Organometallic Compounds for Nonlinear Optics—The Search for En-light-enment!

Nicholas J. Long*

The importance of nonlinear optical phenomena has been known for some time, however, since the mid-1980s, there has been an explosion of interest in the search for and development of nonlinear optical materials that possess commercial device applications. To date, the systems have been utilized in information processing, optical switching, optical frequency conversion, and telecommunications, and with the advancing development of optotechnology, burgeoning demands for suitable materials are becoming apparent. Of the many systems studied for example inorganic crystals and semiconductors, organic crystalline monomers, and long-chain polymers with delocalized π electrons, no one species has proved to be all-encompassing, with advantages for one application being negated by disadvantages for another. This is likely to remain the case for the foreseeable future with the criteria of the application governing the type of material used. However, chemists are gradually elucidating what actually governs second- and third-order nonlinear activity and thereby, tailoring species to show greater effects. In recent years, organometallic compounds, through their unique characteristics such as diversity of metals, oxidation states, ligands, and geometries, have found success and brought a new dimension to the area. This review attempts, with critical appraisal, to bring the discussion of organometallic nonlinear optical systems up to date, as well as giving a brief but general introduction to the field of nonlinear optics.

Keywords: NLO materials · polyacetylenes · sandwich complexes

1. Introduction

The interaction of the electromagnetic field of light (normally high intensity laser light) with a nonlinear optical (NLO) material can result in the generation of new electromagnetic fields. As light passes through a species, its electric field interacts with inherent charges in the material causing the original beam to be altered in phase, frequency, amplitude or polarization. The study of such interactions is the field of *"nonlinear optics"*, and describes deviations from linear behavior as defined by the laws of classical optics.[1]

Such media are now creating intense interest not only due to their NLO properties, but also due to attempts to control other characteristics such as solubility, processability, optical clarity, absorption, and thermal stability, as these will obviously determine technological utility. Initial developments have already given rise to NLO devices, such as frequency doubling crystals useful in laser experimentation. However, there remain enormous possibilities in the field of telecommunications, computer and optical signal processing devices[2, 3] through a) optical phase conjugation and image processing, b) optical switching (i.e. transmission of light depending on the refractive index of the material), c) optical data processing (for computers, where incredibly rapid movements are needed), and d) new frequency generation.

1.1. Inorganic and Organic Materials

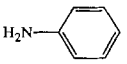
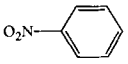
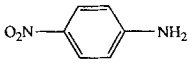
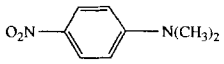
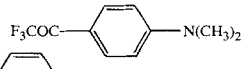
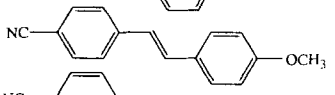
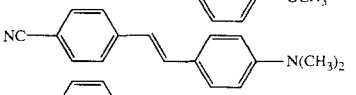
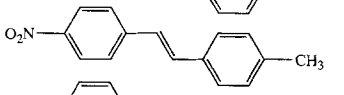
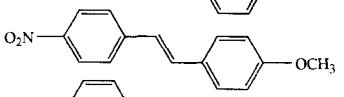
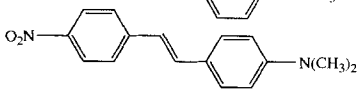
Investigations were initially focused on purely inorganic and organic systems, and the first solids to demonstrate second-order NLO properties were inorganic crystals (e.g. quartz, $LiNbO_3$, and KH_2PO_4),[4] where a photoinduced change in refractive index and later, a photorefractive effect were observed. Inorganic semiconductors followed, such as gallium arsenide (GaAs) and indium antimonide (InSb), which displayed large optical nonlinearities. Multilayer semiconductor materials, which were synthesized by using new crystal growth techniques,[5] exhibited special optical properties not apparent in the bulk material.[6] Both types of NLO materials are used in commercial applications (modulators, optical switches etc.)[7, 8] but they also have drawbacks: the crystals face a "trade-off" problem between response time and magnitude of optical nonlinearity, and the semiconductors are costly and difficult to produce; furthermore, they absorb strongly in the visible region and are of poor optical quality, thereby discounting many possible applications.

[*] Dr. N. J. Long[+]
University Chemical Laboratories,
Lensfield Road, GB-Cambridge CB2 1EW (UK)
[+] New address: Department of Chemistry
Imperial College of Science, Technology and Medicine
South Kensington, GB-London SW7 2AY (UK)

 © VCH Verlagsgesellschaft mbH, D-69451 Weinheim, 1995 0570-0834/95/0101-0021 $ 10.00+.25/0

Several years later, organic systems were investigated as an alternative to inorganic species because of their low cost, fast and large nonlinear response over a broad frequency range, inherent synthetic flexibility, high optical damage thresholds, and intrinsic tailorability.[9-12] It was proposed[13] that the presence of electron-donating and electron-accepting groups on benzene and stilbene systems would result in strong second harmonic generation (SHG). Table 1 gives a list of highly polar

Table 1. The effect of organic end groups on first molecular hyperpolarizabilities (β).

Compound	β ($\times 10^{-30}$ esu)
	1.1
	2.2
	9.2
	12.0
	10.0
	19.0
	36.0
	15.0
	28.0
	73.0

aromatic compounds of benzene and stilbene.[14,15] For example, 2-methyl-4-nitroaniline (MNA, see Fig. 1) produced large values of $\chi^{(2)}$ due to the presence of the methyl substituent on the aromatic ring, inducing non-centrosymmetric crystal packing.[16] This was followed by *trans*-4-dimethylamino-*N*-methyl stilbazolium methyl sulfate which showed a $\chi^{(2)}$ value three hundred times greater than that of MNA.[17] Further investigations have been carried out in an attempt to produce thin film systems, since the crystalline state imposes limitations on the applications. The two main methods for producing such films are polymer poling[18] and Langmuir–Blodgett film formation.[19]

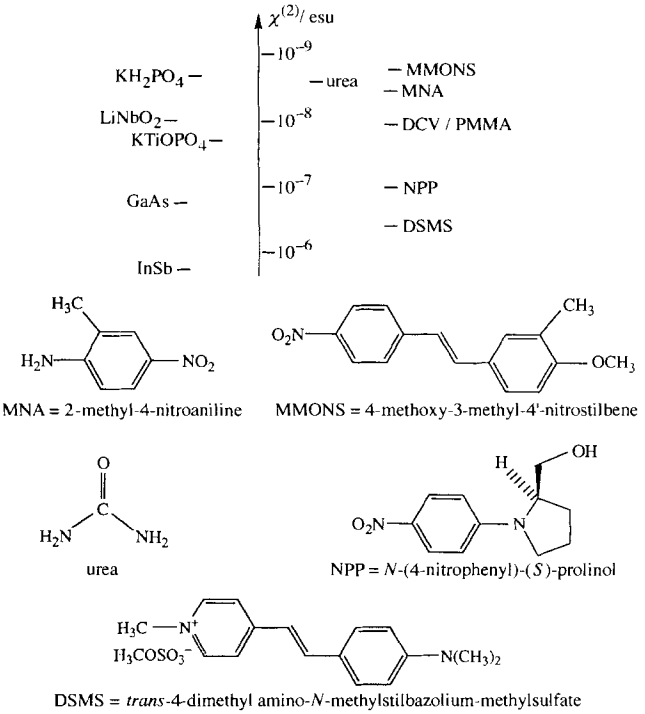
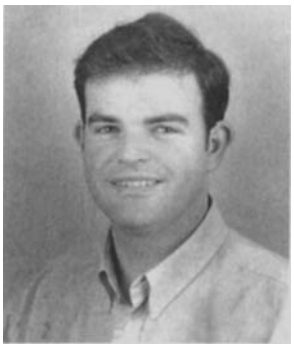


Fig. 1. Top: $\chi^{(2)}$ values for some industrially important inorganic and organic NLO systems. Bottom: Chemical formulas of the systems. For the definition of $\chi^{(2)}$ see Equation (d) (Section 2).

Conjugated organic polymer systems have been of interest in third-order nonlinearity studies; polydiacetylene is the most important.[20] The delocalized π-electron backbone is responsible for the NLO activity, and through a wide range of substitutional side groups, there is structural control and material processability. Poly(2,4-hexadiyne-1,6-diyl-*p*-toluenesulfonate) was synthesized in the solid state by irradiation of crystals of the



Nick Long, born in 1965, in Bristol, studied chemistry at the University of Durham from 1983–1986, and then obtained his Ph.D. from the University of Exeter in 1989 under the supervision of Eddie Abel and Tony Osborne. After staying in Exeter to take up a two-year appointment as "Demonstrator in Inorganic Chemistry", he then moved to the University of Cambridge to become the "Adrian Research Fellow" with Darwin College. In 1993, he was appointed as "Temporary Lecturer in Inorganic Chemistry" at the University of Cambridge. In January 1995 he took up his current position as "Lecturer in Inorganic Chemistry" at Imperial College, London. His interests include transition metal- and/or chalcogen-bridged metallocenophanes, the coordination chemistry of multidentate chalcogeno ligands and novel metallocenyl-acetylide metal complexes. Through close collaboration with Jack Lewis and Paul Raithby, he has become excited by organometallic nonlinear optics, the subject of this review.

monomer with UV, X-, or γ-rays. Formation of many other polydiacetylenes can be completed by this method, and soluble species, such as poly(*N*-*tert*-butoxycarbonyl-*N*-methyl urethane) have improved optical third-order nonlinearity.[21] Other conjugated polymers investigated include polythiophenes, polybenzothiophenes, polyphenylenes, and polyanilines.[2, 22] However, organic systems can suffer from problems, such as volatility, low thermal stability, and mechanical weakness.

Several inorganic and organic materials have found success in NLO (Fig. 1); more information is available in review articles concerned with inorganic,[23, 24] organic,[3, 25–30] polymeric,[31] and general[32] NLO systems. However, recent interest has been engendered by studying organometallic and coordination compounds. There has been scant in-depth discussion of the rapidly expanding area of organometallic NLO materials, with the notable exception of articles by Nalwa[33] and Marder.[34] Therefore, this review attempts to bring the field up to date and discuss the salient points arising from the exciting studies in this area.

1.2. Why Organometallic Compounds?

As data and understanding of inorganic and organic NLO materials have accumulated, corresponding information regarding the behavior of organometallic compounds has not developed. Nevertheless, in the last six years, investigations of organometallic systems have been greatly intensified. Incorporation of metals into NLO systems gives a new dimension of study and introduces many new variables. The metals can have a large diversity of oxidation states and ligand environments, and due to the polarizable d electrons, a number of interesting effects and greater nonlinear activity are likely to be observed. Reasons for this have been postulated:[34–36]

a) Organometallic systems can possess metal → ligand or ligand → metal charge transfer bands in the visible region of the spectrum. These optical absorption bands are usually associated with large second-order activity (although, they can also lead to "transparency" problems—see later).

b) The compounds have great possibilities for redox changes, a property largely associated with the metal center, which can be electron-poor or electron-rich depending on the oxidation state and ligand environment. Facile redox ability can be envisaged as leading to large hyperpolarizability, with the metal center being an extremely strong donor or acceptor in comparison to conventional organic systems.

c) Chromophores, such as phthalocyanines, containing metal ions are amongst the most intensely colored materials known. The strength of the optical absorption band (related to its transition dipole moment) is also associated with large optical nonlinearities.[37]

d) Many organometallic compounds have low-energy excited states with excited-state dipole moments significantly different from their respective ground-state dipole moments (Fig. 2). Most of these excited states involve transfer of electron density between the central metal and one or more of the associated ligands and have large oscillator strength. This charge transfer will provide a substantial contribution to β (defined in Equation (c); Section 2).

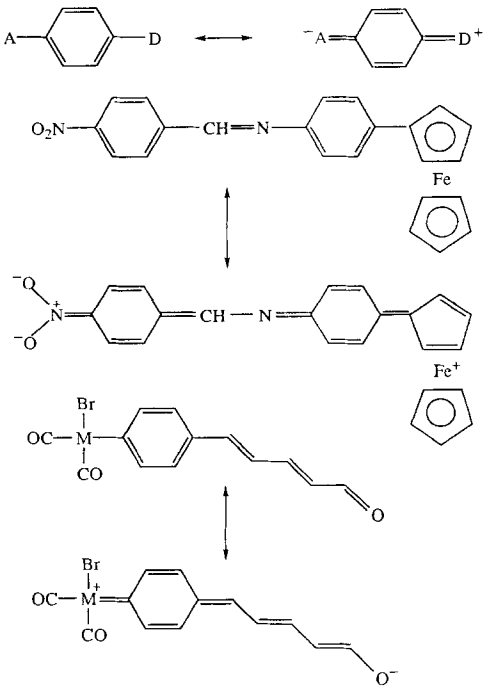


Fig. 2. Ground state and lowest energy excited state structures for some conjugated aromatic systems.

e) Organometallics compounds also have important advantages in the range and mix of non-aromatic ligands that can be attached to the metals. These ligands can shift the occupied and unoccupied metal d orbitals that interact with the π-electron orbitals of the conjugated ligand system. This provides a mechanism for fine-tuning and optimizing β or the crystallographic factors that control the bulk susceptibility.

f) Additionally, the metal centers in these molecules can constitute chiral species[38] so that if resolved, they must form materials that crystallize in non-centrosymmetric space groups, essential for non-zero β values.

g) Incorporation of transition metal ions can also be expected in some cases to increase the solubility of a material in common organic solvents, thereby enhancing its processability.

The only foreseeable problem is the low energy d-d transitions present in nearly all organometallic compounds, normally observed in the visible light region. This gives rise to what is termed a "nonlinearity/transparency trade-off". If a material is to be used in a frequency-doubling or -tripling capacity, then obviously, an aborption of the harmonic light that is produced will limit the usefulness of these materials. Depending upon the location of these bands, the "transparency window" can be large or small, but clearly, the larger a material's transparency range the greater the number of potential applications.

Overall, it is clear that there is plenty of scope for investigation of organometallic NLO compounds and a justified amount of great expectation.

2. The Theory of Nonlinear Optics

The interaction of an electromagnetic field with matter induces a polarization in that matter. In linear optics there is an

instantaneous displacement (polarization) of the electron density of an atom by the electric field E of the light wave. The displacement of the electron density away from the nucleus results in a charge separation (an induced dipole), with moment, μ. With small fields, the strength of the applied field is proportional to the displacement of charge from the equilibrium position, and leads to the relation (a), in which α is the linear polar-

$$\text{Polarization} = \mu = \alpha E \quad \text{(a)}$$

izability of the molecule or atom. If the field oscillates with a frequency, then the induced polarization will have the same frequency and phase, if the response is instantaneous.

Most applications of experiments with NLO are carried out on bulk or macroscopic materials and, in this case, the linear polarization is shown in Equation (b), where χ is the linear

$$P = \chi E \quad \text{(b)}$$

susceptibility of a collection of molecules (on which the parameters of the dielectric constant and refractive index have a bearing).

When a molecule is subjected to laser light (i.e. a very high intensity electric field), the molecule's polarizability can change and be driven beyond the linear regime. Therefore, the now nonlinear molecular polarization P_M (which is a function of the applied field and leads to nonlinear effects) can be expressed by Equation (c), where β = first molecular hyperpolarizability

$$P_M = \alpha E + \beta E^2 + \gamma E^3 + \ldots. \quad \text{(c)}$$

(second order effect) and γ = second molecular hyperpolarizability (third order effect). With increasing field strength, nonlinear effects become more important due to the higher powers of the field E [Eq. (c)]. Since α is much greater than β and γ NLO was not commonly observed before the introduction of the laser and its associated large electric fields.

The polarization of a material is again given by an analogous expression [Eq. (d)], where P_0 is the static dipole of the sample.

$$P = P_0 + \chi^{(1)}E + \chi^{(2)}E^2 + \chi^{(3)}E^3 + \ldots. \quad \text{(d)}$$

$\chi^{(n)}$ is the nth order NLO suspectibility and is analogous to the molecular coefficients in Equation (c) (except that with the χ terms, local field effects, which are consequences of the surrounding medium, are taken into account).

An important point to note is that for β (or $\chi^{(2)}$) to be non-zero, the molecules (or material) need to be non-centrosymmetric. This can be explained by the fact that if a field $+E$ is applied to a molecule, then from Equation (c), the first nonlinear term will induce a polarization of $+\beta E^2$. If a field $-E$ is applied, the predicted polarization would still be $+\beta E^2$, but this should be $-\beta E^2$ if the molecules are centrosymmetric. This contradiction can only be rationalized if $\beta = 0$ in centrosymmetric media. Conversely, γ can be shown to be the first non-zero nonlinear term in centrosymmetric and, indeed, all media, as $+E$ gives $+\gamma E^3$ whilst $-E$ produces $-\gamma E^3$.

Although γ has the properties of a scalar quantity,[39] β cannot also be assumed to be a scalar quantity and in fact, β behaves as a vector.[40] This is important in experiments where the applied field points along a molecular axis and therefore, the hyperpolarizability in that direction will be the dominant component (i.e. the EFISH experiment, see Section 3).

The principle of second harmonic generation (SHG) is that if an intense light beam passes through a second-order NLO species, then light at twice the input frequency will be produced. This can be shown mathematically be expressing the electric field of a plane light wave according to Equation (e), and then introducing this into Equation (d) to give the Equation (f) for the polarization since $\cos^2(\omega t)$ is also $1/2 + 1/2\cos(2\omega t)$ then Equation (f) becomes Equation (g).

$$E = E_0\cos(\omega t) \quad \text{(e)}$$

$$P = P_0 + \chi^{(1)}E_0\cos(\omega t) + \chi^{(2)}E_0^2\cos^2(\omega t) + \chi^{(3)}\cos^3(\omega t)\ldots. \quad \text{(f)}$$

$$P = (P_0 + 1/2\chi^{(2)}E_0^2) + \chi^{(1)}E_0\cos(\omega t) + 1/2\chi^{(2)}E_0^2\cos(2\omega t) + \ldots.. \quad \text{(g)}$$

So, now the polarization consists of a new *"frequency doubled"* component, 2ω. This is called a "three-wave mixing" process, since two photons with frequency ω have combined to generate a single photon with frequency 2ω. This analysis can be extended to third and higher order terms, thus, third-order processes involve "four-wave mixing".

Generally, second-order NLO effects involve the interaction of two distinct waves of electric fields E_1 and E_2 with the electrons of the NLO material. Therefore, with two beams of different frequencies, the second-order term of Equation (g) becomes the left hand side of Equation (h). The right-hand side can be deduced from further mathematics or trigonometry.

$$\chi^{(2)}E_1\cos(\omega_1 t)E_2\cos(\omega_2 t) = 1/2\chi^{(2)}E_1E_2\cos[(\omega_1 + \omega_2)t] + 1/2\chi^{(2)}E_1E_2\cos[(\omega_1 - \omega_2)t] \quad \text{(h)}$$

This indicates that when two beams of light of frequencies ω_1 and ω_2 interact with an NLO material, polarization occurs at sum $(\omega_1 + \omega_2)$ and difference $(\omega_1 - \omega_2)$ frequencies. SHG is the case where the two frequencies are equal. Terms with frequencies that are the sum or difference of two input frequencies or twice the frequency of the input radiation are generated by second-order nonlinear susceptibility.

Third-order optical nonlinearities result from the introduction of a quartic term. By returning to Equation (g) and considering the polarization of a *molecule* [Eq. (c)] (and assuming that the even order terms are zero i.e. the molecule is centrosymmetric), this gives Equation (i) and with trigonometry $(\gamma/6)E_0^3\cos^3(\omega t) = (\gamma/6)E_0^3[3/4\cos(\omega t) + 1/4\cos(3\omega t)]$ this leads to Equation (j).

$$\mu = \mu_0 + \alpha E_0\cos(\omega t) + (\gamma/6)E_0^3\cos^3(\omega t) + \ldots \quad \text{(i)}$$

$$\mu = \mu_0 + \alpha E_0\cos(\omega t) + (\gamma/8)E_0^3\cos(\omega t) + (\gamma/24)E_0^3\cos(3\omega t) + \ldots \quad \text{(j)}$$

Therefore, the interaction of an intense beam of light with a third-order NLO material creates a polarization component at

the third harmonic. Similarly, for a bulk material, the third harmonic generation is represented by $\chi^{(3)}$, the material susceptibility. It should be noted that whilst negative and positive β values give rise to the same potential and physical effects, a positive γ leads to a different electron potential than a negative one would. The application of an intense voltage to a third-order NLO material will induce a refractive index change in that material, and the sign of γ determines whether the third-order contribution to the refractive index is positive or negative. For more in-depth discussion, please consult references[2b, 26, 32, 34].

3. Experiments for Nonlinear Optics

A crucial aspect in the progression of NLO studies has been the development of experimental techniques available for investigating and measuring a material's NLO activity. Over the years, several methods have been widely employed and are briefly discussed here:

1. *Kurtz Powder Technique*:[41-44] This technique was the first used in the study of organometallic materials. A laser is directed onto a powdered sample and, assuming that the material is SHG active, the emitted light at the second harmonic frequency is collected and compared to that of a reference sample, such as quartz or urea, to obtain a measure of the SHG efficiency. It is an excellent method for testing large numbers of powdered materials, but is recognized as semi-quantitative, and minor variations in relative efficiencies are probably not significant.[45] Results are dependent on the particle size, and recrystallization from a range of solvents can lead to different SHG efficiencies. The efficiency measured depends upon both the molecular (β) and bulk (or macroscopic) ($\chi^{(2)}$) polarizabilities, and powder testing is not a reliable probe of structure–property relationships.[34]

2. *Electric Field Induced Second Harmonic Generation (EFISH)*: The EFISH experiment[46-49] allows for a structure–property understanding and gives a projection of the β vector along the molecule dipole (μ) direction. A strong direct current electric field is applied to the gas, liquid, or solution of interest in order to remove the orientational averaging caused by statistical alignment of molecular dipoles in the medium.[40] The components of the experiment are shown in Figure 3.[46, 50, 51] Most materials are dissolved in an appropriate solvent, and methods have been developed[46] to distinguish between the contributions from the solvent and solute. Interpretation of EFISH results can also be difficult if the molecule lacks a clear charge transfer axis along the dipole direction.[35, 52] The experiment generates a harmonic field from three waves, so the induced nonlinear polarization arises from a third-order process and, as such, the second molecular hyperpolarizability (γ) is a component.[26, 35, 45] However, γ is normally determined from third harmonic generation (THG) experiments and then subtracted from the EFISH response to determine β. Yet, in compounds exhibiting significant charge transfer, $\mu\beta$ is much greater than γ and the third-order contribution is often ignored.

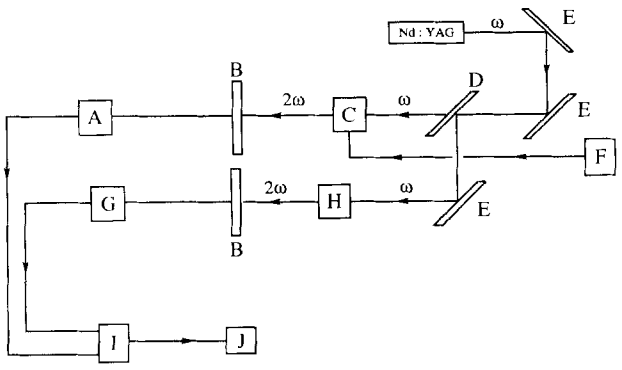


Fig. 3. Schematic diagram of the setup for an EFISH experiment. A = reference photomultiplier tube, B = filter, C = cell, D = beam splitter, E = mirror, F = high-voltage pulse generator, G = signal photomultiplier tube and monochromator, H = reference crystal, I = box car integrator, J = recorder.

3. *Hyper-Rayleigh Scattering (HRS)*: This newly developed technique[53, 54] is used for the determination of the first molecular hyperpolarizability β (second-order NLO polarizability) of NLO molecules. Values of β can be obtained without having to independently determine the dipole moment μ and the second hyperpolarizability γ, and thus this method has an advantage over the EFISH technique.

Intense infrared light pulses of a Nd-doped YAG laser are focused in a thermostated cylindrical cell. A small fraction of the incident light beam is directed on a fast photodiode for monitoring pulse shape and stability, and incident light intensity. The scattered light is collected by an efficient condenser system and gated integrators are used to retrieve actual values for the intensities of the incident and second-order scattered light pulses. HRS is the only method available for determining the β values of salts in solution (as EFISH cannot be applied to conducting solutions), and remarkable results for some mixed-valency metal complexes have been recently reported[55] (see Section 4.3).

4. *Third Harmonic Generation* (THG):[45, 56] This describes the process in which a fundamental laser field of frequency (ω) generates, through nonlinear polarization in the material, a coherent optical field at 3ω. It allows for the determination of the purely third-order electronic nonlinearity of molecules, without complications due to orientational or other motional contributions,[22, 57, 58] and is acknowledged as a rapid, reliable method for determination of γ for molecules in liquids and solutions. However, it should be borne in mind that many third-order NLO materials absorb in the visible and near IR regions, thus hampering assessment of their electronic hyperpolarizabilities.[45]

5. *Degenerate Four-Wave Mixing (DFWM)*[14, 15, 59, 60] is the other most commonly used technique to study third-order NLO materials. Here, three laser beams of the same frequency interact in a material. The nonlinear interaction produces a fourth beam and its intensity is proportional to the product of the input intensities and the square of the bulk susceptibility, $\chi^{(3)}$. If required, the second molecular hyperpolarizability, γ, can be obtained from the relation where N is the density of molecules and L is the local field factor. The capability to obtain measurements with ultra-short pulses is crucial in separating the various contributions to the DFWM signals. Vibrational and orientational mechanisms can contribute to the observed nonlinearity and this creates a problem when developing structure–property relationships of the purely electronic part of γ.[45]

Methods such as optical Kerr gate,[61] linear electro-optic (LEO) modulation,[62] and Maker fringe and wedge techniques[63-65] have also been used for the measurement of opti-

cal nonlinearity. Commonly, a combination of techniques is necessary for complete investigation of a material's NLO behavior, though care should be taken in automatic comparison of NLO values resulting from different techniques due to the various conditions and mechanisms used. For complete and detailed discussion of all the methods, consultation of the listed references is encouraged.

4. Materials for Second-Order Nonlinear Optics

Design of second-order NLO materials is now quite advanced, as over the years, criteria have been discovered that are essential for exhibition of large hyperpolarizabilities. Whilst there is discussion on the importance and variation of these points, the basic tenets are universally accepted and are as follows:

1. polarizable material (the electrons need to be greatly perturbed from their equilibrium positions)
2. asymmetric charge distribution (incorporation of donor–acceptor molecules)
3. a pathway of π-conjugated electrons
4. acentric crystal packing (introduction of a chiral center should guarantee this).

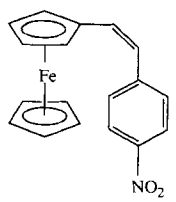
A two-step model concerned with electronic properties[14, 15] has been important in predicting the usefulness of new materials. This suggests that molecules must possess a) excited states close in energy to the ground state, b) large oscillator strengths for electronic transitions from ground to excited states, and c) a large difference between ground and excited state dipole moments.[15a, 66, 67] Such requirements are thus, best met by dipolar, highly polarizable, donor-π-acceptor systems, showing charge transfer between electron-donating and electron-withdrawing groups. Much effort[22, 49, 68] has been exerted into finding the optimum combinations of acceptor and donor groups, especially with organic compounds that are easily substituted. The general conclusion is that the first molecular hyperpolarizability (β) increases with increasing conjugation length. However, using the two-step model, it was shown that there is an optimal combination of donor and acceptor species that maximizes β[69] and, indeed, the strongest acceptor does not necessarily lead to the largest nonlinearity.[68a] Theoretical work[69–71] has also predicted this β maximum and then a decrease, and suggests that for any donor–acceptor pair, there is a certain bridge of a given length that maximizes β. Over the years, research has mainly concentrated on development of stronger acceptors and donors, and the structure of the molecular bridge connecting the two end groups has been rather neglected. Latest results suggest that this is unwise, and an optimal degree of bond length alternation in a polyene-type bridge[52, 72] and the importance of the donor and acceptor orbitals to those of the bridge[73] have been discovered.

A significant enhancement of polarizability has been demonstrated on extending the conjugation length between the donor and acceptor. This generally results from decreasing the energy gap and increasing the transition dipole moment between the relevant states. The effectiveness of various conjugated backbones has been well-studied.[74–76] From reports on some polyene, stilbene, and phenylhexatriene derivatives, it has become clear that phenyl ring-based conjugated linkers should be avoided when designing materials with high β values for NLO.[52]

However, even if a molecule has a large β value, it might fail to exhibit SHG activity. Crystallization in a non-centrosymmetric fashion is also required, and since about 70% of all achiral molecules crystallize in centrosymmetric space groups it is a major problem. To counter this, many strategies for forming acentric crystals capable of showing SHG activity have been employed: 1) incorporation of chiral molecules,[77, 78] 2) hydrogen bonding,[77, 79–81] 3) ionic chromophores,[82, 83] 4) steric hindrance,[16] 5) inclusion phenomena,[84–87] 6) Langmuir–Blodgett techniques,[19] 7) cocrystallization,[88] and 8) dipole–dipole interaction reduction,[89] and these methods have met with varying degrees of success in ensuring a dipolar alignment favorable for SHG.

4.1. Metallocenes

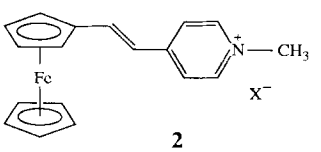
The report in 1987 by Green et al.[90] that a ferrocene derivative had an excellent SHG efficiency, first demonstrated that organometallic compounds could have great potential in the field of second-order NLO. This has led to metallocenes being the most thoroughly studied compounds to date with regard to this field of study. The *cis*-ferrocene derivative **1** was analyzed, since it crystallizes in a non-centrosymmetric space group (in contrast the *trans* isomer shows no SHG signal, because of its center of symmetry). Solvatochromatic behavior was observed in the UV/Vis spectra of **1**; two absorptions (at 340 and 492 nm) are observed in *N,N'*-dimethyl formamide, as opposed to the three (at 320, 406, and 462 nm) in heptane. It should be noted that marked differences in the UV/Vis spectrum of a compound on varying the solvent (i.e. solvatochromatic behavior) is a good initial indicator of potential NLO activity. Kurtz powder measurements at 1.064 μm for the compound gave an SHG efficiency 62 times that of the urea reference sample.[90] It is thought that the facile redox ability exhibited by the metallocene derivatives leads to large values of β by charge transfer through the π-electron conjugation system. The donating strengths of the metallocenes are attributed to the low binding energy of metal electrons, and their effectiveness is responsive to structural modifications which also influence their redox potentials. However, on the basis of binding energies and redox potentials, it was expected that the molecular hyperpolarizabilities would be larger than the observed values.[35] The authors state that poor coupling between the metal center and the substituents due to the π geometry lowers the donating ability of the metal center. Improved coupling and a direct bonding of the metal to the organic acceptor system was effected in a series of alkenylidyne diiron complexes.[91] Compounds such as $[(\eta^5\text{-}C_5H_5)_2Fe_2(CO)_2(\mu\text{-}CO)(\mu\text{-}(E)\text{-}C\text{-}CH{=}CH\text{-}C_6H_4\text{-}p\text{-}N(CH_3)_2)]\,CF_3SO_3$ exhibit large molecular second-order hyperpolarizabilities but lower than expected SHG efficiencies (Kurtz), due to unfavorable alignment of the chromophores in the crystal lattice.



1

This led to reports on similar ferrocenyl compounds by Bandy et al.[92] and Marder et al.[93,94] Species of the formula $[(\eta^5\text{-}C_5H_5)Fe(\eta^5\text{-}C_5H_3(CH_3)CH{=}CHR)]$, where R = *p*-$NO_2C_6H_4$, *p*-$CNC_6H_4$, *p*-$CHOC_6H_4$, -(*E*)-CH=CH-*p*-$NO_2C_6H_4$ and $-\overline{C{=}CH{-}CH{=}C(NO_2)O}$ exhibited powder SHG efficiencies ranging from 1.2 to 17.0 times that of urea.[92] Substitution of a methyl group onto the cyclopentadienyl (Cp) ring containing the acceptor moiety resulted in asymmetry and optical activity and was instrumental in a larger SHG value being observed than for the analogous $(\eta^5\text{-}C_5H_4CH{=}CHR)$ compounds.

The largest SHG value to date for an organometallic compound came from a series of salts of the form **2**, where the counterion is I^-, Br^-, Cl^-, $CF_3SO_3^-$, BF_4^-, PF_6^-, *p*-$CH_3C_6H_4SO_3^-$, NO_3^-, $B(C_6H_5)_4^-$.[93,94] The value of the powder SHG signals depends on the counterion (as was found for organic salts[82,83]), with I^- giving a value 220 times that of the urea standard (Table 2). It is interesting to note that substitution of ruthenium for iron leads to smaller powder efficiencies. This is rationalized as being due to the less electron-rich and, therefore, less effective donor ruthenium, and that the ruthenium compounds examined tend to crystallize in centrosymmetric orientations.[94]



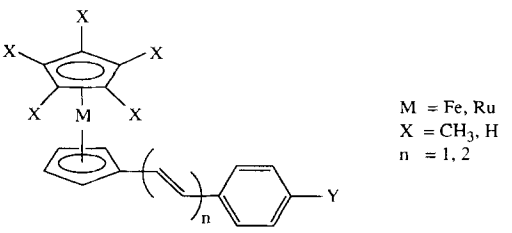
2

Table 2. The powder SHG efficiencies of a series of salts of type **2** [94].

X	SHG efficiency [a]
I	220
Br	165
Cl	0
BF_4	50
NO_3	120
$B(C_6H_5)_4$	13
PF_6	0.05
CF_3SO_3	0
p-$CH_3C_6H_4SO_3$	13

[a] Intensity measured with 1907 nm fundamental radiation. SHG efficiency measured relative to urea.

A systematic study of the molecular hyperpolarizabilities of some ferrocene and ruthenocene derivatives has been recently carried out.[35,95,96] The compounds were of the form $[(\eta^5\text{-}C_5X_5)M(\eta^5\text{-}C_5H_4{-}(CH{=}CH)_n{-}C_6H_4Y)]$ and are depicted in Figure 4. Variations incorporating different metal centers M and acceptor groups Y, (NO_2, $COCH_3$, CN, CHO), *cis* and *trans* isomers, exten-sion of conjugation and electron-donating substituents on the Cp rings were studied to obtain a detailed understanding of the structural factors that affect molecular hyperpolarizabilities. It was shown that 1) substitution of pentamethyl groups (X = Me) leads to an increase in dipole moment and nonlinearity, 2) the β value of ferrocenes is greater than that for ruthenocenes and 3) the effect of the conjugation length is great, with a compound featuring two double bonds having a much higher β value ($\beta = 66.0 \times 10^{-30}$ esu) than the analogous species with one alkenene bond ($\beta = 31.0 \times 10^{-30}$ esu).



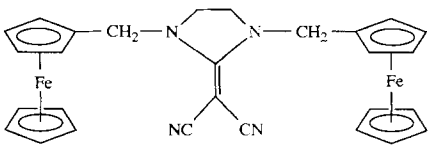
M = Fe, Ru
X = CH_3, H
n = 1, 2

Fig. 4. Metallocenes with conjugated alkenic substituents.

From ferrocenecarbaldehyde, a series of ferrocenyl Schiff bases of the form $[(\eta^5\text{-}C_5H_5)Fe(\eta^5\text{-}C_5H_4CH{=}NR)]$ (e.g. R = $NCH(C_6H_4\text{-}p\text{-}NO_2)$ and C_6H_4-*p*-CN) were prepared.[97,98] Although, considerable solvatochromism was observed, crystallization was in a centrosymmetric space group. The ferrocenyl imine, $[(\eta^5\text{-}C_5H_5)Fe(\eta^5\text{-}C_5H_4)CH{=}N(C_6H_4\text{-}p\text{-}NO_2)]$, did show some nonlinear activity, however, it was not large, being a third times that of the urea reference. The compound has a non-centrosymmetric crystal arrangement but, the $P2_12_12_1$ space group ensures a cancelling of the dipolar nature of the molecule.

Marder et al.[99-101] have utilized the ferrocenyl group as an electron donor in some "push-pull" organoboranes, [(*E*)-D-CH=CH-$B(Mes)_2$] and [D-C≡C-$B(Mes)_2$] (D = $P(C_6H_5)_2$, $(\eta^5\text{-}C_5H_5)Fe(\eta^5\text{-}C_5H_4)$, and Mes = mesityl). Three-coordinate boron has an empty p orbital making it a powerful π acceptor, and some π-conjugated organoboranes were known to exhibit large β coefficients. As a result of the low-lying charge transfer from electron-rich iron to electron-deficient boron, a β value of 24×10^{-30} esu was observed for $[(E)\text{-}(\eta^5\text{-}C_5H_5)Fe\{\eta^5\text{-}C_5H_4{-}CH{=}CH\text{-}B(Mes)_2\}]$.

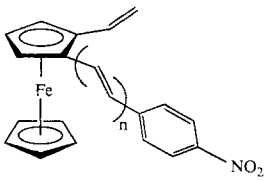
Several other donor (ferrocene)-acceptor compounds have been investigated recently. 1) 4-Ferrocenyl-2′-methyl-4′-nitroazobenzene[102] is a polarizable dipolar molecule; however, the crystal packing involves a centrosymmetric head-to-tail pairing of molecules resulting in no NLO behavior. 2) A SHG signal for the 1,3-diazolidine **3** was detected by powder techniques but it had a low efficiency.[103] 3) Similar results have been reported for donor-acceptor substituted acetylenes.[104,105] For example, the SHG efficiency of ferrocenyl(phenyl)acetylene is 3.7 times that of urea at 1907 nm. However, it is about 15 times lower than the previously described analogous ferrocenyl *ethylenic* compound (**1**).[90]



3

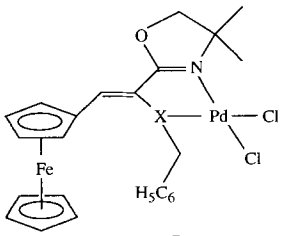
In order to ensure crystallization of a material in a non-centrosymmetric space group, Green et al.[106] have incorporated the chiral ligand (+)-DIOP (DIOP = 2,3-*O*-isopropylidene-2,3-dihydroxy-1,4-bis(diphenylphosphino)butane) into a sequence of compounds of general formula $[(\eta^5\text{-}C_5H_5)Fe\{(+)\text{-}$

diop}(*p*-NCC_6H_4R')]PF_6 (R' = donor or acceptor group). When R = NO_2, the ferrocenyl fragment acts as a π donor through d-π* (NC) orbitals towards the NO_2 acceptor group, and leads to an SHG efficiency 38 times that of urea. After considering that the absence of inversion symmetry is a property of chiral, enantiomerically pure compounds, Togni and Rihs[107] have synthesized some enantiomerically pure ferrocene derivatives **4** for NLO. By also possessing conjugated donor–acceptor systems, large SHG values were expected, unfortunately, the species show a pairwise antiparallel arrangement of the molecules in the solid state, leading to poor SHG efficiencies.



4

Some bimetallic complexes featuring iron (ferrocenyl) and palladium have been formed,[108] where the ferrocenyl group is attached to an electron-attracting oxazoline group through an ethylene linkage (**5**). EFISH measurements of the ferrocenyl ligands gave reasonable values of β, yet the NLO properties were enhanced upon coordination with Pd^{II} by a factor of 2. It is thought that the metal ion withdraws electrons from the lone pairs of the heteroatoms. Other studies on metallocenes such as polymeric materials with pendant ferrocenyl-acceptor moieties[109] and novel arene-Cp-ruthenium complexes(arene = thiophene, nitrobenzene, *N*,*N*-dimethyl-4-nitroaniline, 2-methyl-4-nitroaniline)[110] have recently been communicated. Whilst the ferrocenyl methylmethacrylate[111] polymer has been found to display an SHG efficiency four times that of the quartz standard, NLO activity has yet to be demonstrated for the other species.



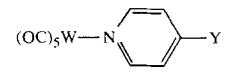
5, X = S, SO

Elegant and thorough theoretical investigations of organometallic structures as second-order NLO chromophores have recently been communicated by Marks, Ratner, and Kanis.[112] Using accurate, chemically orientated, computationally efficient ZINDO-SOS quantum chemical formalism, ferrocenyl molecules such as **2**,[113] (arene)chromium tricarbonyl complexes,[113] and Group VI stilbazole and pyridine pentacarbonyl derivatives[114] have been examined. By comparing computed quadratic hyperpolarizabilities with recent organometallic solution phase EFISH data, the authors were able to demonstrate the reliability of this theoretical approach, rationalize known molecular responses, and suggest chemical modifications in order to optimize hyperpolarizabilities in metal-containing chromophoric species.

One of the conclusions was that organometallic chromophores must possess a highly polarized, strongly coupled ligation sphere around a given metal for effective second-order NLO behavior. More importantly, it was shown that efficient quantum chemical methods can be used to understand hyperpolarizabilities and thus, be utilized in designing new chromophoric units possessing optimal NLO characteristics.

4.2. Metal Carbonyl and Metal Carbonyl Pyridine Complexes

In 1986, a large number of transition metal organometallic complexes of Group VI metal carbonyl arenes, pyridines, and chiral phosphanes were studied by powder techniques for SHG activity.[36] The metal carbonyl arene complexes have the formula $[M(CO)_n(\eta\text{-arene})L_{3-n}]$ (where M = Cr, Mo, W; L = phosphane; $n = 0-3$) but generally crystallize in centrosymmetric space groups, giving vanishing $\chi^{(2)}$ values. This was also the problem with the metal carbonyl pyridine species, the SHG efficiencies ranging between 0.04 and 1.0 (relative to urea). There are several reasons why metal carbonyl arene complexes were expected to show significant NLO response. Intense metal → ligand charge transfer absorptions are observed in the low-energy absorption spectra increasing the dipole moment, and the arenes introduce a number of delocalized electrons and, therefore, conjugation. With this in mind, Cheng et al.[95] examined a series of (η^6-arene) tricarbonylchromium complexes $[Cr(\eta^6\text{-}C_6H_5X)(CO)_3]$ (X = H, OCH_3, $COOCH_3$, NH_2, and $N(CH_3)_2$). However, β values were again small, with little effect on changing the substituents due to poor linking conjugation through the system. Some metal bipyridine complexes $[M(bpy)(CO)_4]$ (M = Mo, Cr, W) and $[M(bpy)Cl_4]$ (M = Pt, Pd) also showed SHG values similar to that of urea. In contrast, a series of pentacarbonyl(pyridine)tungsten σ-complexes **6** gave some interesting EFISH results.[95, 115] These compounds possess a σ linkage as the nitrogen lone pair donates to the empty d-orbital of tungsten. Efficient overlap of the pyridine π orbitals with the d_{xz} and d_{yz} orbitals also allows π donation toward the metal center which acts as a ground state π-acceptor due to the pentacarbonyl ligands. Compared to the (π-arene)tricarbonylchromium species, there was a good degree of nonlinearity shown here (values are comparable to well-known organic systems such as *p*-nitroaniline[15b]) and the β values were sensitive to substitution at the 4-position.

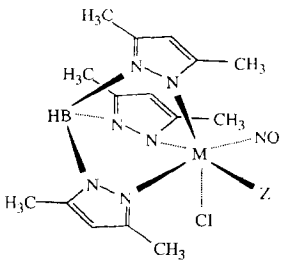


6, Y = H, NH_2, C_6H_5, CHO, $COCH_3$

Metal carbonyl complexes have been utilized in "guest–host" inclusion chemistry. Zero SHG results from the strong tendency of dipoles to dimerize in an antiparallel (centrosymmetric) orientation. If channel dimensions can be controlled and maintained small, relative to guest dimensions, then head-to-tail dipolar orientation becomes electrostatically preferred, leading to SHG active materials. Inclusion hosts such as thiourea, tris-*o*-thymotide and clathrates form polar inclusion complexes with organometallic compounds, and over 60% were found to be SHG active.[116, 117] Depending on the ratio of the host–guest, crystallization of the materials in non-centrosymmetric space groups can be observed. For example, a thiourea: $[(\eta^6\text{-}C_6H_6)Cr(CO)_3]$ inclusion complex (3:1) has an SHG efficiency 2.3 times that of urea, whereas the uncomplexed material is inactive. Inclusion of [(η^4-trimethylenemethane)$Fe(CO)_3$] and [(cyclohexadienyl)$Mn(CO)_3$] has also met with some success.[84]

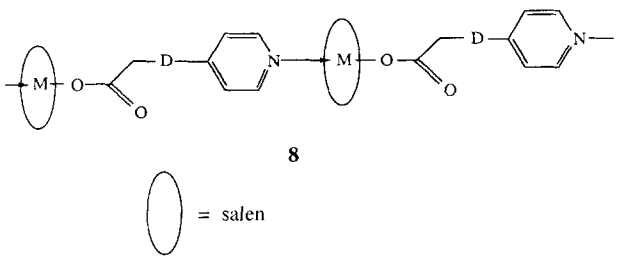
4.3. Octahedral Metal Complexes

In recent years, complexes of the form [M(NO)LXZ] (M = Mo, W; L = tris(3,5-dimethylpyrazolyl)borate; X = I, Cl; Z = O, NH, OPh, NC_4H_4, NHPh, SPh) have been shown to exhibit excellent SHG properties. The redox activities of these species are crucial with the 16e$^-$ [M(NO)LClZ] (Z = O or NH) and the 17e$^-$ [M(NO)LClZ]$^-$ moieties acting as electron-withdrawing and -donating substituents, respectively.[118, 119] With metal centers and ligands that are chiral,[38] it was perhaps surprising that only small SHG efficiencies were observed, until it was discovered that one molecule in the unit cell is orientated so that it opposes the other. Introduction of the bulky and electron-donating ferrocenyl group was more effective and complexes of the type **7** with M = Mo, Z = 4-NHC_6H_4-N=N-C_6H_4-4'-Fc as well as M = W, Mo, Z = 4-NHC_6H_3-(3-Me)-N=N-C_6H_4-4'-Fc (Fc = $(\eta^5$-$C_5H_5)Fe(\eta^5$-$C_5H_4)$), gave respective SHG efficiencies of 59, 53, and 123 times that of urea. Modification of various parts of the complexes indicated that without the [M(NO)LCl]$^-$ and, in particular, the [Fc-$C_6H_4N_2C_6H_4$] fragments, little or no SHG activity would be observed.[38]



7

Thompson et al.[120, 121] have investigated monomeric, dimeric, and oligomeric metal (primarily manganese) complexes **8** of the tetradentate salen ligand (*N*,*N*'-bis(salicylideneaminato)ethylene). The ligand was chosen due to its low optical absorption and propensity for planar

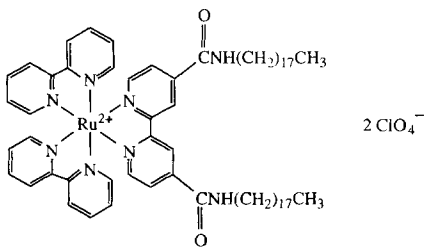


8

= salen

coordination geometries. Additionally, a bifunctional ligand is incorporated in these complexes which is capable of bonding to the metal in both a dative and covalent fashion. Initial results were not encouraging due to structural factors, but introduction of chirality into the organic bridging ligand should solve such problems.

Sakaguchi et al.[122] have demonstrated that metal → ligand charge transfer transitions are important for SHG by forming a ruthenium(II) tris(2,2'-bipyridine) complex **9**. The β value for this compound is around 70×10^{-30} esu which is comparable to the previously tested organic system, 2-methyl-4-nitroaniline.[123] Ruthenium has also been incorporated in complexes of the form $[(\eta^5$-$C_5H_5)Ru(PPh_3)_2L]PF_6$, where L can be various ligands including substituted nitriles.[124] EFISH measurements at 1.064 μm of second-order hyperpolarizabilities revealed a significant effect of type and length of conjugation. For example,



9

the biphenyl system (-C_6H_4-C_6H_4-$OC_{12}H_{25}$) gives a β value of 20×10^{-30} esu, whilst the single phenyl ring system shows one of 3.5×10^{-30} esu.

Recent measurements on mixed-valence metal complexes using the hyper-Rayleigh scattering technique have proved very interesting.[55] It was postulated that mixed-valence compounds characterized by an intervalence charge transfer transition, in which the donor and acceptor centers are both metal atoms, may well provide a large second-order response. Measurements of β of a bimetallic complex ion, $[(CN)_5Ru(\mu$-$CN)Ru(NH_3)_5]^-$ and an organometallic analogue, $[(\eta^5$-$C_5H_5)Ru(PPh_3)_2(\mu$-$CN)Ru(NH_3)_5]^{3+}$, gave values greater than 10^{-27} esu., which are among the largest recorded for solution species. The energy of the charge transfer transition is easily modified, suggesting that there is considerable NLO potential for this type of chromophore.

Independent studies have also investigated unsymmetrical ruthenium[125, 126] and osmium[126] acetylide complexes with donating and accepting groups (Fig. 5). Initial powder SHG

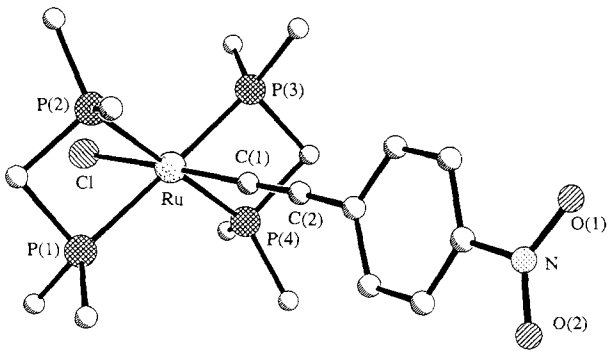


Fig. 5. Crystal structure of the donor-acceptor compound [ClRu(dppm)$_2$-(C≡C-C_6H_4-*p*-NO_2)]. (Hydrogen atoms and phenyl groups on the phosphane ligands are omitted for clarity).

measurements[126] have proved disappointing due to the materials crystallizing in centrosymmetric space groups.

4.4. Square-Planar Metal Complexes

Due to the excellent electron-donating ability of square-planar metal fragments, such as $[M(PEt_3)_2X]$ (M = Ni, Pd, Pt; X = Cl, Br, I), in donor-acceptor aromatic complexes, materials suitable for SHG have been yielded.[127] A list of the powder SHG efficiencies for these compounds featuring a substituted aromatic electron-accepting species is shown in Table 3. The

Table 3. Second harmonic generation efficiencies of complexes of the form *trans*-$[M(PEt_3)_2X(2\text{-}Y\text{-}4\text{-}Z\text{-}C_6H_3)]$.

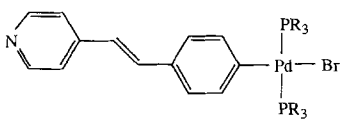
M	X	Y	Z	SHG efficiency β [a]
Pt	Br	H	NO_2	4.2
Pt	I	H	NO_2	5.0–8.0 [b]
Pt	Br	H	CHO	1.5–3.4 [b]
Pt	Br	CH_3	NO_2	2.0–14.0 [b]
Pt	Br	NO_2	H	0.8
Pd	I	H	NO_2	2.3
Pd	Br	CH_3	NO_2	5.0–10.0 [b]
Pd	Br	H	CHO	2.3

[a] Relative to urea. [b] Range due to values obtained from several preparations and probably dependent upon particle size.

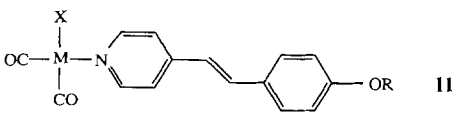
para-orientated nitro-compounds showed the largest SHG signals, in one case up to 14 times that of urea. The values are also influenced by the nature of the metal atom, the halogen, and the substituent on the phenyl ring. EFISH measurements on related palladium and platinum derivatives of the formula $[ML_2XY]$ (where L = PEt_3; X = Br, I; Y = σ-$C_6H_4NO_2$ and σ-C_6H_4CHO) have reinforced these trends.[95] Here, the *para*-substituent is in conjugation with the metal center, and, as is expected, it has a significant effect on the hyperpolarizability, with $\beta(NO)_2 > \beta(CHO)$ due to greater electron acceptance of the former substituent. To a lesser extent, the metal, halide, and phosphane again influence the magnitude of β.

Some linear donor–acceptor substituted platinum bis(acetylides) of the form *trans*-$[Pt(PMe_2Ph)(C{\equiv}CX)(C{\equiv}CY)]$ (X = π donor e.g. MeO, MeS, Me_2N and Y = π acceptor e.g. CN, NO_2)[128, 129] crystallize in a non-centrosymmetric mode and exhibit reasonable SHG efficiencies. It was of interest to study the effect of the metal centers as a linker between the organic-donors and -acceptors. Similar donor–acceptor metal acetylides of the form $[(CO)_5Mn{-}C{\equiv}C{-}C_6H_4{-}C{\equiv}C{-}Pd(PBu_3)_2Cl]$ have been synthesized[130] and, although these species are expected to show interesting second-order NLO behavior, this has yet to be demonstrated.

Stilbazole-based square-planar metal complexes have been of recent interest. Addition of *trans*-4′-bromo-4-stilbazole to $[Pd(PR_3)_4]$ yields the corresponding Pd^{II} complexes **10**.[131] Although the compounds feature conjugated systems with an asymmetric charge distribution, powder SHG values, lower or comparable with that of urea, were obtained due to centrosymmetric crystallization. The situation is more positive when a *cis*-$[MX(CO)_2]$ group (M = Ir^I, Rh^I; X = Cl, Br) is bound to the N atom of the stilbazole-pyridine ring and R is a chiral, long-chain alkyl group (**11**).[132, 133] The β value of the free stilbazole increases on coordination of the *cis*-$[MX(CO)_2]$ species indicating that this metal fragment is a better acceptor than the heteroatom of the pyridine ring. It is advantageous that the compounds are not strongly colored but still possess reasonably large hyperpolarizabilities (species where a charge transfer term is the main component of the β value are normally highly colored), since this gives the material a wider transparency range and hence, more varied potential device applications. The SHG values are small but non-zero, showing that the chiral alkyl group R has little influence on the molecular packing.



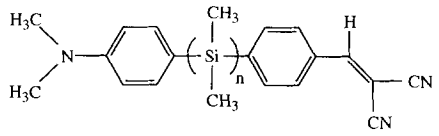
10, R = CH_3, C_2H_5, C_3H_7



11

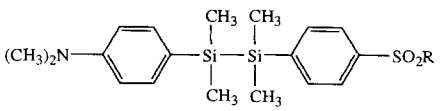
4.5. Silicon Complexes

In 1990, a series of substituted silanes (**12**) were formed, where the electron-donor and electron-acceptor groups were separated by silicon atoms.[134, 135] EFISH studies showed that the hyperpolarizability increases with increasing number of Si atoms due to the σ delocalization along the Si–Si backbone and, in addition, there was increased polarizability of the silicon backbone compared to that of carbon. Another important characteristic of these compounds is their optical transparency. For example, addition of silicon atoms to the chain lowers absorption maxima to 276 nm which is significantly lower than a standard donor–acceptor polyene like *p*-nitroaniline (λ_{max} = 365 nm).



12, n = 1, 2, 6

Polycarbosilanes[136] with main chain arylene and acetylene groups, $[-C{\equiv}C{-}SiPh_2{-}C{\equiv}C{-}Z{-}]_n$, have been prepared with a wide variety of arene groups, Z, for example fluorene-2,7-bipyridine-2,2′, anthracene-9,10, thiophene-2,5, and 5-cyano-2-hydroxybenzene-1,3-diyl. The NLO-active donor–acceptor groups are contained in a segment in the main polymer chain and although detailed results are awaited, promising NLO activity has been observed. Finally, a series of *p*-substituted diphenylsilanes have been formed with dimethylamino (donor) and sulfonyl (acceptor) groups (**13**),[137] and the β values obtained were close to those found for the compounds **12**.[134]

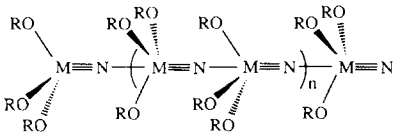


13, R = C_6H_5, C_4F_9

4.6. Metal Nitrido Compounds

Nitrido compounds of the type $[(RO)_3M{\equiv}N]$ have been known for some time.[138, 139] They crystallize in non-centrosymmetric space groups and exist as long chains of alternating short (triple) and long (single) bonds. Hopkins et al.[140] have since formed one-dimensional polymers of the

form $[(RO)_3M{\equiv}N]_n$ (M = Mo, W; R = CMe_3, CMe_2CF_3, CMe_2Et) **14** and studied their powder SHG efficiencies. Surprisingly, only small values were obtained, but they have been shown to be influenced by the nature of the alkoxido ligands and the length of the conjugated $[MN]_n$ backbone.



14

Finally, pentaamine ruthenium complexes, $[(NH_3)_5RuN{\equiv}C\text{-}R\text{-}C{\equiv}NRu(NH_3)_5](PF_6)_5$ (R = C_6H_4, $C_6H_2(CH_3)_2$ are thought to be potential NLO species, but this has not been proved due to decomposition upon irradiation of laser light.[141]

5. Materials for Third-Order Nonlinear Optics

The structure–property relationships that govern third-order NLO polarization are a little vague. Unlike the design of second-order NLO materials, which follow some well-defined guidelines, models for the synthesis of third-order species are much less well-developed. However, polymeric materials with extended π conjugation are known to be important, and an increased effective conjugation and hence, large π delocalization length has been recognized as a way of achieving large third-order nonlinearities.[10, 142, 143] Extended π-electron delocalization creates a large anharmonic component in the nonresonant electron oscillations.[144] In 1973, it was reported that $\chi^{(3)}$ increases with the number of atoms in long-chain molecules.[145] This was followed later by the suggestion that long π-electron conjugated structures are ideal for $\chi^{(3)}$.[146] The discovery of π-electron delocalized conducting polymers in the 1980s created further interest in third-order NLO properties and, to date, much of the research has focused on conjugated polymers such as polyacetylenes, polythiophenes, and various semiconductors.[2a] These organic enyne systems reach a saturation in material nonlinearity, so consideration needs to be given to ways of modifying the electronic and lattice configurations. Organometallic polymers have extended π-electron delocalization plus extra features which could enhance $\chi^{(3)}$. Transition metals are incorporated in such a way that some of their d orbitals interact with the conjugated π-electron orbitals of the organic repeating unit. Therefore, an extended, delocalized electronic system within the polymer chain is formed. Electronic features can be manipulated by varying the ligands attached to the metal center. Also, many organometallic polymers have low-lying charge transfer transitions not present in organic systems.

For third-order effects, there is no inherent symmetry restriction, and it is hoped that judicious use of metal moieties will further the design of radically different third-order species that perhaps do not involve large delocalized electronic systems.

5.1. Metallocenes

As was discussed in Section 4.1, metallocene derivatives are known to be important NLO materials. Less work has been completed featuring third-order materials than second-order ones, but metallocenes allow direct comparisons to be made between organic and organometallic compounds. The third-order optical nonlinearity of metallocenes such as ferrocene, hafnocene, ruthenocene, zirconocene, and bis(trimethylsilyl)ferrocene has been initially investigated by optical power limiting measurements.[147, 148] The values of γ obtained by using this technique were quite high and possibly electronic in origin. Similar experiments have focused on some lanthanide tris(cyclopentadienyl)metallocenes $(\eta^5\text{-}C_5H_5)_3M$ (M = Yb, Nd, Dy, Er, Pr).[149] Although the species did exhibit third-order NLO behavior, two-photon absorption takes place, thus limiting the suitability of the material for device applications.[150, 151]

Some symmetric end-capped acetylenes have undergone THG analysis.[104] One of the compounds, 1,4-bis(ferrocenyl)butadiyne, showed a $\chi^{(3)}$ value of 225×10^{-14} esu, which is more than double that of the organic species 1,4-diphenylbutadiyne.

To help elucidate the NLO properties of organometallic structures, a series of aryl and vinyl derivatives of ferrocene have been synthesized (Fig. 6).[152] The second molecular hyperpolarizabilities γ, determined by degenerate four-wave mixing at 602 nm, were overall fairly low. Nevertheless, some important points could be gleaned from the data: 1) The γ value increases strongly with the length of the conjugated π-electron system (a feature also found in organic polyenes) until a large limiting value is reached, where additional conjugation is ineffective with

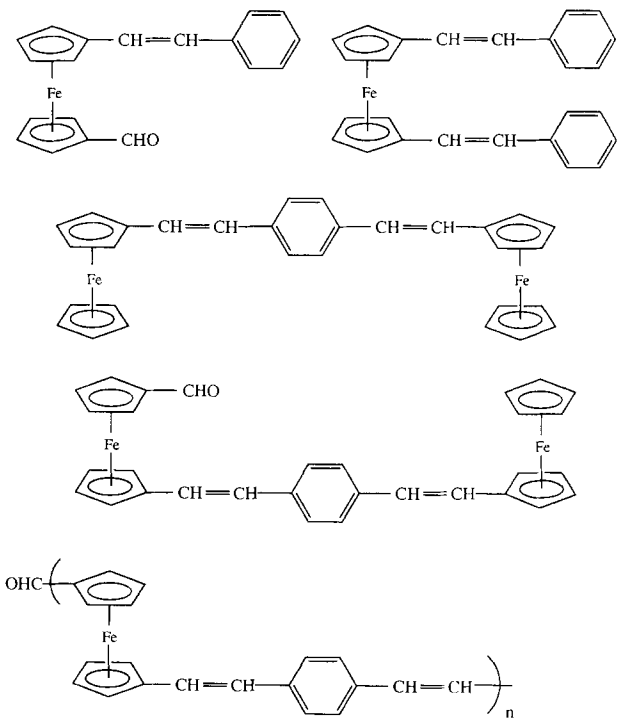


Fig. 6. The structures of some arylvinyl- and vinylferrocene derivatives studied for third-order NLO.

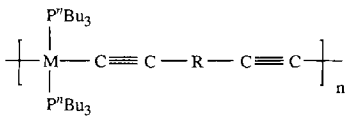
regard to γ.[151] 2) The effective conjugation is determined by the length of the arylvinyl system, the ferrocenyl group not being very significant in this respect. 3) The π-electron delocalization through the ferrocene center is less effective than through a double bond or phenyl group. 4) The d-d transition of the metal in the ferrocene moiety does not make a significant contribution to the optical nonlinearity, as opposed to the d-π* and π-π* transitions.

Ferrocenyl- and bis(ferrocenyl)alkynes and -polyynes are of interest and the 1,8-bis(ferrocenyl)octatetrayne has been examined for third-order NLO activity.[153] EFISH techniques (THG measurements on colored compounds have the potential to be affected by resonance enhancement) gave a value of γ of 110×10^{-34} esu which is comparable to linearly conjugated species of a similar length.[154] It is suggested that when considering γ, the conjugated triple bond linkage is poorer than a double bonded one of similar length.

The attractiveness of ferrocenyl-based NLO materials (due to the air-, thermal-, and photochemical stability and synthetic versatility) has led to other ferrocenyl polymers, namely 1) a main-chain homopolymeric system[109, 111] and 2) ferrocenylacetylenes being synthesized.[155] However, in both of these cases, the second molecular hyperpolarizabilities have yet to be determined.

5.2. Metallapolyyne Polymers

Metal-containing organic acetylene polymers were first synthesized by Hagihara et al.[156, 157] when Group 10 metals (Ni, Pd, Pt) were incorporated into conjugated acetylenic backbones (**15**). These materials were shown to possess interesting liquid

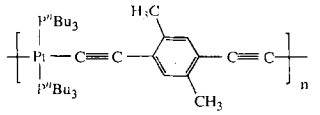
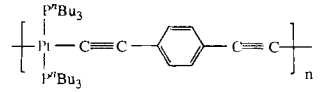
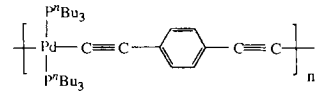
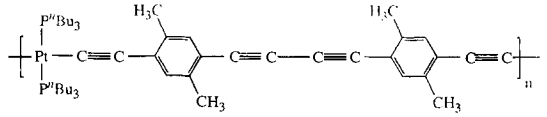
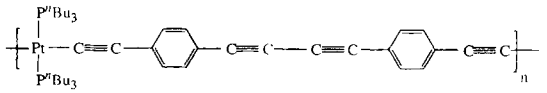


15, M = Ni, Pd, Pt, R = *p*-C_6H_4, *p*-C_6H_4-C_6H_4-*p*,

crystalline,[158] magnetic, and electronic properties. They were subsequently investigated for third-order NLO activities.[159–161] Hyperpolarizabilities (and, in many cases, solubilities) were found to be much higher than those of purely organic counterparts. Measurements were taken by THG and DFWM techniques, and Table 4 lists the γ values for some metallapolyynes. The type of metal, arene spacer, and length of conjugation were all shown to be of importance.

In recent years, reports of other metal-containing acetylide polymers have been quite plentiful. Lewis et al.[162] have formed square-planar (Ni, Pd, Pt) and octahedral (Fe, Ru, Os, Rh, Co) metal polymers by using bis(trimethylstannyl)diyne, $Me_3Sn-C\equiv C-R-C\equiv C-SnMe_3$ (R = C_6H_4, $C_6H_4-C_6H_4$), ligands. Figure 7 shows ruthenium precursor for the synthesis of such polymers. Principal interest has focused on the possibility of these polymeric complexes acting as electronic conductors and, as such, optical and band gap studies (π-π*) have been extensive. To date, no third-order NLO studies have been reported; however, other physical studies concerned with the delocalization of the π system along the polymer chain, point to these compounds having great potential as NLO materials.

Table 4. Third-order hyperpolarizability values γ of some platina- and palladapolyynes.

Compound	γ ($\times 10^{-36}$ esu)
	56
	102
	390
	181
	856

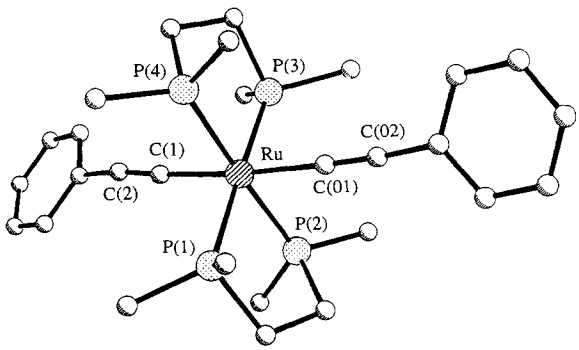


Fig. 7. Crystal structure of $[Ru(dppe)_2(C\equiv C-C_6H_5)_2]$, a precursor to metal-containing acetylide polymers. (Hydrogen atoms and phenyl groups on the phosphane ligands are omitted for clarity).

Carty et al.[163] report the synthesis of linear acetylides of the form $[Ru(CO)_2(PEt_3)_2(C\equiv C)_nR]$, whilst Marder et al.[129, 164, 165] have formed a series of metallapolyynes produced from direct alkyne C–H addition to low-valent metal complexes. Metal-to-ligand d_π-$p_{\pi*}$ charge transfer capabilities should result in excellent third-order behavior.

5.3. Polysilanes and -germanes

These compounds are conjugated polymers markedly different from carbon-based π-conjugated species and have been shown to exhibit interesting NLO properties.[166–170] The silane (or germane) polymers consist of a backbone of silicon (or germanium) with two organic side chains attached to every backbone atom. It is a σ-bonded fragment, but there is suffi-

cient orbital overlap for it to be considered a σ-delocalized system,[166] thus leading to some useful properties: a) The materials are transparent at visible wavelengths, absorbing strongly in the near ultraviolet region (as opposed to π-conjugated polymers that normally absorb in the visible). b) They are highly soluble and exhibit excellent processability and can form thin films of very good optical quality. c) They are thermally and environmentally stable. This combined with NLO activity gives them great potential for device applications. Initial THG studies[167, 168] first indicated that silicon $[Si(n\text{-}C_6H_{13})_2]_n$ ($\chi^{(3)} = 1.3 \times 10^{-12}$ esu) and germanium $[Ge(n\text{-}C_6H_{13})_2]_n$ polymers were comparable to organic species such as poly(phenylenevinylene) ($\chi^{(3)} = 7.8 \times 10^{-12}$ esu). It was also found that the $\chi^{(3)}$ value of $[MeSiPh]_n$ did not change with temperature, but did on variation of film thickness. For instance, as the thickness increases from 120 to 1200 nm so does $\chi^{(3)}$, going from 1.9×10^{-12} to 4.2×10^{-12} esu. $[Si(n\text{-}C_6H_{13})_2]_n$ did, however, show some $\chi^{(3)}$ temperature dependence, with a lower value found at 53 °C than at 23 °C, due to a conformationally more mobile and, therefore, disordered structure at the higher temperature. A series of compounds have been reported where the alkyl substituents have been varied and the data are listed in Table 5.[171] The value of

Table 5. Absorption maxima and $\chi^{(3)}$ values for a series of polysilanes.

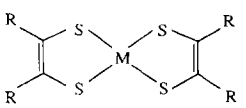
Polymer	λ_{max} [nm]	$\chi^{(3)}$ ($\times 10^{-12}$ esu) [a]
poly(methylphenylsilane)	339	7.2
poly(ethylphenylsilane)	338	5.3
poly(*n*-hexylphenylsilane)	346	6.2
poly(*para-tert*-butylphenyl)methylsilane)	332	4.9
poly(*n*-hexyl-*n*-pentylsilane)	318	2.3
poly((4-methylpentyl)silane)	319	1.8

[a] Measured at 23 °C and at a wavelength of 1064 nm.

$\chi^{(3)}$ appears to depend on polymer orientation; for simple alkyl substitution, there is little difference between polysilanes and -germanes. Addition of conjugated side chains and optimizing polymer orientation will make them even more important NLO materials.

5.4. Metal Dithiolene Complexes

Transition metal dithiolenes (enedithiolato metal complexes) possess a strong, low-energy π-π* transition in the near IR,[172] which can be tuned by altering the metal ion, substituents, or charge state of the dithiolene. They have been used as laser Q-switch materials because of their optical stability. A series of metal dithiolenes (**16**) have featured in third-order NLO studies,[149, 173] and $\chi^{(3)}$ values were found to range from 7.16×10^{-14} to 3.8×10^{-11} esu. For instance, a platinum dithiolene complex with cyano substituents gives a $\chi^{(3)}$ value of 4.2×10^{-12} esu compared to a value of 1.4×10^{-13} esu exhibited by an analogous nickel diselenolene complex possessing CF_3 groups. Similarly, a large $\chi^{(3)}$ figure (3.67×10^{-11} esu) was obtained from a nickel dithiolene species with phenyl substituents (**16**; M = Ni, R = C_6H_5), however, it should be noted that resonant enhancement of these values can occur as the dithiolenes absorb between 700 and 1400 nm.



16, M = Ni, Pt, R = CH_3, C_6H_5

As large one- or two-photon absorptions can render a material useless with regard to all-optical switching applications, a figure of merit has been introduced as a guide.[34, 149] A low value (preferably less than 1) of $2\lambda\beta/n_z$ (λ is the wavelength of the laser, β the two-photon absorption coefficient, and n_z is the nonlinear refractive index) is required for waveguide device switching. It was shown that the dimethyldithiolate complex (**16**; M = Ni, R = CH_3) has great device application potential, whilst the analogous diphenyl species does not. Work is now in progress to form polymeric thiolene systems and to include them in host–guest or side chain polymer systems to improve processability.

Metal complexes of the related species, *o*-aminobenzenethiol (ABT) and benzenethiol have also proved very interesting.[174] Metal substitution increases the $\chi^{(3)}$ value of ABT, and an excellent figure of 2.0×10^{-9} esu for $\chi^{(3)}$ results from a nickel complex of ABT.

5.5. Phthalocyaninato metal Complexes

The phthalocyanines are an extremely interesting and useful class of compounds. They feature an extensively delocalized π system and can be thought of as two-dimensional. Most other third-order NLO compounds feature π-electron conjugation along a backbone and are pseudo-one-dimensional. This imposes some limitations and whilst γ increases with the length of the one-dimensional π-conjugated system, there is a saturation of the parameter (per repeat unit) at some length of the polymeric chain.[72] This may be due to defects in the polymeric chain but, perhaps, also to the limitations of the one-dimensional systems. This had led to considerable interest in the two-dimensional π-conjugated phthalocyanine systems and, in particular, the complexes with a wide variety of metals (Fig. 8).

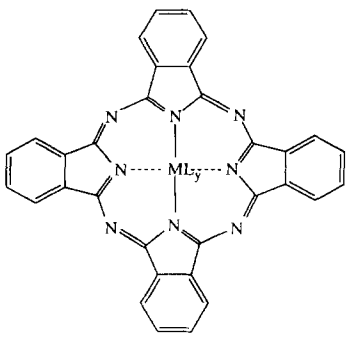


Fig. 8. The general structure of a metallaphthalocyanine complex.

A common property of most phthalocyanines is their chemical and thermal stability. They are versatile, flexible, and modifications are easily made by changing the central metal atoms or the side groups at the edge of the macrocycle. With a choice of up to 70 different metal atoms for incorporation, parameters can be carefully tailored. Several groups have studied various phthalocyanines (H_2Pc) and their metalated analogous (MPc) over recent yeast. Ho et al.[175] investigated thin polycrystalline films of chlorogallium and fluoroaluminum phthalocyanines, where the halogeno ligands were bonded to the metal atom. Different crystal structures were apparent, leading to a change in $\chi^{(3)}$ values.

Third-order nonlinear activity is known to be considerably enhanced by incorporation of the central metal atom, by the introduction of metal → ligand and ligand-metal charge transfer states. For example, the THG of alkoxy derivatives of vanadyl phthalocyanine (VOPc) is two orders of magnitude greater than that of the metal-free species.[176] This trend is also seen following DFWM measurements on metal-free tetrakis-(cumylphenoxy) phthalocyanines and the platinum and lead complexes (see Table 6). The platinum derivative gave a $\chi^{(3)}$ value

Table 6. The third-order susceptibilities of some metallophthalocyanines (after ref. [33]).

Compound [a]	Experimental Technique	$\chi^{(3)}(\times 10^{-12}$ esu)
H_2PcCP4	DFWM	4.0
PbPcCP4	DFWM	20.0
PtPcCP4	DFWM	200.0
RSiPc	DFWM	1800.0
PtPc	DFWM	200.0
$Sc(Pc)_2$	DFWM	1700.0
ClGaPc	THG	25.0
FAlPc	THG	50.0
CuPc	THG	4.0
ClInPc	THG	130.0
VOPc	THG	18.5
TiOPc	THG	27.0
CoPc	THG	0.76
NiPc	THG	0.80
$CuPc(C_4H_9S)_4$	THG	3.7
$CuPc(C_{10}H_{21}S)_4$	THG	26.0
$VOPc(C_6H_{13}S)_4$	THG	9.8

[a] CP4 = Tetrakis(cumylphenoxy), R = $(OSiMe(Ph)OH)_2$.

(2×10^{-10} esu), an order of magnitude greater than the lead derivative ($\sim2\times10^{-11}$ esu) and 50 times that of the parent phthalocyanine. The variations are due to the low-lying charge transfer states in the molecule. Transition metals, such as Pt, with valence d orbitals, introduce many more such states than the main group Pb. These states are not present in the metal-free species and contribute to the observed enhancement of nonlinear susceptibility. Other investigations have focussed on metal species involving Co, Ni, Cu, Zn, Pd, and Pt. With the first row metals, a decrease in γ was observed with an increased number of d electrons.[177, 178] Similar observations and results on various metallophthalocyanines are collected in Table 6.

Other investigations have focused on the role of the substituents on the aromatic rings in the phthalocyanine. The long alkylthio chain in $[VOPc(C_8H_{17}S)_4]$,[179] lowers the $\chi^{(3)}$ value (31.0×10^{-12} esu) due to a disruption of the π-electron system. Conversely, larger $\chi^{(3)}$ values can be observed for metallophthalocyanines with long alkyl chain substituents, since these result in increased steric hindrance and therefore, poorer packing or aggregation of the molecules.

The largest hyperpolarizabilities, to date, for metallophthalocyanines have been reported by Rao et al.[180] for some metal tetrabenzoporphyrin derivatives (Fig. 9). The R groups substituted at the *meso*-positions 5, 10, 15, and 20 were varied and the outer benzene rings were flourinated (X). In most cases, the coordinated metal was zinc, but magnesium was also tested. The $\chi^{(3)}$ values were in the range 1.2×10^{-8}–2.8×10^{-8} esu. A 5,10,15,20-tetra(*para*-dimethylaminophenyl)tetrabenzoporphyrinatozinc species exhibiting the greatest value due to strong electron-donating groups at the *meso* positions.

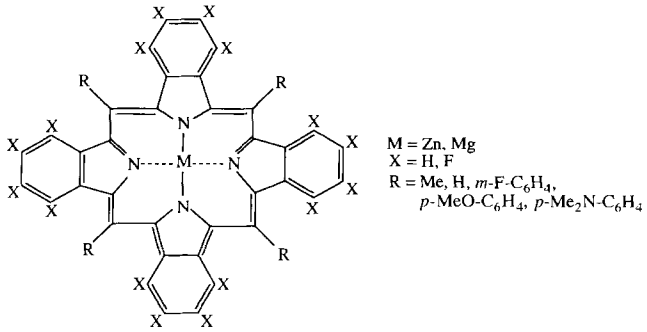


Fig. 9. The general structure of metallotetrabenzoporphyrins.

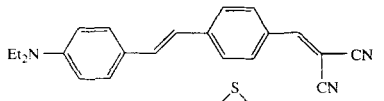
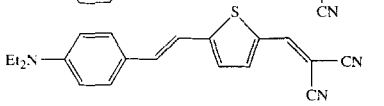
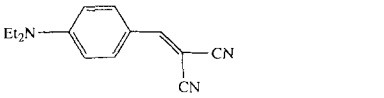
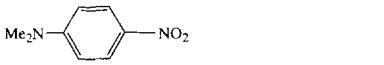
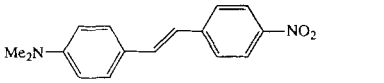
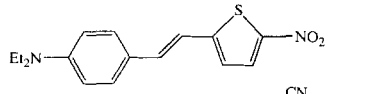
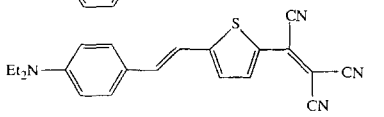
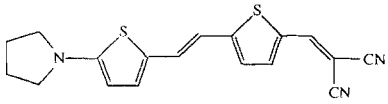
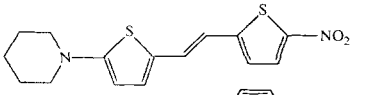
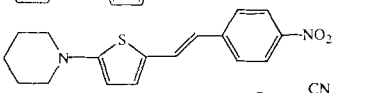
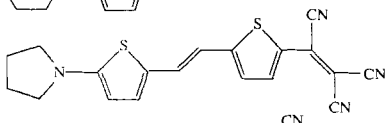
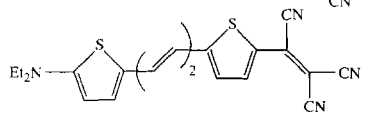
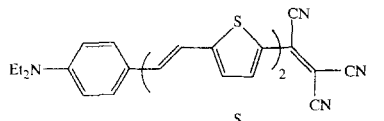
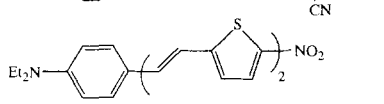
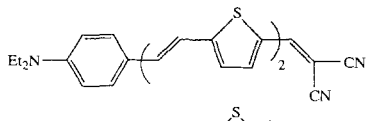
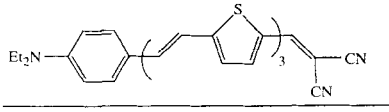
Due to other properties, phthalocyanines have become important as optical limiters.[181] Light of low incident intensity is transmitted through a sample as a linear function of the input intensity; however, at very high input intensities, a nonlinear medium will cause the output intensity to saturate at a particular value. Therefore, detectors and, in particular, eyes can be protected from bright light.

5.6. Thiophenes

Whilst these species do not really feature within the remit of this review, there has been so much recent interest in them with regard to NLO effects that brief mention should be made. Thiophenes and polythiophenes have been investigated for second- and third-order activity, respectively; the main motivation being that thiophene has a lower delocalization energy (117 kJ mol^{-1}) than that of benzene (151 kJ mol^{-1}) (the main spacer or conjugated linking group in NLO materials) and consequently, it offers better effective conjugation.[68d] Initial studies[49, 182] on replacement of a benzene ring with a thiophene ring in donor–acceptor compounds met with no significant enhancement of molecular nonlinearity ($\beta\mu$). However, investigation of some stilbene-type donor-acceptor molecules has revealed that thiophene substitution is highly important and the data obtained are listed in Table 7.[68d, 183, 184]

Obviously, the nature of the donor–acceptor end groups is important, as is illustrated in Table 7, where tricyanovinyl acceptors enhance the molecular nonlinearity far better than dicyanovinyl and nitro species. Additionally, there is a substantially red-shifted charge transfer band connected with the better charge-asymmetry in the tricyanovinyl derivatives. However, it is clear that replacement of the benzene rings with thiophene moieties has a similar effect on the nonlinearity and the charge transfer absorption band (replacement of both benzene rings in a two-ring system is far more significant than changing just one). A noticeable increase in $\beta\mu$ with increase in thiophene chain length is also observed in contrast to the benzenoid situation. In the latter, a definite saturation of $\beta\mu$ with length has been reported,[185] however, from Table 7, the values for the two-ring, three-ring, and four-ring systems (second, second-last, and last entry in Table 7, respectively) show an almost linear increase. Indeed, there is no significant saturation at the length scale considered.

Table 7. Absorption maxima and molecular nonlinearities [a] of some thiophene derivatives; showing the effect of end groups and conjugation.

Compound	λ_{max} [nm]	$\beta\mu$ ($\times 10^{-48}$ esu)
	468	1100
	513	1300
	419	300
	370	110
	424	580
	478	600
	640	6200
	584	2600
	516	1040
	460	660
	718	6900
	662	9100
	653	7400
	506	1400
	547	2300
	556	3800

[a] Values measured with 1907 nm fundamental radiation in dioxane.

The same motivation of better π-electron delocalization and increased effective conjugation has been employed in the formation of polythiophene materials. They have long been known to be conductive polymers, but due to the extended π-conjugation have recently been recognized as an important class of third-order NLO media. Various studies[186, 187] have produced very reasonable third-order susceptibilities for example a $\chi^{(3)}$ of 2700×10^{-10} esu for the polythiophene superlattice, PBTBQ (= poly(α-[5,5′-bithiophenediyl]benzylidene-block-α-[5,5′-bithiophenequinodimethanediyl]).[186] Similar traits to those observed in the second-order NLO studies have been found during the third-order (γ) investigations of some systematically derivatized α-terthiophenes.[188] The limiting conjugation length is much shorter for polyphenylenes than that for polythiophenes, and if the levelling off of the nonlinearity does happen, it occurs after at least a conjugation where $n = 6$. Substitution with a pyrrole or benzene unit of a central thiophene ring reduces the γ value due to a hindering of the conjugation. Finally, addition of polarizable moieties such as iodine or nitro groups at the end of the thiophene chains increases the hyperpolarizability due to an extension of the π-electron backbone by incorporation of these groups.

Therefore, incorporation of metallic moieties with various thiophene derivatives should have great potential in improving the NLO properties of many previously synthesized benzenoid compounds. Indeed, preliminary studies[189] concerned with band gap measurements on the platina polymers shown in Figure 10 have reinforced this opinion.

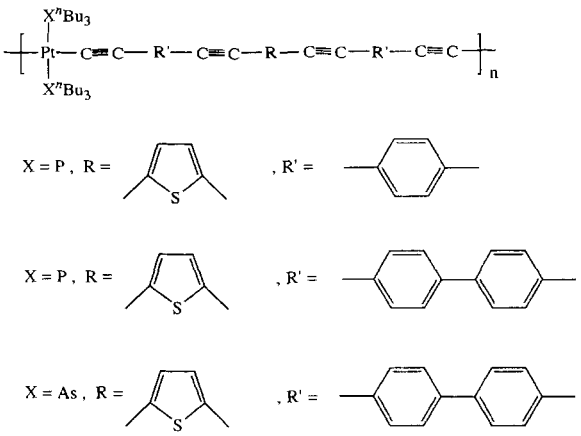


Fig. 10. Platina polymers with thiophene and benzene rings as members of the chain. $n = 24-63$.

6. Summary and Outlook

From the research detailed, it is clear that organometallic compounds are very versatile and have potential as NLO materials. By changing the transition metal, its oxidation state and incorporation of different bond geometries and coordination patterns, NLO properties can be modified. The design of second-order NLO materials continues apace as the guidelines are well understood; however, things are far less certain in the case of third-order materials and any structure–property relationships really are in their infancy. Conjugated systems have been successful but saturation points have been reached, so new designs are needed with perhaps, incorporation of polarizable heavy atoms being a step forward to increase the hyperpolarizability. Some points can be picked up, for instance, factors that

influence β in organic systems (nature of the bridge and donor–acceptor strengths) are relevant to metal-containing systems and values are quite encouraging with some phthalocyanines and dithiolenes exhibiting figures not too far from those needed for device application. Synthetic and solubility constraints have hampered the development of efficient materials but improvements continue to be made, for example thiophene substitution of benzene linking groups has recently demonstrated enhanced molecular nonlinearity, improved solubility, and ease of synthesis.

However, whilst there is great activity in this area, there is still a good deal of progress to be made. An improved understanding of the relationship between the molecular structure and the microscopic optical nonlinearities is crucial for a broadening of thought and incorporation of novel molecules. Theoretical and computational methods can be developed for predicting structural requirements necessary for large nonlinearities. To facilitate this, formation of databases will be vital. Only a very few systematic investigations covering a diversity of species and sequentially built structures have been reported. Due to the sparsity and inconsistency (different experimental and theoretical methodologies) of the available data, it is difficult to draw conclusions concerning many important points of molecular hyperpolarizability. Obviously, reliable, rapid and compatible determination of the NLO properties of the molecules and bulk materials would be helpful here.

More attention needs to be focused on the physical properties of a material, if they are to be successfully incorporated into commercially viable devices. The characteristics of a device application are important as these will dictate what is actually needed from a nonlinear material. Optical transparency, processability and speed of nonlinear response could all be crucial and indeed, the magnitude of the nonlinear response may not be the most important factor. It is unlikely that there is an ideal NLO material, just one which is most effective for a particular scenario.

It is hoped that this review will stimulate interest, as more research is vital for increasing the understanding of optical nonlinearities as well as the development of useful NLO materials. The unique characteristics of metal-containing materials mean that they, undoubtedly, have an important role to play in this area. Nevertheless, there is still scope for a leap of imagination in the design and synthesis of new and striking NLO materials, and the organometallic chemist, with a knowledge of organic chemistry and over 100 elements to choose from could be just the person to do this.

I would very much like to thank Professor, the Lord Lewis and Dr. Paul Raithby for their stimulating help and advice and introducing me to this area of chemistry. Thanks are also due to the group in Cambridge for their comments, computing skills and, in particular, encouragement along the way. Finally, I am very grateful to Darwin College, Cambridge for the award of the "Adrian Research Fellowship".

Received: November 12, 1993 [A 36 IE]
German version: *Angew. Chem.* **1995**, *107*, 37

[1] For a molecule oriented introduction see G. H. Wagnière, *Linear and Nonlinear Optical Properties of Molecules*, VCH, Weinheim/Helvetica Chimica Acta, Basel, **1993**.

[2] a) *Nonlinear Optical Properties of Organic and Polymeric Materials* (Ed.: D. J. Williams) (*ACS Symp. Ser.* **1983**; *233*); b) *Materials for Nonlinear Optics: Chemical Perspectives* (Eds.: S. R. Marder, J. E. Sohn, G. D. Stucky) (*ACS Symp. Ser.* **1991**, *455*).

[3] *Nonlinear Optical Properties of Organic Molecules and Crystals, Vols. 1, 2* (Eds.: D. S. Chemla, J. Zyss), Academic Press, New York, **1987**.

[4] a) P. A. Franken, A. E. Hill, C. W. Peters, *Phys. Rev. Lett.* **1961**, *7*, 118; b) R. C. Miller, D. A. Kleinman, A. Savage, *ibid.* **1963**, *11*, 146; c) R. C. Miller, *Appl. Phys. Lett.* **1964**, *5*, 17; d) G. D. Boyd, R. C. Miller, K. Nassau, W. L. Bond, A. Savage, *Appl. Phys. Lett.* **1964**, *5*, 234; e) R. C. Miller, G. D. Boyd, A. Savage, *ibid.* **1965**, *6*, 77; f) C. Chen, G. Liu, *Annu. Rev. Mater. Sci.* **1986**, *16*, 203.

[5] A. Ashkin, G. D. Boyd, J. M. Dziezik, R. G. Smith, A. A. Ballman, K. Nassan, *Appl. Phys. Lett.* **1966**, *9*, 72.

[6] a) *Molecular Beam Epitaxy and Heterostructures* (Eds.: L. L. Chang, K. Ploog), Nijhoff, Netherlands, **1985**; b) K. Plog, *Angew. Chem. Adv. Mater.* **1989**, *101*, 839; *Angew. Chem. Int. Ed. Engl. Adv. Mater.* **1989**, *28*, 819; *Adv. Mater.* **1989**, *1*, 205.

[7] A. M. Glass, *MRS Bull.* **1988**, *13*, 16.

[8] Y. X. Fan, R. C. Eckhardt, R. L. Byer, R. K. Route, R. S. Fiegelson, *Appl. Phys. Lett.* **1984**, *45*, 313.

[9] a) G. F. Lipscomb, A. F. Garrito, R. S. Narang, *J. Chem. Phys.* **1981**, *75*, 1509; b) J. C. Baumert, R. J. Twieg, G. C. Bjorklund, J. A. Logan, C. W. Dirk, *Appl. Phys. Lett.* **1987**, *51*, 1484; c) P. G. Hugard, W. Blau, D. Schweitzer, *ibid.* **1987**, *51*, 2183; d) J. Zyss, *J. Mol. Electron.* **1985**, *1*, 24; e) C. Dehu, F. Meyers, J. L. Bredas, *J. Am. Chem. Soc.* **1993**, *115*, 6198.

[10] *Nonlinear Optical and Electroactive Polymers* (Eds.: P. N. Prasad, D. R. Ulrich), Plenum, New York, **1988**.

[11] *Nonlinear Optical Properties of Organic Molecules* (Ed.: G. Khanarian), SPIE, Bellingham, WA, USA, **1988**, p. 971.

[12] *Spec. Publ. R. Soc. Chem.* **1989**, *69*.

[13] a) B. L. Davydov, L. D. Derkacheva, V. V. Dunina, M. E. Zhabotinskii, V. F. Zolin, L. G. Koreneva, M. A. Samokhina, *Opt. Spectrosc. Engl. Trans.* **1971**, *30*, 503; b) B. L. Davydov, V. V. Dunina, V. F. Zolin, L. G. Koreneva, *ibid.* **1973**, *34*, 267.

[14] J. L. Oudar, *J. Chem. Phys.* **1977**, *67*, 446.

[15] a) J. L. Oudar, D. S. Chemla, *J. Chem. Phys.* **1977**, *66*, 2664; b) L.-T. Cheng, W. Tam, S. H. Stevenson, G. R. Meredith, G. Rikken, S. R. Marder, *J. Phys. Chem.* **1991**, *95*, 10631.

[16] B. F. Levine, C. G. Bethea, C. D. Thurmond, R. T. Lynch, J. L. Bernstein, *J. Appl. Phys.* **1979**, *50*, 2523.

[17] G. R. Meredith in ref. [2b], p. 27.

[18] a) C. Ye, N. Minami, T. J. Marks, J. Yang, G. K. Wong, *Macromolecules* **1988**, *21*, 2901; b) H. L. Hampsch, J. Yang, C. K. Wong, J. M. Torkelson, *ibid.* **1988**, *21*, 526; c) G. R. Meredith, J. G. Van Dusen, D. J. Williams, *ibid.* **1982**, *15*, 1385.

[19] a) R. Popovitz-Biro, K. Hill, E. M. Landau, M. Lahav, L. Leiserowitz, J. Sagiv, *J. Am. Chem. Soc.* **1988**, *110*, 2672; b) G. H. Cross, I. R. Peterson, I. R. Girling, N. A. Cade, M. J. Goodwin, N. Carr, R. S. Sethi, R. Marsen, G. W. Gray, D. Lacey, M. McRoberts, R. M. Scrowston, K. J. Toyne, *Thin Solid Films* **1988**, *156*, 39; c) T. Richardson, C. G. Roberts, M. E. C. Polywka, S. G. Davies, *ibid.* **1988**, *160*, 231; d) I. Ledoux, P. Fremaux, J. P. Piel, G. Post, J. Zyss, T. McLean, R. A. Hann, P. F. Gordon, S. Allen, *ibid.* **1988**, *160*, 217; e) J. D. Swalen, *ibid.* **1988**, *160*, 197.

[20] C. Sauteret, J. P. Hermann, R. Frey, F. Pradere, J. Ducuing, L. H. Baughman, R. R. Chance, *Phys. Rev. Lett.* **1976**, *36*, 956.

[21] G. N. Patel, *J. Polym. Sci. Polym. Lett. Ed.* **1978**, *16*, 609.

[22] P. N. Prasad, D. J. Williams, *Nonlinear Optical Effects in Molecules and Polymers*, Wiley, New York, **1991**.

[23] S. K. Kurtz in *Nonlinear Optical Materials – Laser Handbook, Vol. 1* (Eds.: F. T. Arecchi, E. O. Schultz-DuBois), North-Holland, Amsterdam, **1972**, p. 923.

[24] S. Singh in *Handbook of Laser Science and Technology, Part 2* (Ed.: R. J. Pressley), Chem. Rubber, Boca Raton, FL, USA, **1971**, p. 3.

[25] J. Zyss, *J. Non-Cryst. Solids* **1982**, *47*, 211.

[26] D. J. Williams, *Angew. Chem.* **1984**, *96*, 637; *Angew. Chem. Int. Ed. Engl.* **1984**, *23*, 690.

[27] S. Tripathy, E. Cavicchi, J. Kumar, R. S. Kumar, *Chemtech* **1989**, *19*, 747.

[28] C. Flytzanis, J. L. Oudar, *Nonlinear Optics Materials and Devices*, Springer, New York, **1986**.

[29] G. R. Meredith, *MRS Bull.* **1988**, *13*, 24.

[30] H. S. Nalwa, T. Watanabe, S. Miyata in *Photochemistry and Photophysics, Vol. 5* (Eds.: J. F. Rubek, G. W. Scott), Chem. Rubber, Boca Raton, FL, USA, **1991**.

[31] T. J. Marks, M. A. Ratner, *Angew. Chem.* **1995**, *107*, no. 2; *Angew. Chem. Int. Ed. Engl.* **1995**, *34*, no. 2.

[32] D. M. Burland, *Chem. Rev.* **1994**, *94*, 1.

[33] H. S. Nalwa, *Appl. Organomet. Chem.* **1991**, *5*, 349.

[34] S. R. Marder in *Inorganic Materials* (Eds.: D. W. Bruce, D. O'Hare), Wiley, Chichester, **1992**, p. 136.

[35] J. C. Calabrese, L.-T. Cheng, J. C. Green, S. R. Marder, W. Tam, *J. Am. Chem. Soc.* **1991**, *113*, 7227.

[36] C. C. Frazier, M. A. Harvey, M. P. Cockerham, H. M. Hand, E. A. Chauchard, C. H. Lee, *J. Phys. Chem.* **1986**, *90*, 5703.

[37] G. L. Geoffrey, M. S. Wrighton, *Organometallic Photochemistry*, Academic Press, New York, **1979**.
[38] B. J. Coe, C. J. Jones, J. A. McCleverty, D. Bloor, P. V. Kolinsky, R. J. Jones, *J. Chem. Soc. Chem. Commun.* **1989**, 1485.
[39] B. F. Levine, C. G. Bethea, *J. Chem. Phys.* **1975**, *63*, 2666.
[40] C. Flytzanis in *Quantum Electronics: A Treatise, Vol. 1* (Eds.: H. Rabin, C. L. Tang), Academic Press, New York, **1975**.
[41] S. K. Kurtz, T. T. Perry, *J. Appl. Phys.* **1968**, *39*, 3798.
[42] J. P. Dougherty, S. K. Kurtz, *J. Appl. Crystallogr.* **1976**, *9*, 145.
[43] J. M. Halbout, S. Blit, C. L. Tang, *IEEE J. Quantum Electron.* **1981**, *QE-17*, 513.
[44] M. J. Rosker, C. L. Tang, *IEEE J. Quantum Electron.* **1984**, *QE-20*, 334.
[45] J. W. Perry, *ACS Symp. Ser.* **1991**, *455*, 71.
[46] K. D. Singer, A. F. Garito, *J. Chem. Phys.* **1981**, *75*, 3572.
[47] J. L. Oudar, H. Le Person, *Opt. Commun.* **1975**, *15*, 258.
[48] B. F. Levine, C. G. Bethea, *Appl. Phys. Lett.* **1974**, *24*, 445.
[49] L.-T. Cheng, W. Tam, S. R. Marder, A. E. Stiegman, G. Rikken, C. W. Spangler, *J. Phys. Chem.* **1991**, *95*, 10643.
[50] C. G. Bethea, *Appl. Opt.* **1975**, *14*, 1447.
[51] R. S. Finn, J. F. Ward, *Phys. Rev. Lett.* **1971**, *26*, 285.
[52] B. G. Tiemann, L.-T. Cheng, S. R. Marder, *J. Chem. Soc. Chem. Commun.* **1993**, 735.
[53] K. Clays, A. Persoons, *Rev. Sci. Instrum.* **1992**, *63*, 3285.
[54] K. Clays, A. Persoons, *Phys. Rev. Lett.* **1991**, *66*, 2980.
[55] W. M. Laidlaw, R. G. Denning, T. Verbiest, E. Chauchard, A. Persoons, *Nature (London)* **1993**, *363*, 59.
[56] F. Kajzar, J. Messier, *Phys. Rev. A* **1985**, *32*, 2352.
[57] P. D. Maker, R. W. Terhune, *Phys. Rev. [Sect.] A* **1965**, *137*, 801.
[58] P. N. Prasad, *ACS Symp. Ser.* **1991**, *455*, 50.
[59] R. W. Hellwarth, *Prog. Quantum Electron.* **1977**, *5*, 1.
[60] M. D. Levenson, *IEEE J. Quantum Electron.* **1974**, *10*, 110.
[61] H. Kambara, H. Kobayashi, K. Kubodera, *IEEE Photonics Tech. Lett.* **1989**, *1*, 149.
[62] I. P. Kaminov, *An Introduction to Electro-Optic Devices*, Academic Press, New York, **1974**.
[63] P. D. Maker, R. W. Terhune, N. Nisenhoff, C. M. Savage, *Phys. Rev. Lett.* **1962**, *8*, 21.
[64] S. K. Kurtz in *Quantum Electronics* (Eds.: H. Rabin, C. L. Tang), Academic Press, New York, **1975**.
[65] J. Jerphagnon, S. K. Kurtz, *J. Appl. Phys.* **1970**, *41*, 1667.
[66] B. F. Levine, C. G. Bethea, *J. Chem. Phys.* **1977**, *66*, 1070.
[67] S. J. Lalama, A. F. Garito, *Phys. Rev. A* **1979**, *20*, 1179.
[68] Recent examples: a) S. R. Marder, C. B. Gorman, B. G. Tiemann, L.-T. Cheng, *J. Am. Chem. Soc.* **1993**, *115*, 3006; b) S. R. Marder, L.-T. Cheng, B. G. Tiemann, *J. Chem. Soc. Chem. Commun.* **1992**, 672; c) A. E. Stiegman, E. Graham, K. J. Perry, L. R. Khundkar, J. W. Perry, L.-T. Cheng, *J. Am. Chem. Soc.* **1991**, *113*, 7568; d) V. P. Rao, A. K.-Y. Jen, K. Y. Wong, K. J. Drost, *J. Chem. Soc. Chem. Commun.* **1993**, 1119.
[69] S. R. Marder, D. N. Beratan, L.-T. Cheng, *Science* **1991**, *252*, 103.
[70] M. Stahelin, D. M. Burland, J. E. Rice, *Chem. Phys. Lett.* **1992**, *191*, 245.
[71] S. Ramasesha, P. K. Das, *Chem. Phys.* **1990**, *145*, 343.
[72] S. R. Marder, L.-T. Cheng, C. G. Gorman, B. G. Tiemann, *Proc. SPIE Int. Soc. Opt. Eng.* **1993**, *1775*, 19.
[73] S. M. Risser, D. N. Beratan, S. R. Marder, *J. Am. Chem. Soc.* **1993**, *115*, 7719.
[74] J. F. Nicoud, R. J. Twieg in ref. [3], p. 227.
[75] R. A. Huijts, G. A. Hasselink, *Chem. Phys. Lett.* **1989**, *156*, 209.
[76] M. Barzoukas, M. Blanchard-Desce, D. Josse, J.-M. Lehn, J. Zyss, *J. Chem. Phys.* **1989**, *133*, 323.
[77] J. Zyss, J. F. Nicoud, M. Coquillay, *J. Chem. Phys.* **1984**, *81*, 4160.
[78] R. J. Twieg, K. Jain, *ACS Symp. Ser.* **1983**, *233*, 57.
[79] J. Zyss, G. Berthier, *J. Chem. Phys.* **1982**, *77*, 3635.
[80] M. C. Etter, G. M. Frankenbach, *Chem. Mater.* **1989**, *1*, 10.
[81] T. W. Panunto, Z. Urbanczk-Lipowska, R. Johnson, M. C. Etter, *J. Am. Chem. Soc.* **1987**, *109*, 7786.
[82] S. R. Marder, J. W. Perry, W. P. Schaefer, *Science* **1989**, *245*, 626.
[83] S. R. Marder, J. W. Perry, B. G. Tiemann, R. E. Marsh, W. P. Schaefer, *Chem. Mater.* **1990**, *2*, 685.
[84] W. Tam, D. F. Eaton, J. C. Calabrese, I. D. Williams, Y. Wang, A. G. Anderson, *Chem. Mater.* **1989**, *1*, 128.
[85] Y. Wang, D. F. Eaton, *Chem. Phys. Lett.* **1985**, *120*, 441.
[86] S. Tomaru, S. Zembutsu, M. Kawachi, M. Kobayashi, *J. Chem. Soc. Chem. Commun.* **1984**, 1207.
[87] S. D. Cox, T. E. Gier, J. D. Bierlein, G. D. Stucky, *J. Am. Chem. Soc.* **1989**, *110*, 2986.
[88] N. Okamoto, T. Abe, D. Chen, H. Fujimara, R. Matsushima, *Opt. Commun.* **1990**, *74*, 421.
[89] J. Zyss, D. S. Chemla, J. F. Nicoud, *J. Chem. Phys.* **1981**, *74*, 4800.
[90] M. L. H. Green, S. R. Marder, M. E. Thompson, J. A. Bandy, D. Bloor, P. V. Kolinsky, R. J. Jones, *Nature (London)* **1987**, *330*, 360.
[91] J. A. Bandy, H. E. Bunting, M. H. Garcia, M. L. H. Green, S. R. Marder, M. E. Thompson, D. Bloor, P. V. Kolinsky, R. J. Jones, J. W. Perry, *Polyhedron* **1992**, *11*, 1429.
[92] J. A. Bandy, H. E. Bunting, M. L. H. Green, S. R. Marder, M. E. Thompson, D. Bloor, P. V. Kolinsky, R. J. Jones, *Spec. Publ. R. Soc. Chem.* **1989**, *69*, 219.
[93] S. R. Marder, J. W. Perry, W. P. Schaefer, B. G. Tiemann, P. C. Groves, K. J. Perry, *Proc. SPIE Int. Soc. Opt. Eng.* **1989**, *1147*, 108.
[94] S. R. Marder, J. W. Perry, B. G. Tiemann, W. P. Schaefer, *Organometallics* **1991**, *10*, 1896.
[95] L.-T. Cheng, W. Tam, G. R. Meredith, S. R. Marder, *Mol. Cryst. Liq. Cryst.* **1990**, *189*, 137.
[96] S. R. Marder, B. G. Tiemann, J. W. Perry, L.-T. Cheng, W. Tam, W. P. Schaefer, R. E. Marsh, *ACS Symp. Ser.* **1991**, *455*, 636.
[97] A. Houlton, N. Jassim, R. M. G. Roberts, J. Silver, D. Cunningham, P. McArdle, T. Higgins, *J. Chem. Soc. Dalton Trans.* **1992**, 2235.
[98] A. Houlton, J. R. Miller, J. Silver, N. Jassim, M. J. Ahmed, T. L. Axon, D. Bloor, G. H. Cross, *Inorg. Chim. Acta* **1993**, *205*, 67.
[99] Z. Yuan, N. J. Taylor, T. B. Marder, I. D. Williams, S. K. Kurtz, L.-T. Cheng, *J. Chem. Soc. Chem. Commun.* **1990**, 1489.
[100] Z. Yuan, N. J. Taylor, T. B. Marder, I. D. Williams, S. K. Kurtz, L.-T. Cheng, *Spec. Publ. R. Soc. Chem.* **1991**, *91*, 190.
[101] Z. Yuan, N. J. Taylor, Y. San, T. B. Marder, I. D. Williams, L.-T. Cheng, *J. Organomet. Chem.* **1993**, *449*, 27.
[102] B. J. Coe, J. D. Foulon, T. A. Hamor, C. J. Jones, J. A. McCleverty, *Acta Crystallogr. Sect. C* **1991**, *47*, 2032.
[103] A. Benito, J. Cano, R. Martinez-Manez, J. Paya, J. Soto, M. Julve, F. Lloret, M. D. Marcos, E. Sinn, *J. Chem. Soc. Dalton Trans.* **1993**, 1999.
[104] J. W. Perry, A. E. Stiegman, S. R. Marder, D. R. Coulter, *Spec. Publ. R. Soc. Chem.* **1989**, *69*, 189.
[105] J. W. Perry, A. E. Stiegman, S. R. Marder, D. R. Coulter, D. N. Beratan, D. E. Brinza, F. L. Klavetter, R. H. Grubbs, *Proc. SPIE Int. Soc. Opt. Eng.* **1988**, *971*, 17.
[106] A. R. Dias, M. H. Garcia, M. P. Robato, M. L. H. Green, K. K. Lai, A. J. Pulham, S. M. Klueber, G. Galavoine, *J. Organomet. Chem.* **1993**, *453*, 241.
[107] A. Togni, G. Rihs, *Organometallics* **1993**, *12*, 3368.
[108] G. Doisneau, G. Balavoine, T. F. Fillebeen-Khan, J.-C. Clinet, J. Delaire, I. Ledoux, R. Loucif, G. Puccetti, *J. Organomet. Chem.* **1991**, *421*, 299.
[109] M. E. Wright, S. A. Svejda, *ACS Symp. Ser.* **1991**, *455*, 602.
[110] M. Kimura, H. Abdel-Halim, D. W. Robinson, D. O. Cowan, *J. Organomet. Chem.* **1991**, *403*, 365.
[111] M. E. Wright, E. G. Toplikar, R. F. Kubin, M. D. Saltzer, *Macromolecules* **1992**, *25*, 1838.
[112] D. R. Kanis, M. A. Ratner, T. J. Marks, *Chem. Rev.* **1994**, *94*, 195.
[113] D. R. Kanis, M. A. Ratner, T. J. Marks, *J. Am. Chem. Soc.* **1992**, *114*, 10338.
[114] D. R. Kanis, P. G. Lacroix, M. A. Ratner, T. J. Marks, *J. Am. Chem. Soc.*, in press.
[115] W. Tam, L.-T. Cheng, J. D. Bierlein, L. K. Cheng, Y. Wang, A. E. Feirling, G. R. Meredith, D. F. Eaton, J. C. Calabrese, G. L. J. A. Rikken, *ACS Symp. Ser.* **1991**, *455*, 158.
[116] A. G. Anderson, J. C. Calabrese, W. Tamand, I. D. Williams, *Chem. Phys. Lett.* **1987**, *134*, 392.
[117] D. F. Eaton, A. G. Anderson, W. Tamand, Y. Wang, *J. Am. Chem. Soc.* **1987**, *109*, 1886.
[118] T. N. Briggs, C. J. Jones, J. A. McCleverty, B. D. Neaves, H. M. Colquhoum, *J. Chem. Soc. Dalton Trans.* **1985**, 1249.
[119] J. A. McCleverty, *Polyhedron* **1989**, *8*, 1669, and references therein.
[120] W. Chiang, M. E. Thompson, D. VanEngen, J. W. Perry, *Spec. Publ. R. Soc. Chem.* **1991**, *91*, 210.
[121] W. Chiang, D. M. Ho, D. VanEngen, M. E. Thompson, *Inorg. Chem.* **1993**, *32*, 2886.
[122] H. Sakaguchi, H. Nakamura, T. Nagamura, T. Ogawa, T. Matsuo, *Chem. Lett.* **1989**, 1715.
[123] C. C. Teng, A. F. Garito, *Phys. Rev. B* **1983**, *28*, 6766.
[124] T. Richardson, C. G. Roberts, M. E. C. Polywka, S. G. Davies, *Thin Solid Films* **1989**, *179*, 405.
[125] D. Touchard, P. Haquette, N. Pirio, L. Toupet, P. H. Dixneuf, *Organometallics* **1993**, *12*, 3132.
[126] A. J. Hodge, S. L. Ingham, M. S. Khan, J. Lewis, N. J. Long, P. R. Raithby, *J. Organomet. Chem.*, in press.
[127] W. Tam, J. C. Calabrese, *Chem. Phys. Lett.* **1988**, *144*, 79.
[128] T. B. Marder, G. Lesley, Z. Yuan, H. B. Fyfe, P. Chow, G. Stringer, T. R. Jobe, N. J. Taylor, I. D. Williams, S. K. Kurtz, *ACS Symp. Ser.* **1991**, *455*, 605.
[129] H. B. Fyfe, M. Mlekuz, G. Stringer, N. J. Taylor, T. B. Marder, *Inorganic and Organometallic Polymers with Special Properties* (Ed.: R. M. Laine) (*NATO ASI Ser. Ser. E*, **1992**, *206*), p. 331.
[130] S. J. Davies, B. F. G. Johnson, J. Lewis, M. S. Khan, *J. Organomet. Chem.* **1991**, *451*, C43.
[131] J. Burdeniuk, D. Milstein, *J. Organomet. Chem.* **1993**, *451*, 213.
[132] D. W. Bruce, A. Thornton, *Mol. Cryst. Liq. Cryst.* **1993**, *231*, 253.
[133] D. W. Bruce, L.-T. Cheng, G. H. Cross, M. Barzoukas, A. Fort, A. Thornton, paper presented at the *5th Int. Conf. Chem. Platinum Group Metals*, University of St. Andrews, UK, **1993**.

[134] G. Mignani, M. Barzoukas, J. Zyss, G. Soula, F. Balegroune, D. Grandjean, D. Josse, *Organometallics* **1991**, *10*, 3660.
[135] G. Mignani, A. Kramer, G. Puccetti, I. Ledoux, G. Soula, J. Zyss, R. Meyrueix, *Organometallics* **1990**, *9*, 2640.
[136] R. J. P. Corriu, W. E. Douglas, Z. Yang, Y. Karakus, G. H. Cross, D. Bloor, *J. Organomet. Chem.* **1993**, *455*, 69.
[137] D. Hissink, P. F. VanHutten, G. Hadziionnou, F. VanBolhuis, *J. Organomet. Chem.* **1993**, *454*, 25.
[138] M. H. Chisholm, D. M. Hoffman, J. C. Huffman, *Inorg. Chem.* **1983**, *22*, 2903.
[139] D. M. T. Chen, M. H. Chishom, K. Folting, J. C. Huffman, N. S. Marchant, *Inorg. Chem.* **1986**, *25*, 4170.
[140] T. P. Pollagi, T. C. Stoner, R. F. Dallinger, T. M. Gilbert, M. D. Hopkins, *J. Am. Chem. Soc.* **1991**, *115*, 703.
[141] P. A. Cahill, *Mater. Res. Soc. Symp. Proc.* **1988**, *109*, 319.
[142] A. J. Heeger, J. Orenstein, D. R. Ulrich in *Nonlinear Optical Properties of Polymers* (*Mater. Res. Soc. Symp. Proc.* **1987**, *109*).
[143] P. N. Prasad, *Thin Solid Films* **1987**, *152*, 275.
[144] G. P. Agrawal, C. Cojan, C. Flytzanis, *Phys. Rev. B* **1978**, *17*, 776.
[145] J. P. Hermann, D. Ricard, J. Ducuing, *Appl. Phys. Lett.* **1973**, *23*, 178.
[146] C. Flytzanis, *Mater. Res. Soc. Symp. Proc.* **1987**, *109*, 167.
[147] C. S. Winter, S. N. Oliver, J. D. Rush, *Opt. Commun.* **1988**, *69*, 45.
[148] C. S. Winter, S. N. Oliver, J. D. Rush, *Spec. Publ. R. Soc. Chem.* **1989**, *69*, 232.
[149] C. S. Winter, S. N. Oliver, J. D. Rush, R. J. Manning, C. Hill, A. Underhill, *ACS Symp. Ser.* **1991**, *455*, 616.
[150] V. Mizrahi, K. W. DeLong, G. I. Stegeman, M. A. Saifi, M. J. Andrejco, *Opt. Lett.* **1989**, *14*, 1140.
[151] D. N. Beratan, J. N. Onuchic, J. W. Perry, *J. Phys. Chem.* **1987**, *91*, 2696.
[152] S. Ghoshal, M. Samoc, P. N. Prasad, J. J. Tufariello, *J. Phys. Chem.* **1990**, *94*, 2847.
[153] Z. Yuan, G. Stringer, I. R. Jobe, D. Kreller, K. Scott, L. Koch, N. J. Taylor, T. B. Marder, *J. Organomet. Chem.* **1993**, *452*, 115.
[154] C. W. Spangler, K. O. Havelka, M. W. Becker, T. A. Kelleher, L.-T. Cheng, *Proc. SPIE Int. Soc. Opt. Eng.* **1991**, *1569*, 129.
[155] S. L. Ingham, M. S. Khan, J. Lewis, N. J. Long, P. R. Raithby, *J. Organomet. Chem.*, in press.
[156] S. Takahashi, M. Kariya, T. Yatake, K. Sonogashira, N. Hagihara, *Macromolecules* **1978**, *11*, 1063.
[157] K. Sonogashira, K. Ohga, S. Takahashi, N. Hagihara, *J. Organomet. Chem.* **1980**, *188*, 237.
[158] S. Takahashi, Y. Takai, H. Morimoto, K. Sonogashira, N. Hagihara, *Mol. Cryst. Liq. Cryst.* **1982**, *32*, 139.
[159] C. C. Frazier, S. Guha, W. P. Chen, M. P. Cockerham, P. L. Porter, E. A. Chauchard, C. H. Lee, *Polymer* **1987**, *28*, 553.
[160] S. Guha, C. C. Frazier, P. L. Porter, K. Kang, S. E. Finberg, *Opt. Lett.* **1989**, *14*, 952.
[161] W. J. Blau, H. J. Byrne, D. J. Cardin, A. P. Davey, *J. Mater. Chem.* **1991**, *1*, 245.
[162] Z. Atherton, C. W. Faulkner, S. L. Ingham, A. K. Kakkar, M. S. Khan, J. Lewis, N. J. Long, P. R. Raithby, *J. Organomet. Chem.* **1993**, *462*, 265; and references therein.
[163] Y. Sun, N. J. Taylor, A. J. Carty, *Organometallics* **1992**, *11*, 4293; *J. Organomet. Chem.* **1992**, *423*, C43.
[164] H. B. Fyfe, M. Mlekuz, D. Zargarian, N. J. Taylor, T. B. Marder, *J. Chem. Soc. Chem. Commun.* **1991**, 188.
[165] H. B. Fyfe, M. Mlekuz, D. Zargarian, T. B. Marder, *Organometallics* **1991**, *10*, 204.
[166] R. D. Miller, J. Michl, *Chem. Rev.* **1989**, *89*, 1359.
[167] F. Kajzar, J. Messier, C. Rosilio, *J. Appl. Phys.* **1986**, *60*, 3040.
[168] L. Yang, Q. Z. Wang, P. P. Ho, R. Dorsenville, R. R. Alfano, W. K. Zou, N. L. Yang, *Appl. Phys. Lett.* **1988**, *53*, 1245.
[169] J.-C. Baumert, G. C. Bjorklund, D. H. Jundt, M. C. Jurich, H. Looser, R. D. Miller, J. Rabolt, R. Sooriyakumaran, J. D. Swalen, R. J. Twieg, *Appl. Phys. Lett.* **1988**, *53*, 1147.
[170] D. J. McGraw, A. E. Siegman, G. M. Wallruff, R. D. Miller, *Appl. Phys. Lett.* **1989**, *54*, 1713.
[171] R. D. Miller, F. M. Schellenberg, J.-C. Baumert, H. Looser, P. Shukla, W. Torruellas, G. Bjorklund, S. Kano, Y. Takahashi, *ACS Symp. Ser.* **1991**, *455*, 636.
[172] J. A. McCleverty, *Prog. Inorg. Chem.* **1968**, *10*, 49.
[173] S. N. Oliver, C. S. Winter, J. D. Rush, A. E. Underhill, C. Hill, *Proc. SPIE Int. Soc. Opt. Eng.* **1990**, *1337*, 81.
[174] J. R. Lindle, C. S. Weisbecker, F. J. Bartoli, J. S. Shirk, T. H. Yoon, O. K. Kim, Z. H. Kafafi, *Proc. Conf. on Lasers and Electro-Optics* **1991**.
[175] Z. Z. Ho, C. Y. Ju, W. M. Hetherington III, *J. Appl. Phys.* **1987**, *62*, 716.
[176] T. Wada, S. Yamada, Y. Matsuoka, C. H. Grossman, K. Shigehara, H. Sasube, A. Yamada, A. F. Garito, *Spec. Publ. R. Soc. Chem.* **1991**, *91*, 292.
[177] J. S. Shirk, J. R. Lindle, F. J. Bartoli, C. A. Hoffman, Z. H. Kafafi, A. W. Snow, *Appl. Phys. Lett.* **1989**, *55*, 1287.
[178] J. S. Shirk, J. R. Lindle, F. J. Bartoli, Z. H. Kafafi, A. W. Snow, *ACS Symp. Ser.* **1991**, *455*, 626.
[179] H. Matsuda, S. Okada, A. Mataki, H. Nakanishi, Y. Suda, K. Sluigehera, A. Yamada, *Proc. SPIE Int. Soc. Opt. Eng.* **1990**, *1337*, 105.
[180] D. V. G. L. N. Rao, F. J. Aranda, J. F. Roach, D. E. Remy, *Appl. Phys. Lett.* **1991**, *58*, 1241.
[181] J. W. Perry, L. R. Khundkar, D. R. Coulter, D. Alvarez, S. R. Marder, T. H. Pei, M. J. Sence, E. W. VanStryland, D. J. Hagan, *Organic Molecules for Nonlinear Optics and Photonics* (Eds.: J. Messier, F. Kajzar, P. N. Prasad) (*NATO ASI Ser. Ser.* **1991**, *194*, 369).
[182] G. Mignani, F. Leising, R. Meyrueix, H. Samson, *Tetrahedron Lett.* **1990**, *31*, 4743.
[183] A. K.-Y. Jen, V. P. Rao, K. Y. Wong, K. J. Drost, *J. Chem. Soc. Chem. Commun.* **1993**, 90.
[184] V. P. Rao, A. K.-Y. Jen, K. Y. Wong, K. J. Drost, *Tetrahedron Lett.* **1993**, *34*, 1747.
[185] L.-T. Cheng, W. Tam, G. R. Meredith, G. Rikken, E. W. Meijer, *Proc. SPIE Int. Soc. Opt. Eng.* **1989**, *1147*, 61.
[186] S. A. Jenekhe, W. C. Chen, S. Lo, S. R. Flom, *Appl. Phys. Lett.* **1990**, *57*, 126.
[187] Y. Wei, R. Hariharan, R. Bakthavatchalam, *J. Chem. Soc. Chem. Commun.* **1993**, 1161.
[188] M. T. Zhao, M. Samoc, B. P. Singh, P. N. Prasad, *J. Phys. Chem.* **1989**, *93*, 7916.
[189] M. S. Khan, A. K. Kakkar, N. J. Long, J. Lewis, P. Raithby, P. Nguyan, T. B. Marder, F. Wittman, R. H. Friend, *J. Mater. Chem.*, in press.

Toxins as Tools in Neurochemistry

Ferdinand Hucho*

Neurotoxins have evolved as molecules targeted specifically against molecules with an important function in the nervous system. Because of their selectivity they have been used as probes for detecting and characterizing key proteins of the nerve cell. Ion channels involved in the propagation of the action potential, proteins of presynaptic neurotransmitter exocytosis, and most importantly, neurotransmitter receptors have been and are presently being analyzed, in some cases already at atomic level by a combination of the tools of neurotoxins, molecular biology, and patch clamp electrophysiology. In this review a selection of these toxins is presented, together with their targets in the nervous system. Special emphasis is given to the recent breakthroughs in our understanding of the mechanism of action of tetanus and botulinum toxins and to the neurotoxins ranging from the plant alkaloid strychnine to the peptide toxins from poisonous snakes, which were fundamental in elucidating ligand-gated ion channels like the glycine and nicotinic acetylcholine receptors.

Keywords: neurotoxins · ion channels · biomembranes · acetylcholine receptor

1. Introduction

Progress in methodology parallels progress in science. Three methods form the basis of the present upsurge in neurochemistry: recombinant gene technology (especially in collaboration with patch-clamp electrophysiology),[1] immunology, and finally, neurotoxinology.[2, 3] Neurotoxins are components of venoms from the animal or plant kingdom that are specifically directed against the nervous system. During evolution many compounds arose, which are used by plants to protect themselves from being eaten, or by animals to defend themselves or to stop and kill their prey. The molecular variety of these substances extends from low molecular weight alkaloids to peptides and complex proteins.

Neurotoxins are molecules that are often targeted against only one function of the nervous system and thereby against one key molecule. Because of this specificity they are ideal tools[4, 5] for the neurochemist who wants to find key molecules in the nervous system and elucidate basic mechanisms of nerve functions. Nature is not wasteful: when, for example, a cobra bites its prey, it injects into it an impressive mixture of deadly substances. But they would be wasted if the wounded mouse escapes and dies in its hole from the cytotoxic, hemolytic, and cardiotoxic proteins contained in the cobra venom. Therefore the animal is first prevented from escaping by a small protein called α-neurotoxin. As we shall see below, this protein blocks with enormous efficiency the transfer of nerve impulses to the muscle needed for fleeing (or fighting). This is one example where neurochemists learned from the cobra and used an α-neurotoxin as a tool for elucidating one of the most important molecular mechanisms of transmission of nerve impulses from cell to cell.[6, 7] Neurotoxins are probes leading the scientist to structures and molecules that are fundamental for nerve activities.

2. Nerve Impulses: Electrical and Chemical

The main activity of a nerve cell is the transport of signals from one place to another.[1, 8] This transport occurs by electrical means *within* cells and (in most cases) by chemical means *between* cells. The crucial event in electrical nerve impulse *conduction* is the action potential. Chemical nerve impulse *transmission* takes place at specialized structures called synapses connecting nerve cells with others. Many of the key molecular structures and mechanisms underlying both the electrical and the chemical nerve impulse conduction have been and are still elucidated by electrophysiologists and biochemists who apply toxins as tools, amongst other techniques. Here I shall review only briefly the application of toxins in unraveling the molecular machinery propagating the action potential, because this is mostly history, while the second part of the story, the elucidation of synaptic nerve impulse transmission, is presently one of the most active topics of neurochemical research. This aspect will therefore be dealt with more extensively.

[*] Prof. Dr. F. Hucho
Freie Universität Berlin
Institut für Biochemie
Arbeitsgruppe Neurochemie
Thielallee 63; 14195 Berlin (Germany)

2.1. The Action Potential Is Based on the Different Kinetics of Two Types of Ion Channels

An electrical potential exists across the plasma membrane of nerve cells at rest, as for most cells, and is called the resting potential. It is a diffusion potential based on ion gradients and different permeabilities of the membrane for Na^+ and K^+ ions. The plasma membrane at rest shows only low permeability for sodium, but considerable permeability for potassium ions. The resting potential is therefore basically a potassium potential described by the Nernst equation. Upon stimulation an action potential is triggered, which is an "all-or-nothing" event self-propagating along the plasma membrane until it reaches the nerve ending. There it is converted into the chemical events forming the synaptic impulse transmission, which is the second half of our story (Section 3).

More than forty years ago, the electrophysiologists Hodgkin and Huxley showed that the action potential is the result of an early influx of sodium ions into the nerve cell and a delayed efflux of potassium ions.[1, 8, 9] These ion currents are mediated by distinct molecular entities called voltage-dependent sodium and potassium channels.[10] These ion channels have in effect been "dissected" by means of neurotoxins: First of all, some toxins interact specifically and with impressive potency with voltage-dependent sodium channels (Fig. 1). They do not influence any other type of channel. Others exclusively affect potassium channels and leave the sodium channels unchanged. Classical blockers of the voltage-dependent sodium channels are the heterocyclic guanidines tetrodotoxin (TTX, extracted originally from certain organs of the puffer fish *Tetraodon* and later found in other poisonous organisms as well)[11, 12] and saxitoxin (STX, found in the dinoflagellate *Gonyaulax*, which occasionally makes a meal for humans of the shellfish that feed on *Gonyaulax* very dangerous).

Interestingly, there are only relatively few toxins affecting voltage-dependent potassium channels.[13, 14] The electrophysiologists investigating action potentials therefore resorted mostly to tetraethylammonium (TEA) and to the amino pyridines as simple, albeit less effective, tools (which inhibit potassium current at μM–mM rather than at nM concentrations). The best natural blockers of voltage-dependent K^+ channels described to date are proteins found in scorpion venoms: noxius toxin (NTX) from *Centruroides noxius*[15] and one toxin from the scorpion *Tityus serrulatus*.[16] I should emphasize that here I am talking about effects on one specific type of potassium channel, the so-called delayed rectifier or "Hodgkin–Huxley" channel. Many other potassium channels[13] are also voltage-gated (although transiently and with differents kinetics), or gated by Na^+, Ca^{2+}, ATP or indirectly by neurotransmitters like acetylcholine (M channel) or serotonin (S channel), and there are specific toxins for them as well. We return to one of them below, when I discuss presynaptic events (Section 3), but for the complete picture of this very complex topic the reader is referred to specialized reviews.[13, 14]

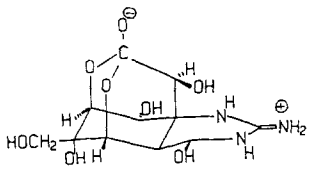
2.2. The Dissection of Sodium Channels by Means of Neurotoxins

Besides the discrimination of these two types of cation channel (the Hodgkin–Huxley sodium and potassium channels), neurotoxins have been used as tools for much more detailed research:[12, 17] Voltage-dependent sodium channels exhibit complicated kinetics with three distinct phases. Upon depolarization of the membrane the channel is rapidly opened (gated), reaches a peak permeability, and then closes (inactivates) spontaneously. Accordingly, one class of toxins promotes gating (Table 1). Representatives of these are the lipophilic alkaloids batrachotoxin, grayanotoxin, aconitine, and veratridine (Fig. 1). Others, like TTX and STX (already mentioned) block the open channel, and a third class, mainly peptide toxins from sea anemones (anemone toxins ATX I-IV) and from various scorpions (ScTX), affects the inactivation. Important in a neurochemical sense is the observation that most of these toxins bind independently to separate sites on the sodium channel protein. They can be grouped into five sets, of which each seems to have its own nonoverlapping binding site (Fig. 2 and Table 1). To accommodate so many independent binding sites, the sodium channel had to be a very large molecule.

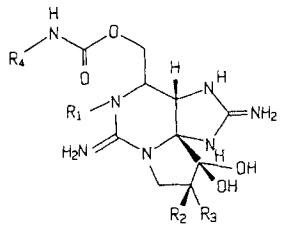
With the help of these toxins, not only the functional domains of the Na^+ channel were defined, but also channel protein was isolated and characterized in reconstituted systems.[18–20] And finally, cDNA coding for sodium channels from various tissues was cloned and sequenced.[21] But even when recombinant



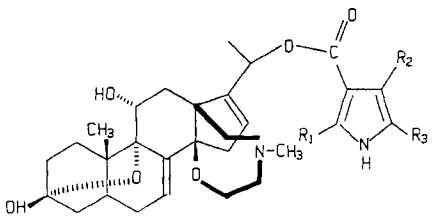
Ferdinand Hucho was born in 1939 in Berlin and is professor of biochemistry at the Freie Universität Berlin. He studied chemistry in Freiburg/Breisgau, where he also did his doctoral work on enzyme kinetics under the supervision of Kurt Wallenfels. After postdoctoral work on the regulation of pyruvate dehydrogenase multi-enzyme complexes with Lester Reed at the University of Texas at Austin, he was assistent of Horst Sund at the Universität Konstanz. He obtained his venia legendi in Konstanz in 1974 and became a professor there in 1979. In the same year he moved to Berlin. His main field of research is neurochemistry, with special emphasis on receptors, ion channels, and signal transduction mechanisms. He is an enthusiastic teacher of biochemistry.



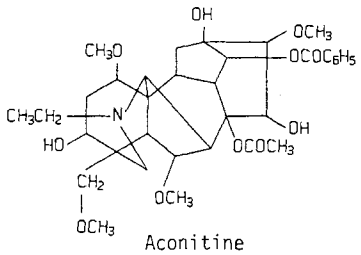
Tetrodotoxin (TTX)



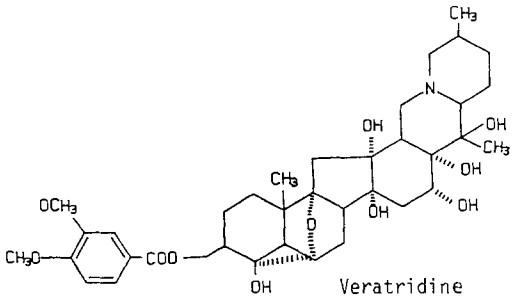
Axitoxin (STX)



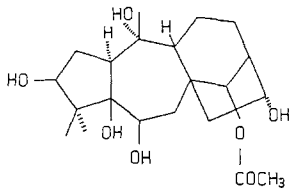
Batrachotoxin



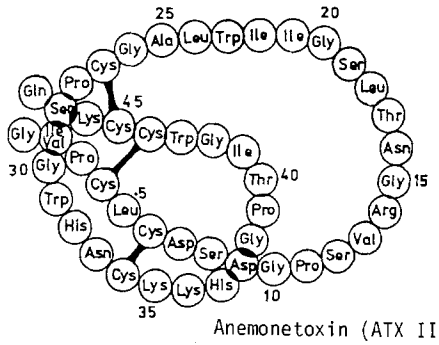
Aconitine



Veratridine



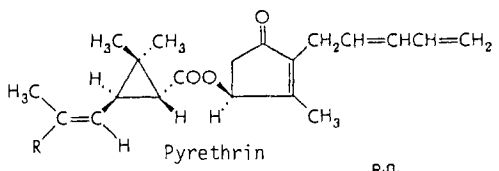
Grayanotoxin



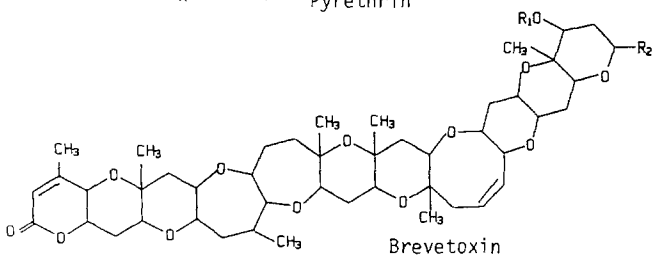
Anemonetoxin (ATX II)

GIIIA: RDCCTHyHyKKCKDRQCKHyQRCCA*
GIIIB: RDCCTHyHyRKCKDRRCKHyMKCCA*
GIIIC: RDCCTHyHyKKCKDRRCKHyLKCCA

μ-Conotoxines



Pyrethrin



Brevetoxin

DNA technologies come into play, toxins are indispensible tools. The cloned channels must be expressed, for example in oocytes from the toad *Xenopus*;[22] and proof that the correct and complete channel was identified comes by comparing the electrophysiology and toxinology of the cloned with the true channel. This was essential with the sodium channel, because the protein isolated biochemically from vertebrate brain as a ^{3}H-TTX-binding protein contained (in addition to a very large α-subunit of 260 kDa) two smaller (39 kDa) β-subunits.[20] The expression studies mentioned above have shown that the cDNA coding for the α-subunit alone contains all the information for the channel properties, including its electrical characteristics and its sensitivity to the various neurotoxins. The function of the small subunits is therefore still open to debate.

The primary structure of the sodium channel α-subunit, as deduced from the cloned and sequenced cDNA, is composed of four repeats of similar amino acid sequences.[21, 22] Each repeat contains six hydrophobic sequences thought to form membrane-spanning helices (Fig. 3 top). The fourth of these putative transmembrane helices, called S4, is especially rich in amino acids with positively charged side chains (located at every third position). It is assumed to be the voltage sensor responsible for opening the channel upon changes of the negative membrane potential. The exact location of the binding sites of the various toxins is largely unknown and is presently under investigation by site-directed mutagenesis in connection with expression studies. The expressed mutated channel is characterized with regard to its electrical properties and its response to the toxins. One point mutation, replacing by site-directed mutagenesis the glutamate residue in position 387 of the rat brain sodium channel by a glutamine residue, renders the channel insensitive to TTX.[23] This residue is located on the loop connecting the presumed transmembrane domains 5 and 6 of repeat I. It was concluded that the TTX-binding site is located on this loop.

Fig. 1. Toxins used as tools for characterizing voltage-dependent Na^+ channels. The chemical diversity of the toxic molecules is impressive; unfortunately, with the present state of knowledge on the three-dimensional structure of the toxins and of their target molecules, we are only beginning to predict from looking at a formula where exactly a substance binds and how it acts.

Table 1. Toxin-binding sites of the voltage-dependent sodium channel [17].

Binding Site	Ligands	Physiological Effect
1	Tetrodotoxin Saxitoxin μ-Conotoxins	inhibit ion transport
2	Veratridine Batrachotoxin Aconitine Grayanotoxin	persistent activation
3	North African α-scorpion toxins Sea-anemone toxins	inhibit inactivation enhance persistent activation
4	American β-scorpion toxins	shift activation
5	*Ptychodiscus brevis* toxin Ciguatoxins	repetitive firing persistent activation

Just to complete the picture (see Fig. 2) I should add some information concerning the voltage-dependent K^+ channel: Its primary structure suggests a similar transmembrane folding pattern.[24] But its size is only about one-fourth that of the Na^+ channel. There seems to be only one instead of four groups of six transmembrane domains (Fig. 3 bottom). Therefore, probably four of these molecules form one K^+ channel, while the Na^+ channel most likely is formed by one of the giant molecules with its four repeats. One other interesting finding should be mentioned: The loop between the presumed transmembrane domains 5 and 6 which is too short to form a membrane-spanning α-helix forms a β-strand immersed into the membrane. Four K^+ channel molecules probably contribute this structure, called the P-loop, to form the wall of the channel.[25]

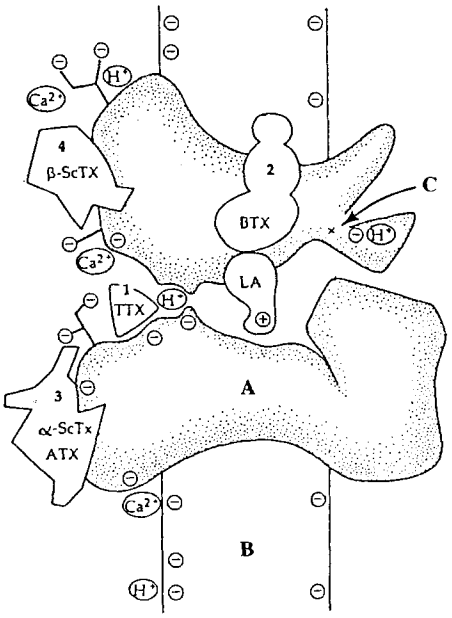


Fig. 2. Schematic drawing of the voltage-dependent Na^+ channel indicating the different binding sites of neurotoxins. The channel protein **A** (dotted region) is large enough (260 kDa) to accommodate binding sites for a variety of low and high molecular weight toxin molecules. By means of the toxins of Figure 1 it was possible to "dissect" various functional moieties of the channel protein (see also Table 2). **B**: membrane lipid, **C**: attack by pronase, iodate, and NBA. (From ref. [10], with kind permission from the publisher, Sinauer).

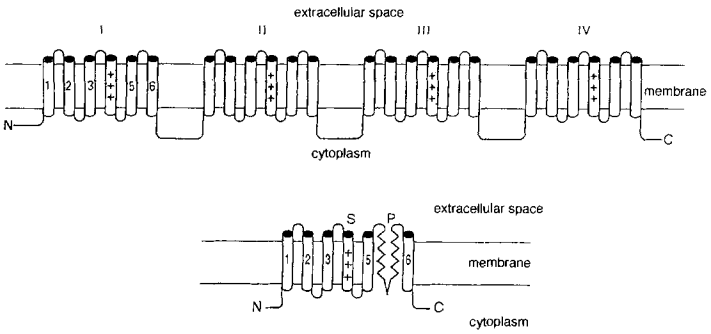


Fig. 3. Schematic representation of the primary structures of voltage-dependent Na^+ channels and Ca^+ channels (top) and K^+ channels (bottom). The cylinders represent membrane-spanning amino acid sequences, which are assumed to form α-helices. The sodium channel protein consists of one very long polypeptide chain, composed of four stretches with similar amino acid sequences (so-called repeats). These repeats probably are arranged within the neuronal membrane to form a ore, the channel proper. The potassium channel protein (bottom) consists of only one repeat. Probably four of these smaller molecules are necessary to form a channel.

3. Synaptic Transmission of Nerve Impulses

The action potential travels along the axonal membrane by opening and closing voltage-dependent Na^+ and K^+ channels and finally arrives at the nerve ending where it causes the transmission of the nerve impulse to the next cell by releasing a substance called a neurotransmitter (Fig. 4). This substance diffuses from its release site at the presynaptic side across the synaptic cleft to the postsynaptic membrane of the next cell about 20–30 nm away. Transmitter release is of great interest from various points of view for current neurochemical and cell biological research and is presently dissected by means of neurotoxins.[26]

3.1. Events on the Presynaptic Side

Transmitter molecules in nerve endings are packaged and stored in small vesicles (Fig. 5). Upon arrival of an action potential, those vesicles, located at special release sites that line up with active zones of the presynaptic membrane, fuse with the presynaptic membrane, thereby opening up and letting the transmitter escape into the synaptic cleft. The empty vesicle is retracted afterwards and refilled with transmitter. Cell biologists call this process "regulated exocytosis" to distinguish it from "constitutive exocytosis", the process that involves the cellular export of many proteins and peptides. Researchers are now asking whether the two processes might have more in common than they had previously thought. Recently, Rothman and co-workers[27a, 27b] identified various proteins, called NSF (*N*-ethylmaleimide-sensitive fusion protein) and SNAP (NSF attachment protein), which seem to be common components of the fusion apparatus involved both in intracellular vesicle traffic from the endoplasmic reticulum (ER) through the golgi apparatus to the plasma membrane and in the regulated exocytosis of synaptic vesicles. The specificity of this otherwise similar membrane transport is secured by selective "SNAP receptors" (SNAREs) directing each vesicle to its proper target. This picture of a widespread basic mechanism is strengthened by the

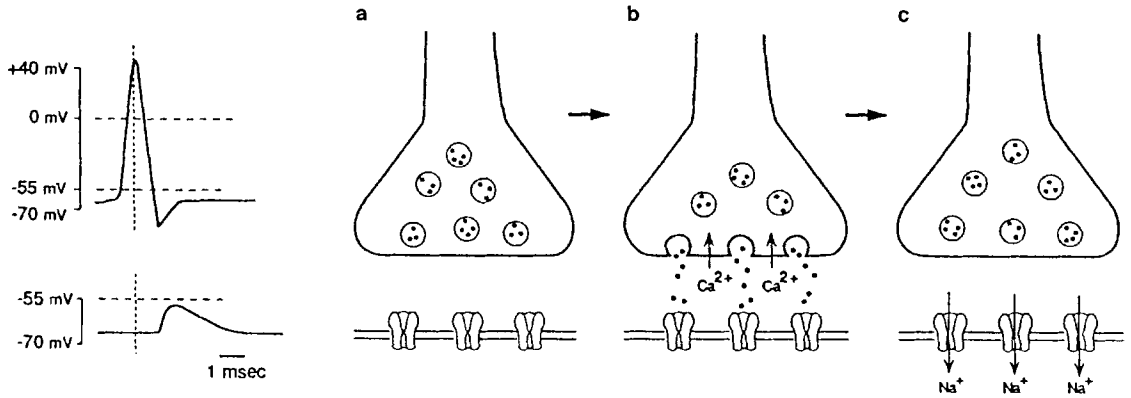


Fig. 4. Chemical nerve impulse transmission at a synapse. Left: electrical events (top diagram: presynaptic action potential; bottom diagram: postsynaptic potential; dashed horizontal lines indicate the required threshhold values). a–c) Top: Molecular events on the presynaptic side. Bottom: Response on the postsynaptic side. A large depolarizing spike, the action potential, travels down the nerve axon. Upon arrival in the nerve ending it triggers a cascade of molecular events leading to the release of neurotransmitter from the presynaptic membrane. The transmitter causes a transient depolarization through specific receptors in the postsynaptic membrane. If this depolarization reaches a threshold, an action potential is initiated postsynaptically (reproduced from ref. [28], with kind permission from Dr. E. R. Kandel).

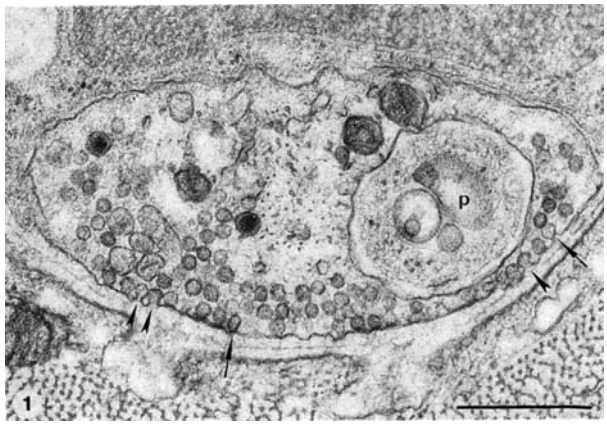


Fig. 5. Electron micrograph of a frog neuromuscular junction. The sample was quick-frozen 2.5 ms after electric stimulation in the presence of the K^+ channel blocker 4-aminopyridine. Clearly visible are some transmitter-containing vesicles in the process of fusion with the presynaptic membrane (arrow heads). Other vesicles seem to be in an earlier or later stage of the process of exocytosis (arrows). The image is reproduced from ref. [121], with kind permission from Springer-Verlag. p: Schwann cell projection invaginated by the nerve ending. Calibration bar: 0.5 μm.

observation that key features of the molecular machinery for secretion are conserved from yeast to neurons.[27c] The process has at least four steps,[28, 29] the molecular components and mechanisms of which are far from understood (Fig. 4; Fig. 6A): the mobilization and transport of vesicles from storage sites to the release sites; the docking of the vesicles to these sites; the fusion of the vesicle membrane with the presynaptic plasma membrane, triggered by Ca^{2+}; and the retraction and recycling of the empty vesicle membrane after exocytosis. Toxins are guiding us to some of the centerpieces of this complex picture.

Three sets of molecules are in the focus of research (Fig. 7): the first group are molecules of the presynaptic membrane (because it is here that docking of the vesicle, fusion, and recycling takes place); the second are proteins of the vesicular membrane (because among them must be the counterparts of the docking and fusion molecules found in the presynaptic membrane); and the third and final group are various regulators loosely associated with the vesicles, the docking sites, the cytoskeleton, or with hitherto unknown intracellular structures.

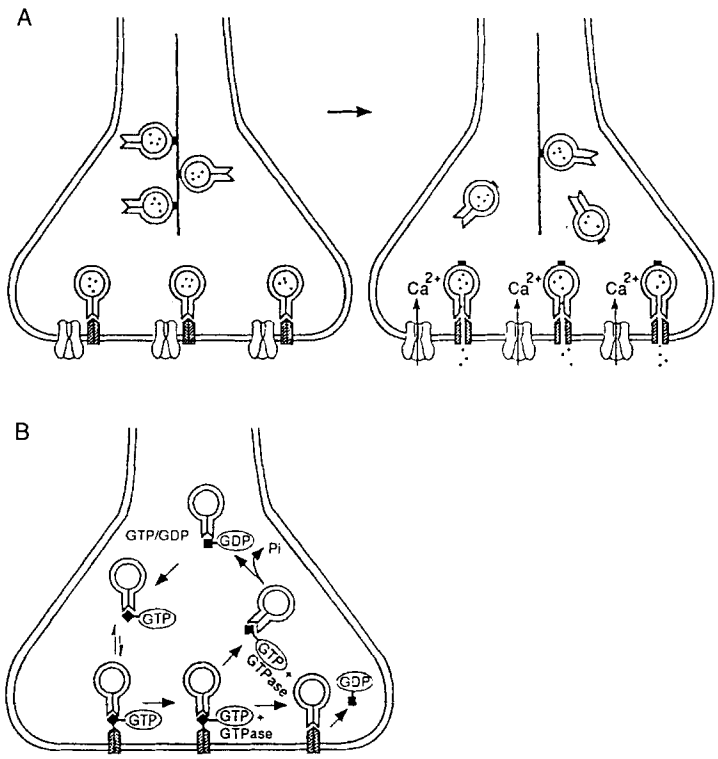


Fig. 6. Schematic drawing of key events in transmitter release from the nerve ending. A: Mobilization and fusion of vesicles triggered by Ca^{2+} influx (right). B: Control of vesicle fusion by rab, a guanine nucleotide-binding and GTP-hydrolyzing protein. (Reproduced from ref. [28], with kind permission from Dr. E. R. Kandel.)

3.2. ω-Conotoxins and N-Type Ca^{2+} Channels

Starting with the presynaptic membrane, we again encounter voltage-dependent ion channels. A key event in presynaptic transmitter release is the influx of Ca^{2+} through specific channels that are opened up by the depolarization caused by the invading action potential (Fig. 6A). Removing Ca^{2+} from the extracellular space or replacing it by Mg^{2+} causes a complete block of synaptic transmission by blocking transmitter release.

It would have been surprising if there were no neurotoxin targeted against this channel that is so instrumental for trans-

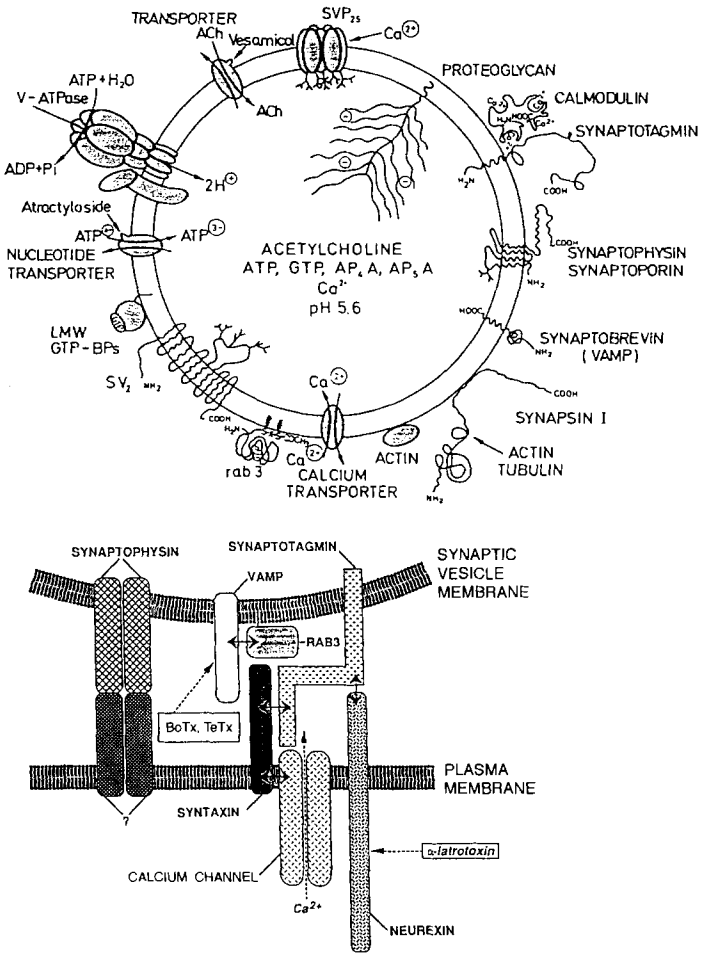


Fig. 7. Proteins of the synaptic vesicles and the presynaptic membrane. A: Schematic drawing of an acetylcholine-storing vesicle with membrane proteins identified to date. Reproduced with kind permission from Dr. H. Zimmermann (Frankfurt) from ref. [122]. B: Proteins involved in the fusion process between vesicle and presynaptic plasma membrane, including the site of action of some of the neurotoxins mentioned in the text. Reproduced from ref. [27], with kind permission from Dr. R. Scheller.

mitter release. Indeed, the marine snails of the genus *Conus* produce a venom full of such neurotoxins.[30] Besides several peptides blocking the voltage-dependent sodium channel like TTX and STX, one group of peptides called ω-conotoxins blocks voltage-dependent Ca^{2+} channels. (The Na^+ channel blockers are called μ-conotoxins (Fig. 1). There are even peptides acting on the postsynaptic nicotinic acetylcholine receptor. They are called α-conotoxins. The three groups are between ten and around thirty amino acids long.[31]) ω-Conotoxins were the first natural substances discovered which affect voltage-dependent calcium channels. They can be used to differentiate the calcium channel subtypes. One ω-conotoxin (code number GVIA) is specific for the N-type calcium channel, the subtype involved in transmitter release.[32] It has little if any effect on the L- and T-type channels. Conotoxins will no doubt be useful for elucidating the topography of ion channels: they are small enough to be easily synthesized. This makes "wild type" and synthetic "mutant" toxins available. They can be labeled radioactively[33] and derivatized for use as photoaffinity labels.[34] Cross-linked covalently to its target protein in situ, they make possible the characterization of functional domains.

Up to now, voltage-dependent calcium channels have been biochemically investigated mainly with other tools such as synthetic drugs and cDNA cloning and sequencing. Interestingly, they turned out to be similar to the sodium channels (Fig. 3): Their largest chain (α_1, $M_r = 230$ kDa) is composed of four repeats with six hydrophobic amino acid stretches each. The S4 regions are believed to be the voltage sensors. Several other subunits are associated with the α_1 chain.[17]

3.3. Black Widow Spider Toxin

The venom of the Black Widow spider *Latrodectus tredecimguttatus* has helped researchers detect another important molecular component of the transmitter-release machinery. It contains a protein of $M_r = 125$ kDa called α-latrotoxin, which is highly poisonous (ED_{50} in mice 20 ng g^{-1}), because it causes unrestricted Ca^{2+}-independent transmitter release and complete depletion of presynaptic transmitter stores.[35] (At the neuromuscular endplate, the peptide-containing vesicles with a large dense core are not released. α-Latrotoxin seems to be a tool for discriminating constitutive and regulated exocytosis.[36]) Its binding site at the presynaptic membrane was identified as a member of the family of proteins known as neurexins.[37, 38] Neurexin may interact through its intracellular domain with proteins like synaptotagmin (Fig. 7) of the vesicle membrane.[39]

3.4. Snake Toxins Acting Presynaptically

Another component of the vesicle exocytosis machinery detected through toxins[40] is a voltage-dependent, but in contrast to the Hodgkin–Huxley channel, inactivating K^+ channel. It was found to be the target of several toxins. The most prominent of these is a group of small proteins (59–61 amino acids long) from the venom of mamba snakes, for example the α,β,γ-dendrotoxins (DTX) and toxin I. As shown first with hippocampal neurons, DTX (and toxin I even more so) facilitates transmitter release by blocking this transient K^+ channel.[41] A block of a K^+ channel means prolonged depolarization by inhibition of the repolarizing outward K^+ current. The consequence of this is a prolonged opening of the voltage-dependent Ca^{2+} channel supplying the exocytosis machinery with Ca^{2+} ions. Facilitation of exocytosis by DTX is therefore caused in the final event by increasing the calcium concentration in the nerve ending.

Perhaps the same target though on cholinergic synapses only (in the peripheral nervous system—in the CNS transmitter specificity is much less pronounced) has to be considered for the effects of β-bungarotoxin. β-Bungarotoxin is a member of the group of "phospholipase A_2 toxins" (β-bungarotoxin, notexin from the Australian tiger snake, crotoxin from the South American rattlesnake, taipoxin from the Australian Taipan, Figure 8). These are proteins from snake venoms that preferentially act presynaptically. Some of them are composed of two disulfide-linked subunits, one of which binds the target and conveys synapse specificity and the other is catalytically active, cleaving phospholipids in a Ca^{2+}-dependent way. Their action on the synapse follows a characteristic triphasic pattern:[42] an initial

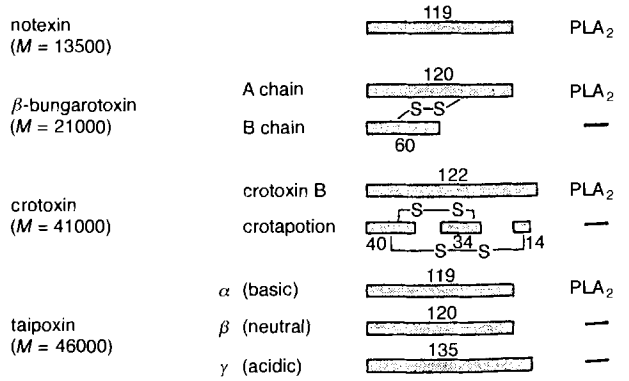


Fig. 8. Neurotoxins from poisonous snakes, with phospholipase A_2 activity. The figure shows the molecular weight, the subunit composition, the number of aminoacids in each subunit, and which subunit contains the lipase activity. Reproduced from ref. [40], with kind permission from Springer-Verlag.

depression is followed by transient facilitation and finally an irreversible blockade. β-Bungarotoxin is thought to bind to the same K^+ channel as DTX,[41,43] though at a different site. Together they may be tools for identifying this channel as a multiprotein complex with interesting regulatory properties. The phospholipase A_2 toxins also serve as tools for elucidating the role of phospholipids in exocytosis.[44]

3.5. Botulinum and Tetanus Toxin

Now, with the help of neurotoxins, we have identified three components of what we call the exocytosis machinery: an N-type voltage-dependent Ca^{2+} channel, an inactivating (A-type) K^+ channel, and neurexin, the α-latrotoxin-binding protein that is somehow involved in the calcium-dependent vesicle docking and/or fusion. A fourth protein, synaptobrevin, achieved prominence through two well-known neurotoxins from clostridia: botulinum toxin (BoTx) and tetanus toxin (TeTx) have long been studied as presynaptic blockers of transmitter release.[45] BoTx specifically blocks acetylcholine release at peripheral synapses, whereas TeTx is less selective and acts at sites in the central nervous system (CNS). But it was shown that this difference is due to the specificity of binding and uptake[46] into neurons rather than to specific toxic mechanisms at the intracellular target: when injected into neurons, both toxins prevent Ca^{2+}-dependent release of catecholamines in addition to acetylcholine.[47] More specifically, it was the light chain (M_r = 55 kDa) of the double-chain BoTx which caused the block after injection; the heavy chain (M_r = 100 kDa) is probably involved in binding to and transport through the plasma membrane. Recently the capacity of Botx to form channels in phospholipid vesicle membranes was visualized by electron cryomicroscopy and image processing.[48]

But which protein is the intracellular target and how is blockage of transmitter release brought about? These toxins led to the discovery of the central role in exocytosis of a protein from the vesicle membrane: the light chains of both BoTx and TeTx were shown to contain Zn^{2+}, and both had amino acid sequences characteristic for Zn-proteases.[49] And indeed, inhibition of their proteolytic activity by chelating the zinc ions destroyed their exocytosis-inhibiting activity. From this discovery, it was a short path to identifying the vesicle protein synaptobrevin, also called VAMP (from "*v*esicle-*a*ssociated *m*embrane *p*rotein") as the natural substrate of both enzyme toxins (Fig. 7).[50,51]

This is, however, only the introduction to an evermore complicated story. In fact there are seven isoforms of botulinum toxin, among which are BoTx A, B, C, E, F, and G. The one mentioned above that cleaves VAMP/synaptobrevin is BoTx B. Others are also zinc proteases. BoTx F cleaves VAMP/synaptobrevin too,[52] and it was shown that BoTx C cleaves syntaxin, a 35 kDa protein anchored to the presynaptic membrane and presumably participating in vesicle-docking;[53] and BoTx A blocks neurotransmitter release by selective cleavage of SNAP 25 (a synaptosomal-associated protein of M_r 25000. SNAP 25 is a member of a family of soluble, *N*SF *a*ccessory *p*roteins).[54] Actually the clostridial toxins together have among their targets important proteins involved in vesicle docking and fusion, not only in regulated but also in constitutive vesicle trafficking and exocytosis[55,56] (Table 2). SNAP 25, for example, was known as a protein involved in constitutive exocytosis. Inhibition of transmitter release by BoTx A proved that it operates in regulated exocytosis as well. They are presently used as a powerful tool kit for dissecting the molecular machinery of exocytosis. W. Huttner[26] gave credit to their importance by coining the term "exocytoxins".

Table 2. Target proteins of clostridial toxins [26].

Neurotoxin	Target	Cleavage Site	Cell type	Intracellular Localization
Tetanus toxin	VAMP/synaptobrevin	Gln76-Phe77	Neuron	Synaptic vesicle
	Cellubrevin	Not identified	All cells	Vesicles of the endocytosing/recycling system
Botulinum neurotoxin A	SNAP 25	Near C terminus	Neuron	Presynaptic plasma membrane, elsewhere?
BoTXB	VAMP/synaptobrevin	Gln76-Phe77	Neuron	Synaptic vesicle
BoTXC	Syntaxin	Near C-terminal membrane anchor, cleavage generates soluble fragment	Neuron	Presynaptic plasma membrane, elsewhere?
BoTXD	VAMP/synaptobrevin	Lys59-Leu60 Ala67-Asp68	Neuron	Synaptic vesicle
	Cellubrevin	Not identified	All cells	Vesicles of the endocytosing/recycling system
BoTXE	SNAP 25	Not identififed	Neuron	Presynaptic plasma membrane, elsewhere?
BoTXF	VAMP/synaptobrevin	Gln58-Lys59	Neuron	Synaptic vesicle
	Cellubrevin	Not identified	All cells	Vesicles of the endocytosing/recycling system
BoTXG	?	–		

Figure 7 gives a simplified view of our present picture of regulated exocytosis, including the proteins identified as playing an

important role. In addition to the molecules identified through the application of toxins as tools, there are others which are equally important—like the synapsins which are protein kinase substrates—and seem to be responsible for vesicle storage and mobilization. Furthermore, RAB3, a small G protein, is thought to play a regulatory role in vesicle trafficking and docking (see also Figure 6B). And finally, there are the docking proteins syntaxin and synaptotagmin. But despite this wealth of molecules and information, we still only have a relatively vague idea about the mechanisms triggering and performing vesicle transport, docking, fusion, and recycling. Toxins, because of their specific action on only one or a few key target molecules, have been and will be indispensible in unraveling this fundamental life process.

3.6. Transmitter Receptors as Postsynaptic Targets of Toxins

The transmitter released from the presynaptic nerve ending diffuses across the synaptic cleft to the postsynaptic membrane. There it is received by specific receptor proteins and triggers an effect in the receiving cell. This effect can be complex, but in the simplest case considered in this article, it is again due to an action potential. The action potential is started by a depolarization of the plasma membrane caused by an influx of sodium ions through an ion channel. To this end transmitter receptors that trigger action potentials are themselves ion channels; to distinguish them from the voltage-dependent ion channels discussed above they are called ligand-gated ion channels.[57] Ligand-gated ion channels are members of the group of type I receptors, as opposed to type II receptors which act on second messenger-producing enzymes through coupling (G) proteins. The ligand-gated ion channel can be specific for cations (Na^+, K^+, Ca^{2+}) or anions (Cl^-). An influx of negative charge into the cell would hyperpolarize it, thereby preventing the triggering of an action potential. Synapses with ligand-gated anion channels are therefore inhibitory; those with cation channels are excitatory synapses. Excitatory synapses use neurotransmitters such as acetylcholine and glutamate; inhibitory synapses use glycine or GABA (γ-amino butyric acid).[58]

So much for the neurobiological background. To return to the toxins-as-tools concept, I would like to restrict myself to a few selected systems, that is, the type I receptors for the transmitters glycine and acetylcholine. I chose the first because it shows in a very straightforward manner the successful procedure leading from applying a toxin to elucidating much of the receptor structure and the second, the nicotinic acetylcholine receptor, because it was the first and still is the best-characterized, a model for the other receptors of its class and an especially convincing example for toxins-as-tools technology.

3.7. Strychnine and the Glycine Receptor

Strychnine is not only a means for murder in many crime stories. It was also the handle which enabled the glycine receptor to be extracted from biological material and purified to homogeneity, prerequisites for partial sequencing, cloning, and cDNA sequencing, which finally led to the primary structure.[59a, 60] Strychnine as a toxin ($LD_{50} = 1\ mg\,kg^{-1}$ in man) causes motor disturbances, convulsions, and death through arrest of respiration.[2, 89] The convulsive action is based on its antagonistic effect on the inhibitory glycinergic synapses in the spinal cord.[59b] Glycine is the predominant inhibitory transmitter in the spinal chord and brain stem, while GABA plays this role mainly in the cortex and cerebellum. In 1982 the glycine receptor was isolated by affinity chromatography on a resin containing immobilized strychnine.[61] The protein is composed of three types of polypeptide chains with molecular weights of 93, 58 (β), and 48 kDa (α_1). The total M_r was about 250 kDa, representing a pentamer[62, 63] comprising the 48 and 58 kDa subunits. The 93 kDa subunit, unlike the other polypeptide chains, is a peripheral protein located at the cytoplasmic surface of the membrane and mediating the interaction of the receptor with the cytoskeleton.[64] Because of this bridging function it was recently named gephyrine.[66] ^{3}H-strychnine helped to detect the ligand binding site in the receptor complex. It can be used as a photoaffinity label and on UV irradiation is irreversibly incorporated into the 48 kDa subunit.[61, 66] Glycine competes with strychnine,[67] but though the binding sites for these two ligands seem to overlap, they are not identical.[68]

Several isoforms of the α- and β-subunits, products of different genes as well of alternative splicing, have been detected.[69, 70] Among these, a neonatally expressed isoform α_2 is especially interesting because its regulation depends on the development of the animal and its low affinity for strychnine.[71, 72] Newly born mice are relatively insensitive to strychnine, because of a single amino acid exchange in the glycine recpetor's α-subunit.[72]

The most interesting finding with the glycine receptor was its similarity with the nicotinic acetylcholine receptor.[60, 62] The primary structures of the subunits are homologous, not only to each other, but also to the other type II receptors (with the exception of the glutamate receptors). Hydropathy plots show that they are also similar in their putative transmembrane folding. Glycine, GABA, and nicotinic acetylcholine receptors are therefore grouped into one "super family" whose members may have evolved from one common ancestral receptor.[73]

These details and many more are, however, the subject of specialized reviews. In the context of this article I want to point out the role toxins play in receptor research: through binding assays and photoaffinity labeling, the toxin aids in defining receptor subunits and isolating the protein. This is a prerequisite for molecular cloning and sequencing either of genomic DNA or of cDNA, (because needed for this are oligonucleotide probes that are deduced from amino acid sequences gained from one or several receptor peptides). To prove that the DNA properly cloned and sequenced codes for the receptor under investigation, expression in a heterologous system, for example in *xenopus* oocytes, is required. There the identity of the receptor is tested electrophysiologically; one criterium for testing whether the right and complete receptor was obtained is its susceptibility to ligands including toxins. This step by step approach has now become routine in receptor research, and we shall see another classical example for this below.

3.8. α-Neurotoxins and the Nicotinic Acetylcholine Receptor

One transmitter receptor exists which we know very well, mainly because the tool kit provided by nature is especially rich in specific toxins.[74] This is the nicotinic acetylcholine receptor of the vertebrate peripheral[7] and central nervous system.[75] As I proceed in briefly reviewing some of the biochemical data collected by neurochemists (mainly over the past two decades), I shall try to enlarge upon the efficiency of some of these tools.

By the middle of the nineteenth century, more than fifty years before scientists knew anything about synapses and receptors, Claude Bernard identified the neuromuscular junction as the site of action of the arrow poison curare.[76] This can be seen as the first step in unraveling the machinery of nerve impulse transmission. But it was not before the early nineteen-seventies that another toxin became crucial for identifying, isolating, and finally characterizing in great structural detail the molecular target of D-tubocurarine, one of the neurotoxic components of the arrow poison.

This other toxin was α-bungarotoxin from the krait *Bungarus multicinctus* (a venomous snake) and a whole family of homologous peptide toxins from poisonous snakes of the genus *Elapidae* and *Hydrophiidae* (whose members include the many species of cobra and sea snakes). Chang and Lee[77] showed that it blocks synaptic transmission at the neuromuscular endplate, the synapse that uses the neurotransmitter acetylcholine for conveying nerve impulses to striated muscle. (At smooth muscle and at heart muscle another type of synapse that also uses acetylcholine is involved in nerve impulse transmission. These synapses respond to different toxins, mainly mushroom and plant alkaloids like muscarine and atropine. They are called "muscarinic cholinergic"[78] as opposed to the "nicotinic cholinergic" synapse discussed in this article; Figure 9).

α-Bungarotoxin was in effect the handle by which the nicotinic acetylcholine receptor was extracted from its membrane environment.[7, 77] It binds with very high affinity ($K_D = 10^{-11}$ M) and extreme specificity to one of the many proteins in the postsynaptic membrane (which in the case of the neuromuscular endplate is the muscle membrane). This integral membrane protein is the nicotinic acetylcholine receptor, the molecule that binds the transmitter acetylcholine released from the nerve ending when an invading action potential arrives. There are other acetylcholine-binding proteins nearby, for example, the acetylcholine esterase, which terminates the nerve impulse by hydrolyzing the transmitter, but this enzyme has no affinity towards α-bungarotoxin. Moreover, α-bungaratoxin was the tool to prove that the acetylcholinesterase and the acetylcholine receptor are different entities.[79] Initially the esterase was thought to simultaneously be the "receptor", possibly causing depolarization of the muscle membrane by letting cations pass at the interface between the protein and its lipid environment.[80]

The method by which a receptor is defined and quantitated is the binding assay. Tritiated α-bungarotoxin[81] was used for quantitative determinations of the amount of receptor protein present, for example, in the different fractions of affinity chromatography of membrane proteins solubilized in detergents. In a typical binding assay,[82] a protein fraction is incubated with

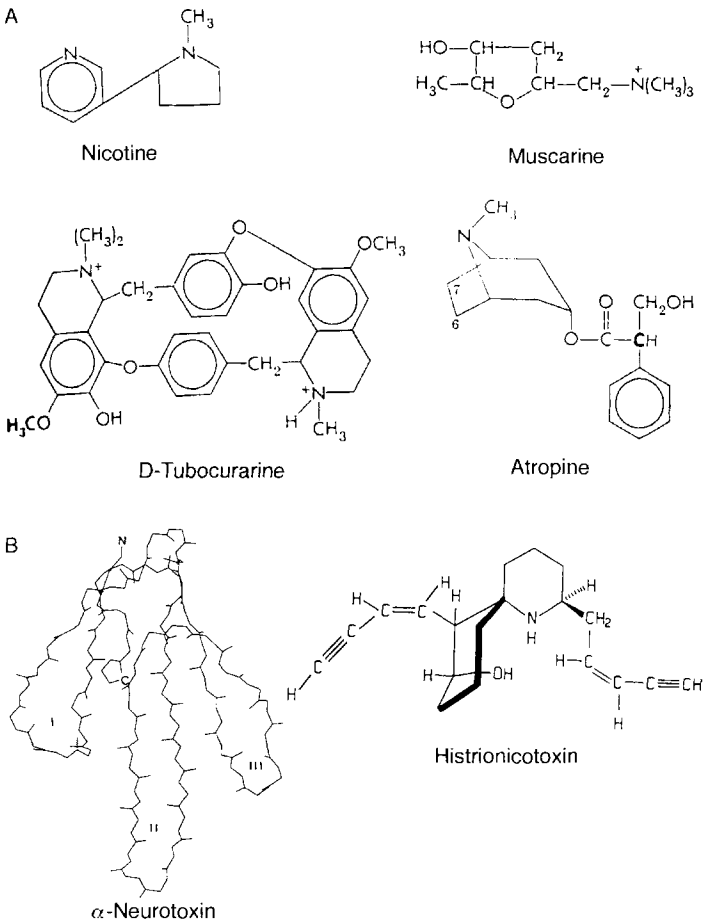


Fig. 9. Neurotoxins of cholinergic synapses. A: Toxins used for discriminating receptor types (nicotinic versus muscarinic acetylcholine receptors). B: Toxins used for discriminating receptor subsites (R versus E of the nicotinic acetylcholine receptor; see text).

^{3}H-α-bungarotoxin. After equilibration the mixture is filtered through a cation exchanger, on which the receptor and its bound radioactive toxin are retained. Unbound toxin is eluted. The radioactivity retained on the filter gives a direct estimate of the number of "binding sites" (= receptor molecules or, if one receptor binds more than one toxin molecule, fractions of this number) present in the protein mixture.

Likewise, fluorescently or radioactively labeled α-bungarotoxin was used to localize and count the receptors in the extra- and subsynaptic part of the endplate, respectively. (Subsynaptically, there are about 20000 receptors per μm^2).

With this tool at hand, the nicotinic acetylcholine receptor was rapidly purified to homogeneity and characterized biochemically. This work was primarily done by Jean-Pierre Changeux and his co-workers at the Institut Pasteur in Paris, but also—sometimes in fierce competition—by Arthur Karlin (New York), Michael Raftery (Pasadena), the Eldefrawis (Baltimore), Eric Barnard (London), and many others. Besides the toxin tool, another help was supplied by nature: the electric tissue of electric eel (*Electrophorus electricus*) and electric ray (*Torpedo spc.*). David Nachmansohn[83] had discovered that this tissue is extremely rich in cholinergic innervation. It made the isolation of receptor protein in mg quantities possible. It turned out that the fish receptor is well conserved during evolu-

tion and in its biochemistry, electrophysiology, immunology, pharmacology, and toxicology very similar to the receptor of higher vertebrates including humans.

Before I continue with the toxin-as-tool theme, I want to summarize some of the biochemical features of the nicotinic acetylcholine receptor that are the basis for the discussion of present applications of toxins in the investigation of structure–function relationships.

The nicotinic acetylcholine receptor[6, 7, 84–88] from *Torpedo californica* is a heteropentameric glycoprotein of M_r 290000. It is composed of two identical polypeptide chains (α, apparent M_r 40000, 437 amino acids) and three different ones (β, apparent M_r 50000, 469 amino acids; γ, apparent M_r 60000, 489 amino acids, and δ, apparent M_r 65000, 501 amino acids). The quaternary structure therefore is $\alpha_2\beta\gamma\delta$. All subunits are glycosylated, all are phosphorylated, and all span the membrane. Since the primary structures of the polypeptide chains was deduced from the cloned and sequenced cDNAs,[89–92] it was assumed that the four stretches of hydrophobic amino acids, each about 22 amino acids long, which are observed in all polypeptide chains, indicate that the chains span the membrane four times.[93]. Until recently it was predicted that the transmembrane part of the receptor is formed by α-helices,[94] but now we are sure that part of the transmembrane domain is formed by β-strands. Both the N- and the C-termini of the chains are extracellular. The primary structures of the four different subunits are similar, which indicates that they may have originated early in evolution from a common ancestral gene.[95] I already mentioned their similarity with other members of the superfamily of ligand-gated ion channels.[60]

So much for the structure. As to the functions, I have mentioned that the nicotinic acetylcholine receptor regulates the cation permeability of the postsynaptic membrane. Therefore, within the protein structure described above there must be at least two functional moieties, an acetylcholine- (and α-neurotoxin-) binding pocket and an ion channel regulated by it. Since the ligand-binding site and the channel interact in the same manner as interactions previously found with allosteric enzymes and transport proteins,[96, 97] there must be a third functional moiety mediating ("transducing") this interaction. This tripartite operational structure is in compliance with the general scheme of all receptor architectures.[57] They are composed of a signal-receiving (ligand-binding) part R, an effector part E that mediates the effect the signal is supposed to have on the target cell, and a transducer structure T, which couples R and E. This RTE-triune receptor concept is the basis of receptor classification into three types: type I, II, and III. The latter type comprises the growth hormone receptors, which are not the concern of this article. With the neurotransmitter receptors the type I receptors are defined as those proteins that contain R,T, and E (usually an ion channel) integrated into one protein. Type II receptors on the other hand contain R,T, and E (which is here an enzyme in most cases, although recently several ion channels have been found in this class too) on distinct and separable proteins. Examples of type I receptors are the nicotinic acetylcholine receptor, the $GABA_A$ and glycine receptors and some subtypes of the serotonine and glutamate receptors. Type II receptors are the β-adrenergic and muscarinic acetylcholine receptors, the receptors for opiates and other peptides, the dopamine receptors etc.[57]

If R, T, and E in type I receptors are not separate molecules, it is an even more difficult task to detect them within the integral protein structure. Here again toxins were indispensible tools, and again I shall prove this point using the nicotinic acetylcholine receptor as an example. The α-neurotoxins are antagonistic ligands of R,[74] while other, mostly low molecular weight, toxins bind specifically to the ion channel E.[97] It turned out that T, the part of the receptor structure transducing the ligand-binding effect to the ion channel, is located at or near this latter toxin-binding site as well.[98]

3.9. Dissection of a Receptor: 'R', the Signal-Receiving Site

The nicotinic acetylcholine receptor has its name from nicotine, a toxic plant alkaloid which, like acetylcholine, acts as an agonist (Fig. 9). Competing for the same ligand-binding site are antagonists, the most powerful of which are the toxic compounds like the arrow poison D-tubocurarine and the snake venom peptide α-neurotoxins. Agonist- and competitive antagonist-binding sites are presently mapped by affinity labeling in connection with microsequencing and by site-directed mutagenesis experiments. There are two binding sites per receptor molecule, one on each of the two α-subunits. By using ^{3}H-α-bungarotoxin in combination with other techniques (reviewed in ref. [7]) the amino acid sequence α180–200 was shown to participate directly in the toxin binding. Interestingly, the receptor from snakes has several mutations in this sequence, lowering the affinity and thereby the toxicity of its own α-neurotoxin.[99]

Recently it became apparent that other subunits participate in toxin binding as well. Photoaffinity labeling of the membrane-bound receptor with radioactive derivatives of D-tubocurarine[100] and α-neurotoxin II from a cobra venom[101] showed that the γ- and δ-subunits incorporate these toxins as well. More specifically, labeling of neighboring subunits with cobra toxin was only achieved when the photoreactive group was attached to one specific residue, lysine 26, of the peptide toxin (Fig. 10).[102] If the photo group was on lys 46, only the

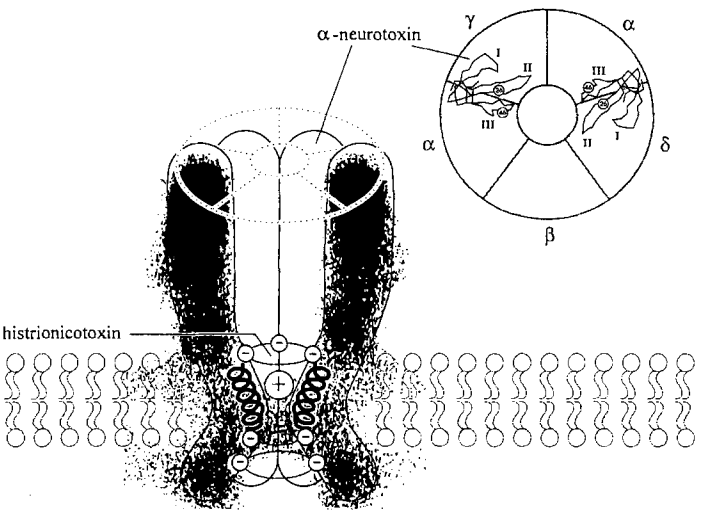


Fig. 10. Model of the nicotinic acetylcholine receptor, the prototype of a ligand-gated ion channel, which was characterized to a large extent by the use of neurotoxins.

α-subunits could be labeled. Moreover, binding studies with D-tubocurarine showed that the two α-subunits have different affinities for their ligands,[103] and competition experiments with photolabeling derivatives of cobra toxin (the lys 26 derivative) indicated that the high affinity α-subunit is located next to the γ- and the low affinity subunit to the δ-subunit. These (and other experiments reviewed elsewhere) allow several conclusions: The antagonist and agonist binding sites are located at the interface of the α- and δ-, and the α- and γ-subunits, respectively. Symmetry considerations demand an $\alpha\gamma\alpha\beta\delta$[87] rather than an $\alpha\beta\alpha\gamma\delta$[104] quaternary structure (Fig. 10).

At present the receptor surface and the quaternary structure are being mapped with α-neurotoxins as tools. In the absence of an X-ray structure this will supply us with a three-dimensional image of at least part of the receptor. This approach is especially promising since the exact tertiary structure of the toxins are known (Fig. 9B) from X-ray analysis of the crystalline proteins[104-106] and from NMR studies.[107-109] If photoreactive groups are introduced to defined side chains, these toxin derivatives can be used as yard sticks for mapping the receptor topography.[102, 110]

3.10. The Ion Channel E as the Receptor's Effector Site

Besides the competitive antagonists there are noncompetitive antagonists (Fig. 9B). These compounds do not prevent the agonist from binding to its sites on the receptor, but still block the response, that is, the ion flux through the channel. Neurotoxins helped to show that noncompetitive antagonists bind directly to the ion channel, blocking it sterically (or allosterically).[7, 96, 97] One such channel-blocking toxin is histrionicotoxin, which is isolated from the skin of South American frogs of the genus *Dendrobates*. Histrionicotoxin became the principal tool in attempts to identify the ion channel within the receptor protein.[111, 112] The main criteria for assigning any compound as a ligand of a site in the ion channel is its voltage-dependent blocking activity and its competition with the proven ion channel ligand histrionicotoxin.[97] According to these criteria[113, 114] a small organic cation, the triphenymethylphosphonium ($TPMP^+$) ion, was used to covalently photolabel the wall of the ion channel and to identify it using protein chemistry methods.[114, 115] The surprising result of these experiments was that each subunit was labeled by $TPMP^+$ in a homologous position.[115] This means that the five subunits contribute a homologous amino acid sequence to the channel wall. This sequence is one of the four hydrophobic stretches thought to span the membrane.[92] Specifically, it is the putative transmembrane helix M2. Therefore, (with the help of histrionicotoxin as a tool) for the first time a receptor's ion channel was identified (Fig. 10): E, the acetylcholine receptor's ion channel, is formed at least in part by the five putative transmembrane helices M2 of the receptor's subunits.[115, 116]

This result was compatible with experiments using quite different techniques, for example, the recombinant DNA technique in combination with patch clamp electrophysiology.[117, 118]

3.11. T, the Receptor's Transducer?

The transducer, the part of the protein coupling R to E, was found by photo affinity labeling and by site directed mutagenesis rather than with the help of neurotoxins. It is located on the same structures which form the wall of the ion channel, that is, on the helix M2.[119, 120]

4. Conclusion

This review of the recent upsurge of neurochemical discoveries due to the use of toxins as tools may give a false impression. It may seem that these tools are restricted to the elucidation of synaptic mechanisms. This is not the case. If space would allow it, I could expand to completely different areas of research such as axonal transport, neuronal development, etc. Given the success of this approach in some fields, and given the continuous discovery of new neurotoxins, it is safe to predict exciting applications of this tool-kit in future neurochemical research.

I thank Prof. Dr. Victor Tsetlin for fruitful cooperation and discussions. Part of the artwork (Figs. 3 and 10) was executed by Ms. K. von Etzel. Work from my laboratory mentioned in this article was financed by the State of Berlin, the Deutsche Forschungsgemeinschaft (SFB 312), and the Fonds der Chemischen Industrie.

Received: November 29, 1993 [A 39 IE]
German version: *Angew. Chem.* **1994**, *106*, 23

[1] Z. W. Hall, *Molecular Neurobiology*, Sinauer, Sunderland, MA, **1992**.
[2] *Handbook of Toxinology* (Eds.: W. T. Shier, D. Mebs), Dekker, New York, **1990**.
[3] H. Herken, F. Hucho, *Handb. Exp. Pharmacol.* **1992**, *102*.
[4] *Toxins as Tools in Neurochemistry* (Eds.: F. Hucho, Yu. A. Ovchinnikov), de Gruyter, Berlin, **1983**.
[5] *Neurotoxins in Neurochemistry* (Ed.: J. O. Dolly), Horwood, Chichester, **1988**.
[6] A. Maelicke, *Angew. Chem.* **1984**, *96*, 193–219; *Angew. Chem. Int. Ed. Engl.* **1984**, *23*, 195–221.
[7] J.-P. Changeux, *Fidia Research Foundation Neuroscience Award Lectures, Vol. 4*, Raven Press, New York, **1990**, pp. 21–168.
[8] F. Hucho, *Neurochemistry—Fundamentals and Concepts*, VCH, Weinheim, **1986**.
[9] A. L. Hodgkin, A. F. Huxley, *J. Physiol. (London)* **1952**, *116*, 473–496.
[10] B. Hille, *Ionic Channels of ExciTable Membranes*, 2nd ed., Sinauer, Sunderland, MA, **1992**.
[11] M. Lazdunski, J. F. Renead, *Annu. Rev. Physiol.* **1982**, *44*, 463–473.
[12] S. Becker, R. D. Gordon, *Handb. Exp. Pharmacol.* **1992**, *102*, 719–737.
[13] N. S. Cook, *Potassium Channels*, Horwood, Chichester, **1990**.
[14] H. Meves, *Handb. Exp. Pharmacol.* **1992**, *102*, 739–774.
[15] E. Carbone, E. Wanke, G. Prestipino, L. D. Possani, A. Maelicke, *Nature* **1982**, *296*, 90–91.
[16] E. Carbone, G. Prestipino, E. Wanke, L. D. Possani, A. Maelicke, *Toxicon* **1983**, *3*, 57–60.
[17] W. Catterall, *Science* **1988**, *242*, 50–61.
[18] W. S. Agnew, *Annu. Rev. Physiol.* **1984**, *46*, 517–530.
[19] J. C. Tanaka, R. E. Furman, R. L. Barchi in *Ion Channel Reconstitution* (Ed.: C. Miller), Plenum, New York, **1986**, pp. 307–336.
[20] W. Catterall, *Annu. Rev. Biochem.* **1986**, *55*, 953–985.
[21] M. Noda, S. Shimizu, T. Tanabe, T. Takai, T. Kayano, T. Ikeda, H. Takahashi, H. Nakayama, Y. Kanoka, N. Minamino, K. Kangawa, H. Matsuo, M. S. Raftery, T. Hirose, S. Inayama, H. Hayashida, T. Miyata, S. Numa, *Nature* **1984**, *312*, 121–127.
[22] M. Noda, T. Ikeda, H. Suzuki, H. Takeshima, T. Takahashi, M. Kuno, S. Numa, *Nature* **1986**, *322*, 826–828.
[23] M. Noda, H. Suzuki, S. Numa, W. Stühmer, *FEBS Lett.* **1989**, *259*, 213–216.
[24] O. Pongs, *Pflügers Arch.* **1989**, *414*, 71–75.
[25] A. J. Yool, T. L. Schwarz, *Nature* **1991**, *349*, 700–704.
[26] W. B. Huttner, *Nature* **1993**, *365*, 104–105.
[27] a) T. Söllner, S. W. Whiteheart, M. Brunner, H. Erdjument-Bromage, S. Geromanos, P. Tempst, J. E. Rothman, *Nature* **1993**, *362*, 318–324; b) S. W. Whiteheart, I. C. Griff, M. Brunner, D. O. Clary, T. Mayer, S. A. Buhrow, J. E.

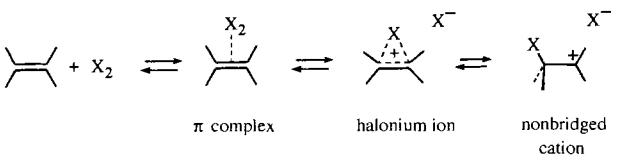
Rothman, *ibid.* **1993**, *362*, 353–355; c) M. K. Bennet, R. H. Scheller, *Proc. Natl. Acad. Sci. USA* **1993**, *90*, 2559–2563.
[28] T. M. Jessell, E. R. Kandel, *Cell* **1993**, *10*, 1–30.
[29] R. B. Kelly, *Cell* **1993**, *10*, 43–53.
[30] J. Striessnig, H. Glossmann, *Handb. Exp. Pharmacol.* **1992**, *102*, 775–805.
[31] B. M. Olivera, J. Rivier, J. K. Scott, D. R. Hillyard, L. J. Cruz, *J. Biol. Chem.* **1991**, *266*, 22067-22070.
[32] M. R. Plummer, D. E. Logothetis, D. Hess, *Neuron* **1989**, *2*, 1453–1463.
[33] H. Glossmann, J. Striessnig, *Rev. Physiol. Biochem. Pharmacol.* **1990**, *114*, 1–105.
[34] J. L. Cruz, B. M. Olivera, *J. Biol. Chem.* **1986**, *201*, 6230–6233.
[35] A. Grasso in *Neurotoxins in Neurochemistry* (Ed.: J. O. Dolly), Horwood, Chichester, **1988**, pp. 67–78.
[36] M. Matteoli, C. Haimann, F. Torri-Tarelli, J. M. Polak, B. Ceccarelli, P. de Camilli, *Proc. Natl. Acad. Sci. USA* **1988**, *85*, 7366–7370.
[37] A. G. Petrenko, V. A. Kovalenko, O. G. Shamotienko, I. N. Surkova, T. A. Tarasyuk, Y. A. Ushkaryov, E. V. Grishin, *EMBO J.* **1990**, *9*, 2023–2027.
[38] Y. A. Ushkaryov, A. G. Petrenko, M. Geppert, T. C. Südhof, *Science* **1992**, *257*, 50–56.
[39] A. G. Petrenko, M. S. Perin, B. A. Davletov, Y. A. Ushkanyov, M. Geppert, T. C. Südhof, *Nature* **1991**, *353*, 65–68.
[40] J. O. Dolly, *Handb. Exp. Pharmacol.* **1992**, *102*, 681–717.
[41] J. O. Dolly, J. V. Halliwell, J. D. Black, R. S. William, A. Pelchen-Matthews, A. L. Breeze, F. Mehraban, I. B. Othman, A. R. Black, *J. Physiol. (Paris)* **1984**, *79*, 280–303.
[42] F. Dreyer, *Rev. Physiol. Biochem. Pharmacol.* **1990**, *115*, 93–136.
[43] A. L. Breeze, J. O. Dolly, *Eur. J. Biochem.* **1989**, *178*, 771–778.
[44] P. Rosenberg in *Neurotoxins in Neurochemistry* (Ed.: J. O. Dolly), Horwood, Chichester, **1988**, pp. 27–42.
[45] H. H. Wellhöner, *Handb. Exp. Pharmacol.* **1992**, *102*, 357–417.
[46] C. Montecucco, *Trends Biochem. Sci.* **1986**, *11*, 314–317.
[47] B. Poulain, S. Mochida, M. Weller, B. Högy, E. Habermann, J. D. F. Wadsworth, C. C. Shone, J. O. Dolly, L. Tauc, *J. Biol. Chem.* **1991**, *266*, 9580–9585.
[48] M. F. Schmid, J. P. Robinson, B. R. DasGupta, *Nature* **1993**, *364*, 827–830.
[49] C. Montecucco, G. Schiavo, *Trends Biochem. Sci.* **1993**, *18*, 324–327.
[50] G. Schiavo, F. Benfenati, B. Poulain, O. Rossetto, P. Polverino de Laureto, B. R. DasGupta, C. Montecucco, *Nature* **1992**, *359*, 832–834.
[51] E. Link, L. Edelmann, J. H. Chou, T. Binz, S. Yamasaki, U. Eisel, M. Baumert, T. C. Südhof, H. Niemann, R. Jahn, *Biochem. Biophys. Res. Commun.* **1992**, *189*, 1017–1023.
[52] G. Schiavo, C. C. Shone, O. Rossetto, F. C. G. Alexander, C. Montecucco, *J. Biol. Chem.* **1993**, *268*, 11516–11519.
[53] J. Blasi, *EMBO J.* **1993**, *12*, 4821–4828.
[54] J. Blasi, E. R. Chapman, E. Link, T. Binz, S. Yamasaki, P. De Camilli, T. C. Südhof, H. Niemann, R. Jahn, *Nature* **1993**, *365*, 160–163.
[55] S. W. Whiteheart, J. C. Griff, M. Brunner, D. O. Clary, T. Mayer, S. A. Buchrow, J. E. Rothman, *Nature* **1993**, *362*, 353–355.
[56] T. Söllner, S. W. Whiteheart, M. Brunner, H. Erdjumant-Bromage, S. Geromanos, P. Tempst, J. E. Rothman, *Nature* **1993**, *362*, 318–324.
[57] F. Hucho, *New Compr. Biochem.* **1994**, *24*, 3–14.
[58] H. Betz, *Neuron* **1993**, *5*, 383–392.
[59] a) H. Betz, *Angew. Chem.* **1985**, *97*, 363–368; *Angew. Chem. Int. Ed. Engl.* **1985**, *24*, 365–370; b) C.-M. Becker, *Handb. Exp. Pharmacol.* **1992**, *102*, 539–575.
[60] G. Grenningloh, A. Rienitz, B. Schmitt, C. Methfessel, M. Zensen, K. Beyreuther, E. D. Gundelfinger, H. Betz, *Nature* **1987**, *328*, 215–220.
[61] F. Pfeiffer, D. Graham, H. Betz, *J. Biol. Chem.* **1982**, *257*, 9389–9393.
[62] D. Langosch, L. Thomas, H. Betz, *Proc. Natl. Acad. Sci. USA* **1988**, *85*, 7394–7398.
[63] D. Langosch, C.-M. Becker, H. Betz, *Eur. J. Biochem.* **1990**, *194*, 1–8.
[64] J. Kirsch, D. Langosch, P. Prior, U. Z. Littauer, B. Schmitt, H. Betz, *J. Biol. Chem.* **1991**, *266*, 22242–22245.
[65] P. Prior, B. Schmitt, G. Grenningloh, I. Pribilla, G. Multhaupt, K. Beyreuther, Y. Maulet, P. Werner, D. Langosch, J. Kirsch, H. Betz, *Neuron* **1992**, *8*, 1161–1170.
[66] D. Graham, F. Pfeiffer, R. Simler, H. Betz, *Biochemistry* **1985**, *24*, 990–994.
[67] D. Graham, F. Pfeiffer, H. Betz, *Eur. J. Biochem.* **1983**, *131*, 519–525.
[68] J. C. Marvizón, J. Vazquez, M. Garcia-Calvo, F. Mayor, Jr., A. Ruiz-Gomez, F. Valdivieso, J. Benavides, *Mol. Pharmacol.* **1986**, *30*, 590–597.
[69] G. Grenningloh, V. Schmieden, P. Schofield, P. H. Seeburg, T. Siddique, T. K. Mohandas, C.-M. Becker, H. Betz, *EMBO J.* **1990**, *9*, 771–776.
[70] G. Grenningloh, I. Pribilla, P. Prior, G. Multhaupt, K. Beyreuther, O. Taleb, H. Betz, *Neuron* **1990**, *4*, 963–970.
[71] C.-M. Becker, W. Hoch, H. Betz, *EMBO J.* **1988**, *7*, 3717–3726.
[72] J. Kuhse, V. Schmieden, H. Betz, *Neuron* **1990**, *5*, 867–873.
[73] P. R. Schofield, M. G. Darlison, N. Fujita, D. R. Burt, F. A. Stephenson, H. Rodriguez, L. M. Rhee, J. Ramachandran, V. Reale, T. A. Glencorse, P. H. Seeburg, E. A. Barnard, *Nature* **1987**, *328*, 221–227.
[74] F. Hucho, *Handb. Exp. Pharmacol.* **1992**, *102*, 577–610.
[75] E. S. Deneris, J. Conolly, S. W. Rogers, R. Duvoisin, *Trends Biochem. Sci.* **1991**, *12*, 34–40.
[76] C. Bernard *Leçon sur les Effets des Substances Toxiques et Medicamenteuse*, Beilliere, Paris, **1857**, pp. 238–306.
[77] C. C. Chang, C. Y. Lee, *Arch. Int. Pharmacodyn. Ther.* **1963**, *144*, 316–332.
[78] J. Järv, A. Rinken, *New Compr. Biochem.* **1994**, *24*, 199–220.
[79] R. Olsen, J. C. Meunier, J.-P. Changeux, *FEBS Lett.* **1972**, *28*, 96–100.
[80] J.-P. Changeux, *Mol. Pharmacol.* **1966**, *2*, 369–392.
[81] A. Menez, J. L. Mongat, P. Fromageot, A. M. Ronseray, P. Boquet, J.-P. Changeux, *FEBS Lett.* **1971**, *17*, 333–338.
[82] J. C. Meunier, R. W. Olsen, J.-P. Changeux, *FEBS Lett.* **1972**, *24*, 63–68.
[83] D. Nachmansohn, *Harvey Lect.* **1955**, 57–99.
[84] J.-P. Changeux, *Harvey Lect.* **1981**, 85–254.
[85] F. Hucho, *Eur. J. Biochem.* **1986**, *158*, 211–226.
[86] T. Claudio in *Frontiers in Molecular Biology: Molecular Neurobiology Volume* (Eds.: D. M. Glover, B. C. Hames), IRL, Oxford University Press, Oxford, **1989**, pp. 63–142.
[87] A. Karlin, *Harvey Lect.* **1991**, 71–107.
[88] F. Hucho, *New Compr. Biochem.* **1994**, *24*, 113–135.
[89] M. Noda, H. Takahashi, T. Tanabe, M. Toyosato, Y. Furutani, T. Hirose, M. Asai, S. Inayama, S. Numa, *Nature* **1982**, *299*, 793–797.
[90] M. Noda, H. Takahashi, T. Tanabe, M. Toyosato, S. Kikyotani, Y. Furutani, T. Horose, H. Takashima, S. Inayama, T. Miyata, S. Numa, *Nature* **1983**, *301*, 251–255.
[91] M. Noda, H. Takahashi, T. Tanabe, M. Toyosato, S. Kikyotani, Y. Furutani, T. Horose, H. Takashima, S. Inayama, T. Miyata, S. Numa, *Nature* **1983**, *302*, 528–532.
[92] T. Claudio, M. Ballivet, J. Patrick, S. Heinemann, *Proc. Natl. Acad. Sci. USA* **1983**, *80*, 1111–1115.
[93] J. Finer-Moore, R. M. Stroud, *Proc. Natl. Acad. Sci. USA* **1984**, *81*, 155–159.
[94] M. A. Raftery, M. Hunkapiller, C. D. Strader, L. E. Hood, *Science* **1980**, *208*, 1454–1457.
[95] A. Karlin, *J. Theor. Biol.* **1967**, *16*, 306–320.
[96] J.-P. Changeux, A. Devillers-Thiéry, P. Chemouilli, *Science* **1984**, *225*, 1335–1345.
[97] K. L. Swanson, E. X. Albuquerque, *Handb. Exp. Pharmacol.* **1992**, *102*, 611–658.
[98] J. Giraudat, M. Dennis, T. Heidmann, J. Y. Chang, J.-P. Changeux, *Proc. Natl. Acad. Sci. USA* **1986**, *83*, 2719–2723.
[99] D. Neumann, D. Barchan, M. Horowitz, E. Kochva, S. Fuchs, *Proc. Natl. Acad. Sci. USA* **1989**, *86*, 7255–7259.
[100] S. E. Pedersen, J. B. Cohen, *Proc. Natl. Acad. Sci. USA* **1990**, *87*, 2785–2789.
[101] V. Tsetlin, K. Pluzhikov, A. Karelin, V. Ivanov in *Toxins as Tools in Neurochemistry* (Eds.: Yu. A. Ovchinnikov, F. Hucho), de Gruyter, Berlin, **1983**, pp. 159–169.
[102] H.-J. Kreienkamp, Yu. N. Utkin, C. Weise, J. Machold, V. Tsetlin, F. Hucho, *Biochemistry* **1992**, *31*, 8239–8244.
[103] R. R. Neubig, J. B. Cohen, *Biochemistry* **1979**, *18*, 5464–5475.
[104] E. Kubalek, S. Ralston, J. Lindstrom, N. Unwin, *J. Cell Biol.* **1987**, *105*, 9–18.
[105] B. Low, H. S. Preston, A. Sato, L. S. Rosen, J. E. Searl, A. D. Rudko, J. S. Richardson, *Proc. Natl. Acad. Sci. USA* **1976**, *73*, 2991–2994.
[106] D. Tsernoglou, G. A. Petsko, *FEBS Lett.* **1976**, *68*, 1–4.
[107] R. A. Love, R. M. Stroud, *Protein Eng.* **1986**, *1*, 37–46.
[108] R. C. Hider, A. F. Drake, F. Inagaki, R. J. P. Williams, T. Endo, T. Miyazawa, *J. Mol. Biol.* **1982**, *158*, 275–291.
[109] A. P. Golavanov, A. L. Lomize, A. S. Arseniev, Yu. N. Utkin, V. I. Tsetlin, *Eur. J. Biochem.* **1993**, *213*, 1213–1223.
[110] B. Chatrenet, O. Tremeau, F. Bontems, M. P. Goeldner, C. G. Hirth, A. Menez, *Proc. Natl. Acad. Sci. USA* **1990**, *87*, 3378–3382.
[111] E. X. Albuquerque, E. A. Barnard, T. H. Chun, A. J. Lapa, J. O. Dolly, S. E. Jansson, J. Daly, B. Witkop, *Proc. Natl. Acad. Sci. USA* **1973**, *70*, 949–953.
[112] T. Heidmann, R. E. Oswald, J.-P. Changeux, *Biochemistry* **1983**, *22*, 3112–3127.
[113] C. E. Spivak, E. X. Albuquerque, *Mol. Pharmacol.* **1985**, *27*, 246–255.
[114] W. Oberthür, P. Muhn, H. Baumann, F. Lottspeich, B. Wittmann-Liebold, F. Hucho, *EMBO J.* **1986**, *5*, 1815–1819.
[115] F. Hucho, W. Oberthür, F. Lottspeich, *FEBS Lett.* **1986**, *205*, 137–142.
[116] F. Hucho, R. Hilgenfeld, *FEBS Lett.* **1989**, *257*, 17–23.
[117] K. Imoto, C. Methfessel, B. Sakmann, M. Mishina, Y. Mori, T. Konno, K. Fukuda, M. Kurasaki, H. Bujo, Y. Fujita, S. Numa, *Nature* **1986**, *324*, 670–674.
[118] J. A. Dani, *Trends Neurosci.* **1989**, *12*, 125–130.
[119] J. Giraudat, M. Dennis, T. Heidmann, J. Y. Chang, J.-P. Changeux, *Proc. Natl. Acad. Sci. USA* **1986**, *83*, 2719–2723.
[120] F. Revah, D. Bertrand, J.-L. Galzi, A. Devillers-Thiéry, C. Mulle, N. Hussy, S. Bertrand, M. Ballivet, J.-P. Changeux, *Nature* **1991**, *353*, 846–849.
[121] B. Ceccarelli, F. Valtorta, W. P. Hurlbut in *Cellular and Molecular Basis of Synaptic Transmission* (Ed.: H. Zimmermann), Springer, Berlin, **1988**, pp. 55.
[122] H. Zimmermann, W. Volknandt, B. Wittich, A. Hausinger, *J. Physiol. (Paris)* **1993**, *87*, 159–170.

New Findings in the Electrophilic Addition of Halogens to Olefins

Rainer Herges*

According to the textbooks, both the mechanism and the theory of electrophilic addition of halogens to olefins are well understood.[1] It is all the more surprising that there is still some groundwork to be done in this field, as was demonstrated by recent synthetic, spectroscopic, and theoretical publications.

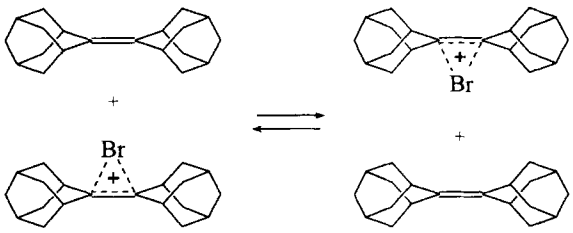
As early as 1937, Roberts and Kimball[2] explained the *anti* selectivity of the bromination of olefins by invoking a bridged bromonium ion as intermediate. Thirty years later, such intermediates were detected under "stable ion conditions" by NMR spectroscopy.[3] The halonium ions of chlorine,[4] bromine,[5] and iodine[6] with adamantylideneadamantane are even isolable as stable salts, because the subsequent nucleophilic attack of the counterion is prevented by steric hindrance in the substrate. It is generally accepted that a π complex precedes formation of such halonium ions,[7–9] and it is supposed that cation-stabilizing substituents (e.g., phenyl) at the olefin lead to distorted or even nonbridged cations (Scheme 1).



Scheme 1.

In the case of adamantylideneadamantane and some other sterically hindered olefins, the free olefin and bromine are in rapid equilibrium with the π complex and the bromonium ion.[6, 10, 11] The equilibrium constant for the formation of the π complex from olefin and bromine strongly depends on the substituents. Moreover, it was demonstrated by NMR that there is a rapid, degenerate transfer of Br^+ from the bromonium ion to the free olefin in the adamantylideneadamantane system (Scheme 2).[6, 12] According to ab initio calculations the transfer proceeds via a "spiro" transition state.

Whereas crystal structures are available for bromonium and iodonium salts,[13, 6] little experimental data exists for the π complexes. According to calculations by Cossi et al.[14] and earlier theoretical work,[15] the π complex of ethene and



Scheme 2.

bromine is about 3–4 kcal mol^{-1} more stable than the starting materials. The axis joining the nuclei in the halogen molecule is perpendicular to the molecular plane of ethene and intersects the midpoint of the double bond. No charge is transferred during complex formation.[16] The frequently used term "charge-transfer complex" is therefore not correct. Since dispersion energy is the main driving force for binding, "van der Waals complex" would be a better description. Compared to the π complex, the bromonium ion is mucher higher in energy. In vacuo (and with bromide as the counterion) the free energy difference is 40 kcal mol^{-1}. Under these conditions the bromonium ion is not likely to be formed by simple thermal activation. However, polar media like methanol lower the free energy of reaction to about +10 kcal mol^{-1}, because the very polar bromonium ion is much better solvated than the nonpolar π complex.

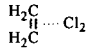
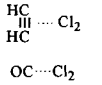
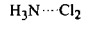
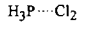
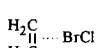
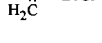
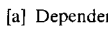
A nonpolar environment and low temperatures should therefore allow the π complex to be observed as a long-lived species. Indeed, as far back as the seventies, the π complex of chlorine and ethene was detected by IR spectroscopy in a nitrogen matrix at 20 K.[17, 18] A totally different and probably revolutionary method for the structural investigation of such labile molecular complexes in the gas phase was reported recently by Legon et al. in a series of papers: Both components (halogen and Lewis base) are expanded separately through a fast-mixing nozzle into the evacuated Fabry–Pérot cavity of a Fourier transform microwave spectrometer.[19] The gases mix, and the supersonic and collision-free expansion results in the molecular complexes being frozen with very low internal energies. Thus, subsequent reaction to form the usual products observed under normal conditions is prohibited. Even complexes such as $H_3P\cdots Cl_2$ can be investigated—the normally explosive course of reaction is avoided.

The rotational spectra do not only give structural information; the intermolecular (quadratic) force constants are related

[*] Priv.-Doz. Dr. R. Herges
Institut für Organische Chemie der Universität Erlangen-Nürnberg
Henkestrasse 42, D-91054 Erlangen (Germany)
Telefax: Int. code + (9131)85-9132
e-mail: herges@organik.uni-erlangen.de

to the centrifugal distortion constants, and the charge distribution can be derived from the nuclear quadrupole coupling constants. Table 1 shows an overview of halogen/Lewis base complexes investigated recently.[20]

Table 1. Bond lengths $r(B\cdots X)$ and force constants k_σ for the $B\cdots X$ bond in the halogen/Lewis base complexes $B\cdots XY$, characterized by rotational spectroscopy.

B···XY	Point group	$r(B\cdots X)$ [Å]	k_σ [N m^{-1}]	Ref.
	C_{2v}	3.128	7.1	[21]
	C_{2v}	3.165	6.8	[22]
	$C_{\infty h}$	3.134	3.7	[23]
	C_{3v}	2.724	12.7	[24]
	C_{3v}	3.240	5.5	[25]
	$C_{\infty h}$	2.915	6.6	[26]
	C_{2v}	2.979	10.5	[27]
	C_{2v}	3.059	9.4	[28]
	$C_{\infty h}$	4.272–4.332 [a]	6.18–6.34 [a]	[29]

[a] Dependent on the isotopic composition.

From a mechanistic point of view, the complexes of ethene and ethyne are most interesting. The axis joining the nuclei in the halogen molecule is perpendicular to and intersects the midpoint of the double or triple bond (Fig. 1). The structural parameters of both the halogen and ethene or ethyne are not significantly changed by complexation. The small force constants k_σ (Table 1) also indicate a very weak interaction between π bond and halogen.[30] The nuclear quadrupole coupling constants of the chlorine atoms differ only slightly and are almost equal to the values observed for free chlorine. This means that there is only a small perturbation in the charge distribution on moving from the separate components to the complex. No significant polarization within the bound halogen is observed. Hence, the microwave investigations provide an impressive confirmation of the properties predicted earlier by theoretical calculations and matrix isolation.

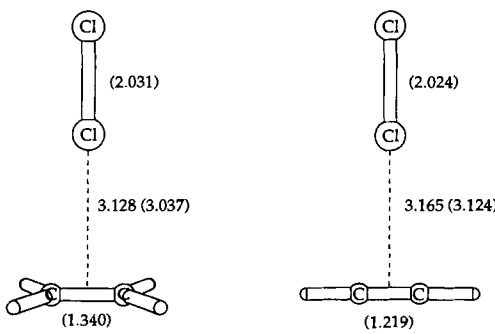
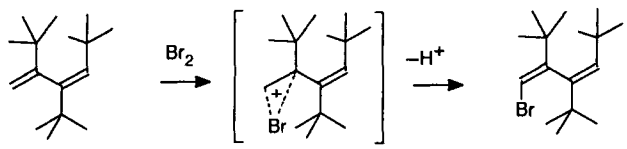


Fig. 1. Structures of the π complexes of chlorine with ethene [21] (left) and ethyne [22] (right). Bond lengths in Å (ab initio values [31] in parentheses).

Hopf et al. recently reported a fascinating, sterically hindered system that, in solution at room temperature, prevents further reaction of the π complex and bromonium ion to form the usual dihalogenated products.[32] With 1,2,3-tri-*tert*-butyl substituted butadiene, the cationic intermediate is stabilized by loss of an α proton. Thus, the overall course of reaction corresponds to that observed for aromatic electrophilic substitutions, which also proceed via a π complex and cationic intermediate (Scheme 3). In the bromination of 2,2,5,5-tetramethyl-3-hexene, the intermediate bromonium ion is stabilized by loss of a β proton. Subsequent HBr elimination yields 2,3-di-*tert*-butyl-1,3-butadiene.[33]



Scheme 3.

The examples show that long-known reactions are also worthy of closer inspection. Modern theoretical, analytical, and synthetic methods not only open novel fields of application, they are also able to contribute to the basic knowledge of mechanistic chemistry.

German version: *Angew. Chem.* **1995**, *107*, 57

Keywords: alkene–halogen complexes · alkyne–halogen complexes · electrophilic addition · reaction mechanisms

[1] For a very detailed review of the mechanism of the bromination of olefins, see M.-F. Ruasse, *Adv. Phys. Org. Chem.* **1993**, *28*, 207.
[2] I. Roberts, G. E. Kimball, *J. Am. Chem. Soc.* **1937**, *59*, 947
[3] a) G. A. Olah, J. M. Bollinger, J. Brinich, *J. Am. Chem. Soc.* **1968**, *90*, 2587; b) G. A. Olah, P. Schilling, P. W. Westerman, H. C. Lin, *ibid.* **1974**, *96*, 3581.
[4] J. H. Wieringa, J. Strating, H. Wynberg, Tetrahedron Lett. **1970**, 4579.
[5] J. Strating, J. H. Wieringa, H. Wynberg, *J. Chem. Soc. Chem. Commun* **1969**, 907.
[6] R. S. Brown, R. W. Nagorski, A. J. Bennet, R. E. D. McClung, G. H. M. Aarts, M Klobukowski, R. McDonald, B. D. Santasiero, *J. Am. Chem. Soc.* **1994**, *116*, 2448
[7] For the first unambiguous spectroscopic evidence for the formation of a π complex as intermediate in the electrophilic addition of chlorine and bromine to olefins, see a) J. E. Dubois, F. Garnier, *Spectrochim. Acta Part A* **1967**, *23*, 2288; b) R. S. Brown, H. Slebocka-Tilk, A. J. Bennet, G. Bellucci, R. Bianchini, R. Ambrosetti, *J. Am. Chem. Soc.* **1990**, *112*, 6310; c) G. Bellucci, R. Bianchini R. J. Ambrosetti, *ibid.* **1985**, *107*, 2464; d) S. Fukuzumi, J. K. Kochi, *J. Org. Chem.* **1981**, *46*, 4116.
[8] From the very strong dependance of the reaction rate, Dubois and Garnier conclude that the nucleophilic attack of the counterion or the solvent takes place at the stage of the bromonium ion, rather than at that of the π complex. The unusually strong solvent isotope effect also suggests that the transition state of the rate-determining step is strongly polarized and most probably corresponds to the formation of the bomonium ion from the π complex: a) J. E. Dubois, F. Garnier, *J. Chem. Soc. Chem. Commun.* **1968**, 241; b) F. Garnier, R. H. Donnay, J. E. Dubois, *ibid.* **1971**, 829.
[9] There are (mostly arene-substituted) olefins that are probably not chlorinated via cationic intermediates, since the *cis* products are formed stereospifically. Not much is known about the mechanism of this "direct" addition, which probably involves the *cis* collapse of the π complex: a) S. J. Cristol, F. R. Stermitz, P. S. Ramey, *J. Am. Chem. Soc.* **1958**, *78*, 4939; b) P. B. D. de la Mare, N. V. Klassen, R. Koenigsberger, *J. Chem. Soc.* **1961**, 5285; c) P. B. D. de la Mare, R. Koenigsberger, *ibid.* **1964**, 5327; d) R. C. Fahey, C. Schubert, *J. Am. Chem. Soc.* **1965**, *87*, 5172; e) M. D. Johnson, E. N. Trachtenberg, *J. Chem. Soc. B* **1968**, 1018.

[10] G. Bellucci, R. Bianchini, C. Chiappe, V. R. Gadgil, A. P. Marchand, *J. Org. Chem.* **1993**, *58*, 3575.
[11] G. Bellucci, R. Bianchini, C. Chiappe, F. Marioni, R. Ambrosetti, R. S. Brown, H. Slebocka-Tilk, *J. Am. Chem. Soc.* **1989**, *111*, 2640.
[12] Bromonium ions of cyclohexene and cyclopentene generated by solvolysis can also transfer Br^+ to other olefins: R. S. Brown, R. Gedye, H. Slebocka-Tilk, J. M. Buschek, K. R. Kopecky, *J. Am. Chem. Soc.* **1984**, *106*, 4515.
[13] H. Slebocka-Tilk, R. G. Ball, R. S. Brown, *J. Am. Chem. Soc.* **1985**, *107*, 4504.
[14] M. Cossi, M. Persico, J. Tomasi, *J. Am. Chem. Soc.* **1994**, *116*, 5373.
[15] a) E. Kochanski, *Quantum Theory Chem. React. 1980–1982* **1981**, *2*, 177–91; b) J. Prisette, G. Seger, E. Kochanski, *J. Am. Chem. Soc.* **1978**, *100*, 6942; c) R. A. Poirier, P. G. Mezey, K. Yates, I. G. Csizmadia, *J. Mol. Struct.* **1981**, *85*, 153; d) A. C. Hopkinson, M. H. Lien, K. Yates, I. G. Csizmadia, *Theor. Chim. Acta* **1977**, *44*, 385; e) S. Yamabe, T. Minato, S. Inagaki, *J. Chem. Soc. Chem. Commun.* **1988**, 532.
[16] According to calculations by E. Kochanski, less than 0.04 electrons are transferred. The main contribution to the stabilization of 3.7 kcal mol^{-1} is due to the dispersion energy; see ref. [15a].
[17] L. Fredin, B. Nelander, *J. Mol. Struct.* **1973**, *16*, 205.
[18] The intermediacy of the complex at room temperature in solution was also demonstrated by UV spectroscopy: ref. [7]; see also a) R. S. Brown, H. Slebocka-Tilk, A. J. Bennet, G. Bellucci, R. Bianchini, R. Ambrosetti, *J. Am. Chem. Soc.* **1990**, *112*, 6310; b) S. Fukuzumi, J. K. Kochi, *J. Org. Chem.* **1981**, *46*, 4116.
[19] A. C. Legon, C. A. Rego, *J. Chem. Soc. Faraday Trans.* **1990**, *86*, 1915.
[20] Some HX/Lewis base complexes were investigated by the same method: a) A. C. Legon, D. G. Lister, H. E. Warner *J. Am. Chem. Soc.* **1992**, *114*, 8177; b) A. C. Legon, C. A. Rego, A. L. Wallwork, *J. Chem. Phys.* **1992**, *97*, 3050.
[21] H. I. Bloemink, K. Hinds, A. C. Legon, J. C. Thorn, *J. Chem. Soc. Chem. Commun.* **1994**, 1321.
[22] H. I. Bloemink, K. Hinds, A. C. Legon, J. C. Thorn, *Chem. Phys. Lett.* **1994**, *223*, 162.
[23] a)W. Jäger, Y. Xu, M. C. L. Gerry, *J. Phys. Chem.* **1993**, *97*, 3685; b) S. Blanco, A. C. Legon, J. C. Thorn, *J. Chem. Soc. Faraday Trans.*, in press.
[24] A. C. Legon, D. G. Lister, J. C. Thorn, *J. Chem. Soc. Chem. Commun.* **1994**, 757.
[25] A. C. Legon, H. E. Warner, *J. Chem. Phys.* **1993**, *98*, 3827
[26] A. C. Legon, J. C. Thorn, *J. Chem. Soc. Faraday Trans.* **1993**, *89*, 4157
[27] H. Bloemink, K. Hinds, A. C. Legon, J. C. Thorn, *Angew. Chem.* **1994**, *106*, 1577; *Angew. Chem. Int. Ed. Engl.* **1994**, *33*, 1512.
[28] H. I. Bloemink, K. Hinds, A. C. Legon, J. C. Thorn, *J. Chem. Soc. Chem. Commun.* **1994**, 1229.
[29] S. Blanco, A. C. Legon, J. C. Thorn, *J. Chem. Soc. Faraday Trans.* **1994**, *90*, 1365.
[30] Cf.: the force constant k_σ of a C–C bond is about 450 Nm^{-1}.
[31] R. Herges, unpublished, MP2/6-31G* level.
[32] H. Hopf, R. Hänel, P. G. Jones, P. Bubenitschek, *Angew. Chem.* **1994**, *106*, 1444; *Angew. Chem. Int. Ed. Engl.* **1994**, *33*, 1369.
[33] G. Bellucci, R. Bianchini, C. Chiappe, D. Lenoir, *12th Conference on Physical Organic Chemistry (IUPAC)* Aug. 29, Padova, Italy, **1994**.

Mononuclear Tris(arene)–Metal Complexes

Ulrich Zenneck*

The first π-arene complex, bis(η^6-benzene)chromium, was synthesized and characterized by Fischer and Hafner almost forty years ago.[1] Are any remarkable discoveries in this area of chemistry still possible today? Since that pioneering work numerous attempts have been made to vary the bonding mode and the number of arene ligands per metal atom. Although the former was achieved after some time, a mononuclear complex with three arene ligands was synthesized for the first time only recently.[2] Considering the intensity of research in organometallic chemistry, this is quite remarkable and calls for closer examination.

If the electronic demand of a metal center is low, the cyclic delocalization of the π electrons in the arene ligands may be interrupted such that only a portion of these electrons interact with the metal. Arenes can coordinate, for example, as η^4 ligands with loss of planarity, if this assures that the 18 valence electron (VE) configuration of the transition metal complex is not exceeded. This occurs relatively easily for condensed arenes, but stable complexes with monocyclic arene ligands having analogous η^4 coordination are also known and have been structurally characterized.[3] The preferred η^4 coordination of polycyclic ligands can be explained by the difference in the resonance energies of the π electrons in the η^4-coordinated arenes, which are especially unfavorable for benzene and its derivatives.[4] In η^4-naphthalene complexes the bound 4π unit is electronically almost completely separated from the 6π unit, which is reflected in the spectroscopic and structural properties. Thus these compounds can be considered benzannelated 1,3-cyclohexadiene complexes; the NMR and UV spectra of 1,3-cyclohexadiene complexes closely resemble those of the related subunits in η^4-naphthalene complexes. The dihedral angles formed between the bound and not bound portions of the ligands are also in the same range for both types of compounds.[5]

Generally the stability of η^4-arene complexes increase within a transition metal triad with the atomic number of the metal center. The decomposition points of the (η^4-benzene)(η^6-benzene)metal(0) complexes (metal = Fe, Ru, Os) serve as an example. The iron complex decomposes at roughly −50 °C, the ruthenium complex at 0 °C, and the dynamic behavior of the osmium complex can be observed by NMR spectroscopy at up to 100 °C.[6] In addition 3d metals sometimes tend to avoid forming η^4-arene complexes; in contrast to the heavier homologues they give rise to paramagnetic 20 VE complexes with a ligand bound η^6 fashion. Thus bis(hexamethylbenzene)iron is a 20 VE sandwich complex with two unpaired electrons, whereas the diamagnetic bis(hexamethylbenzene)ruthenium is a typical (η^4-arene)(η^6-arene)metal complex.[7]

π-Arene complexes can be synthesized by three principle routes: ligand exchange maintaining the oxidation state of the metal center (suitable for cationic complexes), ligand exchange under reducing conditions (for cationic, anionic, and neutral complexes), and direct synthesis by cocondensation of metal

[*] Prof. Dr. U. Zenneck
Institut für Anorganische Chemie der Universität Erlangen-Nürnberg
Egerlandstrasse 1, D-91058 Erlangen (Germany)
Telefax: Int. code + (9131)857367

 © VCH Verlagsgesellschaft mbH, D-69451 Weinheim, 1995 0570-0833/95/0101-0053 $ 10.00+.25/0

vapor and ligand (for neutral complexes). In the reactions under reducing conditions the use of arene anions has been particularly successful recently, since the anions are responsible for both the reduction and halogen–arene exchange of the metal halides typically used as starting materials. When an excess of this reducing agent based on the oxidation state of the metal is used, the elegant formation of arene metalates results.

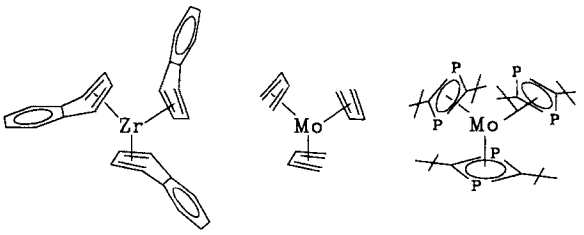
The synthesis of bis(η^6-arene)titanates(1–) from $TiCl_4 \cdot 2THF$ and biphenyl anions[8] was the first alternative to metal vapor synthesis for the preparation of bis(arene)titanium derivatives as potential catalysts.

Surprisingly in the reaction of $ZrCl_4 \cdot 2THF$ with $KC_{10}H_8$ in the presence of [2.2.2]cryptand or [15]crown-5 (Scheme 1) Ellis

$$ZrCl_4 \cdot 2THF + 6KC_{10}H_8 + nL \xrightarrow[-60 \rightarrow 0\,^{\circ}C]{DME} [KL_n]_2[Zr(C_{10}H_8)_3] + 3C_{10}H_8 + 4KCl + 2THF$$
$$[KL_n]_2\text{-}\mathbf{1}$$

Scheme 1. $n = 1$, L = [2.2.2]cryptand; $n = 2$, L = [15]crown-5; DME = 1,2-dimethoxy methane.

and Jang obtained polyether-stabilized dipotassium salts of tris(η^4-naphthalene)zirconates(2–) **1**,[2] which deserve special attention for a number of reasons.



1 **2** **3**

– These are the first tris(arene) complexes with three independent arene ligands; the only previous example of coordination of three neutral arene ligands was the η^{18} coordination of the main group element cations Ga^+, Ge^{2+}, and Sn^{2+} in the cavity of a [2.2.2]paracyclophane.[9] This macrocyclic ligand forms a flexible cage supporting the relatively weak interactions with the cations.

– The zirconates contradict previous findings for η^4-arene coordination without immediately apparent electronic reasons. The expected product of the reaction outlined in Scheme 1 was the still-unknown bis(η^6-naphthalene)zirconate(2–), which should be analogous to bis(η^6-naphthalene)molybdenum[10] and bis(naphthalene)titanate(2–).[11]

– Based on the previously discussed relationship of η^4-bound naphthalene ligands with coordinated *cis*-1,3-dienes, one would expect the zirconates to display analogies with tris(diene)metal complexes. Although corresponding diene metalates are not yet known, molybdenum(0) in tris(butadiene)molybdenum **2**, which is isoelectronic with zirconate(2–), shows the same structural features as **1**.[12] In both cases the donor centers have a trigonal-prismatic arrangement about the metal center with metal–C distances in the range typical for coordinated olefins.

– The readily accessible salt K_2-**1** is an interesting precursor for anionic zirconium compounds such as $[Zr(CO)_6]^{2-}$.[2] Owing to the naphthalene effect,[10] the arene ligands are easily substituted. In general this is expected for naphthalene metalates, which should now be available in greater variety than by previously known analogous routes.

– The isoelectronic relationship Zr^{-II}/Mo^0 raises speculations on the further chemistry of metalates. The preparation of the tris(η^4-1,3-diphosphete)molybdenum derivative **3** was recently reported,[13] in which the Mo^0 center is surrounded by three heterocycles.

Summary: We can look forward to the rapid and highly interesting development of the chemistry of arene metalates.

German version: *Angew. Chem.* **1995**, *107*, 59

Keywords: arene complexes · metalates · titanium compounds · zirconium compounds

[1] E. O. Fischer, W. Hafner, *Z. Naturforsch. B* **1955**, *10*, 665.
[2] M. Jang, J. E. Ellis, *Angew. Chem.* **1994**, *106*, 2036; *Angew. Chem. Int. Ed. Engl.* **1994**, *33*, 1965.
[3] Review: E. L. Muetterties, J. R. Bleeke, E. J. Wucherer, T. A. Albright, *Chem. Rev.* **1982**, *82*, 499; Selected examples: J. O. Albright, L. D. Brown, S. Datta, J. K. Kouba, S. S. Wreford, B. M. Foxman, *J. Am. Chem. Soc.* **1977**, *99*, 5518; W. L. Gladfelter, J. W. Hull, *Organometallics* **1984**, *3*, 605; R. D. Rieke, W. P. Henry, J. S. Arney, *Inorg. Chem.* **1987**, *26*, 420.
[4] W. C. Herndon, *J. Am. Chem. Soc.* **1980**, *102*, 1538.
[5] H. Schäufele, D. Hu, H. Pritzkow, U. Zenneck, *Organometallics* **1989**, *8*, 396.
[6] M = Fe: P. L. Timms, *J. Chem. Soc. Chem. Commun.* **1969**, 1033; P. D. Morand, C. G. Francis, *Organometallics* **1985**, *4*, 1653; M = Ru: E. O. Fischer, C. Elschenbroich, *Chem. Ber.* **1970**, *103*, 162.; P. L. Timms, R. B. King, *J. Chem. Soc. Chem. Commun.* **1978**, 896; M = Os: J. A. Bandy, M. L. H. Green, D. O'Hare, *J. Chem. Soc. Dalton Trans.* **1986**, 2477.
[7] $[(\eta^6\text{-}C_6Me_6)_2Fe]$: E. O. Fischer, F. Röhrscheid, *Z. Naturforsch. B* **1962**, *17*, 483. $[(\eta^6\text{-}C_6Me_6)_2Ru]$: G. Huttner, S. Lange, *Acta Crystallogr. Sect. B* **1972**, *28*, 2049.
[8] D. W. Blackburn, D. Britton, J. E. Ellis, *Angew. Chem.* **1992**, *104*, 1520; *Angew. Chem. Int. Ed. Engl.* **1992**, *31*, 1495. At roughly the same time the reduction of $TiCl_4$ with $K[BEt_3H]$ in the presence of arenes leading to bis(arene)titanium derivates was described: H. Bönnemann, B. Korall, *ibid.* **1992**, *104*, 1506 and **1992**, *31*, 1490.
[9] H. Schmidbaur, R. Hager, B. Huber, G. Müller, *Angew. Chem.* **1987**, *99*, 354; *Angew. Chem. Int. Ed. Engl.* **1987**, *26*, 338; T. Probst, O. Steigelmann, J. Riede, H. Schmidbaur, *ibid.* **1990**, *102*, 1471 and **1990**, *29*, 1397.
[10] N. P. D. Thi, S. Spichiger, P. Paglia, G. Bernardinelli, E. P. Kündig, P. L. Timms, *Helv. Chim. Acta* **1992**, *75*, 2593, and references therein.
[11] J. E. Ellis, D. W. Blackburn, P. Yuen, M. Jang, *J. Am. Chem. Soc.* **1993**, *115*, 11616. The bonding mode of the ligands in $[Ti(C_8H_{10})_2]^2$ has not been determined yet.
[12] P. S. Skell, M. J. McGlinchey, *Angew. Chem.* **1975**, *87*, 215; *Angew. Chem. Int. Ed. Engl.* **1975**, *14*, 195.
[13] F. G. N. Cloke, K. R. Flower, P. B. Hitchcock, J. F. Nixon, *J. Chem. Soc. Chem. Commun.* **1994**, 489.

 © VCH Verlagsgesellschaft mbH, D-69451 Weinheim, 1995 0570-0833/95/0101-0054 $ 10.00+.25/0

Structure Determination from Powder X-Ray Diffraction Data of a Hydrogen-Bonded Molecular Solid with Competing Ferromagnetic and Antiferromagnetic Interactions: The 2-(3,4-Dihydroxyphenyl)-α-Nitronyl Nitroxide Radical**

Joan Cirujeda, Luis Enrique Ochando, Jose Maria Amigó, Concepció Rovira, Jordi Rius, and Jaume Veciana*

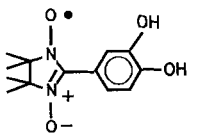
Dedicated to Professor Dwaine O. Cowan

Macroscopic physical properties of molecular solids—magnetic, electrical, and optical—are generally controlled by intermolecular electronic interactions. Therefore, the knowledge of the molecular packing is crucial in order to understand and correlate the bulk properties of a given material with its microscopic characteristics. When no single crystals with suitable size and/or good quality can be grown and the crystal structure of a given compound is needed, one is forced to use the X-ray diffraction data obtained from powder samples. Consequently, the development and improvement of methods allowing structure determinations from powder diffraction data are nowadays strongly demanded.[1]

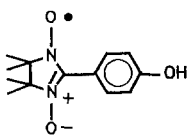
To our knowledge these methods have been used mainly to determine the crystal structures of some inorganic solids, while only very few structures of organic compounds, most having heavy atoms, have been resolved.[2] The solution of crystal structures of purely organic molecular solids from powder X-ray diffraction data measured with laboratory X-ray sources is a difficult task because the number of measurable intensities at high diffraction angles is considerably reduced. In addition, the absence of strong scatterers and the large number of light atoms prevents the direct interpretation of the Patterson function. As previously shown, one of the simplest ways of circumventing these limitations is through the combined use of molecular replacement methods and rigid-body Rietveld refinements.[1a, 3] The extension of this method to all kinds of organic compounds would be very beneficial.

Herein we present the first application of this method for the determination of the molecular packing of a complex organic compound having only s and p electrons and more than ten atoms in the asymmetric unit. We chose the molecular solid formed by the 2-(3,4-dihydroxyphenyl)-α-nitronyl nitroxide radical (**1**).[4] This open-shell molecule deserved a priori to be studied in solid form since it showed significant ferromagnetic interactions and must be an example of a molecular solid whose self-assembly is directed by hydrogen bonds. The synthesis and a detailed magneto-structural correlation of this molecular solid are also reported and discussed here.[5]

The use of hydrogen bonds as a crystal design element in the preparation of magnetic molecular materials has great potential.[6, 7] Very recently it was demonstrated that the 2-(4-hydroxyphenyl)-α-nitronyl nitroxide radical (**2**) forms a two-dimen-



1



2

sional network through hydrogen bonds and that ferromagnetic interactions are propagated along these two directions.[7] Therefore, it seemed interesting to prepare new nitronyl nitroxide radicals similar to **2** but having an additional OH group on the benzene ring, for example, radical **1**. Because this radical contains an equal number of hydrogen bond acceptor (N–O) and donor (O–H) groups that have noncollinear relative orientations and point in all three directions, we expected that these molecules would self-assemble. The resulting molecular solid, a high-dimensional hydrogen-bonded network, may have enhanced magnetic dimensionality.

Radical **1** was prepared following the usual procedure.[8] Thus, the reaction of 2,3-dimethylbutane-2,3-bis(hydroxylamine) with 3,4-dihydroxybenzaldehyde followed by the oxidation of the resulting addition product with lead dioxide yielded the radical **1**.[9] Like most catechol derivatives[10] this open-shell compound is very unstable in solution in a wide variety of solvents. This intrinsic instability, which is probably assisted by the radical character, prevents preparation of large single crystals. For this reason, only polycrystalline samples of **1** were obtained by a rapid precipitation with *n*-pentane from a concentrated chloroform solution.

One of these samples was used for the X-ray powder diffraction measurements.[11–13] The experimental and calculated diffraction patterns and the corresponding difference profile are shown in Figure 1. The crystal packing of radical **1** obtained shows some outstanding features that confirm the initial expectations based on the presence in its skeleton of two hydrogen bond acceptors, one for each of the two hydrogen bond donors. As is shown in Figure 2a, the molecules form double corrugated layers parallel to the (001) plane, which are held together by two types of strong hydrogen bonds. One type of hydrogen bond connects the OH groups at the *meta* positions of benzene rings of two neighboring radicals with the two NO groups on the same side as these OH groups. These hydrogen bonds give rise to dimers, in which molecules are arranged side by side and head to tail ($O_{meta} \cdots ON = 2.6(1)$ Å). The second type of hydrogen bonds links the neighboring dimers through the remaining OH groups in the *para* positions and the other NO groups

[*] Dr. J. Veciana, J. Cirujeda, Dr. C. Rovira, Dr. J. Rius
Institut de Ciència de Materials de Barcelona (CSIC)
Campus de la U. A. B., E-08193-Bellaterra (Spain)
Telefax: Int. code + (3) 580-5729
L. E. Ochando, Prof. J. M. Amigó
Departament de Geologia, Universitat de València
E-47100-Burjassot (Spain)

[**] This work was supported by the Programa Nacional de Nuevos Materiales, Spain (CICyT, Grant No. MAT 91/0553), the New Energy and Development Organization (NEDO) of the Ministry of International Trade and Industry (MITI) of Japan, and the Programa General del Conocimiento, Spain (DGICyT, Grant No. PB92-0010).

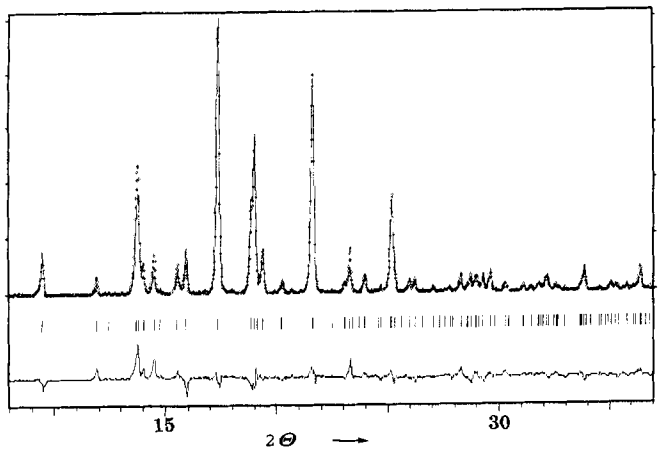


Fig. 1. Observed and calculated X-ray powder diffraction patterns for **1**, and the corresponding difference profile (bottom).

[$O_{para}\cdots ON = 2.7(1)$ Å]. The resulting relative molecular arrangement of these dimers is very similar to that observed for the molecules of radical **2** linked through similar hydrogen bonds between the *para*-OH and NO groups.[7] The shortest intermolecular contacts in **1** are found within the two-dimensional hydrogen-bonded layers; however, the forces operating between these sheets are only weaker van der Waals forces, and accordingly the intermolecular distances are greater (3.1 Å $< d \ll 4.0$ Å). The most relevant structural features in these 2D layers are the head-to-tail overlaps between the molecules of a given dimer with those located on the upper and lower layers (Fig. 2b, c). This relative arrangment gives rise to stair-shaped molecular chains parallel to the c axis.

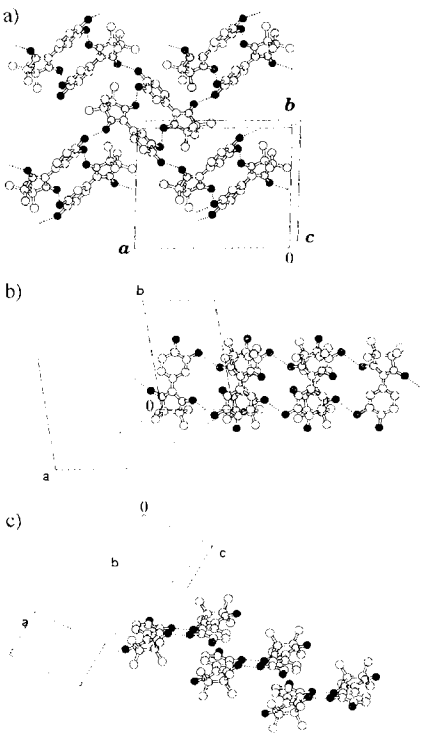


Fig. 2. Crystal structure of **1**. a) View of a two-dimensional corrugated layer parallel to the (001) plane. b) and c) Stacking of molecules in adjacent corrugated planes viewed perpendicular and parallel to the mean planes though the atoms ONCNO. Hydrogen bonds are depicted by dotted lines.

In order to rationalize the magnetic properties of **1**, we have made a detailed analysis of the intermolecular short contacts and the relative molecular orientations present in this molecular solid, taking into account the widely accepted charge transfer mechanism involving frontier orbitals.[16] This analysis suggests the presence of antiferromagnetic (AFM) interactions between the molecules of each dimer and also ferromagnetic (FM) interactions between head-to-tail overlapping molecules of contiguous layers.[17] Furthermore, very weak FM interactions are also expected to be transmitted through the hydrogen bonds involving the *para* OH groups, as occurs in the radical **2**, since both radicals have similar relative orientations in the solid. In conclusion, the molecular packing observed for **1** indicates the presence of predominant alternating FM and AFM interactions along the stair-shaped molecular chains together with other FM interactions of minor importance along other directions perpendicular to the c axis.

The temperature dependence of the static magnetic susceptibility of a polycrystalline sample of **1** was measured in the range $2 \le T \le 300$ K using a SQUID magnetometer. The plot of $\chi_m T$ versus T (Fig. 3) (χ_m = molar magnetic susceptibility) clearly

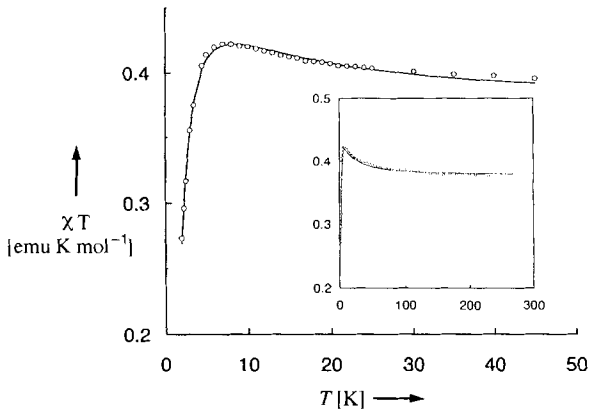


Fig. 3. Temperature dependence of $\chi_m T$ for radical **1**. The solid line corresponds to the least-squares fit (see text).

reveals an increase of the effective magnetic moment of the sample with decreasing temperature until it reaches a maximum at about 7 K. At lower temperatures the value of $\chi_m T$ decreases quite rapidly. This result indicates the simultaneous presence of both FM and AFM intermolecular interactions and confirms expectations based on the observed molecular packing. The experimental susceptibility data were then rationalized with the magnetic model suggested by this molecular packing, in other words, a linear 1D Heisenberg chain of $S = 1/2$ spins with alternating FM and AFM intermolecular exchange interactions: $\cdots$-J_{FM}-J_{AFM}-J_{FM}-J_{AFM}-$\cdots$. For this kind of chain the theory predicts a maximum in the plot of $\chi_m T$ versus T when the FM interaction dominates (i.e. when the alternating parameter, defined as $\alpha = J_{FM}/|J_{AFM}|$, is larger than one). The resulting magnetic behavior is fairly well described by the Equations (a) and (b).[18] Here $T_R = T/|J_{AFM}|$ and χ^{chain} and χ_R^{chain} are the molar and

$$\chi^{chain} T = \chi_R^{chain} T(3g^2/32|J_{AFM}|) \quad \text{(a)}$$

$$\chi_R^{chain} = \frac{AT_R^3 + BT_R^2 + CT_R^2 + D}{T_R^4 + ET_R^3 + FT_R^2 + GT_R + H} \quad \text{(b)}$$

reduced magnetic susceptibilities, respectively, of the repeating units of the chain.[19] In order to consider the weak FM ex-

change interactions, J^{inter}, between a given chain and its $z = 4$ nearest neighboring chains, occurring through the molecules linked by the *para*-O-H ··· O-N hydrogen bonds, Equation (c) was also used.[20]

$$\chi_m = \chi^{chain}/[1 - (2zJ^{inter}\chi^{chain}/Ng^2\beta^2)] \quad (c)$$

Fitting Equations (a)–(c) to the the experimental data yielded the following best-fit parameters: $J_{FM}/k_B = 9.28$, $J_{AFM}/k_B = -3.78$ ($\alpha = 2.45$), and $J^{inter}/k_B = 0.34$ K. Both the signs and the magnitudes of these values are in accord with that expected from the molecular packing and from the results for the related radical **2**.[21]

In conclusion it is shown that powder X-ray diffraction data can be used to elucidate the crystal packing of relatively complex purely organic molecular solids, including those having only s and p electrons. For this purpose it is necessary to know the molecular structure of a related parent compound as an appropriate model system. In addition, our results here confirm the ability of hydrogen bonds to connect correctly functionalized radical molecules in a controlled fashion, thus generating ferromagnetic interactions with a high degree of directionality.

Received: May 3, 1994
Revised version: July 8, 1994 [Z68971E]
German version: *Angew. Chem.* **1995**, *107*, 99

Keywords: electronic structure · magnetic properties · nitroxides · radicals

[1] a) J. Rius, C. Miravitlles, *J. Appl. Cryst.* **1988**, *21*, 224; b) W. I. F. David, *Nature* **1990**, *346*, 731; c) C. J. Gilmore, K. Henderson, G. Bricogne, *Acta Crystallogr. Sect. A.* **1991**, *47*, 830; d) P. R. Rudolf, *Mater. Chem. Phys.* **1993**, *35*, 267.

[2] Previous crystal structure determinations of purely organic compounds containing heavy atoms or less than 10 atoms from X-ray powder diffraction data include: a) G. Reck, R.-G. Kretschmer, L. Kutschabsky, W. Pritzkow, *Acta Crystallogr. Sect. A.* **1988**, *44*, 417; b) J. Rius, C. Miravitlles, E. Molins, I. Crespo, J. Veciana, *Mol. Cryst. Liq. Cryst.* **1990**, *187*, 155; c) K. Honda, M. Goto, M. Kurahashi, *Chem. Lett.* **1990**, 13; d) M. Tremayne, P. Lightfoot, C. Glidewell, K. D. M. Harris, K. Shankland, C. J. Gilmore, G. Bricogne, P. G. Bruce, *J. Mater. Chem.* **1992**, *2*, 1301; e) M. Tremayne, P. Lightfoot, M. A. Metha, P. G. Bruce, K. D. M. Harris, K. Shankland, C. J. Gilmore, G. Bricogne, *J. Solid State Chem.* **1992**, *100*, 191; f) P. Lightfoot, C. Glidewell, P. G. Bruce, *J. Mater. Chem.* **1992**, *2*, 361; g) S. Petit, G. Coquerel, G. Perez, D. Louer, M. Louer, *New J. Chem.* **1993**, *17*, 187; h) *Chem. Mater.* **1994**, *6*, 116.

[3] J. Rius, RIBOLS 90, a rigid-body Rietveld least-squares refinement program, ICMAB (CSIC), Catalunya (Spain), **1990**.

[4] The IUPAC name of **1** is 2-(3,4-dihydroxyphenyl)-4,4,5,5-tetramethyl-4,5-dihydro-1*H*-imidazolyl-1-oxy-3-oxide.

[5] The synthesis, magnetic properties, and crystal structures of **1**, the isomeric radical 2-(3,5-dihydroxyphenyl)-α-nitronyl nitroxide, and the monohydroxilated analogues **2** and 2-(3-hydroxyphenyl)-α-nitronyl nitroxide radical were reported for the first time at the 1st European Workshop on Magnetic Molecular Materials, Castiglione della Pescaia, Grosseto (Italy), May, 1993 and will be published elsewhere.

[6] B. N. Figgis, E. S. Kucharski, M. Vrtis, *J. Am. Chem. Soc.* **1993**, *115*, 176; H. O. Stumpf, L. Ouahab, Y. Pei, D. Greandjean, O. Kahn, *Science* **1993**, *261*, 447; D. Bordeaux, J. X. Boucherle, B. Delley, B. Gillon, E. Ressouche, J. Z. Schweizer, *Z. Naturforsch. A* **1993**, *48*, 117.

[7] a) E. Hernández, M. Mas, E. Molins, C. Rovira, J. Veciana, *Angew. Chem.* **1993**, *105*, 919; *Angew. Chem. Int. Ed. Engl.* **1993**, *32*, 882; b) J. Cirujeda, E. Hernández, C. Rovira, J. L. Stanger, P. Turek, J. Veciana, *J. Mater. Chem.*, in press.

[8] J. H. Osiecki, E. F. Ullman, *J. Am. Chem. Soc.* **1968**, *90*, 1078; E. F. Ullman, J. H. Osiecki, D. G. B. Boocock, R. J. Darcy, *ibid.* **1972**, *94*, 7049.

[9] **1**: m.p. 147–148 °C; IR (KBr): $\tilde{\nu}$ [cm^{-1}] = 3297 (s), 1603 (s), 1502 (m), 1448 (m), 1371 (vs), 1334 (vs), 1289 (vs), 1211 (s), 1167 (s), 1128 (m), 868 (w), 817 (w), 693 (w), 541 (m); UV/Vis ($C_6H_5CH_3$): λ_{max} [nm] (lg ε [M^{-1}cm^{-1}]) = 619 (2.76), 368 (3.80), 282 (4.02); MS: *m/z*: 265 (M^+, 3%), 177 (70), 136 (48), 84 (100), 69 (51); ESR (CCl_4): $g = 2.0063(3)$, $a_N = 7.55(3)$ G.

[10] J. Thomson in *The Chemistry of Quinoid Compounds, Part 1* (Ed.: S. Patai), Wiley, New York, **1974**, p. 112.

[11] The specimen was prepared by filtration of a suspension of **1** in *n*-pentane on a silver filter. The powder diffraction pattern was measured on an automated RIGAKU RU-200H rotating anode diffractometer equipped with a Ge(111) curved incident beam monochromator ($Cu_{K\alpha 1}$ radiation, $\lambda = 1.5405981$ Å, 50 kV, 120 mA, divergence slit 1°, receiving slit = 0.10 mm, 2θ range measured 5–45°, 2θ range used 8–37°, step scan 0.02°, counting time = 10 s, FWHM (full width at half-maximum) = 0.13 of 2θ).

[12] The following procedure was used in the structure determination of **1** from powder X-ray diffraction data: First, a molecule was selected as a model and positioned in the unit cell. This operation requires the determination of three rotation angles and one translation vector. This six-dimensional search can be split into two successive three-dimensional searches: a) the rotational search, determination of the orientation of the model molecule, and b) the translational search, determination of the correct shift to be applied to the properly oriented model molecule. Once the model molecule is correctly positioned, it is neccessary to refine the complete structure. For such a purpose the rigid-body Rietveld refinement was carried out in which the quantity minimized is $\sum w_i(y_i^o - y_i^c)^2$, where y_i^o is the measured intensity at point $2\vartheta_i$ of the powder diffraction pattern and $y_i^c = \sum_m I_c(m)P_i(m)$ is the sum of the contributions of all the m reflections close to $2\vartheta_i$. The constant K is a scaling factor, j_m is the multiplicity of the reflection m, and $P_i(m)$ is the contribution of $I_c(m)$ to the intensity at point $2\vartheta_i$. In order to reduce the effective number of variables per observation, due to the rather large number of atoms in organic compounds, strict constraints were introduced, see ref. [3].

[13] Crystal data of **1**: $C_{13}H_{17}N_2O_4$, $P2_1/a$, $a = 15.905(3)$, $b = 11.927(3)$, $c = 7.598(1)$ Å, $\beta = 111.83(1)°$, $V = 1338(3)$ Å^3, $\rho = 1.24$ g cm^{-1}, $Z = 4$, $\mu = 0.5$ cm^{-1}, $T = 20$ °C. The X-ray diffraction pattern was indexed with TREOR [14] using 18 reflections ($2\theta < 24°$). Figures of merit (see ref. [14]) for the best solution are $M(18) = 60$ and $F(18) = 143$ (0.0042, 30). The unit cell parameters and the zero position were refined with least-squares methods. The integrated intensities of 70 reflections were extracted by fitting asymmetrical Pearson–VII profile functions. The systematic absences are consistent with the space group $P2_1/a$. The crystal structure was determined by introducing the intensities of 50 reflections into ROTSEARCH [1,3]. The selected model molecule was derived from the previously reported molecular coordinates of radical **2** [7]. The best solution supplied by the program was refined with SHELX76 [15] to a R value of 0.34. The correct position of the missing hydroxyl group from the two possible positions could be established by performing the corresponding two refinements (obtained R values were 0.284 and 0.37). The atomic arrangement with the lower R value was assumed as the correct one. The subsequent full-pattern rigid-body least-squares refinement with RIBOLS [3] converged to $R_{wp} = 0.186$ and $R_p = 0.156$. The estimated standard deviations of the Euler angles describing the orientation of the molecules are 0.63, 0.74, and 0.56°. The estimated standard deviations of the positional parameters of the center of mass of the molecule are $\sigma(x) = 0.035$, $\sigma(y) = 0.019$, $\sigma(z) = 0.031$ Å. Further details of the crystal structure are available on request from the Director of the Cambridge Crystallographic Data Centre, 12 Union Road, GB-Cambridge CB2 1EZ (UK), on quoting the full journal citation.

[14] P. E. Werner, *Z. Kristallogr.* **1964**, *120*, 375.

[15] G. M. Sheldrick, SHELX76. A least-squares refinement Program, University of Cambridge, **1976**.

[16] J. B. Goodenough, *Magnetism and the Chemical Bond*, Interscience, New York, **1963**, p. 163; H. M. McConnell, *Proc. R. A. Welch Found. Conf. Chem. Res.* **1967**, *11*, 144; K. Awaga, T. Sugano, M. Kinoshita, *Chem. Phys. Lett.* **1987**, *141*, 540.

[17] For interacting open-shell molecules the charge transfer mechanism involving frontier orbitals predicts an AFM coupling if there is a direct contact between the semi-occupied molecular orbital (SOMO) of neighboring molecules. This occurs within each dimer of radical **1**. By contrast, if such contacts are not present and only SOMO/LUMO or/and SOMO/NHOMO overlaps occur, this mechanism predicts a FM interaction. The last situation seems to be the case for molecules in adjacent 2D layers.

[18] J. J. Borrás-Almenar, Doctoral Thesis, Departament de Química Inorgànica, Universitat de València (Spain), **1992**; J. J. Borrás-Almenar, E. Coronado, J. Curely, R. Georges, J. C. Gianduzzo, *Inorg. Chem.* **1994**, *33*, 5171.

[19] The values for the polynomial factors A–H depend on the magnitude of the alternation parameter α and are given in ref. [18].

[20] W. E. Hatfield, R. R. Weller, J. W. Hall, *Inorg. Chem.* **1980**, *19*, 3825.

[21] The J^{inter}/k_B exchange interaction for **1** has the same order of magnitude than that observed for **2** ($J/k_B = +0.2$ K), see ref. [7].

 © VCH Verlagsgesellschaft mbH, D-69451 Weinheim, 1995 0570-0833/95/0101-0057 $ 10.00+.25/0

Barbituric Acid/2,4,6-Triaminopyrimidine Aggregates in Water and Their Competitive Interaction with a Monolayer of Barbituric Acid Lipids at the Gas–Water Interface**

Thomas M. Bohanon, Steffen Denzinger, Ralf Fink, Wolfgang Paulus, Helmut Ringsdorf,* and Marcus Weck

The principle of exercising a specific function through molecular recognition, self-organization, and competitive interaction is perfectly realized in numerous supramolecular systems in nature. Examples include cell membranes, the immune cascade, and DNA–protein complexes. Based on the century-old lock and key principle of Emil Fischer,[1] numerous experiments have focused on the transfer of molecular recognition and self-organization to synthetic systems.[2–4]

Work on the construction of tape and membrane structures by molecular recognition of substances in organic solvents, for example, cyanuric acid and melamine derivatives, and barbiturates and triaminopyrimidines,[5–8] led to recent investigations of the insertion of 2,4,6-triaminopyrimidine (**2**) in a monolayer of barbituric acid lipids at the gas–water interface.[9] It was found that a tape structure induced by hydrogen bonding is formed which catalyzes a retro-Knoevenagel reaction at a pH of 5–6 as a consequence of organization through molecular recognition.

In this connection, we describe here the interaction between free barbituric acid (**1**) and 2,4,6-triaminopyrimidine (TAP, **2**) in water without preorientation of either compound, and the formation of aggregates (Fig. 1). We were particularly interested in investigating the competitive interaction between these barbituric acid/TAP aggregates dissolved in water and the ordered, stable monolayer of barbituric acid lipids at the gas–water interface.[9]

The interaction between **1** and **2** in water was characterized in situ by FT-IR spectroscopy. The formation of these highly ordered structures through hydrogen bond formation between the two components is evident in Figures 2a–c. For the 1:1 mixture (Fig. 2c) no characteristic bands of the two uncomplexed components can be seen. The asymmetric and symmetric stretching vibrations of the carbonyl group in **1** (Fig. 2b) are shifted to approximately 1670, 1600, and 1550 cm^{-1} by complexation with **2**. An excess of one component, for example, barbituric acid (**1**), does not interfere with complex formation. This excess can be detected above the 1.1:1 ratio by the typical bands for **1**. The spectrum of the 2:1 mixture of **1** and **2** can be understood unequivocally as the addition spectrum of the complex and free barbituric acid (Fig. 2d).[10]

The structure of the aggregates of **1** and **2** is not yet determined unequivocally; both an open tape structure and a cyclic structure are feasible. Elemental analysis of crystals isolated from aqueous mixtures of the two components indicates a 1:1 ratio of barbituric acid and TAP. Although this result provides no indication of the structure in solution, it is, nevertheless, clear evidence of the ability of this complementary system to form aggregates by hydrogen bonding, even in water, thereby supporting the results obtained from IR spectroscopy.

[*] Prof. Dr. H. Ringsdorf, Dr. T. M. Bohanon, S. Denzinger, R. Fink, Dr. W. Paulus, M. Weck
Institut für Organische Chemie der Universität
J.-J.-Becher-Weg 18–20, D-55099 Mainz (Germany)
Telefax: Int. code + (6131)39-3145

[**] T. M. B. was supported by the National Science Foundation program for Long- and Medium-Term Research at Foreign Centers of Excellence (grant no. 9301706).

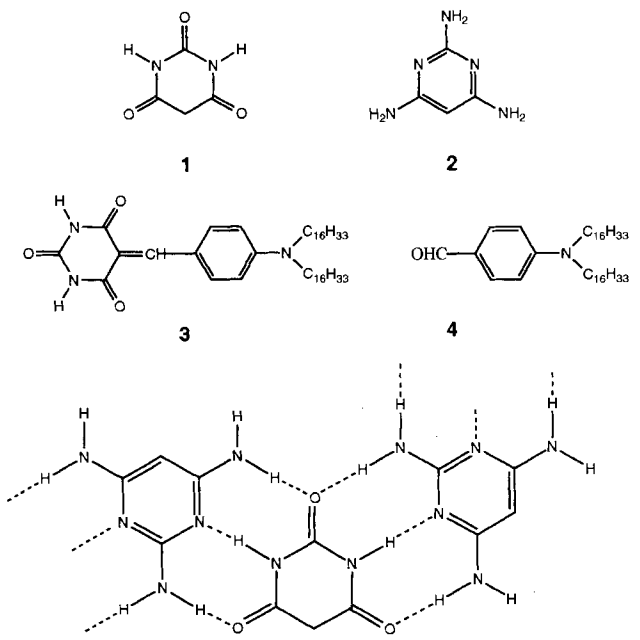


Fig. 1. Barbituric acid (**1**), 2,4,6-triaminopyrimidine (TAP **2**), barbituric acid lipid **3**, and its hydrolysis product **4**. Bottom: Schematic representation of the possible structures of aggregates of **1** and **2**, which are held together in water by hydrogen bonds.

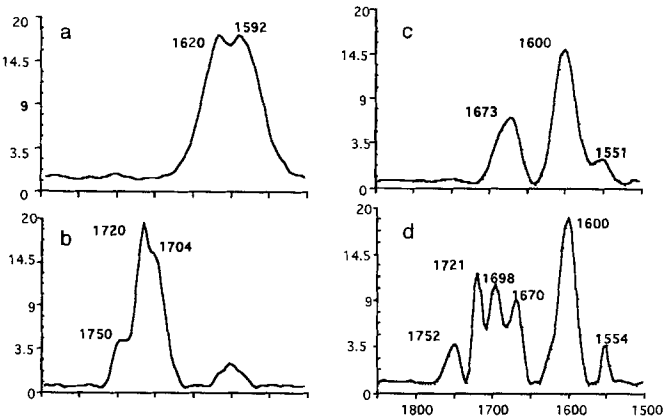


Fig. 2. FT-IR spectra of barbituric acid (**1**), TAP **2**, and mixtures of both in water. a) Spectrum of **2**; b) spectrum of **1**; c) spectrum of a 1:1 mixture of **1** and **2**; d) spectrum of a 2:1 mixture of **1** and **2**. Wavenumbers [cm^{-1}] and absorbance ($\times 10^{-3}$) are given on the abscissa and on the ordinate, respectively.

Competitive processes between systems of varying degrees of order play a decisive role in cell biology. Special examples are recognition- and orientation-induced processes on the membrane surface and, in particular, the immune cascade. Thus, it was of interest to investigate the competitive exchange of TAP **2** between the TAP/barbituric acid aggregates in water (Fig. 1) and a ordered monolayer of barbituric acid lipids at the gas–water interface. One possibility of measuring this exchange arises from the recognition-induced cleavage of barbituric acid lipids at monolayers by TAP, which was reported recently and which was followed by means of UV/Vis reflection spectroscopy.[9] After formation of the tape structure on a 10^{-4} M subphase (pH 6.5) (as shown in Fig. 3a), the C=C bond of the barbituric acid lipid **3**[11] was completely cleaved within 15 min, whereas it is stable on the TAP-free subphase. If the hydrolysis of barbituric acid lipids in monolayers is conducted on a sub-

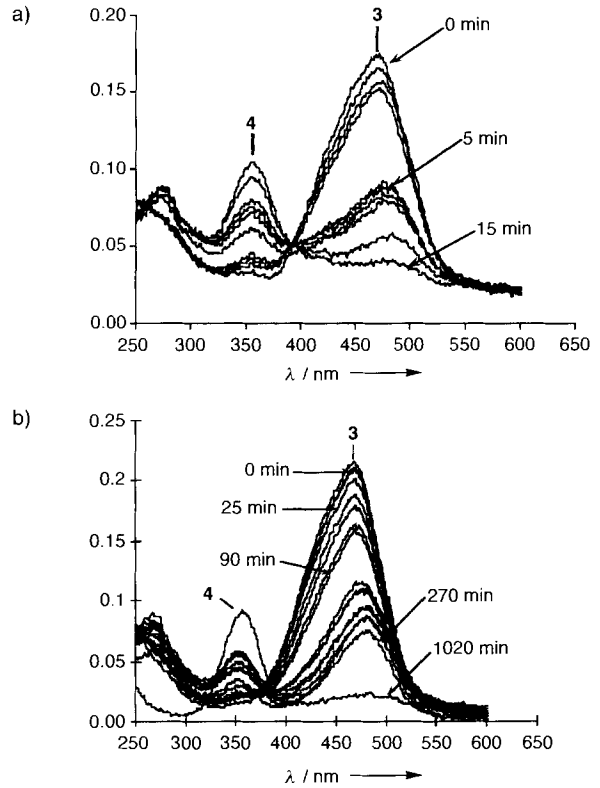


Fig. 3. UV/Vis reflection spectra of barbituric acid lipid **3** at the gas–water interface a) on a 10^{-4} M TAP subphase at pH 6.5; b) in a solution of the 1:1 barbituric acid/TAP aggregate (10^{-4} M, pH 6.5).

phase containing a 1:1 aggregate of barbituric acid and TAP (10^{-4} M, pH 6.5), then the cleavage requires 17 h (Fig. 3b).

This retarded hydrolysis of the barbituric acid lipid **3** indicates a significantly lower concentration of free TAP **2** as a result of its complexation with **1** in water. The course of this cleavage can thus be regarded as a competitive interaction between a fully complexed aggregate of **1** and **2** dissolved in water and a preoriented, highly ordered surface with structures that can recognize TAP **2** (Fig. 4). Thus, the equilibrium of complexed **2** is shifted slowly but completely to the side of the more highly ordered tape structure on the monolayer. Moreover, the barbituric acid (**1**) released by the hydrolysis hinders the insertion of TAP **2** into the monolayer. On the one hand, the acid **1** shifts the initial 1:1 ratio in its favor, but on the other it can enter the monolayer itself and must be displaced there by **2**.[12] This explains the much slower cleavage of the C=C bond towards the end of the reaction.

These IR and UV/Vis spectroscopic investigations show that the system **1**/**2** in water self-organizes to form a supramolecular aggregate stabilized by hydrogen bonding. The structure of this aggregate – whether tape or cyclic, which could be stabilized by H bonds and/or ionic bonds[13] – is not yet clarified. If an aqueous solution of this aggregate is applied to a preoriented, highly ordered surface of barbituric acid lipids, then **2** can be released from the aggregate and bind to the surface. Thus, as already described,[9] a recognition-induced retro-Knoevenagel reaction can take place. The investigation of this type of competitive molecular recognition process and subsequent reactions in water is of great importance, in particular for comparison with biological systems. It cannot be excluded that the interaction of barbituric acid derivatives with hydrogen bond acceptors and/or donors on the cell membrane may also play an important role in the effect of barbiturates as sedatives.

Experimental Procedure

The synthesis and characterization of barbituric acid lipids **3** has already been reported in refs. [9, 12]. All FT-IR spectra were recorded with a Nicolet-5DXC spectrometer equipped with an Ever-Glo light source and a nitrogen-cooled HgCdTe narrow-band detector. The samples were measured with the aid of the attenuated total reflection in a microcircle cell (Spectra-tech; ZnSe crystal) in water ($\varphi \geq 18$ MΩcm) at 20 °C with 5000 scans at 8 cm^{-1} resolution and a Happ-Genzel apodization. The water spectrum served as reference and was subtracted from the spectra of the samples. The concentration of the stock solutions was 10^{-2} M; the mixtures were allowed to stand for about 5 min after preparation before the spectra were recorded.

UV/Vis reflectance measurements on the monolayer were recorded with a spectrometer with a Universal lamp system from Spectroscopy Instruments and an ST-121 diode-array detector from Princeton Instruments. A film balance with a Wilhelmy system was employed.

Elemental analysis of the 1:1 barbituric acid/TAP crystals (dried in vacuum at 100 °C) gave ($C_8H_{11}N_3O_3$): calc.: C 37.95, H 4.38, N 38.72; found: C 37.90, H 4.35, N 38.75.

Received: June 8, 1994
Revised version: September 23, 1994 [Z 7015IE]
German version: *Angew. Chem.* **1995**, *107*, 102

Keywords: barbituric acid · biomembranes · IR spectroscopy · molecular recognition · 2,4,6-triaminopyrimidine · UV/Vis spectroscopy

[1] E. Fischer, *Ber. Dtsch. Chem. Ges.* **1894**, *27*, 2985.
[2] Y. Kyogoku, R. C. Lord, A. Rich, *Science* **1966**, *154*, 518.
[3] J. M. Lehn, *Angew. Chem.* **1988**, *100*, 91–116; *Angew. Chem. Int. Ed. Engl.* **1988**, *27*, 87–112.
[4] H. Ringsdorf, B. Schlarb, J. Venzmer, *Angew. Chem.* **1988**, *100*, 117–162; *Angew. Chem. Int. Ed. Engl.* **1988**, *27*, 113–158.

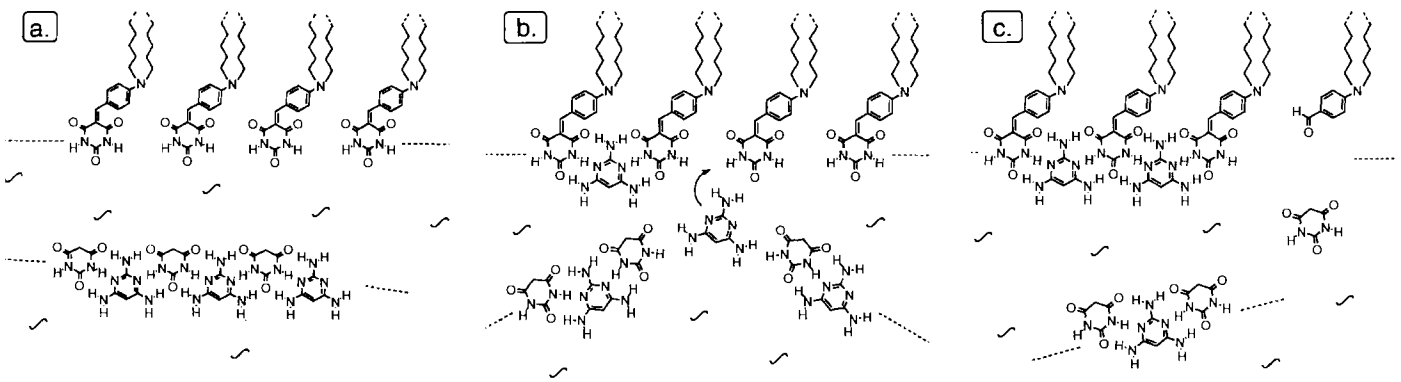


Fig. 4. Schematic representation of the competitive interaction of TAP **2** between barbiturate aggregates of varying degree of organization. a) Barbituric acid lipids at the gas–water interface on a 1:1 subphase of barbituric acid and TAP; b) competitive interaction of TAP between the preoriented monolayer and the aggregates in water; c) hydrolysis of the barbituric acid lipid **3** starts after insertion of TAP into the monolayer.

 © VCH Verlagsgesellschaft mbH, D-69451 Weinheim, 1995 0570-0833/95/0101-0059 $ 10.00+.25/0

[5] K. Kurihara, K. Ohto, Y. Tanaka, Y. Aoyama, T. Kunitake, *J. Am. Chem. Soc.* **1991**, *113*, 444.
[6] Y. Ikeura, K. Kurihara, T. Kunitake, *J. Am. Chem. Soc.* **1991**, *113*, 7342.
[7] J. M. Lehn, M. Mascal, A. Decian, J. Fischer, *J. Chem. Soc. Perkin Trans. 2* **1992**, 461.
[8] C. T. Seto, G. M. Whitesides, *J. Am. Chem. Soc.* **1990**, *112*, 6409; *ibid.* **1991**, *113*, 712; J. A. Zerkowski, C. T. Seto, G. M. Whitesides, *ibid.* **1992**, *114*, 5473; J. P. Mathias, E. E. Simanek, J. A. Zerkowski, C. T. Seto, G. M. Whitesides, *ibid.* **1994**, *116*, 4316.
[9] R. Ahuja, P.-L. Caruso, D. Möbius, W. Paulus, H. Ringsdorf, G. Wildburg, *Angew. Chem.* **1993**, *105*, 1082; *Angew. Chem. Int. Ed. Engl.* **1993**, *32*, 1033–1036.
[10] In analogous investigations of the interaction of barbituric acid with other compounds capable of forming hydrogen bonds, for example urea and 2-aminopyrimidine, 1:1 aggregates were not found. In these cases all the bands of free barbituric acid appeared in addition to weak bands resulting from complex formation.
[11] The isotherm of lipid **3** shows that it has a collapse area of ca. 38 Å^2 per molecule. Above 23 °C the lipid forms a liquid–solid coexistence region; below 23 °C only a gas phase and a solid-analogous phase are observed. The UV/Vis spectra were measured on the monolayer at a subphase temperature of 25 °C and a surface pressure of ca. 5 mN m^{-1}.
[12] Detailed investigations of the cleavage by a retro-Knoevenagel reaction on the lipid monolayer and their influence on the aqueous phase through aggregates will be reported separately (*J. Am. Chem. Soc.*, submitted).
[13] Note added in proof (December 1, 1994): An X-ray structure determination carried out in the meantime by Dr. Dieter Schollmeyer, Institut für Organische Chemie der Universität Mainz, shows that by the incorporation of water molecules the individual components of the system **1**/**2** in the structure are linked to give a network by ionic and hydrogen bonds.

A Versatile Solid-Phase Synthesis of N-Linked Glycopeptides

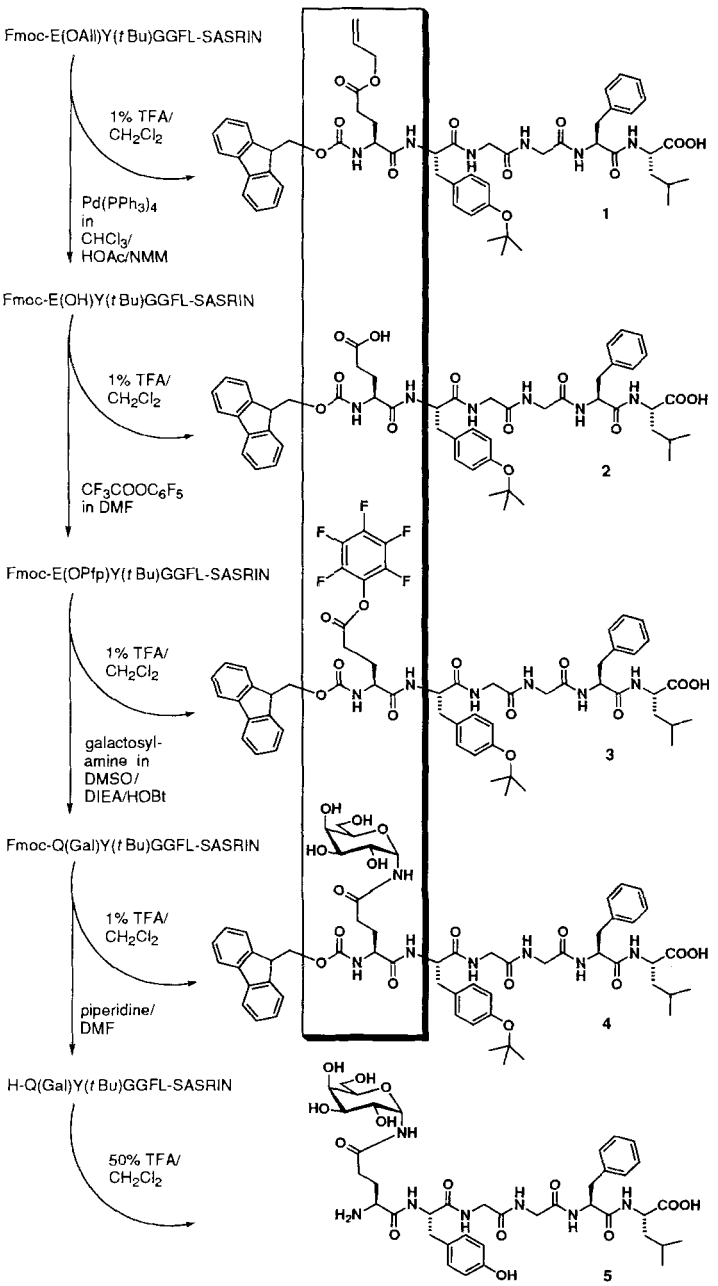
Dirk Vetter,* David Tumelty, Sunil K. Singh, and Mark A. Gallop*

The discovery of novel glycopeptide ligands for relevant biological receptors has been greatly hindered by the difficult syntheses of these complex compounds.[1, 2] A convergent approach to glycopeptide assembly would improve their accessibility, but few studies have addressed this problem. Successful O-glycosylation was reported for the reaction of peracetylated glucose-oxazoline with resin-bound serine-containing peptides.[3] Somewhat surprisingly, complete N-glycosylation has been accomplished only in solution.[4, 5] A recent example was the synthesis of natural glycoprotein fragments by coupling *N*-acetylglucosaminylamine and related oligosaccharidylamines to aspartic acid containing peptides.[6, 7]

In this report we demonstrate a novel method for the solid-phase synthesis of N-linked glycopeptides. Work is currently in progress to apply the outlined approach to the generation of glycopeptide libraries by combinatorial methods.[8]

The key step in our strategy is the coupling of an unprotected glycosylamine to a pentafluorophenyl carboxylate (OPfp) on the side chain of resin-bound peptide. A great variety of glycosylamines are commercially available or accessible from the parent saccharides via a simple one-step derivatization using aqueous ammonia solutions.[9] The resulting 1-amino, 1-deoxysugars are β anomers, except when the neighboring 2-hydroxyl group is axial, as for mannose and lyxose, where the α anomer predominates.[10] The activated fluorenylmethyloxycarbonyl(Fmoc)- and *tert*-butyl(*t*Bu)-protected peptides were prepared by incorporation of aspartic or glutamic acid protected as allyl (OAll) esters at their β- or γ-carboxyl groups, followed by complete deallylation and Pfp ester formation.[11] Protecting group removal and cleavage from the resin afforded the free glycopeptides.

The procedure was optimized on the example Gln(Gal)-Tyr-Gly-Gly-Phe-Leu-OH (**5**).[12] The use of polystyrene resin modified with a highly acid-labile linker (super acid sensitive resin, SASRIN) allowed for the cleavage and characterization of the relevant peptide at each step of the reaction sequence.[13] The reactions are displayed in Scheme 1, and corresponding HPLC traces of the crude cleavage products are shown in Figure 1.



Scheme 1. Example of the generation of N-linked glycopeptides on a solid phase. The reaction sequence deallylation/ester activation/glycosylamine condensation (framed area) was performed on the resin-bound peptide after full assembly. Each step, including Pfp ester formation, was followed by cleavage and characterization of the resulting peptide (**1**–**5**; see Fig. 1).

[*] Dr. D. Vetter,[+] Dr. M. A. Gallop, Dr. D. Tumelty, Dr. S. K. Singh,
Affymax Research Institute
4001 Miranda Avenue, Palo Alto, CA 94304 (USA)
Telefax: Int. code + (415)424-9860

[+] Present address:
Institut für Molekulare Biotechnologie, e. V.
Beutenbergstrasse 11, D-07745 Jena (Germany)
Telefax: Int. code + (3641)656-255
e-mail: 75542.420@compuserve.com

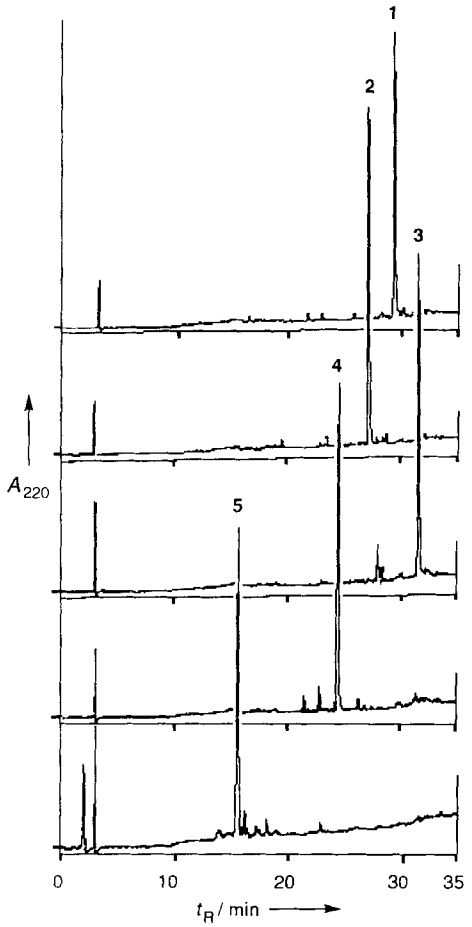


Fig. 1. HPLC traces of the crude products cleaved from the solid phase. The convergent solid-phase synthesis of a glycopeptide can thus be followed stepwise.

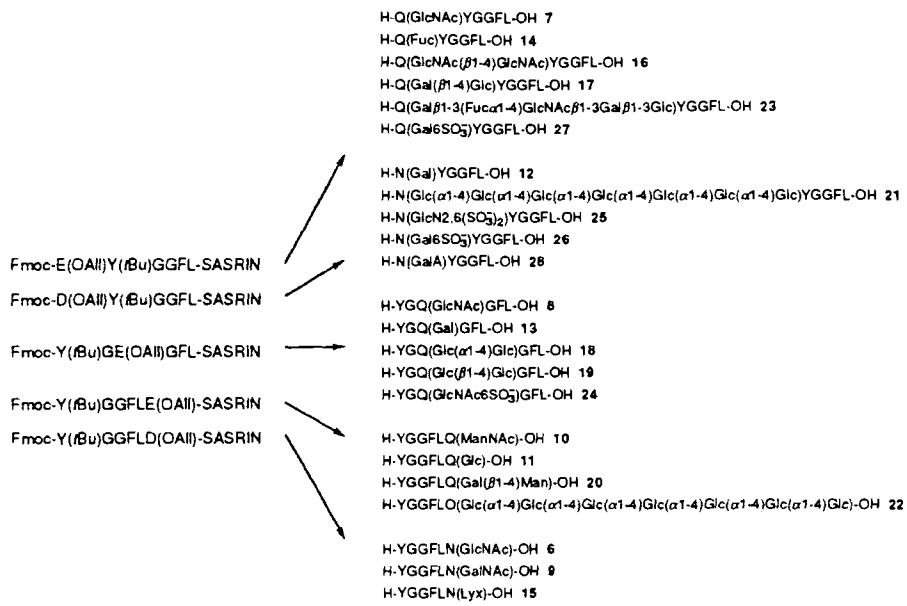
Synthesis commenced with the assembly of the fully protected peptide on the solid phase. Palladium(0)-catalyzed removal of the allyl protecting group without cleavage of the N-terminal Fmoc group was effected with a mixture of chloroform, *N*-methylmorpholine, and acetic acid.[14] Standard deprotection conditions using morpholine as the allyl scavenger consistently caused Fmoc removal.[15]

N-hydroxysuccinimidyl (Su) and pentafluorophenyl esters were each considered for solid-phase activation of the side-chain carboxyl groups of aspartic and glutamic acid; both allow for efficient amidation of the glycosylamines without concomittant esterification of the sugar hydroxyl groups. In practice, formation of the active ester was best accomplished by employing pentafluorophenyl trifluoroacetate in dimethylformamide (DMF)/pyridine. Alternatives such as carbodiimide-mediated esterification with pentafluorophenol as well as activation with bis(*N*-hydroxysuccinimidyl) carbonate were found to be inferior.[16]

Attempts to condense galactosylamine with Fmoc-E(OSu)Y(*t*Bu)GGFL-SASRIN were unsuccessful owing to loss of the Fmoc group and poor reactivity of the succinimidyl ester. Lowering the excess of glycosylamine, shortening reaction times, and using the Pfp active ester resulted in cleaner reactions with only one side product, shown to be the glutamine-containing peptide. This side product is thought to be formed by reaction of the active ester with free ammonia, which could originate from residual traces of ammonium carbonate in the sugar or through hydrolysis of the glycosylamine. A variety of approaches were examined to avoid carboxamide formation. It was found that addition of *N*,*N*-diisopropylethylamine (DIEA) and 1-hydroxybenzotriazole (HOBt) effectively suppressed formation of the side product. Undesired peptide amidation has also been observed by Lansbury et al. in the related *N*-glycopeptide synthetic strategy, where exhaustive lyophilization of the 1-amino sugars was used to remove residual ammonia.[7]

Five support-bound peptides with Glu(OAll) or Asp(OAll) and permutations of the motif Tyr(*t*Bu)-Gly-Gly-Phe-Leu were then synthesized and subsequently condensed with 18 different mono- and oligosaccharidylamines (see Scheme 2). Included in the list of the 23 glycopeptides are to our knowledge the first examples of synthetic peptides bearing carboxylated, mono- and disulfated carbohydrates. The products were purified by HPLC and characterized by FAB-MS and ^{1}H NMR spectroscopy.

The outlined convergent synthesis of glycopeptides proved advantageous in many respects. Protection of saccharide components was obviated because glycosylation was the last bond-forming step in the synthesis. In all cases the stereochemistry of the anomeric center of the parent glycosylamine was retained in the glycopeptide. Yields were quantitative for the glycopeptides prepared from the simple monosaccharides GlcNAc, GalNAc, ManNAc, Glc, Gal, Fuc, and Lyx (→ **6**–**14**) as well as from the disaccharides chitobiose, lactose, maltose, and cellobiose (→ **16**–**19**). A somewhat lower yield was obtained with Gal(β1-4)Man (→ **20**). Conversions of 50 to 80% were obtained for reactions with uncharged oligosaccharides as complex as the penta- and heptasaccharides lacto-*N*-fucopentaose II and maltoheptaose, respectively (→ **21**–**23**). Except for the reaction



Scheme. 2. 23 Glycopeptides obtained by condensing 18 different glycosylamines with five hexapeptides, which contain the motif Tyr-Gly-Gly-Phe-Leu (YGGFL) and the amino acids Glu or Asp in different positions.

 © VCH Verlagsgesellschaft mbH, D-69451 Weinheim, 1995 0570-0833/95/0101-0061 $ 10.00+.25/0

with GlcNAc6SO_3^- (→ **24**, quantitative), generally lower yields of 30 to 50% were encountered with the glycosylamines of charged sugars such as GlcN2,6(SO_3^-)$_2$ (→ **25**), Gal6SO_3^- (→ **26**, **27**), and galacturonic acid (→ **28**). Furthermore, yields were independent of whether the peptides were glycosylated at the N- or C-terminal positions or at the central, glycine-flanked position. Conversions were almost identical for aspartic and for glutamic acid containing peptides.

The intramolecular cyclization of activated aspartic acid containing peptides to yield succinimide or isoaspartic acid products is a well-known side reaction, particularly when the active ester is N-terminal to a small residue like glycine or alanine.[17] The optimal stoichiometry of glycosylamine, DIEA, and HOBt employed in our experimental protocol effectively suppressed aspartimide formation from Asp(OPfp) peptide intermediates.[18] A similar optimization strategy has been described in detail by Lansbury et al.[7]

Common conditions for acidic deprotection of peptide side chains were not employed in this study. Our milder protocol was sufficient to effect removal of standard peptide side chain protecting groups, and O-glycosidic bonds were left intact with one exception: in the synthesis of the representative fucose-containing glycopeptide **23**, 50% of the product was defucosylated.

The orthogonal deprotection and solid-phase activation methodology described here is fully compatible with standard Fmoc/*t*Bu protection schemes and is expected to allow for the introduction of one or more saccharide moieties at a defined position of a peptide or peptide pool. If the sugar is condensed with glutamic rather than aspartic acid, the approach is general and will form the basis for the construction of glycopeptide libraries for massive parallel screening.

Experimental Procedure

General procedures: Fmoc-Glu(OAll)-OH and Fmoc-Asp(OAll)-OH were obtained from Propeptide. Automated peptide synthesis was performed on an ABI 431A using FastMoc cycles on super acid sensitive resin (SASRIN, 0.96 mmol g^{-1}, or Fmoc-Leu-SASRIN, 0.6 mmol g^{-1}, Bachem). Cleavage of resin aliquots was performed in 1% TFA/CH_2Cl_2 as recommended. Analytical HPLC was carried out with a C18 reversed-phase column and a linear gradient of 5–95% acetonitrile in water/TFA at 1 mL min^{-1}. Preparative HPLC was performed with a C18 reversed-phase column and a linear gradient of 0–50% acetonitrile in water/TFA.

2: Deallylation of Fmoc-E[OAll]Y[*t*Bu]GGFL-SASRIN (**1**) was achieved by mixing 5 mL of $CHCl_3$, 0.66 mL of HOAc, and 0.32 mL of *N*-methylmorpholine under nitrogen atmosphere with [Pd(PPh_3)$_4$] (0.4 g, 0.32 mmol), **1** (0.2 g, 0.12 mmol; 0.6 mmol g^{-1}), and PPh_3 (0.4 g, 1.53 mmol). The mixture was stirred vigorously for 2 h at room temperature. The resin was recovered by filtration and washed with $CHCl_3$, DMF, and MeOH. The product consisted of >95% Fmoc-E(OH)Y(*t*Bu)GGFL-OH (**2**) by HPLC (t_R = 27.36 min).

3: To a solution of **2** (20 mg, 12 μmol) in 0.1 mL of anhydrous DMF were added 20 μL of pyridine and pentafluorophenyl trifluoroacetate (40 μL, 0.23 mmol; Aldrich). The mixture was agitated for 2 h at room temperature. The resin was recovered by filtration and washed with DMF and CH_2Cl_2. The product consisted of >95% Fmoc-E(OPfp)Y(*t*Bu)GGFL-OH (**3**) by HPLC (t_R = 31.53 min); FAB-MS: 1129.3 [(M + H^+)].

4: A solution of **3** (20 mg, 12 μmol) in 0.66 mL of anhydrous DMSO was mixed with galactosylamine (8 mg, 45 μmol; Sigma), 4 μL of DIEA, and HOBt (8 mg, 59 μmol; Advanced Chemtech). The mixture was stirred vigorously for 15 min at room temperature. The resin was recovered by filtration and washed with DMSO and CH_2Cl_2. The product consisted of 95% Fmoc-Q(Galβ)Y(*t*Bu)GGFL-OH by HPLC (t_R = 24.36 min); FAB-MS: 1168.5 [(M + Na^+)].

5: A solution of **4** (20 mg, 12 μmol) in 0.4 mL of 20% piperidine/DMF was agitated for 15 min at room temperature. After filtration the procedure was repeated, and the recovered resin was washed with DMF and CH_2Cl_2. The resin was then stirred vigorously with 1 mL of 50% TFA/CH_2Cl_2 for 15 min at room temperature. After filtration the procedure was repeated, and the resin was washed extensively with CH_2Cl_2. The combined filtrates were concentrated in vacuo, and the product was precipitated with ethyl ether and isolated by centrifugation. After dissolution in acetonitrile/water and lyophilization, the crude material was obtained as a white fluffy solid (6.4 mg, 8 μmol, 66% yield). The product consisted of 95% H-Q(Galβ)YGGFL-OH by HPLC (t_R = 15.52 min). Purification was achieved by preparative HPLC. The sample was collected and lyophilized to give **5** (5.6 mg, 7.0 μmol, 58% yield). FAB-MS (calculated/found): 845/868.7 [(M + Na^+)]; FAB-MS (high resolution, calculated/found): 868.3705/868.3708. The β configuration of the Gal-Gln linkage was confirmed by ^{1}H NMR spectroscopy (400 MHz, [D_6]DMSO, 25 °C, TMS): δ = 4.682 (d, J = 9.0 Hz, Gal-H1).

Diagnostic analytical data for representative glycopeptides:

6: H-YGGFLN(GlcNAcβ)-OH, FAB-MS (calculated/found): 872/895.7 [(M + Na^+)]; FAB-MS (high resolution, calculated/found): 895.3814/895.3822; ^{1}H NMR (400 MHz, [D_6]DMSO, 25 °C, TMS): δ = 0.808 (d, J = 6.12 Hz, 3H; Leu-Me), 0.861 (d, J = 6.12 Hz, 3H; Leu-Me), 1.480 (m, 2H; Leu-βHs), 1.540 (m, 1H; Leu-γH), 1.774 (s, 3H; Ac), 4.787 (t, 1H, J = 9.38 Hz, GlcNAc-H1), 6.669 (d, J = 8.48 Hz, 2H; Tyr-H3,H5), 7.006 (d, J = 8.48 Hz, 2H; Tyr-H2,H6), 7.241 (d, J = 4.37 Hz, 5H; Phe), 8.261 (d, J = 8.88 Hz, 1H; Asn-βNH), 9.278 (s, 1H; Tyr-OH).

12: H-N(Galβ)YGGFL-OH, FAB-MS (calculated/found): 831/854.7 [(M + Na^+)]; FAB-MS (high resolution, calculated/found): 854.3548/854.3548; ^{1}H NMR (400 MHz, [D_6]DMSO, 25 °C, TMS): δ = 0.836 (d, J = 6.40 Hz, 3H; Leu-Me), 0.892 (d, J = 6.48, 3H; Leu-Me), 1.530 (m, 2H; Leu-βHs), 1.608 (m, 1H; Leu-γH), 4.031 (m, 1H; Asn-αH), 4.689 (t, J = 8.84 Hz, 1H; Gal-H1), 6.641 (d, J = 8.52 Hz, 2H; Tyr-H3,H5), 7.045 (d, J = 8.52 Hz, 2H; Tyr-H2,H6), 7.243 (d, J = 4.68 Hz, 5H; Phe), 7.944 (t, J = 5.52 Hz, 1H; Gly-NH), 8.346 (t, J = 5.83 Hz, 1H; Gly-NH), 8.810 (d, J = 8.76 Hz, 1H; Asn-βNH), 9.205 (s, 1H; Tyr-OH).

To address the question of succinimide formation and subsequent transpeptidation during activation and condensation of the peptide side chain, compound **12** was investigated by NOE spectroscopy. The isomeric reference glycopeptides H-N(Galβ)YGGFL-OH and H-D(YGGFL-OH)-NH-Galβ were synthesized from the glycosylated amino acids Fmoc-N(Galβ)-OH and Fmoc-D(OH)-NH-Galβ, respectively, with suppression of succinimide formation. Irradiation of the amide proton of the sugar–peptide linkage resulted in a substantial NOE to the α proton of isoasparagine in the isomeric compound. This NOE was completely absent in both the asparagine-containing analogue and glycopeptide **12**. This was taken as evidence that no transpeptidation had occurred during the convergent synthesis of **12**. Details on the NOE study will be published elsewhere.

16: H-Q(GlcNAcβ(1-4)GlcNAcβ)YGGFL-OH, FAB-MS (calculated/found): 1089/1090.6 [(M + H^+)]; FAB-MS (high resolution, calculated/found): 1090.4945/1090.4953;

^{1}H NMR (400 MHz, [D_6]DMSO, 25 °C, TMS): δ = 0.841 (d, J = 6.52 Hz, 3H; Leu-Me), 0.887 (d, J = 6.52 Hz, 3H; Leu-Me), 1.525 (m, 2H; Leu-βHs), 1.620 (m, 1H; Leu-γH), 1.771 (s, 3H; Ac), 1.809 (s, 3H; Ac), 2.156 (t, J = 7.80 Hz, 2H; Gln-γHs), 4.350 (d, J = 8.48 Hz, 1H; GlcNAc-H1'), 4.807 (t, J = 9.20 Hz, 1H; GlcNAc-H1), 6.627 (d, J = 8.44 Hz, 2H; Tyr-H3,H5), 7.028 (d, J = 8.44 Hz, 2H; Tyr-H2,H6), 7.242 (d, J = 4.36 Hz, 5H; Phe), 7.984 (t, J = 5.56 Hz, 1H; Gly-NH), 8.117 (t, J = 7.68 Hz, 1H; Gly-NH), 8.639 (d, J = 7.76 Hz, 1H; Asn-βNH), 9.203 (s, 1H; Tyr-OH).

Chromatographic data (HPLC retention time and percent of product as determined by the absorption at 220 nm) and yields of representative glycopeptides after preparative HPLC (based on 20 mg of resin with the loading specified by the supplier). **8**: 15.48 min, 99%, 7.3 mg (8.2 μmol, 69%); **10**: 14.75 min, 91%, 7.0 mg (7.9 μmol, 41%); **11**: 14.65 min, 99%, 6.5 mg (7.7 μmol, 41%); **19**: 15.21 min, 92%, 7.0 mg (7.0 μmol, 58%); **20**: 14.48 min, 76%, 6.4 mg (6.4 μmol, 33%); **22**: 13.81 min, 89%, 11.7 mg (6.4 μmol, 34%); **26**: 16.95 min, 51%, 3.3 mg (3.6 μmol, 30%).

Received: February 28, 1994
Revised version: July 7, 1994 [Z6717IE]
German version: *Angew. Chem.* **1995**, *107*, 94

Keywords: glycopeptides · peptides · solid-phase synthesis

[1] For an abstract of recent carbohydrate-based drug discovery efforts see J. Alper, *Bio/Technology* **1993**, *11*, 1093.
[2] For a review on glycopeptide synthesis see H. Kunz, *Angew. Chem.* **1987**, *99*, 297; *Angew. Chem. Int. Ed. Engl.* **1987**, *26*, 294–308.
[3] M. Hollósi, E. Kollát, I. Laczkó, K. F. Medzihradszky, J. Thurin, L. Otvös, Jr., *Tetrahedron Lett.* **1991**, *32*, 1531–1534.
[4] A. L. Handlon, B. Fraser-Reid, *J. Am. Chem. Soc.* **1993**, *115*, 3796–3797.
[5] W. T. Shier, *Proc. Nat. Acad. Sci. USA* **1971**, *68*, 2078–2082.
[6] S. T. Anisfeld, P. T. Lansbury, Jr., *J. Org. Chem.* **1990**, *55*, 5560–5561.
[7] S. T. Anisfeld-Cohen, P. T. Lansbury, Jr., *J. Am. Chem. Soc.* **1993**, *115*, 10531–10537.
[8] a) G. Jung, A. G. Beck-Sickinger, *Angew. Chem.* **1992**, *104*, 375; *Angew. Chem. Int. Ed. Engl.* **1992**, *31*, 367–383. b) M. A. Gallop, R. W. Barrett, W. J. Dower, S. P. A. Fodor, E. M. Gordon, *J. Med. Chem.* **1994**, *37*, 1233–1251; E. M. Gordon, R. W. Barrett, W. J. Dower, S. P. A. Fodor, M. A. Gallop, *ibid.* **1994**, *37*, 1385–1401.
[9] L. M. Likhosherstov, O. S. Novikova, V. A. Derevitskaja, N. K. Kochetkov, *Carbohydr. Res.* **1986**, *146*, C1–C5.
[10] The amination and subsequent amidation of a variety of 50 mono- and oligosaccharides will be described in a parallel study. D. Vetter, M. A. Gallop, unpublished.

[11] a) D. Tumelty, D. Vetter, V. Antonenko, *J. Chem. Soc. Chem. Commun.* **1994**, 1067–1068; b) Selective side-chain deallylation was introduced by H. Kunz, H. Waldmann, C. Unverzagt, *Int. J. Pept. Prot. Res.* **1985**, *26*, 493–497.
[12] The leucine enkephalin sequence YGGFL was chosen because glycosylation of a related peptide led to precedented enhancement of biological activity at opioid receptors: R. E. Rodriguez, F. D. Rodriguez, M. P. Sacristán, J. L. Torres, G. Valencia, J. M. García Antón, *Neurosci. Lett.* **1989**, *101*, 89–94.
[13] O-linked glycopeptides have been prepared previously on SASRIN supports, see B. Lüning, T. Norberg, J. Tejbrant, *J. Chem. Soc. Chem. Commun.* **1989**, 1267–1268.
[14] a) F. Albericio, G. Barany, G. B. Fields, D. Hudson, S. A. Kates, M. H. Lyttle, N. A. Solé in *Peptides 1992* (Eds.: C. H. Schneider, A. N. Eberle), ESCOM Science Publishers B. V., Amsterdam, **1993**, pp. 191–193; b) Chemoselective removal of allyl protecting groups in the presence of Fmoc groups has also been described by S. Rio, J. M. Beau, J. C. Jacquinet, *Carbohydr. Res.* **1991**, *219*, 71–90; c) M. Ciommer, H. Kunz, *Synlett* **1991**, *8*, 593–595.
[15] H. Kunz, H. Waldmann, *Angew. Chem.* **1984**, *96*, 49–50; *Angew. Chem. Int. Ed. Engl.* **1984**, *23*, 71–72.
[16] M. Green, J. Berman, *Tetrahedron Lett.* **1990**, *31*, 5851–5852.
[17] M. Bodanszky, J. Z. Kwei, *Int. J. Pept. Prot. Res.* **1978**, *12*, 69–74.
[18] However, assembly of the peptide sequence Fmoc-Y(*t*Bu)GD(OAll)GFL-SASRIN was terminated reproducibly before coupling of the final tyrosine residue. A truncated major side product (70% by HPLC, $m/z = 489$) presumably resulted from lactamization of H-GD(OAll)GFL-SASRIN.

A New Zincosilicate Zeolite with Nine-Ring Channels**

Carsten Röhrig and Hermann Gies*

In recent years zeolites have increasingly found applications as catalysts, molecular sieves, adsorbents, and ion exchangers.[1] The useful properties of these inorganic host–guest systems are based primarily on the structure of the tetrahedral framework of the host of general composition TO_2 and the possible variation of T atoms (T = Si, Al, P, B, Ga, As, Sb, Zn etc.). The guest species fill the pore space of the tetrahedral framework, and for charged frameworks these are the organic or inorganic cations necessary to achieve electroneutrality.

One aim of the synthetic work on zeolites is the search for host structures with low tetrahedral density, that is for frameworks with as few tetrahedral building units [TO_4] per 1000 Å^3 as possible. Furthermore, the materials should contain both catalytically active centers and also pore systems of well-defined geometry. In this context, the topological analysis of known zeolite structures by Brunner and Meier has shown that there is a linear correlation between the smallest ring size occurring in a zeolite structure and the tetrahedral density.[2]

Among zeolite minerals the beryllosilicate lovdarite is of particular interest because its structure contains the spiro-5 building unit, which is built from three-rings, which occur only very rarely in tetrahedral frameworks.[3] Because of the high toxicity of beryllium and the similarity of beryllosilicates and zincosilicates,[4–6] we investigated the possibility of preparing structurally related zincosilicates with low tetrahedral density; in addition, the heteroatom zinc plays an interesting role in the catalytic aromatization of olefins.

For the synthesis, one mol of $Si(OCH_3)_4$ was hydrolyzed in an aqueous solution of 44 mol H_2O, 0.08 mol tetraethylammonium hydroxide (TEAOH), 0.0–0.88 mol NaOH, 0.0–0.88 mol KOH, and 0.0–0.1 mol ZnO (partly undissolved) and placed in a teflon-lined autoclave which was kept at 160–220 °C for 12–14 days.

Depending on the reaction temperature, the concentration ratio of the alkali metal cations, and the amount of ZnO, several different zeolite-like zincosilicate phases of high crystallinity were obtained. These included the already known VPI-7[4–7] and a new phase with the laboratory code RUB-17, which both showed tetragonal-prismatic morphologies. The crystals usually were intergrown to conglomerates so that the analysis and the refinement of the structurs had to be performed on the basis of X-ray powder diffraction data.

In addition to VPI-7 and RUB-17, phases that can be identified unambigiously, a number of other zeolite-like zincosilicates formed whose X-ray powder diffractograms and ^{29}Si NMR spectra show strong similarities, but also distinct differences to those of VPI-7 and RUB-17.

The structure refinement of VPI-7[7] yielded the orthorhombic space group *Fdd*2 with lattice constants $a = 39.88(1)$, $b = 10.326(1)$, and $c = 10.219(1)$ Å, and an idealized composition $Na_{32}(Si_{56}Zn_{16}O_{144})\cdot 42\,H_2O$.

To determine the hitherto unknown structure of RUB-17, a high-resolution powder X-ray diffractogram was indexed. The space groups *C*2, *Cm*, and *C*2/*m* are in agreement with the observed, monoclinic lattice parameters ($a = 7.238(1)$, $b = 40.56(1)$, $c = 7.308(1)$ Å and $\beta = 91.8(1)°$), and the rules for systematic absences. The lattice geometry of RUB-17 is very similar to that of VPI-7, since the diagonals of an orthogonal 7×7 Å^2 plane correspond to the edges of a 10×10 Å^2 plane, that is $a_{RUB-17}\cdot\sqrt{2} \approx c_{RUB-17}\cdot\sqrt{2} \approx b_{VPI-7} \approx c_{VPI-7}$; also, $b_{RUB-17} \approx a_{VPI-7}$ and $\beta_{RUB-17} \approx 90°$. Furthermore, the comparison of the ^{29}Si NMR spectra of VPI-7 and of RUB-17 shows that RUB-17 also contains a signal for a framework silicon atom shifted to unusually low field which can only be ascribed to a Si atom in the spiro center (Fig. 1). We can thus start with the assumption that the structures of RUB-17 and VPI-7 contain similar building units. By structural modeling using the building units of VPI-7, a model for the framework structure of RUB-17 was established. A crystal-chemically acceptable distribution of the tetrahedrally coordinated Si and Zn atoms that are in addition in agreement with the chemical analysis and the NMR measurements was possible only in space group *Cm*.

An optimized DLS model[8] of a hypothetical [SiO_2] framework was used as starting model for the structure refinement with the Rietveld method. The positions of the Zn atoms in the tetrahedral framework were found from difference Fourier syntheses using the Rietveld program XRS-82.[9] This led to the

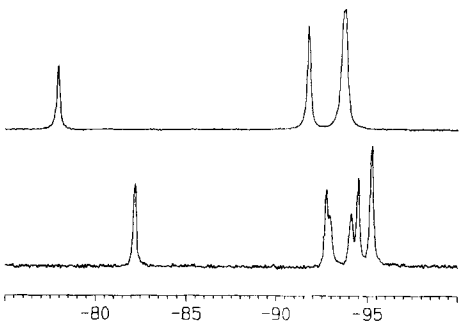


Fig. 1. ^{29}Si NMR spectra of VPI-7 (top) and RUB-17 (bottom). The δ values are plotted on the axis.

[*] Prof. Dr. H. Gies, Dipl.-Min. C. Röhrig
Institut für Mineralogie der Universität
Postfach 10 21 48, D-44801 Bochum (Germany)
Telefax: Int. code + (234) 7094-179

[**] We thank Dr. I. Dierdorf for the measurement of the ^{29}Si NMR spectra. In this communication nine-ring refers to the number of tetrahedral centers that form the ring. Similar terminology is used for three-, four-, five-, and six-rings.

calculation of an improved DLS model of the $[(Zn,Si)O_2]$ framework which took into account the Zn–O bond lengths (1.95 Å). Further refinement (Fig. 2) yielded the positions of the non-framework constituents (Na, K, H_2O) and gave the composition of the unit cell as $K_4Na_{12}[Si_{28}Zn_8O_{72}]\cdot 18H_2O$.[10]

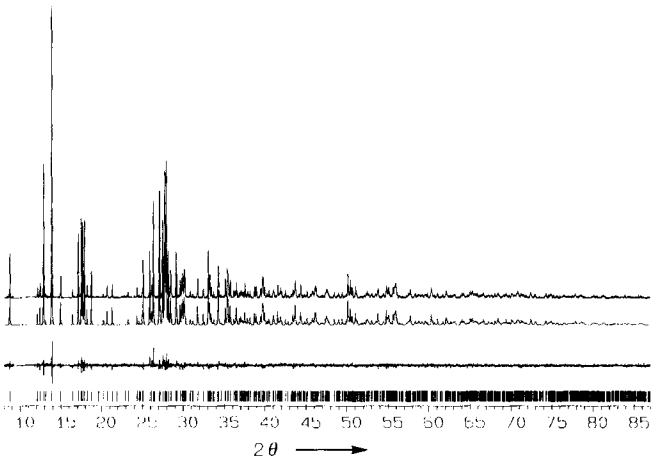


Fig. 2. Observed (top), calculated (center), and difference (bottom) curves of the X-ray diffractogram of RUB-17. Vertical bars indicate the 2θ positions of symmetry-allowed reflections.

The framework structure of RUB-17 is a member of the group of three-dimensional four-connected nets. Neglecting all O atoms, the structure can be constructed from two-dimensional 4.8^2 nets (Fig. 3). Two of these 4.8^2 nets are connected to each other by additional Si atoms and form layer-like building units (LLBUs; Fig. 4). The *spiro*-5 units **1** originate through this form of linkage. The overall structure results from the stacking of the LLBUs. For VPI-7, the LLBUs are linked to each other only by five-rings (Fig. 5 left); in RUB-17, the connection occurs alternately through four-/six-rings and five-rings (Fig. 5 right). The nonframework components Na, K, and H_2O likewise form a three-dimensional network, which is connected to the $[(Zn,Si)O_2]$ tetrahedral framework through Na–O, K–O, and H_2O–O bonds.

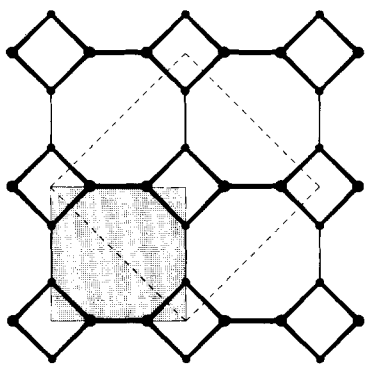
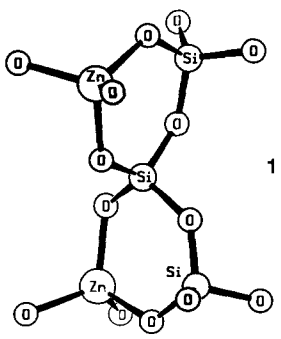


Fig. 3. 4.8^2 layer. Nodes: tetrahedral centers, lines: T-O-T bonds, dashed lines: 10×10 Å^2 plane (VPI-7), dotted area: 7×7 Å^2 plane (RUB-17).



1

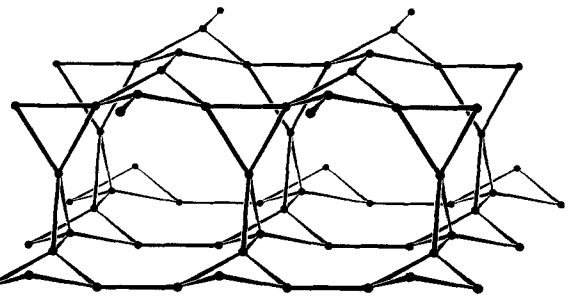


Fig. 4. Layer-like building unit (LLBU). Nodes: tetrahedral centers, lines: T-O-T bonds.

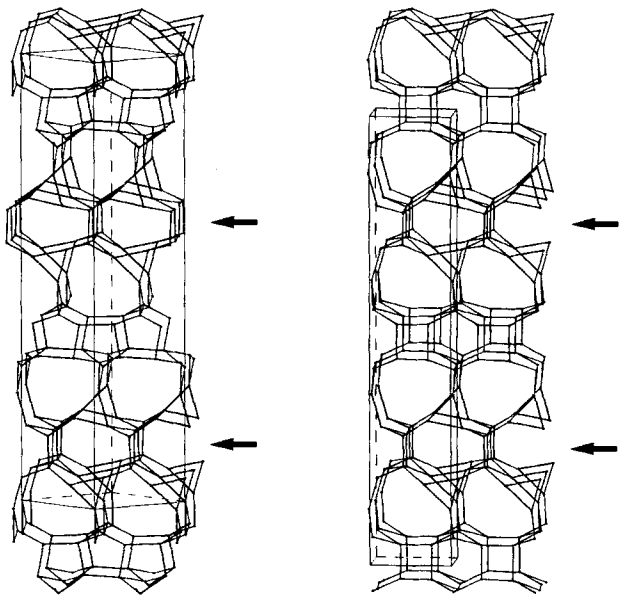


Fig. 5. Tetrahedral framework structure of the unit cell of VPI-7 (left) and RUB-17 (right). The arrows mark five-rings perpendicular to the drawing plane.

The network of alkali metal cations and water molecules plays a decisive role in the stabilization of RUB-17 and VPI-7, since thermal treatment even at relatively low temperatures leads to the breakdown of these structures. Long-term thermal treatment (24 h) at constant temperatures showed that RUB-17 is stable up to about 220 °C, whereas the structure of VPI-7 becomes amorphous already at about 130 °C. It can thus be assumed that the stacking mode of the LLBUs influences the thermal stability of these structures, that is the stacking through four-/six-rings and five-rings (RUB-17) is more stable than the stacking using exclusively five-rings (VPI-7). Accordingly, a structure such as lovdarite in which the LLBUs are connected only through four-/six-rings should be even more thermally stable than RUB-17. The synthesis of a zincosilicate with that structure would probably result in a useful material for commercial catalytic applications.

According to ^{29}Si NMR spectra, it can be assumed that the not yet identified zincosilicates are further members of this polytype series, in which the stacking sequence has not yet been determined.

Experimental Procedure

The chemical analysis of the Si:Zn:Na:K ratio using an ICP spectrometer (Philips PU 7000) gave a composition of 3.5:1:1.3:0.6. The H_2O content was determined by Karl-Fischer titration and TG analyses (Linseis) to be about 10.6 wt%. The morphology of the synthesis products was investigated by scanning electron microscopy

 © VCH Verlagsgesellschaft mbH, D-69451 Weinheim, 1995 0570-0833/95/0101-0064 $ 10.00+.25/0

(Cambridge Stereoscan 250 M3). The density of the synthesized material (ρ = 2.47 g cm^{-3}) was determined with the suspension method using butyl acetate and bromoform as suspension liquids. NMR experiments were carried out on a Bruker ASX 400 spectrometer at 79.495 MHz for Si.

Received: July 2, 1994 [Z 7092 IE]
German version: *Angew. Chem.* **1995**, *107*, 125

Keywords: silicon compounds · structure elucidation · zeolites · zinc compounds

[1] J. V. Smith, *Chem. Rev.* **1988**, *8*, 149.
[2] G. O. Brunner, W. M. Meier, *Nature* **1989**, *337*, 146.
[3] S. Merlino, *Eur. J. Mineral.* **1990**, *2*, 809.
[4] M. J. Annen, M. E. Davis, J. B. Higgins, J. L. Schlenker, *J. Chem. Soc. Chem. Commun.* **1991**, 1175.
[5] M. J. Annen, M. E. Davis, J. B. Higgins, J. L. Schlenker, *Mat. Res. Soc. Symp. Proc.* **1991**, *223*, 245.
[6] M. J. Annen, M. E. Davis, in *Molecular Sieves* (Eds.: M. L. Occelli, H. Robson), van Nostrand Reinhold **1992**, p. 349.
[7] C. Röhrig, H. Gies, B. Marler, *Zeolites* **1994**, *14*, 498.
[8] C. Baerlocher, A. Hepp, W. Meier, Distance Least Squares Refinement Program DLS-76. Institut für Kristallographie & Petrographie, ETH Zürich, **1977**.
[9] C. Baerlocher, X-ray Rietveld System XRS-82, Institut für Kristallographie & Petrographie, ETH Zürich, **1991**.
[10] X-ray structural refinement of RUB-17 $K_4Na_{12}[Si_{28}Zn_8O_{72}]\cdot 18H_2O$: *Cm*, a = 7.238(1), b = 40.56(1), c = 7.308(1) Å, β = 91.8(1)°, Z = 1. Siemens D5000 powder diffractometer with Ge(111) monochromatized $Cu_{K\alpha 1}$ radiation in Debye–Scherrer geometry, 0.3 mm glass capillary, room temperature, scan region: $8 \le 2\theta \le 87$, number of data points: 7516, number of observed reflections: 803, number of refined structure parameters: 107, isotropic temperature factors taken from known zincosilicates and not refined, number of profile parameters: 4, number of geometrical restrictions: 109, Rietveld program XRS-82, R_e = 0.238, R_{wp} = 0.164, R_i = 0.090. Further details of the crystal structure investigation may be obtained from the Fachinformationszentrum Karlsruhe, D-76344 Eggenstein-Leopoldshafen (Germany), on quoting the depository number CSD-58472.

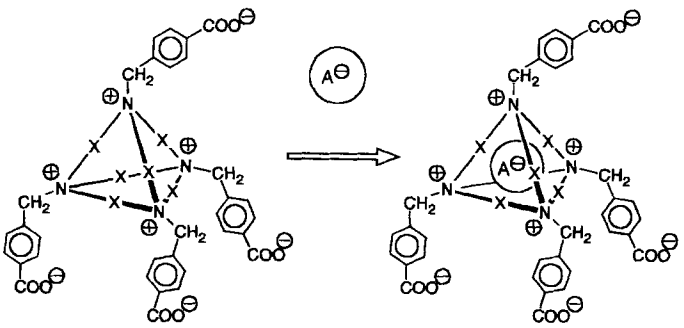
Molecular Recognition of Anions by Zwitterionic Host Molecules in Water**

Karin Worm and Franz P. Schmidtchen*

Cationic artificial molecular hosts are of proven utility in molecular recognition of anions.[1] However, they must inevitably be accompanied by counterions creating competition which disfavors complexation of the desired anionic guest. Electroneutral hosts would avoid this and successful examples employing polytopic Lewis acids[2] or ion–dipole interactions[3, 4] are known. In general these host–guest interactions are quite weak and cannot overcome the competition from protic solvents.

In these protic solvents the natural hosts for anions (e.g. the majority of enzymes) bind the negatively charged guests by direct contact to positively charged anchor groups. An approximately equivalent number of anionic functions are placed somewhat remote from this binding site, yielding a structural pattern with a small overall charge. This zwitterionic character of biogenic hosts combined with a well-defined network of hydrogen bonds results in the specific and enthalpically strong binding of the anionic guest ion.[5, 6]

In order to mimic this natural binding principle we designed the artificial hosts **1** and **2**. By virtue of the electrostatic repulsion of the inner cationic centers these molecules are inclined to adopt inflated conformations with cavities which may encapsulate the guest anion. Rigid substituents extend radially to the exterior carrying a negative charge at their distal ends. Internal collapse by ion pairing is avoided owing to the high connectivity of the molecular skeleton. Preliminary molecular modeling studies[7] in vacuum, however, showed that these hosts acquire an almost spherical shape due to the carboxylates approaching the neighboring quaternary ammonium centers. The arene rings then cover the tetrahedral faces. In molecular dynamics simulations a bromide ion on the outside thus has no chance to make its way into the cavity even when pushed by high kinetic energy (1000 K). Nevertheless molecular mechanics calculations find the inclusion complex more stable by about 23 kcal mol^{-1} than the next best host–guest complex with the guest anion associated from the outside. The results of our calculations support the basic concept underlying the host design, because solvation of the ionic groups most likely will disrupt their mutual interaction and will restore the accessibility of the molecular cage.



1, X = $(CH_2)_6$
2, X = $(CH_2)_8$

3

Starting from the macrotricyclic tertiary amines[8] the target compounds **1** and **2** were obtained by Menshutkin alkylation using α-bromotoluic ester, followed by hydrolysis and desalting by reverse-phase chromatography, in greater than 85% yield. The zwitterionic betaines are only sparingly soluble in water at ambient temperature, but dissolve much better on addition of salt. This correlates with a progressive shift of the ^{1}H NMR signals of the endo- and exocyclic N-CH_2 groups to lower and higher fields, respectively. The picture is compatible with the hosts taking part in chemical exchange processes which are rapid with respect to the NMR time scale. Titrations were performed at 54 °C in homogeneous solution, and the results could be easily fitted to a 1:1 host–guest binding model.[9] The derived association constants K_{ass} and maximum chemical shift differences $\Delta\delta_{max}$ are given in Table 1.[10] With Na_2HPO_4, Na_2S, γ-aminobutyric acid, and trimethylazoniaacetate (betaine) no shifting of NMR signals was observed, which makes inclusion complexation of these substrates highly unlikely. K_{ass} decreases with increasing ionic strength (i.e. 0.2 M NaF) suggesting that electrostatic interactions dominate complexation. The maximum shift difference $\Delta\delta_{max}$ roughly correlates with the size of the anion. Considering that the 1:1 stoichiometry appears to remain fixed even if a high excess of guest is applied, one is forced to assume the penetration of the guest into the molecular cavity

[*] Prof. Dr. F. P. Schmidtchen, Dr. K. Worm
Institut für Organische Chemie und Biochemie
der Technische Universität München
Lichtenbergstrasse 4, D-85747 Garching (Germany)
Telefax: Int. code + (89)3209-3345

[**] This work was supported by the Deutsche Forschungsgemeinschaft and the Fonds der chemischen Industrie.

Table 1. Association constants K_{ass} of various anions with host **1** in D_2O at 327 K.

Anion	Ion radius [pm] [16]	ΔG^0_{hyd} [kcal mol^{-1}] [16]	K_{ass} [M^{-1}]	$\Delta\delta_{max}$ [Hz] [a]
Cl^-	181	−81.2	270	6.3
Br^-	196	−75.2	2150	27.0
I^-	220	−65.7	6480	54.5
I^- [b]	220		1650	55.3
CN^-	191	−70.5	950	6.9

[a] 360 MHz ^{1}H NMR determination. [b] In the presence of 0.2 M NaF.

of the tetrahedral host and consequently the formation of a well-structured complex. Another argument in favor of this view may be drawn from a competition experiment taking chloride as a probe monitoring the ^{35}Cl NMR resonance (Fig. 1). In water the quadrupolar species $^{35}Cl^-$ yields a sharp singlet, due to the rapid interchange of water and the resulting time-averaged high symmetry of the hydration sphere of the Cl^- ion. On addition of host **1** increasing amounts of complex are obtained which has a distinctly lower symmetry. As a corollary the quadrupole relaxation is augmented and leads to severe line broadening or even complete disappearance of the signal.[12] If now iodide, which forms a more stable complex with **1**, is added in portions to this mixture one observes progressive sharpening of the ^{35}Cl peak. Evidently, iodide displaces chloride from the complex. Considering the relationship between the size of host and guests the only plausible location for this process to happen is the central cavity of the host.

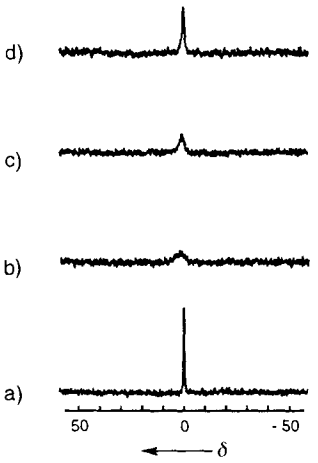


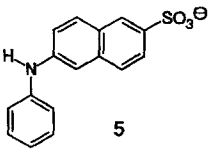
Fig. 1. ^{35}Cl NMR spectra of NaCl in D_2O at 298 K; a) 2.2×10^{-3} M NaCl; b) addition of 1.8×10^{-3} M **1**; c) addition of 5×10^{-4} M NaI to solution b); d) addition of 4×10^{-3} M NaI to solution b).

In the complexation of bromide and iodide by host **1** the ^{1}H NMR peak shift sufficed to determine the enthalpy and entropy of association from the dependence of K_{ass} on temperature (Table 2). For both anions host–guest binding is driven by enthalpy, with iodide exhibiting the distinctly better interaction. In addition negative entropies of association are found which apparently are modulated by enthalpy–entropy compensatory effects.[13] These results may be rationalized qualitatively, if one assumes that the guests have to strip off their solvation shells in the course of complexation. In relation to iodide, bromide requires the higher enthalpic expenditure for this desolvation and consequently shows a smaller overall gain in enthalpy. On the other hand, the release of tightly bound water molecules enhances entropy and thereby counteracts the inherently negative entropy of association. Although this reasoning undoubtedly covers only part of the total interaction, it provides another (though indirect) argument in favor of guest encapsulation, since only this process can serve to explain the loss of the hydration shell. One can extrapolate from the thermodynamic data that host **1** discriminates between the heavy halide ions at 0 °C by a factor of 40, whereas at 85 °C no selectivity is to be seen.

Table 2. Thermodynamic parameters of host-guest binding of bromide and iodide by host **1**.

Anion	ΔG^0 [kcal mol^{-1}]				ΔH°	ΔS°
	312 K	327 K	337 K	347 K	[kcal mol^{-1}]	[cal mol^{-1} K^{-1}]
Br^-	−5.08	−4.98	−4.91	−4.84	−7.6	−8.0
I^-	−6.17	−5.70	−5.38	−5.07	−16.7	−33.9

The bigger tetrahedral host **2**, on titration even with the biggest halide iodide, displays only rather meager shifts of the ^{1}H NMR signals, which did not allow the extraction of meaningful association constants. However, the host–guest complexation could be determined from the fluorescence intensity enhancement of the fluorophoric probe TNS **5** following the Benesi–Hildebrandt protocol.[14] Complex stability ($K_{ass} = 1.46\times10^3$ M^{-1}), which may be attributable to hydrophobic interactions, is similar to that of the complex of **5** with β-cyclodextrin ($K_{ass} = 1.5\times10^3$ M^{-1}),[15] but much weaker than with certain cyclophanes.[14]

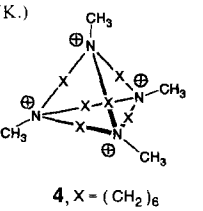


5

The hosts **1** and **2** show that binding of heavily solvated anions is possible, indeed, using abiotic receptors of zero net charge to form well-defined host–guest complexes with respectable affinity. The structurally fixed spatial separation of positively and negatively charged substructures appears to be a mandatory requirement, which in much the same fashion is also realized in the natural receptors.

Received: August 6, 1994 [Z 7214 IE]
German version: *Angew. Chem.* **1995**, *107*, 71

Keywords: anion complexation · host–guest chemistry · molecular recognition



4, X = $(CH_2)_6$

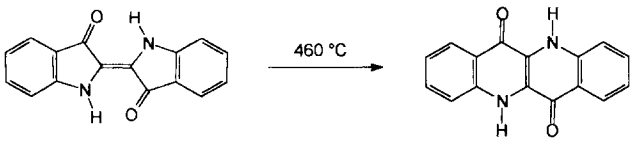
[1] a) F. P. Schmidtchen, *Nachr. Chem. Tech. Lab.* **1988**, *36*, 8-17; b) B. Dietrich, *Pure Appl. Chem.* **1993**, *65*, 1457-1464.
[2] a) H. E. Katz, *J. Org. Chem.* **1989**, *54*, 2179-2183; b) M. T. Reetz, B. M. Johnson, K. Harms, *Tetrahedron Lett.* **1994**, *35*, 2525-2528; c) M. F. Hawthorne, X. Yang, Z. Zeng, *Pure Appl. Chem.*, **1994**, *66*, 245-254; d) S. Aoyagi, K. Tanaka, Y. Takeuchi, *J. Chem. Soc. Perkin Trans. 2*, **1994**, 1549-1553; e) S. Jacobson, R. Pizer, *J. Am. Chem. Soc.* **1993**, *115*, 11216-11221.
[3] K. Worm, F. P. Schmidtchen, A. Schier, A. Schäfer, M. Hesse, *Angew. Chem.* **1994**, *106*, 360-362; *Angew. Chem. Int. Ed. Engl.* **1994**, *33*, 327-329.
[4] P. B. Savage, S. K. Holmgren, S. H. Gellman, *J. Am. Chem. Soc.* **1994**, *116*, 4069-4070.
[5] S. Mangani, M. Ferraroni, P. Orioli, *Inorg. Chem.* **1994**, *33*, 3421-3423.
[6] One of the rare examples of proteins binding anions without the assistance from cationic functional groups is provided by sulfate-binding-protein (SBP): F. A. Quiocho, H. Luecke, J. Åqvist, A. Warshel, *Proc. Natl. Acad. Sci. USA* **1991**, *88*, 2026-2030.
[7] Molecular modeling software Insight II / Discover 2.7 (Biosym), CVFF force field.
[8] F. P. Schmidtchen, *Chem. Ber.* **1980**, *113*, 864-874.
[9] Regression software *Enzfitter* (Biosoft, Cambridge, UK.)
[10] The K_{ass} values communicated here are nominally higher than reported for the tetracationic host **4** [11], which, however, was studied at 25 °C and 0.1 M ionic strength.
[11] F. P. Schmidtchen *Chem. Ber.* **1981**, *114*, 597-607.
[12] The complexation of chloride ion by host **4** was estimated by ^{35}Cl NMR from signal broardening: K. Ichikawa, A. Yamamoto, M. A. Hossain, *Chem. Lett.* **1993**, 2175-2178; cf.: M. W. Hosseini, J. P. Kintzinger, J.-M. Lehn, A. Zahidi, *Helv. Chim. Acta* **1989**, *72*, 1078-1083.
[13] A comprehensive discussion of this phenomenon appeared in the literature recently: a) D. H. Williams, M. S. Searle, J. P. Mackay, U. Gerhard, R. A. Maplestone, *Proc. Natl. Acad. Sci. USA* **1993**, *90*, 1172-1178; b) Y. Inoue, T. Hakushi, Y. Lui, L.-H. Tong, B.-J. Shen, D.-S. Jin, *J. Am. Chem. Soc.* **1993**, *115*, 475-481.
[14] F. Diederich, K. Dick, *J. Am. Chem. Soc.* **1984**, *106*, 8024-8036.
[15] G. Catena, F. V. Bright, *Anal. Chem.* **1989**, *61*, 905-909.
[16] Y. Markus, *J. Chem. Soc. Faraday Trans.* **1991**, *87*, 2995-2999.

 © VCH Verlagsgesellschaft mbH, D-69451 Weinheim, 1995 0570-0833/95/0101-0066 $ 10.00+.25/0

Thermal Isomerization of Indigo

Günter Haucke* and Gerhard Graness

Indigo does not undergo thermal or photochemical *trans-cis* isomerization in contrast, for example, to thioindigo.[1] Dry distillation of indigo produces aniline,[2] and irradiation in the presence of dissolved oxygen, isatin.[3] However, if indigo (**1**) is heated to 450 °C in vacuum in the vapor phase it isomerizes to dibenzonaphthyridindione (**2**) in a suprisingly smooth reaction.



1 **2**

The UV/Vis spectra of this isomerization reaction are shown in Figure 1. The occurrence of an isosbestic point demonstrates the homogeneity of this reaction (yield about 80%; in addition to a carbonized residue the only other product detected is aniline). Compound **2** was synthesized for the first time in 1934 in a relatively complicated multistep reaction.[4] It is extraordinarily thermally stable and can be sublimed at about 1000 °C without degradation.

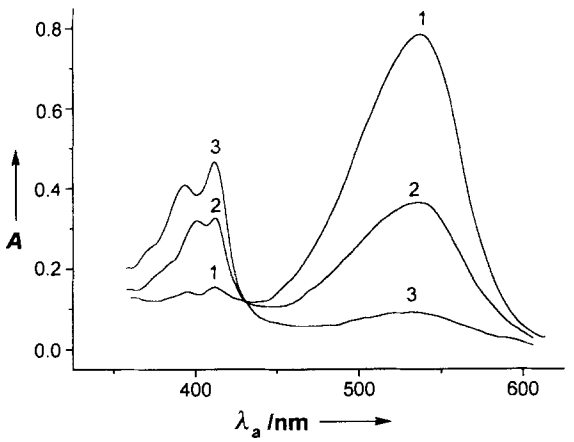


Fig. 1. Spectra recorded during the isomerization of indigo in the gas phase (1: 430 °C, indigo completely vaporized; 2: 480 °C, about 5 min after 1; 3: 500 °C, about 10 min after 1).

To obtain a better understanding of the structure and the spectroscopic properties of both isomers, and also the course of the reaction, quantum chemical calculations using the MNDO-PM3 procedure[5] were carried out.

For both **1** and **2** a nonplanar structure (pyramidalization at the N atom) was calculated. According to the calculations, the energy difference between this and a planar structure was 13.4 kJ mol^{-1} for **1** and 2.3 kJ mol^{-1} for **2**. In contrast, in the electronically excited S_1 state, an almost planar structure resulted for both molecules. The free energy of reaction at 460 °C was calculated to be $\Delta G_R = -62.8$ kJ mol^{-1}.

[*] Doz. Dr. G. Haucke, Dr. G. Graness
Institut für Physikalische Chemie der Universität
Philosophenweg 14, D-07743 Jena (Germany)
Telefax: Int. code + (3641)636118

To explain the mechanism of the isomerization, saddle point calculations were made. A structure for a transition state was found and is illustrated in Figure 2. The mechanism of the isomerization can thus be conceived as follows: The bond between

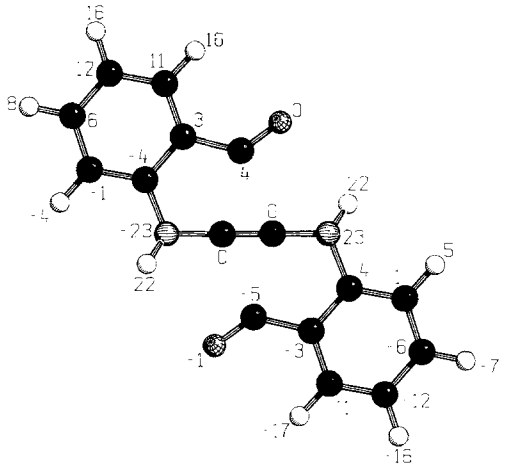
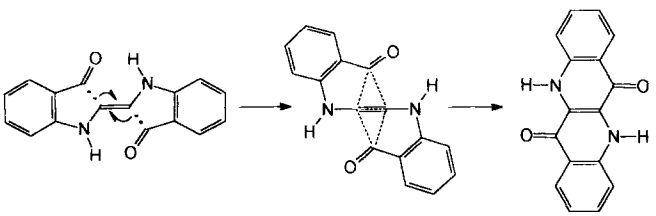


Fig. 2. Structure corresponding to the saddle point of the isomerization of indigo (PM3 calculation); the central C–C bond lies in the plane of the paper; the numbers indicate the deviations vertical to the plane of the paper in pm.

the C atom of the carbonyl group and the central C=C unit is cleaved (weakest bond in **1**). Linearization of both N–C=C units causes a C–C triple bond to be formed from the central C–C double bond. The structure of the indigo molecule changes in such a way that the distances between the C atom of each carbonyl group and both atoms of the central C–C triple bond are approximately the same. Ring formation from this transition state (**TS**) can then lead both to **2** and back to **1**.



1 **TS** **2**

If the orbital symmetry is considered, this process can also be regarded as a dyotrope rearrangement (intramolecular symmetrical transfer of two (σ bonds).[6] Such a [$\sigma_2 + \sigma_2$] process is forbidden by symmetry. However, by including the π-electron system of **1** in the four-membered transition state, the restriction can be relaxed. The very high value of the activation energy (610 kJ mol^{-1}) for the calculated transition state **TS** instead favors a stepwise process. An analogous isomerization was also observed for 5,5'-dibromo-, 4,5,4',5'-tetrabromo-, and 5,7,5',7'-tetrabromoindigo. Thioindigo and thionaphthenindigo (2,2') do not isomerize. Heating **1** in a solvent results in practically no isomerization (in DMSO traces of **2** were detected by its very intense fluorescence).

The spectroscopic properties (UV/Vis absorption and fluorescence) of **1** have been frequently investigated and discussed,[7] also with respect to the differences in absorption behavior between **1** and **2**.[8] A comparison of the absorption and fluores-

 © VCH Verlagsgesellschaft mbH, D-69451 Weinheim, 1995 0570-0833/95/0101-0067 $ 10.00+.25/0

cence of **1** and **2** could lead to a deeper understanding of the chromophoric system of indigoid dyes.

Experimental absorption and fluorescence data together with calculated values of both structural isomers are contrasted in Table 1. The most pronounced differences are: a) **1** absorbs at significantly longer wavelengths than **2**; b) in **1** both λ_a and λ_f are more strongly dependent on the polarity of the solvent than in **2**; c) ϕ_f of **1** is more than two orders of magnitude lower than that of **2**; d) both the absorption and the fluorescence spectrum of **2** show pronounced vibrational structure, and **2** exhibits a distinctly lower Stokes displacement (particularly apparent in benzene) than **1**. Comparison of the experimental data with the results from quantum chemical calculations reveals that the qualitative differences between **1** and **2** are in fact approximately reflected. However, quantitatively the agreement is not good; in particular the longest wavelengths calculated for the transitions of **1** are too short.

Table 1. Experimental and calculated spectroscopic data of **1** and **2** (λ_a: longest wavelength band of the absorption, λ_f: maximum of the fluorescence bands, ϕ_f: fluorescence quantum yields, DMSO: dimethylsulfoxide, TCE: 1,1,2,2-tetrachloroethane).

Compd.	Medium	λ_a/nm	λ_f/nm	Φ_f
1	gaseous, 385 °C	539	564	<0.01
	benzene	598	632	0.0016
	acetonitrile	596	642	0.00096
	DMSO	619	666	0.0011
	TCE	605	653	0.0018
	calculated	422	502	
2	gaseous, 460 °C	412	440 [a]	≈0.1
	benzene	437	445	0.64
	acetonitrile	437	443	0.60
	DMSO	446	454	0.86
	TCE	443	449	0.58
	calculated	368	408	

[a] Shoulder at about 420 nm.

Experimental Procedure

The absorption and fluorescence spectra were recorded on the described compounds in the gas phase in a heated sample chamber with dimensions $5 \times 5 \times 10$ cm^3 fitted with a low-ohm heating element. Thermoelements were used to regulate and control the temperature. A 1.5 cm diameter and about 5 cm long glass tube was charged with the substances (about 0.3 mg), and after several flushes with argon the sample was melted under vacuum. The sample chamber had three mutually perpendicular viewing windows at the level of the optical axes.
The reaction products were identified by mass spectrometry and NMR spectroscopy.

Received: July 19, 1994 [Z7142IE]
German version: *Angew. Chem.* **1995**, *107*, 116

Keywords: indigo · isomerization · semiempirical calculations · spectroscopy

[1] G. M. Wyman, *EPA Newsl.* **1994**, *50*, 9.
[2] P. F. Gordon, P. Gregory, *Organic Chemistry in Colour*, Akademie-Verlag, Berlin, **1983**, p. 13.
[3] N. Kuramoto, T. Kitao, *J. Soc. Dyers Colour.* **1979**, 257.
[4] A. D. Ainley, R. Robinson, *J. Chem. Soc.* **1934**, 1508. An improved synthesis can be found in E. E. Jaffe, H. Matrick, *J. Org. Chem.* **1968**, *33*, 4004.
[5] VAMPC 4.56 from B. Wiedel, Institut für Organische und Makromolekulare Chemie der Universität Jena, 1993. It concerns a PC version of Tim Clark's VAMP 4.5 for Convex C220 which is based on the program packages MOPAC 4.00-6.00 and AMPAC 1.00. The quantum chemical calculations were carried out on a PC 486 DX-66. Geometry optimization was made with the keywords PM3 PRECISE EF (eigenvector following) for S_0 and S_1. With the geometries thus obtained, the electronic transitions were calculated with C. I. = 5 (100 CIs) and 1SCF INTENS. The saddle point calculations were made with the keywords SADDLE XYZ, and the calculation of the thermodynamic data with FORCE THERMO(600).
[6] M. T. Reetz, *Tetrahedron* **1973**, *29*, 2189; *Adv. Organomet. Chem.* **1977**, *16*, 33.
[7] a) M. Klessinger, W. Lüttke, *Tetrahedron* **1963**, *19*, *Suppl. 2*, 315; b) G. Haucke, R. Paetzold, *Nova Acta Leopold.* **1978**, Suppl. *11*, 1–123; c) G. Miehe, P. Süsse, V. Kupcik, E. Egert, M. Nieger, G. Kunz, R. Gerke, B. Knieriem, M. Niemeyer, W. Lüttke, *Angew. Chem.* **1991**, *103*, 1008; *Angew. Chem. Int. Ed. Engl.* **1991**, *30*, 964.
[8] J. Fabian, H. Hartmann, *Light Absorption of Organic Colorants*, Springer, Berlin, **1980**, S. 115–136.

The Novel Copper Polytelluride Salts $NaBa_6Cu_3Te_{14}$ and $(K_{0.60}Ba_{0.40})Ba_6Cu_{2.58}Te_{14}$: Discrete Clusters or Extended Solids?**

Xiang Zhang, Jon L. Schindler, Tim Hogan, Joyce Albritton-Thomas, Carl R. Kannewurf, and Mercouri G. Kanatzidis*

One important difference between the chemistry of Te_x^{2-} and Q_x^{2-} (Q = S, Se) ions is the tendency of the former to associate through Te–Te bonding interactions because of the more diffuse nature of the Te orbitals. While in polysulfides and polyselenides coulombic repulsions dominate their crystal chemistry, polytellurides often show attractions leading to interatomic Te···Te distances much shorter than the van der Waals distance of 4.0 Å. Examples include the alkali metal polytellurides[1] $Na_6Te(Te_5)$,[2a] Na_2Te_6,[2b] A_2Te_3 (A = K, Rb, Cs),[3] A_2Te_5 (A = Rb, Cs),[4] and $CsTe_4$,[5] [TMDH]Te_4 with the organic cation (TMDH = 2,2,5,5-tetramethyl 2,5-diazoniahexane),[6] MTe_2 solids of the pyrite type,[7] and $K_4Hf_3Te_{17}$.[8] However, compounds like $(Ph_4P)_2Te_4 \cdot 2CH_3OH$[9] and $(Me_4N)MTe_4$ (M = Cu, Ag)[10] do not exhibit such Te···Te interactions and behave more like the S and Se counterparts. Apparently interpolytelluride bonding can be turned on and off by choice of the accompanying counterions. Poor coulombic screening of the polytelluride anion and active Te···Te interactions would result with either relatively small counterions or cations with high charge-to-radius ratio (for example dipositive ions). In contrast, good coulombic screening is achieved by larger counterions or more of them in the lattice, which tend to turn inter-Te_x^{2-} interactions off. Recently we reported the compounds $K_2Cu_5Te_5$[11] and $A_3Cu_8Te_{10}$ (A = Rb, Cs),[12] which exhibited no short interpolytelluride contacts. We attempted to test the above counterion hypothesis by employing Ba^{2+} ions in place of alkali metal ions, thus reducing the number of charge-balancing species in the lattice. Here we report preliminary results from these investigations and the synthesis and characterization of **1** and **2**,

$NaBa_6Cu_3Te_{14}$ **1**

$(K_{0.60}Ba_{0.40})Ba_6Cu_{2.58}Te_{14}$ **2**

[*] Prof. Dr. M. G. Kanatzidis, Dr. X. Zhang
Department of Chemistry and Center for Fundamental Materials Research
Michigan State University, East Lansing, MI 48824 (USA)
Telefax: Int. code + (517)353-1793
J. L. Schindler, T. Hogan, J. Albritton-Thomas, Dr. C. R. Kannewurf
Department of Electrical Engineering and Computer Science, Northwestern University, Evanston, IL 60208-3118 (USA)

[**] This work was supported by the National Science Foundation (DMR-92-02428 and DMR-91-20521). MGK is an A. P. Sloan Foundation Fellow (1991–1993), and a Camille and Henry Dreyfus Teacher Scholar (1993–1995).

which possess a novel structure built on discrete Cu/Te clusters held together by intercluster Te···Te bonds.

Single crystal X-ray diffraction studies established that the structures were isomorphous.[13] The framework of **1** is built on a novel cluster of $[Cu_3Te_3(Te_3)_3]^{9-}$ shown in Figure 1. The

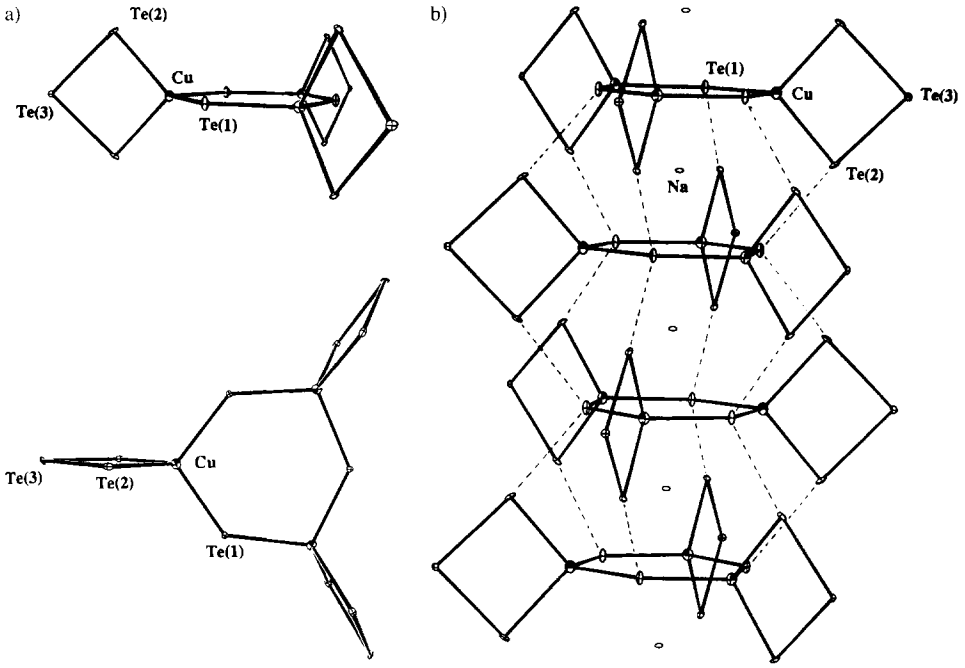


Fig. 1. a) Two views of the structure of the $[Cu_3Te_3(Te_3)_3]^{9-}$ cluster. Selected bond lengths [Å] and angles [°] inside the cluster: Te(1)-Cu, 2.588; Te(2)-Cu, 2.713; Te(2)-Te(3), 2.907(2); Te(1)-Cu-Te(1), 109.6(1); Te(1)-Cu-Te(2), 112.6(1); Te(2)-Cu-Te(2), 96.4; Cu-Te(1)-Cu, 130.4; Te(3)-Te(2)-Cu, 87.67(7); Te(2)-Te(3)-Te(2), 88.22(7). b) Structure of the one-dimensional stack of $[NaCu_3Te_3(Te_3)_3]_n^{8n-}$ clusters. The intercluster Te···Te interactions are shown by the broken lines. The Na^+ ions are sandwiched between the clusters.

entire structure is shown in Figure 2. The cluster consists of four rings, one six-membered and three four-membered. Since the larger six-membered Cu_3Te_3 ring is located on a $\bar{6}2m$ site, it must be strictly planar.[13a] The large amplitude of the anisotropic thermal parameters of all ring atoms in the c direction suggests marked deviations of these atoms from planarity. Each Cu^+ center is further chelated by a Te_3^{2-} ligand to form the four-membered $CuTe_3$ ring, which is also planar and lies perpendicular to the Cu_3Te_3 ring. The Cu^+ center is in a distorted tetrahedral environment; Te-Cu-Te angles range between 96.4(1) and 112.6(1)°. The Cu-Te bond to the monotelluride $Te(1)^{2-}$ at 2.588(6) Å, is quite normal.[11, 12, 14] The Cu-Te bonds to the Te_3^{2-} ligand are much longer (Cu-Te(2) = 2.713(2) Å), while the Te-Te bonds within the ligand are slightly longer than normal (2.907(2) Å). This highly anionic trinuclear copper cluster is unprecedented, but could be compared to the $[In_3Se_3(Se_4)_3]^{3-}$,[15] clusters in which the six-membered In_3Se_3 ring is puckered like cyclohexane. The $[Cu_3Te_3(Te_3)_3]^{9-}$ clusters stack along the c axis in staggered arrangement, and encapsulate Na^+ ions inside the column stack (see Fig. 1b). The packing, at first glance, appears somewhat unusual considering the high negative charge of the clusters. It seems doubtful that Na^+ ions alone can hold them together. A closer examination indicates significant intercluster interactions through the Te atoms. In fact, the Te(1) atom of each of the three monotellurides of one cluster is connected to two Te(2) atoms belonging to two Te_3^{2-} ligands from the neighboring clusters above and below with a Te(1)-Te(2) distance of 3.262(2) Å. This distance is still long compared to a normal Te-Te single bond but significantly shorter than the van der Waals distance (≈4.0 Å). The clusters, linked this way and shaped like a paddle-wheel, form a highly negatively charged, one-dimensional column of $[NaCu_3Te_3(Te_3)_3]_n^{8n-}$ along the c axis. These columns are surrounded by six columns of divalent barium cations. Elsewhere in the lattice discrete Te^{2-} ions (Te(4)) are each surrounded by six Ba^{2+} ions in a trigonal prismatic arrangement. Thus, this compound is a mixed salt of two different anions and two different cations and is best formulated as $NaBa_6[Cu_3(Te)_3\text{-}(Te_3)_3](Te)_2$. Considering the Te···Te interactions only, a novel zigzag $[Te_4]_n^{4n-}$ chain can be visualized with a repeating unit of [Te(1)-Te(2)-Te(3)-Te(2)]$^{4-}$ as illustrated in Figure 1b. The average charge is −1 per Te atom. This $[Te_4]_n^{4n-}$ chain is isoelectronic to the linear chains of $[Te]_n^{n-}$ in CuTe[16] and $[Te_2]_n^{2n-}$ in K_5Te_3.[17] In CuTe a Te-Te single-bond distance of 3.149 Å is present and is considered a bond with bond order 0.5.

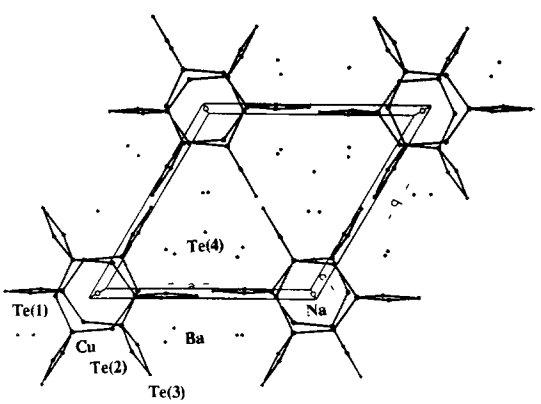


Fig. 2. ORTEP-drawn packing diagram of $NaBa_6Cu_3Te_{14}$ viewed down the c axis. Selected distances [Å] and angles [°] (other than those between clusters): Te(1)-Te(2), 3.262(2); Te(2)-Te(3), 3.912(2); Te(1)-Na, 3.334(1); Cu-Na, 3.536(2); Te(1)-Ba, 3.534(2); Te(2)-Ba, 3.586(2); Te(2)-Ba, 3.614(3); Te(3)-Ba, 3.578(3); Te(3) Ba, 3.627(4); Te(4)-Ba, 3.487(1); Te(2)-Te(1)-Te(2), 100.89(6); Te(1)-Te(2)-Te(3), 173.67(6); Te(1)-Te(2)-Cu, 98.67(6).

The structure of **2** is nearly identical to that of **1**. The primary difference is that in **2** the interstitial position is occupied randomly by K^+ and Ba^{2+} ions. Additional Cu vacancies exist in the Cu/Te framework. The K/Ba ratio of 6:4 and the Cu occupancy of 86% were both determined from the refinement of the X-ray structure analysis.[13] The disorder of K and Ba cations is attributed to the similarity of their ionic radii. This phenomenon has been found to be a common feature for the solid-state structures obtained from mixed K^+/Ba^{2+}-containing fluxes and may have important implications for their properties.[18] While the bond distances and angles found in **2** are mostly similar to those in **1**, a slightly longer Te(1)···Te(2) distance of 3.292(2) Å is

 © VCH Verlagsgesellschaft mbH, D-69451 Weinheim, 1995 0570-0833/95/0101-0069 $ 10.00+.25/0

found in accordance with a slightly shorter Te(2)–Te(3) distance of 2.893(2) Å in the Te_3^{2-} ligand.

In compounds MTe_2 (M = Ti, Nb, Ir) of the CdI_2 type and other layered metal tellurides, interlayer Te···Te interactions were found to play an important role in the electronic structures and physical properties.[19] There is little doubt that the intercluster Te···Te interactions found in our compounds play a similarly crucial role. Without such interactions, these materials would be expected to be insulators assembled just from discrete cluster complexes and charge-compensating ions. Instead, preliminary charge-transport studies suggest that they possess pronounced electrical conductivity. The conductivity of **1** (nearly 0.1 S cm^{-1} at 273 K) decreases with falling temperature to 4×10^{-4} S cm^{-1} (Fig. 3 top), suggesting a semiconductor with a

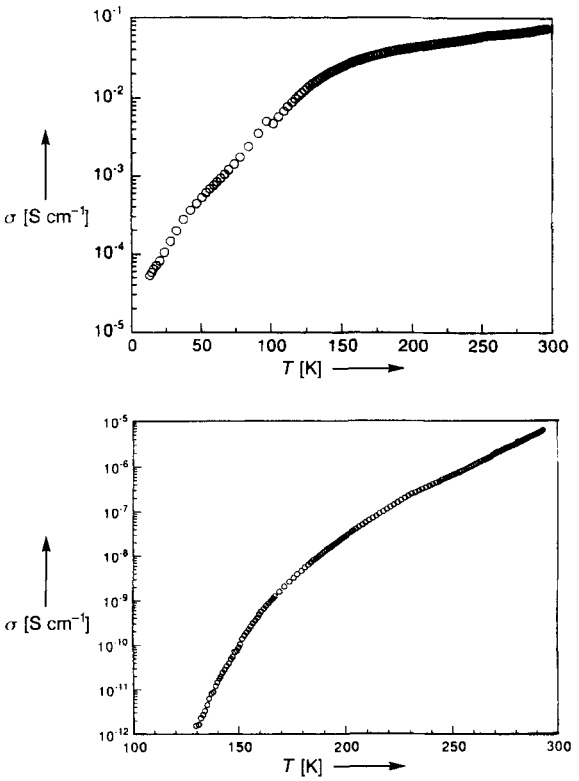


Fig. 3. Four-probe electrical conductivity data as a function of temperature for single crystals of $NaBa_6Cu_3Te_{14}$ (top) and $(K_{0.60}Ba_{0.40})Ba_6Cu_{2.58}Te_{14}$ (bottom).

relatively narrow band gap. As further evidence, diffuse reflectance spectroscopy in the UV/Vis/near-IR region for this phase shows no optical gap, but measurements in the IR region are consistent with a very small band gap. This is confirmed by the thermopower measurements, which show a relatively large Seebeck coefficient (≈ 100 μV K^{-1}) but a positive slope as a function of temperature,[20] which is reminiscent of the behavior of p-type semimetals or narrow band-gap semiconductors. Electrical conductivity and thermoelectric power measurements of **2** also indicate that it is a p-type semiconductor in the temperature range 130–300 K. The conductivity increases with rising temperature from 10^{-12} S cm^{-} at 130 K to 10^{-5} S cm^{-} (Fig. 3, bottom). Both compounds are diamagnetic. More detailed studies of electronic structure and physical properties are under way.

In summary, two novel, one-dimensional, copper polytellurides have been discovered from the reaction of copper with molten polytelluride salts. The construction of extended structures from inter-polytelluride bonding interactions is beautifully manifested in these compounds. Such interactions probably play an important role in influencing the properties. The incorporation of other ions (such as Li^+, Rb^+, Cs^+) into the interstitial positions (sites sandwiched between the Cu/Te clusters) and their effect on intercluster Te···Te bonding is currently under investigation.

Experimental Procedure

Na_2Te and K_2Te were synthesized from a stoichiometric amount of alkali metal and tellurium in liquid ammonia. Cu and BaTe were used as obtained.

1: A Pyrex tube (≈5 mL) containing Cu (0.032 g, 0.5 mmol), Na_2Te (0.261 g, 1.5 mmol), BaTe (0.132 g, 0.5 mmol), and Te (0.510 g, 4 mmol) was sealed under vacuum. The tube was heated at 400 °C for four days, and then slowly cooled at 4 °C h^{-1} to 150 °C. Black chunky crystals were obtained in nearly quantitative yield after removal of the excess $Na_xBa_yTe_z$ flux in *N,N*-dimethylformamide (DMF) under N_2 atmosphere. A composition of $Ba_{5.4}Cu_3Te_{13.2}$ was found from microprobe analysis (energy-dispersive spectroscopy/scanning electron microscopy) of a large number of single crystals. (This technique does not reliably detect Na atoms.)

2: As for **1**. A mixture of Cu (0.032 g, 0.5 mmol), K_2Te (0.206 g, 1 mmol), BaTe (0.132 g, 0.5 mmol) and Te (0.383 g, 3 mmol) was heated at 420 °C for four days. Black chunky crystals were obtained as the major product. Average composition: $K_{0.52}Ba_{5.6}Cu_{2.6}Te_{14}$ (found from the microprobe analysis; average analysis obtained from a large number (>12) of crystals). A minor product in the form of platelets is also present [20].

Received: March 30, 1994
Revised: August 22, 1994 [Z6813IE]
German version: *Angew. Chem.* **1995**, *107*, 117

Keywords: metal–metal bonds · semiconductors · tellurium compounds

[1] P. Böttcher, *Angew. Chem.* **1988**, *100*, 781–794; *Angew. Chem. Int. Ed. Engl.* **1988**, *27*, 759–772.
[2] a) P. Böttcher, R. Keller, *J. Less-Common Met.* **1985**, *109*, 311–321; b) P. Böttcher, *Z. Anorg. Allg. Chem.* **1986**, *542*, 144–152.
[3] a) B. Eisenmann, H. Schäfer, *Angew. Chem.* **1978**, *90*, 731; *Angew. Chem. Int. Ed. Engl.* **1978**, *17*, 684; b) P. Böttcher, *J. Less-Common Met.* **1980**, *70*, 263–271.
[4] a) P. Böttcher, U. Kretschmann, *J. Less-Common Met.* **1983**, *95*, 81–91; b) *Z. Anorg. Allg. Chem.* **1982**, *491*, 39–46.
[5] P. Böttcher, U. Kretschmann, *Z. Anorg. Allg. Chem.* **1985**, *523*, 145–152.
[6] K. W. Klinkhammer, P. Böttcher, *Z. Naturforsch. B* **1990**, *45*, 141–147.
[7] Examples: a) T. A. Bither, R. Bouchard, W. H. Cloud, P. C. Donohue, W. J. Siemons, *Inorg. Chem.* **1968**, *7*, 2208–2220; b) T. A. Bither, P. C. Donohue, W. H. Cloud, P. E. Biestedt, H. S. Young, *J. Solid State Chem.* **1970**, *1*, 526–533.
[8] P. M. Keane, J. A. Ibers, *Inorg. Chem.* **1991**, *30*, 1327–1329.
[9] J. C. Huffman, R. C. Haushalter, *Z. Anorg. Allg. Chem.* **1984**, *518*, 203–206.
[10] K. Kim, M. G. Kanatzidis, *J. Am. Chem. Soc.* **1993**, *115*, 5871–5872.
[11] Y. Park, D. C. Degroot, J. Schindler, C. R. Kannewurf, M. G. Kanatzidis, *Angew. Chem.* **1991**, *103*, 1404–1407; *Angew. Chem. Int. Ed. Engl.* **1991**, *30*, 1325–1328.
[12] X. Zhang, Y. Park, J. L. Schindler, C. R. Kannewurf, M. G. Kanatzidis, unpublished.
[13] a) Crystal data for $NaBa_6Cu_3Te_{14}$ (**1**) at −100 °C ($Mo_{K\alpha}$ radiation): $a = 14.123(2)$, $c = 9.075(1)$ Å, $V = 1567.6(6)$ Å^3, $Z = 2$, $\rho_{calcd} = 5.983$ g cm^{-3}, space group $P6_3/mcm$ (no. 193), $2\theta_{max} = 55°$; number of independent data collected: 765, data observed with $I > 3\sigma(I)$: 504, number of variables: 30, $\mu = 222.39$ cm^{-1}, $R = 0.037$, $R_w = 0.043$, GOF = 1.42. b) Crystal data for $(K_{0.60}Ba_{0.40})Ba_6Cu_{2.58}Te_{14}$ (**2**) at −100 °C ($Mo_{K\alpha}$ radiation): $a = 14.121(3)$, $c = 9.200(5)$ Å, $V = 1589(1)$ Å^3, $Z = 2$, $\rho_{calcd} = 5.963$ g cm^{-3}, space group $P6_3/mcm$ (no. 193), $2\theta_{max} = 60°$; number of independent data collected: 967, data observed with $I > 3\sigma(I)$: 502, number of variables: 31, $\mu = 222.19$ cm^{-1}, exctinction coefficient $= 0.186 \times 10^{-7}$, $R = 0.042$, $R_w = 0.047$, GOF = 1.34. The structures were solved by direct methods from SHELXS-86 [13c] and refined with the TEXSAN [13d] package of crystallographic programs. A DIFABS [13e] correction was applied to the isotropically refined data. All atoms were refined anisotropically. Although the Cu_3Te_3 ring in both compounds is found to be strictly planar, the magnitude of the anisotropic thermal parameters U_{11}, U_{22}, and U_{33}, especially of the Te(1) atom, suggest a slightly puckered conformation. The U_{33} value (thermal vibration amplitude in the *c* direction) is significantly larger than U_{11}. This is particularly true in the Na salt. The observed planar conformation could be the result of averaging over two slightly puckered ones. Attempts to resolve these two conformations were not suc-

 © VCH Verlagsgesellschaft mbH, D-69451 Weinheim, 1995 0570-0833/95/0101-0070 $ 10.00+.25/0

cessful. In the refinement of **2** a random distribution between K and Ba was found in the $-3m$ site. The ratio of Ba to K was refined to 60:40. This ratio was used in the final cycles of refinement. Further details of the crystal structure investigation may be obtained from the Fachinformationszentrum Karlsruhe, D-76344 Eggenstein-Leopoldshafen (Germany), on quoting the depository number CSD-58650. c) G. M. Sheldrick, *Crystallogr. Comput. Data Collect. Determ. Proteins Databases Pap. Int. Summer Sch. 9th 1984* **1985**, 175–189. d) TEXSAN-TEXRAY Structure Analysis Package, Molecular Structure Corporation 1985. e) N. Walker, D. Stuart, *Acta. Crystallogr. Sect. A39* **1983**, 158–166.

[14] a) G. Savelsberg, H. Schäfer, *Mater. Res. Bull.* **1981**, *16*, 1291–1297; b) K. O. Klepp, *J. Less-Common Met.* **1987**, *128*, 79–89; c) G. Savelsberg, H. Schafer, *Z. Naturforsch. B* **1978**, *33*, 370–373.

[15] a) S. Dhingra, M. G. Kanatzidis, *Inorg. Chem.* **1993**, *32*, 1350–1362; b) S. Dhingra, *Dissertation*, Michigan State University, **1992**.

[16] a) I. Patzak, *Z. Metallkd.* **1956**, *47*, 418–420; b) R. V. Baranova, Z. G. Pinsker, *Kristallografiya* **1964**, 9(1), 83–85; c) K. Anderko, K. Schubert, *Z. Metallkd.* **1954**, *45*, 371–378.

[17] I. Schewe, P. Böttcher, *Z. Naturforsch. B* **1990**, *45*, 417–422.

[18] a) J. Li, H. Guo, X. Zhang, M. G. Kanatzidis, *J. Am. Chem. Soc.*, submitted; b) X. Zhang, M. G. Kanatzidis, unpublished.

[19] a) S. Jobic, P. Deniard, R. Brec, J. Rouxel, A. Jouanneaux, A. N. Fitch, *Z. Anorg. Allg. Chem.* **1991**, *598/599*, 199–215; b) E. Canadell, S. Jobic, R. Brec, J. Rouxel, *J. Solid State Chem.* **1992**, *99*, 189–199. c) E. Canadell, L. Monconduit, M. Evain, R. Brec, J. Rouxel, M.-H. Wangbo, *Inorg. Chem.* **1993**, *32*, 10–12.

[20] X. Zhang, M. G. Kanatzidis, unpublished.

$Na_2Ti_3Cl_8$: From Isolated Ti^{2+} Ions to $[Ti_3]^{6+}$ Clusters**

Dirk J. Hinz, Gerd Meyer,* Thorsten Dedecke, and Werner Urland*

For the ternary system Na/Ti/Cl not only the binary chlorides NaCl, $TiCl_2$, $TiCl_3$, and $TiCl_4$, and the mixed valent Ti_7Cl_{16},[1] but also the ternary compounds $NaTiCl_3$, $NaTiCl_4$, and Na_2TiCl_6 have been reported,[2] although existence of the latter has not been confirmed by structure analyses. However, the list of compounds in the Na/Ti/Cl system certainly includes the ternary chlorides Na_2TiCl_4,[3,4] $Na_2Ti_3Cl_8$, and Na_3TiCl_6,[5] which lie on the pseudobinary intersections NaCl/$TiCl_2$ and NaCl/$TiCl_3$, as well as the mixed valent $Na_5Ti_3Cl_{12}$.[5]

Of the newly discovered ternary chlorides of titanium with sodium, $Na_2Ti_3Cl_8$ has surprising properties. This may already be suspected from the nearness of the formula to $Ti_7Cl_{16} = Ti_{0.5}Ti_3Cl_8$ on the one hand and Nb_3Cl_8 [6] on the other. These contain (linked) $[M_3](\mu_1\text{-Cl})_9(\mu_2\text{-Cl})_3(\mu_3\text{-Cl})$ building blocks, within which the metal atoms are connected by means of covalent single bonds; the distances in the $[Ti_3]$ cluster in Ti_7Cl_{16} are 295 pm.[1]

If the titanium with oxidation state IV in $Ti_{0.5}Ti_3Cl_8$ is replaced with Na^+, $Na_2Ti_3Cl_8$ is obtained. In the crystal structure determined at room temperature[7] flat layers of titanium atoms (better: Ti^{2+} ions) are found in the form of a diluted closest packing of spheres, each with four equidistant neighbors ($d = 372$ pm) (Fig. 1, top). $Na_2Ti_3Cl_8$ is isotypic with $Na_2Mn_3Cl_8$:[8] closest packed layers of chloride ions are stacked AABBCC as in 3R–MoS_2; three-quarters of the octahedral sites are filled with Mn^{2+}/Ti^{2+}, one-quarter of all trigonal-prismatic sites are occupied by Na^+ in a similar fashion.

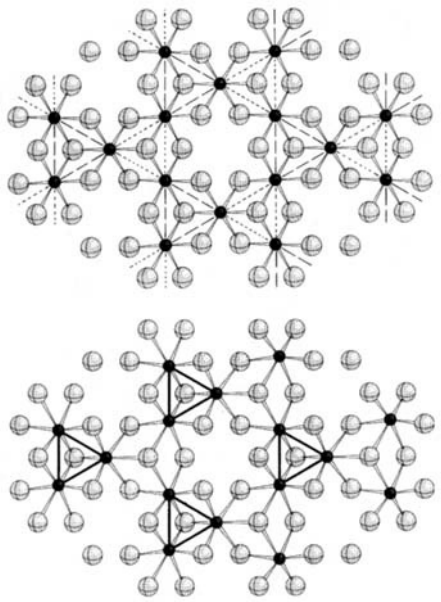


Fig. 1. Cl–Ti–Cl layer in the room-temperature form (top) and low-temperature form (bottom) of $Na_2Ti_3Cl_8$. The phase transition can be interpreted as a Peierls distortion along three directions within the titanium layer.

Magnetic susceptibility measurements were performed on a SQUID magnetometer (Quantum Design, MPMS5) at 2–300 K at a field strength of $H = 1000$ Oe. In order to take into consideration the diamagnetic correction of Na_2TiCl_4 and $Na_2Ti_3Cl_8$, tabular incremental values were employed according to Selwood.[9] The measurements revealed a drastic decrease of the magnetic moment at around 200 K on cooling (cf. Fig. 2). X-ray investigations on powder samples above and below this "critical" temperature also indicated strong alterations, which seems to be confirmed by a comparison of the lattice constants (hexagonal setting): 293 K: $a = 743.32(8)$; $c = 972.1(5)$ pm; 100 K: $a = 697.9(1)$; $c = 2027.1(6)$ pm. Owing to the shrinkage of the a axis (and consequently the dilatation of the c axis), it can be assumed that in the planes of titanium atoms parallel to (001), a transition from *isolated* Ti^{2+} *ions* (d^2 configuration) to $[Ti_3]^{6+}$ *clusters* must have occurred. The magnetic moments at 300 K ($\mu = 2.55\ \mu_B$) and 150 K ($\mu = 1.49\ \mu_B$) correspond well to those observed for Na_2TiCl_4 (300 K; $\mu = 2.56\ \mu_B$; isolated Ti^{2+} ions) and Ti_7Cl_{16} (150 K; $\mu = 1.25\ \mu_B$;[10] $[Ti_3]$ cluster).

Proof for the driving force of the phase transition observed here is provided by a single-crystal structure determination at 183 K.[7] The same crystal was used for this as for the determination at room temperature; astonishingly it was not destroyed by the considerable mechanical stresses accompanying the alteration of the lattice constants already discussed. This is probably because the phase transition, having begun at one point in the crystal, can then propagate throughout the entire crystal. The local changes occurring during the transition are shown in Figure 3. The formation of $[Ti_3]$ clusters in the planes parallel to

[*] Prof. Dr. G. Meyer, Prof. Dr. W. Urland, Dr. D. J. Hinz, Dipl.-Chem. T. Dedecke
Institut für Anorganische Chemie der Universität
Callinstrasse 9, D-30167 Hannover (Germany)
Telefax: Int. code + (511) 762-3006

[**] This work was supported by the Deutsche Forschungsgemeinschaft and the Fonds der Chemischen Industrie.

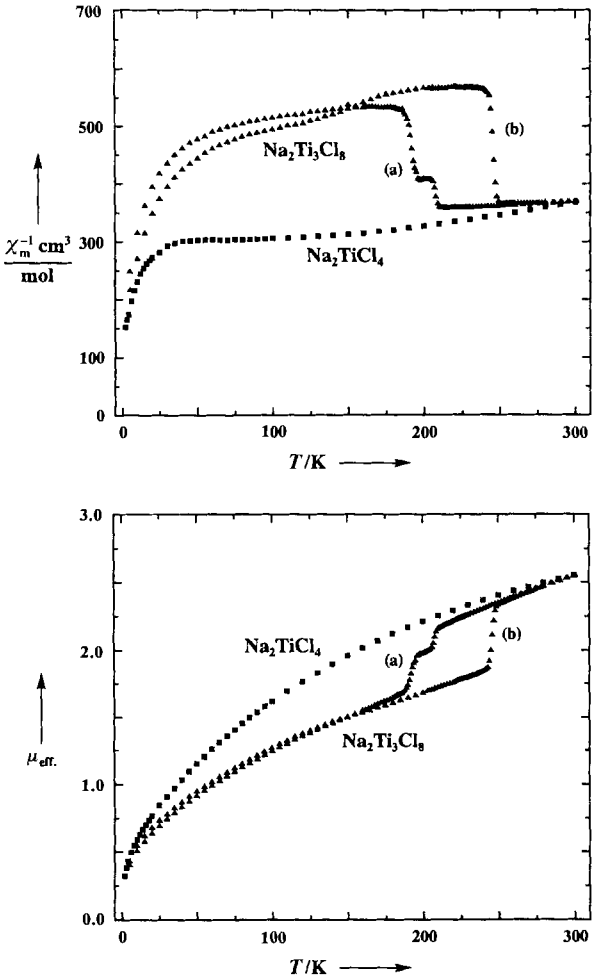


Fig. 2. The reciprocal molar magnetic susceptibility ($H = 1000$ Oe) (top) and the effective magnetic moment (bottom) for $Na_2Ti_3Cl_8$ at 2–300 K. The phase transition displays a distinctive hysteresis. On heating (curve b), the phase transition occurs quickly at about 245 K, whereas this event takes place over a wider temperature range at around 200 K on cooling (curve a). For comparison, the values for Na_2TiCl_4 [4] are also plotted.

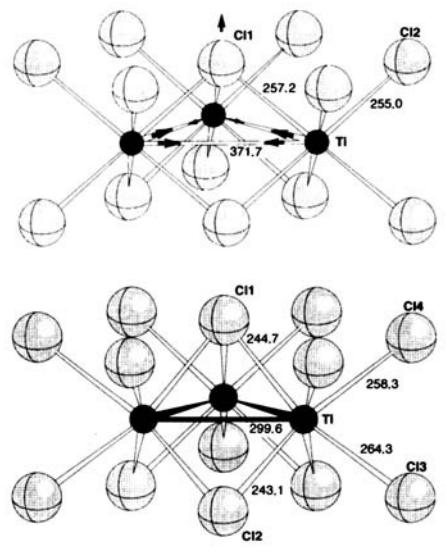


Fig. 3. Ti_3Cl_{13} units in the room-temperature form (top) and low-temperature form (bottom) of $Na_2Ti_3Cl_8$. At the phase transition the titanium atoms shift towards one another out of the octahedral centers of chlorine atoms. In the process the Cl1 atoms are forced far out of the plane of the other chlorine atoms (distances in pm).

(001) (see Fig. 1) leads to the shrinkage of the lattice constant a, the "squeezing out" of μ_3-Cl to the dilatation of the c axis.

According to this, $Na_2Ti_3Cl_8$ demonstrates a thermally activated, reversible transition, observed here for the first time. The transition occurs in a type of two-dimensional Peierls distortion from "isolated" Ti^{2+} ions (d^2 system with $\mu = 2.56\ \mu_B$ (Na_2TiCl_4)) to "discrete" [Ti_3] clusters with covalent "metal–metal single bonds" (6-electron system; $\mu = 1.49\ \mu_B$). Corresponding magnetic transitions with comparable hysteresis behavior are well known from high-spin–low-spin transitions in the transition metals (e.g. spin crossover in Fe^{II} complexes[11]).

The molar volume (V_m) of $Na_2Ti_3Cl_8$ decreases between 293 and 183 K by almost nine percent. The value $V_m = 39.5\ cm^3\ mol^{-1}$ for $TiCl_2$ at 183 K, calculated from $V_m(Na_2Ti_3Cl_8)$ at 183 K (with $V_m(NaCl) = 27.01\ cm^3\ mol^{-1}$) agrees very well with the value calculated from a pyknometrical density determination ($V_m = 38\ cm^3\ mol^{-1}$[12]). From this, and from magnetic measurements,[12, 13] it is possible to deduce that [Ti_3] clusters also exist in $TiCl_2$ at room temperature. Fundamentally, this had already been recognized by Klemm and Grimm. The CdI_2 type assumed by other authors is therefore only correct "in principle".

Experimental Procedure

Single crystals of $Na_2Ti_3Cl_8$ were obtained from the reaction of sodium with $TiCl_3$ (e.g. 44.7 mg Na and 300 mg $TiCl_3$) in the presence of titanium foil (180 mg) in a sealed niobium ampule at 525 °C (three months). Besides $TiCl_2$, NaCl, and turquoise needles of Na_2TiCl_4, the mixture of products contained a small amount of $Na_2Ti_3Cl_8$ in the form of dark green trigonal platelets, which were readily split parallel to (001). Powder preparations suitably pure for X-ray purposes were obtained by the synproportionation of $TiCl_3$ with titanium in the presence of NaCl (e.g. 1 g $TiCl_3$, 379 mg NaCl, approximately 300 mg titanium foil, molar ratio 2:2:>1) in a sealed niobium ampule. The ampule was initially heated slowly to 500 °C and then kept at 750 °C for 24 h. The reaction was then quenched with water and finally tempered at 520 °C for three weeks. The excess titanium foil was easily removed from the reaction mixture.

Received: July 4, 1994 [Z 7096 IE]
German version: *Angew. Chem.* **1995**, *107*, 117

Keywords: clusters · magnetic properties · sodium titanium dichloride · structure elucidation · titanium compounds

[1] H. Schäfer, R. Laumanns, *Z. Anorg. Allg. Chem.* **1981**, *474*, 135–148; B. Krebs, G. Henkel, *ibid.* **1981**, *474*, 149–156.
[2] K. Komarek, P. Herasymenko, *J. Elektrochem. Soc.* **1958**, *105*, 216–219; R. V. Chernov, Y. K. Delimarskii, *Zh. Neorg. Khim.* **1961**, *6*, 2749–2752.
[3] H. D. Lutz, K. Wussow, P. Kuske, *Z. Naturforsch. B* **1987**, *42*, 1379–1386.
[4] D. J. Hinz, T. Dedecke, W. Urland, G. Meyer, *Z. Anorg. Allg. Chem.* **1994**, *620*, 801–804.
[5] D. J. Hinz, Dissertation, Universität Hannover, **1994**.
[6] A. Simon, H. G. von Schnering, *J. Less Common Met.* **1966**, *11*, 31–36; H.-J. Meyer, *Z. Anorg. Allg. Chem.* **1994**, *620*, 81–84.
[7] Crystal structure data for $Na_2Ti_3Cl_8$: a) Room-temperature form: trigonal, space group $R\bar{3}m$ (no. 166), $a = 743.32(8)$, $c = 1972.1(5)$ pm, $V_m = 189.39\ cm^3\ mol^{-1}$, $2\theta_{max} = 70.1°$, $Mo_{K\alpha}$, $\lambda = 71.07$ pm, ω-2θ scan, learnt profile, measurement temperature = 293(1) K, 2922 measured reflections, of which 553 were judged symmetry independent; 552 reflections with $I_o \geq -3\sigma(I_o)$, Lp and empirical absorption correction, structure solution and refinement with SHELXS-86 and SHELXL-93, 18 free parameters refined, R values (all data): $R1|F| = 0.043$, $wR2|F^2| = 0.062$. b) Low-temperature form: trigonal, space group $R3m$ (no. 160), $a = 699.1(1)$, $c = 2031.1(1)$ pm, $V_m = 172.54(6)\ cm^3\ mol^{-1}$, $2\theta_{max} = 50.0°$, $Mo_{K\alpha}$, $\lambda = 71.07$ pm, ω-2θ scan, measurement temperature = 183(1) K, 1241 measured reflections, of which 379 were judged symmetry independent; 379 reflections with $I_o \geq -3\sigma(I_o)$, Lp and empirical absorption correction, structure solution from the room-temperature form, refinement with SHELXL-93, 30 free parameters refined, R values (all data): $R1|F| = 0.070$, $wR2|F^2| = 0.135$. Because of the poor crystal quality (large standard deviations of the intensities) caused by the phase transition, it was not possible to determine the absolute structure of the low-temperature form. It was also not possible to determine whether inversion twins were formed, as was to be expected from this phase transition, as the twin

refinement gave almost identical parameters and R values. Further details of the crystal structure investigation may be obtained from the Fachinformationszentrum Karlsruhe, D-76344 Eggenstein-Leopoldshafen (Germany) on quoting the depository numbers CSD-401026 (room-temperature form) and CSD-401027 (low-temperature form).

[8] C. J. J. van Loon, J. D. Ijdo, *Acta Crystallogr. Sect. B* **1975**, *31*, 770–773.

[9] P. W. Selwood, *Magnetochemistry*, Interscience, New York, **1956**.

[10] H. Lueken, personal Communication; H. Lueken, L. Maque, *Z. Anorg. Allg. Chem.* **1982**, *490*, 64–76.

[11] P. Gütlich, *Angew. Chem.* **1994**, *106*, 2109–2141; *Angew. Chem. Int. Ed. Engl.* **1994**, *33*, 2024–2054.

[12] W. Klemm, L. Grimm, *Z. Anorg. Allg. Chem.* **1942**, *249*, 198–208, 209–218.

[13] J. Lewis, D. J. Machin, I. E. Newnham, R. S. Nyholm, *J. Chem. Soc.* **1962**, 2036–2041.

Homogeneous versus Heterogeneous Zeolite Nucleation

Wim H. Dokter, Harold F. van Garderen, Theo P. M. Beelen,* Rutger A. van Santen, and Wim Bras

A question of considerable debate in zeolite synthesis is the nature of the precursor gel from which the zeolite is formed and whether nucleation occurs within the gel or from the mother liquid of the synthesis mixture.[1, 2] For the synthesis of ZSM-5 and silicalite considerable evidence supports the hypothesis that crystallization occurs by transformation of the precursor gel.[3, 4] On the other hand, it has also been demonstrated that the zeolite can be formed directly from the liquid phase without the intermediacy of a gel phase.[5] Here we report on a silicalite synthesis in which the silicalite crystallites do not nucleate in a separate gel phase, but directly from the liquid phase. Even in this experimental system, in which no gel phase was expected, precursor aggregates were observed with simultaneous, real-time small- and wide-angle X-ray scattering (SAXS-WAXS). These aggregates reorganize in analogy to the heterogeneous reaction mixture before nucleation and subsequent crystallization.[2, 6]

Time-resolved small- and wide-angle X-ray scattering can be applied to study aggregation, gelation, and crystallization processes under in situ conditions. We recently reported a SAXS-WAXS study of the gel morphology changes that occur during silicalite formation in a synthesis mixture with a separate gel phase. We found significant gel transformations before nucleation of silicalite crystallites. The gel morphology could be analyzed in terms of primary particles with a radius of 14 nm and an initial surface fractal dimension of 2.7, indicating a rough surface, which reorganized into smoother particles during reaction.[2, 6] We concluded that nucleation proceeds within the gel.

The simultaneous small- and wide-angle X-ray scattering experiments were performed using beamline 8.2 at the Synchrotron Radiation Source (Daresbury Laboratories, United Kingdom). Details concerning camera geometry and data collection were presented elsewhere.[7] The spatial resolution of the SAXS quadrant detector is 400 μm, and it can handle up to 300000 counts per second.[8] The WAXS detector is a curved knife-edge INEL detector with a spatial resolution of 50 μm and can handle up to 100000 counts per second.[9] The scattering ranges covered are $0.01 < Q < 0.175$ Å^{-1} and $0.8 < Q < 3.4$ Å^{-1} for the SAXS and WAXS detectors, respectively. The SAXS data were corrected for background scattering and solvent using a procedure introduced by Vonk.[10] Fractal dimensions were determined from the parts of the scattering curves where behavior followed the power law, and particle and aggregate sizes were determined from the point of deviation from this behavior. In the determination of the slope of the scattering curve, two possible sources of error may be distinguished. The first is the natural noise present in the data, which is small, however, compared to the error introduced during background subtraction ($D_f \pm 0.05$). The crystallinity of the final product was determined with in-house XRD, which was calibrated with a fully crystalline sample of silicalite.The relation between a scattering spectrum and the species responsible for the scattering is shown in Figures 1a and 1b. For mass fractal aggregates

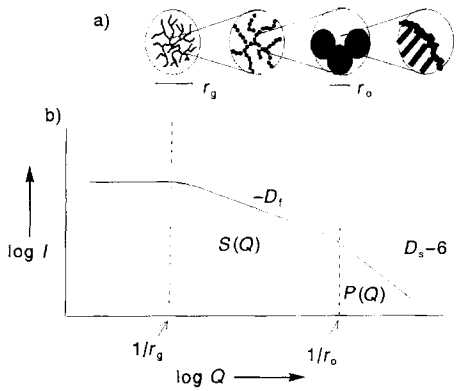


Fig. 1. a) Schematic representation of an aggregate with mass fractal and surface fractal properties; b) the corresponding plot of log I versus log Q of the small-angle scattering spectrum. $S(Q)$ = structure factor, $P(Q)$ = form factor, I = scattered intensity, Q = scattering vector, D_f = mass fractal dimension, D_s = surface fractal dimension, r_g = radius of gyration of the aggregate, r_0 = radius of gyration of primary particles.

the scattered intensity will be dominated by the structure factor, providing information about the correlation between the various primary building units present in the aggregates[11] [Eq. (a)]. Here $Q = 2\pi/\lambda \sin(2\theta)$, λ = wavelength, 2θ = scattering angle, $P(Q)$ = form factor, $S(Q)$ = structure factor, and D_f = mass fractal dimension.

$$I(Q) \sim P(Q)S(Q) \sim S(Q) \sim Q^{-D_f} \quad \text{(a)}$$

On the scale of the primary building units the form factor of the primary building units becomes dominant in the scattering pattern, thus providing information about the surface structure of these units[12] [Eq. (b)], where D_s, the surface fractal

$$I(Q) \sim P(Q) \sim Q^{-(6-D_s)} \quad \text{(b)}$$

dimension, ranges between 2 and 3. The surface fractal dimension equals 2 for a nonfractal, completely smooth surface, thus resulting in the well-known Porod relation[13] [Eq. (c)].

$$I(Q) \sim Q^{-4} \quad \text{(c)}$$

[*] Dr. Ir. T. P. M. Beelen, Dr. Ir. W. H. Dokter, Drs. H. F. van Garderen, Prof. Dr. R. A. Santen
Schuit Institute of Catalysis
Eindhoven University of Technology
P.O. Box 513, NL-5600 MB Eindhoven (Netherlands)
Telefax: Int. code + (40)455054
Drs. W. Bras
Daresbury Laboratory
United Kingdom & Netherlands Organisation for Scientific Research

If D_s increases, the roughness of the surface increases. When $D_s \rightarrow 3$ and $D_f \rightarrow 3$, then a homogeneous distribution of mass and voids (possibly filled) throughout the sample is obtained.[14] Experimentally the parameter D_f (fractal dimension) can be determined from a plot of log $I(Q)$ versus log Q. The slope of the scattering curve α is equivalent to $-D_f$ for mass fractal scattering and equivalent to $-(6 - D_s)$ for surface fractal scattering.

The reaction mixture studied here was prepared from silicic acid powder (Baker 10.2 wt% water), NaOH pellets (Merck, >99 wt%) and tetrapropylammonium hydroxide (TPA) (Fluka 20 wt%) in the following molar ratios: SiO_2/TPA = 4.1, SiO_2/NaOH = 11.5, H_2O/SiO_2 = 11.[15] NaOH was added to the TPAOH solution with gentle stirring. The silicic acid was added to the solution and stirred until a homogeneous dispersion was obtained. This solution was heated for approximately 10 min to obtain a clear synthesis mixture. Water was added to correct for the loss due to evaporation. This synthesis mixture usually remains clear during reaction until crystallization, detectable with standard X-ray diffraction, occurs.[15] The reaction temperature was 120 °C ± 5 °C.

Our results indicate that in the homogeneous system cluster aggregation occurs before crystallization, in analogy to the heterogeneous system.[2, 6] SAXS curves and corresponding schematic aggregate structures are shown in Figures 2 and 3, respectively. As Figures 2a and 3b show, the morphology (D_f = 2.2), observed after a reaction time of 5 min is typical for aggregates condensed according to reaction-limited cluster–cluster aggregation.[16] The low rate of reaction is due to the effect of the structure-directing TPA ions.[17]

The aggregates formed under these conditions have a diameter d of approximately 6.4 nm ($d = 2 \cdot r_g$; r_g = radius of gyration) These aggregates are composed of primary particles with a radius smaller than 1.6 nm, the upper limit of the Q-values of the available SAXS range. These primary particles may be hydrated tetrapropylammonium–silicate clusters. Burkett and Davis have provided evidence for the existence of preorganized organic–inorganic composite structures in the synthesis of ZSM-5.[18] Short-range intermolecular interactions exist between the protons of TPA and silicon atoms of the zeolite precursor phase before development of the long-range order characteristic of the ZSM-5 structure.[18] Other authors observed specific silicate anions in various aqueous silica solutions

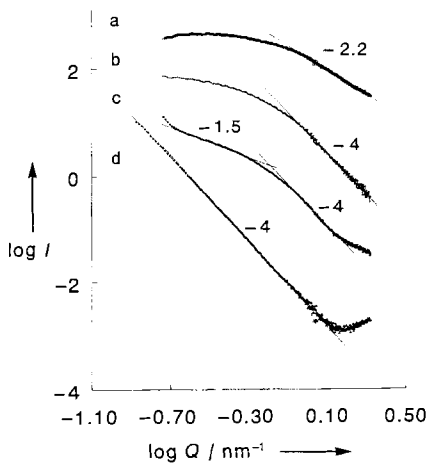


Fig. 2. Plot of log I versus log Q of the small-angle X-ray scattering spectra of the clear silicalite synthesis mixture after reaction times of a) 5 min, b) 35 min, c) 75 min, and d) 105 min.

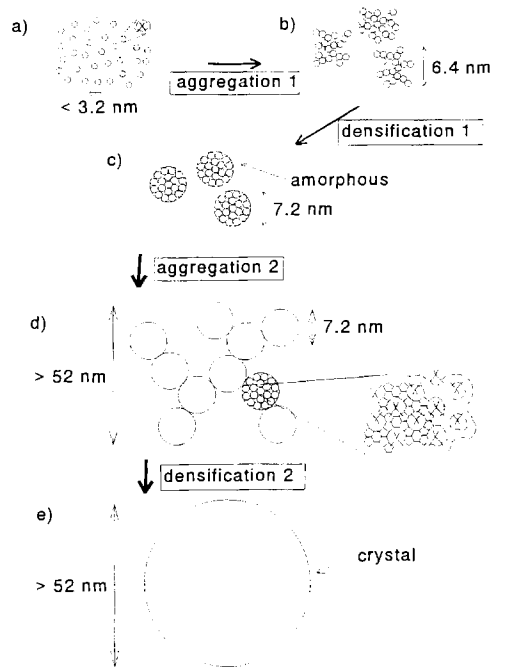


Fig. 3. Mechanism of microstructural random packing, subsequent ordering, and crystallization. a) Silicate/TPA clusters in solution; b) primary fractal aggregates formed from the silicate/TPA clusters (6.4 nm, Fig. 1a); c) densification of these primary fractal aggregates (Fig. 1b); d) combination of the densified aggregates into a secondary fractal structure and crystallization (Fig. 1c); and e) densification of the secondary aggregates and crystal growth.

which may be building blocks for zeolites or precursors of zeolites.[19, 20]

The observed silica/TPA clusters start to densify (Figs. 2b and 3c) with time into denser mass fractal aggregates and subsequently into surface fractal aggregates (Fig. 4). After a reaction

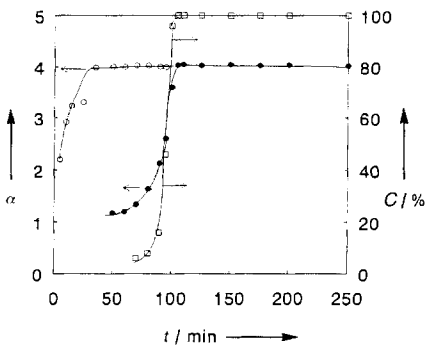


Fig. 4. Plot of crystallinity C (from WAXS) and microstructure (from SAXS) as a function of time t. The scattering slopes α obtained with SAXS are divided in the scattering slope at high Q (small radius) (○) and the scattering slope at small Q (large radius) (●) to clearly demonstrate the consistency between the microstructure and crystallization (□).

time of 35 min at 120 °C the plot of log $I(Q)$ versus log Q shows a Porod slope ($\alpha = -4$), indicative of a homogeneous dense silica/TPA structure with a smooth surface ($D_s = 2$). The size of this structure increases only very slightly (to 7.2 nm) with time. The fact that it does not decrease upon densification indicates that additional primary particles (TPA surrounded with silicate anions) are transported from solution or other silica aggregates to the densifying cluster. The size of these densified silica/TPA

particles is approximately equal to 20 silicalite unit cells. After this densification, the 7.2-nm particles aggregate again into a new, secondary fractal aggregate (Figs. 2c and 3d). The occurrence of crystalline structures is observed simultaneously with WAXS.

Figure 4 shows the time progression of the scattering slope α at large values of Q (small particles) and at small values of Q (large particles or clusters), and the degree of crystallinity as determined with WAXS. The WAXS curves are shown in Figure 5. From these plots we may conclude that crystallization

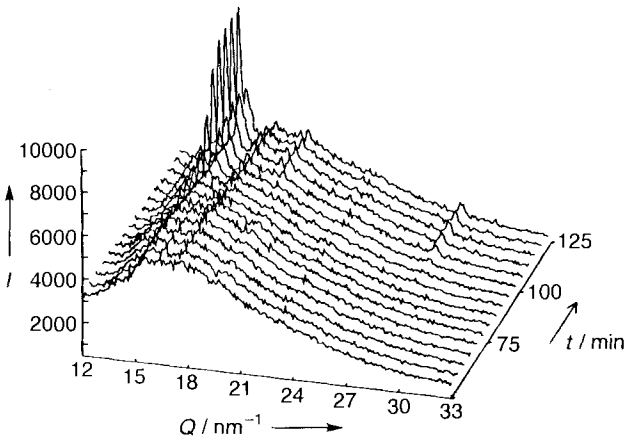


Fig. 5. WAXS spectra of clear silicalite synthesis mixtures demonstrate crystallization beteen 50 and 125 min of reaction. I = intensity, Q = scattering vector, t = time.

starts as soon as the dense silica/TPA particles 7.2 nm in diameter have been formed and aggregation into the larger secondary aggregate starts. Growth of zeolite particles occurs by transformation of the 7.2-nm silica/TPA particles that form the new secondary fractal structure (Fig. 2c). Crystallization occurs again via a surface fractal aggregate (Fig. 4) to a completely smooth (energetically more favorable) structure (Figs. 2d and 3e). They grow rapidly to a size larger than the upper size limit (low Q-limit) of the available SAXS range ($d > 52$ nm).

Crystal growth occurs by combination of the densified primary aggregates into kinetically determined secondary aggregates, indicative for growth by combination of already growing nuclei, which subsequently densify into energetically more favorable, dense, smooth particles. These results are in agreement with the results obtained by Twomey et al. who deduced from size distributions of crystals obtained from light-scattering experiments that nucleation is a continuous process and that growth occurs by agglomeration of nuclei.[21]

One interesting feature of the results presented here is that also in the homogeneous system a precursor aggregate is formed before crystallization, which is indicative of a gel transformation or gel reorganization mechanism of zeolite crystallization even in a clear silicalite solution. This is in contrast to the direct homogeneous crystallization.

For silicalite synthesized from a gelatinous reaction mixture[21] it was concluded that crystallization proceeded also according to a gel transformation mechanism. No mass fractality was observed during these experiments. The different silica source (Aerosil 380) leads to very compact amorphous surface fractal precursor particles with a initial particle size of 14 nm. Crystallization, however, starts only after the surface fractal amorphous particles have been transformed into smooth particles with $D_s = 2$. An analogous feature was observed in this study. The mass fractal aggregate had to transform into smooth, homogeneous, dense structures before crystallization starts. From this we may conclude that homogeneous and heterogeneous crystallization both require an intermediate gel phase before nucleation and crystallization can occur.

In the gel phase nucleation and crystallization occur more slowly than in the homogeneous phase, because the gel formed must first dissolve before a new phase is formed, from which crystallization can occur. This dissolution step is not required in the homogeneous phase, in which the mass transport and subsequent formation of the primary and secondary clusters seem to be the rate-determining steps. Instant crystallization may be achieved when the precursors are prepared in such a way that the desired gel phase for nucleation is obtained directly.

Received: June 30, 1994 [Z 7084 IE]
German version: *Angew. Chem.* **1995**, *107*, 122

Keywords: crystallization · silicon compounds · structure elucidation · zeolites

[1] M. E. Davis, R. F. Lobo, *Chem. Mater.* **1992**, *4*, 756.
[2] Z. Gabelica, J. B. Nagy, G. Debras, E. G. Derouane, *Proc. Int. Zeolite Conf. 6th 1983*, **1984**, 914.
[3] W. H. Dokter, T. P. M. Beelen, H. F. van Garderen, C. P. J. Rummens, R. A. van Santen, J. D. F. Ramsay, *Coll. Surf. A* **1994**, *85*, 89.
[4] W. Xu, J. Li, W. Li, H. Zhang, B. Liang, *Zeolites* **1989**, *9*, 468.
[5] L. E. Iton, F. Trouw, T. O. Brun, J. E. Eperson, J. W. White, S. J. Henderson, *Langmuir* **1992**, *8*, 1045.
[6] W. H. Dokter, T. P. M. Beelen, H. F. van Garderen, R. A. van Santen, W. Bras, G. E. Derbyshire, G. R. Mant, *J. Appl. Crystallogr.* **1994**, *27*, 901.
[7] W. Bras, G. E. Derbyshire, A. J. Ryan, G. R. Mant, A. Felton, R. A. Lewis, C. J. Hall, G. N. Greaves, *Nucl. Instrum. Methods Phys. Res. Sect. A* **1993**, *326*, 587.
[8] R. A. Lewis, N. S. Fore, W. Helsby, C. Hall, A. Jones, B. Parker, I. Sumner, J. S. Worgan, C. Budtz-Jorgensen, *Rev. Sci. Instrum.* **1992**, *63* (1), 642.
[9] M. Evain, P. Deniard, A. Jouanneaux, R. Brec, *J. Appl. Crystallogr.* **1993**, *26*, 563.
[10] C. G. Vonk, *J. Appl. Crystallogr.* **1973**, *6*, 81.
[11] J. E. Martin, A. J. Hurd, *J. Appl. Crystallogr.* **1987**, *20*, 61.
[12] H. D. Bale, P. W. Schmidt, *Phys. Rev. Lett.* **1983**, *53*, 596.
[13] G. Porod, *Kolloid Z.* **1951**, *124*, 83.
[14] D. W. Schaeffer, A. J. Hurd, *Aerosol Sci. Technol.* **1990**, *12*, 876.
[15] J. Verduyn (PCT), **1992**, EP-A02386.
[16] R. Jullien, M. Kolb, *J. Phys. A* **1984**, *17*, L639.
[17] E. M. Flanigan in *Introduction to zeolite science and practice* (Eds.: H. Van Bekkum, E. M. Flanigan, J. C. Jansen), Elsevier, Amsterdam, **1991**, p. 13.
[18] S. L. Burkett, M. E. Davis, *J. Phys. Chem.* **1994**, in press.
[19] P. W. J. G. Wijnen, T. P. M. Beelen, J. W. de Haan, L. J. M. van de Ven, R. A. van Santen, *Colloids Surf.* **1990**, *45*, 255.
[20] D. Hoebbel, A. Vargha, B. Fahlke, G. Engelhardt, *Z. Anorg. Allg. Chem.* **1985**, *521*, 61.
[21] T. A. M. Twomey, M. Mackay, H. P. C. E. Kuipers, R. W. Thompson, *Zeolites* **1994**, *14*, 162.

 © VCH Verlagsgesellschaft mbH, D-69451 Weinheim, 1995 0570-0833/95/0101-0075 $ 10.00+.25/0

Orthorhombic and Monoclinic 2,3,7,8-Tetramethoxythianthrene: Small Structural Difference–Large Lattice Change**

Hans Bock,* Andreas Rauschenbach, Christian Näther, Zdenek Havlas, Angelo Gavezzotti, and Guiseppe Filippini

Dedicated to Professor Wolfgang Hilger on the occasion of his 65th birthday

Molecular compounds can often be isolated in several crystalline modifications that have only small differences in lattice or sublimation energies.[1–3] In addition to serendipitous discoveries,[1, 2a, 3a] frequently crystal growth under skillfully chosen optimal conditions[1, 2b, 3b, 3c]—for instance, from solution or by sublimation,[2c, 3a, 3c] from strongly polar or less polar solvents,[2c, 3c] or in the presence of cation-chelating ligands[3b]—enable certain molecular conformations to be captured "snapshots" of the molecular dynamics.

Here we again report[4a] on 2,3,7,8-tetramethoxythianthrene, which is obtained from diisopropyl ether as monoclinic[4b] and from *n*-hexane as orthorhombic crystals.[5] The structural differences on the molecular level are rather small: comparison reveals that in the orthorhombic modification only the methoxy group in the 3-position is twisted by 79° out of the plane of the adjacent six-membered ring (Fig. 1, top left). However, the small perturbation in the skeletal symmetry from C_{2v} to C_1, which does not apply to the crystallographic site symmetry, formally introduces molecular chirality.

The changes in the crystal lattices on going from the monoclinic modification containing altogether $Z = 12$ molecules of three geometries within the unit cell to the orthorhombic one with $Z = 8$ identical molecules can be plausibly discussed by beginning with the small structural perturbation (Fig. 1, top left). As can be seen from the angles in the planar form (Scheme 1 left), twisting one H_3CO group out of the C_6 plane brings some steric relief especially between the H centers in *ortho* ring position and the methyl groups, since the 228 pm distance between them is within twice the van der Waals radii $2r_H^{vdW}$ of 240 pm.

In contrast, in both the monoclinic and the tetragonal modifications of tetramethoxyselenanthrene all H_3CO substituents lie in the C_6 plane, and a databank search (Cambridge Crystallographic Data Centre),[4c] in complete agreement with PM3 calculations,[6b] suggests that for structures containing methoxy-substituted phenyl rings a planarization should be energetically favorable. Nevertheless, the conformation of the orthorhombic tetramethoxythianthrene (Fig. 1, top left) is supported by geometry-optimized PM3 hypersurface calculations: for the experimentally determined twisting of ω(CC–OC) = 79°[5] above the $O_2C_6S_2$ plane, the (negative) heat of formation is predicted to increase by -3 kJ mol^{-1}, and the local minimum of the rather shallow potential is found at a torsion angle of about 80°.[6] On the contrary, both the turning of a H_3CO

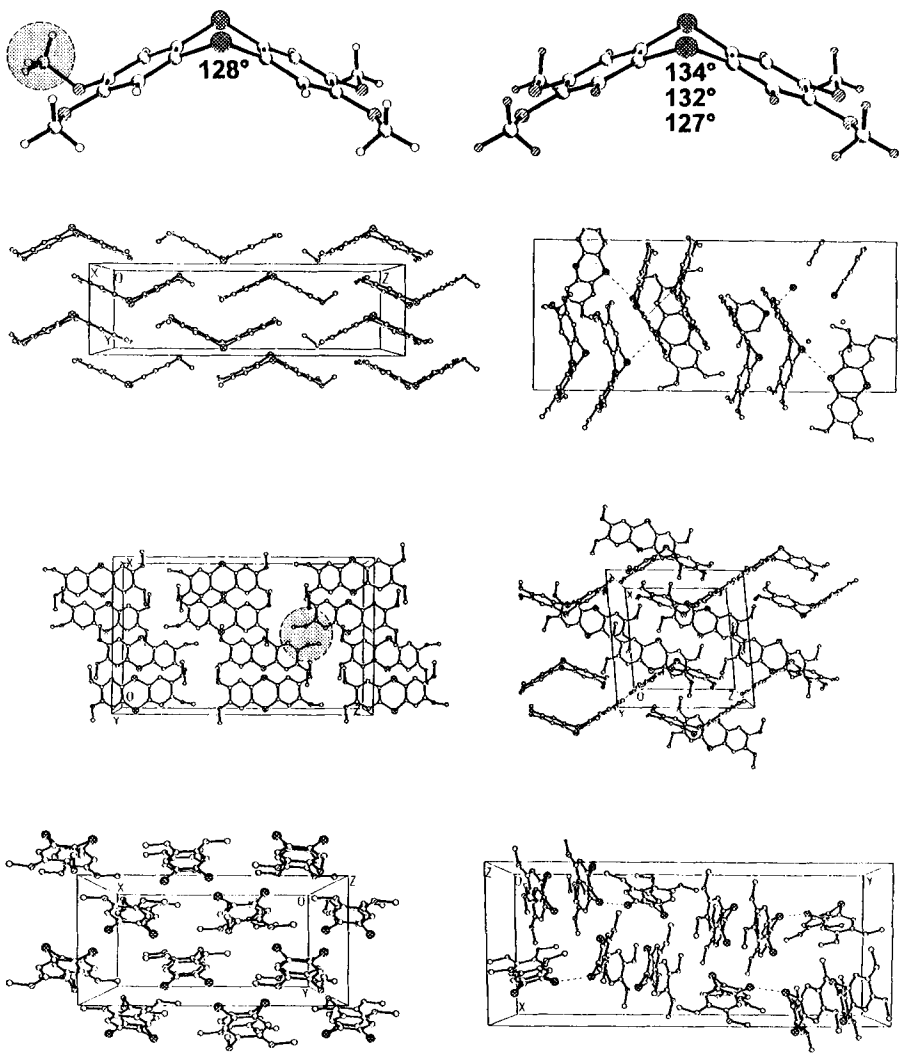


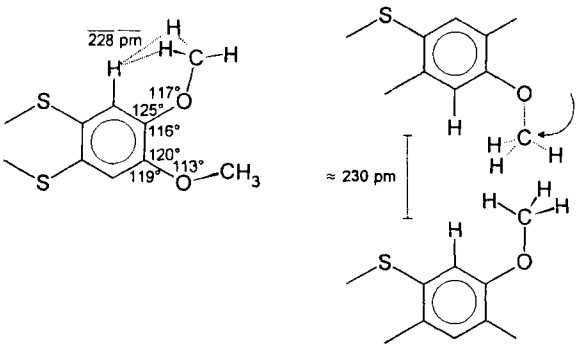
Fig. 1. Single crystal structures of the polymorphic modifications of 2,3,7,8-tetramethoxythianthrene. Left: orthorhombic (*Pbca*, ρ(300 K) = 1.437 g cm^{-3} [5], with an interplanar angle of 128° between the C_6 rings, and unit cell ($Z = 8$) in *a*, *b*, and *c* directions. The shaded circles emphasize the structural distortion by twisting of the methoxy group in 3-position and its effects on the lattice. Right: monoclinic ($P2_1/n$, ρ(300 K) = 1.395 g cm^{-3} [4b]) containing three independent molecules in the asymmetric unit with dihedral angles of 134°, 132°, and 127°, and the unit cell ($Z = 12$) in *a*, *b*, and *c* directions.

[*] Prof. Dr. H. Bock, Dipl.-Chem. A. Rauschenbach, Dipl.-Chem. C. Näther
Chemische Institute der Universität
Marie-Curie-Strasse 11
D-60439 Frankfurt am Main (Germany)
Telefax: Int. code +(69) 5800-9188

Dr. Z. Havlas
Institute of Organic Chemistry and Biochemistry of the Czech Academy of Sciences
Flemingovo Nam 2, CS-16610 Prag (Czech Republic)

Prof. Dr. A. Gavezzotti, Dr. G. Filippini
Institute of Physical Chemistry, University of Milan
Via Golgi, I-20133 Milano (Italy)

[**] Interactions in Crystals, Part 49. The project was supported by the A. Messer-Stiftung, the State of Hesse, the Deutsche Forschungsgemeinschaft, and the Fonds der Chemischen Industrie. Part 48: H. Bock, I. Göbel, C. Näther, B. Solouki, A. John, *Chem. Ber.* **1994**, *127*, 2197.



Scheme 1. Left: Bond angles and H···H distance in 2,3,7,8-tetramethoxythianthrene. Right: hypothetical C···C distance of about 230 pm in the orthorhombic lattice (Fig. 1: left) on attempting to twist the H_3CO group back into the plane of the six-membered ring (cf. text).

substituent below the $O_2C_6S_2$ plane and the dis- or conrotatory movement of two vicinal methoxy groups (H_3CO-CC-OCH_3) require energy.[6a] Altogether therefore, tetramethoxythianthrene displays– in close analogy to the polymorphic conformers of tetraisopropyl-*p*-phenylene diamine[3a]—a delicate balance between n_O/π-delocalization of the oxygen lone pair density and the H/H repulsion especially between H centers of the ring in *ortho*-position and of the methyl group (Scheme 1 left).

Though rather small, the structural distortion is nevertheless connected with a profound lattice change (Fig. 1), which shall be rationalized as follows: a hypothetical attempt to twist the methoxy group of the orthorhombic modification back into the plane of the phenyl ring, would enforce a nonbonding C···C distance of only 230 pm (Scheme 1 right). This would correspond to a prohibitive 42% contraction of the usual van der Waals distance between two methyl groups of 400 pm.[7] This argument explains the increased packing density due to the parallel arrangement of two twisted H_3CO substituents, each from different molecules (Fig. 1, shaded circle in the unit cell second from top, left). On the other hand, the shortest contact distance $(CH_2)H\cdots S$ resulting from the dense packing is only 281 pm and, therefore, smaller than the van der Waals radii sum of $r_H^{vdW} + r_S^{vdW} = 120 + 185 = 305$ pm by only 8%.[7]

Every tetramethoxythianthrene molecule in the orthorhombic modification is surrounded in the *a*, *b* plane by six adjacent ones (Fig. 1, bottom left), and above and below it in the *c* direction are two additional molecules. In contrast, the monoclinic modification (Fig. 1, right) contains relatively loosely packed pairs of the sulfur heterocycles with mean S···S distances of 398 pm; the third molecule lies perpendicular to this pair. The density difference at room temperature between the orthorhombic ($\rho = 1.437\ g\,cm^{-3}$) and the monoclinic ($\rho = 1.395\ g\,cm^{-3}$)[4b] modifications amounts to 2.6%. As expected,[1, 8] this is reflected in the lattice or sublimation energies calculated by the atom/atom potential approximation,[9a, b] which predicts $-34.7\ kJ\,mol^{-1}$ for the orthorhombic and $-32.3\ kJ\,mol^{-1}$ for the monoclinic modification of 2,3,7,8-tetramethoxythianthrene.[9c]

The following proposals are forwarded for discussion of the crystal growth of the two different modifications:[1–3, 10] The monoclinic crystals of lower density and lattice energy should grow from a solution in the polar diisopropyl ether rather fast and in a kinetically controlled way, whereas the orthorhombic crystals with higher density and lattice energy presumably grow under thermodynamical control from a solution in an unpolar hydrocarbon. Whether the symmetry change $C_{2v} \rightarrow C_1$ occurs partly in solution already or only on incorporation into the crystal lattice cannot be answered; however, the existence of the 2,3,7,8-tetramethoxythianthrene modifications is another example—as is the use of the monoethyltetramethylcyclopentadienyl ligand in the rapid crystallization of metal sandwich complexes[10b] –of the often useful rule of thumb that reduced molecular symmetry can promote an energetically favored crystallization.

Received: February 11, 1994
Revised version: July 25, 1994 [Z 6684 IE]
German version: *Angew. Chem.* **1995**, *107*, 120

Keywords: organic solids · polymorphism · structure elucidation · 2,3,7,8-tetramethoxythianthrene

[1] Reviews on crystal investigations of polymorphic molecular conformers: "Conformational Polymorphism": J. Bernstein in *Organic Solid State Chemistry* (Ed.: G. R. Desiraju), Elsevier, Amsterdam, **1987**, pp. 471–517; G. R. Desiraju, *Crystal Engineering* (*Mater. Sci. Monogr.*) **1989**, *54*, pp. 285–301, and references therein; see also refs. [2, 3].

[2] Selected recent publications on polymorphism: a) bis(pyridinium)squarate: M. T. Reetz, S. Höger, K. Harms, *Angew. Chem.* **1994**, *106*, 193; *Angew. Chem. Int. Ed. Engl.* **1994**, *33*, 181; b) lattice energy calculations for monoclinic and orthorhombic modifications of benzene, naphthalene, and anthracene: J. Bernstein, J. A. R. P. Sarma, A. Gavezzotti, *Chem. Phys. Lett.* **1990**, *174*, 361; c) tricycloindane-1,3-dione: J. J. Stezowski, P. U. Biedermann, T. Hildenbrand, J. A. Dorsch, J. Eckhardt, I. Agranat, *J. Chem. Soc. Chem. Commun.* **1993**, 213.

[3] The crystals of polymorphic modifications of molecular conformers grown so far by the Frankfurt group: a) monoclinic and triclinic tetraisopropyl-*p*-phenylenediamine (H. Bock, I. Göbel, C. Näther, Z. Havlas, A. Gavezzotti, G. Filippini, *Angew. Chem.* **1993**, *105*, 1823; *Angew. Chem. Int. Ed. Engl.* **1993**, *32*, 1755; cf. also H. Bock, J. Meuret, C. Näther, U. Krynitz, *Chem. Ber.* **1994**, *127*, 55; b) pseudopolymorphic, orthorhombic, and monoclinic tetraphenyl-*p*-benzosemiquinone sodium containing two or three tetrahydropyran solvent molecules (H. Bock, A. John, C. Näther, *J. Chem. Soc. Chem. Commun.* **1994**, 1939; c) orthorhombic and triclinic bis(pyridylamine): H. Bock, H. Schödel, A. Gavezzotti, G. Filippini, unpublished (cf. H. Bock, *Phosphorus, Sulfur, Silicon Rel. El.*, **1994**, *87*, 23; see in addition J. E. Johnson, R. A. Jacobson, *Acta Crystallogr. Sect. B* **1973**, *29*, 1669 and G. J. Pyrka, A. A. Pinkerton, *Acta Crystallogr. Sect. C* **1992**, *48*, 91; d) isotypic, monoclinic *N,N'*-ditosyl-*p*-phenylendiamine with included solvent molecules such as acetone, cyclopentanone, cyclopent-2-enone, tetrahydrofuran, or 2,5-dihydrofuran: H. Bock, N. Nagel, C. Näther, unpublished (cf. H. Bock, *Mol. Cryst. Liq. Cryst.* **1994**, *240*, 166).

[4] a) H. Bock, A. Rauschenbach, K. Ruppert, Z. Havlas, *Angew. Chem.* **1991**, *103*, 706; *Angew. Chem. Int. Ed. Engl.* **1991**, *30*, 714; b) W. Hinrichs, H.-J. Riedel, G. Klar, *J. Chem. Res. (S)* **1982**, 334; *J. Chem. Res. (M)* **1982**, 3501; c) the thiaseleno and diseleno derivatives crystallize isotypically tetragonal with $Z = 4$ in $P42_1m$: M. Dötze, W. Hinrichs, G. Klar, *J. Chem. Res. (S)* **1991**, 314; *J. Chem. Res. (M)* **1991**, 2861.

[5] The crystal growth of colorless platelets from *n*-hexane can be accomplished after a 24 h Soxhlet-extraction of the raw product [4b] under argon and slow evaporation of the solvent at normal pressure. $C_{16}H_{16}O_4S_2$ (336.4 g mol^{-1}), (150 K) $a = 1549.0(1)$, $b = 752.3(1)$, $c = 2606.4(2)$ pm, $V = 3037.2 \times 10^6$ pm^3, $Z = 8$, $\rho_{calcd} = 1.471\ g\,cm^{-3}$, $\mu = 0.37\ mm^{-1}$, orthorhombic, space group *Pbca* (no. 61). Siemens AED-II four-circle diffractometer ($Mo_{K\alpha}$ radiation), 3405 measured reflections within $3 < 2\theta < 50$, of which 2637 are independent, 2097 with $I > 1.0\sigma(I)$. Structure solution with direct methods and difference-Fourier-technique (SHELXTL-PC), 207 parameters. All heavy atoms were refined anisotropically, all H in ideal positions and refined according to the riding model using isotropic displacement parameters, $R = 0.0445$, $Rw = 0.0372$, $Rg = 0.0394$, $w = 1/\sigma^2(F) + 0.0002\,F^2$, GOF = 1.3757, Shift/Error < 0.0001, residual electron density 0.28/−0.28 e Å^{-3}. Further details of the crystal structure determination may be obtained from the Fachinformationszentrum Karlsruhe, D-76344 Eggenstein-Leopoldshafen (Germany) on quoting the depository number CSD-58 673.

[6] a) The PM3 calculations (program: *J. J. P. Stewart, J. Comput. Chem.* **1989**, *10*, 209) have been performed on the structural data [5] with partial geometry optimization with the program version MOPAC 6.0 (QCPE No. 455) on an IBM RISC 6000/320. The PM3 heats of formation (in kJ mol^{-1}) additionally calculated for the rotation of a H_3CO group below the $O_2C_6S_2$ plane and for the simultaneous dis- and conrotatory rotations of the vicinal substituents, as well as the respective minima (or points of inflection) of the torsion angles (in °) amount to +4/(80), +8/80 and +7/100. b) Cf. W. Hummel, K. Huml, H.-B. Bürgi, *Helv. Chim. Acta* **1988**, *71*, 1291.

 © VCH Verlagsgesellschaft mbH, D-69451 Weinheim, 1995 0570-0833/95/0101-0077 $ 10.00+.25/0

[7] H. Bock, K. Ruppert, C. Näther, Z. Havlas, H.-F.- Herrmann, C. Arad, I. Göbel, A. John, J. Meuret, S. Nick, A. Rauschenbach, W. Seitz, T. Vaupel, B. Solouki, *Angew. Chem.* **1992**, *104*, 564; *Angew. Chem. Int. Ed. Engl.* **1992**, *31*, 550, and references therein.

[8] Cf., for example, I. Bar, J. Bernstein, *J. Phys. Chem.* **1984**, *88*, 243, and references therein.

[9] a) Summary: A. J. Pertsin, A. I. Kitaigorodsky, *The Atom-Atom Potential Method*, Springer, **1987**; b) G. Filippini, A. Gavezzotti, *Acta Crystallogr. Sect. B* **1993**, *49*, 868 (optimized parameter set for atom/atom potential approximation calculations of crystal lattice or sublimation energies). The potential is defined exclusively intermolecularly and contains no intramolecular corrections. Additional lattice vibration calculations yield frequencies within the limits of expectation.

[10] Cf., for example, *a*) P. J. Fagan, M. D. Ward, *Sci. Am.* **1992**, *267*, 28; b) O. J. Scherer, *Angew. Chem.* **1990**, *102*, 1137; *Angew. Chem. Int. Ed. Engl.* **1990**, *29*, 1104.

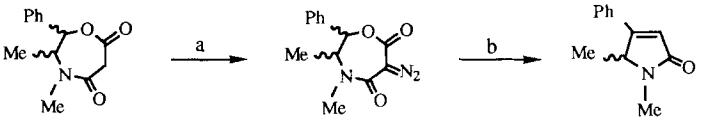
(*S*)-(+)- and (*R*)-(−)-1,5-Dimethyl-4-phenyl-1,5-dihydro-2*H*-pyrrol-2-ones by Carbene Ring Contraction and Decarboxylation of (2*R*,3*S*)-(−)- and (2*S*,3*R*)-(+)-6-Diazo-3,4-dimethyl-2-phenyloxazepane-5,7-diones**

Giorgio Chelucci and Antonio Saba*

The interest in ephedrine enantiomers as chiral auxiliaries increased after oxazepane-5,7-dione **1** was reported by Mukaiyama et al.[1] The 6-benzylidene derivative of **1** has been used as a chiral Michael acceptor,[2] a dienophile in asymmetric Diels–Alder cycloadditions,[3] and an unsaturated substrate in asymmetric cyclopropanation.[4] In the course of our studies in the field of stabilized carbenes and carbenoids generated by decomposition of α-diazocarbonyl compounds,[5] we have devoted our attention to the reactivity of (2*R*,3*S*)-(−)-6-diazo-3,4-dimethyl-2-phenyloxazepane-5,7-dione (**2**) and its enantiomer **2'**. Here we wish to report their catalytic decomposition, which affords exclusively (*S*)-(+)- and (*R*)-(−)-1,5-dimethyl-4-phenyl-1,5-dihydro-2*H*-pyrrol-2-one (**3** and **3'**).

The 6-diazooxazepanediones **2** and **2'** were easily prepared under mild conditions by a "diazo transfer" reaction with *p*-toluenesulfonyl azide (TsN_3);[6] the starting materials oxazepanediones **1** and **1'** were obtained from (−)-ephedrine and (+)-ephedrine, respectively. The decomposition reaction of **2** and **2'** was carried out in the presence of catalytic amounts of copper(I) triflate or rhodium(II) acetate dimer in CH_2Cl_2 at room temperature and was allowed to proceed until the diazo stretching band in the IR spectrum had disappeared. After filtration on neutral Al_2O_3, removal of the solvent, and crystallization of the residue, the 2-pyrrolones **3** and **3'** were obtained in good yield (Scheme 1).

The structure of the ring-contraction product **3** was determined from the mass, ^1H NMR, and ^{13}C NMR spectra

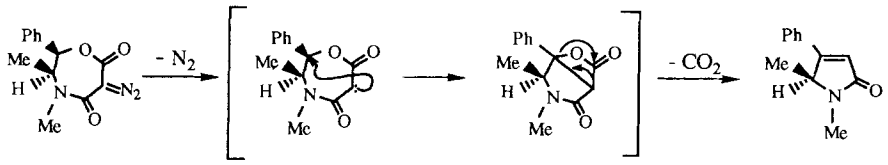


1 : (2*R*)(3*S*) **2** : (2*R*)(3*S*) **3** : (*S*)
1': (2*S*)(3*R*) **2'** : (2*S*)(3*R*) **3'** : (*R*)

Scheme 1. a) TsN_3, NEt_3, CH_3CN, room temperature, 24 h (85%); b) 5% copper(I) triflate or 5% rhodium(II) acetate dimer, CH_2Cl_2, room temperature (95%).

(Table 1), and a single-crystal X-ray diffraction study.[7] The latter confirmed the presence of a single enantiomer in the crystal and consequently the retention of configuration at the carbon bearing the methyl group, which is not involved in the process.

Ring contraction of heterocyclic α-diazo carbonyl compounds mostly proceed via a ketene (Wolff rearrangement[8]) and rarely have any synthetic value.[9] In our case, **3** was formed as a result of a transannular attack in the seven-membered heterocycle by the ketocarbene or ketocarbenoid intermediate. The regiospecific insertion into the benzylic C–H bond of oxazepane **2** can be ascribed to the greater electron density of this bond: electronic activation by the lactone oxygen[10] and by the phenyl group makes this bond more susceptible to attack by the electrophilic carbene species. In addition, it is documented that, in intramolecular C–H insertion reactions of diazoacetamides, a five-membered γ-lactam ring is more likely to be formed than the potentially competitive β-lactam.[11] The suggested straightforward mechanism of regiospecific carbene attack followed by ready CO_2 extrusion from the resulting unstable bicyclic intermediate is shown in Scheme 2.[12] Irradiation of diazo compound **2** with ultraviolet light ($\lambda = 250$ nm, in CH_2Cl_2) led to formation of the same reaction product **3**, although in much lower yield.[13]



2 **3**

Scheme 2.

The enantiomerically pure compounds **3** and **3'** open access to biologically active 4,5-disubstituted 2-pyrrolidinones, which can be considered as precursors to γ-aminobutyric acid (GABA).[14] Thus, catalytic hydrogenation of **3** gave a diastereomeric mixture of (4*S*,5*S*)-(+)- and (4*R*,5*S*)-(−)-1,5-dimethyl-4-phenyl-2-pyrrolidinone (**4a** and **4b**) in a ratio of 5.5:4.5 (Scheme 3).[15] The enantiomer **3'** was submitted to the same reductive procedure. A roughly 1:1 mixture of (4*R*,5*R*)-(−)- and (4*S*,5*R*)-(+)-1,5-dimethyl-4-phenyl-2-pyrrolidinone (**4a'** and **4b'**) were obtained. The diastereoisomeric pairs **4a**/**4b** and **4a'**/**4b'** were readily separated by chromatography on silica gel (eluant: hexane/ethyl acetate 8/2), and their configurations confirmed by NMR spectroscopy. In particular, the resonance for the 5-methyl of **4b** (Table 1) shows the well-known γ-gauche effect in the ^{13}C NMR spectrum[16] and is shifted upfield relative to that of the diastereoisomer **4a** ($\Delta\delta = 4$). Thus, **4b** can be assigned the *cis*- and **4a** the *trans*-pyrrolidinone configuration. Since the carbon bearing the methyl group is unaffected in the reaction,

[*] Prof. Dr. A. Saba, Dr. G. Chelucci
Dipartimento di Chimica, Facoltà di Scienze
Via Vienna 2, I-07100 Sassari (Italy)
Telefax: Int. code + (79)229-559

[**] This work was supported by the Ministero dell' Università e della Ricerca Scientifica e Technologica (MURST) (40% of funding). We thank Mauro Mucedda for experimental assistance.

Table 1. Important physical data for **2**–**5** [a].

2: white crystals; m.p. 119–120 °C (decomp.); $[\alpha]_D^{25} = -122$ ($c = 0.52$ in $CHCl_3$); ^1H NMR ($CDCl_3$): $\delta = 7.42-7.29$ (m, 5H), 5.63 (s, 1H), 3.61 (q, $J = 6.9$ Hz, 1H), 3.13 (s, 3H), 1.20 (d, $J = 6.9$ Hz, 3H); ^{13}C NMR ($CDCl_3$): $\delta = 162.3$, 157.7, 136.8, 128.6, 125.5, 80.7, 62.1, 36.1, 10.5; IR (Nujol): $\tilde{\nu} = 2935$, 2930, 2840, 2142, 1660, 1605, 1302, 1140, 735 cm^{-1}.

3: white crystals; m.p. 143–144 °C (hexane/benzene 8/2); $[\alpha]_D^{25} = +127$ ($c = 0.54$ in $CHCl_3$); ^1H NMR ($CDCl_3$): $\delta = 7.42$ (s, 1H), 6.35 (s, 1H), 4.51 (q, $J = 6.9$ Hz, 1H), 3.06 (s, 3H), 1.34 (d, $J = 6.9$ Hz, 3H); ^{13}C NMR ($CDCl_3$): $\delta = 170.3$, 160.1, 131.6, 129.6, 128.8, 126.7, 120.4, 59.3, 26.7, 17.4; IR (Nujol): $\tilde{\nu} = 3060$, 2995, 2992, 2840, 1670, 1360, 895, 758, 690 cm^{-1}. MS (70 eV); m/z (%): 187 (20) [M^+], 185 (100) [$M^+ - 2H$], 157 (28) [$M^+ - 2CH_3$], 129 (52) [$M^+ - 2CH_3 - CO$].

4a: colorless oil; $[\alpha]_D^{25} = +9.5$ ($c = 0.64$ in $CHCl_3$); ^1H NMR ($CDCl_3$): $\delta = 7.35-7.18$ (m, 5H), 3.52 (quint, $J = 6.6$ Hz, 1H), 2.96 (dq, $J = 6.3$, 2.1 Hz, 1H), 2.85–2.77 (m, 1H), 2.84 (s, 3H), 2.57–2.48 (m, 1H), 1.25 (d, $J = 6.6$ Hz, 3H); ^{13}C NMR ($CDCl_3$): $\delta = 173.4$, 141.4, 128.4, 127.2, 127.1, 62.9, 46.7, 38.9, 27.2, 18.4; IR (neat): $\tilde{\nu} = 2965$, 2913, 1682, 1450, 1414, 1395, 1376, 1071, 762, 703 cm^{-1}.

4b: colorless oil; $[\alpha]_D^{25} = -166.8$ ($c = 0.74$ in $CHCl_3$); ^1H NMR ($CDCl_3$): $\delta = 7.37-7.16$ (s, 5H), 3.86 (quint, $J = 6.6$ Hz, 1H), 3.69 (q, $J = 8.4$ Hz, 1H), 2.86 (s, 3H), 2.80–2.56 (m, 2H), 0.79 (d, $J = 6.6$ Hz, 3H); ^{13}C NMR ($CDCl_3$): $\delta = 173.8$, 138.7, 128.4, 127.7, 126.9, 59.32, 42.3, 34.8, 27.6, 14.4; IR (neat): $\tilde{\nu} = 2968$, 2923, 1683, 1480, 1450, 1396, 1258, 755, 702 cm^{-1}.

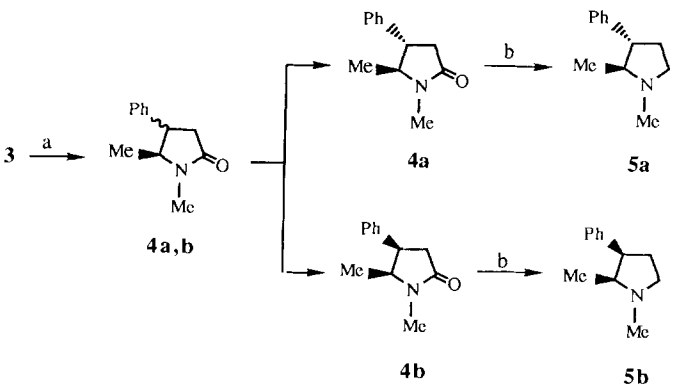
5a: colorless oil; $[\alpha]_D^{25} = -4.4$ ($c = 0.90$ in $CHCl_3$); ^1H NMR ($CDCl_3$): $\delta = 7.25-7.16$ (m, 5H), 3.23 (dt, $J = 9.4$, 2.1 Hz, 1H), 2.80 (dt, $J = 9.9$, 6.9 Hz, 1H), 2.45 (dd, $J = 6.3$, 2.1 Hz, 1H), 2.40–2.29 (m, 1H), 2.33 (s, 3H), 2.14–2.05 (m, 1H), 1.87–1.77 (m, 1H), 1.03 (d, $J = 6.3$ Hz, 3H); ^{13}C NMR ($CDCl_3$): $\delta = 144.2$, 130.1, 128.3, 127.8, 126.2, 69.9, 56.6, 52.8, 40.1, 31.4, 16.5; IR (neat): $\tilde{\nu} = 2961$, 2773, 1498, 1449, 1373, 1167, 754, 700 cm^{-1}.

5b: colorless oil; $[\alpha]_D^{25} = +15.8$ ($c = 0.72$ in $CHCl_3$); ^1H NMR ($CDCl_3$): $\delta = 7.28-7.16$ (m, 5H), 3.29–3.18 (m, 2H); 2.48–2.39 (m, 1H), 2.31 (s, 3H), 2.29–2.18 (m, 2H), 2.08–1.96 (m, 1H), 0.65 (d, $J = 6.6$ Hz, 3H); ^{13}C NMR ($CDCl_3$) $\delta = 143.8$, 138.4, 128.9, 127.8, 125.9, 64.9, 56.5, 48.4, 40.6, 31.2, 15.5.

[a] The NMR spectra were recorded at 300 MHz (^1H) and 75 MHz (^{13}C).

the absolute configurations of the stereoisomers are as shown in Scheme 3.

The analgetic activity of the 3-phenylpyrrolidines, which are analogues of Profadol and the related 3-phenyl-2-substituted pyrrolidines is well documented.[17] They can be prepared by a wide variety of methods, all affording racemates.[18] However, to our knowledge, only a single procedure for the synthesis of the homochiral (−)-*trans*-2-methyl-3-phenylpyrrolidine has been reported, based on the use of a bicyclic lactam, derived from phenylglycinol, as the chiral auxiliary.[19] Starting from enantiomerically pure **4** and **4′**, we obtained (2*S*,3*S*)-(−)- and (2*S*,3*R*)-(+)-1,2-dimethyl-3-phenyl-pyrrolidine (**5a** and **5b**), and (2*R*,3*S*)-(+)- and (2*R*,3*S*)-(−)-1,2-dimethyl-3-phenyl-pyrrolidine (**5a′** and **5b′**), respectively, by reductive cleavage with AlH_3. The absolute configurations of these 2,3-disubstituted pyrrolidines is the same as that of the parent lactams, since



Scheme 3. a) H_2, Pd/C, MeOH, followed by chromatography on silica gel (88%); b) $LiAlH_4/AlCl_3$, THF (93%).

the stereocenters present in the structure are not involved in the reductive process.

In conclusion, the (−)-ephedrine and (+)-ephedrine derivatives (−)- and (+)-6-diazooxazepane-5,7-diones **2** and **2′** can be regarded as convenient homochiral starting materials for the preparation of the four stereoisomeric 4-phenyl-5-methyl-2-pyrrolidinones and the corresponding enantiomerically pure 3-phenyl-2-methyl-pyrrolidines.

Received: July 16, 1994 [Z 7132 IE]
German version: *Angew. Chem.* **1995**, *107*, 104

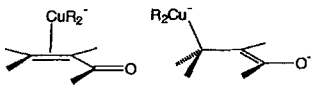
Keywords: carbene reactions · diazo compounds · ephedrine · heterocycles

[1] T. Mukaiyama, T. Takeda, M. Osaki, *Chem. Lett.* **1977**, 1165
[2] T. Mukaiyama, Y. Hirako, T. Takeda, *Chem. Lett.* **1978**, 461.
[3] L. F. Tietze, S. Brand, T. Pfeiffer, J. Antel, K. Harms, G. M. Sheldrick, *J. Am. Chem. Soc.* **1987**, *109*, 921.
[4] T. Mukaiyama, T. Takeda, K. Fujimoto *Bull. Chem. Soc. Jpn.* **1978**, *51*, 3368.
[5] A. Saba, *Synth. Commun.* **1994**, *5*, 695.
[6] M. Regitz, G. Maas, *Diazo Compounds, Properties and Synthesis*, Academic Press, London. **1986**.
[7] Crystal data for **3**: $C_{12}H_{13}NO$, $M_r = 187.24$, orthorhombic, space group $P2_12_12_1$, $a = 11.349(2)$, $b = 13.347(3)$, $c = 6.838(2)$ Å, $V = 1035.8(4)$ Å^3, $Z = 4$, $\rho_{calcd} = 1.201$ g cm^{-3}, $\mu = 6.05$ cm^{-1} ($Cu_{K\alpha}$, $\lambda = 1.54178$ Å). Data were collected at room temperature on a Rigaku AFC6R diffractometer with filtered $Cu_{K\alpha}$ radiation and the ω-2θ scan technique to a maximum 2θ range of 119.3°. 927 reflexions were measured, 420 observed ($I > 3.00\sigma(I)$), $R = 0.057$, $Rw = 0.050$. The structure was solved by direct methods (SHELX-86: G. M. Sheldrick, Institut for Anorganische Chemie der Universitat Gottingen, **1986**), and some non-H atoms were refined anisotropically, while the rest were refined isotropically. Hydrogen atoms were placed in calculated positions and not refined. Further details of the crystal structure investigation may be obtained from the Fachinformationszentrum Karlsruhe, D-76344 Eggenstein-Leopoldshafen (Germany), on quoting the depository number CSD-58 678.
[8] Reviews: H. Meier, P. K. Zeller, *Angew. Chem.* **1975**, *87*, 43; *Angew. Chem. Int. Ed.* **1975**, *14*, 32; T. Ye, A. McKervey, *Chem. Rev.* **1994**, *94*, 1091.
[9] J. T. Carlock, B. Stanovnik, M. Tisler, *Synthesis* **1976**, 754; J. T. Carlock, J. S. Bradshaw, B. Stanovnik, M. Tisler, *J. Org. Chem.* **1977**, *42*, 1883; J. T. Carlock, J. S. Bradshaw, B. Stanovnik, M. Tisler, *J. Heterocycl. Chem.* **1977**, *14*, 519; B. Stanovnik, M. Tisler, E. Voncina, *Heterocycles* **1979**, 761; Y. Tamura, H. Ikeda, C. Mukai, S. M. M. Bayomi, M. Ikeda, *Chem. Pharm. Bull.* **1980**, *28*, 3430.
[10] E. Lee, K. W. Jung, Y. S. Kim, *Tetrahedron Lett.* **1990**, *31*, 1023; J. Adams, M. Poupart, L. Grenier, C. Schaller, N. Onimet, R. Frenette, *Tetrahedron Lett.* **1989**, *30*, 1749.
[11] M. P. Doyle, M. N. Protopopova, W. R. Winchester, L. K. Daniel, *Tetrahedron Lett.* **1992**, *33*, 7819, and references therein.
[12] The formation of the bicyclic intermediate depicted in Scheme 2 was supported by ^1H NMR analysis of the reaction mixture at 50% conversion; so far, all attempts at isolation have failed.
[13] After 60% conversion (20 h, room temperature), the yield decreased and, when the reaction was complete (2 d), a complex mixture of products was obtained.
[14] L. E. Burgess, A. I. Meyers, *J. Am. Chem. Soc.* **1991**, *113*, 9858, and references therein.
[15] Ratio was determined by 300 MHz, ^1H NMR spectroscopy.
[16] R. M. Silverstein, G. C. Bassler, T. C. Morrill, *Spectrometric Identification of Organic Compounds*, Wiley, New York, **1981**, pp. 258–262; R. G. Abraham, J. Fisher, P. Loftus, *Introduction to NMR Spectroscopy*, Wiley, New York, **1988**, pp. 29–33; J. K. Witesell, T. LaCour, R. L. Lowell, J. Pojman, P. Ryan, A. Yamada-Nosaka, *J. Am. Chem. Soc.* **1988**, *110*, 991.
[17] C. V. Winder, M. Wefford, J. Wax, A. H. Kaump, *J. Pharmacol. Exp. Ther.* **1966**, *154*, 161.
[18] J. F. Cavalla, R. A. Selway, J. Wax, L. Scotti, C. W. Winder, *J. Med. Chem.* **1962**, *5*, 441; M. Langlois, J. Maillard, *Bull. Soc. Chim. Fr.* **1971**, 2976, and references therein.
[19] A. I. Meyers, L. Snyder, *J. Org. Chem.* **1992**, *57*, 3814.

Elusiveness of Cu^{III} Complexation; Preference for Trifluoromethyl Oxidation in the Formation of $[Cu^{I}(CF_3)_4]^-$ Salts**

James P. Snyder*

1,4-Addition of organocuprates to α,β-enones is a cornerstone carbon–carbon bond-forming reaction in synthetic chemistry.[1–3] Although the mechanism of delivery of the Cu-bound moiety is not fully understood, the currently ascendent concept postulates the preliminary and reversible formation of a π-olefin complex (**1**),[4–10] transformation to a copper(III) β-adduct (**2**), and collapse to products.[7, 8, 11, 12] Skepticism about the viability of Cu^{III} intermediates has been expressed.[13] In addition, according to recent ab initio calculations using an effective core potential at copper, monoalkylcopper reagents (RCu) may add 1,4 to enones through a six-membered transition state incorporating the carbonyl oxygen atom.[14–16] By implication, copper(III) intermediates are bypassed. In this context the very recent oxidative synthesis and X-ray structure determination of stable, colorless, and presumably diamagnetic salts of the $[Cu(CF_3)_4]^-$ ion (**3**)[17, 18] along with the previously described dithiocarbamate **4**[18] are of singular importance.



1 **2**

Scheme 1.

$[Cat][Cu(CF_3)_4]$ Cat-**3**, Cat = Bu_4N, Ph_4N, $(Ph_3P)_2N$

$[Cu(CF_3)_2SC(S)NEt_2]$ **4**

The anion **3** is nearly square planar in the crystal; the four CF_3 groups are alternately located slightly above and below the mean molecular plane. The substances have been characterized as Cu^{III} salts with a d^8 configuration at the metal. The only other putative copper(III) compound with a perfluoroalkyl substituent (**4**)[18] shares with **3** a distorted square-planar structure and a pair of nearly linear CCuS bonds.

Salts of **3** have been prepared by oxidation of $Cu^{I}CF_3$. Classification of **3** as a Cu^{III} species presupposes that the metal rather than the ligand has relinquished its electrons. Let us presume the opposite, namely that oxidation has resulted in one CF_3^+ moiety in the product along with three CF_3^- units and $Cu^{I}(d^{10})$. Then, to a first approximation, $[Cu(CF_3)_4]^-$ can be considered a normal cuprate $[CF_3\text{-}Cu\text{-}CF_3]^-$ in which the copper is further coordinated to a trifluoromethyl anion and cation. Although the bonding in **3** is highly ionic, the covalent components can be illuminated by a qualitative MO correlation diagram of the ideal square-planar complex (Fig. 1). For simplicity only the Cu–C bonds are considered.

On the left side of Figure 1 four symmetry-adapted molecular orbitals are derived from the sp^3 carbon hybrid orbitals available for bonding from the four trifluoromethyl groups. The bonding and two nonbonding MOs are filled; the fully antibonding orbital is empty. On the right the copper $3d_{x^2-y^2}$ and 4s orbitals are depicted as occupied and virtual, respectively. Interaction of SS_1 orbitals of Cu(4s) and CF_3 results in the fully symmetric MO for **3** delocalized over the metal and the four trifluoromethyl groups. A second bond arises from combination of SS_2 orbitals, the metal $d_{x^2-y^2}$ orbital serving as a lone-pair donor to satisfy the electron deficiency caused by CF_3^+. Nonbonding MOs contain the third and fourth pair of electrons. The MO filling scheme implies that $[Cu(CF_3)_4]^-$ salts are associated covalently by only four bonding electrons. Further refinement of the diagram would include secondary contributions from the copper d orbitals and the fluorine atoms.

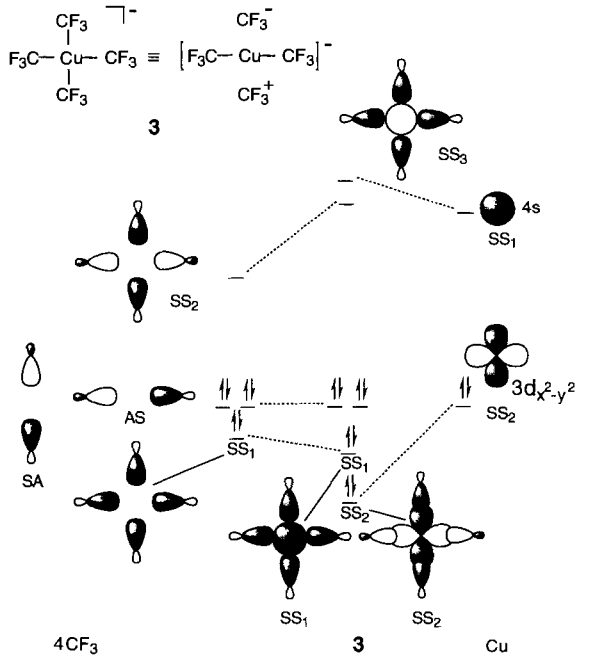


Fig. 1. Idealized MO correlation diagram for the Cu–C bonds of **3**, derived from the symmetry-adapted MOs for four C sp^3 centers (left) and Cu AOs (right). S and A designations refer to the symmetry reflected across, respectively, vertical and horizontal planes orthogonal to the plane of the paper.

In an attempt to verify this picture, calculations have been performed on the experimentally determined geometry of **3** using a 6-31G*(6d) basis set on CF_3, the Hay–Wadt effective core potential (ECP-2)[19] for the ten core electrons of copper, a double-ζ basis set for the remaining metal electrons ((9s5p5d)/[3s4p2d], split (441/2111/41)),[20, 21] and MP2 electron correlation.[22] This prescription has proved to be effective for geometries and energies of both Ti and Cu^{I} complexes.[20, 21, 23] The resulting Hartree–Fock (SCF) and correlated (MP2) wavefunctions were subsequently subjected to a natural population (NPA) and bond orbital (NBO) analysis.[27–30] To test the predicted structure in the present case, anion **3** has been optimized at the SCF level without symmetry constraints. A symmetrical structure with $r(Cu\text{–}C) = 1.967$ Å, $r(C\text{–}F) = 1.338$ and 1.343 Å, $\theta(Cu\text{-}C\text{-}F) = 113.5°$ and $\theta(C\text{-}Cu\text{-}C) = 170.0°$ results in excellent agreement with the X-ray crystal structure (e.g., $r(Cu\text{–}C) = 1.949\text{–}1.983$ Å, $\theta(C\text{-}Cu\text{-}C) = 165.0$ and 172.6°).[17]

At the experimentally determined structure of anion **3**, calculated atomic charges are high (MP2 (SCF): Cu + 0.71 (+1.1), C + 0.74 (+ 0.81), F −0.39 (− 0.44)) and Wiberg Cu–C bond orders moderate (0.29 (0.38)). A considerable degree of ionic character is further reflected by the diminutive 19% contribution of copper to the localized CuC bonding orbitals at the SCF level. It falls away altogether when MP2 correlation is included. According to NPA analysis the copper d orbitals are populated as follows: d_{xy}, d_{xz}, d_{yz}, and d_{z^2} 1.96–1.98, $d_{x^2-y^2}$ 1.77 (1.38)

[*] Prof. Dr. J. P. Snyder
IRBM P. Angeletti
Via Pontina Km 30.600
I-00040 Pomezia, Rome, (Italy)
Telefax: Int. code + (6)91093-654

[**] I am grateful to Dr. Steven Bertz (Lonza Inc.) for stimulating our interest in this problem and to Dr. Gernot Frenking (Marburg) for many helpful discussions on the use of ab initio calculations for treating copper complexes.

electrons. In addition 10.3 (9.88) electrons reside in copper's outer shells: 4s (0.53 (0.49)), 3d (9.7 (9.4)), 4p (0.04 (0.02)), 4d (0.06 (0.02)). A straightforward interpretation of the data is that copper functions as a d-base through the $3d_{x^2-y^2}$ orbital, retrieving lost electronic charge by means of backbonding to the 4s, 4p, and 3d orbitals. The analysis places 3.3 (3.1) and 7.4 (7.5) electrons at carbon and fluorine atoms, respectively. Carbon is thus depleted by +0.7 (+0.9) units of charge, while fluorine gains −0.4 (−0.5). The CF_3 groups carry 25.4 (25.5) electrons, precisely the average of three CF_3^- groups and one CF_3^+ group. Charge neutralization in anion **3** by an ammonium cation to give a contact ion-pair causes no change in the electron distribution.

Attempts were made to force the SCF wavefunction to converge on the Cu^{III} state by switching filled copper d orbitals with the LUMO, the high energy counterpart of **3**'s bonding SS_2 MO in Figure 1. The numerical experiment led to a state with 1.99–2.00 electrons in all d orbitals except d_{xy}, which had 1.1 electrons. The total energy of this state is 250 kcal mol^{-1} above the fully relaxed d_{xy} orbital with 1.97 electrons. This is consistent with the SCF result that the largely localized lone pair Cu d orbitals in **3** are 193–218 kcal mol^{-1} lower in energy than the HOMO. In the naked Cu^I monocation the same orbitals are degenerate and lie at the frontier orbital gap. An empirical argument that might be made against the interpretation of **3** as a Cu^I complex is the appearance of a quasi square-planar structure in the solid state, the common geometry for d^8 metal complexes. Though tetracoordinate d^{10} Cu^I–ligand association ordinarily produces tetrahedral structures, square-planar approximations are not unknown.[31–33]

The picture that emerges for **3** is one in which the bonding between Cu^+ and the average of $(CF_3^-)_3$ and CF_3^+ (i.e. $(CF_3^{-0.5})_4$) is principally ionic. The covalent component derived by the full calculation is in complete accord with Figure 1. Two delocalized five-center, two-electron bonds are accompanied by two nonbonding electron pairs. The description strongly implies that oxidation of $CuCF_3$ has effectively removed electrons from a CF_3 ligand, and the charge depletion is then shared equally by the four trifluoromethyl substituents in product **3**. Furthermore, the electron depletion at CF_3 depicted in Figure 1 suggests CF_3–CF_3 to be an important thermal decomposition product, as has been observed (D. Naumann and T. Roy, private communication). Similar calculations show that analogous concepts apply to **4**.[18]

The apparent willingness of a powerful electronegative moiety such as CF_3^- to undergo oxidation in preference to Cu^I underscores both the importance of the role of ligand in assessing oxidation pathways in metal complexes and the resistance of copper to assume the Cu^{III} state. The principles outlined herein can be expected to apply to the mechanism of cuprate addition as well as to contribute to a deeper understanding of other metals assigned high oxidation states in complexes.

Received: May 13, 1994
Revised: August 4, 1994 [Z6933IE]
German version: *Angew. Chem.* **1995**, *107*, 112

Keywords: ab initio calculations · copper compounds · cuprates · electronic structure

[1] B. E. Rossiter, N. M. Swingle, *Chem. Rev.* **1992**, *92*, 771.
[2] B. H. Lipshutz, S. Sengupta, *Org. React.* **1992**, *41*, 135.
[3] "CuCl": S. H. Bertz, E. H. Fairchild in *Encyclopedia of Reagents for Organic Synthesis* (Ed.: L. Paquette), Wiley, Chichester, in press.
[4] G. Hallnemo, T. Olsson, C. Ullenius, *J. Organomet. Chem.* **1985**, *282*, 133–144.
[5] B. Christenson, T. Olsson, C. Ullenius, *Tetrahedron* **1989**, *45*, 523–534.
[6] S. H. Bertz, R. A. J. Smith, *J. Am. Chem. Soc.* **1989**, *111*, 8276–8277.
[7] E. J. Corey, N. W. Boaz, *Tetrahedron Lett.* **1984**, *25*, (29), 3063–3066.
[8] E. J. Corey, N. W. Boaz, *Tetrahedron Lett.* **1985**, *26*, (49), 6015–6018.
[9] S. Sharma, A. C. Oehlschlager, *Tetrahedron* **1991**, *47*, 1177–1184.
[10] N. Krause, R. Wagner, A. Gerold, *J. Am. Chem. Soc.* **1994**, *116*, 381–382.
[11] S. R. Krauss, S. G. Smith, *J. Am. Chem. Soc.* **1981**, *103*, 141–148.
[12] C. R. Johnson, G. A. Dutra, *J. Am. Chem. Soc.* **1973**, *95*, 7783.
[13] J. P. Collman, L. S. Hegedus, *Principles and Applications of Organotransition Metal Chemistry*, University Science Books, Mill Valley, CA, **1980**.
[14] A. E. Dorigo, K. Morokuma, *J. Am. Chem. Soc.* **1989**, *111*, 4635–4643.
[15] A. E. Dorigo, K. Morokuma, *J. Am. Chem. Soc.* **1989**, *111*, 6524–6536.
[16] H. O. House, W. L. Respess, G. M. Whitesides, *J. Org. Chem.* **1966**, *31*, 3128.
[17] D. Naumann, T. Roy, K.-F. Tebbe, W. Crump, *Angew. Chem.* **1993**, *105*, 1555–1556; *Angew. Chem. Int. Ed. Engl.* **1993**, *32*, 1482–1483. Meanwhile, a superconducting salt with $[Cu(CF_3)_4]^-$ as anion has been reported: J. A. Schleuter, U. Geiser, J. M. Williams, H. H. Wang, W.-K. Kwok, J. A. Fendrich, K. D. Carlson, C. A. Achenbach, J. D. Dudek, D. Naumann, T. Roy, J. E. Schirber, W. R. Bayless, *J. Chem. Soc. Chem. Commun.* **1994**, 1599–1600.
[18] M. A. Willert-Porada, D. J. Burton, N. C. Baenziger, *J. Chem. Soc., Chem. Commun.* **1989**, 1633.
[19] P. J. Hay, W. R. Wadt, *J. Chem. Phys.* **1985**, *82*, 299.
[20] V. Jonas, G. Frenking, M. T. Reetz, *J. Comput. Chem.* **1992**, *13*, (8), 919–934.
[21] M. Böhme, G. Frenking, M. T. Reetz, *Organometallics*, submitted.
[22] M. J. Frisch, G. W. Trucks, M. Head-Gordon, P. M. W. Gill, M. W. Wong, J. B. Foresman, B. G. Johnson, H. B. Schlegel, M. A. Robb, E. S. Replogle, R. Gomperts, J. L. Andres, K. Raghavachari, J. S. Binkley, C. Gonzalez, R. L. Martin, D. J. Fox, D. J. Defrees, J. Baker, J. J. P. Stewart, J. A. Pople, *Gaussian 92*, Revision A ed., Gaussian, Inc., Pittsburg, PA, **1992**.
[23] The ECP-2/MP2 combination used here provides results comparable with all-electron calculations. For Cu–F we find r(Cu–F) = 1.747 Å and μ = 5.21 D. A recent near-Hartree–Fock limit plus MP2 calculation gave 1.786 Å and 6.12 D [24] (vs. experimental values of 1.745 Å and 5.77 D [25]). For Cu–CH_3 we obtain r(Cu–C) = 1.913 Å and μ = 2.29 D. An all-electron triple-ζ optimization with correlation yielded 1.936 Å and 2.41 D, respectively [26].
[24] P. Schwerdtfeger, P. D. W. Boyd, G. A. Bowmaker, L. P. Aldridge, *Struct. Chem.* **1990**, *1*, 405–415.
[25] K. P. Huber, G. Herzberg, *Molecular Spectra and Molecular Structure. Constants of Diatomic Molecules*, Van Nostrand, New York, **1979**.
[26] C. W. Bauschlicher Jr., S. R. Langhoff, H. Partridge, L. A. Barnes, *J. Chem. Phys.* **1989**, *91*, 2399–2411.
[27] A. E. Reed, R. B. Weinstock, F. Weinhold, *J. Chem. Phys.* **1985**, *83*, 735.
[28] A. E. Reed, F. Weinhold, *J. Chem. Phys.* **1985**, *83*, 1736.
[29] A. E. Reed, F. Weinhold, *J. Am. Chem. Soc.* **1986**, *108*, 3586–3593 and references therein.
[30] A. E. Reed, L. A. Curtis, F. Weinhold, *Chem. Rev.* **1988**, *88*, 899.
[31] B. Chiari, U. Piovesana, T. Tarantelli, P. F. Zanazzi, *Inorg. Chem.* **1984**, *23*, 2542–2547.
[32] J. C. Dyason, P. C. Healy, L. M. Engelhardt, C. Pakawatchai, V. A. Patrick, A. H. White, *J. Chem. Soc. Dalton Trans.* **1985**, *4*, 839–844.
[33] M. Hakansson, S. Jagner, M. Nilsson, *J. Organomet. Chem.* **1987**, *336*, 279–285.

1,3,5,7-Tetraphosphabarrelene: A New Cyclic Phosphaalkyne Tetramer**

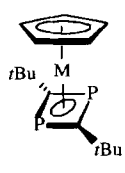
Paul Binger,* Gerald Glaser, Barbara Gabor, and Richard Mynott

The chemistry of phosphaalkynes (RC≡P) has gained considerable momentum through the use of transition-metal templates in cyclooligomerizations.[1] The cyclodimerization of *tert*-butylphosphaacetylene **5** to give the cobalt[2] and rhodium[3] η^4-1,3-diphosphacyclobutadiene complexes **1**, the unexpected formation of the tricyclic zirconium and hafnium complexes **2**

[*] Prof. Dr. P. Binger, Dr. G. Glaser, B. Gabor, Dr. R. Mynott
Max-Planck Institut für Kohlenforschung
Kaiser-Wilhelm-Platz 1, D-45470 Mülheim an der Ruhr (Germany)
Telefax: Int. code + (208)306-2980

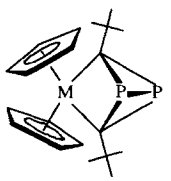
[**] This work was supported by the Volkswagen-Stiftung and the Deutsche Forschungsgemeinschaft (Graduiertenkolleg: phosphorus as a connecting link between different chemical disciplines).

from **5**,[4] and the cyclotrimerization of **5** to yield the 1,3,5-triphosphadewarbenzene complex **3** with vanadium as the central atom[5] are important milestones in an area that is still rapidly developing.



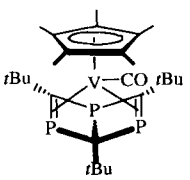
1

M = Co, Rh



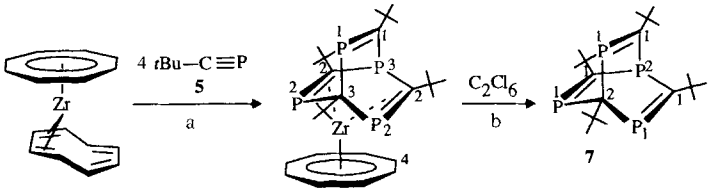
2

M = Zr, Hf



3

Of these metal complexes with heterocyclic ligands, only the zirconium and hafnium compounds **2** have thus far emerged as viable starting materials for the synthesis of novel phosphaheterocycles.[4b, 6] In this context, the remarkable synthesis of a symmetrical tetraphosphacubane from **2** deserves a special mention.[7] We report here the first successful cyclotetramerization of the phosphaalkyne **5** with the bis(cyclooctatetraene)–zirconium complex **4** to yield the η^4-1,3,5,7-tetraphosphabarrelene–zirconium complex **6** and the reaction of **6** with hexachloroethane to liberate the 1,3,5,7-tetraphosphabarrelene derivative **7**, a novel, cyclic tetramer of phosphaalkyne **5** (Scheme 1).



4 **6** **7**

Scheme 1. a: toluene, 2 d, 70 °C, −cot; b: pentane, 12 h, −78–20 °C, $-C_2Cl_4$, $-[(cot)ZrCl_2]$

The zirconium complex **6** was obtained as a dark green, microcrystalline solid in 81% yield after prolonged heating of **4**[8] with excess *tert*-butylphosphaacetylene **5** at 70 °C. Although we have not yet been able to grow crystals suitable for a crystal structure analysis, the structure of **6** could nevertheless be established unambiguously through spectroscopic methods (mass spectrometry; ^1H, ^{13}C, and ^{31}P NMR spectroscopy).

The mass spectrum of **6** exhibits a molecular ion peak at *m/z* 594 and a base peak at *m/z* 400 corresponding to a tetramer of **5** (Table 1). This was the first significant clue that complex **6** contained a tetramer of **5** that could be cleaved from **6** as a stable compound. In the ^{31}P NMR spectrum of **6**, three signals are observed for the four phosphorus atoms, in a ratio of 1:2:1 at $\delta = 285.3$, -113.4, and -137.6; these are assigned to the phosphorus atoms 1, 2, and 3, respectively (for the atomic numbering, see the structure formula for **6**). As a result of the very similar coupling constants ($J(P1,P2) = 8.8$, $J(P1,P3) = 7.8$ Hz), the signal for the P1 atom appears as a pseudoquartet, whereas a doublet of doublets ($J(P2,P3) = 16$ Hz) is observed for the P2 center, and a triplet of doublets for P3.

As anticipated, the ^1H NMR spectrum of **6** features three singlets for the *tert*-butyl groups in the expected region and in a ratio of 2:1:1; the protons of the η^8-bound cyclooctatetraene ligand (cot) are assigned to a singlet at $\delta = 6.89$. The ^{13}C NMR spectrum completes the structure determination for the η^4-bound 1,3,5,7-tetraphosphabarrelene in complex **6**: The four carbon atoms of the bicyclic system (C1–C3) give rise to three groups of signals. The sp^3 C atom (C3) resonates at highest field ($\delta = 37.7$). The coupling constants to the four P atoms are $J(C3,P1) = 84$ Hz (d), $J(C3,P2) = 69.6$ Hz (t), and $J(C3,P3) = 2.6$ Hz (d). As expected, the largest downfield shift to $\delta = 219.8$ is observed for the signal arising from the uncomplexed P=C bond (C1), which is split into a doublet of doublets of triplets (see Table 1). The C atoms of the π-coordinated P=C bonds (C2) give rise to a multiplet at $\delta = 76.7$, which corresponds to the X component of an ABMX system (A, B, M = ^{31}P; X = ^{13}C; $J(P1,C2)$ not detectable). A simulation of the multiplet generates a value of 56.8 Hz for $J(P2_A,P2_B)$ (for $J(C,P)$, see Table 1). The large upfield shift relative to the P=C signal in free tetraphosphabarrelene supports the presence of a strong interaction with the zirconium atom.

The η^4-bound tetraphosphabarrelene could be removed from complex **6** with the help of hexachloroethane. After the reaction mixture had been stirred for 12 h at 20 °C, **7** was obtained as a yellow microcrystalline solid in 88% yield. Compound **7** was found to be sensitive to oxidation, but surprisingly thermally stable: for example, it sublimes unchanged in vacuo above approximately 250 °C. In the absence of crystals suitable for a crystal structure analysis, the structure of **7** was determined spectroscopically. Both a correct elemental analysis and the molecular mass of 400 obtained by mass spectrometry confirm that **7** is a tetramer of **5**. Because of the symmetry of the molecule, the ^{31}P NMR spectrum shows only two sets of signals for the four P atoms in an intensity ratio of 3:1. The doublet at $\delta = 324.1$ ($J(P,P) = 13.0$ Hz) is assigned to the three equivalent phosphorus atoms of the P=C bonds, whilst the quartet at $\delta = -87.0$ corresponds to the triply coordinated P2 atom (see Table 1). Both signals lie in the expected region. The ^1H NMR spectrum of **7** contains equally few signals: two singlets are found at $\delta = 1.52$ and 2.01 in a ratio of 3:1, corresponding to the

Table 1. Selected physical data for **6** and **7** [a,b].

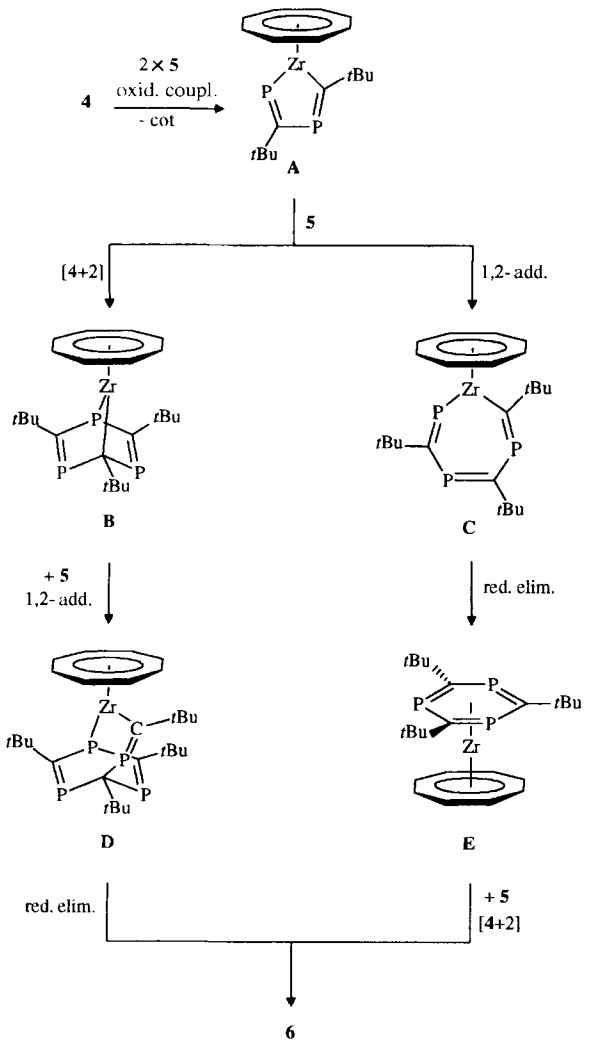
6: ^1H NMR [c]: $\delta = 1.08$ (s, 18H, *t*Bu at C-2), 1.23 (s, 9H, *t*Bu at C-3) 1.29 (s, 9H, *t*Bu at C-1), 6.89 (s, 8H, cot); ^{13}C NMR: $\delta = 37.72$ ($J_{(C,P1)} = 84.0$, $J_{(C,P2)} = 69.6$, $J_{(C,P3)} = 2.6$ Hz, C-3), 37.70 ($J_{(C,P1)} = 21.0$, $J_{(C,P2)} = 12.4$, $J_{(C,P3)} = 2.8$ Hz, $C(CH_3)_3$ at C-3), 31.3 ($^1J_{(C,H)} = 125$, $J_{(C,P1)} = 12.0$, $J_{(C,P2)} = 6.9$ Hz, $C(CH_3)_3$ at C-3), 76.7 (X component of a ABMX spin system [d]; $^1J_{(P2_A,C)} = 97.0$, $^3J(P2_B,C) = 3.7$, $J_{(C,P3)} = 42.8$ Hz, C-2), 38.0 ($J_{(C,P2_A)} + J_{(C,P2_B)} = 22.4$, $J_{(C,P3)} = 14.3$ Hz, $C(CH_3)_3$ at C-2), 35.9 ($^1J_{(C,H)} = 125$, $J_{(C,P2_A)} + J_{(C,P2_B)} = 10.0$, $J_{(C,P3)} = 10.1$ Hz, $C(CH_3)$ at C-2), 219.8 ($J_{(C,P1)} = 97.6$, $J_{(C,P2)} = 5.6$, $J_{(C,P3)} = 58.6$ Hz, C-1), 43.6 ($J_{(C,P1)}$, $J_{(C,P3)} = 22.7$, 25.2 Hz, $C(CH_3)_3$ at C-1), 35.7 ($^1J_{(C,H)} = 125$, $J_{(C,P1)}$, $J_{(C,P3)} = 14.8$, 9.1 Hz, $C(CH_3)_3$ at C-1), 97.2 ($^1J_{(C,H)} = 168$ Hz, C-4); ^{31}P NMR: $\delta = 285.3$ ($J_{(P1,P2)} = 8.8$, $J_{(P1,P3)} = 7.8$ Hz, P-1), -113.4 ($J_{(P1,P2)} = 8.8$, $J_{(P2,P3)} = 16.0$ Hz, P-2), -137.6 ($J_{(P1,P3)} = 7.8$, $J_{(P2,P3)} = 16.0$ Hz, P-3); MS (70 eV): *m/z* [%]: 594 (M^+) [16], 537 ($M^+ - t$Bu) [19], 463 ($M^+ - t$BuC≡P − P) [16], 425 ($M^+ - t$BuC≡P − *t*BuC) [21], 400 (M^+ − cotZr) [100], 300 ((*t*BuP≡C)$_3^+$) [10], 262 ((*t*BuC≡P)$_4^+ - t$Bu$_2$C$_2$) [92], 169 [83]

7: ^1H NMR: $\delta = 2.01$ (s, 9H, *t*Bu), 1.52 (s, 27H, *t*Bu); ^{13}C NMR: $\delta = 229.6$ (X component of a AB_2MX spin system [d]; $^1J(C,P1_A) = \pm 55.8$, $^3J(C,P1_B) = \pm 4.9$, $^1J(C,P2) = 45.8$ Hz, C-1), 43.7 (m, $C(CH_3)_3$ at C-1), 32.7 (m, $C(CH_3)_3$ at C-1), 102.7 (dq, $J_{(C,P1)} = 70.8$, $J_{(C,P2)} = 7.5$ Hz, C-2), 38.0 (q, $J_{(C,P1)} = 16.1$ Hz, $C(CH_3)_3$ at C-2), 32.7 (m, $C(CH_3)_3$ at C-2); ^{31}P NMR: $\delta = 324.1$ (d, $J_{(P,P)} = 13.0$ Hz), −87.0 (q, $J_{(P,P)} = 13.0$ Hz); MS (70 eV): *m/z* (%): 400 (M)$^+$ [41], 300 (M − P≡C*t*Bu)$^+$ [6], 262 ($M - C_2t$Bu$_2$)$^+$ [100], 200 ($P_2C_2(t$Bu)$_2$)$^+$ [14], 169 [73]

[a] ^1H (300 MHz, TMS), ^{13}C (75.5 MHz, TMS), ^{31}P NMR spectra (121.5 MHz, 85% H_3PO_4); **6** in [D$_8$]THF; **7** in C_6D_6; MS: Varian-CH5. [b] For numbering of the C and P atoms, see structural formulae of **6** and **7**. [c] Assignments by $^{31}P-^1H$ and $^{13}C-^1H$ correlation. [d] From simulation of the multiplets. The chemical shifts of **A** and **B** are different owing to ^{13}C isotope effects.

two distinct *tert*-butyl groups bound to C1 and C2 (see structural formula of **7** for atomic numbering). In agreement with our proposed structure, only two sets of signals are observed in the ^{13}C NMR spectrum of **7** for the four carbon atoms of the bicyclic structure: a multiplet at $\delta = 229.6$ for the three sp^2 carbon atoms (C1) and a quartet of doublets at $\delta = 102.7$ (J(C,P1) = 70.8, J(C,P2) = 7.5 Hz) for the sp^3 carbon atom (C2). The multiplet assigned to C1 is the X component of an AB_2MX spin system (A, B, M = ^{31}P; X = ^{13}C), which was likewise simulated. The chemical shifts of the *tert*-butyl signals (see Table 1) require no further explanation. Thus, the structure of **7** corresponds to that of 1,3,5,7-tetraphosphabarrelene (1,3,5,7-tetraphosphabicyclo[2.2.2]octatriene).

With the synthesis of tetraphosphabarrelene complex **6**, it has for the first time been possible to cyclotetramerize four phosphaalkyne units at a metal center. The previously known phosphaalkyne tetramers, such as, tetraphosphacubane[7] or tetraphosphatricyclooctadiene,[9] were accessed through the cycloaddition reactions of 1,3- or 1,2-diphosphets, which were in turn liberated from the corresponding metal–phosphaalkyne dimer complex (e.g., **2**). The uniformity with which the cyclotetramerization of **5** proceeds is remarkable. Comparable cyclotetramerizations of alkynes at transition-metal centers to yield barrelenes are not known, although certain metal complexes do catalyze the cyclotetramerization of alkynes to cyclooctatetraene.[10]



The question as to the pathway of this unusual tetramerization of **5** cannot be answered conclusively. A stepwise process seems plausible, with an oxidative coupling of two phosphaalkyne molecules to give the 2-zircona-1,4-diphosphacyclopentadiene **A** as the initial step. This might be followed either by a 1,2-addition of **5** to give **C** or by a [4 + 2] cycloaddition of **5** to **A** to yield **B**. Complex **6** would then be formed by a 1,2-addition of a fourth molecule of **5** to intermediate **B** and reductive elimination from **D**, or alternatively by a [4 + 2] cycloaddition of **5** to the 1,3,5-triphosphabenzene complex **E**.

Experimental Procedure

6: A solution of **4** (0.92 g, 3.1 mmol) and **5** (1.3 g, 13 mmol) in toluene (60 mL) was heated for 2 d at 70 °C. A change in color from dark violet to dark green was observed. After removal of solvent, the residue was taken up in ether (40 mL). Small amounts of insoluble material were removed by filtration through a D3 frit, and the clear solution was kept at −78 °C. After 2 d, **6** was filtered off as a dark green microcrystalline solid. Yield: 1.50 g (81%); m.p. 175 °C (decomp.).

7 from **6**: Hexachloroethane (0.47 g, 2 mmol) was added to a suspension of **6** (1.0 g, 1.68 mmol) in pentane (50 mL) at −78 °C. The mixture was allowed to warm to room temperature and was then stirred for 12 h. Insoluble [(cot)$ZrCl_2$] and excess C_2Cl_6 were filtered off, and solvent was removed from the filtrate at 0.5 mbar. The yellow-red solid residue was dissolved in ether (5 mL) and cooled to −78 °C. After 3 d, a microcrystalline yellow precipitate was filtered off and dried at 10^{-3} mbar. Yield: 538 mg (88%); m.p. 93 °C.

Received: 25 August, 1994 [Z 7265IE]
German version: *Angew. Chem.* **1995**, *107*, 114

Keywords: cyclizations oligomerizations · phosphaalkynes · tetraphosphabarrelene · zirconium compounds

[1] Reviews: a) J. F. Nixon, *Chem. Rev.* **1988**, *88*, 1327–1362; b) M. Regitz, P. Binger, *Angew. Chem.* **1988**, *100*, 1541–1565; *Angew. Chem. Int. Ed. Engl.* **1988**, *27*, 1484–1508; c) P. Binger in *Multiple Bonds and Low Coordination in Phosphorus Chemistry* (Eds.: M. Regitz, O. J. Scherer), 1st ed., Thieme, Stuttgart, **1990**, pp. 90–111; d) M. Regitz in *Organic Synthesis via Organometallics* (OSM 4, Aachen) (Eds.: D. Enders, H.-J. Gais, W. Keim), Vieweg, Wiesbaden, **1993**, pp. 93–113; e) latest publication: V. Caliman, P. B. Hitchcock, J. F. Nixon, M. Hofmann, P. von R. Schleyer, *Angew. Chem.* **1994**, *106*, 2284–2286; *Angew. Chem. Int. Ed. Engl.* **1994**, *33*, 2202–2204.

[2] a) P. Binger, R. Milczarek, R. Mynott, M. Regitz, W. Rösch, *Angew. Chem.* **1986**, *98*, 645–646; *Angew. Chem. Int. Ed. Engl.* **1986**, *25*, 644–645; b) P. Binger, R. Milczarek, R. Mynott, C. Krüger, Y.-H. Tsay, E. Raabe, M. Regitz, *Chem. Ber.* **1988**, *121*, 637–645.

[3] a) P. B. Hitchcock, M. J. Maah, J. F. Nixon, *J. Chem. Soc. Chem. Commun.* **1986**, 737–738; b) P. Binger, B. Biedenbach, R. Mynott, C. Krüger, P. Betz, M. Regitz, *Angew. Chem.* **1988**, *100*, 1219–1221; *Angew. Chem. Int. Ed. Engl.* **1988**, *27*, 1158–1160.

[4] a) P. Binger, B. Biedenbach, C. Krüger, M. Regitz, *Angew. Chem.* **1987**, *99*, 798–799; *Angew. Chem. Int. Ed. Engl.* **1987**, *26*, 764–765; b) S. Barth, Dissertation, Universität Kaiserslauten, **1993**.

[5] R. Milczarek, W. Rüsseler, P. Binger, K. Jonas, K. Angermund, C. Krüger, M. Regitz, *Angew. Chem.* **1987**, *99*, 957–958; *Angew. Chem. Int. Ed. Engl.* **1987**, *26*, 908–909.

[6] P. Binger, T. Wettling, R. Schneider, F. Zurmühlen, U. Bergsträsser, J. Hoffmann, G. Maas, M. Regitz, *Angew. Chem.* **1991**, *103*, 208–211; *Angew. Chem. Int. Ed. Engl.* **1991**, *30*, 207–210.

[7] T. Wettling, B. Geißler, R. Schneider, S. Barth, P. Binger, M. Regitz, *Angew. Chem.* **1992**, *104*, 761–762; *Angew. Chem. Int. Ed. Engl.* **1992**, *31*, 758–759.

[8] H.-J. Kablitz, G. Wilke, *J. Organomet. Chem.* **1973**, *51*, 241–271.

[9] B. Geißler, S. Barth, U. Bergsträßer, M. Slany, J. Durkin, P. B. Hitchcock, M. Hofmann, P. Binger, J. F. Nixon, P. von R. Schleyer, M. Regitz, *Angew. Chem.* in press.

[10] a) W. Reppe, O. Schlichting, K. Klager, T. Toepel, *Justus Liebigs Ann. Chem.* **1948**, *560*, 1–92; b) review: N. E. Schore, *Chem. Rev.* **1988**, *88*, 1081–1119.

 © VCH Verlagsgesellschaft mbH, D-69451 Weinheim, 1995 0570-0833/95/0101-0083 $ 10.00+.25/0

Oligomethylene-Bridged Vitamin B_{12} Dimers**

Bernhard Kräutler,* Tomas Dérer, Pingli Liu, Walter Mühlecker, Michael Puchberger, Karl Gruber, and Christoph Kratky*

Dedicated to Professor Karl Schlögl on the occasion of his 70th birthday

Organometallic vitamin B_{12} derivatives such as coenzyme B_{12} and methylcobalamin are cofactors of considerable biological importance either as "reversible sources of an alkyl radical"[1] or as intermediates in methyl group transfer reactions.[2] Owing to their stability in protic environment, organometallic B_{12} derivatives also hold a large potential for preparative radical reactions.[3] We report here on oligomethylene-bridged B_{12} dimers such as the tetramethylene-1,4-di-Co_β-cobalamin **D4**,[4] organometallic B_{12} derivatives of a novel structural type. Such binuclear B_{12} derivatives, which contain two thermally and photochemically labile organometallic bonds, may be considered "latent alkanediyl diradicals".[5]

In methanolic solution and under inert atmosphere 0.5 mole equivalents of 1,4-dibromobutane were added to electrochemically produced Co^I cobalamin. The color of the reaction mixture changed rapidly from green to red, indicating the alkylation of cobalt. Upon aqueous workup under exclusion of light, dark red, prismatic crystals of chromatographically uniform dimer **D4** were obtained (60% yield).

In contrast and as expected, the addition of 1,4-dibromobutane in about a hundredfold excess and under inert atmosphere to electrochemically produced Co^I cobalamin led to the almost exclusive formation of monomeric Co_β-4-bromobutylcobalamin **M4**. After crystallization, **M4** was isolated in about 80% yield.[6] Use of homologous 1,5-dibromopentane and 1,6-dibromohexane, but not of 1,3-dibromopropane,[7] resulted in analogous organometallic B_{12} dimers (**D5** in 75% yield, **D6** in 78% yield).

Characteristic UV/Vis and CD spectra of the dimers **D4**–**D6** as well as of the monomer **M4** indicated the presence of organometallic B_{12} derivatives with only weak interactions between the chromophores of the dimer moieties. In the FAB mass spectra (besides signals of fragments) the diagnostic signals of the respective molecule ions were observed (in the case of **D4** at $m/z = 2714$).

Owing to the effective C_2 symmetry of the dimers **D4**–**D6**, the number of signals of chemically inequivalent protons in the ^1H NMR spectra was reduced (Fig. 1). The NMR spectroscopic analysis of dimer **D4** by means of homonuclear (DQF-COSY and ROESY) and heteronuclear correlations (HMQC and HMBC spectra)[8] allowed complete assignment of the ^1H and ^{13}C signals; for example, the signals at high field were attributed to the protons of the cobalt-bound alkanediyl chain (four broad signals at $\delta = -0.50$ [H_a(A2)], -0.04 [H_b(A2)], 0.20 [H_a(A1)], and 0.97 [H_b(A1)]). The observation of NOE effects between groups bonded on the *endo* side of the hydrocarbon-bridged cobalamin halves of **D4** (for example, between the singlet at $\delta = 1.23$ [CH_3(17B)] and the signals at $\delta = 2.56$ [s, $CH_3(5^1)$] and $\delta = 1.85/2.20$ [AB system, $CH_2(7^1)$]), indicated spatial prox-

M3 : $n = 3$
M4 : $n = 4$
M5 : $n = 5$
M6 : $n = 6$

D4 : $n = 4$
D5 : $n = 5$
D6 : $n = 6$

D4

[*] Prof. Dr. B. Kräutler, Dipl.-Ing. T. Dérer, Dr. M. Puchberger, Mag. W. Mühlecker
Institut für Organische Chemie der Universität
Innrain 52a, A-6020 Innsbruck (Austria)
Telefax: Int. code + (512) 507-2892
Prof. Dr. C. Kratky, Mag. K. Gruber
Institut für Physikalische Chemie der Universität
Heinrichstrasse 28, A-8010 Graz (Austria)
Telefax: Int. code + (316) 322248
Dr. P. Liu
Département de Chimie Organique, Université de Genève, (Switzerland)

[**] We would like to thank Dr. E. Hoffmann (Varian, Darmstadt, Germany) and Dr. D. Moskau (Bruker-Spektrospin, Fällanden, Switzerland) for measuring the 500 MHz ^1H NMR spectra, Dr. W. Amrein and R. Häfliger (ETH, Zürich) for the FAB mass spectra, and H. Hediger and R. Dohner (ETH, Zürich) for recording the CD spectra. This work was supported financially by the Swiss National Science Foundation (Proj.-Nr. 20.29850.90) and by the Austrian National Science Foundation FWF (Proj.-Nr. P-9334 and P-9542). – FAB = fast atom bombardment, CD = circular dichroism, NOE = nuclear Overhauser enhancement, NOBA = *ortho*-nitrobenzyl alcohol.

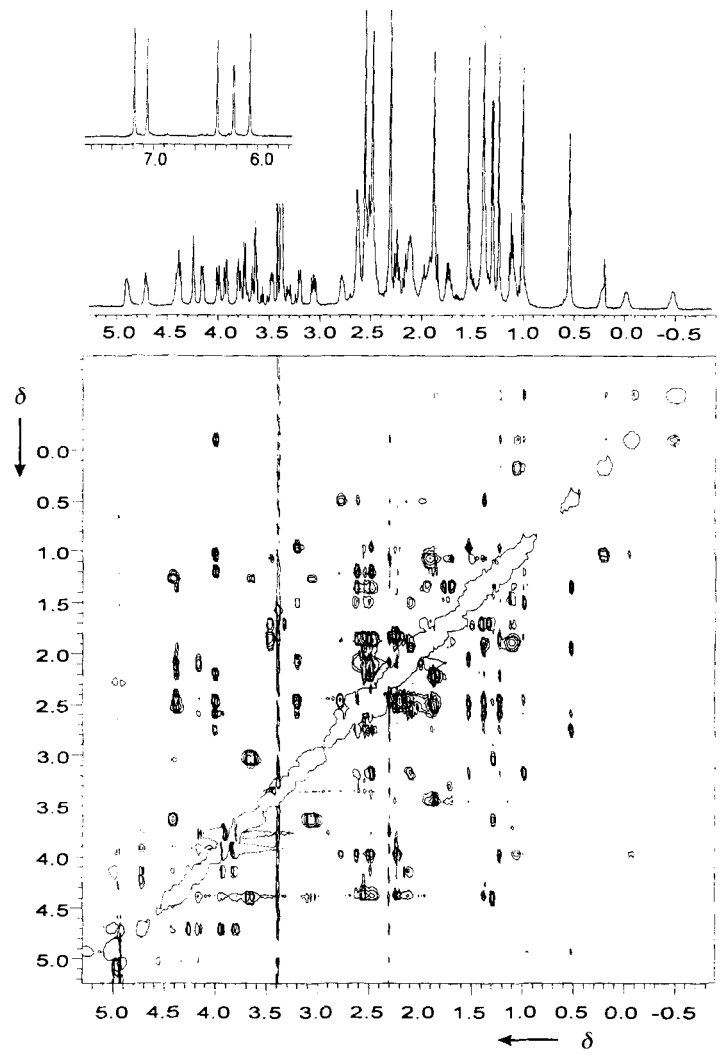


Fig. 1. Top: 500 MHz ^{1}H NMR spectrum of **D4** in CD_3OD; bottom: ROESY spectrum of **D4** in CD_3OD (see text and Table 1 for further details).

imity of these groups in **D4** (Fig. 1, bottom) due to the tetramethylene bridge.

The X-ray analysis of a single crystal of **D4** confirmed the spectroscopically deduced constitution and configuration of this dimer, as well as its effective C_2-symmetric conformation (Fig. 2).[9] The structure of the cobalamin moieties of **D4** is similar to that of monomeric, organometallic B_{12} derivatives. The ligand planes of the two cobalamin halves of **D4** are almost parallel (tilt of 2.3°). The corrin ligands form a torsional angle of about 27° with respect to the cobalt–cobalt axis, which is close to perpendicular with respect to the ligand planes. This arrangement results in a rather tight packing of the two substituted corrin units without any noticeable buildup of strain on the *endo* side. Indeed, the folding[10a] of the corrin ligands in **D4** amounts to 16.5° and is practically identical to that of methylcobalamin.[10b]

The tetramethylene chain that bridges the two cobalt centers at a distance of 6.95 Å is shielded laterally by the corrin substituents located on the *endo* side. The tetramethylene chain occurs in a close-to-staggered conformation. The two terminal C–Co bonds are both 2.00 Å long and positioned antiperiplanar with respect to the central C(A2)–C(A2′) bond. The torsion angle with respect to the latter bond amounts to 50(2)°, such that in this open-chain system an unusual synclinal conformation is observed.

Table 1. Selected spectroscopic data for **D4**, **D5**, **D6**, and **M4** [a].

D4: red crystals. UV/Vis: λ_{max}(lgε) = 264 (4.60), 279 (4.53), 289 (4.50), 310s (4.36), 318 (4.38), 373s (4.21), 450s (3.81), 514 (4.13); CD: $\lambda(\Delta\varepsilon)$ = 252 (−5.76), 270 (19.5), 298 (9.67), 329 (−8.23), 355 (−18.10), 388 (13.60), 435 (−11.10), 496 (17.90), 557 (−17.50); λ_0: 259, 316, 373, 405, 457, 524; ^{1}H NMR: δ = −0.50 (m, 2H), −0.04 (m, 2H), 0.20 (m, 2H), 0.53 (s, 6H), 0.97 (m, 2H), 1.00 (s, 6H), 1.10 (m, 4H), 1.23 (s, 6H), 1.29 (d, 6H), 1.38 (s + m, 8H), 1.53 (s, 6H), 1.73 (m, 2H), 1.8–2.0 (m, 6H) und 1.88 (s, 6H), 2.0–2.2 (m, 8H), 2.24 (m, 4H), 2.30 (s, 12H), 2.35–2.6 (m, 4H), 2.49 (s, 6H) und 2.56 (s, 6H), 2.63 (m, 4H), 2.80 (m, 2H), 3.07 (dd, 2H), 3.21 (d, 2H), 3.49 (m, 2H), 3.60–3.80 (m, 8H), 3.94 (d, 2H), 4.0 (d, 2H), 4.17 (m, 2H), 4.26 (m, 2H), 4.3–4.5 (m, 4H), 4.73 (m, 2H), 6.08 (s, 2H), 6.23 (d, 2H), 6.39 (s, 2H), 7.06 (s, 2H), 7.20 (s, 2H); ^{13}C NMR: δ: 16.6 (2q), 18.4 (q), 18.6 (q), 19.9 (q), 20.1 (q), 20.3 (q), 20.6 (q), 20.9 (q), 22.2 (q), 27.4 (t), 27.6 (t), 28.7 (t), 29.1 (t), 32.4 (t), 32.9 (t), 33.0 (q), 33.3 (t), 33.4 (t), 33.6 (t), 35.5 (t), 36.7 (t), 40.6 (d), 44.3 (t), 45.1 (t), 46.4 (t), 47.9 (s), 48.0 (s), 52.0 (s), 54.3 (d), 57.0 (d), 57.5 (d), 59.0 (s), 62.9 (t), 71.1 (d), 73.4 (d), 75.0 (d), 75.9 (d), 83.4 (d), 87.0 (s), 87.5 (d), 95.5 (d), 105 (s), 108 (s), 112 (d), 120 (d), 133 (2s), 135 (s), 141 (s), 143 (d), 164 (s), 165 (s), 171 (s); 175 (s), 177 (2s); FAB-MS: *m/z* (%): 2716.5(12), 2715.8(29), 2714.0(25), 2657.9(5), 1330.3(100) [$C_{128}H_{184}Co_2N_{26}O_{28}P_2$: *m/z* = 2713.19].

D5: red crystals. UV/Vis: λ_{max}(lgε) = 240 (4.65), 265 (4.59), 310s (4.39), 318 (4.40), 343 (4.34), 370s (4.22), 450s (3.83), 514 (4.16); CD: $\lambda(\Delta\varepsilon)$ = 258 (−16.0), 272 (8.5), 287 (3.5), 298 (12.5), 330 (−6.5), 358 (−16.0), 387 (16.0), 438 (−9.5), 498 (12.5), 554 (−18.0); FAB-MS: *m/z* (%): 2729.5 (8.1), 2728.5 (8.5), 2727.5 (3.7), 2658.6 (3.6), 1330.3 (100) [$C_{129}H_{186}Co_2N_{26}O_{28}P_2$: *m/z* = 2727.203].

D6: red crystals. UV/Vis: λ_{max}(lgε) = 266 (4.56), 279 (4.51), 289 (4.49), 310s (4.40), 315 (4.41), 344 (4.34), 370s (4.21), 450s (3.85), 511 (4.17); CD: $\lambda(\Delta\varepsilon)$ = 256 (−11.7), 298 (10.1), 329 (−6.1), 358 (−14.4), 388 (14.4), 438 (−11.4), 496 (15.5), 555 (−16.8); FAB-MS: *m/z* (%): 2744.5 (8.7), 2743.5 (6.3), 2741.5 (6.4), 2658.6 (1.7), 1330.3 (100) [$C_{130}H_{188}Co_2N_{26}O_{28}P_2$: *m/z* = 2741.22].

M4: red crystals. UV/Vis: λ_{max}(lgε) = 266 (4.21), 280 (4.16), 289 (4.14), 309 (4.06), 316 (4.06), 343 (3.99), 372s (3.88), 450s (3.53), 512 (3.83); CD: $\lambda(\Delta\varepsilon)$ = 256 (−8.2), 273 (2.3), 297 (4.6), 327 (−2.9), 358 (−6.9), 387 (5.7), 438 (−5.2), 496 (9.2), 558 (−5.0); FAB MS: *m/z* (%): 1466.2(32), 1465.2(28), 1329.3(100) [$C_{66}H_{96}{}^{79}Br$-$CoN_{13}O_{14}P$: *m/z* = 1463.54].

[a]: UV/VIS: ca. 5×10^{-5} M in H_2O: KONTRON-UVIKON860; CD spectra: ca. 5×10^{-5} M in H_2O: JOBIN-YVON Dichrograph, MarkIII; NMR in CD_3OD, ca. 26°C: Varian UNITYplus (500 MHz); ^{1}H: $\delta(CD_2HOD)$ = 3.35; ^{13}C: $\delta(CD_3OD)$ = 49.0; FAB-MS: ZAB-2SEQ (NOBA matrix).

Exploratory thermolytic investigations provided no hint of possible strain that might accelerate the decomposition of **D4**. This dimer decomposed five and eight times slower than its homologues **D5** and **D6**, respectively,[11] when heated at 110°C in oxygen-free ethylene glycol solution. Under these conditions the dimers **D5** and **D6** decomposed into Co^{II} cobalamin (UV/Vis) and cyclopentane or cyclohexane, respectively (^{1}H NMR). Photolysis of **D5** (oxygen-free aqueous solution, room temperature) also led to cyclopentane (^{1}H NMR, GC/MS) and Co^{II} cobalamin (UV/Vis).[12] Formation of cycloalkanes from the penta- and hexamethylene bridges of **D5** and **D6**, respectively, most probably proceeds by a yet-undocumented, but thermodynamically favorable route leading to the formation of a C–C bond by homolytic substitution: It results from the attack of an alkyl radical at the saturated carbon center of the metal-bonded alkyl ligand and occurs with simultaneous loss of a Co^{II} corrin.

Dinuclear hydrocarbon-bridged complexes often display unusual reactivities.[5, 13] The bridging tetramethylene ligand of the dimer **D4** appears to be conformationally strained as a result of its constitution and of intramolecular packing effects. In **D4** a remarkable situation therefore exists that may model possible mechanisms of enzyme activation.[1, 14]

Oligomethylene-bridged B_{12} dimers such as **D5** and **D6** may also allow the study of the formation of C–C bonds by reactions between alkyl radical and saturated organometallic functions, a subject that appears to be of interest from mechanistic and biological points of view.[15] Under mild conditions and in aqueous media **D5** and **D6** provide easy access to an extraordinary range of radical chemistry. Indeed, homolysis of the two C–Co bonds of such dimers can be initiated thermally and with

 © VCH Verlagsgesellschaft mbH, D-69451 Weinheim, 1995 0570-0833/95/0101-0085 $ 10.00+.25/0

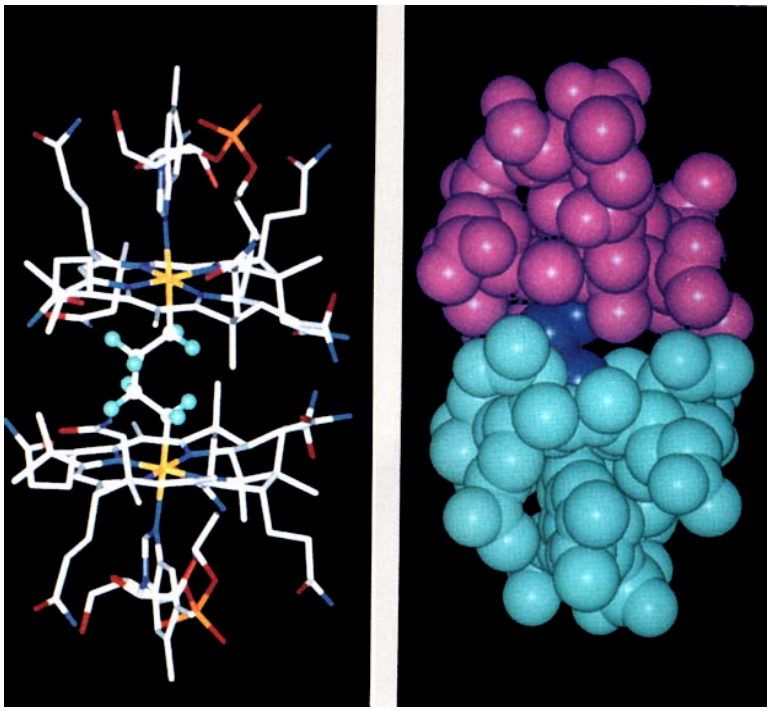


Fig. 2. Crystal structure of the dimer **D4** [9]. Left: ball-and-stick model; right: space-filling model.

visible light, and (formally) releases two organic radical centers. Depending on the sequence of homolysis events (either stepwise or synchronous), the oligomethylene bridge leads either to an (intermediate) organometallic alkyl radical or to a (1,ω)-alkyl diradical.

Experimental Procedure

D4: Under inert gas (glovebox, <10 ppm O_2), aquocobalamin chloride (100 mg, 7.23×10^{-5} mol; Roussel Uclaf apyrogene) was dissolved in 4 mL of a 0.1 M solution of tetrabutylammonium hexafluorophosphate in methanol and reduced with stirring at a mercury cathode (-1.1 V versus 0.1 V calomel electrode; residual current: approximately 0.05 mA). The solution then contained Co^I cobalamin (UV/Vis). It was protected from light and 1,4-dibromobutane (4.3 µL, 0.5 mol equiv) was added. The reaction mixture was reduced further at -1.0 V (total consumption: 16.5 C versus 14.0 C in theory). Under protection from light, the solution was added to 20 mL of distilled water and extracted with three portions of 20 mL of methylene chloride. The dark red, aqueous phase was then concentrated. Dimer **D4** crystallized at 0–5 °C from concentrated, aqueous solutions to give 58.5 mg of **D4** (60% yield).

D5 was prepared in analogy to **D4** with 0.5 equivalents of 1,5-dibromopentane. Crystallization from water/acetone yielded 74 mg (75.5%) of **D5**.

D6 was prepared in analogy to **D4** with 0.5 equivalents of 1,6-dibromohexane. Crystallization from water/acetone yielded 78 mg (78.5%) of **D6**.

M4 was prepared in analogy to **D4**, except for the addition of 100 equivalents of 1,4-dibromobutane at the beginning of the electrochemical reduction at -1.0 V. The yield of **M4** obtained from water/acetone was 83.5 mg (79%).

Received: July 21, 1994 [Z 7152 IE]
German version: *Angew. Chem.* **1995**, *107*, 66

Keywords: alkanediyl-bridged complexes · cobalt compounds · vitamin B_{12}

[1] a) J. Halpern, *Science* **1985**, *227*, 869–875; b) B. T. Golding, D. N. R. Rao in *Enzyme Mechanisms* (Eds.: M. I. Page, A. Williams), Royal Society of Chemistry, London, **1987**, p. 404.

[2] a) R. G. Matthews, V. J. Banerjee, S. W. Ragsdale, *BioFactors* **1990**, *2*, 147; b) B. Kräutler in *The Biological Alkylation of Heavy Elements* (Eds.: P. J. Craig, F. Glockling), Royal Society of Chemistry, London, **1988**, p. 168.

[3] S. Busato, O. Tinembart, Z. Thang, R. Scheffold, *Tetrahedron* **1990**, *46*, 3155–3166.

[4] Formation of dimer **D4** through a reaction of Co^I cobalamin with 1,4-dibromobutane was first suggested in 1964, although with no evidence concerning its structure: E. L. Smith, L. Mervin, P. W. Muggleton, A. W. Johnson, N. Shaw, *Ann. N. Y. Acad. Sci.* **1974**, 565–574.

[5] a) A summary of alkanediyl-bridged metal complexes: C. P. Casey, J. D. Audett, *Chem. Rev.* **1986**, *86*, 339–352; W. Beck, B. Niemer, M. Wieser, *Angew. Chem.* **1993**, *197*, 969–996; *Angew. Chem. Int. Ed. Engl.* **1993**, *32*, 923; b) alkanediyl-bridged porphinoid iron complexes: K. Shin, B.-S. Yu, H. M. Goff, *Inorg. Chem.* **1990**, *29*, 889–890; c) oligomethylene-bridged cobaloxime dimers: K. P. Finch, J. R. Moss, *J. Organomet. Chem.* **1988**, *346*, 253–266.

[6] The addition of one mole equivalent of Co_β-4′-bromobutylcobalamin **M4** to a solution of electrochemically produced Co^I cobalamin similarly led to the formation of the dimer **D4** in approximately 70% yield; the use of Co_β-3′-bromopropylcobalamin **M3** led only to dealkylation.

[7] A bridging trimethylene group would be expected to result in a considerable increase of strain (cf. discussion in ref. [4]).

[8] NMR techniques: cf. for example: H. Kessler, M. Gehrke, C. Griesinger, *Ang. Chem.* **1988**, *100*, 507; *Angew. Chem. Int. Ed. Engl.* **1988**, *27*, 490; DQF-COSY (Double Quantum Filtered Correlation Spectroscopy): U. Piantini, W. O. Sorensen, R. R. Ernst, *J. Am. Chem. Soc.* **1982**, *104*, 6800; ROESY (Rotating Frame Nuclear Overhauser Spectroscopy): A. A. Bothner-By, R. L. Stephens, J. M. Lee, *ibid.* **1984**, *106*, 811; HMQC (Heteronuclear Multiple Quantum Coherence): M. F. Summers, G. L. Marzilli, A. Bax, *ibid.* **1986**, *108*, 2093; HMBC (Heteronuclear Multiple Bond Correlation): A. Bax, M. F. Summers, *ibid.* **1986**, *108*, 2093.

[9] a) X-ray analysis of **D4**·63 H_2O: prismatic crystals from H_2O; space group $P4_12_12$, $a=16.135(4)$, $c=70.902(14)$ Å, $V=18461(7)$ Å^3, $Z=4$, $\rho_{calcd}=1.385$ g cm^{-3}, $\mu(Cu_{K\alpha})=2.48$ mm^{-1}, $T=88(2)$ K. Data collection on a modified STOE diffractometer ($Cu_{K\alpha}$ radiation $\lambda=1.5418$ Å, Ni filter); Structure determination with a total of 12540 measured reflections, 11389 unique ($R_{int}=0.0616$); structure solution with Patterson methods; refinement versus F_o^2, $\omega R_2=0.275$ for all 11389 reflections ($\omega^{-1}=\sigma^2(F_o^2)+(0.18P)^2$, $P=1/3\max(0,F_o^2)+2/3F_c^2$); $R1=0.097$ for 6263 observed reflections ($F_o^2>4\sigma(F_o^2)$); empirical absorption and volume corrections [9c], computer programs in ref. [9a-c]. Further details of the crystal structure investigation are available on request from the Director of the Cambridge Crystallographic Data Centre, 12 Union Road, GB-Cambridge CB2 1EZ (UK), on quoting the full journal citation. b) SHELXTL 4.1, Siemens Crystallographic Research System, **1990**; c) SHELXL-93: G. Sheldrick, University of Göttingen, **1993**; d) DIFABS: N. Walker, D. Stuart, *Acta Crystallogr. Sect. A* **1983**, *39*, 158–166.

[10] a) V. B. Pett, M. N. Liebman, P. Murray-Rust, K. Prasad, J. Glusker, *J. Am. Chem. Soc.* **1987**, *109*, 3207; b) M. Rossi, J. P. Glusker, L. Randaccio, M. F. Summers, P. J. Toscano, L. G. Marzilli, *ibid.* **1985**, *109*, 7894.

[11] Rates of decomposition [s^{-1}] during thermolysis (110 °C, ethylene glycol): **D4**: $\lg k=-4.09$; **D5**: $\lg k=-3.38$; **D6**: $\lg k=-3.17$.

[12] Interestingly, an analogous formation of cyclohexane could not be observed in exploratory photolysis experiments with **D6**.

[13] See for example H. Lang, *Angew. Chem.* **1994**, *106*, 569; *Angew. Chem. Int. Ed. Engl.* **1994**, *33*, 547.

[14] J. Rétey, *Angew. Chem.* **1990**, *102*, 573–379; *Angew. Chem. Int. Ed. Engl.* **1990**, *29*, 355.

[15] See D. Arigoni, P. K. Galliker, unpublished; cf. P. K. Galliker "Zur Biosynthese der Etherlipide aus Methanobacterium thermoautotrophicum", Dissertation ETH-Zürich, Nr. 9119, **1990**.

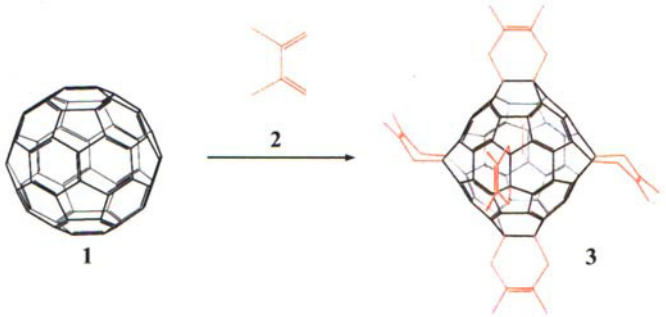
A Highly Symmetric Sixfold Cycloaddition Product of Fullerene C_{60}**

Bernhard Kräutler* and Josef Maynollo

Fullerenes[1] provide fascinating carbon skeletons for endo- and exohedral chemical modifications.[2, 3] Owing to their spherical structure of regularly arranged, unsaturated carbon centers, they are functionalizable in three dimensions. In recent years an increasing number of fullerene derivatives, monofunctionalized on the *exo* surface, have been produced on a preparative scale.[3, 4] A complication in the synthesis of multiple addition products at the fullerene skeleton has been the problem of regioselectivity.[5, 6] For organometallic fullerene derivatives the production and characterization of specific (often thermally labile and oxygen-sensitive) twofold and sixfold adducts have been achieved.[7]

We have been exploring Diels–Alder reactions[4] of fullerenes and report on a hydrocarbon compound with unusual symmetry properties that can be produced through a remarkably regioselective sixfold [4 + 2] cycloaddition of a 1,3-diene to fullerene C_{60}.

When an Ar_2-saturated solution of fullerene C_{60} (**1**) and an excess of 2,3-dimethyl-1,3-butadiene (**2**) in 1,2-dichlorobenzene was heated for several days under protection from light, a change of color from reddish purple to brown and, eventually, to light red-orange could be observed. Besides several other, colored products[8] in the reaction mixture, the almost colorless hexaaddition product **3** was found.[9] The mixture was separated by column chromatography (silica gel). A uniform sample of the hexaaddition product **3** was isolated in 26% yield, and its structure was secured by spectroscopic means.



The ^1H NMR spectrum ($CDCl_3$) of **3** shows only two singlets, at $\delta = 1.85$ and 2.90, due to its twelve symmetry-equivalent methyl and methylene groups.[10] The ^{13}C NMR spectrum **3** consists of only six signals: three signals at $\delta = 19.1$, 45.7, and 129.0, each for the set of twelve symmetry-equivalent carbon atoms of the six [2]buteno bridges, and three signals at $\delta = 60.1$, 142.0, and 152.0, due to twelve (twenty-four) symmetry-equivalent, saturated (unsaturated) fullerene carbon centers.[10] The C,C connectivity in **3** was deduced from C,H long-range correlations observed in the HMBC spectrum (HMBC = heteronuclear multiple bond correlation).[11] In the UV/Vis spectrum of **3** absorption bands in the visible range characteristic of fullerenes do not appear. This finding is consistent with the high degree of deconjugation of the unsaturated carbon skeleton in **3**. The absorption maximum at longest wavelength of a solution of **3** appears in the UV region at $\lambda = 348$ nm ($\lg \varepsilon = 3.87$). The positive-ion FAB mass spectrum of **3** shows a base peak at $m/z = 720$ (C_{60}^+) and signals at $m/z = 1213.5$ (6%, M^+) and 1212.5 (8%), as well as weaker signals at $m/z = 1131$, 1048, 966, 884, and 802, due to fragments from sequential loss of the butadiene addends of **3**.

The extraordinary high effective symmetry of **3** (T_h)[10] results from a sixfold Diels–Alder reaction of the 1,3-diene **2** at the six symmetry-equivalent "6-6 bonds" located between the six-membered rings of fullerene C_{60} (**1**). Whether the remarkable regiocontrol observed in the multiple Diels–Alder reaction with **1** (average effective selectivity >80% for each addition step)[12] results from thermodynamic or kinetic factors, remains to be investigated. Unlike the organometallic multiple adducts, which were reported to be thermally labile and extremely sensitive to oxidation in solution,[7] a solution of **3** stored under N_2 for twelve hours at room temperature showed no sign of decomposition according to its ^1H NMR spectrum.

The partial saturation of the carbon skeleton of the fullerene through sixfold addition results in a chromophore structure of eight completely symmetry-equivalent, strained benzene rings, each of them bridged six times. Therefore, **3** is apparently a new type of multiply bridged cyclophane.[13]

The framework of **3** shows two basic constitutional patterns, which, as far as hydrocarbons are concerned, represent a previously unknown superposition[14] of two basic, platonic bodies: the [2]buteno bridges of **3** span the network of an octahedron and the cyclically conjugated six-membered rings, that of a cube (Fig. 1).

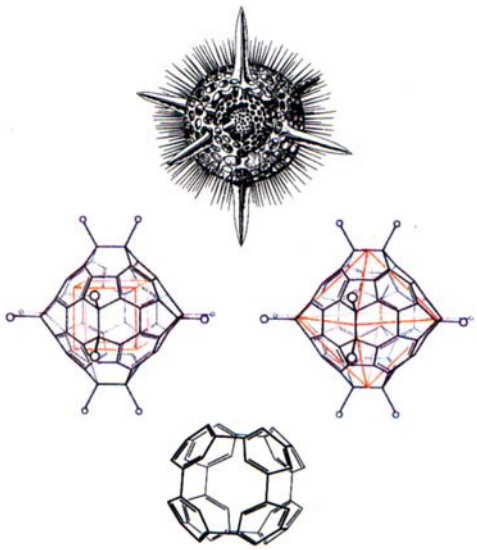


Fig. 1. Skeletal structure of the radiolarian *Hexacontium asteracanthion* (top, according to Haeckel, ref. [15]); superposition of the framework of T_h-symmetric hexaadducts (such as **3**) with a cube (middle left) and with an octahedron (middle right); structure of the residual chromophore in **3** (bottom).

The carbon skeleton of the fullerenes provides a unique basis for the formation of a great variety of molecular structures with spherical cores.[3–7] Through exohedral, covalent modification, new carbon compounds can be produced whose variety of forms and frameworks can be modeled after the (natural) structures of the silicate skeletons of radiolaria.[15] Accordingly, partially unsaturated carbon compounds such as **3** with spherical cores

[*] Prof. Dr. B. Kräutler, Mag. J. Maynollo
Institut für Organische Chemie der Universität
Innrain 52a, A-6020 Innsbruck (Austria)
Telefax: Int. code + (512) 507-2892

[**] We would like to thank Dr. Robert Konrat and Mag. Walter Mühlecker for measuring NMR spectra, Rolf Häfliger and Dr. Walter Amrein (ETH, Zürich) for FAB mass spectra, Dr. Ludwig Call for his pertinent comments, Mag. Michael Schranz and Dr. Michael Puchberger for researching bibliographical data, and Fluka AG (Buchs, Switzerland) for providing a sample of C_{60}. – FAB = fast atom bombardment, NOBA = *ortho*-nitrobenzyl alcohol.

 © VCH Verlagsgesellschaft mbH, D-69451 Weinheim, 1995 0570-0833/95/0101-0087 $ 10.00+.25/0

derived from fullerenes through multiple, exohedral functionalization might be classified generally as "radiolarenes".

Hexaadduct **3** is an unusual hydrocarbon in many respects; its new, highly strained, multiply bridged 1,2,3,4,5,6-cyclophane structure can be constructed through "conventional" Diels–Alder reactions[4a] thanks to the high degree of strain[16] already existing in the fullerene unit.

Experimental Procedure

In a gas-tight ampule protected from light, fullerene C_{60} [4a] (**1**; 20.0 mg, 2.77×10^{-2} mol), 2,3-dimethyl-1,3-butadiene (**2**; 2.28 g, 2.77×10^{-2} mol), and hydroquinone (6.1 mg, 5.54×10^{-5} mol) [17] were dissolved in 0.5 mL of *o*-dichlorobenzene and deoxygenated by three freeze-pump-thaw cycles. The reaction mixture was then saturated with Ar and heated for 234 h at 110 °C. The reaction mixture was cooled, concentrated under vacuum (maximum temperature 35 °C), and purified by column chromatography under inert gas (silica gel, hexane/CH_2Cl_2 9:1) to give a colorless and chromatographically uniform sample of the hexaaddition product **3** besides other products. After filtration through cotton wool, addition of cyclohexane, evaporation of the solvent, and drying under high vacuum, 8.8 mg of the slightly yellow hexaaddition product **3** was obtained (7.25×10^{-6} mol, 26%). Light yellow solid, m.p. > 275 °C (decomp); ^{1}H NMR (200 MHz, $CDCl_3$, 30 °C): δ = 1.85 (s, 3*n*H), 2.90 (s, 2*n*H); ^{13}C NMR (125.7 MHz, $CDCl_3$, 30 °C): δ = 19.1, 45.7, 60.1, 129.0, 142.0, 152.0; UV/Vis (CH_2Cl_2): λ_{max} (lg ε) = 290.5 (4.21), 308 sh (4.13), 348 (3.87) nm; IR($CDCl_3$): ν = 2874, 2854, 1722, 1672, 1441, 1379, 1261, 1099, 1024 cm^{-1}; Positive-ion FAB-MS (NOBA matrix): *m/z* (%): 1214 (7.5), 1213(5.9), 1212(8.5) [1212.471, M^+, calculated for $C_{69}H_{60}$: 1212.468], 1048 (3.7) [$M^+ - C_{12}H_{20}$], 967 (4.3) [$M^+ - C_{18}H_{30}$], 884 (5.7) [$M^+ - C_{24}H_{40}$], 802 (11.7) [$M^+ - C_{30}H_{50}$], 720 (100) [C_{60}^+].

Received: August 10, 1994 [Z 7229 IE]
German version: *Angew. Chem.* **1995**, *107*, 69

Keywords: Diels–Alder reactions · fullerenes

[1] a) H. W. Kroto, *Angew. Chem.* **1992**, *104*, 113; *Angew. Chem. Int. Ed. Engl.* **1992**, *31*, 111; b) R. F. Curl, R. E. Smalley, *Sci. Am.* **1991**, *265*(10), 32; c) W. Krätschmer, L. D. Lamb, K. Fostiropoulos, D. R. Huffman, *Nature* **1990**, *347*, 354; d) F. Diederich, Y. Rubin, *Angew. Chem.* **1992**, *104*, 1123; *Angew. Chem. Int. Ed. Engl.* **1992**, *31*, 1101; e) *Fullerenes* (Eds.: G. S. Hammond, V. J. Kuck) (*ACS Symp. Ser.* **1992**, *481*).

[2] a) H. Schwarz, *Angew. Chem.* **1992**, *104*, 301; *Angew. Chem. Int. Ed. Engl.* **1992**, *31*, 293; b) *Nova Acta Leopold. NF* 285, 167, **1993**; c) M. Sanders, H. A. Jimenez-Vasquez, R. J. Cross, S. Mroczkowski, D. I. Freedberg, F. A. Anet, *Nature* **1994**, *367*, 256.

[3] See, for example a) J. M. Hawkins, *Acc. Chem. Res.* **1992**, *25*, 150; b) T. Suzuki, Q. Li, K. C. Khemani, F. Wudl, *J. Am. Chem. Soc.* **1992**, *114*, 7301; c) A. Vasella, P. Uhlmann, C. A. A. Waldraff, F. Diederich, C. Thilgen, *Angew. Chem.* **1992**, *104*, 1383; *Angew. Chem. Int. Ed. Engl.* **1992**, *31*, 1388; d) A. Hirsch, *ibid.* **1993**, *105*, 1189 and **1993**, *32*, 1138; e) *Chem. Unserer Zeit* **1994**, *18*, 79; f) R. Taylor, D. R. M. Walton, *Nature* **1993**, *363*, 685; g) J. Osterodt, M. Nieger, P.-M. Windscheif, F. Vögtle, *Chem. Ber.* **1993**, *126*, 2331.

[4] a) B. Kräutler, M. Puchberger, *Helv. Chim. Acta* **1993**, *76*, 1626; b) Y. Rubin, S. Khan, D. I. Freedberg, C. Yeretzian, *J. Am. Chem. Soc.* **1993**, *115*, 344; c) P. Belik, A. Gügel, J. Spickermann, K. Müllen, *Angew. Chem.* **1993**, *105*, 95; *Angew. Chem. Int. Ed. Engl.* **1993**, *32*, 78; d) S. I. Khan, A. M. Oliver, M. N. Paddon-Row, Y. Rubin, *J. Am. Chem. Soc.* **1993**, *115*, 4919; e) M. Tsuda, T. Ishida, T. Nogami, S. Kurono, M. Ohashi, *J. Chem. Soc. Chem. Commun.* **1993**, 1296; f) J. A. Schlueter, J. M. Seaman, S. Taha, H. Cohen, K. R. Lykke, H. H. Wang, J. M. Williams, *ibid.* **1993**, 972; g) M. F. Meidine, R. Roers, G. J. Langley, A. G. Avent, A. D. Darwish, S. Firth, H. W. Kroto, R. Taylor, D. R. M. Walton, *ibid.* **1993**, 1342; h) F. Diederich, U. Jonas, V. Gramlich, A. Herrmann, H. Ringsdorf, C. Thilgen, *Helv. Chim. Acta* **1993**, *76*, 2445; i) P. Belik, A. Gügel, A. Kraus, J. Spickermann, V. Enkelmann, G. Frank, K. Müllen, *Adv. Mater.* **1993**, *5*, 854.

[5] a) F. N. Tebbe, R. L. Harlow, D. B. Chase, D. L. Thorn, G. C. Campbell, Jr., J. C. Calabrese, N. Herron, R. J. Young, Jr., E. Wasserman, *Science* **1992**, *256*, 822; b) A. Hirsch, I. Lamparth, H. R. Karfunkel, *Angew. Chem.* **1994**, *106*, 453; *Angew. Chem. Int. Ed. Engl.* **1994**, *33*, 437; c) J. M. Hawkins, A. Meyer, M. Nambu, *J. Am. Chem. Soc.* **1993**, *115*, 9844; d) C. Caron, R. Subramanian, F. D'Souza, J. Kim, W. Kutner, M. T. Jones, K. M. Kadish, *ibid.* **1993**, *115*, 8505; e) P. R. Birkett, P. B. Hitchcock, H. W. Kroto, R. Taylor, D. R. M. Walton, *Nature* **1992**, *357*, 479.

[6] An elegant (stepwise) solution of this problem through an intramolecular ("tether-directed") Diels–Alder reaction was recently reported: L. Isaacs, R. F. Haldimann, F. Diederich, *Angew. Chem.* **1994**, *106*, 2434; *Angew. Chem. Int. Ed. Engl.* **1994**, *33*, 2339.

[7] a) P. J. Fagan, J. C. Calabrese, B. Malone, *J. Am. Chem. Soc.* **1991**, *113*, 9408; b) P. J. Fagan, J. C. Calabrese, B. Malone, *Acc. Chem. Res.* **1992**, *25*, 134; c) A. L. Balch, J. W. Lee, B. C. Noll, M. M. Olmstead, *J. Am. Chem. Soc.* **1992**, *114*, 10984; d) A. L. Balch, J. W. Lee, M. M. Olmstead, *Angew. Chem.* **1992**, *104*, 1400; *Angew. Chem. Int. Ed. Engl.* **1992**, *31*, 1356; e) M. Rasinkangas, T. T. Pakkanen, T. A. Pakkanen, M. Ahlgren, J. Rouvinen, *J. Am. Chem. Soc.* **1993**, *115*, 4901. f) Editor's note: After this manuscript was accepted, a report on the stepwise sixfold addtion of $(EtO_2C)_2C$ to C_{60} appeared: A. Hirsch, I. Lamparth, T. Grösser, H. R. Karfunkel *J. Am. Chem. Soc.* **1994**, *116*, 9385.

[8] According to NMR and FAB mass spectra of incompletely separated samples, they were actually twofold to fivefold addition products of **1** and **2**.

[9] According to the nomenclature for **1** suggested in Chemical Abstracts (cf. *Chem. Abstr.* **1993**, *119*, 4461CS and *ibid.* **1992**, *116*, Index Guide, 155I), hexaadduct **3** should be named 1,9;16,17; 30,31;21,40;44,45;52,60-hexa-(2,3-dimethyl-[2]buteno)-1,9,16,17,30, 31,21,40,44,45,52,60-dodecahydro-[5,6]fullerene-C_{60}.

[10] The room-temperature NMR spectra of **3** are compatible with an effective T_h symmetry.

[11] A. Bax, M. F. J. Summers, *J. Am. Chem. Soc.* **1986**, *108*, 2093; b) cf. H. Kessler, M. Gehrke, C. Griesinger, *Angew. Chem.* **1988**, *100*, 507; *Angew. Chem. Int. Ed. Engl.* **1988**, *27*, 490.

[12] The formation of **3** corroborates previous findings [3e,4,6] on the considerable selectivity of [4 + 2] cycloadditions at **1** at one of the thirty 6-6 bonds. Notwithstanding this rule, synthesis of **3** from **1** supposes a high effective regioselectivity: indeed, of the eight possible, constitutionally isomeric bisadducts, no more than two (which might be qualified as "antipodal" and "orthogonal") actually lead to the formation of **3** via three out of 46 possible regioisomeric trisadducts. Besides, the formation of **3** can only be achieved via one particular route out of 25 routes for the sixth addition of diene **2** to the constitutionally correct pentaadduct.

[13] a) F. Diederich, *Cyclophanes*, The Royal Society of Chemistry, Cambridge, **1991**; b) F. Vögtle, *Cyclophan-Chemie*, Teubner, Stuttgart, **1990**.

[14] Comparable skeleton structures also exist in the reversibly formed organometallic hexaadduct of C_{60} and $[(Et_3P)_2Pt]$ or $[(Et_3P)_2Pd]$ [7a] as well as in the multiple addition product of **1** described by Diederich et al. (ref. [6]). See also ref. [7f].

[15] Cf. K. G. Grell, *Protozoologie* (Ed.: H.-E. Gruner), Springer, Berlin, **1956**, p. 218.

[16] H.-D. Beckhaus, S. Verevkin, C. Rüchardt, F. Diederich, C. Tilgen, H.-U. ter Meer, H. Mohn, W. Müller, *Angew. Chem.* **1994**, *106*, 1033; *Angew. Chem. Int. Ed. Engl.* **1994**, *33*, 996.

[17] Preparations without addition of hydroquinone gave notably lower yields of **3**.

Photoswitchable Phase Separation in Hydrophobically Modified Poly(acrylamide)/Surfactant Systems**

Jochem J. Effing and Jan C. T. Kwak*

Self-assembling systems have been the subject of increasing interest in recent years. In aqueous systems typical building blocks for supramolecular structures are surfactants or more generally amphiphilic molecules. The self-organizing properties of these amphiphiles can be can be influenced externally by incorporating functionalities into the molecules (eg., photoactive[1] or redoxactive groups[2]). The interactions between polymers and surfactants in aqueous solutions lead to the formation of complexes with special physical properties. The resulting systems are of interest in various fields like detergency, drug delivery, and enhancement of oil recovery.[3] Of special interest are hydrophobically modified polymers that allow the strength of the hydrophobic interaction between polymer and surfactant and the structure of the complexes to be tailored to different applications.

[*] Prof. Dr. J. C. T. Kwak, Dr. J. J. Effing
Department of Chemistry, Dalhousie University
Halifax, B3H 4J3, (Canada)
Telefax: Int. code + (902)494-1310

[**] This work was supported by the Natural Sciences and Engineering Research Council of Canada (NSERC) and by fellowships to J.J.E. from the Killam Trust (Dalhousie University) and the Deutsche Forschungsgemeinschaft. The authors acknowledge useful discussions with I. J. McLennan.

We have recently reported evidence for an associative phase separation in a mixture of hydrophobically modified poly(acrylamide) (HPAM) and sodium dodecylsulfate (SDS).[4] The polymer was a copolymer of acrylamide and *N*-decylacrylamide with a hydrophobic monomer content of 2 mol%. Phase separation is induced by the addition of salt (Na_2SO_4); the two-phase region occurs at lower temperature. Both gel phase and supernatant phase contain surfactant and polymer. In this paper we report unusual, light-induced phase separation for aqueous polymer/surfactant systems where the polymer incorporates monomers with azobenzene groups. The idea to incorporate an azobenzene moiety as the hydrophobic side group into the poly(acrylamide)s was initiated by both the work of Shinkai et al. on photoactive surfactants[5] and of Irie et al. on the solubility properties of azobenzene-containing polymers.[6] The *trans–cis* isomerization of the chromophore results in a large change in its geometry and polarity, and therefore leads to a different strength of interaction between polymer and surfactant, which influences the phase behavior of the mixtures. Such light-induced phase separations open interesting possibilities for the design of materials (including optical switches, electrorheological fluids, etc.) with either linear or cross-linked polymers.

The hydrophobically modified poly(acrylamide)s were prepared by radical copolymerization of acrylamide and 4-acrylamidoazobenzene (2 mol% with respect to acrylamide) at 60 °C in *tert*-butylalcohol or dimethyl sulfoxide (DMSO). The initiator azobis(isobutyronitrile) (AIBN) was used in a concentration of 0.5 mol% with respect to acrylamide.[7] The composition of the copolymers was determined by UV/Vis spectroscopy.[8] For the polymer in *tert*-butylalcohol a degree of substitution of 1.2 mol% was obtained, whereas in the DMSO polymerization only 0.9 mol% azobenzene monomer was incorporated. The intrinsic viscosity (in DMSO) and thereby the molecular weight of the copolymer polymerized in DMSO is higher than the polymer obtained in *tert*-butylalcohol. The latter copolymer will be called PAM-Azo-1.2, and the former PAM-Azo-0.9.

Mixtures of ionic surfactants and these new copolymers show the same type of phase behavior as the alkyl substituted poly(acrylamide)s.[4] Figure 1 shows a series of plots of the transition (clearing) temperatures for 1 wt% solutions of PAM-Azo-0.9 and PAM-Azo-1.2 (from the two-phase region at lower temperature to the one-phase region) versus SDS concentration at different Na_2SO_4 concentrations. In the case of mixtures of the lower molecular weight PAM-Azo-1.2 with SDS, phase separation at room temperature was only observed at Na_2SO_4 concentrations above 0.4 M. For the PAM-Azo-0.9 polymer, phase separation in the presence of SDS was already observed over a small surfactant concentration range with 0.07 M Na_2SO_4 and transition temperatures to the one-phase region of 23–25 °C. With increasing salt concentration, the transition temperatures increased and the surfactant concentration range at which phase separation took place broadened. The transition temperatures for the PAM-Azo-0.9/SDS mixtures at salt concentration of 0.5 M were significantly higher than for PAM-Azo-1.2. In addition, the transition temperatures for PAM-Azo-0.9 reached their highest values at approximately half the SDS concentration relative to PAM-Azo-1.2, and the maximum was much more pronounced. The concentration range over which a two-phase region existed was, on the other hand, comparable for both polymers. The higher transition temperatures for PAM-Azo-0.9 mixtures may be a result of its higher molecular weight compared to that of the polymer formed in *tert*-butylalcohol, whereas the lower SDS concentration at which the maximum in the clearing temperature occurs may be related to the lower degree of substition with hydrophobic azobenzene units. For both polymers, phase separation was also observed in a mixture with the cationic surfactant tetradecyltrimethylammonium bromide (TTAB) when $MgSO_4$ was added, whereas only the higher molecular weight PAM-Azo-0.9 exhibited a two-phase region with TTAB in the presence of 0.5 M Na_2SO_4. Complete phase-diagram studies on these systems are in progress.

The dramatic effect on phase separation of irradiation, which leads to *trans–cis* isomerization of the azobenzene side groups, is shown in Figure 2. The phase-separated systems before irradiation are depicted on the left, and the one-phase systems after irradiation at 350 nm on the right.[9] The top system is composed of PAM-Azo-1.2 (3 wt%), SDS (32 mM), and Na_2SO_4 (0.5 M); the bottom system contains PAM-Azo-0.9 (1 wt%) in a solution of TTAB (4.5 mM) and $MgSO_4$ (0.5 M). It is important to note that this light-induced phase transition is fully reversible,

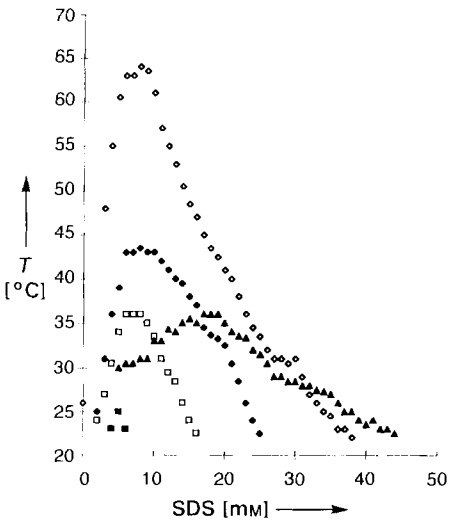


Fig. 1. Plot of the transition temperatures from the two-phase to the one-phase region for PAM-Azo-0.9 and PAM-Azo-1.2 as a function of SDS concentration at different Na_2SO_4 concentrations: PAM-Azo-0.9: ■ = 0.07 M, □ = 0.1 M, ● = 0.2 M, ○ = 0.5 M Na_2SO_4; PAM-Azo-1.2: ▲ = 0.5 M Na_2SO_4; the polymer concentration is 1 wt%.

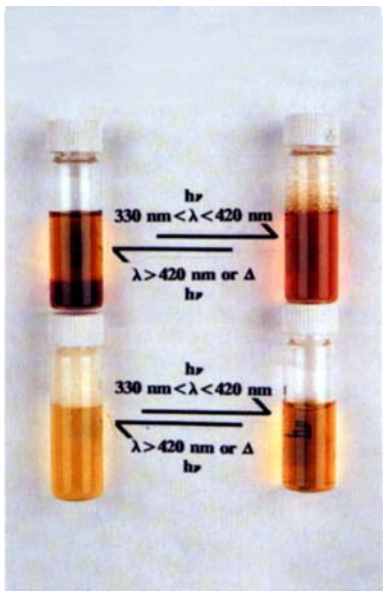


Fig. 2. Reversible transition from two-phase systems to one-phase systems on irradiation at 25 °C. Top: 3 wt% PAM-Azo-1.2, 32 mM SDS, and 0.5 M Na_2SO_4; bottom: 1 wt% PAM-Azo-0.9, 4.5 mM TTAB, and 0.5 M $MgSO_4$.

 © VCH Verlagsgesellschaft mbH, D-69451 Weinheim, 1995 0570-0833/95/0101-0089 $ 10.00+.25/0

and can be repeated indefinitely. To our knowledge this is the first time that such a phenomenon has been reported for polymer/surfactant assemblies.

The binding of the surfactant molecules to the copolymers and the influence of the *trans–cis* isomerization on the strength of the hydrophobic interaction can be monitored by ^{1}H NMR spectroscopy. On binding to the azobenzene moieties, the surfactant proton peaks experience a chemical shift induced by an aromatic ring current. Figure 3 shows the changes in the chemical shifts of the methylene protons at positions 3–11 in the case of SDS and 3–13 in the case of TTAB (position 1 is defined as the carbon directly attached to the sulfate or ammonium group, respectively) in the presence of 1.5 wt% PAM-Azo-1.2 at 25 °C. Already at low concentrations (0.4 mM), the surfactants bind to the copolymer; this leads to initial chemical shift differences of $\Delta\delta = 0.23$ for SDS and $\Delta\delta = 0.13$ for TTAB. With increasing surfactant concentration, the changes become smaller as a result of the increasing ratio of bound surfactant to azobenzene moieties until the hydrophobic azobenzene groups are saturated. The concentration of free surfactant molecules then increases. For TTAB $\Delta\delta$ is already 0 at concentrations of 10–12 mM, whereas $\Delta\delta$ is still 0.07 for SDS even at 20 mM.

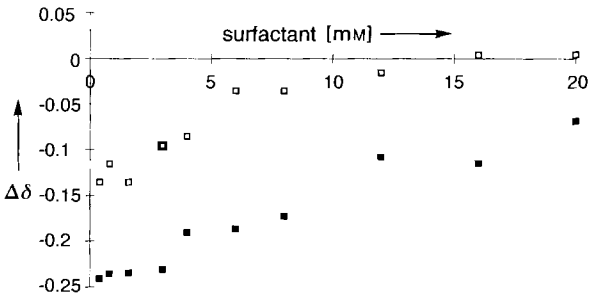


Fig. 3. Changes in ^{1}H NMR chemical shifts of SDS (methylene protons at positions 3–11) and of TTAB (methylene protons at positions 3–13) at 25 °C. ■ = SDS; □ = TTAB; $\Delta\delta = \delta$(in 1.5 wt% PAM-Azo-1.2) $- \delta$(in water).

That the binding of the surfactants is weakened if not suppressed by converting the *trans* azobenzene into its *cis* isomer can be seen from the ^{1}H NMR spectra (Fig. 4) of PAM-Azo-1.2/surfactant mixtures (0.5 wt% polymer in 2 mM surfactant solutions) before (bottom spectrum) and after (middle spectrum) irradiation of the samples at 350 nm. For comparison the spectra of the free surfactants (2 mM solutions) are also shown (top spectrum). Upon irradiation the chemical shifts of the surfactant protons move towards the values for the free surfactants and sharpen up, as can be seen most clearly for the α protons at $\delta = 3.93$ (SDS) and 3.17 (TTAB). In the case of TTAB, the peak at $\delta = 1.117$ splits upon *trans* to *cis* isomerization, so that the peak of the γ protons (at C-3) is well separated ($\delta = 1.219$) from the peak of the methylene protons at positions 4–13 ($\delta = 1.147$).

In conclusion, we have shown that light-switchable phase transitions can be obtained in polymer/surfactant systems containing azobenzene-modified poly(acrylamide)s. These hydrophobically modified polymers undergo an associative phase separation in mixtures with SDS and TTAB in the presence of salt when the azobenzene moiety is in the *trans* form. On isomerization to the *cis* form, the two-phase system clears to a single phase.

Received: June 22, 1994 [Z 7061 IE]
German version: *Angew. Chem.* **1995**, *107*, 88

Keywords: azo compounds · *trans–cis* isomerization · phase separation · poly(acrylamide)s · surfactants

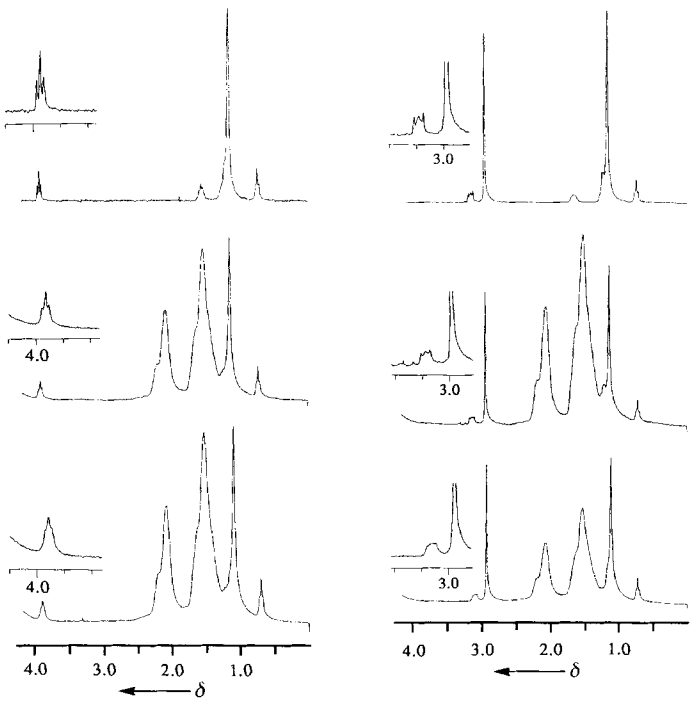


Fig. 4. Left: ^{1}H NMR spectra (250 MHz, D_2O) of PAM-Azo-1.2/SDS mixtures at 25 °C before (bottom spectrum) and after irradiation at 350 nm (middle spectrum), and of pure SDS (top spectrum); right: ^{1}H NMR spectra of PAM-Azo-1.2/TTAB mixtures before (bottom spectrum) and after irradiation at 350 nm (middle spectrum), and of pure TTAB (top spectrum). In both cases the polymer concentration was 0.5 wt%, and the solutions were 2 mM in surfactants.

[1] S. Tazuke, S. Kurihara, H. Yamaguchi, T. Ikeda, *J. Phys. Chem.* **1987**, *91*, 249–251
[2] T. Saji, K. Hoshino, S. Aoyagui, *J. Am. Chem. Soc.* **1985**, *107*, 6865–6868.
[3] a) E. D. Goddard in "*Surfactants in Solution, Vol. 11* (Eds.: K. L. Mittal, D. O. Shah), Plenum Press, New York, **1991**, p. 219; b) "*Polymers in Aqueous Media* (J. E. Glass) (*Adv. Chem. Ser.* **1989**, *223*).
[4] J. J. Effing, I. J. McLennan, J. C. T. Kwak, *J. Phys. Chem.* **1994**, *98*, 2499–2502.
[5] S. Shinkai, K. Matsuo, A. Harada, O. Manabe, *J. Chem. Soc. Perkin Trans. 2*, **1982**, 1261–1265.
[6] a) M. Irie, H. Tanaka, *Macromolecules* **1983**, *16*, 210–214; b) D. Kungwatchakun, M. Irie, *Makromol. Chem. Rapid Commun.* **1988**, *9*, 243–246.
[7] In *tert*-butylalcohol the copolymer precipitated during the polymerization. After 8 h reaction time the solutions were cooled down, and the polymer filtered off. In the case of the DMSO reaction, the polymer was first precipitated in ethanol. In order to remove residual monomer from the polymer, the precipitates were each stirred in acetone for 12 h and then filtered. This process was repeated three times. Before use the copolymers were freeze-dried from an aqueous solution.
[8] For calibration we synthesized the model compound 4-propionamidoazobenzene, which has a UV absorption spectrum identical to that of the copolymer. Assuming that the extinction coefficient of the model compound and polymer bound chromophore are identical, we set up a calibration curve with the help of the model compound.
[9] A Spectroline Miniature UV Quartz Pencil Lamp (Type 36-380) was used for the irradiation. The lamp emits light from 310 to 410 nm with maxima at 350 nm (0.78 μWcm^{-2}nm^{-1}) and 365 nm (1 μWcm^{-2}nm^{-1}).

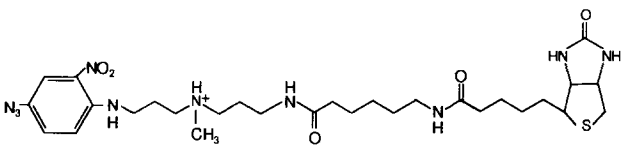
Micron-Scale Patterning of Biological Molecules**

David John Pritchard, Hywel Morgan*, and Jonathan Mark Cooper*

Techniques for controlling the architecture of immobilized biomolecular films on surfaces have a wide range of potential applications in biosensing, cell guidance, and molecular electronics. Previously, films with a predetermined molecular composition in the z direction have been produced by, for example, either Langmuir-Blodgett technology or self-assembly.[1] To date, however, it has not been possible to selectively pattern more than one type of biological molecule on the x,y plane of a surface, although Fodor et al. have synthesized multiple arrays of different oligopeptides or oligonucleotides on glass surfaces.[2] We describe here for the first time a method for patterning two or more functional proteins on a surface whilst minimizing nonspecific binding (NSB). Such a technology is important in the development of multianalyte microsensors, and we illustrate a possible application by immobilizing antibodies.

At present, patterning of molecules may be performed by using photolithographic procedures with lift-off,[3] methods that are not appropriate for biologically active molecules. Alternatively, photoactivation or photodeactivation of surface-bound coupling molecules has been used for immobilizing proteins on surfaces (e.g., with organosilanes or aryl azides).[3-6] These approaches have not, however, been used for immobilization of more than one type of functional molecule.[2-6]

We show in this paper that it is possible to selectively attach different biological molecules in precise areas of a surface by using a combination of self-assembly and photactivation. The method is based on the interaction between streptavidin (or a deglycosylated form of avidin, avidin D) and the analogue **1** (counterion: citrate) of the ligand biotin, which is functionalized with a photoactive group and is thus referred to as a photobiotin (obtained from Vector Laboratories, Peterborough, UK).



1

Photobiotin was first developed as a nucleic acid hybridization probe,[7] and has also been used to label proteins.[8] It has a terminal aryl azide group, which is stable in the dark, but forms a reactive aryl nitrene group upon exposure to light (340–375 nm) with the potential to bind an organic species.[9] The photobiotin molecule used in this study incorporates a spacer arm to minimize steric hindrance to binding. By combining the NSB properties of avidin D with the activation of photobiotin, we are able to produce discrete molecular patterning in the plane of a molecular film.

[*] Dr. J. M. Cooper, Dr. H. Morgan, D. J. Pritchard
Department of Electronics & Electrical Engineering
University of Glasgow, G128LT (UK)
Telefax: Int. code + (41)330-4907

[**] This work was supported by Biotechnology and Biological Sciences Research Council (BBSRC) (Grant No GR/H31967).

The immobilization procedure is represented by Figure 1 and involves the modification of a surface with avidin D, followed by the binding of photobiotin **1** to provide a matrix onto which molecules can be "written" by means of light and a mask.

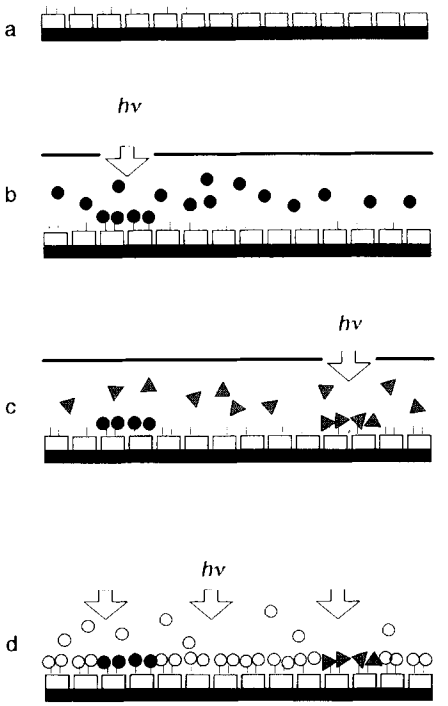


Fig. 1. A schematic representation of the immobilization procedure: a) avidin D (□) with photobiotin **1** (|) immobilized onto a surface; b) exposure of selected areas to light through a mask results in activation of the photobiotin molecule, and a protein (●) in the solution is immobilized specifically; c) unbound material is removed by washing, and the procedure repeated with a second protein (▲); d) the entire surface is exposed to light and unreacted photobiotin is blocked with casein (○).

Protein can be immobilized onto both gold and SiO_2 by this method. In the case of gold, the surface was first modified with a thiol monolayer, onto which avidin D was bound by means of a carbodiimide coupling agent. Alternatively, avidin could be immobilized onto SiO_2 by using a suitable silanization procedure and a protein coupling reagent. In either case, the avidin-modified surface was incubated in a solution of photobiotin (Fig. 1a), and selected areas of this surface were exposed to light, resulting in the activation of the photobiotin molecule. The aryl nitrene which was formed reacted with any protein present in solution and thus immobilized it onto the surface (Fig. 1b).

Patterns were "written" by exposing the surface to light through a mask in the presence of a second protein (Fig. 1c) or, further, with a *sequence* of proteins. After patterning, all unreacted photobiotin groups were neutralized by exposing the whole surface to light in the presence of a blocking molecule such as casein (Fig. 1d). The technique has the advantage that any protein that is not immobilized can be recovered, unaltered.

Biomolecular patterns were written by these techniques. The fluorescent micrographs of two proteins, rabbit IgG and rat IgG, coupled to SiO_2 are presented in Figure 2. These proteins were immobilized onto the surface, which was then exposed to goat anti-rabbit IgG labeled with tetramethylrhodamine isothiocyanate (TRITC) and rabbit anti-rat labeled with IgG fluorescein isothiocyanate (FITC), and the pattern was thus developed. Figure 2 shows that both antibodies are only immobilized onto the surface where the photobiotin had been exposed to light. The resolution of the lithographic patterning technique is limit-

 © VCH Verlagsgesellschaft mbH, D-69451 Weinheim, 1995 0570-0833/95/0101-0091 $ 10.00+.25/0



Fig. 2. A photograph of SiO_2 patterned with two fluorescently labeled antibodies. The antibodies were immobilized by the photoactivation procedure described previously. Red fluorescence indicates the presence of bound rabbit IgG, and green fluorescence the presence of bound rat IgG. The lines are 10 μm wide separated by 10 μm gaps. Black areas indicate minimal nonspecific binding of antibodies. The length of the bar represents 10 μm.

ed by diffraction of light. This effect is exaggerated, since the mask is not in direct contact with the SiO_2, but is separated by a film of buffered protein solution, estimated to be 1 μm thick. Nevertheless, Figure 3 shows that 1.5 μm lines can be written by using a TRITC-labeled IgG. It should be noted that in Figure 2 the TRITC lines are less red than in Figure 3 owing to the fact that a double exposure (TRITC and FITC filters) was needed to obtain the former. This color change is not due to NSB of the FITC probe, as it occurs in the absence of the FITC label.

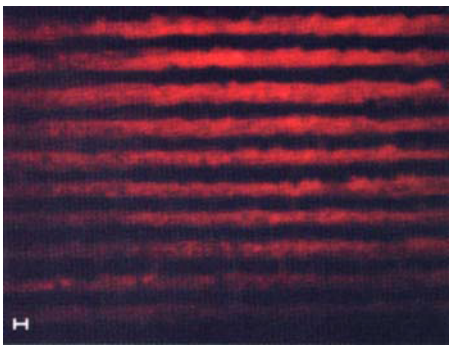


Fig. 3. Photograph of SiO_2 patterned with TRITC-labeled IgG. This illustrates the resolution obtainable with this technique. The lines are 1.5 μm wide separated by 1.5 μm gaps, and were written with a 1.5 μm mark-space mask. The length of the bar represents 1 μm.

Nonspecific binding of antibodies to other regions of the SiO_2 surface was not detectable by fluorescence microscopy. It was, however, possible to use a sensitive electrochemical assay for IgG labeled with an alkaline phosphatase (ALP) to estimate the size of NSB effects on a modified gold surface (Fig. 4). The total charge density generated as a result of NSB (trace b) was 0.43 $mC\,cm^{-2}$, whilst that for the specific binding reaction (trace a) was 23.9 $mC\,cm^{-2}$; this indicates that NSB is limited to 1.8% of total binding. Measurement of the extent of NSB with steady-state currents (minus the background reading in buffer) gave a similar value (1.9%). This value includes cross-reactivity between different antibodies as well as NSB.

The binding of ALP-labeled IgG directly onto an avidin D-coated gold electrode was also measured in an electrochemical ALP assay, and the charge density was 0.17 $mC\,cm^{-2}$, equivalent to 0.7% NSB. Such values represent a significant advance on those presently obtainable and now allow patterning of biological molecules to be carried out at microsensor arrays. The technique also has the advantage that it may be integrated with lithographic processes currently in use in device fabrication in the electronics industry.

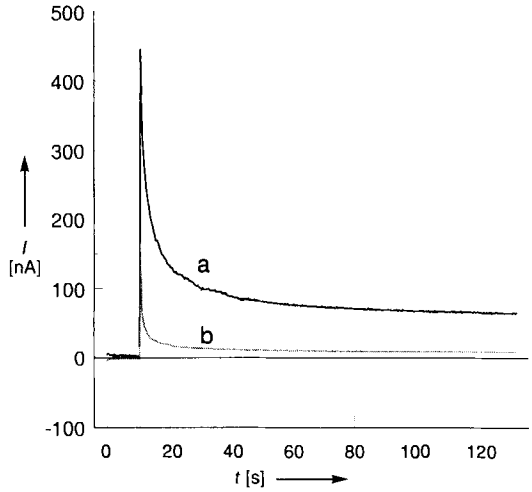


Fig. 4. Responses from two gold electrodes patterned with immobilized antibodies. Further details see Experimental Procedure.

Experimental Procedure

Antibody patterning on a SiO_2 surface: Avidin D (0.2 mg mL^{-1}) in phosphate buffered saline (10 mM phosphate buffer, 2.7 mM KCl, 137 mM NaCl), pH 7.4 (PBS buffer), was immobilized onto a 1 cm^2 disc of silanized SiO_2 [3], which was subsequently incubated in bovine serum albumin in PBS (0.2 mg mL^{-1}) at room temperature for 1 h. PBS was also used for washing between each step. The wafer was then incubated in long-arm photobiotin **1** in PBS (10 μg mL^{-1}) for 20 min in the dark, and was covered with rabbit IgG (10 μg mL^{-1}). Light activation of the photobiotin and coupling of the respective antibodies was performed with a 100 W, high-pressure mercury vapor lamp (185 mm from the surface, irradiance = 9 $mW\,cm^{-2}$) for 15 min through a mask and a Hoya SL glass filter, which removed radiation below 300 nm. No decrease in the activity of the polyclonal IgGs used in this work or of ALP was observed upon exposure to the filtered light.

The patterning process was then repeated with rat IgG (10 μg mL^{-1}). During the course of the light-activation experiment, the temperature of the wafer did not increase by more than 5°C. In order to "block" unreacted photobiotin sites, the wafer was immersed in casein in PBS (10 mg mL^{-1}) and was exposed to light for 15 min. The pattern was then "developed" in TRITC-labeled goat anti-rabbit IgG in PBS (10 μg mL^{-1}) for 60 min and then in FITC-labeled rabbit anti-rat IgG in PBS (10 μg mL^{-1}) for 60 min. All IgGs were polyclonal and were obtained from Sigma (UK).

Antibody patterning on a gold surface: Gold was modified with *N*-acetyl cysteine, onto which avidin D was bound by means of a carbodiimide coupling agent [10]. The method for immobilization of IgG was, otherwise, as described previously.

Electrochemical measurements: The gold electrodes (0.2 cm diameter) were first modified in 5 mM *N*-acetyl cysteine (Sigma) in 10 mM phosphate buffer (pH 7.0) for 2 h, and were then washed in water. The *N*-acetyl cysteine modified electrodes were incubated in a 10% (w/v) solution of 1-ethyl-3-(3-dimethylaminopropyl)carbodiimide (EDC) in 10 mM phosphate buffer for 2 h at 25°C, and were washed in water. The EDC-activated electrodes were placed in a solution of avidin D in 10 mM phosphate buffer (0.2 mg mL^{-1}) for 16 h at 4°C before washing. The electrodes were then incubated in casein in 10 mM phosphate buffer (0.2 mg mL^{-1}) for 1 h at room temperature. Photobiotin **1** was assembled on the avidinated gold, and both electrodes were patterned with a goat anti-rabbit IgG. One electrode was subsequently exposed to an excess of antigen rabbit IgG (trace a), and the other to rat IgG (trace b) Finally both electrodes were incubated in the presence of an excess of ALP-labeled goat anti-rabbit IgG for 120 min and were washed. A solution of 10 mM 1-naphthyl phosphate in 100 mM tris(hydroxymethyl)aminomethane (Tris) containing 2.7 mM KCl and 137 mM NaCl was added to the electrodes, and after 5 min the electrodes were poised at + 320 mV vs. Ag/AgCl. A current was measured for 2 min owing to the electrochemical oxidation of enzymically produced 1-naphthol (which, unlike 1-naphthyl phosphate, is electroactive at this potential). When ALP-labeled goat anti-rat IgG was used in place of ALP-labeled goat anti-rabbit IgG, then both electrodes exhibited behavior similar to that seen in trace b. This demonstrates that nonspecific binding of rat IgG to electrodes coated with goat anti-rabbit IgG is minimal.

Received: June 28, 1994
Revised version: September 5, 1994 [Z 7081 IE]
German version: *Angew. Chem.* **1995**, *107*, 84

Keywords: antibodies · immobilization · immunosensors · photolithography

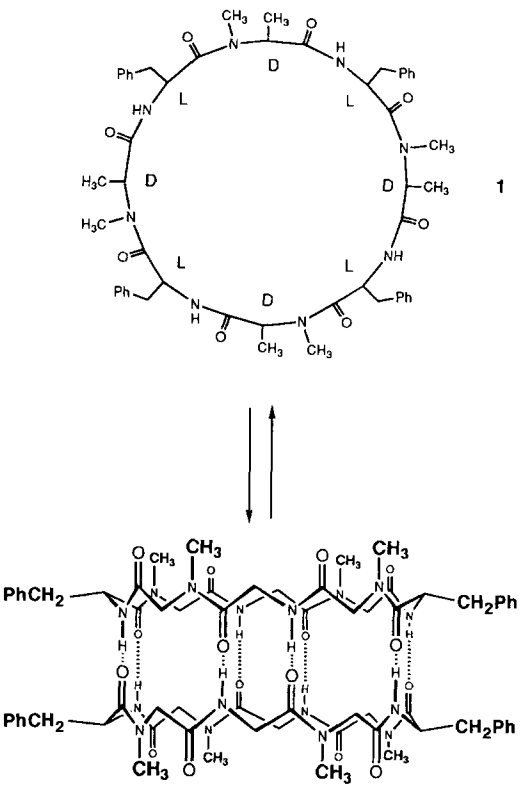
[1] P. E. Laibinis, J. J. Hickman, M. S. Wrighton, G. M. Whitesides, *Science* **1989**, *245*, 845–847.
[2] S. P. A. Fodor, J. L. Reid, M. C. Pirrung, L. Stryer, A. T. Lu, D. Solas, *Science* **1991**, *251*, 767–773.
[3] P. Connolly, J. M. Cooper, G. M. Moores, J. Shen, G. Thompson, *Nanotechnology* **1991**, *2*, 160–163.
[4] C. S. Dulcey, J. H. Georger, V. Krauthmaer, D. A. Stenger, T. L. Fare, J. M. Calvert, *Science* **1991**, *252*, 551–554.
[5] C. R. Lowe, F. G. P. Earley, US-A 4562157, **1985**.
[6] S. K. Bhatia, J. L. Teixeira, M. Anderson, L. C. Shriver-Lake, J. M. Calvert, J. H. Georger, J. J. Hickman, C. S. Dulcey, P. E. Schoen, F. S. Ligler, *Anal. Biochem.* **1993**, *208*, 197–205.
[7] A. C. Forster, J. L. McInnes, D. C. Skingle, R. H. Symons, *Nucleic Acids Res.* **1985**, *13*, 745–776.
[8] E. Lacey, W. N. Grant, *Anal. Biochem.* **1987**, *163*, 151–158.
[9] P. A. S. Smith in *Azides and Nitrenes. Reactivity and Utility* (Ed.: E. F. V. Scriven), Academic Press, London, **1984**, p. 95.
[10] J. M. Cooper, K. Greenough, C. J. McNeil, *J. Electroanal. Chem. Interfacial Electrochem.* **1993**, *347*, 267–275.

The Structural and Thermodynamic Basis for the Formation of Self-Assembled Peptide Nanotubes**

M. Reza Ghadiri,* Kenji Kobayashi, Juan R. Granja, Raj K. Chadha, and Duncan E. McRee

Design of molecular objects with predefined shapes and functions has come to the forefront of chemistry and materials research lately.[1–14] In particular, considerable effort has been devoted toward the rational design of tubular structures because of their potential utility in molecular transport, inclusion chemistry, chemical catalysis, and manufacture of novel optical and electronic devices.[15–24] Here, in the context of a new design, we provide a detailed analysis of the conformation in solution and thermodynamic basis for the peptide self-assembly process, and present the first definitive high-resolution structural model in support of the recently reported peptide nanotubes and transmembrane ion channel structures.[15–17] A cyclic peptide with a selectively N-methylated backbone has been designed and shown to self-assemble into a discrete soluble cylindrical dimer in nonpolar organic solvents. Under appropriate conditions, the peptide also assembles to produce a unique porous crystalline object having an ordered parallel array of water-filled channels of 7–8 Å diameter, the interior amphiphilic surface of which has alternating hydrophobic and hydrophilic domains approximately every 11 Å. The structural assignments and thermodynamic characterizations are supported by a variety of ^{1}H NMR techniques, FT-IR spectroscopy, and high-resolution X-ray crystallography.

Recent designs of peptide nanotubes were based on the central premise that cyclic peptides made up of alternating D- and L-amino acid residues can adopt a flat ring-shaped conformation in which the backbone amide groups are approximately perpendicular to the plane of the ring.[15–17] Furthermore, it was postulated that intermolecular hydrogen bonding and ring stacking interactions of peptide subunits in this conformation would be energetically favored under appropriate conditions and would thus produce open-ended, hollow, tubular ensembles. The key structural requirement for producing a multiply ring-stacked tubular structure was the spatial disposition of the hydrogen-bond donor and acceptor sites of the backbone on *both* faces of the (monomeric) peptide ring structure.[15–17] In the present design, however, the cyclic peptide subunit is devoid of hydrogen-bond donation from one face of the ring structure because of selective methylation of backbone amide nitrogen functionalities. Such a ring-shaped peptide subunit cannot participate in an extended hydrogen-bonded network and is therefore predisposed toward the dimeric, antiparallel stacked, cyclindrical structure—the key fundamental repeating structural motif of the larger peptide nanotube counterparts. The eight-residue cyclic peptide *cyclo*[(–L-Phe–D-*N*-MeAla–)$_4$-] (**1**) was designed for the task in hand[25] (Scheme 1). The sequence and



Scheme 1. A two-dimensional representation of the chemical structure of the peptide subunit (D and L refers to the amino acid chirality) and the self-assembled cylindrical ensemble (for clarity only four of the eight CH_2Ph groups are represented).

the choice of amino acid residues were based on the following considerations: Molecular modeling indicated that methylation of backbone amide nitrogen functionalities at all alanine residues would be sufficient to effectively prevent one face of the putative peptide ring structure from participating in intermolecular hydrogen-bonding and ring-stacking interactions. The peptide was also designed to have an allowed symmetry for favorable intermolecular packing interactions in the solid state thus permitting its detailed structural characterization by X-ray crys-

[*] Prof. M. R. Ghadiri, Dr. K. Kobayashi, Dr. J. R. Granja, Dr. R. K. Chadha, Dr. D. E. McRee
Departments of Chemistry and Molecular Biology
The Scripps Research Institute
10666 North Torrey Pines Road, La Jolla, CA 92307 (USA)
Telefax: Int. code + (619)554-6656

[**] This work was supported by the U.S. Office of Naval Research. We thank D.-H. Huang and M. A. Case for their assistance with NMR spectroscopy, G. Siuzdak for mass spectrometric analysis, G. M. Morris for assistance with computer graphics representations, and Professor G. Sheldrick for valuable suggestions regarding the X-ray crystallographic analysis. K. K. acknowledges the Ministry of Education, Science, and Culture of Japan for a postdoctoral Fellowship. J. R. G. thanks NSCORT for a summer fellowship. M. R. G. is a Searle Scholar (1991–94) and Alfred P. Sloan Research Fellow (1993–1995).

tallographic techniques. In addition, to gain a better understanding of the structural basis and the thermodynamics of the peptide self-assembly process in nonpolar media—a situation recently encountered in the design of transmembrane ion channel structures[16]—the putative peptide ring structure was decorated with hydrophobic residues to render the subunit and the resulting ensemble soluble in nonpolar organic solvents. The following studies, using ^{1}H NMR techniques, FT-IR spectroscopy, and single-crystal X-ray structural analysis, unequivocally establish the validity of our basic design hypothesis.

The ^{1}H NMR spectrum of the peptide subunit **1** in polar solvents such as deuterated methanol or dimethylsulfoxide (DMSO) displays several conformational isomers which slowly interconvert as a result of the well-known propensity of secondary amides toward *cis–trans* isomerization. Variable-temperature NMR experiments in DMSO indicate *cis–trans* conformational activation barriers on the order of 16 to 17 kcal mol^{-1}. However, in nonpolar solvents such as carbon tetrachloride (CCl_4) or deuterochloroform ($CDCl_3$) the peptide **1** exists in an all-*trans* conformation with a flat-ring-shaped backbone, which is in dynamic equilibrium with the expected cylindrical dimer (Scheme 1). Monomeric **1** displays a temperature-independent (from -40 to 55 °C in $CDCl_3$) and highly symmetrical ^{1}H NMR spectrum excluding the possibility of an intramolecularly hydrogen-bonded conformation. The preponderance of a flat-ring-shaped backbone conformation is also indicated by the observed $J_{NH,\alpha H}$ coupling constant of 7.5 Hz. Intermolecular hydrogen-bonding interactions producing the stacked dimeric ensemble are signified by the expected downfield shift of the phenylalanine N-H resonance from $\delta = 6.98$ to 8.73 ($J_{NH,\alpha H} = 8.8$ Hz) and are unequivocally established by the observed exchange and NOE cross peaks in the ROESY spectrum (Fig. 1).[26, 27] Formation of a tight hydrogen-bonded ensemble with an average intersubunit N–O distance of 2.95 Å is also evidenced by the appearance of an N–H stretching band in the infrared spectrum at 3309 cm^{-1}. As expected, the self-assembly process displays concentration- and solvent-dependent spectra with the association constants $K_a(CCl_4) = 1.4 \times 10^4$ M^{-1} and $K_a(CDCl_3) = (1.26 \pm 0.13) \times 10^3$ M^{-1} at 293 K.[28]

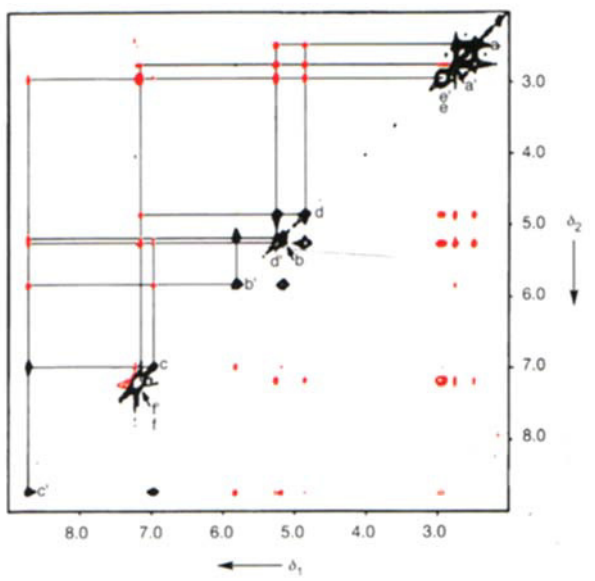


Fig. 1. Two-dimensional phase-sensitive (TPPI) ROESY NMR spectrum of the peptide in $CDCl_3$ (2.0 mM) at 298 K (exchange cross peaks are in black and the NOE cross peaks in red). Letters a–f and a′–f′ mark resonances for the monomeric peptide subunit and the dimeric cylindrical ensemble, respectively (a = NMe, b = α-H(ala), c = NH, d = α-H(Phe), e = β-H(Phe), f = Ph).

Variable-temperature studies (van't Hoff plots) establish the following thermodynamic parameters for the dimerization process in chloroform: $\Delta C_p = -203.1$ cal K^{-1} mol^{-1}, $\Delta H^\circ_{298} = -11.0$ kcal mol^{-1}, and $\Delta S^\circ_{298} = -23.7$ cal K^{-1} mol^{-1}, which clearly supports the expected enthalpic contribution of intermolecular hydrogen-bonding interactions (0.5 to 0.7 kcal mol^{-1} for each hydrogen-bonding interaction) as the major driving force in the self-assembly process. The above experiments indicate that in solution the peptide subunit adopts a flat-ring-shaped conformation, which energetically favors ring stacking and intermolecular hydrogen-bonding interactions over the nonassembled form by 4.0 to 5.6 kcal mol^{-1}, depending on the solvent employed. It follows then that the gain in free energy of stabilization will be additive as the number of ring-stacking interactions increase. This is particularly relevant to the structures of the recently designed self-assembled nanotubes and transmembrane ion channels.[15–17]

Colorless prismatic crystals suitable for X-ray analysis were obtained from the solutions of **1** in water-saturated dichloromethane by vapor-phase equilibration with hexane. The solid-state structure[29] is a cylindrical dimeric ensemble, analogous to the solution structure deduced from the ^{1}H NMR and FT-IR analyses, and thus corroborates very well the nanotube structures previously derived primarily from the analysis of electron diffraction patterns[15, 17] (Fig. 2). It consists of a flat-ring-shaped cyclic peptide subunit with backbone amide groups perpendicular to the plane of the ring and a crystallographic four-

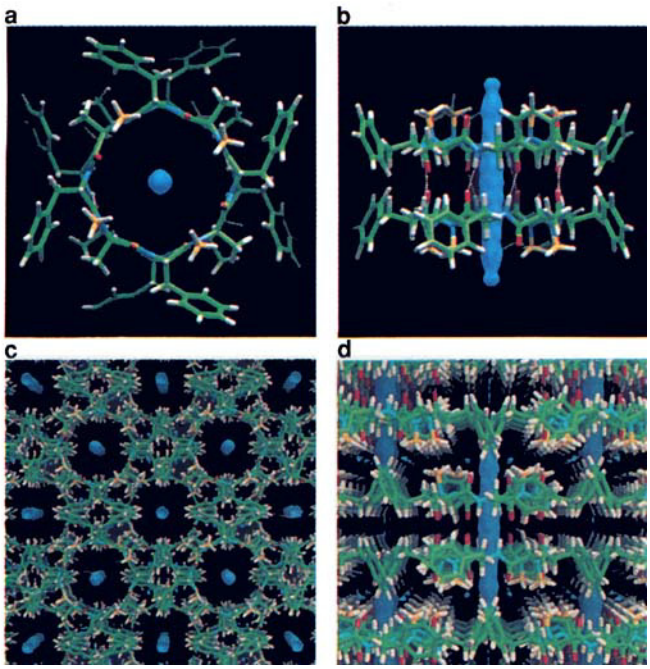


Fig. 2. Crystal structure of the cylindrical dimer and the crystal lattice showing the electron density for water. In order to display the positions of water molecules, the solvent was omitted from the model and an $F_o - F_c$ electron density map calculated. The map shows the position of solvent atoms and is illustrated as a blue isosurface at the level of 4 σ. a) View of the dimer down the crystallographic fourfold axis, *c* (space group *I*422). b) View of the dimer along the twofold axis, *a* or *b*. The rod-shaped solvent electron density in the center of the cylindrical ensemble represents the time-averaged position of several overlapping water binding sites. c) Crystal lattice with solvent electron density viewed along the *c* axis, showing the channels traversing the crystal. The figure is two unit cells wide, two unit cells high, and 1.5 unit cells deep. d) As in c) but viewed along the *a* or *b* axis. The solvent density is much reduced in the proximity of the hydrophobic phenyl groups and is fairly uniform in the center of the dimer. In the extended nanotube structures, which are not interrupted by N-methylated amide groups, the water electron density would form a continuous tube throughout the entire nanotube.

 © VCH Verlagsgesellschaft mbH, D-69451 Weinheim, 1995 0570-0833/95/0101-0094 $ 10.00+.25/0

fold rotation axis parallel to the c axis passing through the center of the peptide ring (Fig. 2a). Two peptide subunits (**1**) are closely stacked in an antiparallel orientation and are related by a twofold rotation along either the a or b axis (Fig. 2b). The β-sheet-like cylindrical ensemble is stabilized by eight intersubunit hydrogen-bonding interactions with an intersubunit N–O distance of 2.90 Å. The distance of 2.95 Å inferred from the observed N–H stretching band at 3312 cm^{-1} in the FT-IR spectrum is remarkably consistent with the crystallographic measurements. The cylindrical dimer has an approximate van der Waals internal diameter of 7.5 Å and a volume of 450 $Å^3$. The tubular cavity is filled with partially disordered water molecules, establishing the hydrophilic internal characteristics of the peptide nanotube structures (Fig. 2). The dimer packs in the crystal in a body-centered fashion to produce a continuously channeled superlattice along the c axis (Fig. 2c and d). The interior surface characteristics of the channels alternate approximately every 11 Å between the hydrophobic domains, created by the aromatic phenyl moieties and the hydrophilic interior of the peptide dimer. Water molecules near the hydrophobic domains are considerably more disordered, displaying only a weak residual electron density. The observed electron density for water is the time-average of water molecules binding at several overlapping sites, which suggests a facile movement of loosely held water molecules within the cavity. This observation, which can be attributed to the lack of a discrete, strong binding site (or sites), is an important attribute of the peptide nanotube structures and may be useful for rationalizing the remarkable transport efficiencies of the recently described transmembrane ion channels.[16]

The design principle described above is expected to have a number of potential applications. Appropriately designed subunits with hydrogen bonding possible only in one direction can be used as tube terminators or capping agents and may be used to gate the self-assembled transmembrane ion channel structures. The unique amphiphilicity of the noncentrosymmetric channeled crystals may be useful for binding both hydrophobic and hydrophilic substrates, thus extending the potential utility of peptide nanotubes as molecular inclusion devices and nonlinear optical materials.

Received: July 8, 1994 [Z 7113 IE]
German version: *Angew. Chem.* **1995**, *107*, 76

Keywords: nanostructures · peptides · self-assembly

[1] D. J. Cram, *Nature (London)* **1992**, *356*, 29–36.
[2] J.-M. Lehn, *Science* **1993**, *260*, 1762–1763.
[3] G. M. Whitesides, J. P. Mathias, C. T. Seto, *Science* **1991**, *254*, 1312–1319.
[4] M. R. Ghadiri, M. A. Case, *Angew. Chem.* **1993**, *105*, 1663–1667; *Angew. Chem. Int. Ed. Engl.* **1993**, *32*, 1594–1597.
[5] R. Wyler, J. de Mendoza, J. Rebek, Jr., *Angew. Chem.* **1993**, *105*, 1820–1821; *Angew. Chem. Int. Ed. Engl.* **1993**, *32*, 1699–1701.
[6] R. A. Bissell, E. Cordova, A. E. Kaifer, J. F. Stoddart, *Nature (London)* **1994**, *369*, 133–137.
[7] F. Diederich, *Nature (London)* **1994**, *369*, 199–207.
[8] B. J. Whitlock, H. W. Whitlock, *J. Am. Chem. Soc.* **1990**, *112*, 3910–3915.
[9] S. Mann, *Nature (London)* **1993**, *365*, 499–505.
[10] J. M. J. Fréchet, *Science* **1994**, *263*, 1710–1715.
[11] G. R. Newkome, C. N. Moorefield, G. R. Baker, R. K. Behera, G. H. Escamilla, M. J. Saunders, *Angew. Chem.* **1992**, *104*, 901–903; *Angew. Chem. Int. Ed. Engl.* **1992**, *31*, 917–919.
[12] H. B. Mekelburger, W. Jaworek, F. Vögtle, *Angew. Chem.* **1992**, *103*, 1609–1614; *Angew. Chem. Int. Ed. Engl.* **1992**, *31*, 1571–1576.
[13] Z. Xu, J. S. Moore, *Angew. Chem.* **1993**, *105*, 1394–1396; *Angew. Chem. Int. Ed. Engl.* **1993**, *32*, 1354–1357.
[14] V. Balzani, S. Campagna, G. Denti, A. Juris, S. Serroni, M. Venturi, *Coord. Chem. Rev.* **1994**, *132*, 1–13.
[15] M. R. Ghadiri, J. R. Granja, R. A. Milligan, D. E. McRee, N. Khazanovich, *Nature (London)* **1993**, *366*, 324–327. For an earlier theoretical investigation see: P. De Santis, S. Morosetti, R. Rizzo, *Macromolecules* **1974**, *7*, 52–58. For the syntheses of some cyclic oligopeptides with S_{2n} symmetry with the construction of tubular structures as the stated goal see: L. Tomasic, G. P. Lorenzi, *Helv. Chim. Acta* **1987**, *70*, 1012–1016.
[16] M. R. Ghadiri, J. R. Granja, L. K. Buehler, *Nature (London)* **1994**, *369*, 301–304.
[17] N. Khazanovich, J. R. Granja, D. E. McRee, R. A. Milligan, M. R. Ghadiri, *J. Am. Chem. Soc.* **1994**, *116*, 6011–6012.
[18] S. Iijima, *Nature (London)* **1991**, *354*, 56–58.
[19] J. M. Schnur, *Science* **1993**, *262*, 1669–1676.
[20] J.-H. Fuhrhop, D. Spiroski, C. Boettcher, *J. Am. Chem. Soc.* **1993**, *115*, 1600–1601.
[21] A. Harada, J. Li, M. Kamachi, *Nature (London)* **1993**, *364*, 516–518.
[22] C. T. Kresge, M. E. Leonowicz, W. J. Roth, J. C. Vartuli, J. S. Beck, *Nature (London)* **1992**, *359*, 710–712.
[23] M. F. M. Roks, R. J. M. Nolte, *Macromolecules* **1992**, *25*, 5398–5407.
[24] Q. S. Huo, D. I. Margolese, U. Ciesla, P. Feng, T. E. Gier, P. Sieger, R. Leon, P. M. Petroff, F. Schüth, G. D. Stucky, *Nature (London)* **1994**, *368*, 317–321.
[25] The linear form of the target sequene H(-L-Phe-D-N^2-Me-Ala-)$_4CO_2H$ was synthesized according to standard solid-phase methods and then cyclized in solution to furnish the desired cyclic peptide subunit using the following procedure: A solution of the linear peptide in DMF (1 mM) was treated with 2-(1-H-benzotriazol-1-yl)-1,1,3,3-tetramethyluronium hexafluorophosphate (3 mM), 1-hydroxybenzotriazole (3 mM), and diisopropylethylamine (1% v/v) at 5 °C for 12 h to give the desired cyclic peptide in 70% yield after reverse-phase HPLC purification.
[26] A. Bax, D. G. Davis, *J. Magn. Reson.* **1985**, *63*, 207–213.
[27] ROESY experiments were performed on a Bruker AMX-500 with 300 ms spin lock (mixing) time using Bruker's standard pulse program. Data were processed with FELIX software. Time domain data was apodized with skewed sine-bell squared window functions. Zero-filling was used to obtain the final data size of the 1024 × 1024 complex matrix.
[28] The association constants reported are the lower limits because of the presence of small amounts of included water in the peptide samples. When water is rigorously excluded (4 Å molecular sieves) the association constant $K_a(CDCl_3) = 1260\,M^{-1}$ is approximately doubled to $K_a(CDCl_3) = 2540\,M^{-1}$. The value of $K_a(CCl_4)$ reported was measured in a mixture of 84% CCl_4 and 16% $CDCl_3$ for reasons of solubility.
[29] Data were collected on a Rigaku AFC6R diffractometer equipped with a rotating copper anode ($Cu_{K\alpha}$) and a highly oriented graphite monochromator. The structure was solved in the space group $I422$ with a final R factor of 8.87%, weighted R factor of 10.35%, and residual electron density of 0.64 $e\,Å^{-3}$ for 983 unique reflections with $F > 4.0\sigma(F)$. The unit cell parameters are $a = b = 16.78$, and $c = 21.97$ Å.

β-Sheet Peptide Architecture: Measuring the Relative Stability of Parallel vs. Antiparallel β-Sheets**

Kenji Kobayashi, Juan R. Granja, and M. Reza Ghadiri*

In memory of Professor Linus C. Pauling

Among the most commonly occurring protein secondary structures, β-sheets are the least studied because well-characterized peptide model systems are not available.[1–3] In particular, despite a number of theoretical studies implicating the possible role of amino acid residues and cross-strand interactions between side chains in directing the folding characteristics of β-sheet structures,[4] to date no direct experimental evidence has been forthcoming to establish the underlying energetic factors

[*] Prof. M. R. Ghadiri, Dr. K. Kobayashi, Dr. J. R. Granja
Departments of Chemistry and Molecular Biology
The Scripps Research Institute
10666 North Torrey Pines Road, La Jolla, CA 92307 (USA)
Telefax: Int. code + (619)554-6656

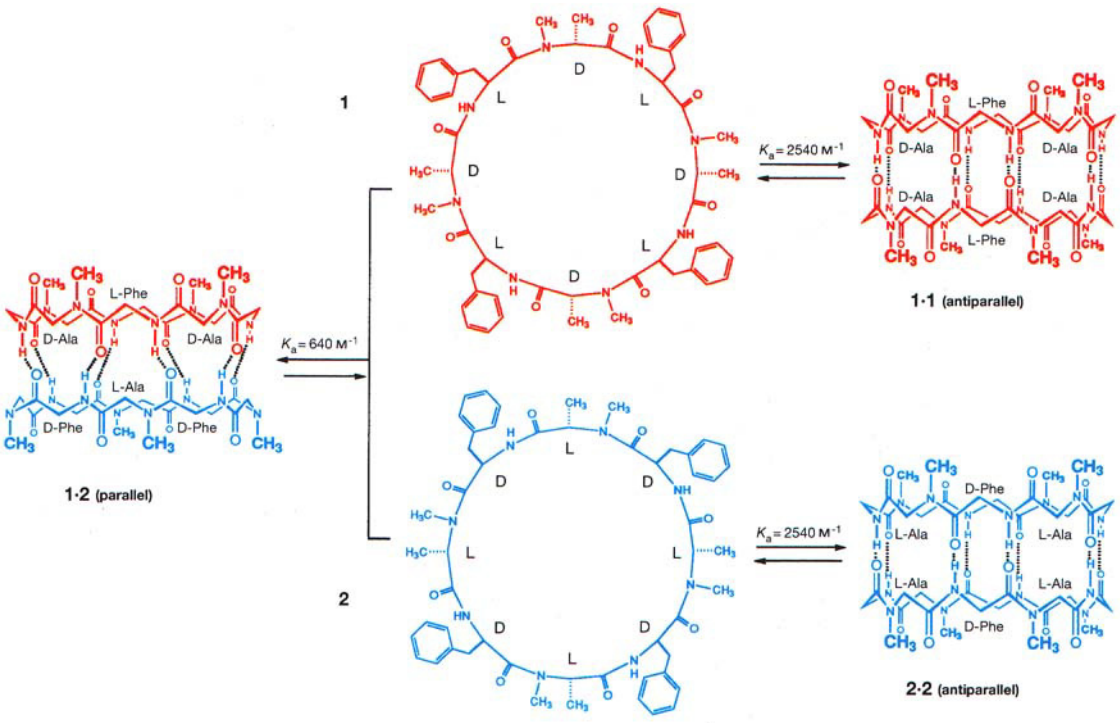
[**] This work was supported in part by the U.S. Office of Naval Research and the National Institute of General Medicine. We thank colleagues D. H. Huang and M. A. Case for their assistance in NMR spectroscopy. K. K. acknowledges the Ministry of Education, Science, and Culture of Japan for a postdoctoral fellowship. J. R. G. thanks NSCORT for a summer fellowship. M. R. G. is a Searle Scholar (1991–1994) and Alfred P. Sloan Research Fellow (1993–1995).

that may favor the formation of parallel or antiparallel arrangements. Here we describe the design, synthesis, and characterization of a novel model structure for β-sheets and provide the first direct evaluation of the thermodynamic preference for the antiparallel vs. parallel β-sheet formation. Within the constraints of the present model, our studies establish for the first time the significant role of backbone–backbone hydrogen-bonding interactions in favoring the formation of the antiparallel β-sheet structure.

The de novo design of peptides with well-defined β-sheet structures has been hampered primarily by the propensity of extended hydrophobic or amphiphilic polypeptides toward nonspecific intermolecular aggregation, by lack of control over the relative sheet register, and by the inability to predict or control the extent of the backbone twist in such structures.[5] Moreover, there has been no study to date that documents the formation of parallel and antiparallel β-sheet structures starting with the same or similar peptide sequence(s), which might allow direct assessment of the role of backbone–backbone interactions and cross-strand interactions between side chains in such arrangements. In the preceding article, we described the design of an antiparallel β-sheet cylindrical ensemble based on the self-assembly of flat ring-shaped cyclic peptide subunits with a specifically N-methylated backbone.[6] This unique β-sheet ensemble is free of the complications commonly plaguing β-sheet model systems and constitutes the basis structure for the present study.

The cyclic octapeptides **1**–**3** were designed for the task in hand. They all share the following basic design principles: The peptides are made up of eight alternating D- and L-amino acids which adopt a flat ring-shaped conformation in nonpolar organic solvents and stack to form cylindrical β-sheet arrangements.[6, 7] Solution-phase ^{1}H NMR studies as well as high-resolution X-ray structural analysis have indicated that all backbone ϕ and ψ dihedral angles reside within the accessible β-sheet regions of the Ramachandran map.[8] The present design satisfies the two criteria essential for directing the formation of parallel and/or antiparallel β-sheet ensembles. It provides absolute control over the facial selectivity of the strand in intermolecular hydrogen-bonding interactions between the backbones and the means of rigorously regulating the relative sheet register thereby setting the identity of the cross-strand nearest neighbor residues. The facial selectivity is directed by the N-methylated amide functionalities of the backbone, which prevent one face of the peptide ring structure from participating in intermolecular hydrogen bonding. Control over the sheet register is the direct consequence of the alternating D- and L-conformations of the backbone, which constrains the β-sheet structure so that only homochiral residues can make up the cross-strand β-sheet neare pairs. This restriction is engendered by the requirement for the intermolecular hydrogen-bonding pattern which is dictated by the juxtaposition of amide hydrogen-bond donor and acceptor sites, as well as by the large steric interactions between side chain and backbone in alternative sheet-register and side-chain arrangements. Therefore, as the result of the above design features, enantiomerically pure peptides such as **1**–**3** can only form homodimeric antiparallel β-sheet structures. However, the same structural reasoning would dictate that a β-sheet structure made up of two enantiomeric peptide subunits must necessarily form the corresponding heterodimeric *parallel* β-sheet arrangement.

With this basic design notion in hand, we set out to measure the relative stability of parallel vs. antiparallel β-sheet structures using the two enantiomeric forms of the same peptide sequence (peptides **1** and **2**). A racemic solution containing an equal amount of peptides **1** and **2** can produce an equilibrium mixture of the parallel ensemble **1** · **2** and the enantiomeric antiparallel **1** · **1** and **2** · **2** β-sheet structures (Scheme 1). Formation of diastereomeric **1** · **2** and **1** · **1** (or its enantiomer **2** · **2**) complexes can be conveniently monitored by ^{1}H NMR spectroscopy. Previously, we have shown that peptide **1** or **2** can self-assemble in nonpolar organic solvents to form the predicted antiparallel β-sheet structure.[6] The structural and thermodynamic characteristics of the β-sheet structure have been established with high-resolution X-ray crystallography and 1D and 2D ^{1}H NMR spectroscopy. A particularly diagnostic feature in the ^{1}H NMR spectrum of peptide **1** or **2**, which signifies formation of the antiparallel β-sheet structure, is the resonance for the intermolecularly hydrogen-bonded NH proton at $\delta = 8.73$ having a



Scheme 1. The strategy employed for measuring the relative stability of the parallel and antiparallel β-sheet structures is schematically illustrated. For simplicity, only the backbone structures of the ensembles are illustrated (D and L refer to the chirality of the amino acid residues). Note that in all three ensembles only homochiral residues make up the nearest neighbor cross-strand pairs as indicated by the partial labeling of the αH_a positions. Association constants (K_a) were measured directly by analyzing the ^{1}H NMR spectra [6].

 © VCH Verlagsgesellschaft mbH, D-69451 Weinheim, 1995 0570-0833/95/0101-0096 $ 10.00+.25/0

$J_{NH,zH}$ coupling constant of 8.8 Hz (the NH proton of the free peptide subunit resonates at $\delta = 6.98$ with $J_{NH,zH} = 7.5$ Hz) (Fig. 1a). However, an equal mixture of the enantiomeric peptides **1** and **2**, in addition to the previously assigned ^{1}H NMR peaks for the antiparallel structure (**1** · **1** and **2** · **2**), displays a new set of ^{1}H NMR resonances for the parallel structure (**1** · **2**).[9] The NH proton's signal for the parallel β-sheet structure appears at $\delta = 8.49$ with the $J_{NH,zH}$ coupling constant of 8.8 Hz signifying the similarity of the backbone conformation in both parallel and antiparallel β-sheet structures (Fig. 1b). The

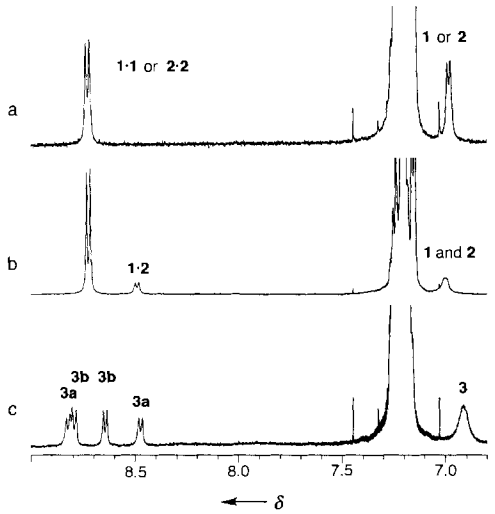
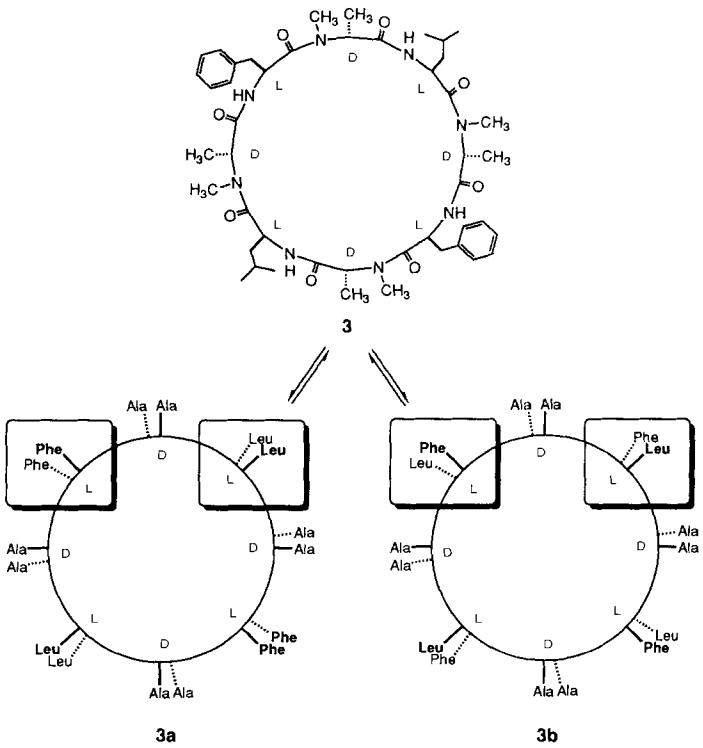


Fig. 1. The NH signals of the ^{1}H NMR spectrum (500 MHz in $CDCl_3$ at 293 K) of a) enantiomerically pure peptides **1** or **2** (1 mM), b) a racemic mixture of peptides **1** and **2** (10 mM), and c) peptide **3** (3.0 mM). All resonances were assigned based on the analysis of the ROESY spectra [6]. The labels refer to the position of the NH resonances: $\delta(\mathbf{1}) = \delta(\mathbf{2}) = 6.98$, $\delta(\mathbf{3}) = 6.92$; $\delta(\mathbf{1} \cdot \mathbf{1}) = \delta(\mathbf{2} \cdot \mathbf{2}) = 8.73$; $\delta(\mathbf{3a}) = 8.48$ and 8.83, and $\delta(\mathbf{3b}) = 8.65$ and 8.80; $\delta(\mathbf{1} \cdot \mathbf{2}) = 8.49$. All β-sheet ensembles display $J_{NH,zH}$ coupling constants of 8.8 Hz.

relative intensity of the ^{1}H NMR resonances was used to assess the free energy of stabilization of the two β-sheet arrangements. The above studies indicate that the antiparallel β-sheet structure ($\Delta G_{293} = 4.56$ kcal mol^{-1}, $K_a(CDCl_3) = 2540$ M^{-1} at 293 K)[6] is more stable by 0.8 kcal mol^{-1} than the parallel arrangment ($\Delta G_{293} = 3.76$ kcal mol^{-1}, $K_a(CDCl_3) = 640$ M^{-1} at 293 K).

An important consideration is whether the measured stability difference between the parallel and the antiparallel β-sheet structures is due to the difference in the backbone–backbone hydrogen-bonding pattern, or whether there exists a significant energetic contribution from the cross-strand side chain–side chain interactions,[4] which may favor a particular β-sheet arrangement. Peptide **3** was designed to probe the origin of the observed structural selectivity. In addition to the phenylalanine and alanine residues, the peptide contains two leucine residues in order to exaggerate any existing cross-strand interactions between side chains. The peptide subunit **3**, unlike peptides **1** and **2** which are fourfold symmetric, has only a twofold symmetry along the axis perpendicular to the plane of the ring structure.[10] Therefore, two diastereomeric antiparallel β-sheet ensembles can be formed: in one isomer (**3a**) D-Ala ··· D-Ala, L-Leu ··· L-Leu, and L-Phe ··· L-Phe residues form the cross-strand pairs, while in the other isomer (**3b**) D-Ala ··· D-Ala, and L-Leu ··· L-Phe residues make up the nearest neighbor pairs (Fig. 2). If significant cross-strand interactions between side chains exist, then formation of one ensemble should predominate.[10] Analysis of the ^{1}H NMR spectrum of the peptide **3** is



Scheme 2. Schematic representation of the self-assembly of peptide **3** producing two diastereomeric antiparallel β-sheet ensembles **3a** and **3b** (amino acid side-chain positions in the top strand are indicated by the solid lines and the bottom strand by the dashed lines). Boxed residues emphasize the differences between the two β-sheet ensembles **3a** and **3b** in the juxtapositioning of cross-strand nearest neighbor side chains.

indicative of an almost equal mixture of the two expected **3a** and **3b** isomers (Fig. 1c).[11] This study clearly establishes lack of any significant contribution (~ 50 cal mol^{-1} at 293 K) from interactions between side chains toward structural stability, which is the expected outcome considering the hydrophobic side chains and the nonpolar solvents employed in the above studies. Therefore, the observed thermodynamic preference for the antiparallel structure reflects the underlying differences in the recognition of the backbone–backbone pattern in the parallel vs. antiparallel β-sheet arrangements.

In summary, the present study provides the first rigorously characterized model for β-sheet structure that assesses the contribution of backbone–backbone interactions and cross-strand interactions between side chains in directing the formation of parallel and antiparallel β-sheet arrangements. It should be expected that changes in the polarity of the medium may produce significant and additive energetic contributions, emanating from cross-strand interactions between side chains, toward stabilizing a particular β-sheet arrangement. The availability of the simple β-sheet model system presented here may now provide the means for the detailed characterization of underlying factors which favor the β-sheet structural fold.

Received: September 5, 1994 [Z 7292 IE]
German version: *Angew. Chem.* **1995**, *107*, 79

Keywords: peptides · self-assembly · β-sheet structures

[1] a) L. Pauling, R. B. Corey, *Proc. Natl. Acad. Aci. USA* **1951**, *37*, 251–256; b) *ibid.* **1953**, *39*, 253–256; c) F. R. Salemme, *Prog. Biophys. Molec. Biol.* **1983**, *42*, 95–133.

[2] a) C. A. Kim, J. M. Berg, *Nature (London)* **1993**, *362*, 267–270; b) D. L. Minor, Jr., P. S. Kim, *ibid.* **1994**, *367*, 660–663; c) C. K. Smith, J. M. Withka, L. Regan, *Biochemistry* **1994**, *33*, 5510–5517.

 © VCH Verlagsgesellschaft mbH, D-69451 Weinheim, 1995 0570-0833/95/0101-0097 $ 10.00+.25/0

[3] a) J. S. Balcerski, E. S. Pysh, G. M. Bonora, C. Toniolo, *J. Am. Chem. Soc.* **1976**, *98*, 3470–3473; b) D. S. Kemp, B. R. Bowen, *Tetrahedron Lett.* **1988**, *29*, 5081–5082; c) D. S. Kemp, B. R. Bowen, C. C. Muendel, *J. Org. Chem.* **1990**, *55*, 4650–4657; d) K. Y. Tsang, H. Diaz, N. Graciani, J. W. Kelly, *J. Am. Chem. Soc.* **1994**, *116*, 3988–4005.

[4] a) K.-C. Chou, G. Némethy, H. A. Scheraga, *Biochemistry* **1983**, *22*, 6213–6221; b) S. Lifson, C. Sander, *Nature (London)* **1979**, *282*, 109–111; c) K.-C. Chou, G. Némethy, H. A. Scheraga, *Acc. Chem. Res.* **1990**, *23*, 134–141.

[5] a) G. Seipke, H. A. Arfmann, K. G. Wagner, *Biopolymers* **1974**, *13*, 1621–1633; b) A. Brack, L. Orgel, *Nature (London)* **1975**, *256*, 383–387; c) S. S. Pierree, R. T. Ingwall, M. S. Varlander, M. Goodman, *Biopolymers* **1978**, *17*, 1837–1847; d) D. G. Osterman, E. T. Kaiser, *J. Cell. Biochem.* **1985**, *29*, 57–72; e) K.-H. Altmann, A. Flörsheimer, M. Mutter, *Int. J. Pept. Protein Res.* **1986**, *27*, 314–319; e) M. Mutter, R. Gassmann, U. Buttkus, K.-H. Altmann, *Angew. Chem.* **1991**, *103*, 1504–1506; *Angew. Chem. Int. Ed. Engl.* **1991**, *30*, 1514–1516; f) S. Zhang, T. Holmes, C. Lockshin, A. Rich, *Proc. Natl. Acad. Sci. USA* **1993**, *90*, 3334–3338.

[6] M. R. Ghadiri, K. Kobayashi, J. R. Granja, R. K. Chadha, D. E. McRee, *Angew. Chem.* **1995**, *107*, 76–78; *Angew. Chem. Int. Ed. Engl.* **1995**, *34*, 93–95.

[7] a) M. R. Ghadiri, J. R. Granja, R. A. Milligan, D. E. McRee, N. Khazanovich, *Nature (London)* **1993**, *366*, 324–327; b) M. R. Ghadiri, J. R. Granja, L. K. Buehler, *ibid.* **1994**, *369*, 301–304; c) N. Khazanovich, J. R. Granja, D. E. McRee, R. A. Milligan, M. R. Ghadiri, *J. Am. Chem. Soc.* **1994**, *116*, 6011–6012.

[8] The cyclic peptide structure, although representing a limiting form of backbone twist, has backbone ϕ and φ angles (-128.4 and 126.7°, respectively, for Phe and 131.5 and $-146.2°$, respectively, for Ala) that are well within the allowed β-sheet regions of the Ramachandran map.

[9] This species has been fully characterized by the observed exchange and NOE cross peaks in the ROESY spectrum. Additional support for the formation of this new dimeric ensemble was provided by deuterium labeling studies. The amide backbone protons of peptide **1** were first exchanged with deuterium ($96 \pm 2\%$ incorporation) and then mixed with an equal amount of peptide **2**. Analysis of the ^{1}H NMR spectrum, comparing the intensity of the NH resonances to those of the α and β protons and of the side chain, indicated a $50 \pm 4\%$ reduction in the NH signal intensity, thus unequivocally establishing the dimeric state of the new β-sheet ensemble.

[10] Because of the fourfold symmetry along the axis perpendicular to the plane of the ring, the enantiomeric peptides **1** and **2** can only form one type of antiparallel β-sheet ensemble (four equivalent hydrogen-bonding positions) in which Ala-Ala and Phe-Phe residues make up the near neighbor cross-strand pairs. However, in the case of peptide **3** in which only a twofold symmetry along the same axis exists, two diastereomeric β-sheet structures are possible. Because both ensembles have identical hydrogen-bonding interactions between the backbones, the relative population of the two diastereomers will be dictated by the difference in the energetic contributions of the nearest neighbor cross-strand interactions between side chains.

[11] All NMR resonances, including the sets belonging to **3a** and **3b** ensembles, were assigned with the aid of ROESY spectroscopy. ^{1}H NMR studies indicate the formation of a 48:52 (± 0.5) mixture of the two diastereomers corresponding to $\Delta\Delta G_{293} = 48 \pm 14$ cal mol^{-1}. We were unable to assign with high confidence which set of signals belonged to the diastereomers **3a** or **3b**. Therefore, for illustrative simplicity we have arbitrarily assigned each set of resonances to **3a** or **3b** in Figure 1.

Synthesis and Structure of a Dendritic Polysilane**

Joseph B. Lambert,* Jodi L. Pflug, and Charlotte L. Stern

The chemistry of oligo- and polymeric silanes, $(-SiR_2-)_n$, has blossomed over the last 20 years.[1] These molecules are of interest for their structural, electronic, optical, and chemical properties. These advantageous properties, however, can be offset by the lability of the Si–Si bonds, which have low bond dissociation energy in polysilane chains compared with C–C bonds in hydrocarbon chains.[1] The Si–Si bonds can be isomerized by acid catalysts and can be cleaved by nucleophiles, electrophiles, or light.[2] On a different front, the last 10 years have seen the rapid rise in the study of dendritic polymers, whose repeatedly branched structure emanates from a single core.[3] Such materials tend toward the shape of a sphere, and many bonds are inaccessible to attack by reagents in solution.

We have sought to prepare dendrimers composed entirely of polysilane chains, with the expectation that the less accessible inner Si–Si bonds would exhibit high stability. Because the dendritic structure contains a multiplicity of branching sites, the longest polysilane chain is repeated many times. Such structural redundancy means that a single Si–Si scission most likely will not alter the optical or electronic properties that make polysilanes important.

Except for a few simple compounds with a core Si bonded to three or four Si atoms, that is, so-called zeroth generation dendrimers such as $(Me_3Si)_4Si$, to our knowledge there are no known dendritic polysilanes. We report herein the preparation and crystal structure of the first such example, methyl[tris(permethylneopentasilyl)]silane (**1**),[4] in which the longest poly-

$[(Me_3Si)_3SiSiMe_2]_3SiMe$ **1**

silane chain of seven silicon atoms is repeated 27 times in the dendritic structure. The core silicon atom in **1** is bonded to a methyl group and to three dimethylsilyl groups that serve as spacers to the next branching point, which is a silicon atom to which three trimethylsilyl groups are attached. Scission of one of the peripheral Si–Si bonds in a tris(trimethylsilyl)silyl group still would leave 21 intact Si_7 pathways. Even scission of two such Si–Si bonds would leave 15 or 16 Si_7 pathways, depending on whether the two Si–Si bonds are in respectively the same or different tris(trimethylsilyl)silyl groups. Scission of a Si–Si bond on either side of a spacer dimethylsilanediyl group would remove one of the three dendrons or wedges but still leave nine Si_7 pathways. This molecule therefore illustrates the redundancy present in dendritic polysilanes.

The dendrimer **1** was prepared starting from commercially available tris(trimethylsilyl)silane, which was converted in 90% yield to methyl[tris(trimethylsilyl)]silane by sequential treatment with chloroform (or carbon tetrachloride) and methyllithium. Treatment of the resulting silane with chlorotrimethylsilane and aluminum trichloride according to the method of Ishikawa et al.[5] yielded methyl[tris(chlorodimethylsilyl)]silane in 75% yield after purification by distillation. A single chlorine atom on one of the $SiMe_3$ substituents deactivates the group to further demethylation/chlorination; thus the reaction time and temperature were chosen to ensure that the trichlorinated level was reached. Subsequent reaction of the trichlorinated silane with tris(trimethylsilyl)silyllithium[6] in methyltetrahydrofuran at -15 °C yielded the dendrimer **1** in 85% yield after recrystallization.

The white solid **1** does not sublime but softens around 150 °C. The highest cluster in the mass spectrum has its largest peak at m/z 945, which corresponds to loss of methyl from the expected largest peak in the parent isotopic cluster, which would occur at $(M + 2)$ or 960. The most abundant peak, at m/z 305, corresponds to the permethylneopentasilyl group (one wedge). The ^{29}Si NMR spectrum contains peaks at $\delta = -69.6$ from the core silicon, at $\delta = -26.7$ for the silicon atoms of the spacer (Me_2Si), at $\delta = -124$ for the silicon atoms at the first generation branching point, and at $\delta = -9.44$ for the peripheral

[*] Prof. J. B. Lambert, J. L. Pflug, C. L. Stern
Department of Chemistry
Northwestern University
Evanston, IL 60208-3113 (USA)
Telefax: Int. code +708-491-7713

[**] This work was supported by the National Science Foundation (Grant No. CHE-9302747). We thank Mr. J. M. Denari for measuring the extinction coefficients.

trimethylsilyl silicon atoms. To form a second generation dendrimer, each of the nine trimethylsilyl groups could be converted to dimethylsilyl spacer groups which could then bind to new tris(trimethylsilyl)silyl groups.

The structure of dendrimer **1** was confirmed by X-ray crystallography (Fig. 1).[7] The three neopentasilyl groups are arranged so that the molecule has a threefold axis of symmetry through the Si–C bond of the core silicon atom. There are two equally populated arrangements present in the asymmetric unit, differing in configuration at the core silicon. As a result, there is an effective mirror plane perpendicular to the C_3 axis, and the molecule appears to lie on a sixfold inversion center. There is slight disorder of the trimethylsilyl groups, which enlarges the thermal ellipsoids and raises the *R* factor.

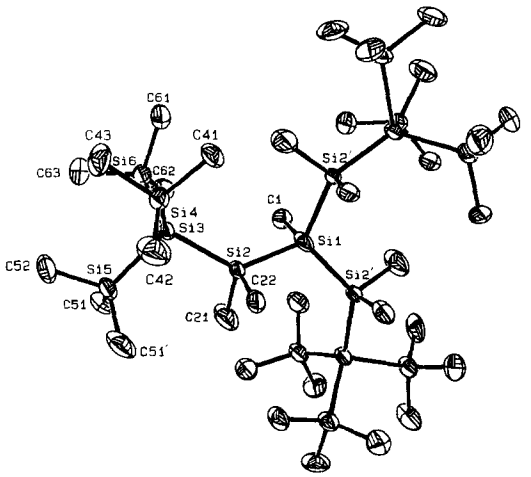


Fig. 1. The crystal structure of **1**.

There is considerable steric interaction between the three permethylneopentasilyl groups. As a result, the three dimethylsilyl groups around the central Si atom flatten toward the methyl group, as indicated by the enlarged Si2-Si1-Si2′ angle (116.10(4)°) and the diminished Si2-Si1-CH_3 angle (101.54(7)°). The most significant distortion that relieves the steric interaction is the considerable increase in the Si1-Si2-Si3 angle (130.4(1)°), which is largely compensated for by the decrease in the CH_3-Si2-CH_3 angle (97.8(3)°). The only other significant (>5°) angular distortion is of Si2-Si3-Si6, which opens up to 119.9(1)°. Steric congestion in **1** also is reduced by stretching Si2–Si3 (2.390(3) Å) (no other Si–Si distortions differ by more than 0.03 Å from the normal length of 2.340 Å as found for example in hexamethyldisilane[8]). Extreme bond stretching has been found in hexa-*tert*-butyldisilane (2.697 Å),[9] but this molecule does not have easily distortable Si-Si-Si angles and therefore is forced to take the more expensive route of bond stretching. These results suggest that two dimethylsilyl spacers between branching points would provide a more strain-free molecule.

The 27 Si_7 pathways in the dendrimer are not equivalent in the solid. Each pathway is defined by four dihedral angles. Although not always exactly 60 or 180°, they nonetheless may be broadly classified as *gauche* (G) or *anti* (A). In the crystal there are three AGAA, six GGAA, six GAGA, and twelve GAGG pathways (see Fig. 1). There is no all-*anti* pathway, usually associated with optimal electronic delocalization. Nonetheless, the λ_{max} at 272 nm is lower in energy than that of the linear heptasilane (266 nm), and almost identical to that of octasilane (272.5 nm),[10] which presumably exist predominantly in *anti* forms.[11] At least as measured by UV absorption, this dendrimer with its multiplicity of conformational pathways has molecular orbitals with similar delocalization to that of linear polysilanes of the same length.

The redundancy of pathways is most remarkably manifested by the extinction coefficient of the absorption maximum at 272 nm. Linear polysilanes of length six to eight have extinction coefficients in the range $2-4\times10^4$,[10] but the dendrimer **1** exhibits an extinction coefficient of 3.4×10^5, more than an order of magnitude larger than that of the linear heptasilane. Thus, the multiplicity of pathways dramatically enhances the extinction coefficient without appreciably changing the absorption maximum.

We are currently engaged in the preparation and characterization of other dendritic polysilanes, whose electronic properties should be as interesting as those of linear polysilanes and whose chemical and environmental stability should exceed that of linear polysilanes, because of steric inaccessibility of many of the Si–Si bonds and redundancy of pathways.

Received: June 30, 1994 [Z 7083 IE]
German version: *Angew. Chem.* **1995**, *107*, 106

Keywords: dendrimers · polysilanes · silicon compounds

[1] R. Walsh, *Acc. Chem. Res.* **1981**, *14*, 246–252.
[2] R. West in *The Chemistry of Organic Silicon Compounds, Part 2* (Eds.: S. Patai, Z. Rappoport), Wiley, Chichester, **1989**, Ch. 19, pp. 1207–1240.
[3] D. A. Tomalia, H. D. Durst, *Top. Curr. Chem.* **1993**, *165*, 193–313.
[4] Named as a substituted Si_7 chain, this molecule is 1,1,1,3,3,4,5,5,7,7,7-undecamethyl-2,2,6,6-tetrakis(trimethylsilyl)-4-(1,1,3,3,3-pentamethyl-2,2-bis(trimethylsilyl)trisilyl)heptasilane.
[5] M. Ishikawa, M. Kumada, H. Sakurai, *J. Organomet. Chem.* **1970**, *23*, 63–69.
[6] G. Gutekunst, A. G. Brook, *J. Organomet. Chem.* **1982**, *225*, 1–3.
[7] $Si_{16}C_{34}H_{102}$; $M_r = 960.55$, $a = 15.020(3)$, $c = 16.016(4)$ Å, $V = 3129(2)$ Å^3, space group $P6_3/m$, $Z = 2$, $\rho_{calcd} = 1.019$ g cm^{-3}, $2\theta_{max} = 46.0°$, $Mo_{K\alpha}$ ($\lambda = 0.71069$ Å), -120 °C; 2627 unique reflections, 1330 reflections with $I > 3\sigma$, $R = 0.059$, $R_w = 0.061$ (129 parameters). The structure was solved by the SHELXS-86 direct methods, and all non-hydrogen atoms were refined anisotropically (Texsan 5.0). Hydrogen atoms were fixed at idealized positions, except for those on the methyl C1 on the core silicon Si1. The maximum and minimum peaks on the final difference Fourier map corresponded to 0.51 and -0.46 e Å^{-3}, respectively. Further details of the crystal structure are available on request from the Director of the Cambridge Crystallographic Data Centre, 12 Union Road, GB-Cambridge CB21EZ (UK).
[8] B. Beagley, J. J. Monaghan, T. G. Hewitt, *J. Mol. Struct.* **1971**, *8*, 401–411.
[9] N. Wiberg, H. Schuster, A. Simon, K. Peters, *Angew. Chem.* **1986**, *98*, 100–101; *Angew. Chem. Int. Ed. Engl.* **1986**, *25*, 79–80.
[10] H. Gilman, W. H. Atwell, G. L. Schwebke, *J. Organomet. Chem.* **1964**, *2*, 369–371.
[11] H. S. Plitt, J. W. Downing, M. K. Raymond, V. Balaji, J. Michl, *J. Chem. Soc. Faraday Trans.* **1994**, *90*, 1653–1662.

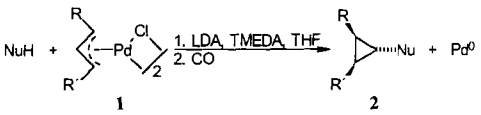
 © VCH Verlagsgesellschaft mbH, D-69451 Weinheim, 1995 0570-0833/95/0101-0099 $ 10.00+.25/0

Isolation and X-Ray Crystal Structure of a Palladacyclobutane: Insight into the Mechanism of Cyclopropanation**

H. M. R. Hoffmann,* Andreas R. Otte, Andreas Wilde, Stephan Menzer, and David J. Williams

The reaction of (η^3-allyl)palladium complexes with nucleophiles is of general synthetic and fundamental, mechanistic interest.[1] We report here on the preparation, isolation, and full characterization of a palladacyclobutane, the structure of which affords insight into the mechanism of cyclopropane formation.

We have previously shown that a nucleophilic cyclopropanation of (η^3-allyl)palladium complexes is feasible (Scheme 1),[2-4] provided that the following is taken into account: 1) Sterically hindered, less stabilized nucleophiles (pK_a range of protonated carbanions 20–30) give the highest yields;

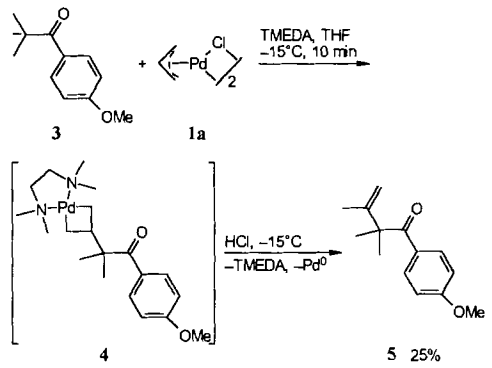


Scheme 1. R = H, aryl, alkyl; R′ = H, aryl, *not* alkyl. LDA = lithium diisopropylamide, TMEDA = *N,N,N′,N′*-tetramethylethylenediamine.

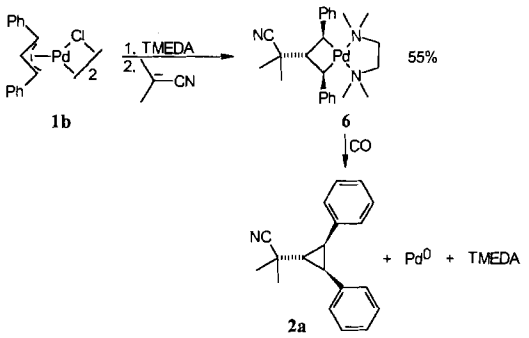
2) TMEDA is the most successful ligand and cosolvent—other bidentate N,N-donors (e.g., sparteine) provide lower yields; 3) added carbon monoxide accelerates and facilitates cyclopropane formation; and 4) the reaction temperature must be carefully optimized and depends on the pK_a and reactivity of the attacking nucleophile (e.g., deprotonated esters, amides, sulfones, fluorene, nitriles, and deprotonated ketones). The electrophilicity of the (η^3-allyl)palladium complex also varies depending on the structure of the allyl ligand. The optimum temperature is in the range −60 °C to −15 °C.

It has been suggested that "reductive elimination of cyclopropane is a fast process, as no palladacyclobutane has been isolated."[5] Indeed, attempts to isolate palladacyclobutanes from the reaction of η^3-allyl complex **1a** and benzenologous ester enolate **3** at −15 °C were not successful (Scheme 2). However, we assumed metallacyclobutane **4** to be the reactive intermediate, since addition of concentrated aqueous HCl at −15 °C caused an immediate precipitation of palladium black. On workup olefin **5** was isolated. This product is thought to arise as a result of monoprotonation of a carbon–palladium σ bond in **4** and β-hydride elimination. We then tried to prepare palladacyclobutanes with two secondary rather than two primary (cf. **4**) alkylpalladium bonds; this would allow us to take advantage of the "aryl effect".[4]

The reaction of (η^3-1,3-diphenylallyl)palladium with deprotonated isobutyronitrile in THF/TMEDA[6] at −15 °C (Scheme 3) gave a yellow solution, which, on warming to room temperature, furnished a yellow powder. This was isolated, purified and identified by chemical and spectroscopic means. A cyclopropane product was not observed. The compound was kinetically inert at room temperature, and also stable to air and water. When carbon monoxide was passed over a dichloromethane solution of these crystals, palladium precipitated and the substituted cyclopropane **2a** was formed (by reductive elimination). ^{1}H and ^{13}C NMR data suggested that palladacyclobutane **6** was the isolated intermediate (Scheme 3, Table 1).



Scheme 2.



Scheme 3.

Table 1. Physical and spectroscopic data for **6**.

M.p. 128 °C (decomp.); IR: ($CHCl_3$): $\tilde{\nu}$[cm^{-1}] = 3000, 2972, 2912, 2228, 1586, 1484, 1460; ^{1}H NMR (200 MHz, CD_2Cl_2): δ = 7.49 (d, J = 7 Hz, 4H, H_{arom}), 7.12 (t, J = 7.7 Hz, 4H, H_{arom}), 6.86 (tt, J = 7 Hz, 1 Hz, 2H, H_{arom}), 3.22 (t, J = 9.5 Hz, 1H, CH), 2.36 (s, 6H, 2 NCH_3), 2.55–2.40, 2.17–2.02 (m, 4H, CH_2-CH_2), 1.56 (d, J = 9.5 Hz, 2H, PhC*H*), 1.44 (s, 6H, 2 NCH_3), 0.98 [s, 6H, 2 $(CH_3)_2CCN$]

^{13}C NMR [a]: (CD_2Cl_2): δ = 154.47 (↑), 128.35 (↓), 127.58 (↓), 126.34 (↑), 121.44 (↓), 63.23 (↓), 60.05 (↑), 48.66 (↓), 47.71 (↓), 45.20 (↑), 24.51 (↓), 5.21 (↓); MS (70 eV): m/z (%): 261 (4), 193 (76), 115 (100), 91 (30)

[a] APT (*a*ttached *p*roton *t*est): spin echo based selection of multiplicities of ^{13}C NMR signals. Quaternary C and CH_2 carbon atoms give positive signals (↑), while CH and CH_3 give negative signals (↓).

Slow evaporation of a dichloromethane solution of **6** at room temperature provided single crystals suitable for X-ray crystallography (Fig. 1).[7] The molecule is virtually symmetric and has an average noncrystallographic C_s symmetry about the plane perpendicular to the coordination plane and bisecting the C(6)–C(7) bond (Fig. 2, top). The two phenyl rings are approximately coplanar (5° between their mean planes) and oriented orthogonally (89°) with respect to the C(2)-Pd-C(4) plane. This arrangement of the two phenyl rings optimizes orbital overlap of the two Pd–C σ bonds with the aromatic π electron systems.

[*] Prof. H. M. R. Hoffmann, Dr. A. R. Otte, Dr. A. Wilde
Department of Organic Chemistry, University of Hannover
Schneiderberg 1 B, D-30167 Hannover (Germany)
Telefax: Int. code + (511)762-3011
Dr. S. Menzer, Dr. D. J. Williams
Chemical Crystallography Laboratory, Imperial College of Science Technology and Medicine, South Kensington, London, SW7 2AY (UK)

[**] We thank Prof. H. Duddeck for advice with the NMR spectra. Our work was supported by the Deutsche Forschungsgemeinschaft and Degussa by a generous gift of palladium salts. The Fonds der Chemischen Industrie provided a PhD fellowship to A. Wilde.

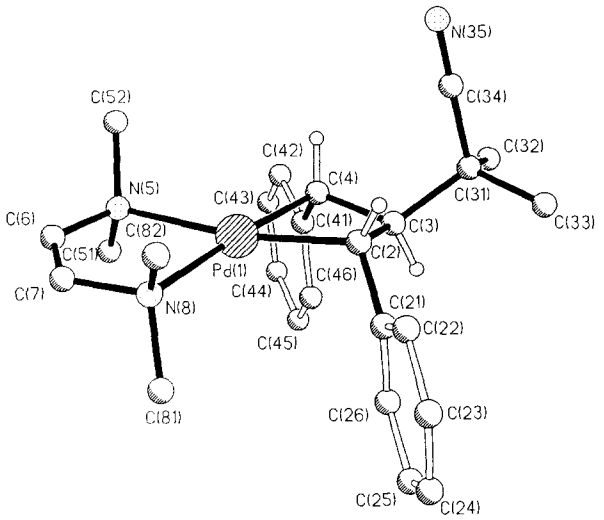
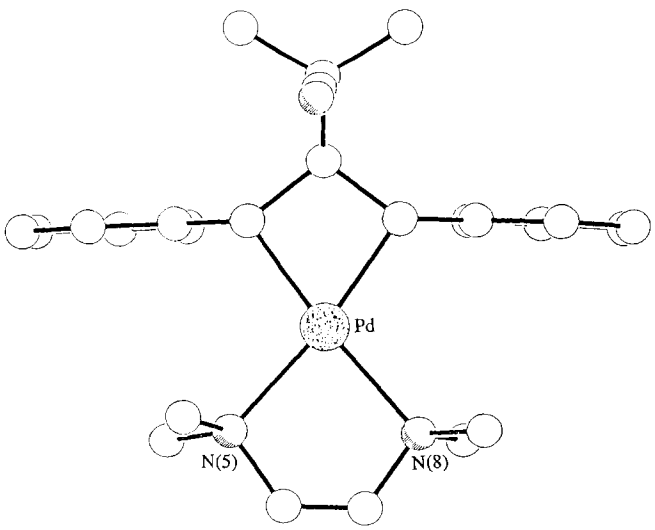


Fig. 1. Crystal structure of **6**. Hydrogen atoms only shown at C(2), C(3), and C(4). The numbering of the atoms does not conform to IUPAC conventions. Important bond lengths [Å] and angles [°]: Pd-C(2) 2.060(5), Pd-C(4) 2.048(4), Pd-N(5) 2.230(4), Pd-N(8) 2.233(4), C(2)-C(3) 1.535(6), C(3)-C(4) 1.532(6); C(2)-Pd-C(4) 69.8(2), N(5)-Pd-N(8) 81.7(2), Pd-C(2)-C(3) 93.2(3), Pd-C(2)-C(21) 115.3(3), C(21)-C(2)-C(39) 119.0(4), C(2)-C(3)-C(4) 100.1(3), C(2)-C(3)-C(31) 116.5(4), C(4)-C(3)-C(31) 116.3(4), C(3)-C(4)-Pd 93.7(3), C(3)-C(4)-C(41) 117.3(4), C(41)-C(4)-Pd 114.3(3).



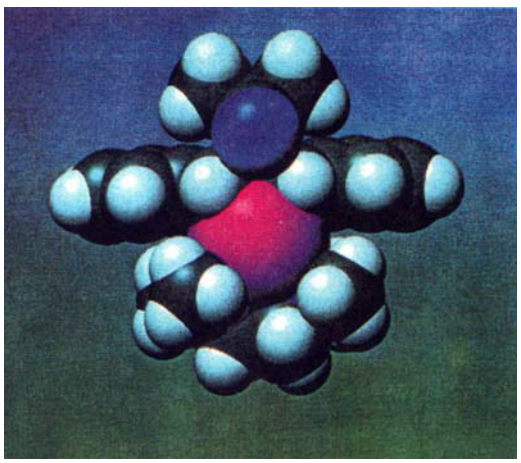


Fig. 2. Crystal structure of **6** (top view). Top: ball-and-stick representation. Bottom: space-filling model.

The ligands around the Pd atom adopt a distorted square-planar geometry with internal ligand angles at Pd of 69.8(2)° within the palladacyclobutane moiety and 81.7(2)° within diazapalladacyclopentane. The palladacyclobutane ring is not flat, but slightly folded at a fold angle of 161.4° about the C(2)–C(4) diagonal (i.e., 18.6° out of plane). As a consequence of this slight folding,[8] there is unfavorable near-eclipsing of the substituents attached to C(2) and C(3) and of those at C(3) and C(4) (Fig. 3).[9, 10] The Pd–C bond lengths [Pd–C(4) 2.048(4), Pd–C(2) 2.060(5) Å] are within the normal range. However, the Pd–N bonds [2.230(4) and 2.233(4) Å], which are *trans* to a Pd–C sp^3 bond, are unusually long; this is consistent with a *trans* effect.[11]

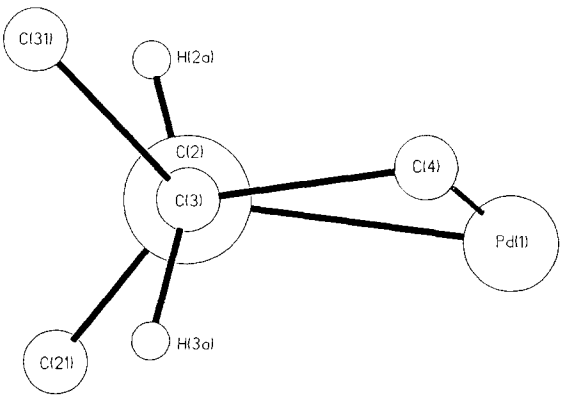


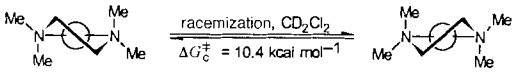
Fig. 3. Selected torsion angles in **6**.

The distance between the two *ortho* aromatic hydrogens pointing inwards is small (2.57 Å); the palladium atom is therefore screened from attack from the bottom face of the molecule. However, the top face is comparatively accessible (Fig. 2, bottom), and reaction of the palladium center with carbon monoxide is thus possible.[12] β-Hydride eliminations are generally fast reactions, but require a synperiplanar conformation. In the case at hand, the torsion angles are not far from 90° (Pd-C(4)-C(3)-H(3) 107° and Pd-C(2)-C(3)-H(3) −107°), and alkene formation is thus effectively blocked.

The NMR spectrum (solvent CD_2Cl_2) of **6** is temperature-dependent. The ^{13}C signals of the four $N(CH_3)_2$ carbon atoms are not equivalent and appear as two singlets; this is consistent with the ^1H NMR spectrum (two singlets, 6H; cf. ref. [9]). At −80 °C the two ^{13}C signals of the $N(CH_3)_2$ carbons split into four signals ($T_c \approx 233$ °K; $\Delta G_c^{\ddagger} = 10.5 \pm 0.5$ kcal mol^{-1}), and the singlet corresponding to the CH_2CH_2 group is transformed into two singlets ($T_c \approx 208$ °K; $\Delta G_c^{\ddagger} = 10.4 \pm 0.5$ kcal mol^{-1}). Moreover, there are two Pd*C*HPh singlets ($T_c \approx 218$ °K; $\Delta G_c^{\ddagger} = 10.3 \pm 0.5$ kcal mol^{-1}), and the singlet due to the geminal dimethyl carbon atoms ($C(CH_3)_2CN$) splits into two singlets. However, the singlets assigned to the quaternary ($C(CH_3)_2CN$), cyano, and ring (C(3)) carbon atoms remain sharp down to −90 °C. These results are consistent with the following conformational fluctuations: The molecule loses its "dynamic C_s symmetry"; instead, two equally populated enantiomers (C_2 symmetry) appear, which interconvert (racemize) (Scheme 4).[13]

At room temperature the aromatic carbons appear as four discrete signals (2 × *ipso*, 4 × *ortho*, 4 × *meta*, 2 × *para*). At −80 °C signals of the *ipso* and the *para* C atoms are each split into two, as expected for the hindered racemization discussed

 © VCH Verlagsgesellschaft mbH, D-69451 Weinheim, 1995 0570-0833/95/0101-0101 $ 10.00+.25/0

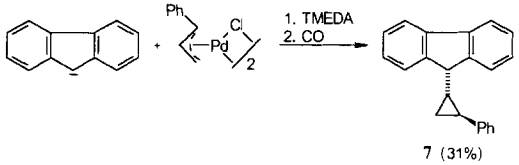


Scheme 4. Racemization of **6** in CD_2Cl_2 (the broken circle denotes the Pd atom; other atoms omitted). Schematic representation: The deviation of the methylene carbons from the N-Pd-N plane is only about 0.026–0.05 Å.

above. However, signals corresponding to the *ortho* and *meta* C atoms each split not into two, but four signals. Thus, all twelve aromatic carbon atoms become inequivalent. Hindered racemization is accompanied by a freezing of the phenyl group rotation. We assume that the barrier to rotation of the phenyl group is comparable to that of racemization. The barrier to rotation about the C–Ph ($\Delta G_c^{\ddagger} = 10$ kcal mol^{-1}) indicates a significant steric hindrance. Each phenyl group is jammed by one opposing N-methyl group.[9]

The crystal structures of **6** and the final product **2a**[14] allow us to map out the reaction pathway of (η^3-1,3-diphenylallyl)palladium complex **1b** with deprotonated isobutyronitrile in the presence of TMEDA. The bulky nucleophile does not attack the electron-rich metal center, but instead the central carbon atom of the allyl ligand, and palladacyclobutane **6** is formed. Because of the mutual repulsion between the two phenyl groups in **6**, the spontaneous reductive elimination to the *cis*-diphenyl cyclopropane **2a** from palladacyclobutane **6** is impeded. However, cyclopropanation is accelerated, and yields are generally improved by passing carbon monoxide over the reaction solution.[12, 15] Carbon monoxide is not only sterically accessible, but also a strong π acid. By attacking the 16-electron metallacycle from the top face (Fig. 2, bottom) carbon monoxide removes electron density from palladium and thus facilitates reductive elimination and conversion of the 1,3-propanediyl ligand into the corresponding cyclopropane. It seems likely that the transformation of **6** to **2a** in the presence of carbon monoxide proceeds via an 18-electron transition state or intermediate.[12] In any event, the transannular C(2)···C(4) distance in **6** (2.35 Å) must be contracted substantially to approximately 1.55 Å in **2a**, corresponding to the new C–C bond.[14]

The question arises as to whether the nucleophilic enolate initially attacks the η^3-allyl complex at palladium through its heteroatom (i.e., oxygen), and the palladacyclobutane is subsequently formed by a favorable intramolecular pathway. We have found that the anion of fluorene ($pK_a = 23$), which is devoid of all heteroatoms, is also capable of inducing cyclopropanation (Scheme 5). Thus direct attack of the hindered nucleophilic carbon at the central position of the allyl ligand seems to be the more likely mechanism.



Scheme 5.

In summary, we have established the experimental conditions for converting a range of η^3-allyl Pd complexes into cyclopropanes. Palladacyclobutane is a key intermediate, the structure of which permits an in-depth analysis of the reaction pathway. With the synthesis and full characterization of the title heterocycle, we have contributed a new type of metallacycle to the growing class of metallacyclobutanes, which are of general relevance in catalysis.[16]

Received: July 4, 1994 [Z 7095 IE]
German version: *Angew. Chem.* **1995**, *107*, 73

Keywords: cyclopropanation · palladacyclobutanes · palladium compounds

[1] J. P. Collman, L. S. Hegedus, J. R. Norton, R. G. Finke, *Principles and Applications of Organotransition Metal Chemistry*, University Science Books, Mill Valley, CA, **1987**, pp. 881–919; B. M. Trost, *Angew. Chem.* **1989**, *101*, 1199; *Angew. Chem. Int. Ed. Engl.* **1989**, *28*, 1173; C. Elschenbroich, A. Salzer, *Organometallics – A Concise Introduction*, 2nd ed, VCH, Weinheim, **1992**.

[2] H. M. R. Hoffmann, A. R. Otte, A. Wilde, *Angew. Chem.* **1992**, *104*, 224; *Angew. Chem. Int. Ed. Engl.* **1992**, *31*, 234.

[3] A. Wilde, A. R. Otte, H. M. R. Hoffmann, *J. Chem. Soc. Chem. Commun.* **1993**, 615.

[4] A. R. Otte, A. Wilde, H. M. R. Hoffmann, *Angew. Chem.* **1994**, *106*, 1352; *Angew. Chem. Int. Ed. Engl.* **1994**, *33*, 1280.

[5] Homologous platinacyclobutanes are stable and known: C. Carfagna, R. Galarini, A. Musco, R. Santi, *Organometallics* **1991**, *10*, 3956, zit. Lit.

[6] The reaction of (η^3-allyl)palladium complexes with TMEDA has been studied: L. S. Hegedus, B. Åkermark, D. J. Olsen, O. P. Anderson, K. Zetterberg, *J. Am. Chem. Soc.* **1982**, *104*, 697.

[7] Crystal data for **6**: orthorhombic, $a = 10.737(4)$, $b = 11.023(2)$, $c = 20.284(7)$ Å, $V = 2400.5(14)$ Å^3, space group $P2_12_12_1$, $Z = 4$, $\rho_{calcd} = 1.34$ g cm^{-3}, $\mu(Mo_{K\alpha}) = 7.9$ cm^{-1}, 2507 independent observed reflections with [($|F_o| > \sigma|F_o|$), $2\theta \leq 55°$], refined to $R = 0.032$, $R_w = 0.032$. Siemens P4 diffractometer, ω scans, $Mo_{K\alpha}$ radiation (graphite monochromator). The structure was solved by direct methods, and the non-hydrogen atoms refined anisotropically. There is a 50:50 up–down/down–up disorder (static rather than dynamic) of the C(6)–C(7) bond; these atoms were refined subject to refined C–C and C–N distance constraints. H atoms were assigned isotropic thermal parameters and allowed to ride on their parent carbon atoms. Further details of the crystal structure investigation are available from the Cambridge Crystallographic Data Centre, 12 Union Road, Cambridge CB2 1EZ (UK), on quoting the full journal citation.

[8] Conformational analysis of cyclobutane and heterocyclic analogues: R. M. Moriarty, *Top. Stereochem.* **1974**, *8*, pp. 271–421. A square-planar, D_{4h}-symmetric cyclobutane is fully eclipsed and has internal angles of $4 \times 90°$ (= 360°). Usually cyclobutanes try to escape this unfavorable conformation by puckering.

[9] The slight puckering of the palladacyclobutane ring is accompanied by approach of one of the N-methyl groups N(5) and N(8) towards the π faces of the adjacent phenyl groups (2.58 Å and 2.67 Å, respectively). ^{1}H NMR evidence indicates that this close contact persists in solution [the signals of $N(CH_3)_2$ are inequivalent ($\delta = 2.36$ (6H, s), 1.44 (6H, s)); i.e., anisotropic shielding by two facing phenyl rings causes an upfield shift of almost 1 ppm].

[10] The only related system is a bis(methoxycarbonyl)-substituted palladacyclobutan-3-one (a substituted 2-oxopropanediyl); however, this exhibits substantial folding (53°) of the four-membered ring, accompanied by pyramidalization at the carbonyl center. Furthermore, a β-hydride elimination is structurally impossible in this case. R. D. W. Kemmitt, P. McKenna, D. R. Russell, L. J. S. Sherry, *J. Chem. Soc. Dalton Trans.* **1985**, 259.

[11] W. de Graaf, J. Boersma, W. J. J. Smeets, A. L. Spek, G. van Koten, *Organometallics* **1989**, *8*, 2907. [Similar Pd–N bond lengths (2.23 Å) have been observed when the bonds are *trans* to vinylic, sp^2 carbons: C. Arlen, M. Pfeffer, O. Bars, D. Grandjean, *J. Chem. Soc. Dalton Trans.* **1983**, 1535].

[12] Reductive elimination of Pt^{II} in platina(IV)cyclobutanes mediated by a π acceptor: F. J. McQuillin, K. G. Powell, *J. Chem. Soc. Dalton Trans.* **1972**, 2123. π Acceptor mediated reductive elimination ($Ni^{2+} \rightarrow Ni$) with C–C bond formation: T. Yamamoto, A. Yamamoto, S. Ikeda, *J. Am. Chem. Soc.* **1971**, *93*, 3350; ibid., 3360. Carbon monoxide promoted reductive elimination ($Pd^{2+} \rightarrow Pd$) in dimethylpalladium(II) complexes: T. Ito, H. Tsuchiya, A. Yamamoto, *Bull. Chem. Soc. Jpn.* **1977**, *77*, 1319.

[13] Racemization may take place by reversible Pd–N bond cleavage. Since the palladacyclobutane moiety is symmetrical, the mechanism of racemization cannot be identified. See also, A. Gogoll, J. Örnebro, H. Grennberg, J.-E. Bäckvall, *J. Am. Chem. Soc.* **1994**, *116*, 3631.

[14] The structural analysis of **2a** is currently in progress.

[15] The conversion of isolated palladacyclobutane **6** into **2a** has also been brought about by reaction with isoelectronic NO^+ (from $NO^+PF_6^-$ in CH_2Cl_2) and by oxidative addition of iodine (or methyl iodide), presumably via a Pd^{IV} intermediate.

[16] Metallacyclobutanes of early transition metals as reactive intermediates in olefin metathesis: J. Feldman, R. R. Schrock, *Prog. Inorg. Chem.* **1991**, *39*, 1–74; see also E. B. Tjaden, G. L. Casty, J. M. Stryker, *J. Am. Chem. Soc.* **1993**, *115*, 9814; K. Ohe, H. Matsuda, T. Morimoto, S. Ogoshi, N. Chatani, S. Murai, *ibid.* **1994**, *116*, 425.

The Stabilization of the Rb^- Ion in $Na_{16}Rb_7Sb_7 = Na_{16}(RbRb_6)Sb_7$**

Hans Georg von Schnering,* Raúl Hector Cardoso Gil, Wolfgang Hönle, Armin Burkhardt,* Georges Krier, and Ole Krogh Andersen

Dedicated to Professor Manuel Cardona on the occasion of his 60th birthday

We have started to reexamine binary compounds of the alkali metals with elements of the fifth main group (pnictides M_3X),[1] because great controversy surrounds the details of these simple structures (exact composition, superstructures, symmetry). In both structure types, Li_3Bi and Na_3As, the E1 atoms each occupy two structurally and chemically different positions in the ratio of 2:1, and, therefore, we also tried to prepare ternary compounds. Considering that both Na_3Sb and Rb_3Sb crystallize in the hexagonal Na_3As structure type, the preparation of "Na_2RbSb" should show if and how the structure adapts to the different sizes of Na and Rb.

However, during the synthesis $Na_{16}Rb_7Sb_7 \triangleq Na_{2.29}RbSb$ crystallized in the form of brittle, silver shiny cuboctahedra with metallic luster.[2] The compound was characterized by chemical analysis,[3] structural determination,[4] and electrical conductivity measurements.[4] Also, to better understand the results obtained, crystal chemical considerations and quantum chemical calculations were carried out. The compound, which readily decomposes in air to give a gray material that has not yet been characterized, was found to be a semiconductor, with $E_g = 0.33$ eV. The composition itself is indicative of an unusual electron distribution, since in a semiconducting antimonide, all of the valence electrons should be localized by forming Sb^{3-} ions, which, however, in $Na_{16}Rb_7Sb_7$ would only require 21 of the 23 valence electrons of the alkali metal atoms.

$Na_{16}Rb_7Sb_7$ crystallizes cubically in the space group $Fm\bar{3}m$ (no. 225), isotypical to $Sc_{11}Ir_4$,[6] and is the first representative of this $cF120$ structure type with main group elements. Indeed, this structure is similar to the Li_3Bi type ($a' = 2a$), as the following comparison will show: $[(Li_{16}(Li_8))Bi_8]_4 \triangleq [(Na_{16})(Rb_6\square_2)(Sb_7Rb)]_4 \triangleq [(Sc_{16})(Sc_6\square_2)(Ir_8)]_4$. The Li_3Bi structure is built of condensed Bi_{12} cuboctahedra, each centered by one further Bi atom, which is enveloped by a Li_8 cube ($Bi_{12/4}BiLi_8$). The remaining Li atoms ($Li_{8/8} + Li_{6/2}$) are located in the octahedral holes of the Bi packing. In the $cF120$ structure of $Na_{16}Rb_7Sb_7$, six of the Sb atoms form a three-dimensional net of condensed Sb_{12} cuboctahedra. However, only every second cuboctahedron is occupied by the seventh Sb atom, surrounded by a Na_8 cube. A Rb_6 octahedron is located in the other cuboctahedron, and in its center lies the seventh Rb atom (instead of a Sb atom). This centered $[RbRb_6]$ octahedron is also surrounded by eight Na atoms, but they are shifted to the periphery of the Sb_{12} cuboctahedron, namely into its eight triangular faces. By this shift, precisely the defects in comparison to the initial Li_3Bi structure are forced: $[(Li_8)(Li_{6/2}Li_{8/8})(Bi_{12/4}Bi)] + [(Li_8)(Li_{6/2}Li_{8/8})(Bi_{12/4}Bi)] \rightarrow [(Na_8)(\square\square_3)(Sb_{12/4}Sb)] + [(Na_8)(\square Rb_6)(Sb_{12/4}Rb)]$. Structure and electron distribution are immediately explained with the assumption that in this compound a Rb^- ion is stabilized: $(Na^+)_{16}(Rb^+)_6Rb^-(Sb^{3-})_7 = (Na^+)_{16}(RbRb_6)^{5+}(Sb^{3-})_7$!

The coordination of the individual atoms can be seen in Figure 1. The distances d(Sb–Na) and d(Na–Na) correspond to those in Na_3Sb, if the trigonal-planar coordination at Na2 is considered. The distances d(Rb1–Rb2) in the $(RbRb_6)$ octahedron, with the Rb^- ion in the center of a two-electron cluster Rb_5^{5+}, are 3.580 Å, which is significantly less than those found in Rb_3Sb (3.83–4.42 Å). The enormous expansion of the Na2 cube around this cluster, a distinct sign of the reduced attractive forces by the formal substitution of Sb^{3-} by Rb^-, is made especially clear by comparing the distances between the atoms of the cuboctahedral centers and the atoms of the surrounding Na_8 cube: d(Rb2–Na) = 4.48 Å $\gg$ d(Sb2–Na1) = 3.449 Å.

Even though the existence of the Rb^- ion with cryptands is known through the work of Dye et al.,[7] for $Na_{16}Rb_7Sb_7$ extensive studies are necessary to justify such an assumption. These

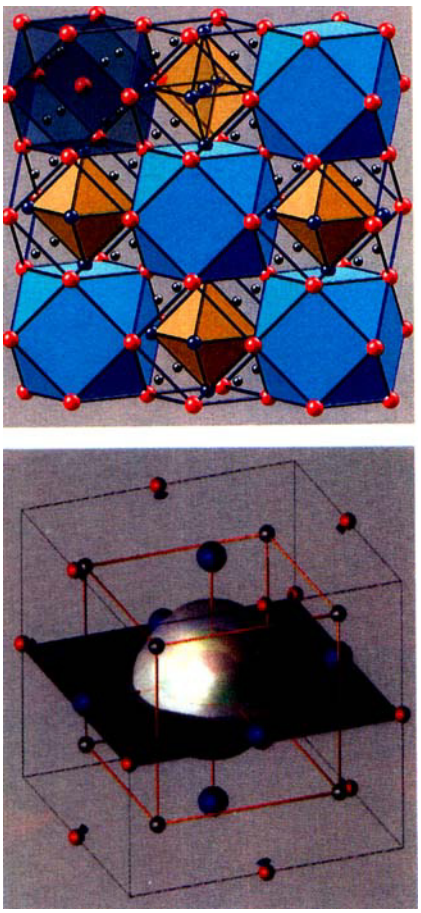


Fig. 1. Top: Segment of the cubic $Na_{16}Rb_7Sb_7$ structure parallel to a (100) face. Condensed Sb_{12} cuboctahedra (blue) are centered alternating by Sb (red spheres) and the octahedral $(RbRb_6)^{5+}$ cluster (yellow octahedra) inside transparent cuboctahedra; Rb = blue spheres. The Na atoms (silver colored) surround the two different centers Sb and $RbRb_6$ as cubes of different size. Na1 is coordinated tetrahedrally by four Sb atoms, Na2 trigonally planar by three Sb atoms. Bottom: One eigth of the unit cell with origin in $(\frac{1}{4}\frac{1}{4}\frac{1}{4})$. Rb2 in the center is surrounded octahedrally by Rb1 atoms (blue). The ELF is represented on a cross section running through the octahedral basis using the color table given in reference [12]. The iso density values extending nearly spherically around Rb2 are colored according to ELF. The two outer isosurfaces (0.002 ea_0^{-3}) mark the region of high density accumulation labeled with an arrow in Fig. 3 between Rb1 and Rb2. This region is characterized by high ELF values (white).

[*] Prof. Dr. H. G. von Schnering, Dr. A. Burkhardt, Dr. R. H. Cardoso Gil, Dr. W. Hönle, Dr. G. Krier, Prof. O. K. Andersen
Max-Planck-Institut für Festkörperforschung
Heisenbergstrasse 1, D-70569 Stuttgart (Germany)

[**] Thanks are due to the Fonds der Chemischen Industrie for financial support. We would also like to thank Andreas Savin, Olle Gunnarsson, Volker Eyert and Ove Jepsen for fruitful discussions, as well as Yuri Grin and Ortrud Buresch for the polyhedral representation and for the chemical analysis, respectively.

 © VCH Verlagsgesellschaft mbH, D-69451 Weinheim, 1995 0570-0833/95/0101-0103 $ 10.00+.25/0

were carried out experimentally and theoretically. By direct reaction of Na, Rb, Sb, and NaI, the isotypic compound, $Na_{16}Rb_6ISb_7$ is formed quantitatively. With I^- at the Rb2 position a structure is formed which can be accepted without further discussion. Corresponding reactions also result in the formation of isotypic compounds with Au^- and Na^-.[11]

In the same way, calculations of the electrostatic lattice potentials by the Ewald method[8] give a positive potential at the Rb2 site for the $Na_{16}Rb_7Sb_7$ structure (c.f. for Li_3Bi as well), suitable only for a E^- particle, even at variation of the charges. The tight-binding LMTO band structure, and the electron localization function ELF[9, 10] were calculated with the program package TB-LMTO.[11, 12] The exchange correlations potential from reference [13] have been used; gradient corrections according to reference [14] were also considered. Figure 2 shows the calculated band structure of $Na_{16}Rb_7Sb_7$. The 21 low-lying bands, with mainly Sb-p character between -0.9 and -3.4 eV are completely filled. From the above-lying broad band continuum of Na and Rb states one impurity band is split off, extending from the Fermi edge to the upper edge of the Sb bands. This band is formed predominantly by the 5s orbitals of the Rb2 atoms.

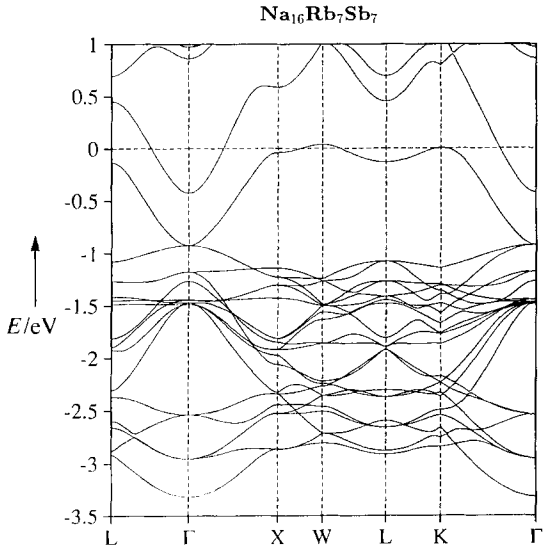


Fig. 2. The band structure of $Na_{16}Rb_7Sb_7$; all energies are given relative to the Fermi level. The crystallographic coordinates of the special k points are: Γ (000), L ($\frac{1}{2}\frac{1}{2}\frac{1}{2}$), X (010), W ($\frac{1}{2}$10), K ($0\frac{3}{4}\frac{3}{4}$).

Almost parallel to this band, about 0.5 eV higher, extends a band of Na2 character. This band, which crosses the Fermi energy around the Γ point, would lead to the conclusion that $Na_{16}Rb_7Sb_7$ should exhibit semi-metallic behavior with an indirect band gap of -0.4 eV, which is contrary to the observed semiconducting behavior. This discrepancy arises from the use of the local density approximation (LDA), which tends to underestimate the band gap, as well documented in the case of silicon.[15, 16] However, this error does not change the overall ground state properties (i.e. electron density).

By comparing the SCF-LMTO potential character C, it can be seen that compared to the surrounding Rb1 atoms (-1.19 eV) the 5s orbital of the central Rb2 atom (-2.54 eV) is lowered by 1.35 eV due to the Madelung contribution of its environment. Therefore, it lies close to the 3s orbitals of Na1 (-2.70 eV) and Na2 (-2.64 eV). This Madelung induced lowering of the Rb2 potential causes the impurity band together with the, compared to the Na 3s orbital, larger range of the Rb 5s orbitals.

Figure 3 shows along the Sb1–Rb1–Rb2 line the density of those electrons, whose energy lies between the Fermi energy and the upper edge of the Sb bands. Besides strong density oscillations in the region of the cores, a density accumulation between the rubidium atoms is clearly noticeable (arrow in Fig. 3). Its maximum is moved from the bond center by approximately 13% towards the central Rb2 atom. To investigate whether directed Rb–Rb bonds are present, a three-dimensional density grid was calculated.

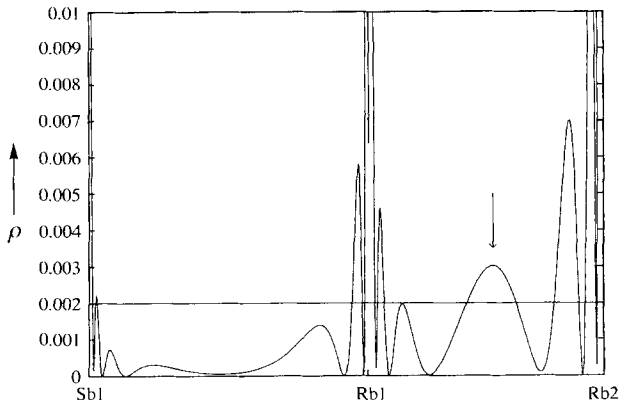


Fig. 3. The electron density resulting from the impurity band along the line Sb1 (center of the neighboring cuboctahedron)–Rb1 (corner of the octahedron)–Rb2 (center of the octahedron). The density ϱ is given in atomic units $e\,a_0^{-3}$. The iso value ($0.002\ e\,a_0^{-3}$) used for the representation of the partial charge density (bottom of Fig. 1) resulting from the impurity band is marked as a horizontal line.

Figure 1 (bottom) shows a section of the structure, which corresponds to one eighth of the unit cell. In its center is Rb2, octahedrally surrounded by Rb1 atoms. The Na2 atoms form a cube with the corner points above the octahedral faces. The Sb2 atoms form a cuboctahedron with the corner points above the edges of the octahedron. To illustrate the course of the ELF besides the isodensity surfaces, a sectional plane runs through the basis of the Rb_6 octahedron, colored by the ELF with the aid of a color scale. A ring of high localization (white) around Rb2 is clearly noticeable. The high ELF values (white) coincide with the marked (arrow) density accumulation between Rb1 and Rb2 in Figure 3, which extends almost spherically around the central Rb2 atom (Fig. 1, bottom). Thus, no directed Rb–Rb bonds are present. Furthermore, no considerable contributions of other atoms are indicated.

The crystal chemical interpretation, the successful substitution of Rb^- by I^- and by Au^-, and the electrostatical analysis, as well as the calculated band structure, allow the formal description of Rb2 as a stabilized and polarized Rb^-. However, the majority of this charge is located in the overlap area between Rb1 and Rb2. To avoid the suggestion of extreme charge separation, the additional density can be assigned to the lowest a_{1g} orbital of the cluster Rb_7^{5+}. Both descriptions are equivalent, since the contribution of the Rb2–5s orbital, due to its location in the cluster interior, is expected to dominate this cluster orbital.

Received: July 16/July 27, 1994,
Revised version: August 26, 1994 [Z7134 IE/7175 IE]
German version: *Angew. Chem.* **1995**, *107*, 81

Keywords: alkali metal compounds · antimony compounds · electron localization · Zintl phases

 © VCH Verlagsgesellschaft mbH, D-69451 Weinheim, 1995 0570-0833/95/0101-0104 $ 10.00+.25/0

[1] R. H. Cardoso Gil, Thesis, University of Stuttgart, **1994**.
[2] The elements (molar ratio Na:Rb:Sb = 2.29:1:1; batch size 1 g) were heated under inert conditions (glove box: $c_{H_2O} \leq 0.1$ ppm; $c_{O_2} \leq 0.1$ ppm) in sealed Nb ampoules (15 mm diameter, 0.5 mm wall thickness, ca. 5 cm in length) in evacuated quartz jackets (within 12 h heating up to 873 K, tempered 120 h at this temperature, cooling down to room temperature within 48 h). Handling under inert conditions.
[3] Chemical analysis with ICP-AES: 16.2 (20.23 calcd.) wt.% Na; 37.1 (32.90 calcd) wt.% Rb; 46.7 (46.87 calcd) wt.% Sb. The discrepancies between experimental and calculated values are due to the analytical method not well suited for the alkali metals and the small sample size (up to 10 mg).
[4] Crystal structure of $Na_{16}Rb_8Sb_8$: Single crystal, $M = 1818.36$; $a = 15.658(2)$ pm; space group $Fm\bar{3}m$ (no. 225); $Z = 4$; $V = 578.0$ cm^3 mol^{-1}; $N(hkl) = 270$, thereof 253 with $F \geq 3\sigma(F)$; 19 variables, $R_{aniso} = 0.044$. Measurement: Siemens P3 four-circle diffractometer, graphite monochromator, scintillation counter, ω scan $5 \leq 2\theta \leq 60$, 293 K; Mo_{K_α} radiation. Refinement: empirical absorption correction with 11 reflections hkl in ψ scan mode, program system SHELX 76, least-squares refinement. Further details of the crystal structure investigation may be obtained from the Fachinformationszentrum Karlsruhe, D-76344 Eggenstein-Leopoldshafen (Germany), on quoting the depository number CSD-58632.
[5] Temperature-dependent measurement of the electrical conductivity on pressed powder pellets under inert conditions: $E_g = 0.33$ eV using the Van der Pauw method: L. J. Van der Pauw, *Philips Res. Rep.* **1958**, *13*, 1.
[6] B. Chabot, K. Cenzual, E. Parthé, *Acta Crystallogr. Sect. B* **1980**, *36*, 7.
[7] M. J. Wagner, J. L. Dye, *Annu. Rev. Mater. Sci.* **1993**, *23*, 223; D. L. Ward, R. H. Huang, J. L. Dye, *Acta Crystallogr. Sect. C* **1990**, *46*, 1838; R. H. Huang, D. L. Ward, J. L. Dye, *J. Am. Chem. Soc.* **1989**, *111*, 5707; J. L. Dye, M. G. DeBacker, *Annu. Rev. Phys. Chem.* **1987**, *38*, 271.
[8] R. Hoppe, *Angew. Chem.* **1966**, *78*, 52; *Angew. Chem. Int. Ed. Engl.* **1966**, *5*, 95; G. Roch, W. Neukäter, H. G. von Schnering, "Programm zur Berechnung von Gitterpotentialen und Madelungfaktoren", Universität Münster, **1962**; R. Nesper, "Modifizierungen zur Berechnung von Potentialdichten", Max-Planck-Institut für Festkörperforschung, Stuttgart, **1984**, unpublished.
[9] A. Savin, A. D. Becke, J. Flad, R. Nesper, H. Preuss, H. G. von Schnering, *Angew. Chem.* **1991**, *103*, 421; *Angew. Chem. Int. Ed. Engl.* **1991**, *30*, 409.
[10] A. Savin, O. Jepsen, J. Flad, O. K. Andersen, H. Preuss, H. G. von Schnering, *Angew. Chem.* **1992**, *104*, 186; *Angew. Chem. Int. Ed. Engl.* **1992**, *31*, 187.
[11] G. Krier, M. van Schilfgaarde, T. A. Paxton, O. Jepsen, O. K. Andersen, Program TB-LMTO.
[12] To keep the calculation effort for 30 atoms of the third and fifth period in the primitive unit cell within reasonable bounds an efficient linear muffin tin orbital (LMTO) basis set consisting of 44 basis functions (16 Na 3s + 7 Rb 5s + 21 Sb 5p, Sb 5s in core) was used. Orbitals with higher l value were downfolded. The band character was determined by projection onto orthonormal orbitals. The atomic sphere approximation (ASA) requires the representation of the unit cell volume as sphere packing. Since $Na_{16}Rb_8Sb_8$ is almost closely packed no empty spheres were necessary. The sphere radii have been chosen in such a way that the overlapping muffin tin potential reproduces the full potential as good as possible (Na1: 1.94, Na2: 1.90, Rb1: 2.12, Rb2: 2.15, Sb1: 1.94, Sb2: 1.90 Å). The charge density as well as the electron localization function (ELF) were calculated from the resulting wave functions. For the three-dimensional representation of these quantities the density is displayed as isosurface colored by the corresponding ELF values ($0 \leq$ ELF ≤ 1). Regions of high localization appear in white, towards lower values the colors change from brown over yellow and green to blue (topological color table).
[13] U. Barth, L. Hedin, *J. Phys. C* **1972**, *5*, 1629.
[14] D. C. Langreth, M. J. Mehl, *Phys. Rev. Lett.* **1981**, *47*, 446; *Phys. Rev. B* **1983**, *28*.
[15] L. J. Sham, M. Schlüter, *Phys. Rev. Lett.* **1983**, *51*, 1888.
[16] G. A. Baraff, M. Schlüter, *Phys. Rev. B* **1984**, *30*, 3460.

The Colors of C_{60} Solutions**

Javier Catalán,* José L. Saiz,* José L. Laynez, Nadine Jagerovic, and José Elguero*

It is surprising that solutions of an apolar compound like C_{60} are different colors, depending on the solvent used.[1, 2] For instance, it has been described that C_{60} solutions are pink in fluorobenzene (FB), magenta in toluene (T), bluish-violet in methoxybenzene (MOB), brownish in 1,2-dimethoxybenzene (12DMOB), and brown-yellow in 1,2,3,5-tetramethylbenzene (1235TMB). These observations cannot be explained by the influence of the solvent; neither the solvent polarity nor the solvent polarizability play a role.

Ermer[1] reported the color of C_{60} solutions in a series of aromatic solvents with different π-donating ability (nitrobenzene, benzene, anisole, and 12DMOB) and suggested that the UV/Vis spectra of these solutions should be analyzed with regard to charge transfer (CT) effects. CT complexes have been proposed by Wang et al.[3, 4] and by Rao et al.[5, 6] to explain the interaction between C_{60} and *N,N*-dimethylaniline, and by Williams and Verhoeven to explain the interaction between C_{60} and 12DMOB or an alkoxicalix[8]arene sulfonate.[7]

Independently, Scrivens and Tour[2] have studied the solubility of C_{60} in a series of 30 aromatic solvents (benzene and naphthalene derivatives) and reported the color of the corresponding saturated solutions. If one examines these data, it appears that, with some exceptions, there is a correlation between color and solubility. Thus, in those solvents where C_{60} is less soluble (from 0.3 mg mL^{-1} in pyridine to 1.4 mg mL^{-1} in *tert*-butylbenzene) the saturated solutions are pink. In the intermediate zone (from 1.5 mg mL^{-1} in benzene to 17.9 mg mL^{-1} in 1,2,4-trimethylbenzene) the saturated solutions are magenta. Finally, for the solvents in which C_{60} is most soluble, for instance 1235TMB (20.8 mg mL^{-1}) and 1-bromo-2-methylnaphthalene (34.8 mg mL^{-1}), the saturated solutions are brownish. Quinoline is an exception since, although the solubility of C_{60} is only 7.2 mg mL^{-1}, the color of the solution is brownish.

Ruoff et al.[8] in a study of the solubility of C_{60} in a series of 47 solvents, aromatic as well as non-aromatic, do not discuss the color of the solutions but report that "in the case of cyclohexane, we noticed that initial addition of the solvent to C_{60} resulted in a fairly intense purple color, which would indicate a high solubility. However, upon filtration through the 0.45 mm filter, only a faintly colored solution was obtained. Most of the color was from a fluffy purple solid that remained suspended in the solution for long periods". The solubility of C_{60} in cyclohexane is very low, 0.002 mg mL^{-1}.[8]

Considering all these reports, we will try in this paper to answer two fundamental questions: 1) Does the color of a saturated solution of C_{60} change by dilution or on standing? 2) In the zone of concentrations explored, does C_{60} obey the Lambert–Beer law? This last question is related to the possibility that C_{60} should be partly monomeric and partly aggregated or

[*] Prof. Dr. J. Catalán
Departamento de Química Física Aplicada
Universidad Autónoma de Madrid
Cantoblanco, E-28049 Madrid (Spain)
Telefax: Int. code + (91)3974-187
Dr. J. L. Saiz, Dr. J. L. Laynez
Instituto de Química Física "Rocasolano" Madrid (Spain)
Dr. J. Elguero, Dr. N. Jagerovic
Instituto de Química Médica Madrid (Spain)

[**] This work was supported by the Consejo Superior de Investigaciones Científicas (Special Action "Fullerenes") and by the Spanish Dirección General de Investigación Científica y Técnica (project no. PB90-0117).

in suspension depending on the concentration. Answering these two questions will help to understand why C_{60} changes in color with the solvent.

Figures 1, 2, and 3 show a series of solutions of C_{60} in 12DCB (1,2-dichlorobenzene), 1235TMB, and 12DMOB, respectively. The corresponding concentrations for tubes 1 to 10 are given in Table 1. In the three series, the tubes with the same numbers have approximately the same concentration.

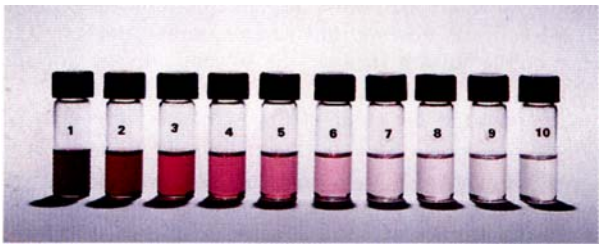


Fig. 1. Solutions of C_{60} in 12DCB. Concentrations see Table 1.

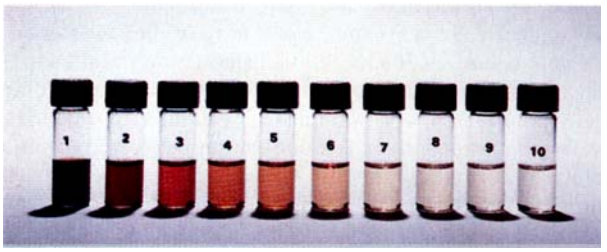


Fig. 2. Solutions of C_{60} in 1235TMB. Concentrations see Table 1.

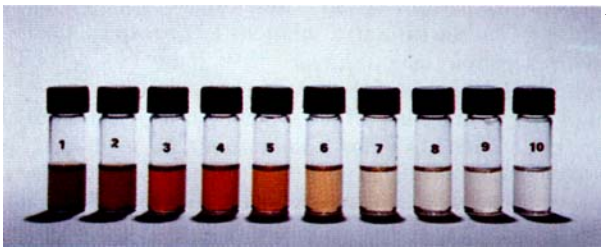


Fig. 3. Solutions of C_{60} in 12DMOB. Concentrations see Table 1.

As Figure 1 shows, the concentrated solutions of C_{60} in 12DCB are a beautiful magenta color which fades but does not change on dilution. All these solutions have *identical* UV/Vis spectra between 700 and 300 nm which almost perfectly superimpose when they are standardized for an optical path of 1 cm and a 1 M concentration. Consequently, the Lambert–Beer law is obeyed.

Concentrated solutions of C_{60} in 12DMOB (Fig. 3) have a red-brownish color which on dilution initially turns red (up to 2×10^{-3} M), then orange (1×10^{-3} M), and finally yellow (from 1×10^{-4} M downwards). Nevertheless, the corresponding spectra obey the Lambert–Beer law and this is the reason why, when standardized to an optical path of 1 cm and a 1 M concentration, all of them are *identical*. We have checked that the most concentrated solutions do not contain aggregates larger than 0.45 mm, since neither the color nor the spectra change when these solutions are filtered through a 0.45 mm filter.

A similar phenomenon happens with solutions of C_{60} in 1235 TMB (Fig. 2), where the color changes from brownish to yellow when the concentration changes from 5×10^{-3} M to 2×10^{-5} M.

In all cases, the Lambert–Beer law is obeyed. If the absorbance is plotted against molar concentration (14 points), for instance, at 333 nm, the values $R = 0.994$ for 12DCB, $R = 0.998$ for 1235TMB, and $R = 0.990$ for 12DMOB are obtained. The extinction coefficients have been determined at 410, 470, 520, 580, 600, and 650 nm, wavelengths which correspond to the violet, blue, green, yellow, orange, and red zones of the spectrum, respectively. These values and those for other solvents are given in Table 2.

Table 2. Molar extinction coefficients ε [L mol^{-1} cm^{-1}] of C_{60} in different solvents.

Solvent	ε_{410}	ε_{470}	ε_{520}	ε_{580}	ε_{600}	Color
toluene (T)	2561	438	826	678	788	magenta
isopropyl-benzene (IPB)	1834	338	623	514	609	magenta
chlorobenzene (CB)	2313	444	843	662	794	magenta
1,2-dichloro-benzene (12DCB)	3170	616	979	786	887	magenta
fluorobenzene (FB)	3224	976	847	572	548	pink
methoxy-benzene (MOB)	5744	423	773	691	769	bluish-violet
1,2-dimethoxy-benzene (12DMOB)	6600	3570	1725	1060	1050	brownish
1,2,3,5-tetramethyl-benzene (1235TMB)	10332	734	1040	827	917	brown-yellow

For the same concentration (7×10^{-4} M), the three solvents 12DCB, 1235TMB, and 12DMOB show differences in color which are clearly apparent in Figure 4. Figure 5 shows the differences in color for a 1.1×10^{-4} M concentration of C_{60} in a wide range of solvents. These colors remain unaltered for several weeks. Concerning the relationship between color and solubility,[2] it must be pointed out that the color of C_{60} solutions depends on both the solvent and the concentration.

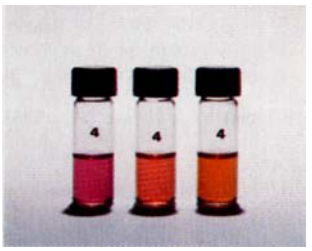


Fig. 4. From left to right: Solutions of C_{60} in 12DCB, in 1235TMB, and in 12DMOB. Concentrations: 7.1×10^{-4} M.

Table 1. C_{60} concentration in 1,2-dichlorobenzene (Fig. 1), 1,2,3,5-tetramethylbenzene (Fig. 2), and 1,2-dimethoxybenzene (Fig. 3).

Tube no.	1	2	3	4	5	6	7	8	9	10
Conc. [M]	5.08×10^{-3}	2.54×10^{-3}	1.07×10^{-3}	7.11×10^{-4}	5.08×10^{-4}	2.54×10^{-4}	1.05×10^{-4}	7.37×10^{-5}	5.27×10^{-5}	2.63×10^{-5}

 © VCH Verlagsgesellschaft mbH, D-69451 Weinheim, 1995 0570-0833/95/0101-0106 $ 10.00+.25/0



Fig. 5. From left to right: Solutions of C_{60} (1.1×10^{-4} M) in the solvents, T, FB, CB, MOB, IPB, 12DCB, 12DMOB, and 1235TMB. Abbreviations see Table 2.

The UV/Vis absorption spectrum of C_{60} in an "inert" solvent like *n*-hexane for wavelengths higher than 300 nm is characterized by an intense peak at 332 nm. In the visible part, in which C_{60} absorbs near 630 nm, the most noticeable features are the transparency in the blue (424–492 nm), already noted by Ajie et al.,[9] as well as in the red (650 nm). *The human eye sees a beautiful purple color as a consequence of the combination of lack of both these absorptions.*

The results of our experiments rule out 1) the existence of aggregates or suspensions in the zone of higher concentrations, because in these solutions there are no changes due to filtration and also because the Lambert–Beer law is always obeyed, and 2) that the color changes of C_{60} with the concentration are due to the existence of CT complexes between C_{60} and some aromatic compounds, because in these solvents the spectra are superimposable if the concentrations are scaled (this eliminates an effect of the concentration on the proportions of species optically active in the visible region).

Since due to the apolar nature of the fullerene C_{60} the absorption spectra are rather insensitive to solvents, neither significant bathochromic nor hypsochromic shifts are observed. Figure 6

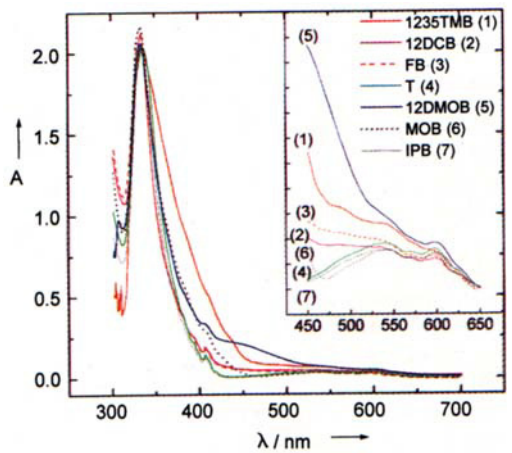


Fig. 6. UV/Vis spectra of C_{60} in several solvents (7×10^{-5} M).

shows the UV/Vis spectra for the different solvents used in this study at the same concentration (7.3×10^{-5} M). Consequently, we conclude that the phenomenon originates mainly from differences in the absorption intensity in the 400–500 nm range, which are perceived by the human eye as differences in color.

Experimental Procedure

The C_{60} used was obtained from MER Co. and has a degree of purity of >99.5%. Solvents with a purity better than 99% (Aldrich) were used when available (fluorobenzene (FB), toluene (T), chlorobenzene (CB), methoxybenzene (MOB), isopropylbenzene (IPB), 1,2-dichlorobenzene (12DCB), 1,2-dimethoxybenzene (12DMOB). The solvent 1,2,3,5-tetramethylbenzene (1235TMB) was also obtained from Aldrich but of technical grade.

The UV/Vis spectra of C_{60} solutions were recorded in a Cary 210 spectrophotometer using cells with an optical path of 0.1 or 1.0 cm. For the most concentrated solutions the instrument becomes saturated due to the large values of the absorbances; in these cases, a Cary 5 spectrophotometer and a variable optical path cell were used (optical path = 0.005 cm).

Received: June 23, 1994 [Z 7068 IE]
German version: *Angew. Chem.* **1995**, *107*, 86

Keywords: color · fullerenes · solvent effects · UV/Vis spectroscopy

[1] O. Ermer, *Helv. Chim. Acta* **1991**, *74*, 1339–1351.
[2] W. A. Scrivens, J. M. Tour, *J. Chem. Soc. Chem. Commun.* **1993**, 1207–1209.
[3] Y. Wang, *J. Phys. Chem.* **1992**, *96*, 764–767.
[4] Y. Wang, L. T. Cheng, *J. Phys. Chem.* **1992**, *96*, 1530–1532.
[5] C. N. R. Rao, R. Seshadri, A. Govindaraj, J. P. Mittal, H. Pal, T. Mukherjee, *J. Mol. Struct.* **1993**, *300*, 289–301; R. Seshadri, F. D'Souza, V. Krishnan, C. N. R. Rao, *Chem. Lett.* **1993**, 217–220.
[6] R. Seshadri, C. N. R. Rao, H. Pal, T. Mukherjee, J. P. Mittal, *Chem. Phys. Lett.* **1993**, *205*, 395–398.
[7] R. M. Williams, J. W. Verhoeven, *Recl. Trav. Chim. Pays-Bas* **1992**, *111*, 531–532.
[8] R. S. Ruoff, D. S. Tse, R. Malhotra, D. C. Lorents, *J. Phys. Chem.* **1993**, *97*, 3379–3383.
[9] H. Ajie, M. M. Alvarez, S. J. Anz, R. D. Beck, F. Diederich, K. Fostiropoulos, D. R. Huffman, W. Krätschmer, Y. Rubin, K. E. Schriver, D. Sensharma, R. L. Whetten, *J. Phys. Chem.* **1990**, *94*, 8630–8633.

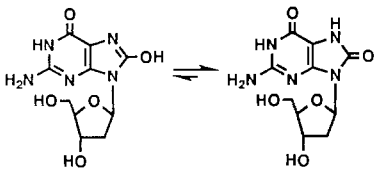
Photosensitized Formation of 8-Hydroxy-2′-deoxyguanosine in Salmon Testes DNA by Furocoumarin Hydroperoxides: A Novel, Intercalating "Photo-Fenton" Reagent for Oxidative DNA Damage**

Waldemar Adam,* Jean Cadet, Francesco Dall'Acqua, Bernd Epe, Danaboyina Ramaiah, and Chantu R. Saha-Möller

Oxidative DNA damage plays a significant role in mutagenesis and carcinogenesis,[1] in which oxidation products of the DNA bases are formed by reactive oxygen species such as hydroxyl and alkoxyl radicals,[2] singlet oxygen,[3] and even the superoxide ion.[2a] The mutagenic[4–6] DNA oxidation product 8-hydroxy-2′-deoxyguanosine (8-OHdG)[7] has been studied intensively in recent years.[2] Since hydroxyl radicals are implicated as the reactive species in oxidative DNA damage,[1] it was of

[*] Prof. Dr. W. Adam, Dr. D. Ramaiah, Dr. C. R. Saha-Möller
Institut für Organische Chemie der Universität
Am Hubland, D-97074 Würzburg (Germany)
Telefax: Int. code + (931)888-4606
Dr. J. Cadet
CEA/Département de Recherche Fondamentale sur la Matière Condensée
SESAM/Lésions des Acides Nucléiques, Grenoble (France)
Prof. Dr. F. Dall'Acqua
Department of Pharmaceutical Sciences, University of Padova (Italy)
Prof. Dr. B. Epe
Institut für Pharmakologie und Toxikologie der Universität Würzburg (Germany)

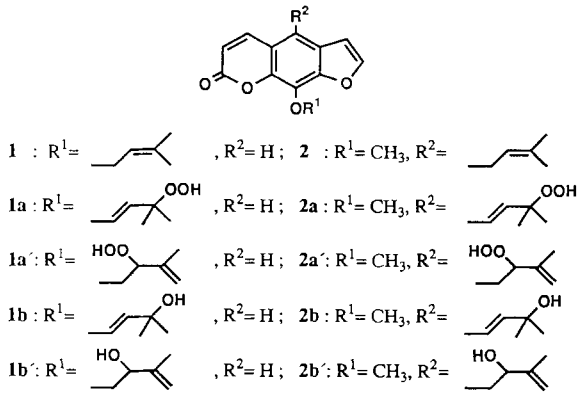
[**] We thank Dr. T. Linker for recording the ESR spectra. D. R. expresses his gratitude to the Alexander von Humboldt Foundation for a Postdoctoral Fellowship (1992–1993). The work was supported by the Deutsche Forschungsgemeinschaft (SFB 172 "Molekulare Mechanismen kanzerogener Primärveränderungen") and the Fonds der Chemischen Industrie.



8-OHdG 8-OxodG

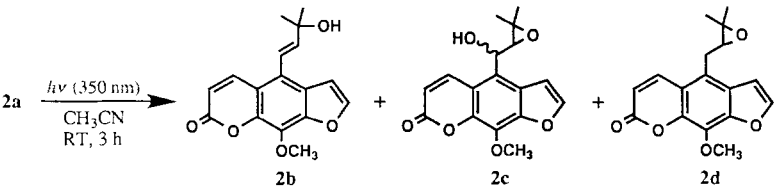
interest to assess the role of hydroxyl radicals in the formation of 8-OHdG. The conventional chemical sources of hydroxyl radical, for example, Fe^{2+}/H_2O_2 (Fenton reaction),[9] are not properly suited for such investigations because they generate, besides hydroxyl radicals, other reactive intermediates such as superoxide ion or metal oxygen species.[10] Therefore, efficient methods for the generation of hydroxyl radicals are required, which circumvent the use of transition metals.

Recently we reported[11] that the furocoumarin hydroperoxides **1a** and **1a′** as well as **2a**, and **2a′**, readily available by photooxygenation[12] of imperatorin (**1**) or the alloimperation derivative **2**, cause single strand breaks and endonuclease-sensitive DNA modifications in supercoiled bacteriophage PM2 DNA upon UV irradiation ($\lambda = 360$ nm). Presumably these lesions derive from hydroxyl radical-type oxidative activity, since the different modifications are formed in the same ratio as for the γ irradiation of dilute DNA solutions.[11] Here we present our new results, which substantiate unequivocally that these DNA-intercalating furocoumarin hydroperoxides are indeed effective photochemical sources for hydroxyl radicals. Hence, these novel furocoumarin hydroperoxides constitute the first intercalating "photo-Fenton"[13] reagents and they induce significant amounts of the DNA oxidation product 8-OHdG in salmon testes DNA on UVA irradiation ($\lambda = 350$ nm).



Among the furocoumarin hydroperoxides **1a**,**a′** and **2a**,**a′**, the derivative **2a** was the most active DNA-damaging agent in endonuclease assays.[11] Therefore, as representative example, the photochemistry of **2a** was studied in detail to corroborate the formation of hydroxyl radicals in the photolysis of this hydroperoxide and to provide mechanistic insight for their generation. Thus, irradiation of **2a** (105 mg, 0.330 mmol) in acetonitrile (70 mL) at 350 nm (Rayonet photoreactor) for 3 h at ambient temperature under a nitrogen gas atmosphere led to complete conversion of the hydroperoxide affording the alcohol **2b** (2%), a 80:20 diastereomeric mixture of hydroxy epoxide **2c** (40%), and the epoxide **2d** (8%), along with substantial amounts (25%) of undefined material of higher molecular weight (Scheme 1). The quantum yield ($\phi = 0.85 \pm 0.04$) of the photochemical decomposition of **2a** was determined by the potassium ferrioxalate actinometry.[14] The formation of these photoproducts is explained in terms of the homolysis of the hydroperoxide moiety initiated by intramolecular energy transfer from the photoexcited furocoumarin chromophore. The prerequisite exothermicity for efficient energy transfer is fulfilled in that the triplet energy E_T of the furocoumarin chromophore (cf. for 8-methoxypsoralen $E_T = 63$ kcal mol^{-1})[15] is higher than that of the hydroperoxide moiety.[16]

The generation of hydroxyl radicals in the photolysis[17] of hydroperoxide **2a** (3.16 mg, 10 μmol) in benzene under a nitrogen gas atmosphere was confirmed by detection of phenol (1.6% based on hydroperoxide consumption). The low yield of phenol in this reaction can be rationalized in terms of further



Scheme 1.

oxidation by hydroxyl radicals to catechol and 1,4-hydroquinone.[18]

It was reported that adamantane is oxidized by hydroxyl radicals to 1-adamantanol, 2-adamantanol, and adamantanone.[13, 19] However, we could not detect any oxidation product of adamantane when **2a** (3.16 mg, 10 μmol) was irradiated[17] in the presence of adamantane (13.6 mg, 100 μmol) in acetonitrile (70 mL, degassed) under a nitrogen gas atmosphere. On the other hand, the photolysis under atmospheric conditions afforded 1-adamantanol (3.3%), 2-adamantanol (0.3%), and adamantanone (1.7%).[15] Presumably the adamantane oxidation products were formed by the reaction of molecular oxygen with the initially generated adamantyl radicals.[18b]

Furthermore, ESR-spectral evidence for hydroxyl radicals was obtained by spin trapping with 5,5-dimethyl-1-pyrroline-*N*-oxide (DMPO). Thus, on irradiation of hydroperoxide **2a** in the presence of DMPO,[20] the characteristic[21] 1:2:2:1 quartet ($a_N = a_H = 14.90$ G and $g = 2.0053$) was observed in the ESR spectrum for the resulting nitroxyl radical. A similar spectrum was obtained for hydroperoxide **2a′**.

Once it had been established that the furocoumarin hydroperoxides are efficient photochemical hydroxyl radical sources, we investigated the formation of 8-hydroxy-2′-deoxyguanosine (8-OHdG) by this novel intercalating photo-Fenton reagent. For this purpose a solution of salmon testes DNA (50 μg mL^{-1}) and furocoumarin hydroperoxide (20–50 μM) **1a′** or **2a** in 5 mM phosphate buffer (1 mL) at pH 7 was irradiated ($\lambda = 350$ nm) at 0 °C for 15 to 30 min (Table 1). After irradiation, the modified DNA was digested by nuclease P1 and alkaline phosphatase and subsequently analyzed by HPLC (amperometric detection at 650 mV)[22] by using a 80:20 mixture of 0.05 M citrate buffer (pH 5) and methanol as eluent. The results are given in Table 1.

As the data in Table 1 reveal, the hydroperoxide **2a** is more efficient than **1a′** in forming 8-OHdG in DNA. Furthermore, control experiments showed that the extent of 8-OHdG formation was not influenced by D_2O, whereas in the presence of 2% *tert*-butyl alcohol about 30% inhibition occurred (Table 1, entries 3–5 and 9–12). Since for the corresponding furocoumarin alcohols **1b′** and **2b** under similar photolysis conditions only insignificant amounts of 8-OHdG were observed (Table 1, entries 7 and 13), and the furocoumarin hydroperoxides **1a′** and

Table 1. 8-OHdG formation photoinduced by furocoumarin hydroperoxide in salmon testes DNA [a].

Entry	Hydroperoxide [b] structure	conc. [μM]	*t*BuOH [%] [c]	Irradiation time [min]	8-OHdG Yield pmol per 50 μg DNA [d]	[%] [e]
1	**1a′**	20	0.0	15	48 (0.15)	0.24
2	**1a′**	20	0.0	30	58 (0.18)	0.29
3	**1a′**	30	0.0	30	72 (0.23)	0.24
4	**1a′**	30	0.5	30	62 (0.19)	0.20
5	**1a′**	30	2.0	30	48 (0.15)	0.16
6	**1a′**	50	0.0	30	100 (0.32)	0.20
7	**1b′**	20	0.0	30	20 (0.06)	0.10
8	**2a**	20	0.0	15	328 (1.05)	1.64
9	**2a**	20	0.0	30	364 (1.16)	1.82
10	**2a**	20	0.5	30	300 (0.96)	1.50
11	**2a**	20	2.0	30	254 (0.81)	1.27
12	**2a**	50	0.0	30	420 (1.34)	0.84
13	**2b**	20	30	30	24 (0.07)	0.12

[a] DNA (50 μg mL^{-1}) was irradiated in 5 mM phosphate buffer (1 mL) at pH 7.0 with furocoumarin hydroperoxide at 0 °C. [b] For comparison, the furocoumarin alcohols **1b′** and **2b** were also investigated. [c] Volume% of reaction solution. [d] Blank was 6 pmol per 50 μg DNA, in parentheses the yields in percent based on guanine consumption are given (50 μg DNA contains ca. 31.2 nmol of guanine); error ca. ±10% of the stated values. [e] Yield based on furocoumarin hydroperoxide consumption.

2a did not form any 8-OHdG without irradiation, the DNA oxidation product 8-OHdG generated in the photolysis of **1a′** and **2a** derives mainly from hydroxyl radicals produced by photosensitized homolysis of the hydroperoxide bond.

For the furocoumarin hydroperoxide **2a** the maximum yield of 8-OHdG (1.82% based on hydroperoxide consumption) was achieved at a hydroperoxide concentration of 20 μM after 30 min irradiation (Table 1, entry 9). Prolonged irradiation (up to 90 min) did not change the yield of 8-OHdG significantly. In fact no peroxide could be detected in the reaction solution by KI test after 30 min irradiation time. The reason for the low yield of 8-OHdG may be due to other DNA modifications such as strand breaks, base-free sites, and oxidation products of DNA bases other than 8-OHdG.[23, 24]

Recently it was reported that irradiation of DNA (260 mg mL^{-1}) in phosphate buffer with γ radiation (50 Gy) under an oxygen gas atmosphere induced 8-OHdG in 0.14% yield.[25] Since the photolysis of **2a** (Table 1, entries 9 and 12) produced 8-OHdG in higher yield (1.8% for **2a** based on hydroperoxide consumption), we suspected that the hydroxyl radicals were formed at least partly in the DNA matrix by photolysis of the DNA-intercalated hydroperoxide **2a**. The quite inefficient inhibition of 8-OHdG formation (ca. 30%) in the photolysis of furocoumarin hydroperoxides versus about 70% inhibition of this DNA damage induced by γ radiation (free hydroxyl radicals),[11] substantiates also intercalation of these hydroperoxides and is in accord with our previous results[11] on DNA damage caused by furocoumarin hydroperoxides.

Therefore, we have examined whether the furocoumarin hydroperoxides investigated herein undergo intercalation, a prerequisite for photoactivity directly in the DNA matrix.[26, 27] Indeed, the formation of a molecular complex between salmon testes DNA and furocoumarins **1a′** and **1b′** was confirmed by strong quenching of the fluorescence,[28] as had been observed previously for other intercalating furocoumarins.[21] From the fluorescence data, the binding parameters of the DNA complexes were calculated according to McGhee and von Hippel[29] (Table 2). As the data reveal, the furocoumarins examined herein form molecular complexes with DNA at least as efficiently as 8-methoxypsoralen (8-MOP). Furthermore, **2a** binds more strongly with DNA than **1a′**. Presumably, the higher efficiency of the hydroperoxide **2a** in comparison to **1a′** to form 8-OHdG (Table 1, entries 2 and 9) is due to its higher DNA binding constant (Table 2).

Table 2. Binding parameters [a] of furocoumarins with salmon testes DNA.

Furocoumarin	K [M^{-1}] [b]	n [c]	$1/n$ [d] 10^{-2}
1a′	6130	60	1.7
1b′	3900	45	2.2
2a	23900	22	4.5
8-MOP [e]	740	8	12.8

[a] Calculated according to McGhee and von Hippel [29]. [b] Association constant. [c] Number of nucleotides occluded by a bound furocoumarin. [d] Frequency of binding sites. [e] Taken from ref. [27].

To assess whether the present furocoumarins, like psoralen,[30] indeed intercalate into DNA when complexed with the macromolecule, we carried out linear flow dichroism (LD) measurements. The LD spectrum[31] of an aqueous solution of the hydroperoxide **2a** in the presence of DNA exhibited a characteristic negative dichroism between 310 and 360 nm, which indicates that the complexed **2a** assumes a position parallel to the DNA bases.[30] Similar negative LD spectra were observed for the furocoumarins **1a′** and **1b′**.

In summary, the results demonstrate that the readily available intercalating and photosensitizing furocoumarin hydroperoxides **1a′** and **2a** serve as convenient sources for the generation of hydroxyl radicals. On near-UVA irradiation these novel photo-Fenton reagents promote efficiently the mutagenic DNA oxidation product 8-hydroxy-2′-deoxyguanosine (8-OHdG). The advantage of this new type of photo-Fenton reagent lies in the fact that hydroxyl radicals can be generated directly in the DNA matrix by photosensitization and the concentration-dependent formation of 8-OHdG can be quantitatively assessed. Because of these favorable properties, the furocoumarin hydroperoxides, in particular the 8-methoxypsoralen derivative **2a**, can be applied as effective hydroxyl radical sources for the investigation of biologically important reactions such as DNA oxidation and cleavage,[23, 32] protein cleavage,[33] crosslinking of biopolymers,[34] and lipid peroxidation.[35] To develop still more effective photoactive hydroxyl radical sources, the optimization of the photosensitizing and intercalating properties of such reagents will be required.

Received: May 4, 1994
Revised version: August 20, 1994 [Z 6895 IE]
German version: *Angew. Chem.* **1995**, *107*, 91

Keywords: DNA oxidation · furocoumarins · hydroperoxides · 8-hydroxy-2′-deoxyguanosine · hydroxyl radicals

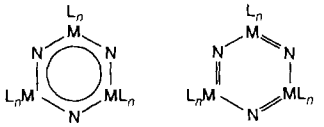
[1] a) *Oxidative Stress: Oxidants and Antioxidants* (Ed.: H. Sies), Academic Press, London, **1991**; b) D. Schulte-Frohlinde, C. von Sonntag in *Oxidative Stress* (Ed.: H. Sies), Academic Press, London, **1985**, pp. 11–40.
[2] a) H. Kasai, S. Nishimura in ref. [1a], pp. 99–116; b) R. A. Floyd, *Carcinogenesis* **1990**, *11*, 1447–1450.
[3] T. P. A. Devasagayam, S. Steenken, M. S. W. Obendorf, W. A. Schulz, H. Sies, *Biochemistry* **1991**, *30*, 6283–6289.
[4] E. Gajewski, G. Rao, Z. Nackerdien, M. Dizdaroglu, *Biochemistry* **1990**, *29*, 7876–7882.
[5] S. Shibutani, M. Takeshita, A. P. Grollmann, *Nature (London)* **1991**, *349*, 431–434.
[6] M. L. Wood, M. Dizdaroglu, E. Gajewski, J. M. Essigmann, *Biochemistry* **1990**, *29*, 7024–7032.

[7] In aqueous solution 8-OHdG exists predominantly in the keto form 7,8-dihydro-8-oxo-2'-deoxyguanosine (8-OxodG) [8].
[8] J. Tchou, H. Kasai, S. Shibutani, M.-H. Chung, J. Laval, A. P. Grollmann, S. Nishimura, *Proc. Natl. Acad. Sci. USA* **1991**, *88*, 4690–4694.
[9] a) C. Walling, *Acc. Chem. Res.* **1975**, *8*, 125–132; b) R. P. Hertzberg, P. B. Dervan, *J. Am. Chem. Soc.* **1982**, *104*, 313–315; c) B. Halliwell, J. M. C. Gutteridge, *Biochem. J.* **1984**, *219*, 1–14.
[10] B. Halliwell, J. M. Gutteridge, *Free Radicals in Biology and Medicine*, 2nd ed., Oxford Univ. Press (Clarendon), New York, **1989**.
[11] B. Epe, M. Häring, D. Ramaiah, H. Stopper, M. M. Abou-Elzahab, W. Adam, C. R. Saha-Möller, *Carcinogenesis* **1993**, *14*, 2271–2276.
[12] M. M. Abou-Elzahab, W. Adam, C. R. Saha-Möller, *Liebigs Ann. Chem.* **1991**, 967–970.
[13] S. Matsugo, S. Kawanishi, K. Yamamoto, H. Sugiyama, T. Matsuura, I. Saito, *Angew. Chem.* **1991**, *103*, 1343–1344; *Angew. Chem. Int. Ed. Engl.* **1991**, *30*, 1351–1353.
[14] C. G. Hatchard, C. A. Parker, *Proc. R. Soc. London A* **1956**, *235*, 518–536.
[15] Y. Sawaki, Y. Ogata, *J. Am. Chem. Soc.* **1976**, *98*, 7324–7327.
[16] R. V. Bensasson, E. J. Land, C. Salet, *Photochem. Photobiol.* **1978**, *27*, 273–280.
[17] The photolyses were conducted for 3 h and the yields determined by GC analysis, calibrated against naphthalene for phenol and dodecane for adamantane-oxidized products.
[18] a) K. Omura, T. Matsuura, *Tetrahedron* **1968**, *24*, 3475–3487; b) X.-M. Pan, M. N. Schuchmann, C. von Sonntag, *J. Chem. Soc. Perkin Trans. 2* **1993**, 289–297.
[19] I. Saito, M. Takayama, T. Matsuura, S. Matsugo, S. Kawanishi, *J. Am. Chem. Soc.* **1990**, *112*, 883–884.
[20] A solution of furocoumarin hydroperoxide (30–120 μM) and DMPO (50 mM) in acetonitrile and sodium cacodylate buffer (20 mM) was irradiated at 350 nm (Rayonet photoreactor) and immediately afterwards the spectrum recorded on a Bruker ESP 300 spectrometer.
[21] E. Finkelstein, G. M. Rosen, E. J. Rauckman, *Arch. Biochem. Biophys.* **1980**, *200*, 1–16.
[22] a) R. A. Floyd, J. J. Watson, P. K. Wong, D. H. Altmiller, R. C. Rickard, *Free Radical Res. Commun.* **1986**, *6*, 163–172; b) M. Berger, C. Anselmino, J.-F. Mouret, J. Cadet, *J. Liq. Chromatogr.* **1990**, *13*, 929–941.
[23] C. von Sonntag, *The Chemical Basis of Radiation Biology*, Taylor and Francis, London, **1987**.
[24] a) A. F. Fuciarelli, B. J. Wegher, F. Gajewski, M. Dizdaroglu, W. F. Blankely, *Radiat. Res.* **1989**, *119*, 219–231; b) A. F. Fuciarelli, B. J. Wegher, W. F. Blankely, M. Dizdaroglu, *Int. J. Radiat. Biol.* **1990**, *58*, 397–415.
[25] H. Kasai, Z. Yamaizumi, M. Berger, J. Cadet, *J. Am. Chem. Soc.* **1992**, *114*, 9692–9694.
[26] a) M. A. Pathak, T. B. Fitzpatrick, *J. Photochem. Photobiol. B* **1992**, *14*, 3–22; b) G. Rodighiero, F. Dall'Acqua, D. Averbeck in *Psoralen DNA Photobiology*, Vol. *1* (Ed.: F. P. Gasparro), CRC, Boca Raton, FL, USA, **1988**, pp. 37–114.
[27] F. Dall'Acqua, M. Terbojevich, S. Marciani, D. Vedaldi, M. Recher, *Chem. Biol. Interact.* **1978**, *21*, 103–115.
[28] Fluorescence data: **1a'** (λ_{ex} = 302 nm); λ_{fl} = 482 nm), **1b'** (λ_{ex} = 304 nm; λ_{fl} = 502 nm), **2a** (λ_{ex} = 335 nm; λ_{fl} = 512 nm).
[29] J. D. McGhee, P. H. von Hippel, *J. Mol. Biol.* **1974**, *86*, 469–489.
[30] F. Tjerneld, B. Nordén, B. Ljunggren, *Photochem. Photobiol.* **1979**, *29*, 1115–1118.
[31] The spectra were measured on a Jasco J500 circular dichroism spectrometer converted for LD, a constant shear gradient of 500 sec^{-1} was used for recording the LD spectra.
[32] R. V. Prigodich, C. T. Martin, *Biochemistry* **1990**, *29*, 8017–8019.
[33] T. M. Rana, C. F. Meares, *J. Am. Chem. Soc.* **1990**, *112*, 2457–2458.
[34] K. J. A. Davis, *J. Biol. Chem.* **1987**, *262*, 9895–9901.
[35] T. A. Dix, J. Aikens, *Chem. Res. Toxicol.* **1993**, *6*, 218.

Solid-State and Solution Structures of $[\{NW(OC(CH_3)_2CF_3)_3\}_3]$ and Factors Favoring the Metathesis of C–N and W–W Triple Bonds in Reactions Involving Organic Nitriles and Ditungsten Hexaalkoxides**

Malcolm H. Chisholm,* Kirsten Folting-Streib, Darin B. Tiedtke, Frédéric Lemoigno, and Odile Eisenstein*

In a paper entitled "Transition Metal Nitrides, Organic Polyenes and Phosphazenes. A Structural and Orbital Analogy"[1] the authors stated, "Perhaps the most interesting conclusion we can draw for transition metal nitrides is that there should be substantial stability for a benzene analogue. Does this mean that the benzene analogue will have all equal bond lengths? We are not sure." Hoffmann et al. drew the limiting structures **A**.[1]



A

Following this theoretical prediction, Roesky et al.[2] reported the synthesis of the first trimeric metal nitride $[\{Cp^*Ta(Cl)N\}_3]$ ($Cp^* = \eta^5$-C_5Me_5), a triazatrimetallabenzene containing a central planar Ta_3N_3 moiety with Ta–N bond lengths that were statistically equivalent (Ta–N = 1.84(2) to 1.90(2) Å). Subsequently, Wolczanski et al. reported the structure of a related trimeric nitride $[\{Cp^*Ta(Me)N\}_3]$ having a similar planar, symmetrical Ta_3N_3 core.[3] They carried out an extended Hückel molecular orbital (EHMO) calculation on an idealized molecule $[(X_2TaN)_3]$ of C_{3v} symmetry and established that the trimer had the familiar π-type MOs with *a* and *e* symmetry as in benzene. These $[(X_2TaN)_3]$ molecules (d^0 tantalum center) with idealized tetrahedral metal centers are analogues of the trimeric phosphazenes $(X_2PN)_3$. We describe here the preparation and structure of a trimer of type $[(X_3WN)_3]$ (d^0 tungsten center) that has a quite different structure to the tantalum trimers above involving a planar W_3N_3 ring with alternating short and long W–N distances.

Whereas $[W_2(OtBu)_6]$ and nitriles react rapidly in hydrocarbon solutions to give $[N{\equiv}W(OtBu)_3]$ and $[R'C{\equiv}W(OtBu)_3]$ (R' = Me, Ph),[4] the related compounds $[W_2(OR)_6]$, where $R = tBuMe_2Si$[5] and $(CF_3)(CH_3)_2C$, are inert toward acetonitrile, except for the reversible, low-temperature formation of adducts $[W_2(OR)_6(NCMe)_2]$.[6] However, we found that benzonitrile and aryl nitriles (ArC≡N) reacted under similar conditions to give nitrides $[\{NW(OR)_3\}_x]$ and PhC≡CPh or ArC≡CAr.[7] For *p*-X-C_6H_4C≡N, we found that the rate was significantly influenced by X and followed the order X = Cl > H > OMe. These reactions were followed with ^{13}C- and ^{15}N-labeled nitriles by NMR spectroscopy. In the presence of

[*] Prof. M. H. Chisholm, Dr. K. Folting-Streib, D. B. Tiedtke
Department of Chemistry and Molecular Structure Center, Indiana University
Bloomington, IN 47405 (USA)
Telefax: Int. code +(812) 855-7148
Prof. O. Eisenstein, F. Lemoigno
Laboratoire de Chimie Théorique, Bâtiment 490
Université de Paris-Sud
F-91405 Orsay (France)

[**] We thank the National Science Foundation and the CNRS for support of this work, Dr. Theodore A. Budzichowski for helpful and encouraging discussions, and Dr. Jodi Wesemann for her help with the cryoscopic molecular weight determination.

ten equivalents of PhC≡N, there was no evidence for an intermediate, and we presume that [PhC≡W(OR)$_3$] reacts rapidly with the excess PhC≡N to give PhC≡CPh and [{N≡W(OR)$_3$}$_x$].[7]

The molecular structure of the fluoroalkoxide derivative **1** was determined in the solid state from a single-crystal X-ray study (Fig. 1).[8] There is a central planar W_3N_3 moiety in **1**, and

[{NW(OC(CH$_3$)$_2$CF$_3$)$_3$}$_3$] **1**

the local geometry about the tungsten can be described in terms of a distorted trigonal bipyramid. The W–N bond lengths alter-

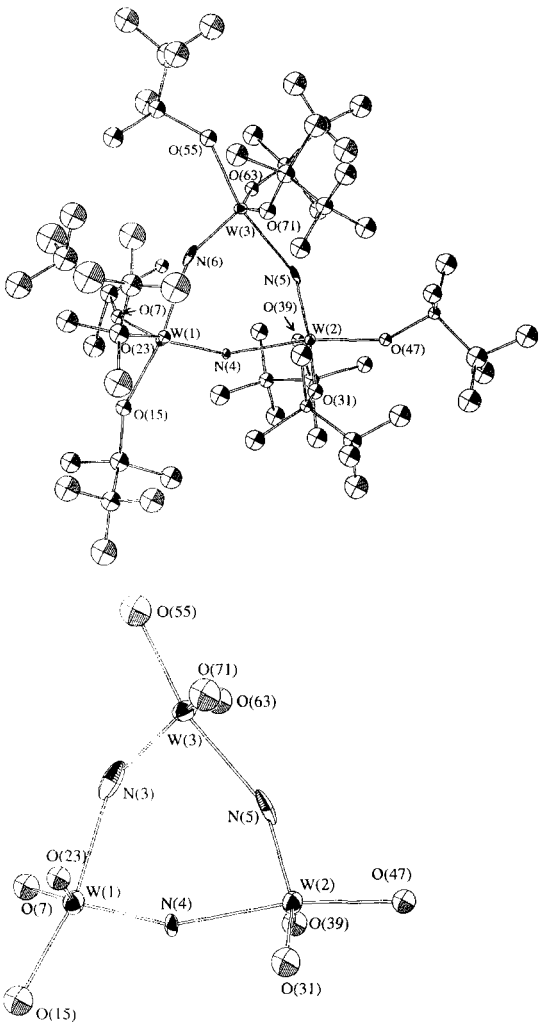
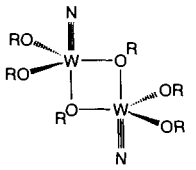


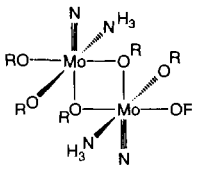
Fig. 1. Crystal structure of **1** (ORTEP representation). Top: view of the complete molecule. Bottom: view of the central $N_3W_3O_6$ skeleton. Selected bond lengths [Å] and angles [°]: W(1)-N(4) 1.732(15), W(2)-N(5) 1.682(19), W(3)-N(6) 1.717(19), W(1)-N(6) 2.159(20), W(2)-N(4) 2.125(5), W(3)-N(5) 2.159(18), W-O_{eq} 1.904–1.913 (1.907 average), W-O_{eq} 1.860–1.909 (1.891 average); N(4)-W(1)-N(6) 84.9(7), N(4)-W(2)-N(5) 84.9(7), N(5)-W(3)-N(6) 87.6(7), W(1)-N(4)-W(2) 154.5(10), W(2)-N(5)-W(3) 153.6(9), W(1)-N(6)-W(3) 150.7(9), O_{eq}-W-N_{eq} 167.6 (average), O_{axial}-W-N_{eq} 106.4 (average), O_{axial}-W-O_{eq} 90.8 (average), O_{eq}-W-O_{eq} 141.8 (average), O_{eq}-W-N_{eq} 109.6 (average).

nate markedly between 1.72(2) (average) and 2.14(2) Å (average), and the N-W-N angles are acute (85–88°), while the W-N-W angles are obtuse. Three fluoroalkoxido ligands lie in the W_3N_3 plane, while three of the remaining six lie above and three below the plane. About each tungsten, the fluoroalkoxido ligand in the W_3N_3 plane is located in a near *trans* configuration to the long W–N bond, while the short W–N bond and the remaining two alkoxido ligands define the equatorial plane of the trigonal bipyramid. ^{15}N NMR studies have shown that the trimeric structure remains intact in solution, as a central resonance is observed flanked by two sets of satellites due to coupling to ^{183}W (I = 1/2, 14% natural abundance; ^1J = 84 and 40 Hz).[10]

The crystal structure of **1** is in marked contrast to that of the symmetrical triazatrimetallabenzene of [(Cp*TaXN)$_3$].[2, 3] It is also different from the infinite polymeric compound [(*t*BuO)$_3$W≡N]$_x$[9] with its alternating short triple and long dative bonds. However, for R = *t*BuMe$_2$Si, solution NMR data reveal that the product is dimeric in solution and has terminal, rather than bridging nitrides. We propose that the dimer in solution has the structure **2**.



2:R = Si*t*BuMe$_2$



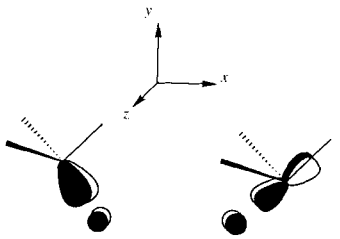
3:R = SiMe$_3$

Of particular relevance to our claim that there are terminal nitrido ligands are the values of $\tilde{\nu}$(W–N) = 1169 (^{14}N) and 1138 cm^{-1} (^{15}N), which may be compared with $\tilde{\nu}$(W–N) = 1014 (^{14}N) and 993 cm^{-1} (^{15}N) for [N≡W(O*t*Bu)$_3$]$_n$ and $\tilde{\nu}$(Ta–N) = 960 (^{14}N) and 930 cm^{-1} (^{15}N) for [Cp*Ta(Me)N]$_3$.[3] Furthermore, the ^{15}N NMR signal[10] shows one set of satellites of 14% intensity due to ^{183}W coupling (^1J = 103 Hz). This is further supported by the structure **3** (shown above), which was determined by DeCock et al.[11] and may be viewed as a bis(amino) adduct of a molybdenum analogue. Cryoscopic molecular weight determinations in benzene (1052 g mol^{-1}) also confirmed the dimeric nature of the siloxide compound in solution.

Thus, complex **1** is a cyclic trimer with alternating long and short W–N bonds whose structure persists in solution.[12] The related siloxide adopts a dimeric structure (akin to that seen for [{MeC≡W(O*t*Bu)$_3$}$_2$]) with terminal nitrido ligands. We now return to the structural nature of the W_3N_3 ring and the factors influencing the geometry of the six-membered ring. Two factors can induce an alternation of the bond length in a planar six-membered ring [(L$_n$M)$_3$N$_3$]. The orbitals of the T-shaped ML$_3$ fragment, even if symmetrically positioned with respect to the plane bisecting the N-M-N angle, can induce a second-order Jahn–Teller distortion of the π electron system that favors M–N bond alternation. Alternatively, a *fac* ML$_3$ fragment can bond to the two nitrogen centers; the M–N bonds are then intrinsically nonequivalent. This leads naturally to bond alternation within the six-membered ring. The fragment [Cp*TaX] (X = Cl and Me) forms two equivalent Ta–N bonds. As mentioned by Wolczanski et al.,[3] the second-order Jahn–Teller effect in [(Cp*TaMe)$_3$N$_3$] is too small owing to the large energy gap between the a_2 and a_1 orbitals, which could otherwise induce bond alternation in the six-membered ring. EH calculations[13] on other model compounds of type [(L$_n$M)$_3$N$_3$] (ML$_n$ = d^0-ML$_2$ and d^0-ML$_3$, where ML$_3$ is a T-shaped fragment situated in the bisector plane of the N-M-N angle) show that the energy difference between the corresponding a_2 and a_1 is similar

to that obtained in the case of [Cp*MX] (d^0 metal center). Small differences are observed in the overlap factor, which is found to favor a slightly larger mixing of a_2 and a_1 in the distorted C_3 structure in the case of T-shaped ML_3. This is due to the fact that the d_{xz} and d_{yz} metal orbitals can both overlap equally well with the nitrogen p_z orbitals, since they both are equivalent nonbonding orbitals in a local trigonal bipyramid. However, this effect remains small.

A more noticeable difference is associated with the intrinsic site preference for ligands in a trigonal bipyramid, which results from σ and π effects. Although OR groups have been seen to be *trans* to each other in some complexes,[14] the strong *trans* influence[15] of the alkoxide ligand should result in a preference for a *fac* over a *mer* geometry. Therefore, one of the OR ligands on each W is apical and the other two are equatorial; as a result, one nitride is equatorial and one apical. The equatorial nitride forms a stronger π bond to the metal than the axial nitride, since the unoccupied metal orbital **I** is strongly hybridized away from the equatorial alkoxide and overlaps strongly with nitrogen π orbital. In contrast, the unoccupied orbital **II** involved in π bonding with the axial nitride is a pure d orbital, which overlaps less with nitrogen p_z orbital.



I **II**

An EH calculation on the model compound $[\{W(OH)_3\}_3N_3]$ with W–N bond lengths that are all identical confirms this analysis: the π-overlap population is larger for the equatorial N (0.29) than for the apical N (0.25). The WN total overlap populations differ by the same amount. The orientation of the $W(OR)_3$ group with one apical OR in the plane of the ring does not seem to be a consequence of the WN bond alternations. In the cyclotungstaphosphazene $[(NPPh_2NPPh_2N)WF_3]$, the authors suggest that one F occupies an apical site and the two others, equatorial sites of the pentacoordinated W center. These conclusions were based on the ^{19}F NMR spectra.[16]

In conclusion, the present work reports the first example of the alternation of long and short M–N bond within a six-membered, M_3N_3-containing ring and reveals how subtle electronic factors associated with the steric and electronic requirements of a d^0-ML_n fragment greatly influence whether the metal nitride structure is an infinite polymer, a dimer, or a cyclotrimer or -tetramer.[17] The electronic factors that influence the metathesis of the M≡M and C≡N bonds are under investigation.

Experimental Procedure

1: Benzonitrile (150 μL, 1.5 mmol) was added to a solution of $[W_2(OC(CH_3)_2CF_3)_6]$ (175 mg, 0.15 mmol) in 10 mL of dry, degassed benzene at 25 °C. The solution was stirred at 25 °C for 24 h, and the solvent removed under vacuum. Sublimation of the impurities followed by recrystallization in dry, degassed hexanes gave X-ray quality, pale yellow crystals in 68% yield.

2: Benzonitrile (150 μL, 1.5 mmol) was added to a solution of $[W_2(OSi^tBuMe_2)_6]$ (175 mg, 0.15 mmol) in 10 mL of dry, degassed benzene at 25 °C. The solution was stirred at 25 °C for 24 h, and the solvent was reduced to 2 mL under vacuum. Dry, degassed acetonitrile (10 mL) was added, the solution filtered under an inert atmosphere, and the solid washed with 2 mL of dry, degassed acetonitrile to afford the product in 78% yield.

Received: June 6, 1994 [Z 7038 IE]
German version: *Angew. Chem.* **1995**, *107*, 61

Keywords: complexes with oxygen ligands · metallabenzenes · metathesis · nitrido complexes · tungsten compounds

[1] R. A. Wheeler, R. Hoffmann, J. Strähle, *J. Am. Chem. Soc.* **1986**, *108*, 5381.
[2] H. Plenio, H. W. Roesky, M. Noltemeyer, G. M. Sheldrick, *Angew. Chem.* **1988**, *100*, 1377; *Angew. Chem. Int. Ed. Engl.* **1988**, *27*, 1330.
[3] M. M. Banaszak-Holl, M. Kersting, B. D. Pendley, P. T. Wolczanski, *Inorg. Chem.* **1990**, *29*, 1518.
[4] R. R. Schrock, M. L. Listemann, L. G. Sturgeoff, *J. Am. Chem. Soc.* **1982**, *104*, 4291.
[5] NMR data for $[W_2(OSi^tBuMe_2)_6(NCMe)_2]$: ^1H NMR (300 MHz, C_7D_8, −40 °C): δ = 1.27 (6H), 1.04 (18H), 0.88 (36H), 0.25 (24H), 0.18 (12H).
[6] J. H. Freudenberger, S. F. Pedersen, R. R. Schrock, *Bull. Soc. Chim. Fr.* **1985**, 349.
[7] For formation of PhC≡CPh from the reaction between $[PhC{\equiv}W(OR)_3]$ and PhC≡N, see ref. [8] in M. L. Listemann, R. R. Schrock, *Organometallics* **1985**, *4*, 74.
[8] Summary of crystal data for **1**: M = 1744.40, monoclinic, $P2_1/c$, a = 22.481(5), b = 11.367(2), c = 22.573(2), β = 94.60°, V = 5749.66 Å^3, Z = 4, ρ_{calcd} = 2.015 g cm^{-3}. The structure was solved by locating the three W atoms by the Patterson method with SHELXS-86. The remaining non-hydrogen atoms were located in successive iterations of least-squares refinement and difference Fourier calculations. Almost all of the hydrogen atoms on the main molecule were evident in a later difference map. The full-matrix least-squares refinement was completed with anisotropic thermal parameters, and the hydrogen atoms were in fixed, idealized positions. The final $R(F)$ was 0.0503 and $R_w(F)$ was 0.0513 for 356 variables and 3827 reflections considered observed. The asymmetric unit contained one half molecule of hexane located at a center of symmetry. Further details of the crystal structure investigation may be obtained from the Fachinformationszentrum Karlsruhe, D-76344 Eggenstein-Leopoldshafen (Germany), on quoting the depository number CSD-58362.
[9] M. H. Chisholm, D. M. Hoffman, J. C. Huffman, *Inorg. Chem.* **1983**, *22*, 2903.
[10] NMR data for **1**: ^1H NMR (300 MHz, C_6D_6, 24 °C): δ = 1.52 (6H), 1.54 (6H), 1.60 (6H); ^{15}N NMR (36.6 MHz, C_6D_6, 24 °C, external reference $^{15}NCMe$, δ = −135.29): δ = 216.6 ($^1J(^{183}W^{15}N)$ = 84 Hz (12%), 40 Hz (12%); ^{19}F NMR (340 MHz, C_6D_6, 24 °C, external reference CF_3CO_2H, δ = 78.45): δ = −84.2 (3F), −83.6 (6F). NMR data von **2**: ^1H NMR (300 MHz, C_6D_6, 24 °C): δ = 0.23 (12H), 0.31 (12H), 0.32 (12H), 1.09 (18H), 1.12 (36H); ^{15}N NMR (36.6 MHz, C_6D_6, 24 °C, external reference $^{15}NCMe$, δ = −135.29): δ = −6.5 ($^1J(^{183}W^{15}N)$ = 103 Hz (14%).
[11] G.-S. Kim, C. W. DeKock, *J. Chem. Soc. Chem. Commun.* **1989**, 1166.
[12] We have been unable to make an unambiguous assignment of ν(W–N) for **1** in the solid state and, therefore, are not able to make a comparison with the tetranuclear complex $[\{NWCl_3(POCl_3)\}_4]$: $\tilde{\nu}$(W–N) = 1087, 1074 cm^{-1}; W. Musterle, J. Strähle, W. Liebelt, K. Dehnicke, *Z. Naturforsch. B* **1979**, *34*, 942.
[13] The weighted H_{ij} formula has been used: J. H. Ammeter, H.-B. Bürgi, J. C. Thibeault, R. Hoffmann, *J. Am. Chem. Soc.* **1978**, *100*, 3686. Parameters of tungsten: A. Dedieu, T. A. Albright, R. Hoffmann, *J. Am. Chem. Soc.* **1979**, *101*, 3141.
[14] For example, in $[Mo_2X_4(OiPr)_6]$ compounds where X = Cl and Br: M. H. Chisholm, C. C. Kirkpatrick, J. C. Huffman, *Inorg. Chem.* **1981**, *20*, 871.
[15] T. G. Appleton, H. C. Clark, L. E. Manzer, *Coord. Chem. Rev.* **1973**, *10*, 352.
[16] K. V. Katti, H. W. Roesky, M. Rietzel, *Inorg. Chem.* **1987**, *26*, 4032.
[17] For a recent review on transition metal nitrides, see: K. Dehnicke, J. Strähle, *Angew. Chem.* **1992**, *104*, 978; *Angew. Chem. Int. Ed. Engl.* **1992**, *31*, 955.

Aggregation of Nitrido–Metal Complexes: The Example of $[(\eta^5\text{-}C_5Me_5)Mo(N)Cl_2]$

Wolfgang A. Herrmann,* Sandra Bogdanovic, Thomas Priermeier, Rinaldo Poli,* and James C. Fettinger

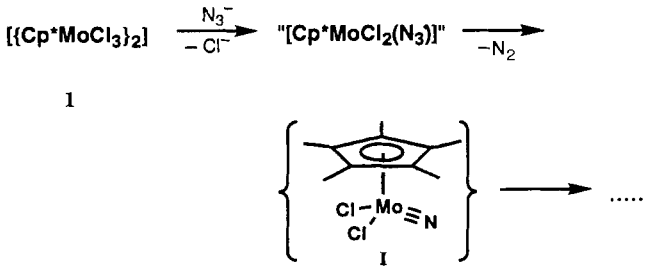
Whereas the chemistry of high-oxidation state cyclopentadienyl transition metal oxides has been the subject of intensive study,[1] the corresponding nitrido complexes have only

[*] Prof. Dr. W. A. Herrmann, S. Bogdanovic, T. Priermeier
Anorganisch-chemisches Institut der Technischen Universität München
Lichtenbergstrasse 4, D-85747 Garching (Germany)
Telefax: Int. code + (89)3209-3473
Prof. Dr. R. Poli, Dr. J. C. Fettinger
Department of Chemistry, University of Maryland
College Park, MD 20742 (USA)
Telefax: Int. code + (301)314-9121

[**] This work was supported by the Fonds der Chemischen Industrie (Ph.D. Fellowship to S. B.), the Alexander von Humboldt-Stiftung (Research Fellowship to R. P.), and the Deutsche Forschungsgemeinschaft.

received little attention; the only examples are $[\{Cp^*Ta(N)Cl\}_n]$ ($n = 3,4$) $[\{Cp^*V(N)Cl\}_2]$, $[CpOs(N)(CH_2SiMe_3)_2]$ and $Li[Cp^*W(N)Me_3]$ ($Cp = \eta^5\text{-}C_5H_5$, $Cp^* = \eta^5\text{-}C_5Me_5$).[2a-e] The tantalum and vanadium compounds can be thought of as aggregates of varying nuclearity of the hypothetical mononuclear fragments $\{Cp^*M(N)Cl\}$ (M = V, Ta). Here we report on the aggregation of a $\{Cp^*Mo(N)Cl_2\}$ transient to form the first examples of Cp^*Mo^{VI} nitrido complexes, which illustrate the electronic and steric effects of the Cp* ligand in the chemistry of nitrido complexes. The general interest is related to the search for stable models[3] of poorly understood metathesis catalysts obtained by in situ alkylation of nitridomolybdenum(VI) complexes.[4] Another point of interest is the reactivity of the nitrido ligand[5] and how this is influenced by the presence of the cyclopentadienyl ring.

The standard synthetic strategy (Scheme 1)[5] introduces the nitrido ligand and two oxidizing equivalents from an azide. Our



Scheme 1.

starting material is the recently reported **1**.[6] When NaN_3 in acetonitrile was employed as the azide source, gas evolution ensues and a purple solution is obtained, from which purple crystals of **2** · 0.25 CH_2Cl_2 (see Scheme 2) are collected in 39% yield after crystallization from dichloromethane/ether/pentane. Elemental analyses and NMR spectra indicate that the compound has incorporated one CH_3CN molecule per two $\{Cp^*Mo(N)Cl_2\}$ units (see Scheme 2). Reaction of **1** with $(CH_3)_3SiN_3$ in CH_2Cl_2 also proceeds with gas evolution, but a emerald-green solution is now obtained. Crystals of paramagnetic (EPR) **3** (see Scheme 2) were isolated in 43% yield by diffusion of *n*-hexane; **3** crystallizes with two molecules of CH_2Cl_2. The structures of both compounds were elucidated by X-ray crystallography.

$[\{Cp^*MoCl_3\}_2]$ **1**

$[Cp^*_2Mo_2Cl_4(N)(N_2CCH_3)]$ **2**

$[Cp^*_4Mo_5N_5Cl_{10}]$ **3**

The structure analysis of **2** (Fig. 1)[7] shows that acetonitrile forms part of a symmetric six-membered Mo_2N_3C ring, which is the first known example of a dimetallatriazene. The molecule can also be described as a dinuclear molybdenum complex with nitrido and acetamidinato(3−) bridging ligands. The planes defined by C1, C2, N2, N3 and Mo1, N1, Mo2 are twisted by an angle of 16.7° along the virtual twofold axis N1-C1-C2. Although the ring is hence not quite planar, the π-electron density is evidently delocalized: the Mo−N1 distances of 1.790(7) Å (Mo1−N1) and 1.851(7) Å (Mo2−N1) are intermediate between those for the typical Mo≡N bond (1.64 Å)[8] and a Mo−N dative bond [e.g., 2.16(1) Å in $[\{MoNCl_3(OPCl_3)\}_4]$;[9] 2.18(3) Å in $[\{MoNMe_2(OtBu)\}_4]$ $(tBuC_5H_4N)_2$[3a]] and slightly shorter than those for the Mo=N double bonds, as for instance

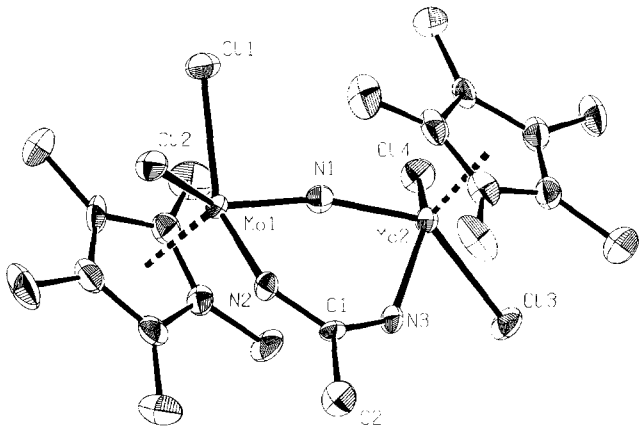


Fig. 1. PLATON diagram of the molecular structure of **2**. Relevant distances [Å] and angles [°]: Mo1-N1 1.790(7), Mo2-N1 1.851(7), Mo1-N2 2.089(8), Mo2-N3 2.082(7), N2-C1 1.34(1), N3-C1 1.33(1), Mo-Cl (average for Mo1 and Mo2) 2.432(2), Mo1-N1-Mo2 161.4(4), Mo1-N2-C1 132.8(6), Mo2-N3-C1 131.9(6), N2-C1-N3 123.6(7)

in $[\{MoN[S_2P(OCH_3)_2]_2\}_4]$ (av 1.868(12) Å).[10] The open Mo1-N1-Mo2 angle of 161.4(4)° indicates strong participation of the π electrons to the Mo−N1 bonding. The other two Mo−N bond lengths (Mo1−N2 and Mo2−N3) are considerably longer (av 2.086(8) Å) and the Mo-N-C angles more closed (av 132.4(6)°), consistent with less multiple bond character for the bonds between the Mo centers and the $(CH_3CN_2)^{3-}$ nitrogen donors. The C−N bonds (av 1.34(1) Å) are typical of partial double bond character, as found for instance in aromatic N-heterocycles (in the 1.32−1.35 Å range).[11] The coordination geometry around the Mo atoms can be described as a four-legged piano stool with two *cis*-chloro ligands, the bridging nitrido ligand, and one of the CH_3CN_2 nitrogen atoms occupying the four basal positions. The two four-legged piano stools share a common vertex identified by the nitrido ligand in such a way that the two Cp* ligands are *anti* with respect to each other.

The structure of the pentanuclear mixed-valence complex **3**[12] (Fig. 2) is unusual and shows that the molecule can be

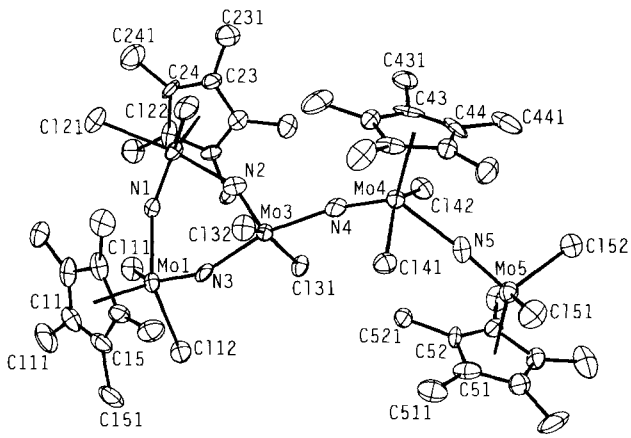
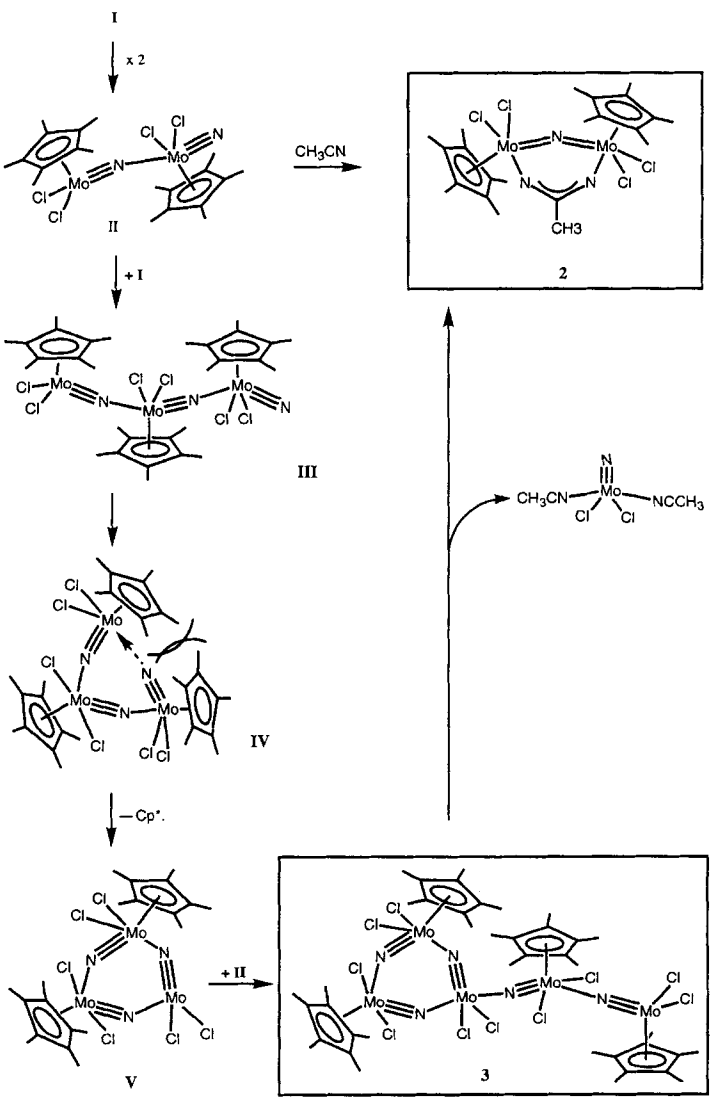


Fig. 2. ORTEP diagram of the molecular structure of **3**. Relevant distances [Å] and angles [°]: Mo1-N1 2.14(2), Mo1-N3 1.70(2), Mo2-N1 1.73(2), Mo2-N2 2.12(2), Mo3-N2 1.68(2), Mo3-N3 2.09(2), Mo3-N4 2.13(2), Mo4-N4 1.69(2), Mo4-N5 2.21(2), Mo5-N5 1.69(2), Mo-Cl (average for Mo1, Mo2 and Mo4) 2.407(10), Mo-Cl (average for Mo3) 2.378(6), Mo-Cl (average for Mo5) 2.284(7), N1-Mo1-N3 80.9(7), N1-Mo2-N2 81.8(7), N2-Mo3-N3 85.3(8), N2-Mo3-N4 107.7(8), N3-Mo3-N4 166.4(7), Cl31-Mo3-Cl32 155.0(2), N4-Mo4-N5 130.7(7), Mo1-N1-Mo2 158.5(9), Mo2-N2-Mo3 154.4(11), Mo1-N3-Mo3 157.2(11), Mo3-N4-Mo4 167.0(12), Mo4-N5-Mo5 175.3(11).

described as an aggregate of four $Cp^*Mo(N)Cl_2$ moieties and a central $Mo(N)Cl_2$ unit. One $Cp^*Mo(N)Cl_2$ dimer forms a trimetallatriazene together with the nitridomolybdenum(v) center, whereas the other dinuclear unit is coordinated in a chain-like fashion to the central Mo atom. The assignment of the oxidation state v to Mo3 is in agreement with the geometry and structural parameters of comparable compounds such as $[Mo(N)X_2L_2]$ ($X^- = L = Cl^-$; $X = N_3^-$, $L = N{\equiv}Mo(N_3)(Et_2PCH_2CH_2PEt_2)_2$).[13]

The Mo_3N_3 cycle in **3** is almost planar (the largest distances from the least-squares plane are 0.098 Å for N2, and −0.051 Å for N3) and contains localized, alternating Mo≡N triple (av 1.70(3) Å) and N → Mo dative bonds (av 2.12(3) Å). Theoretical work predicts particular stability for compounds containing a cyclic M_3N_3 moiety,[14] regardless of whether the Mo–N multiple bonds are delocalized or not. Compound **3** is the first example of a cyclic M_3N_3 unit with localized bonds. This localization is probably the result of the single d electron on Mo3, which encourages square-pyramidal coordination geometry for Mo3 and the presence of only one multiple bond in the apical position at this metal center. The Mo–N bonds are also localized in the lateral chain, as illustrated in the drawing of **3** in Scheme 2. There are four different coordination geometries in **3**: *cis*-$Cp^*MoN_2Cl_2$ for the Mo1 and Mo2 centers (analogous to the Mo centers in **2**), square-pyramidal (MoN_3Cl_2) for Mo3, *trans*-$Cp^*MoN_2Cl_2$ for Mo4, and an unprecedented three-legged piano stool (Cp^*MoNCl_2) for Mo5. The existence of the latter geometry in **3** suggests that the mononuclear species $[Cp^*MoNCl_2]$ **I** is more nucleophilic at the nitrido ligand than it is electrophilic at the metal.



Scheme 2.

As in the structure of **2**, the six-membered ring in **3** has the two Cp* rings on opposite sides of the Mo_3N_3 plane. A molecular model where the two Cp* ligands are placed on the same side of the ring reveals an unbearable steric situation. This is because the four-legged piano stool geometry forces the Mo–Cp* vectors to lie almost perpendicular to the Mo_3N_3 plane. Based on this observation, we suggest that a trinuclear $(Cp^*MoCl_2N)_3$ compound, in which two Cp* rings would be forced to reside on the same side of the three-membered ring, cannot exist. In the related trimer of tantalum reported by Roesky et al.,[2a] a greater distance between the Cp* rings is allowed by the three-legged piano stool geometry around the metals.

A possible route for the formation of compounds **2** and **3** follows from Scheme 2. The hypothetical $Cp^*Mo(N)Cl_2$ intermediate **I** oligomerizes to **II** and **III** because of the pronounced basicity of the nitrido ligand. In acetonitrile, these intermediates are likely to be coordinated by a solvent molecule at the unsaturated metal center. Subsequent addition of **II** could lead to a $[Cp^*MoCl_2N]_\infty$ polymer (a polymeric Cp* metal nitride, e.g. $[Cp^*Ta(N)Cl]_\infty$, has been observed[2b]) but other alternatives are available to intermediates **II** and **III**. A CH_3CN adduct of **II** can cyclize to afford **2** directly through attack of the nucleophilic nitrido ligand at the C atom of the ligand. In CH_2Cl_2, **III** can cyclize but, in doing so, a strong steric interaction is established between two Cp* rings (e.g. see **IV**). Therefore, one Cp* ring is likely to be lost at this stage to give **V**. The reaction is completed by coordination of **II** to the unsaturated Mo^V center.

The EPR spectrum of **3** in CH_2Cl_2 shows a resonance at $g = 1.965$ ($a_{Mo} = 46.0$ G), similar to those reported for other pentacoordinated Mo^V nitrido complexes.[13, 15] Compound **3** reacts with THF to form a yellow solution with a new EPR resonance at $g = 1.957$ ($a_{Mo} = 48.5$ G), which we assign to $[MoNCl_2(thf)_2]$. On the other hand, acetonitrile reacts with **3** to form a purple solution containing **2** as shown by NMR spectroscopy and exhibiting an EPR spectrum ($g = 1.957$, $a_{Mo} = 48.9$ G) which we assign to $[MoNCl_2(CH_3CN)_2]$.

Our results indicate that the less encumbering Cp ligand should be capable of stabilizing a trimeric $[\{CpMoNCl_2\}_3]$ structure, while Cp* is not. With regard to the possible existence of a dinuclear $[\{Cp^*Mo(\mu\text{-}N)Cl_2\}_2]$ structure analogous to that of Doherty's vanadium compound,[2c] no evidence of such a structure exists and the observation of an open-chain dinuclear unit in the structure of **3** suggests that it is unstable. Important factors may be the greater tendency of Mo (with respect to V) to reach an electronically saturated configuration, and the ability of all bridging N atoms to act as eight-electron donors in **3**, whereas in a (hypothetical) $[\{Cp^*Mo(\mu\text{-}N)Cl_2\}_2]$ structure with a Mo-N-Mo angle smaller than 120° the N atoms could at best provide six electrons to the metal centers.

In conclusion, the electron-donating character of Cp* and the availability of lone pairs for π bonding on the chloro ligands enhance the nitrido nucleophilicity and suppress electrophilicity at the electronically unsaturated metal center. Based on these principles, compounds of type $[Cp^*Mo(\equiv N \rightarrow A)Cl_2]$ (A = Lewis acid) appear to be reasonable synthetic targets.

Experimental Procedure

2: A suspension of $[Cp^*Mo(CO)_2Cl_3]$ (207 mg, 0.53 mmol) in CH_3CN (30 mL) was kept at 60 °C for 30 min. NaN_3 (34 mg, 0.52 mmol) was added to the resulting burgundy solution and the mixture was stirred at 25 °C for 30 min (gas evolution and color change to purple). The mixture was evaporated to dryness and the residue was extracted with CH_2Cl_2. After filtration, the solution was layered with a mixture of Et_2O (15 mL) and pentane (15 mL) and cooled slowly to −35 °C. Purple crystals of $\mathbf{2} \cdot 0.25\,CH_2Cl_2$ (67 mg, 39%) were isolated by decanting off the mother liquor and drying the solid under vacuum. ^1H NMR (CD_2Cl_2, 25 °C): $\delta = 2.52$ (s, 3H, N_2CCH_3), 1.99 (s, 30H, Cp*). Analysis for $C_{22.25}H_{33.5}Cl_{4.25}Mo_2N_3$ ($= \mathbf{2} \cdot 0.25\,CH_2Cl_2$). Calc.: C, 38.48; H, 4.86; N, 6.05, Cl 22.97. Found: C, 38.18; H, 4.96; N, 5.88, Cl 22.49. A crystal suitable for X-ray analysis was chosen under mother liquor.

3: A suspension of $[Cp^*Mo(CO)_2Cl_3]$ (351 mg, 0.892 mmol) in CH_2Cl_2 (30 mL) was heated under reflux for 2 h. To the resulting solution of $[\{Cp^*MoCl_3\}_2]$ [6], $(CH_3)_3SiN_3$ (125 μL, 108 mg, 0.94 mmol) was added and the mixture was stirred at 25 °C for 30 min (gas evolution and color change to emerald green). Diffusion of a 50 mL *n*-hexane layer gave black crystals of $\mathbf{3} \cdot 2\,CH_2Cl_2$ (124 mg, 43%). EPR (CH_2Cl_2, 25 °C): $g = 1.965$, $a_{Mo} = 46.0$ G. Analysis for $C_{42}H_{64}Cl_{14}Mo_5N_5$ ($= \mathbf{3} \cdot 2\,CH_2Cl_2$): Calc.: C, 31.24; H, 3.99; N, 4.34. Found: C, 31.17; H, 4.29; N, 4.34.

Received: July 7, 1994 [Z 7110 IE]
German version: *Angew. Chem.* **1995**, *107*, 63

Keywords: cyclopentadienyl complexes · molybdenum compounds · nitrido complexes

[1] Reviews: a) W. A. Herrmann, *Angew. Chem.* **1988**, *100*, 1269–1286; *Angew. Chem. Int. Ed. Engl.* **1988**, *27*, 1297–1313; b) F. Bottomley, *Polyhedron* **1992**, *11*, 1707–1731.

[2] a) H. Plenio, H. W. Roesky, M. Noltemeyer, G. M. Sheldrick, *Angew. Chem.* **1988**, *100*, 1377–1378; *Angew. Chem. Int. Ed. Engl.* **1988**, *27*, 1330–1331; b) H. W. Roesky, M. Lücke, *J. Chem. Soc. Chem. Commun.* **1989**, 748; c) T. S. Haddad, A. Aistars, J. W. Ziller, N. M. Doherty, *Organometallics* **1993**, *12*, 2420–2422; d) R. W. Marshman, J. M. Shusta, S. R. Wilson, P. A. Shapley *ibid.* **1991**, *10*, 1671–1676; e) T. Glassman, M. G. Vale, R. R. Schrock, *ibid.* 4046–4057.

[3] a) W. A. Herrmann, S. Bogdanovic, J. Behm, M. Denk, *J. Organomet. Chem.* **1992**, *430*, C33–38; W. A. Herrmann, S. Bogdanovic, R. Poli, T. Priermeier, *J. Am. Chem. Soc.* **1994**, *116*, 4989–4990.

[4] K. Seyferth, R. Taube, *J. Organomet. Chem.* **1982**, *229*, C19–23.

[5] Review: K. Dehnicke, J. Strähle, *Angew. Chem.* **1992**, *104*, 978–1000; *Angew. Chem. Int. Ed. Engl.* **1992**, *31*, 955–978.

[6] F. Abugideiri, G. A. Brewer, J. U. Desai, J. C. Gordon, R. Poli, *Inorg. Chem.* **1994**, *33*, 3745–3751.

[7] Crystal structure data of $\mathbf{2} \cdot 1.4\,CH_2Cl_2$: $a = 14.486(3)$, $b = 14.814(2)$, $c = 17.002(3)$ Å, $\beta = 110.62(1)°$, $V = 3415(1)$ Å^3, space group $P2_1/c$ (no. 14). The single crystals for X-ray analysis were chosen under mother liquor. The asymmetric unit contains 1.4 additional molecules of CH_2Cl_2. The structure was solved by the Patterson method and refined by full-matrix least-squares methods and subsequent difference Fourier techniques for 317 parameters and 3876 observed reflections ($I > 3\sigma(I)$). $R = 0.067$, $R_w = 0.072$. Further details of the crystal structure investigation are available on request from the Director of the Cambridge Crystallographic Data Centre, 12 Union Road, GB-Cambridge CB2 1EZ (UK), on quoting the full journal citation.

[8] W. A. Nugent, J. M. Mayer, *Metal-Ligand Multiple Bonds*, Wiley, New York, **1988**, Chapter 5.

[9] K. Dehnicke, J. Strähle, *Angew. Chem.* **1981**, *93*, 451–464; *Angew. Chem. Int. Ed. Engl.* **1981**, *20*, 413–426.

[10] M. E. Noble, K. Folting, J. C. Huffmann, R. A. D. Wentworth, *Inorg. Chem.*, **1982**, *21*, 3772–3776.

[11] R. C. Weast, *Handbook of Chemistry and Physics*, 57th ed., CRC Press, Cleveland, Ohio, USA, **1976**, F212.

[12] Crystal structure data of $\mathbf{3} \cdot 2\,CH_2Cl_2$: $a = 16.842(2)$, $b = 18.829(2)$, $c = 19.016(2)$ Å, $V = 6030.2(12)$ Å^3, $Z = 4$, orthorhombic, space group $P2_12_12_1$. The structure was solved by direct methods and refined by alternating full-matrix least-squares methods and difference Fourier maps for 615 parameters and 5979 observed reflections ($I > 2\sigma(I)$). $R = 0.0689$, $R_w = 0.168$, GOF = 1.102 [7].

[13] a) J. Schmitte, C. Friebel, F. Weller, K. Dehnicke, *Z. Anorg. Allg. Chem.* **1982**, *495*, 148–156. b) D. L. Hughes, M. Y. Mohammed, C. J. Pickett, *J. Chem. Soc. Dalton Trans.* **1990**, 2013–2019.

[14] R. A. Wheeler, R. Hoffmann, J. Strähle, *J. Am. Chem. Soc.* **1986**, *108*, 5381–5387.

[15] J. Chatt, J. R. Dilworth, *J. Chem. Soc. Chem. Commun.* **1974**, 517–518.

An Ab Initio Investigation of the Rh^I-Catalyzed Hydroboration of C=C Bonds: Evidence for Hydrogen Migration in the Key Step**

Andrea E. Dorigo and Paul von Ragué Schleyer*

The uncatalyzed hydroboration of alkenes has been studied extensively experimentally[1] and theoretically,[2, 3] and its mechanism is understood in detail. The synthetic usefulness of the Rh^I-catalyzed hydroboration reaction has been demonstrated by Evans recently.[4, 5] That the diastereoselectivity of the reaction is opposite to that observed for uncatalyzed hydroborations is of particular interest. While a mechanism[5–7] (Fig. 1)

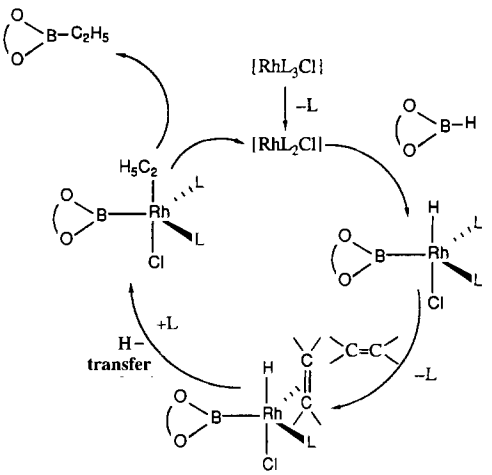


Fig. 1. Proposed mechanism [4, 5] for Rh^I-catalyzed hydroboration of C=C bonds.

has been proposed, the nature of the intermediates involved and the key step in the reaction are uncertain. Here we describe an ab initio study[8] of the potential energy surface for the addition of BH_3 to C_2H_4 catalyzed by $[Rh(PH_3)_3Cl]$. Our calculations show that hydrogen, rather than BH_2, migrates to the double bond in the key step. The results also support the existence of several 14-electron complexes as reaction intermediates and provide a possible explanation for the reaction diastereoselectivity.

Initial pseudopotential HF/LANL1DZ[8, 9] geometry optimizations followed by RMP2/LANL1DZ optimizations were carried out for all stationary points. The resulting structures are shown in Figures 2–5. All the RHF wavefunctions were stable to UHF expansion. Single-point MP4(SDQ) energies on the MP2/LANL1DZ geometries used the LANL1DZ basis set augmented with f functions on rhodium (f exponent = 0.35[9]), d functions[10] on the carbon and boron atoms, and p functions[10] on the H atom being transferred from the BH_3 unit to the C=C bond. This basis set is denoted as LANL1DZ(POL) here. Single-point MP4(SDQ) calculations were also carried out using a basis set (referred to as basis set II in the following) differing from LANL1DZ in that the 4s and 4p electrons of Rh

[*] Prof. Dr. P. von R. Schleyer, Dr. A. E. Dorigo
Computer-Chemie-Centrum
Institut für Organische Chemie I
der Universität Erlangen-Nürnberg
Henkestrasse 40, D-91054 Erlangen (Germany)
Telefax: Int. code + (9131)85-9132

[**] This work was supported by the Volkswagen-Stiftung, the Fonds der Chemischen Industrie, the Convex Computer Corporation, and the Deutsche Forschungsgemeinschaft.

are included in the valence space instead of being described by the effective core potential; the relative energies at both the MP2/II//MP2/LANL1DZ and the MP4(SDQ)/II//MP2/LANL1DZ levels were similar to those at the MP2/LANL1DZ level. For the first step of the reaction—the addition of BH_3 to **1** to give **2**—QCISD(T)/LANL1DZ(POL) single-point calculations were also performed. Absolute energies at MP2/LANL1DZ, MP4(SDQ)/II, and MP4(SDQ)/LANL1DZ(POL) are given in Table 1 for all the reaction intermediates as well as for BH_3, PH_3, and C_2H_4; QCISD(T)/LANL1DZ(POL) energies are given for **1**, **2**, and BH_3. We discuss the MP2/LANL1DZ-optimized structures and the relative energies at the MP4(SDQ)/LANL1DZ(POL) level, unless otherwise noted.

Table 1. a) Absolute energies [−a.u.] at the MP2/LANL1DZ (**1**–**14**), MP4(SDQ)//II, MP2/LANL1DZ(POL), and MP4(SDQ)/LANL1DZ(POL) levels (**1**–**12**). b) Absolute energies [−a.u.] of **1**, **2**, and BH_3 at the QCISD(T)/LANL1DZ(POL) level.

Cmpd.	MP2/ LANL1DZ	MP4(SDQ) II//MP2/ LANL1DZ	MP2/ LANL1DZ(POL) //MP2/ LANL1DZ	MP4(SDQ)/ LANL1DZ(POL) //MP2/ LANL1DZ
1	53.20307	139.82073	53.28177	53.32244
2	79.73001	166.33234	79.87250	79.92649
3	71.59258	158.17367	71.73230	71.76926
4	149.82698	236.41973	150.08410	150.13417
5	149.81833	236.41119	150.07784	150.12767
6	149.82257	236.41852	150.07780	150.13053
7	149.80158	236.40157	150.05238	150.11050
8	149.81288	236.41392	150.05956	150.11494
9	149.83536	236.43761	150.08275	150.14119
10	157.96631	244.58736	158.20990	158.28719
10	157.92520	244.54389	158.17818	158.25055
12	157.92103	244.54334	158.16593	158.24013
BH_3	26.42640	26.44232	26.46362	26.48233
PH_3	8.08517	8.10462	8.08517	8.10462
C_2H_4	78.18265	78.20729	78.28366	78.31050
$EtBH_2$	104.65956	104.69882	104.80160	104.84500
13	157.93321	–	–	–
14	157.92180	–	–	–
			QCISD(T)/ LANL1DZ(POL) //MP2/ LANL1DZ	
1			53.35842	
2			79.94640	
BH_3			26.48462	

In accord with the proposed mechanism[5, 6] (Fig. 1), we assumed the active catalytic species to be $[Rh(PH_3)_2Cl]$[11] (**1**, Fig. 2). Addition of BH_3 to **1** gives the 16-electron complex **2**, which is more stable than the reactants by 76.4 kcal mol^{-1} at MP4(SDQ)/LANL1DZ(POL), and by 64.9 kcal mol^{-1} at QCISD(T)/LANL1DZ(POL). Entropically, the reaction is disfavored by 37.5 cal mol^{-1} K^{-1},[13] which corresponds to a $T\Delta S$ value of 11.2 kcal mol^{-1} at 298 K. The free energy of **2**, based on the difference of 64.9 kcal mol^{-1} at QCISD(T)/LANL1DZ-(POL), is therefore 53.7 kcal mol^{-1} lower than that of **1** and BH_3. Formation of **2** is followed by loss of a PH_3 unit to give **3**, which is 33.0 kcal mol^{-1} higher in energy than **2** and PH_3, and by addition of C_2H_4 to **3** to give **4**, which is 34.1 kcal mol^{-1} lower in energy than isolated **3** and C_2H_4 molecules. No barrier was found for the formation of **4**, a 16-electron species, from the 14-electron complex **3**.[12, 13]

The C_2H_4 unit of **4** can be attacked intramolecularly, either by a hydrogen atom or by the BH_2 group of the BH_3 fragment, to give, respectively, **6** and **7** (Fig. 3). Structure **6** is strongly favored at all levels of theory (Table 1); indeed, **7** is even less

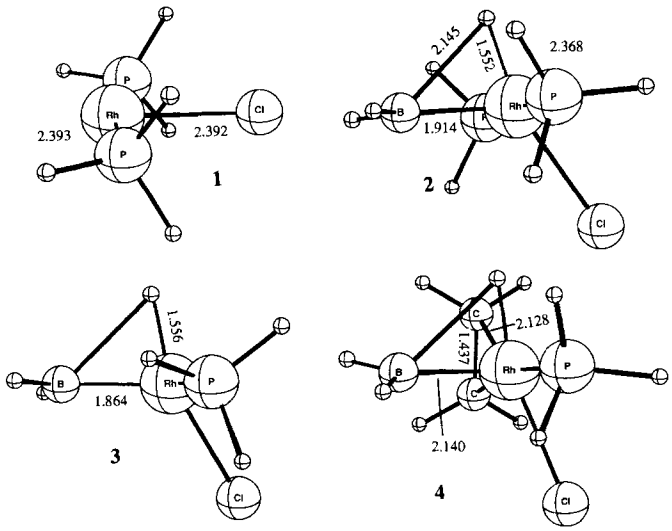


Fig. 2. MP2/LANL1DZ-optimized structures for **1**–**4**.

stable (by 10.8 kcal mol^{-1}) than the transition structure **5** that connects **4** and **6**. This result indicates, in agreement with the experimental proposal,[5] that H migration is favored both kinetically and thermodynamically over BH_2 migration. Structure **5** is only 4.1 kcal mol^{-1} higher in energy than **4** and 1.8 kcal mol^{-1} higher than **6**; the negative eigenvalue of **5** (transition structure vector) corresponds to lengthening of the breaking[14] B—H bond and of the C=C bond. We note that **6**, though formally a 14-electron species, is not a high-energy intermediate, since it benefits from the agostic interaction involving donation of the electrons of a C—H bond to the electron-deficient Rh center. In fact, the resulting Rh—H distance in **6** (1.832 Å) is not much greater than the length of the fully formed Rh—H bond in **7** (1.497 Å). This agostic interaction also explains the greater stability of **6** relative to **7**. Both species are 14-electron complexes, and the electron-deficient rhodium center is stabilized more effectively by the agostic interaction with the C—H bond (in **6**) than by the analogous interaction with the B—H bond (in **7**).

Formation of **6** may be followed either by addition of PH_3, with a subsequent internal rearrangement to give the hydroborated product, or by internal rearrangement to give **9**, followed by PH_3 addition yielding the product complex, **10**. We consider the latter possibility first. Rearrangement of **6** to **9** is exothermic by 6.7 kcal mol^{-1}, and takes place via transition structure **8**, which lies 9.8 kcal mol^{-1} above **6**. Addition of PH_3 to **9**, giving **10**, is exothermic by 26.0 kcal mol^{-1} at MP4(SDQ)/LANL1DZ(POL). No attempts were made to locate a transition structure between **9** and **10**, since the barrier is not expected to be significant. Structure **10** is substantially more stable than the isolated **9** and PH_3 molecules; moreover, addition of PH_3 to **9** is not expected to be the rate-determining step, given that intermediate **9** is substantially lower in energy than intermediate **6**. Loss of $C_2H_5BH_2$ from **10** gives back **1**, which reenters the catalytic cycle. At MP4(SDQ)/LANL1DZ(POL), **10** is more stable than **1** and $C_2H_5BH_2$ by 75.1 kcal mol^{-1}. A better estimate of the energy required for this step can be obtained by considering that the QCISD(T)/LANL1DZ(POL) stabilization (64.9 kcal mol^{-1}) of **2** relative to BH_3 and **1** is smaller than the MP4(SDQ)/LANL1DZ(POL) value (76.4 kcal mol^{-1}) by 11.5 kcal mol^{-1}, and that the $T\Delta S$ value for this process is −11.2 kcal mol^{-1}. Thus, we estimate the free energy of the formation of $C_2H_5BH_2$ and **1** to be (75.1 − 11.5 − 11.2), or 52.4 kcal mol^{-1}.[15] The computed stability of $C_2H_5BH_2$ with respect to BH_3 and C_2H_4 is 32.7 kcal mol^{-1}.

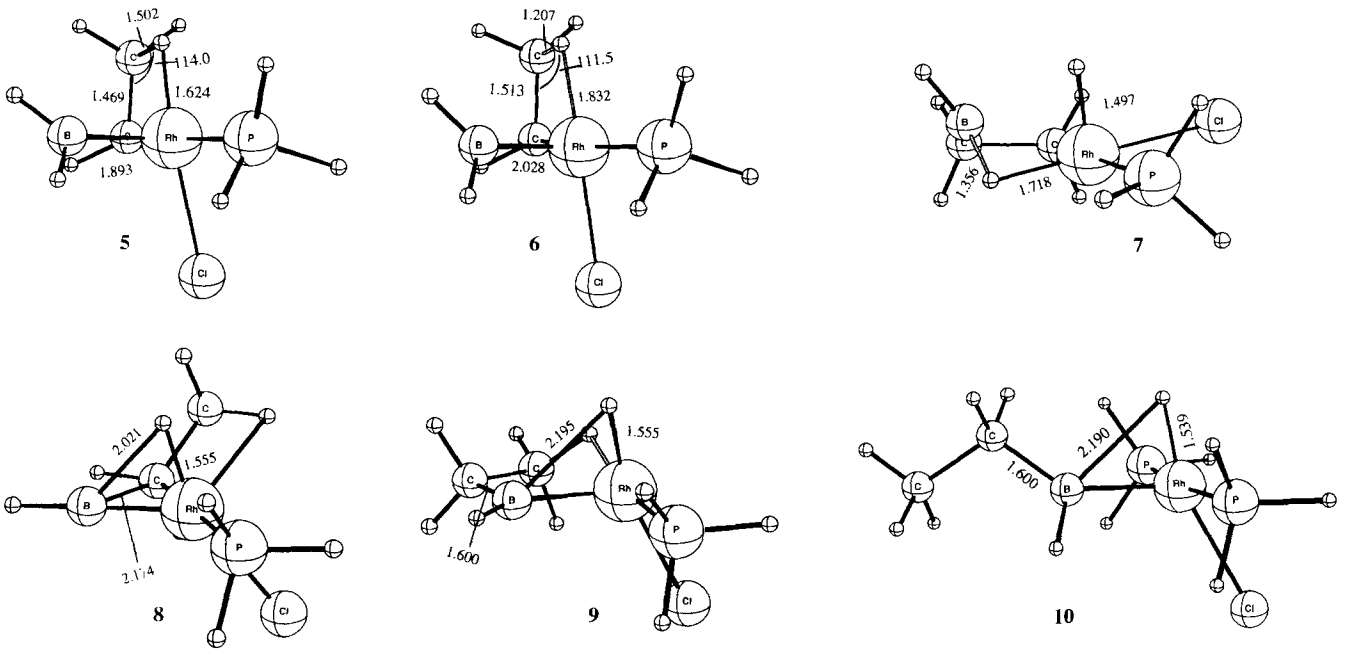


Fig. 3. MP2/LANL1DZ-optimized structures for **5**–**10**.

The alternative to the **6** → **8** → **9** → **10** pathway first involves addition of PH_3 to **6**, followed by intramolecular B–C bond formation leading to **10**. Addition of PH_3 to **6** leads to a complex (**11**, Fig. 4) with an association energy of 9.6 kcal mol^{-1}. Intermediate **11** then rearranges to **10** via transition structure **12**. The latter is only 6.5 kcal mol^{-1} higher in energy than **11**. Hence, the **6** → **11** → **12** → **10** pathway appears to be more favorable than the **6** → **8** → **9** → **10** pathway, which involves initial C–B bond formation followed by PH_3 addition.

Another pathway is possible in principle: starting from **2**, addition of C_2H_4 might give **13** (Fig. 5). This species can either lose PH_3 (to give **4**), or undergo a rearrangement with H migration similar to that described for **4**. Energies for an analogous "associative"[12] mechanism have been computed for the hydrogenation of ethylene; however, both experimental and computational evidence militates against the involvement of such processes. Both Nöth[6] and Evans[5] favor a dissociative mechanism such as the one leading to **4**; kinetic evidence in favor of this is described by Evans. Moreover, the related hydrosilylation reaction[16] can take place *intra*molecularly, and with initial migration of the silyl group according to Bosnich.[16] Inspection of **13** shows that the only Rh-bound group that can migrate to the C=C bond is the hydrogen atom, since the other moiety ($-BH_2$ in the case of **13**, or $-SiR_3$ for hydrosilylation reactions) lies *trans* to the C=C group. Indeed, even formation of a structure analogous to **13**—in which an SiR_3 groups replaces a BH_2 group—would be impossible for a molecule in which the silicon atom were connected by a three-atom chain[16] to the C=C bond.

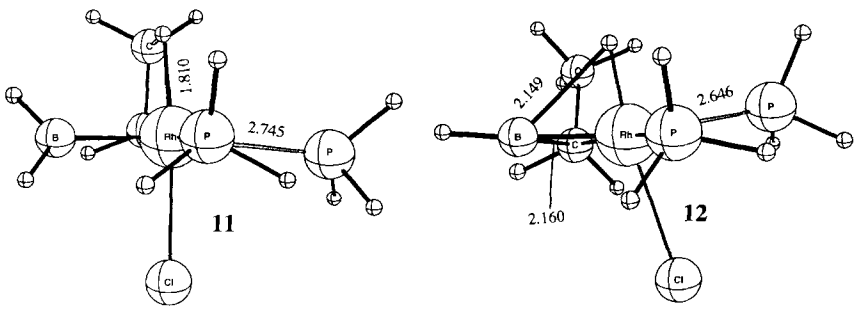


Fig. 4. MP2/LANL1DZ-optimized structures for **11** and **12**.

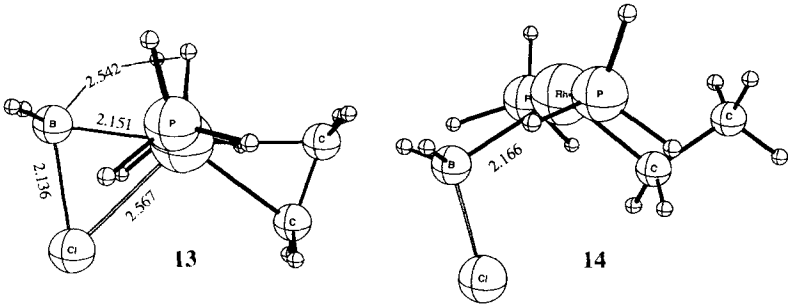
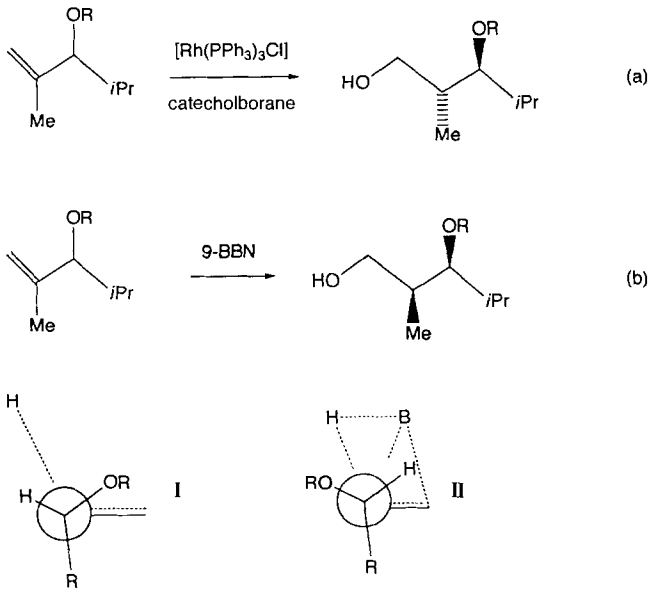


Fig. 5. MP2/LANL1DZ-optimized structures for **13** and **14**.

Evidence against the associative mechanism also comes from computation of both **13** and **14**, which is analogous to the computation of a key intermediate[12] for the associative pathway in the hydrogenation reaction. Although both species are thermodynamically quite stable—**13** is 12.9 kcal mol^{-1} more stable than **2** and ethylene, while **14** is 7.2 kcal mol^{-1} less stable than **13** (only MP2/LANL1DZ//MP2/LANL1DZ energies were calculated for these species)—the structures and bonding analysis of both species, but of **14** in particular, indicate that they are complexes of BH_2Cl with a rhodium species. In contrast to the hydrogenation study, for an associative hydroboration no minimum could be found corresponding to a complex retaining Rh–Cl bonding.[12] Thus, while **14** is a fairly stable isomer on the potential energy surface, we do not believe that it is an intermediate.

 © VCH Verlagsgesellschaft mbH, D-69451 Weinheim, 1995 0570-0833/95/0101-0117 $ 10.00+.25/0

Experimentally,[4] the catalyzed hydroboration of chiral allylic alcohols and ethers gives diastereoselectivity opposite to that observed without catalysis.[4, 17] A representative example is shown in Scheme 1. While we have not examined the reaction



Scheme 1. Stereoselectivity of the uncatalyzed [Eq. (a)] and catalyzed [Eq. (b)] hydroboration of chiral ethers, and proposed transition structure models (**I** and **II**, respectively) for the two reactions. 9-BBN = 9-borabicyclo[3.3.1]nonane.

of chiral alkenes, the switch in diastereoselectivity due to Rh^I catalysis can be rationalized by considering transition structure **5**, where the angle of attack of the hydrogen atom is about 114° (Fig. 3). Allylic substituents are expected to adopt a conformation that minimizes repulsive steric interactions with the incoming hydrogen atom, like conformation **I** shown in Scheme 1. Here, the alkyl group occupies the least hindered position (*anti* to the attacking hydrogen), while the allylic hydrogen atom occupies the most hindered position (inside). In contrast, the conformation **II** preferred in the uncatalyzed hydroboration leads to the opposite diastereomer.[2] The different conformational preferences in the two transition structures are due to the steric and electronic requirements of the electron-deficient BR_2 group. In the catalyzed reaction this group is not involved in the attack of hydrogen on the C=C bond.

In conclusion, our study[18] confirms the suggestion[4] that H migration is preferred to BH_2 migration in the key step of the Rh^I-catalyzed reaction. This step helps explain the reaction diastereoselectivity. Our study also lends support more generally to the intermediacy of 14-electron intermediates, which also may be involved in related reactions such as Rh^I-catalyzed hydrosilylations of C=C bonds.[16] For the latter it has been suggested[16] that the trialkylsilyl group migrates first, followed by the hydrogen in a later step. This mechanistic preference may be explained in the same way as the preference for H migration over BR_2 migration: the silyl group migrates because it can stabilize the electron-deficient metal center more effectively. The results of our investigations into these silyl systems will be reported subsequently.

Received: March 12, 1994
Revised version: September 20, 1994 [Z 6754 IE]
German version: *Angew. Chem.* **1995**, *107*, 108

Keywords: ab initio calculations · rhodium compounds · catalysis · hydroborations

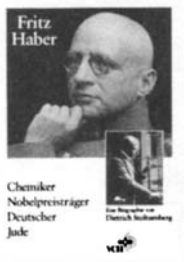
[1] H. C. Brown, *Boranes in Organic Chemistry*, Cornell University Press, Ithaca, NY, **1972**.
[2] K. N. Houk, N. G. Rondan, Y. D. Wu, J. T. Metz, M. N. Paddon-Row, *Tetrahedron*, **1984**, *40*, 2257.
[3] N. J. van Eikema Hommes, P. von R. Schleyer, *J. Org. Chem.* **1991**, *56*, 4074.
[4] D. A. Evans, G. C. Fu, A. H. Hoveyda, *J. Am. Chem. Soc.* **1992**, *114*, 6671.
[5] D. A. Evans, G. C. Fu, B. A. Anderson, *J. Am. Chem. Soc.* **1992**, *114*, 6679.
[6] D. Männig, H. Nöth, *Angew. Chem.* **1985**, *97*, 854; *Angew. Chem. Int. Ed. Engl.* **1985**, *24*, 878.
[7] Brown and Lloyd-Jones have suggested that, for the reaction of catecholborane with phosphane-free rhodium catalysts, β-hydride elimination competes with addition of a second molecule of borane: J. M. Brown, G. C. Lloyd-Jones, *J. Am. Chem. Soc.* **1994**, *116*, 866.
[8] All calculations used the Gaussian 92 program: M. J. Frisch, G. W. Trucks, M. Head-Gordon, P. M. W. Gill, M. W. Wong, J. B. Foresman, B. G. Johnson, H. B. Schlegel, M. A. Robb, E. S. Replogle, R. Gomperts, J. L. Andres, K. Raghavachari, J. S. Binkley, C. Gonzales, R. L. Martin, D. J. Fox, D. J. Defrees, J. Baker, J. J. P. Stewart, J. A. Pople, Gaussian Inc., Pittsburgh, PA, **1992**. See also J. B. Foresman, Æ. Frisch, *Exploring Chemistry with Electronic Structure Methods: A Guide to using Gaussian*, Gaussian Inc., Pittsburgh, PA, **1993**.
[9] An effective core potential was employed for rhodium in which the nine valence electrons were described by a double-ζ basis set. See: P. J. Hay, R. W. Wadt, *J. Chem. Phys.* **1985**, *82*, 270.
[10] The f exponent of 0.35 for Rh is also used in K. Balasubramanian, D. W. Liao, *J. Chem. Phys.* **1988**, *92*, 6259. C d exponent: 0.8; B d exponent: 0.6; H p exponent: 0.11.
[11] a) Detailed calculations on **1** have also been reported by N. Koga, K. Morokuma, *J. Am. Chem. Soc.* **1993**, *115*, 6883. See also *J. Phys. Chem.* **1990**, *94*, 5454. Note added in proof (September 20, 1994): we found that the triplet state of **1** is lower in energy than the singlet; however, as one of the referees also pointed out, facile intersystem crossing in **1** implies that computation of subsequent steps on the singlet surface is justified. The value which we calculate for the free energy of the final elimination step (52.4 kcal mol^{-1}) is based on the energy of singlet **1**. Assuming the triplet to be 9.7 kcal mol^{-1} more stable than the singlet (as calculated by Koga and Morokuma) the free energy of the final elimination step becomes 42.7 kcal mol^{-1}. Other factors [15] may lower this value further. b) According to Dedieu, the *cis* isomer of **1** is favored (A. Dedieu, *Inorg. Chem.* **1980**, *19*, 375); this isomer is also favored at HF/LANL1DZ, and is close in energy to **1** at all levels considered. However, an attempt to optimize the complex of BH_3 with the *cis* isomer of **1** led to the formation of a structure having a B–Cl bond, which is clearly not involved in the addition of BH_3 to C_2H_4.
[12] Similarly, no barrier has been found for the addition of C_2H_4 to a 16-electron intermediate in the Rh^I-catalyzed hydrogenation of C=C bonds: C. Daniel, N. Koga, J. Han, X. Y. Fu, K. Morokuma, *J. Am. Chem. Soc.* **1988**, *110*, 3773.
[13] a) The entropies of **1**, BH_3, and **2** are 96.1, 46.4, and 105.0 cal mol^{-1} K^{-1}, respectively. b) While formation of **3** is disfavored enthalpically, it is favored entropically. The entropies of **2**, **3**, and PH_3, calculated from numerical frequency computations, are 105.0, 89.6, and 50.3 cal mol^{-1} K^{-1}; thus, dissociation of **3** into **2** and PH_3 is favored by 34.9 cal mol^{-1} K^{-1}, which corresponds to 10.4 kcal mol^{-1} at 298 K. The free energy for the dissociation of **2** can be thus estimated to be 22.6 (= 33.0 − 10.4) kcal mol^{-1}. Similarly, the entropies of **3**, C_2H_4, and **4** are 89.6, 52.5, and 106.7 cal mol^{-1} K^{-1}; **4** is therefore formed with a loss of entropy of 35.4 cal mol^{-1} K^{-1}, corresponding to 10.5 kcal mol^{-1} at 298 K. Thus, the free energy for the formation of **4** can be estimated at −23.6 (− 34.1 + 10.5) kcal mol^{-1}.
[14] Some residual B–H bonding is present in **2**, **3**, and **4**, in spite of the fairly large B–H distance. The Wiberg bond index is 0.13, 0.14, and 0.13, respectively.
[15] Experimental systems involve stabilized boranes, such as catecholborane or 4,4,6-trimethyl-1,3,2-dioxaborane (TMDB) (for a review, see K. Burgess, M. J. Ohlmeyer, *Chem. Rev.* **1991**, *91*, 1179). For these systems the interaction with **1** or analogous rhodium catalysts is certainly smaller than the values which we calculate for BH_3. Likewise the final reductive elimination step should be energetically less unfavorable than calculated here.
[16] S. H. Bergens, P. Noheda, J. Whelan, B. Bosnich, *J. Am. Chem. Soc.* **1992**, *114*, 2121.
[17] W. C. Still, J. C. Barrish, *J. Am. Chem. Soc.* **1983**, *105*, 2487.
[18] Note added in proof (December 12, 1994): A recently published theoretical mechanism (D. G. Musaev, A. M. Mebel, K. Morokuma, *J. Am. Chem. Soc.* **1994**, *116*, 10693) differs significantly from our proposal. The dissociative mechanism [5, 6] we favor was not computed. Moreover, BR_2 migration was favored over H migration in the key step, in contrast with the experiments by Evans et al. [5] and our conclusions.

 © VCH Verlagsgesellschaft mbH, D-69451 Weinheim, 1995 0570-0833/95/0101-0118 $ 10.00+.25/0

Conflicts of Conscience

Fritz Haber—Chemiker, Nobelpreisträger, Deutscher, Jude. By *D. Stoltzenberg*. VCH Verlagsgesellschaft, Weinheim, 1994. XIV, 669 pp., 93 figures, 8 tables, hardcover DM 98.00.—ISBN 3-527-29206-3

Dietrich Stoltzenberg's new book is the first substantial and truly comprehensive biography of Fritz Haber (1868–1934) ever published—sixty years after Haber's death and at a time when German literature is the forum for a lively debate about the subject.



The author of his biography is himself a chemist, as well as a son of the industrialist Hugo Stoltzenberg (one of Haber's co-workers as early as the gas-warfare days of World War I) and the chemist Margarethe Stoltzenberg-Bergius (a sister of F. Bergius, developer of the coal-hydrogenation process and one-time assistant to Haber). Stoltzenberg has therefore been familiar with Haber and his career since childhood, a genuine stroke of luck for this particular biographer of the Nobel laureate. The resulting account of Fritz Haber's career is as well-informed, engaging, and authoritative as one would expect, and it offers a balanced and fair examination of every stage of the subject's life. Despite his obvious empathy with Haber the man, Stoltzenberg is not uncritical, and he is certainly not deferential—a temptation to which many biographers unfortunately succumb. Nevertheless, Stoltzenberg often introduces his criticism in subtle ways and between the lines. The overall treatment is to the point, albeit occasionally very detailed.

Haber's career is examined very thoroughly and documented by many new sources, with appropriate attention to his origins in a Jewish family, his early schooling and education at a number of universities, and his doctoral work in the field of organic chemistry. Haber undertook several years of academic and practical apprenticeship followed by internships in various industries before finally presenting a habilitation thesis in physical chemistry to the University of Karlsruhe (1896). A 17-year sojourn in Karlsruhe, rightfully characterized by Stoltzenberg as Haber's "personal and scientific climax," earned for him a reputation as an outstanding electrochemist, and it led to the creation of a chair in physical chemistry equipped with all the facilities necessary for industrially oriented research. The Karlsruhe years also witnessed the solution to the nitrogen-fixation problem, ensuring the availability for the first time of an adequate supply of nitrogenous fertilizers for agriculture through Haber's epochal development of an ammonia synthesis based on the catalytic hydrogenation of nitrogen. This was the famous Haber process, later known as the Haber–Bosch process, for which a Nobel Prize was awarded in 1918. The ammonia work necessarily entailed close and fruitful collaboration with chemical industry, an involvement which together with the Janus-faced character of ammonia itself (a starting material not only for fertilizers but also explosives) and Haber's own intellectual propensities (C. Engler described him in a letter to BASF as "a sharp and adroit dialectician") laid the groundwork for points of friction that certain contemporary critics and their present-day apologists subsequently transformed into major stumbling blocks.

In 1911 Haber became director of the newly created Kaiser Wilhelm Institute for Physical Chemistry and Electrochemistry in Berlin-Dahlem. The Institute personnel were later merged with staff from the War Ministry, after which Haber occupied various official positions within the Ministry itself, eventually becoming director of the Chemical Division ("Haber's Office")—and thereby the "instigator of chemical warfare." His tireless and ultimately self-destructive efforts in this capacity led to the systematic development and subsequent battlefield deployment of poison gas, which was to become another stumbling block for Haber and a major source of the controversy that continues to surround him. After World War I he occupied himself with various chemical projects (including attempts to exploit the gold reserves in sea water) and miscellaneous contributions to scientific policy and the support of scientific research. On April 30, 1933, at the age of 64, he submitted his formal resignation, expressed in the most emphatic of terms both verbally and in writing—one month after the government organized its first boycott and enacted the first of the laws directed against the Jews. Haber died in 1934.

Based on Haber's curriculum vitae alone it is difficult to understand the intensity of the dissonant debate over guilt and entanglement provoked by his career, or to explain the current renaissance of the controversy, but the extent of the polarization itself is readily demonstrated. "Haber was more than a great leader of science—he was a great man. His rich, full life, the institutions he made, his service to his country, even his failures—all were on the grand scale." These noble words were delivered by J. E. Coates on the occasion of the 1937 Haber Memorial Lecture (*J. Chem. Soc.*, 1939). Coates was a student of Haber's, but he was also an Englishman, and the sentiments quoted above were expressed on the eve of yet another war. How different they are from the charges of Haber's critics (often non-chemists), typical exponents of "the modern interpretation of history" and "flagbearers of enlightenment" who reinterpret lives lived in the past "from the perspective of the present," or even "in the spirit of a modern approach to life." Here the talk is all of "scandal," with Haber's life portrayed and interpreted in a temporal context devoid of all trace of understanding, even understanding with respect to Haber's unique aberrations, which are

This section contains book reviews and a list of new books received by the editor. Book reviews are written by invitation from the editor. Suggestions for books to be reviewed and for book reviewers are welcome. Publishers should send brochures or (better) books to Dr. Ralf Baumann, Redaktion Angewandte Chemie, Postfach 101161, D-69451 Weinheim, Federal Republic of Germany. The editor reserves the right of selecting which books will be reviewed. Uninvited books not chosen for review will not be returned.

 © VCH Verlagsgesellschaft mbH, D-69451 Weinheim, 1995 0570-0833/95/0101-0119 $ 10.00+.25/0

said to "cast a deep shadow over his life and work" (Stoltzenberg).

What purpose do such comments serve, and what do they add to the discussion concerning Fritz Haber, a discussion in which we are still engaged 60 years after his death? Fritz Haber was not simply a highly respected chemist; he was also a divided and torn human being whose legacy to mankind includes both an ingenious procedure for synthesizing ammonia and the "Haber product," $W = c \times t$, intended for use as a standard in assessing the lethal power of chemical weapons. The study of Haber's life and character anticipates in an exemplary way the broader debate over guilt and entanglement as it applies to scientists generally, including the progenitors of the atomic and hydrogen bombs: Otto Hahn, Robert J. Oppenheimer, and Edward Teller. Haber serves as an especially attractive case-study for ideologues, because through him they purport to be able to construct the continuous and calamitous sequence: Haber = criminal = chemical industry = industry in general = capitalism = evil = antisocial.

Several biographies, including Stoltzenberg's, make explicit reference to one particular saying attributed to Haber: "im Frieden für die Menschen, im Krieg für das Vaterland" ("in peacetime for mankind, in war for the Fatherland"), words that are no more but at the same time no less valid or repulsive than the British "Right or wrong: my country." Limitations that may also have been implicit in the sentiments so expressed—once a topic of national debate that has since turned global—no longer lend themselves to accurate reconstruction, but fairness demands that the remark at least be viewed against the background of the times. Haber was a converted Jew; at various stages in his life he was subjected to all the misgivings Jewishness evoked in Germany even during the reign of the Kaisers. Like many others he attempted to confront prejudice with extraordinary personal deeds coupled with an ardent display of "Germanness," perhaps even with a rash and precipitous form of patriotism. This problematic situation was a matter of some discussion subsequent to 1918 in connection with responsibility for the Great War. Haber believed there had been solid grounds for introducing poison gas into the fighting, especially on the German side. He never denied or repudiated this stance, and he accepted full responsibility for it. Stoltzenberg thoroughly explores this important facet of Haber's understanding of the very personal meaning of Germanness.

Stoltzenberg's biography also conveys—as far as possible 60 years after the protagonist's death—a sense of Haber's fate as that of an understanding, sensitive, and at the same time tragic individual: tragic in terms of his association with weapons that have since been outlawed and problems peculiar to the intersection of science with politics; tragic also in the personal sphere, with two unhappy marriages, the first of which ended in his wife's suicide, and the experience of being hounded out of office just six months short of retirement. Today we can only speculate about the extent to which all of this led to a guilt complex evolving gradually and through psychosomatic processes into a state of autostress, which perhaps culminated in his precarious state of health and early death.

But why is there so much posthumous hate, or at best such posthumous lack of understanding? Ideologues and others not given to reflection find it child's play to label Fritz Haber posthumously as a criminal, because by present-day standards he did assume a tremendous burden of personal guilt; besides, he is no longer able to defend himself. The fact that he was also a scientist—indeed, an outstanding scientist: a Nobel laureate—makes Haber a particularly valuable commodity for ideologues; they can attack Fritz Haber the personally vulnerable individual, and then transform him into a symbol for science, industry, and capitalism generally. For champions of a simplistic point of view the conclusion is perfectly straightforward: anyone not opposed to Haber and gas warfare and the synthesis of ammonia must automatically be an enemy of socialism and peace—ergo, a vile human being.

Another phenomenon that must also be taken into account is the way Haber's opponents present their retrospective interpretation of a life lived at another time, with the subject of a biography used essentially as a vehicle for criticizing the history and conditions of another era. As Stoltzenberg's biography makes clear, it is simply dishonest to ignore influences of the times and the circumstances that prevailed, including in this case a restrictive national perspective and the situation inevitably facing a baptized Jew. In short, one cannot overlook the cumulative effect of a host of political currents, cultural influences, questions related to an individual's personal origins, historical consciousness, and the like. Moreover, Fritz Haber cannot be regarded as representative simply because contrasts may be apparent between certain aspects of his behavior then and what we might regard as permissible today with our (superior!) wisdom and understanding. This would be tantamount to denying the temporal qualities associated with every human life, and critiquing every utterance from the past according to the standards of today. Doing so requires that we abandon all sympathy for the world of our parents and grandparents, and a lack of sympathy is equivalent to a lack of understanding. Stoltzenberg does demonstrate sympathy in his writing, and with it a measure of anxiety, and he transmits his feelings to the reader. It is also important to reiterate that Haber's own contemporaries and colleagues viewed him with considerably more understanding, and despite the difficult circumstances of the time the obituaries they prepared articulate far more *noblesse* than the words of many of today's "know-it-alls."

What remains is the recognition that we can only *attempt* to understand Fritz Haber. We cannot relieve him of his tragedy, nor of his entanglements with guilt. He anticipated in encapsulated form that which should characterize every scientist: the upright integrity of a researcher who knows himself to be one with the spirit and morals of his age and of his contemporaries of all nationalities. A tendency to cast this premise in doubt, as some now do, is one of those inexplicable, irrational manifestations of the German soul. That Haber was also the victim of disdain and a political movement's will to exterminate physically those whom it dismissed on ethnic grounds should actually be regarded as an honor.

Haber also leaves us with a question, one that needs to be addressed by every scientist: precisely when does progress become transformed into a weapon, thus triggering an obligation on the part of the individual scientist to engage in emphatic and articulate opposition? Progress cannot be prevented, but one can most assuredly insist that it not be misused. Haber's ultimate tragedy lies in the fact that he failed to recognize this distinction.

Boy Cornils
Hoechst AG, Frankfurt/Main (Germany)

FT-NIR Atlas. By *M. Buback* and *H. P. Vögele*. VCH Verlagsgesellschaft, Weinheim/VCH Publishers, New York, 1993. 1067 pp., hardcover DM 880.00, $ 570.00.—ISBN 3-527-28567-9/1-56081-744-5

With the increasing use of modern Fourier transform (FT) infrared spectrometers, the NIR spectral region (4000–

 © VCH Verlagsgesellschaft mbH, D-69451 Weinheim, 1995 0570-0833/95/0101-0120 $ 10.00+.25/0

10000 cm^{-1}), which was previously rather neglected, has become readily accessible and is of interest to many analytical laboratories. This *FT-NIR Atlas* is the first volume in a series of "SpecBooks" which are planned to cover all the most important spectroscopic methods. It contains the first ever collection of digital NIR spectra. Unlike the many conventional spectra atlases that have a long tradition based on "analog" spectra, the *FT-NIR Atlas* is a "hard copy" which has been generated, largely automatically, from a digital data bank to produce a collection of NIR spectra of 1957 compounds.

The arrangement of this spectra collection is similar to that in the *Merck FT-IR Atlas*. For each substance two spectra are shown separately, covering the ranges 3800–7200 cm^{-1} (NIR I, on a scale of about 250 cm^{-1} per cm) and 6300–10500 cm^{-1} (NIR II, on a scale of about 625 cm^{-1} per cm), which results in a very clear presentation. Alongside each spectrum are listed up to seven of the strongest peaks, which considerably simplifies making comparisons with experimentally observed spectra. Each compound is identified by its structural formula, systematic name, and molecular formula. The CAS Registry number, manufacturer's catalog number, and physical properties such as molar mass, density, melting point, etc. are also listed. In cases where the compound was not available in a sufficiently pure form for recording a true spectrum, the exact composition of the mixture is given in an appendix. The selection of the 1957 compounds included is, of course, arbitrary; however, as it is based on collecting together compounds from current catalogs of chemicals this ensures that it includes many of the compounds most commonly found in laboratories.

The volume is very well produced, and even fine details of the spectra are clearly discernible. The introduction gives a short and succinct account of the experimental and theoretical background. Separate indexes according to molecular formula, compound name, and CAS Registry number are provided. However, many users will have difficulties in locating compounds by name; for example, triphenylmethane is listed as "Benzene, 1,1′,1″-methylidynetris-". Here it would definitely have been sensible to also include common trivial names in the index. A further criticism concerns the structural formulas; these are shown without the hydrogen atoms, a convention which takes a little getting used to.

Despite the fact that this presentation in book form is in competition with the electronic data bank, with all the latter's advantages, it will certainly find an established place in spectroscopic and analytical laboratories. Its advantages are that the spectra are simply within arm's reach, without the bother of a flickering VDU screen, and several spectra can be directly compared. The only obstacle to its becoming widely available will be the present impoverished state of many university libraries.

Wolfram Sander
Organische Chemie II
der Universität Bochum (Germany)

Activated Metals in Organic Synthesis. By *P. Cintas*. CRC Press, Boca Raton, USA, 1993. 236 pp., hardcover $ 59.95.—ISBN 0-8493-7863-X

This book describes in detail the applications of activated metals in organic and organometallic chemistry. The first part (Chapters 1–3) covers metal vaporization methods, a number of other metal activation methods (such as the Rieke, metal–anthracene, and ultrasonic methods), and the use of metal–graphite compounds. Each method is discussed in considerable detail, clearly explaining its advantages and disadvantages. The most important reactions are collected together in equation form, and the experimental details of the most useful activation methods are described clearly and concisely (including, for example, the preparation of Rieke zinc, of iodine-activated magnesium, and of activated nickel from nickel diisopropoxides).

The second part (Chapters 4–8) is concerned with the use of activated metals in organic synthesis. Many examples are given together with references to recent work (150–200 literature citations per chapter), providing an important and valuable resource for the preparative organic chemist and for everyone who uses metals in synthesis. Chapter 4 describes the use of activated metals in reductions. Chapter 5 then deals with reductive couplings of carbonyl compounds, giving a very good review which ranges from the classical pinacol coupling to the McMurry coupling. Additions to carbonyl compounds are described in Chapter 6, treating the Barbier reaction (in which the reactive organometallic species is generated in the presence of the electrophile) and reactions of the Reformatsky type in separate sections. However, this classification is not followed consistently, as the section on the Barbier reaction also includes two-stage organometallic reactions. The treatment of the important reactions is very good, with clearly set out equations to give the reader a sound grasp of the principles. The discussion of the Reformatsky reaction is especially detailed (including the structures of the reagents, the role of zinc activation, the extension to other metals, and the stereoselectivity of the reaction). Chapter 7 is devoted to cyclizations, in which activated metals offer an important means of generating reactive intermediates (e.g. Simmons–Smith reactions and metal-initiated free radical cyclizations). The final chapter describes zinc-mediated ring-opening reactions of sugar derivatives and applications to the stereoselective synthesis of chiral acyclic polyhydroxy building blocks.

To summarize, the book gives a good overview of synthetic applications of activated metals, which is an important area of modern organic chemistry. It makes easy reading, is very detailed, and is suitable for post-graduate and advanced chemistry students, as well as for industrial chemists involved in research and development. It should be available in every university library.

Paul Knochel
Fachbereich Chemie
der Universität Marburg (Germany)

Cluster Chemistry. By *G. González-Morega*. Springer, Heidelberg, 1993. 302 pp., paperback DM 98.00.—ISBN 3-540-56470-5

Cluster Chemistry by G. González-Morega was announced as "the first (book) to be appropriate for disseminating and especially for teaching this contemporary topic." Notwithstanding an ever growing number of monographs covering various aspects of this field of science, there is indeed a need for a textbook which can form the basis of an advanced undergraduate or graduate course and, most of all, lead the "novice" who is familiar with the basic principles on to the more advanced topics.

The introductory section (Ch. 1) on "Current Concepts in Modern Chemistry" is concerned with the fundamental aspects of the theory of atomic structure and chemical bonding as may be found in most textbooks on general and/or inorganic chemistry. The following chapter on "Transition Metal Cluster Chemistry" is the first major section dealing with the topic of the book. Beginning with a discussion on the classification of clusters (naked/ligated, high valence/low valence) and the principal types of ligands, a sur-

 © VCH Verlagsgesellschaft mbH, D-69451 Weinheim, 1995 0570-0833/95/0101-0121 $ 10.00+.25/0

vey of (primarily) molecular clusters according to their nuclearity is given. The coverage is extensive rather than intensive, and it is arguable whether long reference lists of compounds are particularly useful at this stage. There are several confusing statements, such as: (p. 68) "The study of cluster hydrides is of considerable interest since ... they are intimately associated with important catalytic processes, e.g. Fischer Troppch (!) processes for ammonia and methane synthesis"; (p. 76) "Solid angles and distortion degree in open structures depend on a number of factors as, for instance, the number of electrons, the nature of disposable orbitals, and the properties of ligands" ... and so on ...

Instead of reading the section on "Bonding in Metal Clusters", those who wish to get familiar with this very important aspect of cluster chemistry should rather consult the original papers cited by the author. In Sections 2.4 ("Synthesis of Cluster Compounds"), 2.5 ("Cluster Reactivity") and 2.6 ("Cluster Catalysis") various aspects of these topics are discussed on the basis of the review literature of the 1980s. Chapter 3 is devoted to "Main Group–Transition Metal Mixed Clusters", a chapter which "deals mainly with compounds in which the main group elements may be considered as cluster vertexes of the polyhedron." I found it difficult to appreciate why hydrido clusters, clusters with interstitial atoms, etc., which were already in part covered in the previous chapter require a separate section. The statements in the sub-section 3.1.3 on "Proton Magnetic Resonance" of hydrido clusters are entirely incorrect and should be avoided by the reader.

In Chapter 4 several aspects of (among others) alkali metal suboxides, boranes, Zintl ions and, more extensively, fullerenes are discussed. The book concludes with a brief section on iron–sulfur cages in proteins.

Unfortunately, this book is riddled with typographical errors, incorrect citations, journal hybridizations (there are 15 references to "*J. Am. Chem. Soc., Dalton Trans.*" in Table 3.2 alone) as well as several factual errors (too many to list in a review). It is only with these reservations that it might be useful to the graduate student interested in cluster chemistry.

Clusters and Colloids. From Theory to Applications. Edited by *G. Schmid.* VCH Verlagsgesellschaft, Weinheim/ VCH Publishers, New York, 1994. 555 pp., hardcover DM 249.00.— ISBN 3-527-29043-5/1-56081-753-4

Clusters and Colloids edited by G. Schmid is clearly written for a readership familiar with the fundamental aspects of cluster chemistry and colloid science (as is pointed out by the editor in the introductory chapter). The choice of the topics is such that this book may complement other currently available monographs on clusters but, most of all, takes into account the very recent developments in this area of science. Distinguished researchers in the fields of high nuclearity cluster chemistry and colloid science offer a multifaceted and in depth account of the current state of the art.

In the first main section of the book (Ch. 2) N. Rösch and G. Pacchioni give a clearly structured and critical survey of the theoretical methods employed in the investigation of naked and ligated metal clusters. The potential and weaknesses of the different approaches are outlined and compared, which makes this section excellent reading for those (experimentalists, in particular) who wish to acquire a sound "second level" knowledge in this area. A concise overview of the physical methods for the investigation of the electronic structures of clusters is also given, although this part of the chapter is somewhat less critical towards the original literature.

Chapter 3 by D. Fenske, G. Longoni and G. Schmid is devoted to the whole area of ligated high nuclearity clusters ("Clusters in Ligand Shells"). Longoni's survey of low-valent organometallic clusters is probably the best contemporary review of the area of high nuclearity carbonyl clusters, while Fenske gives a well structured account of the rapidly expanding area of the structural chemistry of transition metal clusters containing bridging main group elements. Whether Schmid's section on "super clusters", which clearly lie outside the regime of "conventional" molecular clusters, would have been more appropriately placed next to (or before) the chapter on transition metal colloids at the end of the book is a matter of personal taste. The clarity of the presentation in this section should, however, be commended.

In "Clusters in Cages" (Ch. 4) S. Kawi and B. C. Gates review investigations of clusters encapsulated in zeolite cages. Particular emphasis is placed upon the analytical methods used, as is also the case in J. S. Bradley's section on "The Chemistry of Transition Metal Colloids" (Ch. 6). Both emphasize the importance of methodological aspects in the development of a field of research, a notion which is particularly apparent in the long history of research in colloid chemistry and physics.

Sandwiched between these two chapters is a survey of "Discrete and Condensed Transition Metal Clusters in Solids" by A. Simon, covering not only the structural systematics but also the structure–property relationships in this important area of solid state chemistry. This section is extremely well written and offers both the "non-solid state" cluster chemist and the specialist in that area the quintessence of more than two decades of research on clusters in solids.

As a whole, this is indeed a well-integrated, readable book and the editor and contributors are to be congratulated on their achievement. It is strongly recommended to anyone who wishes to learn about the more advanced aspects of cluster chemistry and to become addicted to the beauty of cluster compounds.

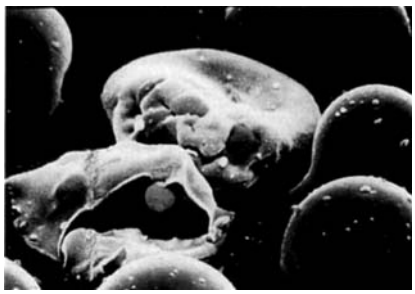
Lutz H. Gade
Institut für Anorganische Chemie der Universität Würzburg (Germany)

 © VCH Verlagsgesellschaft mbH, D-69451 Weinheim, 1995 0570-0833/95/0101-0122 $ 10.00+.25/0

Disulfide-Reductase Inhibitors as Chemotherapeutic Agents: The Design of Drugs for Trypanosomiasis and Malaria

R. Heiner Schirmer,* Joachim G. Müller, and R. Luise Krauth-Siegel

Viewed globally, parasitic diseases such as malaria and Chagas' cardiopathy pose an increasing threat to human health and welfare. Recognition of this problem and the challenge of synthesizing a quinine-like antimalarial agent sparked off the development of the chemical industry about 100 years ago. Our contribution deals with aspects of drug design, a young branch of pharmaceutical chemistry. As drug targets the flavoenzyme, glutathione reductase, and the recently discovered parasite enzyme, trypanothione reductase, were chosen. Based on the knowledge of the structure of these molecules, the modeling of enzyme inhibitors as potential chemotherapeutic agents against parasites has become possible. In addition, biochemical and clinical observations are considered since chemical principles of biological evolution can serve as guidelines for the pharmaceutical chemists. The picture shows two erythrocytes destroyed by malaria parasites. In the center of the photograph a parasite is just leaving its host cell through the ruptured cell membrane. Its target could be a neighboring healthy erythrocyte.



Keywords: drug design · enzyme inhibitors

1. Introduction

Drug design applies biomolecular recognition mechanisms to chemotherapeutic problems.[1] The first step is always the determination of the three-dimensional structure of a protein or another macromolecule that plays an important role for a particular pathogen or disease process. Then by means of computer modeling, inhibitors of this target molecule can be proposed.[2] These molecules are synthesized, tested for their chemotherapeutic activity, and if they are promising, improved further. An example of this principle was the development of the peptidase blocker Captopril, an important compound for the treatment of hypertension.[3] The latest success of drug design is guanidinoglycal, an enzyme inhibitor that is active against influenza viruses.[4, 5]

Our review deals with the need to develop novel compounds to combat parasitic infectious diseases. Two disulfide reductases, the antioxidative enzymes trypanothione reductase and glutathione reductase, were chosen as target molecules for the design of parasiticidal drugs.

[*] Prof. Dr. R. H. Schirmer, Dr. J. G. Müller, and Priv.-Doz. R. L. Krauth-Siegel
Institut für Biochemie II der Universität
Im Neuenheimer Feld 328, D-69120 Heidelberg (Germany)
Telefax: Int. code + (6221)56-5586

2. Clinical Pictures of Malaria

In the last 25 years malaria has regained its former position as the greatest threat to the health and economic prosperity of mankind.[6, 7] According to figures published by the World Health Organization, 1500 million people live in areas where malaria is endemic, 300 million cases are recorded each year, and more than 2 million—mostly children under five years of age—die from malaria; an unknown number of children are left crippled or chronically ill.

The causative agents of malaria are protozoa (*Plasmodium species*) that are transmitted through the blood-sucking anopheles mosquitoes. Humans become ill when the malaria parasites multiply in the erythrocytes (the red blood cells). The clinical picture is dominated by high fever and a debilitating feeling of illness. The *vivax malaria* is known to give rise to a bout of fever every 48 h. Each fever attack requires from the infected patient an energy expenditure of up to 20000 kJ. When undernourished children are affected, the exhaustion from the bouts of fever can starve them to death.

A severe burden is also placed on the immune system. If only 1% of erythrocytes are affected by malaria, every 48 hours the rupture of the infected cells will release 10–20 g of foreign proteins directly into the bloodstream. Thus malaria is the septicaemia par excellence. Many lines of evidence indicate that the

 © VCH Verlagsgesellschaft mbH, D-69451 Weinheim, 1995 0570-0833/95/0202-0141 $ 10.00+.25/0

immune system, in particular the network of interleukins, was programmed during evolution to be highly effective in combating not bacteria and tumor cells, but intracellular parasites.

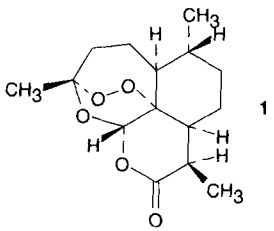
Consequently, basic principles of the body's defence against tumor cells are expected to be revealed by studying parasitic diseases. Our recommendation that cancer research should include parasitic diseases also has a political dimension: a much greater proportion of research funding is spent on each patient suffering from cancer than is spent on each human being dying of malaria.

Even more perilous than *vivax malaria* is *malaria tropica* which is caused by *Plasmodium falciparum*. In this form of the disease the course of the fever is less characteristic, and the feared complication is cerebral malaria, which manifests itself as hallucinations, headaches, convulsions, and severe disturbances of consciousness. Five percent of the children who survive cerebral malaria suffer permanent neurological damage such as hemiplegia, blindness, or speech impairment.[8a] On account of its widespread distribution, malaria is the most serious brain disease in the world.

Chronic malaria is a serious health problem principally because of the resulting anaemia. The mental changes accompanying it led to the colloquial use of the word "spleen", which originally referred to the peculiarities of a person with an enlarged spleen caused by malaria.

The development of a vaccine against malaria has so far not fulfilled expectations. Nevertheless, a synthetic peptide vaccine developed by Patarroyo and colleagues in Colombia has procured partial protection against *P. falciparum* infection in field trials.[8b]

Malaria pathogens are most adaptable to chemical changes in their environment. Following the introduction of a new drug, it can be anticipated that *Plasmodium falciparum* will develop resistance within a few years. Chloroquine (resochin), the drug of choice a decade ago, is ineffective today in most regions where malaria is endemic. Only with the worldwide appearance of resistant strains of the parasite did scientists become interested in the mechanism of action of this compound. At present the most attractive hypothesis is that chloroquine blocks a parasite-specific heme polymerase.[8c] Tourism and, above all, military travel to distant regions were largely responsible for the spread of chloroquine-resistant pathogens.



1

At the present time there is no agent that can offer protection against malaria in all regions of the world; the need for novel chemotherapeutic agents is therefore acute. The most promising compounds now are derivatives of Qinghaosu (Artemisinin, **1**), which was isolated in 1971 by Chinese chemists from the leaves of Artemisia species.[9b]

3. Chagas' Heart Disease (American Trypanosomiasis)

Like the plasmodia, the interrelated Trypanosomes, Leishmanias, and Crithidias are also unicellular parasites. These three protozoa belong to another order, the Kinetoplastida; the name refers to their typical propeller-like flagellum (Fig. 1, left). Crithidias are only pathogenic for insects. Trypanosomes and leishmanias, on the other hand, cause severe infectious diseases of man and domestic animals in tropical countries. Examples of

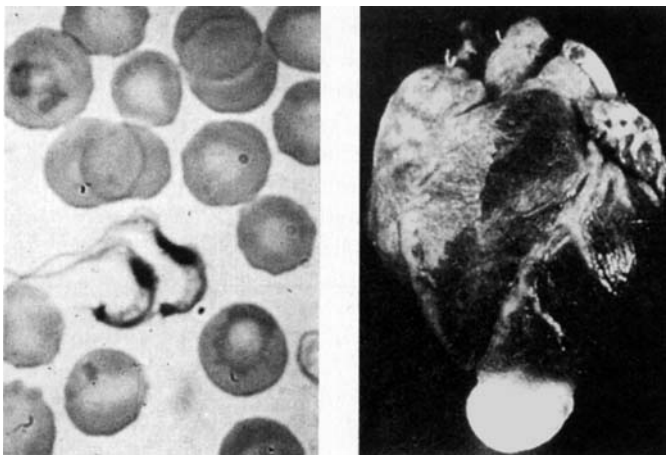


Fig. 1. The causative agent of Chagas' disease, the scourge of South America, is *Trypanosoma cruzi*. In the center of the left hand photograph two trypanosomes can be seen surrounded by erythrocytes; their destinations are, for instance, heart muscle and nerve cells. In many patients the disease becomes chronic, leading to complete destruction of the heart. After years or decades, sudden death can occur due to conduction disorders or rupture of the heart. Typical for Chagas' disease is the bulging and thinning of the apical region of the left heart ventricle (see bottom of the right-hand photograph). The pathogenesis of the disease with its insidious cell destruction resembles the "broken heart" described in fiction [e.g., The Lady of the Camelias by A. Dumas fils (1848) which formed the subject of the opera "La Traviata" by F. M. Piave and G. Verdi (1853)].



Heiner Schirmer was born in 1942 and studied medicine and philosophy in Basle and Heidelberg. In 1966 he obtained a doctorate under Caspar Rüegg with a thesis entitled "Arterial contractile protein". After clinical work and postdoctoral research at Dartmouth Medical School, NH, he went to the Max Planck Institute for Medical Research in 1970, where he worked together with Georg Schulz on the structural analysis of nucleotide-binding proteins. In 1976 he was Bicentennial Lecturer in Boston and Philadelphia. Since 1980 he has been professor at the Biochemical Institute II, University of Heidelberg; his major research interest is the biochemistry of intracellular parasites.

these are Chagas' disease, which occurs in Latin America (pathogen: *Trypanosoma cruzi*), African sleeping sickness (*Trypanosoma brucei gambiense* and *Trypanosoma brucei rhodesiense*), oriental sore (*Leishmania tropica*), Kala azar (*Leishmania donovani*), as well as the devastating cattle disease Nagana (*Trypanosoma congolense*).

In collaboration with Klaus-Dieter Hungerer, Behringwerke Marburg, we have mainly worked on *Trypanosoma cruzi*, the causative agent of a chronic disease affecting the heart and other organs (Fig. 1, right). Blood-sucking bugs act as vectors. The disease—described by Carlos Chagas in 1909 and named after him—is the most serious socio-medical problem in South America. According to an estimate by the World Health Organization more than 20 million people from the lower socio-economic groups are infected with *T. cruzi*. In the USA about 100000 people are affected, probably due to transfusion of blood and blood products originating from South America.

In biochemical terms a common feature of trypanosomes and malaria parasites is their need for a highly efficient thiol metabolism to protect them from reactive O_2 derivatives and other oxidants.[9a] This Achilles heel of parasites, their sensitivity to oxidative stress,[10, 11] is a promising point of attack for drug design.

4. Oxidative Stress as a Chemotherapeutic Strategy

Per day a human being consumes 800 litres of oxygen, 5% of which (that is, 50 g) is converted by side reactions into reactive oxygen species such as $O_2^{\bullet-}$, $HO_2^{\bullet}$, $ONOO^-$ (pernitrite), $HO^{\bullet}$, and H_2O_2.[12] These compounds are cytotoxic because of their ability to modify nucleic acids, thiol-containing proteins, and membrane lipids. There are numerous metabolic pathways for the detoxication of reactive oxygen species; when these antioxidative systems are challenged, the cell or the tissue is regarded as being under "oxidative stress".[12]

Oxidative stress is not simply an undesirable consequence of aerobic life; it also represents an important principle of the organism's chemical defense against invaders: during the "respiratory burst" reaction of activated leukocytes and macrophages, specific membrane-bound oxidases ($NADPH + 2O_2 \rightarrow NADP^+ + H^+ + 2O_2^{\bullet-}$) produce superoxide anions. These radicals serve as starting material for the synthesis of chemical agents that combat bacteria, parasites, and tumour cells. In the Haber–Weiss reaction ($O_2^{\bullet-} + H_2O_2 \rightarrow O_2 + HO^- + HO^{\bullet}$), for instance, highly toxic OH radicals are generated from $O_2^{\bullet-}$.[12d]

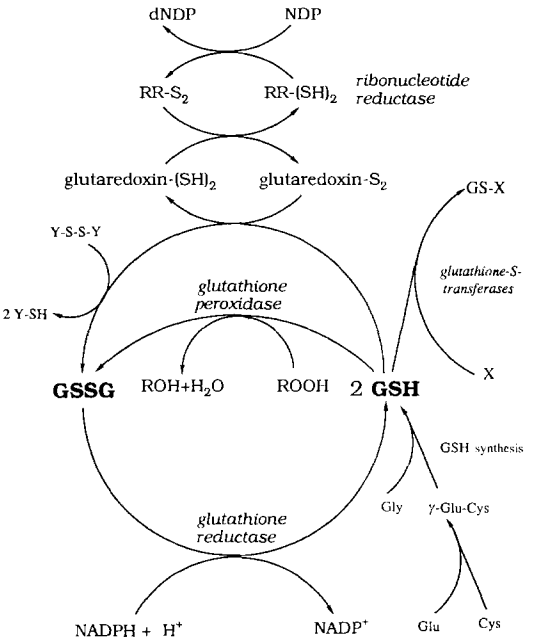
Furthermore, numerous pharmacologically and toxicologically active compounds exert their effects, as so-called redox cyclers, by producing reactive oxygen species. For example, a redox cycler X can be reduced by flavoenzymes to the radical anion $X^{\bullet-}$ [Eq. (a)], which then reacts with oxygen [Eq. (b)].

$$NADPH + 2X \longrightarrow 2X^{\bullet-} + NADP^+ + H^+ \quad (a)$$

$$2X^{\bullet-} + 2O_2 \longrightarrow 2X + 2O_2^{\bullet-} \quad (b)$$

Thus the net reaction catalyzed by the redox cycler X is that of leukocyte respiratory burst oxidase. Known redox cyclers are nifurtimox, a drug used in the treatment of Chagas' disease,[9a] the cytostatic agents mitomycin C and doxorubicin, as well as the herbicides paraquat[13a] and diquat. It is noteworthy in this context that the antimalarial agent Qinghaosu (**1**) contains an *endo* peroxide group which is essential for its action.[9b]

Clinical and epidemiological observations have provided further evidence that oxidative stress is an important mechanism for the destruction of parasites and tumour cells.[12c] Specifically, congenital as well as acquired factors that produce oxidative stress in erythrocytes offer partial protection against malaria.[10] The best known example is glucose-6-phosphate dehydrogenase deficiency ($G6PDH^-$; the minus sign of the superscript denotes the deficiency). $G6PDH^-$ is the most common inherited enzyme abnormality in man. It exists in more than 300 genetic variants and affects 400 million people worldwide.[14a] The functional defect involves limited availability of NADPH through the hexosemonophosphate pathway. In erythrocytes this leads to an impairment of the glutathione redox system (Scheme 1) with a consequent marked increase in oxidative stress.[14b] The additional oxidative load due to the parasite[15a] may lead to premature liberation of immature nonviable parasites.



Scheme 1. The glutathione redox cycle. In the center of the cycle is the tripeptide glutathione (GSH, γ-glutamylcysteinylglycine) that is formed from the amino acids in an ATP-dependent pathway. GSH takes part in the detoxication of organic hydroperoxides (ROOH), in the production of deoxyribonucleotides (deoxynucleosidediphosphates, dNDP) for DNA synthesis [18] as well as in thiol–disulfide exchange reactions. In these reactions two GSH molecules are oxidized to the disulfide (GSSG). GSH is regenerated by reduction with NADPH (catalyzed by glutathione reductase). In erythrocytes NADPH is supplied by the enzyme glucose-6-phosphate dehydrogenase (G6PDH). GSH not only detoxicates peroxides. So-called glutathione-S-transferases allow the elimination of a variety of cytotoxic substances by conjugation with glutathione. In addition these enzymes take part in the synthesis of certain leukotrienes and hence in the control of many (patho)physiological processes [19b].

Favism is a special form of glucose-6-phosphate deficiency which is restricted to regions where malaria was or is endemic. It is characterized by episodes of hemolytic anemia, which are often precipitated by a meal of fava beans. Since these beans (*Vicia faba*) have been a principal source of protein in Mediter-

ranean countries from time immemorial, this food source might be expected to have led to a natural selection against glucose-6-phosphate-dehydrogenase deficiency. In actual fact, however, the frequency of the mutated G6PDH gene is at its highest in these countries.[14c] The inborn enzyme defect and the nutritional factor exert a synergistic effect in the protection against *P. falciparum*. The antimalarial principles of the fava bean, namely the β-glucosides of the pyrimidines isouramil and divicine have been isolated. These compounds act as redox cyclers producing H_2O_2, which in turn leads to oxidative stress in $G6PDH^-$ cells.[14b] Thus it is likely that fava beans confer some protection from malaria also in persons with normal G6PDH genes.[*]

Since the $G6PDH^-$ phenotype results in a deficiency of NADPH, the substrate of glutathione reductase, favism corresponds clinically to functional insufficiency of glutathione reductase in erythrocytes.[12e] This is also consistent with the observation that inherited glutathione reductase deficiency, a rare condition, results in a disease resembling favism.[16] On this basis the inhibition of glutathione reductase, a pharmacological phenocopy of G6PDH-deficiency, represents a promising approach towards the chemotherapy of malaria.[10, 13b, 17]

4.1. Detoxication of H_2O_2 and Organic Peroxides by the Glutathione Reductase Cycle

The main defence system against reactive oxygen species is the glutathione redox cycle, which involves the enzymes glutathione reductase (GR) and glutathione peroxidase (Scheme 1). The flavoenzyme glutathione reductase [EC 1.6.4.2] catalyzes the NADPH-dependent reduction of glutathione disulfide (GSSG, oxidized glutathione) to glutathione (GSH) [Eq. (c)]. Thus GR

$$GSSG + NADPH + H^+ \xrightleftharpoons{GR} 2GSH + NADP^+ \quad (c)$$

is the link between a pyrimidine nucleotide redox system and a thiol/disulfide redox system in the cell.[16, 19a, 20] By means of the GR-catalyzed reaction the ratio of the intracellular concentration of GSM to that of GSSG is maintained at greater than 20,[12a] while the GSH concentration in animal cells is about 3 mM. GSH takes part in many biological functions, including the detoxication of cytosolic hydrogen peroxide and organic peroxides by means of the selenium-dependent glutathione peroxidase (Scheme 1). Superoxide radicals and hydrogen peroxide are reduced by the combined action of this enzyme and two other antioxidative enzymes, namely, superoxide dismutase [EC 1.15.1.1] and catalase [EC 1.11.1.6] [Eqs. (d)–(f)].[12a]

$$2O_2^{\cdot-} + 2H^+ \xrightarrow{\text{superoxide dismutase}} O_2 + H_2O_2 \quad (d)$$

$$2H_2O_2 \xrightarrow{\text{catalase}} O_2 + 2H_2O \quad (e)$$

$$H_2O_2 + 2GSH \xrightarrow{\text{glutathione peroxidase}} GSSG + 2H_2O \quad (f)$$

[*] It has been suggested that chimpanzees use certain plants not only for food but mainly as a prophylaxis against pathogens. The antimalarial principles in these plants are under investigation at present [15b]; vernodalin, a sesquiterpene from *Veronia amygdalina*, is a particularly promising compound.

A comparison of the two H_2O_2-scavenging enzymes in red blood cells showed that glutathione peroxidase [Eq. (f)] is active at much lower H_2O_2 concentrations than catalase [Eq. (e)].

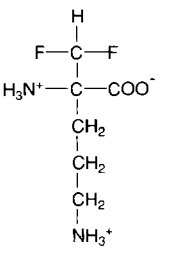
4.2. Trypanothione and Other Glutathionylspermidines in Trypanosomes and Leishmanias

Trypanosomes and their relatives exhibit a large number of metabolic reactions not seen in other microorganisms and higher organisms.[21] One possible explanation for this is the long period of independent evolution (300 million years) of the Kinetoplastida, which are one of the oldest eukaryotic lineages. Be that as it may, the metabolic pathways specific to these parasites, for example the trypanothione metabolism,[22, 23] constitute promising targets for the rational development of therapeutic agents.

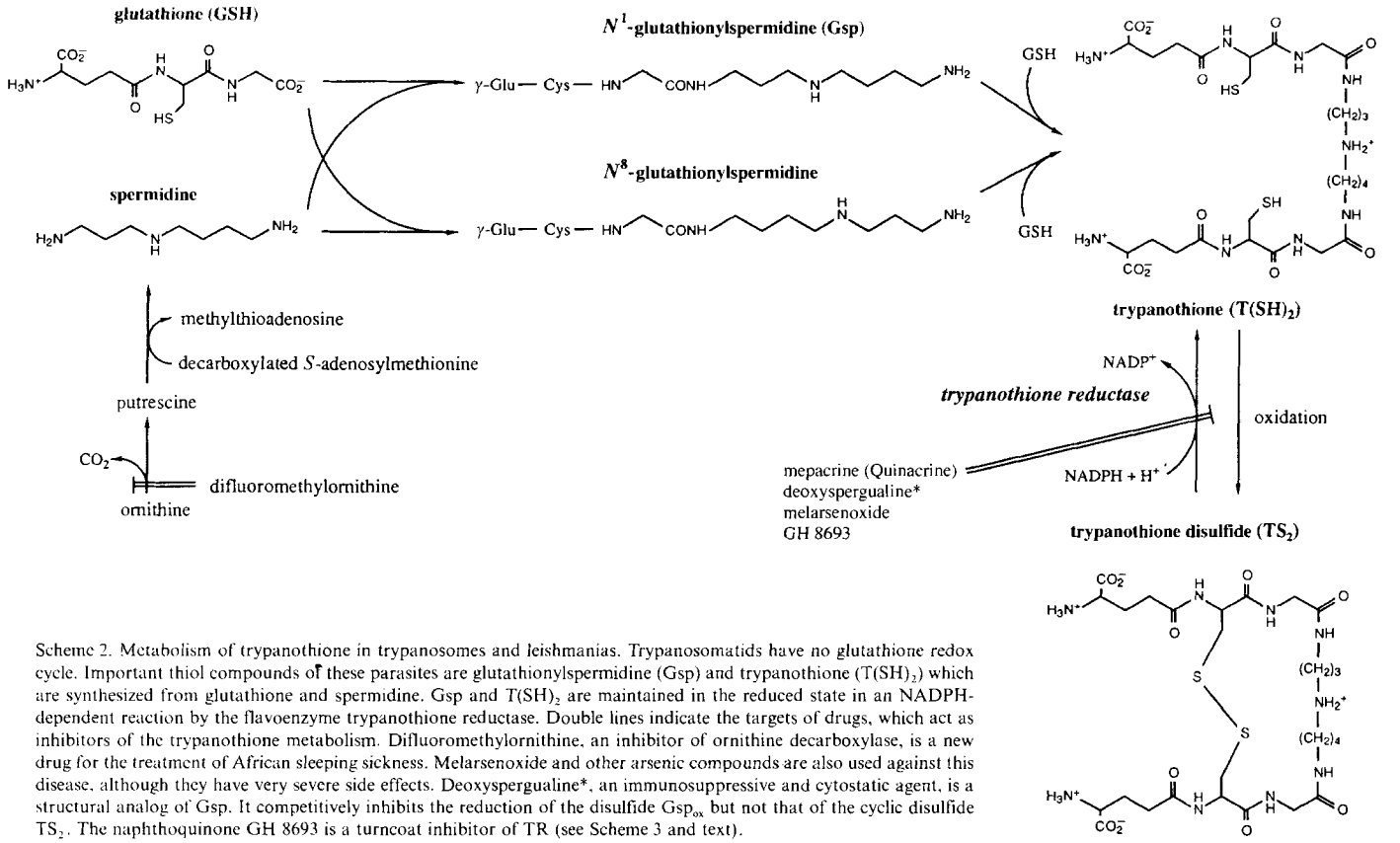
In contrast to almost all other organisms whose intracellular redox equilibrium depends on the glutathione/glutathione reductase system (Scheme 1), trypanosomatids have no glutathione reductase. Their most important thiols are compounds in which the tripeptide glutathione is linked by an amide bond to the triamine spermidine (Scheme 2).[24] Trypanothione [$T(SH)_2$] and monoglutathionylspermidine (Gsp) are maintained in the reduced state by the NADPH-dependent enzyme trypanothione reductase.[25, 26] At least in some trypanosomatids, 4-mercaptohistidine (ovothiol A) is another major thiol compound.[27a, b] Trypanosomes lack the enzymes catalase and glutathione peroxidase, which in other organisms degrade H_2O_2 and organic hydroperoxides. H_2O_2 might be detoxicated in uncatalyzed reactions (for example, $H_2O_2 + T(SH)_2 \rightarrow 2H_2O + TS_2$).[27c]

Trypanosomes and leishmanias are substantially more sensitive to oxidative stress than their biological hosts. This is consistent with the fact that nifurtimox (Lampit) and benznidazol (Radanil), the only drugs available for the treatment of Chagas' disease, are redox cyclers. As nitroarenes, they give rise to the formation of reactive oxygen species.[9a] Both compounds are, however, only effective in the acute stage of Chagas' disease, and they have serious side effects. There is also a need for new compounds against other forms of trypanosomiasis.

Surprisingly, most of the agents with known activity against trypanosomes affect the recently discovered trypanothione metabolism (Scheme 2). A case in point is the treatment of sleeping sickness with arsenic compounds developed by Paul Ehrlich. Fairlamb et al.[28] were able to show that melarsen-oxide forms a 1:1 stoichiometric adduct with the dithiol trypanothione. In addition, enzymes with spatially adjacent thiol groups (for example, TR and GR) are inhibited by trivalent aromatic arsenicals. The naphthoquinone GH 8693, synthesized by the late Graeme Henderson of the Rockefeller University, acts in vitro as a trypanocide against *T. cruzi* and is a turncoat inhibitor of TR (see Scheme 3).[29] A major breakthrough was achieved in 1990 with the introduction of difluoromethylornithine (eflornithine, **2**) as a most effective drug against the chronic form of sleeping



2



Scheme 2. Metabolism of trypanothione in trypanosomes and leishmanias. Trypanosomatids have no glutathione redox cycle. Important thiol compounds of these parasites are glutathionylspermidine (Gsp) and trypanothione ($T(SH)_2$) which are synthesized from glutathione and spermidine. Gsp and $T(SH)_2$ are maintained in the reduced state in an NADPH-dependent reaction by the flavoenzyme trypanothione reductase. Double lines indicate the targets of drugs, which act as inhibitors of the trypanothione metabolism. Difluoromethylornithine, an inhibitor of ornithine decarboxylase, is a new drug for the treatment of African sleeping sickness. Melarsenoxide and other arsenic compounds are also used against this disease, although they have very severe side effects. Deoxyspergualine*, an immunosuppressive and cytostatic agent, is a structural analog of Gsp. It competitively inhibits the reduction of the disulfide Gsp_{ox} but not that of the cyclic disulfide TS_2. The naphthoquinone GH 8693 is a turncoat inhibitor of TR (see Scheme 3 and text).

sickness. Unfortunately, the example of eflornithine also illustrates the difficulties of financing the production of a compound for exclusive use in the so-called Third World.[30a] Difluoromethylornithine inhibits spermidine synthesis by the parasite (Scheme 2); due to the short in vivo half-life of human ornithine decarboxylase, the polyamine metabolism of the host is unaffected.[21] Eflornithine is also completely inactive against the pathogens responsible for South American trypanosomiasis because *T. cruzi* produces spermidine by another pathway[21, 22, 30b] or obtains it from the patient's blood.

5. The Three-Dimensional Structures of Glutathione and Trypanothione Reductase as a Basis for Drug Design

Trypanothione reductase is an obvious choice for drug design, since it is pathogen-specific and does not occur in man. In contrast, the selection of human erythrocyte glutathione reductase as a target for antimalarial agents requires some explanation. Firstly, as set out in Section 4, we follow a principle provided by nature itself. Secondly, it was shown for many patients treated with 1,3-bis(2-chloroethyl)-1-nitrosourea (BCNU or carmustine; see Section 6.1) that GR is not essential for normal erythrocyte function; the reduced lifespan of GR-deficient red blood cells (30 days instead of 100 days) is tolerable.[16] Thirdly, the problem of unfavorable evolutionary selection is avoided: drugs directed against parasite structures also select for drug-resistance among parasites.[31] This, of course, is much less pronounced for chemotherapeutic agents directed against a host protein. Finally, the membranes of parasitized erythrocytes become permeable to relatively large anionic compounds ($M_r < 600$).[32] Many of the known inhibitors of glutathione reductase fall into this category.[*]

It should also be noted that tailored inhibitors of glutathione reductase are not only of interest as drugs for the treatment of malaria but also as cytostatics, as probes for studying the detoxication metabolism, and as herbicides.[23]

Human glutathione reductase is one of the most thoroughly studied enzymes. The amino acid sequence[33a] and the three-dimensional structure at 1.5 Å resolution are known.[33b] The binding of the substrates,[34] substrate analogs, and inhibitors,[16, 35, 36] as well as the stereochemistry of catalysis[37] have been studied in great detail. The cDNA of glutathione reductase was cloned and sequenced with the result that an even more detailed structure–mechanism analysis of the enzyme has become possible with site-directed mutagenesis.[38]

GR is a homodimer consisting of subunits with an M_r of 52000. The enzyme has two identical active sites; amino acids of both protein subunits are involved at each catalytic site. As shown in Figure 2, the isoalloxazine ring of the prosthetic FAD group forms a barrier between the substrate compartments: NADPH binds to the *re* side and glutathione disulfide (GSSG) to the *si* side of the flavin ring. The *si* side of the flavin is also in close contact with the redox-active dithiol/disulfide of the protein. Catalysis takes place in such a way that the reduction

[*] We have isolated glutathione reductase from *Plasmodium falciparum* in pure form and characterized it, but it has not yet been obtained in crystalline form. The corresponding gene segment has recently been sequenced by S. Müller and R. Walter at the Bernhard-Nacht-Institut in Hamburg, Germany. It may be possible to use differences between the host and parasite glutathione reductases for designing drugs against the enzyme of the malaria parasite.

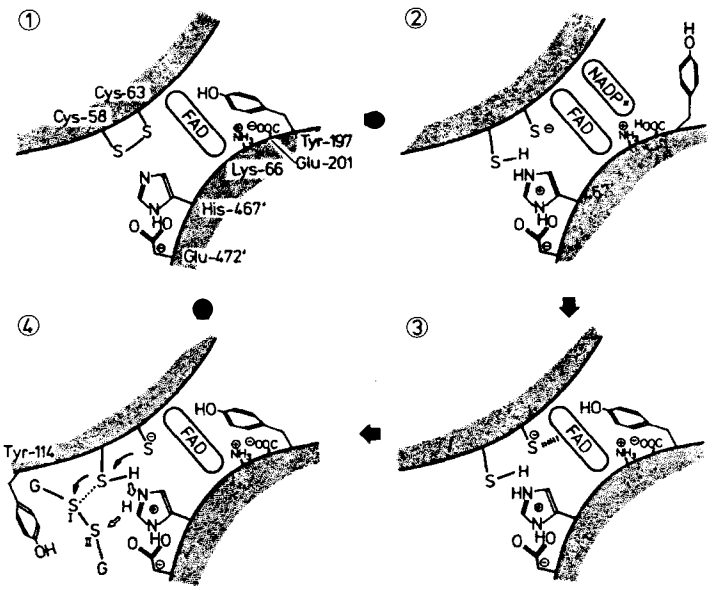


Fig. 2. Catalytic cycle of glutathione reductase [19a, 34, 37]. The enzyme glutathione reductase (GR) cycles during catalysis between the oxidized form E and the two-electron reduced form EH_2. ① The oxidized form of GR, E_{ox}, is characterized by a closed disulfide bridge between Cys 58 and Cys 63. ② Reduction of the disulfide with the coenzyme NADPH. Here the complex between the reduced enzyme EH_2 and the product $NADP^+$ is shown. ③ Release of $NADP^+$ results in formation of EH_2. This state is characterized by a charge-transfer interaction between the thiolate form of Cys 63 and the flavin ring (||||). ④ The three catalytic steps leading to the formation of two molecules of GSH from GSSG. The light arrows depict presumed proton shifts during the formation of the mixed disulfide between Cys 58 and glutathione I; this reaction leads to the liberation of one molecule of glutathione (GSH II). The solid arrows indicate the movement of electrons during the cleavage of the mixed disulfide. This causes the release of GSH I and converts the enzyme back to its oxidized form E_{ox}.

equivalents of NADPH are carried via the flavin ring to the disulfide bridge of the protein with the result that the dithiol Cys 58 – Cys 63 is formed. After binding of glutathione disulfide (GSSG) a series of thiol-disulfide exchanges leads to the release of two molecules of GSH and to reoxidation of the active site dithiol to give the disulfide. This completes the catalytic cycle.

The three-dimensional structures of trypanothione reductase from *Crithidia fasciculata*[39, 40] and *Trypanosoma cruzi*[42] have recently been elucidated. This is also the case for the binary complexes *C. fasciculata* TR – Gsp_{ox},[40b] *C. fasciculata* TR – $NADP^+$,[40c] and *T. cruzi* TR · NADPH.[42] TR is an FAD- and NADPH-dependent disulfide reductase[19a] and hence shares many physical and chemical properties with GR, the closely related host enzyme.[26] The most important difference between the two reductases is the mutually exclusive specificity for the disulfide substrate: TR reduces only the glutathionylspermidine conjugate, whereas GR is specific for glutathione disulfide.

The active site of TR with the redox-active disulfide/dithiol and the flavin ring in the center is very similar to that of GR (Fig. 3). All amino acid residues of GR that are directly involved in catalysis are conserved in TR.[41, 42] The binding region for the disulfide substrate is—by virtue of the different orientation of two α-helices—more spacious in TR than in GR.

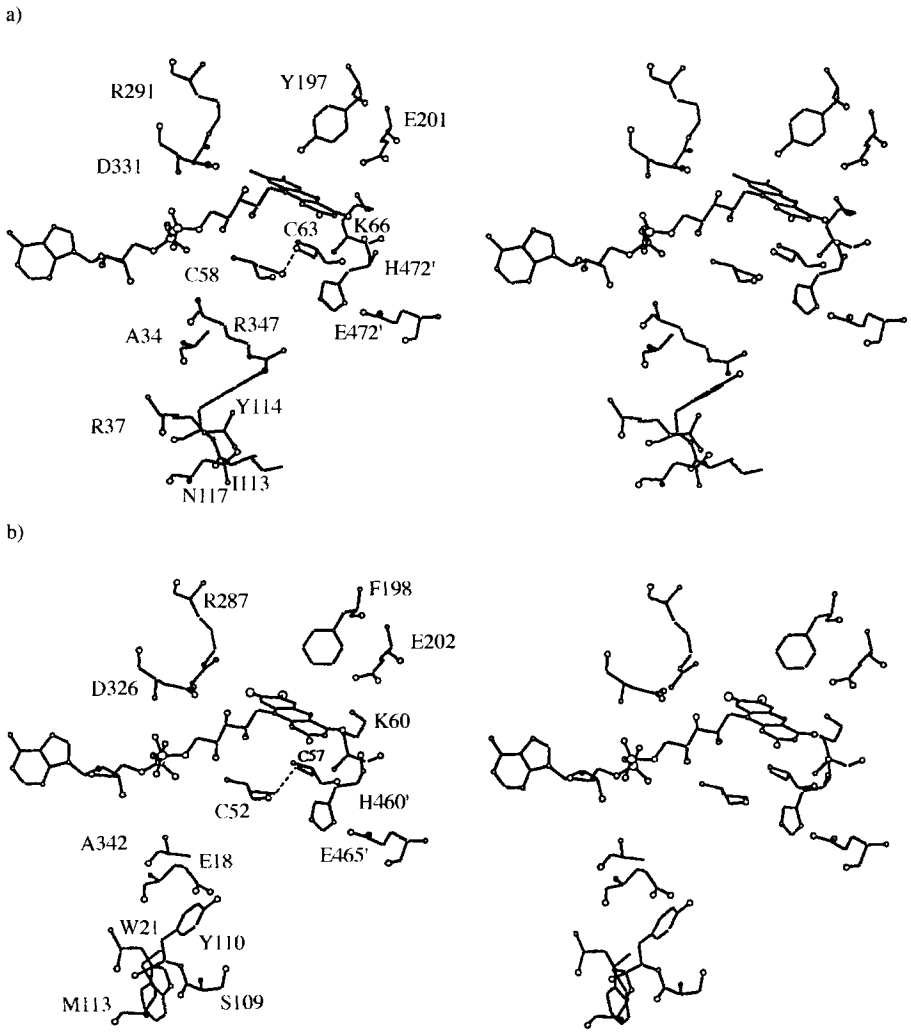


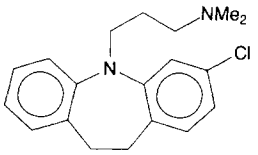
Fig. 3. A comparison of the active sites of glutathione reductase (a) and trypanothione reductase (b) [42, 43]. The isoalloxazine ring of FAD forms the center of the active site. The redox-active disulfide bridge of the protein is represented by a broken line. At several equivalent positions, TR from *Trypanosoma cruzi* and human GR contain different amino acids, namely: Glu18 (corresponding to Ala34 in GR), Trp21 (Arg37), Ser109 (Ile113), Met113 (Asn117) and Ala342 (Arg347). (The numbering is different for the two proteins because of amino acid insertions and/or deletions along the polypeptide chains.)

Of the 19 residues which in GR participate in the binding of GSSG, only five are not conserved in TR (legend to Fig. 3). Remarkably, three arginine residues at the active site of GR are replaced by neutral or acidic residues in TR.[42,43] These exchanges reflect the different charges on the substrates. Whereas GSSG when bound to GR has two negative C-terminal ends (the carboxylate groups of the glycine residues), the TR substrates TS_2 and Gsp_{ox} (Scheme 2) have one and four positive charges, respectively, in the corresponding region. Site-directed mutagenesis of TR and GR,[41,44,45] as well as the structural analysis of the TR·Gsp_{ox} complex[40b] have confirmed the importance of certain amino acid positions for substrate specificity. Indeed, exchanging only a few amino acid residues is sufficient to convert a TR into a GR and vice versa.

The next goal is the crystallographic investigation of enzyme–inhibitor complexes. An understanding of the interactions between protein and ligands is fundamental for the synthesis of specific, high-affinity inhibitors.

5.1. Derivatives of Tricyclic Antidepressants Fitting the Spermidine Niche of Trypanothione Reductase

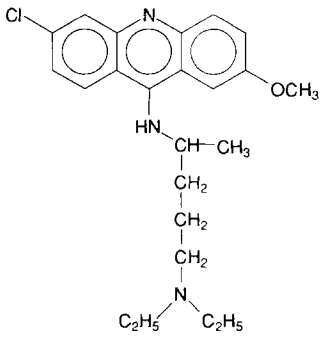
By comparing the substrate-binding sites of trypanothione reductase and glutathione reductase, Benson et al.[46a] discovered a hydrophobic niche in TR. The GR structure contains polar residues in the corresponding region. Using the computer-assisted programs of Goodford,[2] the authors probed this niche with different molecular fragments and classified the probes according to energetically and geometrically favored binding positions in TR. The subsequent molecular modeling showed that tricyclic compounds of the phenothiazine type—well known as antidepressant drugs—happened to contain the best-fitting probes as part of their structure. Enzyme kinetic studies confirmed that compounds such as clomipramine (**3**) are competitive inhibitors of trypanothione reductase and are therefore candidates for lead substances for the synthesis of novel trypanothione reductase inhibitors. It had long been known that these compounds do not inhibit glutathione reductase.[46b]



3

First experiments with the phenothiazines showed promising results in terms of their ability to kill trypanosomes in stored blood. The advantage of these agents as lead compounds in drug design lies in the fact that their toxicology and pharmacology have been thoroughly studied, and a few have already been approved for clinical use although at a low dosage. One possibility of improving on the lead compound, clomipramine, is obvious. On binding to TR, the tricyclic system is apparently held in a form twisted around its middle axis.[46a] All other parameters being equal, a synthetic derivative that could achieve receptor complementarity without conformational strain would bind to TR with much higher affinity. As the next step, of course, the nature of the binding of these drugs to the enzyme needs to be confirmed by X-ray diffraction analysis of crystalline TR–inhibitor complexes.

Another tricyclic compound with trypanocidal properties is the acridine derivative, mepacrine (Primaquine, Atebrin; **4**). Like chlomipramine it is a competitive inhibitor of TR but not of GR.[31] Recently we managed to bind mepacrine to crystalline TR and to elucidate the structure of the enzyme–inhibitor complex.[46c]



4

Studies on a number of riboflavin analogs that are more potent inhibitors of GR[47a] than TR showed that the selectivity of the TR inhibitors described above depends not simply on the presence of a tricyclic ring system. The riboflavin analogs most likely bind between the subunits of glutathione reductase in a cavity larger than that in trypanothione reductase.[47b]

5.2. Communication Policy of Organisms: Flexible Compounds Inside—Rigid Ring Systems for the Environment

The examples of mepacrine and clomipramine show that a rigid ring system fits into a protein niche whose biological function is the binding of a *flexible* structure, namely the spermidine chain of trypanothione. This finding is consistent with the rule that for its own housekeeping functions each organism favors compounds that do not bind too tightly to their physiological partners. The weak binding is due to the loss in entropy when many rotations around single bonds in the ligand are arrested.[48,49] The reversibility of complex formation appears to be fundamental for the biochemistry of an organism.

In contrast, biomolecules that are synthesized in order to exert effects on other individuals often form rigid cyclic structures. In many cases these structures are further stabilized by bridging atomic groups. Cyclization leads to order in a chemical structure; the entropy costs associated with the binding of such a molecule to a receptor are relatively small, and the free energy of binding is thereby shifted to negative, that is, more favorable values. Examples of ligands for "foreign" receptors include antibiotics, pheromones and other aromatic attractants, plant alkaloids, as well as animal poisons. Many drugs are also polycyclic compounds with restricted conformational freedom. Such compounds are not only suitable as tightly binding ligands; in addition they are resistant to degradation by hydrolytic enzymes. This is particularly true for rigid peptide mimetics; the analogous flexible structures are hydrolyzed within seconds by peptidases of the target organism: peptidases and other hydrolases preferably attack molecules that have great conformational freedom.

The degree of ring formation and bridging in otherwise similar ligands allows subtle control of binding to a receptor and hence of a physiological function. Even the introduction of a double bond in the alkyl moiety of a ligand can increase the affinity constant by an order of magnitude (see Appendix). Much of this knowledge is derived from a model system in which the interactions of the antibiotic ristocetin A with *N*-acetyl-D-alanyl-D-alanine, a fragment of the bacterial cell wall, can be analyzed and quantified in a systematic way.[48,49]

Table 1. Aspects of enzyme inhibition with reference to chemotherapy.

Inhibitor type	Principle	Examples
Polycyclic compounds with five- and six-membered aromatic rings (see Sections 5.1 and 5.2 and Appendix).	The limited number of single bonds with free rotation reduces the entropy costs for complex formation. In addition, rigid compounds are resistant to destruction by hydrolytic enzymes [48,49].	– Active principle of many natural products (antibiotics, alkaloids, pheromones) – competitive inhibition of TR by mepacrine [31] and tricyclic antidepressants [46a] – inhibition of GR by flavin analogs [47].
Slowly dissociating ligands (see Section 6.1).	K_{diss} (as quotient of the half-lives of complex formation and dissociation) should be $<10^{-8}$ M. If the $t_{\frac{1}{2}}$ of complex formation is >100 ms, the complex is infinitely stable on a biological time scale [52].	– Half-life of the physiological GR-FAD complex >1 month – Kinetic stabilization due to slow conformational changes [4] of the guanidinoglycal–sialidase complex (treatment of influenza).
Substrate analogs (see Section 6.1).	Computer-assisted studies of the active site using functional groups provide short cuts to appropriate substitutions in the substrate molecule [2,4].	– Inactivation of the sialidase of influenza viruses by guanidinoglycal [4,5]. – Inhibition of GR by dinitrophenylglutathione (Fig. 4).
Suicide inhibitors (see Section 6.1).	A substrate analog is converted by the enzyme into a reactive intermediate, which then blocks the enzyme irreversibly [52].	– difluoromethylornithine (**2**) as an inhibitor of ornithine decarboxylase (chemotherapy of African sleeping sickness) – allopurinol as an inhibitor of xanthine oxidase (pharmacological prevention of gout).
Syncatalytic inhibitors (see Section 6.1).	A reactive group of the enzyme becomes exposed during the course of the catalytic cycle and is then modified by the inhibitor.	– Covalent modification of Cys 58 of GR by BCNU (chemotherapy of tumors and malaria) and of Cys 52 of TR [29,35].
Turncoat inhibitors (see Section 6.1).	The ligand inhibits the physiological reaction of the enzyme and promotes an unwanted side reaction.	– induction of oxidase activity of GR by the herbicide paraquat (methylviologen; 1,1′-dimethyl-4,4′-bipyridinium dichloride) [13a]. – induction of oxidase activity in TR by GH 8693, a trypanocidal naphthoquinone [29,55b] (see Scheme 3).
Ligand chimeras (see Section 6.2).	Two ligands of the enzyme are bridged by a suitable linker, which is tailored on the basis of the known protein structure. The K_{diss} of a ligand chimera represents the product of the individual dissociation constants.	– specific inhibition of adenylate kinase by diadenosine pentaphosphate (**5**), a compound in which an additional phosphate forms a bridge between the two substrates ATP and AMP [55a]. – affinity labeling of glutathione synthetase by adenosine-5′-polyphospho-5′-pyridoxal [56] [a].
Peptide mimetics (see Section 6.3).	Rigid peptide analogs inhibit the physiological enzyme-peptide interaction.	– inactivation of angiotensin-converting enzyme (ACE) by captopril (treatment of hypertension; treatment of cardiac insufficiency in Chagas' disease) [3]. – inhibition of plasmodium hemoglobinase by a peptide mimetic with antimalarial activity [57a].
	Peptides and peptide analogs prevent the intra- or intermolecular interactions of a protein. This can lead to destabilization and intracellular degradation of the protein [59].	– dimerization inhibitors of the ribonucleotide reductase of herpes simplex virus [58] and of human GR [59]. – association inhibitors of a protein assembly that amplifies cellular signalling [60].

[a] The principle of connecting two molecular groups by a designed bridge has also been used for stabilizing the quaternary structure of hemoglobin [57b]. This was a critical step for the development of blood substitutes.

6. Design of Inhibitors with High Affinity and Selectivity

What are the prospects of developing drugs with high affinity and selectivity, that is, agents which can be administered in almost stoichiometric or even substoichiometric amounts relative to their receptors? Examples and the principles involved are discussed in the following sections and listed in Table 1.

6.1. Substrates as Lead Compounds

6.1.1. Reversibly Binding Inhibitors

Typical examples of inhibitors that are substrate analogs are the antimalarial pyrimethamine, which binds to dihydrofolate reductase from *P. falciparum* with a K_{diss} of 10^{-10} M,[52] and guanidinoglycal, an inhibitor of influenza virus sialidase developed by drug design.[4,5] Since in the development of such reversibly binding inhibitors the law of mass action serves as a guide, let us consider the binding of the ligand L to the receptor R.

From Equation (g) it follows that K_{diss} is that concentration of free ligand L at which the concentrations of RL and R are

$$K_{diss} = [R][L]/[RL] = k_{diss}/k_{ass} \quad (g)$$

equal. Thus, when $[L] = 100\,K_{diss}$, the enzyme is inhibited to greater than 99%.[*] Drug design should aim at inhibitors with

[*] In this context the volume of the relevant cells is significant: the volume of the bacterium *Escherichia coli* is 10^{-15} L, of the malaria pathogen *Plasmodium falciparum* about 10^{-14} L, and of a human erythrocyte 10^{-13} L. According to the law of mass action, if K_{diss} for a given enzyme–inhibitor complex is 10^{-11} M, only 0.6 of a free L molecule will be required to produce 99% enzyme inhibition in the bacterial cell, whereas the corresponding figures in Plasmodium and erythrocytes are 6 and 60 molecules, respectively. Furthermore, it is worth noting that many enzymes are present only in very low numbers per cell. In view of these small numbers, it is doubtful whether the law of mass action is applicable at all. In the case considered here, however, about 10000 molecules of the enzyme glutathione reductase are present in each erythrocyte, and the concentration of TR in trypanosomes is even 10 times greater.

a K_{diss} of less than 10^{-8} M, otherwise [L] must be very high in order to sustain the inactive complex, which could lead to an unacceptable dosage regimen, rapid excretion, or unwanted side effects of the ligand L.

In addition, for the treatment of infectious diseases, slowly dissociating compounds are desirable in order to switch off an enzyme molecule "permanently" once it has been complexed. An RL complex is kinetically stabilized if k_{diss}, the rate constant for dissociation, is small; k_{diss} values less than 10^{-5} s^{-1} mean that the half-life of the RL complex is greater than 18 h. For synthetic[4] as well as physiologically important ligands (for instance, specific peptids as inhibitors of proteases), a slow conformational change of the complex (RL → R*L*) often takes place. In this way the half-life of the complex ranges from days to months; the complex can hence no longer decompose within a biologically meaningful time period. (When treating diseases one must, of course, bear in mind that the target R may continue to be produced by surviving cells.)

6.1.2. *Suicide Inhibitors*

A variation of this theme is the possibility that a substrate analog is converted by the target enzyme to a product which forms an extremely long-lasting complex with the enzyme or covalently blocks the active site. Well-known suicide inhibitors are the anti-sleeping sickness drug difluoromethylornithine (**2**), which blocks ornithine decarboxylase of *Trypanosoma brucei gambiense* (see Scheme 2), and the antiviral agent fluorouracil, an inhibitor of thymidylate synthase.[52]

6.1.3. *Syncatalytic Inhibition*

The principle resembles suicide inhibition in that only the actually performing enzyme is blocked, but not the enzyme in its resting state. For example, GR and also TR are inhibited by the cytostatic agent 1,3-bis(2-chloroethyl)-1-nitrosourea (BCNU = carmustine). However, this does not apply to the form of the enzyme normally present in vitro (E_{ox}), but only to the NADPH-reduced EH_2 (Fig. 2): In statu nascendi the thiolate group of Cys 58 reacts with chloroethyl isocyanate, a decomposition product of BCNU, to give the chloroethylcarbamoyl ester. X-ray diffraction analysis of the covalently inhibited enzyme shows that the carbamoyl group—attached by hydrogen bonds and van der Waals forces—fits snugly into its binding site.[35] These additional noncovalent interactions between enzyme and inhibitor ensure the stability of the carbamoyl ester. In the case of low molecular weight thiol compounds, the carbamoylation by BCNU is easily reversible.[53]

BCNU and the better tolerated 1-(2-chloroethyl)-3-(2-hydroxyethyl)-1-nitrosourea (HeCNU) are active antimalarials when tested in cell culture and on animals. (Interestingly, HeCNU does not produce carbamoylation but alkylation of Cys 58 in GR.[11]) Furthermore, tumor patients treated with BCNU are susceptible to numerous other infectious diseases but, to our knowledge, not to malaria.

These observations suggest the design of carbamoylating drugs, which in contrast to BCNU itself, are capable of differentiating between the active sites of human glutathione reductase, trypanothione reductase, and liponamide dehydrogenase of *T. cruzi*, an enzyme related mechanistically to TR and GR.[31,43b]

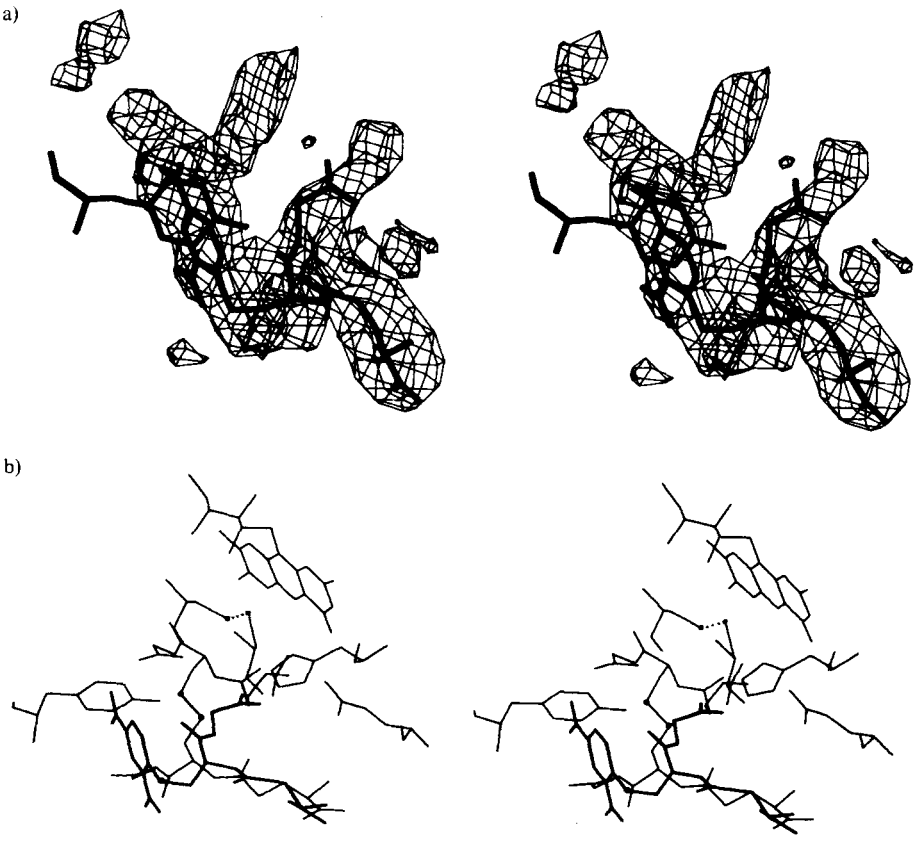


Fig. 4. a) Stereoview of the binding of 2,4-dinitrophenylglutathione (DNPG) to the GSSG binding site of glutathione reductase [36]. The difference electron density is given in bird-cage representation. Tyr 114 is shown in its undisturbed position. On binding DNPG the ring of Tyr 114 rotates about the C_α–C_β bond. The positive electron density, which arises from this movement, appears above and behind the tyrosine ring. The γ-glutamyl part of DNP-glutathione with its characteristic free α-L-amino acid moiety is located at the lower right-hand side. b) Comparison of the binding of GSSG and DNPG (stereoview). DNPG is represented in bold (with the γ-glutamyl at the lower right). The remaining structures drawn as thin lines are sections of glutathione reductase with bound GSSG. All molecular parts drawn as thin lines can be identified in Fig. 2, where they are given in approximately the same view, that is, the riboflavin moiety of FAD (at the top), Tyr 114 (outside left), the redox active dithiol Cys 58–Cys 63, His 467', and Glu 472'. (Residues of the other subunit are primed.) Comparison of the binding of GSSG and DNPG shows that only the γ-glutamyl parts—held in position by Lys 67 and Glu 473' (not shown)—do overlap. The position of the sulfur atom in DNPG is different from both sulfur atoms of bound GSSG. If the structure of the inhibitor–GR complex had been elucidated before the enzyme–substrate complex, we would probably have predicted the substrate binding incorrectly.

6.1.4. *Paradoxically Binding Substrate Analogs*

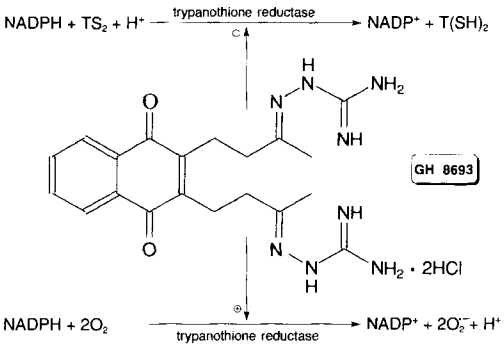
In choosing compounds as leads for inhibitor design, one should take into account that the individual atomic groups of the substrate are not equally important for the molecular recognition process.[51] In compounds with great conformational freedom only a few clearly defined fragments bind to the enzyme with high affinity, and that not all bond rotors are fixed on complex formation. In this context the approach of Goodford[2] is particularly successful for probing the binding sites of a receptor using, for example, single NH_3^+ groups or carboxylate groups instead of complete ligands.

As an example of the unexpected binding of a substrate analog to an enzyme, let us consider the action of 2,4-dinitrophenylglutathione (DNPG) as an inhibitor of GR[36] (Fig. 4). DNPG is formed in the liver from 1-chloro-2,4-dinitrobenzene by conjugation with glutathione. The DNP-glutathione conjugate is fixed to the GSSG binding site but the glutathione part is bound, unlike the two glutathione residues of GSSG. Only the γ-glutamyl part of DNP-glutathione adopts an expected position (Fig. 4b). In retrospect, this is not surprising since the γ-glutamyl part contains that characteristic part of the glutathione molecule which is not present in other peptides: a negatively charged carboxylate and a positively charged ammonium group in a rigid steric configuration.

The overall binding mode of the glutathione moiety of DNPG is thus determined by the non-glutathione part of the molecule. This is probably true for many other glutathione derivatives as well. In a crystallographic study, Janes and Schulz[54b] showed that the imprecise binding of substrate analogs to GR is a biologically meaningful molecular mechanism which prevents processing of nonphysiological substrates. It is worth emphasizing that the γ-glutamyl group with its α-amino acid moiety is a characteristic feature of glutathione and can therefore be used for probing putative glutathione-dependent enzymes.

6.1.5. *Turncoat Inhibitors*

A strong impact on the redox metabolism of trypanosomes is expected from GH 8693 and other "turncoat inhibitors". This concept[11, 29] is illustrated in Table 1 and Scheme 3. GH 8693



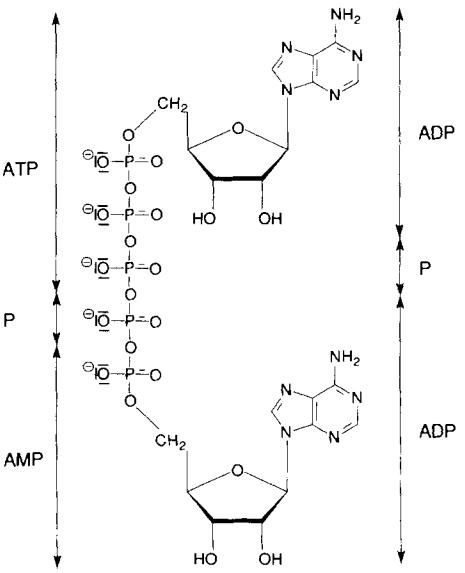
Scheme 3. The trypanocidal compound GH 8693 as a turncoat inhibitor of trypanothione reductase. At micromolar concentrations GH 8693 [55b] acts as an inhibitor of trypanothione reductase [29] (upper equation, inhibition constant $K_i = 1$ μM). At higher concentrations of GH 8693, trypanothione reductase catalyzes the reduction of O_2 to give a superoxide radical (lower equation, Michaelis constant $K_m = 15$ μM). Thus binding of GH 8693 to TR changes the antioxidative function of the enzyme into a prooxidative one—hence the name turncoat inhibitor [11, 29], sabotage inhibitor, or subversive substrate [55b].

binds to NADPH-reduced trypanothione reductase from where it transfers electrons to molecular oxygen to create two superoxide radicals. Concomitantly the reduction of the cognate substrate TS_2 is inhibited. Thus, in terms of overall balance, an antioxidative enzyme is converted into a prooxidative one.

Turncoat inhibitors exert a variety of effects that can be exploited for the chemotherapy of parasitic diseases:[31] NADPH and O_2 are wasted, the thiol/disulfide ratio is lowered, and the resulting reactive oxygen species can trigger lipid peroxidation and other chain reactions. Since turncoat inhibitors undergo redox cycling, they act as catalysts.

6.2. Ligand Chimeras

Most proteins bind very different types of ligands at sites physically separated from one another. Two ligands can be chemically linked by an adaptor moiety whose length and chemical criteria must be tailored to the protein structure. This molecular modeling leads to ligand chimeras with high affinity for the receptor.[55a, 56] In Table 1 diadenosinepentaphosphate (**5**), a disubstrate analog of adenylate kinase (ATP + AMP $\rightleftharpoons$ 2 ADP), is shown. For GR and TR, numerous combinations are conceivable in view of the many known ligands—substrates, cofactors, and inhibitors. A case in point is a chimera containing a tricyclic ring system (see Section 5.1) and a turncoat inhibitor (see Section 6.1) at an appropriate distance.



5

The kinetic stability of the enzyme–ligand complex also needs to be considered (Table 1). The half-life of the diadenosinepentaphosphate–adenylate kinase complex is only about 1 s. For this reason unmodified diadenosinepentaphosphate is more suited to diagnostic or emergency medicine than to long-term chemotherapy of infectious diseases.

6.3. Blocking Protein Folding and Organization by Catalytically Acting Peptide Mimetics

Many pathogen proteins such as trypanothione reductase from *T. cruzi*,[42] the enzymes of the AIDS virus, or ribonucleotide reductase of the herpes simplex virus are obligatory dimers; each subunit is inactive in itself. Since compounds that affect protein–protein interactions are highly specific inhibitors, dimeric proteins are especially interesting as target molecules for drugs.

The ribonucleotide reductase of the herpes simplex virus[58] consists of two subunits, one large and one small. A nonapeptide whose sequence corresponds to the C-terminal region of the small subunit displaces the small from the large subunit thereby separating the two. In this way ribonucleotide reductase is inactivated. In principle, such inhibitory peptides could act catalytically, that is, even in substoichiometric amounts: the separated subunits are often unstable and are degraded by the proteases of the cell. The more stable contact surface inhibitor is then released and can attack the next dimer.

We have carried out detailed studies on the inhibition of dimerization and its consequences for human glutathione reductase.[59] Each subunit contributes essential functional groups to both catalytic sites; the monomer thus cannot be active. In addition, peptides that correspond to the complementary contact surfaces of the protein subunits appear to inhibit the formation of the active enzyme. The site at which the subunits are in closest contact was chosen for mutagenesis (Fig. 5); it is formed by the parallel helices 439–454 and 439′–454′.[33b] By means of the exchanges (Gly446 → Glu and Gly446′ → Glu′) the smallest side chains (the H atoms of the glycine residues) were replaced by bulky negatively charged groups at positions of the contact surface facing each other.[59] This mutation not only prevented dimer formation; each monomer behaved like an unordered polypeptide chain, that is, in none of the four domains were structural elements detectable by physical and chemical methods. The biological stability of this protein was investigated in bacterial cells. While normal human glutathione reductase remains stable and active over many hours, the protein mutant was quantitatively degraded within minutes.

As a first step towards the development of dimerization inhibitors of glutathione reductase we plan to synthesize analogs of the peptide 439-454 and to fix them in their native conformation (which is a slightly deformed α-helix) (Fig. 5). The principles and methods for the synthesis of stable peptide mimetics have been summarized in monographs by Wieland[61] as well as in several recent reviews.[62–65]

The dimerization of proteins can be seen on the one hand as a special case of protein folding and on the other as an example for the formation of protein ensembles. The development of peptide mimetics is therefore an especially promising field for drug design as such compounds can exert effects both on the folding process and on protein–protein interactions. Since peptide mimetics normally lead to destabilization and subsequently to degradation of the target protein, they can affect pathophysiological processes at very low doses.

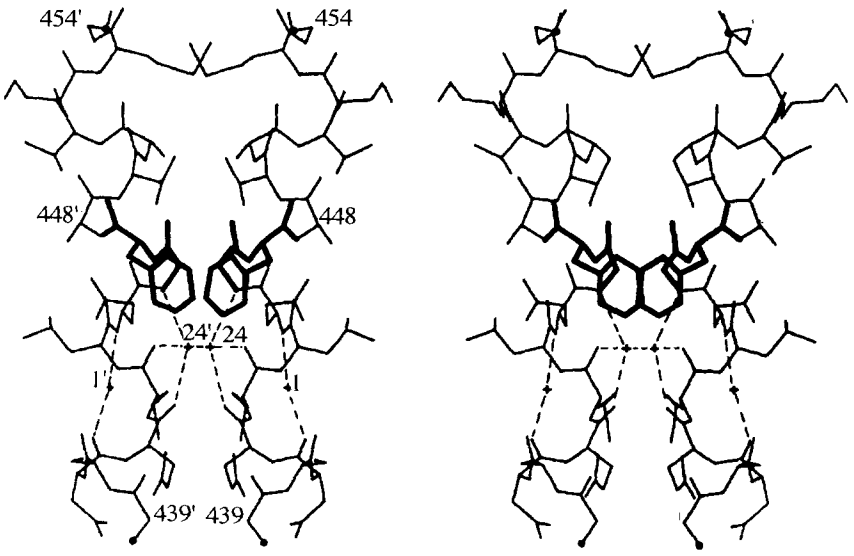


Fig. 5. Stereoview of the closest contact between the subunits of glutathione reductase. The helices 439–454 and 439′–454′ are shown. The amino acid residues Gly446 and Phe447 of both chains are indicated in bold. The exchange of Gly446 and 446′ for Glu residues results in a disordered GR-mutant which is degraded by intracellular proteases [59]. A peptide analog preventing the contact of the subunits at this site would probably have the same effect as the mutation and suppress intracellular glutathione reductase activity even in catalytic amounts.

7. Future Prospects

Drug design is not simply an extension of the repertoire of pharmaceutical chemistry. The analysis of ligand–receptor interactions leads in many ways to new concepts in structural chemistry and molecular biology. Not least because of its importance for medicine, glutathione reductase is one of the best understood enzymes[66] and a promising protein for industrial applications.[16, 67]

Research on parasites is not only necessary on humanitarian grounds. It also serves as a driving force for progress, since only interdisciplinary efforts will lead to a better knowledge and control of these mysterious pathogens.[67d] In developed countries the major parasitoses are mistakenly ignored. Parasitic diseases are not only of interest to Western societies as life-threatening complications of AIDS. Other problems like allergies, cancer, and hereditary diseases assume their own perspectives only against a background of man's natural situation, which was and is largely primed by the confrontation with challenges like starvation and parasitic diseases.[6, 7]

Appendix: On the Stability of a Protein–Ligand Complex

The Gibbs–Helmholtz Equation (h), gives the free energy of binding of a ligand to a macromolecule in which $\sum\Delta G$ consists

$$\sum\Delta G = \sum\Delta H - \sum T\Delta S \qquad \text{(h)}$$

of numerous negative (that is, favorable) and positive (that is, unfavorable) elements.

According to our present state of knowledge it is not possible to calculate with sufficient accuracy the free energy of biologically or pharmacologically interesting interactions. The following considerations[48-51, 68-72] are, however, useful if $\sum\Delta G_0$ is known for a lead compound and only one chemical grouping of the ligand is to be changed at a time. According to Equation (i),

$$\Delta G_0 = 2.3\,RT\lg K_{diss} \quad \text{(i)}$$

a change in ΔG_0 of 5.7 kJ mol^{-1} at 300 K signifies a change in the inhibitor constant K_{diss} of 10. Fixing a single bond rotor of the ligand in the right configuration—for example by introducing a double bond[70]—can result in a reduction (that is, an improvement) of the inhibitor constant by a factor of 10 [see c)]. The following contributions to ΔG need to be taken into account (all the values refer to 300 K):

a) ΔG_{R+T}, the overall entropy loss due to bimolecular association: Ligand and macromolecule, each regarded as rigid, lose their entropies of translation and rotation on forming a complex. ΔG_{R+T} is unfavorable and can be estimated from Equation (j),[70] where M_r is the relative molecular mass of the ligand.

$$\Delta G_{R+T} = (20\lg M_r + 10)\ \text{kJ mol}^{-1} \quad \text{(j)}$$

b) ΔG_h, the entropy gain of water (hydrophobic effect): On complex formation, hydrocarbon groups are often withdrawn from contact with water. ΔG_h is negative (favorable) and amounts to about -20 kJ mol^{-1} per nm^2 of hydrophobic area.[49, 71] It is very difficult to estimate the entropy gain of H_2O molecules released to bulk water when a hydrogen bond between ligand and protein is formed (for this aspect see two controversial papers[49, 70] by Williams).

c) ΔG_r, the entropy loss due to restricted rotation about single bonds: Complex formation arrests rotation for numerous single bonds; the free energy ΔG_r required is 3.5–6.0 kJ for each rotor.[49, 70] When rigid ligands are bound, no bond rotors of the ligand are fixed. This explains the prevalence of aromatic and other rigid molecular structures among drugs and poisons.

d) ΔG_i, the free energy of interaction between complementary groups: ΔG_i relates to the situation when ligand and protein are already oriented in the optimal position for noncovalent interactions. Thus ΔG_i can be regarded as the "intrinsic binding energy". Water molecules are often integral parts of the contact surfaces. For instance, in the glutathione reductase–GSSG complex, there are ten "direct" and 14 water-mediated interactions between ligand and enzyme.[34, 54]

Complementarity and hence selective binding means that many pairs are formed between the contact surfaces, each pair consisting of two dipoles, or two electrically counter-charged groups, or two nonpolar groups. The dipoles normally form hydrogen bonds and the electric charges salt bridges; the nonpolar pairs are held together by dispersion forces. The ΔG_i value (-2 to -20 kJ mol^{-1} for hydrogen bonds, up to -30 kJ mol^{-1} for salt bridges, and -0.1 kJ mol^{-1} for a pair of nonpolar partner atoms[50, 70, 71]) are determined by Coulomb's law. Consequently, the attractive forces also depend on the relative orientation of the partners and on the microscopic dielectric constant, ε, which as a rule is unknown. For the interior of a protein, ε is assumed to be 10 to 20 times smaller than for water.

To improve the polarization of a chemical group it is often favorable to have a metal ion as a partner on the complementary surface. Examples are the binding of O_2 to the iron ion of hemoglobin and the fixation of the methyl group of ethanol by the zinc ion of alcohol dehydrogenase.[70]

Although salt bridges (ion pair bonds) have favorable ΔG_i values, their contribution to the stabilization of a receptor–ligand complex is in general small. The reason is that numerous bond rotors must be oriented and arrested [see c)] before the ionic groups can come together at the optimal salt bridge distance.[72]

e) ΔG_{vdW}, the change in van der Waals energy: One must also take into account the change in the van der Waals interaction energy[50] that occurs on a complex formation. The rule is that attractive forces are weak and repulsive forces very strong. A single unfavorable van der Waals contact can prevent the formation of a complex that otherwise would be favorable.

f) ΔG_{conf}, the change in conformational energy:
Before or after binding the ligand, the receptor can find itself in a conformation with strained bond angles or interatomic distances. Consequently the formation of a low affinity complex in rapid preequilibrium can be followed by slow conversion into a high affinity complex.[4, 54] The formation of such kinetically stabilized complexes are irreversible on a biological time scale (see also Section 6.1).

The factorization of the binding energy as discussed in a) to f) indicates that molecular recognition has not yet achieved the status of a science, that is, we are generally not in a position to make reliable predictions. Therefore, new approaches such as the problem-oriented use of genetic algorithms[73, 74] are urgently required.

A problem which is often overlooked is that of specifically bound water molecules. In the structure of glutathione reductase there are more than 100 of these molecules, some of which even do not exchange with the bulk aqueous phase.[33b] Many intra- and intermolecular contacts of macromolecules are mediated by individual molecules or even networks of water. Recently it has been shown that H_2O molecules—as noncovalent extensions of DNA bases—even serve as selective recognition structures for a specific protein–DNA interaction.[75] These facts must be accounted for in ligand design and in estimations of interaction energies. All energy terms discussed above, as well as the microscopic dielectric constant may be influenced by bound water molecules. For these reasons we suggest that each structurally defined water molecule in a receptor should be given the status of a *cofactor*, as it is accepted for bound metal ions such as the zinc ions in alcohol dehydrogenase. Apart from remaining (type 1) water molecules, there can also be type 2 water molecules coming in with the ligand.[34] This implies that a receptor–ligand complex is only described satisfactorily when all water molecules with a structural or functional role have been identified.

The colleagues to whom we are indebted are listed as authors in the Reference section. In particular we would like to thank Dr. K.-D. Hungerer, Behringerwerke Marburg, Frau Irene König, Heidelberg, and Prof. K. Lingelbach, Hamburg. Frau Helga Alt

was responsible for the preparation of the manuscript. Our work has been supported by the Deutsche Forschungsgemeinschaft, the Fonds der Chemischen Industrie, and the Federal Ministry for Research and Technology (BMFT).

Received: September 20, 1993 [A271E]
German version: *Angew. Chem.* **1994**, *106*, 153
Translated by Dr. D. Jack, Glasgow, Scotland

[1] W. G. J. Hol, *Angew. Chem.* **1986**, *98*, 765–777; *Angew. Chem. Int. Ed. Engl.* **1986**, *25*, 767–778.
[2] P. J. Goodford, *J. Med. Chem.* **1985**, *28*, 849–857.
[3] D. W. Cushman, H. S. Cheung, E. F. Sabo, M. A. Ondetti, *Biochemistry* **1977**, *16*, 5484–5491.
[4] M. von Itzstein, K.-Y. Wu, G. B. Kok, M. S. Pegg, J. C. Dyason, B. Jin, T. V. Phan, M. L. Smythe, H. F. White, S. W. Oliver, P. M. Colman, J. N. Varghese, D. M. Ryan, J. M. Woods, R. C. Bethell, V. J. Hotham, J. M. Cameron, C. R. Penn, *Nature (London)* **1993**, *363*, 418–423.
[5] C. Unverzagt, *Angew. Chem.* **1993**, *105*, 1762–1764; *Angew. Chem. Int. Ed. Engl.* **1993**, *32*, 1691–1693.
[6] a) H. M. Gilles, D. A. Warrell, *Bruce-Chwatt's Essential Malariology*, 3. Aufl., Edward Arnold, London, **1993**; b) D. J. Wyler, *N. Engl. J. Med.* **1992**, *327*, 1519–1521.
[7] R. H. Schirmer, K. Becker, *Futura* **1993**, *4*, 15–21.
[8] a) D. R. Brewster, D. Kwiatkowski, N. J. White, *Lancet* **1990**, *336*, 1039–1043; b) M. V. Valero, L. R. Amador, C. Galindo, J. Figueroa, M. S. Bello, L. A. Murillo, A. L. Mora, G. Patarroyo, C. L. Rocha, M. Rojas, J. J. Aponte, L. E. Sarmiento, D. M. Lozada, C. G. Coronell, N. M. Ortega, J. E. Rosas, P. L. Alonso, M. E. Patarroyo, *ibid.* **1993**, *341*, 705–710; c) A. F. G. Slater, A. Cerami, *Nature (London)* **1992**, *355*, 167–169.
[9] a) R. Docampo, S. N. J. Moreno, *Rev. Infect. Dis.* **1984**, *6*, 223–238; b) X. D. Luo, C. C. Shen, *Med. Res. Rev.* **1987**, *7*, 29–52. Qinghaosu is pronounced as if it were written ching-how-sue in English. This conforms with the Pinyin system of transliteration of Chinese chracters which was officially adopted in 1975.
[10] N. H. Hunt, R. Stocker, *Blood Cells* **1990**, *16*, 499–530.
[11] R. H. Schirmer, T. Schöllhammer, G. Eisenbrand, R. L. Krauth-Siegel, *Free Rad. Res. Commun.* **1987**, *3*, 3–12.
[12] a) H. Sies, *Angew. Chem.* **1986**, *98*, 1061–1075; *Angew. Chem. Int. Ed. Engl.* **1986**, *25*, 1058–1070; b) B. Halliwell, J. M. C. Gutteridge, C. E. Cross, *J. Lab. Clin. Med.* **1992**, *119*, 598–620; c) J. G. Müller, U. S. Bücheler, K. Kayser, R. H. Schirmer, D. Werner, R. L. Krauth-Siegel, *Cell. Mol. Biol.* **1993**, *39*, 389–396; d) F. Haber, J. Weiss, *Proc. R. Soc. London Ser. A* **1934**, *147*, 332. e) K. Becker, M. Gui, A. Traxler, C. Kirsten, R. H. Schirmer, *Histochem.* **1994**, *102*, 389–396.
[13] a) R. Richmond, B. Halliwell, *J. Inorg. Biochem.* **1982**, *17*, 95–107; b) B. Bayer, A. Dieckmann, K.-G. Fritsch, R. Kientsch, D. von Cunow, D. T. Spira, R. H. Schirmer, A. Wendel, A. Jung, *Biol. Chem. Hoppe-Seyler* **1984**, *365*, 965.
[14] a) T. Vulliamy, P. Mason, L. Luzzatto, *Trends Genet.* **1992**, *8*, 138–143; b) M. Chevion, T. Novak, G. Glaser, J. Mager, *Eur. J. Biochem.* **1982**, *127*, 405–409; c) S. K. Martin, *Parasitol. Today* **1994**, *10*, 251–252.
[15] a) H. Atamni, H. Ginsburg, *Molec. Biochem. Parasitol.* **1993**, *61*, 231–242; b) C. W. Wright, I. D. Phillipsen, G. C. Kirby, D. C. Warhurst, M. A. Huffman, W. Ohigashi, *Proc. 5th Malaria Meeting* (Oxford) **1993**, *22*.
[16] R. H. Schirmer, R. L. Krauth-Siegel, G. E. Schulz in *Glutathione, Part A* (Eds.: D. Dolphin, R. Poulson, O. Avramovic), Wiley, New York, **1989**, pp. 553–596.
[17] Y. Zhang, E. Hempelmann, R. H. Schirmer, *Biochem. Pharmacol.* **1988**, *37*, 855–860.
[18] A. Holmgren, *J. Biol. Chem.* **1979**, *254*, 3672–3678.
[19] a) C. H. Williams, Jr. in *Chemistry and Biochemistry of Flavoenzymes, Vol. III* (Ed. F. Müller), CRC, Boca Raton, FL, **1992**, pp. 121–211; b) T. Ishikawa, *Trends Biochem. Sci.* **1992**, *17*, 463–468.
[20] R. H. Schirmer, G. E. Schulz in *Pyridine Nucleotide Coenzymes, Part B* (Eds.: D. Dolphin, R. Poulson, O. Avramovic), Wiley, New York, **1987**, pp. 333–379.
[21] A. H. Fairlamb, *Parasitology* **1989**, *99*, 93–112.
[22] A. H. Fairlamb, A. Cerami, *Annu. Rev. Microbiol.* **1992**, *46*, 695–729.
[23] R. L. Krauth-Siegel, R. H. Schirmer, *Nachr. Chem. Tech. Lab.* **1989**, *37*, 1026–1034.
[24] A. H. Fairlamb, P. Blackburn, P. Ulrich, B. T. Chait, A. Cerami, *Science* **1985**, *227*, 1485–1487.
[25] S. L. Shames, A. H. Fairlamb, A. Cerami, C. T. Walsh, *Biochemistry* **1986**, *25*, 3519–3526.
[26] R. L. Krauth-Siegel, B. Enders, G. B. Henderson, A. H. Fairlamb, R. H. Schirmer, *Eur. J. Biochem.* **1987**, *164*, 123–128.
[27] a) D. J. Steenkamp, H. S. C. Spies, *Eur. J. Biochem.* **1994**, *223*, 43–50; b) H. S. C. Spies, D. J. Steenkamp, *ibid* **1994**, *224*, 203–213; c) E. G. S. Carnieri, S. N. J. Moreno, R. Docampo, *Mol. Biochem. Parasitol.* **1993**, *61*, 79–86.
[28] A. H. Fairlamb, G. B. Henderson, A. Cerami, *Proc. Natl. Acad. Sci. USA* **1989**, *86*, 2607–2611.
[29] M. C. Jockers-Scherübl, R. H. Schirmer, R. L. Krauth-Siegel, *Eur. J. Biochem.* **1989**, *180*, 267–272.
[30] a) T. Godal, *TDR news* (Ed.: World Health Organization), **1992**, *38*, 1–2; b) S. Majumder, J. J. Wirth, A. J. Bitonti, P. P. McCann, F. Kierszenbaum, *J. Parasitol.* **1992**, *78*, 371–374.
[31] R. L. Krauth-Siegel, H. Lohrer, U. S. Bücheler, R. H. Schirmer in *Biochemical Protozoology* (Eds.: G. H. Coombs, M. North), Taylor and Francis, London, **1991**, pp. 493–505.
[32] S. Kutner, W. V. Breuer, H. Ginsburg, S. B. Aley, Z. I. Cabantchik, *J. Cell. Physiol.* **1985**, *125*, 521–527.
[33] a) R. L. Krauth-Siegel, R. Blatterspiel, M. Saleh, E. Schiltz, R. H. Schirmer, R. Untucht-Grau, *Eur. J. Biochem.* **1982**, *121*, 259–267; b) P. A. Karplus, G. E. Schulz, *J. Mol. Biol.* **1987**, *195*, 701–729.
[34] P. A. Karplus, G. E. Schulz, *J. Mol. Biol.* **1989**, *210*, 163–180.
[35] P. A. Karplus, R. L. Krauth-Siegel, R. H. Schirmer, G. E. Schulz, *Eur. J. Biochem.* **1988**, *171*, 193–198.
[36] M. Bilzer, R. L. Krauth-Siegel, R. H. Schirmer, T. P. Akerboom, H. Sies, G. E. Schulz, *Eur. J. Biochem.* **1984**, *138*, 373–378.
[37] E. F. Pai, G. E. Schulz, *J. Biol. Chem.* **1983**, *258*, 1752–1757.
[38] a) U. S. Bücheler, D. Werner, R. H. Schirmer, *Nucleic Acids Res.* **1992**, *20*, 3127–3133; b) B. Leistler, R. N. Perham, *Biochemistry* **1994**, *33*, 2773–2781.
[39] J. Kuriyan, X. P. Kong, T. S. R. Krishna, R. M. Sweet, N. J. Murgolo, H. Field, A. Cerami, G. B. Henderson, *Proc. Natl. Acad. Sci. USA* **1991**, *88*, 8764–8768.
[40] a) W. N. Hunter, S. Bailey, J. Habash, S. J. Harrop, J. R. Helliwell, T. Aboagye-Kwarteng, K. Smith, A. H. Fairlamb, *J. Mol. Biol.* **1992**, *227*, 322–333; b) S. Bailey, K. Smith, A. H. Fairlamb, W. N. Hunter, *Eur. J. Biochem.* **1993**, *213*, 67–75; c) S. Bailey, K. Smith, A. H. Fairlamb, W. N. Hunter, *Acta Crystallogr. B* **1994**, *50*, 139–154.
[41] F. X. Sullivan, S. B. Sobolov, M. Bradley, C. T. Walsh, *Biochemistry* **1991**, *30*, 2761–2767.
[42] C. B. Lantwin, I. Schlichting, W. Kabsch, E. F. Pai, R. L. Krauth-Siegel, *Proteins Struct. Funct. Genet.* **1994**, *18*, 161–173.
[43] a) R. L. Krauth-Siegel, E. M. Jacoby, C. B. Lantwin in *Flavins and Flavoproteins, Vol. 11* (Ed.: K. Yagi), de Gruyter, Berlin, **1993**, pp. 258–268; b) R. L. Krauth-Siegel, R. Schöneck, *FASEB J.* **1995**, in press.
[44] M. Bradley, U. S. Bücheler, C. T. Walsh, *Biochemistry* **1991**, *30*, 6124–6127.
[45] G. B. Henderson, N. J. Murgolo, J. Kuriyan, K. Osapay, D. Kominos, A. Berry, N. S. Scrutton, N. W. Hinchliffe, R. N. Perham, A. Cerami, *Proc. Natl. Acad. Sci. USA* **1991**, *88*, 8769–8773.
[46] a) T. J. Benson, J. H. McKie, J. Garforth, A. Borges, A. H. Fairlamb, K. T. Douglas, *Biochem. J.* **1992**, *286*, 9–11; b) K.-G. E. Fritsch, *Biol. Chem. Hoppe-Seyler* **1982**, *363*, 1302; c) E. M. Jacoby, I. Schlichting, R. L. Krauth-Siegel, unpublished.
[47] a) K. Becker, R. I. Christopherson, W. B. Cowden, N. H. Hunt, R. H. Schirmer, *Biochem. Pharmacol.* **1990**, *39*, 59–65; b) A. Schönleben-Janas, P. Kirsch, P. Mittl, R. H. Schirmer, R. L. Krauth-Siegel, unpublished.
[48] D. H. Williams, J. P. L. Cox, A. J. Doig, M. Gardner, U. Gerhard, P. T. Kaye, A. R. Lal, I. A. Nicholls, C. J. Salter, R. C. Mitchell, *J. Am. Chem. Soc.* **1991**, *113*, 7020–7030.
[49] D. H. Williams, *Proc. Natl. Acad. Sci. USA* **1993**, *90*, 1172–1178.
[50] G. E. Schulz, R. H. Schirmer, *Principles of Protein Structure*, Springer, New York, **1979**.
[51] G. E. Schulz, *Biol. Unserer Zeit* **1984**, *4*, 121–124.
[52] C. T. Walsh in *Modern Design of Antimalarial Drugs* (Ed.: World Health Organization), WHO, Geneva, **1982**, pp. 95–109.
[53] a) M. R. Davis, K. Kassahun, C. M. Jochheim, K. M. Brandt, T. A. Baillie, *Chem. Res. Toxicol.* **1993**, *6*, 376–383; b) K. Becker, R. H. Schirmer, *Methods Enzymol.* **1994**, in press.
[54] a) P. A. Karplus, G. E. Schulz, *J. Mol. Biol.* **1989**, *210*, 163–180; b) W. Janes, G. E. Schulz, *Biochemistry* **1990**, *29*, 4022–4030.
[55] a) P. Feldhaus, T. Fröhlich, R. S. Goody, M. Isakov, R. H. Schirmer, *Eur. J. Biochem.* **1975**, *57*, 197–204; b) G. B. Henderson, P. Ulrich, A. H. Fairlamb, J. Rosenberg, M. Pereira, M. Sela, A. Cerami, *Proc. Natl. Acad. Sci. USA* **1988**, *85*, 5374–5378.
[56] T. Hibi, H. Kato, T. Nishioka, J. Oda, H. Yamaguchi, Y. Katsube, K. Tanizawa, T. Fukui, *Biochemistry* **1993**, *32*, 1548–1554.
[57] a) S. E. Francis, I. Y. Gluzman, A. Oksman, A. Knickerbocker, R. Mueller, M. L. Bryant, D. R. Sherman, D. G. Russell, D. E. Goldberg, *EMBO J.* **1994**, *13*, 306–317; b) T.-H. Jessen, R. Hilgenfeld, *Angew. Chem.* **1992**, *104*, 862–863; *Angew. Chem. Int. Ed. Engl.* **1992**, *31*, 848–849.
[58] W. McClements, G. Yamanaka, V. Garsky, H. Perry, S. Bacchetti, R. Colonno, R. B. Stein, *Virology* **1988**, *162*, 270–273.
[59] A. Nordhoff, U. S. Bücheler, D. Werner, R. H. Schirmer, *Biochemistry* **1993**, *32*, 4060–4066.
[60] N. Li, A. Batzer, R. Daly, V. Yajnik, E. Skolnik, P. Chardin, D. Bar-Sagi, B. Margolis, J. Schlessinger, *Nature (London)* **1993**, *363*, 85–88.

[61] T. Wieland in *Peptides of Poisonous Aminita Mushrooms* (Ed.: T. Wieland), Springer, New York, **1986**, pp. 22–100.
[62] R. S. Struthers, G. Tanaka, S. C. Koerber, T. Solmajer, E. L. Baniak, L. M. Gierasch, W. Vale, J. River, A. T. Hagler, *Proteins Struct. Funct. Genet.* **1990**, *8*, 295–304.
[63] R. Hirschmann, *Angew. Chem.* **1991**, *103*, 1305–1330; *Angew. Chem. Int. Ed. Engl.* **1991**, *30*, 1278.
[64] A. Giannis, T. Kolter, *Angew. Chem.* **1993**, *105*, 1303–1326; *Angew. Chem. Int. Ed. Engl.* **1993**, *32*, 1244–1267.
[65] R. A. Wiley, D. H. Rich, *Med. Res. Rev.* **1993**, *13*, 327–348.
[66] D. Voet, J. G. Voet, *Biochemistry*, Wiley, New York, **1990**, pp. 382–389; *Biochemie*, VCH, Weinheim, **1992**, pp. 376–382.
[67] a) N. S. Scrutton, A. Berry, R. N. Perham, *Nature (London)* **1993**, *343*, 38–43; b) I. Willner, E. Katz, A. Riklin, R. Kasher, *J. Am. Chem. Soc.* **1992**, *114*, 10965–10966; c) S. M. Brocklehurst, Y. N. Kalia, R. N. Perham, *Trends in Biochem. Sci.* **1994**, *19*, 360–361.
[68] W. P. Jencks, *Proc. Natl. Acad. Sci. USA* **1981**, *78*, 4046–4050.
[69] C. N. Pace, U. Heinemann, U. Hahn, W. Saenger, *Angew. Chem.* **1991**, *103*, 351–369; *Angew. Chem. Int. Ed. Engl.* **1991**, *24*, 71–80.
[70] D. H. Williams, *Aldrichim. Acta* **1991**, *24*, 71–80.
[71] L. Serrano, J. L. Neira, J. Sancho, A. R. Fersht, *Nature (London)* **1992**, *356*, 453–455.
[72] S. Dao-pin, U. Sauer, H. Nicholson, B. W. Matthews, *Biochemistry* **1991**, *30*, 7142–7153.
[73] T. Dandekar, P. Argos, *Prot. Eng.* **1992**, *5*, 637–645.
[74] T. Dandekar, P. Argos, *J. Mol. Biol.* **1994**, *236*, 844–861.
[75] Z. Shakked, G. Guzikevich-Guerstein, F. Frolow, D. Rabinovich, A. Joachimiak, P. B. Sigler, *Nature (London)* **1994**, *368*, 469–473.

Design, Synthesis, and Properties of Molecule-Based Assemblies with Large Second-Order Optical Nonlinearities

Tobin J. Marks* and Mark A. Ratner*

The design, synthesis, characterization, and understanding of new molecular and macromolecular assemblies with large macroscopic optical nonlinearities represents an active field of research at the interface of modern chemistry, physics, and materials science. Challenges in this area of photonic materials typify an important theme in contemporary chemistry: to create new types of functional materials by the rational construction of supramolecular assemblies exhibiting preordained collective phenomena by virtue of "engineered" molecule–molecule interactions and spatial relationships. This review surveys several approaches to, and the microstructural and optical properties of, second-order nonlinear optical materials built from noncentrosymmetric assemblies of chromophores having large molecular hyperpolarizabilities. Such types of materials can efficiently double the frequency of incident light, exhibit other second-order nonlinear optical effects, and contribute to the knowledge base needed for new photonic device technologies. Systems described include chromophore macromolecule guest–host matrices, chromophore-functionalized glassy macromolecules, thermally crosslinked chromophore–macromolecule matrices, and intrinsically acentric self-assembled chromophoric superlattices.

Keywords: NLO materials · nonlinear optics · polymers · self-assembly · thin films

1. Introduction

One of the great challenges in contemporary chemical synthesis is the construction of multimolecular arrays with preordained collective properties by virtue of "engineered" interactions/spatial relationships between preselected constituent molecular building blocks. Although the art of chemical synthesis has advanced to the point in which many classes of complex molecules are now readily accessible, rational approaches to the production of structurally controlled multimolecular assemblies is at a far more primitive level.[1] Second-order molecule-based nonlinear optical (NLO) materials,[2] in which microstructural acentricity is a key design requirement, represent one such chemical challenge and are the subject of the present review. However, it must be emphasized that similar synthetic issues are relevant in the design and construction of molecular "metals"[3] and "ferromagnets",[4] as well as biomimetic photosynthetic structures,[5] self-assembling catalytic/enzymatic ensembles, and a host of other fascinating problems in supramolecular science.[1]

The large current scientific and technological interest in NLO materials[6] based upon electronically delocalized organic and metal-organic molecular chromophoric[2] building blocks stems from the demonstrated possibilities of very large nonresonant responses, ultrafast response times, low dielectric constants and dielectric losses, high optical damage thresholds, and the intrinsic tailorability of the constituent molecular structures.[2] When such materials are incorporated into glassy polymeric structures, the additional attractions of supramolecular organization, improved mechanical/dimensional stability, improved optical transparency (versus typical organic single crystals), and ready processability into thin-film waveguiding structures can be envisioned. Such characteristics are attractive for the fabrication of high-performance photonic devices for optical signal processing, telecommunications, computing, data storage; indeed the first prototype devices have recently been demonstrated.[2, 7] Needless to say, many basic scientific issues and challenges constitute the fundamental knowledge base that must be acquired before such experimental results can become viable technologies.

The purpose of this article is to review synthetic and physicochemical efforts to rationally design, construct, and understand new classes of molecule/macromolecule-based second-order NLO materials. Space limitations do not permit exhaustive discussion of all research being performed at academic and industrial laboratories worldwide. Therefore, the present discussion is necessarily selective and oriented toward the interests of the authors, focussing most heavily upon recent activities closest to the central theme of this article: construction of acentric chro-

[*] Prof. T. J. Marks, Prof. M. A. Ratner
Department of Chemistry and the Materials Research Center
Northwestern University
Evanston, IL 60208-3113 (USA)
Telefax: Int. code + (708)491-2990

mophore–polymer assemblies. As the present discussion unfolds, it will also be seen that modern quantum chemical formalisms can, and we believe should, play a key role in the design and understanding of new NLO materials. While reference to these activities is made in the present review, a full discussion of what is becoming a very active field can be found in reference.[8]

2. Origin of Molecular/Multimolecular NLO Phenomena

The fundamental relationship describing the induced change in molecular dipole moment (polarization) upon interaction with an oscillating external electric field (light) can be expressed in a power series [Eq. (a)].[2, 6] Here p_i is the electronic polariza-

$$p_i = \sum_j \alpha_{ij} E_j + \sum_{j \leq k} \beta_{ijk} E_j E_k + \sum_{j \leq k \leq l} \gamma_{ijkl} E_j E_k E_l + \ldots \qquad \text{(a)}$$

tion induced along the ith molecular axis, E_j is the jth component of the applied electric field, α is the linear polarizability, β the quadratic hyperpolarizability, and γ the cubic hyperpolarizability. The terms beyond the first describe a nonlinear response to the radiation field and account for the terminology "nonlinear optics." Importantly, the even order tensor, β, which is responsible for doubling the frequency of incident light (second harmonic generation, SHG), linear electrooptic effects, and frequency mixing, vanishes in a centrosymmetric environment.

The macroscopic polarization arising from an *array* of molecules is given by Equation (b), where the χ's are macroscopic

$$p_I = \sum_J \chi^{(1)}_{IJ} E_j + \sum_{J \leq K} \chi^{(2)}_{IJK} E_J E_K + \sum_{J \leq K \leq L} \chi^{(3)}_{IJKL} E_J E_K E_L + \ldots \qquad \text{(b)}$$

susceptibilities. The macroscopic susceptibilities are related to the corresponding molecular terms α, β, γ, etc. by local field corrections (intermolecular interactions) and the density of chromophores as in Equation (c) for frequency doubling. Here

$$\chi^{(2)}_{IJK}(-2\omega;\omega,\omega) = N \sum_{ijk} f_{Ii} f_{Jj} f_{Kk} \beta_{ijk}(-2\omega;\omega,\omega) \langle a_{Ii} a_{Jj} a_{Kk} \rangle \qquad \text{(c)}$$

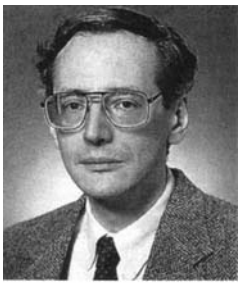
N is the number of molecules per unit volume, the f's are poorly understood local field corrections, and the a's are projectors of unit vectors along the molecular axes onto the laboratory axes.

How the second-order molecular response depends upon the frequency of input radiation (the dispersion) is an important consideration and one that only recently has been investigated in experimental detail (see Section 6). The simplest theoretical description (the "two-level model") pragmatically describes the second-order molecular response in terms of electronic charge transfer excitation between the ground state g and an electronically excited state e [Eq.(d)].[2] Here f is the oscillator strength

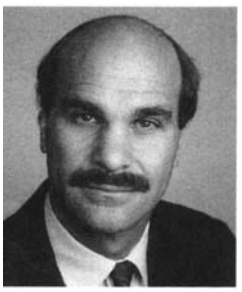
$$\beta_i(-2\omega;\omega,\omega) = \frac{3e^2}{2} \frac{\hbar\omega_{ge} f \Delta\mu_{ge}}{[(\hbar\omega_{ge})^2 - (\hbar\omega)^2][(\hbar\omega_{ge})^2 - (2\hbar\omega)^2]} \qquad \text{(d)}$$

and $\hbar\omega_{ge}$ is the energy of the charge transfer optical excitation between the ground the excited state, and $\Delta\mu_{ge}$ is the difference in dipole moment between the two states. The two-level formula predicts a pair of NLO resonances (enhancements) for each input frequency ω; one at the fundamental energy ($\hbar\omega$) and the other at twice the incident frequency ($2\hbar\omega$). Clearly the nonlinear response will be largest near these resonant frequencies; however, for actual devices it is usually desirable to avoid extensive absorption of the generated light and/or photochemical damage of the sample.

From the foregoing discussion, it can be seen that the observed nonlinear response of a material is ultimately governed by the optical characteristics of constituent molecular chromophores, the frequencies of the input radiation, and the overall



Tobin J. Marks was born in Washington, D. C., in 1944. He received a B. Sc. degree in chemistry from the Unversity of Maryland in 1966 and a Ph.D. degree in inorganic chemistry from the Massachusetts Institute of Technology in 1970, working with F. A. Cotton. He moved to Northwestern University as an assistant professor in 1970. He is currently Charles E. and Emma H. Morrison Professor of Chemistry and Professor of Materials Science and Engineering at Northwestern. His research interests include the design, synthesis, and physicochemical properties of unusual molecules and molecule-derived materials.

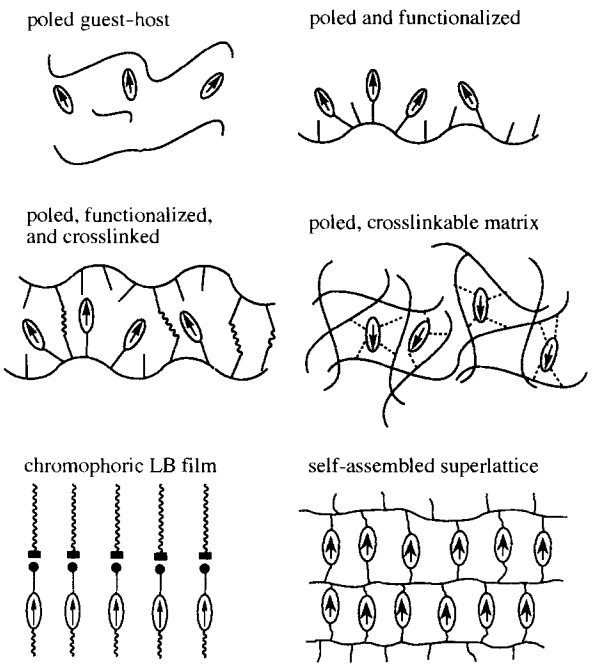


Mark A. Ratner, Professor of Chemistry at Northwestern University, was educated at Harvard, Northwestern, Aarhus, Munich, and New York. His research centers on the use of theoretical methods and insights to understand, to correlate, and to predict experimental behaviors. Current interests in his research group center on transport and mesoscopic phenomena in molecular materials.

spatial organization (e.g., noncentrosymmetry for $\chi^{(2)}$) that can be imposed upon large ensembles of these constituents. The scientific challenge here lies in devising new and more efficient approaches to the synthesis and processing of polymeric NLO systems for maximum performance characteristics as well as in developing deeper understandings of organizational and motional processes within polymer films, of interfaces between polymers and other surfaces, and of the electronic structural aspects of how single molecules and molecule ensembles interact with electromagnetic radiation.

3. General Synthetic Strategies for Polymeric NLO Materials

For polymer-based second-order ($\chi^{(2)}$) materials, the crucial synthetic problem, beyond optimizing the individual responses of the constituent chromophores (not a topic of this article), is to maximize the chromophore number density (cf., Eq.(c)), while achieving and preserving maximum acentricity of the microstructure. Various strategies to achieve these ends are depicted in Scheme 1, and will be discussed in the approximate order in which they have been investigated.



Scheme 1. Design motifs for molecular/polymer NLO materials.

One pioneering approach to polymeric second-order materials was to dissolve ("dope") NLO chromophores in glassy polymer matrices and then to align the dipolar chromophore molecules with a strong orienting electric field (poling), while heating near the matrix glass transition temperature T_g (the temperature at which the material undergoes a transition from the glassy to rubbery state).[9] The performance of such materials after cooling and removal of the electric field is limited by the low chromophore number densities which can usually be achieved before phase separation occurs and by the physical aging/structural relaxation characteristics inherent to all glassy polymers.[10, 11] These lead to loss of free volume and eventual randomization of the poling-induced preferential chromophore orientation. Hence, the SHG efficiency of such "guest–host" materials (Scheme 1 top left) is generally short-lived except in cases of extremely high matrix T_g values. In addition, we have observed that the chromophore constituents are not strongly bound in such matrices (they frequently sublime out during poling at higher temperatures) and that these materials readily undergo dielectric breakdown[12] during poling (possibly due to the mobility of ionized molecular constituents).[13]

A second traditional approach to the construction of efficient film-based SHG materials has been to incorporate NLO chromophores into acentric Y-type Langmuir–Blodgett (LB) films (Scheme 1 bottom left).[14, 15] A priori, such an approach offers far greater net chromophore alignment than is possible in a poling field (where net alignment is Boltzmann statistically determined), temporal stability of the chromophore alignment, and controlled film thickness. While recent results with LB film-based NLO films have been encouraging, significant problems appear to arise in many cases from the fragility of the films, the temporal instability of chromophore alignment (even near room temperature), the problem of scattering microdomains, and the structural regularity of layer deposition that is possible.[14, 15]

Covalently linking selected high-β chromophores to the backbones of high-T_g glassy polymers (Scheme 1 top right) potentially offers several advances over poled chromophore–polymer guest–host systems.[16] These include achieving considerably higher chromophore number densities without chromophore phase separation, greater thermal and chemical stability of the chromophore–polymer structure, and possible hindrance of dielectric breakdown processes. Moreover, initial design plans envisioned that covalent attachment to the polymer backbone might impede acentricity-degrading chromophore reorientation processes. Many of these advantages have indeed been realized (see Section 4.2 and 4.3). Nevertheless, all poled chromophore–glassy polymer ensembles are kinetically unstable with respect to relaxation to the thermodynamic equilibrium state of globally random orientation. Thus, the need for complete immobilization under the most adverse of anticipated device operating conditions (perhaps 70 °C or greater for five years; perhaps brief excursions to 300 °C or more during fabrication) has stimulated efforts to achieve even greater chemical control over polymer chain dynamics. The question was therefore asked as to whether chromophore–polymer structures could be aligned in an electric field while *simultaneously* effecting crosslinking reactions which would "lock" the chromophore units in their aligned orientations (Scheme 1 middle).[17] The progress made toward these goals will be discussed in Section 5.

A totally different strategy for the synthesis of second-order chromophore–polymer matrices is one in which artificial superlattices would be constructed in a layer-by-layer fashion using covalent self-assembly techniques (Scheme 1 bottom right).[18] In principle, such an approach could achieve far higher degrees of net chromophore alignment than electric field poling, and far greater alignment temporal stability than a typical glassy polymer which is subject to physical aging. However, such an approach places considerable demands on the design of the

appropriate chromophoric building blocks and assembly methodologies, not to mention physical characterization techniques that must provide information on the state of completion of microstructures evolving on the dimensional scale of 10–20 Å per synthetic operation. Nevertheless, such superlattices can be synthesized and preliminary data reveals structural regularity and *very large* $\chi^{(2)}$ responses (see Section 6).

In the following sections we survey by class, some highlights in the synthesis and characterization of the second-order chromophore–polymer structure classes introduced above.

4. Poled Chromophore-Functionalized Polymers

4.1. Response of Functionalized Polymer to Electric Field Poling

The response of embedded chromophores to a poling field has been described by Singer et al. for the simplified case of isolated molecules in the gas phase ("the oriented chromophore gas model", Eqs. (e) and (f)).[9a, b] An excellent overview of the

$$d_{33} = 1/2[Nf^{2\omega}f^{\omega}f^{\omega}\beta_{zzz}L_3(p)] \quad \text{(e)}$$

$$p = \frac{f^0\mu E_p}{kT} \quad \text{(f)}$$

theory can be found in reference [2g]. Here d_{33} is the second harmonic index (formally $1/2\ \chi^{(2)}_{333}(-2\omega;\omega,\omega)$), which expresses the efficiency of second harmonic generation by the material (two input photons of frequency ω produce an output photon of frequency 2ω) and $L_3(p)$ is the third order Langevin function. The 3-axis is the uniaxial axis defined by the direction of the poling field [Eqs. (g)–(i); $P^{2\omega}$ is the second harmonic polarization].[6] It is assumed that the poled glassy thin film is uniaxial and belongs to point group ∞mm. It can be shown by symmetry that $d_{31} = d_{15}$. It is pragmatically assumed that the chromophore molecules are rodlike with the dipole moment along the molecular long axis and that β_{zzz} (z refers to the molecular axis) is the only nonzero element of the molecular hyperpolarizability tensor. N in Equation (e) is again the chromophore number density, the f stands for the local field (environmental) factor at the indicated frequencies, μ in Equation (f) is the chromophore dipole moment, and E_p is the poling field. This noninteracting chromophore model also predicts that $d_{33} = 3d_{31}$.

$$P_x^{2\omega} = 2d_{15}E_xE_z \quad \text{(g)}$$

$$P_y^{2\omega} = 2d_{15}E_yE_z \quad \text{(h)}$$

$$P_z^{2\omega} = d_{31}E_x^2 + d_{31}E_y^2 + d_{33}E_z^2 \quad \text{(i)}$$

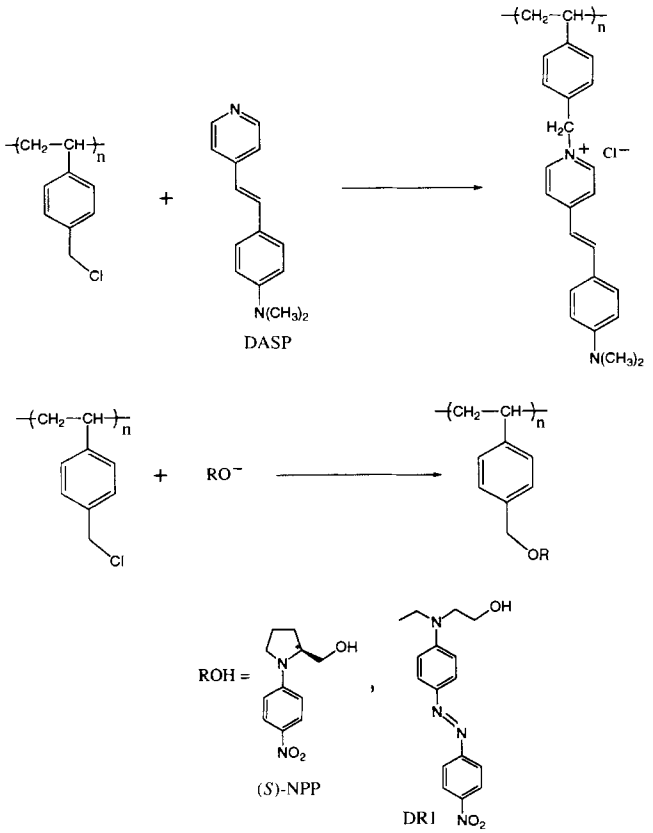
In terms of chromophore design, Equations (e) and (f) predict that β_{zzz} and μ should be maximized for optimum NLO response. While the applicability of Equations (e) and (f) to real systems is an important, incompletely resolved question, chemically oriented semiempirical formalisms are now available that allow efficient computation and origin analysis of β_{ijk}, μ, and λ_{max} (the latter is crucial for laser compatibility optimization) for both organic and metal-organic chromophore molecules, without resort to tedious empirical synthetic efforts.[8, 19] The degree to which d_{33} conforms to Equations (e) and (f) is most relevant at (desired) high N values, where chromophore–chromophore interactions become non-negligible. The macroscopic aspects of these effects are addressable by synthesis, spectroscopy, and poling/NLO characterization (see Section 4.2 and 4.3). Theoretical studies on multichromophore clusters have also proven valuable in analyzing the consequences of close, chromophore–chromophore interactions in determining β for local clusters.[20] These are summarized in another review.[8] The "oriented chromophore gas" model must also be generalized for high chromophore number densities, where the orientations may be attenuated by interchromophore dipolar interactions.[21]

The most detrimental aspect of chromophore–chromophore interactions is likely to be the formation of statistically centrosymmetric aggregates when N becomes large. One way to frustrate this might be to employ chiral chromophores, since chiral molecules must necessarily crystallize in acentric space groups.[2] The importance of chromophore–chromophore interactions can also be probed by comparing the properties of polymers functionalized with both homochiral and racemic chromophore molecules (see Section 4.2). Another issue in chromophore design arises when immobilizing, crosslinking processes are desired. Synthetic approaches must imbue the chromophores with chemical functionality appropriate for crosslinking, with both protected and unmasked forms of the crosslinking functional groups ideally available. Needless to say, useful chromophores should have acceptable environmental stability.

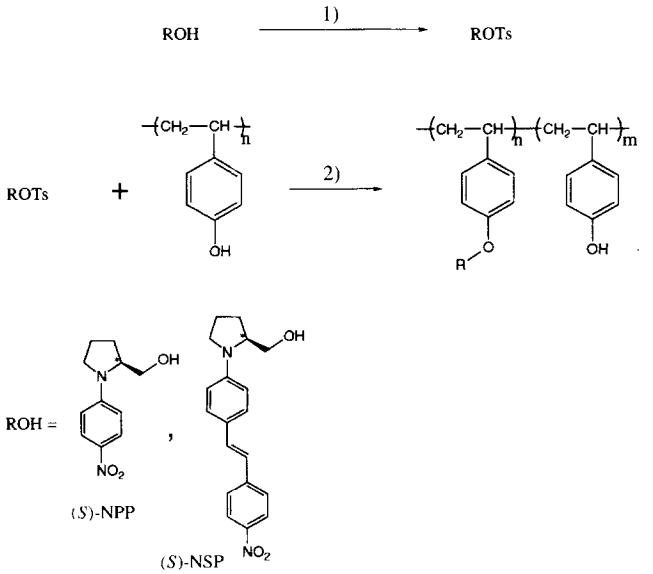
Polymer backbones suitable for NLO chromophore functionalization should have good film-forming characteristics, good optical transparency (preferably amorphous microstructures), appropriate reactivity for functionalization and/or crosslinking, good environmental stability (including dielectric breakdown strength), and minimum microstructural mobility (as judged by T_g, T_β (T_β = the temperature of the highest secondary transition, frequently associated with side-group rotations), and other chain/sidechain motional indices).

4.2. Poled Polystyrenes and Related Backbones

Initial systems investigated included functionalized polystyrenes derived from chloromethylated polystyrene (PS)[16] and functionalized poly(*para*-hydroxystyrene)[13a] (PHS). The former was straightforwardly functionalized with the high-β chromophore Disperse Red 1 (DR1) and the chiral prolinol chromophores NPP by a Williamson ether synthesis, while a saltlike, high-β stilbazolium group (DASP) was introduced by quaternization (Scheme 2). PHS forms tenacious coatings on many substrates and exhibits higher T_g values than PS (ca. 155–180 °C vs. ca. 105 °C, presumably due to the extensive hydrogen bonding network)[22] and can be readily functionalized using the *para*-toluenesulfonates of chiral (*S*)-NPP[17c, 23, 24a, b] and (*S*)-NSP[24c, d] (Scheme 3) in yields of up to about 90% of the phenol groups. Table 1 summarizes d_{33} and other data for these polymers subsequent to film casting, annealing (to remove volatile impurities), and poling by either contacting electrodes or a corona discharge.[25] (The former allows more precise control of the poling field but is more subject to film dielectric breakdown.



Scheme 2. Synthesis of chromophore-functionalized polystyrenes.



Scheme 3. Synthesis of chromophore-functionalized PHS. 1) *p*TsCl, pyridine, 0 °C; 2) NaH, N-methylpyrrolidone (NMP).

The latter achieves greater but less readily quantified poling fields, but may leave small amounts of residual charge on the surface.[10c] Importantly, largely nonresonant (cf. Eq. (e)) d_{33} values (up to 80×10^{-9} esu) considerably in excess of the d_{36} of KH_2PO_4 (1.1×10^{-9} esu) and the d_{31} of $LiNbO_3$ (14.2×10^{-9} esu) can be achieved. At high functionalization levels, the chromophore number density of NPP-PHS is about 60% of that of crystalline NPP.[23]

Table 1. SHG coefficients for chromophore-functionalized polystyrenes [a].

Material	Functionalization level (% phenyl rings)	$d_{33}\times10^9$ [esu] [b]
(PS)CH_2-DR1	12.5	2.7 [c]
(PS)CH_2-DASP	4.5	0.12 [c]
(PS)CH_2-(*S*)-NPP	36.0	3.8 [c]
(*S*)-NPP-PHS	16	13 [d]
(*S*)-NPP-PHS	36	45 [d]
(*S*)-NPP-PHS	48	58 [d]
(*S*)-NPP-PHS	62	66 [d]
(*S*)-NPP-PHS	75	72 [d]
(*S*)-NPP-PHS	90	80 [d]
(*S*)-NSP-PHS	42	50 [d]
(*S*)-NSP-PHS	77	160 [d]

[a] Measured within 30 min of poling; $\lambda = 1064$ nm. [b] Experimental SHG coefficients. [c] Contact poling; $E_p = 0.8-1.2$ MVcm^{-1}. [d] Corona poling; $E_p = 3-4$ MVcm^{-1}.

The (*S*)-NPP-PHS model system[17c, 24a, b] has been studied in detail with respect to the validity of the chromophore gas model. There is an approximately linear relationship between d_{33} and N, which is *independent* of whether the chromophore is homochiral or racemic (Fig. 1). The form of Equations (e) and

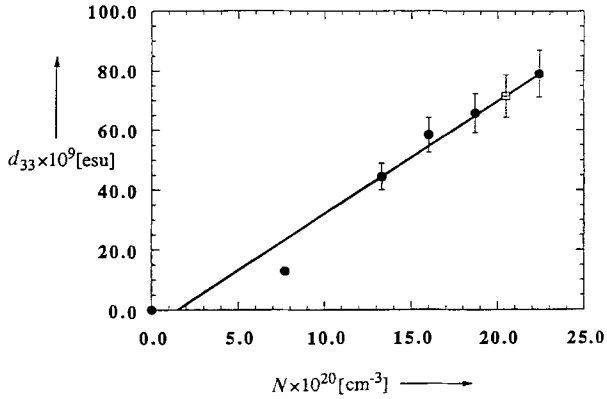


Fig. 1. SHG coefficients of (*S*)-NPP-PHS films poled at 0.3 MVcm^{-1} as a function of chromophore number density N. The value marked with ⊟ is for a polymer prepared from racemic NPPOH.

(f) also predicts that d_{33} will scale linearly with poling field at relatively low fields, but will saturate when $f^0\mu E_p \approx kT$. This point will be reached in the case of the (*S*)-NPP-PHS model system when $E_p > 1.3$ MVcm^{-1} and Figure 2 shows that d_{33} does indeed "saturate" at higher poling fields. While these NLO results and transmission optical spectra are in accord with minimal chromophore–chromophore interaction effects, various polymer dynamic properties are markedly sensitive to the chromophore functionalization level (see Fig. 3a).

Figure 3 shows d_{33} temporal stability data for representative poled (*S*)-NPP-PHS films. Four factors influence the rate of SHG decay: 1. Traces of residual solvent (THF) are detected by FT-IR spectroscopy and have a plasticizing effect on the polymer matrix (verified by DSC). Annealing the films at high temperatures removes THF and enhances the temporal stability. 2. Increasing chromophore functionalization levels has a deleteri-

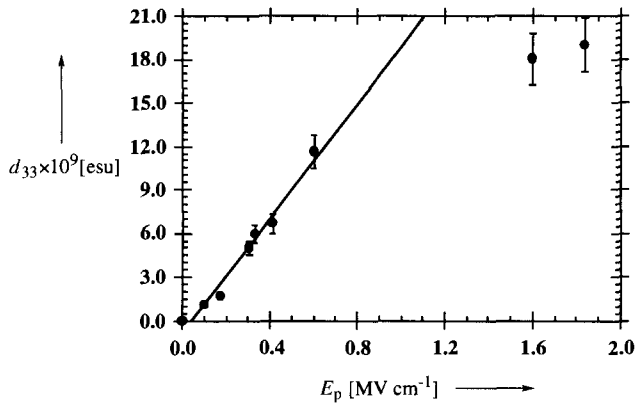


Fig. 2. SHG coefficient of (*S*)-NPP-PHS films (48% chromophore functionalization level) as a function of contact poling field, E_p. The line is a least-squares fit to the low-field data points.

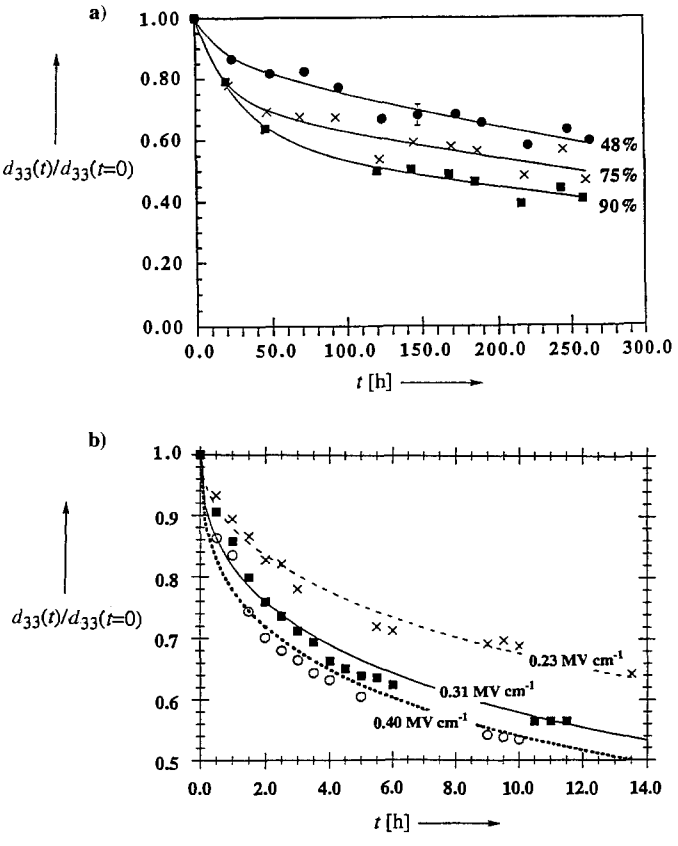


Fig. 3. a) The effect of the functionalization level on the SHG temporal characteristics of poled (*S*)-NPP-PHS films. Samples were corona poled at 133 °C. Curves represent least-squares fits to a biexponential function [Eq. (j)]. A representative error bar is provided on the 48% (*S*)-NPP-PHS transient. Decay measurements taken at 25 °C. b) Effect of applied poling field strength on the temporal characteristics of d_{33} for a contact-poled (*S*)-NPP-PHS film (36% functionalization level) after cessation of poling. Electric field poling was terminated at $t = 0$. Lines through data points represent nonlinear least-squares fit to Equation (j).

ous effect on d_{33} temporal stability (Fig. 3a), and enhanced mobility of the chain structure is also mirrored in falling T_g values and FT-IR spectroscopic evidence for diminished ArOH ··· HOAr hydrogen bonding.[13, 24] 3. Increasing poling field magnitudes, which displace the microstructure in increasing degrees from thermodynamic equilibrium, also result in lowered d_{33} temporal stability (Fig. 3b; greater driving force to return to equilibrium). 4. Physical aging of the film in the poling field and attendant reduction in free volume leads to enhanced d_{33} temporal stability.[24a, b]

Data of the type shown in Figure 3 convey much fundamental information on macromolecule dynamics and how it depends on polymer architecture, processing, physical aging, etc. In most cases, a biexponential [Eq. (j)] or phenomenological Kohlrausch–Williams–Watts (KWW) stretched exponential expression [Eq. (k)] can be successfully fit by numerical regression techniques to the $d_{33}(t)$ decay data (comparable statistical r values).[26, 27]

$$d_{33} = [Ae^{-t/\tau_1} + (1 - A)e^{-t/\tau_2}]d_{33}(0) \quad \text{(j)}$$

$$d_{33} = e^{-(t/\tau)^{\beta}}d_{33}(0)(0 < \beta \leq 1) \quad \text{(k)}$$

The biexponential expression can be viewed as a "two-state" description of chromophore reorientation dynamics, for example in liquidlike/large free volume and glasslike/small free volume matrix microenvironments.[28] The KWW expression describes the dynamics in terms of a manifold of relaxation processes.[26, 27] It will be seen that the below-T_g relaxation of most poled NLO polymers can usually be simulated by either of these simple models. Fitting (*S*)-NPP-PHS $d_{33}(t)$ data to Equation (k) yields τ and β parameters[24a, b] which reveal a strikingly narrower distribution of relaxation times and considerably reduced rotational mobility than found in typical guest–host systems.[26, 27] Similar conclusions have been reached by researchers at IBM in studies of chromophore-functionalized polyacrylates.[27e] In regard to temperature dependence, conventional liquid diffusion-like descriptions for polymer motion such as the Williams–Landel–Ferry (or equivalent Vogel–Tamman–Fulcher) equation [Eq. (l); where τ is the relaxation

$$\lg\frac{\tau(T)}{\tau(T_g)} = \frac{-C_1(T - T_g)}{C_2 + (T - T_g)} \quad \text{(l)}$$

time; and C_1, C_2 arbitrary, but well-studied constants] are not strictly applicable to systems far below T_g.[27] Apparent activation energies for chromophore reorientation above T_g in (*S*)-NPP-PHS[24a, b] are considerably greater than in typical guest–host materials.[26, 27] Application of Equation (l) argues that poled polymer T_g values must be in excess of 250–300 °C for practical device lifetimes at operating temperatures on the order of 70 °C.[27e] The development of polymer dynamic theories applicable to the present NLO polymer systems is in an early stage.

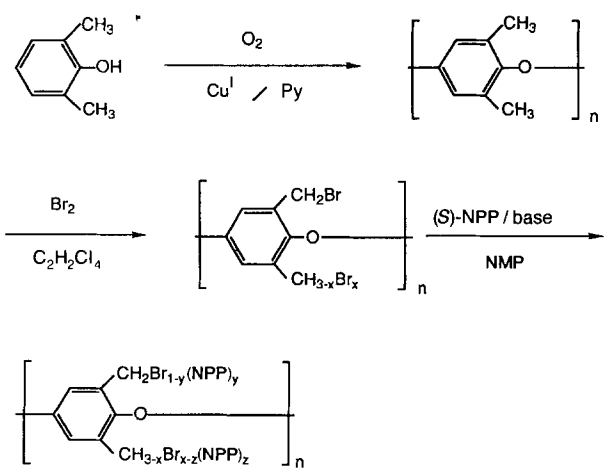
In contrast to the above findings on chromophore-functionalized (*S*)-NPP-PHS, attempts to prepare NLO-active NPP + PS and NPP + PHS guest–host materials were less successful.[13] Phase separation and matrix opacity were observed at chromophore concentrations as low as about 5 mol%. Dielectric breakdown was frequently observed at low poling fields, and d_{33} decay was more rapid than all but the most highly functionalized/lowest T_g NPP-PHS matrices.

(*S*)-NSP-PHS (Scheme 3) specimens have also been prepared over a range of functionalization levels.[24c, d] T_g parame-

ters are as high as 185 °C and corona-poled film d_{33} values (partly resonant-enhanced) are as high as about 160×10^{-9} esu (Table 1).[24c, d]

4.3. Polyphenylene Ethers

Holding the (*S*)-NPP chromophore moiety constant, polyphenylene ethers have been investigated with the goal of learning the effects of increasing matrix T_g values, while achieving similar or higher chromophore number densities than the NPP-PHS system. Poly(2,6-dimethyl-1,4-phenylene oxide) (PPO) is a high-strength, amorphous engineering thermoplastic with T_g about 205–210 °C and excellent film-forming characteristics.[29] PPO can be prepared by the oxidative coupling of 2,6-dimethylphenol[30] (Scheme 4). Bromination[31] yields



Scheme 4. Synthesis of chromophore-functionalized PO.

PPO-Br_x materials with functionalization levels on the order of 1.6–1.8 Br per repeat unit. (*S*)-NPP can then be introduced as shown in Scheme 4 to obtain 1.4–1.6 NPP per repeat unit with T_g values near 173 °C.[32] Film casting followed by annealing and either contact or corona poling affords nonresonant d_{33} values as high as 65×10^{-9} esu. Assuming approximate additivity of PPO and NPP densities, it is estimated that the chromophore number densities are about 70% of that of crystalline (*S*)-NPP.

SHG temporal stability data for representative poled (*S*)-NPP-PPO films are shown in Figure 4. Fitting a biexponential expression to the data [Eq. (j)] yields rather large τ_2 values, especially for the contact-poled film (ca. 400 days).[32] In situ SHG poling experiments have also been carried out on NPP-PPO films.[32] Importantly, chromophore orientational response begins far below the experimental T_g value. Furthermore, d_{33} increases more rapidly as T_g is approached (in accord with greater polymer mobility) and reaches a maximum as the temperature begins to decrease (in accord with the temperature-dependence of Equations (e) and (f)).

Slab waveguiding structures have been fabricated from (*S*)-NPP-PPO films.[32] Using standard prism coupling techniques, two TE modes are observed. The refractive index at 0.633 μm

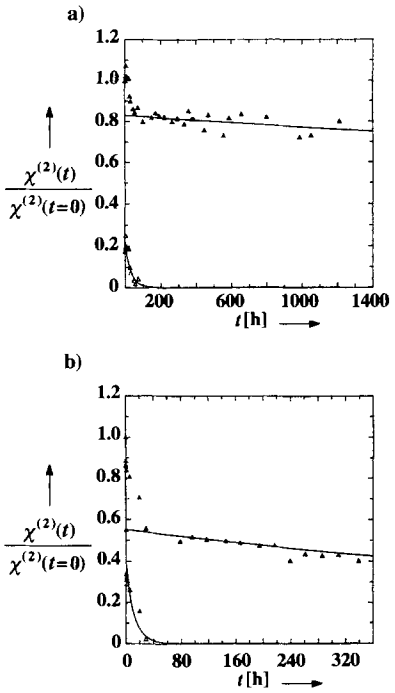


Fig. 4. Temporal characteristics of the SHG coefficient of (*S*)-NPP-PPO films (1.43 NPP moieties per repeat unit). Decay data taken at 25 °C. The solid lines each show the two exponential components of the least-squares fit of Equation (j). a). Contact poled at 2.1 $MVcm^{-1}$; b) corona poled.

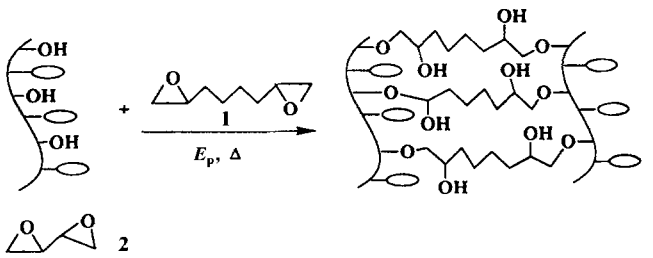
is 1.584 ± 0.001 and the loss coefficient, α, is estimated to be $\leq 1\ dBcm^{-1}$ at $= 0.633\ \mu m$ (dB = decibel). This degree of transparency is compatible with waveguiding device requirements.[7]

5. Poled, Thermally Crosslinked NLO Polymers

Further chemical control over the randomization of poling aligned chromophore dipoles can be achieved by "locking" them in place simultaneous with poling. Thermal crosslinking of polymer structures is known to effect the densification/vitrification/free volume decrease of reactive matrices to a degree that can be controlled by the temperature and duration of curing. Initially, this approach was pursued with chromophore-functionalized PHS[17c] and with chromophore-embedded matrices; however, impressive advances have also been achieved by other groups using complementary strategies (see Sections 5.2–5.4).[17a, b, 33] Several other dividends of this approach include greater film resistance to dielectric breakdown, cracking, and delamination.

5.1. Crosslinked, Chromophore-Functionalized Polystyrenes

Films of (*S*)-NPP-PHS were cast from solutions also containing 1,2,7,8-diepoxyoctane (**1**, DEO) or 1,2,3,4-diepoxybutane (**2**), (Scheme 5).[17c, 24a] Optimum epoxy crosslinking conditions[34, 35] can be established by parallel experiments in which the ring-opening process is monitored by FT-IR spectroscopy[36] of films cast on KBr plates. The films from NPP-



Scheme 5. Simultaneous poling and crosslinking of chromophore-functionalized PHS.

PHS and **1** or **2** were partially cured at 100 °C for 1 h and then at 100 °C and 10^{-4} Torr for 24 h. This procedure brings about partial crosslinking as well as removal of residual traces of solvent and other plasticizing volatiles. The annealed NPP-PHS films were next corona poled at 180 °C for 1 h. For optimum polymer/diepoxide stoichiometries (see Fig. 6), such conditions induce high degrees of crosslinking, while as noted above, corona poling provides higher electric fields than contact poling techniques without ready dielectric breakdown. The poled films were then cooled to room temperature and physically aged for 1 h prior to removal of the corona field. The crosslinked films are impervious to organic solvents and more resistant to cracking than noncrosslinked films. Good transparency characteristics are illustrated by the successful fabrication of waveguides of the type described in Section 4.3 for NPP-PPO.

SHG temporal decay data for the poled, crosslinked NPP-PHS films were fit by least-squares techniques to the aforementioned, phenomenological biexponential expression of [Eq. (j)]. In Table 2 are set out d_{33}, τ_1, τ_2 data for NPP-PHS films as a

Table 2. SHG coefficients (d_{33}) and temporal decay parameters for corona-poled, NPP-PHS films as a function of thermal crosslinking [a].

Crosslinking agent	Diepoxide/ OH [b]	$d_{33} \times 10^9$ [esu] [c]	τ_1 [days] [d]	τ_2 [days] [e]
-	-	8.8	26	30
-	-	8.6 [f]	36 [f]	26 [f]
1	0.50	7.0	79	100
2	0.25	3.8	18	74
2	0.50	5.5	20	53
2	0.75	2.1	11	51
2	1.00	1.4	9	46

[a] Films poled at 180 °C ($E_p = 3-4$ MVcm^{-1} unless otherwise indicated. [b] Equivalents of the crosslinking reagent **1** or **2** per equivalent available phenol OH. [c] At $\lambda = 1064$ nm. [d] Short-term SHG decay constant from Equation (j). Data taken at 25 °C. [e] Long-term SHG decay constant from Equation (j). Data taken at 25 °C. [f] Poled at 150 °C.

function of crosslinking procedure. The corona-poled nonresonant d_{33} values are generally comparable to those previously achieved for contact-poled NPP-PHS samples at comparable functionalization levels. Equally important, SHG efficiency is not adversely affected by the crosslinking chemistry, except at very high levels of crosslinking agent (see Fig. 6). In regard to d_{33} temporal stability, Figure 5 compares the effects of simultaneously corona poling and crosslinking (*S*)-NPP-PHS with 0.5 equivalents **1** per available phenol OH group to two films poled in an essentially identical manner but without an epoxy

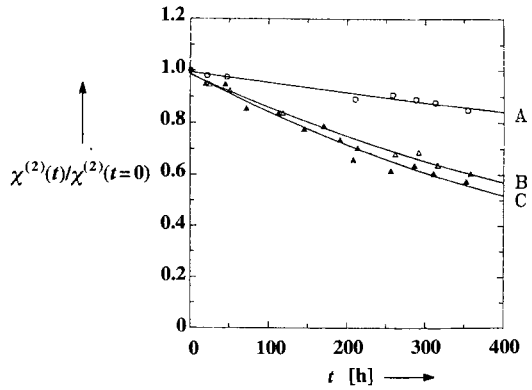


Fig. 5. Temporal characteristics of the SHG coefficient d_{33} for corona-poled (*S*)-NPP-PHS films. A: Simultaneously poled (180 °C) and crosslinked with 0.5 equiv **1** per phenol OH; B: Poled at 180 °C. C:) Poled at 150 °C. The solid lines are from fits of Equation (j).

crosslinking agent. The increase in SHG temporal stability is clearly evident and translates into 3.0-fold and 3.3-fold increases in τ_1 and τ_2, respectively. For the films that have not been crosslinked, higher poling temperatures (150–180 °C) result in a decrease in the short-term decay component of $d_{33}(t)$ versus samples annealed at lower temperatures (cf. B and C in Fig. 5). The effect of the epoxy crosslinking/densification methodology on chromophore mobility should be a complex function of crosslinking temperature, stoichiometry, and diepoxide reagent. Figure 6 shows the effect on the $d_{33}(t)$ τ_2 parameter of increasing

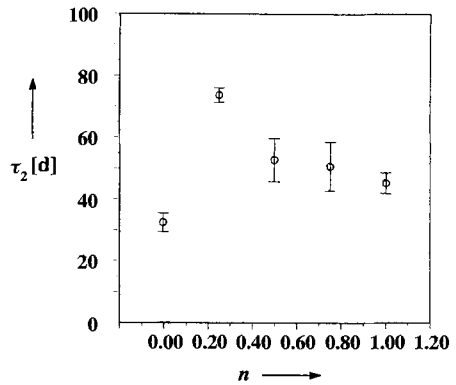
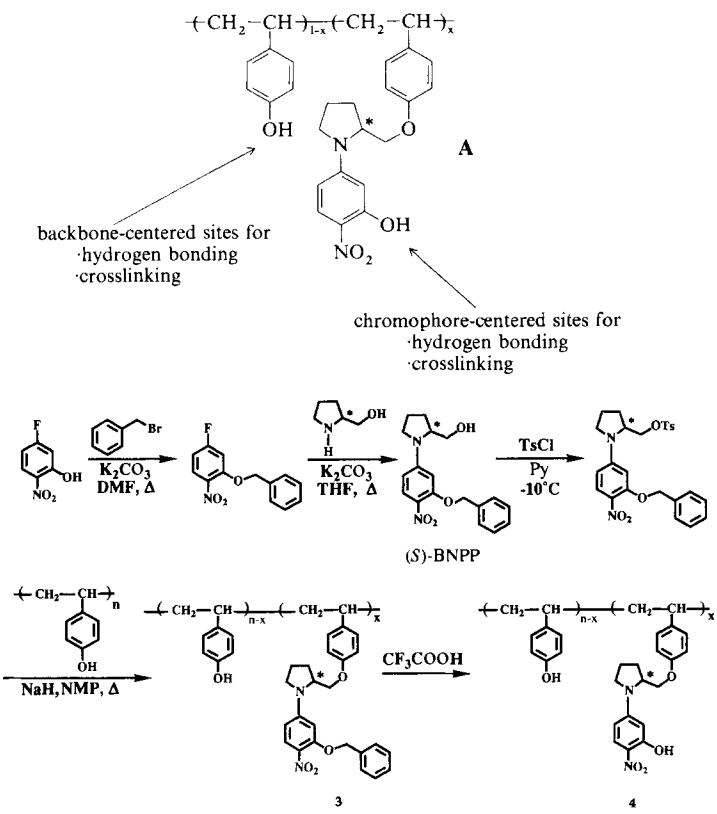


Fig. 6. Long-term SHG decay parameters [Eq. (j)] of poled (*S*)-NPP-PHS films simultaneously corona poled and crosslinked with the indicated equivalents n of **2** per available phenol OH.

the stoichiometric ratio of crosslinking agent for constant poling procedure. Note that τ_2 rises to a maximum at relatively low diepoxide to available phenol OH ratios, then declines at higher ratios. FT-IR spectroscopy reveals residual, unreacted epoxide groups (incomplete crosslinking) at the higher **2** to OH ratios, and it is reasonable that dangling, unreacted epoxide sidechains have a plasticizing effect on the matrix. At **2** to OH ratios greater than about 0.5, the matrix becomes opaque after casting and curing, indicating phase separation and leading to a decrease in measured d_{33} values.

The NPP-PHS results raise questions as to the optimum polymer architectural strategies for crosslinking (both covalent and hydrogen bonding) to achieve maximum chromophore immobi-



Scheme 6. Top: NPP-PHS polymers **A** with different crosslinking possibilities. Bottom: Synthetic approach to polymers of type **A** with site-selective hydrogen bonding or crosslinking. DMF = dimethylformamide.

lization. This issue was systematically addressed with a modified family of NPP-PHS structures **A** with both backbone only and backbone + chromophore-centered crosslinking (Scheme 6 top).[37] The synthetic approach to these polymers is shown in Scheme 6 bottom. An hydroxyl-functionalized analogue of (*S*)-NPP (HNPP), protected with a benzyl group ((*S*)-BNPP), was synthesized as shown in Scheme 6. Tosylation and reaction with deprotonated PHS yields (*S*)-BNPP-PHS (**3**). Subsequent deprotection with trifluoroacetic acid then yields (*S*)-NHPP-PHS (**4**). Polymers **3** and **4** were purified by repeated precipitation and drying under high vacuum at elevated temperatures.

Films of polymers **3** and **4** were cast from THF solutions and dried under high vacuum. Crosslinking experiments were carried out by introducing an equimolar (1:1 epoxy unit/OH group) quantity of **1** or polyepoxide **5** into the polymer/THF solutions. Optimum crosslinking conditions were established through independent experiments monitored by FT-IR spectroscopy (vide supra). All films were corona-poled (1 h, $T \geq 140\,^{\circ}C$.

In Table 3 are compiled T_g data and initial d_{33} coefficients for the films examined in this study. The T_g data reflect the consequences of benzylation (**3**), which diminishes matrix-immobilizing hydrogen bonding,[22] of increasing backbone functionalization, which not unexpectedly enhances chain mobility,[38] and of thermal epoxide crosslinking, which clearly has the greatest inhibitory effect on chain mobility. The SHG coefficients, measured at 25 °C within 10 min of cessation of poling, are relatively large, reflecting both the substantial chromophore number densities as well as the anticipated $\mu\beta_{vec}$ value (β_{vec} = vector component of β in the direction of the dipole moment) of HNPP.[37] Film d_{33} temporal characteristics for the following six HNPP-PHS-based systems are compared in Figure 7: a) no protection

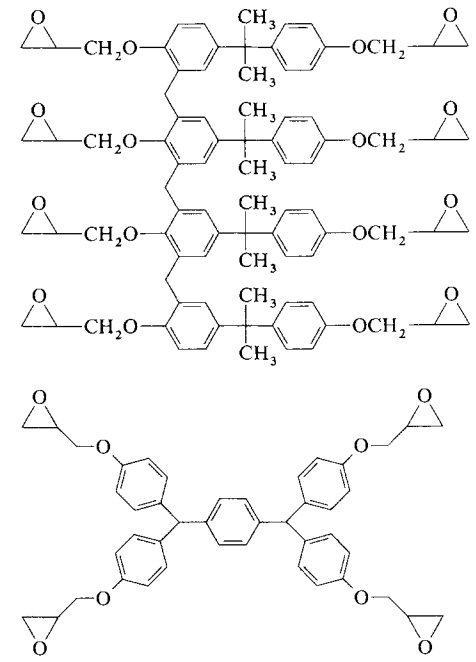


Table 3. SHG frequency doubling efficiency and temporal stability parameters for corona-poled [a] HNPP-PHS films.

Material	Functionalization level [%]	T_g [°C]	$d_{33} \times 10^9$ [esu] [b]	τ_1 [days] [c]	τ_2 [days] [c]
cross linked systems					
1 + **4**	35	144	14	35	> 1 yr
1 + **3**	35	108	24	30	> 1 yr
5 + **4**	35	152	9	4	> 1 yr
5 + **3**	35	131	14	0.4	> 1 yr
hydrogen-bonded systems					
4	35	137	22	4	120
3	35	97	23	4	80
4	88	114	34	4	110

[a] $E_p = 3\text{–}4\ MVcm^{-1}$. [b] At $\lambda = 1064$ nm. [c] See Equation (j).

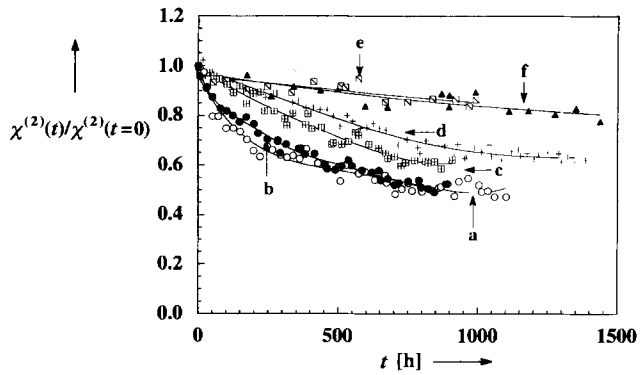


Fig. 7. Temporal characteristics at 25 °C of the SHG coefficient of six corona-poled films from **3** or **4** (35% functionalization level) having differing degrees of HNPP/PHS protection and/or either **1** or **5** crosslinking. The solid lines represent fits of Equation (j).

or crosslinking; b) HNPP protection (BNPP derivatives) but no crosslinking; c) BNPP derivatives and **1**-crosslinking at the PHS backbone hydroxyl residues only; d) **1**-crosslinking at both HNPP and PHS positions; e) BNPP derivatives and **5**-crosslinking at the PHS backbone; f) **5**-crosslinking at both HNPP and PHS positions. Several trends are evident. First, while T_g values afford a gross measure of matrix mobility, they only provide a qualitative guide to the temporal stability of SHG efficiency (cf., a) versus b)). The data also demonstrate that any ArOH ··· HOAr hydrogen bonding interactions involving the chromophore moieties have little if any effect on $d_{33}(t)$ over and above those provided by the polymer backbone OH groups. Although crosslinking at the PHS functionalities alone (c) affords a significantly lower T_g material than HNPP-PHS (a), the effect on $d_{33}(t)$ is clearly opposite and large. Bifunctional crosslinking that *directly involves* the chromophore substituent affords the greatest stabilization of SHG efficiency (and correspondingly, the highest T_g). However, it is also evident that polyepoxide crosslinkers effect the greatest degree of SHG temporal stabilization and that the effect appears less sensitive to local crosslink architecture.

The $d_{33}(t)$ data are satisfactorily fit to either biexponential [Eq. (j)] or stretched exponential [Eq. (k)] decay functions. Time constants derived from the former model are compiled in Table 3. These quantitatively amplify the above discussion, with the τ_2 values/SHG temporal stability parameters rivalling those of many stable NLO chromophore-functionalized glassy polymer systems. Fitting at the same level of confidence ($r = 0.98-0.99$) to the more phenomenological KWW stretched exponential [Eq. (k)] yields β values which support considerably higher degrees of immobilization than in NPP-PHS.[24a, b] The knowledge base from the above experiments has now been applied to crosslinking (*S*)-NSP-PHS (see Scheme 3) with polyepoxides **5** and **6**.[24c, d] T_g values as high as 260 °C have been achieved with partially resonant-enhanced d_{33} values of about 100×10^{-9} esu. As can be seen in Figure 8, the SHG temporal stability of corona-poled **6**-(*S*)-NSP-PHS films at 100 °C *in air* is excellent.

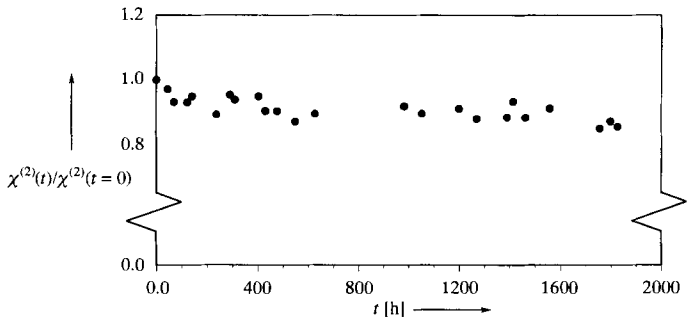
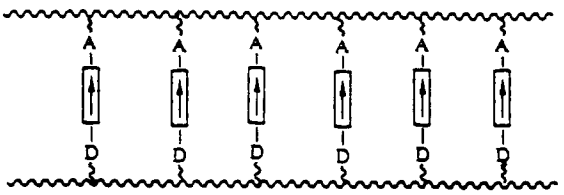


Fig. 8. Temporal characteristics of the SHG coefficient at 100 °C in air of a corona-poled (*S*)-NSP-PHS film crosslinked with polyepoxide **6**.

Dalton et al.[33b, c, g, i] have made important advances in poled second-order materials using a "double-ended" chromophore approach (**7**). As in the functionalized PHS systems, a chromophore-functionalized macromolecule (in this case, a donor–acceptor substituted azo chromophore appended to a polyacrylate) is crosslinked with a difunctional isocyanate. After corona

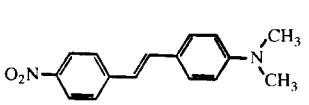


7

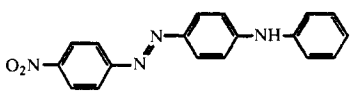
poling, impressive SHG temporal stabilities are observed at 90 °C in air, with d_{33} values (partially resonant-enhanced) of $120 \times 10^{-9}-150 \times 10^{-9}$ esu.

5.2. Embedding Chromophores in Totally Crosslinked Matrices

To determine whether NLO guest chromophores can be immobilized in highly crosslinked matrices, experiments were carried out in which high-β 4-(dimethylamino)-4′-nitrostilbene (DANS, **8**) and Disperse Orange 1 (DO1, **9**) were dispersed in an



8



9

optical grade epoxy resin, which could then be simultaneously poled and thermally cured.[17a, b] In such experiments, solutions of the chromophores were mixed with the epoxy resin and the solvent stripped from the solution. The chromophore-doped resin was next mixed with the amine crosslinker and the resulting fluid introduced between transparent ITO glass electrodes. Partial crosslinking of the matrix at 80 °C prior to poling is required to avoid dielectric breakdown. Poling fields were next gradually applied and maintained for measured periods of time at 80–150 °C. Films were cooled to room temperature prior to removal of the field. Typical d_{33} values at zero time are in the range $0.1 \times 10^{-9}-1.0 \times 10^{-9}$ esu. These magnitudes agree well with those expected for the (relatively low) chromophore number densities employed ($N = 0.4 \times 10^{19}-1.9 \times 10^{19}\,cm^{-3}$), assuming literature $\mu_z\beta_{zzz}$ values for the chromophore and the applicability of Equation (e).

The SHG temporal characteristics of the chromophore-doped/epoxy matrices depend strongly upon the crosslinking conditions. In poling field/temperature cycling experiments carried out as a function of curing time, the decay rate of d_{33} gradually declines as progressive crosslinking increases the degree of chromophore immobilization. After long curing times at 80 °C, for $d_{33}(t)$ Equation (j) yields $\tau_1 = 7$, $\tau_2 = 72$ days for the DANS-doped epoxy matrix and $\tau_1 = 8$, $\tau_2 = 142$ days for the DO1-doped epoxy matrix. The lower d_{33} decay rate of the latter matrix presumably reflects a slower reorientation rate for the larger DO1 chromophore. Furthermore, simultaneous curing and contact poling of a DO1-doped matrix at 150 °C yields a chromophoric matrix for which only minor decay in d_{33} can be detected over a period of many days at room temperature (Fig. 9).

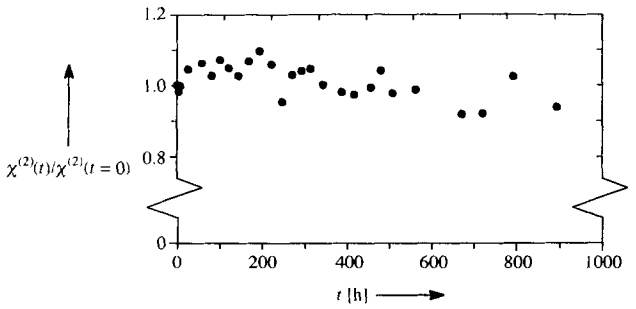
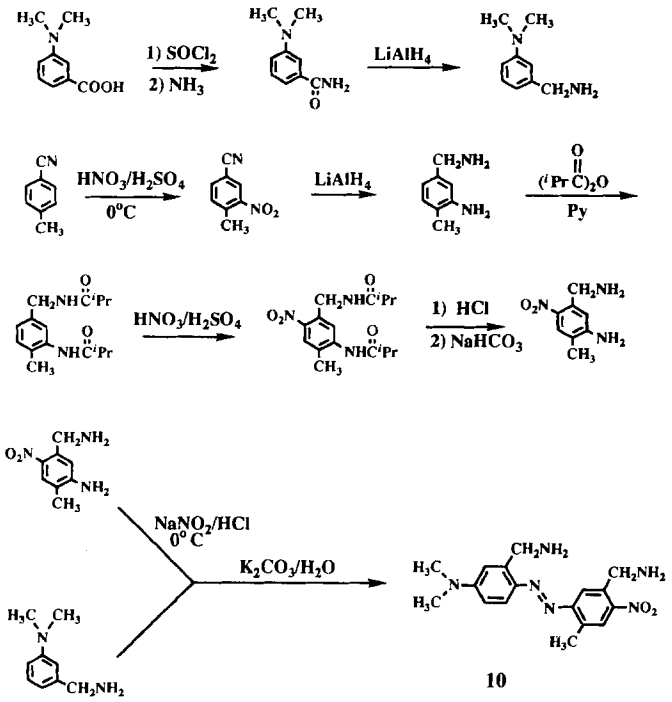


Fig. 9. Temporal characteristics at room temperature of the SHG coefficient d_{33} of epoxy films containing **9** and simultaneously corona poled and cured at 150 °C.

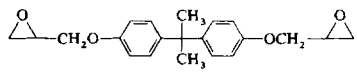
5.3. Matrices with Chromophoric Co-Monomers

While the strategy in Section 5.2 achieves significant chromophore immobilization, it also suffers from the low chromophore number densities which can be achieved. An attractive alternative would be to design a crosslinkable matrix in which one active component was a high-β chromophore molecule. Simultaneous poling and thermal crosslinking would then lead to an acentric matrix with a very high NLO chromophore number density. One synthetic approach is illustrated in Scheme 7.[39] Three design issues were addressed in the invention of **10** as a reactive co-monomer: 1) Substituted azo compounds with electron donating and accepting substituents in the 4,4′ positions were selected since such structures are known to exhibit large π-electron-based β_{vec} values. 2) Two reactive amine functionalities were placed along the direction of the chromophore dipole moment to maximize incorporation of the chromophore into the matrix and to impede d_{33}-eroding reorientation processes transverse to the dipole moment direction. 3) Aminomethyl rather than amino moieties were chosen so that the reactive functional groups would be electronically decoupled from the chromophore π-electron system.



Scheme 7. Synthetic approach to a high-β epoxy co-monomer (**10**).

The effects of both difunctional (**11**) and polyfunctional (**5**) epoxide reagents were investigated. Reaction mixtures of the difunctional chromophoric co-monomer **10** and the appropriate di- or polyepoxide were prepared by dissolving both components in THF (1:1 stoichiometric ratio of N–H bonds to epoxide moieties). After evaporation, the resulting films were partially crosslinked by heating in vacuo to remove any residual solvent and to improve dielectric stability. Parallel T_g and FT-IR-monitored experiments established optimum crosslinking conditions.[39] After corona poling at 130 °C for 2 h, the films were cooled to room temperature over a period of 1 h before removing the poling field. T_g data for these films reflect both a high degree of vitrification/immobilization as well as documented effects of epoxide multifunctionality. The d_{33} values are relatively high (7×10^{-9}–20×10^{-9} esu), exceeding those of the previously discussed guest–host materials by more than a factor of 10 (see Section 5.2). Nevertheless, the present film SHG efficiencies are somewhat less than might be expected on the basis of the chromophore $\mu\beta_{vec}$ value and estimated number density (ca. 6×10^{20} cm^{-3}). Film optical spectra and the effects of varying the poling atmosphere argue that this result is unlikely to be a consequence of chemical degradation. Rather, it appears that a non-negligible fraction of the chromophores are partially immobilized under the prepole crosslinking conditions (necessary to support the corona charge), hence slowly responsive or unresponsive to the poling field. Alternatively, the matrix densification process may be accompanied by a β_{vec} decreasing[40] twist of the chromophore structure from aryl ring coplanarity (not, however, obvious from the UV/Vis spectra).



The temporal stability of the SHG efficency at room temperature of poled, crosslinked **10** + **11** and **10** + **5** films (Fig. 10) reveals that $d_{33}(t)$ stabilities equal or exceed those of many pre-

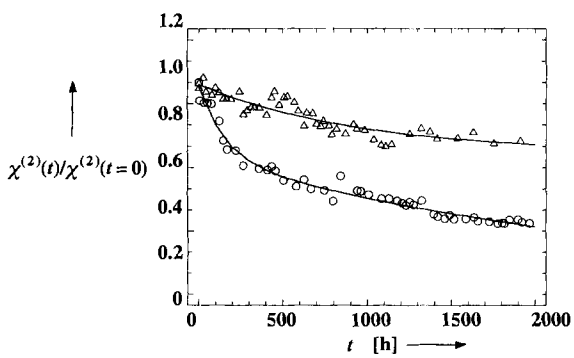
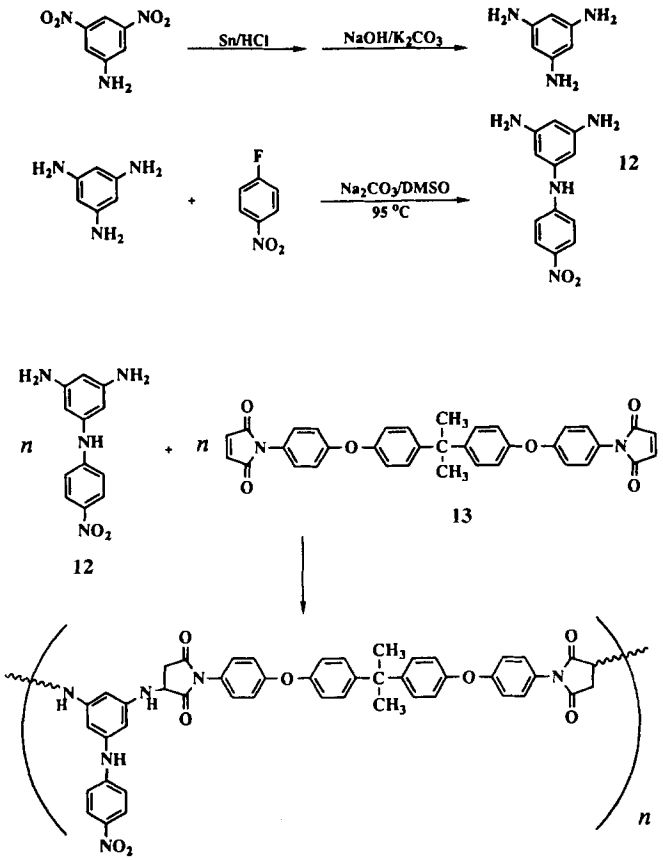


Fig. 10. SHG temporal characteristics at 25 °C for crosslinked, corona-poled films prepared from the reactive chromophoric co-monomer **10** (see Scheme 7) and polyepoxide reagent **5** (△) and the diepoxide **11** (○). Solid lines represent fits of Equation (j). Samples were stored at room temperature.

viously described guest–host systems. Furthermore, the superior immobilization characteristics of the polyepoxide-based matrices are evident. A biexponential [Eq. (j)] or stretched exponential [Eq. (k)] model can be fit to the $d_{33}(t)$ data by nonlinear regression techniques. The impressive SHG temporal stability of the **10** + **5** crosslinked matrices prompted additional quantitative temporal stability measurements at elevated temperatures.[39] The d_{33} decay (especially the initial decay) is, as expected, more rapid at 85 °C. Nevertheless, the long-term decay time constant is still on the order of four months. The KWW model [Eq. (k)] yields β values in accord with a narrower distribution of relaxation times than found for simple guest–host systems.

5.4. Crosslinked Polyimide Systems

As polymeric materials, polyimides[41] display great structural versatility as well as impressive thermal stability, T_g values, processability, and optical transparency (high-quality waveguides can be fabricated from polyimides).[42] Furthermore, polyimides have recently been utilized as presumably noninteracting hosts in poled, high-T_g guest–host NLO materials.[43] Chromophoric co-monomer **12** was designed for compatibility with polyimide polyadditions and was straightforwardly synthesized as shown in Scheme 8.[44] Films containing **12** and bismaleimide co-monomer **13** were cast from THF and thermally prepolymerized prior to poling. Verification of the course of the polymerization is provided by IR and NMR spectroscopy.



Scheme 8. Synthesis and implementation of a bismaleimide-compatible chromophoric co-monomer. DMSO = dimethylsulfoxide.

Independent thermal crosslinking experiments establish the DSC-derived T_g-curing temperature T characteristics shown in Figure 11. The near linearity of the plot is a further indication that the polymerization chemistry is well-behaved, and T_g values

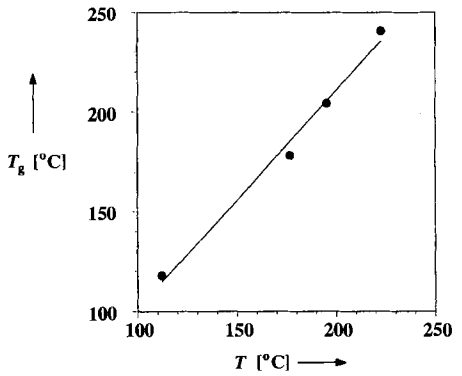


Fig. 11. DSC-determined glass transition temperature T_g as a function of polymerization temperature for **12**-doped polyimide specimens. Polymerization reactions were carried out at each temperature for 1 h. The symbol • denotes an experimental data point. The solid line is drawn as a visual aid. The T_g values were measured at a heating rate of 10 K min^{-1}.

as high as 240 °C rival the highest achieved to date. Corona poling of the **12** + **13** films was carried out over a range of temperatures (vide infra). SHG indices ($\lambda = 1064$ nm) are in the range of 11×10^{-9}–15×10^{-9} esu; these are reasonable for model chromophores with this architecture and number density. They are higher than those exhibited by typical guest–host polyimides[43] and can likely be increased as poling/crosslinking procedures are refined. SHG temporal stability data at 120 °C in air for a **12** + **13** polyimide film are shown in Figure 12. It was

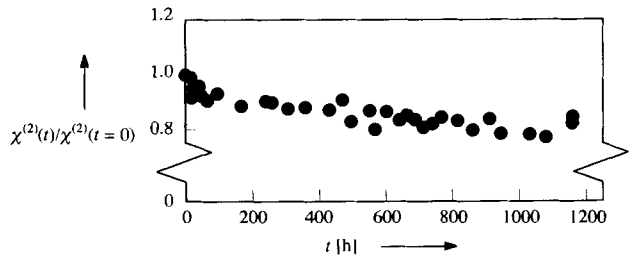


Fig. 12. SHG temporal characteristics at 120 °C in air for a corona-poled film prepared from reactive NLO chromophore **12** and bismaleimide **13** (see Scheme 8).

found that increases in the prepoling temperature are accompanied by increases in the achievable poling temperature, above which SHG signal loss and film damage become apparent. At 85 °C in air, there is only minor (ca. 10–15%) decay in SHG efficiency over the first 24 h, and within the precision of the measurements, negligible to very minor decay over several months.

Ultra-high-T_g polyimides can also be prepared using addition reactions between bismaleimides and diallylarenes.[41] While details of the mechanism have not been fully elucidated, addition and crosslinking appears to involve both "ene" reactions and sequential Diels–Alder additions.[45] Application of this approach to poled, NLO-active polymers has recently

been carried out using *N*,*N*-diallyl-*p*-nitroaniline and a bismaleimide (Fig. 13).[46] T_g values as high as 350°C have been measured, and SHG temporal stability is reasonably good *in air at 150°C*.

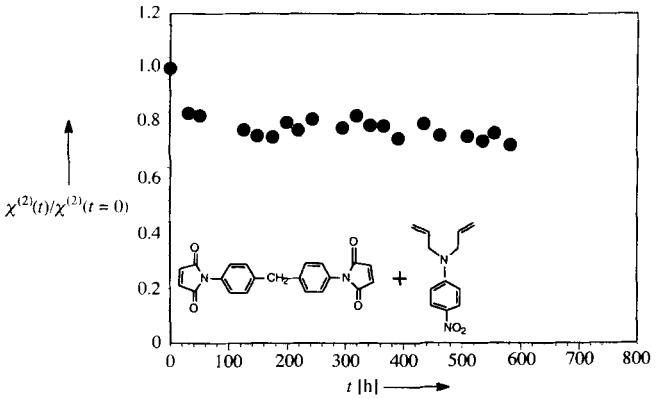
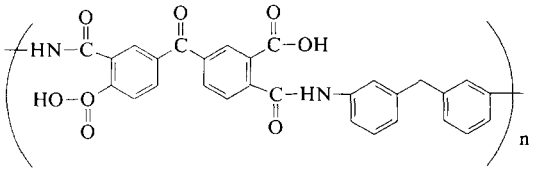
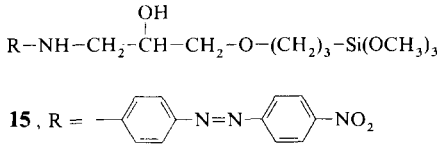


Fig. 13. SHG temporal characteristics at 150°C in air of a corona-poled film prepared from *N*,*N*-diallyl-*p*-nitroaniline and a reactive bismaleimide.

Tripathy et al. have taken a different approach to NLO-active polyimides in which a "polyamic acid" polyimide precursor (**14**) is condensed with a chromophoric siloxane (**15**).[33d] Good



14

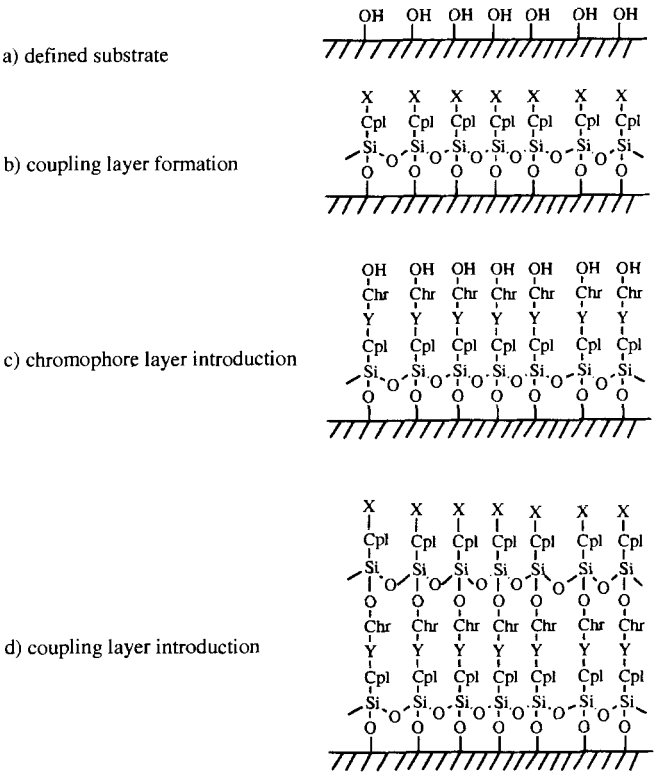


15, R =

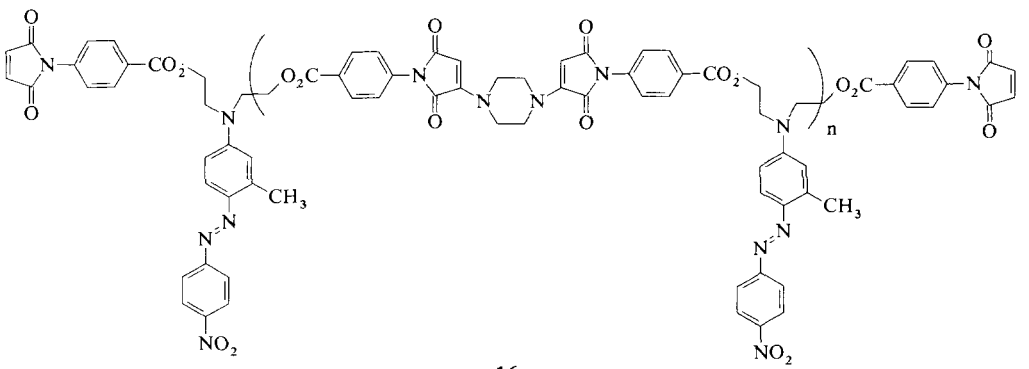
SHG temporal stability is observed for fully crosslinked samples (ca. 20% decay after 150 h in air). Resonant-enhanced d_{33} values are comparable to those of other poled polymers with donor–acceptor substituted stilbene and azo chromophores (see Section 5.1). Topolsky et al.[33j] reported another type of crosslinkable, chromophore-functionalized bismaleimide (**16**). T_g values are about 180°C, while d_{33} values appear comparable to the other examples mentioned above. Temporal stability plots are only reported for several hours at 200°C (ca. 30% decay), so that it is difficult to compare these materials to other crosslinked systems.

6. Chromophoric Self-Assembled Superlattices

An alternative approach to poled polymers and LB films would be the construction of covalently linked, chromophore-containing multilayer structures (see Scheme 1 bottom right). In principle, such materials offer greater net chromophore alignment and number densities than poled films and far greater structural control and stability than LB films. The general strategy employed for superlattice construction is shown in Scheme 9,



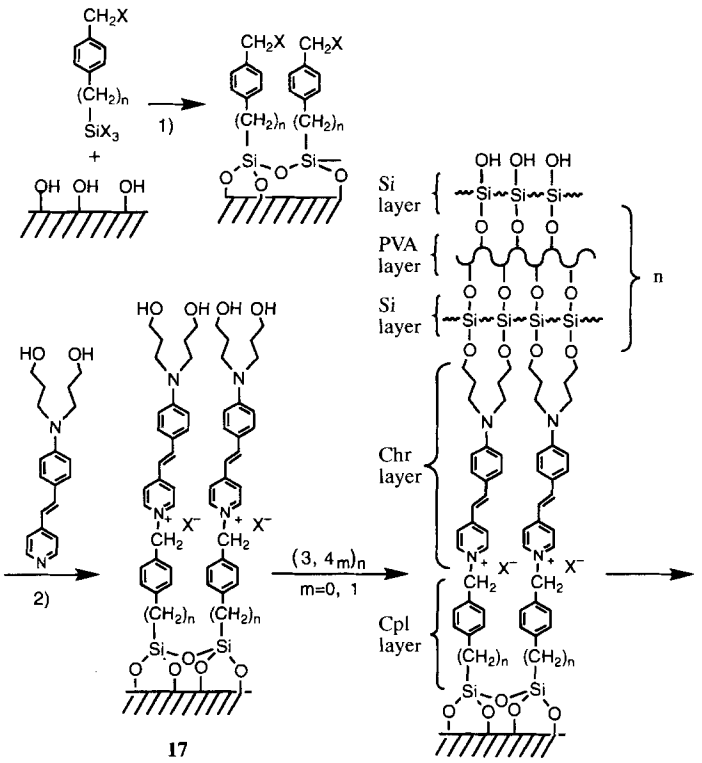
Scheme 9. Strategy for covalently linked NLO multilayers. Cpl = spacer for the coupling reaction, Chr = chromophore.



16

where the basic siloxane technology follows from reactions originally developed by Sagiv et al.,[47,48] and refined by Ulman, Whitesides, and others.[49–51]

A first-generation, test-of-concept synthetic approach to multilayer NLO materials is shown in Scheme 10.[18] Noteworthy features include a stilbazole



Scheme 10. Strategy for the synthesis of self-assembled NLO multilayer materials. 1) Benzene, 25 °C, 115 °C cure; 2) reflux in *n*PrOH; 3) $Cl_3SiOSiCl_2OSiCl_3$ in THF, 115 °C cure; 4) polyvinyl alcohol (PVA) in DMSO. X = I, Cl.

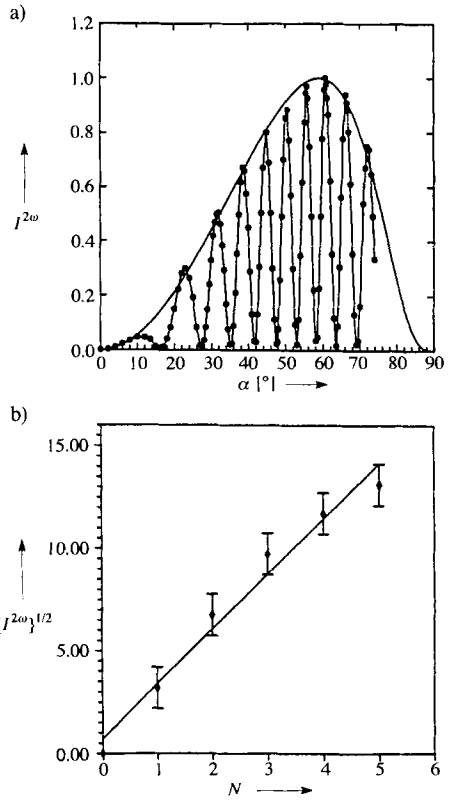


Fig. 14. a) SHG intensity $I^{2\omega}$ in arbitrary units as a function of fundamental beam incident angle α from a glass slide having a self-assembled CplChr monolayer on both sides. The interference pattern arises from the phase difference between the SHG waves generated at either side of the substrate during propagation of the fundamental wave. The solid envelope is a theoretical curve generated for $\chi^{(2)}_{zzz}/\chi^{(2)}_{zyy} = 3$. b) Plot of the square root of SHG intensity versus the number of chromophore layers *N* in the multilayer superlattice. The straight line is the fit to the experimental data.

chromophore precursor in which layer-building quaternization (step 2) affords both an anchored high-β center (**17**; β_{vec} (0.65 eV) $\approx 180 \times 10^{-30}$ cm^5 esu^{-1}) and diagnostic changes in the optical spectrum. In addition, soft polymeric layers are introduced transverse to the stacking direction (steps 3 and 4) to promote structural stability. The course of multilayer evolution on clean SiO_2 substrates can be monitored by optical spectroscopy (growth of chromophore absorption at 510 nm); XPS spectroscopy (initial diminution of Si, O signals; growth and persistence of C, N, I signals); advancing contact angles in accord with expected surface functionalities and which repeat in each 1–4 cycle; null ellipsometry in general accord with expected layer dimensions (thickness in notation of Scheme 9: CplChrSi ca. 34 Å; CplChrSi(PVA)Si(PVA)SiCplChr ca. 100 Å; CplChrSi(PVA)Si(PVA)SiCplChrSi(PVA)Si(PVA)SiCplChrSi(PVA)Si(PVA)Si ca. 235 Å), and NLO characteristics (vide infra). These films adhere strongly to glass, are insoluble in common organic solvents and strong acids, and at first were only effectively removed by diamond polishing. In initial research, assemblies with up to five chromophore layers were constructed.[18, 52]

Transmission SHG measurements (parallel-polarized geometry, $\lambda = 1064$ nm) reveal no in-plane anisotropy in the signal as samples are rotated about the film normal. This indicates that the films possess uniaxial symmetry about the normal and that the distribution of chromophore molecular orientations does not have an azimuthal dependence. Figure 14a shows SHG intensity as a function of incident angle for a glass slide coated on both sides with a self-assembled monolayer (CplChr). Two features are noteworthy. First, nearly complete destructive interference is observed over many randomly selected locations on the films, indicating that the quality of the structures on the two sides of the substrate is nearly identical and uniform. Second, the data envelope from the transmission SHG measurements can be described very well by Equation (m).[53] Here ψ is the average

$$\chi^{(2)}_{zzz}/\chi^{(2)}_{zyy} = 2\cot^2\psi \qquad \text{(m)}$$

angle between the surface normal and the chromophore molecular orientation (β_{zzz}), and, in early work, was found to be in the range 35–39° from both transmission and reflection measurements.

It is found that $d_{33} \approx 200 \times 10^{-9}$ esu for these multilayer materials and $d_{33} \approx 700 \times 10^{-9}$ esu for a single CplChr monolayer of 22 Å estimated thickness. This SHG efficiency considerably exceeds that of typical poled polymers, compares favorably with the best LB films,[14, 15] and is consistent with high chromophore number densities and degrees of acentric alignment. Moreover, the large magnitude of d_{33} suggests that the formation of centrosymmetric aggregates, which commonly occurs in LB films and which greatly depresses achievable bulk nonlinearities, is not important here. Temporal stability studies reveal less than 10% decline in the SHG efficiency of a five-layer structure in the course of six weeks. Since these multilayers are extremely thin in comparison to the wavelength $\lambda = 1064$ nm and hence to the expected coherence length, the SHG signal intensity should scale quadratically with the number of chromophore layers.

This is diagnostic and is commonly employed to assess structural regularity in LB films.[14, 15] As can be seen in Figure 14b, the adherence to quadratic behavior is good, indicating that it is possible to maintain the same degree of noncentrosymmetric chromophore ordering in the additions of successive layers.

These initial results raised key questions about the scope and mechanism(s) of the multilayer assembly process. In terms of substrate scope, it has been found that the multilayer structures can be assembled on borosilicate glass, float (ultra-smooth) glass, ITO surfaces, as well as on the native oxide coatings of single crystal Si and Ge.[52] By modifying deposition and curing conditions, the commercially available chloro coupling reagent (X = Cl in Scheme 10) can be substituted for the difficultly handled iodo reagent (X = I).[18] Since the commercial reagent is a mixture of *meta* and *para* isomers, a synthetic route to the pure *para* isomer was also developed.[54] In preliminary studies, it was found that multiple immersions[52c] interspersed with brief exposure to ambient temperatures form Cp layers with higher and more uniform functional group coverage as judged by XPS, advancing contact angles, and the d_{33} of the resulting chromophore-functionalized surfaces.[55] This preliminary result can be understood in terms of the limited availability (ca. 5 nm^{-2}) of surface SiOH groups, requiring additional water for interchromophore Si-O-Si condensation.[49] When this methodology is employed, the PVA layer in Scheme 10 is no longer required to form robust multilayers.[54]

To better understand the chromophore incorporation step 2 (Scheme 10) in situ SHG techniques have been employed to monitor the quaternization process in real time.[56] This approach allows real time studies of the quaternization kinetics and the average chromophore tilt angle [ψ, Eq. (m)] as a function of reaction extent and conditions. In the first experiments (Fig. 15), it was found that the assembly kinetics do not con-

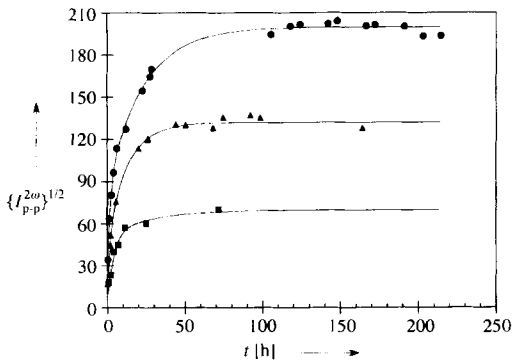


Fig. 15. In situ analyzed time evolution of the SHG signal resulting from step 2 in Scheme 10 in *n*PrOH at 60 °C. The SHG (only the I_{p-p} is presented) data are shown for different prefunctionalization conditions (step 1, Scheme 10, 2 × 18 h (●), 64 h (▲), 18 h (■)); the solid lines are theoretical curves [Eq. (n)].

form to a simple Langmuir model, but rather are better described by a biexponential expression [Eq. (n)] involving rapid

$$(I^{2\omega})^{1/2}(t) = (I^{2\omega})^{1/2}(t = \infty)\,(1 - \alpha_1\, e^{-k_1 t} - \alpha_2\, e^{-k_2 t}) \qquad \text{(n)}$$

initial coverage (k_1) followed by a slower second phase (k_2). Evidence for "fast" and "slow" phases in alkylthiol self-assembly kinetics on gold (as well as Langmuirian behavior) has been reported previously,[57] and deviations from Langmuirian kinetic behavior in other chemisorption processes are not uncommon.[58] Calibrated transmission SHG measurements on completely functionalized films yield, in combination with β_{zzz}^{calcd}[19] and an estimated film thickness of about 25 Å, d_{33} and the chromophore surface density, N_s.[56] For the substrates exposed to 2 × 18 h silanization followed by the stilbazole chromophore precursor, these quantities are 150×10^{-9} esu and 2×10^{14} molecules per cm^2, respectively. The latter value, 49 $Å^2$ per molecule, compares favorably with that for LB films containing essentially the same chromophore substituent,[59] and allows estimation of the actual initial Langmuirian adsorption rate constant, $k_1 = 5.4 \times 10^{-12}\ cm\,s^{-1}$.

By monitoring p-polarized SHG intensity as a function of incident light polarization and assuming a one-dimensional chromophore (a single, dominant β component), the average tilt angle of the principal chromophore β component with respect to the surface normal can be determined in situ [Eq. (m)]. Measurements on the self-assembly process (Fig. 16) reveal that ψ increases rapidly in the early stages of monolayer formation and then reaches a plateau somewhat sooner than $(I^{2\omega})^{1/2}$ (Fig. 15). A significant tilt angle increase with increasing chromophore coverage suggests a collective response to packing forces.

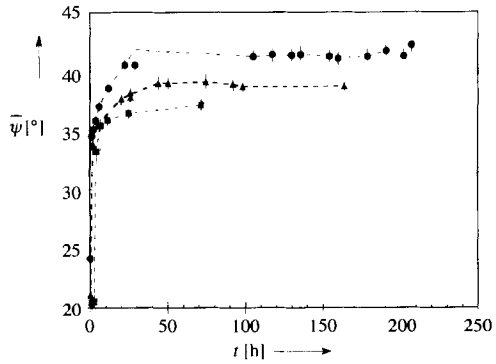
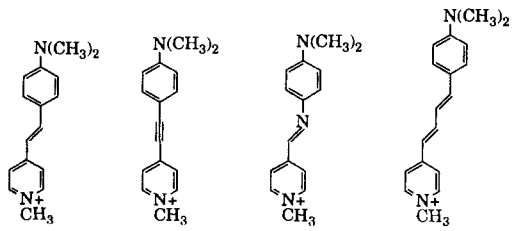


Fig. 16. Average chromophore tilt angle Ψ as a function of reaction time for the in situ data sets of Fig. 15 (2 × 18 h (●), 64 h (▲), 18 h (■)). Error bars represent the dispersity in 10–20 measurements (the dashed lines serve as a visual aid).

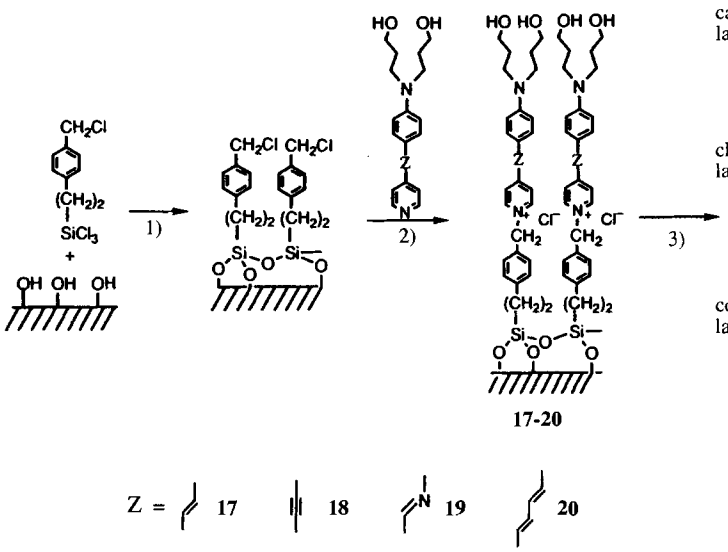
These in situ SHG results suggest a qualitatively two-stage monolayer assembly process for step 2 Scheme 10: Initial, rapid coverage in which isolated chromophore dipoles are reoriented away from the surface normal direction with increasing coverage, presumably due to chromophore–chromophore electrostatic/steric interactions. Subsequent slower, presumably electrostatically/sterically encumbered assembly in which the chromophore tilt angle changes little. These results furthermore illustrate the general efficacy of SHG techniques in probing the microstructural evolution of thin film materials in situ.

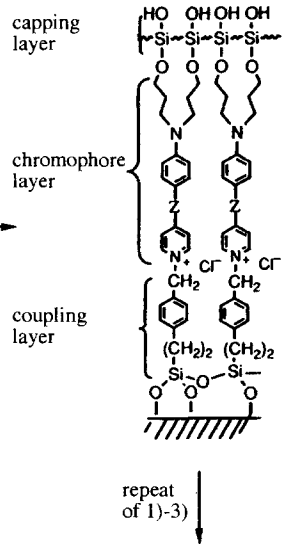
There is no reason to believe that stilbazolium chromophores will be optimum in Scheme 9, and a major effort has been made to target improved chromophore architectures in terms of transparency considerations, shape, enhanced optical nonlinearities, and amenability to additional chemical modification. Scheme 11 summarizes the chromophore structures in various stages of investigation,[60] tabulating semiempirical ZINDO-derived[19] linear and nonlinear optical properties; Scheme 12 shows the



β_{vec} (0.65 eV)	178	171	92.6	343
λ_{max}, ZINDO [nm]	479	466	400	526
λ_{max}, exp. [nm]	509	472	516	498

Scheme 11. Chromophores for self-assembled NLO materials. β_{vec} in units of 10^{-30} cm^{5}esu^{-1}.





Scheme 12. Construction of chromophoric self-assembled multilayer NLO materials. 1) Toluene, 25 °C; 115 °C cure; 2) reflux in *n*PrOH/toluene (80°C); 3) $Cl_3SiOSiCl_2OSiCl_3$ in THF, 115 °C.

construction of multilayers with the analogous chromophores. Since the alkynyl-containing structure **18** offers a rigid-rod geometry (suggesting potentially denser packing) and a blue-shifted λ_{max} (hence greater transparency), it has been the subject of recent investigation. Quaternization on a moderately covered substrate initially affords a monolayer exhibiting a rather modest NLO response; however, addition of the capping layer results in a major increase in SHG efficiency (Fig. 17).[52e] This observation can be interpreted in terms of a major monolayer structural reorganization in which introduction of the siloxane layer brings the average chromophore alignment closer to the direction of the substrate normal (Scheme 13). The structural picture is also supported by optical spectroscopic and grazing angle X-ray reflectivity measurements.[52d, e] As can be seen in Figure 18, alkynyl-derived NLO superlattices with nine layers can be constructed with good structural regularity.

As noted above, there is little experimental information on the input frequency dependence of NLO response for second-order polymeric materials. Such information is essential to a fundamental understanding of NLO phenomena as well as to engineering a device. Optical parametric amplification (OPA) instrumentation, which provides tunable input radiation over a broad range, has recently been designed at Northwestern University with this issue in mind.[60] Figure 19 shows the input frequency dependence of $\chi^{(2)}$ for a self-assembled structure based on chromophore **18**. It can be seen that the response does not adhere to the simple form implied by Equation (d). More importantly, the on-resonance re-



Scheme 13. Influence of a capping layer on the orientation of the chromophores in a monolayer.

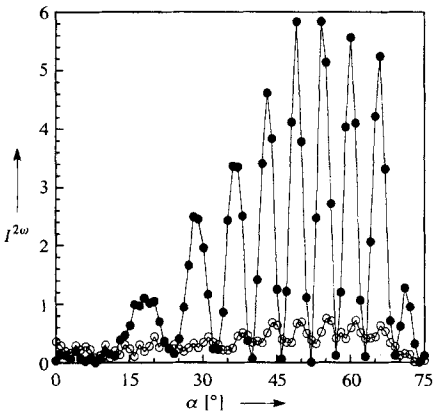


Fig. 17. SHG intensity $I^{2\omega}$ as a function of fundamental beam incident angle α from a glass slide having a self-assembled alkynyl chromophore **18**-derived monolayer on both sides. The interference pattern arises from the phase difference between the SHG waves generated at either side of the substrate during propagation of the fundamental wave. ○: Before the capping with $Cl_3SiOSiCl_2OSiCl_3$ step. ●: After the capping step.

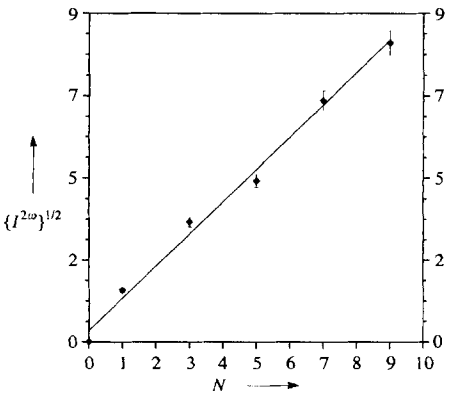


Fig. 18. Plot of the square root of SHG intensity versus the number of chromophore layers *N* in alkynyl chromophore **18**-derived multilayer superlattices. The straight line is the fit to the experimental data.

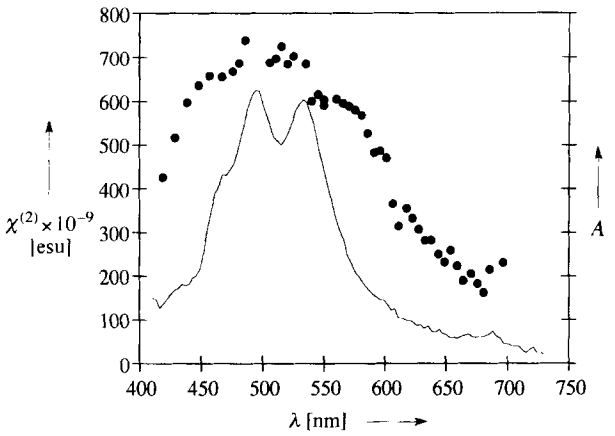
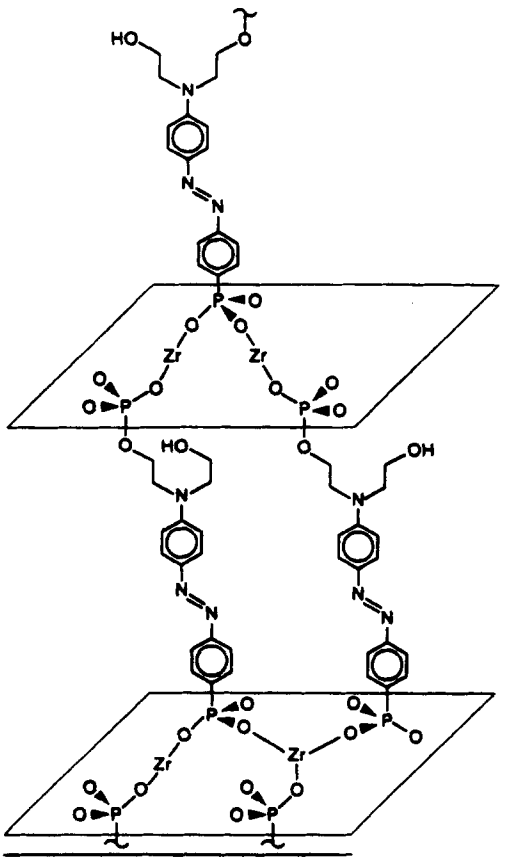


Fig. 19. SHG wavelength λ dependence of $\chi^{(2)}$ (dark points) for a self-assembled film constructed from chromophore **18** and the linear absorption spectrum (solid line, A = absorption in arbitrary units). Note that $\chi^{(2)}$ dispersion is plotted as a function of the *output* wavelength for comparative purposes. Thus, the resonances at about 500 nm in the optical spectrum correspond to the about 1000 nm resonance in the $\chi^{(2)}$ dispersion.

sponse approaches 10^{-6} esu while even the off-resonance response is near 10^{-7} esu![60]

Another self-assembly approach to intrinsically acentric chromophoric multilayer has been reported by Katz et al.[51a,b] Alternating layers of donor–acceptor phosphonate-substituted azo chromophore molecules and zirconyl salts[51c,d] are deposited from aqueous solution (**21**). Up to 32 layers were deposited. Good structural regularity is suggested by linear $(I^{2\omega})^{1/2}$ vs. number of layer plots, while partly resonant-enhanced d_{33} values are about 25×10^{-9} esu (the β for this chromophore is rather low). The SHG signal of this material is reported to be stable to 150 °C, at which point chromophore decomposition occurs.



21

7. Summary and Outlook

Major advances in the construction and performance of polymer-based NLO materials have been made in the past six years. Key developments in the poled polymer area have included the progression from guest–host to chromophore-functionalized to crosslinked systems. It is now known that chromophore number densities approaching those of molecular crystals can be achieved and that these modifications can be compatible with good processability. High T_g materials can now be prepared and further chromophore immobilization can be achieved with simultaneous poling and crosslinking. The first devices (e.g., spatial light modulators) have been fabricated with non-crosslinked chromophore-functionalized polymers, and their performance is encouraging with respect to competing inorganic materials/technologies.[7] Nevertheless, many fundamental, knowledge base issues must be addressed before ultimate materials can be constructed.

The constraints on the degree to which poling-induced chromophore orientation can be maintained over long periods of time above room temperature in glassy polymer-chromophore matrices are not well-understood and present a daunting challenge to polymer synthesis, processing, and theory. How high can T_g values be pushed and to what degree will T_g, T_β, etc., be an accurate measure of chromophore/backbone mobility? What theoretical descriptions are appropriate for physical aging/polymer relaxation far below T_g? Finally, we do not understand which poling/physical aging/curing protocols are most appropriate for maximum microstructural alignment and the temporal stability thereof. For devices fabricated from poled polymers, we need to know more about optical loss, dielectric breakdown, $\chi^{(2)}$ dispersion, and optical damage mechanisms, active layer-buffer layer compatibility, the uniformity, isotropy, and temperature/thermal expansion dependencies of the refractive indices, as well as the thermal stability limits of many polymer structural linkages. We have very little data on the NLO response of real chromophore–polymer matrices as a function of laser input wavelength (dispersion).[60] Many of these answers can only come from carefully planned syntheses, fastidious data collection, and an active interface with strong theoretical capabilities.

In the chromophore design sphere, major advances have been made in developing computationally efficient chemically-oriented theoretical formalisms for targetting new chromophores and understanding which structural and electronic features control linear and NLO response. What is not understood for real materials is how medium and chromophore–chromophore interactions modify/can be used to tune, the response of the individual chromophore molecules. Equally intriguing is the prospect of fundamentally new mechanisms (e.g., octupolar[61]) which might further enhance second-order NLO response. From a chromophore synthetic standpoint, the limits of thermal/environmental stability that can be achieved in highly polar, conju-

gated, donor–acceptor π-electron systems have yet to be defined and is a crucial issue.

Self-assembled chromophore multilayer structures have now been demonstrated which do not require electric field poling to achieve a highly acentric microstructure. Several systems display very large optical nonlinearities, frequently exceeding those of poled polymers. Key questions which must be addressed concern the thermal/chemical robustness of such structures, the structural regularity which can be achieved, the efficiency with which multilayer construction can be achieved, and ultimate film morphology (smoothness). Other optical and NLO questions about the constituent building blocks and aggregates are essentially the same as for poled polymer matrices (vide supra).

It is important to close by emphasizing that besides obvious technological attractions, the study of molecule–macromolecule-based NLO materials grapples with fundamental synthetic and theoretical questions generic to many other areas of contemporary materials chemistry. All involve the rational construction and attendent physical characteristics of structurally precise multimolecular assemblies. These are new, difficult types of problems for chemists, and ones the investigation of which will no doubt produce very large knowledge dividends for decades to come.

This work would not have been possible without the generous financial support of the National Science Foundation through the Northwestern Materials Research Center (grant DMR-9120521) and the Air Force Office of Scientific Research (contracts 90-0071 and 93-1-0114). The contributions of our enthusiastic and dedicated coworkers and colleagues have been inestimable. Their names can be found in the references cited.

Received: August 14, 1993
Revised version: February 16, 1994 [A181E]
German version: *Angew. Chem.* **1995**, *107*, 167

[1] a) J.-M. Lehn, *Science* **1993**, *260*, 1762-1763, and references therein; b) *Top. Curr. Chem.* **1993**, *165*, and articles therein; c) J.-M. Lehn, *Angew. Chem.* **1988**, *100*, 91-116; *Angew. Chem. Int. Ed. Engl.*, **1988**, *27*, 89-112, and references therein; d) D. T. Seto, G. M. Whitesides, *J. Am. Chem. Soc.* **1993**, *115*, 905-916, and references therein.

[2] a) *Optical Nonlinearities in Chemistry* (Ed.: D. M. Burland) (*Chem. Rev.* **1994**, *94*); b) T. Kaino, S. Tomaru, *Adv. Mater.* **1993**, *5*, 172-178, and references therein; c) *Nonlinear Optical Properties of Organic Materials VI* (*Proc. SPIE Int. Soc. Opt. Eng.* **1993**, 2025); d) *Nonlinear Optical Properties of Organic Materials V* (*ibid.* **1992**, *1775*); e) *Materials for Nonlinear Optics: Chemical Perspectives* (*ACS Symp. Ser.* **1991**, 455); f) *Nonlinear Optical Properties of Organic Materials IV*, (*Proc. SPIE Int. Soc. Opt. Eng.* **1991**, *1560*); g) P. N. Prasad, D. J. Williams, *Introduction to Nonlinear Optical Effects in Molecules and Polymers*, Wiley, New York, **1991**. h) *Nonlinear Optical Properties of Organic Materials III*, (*Proc. SPIE Int. Soc. Opt. Eng.* **1991**, *1337*); i) *Nonlinear Optical Effects in Organic Polymers* (Eds.: J. Messier, F. Kajar, P. N. Prasad, D. Ulrich) Kluwer, Dordrecht, **1989**. j) *Organic Materials for Nonlinear Optics* (Eds.: R. A. Hann, D. Bloor) Royal Society of Chemistry, London, **1988**. k) *Nonlinear Optical Properties of Organic Molecules and Crystals Vol. 1,2*. (Eds.: D. S. Chemla, J. Zyss) Academic Press, New York, **1987**; l) for organometallic NLO materials see also N. J. Long, *Angew. Chem.* **1995**, *107*, 37–56; *Angew. Chem. Int. Ed. Engl.* **1995**, *34*, 21–38; m) for a molecule-oriented introduction into the field of nonlinear optical materials see G. H. Wagmiere, *Linear and Nonlinear Optical Properties of Molecules*, VCH/Helvetica Chimica Acta, Weinheim/Basel, **1993**.

[3] a) T. Ishiguro, K. Yamija, *Organic Superconductors*, *Vol. 88*, Springer, Berlin, **1990**, p. 288; b) *The Physics and Chemistry of Organic Superconductors*, *Vol. 51* (Eds.: G. Saito, S. Kagoshima) Springer, Berlin, **1990**, p. 476. c) T. J. Marks, *Angew. Chem.* **1990**, *102*, 886-908; *Angew. Chem. Int. Ed. Engl.* **1990**, *29*, 857-879, and references therein. d) J. R. Ferraro, J. M. Williams, *Introduction to Synthetic Organic Conductors*, Academic Press: Orlando, FL, USA, **1987**.

[4] a) J. S. Miller, A. J. Epstein, *Angew. Chem.* **1994**, *106*, 399-432; *Angew. Chem. Int. Ed. Engl.*, **1994**, *33*, 385-415. b) J. S. Miller, A. J. Epstein, W. M. Reiff, *Accts. Chem. Res.* **1988**, *21*, 114-120, and references therein.

[5] a) M. R. Wasielewski, *Chem. Rev.*, **1992**, *92*, 435-461, and references therein; b) J. Deisenhofer, H. Michel, *Angew. Chem.* **1989**, *101*, 872-892; *Angew. Chem. Int. Ed. Engl.* **1989**, *28*, 829-847; c) R. Huber, *ibid.* **1989**, *101*, 849-871 and **1989**, *28*, 848-869.

[6] a) R. W. Boyd, *Nonlinear Optics*, Academic Press, New York, **1992**; b) Y. R. Shen, *The Principles of Nonlinear Optics*, Wiley, New York, **1984**.

[7] a) K. W. Beeson, P. M. Ferm, K. A. Horn, C. W. Knapp, M. J. McFarland, A. Nabata, J. Shan, C. Wu, J. T. Yardley, *Proc. SPIE Int. Soc. Opt. Eng.* **1993**, *2025*, 488-506; b) T. A. Tumolillo, Jr., P. R. Ashley, *Proc. SPIE Int. Soc. Opt. Eng.* **1993**, *2205*, 507-515; c) W. H. G. Horsthuis, M. M. K. Koerkamp, J.-L. Heidemann, H. W. Mertens, B. H. Hams, *Proc. SPIE Int. Soc. Opt. Eng.* **1993**, *2205*, 516-523; d) C. C. Teng, *Appl. Phys. Lett.* **1992**, *60*, 1538-1540; e) D. E. Bossi, R. W. Ade, *Laser Focus World*, **1992**, September, 135-142; f) J. D. Swalen, G. C. Bjorklund, W. Fleming, R. Hung, M. Jurich, V. Y. Lee, R. D. Miller, W. E. Moener, D. Y. Morichere, A. Skamanich, B. A. Smith *Proc. SPIE Int. Soc. Opt. Eng.* **1993**, *2205*, pp. 369-378; g) G. R. Möhlmann, W. H. G. Horsthuis, H. W. Mertens, A. McDonach, M. J. B. Diemeer, F. M. M. Suyten, B. Hendricksen, C. Duchet, P. Fabre, C. Brot, J. M. Copeland, J. R. Mellor, E. van Tomme, P. van Daek, R. Baets *ACS Symp. Ser.* **1991**, *455*, 426-433; h) D. G. Girton, S. L. Kwiatkowski, G. L. Lipscomb, R. S. Lytel, *Appl. Phys. Lett.* **1991**, *58*, 1730-1732.

[8] D. R. Kanis, M. A. Ratner, T. J. Marks, *Chem. Rev.* **1994**. *94*. 195-242.

[9] a) K. D. Singer, J. E. Sohn, S. J. Lalama, *Appl. Phys. Lett.* **1986**, *49*, 248-250; b) K. D. Singer, M. G. Kuzyk, J. E. Sohn, *J. Opt. Soc. Am. B*, **1987**, *4*, 968-975; c) G. A. Meredith, J. G. Van Dusen, D. J. Williams, *Macromolecules* **1982**, *15*, 1385-1389.

[10] a) H. L. Hampsch, J. Yang, G. K. Wong, J. M. Torkelson, *Macromolecules*, **1988**, *21*, 526-528; b) J. G. Victor, J. M. Torkelson, *ibid.* **1987**, *20*, 2241-2250; c) H. L. Hampsch, J. Yang, G. K. Wong, J. M. Torkelson, *ibid.* **1990**, *23*, 3540-3647 and 3648-3654, and references therein; d) S. Schüssler, R. Richert, H. Bässler, *ibid.* **1994**, *27*, 4318-4326.

[11] L. C. E. Struik, *Physical Aging in Amorphous Polymers and Other Materials*, Elsevier, Amsterdam, **1978**.

[12] a) T. Hibma, P. Pfluger, H. R. Zeller, H. Kuzmany, M. Mehring, S. Roth *Electronic Properties of Polymers and Related Compounds*, Springer, Berlin, **1985**, pp. 317-326, and references therein; b) B. A. Newman, P. Chen, K. D. Pae, J. I. Scheinbeim, *J. Appl. Phys.* **1980**, *51*, 5161-5164, and references therein; c) A. R. Blythe, *Electrical Properties of Polymers*, Cambridge University Press, Cambridge, **1979**, Chap. 6; d) K. N. Mathes, *Encycl. Polym. Sci. Eng.* **1986**, *5*, 512-593. e) H. Block, *Adv. Polym. Sci.* **1979**, *33*, 93-167, and references therein.

[13] a) C. Ye, N. Minami, T. J. Marks, J. Yang, G. K. Wong, *Macromolecules* **1988**, *21* 2901-2904; b) in ref. [2f], pp. 173-183.

[14] a) T. L. Penner, H. R. Motschmann, N. J. Armstrong, M. C. Ezenyilimba, D. J. Williams, *Nature* (*London*) **1993**, *367*, 49-51, and references therein; b) W. M. K. P. Wijekoon, B. Asghorian, P. N. Prasad, T. Geisler, S. Rosenkilde, *Thin Solid Films*. **1992**, *208*. 137-144; c) V. A. Howarth, N. Asai, N. Kishii, I. Fujiwara, *Appl. Phys. Lett.* **1992**, *61*, 1616-1618; d) C. Bosshard, M. Küpfer, P. Günter, C. Pasquier, S. Zahir, M. Seifert, *Appl. Phys. Lett.* **1990**, *56*, 1204-1206, and references therein; e) R. Popvitz-Biro, K. Hill, E. M. Landau, M. Lahav, L. Leiserowitz, J. Sagiv, H. Haiung, G. R. Meredith, H. Vanherzeele, *J. Am. Chem. Soc.* **1988**, *110*, 2672-2674.

[15] a) D. J. Williams, T. L. Penner, J. S. Schildkraut, N. Tillman, A. Ulman, *Adv. Mater.* **1993**, *5*, 195-218; b) C. Bubeck, F. Effenberger, L. Häussling, D. Neher, C.-P. Niesert, H. Ringsdorf, *ibid.* **1992**, *4*, 413-416; c) G. J. Ashwell, R. C. Hargreaves, C. E. Baldwin, G. S. Bahra, C. R. Brown, *Nature* (*London*), **1992**, *357*, 393-395; d) S. Allen, T. D. McLean, P. F. Gordon, B. D. Bothwell, P. Robein, I. Ledoux, *Proc. SPIE Int. Soc. Opt. Eng.* **1988**, *971*, 206-215; e) J. S. Schildkraut, T. L. Penner, C. S. Willand, A. Ulman, *Opt. Lett.* **1988**, *13*, 134-136; f) D. Lupo, W. Prass, U. Schunemann, A. Laschewsky, H. Ringsdorf, I. Ledoux, *J. Opt. Soc. Am. B*, **1988**, *5*, 300-308; g) The most promising of the Eastman Kodak chromphoric LB films irreversibly lose their SHG capacity at 50 °C: T. L. Penner, Fall MRS Meeting, Boston, MA, November 1992, Symposium R.

[16] C. Ye, T. J. Marks, J. Yang, G. K. Wong, *Macromolecules* **1987**, *20*, 2322-2324.

[17] a) M. A. Hubbard, N. Minami, C. Ye, T. J. Marks, J. Yang, G. K. Wong, *Proc. SPIE Int. Soc. Opt. Eng.* **1988**, *971*, 136-143; b) M. A. Hubbard, T. J. Marks, J. Yang, G. K. Wong, *Chem. Mater.* **1989**, *1*, 167-169; c) J. Park, T. J. Marks, J. Yang, G. K. Wong, *ibid.* **1990**, *2*, 229-231.

[18] D. Li, M. A. Ratner, T. J. Marks, C. Zhang, J. Yang, G. K. Wong, *J. Am. Chem. Soc.* **1990**, *112*, 7389-7390.

[19] a) D. R. Kanis, M. A. Ratner, T. J. Marks, M. C. Zerner, *Chem. Mater.* **1991**, *3*, 19-21; b) D. R. Kanis, M. A. Ratner, T. J. Marks, *J. Am. Chem. Soc.* **1990**, *112*, 8203-8204; c) *Int. J. Quantum Chem.* **1992**, *43*, 61-82.

[20] a) S. DiBella, M. A. Ratner, T. J. Marks, *J. Am. Chem. Soc.* **1992**, *114*, 5842-5849; b) S. DiBella, I. L. Fragala, M. A. Ratner, T. J. Marks, *ibid.* **1993**, *115*, 682-686.

[21] a) C. H. Wang, *J. Chem. Phys.* **1993**, *98*, 3457-3462; b) H. W. Guan, C. H. Wang, *ibid.* **1993**, *98*, 3463-3468.

[22] a) E. J. Moskala, D. F. Varnell, M. M. Coleman, *Polymer*, **1985**, *26*, 228-234; b) A. Nakamura, T. Hatakeyama, H. Hatakeyama, *ibid.* **1981**, *22*, 473-476; c) T. Hatakeyama, A. Nakamura, H. Hatakeyama, *ibid.* **1978**, *19*, 593-594.

[23] a) M. Barzoukas, D. Josse, P. Fremaux, J. Zyss, J. F. Nicoud, J. Morely, *J. Opt. Soc. Am. B*, **1987**, *4*, 977-986; b) J. Zyss, J. F. Nicoud, M. Coquillay, *J. Chem. Phys.* **1984**, *81*, 4160-4167.

[24] a) M. A. Firestone, J. Park, N. Minami, M. A. Ratner, J. Yang, T. J. Marks, W. Lin, G. K. Wong, *Macromolecules*, in press; b) M. A. Firestone, M. A. Ratner, T. J. Marks, W. Lin, G. K. Wong, *ibid.*, in press; c) E. T. Crumpler, D. Li, T. J. Marks, M. A. Ratner, W. Lin, G. K. Wong, *Abst. 207th Nat. Meet. Am. Chem. Soc.*, San Diego, CA, USA, **1994**, INOR 521; d) E. T. Crumpler, T. J. Marks, W. Lin, G. K. Wong, *Chem. Mater.*, submitted.

[25] R. B. Comizzoli, *J. Electrochem. Soc.* **1987**, *134*, 424-429.

[26] a) G. H. Fredrickson, *Annu. Rev. Phys. Chem.* **1988**, *39*, 149-180; b) G. H. Fredrickson, S. A. Brawer, *J. Chem. Phys.* **1986**, *84*, 3351-3366; c) M. F. Shlesinger, E. W. Montroll, *Proc. Natl. Acad. Sci USA*, **1984**, *81*, 1280-1283; d) E. W. Montroll, J. T. Bendler, *J. Stat. Phys.* **1984**, *34*, 129-162; e) G. Williams, D. C. Watts, *Trans. Faraday Soc.* **1970**, *66*, 80-87.

[27] a) G. T. Boyd, C. V. Francis, J. E. Trend, D. A. Ender, *J. Opt. Soc. Am. B*, **1991**, *8*, 887-894; b) K. D. Singer, L. A. King, *J. Appl. Phys.* **1991**, *70*, 3251-3255; c) W. Köhler, D. R. Robello, C. S. Willand, D. J. Williams, *Macromolecules* **1991**, *24*, 4589-4599; d) A. Dhinojwala, G. K. Wong, J. M. Torkelson, *ibid.* **1992**, *25*, 7395-7397; e) M. Stahelin, C. A. Walsh, D. M. Burland, R. D. Miller, R. J. Twieg, W. Volksen, *J. Appl. Phys.* **1993**, *73*, 8471-8479, and references therein.

[28] a) W.-E. Yu, C. S. P. Sung, R. E. Robertson, *Macromolecules* **1988**, *21*, 355-364, and references therein; b) W.-E. Yu, C. S. P. Sung, *ibid.* **1988**, *21*, 365-371; c) C. S. P. Sung, E. Pyun, H.-L. Sun, *ibid.* **1986**, *19*, 3922-3929.

[29] D. Aycock, V. Abolins, D. M. White, *Encycl. Polym. Sci. Eng. 1985-, Vol. 13*, **1988**, pp. 1-30, and references therein.

[30] D. M. White, *J. Org. Chem.* **1969**, *34*, 297-303.

[31] I. Cabasso, J. Jagur-Grodzinski, D. Vofsi, *J. Appl. Polym. Sci.* **1974**, *18*, 1969-1986.

[32] D. Dai, T. J. Marks, J. Yang, P. M. Lundquist, G. K. Wong, *Macromolecules* **1990**, *23*, 1894-1896.

[33] For some recent, complementary thermal crosslinking approaches, see: a) D. Jungbauer, B. Reck, R. Twieg, D. Y. Yoon, C. G. Willson, J. D. Swalen, *Appl. Phys. Lett.* **1990**, *56*, 2610-2612; b) M. Chen, L. Yu, L. Dalton, Y. Shi, W. H. Steier, *Macromolecules* **1991**, *24*, 5421-5428; c) L. Yu, W. Chan, S. Dikshit, Z. Bao, Y. Shi, W. H. Steier, *Appl. Phys. Lett.* **1992**, *60*, 1655-1657; d) R. J. Jeng, Y. M. Chen, A. K. Jain, J. Kumar, S. K. Tripathy, *Chem. Mater.* **1992**, *4*, 1141-1144; e) L.-T. Cheng, R. P. Foss, G. R. Meredith, W. Tam, F. C. Zumsteg, *Mater. Res. Soc. Symp. Proc.* **1992**, *247*, 27-38; f) S. Marturankakul, J. I. Chen, L. Li, R. J. Jeng, J. Kumar, S. K. Tripathy, *Chem. Mater.* **1993**, *5*, 592-594; g) P. Ranon, Y. Shi, W. H. Steier, C. Xu, B. Wu, L. R. Dalton, *Appl. Phys. Lett.* **1993**, *62*, 2605-2607; h) C. V. Francis, K. M. White, G. T. Boyd, R. S. Moshrefzadeh, S. K. Mohapatra, M. D. Radcliffe, J. E. Trend, R. C. Williams, *Chem. Mater.* **1993**, *5*, 506-510; i) C. Xu, B. Wu, O. Todorova, L. R. Dalton, Y. Shi, P. M. Ranon, W. H. Steier, *Macromolecules* **1993**, *26*, 5303-5309; j) G. Topolsky, J.-P. Lecomte, R. Meyrueix, *ibid.* **1993**, *26*, 7383-7385; k) Z. Peng, L. Yu, *Macromolecules* **1994**, *27*, 2638-2640.

[34] a) F. Lohse, *Makromol. Chem. Macro. Symp.* **1987**, *7*, 1-16; b) E. F. Oleinik, *Adv. Polym. Sci.* **1986**, *80*, 49-99; c) K. Dušek, *ibid.* **1986**, *78*, 1-59; d) B. A. Rozenberg, *ibid.* **1986**, *75*, 113-165.

[35] a) X. Wang, J. K. Gillham, *J. Coatings Technol.* **1992**, *64*, 37-45; b) G. Wisanrakkit, J. K. Gillham, *ibid.* **1990**, *62*, 35-50.

[36] a) L. V. McAdams, J. A. Gannon, *Encycl. Polym. Sci. Eng. Vol. 6*, **1986**, pp. 322-382, and references therein; b) E. Mertzel, J. L. Koenig, *Adv. Polym. Sci.* **1986**, *75*, 74-112.

[37] a) Y. Jin, S. H. Carr, T. J. Marks, W. Lin, G. K. Wong, *Chem. Mater.* **1992**, *4*, 963-965; b) Y. Jin, S. H. Carr, T. J. Marks, W. Lin, G. K. Wong, *Mats. Res. Soc. Sympos. Proc.* **1992**, *247*, 39-42; c) Y. Jin, T. J. Marks, W. Lin, G. K. Wong, *Macromolecules*, submitted.

[38] a) A. Rudin, *The Elements of Polymer Science and Engineering*, Academic Press, New York, **1982**, Chapt. 11; b) J. T. Rabek, *Experimental Methods in Polymer Chemistry*, Wiley, New York, **1980**, Chapt. 32.

[39] a) M. A. Hubbard, T. J. Marks, W. Lin, G. K. Wong, *Chem. Mater.* **1992**, *4*, 965-968; b) M. A. Hubbard, T. J. Marks, W. Lin, G. K. Wong, *Chem. Mater.*, submitted.

[40] a) D. Li, T. J. Marks, M. A. Ratner, *J. Phys. Chem.* **1992**, *96*, 4325-4336; b) *Mater. Res. Soc. Symp. Proc.* **1989**, *134*, 665-671.

[41] a) T. Takekoshi, *Adv. Polym. Sci.* **1990**, *94*, 1-25; b) B. Sillion in *Comprehensive Polymer Science*, (Eds.: G. Allen, J. C. Bevington), Pergamon, Oxford, **1989**, Chapt. 30; c) J. E. White, *Ind. Eng. Chem. Prod. Res. Dev.* **1986**, *25*, 395-400; d) C. E. Sroog, *Macromol. Rev.* **1976**, *11*, 161-203; e) J. V. Crivello, *J. Polym. Sci.* **1973**, *11*, 1185-1193.

[42] a) K. K. Chakravorty, *Appl. Phys. Lett.* **1992**, *61*, 1163-1165; b) C. P. Chien, K. K. Chakravorty, *Proc. SPIE Int. Soc. Opt. Eng.* **1990**, *1323*, 338-347; c) R. Reuter, H. Franke, C. Feger, *Appl. Opt.* **1988**, *27*, 4565-4571; d) R. Selvraj, H. T. Lin, J. F. McDonald, *J. Lightwave Technol.* **1988**, *6*, 1034-1039; e) R. D. Rossi *Engineered Materials Handbook, Vol. 3*, ASM, Materials Park, OH, USA, **1992**, p. 151-162.

[43] a) S. Ermer, J. F. Valley, R. Lytel, G. F. Lipscomb, T. E. VanEck, D. G. Girton, *Appl. Phys. Lett.* **1992**, *61*, 2272-2275; b) J. F. Valley, J. W. Wu, S. Ermer, M. Stiller, E. S. Binkley, J. T. Kenney, G. F. Lipscomb, R. Lytel, *ibid.* **1992**, *60*, 160-163; c) J. W. Wu, J. F. Valley, M. Stiller, S. Ermer, E. S. Binkley, J. T. Kenney, G. F. Lipscomb, R. Lytel, *Proc. SPIE Int. Soc. Opt. Eng.* **1991**, *1560*, 196-205; d) J. W. Wu, E. S. Binkley, J. T. Kenney, R. Lytel, A. F. Garito, *J. Appl. Phys.* **1991**, *69*, 7366-7369; e) J. W. Wu, J. F. Valley, S. Ermer, E. S. Binkley, J. T. Kenney, G. F. Lipscomb, R. Lytel, *Appl. Phys. Lett.* **1991**, *58*, 225-227; f) M. Stähelin, D. M. Burland, M. Ebert, R. D. Miller, B. A. Smith, R. J. Twieg, W. Volksen, C. A. Walsh, *ibid.* **1992**, *61*, 1626-1629.

[44] a) J. T. Lin, M. A. Hubbard, T. J. Marks, W. Lin, G. K. Wong, *Chem. Mater.* **1992**, *4*, 1148-1150; b) J.-F. Wang, M. A. Hubbard, J. Lin, T. J. Marks, W. P. Lin, G. K. Wong, *Proc. SPIE Int. Soc. Opt. Eng.* **1993**, *2025*, 62-68; c) J.-F. Wang, T. J. Marks, W. Lin, G. K. Wong, *Chem. Mater.*, submitted.

[45] a) R. J. Morgan, R. J. Jurek, T. Donnellan, A. Yen, *Polym. Prepr.* **1992**, *33*, 426-427, and references therein; b) S. Zahir, M. A. Chaudhari, J. King, *Makromol. Chem. Macromol. Symp.* **1989**, *25*, 141-154.

[46] J.-F. Wang, T. J. Marks, W. Lin, G. K. Wong, *Macromolecules*, submitted.

[47] a) M. Pomerantz, A. Segmuller, L. Netzer, J. Sagiv, *Thin Solid Films*, **1985**, *132*, 153-162; b) L. Netzer, R. Iscovici, J. Sagiv, *ibid.* **1983**, *100*, 67-76; c) L. Netzer, R. Iscovici, J. Sagiv, *ibid.* **1983**, *99*, 235-241.

[48] a) R. Maoz, J. Sagiv, *Langmuir* **1987**, *3*, 1034-1044, 1045-1051; b) C. R. Kessel, S. Granki, *ibid.* **1991**, *7*, 532-538.

[49] a) S. R. Wasserman, G. M. Whitesides, I. M. Tidswell, B. M. Ocko, P. S. Pershan, J. D. Axe, *J. Am. Chem. Soc.* **1989**, *111*, 5852-5861; b) S. R. Wasserman, Y.-T. Tao, G. M. Whitesides, *Langmuir* **1989**, *5*, 1074-1087.

[50] a) N. Tillman, A. Ulman, T. L. Penner, *Langmuir* **1989**, *5*, 101-111; b) A. Ulman, N. Tillman, *ibid.* **1989**, *5*, 1418-1420; c) N. Tillman, A. Ulman, J. S. Schildkruat, T. L. Penner, *J. Am. Chem. Soc.* **1988**, *110*, 6136-6144; d) A. Ulman, *Adv. Mater.* **1990**, *2*, 573-582, and references therein; e) *An Introduction to Ultrathin Organic Films, Part 3*, Academic Press, New York, **1991**.

[51] For complementary self-assembly approaches, see: a) H. E. Katz, W. L. Wilson, G. Scheller, *J. Am. Chem. Soc.* **1994**, *116*, 6636-6640; b) H. E. Katz, G. Scheller, T. J. Putvinski, M. L. Schilling, W. L. Wilson, C. E. D. Chidsey, *Science* **1991**, *254*, 1485-1487; c) H. Lee, L. J. Kepley, H.-G. Hong, T. E. Mallouk, *J. Am. Chem. Soc.* **1988**, *110*, 618-620; d) H. Lee, L. J. Kepley, H.-G. Hong, S. Akhter, T. E. Mallouk, *J. Phys. Chem.* **1988**, *92*, 2597-2601.

[52] a) D. Li, T. J. Marks, C. Zhang, J. Yang, G. K. Wong, *Proc. SPIE Int. Soc. Opt. Eng.* **1991**, *1560*, 341-347; b) D. S. Allan, F. Kubota, T. J. Marks, C. Zhang, W. P. Lin, G. K. Wong, *ibid.* **1993**, *2025*, 362-369; c) D. S. Allan, F. Kubota, Y. Orihaski, D. Li, T. J. Marks, T. G. Zhang, W. P. Lin, G. K. Wong, *Polym. Prepr.* **1991**, *32*, 86-87; d) D. S. Allan, F. Kubota, A. K. Kakkar, T. J. Marks, T. G. Zhang, W. P. Lin, M. Shih, G. K. Wong, P. Dutta, *Mater. Res. Soc. Symp. Proc.* **1992**, *247*, 779-786; e) A. K. Kakkar, S. Yitzchaik, S. B. Roscoe, F. Kubota, D. S. Allan, T. J. Marks, W. Lin, G. Wong, *Langmuir*, **1993**, *9*, 388-390; f) D. Li, D. C. Smith, B. I. Swanson, J. D. Farr, M. T. Paffett, M. E. Hawley, *Chem. Mater.* **1992**, *4*, 1047-1053.

[53] a) Y. R. Shen, *The Principles of Nonlinear Optics*, Wiley, New York, Chapt. 2; b) T. G. Zhang, C. H. Zhang, G. K. Wong, *J. Opt. Soc. Am. B*, **1990**, *7*, 902-907.

[54] F. Kubota, D. S. Allan, T. J. Marks, unpublished.

[55] S. Yitzchaik, A. K. Kakkar, T. J. Marks, unpublished.

[56] S. Yitzchaik, S. B. Roscoe, D. S. Allan, A. K. Kakkar, T. J. Marks, Z. Xu, T. G. Zhang, W. Lin, G. K. Wong, *J. Phys. Chem.* **1993**, *97*, 6958-6960.

[57] a) R. C. Thomas, L. Sun, R. M. Crooks, A. J. Ricco, *Langmuir* **1991**, *7*, 620-622; b) C. D. Bain, E. B. Troughton, Y.-T. Tao, J. Evall, G. M. Whitsides, R. G. Nuzzo, *J. Am. Chem. Soc.* **1989**, *111*, 321-335.

[58] a) P. N. T. van Velzen, J. J. Ponjee, A. Benninghoven, *Appl. Surf. Sci.* **1987**, *37*, 147-159; b) A. W. Adamson, *Physical Chemistry of Surfaces*, 5th ed. Wiley, New York, 1990, Chapt. 14, 15.

[59] G. J. Ashwell, R. C. Hargreaves, C. E. Baldwin, G. S. Bahra, C. R. Brown *Nature (London)* **1992**, *357*, 393-395.

[60] P. M. Lundquist, S. Yitzchaik, T. G. Zhang, D. R. Kanis, M. A. Ratner, T. J. Marks, G. K. Wong *Appl. Phys. Lett.* **1994**, *64*, 2194-2196.

[61] a) J. Zyss, *Nonlinear Opt.* **1991**, *1*, 3-15; b) J. L. Brèdas, F. Meyers, B. M. Pierce, J. Zyss, *J. Am. Chem. Soc.* **1992**, *114*, 4928-4929.

Peptide Ligases—Tools for Peptide Synthesis

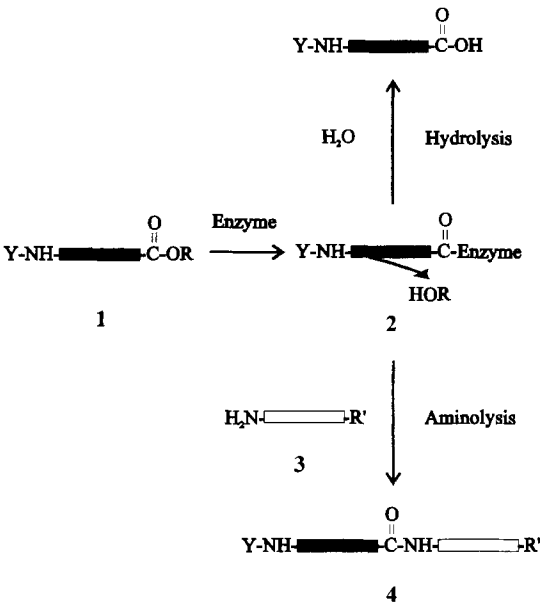
Hans-Dieter Jakubke*

Following the first chemical formation of a peptide bond by Theodor Curtius in 1881 in the laboratory of Hermann Kolbe in Leipzig, chemical peptide synthesis[1] developed over the next ninety years culminating in the first total synthesis of an enzyme. Ribonuclease A (RNase A), composed of 124 amino acid residues, was constructed by condensation of fragments in solution[2] as well as by solid-phase synthesis.[3] Roughly ten years later Yajima and Fujii[4] synthesized RNase A according to an improved conventional synthetic strategy and obtained the first crystalline synthetic enzyme having full enzymatic activity. But an ideal, universally applicable method for chemical formation of the peptide bond has still not been found. Since chemosynthetic reactions are typically conducted with residues having chiral centers, racemization is a constant concern. Even stepwise chain extension using urethane protecting groups, which are supposed to prevent racemization, may be affected; chemical linkage of peptide fragments is yet more unreliable.

A recent paper[5] describes a new synthesis of RNase A, in which an enzyme was used for the first time to couple fragments obtained by solid-phase synthesis to form a protein. The idea of using enzymes to make peptide bonds is about as old as chemical peptide synthesis itself. In 1898, evoking the reversibility of chemical reactions, van't Hoff predicted that enzymes could be used to catalyze the formation of peptide bonds. This idea was first taken up in 1938 by Max Bergmann and confirmed experimentally.

Owing to the stereo- and regiospecificity of enzymes, their application for the formation of peptide bonds certainly offers a list of advantages over chemical procedures, for example mild reaction conditions, no need for permanent protection of functional groups in side chains, racemization-free course of reaction, and simple scale-up after optimization of the process. To make full use of these advantages, however, a close to universally applicable peptide ligase is needed,[**] which in principle would display high catalytic efficiency for all theoretically possible combinations of amino acids; in other words, it should be nonspecific and not affected by the side chain functions of the amino acids to be coupled. Since an ideal biocatalyst like the ribosomal peptidyl transferase is not available, and multienzyme complexes in bacterial peptide synthesis are limited to specific purposes, only proteases can be used for formation of the peptide bond. Two different mechanistic strategies for the application of proteases can be described.[6]

In comparison to equilibrium-controlled peptide synthesis, kinetically controlled synthesis[7] offers the possibility of more targeted manipulations. Following this approach for reactions with low enzyme requirements and short reaction times, mechanistic considerations limit the enzymes employed to serine and cysteine proteases. Unfortunately, proteases are not perfect acyl transferases; owing to their limited specificity, other undesired reactions may take place parallel to acyl transfer, for example hydrolysis of the acyl enzyme **2**, secondary hydrolysis of the peptide product **4**, and other undesired cleavages of possible protease-labile bonds in **1**, **3**, and **4** (Scheme 1).



Scheme 1.

To eliminate or minimize these disadvantages, the enzyme can be engineered and/or the reaction medium and the mechanistic features of the process can be adjusted as shown schematically in Figure 1.[8] Undesired hydrolytic side reactions may be eliminated by adapting the medium. Protease-catalyzed syntheses in monophasic organic solvents or in biphasic aqueous–organic

[*] Prof. Dr. H.-D. Jakubke
Institut für Biochemie
Fakultät für Biowissenschaften, Pharmazie und Psychologie der Universität
Talstrasse 33, D-04103 Leipzig (Germany)
Telefax: Int. code + (341)960-3099

[**] In deviation from EC nomenclature, the term peptide ligase here refers to a biocatalyst for the formation of the peptide bond.

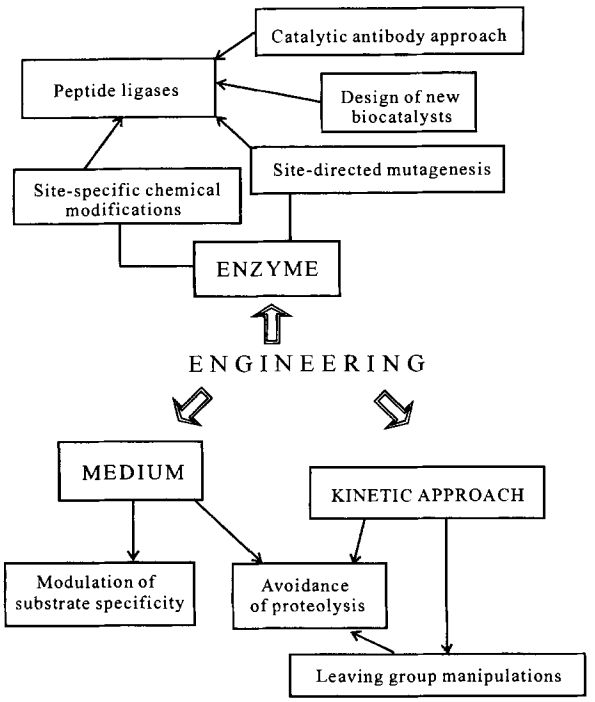
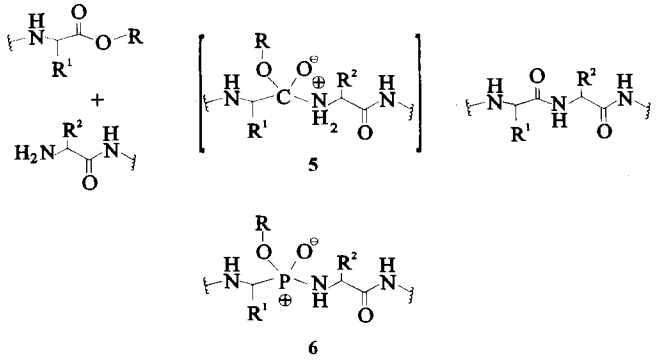


Fig. 1. Possibilities for engineering enzymatic peptide synthesis at different levels.

systems proceed with minimal proteolytic side reactions. Since the reactants are better soluble in organic media, the chemical and enzymatic steps can be accomodated. Side reactions can also be eliminated and yields of peptides increased by direct reduction of the water content of the reaction medium, for example in syntheses in frozen aqueous systems and reactions in dense media. Another option in modifying a kinetically controlled reaction is manipulating the leaving group so that the enzyme reacts exclusively with the acyl donor **1** and not with the peptide product **4** or the amino component **3**. Then even protease-labile products can be obtained in good yields. Two recent reviews give an overview of the current possibilities for manipulation.[8, 9]

The term enzyme engineering[10] (see Fig. 1) describes a range of techniques from deliberate chemical modification to remodeling a wild-type enzyme by gene technology. "Subtiligase", a mutant of subtilisin BNP', was prepared by Jackson et al.[5] by protein design and used in a further total synthesis of RNase A. This work, which combines solid-phase synthesis of oligopeptides and enzymatic coupling of these fragments, demonstrates the state of the art in peptide synthesis and proves impressively the potential of enzymes for the formation of peptide bonds. Average yields of roughly 75% were obtained in the fragment condensations. The excellent leaving group of the Phe-NH_2-modified carboxamido methyl ester, which even in unmodified form was found to be a very good acyl donor in other syntheses,[11] and the use of a considerable excess of acyl donor ensured that most of the side reactions were suppressed. The total yield after the five fragment condensations was 15%, and after the folding of the final product, 8%. Thus starting with 100 mg of the initial peptide (residues 98–124), RNase A can be obtained on a 10-mg scale. The fragments (77–97, 64–76, 52–63, 21–51, 1–20) were chosen such that the C-terminal residues, Tyr^{97}, Tyr^{76}, Val^{63}, and Ala^{20}, were the closest to matching the substrate specificity of the subtilisin mutant. A similar strategy was also used in the synthesis of three variants of RNase A, in which the two histidine residues His^{12} and His^{119} at the active center were exchanged individually and simultaneously for L-4-fluorohistidine; the affect of these substitutions in the three analogues of RNase A was studied in detail.

Substrate binding at the active site[7] plays a crucial role in protease-catalyzed peptide bond formation. Unfortunately, a simple C-N ligase is not capable of developing different substrate binding regions, for example by induced fit, for the structurally diverse amino acid side chain functionalities. According to Linus Pauling the action of an enzyme depends on the complementarity of the active site to the transition state structure of a reaction, as shown in Scheme 2 for peptide bond formation.

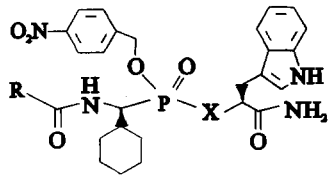


Scheme 2.

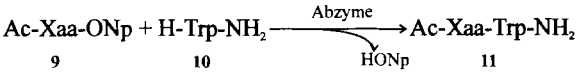
Given the fact that the enzyme should not bind the substrate very strongly but must stabilize the transition state considerably, it is unlikely that a relatively simple enzyme can act as a universal peptide ligase. This premise was recently confirmed by reports by Hirschmann et al.[12] and by Jacobsen and Schultz[13] on peptide bond formation with catalytic antibodies (abzymes). Analogues of the transition state were used as haptens to induce antibodies with the correct arrangement of catalytic groups. The idea behind both strategies is illustrated in Scheme 2 by the transition state analogue **6** synthesized by Hirschmann et al.[12] When these haptens are injected in animals, their immune systems generate antibodies against them. Since the structure of the tetrahedral intermediate **5** is also greatly affected by the amino acid side chains R^1 and R^2, it is doubtful whether a universally applicable catalytic antibody can be generated for peptide bond formation. The structures of the transition state analogues **7**, **8a**, and **8b** were changed deliberately, in particular by incorporation of a cyclohexyl group, such that the abzymes that catalyzed the reaction of **9** and **10** would have broad substrate specificity (Scheme 3).

The abzyme-catalyzed dipeptide syntheses gave all possible stereoisomers in yields of 44 to 94%. The abzymes did not catalyze the hydrolysis of either the dipeptide products or the activated esters employed. Jacobsen and Schultz[13] elicited antibodies against a neutral phosphonate diester transition state analogue, which significantly accelerated the coupling of an N^{α}-acylalanine azide with a phenylalanine derivative relative to the

 © VCH Verlagsgesellschaft mbH, D-69451 Weinheim, 1995 0570-0833/95/0202-0176 $ 10.00+.25/0



7 X= NH, R= -$(CH_2)_3$COOH
8a X= O, R= -$(CH_2)_3$COOH
8b X= O, R= Me



9 **10** **11**

(Xaa = Val, Leu, Phe)

Scheme 3.

uncatalyzed reaction. The application of catalytic antibodies exploits the fundamental property of the immune system, generating binding sites in the folds of the antibodies which are analogous to the active sites in enzymes. Proof of this is provided by the determination of the three-dimensional structure of a catalytic antibody developed for peptide cleavage.[14] The active site of this antibody contains a Ser-His dyad and thus has great similarities with the active sites of serine proteases.

These sensational findings will certainly initiate a new era in the construction of peptide ligases. Now with the emergence of catalytic antibodies for peptide synthesis, the arsenal of methods is augmented, and the prospects for future progress are bright. However, extensive development is needed before this approach is applied as routinely as enzymatic peptide synthesis currently is, and this perspective emphasizes the importance of the chemoenzymatic synthesis of RNase A.

Keywords: catalytic antibodies · ligases · peptide synthesis · RNase A · subtilisin

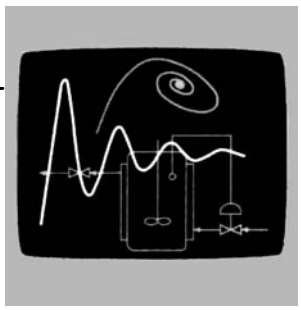
German version: *Angew. Chem.* **1995**, *107*, 189

[1] K.-H. Altmann, M. Mutter, *Chem. Unserer Zeit* **1993**, *27*, 274–286.
[2] R. Hirschmann, R. F. Nutt, D. F. Veber, R. A. Vitali, S. L. Varga, T. A. Jacob, F. W. Holly, R. G. Denkewalter, *J. Am. Chem. Soc.* **1969**, *91*, 507–508.
[3] B. Gutte, R. B. Merrifield, *J. Am. Chem. Soc.* **1969**, *91*, 501–502.
[4] H. Yajima, N. Fujii, *J. Am. Chem. Soc.* **1981**, *103*, 5867–5871.
[5] D. Y. Jackson, J. Vurnier, C. Quan, M. Stanley, J. Tom, J. A. Wells, *Science* **1994**, *266*, 243–247.
[6] Selected reviews: a) J. S. Fruton, *Adv. Enzymol. Relat. Areas Mol. Biol.* **1982**, 239–306; b) H.-D. Jakubke, P. Kuhl, A. Könnecke, *Angew. Chem.* **1985**, *97*, 79–87; *Angew. Chem. Int. Ed. Engl.* **1985**, *24*, 85–93; c) W. Kullmann, *Enzymatic Peptide Synthesis*, CRC, Boca Raton, FL, USA, **1987**; d) H.-D. Jakubke in *The Peptides: Analysis, Synthesis, Biology* (Eds.: S. Udenfriend, J. Meienhofer), Band 9, Academic Press, New York, **1987**, pp. 103–165; e) K. Morihara, *Trends Biotechnol.* **1987**, *5*, 164–170; f) C.-H. Wong, K.-T. Wang, *Experientia* **1991**, *47*, 1123–1129; g) A. J. Andersen, J. Fromsgaard, P. Thorbeck, S. Aasmul-Olsen, *Chim. Oggi* **1991**, *9*(3), 17–24; *ibid.* **1991**, *9*(4), 17–23.
[7] V. Schellenberger, H.-D. Jakubke, *Angew. Chem.* **1991**, *103*, 1440–1452; *Angew. Chem. Int. Ed. Engl.* **1991**, *30*, 1437–1449.
[8] H.-D. Jakubke, *J. Chin. Chem. Soc.* **1994**, *41*, 355–370.
[9] J. Bongers, E. P. Heimer, *Peptides* **1994**, *15*, 183–193.
[10] C.-H. Wong, *Chimia* **1993**, *47*, 127–132.
[11] P. Kuhl, U. Zacharias, H. Burckhardt, H.-D. Jakubke, *Monatsh. Chem.* **1986**, *117*, 1195–1204.
[12] R. Hirschmann, A. B. Smith III, C. M. Taylor, P. A. Benkovic, S. D. Taylor, K. M. Yager, P. A. Sprengeler, S. J. Benkovic, *Science* **1994**, *265*, 234–237.
[13] J. R. Jacobsen, P. G. Schultz, *Proc. Natl. Acad. Sci. USA* **1994**, *91*, 5888–5892.
[14] G. W. Zhou, J. Guo, W. Huang, R. J. Fletterick, T. S. Scanlan, *Science* **1994**, *265*, 1059–1064.

Ingham, J. et al.

Chemical Engineering Dynamics

Modelling with PC Simulation



1994. XX, 701 pages with 430 figures.
Hardcover. DM 276.-/ öS 2153.-/ sFr. 256.-.
ISBN 3-527-28577-6

In this book, the reader is guided through the complex study of dynamic chemical engineering systems by the unique combination of a simplified presentation of the fundamental theory (Part 1) and direct hands-on computer experimentation with the provision of 85 accompanying computer-based simulation examples (Part 2) supplied on diskette.

The ISIM digital simulation language is very simple to use and its powerful interactive nature enables the readers to create their own simulations, based on their own specific problems. This powerful dynamic ISIM software is ready to run on any DOS personal computer.

The treatment employed in this book is well tried and tested, based on over 20 years experience in teaching an international post-experience course. Whether for the teacher, the student, the chemist or engineer, this book serves as the key to a greater understanding of chemical engineering dynamics through the fun and enjoyment of active learning.

To order please contact your bookseller or:

VCH, P.O. Box 10 11 61, D-69451 Weinheim, Telefax (0) 62 01 - 60 61 84

VCH, Hardstrasse 10, P.O. Box, CH-4020 Basel

VCH, 8 Wellington Court, Cambridge CB1 1HZ, UK

VCH, 220 East 23rd Street, New York, NY 10010-4606, USA (toll free: 1-800-367-8249)

VCH, Eikow Building, 10-9 Hongo 1-chome, Bunkyo-ku, Tokyo 113 Japan

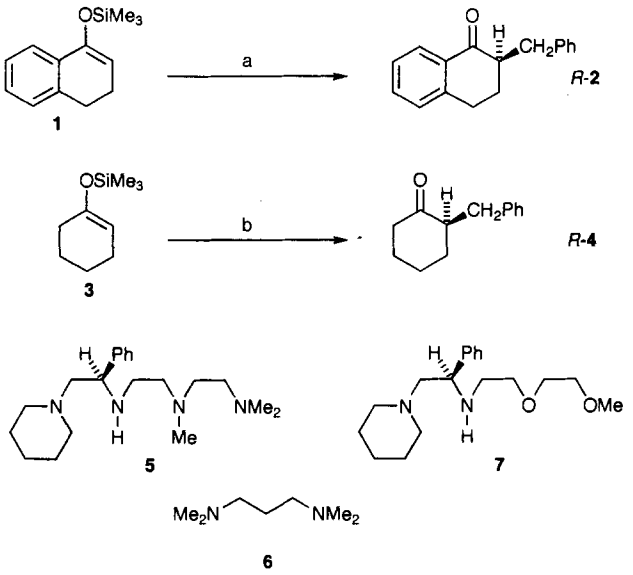
VCH

Catalytic Asymmetric C–C Bond Formation: New Enolato- and Organolithium Chemistry

David J. Berrisford*

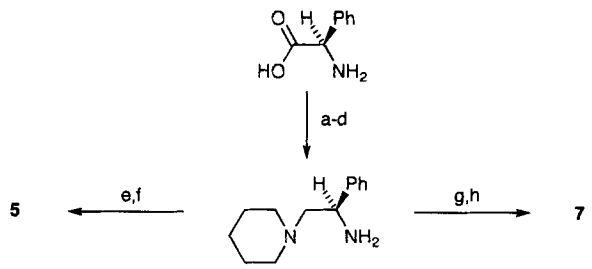
Organolithium reagents are a cornerstone of the development and practice of modern organic chemistry. The pivotal role of these reagents reflects their early introduction in undergraduate chemistry courses. Although the enormous interest in catalytic asymmetric C–C bond formation[1, 2] has provided a number of practical solutions in other areas, highly enantioselective, *catalytic* reactions of organolithium reagents generally remain elusive. The complex solution equilibria,[3] so characteristic of lithioanions, continually frustrate attempts to discover viable catalytic processes. Two recent pieces of work[4, 5] have made valuable advances towards this goal.

Koga et al. have discovered[4] a remarkable catalytic process for the asymmetric benzylation of lithium enolates derived from silyl enol ethers **1** and **3** (Scheme 1). Previously, stereocontrolled



Scheme 1. Asymmetric benzylation of lithium enolates. a) 1. MeLi/LiBr, toluene; 2. 5 mol% **5**, 2 equiv **6**, 10 equiv $PhCH_2Br$, −45 °C, 18 h (76%, 96% *ee*); b) 1. MeLi/LiBr, Et_2O; 2. 10 mol% **5**, 2 equiv **6**, 10 equiv $PhCH_2Br$, −45 °C, 18 h (52%, 90% *ee*).

lithium enolate alkylation has been restricted to either diastereoselective processes[2a, c] requiring the covalent attachment of a chiral auxiliary, or to reactions with stoichiometric amounts of external ligands.[2b] Indeed, the new catalytic reaction is a development of an earlier stoichiometric benzylation of **1** which achieves a 92% *ee* of **2** using ligand **7**.[6] The new process differs from the former stoichiometric procedure in a number of respects. The structure of the chiral ligand is modified to **5**. This ligand must be used in conjunction with an excess of an additional achiral ligand exemplified (Scheme 1) by the optimum choice **6**. Both polydentate chiral ligands (**5**/**7**) are prepared[7] in straightforward manner from phenylglycine (Scheme 2). The new ligand **5** delivers increased enantioselectivity under stoichiometric conditions (up to 97% *ee* for **2**) and maintains the level of asymmetric induction under defined catalytic conditions. Under optimal conditions, a 96% *ee* (76% yield) of **2** can be realized using 5 mol% of **5** in toluene. Careful experimentation has shown that switching to 1,2-dimethoxyethane (DME) as solvent retains almost all the high enantioselectivity and has a beneficial effect on conversion (90% *ee*/91% yield). Lower ligand loading (< 5 mol%) has a deleterious effect on both conversion and enantioselectivity.



Scheme 2. a) CBZ-protection; b) piperidine/$PO(OEt)_2CN$ (76%); c) HBr/AcOH (100%); d) $LiAlH_4$ (67%); e) $Me_2N(CH_2)_2N(Me)CH_2CO_2H/PO(OEt)_2CN$ (69%); f) BH_3·THF (63%); g) $MeO(CH_2)_2OCH_2CO_2H/PO(OEt)_2CN$ (83%); h) BH_3·THF (74%).

The study constitutes a further example of how efficient catalytic reactions can be achieved despite the presence of complex solution equilibria.[8] Originally, this chemistry was developed in a nondonor solvent rather than using an excess of donor as solvent. In so doing, the effects of additives, both chiral and achiral, are maximized. Enolate generation in the catalytic system is accomplished by the reaction of silyl enol ethers with methyllithium. This procedure avoids the formation of an additional secondary amine, which, in principle, could compromise the asymmetric induction by forming mixed aggregates[9] with the lithium enolate.

Incorporation of lithium bromide and an achiral, bidentate ligand in addition to **5** are essential for selectivity. The effects of the achiral ligands are the most revealing part of the study. The bidentate ligand **6** and its analogues provide a substantial rate acceleration. Without the additional ligand, conversion drops precipitously under catalytic conditions. Simple tertiary diamines are the most effective additives, tetramethylethylenediamine being slightly inferior to the preferred propyl analogue **6**. Use of DME as an additive does not accelerate the reaction. However, the presence of DME has little effect on the enantiomeric excess and hence can substitute for toluene as the reac-

[*] Dr. D. J. Berrisford
Department of Chemistry
University of Manchester Institute of Science and Technology
PO Box 88, Manchester M60 1QD (UK)
Telefax: Int. code + (061) 236 7677

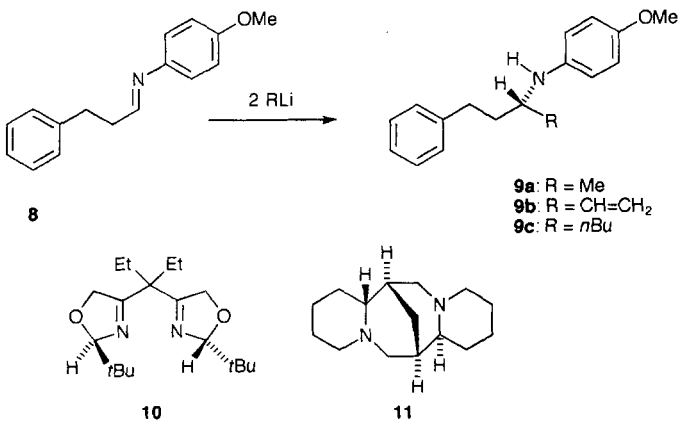
 © VCH Verlagsgesellschaft mbH, D-69451 Weinheim, 1995 0570-0833/95/0202-0178 $ 10.00+.25/0

tion solvent. It is proposed that the achiral additive sequesters[10] the excess of LiBr that is generated as the benzylation reaction proceeds. Under stoichiometric conditions without additional LiBr, the enantiomeric excess increases with time and conversion, indicating the beneficial *in situ* role of the salt. However, excess of LiBr slows the reaction prohibitively (< 1% conversion). The results implicate a kinetically dominant mixed aggregate comprising lithium halide, lithium enolate, and chiral ligand. The subtleties of the mechanism clearly warrant considerable further investigation.

These intriguing effects of the additive ligands on the reaction rate and stereoselectivity are reminiscent of those discovered[11] in simple lithium enolate aldol reactions. Related halide effects[12] are reported in other enolate reactions. The addition of lithium chloride has a beneficial effect on the asymmetric deprotonation[13] of ketones by chiral lithium amides, so implicating a reactive lithium amide–lithium chloride aggregate.[14]

Although, the catalytic procedure uses a two-stage method to generate the enolate, it should be possible to use direct ketone enolization by an appropriate lithium amide base. The catalytic alkylation reaction is limited as yet to two enolates and a single example of a reactive alkyl halide. The full scope of this process remains to be determined, particularly with respect to the range of compatible substrates and electrophiles. Nevertheless, Koga et al. have discovered a significant example of catalytic lithium enolate chemistry and one that holds considerable promise for future development.

Another recent contribution[5] by Denmark et al. illustrates an effective method for promoting the nucleophilic addition reactions[2] of organolithium reagents to imines. The chemistry is a development of earlier methodology.[15] The organolithium additions to *N*-aryl imines, for example **8**, are promoted by C_2-symmetric bis(oxazoline) ligands, such as **10**, or (−)-sparteine **11** (Scheme 3) with high asymmetric induction. Notably, the oxazoline ligands deliver excellent selectivities for aliphatic imines. Both methyl- and vinyllithium additions can be promoted by **10** with significant enantioselectivities (**9a**, R = Me: 91% *ee*, Table 1). However, ligand **11** is beneficial for the *n*-butyl- and phenyllithium additions (**9c**, R = *n*Bu: 91% *ee*, Table 1). In certain cases, decreasing the ligand loading to a practical 20 mol% retains most of the ceiling enantiomeric excess. Substrate enolization, which is often a problem for aliphatic imines, does not compete to a significant extent. Moreover, the *N*-aryl amine products can be deprotected by using published methodology[15] to afford the corresponding primary amines. This chemistry is, therefore, complementary to asymmetric hydrogenation[16] of imines, and offers an alternative entry into important amino compounds.



Scheme 3. Asymmetric nucleophilic addition to an aliphatic imine.

Table 1. Reaction conditions for the nucleophilic addition of RLi to **8** as well as yields and enantiomeric excesses *ee* of the products **9**.

R	*T* [°C]	Ligand (equiv.)	Yield [%]	*ee* [%]
Me	−63	**10** (1.0)	96	91
Me	−63	**10** (0.2)	81	82
$CH=CH_2$	−78	**10** (1.0)	95	89
$CH=CH_2$	−78	**10** (0.2)	82	82
*n*Bu	−94	**11** (1.0)	90	91
*n*Bu	−78	**11** (0.2)	91	79

The chemistry is further proof of the utility of naturally occurring (−)-sparteine.[17] The oxazoline ligands are prepared from *tert*-leucine. An important issue currently being addressed[5] is the structure of the active organometallic complex. The disparity between the enantioselectivity of the stoichiometric and catalytic runs could result from competing "uncatalyzed" addition. It is also possible that the product[18] lithium amide affects the selectivity to some degree through mixed aggregation phenomena.

These studies are beneficial in two respects. Efficient or improving asymmetric methodology is of primary importance, especially in such a fundamental area. Additionally, this work provides new insights[3] into the complex solution behavior of these commonplace organometallic reagents.

German version: *Angew. Chem.* **1995**, *107*, 192

Keywords: asymmetric synthesis · catalysis · lithium compounds

[1] R. Noyori, *Asymmetric Catalysis in Organic Synthesis*, Wiley, New York, **1994**; *Catalytic Asymmetric Synthesis* (Ed.: I. Ojima), VCH, Weinheim, **1993**.
[2] a) D. Seebach, *Angew. Chem.* **1990**, *102*, 1363; *Angew. Chem. Int. Ed. Engl.* **1990**, *29*, 1320; b) K. Tomioka, *Synthesis* **1990**, 541; c) P. G. Willard in *Comprehensive Organic Synthesis, Vol. 1* (Eds.: B. M. Trost, I. Fleming), Pergamon, Oxford, **1991**, p. 1; D. M. Huryn in *Comprehensive Organic Synthesis, Vol. 1* (Eds.: B. M. Trost, I. Fleming), Pergamon, Oxford, **1991**, p. 49.
[3] D. Seebach, *Angew. Chem.* **1988**, *100*, 1685; *Angew. Chem. Int. Ed. Engl.* **1988**, *27*, 1624.
[4] M. Imai, A. Hagihara, H. Kawasaki, K. Manabe, K. Koga, *J. Am. Chem. Soc.* **1994**, *116*, 8829.
[5] S. E. Denmark, N. Nakajima, O. J.-C. Nicaise, *J. Am. Chem. Soc.* **1994**, *116*, 8797.
[6] a) M. Murakata, M. Nakajima, K. Koga, *J. Chem. Soc. Chem. Commun.* **1990**, 1657; b) Y. Hasegawa, H. Kawasaki, K. Koga, *Tetrahedron Lett.* **1993**, *34*, 1963.
[7] R. Shirai, K. Aoki, D. Sato, H.-D. Kim, M. Murakata, T. Yasukata, K. Koga, *Chem. Pharm. Bull.* **1994**, *42*, 690.
[8] R. Noyori, H. Takaya, *Chemica Scripta* **1985**, *25*, 83.
[9] a) P. J. Cox, N. S. Simpkins, *Tetrahedron: Asymmetry* **1991**, *2*, 1; b) E. Vedejs, N. Lee, *J. Am. Chem. Soc.* **1991**, *113*, 5483.
[10] Powerful donors such as hexamethylphosphoramide are known to suppress mixed aggregation between MeLi and LiCl; H. J. Reich, J. P. Borst, R. R. Dykstra, D. P. Green, *J. Am. Chem. Soc.* **1993**, *115*, 8728.
[11] P. J. Pospisil, S. R. Wilson, E. N. Jacobsen, *J. Am. Chem. Soc.* **1992**, *114*, 7585.
[12] a) P. L. Hall, J. H. Gilchrist, A. T. Harrison, D. J. Fuller, D. B. Collum, *J. Am. Chem. Soc.* **1991**, *113*, 9575; b) F. E. Romesberg, D. B. Collum, *ibid.* **1994**, *116*, 9187; c) *ibid.* 9198; d) A. Loupy, B. Tchoubar, *Salt Effects in Organic and*

Organometallic Chemistry, VCH, Weinheim, **1991**; e) J. Corset, F. Froment, M.-F. Lautié, N. Ratovelomanana, J. Seyden-Penne, T. Strzalko, M.-C. Roux-Schmitt, *J. Am. Chem. Soc.* **1993**, *115*, 1684; f) L. M. Jackman, T. S. Dunne, *J. Am. Chem. Soc.* **1985**, *107*, 2805.

[13] a) B. J. Bunn, N. S. Simpkins, *J. Org. Chem.* **1993**, *58*, 1847; b) B. J. Bunn, N. S. Simpkins, Z. Spavold, M. J. Crimmin, *J. Chem. Soc. Perkin Trans. 1* **1993**, 3113.

[14] F. S. Mair, W. Clegg, P. A. O'Neil, *J. Am. Chem. Soc.* **1993**, *115*, 3388.

[15] a) K. Tomioka, M. Shindo, K. Koga, *J. Am. Chem. Soc.* **1989**, *111*, 8266; b) K. Tomioka, I. Inoue, M. Shindo, K. Koga, *Tetrahedron Lett.* **1990**, *31*, 6681; c) *ibid.* **1991**, *32*, 3095; d) I. Inoue, M. Shindo, K. Koga, K. Tomioka, *Tetrahedron: Asymmetry* **1993**, *4*, 1603; e) I. Inoue, M. Shindo, K. Koga, K. Tomioka, *Tetrahedron* **1994**, *50*, 4429.

[16] For leading references see: a) M. J. Burk, J. P. Martinez, J. E. Feaster, N. Cosford, *Tetrahedron* **1994**, *50*, 4399; b) A. Viso, N. E. Lee, S. L. Buchwald, *J. Am. Chem. Soc.* **1994**, *116*, 9373.

[17] S. Thayumanavan, S. Lee, C. Liu, P. Beak, *J. Am. Chem. Soc.* **1994**, *116*, 9755, and references therein; A. Carstens, D. Hoppe, *Tetrahedron* **1994**, *50*, 6097.

[18] a) A. H. Alberts, H. Wynberg, *J. Am. Chem. Soc.* **1989**, *111*, 7265; b) *J. Chem. Soc. Chem. Commun.* **1990**, 453.

 © VCH Verlagsgesellschaft mbH, D-69451 Weinheim, 1995 0570-0833/95/0202-0180 $ 10.00+.25/0

Trace Analysis of the Radionuclides ^{90}Sr and ^{89}Sr in Environmental Samples I: Laser Mass Spectrometry**

Jörg Lantzsch, Bruce A. Bushaw, Günter Herrmann, Heinz-Jürgen Kluge, Ludwin Monz, Sabine Niess, Ernst W. Otten, Richard Schwalbach, Martin Schwarz, Judith Stenner, Norbert Trautmann, Klaus Walter, Klaus Wendt,* and Klaus Zimmer

Strontium-90 is one of the most toxic radionuclides known; only naturally occurring polonium-210 (from lead-210), radium-226, and several nuclides of the actinides have a greater toxicity.[1] The reason for the toxicity of strontium-90 is its long half-life of 28.5 years combined with its permanent and complex accumulation occurring in bones.[2] Strontium-90 is a high yield nuclear fission product of both uranium-235 and of plutonium-239, and was distributed worldwide during the above-ground nuclear weapon tests in the 1950s and 1960s. In the Federal Republic of Germany the average surface coverage of strontium-90 at the beginning of the 1980s was 2 kBq m^{-2}.[3] This value increased only marginally due to the deposition of strontium-90 from the Chernobyl accident at the end of April 1986; measurements from air filters and rainwater in the Mainz region indicated an increase of 0.02 kBq m^{-2}.[4] However, it took two weeks before reliable data on the deposition were available—much too long in the case of acute contamination. It became clear just how inadequate the usual radioactivity measurements are for the determination of strontium-90 in environmental samples containing a mixture of fresh fission products.

In this and the two following communications[5, 6] alternative physical detection methods and chemical separation techniques are reported for strontium-90 and -89 in fresh fallout. These methods and procedures were developed in a coordinated approach by three groups, with the goal of producing reliable analytical results within one day. Two procedures were tested as alternatives to the radiometric methods: resonance ionization spectroscopy using lasers in a collinear geometry on a mass-separated atomic beam and accelerator mass spectrometry.[5] Furthermore, a chemical separation technique was devised using liquid–liquid extraction with crown ethers. A rapid method was also developed for the determination of radioactive strontium isotopes by ion exchange chromatography with subsequent on-line β-detection.[6]

The determination of strontium-90 in fresh fallout is difficult, since it is obscured by the shorter lived strontium-89 ($t_{1/2}$ = 50.5 d); the $^{89}Sr/^{90}Sr$ activity ratio in Chernobyl fallout was between 11/1[7] and 17/1[4] compared to about 200/1 for fallout from nuclear weapon tests.[8] Since the two strontium isotopes are pure β^- emitters they are not detected by the otherwise powerful analysis of fallout mixtures by high resolution γ radiation spectroscopy. Rather, they must be chemically isolated and analyzed by a far less specific measurement of β^- rays. For detection of small amounts of strontium-90 in an excess of strontium-89 at an overall low level of activity, different properties of the decay products have long been used:[9] Yttrium-90 is a β^- emitter with $t_{1/2}$ = 64 h, while yttrium-89 is, in contrast, stable. Yttrium-90 grows from strontium-90 in the purified strontium fraction, and after several days it is chemically separated, measured, and the activity decay followed over a few days, to confirm its identity. This yields the strontium-90 activity; the difference between this and the total β^- activity of the purified strontium fraction gives the strontium-89 activity.

The delay in waiting for the formation and decay of yttrium-90 can be avoided by using the differences in β^- decay energies (^{90}Sr 0.55 MeV, ^{89}Sr 1.49 MeV) to simultaneously measure both strontium isotopes. Both nuclides are counted together using a liquid scintillator, but only strontium-89 is registered by means of Cherenkov radiation. This procedure reaches its limit at a high $^{89}Sr/^{90}Sr$ ratio and low activity.[10]

The usual chemical separation process[9] for strontium is inadequate for fresh fallout. The strontium and barium in the sample solution are precipitated with concentrated nitric acid as nitrates; this removes among other components inactive calcium, which can be present in significant amounts. Barium is then separated from strontium by chromate precipitation. This step is particularly critical, because in fresh fallout the fission product barium-140 ($t_{1/2}$ = 12.8 d) is about four times more abundant than strontium-89, and its daughter product lanthanum-140 ($t_{1/2}$ = 40 h) accompanies yttrium-90 in the separation thus resulting in a false measurement of the yttrium-90 activity.

In the following, a procedure is presented for the detection of strontium-90 and -89 by a combination of laser spectroscopy and mass spectrometry.[11a] The technique was developed for air-filter samples, since here the presence of fresh fission products is the easiest to recognize. With the method, it should be possible to record concentrations of 1×10^8 atoms per 1000 m^3 air, corresponding to 1.5×10^{-14} g and activities of 80 mBq ^{90}Sr and 16 Bq ^{89}Sr. These were typical concentrations found in Germany after the Chernobyl accident. The main problem with mass spectrometric and optical detection is the presence of up to 10^{18} stable strontium atoms (150 µg)—up to 82.6% ^{88}Sr—in such samples. Therefore, a selectivity of 10^{10} is required for the radioisotopes to be detected over the stable strontium-88. Furthermore, an efficiency of 10^{-5} is necessary for the overall process to keep the statistical error small for a sample of 10^8 atoms. The implementation of the procedure including sampling and chemical treatment should require a maximum of one day and allow the simultaneous measurement of both isotopes strontium-89 and -90.

We use a combination of conventional magnetic mass separation, collinear laser excitation of a fast atomic beam, field ion-

[*] Dr. K. Wendt, Dipl.-Phys. J. Lantzsch, B. A. Bushaw M. Sc., Prof. Dr. H.-J. Kluge, Dr. L. Monz, Prof. Dr. E. W. Otten, Dipl.-Phys. R. Schwalbach, Dipl.-Phys. M. Schwarz, Dipl.-Phys. J. Stenner, Dipl.-Phys. K. Zimmer
Institut für Physik der Universität
Staudingerweg 7, D-55099 Mainz (Germany)
Telefax: Int. code + (6131)39-2991

Prof. Dr. G. Herrmann, Dipl.-Chem. S. Niess, Dr. N. Trautmann, Dr. K. Walter
Institut für Kernchemie der Universität Mainz (Germany)

[**] This work was supported by the Bundesministerium für Umwelt, Naturschutz und Reaktorsicherheit, by the Bundesamt für Strahlenschutz, and the Umweltzentrum der Universität Mainz.

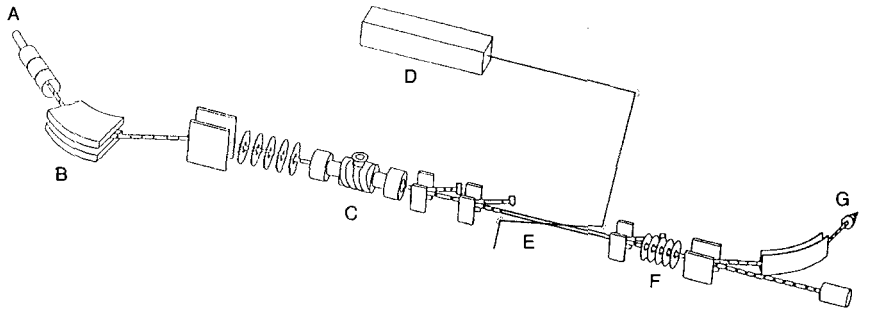


Fig. 1. Schematic representation of the apparatus for laser mass spectrometry. A = 33 keV ion source, B = mass separator, C = charge exchange cell, D = argon ion laser, E = optical excitation, F = field ionization, G detector.

ization of the excited atoms, and particle detection of the ions (Fig. 1).[11b]

The chemically isolated strontium from an air sampling filter is loaded into an ion source where it is reduced, vaporized, and then ionized on a hot tungsten surface. The positive ions are extracted and accelerated to an energy of 33 keV. Mass separation in a 60° sector field magnet provides an inital suppression of the stable isotopes by up to seven orders of magnitude. The ion beam is then neutralized by charge exchange with cesium vapor in a heated cell to produce a beam of fast atoms. The different velocities of the isotopes in this beam cause an artificial isotope shift (Doppler shift) of the resonance frequency in the subsequent optical excitation. In addition this results in very narrow linewidths,[12] and leads to the required isotopic selectivity. The velocity of the ion beam is adjusted by applying a potential to the charge exchange cell to achieve a match to the resonance frequencies of the desired isotopes. In the next stage, where the optical excitation occurs, the atomic beam is superimposed at an angle of 2° with a UV laser beam from a continuous argon ion laser at a fixed wavelength (364 nm). This geometry allows all the advantages of collinear laser spectroscopy, while preventing a loss of selectivity due to the Stark effect in the electric fields.[11b] The absorption of a laser photon causes a resonant and selective excitation of the desired strontium isotope into a high-energy Rydberg state. These excited atoms are then ionized in an electric field. The resulting ions are deflected from the beam path and energy analyzed by a cylindrical condensor and then counted by means of a particle detector. The necessary high efficiency is achieved by the particle detection.[13]

The method was first tested by using synthetic samples with known levels of strontium-90 in the presence of high levels of stable strontium (up to 10^{18} atoms). The lines of optical resonance for strontium-90 and for the naturally occurring reference isotope strontium-84 (0.56% abundance) were measured alternately over a period of about one hour, with ^{90}Sr measured 90% of the time. The number of events obtained at the two resonance frequencies yields the ratio $^{90}Sr/^{84}Sr$. Since the amount of stable strontium in the original sample is known from X-ray fluorescence spectroscopy, the absolute amount of strontium-90 in the sample can be ascertained. A systematic error of about 10% is associated with the method, the statistical error is limited only by counting statistics. With this method it was possible to detect 10^7 atoms of ^{90}Sr in 10^{17} atoms of stable strontium. The required isotopic selectivity of 10^{10} is thus achieved and the limit of detection is even lower than required.

For strontium-89 its nuclear spin of 5/2 makes determination difficult, since it leads to complex hyperfine splitting of the optical resonance. Moreover, in the mass separation strontium-89 lies directly adjacent to the most abundant stable isotope strontium-88. This results in a reduction in selectivity and worsens the limit of detection by an order of magnitude. With synthetic samples it has so far been possible to measure 10^9 atoms of ^{89}Sr in 10^{16} atoms of stable strontium.

To demonstrate the usefulness of the procedure parts of an air filter that was exposed to the passage of the Chernobyl clouds between April 15–30, 1986, at the GSF in Neuherberg near München were processed and measured. The total sampling volume was about 2×10^5 m^3 air, while each measured segment corresponded to a volume of about 1000 m^3. Figure 2 shows typical results. The level of ^{90}Sr measured was 1.5×10^9 atoms, corresponding to a ^{90}Sr concentration of 1.2 mBq m^{-3} at the time of sampling. This result is in good agreement with radiometric measurements[14] performed with a much larger section of the air filter.

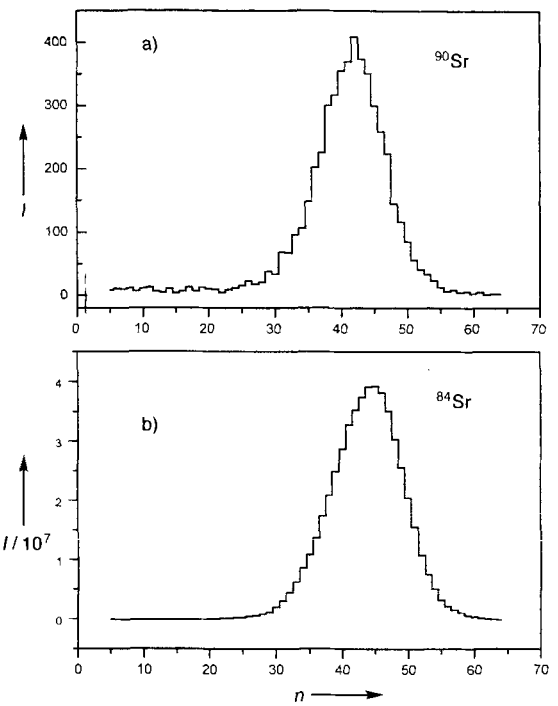


Fig. 2. Strontium-90 in an air filter exposed at the GSF Neuherberg (near München) during and after the reactor accident in Chernobyl. Resonance signals (plot of the intensity I [number of the events measured] against the channel number n) a) for ^{90}Sr and b) for the reference isotope, stable ^{84}Sr. A level of 1.5×10^9 atoms ^{90}Sr, corresponding to a concentration in the air of 1.2 mBq m^{-3} at the time of sampling, was recorded.

The initial chemical separation of strontium used for the above measurements does not have to be especially selective, since fission products in other mass ranges, such as barium-140, are separated during mass selection. Also isobaric stable impurities, such as zirconium-90, do not lead to significant interference because of the high elemental selectivity of laser excitation. This is in contrast to accelerator mass spectrometry which has also been suggested for the detection of strontium isotopes.[5, 15] The essential requirement for the chemical separation is eliminating large additions of carrier for strontium and barium. Such a procedure has been devised based on liquid–liquid extraction with crown ethers.

 © VCH Verlagsgesellschaft mbH, D-69451 Weinheim, 1995 0570-0833/95/0202-0182 $ 10.00+.25/0

This process begins with ashing the air filter at 700 °C and then dissolving the ash in 3 M nitric acid. After spiking with 10^{17} atoms of stable strontium the total strontium content is determined by X-ray fluorescence with an accuracy of better than 5%. The alkaline earth metal carbonates are precipitated from the dilute sample solutions by addition of ammonium carbonate. The precipitate is dissolved in 6 M nitric acid and the pH of the solution adjusted to 3–5 with lithium hydroxide. After addition of picrate as counterion Sr^{2+} and Ba^{2+} are separated from Ca^{2+} by extraction into dicyclohexano[18]crown-6. After back-extraction with 3 M hydrochloric acid Ba^{2+} is removed with dibenzo[24]crown-8, again in the presence of picrate. The Sr^{2+} remaining in the aqueous phase is purified from residual picrate on a cation exchange column, eluted with 6 M hydrochloric acid and the eluate is evaporated. After dissolution in 20 µL 3 M nitric acid the strontium fraction is loaded into the ion source for measurement. An average chemical yield of 70% was measured by using radiotracers. This separation procedure is also suitable for radiometric methods which require larger amounts of carrier material.

Details of the laser spectroscopy results and the chemical separation process will be published in the near future.

Received: June 11, 1994 [Z 7031 IE]
German version: *Angew. Chem.* **1995**, *107*, 202

Keywords: mass spectrometry · radionuclides · strontium

[1] a) M. Eisenbud, *Environmental Radioactivity*, Academic Press, Orlando, **1987**; b) ref. [1a], pp. 405–424.
[2] Ref. [1a], pp. 320–331.
[3] *Umweltradioaktivität und Strahlenbelastung, Jahresbericht 1983* (Ed.: Bundesminister des Inneren), Bonn, **1983**, p. 72.
[4] H. O. Denschlag, A. Diel, K.-H. Gläsel, R. Heimann, N. Kaffrell, U. Knitz, H. Menke, N. Trautmann, M. Weber, G. Herrmann, *Radiochim. Acta* **1987**, *41*, 163–172.
[5] F. Arslan, M. Behrendt, W. Ernst, E. Finckh, G. Greb, F. Gumbmann, M. Haller, S. Hofmann, R. Karschnick, M. Klein, W. Kretschmer, J. Mackiol, G. Morgenroth, C. Pagels, M. Schleicher, *Angew. Chem.* **1995**, *107*, 205–207; *Angew. Chem. Int. Ed. Engl.* **1995**, *34*, 183–186.
[6] J. Alfaro, T. Apfel, H. Diercks, A. Knöchel, R. Sen Gupta, K. Tödter, *Angew. Chem.* **1995**, *107*, 207–210; *Angew. Chem. Int. Ed. Engl.* **1995**, *34*, 186–189.
[7] H. Hötzl, G. Rosner, R. Winkler, *Radiochim. Acta* **1987**, *41*, 181–190.
[8] Ref. [1a], p. 280.
[9] G. Herrmann, G. Erdelen, *Radiochemische Methoden zur Bestimmung von Radionukliden* (Arbeitsanleitungen): *Strontium 89 und 90*, (Ed.: Bundesminister für Atomenergie und Wasserwirtschaft), Gernsbach, Braunschweig, **1959**.
[10] K. Walter, G. Herrmann, N. Trautmann, *Radiochim. Acta* **1993**, *62*, 207–212.
[11] a) G. Herrmann, H.-J. Kluge, G. Passler, N. Trautmann, K. Wendt, *Phys. Bl.* **1994**, *50*, 929–933; b) L. Monz, R. Hohmann, H.-J. Kluge, S. Kunze, J. Lantzsch, E. W. Otten, G. Passler, P. Senne, J. Stenner, K. Stratmann, K. Wendt, K. Zimmer, G. Herrmann, N. Trautmann, K. Walter, *Spectrochim. Acta Part B* **1993**, *48*, 1655–1671.
[12] R. Neugart in *Progress in Atomic Spectroscopy, Part D* (Eds.: H. J. Beyer, H. Kleinpoppen), Plenum, New York, **1987**, pp. 75–126.
[13] a) V. S. Letokhov, *Laser Photoionization Spectroscopy*, Academic Press, Orlando, **1987**; b) G. S. Hurst, M. G. Payne, *Principles and Applications of Resonance Ionization Spectroscopy*, Hilger, Bristol, **1988**.
[14] G. Rosner, personal communication, **1993**. We would like to thank Dr. Rosner at GSF Neuherberg for supplying the filter samples.
[15] a) M. Baumgärtner, U. Emmerling, W. Ernst, E. Finckh, G. Fuchs, F. Gumbmann, M. Haller, R. Höpfl, R. Karschnick, W. Kretschmer, A. Rauscher, M. Schleicher, W. Schuster, *Nucl. Instrum. Methods Phys. Res. Sect. B* **1990**, *50*, 286–290; b) D. Müller, B. Bante, T. Faestermann, A. Gillitzer, H. J. Körner, G. Korschinek, U. Büttner, *ibid.* **1992**, *68*, 313–318.
[16] a) K. Zimmer, J. Stenner, H.-J. Kluge, J. Lantzsch, L. Monz, E. W. Otten, G. Passler, R. Schwalbach, M. Schwarz, H. Stevens, K. Wendt, G. Herrmann, S. Nieß, N. Trautmann, K. Walter, B. A. Bushaw, *Appl. Phys. Sect. B* **1994**, *59*, 117–121; b) K. Walter, K. Christian, S. Nieß, G. Herrmann, N. Trautmann, unpublished.

Trace Analysis of the Radionuclides ^{90}Sr and ^{89}Sr in Environmental Samples II: Accelerator Mass Spectrometry (AMS)**

Fatma Arslan, Martin Behrendt, Werner Ernst, Eberhard Finckh,* Gunther Greb, Friedrich Gumbmann, Martin Haller, Stefan Hofmann, Ralf Karschnick, Matthias Klein, Wolfgang Kretschmer, Jochen Mackiol, Gerhard Morgenroth, Christian Pagels, and Markus Schleicher

The quantitative determination of extremely small quantities of rare isotopes is conveniently performed by accelerator mass spectrometry (AMS), which is also operated in the Tandem Accelerator Laboratory of the Universität Erlangen–Nürnberg. The measured ratio of the concentrations of the rare and the abundant isotopes can be in the range 10^{-9} to 10^{-15}. Such ratios cannot be satisfactorily determined by conventional mass spectrometry. Instead, special nuclear physical methods must be applied that require energies in the MeV range only achievable using an accelerator. One of these methods has been used routinely for several years for the determination of ^{10}Be and ^{14}C;[1, 2] it is also suitable for elementary analysis.[3]

The equipment at Erlangen is schematically illustrated in Figure 1.[4, 5] In the sputter ion source, Cs vapor is thermally ionized (about 1000 °C) at a spherical Ta surface, and the Cs^+ ions

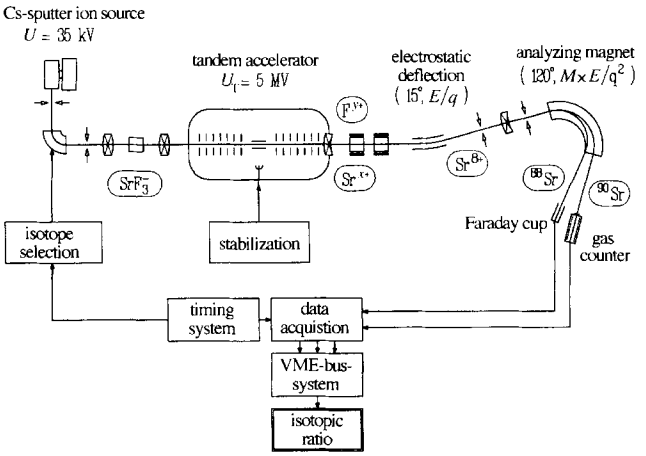


Fig. 1. Schematic representation of the AMS equipment at Erlangen (see text for further details).

are focused on the sample by suitable electric fields. This causes negative ions to be expelled from the sample. In order to achieve an ion beam of optimum quality (i.e., a high ionic current with low emittance), the electric fields in the source were optimized by computer simulations.[6] The negative ions are separated according to their mass in the 90° injection magnet. The isotopes

[*] Prof. Dr. E. Finckh, F. Arslan, M. Behrendt, W. Ernst, G. Greb, F. Gumbmann, M. Haller, S. Hofmann, R. Karschnick, M. Klein, W. Kretschmer, J. Mackiol, G. Morgenroth, C. Pagels, M. Schleicher
Physikalisches Institut der Universität Erlangen-Nürnberg
Erwin-Rommel-Strasse 1, D-91058 Erlangen (Germany)
Telefax: Int. code + (9131)15249

[**] This work was supported by the Bundesministerium für Umwelt, Naturschutz, und Reaktorsicherheit. We thank Siemens AG, Erlangen for the ^{90}Sr activity and Dipl.-Chem. Rahul Sen Gupta, Universität Hamburg, for the preparation of the calibrated samples.

to be measured are injected cyclically into the tandem accelerator, where they undergo a charge reversal at a typical energy of 5 MeV, giving an n-fold positively charged state, and are then accelerated to $(n+1)\times 5$ MeV. The molecular ions resulting from the charge reversal are in a highly positively charged state, and decompose to form positively charged atoms.

The mass spectrometer consists of an electrostatic deflecting field (15°) and a 120° analyzing magnet. This magnet is equipped with second order (split pole) image correction, and optimized for high mass dispersion. In the focal plane 3 m beyond the end of the magnetic field the ^{88}Sr and ^{90}Sr isotopes are separated by 8 cm from each other. The imaging properties of this spectrometer were calculated by us, and the results of tests with various Sr and Zr isotopes were in agreement with predictions.

Furthermore, in the beam path before and after the accelerator are several electrostatic focusing lenses, deflection plates for adjusting the beam, and beam-defining slits. The beam tubes of the equipment are evacuated by several mechanical and cryogenic pumps ($p < 10^{-3}$ Pa).

The ions of the more abundant isotope are measured as an ionic current in a Faraday cup in the focal plane of the 120° magnet. The less abundant ions are detected separately in a $\Delta E - E$ gas detector. In this way, the energy loss ΔE in the first part and the residual energy E in the second part of the gas-filled ionization chamber are determined simultaneously. The number of events is then plotted versus the ΔE-E plane. The signal due to the ions of the isotope being determined appears at a definite position in this plane. Background ions, which appear in the detector because of rare events such as scattering by the residual gas, give other ΔE and E values and can be distinguished. For light ions, the separation of isobaric ions is also possible. These differ only in energy loss, so that there is no residual background. In the case of the heavy ^{90}Sr ions, the ΔE measurement is not sufficient to separate them from the isobaric ^{90}Zr ions. A limit of detection of ^{90}Sr ions is thus imposed by the effectiveness with which it is possible to remove the ^{90}Zr present in the sample by chemical pretreatment of the sample. Therefore, a high standard of sample preparation is required (see also ref. [7]).

The basic difference from secondary ion mass spectrometry (SIMS) consists in the decomposition of the molecular ions during charge reversal in the accelerator and in the special methods for detecting the ionized atoms, which, at the high energies used, are very sensitive to atomic number Z and mass number A of the ions. However, the great technical complexity of AMS is only acceptable if simpler methods are not adequate.

Only negative ions can be accelerated in the tandem accelerator. As Sr does not form negative ions, a negative molecular ion must first be formed, which then decomposes into its components on charge reversal in the accelerator. Extensive testing has been carried out to determine the most suitable molecule (Table 1) and hence to establish the chemical nature of the AMS sample. The optimum molecular ion is SrF_3^-, which can be extracted from a SrF_2 sample producing relatively high currents. For the sputtering process, the sample must have good thermal and electrical conductivity. The SrF_2 is therefore mixed with a suitable powdered metal (high purity Au; mass ratio SrF_2:Au = 1:2), ground in a pestle and mortar, and compressed in the sample holder at a pressure of 1500 MPa (15 kbar). A target that contains 10 mg SrF_2 yields negative ions in the sputtering source for a period of 2–3 h.

Table 1. Electric currents of negative ions from various strontium compounds. Powdered Au or Ta must be added to cause electrical conductivity.

Test material	Ion	Current [nA]	Test material	Ion	Current [nA]
SrF_2 + Ta	SrF^-	150	$SrCl_2$ + Au	$SrCl^-$	150
SrF_2 + Au	SrF^-	200	SrS	SrS^-	100
	SrF_3^-	300	$SrCO_3$ + Au	SrO^-	<2

Ions of different masses are already well separated after the 90° injection magnet. A mass spectrum recorded after this magnet (Fig. 2) contains not only the signals for SrF^- and SrF_3^-, but

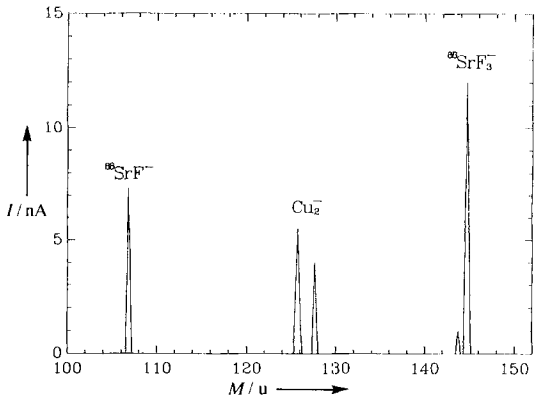


Fig. 2. Section of the mass spectrum recorded after the 90° injection magnet. I is the ionic current.

also two signals for Cu_2^-. For the ^{90}Sr measurement, the magnetic field of the injection magnet is set for $^{90}SrF_3^-$ ions. As a determination of the abundant $^{88}SrF_3^-$ ions is also necessary as a reference value, these ions are injected every 30 ms for 5 ms instead of $^{90}SrF_3^-$. Switching between the two types of ion takes place by applying a suitable high voltage to the chamber inside the 90° magnet at a constant magnetic field. Since this can occur very rapidly, slow changes of the ion transmission through the accelerator can be eliminated.

Decomposition of the injected SrF_3^- ions takes place after charge reversal, and ionized atoms with various positive charges are formed. These cations are then separated (Fig. 3) in the

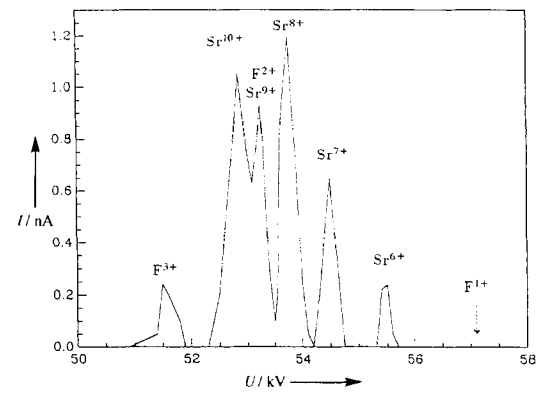
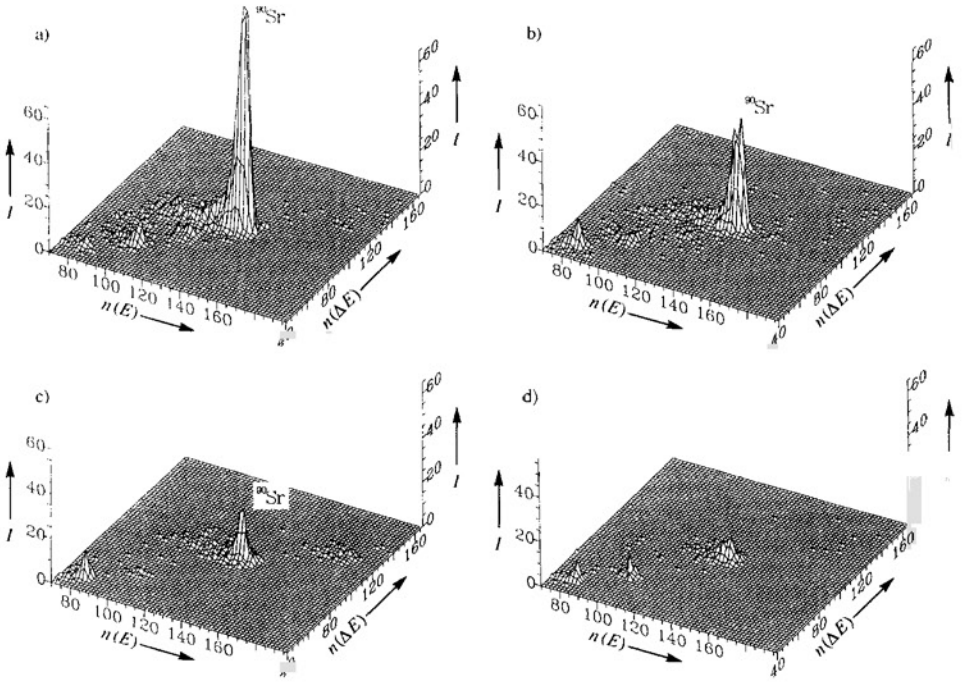


Fig. 3. Separation of the ionized atoms with various positive charges by the electrostatic sector field. The ionic current I due to the molecular fragments is plotted against the applied voltage U.

electrical sector field (see Fig. 1). The signal for Sr^{8+} is intense, and is well separated from its neighbors. It is therefore used for the ^{90}Sr measurements.

This method of analysis was tested by using samples containing known concentrations of ^{90}Sr taken from a commercially available standard material. Two inactive reference samples and three



The intensity I (number of measured events) is plotted versus the channel number $n(\Delta E)$ which is proportional to the energy loss ΔE, and versus the channel number $n(E)$, which is proportional to the residual energy E. ^{90}Sr ions appear at a definite energy loss ΔE and a certain residual energy E. The background contribution is determined from the spectrum of the inactive sample (below right).

^{90}Sr samples were investigated: high purity ("Optipur") SrF_2, inactive SrF_2 prepared from $SrCO_3$ by treatment with high purity HF, and three samples of SrF_2 of different activity prepared from $SrCO_3$ ("Suprapur") with addition of a ^{90}Sr standard. This was obtained by diluting 1 mL of $^{90}SrCl_2$ solution which had an activity of 7700 Bq with H_2O ("Nanopur"). The $^{90}Sr/^{88}Sr$ ratios for the three active samples were 1.4×10^{-9}, 7×10^{-9}, and 14×10^{-9}.

For the measurements, a source voltage of $U = 35$ kV was used, with an acceleration voltage of $U_T = 5$ MV in the tandem accelerator. With the selected ion (Sr^{8+}), this corresponds to a beam energy of 43 MeV after the charge reversal and the second acceleration. Because of the energy losses on decomposition of the molecule, the energy of the Sr ions is somewhat less than $(8+1) \times 5$ MeV. The measured ^{88}Sr ionic current in the focal plane of the 120° analyzing magnet was 1.5 nA. Typical ΔE–E spectra for the inactive sample and the three active samples are shown in Figure 4. From the intensity of the ^{90}Sr signal, the activity of each sample can be calculated after normalization based on the number of ^{88}Sr ions. As can be seen from the spectrum of the inactive sample, a small background due to ^{90}Zr is present which cannot be distinguished from the ^{90}Sr. This limits the sensitivity of the ^{90}Sr determination.

Other impurities in the sample (e.g., Ag, Al, Cu) are only noticeable at higher concentrations, and can be avoided by a suitable pretreatment. This background was minimized in a large number of measurements; considerable improvements resulted from the use of Au as a mixed substance (instead of Ag as is used in ^{14}C determinations) and of a Ta insert in the copper sample holder. The advantage of using the heavy elements Au and Ta is that they can be completely removed in the injection magnet due to their high mass. Light elements, on the other hand, can form molecular ions (e.g., with F) with a mass similar to that of the SrF_3^- ions, and these consequently appear in the accelerator.

The isotope ratios $^{90}Sr/^{88}Sr$ were determined from the 6–10 separate measurements (10 min measuring time per sample). The results are listed in Table 2. The stated measuring errors were determined from the spread of the data. The values for the inactive sample must be taken as the background measurement which must be subtracted from the values for the active samples. The results, corrected in this way, agree well with the isotope ratios calculated from the activity of the standard within the limits of error.

Table 2. Results of measurements on samples of known activity, and two inactive samples (blank and "Optipur"). The result for the blank is the value for the background, presumably due to zirconium, and must be subtracted from the values for the calibrated samples. The errors ($\pm 1\sigma$) are determined from several individual measurements.

Sample [a]	measured	after subtracting background
1(14)	14.4 ± 0.9	13.12 ± 0.94
2(7)	7.09 ± 0.5	5.81 ± 0.57
3(1.4)	2.25 ± 0.13	0.97 ± 0.31
blank	1.28 ± 0.28	
Optipur	1.15 ± 0.15	

[a] Values in parentheses give the $^{90}Sr/^{88}Sr$ ratio $\times 10^9$.

The measurements carried out with the AMS equipment in Erlangen have shown that rapid ^{90}Sr analyses are possible at levels as low as 10^{-9} using pure starting materials. However, using environmental samples containing fission products, for example those prepared from air filters, an optimized chemical pretreatment is necessary. The level of ^{90}Zr must be reduced below 10^{-9}, and other impurities (e.g., Al, Cu, Ag) must be effectively removed.

Received: June 11, 1994 [Z 7030 IE]
German version: *Angew. Chem.* **1995**, *107*, 205

[1] "Proceedings Sixth International Conference on AMS, 1993" in *Nucl. Instrum. Methods Phys. Res. Sect. B* **1994**, *94*, 1–524.
[2] "14th International Radiocarbon Conference, 1991" in *Radiocarbon* **1992**, *34*, 279–942.

[3] J. M. Anthony, S. Matteson, J. L. Duggan, P. Elliot, D. Marble, F. D. McDaniels, D. Weathers, *Nucl. Instrum. Methods Phys. Res. Sect. B* **1990**, *52*, 493–497; M. Döbeli, P. W. Nebiker, M. Suter, H. A. Synal, D. Vetterli, *ibid.* **1994**, *85*, 770–774.

[4] M. Baumgärtner, U. Emmerling, W. Ernst, E. Finckh, G. Fuchs, F. Gumbmann, M. Haller, R. Höpfl, R. Karschnick, W. Kretschmer, A. Rauscher, M. Schleicher, W. Schuster, *Nucl. Instrum. Methods Phys. Res. Sect. B* **1990**, *50*, 286–290 and **1990**, *52*, 273–277.

[5] F. Arslan, M. Behrendt, W. Ernst, E. Finckh, G. Greb, F. Gumbmann, M. Haller, S. Hofmann, R. Karschnick, M. Klein, W. Kretschmer, J. Mackiol, G. Morgenroth, C. Pagels, M. Schleicher, *Nucl. Instrum. Methods Phys. Res. Sect. B* **1994**, *92*, 39–42.

[6] R. Höpfl, T. Bretschneider, A. Buchler, Y. Charasse, W. Ernst, E. Finckh, R. Goblirsch, F. Gumbmann, M. Haller, R. Karschnick, W. Kretschmer, A. Rauscher, H. Schielein, M. Schleicher, *Rev. Sci. Instrum.* **1992**, *63*, 2469–2471.

[7] J. Alfaro, T. Apfel, H. Diercks, A. Knöchel, R. Sen Gupta, K. Tödter, *Angew. Chem.* **1995**, *107*, 207–210; *Angew. Chem. Int. Ed. Engl.* **1995**, *34*, 186–189.

Trace Analysis of the Radionuclides ^{90}Sr and ^{89}Sr in Environmental Samples III: Development of a Fast Analytical Method**

Juan Alfaro, Thomas Apfel, Herbert Diercks, Arndt Knöchel,* Rahul Sen Gupta, and Klaus Tödter

The nondestructive determination of the ^{90}Sr and ^{89}Sr content in a given sample is impossible due to the lack of characteristic γ-lines for these pure β^- emitters. This determination, however, is especially important in the case of nuclear accidents as Sr^{2+} isotopes are deposited, like Ca^{2+}, into the bones where they damage the blood-forming organs, an effect that is worsened by their long biological half-life. In combination with the relatively high ionization density of the β^- radiation released and the long physical half-life, this leads to a high radiotoxicity, especially for ^{90}Sr.

As other nuclides contribute to the essentially nonspecific β^- radiation, it is necessary to remove all accompanying nuclides before analyzing the Sr isotopes. The established standard method consists of a series of precipitation steps, the quality of which is crucially dependent on the exact precipitation conditions.[1] The ^{90}Sr content is then determined from the daughter nuclide ^{90}Y, which must first be formed and separated. The accuracy and the detection limit is therefore dependent on reaching the equilibrium between the radioactive Sr and Y isotopes. A detection limit of 1 mBq kg^{-1} is possible, but this requires an analysis time of 2–3 weeks, unacceptably long in the case of accidents.

This became apparent shortly after the reactor accident at Chernobyl when there were no analytical techniques for the determination of $^{89}Sr/^{90}Sr$ contents that where sufficiently fast and reliable to estimate the spread and extent of the Sr contamination.[2] The separation of strontium by personnel unaccustomed to the technique was especially problematic. Even the presence of additional equipment did not allow an increase in sample throughput to meet the short-term need.[3]

[*] Prof. Dr. A. Knöchel, J. Alfaro, T. Apfel, H. Diercks, R. Sen Gupta, K. Tödter
Institut für Anorganische und Angewandte Chemie der Universität
Martin-Luther-King-Platz 6, D-21049 Hamburg (Germany)
Telefax: Int. code + (40)4123-2893

[**] This work was supported by the Bundesministerium für Umwelt, Naturschutz und Reaktorsicherheit as well as the Fonds der Chemischen Industrie. We thank Dr. Heinemann, KFA Jülich, and Dr. Vogl, Bundesamt für Strahlenschutz, for providing us with samples and some measurements.

In order to overcome these shortcomings, the German Federal Minister of the Environment, Nature Conservation, and Nuclear Safety (Bundesminister für Umwelt, Naturschutz und Reaktorsicherheit) stimulated the development of methodologies to enable the collection of data by precision analyses which would allow model calculations of the spread of contaminated aerosols. The results of these calculations were then to be used to perform well-targeted, rapid analyses of food, soil, and plant samples. For the detection of radioactive strontium isotopes, a rapid method was developed that lends itself to automation, performs an on-line measurement of the Sr isotope contents, minimizes the educational requirements for the operators, and minimizes possible sources of errors. The analytical techniques developed under these premises are based on ion chromatographic separation[4] of Sr with a subsequent flow detection.[5] They are schematically summarized in Figure 1.

It was necessary to optimize existing sample preparation steps or even to develop new ones in some cases in order to be able to exploit the full capabilities of ion chromatography coupled with on-line detection.

Milk samples are ashed without time-consuming drying steps directly in an electrically heated, quartz-glass fluidized bed reactor at 650 °C.[6] Using a special injection system, the milk is added with a flow rate of 5 mL min^{-1}—the flow rate is limited by the size of the reactor—directly into the heated fluidized bed of quartz sand. The use of compressed air to generate the fluidized bed leads to a soot-free ash which can be removed together with the sand from the reactor, after a cool-down period of approximately 20 minutes. The strontium can be extracted from this mixture with 20% HCl with a yield of over 99%. The solution is then evaporated to dryness and the residue is taken up in a 2% $(NH_4)_2H_2EDTA$ solution (pH = 5). This solution is subjected to ion chromatography in order to separate Sr^{2+}.

Airborne dust samples, together with the filter material, are either oxidatively pyrolyzed in the newly developed fluidized bed apparatus[7] or ashed in a muffle oven. The residue is solubilized in a microwave-assisted system (MLS-1200, Milestone) using a mixture of three parts HCl, one part HNO_3, and 1/30 part HF over a period of 45 minutes. The solution is evaporated to dryness, the residue is then taken up in a 2% $(NH_4)_2H_2EDTA$ solution (pH = 5) and ion chromatography is used to separate Sr^{2+} from this solution.

For the examination of soil samples, 100 g of the homogenized and ashed sample are subjected to Soxhlet extraction with 20% HCl. Subsequently, iron is removed to about 99% from the solution in the form of the hexachloro complex using an anion exchange resin (Dowex 1X-4). This is necessary because iron interferes with the further treatment of the sample. The iron-free solution is then evaporated to dryness in a rotary evaporator. The residue is taken up, with mild heating, in the 2% $(NH_4)_2H_2EDTA$ solution (pH = 5) and ion chromatography is again used to separate Sr^{2+} from this solution. (The residual iron left on the column can be removed by washing with water.)

The ion chromatographic separation of strontium isotopes exploits the strong affinity of Sr^{2+} ions to a highly acidic cation exchange resin[8] in combination with the formation of, compared to other cations, less stable Sr^{2+}–EDTA complexes.[9]

After the solubilized and conditioned sample solution is put onto a cation exchange column, metal ions such as ZrO^{2+}, Y^{3+}, Fe^{3+}, Cu^{2+}, Zn^{2+}, Pb^{2+}, Mn^{2+}, Ru^{3+}, Co^{2+}, and Ln^{3+} (Ln = rare earth element) do not interact with the exchange resin at this pH due to the high stability of their EDTA complexes. These ions therefore pass freely through the column. Ca^{2+}

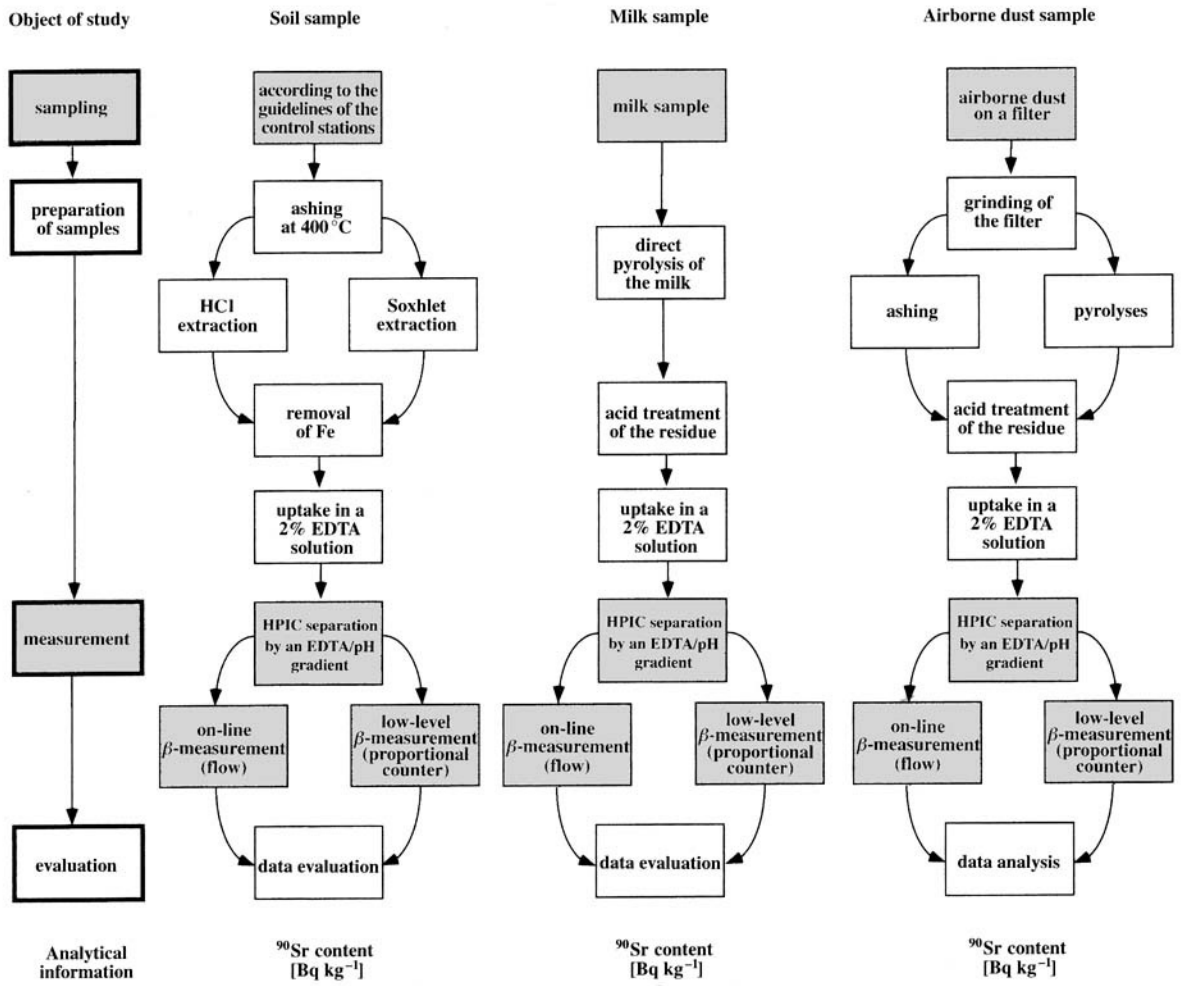


Fig. 1. Analytical method for the determination of ^{90}Sr. EDTA = ethylenediaminetetraacetate, HPIC = high performance ion chromatography.

forms less stable EDTA complexes and is retained to a small degree, while Sr^{2+}, Ba^{2+}, and Ra^{2+} are retained quantitatively on the column.

Using an EDTA-controlled pH gradient, these nuclides can by eluted in a stepwise manner. The completeness of the separation was tested with the radiotracers $^{54}Mn^{2+}$, $^{59}Fe^{3+}$, $^{65}Zn^{2+}$, $^{60}Co^{2+}$, $^{22}Na^{+}$, $^{85}Sr^{2+}$, $^{137}Cs^{+}$, $^{131}Ba^{2+}$, $^{140}La^{3+}$, $^{103}Ru^{3+}$, and $^{95}Zr^{4+}$. It was possible to demonstrate that the separation is quantitative at the concentration levels that typically occur in accident situations.

A glass column with a volume of 2 mL allows, at pH = 6, the complete separation of 0.2–4 mg of Sr^{2+} in a maximum volume 4 mL, from 200 mg of Ca^{2+}; Ba^{2+} only elutes at pH > 7. High matrix element concentrations, typically found in soil samples, require correspondingly larger columns.

Figure 2 shows a typical result of the analysis of a simulated airborne dust sample. A 2 mL column was used. The 5 mL sample contained 200 μg of Sr^{2+} and a total of 18 mg of other ions. Owing to the very small eluted volume, the immediate subsequent on-line detection of strontium is possible, using a β^--HPLC detector, without having to take the formation of the daughter nuclide ^{90}Y into consideration. Optimized detector settings and parameters made it feasible to simultaneously detect ^{90}Sr (E_{max} = 0.5 MeV) and ^{89}Sr (E_{max} = 1.5 MeV) in the two independent monitor channels, up to a ratio of 1/20. When less favorable $^{90}Sr/^{89}Sr$ ratios are present, the ^{90}Sr content can be determined via subsequently formed ^{90}Y. In this case, after

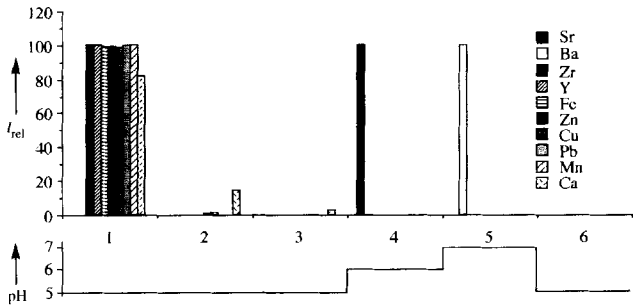


Fig. 2. Separation of strontium from a simulated airborne dust sample using an EDTA/pH gradient. The recurrence I_{rel} [%] is plotted versus the number of the fraction; the fraction volume was 10 mL. The ions were detected by total reflection X-ray fluorescence analysis (TRFA) [10] (Seifert, Ahrensburg).

the removal of accompanying elements, the strontium is left on the column overnight; ^{90}Y is eluted immediately when the system is re-started and comes off in a narrow band and can be detected in the stream.

Figure 3 shows the schematic setup of the automated HPLC apparatus. It is controlled by a computer and consists of two high-pressure gradient pumps, an autosampler, a motorized switching valve, separation columns with volumes of 15 and 2 mL for preseparation and focusing, a β^--detector, and a fraction collector.

 © VCH Verlagsgesellschaft mbH, D-69451 Weinheim, 1995 0570-0833/95/0202-0187 $ 10.00+.25/0

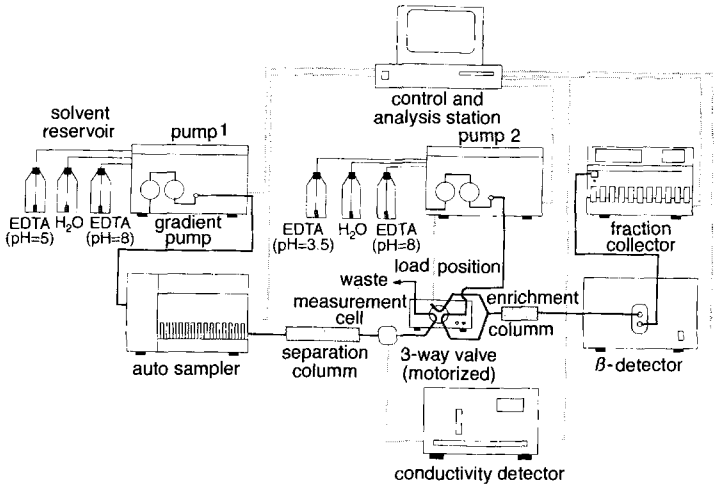


Fig. 3. HPLC apparatus for the separation and determination of radioactive strontium isotopes (HPLC components obtained from Gynkotek, Munich; flow β^--detector LB 506-C, laboratory of Prof. Berthold, Wildbad).

The complete set of procedures listed in Figure 1 was tested by using standard solutions; the method for soil samples has been applied to Russian samples from the area of Clincy as well as to strontium-doped reference samples provided by the Federal Agency for Nuclear Safety (Bundesamt für Strahlenschutz).

The soil samples were first ashed at 450 °C and subsequently, in accordance with the published official requirements,[11] either extracted directly with HCl or subjected to an HCl Soxhlet extraction. The iron matrix was removed from the HCl solution in the form of hexachloroferrate(III) by anion exchange. After complete evaporation of the solvent and redissolution in 2% $(NH_4)_2H_2EDTA$, the pH was adjusted to 5. As described above, Sr^{2+} is preseparated on the 15 mL column, focused on the second ion exchange column (2 mL), and the $^{90}Sr^{2+}$ was detected online in the throughput. For control purposes, the Sr fractions were collected immediately after the separation and subjected to off-line measurements using a low-level counter equipped with 10 proportional counting tubes.

In addition, the soil samples were examined by γ-spectroscopy before the extraction, after the drying and homogenizing steps. The recovery was determined after each step using TRFA.[10]

Table 1. β^-- and γ-measurements of Russian soil samples.

Sample	γ-Measurements [Bq kg^{-1}]				β^--Measurements ^{90}Sr [Bq kg^{-1}]		
no.	^{137}Cs	^{137}Cs [a]	^{134}Cs	^{134}Cs [a]	flow	low-level [b]	standard [a]
1586	709	760	66	81	10	15	14
1587	1150	1100	117	110	17	20	23
1588	2610	2500	265	260	39	41	36
1589	658	700	67	76	19	20	20
1590	2280	2300	235	220	–	9	9.2
1591	92	99	8	10	–	4	4.1
1592	7870	7300	805	790	70	65	69
1593	4400	4700	452	500	54	66	50
1594	5350	5700	504	580	55	61	59
1595	7400	7500	737	760	88	79	150
1597	78	80	6	7	12	10	14
1598	1980	1900	203	200	26	28	26
1599	6790	7700	694	830	81	87	88
1600	165	160	14	15	–	2	5.4
1601	2570	3000	265	320	30	31	27
1614	2730	3000	258	290	48	45	50
1615	1010	1100	104	104	–	–	10

[a] Data from KFA-Jülich. [b] Low-level counter LB 770-2 (Labor Prof. Berthold).

Table 1 summarizes the results of the β^-- and γ-measurements of the Russian soil samples.

The results obtained by the rapid technique (flow detection) agree well with those obtained with the standard method and the low-level measurements. Table 2 summarizes the results obtained for the reference samples.

Table 2. Results obtained for the reference samples.

Sample no.	Doping BFS [a] [Bq]	Flow [Bq]	Low-level [Bq]	Scintillation [Bq]
11	9	7 ± 2,5	8 ± 3	7 ± 2
12	76	75 ± 1	72 ± 8	72 ± 10
13	54	57 ± 7	54 ± 12	53 ± 8
14	99	99 ± 12	99 ± 12	99 ± 11
15	31	29 ± 4	26 ± 8	27 ± 6
16	76	72 ± 11	66 ± 11	67 ± 14
17	23	21 ± 7	21 ± 3	20 ± 4
18	107	114 ± 7	111 ± 16	107 ± 11
19	10	10 ± 1	10 ± 3	10 ± 3
20	46	46 ± 1	47 ± 5	45 ± 5

[a] Bundesamt für Strahlenschutz, Neuherberg.

It is obvious that the new technique is able to quantitatively detect ^{90}Sr in soil samples. The deviations (68.3%) are in the usual error range of 10–15%; however, it should be noted that the stated confidence intervals are based on only two parallel determinations, assuming the t-distribution.[12]

Figure 4 shows the chromatogram for a separation of a standard sample doped with ^{90}Sr/Y, ^{103}Ru and ^{137}Cs.

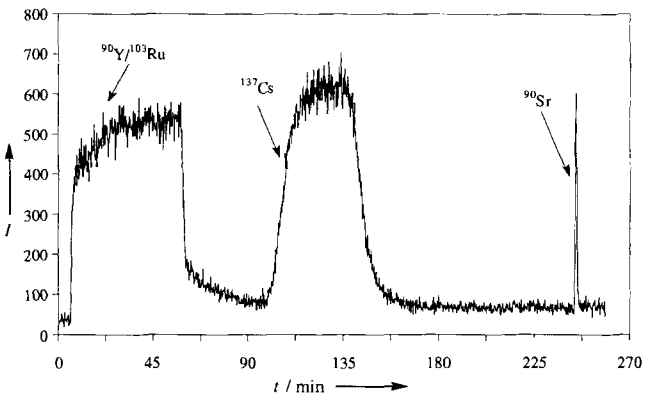


Fig. 4. Chromatogram (β^--HPLC detector) of a standard soil sample treated with ^{90}Sr/Y, ^{103}Ru, and ^{137}Cs.

The characteristic data for these analytical procedures, obtained by calibration methods,[11] indicate that in the studied range of activities (9–150 Bq), systematic errors can be excluded with a statistical certainty of 95%. An additional F-test[12] allows the exclusion of systematic deviations between the measured data with a statistical certainty of 99%.

The newly developed method for the separation of Sr isotopes is also suitable for sample preparation needed for accelerator mass spectrometry (AMS)[13] and resonance ionization mass spectrometry.[14]

Received: June 11, 1994 [Z 7029 IE]
German version: *Angew. Chem.* **1995**, *107*, 207

Keywords: chromatography · ion chromatography · on-line detectors · radionuclides · strontium

 © VCH Verlagsgesellschaft mbH, D-69451 Weinheim, 1995 0570-0833/95/0202-0188 $ 10.00+.25/0

[1] *Meßanleitungen for die Überwachung der Radioaktivität in der Umwelt and zur Erfassung radioaktiver Emissionen aus kerntechnischen Anlagen* (Ed.: Bundesminister for Umwelt, Naturschutz and Reaktorsicherheit), Fischer, Stuttgart, **1992**.
[2] *Veröffentlichungen der Strahlenschutzkommission, Vol. 7* (Ed.: Bundesminister for Umwelt, Naturschutz and Reaktorsicherheit), Fischer, Stuttgart, **1987**.
[3] Hamburg Workshop "Radiologische Auswirkungen des Tschernobyl-Unfalls auf die Bundesrepublik Deutschland", 20./21. November 1986, Hamburg.
[4] M. A. Wade, H. J. Seim, *Anal. Chem.* **1961**, *33*, 793.
[5] For a definition of the analytical terms: K. Danzer, E. Than, D. Molch, L. Küchler, *Analytik*, Wissenschaftliche Verlagsgesellschaft, Stuttgart, **1987**.
[6] R. Sen Gupta, Dissertation, Universität Hamburg, **1995**.
[7] R. Sen Gupta, Diplomarbeit, Universität Hamburg, **1992**.
[8] Cation Exchange Resin Instructions, BIO-RAD Laboratories, Richmond.
[9] F. Umland, *Theorie und praktische Anwendung von Komplexbildnern*, Akademische Verlagsgesellschaft, Frankfurt am Main, **1971**.
[10] R. Klockenkämper in *Analytiker Taschenbuch, Vol. 10* (Ed.: H. Günzler), Springer, Berlin, **1991**.
[11] W. Funk, V. Dammann, G. Donnevert, *Qualitätssicherung in der Analytischen Chemie*, VCH, Weinheim, **1992**.
[12] K. Doerfel, *Statistik in der Analytischen Chemie*, 3rd ed., VCH, Weinheim, **1990**.
[13] M. Baumgärtner, U. Emmerling, W. Ernst, E. Finckh, G. Fuchs, F. Gumbmann, M. Haller, R. Höpfl, R. Karschnick, W. Kretschmer, A. Rauscher, M. Schleicher, W. Schuster, *Nucl. Instrum. Methods Phys. Res. B* **1990**, *50*, 286; F. Arslan, M. Behrendt, W. Ernst, E. Finckh, G. Greb, F. Gumbmann, M. Haller, S. Hofmann, R. Karschnick, M. Klein, W. Kretschmer, J. Mackiol, G. Morgenroth, C. Pagels, M. Schleicher, *Angew. Chem.* **1995**, *107*, 205–207; *Angew. Chem. Int. Ed. Engl.* **1995**, *34*, 183–186.
[14] L. Monz, R. Hohmann, H.-J. Kluge, S. Kunze, J. Lantzsch, E. W. Otten, G. Passler, P. Senne, J. Stenner, K. Stratmann, K. Wendt, K. Zimmer, *Spectrochim. Acta* **1993**, *48*, 1655; J. Lantzsch, B. A. Bushaw, G. Herrmann, H.-J. Kluge, L. Monz, S. Niess, E. W. Otten, R. Schwalbach, M. Schwarz, J. Stenner, N. Trautmann, K. Walter, K. Wendt, K. Zimmer, *Angew. Chem.* **1995**, *107*, 202–204; *Angew. Chem. Int. Ed. Engl.* **1995**, *34*, 181–183.

Diastereoselective Coupling of Anodically Generated Radicals Bearing Chiral Amide Groups**

Bruno Klotz-Berendes, Hans J. Schäfer,* Matthias Grehl, and Roland Fröhlich

Dedicated to Professor Wolfgang Lüttke on the occasion of his 75th birthday

Anodic decarboxylation of carboxylic acids provides radicals (Kolbe electrolysis) and carbocations (non-Kolbe electrolysis) selectively and directly for synthesis.[1] The radicals may be used for homo- or heterocoupling reactions and for inter- or intramolecular additions to double bonds. The configurations of stereogenic centers at C3 or more distant positions of the carboxylic acids are retained, while those at C2 are completely lost.[2] By contrast, the use of chiral auxiliaries could lead to the formation of a stereogenic center at C2. Such induction has not yet been described for Kolbe electrolysis, whilst some cases are known for non-Kolbe electrolyses.[3] Recently diastereoselective cyclizations by the coupling of photochemically generated radicals have also been described.[4]

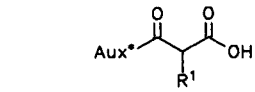
[*] Prof. Dr. H. J. Schäfer, Dipl.-Chem. B. Klotz-Berendes, Dr. M. Grehl,[+] Dr. R. Fröhlich[+]
Organisch-chemisches Institut der Univesität
Corrensstrasse 40, D-48149 Münster (Germany)
Telefax: Int. code + (251)83-9772

[+] X-ray structure analyses

[**] Electroorganic Syntheses, Part 60. This work was supported by the Fonds der Chemischen Industrie and the EC Human Capital and Mobility Programme (no. ERBCHRXCT 920073). Part 59: C. Zielinski, H. J. Schäfer, *Tetrahedron Lett.* **1994**, *35*, 5621–5624.

We report here on diastereoselective radical couplings by means of Kolbe electrolysis with formation of a stereogenic center. This was achieved by electrolyzing 2-substituted malonic acid amides **1**, which have a chiral auxiliary linked through the amide function, in the presence of co-acids **2**. Seven auxiliary groups **A**–**G** in malonic acid amides **1** and carboxylic acids **2** with substituents of varying size at C2 were used to check their effect on the diastereoisomeric ratio of the coupling product (**5**:**6**).

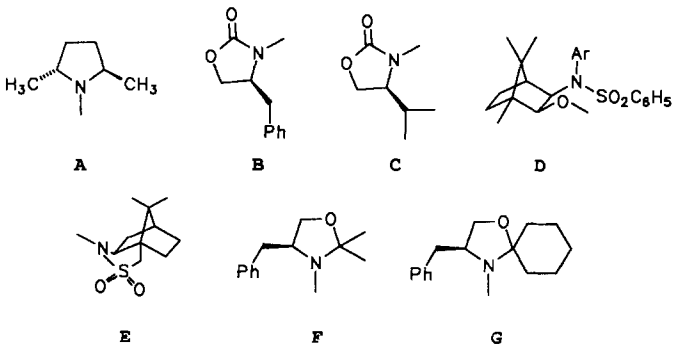
Malonic acid amides **1a** and **1b** were prepared in 58–73% yields by partial hydrolysis of the appropriate diethyl malonates (with KOH in ethanol), followed by acid chloride formation (with $SOCl_2$), reaction with the hydrochloride of **A**–**H** (in the presence of triethylamine in absolute dichloromethane), and subsequent hydrolysis of the ester group (with 20% KOH in ethanol). The **A**–**H** auxiliary was prepared by the method of



	R^1	Auxiliary
a	$CH_2C_6H_5$	**A**
b	C_4H_9	**A**
c	tC_4H_9	**A**
d	$C_2H_5C(CH_3)_2$	*rac*-**A**
e	tC_4H_9	**B**
f	tC_4H_9	**C**
g	tC_4H_9	**D**
h	tC_4H_9	**E**
i	tC_4H_9	**F**
j	tC_4H_9	**G**

R^2–CO_2H **2**

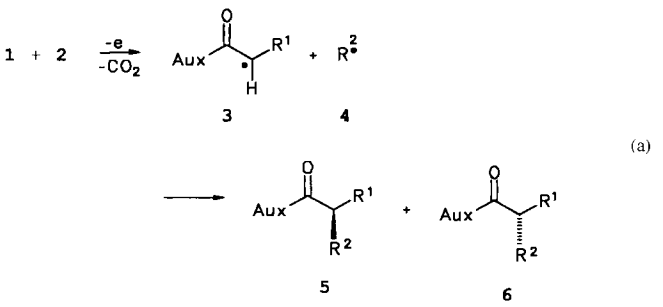
	R^2
a	C_6H_{13}
b	C_4H_9
c	$tC_4H_9CH_2$
d	$(C_3H_7)_2CH$
e	$C_2H_5O_2C(CH_3)_2C$



Masamune et al.[5] Precursors of **1c** and **1d** were prepared in 26 and 21% yields, respectively, by first condensing the corresponding diethyl malonate with acetone (zinc chloride in Ac_2O),[6a] treating the product with ethyl- or methylmagnesium iodide in the presence of CuCl,[6a] and finally, partially hydrolyzing the ester.[6b] In analogy to the synthesis of **1a**, **b**, these malonates were then converted to **1c**, **d** via the acid chlorides with yields of 75–84%. **1e** could not be prepared in the way described for **1a**–**d**. The ethyl ester of the corresponding ethyl 2-*tert*-butylmalonamide with auxiliary **B**[7] could not be selectively hydrolyzed.[8] Therefore, **1e** was prepared by treating the dianion of 3,3-dimethylbutanoic acid with benzyl chloroformate (87%). The acid was converted to the acid chloride and

then, by means of the lithium salt of **B**, into the amide (93%), from which the benzyl group was removed by hydrogenation (56–58%). For the syntheses of **1f–i** the above-mentioned acid chloride was treated with either lithium salts of **C**[9] and **D**[10] or with the non-lithiated auxiliaries **E**,[11] **F**,[12] and **G**[13] to give the corresponding amides; again the benzyl groups were removed by hydrogenation.

Carboxylic acids **1** were electrolyzed in a one-compartment cell together with a five- to tenfold excess of the co-acid **2**. The diastereomers **5** and **6** [Eq. (a)] were isolated in yields from 13 to



(a)

69% (based on **1**) (Table 1). The main by-products arise from disproportionation of radical **3** formed from **1**. During the electrolysis of **1g** with **2** no conversion was observed.

Table 1. Diastereoselective mixed Kolbe electrolyses between 2-substituted malonic acid amides **1** and co-acids **2**.

Entry	1	2	5, 6 (5:6)	Yield 5 + 6 [%]	*de* of 5, 6 [%]
1	**a**	**b**	**a** (1.7:1) [a]	38	26
2	**a**	**a**	**b** (1.5:1) [b]	32	20
3	**b**	**a**	**c** (1.6:1) [c]	38	22
4	**c**	**b**	**d** (2.9:1) [d]	36	49
5	**c**	**c**	**e** (4.7:1) [d]	39	65
6	**c**	**d**	**f** (4.5:1) [d]	40	64
7	**d**	**b**	**g** (3.3:1) [d]	69	53
8	**d**	**c**	**h** (5.5:1) [d]	42	69
9	**d**	**d**	**i** (5.6:1) [d]	37	70
10	**d**	**e**	**j** (13.4:1) [d]	13	86
11	**h**	**c**	**k** (1:4.1) [e]	51	60
12	**i**	**c**	**l** (1:2.7) [e]	33	46
13	**j**	**c**	**m** (1:2.6) [f]	20	45

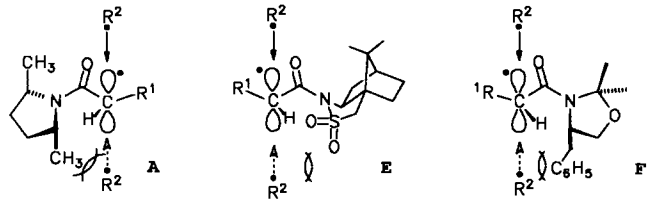
[a] The assignment of the stereochemistry at C2 was based on an independent asymmetric synthesis [14]. [b] The configuration of **5b** was assigned based on a ^{1}H NMR spectrum corresponding to that of **5a**. [c] Unequivocal assignment of the configuration at the new stereogenic center could not be made since neither an independent synthesis, as in [a], was possible nor did the positions of the signals in the ^{1}H NMR spectrum differ characteristically. [d] The assignment of the configuration at C2 is supported by three characteristic signal shifts in the ^{1}H NMR spectrum of **5** compared with those of **6**: a) the high-field shift of the methine protons in auxiliary **A**, b) the low-field shift of the methine protons on C2, and c) the high-field shift of the protons in the methyl groups of the *t*Bu and the *iso*-pentyl residues. [e] The configuration at C2 has been confirmed by an X-ray structure analysis [15]. [f] The configuration of **6m** was assigned based on a ^{1}H NMR spectrum corresponding to that **6l**.

The coupling most likely occurs through free radicals. Since carboxylic acids with a stereogenic center at C2 yield completely racemic products in Kolbe electrolysis,[2a] participation of the electrode by means of adsorption or face-selective shielding of the intermediate radical is largely excluded. The diastereoselectivity is, therefore, induced by the chiral amide group. The intermediate radical **3** occurs preferentially in the (*Z*) configuration [Eq. (b)],[16] in which the stereogenic center of the chiral auxiliary shields one face more effectively than the other.[16b]



(b)

As can be seen from Table 1, the chiral, C_2-symmetrical *trans*-2,5-dimethylpyrrolidine[17] **A** is the most effective auxiliary (entries 1–10), followed by Oppolzer's camphor sultam[18] **E** (entry 11), and the oxazolidines **F** and **G**[19] (entries 12, 13). With the oxazolidines **B** and **C** practically no face differentiation was observed. Thus in the electrolysis of **1e** or **1f** with **2b–d** diastereoisomeric excesses of 0–13% were achieved. The configuration at the stereogenic carbon atom of the predominant diastereoisomer arising from radical combination is in accord with the mechanistic picture developed for the addition of radicals substituted with an auxiliary.[20] Accordingly, the groups and atoms R^1, C$^\cdot$, C(=O), and N lie in a plane (Scheme 1). In



Scheme 1. Preferred direction for the approach of the co-radical to the auxiliary-substituted radical.

auxiliary **A** coupling from the *si* face is hindered by the axial 2-methyl group on the pyrrolidine[17] such that coupling of the co-radical occurs more or less preferentially on the *re* face. In **E** the axial oxygen atom of the sulfonyl group,[18] and in **F** and **G** the axial benzyl groups, exert the opposite effect.

The structure of the predominant diastereomer **6k** (Fig. 1)[15] reflects the preferred configuration of the intermediate radical **3** and the favored *si* coupling with **4**. Diastereoselectivity with auxiliaries **B** and **C** is small; here, obviously, the carbonyl group and not the benzyl residue of the auxiliary is oriented *syn* to the

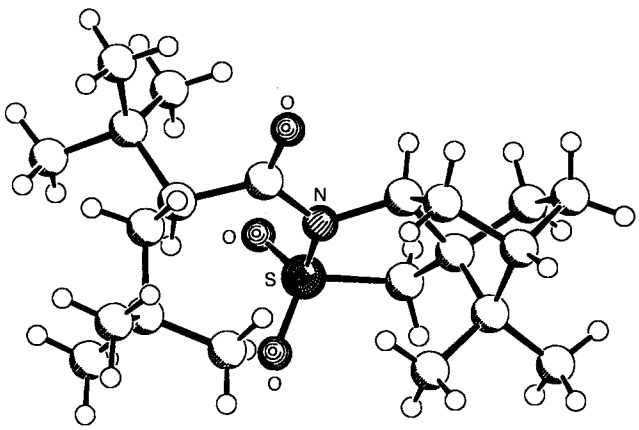


Fig. 1. Schakal plot of the crystal structure of **6k**.

 © VCH Verlagsgesellschaft mbH, D-69451 Weinheim, 1995 0570-0833/95/0202-0190 $ 10.00+.25/0

radical C atom such that face differentiation is hardly possible. As expected, the diastereoselectivity of the coupling increases with an increase in size of the co-radical (entry 7 < 8 < 9 < 10).

Since radical coupling is very fast,[21] that means with a very low activation energy, according to the Hammond principle a very early transition state is to be expected, in which steric interaction between radicals **3** and **4** is still minimal. Nevertheless, the use of proven auxiliaries and large co-radicals leads to a remarkable diastereoselectivity even in intermolecular radical coupling.

Experimental Procedure

5k, **6k**: Carboxylic acid **1h** (203 mg, 0.568 mmol) and co-acid **2c** (660 mg, 5.68 mmol) were dissolved in 13 mL of dry methanol, neutralized to an extent of 5% with 0.31 mL of a 1 M solution of KOH in dry methanol, and electrolyzed in a circulation cell with a steel cathode and a platinum anode (4 cm^2) (electrode distance: 0.5 mm) at a current density of 600 mA cm^{-2} at 30–35 °C. The electrolysis was stopped when the pH reached 8–9, and the solvent was distilled off. The residue was taken up in diethyl ether, washed with saturated sodium hydrogen carbonate solution, and dried ($MgSO_4$). The diastereomeric excess in the residue was determined by capillary gas chromatography, and the diastereoisomers were isolated by flash chromatography and HPLC. ^1H NMR of **6k**: δ = 0.89 (s, 9H, $CH_2C(CH_3)_3$), 0.96 (s, 3H, $C(CH_3)_2$), 1.00 (s, 9H, $CHC(CH_3)_3$), 1.15 (s, 3H, $C(CH_3)_2$), 1.30–1.48 (m, 2H, camphor; dd, J = 14.0, 1.2 Hz, 1H, $CH_2C(CH_3)_3$), 1.82–1.99 (m, 3H, camphor; not completely resolved dd, J = 14.0, J = 10.7 Hz, 1H, $CH_2C(CH_3)_3$), 2.12–2.16 (m, 2H, camphor), 2.74 (dd, J = 10.7, J = 1.2 Hz, 1H, $CHC(CH_3)_3$), 3.47 (d, 2H, J_{AB} = 13.8 Hz, SCH_2), 3.83 (dd, J = 7.3, J = 5.8 Hz, 1H, CH_2CHN). ^{13}C NMR of **6k**: δ = 20.0 (q, $C(CH_3)_2$), 20.9 (q, $C(CH_3)_2$), 26.1 (t, CH_2), 27.6 (q, $CH_2C(CH_3)_3$), 29.3 (q, $CHC(CH_3)_3$), 30.5 (s, $CH_2C(CH_3)_3$), 33.6 (t, CH_2), 35.7 (s, $CHC(CH_3)_3$), 39.1 (t, CH_2), 44.5 (d, CH_2CHCH_2), 44.8 (t, $CH_2C(CH_3)_3$), 47.3 (s, C1, $C(CH_3)_2$), 49.5 (d, CHCO), 53.4 (t, SCH_2), 66.7 (d, CHN), 176.0 (s, CO-amide).

Received: August 27, 1994 [Z 7275 IE]
German version: *Angew. Chem.* **1995**, *107*, 218

Keywords: asymmetric synthesis · auxiliaries · Kolbe electrolysis · radicals

[1] H. J. Schäfer, *Top. Curr. Chem.* **1990**, *152*, 91–151.
[2] L. Eberson, G. Ryde-Petterson, *Acta Chem. Scand.* **1973**, *27*, 1159–1161; L. Eberson, K. Nyberg, R. Servin, *Acta Chem. Scand. Ser. B* **1976** *30*, 906–907; G. E. Hawkes, J. H. P. Utley, G. B. Yates, *J. Chem. Soc. Perkin Trans. 2* **1976**, 1709–1716.
[3] D. Seebach, P. Renaud, *Angew. Chem.* **1986**, *98*, 836–838; *Angew. Chem. Int. Ed. Engl.* **1986**, *25*, 843–845.
[4] P. Wessig, P. Wettstein, B. Giese, M. Neuburger, M. Zehnder, *Helv. Chim. Acta* **1994**, *77*, 829–837.
[5] S. Masamune, R. P. Short, R. M. Kennedy, *J. Org. Chem.* **1989**, *54*, 1755–1756.
[6] a) E. L. Eliel, R. O. Hutchins, Sr. M. Knoeber, *Org. Synth.* **1970**, *50*, 38–42; b) F. W. Nader, A. Brecht, S. Kreisz, *Chem. Ber.* **1986**, *119*, 1196–1207.
[7] D. Evans, J. R. Gage, *Org. Synth.* **1990**, *68*, 77–82.
[8] In alkaline media only the oxazolidone residue is hydrolyzed; with pig liver esterase and in acid media no conversion occurs.
[9] M. S. Newman, A. Kutner, *J. Am. Chem. Soc.* **1951**, *73*, 4199–4204.
[10] G. Helmchen, A. Selim, D. Dorsch, I. Taufer, *Tetrahedron Lett.* **1983**, *24*, 3213–3216.
[11] Available from Merck.
[12] Synthesized as a new auxiliary in analogy to the method of N. A. Porter, I. J. Rosenstein, R. A. Breyer, J. D. Brunke, W. Wu, A. T. McPhail, *J. Am. Chem. Soc.* **1992**, *114*, 7664–7676.
[13] Obtained as a new auxiliary by a modification of a method for preparing oxazolidones by P. Michon, A. Rassat, *Bull. Soc. Chim. Fr.* **1971**, 3561–3567.
[14] For the independent synthesis of **5a** the lithium salt of (*S*)-3-(1-oxohexyl)-4-(phenylmethyl)-2-oxazolidinone was alkylated with benzyl bromide with 98% *de* according to the method of D. A. Evans, M. D. Ennis, D. J. Mathre, *J. Am. Chem. Soc.* **1982**, *104*, 1737–1739. On the grounds of the mechanism of the reaction, the newly formed stereogenic center has (*R*) configuration. Removal of the auxiliary without racemization was carried out according to the method of D. A. Evans, J. Gage, *Org. Synth.* **1990**, *68*, 83–91. Auxiliary **A** was subsequently coupled without racemization to the acid chloride. The product is identical with **5a** according to gas chromatography and ^1H NMR spectroscopy.
[15] Crystal structure data for **6k**: $C_{21}H_{37}NO_3S$, M = 383.58, crystal dimensions 0.3 × 0.25 × 0.2 mm, a = 8.718(1), b = 11.861(3), c = 11.137(2) Å, β = 108.02(1)°, V = 1095.1(4) Å^3, ρ_{calcd} = 1.163 g cm^{-3}, μ = 14.6 cm^{-1}, Z = 2, monoclinic, space group $P2_1$ (no. 4), Enraf-Nonius CAD4 diffractometer, λ = 1.54178 Å, T = 223 K, ω–2θ scan, 2455 measured reflections ($\pm h$, $-k$, $+l$), 2337 independent and 2151 observed [$I \geq 2\sigma(I)$] reflections, 244 refined parameters, R = 0.068, wR^2 = 0.172, Flack parameter 0.00(3), max. residual electron density 0.85(–0.61) e Å^3, solution by direct methods, hydrogen atoms in calculated positions. Crystal structure data for **6n** (reaction of **1e** with **2c**): $C_{21}H_{31}NO_3$, M = 345.47, crystal dimensions 0.4 × 0.4 × 0.4 mm, a = 9.501(2), b = 11.489(2), c = 18.756(4) Å, V = 2047.3(7) Å^3, ρ_{calcd} = 1.121 g cm^{-3}, μ = 5.9 cm^{-1}, Z = 4, orthorhombic, space group $P2_12_12_1$ (no. 19), Enraf-Nonius CAD4 diffractometer, λ = 1.54178 Å, T = 293 K, ω–2θ scan, 4802 measured reflections ($-h$, $+k$, $\pm l$), 4210 independent and 4028 observed [$I \geq 2\sigma(I)$] reflections, 233 refined parameters, R = 0.042, wR^2 = 0.116, Flack parameter –0.2(2), max. residual electron density 0.21(–0.14) e Å^3, solution by direct methods, hydrogen atoms in calculated positions. Crystal data for **6l**: $C_{23}H_{37}NO_2$, M = 359.54, crystal dimensions 0.25 × 0.2 × 0.4 mm, a = 9.182(4), b = 13.564(4), c = 17.965(2) Å, V = 2237.4(12) Å^3, ρ_{calcd} = 1.067 g cm^{-3}, μ = 5.1 cm^{-1}, Z = 4, orthorhombic, space group $P2_12_12_1$ (no. 4), Enraf-Nonius CAD4 diffractometer, λ = 1.54178 Å, T = 223 K, ω–2θ scan, 4213 measured reflections ($+h$, $-k$, $\pm l$), 3793 independent and 2187 observed [$I \geq 2\sigma(I)$] reflections, 244 refined parameters R = 0.061, wR^2 = 0.144, Flack parameter –2.0(6), max. residual electron density 0.28(–0.16) e Å^3, solution by direct methods, hydrogen atoms in calculated positions. Programs used: SHELX-86, SHELX-93, SCHAKAL-92. Further details of the crystal structure investigation may be obtained from the Fachinformationszentrum Karlsruhe, D-76344 Eggenstein-Leopoldshafen (Germany) on quoting the depository numbers CSD-401246 for **6k**, CSD-401247 for **6n**, and CSD-401248 for **6l**.
[16] a) W. Strub, E. Roduner, H. Fischer, *J. Phys. Chem.* **1987**, *91*, 4379–4383; b) N. A. Porter, I. J. Rosenstein, R. A. Breyer, J. D. Bruhnke, W.-X. Wu, A. T. McPhail, *J. Am. Chem. Soc.* **1992**, *114*, 7664–7676.
[17] For applications of auxiliary **A** in diastereoselective radical additions see: N. A. Porter, D. M. Scott, I. J. Rosenstein, B. Giese, H. G. Zeitz, A. Veit, *J. Am. Chem. Soc.* **1991**, *113*, 1791–1799; N. A. Porter, D. M. Scott, A. T. McPhail, *Tetrahedron Lett.* **1990**, *31*, 1679–1682.
[18] For applications of auxiliary **E** in diastereoselective radical additions see: D. Curran, W. Shen, W. Zhang, T. A. Heffner, *J. Am. Chem. Soc.* **1990**, *112*, 6738–6740.
[19] For applications of oxazolidines as chiral auxiliaries in diastereoselective radical additions see: N. A. Porter, I. J. Rosenstein, R. A. Breyer, J. D. Bruhnke, W. Wu, *J. Am. Chem. Soc.* **1991**, *113*, 7788.
[20] a) N. A. Porter, B. Giese, D. P. Curran, *Acc. Chem. Res.* **1991**, *24*, 296–304; b) W. Smadja, *Synlett* **1994**, 1–26.
[21] K. K. Ingold in *Free Radicals, Vol. I* (Ed.: J. K. Kochi), Wiley, New York, **1973**, p. 37.

A Rhodium-Mediated, Stepwise Trimerization of an Alkyne That Does Not Lead to a Benzene but Selectively to a Hexadienyne Derivative**

Helmut Werner,* Martin Schäfer, Justin Wolf, Karl Peters, and Hans Georg von Schnering

Dedicated to Professor Günther Wilke on the occasion of his 70th birthday

Since the pioneering work by Reppe et al.[1] it is well known that various transition metal compounds catalyze the cyclotrimerization of alkynes to benzene derivatives.[2] With regard to the mechanism of the reaction, it is generally assumed that initially two alkyne molecules coordinate to the metal atom, that in the

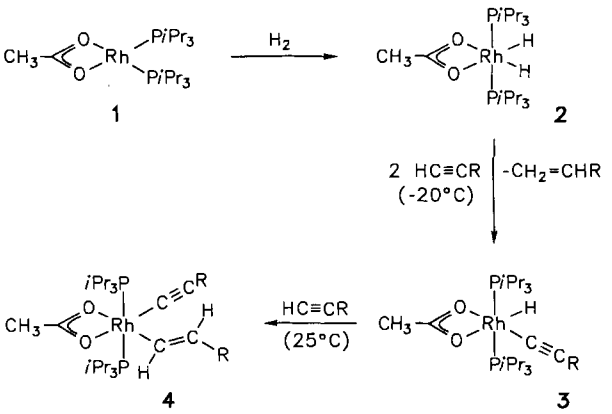
[*] Prof. Dr. H. Werner, Dr. M. Schäfer, Dr. J. Wolf
Institut für Anorganische Chemie der Universität
Am Hubland, D-97074 Würzburg (Germany)
Telefax: Int. code + (931)888-4605
Prof. Dr. H. G. von Schnering, Dr. K. Peters
Max-Planck-Institut für Festkörperforschung
Heisenbergstrasse 1, D-70506 Stuttgart (Germany)
Telefax: Int. code + (711)689-1562

[**] This work has been supported by the Volkswagen Stiftung, the Deutsche Forschungsgemeinschaft (SFB 347), and Degussa AG.

next step by oxidative coupling the formation of a metallacyclopentadiene occurs, and that finally this reactive intermediate reacts with another alkyne to give the cyclic trimer. Vollhardt in particular has transformed the [2 + 2 + 2] cycloaddition of alkynes or of alkynes and olefins mediated by cyclopentadienylcobalt compounds into a useful and widespread synthetic methodology.[3]

We have recently shown that the dimerization of two 1-alkynes in the coordination sphere of rhodium can lead to the formation of either enynes (e.g., (*Z*)-PhCH=CHC≡CPh) or butatrienes (e.g., (*E*,*Z*)-PhCH=C=C=CHPh).[4] Key intermediates are the alkynyl(vinylidene) metal complexes *trans*-[Rh(C≡CR)(=C=CHR)($P i Pr_3$)$_2$], which are formed from [Rh(η^3-$CH_2C_6H_5$)($P i Pr_3$)$_2$] and two equivalents of HC≡CR (R = Ph, *t*Bu), and which react with CO or HCl by C–C coupling. In the continuation of this work, by using the acetatorhodium(I) complex **1**[5] as the starting material we have now achieved the trimerization of a 1-alkyne that selectively yields a hexadienyne instead of a benzene derivative.

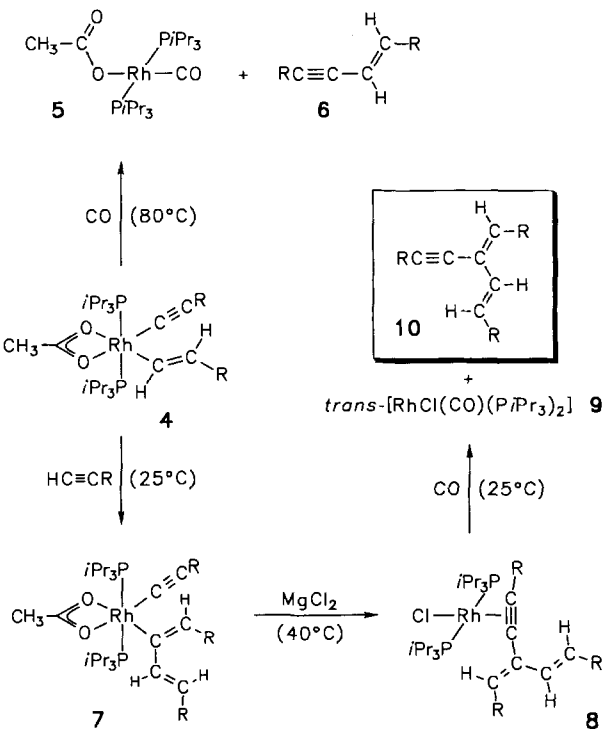
The preparation of the intermediate **4**, which plays a decisive role in the C–C bond formation, is outlined in Scheme 1. Com-



Scheme 1. R = CO_2Me.

pound **2**, formed on oxidative addition of H_2 to **1**,[6] reacts first with HC≡CCO_2Me in pentane at −20 °C to yield the alkynyl(hydrido) complex **3**, which on further treatment with an equimolar amount of methyl propiolate (pentane, 25 °C) quantitatively gives the alkynyl(vinyl)rhodium(III) derivative **4**. Due to the ^{1}H and ^{31}P NMR spectroscopic data there is no doubt that the two substituents at the C=C bond as well as the two phosphane ligands at the rhodium center are *trans* disposed.[7]

Compound **4** is thermally quite stable and under normal conditions inert in presence of carbon monoxide. If, however, a solution of **4** in benzene under a CO atmosphere is warmed to 80 °C, a reaction takes place giving complex **5**[6] and the (*E*)-butenyne **6** almost quantitatively (Scheme 2). Surprisingly, compound **4** reacts with methyl propiolate (also in benzene) even at room temperature. In contrast to the reaction with CO, a colorless crystalline solid **7** is isolated in 78% yield instead of a butenyne. Compound **7** was found to be a derivative of **4** with a 2-butadienyl instead of a vinyl group as a substituent. As Figure 1 illustrates[8] the metal center of **7** is octahedrally coordinated with the two phosphane ligands in *trans* position. The atoms O1, O3, C4, and C9 are in a plane but are not located at the corners of a square due to the small bite angle of the acetato ligand (O1-Rh-O3 58.8(2)°). Most noteworthy is the unsymmetrical coordination of the CH_3CO_2 group; while the distance Rh–O3 (2.151(5) Å) is similar to the Rh–O distances of **1** (2.170(3) and



Scheme 2. R = CO_2Me.

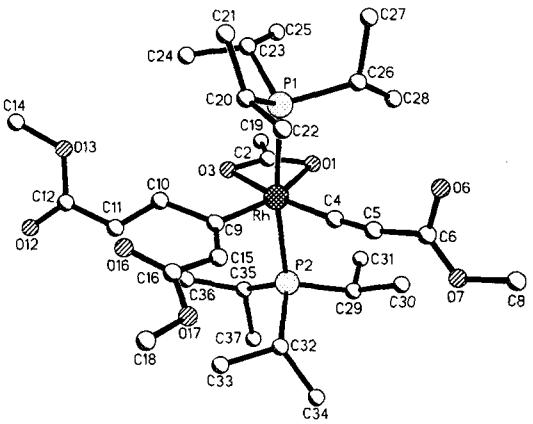


Fig. 1. Crystal structure of **7**. Selected bond lengths [Å] and angles [°]: Rh-P1 2.431(3), Rh-P2 2.407(3), Rh-O1 2.260(6), Rh-O3 2.151(5), Rh-C4 1.937(8), Rh-C9 2.015(9), C4-C5 1.195(11), C5-C6 1.46(1), C9-C10 1.48(1), C9-C15 1.35(1), C10-C11 1.32 (1), C11-C12 1.43(1), C15-C16 1.43(1), C2-O1 1.25(1), C2-O3 1.27(1); P1-Rh-P2 171.5(1), O1-Rh-C9 159.5(3), O3-Rh-C4 170.0(4), O3-Rh-C9 100.7(3), O1-Rh-O3 58.8(2), O1-Rh-C4 111.4(3), C4-Rh-C9 89.1(4), P1-Rh-O1 90.8(2), P1-Rh-O3 93.3(2), P1-Rh-C4 85.0(3), P1-Rh-C9 90.5(3), P2-Rh-O1 85.7(2), P2-Rh-O3 91.6(2), P2-Rh-C4 89.0(3), P2-Rh-C9 95.5(3), Rh-C4-C5 176.9(7), C4-C5-C6 169.0(9), Rh-C9-C10 109.5(6), Rh-C9-C15 129.5(7), C9-C10-C11 128.9(8), C9-C15-C16 130.0(8), C10-C11-C12 124.8(9), C10-C9-C15 120.9(8), Rh-O1-C2 88.6(6), Rh-O3-C2 93.1(5), O1-C2-O3 119.4(8).

2.174(3) Å)[5], the Rh–O1 bond length (2.260(6) Å) is significantly longer. The C_4 unit is linked through C9 to the metal center and has the thermodynamically more favored (*E*) configuration at both C=C bonds (C9–C15 and C10–C11). Both halves of the butadienyl ligand are twisted around the C9–C10 bond, the torsion angle (61.8°) being distinctly larger than in the square-planar complex *trans*-[Rh{η^1-(*Z*)-C(=CHPh)CH=CH_2}(CO)($P i Pr_3$)$_2$] (46.5°).[9] With regard to the mechanism of formation of **7** we assume that initially by partial cleavage of the CH_3CO_2-Rh chelate bond one molecule of HC≡CCO_2Me is added to the

 © VCH Verlagsgesellschaft mbH, D-69451 Weinheim, 1995 0570-0833/95/0202-0192 $ 10.00+.25/0

rhodium center. This step is followed by a rearrangement of the 1-alkyne to the isomeric vinylidene ligand, and finally a vinyl-vinylidene coupling analogous to the reaction of *trans*-[Rh(CH=CH$_2$)(=C=CHPh)(P*i*Pr$_3$)$_2$] with CO[9] occurs.

Similar to **4**, compound **7** is thermally stable and even on heating to 60 °C no C–C coupling takes place. However, the coupling of the butadienyl and the alkynyl ligands at rhodium can be easily achieved if a solution of **7** in diethyl ether is treated with an excess of $MgCl_2 \cdot 6H_2O$ and Na_2CO_3 and then stirred for 4 h at 40 °C. From the crude reaction product, deep red air-stable crystals of **8** have been isolated in 79% yield, the spectroscopic data of which are closely related to those of alkynerhodium(I) complexes of general composition *trans*-[RhCl(RC≡CR′)(P*i*Pr$_3$)$_2$].[10] The X-ray crystal structure analysis of **8** (see Fig. 2)[8] reveals a somewhat distorted square-planar coordination around the metal center with the atoms Cl, P1, P2, C2, and Rh in the same plane. The C1 atom of the alkyne unit is located significantly above this plane. Despite of the unsymmetrical coordination of the RC≡CR′ ligand to the metal center, the bond lengths Rh–C1 (2.02(1) Å) and Rh–C2 (2.00(1) Å) are nearly identical, a situation which is different to that of the structurally related diynerhodium(I) compound *trans*-[RhCl(η^2-Me$_3$SiC≡CC≡CSiMe$_3$)(P*i*Pr$_3$)$_2$].[11] We note that the butadienyl substituent at the C≡C bond still has the (*E*,*E*) configuration which proves that during the C–C coupling no (*E*)/(*Z*) isomerization takes place. In contrast to **7**, however, the C_4 unit in **8** is *s-trans*. The torsion angle [C8-C7-C6-C12] (4.9°) as well as the dihedral angles between the planes [C1,C2,C3]/[C6,C12,C13] (1.4°) and [C1,C2,C3]/[C7,C8,C9] (4.7°) confirm that the C_6 core of the hexadienyne ligand is almost coplanar. The C≡C bond lies perpendicular to the plane [Cl,Rh,P1,P2], as is expected according to the Dewar/Chatt/Duncanson bonding scheme.

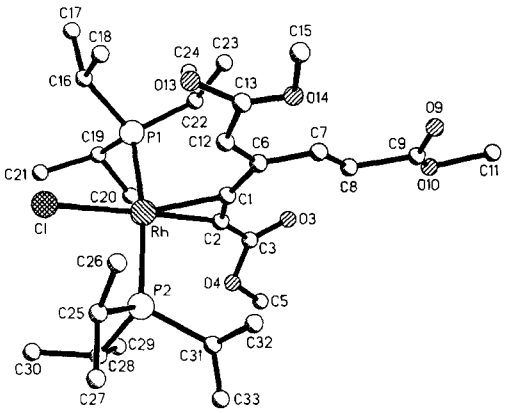


Fig. 2. Crystal structure of **8**. Selected bond lengths [Å] and angles [°]: Rh-P1 2.371(3), Rh-P2 2.369(3), Rh-Cl 2.337(3), Rh-C1 2.02(1), Rh-C2 2.00(1), C1-C2 1.21(2), C2-C3 1.40(2), C1-C6 1.54(2), C6-C7 1.38(2), C6-C12 1.35(2), C7-C8 1.34(2); P1-Rh-P2 168.9(1), Cl-Rh-C1 149.9(3), Cl-Rh-C2 174.8(3), Cl-Rh-P1 88.5(1), Cl-Rh-P2 86.0(1), P1-Rh-C1 92.6(3), P1-Rh-C2 89.9(3), P2-Rh-C1 96.9(3), P2-Rh-C2 94.6(3), C1-Rh-C2 35.1(5), C1-C2-C3 140.9(12), C2-C1-C6 160.4(10), C1-C6-C7 118.9(13), C1-C6-C12 118.3(11), C7-C6-C12 122.6(13), C6-C7-C8 125.5(15), C7-C8-C9 129.0(15).

Similar to the butenyne complex *trans*-[RhCl(η^2-PhC≡CCH=CHPh)(P*i*Pr$_3$)$_2$][4] compound **8** also reacts with CO at room temperature, the ligand displacement being indicated by an instantaneous change of color from deep red to light yellow. Equimolar amounts of both the rhodium carbonyl compound **9**[12] and the hexadienyne derivative **10** are obtained in quantitative yield, the latter of which has been characterized by GC/MS and ^{1}H NMR spectroscopy (Table 1). It should be emphasized that in contrast to the reaction of [Ni(CO)$_2$(PPh$_3$)$_2$] with methyl propiolate,[2b] in the stepwise rhodium-mediated trimerization of HC≡CCO$_2$Me no cyclic $C_6H_3(CO_2Me)_3$ isomer can be detected. As far as we know only in the oligomerization of ferrocenylethyne, catalyzed by [Ni(CO)$_2$(PPh$_3$)$_2$], a branched trimer (*E*,*E*)-FcC≡C-C(=CHFc)CH=CHFc [Fc = (η^5-C$_5$H$_5$)-Fe(η^5-C$_5$H$_4$-)], structurally related to **10**, is formed apart from the corresponding butenyne and benzene derivatives but merely in 45% yield.[13]

Table 1. Selected spectroscopic data of compounds **7**, **8**, and **10** (omitting the ^{1}H and ^{13}C NMR data for phosphane ligands).

7: IR (C_6H_6): $\tilde{\nu}$ = 2100 (C≡C), 1710, 1683 (C=O), 1565, 1530 (C=C and OCO) cm^{-1}; ^{1}H NMR (400 MHz, C_6D_6): δ = 8.36 [d, *J*(H,H) = 15.8 Hz, C*H*=CHCO$_2$Me], 6.72 [m, d in ^{1}H{^{31}P}, *J*(Rh,H) = 2.4 Hz, RhC=C*H*CO$_2$Me], 6.34 [d, *J*(H,H) = 15.8 Hz, CH=C*H*CO$_2$Me], 3.44, 3.38, 3.37 (all s, CO$_2$CH$_3$), 1.68 (s, RhO$_2$CCH$_3$); ^{13}C NMR (100.6 MHz, C_6D_6): δ = 184.32 [dt, *J*(Rh,C) = 1.2, *J*(P,C) = 1.2 Hz, RhO$_2$CCH$_3$], 167.04 (s, CH=CHCO$_2$Me), 163.85 [dt, *J*(Rh,C) = 3.5, *J*(P,C) = 0.7 Hz, RhC=CHCO$_2$Me], 163.57 [dt, *J*(Rh,C) = 30.6, *J*(P,C) = 7.8 Hz, Rh*C*], 153.67 [d, br, *J*(Rh,C) = 1.4 Hz, RhC=CCO$_2$Me], 147.95 (s, br, *C*H=CHCO$_2$Me), 126.90 [t, br, *J*(P,C) = 2.5 Hz, RhC=*C*HCO$_2$Me], 118.26 (s, CH = *C*HCO$_2$Me), 111.81 [dt, *J*(Rh,C) = 51.4, *J*(P,C) = 16.8 Hz, Rh*C*≡C], 100.46 [dt, *J*(Rh,C) = 10.1, *J*(P,C) = 2.0 Hz, RhC≡*C*], 51.19, 51.06, 50.61 (all s, CO$_2$*C*H$_3$), 24.81 (s, RhO$_2$*C*CH$_3$); ^{31}P NMR (162.0 MHz, C_6D_6): δ = 26.28 [d, *J*(Rh,P) = 93.2 Hz].

8: IR (hexane): $\tilde{\nu}$ = 1845 (C≡C), 1725, 1715, 1700 (C=O) cm^{-1}; ^{1}H NMR (400 MHz, C_6D_6): δ = 9.11 [d, *J*(H,H) = 16.0 Hz, C*H*=CHCO$_2$Me], 8.00 (s, C≡CC=C*H*CO$_2$Me), 7.40 [d, br, *J*(H,H) = 16.0 Hz, CH=C*H*CO$_2$Me], 3.49, 3.37, 3.35 (all s, CO$_2$CH$_3$); ^{13}C NMR (100.6 MHz, C_6D_6): δ = 166.71, 166.46 (both s, = CH*C*O$_2$Me), 158.80 (s, br, C≡*C*CO$_2$Me), 138.59 (s, C≡*C*C), 137.01 (s, *C*H=CHCO$_2$Me), 130.66 (s, C=*C*HCO$_2$Me), 128.02 (s, CH=*C*HCO$_2$Me), 93.14 [dt, *J*(Rh,C) = 17.9, *J*(P,C) = 2.6 Hz, C≡*C*CO$_2$Me], 88.21 [d, br, *J*(Rh,C) = 16.5 Hz, *C*≡CCO$_2$Me], 51.70, 51.51, 51.31 (all s, CO$_2$CH$_3$); ^{31}P NMR (162.0 MHz, C_6D_6): δ = 33.63 [d, *J*(Rh,P) = 110.6 Hz].

10: ^{1}H NMR (200 MHz, C_6D_6): δ = 8.78 [d, *J*(H,H) = 15.9 Hz, C*H*=CHCO$_2$Me], 6.66 [d, *J*(H,H) = 15.9 Hz, CH=C*H*CO$_2$Me], 5.95 (s, C=C*H*CO$_2$Me), 3.28, 3.20, 3.15 (all s, CO$_2$CH$_3$).

We are currently investigating whether the generation of the hexadienyne **10** from compound **8** is also possible with methyl propiolate. If this can be achieved, the ligand displacement process should generate instead of **9** the alkynyl(hydrido)rhodium(III) complex **3** which could initiate a catalytic cycle. In this context we note that Klein et al.[14] have recently shown that the cobalt cluster [Co$_3$(μ_3-H)(μ_2-CO)$_3$(PMe$_3$)$_6$] reacts catalytically with phenylacetylene at 100 °C to give the linear hexadienyne PhC≡CC(Ph)=CHCH=CHPh which stereochemically is different from **10**. The mechanistic route leading to this trimer is unknown. Therefore, to the best of our knowledge the formation of **10** from three molecules of a 1-alkyne represents the first example of an oligomerization reaction for which the stepwise course has been largely elucidated by the isolation and structural characterization of several important intermediates.

Received: August 2, 1994 [Z 7201 IE]
German version: *Angew. Chem.* **1995**, *107*, 213

Keywords: alkynetrimerization · complexes with carbon ligands · dienynes · rhodium compounds

[1] W. Reppe, N. von Kutepow, A. Magin, *Angew. Chem.* **1969**, *81*, 717–723; *Angew. Chem. Int. Ed. Engl.* **1969**, *8*, 722–728.

[2] See for example: a) L. S. Meriwether, E. C. Colthup, G. W. Kennerly, R. N. Reusch, *J. Org. Chem.* **1961**, *26*, 5155–5163; b) L. S. Meriwether, M. F. Leto, E. C. Colthup, G. W. Kennerly, *ibid.* **1962**, *27*, 3930–3941; c) J. P. Collman, J. W. Kang, W. F. Little, M. F. Sullivan, *Inorg. Chem.* **1968**, *7*, 1298–1303; d) G.

M. Whitesides, W. J. Ehmann, *J. Am. Chem. Soc.* **1969**, *91*, 3800–3807; e) C. Hoogzand, W. Hübel in *Organic Synthesis via Metal Carbonyls* (Eds.: I. Wender, P. Pino), Wiley, New York, **1968**, Chap. 3; f) D. R. McAlister, J. E. Bercaw, R. G. Bergman, *J. Am. Chem. Soc.* **1977**, *99*, 1666–1668; g) N. E. Schore, *Chem. Rev.* **1988**, *88*, 1081–1119; h) D. P. Smith, J. R. Strickler, S. D. Gray, M. A. Bruck, R. S. Holmes, D. E. Wigley, *Organometallics* **1992**, *11*, 1275–1288.

[3] K. P. C. Vollhardt, *Angew. Chem.* **1984**, *96*, 525–541; *Angew. Chem. Int. Ed. Engl.* **1984**, *23*, 539–555; see also: H. Bönnemann, *ibid.* **1985**, *97*, 264–279 and **1985**, *24*, 248–263.

[4] M. Schäfer, N. Mahr, J. Wolf, H. Werner, *Angew. Chem.* **1993**, *105*, 1377–1379; *Angew. Chem. Int. Ed. Engl.* **1993**, *32*, 1315–1318.

[5] H. Werner, M. Schäfer, O. Nürnberg, J. Wolf, *Chem. Ber.* **1994**, *127*, 27–38.

[6] M. Schäfer, J. Wolf, H. Werner, *J. Organomet. Chem.* **1994**, *476*, 85–91.

[7] M. Schäfer, Dissertation, Universität Würzburg, **1994**.

[8] Data of the X-ray structural analyses. **7**: Crystals from methanol/water (3:1); crystal size $0.4 \times 0.5 \times 0.25$ mm; monoclinic, space group $P2_1/a$; $Z = 4$, $a = 18.442(2)$, $b = 10.448(1)$, $c = 19.148(3)$ Å, $\beta = 91.17(1)^\circ$, $V = 3688.7(4)$ Å^3; $\rho_{calcd} = 1.323$ g cm^{-3}; max $2\omega = 50^\circ$; 5903 reflections measured, 5384 independent, 3525 observed [$F > 3\sigma(F)$]. **8**: Crystals from pentane ($-30\,^\circ$C); crystal size $0.2 \times 0.3 \times 0.15$ mm; triclinic, space group $P\bar{1}$; $Z = 2$, $a = 12.011(2)$, $b = 14.538(3)$, $c = 10.504(2)$ Å, $\alpha = 91.50(1)^\circ$, $\beta = 100.42(1)^\circ$, $\gamma = 84.20(1)^\circ$, $V = 1794.6(5)$ Å^3; $\rho_{calcd} = 1.316$ g cm^{-3}; max $2\omega = 45^\circ$; 4705 reflections measured, 4705 independent, 3473 observed [$F > 3\sigma(F)$]. For **7** and **8**: Philips/STOE diffractometer, $Mo_{K\alpha}$, graphite monochromator, Lorentzian polarization and empirical absorption corrections (ψ-scan method); direct methods [Siemens SHELXTL PLUS (PC)], refinement with full-matrix, least-squares method; for **7**: $R = 0.083$, $R_w = 0.049$; reflection/parameter ratio 15.00; residual electron density $+1.02/-1.21$ eÅ^{-3}; for **8**: $R = 0.072$, $R_w = 0.055$; reflection/parameter ratio 17.45; residual electron density $+0.89/-1.11$ eÅ^{-3}. Further details of the X-ray structure analyses may be obtained from the Fachinformationszentrum Karlsruhe, D-76344 Eggenstein-Leopoldshafen (Germany), on quoting the depository numbers CSD-401093 (**7**) and 401094 (**8**).

[9] R. Wiedemann, P. Steinert, M. Schäfer, H. Werner, *J. Am. Chem. Soc.* **1993**, *115*, 9864–9865.

[10] a) H. Werner, J. Wolf, U. Schubert, K. Ackermann, *J. Organomet. Chem.* **1986**, *317*, 327–356; b) H. Werner, M. Baum, D. Schneider, B. Windmüller, *Organometallics* **1994**, *13*, 1089–1097.

[11] T. Rappert, O. Nürnberg, H. Werner, *Organometallics* **1993**, *12*, 1359–1364.

[12] C. Busetto, A. D'Alfonso, F. Maspero, G. Perego, A. Zazzetta, *J. Chem. Soc. Dalton Trans.* **1977**, 1828–1834.

[13] C. U. Pittman Jr., L. R. Smith, *J. Organomet. Chem.* **1975**, *90*, 203–210.

[14] H. F. Klein, M. Mager, S. Isringhausen-Bley, U. Flörke, H.-J. Haupt, *Organometallics* **1992**, *11*, 3174–3175.

Electrochemical Synthesis of a Redox-Active Polymer Based on Buckminsterfullerene Epoxide**

Milan Fedurco, David A. Costa, Alan L. Balch,* and W. Ronald Fawcett*

Despite the interest in forming polymeric materials containing C_{60} units, little progress toward preparation of such substances has been made. Rao et al.[1a] described the photoinduced polymerization of solid C_{60} films. Takahasi et al.[1b] used a high-frequency plasma to induce polymerization in a sublimed film containing C_{60} and C_{70}. Diederich et al. recently described the electrochemical conversion of a dihydromethanofullerene into a conducting polymer.[2] Copolymers between C_{60} and the diradical xylylene have also been formed in toluene solution.[3]

[*] Prof. A. L. Balch, M. Fedurco, D. A. Costa, Prof. W. R. Fawcett
Department of Chemistry, University of California
Davis, CA 95616 (USA)
Telefax: Int. code + (916) 752-8995

[**] This research was supported by the National Science Foundation (ALB, grant nos. CHE9022909 and CHE9321257) and the Office of Naval Research (WRF).

We describe here the formation of an insoluble conducting film on an electrode from fullerene epoxide $C_{60}O$.[4–6] Unlike most other conducting polymers formed electrochemically,[7, 8] this film is grown in a cathodic reaction and incorporates cations. Combination of cationic conducting material with anionic conducting material, for example that based on polypyrrole,[9] is of potential importance in the production of microelectronic devices such as transistors. In addition, conducting polymers have been extensively studied for use in high energy density batteries.[8]

Initial experiments were carried out by means of cyclic voltammetry at a gold electrode (area ca. 7×10^{-3} cm^2) in a toluene/acetonitrile solution (4/1 volume ratio) containing 0.1 M tetrabutylammonium perchlorate (TBAP) and 0.4 mM $C_{60}O$.[10] Current–potential data on the forward sweep using square-wave voltammetry were similar to those reported by Suzuki et. al[11] with four irreversible reduction steps at potentials roughly equal to those for C_{60}. These authors used 1,2-dichlorobenzene as solvent, a system in which electropolymerization does not occur. Current–potential data obtained at a sweep rate of 100 mV s^{-1} are shown for the first 17 cycles in Figure 1a. The

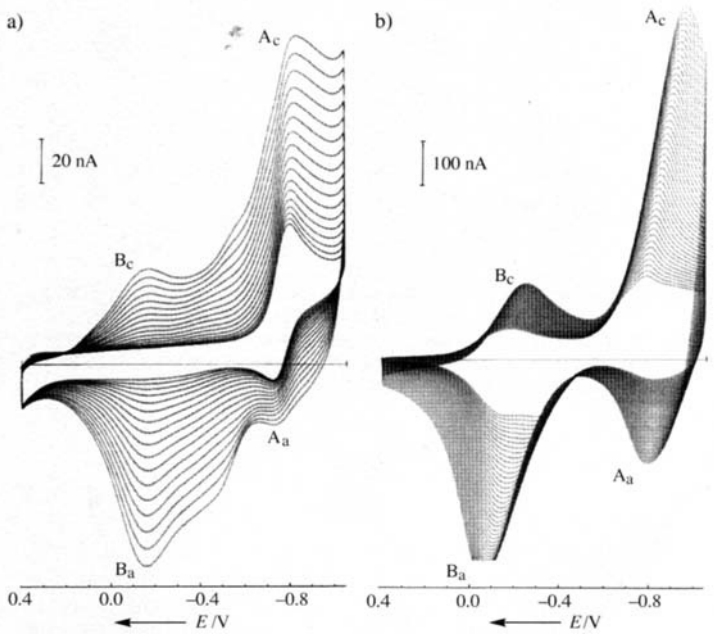


Fig. 1. a) Cyclic voltammograms (scan rate 100 mV s^{-1}) between +0.4 and −1.05 V for the reduction of $C_{60}O$ at a gold electrode in a toluene/acetonitrile mixture containing 0.1 M TBAP. The current at the initial reduction peak A_c (−0.79 V) increases in subsequent cycles, and new peaks (B_a and B_c) appear at more positive potentials. Data are shown for the first 17 cycles. b) As in (a) but for the 33rd to 75th cycle.

current peak A_c on the first sweep toward negative potentials (−0.79 V vs the Ag/Ag$^+$ reference) is attributed to formation of the anion radical $C_{60}O^{\cdot -}$. Its anodic counterpart A_a observed on the return sweep is considerably reduced in magnitude, presumably because of a follow-up chemical reaction involving polymerization [Eq. (a)].

$$C_{60} + C_{60}O^{\cdot -} \longrightarrow C_{60}\text{–}O\text{–}C_{60}\text{–}O^{\cdot -} \qquad \text{(a)}$$

After several cycles major peaks B_c and B_a develop at more positive potentials (−0.15 V), and a orange-brown film can be seen forming on the electrode. The fact that peaks B_c and B_a

occur at the same potential demonstrates that they arise from a process involving material attached to the electrode. They are attributed to incorporation of TBA^+ ions into the film on the negative sweep (B_c) and expulsion of same ions on the positive sweep (B_a). The minor peaks that develop between peaks A and B are associated with electrode reactions involving dimers or trimers, which are in the solution near the electrode and eventually become incorporated in the film. The development of the cyclic voltammetric curves up to 75 cycles is shown in Figure 1b. It is clear that the film continues to grow in thickness due to formation of $C_{60}O^{\bullet -}$ during the sweeps toward negative potentials, but the shape and position of the waves at more positive potentials are distorted owing to the increasing resistance of the deposited film. Similar results were obtained on other electrodes including glassy carbon, graphite, mercury, platinum, and glass coated with indium-doped tin oxide (ITO). Thick films were brown in color, and uniform in thickness (3–5 μm) according to depth profilometry. The deposit adhered very strongly to solid electrodes but formed as a powder on mercury. The measured current densities are smaller than those obtained earlier for the formation of polypyrrole.[8, 9] This probably reflects a lower conductivity of the $C_{60}O$ polymer due to differences in structure and the nature of the ion moving.

Additional experiments performed with a gold electrode modified with the deposit demonstrated that the film has both ionic and electronic conductivity. When an electrode with a thick film is transferred to a toluene/acetonitrile solution containing 0.1 M TBAP but no $C_{60}O$, continuous cycling in the potential region from 0.4 to −1.2 V resulted in cyclic voltammograms with the same peaks as those in Figure 1, whose heights now remained constant with further cycling (see Fig. 2).

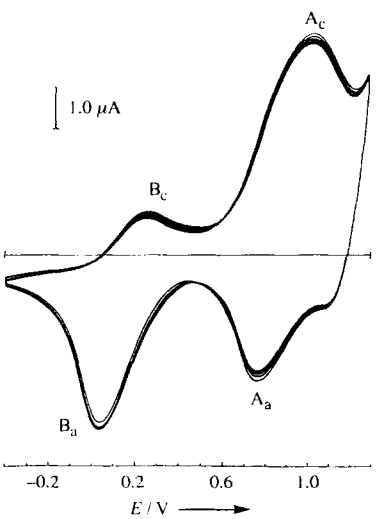


Fig. 2. Cyclic voltammograms obtained at a gold electrode covered by a $C_{60}O$ polymer film in a toluene/acetonitrile solution containing 0.1 M TBAP but no $C_{60}O$ (scan rate 100 mVs^{-1} between 0.4 and −1.2 V, Ag/Ag^+ reference electrode).

The processes leading to current at A and B now do not involve further growth of the film. However, if the potential range for cycling is restricted to the range 0.4 to −0.5 V, the peaks at B_c and B_a disappear after a few cycles. This suggests that maintaining the electrode potential at positive potentials results in the ejection of TBA^+ ions from the film and a reduction in its ionic conductivity. When the potential range is extended again in the negative direction to −1.2 V, the current peaks A reappear and the current at B is restored after roughly ten cycles. The current at A_c is now attributed to reduction of the polymer to give it a net negative charge, and the return of the features at B, to the resumption of the process by which TBA^+ ions move in and out of the polymer film. Reversible voltammetric waves for the oxidation of ferrocene are observed both at the unmodified and modified electrode, suggesting that the film is also electronically conducting.[9]

The role of ionic conductivity was also demonstrated in a transfer experiment in which a well-developed polymer film (ca. 50 cycles) was transferred from the toluene/acetronitrile solution to an acetonitrile solution containing 0.1 M $LiClO_4$ but no $C_{60}O$. All cathodic and anodic peaks decreased continuously in this medium when the electrode was cycled at the same scan rate (100 mVs^{-1}). This result can be attributed to the poor solubility of the Li^+ ion in the hydrophobic polymer environment. When the electrode is returned to the toluene/acetonitrile solution containing TBAP, the current–potential characteristics are restored after a few cycles. Presumably TBA^+ is better able to move in the hydrophobic environment created by the $C_{60}O$ polymer units.

It was also noted that the polymer can be deposited from the toluene/acetonitrile solution containing 0.1 M TBAP with the electrode potential of −1.2 V. This supports our conclusion that the mechanism involves polymerization of a species produced by reduction of $C_{60}O$.

The brown film has been characterized by a variety of techniques. Laser desorption time-of-flight mass spectrometry in the negative-ion mode confirms the presence of fullerene units within the polymer. The spectrum obtained under high laser power shows a prominent signal at m/z 720 due to C_{60}^- as well as a signal due to $[(C_{60})_2O_2]^{\bullet -}$; other signals occurred up to m/z 400 000. Mass spectra in the positive-ion mode confirm the presence of TBA^+ ions in the film, since an intense peak at m/z 242 is observed. The IR spectrum of the film dispersed in potassium bromide shows absorptions at 2962, 2879, 1460, 1396, and 802 cm^{-1}, which arise from the TBA^+ ion, at 1095, 1026, and 617 cm^{-1} due to perchlorate anions, a weak band at 517 cm^{-1}, which is the prominent band in C_{60} and $C_{60}O$ (the other fullerene features are covered by the absorptions listed above), a sharp band at 1257 cm^{-1} assigned to the C-O-C stretch of the polymer, and bands at 3425, 3131, and 1620 cm^{-1} ascribed to water molecules that may be present due to absorption from air. The UV/Vis absorption spectrum of the film is dominated by fullerene-like features with three prominent absorptions at 224, 272, and 342 nm and a broad weaker shoulder at approximately 490 nm.

Polymer films prepared on polycrystalline gold and ITO electrodes were further studied by scanning electron microscopy (SEM) and scanning tunneling microscopy. Figure 3 shows an SEM image of the $(C_{60}O)_n$ polymer grown to a thickness of 3 μm on polycrystalline gold by electrochemical deposition. The bubblelike structures on the surface result from the formation of new nuclei in the cathodic sweep of the cyclic voltammogram. Micrographs of polymer deposited on ITO electrodes were quite different; the polymer surface was almost featureless at the same magnification. The same system was examined by scanning tunneling microscopy with films 3 μm thick, and equivalent results were obtained. The fact that these experiments are possible provides further evidence of the conductivity of the electrochemically deposited layer. Electronic conductivity, probably involving a hopping mechanism, must be assumed in films of this thickness. SEM studies were also carried out with electrochemically deposited films consisting of polypyrrole, and polypyrrole on $(C_{60}O)_n$. The polypyrrole film was formed on an ITO electrode by cycling the potential between −0.5 and 0.8 V

 © VCH Verlagsgesellschaft mbH, D-69451 Weinheim, 1995 0570-0833/95/0202-0195 $ 10.00+.25/0

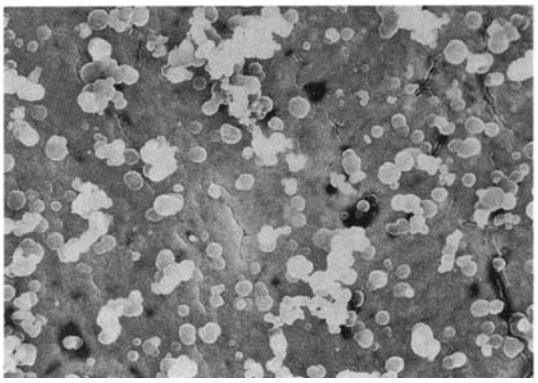


Fig. 3. Scanning electron micrograph of the $(C_{60}O)_n$ polymer film formed electrochemically on a gold disc (the length of the bar corresponds to 1.7 μm). The bubblelike structures on the surface are characteristic of the nucleation and growth processes from the toluene/acetonitrile solution containing TBAP.

in the same toluene/acetonitrile mixture containing 0.1 M TBAP and 0.01 M pyrrole. The morphology of these films was clearly different from that of the $(C_{60}O)_n$ polymer. An electron micrograph of a $(C_{60}O)_n$ polymer film on ITO with a subsequent deposit of polypyrrole is shown in Figure 4. The original $C_{60}O$ film was grown electrochemically under the same conditions

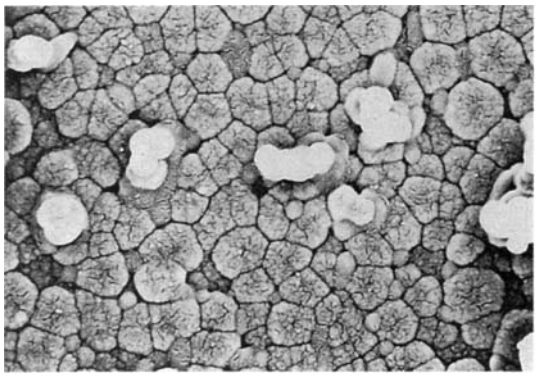


Fig. 4. Scanning electron micrograph of a $(C_{60}O)_n$ polymer film formed electrochemically on an ITO electrode with a subsequent deposit of polypyrrole (see text; the length of the bar corresponds to 1.1 μm)). The polypyrrole nuclei appear as bubblelike structures on the surface with a clearly different morphology from the $(C_{60}O)_n$ substrate polymer.

described above to a thickness of roughly 3 μm. It was then placed in a pyrrole solution for electrochemical deposition of polypyrrole and cycled in the potential range from −0.5 to 0.8 V ten times. The bubblelike nuclei formed on a background of different morphology are clearly visible on the micrograph. The reverse process, deposition of the $C_{60}O$ polymer on a polypyrrole substrate, was also carried out successfully. These results are clearly important with respect to the possible development of microelectronic devices, since the nature of the ionic conductors in the two polymers is clearly different.

In conclusion, the present study has shown that a covalently linked, redox-active fullerene polymer can be obtained through electrochemical reduction of $C_{60}O$. The electrochemically deposited films have mechanical and electrical properties that may make this material technologically important. Further studies of their properties and the electrochemical polymerization of other derivatized fullerenes are in progress.

Received: June 28, 1994
Revised version: October 6, 1994 [Z 7080 IE]
German version: *Angew. Chem.* **1995**, *107*, 220

Keywords: electrochemistry · fullerenes · organic conductors · polymers

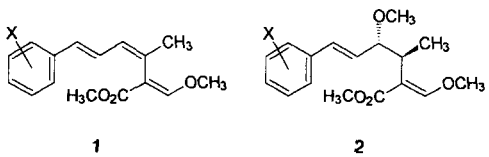
[1] a) A. M. Rao, P. Zhou, K.-A. Wang, G. T. Hager, J. M. Holden, Y. Wang, W. T. Lee, X.-X. Bi, P. C. Eklund, D. S. Cornett, M. A. Duncan, I. J. Amster, *Science* **1993**, *259*, 955–957; b) N. Takahasi, H. Dock, N. Matsuzawa, M. Ata, J. *Appl. Phys.* **1993**, *74*, 5790–5798.
[2] H. L. Anderson, C. Boudon, F. Diederich, J.-P. Gisselbrecht, M. Gross, P. Seiler, *Angew. Chem.* **1994**, *106*, 1691; *Angew. Chem. Int. Ed. Engl.* **1994**, *33*, 1628.
[3] D. Loy, R. Assink, *J. Am. Chem. Soc.* **1992**, *114*, 3977–3978.
[4] K. M. Creegan, J. L. Robbins, W. K. Robbins, J. M. Millar, R. D. Sherwood, P. J. Tindall, D. M. Cox, A. B. Smith III, J. P. McCauley, Jr., D. R. Jones, R. T. Gallagher, *J. Am. Chem. Soc.* **1992**, *114*, 1103–1105.
[5] Y. Elemes, S. K. Silverman, C. Shen, M. Kao, C. S. Foote, M. M. Alvarez, R. L. Whetten, *Angew. Chem.* **1992**, *104*, 364; *Angew. Chem., Int. Ed. Engl.* **1992**, *31*, 351–353.
[6] A. L. Balch, D. A. Costa, J. W. Lee, B. C. Noll, M. M. Olmstead, *Inorg. Chem.* **1994**, *33*, 2071–2072.
[7] T. A. Skotheim, *Handbook of Conducting Polymers Vols. 1, 2*, Dekker, New York, **1986**.
[8] A. F. Diaz, J. F. Rubinson, H. B. Mark, Jr., *Adv. Polym. Sci.* **1988**, *84*, 113.
[9] A. F. Diaz, K. K. Kanazawa, *J. Chem. Soc. Chem. Comm.* **1979**, 635–636.
[10] The voltammetry was carried out with a PAR 273 potentiostat interfaced to a microcomputer. Positive feedback was used to compensate for iR drop between the Au working electrode and the reference electrode (Ag/Ag^+ in acetonitrile containing 0.01 M $AgClO_4$ and 0.09 M TBAP). The counter electrode was also made of Au.
[11] T. Suzuki, Y. Maruyama, T. Akasaka, W. Ando, K. Kobayashi, S. Nagase, *J. Am. Chem. Soc.* **1994**, *116*, 1359–1363.

9-Methoxystrobilurins—A Link Between Strobilurins and Oudemansins**

Silvia Zapf, Andreas Werle, Timm Anke,* Dörte Klostermeyer, Bert Steffan, and Wolfgang Steglich*

Dedicated to Professor Werner Tochtermann on the occasion of his 60th birthday

Strobilurins **1** and oudemansins **2** from cultures of basidiomycetes are of great interest as potent fungicides.[1] The discovery that their fungicidal action is determined by the (*E*)-β-methoxy-



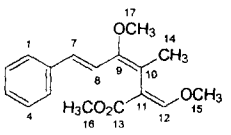
1 **2**

[*] Prof. Dr. T. Anke, Dipl.-Biol. S. Zapf, A. Werle
Lehrbereich Biotechnologie der Universität
Paul-Ehrlich-Strasse 23, D-67663 Kaiserslautern (Germany)
Telefax: Int. code + (631) 205-2999
Prof. Dr. W. Steglich, Dipl.-Chem. D. Klostermeyer, Dr. B. Steffan
Institut für Organische Chemie der Universität
Karlstrasse 23, D-80333 München (Germany)
Telefax: Int. code + (89) 5902-604

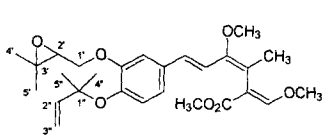
[**] Antibiotics from Basidiomycetes, Part 48. This work was supported by the Deutsche Forschungsgemeinschaft. Part 47: R. Velten, D. Klostermeyer, B. Steffen, W. Steglich, A. Kuschel, T. Anke, *J. Antibiot.*, **1994**, *47*, 1017–1024.

acrylate unit[2] led to the synthesis of a large number of analogues, culminating recently in the first presentation of products for commercial development.[3]

We have discovered a new class of β-methoxyacrylate antibiotics, 9-methoxystrobilurins **3** and **4**, which combine the structural features of **1** and **2** and have fungicidal activity.



3



4

9-Methoxystrobilurin A (**3**) was isolated from the culture filtrate (CF) of an Ethiopian *Favolaschia* species[4] by adsorption on Mitsubishi resin (Diaion HP21) and subsequent elution with acetone. Pure **3** was obtained by chromatography of the crude product (92.2 mg L^{-1} CF) on silica gel (Kieselgel 60, Merck; cyclohexane/EtOAc = 7:3), followed by preparative high-performance liquid chromatography (Merck Lichrosorb Diol, 7 μm, cyclohexane/*tert*-butyl methyl ether = 95:5) with a yield of 2.4 mg L^{-1} CF.

According to its high-resolution electron-impact (EI) ionization mass spectrum, **3** has the empirical formula $C_{17}H_{20}O_4$; the fragment ions *m/z* 121 and 75, which are characteristic for strobilurin A (**1**; X = H), are present in the spectrum.[5] The signals of the (*E*)-β-methoxyacrylate unit can be identified in the NMR spectra (Table 1),[5] whilst the 9-H signal of the strobilurin side chain is absent. An additional methoxy signal at $\delta_H = 3.61$ and the chemical shifts of C-9 and C-10 typical of conjugated vinyl ethers at $\delta_C = 152.7$ and 118.1 indicate that the antibiotic is 9-methoxystrobilurin A (**3**). The (*E*) configuration of the C-9 double bond is verified by the nuclear Overhauser enhancement (NOE) between the methyl and methoxy groups. The *cis* configuration of these groups causes an upfield shift of the ^{13}C NMR signal of the methyl group at position 14 compared with that of strobilurin A, from $\delta_C = 23.9$ to $\delta_C = 16.3$.

9-Methoxystrobilurin K (**4**), $C_{27}H_{36}O_7$, was isolated from the lyophilized mycelium of the *Favolaschia* culture by extraction with methanol, and was purified following the same procedure as for **3** (yield 2.8 mg L^{-1} culture). According to its ^1H and ^{13}C NMR spectra (Table 1), the compound is a 9-methoxystrobilurin with a 1,1-dimethyl-2-propenyloxy and a 3-methyl-2,3-epoxybutyloxy group at the 2- and 3-position, respectively, of the central phenyl unit. The position of the substituents was obtained from the inversely detected heteronuclear multiple-bond correlation spectrum (HMBC spectrum,[6] Fig. 1) and

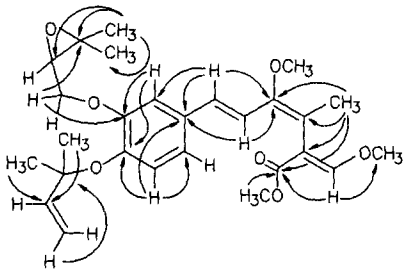


Fig. 1. ^1H-^{13}C long-range couplings for **4** from the HMBC spectrum.

^{13}C–^1H decoupling experiments. The stereochemistry of the hexatrienyl side chain was obtained from the NOESY spectrum (Fig. 2). This leads to structure **4** for 9-methoxystrobilurin K.

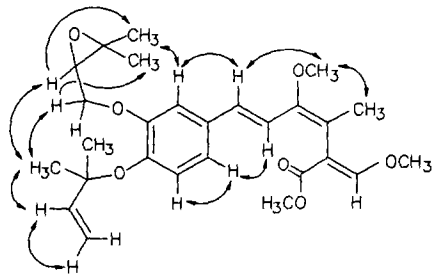
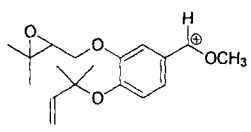


Fig. 2. Selected NOE correlations for **4**.

The typical fragmentation of the strobilurins[5] in the EI mass spectrum of **4** results in fragment **5** (base peak *m/z* 305); consecutive loss of the dimethyl and epoxyalkyl groups from **5** produces the intense fragment ions at *m/z* 237 and 153.



5

The fact that the 9-methoxystrobilurins **3** and **4** occur together with the oudemansins and strobilurins in the *Favolaschia* culture indicates that these compounds are biosynthetically related.[8]

Like the strobilurins and oudemansins, **3** and **4** inhibit a large number of fungi and yeasts in plate diffusion tests at low concentrations (Table 2). No antibacterial activity could be detected. The 9-methoxy derivatives like other strobilurins[10] are strong respiratory inhibitors. Respiration of *Penicillium notatum* is completely inhibited by 0.3 μg mL^{-1} 9-methoxystrobilurin A (1.04 μM) and 9-methoxystrobilurin K (0.64 μM). The

Table 1. Physical and spectroscopic data for compounds **3** and **4**.

3: colorless oil; $R_f = 0.72$ (toluene/acetone 70:30); UV/Vis (MeOH): $\lambda_{max}(\lg\varepsilon) =$ 301 (4.39), 230 nm (4.34); IR (KBr): $\tilde{\nu} =$ 3423, 2942, 1709, 1628, 1449, 1435, 1250, 1127, 1071 cm^{-1}; ^1H NMR (300 MHz, $CDCl_3$): $\delta = 1.84$ (s, 14-H), 3.61 (s, 17-H), 3.65 (s, 16-H), 3.75 (s, 15-H), 6.45 (d, $J = 15.9$ Hz, 8-H), 6.64 (d, $J = 15.9$ Hz, 7-H), 7.13 (dddd, $J = 7.1$, 7.1, 1.5, 1.5 Hz, 3-H), 7.22 (ddd, $J = 7.2$, 7.1, 1.5 Hz, 2-H and 4-H), 7.30 (dd, $J = 7.2$, 1.5 Hz, 1-H and 5-H), 7.33 (s, 12-H); ^{13}C NMR (75 MHz, $CDCl_3$): $\delta = 16.3$ (C-14), 51.6 (C-16), 59.5 (C-17), 61.8 (C-15), 110.6 (C-11), 118.8 (C-10), 121.6 (C-8), 126.6 (C-1, C-5), 127.3 (C-3), 127.6 (C-7), 128.5 (C-2, C-4), 137.5 (C-6), 152.7 (C-9), 159.3 (C-12), 168.1 (C-13); EI-MS (70 eV): *m/z*(%) 288.1397 (28) [M^+], calcd. ($C_{17}H_{20}O_4$) 288.3444, 273 (46), 245 (11), 241 (14), 213 (36), 209 (13), 197 (15), 185 (17), 181 (18), 170 (71), 153 (28), 131 (29), 121 (100), 105 (40), 103 (25), 91 (21), 77 (37), 75 (36).

4: yellowish oil; $R_f = 0.77$ (toluene/acetone 70:30); $[\alpha]_D^{23} = -8.8$ ($c = 0.8$ in chloroform); UV/Vis (MeOH): $\lambda_{max}(\lg\varepsilon) = 306$ (4.39), 230 nm (4.37); CD (MeOH): $\lambda_{max}(\Delta\varepsilon) = 307 (-0.38)$, 260 (−0.33), 222 nm (+1.53); IR (KBr): $\tilde{\nu} =$ 3424, 2980, 2940, 1710, 1629, 1503, 1437, 1267, 1196, 1127, 1068, 1020 cm^{-1}; ^1H NMR (300 MHz, $CDCl_3$): $\delta = 1.23$ (s, 4′-H), 1.32 (s, 4″-H, 5″-H), 1.43 (s, 5′-H), 1.89 (s, 14-H), 3.66 (s, 17-H), 3.68 (dd, $J = 7.8$, 3.4 Hz, 2′-H), 3.72 (s, 16-H), 3.81 (s, 15-H), 3.98 (dd, $J = 12.3$, 7.8 Hz, 1′-H), 4.22 (dd, $J = 12.3$, 3.4 Hz, 1′-H), 5.15 (dd, $J = 10.7$, 1.0 Hz, 3″-H), 5.18 (dd, $J = 17.6$, 1.0 Hz, 3″-H), 5.88 (dd, $J = 17.6$, 10.7 Hz, 2″-H), 6.37 (d, $J = 15.9$ Hz, 8-H), 6.59 (d, $J = 15.9$ Hz, 7-H), 6.82 (d, $J = 8.8$ Hz, 4-H), 6.94 (dd, $J = 8.8$, 2.2 Hz, 5-H), 6.95 (d, $J = 2.2$ Hz, 1-H), 7.39 (s, 12-H); ^{13}C NMR (75 MHz, $CDCl_3$): $\delta = 16.3$ (C-14), 21.8 (C-4′), 26.3 (C-4″ or C-5″), 26.7 (C-4″ or C-5″), 28.1 (C-5′), 51.5 (C-16), 59.5 (C-17), 61.8 (C-15), 71.8 (C-1′), 75.5 (C-2′), 76.1 (C-1″), 81.7 (C-3′), 110.6 (C-11), 114.4 (C-3″), 118.1 (C-10), 120.1 (C-4), 120.4 (C-8), 121.6 (C-1 or C-5), 122.5 (C-1 or C-5), 126.8 (C-7), 132.9 (C-6), 143.6 (C-2″), 146.4 (C-3), 150.7 (C-2), 152.7 (C-9), 159.3 (C-12), 168.1 (C-13); EI-MS (70 eV): *m/z*(%) 472.2492 (17) [M^+], calcd. ($C_{27}H_{36}O_7$) 472.5801, 440 (6) [M^+ − MeOH], 372 (7), 306 (37), 305 (100), 288 (10), 237 (23), 235 (14), 193 (8), 153 (48), 121 (18), 97 (19), 75 (15), 69 (44).

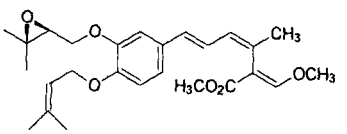
 © VCH Verlagsgesellschaft mbH, D-69451 Weinheim, 1995 0570-0833/95/0202-0197 $ 10.00+.25/0

Table 2. Spectrum of fungicidal action of 9-methoxystrobilurin A and K (– : no inhibition observed; values with i: incomplete inhibition).

Test organism	Diameter of inhibition zone [mm] 9-Methoxystrobilurin A (3) µg per disc [a] 0.1	1	9-Methoxystrobilurin K (4) 0.1	1
Absidia glauca (+)	–	15 i	–	10
Absidia glauca (–)	17 i	26 i	14	20
Alternaria porri	35 i	52 i	18 i	28 i
Aspergillus ochraceus	18 i	34 i	15 i	24 i
Epicoccum purpurascens	22 i	24 i	10 i	15 i
Fusarium oxysporum	24 i	35 i	–	12 i
Fusarium fujikuroi	32 i	40 i	12 i	15 i
Mucor miehei	23	37	14	20
Paecilomyces variotii	21 i	36 i	15 i	22 i
Penicillium islandicum	11 i	17 i	10 i	18 i
Penicillium notatum	26 i	37 i	15 i	21 i
Rhodotorula glutinis	15 i	25 i	10 i	17 i
Ustilago nuda	20 i	28 i	14 i	20 i
Zygorrhynchus moelleri	13 i	20 i	–	13 i

[a] Diameter 6 mm.

respiratory inhibition due to 9-methoxystrobilurin resembles that of strobilurin A and oudemansin A, which shows that substitution of a methoxy group at C-9 on strobilurin A does not influence its effect on respiration. The 9-methoxy derivatives, like strobilurin E,[11] have cytostatic properties. HeLa S3 cells show pronounced inhibition of growth and changes in morphology in the presence of 2 µg mL^{-1} (6.94 µM) **3** and 4 ng mL^{-1} (8.47 nM) **4**. Whilst the cytostatic activity of **3** is similar to that of strobilurin A in this test system, the extraordinarily large effect of **4** on the HeLa S3 cells is comparable with that of strobilurin D (**6**).



6

Received: June 24, 1994 [Z 7071 IE]
German version: *Angew. Chem.* **1995**, *107*, 255

Keywords: strobilurins · oudemansins · fungicides · antibiotics

[1] Reviews: a) T. Anke, W. Steglich in *Biologically Active Molecules* (Ed.: U. P. Schlunegger), Springer, Berlin, **1989**, pp. 9–25; b) K. Beautement, J. M. Clough, P. J. de Fraine, C. R. A. Godfrey, *Pestic. Sci.* **1991**, *31*, 499–519; c) H. Sauter, E. Ammermann, F. Roehl in *Crop Protection Agents from Nature: Natural Products and Analogues* (Ed.: L. G. Copping), Royal Society of Chemistry, Cambridge, **1995**; d) J. M. Clough, *Nat. Prod. Rep.* **1993**, *10*, 565–574.

[2] a) G. Schramm, Dissertation, Universität Bonn, **1980**; T. Anke, G. Schramm, W. Steglich, G. von Jagow in *Roots of Modern Biochemistry* (Eds.: H. Kleinkauf, H.-H. von Döhren, L. Jaenicke), de Gruyter, Berlin, **1988**, pp. 657–662.

[3] a) E. Ammermann, G. Lorenz, K. Schelberger, B. Wenderoth, H. Sauter, C. Rentzea, *Proc. Brighton Crop Prot. Conf. Pests Dis. Vol. 1*, The British Crop Protection Council, Brighton, **1992**, pp. 403–410; b) J. R. Godwin, V. M. Anthony, J. M. Clough, C. R. A. Godfrey, *ibid.*, p. 435–442.

[4] The bright yellow fruiting bodies of the yet-unidentified species of *Favolaschia* (sp. 87129) were collected in Kolobo, Ethiopia, in 1991, and were used to establish the mycelial culture by means of spore replication. Culture conditions on a 100 L scale: HMP medium (yeast extract 4, malt extract 10, glucose 4 g l^{-1}; pH 5.5). The fermentation was ended after five to seven days.

[5] G. Schramm, W. Steglich, T. Anke, F. Oberwinkler, *Chem. Ber.* **1978**, *111*, 2779–2784.

[6] A. Bax, D. Marion, *J. Magn. Reson.* **1988**, *78*, 186–191.

[7] 4-Hydroxystrobilurin D, which is related and has an (*S*)-2-(3-methyl-2,3-epoxybutyloxy) substituent [8], exhibits an optical rotation of $[\alpha]_D^{22} = +22$ ($c = 0.3$, $CHCl_3$). Because of the different chromophore, the negative rotation of **4** ($[\alpha]_D^{22} = -8.8$ ($c = 0.8$, $CHCl_3$)) does not allow any reliable conclusions about the absolute configuration to be drawn. The CD curves also show no obvious mirror-image trend.

[8] S. Backens, W. Steglich, J. Bäuerle, T. Anke, *Liebigs Ann. Chem.* **1988**, 405–409.

[9] T. Anke and S. Zapf were able to isolate the strobilurins A, C, E, and F and oudemansin A from the *Favolaschia* culture, in addition to **3** and **4**.

[10] W. F. Becker, G. von Jagow, T. Anke, W. Steglich, *FEBS Lett.* **1981**, *132*, 329–333.

[11] W. Weber, T. Anke, B. Steffan, W. Steglich, *J. Antibiot.* **1990**, *43*, 207–212.

2,4-Di-*tert*-butyl-1λ^3,3λ^3-diphosphinines: Targeted Synthesis at Iron(0) Centers and Oxidative Release**

Dieter Böhm, Falk Knoch, Susanne Kummer, Uwe Schmidt, and Ulrich Zenneck*

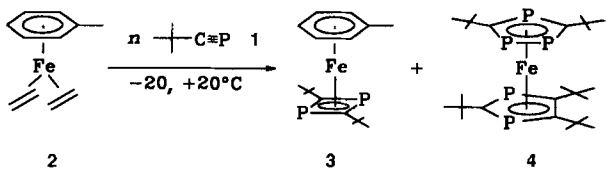
Dedicated to Professor Peter Paetzold on the occasion of his 60th birthday

Trivalent phosphorus atoms and CR fragments are isoelectronic building blocks that can occupy equivalent positions in many organophosphorus compounds, for example in heteroarenes. The simplest member of this group, λ^3-phosphinine (phosphabenzene)[1] is known, as well as many of its substitution products.[2] Phosphinines can act as σ-donor ligands, utilizing the lone pair on phosphorus, and also as cyclic η^6 ligands.[2] Of the three possible diphosphinine isomers, only 2,3,5,6-tetrakis(trifluoromethyl)-1λ^3,4λ^3-diphosphinine has so far been prepared in solution and spectroscopically characterized.[3] There is also very little known about phosphorus-rich benzene analogues. A cyclotrimerization product of *tert*-butylphosphaethyne **1**[4] has been characterized as a π-bound triphosphadewarbenzene.[5] A second trimerization product of **1** was postulated to be a coordinated 1,3,5-triphosphinine;[6] this, however, has not yet been definitively proven.[7] We report here an efficient synthesis of 1λ^3,3λ^3-diphosphinines in the coordination sphere of iron(0) by [2 + 2 + 2] cycloaddition of two phosphaalkynes and a terminal alkyne. The release of these 1λ^3,3λ^3-diphosphinines under oxidative conditions is also discussed.

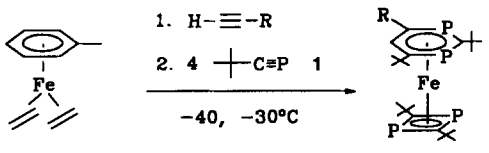
The reaction of bis(η^2-ethylene)(η^6-toluene)iron **2**[8] with *tert*-butylphosphaethyne **1** at moderate temperatures (maximum room temperature) yields, apart from the cyclodimerization of **1** to a coordinated 1,3-diphosphete in (η^4-2,4-di-*tert*-butyl-1,3-diphosphete)(η^6-toluene)iron **3**, a surprising formation of five-membered rings. This leads to a pentaphosphaferrocene, penta-*tert*-butyl-(1,2,4-triphospholyl)(1,3-diphospholyl)iron (**4**).[9] During this reaction, at least one phosphaalkyne molecule must undergo cleavage of the triple bond,[9] and the trimerization of the phosphaalkyne **1** is avoided in this case. Normally, this reaction predominates during the interaction of **2** with alkynes.[10]

[*] Prof. Dr. U. Zenneck, Dipl.-Chem. D. Böhm, Dr. F. Knoch, Dipl.-Chem. S. Kummer, Dipl.-Chem. U. Schmidt
Institut für Anorganische Chemie der Universität Erlangen-Nürnberg
Egerlandstrasse 1, D-91058 Erlangen (Germany)
Telefax: Int. code + (9131)85-7367

[**] Reactive π Complexes of Electron-Rich Transition Metals, Part 14. This work was supported by the Deutsche Forschungsgemeinschaft and the Fonds der Chemischen Industrie. We thank Prof. Dr. D. Sellman for the time on the X-ray diffractometer. Part 13: C. Brodt, S. Niu, H. Pritzkow, M. Stephan, U. Zenneck, *J. Organomet. Chem.* **1993**, *459*, 283.



The reaction of **2** with acetylene at −40 °C or with terminal alkynes at −30 °C, followed by a reaction with **1**, leads to a suppression of the five-membered ring formation, and apart from small quantities of **3** and **4**, the stable sandwich complexes **5a–e**, which contain 2,4-di-*tert*-butyl-1λ^3,3λ^3-diphosphinines



5a, R = H (55%)
5b, R = $CH_2OC(O)CH_3$ (35%)
5c, R = n-C_4H_9 (40%)
5d, R = CH_2OH (35%)
5e, R = CH_2OCH_3 (35%)

and 2,4-di-*tert*-butyl-1λ^3,3λ^3-diphosphete as ligands, are obtained. If **1** is added to **2** before the addition of the alkyne, the same products result; however, the yields of **5a–e** are significantly lower. The [2 + 2 + 2] cycloaddition of two molecules of **1** and one acetylene molecule (or a different alkyne) is regiospecific in two ways: only 1,3-diphosphinines are formed, but no 1,4-derivatives, and the substituent introduced with the alkyne always ends up in the position neighboring the P atom. The reaction fails with 3,3-dimethylbutyne and internal alkynes; functional groups on 1-alkynes, such as hydroxyl, ethers, or esters, are tolerated.

According to the spectroscopic data (Table 1) and the single-crystal X-ray structure analyses of **5a** (Fig. 1) and **5b**,[11] the

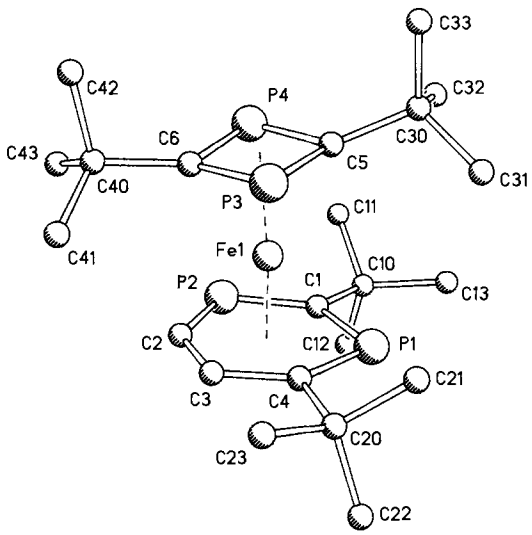


Fig 1. Structure of **5a** in the crystal. Selected bond lengths [Å] and angles [°]: Fe–P1 2.388(5), Fe–P2 2.387(6), Fe–P3 2.288(5), Fe–P4 2.306(5), Fe–C1 2.218(14), Fe–C2 2.163(17), Fe–C3 2.223(16), Fe–C4 2.173(15), Fe–C5 2.166(16), Fe–C6 2.110(14), P1–C1 1.738(16), P1–C4 1.763(16), P2–C1 1.760(15), P2–C2 1.769(17), P3–C5 1.769(17), P3–C6 1.770(15), P4–C5 1.782(17), P4–C6 1.774(17), C1–C10 1.584(23), C2–C3 1.436(23), C3–C4 1.510(22), C4–C20 1.519(23), C5–C30 1.524(24), C6–C40 1.542(20); C1-P1-C4 105.7(7), C1-P2-C2 103.0(8), C5-P3-C6 80.9(8), C5-P4-C6 80.5(7), P1-C1-P2 131.0(10), P2-C2-C3 131.8(13), C2-C3-C4 120.8(14), P1-C4-C3 127.5(12), P3-C5-P4 99.1(9), P3-C6-P4 99.3(7).

η^6-ligated 1,3-diphosphinines are essentially planar six-membered heteroarenes. The deviations of the ring atoms from the least-squares planes of the 1,3-diphosphinines range from + 3.1 to −1.9 pm for **5a** and +1.8 to −1.6 pm for **5b**. The data agree well with those obtained for η^6-coordinated phosphinines.[1,2] The distance between two of the sp^2 ring carbon atoms of **5a** (C3 and C4) is surprisingly large (151 pm), the same length as the single bond between C4 and C20. In contrast, the equivalent C3–C4 distance in **5b** (142 pm) is in the expected range. The reasons behind the large C–C distance in the ring of **5a** are not yet clear.

Table 1. Selected spectroscopic data for **5a,b** and **6a,b** [a].

5a: All NMR spectra represent the slow exchange limit. ^{1}H NMR (269.60 MHz, C_7D_8, 243 K, TMS): δ = 1.55 (s, 18H, Me at C10 and C20), 0.86 (s, 9H, Me at C30), 1.07 (s, 9H, Me at C40), 5.53 (ddd, 1H, H at C2, J(H,H) = 9.4, J(H,P) = 35.5, J(H,P) = 0.7 Hz), 6.10 (ddd, 1H, H at C3, J(H,P) = 5.5, J(H,P) = 8.5 Hz); ^{31}P{^{1}H} NMR (109.37 MHz, C_7H_8, 295 K, 85% H_3PO_4 (ext.)): δ = 10.8 (ddd, 1P, P2, J(P,P) = 12.4, J(P,P) = 8.7, J(P,P) = 5.4 Hz), 27.8 (d, 1P, P1, J(P,P) = 12.4 Hz), 30.7 (br, 1P, P4), 40.0 (br, 1P, P3); ^{13}C{^{1}H} NMR (67.7 MHz, C_7D_8, 298 K, TMS): δ = 34.8 (t, Me a C10, J(C,P) = 19.7 Hz), 32.8 (d, Me at C20, J(C,P) = 16.9 Hz), 30.8 (s, Me at C30), 33.3 (s, Me at C40), 40.7 (t, C10, J(C,P) = 36.7 Hz), 39.0 (d, C20, J(C,P) = 38.4 Hz), 35.2 (t, C30, J(C,P) = 11.3 Hz), 35.7 (t, C40, J(C,P) = 11.3 Hz), 133.5(dd, C1, J(C,P) = 73.3, J(C,P) = 84.6 Hz), 122.8 (dd, C4, J(C,P) = 71.1, J(C,P) = 4.5 Hz), 101.5 (t, C5, J(C,P) = 57.5Hz), 107.9 (t, C6, J(C,P) = 57.5 Hz), 90.7 (dd, C2, J(C,P) = 62.1, J(C,P) = 3.1 Hz), 91.3 (t, C3, J(C,P) = 8.5 Hz); EI-MS (70 eV): m/z (%): 482 (73) [M^+], 28 (100).

5b: ^{1}H NMR (60 MHz, $CDCl_3$, 295 K, TMS): δ = 1.00 (s, 18H, 2 tBu), 1.55 (s, 9H, tBu), 1.65 (s, 9H, tBu), 2.10 (s, CH_3), 5.15 (d, 2H, CH_2, J(H,P) = 14.0 Hz), 7.00 (t, 1H, H at C3, J(H,P) = 6.0 Hz); ^{31}P{^{1}H} NMR (109.37 MHz, $CDCl_3$, 295 K, 85% H_3PO_4 (ext.)): δ = 14.1 (d, 1P, P2, J(P,P) = 18.22 Hz), 16.1 (d, 1P, P1), 35.0 (s, 2P, P3 and P4); ^{13}C{^{1}H} NMR (67.7 MHz, $CDCl_3$, 295 K, TMS): δ = 22.0 (s, C9), 31.5 (d, Me at C20, J(C,P) = 11.3 Hz), 33.0 (s, Me at C30 and C40), 35.5 (t, Me at C10, J(C,P) = 19.9 Hz), 36.5 (d, C30 and C40, J(C,P) = 11.3 Hz), 39.5 (d, C20, J(C,P) = 19.8 Hz), 42.0 (t, C10, J(C,P) = 22.6 Hz), 73.0 (d, C7, J(C,P) = 19.6 Hz), 97.0 (s, C8), 102.0 (dd, C4, J(C,P) = 63.9, J(C,P) = 7.5 Hz), 111.0 (t, C3, J(C,P) = 25.3 Hz), 127.0 (dd, C2, J(C,P) = 73.9, J(C,P) = 3.1 Hz), 137.0 (dd, C1, J(C,P) = 82.1, J(C,P) = 73.9 Hz); EI-MS (70 eV): m/z (%): 554 (98) [M^+], 354 (100) [M^+−(tBuCP)$_2$].

6a: ^{1}H NMR (269.60 MHz, $CDCl_3$, 295 K, TMS): δ = 1.52 (d, 9H, Me at C20, J(H,P) = 1.5 Hz), 1.67 (t, 9H, Me at C10, J(H,P) = 1.5 Hz), 8.06 (ddd, 1H, H at C3, J(H,P) = 11.1, J (H,P) = 6.8, J(H,H) = 11.1 Hz), 8.78 (ddd, 1H, H at C2, J(H,P) = 41.8, J(H,H) = 4.3, J(H,H) 11.1 Hz); ^{31}P{^{1}H} NMR (109.37 MHz, $CDCl_3$, 295 K, 85% H_3PO_4 (ext.)): δ = 220.2 (d, P2, J(P,P) = 24.7 Hz), 237.9 (d, P1, J(P,P) = 24.7 Hz); ^{13}C{^{1}H} NMR (67.7 MHz, $CDCl_3$, 295 K, TMS): δ = 33.0 (d, 3C, C21, C22, and C23, J(C,P) = 12.2 Hz), 35.4 (t, C11, C12, and C13, J(C,P) = 13.0 Hz), 40.0 (d, C20, J(C,P) = 24.4 Hz), 43.1 (d, C10, J(C,P) = 20.5 Hz), 129.9 (dd, C3, J(C,P) = 13.5, J(C,P) = 9.9 Hz), 150.7 (dd, C2, J(C,P) = 51.8, J(C,P) = 15.2 Hz), 181.2 (dd, C2, J(C,P) = 63.9, J(C,P) = 18.3 Hz), 217.1 (dd, C1, J(C,P) = 76.9, J(C,P) = 70.8 Hz).

6b: ^{1}H NMR (60 MHz, $CDCl_3$, 295 K, TMS): δ = 1.89 (t, 9H, Me at C20, J(H,P) = 6.0 Hz), 1.73 (t, 9H, Me at C10, J(H,P) = 8.0 Hz), 2.08 (s, 3H, Me at C9), 5.47 (dd, 2H, at C7, J(H,P) = 14.0, J(H,P) = 4.0 Hz), 8.03 (t, 1H at C3, J(H,P) = 8.0 Hz); ^{31}P{^{1}H} NMR (109.37 MHz, $CDCl_3$, 295 K, 85% H_3PO_4 (ext.)): δ = 222.5 (d, P2, J(P,P) = 21.0 Hz), 235.5 (d, P2, J(P,P) = 21.0 Hz); ^{13}C{^{1}H} NMR (67.7 MHz, $CDCl_3$, 295 K, TMS): δ = 20.0 (s, C9), 31.0 (d, C21, C22, and C23, J(C,P) = 12.2 Hz), 34.0 (t, C11, C12, and C13, J(C,P) = 12.9 Hz), 39.0 (d, C20, J(C,P) = 22.9 Hz), 42.0 (t, C10, J(C,P) = 21.3 Hz), 69.0 (d, C7, J(C,P) = 47.3 Hz), 131.0 (t, C3, J(C,P) = 10.7 Hz), 160.0 (dd, C4, J(C,P) = 50.3, J(C,P) = 15.2 Hz), 169.0 (s, C8), 181.0 (dd, C2, J(C,P) = 64.0, J(C,P) = 15.2 Hz), 216.0 (dd, C1, J(C,P) = 76.2, J(C,P) = 70.1 Hz).

[a] Atom numbering as in Fig. 1.

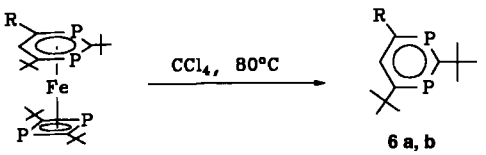
 © VCH Verlagsgesellschaft mbH, D-69451 Weinheim, 1995 0570-0833/95/0202-0199 $ 10.00+.25/0

The NMR spectra (^1H, ^{13}C, ^{31}P) of **5a** are temperature-dependent owing to the hindered rotation of both cyclic ligands, which carry two *tert*-butyl groups each. The rotation barrier $\Delta G^{\ddagger}_{rot}$ is 55 kJ mol^{-1}. For **5b–e**, the NMR spectra represent the rapid exchange limit. Line broadening is observed for some signals only below $-80\,^{\circ}C$, hence $\Delta G^{\ddagger}_{rot}$ is smaller than 30 kJ mol^{-1}. This can be explained by the interaction between the R substituents and one of the *tert*-butyl groups of the diphosphete.

The compounds **3** and **5a–e** are structurally analogous complexes in which the toluene and the diphosphinine ligands, which, to our knowledge, are described here for the first time, occupy equivalent positions. Consequently, the spectroscopic properties of these species are quite similar.[9] There are, however, big differences in the redox behavior: while **3** can be reversibly oxidized and, at low temperatures, reduced electrochemically, the anions and cations of **5a** are so short-lived that on the time scale of cyclic voltammetry, they decompose completely even at low temperatures.[12] Only in situ EPR spectroscopy on the redox products yielded indications of the existence of the ions 5^+ and 5^-. A similar difference has been observed for ferrocene and the pentaphosphaferrocene derivatives **4**[13] as well as (pentamethylcyclopentadienyl)(pentaphospholyl)iron.[14] The latter two species do not yield stable cations, while the ferrocenium ion can be isolated in the form of salts.

We assume the mechanism of formation to proceed by an initial replacement of one or both ethylene ligands in **2** by the alkyne. Subsequently, four molecules of **1** are added in a stepwise fashion and the toluene ligand is lost. The two heterocycles are probably formed via ferraphospha- and ferradiphosphacyclopentadiene intermediates, respectively. Stable cycloaddition products of this type have been demonstrated for a $1\lambda^3$-phospha-3-zirconacyclopenta-1,4-diene[15] and a $1\lambda^3,4\lambda^3$-diphospha-2-rhodacyclopenta-3,5-diene.[16]

The oxidative decomplexation of the 1,3-diphosphinines succeeds with $FeCl_3$ or halogenated hydrocarbons at elevated temperatures. The most useful reaction for preparative purposes is the treatment of **5a** and **5b** with CCl_4, which releases **6a** and **6b**, respectively.



a, R = H

b, R = $CH_2OC(O)CH_3$

According to their NMR spectra (^1H, ^{13}C, ^{31}P), the stable free 1,3-diphosphinines **6a,b** can be classified as π^6 heteroarenes (Table 1). The relationship to phosphinines is clearly apparent and the spectroscopic findings are incompatible with alternative structures, such as Dewar-diphosphinine, diphosphaprismane, or diphosphabenzvalene. This has also been confirmed by comparing the ^1H, ^{13}C, and ^{31}P NMR spectra of **6a** and **6b** with those of the isomers of phosphinine.[17] The successful release of **6a** and **6b** completes their synthesis from simple precursors at the transition metal center. The novel rings are now available for further work. Studies concerning their organoelement and coordination chemistry are currently underway. Metal complexes of **6a** and **6b** with labile co-ligands are of particular interest as potential catalysts, for instance for the synthesis of pyridines.[18]

Experimental Procedure

5a–e: A solution of **2** (0.52 g, 2.5 mmol) was prepared in toluene (70 mL) at $-40\,^{\circ}C$, under an inert gas atmosphere. The mixture was either saturated with acetylene or treated at $-30\,^{\circ}C$ with 2-propynyl acetate (0.74 g, 7.5 mmol). At $-30\,^{\circ}C$, **1** (1.0 g, 10 mmol) in toluene (20 mL) was added, and the solution was allowed to warm to room temperature over a period of 3 h. The solvent was subsequently removed under vacuum (0.01 mbar). The black residue was taken up in petroleum ether and filtered through a small amount of Al_2O_3 (5% H_2O), which was washed with petroleum ether. The solution was reduced in volume and subjected to chromatography on SiO_2 (5% H_2O).

The reaction with acetylene and the use of petroleum ether as eluant yielded **5a** (662 mg, 1.37 mmol, 55%) as dark red, analytically pure crystals. A second fraction afforded the isolation of **3** in 12% yield.

The reaction with 2-propynyl acetate combined with the use of petroleum acetate/toluene (5:1) as eluant led to the isolation of **5b**. After recrystallization, **5b** was obtained in an analytically pure form (387 mg, 0.7 mmol, 35%).

Compounds **5c–e** can be prepared in an analogous manner (see Scheme 2 for yields).

6b: **5b** (1.06 g, 1.9 mmol) was dissolved in CCl_4 (20 mL), and the solution was heated to reflux. After 1 h the solution was filtered through Al_2O_3 and the solvent was distilled off. Subsequent vacuum distillation (2 Pa) yielded **6b** as the first fraction (130 °C) in the form of a yellow oil (143 mg, 0.48 mmol, 25%). Further fractions collected at higher temperatures contained only small portions of **6b**. The diphosphinine **6a** was obtained from **5a** in an analogous manner.

Received: July 29, 1994 [Z 7186 IE]
German version: *Angew. Chem.* **1995**, *107*, 251

Keywords: complexes with phosphorus ligands · heteroarenes · phosphaalkynes

[1] A. J. Ashe III, *J. Am. Chem. Soc.* **1971**, *93*, 3293.
[2] G. Märkl in *Multiple Bonds and Low Coordination in Phosphorus Chemistry* (Eds.: M. Regitz, O. J. Scherer), Thieme, Stuttgart, **1990**, pp. 220-257, and references therein; C. Elschenbroich, M. Nowotny, A. Behrendt, K. Harms, S. Wocadlo, J. Pebler, *J. Am. Chem. Soc.* **1994**, *116*, 6217.
[3] Y. Kobayashi, J. Kumadaki, A. Ohsawa, H. Hamana, *Tetrahedron Lett.* **1976**, 3715; *ibid.* **1977**, 867; C. G. Krespan, B. C. McKusick, T. L. Cairns, *J. Am. Chem. Soc.* **1960**, *82*, 1515; C. G. Krespan, *ibid.* **1961**, *83*, 3432.
[4] G. Becker, G. Gresser, W. Uhl, *Z. Naturforsch. B* **1981**, *36*, 16.
[5] R. Milczarek, W. Rüsseler, P. Binger, K. Jonas, K. Angermund, C. Krüger, M. Regitz, *Angew. Chem.* **1987**, *99*, 957; *Angew. Chem. Int. Ed. Engl.* **1987**, *26*, 908.
[6] A. R. Barron, A. H. Cowley, *Angew. Chem.* **1987**, *99*, 956; *Angew. Chem. Int. Ed. Engl.* **1987**, *26*, 907.
[7] P. Binger, paper presented at the PSIBLOCS meeting, Paris, August 1988. J. F. Nixon, *Chem. Rev.* **1988**, *88*, 1327.
[8] U. Zenneck, W. Frank, *Angew. Chem.* **1986**, *98*, 806; *Angew. Chem. Int. Ed. Engl.* **1986**, *25*, 831.
[9] M. Driess, D. Hu, H. Pritzkow, H. Schäufele, U. Zenneck, M. Regitz, W. Rösch, *J. Organomet. Chem.* **1987**, *334*, C35.
[10] U. Zenneck, *Angew. Chem.* **1990**, *102*, 171; *Angew. Chem. Int. Ed. Engl.* **1990**, *29*, 126.
[11] The crystal structure analysis was performed using an automatic four-circle diffractometer (Siemens P4). $T = 293$ K, $Mo_{K\alpha}$ radiation, graphite monochromator, unit cell determined with 18 reflections, ω scans with 3.0–30° min^{-1}. Structure solution by direct methods (SHELXTL-PLUS), anisotropic refinement of the non-hydrogen atoms. The positions of the hydrogen atoms were taken from difference Fourier maps and fixed during the refinement; hydrogen atoms were given common isotropic temperature factors. Crystal structure data for **5a**: single crystal from hexane, red parallelepiped 0.4 × 0.2 × 0.2 mm^3. Scan range $3° < 2\theta < 60°$, 9289 reflections, of which 7541 were symmetry-independent, 1644 reflections with $F > 4\sigma(F)$ were classified as observed. Orthorhombic, space group $P2_12_12_1$, $a = 1050.2(2)$, $b = 1112.8(2)$, $c = 2194.0(4)$ pm, $V = 2.563(1)$ nm^3, $\rho_{calcd} = 1.25$ g cm^{-3}, $Z = 4$. $R = 0.058$, $R_w = 0.052$, 244 refined parameters. A crystal structure analysis of **5b** with $R = 0.038$ and $R_w = 0.034$ has also been performed; D. Böhm, S. Kummer, F. Knoch, U. Zenneck, unpublished results. Further details regarding the crystal structure determination can be obtained from the Fachinformationszentrum Karlsruhe, D-76344 Eggenstein-Leopoldshafen (Germany), on quoting the depository number CSD-58483.

[12] By cyclic voltammetry, only irreversible electron transfer reactions were found for **5a** and **5b**: for instance, for **5a** at a glassy carbon electrode in 1,2-dimethoxyethane, using $(n\mathrm{Bu})_4\mathrm{NPF}_6$ as supporting electrolyte, at $E_{p(ox)} = 0.86$ V and $E_{p(red)} = -1.84$ V (referenced to the saturated calomel electrode); D. Böhm, H. Meth, U. Zenneck, unpublished results.
[13] D. Hu, Dissertation, Universität Heidelberg, **1990**.
[14] O. J. Scherer, Universität Kaiserslautern, W. Kaim, Universität Stuttgart, personal communication, **1987**.
[15] P. Binger, B. Biedenbach, A. Herrmann, R. Milczarek, R. Schneider, *Phosphorus Sulfur Silicon Relat. Elem.* **1990**, *49/50*, 337; A. Herrmann, Dissertation, Universität Kaiserslautern, **1990**.
[16] P. Binger, B. Biedenbach, R. Mynott, C. Krüger, P. Betz, M. Regitz, *Angew. Chem.* **1988**, *100*, 1219; *Angew. Chem. Int. Ed. Engl.* **1988**, *27*, 1158.
[17] K. Blatter, W. Rösch, U.-J. Vogelbacher, J. Fink, M. Regitz, *Angew. Chem.* **1987**, *99*, 67; *Angew. Chem. Int. Ed. Engl.* **1987**, *26*, 85.
[18] U. Schmidt, U. Zenneck, *J. Organomet. Chem.* **1992**, *440*, 187; F. Knoch, F. Kremer, P. Le Floch, F. Mathey, U. Schmidt, U. Zenneck, unpublished results.

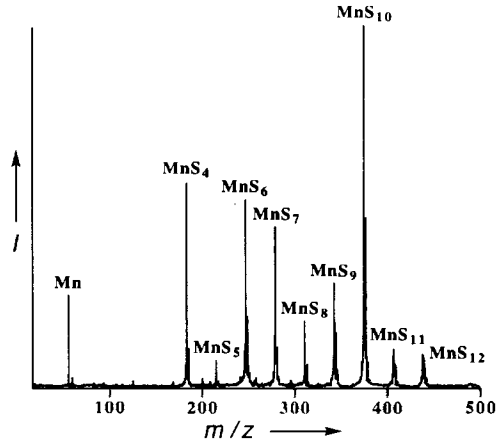


Fig. 1. Mass spectrum of the (positive) products of the reaction between Mn^+ and S_8 at $2-3\times10^{-8}$ mbar. The spectrum was recorded after a reaction period of 10 s, that is, after all of the Mn^+ has reacted.

Formation and Structures of New Metallo- and Metallapolysulfanes, $[MS_y]^+$ ($y = 2-16$)**

Ian Dance,* Keith Fisher, and Gary Willett

Amongst the growing knowledge and understanding of the reactions of ligands with bare metal ions in the gas phase[1] there is scanty information about reactions with sulfur,[2, 3] although metallapolysulfane ions are known to be formed in reactions with ethylenesulfide.[3, 4] While investigating the formation and structures of clusters $[M_xS_y]^-$ generated subsequent to laser ablation of metal sulfides,[5] we observed the formation of $[MS_y]^+$ ions, presumably from elemental sulfur released during laser ablation. Subsequently we discovered that there is a general reaction of $M^+_{(g)}$ with $S_{8(g)}$ to form series of metallapolysulfane complexes $[MS_y]^+$ for most elements of the periodic table. We report here on the ions $[MS_y]^+$ ($y = 2-16$) for first row transition metals, and present some results of density functional computations of the structures of major species.

The metal ions $M^+_{(g)}$ were generated by laser ablation of the metal (Ti, V, Cr, Co, Ni, Cu, Zn), metal oxide (Sc), or the metal sulfide (Mn, Fe) in the ion trap of a Fourier transform ion cyclotron resonance (FTICR) mass spectrometer, while a capillary containing sulfur provided a background sulfur pressure of $2-3\times10^{-8}$ mbar. The trapped metal ions M^+ were allowed to undergo collisional cooling for periods of 0.1–2 s, then all other ions were ejected from the cell, and the reactions of the thermalized M^+ ions with the excess S_8 [6] were monitored for periods of up to 100 s. A representative spectrum for Mn is shown in Figure 1.

The major and minor products for all of the first row transition metals are listed in Table 1, with indications of the reaction time scales. The conversion of the M^+ ions appears to be pseudo first order for all metals. Only in the case of Zn^+ ions is the S_8^+ ion a major product. This is probably formed by charge transfer between the S_8 molecules and one of the zinc polysulfanes, not by rapid resonant charge transfer with the Zn^+ ions.[7]

Table 1. Positive ion products of the reactions of thermalized metal ions $M^+_{(g)}$ with excess sulfur vapor at $2-3\times10^{-8}$ mbar.

Metall	Major products (t/s)	Minor products
Sc^+	$[ScS_4]^+$ (1–5), $[ScS_{10}]^+$ (5–50), $[ScS_{12}]^+$ (>50)	$[ScS_2]^+$, $[ScS_6]^+$, $[ScS_8]^+$, $[ScS_9]^+$, $[ScS_{11}]^+$, $[ScS_{13}]^+$, $[ScS_{14}]^+$ [a]
Ti^+	$[TiS_4]^+$ (<8), $[TiS_8]^+$ (>8)	$[TiS_6]^+$, $[TiOS_6]^+$ [b], $[TiS_{10}]^+$, $[TiS_{12}]^+$ [a]
V^+	$[VS_4]^+$ (<8), $[VS_8]^+$ (>8)	$[VS_2]^+$, $[VS_5]^+$, $[VS_6]^+$, $[VS_7]^+$, $[VS_9]^+$, $[VS_{10}]^+$
Cr^+	$[CrS_4]^+$ (<10), $[CrS_8]^+$ (>10)	$[CrS_6]^+$, $[CrS_{10}]^+$
Mn^+	$[MnS_4]^+$ (<8), $[MnS_{10}]^+$ (>8)	$[MnS_5]^+$ [a], $[MnS_6]^+$, $[MnS_7]^+$, $[MnS_8]^+$, $[MnS_9]^+$, $[MnS_{11}]^+$, $[MnS_{12}]^+$
Fe^+	$[FeS_4]^+$ (<5), $[FeS_{10}]^+$ (>5)	$[FeS_6]^+$, $[FeS_7]^+$, $[FeS_8]^+$
Co^+	$[CoS_4]^+$ (<30), $[CoS_6]^+$ (30–50), $[CoS_{10}]^+$ (>50)	$[CoS_5]^+$, $[CoS_7]^+$, $[CoS_8]^+$
Ni^+	$[NiS_4]^+$ (<15), $[NiS_{10}]^+$ (>15)	$[NiS_5]^+$, $[NiS_6]^+$, $[NiS_8]^+$
Cu^+	$[CuS_4]^+$ (<20), $[CuS_{12}]^+$ (>20)	$[CuS_4(H_2O)]^+$ [b], $[CuS_8]^+$, $[CuS_{10}]^+$, $[CuS_{13}]^+$, $[CuS_{16}]^+$
Zn^+	$[S_8]^+$	$[ZnS_4]^+$, $[ZnS_4(H_2O)]^+$ [b], $[ZnS_{10}]^+$, $[ZnS_{12}]^+$

[a] Formed in traces. [b] Formed from adventitious water.

The reactivity patterns for M^+ plus S_8 can be summarized as: 1. The relative rates of reaction of M^+ with S_8 are $(Fe \approx Sc) > (Ti \approx V \approx Cr \approx Mn) > (Co \approx Ni) > (Cu \approx Zn)$. These follow atomic number, except for the enhanced reactivity of Fe^+. 2. For all metals except Zn, $[MS_4]^+$ is the first major product. 3. At longer times the major products are $[MS_6]^+$ for M = Co; $[MS_8]^+$ for M = Ti, V, and Cr; $[MS_{10}]^+$ for M = Sc, Mn, Fe, and Ni; and $[MS_{12}]^+$ for M = Sc and Cu. 4. The highest mass ions are $[MS_{10}]^+$ for M = V, Cr, Fe, Co, and Ni; $[MS_{12}]^+$ for M = Ti, Mn, and Zn; $[MS_{14}]^+$ for M = Sc; and $[MS_{16}]^+$ for M = Cu. 5. $[MS_y]^+$ with y odd are not abundant, except for $[VS_7]^+$ and $[MnS_7]^+$.

What are the structures and structural principles for these new complexes? In order to answer this question we used established ab initio density functional theory[8] to explore the structure-energy surfaces of the complexes by optimization of a variety of postulated structures. Jones et al., for example, used local density functional methods coupled with molecular dynamics to map the energy surfaces for sulfur molecules.[9] Here we outline key results for the ions $[MS_4]^+$, $[MS_8]^+$, and $[MS_{12}]^+$: details of all calculated geometrical and electronic structures will be presented separately.

[*] Prof. I. Dance, Dr. K. Fisher, Dr. G. Willett
School of Chemistry, University of New South Wales,
Sydney 2052 (Australia)
Telefax: Int. code + (2) 662 2835
e-mail: I. Dance@unsw.edu.au

[**] Financial support from the Australian Research Council is gratefully acknowledged, as is the generous provision of computing resources by Australian Numerical Simulation and Modelling Services.

For the ubiquitous small complex $[MS_4]^+$, we first explored the obvious structural possibilities, namely tetrahedral $[M(S)_4]$, pseudo-tetrahedral $[M(S_2)_2]$, the monocyclic chelate $[MS_4]$, and $[M(\eta^4\text{-}S_4)]$, in which the number of S–S bonds ranges from 0 to 4. During energy minimizations of these isomers for M = Sc, V, Mn, Co, and Cu, it became apparent that the most favorable binding energies often occurred for low symmetry arrangements of S_2 groups around the metal atom. The principal geometrical features for the $[MS_4]^+$ ion can be described in terms of the six structures **1a–f** shown in Figure 2. The D_2 symmetric structure

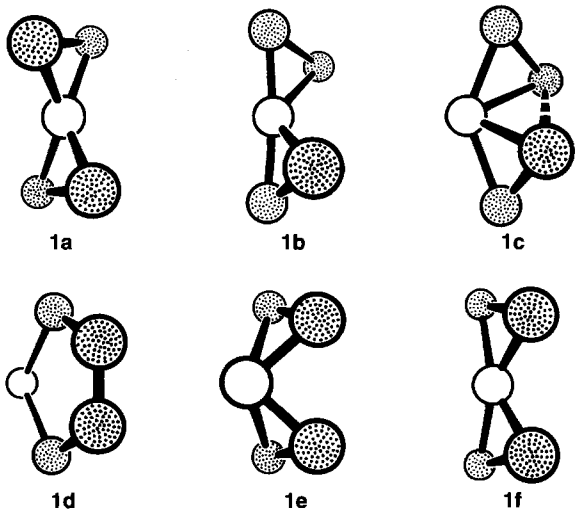


Fig. 2. Stable structures 1 for $[MS_4]^+$ ions.

1a is a pseudo-tetrahedral complex $[M(S_2)_2]$ in which the S_2 groups are most separated, while in **1b** (C_2 symmetry) the S_2 groups approach such that one S-M-S angle is close to 180°. The complex **1c** (C_2 symmetry) exhibits secondary bonding (ca. 2.5 Å) between two S_2 groups, while in **1d** (C_{2v} symmetry) the S_2 have joined to form an S_4 group which chelates the metal atom. In the C_s symmetric isomer **1f** the coordination of the metal atom approaches rectangular planar, while in **1e** (C_s symmetry) the metal atom lies out of the plane of the two S_2 groups. For Sc, isomers **1a**, **1c**, and **1e** have very similar energies and are the most stable; for V and Mn, isomer **1b** is the most stable, about 28 kJ mol^{-1} more stable than isomer **1a**; for Co, isomers **1a,b** are close in energy and isomer **1f** is about 20 kJ mol^{-1} less stable; and for Cu, isomer **1d** is most stable . The general preference for coordination of η^2-S_2 units, except at the end of the transition series, is consistent with the dissociation of S_2 units from $[FeS_y]^+$ on collisional activation.[3, 4b]

The structures of the complexes $[MS_8]^+$, which are prominent for the earlier transition metals, have been investigated by calculations on $[VS_8]^+$. The most stable isomer is **2a**, in which four η^2-S_2 groups are arrayed around V in stereochemistry intermediate between square planar and tetrahedral (see Fig. 3). The isomer **2b** with a relative energy of + 41 kJ mol^{-1} is similar geometrically but has two secondary S–S interactions (2.45 Å) connecting the S_2 groups as two pairs. Closure of these secondary interactions leads to the bis-chelate $[V(S_4)_2]^+$ structure **2c** with an energy of + 83 kJ mol^{-1}. The structure **2d** (V-centered *cyclo*-S_8) is geometrically feasible, but very much less stable at + 400 kJ mol^{-1}. The stability order for the isomers of $[MS_8]^+$ is metal dependent, and for $[CuS_8]^+$ the bis-chelate isomer **2c** is the most stable. Isomer **2a** is geometrically similar to the homoleptic peroxo-complexes $[M(O_2)_4]^{z-}$ of Cr, Mo, and Nb.[10]

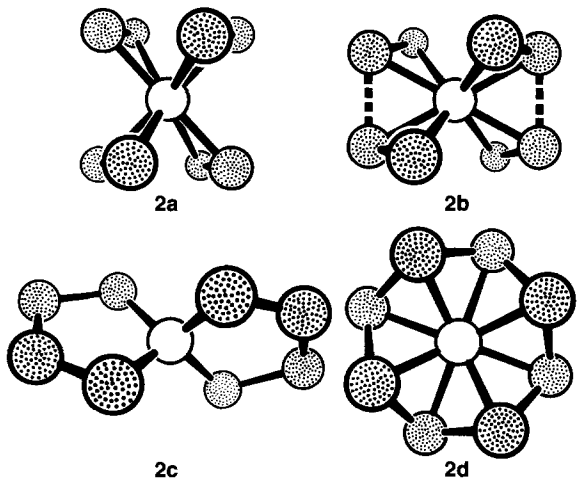


Fig. 3. The structures of four isomers for $[VS_8]^+$. **2a**: $E_{rel} = 0$, V–S 2.45 Å, S–S 2.02 Å; **2b**: $E_{rel} = +41$ kJ mol^{-1}, V–S 2.43, 2.52 Å, S–S 2.04, 2.45 (broken line) Å; **2c**: $E_{rel} = +83$ kJ mol^{-1}, V–S 2.25 Å, S–S 2.15 (1–2, 3–4), 2.08 (2–3) Å; **2d**: $E_{rel} = +400$ kJ mol^{-1}, V–S 2.58 Å, S–S 2.22, 2.25 Å.

As the number of S atoms increases, the structure-energy surface flattens. Figure 4 shows six optimized stationary points (structures **3**) for the $[CuS_{12}]^+$ ion. The isomer **3a** with a six-co-

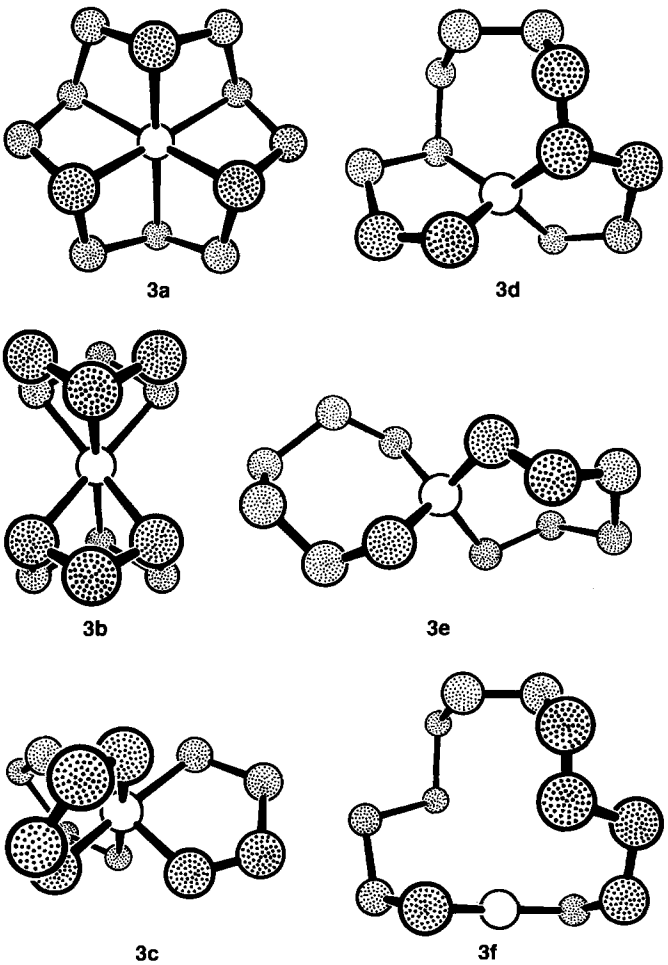


Fig. 4. The optimized structures of six isomers for $[CuS_{12}]^+$. **3a**: $E_{rel} = 0$, Cu–S 2.77 Å, S–S alternate 2.09, 2.25 Å; **3b**: $E_{rel} = +19$ kJ mol^{-1}, Cu–S 2.78 Å, S–S 2.16 Å; **3c**: $E_{rel} = +76$ kJ mol^{-1}, Cu–S 2.60 Å, S–S 1.97, 2.30 Å; **3d**: $E_{rel} = +34$ kJ mol^{-1}, Cu–S 2.34, 2.53 Å; **3e**: $E_{rel} = +86$ kJ mol^{-1}, Cu–S 2.40 Å, S–S alternate 2.04, 2.30 Å; **3f**: $E_{rel} = +83$ kcal mol^{-1}, Cu–S 2.24 Å.

 © VCH Verlagsgesellschaft mbH, D-69451 Weinheim, 1995 0570-0833/95/0202-0202 $ 10.00+.25/0

ordinate Cu atom within a *cyclo*-S_{12} ring is the most stable. Two other isomers with a six-coordinate Cu atom are **3b** with two *cyclo*-S_6 ligands (1,3,5 connections) at relative energy $+19\ kJ\,mol^{-1}$ and **3c**, a tris-S_4 chelate complex ($+76\ kJ\,mol^{-1}$). A four-coordinate Cu atom is found in **3d** with a single chelating S_{12} ligand (1,4,9,12 connections) and in **3e** with two S_6 chelate ligands, which occur at $+34$ and $+86\ kJ\,mol^{-1}$, respectively. The isomer **3f** is a CuS_{12} monocycle with linear coordination of Cu, and has an energy of $+83\ kJ\,mol^{-1}$ relative to **3a**. There are many other feasible configurations and conformations under investigation, but it appears that here chelating structures with shorter S_y chains are less stable than structures which maximize the number of S–S bonds.

An obvious structure for the $[CuS_{16}]^+$ ion is a sandwich of the Cu^+ ion between two S_8 cycles: precedent for this is found in the $[Ag(S_8)_2]^+$ ion crystallized with AsF_6^-.[11] We note another interesting possible structure type for $[CuS_{16}]^+$ and $[CuS_{13}]^+$: when Cu^+ is tetrahedrally coordinated it fits well within *cyclo*-S_{16}, generating four fused CuS_5 cycles with multiple conformations. Excision of the central S_3 of one cycle yields a chelated structure for the $[CuS_{13}]^+$ ion with the same tetrahedral coordination.

We recognize the connections of this new metallo-/metallapolysulfane chemistry to the metal plus S_8 reactions of Rauchfuss et al.,[12] and to the structures of metal complexes of polythiacycloalkanes.[13, 14] The difference is that our metal reactants are all formally oxidation state +1. Finally, we note that this is the third phase of general metal polysulfide chemistry, which diversified immensely when it was transferred from protic to aprotic media,[15–17] and is now diversifying further on transport to the pristine gas phase.

Received: July 26, 1994 [Z 7173 IE]
German version: *Angew. Chem.* **1995**, *107*, 215

Keywords: ab initio calculations · laser ablation · mass spectrometry · metallapolysulfanes

[1] K. Eller, H. Schwarz, *Chem. Rev.* **1991**, *91*, 1121.
[2] J. E. Bartmess, J. G. Kester, *Inorg. Chem.* **1984**, *23*, 1877–1880.
[3] J. R. Gord, B. S. Freiser, *Anal. Chim. Acta*, **1989**, *225*, 11–24.
[4] a) T. J. Carlin, M. B. Wise, B. S. Freiser, *Inorg. Chem.* **1981**, *20*, 2743–2745; b) M. B. Wise, D. B. Jacobsen, B. S. Freiser, *J. Am. Chem. Soc.* **1985**, *107*, 1590, 6744; c) R. L. Hettich, T. C. Jackson, E. M. Stanko, B. S. Freiser, *ibid.* **1986**, *108*, 5086 5093; d) T. C. Jackson, T. J. Carlin, B. S. Freiser, *Int. J. Mass Spectrom. Ion Processes* **1986**, 72, 169–185; e) T. J. MacMahon, B. S. Freiser *J. Am. Chem. Soc.* **1989**, *111*, 421–427.
[5] a) I. G. Dance, K. J. Fisher, D. Rice, G. D. Willett, *J. Am. Chem. Soc.* **1991**, *113*, 5141. b) J. H. El Nakat, I. G. Dance, K. J. Fisher, G. D. Willett, *J. Chem. Soc. Chem. Commun.* **1991**, 746–748. c) *Inorg. Chem.* **1991**, *30*, 2957–2958.
[6] Low energy electron impact mass spectra of the sulfur atmosphere showed that it contained >80% S_8, with some S_5^+ and S_6^+: H. M. Fales, Q.-L. Pu, R. T. Mason, L. K. Pannell *Int. J. Mass Spectrom. Ion Processes*, **1991**, *106*, 273–281.
[7] Unreacted Zn^+ ions remain after 50s. The relevant ionization potentials are: Zn 9.4, S_8 9.04. S. G. Lias, J. E. Bartmess, J. F. Liebman, J. L. Holmes, R. D. Levin, W. G. Mallard, *J. Phys. Chem. Ref. Data* **1988**, *17*, Suppl. 1.
[8] Program DMol.v 2.3, Biosym Technologies Inc, San Diego, USA. Double numerical basis sets with polarization functions are used, with core orbitals frozen. The Vosko–Wilk–Nusair [8a] correlation functional and the Becke [8b] exchange functional with nonlocal corrections are employed. Spin restricted calculations on even-electron monopositive ions only are reported here. Details of the electronic structures will follow. a) S. J. Vosko, L. Wilk, M. Nusair, *Can. J. Phys.* **1980**, *58*, 1200; b) A. D. Becke, *J. Chem. Phys.* **1988**, *88*, 2547.
[9] D. Hohl, R. O. Jones, R. Car, M. Parrinello, *J. Chem. Phys.* **1989**, *89*, 6823.
[10] M. Roch, J. Weber, A. F. Williams, *Inorg. Chem.* **1984**, 23, 4571–4580, and references cited therein.
[11] H. W. Roesky, M. Thomas, J. Schimkowiak, P. G. Jones, W. Pinkert, G. M. Sheldrick, *J. Chem. Soc. Chem. Commun.* **1982**, 895.
[12] P. P. Paul, T. B. Rauchfuss, S. R. Wilson, *J. Am. Chem. Soc.* **1993**, *115*, 3316–3317; S. Dev, E. Ramli, T. B. Rauchfuss, S. R. Wilson, *Inorg. Chem.* **1991**, *30*, 2514–2519; E. Ramli, T. B. Rauchfuss, C. A. Stern, *J. Am. Chem. Soc.* **1990**, *112*, 4043–4044.
[13] A. J. Blake, M. Schroeder, *Adv. Inorg. Chem.* **1990**, 35, 1.
[14] S. C. Rawle, S. R. Cooper, *Struct. Bonding (Berlin)* **1991**, *72*, 1.
[15] M. Draganjac, T. B. Rauchfuss, *Angew. Chem.* **1985**, *97*, 745–760; *Angew. Chem. Int. Ed. Engl.* **1985**, *24*, 742.
[16] A. Müller, *Polyhedron*, **1986**, *5*, 323; A. Müller, E. Dieman, *Adv. Inorg. Chem.*, **1987**, *31*, 89.
[17] M. G. Kanatzidis, S.-P. Huang, *Coord. Chem. Rev.* **1994**, *130*, 509–621.

Formation of an Alkylperoxoiron(III) Complex during Oxidations Catalyzed by μ-Oxodiiron(III) Complexes**

Stéphane Ménage, Elizabeth C. Wilkinson, Lawrence Que, Jr., and Marc Fontecave*

Mononuclear[1] and binuclear non-heme iron complexes[2] have been recently shown to catalyze the oxidation of hydrocarbons by alkyl hydroperoxides such as *tert*-butyl hydroperoxide (TBHP) and cumene hydroperoxide (CHP) and thus provide good models of non-heme iron-based monooxygenases like methane monooxygenase.[3] It has been suggested that the catalytic activity of these systems depends on the ability of the iron sites to bind the peroxide and generate oxidizing high-valent iron species.[4] While a peroxoiron(III) intermediate is likely to be a key intermediate in oxygenations catalyzed by enzymes or model systems, such a complex has never been observed during catalysis and characterized. Recently, a transient, highly unstable, high-spin alkylperoxo complex of iron in a non-heme environment was observed and characterized during reactions of a mononuclear iron(II) complex with TBHP or CHP.[5] Whether this complex catalyzes alkane functionalization was not specified. We have observed a transient complex during oxidation of alcohols by TBHP or CHP catalyzed by a non-heme oxo-bridged diiron(III) complex, and herein we report its spectroscopic characterization as an alkylperoxoiron(III) complex.

We have previously demonstrated that complex **1**, in which two $[Fe(bpy)_2(H_2O)]$ units (bpy = 2,2′-bipyridine) are bridged

$[Fe_2O(bpy)_4(H_2O)_2(ClO_4)_4]$ **1**

by an oxo group, is a very efficient catalyst for the oxidation of alkanes and alcohols by TBHP.[4] At room temperature, in acetonitrile as solvent, and with benzyl alcohol as substrate, a deep bluish green complex **2** appeared almost instantaneously after the addition of the peroxide and then slowly disappeared after one minute, when all of the oxidant had been consumed.[6] Running the experiment at $-10\,^{\circ}C$ allowed slower accumulation of

[*] Prof. M. Fontecave, Dr. S. Ménage
L. E. D. S. S., URA 332, Université J. Fourier, BP53X
F-38052 Grenoble Cedex 09 (France)
Telefax: Int. code +76 51 43 82
E. Wilkinson, Prof. L. Que, Jr.
Department of Chemistry, University of Minnesota
Minneapolis, MN 55455 (USA)

[**] This work was supported by NATO (M. F. and L. Q., grant CRG-930188) and by the U.S. National Institutes of Health (L. Q., grant GM-38767).

complex **2** and permitted its spectroscopic characterization. The UV/VIS spectrum of **2** exhibits a broad absorption band at 640 nm (ε/Fe = 1700 ± 200 $M^{-1}cm^{-1}$; Fig. 1). In the analogous reaction with CHP the absorption band was blue-shifted to 627 nm. Resonance Raman spectra of frozen complex **2** at 77 K with 628-nm laser excitation revealed two strong res-

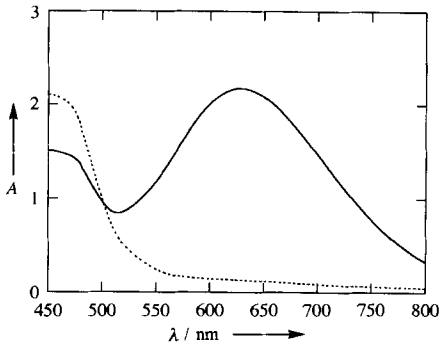


Fig. 1. Electronic spectra of complex **1** (0.7 mM; ···) and complex **2** (——) in the presence of 200 equiv benzyl alcohol. **2** was generated by addition of 50 equiv CHP to the solution of **1** at −10 °C.

onance-enhanced Raman features at 808 and 678 cm^{-1} (Fig. 2), which were not affected by the presence of $H_2{}^{18}O$. These bands shifted to 805 and 696 cm^{-1} when CHP was used, and to 814, 742, 696, and 668 cm^{-1} when [D_9]TBHP was used, demonstrating that the alkylperoxo moiety remains intact in intermediate **2**. The energies of these bands are in the range characteristic for O–O vibrations for peroxides (750–950 cm^{-1}) and comparable to those found for the only characterized alkylperoxoiron(III) complex.[5, 7] Though a precise assignment of these vibrations has not been made, the accumulated data suggest that these features arise from an iron-bound alkylperoxo moiety and that the longest wavelength band arises from an alkylperoxo-to-iron(III) charge transfer transition.

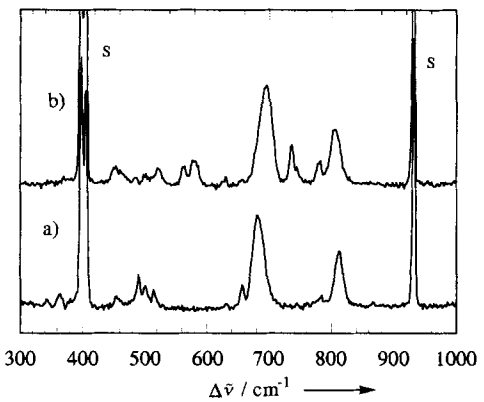


Fig. 2. Resonance Raman spectra (excitation at λ = 627.6 nm, 77 K) of complex **2** obtained with a) TBHP and b) CHP as oxidant in acetonitrile in the presence of benzyl alcohol. Peaks labeled with S arise from solvent.

When the reaction was monitored by EPR spectroscopy, a rhombic EPR signal (g_1 = 2.18, g_2 = 2.12, g_3 = 1.98) appeared during the reaction (Fig. 3). The time-dependent variation of the intensity of this EPR signal strictly coincided with the variation of the 640-nm absorption band, strongly suggesting that

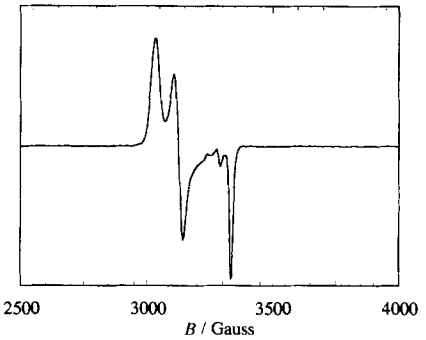
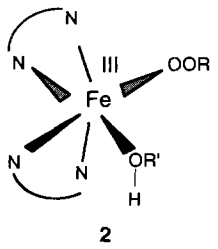


Fig. 3. EPR spectra of complex **2** at 100 K in acetonitrile. Experimental conditions: power 5 mW; modulation 3.2; time constant 0.128 s.

the blue-green complex **2** is also the EPR-active species. The characteristic features of the EPR signal demonstrate that complex **2** is not a binuclear species but rather a mononuclear low-spin rhombic (with reference to its EPR spectrum) iron(III) complex. Such a spectrum has also been observed for synthetic heme–peroxide complexes,[8] "activated bleomycin",[9] and related models.[10] Its intensity accounts for as much as 0.8 spin per iron atom.[11] Our spectroscopic studies strongly suggest that complex **2** contains an alkylperoxo moiety bound to a mononuclear iron(III) center.

There are still some questions regarding the nature of the sixth ligand. A possibility is that the alkylperoxo moiety binds to the metal center in an η^2 coordination mode as proposed for the high-spin iron(III) complex [Fe(6TLA)OO*t*Bu]$^{2+}$ (6TLA = tris[(6-methyl-2-pyridyl)methyl]amine).[5] However, the spectroscopic properties of complex **2** differ markedly from those of [Fe(6TLA)OO*t*Bu]$^{2+}$, and we suggest that in our case η^1 coordination is more likely. Since complex **2** is observable only in the presence of alcohols (methanol, cyclohexanol, phenol), it is likely that an alcohol occupies the sixth coordination site. The following observations are consistent with this hypothesis. First, the shape of the $S = 1/2$ EPR signal varies depending on the alcohol. Secondly, the absorption maximum of the intermediate shifted to 620 nm when phenol was used.[12, 13] Thirdly, the intermediate did not form with sterically hindered phenols such as 2,3,4-trimethylphenol. We thus propose the structure shown in Scheme 1 for complex **2**.



2

Scheme 1. Proposed structure for complex **2**. $\overset{\frown}{N\,N}$ = bpy.

Our data demonstrate for the first time that during oxidations of substrates by alkyl hydroperoxides catalyzed by a binuclear iron(III) complex, a mononuclear peroxoiron(III) intermediate is formed. The binding of the peroxide to the metal center is probably essential for its activation. Whether this complex is the active species or a precursor of a more oxidizing intermediate remains to be firmly established.

Received: May 20, 1994
Revised version: September 14, 1994 [Z 6956 IE]
German version: *Angew. Chem.* **1995**, *107*, 198

Keywords: complexes with oxygen ligands · enzyme models · iron compounds · oxidations

 © VCH Verlagsgesellschaft mbH, D-69451 Weinheim, 1995 0570-0833/95/0202-0204 $ 10.00+.25/0

[1] a) D. R. H. Barton, S. D. Bévière, W. Chavasiri, D. Doller, B. Hu, *Tetrahedron Lett.* **1992**, *25*, 504; b) L. Saussine, E. Brazil, A. Robine, H. Mimoun, J. Fisher, R. Weiss, *J. Am. Chem. Soc.* **1985**, *107*, 3534; c) J. D. Koola, J. K. Kochi, *Inorg. Chem.* **1987**, *26*, 908; d) T. Kojima, R. A. Leising, S. Yan, L. Que, Jr., *J. Am. Chem. Soc.* **1993**, *115*, 11328.

[2] a) R. H. Fish, M. S. Konings, K. J. Oberhausen, R. H. Fong, W. M. Yu, G. Christou, J. B. Vincent, D. K. Coggin, R. M. Buchanan, *Inorg. Chem.* **1991**, *30*, 3002; b) R. A. Leising, J. Kim, M. A. Pérez, L. Que, Jr., *J. Am. Chem. Soc.* **1993**, *115*, 618, and references therein.

[3] a) A. C. Rosenzweig, C. A. Frederick, S. J. Lippard, P. Norlund, *Nature* **1993**, *366*, 537; b) J. Green, H. Dalton, *Biochem. J.* **1986**, *236*, 155; c) J. D. Lipscomb, *Annu. Rev. Microbiol.*, in press.

[4] S. Ménage, J.-M. Vincent, C. Lambeaux, G. Chottard, A. Grand, M. Fontecave, *Inorg. Chem.* **1993**, *32*, 4766.

[5] Y. Zang, T. E. Elgren, Y. Dong, L. Que, Jr., *J. Am. Chem. Soc.* **1993**, *115*, 811.

[6] The reaction of **1** (0.7 mM), 50 equiv of 80% CHP, and 200 equiv benzyl alcohol for 90 s produced 35 equiv benzaldehyde. The yield of the reaction based on the oxidant is 35%.

[7] S. Ahmad, J. D. McCallum, A. K. Shiemke, E. H. Appelman, T. M. Loehr, J. Sanders-Loehr, *Inorg. Chem.* **1988**, *27*, 2230.

[8] K. Tajima, T. Edo, K. Ishizy, S. Imaoka, Y. Funae, S. Oka, H. Sakurai, *Biochem. Biophys. Res. Commun.* **1993**, *191*, 157.

[9] R. M. Burger, J. Peisach, S. B. Horwitz, *J. Biol. Chem.* **1981**, *256*, 11636.

[10] R. J. Guajardo, S. E. Hudson, S. J. Brown, P. K. Mascharak, *J. Am. Chem. Soc.* **1993**, *115*, 7971.

[11] The EPR signal was quantified by double integration with copper sulfate as a standard at 100 K.

[12] The transient species can be generated by using 30 equiv phenol or 4-methylphenol instead of 200 equiv benzyl alcohol. All the phenol was consumed during the oxidation process, and 1,4-benzoquinone and 1,4-hydroquinone were obtained as major products.

[13] This band was not observed in the absence of TBHP, indicating that it does not arise from a phenolate-to-iron(III) charge transfer transition.

A New Type of Trinuclear Oxoiron(III) Cluster**

Jean-Marc Vincent, Stéphane Ménage, Jean-Marc Latour, Azzedine Bousseksou, Jean-Pierre Tuchagues, André Decian, and Marc Fontecave*

The search for polynuclear oxo- and/or hydroxo-bridged iron complexes has been motivated by their implications in natural systems.[1] The simplest diiron(III) centers have been structurally identified in the active site of hemerythrin, methane monooxygenase, and ribonucleotide reductase, in which they are involved in dioxygen transport or activation.[2] Recent studies have revealed the potential of synthetic model complexes containing a Fe-O-Fe unit as catalysts for the oxidation of alkanes by peroxides.[3] Moreover, such centers are early intermediates in the formation of large hydroxo(oxo)iron aggregates in the interior of ferritin, the multisubunit iron-storage protein.[4] Information on the transition of binuclear oxo-bridged iron(III) complexes into clusters of higher nuclearity is sparse, and mechanisms of the first steps of the formation of the ferritin iron core are still ill-defined. Our recent investigations of the chemical reactivity of dibridged μ-acetato(μ-oxo)diiron(III) model complexes showed that complex **1** could, in the presence of an organic base, generate complex **2**, which has an unprecedented triiron core.[5] Herein we report the preparation, the X-ray structure, and the spectroscopic and magnetic properties of this new type of carboxylato(oxo)iron cluster.

$[Fe_2O(phen)_4(OAc)](ClO_4)_3$ **1** $[Fe_3O_2(phen)_6(OAc)_2](ClO_4)_3$ **2**

The core of the cation of **2** · EtOAc shown in Figure 1 consists of a bent triiron chain[6] which can be described as two identical (μ-oxo)diiron(III) units with a common central iron atom. As a result there is a pseudo-C_2 axis within the molecule passing through the central Fe2 atom. All three metal centers have a N_4O_2 coordination environment with pseudo-octahedral symmetry. Each Fe center coordinates the nitrogen atoms of two bidentate phenanthroline ligands. One oxo and one monodentate acetato ligand complete the coordination sphere of the terminal iron atoms, and two μ-oxo ligands that of the central iron atom. The distances and angles are comparable to those observed in (μ-oxo)diiron(III) complexes (average Fe-O-Fe angle 160.6°, average Fe···Fe distance 3.536 Å).[2] The length of the Fe–O bonds to the acetato ligand (average Fe–O distance 1.965 Å) are in the usual range. As previously observed for $[Fe_2O(Me_2bpy)_4(CF_3CO_2)_2]$, in which the trifluoroacetato ligand is also monodentate, the carbonyl oxygen atom of the carboxyl group lies above the phenanthroline plane, suggesting $\pi-\pi$ interactions.[3e] As expected, the Fe–N bonds *trans* to the strong electron-donating μ-oxo ligand are longer (2.271(8) and 2.283(8) Å for the terminal Fe atoms and 2.337(8) Å for the central one) than those *cis* (average 2.164 Å), because of the *trans* effect. The presence of two oxo ligands at the central iron atom is responsible for longer Fe–O_{oxo} bonds (1.814(7) and 1.823(7) Å compared to 1.771(7) and 1.775(6) Å at the terminal iron atoms). The *trans* effect also explains why the configuration in which the two oxo ligands are *cis* with respect to the central iron is favored (O1-Fe2-O4 104.7°). This configuration

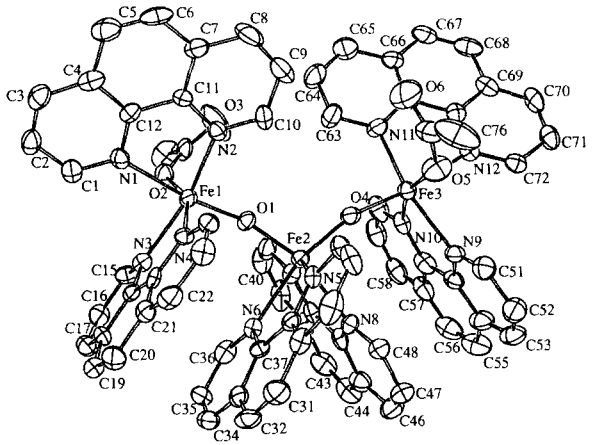


Fig. 1. ORTEP representation of the structure of the cation of **2** (ellipsoids at 50% probability). Hydrogen atoms have been omitted for clarity. Selected bond lengths [Å] and angles [°]: Fe1-O1 1.775(6), Fe1-O2 1.971(7), Fe1-N1 2.283(8), Fe1-N2 2.164(8), Fe2-O1 1.814(7), Fe2-O4 1.823(7), Fe1-N5 2.140(8), Fe2-N6 2.337(8), Fe2-N8 2.329(8), Fe3-O4 1.771(7), Fe3-N9 2.189(8), Fe3-N10 2.260(9), Fe3-N11 2.142(9), Fe3-N12 2.271(8), Fe3-O5 1.961(8); Fe1-O1-Fe2 160.3(4), Fe2-O4-Fe3 161.1(4).

[*] Prof. M. Fontecave, J.-M. Vincent, S. Ménage
L. E. D. S. S., URA 332, Université J. Fourier, BP53X
F-38052 Grenoble (France)
Telefax: Int. code +76 51 43 82
J.-M. Latour
Département de Recherche Fondamentale sur la Matière Condensée
Laboratoire SESAM/CC (URA 1194), Centre d'Etudes de Grenoble
A. Bousseksou, J.-P. Tuchagues
Laboratoire de Chimie de Coordination du CNRS, UPR 8241, Toulouse
A. Decian
Laboratoire de Chimie des Métaux de Transition et Catalyse
URA 424, Université Strasbourg I

[**] This research was supported by the Centre National de la Recherche Scientifique (URA 332 and GDR Métalloprotéines et Analogues de Synthèses). We are grateful to Professor F. Varret for helpful discussions.

also allows stacking of the phenanthroline rings, which probably contributes to the stability of the structure. As a result, the triiron chain is bent with an Fe-Fe-Fe angle close to 120°, affording a 6.135-Å separation between the terminal iron atoms. Only two other triiron(III) complexes with similar structures have been reported.[7, 8] One contains two bis(μ-carboxylato)(μ-hydroxo) bridges and the second, one bis(μ-carboxylato)(μ-hydroxo) bridge and one bis(μ-carboxylato)(μ-oxo) bridge; however, in both complexes the three iron atoms are perfectly aligned. In both cases, the oxo and hydroxo ligands are *trans* with respect to the central iron, and the Fe–O(H) distances are longer than those in **2**. Complex **2** is thus the first trinuclear complex with two μ-oxo and no carboxylato bridges.

The magnetic susceptibility of **2** has been measured from 2 to 300 K at field strengths of 0.5, 1, 2, and 3 Tesla.[9] The value of the $\chi_M T$ product (4.24 $cm^3 K mol^{-1}$ at 300 K) decreases to a minimum value of 4.19 $cm^3 K mol^{-1}$ at around 200 K and increases again to a plateau at 4.21 $cm^3 K mol^{-1}$ from 100 to 25 K (Fig. 2). At lower temperatures the $\chi_M T$ product exhibits a steep

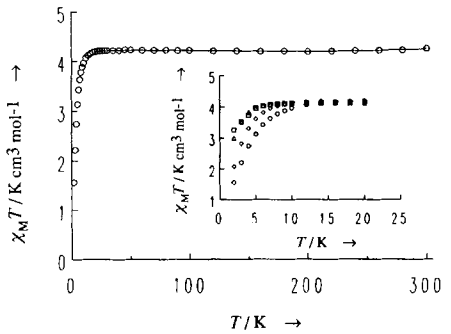


Fig. 2. Temperature dependence of the product of the molar susceptibility χ_M and the temperature T at 3 Tesla. The solid line is the result of the simulation over the range 30–300 K with the parameters indicated in the text. The inset shows the same data in the range 2–20 K at field strengths of 0.5 (□), 1 (△), 2 (◇), and 3 (○) Tesla.

decrease which is strongly field dependent. This behavior is consistent with a strong antiferromagnetic coupling of the Fe_3^{III} unit, leading to a $S = 5/2$ ground state which is disturbed by zero-field effects at low temperature. The high-temperature data ($T \geq 30$ K) can be described with the Heisenberg exchange Hamiltonian [Eq. (a)], which takes into account both the ex-

$$\mathcal{H} = -J[S_1S_2 + S_2S_3] - J'S_1S_3 \qquad \text{(a)}$$

change interaction (J) between vicinal iron atoms and that (J') between the terminal iron atoms. The calculation led to the following best-fit values: $g = 1.96$, $J = -168\ cm^{-1}$, $J' = +5\ cm^{-1}$. The large absolute value of J is quite in line with the short Fe–O distances (1.771–1.824 Å).[10] To confirm the value of the external coupling constant J', the fitting was repeated with $J' = 0$; this resulted in a significantly poorer fit and a larger value for the exchange interaction, $J = -183\ cm^{-1}$. In the related (μ-hydroxo)(μ-oxo)triiron complex the J' value was three times larger ($11\ cm^{-1} < J' < 24\ cm^{-1}$).[8]

No satisfactory simulation of the low-temperature data was obtained upon treating **2** as a $S = 5/2$ spin system with axial and rhombic zero-field splittings. This discrepancy might be explained by local anisotropies and the possible misalignment of the g tensors of the three Fe atoms, owing to the low symmetry of the complex.

The X-band EPR spectrum of complex **2** at 90 K in frozen acetonitrile (Fig. 3) displays three features centered at $g = 8.5$,

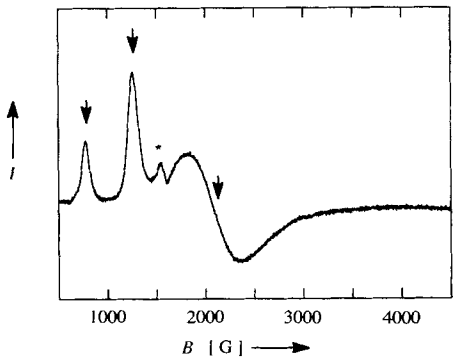


Fig. 3. X-band EPR spectrum of complex **2** in acetonitrile (2 mM) at 90 K. Experimental conditions: gain = 5×10^4; microwave power = 10 mW; modulation = 3.2; frequency = 9.411 GHz; time constant = 1.28 ms. The g values in the text were calculated from the signals marked with arrows. The signal marked with an asterisk is attributed to an impurity.

5.3, and 3.0. This differs greatly from the spectra of the two other bridged Fe_3 complexes and the linear cluster $[Fe_3S_4(SR)_4](Et_4N)_3$, in which only one strong feature is observed at $g = 4.3$.[11, 12] Lowering the recording temperature from 90 to 6 K led to an increase of the relative intensity of the $g = 8.5$ transition and a decrease of the other signals, demonstrating that the former derives from the ground state of the magnetic system (data not shown in Fig. 3). This spectrum may be consistent with an overall $S = 5/2$ ground state with $E/D < 1/3$. According to the $S = 5/2$ rhombograms, a graphic solution gives an E/D value of roughly 0.15.[13] This result explains the difficulty in fitting the magnetic data at low temperature when only an axial zero-field splitting parameter is applied. The use of E and D tensors in the exchange Hamiltonian will require further investigation.

The Mössbauer spectra of complex **2** recorded at 293, 80, and 4.2 K are consistent with the presence of two nonequivalent structural units associated with two different values of the quadrupole splitting (ΔE_Q) parameter (Fig. 4).[14] Line broad-

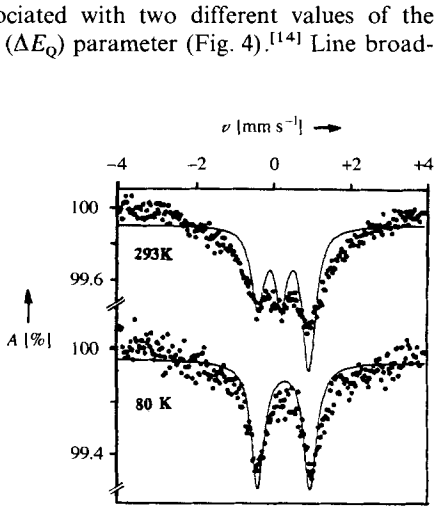


Fig. 4. Mössbauer spectra for a microcrystalline sample of complex **2** at 293 and 80 K.

ening arising from magnetic relaxation effects, which are often observed in paramagnetic high-spin Fe^{III} complexes,[15] does not allow straightforward analysis of the Mössbauer spectra. It is worth noticing that the line broadenings are different for the two sites: the pattern exhibiting a large quadrupole splitting is weakly temperature dependent, while the pattern characterized by a small ΔE_Q becomes increasingly ill defined with decreasing

 © VCH Verlagsgesellschaft mbH, D-69451 Weinheim, 1995 0570-0833/95/0202-0206 $ 10.00+.25/0

temperature, without reaching, however, the static situation of a well-resolved paramagnetic hyperfine structure at 4.2 K.[16] The parameters of the doublet characterized by the larger quadrupole separation have been measured from the spectrum recorded at 80 K (δ/iron foil at 293 K = 0.50(1) mm s^{-1}, ΔE_Q = 1.39(2) mm s^{-1}) and are consistent with those of (μ-oxo)diiron(III) complexes (δ = 0.36–0.56(1) mm s^{-1}, ΔE_Q = 1.3–1.8 mm s^{-1}).[1, 2] Those of the doublet characterized by the smaller separation have been obtained only from the spectrum recorded at 293 K and not that at 80 K because of line broadening (δ = 0.72(1) mm s^{-1}, ΔE_Q = 0.67(2) mm s^{-1}). These parameters indicate that the corresponding iron site is in a less distorted octahedral environment. Close inspection of the structural data shows that though the N_4O_2 coordination environments of the three iron atoms are roughly equivalent, the central iron atom has the most distorted octahedral coordination (based on the standard deviation for the Fe–N distances and the average L-Fe-L angle deviation from 90°) and should thus be associated with the doublet exhibiting the larger quadrupole splitting (ΔE_Q = 1.39(2) mm s^{-1}). The crystallographically pseudo-equivalent terminal iron atoms have less distorted ligand environments and are not distinguished from each other in the Mössbauer spectra.

Complex **2** further illustrates the rich and growing chemistry of carboxylato(oxo)iron compounds. Its unprecedented structure with a bent triiron unit gives rise to unusual spectroscopic and magnetic properties. This is the first example of the transformation of a (μ-oxo)diiron(III) unit into a complex with a triiron chain. Complex **2** may represent a missing link in the series of precursors for mineralized iron(III) compounds (e.g., the polyiron core of ferritin).[1e] The presence of an exchangeable acetato ligand might allow further controlled polymerization of the iron chain.

Experimental Procedure

The synthesis of **1** is described in ref. [3e]. **2** · EtOAc: Addition of 1,2-dimethylimidazole (4.5 µL, 1.5 equiv) to **1** (30 mg, 25 µmol) in 3 mL of acetonitrile resulted in a red solution. Crystals were obtained by vapor diffusion of ethyl acetate into the mother liquor and gave satisfactory analysis (60% yield). Anal. calcd for $[Fe_3O_2(C_{12}H_8N_2)_6(CH_3CO_2)_2](ClO_4)_3 \cdot C_4O_2H_8$: C 53.82, H 3.47, N 9.42, Cl 5.95, Fe 9.38. Found: C 53.44, H 3.58, N 9.62, Cl 5.97, Fe 9.20. UV/VIS (CH_3CN, 25 °C): 378 nm (12700 M^{-1} cm^{-1}).

Received: June 3, 1994
Revised version: September 12, 1994 [Z 6990 IE]
German version: *Angew. Chem.* **1995**, *107*, 199

Keywords: complexes with oxygen ligands · EPR spectroscopy · iron compounds · magnetic properties · Mössbauer spectroscopy

[1] a) D. M. Kurtz, Jr., *Chem. Rev.* **1990**, *90*, 585; b) J. S. Lippard, *Angew. Chem.* **1988**, *100*, 353; *Angew. Chem. Int. Ed. Engl.* **1988**, *27*, 344; c) K. S. Hagen, *ibid.* **1992**, *104*, 1036 and **1992**, *31*, 1010, and references therein.

[2] a) L. Que, Jr., A. E. True, *Prog. Inorg. Chem.* **1990**, *38*, 97; b) J. Sanders-Loehr in *Iron Carriers and Iron Proteins* (Ed.: T. M. Loehr), VCH, New York, **1989**, p. 373.

[3] a) J. B. Vincent, J. C. Huffman, G. Christou, Q. Li, M. A. Nanny, D. N. Hendrickson, R. H. Fong, R. H. Fish, *J. Am. Chem. Soc.* **1988**, *110*, 6898; b) R. H. Fish, M. S. Konings, K. J. Oberhausen, R. H. Fong, W. M. Yu, G. Christou, J. B. Vincent, D. K. Coggin, R. M. Buchanan, *Inorg. Chem.* **1991**, *30*, 3002; and references therein; c) N. Kitajima, H. Fukui, Y. Moro-oka, *J. Chem. Soc. Chem. Commun.* **1988**, 485; d) R. A. Leising, J. Kim, M. A. Pérez, L. Que, Jr., *J. Am. Chem. Soc.* **1993**, *115*, 9524; e) S. Ménage, J. M. Vincent, C. Lambeaux, G. Chottard, A. Grand, M. Fontecave, *Inorg. Chem.* **1993**, *32*, 4766.

[4] A. Treffry, J. Hirzmann, S. J. Yewdall, P. M. Harrison, *FEBS Lett.* **1992**, *302*, 108.

[5] Abbreviations used: OAc = acetate, phen = 1,10-phenanthroline, Me_2bpy = 4,4'-dimethyl-2,2'-bipyridine, EtOAc = ethyl acetate, T1,4DMIP = tris(1,4-dimethylimidazol-2-yl)phosphane.

[6] Diffraction-quality red crystals (0.4 × 0.2 × 0.1 mm) were obtained from ethyl acetate/acetonitrile. The complex **2** · EtOAc crystallizes in the monoclinic system, space group $P2_1/c$, with a = 13.336(4), b = 22.804(6), c = 25.181(7) Å, β = 92.41(2), V = 7668.7 Å^3, Z = 4. 5299 Unique observed reflections, for which $I > 3.0\sigma(I)$, were collected at 293 K with $Mo_{K\alpha}$ radiation (λ = 0.71069 Å) to $2\theta_{max}$ = 26° on an Enraf-Nonius CAD4F X-ray diffractometer. The structure was solved by direct methods and refined to R = 0.074, R_w = 0.099. Further details of the crystal structure investigation may be obtained from the Director of the Cambridge Crystallographic Data Centre, 12 Union Road, GB-Cambridge CB21EZ (UK), on quoting the full journal citation.

[7] V. Vonkai, G. Newton, D. M. Kurtz, *Inorg. Chem.* **1992**, *31*, 34.

[8] N. Kitajima, H. Amagai, N. Tamura, M. Ito, Y. Moro-oka, K. Heerwergh, A. Pénicaud, R. Mathur, C. A. Reed, P. D. Boyd, *Inorg. Chem.* **1993**, *32*, 3583.

[9] Magnetic susceptibility data were measured on 17.44-mg microcrystalline sample with a Quantum Design MPMS SQUID magnetometer. Data were collected over the temperature range 2–300 K at field strengths of 3, 2, 1, and 0.5 Tesla.

[10] S. M. Gorun, S. J. Lippard, *Inorg. Chem.* **1991**, *30*, 1625.

[11] EPR spectra of **2** in the solid state and in acetonitrile were similar, which shows that **2** does not dissociate in solution. In contrast to the ^{1}H NMR spectra of $[Fe_3(\mu\text{-}OH)_2(\mu\text{-}OAc)_4(T1,4DMIP)_2](PF_6)_3$ and other oxoiron(III) complexes like **1**, the spectrum of **2** is very complex with resonances in the range $90 \geq \delta \geq -60$. The signal of the methyl acetato ligand has been assigned by comparison with the trifluoroacetato derivative (δ_{CH_3} = 39). Also resonance Raman spectra show a Fe–O vibration from a linear Fe-O-Fe unit.

[12] J. J. Girerd, G. C. Papaefthymiou, A. D. Watson, E. Gamp, K. S. Hagen, N. Edelstein, R. B. Frankel, R. H. Holm, *J. Am. Chem. Soc.* **1984**, *106*, 5941.

[13] a) W. R. Hagen, *Adv. Inorg. Chem.* **1992**, *38*, 165; b) S. Wickman, *J. Chem. Phys.* **1965**, *42*, 2113.

[14] Mössbauer measurements were made with conventional constant-acceleration spectrometer with a 50-mCi source of ^{57}Co (Rh matrix). The absorber was a microcrystalline powder sample (120 mg) of **2**. Variable-temperature spectra were obtained in the 4–300 K range by using a MD 306 Oxford cryostat.

[15] N. N. Greenwood, T. C. Gibbs, in *Mössbauer Spectroscopy*, Chapman & Hall, New York, **1971**.

[16] To prove these relaxation phenomena it is necessary to reach a static state and observe the internal magnetic field. This can be obtained by applying a weak magnetic field. When an external magnetic field of 2 Tesla was applied at 7 K, the magnetic fluctuations were frozen, and analysis of the resulting Zeeman spectrum allowed us to measure an internal effective magnetic field of roughly 3.9 T.

Mutually Interpenetrating Sheets and Channels in the Extended Structure of [Cu(4,4'-bpy)Cl]**

O. M. Yaghi* and Guangming Li

In memory of Mouannes A.-F. Yaghi

The development of synthetic strategies for the design of solid-state structures from soluble components is of intense current interest.[1] The building-block approach has been utilized for the rational assembly of inorganic[2] and organometallic[3, 4] crystalline solids. We have initiated a program aimed at using this approach in the preparation of crystalline materials possessing open-framework structures with cavities or channels. Simple ligands such as 4,4'-bipyridine (4,4'-bpy) are chosen for their demonstrated ability to act as rods linking together metal centers to give extended solids with diverse topologies.[5] This report shows how chloro-bridged Cu^I dimers with M–M bonding may be combined with 4,4'-bpy to form sheets of [Cu(4,4'-bpy)Cl]-containing cavities with dimensions of nearly 16 × 26 Å.

[*] Prof. O. M. Yaghi, G. Li
Department of Chemistry and Biochemistry
Goldwater Center for Science and Engineering
Arizona State University
Tempe, AZ 85287 (USA)
Telefax: Int. code + (602)965-2747

[**] This work was supported by the U. S. National Science Foundation (Grant CHE-9224279) and the Petroleum Research Fund, administered by the American Chemical Society (PRF No. 28175-G3); 4,4'-bpy = 4,4'-bipyridine.

In the overall structure, these sheets are interlocked with other sheets to form a three-dimensional, neutral network containing a two-dimensional, intersecting system of channels of smaller aperture.

Crystals of [Cu(4,4′-bpy)Cl] were obtained by diffusing solutions of CuCl and 4,4′-bpy into ethylene glycol. The compound was formulated by elemental analysis[6] and characterized by X-ray single-crystal analysis.[7, 8] The extended structure is made up of the building-block unit shown in Figure 1: dimeric

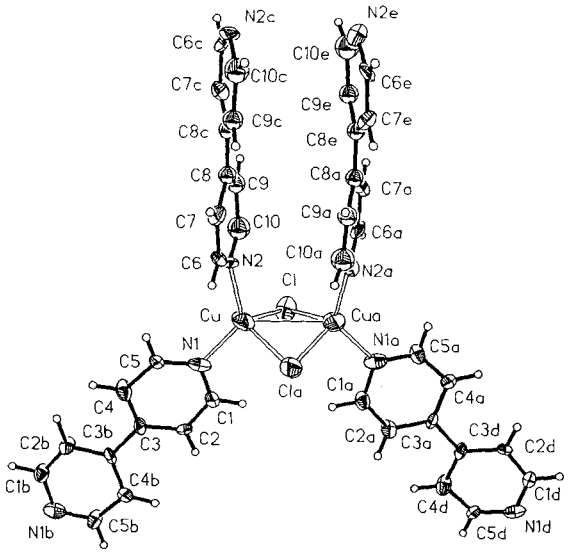


Fig. 1. A perspective drawing of the μ_2-chloro-bridged dinuclear building-block unit present in crystalline [Cu(4,4′-bpy)Cl] Non-hydrogen atoms are represented by thermal vibration ellipsoids drawn to encompass 50% of electron density. Hydrogen atoms are represented by arbitrarily small spheres. Atoms labeled with a–e are related to atoms without these letters by the following symmetry operations: for a, $1-x, 1/2-y, z$; b, $-1/4+y, 1/4+x, 1/4-z$; c, $3/4-y, 3/4-x, -1/4-z$; d, $5/4-y, 1/4-x, 1/4-z$; and e, $1/4+y, -1/4+x, -1/4-z$. Selected interatomic distances [Å] and angles [°]: Cu-Cl 2.415(6), Cu-Cla 2.475(6), Cu-Cua 2.763(7), Cu-N1 1.97(1), Cl-Cu-N1 105.1(5), Cl-Cu-N2 108.3(4), Cl-Cu-Cla 104.9(2), N1-Cu-Cla 99.6(4), N2-Cu-Cla 115.5(5), N1-Cu-N2 125.6(6), Cl-Cu-Cua 56.6(2), Cu-Cl-Cua 68.8(2), Cua-Cu-Cla 54.6(2), N1-Cu-Cua 101.9(4) (cf. ref. [8]).

Cu^I centers are bridged by two chloro ligands, and each metal atom is linked to two 4,4′-bpy ligands to form a slightly distorted tetrahedron with N2-Cu-N1 = 125.6(6)°, N1-Cu-Cla = 99.6(4)°, and Cl-Cu-Cla = 104.9(4)°. In addition, the N1 and N2 pyridine rings are twisted by 22.0(5)° and 15.60(4)° relative to the N1b and N2c rings. These distortions are due to the fact that each 4,4′-bpy acts as a bismonodentate ligand linking two Cu^I dimeric units, as shown in Figure 2; this results in formation of an infinite hexagonal array made up of Cu^I dimers with M–M bonding and 4,4′-bpy ligands, and containing pores measuring around 16 × 26 Å. However, in the absence of large guest molecules to fill the pores during the molecular assembly process, other perpendicular and symmetry-equivalent sheets of the same structure and composition are found to occupy the pores. Although, these two infinite sheet arrays are mutually perpendicular, they are not bound to each other, but are instead interlocked, like catenanes, as independent two-dimensional networks.[9]

The overall structure thus formed is a neutral three-dimensional framework, in which the interpenetrating two-dimensional networks fill up most of the pore space with channels of only small diameter (≈ 2 × 4 Å) remaining open (Figs. 3 and 4). It was

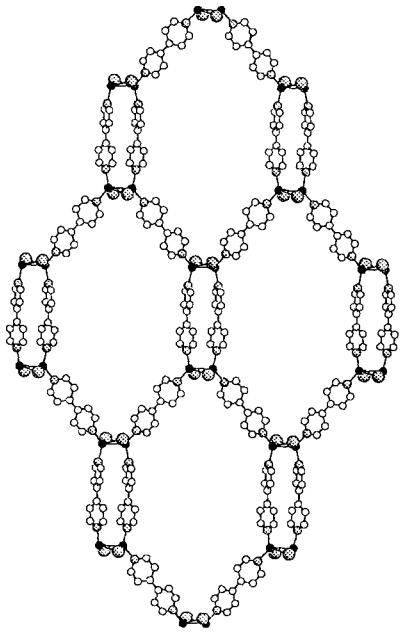


Fig. 2. A SCHAKAL drawing showing how the organization of the building-block unit $[Cu(4,4'\text{-bpy})Cl]_4$ results in the construction of infinite porous sheets that are a fragment of the crystal structure of [Cu(4,4′-bpy)Cl]. The hydrogen atoms on the bipyridine units have been omitted for clarity. Dark spheres, Cu; large shaded spheres, Cl; small shaded spheres, N; and open spheres, C.

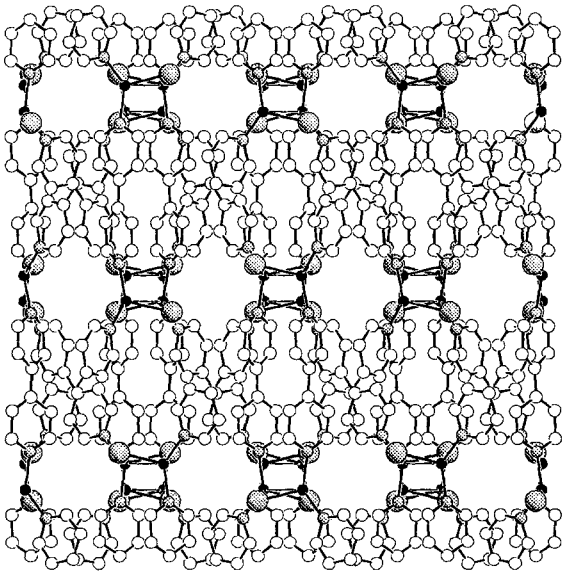


Fig. 3. A SCHAKAL drawing of the overall crystal structure of [Cu(4,4′-bpy)Cl] showing how infinite sheets are interlocked to fill the pores (shown in Fig. 2) leaving only small empty channels in the structure. The omissions and shadings are as in Figure 2.

found from the X-ray analysis that these channels are too small to accommodate acetonitrile or dimethyl sulfoxide (DMSO) solvent molecules as guests in the crystal. This was confirmed by thermal gravimetric analysis performed on a 35.306 mg sample, which showed that the material begins to degenerate at 175 °C to give only pyridine, chloride, and copper metal. Also, ^{13}C CPMAS (cross polarization magic angle spinning) solid-state NMR data showed only resonances due to the 4,4′-bpy carbon atoms and none that could be attributed to possible guest species.

 © VCH Verlagsgesellschaft mbH, D-69451 Weinheim, 1995 0570-0833/95/0202-0208 $ 10.00+.25/0

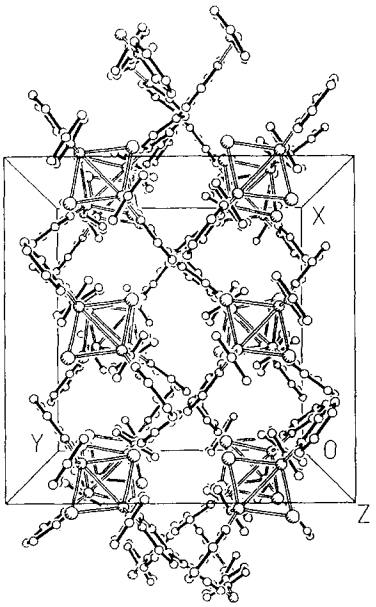


Fig. 4. A plot of the structure showing the unit cell packing and the perpendicular interpenetrating arrangement of the Cu–Cu units. Small partially shaded spheres, N; medium-sized partially shaded spheres, Cu; large partially shaded spheres, Cl; open spheres, C.

The size of the channel openings is very similar to those observed in some zeolite molecular sieves, such as, analcime (2.2–2.4 Å) and natrolite (2.6 × 3.9 Å),[10, 11] where water (kinetic diameter ≈ 2.8 Å) is known to penetrate and diffuse into the channels. We found that the material synthesized is stable in air indefinitely and in boiling water for up to 1 h. Currently, we are attempting to evaluate its potential use in water adsorption and in gas separation processes.

Experimental Procedure

[Cu(4,4′-bpy)Cl]: The addition of an acetonitrile solution (10 mL) of 4,4′-bpy (0.78 g, 5.0 mmol) to an acetonitrile solution (50 mL) of CuCl (0.50 g, 5.0 mmol) resulted in the immediate formation of a dark red, microcrystalline material. This solid was collected and washed with ethanol (3 × 20 mL) followed by diethyl ether (3 × 20 mL), and dried under vacuum for 24 h to give 1.2 g (94%) [7]. Crystals suitable for X-ray single-crystal analysis were obtained by diffusing a DMSO solution of 4,4′-bpy (0.10 M) into an acetonitrile solution of CuCl (0.10 M) through ethylene glycol (3 mL). This results in the formation of red, rectangular parallelepiped-shaped crystals at the acetonitrile/ethylene glycol interface. Alternatively, large crystals were obtained by diffusing solutions of the reactants in a 5 mm thick mineral oil.

Received: July 20, 1994 [Z 7145 IE]
German version: *Angew. Chem.* **1995**, *107*, 232

Keywords: complexes with nitrogen ligands · copper compounds · zeolite analogues

[1] a) *Supramolecular Architecture: Synthetic Control in Thin Films and Solids* (Ed.: T. Bein) (*ACS Symp. Ser.* **1992**, *499*); b) T. E. Mallouk, H. Lee, *J. Chem. Educ.* **1990**, *67*, 829–834.

[2] O. M. Yaghi, Z. Sun, D. A. Richardson, T. L. Groy, *J. Am. Chem. Soc.* **1994**, *116*, 807–808.

[3] See for example, a) K.-M. Park, R. Kuroda, T. Iwamoto, *Angew. Chem.* **1993**, *105*, 939–941; *Angew. Chem. Int. Ed. Engl.* **1993**, *32*, 884–886; b) T. Kitazawa, H. Sugisawa, M. Takeda, T. Iwamoto, *J. Chem. Soc. Chem. Commun.* **1993**, 1855–1856; c) T. Iwamoto in *Inclusion Compounds, Vol. 5* (Eds.: J. L. Atwood, J. E. D. Davies, D. D. Macnicol), Oxford University Press, Oxford, **1991**, p. 177, and references therein; d) R. Robson, B. F. Abrahams, S. R. Batten, R. W. Gable, B. F. Hoskins, J. Liu in ref. [1a], p. 256.

[4] U. Behrens, A. K. Brimah, K. Yünlü, R. D. Fischer, *Angew. Chem.* **1993**, *105*, 117–119; *Angew. Chem. Int. Ed. Engl.* **1993**, *32*, 82–83.

[5] M. Fujita, Y. J. Kwon, S. Washizu, K. Ogura, *J. Am. Chem. Soc.* **1994**, *116*, 1151–1152; see also ref. [3d].

[6] Elemental analysis: $C_{10}H_8N_2CuCl$: calcd.: C 47.06, H, 3.16, N 10.98, Cu, 24.90, Cl, 13.89; found.: C 47.34, H, 3.03, N 11.11, Cu 25.84, Cl, 13.00.

[7] The homogeniety of the bulk product was confirmed by comparison of the observed and calculated X-ray powder diffraction patterns. The calculated pattern was produced by using the SHELXTL-XPOW program with the single-crystal data.

[8] Single crystals of [Cu(4,4′-bpy)Cl] were analyzed at 20 °C. Tetragonal, space group $I4_1/acd$, (no. 142) with $a = 14.246(4)$, $c = 38.596(12)$ Å, $V = 7833(3)$ Å^3, $Z = 16$, $\rho_{calcd} = 1.731$ g cm^{-3} and $\mu_a(Mo_{K\alpha}) = 2.46$ mm^{-1}. A total of 1345 independent absorption-corrected reflections having $2\theta(Mo_{K\alpha}) < 45.8°$ (the equivalent of 0.6 $Cu_{K\alpha}$ spheres) were collected on a computer-controlled Nicolet autodiffractometer with full 2.00° wide ω scans and graphite-monochromated $Mo_{K\alpha}$ radiation. The structure was solved by direct methods (SHELXTL-PC) and the resulting structural parameters were refined by least-squares techniques to converge ($R1$ (unweighted, based on $|F|$) = 0.050 for 465 independent absorption-correction reflections having $2\theta < 45.8°$ and $I > 2\sigma(I)$) using counter-weighted full-matrix least-square techniques and a structural model which incorporated anisotropic thermal parameters for C8, C9, and C10 and for all hydrogen atoms. The hydrogen atoms were fixed at idealized sp^2-hybridized positions with C–H bond lengths of 0.96 Å, and their isotropic thermal parameters were fixed at values 1.2 times the equivalent isotropic thermal parameters of the carbon atoms to which they are covalently bonded. Further details on the crystal structure investigation may be obtained from the Fachinformationszentrum Karlsruhe, D-76344 Eggenstein-Leopoldshafen (Germany), on quoting the depository number CSD-58460.

[9] Interlocking of supramolecular structures is an interesting area in chemical topology, and it has been observed in molecular organic and very few extended inorganic systems: a) J. P. Sauvage, *Acc. Chem. Res.* **1990**, *23*, 319–327; b) G. Schill, *Catenanes, Rotaxanes, and Knots*, Academic Press, New York, **1988**; c) A. Michaelides, V. Kiritsis, S. Skoulika, A. Aubry, *Angew. Chem.* **1993**, *105*, 1525–1526; *Angew. Chem. Int. Ed. Engl.* **1993**, *32*, 1495–1497; d) S. R. Batten, B. F. Hoskins, R. Robson, *J. Chem. Soc. Chem. Commun.* **1991**, 445–447; e) R. W. Gable, B. F. Hoskins, R. Robson, *ibid.* **1990**, 1677–1678.

[10] A. Dyer, A. Molyneux, *J. Inorg. Nucl. Chem.* **1968**, *30*, 829–837.

[11] S. P. Gabuda, *Dokl. Akad. Nauk SSSR* **1962**, *146*, 840–843.

Investigation of Self-Assembled Supramolecular Species in Solution by IL-ESMS, a New Mass Spectrometric Technique**

Keith C. Russell, Emmanuelle Leize, Alain Van Dorsselaer, and Jean-Marie Lehn*

The spontaneous assembly of complementary components into designed architectures has developed recently into a central theme of supramolecular chemistry.[1] In particular, hydrogen bonding has been used for the generation of supramolecular assemblies in solution, in liquid crystals, and in the solid state.[2–5] Whereas solid-state structures may be determined by X-ray crystallography, procedures are greatly needed for investigation of organized species formed in solution, in particular to determine whether their structures are the same as in the solid. Vapor-phase osmometry, membrane osmometry, and gel permeation chromatography have been used and generally yield molecular weights with degrees of error that can be as large as

[*] Prof. Dr. J.-M. Lehn, Dr. K. C. Russell
Laboratoire de Chimie Supramoléculaire, Institut Le Bel
Université Louis Pasteur
4 rue Blaise Pascal, F-67000 Strasbourg (France)
Telefax: Int. code +88 41 10 20
Dr. E. Leize, Dr. A. Van Dorsselaer
Laboratoire de Spectrométrie de Masse Bio-organique
Centre de Recherche Chimie
Université Louis Pasteur
1 rue Blaise Pascal, F-67008 Strasbourg (France)

[**] We thank the Centre National de la Recherche Scientifique (URA 422 and URA 31) and the Research and Development Corporation of Japan for support of this work, the Collège de France for a postdoctoral fellowship to K. C. R., and the Conseil Régional d'Alsace for financial support for E. L. and for partial financing of an ES mass spectrometer. The financial support of Bioavenir (Rhône Poulenc Santé) is also gratefully acknowledged.

a single assembly unit; in addition they only give an average of all species in solution.

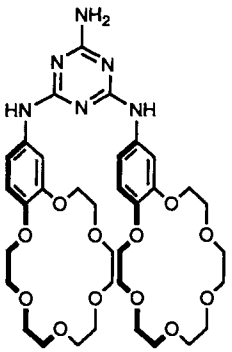
Electrospray mass spectrometry (ESMS)[6] has emerged as a mild method for the characterization of a large range of molecules such as proteins,[7] oligonucleotides,[8] and coordination compounds.[9] No energy is required to ionize the sample, since a solution of preformed ions is used, and only minimal energy is necessary for transferring the ions from solution into the gas phase. A number of noncovalent association complexes have also been examined by ESMS. They include enzyme–substrate, enzyme–product, receptor–ligand, and oligonucleotide associations.[10] Moreover, it is possible to follow by ESMS the formation of metal coordination assemblies under equilibrium conditions and obtain information about the different species present in solution.[11]

Hydrogen-bonded supramolecular assemblies, which are usually stable only in solvents of low polarity, are uncharged in these solutions and thus cannot be studied by ESMS. It is therefore crucial to develop a general method for the examination of such neutral associations in solution. The use of ESMS-active tags, for example cation-binding crown ethers and protonatable dimethylaniline groups, has permitted the characterization of neutral organic molecules such as vitamin D and fullerene derivatives.[12, 13]

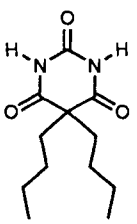
We describe here an ion-labeling electrospray mass spectrometry (IL-ESMS) method for the characterization of self-assembled species formed from complementary hydrogen-bonding components in organic solution.

The complementary partners barbituric acid and triaminopyrimidine or triaminotriazine assemble through formation of six hydrogen bonds into species that have been characterized in the solid state by X-ray crystallography. Three types of supramolecular structures have been found depending on the nature of the components: a linear strand (ribbon or tape),[14–16] an undulating strand (or crinkled tape),[16] and a macrocycle (or rosette).[16]

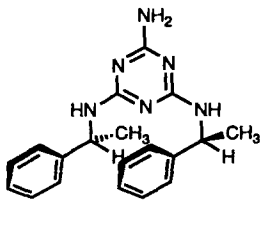
Our goal was to develop ESMS-active tags for the study of hydrogen-bonded supramolecular assemblies with the intent of observing the individual species present in a solution of the self-assembling complementary components **A** and **B**. This may also permit us to estimate the ability of ESMS to characterize labile polyassociated species. Related systems include oligonucleotide duplexes, which are considerably more stable, since the smallest ones studied by ESMS thus far comprised eight base pairs; the partners were held together by a total of 18–24 hydrogen bonds as well as stacking interactions.[10f].



A



B



C

The triazines **A** and **C** were synthesized by reaction of 4′-aminobenzo[18]crown-6 (2 equiv, Janssen Chemicals), or (*R*)- then (*S*)-α-methylbenzylamine (1 equiv each) with 6-amino-2,4-dichloro-1,3,5-triazine[17] at high concentration (76 and 85% yield, respectively). The barbiturate **B** was obtained as previously described.[18] All materials gave the expected spectroscopic data.[19]

Since hydrogen-bonded assemblies such as those formed by the **A**/**B** pair are expected to be destroyed on protonation, ionization was achieved by complexation of potassium ions by the crown ether groups of component **A**. Equimolar mixtures of the partners **A** and **B** (10^{-2} M) in dichloromethane were treated with KPF_6 ($M = 184.1$ Da) (solution S_1, Table 1) and then studied by ESMS. The compositions of the ions observed are listed in Table 2.

Table 1. Composition of the solutions studied by ESMS.

Solution	Components, stoichiometry	Solvent	Concentration [a]	Salt [b]
S_1	**A** + **B**	CH_2Cl_2	10^{-2}	KPF_6
S_2	**A** + **B**	CH_2Cl_2	10^{-3}	KPF_6
S_3	**A** + **B**	CH_2Cl_2	10^{-2}	KPF_6 [c]
S_4	**A** + **B**	benzene	10^{-2}	KPF_6
S_5	**A** + **B**	CH_2Cl_2/pentane (1/1)	10^{-2}	KPF_6
S_6	**B** + **C**	CH_2Cl_2	10^{-2}	–
S_{6a}	**A** + **B** + **C**	CH_2Cl_2	10^{-2}	KPF_6
S_{6b}	**A** + 20**B** + 20**C**	CH_2Cl_2	10^{-2}	KPF_6
S_{6c}	**A** + 20**B** + 20**C**	CH_2Cl_2	10^{-3}	KPF_6
S_7	**A**	CH_2Cl_2	10^{-2}	–

[a] Single-component solutions; in M. [b] Saturated salt solution unless indicated otherwise. [c] Solution half-saturated with salt.

The ES mass spectrum of S_1 (Fig. 1) was measured at $V_c = 10$ V to minimize possible fragmentation of the assemblies. Indeed, at $V_c > 20$ V hydrogen-bonded complexes began to fragment owing to their relatively weak association.[20] Peaks at m/z 412.4 and 969.4 correspond to the differently charged molecules of **A**; the more abundant species is [**A**, $2K^+$, PF_6^-]. As partner **B** was not ionized, it was not detected. Peaks at m/z 1209.7 and 1886.9 correspond to an $\mathbf{A_3B_3}$ complex. The ion giving the peak at m/z 1209.7 is not an unspecific aggregate of **A** and **B**, because it is not a singly charged ion (isotope pattern not resolved with a resolution of 1500 at m/z 1300). A less intense peak at m/z 1329.8 is observed for the doubly charged ion of $\mathbf{A_2B_3}$. The same signals were found for the **A**/**B** mixture at 10^{-3} M (S_2), although the peaks were less intense.

The charge state of these three peaks was confirmed by the ESMS study of S_3 (Fig. 2). S_3 contains half as much KPF_6 as S_1 does, and thus more peaks corresponding to complexes of composition $\mathbf{A_3B_3}$ and $\mathbf{A_2B_3}$ occur, by the loss of one or more KPF_6 units (m/z 1148.5, 1087.3, 1025.7, and 1237.9, respectively). The detection of the ion [**A** + K^+] (m/z 785.5) as the base peak indicates a redistribution of charge states of **A** by loss of KPF_6. A m/z difference of 61.2 (= $M(KPF_6)/3$) obtained between the four peaks at m/z 1025.7, 1087.3, 1148.5, and 1209.7

 © VCH Verlagsgesellschaft mbH, D-69451 Weinheim, 1995 0570-0833/95/0202-0210 $ 10.00+.25/0 Angew. Chem. Int. Ed. Engl. 1995, 34, No. 2

Table 2. Summary of m/z values of ions detected by ESMS for **A** and the complexes **M** (= $\mathbf{A_3B_2}$, $\mathbf{A_2B_3}$, and $\mathbf{A_3B_3}$) [a].

	A	$\mathbf{A_2B_3}$	$\mathbf{A_3B_2}$	$\mathbf{A_3B_3}$
M [b]	746.8	2214.5	2721.0	2961.3
$\mathbf{M} + K^+$	785.5	–	–	–
$\mathbf{M} + K^+ + KPF_6$	969.4	–	–	–
$\mathbf{M} + 2K^+$	412.4	–	1399.0	1519.1
$\mathbf{M} + 2K^+ + KPF_6$	–	1237.9	1491.0	1611.0
$\mathbf{M} + 2K^+ + 2KPF_6$	–	1329.8	1582.9	1703.0
$\mathbf{M} + 2K^+ + 3KPF_6$	–	–	1674.9	1794.9
$\mathbf{M} + 2K^+ + 4KPF_6$	–	–	–	1886.9
$\mathbf{M} + 3K^+$	–	–	–	1025.7
$\mathbf{M} + 3K^+ + KPF_6$	–	–	–	1087.3
$\mathbf{M} + 3K^+ + 2KPF_6$	–	–	–	1148.5
$\mathbf{M} + 3K^+ + 3KPF_6$	–	–	–	1209.7

[a] Graphic representations of the assemblies are given in Figs. 1–3. For the 2:3 assemblies (second and third columns) only one of the possible superstructures is shown. [b] Calculated molecular weights of complexes **M**.

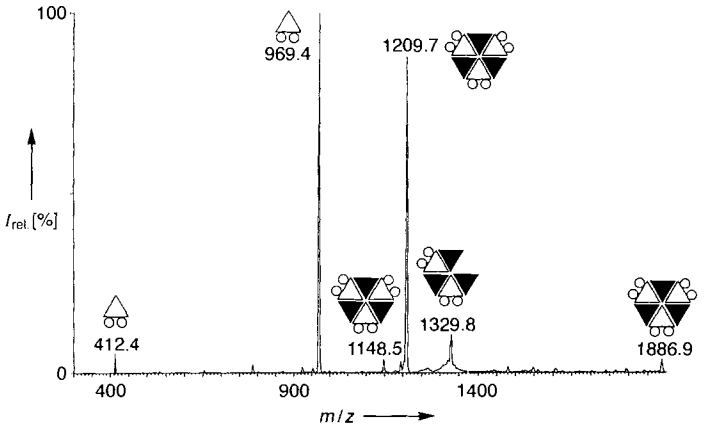


Fig. 1. ES mass spectrum of S_1 (Table 1). The observed ions are summarized in Table 2. The schematic representations of the complexes composed of **A** and **B** do not indicate the contributions of the K^+ ions and KPF_6 molecules to the m/z values.

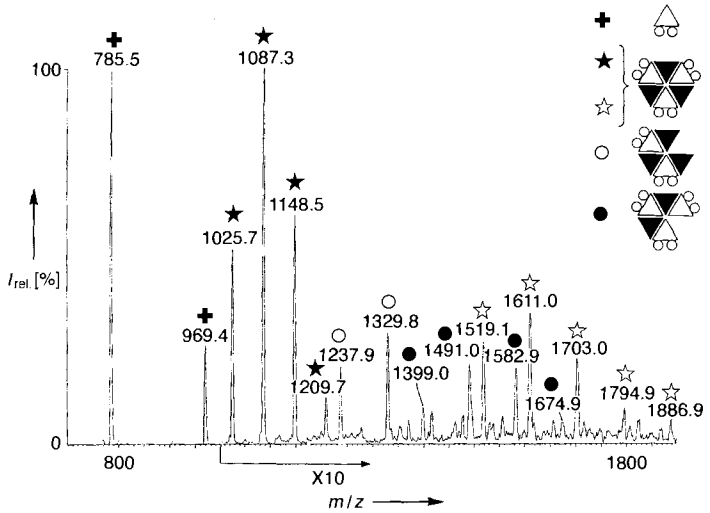


Fig. 2. ES mass spectrum of S_3 (Table 1). The observed ions are summarized in Table 2.

(Table 2) corresponds to the loss of three, two, and one KPF_6, respectively, from the ion at m/z 1209.7, indicating that these peaks indeed arise from triply charged ions. A m/z difference of 92.5 (= $M(KPF_6)/2$) for the series of peaks m/z 1519.1, 1611.0, 1703.0, 1794.9, and 1886.9 (Table 2) corresponding to the loss of four, three, two, and one KPF_6, respectively, from the ion at m/z 1886.9, and for peaks m/z 1237.9 and 1329.8 (Table 2) corresponding to the loss of one KPF_6 from the ion at m/z 1329.8, confirm the doubly charged state of these ions. The peaks at m/z 1399.0, 1491.0, 1582.9, and 1674.9 (Table 2) result from the doubly charged ions of the complex $\mathbf{A_3B_2}$, which were not present in the spectrum of S_1.

The addition of 10% MeOH (a solvent known to disrupt hydrogen-bonded assemblies) to S_1 eliminated all peaks from the mass spectrum corresponding to assemblies of **A** and **B**; only a single intense peak at m/z 969.7 for $[\mathbf{A} + 2K^+ + PF_6^-]$ was seen. The results obtained provide evidence that the assemblies observed were indeed those present in solution (no additional assembly in the gas phase), and that ion–molecule reactions were not taking place.[21]

The ES mass spectra recorded in less polar solvents such as benzene (S_4, Fig. 3) and pentane/dichloromethane 1/1 (S_5)

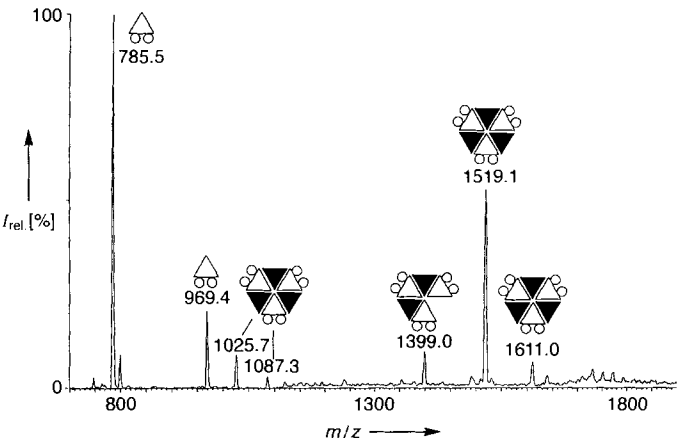
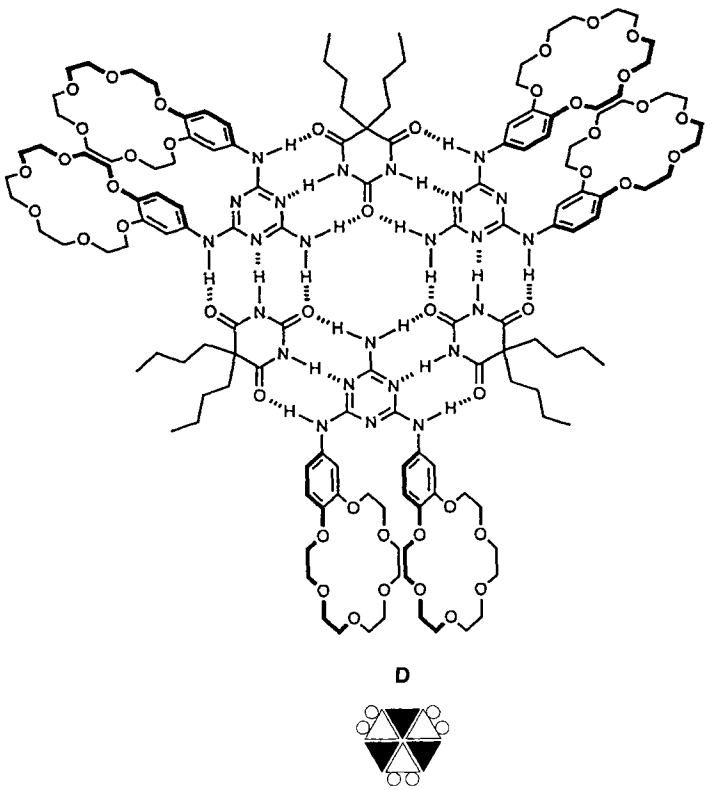


Fig. 3. ES mass spectrum of S_4 (Table 1). The observed ions are summarized in Table 2.

showed the characteristic doubly charged ions (m/z 1519.1, 1611.0) and triply charged ions (m/z 1025.7, 1087.3) of the complex $\mathbf{A_3B_3}$, as well as the doubly charged ion (m/z 1399.0) of $\mathbf{A_3B_2}$ (Table 2). In contrast to the spectra obtained in dichloromethane, no adducts of KPF_6 were found for these ions, and the doubly charged state was most abundant. This difference can be explained by poorer solvation of KPF_6 by these solvents as compared to dichloromethane.[22]

These ESMS studies have thus allowed the characterization of three complexes in solution: $\mathbf{A_3B_3}$, $\mathbf{A_2B_3}$, and $\mathbf{A_3B_2}$. Assembly $\mathbf{A_3B_3}$ was the predominant species detected. Since no larger complexes were observed, we can attribute to $\mathbf{A_3B_3}$ a closed structure of a supramolecular macrocycle (**D**), similar to that observed for related systems in the solid state.[16] Such a structure could explain the higher stability of $\mathbf{A_3B_3}$ relative to that of $\mathbf{A_3B_2}$ and $\mathbf{A_2B_3}$. Indeed, in contrast to $\mathbf{A_3B_2}$ and $\mathbf{A_2B_3}$, the $\mathbf{A_3B_3}$ assembly was not influenced by the amount of salt introduced to ionize the complexes.[23] The possible structures for $\mathbf{A_3B_2}$ and $\mathbf{A_2B_3}$ in solution again could be a linear ribbon, and undulating ribbon, or a partial rosette (Fig. 4).

ESMS has proved its utility for the characterization of hydrogen-bonded complexes, but only species containing charged groups under near physiological conditions have previously been observed. For neutral assemblies that are destroyed by protonation the present results indicate that charge may be introduced through ion binding to a suitably designed compo-



nent. Thus component **A** in the presence of a complexable salt allows neutral species that would otherwise not be evident to be characterized by ESMS. By extension, this points to an *ion labeling method* applicable to the study of any self-assembled structure in solution capable of incorporating the labeling agent **A** added in trace amounts. In the absence of salts the label **A**, as well as any assembly it is part of, is invisible to ESMS, since it has no charge ("ion label" OFF). But in the presence of a salt, **A** coordinates a cation and the "ion label" containing species become visible by ESMS ("ion label" ON). This was tested by the introduction of **A** into a preformed assembly of **B** · **C**.



Fig. 4. Possible architectures of the assemblies composed of 2×3 units: supramolecular macrocycle or rosette (left), ribbon or tape (center), undulating ribbon (right). White and black triangles represent components **A** or **C** and **B**, respectively.

The ESMS study of the species present in an equimolar mixture of **B** and **C** (10^{-2} M in dichloromethane; S_6) was performed by mixing with label **A** (10^{-2} M in dichloromethane; S_7) in two proportions, S_6:S_7 = 1:1 (S_{6a}) and 20:1 (S_{6b}). No peaks were observed in the spectrum of S_{6a} before addition of salt (label OFF). After the addition of KPF_6 to the solution (label ON), the spectrum (Fig. 5a) showed two major species, the ion label **A** (*m/z* 969.4) and the complex $\mathbf{A_2B_3C}$ (*m/z* 1497.1), as well as three other complexes, $\mathbf{A_3B_3}$ (*m/z* 1209.7), $\mathbf{AB_2C}$ (*m/z* 1784.4) and $\mathbf{AB_3C_2}$ (*m/z* 2359.2). In the spectrum of S_{6b} (Fig. 5b) the major species observed were **A** and $\mathbf{AB_3C_2}$; as expected the intensity of the peak corresponding to $\mathbf{A_2B_3C}$ was very weak. The peaks for assemblies $\mathbf{A_3B_3}$ and $\mathbf{AB_2C}$ disappeared, and two new species were present: **ABC** (*m/z* 1544.3) and $\mathbf{AB_2C_2}$ (*m/z* 2119.0).

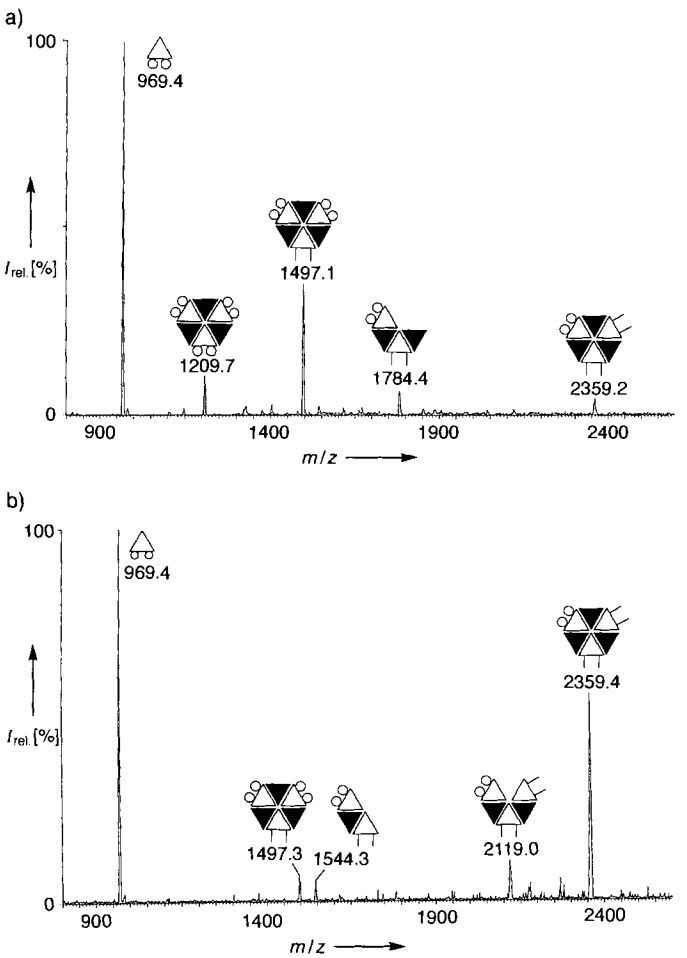


Fig. 5. ES mass spectra of solutions S_{6a} (a) and S_{6b} (b). **A** (M = 746.8) is characterized by the peak *m/z* 969.4 [$\mathbf{A} + 2K^+ + PF_6^-$], $\mathbf{A_3B_3}$ (M = 2961.3) by *m/z* 1209.7 [$\mathbf{A_3B_3} + 6K^+ + 3PF_6^-$], $\mathbf{A_2B_3C}$ (M = 2548.9) by *m/z* 1497.1 [$\mathbf{A_2B_3C} + 4K^+ + 2PF_6^-$], $\mathbf{AB_2C}$ (M = 1561.8) by *m/z* 1784.4 [$\mathbf{AB_2C} + 2K^+ + PF_6^-$], $\mathbf{AB_3C_2}$ (M = 2136.5) by *m/z* 2359.2 [$\mathbf{AB_3C_2} + 2K^+ + PF_6^-$], **ABC** ($M$ = 1321.5) by *m/z* 1544.3 [$\mathbf{ABC} + 2K^+ + PF_6^-$], $\mathbf{AB_2C_2}$ (M = 1896.2) by *m/z* 2119.0 [$\mathbf{AB_2C_2} + 2K^+ + PF_6^-$].

Thus, when a large proportion of ion label was introduced, the major species was $\mathbf{A_2B_3C}$, whereas when the proportion of **A** was low, the $\mathbf{AB_3C_2}$ complex became most abundant. These observations are in agreement with a statistical incorporation of the ion label **A** into the neutral assembly. Again, no assemblies with molecular weights greater than that of a six-component species were observed, suggesting that this assembly also prefers a macrocyclic rosette architecture (Fig. 4). The same species were found for the 1/20/20 **A**/**B**/**C** mixture at 10^{-3} M (S_{6c}).

In conclusion, we have shown that electrospray mass spectrometry can be used to study hydrogen-bonded self-assembled species. We have developed a new methodology for which we suggest the name ion-labeling electrospray mass spectrometry (IL-ESMS), which can be used to observe discrete neutral assemblies in solution. The present results indicate that the range of species likely to be studied by ESMS can be extended to labile supramolecular species formed by self-assembly. In the cases studied the highest molecular weight species observed is a six-component entity, most likely possessing the closed structure of a supramolecular macrocycle **D**. By designing appropriate ion-labeling components that combine an ion binding site (such as a crown ether or a cryptand) with specific recognition groups, it should become feasible to extend this IL-ESMS procedure to

the investigation of a wide variety of hydrogen-bonded supramolecular assemblies and more generally of self-assembly through any type of intermolecular interaction. Such work is currently in progress in our laboratory.

Experimental Procedure

Positive-ion ES mass spectra were obtained on a VG BioQ triple quadrupole apparatus with a mass-to-charge (m/z) range up to 4000 (VG Bio Tech Ltd, Altrincham, UK). The electrospray source was heated to 50 °C. The sampling cone voltage (V_c) [6] was at 10 V to avoid fragmentation of the assemblies. Sample solutions were introduced into the mass spectrometer source with a syringe pump (Harvard type 55 1111; Harvard Apparatus Inc., South Natick, MA, USA) at a flow rate of 6 $\mu L\,min^{-1}$. Calibration was performed using protonated horse myoglobin. The resolution was usually about 500 at m/z 1000 (10% height). Scanning was performed from m/z 200 to 2200 in 15 s. The data system was operated as a multichannel analyzer, and several scans were summed to obtain the final spectrum. Samples for ESMS were prepared by dissolving equimolar amounts of the components in the appropriate solvent (dichloromethane, benzene, pentane) to achieve the concentrations listed in Table 1. Solutions containing salts were prepared by adding 0.5 mg of salt (KPF_6, $NaClO_4$, CsCl) in 0.5 mL of solution and sonicating briefly. The solution was removed from the excess salt with a pipette and directly analyzed. Labeling experiments were performed by adding the desired ratio of equimolar solutions of the inactive label (**A** without KPF_6) and the assembly of interest, and then adding KPF_6 as previously described.

Received: July 9, 1994
Revised version: September 21, 1994 [Z 7116 IE]
German version: *Angew. Chem.* **1995**, *107*, 244

Keywords: crown ethers · mass spectrometry · supramolecular chemistry

[1] J.-M. Lehn, *Angew. Chem.* **1990**, *102*, 1347; *Angew. Chem. Int. Ed. Engl.* **1990**, *29*, 1304.
[2] G. M. Whitesides, J. P. Mathias, C. T. Seto, *Science* **1991**, *254*, 1312.
[3] C. Fouquey, J.-M. Lehn, A. M. Levelut, *Adv. Mater.* **1990**, *2*, 254.
[4] T. Gulik-Krzywicki, C. Fouquey, J.-M. Lehn, *Proc. Natl. Acad. Sci. USA* **1993**, *90*, 163.
[5] J.-M. Lehn, *Makromol. Chem. Macromol. Symp.* **1993**, *69*, 1.
[6] a) A. P. Bruins, T. R. Covey, J. D. Henion, *Anal. Chem.* **1987**, *59*, 2642; b) J. B. Fenn, M. Mann, C. K. Meng, S. F. Wong, C. M. Whitehouse, *Mass Spectrom. Rev.* **1990**, *9*, 37; c) A. P. Bruins, *ibid.* **1991**, *10*, 53.
[7] J. B. Fenn, M. Mann, C. K. Meng, S. F. Wong, C. M. Whitehouse, *Science* **1989**, *246*, 64.
[8] J. T. Stults, J. C. Marsters, *Rapid Commun. Mass Spectrom.* **1991**, *5*, 359.
[9] a) V. Katta, S. K. Chowdhury, B. T. Chait, *J. Am. Chem. Soc.* **1990**, *112*, 5348; b) F. Bitsch, C. O. Dietrich-Buchecker, A. K. Khémiss, J.-P. Sauvage, A. Van Dorsselaer, *ibid.* **1991**, *113*, 4023; c) F. Bitsch, G. Hegy, C. O. Dietrich-Buchecker, E. Leize, J.-P. Sauvage, A. Van Dorsselaer, *New J. Chem.* **1994**, in press.
[10] a) B. Ganem, Y. T. Li, J. D. Henion, *J. Am. Chem. Soc.* **1991**, *113*, 6294; b) *ibid.* **1991**, *113*, 7818; c) V. Katta, B. T. Chait, *ibid.* **1991**, *113*, 8534; d) M. Baca, S. B. H. Kent, *ibid.* **1992**, *114*, 3992; e) A. K. Ganguly, B. N. Pramanik, A. Tsarbopoulos, T. R. Covey, E. Huang, S. A. Fuhrman, *ibid.* **1992**, *114*, 6559; f) B. Ganem, Y. T. Li, J. D. Henion, *Tetrahedron Lett.* **1993**, *34*, 1445; g) M. Jaquinod, E. Leize, N. Potier, A. M. Albrecht, A. Shanzer, A. Van Dorsselaer, *ibid.* **1993**, *34*, 2771; h) M. Przybylski, M. O. Glocker, *Angew. Chem.* **1995**, in press.
[11] E. Leize, A. Van Dorsselaer, R. Krämer, J.-M. Lehn, *J. Chem. Soc. Chem. Commun.* **1993**, 990.
[12] S. R. Wilson, Q. Lu, M. L. Tulchinsky, Y. Wu, *J. Chem. Soc. Chem. Commun.* **1993**, 664.
[13] S. R. Wilson, M. L. Tulchinsky, Y. Wu, *Bioorg. Med. Chem. Lett.* **1993**, *3*, 1805.
[14] J.-M. Lehn, M. Mascal, A. DeCian, J. Fischer, *J. Chem. Soc. Chem. Commun.* **1990**, 479.
[15] J. A. Zerkowski, C. T. Seto, D. A. Wierda, G. M. Whitesides, *J. Am. Chem. Soc.* **1990**, *112*, 9025.
[16] J. A. Zerkowski, C. T. Seto, G. M. Whitesides, *J. Am. Chem. Soc.* **1992**, *114*, 5473.
[17] O. Diels, *Ber. Dtsch. Chem. Ges.* **1899**, *32*, 691.
[18] E. Fischer, A. Dilthey, *Justus Liebigs Ann. Chem.* **1904**, *335*, 334.
[19] Compound **B** also gave satisfactory microanalytical data. Triazines **A** and **C** were not crystalline, and it was not possible to obtain satisfactory microanalyses.
[20] R. D. Smith, J. A. Loo, C. J. Barinaga, G. G. Edmonds, H. R. Udseth, *J. Am. Chem. Soc. Mass. Spectrom.* **1990**, *1*, 53; V. Katta, S. K. Chowdhury, B. T. Chait, *Anal. Chem.* **1991**, *63*, 174.
[21] For studies at the rather high concentration (10^{-2} M) used in this work, ion–molecule reactions in the gas phase might occur in the ES source. To be certain that peaks observed for assemblies $\mathbf{A_3B_3}$, $\mathbf{A_2B_3}$, and $\mathbf{A_3B_2}$ were not an artifact of ESMS, we studied a solution in which **A** was replaced by benzo[18]crown-6 (18C6), a compound unable to form hydrogen bonds. The only peaks observed in the ES mass spectrum of this solution corresponded to ions $18C6/K^+$, $(18C6)_2/K^+$ and $(18C6)_2/2K^+$. No peaks for possible assemblies of **B** and macrocycle were observed.
[22] The ionization of the complexes in S_1 was also examined by adding $NaClO_4$ and CsCl, instead of KPF_6. With $NaClO_4$ the results were similar to those obtained with KPF_6: adducts of KPF_6/K^+ were replaced by adducts of $NaClO_4/Na^+$. In contrast, with CsCl, $\mathbf{A_3B_3}$ was the only complex detected, but in two charge states: $[\mathbf{A_3B_3} + 3Cs^+]$ and $[\mathbf{A_3B_3} + 2Cs^+]$. The difference in the ionization might be explained by the specific complexation of the alkali metal ions by the crown ether. Indeed, Cs^+ is known to form the sandwich complex $(18C6)_2/Cs^+$, while Na^+ and K^+ give the complexes $18C6/Na^+$ and $18C6/K^+$.
[23] Interestingly, $\mathbf{A_2B_3}$ was present only for large amounts of salt and $\mathbf{A_3B_2}$ only for smaller quantities of salt.

Gas-Phase Activation of Fluorocarbons by "Bare" and Coordinated Praseodymium Cations**

Christoph Heinemann, Norman Goldberg, Inis C. Tornieporth-Oetting, Thomas M. Klapötke, and Helmut Schwarz*

Dedicated to Professor Josef Seibl on the occasion of his 70th birthday

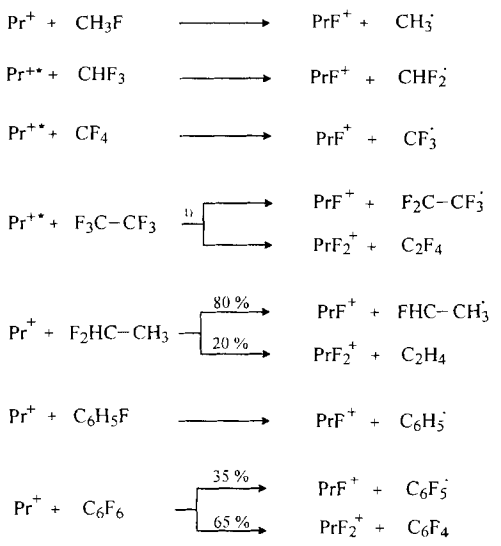
The activation of the strong carbon–fluorine bond by transition metal complexes is a formidable task in organometallic chemistry.[1] Immense industrial interest in this field is due to the widespread use of fluorocarbons and mixed fluorohalocarbons, which takes advantage of their high thermal and chemical stability. Evidence for the involvement of these substances in the mechanisms of stratospheric ozone depletion has made their future use questionable, and there is now a need for selective and efficient chemical conversion. Similar to the growing body of information on C–H and C–C activation of hydrocarbons, gas-phase studies on the intrinsic reactivities of "bare" and ligated transition metal cations[2] are expected to help in the understanding of the molecular mechanisms in the transition metal assisted cleavage of a C–F bond. In this vein, we report on the activation of various aliphatic and aromatic C–F bonds by "bare" Pr^+ ions and small praseodymium complexes PrL^+ (L = O, F) as observed by Fourier transform ion cyclotron resonance mass spectrometry (FT-ICR-MS). Furthermore, we present the first observation of *neutral* praseodymium monofluoride PrF and praseodymium difluoride PrF_2 in the gas phase by means of neutralization–reionization mass spectrometry (NRMS).

In solution-phase chemistry, the homolytic cleavage of C–F bonds in perfluorinated olefins has been achieved with electrophilic divalent lanthanide reagents of the type $LnCp^*_2$ (Ln = Eu, Sm, Yb; $Cp^* = C_5Me_5$).[3] As a first example for

[*] Prof. Dr. H. Schwarz, Dipl.-Chem. C. Heinemann, Dr. N. Goldberg
Institut für Organische Chemie der Technischen Universität
Strasse des 17. Juni 135, D-10623 Berlin (Germany)
Telefax: Int. code +(30) 31421102
Dr. I. C. Tornieporth-Oetting, Priv.-Doz. Dr. T. M. Klapötke
Institut für Anorganische und Analytische Chemie
der Technischen Universität Berlin

[**] This work was supported by the Deutsche Forschungsgemeinschaft, the Volkswagen-Stiftung, and the Fonds der Chemischen Industrie. We thank Dr. D. Schröder and Dipl.-Chem. N. Raabe for helpful discussions and technical assistance.

intermolecular activation of saturated fluorocarbons, Bergman et al. reported recently that the actinide complex $[(MeC_5H_4)_3U(tBu)]$ can abstract a fluorine radical from a variety of fluoroalkanes.[4] In the gas phase the anionic tricarbonylmanganese complex $[Mn(CO)_3]^-$ was shown to activate C–F bonds,[5] and cationic fluorolanthanide complexes LnF^+ (Ln = La, Ce, Pr) as well as UF^+ have been observed in nuclear fission experiments with ^{235}U in the presence of CF_4.[6] In line with these observations we find that in ion/molecule reactions of Pr^+ and a variety of fluorocarbons, homolytic cleavage of C–F bonds is a quite general phenomenon (Scheme 1).

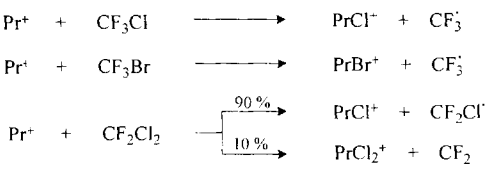


Scheme 1. Pr^{+*} represents a Pr^+ ion that is kinetically or electronically excited prior to reaction. Thermally excited Pr^+ does not react. 1) Because this reaction is endothermic no relative intensities can be given.

In the simplest example Pr^+ formally abstracts a fluorine atom from methyl fluoride (bond dissociation energy, $E_B(H_3C-F) = 112.8 \pm 0.3$ kcal mol^{-1})[7] to form the PrF^+ ion. The reaction rate is 16% of the theoretical collision rate k_{coll}[8] ($k_{exp} = 3 \times 10^{-10}$ cm^3 s^{-1} molecule^{-1}; $k_{coll} = 19 \times 10^{-10}$ cm^3 s^{-1} molecule^{-1}). In the corresponding reaction with 1,1-difluoroethane ($E_B(H_3CFHC-F) = 113$ kcal mol^{-1}) an additional double defluorination pathway gives rise to PrF_2^+ ($PrF^+ : PrF_2^+ = 4:1$). However, fluorine abstraction from CF_3H ($E_B(F_2HC-F) = 128 \pm 3$ kcal mol^{-1}), CF_4 ($E_B(F_3C-F) = 132.4$ kcal mol^{-1}), and C_2F_6 ($E_B(F_3CF_2C-F) = 127$ kcal mol^{-1}) is observed only if the Pr^+ ions are not properly thermalized prior to reaction, that is, if they are kinetically or electronically excited. Since a reliable value for the bond dissociation energy of PrF^+ is not available, it remains unclear whether cleavage at the C–F bond is endothermic, whether the initially formed ion/molecule complex has too short a lifetime (this may especially apply for the unpolar and unpolarizable CF_4 and C_2F_6 molecules), or whether a substantial activation barrier is operative. However, assuming that for cleavage of a simple single bond the barrier should be at most very small, one may tentatively derive an upper value of 131 kcal mol^{-1} for $E_B(Pr^+-F)$ from the *non*observation of C–F bond activation in CHF_3.

Similar to its reactions with aliphatic fluorocarbons Pr^+ cleaves the aromatic C–F bond in fluorobenzene ($E_B(C_6H_5-F) = 125.3 \pm 2.3$ kcal mol^{-1}) at nearly 80% of the theoretical collision rate ($k_{exp} = 11 \times 10^{-10}$ cm^3 s^{-1} molecule^{-1}; $k_{coll} = 14 \times 10^{-10}$ cm^3 s^{-1} molecule^{-1}). For comparison, this lanthanide cation is unreactive towards benzene. The reaction with C_6H_5F provides a lower limit for the bond strength of PrF^+, from which we derive an experimental bracketing value of 127 ± 4 kcal mol^{-1}. In contrast to Pr^+, the less "fluorophilic" Fe^+ ion promotes the loss of hydrogen fluoride from fluorobenzene, resulting in the formation of the cationic iron–benzyne complex $[FeC_6H_4]^+$[9]. In the reaction of Pr^+ with hexafluorobenzene ($E_B(C_6F_5-F) = 116.6 \pm 16$ kcal mol^{-1}), the double defluorination pathway resulting in the formation of PrF_2^+ and C_6F_4 predominates over the abstraction of a single fluorine atom. This experiment supports earlier conjectures from solution chemistry[1, 10] that tetrafluorobenzyne, the existence of which is still unproved to the best of our knowledge, is an intermediate in the activation of hexafluorobenzene by electron-deficient lanthanide complexes.

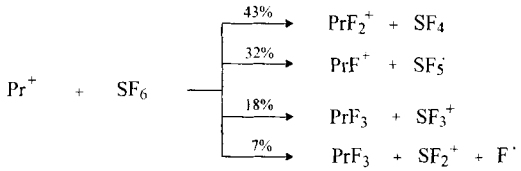
In the reactions of mixed fluorohalocarbons with Pr^+ (Scheme 2), we observed exclusive activation of the weaker



Scheme 2.

C–Cl or C–Br bonds of the substrate (e.g. $E_B(Cl_2FC-F) = 122.7$ kcal mol^{-1}, $E_B(ClF_2C-Cl) = 88.7$ kcal mol^{-1}), although C–F bond activation is thermochemically possible. These experiments provide lower limits of 88.7 and 56.8 kcal mol^{-1} for the bond dissociation energies of Pr^+-Cl and Pr^+-Br, respectively.

Finally, the unpolar and highly unreactive sulfur hexafluoride molecule SF_6 is also activated by Pr^+ in a kinetically efficient process ($k_{exp} = 7.8 \times 10^{-10}$ cm^3 s^{-1} molecule^{-1}; $k_{coll} = 7.1 \times 10^{-10}$ cm^3 s^{-1} molecule^{-1}) (Scheme 3). Here we observe,



Scheme 3.

in addition to PrF^+ and PrF_2^+, the sulfur fluoride ions SF_3^+ and SF_2^+ as primary reaction products, similar to the results recently reported for the corresponding reaction of Sc^+.[11] The exothermic formation of the SF_x^+ species is in accord with their experimental heats of formation[7] and appears to be driven by the stability of neutral PrF_3.

If one follows the commonly accepted view[12] that the 4f electrons of the lanthanide elements are usually chemically inert, then it is indeed quite remarkable that Pr^+ shows the observed reactivity towards fluorocarbons. In particular, the electronic ground state configuration of this cation[13] ($4f^3 5d^0 6s^1$) should not be suitable for insertion into a single bond, a process for which a minimum of *two* valence electrons (i.e. *non*-f electrons) appears necessary.[14] Formally, one may think of a two-electron donation from the metal cation to the σ^* orbital of the

C–X bond to be activated. In accord with this argument, Pr^+ has been shown to be unreactive with most hydrocarbon substrates.[14, 15] Since we have no indication that excited states of Pr^+ were not efficiently quenched in our experiments, we propose two possible mechanistic scenarios (Fig. 1) to explain the observed ground-state reactivity of Pr^+ with fluorocarbons.

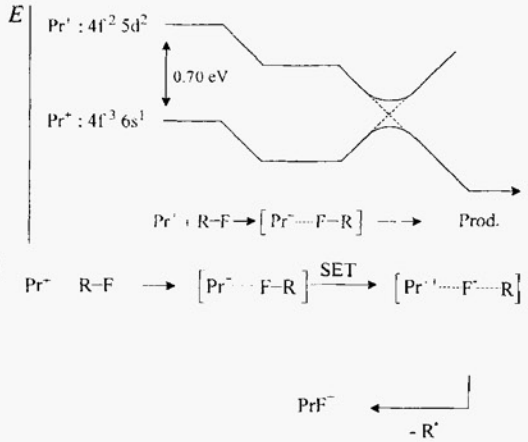


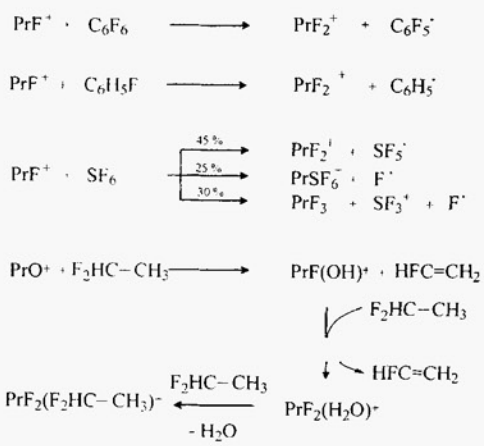
Fig. 1. Mechanisms for C–F bond activation by ground-state Pr^+ ions. a) Curve-crossing model involving the low-lying $4f^25d^2$ electronic configuration of Pr^+ (Prod. = products); b) Single electron transfer (SET) followed by fluorine transfer in the initially formed ion/molecule complex.

1) A curve-crossing model, favored by the strong spin–orbit coupling present in the lanthanide series (Fig. 1a):[13] Here, transitions from the potential energy surface of the Pr^+ ground state to a potential energy surface of an appropriate low-lying excited state of Pr^+ (lowest state with $4f^25d^2$ configuration: +0.70 eV; lowest state with $4f^25d^16s^1$ configuration: +0.94 eV[13]) can occur due to avoided crossings. Essentially, this results in a lowering of the activation barrier for the insertion of the ground state metal cation into the activated bond.[16] 2) Single-electron transfer (SET) from Pr^+ to the fluorine atom of the substrate in the initial ion/molecule complex (Fig. 1b): This step is followed by C–F bond cleavage, as postulated in similar cases in solution chemistry.[1]

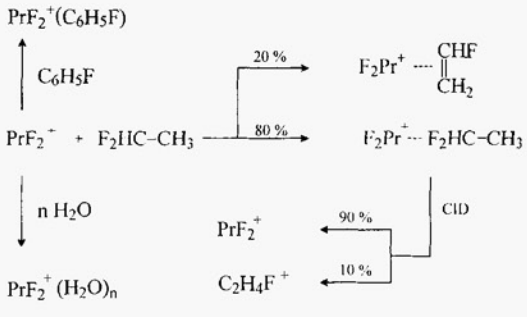
In addition to the reactions of "bare" Pr^+ ions, small praseodymium complexes PrL^+ (L = O, F) also induce C–F bond activation in various substrates (Scheme 4). PrF^+ reacts with C_6H_5F by abstraction of a fluorine atom, indicating that the second fluorine atom in PrF_2^+ has a bond dissociation energy comparable to the first one ($E_B(FPr^+-F) > 125$ kcal mol^{-1}). However, the secondary processes are often significantly slower than the primary reactions (e.g. for $Pr^+ + SF_6$ $k = 7.8 \times 10^{-10}$ cm^3 s^{-1} molecule^{-1}; for $PrF^+ + SF_6$ $k = 5 \times 10^{-11}$ cm^3 s^{-1} molecule^{-1}). Since PrF^+ has a open-shell $4f^3$ electronic configuration,[17] its reactivity is even more surprising than that of Pr^+ and indicates that the 4f electrons of lanthanide ions can in fact be chemically active if the driving force for the reaction is sufficiently large and solvation effects are absent. We note in passing that PrF^+ can be oxidized by N_2O to form the mixed fluorooxo complex $PrOF^+$ with praseodymium in a formal oxidation state of +IV.

Even more interesting is the reactivity of PrO^+ (generated from Pr^+ and N_2O), a species with an extremely strong Pr^+–O bond ($E_B(Pr^+-O) = 191$ kcal mol^{-1}[7]), which is generally unreactive with hydrocarbons. For example, we only observed formation of an adduct complex when this cationic oxide was exposed to benzene, while for the less oxophilic FeO^+ oxygen transfer to the unsaturated substrate has been reported.[18] However, upon reaction of PrO^+ with 1,1-difluoroethane, very slow (relative reaction rate 1% compared to the "bare" Pr^+ cation) addition of hydrogen fluoride to PrO^+ takes place (Scheme 4). In kinetically more efficient subsequent reaction steps an additional molecule of HF is added to this complex, and H_2O is replaced by one molecule of the substrate. These observations suggest that the overall reaction proceeds via a mixed cationic fluorohydroxo complex and the cationic difluoropraseodymium complex, whereby the formerly strongly bound oxygen ligand becomes part of the loosely bound water molecule. Elimination of HF from the substrate proceeds presumably by a 1,2 mechanism, since the most promising substrate for 1,1 elimination of HF, trifluoromethane, is not activated by PrO^+. With reference to the theoretical analysis of other surprisingly slow ion/molecule reactions involving transition metal oxo cations,[16] the very small reaction efficiency in the PrO^+/1,1-difluoroethane system suggests that a spin–orbit-mediated curve-crossing mechanism (Fig. 1) may be operative in this case as well.

While PrF_2^+ is unreactive with CF_4 and SF_6, we observed formation of adduct complexes with water, fluorobenzene, and 1,1-difluoroethane (Scheme 5). Collision-induced dissociation of the $F_2Pr^+-F_2HC-CH_3$ adduct complex at low energies leads only to PrF_2^+. At higher collision energies the appearance of the $C_2H_4F^+$ ion (accompanied by formation of the neutral PrF_3) suggests that in the adduct 1,1-difluoroethane coordinates to the cationic transition metal center through a fluorine atom. These observations point to results from solution-phase chemistry, where precoordination of the substrate molecule to the transi-



Scheme 4.



Scheme 5. n = 1,2

tion metal center prior to activation of the C–F bond has been deduced from solvation effects.[3] In addition to adduct formation, PrF_2^+ also induces loss of hydrogen fluoride from this substrate, resulting in the formation of the $CHF{=}CH_2{-}PrF_2^+$ complex.

As a general conclusion we note that the strength of the praseodymium–fluorine bond is apparently the driving force in the reactions of the praseodymium cation with different fluorocarbons. Overall, Pr^+ activates exclusively C–F and not C–H or C–C bonds. However, as already stressed in a recent review,[1] the unfavorable thermodynamics of these systems severely restrict the design of *catalytic* cycles[1b] for C–F bond activation.

The stability of rare earth fluorides is not restricted to the most common +III oxidation state, as shown by the characterization of various lanthanide subfluorides by spectroscopic techniques[19] and their preparative-scale synthesis.[20] However, neutral praseodymium(I) fluoride and praseodymium(II) fluoride are unknown in the condensed phase, and solid lanthanide(II)fluorides with exact LnF_2 stoichiometry have only been characterized for Ln = Sm, Eu, Yb, and presumably Tm.[20] Among the lanthanide fluorides studied in the gas phase,[17a, 19] neutral PrF and PrF_2 are still missing. In this context, we have applied the technique of neutralization–reionization mass spectrometry (NRMS)[21] to PrF^+ and PrF_2^+. The NRMS spectra (Fig. 2) give clear evidence that neutral

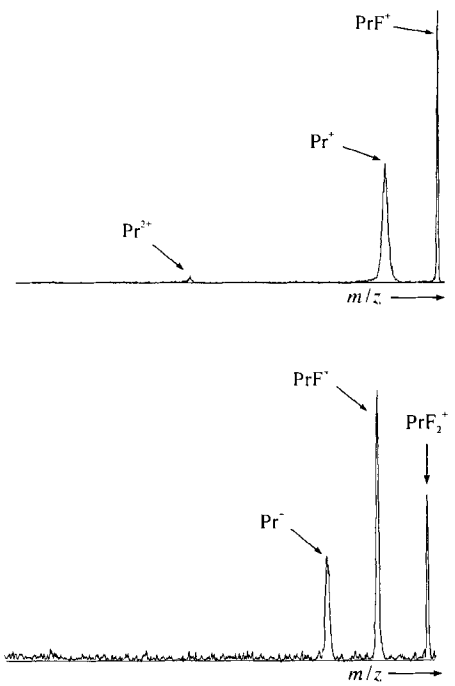


Fig. 2. Neutralization–reionization mass spectra (NRMS) of PrF^+ (top) and PrF_2^+ (bottom). The signals labeled PrF^+ (top) and PrF_2^+ (bottom) are recovery signals.

praseodymium mono- and difluoride are in fact stable chemical species, at least under gas-phase conditions.

Experimental Procedure

Ion/molecule reactions under thermal conditions were performed using a Spectrospin CMS-47X Fourier transform ion cyclotron resonance mass spectrometer equipped with an external ion source (for details see ref. [22]). $^{141}Pr^+$ ions were generated by laser desorption/laser ionization by focusing the beam of a Nd:YAG laser (Spectron Systems; $\lambda = 1064$ nm) onto a piece of pure praseodymium metal (Strem, 3N REO). The ions were transferred to the analyzer cell by a system of electrostatic potentials and lenses, decelerated, trapped in the field of a superconductive magnet (Oxford Instruments, maximum field strength: 7.05 T), and thermalized with pulsed-in argon (maximum pressure ca. 5×10^{-5} mbar). Reactants were admitted to the cell by means of a leak valve at a stationary pressure of $(1-5) \times 10^{-8}$ mbar (as measured by an uncalibrated ion gauge, BALZERS IMG070). Reaction products were analyzed by their high-resolution mass spectra, and their pathways were investigated by using MS/MS and double-resonance techniques. All rate constants were derived from the pseudo-first-order decay of the starting ion and are reported with an estimated accuracy of ±30%.

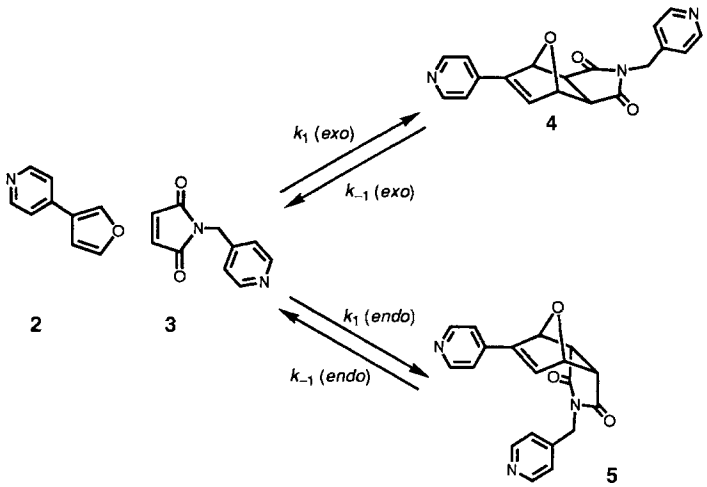
For the neutralization–reionization (NRMS) experiments a large-scale four-sector tandem mass spectrometer was used [23]. The PrF^+ ions were produced by fast-atom bombardment (FAB) of PrF_3 [24], whereas PrF_2^+ was generated in a chemical ionization source by ionizing tris(hexafluoroacetylacetonato)-praseodymium (Strem) in the presence of NF_3. The mass-selected ions were neutralized in the first part of a tandem collision cell upon collisions with xenon (80% transmission, T). Ions that did not undergo neutralization in this region were deflected from the beam of neutral molecules by an electrode (charged at 1000 V) situated between the two collision cells. Neutralized molecules were reionized by colliding them with oxygen (80% T). The *minimal* life time t, which can be derived from the transit time of the neutral particles to travel from the first to the second part of the tandem-collision cell, is of the order of 10 μs.

Received: July 6, 1994 [Z 7097 IE]
German version: *Angew. Chem.* **1995**, *107*, 225

Keywords: fluorocarbons · lanthanide compounds · mass spectrometry

[1] a) J. L. Kiplinger, T. G. Richmond, C. E. Osterberg, *Chem. Rev.* **1994**, *94*, 373. b) For a remarkable recent example of *catalytic* activation of a C–F bond, see: M. Aizenberg, D. Milstein, *Science* **1994**, *265*, 359. c) For reactions of metal ions at fluorinated surfaces, see: T. Pradeep, D. E. Riederer, S. H. Hoke, T. Ast, R. G. Cooks, M. R. Linsford, *J. Am. Chem. Soc.* **1994**, *116*, 8658.
[2] Recent reviews: a) P. B. Armentrout, *Annu. Rev. Phys. Chem.* **1990**, *41*, 313; b) K. Eller, H. Schwarz, *Chem. Rev.* **1991**, *91*, 1121; c) J. C. Weishaar, *Acc. Chem. Res.* **1993**, *26*, 213.
[3] P. L. Watson, T. H. Tulip, I. Williams, *Organometallics* **1990**, *9*, 1999.
[4] M. Weydart, P. A. Andersen, R. G. Bergman, *J. Am. Chem. Soc.* **1993**, *115*, 8837. In the gas phase UF^+ is generated upon reaction of U^+ with methyl fluoride: P. B. Armentrout, J. L. Beauchamp, *J. Phys. Chem.* **1981**, *85*, 4103.
[5] M. T. Jones, R. N. MacDonald, *Organometallics* **1988**, *7*, 1221.
[6] P. Hoff, L. Jacobsson, B. Johansson, P. Aagard, G. Rudstam, H.-U. Zwicky, *Nucl. Instrum. Methods* **1980**, *172*, 413.
[7] Thermochemical data from: a) S. G. Lias, J. F. Liebman, R. D. Levin, S. A. Kafafi, *NIST Standard Reference Database, Positive Ion Energetics*, Version 2.01, January 1994; b) S. G. Lias, J. E. Bartmess, J. F. Liebman, J. L. Holmes, R. D. Levin, W. G. Mallard, *J. Phys. Chem. Ref. Data* **1988**, *17*, Suppl. 1.
[8] T. Su, W. J. Chesnavich, *J. Chem. Phys.* **1982**, *76*, 5183.
[9] a) T. G. Dietz, D. S. Chatellier, D. P. Ridge, *J. Am. Chem. Soc.* **1978**, *100*, 4905; b) A. Bjarnason, J. W. Taylor, *Organometallics* **1988**, *8*, 2020; *ibid.* **1990**, *9*, 1493; c) A. Bjarnason, *ibid.* **1991**, *10*, 1244; d) A. Bjarnason, *Rapid. Commun. Mass Spectrom.* **1994**, *8*, 366.
[10] G. B. Deacon, P. I. Mackinnon, T. D. Tuong, *Aust. J. Chem.* **1983**, *36*, 43.
[11] C. Q. Jiao, B. S. Freiser, *J. Am. Chem. Soc.* **1993**, *115*, 6268.
[12] See for example: a) J. E. Huheey *Inorganic Chemistry – Principles of Structure and Reactivity*, 3rd ed. Harper & Row, New York, **1983**. b) For an excellent review on organolanthanide chemistry, see: T. J. Marks, R. D. Ernst in *Comprehensive Organometallic Chemistry* (Eds.: G. Wilkinson, F. G. A. Stone, E. W. Ebel), Pergamon, Oxford, **1982**, Chapter 21.
[13] W. C. Martin, R. Zalubas, L. Hagan, *Atomic Energy Levels – The Rare Earth Elements*, NSRDS-NBS 60, National Bureau of Standards, Washington, **1978**.
[14] J. B. Schilling, J. L. Beauchamp, *J. Am. Chem. Soc.* **1988**, *110*, 15.
[15] Recent work on gas-phase chemistry of lanthanide cations: a) C. Heinemann, D. Schröder, H. Schwarz, *Chem. Ber.* **1994**, *127*, 1807; b) W. W. Yin, A. G. Marshall, J. Marçalo, A. Pires de Matos, *J. Am. Chem. Soc.*, **1994**, *116*, 8666; c) H. H. Cornehl, C. Heinemann, D. Schröder, H. Schwarz, *Organometallics*, in press.
[16] For a recent analysis of a spin-orbit-mediated curve-crossing mechanism, see: a) D. Schröder, A. Fiedler, M. F. Ryan, H. Schwarz, *J. Phys. Chem.* **1994**, *98*, 68; b) A. Fiedler, D. Schröder, S. Shaik, H. Schwarz, *J. Am. Chem. Soc.*, in press.
[17] a) I. Gotkis, *J. Phys. Chem.* **1991**, *95*, 6086; b) C. Heinemann, H. Schwarz, unpublished theoretical results.
[18] a) D. Schröder, H. Schwarz, *Helv. Chim. Acta* **1992**, *75*, 1281; b) H. Becker, D. Schröder, W. Zummack, H. Schwarz, *J. Am. Chem. Soc.* **1994**, *116*, 1096.
[19] For a review on comprehensive mass-spectrometric studies, see: K. F. Zmbov, J. L. Margrave, *Mass Spectrometry in Inorganic Chemistry* (Ed.: J. L. Margrave) *Adv. Chem. Ser.* **1968**, *72*, 267.

[20] *Gmelin Handbook of Inorganic Chemistry, No. 39C*, Springer, Berlin **1976**.
[21] NRMS has been successful in probing the existence of elusive inorganic molecules: a) M. Iraqi, N. Goldberg, H. Schwarz, *J. Phys. Chem.* **1993**, *97*, 11371; b) D. Schröder, J. Hrušák, I. C. Tornieporth-Oetting, T. M. Klapötke, H. Schwarz, *Angew. Chem.* **1994**, *106*, 223; *Angew. Chem. Int. Ed. Engl.* **1994**, *33*, 212; c) N. Goldberg, M. Iraqi, H. Schwarz, A. Boldyrev, J. Simons, *J. Chem. Phys.* **1994**, *101*, 2871; d) D. Schröder, A. Fiedler, H. Schwarz, *Int. J. Mass Spectrom. Ion Processes* **1994**, *134*, 239; e) for a recent review on NRMS, see: N. Goldberg, H. Schwarz, *Acc. Chem. Res.* **1994**, *27*, 347.
[22] a) K. Eller, H. Schwarz, *Int. J. Mass. Spectrom. Ion Processes* **1989**, *93*, 243; b) K. Eller, W. Zummack, H. Schwarz, *J. Am. Chem. Soc.* **1990**, *112*, 621.
[23] For a description of the apparatus, see: a) R. Srinivas, D. Sülze, T. Weiske, H. Schwarz, *Int. J. Mass Spectrom. Ion Processes* **1990**, *107*, 369; b) R. Srinivas, D. Sülze, W. Koch, C. H. DePuy, H. Schwarz, *J. Am. Chem. Soc.* **1991**, *113*, 5970; c) R. Srinivas, D. K. Böhme, D. Sülze, H. Schwarz, *J. Phys. Chem.* **1991**, *95*, 9836.
[24] Synthesis of praseodymium trifluoride from the elements: I. C. Tornieporth-Oetting, T. M. Klapötke, unpublished results (for an earlier synthesis, see: E. L. Muetterties, L. E. Castle, *J. Inorg. Nucl. Chem.* **1961**, *18*, 148).

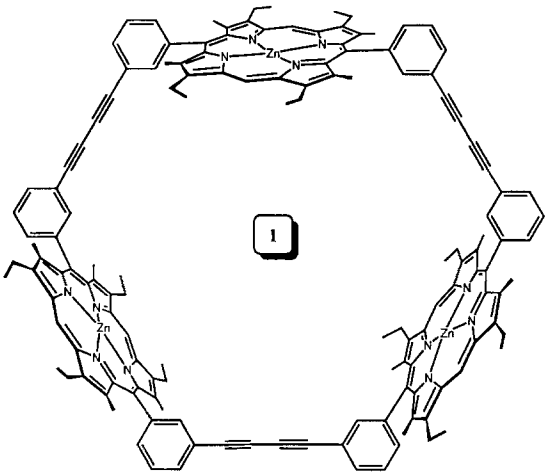


Scheme 1. Diels–Alder reaction between diene **2** and dienophile **3** to give *exo* adduct **4** and *endo* adduct **5**. The structures of **4** and **5** were distinguished unambiguously by NOE difference spectroscopy.

Free-Energy Profile for a Host-Accelerated Diels–Alder Reaction: The Sources of *exo* Selectivity**

Christopher J. Walter and Jeremy K. M. Sanders*

The use of free-energy profiles[1] for enzyme-catalyzed reactions has transformed the study of enzyme mechanisms, because the dependence of the height of the energy barrier on substrate variation and on enzyme mutation allows one to dissect out rationally the important contributions to binding and catalysis.[2] We have now applied this approach to enzyme mimics as exemplified by the porphyrin trimer **1**[3] and have examined its



exo-selective acceleration of the Diels–Alder reaction shown in Scheme 1.[4, 5] There are as yet few effective enzyme mimics for bimolecular reactions, because the design rules governing their operation are not understood;[6, 7] in particular the importance of factors such as substrate strain, host flexibility, solvation, and quality of fit is not yet clear. We have begun to uncover the rules for our hosts by elucidating some of the binding and kinetic parameters for the reactions in Scheme 1, and in doing so have acquired some insight into the *exo* selectivity of **1**. We also demonstrate the accelerated conversion of *endo* adduct to *exo* adduct by **1**.

The Diels–Alder reaction has rich stereo- and regiochemistry, stringent geometrical requirements, and no need for external reagents, and it has been the subject of related studies using catalytic antibodies.[8] The reaction also offers the possibility of altering stereo- and regiochemistry through controlling the transition state within a cavity. We have used a furan-derived diene and maleimide-derived dienophile, because this combination reacts reversibly,[9] giving the opportunity of studying the kinetics, and therefore the approach to the transition states, in both the forward and reverse directions.[10] The reaction in Scheme 1 was inhibited by strongly bound products; this could have been avoided by engineering a second step,[8] but the apparent disadvantage of lack of turnover is outweighed by the direct access to the transition state energies available from a study of the unimolecular reverse reactions as described below.

The equilibrium constant for the reaction shown in Scheme 1 is quite large (k_1 (*exo*)/k_{-1} (*exo*) is approximately 5000 M^{-1} in $C_2H_2Cl_4$ at 30 °C, decreasing to 400 at 60 °C), but the equilibrium at millimolar concentrations lies on the side of the starting compounds. The relative orientations of the pyridine groups in the two adducts are very different, and molecular models suggested that the *endo* adduct would fit less well into the cavity of the trimer than the *exo* adduct would. The measured binding constants confirm this; the *exo* adduct binds around 15 times more strongly in $C_2H_2Cl_4$ at 30 °C (9×10^6 M^{-1} vs 6×10^5 M^{-1}) and six times more strongly at 60 °C (4.6×10^5 M^{-1} vs 8×10^4 M^{-1}). In the absence of porphyrin trimer, the *endo* adduct obtained by kinetic control is a significant product at low temperature, while the *exo* adduct obtained by thermodynamic control is the only product detected at high temperatures; at 60 °C the *exo*/*endo* ratio is roughly 4 initially, but the *endo* adduct then disappears.

Addition of one equivalent of trimer to the two reactants (0.9 mM each in $C_2H_2Cl_4$) accelerates the forward Diels–Alder reaction around 1000-fold at 30 °C and 200-fold at 60 °C, yielding the *exo* adduct as the only detectable product.[4, 5] The initial

[*] Dr. J. K. M. Sanders, Dr. C. J. Walter
Cambridge Centre for Molecular Recognition
University Chemical Laboratory
Lensfield Road, GB-Cambridge CB2 1EW (UK)
Telefax: Int. code +(1223) 336913
e-mail: JKMS@cus.cam.ac.uk

[**] We thank the Science and Engineering Research Council for financial support and Dr. R. S. Wylie for valuable advice.

reaction rate in the presence of trimer is almost temperature independent under these conditions, because as the temperature is raised, the increase in the intrinsic rate of the reaction inside the porphyrin cavity is almost exactly offset by weaker substrate binding.[5]

The forward and reverse reactions shown in Scheme 1 were followed at 60 °C by NMR spectroscopy in the absence of trimer. The derived rate constants (Table 1) were obtained by

Table 1. Rate constants for the forward and reverse Diels–Alder reaction in the presence (+) and absence (−) of trimer **1** [a].

	− Trimer	+ Trimer
$k_1(exo)$	220 (±40) $s^{-1} mol^{-1} dm^3$	ca. 1000 s^{-1} [b]
$k_{-1}(exo)$	0.55 (±0.1) s^{-1}	0.7 (±0.2) s^{-1}
$k_1(endo)$	50 (±20) $s^{-1} mol^{-1} dm^3$	ca. 10 s^{-1} [b]
$k_{-1}(endo)$	12 (±5) s^{-1}	4 (±2) s^{-1}

[a] At 60 °C in $C_2D_2Cl_4$. All rate constants have been multiplied by 10^6. [b] Estimated from heights of the energy barriers in Fig. 1; the value for $k_1(exo)$ within the cavity is a lower limit.

curve fitting and allowed the fixing of the levels of the *endo* and *exo* products and transition states in the energy profile relative to those of the starting materials (Fig. 1). The binding constants at 60 °C for substrates and products were also converted to free energies to give the energy levels for the bound species. Finally the rates for the unimolecular reverse reaction for each bound adduct (k_{-1} (*exo*) and k_{-1} (*endo*)) within the trimer cavity were measured by NMR spectroscopy as described in the experimental section. These rates provide the activation energies for reaching the bound transition states from the bound Diels–Alder adducts.[11] The resulting complete free energy profile for the reaction at 60 °C is shown in Figure 1.

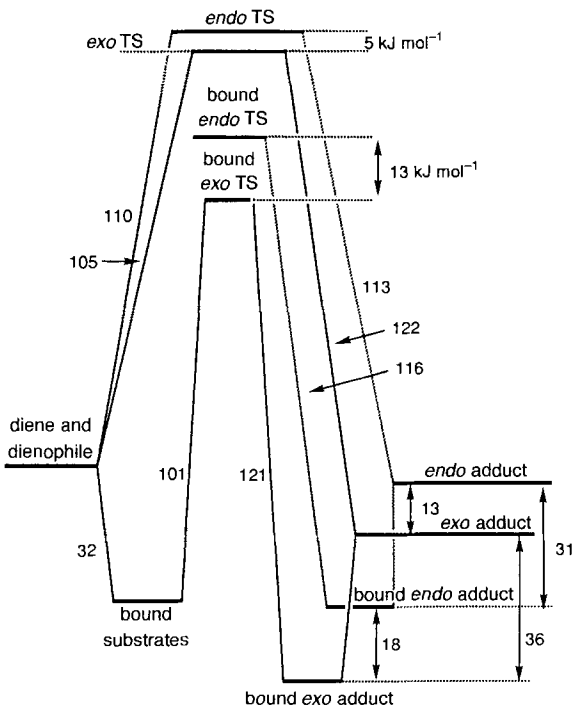


Fig. 1. Free-energy profiles for the Diels–Alder reaction at 60 °C in $C_2H_2Cl_4$ solution. TS = transition state.

The profile identifies three sources of the *exo* selectivity in the trimer-accelerated reaction: 1) the *endo* adduct is less stable thermodynamically by about 13 kJ mol^{-1}; 2) since trimer **1** binds the *endo* adduct less strongly, the *endo* complex is 18 kJ mol^{-1} less favorable than the *exo* complex; 3) the trimer slows the reverse reaction of the *endo* adduct by threefold (Table 1), showing that the *endo* transition state is less well recognized by the trimer than the *endo* adduct. By contrast, the reverse reaction of the *exo* adduct is not slowed by trimer: the *exo* transition state is as well recognized as the *exo* adduct.

These three factors combine such that the *endo* transition state within the trimer cavity is some 13 kJ mol^{-1} higher in energy than the *exo* transition state, giving a predicted difference of more than 100-fold in the forward rates for formation of the two adducts inside the cavity. This prediction is consistent with our inability to detect *endo* product. The energies of the bound transition states derived by this indirect route correspond to an increase in the activation energy for the forward *endo* reaction from 110 to 114 kJ mol^{-1} and a decrease in activation energy for the *exo* reaction from 105 to 101 kJ mol^{-1}.[11] The decreased activation energy for the forward *exo* reaction inside the cavity corresponds to an effective molarity[12] of at least 4 M; the reaction is accelerated by a positive templating effect.[13] It appears therefore that the macroscopic acceleration observed is partly the result of concentrating the diene and dienophile within the same cavity, and partly the result of a reduced activation energy once the starting compounds are bound. In contrast, the larger activation energy (Table 1) of the forward *endo* reaction within the cavity corresponds to an effective molarity within the cavity of 0.2 M. Since this effective molarity is greater than the concentration of the free substrates, a macroscopic acceleration of the forward *endo* reaction is predicted by virtue of the high concentration of substrate pairs in the cavity. However, it cannot be observed experimentally because the *exo* reaction is so dominant.

One consequence of these energetics is that the trimer effectively encourages conversion of the *endo* adduct to its *exo* isomer: the reverse reaction is marginally slowed, but as soon as the (very dilute) diene and dienophile are created, they bind within the cavity and react to form *exo* adduct. Thus, a 0.9 mM solution of *endo* adduct in the absence of trimer is converted over a period of hours to a largely dissociated diene–dienophile pair, while in the presence of trimer it is converted instead into roughly 55% *exo* adduct in 100 hours.

Trimer **1** represents an important step in the development of enzyme mimics, because its major role is in recognition and orientation events that are decoupled from the reaction itself: one should be able to bring together a wide range of different reactive pairs simply by changing the substituents on the amine ligand. The ability of **1** to catalyze acyl transfer reactions has been described elsewhere.[6] Furthermore, rational changes in synthetic design should allow systematic study of the importance of such factors as host flexibility and quality of fit in supramolecular catalysis.

Experimental Procedure

Binding constants were measured by UV/Vis spectroscopy as described previously [3]. Forward and reverse reaction rates of the control reactions (in the absence of **1**) were determined from NMR spectra of reaction mixtures. Rates of reactions in the presence of trimer **1** were measured by removing aliquots (0.5 mL) of reaction mixture, quenching by addition of several drops of 1:1 trifluoroacetic acid/CD_3OD (to remove the zinc ion from **1**), and then neutralizing by addition of solid potassium carbonate before transfer to an NMR tube for spectroscopic assay. All rate constants were derived by following the reaction to completion and by obtaining the best-fit computer simulation of the kinetics over the whole reaction curve.

exo Adduct **4**: 4-(3-Furyl)pyridine hydrochloride (80 mg, 0.44 mmol) [14] was added to a solution of 4-(maleimidomethyl)pyridine (80 mg, 0.43 mmol) in distilled toluene (10 mL). The suspension was stirred with potassium carbonate for 2 h at room temperature and filtered. The resulting solution of **2** and **3** was flushed with argon and heated at 60 °C in the dark for 5 d. The crystals of *exo* adduct that formed were then collected by filtration. Yield: 65 mg (41%) ^{1}H NMR (250 MHz, $CDCl_3$): δ = 3.02 (d, J = 8 Hz, 1H), 3.08 (d, J = 8 Hz, 1H), 4.68 (s, 2H), 5.47 (d, J = 3 Hz, 1H), 5.65 (s, 1H), 6.92 (d, J = 3 Hz, 1H), 7.19 (d, J = 6 Hz, 2H), 7.27 (d, J = 6 Hz, 2H), 8.55 (d, J = 6 Hz, 2H), 8.66 (d, J = 6 Hz, 2H); ^{13}C NMR (100 MHz, $CDCl_3$): δ = 41.5, 47.5, 48.8, 81.3, 82.7, 119.7, 122.4, 133.1, 150.3, 150.8, 175.0, 175.2. Anal. calcd for $C_{14}H_{15}N_3O_3$: C 68.46, H 4.54, N 12.61. Found: C 68.37, H 4.57, N 12.62. Neither the mass spectrum nor melting point could be obtained owing to rapid reverse Diels-Alder reaction on ionization or heating.

endo Adduct **5**: An identical reaction mixture to that above was kept at room temperature in the dark for 10 d. White crystals of **4** were removed by filtration, and **5** was separated from the filtrate by preparative thin-layer chromatography (7% methanol in chloroform). Yield: 5 mg (3%) ^{1}H NMR (250 MHz, $CDCl_3$): δ = 3.75 (m, 2H), 4.29 (s, 2H), 5.43 (m, 1H), 5.62 (m, 1H), 6.22 (s, 1H), 6.84 (d, J = 6 Hz, 2H), 6.94 (d, J = 6 Hz, 2H), 8.27 (d, J = 6 Hz, 2H), 8.52 (d, J = 6 Hz, 2H); ^{13}C NMR (100 MHz, $CDCl_3$): δ = 41.1, 46.3, 47.4, 80.2, 81.7, 120.0, 123.5, 130.8, 149.8, 150.1. Neither the mass spectrum nor melting point could be obtained owing to rapid reverse Diels-Alder reaction on ionization or heating.

Received: July 22, 1994 [Z 7157 IE]
German version: *Angew. Chem.* **1995**, *107*, 223

Keywords: Diels–Alder reactions · enzyme models · host–guest chemistry · kinetics · porphyrinoids

[1] W. J. Albery, J. R. Knowles, *Biochemistry* **1976**, *15*, 5627.
[2] J. M. Avis, A. R. Fersht, *Biochemistry* **1993**, *32*, 5321; K. Johnsson, R. K. Allemann, H. Widmer, S. A. Benner, *Nature (London)* **1993**, *365*, 530.
[3] H. L. Anderson, J. K. M. Sanders, *J. Chem. Soc. Chem. Commun.* **1989**, 1714.
[4] C. J. Walter, H. L. Anderson, J. K. M. Sanders, *J. Chem. Soc. Chem. Commun.* **1993**, 458.
[5] R. P. Bonar-Law, L. G. Mackay, C. J. Walter, V. Marvaud, J. K. M. Sanders, *Pure Appl. Chem.* **1994**, *66*, 803.
[6] L. G. Mackay, R. S. Wylie, J. K. M. Sanders, *J. Am. Chem. Soc.* **1994**, *116*, 3141; T. R. Kelly, G. J. Bridger, C. Zhao, *ibid.* **1990**, *112*, 8024; J. S. Nowick, Q. Feng, T. Tjivikua, P. Ballester, J. Rebek, Jr., *ibid.* **1991**, *113*, 8831; W. L. Mock, T. A. Irra, J. P. Wepsiec, M. Adhya, *J. Org. Chem.* **1989**, *54*, 5032.
[7] H.-J. Schneider, R. Kramer, J. Rammo, *J. Am. Chem. Soc.* **1993**, *115*, 8980.
[8] D. Hilvert, K. W. Hill, K. D. Nared, M.-T. M. Auditor, *J. Am. Chem. Soc.* **1989**, *111*, 9261; A. C. Braisted, P. G. Schultz, *ibid.* **1990**, *112*, 7430; V. E. Gouverneur, K. N. Houk, B. de Pascual-Teresa, B. Beno, K. D. Janda, R. A. Lerner, *Science* **1993**, *262*, 204.
[9] F. Fringuelli, A. Taticchi, *Dienes in the Diels-Alder Reaction*, Wiley, Chichester, **1990**.
[10] The kinetics of a thiazolium-cyclophane which mimics the reversible benzoin condensation of thiamine pyrophosphate have also been studied in both directions: F. Diederich, H.-D. Lutter, *J. Am. Chem. Soc.* **1989**, *111*, 8438.
[11] It is difficult to extract directly experimental values for the rate of the forward *exo* reaction within the cavity, because the binding equilibria in this system are very complicated. This is often the case for enzyme mimics that have not had the benefit of millions of years of evolution to optimize their catalytic abilities [7]. A general computer model of the binding and kinetics has been developed in this laboratory (R. S. Wylie, J. K. M. Sanders, *Tetrahedron* **1994**, in press) and may well allow more direct access to such rate constants in the near future.
[12] A. J. Kirby, *Adv. Phys. Org. Chem.* **1980** *17*, 183.
[13] S. Anderson, H. L. Anderson, J. K. M. Sanders, *Acc. Chem. Res.* **1993**, *26*, 469.
[14] P. Ribereau, G. Queguiner, *Can. J. Chem.* **1983**, *61*, 334.

The Formation of a Mixed Organolithium Aggregate $Li_4R_2nBu_2$ during the Heteroatom-Assisted Lithiation of 1,3-Bis(dimethylaminomethyl)-2,4,6-trimethylbenzene (R = 2,6-$(CH_2NMe_2)_2$-3,5-$Me_2C_6HCH_2$)

Peter Wijkens, Ernout M. van Koten, Maurits D. Janssen, Johann T. B. H. Jastrzebski, Anthony L. Spek, and Gerard van Koten*

Dedicated to Professor Ekkehard Lindner on the occasion of his 60th birthday

In the course of our studies into the organometallic chemistry of the potentially tridentate monoanionic 2,6-bis(dimethylaminomethyl)phenyl ligand, compounds having special properties and reactivities were obtained:[1, 2] 1) metals stabilized in unusual oxidation states,[3] 2) stabilized reactive intermediates,[4] and 3) species showing catalytic activity.[5] Such organometallic compounds have related structures in which two five-membered M-C-C-C-N chelate rings share a common M–C bond.

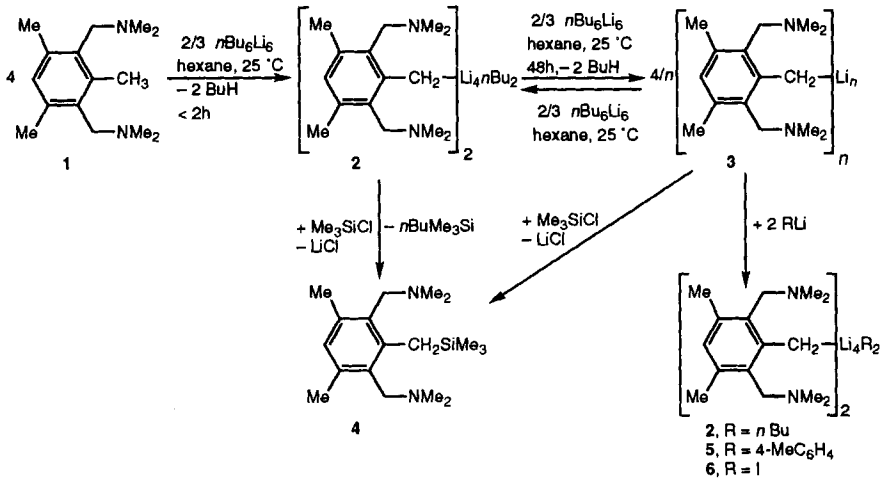
In order to fine-tune the metal environment, we decided to investigate the properties of compounds in which the two five-membered chelate rings are extended to six-membered ones having an M-C-C unit in common. Heteroatom-assisted lithiation is, especially when the heteroatom belongs to a tertiary amino group, a valuable reaction for the synthesis of heteroatom-containing organolithium compounds, and usually provides products of high purity with excellent yield.[6, 7] We therefore started our investigations with the attempted metalation of 1,3-bis(dimethylaminomethyl)-2,4,6-trimethylbenzene (**1**) at the 2-methyl group.

The lithiation of **1** with *n*BuLi in a 1:1 molar ratio at room temperature afforded a white, crystalline precipitate within two hours. According to its ^{1}H NMR spectrum this precipitate appeared to be a unique aggregate **2** of the parent lithiated ligand and unreacted *n*BuLi in a 1:1 ratio (Scheme 1).[8] Compound **2** was characterized by elemental analysis, ^{1}H, ^{13}C, and ^{6}Li NMR spectroscopy, and an X-ray crystal structure determination.[9]

Prolonged reaction times (two days) afforded a yellow compound **3**, tentatively assigned the structure of the pure lithiated ligand. Its insolubility in both apolar and polar solvents hampered characterization of **3**. Alternatively, **3** could be prepared in high yield within two hours by the reaction of **1** with *t*BuLi in a 1:1 molar ratio (see *Experimental Procedure*). According to the ^{1}H NMR and mass spectra (see *Experimental Procedure*), reaction of both **2** and **3** with D_2O afforded exclusively the α-monodeuteriobenzyl derivative; this indicated that quantitative regioselective lithiation at the 2-methyl group had occurred. This was furthermore confirmed by the exclusive formation of the α-trimethylsilylbenzyl derivative **4** from the reaction of both **2** and **3** with Me_3SiCl (Scheme 1). Moreover, reaction of **2** with Me_3SiCl afforded the α-trimethylsilylbenzyl derivative and *n*$BuMe_3Si$ in a 1:1 molar ratio, while the same reaction of **3** afforded only trace amounts (< 1%) of *n*$BuMe_3Si$. That **2** may

[*] Prof. Dr. G. van Koten, P. Wijkens, E. M. van Koten, M. D. Janssen, Dr. J. T. B. H. Jastrzebski
Debye Institute, Department of Metal-Mediated Synthesis
Utrecht University
Padualaan 8, NL-3584 CH Utrecht (The Netherlands)
Telefax: Int. code +(30) 523-615

Dr. A. L. Spek
Bijvoet Center for Biomolecular Research
Laboratory of Crystal and Structural Chemistry, Utrecht University



Scheme 1.

be regarded as an intermediate in the heteroatom-assisted lithiation of **1** to give **3** became evident from the initially surprising observation that reaction of pure **3** with one equivalent of *n*BuLi led to selective re-formation of **2**.

An X-ray crystal structure determination of **2** revealed an overall structural geometry based on a central, almost regular Li_4 tetrahedron.[9] Two of the four Li_3 faces of the Li_4 tetrahedron are each bound to an anionic tridentate ligand ($C\widehat{N}_2$) through the benzylic carbon atom in a four-center two-electron (4c–2e) interaction (C–Li 2.319(7) Å, mean value). The two butyl groups are likewise 4c–2e-bound through the α-carbon atom (C–Li 2.215(7) Å, mean value) to the other two Li_3 faces (Fig. 1).[10] Coordinative saturation for each lithium atom is achieved by intramolecular coordination of the four nitrogen atoms (N–Li 2.079(7) Å, mean value), two from each of the heteroatom-containing ligands. The two tridentate anionic ligands may be arranged in two different ways at the faces of the Li_4 tetrahedron, and two enantiomeric aggregates thus exist. As a consequence of the crystal space-group symmetry, both are present in the unit cell.

The bonding of the benzylic group to the Li_3 face is slightly asymmetric, as is reflected by the three different C–Li distances (2.204(6), 2.348(7), and 2.407(7) Å). However, there seems to be no significant interaction between the aromatic C1 atom attached to C_α and one of the Li atoms (shortest C1–Li distance 2.782 Å). This conclusion seems to be corroborated by the angle of 113° between the C1–C7 bond and the center of the plane defined by Li1, Li2, and Li4. This points to a tetrahedral geometry around the benzylic carbon atom. These structural features of **2** are rather surprising since numerous X-ray crystal structure determinations have shown that aggregated benzyllithium compounds have planar benzyl ligands in which both the benzylic C_α and the aromatic C(*ipso*) atoms interact with lithium, as in $[PhCH_2Li(N(CH_2CH_2)_3N)_2]_n$[11] and $[PhCH_2Li(Et_2O)]_n$.[12] Only in monomeric $[PhCH_2Li(tmeda)(thf)]$ (tmeda = *N*,*N*,*N*′,*N*′-tetramethylethylenediamine)[13] and $[PhCH(SPh)Li(thf)_3]$[14] is the benzylic group η^1-bound.

The overall structural geometry of **2** is closely related to that found for other tetranuclear alkyl- and aryllithium aggregates:[15] each of the organic groups is 4c–2e-bound to a Li_3 face of the central Li_4 tetrahedron; the fourth coordination site of each lithium atom is occupied by either an intramolecularly coordinating substituent (i.e., a well-positioned solvent molecule)[16, 17] or an additional donor molecule.[18, 19]

The ^1H, ^{13}C, and ^6Li NMR spectra of **2**, recorded in solution ([D_8]toluene) and at low temperature (– 30 °C), are consistent with a structure in solution analogous to that found in the solid state. Furthermore, the molecular weight of 587 measured by cryoscopy in benzene agrees with this tetranuclear aggregation state (calcd 608). Below –10 °C the ^1H NMR spectrum of **2** shows four resonances for the two NMe_2 groups, two AB patterns for the two CH_2N groups, and two resonances for the two Me substituents; the H4 resonance is, on the other hand, a singlet (Table 1). These results indicate the lack of a symmetry plane perpendicular to the plane of the aryl ring that also contains C(benzyl)–C4 as well as the lack of a symmetry plane containing the aryl ring. Accordingly, the CH_2NMe_2 substituents are diastereotopic as are the methyl groups in each NMe_2 group. This diastereotopicity also indicates that the N–Li coordination is nonfluxional on the NMR timescale at this temperature. A similar conclusion can be drawn from ^{13}C NMR data obtained at –20 °C. Moreover, the ^6Li NMR spectrum at –20 °C shows two distinct resonances at $\delta = 1.36$ and 1.44, respectively, in a 1:1 intensity ratio; this indicates the presence of two magnetically inequivalent lithium atoms in the Li_4 tetrahedron (the two benzylic ligands and the two butyl groups are enantiotopic as a result of twofold axial symmetry).

At higher temperatures (20 °C) a process becomes operative on the NMR timescale that generates a virtual symmetry plane perpendicular to the plane of the aryl ring; in

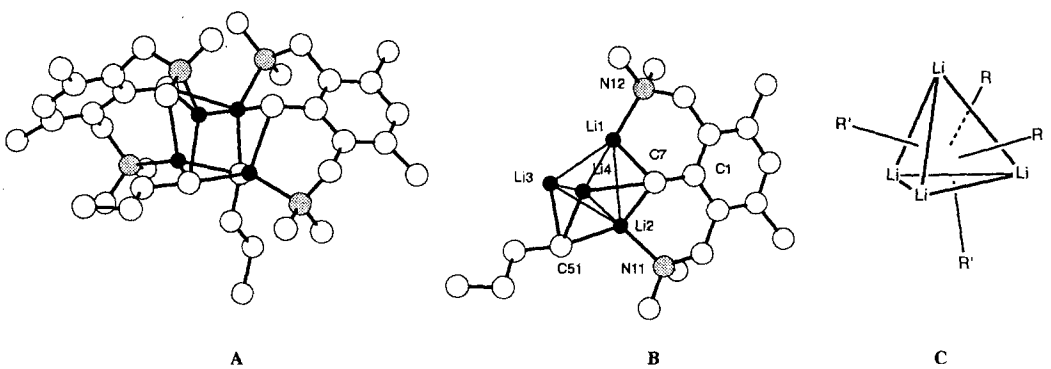


Fig. 1. A: crystal structure of **2**; B: part of the structure of **2** (one of the benzylic ligands and one of the butyl groups are omitted for clarity) with the adopted numbering scheme; C: schematical representation showing the orientation of the two different groups R ($C\widehat{N}_2$) and R′ (*n*Bu) over the Li_4 tetrahedron. Important bond lengths [Å]: Li1-Li2 2.544(8), Li2-Li3 2.582(9), Li1-Li4 2.571(8), Li2-Li3 2.585(8), Li2-Li4 2.510(8), Li3-Li4 2.494(8), C7-Li1 2.204(6), C7-Li2 2.348(7), C7-Li4 2.407(7), C51-Li1 2.198(8), C51-Li2 2.338(6), C51-Li3 2.211(7), N11-Li2 2.123(6), N12-Li1 2.045(7).

 © VCH Verlagsgesellschaft mbH, D-69451 Weinheim, 1995 0570-0833/95/0202-0220 $ 10.00+.25/0

Table 1. Relevant ^1H and ^{13}C NMR data in [D$_8$]toluene for [D]-**1**, **2**, **4**, **5**, and **6** (in [D$_8$]toluene).

Cmpd.	T[°C]	$\delta(^1H)$ 3,5-ArMe$_2$	$\delta(^1H)$ NMe$_2$	$\delta(^1H)$ CH$_2$N	$\delta(^{13}C)$ 3,5-ArMe$_2$	$\delta(^{13}C)$ NMe$_2$	$\delta(^{13}C)$ CH$_2$N	$\delta(^{13}C)$ ArCH$_2$X
2	−20	2.24, 2.26	2.00, 2.11, 2.19, 2.26	3.15, 3.40 [a]; 3.15, 3.50 [a]	21.7, 22.1	44.0, 44.4, 47.9, 48.7	59.4, 59.9	24.5 [b]
2	25	2.22	2.06, 2.25	3.18, 3.49 [a]	21.8	44.2, 48.3	59.7	24.3 [b]
2	100	2.15	2.08	3.30				
5	−20	2.15, 2.35	1.50, 1.60, 1.88, 2.35	2.98, 3.52 [a]; 3.15, 3.71 [a]	22.0, 22.3	43.7, 44.3, 45.3, 49.3	58.6, 60.0	23.3 [b]
5	25	2.17	1.72, 2.00	3.14, 3.64 [a]	21.7	43.9, 47.8	59.4	23.2[b]
5	100	2.11	1.95	3.35				
6	25	2.35	2.07, 2.19	3.19, 3.51 [a]	22.0	44.7, 49.4	59.1	26.0 [b]
[D]-**1**	25	2.34	2.11	3.34	20.5	44.9	57.6	15.7 [c]
4	25	2.31	2.11	3.35	20.7	44.9	57.9	19.3 [d]

[a] $^2J(HH) = 12$ Hz. [b] X = Li, the line width of 80 Hz, due to coupling of three lithium atoms with carbon, corresponds to an average $^1J(^{13}C^7Li)$ of about 9 Hz. [c] X = D, $^1J(CD) = 19$ Hz. [d] X = SiMe$_3$.

the ^1H NMR spectrum there is one AB pattern, two NMe resonances, and one Ar–CH$_3$ resonance. A possible explanation might be a process involving the pairwise exchange of coordinating nitrogen atoms. Finally, at elevated temperatures (above 100 °C) there is also coalescence of the AB pattern and the two NMe resonances coalesce to single lines. The ^6Li NMR spectrum shows a single resonance; this indicates that the Li atoms have become equivalent. These observations are probably explained by process involving fast scrambling of the organic groups over the Li$_3$ faces of the Li$_4$ tetrahedron (alternatively interaggregate exchange may occur). Similar process have been proposed for other tetranuclear organolithium compounds in which the organic group contains one heteroatom substituent.[16, 17]

Previously we suggested a possible mechanism for the heteroatom-assisted lithiation of substituted *N,N*-dimethylbenzylamines with *n*BuLi that involves the successive replacement of *n*Bu groups on the Li$_3$ faces of the solvated Li$_4$(*n*Bu)$_4$ aggregate. The first step was the anchoring of the substrate through its heteroatom to a vertex of the Li$_4$ tetrahedron.[20] Based on chemical evidence Li$_4$(*n*Bu)$_2$(C$_6$H$_4$-2-CH$_2$NMe$_2$)$_2$ was proposed to be a stable intermediate in the lithiation reaction of C$_6$H$_5$CH$_2$NMe$_2$ with *n*BuLi.[21, 22] The isolation of **2** provides additional evidence for the mechanism outlined above. The conversion of **2** to **3** proceeds much slower than that of **1** to **2**, since, in order to anchor the substrate, the reaction beyond **2** requires cleavage of the intramolecular Li–N bond.

This reasoning points the way for the rational construction of mixed organolithium clusters by design of organic ligands, that is to say, the two benzylic diamine anions in **2** stabilize a dicationic Li$_4$ tetrahedron $[(\overset{\frown}{C}\overset{\frown}{N}_2)_2Li_4]^{2+}$ that can bind two monodentate anions R$^-$. The selective synthesis of the $[(\overset{\frown}{C}\overset{\frown}{N}_2)_2Li_4X_2]$ aggregates with X = *n*Bu (**2**), or *p*Tolyl (**5**), or halide (**6**) (Scheme 1 and *Experimental Procedure*) is proof of the potential of this method. Recent examples of this exciting area in organolithium chemistry is the selective synthesis of RLi$_2$X aggregates in which R is the pentadentate monoanionic organic group [C$_6$H$_3$-2,6-(CH$_2$N(Me)CH$_2$CH$_2$NMe$_2$)$_2$]$^-$.[23]

Owing to the presence of two different organic groups in **2**, this material is obviously not well suited as a starting material for the synthesis of other organometallic compounds, and it has already been shown that its reaction with Me$_3$SiCl affords two products. For the synthesis of organometallic compounds containing the [1,3-bis(dimethylaminomethyl)-4,6-dimethylphenyl)methyl tridentate monoanionic ligand, compound **6** (which may be regarded as a soluble modification of **3**) seems to be a better choice. This topic will be the subject of a forthcoming study.

Experimental Procedure

2: A hexane solution (16 mL) of 1.6 M *n*BuLi (25.6 mmol) was added at room temperature to a solution (30 mL) of **1** [24] in hexane. After 1 h the clear yellow solution was concentrated to ca. 20 mL. After 2 h pale yellow crystals were formed. These were isolated by centrifugation, washed with pentane, and dried in vacuo to afford **2** (2.56 g, 70% yield). Relevant ^1H and ^{13}C NMR data are given in Table 1 [26]. Reaction of **2** with Me$_3$SiCl afforded **4** and BuMe$_3$Si in a 1:1 molar ratio according to ^1H and ^{13}C NMR, and GCMS analysis.

3: A pentane solution (6.2 mL) of 1.5 M *t*BuLi (9.3 mmol) was added at −50 °C to a solution (20 mL) of **1** in pentane. The reaction mixture was stirred at room temperature for 1 h, during which time a yellow solid material was formed. This solid material was isolated by centrifugation, washed with pentane, and dried in vacuo to afford **3** (1.92 g, 87% yield). Reaction of a suspension of **3** in D_2O afforded, according to ^1H and ^{13}C NMR, and GCMS analysis, exclusively 1,3-bis-(dimethylaminomethyl)-4,6-dimethyl-2-monodeuteriomethylbenzene. Reaction of a suspension of **3** with Me$_3$SiCl afforded exclusively **4**.

Reaction of a suspension of **3** in benzene or diethyl ether with *n*BuLi, 4-MePhLi, and LiI (1:1 molar ratio) afforded **2**, **5**, and **6**, respectively. All compounds were characterized by elemental analysis, and ^1H and ^{13}C NMR spectroscopy. Relevant ^1H and ^{13}C NMR data are given in Table 1 [26].

Received: July 23, 1994 [Z 7164 IE]
German version: *Angew. Chem.* **1995**, *107*, 239

Keywords: chelate ligands · lithium compounds · metalation

[1] G. van Koten, *Pure Appl. Chem.* **1989**, *61*, 1681.
[2] G. van Koten, *Pure Appl. Chem.* **1990**, *62*, 1155.
[3] A. de Koster, J. A. Kanters, A. L. Spek, A. A. H. van der Zeijden, G. van Koten, K. Vrieze, *Acta Crystallogr. Sect. C* **1985**, *41*, 893.
[4] J. A. M. van Beek, G. van Koten, W. J. J. Smeets, A. L. Spek, *J. Am. Chem. Soc.* **1986**, *108*, 5010.
[5] D. M. Grove, G. van Koten, A. H. M. Verschuren, *J. Mol. Catal.* **1988**, *45*, 169.
[6] H. W. Gschwend, H. R. Rodriguez, *Org. React.* **1979**, *26*, 1.
[7] J. T. B. H. Jastrzebski, G. van Koten, *Inorg. Synth.* **1989**, *26*, 150.
[8] With this knowledge in mind, it is obvious that reaction of **1** with 2 equiv of *n*BuLi would afford **2** in quantitative yield (see *Experimental Procedure*).
[9] X-ray crystal structure data for **2**: $C_{38}H_{68}Li_4N_4$, monoclinic, space group $P2_1/c$, $a = 10.8476(7)$, $b = 16.5638(11)$, $c = 22.3064(12)$ Å, $\beta = 101.525(5)°$, $V = 3927.1(4)$ Å^3, $\rho_{calcd} = 1.030$ g cm^{-3}, $\mu(Mo_{K\alpha}) = 0.5$ cm^{-1}, $Z = 4$, 8946 unique reflections ($1.5 < \theta < 27.4$), 3800 with $F_o > 4.0\sigma(F_o)$. Enraf-Nonius CAD4T rotating anode diffractometer, graphite monochromated $Mo_{K\alpha}$ radiation, $\lambda = 0.71073$ Å, $T = -123$ °C. Solution by direct methods (SHELXS86), refinement of F^2 with SHELXL-93 converged at R_1 (wR_2) = 0.088 (0.242), $w = 1/(\sigma^2(F_o^2) + (0.1124P)^2)$ for 416 refined parameters (anisotropic temperature factors for the nonhydrogen atoms). Hydrogen atoms were included at calculated positions (C–H = 0.98 Å), riding on their carrier atoms. Further details of the crystal structure investigation are available on request from the Cambridge Crystallographic Data Centre, University Chemical Laboratory, 12 Union Road, Cambridge CB2 1EZ (UK), on quoting the full journal citation.
[10] The two benzylic and the two butyl groups are crystallographically inequivalent and afford slightly but not significantly different bond lengths and angles.
[11] S. P. Patterman, I. L. Karle, G. D. Stucky, *J. Am. Chem. Soc.* **1970**, *92*, 1150.
[12] M. A. Beno, H. Hope, M. M. Olmstead, P. P. Power, *Organometallics* **1985**, *4*, 2117.
[13] W. Zarges, M. Marsch, K. Harms, G. Boche, *Chem. Ber.* **1989**, *122*, 2303.

[14] W. Zarges, M. Marsch, K. Harms, W. Koch, G. Frenking, G. Boche, *Chem. Ber.* **1991**, *124*, 543.
[15] E. Weiss, *Angew. Chem.* **1993**, *105*, 1565; *Angew. Chem. Int. Ed. Engl.* **1993**, *32*, 1501.
[16] G. W. Klumpp, *Recl. Trav. Chim. Pays-Bas* **1986**, *105*, 1.
[17] J. T. B. H. Jastrzebski, G. van Koten, M. Konijn, C. H. Stam, *J. Am. Chem. Soc.* **1982**, *104*, 5490.
[18] H. Köster, D. Thoenes, E. Weiss, *J. Organomet. Chem.* **1978**, *160*, 1.
[19] H. Hope, P. P. Power, *J. Am. Chem. Soc.* **1983**, *105*, 5320.
[20] The kinetic intermediates are most likely smaller aggregates. The tetranuclear lithium aggregates are the thermodynamically most stable species.
[21] G. van Koten, J. T. B. H. Jastrzebski, *Tetrahedron* **1989**, *45*, 569.
[22] However, in the case of the present benzylic diamine chelate the $Li_4Bu_2(\overset{\frown}{C}\,\overset{\frown}{N})_2$ aggregate is further stabilized, since the two $\overset{\frown}{C}\,\overset{\frown}{N}$ groups effectively cap the four Li atoms and prevent further attack by the free benzylic diamine ligands.
[23] I. C. M. Wehman-Ooyevaar, G. M. Kapteijn, D. M. Grove, A. L. Spek, G. van Koten, *J. Organomet. Chem.* **1993**, *452*, C1.
[24] Obtained in almost quantitative yield by reaction of 1,3-bis(bromomethyl)-2,4,6-trimethylbenzene [25] with 4 equiv of Me_2NH; characterized by ^1H and ^{13}C NMR spectroscopy and GCMS.
[25] A. W. van der Made, R. H. van der Made, *J. Org. Chem.* **1993**, *58*, 1262.
[26] Detailed ^1H, ^{13}C, and ^6Li NMR data are available upon request from the authors.

Carbon–Carbon Bond Cleavage with Inversion of Configuration: Conversion of (*R*)-(+)-1-Methoxytetrafluoropropionic Acid to (*S*)-(−)-1,2,2,2-Tetrafluoroethyl Methyl Ether

Keith Ramig,* Linda Brockunier,
Patrice W. Rafalko, and Leonid A. Rozov

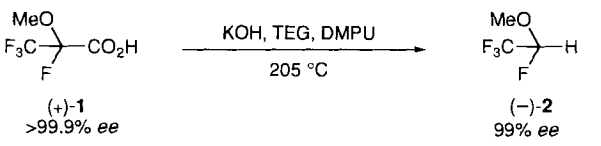
Dedicated to Professor Theodore Cohen on the occasion of his 65th birthday

Asymmetric synthesis of pharmaceuticals is of increasing interest, because in many cases only one enantiomer of a chiral drug may be effective. In the field of inhalational anesthetics differences in the pharmacological profiles of enantiomers have been noted.[1] However, access to these small, highly fluorinated compounds in optically active form has been limited owing to the scarcity of suitable synthetic methods.[2] Enantiomeric separation of some of these compounds on a preparative scale has only recently been accomplished.[3]

A recent report[4] has detailed the asymmetric synthesis of 1,2,2,2-tetrafluoroethyl methyl ether (**2**),[5] an intermediate in the synthesis of the anesthetic compounds 1,2,2,2-tetrafluoroethyl difluoromethyl ether (desflurane, Suprane, **6**),[6] and 1,2,2,2-tetrafluoroethyl chlorofluoromethyl ether.[7] The key reaction was stereospecific decarboxylation of enantiomerically pure 1-methoxytetrafluoropropionic acid (**1**),[8] yielding ether **2** with 99% enantiomeric excess (*ee*) (Scheme 1). Important data lacking in that paper were the absolute configurations of the starting material and the product. We wish to report that we have determined the absolute configurations of both acid **1** and ether **2**. This data, which will establish the stereochemical direction of C–C bond cleavage, is important if these types of reactions are to become viable in asymmetric synthesis.

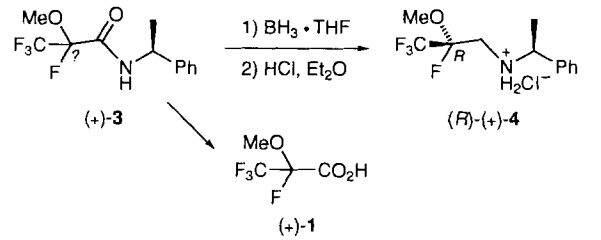
[*] Dr. K. Ramig, L. Brockunier, Dr. L. A. Rozov
Ohmeda Pharmaceutical Products Division Inc.
100 Mountain Avenue, Murray Hill, NJ 07974 (USA)
Telefax: Int. code +(908) 771-6161

P. W. Rafalko
BOC Group Technical Center, Murray Hill, NJ (USA)



Scheme 1. Decarboxylation of acid **1** [4]. TEG = triethylene glycol, DMPU = dimethylpropylene urea = 1,3-dimethyl-3,4,5,6-tetrahydro-1*H*-2-pyrimidinone.

The absolute configuration of acid **1** is established by an X-ray crystallographic structure determination of a derivative. Amide (+)-**3** (>99.9% diastereomeric excess),[4] an intermediate in the optical resolution of acid (±)-**1**, is treated sequentially with $BH_3 \cdot THF$ complex[9] and ethereal HCl, affording amine salt (+)-**4**[10] (Scheme 2). The X-ray crystal structure[11]



Scheme 2. Establishment of the absolute configuration of acid **1**.

(Fig. 1) shows that the chiral fluorine-bearing carbon atom has the (*R*) configuration. Thus, it is established that acid **1** has the (*R*)-(+) configuration.

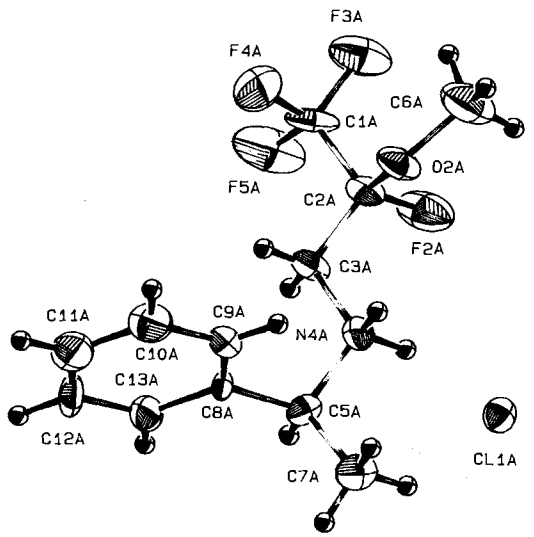
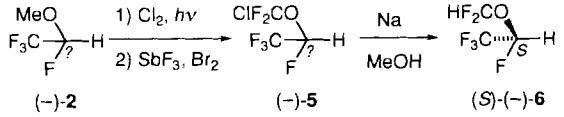


Fig. 1. ORTEP drawing of one of the two (*R*)-(+)-**4** molecules [11] in the asymmetric unit.

Establishment of the absolute configuration of ether **2** relies upon its conversion to a compound of known absolute configuration (Scheme 3). Trichlorination of the methoxy group of ether (−)-**2**[4] with Cl_2/incandescent light followed by difluorination with SbF_3/Br_2[12] gives chloroether (−)-**5** (bp 22–24 °C, $[\alpha]_D^{25} = -33$ ($c = 1$ in $CHCl_3$)). Chloroether (−)-**5** is converted to the anesthetic (−)-desflurane ((−)-**6**) by the action of Na in MeOH. According to ^1H and ^{19}F NMR analyses, the reaction results in a 1.5:1 mixture of chloroether **5** and desflurane. Chiral



(−)-**2** (−)-**5** (*S*)-(−)-**6**

Scheme 3. Establishment of the absolute configuration of ether **2**.

capillary GC analysis at 35 °C on a Chiraldex G-TA column (ASTEC, Whippany, NJ, USA) shows that the anesthetic **6** produced from the reaction is the levorotatory isomer, based on its longer retention time.[13] Because it is known[14] that the absolute configuration of (−)-**6** is (*S*), it is now certain that the absolute configuration of ether (−)-**2** is also (*S*).

The above data indicate that acid **1** undergoes highly stereospecific C–C bond cleavage, producing ether **2** with 99.5% inversion of configuration at the chiral carbon atom. This result is surprising, considering that in acyclic systems certain decarboxylations[15] and such related C–C bond breaking processes as the cleavage of tertiary alcohols[16] and Haller–Bauer cleavage[17] in most cases exhibit retention of configuration in the product, sometimes as high as 98%. The reaction is less selective in other solvents. In the present case, the very high level of inversion of configuration may be due to the highly electronegative α substituents of acid **1**. These, through hydrogen bonding, may cause the quenching proton of triethylene glycol to be in the required position opposite the carboxyl leaving group, assuming decarboxylation and quenching of the resultant organopotassium intermediate occur heterolytically; a concerted mechanism is also possible.

We have shown that under relatively harsh conditions an enantiomerically pure acyclic carboxylic acid can be decarboxylated to give a product with nearly complete inversion of configuration. This result is especially significant considering that carboxylic acids are known to produce products with a medium to high degree of configurational retention or racemization when subjected to much less drastic conditions.[15] To our knowledge, this is the most stereospecific C–C bond cleavage ever seen in an acyclic system. Future reports from this laboratory will describe use of this reaction in the synthesis of optically active anesthetics as well as new mechanistic data which will clarify the basic concept of configurational retention versus inversion in these systems.

Received: August 15, 1994 [Z 7238 IE]
German version: *Angew. Chem.* **1995**, *107*, 254

Keywords: configuration determination · fluorohydrocarbons · inhalational anesthetics

[1] A. C. Hall, W. R. Lieb, N. P. Franks, *Br. J. Pharmacol.* **1994**, *112*, 906; B. D. Harris, E. J. Moody, A. S. Basile, P. Skolnick, *Eur. J. Pharmacol.* **1994**, *267*, 269; G. Lysko, J. Robinson, R. Casto, R. Ferrone, *ibid.*, **1994**, *213*, 25.

[2] D. L. Pearson, Dissertation, Cornell University, **1990**; *Diss. Abstr. Int. B* **1992**, *52*, 6400; C. G. Huang, L. A. Rozov, D. F. Halpern, G. G. Vernice, *J. Org. Chem.* **1993**, *58*, 7382; L. A. Rozov, C. G. Huang, D. F. Halpern, G. G. Vernice (Anaquest) US-A 5283372, **1994** [*Chem. Abstr.* **1994**, *120*, 322704v].

[3] D. U. Staerk, A. Shitangkoon, G. Vigh, *J. Chromatogr. A* **1994**, *663*, 79; F. V. Schurig, H. Grosenick, *ibid.* **1994**, *666*, 617.

[4] L. A. Rozov, K. Ramig, *Tetrahedron Lett.* **1994**, *35*, 4501.

[5] G. Siegemund, R. Muschaweck (Hoechst) US-A 3981927, **1976** [*Chem. Abstr.* **1976**, *82*, 155327d].

[6] L. A. Rozov, C. G. Huang, G. G. Vernice (Anaquest) US-A 5205914, **1993** [*Chem. Abstr.* **1993**, *119*, 116811v].

[7] G. Siegemund, R. Muschaweck (Hoechst) DE-B 2361058, **1975** [*Chem. Abstr.* **1975**, *83*, 163636q].

[8] D. Sianesi, A. Pasetti, F. Tarli, *J. Org. Chem.* **1966**, *31*, 2312.

[9] H. C. Brown, P. Heim, *J. Org. Chem.* **1973**, *38*, 912.

[10] All new compounds provided satisfactory spectral data and correct combustion analyses.

[11] Single crystals of amine (*R*)-(+)-**4** were grown by slow evaporation from a solution of 12% v/v water in acetone. In the crystal structure determination the asymmetric unit contains two crystallographically independent molecules exhibiting similar configurational and geometric parameters. Representative molecule A is depicted in Figure 1. All bond lengths and bond angles are as expected. $M_r = 301.71$, monoclinic, space group $P2_1$, $a = 11.140(6)$, $b = 17.275(5)$, $c = 7.290(4)$ Å, $\beta = 90.19(5)°$, $V = 1403(2)$ Å^3, $Z = 4$, $\rho_{calc} = 1.43$ g cm^{-3}, $\mu = 28.28$ cm^{-1}. Data were collected on a colorless crystal measuring $0.25 \times 0.25 \times 0.10$ mm at $T = -160$ °C with a Rigaku AFC5S diffractometer; $\omega/2\theta$ scans with a scan speed of 8–32°/min in ω and a scan width of $(1.47 + 0.30 \tan\theta)°$ using graphite-monochromated $Cu_{K\alpha}$ radiation. Lattice parameters were determined by least squares using 25 reflections with $37.3° < 2\theta < 77.2°$. Three standards monitored every 150 reflections indicated no significant decay. A full set of Friedel mates was collected totaling 3918 reflections ($\sin\theta_{max}/\lambda = 0.56$ Å^{-1}; $0 \le h \le 13$, $0 \le k \le 19$, $-8 \le l \le 8$), 3535 of which were unique with merging $R = 0.055$. (The Friedel mates were not merged.) The structure was solved using MITHRIL and refined (P. W. Rafalko, R. I. Fryer, L. V. Kudzma, *Acta Crystallogr. Sect. C* **1993**, *49*, 116, and references therein) using 2706 reflections with $I > 3.00\sigma(I)$. All non-hydrogen atoms were refined anisotropically. The hydrogen atoms were assigned calculated positions and temperature factors (H–C = 0.95 Å; $B_{eq}(H) = 1.2\,B_{eq}$ (C or N)). The final R and R_w values $R^R = 0.086$ and $R_w^R = 0.116$, respectively, with GOF = 2.64. The Hamilton R-test (D. Rogers, *Acta Crystallogr. Sect. A* **1981**, *37*, 734) confirms that the absolute configuration of amine (*R*)-(+)-**4** is as shown. Both data for stereoisomers (*R*)-(+)-**4** and (*S*)-(−)-**4** were fully refined: $R^S/R^R \sim R_w^S/R_w^R = 1.07$ ($R^S = 0.093$, $R_w^S = 0.124$, GOF = 2.82 for (*S*)-(−)-**4**. Calculated $\alpha < 10^{-10}$ for $N = 2364$ establishes the validity of the assignment. Further details of the crystal structure investigation are available from the Director of the Cambridge Crystallographic Data Centre, 12 Union Road, GB-Cambridge, CB2 1EZ (UK), on quoting the full journal citation.

[12] T. Ishihara, M. Kuroboshi, *Chem. Lett.* **1987**, 1145.

[13] It has been established that (−)-**6** elutes after its (+) enantiomer on this stationary phase: L. A. Rozov, C. G. Huang, D. F. Halpern, G. G. Vernice, abstract FLUO #19 presented at the 206th ACS National Meeting, Chicago, IL, August, 1993. Coinjection of the reaction product with authentic (±)-desflurane verifies the peak assignment.

[14] P. L. Polavarapu, A. L. Cholli, G. G. Vernice, *J. Pharm. Sci.* **1993**, *82*, 791.

[15] T. R. Doyle, O. Vogl, *J. Am. Chem. Soc.* **1989**, *111*, 8510; D. J. Cram, A. S. Wingrove, *ibid.* **1963**, *85*, 1100, and references therein.

[16] T. D. Hoffmann, D. J. Cram, *J. Am. Chem. Soc.* **1969**, *91*, 1009, and earlier papers in this series; D. J. Cram, *Fundamentals of Carbanion Chemistry*, Academic Press, **1965**, Chapter 4.

[17] J. P. Gilday, L. A. Paquette, *Org. Prep. Proc. Int.* **1990**, *22*, 169.

Investigations into the Targeted Design of Solids: Hydrothermal Synthesis and Structures of One-, Two-, and Three-Dimensional Phases of the Oxovanadium–Organodiphosphonate System**

Victoria Soghomonian, Qin Chen, Robert C. Haushalter,* and Jon Zubieta*

The recent expansion of the chemistry of the metal organophosphonate systems[1–3] reflects their practical applications as catalysts, hosts in intercalation compounds, and protonic conductors.[4–7] Vanadyl organophosphonates such as $[VO(RPO_3)] \cdot x H_2O$[8–11] and $[(VO)_2\{(O_3P)_2CH_2\}] \cdot 4H_2O$,[10] possess structurally well-defined internal void spaces

[*] Prof. J. Zubieta, V. Soghomonian, Q. Chen
Department of Chemistry, Syracuse University
Syracuse, NY 13244-4100 (USA)
Telefax: Int. code +(315) 443-4070
e-mail: jazubiet@mailbox.syr.edu
Dr. R. C. Haushalter
NEC Research Institute, 4 Independence Way
Princeton, NJ 08540 (USA)
Telefax: Int. code +(609) 951-2483
e-mail: haushalter@research.nj.nec.com

[**] The work at Syracuse was supported by the National Science Foundation (Grant CHE 9318824).

and coordination sites which allow such materials to intercalate alcohols by coordination of the substrate molecule to the vanadium sites of the V-P-O layer. When combined with readily modified organic substituents, the thermal stability and reactivity of transition metal oxide moieties, and the interplay of hydrophilic and hydrophobic domains, such substrate-specific recognition and incipient coordinative unsaturation of the vanadium sites offers an approach to the design of highly selective oxidation catalysts.[12–14] We have sought to expand the chemistry of the V-O-RPO_3^{2-} system by the introduction of various templates as structure-directing units, a methodology which results in a dramatic expansion of the range of materials (with respect to structure and composition) of the analogous oxovanadium phosphate phases.[15–18] Encouraged by our success in introducing progressively more radical modifications in the layered structures of V-O-RPO_3^{2-} phases by exploitation of appropriate templates,[19–21] we have turned our attention to the oxovanadium diphosphonate system, V-O-$[O_3P(CH_2)_nPO_3]^{4-}$, where "engineering" of the material could be accomplished both by introduction of different templates and by changes in the length of the diphosphonate space group R. Pursuing this strategy, one-, two- and pillared two- or three-dimensional phases, **1**, **2**, and **3** respectively, have been synthesized and structurally characterized.

$[H_2N(CH_2CH_2)_2NH_2][(VO)(O_3P(CH_2)PO_3)]$ **1**

$[H_3N(CH_2)_2NH_3][(VO)(O_3P(CH_2)_2PO_3)]$ **2**

$[H_3N(CH_2)_2NH_3][(VO)_4(OH)_2(H_2O)_2\{O_3P(CH_2)_3PO_3\}_2]\cdot 4H_2O$ **3**

The materials **1**–**3** were prepared by hydrothermal synthesis.[22–24] By employing temperatures in the 150 °C to 250 °C range under autogenous pressures, self-assembly from simple molecular precursors of metastable phases which retain the bond relationships between most of the constituent atoms may be accomplished. A variety of precursors may be introduced since all precursors are soluble under the conditions of the synthesis. Furthermore, a variety of templating cations may be employed to direct the organization of the solid and to induce crystallization, since templates of appropriate size or geometry may be selected from the reaction mixture to fill the crystal vacancies. In this way, compounds **1**–**3** were prepared from mixtures of VCl_4, H_2O, the appropriate diphosphonates, and templates at 200 °C for periods of 50–96 h. The IR spectra of each of the materials exhibited a band in the 968 to 985 cm^{-1} range assigned to ν(V=O) and several bands in the 1000 to 1200 cm^{-1} region characteristic of the (PO_3) group.

As shown in Figure 1, the structure of **1**[25] consists of infinite puckered chains of $[(VO)(O_3P(CH_2)PO_3)]^{2-}$ units with piperazinium ions occupying the interstrand regions. The V^{IV} sites exhibit square pyramidal coordination geometry with the apical position occupied by a terminal oxygen atom and the four equatorial positions defined by phosphonate oxygen atoms, two from each of two diphosphonato ligands. Each diphosphonate group symmetrically bridges two vanadium centers, and each PO_3 unit of the ligand retains a pendant (P–O) group. While pendant (P–OH) groups are more common in organophosphonate coordination chemistry, the uncoordinated (P=O) group has been demonstrated in the structure of $[nBu_4N]_2[V_2O_4(RPO_3)_2]$.[2] The structure of this (P–O) moiety in **1** receives contributions from the multiply bonded (P=O) form, as suggested by the relatively short P–O distance of 1.518(6) Å, and more significantly from the charge interaction [$-PO^- \cdots {}^+HN-$] with the cation in **1** as indicated by O···H distances in the 2.1–2.5 Å range. This diphosphonate coordination mode contrasts with that of the layered solid $[(VO)_2(O_3P(CH_2)PO_3)(H_2O)_4]$ wherein all phosphonate oxygen donors are coordinated to metal centers. The unusual chain-puckering in **1** is attributed to the long-range axial interactions between adjacent (VO) sites which cause folding of the one-dimensional strands through an alternating short–long (V=O···V=O···V=O) zigzag motif. This structural feature is also observed in the structure of the V-P-O plane of $[(VO)(O_3PC_6H_5)(H_2O)]$. Valence sum calculations[26] confirm that vanadium is in the +IV oxidation state.

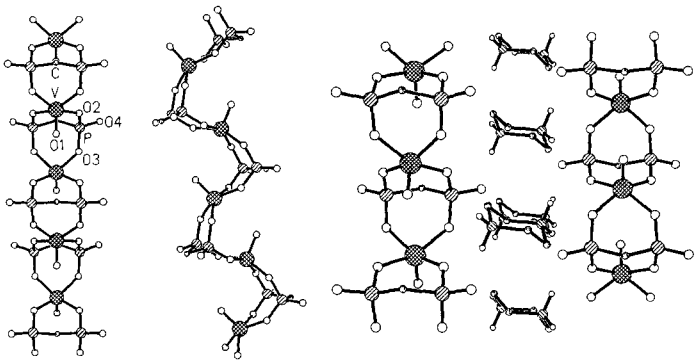


Fig. 1. Two views of the $[(VO)(O_3PCH_2PO_3)]_n^{2n-}$ chains of **1**. Middle: View of the zigzag pattern adopted as a result of folding of (V=O) groups into the vacant coordination site of the neighboring vanadyl unit. Left: View of the chain showing the atom-labeling scheme, which is also applicable in all subsequent figures: V atoms are crosshatched, P atoms are lined bottom left to top right, O atoms are open circles, and C atoms are lightly shaded small circles. Right: A view of neighboring $[(VO)(O_3PCH_2PO_3)]_n^{2n-}$ chains and the intervening piperazinium ions.

The structure of **2**[27] consists of layers of square pyramidally surrounded V^{IV} sites; the pyramids corner-sharing with diphosphonate tetrahedra to produce $[(VO)(O_3PCH_2CH_2PO_3)]_n^{2n-}$ layers. The ethylenediammonium ions occupy the interlamellar regions (Fig. 2). In addition to the apical oxygen atom, each vanadium(IV) site is bonded in the equatorial positions to four diphosphonate oxygen donors, one from each of four diphosphonate groups. Hence, each diphosphonato ligand bridges four vanadium centers in a monodentate fashion through two oxygen donors of each (PO_3) unit. In a fashion akin to that in **1**, each PO_3 group exhibits a pendant (P–O) group, which projects into the interlamellar space, as do the vanadyl oxygen atoms. Again, the structure exhibits hydrogen bonding between the pendant group and the organic cations. In comparison to the prototypical layered structures $[(VO)(O_3PC_6H_5)(H_2O)]$[9] and $[(VO)_2\{(O_3PCH_2PO_3)\}(H_2O)_4]$,[10] and V-O-$RPO_3^{2-}$ layer of **2** exhibits a more open net as a consequence of the presence of 14-membered (V-O-P-C-C-P-O)$_2$ rings (see Fig. 4b). The layer also exhibits eight-membered (V-O-P-O-V-O-P-O-) rings, char-

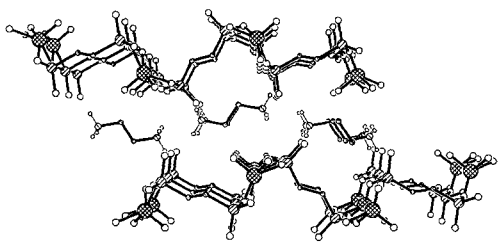


Fig. 2. The structure of **2** viewed along the crystallographic a axis, illustrating the interlamellar location of the organic cations.

acteristic of both molecular and solid-phase structures of the V-O-RPO_3^{2-} system.

The dramatic structural variations attendant to expansion of the phosphonate tether group are evident in the "pillared" structure adopted by **3** (Fig. 3). The structure of **3**[28] may be described in terms of inorganic V-P-O layers joined covalently

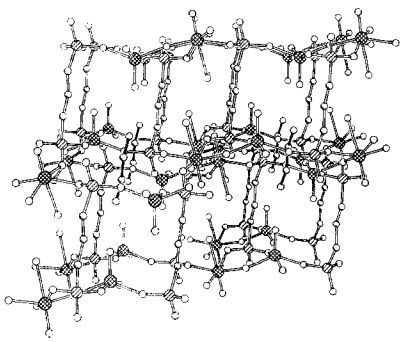


Fig. 3. A view of the three-dimensional V-O-P-C framework adopted by **3**, highlighting the positions of the organic cations which penetrate the inorganic V-O-P layers. Dotted circles are N atoms.

by the trimethylene bridges of the diphosphonate groups. Since the covalently linked framework includes the ligand carbon framework, the solid may alternatively be described as a three-dimensional V-P-O-C framwork with ethylenediammonium cations occupying the channels parallel to the crystallographic *a* axis. There are two distinct vanadium(IV) environments (see Fig. 4c): the V1 site is square pyramidal, surrounded by an apical oxygen atom, three oxygen donors of PO_3 groups and an oxygen atom of a bridging hydroxy group, while the V2 site is distorted octahedral, surrounded by an apical oxygen atom, three oxygen donors of PO_3 groups, the oxygen atom of a bridging hydroxy group, and an oxygen atom of a terminal aquo ligand. The binuclear $[V^{IV}_2O_2(OH)]$ unit provides an unusual structural motif within the V-P-O layers. The diphosphonato ligands span adjacent layers such that one of the PO_3 groups symmetrically bridges the V^{IV} sites of a $[V_2O_2(OH)]$ unit and coordinates through the remaining oxygen donor to the V2 site of an adjacent binuclear unit, while the second (PO_3) group bonds to two V1 sites and one V2 site of three proximal $[V_2O_2(OH)]$ units from a neighboring layer. In contrast to the structures of **1** and **2**, all the oxygen donors of the diphosphonato ligand in **3** coordinate to metal centers.

An unusual feature of the V-O-RPO_3^{2-} system is the range of connectivity patterns which are beginning to emerge for vanadium polyhedra and phosphonate tetrahedra within the V-P-O layers. As shown in Figure 4a, $[(VO)(O_3PC_6H_5)(H_2O)]$ exhibits vanadium octahedra corner-sharing through short–long V–O interactions into infinite chains, while $[(VO)\{(O_3P)_2CH_2\}(H_2O)_4]$ contains isolated (VO_6) octahedra, that is, no V-O-V bonding. While the structure of **2** resembles the latter with respect to the absence of V-O-V bonds, the vanadium sites are square pyramidal and as noted previously the details of the polyhedral connectivity are quite distinct. The V-P-O structure of **3** is unique in presenting $[V_2O_2(OH)]$ binuclear units with both octahedral and square-pyramidal vanadium sites. While the structure of $(Et_4N)[(VO)_3(OH)(H_2O)(O_3PEt)_3]\cdot H_2O$[21] also displays the $[V_2O_2(OH)]$ motif, the detailed connectivity within the plane is quite distinct from that of **3**.

The preparation of compounds **1**–**3** illustrates the power of hydrothermal synthesis, since in this way compounds can be formed by "self-assembly" from molecular precursors of metastable phases not accessible through conventional high-temperature solid-state techniques. While "designed" synthesis in the sense of predictability of product identity has yet to be achieved, it is clear that the combination of hydrothermal synthesis methods, appropriate adjustment of organic spacers in the ligand component, and suitable templates for framework organization allows modification both of framework dimensionality, and of V-P-O layer separation, and isolation of a range of phase compositions of dramatic structural variability limited only by the flexibility of polyhedral connectivity of the component moieties. Modification of the length of the organic buttress of the diphosphonato ligand should allow the engineering of materials with specific interlayer spacings and hence tailored microporosities.[4, 29]

Experimental Procedure

1: A mixture of VCl_4, methylenediphosphonic acid, piperazine, and water in the mole ratio 1:1:1.93:945 was heated at 200 °C and autogenous pressure for 50 h in a 23 mL Teflon-lined Parr acid digestion bomb (50% fill volume). Green crystals of **1** were isolated in 80% yield. IR (KBr pellet) $\tilde{\nu}$[cm^{-1}] = 3024 (w), 2958 (w), 2758 (m), 2626 (n), 1621 (m), 1505 (m), 1449 (m), 1156 (s), 1084 (s), 1029 (vs), 968 (s), 907 (w), 785 (s), 630 (m), 475 (w). Anal. calcd. for $C_5H_{14}N_2O_7P_2V$: C 18.3; H 4.28; N 8.56; found: C 18.3; H 4.39; N 8.55.

2: A mixture of VCl_4, ethylenediphosphonic acid, ethylenediamine, and water in the mole ratio 1:3.11:5.1:1890 was heated at 200 °C and autogenous pressure for 96 h in a quartz glass tube. Green crystals of **2** were collected in 90% yield. IR (KBr pellet) $\tilde{\nu}$[cm^{-1}] = 3448 (w), 2925 (m), 1181 (w), 1109 (s), 1076 (s), 1037 (sh), 1014 (vs), 975 (s), 775 (m), 546 (m), 463 (w). Anal. calcd. for $C_4H_{14}N_2O_7P_2V$: C 15.2; H 4.44; N 8.89; found: C 14.9; H 4.14; N 8.67.

3: A mixture of VCl_4, propylenediphosphonic acid, ethylenediamine, piperazine, and H_2O in the mole ratio 1:1.47:4.8:945 was heated at 200 °C and autogenous pressure for 80 h in a quartz glass tube. Blue crystals of **3** were isolated in 40% yield along with $[H_2N(CH_2CH_2)_2NH_2][(VO)_2(HO_3PCH_2CH_2CH_2PO_3)_2]$ (**4**), a layered material whose properties will be discussed elsewhere. While the piperazine template does not appear in the product **3**, it is necessary for the isolation of crystals suitable for X-ray crystallography. In the absence of piperazine, compound **3** was obtained

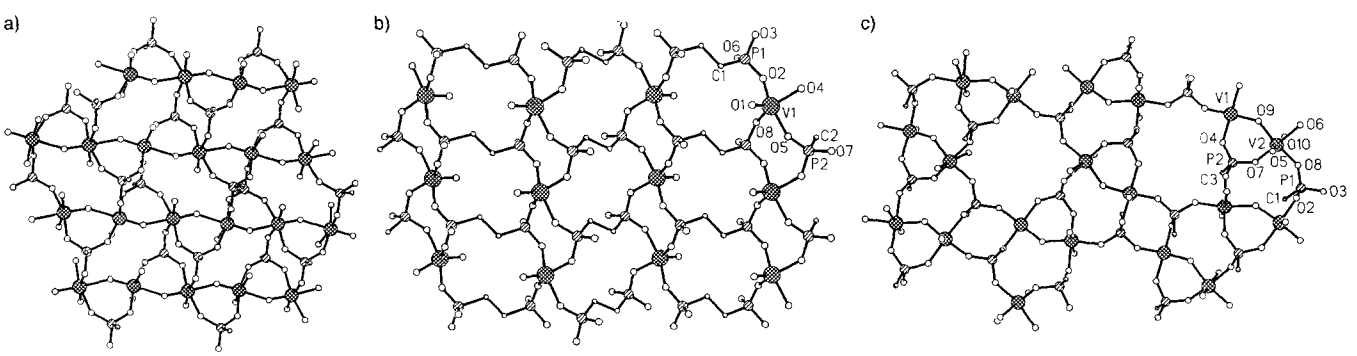


Fig. 4. The V-P-O layers of a) $[(VO)(O_3PC_6H_5)(H_2O)]$, b) of **2**, and c) of **3**.

 © VCH Verlagsgesellschaft mbH, D-69451 Weinheim, 1995 0570-0833/95/0202-0225 $ 10.00+.25/0

as a microcrystalline material whose identity has been confirmed by powder diffraction. IR (KBr pellet) $\tilde{\nu}$[cm^{-1}] = 3433 (s, br), 2757 (w), 1250 (w), 1144 (m), 1072 (s), 1034 (vs), 1012 (sh), 985 (w), 801 (w). Anal. calcd. for $C_8H_{36}N_2O_{24}P_4V_4$: C 11.0; H 4.13; N 3.21; found: C 11.6; H 3.11; N 3.00. Heating of **3** at 100 °C for 5 h results in removal of six equivalents of water to give the material $(H_3NCH_2CH_2NH_3)[(VO)_4(OH)_2(O_3PCH_2CH_2CH_2PO_3)_2]$ (**3a**). Anal. calcd. for $C_8H_{24}N_2O_{18}P_4V_4$: C 12.6; H 3.14; N 3.66; found: C 12.3; H 3.02; N 3.41.

Received: July 4, 1994
Revised version: September 6, 1994 [Z 7093 IE]
German version: *Angew. Chem.* **1995**, *107*, 229

Keywords: hydrothermal synthesis · polyoxometalates · solid-state structures · vanadium compounds

[1] J. Zubieta, *Comments Inorg. Chem.* **1994**, *16*, 153, and references therein
[2] Q. Chen, J. Salta, J. Zubieta, *Inorg. Chem.* **1993**, *32*, 4485.
[3] C. Bhardwaj, H. Hu, A. Clearfield, *Inorg. Chem.* **1993**, *32*, 4294, and references therein.
[4] G. Alberti, U. Constantino, F. Marmottini, R. Vivani, P. Zappelli, *Angew. Chem.* **1993**, *105*, 1396; *Angew. Chem. Int. Ed. Engl.* **1993**, *32*, 1357, and references therein.
[5] G. Alberti, U. Constantino in *Inclusion Compounds 5* (Eds.: J. L. Atwood, J. E. D. Davis, D. D. MacNicol), Oxford University Press, Oxford, **1991**, Chapter 5.
[6] D. A. Burwell, M. E. Thompson, *Supramolecular Architecture* (*ACS Symp. Ser.* **1992**, *499*, 166).
[7] A. Clearfield, C. Y. Ortiz-Avila, *Supramolecular Architecture* (*ACS Symp. Ser.* **1992**, *499*, 178).
[8] J. W. Johnson, A. J. Jacobson, W. M. Butler, S. E. Rosenthal, J. F. Brody, J. T. Lewandowski, *J. Am. Chem. Soc.* **1989**, *111*, 381.
[9] G. H. Huan, A. J. Jacobson, J. W. Johnson, E. W. Corcoran, Jr., *Chem. Mater.* **1990**, *2*, 2.
[10] G. H. Huan, J. W. Johnson, A. J. Jacobson, J. S. Merola, *J. Solid State Chem.* **1990**, *89*, 220.
[11] G. Huan, A. J. Jacobson, J. W. Johnson, D. P. Goshorn, *Chem. Mater.* **1992**, *4*, 661.
[12] T. E. Mallouk, H. Lee, *J. Chem. Educ.* **1990**, *67*, 829.
[13] R. C. Haushalter, L. A. Mundi, *Chem. Mater.* **1992**, *4*, 31.
[14] A. Stein, S. W. Keller, T. E. Mallouk, *Science* **1993**, *259*, 1558.
[15] V. Soghomonian, Q. Chen, R. C. Haushalter, J. Zubieta, C. J. O'Connor, *Science* **1993**, *259*, 1596.
[16] V. Soghomonian, Q. Chen, R. C. Haushalter, J. Zubieta, *Angew. Chem.* **1993**, *105*, 601; *Angew. Chem. Int. Ed. Engl.* **1993**, *32*, 610.
[17] V. Soghomonian, Q. Chen, R. C. Haushalter, J. Zubieta, *Chem. Mater.* **1993**, *5*, 1595.
[18] V. Soghomonian, Q. Chen, R. C. Haushalter, J. Zubieta, C. J. O'Connor, *Chem. Mater.* **1993**, *5*, 1690.
[19] $[Et_2NH_2][Me_2NH_2][(VO)_4(OH)_2(O_3PC_6H_5)_4]$: M. I. Khan, Y.-S. Lee, C. J. O'Connor, R. C. Haushalter, J. Zubieta, *J. Am. Chem. Soc.* **1994**, *116*, in press.
[20] $[EtNH_3]_2[(VO)_3(H_2O)(O_3PC_6H_5)_4]$: M. I. Khan, Y.-S. Lee, C. J. O'Connor, R. C. Haushalter, J. Zubieta, *Inorg. Chem.* **1994**, *33*, 3855.
[21] $[Et_4N][(VO)_3(OH)(H_2O)(O_3PC_2H_5)_3]\cdot H_2O$: M. I. Khan, Y.-S. Lee, C. J. O'Connor, R. C. Haushalter, J. Zubieta, *Chem. Mater.* **1994**, *6*, in press.
[22] M. Figlarz, *Chem. Scr.* **1988**, *28*, 3.
[23] J. Rouxel, *Chem. Scr.* **1988**, *28*, 33.
[24] R. A. Laudise, *Chem. Eng. News* **1987**, Sept. 8, 30.
[25] **1**: orthorhombic *Pnma*, $a = 8.012(2)$, $b = 18.191(4)$, $c = 7.744(2)$ Å, $V = 1128.7(5)$ Å^3, $Z = 4$, $\rho_{calcd} = 1.925$ gcm^{-3}; structure solution and refinement based on 1452 reflections with $I_o \geq 3\sigma(I_o)$ ($Mo_{K\alpha}$, $\lambda = 0.71073$ Å) converged at $R = 0.0374$. Further details of the crystal structure investigations of **1**–**3** may be obtained from the Fachinformationszentrum Karlsruhe, D-76344 Eggenstein-Leopoldshafen (Germany), on quoting the depository number CSD-58635.
[26] I. D. Brown in *Structure and Bonding in Crystals, Vol. 2* (Eds.: M. O'Keeffe, A. Navrotsky), Academic Press, New York, **1981**, p. 1.
[27] **2**: monoclinic $P2_1/n$, $a = 5.023(1)$, $b = 16.306(3)$, $c = 13.304(2)$ Å, $\beta = 92.54(3)°$, $V = 1088.9(7)$ Å^3, $Z = 4$, $\rho_{calcd} = 1.919$ gcm^{-3}; structure solution and refinement based on 1358 reflections with $I_o \geq 3\sigma(I_o)$ ($Mo_{K\alpha}$, $\lambda = 0.71073$ Å) converged at $R = 0.0557$ [25].
[28] **3**: monoclinic $C2/c$, $a = 14.870(3)$, $b = 10.245(2)$, $c = 18.868(4)$ Å, $\beta = 99.50(3)°$, $V = 2835.0(12)$ Å^3, $Z = 4$, $\rho_{calcd} = 2.015$ gcm^{-3}; structure solution and refinement based on 1266 reflections with $I_o \geq 3\sigma(I_o)$ ($Mo_{K\alpha}$, $\lambda = 0.71073$ Å) converged at $R = 0.0533$ [25].
[29] J. Alper, *Chem. Ind. (London)* **1986**, 335.

Dimensional Reduction of $Re_6Se_8Cl_2$: Sheets, Chains, and Discrete Clusters Composed of Chloride-Terminated $[Re_6Q_8]^{2+}$ (Q = S, Se) Cores**

Jeffrey R. Long, Andrew S. Williamson, and Richard H. Holm*

Lack of access to certain transition metal halide and chalcohalide clusters through self-assembly methods has enkindled interest in cluster excision, a low-temperature procedure in which the desired cluster is removed intact in molecular form from its covalently bound environment within an extended solid framework.[1] As demonstrated for the *n*-dimensional phases $Re_6Se_{4+n}Cl_{10-2n}$ ($n = 1 - 3$),[2] the effective use of current excision methodology is largely contingent upon the clusters being loosely bound in one or two dimensions.[3] This, however, is not always the case, and many clusters exist in a three-dimensional and/or more tightly bound framework. Our recent efforts have therefore focused on the development of a general high-temperature technique for producing frameworks of reduced connectivity, in hope of thereby gaining entry to a wealth of formerly inaccessible cluster chemistry. Herein, we describe such a technique, and demonstrate its efficacy by application to the $Re_6Se_8Cl_2$ parent structure.

The premise underlying our approach is exemplified in Figure 1, which illustrates the stepwise deconstruction of a rudimentary three-dimensional cluster framework. The initial structure consists of $[M_mQ_q]$ cluster cores linked in three dimensions by bridging anions X. Successive incorporation of additional equivalents of X reduces the overall dimensionality of the framework by terminating intercluster bridges, producing structures containing sheets, chains and, finally, discrete clusters. To preserve the original cluster electron count, each X added is accompanied by a charge-compensating cation A, which resides external to the framework (i.e., between sheets, chains, or isolated clusters). The scheme presented in Figure 1 is not necessarily intended to imply a specific reaction pathway (although it may do so in some cases), but rather to provide a formalism with which new lower dimensional compounds may be derived from existing structures. Thus, this process of *dimensional reduction*, when applied to a known parent phase, serves as a means of formulating synthetic targets with structures amenable to excision or direct dissolution, ultimately affording the desired cluster in molecular form. Substitution of single metal centers M for the $[M_mQ_q]$ cores in Figure 1 creates an analogous formalism for metal–anion frameworks, useful in relating covalent structures throughout the solid state.[4]

Many of the more intractable cluster frameworks are partially or entirely linked by bonding interactions directly between cores, rather than through some intermediate bridging ligand, as in Figure 1.[1] The two-dimensional framework in $Re_6Se_8Cl_2$ ($\triangleq [Re_6Se^i_4Se^{i-a}_{4/2}]Se^{a-i}_{4/2}Cl^a_2$)[5] provides such an example. Its structure[6] (Fig. 2) is built up from electron-precise, face-capped octahedral $[Re_6Se_8]^{2+}$ cluster cores, each with two attendant terminal chlorides at *trans* rhenium apices and four

[*] Prof. R. H. Holm, J. R. Long, A. S. Williamson
Department of Chemistry, Harvard University
Cambridge, MA 02138 (USA)
Telefax: Int. code + (617)496-9289

[**] This work was supported by the National Science Foundation (Grant CHE 92-08387). X-ray equipment was obtained through the National Institutes of Health (Grant 1 S10 RR 02247). We thank the Office of Naval Research for their support of J. R. L. in the form of a predoctoral fellowship (1991–1994), and M. J. Scott, D. Lange, and B. Souza for technical assistance.

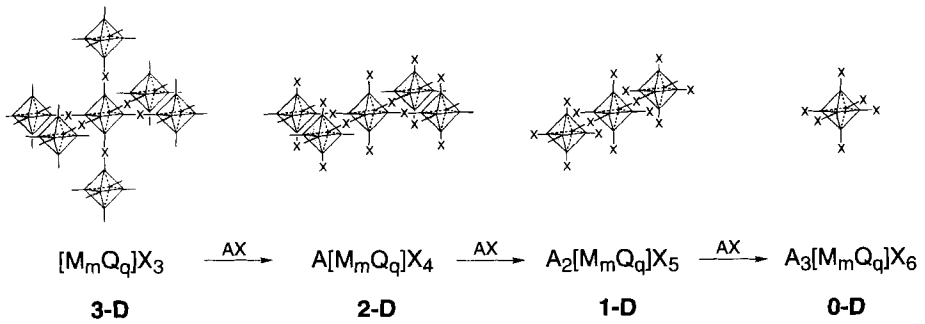


Fig. 1. Dimensional reduction of a simple three-dimensional cluster framework, $[M_mQ_q]X_3$. Anions X bridging cluster cores $[M_mQ_q]$ (arbitrarily represented by shaded octahedra) are rendered terminal through the incorporation of additional equivalents of X, reducing the overall dimensionality of the structure. Cations A (not shown) are simultaneously introduced to balance the negative charge accrued by the framework.

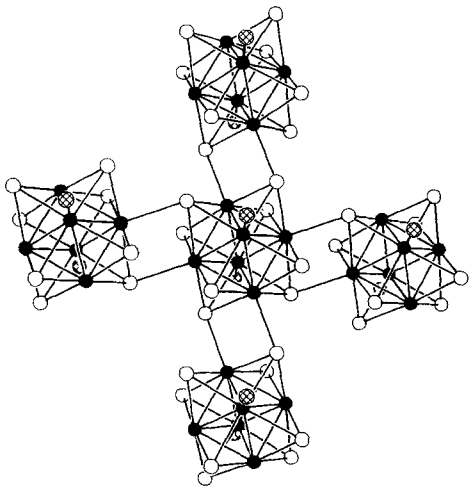
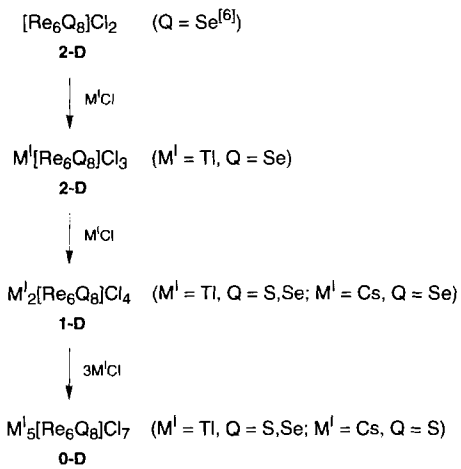


Fig. 2. Local cluster environment in the $Re_6Se_8Cl_2$ parent structure; its sheetlike cluster framework extends within the plane of the page. Black, white and cross-hatched spheres represent Re, Se, and Cl atoms, respectively. Selected mean interatomic distances [Å] and angles [°]: Re–Re 2.64(2), non-rhomb Re–Se^i 2.52(1), Re–Se^a 2.62(2), Re–Cl 2.38(1), Re-Re-Re 60.0(5); within Re_2Se_2 rhombs Re–Se 2.62(1), Re–Re 3.43(2) [6].

rhombic Re_2Se_2 interactions linking neighboring cores. The rigidity inherent in these Re_2Se_2 rhombs lends itself to the overall framework, rendering the chloride-terminated sheets impervious to excision. In view of the multitude of solids exhibiting $[Re_6Q_8]^{2+}$ (Q = S, Se) cluster cores,[1] and the lack of any corresponding species in solution, the $Re_6Se_8Cl_2$ structure was chosen as a prototype for testing the validity of the dimensional reduction approach. Seven new phases containing this core motif were synthesized and structurally characterized by single-crystal X-ray methods.[7] Their relations to the $Re_6Se_8Cl_2$ parent phase[8] through extent of M^ICl (M^I = Cs, Tl)[9] uptake are presented in Scheme 1.

The first step in Scheme 1 proceeds with the incorporation of one equivalent of TlCl to yield $TlRe_6Se_8Cl_3$ ($\triangleq$ $Tl[Re_6Se^i_5Se^{i-a}_{3/2}]Se^{a-i}_{3/2}Cl^a_3$). Here the overall dimensionality of the cluster framework has not been reduced; however, the rigidity of the sheets has relaxed substantially. Figure 3 shows the structure and local surroundings of the $[Re_6Se_8]^{2+}$ cores in the new two-dimensional phase. Each core now has three associated terminal chlorides (*fac* arrangement) and three rhombic Re_2Se_2 interactions with neighboring cores. As in $Re_6Se_8Cl_2$, the clusters achieve an ideal configuration of 24 metal-based electrons corresponding to twelve Re–Re bonds, and consequently display no significant distortion away from a perfectly regular Re_6 octahedron (an observation which holds for the entire series of compounds listed in Scheme 1). Similarly, the sole core irregularity, an approximate 0.1 Å lengthening in those Re–Se bonds integral to the Re_2Se_2 rhombs, is retained in $TlRe_6Se_8Cl_3$, as are the other core interatomic distances and angles. Although it contains one fewer linkage per cluster, the sheetlike framework of $TlRe_6Se_8Cl_3$ is slightly more complicated than that of $Re_6Se_8Cl_2$. While the lower two Re_2Se_2 rhombs in Figure 3 are perpendicular to the plane of the page, the upper one is situated within the plane. The choice of atom Se(7) over Se(4) in forging an intercore bond effectively destroys



Scheme 1. Dimensional reduction of the $Re_6Se_8Cl_2$ parent structure.

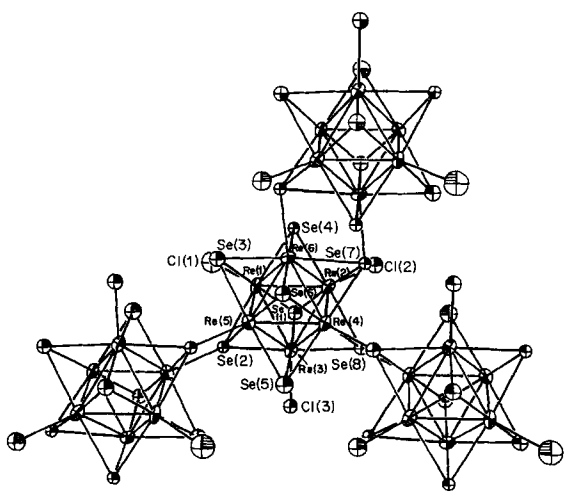


Fig. 3. Local cluster environment in the structure of two-dimensional $TlRe_6Se_8Cl_3$ (70% probability ellipsoids). Inversion centers are situated in the middle of each Re_2Se_2 rhomb; lower two rhombs are perpendicular to the plane of the page. Selected interatomic distances [Å] and angles [°]: mean Re–Re 2.64(2), Re(4)–Se(8) 2.63(2), Re(5)–Se(2) 2.62(2), Re(6)–Se(7) 2.67(2), mean of other Re–Se^i 2.51(2), mean Re–Se^a 2.62(2), mean Re–Cl 2.39(5), mean Re–Re–Re 60.0(5) and 90.0(4), mean Re–Re–Cl 135(2), mean Re–Se^i–R 63(1), mean Se–Re–Cl 91(2); within Re_2Se_2 rhombs mean values are Re–Se 2.63(2), Re–Re 3.41(3), Re–Se–Re 81.0(3), Se–Re–Se 99.0(3).

a potential threefold rotational axis running through atoms Se(1) and Se(6), preempting the simpler alternative structure in favor of a more densely packed, but corrugated sheet. The thallium cations sandwiched between these $[Re_6Se_8Cl_3]^-$ sheets interact with the exposed chlorine and selenium atoms on their surfaces.[10]

Incorporation of one more equivalent of TlCl gives rise to $Tl_2Re_6Se_8Cl_4$ ($\hat{=} Tl_2[Re_6Se^i_6Se^{i-a}_{2/2}]Se^{a-i}_{2/2}Cl^a_4$), wherein the dimensionality of the cluster framework has now been reduced by one. In this phase, neighboring $[Re_6Se_8]^{2+}$ cores are linked by Re_2Se_2 rhombs at *trans* rhenium apices to form a one-dimensional chain (Fig. 4). The chains are sheathed with terminal

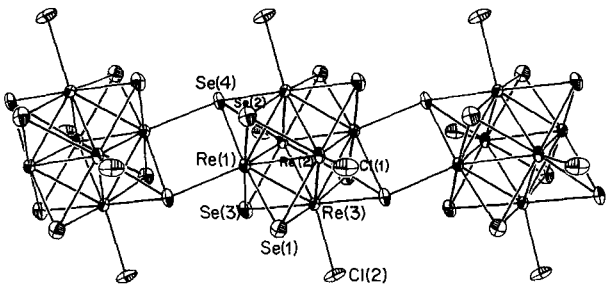


Fig. 4. Local cluster environment in the structure of one-dimensional $Tl_2Re_6Se_8Cl_4$ (70% probability ellipsoids). Inversion centers are located at the center of each cluster and each Re_2Se_2 rhomb. Selected interatomic distances [Å] and angles [°]: mean Re–Re 2.63(2), Re(1)–Se(4) 2.635(5), mean of other Re–Se^i 2.510(5), Re–Se^a 2.600(7), mean Re–Cl 2.413(2), mean Re-Re-Re 60.0(5) and 90.0(5), mean Re-Re-Cl 135.2(7), mean Re-Se^i-Re 63.0(8), mean Se-Re-Cl 92.2(6); within Re_2Se_2 rhombs mean Re–Se 2.62(2), Re–Re 3.407, Re-Se-Re 81.3(2), Se-Re-Se 98.7(2).

chlorides, which ligate the remaining four rhenium atoms of each cluster core. $Cs_2Re_6Se_8Cl_4$ contains virtually identical cluster chains, with only a slight increase in interchain separations due to the larger intermediate Cs cations. For both structures, the bond lengths and angles within clusters and rhombs do not significantly deviate from the corresponding parameters in $Re_6Se_8Cl_2$. Another closely related phase, $Tl_2Re_6S_8Cl_4$, features $[Re_6S_8]^{2+}$ cores linked to form an analogous chain structure. Here, the shorter Re–S bonds induce a contraction in the Re_2S_2 rhombs (mean interatomic distances [Å] and angles [°]: Re–S 2.52(3), Re–Re 3.24(2), Re-S-Re 80.2(2), S-Re-S 99.8(2)), drawing cluster cores within chains closer together. In other regards, the clusters differ unremarkably from those of $Cs_5Re_6S_8Cl_7$ described below. Interestingly, none of these phases assumes the isomeric two-dimensional cluster framework of Figure 1 (X = Cl), as adopted by $Re_6Se_6Cl_6$ ($\hat{=} [Re_6Se^i_6Cl^i_2]Cl^a_2Cl^{a-a}_{4/2}$).[11] Very likely, this is a result of the electrostatics involved in accommodating two large cations per cluster unit.

The terminus in the dimensional reduction of $Re_6Se_8Cl_2$ is attained with the incorporation of five total equivalents of TlCl to form zero-dimensional $Tl_5Re_6Se_8Cl_7$ (or, more precisely, $Tl_4[Re_6Se_8Cl_6] \cdot TlCl$). The discrete $[Re_6Se_8Cl_6]^{4-}$ clusters in this phase accomplish our immediate goal of breaking down the two-dimensional framework of $Re_6Se_8Cl_2$. Once again, the geometry of the clusters in the parent phase is preserved, barring those effects which arise from the presence of core-linking Re_2Se_2 rhombs. Exchange[12] of an alkali metal for Tl in this structure should provide the cluster in soluble form, however, such experiments await a more efficient synthesis of $Tl_5Re_6Se_8Cl_7$. Attempts at preparing a cesium-substituted analogue, invariably resulted in formation of large quantities of Cs_2ReCl_6, among other phases. In direct contrast, the parallel phases $Tl_5Re_6S_8Cl_7$ and $Cs_5Re_6S_8Cl_7$, containing unprecedented $[Re_6S_8Cl_6]^{4-}$ clusters (Fig. 5), are both produced very near quantitatively.[13] A comparison of the $[Re_6Se_8]^{2+}$ and $[Re_6S_8]^{2+}$ cores, reveals that the expected differences due to the shorter Re–S bonds are accompanied by a subtle isotropic con-

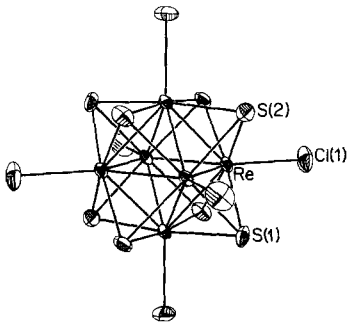


Fig. 5. Structure of the discrete $[Re_6S_8Cl_6]^{4-}$ cluster in $Cs_5Re_6S_8Cl_7$ (70% probability ellipsoids). The cluster resides on a $\bar{3}$ symmetry site, with atom S(2) on the threefold rotation axis. Selected interatomic distances [Å] and angles [°]: mean Re–Re 2.597(3), mean Re–S 2.399(3), Re–Cl 2.42(1), Re-Re-Re 60.0(1) (mean) and 90.0(1), mean Re-Re-Cl 135(1), mean Re-S-Re 65.5(1), mean S-Re-Cl 93.4(9).

traction of the Re_6 octahedron. $Cs_5Re_6S_8Cl_7$ readily dissolves in acidic media to afford a bright yellow solution, the chemical properties of which are currently under investigation. Preliminary X-ray studies confirm retention of the hexanuclear rhenium cores recovered from these solutions.

Experimental Procedure

Stoichiometric 0.500 g mixtures of Re (– 325 mesh, Cerac), Q (S: –100 mesh, Aldrich; Se: –325 mesh, Strem), $ReCl_5$ (– 40 mesh, Cerac), and M^ICl (TlCl: Strem; CsCl: Baker, dried for two days at 200 °C) were intimately ground in a pure dinitrogen atmosphere, and sealed in fused silica ampules (id × od × l = 7 × 10 × 120 mm) under vacuum. Reactions were carried out at 900 °C for 7000 min, cooled at 0.2 °C per min to about 500 °C, and air-quenched. Product identity and purity was confirmed by comparison of the observed X-ray powder diffraction (Scintag XDS-2000, $Cu_{K\alpha}$ radiation) pattern with calculated patterns generated from single-crystal results. Samples exhibiting large crystal faces were analyzed (EMPA) with a Cameca MBX electron microprobe employing a Tracor Northern TN-1310 wavelength-dispersive spectrometer.

$TlRe_6Se_8Cl_3$ (EMPA: $Tl_{0.95(1)}Re_{6.00(4)}Se_{8.31(7)}Cl_{2.90(8)}$) forms as black hexagonal prisms which are not single crystals, but rather consist of a large number of slightly misfit stacked plates. With considerable difficulty, a razor blade was employed in slicing a single plate off of one of these stacks for X-ray analysis. Reactions targeting $Tl_2Re_6Se_8Cl_4$ (small black parallelpipeds) and $Tl_5Re_6Se_8Cl_7$ (EMPA: $Tl_{4.70(6)}Re_{6.00(5)}Se_{8.2(1)}Cl_{6.80(6)}$; large, irregular red blocks) gave very low yields (typically 5 and 10 mg of mechanically sorted crystals, respectively), the major products being $TlRe_6Se_8Cl_3$ and TlCl. Attempts at improving these yields by varying reaction conditions or including transport agents were not successful. Red $Tl_2Re_6S_8Cl_4$ and black $Cs_2Re_6Se_8Cl_4$ both crystallize in densely packed clumps of thin needles. $Tl_5Re_6S_8Cl_7$ (EMPA: $Tl_{4.7(2)}Re_{6.00(7)}S_{7.93(8)}Cl_{6.8(1)}$) and $Cs_5Re_6S_8Cl_7$ (EMPA: $Cs_{5.10(6)}Re_{6.01(1)}S_{7.88(6)}Cl_{6.75(6)}$) occur as thick hexagonal plates, of respective orange-red and yellow-orange color. The latter phase dissolves in dilute $HCl_{(aq)}$ and EtOH/$HCl_{(aq)}$ to yield a bright yellow solution.

Received: September 12, 1994 [Z 7309 IE]
German version: *Angew. Chem.* **1995**, *107*, 248

Keywords: clusters · rhenium compounds · solid-state chemistry

[1] S. C. Lee, R. H. Holm, *Angew. Chem.* **1990**, *102*, 868; *Angew. Chem. Int. Ed. Engl.* **1990**, *29*, 840.

[2] O. M. Yaghi, M. J. Scott, R. H. Holm, *Inorg. Chem.* **1992**, *31*, 4778. For a detailed structural analysis of these and related phases, see: A. Perrin, M. Sergent, *New J. Chem.* **1988**, *12*, 337.

[3] There are only three reports of cluster excision from three-dimensional solids: F. Stollmaier, A. Simon, *Inorg. Chem.* **1985**, *24*, 168; F. Rogel, J. D. Corbett, *J. Am. Chem. Soc.* **1990**, *112*, 8198; C. E. Runyan, T. Hughbanks, *ibid.* **1994**, *116*, 7909.

[4] The correlation between cation/anion incorporation and dimensionality has been specifically recognized in the structures of certain metal-chalcogenides: M. G. Kanatzidis, Y. Park, *Chem. Mater.* **1990**, *2*, 99; E. A. Axtell, J.-H. Liao, Z. Pikramenou, Y. Park, M. G. Kanatzidis, *J. Am. Chem. Soc.* **1993**, *115*, 12191; Y.-J. Lu, J. A. Ibers, *Comments Inorg. Chem.* **1993**, *14*, 229.

[5] The notation employed here is defined in H. Schäfer, H. G. von Schnering, *Angew. Chem.* **1964**, *76*, 833.

[6] L. Leduc, A. Perrin, M. Sergent, *Acta Cryst.* **1983**, *C39*, 1503.

[7] Crystallographic data: $TlRe_6Se_8Cl_3$, $P\bar{1}$, $a = 8.885(4)$, $b = 8.978(4)$, $c = 11.039(5)$ Å, $\alpha = 109.66(3)$, $\beta = 90.21(4)$, $\gamma = 94.74(4)°$, $V = 826.0(6)$ Å^3, $Z = 2$, $\mu = 71.58$ mm^{-1}, $R = 0.1021$, $R_w = 0.0999$; $Tl_2Re_6Se_8Cl_4$, $P\bar{1}$, $a = 6.569(3)$, $b = 8.764(4)$, $c = 8.873(3)$ Å, $\alpha = 85.09(3)$, $\beta = 82.31(3)$, $\gamma = 69.18(3)$, $V = 427.8(3)$ Å^3, $Z = 1$, $\mu = 71.15$ mm^{-1}, $R = 0.0810$, $R_w = 0.0803$; $Tl_2Re_6S_8Cl_4$, $P\bar{1}$, $a = 6.360(3)$, $b = 8.777(3)$, $c = 16.363(3)$ Å, $\alpha = 94.85(2)$, $\beta = 92.70(3)$, $\gamma = 96.39(3)°$, $V = 903.1(5)$ Å^3, $Z = 2$, $\mu = 59.30$ mm^{-1}, $R = 0.0799$, $R_w = 0.0778$; $Cs_2Re_6Se_8Cl_4$, $P\bar{1}$, $a = 6.531(2)$, $b = 9.128(4)$, $c = 10.005(5)$ Å, $\alpha = 107.80(4)$, $\beta = 105.38(3)$, $\gamma = 102.78(3)°$, $V = 517.0(4)$ Å^3, $Z = 1$, $\mu = 53.03$ mm^{-1}, $R = 0.1397$; $Tl_3Re_6Se_8Cl_7$, $R\bar{3}c$, $a = 9.397(3)$, $c = 51.895(23)$ Å, $Z = 6$, $\mu = 69.34$ mm^{-1}, $R = 0.0668$, $R_w = 0.0637$; $Tl_3Re_6S_8Cl_7$, $R\bar{3}c$, $a = 9.312(2)$, $c = 50.823(15)$ Å, $Z = 6$, $\mu = 61.34$ mm^{-1}, $R = 0.0670$, $R_w = 0.0635$; $Cs_5Re_6S_8Cl_7$, $R\bar{3}c$, $a = 9.742(2)$, $c = 53.479(17)$ Å, $Z = 6$, $\mu = 32.01$ mm^{-1}, $R = 0.0585$, $R_w = 0.0523$. Data were collected at 223 K (295 K for $Tl_2Re_6Se_8Cl_4$) on a Nicolet P3f diffractometer employing graphite-monochromated $Mo_{K\alpha}$ radiation ($\lambda = 0.71073$ Å). Structures were solved by direct methods with the aid of difference Fourier maps, and refined ($F_0 > 6\sigma F_0$) with successive full-matrix least-squares cycles (SHELXTL PLUS). All of the compounds absorb X-rays heavily, and an empirical correction (XEMP) based on azimuthal Ψ-scans was applied to each data set. For the rhombohedral crystals, this correction proved adequate when combined with collection of excess data used to average equivalent reflection intensities. However, the lack of (non-Friedel) equivalent data for triclinic crystals led to remanent absorption effects; as a result, the Se and Cl atoms in $TlRe_6Se_8Cl_3$ and two of the S atoms in $Tl_2Re_6S_8Cl_4$ could not be refined anisotropically. The structure of $Cs_2Re_6Se_8Cl_4$ was solved, but would not refine satisfactorily. An analytical absorption correction (six crystal faces were indexed as {100}, {010} and {001}) was successfully applied to $Tl_2Re_6Se_8Cl_4$. Further details of the crystal structure investigations are available on request from the Fachinformationszentrum Karlsruhe, D-76344 Eggenstein-Leopoldshafen (Germany), on quoting the depository number CSD-58636.

[8] Alternatively, the three-dimensional $Re_6S_8Cl_2$ ($\triangleq [Re_6S_6^{i-a}]S_{2/2}^{a-i}Cl_{4/2}^{a-a}$) structure may serve as a parent for the $[Re_6S_8]^{2+}$ core-containing phases: C. Fischer, S. Fiechter, H. Tributsch, G. Reck, B. Schultz, *Ber. Bunsenges. Phys. Chem.* **1992**, *96*, 1652.

[9] In general, smaller monocations M^I were found to be considerably less effective.

[10] The M^I cations in all of the seven new phases display complex coordination environments involving both Q and Cl atoms.

[11] A. Perrin, L. Leduc, M. Sergent, *Eur. J. Solid State Inorg. Chem.* **1991**, *28*, 919.

[12] Similar exchanges have been performed in $Tl_4Re_6Se_{12}$: G. Huan, M. Greaney, M. Greenblatt, G. Liang, M. Croft, *Solid State Ionics* **1989**, *32*, 134.

[13] Solids containing discrete $[Re_6S_{14}]^{10-}$ clusters have also been recently reported: W. Bronger, M. Kanert, M. Loevenich, D. Schmitz, *Z. Anorg. Allg. Chem.* **1993**, *619*, 2015.

Direct Observation of O–H Reductive Elimination from Ir^{III} Complexes**

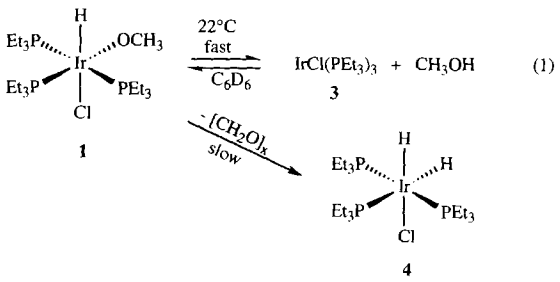
Ofer Blum and David Milstein*

Hydrido(hydroxo) and -(alkoxo) complexes are postulated as intermediates in various transition metal mediated catalytic transformations.[1] Formation of O–H bonds by reductive elimination from such complexes is suggested as the product-forming step in several reactions, such as the hydrogenation of CO to methanol,[2] hydrogen transfer reactions,[1e] and alcohol homologation.[1f] O–H bond formation by reductive elimination is rarely observed, and was so far found to require ligand addition,[1c, 3] UV irradiation,[3a] or oxidation.[4] In other examples, the H–M–OR (R = H, alkyl or aryl) species was generated in situ but was not observed.[2, 5] In all these cases, O–H bond formation was not rate determining. Here we report the reversible, unassisted reductive elimination of water and methanol from *mer-cis*-$[HIr(OR)Cl(PR'_3)_3]$ (R = H, Me; R' = Me, Et), which takes place without prior ligand dissociation. The results of this study lead to the conclusion that for hydrido(alkoxo) complexes, O–H reductive elimination is preferred over β-hydride elimination.

The compounds **1** and **2** are prepared by oxidative addition of

mer-cis-$[HIr(OR)Cl(PEt_3)_3]$ **1**, R = CH_3; **2**, R = H

methanol or water to $[IrCl(PEt_3)_3]$ (**3**)[6] at −30 °C.[7, 8] Both **1** and **2** undergo HOR reductive elimination in pure benzene at room temperature, generating **3**. Fast equilibrium between **1** and **3** is observed (Scheme 1) at 22 °C in a 9.36 mM solution of



Scheme 1. Reactions of **1**.

3 in C_6D_6 containing methanol ($c_{CH_3OH} = 223$ mM). Concomitantly, slow, irreversible β-hydride elimination from **1** generates the complex **4**[9] and decreases the concentrations of **1** and **3** (Scheme 1). Nevertheless, the ratio of these concentrations remains unaffected. The same c_1/c_3 ratio was obtained when starting with a 9.36 mM solution of **1** under otherwise identical conditions.[10] This corroborates the establishment of a fast equilibrium between **3** and **1**, and that the O–H reductive elimination from **1** is substantially faster than the β-H elimination.

As expected, the reductive elimination process (Scheme 1) is entropically driven ($\Delta S^0 = 67(4)$ cal K^{-1} mol^{-1}) (Fig. 1).[11]

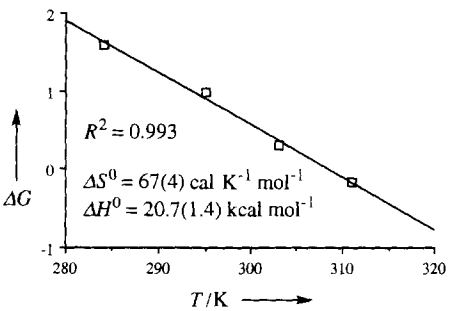


Fig. 1. The temperature dependence of ΔG [kcal mol^{-1}] of the O–H reductive elimination from **1**.

From the value of the reaction enthalpy ($\Delta H^0 = 20.7(1.4)$ kcal mol^{-1}) it is possible to estimate the sum of the Ir–H and Ir–OCH_3 bond energies D of **1** as 125 kcal mol^{-1}.[12] Based on previously determined D(Ir–H) values,[13] the Ir–H bond strength in **1** is estimated to be between 57 and

[*] Prof. D. Milstein, O. Blum
Department of Organic Chemistry, The Weizmann Institute of Science
Rehovot 76100 (Israel)
Telefax: Int. code +(8) 34-4142

[**] This work was supported by the US–Israel Binational Science foundation. We thank Hoechst, A.G. for a gift of chemicals.

64 kcal mol^{-1} resulting in $D(\mathrm{Ir-OCH_3}) \approx 68-61$ kcal mol^{-1}. To our knowledge, this is the first experimentally determined bond strength for the bond between an alkoxo group and a late transition metal.[14] The observation that $D(\mathrm{M-H}) \sim D(\mathrm{M-OCH_3})$ is in agreement with the relative M–X bond strengths (X = anionic ligand) reported by Bryndza, Bercaw and coworkers.[14]

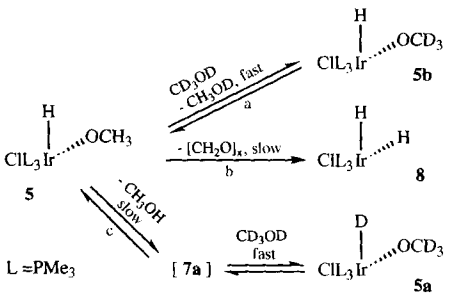
The PMe_3 complexes **5** and **6**[15] were prepared in a similar manner to **1** and **2** from **7**[16] and methanol or water, respectively. Interestingly, only **5** and **6** (but not the Ir^{I} complex **7a**[17]) are present after completion of the oxidative addition under the conditions mentioned above, indicating strong dependence of the equilibrium in Scheme 1 on the phosphane ligand size.[18]

mer-cis-[HIr(OR)Cl(PMe$_3$)$_3$] **5**, R = CH$_3$; **6**, R = H

[(C$_8$H$_{14}$)IrCl(PMe$_3$)$_3$] **7**

[IrCl(PMe$_3$)$_3$] **7a**

The addition of CD_3OD (2.24 M) to a solution of **5** (32.1 mM) in C_6D_6 at 22 °C gives rise to three competing reactions (Scheme 2, a–c). The fast anionic ligand exchange (a) has



Scheme 2. Reactions of **5**.

a pseudo first order rate constant ($k_2c_{CD_3OD}$) of 7.85×10^{-4} s^{-1}.[19] The rate constant of the β-hydride elimination to give **8** (b) (in CH_3OH and not CD_3OD under otherwise the same conditions) is 3.28×10^{-5} s^{-1}.[20] The rate-determining reductive elimination[21] step in reaction c has a rate constant of 1.22×10^{-4} s^{-1},[22] about 3.7 times faster than the β-hydride elimination. Reaction c takes place (albeit slowly) also under conditions in which the β-hydride elimination from **5** is not observed (at −30 °C or in the presence of lower methanol concentration (89.2 mM)).[9] The hydrido(hydroxo) complex **6** also undergoes Ir–H to Ir–D exchange (in D_2O/THF).

The rate of the oxidative addition to **3** in Scheme 1 was not influenced by the addition of a tenfold excess of triethylphosphane. Similarly, the rate of methanol oxidative addition to **7a** was not affected by a fifteenfold excess of LiCl.[23] These results indicate that the O–H reductive elimination from **1**, **2**, **5**, and **6** proceeds without prior chloride or phosphane dissociation.[25]

Surprisingly, the cation in **9** does not undergo exchange of Ir–H in D_2O/THF, and **10** is stable towards thermal reductive elimination at 70 °C.[4] This result contradicts the expectations that reductive elimination is facilitated by lower electron density[26] or by higher steric hindrance.[18] (The cationic complexes in **9** and **10** are less electron-rich than the neutral complexes **6** and **5**, respectively, and the PMe_3 ligand is bulkier than the chloro ligand). It is possible that the chloro ligand in **5** and **6** stabilizes the pentacoordinate transition state of the reductive elimination by π donation. The effect of π donation on pentacoordinate d^6 iridium complexes was recently discussed.[9, 27] We are currently trying to clarify this point.

cis-[HIr(OH)(PMe$_3$)$_4$]PF$_6$ **9**

cis-[HIr(OCH$_3$)(PMe$_3$)$_4$]PF$_6$ **10**

In conclusion, this study demonstrates that formation of alcohols (and water) by O–H reductive elimination is feasible and can compete favorably with β-H elimination. This supports proposals of O–H bond formation as the product-forming step in industrially important processes such as CO hydrogenation[1d] and alcohol homologation.[1f, 2]

Received: July 25, 1994 [Z 7170 IE]
German version: *Angew. Chem.* **1995**, *107*, 210

Keywords: iridium compounds · O–H bond formation · reductive elimination

[1] a) T. Yoshida, Y. Ueda, S. Otsuka, *J. Am. Chem. Soc.* **1978**, *100*, 3941; b) T. Yoshida, T. Okano, Y. Ueda, S. Otsuka, *ibid.* **1981**, *103*, 3411; c) T. Yoshida, T. Matsuda, T. Okano, T. Kitani, S. Otsuka, *ibid.* **1979**, *101*, 2027; d) H. E. Bryndza, W. Tam, *Chem. Rev.* **1988**, *88*, 1163; e) Y. J. Kim, K. Osakada, A. Takenaka, A. Yamamoto, *J. Am. Chem. Soc.* **1990**, *112*, 1096, and references therein; f) H. Bahrmann, B. Cornils in *New Synthesis with Carbon Monoxide* (Ed.: J. Falbe), Springer, Berlin, **1980**, p. 226; g) T. Yoshida, T. Okano, T. Saito, S. Otsuka, *Inorg. Chim. Acta* **1980**, *44*, L135.

[2] D. Milstein, *J. Am. Chem. Soc.* **1986**, *108*, 3525, and references therein.

[3] a) D. S. Glueck, L. J. Newman-Winslow, R. G. Bergman, *Organometallics* **1991**, *10*, 1462; b) J. F. Hartwig, R. A. Andersen, R. G. Bergman, *ibid.* **1991**, *10*, 1875; c) M. D. Fryzuk, M.-L. Jang, T. Jones, F. W. B. Einstein, *Can. J. Chem.* **1986**, *64*, 174; d) W. C. Kaska, S. Nemeh, A. Shirazi, S. Potuznik, *Organometallics* **1988**, *7*, 13; e) C. Di Bugano, M. Pasquali, P. Leoni, P. Sabatino, D. Braga, *Inorg. Chem.* **1989**, *28*, 1390; f) B. Hauger, K. G. Caulton, *J. Organomet. Chem.* **1993**, *450*, 253; g) T. Yamamoto, K. Sano, A. Yamamoto, *Chem. Lett.* **1982**, 907.

[4] $C(NO_2)_4$ oxidatively induces methanol liberation from **10**: D. Milstein, J. C. Calabrese, I. D. Williams, *J. Am. Chem. Soc.* **1986**, *108*, 6387.

[5] a) J. S. Thompson, K. A. Bernard, B. J. Rappoli, J. D. Atwood, *Organometallics* **1990**, *9*, 2727; b) J. S. Thompson, S. L. Randall, J. D. Atwood, *ibid.* **1991**, *10*, 3906; c) H. E. Bryndza, J. S. Calabrese, M. Marsi, D. C. Roe, W. Tam, J. E. Bercaw, *J. Am. Chem. Soc.* **1986**, *108*, 4805.

[6] A. L. Casalnuovo, J. C. Calabrese, D. Milstein, *Inorg. Chem.* **1987**, *26*, 971; *J. Am. Chem. Soc.* **1988**, *110*, 6738.

[7] **1**: ^{1}H NMR (400 MHz, C_6D_6, 22 °C, referenced to residual solvent peak): $\delta = 4.01$ (d, ^4J(H,P,*trans*) = 5.7 Hz, 3H; OC*H*$_3$), 2.09 (m, (= d·q·virt. t), $J = 3.7$ Hz, 6H; 2P(*H*-C(H)-CH$_3$)$_3$), 1.71 (m, (= d·q·virt. t), $J = 3.7$ Hz, 6H; 2P(H-C(*H*)-CH$_3$)$_3$), 1.67 (dq, ^2J(H,P) = ^3J(H,H) = 7.2 Hz, 6H; P(C*H*$_2$CH$_3$)$_3$), 1.11 (tt (apparent quintet), $^{virt.}J$(H,P) = ^3J(H,H) = 7.4 Hz, 18H; 2P(CH$_2$C*H*$_3$)$_3$), 0.86 (dt, ^3J(H,P) = 14.4, ^3J(H,H) = 7.6 Hz, 9H; P(CH$_2$C*H*$_3$)$_3$), −21.60 (dt, $^2J^d$(H,P,*cis*) = 16.7, $^2J^t$(H,P,*cis*) = 14.6 Hz, 1H; Ir*H*). ^{31}P{^{1}H} NMR (C_6D_6, referenced to external 85% solution of H_3PO_4 in D_2O): $\delta = -6.9$ (d, ^2J(P,P,*cis*) = 16 Hz, 2P), −20.4 (t, ^2J(P,P,*cis*) = 16 Hz, 1P). The ^{1}H and ^{31}P{^{1}H} NMR of **1** are similar to those of **2** [8], that was also characterized crystallographically.

[8] **2**: IR (nujol): $\tilde{\nu} = 3463$ (m, OH), 2184 cm^{-1} (m, IrH). The complex is highly hygroscopic. ^{1}H NMR (400 MHz, C_6D_6, 22 °C, referenced to the residual solvent peak): $\delta = 2.10$ (m (13 lines), J(apparent) = 3.6 Hz, 6H; 2P(C(*H*)HCH$_3$)$_3$), 1.73 (m (13 lines), J(apparent) = 3.6 Hz, 6H; 2P(C(H)*H*CH$_3$)$_3$), 1.61 (apparent quintet, $^2J^d$(H,P) = $^3J^q$(H,H) = 8.0 Hz, 6H; P(C*H*$_2$CH$_3$)$_3$), 1.09 (m (apparent quintet), J(apparent) = 7.4 Hz, 18H; 2P(C(H)HC*H*$_3$)$_3$), 0.89 (dt, $^3J^d$(H,P) = 14.7 Hz, $^3J^t$(H,H) = 7.5 Hz, 9H; P(CH$_2$C*H*$_3$)$_3$), −2.07 (d, $^3J^d$(H,P,*trans*) = 5.5 Hz, 1H; IrO*H*), −21.72 (dt, $^2J^d$(H,P,*cis*) = 17.6 Hz, $^2J^t$(H,P,*cis*) = 15.3 Hz, 1H; Ir*H*). ^{31}P{^{1}H} NMR (C_6D_6 referenced to external 85% solution of H_3PO_4 in D_2O): $\delta = -17.4$ (t, ^2J(P,P,*cis*) = 15 Hz, 1P), −8.0 (d, ^2J(P,P,*cis*) = 15 Hz, 2P). Crystals of **2** suitable for low-temperature X-ray examination were obtained by slow evaporation of a 1/1 benzene/pentane solution. A detailed discussion of the interesting features of this structure will be given elsewhere.

[9] **4** and **8** are fully characterized and the β-H elimination from **1** and **5** is discussed in detail: O. Blum, D. Milstein, *J. Am. Chem. Soc.* submitted.

[10] The ratio of concentrations of **1** and **3** under the specified conditions is 1.203 ± 0.05, starting from pure **3**. The starting solution of pure **1** provided a ratio of 1.20 ± 0.09.

[11] The value of ΔS^0 seems high. A typical value of only 30 cal K^{-1} mol^{-1} is dictated by translational entropy upon formation of two molecules from one.

It is possible that loss of the relatively strong hydrogen bond between methanol and the methoxo ligand of **1** (which is expected to be much stronger than between two methanol molecules) accounts for the additional ΔS^0 release. We thank the referee for bringing this point to our attention.

[12] $\Delta H^0 + D(H-OCH_3) \approx D(Ir-H) + D(Ir-OCH_3)$. $D(H-OCH_3) = 104.4 \pm 1$ kcal mol^{-1}: L. Batt, R. D. McCulloch, *Int. J. Chem. Kinet.* **1976**, *8*, 491. For a discussion concerning such calculations see footnote 34 in ref. [3b].

[13] D(Ir–H) values of 57 to 64 kcal mol^{-1} have been reported for iridium phosphane complexes with phosphanes of a cone angle larger than 125°: J. A. Martinho-Simões, J. L. Beauchamp, *Chem. Rev.* **1990**, *90*, 629.

[14] Relative M–X bond strengths (X^- = anionic ligand as H^-, CH_3^-, MeO^-, Cl^- etc.) were experimentally determined for [Cp*(PMe_3)$_2$RuX] and for [{Ph$_2$P(CH$_2$)$_2$PPh$_2$}MePtX]: H. E. Bryndza, L. K. Fong, R. A. Paciello, W. Tam, J. E. Bercaw, *J. Am. Chem. Soc.* **1987**, *109*, 1444. From a best fit to an ECT model, the values 33.9 kcal mol^{-1} and 24.7 kcal mol^{-1}, respectively, were determined for X = OCH_3: R. S. Drago, N. M. Wong, D. C. Ferris, *ibid.* **1992**, *114*, 91.

[15] **5**: IR (neat): $\tilde{\nu}$ = 2165 (s, IrH), 1077 cm^{-1} (s, CO). Upon exposure to air, the CO peak disappears immediately and a broad OH signal, centered around 3400 cm^{-1} appears. ^{1}H NMR (400 MHz, C_6D_6, 22 °C, referenced to the residual solvent peak): δ = 4.09 (d, $^4J^d$(H,P,*trans*) = 5.6 Hz, 3H; OCH_3) 1.40 (t, J(apparent)(H,P) = 3.6 Hz, 18H; 2P(CH_3)$_3$), 1.13 (d, ^2J(H,P) = 10.5 Hz, 9H; P(CH_3)$_3$), −21.56 (dt, $^2J^d$(H,P) = 19.2, $^2J'$(H,P) = 14.7 Hz; 1H; Ir*H*). ^{1}H{^{31}P} NMR (C_6D_6): δ = 4.09 (s, 3H), 1.40 (s, 18H), 1.13 (s, 9H), −21.56 (s, 1H). ^{31}P{^{1}H} NMR (C_6D_6, referenced to external 85% solution of H_3PO_4 in D_2O): δ = −30.9 (d, ^2J(P,P,*cis*) = 18.5 Hz, 2P), −50.6 (t, ^2J(P,P,*cis*) = 18.5 Hz, 1P). ^{13}C{^{1}H} NMR (C_6D_6, referenced to the solvent peak): δ = 65.3 (br.s; OCH_3), 21.2 (d, ^1J(C,P) = 37 Hz; P(CH_3)$_3$), 16.2 (t, ^{virt}J(C,P) = 18 Hz; 2P(CH_3)$_3$). **6**: ^{1}H NMR (400 MHz, C_6D_6, 22 °C, referenced to the residual solvent peak): δ = 1.36 (t, J(apparent)(H,P) = 3.6 Hz, 18H; 2P(CH_3)$_3$), 1.19 (d, ^2J(H,P) = 9.6 Hz, 9H; P(CH_3)$_3$), −2.15 (d, ^3J(H,P,*trans*) = 5.8 Hz, 1H; IrOH), −21.73 (dt, $^2J^d$(H,P,*cis*) = 17.7, $^2J'$(H,P,*cis*) = 16.8 Hz, 1H; Ir*H*). ^{31}P{^{1}H} NMR (C_6D_6, referenced to the solvent peak): δ = −33.0 (d, ^2J(H,P,*cis*) = 18 Hz, 2P), −49.3 (t, ^2J(H,P,*cis*) = 18 Hz, 1P).

[16] T. Herskovitz, *Inorg. Synth.* **1982**, *21*, 99.

[17] We found that **7** is completely dissociated into **7a** and cyclooctene at room temperature in C_6D_6.

[18] a) W. D. Jones, V. L. Kuykendall, *Inorg. Chem.* **1991**, *30*, 2615; b) P. L. Kuch, R. S. Tobias, *J. Organomet. Chem.* **1976**, *122*, 429.

[19] The second order rate constant is 3.50×10^{-4} M^{-1} s^{-1}. This reaction was discussed in detail in ref. [9] and in references therein.

[20] As the exchange reaction is fast, practically only **5b** is available for the β-hydride elimination. Yet, since deuterium substitution α to the oxygen atom is not expected to influence the reductive elimination rate by much, the comparison to **5** is relevant.

[21] A mechanism involving H/D exchange with C_6D_6 is unlikely since **5** is unreactive in neat C_6D_6, and since also in [H_8]THF reaction c in Scheme 2 yields only **5a**.

[22] In CD_3OD the observed rate constant for the disappearance of the IrH signal in ^{1}H NMR spectrum is the simple sum of the first order rate constants of the reductive elimination to **7a** and the β-H elimination to **8**. The rate constant of reaction b in Scheme 2 was obtained by following the disappearance of the overlapping signals of the aliphatic protons of **5** and **5b**.

[23] *mer-cis*-[HIrCl$_3$(PMe_3)$_3$] [24] is obtained. Yet, since the presence of LiCl does not change the oxidative addition rate, it has the same rate-determining step as the methanol oxidative addition in absence of LiCl.

[24] A. A. Zlota, F. Frolow, D. Milstein, *J. Chem. Soc. Chem. Commun.* **1989**, 1826.

[25] These rule out reversible, non-rate-determining phosphane or chloride dissociation, followed by O–H reductive elimination. Experiments reported in ref. [9] exclude also mechanisms involving rate-determining initial dissociation of phosphane or chloride. Repeating reaction b in Scheme 2 in presence of [D_6]PMe_3 brought to no incorporation of labeled phosphane into **8**. As reaction c in Scheme 2 is faster and reversible under the conditions applied, this result indicates that any phosphane dissociation from **5** must be very slow, and not on the reaction pathway. Chloride heterolysis from **5** is on the pathway of reaction b in Scheme 2, and is methanol catalyzed. As a minimum amount of methanol is necessary to solvate the basic methoxo ligand (and possibly to participate in relatively strong hydrogen bonding with it), a methanol concentration threshold was observed for this reaction. The equilibrium in Scheme 1 and the reaction c in Scheme 2 are not catalyzed by methanol, implying that rate-determining chloride dissociation is not on the O–H reductive elimination pathway.

[26] J. P. Collman, L. S. Hegedus, J. R. Norton, R. G. Finke, *Principles and Applications of Organotransition Metal Chemistry*, University Science, Mill Valley, CA, USA, **1987**, pp. 322–333.

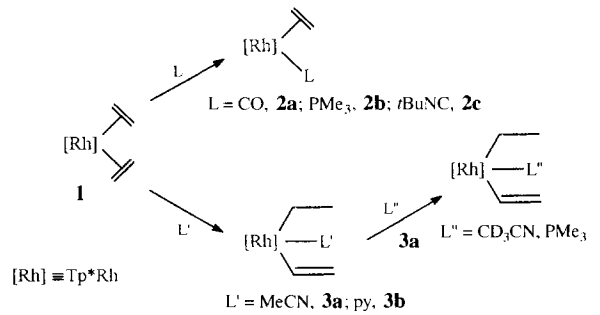
[27] a) J. F. Riehl, Y. Jean, O. Eisenstein, M. Pélissier, *Organometallics* **1992**, *11*, 729; b) H. E. Bryndza, P. J. Domaille, R. A. Paciello, J. E. Bercaw, *ibid.* **1989**, *8*, 379.

Does the Facile Inter- and Intramolecular C–H Bond Activation by Tp*–Rh Complexes Proceed via Rh^I or Rh^{III} Intermediates?**

Pedro J. Pérez, Manuel L. Poveda, and Ernesto Carmona*

The majority of C–H activation processes in arenes that are induced by Rh or Ir complexes of cyclopentadienyl or related ligands involve low-valent, electron-rich Rh^I or Ir^I centers as the reactive intermediates.[1, 2] Recent work from our laboratory[3] and from Bergman's group[4] has shown that more electrophilic Ir^{III} species are able to promote C–H activation under very mild conditions. In our case, as in a similar example reported by Graham et al.[5] the use of a hard, N-donor ligand, the tris(3,5-dimethylpyrazol-1-yl)hydroborate (Tp*), which is in addition known to enforce sixfold coordination,[6] contributes to the stabilization of the Ir^{III} oxidation state and drives, for example, the conversion of [Tp*Ir(C_2H_4)$_2$] into the thermodynamically more stable hydridovinyl Ir^{III} isomer [Tp*Ir(H)(CH=CH_2)(C_2H_4)].[7] We have now prepared the Rh analogue [Tp*Rh(C_2H_4)$_2$] (**1**) and would like to report preliminary studies which reveal intriguing and unexpected reactivity patterns in the thermal C–H activation.

Following Trofimenko's synthesis[8] of the unsubstituted Tp analogue, complex **1** was prepared in approximately 70% yield by reacting KTp* with [{RhCl(C_2H_4)$_2$}$_2$]. In solution **1** was found to be a highly fluxional molecule that exhibited an interesting behavior towards Lewis bases: Treatment of solutions of **1** in benzene at 20 °C with the soft donors CO, PMe_3, or *t*BuNC resulted in fast extrusion of one of the molecules of C_2H_4 and formation of the adducts **2** (Scheme 1).[9] However, under the



Scheme 1. Reactions of **1** with Lewis bases.

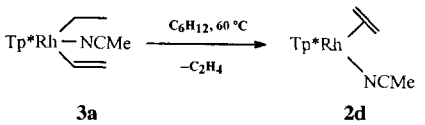
same conditions, the harder N-bases NCMe and C_5H_5N(py) produced the Rh^{III} complexes **3**, which contain ethyl and vinyl fragments derived from the original ethylene ligands. In com-

[*] Prof. Dr. E. Carmona, Dr. M. L. Poveda
Departamento de Química Inorgánica
Instituto de Ciencia de Materiales
Universidad de Sevilla-Consejo Superior de Investigaciones Científicas
E-41071 Sevilla (Spain)
Dr. P. J. Pérez
Departamento de Química y Ciencias de los Materiales
Universidad de Huelva (Spain)

[**] This work was supported by the Dirección General de Investigación Científica y Técnica and Junta de Andalucía. We also acknowledge support from the European Union (ERB4050PL920650) and thank Dr. M. A. Esteruelas (Universidad de Zaragoza, Spain) for GC-MS facilities and the Universidad de Sevilla (NMR and analytical services). Compounds **1** and **2b** were originally prepared in this laboratory by Dr. M. C. Nicasio and S. Taboada, respectively. Tp* = HB(3,5-$Me_2C_3N_2H_2$)$_3$.

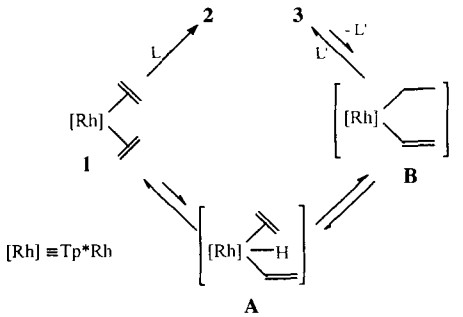
pound **3a** the coordinated NCMe ligand was substituted rapidly at 20 °C by $NCCD_3$ or PMe_3.

A more important observation was that **3a** in a cyclohexane solution maintained at 60 °C for 8 h, reverted to the Rh^I adduct **2d** [Eq. (a)]. Similarly, the CO complex **2a** was formed when the



3a **2d** (a)

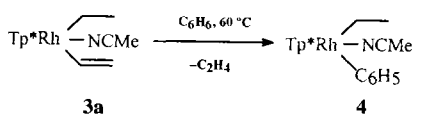
Rh^{III} derivative **3a** was stirred at 20 °C under an atmosphere of carbon monoxide. To account for this behavior, we propose that the bis(ethylene)–Rh^I complex **1** is in equilibrium with undetectable, although kinetically accessible, amounts of the hydridovinyl Rh^{III} isomer **A**, and that the ethylvinyl intermediate **B** is also attainable from **A** at room temperature (Scheme 2). The



Scheme 2. Proposed mechanism for the reactions in the system **1**, **2**, and **3**.

reactions of **1** with the soft donors proceed through the Rh^I route. This route seems to be kinetically disfavored for the harder donors at room temperature, and the corresponding reactions go to completion by the alternative, competitive Rh^{III} pathway. Since the aforementioned reactivity of **3a** suggests that intermediate **B** can also be reached from the Rh^{III} adduct, our results indicate that, at 60 °C, acetonitrile is able to enter the Rh^I pathway and displace one of the C_2H_4 ligands in **1** to afford the Rh^I adduct **2d**, which is obviously the thermodynamic product of the reaction of **1** with NCMe.

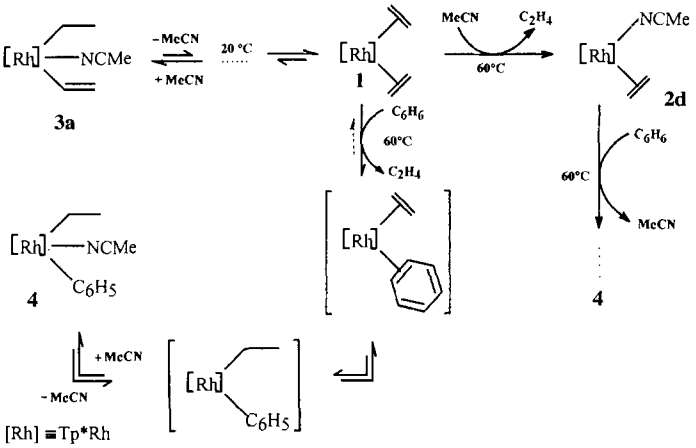
The lability of the acetonitrile ligand in **3a** makes this complex an ideal candidate for promoting intermolecular C–H bond activation reactions. When a benzene solution of **3a** was heated at 60 °C for 8 h, a smooth reaction ensued that furnished the ethylphenyl derivative **4** in almost quantitative yield [Eq. (b)]. With C_6D_6, $[D_{10}]$-**4** was obtained (i.e., the product



3a **4** (b)

was fully deuterated in both the phenyl and the ethyl fragments). The similarity between the starting material and the final product, together with the observation that free MeCN slows down this reaction, may suggest a mechanism involving the Rh^{III} intermediate **B** as the active species (see Scheme 2).

However, GC-MS analysis of the gas evolved in the reaction with C_6D_6 reveals the ethylene produced has normal isotopic composition, and this clearly contradicts the above proposal (see below). Since, as already shown, the bis(ethylene) complex **1** is accessible from **3a** under the reaction conditions, we propose that C_6H_6 activation occurs in an η^2-benzene species[10] resulting from the substitution of C_2H_4 by C_6H_6 in compound **1** (Scheme 3). The proposed reversibility for the C_6H_6 coordina-



Scheme 3. C–H activation with **3a**.

tion and activation steps is supported by the fact that identical products were obtained from the reactions of both **1** and **4** with a large excess of C_2H_4 at 60 °C (the η^4-butadiene complex [Tp*Rh(η^4-C_4H_6)] and two minor species, which have so far not been completely characterized). The mechanism provides a reasonable explanation for the formation of $[D_{10}]$-**4** in C_6D_6. It seems that, under the conditions used for the C_6H_6 activation reaction, the back transformation of the η^2-benzene adduct into **1** (Scheme 3) does not occur to a measurable extent. This explains the fact that only C_2H_4 was detected when C_6D_6 was used. Interestingly, complex **2d** also yielded **4** when heated in C_6H_6, but the conversion rate is lower than that of **3a**; therefore, **2d** cannot be an intermediate in the activation of C_6H_6 by **3a**.

In conclusion, we have demonstrated that: a) Apparently simple, straightforward reactions of the olefin complex **1** can proceed either with C_2H_4 replacement by the donor, in other words, with substitution at the Rh^I–C_2H_4 complex, or via an unsaturated Rh(H)(C_2H_3) species, that is to say, via a Rh^{III} hydridovinyl isomer. Such behavior is, to our knowledge, unprecedented. b) Despite the availability of the Rh^{III} unsaturated intermediates in this system, only Rh^I species seem to be directly involved in the activation of benzene. The implication for Rh^{III} compounds in this kind of reaction must await the design of appropriate model systems.

Experimental Procedure

1: A solution of $[\{RhCl(C_2H_4)_2\}_2]$ (0.79 g, 2 mmol) in THF (50 mL) was cooled to −30 °C and treated with KTp* (1.35 g, 4 mmol). The mixture was stirred for 4 h and volatiles were then removed under reduced pressure at −20 °C (overheating must be avoided up to this stage). The residue was dissolved in CH_2Cl_2/Et_2O (1/1, 40 mL) and filtered through Celite. The resulting yellow-orange solution was evaporated to dryness to give 1.5 g of complex **1** (80% yield). This product must be stored below 0 °C. ^1H NMR (500 MHz, C_6D_6, 25 °C): δ = 5.61 (s, 3H, $H_{arom.}$), 2.59 (d, 8H, $2C_2H_4$, J(H,Rh) = 2 Hz), 2.43 (s, 9H, 3Me), 2.16 (s, 9H, 3*C*-Me); $^{13}C\{^1H\}$ NMR (125 MHz, C_6D_6, 25 °C): δ = 150.4 (3*C*-Me), 143.4 (3*C*-Me), 107.1 ($3C_{arom.}$-H), 47.1 (d, $2C_2H_4$, J(C,Rh) = 12 Hz), 14.4 (3C-*Me*), 12.5 (3C-*Me*).

3a: Upon dissolving complex **1** (0.6 g, 1.3 mmol) in acetonitrile (20 mL) an off-white solution was rapidly formed. After the solution had been stirred for 15 min, it was concentrated until cloudy and cooled overnight at −20 °C. Complex **3a** was

obtained as white crystals in 75% yield. ^{1}H NMR (500 MHz, C_6D_6, 25 °C): δ = 8.36, 6.02, 5.40 (m, 3H, Rh-CH$_A$=CH$_M$H$_X$, J(A,X) = 17, J(A,M) = 9, J(M,X) = 2, J(A,Rh) = 3, J(X,Rh) = 1, J(M,Rh) = 2 Hz), 5.83, 5.76, 5.61 (s, 3H, H$_{arom.}$), 2.80 (m, 1H, CH$_3$CH*H*), 2.70 (m, 1H, CH$_3$C*H*H), 2.55, 2.43, 2.39, 2.27, 2.26, 2.16 (s, 18H, 6Me), 1.09 (t, 3H, C*H*$_3$CH$_2$, J(H,H) = 7.5 Hz), 0.69 (s, 3H, NCMe); ^{13}C{^{1}H} NMR (125 MHz, C_6D_6, 25 °C): δ = 158.8 (d, CH$_2$=*C*H-Rh, J(C,Rh) = 30 Hz), 151.8, 149.1, 149.0, 143.3, 142.6, 142.2 (6*C*-Me), 118.2 (d, N*C*Me, J(C,Rh) = 12 Hz), 117.7 (*C*H$_2$=CHRh), 107.5, 106.0, 105.7 (3$C_{arom.}$-H), 16.8, 14.1, 13.7, 13.1, 13.0, 12.3, 12.1 (6Me and *C*H$_3$CH$_2$), 10.0 (d, CH$_3$*C*H$_2$, J(C,Rh) = 25 Hz), −0.4 (NC*Me*).

4: A solution of **3a** (0.2 g, 0.4 mmol) in benzene was heated at 60 °C for 8 h. Complex **4** was isolated as a white powder in 80% yield upon removing all volatiles under reduced pressure. ^{1}H NMR (500 MHz, C_6D_6, 25 °C): δ = 7.64 (d), 7.42 (t), 7.13 (d), 7.09 (d), 6.94 (t) (5H, C$_6$H$_5$, J(H,H) = 7 Hz), 5.86, 5.77, 5.61 (s, 3H), 2.96 (m, 1H, CH$_3$CH*H*), 2.70 (m, 1H, CH$_3$C*H*H), 2.44, 2.29, 2.28, 2.20, 1.86, 1.69 (s, 18H, 6Me), 1.06 (t, 3H, C*H*$_3$CH$_2$, J(H,H) = 7.5 Hz), 0.51 (s, 3H, NCMe); ^{13}C{^{1}H} NMR (125 MHz, C_6D_6, 25 °C): δ = 159.0 (d, C$_q$Rh, J(C,Rh) = 30 Hz), 152.1, 149.0, 148.9, 143.2, 142.8, 142.0 (6*C*-Me), 140.6, 137.8, 126.0, 125.5, 121.2 (C$_6$H$_5$), 118.4 (d, N*C*Me, J(C,Rh) = 8 Hz), 107.8, 106.0, 105.9 (3$C_{arom.}$-H), 16.9, 14.0, 13.5, 13.2, 13.1, 12.4, 12.2 (6*C*-*Me* and *C*H$_3$CH$_2$), 11.7 (d, CH$_3$*C*H$_2$, J(C,Rh) = 25 Hz), 0.8 (NC*Me*).

Received: June 20, 1994
Revised version: August 16, 1994 [Z 7051 IE]
German version: *Angew. Chem.* **1995**, *107*, 242

Keywords: alkene complexes · C–H activation · rhodium compounds

[1] W. D. Jones, F. J. Feher, *Acc. Chem. Res.* **1989**, *22*, 91; R. G. Bergman, *J. Organomet. Chem.* **1990**, *400*, 273; W. A. G. Graham, *ibid.* **1986**, *300*, 81; I. P. Rothwell, *Polyhedron* **1985**, *4*, 177; R. H. Crabtree, *Chem. Rev.* **1985**, *85*, 245.
[2] *Selective Hydrocarbon Activation* (Eds.: J. A. Davies, P. L. Watson, J. F. Liebman, A. Greenberg), VCH, New York, **1990**; *Activation and Functionalization of Alkanes* (Ed.: C. L. Hill), Wiley, New York, **1989**.
[3] O. Boutry, E. Gutiérrez, A. Monge, M. C. Nicasio, P. J. Pérez, E. Carmona, *J. Am. Chem. Soc.* **1992**, *114*, 7288; E. Gutiérrez, A. Monge, M. C. Nicasio, M. L. Poveda, E. Carmona, *ibid.* **1994**, *116*, 791.
[4] P. Burger, R. G. Bergman, *J. Am. Chem. Soc.* **1993**, *115*, 10462.
[5] C. K. Ghosh, J. K. Hoyano, R. Kreutz, W. A. G. Graham, *J. Am. Chem. Soc.* **1989**, *111*, 5480.
[6] M. D. Curtis, K.-B. Shiu, W. M. Butler, *J. Am. Chem. Soc.* **1986**, *108*, 1550.
[7] P. J. Pérez, M. L. Poveda, E. Carmona, *J. Chem. Soc. Chem. Commun.* **1992**, 8.
[8] S. Trofimenko, *J. Am. Chem. Soc.* **1969**, *91*, 588.
[9] Compound **2a** has been previously reported: C. K. Ghosh, W. A. G. Graham, *J. Am. Chem. Soc.* **1989**, *111*, 375.
[10] This process is probably associative; see W. D. Jones, E. T. Hessell, *J. Am. Chem. Soc.* **1992**, *114*, 6087.

LaI: An Unprecedented Binary Rare Earth Metal Monohalide with a NiAs-Type Structure**

James D. Martin and John D. Corbett*

For more than 30 years, considerable effort has been devoted to the discovery and characterization of binary halides M_aX_b rare earth metals in low oxidation states. Dihalide phases with X = Cl, Br, and I are known for a majority of the rare earth metals. These exhibit saltlike characteristics except for the metallic diiodides of La, Ce, Pr, Gd, and Sc. Other reduced halides M_2X_3 and M_2X_5 seem to be more limited and elusive.[1] Nevertheless, the quest for binary monohalides of the rare earth metals has witnessed a tumultuous history. Numerous reports of supposed binary rare earth monohalides,[2] in which the heavy atom arrangement is the same as in the truly binary phases ZrCl and ZrBr,[3] were later shown to be MXH_n phases ($\approx 0.67 \leq n \leq 1$) stabilized by hydrogen atoms in the tetrahedral interstices between the double layers.[4, 5] As a result, it has been generally concluded that binary monohalide phases of these elements do not exist. But if a monohalide were to exist, chemical experience would predict that the larger, more polarizable iodide should provide the most stable compound either as a conventional salt or, more likely, as a metallic phase like LaI_2.[6]

We report here the first example of a truly binary rare earth metal monohalide, LaI, discovered during our explorations of very reduced lanthanum/iodine/transition metal systems. This unprecedented monohalide is also the first to adopt the NiAs-type structure, as depicted in the [110] projection in Figure 1. Here La occupies all octahedral interstices (site 2*a*; 0, 0, 0) between the hexagonal closes-packed (hcp) iodide layers (2*c*; 1/3, 2/3, 1/4) in the hexagonal space group $P6_3/mmc$.[7] Furthermore, LaI exhibits by far the largest c/a ratio (2.47) of any known compound with a NiAs-type structure. This compares with $c/a = 1.63$ for closest packing of spheres and the previous maximum c/a ratio of 1.93 for TiS, which had been considered anomalously large.[8] The elongation of the c axis is a consequence of an optimization of La–La bonding within the (002) planes under the constraints of reasonable La–I interactions and closed-shell repulsions between iodine ions. The I-La-I angles for I atoms related by the 3 and $\bar{3}$ symmetry operations are 72.50(1) and 107.50(1)°, respectively. The I···I distance (sixfold) of 3.93 Å is a little less than those reported for rare earth metal iodides with cluster or chain structures (3.96 and 3.97 Å in $Y_6I_7C_2$ and $Sc_7I_{12}C$ are the shortest[9]). But the repulsion is offset by an equal number of bonding La–La interactions also at 3.93 Å. This corresponds to a Pauling metallic bond order of 0.128 (× 6), whereas the La–La distance of 4.86 Å along c corresponds to one of 0.004 (× 2). The two observed La–La distances are far different from those predicted for an ideal hcp NiAs-type structure with the same La–I distances namely, 4.7 and 3.8 Å, respectively. The La–I distances of 3.3227(2) Å are 0.09 Å larger than the estimated sum of the radii of the six-coordinate atoms,[10] but close to the 3.35 Å distances reported for LaI_2 ($MoSi_2$-type, eight-coordinate).[11] The NiAs structure is distinctive in its relative flexibility compared with higher symmetry or layered structures and can, as seen, accommodate enhanced metal–metal interactions even in the presence of relatively large anions.[8]

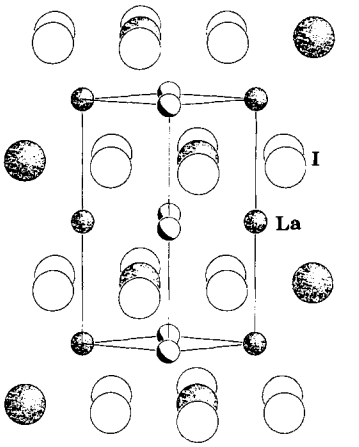


Fig. 1. [110] view of LaI (NiAs-type structure, La: ○, I: ○). The atoms in the [110] section are shaded, while atoms in two additional layers both in front and back are white.

LaI is obtained by reduction of sublimed LaI_3 by La metal (Ames Lab, 99.8 atom% total, 0.07 atom% H) at 750 °C for several weeks in a welded niobium tube that is in turn sealed within a well-baked, evacuated fused silica jacket. Reactions of

[*] Prof. J. D. Corbett, Dr. J. D. Martin
Department of Chemistry, Iowa State University
Ames, IA 50011 (USA)
Telefax: Int. code + (515)294-5718

[**] The authors gratefully acknowledge Prof. M.-H. Whangbo and Dr. E. Canadell for helpful discussions and Dr. Ming Xu for magnetic susceptibility measurements. This research was supported by the National Science Foundation, Solid-State Chemistry (grant DMR-9207361), and was carried out in the facilities of the Ames Laboratory of the U.S. Department of Energy.

binary mixtures with the components in the desired stoichiometry are incomplete and yield a mixture of LaI (≈40%), LaI_2, and La after ten weeks in which the iodides completely cover the metal surfaces. Only LaI_2 has been observed from reactions run at or above 800 °C, implying that the stability range of LaI has been exceeded. LaI that is free of other iodides according to Guinier patterns has been obtained from the same type of reactions with a onefold excess of La. These reaction mixtures also contained Mn or Cr, but these do not yield iodide phases under these conditions and appear to be completely superfluous. Several large single crystals from a reaction with Mn were found to contain only La and I in a 1:1 ratio according to results of scanning electron microscopy with energy dispersive spectroscopy. In the slow reactions that yield LaI from LaI_2 and La, transport appears to be the rate-limiting factor, probably because of low LaI_3(g) pressure above LaI_2(s). Preliminary experiments have not yet revealed similar monoiodide phases for other rare earth elements (Pr, Nd, Gd); however, appropriate reaction conditions may yield positive results. LaI has a metallic appearance with a silver to light gold reflectance and is typically found coating the surface of the metal. It can be readily distinguished from the layered LaI_2 by the latter's violet-purple reflectance and ready cleavage.

The long reaction times, enhanced yields from lanthanum-rich reactions, and the low apparent decomposition temperature are somewhat reminiscent of the earliest reports of numerous rare earth monohalides that later proved to be halide hydrides MXH_n.[2, 4, 5] In those cases hydrogen initially came from adventitious sources, for example from metals prepared by decomposition of MH_2 or from H_2O from the walls of insufficiently baked fused silica reaction jackets. Traces of water in the reaction mixture normally led to an MOI by-product, but LaOI has been notably absent from our reactions. To clarify further the possibility of hydrogen in LaI, several reactions of LaI_3, LaH_2, and La were run at 750 °C for three to four weeks. The reaction with an overall La:I:H mole ratio of 1:1:1 yielded the desired iridescent green phase in 95% yield (plus an unknown black powder). Thus the bona fide $LaIH_n$ ($n \approx 1$) adopts the expected layered ZrCl-type structure for the heavy atoms ($a = 4.2063(4)$, $c = 31.947(7)$ Å). This product was sealed in a Nb container and heated for 9 h at 770 °C in dynamic high vacuum, whereupon ≈40% decomposed to LaI (plus traces of LaOI and LaI_2). That the new LaI must contain very little hydrogen, if any, was confirmed by a similar synthesis reaction with a La:I:H mole ratio of 1:1:0.25, which yielded 45–55% $LaIH_n$, 35–40% LaI, 5–10% LaI_2 (presumably because of incomplete reaction), and ≈5% LaOI. Virtually no hydrogen remains for LaI if the limiting hydride content of $LaIH_n$ is near $n = 0.6$, as reported elsewhere.[12] The overall results are not characteristic of an undetected ternary interstitial atom at significant levels, but very small amounts of hydrogen may never be ruled out.

Actually the NiAs-type structure itself affords strong evidence that interstitial hydrogen atoms cannot be important. Unlike the close-packed, double metal layers in the ZrCl- and ZrBr-type frameworks, where the hydrogen atoms in MXH_n occupy tetrahedral cavities within condensed trigonal antiprisms of M atoms,[5, 12] the NiAs structure type with a trigonal-prismatic arrangement of metal atoms affords no plausible cavities for hydrogen. The heavy atoms in recently described dihalides such as $LaBr_2D_{0.9}$ adopt MoS_2-like layered structures such that a trigonal prism of halogen atoms surrounds each metal atom.[13] This affords each hydrogen atom a trigonal-planar site (c) in the metal layer (b) with no adjacent halogen atoms [Ab(c)A]. In contrast, each hydrogen atom in the equivalent site in an NiAs structure [Ab(c)C] would have three La atoms at a reasonable distance of 2.27 Å, but one coaxial iodine atom only 2.42 Å away. If the hydrogen atom is displaced 0.53 Å from the iodine atom, the I···H distances to all four neighboring iodine atoms would be 2.96 Å. Nonetheless, this is still quite short compared with either the estimated sum of crystal radii (3.16 Å) or, better, the distances derived from the shortest D···Br separations found in this sort of structure, namely in $Th_6Br_{15}D_7$[14] and Zr_2Br_2D (3.13 and 3.18 Å, respectively),[15] when corrected for the 0.24 Å difference in radii of the halogens. Such a cavity with three La and also four close I neighbors does not appear at all suitable for binding hydrogen atoms.

Like the MI_2 phases, LaI is expected to exhibit metallic properties. While sufficient quantities of single-phase LaI have not yet been synthesized for reliable measurements, two-probe conductivity measurements on a single crystal (using La contacts) indicated virtually only contact resistance in the best directions with appreciably higher resistance in others. Magnetic susceptibility measurements from 6 to 300 K on a single-phase sample (by X-ray diffraction) showed a Pauli paramagnetism of 2.0×10^{-4} emu mol^{-1} after core corrections.

Extended Hückel tight-binding (EHTB) band calculations[16] have been carried out to ascertain more about the electronic structure of LaI. The dispersion relations of the d-block bands are shown in Figure 2. The calculated Fermi surface of the

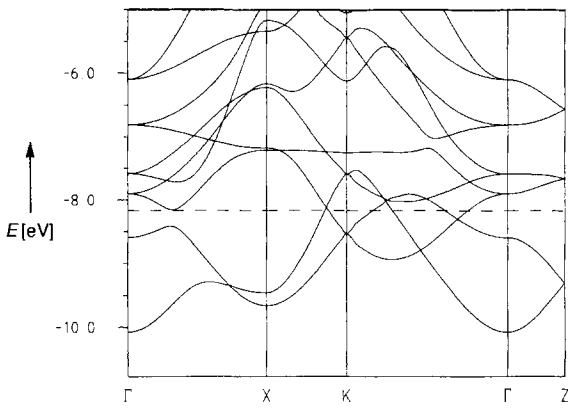


Fig. 2. The La d-block bands in LaI according to EHTB band calculations; the Fermi level is marked by a dashed line. The iodine valence band lies below −12.0 eV. X = $a^*/2$, 0, 0; K = $a^*/3$, $b^*/3$, 0; Z = 0, 0, $c^*/2$. (Parameters from E. Canadell, M.-H. Whangbo, *Inorg. Chem.* **1994**, *33*, 287.)

three-dimensional structure with the large c/a ratio is strongly anisotropic and best described as six warped cylinders oriented along the c^* direction with hole and electron pockets at c^* and $c^*/2$, respectively. (Cross sections of the calculated Fermi surface at 0.1 intervals along 0, 0, c^* are included in the supplementary material). Because of symmetry the two electron surfaces are degenerate at $c^*/2$. Thus, the warped cylinder is closed by the electron pocket. Strongly anisotropic conductivity characteristics are expected. Strong La–La bonding within the *a*, *b* plane is responsible for the extensive mixing of the bands perpendicular to c^* derived from the "t_{2g}-like" d orbitals. This along with poor La–La bonding along *c* creates the strongly anisotropic Fermi surface in spite of the symmetry-required degeneracy which closes the surface along c^*.

Because of the *k*-vector dependent mixing of t_{2g}-like bands, LaI cannot be considered a version of the 1T-MX_2 (CdI_2-type) layered structures in which diverse patterns of metal clustering are driven by charge density waves.[17] The absence of any

superstructure at room temperature has been confirmed by Weissenberg photographs of the *hk*0 and *hk*1 layers, and there is no sign of a transition in the magnetic data >6 K.

Received: July 16, 1994 [Z 7133 IE]
German version: *Angew. Chem.* **1995**, *107*, 234

Keywords: halogen compounds · lanthanide compounds · metallic conductors · semiempirical calculations · solid-state structures

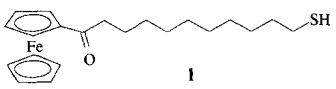
[1] G. Meyer, *Chem. Rev.* **1988**, *88*, 93.
[2] a) A. Simon, H. Mattausch, N. Holzer, *Angew. Chem.* **1976**, *88*, 685; *Angew. Chem. Int. Ed. Engl.* **1976**, *15*, 624; b) K. R. Poppelmeier, J. D. Corbett, *Inorg. Chem.* **1977**, *16*, 294; c) H. Mattausch, J. B. Hendricks, R. Eger, J. D. Corbett, A. Simon, *ibid.* **1980**, *19*, 2128; d) H. Mattausch, A. Simon, N. Holzer, R. Eger, *Z. Anorg. Allg. Chem.* **1980**, *466*, 7; e) R. Araujo, J. D. Corbett, *Inorg. Chem.* **1981**, *20*, 3082.
[3] a) D. G. Adolphson, J. D. Corbett, *Inorg. Chem.* **1976**, *15*, 1820; b) R. L. Daake, J. D. Corbett, *ibid.* **1977**, *16*, 2029.
[4] a) H. Mattausch, W. Schramm, R. Eger, A. Simon, *Z. Anorg. All. Chem.* **1985**, *530*, 43; b) G. Meyer, S.-J. Hwu, S. Wijeyeskera, J. D. Corbett, *Inorg. Chem.* **1986**, *25*, 4811; c) A. Simon, H. Mattausch, R. Eger, *Z. Anorg. Allg. Chem.* **1987**, *550*, 50; d) H. Mattausch, R. Eger, J. D. Corbett, A. Simon, *ibid.* **1992**, *616*, 157.
[5] F. Ueno, K. R. Ziebeck, H. Mattausch, A. Simon, *Rev. Chim. Miner.* **1984**, *21*, 804.
[6] a) J. D. Corbett, R. A. Sallach, D. A. Lokken, *Adv. Chem. Ser.* **1967**, *71*, 56; b) E. Warkentin, H. Bärnighausen, *Z. Anorg. Allg. Chem.* **1979**, *459*, 187.
[7] Crystal structure analysis of LaI: Lattice constants, $a = 3.9297(4)$, $c = 9.710(1)$ Å were obtained from Guinier powder patterns ($\lambda = 1.540562$ Å), $V = 129.86(4)$ Å^3, $Z = 2$, hexagonal space group $P6_3/mmc$ (no. 194). Data were collected on a Rigaku AFC6 diffractometer at 22 °C with monochromated $Mo_{K\alpha}$ radiation ($h,k,\pm l$). The structure was solved by direct methods (SHELXS). The residuals were $R(F) = 0.028$, $R_w = 0.029$ for 49 independent reflections ($2\theta < 50°$, $I > 3\sigma(I)$) and 7 variables. The platelike crystal habit ($0.05 \times 0.15 \times 0.6$ mm) caused significant absorption problems ($\mu = 278.9$ cm^{-1})($R = 0.054$) which were corrected by the DIFABS method (N. Walker, D. Stuart, *Acta Crystallogr. Sect. A* **1983**, *39*, 158; transmission range 0.581–1.175). This removed the anisotropy in thermal parameters of both atoms and the corresponding "ghost peaks" (3.0–2.1 e Å^{-3}) in the difference Fourier map. An inverse NiAs structure can clearly be ruled out, since it gave a poorer refinement and disparate temperature factors (B-values). Further details of the crystal structure investigation may be obtained from the Fachinformationszentrum Karlsruhe, D-76344 Eggenstein-Leopoldshafen (Germany) on quoting the depository number CSD-58 680.
[8] J. Nakahara, H. Franzen, D. K. Misemer, *J. Chem. Phys.* **1982**, *76*, 4080.
[9] a) D. S. Dudis, J. D. Corbett, S.-J. Hwu, *Inorg. Chem.* **1986**, *25*, 3434; b) S. M. Kauzlarich, T. Hughbanks, J. D. Corbett, P. Klavins, R. N. Shelton, *ibid.* **1988**, *27*, 1791.
[10] R. P. Shannon, *Acta Crystallogr. Sect. A* **1976**, *37*, 751.
[11] E. Warkentin, H. Bärnighausen, *Third European Crystallographic Meeting*, Zürich, Switzerland, September, **1976**, p. 356.
[12] A. Simon, H. Mattausch, G. J. Miller, W. Bauhofer, R. K. Kremer, *Handb. Phys. Chem. Rare Earths*, **1991**, *15*, 191.
[13] C. Michaelis, H. Mattausch, H. Borrmann, A. Simon, J. K. Cockcroft, *Z. Anorg. Allg. Chem.* **1992**, *607*, 29.
[14] F. Böttcher, A. Simon, R. K. Kremer, H. Buchkremer-Hermanns, J. K. Cockcroft, *Z. Anorg. Allg. Chem.* **1991**, *598/599*, 25.
[15] S. Wijeyesekera, J. D. Corbett, *Solid State Commun.* **1985**, *54*, 657.
[16] M.-H. Whangbo, R. Hoffmann, *J. Am. Chem. Soc.* **1978**, *100*, 6093.
[17] C. Rovira, M.-H. Whangbo, *Inorg. Chem.* **1993**, *32*, 4094.

Molecular Recognition at an Interface: Binding of Monolayer-Anchored Ferrocenyl Groups by an Amphiphilic Calixarene Host**

Litao Zhang, Luis A. Godínez, Tianbao Lu, George W. Gokel, and Angel E. Kaifer*

Self-assembly of alkanethiols on gold surfaces constitutes one the most useful methods for the preparation of supported monolayers exhibiting a high degree of molecular organization.[1] The preparation of similar monolayers incorporating molecular recognition sites is of fundamental as well as practical importance. However, the literature contains only a few reports of binding phenomena in supported monolayer systems.[2] We demonstrate here that ferrocenyl groups covalently attached to a supported alkanethiol monolayer can be complexed effectively by an amphiphilic receptor in the contacting aqueous solution. The major finding of this work is that the receptor must have substantial amphiphilic character in order to bind the guest residues anchored to the monolayer assembly.

Coassembly of the thiolated ferrocene derivative **1** with an alkanethiol yields mixed monolayers in which, by selecting the length of the alkanethiol chain, one can easily vary the degree of accessibility of the ferrocenyl groups to the contacting solution.[3] Exposure of a gold bead electrode to an ethanolic solution containing 0.25 mM **1** and 0.75 mM decanethiol ($C_{10}H_{21}SH$) resulted in the coassembly of a monolayer in which the ferrocenyl groups protrude from the hydrophobic core. The voltammetric response of this supported monolayer in 1.0 M $HClO_4$ (Fig. 1) is characterized by the reversible oxidation of the surface-confined ferrocenyl groups ($Fc \rightleftharpoons Fc^+ + e^-$). The formal oxidation potential measured from the cyclic voltammogram was +0.51 V vs a sodium chloride saturated calomel electrode (SSCE), and the potential difference between the anodic and cathodic peak potentials (ΔE_p) was typically smaller than 10 mV at scan rates of 0.5 V s^{-1} or less. The surface coverage of ferrocenyl groups, as determined from the integration of the anodic wave, was 1.2×10^{-10} mol cm^{-2}, while the maximum coverage obtained in our experiments from self-assembly of pure **1** (no alkanethiol) was 4.3×10^{-10} mol cm^{-2}. All these electrochemical parameters are in agreement with published values for this and similar ferrocenyl-containing, self-assembled monolayer systems.[4]



1

We have recently reported that the sulfonated calix[6]arene **2** is an excellent host for several ferrocene derivatives in aqueous media.[5] Thus, we were interested in probing the interactions of monolayer-anchored ferrocenyl groups with this host. However, we could not find any evidence for binding, as the E° value for the oxidation of the ferrocenyl groups in the monolayer did not change appreciably when the contacting solution contained

[*] Prof. A. E. Kaifer, L. Zhang, L. A. Godínez
Department of Chemistry, University of Miami
Coral Gables, FL 33124 (USA)
Telefax: Int. code +(305)662-4007
Prof. G. W. Gokel, Dr. T. Lu
Department of Molecular Biology and Pharmacology
Washington University School of Medicine
Campus Box 8020, 660 S. Euclid Avenue, St. Louis, MO 63110 (USA)

[**] This work was supported by the National Science Foundation (grant nos. CHE-9000532 and CHE-9304262 to A. E. K.) and the National Institutes of Health (grant nos. GM-36262 and AI-27179 to G. W. G.). L. Z. thanks the University of Miami for a Maytag Fellowship and L. A. G. thanks the Universidad Nacional Autónoma de México for a graduate fellowship.

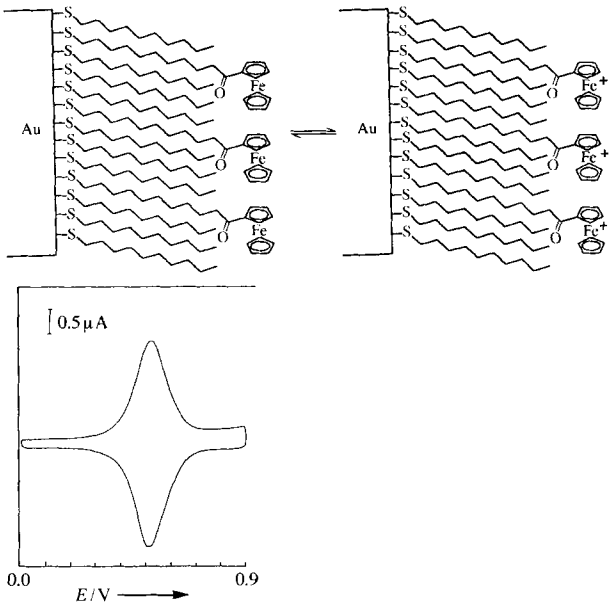
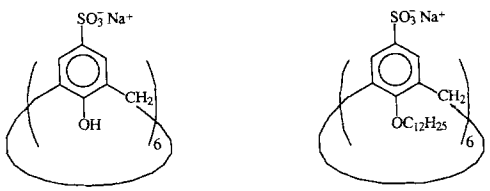


Fig. 1. Voltammetric response of a mixed monolayer formed by the coassembly of **1** and $C_{10}H_{21}SH$ on a gold bead electrode. The voltammogram was recorded with the monolayer-modified electrode immersed in 1.0 M $HClO_4$. Initial potential: 0.0 V vs SSCE; scan rate: 0.5 $V s^{-1}$.

the calixarene host, even at concentrations as high as 1–2 mM. This highly charged, anionic host must be strongly solvated by water molecules,[6] which seems to prevent its effective approach to the ferrocenyl groups residing in the monolayer/solution interface.

Thus we turned our attention to an amphiphilic analogue of **2**, the dodecyl derivative **3**, which is prepared by O-alkylation of



2 **3**

the parent calixarene.[7] Very low concentrations of **3** have a profound effect on the voltammetric response of the $C_{10}H_{21}SH$/**1** monolayer. For instance, in the presence of 0.4 μM **3** the anodic peak for ferrocene oxidation splits into two well-resolved peaks (Fig. 2 top). The first one remains at approximately the same potential as that observed in the absence of **3**, while the second one is shifted in the positive direction by about 90 mV. The latter peak increases with the concentration of **3** at the expense of the original peak. In the presence of 2 μM **3**, only the calixarene-induced peak is observed. We thus assign this new redox couple to the oxidation of the monolayer-anchored ferrocenyl groups complexed by the amphiphilic calixarene hosts. Figure 2 bottom shows a comparison of the initial (no **3** added) and final (in the presence of 2.0 μM **3**) voltammetric responses. Further additions of **3** do not affect the voltammetric response of the monolayer.

Potential cycling of a gold electrode derivatized with a $C_{10}H_{21}SH$/**1** monolayer results in a gradual loss of ferrocene coverage due to the slow decomposition of the oxidized ferrocenyl sites.[8] This decomposition reaction is responsible for the decreased peak currents observed in the presence of 2 μM **3** (see Fig. 2 bottom), as this voltammogram was recorded after several additions of calixarene and several potential cycles to monitor their effects. As a control experiment, a gold electrode derivatized with a $C_{10}H_{21}SH$/**1** monolayer was submitted to prolonged potential cycling between 0.0 and 0.9 V vs SSCE in a 1.0 M $HClO_4$ solution (no calixarene). As expected, the currents associated with the ferrocene redox couple continuously decreased with cycling time, but the oxidation potential remained unaffected at 0.51 V vs SSCE. Therefore, the changes in oxidation potential observed upon addition of calixarene are due to changes in ferrocene's microenvironment, not to variations in the surface density of ferrocenyl sites in the monolayer.

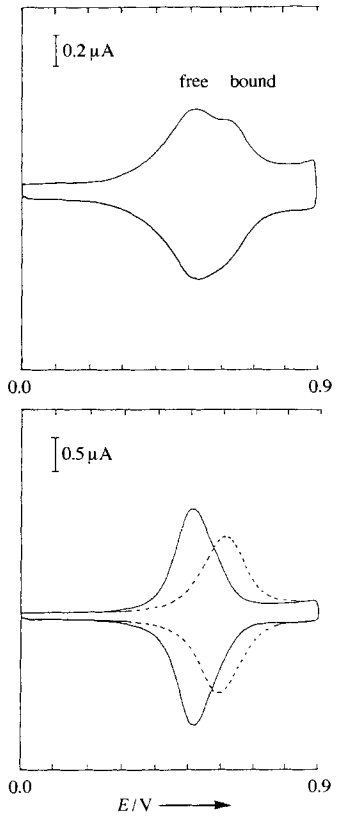


Fig. 2. Top: Voltammetric response of a mixed monolayer prepared like that in Figure 1 in the presence of **3** (0.4 μM) in the contacting solution. Bottom: Comparison of the voltammograms obtained in the absence (continuous line) and in the presence (dotted lined) of **3** (2.0 μM) in the contacting solution. All other conditions were as those used in Figure 1.

Recently, Craeger et al. have shown that the presence of long-chain alcohols in the solution phase causes substantial anodic shifts in the oxidation potential of monolayer-anchored ferrocenyl residues.[9] They interpreted these findings as the result of aggregation of the long-chain alcohol at the monolayer/solution interface which increases the hydrophobic character of the ferrocene microenvironment, thus favoring the reduced neutral form over the oxidized cationic form and shifting the oxidation potential to more positive values. Our results with **3** cannot be explained simply by the aggregation of the amphiphilic calixarene at the monolayer/solution interface because of two key experimental findings: 1) The presence of **3** in the solution causes the split of the ferrocene redox couple into two couples that can be clearly assigned to the oxidation of free and bound ferrocenyl sites. 2) The splitting of the ferrocene redox couple is only detected in the concentration range 0.05–2 μM **3**. At higher concentrations of **3** the voltammetric behavior remains constant, indicating that all the monolayer ferrocenyl groups are bound so that further additions of host have no effect in the observed E° value. These observations are fully consistent with the proposed interfacial binding of the ferrocenyl sites by the amphiphilic calixarene host. We performed several control experiments exposing $C_{10}H_{21}SH$/**1** monolayers to solutions contain-

 © VCH Verlagsgesellschaft mbH, D-69451 Weinheim, 1995 0570-0833/95/0202-0236 $ 10.00+.25/0

ing increasing concentrations of amphiphiles having only one alkyl chain. The results are shown in Figure 3. In agreement with Craeger's observations with long-chain alcohols,[9] both amphiphiles surveyed (dodecyl sulfate and dodecyltrimethylammonium) caused anodic shifts in the oxidation potential of the monolayer-anchored ferrocenyl groups. However, the redox couple never splits, and the magnitude of the observed potential shifts was smaller than the saturation shift observed with **3**. These findings, as well as the insensitivity of the E° shifts to the amphiphile's positive or negative charge, are consistent with the aggregation of the amphiphiles on the monolayer/solution interface. The differences between these data and those obtained with the amphiphilic calixarene clearly suggest a more specific mechanism for the interaction between the ferrocene groups and these host molecules.

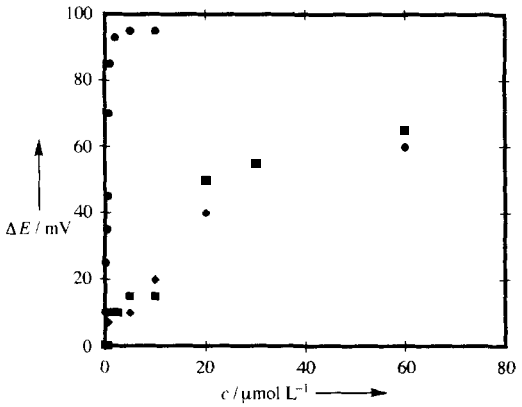


Fig. 3. Oxidation potential shift of the monolayer-anchored ferrocenyl groups induced by the addition of micromolar solutions of **3** (●), sodium dodecyl sulfate (■), and dodecyltrimethylammonium bromide (◆).

The calixarene-induced E° shift of +90 mV is very similar to that observed in solution for the binding of ferrocene derivatives by β-cyclodextrin.[10] This value contrasts with the larger negative shifts observed for the binding of ferrocene derivatives by compound **2** in solution.[5] In the latter case, the calixarene acts as an anionic host. In this work, host **3** probably interacts with the ferrocenyl group primarily by including it "octopus-like" in its aliphatic "tentacles" (Fig. 4). The change in the microenvironment of the ferrocenyl groups upon binding by **3** is thus close to that suffered upon inclusion by cyclodextrin in solution experiments, which explains the similarity in the observed oxidation potentials shifts.

Coassembly of **1** and octadecanethiol ($C_{18}H_{37}SH$) leads to a monolayer in which the formal oxidation potential of the ferrocenyl groups is quite insensitive to the presence of host **3** in the

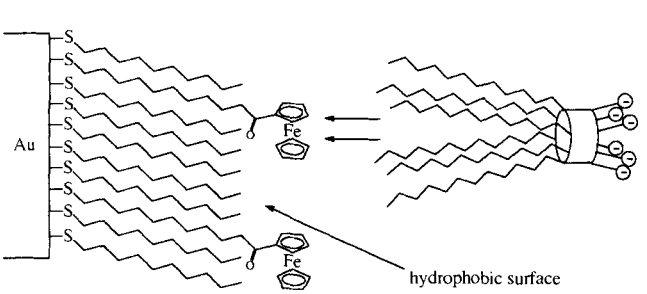


Fig. 4. Schematic representation of the proposed mode of interaction between the monolayer-anchored ferrocenyl groups and the amphiphilic calixarene host **3**.

containing monolayer. In this case, the alkanethiol's chains are long enough to surround the ferrocenyl sites in the hydrophobic core of the monolayer, preventing their interaction with the calixarene host in the contacting solution. Therefore, the location of the ferrocenyl groups in the monolayer assembly plays an important role in their binding by amphiphilic hosts.

In summary, we provide evidence in this work for the complexation of monolayer-anchored ferrocenyl groups at an interface by the sparingly water-soluble, amphiphilic calixarene host **3**. The binding was detected electrochemically from the profound effects that very low concentrations (0.05 - 2.0 μM) of the host exert on the voltammetric response of the ferrocenyl sites at the interface. The parent calixarene **2** lacks the amphiphilic character that seems to be necessary to show effective receptor properties in interfacial environments. The results reported here combined with recently published data[11] establish calixarene **3** as a versatile interfacial host.

Experimental Procedure

Thiol **1** was synthesized according to a reported procedure [4a]. The calixarene hosts were prepared as their corresponding salts (Na_8-**2** and Na_6-**3**) according to the methods described by Shinkai and co-workers [7]. Sodium dodecyl sulfate and dodecyltrimethylammonium bromide were obtained from Fluka and Kodak, respectively, and used without further purification. Gold wire (99.999%) was purchased from Johnson Matthey. All other chemicals and solvents were of the best commercial grade available. Distilled water was further purified by passage through a Barnstead Nanopure four-cartridge system.

The gold bead working electrodes were made as reported elsewhere [12]. The geometric and true surface areas of these electrodes were measured by published methods [12]. The voltammetric response of these electrodes was checked in 1.0 M $HClO_4$. Flat background responses in the potential range 0.0 to +0.90 V vs SSCE were commonly found. Otherwise, the electrode was discarded.

For monolayer preparation the gold bead electrode was immersed overnight in deoxygenated ethanolic solutions containing mixtures of **1** and the appropriate alkanethiol. The total concentration of thiol was always maintained at 1.0 mM. Before the cyclic voltammetric experiments, the gold bead electrode was rinsed with copious amounts of pure ethanol and then purified water. Cyclic voltammetry (single compartment cell, Pt flag counter electrode, homemade SSCE) was performed with the monolayer-covered gold bead working electrode immersed in 1.0 M $HClO_4$ (cell volume 10 mL). As required by the binding studies, the hosts were introduced to this solution by addition of microliter aliquots by syringe from appropriate stock solutions.

Received: July 20, 1994
Revised version: September 13, 1994 [Z 7144IE]
German version: *Angew. Chem.* **1995**, *107*, 236

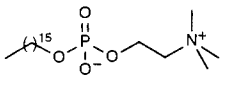
Keywords: calixarenes · cyclic voltammetry · thin films · sandwich complexes · supramolecular chemistry

[1] For reviews, see: a) G. M. Whitesides, P. E. Laibinis, *Langmuir* **1990**, *6*, 87; b) L. H. Dubois, R. G. Nuzzo, *Annu. Rev. Phys. Chem.* **1992**, *43*, 437.
[2] For a recent example, see: E. U. T. van Velzen, J. F. J. Engbersen, D. N. Reinhoudt, *J. Am. Chem. Soc.* **1994**, *116*, 3597.
[3] G. K. Rowe, S. E. Creager, *Langmuir* **1991**, *7*, 2307.
[4] a) C. E. D. Chidsey, C. R. Bertozzi, T. M. Putvinski, A. M. Mujsce, *J. Am. Chem. Soc.* **1990**, *112*, 4301; b) *Langmuir* **1991**, *7*, 1192; c) K. Uoasaki, Y. Sato, H. Kita, *ibid.* **1991**, *7*, 1510.
[5] L. Zhang, A. Macias, T. Lu, J. I. Gordon, G. W. Gokel, A. E. Kaifer, *J. Chem. Soc. Chem. Commun.* **1993**, 1017. In solution at pH 7 calixarene **2** is an octaanion owing to the deprotonation of two of its six phenolic OH groups. In the acidic media utilized in this work all the phenolic OH groups are protonated and both calixarene hosts (compounds **2** and **3**) are likely to be present as hexaanions.
[6] J. L. Atwood, D. L. Clark, R. K. Kuneja, G. W. Orr, K. D. Robinson, R. L. Vincent, *J. Am. Chem. Soc.* **1992**, *114*, 7558.
[7] S. Shinkai, S. Mori, H. Kiroshi, T. Tsukabi, O. Manabe, *J. Am. Chem. Soc.* **1986**, *108*, 2409.
[8] a) D. D. Popenoe, R. S. Deinhammer, M. D. Porter, *Langmuir* **1992**, *8*, 2521; b) N. L. Abbott, G. M. Whitesides, *ibid.* **1994**, *10*, 1493.
[9] S. E. Creager, G. K. Rowe, *Langmuir* **1993**, *9*, 2330.
[10] a) T. Matsue, D. H. Evans, T. Osa, N. Kobayashi, *J. Am. Chem. Soc.* **1985**, *107*, 3411; b) R. Isnin, C. Salam, A. E. Kaifer, *J. Org. Chem.* **1991**, *56*, 35.
[11] A. R. Bernardo, T. Lu, E. Córdova, L. Zhang, G. W. Gokel, A. E. Kaifer, *J. Chem. Soc. Chem. Commun.* **1994**, 529.
[12] M. Gómez, J. Li, A. E. Kaifer, *Langmuir* **1991**, *7*, 1797.

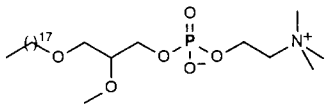
Synthesis, Antitumor Activity, and Tolerability of Phospholipids Containing Nitrogen Homologues**

Jurij Stekar,* Gerhard Nössner, Bernhard Kutscher, Jürgen Engel, and Peter Hilgard

Edelfosine (2-*O*-methyl-1-*O*-octadecyl-*rac*-glyceryl-3-phosphocholine, **2-N**) and miltefosine (hexadecylphosphocholine) are prototypes of new antineoplastically active phospholipids that have been already used clinically. However, oral administration of these drugs to cancer patients was seriously hampered



miltefosine

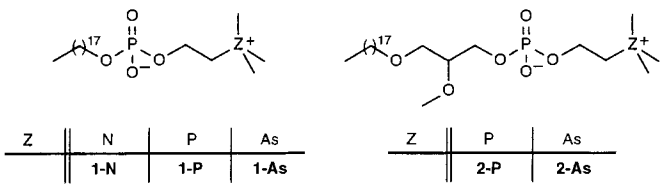


edelfosine 2-N

by side effects in the digestive tract (nausea, vomiting, diarrhea, loss of body weight).[1] Corresponding animal experiments led us to assume that during the metabolism of these phospholipids, choline esters are formed which imitate the effects of the parasympathetic nervous system on the intestine; such compounds might be responsible at least in part for the symptoms observed in patients and animals. This hypothesis has been supported by the finding that a heterocyclic phospholipid in which choline is replaced by *N*-(2-hydroxyethyl)-*N*-methylpiperidine is tolerated much better.[2]

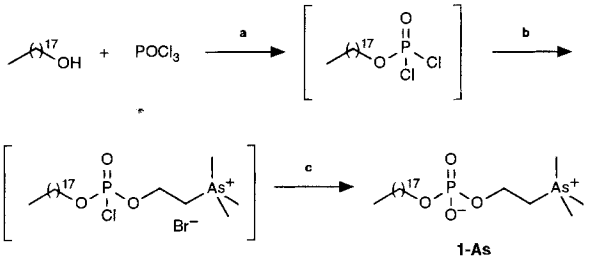
In our search for new phospholipids with better tolerability and higher cytostatic activity, special attention was given to the fact that phosphonium and arsonium homologues of choline esters (e.g. of acetylcholine) exert a considerably weaker parasympathomimetic action than the choline esters themselves.[3] Furthermore, it was recently recognized that large amounts of arsonium compounds are ingested with sea food (lobsters, crabs, and clams contain up to 80 ppm arsenic; As content of sea water is only 0.003 ppm!) mainly in the form of just slightly toxic compounds such as arsonium betaine and arsonium choline.[4, 5] Based on these findings, it seemed possible that replacement of N in choline with As or P would lead to better tolerable but still chemotherapeutically active phospholipids. Accordingly, the biological effects of the new analogues (Scheme 1) synthesized to test this working hypothesis were compared to those of the parent compounds **1-N** (octadecylphosphocholine) and **2-N**. The analogues are derived from the parent compounds by exchange of the central atom of the onium complex while maintaining the hydrophobic octadecyl and octadecylglyceryl residues, respectively. We report here on the syntheses and first results of biological tests with these novel derivatives.

The parent compounds **1-N** and **2-N** were prepared as described previously.[6, 7] In the synthesis of [2-(trimethylarsonio)ethyl]-*n*-octadecylphosphate (**1-As**) (Scheme 1), phosphoryl



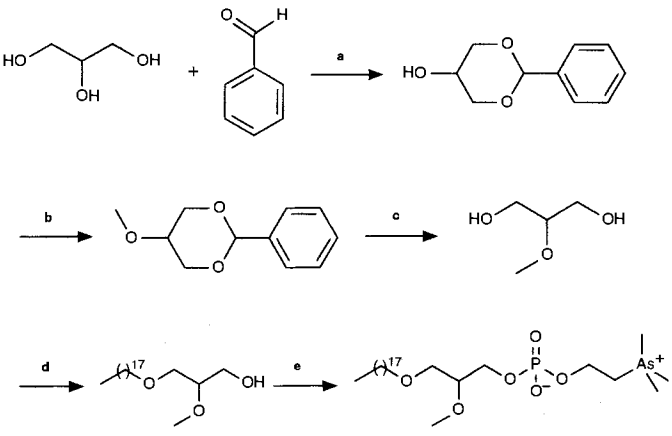
Scheme 1. General formulas and abbreviations for the homologous phospholipids.

chloride was treated with *n*-octadecanol. The resulting *n*-octadecylphosphoric dichloride was not isolated but treated directly with 2-hydroxyethyltrimethylarsonium bromide (prepared from trimethylarsane and bromoethanol according to Irgolic et al.[8]). The phosphoric diester chloride that formed was hydrolyzed to yield **1-As** as an inner salt (Scheme 2). The homologous compound **1-P** was prepared analogously from *n*-octadecanol, $POCl_3$, and 2-hydroxyethyltrimethylphosphonium bromide (yield 24%).



Scheme 2. Synthesis of **1-As**. a) $CHCl_3$/pyridine/0 °C; b) $HO(CH_2)_2As^+(CH_3)_3Br^-$/pyridine/0 °C → 20 °C; c) 10% HCl/purification with ion exchange resin (Amberlite MB3, ethanol)/digestion with acetone; total yield 43%.

In the synthesis of 2-*O*-methyl-1-*O*-octadecyl-*rac*-glyceryl-3-phosphoarsonium choline (**2-As**), methylation of 1,3-benzylideneglycerol with dimethyl sulfate was followed by cleavage of the benzylidene residue and alkylation with methyl octadecylsulfonate to provide 2-*O*-methyl-1-*O*-octadecyl-*rac*-glycerol. Subsequent phosphorylation with $POCl_3$, reaction of the intermediate with arsonium choline bromide, and hydrolysis of the resulting diester led to **2-As** (Scheme 3). The phosphonium ana-



Scheme 3. Synthesis of **2-As**. a) Toluene/*p*-CH_3-$C_6H_4SO_3H$/reflux/−H_2O, yield 60%; b) KO*t*Bu/dimethyl sulfate/toluene/60 °C, yield 83%; c) $CH_3OH/H_2O/H_2SO_4$/70 °C, yield 84%; d) $H_3C(CH_2)_{17}OSO_2CH_3$/KO*t*Bu/*tert*-amyl alcohol/90 °C, yield 81%; e) 1. $POCl_3$/pyridine/$CHCl_3$/0 °C, 2. $HO(CH_2)_2As^+(CH_3)_3Br^-$/pyridine/0 °C → 20 °C, 3. HCl/H_2O, purification with ion exchange resin (Amberlite MB3, ethanol)/digestion with acetone, yield 33%; total yield 11%.

[*] Dr. J. Stekar, Dr. P. Hilgard
Exp. Tumorforschung, ASTA Medica AG
Weismüllerstrasse 45, D-60314 Frankfurt am Main (Germany)
Telefax: Int. code + (69)4001-2745
Dr. G. Nössner, Dr. B. Kutscher, Prof. Dr. J. Engel
Chemische Forschung, ASTA Medica AG

[**] We thank Sandra Nemetz and Thomas Kynast for conducting the syntheses, Eric Thoenes, Waltraud Maschmann, Susanne Vahlenkamp, Anneli Knoop, and Sabine Falk for the biological testing, and Uwe Riemer for evaluating the tests.

logue of **2-As**, **2-P**, was synthesized analogously in 26% yield. The NMR spectroscopic data of the new phospholipids are listed in Table 1.

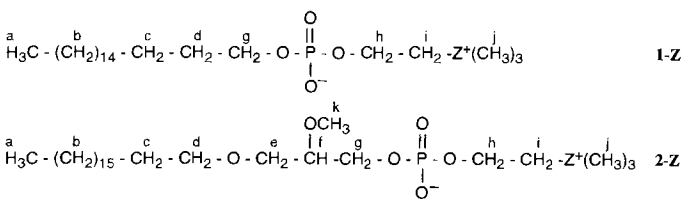


Table 1. Chemical shifts δ from the ^{1}H NMR spectra of compounds **1-N**, **1-P**, **1-As**, **2-N**, **2-P**, and **2-As** (CD_3OD) [a].

	1-N	1-P	1-As	2-N	2-P	2-As
a	0.97	0.99	0.98	0.97	0.97	0.98
	t (3H)	t (3H)	t (3H)	t (3H)	t (3H)	t (3H)
b	1.34	1.37	1.38	1.34	1.38	1.39
	m (28H)	m (28H)	m (28H)	m (30H)	m (30H)	m (30H)
c	1.67	1.67	1.48	1.63	1.65	1.66
	quin (2H)	quin (2H)	quin (2H)	quin (2H)	quin (2H)	quin (2H)
d	1.71	1.71	1.73	3.54	3.55	3.55
	quin (2H)	quin (2H)	quin (2H)	m (2H)	m (2H)	m (2H)
e	-	-	-	3.65	3.65	3.63
				m (2H)	m (2H)	m (2H)
f	-	-	-	3.56	3.58	3.59
				m (1H)	m (1H)	m (1H)
g	3.94	3.93	3.95	3.94; 4.03	3.97; 4.05	3.96; 4.05
	q (2H)	q (2H)	q (2H)	m (2×1H)	m (2×1H)	m (2×1H)
h	4.33	4.27	4.30	4.31	4.31	4.32
	m (2H)	m (2H)	q (2H)	m (2H)	m (2H)	q (2H)
i	3.70	2.65	2.81	3.70	2.67	2.81
	m (2H)	m (2H)	t (2H)	m (2H)	m (2H)	t (2H)
j	3.30	2.01	2.05	3.27	2.02	2.04
	s (9H)	d (9H)	s (9H)	s (9H)	d (9H)	s (9H)
k	-	-	-	3.51	3.55	3.55
				s (3H)	s (3H)	s (3H)

[a] The chemical shifts are relative to external tetramethylsilane (TMS). All spectra were recorded at 25 C and 500 µHz on a Bruker AMX-500 spectrometer. Abbreviations: s singlet, d doublet, t triplet, q quartet, quin quintet. Number of protons in parentheses determined by signal integration. Correct elemental analyses.

As evident from Table 2, the novel phospholipids are less toxic for mice than the two cholinephospholipids **1-N** and **2-N**. This is particularly noteworthy since arsenic compounds are generally quite poisonous. These results indicate that the toxicity of the phospholipids containing hydrophobic regions of the same structure is determined solely by the atomic number of the Group 5 element that is the central atom in the hydrophilic onium complex.

Table 2. Acute oral toxicity (LD_{50} p.o. [a], mmol kg^{-1}) of **1-N**, **2-N**, and the corresponding phosphonium and arsonium phospholipids in mice.

Hydrophobic region	Onium group Me_3N	LD_{50}	Me_3P	LD_{50}	Me_3As	LD_{50}
octadecyl	**1-N**	0.8	**1-P**	1.8 [b]	**1-As**	2.0 [c]
2-*O*-methyl-1-*O*-octadecylglyceryl	**2-N**	0.8	**2-P**	1.8 [b]	**2-As**	1.7 [b]

[a] The acute oral LD_{50} value is the dose per kilogram body weight that results in the death of 50% of the animals (solutions or suspensions are introduced to the stomach by means of a stomach tube). The LD_{50} value serves as a measure of the toxicity of a given compound; a higher value thus indicates lower toxicity. To determine the LD_{50} value, each of four equidistant logarithmic doses were applied to ten mice, and the results were evaluated by using logit analysis. [b] $P < 0.05$ vs LD_{50} of the corresponding N-containing phospholipid. [c] $P = 0.001$ vs LD_{50} of **1-N**.

The comparatively low acute toxicity of **1-P** and **1-As** is not accompanied by reduced cytotoxicity in vitro, as quantified by EC_{90} values. Although the EC_{90} values suggest that the two alkylphospholipids have slightly higher cytotoxic activity, the differences relative to **1-N** are not statistically significant (Table 3). The results of the comparative in vitro examination of the two glycerophospholipids on DS cancer cells were similar (**2-N**: $EC_{90} = 5.5$ µmol L^{-1}; **2-As**: $EC_{90} = 4.8$ µmol L^{-1}).

Table 3. Cytotoxicity of three homologous phospholipids on cell lines L1210, KB, and DS (soft-agar tumor stem-cell assay according to Salmon et al. [11]).

Phospholipid	EC_{90} [a] [µmol L^{-1}] L 1210 cells	KB cells	DS cells
1-N	7.3 ± 1.6	6.4 ± 3.1	7.3 ± 1.9
1-P	6.6 ± 2.9	6.2 ± 3.1	[b]
1-As	5.8 ± 0.6	6.4 ± 0.9	6.2 ± 2.1

[a] The EC_{90} value is the concentration that kills 90% of the treated cells, in other words, only 10% of the cultivated cells survive phospholipid application; the means are given ± s ($n = 6$). The lower the EC_{90} value, the stronger the cytotoxic activity. No significant difference to the corresponding EC_{90} values of **1-N**; ΔEC_{90} for **1-N** and **1-As** in L1210 cells is only marginally significant ($0.10 > P > 0.05$; two-tailed t-test). [b] Not tested.

Experiments on rats bearing DMBA-induced carcinoma[12] show that the arsonium and phosphonium phospholipids have distinctly better tolerability than the corresponding choline compounds. This is illustrated by a comparison between **1-As** and miltefosine (**1-N** is not suitable for clinical applications because of its high toxicity). As can be seen in Figure 1a, when

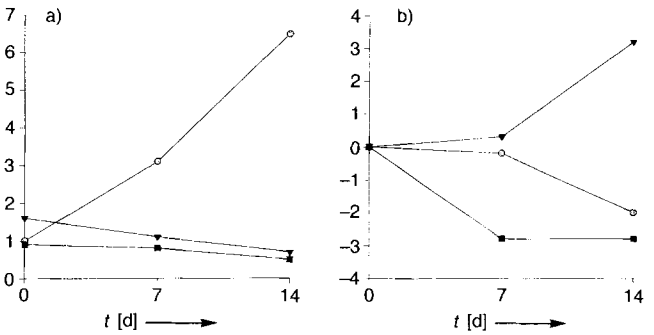


Fig. 1. a) Decrease in the weight of DMBA-induced tumors as a consequence of oral treatment with four doses (given on days 0, 3, 7, 10) of miltefosine (■, 4×68.1 mg per kg body weight) or **1-As** (▼, 4×68.1 mg per kg body weight), as well as tumor growth in untreated animals (●, control). The differences in the intensity of tumor regression between the groups treated with miltefosine and **1-As** are not statistically significant (multivariate rank test according to Koziol). Each of the three test groups consisted of seven rats. The median tumor weight in grams is plotted on the ordinate. b) Comparison of the tolerability of miltefosine and **1-As** based on the change in the mean net body weight in the test groups. The observed differences between the means are statistically significant on day 14 ($P < 0.05$; two-tailed t-test). The decrease in net body weight in the control group is attributed to the toxic effects of the tumor. Each of the three test groups consisted of seven rats. The mean of the change in net body weight in % is plotted on the ordinate. For the assignment of the curves see Fig. 1a.

four oral doses of 68.1 mg of miltefosine per kg body weight (4×167 µmol kg^{-1}) were applied, clear regression of the tumors (to about 56% of the weight registered on day 0) was observed on day 14. However, the general condition of the animals had also deteriorated (3% loss of net body weight (body weight minus tumor weight) on day 14, Fig. 1b). Four applications of 68.1 mg of **1-As** per kg body weight (4×137 µmol kg^{-1}) resulted

in slightly stronger tumor shrinkage on day 14 (to about 45% of the value registered at the start of the experiment, Fig. 1a), although the molar dose amounted to only 82% of that of miltefosine. In contrast to studies with miltefosine, the animals showed a clear-cut gain in net body weight on day 14 (3%, Fig. 1b). Even when $4 \times 100\ mg\,kg^{-1}$ ($4 \times 201.4\ \mu mol\,kg^{-1}$) of **1-As** was administered, an increase (1% on day 14) rather than reduction of the net body weight was registered. At the same time the tumors shrank to 20% of their starting weight (results not shown graphically). The difference between these results and the corresponding data from the experiment with $4 \times 68.1\ mg\,kg^{-1}$ miltefosine was significant both with respect to the net body weight and regression of the tumors (P (probability) < 0.05). Thus, due to its better tolerability, **1-As** could be administered in higher doses which led to a further improvement of the antitumoral effect (i.e. the therapeutic range was increased relative to that of miltefosine). Similar results were obtained also with the other novel analogoues.

In the present experiments we have demonstrated that the new compounds have comparable antineoplastic activity to that of the N-containing parent phospholipids in vitro and in rats bearing DMBA-induced tumors. For a definitive evaluation of cancer-inhibiting potency, further comparative experiments and dose–response curves are necessary. We have also shown that **1-As** is better tolerated by rats than miltefosine. This finding supports the previously mentioned hypothesis. The superiority of arsonium phospholipids over the N-containing parent compounds is due to their broader therapeutic range. Accordingly, by appropriately changing the structure of the molecule, it is possible to mitigate the side effects (e.g. loss of the net body weight) of phospholipids without diminishing their antineoplastic efficacy. This suggests that the (still unknown) mechanism of the anticancer activity may be different from that responsible for the side effects of this new class of anticancer agents.

The weaker parasympathomimetic activity of the arsonium and phosphonium analogues relative to that of acetylcholine[3] was ascribed to the fact that the P and As atoms have greater covalent radii than N atoms. As a result, the corresponding onium complexes are larger.[3] The same explanation might also account for the better tolerability of phosphonium and arsonium phospholipids.

To our knowledge no cancer-inhibiting arsonium derivatives have been prepared so far. Some As^{III} compounds exhibit antineoplastic activity;[9, 10] however, they are much more toxic than the tetracoordinate arsenic containing phospholipids described here. Progress in the synthesis of further biologically active phospholipid derivatives will be described in the near future.

Received: May 21, 1994
Revised version: July 28, 1994 [Z 6958 IE]
German version: *Angew. Chem.* **1995**, *107*, 195

Keywords: antitumor agents · phospholipids

[1] S. Danhauser-Riedl, A. Drozd, M. Zaffernai, U. Bruntsch, M. Peukert, H. Sindermann, H. W. Präuer, J. R. Siewert, J. Rastetter, W. E. Berdel, *Onkologie* **1991**, *14*, 392–396.
[2] J. Stekar, P. Hilgard, R. Voegeli, H. R. Maurer, J. Engel, B. Kutscher, G. Nößner, W. Schumacher, *Cancer Chemother. Pharmacol.* **1993**, *32*, 437–444.
[3] R. B. Barlow, *Introduction to Chemical Pharmacology*, 2nd ed., Methuen, London, **1964**, p. 196.
[4] H. Yamouchi, T. Kaise, Y. Yamamura, *Bull. Environ. Contam. Toxicol.* **1986**, *36*, 350–355.
[5] R. Kruse, U. Ballin, *24. GDCh-Hauptversammlung*, Hamburg 5.–11. September **1993**, p. 134.
[6] J. Engel, B. Kutscher, W. Schumacher, U. Niemeyer, A. Olbrich, G. Nössner (ASTA Medica, Frankfurt am Main), DE-B 4220852, **1991**.
[7] S. Tsushima, Y. Yoshioka, S. Tanida, H. Nomura, S. Nojima, M. Hozumi, *Chem. Pharm. Bull.* **1982**, *30*, 3260–3270.
[8] K. J. Irgolic, T. Junk, C. Kos, W. S. McShare, G. C. Pappalardo, *Appl. Organomet. Chem.* **1987**, *1*, 403–412.
[9] D. Lissauer, *Ber. Klin. Wochenschr.* **1865**, *2*, 403–404.
[10] F. E. Knock, *Anticancer Agents*, 1st ed., Thomas, Springfield, **1967**, p. 139.
[11] S. E. Salmon, A. W. Hamburger, B. Soehnlen, B. G. M. Durie, D. S. Alberts, T. E. Moon, *N. Engl. J. Med.* **1978**, *298*, 1321–1324.
[12] DMBA-induced carcinoma is a breast carcinoma of the rat induced by a single oral dose of dimethylbenz[*a*]anthracene.

Addenda

The authors of the communication "Unequivocal Partitioning of Crystal Structures, Exemplified by Intermetallic Phases Containing Aluminum" by R. Nesper et al. (*Angew. Chem. Int. Ed. Engl.* **1994**, *33*, 2073–2076) would like to make the following addenda:

1. Qualitative and quantitative interpretations of ELF have already been given by A. Savin (A. Savin, H.-J. Flad, J. Flad, H. Preuss, H. G. von Schnering, *Angew. Chem.* **1992**, *104*, 185; *Angew. Chem. Int. Ed. Engl.* **1992**, *31*, 185; A. Savin, P. Kohout, H. G. von Schnering, *Intern. Conf. Inorg. Chem.* Stuttgart, **1993**).
2. In a recent publication by B. Silvi and A. Savin (*Nature*, **1994**, *371*, 683 and cf. D. L. Cooper, *ibid.* **1994**, *371*, 651) there are also attempts at a new interpretation of chemical bonding by means of ELF.
3. A series of hitherto unpublished works by Kohout, Savin, and von Schnering concerning quantifications of ELF, partly on ionic radii and ionic volumes, were performed at the same time as our investigations on the Wirkungsbereiche.
4. We explicitly would like to thank Dr. A. Savin for helpful advice regarding the interpretation of ELF and his support concerning calculations of ELF.

D. A. Dougherty and S. J. Jacobs, authors of the communication "Combination of Superexchange and Spin-Polarization Mechanisms Leads to a Novel Hydrocarbon Tetraradical with a High-Spin Ground State" (*Angew. Chem. Int. Ed. Engl.* **1994**, *33*, 1104–1106), would like to make the following addendum to their work: This work was supported by the National Science Foundation, to whom we are grateful.

Djerassi's Park

The Bourbaki Gambit. By *C. Djerassi.* The University of Georgia Press, Athens (USA), 1994. 230pp., hardcover $ 19.95.—ISBN 0-8203-1652-0

Chemists often complain about their poor public image. Instead of praise or thanks for their achievements they are almost exclusively accused of heinous deeds. Well, a public image, that precarious and ephemeral notion, is influenced by many things, not only by reports of catastrophes, the toxin of the week, or the destruction of the environment. Self-presentation is also important, whether it be in television, film, or aesthetic literature. Compared with doctors and lawyers, the number of chemists who have given up their original career or who write as a hobby is vanishingly small. How Elias Canetti scornfully turned his back on his chemistry studies can be read in "Fackel im Ohr", and what happens when a nonchemist recruits his heroes from our ranks is evident in Heinrich Mann's "Untertan". That Carl Djerassi, after an extremely successful career as organic chemist with hundreds of scientific publications and several chemistry books to his name, has defected from this literature to what he terms Science-in-fiction is just as remarkable as it is welcome from the above-mentioned considerations.



What is Science-in-fiction? On the one hand a genre that enables the link between science and literature to be used to bring scientific knowledge and normally unseen details of the life and career of a scientist to a wider public. On the other hand this concept embodies the claim to provide a "high proportion of truth and fiction", that is, a particular quality of accuracy and credibility, which even the author finds an exacting demand.

In the first book of a planned trilogy, "Cantor's Dilemma", the themes were trust and ambition, truth and fraud in science. Besides the yearning of scientists to be recognized by their peers, "The Bourbaki Gambit" tackles, in particular, the problems that confront aging natural scientists in a society possessed by the idea of perpetual youth. Such a natural scientist is Max Weiss, Professor of Biochemistry at Princeton University, who was manoevered by the skillful tactics of the dean into early retirement. Deeply vexed he decides to take vengeance on the scientific establishment in order to prove that researchers at his age not only can, but are ideally suited to achieve outstanding results. He formulates the plan to work with other like-minded scientists under a pseudonym, just like the group of French mathematicians which has really existed since 1934 under the name Nicolas Bourbaki. The first he can win over to his "Bourbaki concept" is the Innsbruck professor Sepp Krzilska, who has just retired and is particularly piqued that the day after his retirement every one of his nameplates had been removed from the institute. Then there is the Japanese Hiroshi Nishimura of the University of Tokyo, which has a particularly low retirement age limit. At sixty he already has to face retirement in the near future. The author uses his participation to provide the reader with an at times quite protracted discourse on the Japanese scientific establishment. Although Mr. Nishimura actually wants to devote himself to lyric poetry, he is enthusiastic about the Bourbaki idea. As the fourth, and the only scientist not immediately faced with retirement, is the Professor of Mathematical Biophysics, Charlea Cherith Conway, called C_3 by the narrator. Together they form a "biochemical Bourbaki" and name themselves "Diana Skordylis". Although she does not belong to the Bourbaki group in the strictest sense, the list would be incomplete without the historian Diana Doyle-Ditmus, whom the narrator nicknames D_3 (for the first person narrator, these abbreviations are munemonics, which in addition have "something so comfortingly chemical" about them). Max Weiss meets her through her grandchild, Jocelyn Powers, one of his students who is later involved in the project as a post-graduate.

As the notion takes shape, the problems begin to arise: What fields should be covered in the first place, who should have a casting vote in controversial decisions, what topic should take precedence? The intention should, of course, remain largely secret—besides, none of the members have stood at the lab bench for decades. For that reason alone, the topics for consideration must be mainly theoretical. Furthermore, since the four come from different fields of biochemistry and microbiology, it soon becomes clear that a common topic is lacking. Initially, therefore, extensions and corrections of old papers are chosen for publication. Above all, the development of a universally valid theory of epigenetics and the application of catalytic antibodies are discussed as other research areas; incidentally, the latter theme is explained in lucid terms, even for nonscientists. Then one day Sepp Krzilska has the contagious idea, namely the polymerase chain reaction, which was last year acknowledged with the Nobel prize for chemistry. This reaction actually has nothing to do with Carl Djerassi nor with the Bourbaki concept (the true circumstances of its discovery are at least equally spectacular and are described by their discoverer K. B. Mullis in a fascinating article in *Scientific American*). Nevertheless, the theme is eminently suitable for the story—the genial simplicity of PCR enables the novel to present an amazingly in-depth and yet extremely understandable account of the scientific implications. In this way Djerassi succeeds in bringing this important new biochemical development, which has already been widely applied, to a broad circle of readers. In addition the fictional discovery is so spectacular that the plot reaches a climax shortly thereafter. At first the conceit

This section contains book reviews and a list of new books received by the editor. Book reviews are written by invitation from the editor. Suggestions for books to be reviewed and for book reviewers are welcome. Publishers should send brochures or (better) books to Dr. Ralf Baumann, Redaktion Angewandte Chemie, Postfach 101161, D-69451 Weinheim, Federal Republic of Germany. The editor reserves the right of selecting which books will be reviewed. Uninvited books not chosen for review will not be returned.

of researchers is evident. This does not really apply to Hiroshi, whose chief interest anyway is his lyric poetry. Also for Charlea the project is interesting for another reason, namely to explore the limits of the possible. Max is in a somewhat different position, since he is beginning to gather ideas for a later date in order to publish them independently. The crucial stumbling block, however, is Sepp Krzilska, who considers the whole discovery his idea. For him it is a matter of utmost importance, and at all events he wishes to publish under his own name. An additional problem is that the fictional Diana Skordylis is increasingly dragged into the limelight of the scientific public—at first she escapes, pleading "personal circumstances"—until the award of the renowned Levenson Prize exposes the whole affair.

What makes this book a particular pleasure to read is the excellent detailed knowledge of the author. It makes the tale so realistic that it could, in principle, happen at any time (or perhaps has happened somewhere already?). The showplaces of the plot—whether they be the annual conference of the National Academy of Sciences, the Virgin Islands, the Isle of Capri, or the Villa Malaparte—are described with a remarkable precision. In addition, topical themes such as the position of women in the natural sciences are also discussed. Furthermore, the story of the love affair between two septuagenarians is charming.

If one expects to be informed and/or entertained by literature, whatever the genre, this tale by Djerassi from the world of chemistry and biochemistry does both. What more can one hope for? Give us the third volume of the series (i.e. make it a veritable PCR, a *p*oetry *c*hain *r*eaction), which is rumored to appear next year and certainly will extend Djerassi's (science) park by another colorful sector, as soon as possible.

Henning Hopf, Andreas Plagens
Institut für Organische Chemie
der Technischen Universität
Braunschweig (FRG)

Amorphous Inorganic Materials and Glasses. By *A. Feltz*. VCH Verlagsgesellschaft, Weinheim/VCH Publishers, New York, 1993. 440 pp., hardcover DM 198.00.—ISBN 3-527-28421-4/1-56081-212-5

Almost ten years after the publication of the original German edition of this now well-established standard work on the amorphous state of matter, the author and publishers have set out through this English translation to bring it to a wider international readership. Its format and size are largely unchanged, but the style of production is more up-to-date and the new two-column layout emphasizes the author's concise and informative style of writing, and leads the reader in a clear way through the great wealth of data that the book contains.

However, when one begins to examine the contents in detail it becomes evident, if one has not already realized this, that it is essentially just a one-to-one translation of the German version. The list of contents (9 pp.) has exactly the same length and exactly the same unclear structure as its predecessor. It could undoubtedly have been made more useful and informative by putting less emphasis on the fine detail of the less important topics and instead highlighting the main topics. The subject index (11 pp.) is only slightly longer than in the original version and consequently does not contain much more information.

After a brief introduction the second chapter is entitled "The Amorphous and Vitreous State of Inorganic Materials", and deals with the conditions needed for preparing glasses and amorphous solids, the thermodynamic description of the glassy state, and the types of phase transformations that can occur in such systems. In the section on the characterization of the structures of noncrystalline materials the main approaches discussed are the various diffraction methods (X-rays, electrons, and neutrons) and spectroscopic methods (IR, Raman, NMR, UV, Mössbauer, and EXAFS spectroscopies). In the section on the electronic states in noncrystalline solids the author develops theoretical models for describing the phenomenon of electrical conduction in amorphous substances.

The third and longest chapter, "Amorphous and Glass-Forming Substances", begins with elements and alloys, including metallic glasses and amorphous nonmetals ranging from boron to arsenic and antimony. Other glass-forming systems are then discussed, beginning with the various binary compounds and moving on to the ternary chalcogenide systems.

Chapter 4, "Electrical Conductivity and Optical Properties of Glasses and Amorphous Solids", describes these phenomena in detail, covering aspects such as the mechanism of charge transport and photoinduced structural changes in glasses.

The publication of a translation of a ten-year-old book prompts one to ask whether the subject matter remains up-to-date, since even in the field of amorphous materials, research has not stood still during the last decade. The first four chapters have been updated only by briefly outlining the latest developments at the ends of the chapters. Chapter 5, "Applications", is much better in this respect, as it has undergone a considerably more thorough revision. The topics discussed include the latest trends and developments in applications of the semiconducting properties of certain glasses and amorphous films, the use of optical glasses for IR transmission, and information storage based on the structural changes that take place in glasses.

The aspects to be criticized, as in the case of the contents list already mentioned, relate only to the formal presentation. Thus, the bibliographies are, as in the German version, collected together at the ends of the chapters. As a result of this, especially for references that extend across chapters, the corresponding citation in the text can only be found by a time-consuming search through the book or by consulting the not very clear list of contents followed by much flipping of pages. Also the old consecutive numbering system based on the German text has been retained, so that new citations that have been inserted into the text have been assigned numbers that break the original numbering scheme. On the other hand the figures, which have only undergone slight changes, are clear and are a great help to understanding many of the points mentioned in the text.

The information has been assembled with great care, involving an enormous amount of work and attention to detail. This is especially evident in the literature references, of which there are over 2000; their number does not fully reflect the vast amount of individual data, as many of these relate to monographs and review articles. The wealth of information is impressive, and could only be presented in this form through the author's precise and economical style. However, the desire to cover all the results and theories on the amorphous state within a limited space has unfortunately meant that some aspects, such as the sol–gel process or solid-state NMR spectroscopy, could only be treated briefly. The reader who would like to learn more about such topics will certainly be disappointed at first glance on opening this book. But on examining it more carefully he or she will find that the literature references open up access to the whole range of the subject. In any case, everyone interested in obtaining a comprehensive overview of the subject will find this book indispensable. It is to be

 © VCH Verlagsgesellschaft mbH, D-69451 Weinheim, 1995 0570-0833/95/0202-0242 $ 10.00+.25/0

hoped that this English edition will be as well received internationally as the original version has been in the German-speaking world.

Hans Reuter
Institut für Anorganische Chemie
der Universität Osnabrück (FRG)

Methods of Immunological Analysis. VCH Verlagsgesellschaft, Weinheim/ VCH Publishers, New York, 1993. **Vol. 1: Fundamentals.** Edited by *R. F. Masseyeff, W. H. Albert* and *N. A. Staines.* 715 pp., hardcover DM 410.00, $ 265.00.—ISBN 3-527-27906-7/0-89573-902-X; **Vol. 2: Samples and Reagents.** Edited by *W. H. Albert* and *N. A. Staines.* 591 pp., hardcover DM 410.00, $ 265.00.—ISBN 3-527-27907-5/0-89573-903-8; **Vol. 3: Cells and Tissues.** Edited by *R. F. Masseyeff, W. H. Albert* and *N. A. Staines.* 603 pp., hardcover DM 410.00, $ 265.00.—ISBN 3-527-27908-3/0-89573-904-6

This is a very comprehensive work with an excellent arrangement of the contents. In view of the rapid developments occurring in immunochemistry, this three-volume set appears at just the right time. In Volume 1 the basic concepts of immunological analysis are explained, and the most important and well-established methods are described in detail. The chapter entitled "Molecular Basis of Antigen–Antibody Reactions" is especially good, giving a concise but thoroughly comprehensive account of the state of knowledge up to the beginning of 1991. As well as structural aspects of antigen–antibody reactions, the kinetics and thermodynamics of such reactions are discussed in detail. Another important quantity in relation to antigen–antibody reactions is the cross-reactivity, which is discussed using the example of the steroid ring skeleton. This chapter ends with a very nice contribution on "Factors Modulating Antigenicity". The chapters on "Methods Using Labeled Reagents" and "Labels and their Measurement" give an up-to-date survey of important reagents (tracers) and the methods for detecting them. These chapters are indispensable for choosing a suitable detection system. The discussion here is soundly based and thorough, and includes structural formulas.

Volume 2 describes the preparation and characterization of reagents used in immunological analysis. As well as explaining the theory of the methods, the chapters include practical advice on carrying them out and suggestions for overcoming problems, showing that the authors have much experience in everyday laboratory practice. Sections 4.1 to 4.5, devoted entirely to antibodies, deserve a special mention. With over 280 pages these are practically a book in themselves, containing detailed treatments of the advantages and disadvantages of polyclonal and monoclonal antibodies, the modification of antibodies, and antibodies with special properties, e.g. catalytic antibodies. Chapter 5 is concerned with chemical coupling and derivatization methods, which are indispensable for applications in immunochemistry. The various methods are described in a clear and easily understandable way, with selected examples of laboratory procedures based on different chemical approaches. However, some of the most elegant coupling methods that have been reported in the literature are not mentioned. Also the importance of immunoaffinity columns and the methods for preparing them are not given enough emphasis.

Volume 3 gives a comprehensive overview of immunological methods for the analysis of cells and tissues. In addition considerable space is devoted to cell preparation and cell culture, which are very important as preliminaries to the analysis of cells and tissues. The first 90 pages contain very detailed descriptions of the isolation of cells and tissues, which even relatively inexperienced users should be capable of following without difficulty. The main emphasis is on human cell systems, but adequate attention is also given to experimental animal and plant systems. Some basic principles of cell culture for the types of cell systems mentioned above are then explained, with careful distinctions according to the different systems. The chapter on "Methods of Phenotype Analysis" (over 180 pp.) is especially useful, covering all aspects of immunocytochemistry from general principles to detailed laboratory methods, often giving several alternatives and including references. Everyone acquainted with such methods knows that it is necessary to vary a large number of experimental parameters to arrive at conditions giving the best results. Surprisingly, some important new detection methods based on immunohistochemical and, most notably, immunofluorescence techniques, which are also capable of yielding quantitative information at the single cell level (e.g. through the distribution of damage in DNA), are not covered. This is an area which should definitely be included in the next edition.

To sum up, this is a work that will be of value throughout the field of immunological analysis. It includes a wealth of references covering the period up to the beginning of 1991, and thus serves as a guide to the original literature. This series of volumes will be essential for every laboratory concerned with immunochemistry.

Karl-Heinz Glüsenkamp
Institut für Zellbiologie
der Universität-Gesamthochschule
Essen (FRG)

 © *VCH Verlagsgesellschaft mbH, D-69451 Weinheim, 1995* *0570-0833/95/0202-0243 $ 10.00+.25/0*

Atom Economy—A Challenge for Organic Synthesis: Homogeneous Catalysis Leads the Way

Barry M. Trost*

Enhancing the efficiency of the synthesis of complex organic products constitutes one of the most exciting challenges to the synthetic chemist. Increasing the catalogue of reactions that are simple additions or that minimize waste production is the necessary first step. Transition metal complexes, which can be tunable both electronically and sterically by varying the metal and/or ligands, are a focal point for such invention. Except for catalytic hydrogenation, such methods have been rare in complex synthesis and virtually unknown for C–C bond formation until the advent of cross-coupling reactions. These complexes may orchestrate a variety of C–C bond-forming processes, important for creation of the basic skeleton of the organic structure. Their ability to insert into C–H bonds primes a number of different types of additions to relatively nonpolar π-electron systems. Besides imparting selectivity, they make feasible reactions that uncatalyzed were previously unknown. The ability of these complexes to preorganize π-electron systems serves as the basis both of simple additions usually accompanied by subsequent hydrogen shifts and of cycloadditions. The ability to generate "reactive" intermediates under mild conditions also provides prospects for new types of C–C bond-forming reactions. While the examples reveal a diverse array of successes, the opportunities for new invention are vast and largely untapped.

Keywords: carbon–carbon coupling · catalysis · cycloadditions · synthetic methods

1. Introduction

The goal of reducing simultaneously the depletion of raw materials and the generation of waste has taken on new urgency for the chemical community as society places increasing emphasis on environmental concerns. Thus, production of the myriad of substances that are required to serve the needs of society, stretching from the worlds of materials science to health care, must address synthetic efficiency not only in terms of selectivity (chemo-, regio-, diastereo-, and enantioselectivity) but increasingly in terms of atom economy, that is, in terms of maximizing the number of atoms of all raw materials that end up in the product.[1] The ideal chemical reaction is not only selective but is also just a simple addition (either inter- or intramolecular) in which any other reactant is required only in catalytic amounts.

The producers of commodity chemicals have recognized the importance of these issues. Though many existing processes do not meet these objectives, they are mainly rather old technologies. "Newer" processes represented by hydroformylation,[2] Ziegler–Natta polymerization,[3] and hydrocyanation[4] are spectacular illustrations of how practical and important processes that possess these characteristics are. On the other hand, such issues have not been emphasized for production of smaller volume chemicals. Clearly, a high priority goal of any chemical production is an environmentally benign design.

With the increasing sophistication of the types of substances that we must produce to meet society's needs, this task is quite daunting. In many instances, the synthesis of such compounds by any means in an economically viable way is a major accomplishment; to do so with atom economy as well is an almost untenable proposition. Part of the problem lies in the lack of some type of selectivity for processes that meet this definition. For example, apart from catalytic hydrogenation, the Diels–Alder reaction comes closest to representing the ideal chemical reaction in terms of atom economy and chemo-, regio-, and diastereoselectivity.[5] However, achievement of enantioselectivity in a catalytic sense is a major challenge and a subject of intense activity.[6] In most instances, the failure arises from the lack of atom economy. In a practical sense, while we should strive for the ideal in which all reactions are simple additions, we cannot expect to always achieve the ideal. When reactions are of the form A + B → C + D where C is the desired product, the by-product D should be as small and innocuous as possible. Catalysis by transition metal complexes has a major role to play in addressing the issue of atom economy—both from the point of view of improving existing processes and, most importantly, from discovering new ones. This review will focus on the formation of C–C bonds by homogeneous catalysis in complex organ-

[*] Prof. B. M. Trost
Department of Chemistry, Stanford University
Stanford, CA 94305-5080 (USA)
Telefax: Int. code + (415)725-0259

 © *VCH Verlagsgesellschaft mbH, D-69451 Weinheim, 1995* *0570-0833/95/0303-0259 $ 10.00+.25/0*

ic synthesis. Thus, polymerization methods, although extremely important, are outside its scope. Several well established transition metal catalyzed reactions represented by carbonylation are well appreciated and well reviewed; as a result, they are not covered by this overview.

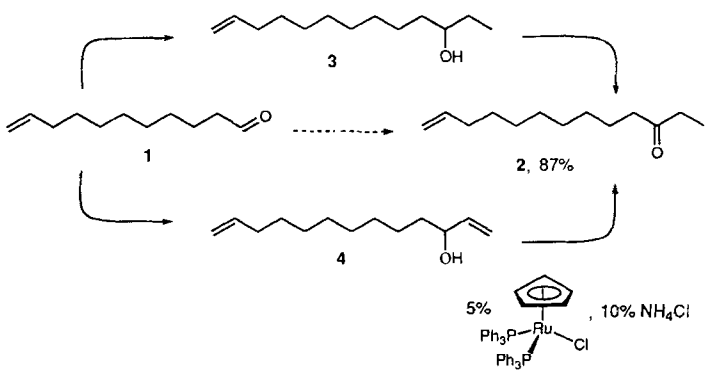
2. Prototropic Rearrangements

The ability of transition metal complexes to make and break C–H bonds forms the basis of many catalytic processes beyond the obvious catalytic hydrogenation. Olefin isomerizations[7] may involve insertion into an allylic C–H bond (Scheme 1),



Scheme 1.

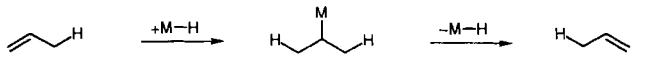
which has been proposed for a ruthenium catalyzed intramolecular redox reaction of an allylic alcohol (Scheme 2, **4** → **2**).[8] While many metal complexes effect olefin isomerizations, their lack of chemoselectivity render them useless with substrates like **4**. This example illustrates the potential such methodology offers in terms of atom economy. Whereas the "normal" conversion of aldehyde **1** to **2** would employ two steps involving stoichiometric organometallic reagents to form **3** followed by



Scheme 2.

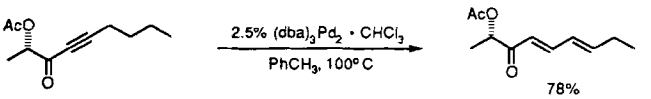
adjustment of the oxidation level with some stoichiometric oxidant, this reaction supplants the latter with a simple prototropic isomerization. While **4** may be formed from **1** by use of a stoichiometric vinyl organometallic reagent, it may also be formed by catalytic additions of acetylene[9] followed by hydrogen thereby transforming aldehyde **1** into ketone **2** with excellent atom economy.

Isomerizations by C–H insertion take advantage of the stability of π-allyl metal complexes. However, such pathways are not always feasible. An alternative mechanism invokes a metal hydride addition followed by a β-elimination (Scheme 3).



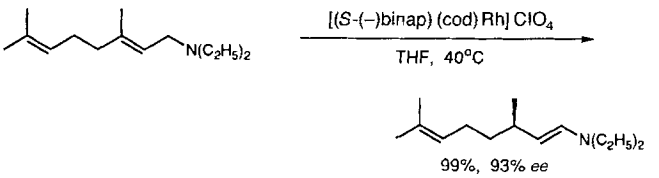
Scheme 3.

This pathway permits isomerizations of alkynes to dienes (Scheme 4), which are geometrically precluded from reacting by a π-allyl mechanism.[10, 11] In addition to palladium complexes, those of iridium,[11] ruthenium,[12] and rhodium[13] also catalyze similar reactions.



Scheme 4. dba = dibenzylidene acetone.

The analogous isomerization of *N*,*N*-diethylgeranylamine with chiral rhodium complexes (Scheme 5) to produce natural citronellal after hydrolysis of the enamine[14, 15] serves as the key step in the synthesis of the side chain of α-tocopherol[16] and a commercial synthesis of menthol.[17]



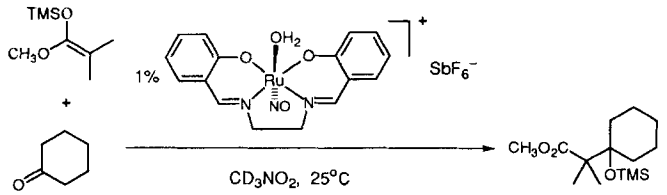
Scheme 5. cod = cyclooctadiene, binap = 2,2'-bis(diphenylphosphino)-1,1'-binaphthyl.



Born in Philadelphia, Pennsylvania in 1941, where he obtained his BA (1962) at the University of Pennsylvania, Barry M. Trost completed his Ph. D degree in Chemistry at the Massachusetts Institute of Technology in 1965 under Professor Herbert O. House. He moved immediately to the University of Wisconsin where he was promoted to Professor of Chemistry in 1969 and subsequently became Vilas Research Professor in 1982. He joined the faculty at Stanford as Professor of Chemistry in 1987 and became Professor of Humanities and Sciences in 1990. In addition, he has been visiting professor in Germany (Marburg, Hamburg, Munich), France (Universities of Paris VI and Paris South), Italy (University of Pisa), Denmark (Copenhagen) and Spain (University of Barcelona). In 1994 he was presented with an honorary doctorate from the Université Claude-Bernard (Lyon I), France. He has garnered numerous awards for both teaching and research, the most recent being the Roger Adams Award of the ACS (1995) and was elected a member of the U. S. National Academy of Sciences (1980) and a fellow of the American Academy of Sciences (1982).

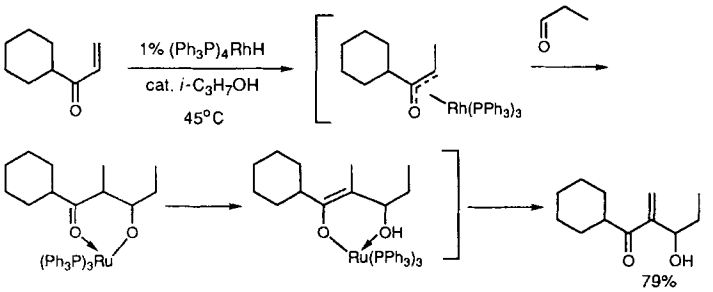
3. Intermolecular Prototropic and Related Additions

The aldol and related addition reactions to the carbonyl group of aldehydes and ketones normally entails use of Brønsted bases or acids, most commonly in stoichiometric amounts. Performing such reactions with transition metal catalysts offers two advantages beyond the avoidance of stoichiometric reagents: 1) more neutral reaction conditions that can enhance chemoselectivity and 2) prospects for asymmetric induction. The enol silyl ether version of the aldol addition may be effectively catalyzed by a ruthenium catalyst (Scheme 6) and



Scheme 6.

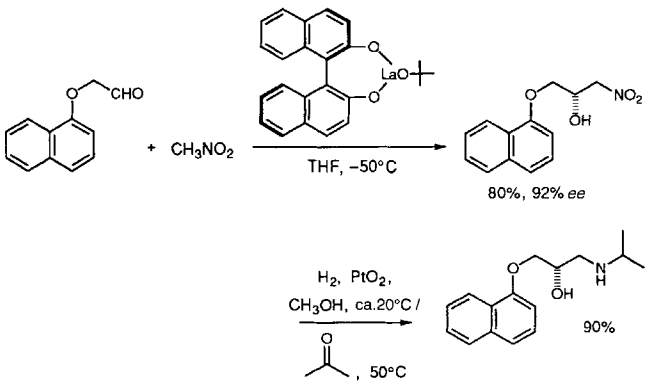
proceeds to > 90% completion in less than 3 minutes. The ruthenium center may be considered to enhance the electrophilicity of the carbonyl partner by coordination; that is, it functions as a Lewis acid.[18] However, mechanistic diversity of transition metal catalyzed reactions permits unorthodox types of aldol reactions. As illustrated in Scheme 7, formation of an enolate by



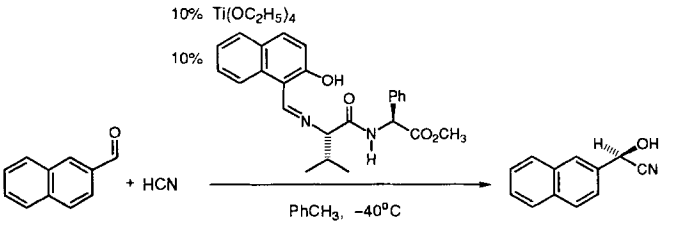
Scheme 7.

hydrometalation of an enone sets the stage for a net aldol reaction of unsaturated ketones as the aldol donor partner—a role they cannot play in simple acid or base catalyzed chemistry.[19]

The promise that such transition metal catalyzed versions may proceed with good enantioselectivity is beginning to be fulfilled. The addition of nitromethane to aldehydes (the Henry reaction) proceeds with good asymmetric induction on use of a catalytic lanthanide base.[20] A simple synthesis of (*S*)-(−)-propranolol utilizes this reaction (Scheme 8).[21] In another variation a titanium complex serves as the equivalent of a chiral Lewis acid in promoting cyanohydrin formation (Scheme 9).[22]

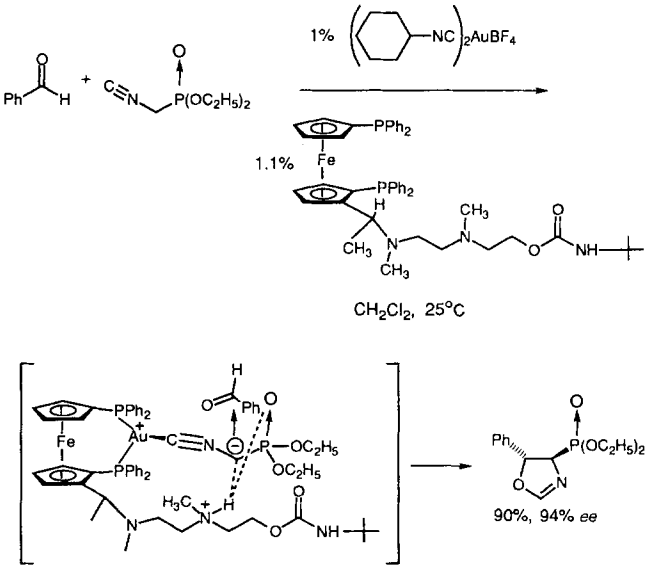


Scheme 8.



Scheme 9.

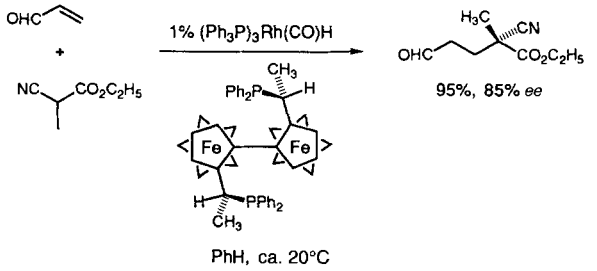
The gold and silver catalyzed aldol addition of isonitriles proceeds with high asymmetric induction in the presence of a chiral ligand. An asymmetric synthesis of α-amino acids ensues on use of α-isocyanocarboxylates.[23] Phosphorus analogues derive from use of α-isocyanophosphonates (Scheme 10).[24]



Scheme 10.

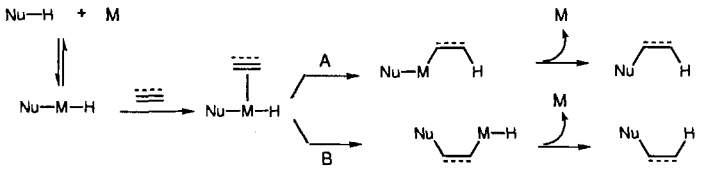
The ability of the isonitrile to coordinate to gold or silver provides the activation of the isonitrile—promoting deprotonation and addition to the carbonyl group.

This same type of activation serves as the basis of the metal catalyzed Michael addition of nitriles in which coordination of the nitrogen of the nitrile initiates the events leading to addition.[25] The asymmetric addition of ethyl α-cyanopropionate to prop-2-enal highlights the utility of this metal catalyzed version of the Michael reaction (Scheme 11).[26]



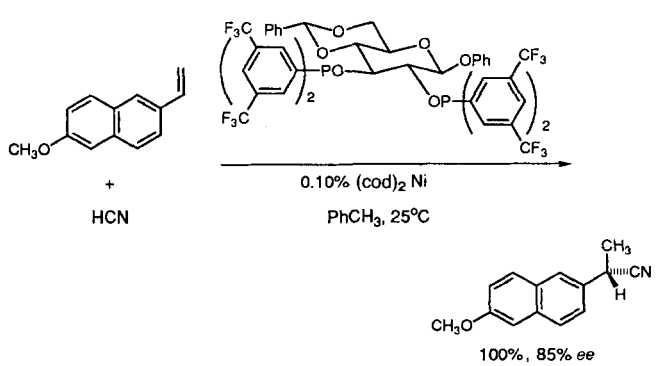
Scheme 11.

Using a transition metal to activate a pronucleophile for addition reactions creates a new level of reactivity that is not present with main group elements, namely the ability to add to nonpolarized unsaturated systems. The important facile processes of hydrometalation and carbametalation, characteristic of the transition elements, initiate additions of a C–H bond across double and triple bonds as formalized in Scheme 12.

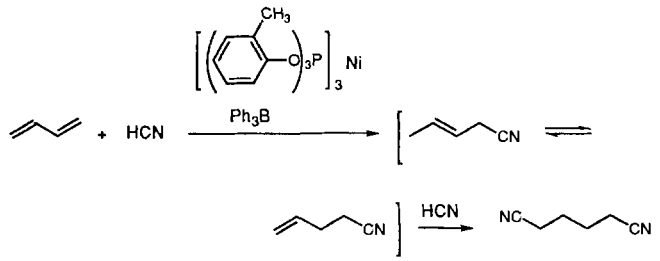


Scheme 12. Formal representation of the hydrometalation A and carbametalation B as routes to the addition of C–H bonds to nonpolar double and triple bonds.

The nickel catalyzed hydrocyanation of olefins[4, 27] is initiated by a hydrometalation (Scheme 12, path A), which may proceed with high asymmetric induction in the presence of a chiral ligand (Scheme 13).[28] The *cis* nature of the addition[29] suggested by (Scheme 12) leads to *E* isomers of substituted acrylonitriles by hydrocyanation of 1-alkynes.[30] Dienes are excellent acceptors, since the intermediate is a π-allylnickel complex.[4, 31] Combining hydrocyanation with olefin isomerization led to a commercially viable synthesis of adiponitrile (Scheme 14).[4, 32]

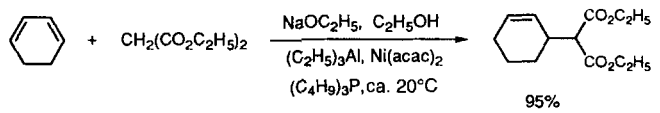


Scheme 13.



Scheme 14.

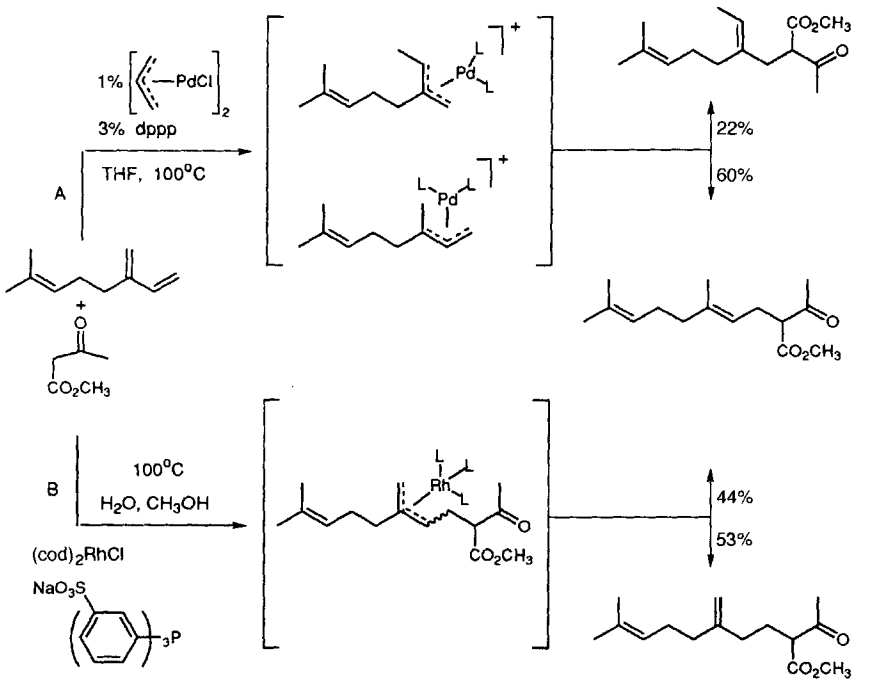
Nickel complexes also catalyze the addition of active methylene compounds like malonic esters and β-ketoesters to cyclic dienes (Scheme 15),[31] which presumably proceed by a similar mechanism (Scheme 12, path A). Extrapolation to acyclic dienes is normally plagued by diene oligomerization, itself an important and interesting process (see Scheme 31). With palladium catalysis such oligomerizations may be suppressed relative to simple additions by use of bidentate ligands (Scheme 16A).[33] With an unsymmetrical diene like myrcene, the two feasibile regioisomeric π-allylpalladium complexes yield two regioisomeric products, although one predominates. The major regioisomer isolated in 60% yield serves as a commercially important intermediate in the synthesis of vitamins A and E.



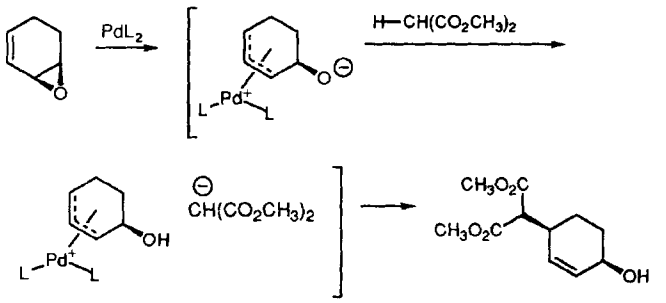
Scheme 15. acac = acetylacetonate.

Switching the catalyst may change the mechanism. Indeed, a rhodium complex catalyzes the same addition by a carbametalation (Scheme 12, path B) to produce a different mixture that results from lack of regioselectivity in the proton transfer step (Scheme 16B).[34] This latter route becomes commercially viable since both products can be taken on to pseudoionone, the key intermediate on the route to vitamins A and E.

A related but mechanistically different process is the palladium catalyzed addition of pronucleophiles to vinyl epoxides (Scheme 17). In this reaction, ionization of the epoxide by palladium creates the base to deprotonate the pronucleophile, setting the stage for the normal nucleophilic attack on a π-allyl complex.[35] The stereochemistry always involves formation of the new C–C bond on the same face of the π system from which the leaving group departed, regardless of regiochemistry. The regiochemistry normally involves attack at the allylic terminus distal to oxygen as depicted. This process differs from the simple base



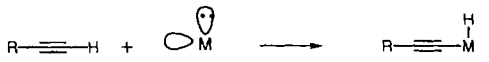
Scheme 16. dppp = 1,3-bis(diphenylphosphino)propane.



Scheme 17.

promoted nucleophilic ring opening of the epoxide in both regio- and diastereoselectivity.

The ability of transition metals to insert readily into acetylenic C–H bonds, as represented formally in Scheme 18,

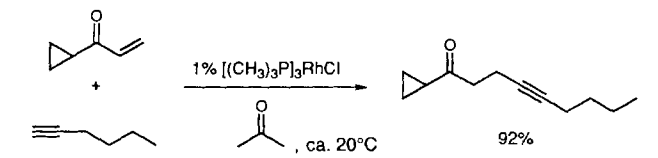


Scheme 18.

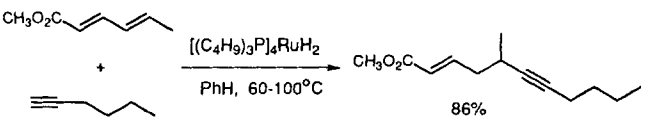
derives both from the acidity of this proton and the excellent coordinating ability of the acetylenic linkage. Thus, a 1-alkyne may function similarly to HCN and active methylene compounds as summarized in Scheme 12.

Rhodium [36] and ruthenium (Schemes 19 and 20)[37] complexes catalyze the addition of terminal alkynes to activated olefins and dienes. Appropriate deuterium labeling experiments demonstrate that with dienes the reaction proceeds by a clean *cis*-1,2-addition. The low conversions of the rhodium catalyzed reaction diminish its utility in spite of the high yields.

The addition to unactivated multiple bonds is complicated by the normally dominant self-addition. For example, with a palladium catalyst the dimerization proceeds well, even in the pres-

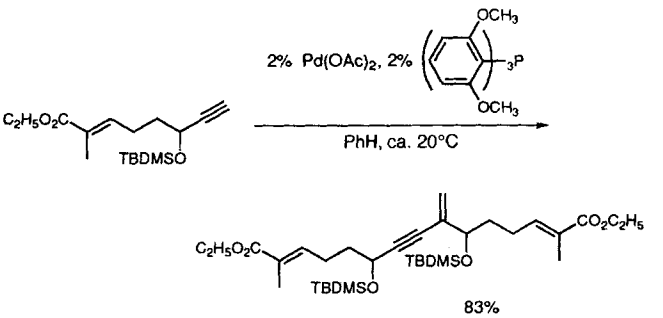


Scheme 19.



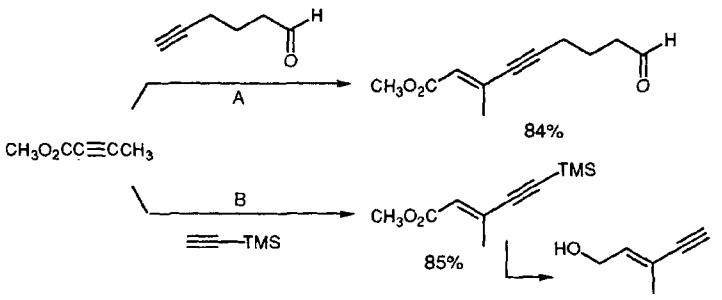
Scheme 20.

ence of an activated olefin (Scheme 21).[38] On the other hand, an activated 1-alkyne completely intercepts the organopalladium intermediate in a highly chemoselective fashion. For ex-



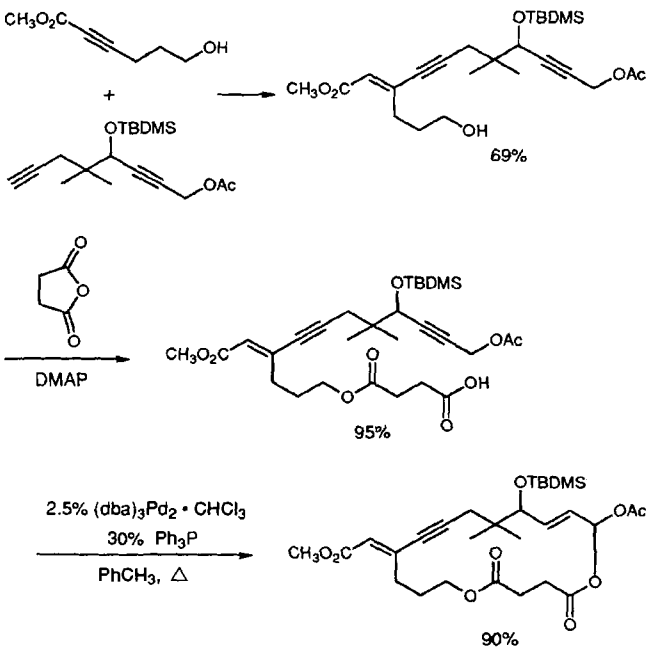
Scheme 21. TBDMS = *tert*-butyldimethylsilyl.

ample, the unsymmetrical cross-coupling occurs even in the presence of an unprotected aldehyde (Scheme 22, path A).[39] The adduct of methyl butynoate and trimethylsilylacetylene (Scheme 22, path B)[40] may be readily transformed into an



Scheme 22. The reaction conditions for A and B are the same as given in Scheme 20. TMS = trimethylsilyl.

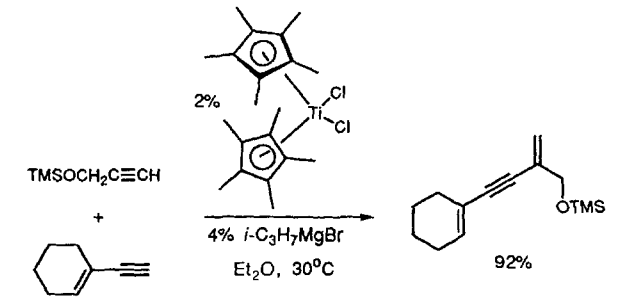
important building block for Vitamin A synthesis.[41] Scheme 23 illustrates the use of this reaction as a key step in constructing an acyclic carboxylic acid that ultimately undergoes a palladium catalyzed lactonization by cycloisomeriza-



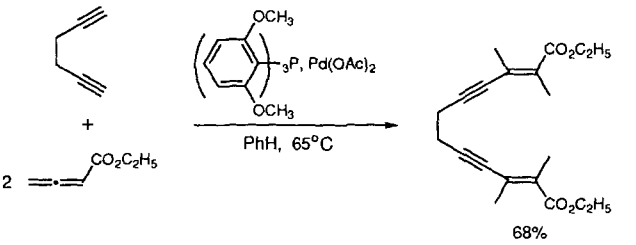
Scheme 23. Conditions for the first step as given in Scheme 20.

tion.[42] Thus, a relatively complicated eighteen-membered macrodiolide arises from two alkyne building blocks by a simple series of inter- and intramolecular additions. A most remarkable selectivity has occurred with a titanium(II) catalyst that promotes the coupling of an unsaturated terminal alkyne as the donor and a saturated terminal alkyne as the acceptor (Scheme 24).[43] Allenes serve as effective acceptors for terminal alkynes, and novel oligo(enyne)s may result (Scheme 25).[44]

Extension of these concepts to other additions depends upon the ability of the transition metal to undergo the C–H insertion.

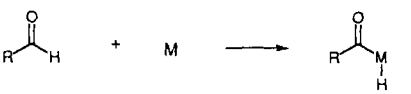


Scheme 24.



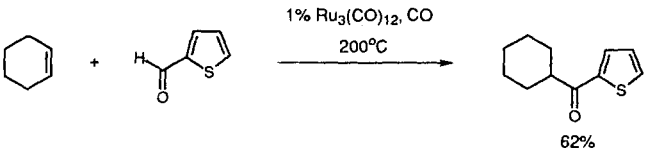
Scheme 25.

The ability of transition metals to decarbonylate aldehydes via an acyl metal hydride intermediate (Scheme 26) suggests the



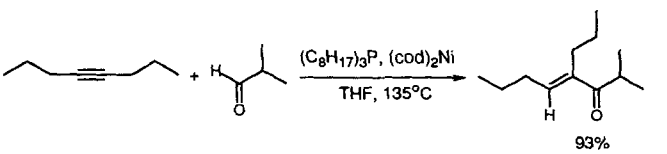
Scheme 26.

prospect of trapping that intermediate as in Scheme 12. Whereas capture with a simple olefin proceeds in only modest yields with a ruthenium complex (Scheme 27),[45] capture by a 1-alkyne occurs in good yields with a nickel catalyst



Scheme 27.

(Scheme 28).[46] Substrates containing sulfur are compatibile with homogeneously catalyzed reactions, which contrasts with their role as poisons for many heterogeneously catalyzed processes. The *E* geometry of the product in Scheme 28 is consistent with a *cis* addition.

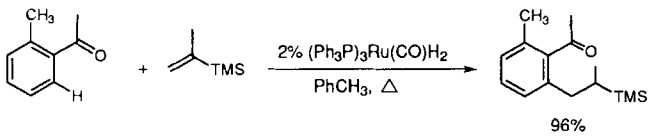


Scheme 28.

Precoordination provides an important kinetic path for many transition metal catalyzed reactions, one of which is *ortho*-metalation (Scheme 29). On use of a ruthenium catalyst which becomes coordinatively unsaturated by loss of hydrogen to promote *ortho*-metalation, aryl ketones add to unhindered olefins, especially vinylsilanes.[47] The example of Scheme 30 reveals the kinetic preference for insertion into a sp^2 C–H bond over a sp^3 C–H bond, in spite of the greater stabilization by conjugation of the benzylic organometallic intermediate that would have formed in the latter case and its lower bond energy.

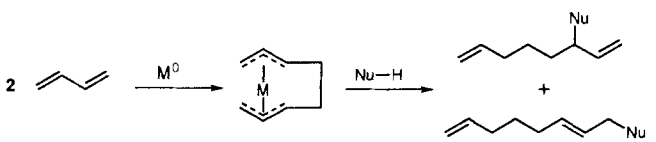


Scheme 29. CG = coordinating group.

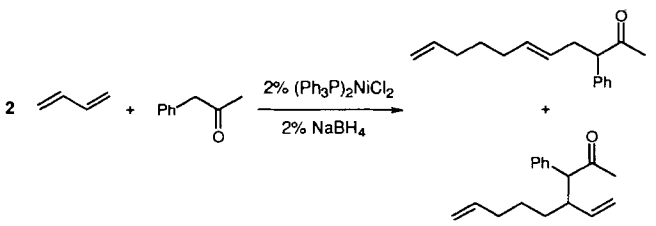


Scheme 30.

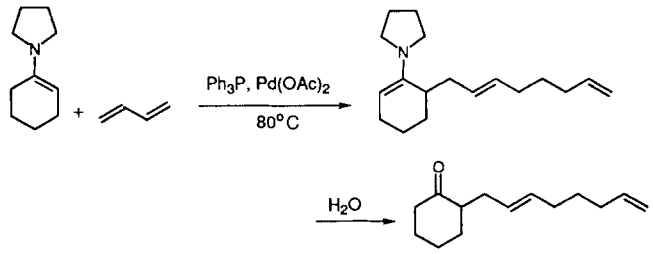
The reactions of simple dienes in additions are frequently complicated by self-oligomerization or telomerization. Such reactions are believed to involve bis(allyl)metal complexes as intermediates, which react with pronucleophiles to give regioisomeric addition products (Scheme 31). Although many metals including Co, Ir, Rh, and Ru promote such reactions, most work centers on Ni[48] and Pd.[49] For example, a Ni^0 catalyst generated in situ from triphenylphosphane and nickel chloride in the presence of sodium borohydride gave an 85:15 mixture of the 2:1 adducts of butadiene and phenylacetone depicted in Scheme 32 (telomers) to the 1:1 adducts.[50] Of the 2:1 adducts, the linear to branched telomer ratio is 8.4:1. Better selectivity for the telomeric products is obtained from the palladium catalyzed reaction (Scheme 33).[51] The adduct of acetic acid (Scheme 34) has proved to be particularly useful for the synthesis of natural products. For example, the linear adduct which may obtained in 88% yield and 28:1 regioselectivity [catalyst (o-$C_7H_7O)_3P$, $Pd(OAc)_2$][52] served as a useful intermediate for the synthesis of the fragrance ingredient muscone[53] and the macrolide diplodialide.[54] The branched product is a convenient source of octa-1,7-dien-3-one, which by a simple sequence is converted into a useful steroid intermediate (Scheme 35).[55]



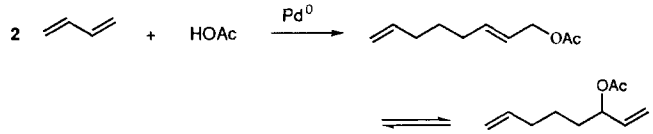
Scheme 31.



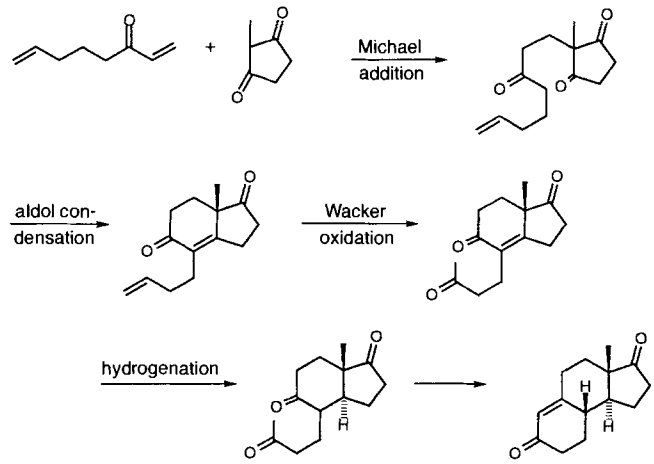
Scheme 32.



Scheme 33.

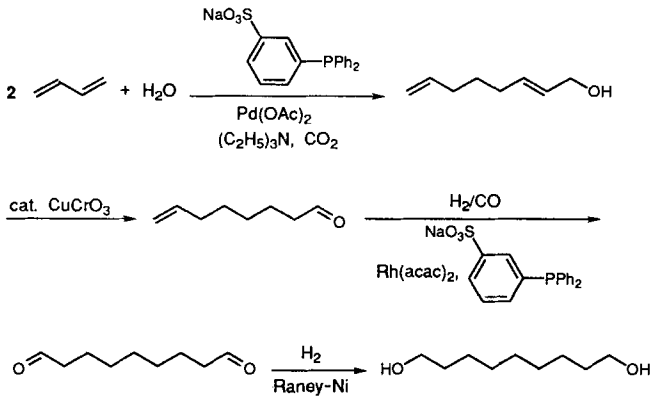


Scheme 34.



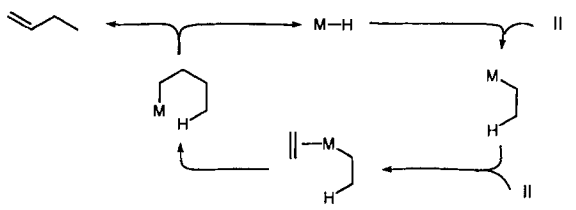
Scheme 35.

Since all the reactions are either simple additions or involve only water as a by-product, this strategy becomes rather atom economical. The commercial synthesis of 1,9-nonanediol (Scheme 36) that combines a prototropic addition and isomerization of the telomer 2,7-octadien-1-ol with hydroformylation and hydrogenation is an ideal synthetic strategy for this commercial target.[56]



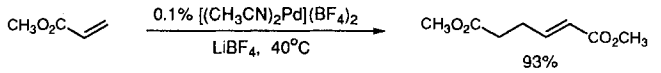
Scheme 36.

The employment of nonacidic reaction partners for additions to π-electron systems requires initiation by a metal hydride (Scheme 37). The dimerization of olefins by complexes of the



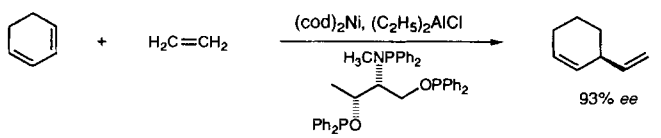
Scheme 37.

later transition metal complexes illustrates this approach. Whereas nickel is normally the preferred catalyst with nonfunctionalized olefins, a "naked" Pd^{2+} catalyst is recommended for the dimerization of methyl acrylate (Scheme 38).[57] Cross-cou-



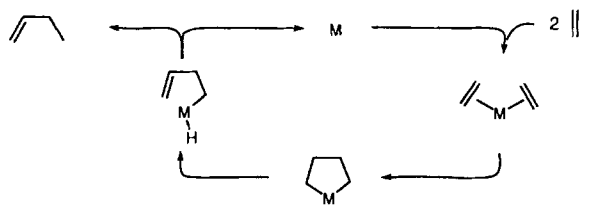
Scheme 38.

pling can occur between simple olefins (e.g. ethylene) and olefins activated either by strain (e.g. norbornene)[58] or electronic factors (e.g. styrene).[59] Alternatively, a diene is an excellent partner for hydrovinylation for which the advantage of transition metal catalysis for asymmetric induction may be exploited (Scheme 39).[60]



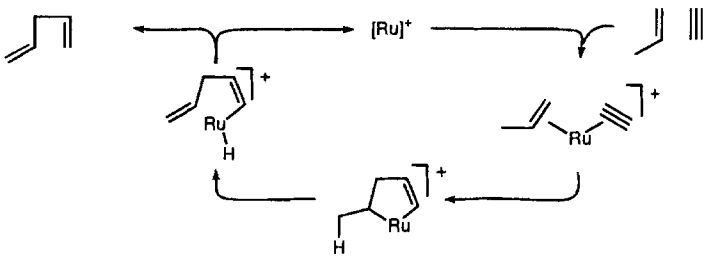
Scheme 39.

An alternative mechanism to that in Scheme 37 invokes a metallacycle (Scheme 40). This pathway requires a geometrically difficult β-hydride elimination in the metallacyclopentane, because the dihedral angle between the C–M and β C–H bonds



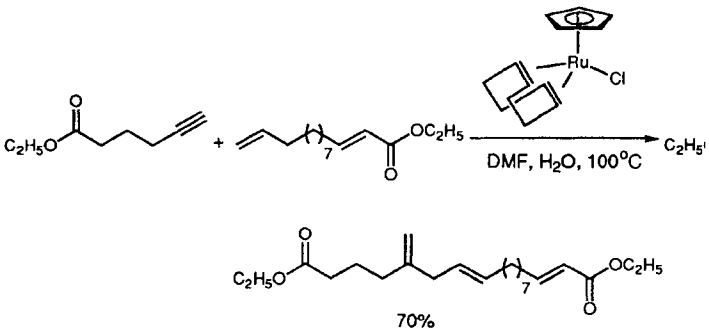
Scheme 40.

cannot readily become 0° as required for such eliminations.[61] On the other hand, such a mechanism seems to operate in a ruthenium catalyzed addition, which obviates the above problem by an elimination exocyclic to the ring according to Scheme 41. Thus, heating an internal or terminal alkyne with



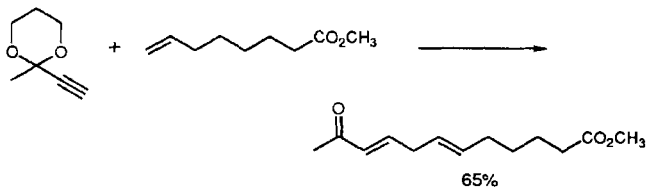
Scheme 41.

a monosubstituted olefin in the presence of a ruthenium complex gives rise to the equivalent of a highly selective Alder ene type reaction (Scheme 42).[62] The high chemoselectivity is exhibited by its compatibility with most functional groups (esters,

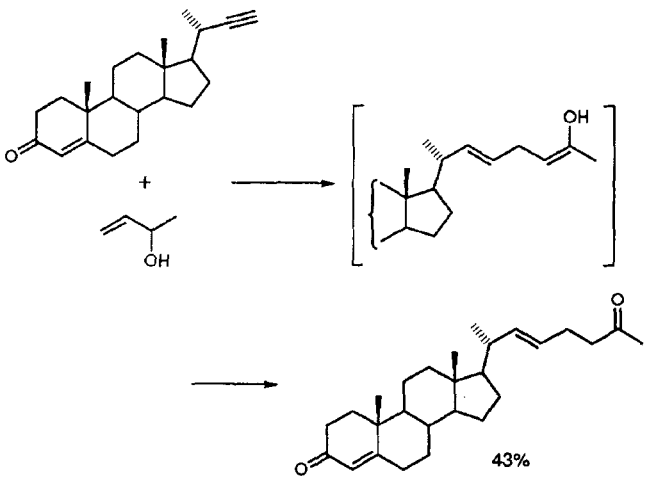


Scheme 42. DMF = dimethylformamide.

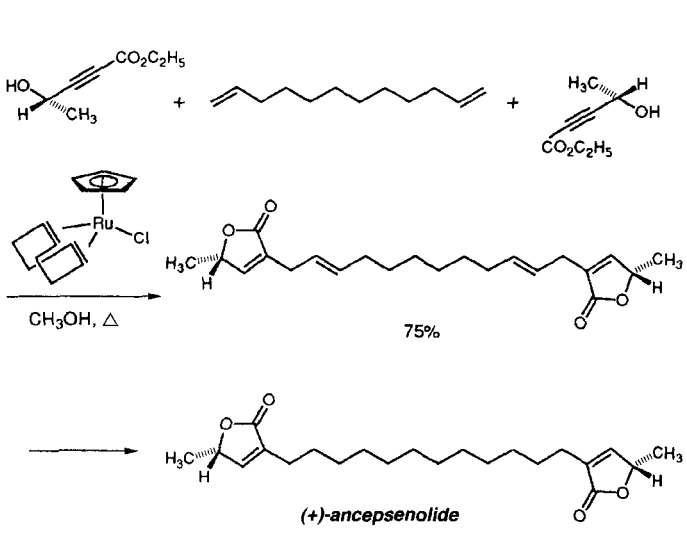
ketones, alcohols, ketals etc.): the "activated" olefin, that is, the conjugated ester, would normally be thought to be the site of reaction. The regioselective preference for formation of the "branched" product changes upon introduction of steric hindrance at the propargylic position (Scheme 43). A similar preference for the "linear" product also results from employment of an allyl alcohol in which the initial product, an enol, tautomerizes to give the γ,δ-unsaturated ketone (Scheme 44).[63] Employing a γ-hydroxybutynoate as the acetylenic partner (Scheme 45) leads to a surprising regioselectivity in which the alkylation occurs at the position α to the carbonyl group, a contra-elec-



Scheme 43. Reaction conditions as in Scheme 39.



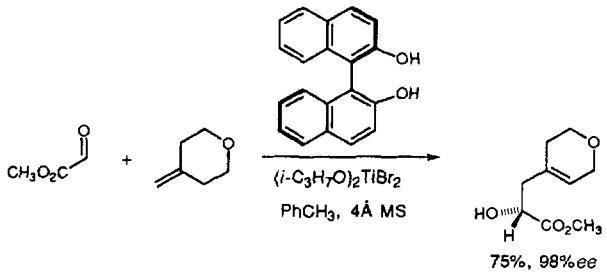
Scheme 44. Reaction conditions as in Scheme 39.



Scheme 45.

tronic orientation with respect to the normal preference in an Alder ene reaction. The *Z* juxtaposition of the hydroxy and ester groups leads to spontaneous lactonization with the expulsion of ethanol under the reaction conditions and thus to a facile synthesis of α-alkylated-γ-butyrolactones. A short route to the acetogenin (+)-ancepsenolide employs a double ruthenium catalyzed addition and establishes the absolute configuration of this natural product (Scheme 45).[64] The regioselectivity is consistent with the metallacycle intermediate proposed in (Scheme 40) in which 1) steric hindrance is minimized and 2) substituents that may coordinate to ruthenium are preferentially proximal to the metal.

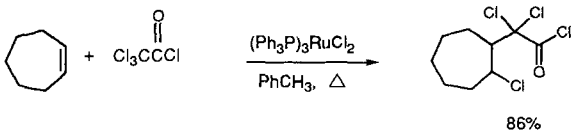
When the enophile is replaced by a carbonyl group, the reaction corresponds to the oxaene reaction. Such reactions have been catalyzed by standard Lewis acids including those of the early transition elements. Chiral titanium complexes as catalysts in these reactions have afforded high enantiomeric excess in selected cases (Scheme 46).[65]



Scheme 46. MS = Molecular sieves.

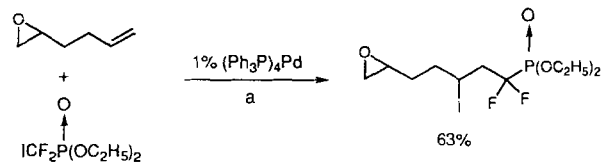
4. Intermolecular Heterotropic Additions

Halotropic additions of polyhalides to olefins have been catalyzed by ruthenium (Scheme 47)[66] and palladium



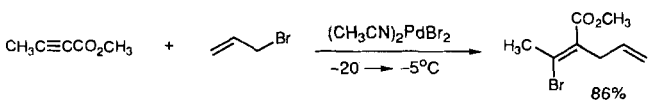
Scheme 47.

(Scheme 48).[67] Such reactions have characteristics very similar to those of radical reactions. The role of the metal may be mainly to serve as an electron shunt. On the other hand, the *cis*



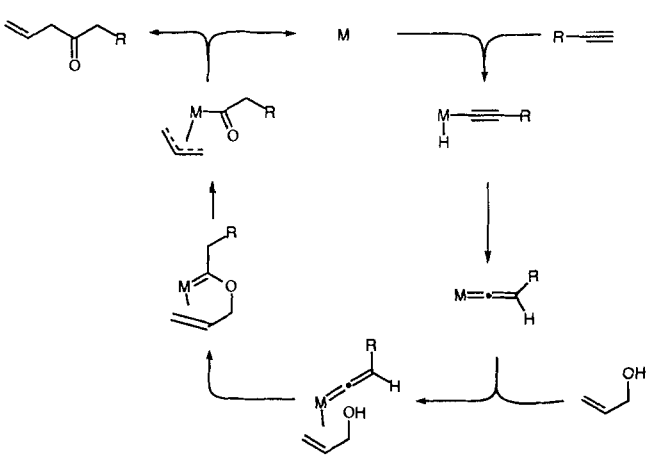
Scheme 48. a: Neat, at room temperature.

addition of allyl chlorides and bromides to alkynes (Scheme 49) appears to involve a halopalladation followed by carbametalation and dehalopalladation, in accord with the observed regioselectivity.[68]



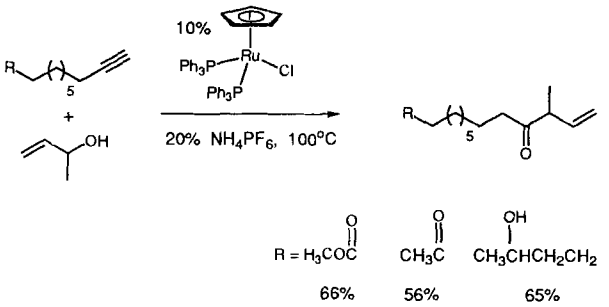
Scheme 49. The reaction was performed without solvent.

Novel transition metal complexes offer a particularly promising approach to new reactions involving heterotropic shifts. The ease of formation of vinylidene complexes from terminal alkynes suggested the catalytic cycle outlined in Scheme 50. Use of



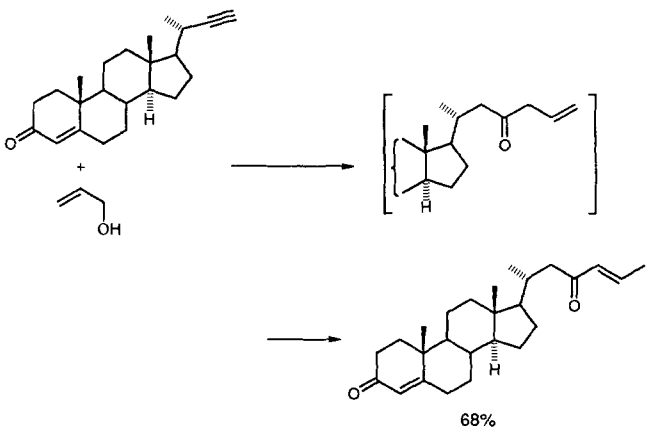
Scheme 50.

an allyl alcohol as the second component promotes a normally sluggish nucleophilic addition by precoordination. The resultant 1-metalla-3-oxa-1,5-hexadiene undergoes a metalla-Claisen rearrangement to set the stage for reductive elimination to form a β,γ-unsaturated ketone. The net result is the conversion of a terminal alkyne and an allyl alcohol into the simple adduct, and involves an oxytropic rearrangement. This process is realized with a ruthenium catalyst in a reaction that exhibited excellent chemo- and regioselectivity (Scheme 51).[69, 70] The dramatic



Scheme 51.

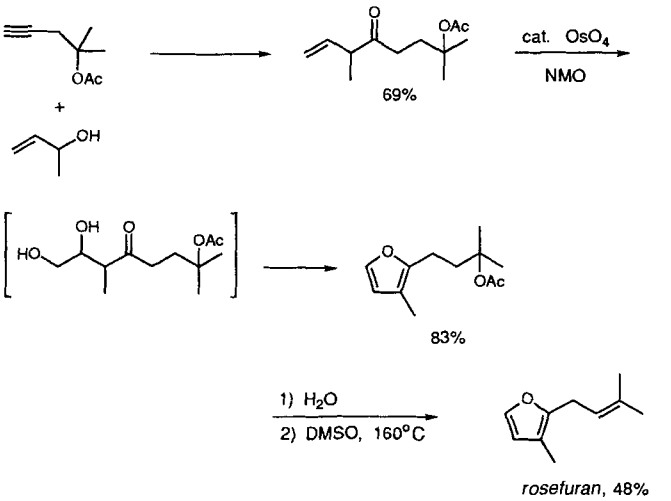
effect of the ligands on the course of the reaction can be seen by comparing Schemes 44 and 52. This latter example illustrates the utility of this methodology for the construction of functionalized steroid side chains such as that of the ganoderic acids, which function as ACE inhibitors.[71] By introducing phosphanes ligated to ruthenium, the pathway switches completely from the metallacycle pathway, which requires coordinative unsaturation, to the vinylidene pathway, which requires an electron-rich ruthenium center. The phosphanes both block coordination sites and enhance the electron-richness of the metal. Thus, from the same two reaction partners, addition may result



Scheme 52. Reaction conditions as in Scheme 48.

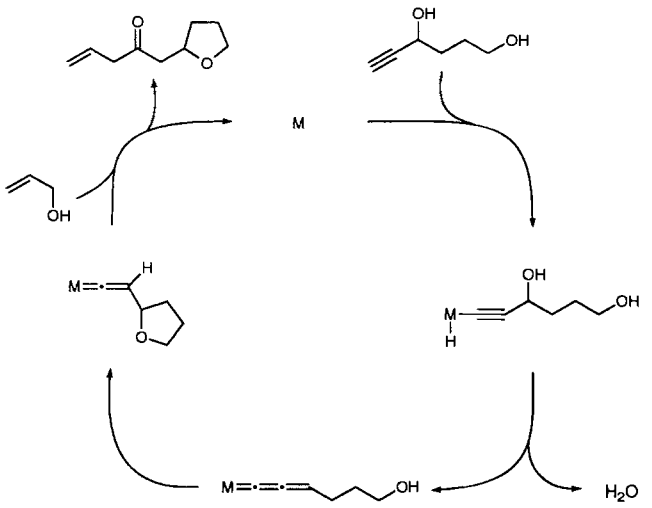
in a γ,δ-unsaturated ketone with no oxytropic rearrangement[63] or a β,γ-unsaturated ketone with oxytropic rearrangement.[69, 71]

The β,γ-unsaturated ketones also function as convenient furan precursors displaying atom economy. The synthesis of rosefuran (Scheme 53) exemplifies this methodology in which the recyclability of the *N*-methylmorpholine-*N*-oxide and acetic acid enables this sequence to be performed with only water as a by-product.[72]

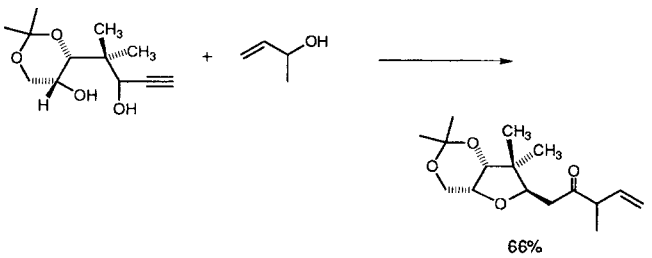


Scheme 53. Reaction conditions for the first step as in Scheme 48. DMSO = dimethylsulfoxide, NMO = *N*-methylmorpholine-*N*-oxide.

If the alkyne partner is a propargylic alcohol, the initial acetylide metal intermediate may undergo dehydration rather than protonation to form an allenylidene complex. Scheme 54 outlines a cyclization accompanying reconstitutive addition in which the only by-product is water.[73] In a model study which culminated in the synthesis of the spiroketal unit of the phosphatase inhibitor calyculin A, an alkyne derived from (*R*)-pantolactone condensed with 1-buten-3-ol to give the highly functionalized tetrahydrofuran unit with exclusive 2,5-*trans* configuration (Scheme 55).[74]



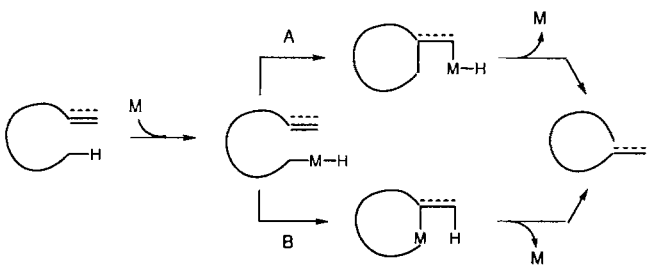
Scheme 54.



Scheme 55. Reaction conditions as in Scheme 48.

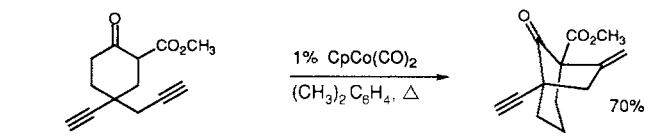
5. Prototropic and Related Cycloisomerizations

When the reactions described in Sections 2–4 are performed intramolecularly, the reaction constitutes a cyclization by isomerization as illustrated in Scheme 56 for a proton shift. Con-

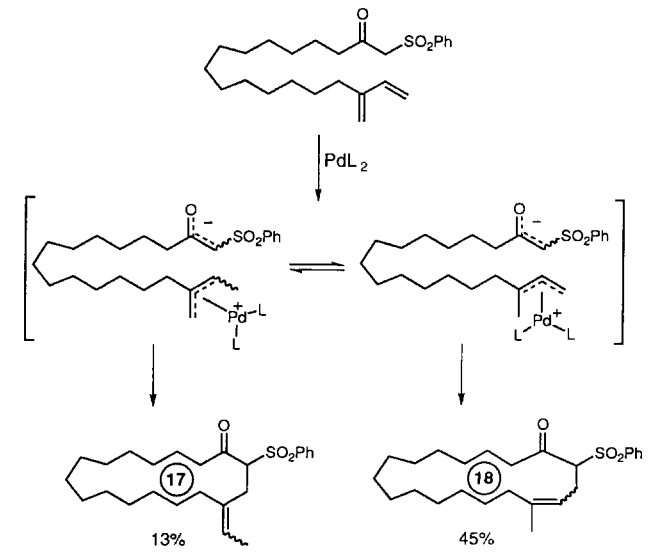


Scheme 56.

sidering the potential in this approach to cyclization, there are relatively few examples. For highly acidic compounds like β-keto esters, a cobalt complex effects addition to an alkyne (Scheme 57), presumably by a mechanism resembling path A in Scheme 56.[75] Additions of similar pronucleophiles to dienes occur with a palladium catalyst (Scheme 58).[76] This process probably involves initial hydropalladation to form π-allylpalladium intermediates (Scheme 56, path B), which undergo cy-

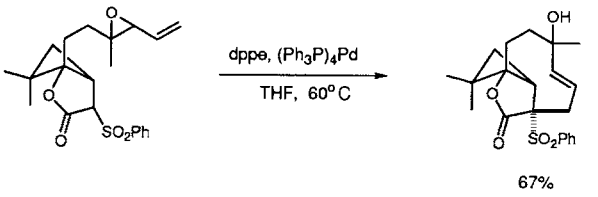


Scheme 57.



Scheme 58.

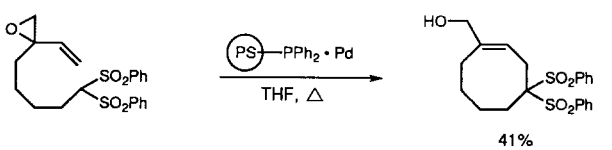
clization. The formation of macrocycles by this process is noteworthy. Initiating the cycloisomerization by deprotonation of the pronucleophile by the initial adduct between the Pd^0 catalyst and the vinyl epoxide has proven a powerful approach to macrocyclizations even for the formation of medium-sized rings.[77, 78] This reaction is a key step in the synthesis of punctaporonin B (Scheme 59).[79] With a polymeric catalyst cycliza-



Scheme 59. dppe = bis(diphenylphosphino)ethane.

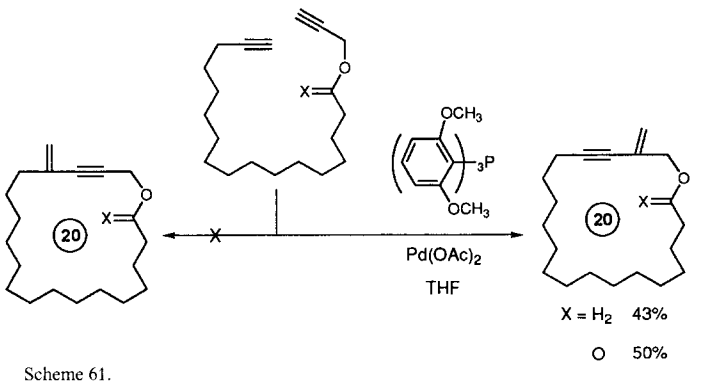
tions to medium as well as large rings can be performed at 0.5 M substrate concentration (Scheme 60).[80]

The ease of insertion of Pd^0 into acetylenic C–H bonds permits macrocyclizations also by a mechanism analogous to path



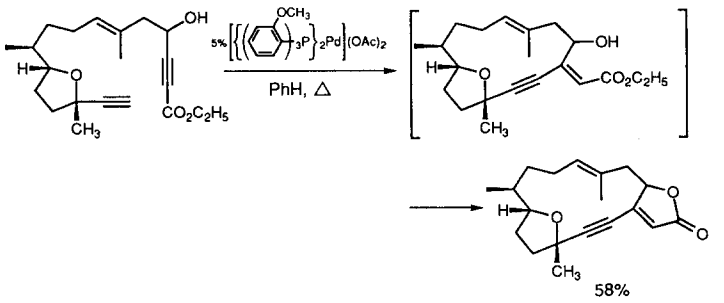
Scheme 60. PS = polystyrene.

B in Scheme 56. In the example of Scheme 61, although cyclization could occur in either direction, it is completely chemoselective: the acetylenic linkage proximal to the electronegative substituent serves as the acceptor.[81] In this reaction an activated



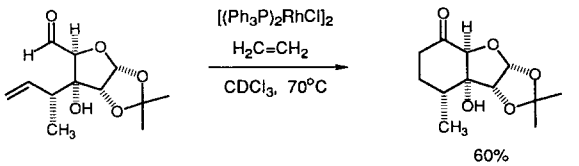
Scheme 61.

alkyne as in Scheme 62 results in cycloisomerization and concomitant butenolide formation.[82] This macrocyclization serves as a key step in a projected synthesis of the cembranoid pachiclavulanolide.



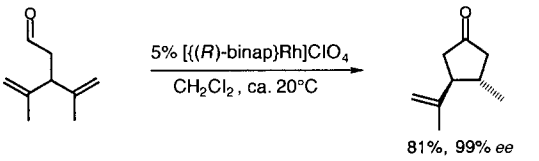
Scheme 62.

If the ability to insert into an aldehydic C–H bond (Scheme 26) is applied to intramolecular additions to unsaturated C–C bonds (intramolecular version of Scheme 12), the result is a novel cycloalkanone synthesis.[83] Although the formation of cyclopentanones proceeds most readily, cyclohexanones may also form (Scheme 63).[84] Excellent asymmetric induction may be observed (Scheme 64).[85]

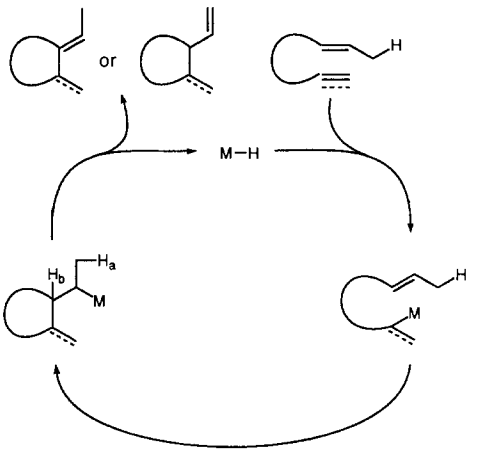


Scheme 63.

Initiating the reaction by hydrometalation and terminating the sequence by β-elimination (Scheme 65) opens a variant on Scheme 56 for cyclization that is a transition metal analogue of the intramolecular Alder ene reaction.[86] A further feature

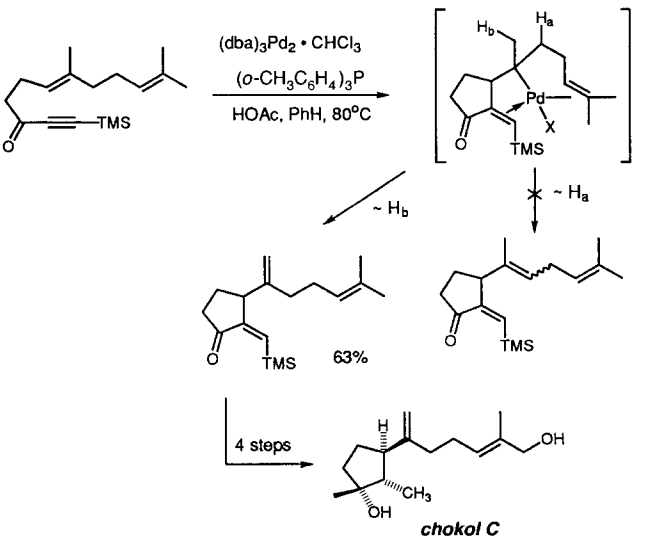


Scheme 64.



Scheme 65.

of this process is the ability to direct regioselectivity.[87] For example, cycloisomerization of the enyne of Scheme 66 may produce two Alder ene type products. Thermal reactions of analogous substrates generally favor migration of H_a. A hydri-

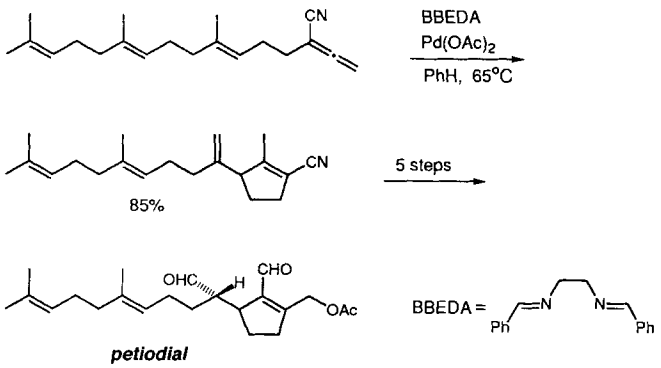


Scheme 66.

dopalladium catalyst, generated in situ from palladium (0) and acetic acid, yields the compound produced exclusively by migration of H_b.[88] This unorthodox regioselectivity derives from coordination of the remote double bond to palladium, thereby fixing the geometry of C–H_a to disfavor its β-elimination. The resultant product is easily converted into the cyclopentanoid antifungal agent chokol C. The total synthesis requires only

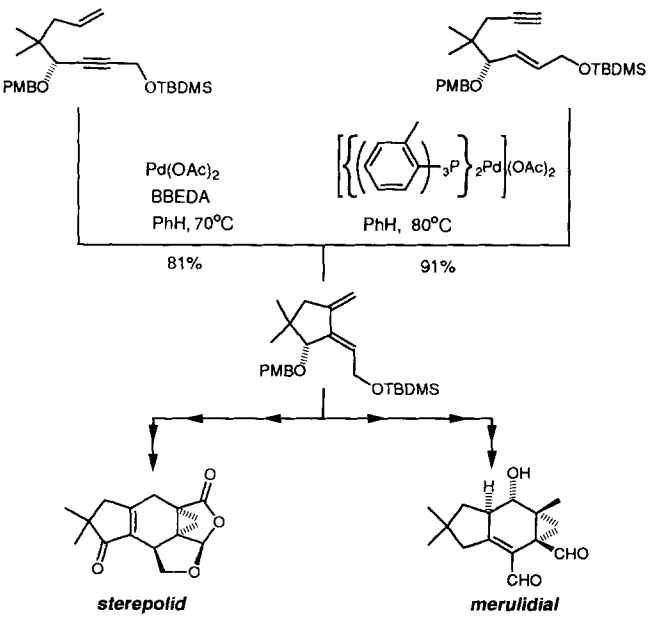
seven steps from commercially available geranyl bromide and *N*,*N*-dimethylacetamide. Syntheses of dendrobine[89] and picrotoxinin[90] utilized this cycloisomerization as a key step.

Replacing an alkyne by an allene may also lead to successful Alder ene type cyclizations. A synthesis of the marine antibiotic petiodial involves such a tranformation to create the properly substituted cyclopentenyl ring (Scheme 67).[91] A nickel-chromium catalyst supported on polystyrene[92] appears to be more general for cyclizations of enallenes.[93]



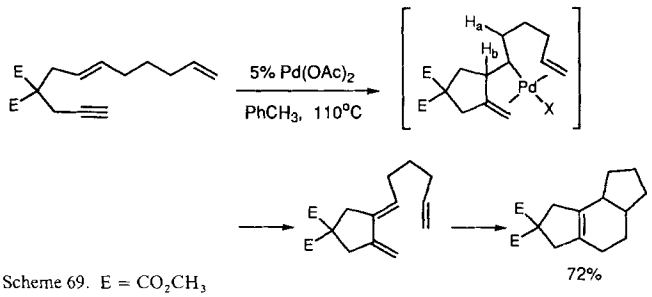
Scheme 67.

A major benefit of this type of transition metal catalyzed reation is the prospect of performing reactions not possible under thermal conditions. In Scheme 65 it is seen that the Alder ene type product derives from β-elimination of H_a in the primary cyclized product. Elimination of H_b to produce the synthetically versatile 1,3-dienes cannot be achieved thermally, but it can be envisioned to occur in this metal catalyzed version. Indeed, such a reaction proceeds in excellent yield[94, 95] and served as the key to a general strategy for the synthesis of the isolactaranes represented by sterepolide[96] and merulidial[97] (Scheme 68). The regioselectivity of the cycloisomerization of the enyne with the terminal triple bond reveals the effect of



Scheme 68. PMB = *para*-methoxybenzyl.

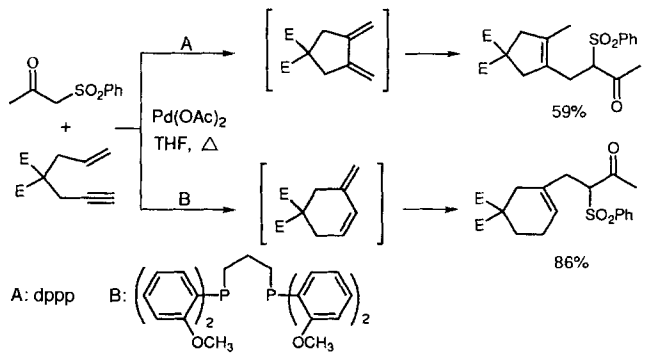
substitution at the allylic position: an alcohol or its derivative functions as a regiochemical control element directing the β-elimination to favor the 1,3-diene.[95, 98] The importance of this cycloisomerization stems from the ability of the 1,3-dienes to function in a second atom economical process, the Diels–Alder reaction. Tethering of remote substituents also favors 1,3-diene formation. Thus, cycloisomerization may be followed by cycloaddition to fold an acyclic polyenyne into a polycycle (Scheme 69).[94] While elimination of neither H_a nor H_b is particularly geometrically favorable, the C–H_b bond can



Scheme 69. E = CO_2CH_3

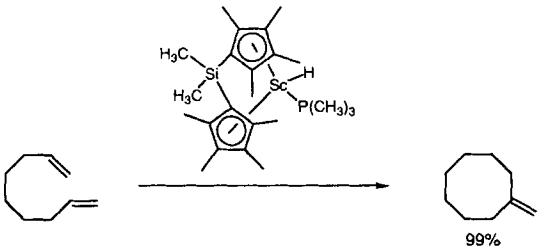
more nearly approach the requisite orientation and, being allylic, is weaker—two factors that favor formation of the 1,3-diene. The remote double bond then functions as the dienophile to form the tricycle. Similar reactions have also been catalyzed by a nickel–chromium complex, preferably supported on polystyrene.

The formation of 1,3-dienes by cycloisomerizations sets the stage for metal catalyzed additions of pronucleophiles as in Scheme 15 and path A in Scheme 16a. Since palladium can catalyze each step separately, finding the right ligand allows the steps to proceed successively in a one-pot reaction (Scheme 70).[99] Surprisingly, changing the ligand completely



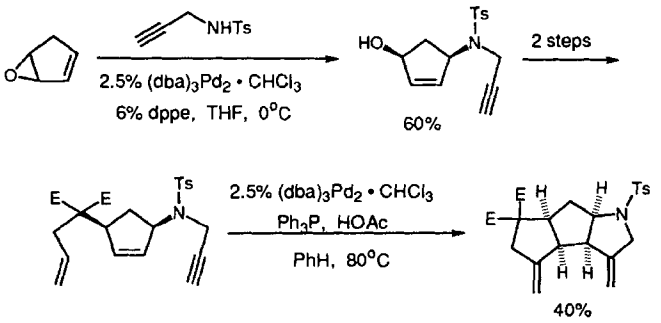
Scheme 70. The ligands for the routes A and B are listed separately. E = CO_2CH_3.

changes the regioselectivity of the initial cyclization from five- (Path A) to six-membered (Path B) ring formation. Path B normally is not observed in the simple cycloisomerizations. A scandium hydride catalyzes the cycloisomerization of α,ω-dienes by a similar mechanism.[100] Remarkably, medium and large rings form readily (Scheme 71), although the catalyst cannot tolerate Lewis basic sites. Other metals including palladium,[101] rhodium,[101] and nickel[102] are reported to cycloisomerize α,ω-dienes with varying success.



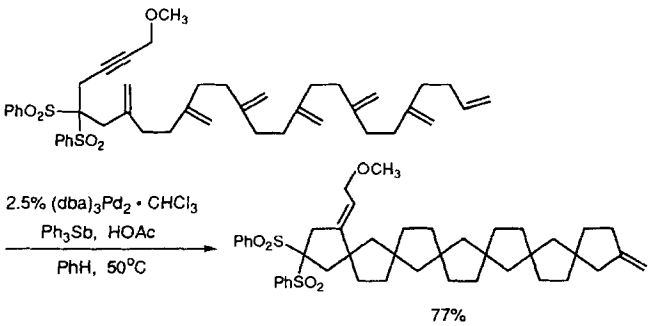
Scheme 71.

Another prospect for invention is the interception of the initial monocycle of Scheme 65 by further unsaturated functional groups. Construction of quinanes and heteroquinanes involves capture by an additional double bond system (Scheme 72) in a



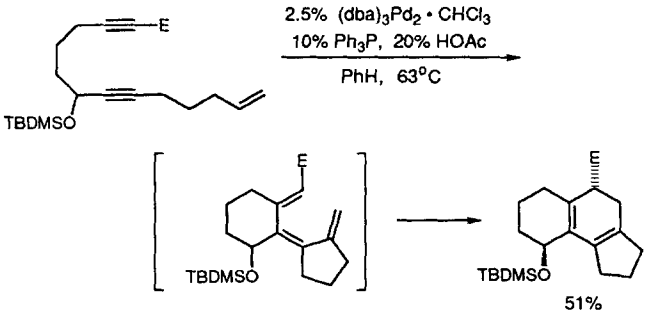
Scheme 72. Ts = *para*-tolylsulfonyl, E = CO_2CH_3.

sequence initiated by a palladium catalyzed addition of a vinyl epoxide and a pronucleophile.[103] The juxtaposition of the unsaturated bonds determines the nature of the ring system that will be created, as illustrated for a linear azatriquinane synthesis in Scheme 72. The number of rings that can be created equals the number of double plus triple bonds minus one. Thus, zipping up the heptaenyne in Scheme 73 with a palladium catalyst creates a heptaspirane that resembles a molecular rope.[104]



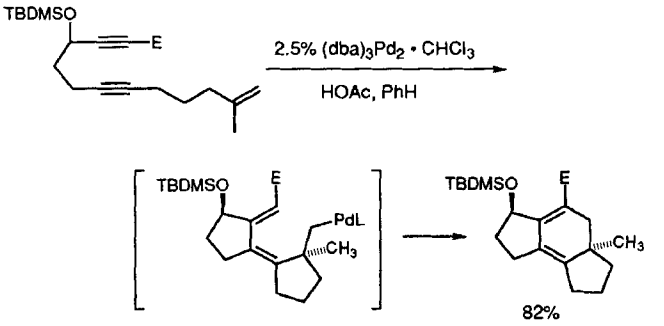
Scheme 73.

Replacing the internal double bond by another triple bond provides a novel strategy for the synthesis of 1,3,5-hexatrienes (Scheme 74). These intermediates further cycloisomerize by a rotoselective disrotation to form a single diastereomeric tricycle. Preclusion of the final β-elimination does not stop cyclization, since the intermediate with a terminal palladium moiety



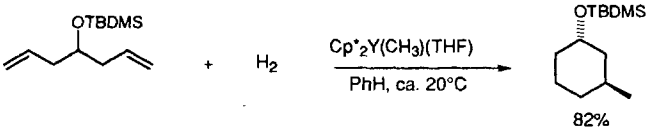
Scheme 74. E = CO_2CH_3.

may bite back on itself to produce a tricycle similar to that derived from electrocyclization of a hexatriene (Scheme 75). Other mechanisms also explain this efficient tricyclization.



Scheme 75.

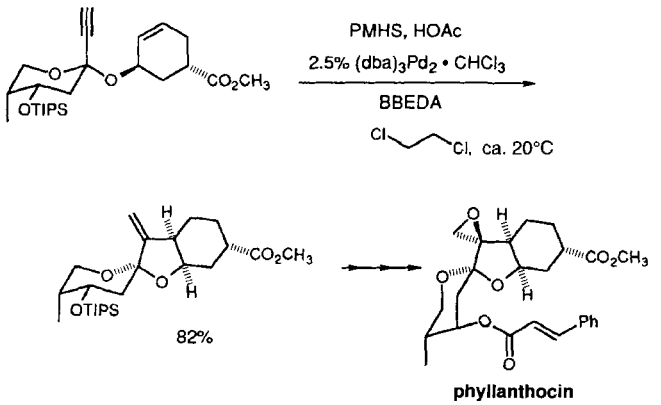
Another opportunity for innovation envisions interception of the C–M bond of the initial monocycle of Scheme 65 by an external trap such as hydrogen to effect a reductive cyclization. Indeed, an yttrium hydride formed in situ permits an atom economical addition of hydrogen with concomittant cyclization, which dominates over simple reduction with appropriate substrates (Scheme 76).[105] A more general but less atom econom-



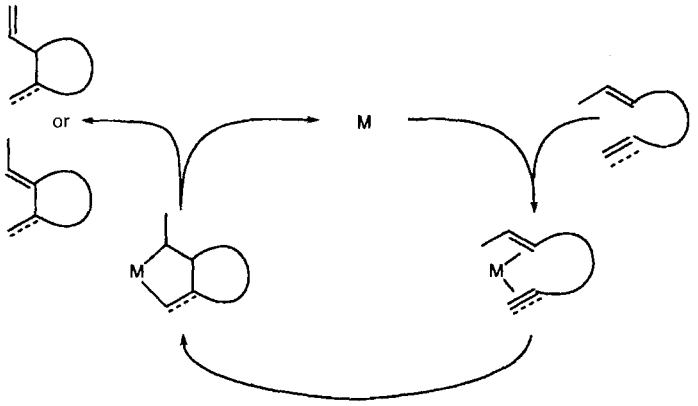
Scheme 76. Cp*.

ical reductive cyclization employs a proton and a hydride source as an equivalent of molecular hydrogen.[106] This palladium catalyzed reductive cyclization of an enyne served as a key step in a synthesis of the clinically useful phyllanthocin (Scheme 77).[107]

An alternative mechanism for cycloisomerization recognizes the chelating potential of α,ω-unsaturation (Scheme 78). In fact, some of the palladium catalyzed cyclizations of Schemes 66–69, 72–75, and 77 may proceed through such a pathway.[86b, 94] Use of "tetramethoxycarbonylpalladacyclopentadiene" (TCPC) as catalyst for such cycloisomerizations is

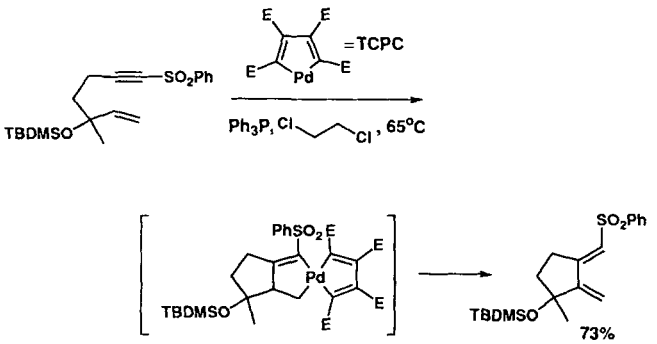


Scheme 77. PMHS = polymethylhydrosiloxane. TIPS = triisopropylsilyl.

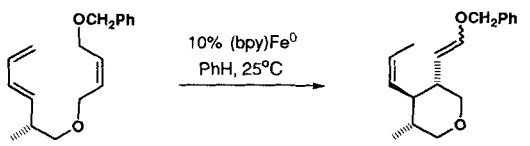


Scheme 78.

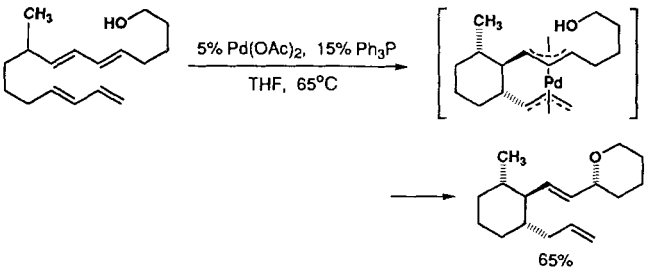
be lieved to involve such a pathway (Scheme 79).[108] The iron(0) catalyzed Alder ene type process (Scheme 80) appears to involve such a mechanism.[109] The intramolecular analogue of the diene telomerization reaction (Scheme 31)[110] also invokes a similar concept (Scheme 81) via a bis(π-allyl)palladium intermediate.



Scheme 79. E = CO_2CH_3.

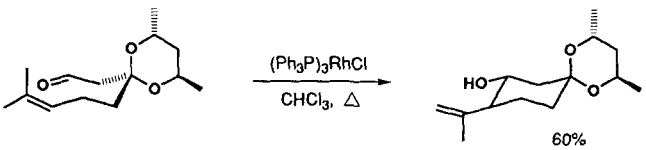


Scheme 80. bpy = bipyridine.



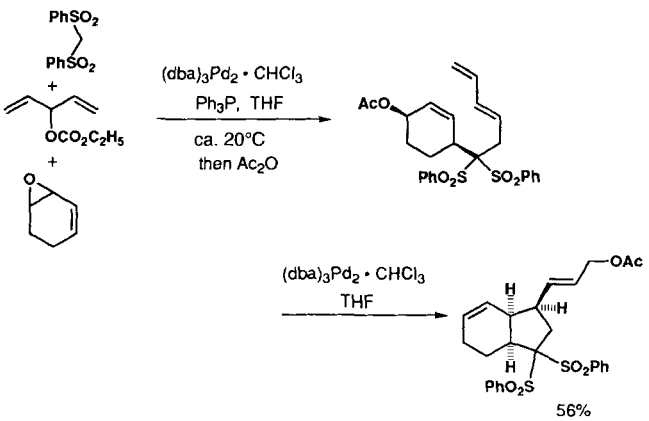
Scheme 81.

Replacment of an olefin by a carbonyl group leads to an oxaene reaction. While typical Lewis acids normally catalyze this reaction, such cycloisomerizations have also been reported with Wilkinson's catalyst (Scheme 82), although the mechanism of this catalysis is obscure.[111, 112]



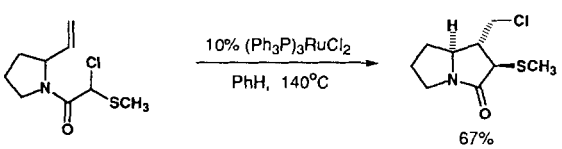
Scheme 82.

Cycloisomerizations can also involve heterotropic rearrangements. An oxytropic cyclization involving π-allylpalladium intermediates proceeds stereospecifically to the bicycle with an *endo*-oriented side chain (Scheme 83).[113] The ruthenium



Scheme 83.

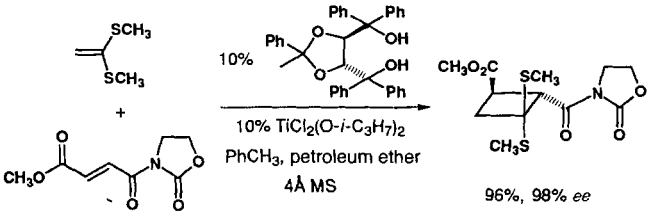
catalyzed halotropic addition occurs intramolecularly (Scheme 84).[114] This reaction may be extendable to form medium and large rings.[115]



Scheme 84. Only the major product is shown.

6. Cycloadditions

The fastest way to increase molecular complexity is to form more than one bond at a time as in cycloadditions. Orbital symmetry reveals that Hückel-like (4n + 2) transition states are favored whereas 4n transition states are forbidden in a geometrically favorable suprafacial conformation. However, metal catalysis may succeed in both cases since it opens a plethora of mechanistic possibilities beyond the concerted cycloaddition. The orbital-symmetry-forbidden [2 + 2] suprafacial cycloaddition is catalyzed by early transition metals which seem to function as Lewis acids. Chiral cyclobutanes (Scheme 85) and cyclobutenes form with excellent enantioselectivity.[116]



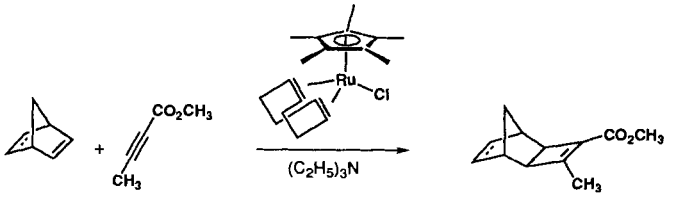
Scheme 85.

A more promising strategy involves reductive elimination of metallacyclopentenes that may form from alkynes and alkenes (Scheme 86). Such an intermediate has been invoked in the



Scheme 86.

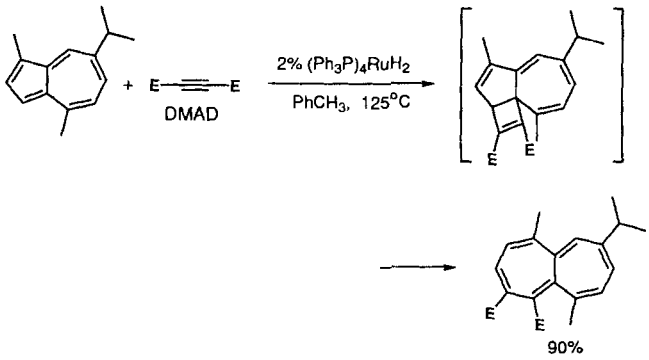
ruthenium catalyzed Alder ene reaction (Scheme 41). With a strained alkene partner such as norbornene or norbornadiene, such a [2 + 2] cycloaddition occurs in the presence of a coordinatively unsaturated ruthenium complex (Scheme 87).[117] In



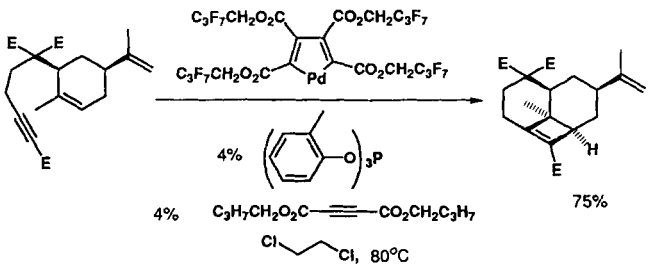
Scheme 87. The yield is 79% relative to norbornene and 87% relative to norbornadiene.

contrast to other diene reaction partners (vide infra), norbornadiene undergoes only [2 + 2] cycloaddition. Other catalysts have been reported to behave similarly.[118] This reaction expanded an azulene into a heptalene with dimethyl acetylenedicarboxylate (DMAD) (Scheme 88).[119]

Palladacyclopentadienes promote [2 + 2] cycloadditions of enynes (Scheme 89).[120] The resulting cyclobutenes undergo

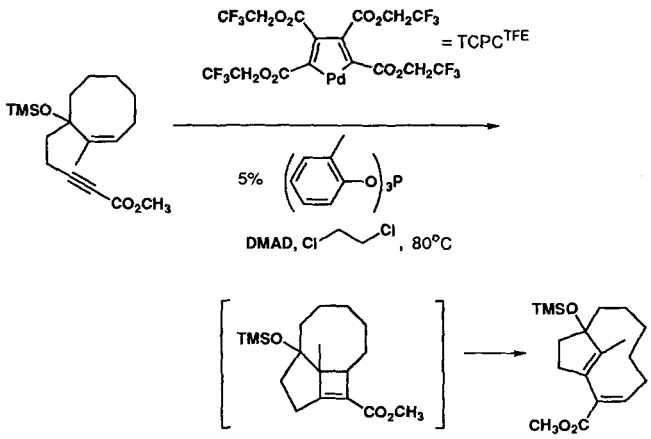


Scheme 88. E = CO_2CH_3.



Scheme 89.

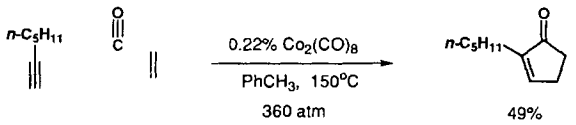
thermal conrotatory ring opening to form 1,3-dienes. Shortening the tether connecting the double and triple bonds of the substrate from four to three atoms lowers the temperature for ring opening so much that only the enyne metathesis product is observed (Scheme 90).[121] The presence of bicyclic structures like those depicted in Scheme 90 in many natural products makes this simple approach for their creation very attractive.



Scheme 90.

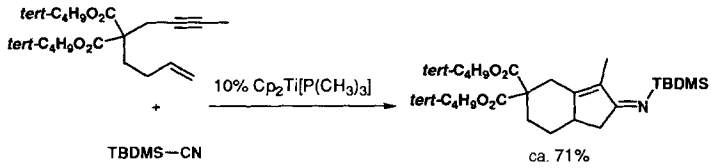
Intercepting the metallacyclopentene by carbon monoxide creates the structurally important cyclopentenones. Surrogates for CO such as isonitriles react analogously. With dicobalt octacarbonyl as the complex, this addition is known as the Pauson–Khand reaction and is an important synthesis of cyclopentenones.[122] Unfortunately, the reaction generally requires a stoichiometric amount of the cobalt complex, although a recent

example has illustrated the potential for a catalytic process (Scheme 91).[123] An analogous process catalytic in a titanium complex traps the cyclopentene with a silylisonitrile generated in



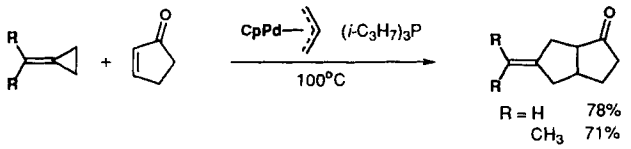
Scheme 91.

situ by isomerization of a silylcyanide (Scheme 92).[124] Ni^0 effects a similar reaction, which, however, requires a stoichiometric amount of the "catalyst."[125] These sequences constitute a [2 + 2 + 1] approach for five-membered ring construction.



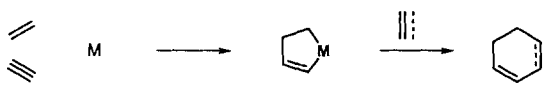
Scheme 92.

A [3 + 2] cycloaddition also generates five-membered rings. A cooligomerization of methylenecyclopropane with electron-deficient or strained alkenes produces methylenecyclopentanes even with substituted substrates (Scheme 93).[126] Whether the reaction involves ring opening to a trimethylenemethane complex or direct oligomerization through a metallacycle has not been elucidated.



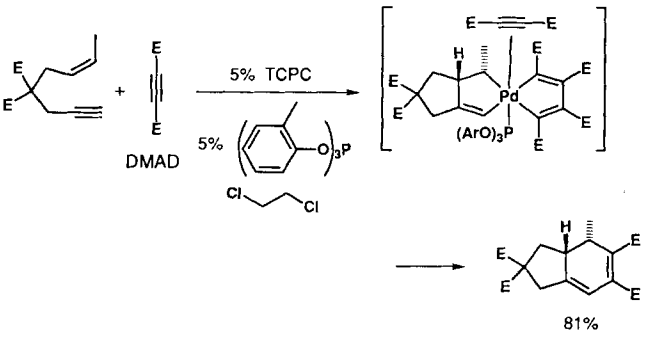
Scheme 93.

Intercepting the metallacycle of Scheme 86 with a two-carbon trap generates six-membered rings in a formal [2 + 2 + 2] type of cycloaddition (Scheme 94). Cycloisomerization of enynes

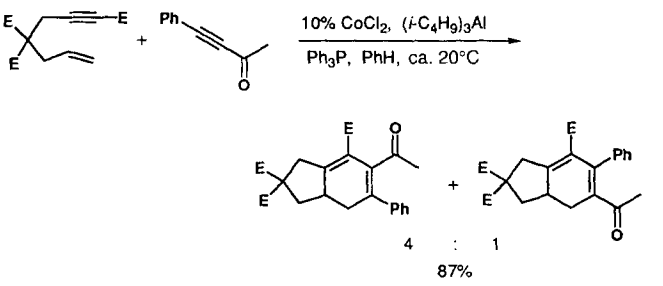


Scheme 94.

with TCPC in the presence of excess dimethyl acetylenedicarboxylate leads to the bicyclic derivative formed by trapping the purported palladacyclopentene intermediate (Scheme 95).[108] A low-valent cobalt complex generated in situ extends this reaction to monoactivated alkynes (Scheme 96),[127] whereas tethering all three unsaturated bonds permits [2 + 2 + 2] cycloaddi-

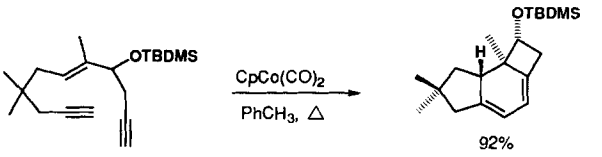


Scheme 95.



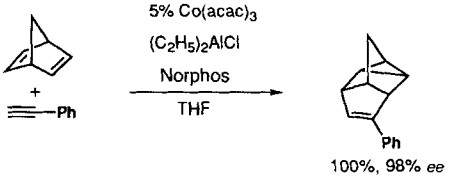
Scheme 96.

tion even without activating groups (Scheme 97),[128] although a stoichiometric amount of the cobalt "catalyst" is required because the product is strongly coordinated to cobalt.



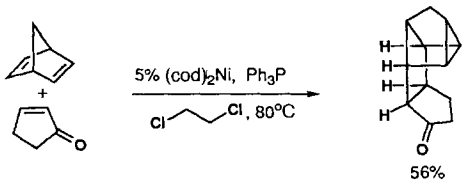
Scheme 97.

Norbornadiene undergoes [2 + 2 + 2] cycloadditions (homo-Diels–Alder reactions) with alkynes in the presence of a cobalt catalyst.[129] Since norbornadiene functions as a bidentate ligand to direct the initial cobaltacycle to the *endo* face, deltacyclenes (Scheme 98) rather than cyclobutenes (Scheme 87)[130]



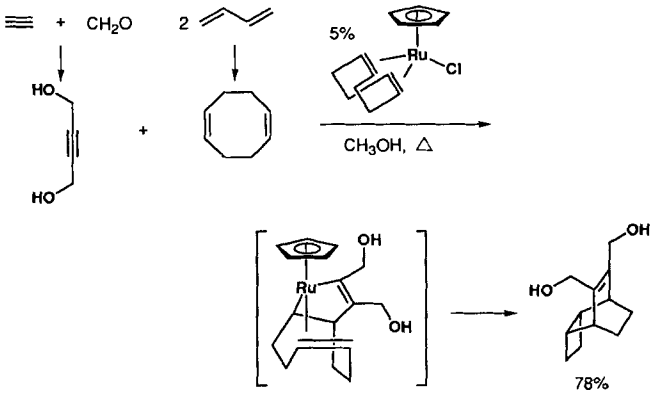
Scheme 98. Norphos = 5,6-bis(diphenylphosphino)norbornene.

result. As illustrated, placing the metal in a chiral ligand environment may impart high enantioselectivity. Using a nickel catalyst enables enones to be used as the "homodienophile" (Scheme 99),[131] which suggests that the course of reaction in Scheme 94 may be applicable to metallacyclopentanes. 1,5-Cy-



Scheme 99.

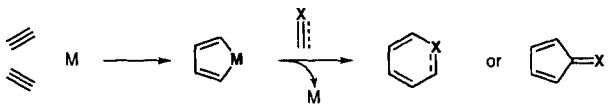
clooctadiene participates efficiently in [2 + 2 + 2] cycloadditions (bis-homo-Diels–Alder reaction) with alkynes in the presence of a ruthenium catalyst in which a ruthenacyclopentene may be postulated as an intermediate (Scheme 100).[132] The



Scheme 100.

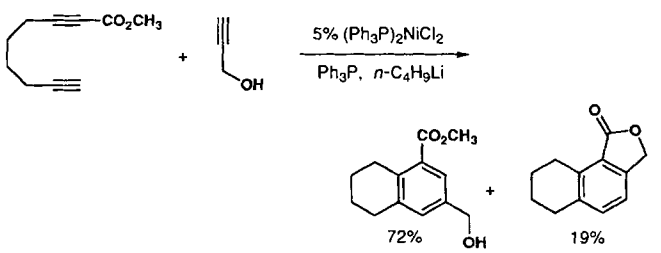
atom efficiency of this process for construction of the energy-rich tricycle becomes evident when it is realized that both reaction partners are synthesized by simple addition reactions. Thus, by a series of three additions, acetylene, formaldehyde (or other aldehydes or ketones), and butadiene combine to form the tricyclo[4.2.2.$0^{2,5}$]dec-7-enes. All other are used catalytically.

The formation of metallacyclopentadienes (Scheme 101) appears to be even more facile than that of metallacyclopentenes.

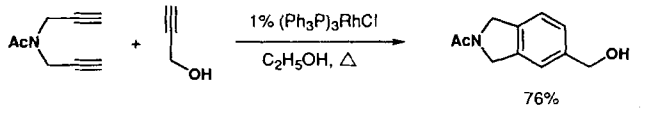


Scheme 101.

The classical example is the construction of benzenoid arenes by cotrimerization of alkynes.[133] Many metals catalyze this process, but nickel (Scheme 102),[134] rhodium (Scheme 103),[135]

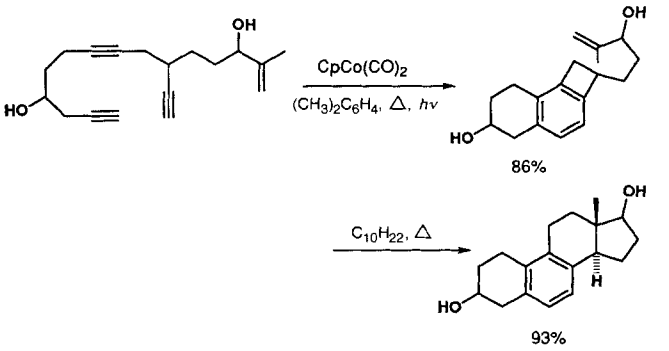


Scheme 102.



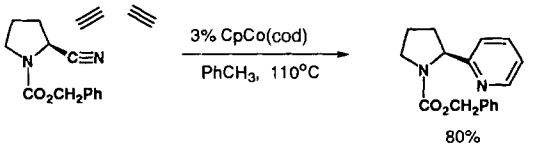
Scheme 103.

and especially cobalt (Scheme 104)[136] have proven particularly effective. In contrast to the reaction in Scheme 97, the cobalt dissociates easily from the arene, and the reaction is truly cata-



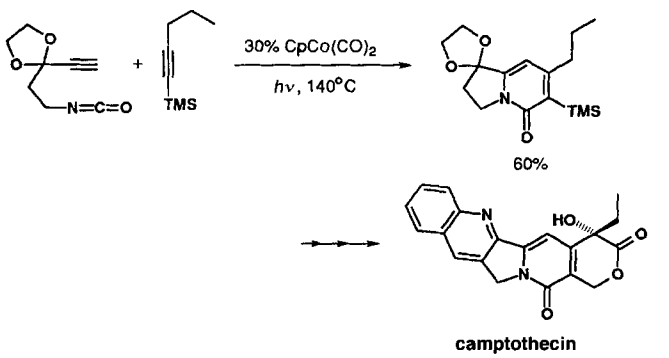
Scheme 104.

lytic in cobalt. This example illustrates the strain that may be incorporated into the cycloaddition product, which is released in a subsequent thermal electrocyclic reaction to set the stage for a final [4 + 2] thermal cycloaddition. Thus, by a series of simple cycloisomerizations, an acyclic precursor is folded into the entire steroid skeleton. Replacing an alkyne by the isoelectronic nitrile leads to a very efficient pyridine synthesis (Scheme 105).[137, 138] Cumulative unsaturation represented by



Scheme 105.

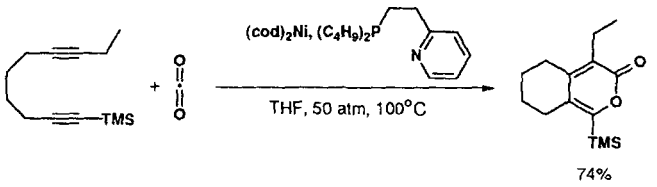
an isocyanate effectively captures the cobaltacyclopentadiene (Scheme 106)—an important step for the synthesis of the antitumor agent camptothecin.[139] Alkenes also function as effective



Scheme 106.

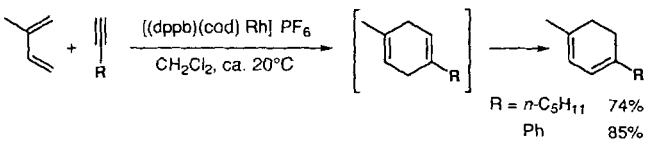
traps. Since the resultant cyclohexadienes coordinate extremely well to cobalt, normally stoichiometric amounts of the "catalyst" are required in such cases. Niobium complexes also initiate [2 + 2 + 2] cycloadditions of alkynes.[140]

With carbon monoxide, capture of the metallacyclopentadiene normally generates the cyclopentadienone rather than pyran derivatives. However, since cyclopentadienones are excellent ligands, the products are normally metal complexes, and thus the reactions require stoichiometric amounts of the metal.[141] On the other hand, carbon dioxide participates in a [2 + 2 + 2] type cycloaddition under the influence of a nickel catalyst (Scheme 107).[142] Aldehydes may function in similar fashion to produce pyrans.[143]



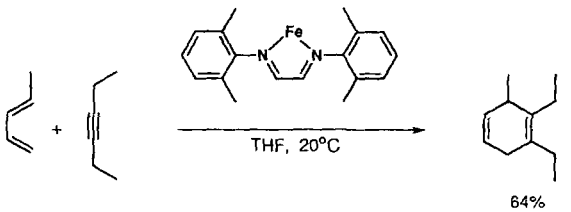
Scheme 107.

Precoordination onto a transition metal promotes [4 + 2] cycloadditions that might not occur thermally or occur only at unacceptably high temperatures. On use of a coordinatively unsaturated electrophilic rhodium complex, dienes react with unactivated alkynes (Scheme 108) to give the adduct in which



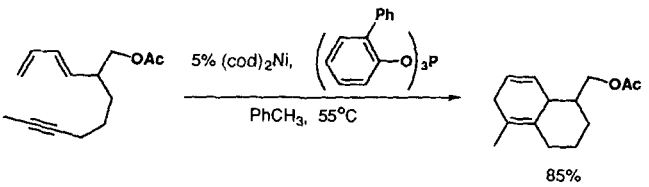
Scheme 108. dppb = 1,4-bis(diphenylphosphino)butane

isomerization of the double bonds to the thermodynamically more stable conjugated isomer accompanies cycloaddition.[144] With an iron(0) complex, catalysis of the cycloaddition occurs without isomerization of the double bonds (Scheme 109).[145]

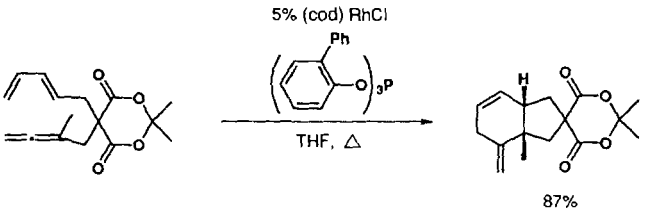


Scheme 109.

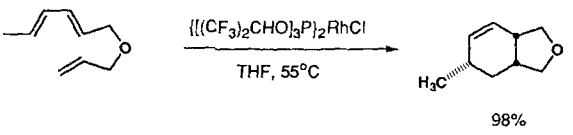
While the "para" type product dominates, other isomers also form. Tethering the partners overcomes the regioselectivity problem, and catalysis may be accomplished both with rhodium[146] and nickel (Scheme 110)[147] complexes. Rhodium catalysts enable both allenes (Scheme 111)[148] and simple olefins (Scheme 112)[148] to serve as "dienophiles." The ability of transition metals to promote ring opening of strained rings has led



Scheme 110.

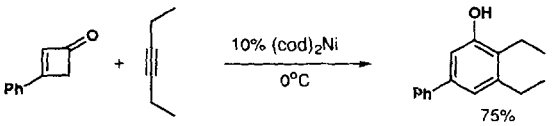


Scheme 111.



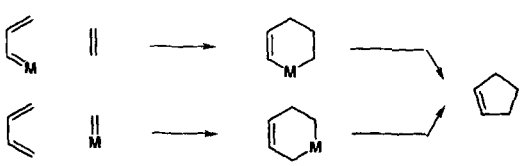
Scheme 112.

to a novel Diels–Alder type cycloaddition of cyclobutenones with alkynes, presumably involving a vinylketene coordinated to the metal as the diene partner (Scheme 113).[149] Unsymmetrical alkynes show no regioselectivity.



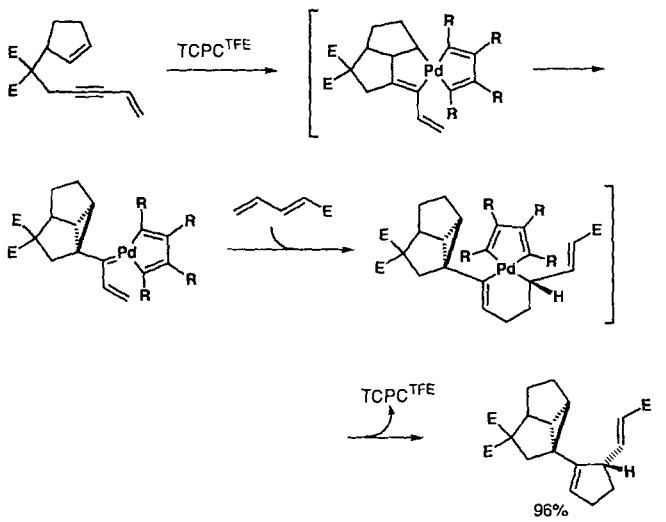
Scheme 113.

A new type of approach for cycloaddition proposes the use of a metalladiene or metallaenophile as reaction partner (Scheme 114). Although such carbenes normally participate in [2 + 2] cycloadditions leading to metathesis type products, the potential for creation of unusual ring systems not directly accessible by Diels–Alder reactions, such as cyclopentenes, make the search for such processes highly worthwhile. In the first example of a metalladiene participating in a cycloaddition, the vinylcar-



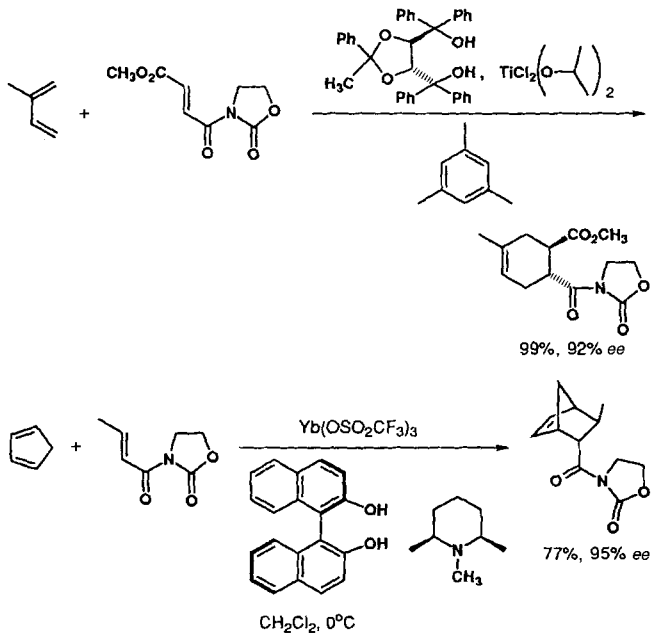
Scheme 114.

bene is generated in situ by a cycloisomerization of an enyne as in Scheme 115.[150] Trapping of the palladadiene intermediate requires a diene or enyne and proceeds with high regio- and diatereoselectivity.[151] Thus, simple metal catalyzed isomerization and addition convert simple building blocks into complex polycycles with high atom economy.



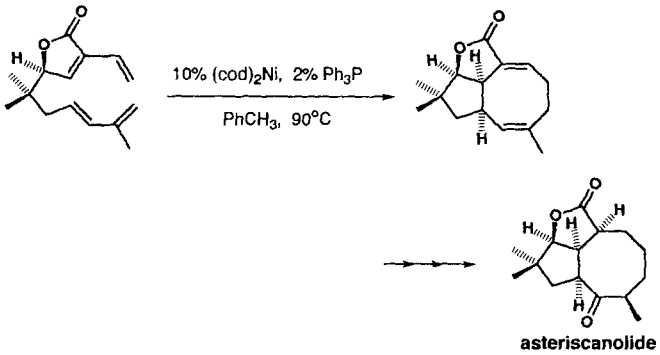
Scheme 115. E = CO_2CH_3, R = $CO_2CH_2CF_3$.

A more traditional catalysis of the Diels–Alder reaction utilizes the transition metal as a Lewis acid. These catalysts offer the advantage of imparting enantioselectivity as exemplified by titanium[152] and lanthanide (Scheme 116)[153] catalysts.



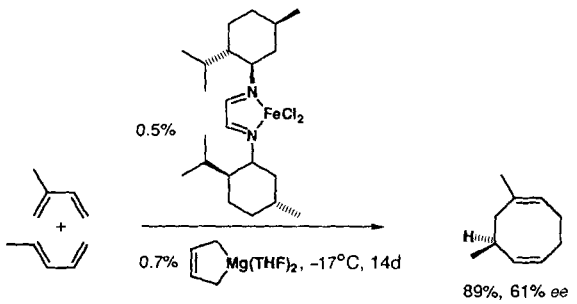
Scheme 116.

Higher order cycloadditions are also promoted by transition metals. The [4 + 4] cycloaddition to cyclooctanes catalyzed by nickel controls regioselectivity by tethering the two groups.[154–156] An effective synthesis of (+)-asteriscanolide highlights the practicality of this cycloaddition (Scheme 117).[157] While intermolecular homocoupling of dienes also



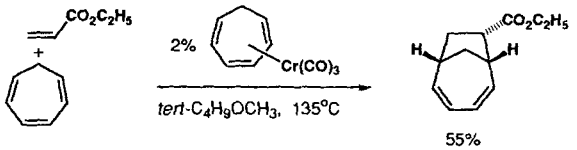
Scheme 117.

may be achieved with the nickel catalyst, an iron catalyst has effected selective cross-coupling of two different dienes asymmetrically (Scheme 118).[158] An alternative paradigm for eight-



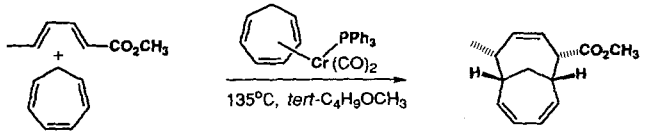
Scheme 118.

membered ring construction is [6 + 2] cycloadditions. On use of a chromium catalyst, cycloheptatriene (Scheme 119) and its heterocyclic variants form cycloadducts with typical dieno-



Scheme 119.

philes.[159] This reaction has been extended to [6 + 4] cycloadditions, which, however, proceed much slower (only 36% complete after 18 h, Scheme 120). Many further prospects for metal assisted cycloadditions not achievable otherwise abound.



Scheme 120.

7. Conclusion

The tremendous strides in organic synthesis in the last several decades have engendered the feeling that no target is too complex to tackle by synthesis. However, such notions founder if the practicality is questioned. It is not adequate only to complete a synthesis; the effectiveness of the route is critical. Improving the ability to design molecular structures more efficiently stems largely from enhancements in the selectivity of available reactions and reagents. Increasingly, transition metal catalyzed reactions are proving their value for such goals. No reaction better exemplifies this point than the transition metal catalyzed cross-coupling. However, in solving such problems of selectivity, the issue of atom economy is normally neglected. The scale-up of a complex synthesis from the research laboratory to the plant cannot ignore this fundamental question. This issue has long been recognized by the commodity chemical industry for obvious reasons. Only recently has the subject become an issue for the synthesis of smaller volume products. As the legitimate concerns of society for wise use of our limited resources with minimal environmental risk grow, the ability to produce the chemicals needed to improve the human condition will hinge on the inventfulness of chemists to design more efficient syntheses.

As a start, the repertoire of reactions that are highly atom economical must increase. The prospects for invention are vast. Clearly, the molecular gymnastics—even acrobatics—for organic molecules that transition metals direct represent promising opportunities for new invention.

Several themes become evident. Many reactive intermediates do not participate usefully in synthetic reactions either because of the harshness of the conditions required to generate them or because their high reactivity makes their trapping impractical. The ability of transition metals to create such "reactive" intermediates under mild conditions promotes specific further reactions with a selectivity tunable by the ligand environment. Precoordination imparts both selectivity and kinetic reactivity to otherwise unselective or unreactive systems. One additional benefit that emerges from this last concept addresses chemical safety. By imparting chemical reactivity only during the synthesis, the chemicals to be handled and/or stored can be more benign.

The reactions described herein represent only a beginning towards achieving these objectives. Clearly, the vastness of the territory to be explored assures exciting opportunities for generations. We still require "functional groups" to assist selective activation for new bond formation. An ideal for which we should strive is the elimination of such a requirement when the functional groups are absent from the ultimate target. We have barely begun to broach such a strategy, which today seems unattainable. Undoubtedly, such pessimism will fade as new breakthroughs emerge, especially those emanating from the domain of transition metal catalysis.

I am thankful for the many coworkers who have contributed both intellectually and experimentally to our program and who have been identified in the references. The National Science Foundation and the National Institutes of Health through the General Medical Science Institute have provided the financial support for our work.

Received: May 13, 1994 [Z66IE]
German version: *Angew. Chem.* **1995**, *107*, 285

[1] B. M. Trost, *Science* **1991**, *254*, 1471.
[2] I. Tkatchenko in *Comprehensive Organometallic Chemistry, Vol. 8* (Ed.: G. Wilkinson), Pergamon, Oxford, **1982**, p. 101; J. K. Stille in *Comprehensive Organometallic Chemistry, Vol. 4* (Eds: B. M. Trost, I. Fleming, M. F. Semmelhack), Pergamon, Oxford, **1991**, p. 913. For recent developments regarding selectivity, see G. D. Cuny, S. L. Buchwald, *J. Am. Chem. Soc.* **1993**, *115*, 2066; M. E. Broussard, B. Juma, S. G. Train, W.-J. Peng, S. A. Laneman, G. G. Stanley, *Science* **1993**, *260*, 1784; N. Sakai, S. Mano, K. Nozaki, H. Takaya, *J. Am. Chem. Soc.* **1993**, *115*, 7033.
[3] J. Boor, *Ziegler–Natta Catalysts and Polymerization*, Academic Press, New York, **1979**; *Transition Metals and Organometallics as Catalysts for Olefin Polymerization* (Eds.: W. Kaminsky, H. Sinn), Springer, Berlin, **1987**; *Transition Metal Catalyzed Polymerizations; Ziegler–Natta and Metathesis Polymerizations* (Ed.: R. P. Quirk), Cambridge University Press, Cambridge, **1988**; *Catalytic Olefin Polymerization* (Eds.: T. Keii, K. Soga), Elsevier, New York, **1990**.
[4] E. S. Brown in *Organic Synthesis via Metal Carbonyls Vol. 2* (Eds.: I. Wender, P. Pino), Wiley-Interscience, New York, **1977**, p. 655; C. A. Tolman, R. J. McKinney, W. C. Seidel, J. D. Druliner, W. R. Stevens, *Adv. Catal.* **1985**, *33*, 1.
[5] a) *Comprehensive Organic Synthesis Vol. 5* (Eds.: B. M. Trost, I. Fleming, L. A. Paquette), Pergamon, Oxford, **1991**; b) W. Oppolzer in ref. [5a], p. 315; c) S. M. Weinreb in ref. [5a], p. 401; d) D. L. Boger in ref. [5a], p. 451; e) W. R. Roush in ref. [5a], p. 513; f) U. Pindur, G. Lutz, C. Otto, *Chem. Rev.* **1993**, *93*, 741.
[6] H. B. Kagan, D. Riant, *Chem. Rev.* **1992**, *92*, 1007.
[7] S. G. Davies, *Organotransition Metal Chemistry. Applications to Organic Synthesis*, Pergamon, Oxford, **1982**, Chapter 7; H. M. Colquhoun, J. Holton, D. J. Thompson, M. V. Twigg, *New Pathways for Organic Synthesis*, Plenum, New York, **1984**, Chapter 5.
[8] B. M. Trost, R. J. Kulawiec, *J. Am. Chem. Soc.* **1993**, *115*, 2027. For other Ru catalyzed isomerizations of allyl alcohols, see J. E. Bäckvall, U. Andreasson, *Tetrahedron Lett.* **1993**, *34*, 5459; D. V. McGrath, R. H. Grubbs, *Organometallics* **1994**, *13*, 224.
[9] W. Ziegenbein in *Chemistry of Acetylenes* (Ed.: H. G. Viehe), Dekker, New York, **1969**, pp. 169–256.
[10] B. M. Trost, T. Schmidt, *J. Am. Chem. Soc.* **1988**, *110*, 2301.
[11] C. Guo, X. Lu, *J. Chem. Soc. Perkin Trans. 1* **1993**, 1921; X. Lu, J. Ji, D. Ma, W. Shen, *J. Org. Chem.* **1991**, *56*, 5774; D. Ma, X. Lu, *Tetrahedron*, **1990**, *46*, 3189, 6319; D. Ma, Y. Yu, X. Lu, *J. Org. Chem.* **1989**, *54*, 1105.
[12] Cf. H. Nemoto, H. N. Jimenez, Y. Yamamoto, *J. Chem. Soc. Chem. Commun.* **1990**, 1304; H. Frauenrath, M. Sawicki, *Tetrahedron Lett.* **1990**, *31*, 649; D. P. Curran, P. B. Jacobs, R. L. Elliott, B. H. Kim, *J. Am. Chem. Soc.* **1987**, *109*, 5280.
[13] S. Sato, H. Okada, I. Matsuda, Y. Izumi, *Tetrahedron Lett.* **1984**, *25*, 769.
[14] K. Tani, T. Yamagata, S. Akutagawa, H. Kumobayashi, T. Taketomi, H. Takaya, A. Miyashita, R. Noyori, S. Otsuka, *J. Am. Chem. Soc.* **1984**, *106*, 5208.
[15] See also R. Schmid, J. Foricher, M. Cereghetti, P. Schönholzer, *Helv. Chim. Acta* **1991**, *74*, 370; R. Schmid, H. J. Hansen, *ibid.* **1990**, *73*, 1258.
[16] K. Takabe, Y. Uchiyama, K. Okisaka, T. Yamada, T. Katigeri, T. Okazaki, Y. Oketa, H. Kumobayashi, S. Akutagawa, *Tetrahedron Lett.* **1985**, *26*, 5153.
[17] S. Akutagawa in *Organic Synthesis in Japan: Past, Present and Future* (Eds.: R. Noyori, T. Hiraoka, K. Mori, S. Murahashi, T. Onoda, K. Suzuki, O. Yonemitsu), Tokyo Kagaku Dodin, Tokyo, **1992**, p. 75.
[18] T. K. Hollis, W. Odenkirk, N. P. Robinson, J. Whelan, B. Bosnich, *Tetrahedron* **1993**, *49*, 5415. For a lanhanide catalyzed process, see S. Kobayashi, I. Hachiya *J. Org. Chem.* **1994**, *59*, 3590.
[19] S. Sato, I. Matsuda, Y. Izumi, *Chem. Lett.* **1985**, 1875. For nonmetal catalyzed reactions of this type, see H. M. R. Hoffmann, J. Rabe, *J. Org. Chem.* **1985**, *50*, 3849.
[20] H. Sasai, T. Suzuki, S. Arai, T. Arai, M. Shibasaki, *J. Am. Chem. Soc.* **1992**, *114*, 4418.
[21] H. Sasai, N. Itoh, T. Suzuki, M. Shibasaki, *Tetrahedron Lett.* **1993**, *34*, 855.
[22] H. Nitta, D. Yu, M. Kudo, A. Mori, S. Inoue, *J. Am. Chem. Soc.* **1992**, *114*, 7969.
[23] Y. Ito, M. Sawamura, T. Hayashi, *J. Am. Chem. Soc.* **1986**, *108*, 6405; T. Hayashi, M. Sawamura, Y. Ito, *Tetrahedron* **1992**, *48*, 1999.
[24] A. Togni, S. D. Pastor, *J. Org. Chem.* **1990**, *55*, 1649; S. D. Pastor, A. Togni, *Helv. Chim. Acta* **1991**, *74*, 905.
[25] T. Naota, H. Taki, M. Mizuno, S. I. Murahashi, *J. Am. Chem. Soc.* **1989**, *111*, 5954; S. Paganelli, A. Schionato, C. Botteghi, *Tetrahedron Lett.* **1991**, *32*, 2807.
[26] M. Sawamura, H. Hamashima, Y. Ito, *J. Am. Chem. Soc.* **1992**, *114*, 8295; *Tetrahedron* **1994**, *50*, 4439. See also H. Brunner, B. Hammer, *Angew. Chem.* **1984**, *96*, 305; *Angew. Chem. Int. Ed. Engl.* **1984**, *23*, 312.
[27] W. A. Nugent, R. J. McKinney, *J. Org. Chem.* **1985**, *50*, 5370.
[28] T. V. RajanBabu, A. L. Casalnouvo, *J. Am. Chem. Soc.* **1992**, *114*, 6265.
[29] J. E. Bäckvall, O. S. Andell, *J. Chem. Soc. Chem. Commun.* **1981**, 1098.

[30] W. R. Jackson, C. G. Lovel, *J. Chem. Soc. Chem. Commun.* **1982**, 1231; G. D. Fallon, N. J. Fitzmaurice, W. R. Jackson, P. Perlmutter, *ibid.* **1985**, 4; W. R. Jackson, P. Perlmutter, A. J. Smallridge, *Tetrahedron Lett.* **1988**, *29*, 1983.

[31] O. S. Andell, J. E. Bäckvall, C. Moberg, *Acta Chem. Scand. Ser. B* **1986**, *40*, 184.

[32] G. W. Parshall, S. D. Ittel, *Homogeneous Catalysis*, Wiley-Interscience, New York, **1992**, pp. 42–45.

[33] B. M. Trost, L. Zhi, *Tetrahedron Lett.* **1992**, *33*, 1831. See also P. W. Jolly, N. Kokel, *Synthesis* **1990**, 771.

[34] C. Mercier, G. Mignani, M. Aufrand, G. Allmang, *Tetrahedron Lett.* **1991**, *32*, 1433. See also G. Mignani, D. Morel, Y. Colleville, *ibid.* **1985**, *26*, 6337.

[35] B. M. Trost, G. A. Molander, *J. Am. Chem. Soc.* **1981**, *103*, 5969. See also J. Tsuji, H. Kataoka, Y. Kobayashi, *Tetrahedron Lett.* **1981**, *22*, 2575.

[36] G. I. Nikishin, I. P. Kovalev, *Tetrahedron Lett.* **1990**, *31*, 7063.

[37] T. Mitsudo, Y. Nakagawa, K. Watanabe, Y. Hori, H. Misawa, H. Watanabe, Y. Watanabe, *J. Org. Chem.* **1985**, *50*, 565.

[38] B. M. Trost, C. Chan, C. Rühter, *J. Am. Chem. Soc.* **1987**, *109*, 3486.

[39] B. M. Trost, J. J. Caringi, unpublished.

[40] B. M. Trost, A. Harms, unpublished.

[41] U. Schwieter, G. Saucy, M. Montavon, C. von Planta, R. Rüegg, O. Isler, *Helv. Chim. Acta* **1962**, *45*, 517; C. von Planta, U. Schwieter, L. Chopard-dit-Jean, R. Rüegg, M. Kofler, O. Isler, *ibid.* **1962**, *45*, 548. For another synthesis and application, see W. R. Roush, B. B. Brown, *J. Am. Chem. Soc.* **1993**, *115*, 2268.

[42] B. M. Trost, W. Brieden, K. H. Baringhaus, *Angew. Chem.* **1992**, *104*, 1392; *Angew. Chem. Int. Ed. Engl.* **1992**, *31*, 1335.

[43] M. Akita, H. Yasuda, A. Nakamura, *Bull. Chem. Soc. Jpn.* **1984**, *57*, 480.

[44] B. M. Trost, G. Kottirsch, *J. Am. Chem. Soc.* **1990**, *112*, 2816.

[45] T. Kondo, M. Akazome, Y. Tsuji, Y. Watanabe, *J. Org. Chem.* **1990**, *55*, 1286. See also T. B. Marder, D. C. Roes, D. Milstein, *Organometallics* **1988**, *7*, 1451.

[46] T. Tsuda, T. Kujor, T. Saegusa, *J. Org. Chem.* **1990**, *55*, 2554.

[47] S. Murai, F. Kakiuchi, S. Sekine, Y. Tanaka, A. Kamatani, M. Sonoda, N. Chatani, *Nature (London)* **1993**, *336*, 529.

[48] P. W. Jolly, G. Wilke, *The Organic Chemistry of Nickel, Vol. II*, Academic Press, New York, **1975**.

[49] J. Tsuji, *Adv. Organometallics Chem.* **1979**, *17*, 141; J. Tsuji, *Organic Synthesis with Palladium Compounds*, Springer, Berlin, **1980**, pp. 90–125.

[50] R. Baker, A. H. Cook, T. N. Smith, *J. Chem. Soc. Perkin Trans. 2* **1974**, 1517.

[51] J. Tsuji, *Bull. Chem. Soc. Jpn.* **1973**, *46*, 1896.

[52] D. Rose, H. Lepper, *J. Organometallics Chem.* **1973**, *49*, 473.

[53] J. Tsuji, K. Mizutani, I. Shimizu, K. Yamamoto, *Chem. Lett.* **1976**, 773.

[54] J. Tsuji, T. Mandai, *Tetrahedron Lett.* **1978**, 1817.

[55] J. Tsuji, I. Shimizu, H. Suzuki, Y. Naito, *J. Am. Chem. Soc.* **1979**, *101*, 5070.

[56] G. W. Parshall, S. D. Ittel, *Homogeneous Catalysis*, Wiley-Interscience, New York, **1992**, pp. 126–127, 680.

[57] W. A. Nugent, F. W. Hobbs, Jr., *J. Org. Chem.* **1983**, *43*, 5364; W. A. Nugent, R. J. McKinney, *J. Mol. Catal.* **1985**, *29*, 65.

[58] B. Bogdanović, B. Henc, B. Meister, H. Pauling, G. Wilke, *Angew. Chem.* **1972**, *84*, 1070; *Angew. Chem. Int. Ed. Engl.* **1972**, *11*, 1023.

[59] G. Wilke, *Angew. Chem.* **1988**, *100*, 189; *Angew. Chem. Int. Ed. Engl.* **1988**, *27*, 185.

[60] G. Buono, C. Siv, G. Peiffer, C. Triantaphylides, P. Denis, A. Mortreux, F. Petit, *J. Org. Chem.* **1985**, *50*, 1781. See also B. Bogdanović, B. Henc, A. Lösler, B. Meister, H. Pauling, G. Wilke, *Angew. Chem.* **1973**, *85*, 1013; *Angew . Chem. Int. Ed. Engl.* **1973**, *12*, 954.

[61] See, however, T. Mitsudo, S. Zhang, M. Nagao, Y. Watanabe, *J. Chem. Soc. Chem. Commun.* **1991**, 598.

[62] B. M. Trost, A. F. Indolese, *J. Am. Chem. Soc.* **1993**, *115*, 4361.

[63] B. M. Trost, J. A. Martinez, R. J. Kulawiec, A. F. Indolese, *J. Am. Chem. Soc.* **1993**, *115*, 10402.

[64] B. M. Trost, T. J. J. Müller, *J. Am. Chem. Soc.* **1994**, *116*, 4985.

[65] M. M. Kabat, M. Lange, P. M. Wovkulich, M. R. Uskokovic, *Tetrahedron Lett.* **1992**, *33*, 7701; K. Mikami, M. Terada, T. Nakai, *J. Am. Chem. Soc.* **1990**, *112*, 3949.

[66] T. Nakano, Y. Shimada, R. Sako, M. Kayama, H. Matsumoto, Y. Nagai, *Chem. Lett.* **1982**, 1255.

[67] Z. Yang, D. J. Burton, *Tetrahedron Lett.* **1991**, *32*, 1019. See also J. Tsuji, K. Sato, H. Nagashima, *Tetrahedron* **1985**, *41*, 393.

[68] K. Kaneda, T. Uchiyama, Y. Fujiwara, T. Imanaka, S. Teranishi, *J. Org. Chem.* **1979**, *44*, 55.

[69] B. M. Trost, G. Dyker, R. J. Kulawiec, *J. Am. Chem. Soc.* **1990**, *112*, 7809.

[70] B. M. Trost, R. J. Kulawiec, *J. Am. Chem. Soc.* **1992**, *114*, 5579.

[71] B. M. Trost, R. J. Kulawiec, A. Hammes, *Tetrahedron Lett.* **1993**, *34*, 587.

[72] B. M. Trost, J. A. Flygare, *J. Org. Chem.* **1994**, *59*, 1078.

[73] B. M. Trost, J. A. Flygare, *J. Am. Chem. Soc.* **1992**, *114*, 5476.

[74] B. M. Trost, J. A. Flygare, *Tetrahedron Lett.* **1994**, *35*, 4059.

[75] R. Stammler, M. Malacria, *Synlett* **1994**, 92.

[76] B. M. Trost, L. Zhi, unpublished.

[77] B. M. Trost, R. W. Warner, *J. Am. Chem. Soc.* **1982**, *104*, 6112; *ibid.* **1983**, *105*, 5940.

[78] B. M. Trost, J. T. Hane, P. Metz, *Tetrahedron Lett.* **1986**, *27*, 5695.

[79] A. S. Kende, I. Kaldor, R. Aslanian, *J. Am. Chem. Soc.* **1988**, *110*, 6265.

[80] B. M. Trost, B. A. Vos, C. M. Brzezowski, D. P. Martina, *Tetrahedron Lett.* **1992**, *33*, 717.

[81] B. M. Trost, S. Matsubara, J. J. Caringi, *J. Am. Chem. Soc.* **1989**, *111*, 8745.

[82] B. M. Trost, S. Mallart, unpublished.

[83] R. E. Campbell, C. F. Lochow, K. P. Vora, R. G. Miller, *J. Am. Chem. Soc.* **1980**, *102*, 5824; R. C. Larock, K. Oertle, G. F. Potter, *ibid.* **1980**, *102*, 190.

[84] K. P. Gable, G. A. Benz, *Tetrahedron Lett.* **1991**, *32*, 3473.

[85] X. M. Wu, K. Funakoshi, K. Sakai, *Tetrahedron Lett.* **1993**, *34*, 5927. See also R. W. Barnhart, X. Wang, P. Noheda, S. H. Bergens, J. Whelan, B. Bosnich, *Tetrahedron* **1994**, *50*, 4335.

[86] a) B. M. Trost, D. C. Lee, F. Rise, *Tetrahedron Lett.* **1989**, *30*, 651. b) See also B. M. Trost, M. Lautens, C. Chan, D. J. Jebaratnam, T. Mueller, *J. Am. Chem. Soc.* **1991**, *113*, 636.

[87] B. M. Trost, M. Lautens, *Tetrahedron Lett.* **1985**, *26*, 4887.

[88] B. M. Trost, L. T. Phan, *Tetrahedron Lett.* **1993**, *34*, 4735.

[89] B. M. Trost, A. S. Tasker, G. Rühter, A. Brandes, *J. Am. Chem. Soc.* **1991**, *113*, 671.

[90] B. M. Trost, D. J. Jebaratnam, *Tetrahedron Lett.* **1987**, *28*, 1611. According to the work of M. Miyashita, T. Suzuki, A. Yoshikoshi, *J. Am. Chem. Soc.* **1989**, *111*, 3728, our synthesis also provides an access to picrotoxinin.

[91] B. M. Trost, K. Matsuda, *J. Am. Chem. Soc.* **1988**, *110*, 5233.

[92] B. M. Trost, J. M. Tour, *J. Am. Chem. Soc.* **1987**, *109*, 5268.

[93] B. M. Trost, J. M. Tour, *J. Am. Chem. Soc.* **1988**, *110*, 5231.

[94] B. M. Trost, G. J. Tanoury, M. Lautens, C. Chan, D. T. MacPherson, *J. Am. Chem. Soc.* **1994**, *116*, 4255.

[95] B. M. Trost, D. L. Romero, F. Rise, *J. Am. Chem. Soc.* **1994**, *116*, 4268.

[96] B. M. Trost, J. Y. L. Chung, *J. Am. Chem. Soc.* **1985**, *107*, 4586; B. M. Trost, P. A. Hipskind, J. Y. L. Chung, C. Chan, *Angew. Chem.* **1989**, *101*, 1559; *Angew. Chem. Int. Ed. Engl.* **1989**, *28*, 1502.

[97] B. M. Trost, P. A. Hipskind, *Tetrahedron Lett.* **1992**, *33*, 4541.

[98] B. M. Trost, D. C. Lee, *J. Org. Chem.* **1989**, *54*, 2271.

[99] B. M. Trost, L. Zhi, K. Imi, *Tetrahedron Lett.* **1994**, *35*, 1361.

[100] W. E. Piers, P. J. Shapiro, E. E. Bunel, J. E. Bercaw, *Synlett* **1990**, 74.

[101] R. Grigg, J. F. Malone, T. R. B. Mitchell, A. Ramasubbu, R. M. Scott, *J. Chem. Soc. Perkin Trans. 1* **1985**, 1745.

[102] B. Bogdanović, *Adv. Organometallics Chem.* **1979**, *17*, 105.

[103] B. M. Trost, Y. Shi, *J. Am. Chem. Soc.* **1991**, *113*, 701; *ibid.* **1993**, *115*, 9421.

[104] B. M. Trost, Y. Shi, *J. Am. Chem. Soc.* **1992**, *114*, 791; *ibid.* **1993**, *115*, 12491.

[105] G. A. Molander, J. O. Hoberg, *J. Am. Chem. Soc.* **1992**, *114*, 3123.

[106] B. M. Trost, F. Rise, *J. Am. Chem. Soc.* **1987**, *109*, 3161.

[107] B. M. Trost, Y. Kondo, *Tetrahedron Lett.* **1991**, *32*, 1613; B. M. Trost, E. D. Edstrom, *Angew. Chem.* **1990**, *102*, 541; *Angew. Chem. Int. Ed. Engl.* **1990**, *29*, 520. See also B. M. Trost, E. D. Edstrom, M. B. Carter–Petillo, *J. Org. Chem.* **1989**, *54*, 4489.

[108] B. M. Trost, G. J. Tanoury, *J. Am. Chem. Soc.* **1987**, *109*, 4753.

[109] J. M. Takacs, L. G. Anderson, M. W. Creswell, B. E. Takacs, *Tetrahedron Lett.* **1987**, *28*, 5627. See also J. M. Takacs, P. W. Newsome, C. Kuehn, F. Takusagawa, *Tetrahedron* **1990**, *46*, 5507; J. M. Takacs, Y. C. Myoung, *Tetrahedron Lett.* **1992**, *33*, 317.

[110] J. M. Takacs, S. V. Chandramouli, *J. Org. Chem.* **1993**, *58*, 7315.

[111] For an asymmetric Alder ene cyclization, see K. Narasaka, Y. Hayashi, S. Shimada, *Chem. Lett.* **1988**, 1609.

[112] K. Sakai, X. M. Wu, T. Hata, N. Marubayashi, K. Funakoshi, *J. Chem. Soc. Perkin Trans. 1* **1991**, 2531; K. Funakoshi, N. Togo, Y. Taura, K. Sakai, *Chem. Parm. Bull.* **1989**, *37*, 1990.

[113] B. M. Trost, J. F. Luengo, *J. Am. Chem. Soc.* **1988**, *110*, 8239.

[114] H. Ishibashi, N. Uemura, H. Nakatani, M. Okazaki, T. Sato, N. Nakamura, M. Ikeda, *J. Org. Chem.* **1993**, *58*, 2360; G. M. Lee, S. M. Weinreb, *ibid.* **1990**, *55*, 1281.

[115] T. Yamamoto, S. Ishibuchi, T. Ishizuka, M. Haratake, T. Kunieda, *J. Org. Chem.* **1993**, *58*, 1997; F. O. H. Pirrung, H. Hiemstra, B. Kaptein, M. E. M. Sobrino, D. G. I. Petra, H. E. Shoemaker, W. N. Sperkamp, *Synlett* **1993**, 739.

[116] K. Narasaka, Y. Hayashi, H. Shimadzu, S. Niihata, *J. Am. Chem. Soc.* **1992**, *114*, 8869.

[117] T. Mitsudo, H. Naruse, T. Kondo, Y. Ozaki, Y. Watanabe, *Angew. Chem.* **1994**, *106*, 595; *Angew. Chem. Int. Ed. Engl.* **1994**, *33*, 580.

[118] H. tom Dieck, M. Mallien, R. Diercks, *J. Mol. Catal.* **1989**, *51*, 53.

[119] A. J. Rippert, H. J. Hansen, *Helv. Chim. Acta* **1992**, *75*, 2219.

[120] B. M. Trost, M. Yanai, K. Hoogsteen, *J. Am. Chem. Soc.* **1993**, *115*, 5294.

[121] B. M. Trost, M. K. Trost, *J. Am. Chem. Soc.* **1991**, *113*, 1850. For a recent report of a Ru catalyzed reaction, see N. Chatani, T. Morimoto, T. Muto, S. Murai, *J. Am. Chem. Soc.* **1994**, *116*, 6049.

[122] N. E. Schore in ref. [5a], Chapter 9.1, pp. 1037–1064.

[123] V. Rautenstrauch, P. Mégard, J. Conesa, W. Küster, *Angew. Chem.* **1990**, *102*, 1441; *Angew. Chem. Int. Ed. Engl.* **1990**, *29*, 1413. See also N. Jeong, S. H. Hwang, Y. Lee, Y. K. Chung, *J. Am. Chem. Soc.* **1994**, *116*, 3159. For an iron catalyzed reaction of diallenes and allenyl carbonyl compounds, see B. Eaton, B. Rollman, J. A. Kaduk, *J. Am. Chem. Soc.* **1992**, *114*, 6245; M. S. Sigman, C. E. Kerr, B. E. Eaton, *ibid.* **1993**, *115*, 7545.

[124] S. C. Berk, R. B. Grossman, S. L. Buchwald, *J. Am. Chem. Soc.* **1993**, *115*, 4912.
[125] K. Tamao, K. Kobayashi, Y. Ito, *J. Am. Chem. Soc.* **1988**, *110*, 1286.
[126] P. Binger, H. M. Büch, *Top. Curr. Chem.* **1987**, *135*, 77. For intramolecular variants, see S. Yamago, E. Nakamura, *Tetrahedron* **1989**, *45*, 3081; R. T. Lewis, W. B. Motherwell, M. Shipman, *J. Chem. Soc. Chem. Commun.* **1988**, 948.
[127] B. M. Trost, T. Naota, unpublished.
[128] E. P. Johnson, K. P. C. Vollhardt, *J. Am. Chem. Soc.* **1991**, *113*, 381.
[129] M. Lautens, C. M. Crudden, *Organometallics* **1989**, *8*, 2733.
[130] H. Brunner, M. Muschiol, F. Prester, *Angew. Chem.* **1990**, *102*, 680; *Angew. Chem. Int. Ed. Engl.* **1990**, *29*, 652; M. Lautens, J. C. Lautens, A. C. Smith, *J. Am. Chem. Soc.* **1990**, *112*, 5627.
[131] M. Lautens, L. G. Edwards, *Tetrahedron Lett.* **1989**, *30*, 6813.
[132] B. M. Trost, K. Imi, A. F. Indolese, *J. Am. Chem. Soc.* **1993**, *115*, 8831.
[133] N. E. Schore, *Chem. Rev.* **1988**, *88*, 1081. For a recent leading reference, see J. E. Hill, G. Balaich, P. E. Fanwick, I. P. Rothwell, *Organometallics* **1993**, *12*, 2911.
[134] P. Bhatarah, E. H. Smith, *J. Chem. Soc. Chem. Commun.* **1991**, 277.
[135] R. Grigg, R. Scott, P. Stevenson, *Tetrahedron Lett.* **1982**, *23*, 2691. See also S. J. Neeson, P. J. Stevenson, *ibid.* **1988**, *29*, 813.
[136] S. H. Lecker, N. H. Nguyen, K. P. C. Vollhardt, *J. Am. Chem. Soc.* **1986**, *108*, 857. See also Z. Zhou, L. P. Battaglia, G. P. Chiusoli, M. Costa, M. Nardelli, C. Pelizzi, G. Predieri, *J. Chem. Soc. Chem. Commun.* **1990**, 1632.
[137] G. Chelucci, M. Falorni, G. Giacomelli, *Synthesis* **1990**, 1121.
[138] See also H. Bönnemann, W. Brijoux, *Bull. Soc. Chim. Belg.* **1985**, *94*, 635; R. E. Geiger, M. Lalonde, H. Stoller, K. Schleich, *Helv. Chim. Acta* **1984**, *67*, 1274; D. J. Brien, A. Naiman, K. P. C. Vollhardt, *J. Chem. Soc. Chem. Commun.* **1982**, 133.
[139] R. A. Earl, K. P. C. Vollhardt, *J. Org. Chem.* **1984**, *49*, 4786. For a review, see K. P. C. Vollhardt, *Angew. Chem.* **1984**, *96*, 525; *Angew. Chem. Int. Ed. Engl.* **1984**, *23*, 539.
[140] A. C. Williams, P. Sheffels, D. Sheehan, T. Livinghouse, *Organometallics* **1989**, *8*, 1566.
[141] See A. J. Pearson, R. J. Shively, Jr., *Organometallics* **1994**, *13*, 578.
[142] T. Tsuda, S. Morikawa, N. Hasegawa, T. Saegusa, *J. Org. Chem.* **1990**, *55*, 2978.
[143] T. Tsuda, T. Kiyoi, T. Miyane, T. Saegusa, *J. Am. Chem. Soc.* **1988**, *110*, 8570.
[144] I. Matsuda, M. Shibata, S. Sata, Y. Izumi, *Tetrahedron Lett.* **1987**, *29*, 3361.
[145] H. tom Dieck, R. Diercks, *Angew. Chem.* **1984**, *95*, 801; *Angew. Chem. Int. Ed. Engl.* **1983**, *22*, 778.
[146] R. S. Jolly, G. Luedtke, D. Sheehan, T. Livinghouse, *J. Am. Chem. Soc.* **1990**, *112*, 4965.
[147] P. A. Wender, T. E. Jenkins, *J. Am. Chem. Soc.* **1989**, *111*, 6432.
[148] T. E. Jenkins, Ph.D. Thesis, Stanford, University, **1992**.
[149] M. A. Huffman, L. S. Liebeskind, *J. Am. Chem. Soc.* **1991**, *113*, 2771.
[150] For an analogous transformation, see B. M. Trost, A. S. K. Hashmi, *Angew. Chem.* **1993**, *105*, 1130; *Angew. Chem. Int. Ed. Engl.* **1993**, *32*, 1085.
[151] B. M. Trost, A. S. K. Hashmi, *J. Am. Chem. Soc.* **1994**, *116*, 2183.
[152] K. Narasaka, N. Iwasawa, M. Inoue, T. Yamada, M. Nakashima, J. Sugimori, *J. Am. Chem. Soc.* **1989**, *111*, 5340.
[153] S. Kobayashi, I. Hachiya, H. Ishitani, M. Araki, *Tetrahedron Lett.* **1993**, *34*, 4535.
[154] K. Tamao, K. Kobayashi, Y. Ito, *Synlett* **1992**, 539.
[155] P. A. Wender, M. L. Snapper, *Tetrahedron Lett.* **1987**, *28*, 2221.
[156] P. Brun, A. Tenaglia, B. Waegell, *Tetrahedron Lett.* **1983**, *24*, 385.
[157] P. A. Wender, N. C. Ihle, C. R. D. Correia, *J. Am. Chem. Soc.* **1988**, *110*, 5904.
[158] K.-U. Baldenius, H. tom Dieck, W. A. König, D. Icheln, T. Runge, *Angew. Chem.* **1992**, *104*, 338; *Angew. Chem. Int. Ed. Engl.* **1992**, *31*, 305.
[159] J. H. Rigby, K. M. Short, H. S. Ateeq, J. A. Henshilwood, *J. Org. Chem.* **1992**, *57*, 5290.

Digitalis Research in Berlin–Buch—Retrospective and Perspective Views**

Kurt R. H. Repke,* Rudolf Megges, Jürgen Weiland, and Rudolf Schön

"The following remarks consist partially of matter of fact, and partially of opinion. The former will be permanent; the latter must vary with the detection of error, or the improvement of knowledge. I hazard them with diffidence, and hope they will be examined with candour." These declarations, which stem from the famous book "An Account of the Foxglove and some of its Medical Uses" by physician William Withering in 1785 in which he introduced preparations from digitalis leaves in the therapy of dropsy (cardiac failure), are cited here by the senior author because of his awareness of the difficulties in presenting a balanced report on his life-long research project on the further development of digitalis. His decision to devote himself to digitalis research originated at the bedside, when as a physician he experienced the grim final stages of cardiac failure in which no real help for the patients is possible. Unfortunately, his research project did not fit into the research program decreed by the Ministry of Science of the German Democratic Republic, so that he was ordered to stop the digitalis project in favor of biomembrane studies. Fortunately, he got round the ban simply by labeling the digitalis-like acting steroids as probes for the cell membrane-located Na^+/K^+-transporting ATPase which he had just recognized as the digitalis target (receptor) enzyme. These and other ventures by the authors are collated here for the first time. The aim of this review is to foster straightforward research for solving a major challenge: the development of steroidal drugs for the prevention and cure of cardiac failure.

Keywords: digitalis · drug design · medicinal chemistry · pharmaceuticals · steroids

1. Introduction: The Challenge of Digitalis Research

The challenge of digitalis research derives from the need for new drugs for the prevention of cardiac failure and the successful treatment of the failing heart. Specifically, the need follows from: the prevalence and mortality of heart failure in developed countries; the fact that the cardiac drugs available are clearly inadequate to restore health or even to minimize discomfort and disability; and the condition that previous research efforts to provide drugs satisfying the above requirements have widely failed. Selected facets of the latter studies were previously reviewed by the authors of this review.[1, 2]

1.1. The Underlying Medical Demand

The incidence and prevalence of congestive heart failure have increased in recent years,[3] and as the average age of the population increases, it is expected to continue to increase. The prognosis after first diagnosis is grim; less than half of the patients survive more than five years.[4] The survival rate depends on several variables, essentially defined in Figure 1.

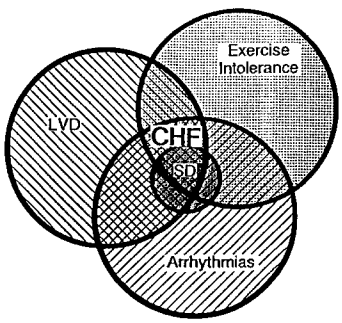
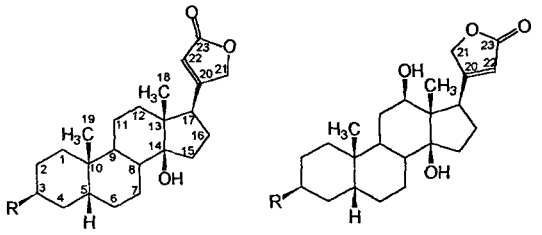


Fig. 1. Clinical manifestations of myocardial disease. The Scheme shows the possible coincidences of left ventricular dysfunction (LVD), exercise intolerance, and ventricular arrhythmias as the most common manifestations of the failing heart syndrome. Clinical heart failure (CHF) corresponds to the coexistence of LVD and exercise intolerance. Sudden death (SD) occurs in patients with arrhythmias and predominantly in those with LVD and CHF (from ref. [5]).

The therapeutic value of preparations from Digitalis plants was discovered by Withering more than 200 years ago.[6] Digitoxin (**1**) and digoxin (**2**) (Fig. 2), the predominant active materials, still belong today to the drugs most common-

[*] Prof. Dr. K. R. H. Repke, Dr. R. Megges, Dr. J. Weiland, Dr. R. Schön
Max-Delbrück-Centrum für Molekulare Medizin
Robert-Rössle-Strasse 10, D-13125 Berlin–Buch (Germany)
Telefax: Int. code +(30) 949-4161

[**] Definitions and abbreviations: Digitalis: generic term to cover all steroids which act cardiotonic by inhibiting Na^+/K^+-ATPase by occupancy of its digitalis recognition matrix and binding cleft; Na^+/K^+-ATPase, the Na^+/K^+-transporting adenosine triphosphate phosphohydrolase (EC 3.6.1.37), residing in the plasma membrane of all mammalian cells, which effects the conversion of scalar phosphoryl energy of ATP into vectorial electrochemical energy; for the molecular mechanism see K. R. H. Repke, R. Schön, *Biol. Rev.* **1992**, *67*, 31–78; *Biochim. Biophys. Acta* **1992**, *1154*, 1–16.



1 2

Fig. 2. Structural formulae of digitoxin (**1**) and digoxin (**2**) (R = tridigitoxosyloxy). Compound **1** is shown in 14/22-conformation and **2** in 14/21-conformation in which the C22 proton or the C21 protons, respectively, are localized opposite to the C14β-OH group. High potency is preserved in conformationally semi-rigid cardenolide derivatives in which the butenolide C21 protons, due to bulky substituents at the C22 atom (cf. Fig. 9), are forced into a potential energy well near C14β-OH. Hence, the 14/21-conformer appears to be the receptor-bound conformer [7]. Note the *cis*-junction of the rings C and D of the steroid framework is not achieved in the biosynthetic pathways of humans and animals (except for a few toads) (cf. Sections 2.5 and 2.6).

ly prescribed for the treatment of cardiac failure.[3, 8] In 1930, the famous heart specialist Wenckebach[9] concluded: "Digitalis treatment is one of the most important and serious duties of the general physician; it demands a great deal of skill, power of observation, keen interest, and experience. A long life is too short to learn enough about this wonderful drug." More recently, however, considerable controversy has arisen about the role and value of digitalis in treating patients with cardiac failure.[3] The open question at present, is that one cannot draw any conclusions about the effects of digitalis on survival.[10] Physicians are looking forward to additional first-line agents that are relatively safe and that can be used as monotherapy to improve the quality of life, retard progression of the disease, and prevent sudden death.[4, 11] One may expect in the coming years that every effort must and will be made to develop new compounds that will not only beneficially affect the hemodynamic and functional impairment of patients with cardiac failure, but will also hopefully contribute to reaching an achievable goal, namely, the prevention of the clinical manifestation of cardiac insufficiency.[4, 11]

1.2. Paradise Postponed

During the last decade many new drugs have been developed and tested on patients with heart failure at a rate of one new agent every month. An overview of the more interesting agents and their putative major mechanisms has been presented in a detailed, but balanced way by G. Grupp.[12] Phosphodiesterase inhibitors such as amrinone and milrinone seemed to hold great promise, but finally yielded disappointing results. In contrast to the digitalis compounds such cardiotonic drugs lose their effectiveness when they are needed most, that is in severe heart failure.[13] Moreover, reports on increased mortality[14-16] have dampened the initial enthusiasm for the use of phosphodiesterase inhibitors: "paradise postponed".[17] The return on the huge investment of money, time, manpower, and resources to develop an orally administrable inotropic drug to supplement or replace digitalis compounds has generally been disappointing. This has had a devastating effect on the further development of this class of non-digitalis inotropic drugs.[18]

Only digitalis, diuretics, and inhibitors of the angiotensin-converting enzyme each fulfill some of the criteria of a first-line agent in the treatment of chronic heart failure. However, none of these drugs satisfies all of the desired characteristics, and none can optimally manage the heart failure state when used alone.[19] Unfortunately, converting enzyme inhibitors and diuretics have the tendency to impair renal function, while digitalis compounds tend to improve renal function. However, digitalis intoxication has continued to be one of the most prevalent adverse drug reactions encountered in clinical practice due to the narrow margin between the therapeutic and toxic doses and the marked variations in individual sensitivity.[20] Nevertheless, there has been little decline in the use of digitalis over the last five years, indicating that the mentioned newer agents for the treatment of cardiac failure have not replaced the widespread use of digitalis.[3]

1.3. Apparent Causes for the Previous Lack of Success

The search for cardiotonic steroids with an increased therapeutic range by modification of the structures of known digitalis



Kurt R. H. Repke, born in 1919, obtained his medical doctor's degree in 1945. Between 1945 and 1950 he trained in various medical disciplines at hospitals in Hamburg and Potsdam as well as, under Professor Gerhardt Katsch, at the Clinic for Internal Medicine of the University in Greifswald. To acquire a profound understanding of the pharmacological and biochemical foundations of drug therapy, he worked and habilitated under Paul Wels at the Institute of Pharmacology of the University in Greifswald (1950–1955), and subsequently until 1963 under Professor Karl Lohmann at the Institute of Biochemistry of the Academy of Sciences in Berlin–Buch. He followed Lohmann as the director of this institute (1964–1971) and then headed the Biomembrane Section of the newly formed Central Institute of Molecular Biology of the Academy (1971–1984). Since he has been an emeritus professor he has pursued with full vigor his research aims which include in addition to digitalis research the elucidation of the complex mechanism of the interconversion of the scalar phosphoryl energy of ATP into the vectorial energy of cation gradients through biomembranes. Professor Repke has been a member of the Deutsche Akademie der Naturforscher Leopoldina and a honorary member of the Cardiac Muscle Society of USA. He devotes his leisure time to the study of Goethe's genius.

compounds appeared unsuccessful for several decades. This has been interpreted as probably reflecting an already insuperably high degree of structural optimization in the therapeutically used natural compounds of herbal origin.[21] However, the lack of progress might have followed from conceptual limitations or experimental weaknesses in the research endeavors.

The synthetic modifications were based on equating the natural compounds with lead structures. Specifically, the derivatizations were focussed on the side chain at C17 in **1** and **2**, erroneously taken to be the pharmacophoric lead structure.[22-25] The activity of the derivatives was primarily evaluated in animal model systems. They allow the measurement of inotropic and toxic effects, but not the discrimination between the diverse molecular mechanisms underlying the observed effects (cf. Section 2.4). Such observations preclude the derivation of self-consistent structure–activity relationships, as emerges from pertinent reviews.[24-26] Thus, the initially untargeted strategy for the chemical modification necessarily resembled a "molecular roulette". However, for a rational approach to the development of drugs, an understanding of the effect-triggering interaction between active agent and receptor on the molecular level is needed, as emphasized by Ariëns in 1976.[27] He felt that basic research into physiological and biochemical processes would become the cornerstone for new drug development in the near future.

1.4. The Early Illusion and the Present Realities

As reviewed by Parascandola[28] very early some attempts were made to relate the pharmacological action of organic compounds to their structure while structural organic chemistry was still in its infancy. Nevertheless, Brown and Fraser began their promising work in 1869 with the following declaration of faith: "There can be no reasonable doubt that a relation exists between the physiological action of a substance and its chemical composition." In 1877, Brunton even speculated that physicians would soon be able to predict the pharmacological action of any compound from its constitution. This early hope turned out to be an illusion that still applies. Consequently, in 1992 Kuntz[29] stated that we cannot design drugs with a specific mode of action and acceptable biological properties from first principles. What we can reliably expect is to be able to design competitive enzyme inhibitors, and to begin the long process of drug development from such a sensible starting point.[29]

The cornerstone of the newest strategy for design of novel drugs has been proclaimed to be the accurate knowledge of the three-dimensional structure of the potential target proteins, which are complexed with a great variety of ligands (inhibitors) in their recognition and triggering place.[29-33] As stated by the staff of a specialist drug design company in 1991[32]—knowledge of the three-dimensional structure of pharmacologically significant receptor-ligand complexes at the level of resolution achieved by X-ray crystallography has the potential for profoundly influencing and speeding the discovery and development of lead compounds. Since the desolvation of ligand and protein in their going from free to bound form are not considered in this procedure, it has been easier to discover various novel lead compounds by satisfying the evident nonpolar and electrostatic requirements for binding to the catalytic center of a target enzyme than it has been to elaborate these lead structures into potent inhibitors with a small number of iterations.[32] The superiority of that "direct" strategy, as described for the discovery of drugs, over existing methods remains to be investigated.[32]

Despite impressive advances in X-ray crystallography of macromolecules, availability of high-quality crystals remains the major limiting factor in the exploitation of this technique. Otherwise, modeling based on the knowledge of homologous proteins is now generally held to provide an insufficiently stable base for rational drug design.[33] In addition, for the majority of protein sequences with little significant homology to known structures, the problem of predicting secondary and tertiary structures[34] accurately enough for drug design applications is felt to be still insurmountable.[33]

As the "direct" strategy in drug design has been mostly not applicable, "indirect" routes based on the analysis of structure–activity relationships have more generally been pursued. These routes had to be followed also in digitalis research (cf. ref. [1, 2, 35–71]). As long as neither the site nor the mechanism of digitalis action were known, we had to discover by "untargeted" strategy the target enzyme (receptor) to clear the path to the targeted strategy (see Sections 2.1 and 2.2). The ensuing multistage development (cf. ref. [72]) of digitalis research in Berlin–Buch led to the targeted strategy, comprising the following stages: the Na^+/K^+-ATPase was identified as the digitalis target (receptor) enzyme and its role in controlling cardiac contractility was derived (Section 2.2); the "microscopic" digitalis mechanism of Na^+/K^+-ATPase inhibition was clarified (Section 2.3); the capabilities and limitations of biological and molecular screening test systems were evaluated (Section 2.4); the lead structures for digitalis-like action were discovered in the course of an extended "chemical hunt"[1, 2, 35-71] (Sections 2.5 and 3); the mystery surrounding the chemical identity of the putative endogenous digitalis was attributed to the lack of specificity of the various analytical procedures applied (Section 2.6). Based on the achieved insights, some facets of the most recent developments of the research will be delineated in Section 3.

2. The Stages of Digitalis Research

Over thirty years, digitalis research has been stimulated by mutual supplement and criticism of the research groups in Sydney and Berlin–Buch. Although both studying the digitalis problem, their research efforts differed in many ways due to different experiences and preferences as well as different methodological and conceptional approaches. The work in Sydney has focussed on the isolation and structure determination of natural substances and, above all, the synthesis of digitalis analogues by substitution of the lactone group at C17 by different open side chains or/and substitution of the sugar component at C3 by different ester groups as well as the determination of the inotropic activity of the compounds on surviving preparations from the cardiac muscle of the guinea-pig. The voluminous results of the Australian groups were comprehensively published by Wright in 1960;[73] Thorp and Cobbin in

1967;[74] Thomas, Boutagy, and Gelbart in 1974;[75] Thomas, Gray, and Andrews in 1990[24] and Thomas in 1991.[25] Thus, their brilliant contributions will not be reviewed here for the sake of brevity, too.

2.1. The Role of Biotransformation

The metabolic transformation of digitalis glycosides (reviewed in refs. [76, 77]) can sometimes render the interpretations of biological potency data in terms of structure–activity relationships more difficult. This becomes evident from the following examples. When orally applied, lanatoside C undergoes deglucosylation and deacetylation by microorganisms in the intestinal tract before the glycoside becomes absorbed in the form of digoxin (**2**).[78–80] Lanatoside C is thus a prodrug. Pentaacetylgitoxin requires deacetylation to 16-acetylgitoxin by microbial and animal hydrolases before it becomes effective; it presents thus an example of drug latentiation.[81–83]

As illustrated in Figure 3, digitoxin (**1**) and digoxin (**2**) undergo, by cleavage of the tridigitoxoside chains, a slow, stepwise degradation to the aglycones which are rapidly inactivated by epimerization and conjugation of the released hydroxy group at C3.[84–90] Taking into account the locus and speed of biotransformation on the one hand and the biological activities of the metabolites on the other (cf. Fig. 3), the following conclusions can be drawn: As a rule, the ultimately active agents are not formed by biotransformation. The biotransformations are rather detoxification reactions.[76, 77] Due to its slow removal, the sugar side chain prolongs the half time of the active molecules in the animal body.[84, 85, 93] However, the large variations in acute potency

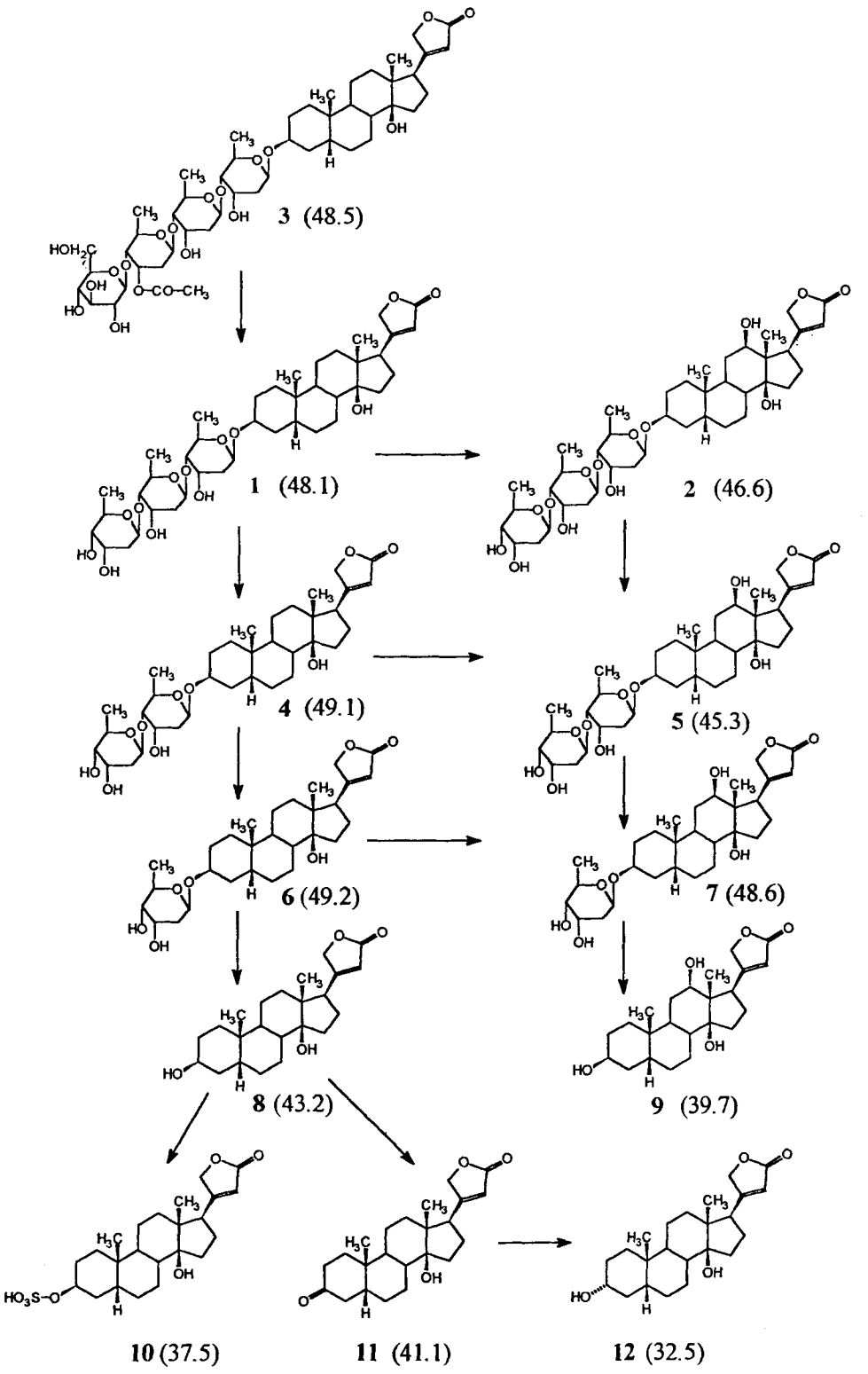


Fig. 3. Biotransformation of lanatoside A (**3**) in the animal body. The deacetylation and deglucosylation (**3** → **1**) are effected by microbial enzymes in the intestinal tract, allowing absorption of **1** [78–80]. Then, liver enzymes bring about C12β-hydroxylation (**1** → **2**), stepwise separation of the three digitoxose residues (**1** → **8**; **2** → **9**), conjugation with sulfuric acid (**8** → **10**) or epimerization of C3β-OH (**8** → **12**) [84–90]. The latter two reactions are the decisive detoxification steps as the drop in the Gibbs energy of interaction with the receptor enzyme (given below the formulae in parentheses, expressed in $-$kJ mol^{-1}) indicates. Scrutiny of the $\Delta G^{0\prime}$ values suggests that the sugar side chain for the most part remains outside the digitalis recognition matrix and binding cleft of the receptor and that the sugar residue next to the steroid nucleus lies at the mouth of the receptor cleft. If so, the lactone function is positioned at the bottom of the cleft such that the cleft length amounts to about 1.88 nm [91, 92].

shown by digitalis glycosides of different constitution and configuration cannot be explained by differences in the biotransformation.[76, 77, 93–96]

The 12β-hydroxylation of digitoxin (**1**) to form digoxin (**2**)[97] is no prerequisite of cardiotonic action;[97] as indicated in Figure 3, it rather involves a small loss of potency. The double bond in the butenolide side chain can be hydrogenated by microorganisms in the intestinal tract.[76, 77, 79] Since this appears to be irreversible in the animal tissues, the lactone residue cannot serve as hydrogen carrier in the intermediary metabolism[76] as suggested earlier. The double bond orients the H-binding acceptor oxygen atoms of the butenolide towards the H-donating amino acid residues of the recognition matrix of Na^+/K^+-ATPase involved in long-range attraction and high potency binding[2] (cf. Fig. 9). Moreover, the double bond is important for stabilizing the lactone side chain against hydrolysis at physiological pH which is accompanied by loss of potency.[98]

2.2. The Target Enzyme and Its Role in Controlling Contractility

The results of our studies on the metabolic fate of digitalis compounds led us to the inviting conclusion that the question as to the biochemical mechanism of digitalis action is not related to the biotransformation of the herbal compounds in the mammalian body, but that this question appears to coincide with the question as to the nature and function of the digitalis receptor.[76] This conception appeared in 1961 rather daring as it emerges from a look back at a symposium on enzymes and drug action held at that time.[99] When asked to comment on receptor models, R. J. P. Williams replied that he understood the word "receptor" as a synonym for lack of knowledge, and Chain added to not believe that the enzyme approach is the right way to discover new drugs nor to understand in a general way the mode of action of drugs.

Nevertheless, our group wanted to test whether the Na^+/K^+-ATPase, only just shown to be inhibited by the digitalis glycoside ouabain,[100] exhibits the characteristics to potentially serve as the digitalis target (receptor) enzyme. To this end, we extensively compared the many conditions under which digitalis compounds act on contractility, Na^+/K^+ transport, and Na^+/K^+-ATPase activity. At each level, correlations were demonstrated for all 20 characteristics of digitalis action examined, for example locus of action, species differences of digitalis sensitivity, structure–activity relationships, ionic antagonism and synergism, cation requirements for action, time course for development of effects, dependence on specific functional states, and range of effective digitalis concentrations.[76, 101–104] Since the early sixties, our findings and conclusions have been confirmed and extended in several ways by various research groups.[105–113] At long last, after decades of controversy, a consensus has emerged that the inotropic effects of digitalis compounds result from binding to and inhibition of Na^+/K^+-ATPase as stated by T. W. Smith in 1988.[20] Okita et al. reported in 1990 that, in accordance with its receptor function, digoxin (**2**), administered therapeutically in the clinical setting, inhibits the Na^+/K^+ pump in the human heart.[114]

The Na^+/K^+-ATPase is the biochemical machinery in the Na^+/K^+ pump which maintains the normally high intracellular concentration of K^+ ions and low intracellular concentration of Na^+ ions in cardiac muscle and other excitable cells. As deduced by Repke in 1964,[115] the actual Na^+ concentration regulates indirectly the Ca^{2+} concentration in cell interior which has been known to be the final regulator of cardiac contractility. More specifically, the integrating assessment of the then available experimental data on the relationship between the contractility of the cardiac muscle cell and the flows of K^+, Na^+, and Ca^+ ions across the cell membrane led him to the hypothesis that a transient increase of the intracellular Na^+ concentration, resulting from the digitalis-produced reduction of the Na^+/K^+ pumping capacity of the cell by inhibition of a portion of the Na^+/K^+-ATPase total, plays the primary role in the control of cardiac force.[115, 116] The indicated interrelationship has often been questioned, but in 1985 it was finally fully corroborated in using Na^+-selective microelectrodes. Lee[117] established the essential role of the increase in the intracellular Na^+ activity for the action of digitalis at low and high concentrations. Specifically, he showed that digitalis produces a parallel increase in Na^+ activity and contractile force, and that these parameters remain closely correlated during the positive inotropic effect. The increase of the chemical activity of Na^+ ions leads, via the Na^+/Ca^{2+} exchanger, to an increase of the chemical activity of the Ca^{2+} ions through enhanced Ca^{2+} influx into and reduced Ca^{2+} efflux from the cardiac muscle cell as reviewed elsewhere.[1]

2.3. The "Microscopic" Mechanism of Na^+/K^+-ATPase Inhibition

In 1953, Wilbrandt et al.[118] accounted for the strong dependence of the cardiac action of digitalis compounds on contraction frequency with the hypothesis that these steroidal agents interfere with cation transmembrane flows occurring during excitation and recovery. This suggestion was based on the knowledge that other steroids, especially corticosteroids, play an important role, possibly as cation carriers (Fig. 4), in cation

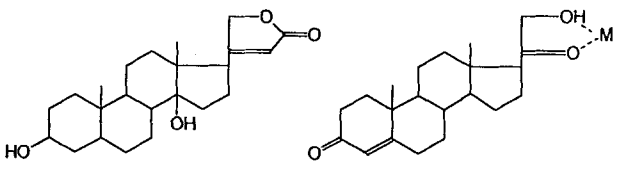


Fig. 4. Assumed structural analogy between a strong inhibitor of Na^+/K^+ transport (digitoxigenin; left) and a presupposed chelate formed between 11-deoxycorticosterone and an alkali metal cation (M; right). On this basis, the action of digitalis compounds was suggested by Wilbrandt [119] to be caused by competitive antagonism towards cation-laden corticosteroids which were thought to be complexed with Na^+/K^+-transporting ATPase and to serve as cation carriers across the membrane of the cell (from ref. [119]).

transport. In support of the above hypothesis, Wilbrandt[120] reported that corticosteroids antagonize the inhibitory action of cardiotonic steroids on cellular Na^+/K^+ transport. Consequently, Wilbrandt[121] considered the possibility that the digitalis effect may be on a corticosteroid-carrier part of Na^+/K^+-ATPase rather than on the enzyme protein. However, our group[122] showed that corticosteroids do not attenuate a digi-

talis-induced Na^+/K^+-ATPase inhibition, and the observations appeared to exclude a direct, functionally antagonistic competition between corticosteroids and cardiotonic steroids for binding to a common site on that enzyme. The antagonistic action of corticosteroids and cardiotonic steroids found by Wilbrandt and Weiss[123] for intact cells appears to be based on the induction of biosynthetic increases of the number of Na^+/K^+-ATPase molecules[124] compensating for the portion of digitalis-inhibited enzyme molecules.

The inhibitory effect of digitalis compounds on Na^+/K^+-ATPase activity arises from their interaction with the recognition part and effect-triggering binding site on the enzyme protein which we have further characterized by the following findings. Large excesses of ATP over digitalis with respect to the concentration do not antagonize digitalis binding to the enzyme.[125] There is a competitive K^+ effect on digitalis binding under certain conditions, but, as shown by us,[125] its molecular basis is not competition for a common binding site on the enzyme, but competition for the ATP- or digitalis-binding enzyme conformation. Using definitions given by Monod et al.,[126] digitalis compounds are thus noncompetitive, heterotropically acting allosteric inhibitors which produce the transition from an active to an inactive conformational state of enzyme protein. More specifically, a common denominator of the inhibitory action of digitalis compounds has been shown by our group[127] to be a large gain in entropy in the enzyme protein associated with a loss of high ATP affinity to the catalytic center.

The search for the proper locality of the digitalis recognition and binding protein matrix has intensively been approached by several groups through elucidation of the connection between distinctions in digitalis affinity (ouabain taken as a prototype) and those in the primary structure of Na^+/K^+-ATPase (Fig. 5). However, with increasing knowledge all hitherto published proposals (see review in ref. [2]) have turned out to be untenable. As we shortly shall show elsewhere, the digitalis binding cleft is formed by two membrane-penetrating peptide sequences (H1 in Fig. 5) which through their association bring about the interplay between the two catalytic α subunits in the diprotomeric holoenzyme $(\alpha\beta)_2$ such that, by intercalation of a digitalis molecule, the catalytic cycle becomes interrupted.

2.4. The Comparison of Biological and Molecular Screening Test Systems

The most suitable method for the quantitative determination of the positive-inotropic (cardiotonic) effect of a cardioactive compound is the assessment of its influence on the isometric contraction curve measured in isolated cardiac muscle preparations from some animal species. However, to obtain reliable data for the comparison of the inotropic potency of the various cardioactive compounds, it is essential to perform the experiments under identical conditions.[131] Because of the variety of test conditions used, it is not easy or is even impossible to integrate in terms of structure–activity relationships the numerical values reported in the literature.[132, 133] A comprehensive survey of the structure–activity relationships found in guinea-pig cardiac preparations under identical conditions has recently been presented by R. Thomas et al.[24]

Important for the realization of the message of this review is the understanding that there are two basic possibilities for misinterpretation of observations with animal model systems. First, all inhibitors of the Na^+/K^+ transport system irrespective of their microscopic inhibitory mechanism (see below) produce positive inotropic effects if they do not additionally affect other biochemical systems which preclude the manifestation of the inotropic action.[110] Second, some inhibitors of Na^+/K^+ transport, even when effective through occupancy of the digitalis binding cleft, can fail to produce a positive inotropic action when they additionally affect biochemical systems which preclude the manifestation of their inotropic faculty. Prominent examples for both cases were diagnosed[2] by successive use of the "macroscopic" and "microscopic" test systems characterized below.

The macroscopic screening with Na^+/K^+-ATPase proved to be an only initially useful test. It restricts itself to the assessment

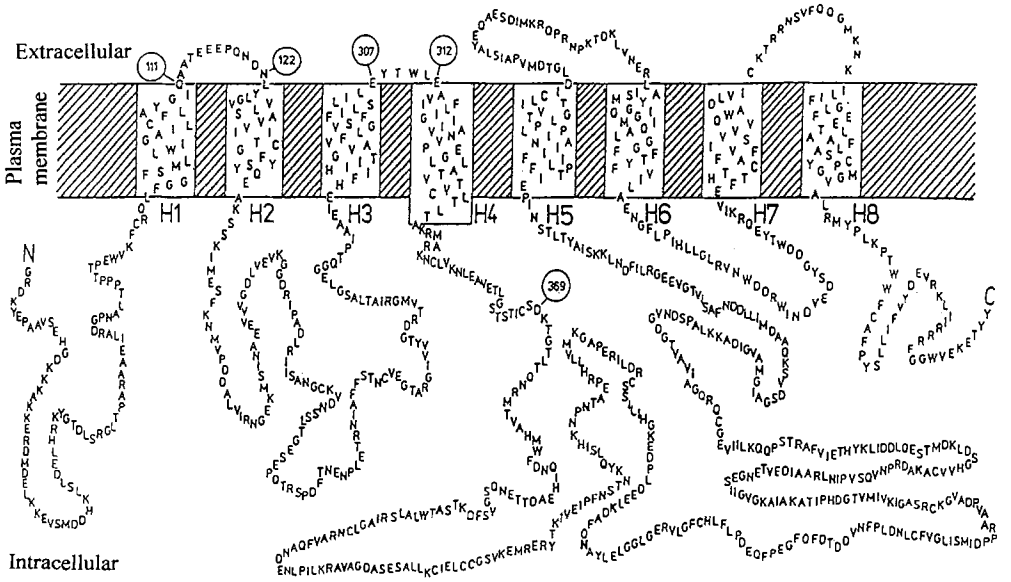


Fig. 5. Schematic representation of the primary structure and spatial organization of the catalytic subunit of Na^+/K^+-ATPase. The amino acid chain penetrates the membrane of the cell eight times. The membrane crossing sequences H1–H4 carry the extracellularly disposed H1–H2 junction (Q111–N122) and H3–H4 junction (E307–E312) which were supposed to interplay in building the digitalis recognition and binding matrix [2]. The H4 stretch directly mediates the communication of the matrix with the phosphorylatable aspartyl residue D369 in the catalytic center of the enzyme. The scheme shown here is a combination of the figures in refs. [128 129].

of the apparent Gibbs energy change ($\Delta G^{0\prime}$) in the formation of the equilibrium complex of an inhibitor with the enzyme under standardized conditions; the experimental details were published elsewhere by us.[92, 134, 135] The availability of the $\Delta G^{0\prime}$ values allowed us to apply the extrathermodynamic approach to the quantitative analysis of structure–activity relationships.[92, 134, 135] This procedure clearly requires that a uniform macroscopic and microscopic mechanism underlies the observed inhibitory effectiveness. However, fulfilment of this prerequisite cannot be derived from studies on the inhibition of Na^+/K^+-ATPase (or Na^+/K^+ transport): therefore the investigation is named a macroscopic screening test. Specifically, many inhibitory-active ligands of any structure (cf. ref. [136]) can interrupt the catalytic cycle of Na^+/K^+-ATPase by binding to quite different binding sites than those occupied by digitalis compounds (Fig. 6). Hence, agents which inhibit the enzyme system through a digitalis-unlike microscopic mechanism will necessarily lead to a null hypothesis concerning structure–activity relationships.

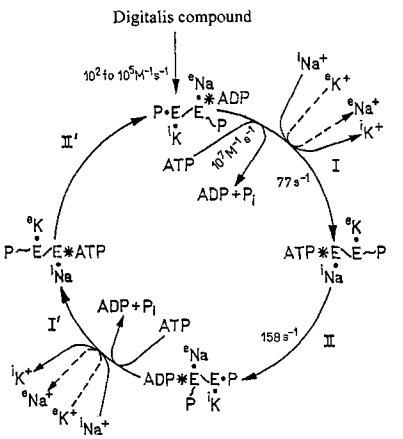


Fig. 6. Reaction and function scheme of Na^+/K^+-ATPase. Noteworthy are the large differences in the association rate constants for the formation of the inhibitory complex between various digitalis compounds and the phosphorylated enzyme intermediate on the one hand, and for the formation of the productive complex between ATP and the same intermediate on the other, during maximum activity of the enzyme. The letters E denote the two catalytic subunits, and the superscripts indicate the locations of the Na^+ or K^+ ions on the intracellular (i) or extracellular (e) side of the enzyme or the cell, respectively. Compared with the diffusional rate constant of slowly diffusing reactants (10^9 M^{-1}s^{-1}), the digitalis association rate constants were found to be 4 - 7 orders of magnitude smaller [127], but similar to the isomerization constant known to characterize the protein conformation change in enzyme–substrate interactions ranging from 10^2–10^4 s^{-1}. The duration of the half-cycle at 37 °C is 6–7 ms (from ref. [137]).

The microscopic screening is based on our experience[66, 130] that the competent occupancy of the digitalis binding cleft by an inhibitor of Na^+/K^+-ATPase, no matter of structure, and hence its quality as a mechanistically digitalis-like compound is proved by its capacity to promote the synthesis of the energy-rich carboxyphosphate–phosphoenzyme from orthophosphate in presence of Mg^{2+} ions. Microscopic screening has therefore been proven as a final test for selecting or rejecting compounds for uncovering the pharmacophoric lead structure in bimolecular recognition studies.[66, 130]

As well-known, man is in many respects a unique species. Therefore it is not really surprising that for the receptor–effector parameters, there are considerable distinctions between the isoforms of Na^+/K^+-ATPase from man and other species.[104, 127, 134, 138] Fortunately, the Na^+/K^+-ATPase preparations from human tissues, suitable for the use in the above molecular test systems, can easily be made.[92, 134] The times are over, in which a surviving heart cut out of a decapitated man had to be used to study the action of digitoxin on human cardiac muscle.[139]

2.5. The Chemical Hunt for the Discovery of Lead Structures and the Functional Classification of the Other Structural Components in Digitalis-Like Acting Inhibitors

The lead structure in complex biologically active compounds is defined as that structural component which shows the minimal, specific recognition requirements and is still able to evoke the biological effect of interest although its potency may be weak.[140, 141] The discovery of the lead structure has been regarded as an essential step in reducing the gamble in drug design.[142] In fact, the development of a novel drug can demand the synthesis of 10000–20000 new compounds and cost more than 200 million German Marks.[143] Also in case of cardiac glycosides such as digitoxin (**1**) or digoxin (**2**) (Fig. 1) the detection of their lead structure proved to be difficult. Digitalis compounds are noncompetitive, heterotropically acting allosteric inhibitors of Na^+/K^+-ATPase as deduced in Section 2.3. This means that they bear no resemblance to the substrate ATP and thus do not provide a sensible starting point in the search for the lead structure. This appears to explain why it took until 1985 before our group detected the proper lead component in cardiac glycosides.[91, 92] Our systematic screening of about seven hundred essentially congeneric digitalis derivatives has been made possible through the donation of numerous rare compounds by many eminent chemists such as K. Meyer, G. R. Pettit, T. Reichstein, D. Satoh, F. Sondheimer, C. Tamm, R. Tschesche, K. Wiesner, and W. W. Zorbach to name but a few. The given rich fund has been supplemented in our laboratory by targeted partial synthesis of steroid derivatives not available from herbal sources.[35–68] The structure of the compounds and the pertinent test data have fully been presented in references [1, 2].

Thus, we have travelled a long distance down the road that has led us to the functional apportionment of the three structural components of ordinary digitalis compounds. As concisely substantiated in Figure 7, the steroid skeleton, 5β,14β-androstane-3β,14-diol (**16**), is the inherently active lead structure in the natural cardiac glycosides. The removal of the hydroxyl group at C3β only lessens the potency slightly and the replacement of C14β-OH by C14β-NH_2 can even considerably increase the inhibitory effect.[2] Hence, the basic lead structure is 5β,14β-androstane (cf. Figs. 7 and 10). The C3β-O and C17β side chains, when separated from the steroid skeleton, are without intrinsic inhibitory action of their own; however, when linked with the steroid lead, the C3β-O and C17β side chains contribute moderately or powerfully, respectively, to the integral interaction energy. This is summarized below.

The tridigitoxoside chain of digitoxin (**1**) and digoxin (**2**) can more than isoenergetically be replaced by several monosides as exemplified in Figure 8. The butenolide substituent of **1** and **2**

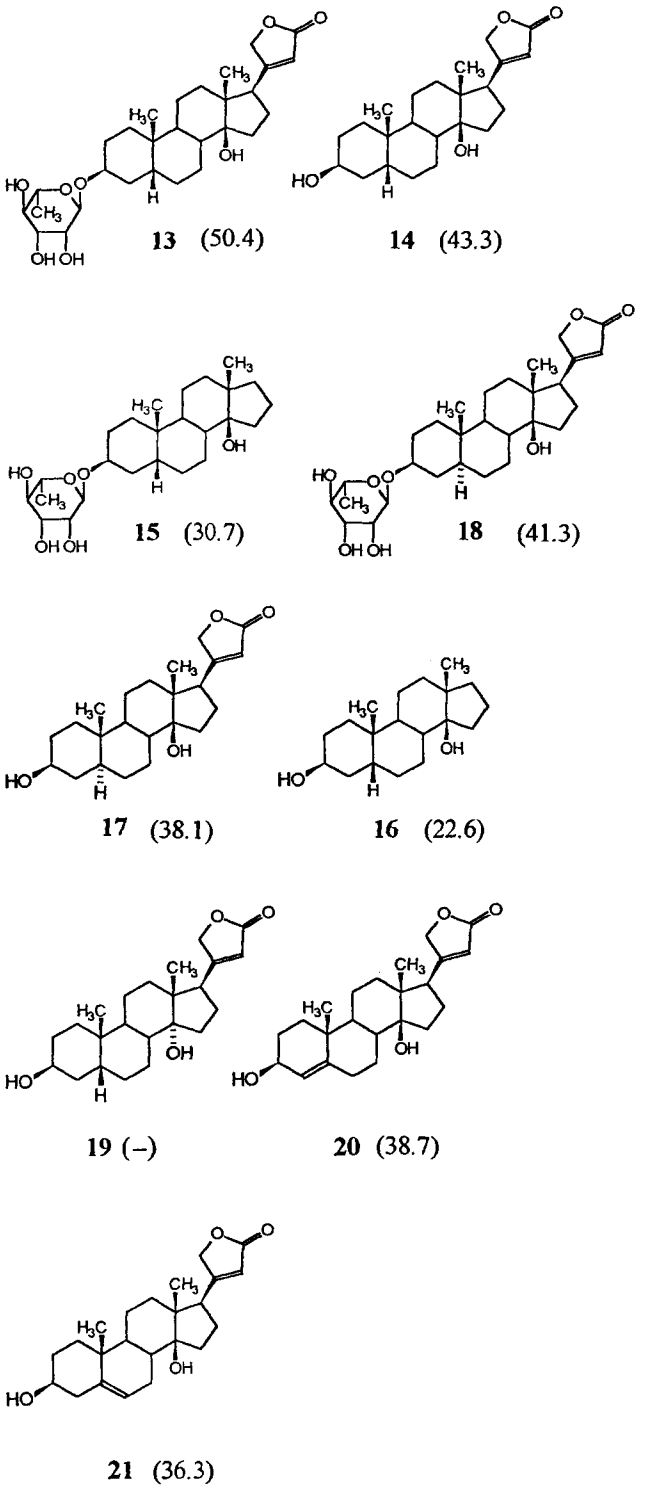


Fig. 7. The impact of stripping the side chains of 3β-*O*-(α-L-rhamnosyl)-digitoxigenin (**13**) (**13** → **14**, **13** → **15**, **13** → **16**) reveals their distinct contributions to the integral Gibbs energy of interaction with Na^+/K^+-ATPase from human cardiac muscle [91, 92]. While the sugar and lactone residues are devoid of inhibitory effect on their own, the steroid skeleton **16** exhibits an intrinsic potency not different from unity [130] and acts thus as the lead structure in the digitalis glycosides [91, 92, 130]. Conversion of the A/B-*cis*- into the A/B-*trans*-ring junction (**14** → **17**) reduces the potency of the aglycon and also diminishes the strengthening of the inhibitory efficacy by glycosidation (cf. **14** → **13** with **17** → **18**). However, conversion of the C/D-*cis*- into the C/D-*trans*-ring junction (**14** → **19**) annuls the potency of the precursor compound. A comparison of the Gibbs interaction energies of the aglycons **14**, **17**, **20**, and **21** shows that **14** with a strongly bent, essentially inflexible steroid skeleton fits best into the digitalis binding cleft. The numbers in parentheses indicate the $\Delta G^{0\prime}$ values in $-kJ\,mol^{-1}$; **19** is inactive.

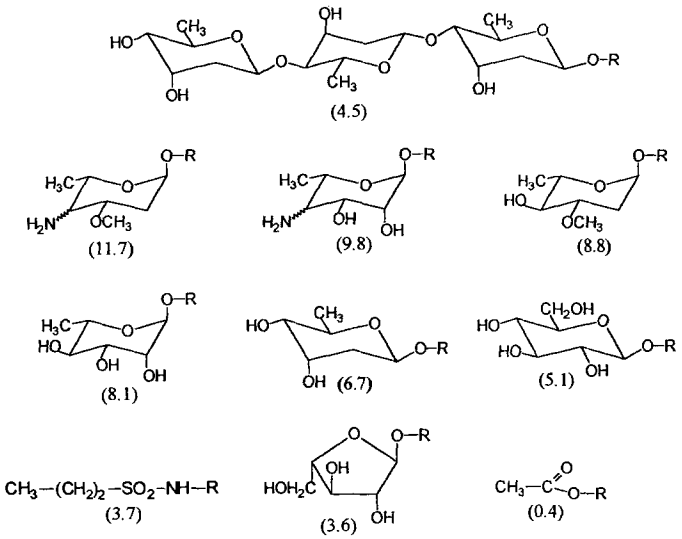


Fig. 8. Differences in the increments of Gibbs energy of the interaction between Na^+/K^+-ATPase from human cardiac muscle and digitoxigenin (**14**) produced by introduction of various substituents at C3β-OH [2]. The conformational flexibility of the sugar residues, arising from the two degrees of rotational freedom about the glycoside bonds, can help to account for the finding that both β-D- and α-L-sugars with C1 or 1C conformation, respectively, increase the interaction energy. In addition, the amino acid sequences involved in forming the sugar binding subsite may have some conformational adaptability. The numbers in parentheses indicate the $\delta\Delta G^{0\prime}$ values in $-kJ\,mol^{-1}$.

also can isoenergetically or even more than isoenergetically be replaced by several heterocycles shown in Figure 9. Attempts have been made to utilize our complete data for the derivation of the chemotopography of the digitalis recognition matrix and binding cleft in the Na^+/K^+-ATPase protein as a step in the rational design of new inotropic steroids.[2]

As shown in Figure 7, the powerful inhibitor digitoxigenin **14** loses its potency already by conversion of the C/D-*cis* ring junction into the C/D-*trans* junction (**14** → **19**). The latter geometry is common in the endogenous hormonal steroids. Due to this early experience, C/D-*trans* steroids were regarded by us as irrelevant in considerations of the relationship between structure and inhibitory potency, although we had found some compounds without lactone substituent at C17β as active or even more active than their C/D-*cis* relatives[92] (cf. the $\Delta G^{0\prime}$ values for **16** and **23** in Figures 7 and 10).

As pointed out by Marshall and Cramer recently,[144] attempts to correlate biological activity with the structure of a compound often have had limited success unless the study has confined itself to congeneric series. However, the inclusion of structurally diverse molecules, interacting at the same receptor site, promises more basic solutions to the problem of structure–activity relationships, which may lead to the development of novel therapeutic agents.[144] Hence, we resumed and systematically extended our studies with C/D-*trans* steroids of hormonal type.

Fundamental for this endeavor was our detection that in the macroscopic and microscopic screening tests (cf. Section 2.4) some progestins such as megestrol acetate (**25**) and chlormadinol acetate (**26**) proved to be effective inhibitors of Na^+/K^+-ATPase (Fig. 10) operating through a digitalis-like microscopic mechanism, that is, competent occupancy of the digitalis binding cleft.[66] Linkage of C3β-OH with a monosaccharide either

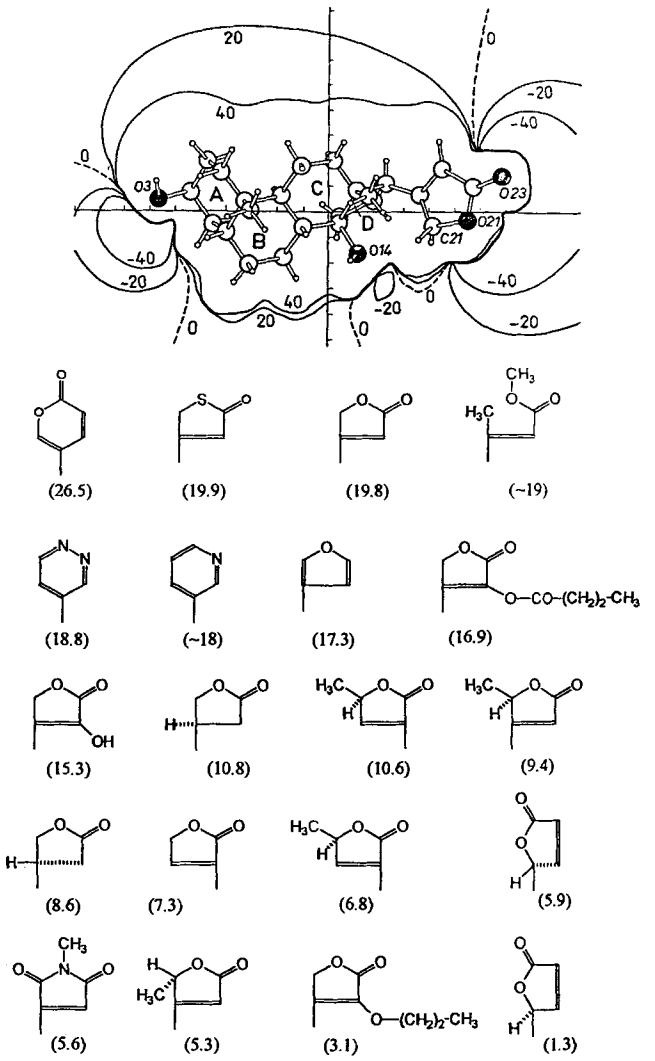


Fig. 9. The kinetic role and energetic contribution of substituents at C17β of 5β,14β-androstane-3β,14-diol in the interaction of the inhibitors with Na^+/K^+-ATPase from human cardiac muscle. The grossly dipolar distribution of the molecular electrostatic potential field in the outer space of digitoxigenin (**14**) shown in the upper part of the figure (from ref. [91]), appears to control the long- and medium-range attraction of the molecule in forming the diffusion complex and to promote the pull of the aglycon, with the lactone ring ahead, into the receptor binding cleft [91, 92]. The formation of the inhibitory complex appears to involve hydrogen bonds between the electron-rich oxygen, sulfur, or nitrogen atoms in the different side chains on the one hand and H-donating amino acid side chains in the pertinent receptor binding subsite on the other. A perusal of the very different contributions of the C17β-substituents to the interaction energy reveals that the sizes of the measured integrals result from an intricate superposition of both attractive and repelling electronic and steric components of their partial structures [1, 2]. The numbers in parentheses indicate the $\delta\Delta G^{0\prime}$ values in $-kJ\,mol^{-1}$.

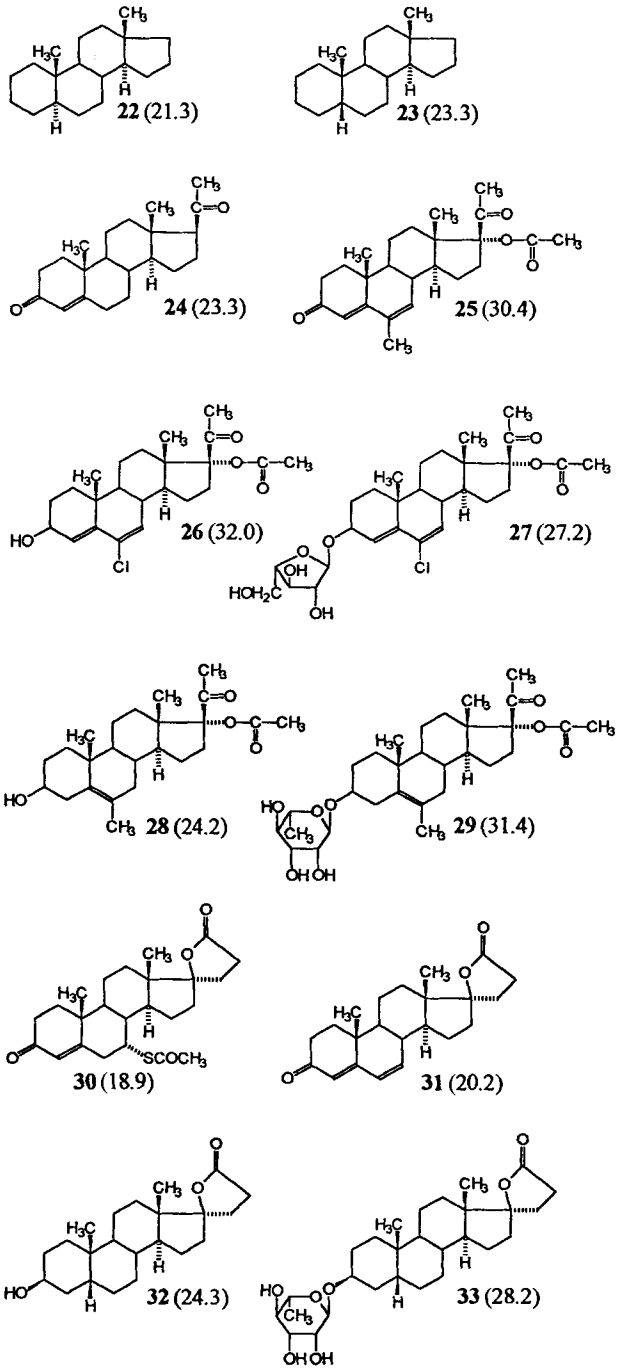


Fig. 10. The Gibbs energy of interaction between Na^+/K^+-ATPase from human cardiac muscle and digitalis-like acting C/D-*trans* steroids of hormonal type: impact of changes in configuration and substitution [2, 64–66, 145]. Applying the definition cited in Section 2.5 [141, 142], the lead structure in these steroids is 5β-androstane when occupying the digitalis binding cleft. The numbers in parentheses give the $\Delta G^{0\prime}$ values in $-kJ\,mol^{-1}$.

decreases (**26** → **27**) or increases (**28** → **29**) the inhibitory potency. This roughly parallels the response of some C/D-*cis* steroids (cf. **17** → **18** with **14** → **13** in Fig. 7). The mentioned differential impact of glycosidation reflects the unwieldy or fitting spatial disposition of the sugar side chain in the sugar subsite of the digitalis binding cleft that is guided by the geometry of the A/B ring junction.[65]

Most remarkably, glycosidation of chlormadinol acetate **26** → **27** transformed its negative-inotropic action[146] into a surprisingly continual, positive-inotropic action.[64] The effects of **27** on cardiac contractility and other circulatory parameters in cats are more favorable than those of digitoxin (**1**). The possibility that this functional distinction is related to the C/D-*trans* or C/D-*cis* ring junction in the two inotropic agents still needs to be verified. The way to the answer of this question will be addressed in Section 3. Here, the primary, most important conclusion from our studies with **27** is that the C/D-*cis* ring junction, known to occur in steroids of some plants and toads only, is—contrary to the present dogma—not an indispensable requirement for cardiotonic action; likewise animal hormone steroids with a C/D-*trans* ring junction can have the capability

of eliciting digitalis-like, positive inotropic actions.[64] The prerequisite for the realization of this potential has been recognized to be the elimination of the hormonal potency by steroid glycosidation which prevents interaction with the intracellularly located hormone receptors.[64] A further potential case for such connection will be considered in Section 3.

2.6. The Mystery of Endogenous Digitalis

Our interest in the exploration of C/D-*trans* steroids of hormone type with regard to possible digitalis-like actions has also been stimulated by their potential relation to endogenous digitalis. The methodical search for its nature was pioneered by Szent-Györgyi[147] who reported in 1953 that normal blood serum contains substances which exert a digitalis-like action. Among 22 steroids probed, deoxycorticosterone and progesterone were found to share with serum and cardiac glycosides the action on the contractility of the heart. Their potency, however, was too low to account for the serum activity. In the above context, Szent-Györgyi reasoned that "the digitalis glycosides are no drugs at all: they are substitutes for a missing screw in our machinery, which had a cardinal role in one of the most basic physiological regulations".

More recently, the search for endogenous digitalis was fuelled by the discovery of endorphins, the endogenous ligands of the opiate receptor. Thus, it became tempting to conclude that a parallel situation might apply to an endogenous analogue of digitalis. This conception appears to be supported by the fact that a specific digitalis-binding site exists on the Na^+/K^+-ATPase of all animal species.

For theoretical and practical reasons, the search for endogenous digitalis has become a challenge to many people in medical and basic research as well as in the pharmaceutical industry. As reviewed by Goto et al.[148] and Hamlyn and Manunta,[149] numerous affirmative reports have provided circumstantial and substantial evidence for the occurrence of endogenous inhibitors of Na^+/K^+-ATPase, but the clarification of their chemical identity has remained elusive. Many candidates for an endogenous digitalis-like factor have been proposed on the basis of the application of nine criteria.[148] However, all underlying assays say little or nothing about the precise binding site of the candidates and the microscopic mechanism of observed effects. The most suitable criterion for classifying a substance or an isolate as digitalis-like acting is by proving its occupancy of the digitalis binding matrix[66, 130] as evidenced by the microscopic test technique (cf. Section 2.4). However, it has hitherto been utilized in one study only.[150] Therein, the well-characterized hypothalamic inhibitor of Na^+/K^+-ATPase has shown, unlike digitalis, a negative response in the microscopic assay. Apparently, some physiological inhibitors of Na^+/K^+-ATPase exist in the animal body which have not necessarily a structural relationship to digitalis compounds.[151]

The reports by Hamlyn et al.[152] and Goto et al.[153] that some Na^+/K^+-ATPase inhibitors isolated from various sources appeared to be identical with ouabain or digoxin were, in fact, most compelling. The serious problem with the acceptance of their identity is that a biosynthetic pathway for such C/D-*cis* steroids, as exists in some rare plants and toads, is unknown in mammals. Our doubt about the identity of the endogenous inhibitor of the Na^+/K^+-ATPase with ouabain has most recently been reinforced.[154] In this context, we are tempted to speculate that some C/D-*trans* hormone steroids, such as the progestins listed in Section 2.5, could serve as models for the chemical nature of endogenous digitalis.[66]

3. The Most Recent Development Stage: Data-Directed Optimization of the Lead Steroid

The major limiting factor of the maximum digitalis dose which can be administered in the treatment of cardiac failure, is the development of ventricular arrhythmias. An essential element contributing to the origin of arrhythmogenic action of cardiac glycosides is cerebral neuroexcitation.[155] The importance of neural digitalis actions follows from the various functions of Na^+/K^+-ATPase in neural tissues.[156] Thus, inhibition of neural Na^+/K^+-ATPase by digitalis compounds plays the causal role in triggering both the therapeutically useful and detrimental, initially neural actions of digitalis.[157] Hence, a promising way to increase the ratio of doses for the therapeutic and toxic digitalis effects appears to be the design of digitalis derivatives with exceptionally different affinities for the isoforms of Na^+/K^+-ATPase in cardiac muscle and brain cells.[1, 2]

An initiating comparison of Na^+/K^+-ATPase preparations from human cardiac muscle and brain cortex with regard to their affinity to 76 C/D-*cis* steroids revealed on average a 1.5-fold lower affinity to the cerebral enzyme preparation.[134] The C/D-*trans* compound **27** showed a 3.2-fold lower affinity to the same enzyme preparation.[64] This possibly explains why **27** did not evoke arrhythmias in cats as observed with **2**.[64] However, both enzyme preparations apparently consisted of a mixture of three Na^+/K^+-ATPase isoforms[158] of unknown individual affinities. The clearcut decision about the relative affinities of C/D-*cis* and C/D-*trans* steroids to particular isoenzymes from cardiac muscle and neural cells requires studies with the isolated isoforms not available as yet. In the light of the knowledge that the steroid skeleton serves as the pharmacophoric lead structure not only for Na^+/K^+-ATPases from human tissues but also from animal tissues of widely differing digitalis affinity,[2, 104, 134] it appears almost certain to suppose that a proportion of Na^+/K^+-ATPase isoforms in human contractile and neural cells differs in the chemotopography of the steroid binding subsite in the digitalis binding cleft.

Our endeavor to clarify the possible suitability of C/D-*trans* hormone steroids as parent structures for the design of novel cardiac drugs has most recently centred on the aldosterone antagonists spironolactone (**30**) and canrenone (**31**) (see Fig. 10). Our interest in these spirosteroids was raised by reports from clinicians and general practitioners that these C/D-*trans* steroids exert a direct positive-inotropic action in the treatment of patients with severe congestive heart failure.[159–164] However, the spirosteroids have been fully effective only in combination therapy with a diuretic, an inhibitor of the angiotensin-activating enzyme or/and digoxin. Hence, the mechanism of the remarkably beneficial cardiac action of the aldosterone antagonists has remained not well understood.[163, 164] For that reason, the unexpected cardiotonic aspects of their action has

been analyzed by us; it turned out to be one of the rare cases of "clinical feedback".

Our analysis of the interaction of **30** and **31** with human Na^+/K^+-ATPase preparations in the macroscopic and microscopic test system (cf. Section 2.4) uncovered that both spirosteroids are digitalis-like acting inhibitors of the receptor enzyme. Their low inhibitory potency (cf. their $\Delta G^{0\prime}$ values shown in Fig. 10 with those of digitoxin (**1**) or digoxin (**2**) given in Fig. 3) accounts for the need of the mentioned combination therapy. Derived from our experience on the impact of glycosidation on the potency of various progesterone derivatives[64, 65] we succeeded in increasing the efficacy of **31** twenty-fold by glycosidation **31** → **33**.[145] The potency of **33** is even somewhat higher than that of **27** which we had shown to exert a favorable positive-inotropic action in cats.[64] Of course, additional studies with **33** and compounds of this type will have to be performed to establish their pharmacological profile and to select those derivatives not with top potency, but with the largest therapeutic dosage range. The experience with the pharmacological profile of **27**[64] gives reasons for the expectation that the adverse hormonal reactions of the aldosterone antagonists[165–167] are reduced or eliminated by their glycosidation, when their interaction with the hormone receptors can be prevented. The probe on the generality of the postulated interrelationships and the further structural and functional optimization of aldosterone antagonists may be studied by exploiting the innovative potential invested in the more comprehensive insight in those problems which is derivable from our studies with C/D-*cis* steroids[1, 2] (cf. Figs. 7–9).

4. Summary and Prospect

The article starts by outlining the reasons why cardiotonic steroids constitute a long-standing and still continuing research challenge, and by disclosing the motivation of the senior author to engage himself in this demanding field 30 years ago. This is followed by detailing the stages and levels of digitalis research in which the authors have extensively been involved, and by outlining the most recent developmental stage opened by their discoveries. The article reveals that even the elementary stages of drug research as treated here are a multifaceted and intricate domain which at last should include pharmacological and clinical feedback "loops" to test the limits of chemical and biochemical patterns of thought suggested by the initiating work of the authors. Any major development as envisaged here is necessarily a long haul and involves extensive investment of resources in the pursuit of the designated concept, the therapeutic merit of which can be judged only at the end of the road (cf. ref. [168]).

The most recent work has been supported by grants from the Deutsche Forschungsgemeinschaft (Re 878/1–4) and the Fonds der Chemischen Industrie.

Received: September 15, 1993 [A 25 IE]
German version: *Angew. Chem.* **1995**, *107*, 308

[1] K. R. H. Repke, W. Schönfeld, J. Weiland, R. Megges, A. Hache in *Design of Enzyme Inhibitors as Drugs* (Eds.: M. Sandler, H. J. Smith), Oxford University Press, Oxford, **1989**, pp. 435–502.
[2] K. R. H. Repke, J. Weiland, R. Megges, R. Schön, *Prog. Med. Chem.* **1993**, *30*, 135–202.
[3] S. Yusuf, R. Garg, P. Held, R. Gorlin, *Am. J. Cardiol.* **1992**, *69*, 64G–70G.
[4] W. M. Smith, *Am. J. Cardiol.* **1985**, *55*, 3A–8A.
[5] J. N. Cohn, *Circulation* **1988**, *78*, 1099–1107.
[6] W. Withering, *An Account of the Foxglove, and some of its Medical Uses; with Practical Remarks on Dropsy, and other Diseases*, Robinson, London, **1785**.
[7] R. Hintsche, R. Megges, D. Pfeiffer, H. J. Portius, W. Schönfeld, K. R. H. Repke, *Eur. J. Med. Chem.* **1985**, *20*, 9–15.
[8] E. Erdmann in *Cardiac Glycosides 1785–1985* (Eds.: E. Erdmann, K. Greeff, J. C. Skou), Steinkopff, Darmstadt, **1986**, p. V.
[9] K. F. Wenckebach, *Br. Med. J.* (Suppl. Epitome) **1930**, *1*, 181.
[10] K. Swedberg, *Circulation* **1993**, *87* (Suppl. IV), IV-126–IV-129.
[11] J. J. Kellermann, *Am. Heart J.* **1990**, *120*, 1529–1531.
[12] G. Grupp, *Mol. Cell. Biochem.* **1987**, *76*, 97–112.
[13] E. Erdmann, M. Böhm in *Inotropic Stimulation and Myocardial Energetics* (Eds.: H. Just, C. Holubarsch, H. Scholz), Steinkopff, Darmstadt, **1989**, pp. 125–133.
[14] R. DiBianco, R. Shabetai, W. Kostuk, J. Moran, R.-C. Schlant, R. Wright, *N. Engl. J. Med.* **1989**, *320*, 677–683.
[15] B. F. Uretsky, M. Jessup, M. A. Konstam, G. W. Dec, C. V. Leier, J. Benotti, S. Murali, H. C. Herrmann, J. A. Sandberg, *Circulation* **1990**, *82*, 774–780.
[16] A. D. Goldberg, J. Nicklas, S. Goldstein, *Am. J. Cardiol.* **1991**, *68*, 631–636.
[17] J. N. Cohn, *N. Engl. J. Med.* **1989**, *320*, 729–731.
[18] C. V. Leier, *Am. J. Cardiol.* **1992**, *69*, 120G–129G.
[19] M. Packer, *Circulation* **1989**, *79*, 198–204.
[20] T. W. Smith, *N. Engl. J. Med.* **1988**, *318*, 358–365.
[21] V. Austel, E. Kutter in *Arzneimittelentwicklung: Grundlagen – Strategien – Perspektiven* (Ed.: E. Kutter), Thieme, Stuttgart, **1978**, pp. 113–139.
[22] H. J. Portius, K. R. H. Repke, *Arzneim. Forsch.* **1964**, *14*, 1073–1077.
[23] D. S. Fullerton, K. Ahmed, A. H. L. From, R. H. McParland, D. C. Rohrer, J. F. Griffin in *Molecular Graphics and Drug Design* (Eds.: A. S. V. Burgen, G. C. K. Roberts, M. S. Tute), Elsevier, Amsterdam, **1986**, pp. 257–284.
[24] R. Thomas, P. Gray, J. Andrews, *Adv. Drug Res.* **1990**, *19*, 313–562.
[25] R. E. Thomas in *Molecular Structure and Biological Activity of Steroids* (Eds.: M. Bohl, W. L. Duax), CRC, Boca Raton, FL, **1992**, pp. 399–464.
[26] T. W. Güntert, H. H. A. Linde, *Cardiac Glycosides, Part I: Experimental Pharmacology* (Ed.: K. Greeff) (*Handb. Exp. Pharmacol.* **1981**, *56/I*, 13–24).
[27] E. J. Ariëns, *Med. Chem. Proc. Int. Symp. 5th 1976* **1977**, 409–412.
[28] J. Parascandola, *Pharm. Hist.* **1971**, *13*, 3–10.
[29] I. D. Kuntz, *Science* **1992**, *257*, 1078–1082.
[30] W. G. J. Hol, *Angew. Chem.* **1986**, *98*, 765–777; *Angew. Chem. Int. Ed. Engl.* **1986**, *25*, 767–778.
[31] N. C. Cohen, J. M. Blaney, C. Humblet, P. Gund, D. C. Barry, *J. Med. Chem.* **1990**, *33*, 883–894.
[32] K. Appelt, R. J. Bacquet, C. A. Bartlett, C. L. J. Booth, S. T. Freer, M. A. M. Fuhry, M. R. Gehring, S. M. Herrmann, E. F. Howland, C. A. Janson, T. R. Jones, C.-C. Kan, V. Kathardekar, K. K. Lewis, G. P. Marzoni, D. A. Matthews, C. Mohr, E. W. Moomaw, C. A. Morse, S. J. Oatley, R. C. Ogden, M. R. Reddy, S. H. Reich, W. S. Schoettlin, W. W. Smith, M. D. Varney, J. E. Villafranca, R. W. Ward, S. Webber, S. E. Webber, K. M. Welsh, J. White, *J. Med. Chem.* **1991**, *34*, 1925–1934.
[33] J. Hodgson, *Bio/Technology* **1991**, *9*, 19–21.
[34] R. Y. Yada, R. L. Jackman, S. Nakai, *Int. J. Pept. Protein Res.* **1988**, *31*, 98–108.
[35] R. Megges, R. Franke, B. Streckenbach, K. Repke, H.-J. Schmidt (VEB Arzneimittelwerk Dresden), DE-OS 1939173, **1970** [*Chem. Abstr.* **1970**, *73*, 131223e].
[36] R. Megges, K. Repke, B. Streckenbach, R. Franke, G. Kammann (VEB Arzneimittelwerk Dresden), DE-OS 2019967, **1970** [*Chem. Abstr.* **1971**, *74*, 31915j].
[37] F. Dittrich, R. Megges, H. J. Portius, K. Repke (Akademie der Wissenschaften der DDR), DD-P 94616, **1972** [*Chem. Abstr.* **1973**, *79*, 42775t].
[38] R. Megges, H. Timm, F. Dittrich, H. J. Portius, K. Repke (Akademie der Wissenschaften der DDR), DD-P 109869, **1974** [*Chem. Abstr.* **1975**, *83*, 179414b].
[39] R. Megges, H. Timm, P. Thiemann, F. Dittrich, P. Franke, H. J. Portius, K. Repke (Akademie der Wissenschaften der DDR), DD-P 109622, **1974** [*Chem. Abstr.* **1975**, *83*, 59166a].
[40] C. Lindig, P. Franke, K. R. H. Repke, *J. Prakt. Chem.* **1975**, *317*, 17–28.
[41] P. Franke, C. Lindig, K. R. H. Repke, *J. Prakt. Chem.* **1975**, *317*, 86–98.
[42] R. Megges, H. J. Portius, K. R. H. Repke, *Pharmazie* **1979**, *34*, 328–329.
[43] R. Megges, H. Kreissl, H. J. Portius, K. Repke (Akademie der Wissenschaften der DDR), DD-P 144060, **1980** [*Chem. Abstr.* **1981**, *95*, 62608z].
[44] C. Lindig, K. R. H. Repke, *J. Prakt. Chem.* **1980**, *322*, 991–1002.
[45] F. Theil, C. Lindig, K. R. H. Repke, *J. Prakt. Chem.* **1980**, *322*, 1003–1011.
[46] F. Theil, C. Lindig, K. R. H. Repke, *J. Prakt. Chem.* **1980**, *322*, 1012–1020.
[47] R. Megges, H. Timm, P. Franke (Akademie der Wissenschaften der DDR), DD-P 148222, **1981** [*Chem. Abstr.* **1982**, *96*, 35645y].
[48] A. Messerschmidt, R. Megges, H. Schrauber, *Cryst. Struct. Commun.* **1981**, *10*, 1041–1051.
[49] E. Höhne, A. Messerschmidt, R. Megges, *Cryst. Struct. Commun.* **1981**, *10*, 407–414.

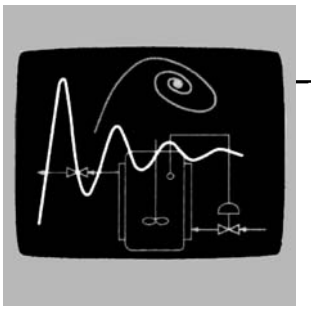
[50] A. Messerschmidt, E. Höhne, R. Megges, *Cryst. Struct. Commun.* **1981**, *10*, 399–406.
[51] R. Megges, I. Eschholz, R. Hintsche, R. Schwensow (Akademie der Wissenschaften der DDR), DD-P 154899, **1982** [*Chem. Abstr.* **1983**, *98*, 54299w].
[52] B. Streckenbach, P. Franke, R. Hintsche, H. J. Portius, K. R. H. Repke, *J. Prakt. Chem.* **1983**, *325*, 599–606.
[53] C. Lindig, K. R. H. Repke, *J. Prakt. Chem.* **1983**, *325*, 574–586.
[54] C. Lindig, *J. Prakt. Chem.* **1983**, *325*, 587–598.
[55] J. Wicha, M. Masnyk, W. Schönfeld, K. R. H. Repke, *Heterocycles* **1983**, *20*, 231–234.
[56] R. Megges, H. Timm, P. Franke, R. Hintsche (Akademie der Wissenschaften der DDR), DD-P 216242, **1984** [*Chem. Abstr.* **1985**, *103*, 142275n].
[57] J. Weiland, R. Schwensow, R. Megges, W. Schönfeld, M. M. Kabat, A. Kurek, J. Wicha (Akademie der Wissenschaften der DDR), DD-P 237170, **1986** [*Chem. Abstr.* **1988**, *108*, 75780m].
[58] C. Lindig, *J. Prakt. Chem.* **1986**, *328*, 682–694.
[59] C. Lindig, K. R. H. Repke, *J. Prakt. Chem.* **1986**, *328*, 695–704.
[60] R. Megges, H. Timm, W. Rollka, P. Franke, J. Weiland, K. R. H. Repke (Akademie der Wissenschaften der DDR), DD-P 233570, **1986** [*Chem. Abstr.* **1987**, *106*, 50557q].
[61] K. Schwabe, J. Weiland, D. Hübler, K. R. H. Repke (Akademie der Wissenschaften der DDR), DD-P 249273, **1987** [*Chem. Abstr.* **1988**, *109*, 211390j].
[62] C. Lindig, K. R. H. Repke, *J. Prakt. Chem.* **1987**, *329*, 841–858.
[63] J. Weiland, D. Pfeiffer, M. Wunderwald, R. Schwensow, R. Megges (Akademie der Wissenschaften der DDR), DD-P 245879, **1987** [*Chem. Abstr.* **1988**, *109*, 6891g].
[64] J. Weiland, K. Schwabe, D. Hübler, W. Schönfeld, K. R. H. Repke, *J. Enzyme Inhib.* **1987**, *2*, 31–36.
[65] J. Weiland, W. Schönfeld, K.-H. Menke, K. R. H. Repke, *Pharmacol. Res.* **1991**, *23*, 27–32.
[66] K. R. H. Repke, J. Weiland, K.-H. Menke, *J. Enzyme Inhib.* **1991**, *5*, 25–32.
[67] J. Weiland, P. Franke, D. Tresselt, M. Nitz, W. Schönfeld (Akademie der Wissenschaften, Berlin), DD-P 290891, **1991** [*Chem. Abstr.* **1991**, *115*, 280473z].
[68] J. Weiland, D. Tresselt, M. Nitz, R. Megges, W. Schönfeld (Akademie der Wissenschaften, Berlin), DD-P 290892, **1991** [*Chem. Abstr.* **1991**, *115*, 256559m].
[69] K. R. H. Repke, W. Schönfeld, *Trends Pharmacol. Sci.* **1984**, *5*, 393–397.
[70] W. Schönfeld, J. Weiland, K. R. H. Repke in *Cardiac Glycosides 1785–1985* (Eds.: E. Erdmann, K. Greeff, J. C. Skou), Steinkopff, Darmstadt, **1986**, pp. 127–134.
[71] K. R. H. Repke, J. Weiland, *Pharmacol. Res. Commun.* **1988**, *20*, 425–450.
[72] T. A. Krenitsky, G. B. Elion in *Strategy in Drug Research* (Ed.: J. A. K. Buisman), Elsevier, Amsterdam, **1982**, pp. 65–87.
[73] S. E. Wright, *The Metabolism of Cardiac Glycosides*, Thomas, Springfield, IL, **1960**.
[74] R. H. Thorp, L. B. Cobbin, *Cardiac Stimulant Substances*, Academic Press, New York, **1967**.
[75] R. Thomas, J. Boutagy, A. Gelbart, *J. Pharm. Sci.* **1974**, *63*, 1649–1683.
[76] K. R. H. Repke, *New Aspects of Cardiac Glycosides* (Eds.: W. Wilbrandt, P. Lindgren) (*Proc. Int. Pharmacol. Meet. 1st 1961* **1963**, *3*, 47–73).
[77] K. R. H. Repke, *OAZ Oesterr. Apoth. Ztg.* **1970**, *24*, 515–522.
[78] F. Lauterbach, K. R. H. Repke, D. Nitz, *Naunyn-Schmiedebergs Arch. Exp. Pathol. Pharmakol.* **1960**, *240*, 45–71.
[79] I. Herrmann, K. R. H. Repke, *Symposium über biochemische Aspekte der Steroidforschung* (Ed.: K. Schubert) (*Abh. Dtsch. Akad. Wiss. Berlin Kl. Med.* **1968**(2)), Akademie-Verlag, Berlin, **1969**, pp. 115–119.
[80] I. Herrmann, K. R. H. Repke, *Acta Microbiol. Acad. Sci. Hung.* **1975**, *22*, 481–485.
[81] K. R. H. Repke, R. Megges, *Dtsch. Gesundheitswes.* **1963**, *18*, 1325–1333.
[82] K. R. H. Repke, R. Megges, *Therapiewoche* **1973**, *23*, 2314–2318.
[83] K.-O. Haustein, C. Pachaly, D. Murawski, *Int. J. Clin. Pharmacol. Biopharm.* **1978**, *16*, 285–289.
[84] K. R. H. Repke, *Naunyn-Schmiedebergs Arch. Exp. Pathol. Pharmakol.* **1958**, *233*, 271–283.
[85] K. R. H. Repke, L. Roth, S. Klesczewski, *Naunyn-Schmiedebergs Arch. Exp. Pathol. Pharmakol.* **1959**, *237*, 155–170.
[86] F. Lauterbach, K. R. H. Repke, D. Nitz, *Naunyn-Schmiedebergs Arch. Exp. Pathol. Pharmakol.* **1960**, *239*, 196–218.
[87] I. Herrmann, K. R. H. Repke, *Naunyn-Schmiedebergs Arch. Exp. Pathol. Pharmakol.* **1964**, *248*, 351–369.
[88] I. Herrmann, K. R. H. Repke, *Naunyn-Schmiedebergs Arch. Exp. Pathol. Pharmakol.* **1964**, *248*, 370–386.
[89] K. R. H. Repke, L. T. Samuels, *Biochemistry* **1964**, *3*, 685–689.
[90] K. R. H. Repke, L. T. Samuels, *Biochemistry* **1964**, *3*, 689–695.
[91] K. R. H. Repke, *Trends Pharmacol. Sci.* **1985**, *6*, 275–278.
[92] W. Schönfeld, J. Weiland, C. Lindig, M. Masnyk, M. M. Kabat, A. Kurek, J. Wicha, K. R. H. Repke, *Naunyn-Schmiedeberg's Arch. Pharmacol.* **1985**, *329*, 414–426.
[93] K. R. H. Repke, *Naunyn-Schmiedebergs Arch. Exp. Pathol. Pharmakol.* **1959**, *236*, 242–245.
[94] I. Herrmann, H. J. Portius, K. R. H. Repke, *Naunyn-Schmiedebergs Arch. Exp. Pathol. Pharmakol.* **1964**, *247*, 1–18.
[95] I. Herrmann, K. R. H. Repke, *Naunyn-Schmiedebergs Arch. Exp. Pathol. Pharmakol.* **1964**, *247*, 19–34.
[96] I. Herrmann, K. R. H. Repke, *Naunyn-Schmiedebergs Arch. Exp. Pathol. Pharmakol.* **1964**, *247*, 35–48.
[97] K. R. H. Repke, S. Klesczewski, L. Roth, *Naunyn-Schmiedebergs Arch. Exp. Pathol. Pharmakol.* **1959**, *237*, 34–48.
[98] C. Lindig, K. R. H. Repke, *Acta Biol. Med. Ger.* **1971**, *26*, 501–512.
[99] *Ciba Foundation Symposium: Enzymes and Drug Action, Panel Discussion*, Churchill, London, **1962**, p. 396, 429.
[100] R. L. Post, C. R. Merritt, C. R. Kinsolving, C. D. Albright, *J. Biol. Chem.* **1960**, *235*, 1796–1802.
[101] K. R. H. Repke, H. J. Portius, *Experientia* **1963**, *19*, 452–458.
[102] K. R. H. Repke, H. J. Portius, *Naunyn-Schmiedebergs Arch. Exp. Pathol. Pharmakol.* **1963**, *245*, 59–61.
[103] K. R. H. Repke, H. J. Portius, *Folia Haematol. (Leipzig)* **1965**, *83*, 28–38.
[104] K. R. H. Repke, M. Est, H. J. Portius, *Biochem. Pharmacol.* **1965**, *14*, 1785–1802.
[105] A. Schwartz, J. C. Allen, W. B. van Winkle, R. Munson, *J. Pharmacol. Exp. Ther.* **1974**, *191*, 119–127.
[106] A. Schwartz, G. E. Lindenmayer, J. C. Allen, *Pharmacol. Rev.* **1975**, *27*, 3–134.
[107] A. Schwartz, K. Whitmer, G. Grupp, I. Grupp, R. J. Adams, S.-W. Lee, *Ann. N. Y. Acad. Sci.* **1982**, *402*, 253–271.
[108] H. Flasch, N. Heinz, *Naunyn-Schmiedeberg's Arch. Pharmacol.* **1978**, *304*, 37–44.
[109] L. H. Michael, A. Schwartz, E. T. Wallick, *Mol. Pharmacol.* **1979**, *16*, 135–146.
[110] T. Akera, *Cardiac Glycosides, Part I: Experimental Pharmacology* (Ed.: K. Greeff) (*Handb. Exp. Pharmacol.* **1981**, *56/I*, 287–336).
[111] E. Erdmann, *Cardiac Glycosides, Part I: Experimental Pharmacology* (Ed.: K. Greeff) (*Handb. Exp. Pharmacol.* **1981**, *56/I*, 337–380).
[112] L. Brown, E. Erdmann, R. Thomas, *Biochem. Pharmacol.* **1983**, *32*, 2767–2774.
[113] T. W. Smith, E. M. Antman, P. L. Friedman, C. M. Blatt, J. D. Marsh, *Prog. Cardiovasc. Dis.* **1984**, *26*, 495–523.
[114] H. H. Rasmussen, G. T. Okita, R. S. Hartz, R. E. ten Eick, *J. Pharmacol. Exp. Ther.* **1990**, *252*, 60–64.
[115] K. R. H. Repke, *Klin. Wochenschr.* **1964**, *42*, 157–165.
[116] K. R. H. Repke, *Drugs and Enzymes* (Eds.: B. B. Brodie, J. R. Gillette, R. Capek) (*Proc. Int. Pharmacol. Meet. 2nd 1963* **1965**, 65–87).
[117] C. O. Lee, *Am. J. Physiol.* **1985**, *249*, C367–C378.
[118] W. Wilbrandt, K. Brawand, P. N. Witt, *Naunyn-Schmiedebergs Arch. Exp. Pathol. Pharmakol.* **1953**, *219*, 397–407.
[119] W. Wilbrandt, *Helv. Physiol. Pharmacol. Acta* **1958**, *16*, 31–43.
[120] W. Wilbrandt, *Dtsch. Med. Wochenschr.* **1957**, *82*, 1153–1158.
[121] W. Wilbrandt, *New Aspects of Cardiac Glycosides* (Eds.: W. Wilbrandt, P. Lindgren) (*Proc. Int. Pharmacol. Meet. 1st 1961* **1963**, *3*, 3–9).
[122] H. J. Portius, K. R. H. Repke, *Symposium über biochemische Aspekte der Steroidforschung* (Ed.: K. Schubert) (*Abh. Dtsch. Akad. Wiss. Berlin Kl. Med.* **1968**(2)), Akademie-Verlag, Berlin, **1969**, p. 180–183.
[123] W. Wilbrandt, E. M. Weiss, *Arzneim. Forsch.* **1960**, *10*, 409–412.
[124] B. C. Rossier, L. G. Palmer in *The Kidney. Physiology and Pathophysiology*, 2nd ed. (Eds.: D. W. Seldin, G. Giebisch), Raven, New York, **1992**, pp. 1373–1409.
[125] W. Schönfeld, R. Schön, K.-H. Menke, K. R. H. Repke, *Acta Biol. Med. Ger.* **1972**, *28*, 935–956.
[126] J. Monod, J. Wyman, J.-P. Changeux, *J. Mol. Biol.* **1965**, *12*, 88–118.
[127] J. Beer, R. Kunze, I. Herrmann, H. J. Portius, N. M. Mirsalichova, N. K. Abubakirov, K. R. H. Repke, *Biochim. Biophys. Acta* **1988**, *937*, 335–346.
[128] Y. A. Ovchinnikov, N. M. Arzamazova, E. A. Arystarkhova, N. M. Gevondyan, N. A. Aldanova, N. N. Modyanov, *FEBS Lett.* **1987**, *217*, 269–274.
[129] J. M. Capasso, S. Hoving, D. M. Tal, R. Goldshleger, S. J. D. Karlish, *J. Biol. Chem.* **1992**, *267*, 1150–1158.
[130] W. Schönfeld, K.-H. Menke, R. Schönfeld, K. R. H. Repke, *J. Enzyme Inhib.* **1987**, *2*, 37–45.
[131] M. Reiter, *Cardiac Glycosides, Part I: Experimental Pharmacology* (Ed.: K. Greeff) (*Handb. Exp. Pharmacol.* **1981**, *56/I*, 153–159).
[132] L. Brown, R. Thomas, *Arzneim. Forsch.* **1983**, *33*, 814–817.
[133] L. Brown, R. Thomas, *Arzneim. Forsch.* **1984**, *34*, 572–574.
[134] W. Schönfeld, R. Schönfeld, K.-H. Menke, J. Weiland, K. R. H. Repke, *Biochem. Pharmacol.* **1986**, *35*, 3221–3231.
[135] W. Schönfeld, K. R. H. Repke, *Quant. Struct. Act. Relat.* **1988**, *7*, 160–165.
[136] H. H. Shlevin, *Drug Dev. Res.* **1984**, *4*, 275–284.
[137] K. R. H. Repke, F. Dittrich, *Trends Pharmacol. Sci.* **1980**, *1*, 398–402.
[138] K. R. H. Repke, W. Schönfeld, R. Schönfeld, K.-H. Menke, *Pharmazie* **1990**, *45*, 237–239.

[139] T. Deneke, H. Adam, *Z. Exp. Pathol. Ther.* **1906**, *2*, 491.
[140] G. R. Marshall, C. D. Barry, H. E. Bosshard, R. A. Dammkoehler, D. A. Dunn, *Computer-Assisted Drug Design* (Eds.: E. C. Olson, R. E. Christoffersen) (*ACS Symp. Ser.* **1979**, *112*, 205–226).
[141] A. J. Stuper, W. E. Brügger, P. C. Jurs, *Computer Assisted Studies of Chemical Structure and Biological Function*, Wiley, New York, **1979**, p. 1.
[142] K. R. H. Wooldridge, *Med. Chem. Proc. Int. Symp. 5th 1976* **1977**, 427–432.
[143] M. Bohl in *Molecular Structure and Biological Activity of Steroids* (Eds.: M. Bohl, W. L. Duax), CRC, Boca Raton, FL, **1992**, pp. 91–155.
[144] G. R. Marshall, R. D. Cramer III, *Trends Pharmacol. Sci.* **1988**, *9*, 285–289.
[145] K. R. H. Repke, J. Weiland, R. Megges, R. Schön, M. Nitz (Max-Delbrück-Centrum für Molekulare Medizin), DE-OS 4321937, **1995**.
[146] F. S. LaBella, I. Bihler, J. Templeton, R.-S. Kim, M. Hnatovich, D. Rohrer, *Fed. Proc.* **1985**, *44*, 2806–2811.
[147] A. Szent-Györgyi, *Chemical Physiology of Contraction in Body and Heart Muscle*, Academic Press, New York, **1953**, pp. 79–88.
[148] A. Goto, K. Yamada, N. Yagi, M. Yoshioka, T. Sugimoto, *Pharmacol. Rev.* **1992**, *44*, 377–399.
[149] J. M. Hamlyn, P. Manunta, *J. Hypertens.* **1992**, *10* (Suppl. 7), S99–S111.
[150] C. T. Carilli, M. Berne, L. C. Cantley, G. T. Haupert, Jr., *J. Biol. Chem.* **1985**, *260*, 1027–1031.
[151] G. T. Haupert, Jr. in *The Na^+,K^+ Pump., Part B: Cellular Aspects* (Eds.: J. C. Skou, J. G. Nørby, A. B. Maunsbach, M. Esmann), Liss, New York, **1988**, pp. 297–320.
[152] J. M. Hamlyn, M. P. Blaustein, S. Bova, D. W. DuCharme, D. W. Harris, F. Mandel, W. R. Mathews, J. H. Ludens, *Proc. Natl. Acad. Sci. USA* **1991**, *88*, 6259–6263.
[153] A. Goto, T. Ishiguro, K. Yamada, M. Ishii, M. Yoshioka, C. Eguchi, M. Shimora, T. Sugimoto, *Biochem. Biophys. Res. Commun.* **1990**, *173*, 1093–1101.
[154] A. A. Tymiak, J. A. Norman, M. Bolgar, G. C. DiDonato, H. Lee, W. L. Parker, L.-C. Lo, N. Berova, K. Nakanishi, E. Haber, G. T. Haupert, Jr., *Proc. Natl. Acad. Sci. USA* **1993**, *90*, 8189–8193.
[155] D. G. Pace, R. A. Gillis, *Arch. Int. Pharmacodyn. Ther.* **1982**, *255*, 103–116.
[156] W. L. Stahl, *Neurochem. Int.* **1986**, *8*, 449–476.
[157] R. A. Gillis, J. A. Quest in *Cardiac Glycosides 1785–1985* (Eds.: E. Erdmann, K. Greeff, J. C. Skou), Steinkopff, Darmstadt, **1986**, pp. 347–356.
[158] R. M. Young, J. B. Lingrel, *Biochem. Biophys. Res. Commun.* **1987**, *145*, 52–58.
[159] R. Schröder, B. Ramdohr, U. Hüttemann, K. P. Schüren, *Dtsch. Med. Wochenschr.* **1972**, *97*, 1535–1538.
[160] U. Ehrlich, H. Klepzig, *Med. Klin. (Munich)* **1976**, *71*, 1546–1554.
[161] U. Lindner in *Therapie mit Aldosteron-Antagonisten* (Ed.: E. Mutschler), Urban & Schwarzenberg, München, **1988**, pp. 71–82.
[162] A. A. van Vliet, A. J. M. Donker, J. J. P. Nauta, F. W. A. Verheugt, *Am. J. Cardiol.* **1993**, *71*, 21A–28A.
[163] U. Dahlström, E. Karlsson, *Am. J. Cardiol.* **1993**, *71*, 29A–33A.
[164] F. Zannad, *Am. J. Cardiol.* **1993**, *71*, 34A–39A.
[165] D. J. Greenblatt, J. Koch-Weser, *JAMA J. Am. Med. Assoc.* **1973**, *225*, 40–43.
[166] H. R. Ochs, D. J. Greenblatt, G. Bodem, T. W. Smith, *Am. Heart J.* **1978**, *96*, 389–400.
[167] Y. Nishino, H. Schröder, M. F. El Etreby, *Arzneim. Forsch.* **1988**, *38*, 1800–1805.
[168] M. Weatherall, *Nature (London)* **1982**, *296*, 387–390.

Ingham, J. et al.

Chemical Engineering Dynamics

Modelling with PC Simulation



1994. XX, 701 pages with 430 figures.
Hardcover. DM 276.-/
öS 2153.-/ sFr. 256.-.
ISBN 3-527-28577-6

In this book, the reader is guided through the complex study of dynamic chemical engineering systems by the unique combination of a simplified presentation of the fundamental theory (Part 1) and direct hands-on computer experimentation with the provision of 85 accompanying computer-based simulation examples (Part 2) supplied on diskette.

The ISIM digital simulation language is very simple to use and its powerful interactive nature enables the readers to create their own simulations, based on their own specific problems. This powerful dynamic ISIM software is ready to run on any DOS personal computer.

The treatment employed in this book is well tried and tested, based on over 20 years experience in teaching an international post-experience course. Whether for the teacher, the student, the chemist or engineer, this book serves as the key to a greater understanding of chemical engineering dynamics through the fun and enjoyment of active learning.

To order please contact your bookseller or:

VCH, P.O. Box 10 11 61, D-69451 Weinheim, Telefax (0) 62 01 - 60 61 84

VCH, Hardstrasse 10, P.O. Box, CH-4020 Basel

VCH, 8 Wellington Court, Cambridge CB1 1HZ, UK

VCH, 220 East 23rd Street, New York, NY 10010-4606, USA (toll free: 1-800-367-8249)

VCH, Eikow Building, 10-9 Hongo 1-chome, Bunkyo-ku, Tokyo 113 Japan

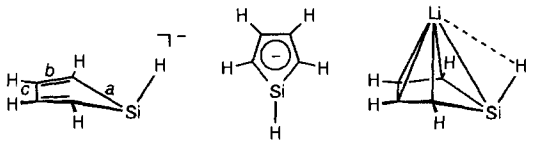
VCH

Five-Membered Aromatic and Antiaromatic Rings with Gallium, Germanium, and Bismuth Centers: A Short March through the Periodic Table

Hansjörg Grützmacher*

The concepts of aromaticity and anti-aromaticity are troublesome,[1] as can also be clearly seen from the examples described here of five-membered 4π and 6π heterocycles XC_4R_4 (4π: X = CR^+, BR, AlR, GaR, InR; 6π: CR^-, SiR^-, GeR^-, N^-, NR, P^-, PR, O, S, Se, etc.). These heterocycles therefore enjoy the attention of many research groups as objects for the study of bonding theory and because of their rich heterocyclic chemistry. At any rate the simple count of π electrons in a ring framework is no sufficient criterion for aromaticity or anti-aromaticity. A concept of Dauben, Jr., for establishing a criterion for aromaticity has now been taken up and extended by Kutzelnigg et al.[1a] and Schleyer et al.[2] An increased magnetic susceptibility Λ of a cyclic π-elcctron system is calculated as the difference ($\chi_M - \chi'_M$) between the susceptibility χ_M of the cycle with *delocalized* electrons and the susceptibility χ'_M with localized electrons. For an aromatic ring Λ is negative (diamagnetic), for an antiaromatic ring positive (paramagnetic).[1b] The susceptibility χ_M is, in principle, also experimentally determinable, while χ' is calculated from increments. The research group of Schleyer can show with a wide range of five-membered rings that the Dauben concept is compatible with aromatic stabilization energies and the geometries of the rings. A planar ring framework and bonds that are to a large extent equal in length indicate delocalization of the electrons, that is, the aromatic character. On the other hand a folded ring framework for 6π heterocycles and, in any case, alternating bond lengths point to localization of the electrons in antiaromatic compounds. The following series along which the aromaticity decreases and the anti-aromaticity increases can be set up: $C_5H_5^- > HNC_4H_4 > SC_4H_4 > OC_4H_4 > HSiC_4H_4^- > HPC_4H_4 > HAlC_4H_4 > HBC_4H_4 > HSiC_4H_4^+ > C_5H_5^+$. The calculations of the gas-phase structure of the silacyclopentadiene anion $HSiC_4H_4^-$ (**1a**) of the 6π aromatic rings will be highlighted here.

The calculation of the structure of this molecule, which had already been undertaken by Gordon et al.,[3] and Damewood, Jr., has now been repeated by Goldfuss and Schleyer with an extended basis set (RMP2(fc)/6-31 + G**).[5] According to these calculations, **1a** has a folded C_s-symmetrical structure [Σ°(Si) = 321.6°] with slightly different C–C lengths (b = 1.399, c = 1.433 Å) and Si–C lengths that are shortened relative to Si–C single bonds (a = 1.847 Å). Calculated to be only 3.8 kcal mol^{-1} more energetic, the planar structure **1b** with C_{2v} symmetry (which corresponds to the transition state for the inversion at the Si center) shows, in addition, a distinctly shortened Si–C bond (1.793 Å) and virtually equal C–C lengths (1.422, 1.414 Å). The new calculations also demonstrate that the stability of silacyclopentadiene anions **1** have previously been substantially underestimated (about 51% of the calculated aromatic stabilization energy of Cp^-). Interestingly, for the solvent-free ion pair silacyclopentadienyllithium (**2**) a structure has been determined



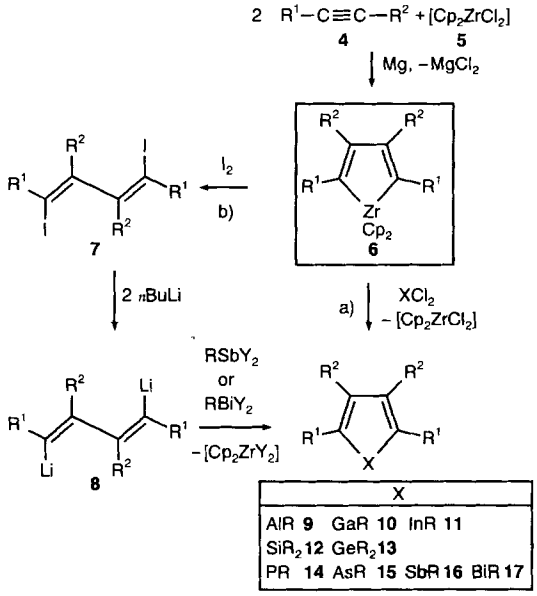
1a C_s **1b** C_{2v} **2**

that approximates even more closely the planar molecular geometry of **1b**.[5] An η^5-coordinated "inverse" lithium silanide with an only slightly pyramidalized silicon center [Σ° = 340.2°, a = 1.823, b = 1.420, c = 1.424 Å] as global minimum resulted from a RMP2/6-31G** calculation. Already 80% of the aromatic stabilization energy calculated for LiCp can be assigned to this molecule.

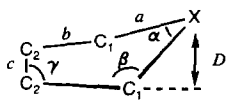
Of the antiaromatic rings, $C_5H_5^+$ (**3**) is particularly interesting as counterpart to $C_5H_5^-$. A laborious ab initio study of the Erlangen group[6] gives the remarkable result that this cation has a planar molecular structure (D_{5h}) with a triplet ground state, and not, as the anticipated according to the Jahn–Teller theorem for a cyclic anti-aromatic π electron system, a molecular structure distorted towards C_{2v} symmetry with a singlet ground state. As early as 1973, Saunders, Breslow et al. could generate the cation $C_5H_5^+$ (**3**) from C_5H_5Br and SbF_5 at low temperatures and prove its triplet state by ESR spectroscopy.[7]

Not only the theoreticians, but also experimentalists refined their methods. The preparation of heterocyclopentadiene was considerably facilitated in particular by a synthetic route developed by Fagan and Nugent,[8] in which two equivalents of an alkyne (**4**) was coupled with [Cp_2ZrCl_2] (**5**) in the presence of magnesium to form zirconacyclopentadienes **6**. Metallacycle **6**

[*] Prof. Dr. H. Grützmacher
Institut für Anorganische und Analytische Chemie der Universität
Albertstrasse 21, D-79104 Freiburg (Germany)
Telefax: Int. code + (761)203-5987
e-mail: gruetzma@sun2.ruf.uni-freiburg.de



reacts with halides according to route a) to form heterocyclopentadienes such as **9**–**15**. Ashe III et al. chose for the synthesis of stibole and bismole derivatives **16** and **17** (X = SbR, BiR; cf. Table 1), a roundabout route b) via a 1,4-diiodobutadiene (**7**) and a 1,4-dilitiobutadiene (**8**) prepared from it by halogen/metal exchange.[9] Cowley et al. also used the Fagan–Nugent synthesis for the preparation of a galla- and an indacyclopentadiene (**10** and **11**, respectively).[10] A single-crystal X-ray structure analysis was possible on **10**. Selected distances and angles (Scheme 1) are listed in Table 1 together with those of other 4π and 6π heterocycles. These compounds extend the neutral class



Scheme 1.

Table 1. Selected structural parameters (see Scheme 1) of some XC_4H_4 heterocycles [21]. The exact description of the substituents are to be found in the cited original references.

	X	*a*	*b*	*c*	α	β	γ	*D*	Ref.
9	AlR [a]	1.97	1.36	1.52	91.6	105.6	118.7	0.04	[12]
10	GaR	1.95	1.31	1.52	90.1	107.5	117.5	0.00	[10]
	CH^-	1.40	1.40	1.40	108.1	108.1	108.1	0.00	[13]
	NR	1.37	1.35	1.42	109.8	107.6	107.5	0.00	[14a]
14	PR	1.78	1.34	1.44	90.7	110.0	114.1	0.21	[14b]
15	AsR	1.94	1.34	1.44	87.1	108.7	117.3	0.17	[14d]
16	SbR	2.14	1.32	1.46	81.5	109.5	120.3	0.08	[9d]
17	BiR	2.24	1.34	1.44	79.3	–	–	–	[9b]

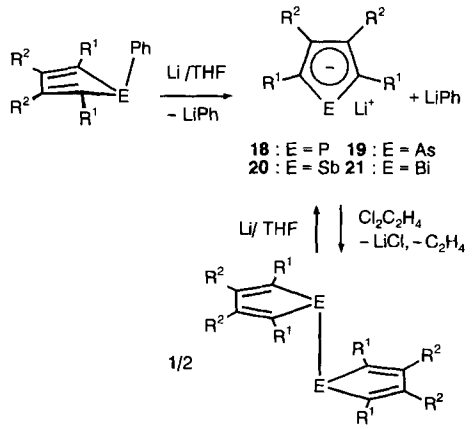
[a] Et_2O adduct; Al–O 1.91 Å.

of five-membered 4π heterocycles obtained by the isovalent electronic replacement of CR^+ by BR, AlR, GaR, or InR. Of these, some deeply colored boroles, RBC_4R_4, have been known the longest, although no structure determination has yet been successful.[11] However, an aluminacyclopentadiene (**9**) could also be structurally characterized as diethyl ether adduct by Krüger, Sekutowski et al. in 1977.[12]

The heteroatom built into the ring frameworks of **9**–**11** forces the heterocycles into C_{2v} symmetry. The rings **9**–**11** are in the singlet state, and the delocalization of the electrons over the ring framework, which is anticipated for an anti-aromatic π system,[2] is lifted. In **9** and **10** the experimetally determined C–C distances *b* (1.31–1.36 Å) and *c* (1.52 Å) are therefore distinctly different. The planarity of the five-membered rings **9** and **10** is remarkable (deviation *D* of the aluminum center in **9** is only 0.04 Å).

The five-membered rings with 6π-electron systems are best exemplified by the cyclopentadienide ion $C_5H_5^-$ (Cp^-), whose planar molecular structure with D_{5h} symmetry has been experimentally determined in uncomplexed form, for instance in the compounds $[(Me_3P)_4(NO)MeRe]^+Cp^-$[13] or $[Cp_2Ta(\mu\text{-}CH_2)_2Pd(Me_2PCH_2CH_2PMe_2]^+Cp^-$.[13b] The length of the C–C bonds (*a*, *b*, and *c*) is about 1.40 Å.[13a] In contrast the C–C bonds *b* (1.32–1.34 Å) and *c* (1.42–1.56 Å) in the phospholes **14**, arsoles **15**, stiboles **16**, and bismoles **17** are very different in length and confirm the localization of the electrons (weak aromatic character).[14] In addition, the rings **14**–**17** containing an element of the third to sixth period are no longer planar (D = 0.21–0.08 Å). For steric reasons the deviation is most pronounced in the phospholes.

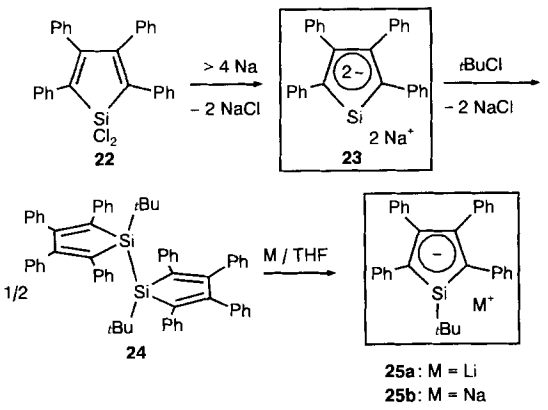
The anions $XC_4H_4^-$ **18**–**21** (X = P, As, Sb, Bi) with lithium ions as counterions can be prepared from suitable pnictogen



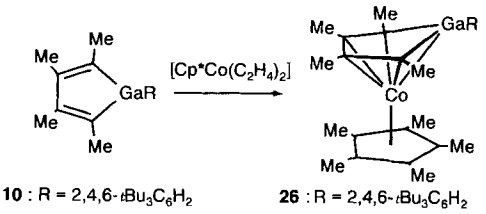
cyclopentadienes. To date only the structural analysis of lithium phospholide $Li(PC_4Me_4)$ (**18**) has been achieved.[15] In **18**, besides relatively long Li–C distances (2.40 Å), almost equal C–C distances *b* (1.40 Å) and *c* (1.42 Å) were found; thus **18** can be assigned an increased aromatic character relative to the neutral phosphole **14** [cf. $HSiC_4H_4^-$ (**1a**) and $LiHSiC_4H_4$ (**2**)].

Despite intensive experimentation[16] no sila-, germa-, stanna-, or plumbacyclopentadienide analogous to Cp^- has previously been able to be characterized. Boudjouk et al. recently presented an efficient synthesis of the sterically demanding substituted lithium and sodium silacyclopentadienide (**25a**, **b**).[17] The anion is prepared via the pyrophoric dianion **23** that W.-C. Joo et al. isolated as red-brown solid and characterized by ^1H and ^{13}C NMR spectroscopy.[18] Also **25a** and **b** could be characterized only by NMR spectra. The resonance signal of the ^{29}Si nucleus was detected at relatively low field [δ = 25.1 (Li counterion, THF); δ = 26.1 (Na counterion, THF)] The authors therefore anticipate a delocalization of the negative charge over the C_4Si ring and a planarization of the coordination geometry at the silicon atom, which was supported by IGLO calculations of the chemical shift of the ^{29}Si nucleus in **2**.

 © VCH Verlagsgesellschaft mbH, D-69451 Weinheim, 1995 0570-0833/95/0303-0296 $ 10.00+.25/0

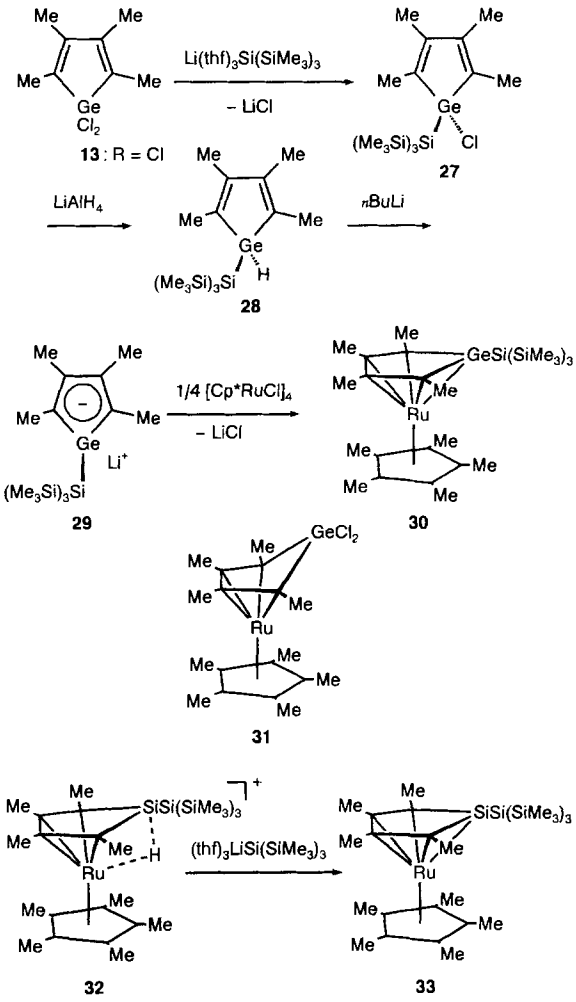


The heterocyclopentadienes and -dienides presented here are suitable as complex ligands. They bind in an η^5 fashion to metal complex fragments like the classical cyclopentadienyl ligand. For example, the complex **26** synthesized by Cowley et al. can

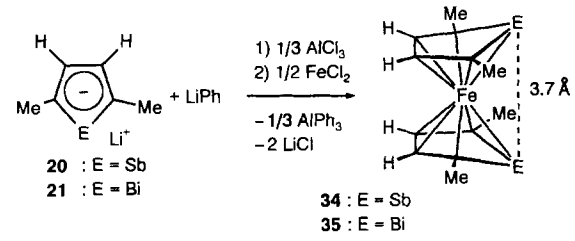


be readily constructed from the substitutionally labile complex $[Cp^*Co(C_2H_4)_2]$ ($Cp^* = C_5Me_5$) and the isolated 4π heterocycle **10** (R = 2,4,6-$tBu_3C_6H_2$).[10] Alternatively, a heterocyclopentadienide like the stibolide **20** or the bismolide **21** can be generated in solution and coupled with a metal halide. The syntheses of **30**[19] and **33**[20] performed by Tilley et al. deserve particular attention in the light of the vain attempts (until recently) to detect unambiguously an η^5-coordinated germa- or silacyclopentadienide in a complex. The synthesis of **30** is achieved by coupling the germacyclopentadienide **29**, prepared in solution, with $[(Cp^*RuCl)_4]$. In contrast, the analogous silacyclopentadienyl complex **33** is obtained by deprotonation of the complex cation **32** with a bent Ru-H-Si bond, because the synthesis of the silacyclopentadienide analogous to **29**, $C_4Me_4SiSi(SiMe_3)_3^-$ failed. The compounds **30** and **32** could be structurally characterized. A planar five-membered C_4Ge or C_4Si ring is observed, and the bulky $Si(SiMe_3)_3$ substituent is hardly twisted out of this plane [12.9° (**30**) and 19.0° (**32**)]. The different lengths of the C–C distances *b* (1.39 Å) and *c* (1.46 Å) in **32** clearly show that the extent of the delocalization of the electrons in **32** is less than that of **30** ($b = 1.40$, $c = 1.41$ Å). The preparation of a pure sample of **33** and its structural characterization has not yet been achieved. The spectroscopic data, in particular the downfield shift of the ^{29}Si NMR resonance signal on deprotonation of **32** ($\delta(^{29}Si) = -27.1$) to **33** ($\delta(^{29}Si) = -7.3$), leave no doubt about the existence of **33**.

Just as remarkable are the sandwich compounds **34** and **35** synthesized by Ashe III et al., in which an unusual ecliptical arrangement of the five-membered rings is observed.[9a, b] The



special arrangement invites speculation about a (binding?) interaction between the antimony and bismuth centers. In the complexes **26** and **30**–**35** in which the heteroatoms of the five-



membered rings are incorporated into the π bonding, a fundamental equalizing of the C–C bond lengths *b* and *c* accompanying a planarization of the ring framework is observed relative to the uncomplexed or η^4-bound heterocycles. Thus, the deviation *D* of the germanium center is 0.97 Å in **31**, but only 0.02 Å in **30**.[19]

In hardly any other branch of chemistry has such a systematic, experimental investigation of the changes in properties of one class of compounds been undertaken by deliberate substitution of a molecular unit by chemical elements from a wide range in the periodic table. By means of the heterocyclopentadienes and

-dienides presented here and their complex compounds, the remarkable validity of experimental concepts, but also of bonding principles can be convincingly tested. Perhaps still open questions, for instance into the interesting structures of silacyclopentadienyl salts like **2** and related compounds or into the dependence of their structures on the counterion, can also be answered by experiment in the near future.

German version: *Angew. Chem.* **1995**, *107*, 323

Keywords: aromaticity · bismuth compounds · cyclopentadienides · gallium compounds · germanium compounds

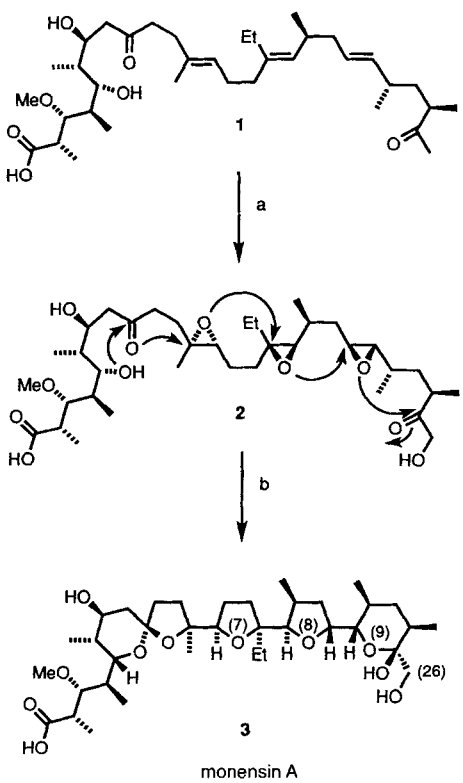
[1] a) U. Fleischer, W. Kutzelnigg, P. Lazzaretti, V. Mühlenkamp, *J. Am. Chem. Soc.* **1994**, *116*, 5298; b) Zusammenfassung: V. I. Minkin, M. N. Glukhovtsev, B. Ya. Simkin, *Aromaticity and Anitaromaticity, Electronic and Structural Aspects*, Wiley, Chichester, **1994**.
[2] P. von R. Schleyer, P. K. Freeman, H. Jiao, B. Goldfuss, *Angew. Chem.* **1995**, *107*, 332; *Angew. Chem. Int. Ed. Engl.* **1995**, *34*, 337.
[3] M. S. Gordon, P. Boudjouk, F. Anwari, *J. Am. Chem. Soc.* **1983**, *105*, 4972.
[4] J. R. Damewood, Jr., *J. Org. Chem.* **1986**, *51*, 5028.
[5] B. Goldfuss, P. v. R. Schleyer, *Organometallics* **1995**, *14*, in press.
[6] M. N. Glukhovtsev, B. Reindl, P. von R. Schleyer, *Mendeleev Commun.* **1993**, 100.
[7] M. Saunders, R. Berger, A. Jaffe, J. M. McBride, J. O'Neill, R. Breslow, J. M. Hoffman, Jr., C. Pechonock, E. Wassermann, R. S. Hutton, V. J. Kuck, *J. Am. Chem. Soc.* **1973**, *95*, 3017.
[8] P. J. Fagan, W. A. Nugent, *J. Am. Chem. Soc.* **1988**, *110*, 2310.
[9] a) A. J. Ashe III, J. W. Kampf, S. M. Al-Taweel, *J. Am. Chem. Soc.* **1992**, *114*, 372; b) A. J. Ashe III, J. W. Kampf, D. B. Puranik, S. M. Al-Taweel, *Organometallics* **1992**, *11*, 2743; c) A. J. Ashe III, J. W. Kampf, S. M. Al-Taweel, *ibid.* **1992**, *11*, 1491; d) A. J. Ashe III, T. R. Diephouse, J. W. Kampf, S. M. Al-Taweel, *ibid.* **1991**, *10*, 2068, and references therein.
[10] A. H. Cowley, F. P. Gabbai, A. Decken, *Angew. Chem.* **1994**, *106*, 1429; *Angew. Chem. Int. Ed. Engl.* **1994**, *33*, 1370.
[11] G. E. Herberich, H. Ohst, *Chem. Ber.* **1985**, *118*, 4303, and references therein.
[12] C. Krüger, J. C. Sekutowski, H. Hoberg, R. Krause-Göing, *J. Organomet. Chem.* **1977**, *141*, 141.
[13] a) C. P. Casey, J. M. O'Connor, K. J. Haller, *J. Am. Chem. Soc.* **1985**, *107*, 1241; b) M. D. Butts, R. G. Bergman, *Organometallics* **1994**, *13*, 1899, and references therein.
[14] a) Pyrroles: N. Kuhn, E.-M. Horn, R. Boese, N. Augart, *Angew. Chem.* **1988**, *100*, 1433; *Angew. Chem. Int. Ed. Engl.* **1988**, *27*, 1368; b) phospholes: P. Coggon, J. F. Engel, A. T. McPhail, L. D. Quin, *J. Am. Chem. Soc.* **1970**, *92*, 5779; c) F. Mathey, *Chem. Rev.* **1988**, *88*, 429; d) arsoles: A. J. Ashe III, W. M. Butler, T. R. Diephouse, *Organometallics* **1983**, *2*, 1005.
[15] T. Douglas, K. H. Theopold, *Angew. Chem.* **1989**, *101*, 1394; *Angew. Chem. Int. Ed. Engl.* **1989**, *28*, 1367.
[16] E. Colomer, R. J. P. Corriu, M. Lheureux, *Chem. Rev.* **1990**, *90*, 265.
[17] J.-H. Hong, P. Boudjouk, *J. Am. Chem. Soc.* **1993**, *115*, 5883.
[18] W.-C. Joo, J.-H. Hong, S.-B. Choi, H.-E. Son, *J. Organomet. Chem.* **1990**, *391*, 27.
[19] W. P. Freeman, T. D. Tilley, A. L. Rheingold, R. L. Ostrander, *Angew. Chem.* **1993**, *105*, 1841; *Angew. Chem. Int. Ed. Engl.* **1993**, *32*, 1744.
[20] W. P. Freeman, T. D. Tilley, A. L. Rheingold, *J. Am. Chem. Soc.* **1994**, *116*, 8428.
[21] The experimental structural parameters of XC_4H_4 heterocycles (X = O, S, Se, Te) were not presented for reasons of space. See R. D. Brown, F. R. Burden, P. D. Godfrey, *J. Mol. Spectrosc.* **1968**, *25*, 415; R. D. Brown, J. G. Crofts, *Chem. Phys.* **1973**, *1*, 217, and references therein.

Oxidative Polycyclization versus the "Polyepoxide Cascade": New Pathways in Polyether (Bio)synthesis?

Ulrich Koert*

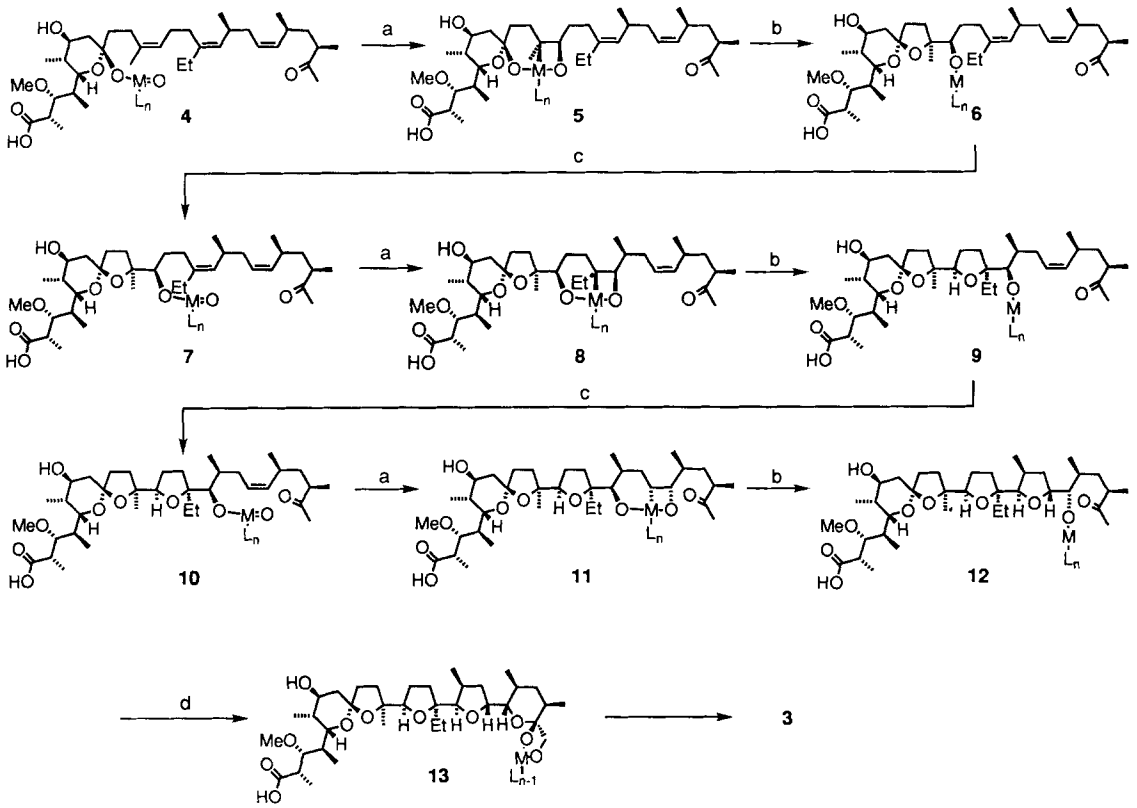
In 1983, Cane et al. postulated that polyether biosynthesis takes place as a two-step process. The first of these steps was proposed to be the enzymatic polyepoxidation of an acyclic hydroxypolyene precursor, and the second comprised a cascade of intramolecular epoxide ring openings with formation of the polyether framework.[1] For monensin A (**3**), for example, this is shown in the following scheme (Scheme 1): the (*E*,*E*,*E*)-triene **1** is transformed biosynthetically into the tris-epoxide **2**, which reacts further in a cascade of epoxide ring openings to yield the natural product **3**.[2]

This biosynthetic scheme gained rapid acceptance, above all because of the elegance of the second step, the "polyepoxide cascade". Polyepoxide cascades of the type **2** → **3** were reproduced in the laboratory[3] and used as key steps in the synthesis of polyethers.[4] The first step in the Cane–Celmer–Westley hypothesis, the stereoselective polyepoxidation, was subject to far less attention, even though it may be regarded as a weak point in the hypothesis. In feeding studies with *Streptomyces cinnamonensis*, no conversion of the (*E*,*E*,*E*)-triene **1** to monensin A (**3**) could be detected.[5] Earlier labeling studies had shown merely that the oxygen atoms in the two tetrahydrofuran rings



Scheme 1. The Cane–Celmer–Westley hypothesis for the biosynthesis of monensin A (**3**); a) stereoselective polyepoxidation; b) polyepoxide cascade; it is assumed that the OH group at C(26) is also introduced during the epoxidation step.

[*] Dr. U. Koert
Fachbereich Chemie der Universität
Hans-Meerwein-Strasse, D-35032 Marburg (Germany)
Telefax: Int. code + (6421)/288917



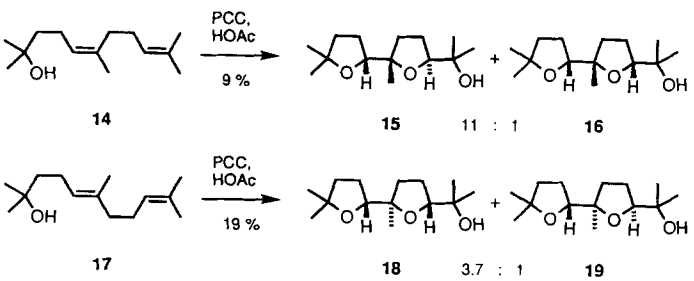
Scheme 2. Townsend–Basak–McDonald hypothesis for the biosynthesis of monensin A (**3**); a) [2 + 2] cycloaddition; b) reductive elimination of the metal with formation of the tetrahydrofuran ring; c) reoxidation of the metal; d) hemiacetal formation and oxidative introduction of the OH group at C(26).

(O-7,8) and in the tetrahydropyran hemiacetal (O-9) were derived from molecular oxygen, and it was unclear whether these were incorporated into the polyether framework by epoxidation or by another oxidation process.[2] Although the second step of the Cane–Celmer–Westley hypothesis, the polyepoxide cascade, is compelling, the initial, polyepoxidation step is still not sufficiently proven experimentally, and hence the entire hypothesis is uncertain.

In a recent publication, McDonald and Towne[6] extended studies of Townsend and Basak,[7] and presented an alternative model to the Cane–Celmer–Westley hypothesis: *syn*-oxidative polycyclization. The Townsend–Basak–McDonald hypothesis for the biosynthesis of monensin A (**3**) is depicted in Scheme 2.

The starting point is the alkoxy-bound oxo metal derivative of a (*Z*,*Z*,*Z*)-triene **4**. Intramolecular [2 + 2] cycloaddition affords a metallaoxetane **5**,[8] and the first tetrahydrofuran ring is then closed by reductive elimination of the metal to form compound **6**. An oxidation step from **6** to **7** activates the alkoxy-bound metal for the next [2 + 2] cycloaddition (**7** → **8**). Reductive elimination of the metal with closure of the second tetrahydrofuran ring leads to compound **9**. The third tetrahydrofuran ring of monensin A is closed in a further, analogous oxidative cyclization sequence (**9** → **10** → **11** → **12**). From compound **12** the natural product **3** can be obtained via the intermediate **13**. The stereochemical course of the oxidative cyclization should be emphasized: because a [2 + 2] cycloaddition is involved, the two oxygen atoms are added to the double bond in *syn* configuration. In order to construct the correct stereochemistry for the polyether framework of monensin A (**3**), the Townsend–Basak–McDonald hypothesis therefore postulates a (*Z*,*Z*,*Z*)-triene of type **4** as a biosynthetic precursor.

Using more simple systems, McDonald and Towne were able to demonstrate that pyridinium chlorochromate (PCC) is a suitable reagent for carrying out *syn*-oxidative polycyclization (Scheme 3).[6] Thus, transformation of the (*Z*)-hydroxydiene **14** yielded the bis-tetrahydrofurans **15** and **16**. Starting with the (*E*)-hydroxydiene **17**, the bis-tetrahydrofurans **18** and **19** were obtained.



Scheme 3. Model reactions of the Townsend–Basak–McDonald hypothesis.

The formation of **15** and **16** from the (*Z*)-diene and of **18** and **19** from the (*E*)-diene support the assumption of a *syn*-oxidative mechanism. The authors present conformational analysis arguments to explain the preferred formation of the *trans*-tetrahydrofurans **15** and **18**.[6]

 © VCH Verlagsgesellschaft mbH, D-69451 Weinheim, 1995 0570-0833/95/0303-0299 $ 10.00+.25/0

The low yields attained for the reactions shown in Scheme 3 call into doubt the usefulness of the *syn*-oxidative polycyclization under the published conditions for preparative purposes. However, the palette of possible oxidation reagents is by no means exhausted. Valuable ideas for a solution of the problem may come from the work of Kennedy et al. with Re_2O_7 as an oxidizing agent for oxidative olefin cyclizations.[9]

A fully satisfying answer to the question of the biosynthesis of polyether compounds such as monensin A (**3**) cannot be given form the results described here. However, it is clear that the new Townsend–Basak–McDonald hypothesis has gained ground on the older Cane–Celmer–Westley hypothesis. A key experiment to test the Townsend–Basak–McDonald hypothesis will be the use of labeled (*Z*,*Z*,*Z*)-trienes of type **4** in feeding experiments with *Streptomyces cinnamonensis*.

German version: *Angew. Chem.* **1995**, *107*, 326

Keywords: biosynthesis · cyclizations · oxidations · polyethers

[1] D. Cane, W. D. Celmer, J. W. Westley, *J. Am. Chem. Soc.* **1983**, *105*, 3594–3600.
[2] J. A. Robinson, *Prog. Chem. Org. Nat. Prod.* **1991**, *58*, 1–81.
[3] a) W. C. Still, A. G. Romero, *J. Am. Chem. Soc.* **1986**, *108*, 2105–2106; b) S. L. Schreiber, T. Sammakia, B. Hulin, G. Schulte, *ibid.* **1986**, *108*, 2106–2108; c) S. A. Russell, J. A. Robinson, D. J. Williams, *J. Chem. Soc. Chem. Commun.* **1987**, 351–352.
[4] For representative examples see: a) T. R. Hoye, J. C. Suhadolnik, *J. Am. Chem. Soc.* **1985**, *107*, 5312–5313; b) K. Nozaki, H. Shirama, *Chem. Lett.* **1988**, 1847–1847; c) I. Paterson, R. D. Tillyer, J. B. Smaill, *Tetrahedron Lett.* **1993**, *34*, 7137–7140; d) U. Koert, H. Wagner, M. Stein, *ibid.* **1994**, *35*, 7629–7632.
[5] D. S. Holmes, J. A. Sherringham, U. C. Dyer, S. T. Russell, J. A. Robinson, *Helv. Chim. Acta* **1990**, *73*, 239–259: the authors point out that solubility problems may have played a role in the failure of the labeling experiment.
[6] F. E. McDonald, T. B. Towne, *J. Am. Chem. Soc.* **1994**, *116*, 7921–7922.
[7] C. A. Townsend, A. Basak, *Tetrahedron* **1991**, *47*, 2591–2602.
[8] Metallaoxetanes have not yet been directly identified. Their role as intermediates in oxidative processes is however the subject of intensive discussion: K. A. Jørgensen, B. Schiøtt, *Chem. Rev.* **1990**, *90*, 1483–1506.
[9] S. Tang, R. M. Kennedy, *Tetrahedron Lett.* **1992**, *33*, 5303–5306.

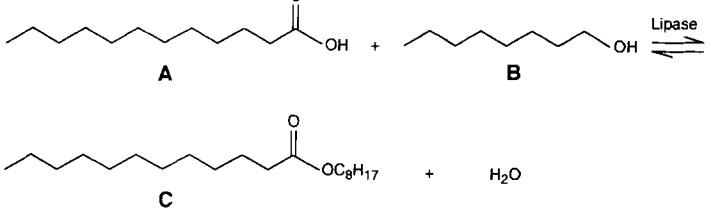
 © *VCH Verlagsgesellschaft mbH, D-69451 Weinheim, 1995* *0570-0833/95/0303-0300 $ 10.00+.25/0*

Efficient Heterogeneous Biocatalysts by Entrapment of Lipases in Hydrophobic Sol–Gel Materials

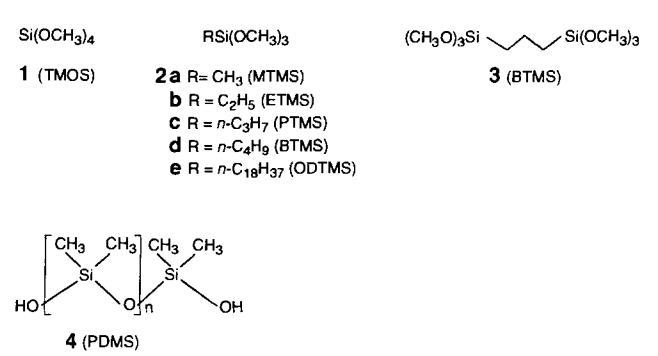
Manfred T. Reetz,* Albin Zonta, and Jörg Simpelkamp

Lipases are amongst the most widely used enzymes in organic chemistry.[1] In aqueous emulsions, they catalyze the chemo-, regio-, and stereospecific hydrolysis of esters, and when suspended in organic solvents[2] they catalyze the reverse reaction, effecting selective esterification.[1] In order to increase the activity and stability of lipases and at the same time to facilitate their recovery, many studies on the immobilization of lipases have been carried out.[3–5] We report here on the entrapment of lipases in hydrophobic sol–gel materials, which results in the formation of highly active, stable and reusable heterogenous biocatalysts.[6]

Following the procedures described earlier for the entrapment of biomolecules in silica gel (SiO_2) using the sol–gel process,[7, 8] tetramethoxysilane (TMOS) **1** was hydrolyzed in the presence of various lipases (e.g. from *Ps. cepacia*, Amano PS). Classical sol–gel processes of this type are acid or base catalyzed; hydrolysis and condensation of TMOS lead to nanometer-sized sol particles which then cross-link to form insoluble amorphous SiO_2 gels.[8] Unfortunately, the immobilized lipases that were produced by this method displayed extremely low activities. For example, relative activities of only 5% were obtained in the esterification of lauric acid (**A**) (0.05 M) with *n*-octanol (**B**) (0.1 M) in isooctane to give octyl laurate (**C**). In this test reaction that was used in all of the following studies, the relative activity x is defined as v(immobilized enzyme)/v(commercial enzyme), where v is the initial rate of the reaction (in μmol(h mg lipase)$^{-1}$).



Since lipases are interphase-active enzymes with hydrophobic domains, they can form ionic as well as hydrophobic interactions with other molecules.[9] For this reason, we speculated that alkyl-modified silica gels[10] with hydrophobic character, produced from silanes of the type $RSi(OCH_3)_3$, might be more suitable host matrices for lipases. In preliminary experiments, we therefore immobilized the lipase from *Ps. cepacia* (Amano PS) in a sol–gel process using $CH_3Si(OCH_3)_3$ (MTMS) (**2a**) or mixtures of TMOS (**1**) and MTMS (**2a**). NaF was used as the catalyst.[11] Figure 1 shows the dependence of the activity on the "methyl content" of the gel. In a mixed gel with 50% MTMS, the relative activity was still only 30%. Further increases in the MTMS content caused the relative activity to rise dramatically, reaching 1300% for a pure MTMS gel.



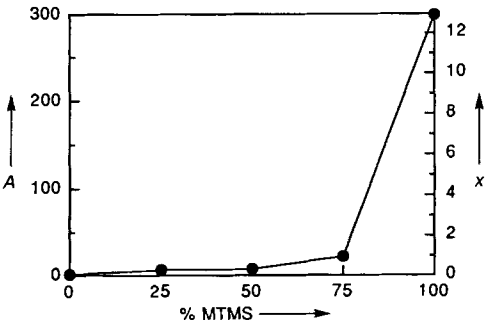


Fig. 1. Dependence of the activity A [μmol(h mg lipase)$^{-1}$] of immobilized *Ps. cepacia* lipase in TMOS/MTMS mixed gels on the gel composition. For the definition of the relative activity x see the text.

Taking a constant $TMOS/RSi(OCH_3)_3$ ratio of 1/1 and varying the R group of the silane, the relative activity sharply rises in the order $CH_3 < C_2H_5 < n\text{-}C_3H_7 < n\text{-}C_4H_9$. In contrast, a further increase in the size of the R group and the associated rise in the lipophilicity by use of *n*-octyl or *n*-octadecyl groups causes only a small additional increase in activity (Fig. 2).

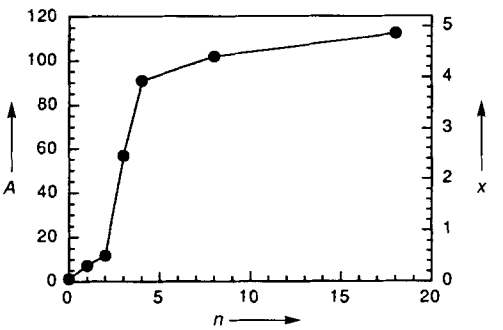


Fig. 2. Influence of the chain length of R on the activity of immobilized *Ps. cepacia* lipase in gels of the type $TMOS/RSi(OMe)_3$ (1/1). n = number of C atoms in R.

[*] Prof. Dr. M. T. Reetz, Dipl.-Biochem. A. Zonta, Dr. J. Simpelkamp
Max-Planck-Institut für Kohlenforschung
Kaiser-Wilhelm-Platz 1, D-45470 Mülheim an der Ruhr (Germany)
Telefax: Int. code + (208)306-2985

The results summarized in Figures 1 and 2 clearly show that the silane component is an important parameter for optimizing the enzymatic activity. We therefore investigated the commercially available silanes **3** and **4**, $n = 5-9$ as gel precursors in combination with TMOS and several lipases.[12] In all cases gel materials were obtained with excellent activities. Up to 93% of the protein was immobilized.

The representative results given in Figure 3 indicate that there is no general recipe for an optimal gel matrix, although in many cases TMOS/PTMS (1/5) gels turned out to be particularly well suited. An increase in activity by a factor of 5 and more (relative to the commercial powders) was achieved with many entrapped lipases. With the lipase SP 523 (Novo) the factor is even 88.

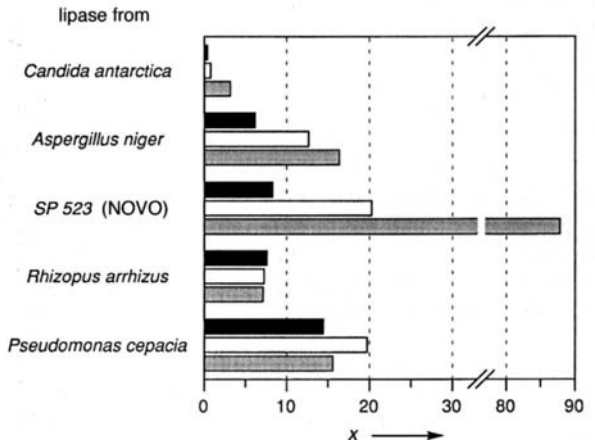


Fig. 3. Relative activity x of immobilized lipases in three different gel materials. Solid: MTMS; outlined: MTMS/PDMS (6/1); shaded: PTMS/TMOS (5/1).

The long-term stability of the entrapped lipases is remarkably high. The test reaction was performed over 30 days in batch reactions, in which the solid catalyst was filtered off after 22 h, washed, and then reused.[13] The activity decreased typically by 15–20% after the first two to three cycles and then remained constant at 80–85% of the initial activity, for example, for Amano PS lipase in pure MTMS or MTMS/PDMS (6/1) gels. In contrast, the same lipase *adsorbed* on a pure MTMS gel lost more than 75% of its initial activity after only eight reaction cycles. Probably only a small fraction of the lipase (15–20%) is adsorbed or only weakly stabilized in the sol–gel process and is hence more easily deactivated or lost.

The morphology of the sol–gel immobilizates was examined by scanning electron microscopy (SEM).[14] Figure 4 shows a typical scanning electron micrograph of a lipase-containing MTMS gel containing amorphous regions as well as spherical particles.

What are the reasons for the increased relative enzyme activities? Since the comparisons are based on suspensions in organic solvents, the primary cause is probably the fine distribution and therefore increased accessibility of the enzyme. It can also be speculated that the hydrophobic groups R in the sol–gel matrix are involved in stabilizing and activating interactions with the hydrophobic domains of the lipases. The observed "alkyl effect" could also be intrinsic during the formation of the gel, possibly by a smaller damaging effect to the enzyme by the hydrophobic silane monomers. An increase in activity caused by a local rise in substrate concentration in the hydrophobic matrix is also conceivable.[5] A favorable influence of possible hydrophobic interactions in the immobilization of lipases on other supports, albeit with much smaller increases in activity, has been described previously.[4]

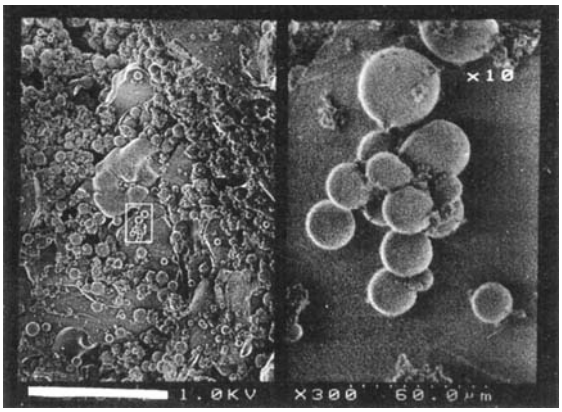
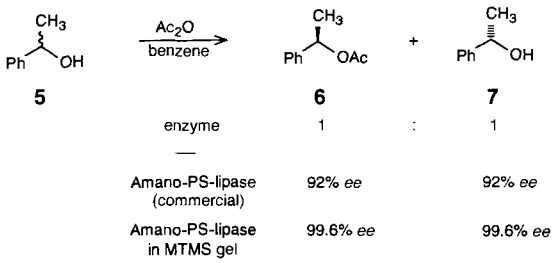


Fig. 4. Scanning electron micrograph of an immobilized lipase (*Ps. cepacia* lipase in MTMS gel). Right: 10x magnification of the area marked on the left. The length of the white bar corresponds to 60 µm.

The first attempts at application of the heterogeneous biocatalysts were carried out in the kinetic resolution of 1-phenylethanol (**5**)[15] using Amano PS lipase in a MTMS gel. The commercial enzyme preparation resulted in 92% *ee*,[16] whereas the same amount of entrapped lipase produced the enantiomerically pure products **6** and **7** (*ee* > 99%).



5		**6**		**7**
	enzyme	1	:	1
	—			
	Amano-PS-lipase (commercial)	92% *ee*		92% *ee*
	Amano-PS-lipase in MTMS gel	99.6% *ee*		99.6% *ee*

The method described herein leads to immobilized lipases with excellent activity and stability. The resulting biocatalysts are easy to reuse[13] and should also be suitable for application in continuous processes. A particular advantage is that by varying a range of parameters[17] it is possible to generate tailor-made gels for each lipase.[6]

Received: July 14, 1994
Revised version: September 17, 1994 [Z 7125 IE]
German version: *Angew. Chem.* **1995**, *107*, 373

Keywords: enzymatic catalysis · immobilization · lipases · sol–gel processes

[1] K. Faber, *Biotransformations in Organic Chemistry*, Springer, Berlin, **1992**; *Enzymes as Catalysts in Organic Synthesis* (Ed.: M. P. Schneider), Reidel, Dordrecht, **1986**; W. Boland, C. Frössl, M. Lorenz, *Synthesis* **1991**, 1049.

[2] A. Zaks, A. M. Klibanov, *Proc. Natl. Acad. Sci. USA* **1985**, *82*, 3192; A. M. Klibanov, *Acc. Chem. Res.* **1990**, *23*, 114.

[3] E. Guibe-Jampel, G. Rousseau, *Tetrahedron Lett.* **1990**, *31*, 112; F. X. Malcata, H. R. Reyes, H. S. Garcia, C. G. Hill, Jr., C. H. Amundson, *J. Am. Oil Chem. Soc.* **1990**, *67*, 890; M. Arroyo, J. M. Moreno, J. V. Sinisterra, *J. Mol. Catal.* **1993**, *83*, 261; see also R. V. Parthasarathy, C. R. Martin, *Nature* **1994**, *369*, 298.

[4] J. A. Bosley, J. C. Clayton, *Biotechnol. Bioeng.* **1994**, *43*, 934; M. Norin, J. Boutelje, E. Holmberg, K. Hult, *Appl. Microbiol. Biotechnol.* **1988**, *28*, 527.

[5] Y. Kimura, A. Tanaka, K. Sonomoto, T. Nihira, S. Fukui, *Appl. Microbiol. Biotechnol.* **1983**, *17*, 107.

[6] „*Immobilisierte Lipasen in hydrophoben Sol-Gel-Materialien*"; M. T. Reetz, A. Zonta, J. Simpelkamp (Max-Planck-Institut für Kohlenforschung), DE-A 4408152.9, **1994**.

[7] F. H. Dickey, *J. Am. Chem. Soc.* **1955**, *59*, 695; P. Johnson, T. L. Whateley, *J. Colloid Interface Sci.* **1971**, 557; L. M. Ellerby, C. R. Nishida, F. Nishida, S. A. Yamanaka, B. Dunn, J. Selverstone Valentine, J. J. Zink, *Science* **1992**, *255*, 1113; Y. Tatsu, K. Yamashita, M. Yamaguchi, S. Yamamura, H. Yamamoto, S. Yoshikawa, *Chem. Lett.* **1992**, 1615; S. Braun, S. Rappoport, S. Shtelzer, R. Zusman, S. Druckmann, D. Avnir, M. Ottolenghi in *Biotechnology: Bridging Research and Application* (Eds.: D. Kamely, A. Shakrabarty, S. E. Kornguth), Kluwer, Boston, **1991**, p. 205; H. Weetall, B. Robertson, D. Cullin, J. Brown, M. Walch, *Biochem. Biophys. Acta* **1993**, *142*, 211.

[8] L. L. Hench, J. K. West, *Chem. Rev.* **1990**, *90*, 33; C. J. Brinker, W. Scherer, *Sol-Gel-Science: The Physics and Chemistry of Sol-Gel-Processing*, Academic Press, Boston, **1990**.

[9] A. M. Brzozowski, U. Derewenda, Z. S. Derewenda, G. G. Dodson, D. W. Lawson, J. P. Turkenburg, F. Bjorkling, B. Huge-Jensen, S. A. Patkar, L. Thim, *Nature (London)* **1991**, *351*, 491; K.-E. Jaeger, S. Ransac, B. W. Dijkstra, C. Colson, M. van Heuvel, O. Missef, *FEMS Microbiol. Rev.* **1994**, *15*, 29.

[10] F. Schwertfeger, W. Glaubitt, U. Schubert, *J. Non-Cryst. Solids* **1992**, *145*, 85; Y. Haruvy, A. Heller, S. E. Weber in *Supramolecular Architecture-Synthetic Control in Thin Films and Solids* (Ed.: T. Bein) (*ACS Symp. Ser.* **1992**, *499*), p. 405.

[11] The lipase was dissolved in water or buffer, centrifuged to remove undissolved solids, and mixed with aqueous solutions of polyvinyl alcohol and sodium fluoride. The silanes were then added in the order of increasing reactivity. The reaction mixture was thoroughly mixed and shaken until gelation occurred (ca. 1 min). The gels thus obtained were allowed to stand in sealed vessels for 24 h, dried for 3 days at 37 °C, washed with water, acetone, and pentane, dried and ground into a powder.

[12] We thank Novo Nordisk A/S (Denmark) for a sample of SP 523 (NOVO) and Amano Enzyme Europe Ltd. (England) for PS lipase.

[13] Whereas the commercial enzyme powder combined with the water produced from the reaction and formed a viscous residue which was difficult to separate, the sol-gel immobilized lipase could be recycled without any difficulty.

[14] We thank Dr. B. Tesche (Fritz Haber Institut, Berlin) for the scanning electron micrographs.

[15] D. Bianchi, P. Cesti, E. Battistel, *J. Org. Chem.* **1988**, *53*, 5531.

[16] According to Cesti et.al. [15] the reaction resulted in 95% *ee*. However, it is known that the enantioselectivity of enzyme-catalyzed reactions can vary for different batchesm of enzyme.

[17] The influence of other parameters, for example the use of additives, the stoichiometry water/silane, the amount of catalyst, and the use of other silane monomers are presently under investigation in our group.

Oligothiophenes—Yet Longer? Synthesis, Characterization, and Scanning Tunneling Microscopy Images of Homologous, Isomerically Pure Oligo(alkylthiophene)s**

Peter Bäuerle,* Thomas Fischer, Bernd Bidlingmeier, Andreas Stabel, and Jürgen P. Rabe*

The synthesis of structurally defined conjugated oligomers with dimensions on the nanometer scale have recently awakened interest not only because of the possibility of investigating transport behavior along the "molecular wire". Interestingly, the lengths of the molecules achieved so far in the series of oligo(tetraethynylethene)s,[1] up to 50 Å, oligo(thienylenethynylene)s,[2] up to 100 Å, and oligo(phenylenethynylene)s,[3] up to 128 Å, have reached the size of the smallest achievable structural dimensions of lithographic nanostructures.[4] Although members of the first series can be charged, preferably by reduction, and are suitable as molecular conductors owing to delocalization, these properties have not yet been established for oligomers linked by alkyne units.

α-Conjugated oligothiophenes are defined model compounds for electrically conducting polythiophenes. Because of their easily oxidized π-electron systems, they exhibit conductivities of up to 20 $S cm^{-1}$, values comparable to those of the corresponding polymers.[5] The correlation between the chain length of oligothiophenes and their electronic properties have already been investigated.[6] The properties of an organic semiconductor are also influenced, however, by the spatial arrangement of the molecules in the solid material.[7] Garnier et al.[7, 8] and Ostoja et al.[9] demonstrated that by improving the molecular order in thin layers of sexithiophene derivatives on silicon, they were able to increase the conductivity and simultaneously improve the mobility of the charge carrier improved. For the transfer of charge from chain to chain (interchain hopping), not only the distance separating the conjugated π-electron systems of the molecules but also their spatial overlap appear to be decisive.[7] The images of poly(3-alkylthiophene)s obtained by high-resolution scanning tunneling microscopy (STM) and atomic force microscopy (AFM) have not been convincing up to now. As Chang and Bard have shown,[10] details in the images recorded by Lacaze et al.[11] of the polymers on graphite cannot readily be distinguished from defects in the graphite structure and assigned to clearly defined molecules. Kamrava et al.[12] used STM to record images of an electrochemically prepared polythiophene film, partially oxidized with $FeCl_4^-$; however, they obtained a resolution of only 5–10 nm. Similarly, AFM investigations did not yield images with molecular resolution.[13]

We report here on the synthesis of a homologous series of isomerically pure α-linked oligo(alkylthiophene)s **1**–**4**. According to calculations, sedecithiophene **4**, the longest known and clearly characterized oligothiophene, should be 64 Å long when extended. Previously, oligo(alkylthiophene)s up to a dodecamer were known,[14] and it is only recently that a pentadecamer has been described.[15] Because of their improved solubility in organic solvents, the new oligothiophenes **1**–**4** can be successfully purified and their physical properties, even those of the longer homologues, were determined in solution. In this way the structure–property relationships can be extended to chain lengths that were previously unobtainable. In addition it was possible to obtain the first STM images of physisorbed two-dimensional (2D) crystalline layers of homologues **1**–**4** with submolecular resolution.

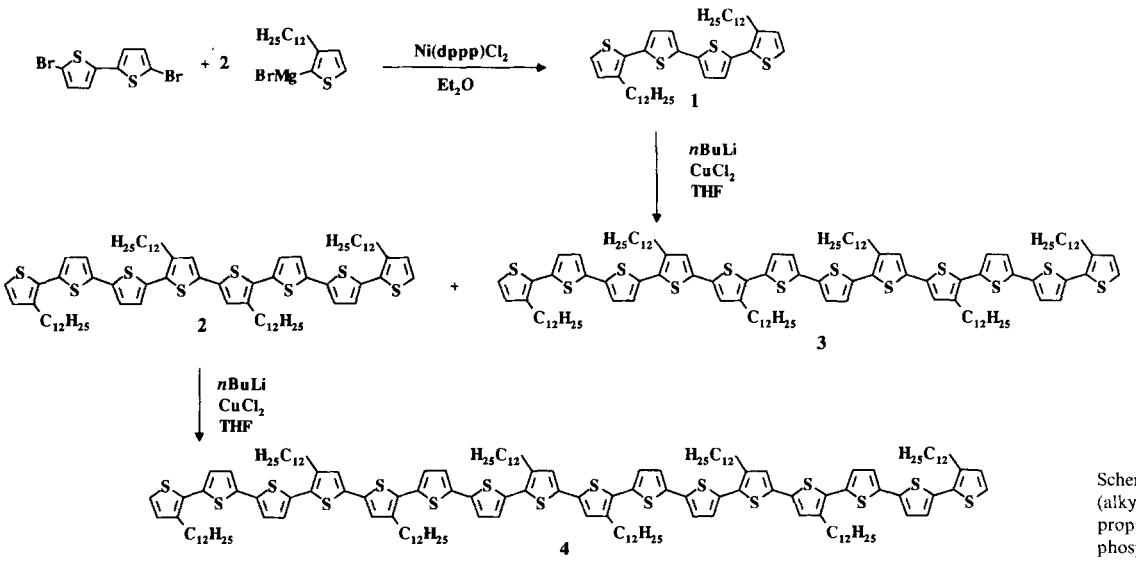
The synthesis of the new oligo(alkylthiophene)s **1**–**4** is shown in Scheme 1. 3,3‴-Didodecylquaterthiophene **1** was obtained in 75% yield by the nickel-catalyzed coupling of two equivalents of the Grignard reagent prepared from 2-bromododecylthiophene[16] with 5,5′-dibromo-2,2′-bithiophene. After the analogous Grignard coupling of an appropriate monobrominated quaterthiophene failed, the conversion of **1** to higher homologues was carried out by oxidative dimerization of the lithiated compound with $CuCl_2$.[17] It had to be taken into account that because of exchange reactions the lithiation of oligothiophenes generally leads to a mixture of mono- and dilithiated products,[17b, 18] and that the yields drop rapidly as the size of the coupling components increases.[19] Thus, the reaction of **1** with equimolar amounts of *n*-butyllithium and $CuCl_2$ yielded as

[*] Prof. Dr. P. Bäuerle, Dipl.-Chem. T. Fischer, B. Bidlingmeier
Institut für Organische Chemie der Universität
Am Hubland, D-97074 Würzburg (Germany)
Telefax: Int. code + (931)888-4606

Prof. Dr. J. P. Rabe
Institut für Physikalische Chemie der Universität
Jakob-Welder-Weg 11, D-55099 Mainz (Germany)
Telefax: Int. code + (6131)39-3768

Dipl.-Chem. A. Stabel
Max-Plank-Institut für Polymerforschung, Mainz (Germany)

[**] We would like to thank the Bundesministerium für Forschung und Technologie ("Transport-Phänomene in Polymer-Substrat-Grenzflächen" and "Muster selbstorganisierender Moleküle") and ESPRIT Basic Research Project 7282 (TOPFIT) for financial support. A. S. thanks the Fonds der Chemischen Industrie for a Kekulé fellowship. We would like to thank Dipl.-Phys. U. Segelbacher (2. Phys. Inst. Universität Stuttgart) for the temperature-dependent spectroelectrochemical measurements.



Scheme 1. Syntheses of oligo(alkylthiophene)s **1**–**4**; dppp = propane-1,2-diylbis(diphenylphosphane).

expected a mixture of starting material, tetradodecyloctithiophene **2**, hexadodecyldodecithiophene **3**, and other higher molecular weight products. Owing to their good solubility, **2** and **3** could be obtained in analytically pure form in yields of 30 and 8%, respectively, by repeated chromatography (purity according to HPLC >99%). Compound **2** was coupled with $BuLi/CuCl_2$ in an analogous manner to give the corresponding octadodecylsedecithiophene, which is the longest known oligothiophene to date (yield of pure material 19%; purity according to HPLC >99%).

The physical properties of the new oligo(alkylthiophene)s **1**–**4** are listed in Table 1. Compounds **1**–**4** are very stable materials; their melting points increase with increasing chain length

Table 1. Physical properties of the substituted oligothiophenes **1**–**4**.

Cmpd.	M.p.[°C]	λ_{max}[nm][a]	ε[L mol^{-1} cm^{-1}]	E_{pa}[V][b]
1	59–60	379	26600	0.51
2	73–74	439	59700	0.34
3	86–87	456	93300	0.19
4	90–91	464	138400	0.12

[a] 10^{-5} M in CH_2Cl_2. [b] 10^{-4} M in dichloroethane, Pt disk electrode ($\varnothing$ = 1 mm), 200 mVs^{-1}, 0.1 M tetrabutylammonium hexafluorophosphate, 40 °C, oxidation potentials E_{pa} vs Fc/Fc^+.

but lie markedly below those of the unsubstituted oligothiophenes.[20] The alkyl side chains lead to increased steric interactions between the conjugated backbones and thus reduce π–π interactions between the molecules in the solid state. In addition the solubility in organic solvents is raised by the presence of the side chains, such that all the homologues are soluble in hexane, aromatic, and chlorinated hydrocarbons and could be fully characterized.

Absorption spectroscop of **1**–**4** showed that not only the energy of the longest wavelength π–π^* transition but also the transition probability increased with increasing chain length (Fig. 1). While a good correlation was found between the absorption energy and the reciprocal of the chain length for other oligothiophene series up to a chain length of eight,[6] the relationship in the series **1**–**4** is not linear (Fig. 2). As a result of the steric influence of the alkyl side chains, the alkyl-substituted thiophene rings in the longer homologues are twisted and the π-conjugated chain appears to deviate increasingly from linearity such that the absorption maxima of **3** and **4** are shifted to higher energies than expected.

Oligothiophenes are ideal model compounds for the charge carriers responsible for the transport of charge in polymers with

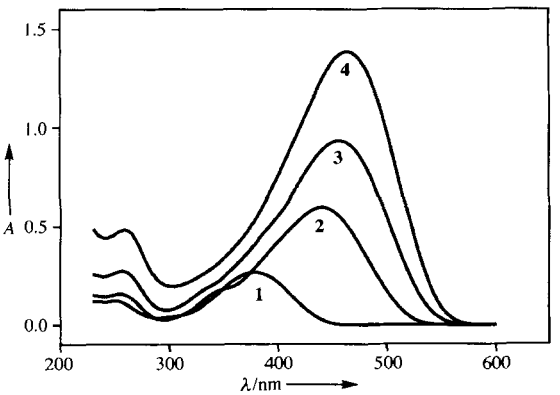


Fig. 1. UV/Vis absorption spectra of the alkyl-substituted oligothiophenes **1**–**4** (10^{-5} M in CH_2Cl_2).

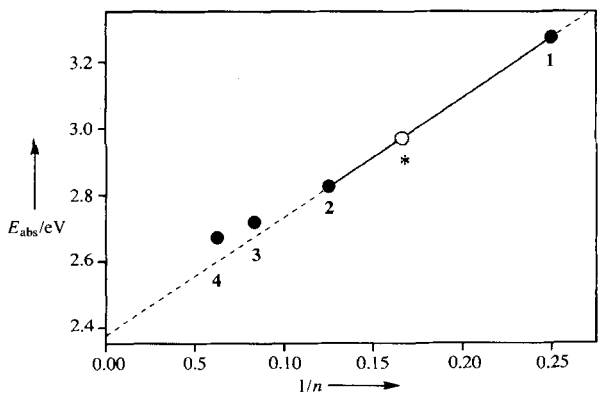


Fig. 2. Dependence of the absorption energies E_{abs} of oligothiophenes **1**–**4** and the hexamer 4′,3″″-didodecylsexithiophene (*) [16, 21] on chain length; E_{abs} is plotted against the reciprocal of the number of thiophene units, $1/n$.

 © VCH Verlagsgesellschaft mbH, D-69451 Weinheim, 1995 0570-0833/95/0303-0304 $ 10.00+.25/0

conjugated π-electron systems. The stable radical cations and dications as well the corresponding anionic species generated specifically from longer oligothiophenes can be regarded as models for polarons and bipolarons.[21] In this context a temperature-dependent reversible dimerization equilibrium of oligothiophene radical cations was studied in detail.[22] The diamagnetic dimeric cations exhibit properties that were previously ascribed to bipolarons, and can therefore be evoked in an alternative description of the mechanism of charge transport in electrically conductive polymers.

The redox properties of **1**–**4**, which were determined by cyclic voltammetry in several solvents, are therefore of special interest. As expected, the first oxidation potential E_{pa} is shifted cathodically with increasing chain length, which is equivalent to a better stabilization of the positive charge in the radical cation (Table 1). The oxidation potentials of **4** ($E_{pa} = 0.12$ V vs ferrocene(Fc)/Fc^+) and **3** ($E_{pa} = 0.19$ V vs Fc/Fc^+) are clearly more negative than those of polythiophene and poly(alkylthiophene)s ($E_{pa} = 0.3$–0.35 V vs Fc/Fc^+).[6b, 23] This indicates that the longer oligomers, in particular, clearly exceed the average chain length of the parent π-conjugated polythiophenes, which typically lie at 8–10 properly linked monomer units. Initial spectroelectrochemical investigations of the radical cations of the new oligomers indicate, in agreement with data from end-capped oligothiophenes,[22b] that the tendency to dimerize increases strongly with increasing chain length. Whereas the monomeric and the dimeric radical cations are in equilbrium at approximately −40 °C for tetramer **1**, equivalent portions of each species are formed at ≈30 °C for octamer **2**, at ≈65–70 °C for dodecamer **3**, and even at >80 °C for hexamer **4**.

In multisweep experiments thin films of controlled thickness of all the homologues could be deposited on the working electrode. The first oxidation potentials of these films with $E_{pa} = -0.11$ to -0.13 V vs Fc/Fc^+ are once again at considerably lower potentials than those of the oligothiophenes **1**–**4**, and indicate the presence of fairly well-defined higher oligomerization products whose characterization is still in progress.

The structures of the oligothiophene films were characterized by the investigation of physisorbed monomolecular layers of **1**–**4** on graphite by STM. Two-dimensional crystals of the two longest compounds, **3** and **4**, which were independent of the concentration of the solution, could be examined, though only during the first half hour after deposition. The mobility and instability of the domain boundaries were found to be very high. We deduce from this that in the case of the longest oligomer **4** in particular, thermodynamic equilibrium had not yet been achieved. 3D crystallization may possibly begin after a longer period, and a macroscopic film is formed on the surface, which inhibits STM imaging because of the low bulk conductivity of the undoped oligothiophene.

Figure 3 shows STM images of 2D crystals of the oligomers **1**–**4** on graphite and the corresponding molecular models. In analogy to earlier work on alkyl(oligothiophenes)[24, 25] we assign the bright areas to the aromatic thiophene skeletons and the darker regions in between to the alkyl chains. The 2D crystals of the four oligothiophenes are based on a common packing pattern in which the molecules are stacked along the length of a lamella. In all four cases the lamellae are separated by roughly 2.2 nm (measured perpendicular to the major axis of the molecule). The degree of overlap between two neighboring thiophene chains in a lamella decreases with increasing chain length. The interpretation of the STM results for **1**–**4** indicates a linearly extended π-electron system in which twisting of the thiophene rings relative to one another is possible. The models in Figure 3 should be understood as schematic representations of a system

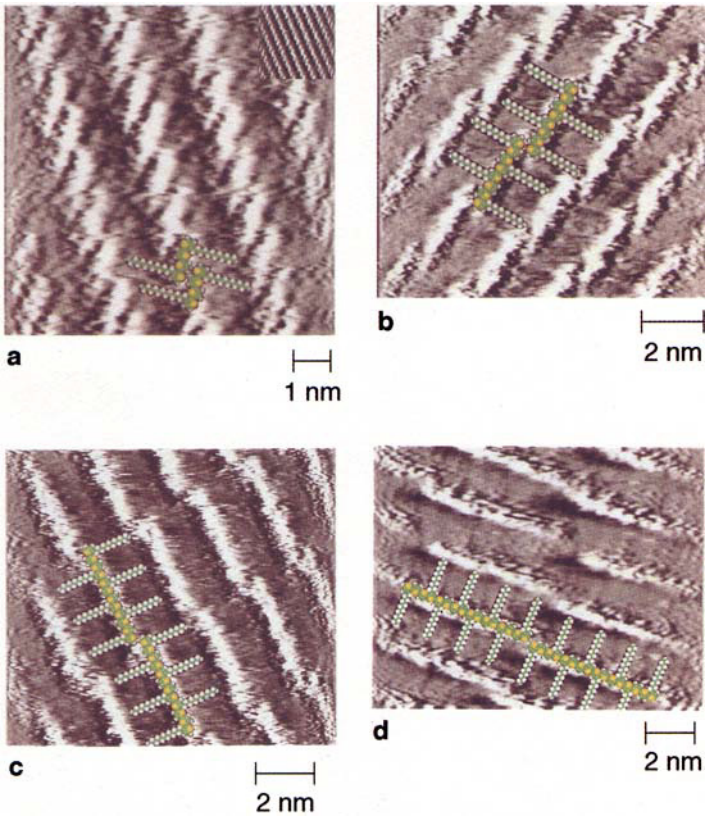


Fig 3. STM images of 2D crystals on HOPG. a) **1**, tunnel potential $U_T = 0.5$ V, tunnel current $I_T = 2.0$ nA; insert upper right: enlarged section; b) **2**, $U_T = 0.4$ V, $I_T = 1$ nA; c) **3**, $U_T = 0.4$ V, $I_T = 0.5$ nA; d) $U_T = 0.5$ V, $I_T = 3$ nA.

subject to rapid configurational molecular dynamics, which at present cannot be resolved on the timescale of STM experiments. For example, the alkyl chains are not found in the all-*trans* conformation shown in the simplified model, but dynamically occupy all of the surface available. By comparison with STM images recorded under conditions in which the graphite surface makes the dominant contribution to the tunnel current I_T and thus to the image,[25] it was established that the alkyl chains are oriented in equilibrium parallel to one of the crystal axes of the graphite. A lamella of adjacent rows of oligothiophenes is shown schematically in Figure 4a. The overlap length defined here Δ of the conjugated aromatic backbone of the thiophenes can be calculated by means of Equation (a), where l is the molecular length, r the distance between two molecules in the direction of the lamella, and ϕ the angle between the lamella direction and the major axis of the molecule.

$$\Delta = l - r \cdot \cos\phi \qquad \text{(a)}$$

The corresponding data for **1**–**4** are given in Table 2. The overlap length Δ and the number of thiophene units n have a linear relationship (Fig. 4b). As expected, Δ depends primarily on the substitution pattern of the oligothiophenes. Thus, for example, the Δ value for 4′,3′′′′-didodecylsexithiophene[25] cannot be predicted on the basis of the slope of the graph in Figure 4b. Comparison with nonregioselectively substituted analogues shows that the thiophene skeleton must be alkylated regioselectively for accurate determination of the overlap length, since the separation δr between the adjacent thiophene skeletons can otherwise vary by up to 30%.[25]

 © VCH Verlagsgesellschaft mbH, D-69451 Weinheim, 1995 0570-0833/95/0303-0305 $ 10.00+.25/0

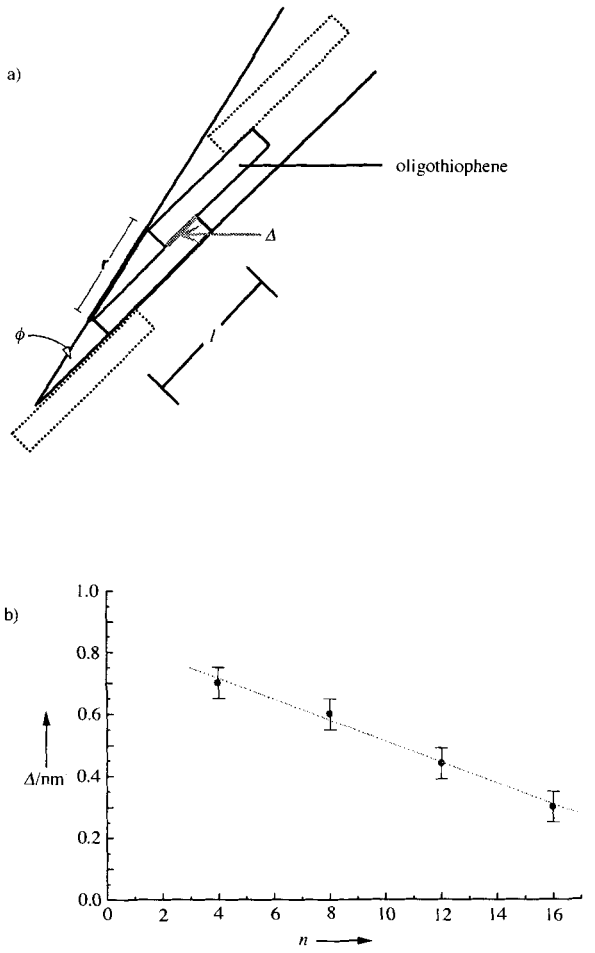


Fig. 4. a) Schematic representation of the adjacent rows of oligothiophenes for the determination of the overlap length Δ, l = length of the molecule, r = distance between two molecules in the direction of the lamella, ϕ = angle between the direction of the lamella and the major axis of the molecule; b) plot of the overlap length Δ versus the number of thiophene units, n.

Table 2. Data from the STM investigation of alkyl-substituted oligothiophenes **1**–**4**.

Cmpd.	r[nm]	ϕ[°]	λ[nm]	Δ[nm]
1	1.22±0.05	35±2	1.7±0.02	0.7±0.05
2	2.67±0.05	12±2	3.2±0.02	0.60±0.05
3	4.35±0.05	8±2	4.8±0.02	0.44±0.05
4	6.1±0.05	5±2	6.4±0.02	0.32±0.05

The synthesis of the soluble oligothiophenes **1**–**4**, which are stable at various oxidation levels, provides the first homologous series of conjugated, easily oxidized molecules with nanometric dimensions, whose conjugation length exceeds that of the previously known oligo- and polythiophenes. Because of the defined geometric and electronic structures and the satisfactory characterizability of oligothiophenes **1**–**4**, the structure–property relationships deduced clearly show longer oligothiophenes may deviate from the linear behavior determined for shorter chains, since the degree of conjugation approaches a limiting value with increasing chain length. The general tendency of the radical cations of the longer chain oligothiophenes to dimerize emphasizes the model character of these compounds with respect to charge carriers and transport phenomena in molecules with conjugated chains and is a further indication of such species in electrically conducting polymers.

In addition, the first STM images of a homologous series of oligomers were recorded. Based on the high-resolution images of isomerically pure oligothiophenes, the relationship between the overlap length of two adjacent thiophene skeletons and the length of the oligothiophene backbone could be determined. Above all, this unexpected supramolecular arrangement of the longer oligomers, in which the molecules are lined up almost ideally for coupling at the α positions, can explain the formation of extremely long molecular wires in electrochemically prepared thin films.

Experimental Procedure

To a solution of 0.35 mmol of the oligothiophene in 20 mL of absolute THF was added dropwise 0.22 mL of a 1.6 M solution of *n*-butyllithium in hexane. A suspension of 0.35 mmol of copper(II) chloride in 8 mL absolute THF was then added. After 4 h the reaction mixture was hydrolyzed with ice water, acidified, and extracted with dichloromethane. The organic phase was neutralized, washed with water, and dried over $MgSO_4$. Oligothiophene **2** was purified several times by chromatography on silica gel eluting with hexane/dichloromethane; **3** and **4** were purified by chromatography on nitrophenol-modified silica gel eluting with hexane/toluene.

1: orange-yellow crystals, m.p. 59–60 °C; ^{1}H NMR (250 MHz, $CDCl_3$): δ = 7.15 (d, 2H; H^1-5, H^4-5), 7.10 (d, 2H; H^2-4, H^3-3), 7.00 (d, 2H; H^2-3, H^3-4), 6.92 (d, 2H; H^1-4, H^4-4), 2.77 (t, 4H; α-CH_2), 1.64 (m, 4H; β-CH_2), 1.24 (m, 36H; CH_2), 0.87 (t, 6H; CH_3); UV/Vis (CH_2Cl_2): λ_{max} [nm] (ε [L mol^{-1} cm^{-1}]) = 251 [12100], 379 [26600]. Elemental analysis: calcd C 72.01, H 8.76, S 19.22; found C 72.12, H 8.81, S 19.99.

(The assignment of the H-atoms to the rings is not indicated here by primes but by the number of the appropriate ring as a superscript e.g. H^4 for H'''.)

2: red crystals, m.p. 73–74 °C. ^{1}H NMR (250 MHz, $CDCl_3$): δ = 7.17 (d, 2H; H^1-5, H^8-5), 7.12 (d, 4H), 7.03 (d, 2H), 7.02 (d, 2H), 7.00 (s, 2H; H^4-4, H^5-3), 6.93 (d, 2H; H^1-4, H^8-4), 2.76 (m, 8H; α-CH_2), 1.65 (m, 8H, β-CH_2), 1.25 (m, 72H; CH_2), 0.87 (m, 12H; CH_3); UV/Vis (CH_2Cl_2): λ_{max} [nm] (ε [L mol^{-1} cm^{-1}]) = 255 [15900], 439 [59700]. Elemental analysis: calcd C 72.13, H 8.63, S 19.26; found C 71.98, H 8.54, S 19.05.

3: small red plates, m.p. 86–87 °C. ^{1}H NMR (250 MHz, $CDCl_3$): δ = 7.18 (d, 2H; H^1-5, H^{12}-5), 7.14 (d, 2H), 7.13 (d, 4H), 7.05 (d, 2H), 7.03 (d, 2H), 7.02 (d, 2H), 7.00 (s, 4H; H^4-4, H^5-3, H^8-4, H^9-3), 6.94 (d, 2H; H^1-4, H^{12}-4), 2.77 (m, 12H; α-CH_2), 1.65 (m, 12H; β-CH_2), 1.26 (m, 108H; CH_2), 0.87 (m, 18H; CH_3); UV/Vis (CH_2Cl_2): λ_{max} [nm] (ε [L mol^{-1} cm^{-1}]) = 255 (27300), 456 (93300). Elemental analysis: calcd C 72.16, H 8.58, S 19.26; found C 72.39, H 8.62, S 19.02.

4: violet microcrystals, m.p. 90–91 °C. ^{1}H NMR (250 MHz, $CDCl_3$): δ = 7.18 (d, 2H; H^1-5, H^{16}-5), 7.14 (d, 4H), 7.13 (d, 4H), 7.05 (d, 4H), 7.04 (d, 2H), 7.03 (d, 2H), 7.01 (s, 6H; H^4-4, H^5-3, H^8-4, H^9-3, H^{12}-4, H^{13}-3), 6.94 (d, 2H; H^1-4, H^{16}-4), 2.77 (m, 16H; α-CH_2), 1.67 (m, 16H; β-CH_2), 1.26 (m, 144H; CH_2), 0.87 (t, 24H; CH_3); UV/Vis (CH_2Cl_2): λ_{max} [nm] (ε [L mol^{-1} cm^{-1}]) = 259 (48400), 464 (138400). Elemental analysis: calcd C 72.18, H 8.55, S 19.27; found C 71.69, H 8.55, S 19.38.

Saturated solutions of **1**–**4** in trichlorobenzene (Aldrich, >99%) were applied to the basal surface of highly oriented pyrolytic graphite (HOPG, Grade ZYB Advanced Ceramics, Cleveland, OH) with a Pasteur pipette. The tunnel tips were etched electrochemically (2 N KOH + 6 N NaCN; Pt/Ir (80/20) wire). Adsorption occurred after a waiting period which was different for each oligomer (ca. 30 min for **1**, 20 min for **2** and about 2–3 min for **3** and **4**). In some cases 2D crystallization was induced by a potential pulse applied between the substrate and the tip (100 ns, 4 V). The images were made with equipment built by us [26]. The STM images were made in current mode (constant height mode) under ambient conditions (scan rate 0.3 Hz per image, positive tip voltage) recorded on videotape, and then digitized. The STM images (Fig. 3) were not digitally processed later. The brightness correlates with the current.

Received: July 27/August 5, 1994
Revised version: October 11, 1994 [Z 7176/Z 7213 IE]
German version: *Angew. Chem.* **1995**, *107*, 335

Keywords: cyclic voltammetry · oligothiophenes · thiophenes · scanning tunneling microscopy

[1] J. Anthony, C. Boudon, F. Diederich, J.-P. Gisselbrecht, V. Gramlich, M. Gross, M. Hobi, P. Seiler, *Angew. Chem.* **1994**, *106*, 794–798; *Angew. Chem. Int. Ed. Engl.* **1994**, *33*, 763–766.

[2] D. L. Pearson, J. S. Schumm, L. Jones II, J. M. Tour, *Polym. Prepr.* **1994**, *35*, 202–203.

[3] J. S. Schumm, D. L. Pearson, J. M. Tour, *Angew. Chem.* **1994**, *106*, 1445–1448; *Angew. Chem. Int. Ed. Engl.* **1994**, *33*, 1360–1363.

[4] Lithographic structural dimensions of <10 nm have been reported recently: C. Joachim, 2nd European Conference on Molecular Electronics, Banz, September 4–9, 1994.

[5] a) E. E. Havinga, I. Rotte, E. W. Meijer, W. Ten Hoeve, H. Wynberg, *Synth. Met.* **1991**, *41*, 473–478; b) D. M. de Leeuw, *ibid.* **1993**, *57*, 3597–3602.
[6] a) D. Fichou, B. Xu, G. Horowitz, F. Garnier, *Synth. Met.* **1991**, *41*, 463–469; b) P. Bäuerle, *Adv. Mater.* **1992**, *4*, 102–107; c) J. Guay, A. Diaz, R. Wu, J. M. Tour, *J. Am. Chem. Soc.* **1993**, *115*, 1869–1874.
[7] F. Garnier, A. Yassar, R. Hajlaoui, G. Horowitz, F. Deloffre, B. Servet, S. Ries, P. Alnot, *J. Am. Chem. Soc.* **1993**, *115*, 8716–8721.
[8] B. Xu, D. Fichou, G. Horowitz, F. Garnier, *Adv. Mater.* **1991**, *3*, 150–153.
[9] P. Ostoja, S. Guerri, S. Rossini, M. Servidori, C. Taliani, R. Zamboni, *Synth. Met.* **1993**, *54*, 447–452.
[10] E. Lacaze, K. Uvdal, P. Bodö, J. Garbarz, W. R. Salaneck, M. Schott, *J. Polym. Sci. Part B: Polym. Phys.* **1993**, *31*, 111–114.
[11] H. Chang, A. Bard, *Langmuir* **1991**, *7*, 1143–1153.
[12] S. J. Kamrava, M. Zagórska, B. Krische, S. Söderholm, *Phys. Scr.* **1991**, *44*, 112–115.
[13] O. Böhme, C. Ziegler, W. Göpel, *Adv. Mater.* **1994**, *6*, 587–589.
[14] a) W. ten Hoeve, H. Wynberg, E. E. Havinga, E. W. Meijer, *J. Am. Chem. Soc.* **1991**, *113*, 5887–5889; b) A. Yassar, D. Delabouglise, M. Hmyene, B. Nessak, G. Horowitz, F. Garnier, *Adv. Mater.* **1992**, *4*, 490–494.
[15] M. Sato, M. Hiroi, *Chem. Lett.* **1994**, 985–988.
[16] P. Bäuerle, F. Pfau, H. Schlupp, F. Würthner, K.-U. Gaudl, M. Balparda Caro, P. Fischer, *J. Chem. Soc. Perkin Trans. 2* **1993**, 489–494.
[17] a) T. Kauffmann, *Angew. Chem.* **1974**, *86*, 321–335; *Angew. Chem. Int. Ed. Engl.* **1974**, *13*, 291–305; b) J. Kagan, S. K. Arora, *Heterocycles* **1983**, *20*, 1937–1940.
[18] R. M. Kellogg, A. P. Schaap, H. Wynberg, *J. Org. Chem.* **1969**, *34*, 343–346.
[19] T. Kauffmann, H. Lexy, *Chem. Ber.* **1981**, *114*, 3674–3683.
[20] The unsubstituted quaterthiophene has a melting point of 215–216 °C; J. Nakayama, T. Konishi, S. Murabayashi, M. Hoshino, *Heterocycles* **1987**, *26*, 1793–1796.
[21] P. Bäuerle, U. Segelbacher, K.-U. Gaudl, D. Huttenlocher, M. Mehring, *Angew. Chem.* **1993**, *105*, 125–127; *Angew. Chem. Int. Ed. Engl.* **1993**, *32*, 76–78.
[22] a) M. G. Hill, K. R. Mann, L. L. Miller, J.-F. Penneau, *J. Am. Chem. Soc.* **1992**, *114*, 2728–2730; b) P. Bäuerle, U. Segelbacher, A. Maier, M. Mehring, *ibid.* **1993**, *115*, 10217–10223.
[23] Polymerization of 3-dodecyl-2,2′-bithiophene [16], which corresponds to half of quaterthiophene **1**, leads to a polymer that also has one solubilizing group per two thiophene units. The polymer has an oxidation potential of $E_{pa} = 0.35$ V vs Fc/Fc^+.
[24] J. P. Rabe, S. Buchholz, L. Askadskaya, *Phys. Scr.* **1993**, *T49*, 260–263.
[25] A. Stabel, J. P. Rabe, *Synth. Met.*, **1994**, *67*, 47–53.
[26] J. P. Rabe, M. Sano, D. Batchelder, A. A. Kalatchev, *J. Microsc. (Oxford)* **1988**, *152*, 573–578.

New Selenolato-Bridged Clusters of Iron and Nickel; the Structures of $[Fe_{12}(SePh)_{24}]$ and $[Na_2(POPh_3)_6][Ni_{20}Se_{12}(SeMe)_{10}]$**

Dieter Fenske* and Andreas Fischer

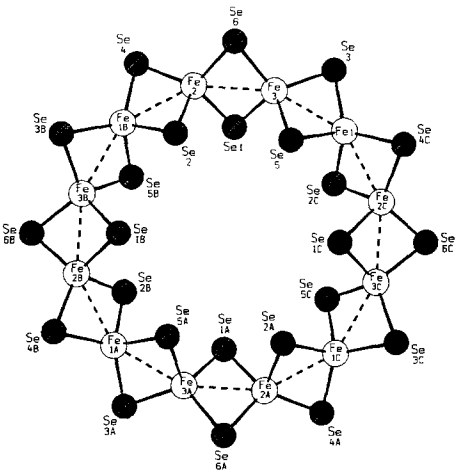
Dedicated to Professor Dr. Gerhard Fritz on the occasion of his 75th birthday

The reactions of phosphane complexes of transition metal halides with $E(SiMe_3)_2$ (E = S, Se, and Te) lead to a great number of multinuclear clusters, whose frameworks contain sections from the structures of binary chalcogenides, which are surrounded by a protecting shell of PR_3 ligands (R = organic group).[1] We have now investigated whether $PhSeSiMe_3$ and NaSeMe can also be used for the synthesis of these types of clusters.

As an example, we found that the Fe_{12} cluster **1** is formed almost quantitatively in the reaction of $FeCl_3$ with PPh_3 and $PhSeSiMe_3$ [Eq. (a)]. In THF and toluene at room temperature, only amorphous powder is obtained, some of which is pyrophoric. In contrast, **1** crystallizes in the form of shiny black needles within 12 h when a suspension of $FeCl_3$ and PPh_3 in dichloroethane is carefully covered with a layer of $PhSeSiMe_3$. Compound **1** decomposes readily on warming in organic solvents releasing elemental selenium. The IR spectrum of **1** contains the characteristic bands of the PhSe group, but further structural information cannot be extracted. An X-ray crystal structure analysis was carried out on **1** to determine the molecular structure.[2] Depending on the conditions of crystallization, crystals containing varying amounts of dichloroethane are formed. $\mathbf{1}\cdot 4C_2H_4Cl_2$ crystallizes in the tetragonal space group $P\bar{4}2_1c$, and $\mathbf{1}\cdot 5C_2H_4Cl_2$ in the orthorhombic space group $Pmmn$; however, this has practically no influence on the bonding parameters of **1**.

$$FeCl_3 \xrightarrow{PPh_3 + PhSeSiMe_3} \underset{\mathbf{1}}{[Fe_{12}(SePh)_{24}]} \qquad (a)$$

Figure 1 shows that a cyclic Fe_{12} cluster is present in **1** which has $\bar{4}$ symmetry in the tetragonal cell. Each Fe atom is surrounded by four Se atoms of the μ_2-SePh ligands in a distorted tetrahedral fashion. As a result, edge-sharing Se_4 tetrahedra connect to form a ring. The Fe atoms are located in the centers of the Se_4 tetrahedra (Se···Se 360–428 pm). The principle of bridging



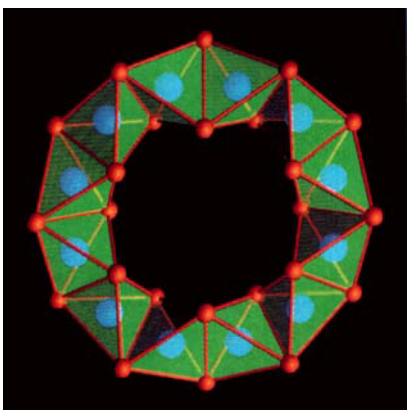


Fig. 1. Top: Ball-and-stick model of **1** (without Ph groups); bottom: polyhedron model of the edge-bridged Se_4 tetrahedra (Fe: blue; Se: orange). Selected distances [±0.2 pm]: Se1-Fe2 242.0, Se1-Fe3 244.6, Se2-Fe2 243.5, Se2-Fe1 243.6, Se3-Fe1 244.8, Se3-Fe3 245.0, Se4-Fe2 243.8, Se4-Fe1 246.6, Se5-Fe3 243.4, Se5-Fe1 244.8, Se6-Fe2 243.4, Se6-Fe3 244.1, Se-C 192–197.

[*] Prof. Dr. D. Fenske, Dipl.-Chem. A. Fischer
Institut für Anorganische Chemie der Universität
Engesserstrasse, Geb.-Nr. 30.45, D-76128 Karlsruhe (Germany)
Telefax: Int. code + (721)661921

[**] This work was supported by the Deutsche Forschungsgemeinschaft (Sonderforschungsbereich 195) and the Fonds der Chemischen Industrie.

chalcogen polyhedra is found in the structures of many ternary chalcogenides. In contrast to **1**, vertex-sharing and edge-sharing E_4 tetrahedra (E = chalcogen) are observed to form dimeric and trimeric units, or even infinite chains in these compounds.[3]

The shortest Fe–Fe distances in **1** are 286.7–290.1 pm. They are thus comparable to the distances in $[Fe_2(SEt)_6]^{2-}$ (Fe–Fe: 297.8 pm) and $Ba_9(Fe_2S_4)_8$ (Fe–Fe: 275.1–286.8 pm),[3,4] as well as those in $[Fe_3S_4(SEt)_4]^{3-}$ (Fe–Fe: 271.4 pm), and $[Na_2Fe_{18}Se_{30}]^{8-}$ and $[Na_9Fe_{20}S_{38}]^{9-}$ (Fe–Fe: 272–289 pm).[5,6]

As in **1**, a ring-shaped cluster is also found in $[Na_2Fe_{18}S_{30}]^{8-}$ which is formed by the connection of S_4 tetrahedra having Fe atoms at their centers. In addition, two Fe_2S units are located at the center of the cluster. These four Fe atoms carry the charge + 2; the remaining 14 Fe atoms occur as Fe^{3+} ions.

In contrast to this, **1** contains iron centers only in the formal oxidation state + 2 (d^6 configuration). Preliminary results from the Mössbauer spectra indicate the presence of Fe^{2+} ions in tetrahedral environments. Obviously, considerable interactions between the Fe^{2+} ions must be considered.[7] This is possibly one explanation for the fact that a magnetic moment of μ_{eff} = 1.51 μB/Fe (at 293 K) was found. In this context, it must be mentioned that investigations have already been performed on ring-shaped iron clusters containing oxygen ligands.[8] The magnetic properties of $[\{Fe(OMe)_2(O_2CCH_2Cl)\}_{10}]$, a compound with octahedrally coordinated Fe^{3+} ions bridged by OMe and O_2CCH_2Cl ligands, are well understood.[8] Just as in **1**, antiferromagnetic coupling between the Fe^{3+} ions is observed (Fe–Fe: 302.8 pm).[8]

A space-filling model of **1** (Fig. 2) clearly shows that the Fe_{12} cluster ring is effectively shielded by the Ph groups bonded to the Se atoms. The Ph groups are arranged in an alternating fashion above and below the Fe_{12} cluster plane. The entire molecule has a diameter of about 12 Å.

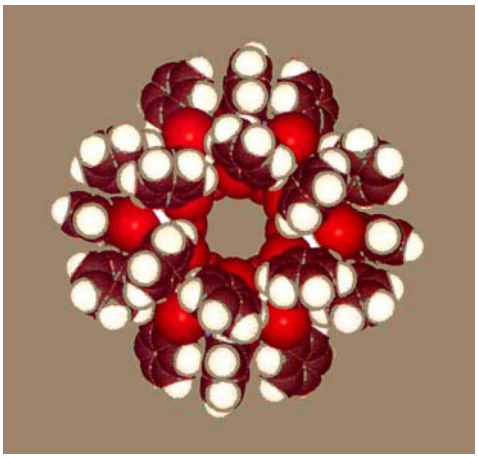


Fig. 2. Space-filling model of **1** (Fe: blue; Se: red; C: black; H: white). The Fe atoms are barely visible.

A further possibility for the synthesis of metal clusters with bridging chalcogen ligands is the reaction of metal halides with NaSR.[5,6,9,10] For example, the reaction of $NiCl_2$ with NaSMe (in the presence of Me_4NCl) leads to the complex $(Me_4N)_2[Ni_3(\mu_3\text{-}S)(\mu_2\text{-}SMe)_3]$.[11] On the other hand, if $[NiCl_2(PPh_3)_2]$ is treated with NaSeMe, black crystals of **2** are obtained in a yield of about 10% [Eq. (b)]. Cluster **2** is formed as a side product in a reaction that has not yet been clarified. The main products of the reaction are NiS and as yet unidentified cluster complexes.

$$[NiCl_2(PPh_3)_2] + NaSeMe \rightarrow \underset{\mathbf{2}}{[Na_2(POPh_3)_6][Ni_{20}Se_{12}(SeMe)_{10}]} \quad (b)$$

Product **2** is an ionic compound consisting of a $[Na_2(POPh_3)_6]^{2+}$ ion and a $[Ni_{20}Se_{12}(SeMe)_{10}]^{2-}$ ion. Two Na^+ ions are found in the centrosymmetrical cation (Fig. 3), each of which is coordinated by the O atoms of the $POPh_3$ ligands in a distorted tetrahedral fashion. The oxygen atoms O3 and O2, which are bonded to P1 and P2, respectively, are about 10 pm closer to Na1 than O1 is (Na1–O1: 227.4; Na1–O2: 218.4; Na1–O3: 216.5 pm). $POPh_3$ is obviously necessary for the formation of this cation; it arises possibly from the reaction of PPh_3 with the solvent or with oxygen.

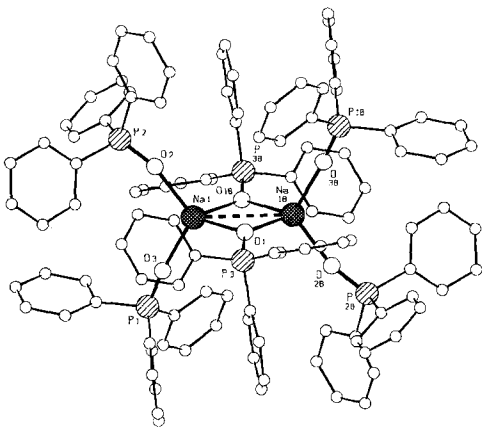


Fig. 3. The structure of the $[Na_2(POPh_3)_6]^{2+}$ ion in **2** (H atoms not shown). Selected distances [± 0.9 pm] and angles [± 0.2°]: Na1-O1 227.4, Na1B-O1 231.5, Na1-O2 218.4, Na1-O3 216.5, Na1 ··· Na1B 333.1, P1-O3 147.9, P2-O2 150.1, P3-O1 149.1; Na1-O1-P3 126.4 (134.3), O2-Na1-O3 115.4, O2-Na1-O1 108.3 (120.5), O3-Na1-O1 110.1 (112.0).

A certain structural relationship can be recognized between the structure of the $[Ni_{20}Se_{12}(SeMe)_{10}]^{2-}$ ion with $\bar{1}$ symmetry (Fig. 4) and that of the (as yet) largest nickel chalcogenide cluster $[Ni_{34}Se_{22}(PPh_3)_{10}]$.[12]

A pentagonal antiprism of Ni atoms (Ni1–Ni5 and atoms at inverted sites) makes up the central unit in the cluster anion of

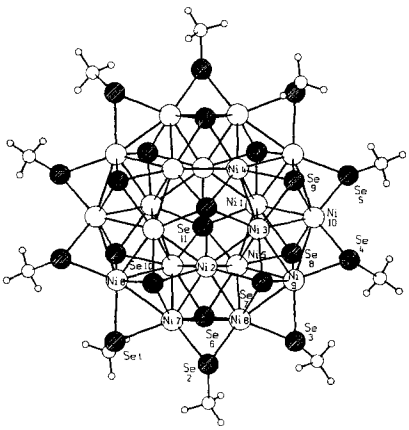


Fig. 4. The structure of the $[Ni_{20}Se_{12}(SeMe)_{10}]^{2-}$ ion in **2**. Selected distances [±0.3 pm]: Ni1-Ni2 248.2, Ni1-Ni5 248.2, Ni2-Ni3 246.2, Ni3-Ni4 248.9, Ni4-Ni5 245.5, Ni6-Ni7 258.9, Ni7-Ni8 257.1, Ni8-Ni9 254.3, Ni9-Ni10 256.3, Ni6-Ni10 259.8, Se11-Ni 235.6–239.1, (μ_4-Se)-Ni 233.9–239.0, (μ_2-Se)-Ni 233.6–238.2.

 © VCH Verlagsgesellschaft mbH, D-69451 Weinheim, 1995 0570-0833/95/0303-0308 $ 10.00+.25/0

2; the Ni–Ni distances (in the pentagonal ring) lie between 245.5 and 248.9 pm. In contrast, the Ni–Ni distances between the pentagonal layers are on average more than 260 pm, and the remaining Ni–Ni distances lie between these values. In the anion of **2** μ_5-Se (Se11, Se11'), μ_4-Se (Se6–Se10), and μ_2-SeMe (Se1–Se5) ligands are present. This shows that the cluster is formed as a result of a complex reaction which takes place partially by cleavage of the Se–C bonds.

Just as in $[Ni_{34}Se_{22}(PPh_3)_{10}]$, two μ_5-Se ligands (Se11) in the anion of **2** cap the top and bottom Ni_5 rings. The remaining Se atoms act as μ_4 ligands, whereas the SeMe groups are μ_2 bridging. As a result of this arrangement, one Ni_2 unit is located over each triangular face of the pentagonal antiprism. These Ni_2 units, together with the μ_4-Se bridging atom and the Ni atoms of the triangular face, give rise to octahedra consisting of five Ni atoms and one Se atom (e.g. Ni1, Ni3, Ni4, Ni6, Ni10, Se9). Thus the cluster can be described as a ring made up of face-sharing Ni_5Se octahedra, in which the Se atoms are arranged in an alternating fashion above and below the ring planes. The outer Ni_{10} ring (Ni6–Ni10 and atoms at inverted sites) is additionally bridged by ten μ_2-SeMe groups and thus sterically saturated. The Ni atoms Ni6–Ni10 are each coordinated by two $SeMe^-$ and two Se^{2-} ligands in a distorted tetrahedral fashion. In contrast, the Ni atoms of the pentagonal antiprism are coordinated by three Se^{2-} ligands.

$[Ni_{20}Se_{12}(SeMe)_{10}]^{2-}$ contains a Ni_{20}^{32+} cluster; the Ni atoms thus have the formal oxidation number 1.6. Mixed-valent states are well known for nickel. For example, the Ni atoms in $[Ni_{34}Se_{22}(PPh_3)_{10}]$ have a formal oxidation number of 1.7, and those in $[Ni_8S(SC_4H_9)_9]^-$ of 1.25.[12, 13] A simple description of the bonding situation in the cluster anion is not possible, as an assignment of Ni–Ni bonds is only possible when arbitrary assumptions are made. We have already had similar difficulties with other chalcogenidonickel cluster complexes.[1] This in mind, it is not surprising that the 18 electron rule and topological rules are not complied with.[14]

Experimental Procedure

1: $FeCl_3$ (0.16 g, 1 mmol) and PPh_3 (0.26 g, 1 mmol) were suspended in dichloroethane (80 mL). Solid undissolved material remained at the bottom of the red solution. The solution was then carefully covered with a layer of $PhSeSiMe_3$ (1 mL, 4 mmol). The solution became colorless at the phase boundary, and a white precipitate was observed. In the course of the following 24 h, the solution turned first dark green and then dark brown. Long dark needles of **1** started to grow on the walls of the reaction vessel along the diffusion boundary. Yield 90%. In contrast, when PPh_3 (0.52 g, 2 mmol) and $PhSeSiMe_3$ (1 mL, 4 mmol) were added to $FeCl_2$ (0.24 g, 2 mmol) in a heterogeneous reaction, in addition to **1**, a pyrophoric residue was also obtained, which was presumably elemental iron.

2: $[NiCl_2(PPh_3)_2]$ (4.44 g, 6.7 mmol) and NaSeMe (2.8 g, 23.9 mmol) were suspended in THF (100 mL) and stirred for several minutes. The suspension turned dark red. After a reaction time of several weeks, a powder was formed containing NaCl and other diverse products. In addition, triclinic crystals of **2** were obtained in the form of black lozenges.

Received: September 2, 1994 [Z 7287 IE]
German version: *Angew. Chem.* **1995**, *107*, 340

Keywords: clusters · complexes with selenium ligands · iron compounds · nickel compounds

[1] D. Fenske, J. Ohmer, J. Hachgenei, K. Merzweiler, *Angew. Chem.* **1988**, *100*, 1300; *Angew. Chem. Int. Ed. Engl.* **1988**, *27*, 1277; H. Krautscheid, D. Fenske, G. Baum, M. Semmelmann, *Angew. Chem.* **1993**, *105*, 1365; *Angew. Chem. Int. Ed. Engl.* **1993**, *32*, 1302; D. Fenske, H. Krautscheid, *ibid.* **1990**, *102*, 1513 and **1990**, *29*, 1453; D. Fenske, J. Steck, *ibid.* **1993**, *105*, 254 and **1993**, *32*, 238; S. Dehnen, A. Schäfer, D. Fenske, R. Ahlrichs, *ibid.* **1994**, *106*, 786 and **1994**, *33*, 746.

[2] Crystal structure analyses: Stoe Stadi-IV and Stoe IPDS diffractometers ($Mo_{K\alpha}$ radiation, empirical absorption correction); data collection and refinement (SHELXS-86, SHELXL-93, SCHAKAL). $\mathbf{1}\cdot 4C_2H_4Cl_2$: lattice constants (200 K): $a = b = 2535.5(12)$, $c = 1391.3(6)$ pm, $\alpha = \beta = \gamma = 90°$, $V = 8944.3 \times 10^6$ pm^3; inversion twin space group $P\bar{4}2_1c$ (no. 114), $Z = 2$, $\mu(Mo_{K\alpha}) = 58.4$ cm^{-1}, $2\theta_{max} = 56°$, 25294 reflections, of which 10556 with $I > 2\sigma(I)$, anisotropic refinement; $R_1 = 0.082$. The phenyl groups are partially disordered. $\mathbf{1}\cdot 5C_2H_4Cl_2$: lattice constants (200 K): $a = 1372.3(9)$, $b = 2542.4(12)$, $c = 2578.3(12)$ pm, $\alpha = \beta = \gamma = 90°$, $V = 8995.5 \times 10^6$ pm^3; space group $Pmmn$ (no. 59), $Z = 2$, $\mu(Mo_{K\alpha}) = 58.7$ cm^{-1}, $2\theta_{max} = 52°$, 9678 reflections, of which 5638 independent with $I > 2\sigma(I)$, Fe, Se anisotropic, C isotropic, $R_1 = 0.086$, $R_2 = 0.082$. **2**: lattice constants (200 K): $a = 1348.7(7)$, $b = 1596.3(11)$, $c = 1847.5(8)$ pm, $\alpha = 97.18(4)$, $\beta = 106.71(4)$, $\gamma = 103.05(3)°$, $V = 3633.5 \times 10^6$ pm^3; space group $P\bar{1}$ (no. 2), $Z = 1$, $\mu(Mo_{K\alpha}) = 79.5$ cm^{-1}, $2\theta_{max} = 52°$, 36312 reflections, of which 15851 independent with $I > 4\sigma(I)$, 801 parameters (Ni, Se, P, O, Na, C anisotropic, the positions of the hydrogen atoms were calculated). $R_1 = 0.080$, $R_2 = 0.076$. Further details of the crystal structure investigation may be obtained from the Fachinformationszentrum Karlsruhe, D-76344 Eggenstein-Leopoldshafen (Germany) on quoting the depository number CSD-58694.

[3] W. Bronger, P. Müller, *J. Less Common Met.* **1984**, *100*, 241; W. Bronger, *Angew. Chem.* **1981**, *93*, 12; *Angew. Chem. Int. Ed. Engl.* **1981**, *20*, 52; J. T. Hoggins, H. Steinfink, *Acta Crystallogr. Sect. B* **1977**, *33*, 673; J. T. Lemley, J. M. Jenks, J. T. Hoggins, Z. Eliezer, H. Steinfink, *J. Solid State Chem.* **1976**, *16*, 117; H. Y. Hong, H. Steinfink, *ibid.* **1972**, *5*, 93; J. S. Swinnea, H. Steinfink, *ibid.* **1980**, *32*, 329.

[4] K. S. Hagen, R. H. Holm, *Inorg. Chem.* **1984**, *23*, 418.

[5] K. S. Hagen, A. D. Watson, R. H. Holm, *J. Am. Chem. Soc.* **1983**, *105*, 3905.

[6] J.-F. You, B. S. Snyder, R. H. Holm, *J. Am. Chem. Soc.* **1988**, *110*, 6589; J.-F. You, R. H. Holm, *Inorg. Chem.* **1991**, *30*, 1431; J.-F. You, G. C. Papaefthymiou, R. H. Holm, *J. Am. Chem. Soc.* **1992**, *114*, 2697.

[7] J. Ensling, Universität Mainz, personal communication.

[8] D. Gatteschi, A. Caneschi, L. Pardi, R. Sessoli, *Science* **1994**, *265*, 1054; K. L. Taft, S. Lippard, *J. Am. Chem. Soc.* **1990**, *112*, 9629.

[9] J. J. Girerd, G. C. Papaefthymiou, A. D. Watson, E. Gamp, K. S. Hagen, N. Edelstein, R. B. Frankel, R. H. Holm, *J. Am. Chem. Soc.* **1984**, *106*, 5941; S. C. Lee, R. H. Holm, *Angew. Chem.* **1990**, *102*, 868; *Angew. Chem. Int. Ed. Engl.* **1990**, *29*, 840.

[10] S. Otsuka, M. Kamata, K. Hirotsu, T. Higuchi, *J. Am. Chem. Soc.* **1981**, *103*, 3011; K. S. Hagen, G. Christou, R. H. Holm, *Inorg. Chem.* **1983**, *22*, 309; G. Christou, K. S. Hagen, J. K. Bashkin, R. H. Holm, *ibid.* **1985**, *24*, 1010; M. Kriege, G. Henkel, *Z. Naturforsch. B.* **1987**, *42*, 1121.

[11] G. Henkel, M. Kriege, K. Matsumoto, *J. Chem. Soc. Dalton Trans.* **1988**, 657.

[12] D. Fenske, J. Ohmer, J. Hachgenei, *Angew. Chem.* **1985**, *97*, 993; *Angew. Chem. Int. Ed. Engl.* **1985**, *24*, 993.

[13] T. Krüger, B. Krebs, G. Henkel, *Angew. Chem.* **1989**, *101*, 54; *Angew. Chem. Int. Ed. Engl.* **1989**, *28*, 61.

[14] B. K. Teo, *Inorg. Chem.* **1984**, *23*, 1251; B. K. Teo, G. Longoni, F. R. K. Chung, *ibid.* **1984**, *23*, 1257; B. K. Teo, *J. Chem. Soc. Chem. Commun.* **1983**, 1362; D. M. P. Mingos, R. L. Johnston, *Struct. Bonding (Berlin)* **1987**, *68*, 29; D. M. P. Mingos, *Chem. Soc. Rev.* **1986**, *15*, 31; *J. Chem. Soc. Chem. Commun.* **1985**, 1352.

Side-Chain Polyrotaxanes with a Tandem Structure Based on Cyclodextrins and a Polymethacrylate Main Chain**

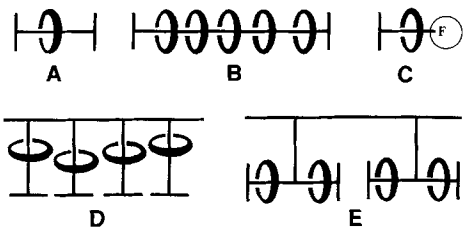
Markus Born and Helmut Ritter*

The chemistry of the rotaxanes has moved out of the area of low molecular weight compounds (Scheme 1, A) in the direction of polymeric structures, in which the linear "thread" molecules pass through a number of crown ethers or cyclodextrins.[1, 2] Recently we extended this group of main-chain polyrotaxanes[3–5] (Scheme 1, B) with a new class of side-chain polyrotaxanes (Scheme 1, D) based on polymethacrylate, polysulfone, and polyether ketone main chains.[6–8]

[*] Prof. Dr. H. Ritter, M. Born
Fachbereich 9, Organische Chemie
und Makromolekulare Chemie der Universität
Gaussstrasse 20, D-42097 Wuppertal (Germany)
Telefax: Int. code + (202) 439-2648

[**] We thank Dr. C. M. Weisshuhn for recording the NMR spectra and the Deutsche Forschungsgemeinschaft for financial support.

 © VCH Verlagsgesellschaft mbH, D-69451 Weinheim, 1995 0570-0833/95/0303-0309 $ 10.00+.25/0



Scheme 1. Rotaxane structures. A = low molecular weight rotaxane; B = main-chain polyrotaxane; C = semirotaxane; D = side-chain polyrotaxane; E = tandem polyrotaxane.

We report here on the synthesis of new tandem polyrotaxanes, in which each branched polymeric side chain has a noncovalently bound cyclodextrin at either end of the side chain (Scheme 1, E). These polymers not only have remarkable structures, but they may also provide fundamental insight for the development of new materials with chiral components which may be useful, for example in the area of chromatography.

Radical copolymerization of 5-[(11-methacryloylamino)-undecanoylamino]isoisophthaloylbis(12-azadodecanoic acid) (**1**) and methyl methacrylate in a ratio of 1:4.1 yielded **2** (Scheme 2). The free acid groups of copolymer **2** were then condensed with the free amino groups of semirotaxane **3a**, which was prepared from 2,6-*O*-dimethyl-*β*-cyclodextrin and 4-amino-*N*-[4-(triphenylmethyl)phenyl]butanamide (**3**). The optically active tandem polyrotaxane **4a** resulted ($[\alpha]_D^{22} = +72.5$ ($CHCl_3$, $c = 10\,g\,L^{-1}$)). The relatively stable semirotaxane[6] **3a** used is similar to a low molecular weight rotaxane that has only one bulky end group and one reactive group (Scheme 1, A, C). In order to characterize **4a**, model polymer **4b**, which has the same structure but without cyclodextrin rings, was prepared analogously.

In the ^1H NMR spectra of **4a** the signals are significantly broadened and shifted relative to those in the spectra of **4b**. The signals of **4a** at $\delta = 7.41-7.43$ corresponding to the anilide segment in 2,6-position ($H_\alpha/H_{\alpha'}$ in Scheme 2) are markedly broadened and shifted downfield by roughly $\Delta\delta = 0.05$, whereas the remaining signals for the triphenylmethyl groups are almost unchanged. The signals of H_a, H_b, and H_c of the isophthaloyl components in **4a** are also broadened. This indicates that the cyclodextrins move readily along the aliphatic side chains at room temperature. In contrast, at $-10\,°C$ the rings are located preferentially near the anilide end groups, according to NMR spectra. The signals of the central isophthaloyl residue are now identical with the corresponding signals of **4a**, and are thus unaffected by the rings at low temperatures.

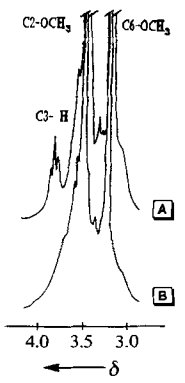
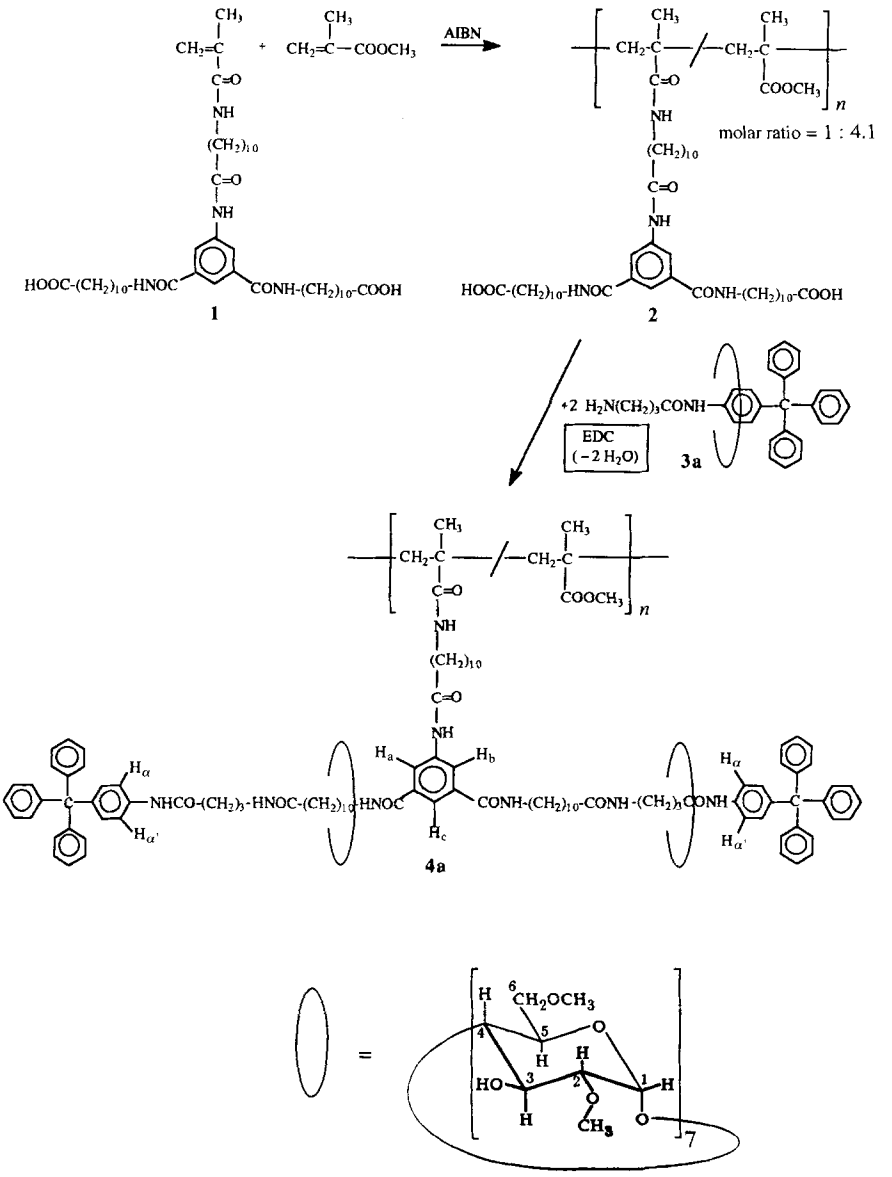


Fig. 1. Sections of the ^1H NMR spectra (250 MHz, $CDCl_3$) near the signals of the C3 protons of the cyclodextrins of a mixture of **4b** and cyclodextrin (A) and **4b** (B). (The signals of the methyl ether protons are cut off for clarity).

As expected, not only do the cyclodextrin rings affect the proton signals of the guests, but also inversely, the guests significantly influence a few signals of the rings. For example, in **4a** the signal of the proton at C3 pointing into the interior of the cage has a marked upfield shift, which is not seen for a simple mixture of **4b** and "free" cyclodextrin (Fig. 1). The original signals of the C3 protons are all shifted in the spectrum of **4a**. This, along with the results of thin-layer chromatography (TLC), indicates that free cyclodextrins are not found with polymer **4a**. Moreover, elemental analysis (see Experimental Procedure, analysis of **4a** and the cyclodextrin-free model compound **4b**) proves that close to all of the side chains are occupied according the proposed structure (Scheme 2).

The cyclodextrin rings of the tandem polyrotaxane **4a** were removed directly by acid glycolysis to give the model polymer **4b**, according to NMR spectroscopy. The characteristic signals of the α,α' protons shift gradually as evident in Figure 2.



Scheme 2. Synthesis of tandem polyrotaxane **4a**. AIBN = α,α'-azodiisobutyronitrile. EDC = *N'*-(3-dimethylaminopropyl)-*N*-ethylcarbodiimide hydrochloride.

 © VCH Verlagsgesellschaft mbH, D-69451 Weinheim, 1995 0570-0833/95/0303-0310 $ 10.00+.25/0

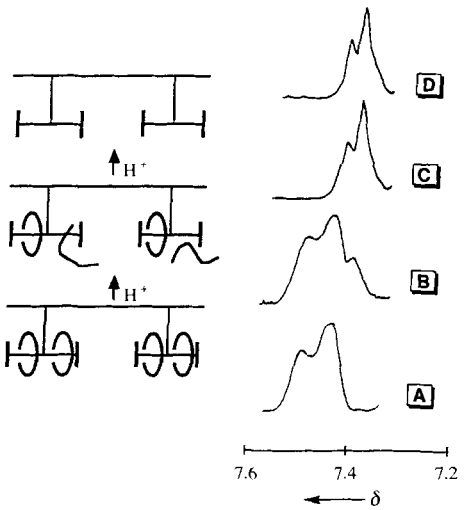


Fig. 2. Progression of the cleavage of cyclodextrin from **4a** in trifluoroacetic acid monitored by ^{1}H NMR. A: **4a**; B: **4a** after 7 h; C: **4a** after 60 h; D: **4b**.

Measurements by differential scanning calorimetry indicated that the glass transition temperature of **4a** is roughly 19 °C higher than that of **4a** (**4a**: 120 °C; **4b**: 101 °C). Apparently the bulky cyclodextrin rings reduce the mobility of the polymer segments.

Experimental Procedure

(11-Methacrylolylamino)undecanamido-1,3-phenylenedicarboxylic acid: A solution of (11-methacryloylamino)undecanecarboxylic acid [9] (6.50 g, 0.02 mol) in THF (30 mL) was treated with triethylamine (2.34 g, 0.02 mol). The resulting solution was cooled to −15 °C, and ethyl chloroformate (2.60 g, 0.02 mol) was added dropwise. After 1 h silylated 5-aminoisophthalic acid (0.02 mol) was added to the suspension, and the reaction mixture was then stirred at room temperature for 2 d.

Silylation: 5-aminoisophthalic acid (4.32 g, 0.02 mol) was suspended in $CHCl_3$ (25 mL) and treated with trimethylchlorosilane (7.60 g, 0.07 mol). Triethylamine (7.08 g, 0.07 mol) was added carefully dropwise. The reaction mixture was then heated at reflux for 3 h. In the workup the solvent was removed and the residue suspended in 200 mL of 2 N HCl. The resulting solid was removed by filtration and washed with water until the rinses were neutral. Yield: 9.04 g (87%).

^{1}H NMR (250 MHz, [D$_6$]DMSO): δ = 1.13–1.74 (m, 16H), 1.83 (s, 3H), 2.29–2.35 (t, 2H), 3.03–3.11 (m, 2H), 5.27 (s, H), 5.60 (s, 1H), 8.14 (s, 1H), 8.44 (s, 2H); IR (KBr): $\tilde{\nu}$[cm^{-1}] = 3300–3600 (OH, NH), 3000–3100 (=C-H), 1655 (amide I), 1535 (amide II); Elemental analysis: calcd. for $C_{23}H_{32}N_2O_6$: C 63.87%, H 7.46%, N 6.48%; found C 63.66%, H 7.33%, N 6.41%.

1: An analogous reaction to that above with the mixed anhydride of (11-methacrylamino)undecanamido-1,3-phenyldicarboxylic acid, two equivalents of 11-aminoundecanoic acid, and four equivalents of trimethylchlorosilane and triethylamine provided **1** in 72% yield.

^{1}H NMR (250 MHz, CD$_3$OD): δ = 1.19–1.73 (m, 48H), 1.92 (s, 3H), 2.27–2.33 (t, 4H), 2.36–2.43 (t, 2H), 3.18–3.24 (t, 2H), 3.34–3.39 (t, 4H), 5.34 (s, 1H), 5.66 (s, 1H), 7.93 (s, 1H), 8.13 (s, 2H); IR (KBr): $\tilde{\nu}$[cm^{-1}] = 3300–3600 (OH, NH), 3000-3100 (=C-H), 2860, 2930 (CH$_2$ valence), 1715 (C=O), 1600 (C=C), 1640–1655 (amide I), 1530–1550 (amide II); Elemental analysis: calcd. for $C_{45}H_{74}N_4O_8$: C 67.63%, H 9.33%, N 7.017%; found C 67.72%, H 9.37%, N 7.16%.

2: Compound **1** (3.34 g, 4.2 mmol) was dissolved in THF (15 mL), and then methyl methacrylate (2.21 mL, 21 mmol), dodecanethiol (0.16 g, 3 mol%), and AIBN (0.13 g, 3 mol%) were added. The mixture was allowed to polymerize at 60 °C for 4 d under N_2. The solution was then added dropwise to acetone (100 mL) and filtered. The solid product was dried at 60 °C ($\eta_{sp}c^{-1}$ = 27 mL g^{-1}; $c = 1.0 \times 10^{-3}$ g mL^{-1}; THF; 25 °C).

^{1}H NMR (250 MHz, [D$_6$]DMSO): δ = 0.73–2.04 (m, 73.5H), 2.14–2.20 (t, 4H), 2.27–2.31 (t, 2H), 2.97–3.07 (m, 2H), 3.22–3.25 (m, 4H), 3.54 (s, 12.3H), 7.89 (s, 1H), 8.12 (s, 2H). The composition ratio of the copolymer was determined to be 1:4.1 from the integration of the signals of the protons adjacent to the carboxylic acid groups at δ = 2.14–2.20 and the ester protons of methyl methacrylate at δ = 3.54. IR (KBr): $\tilde{\nu}$[cm^{-1}] = 3300–3600 (OH, NH), 3000–3100 (=C-H), 2860, 2930 (CH$_2$ valence), 1715–1725 (C=O, acid, ester), 1630–1655 (amide I), 1530–1555 (amide II); Elemental analysis: found C 65.04%, H 8.89%, N 4.63% calcd. for $(C_{45}H_{74}N_4O_8)_1/(C_5H_8O_2)_{4.1}$: C 64.83%, H 8.97%, N 4.51%.

4a: Compound **2** (1.45 g, 1.2 mmol) was dissolved in a mixture of THF (15 mL) and water (5 mL). Then **3a** (4.90 g; contains 1.09 g (2.6 mmol) of **3b**) was added. The solution was cooled to 0 °C and treated with EDC (0.50 g, 2.6 mmol). The reaction mixture was allowed to stir at room temperature for 4 d, then added dropwise to water. The resulting solid was removed by filtration and dried for several days under vacuum over silica gel (η_{spec}/c = 22 mL/g; $c = 1.0 \times 10^{-3}$ g mL^{-1}; THF; 25 °C).

^{1}H NMR (250 MHz, $CDCl_3$): δ = 0.72–2.00 (m, 73.5H), 2.10–2.17 (m, 4H), 2.24–2.51 (m, 6H), 2.67–2.73 (br., 4H), 7.13–7.25 (m, 34H), 7.46–7.51 (br., α-H, α′-H), 7.91–8.34 (br., H$_a$, H$_b$, H$_c$) cyclodextrin signals: δ = 3.39 (s, C6-OCH$_3$), 3.63 (s, C2-OCH$_3$) 4.98–5.07 (m, C1-H, C3-OH); IR (KBr): $\tilde{\nu}$[cm^{-1}] = 3300–3600 (OH-cyclodextrin, NH), 2840–2930 (CH, CH$_2$ valence), 1725 (C=O, ester) 1635–1670 (amide I), 1520–1555 (amide II); Elemental analysis: found C 59.72%, H 8.00%, N 2.58%; calcd. for $(C_{215}H_{322}N_8O_{78})_1/(C_5H_8O_2)_{4.1}$: C 60.47%, H 7.75%, N 2.40%.

4b: An analogous procedure was used as that for **4a** except that **3b** (1.09 g, 2.6 mmol) was the starting material η_{spec}/c = 27 mL g^{-1}; $c = 1.0 \times 10^{-3}$ g mL^{-1}; THF; 25 °C).

^{1}H NMR (250 MHz, $CDCl_3$): δ = 0.72–2.04 (m, 73.5H), 2.12–216 (m, 4H), 2.24–2.55 (m, 6H), 2.65–2.73 (br., 4H), 2.97–3.06 (br., 2H), 3.25–3.49 (m, 10H), 3.59 (s, 12.3H of MMA ester protons), 7.14–7.25 (m, 34H), 7.41–7.43 (d, α-H, α′-H), 8.01 (s, 1H); IR (KBr): $\tilde{\nu}$[cm^{-1}] = 3280–3400 (NH), 3000–3100 (=C-H), 2860, 2920 (CH$_2$ valence), 1725 (C=O, ester), 1630–1655 (amide I), 1530–1555 (amide II); Elemental analysis: found C 72.95%, H 8.02%, N 5.28%; calcd. for $(C_{103}H_{126}N_8O_8)_1/(C_5H_8O_2)_{4.1}$ C 73.63%, H 7.94%, N 5.56%.

Received: April 19, 1994
Revised version: August 30, 1994 [Z68601E]
German version: *Angew. Chem.* **1995**, *107*, 342

Keywords: polymethacrylate · polyrotaxanes · supramolecular chemistry

[1] G. Schill, H. Zollenkopf, *Nachr. Chem. Tech.* **1967**, *79*, 149.
[2] Recent review: I. F. Stoddart, *Angew. Chem.* **1992**, *104*, 860; *Angew. Chem. Int. Ed. Engl.* **1992**, *31*, 846.
[3] G. Wenz, B. Keller, *Angew. Chem.* **1992**, *104*, 201; *Angew. Chem. Int. Ed. Engl.* **1992**, *31*, 197.
[4] A. Harada, M. Kamachi, *Macromolecules* **1990**, *23*, 2821.
[5] Review: H. W. Gibson, H. Marand, *Adv. Mater.* **1993**, *1*, 11; Y. X. Shen, D. Xie, H. W. Gibson, *J. Am. Chem. Soc.* **1994**, *116*, 537.
[6] M. Born, H. Ritter, *Makromol. Chem. Rapid Commun.* **1991**, *12*, 471.
[7] M. Born, T. Koch, H. Ritter, *Acta Polym.* **1994**, *45*, 68.
[8] M. Born, T. Koch, H. Ritter, *Macromol. Chem. Phys.*, in press.
[9] H. Rehse, H. Ritter, *Makromol. Chem.* **1988**, *189*, 529.

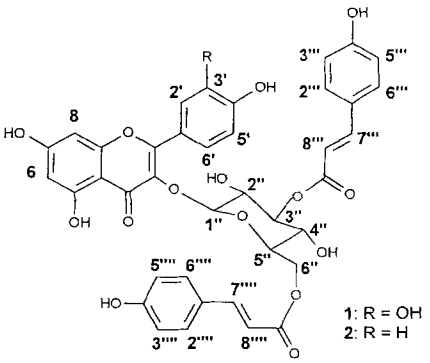
 © VCH Verlagsgesellschaft mbH, D-69451 Weinheim, 1995 0570-0833/95/0303-0311 $ 10.00+.25/0

Structures of UV-B Induced Sunscreen Pigments of the Scots Pine (*Pinus sylvestris* L.)**

Tim P. Jungblut, Jörg-P. Schnitzler, Werner Heller,* Norbert Hertkorn, Jörg W. Metzger, Wilfried Szymczak, and Heinrich Sandermann, Jr.

Owing to increased global UV-B radiation, a consequence of ozone destruction in the stratosphere,[1] living beings need effective protection mechanisms for survival.[2, 3] Most experiments investigating the effect of UV-B radiation have been carried out on cultivated plants,[4] whilst only a few have been performed on trees.[5] Here we report on the structure of sunscreen pigments formed in Scots pine seedlings (*Pinus sylvestris* L.) specifically as a reaction to UV-B irradiation.[6, 7]

Analysis of methanolic extracts of needles from UV-B treated pine seedlings by reversed-phase high-performance liquid chromatography (RP-HPLC) showed that compound **1** in particular was strongly induced in cotyledons, and compound **2** in primary needles (**1** from less than 0.1 to about 0.9 μmol per g fresh weight, and **2** from 0.8 to 2.4 μmol per g fresh weight).[6] Figure 1 shows a typical HPLC elution profile of a methanolic extract from cotyledons after four days of UV-B treatment.



Compounds **1** and **2** were purified and isolated by countercurrent chromatography (MLCCC), gel chromatography on Sephadex LH-20, and preparative RP-HPLC. Their structures were determined by UV and ^{1}H NMR spectroscopy (2D ^{1}H-^{1}H COSY and NOESY), modern techniques in mass spectrometry (TOF-SIMS, electrospray MS in combination with MS/MS), as well as selective chemical degradation. According to these results, **1** is 3″,6″-di-*O*-(*para*-coumaroyl)isoquercitrin, and **2** is 3″,6″-di-*O*-(*para*-coumaroyl)astragalin. These two metabolites belong to a group of diacylated flavonol monoglycosides which have seldom been discussed until now. Compound **1** has already been described; however, there was some uncertainty in the substitution pattern on the sugar moiety.[8] Compound **2** was isolated and characterized for the first time here.

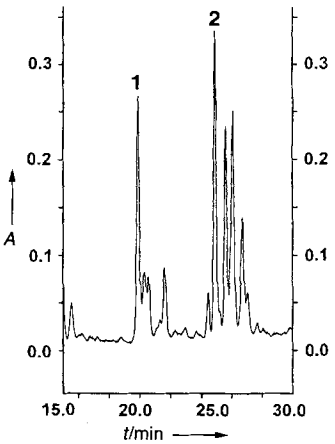


Fig. 1. RP-HPLC trace of a methanolic extract of cotyledons (compound **1** induced) from Scots pine seedlings after four days of UV-B irradiation; detection at 280 nm. t = retention time, A = absorbance in arbitrary units.

The results of the ^{1}H NMR spectroscopic investigations of **1** and **2** are summarized in Table 1. The molecular framework was determined by ^{1}H NMR and 2D ^{1}H-^{1}H COSY NMR spectroscopy. The unequivocal assignment of the aromatic protons was confirmed by NOESY experiments and by comparison with spectra of monoacylated compounds obtained by solvolysis. Selective decoupling experiments enabled unambiguous assignment of the sugar protons and showed the acylation at positions 3″ and 6″.

Structural data obtained from the ^{1}H NMR spectra were confirmed by mass spectrometric measurements. An initial molecular weight determination by time-of-flight secondary ion mass

Table 1 ^{1}H NMR [a], ES-MS, and MS/MS data [b].

1: ^{1}H NMR (400 MHz, CD_3OD (δ = 3.30), 310 K): δ = 8.55 (H, s; OH-7), 7.68 (H, d, ^3J = 15.9 Hz; H-7‴), 7.58 (2H, m; H-2′, H-6′), 7.47 (2H, AA′, ^3J = 8.6 Hz; H-2‴, H-6‴), 7.43 (H, d, ^3J = 15.9 Hz; H-7⁗), 7.33 (2H, AA′, ^3J = 8.6 Hz; H-2⁗, H-6⁗), 6.85 (5H, m (d and 2BB′); H-5′, H-3‴, H-5‴, H-3⁗, H-5⁗), 6.41 (H, d, ^3J = 15.9 Hz; H-8‴), 6.20 (H, d, ^4J = 2.0 Hz; H-8), 6.12 (H, d, ^3J = 15.9 Hz; H-8⁗), 6.06 (H, d, ^4J = 2.0 Hz; H-6), 5.31 (H, d, ^3J = 7.6 Hz; H-1″), 5.13 (H, t, ^3J = 7.9 Hz; H-3″), 4.33 (H, dd, ^2J = 11.8, ^3J = 1.5 Hz; H-6″A), 4.22 (H, dd, ^2J = 11.8, ^3J = 5.9 Hz; H-6″B), 3.73 (H, dd, ^3J = 7.9, ^3J = 9.4 Hz; H-2″), 3.55 (2H, m; H-4″, H-5″); ES-MS: *m/z*: 757 $[M + H]^+$, 455 $[Gl]^+$, 303 $[Agl + 2H]^+$, 165 $[pCOH + H]^+$, 147 $[pC]^+$; ES-MS/MS: daughter ions of *m/z* 757 $[M + H]^+$: *m/z*: 611 $[M - pC + 2H]^+$, 455 $[Gl]^+$, 303 $[Agl + 2H]^+$, 291 $[Gl - pCOH]^+$, 165 $[pCOH + H]^+$, 147 $[pC]^+$; daughter ions of *m/z*: 455 $[Gl]^+$: *m/z*: 291 $[Gl - pCOH]^+$, 165 $[pCOH + H]^+$, 147 $[pC]^+$; parent ions of *m/z*: 303 $[Agl + 2H]^+$: *m/z*: 757 $[M + H]^+$, 611 $[M - pC + 2H]^+$; parent ions of *m/z*: 291 $[Gl - pCOH]^+$: *m/z*: 757 $[M + H]^+$, 455 $[Gl]^+$; parent ions of *m/z* 147 $[pC]^+$: *m/z*: 757 $[M + H]^+$, 611 $[M - pC + 2H]^+$, 455 $[Gl]^+$, 291 $[Gl - pCOH]^+$; neutral loss of 308 *u* $[Gl - pC]$: *m/z*: 611 $[M - pC + 2H]^+$, 455 $[Gl]^+$.

2: ^{1}H NMR (400 MHz, CD_3CN (δ = 1.93), 310 K): δ = 12.26 (H, s; OH-5), 8.40 (H, s; OH-7), 8.04 (2H, AA′, ^3J = 9.0 Hz; H-2′, H-6′), 7.71 (H, d, ^3J = 16.0 Hz; H-7‴), 7.53 (2H, AA′, ^3J = 8.6 Hz; H-2‴, H-6‴), 7.46 (H, d, ^3J = 16.0 Hz; H-7⁗), 7.39 (2H, AA′, ^3J = 8.9 Hz; H-2⁗, H-6⁗), 6.86 (6H, m (3BB′); H-3′, H-5′, H-3‴, H-5‴, H-3⁗, H-5⁗), 6.41 (H, d, ^4J = 2.1 Hz; H-8), 6.40 (H, d, ^3J = 16.0 Hz; H-8⁗), 6.21 (H, d, ^4J = 2.1 Hz; H-6), 6.14 (H, d, ^3J = 16.0 Hz; H-8‴), 5.28 (H, d, ^3J = 7.9 Hz; H-1″), 5.08 (H, t, ^3J = 9.4 Hz; H-3″), 4.24 (H, dd, ^2J = 11.9, ^3J = 1.6 Hz; H-6″A), 4.19 (H, dd, ^2J = 11.9, ^3J = 5.9 Hz; H-6″B), 3.65 (H, dd, ^3J = 7.9, ^3J = 9.4 Hz; H-2″), 3.58 (2H, m; H-4″, H-5″); ES-MS: *m/z*: 741 $[M + H]^+$, 455 $[Gl]^+$, 287 $[Agl + 2H]^+$, 165 $[pCOH + H]^+$, 147 $[pC]^+$; ES-MS/MS: daughter ions of *m/z* 741 $[M + H]^+$: *m/z*: 595 $[M - pC + 2H]^+$, 455 $[Gl]^+$, 291 $[Gl - pCOH]^+$, 287 $[Agl + 2H]^+$, 165 $[pCOH + H]^+$, 147 $[pC]^+$; daughter ions of *m/z* 455 $[Gl]^+$: *m/z*: 291 $[Gl - pCOH]^+$, 165 $[pCOH + H]^+$, 147 $[pC]^+$; parent ions of *m/z* 287 $[Agl + 2H]^+$: *m/z*: 741 $[M + H]^+$; parent ions of *m/z* 291 $[Gl - pCOH]^+$: *m/z*: 741 $[M + H]^+$, 455 $[Gl]^+$; parent ions of *m/z* 147 $[pC]^+$: *m/z*: 741 $[M + H]^+$, 455 $[Gl]^+$, 291 $[Gl - pCOH]^+$; neutral loss of 308 *u* $[Gl - pC]$: *m/z*: 455 $[Gl]^+$.

[a] See structural formula for numbering. [b] Abbreviations: M = molecule = $C_{30}H_{32}O_{16}$ [756] (**1**), $C_{30}H_{32}O_{15}$ [740] (**2**); pC = *para*-coumaroyl group, $C_9H_7O_2$ [147]; pCOH = *para*-coumaric acid, $C_9H_8O_3$ [164]; Gl = glycosyl residue = M − Agl, $C_{24}H_{23}O_9$ [455]; Agl = aglycone, $C_{15}H_9O_7$ [301] (for **1**), $C_{15}H_9O_6$ [285] (for **2**).

[*] Dr. W. Heller, Dipl.-Chem. T. P. Jungblut, Dr. J.-P. Schnitzler, Prof. Dr. H. Sandermann, Jr.
GSF-Forschungszentrum für Umwelt und Gesundheit GmbH
Institut für Biochemische Pflanzenpathologie
Postfach 1129, D-85758 Oberschleissheim (Germany)
Telefax: Int. code + (89) 3187-3383
e-mail: heller@gsf.de
Dr. N. Hertkorn
GSF-Institut für Ökologische Chemie (Germany)
Dr. W. Szymczak
GSF-Institut für Strahlenschutz (Germany)
Dr. J. W. Metzger
Institut für Organische Chemie der Universität Tübingen (Germany)

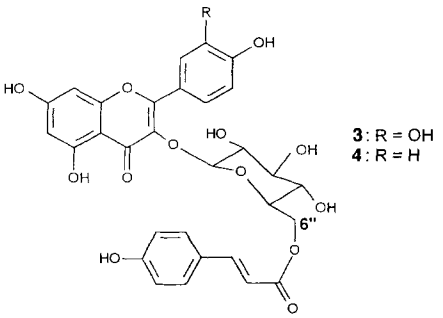
[**] This work was supported by the Fonds der Chemischen Industrie, and by the Deutsche Forschungsgemeinschaft (SFB 323, C-3 Metzger). We thank Dipl.-Phys. M. Köfferlein and Dr. H. Seidlitz (GSF-Arbeitsgruppe Expositionskammern) for recording UV-B radiation during the experiments, and Dr. A. Marston and Prof. Dr. K. Hostettmann (Université de Lausanne, Switzerland) for instruction in advanced techniques in countercurrent chromatography.

spectrometry (TOF-SIMS) was in agreement with the postulated structures.[9] In the negative-ion mode, the base peaks for **1** and **2** at *m/z* 301 and 285, respectively, correspond to the aglycone ions. The quasi molecular ions $[M - H]^-$ at *m/z* 755 and 739 were also observed. Here, the method was used for the first time for analysis of secondary plant substances. Further important structural information was obtained from electrospray MS and MS/MS investigations, after collision-induced dissociation of the protonated molecular ions in a triple quadrupole mass spectrometer (see Table 1). Recently this technique was successfully applied to the analysis of anthocyanins and betacyanins.[10]

In addition to the physicochemical methods mentioned, the following solvolytic degradation reactions were used in the structure determination:

a) Alkaline hydrolysis with NaOH: The products were analyzed directly from the reaction mixture by RP-HPLC and were identified, by co-chromatography and by comparison of the diode array UV spectra with those of authentic samples, as *para*-coumaric acid and isoquercitrin (for **1**), and *para*-coumaric acid and astragalin (for **2**) (molar ratio 2:1 in each case). This confirmed the spectroscopic data, since ester bonds are preferentially cleaved under alkaline conditions.

b) Methanolysis: Continuous degradation of **1** and **2** was observed during the recording of ^{1}H NMR spectra in CD_3OD, indicated by new signals growing in intensity at the expense of the original ones. Analysis of both samples by RP-HPLC showed that two new products had been formed. They were isolated and characterized by UV and ^{1}H NMR spectroscopy as well as by ES mass spectrometry. Apparently transesterification of the diacylated compounds **1** and **2** with the solvent (methanol or perdeuteromethanol) gave rise to the corresponding 6″-monoacyl compounds 6″-*O*-(*para*-coumaroyl)isoquercitrin (**3**) and 6″-*O*-(*para*-coumaroyl)astragalin (tilirosid, **4**), as well as coumaric acid methyl ester and perdeuteromethyl ester.



Compounds **1** and **2** have very similar UV spectra. The maximum of the main absorption band at 315 nm lies right in the region of 290–320 nm expected for effective UV-B absorption. The extinction coefficient was determined in each case as $\varepsilon_{max} = 50\,300$. Thus these compounds offer optimal physiological protection against UV-B radiation. Figure 2 shows the UV spectra of compounds **1**, **3**, and **5** (= **3** with H instead of *para*-coumaroyl at 6″-O).

The absorption behavior of the monoacylated and diacylated metabolites is, as expected, qualitatively similar, but differs quantitatively. The ratios of the absorbances at 315 nm, the absorption maximum for flavonol monoglucosides acylated with coumaric acid, and at 350 nm, the maximum for non-acylated flavonol monoglucosides, are 2.44 (**1**) and 2.33 (**2**) for the diacylated compounds, whereas for the monoacylated compounds the ratios are 1.57 (**3**) and 1.61 (**4**). These values indicate that the

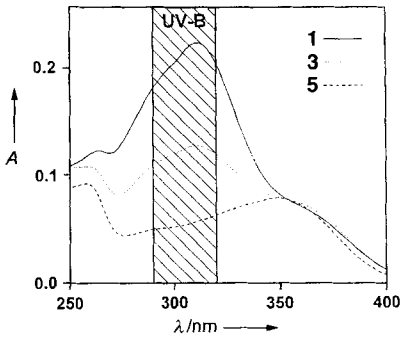


Fig. 2. UV spectra of quercetin derivatives: dicoumaroyl- (**1**), monocoumaroyl- (**3**), and non-acylated quercetin-3-glucoside (**5**) in acetonitrile (normalized to the absorption maximum of the non-acylated flavonol glucoside at 350 nm). The UV spectra of the corresponding kaempferol derivatives (**2**, **4**, and **4** with H instead of *para*-coumaroyl at 6″-O) were very similar; for this reason they are not shown.

irradiation-induced diacylated metabolites exhibit better protection against UV-B radiation than monoacylated compounds at the same molarity.

Respective analyses of enzymatically prepared epidermal tissue[11] and whole needles showed that up to 94% of the diacylated compounds are situated in the epidermis of the pine needle. It can be concluded from this result that the compounds under investigation are compartmented in the epidermis. The absorption behavior at 300 nm of the soluble and the cell wall bound fractions showed that about 80% of the absorption can be attributed to the soluble, and only 20% to the cell wall bound compounds.[12] Thus the soluble diacylated flavonol monoglucosides investigated here provide optimal protection for deeplying tissue against potentially damaging UV-B radiation.

Experimental Procedure

Needles from Scots pine seedlings were homogenized at liquid-nitrogen temperature in a microdismembrator II (Braun, Melsungen, Germany), and extracted in 1.0 mL methanol per 100 mg homogenate for 1 h in the dark at room temperature. After 10 min of centrifugation at 16000 *g* and 4 °C, the supernatant was removed and stored at −80 °C, or analyzed by RP-HPLC using a Beckman HPLC Gold system (Beckman, München, Germany; Nova-Pak (4 μm), 3.9 mm × 300 mm, Waters, Eschborn, Germany). The elution was performed with a gradient of 30–45% acetonitrile in water with 0.1% (w/v) ammonium formate in 2%(v/v) formic acid over 25 min at a flow rate of 1 mL min^{-1}. The elution was monitored with a UV/Vis spectrophotometer (diode array detector 136, Beckman).

The ES-MS measurements were performed with a Sciex API III triple quadrupole mass spectrometer equipped with an ionspray ion source (Sciex, Thornhill, Ontario, Canada). The ES voltage was 4.9 kV and the orifice voltage between 80 and 100 V. Collision-induced dissociation (CID) spectra (daughter ion, parent ion, and neutral loss scans) were obtained with argon as collision gas at a density of 2×10^{14} to 5×10^{14} atoms per cm^2 and a collision energy of 30 to 50 eV. For the ES-MS experiments solutions of the purified substances in acetonitrile were injected directly into the electrospray interface and measured in the positive-ion mode. Addition of ammonium acetate favored formation of $[M + H]^+$ ions and simultaneously suppressed formation of other adduct ions $[M + X]^+$ (X = Na, K). The sample solutions (1 μg mL^{-1}) were injected into the ES interface with a medical syringe infusion pump (Model 22, Harvard Apparatus, South Natik, USA) and a 100 μL microsyringe (Hamilton, Reno, Nevada, USA) at a constant rate of 5 μL min^{-1}.

For the preparation of samples for TOF-SIMS measurements [9] (in negative-ion mode) 35 μg cm^{-2} nitrocellulose (dissolved in acetone) was sprayed onto a polished stainless steel plate with an electrospray setup. The sample was dissolved in *tert*-butyl alcohol (1 μg mL^{-1}), and 1 μL of this was added dropwise to the nitrocellulose. For the ionization, the samples were bombarded with a pulsed 30 keV SF_5^+ beam (3 nA, pulse length 5 ns) at an effective angle of incidence of 42°. The flight length was 60 cm. A transient recorder [13] recorded the complete time-of-flight spectrum for each primary pulse (< 10 primary particles per pulse).

Degradation reactions: a) Alkaline hydrolysis with NaOH: About 20 μg of **1** or **2**, dissolved in methanol, was heated with 100 μL of 0.5% aqueous NaOH for 20 min in a heating block (Liebisch, Bielefeld, Germany) at 45 °C. The reaction mixture was then neutralized with 1 N HCl (pH meter, pH 521, WTW, Weilheim, Germany), and

the resulting reaction products were analyzed by RP-HPLC immediately. b) Methanolysis: Solutions of compounds **1** and **2** in pure methanol were allowed to stand for four weeks, and two new products formed; the reaction was followed by RP-HPLC.

Received: July 12, 1994 [Z 7120IE]
German version: *Angew. Chem.* **1995**, *107*, 376

Keywords: natural products · sunscreen pigments · structure determination

[1] J. B. Kerr, C. T. McElroy, *Science* **1993**, *262*, 1032–1034.
[2] B. Langer, E. Wellmann, *Photochem. Photobiol.* **1990**, *52*, 861–863.
[3] C. J. Beggs, E. Wellmann, H. Grisebach in *Morphogenesis in Plants* (Eds.: R. E. Kendrick, G. H. M. Kronenberg), Martinus Nijhoff, Dordrecht, **1986**, pp. 467–499.
[4] M. Tevini, A. H. Teramura, *Photochem. Photobiol.* **1989**, *50*, 479–487.
[5] a) J. H. Sullivan, A. H. Teramura, *Trees* **1992**, *6*, 115–120; b) E. H. DeLucia, T. A. Day, T. C. Vogelman, *Plant Cell Environ.* **1992**, *15*, 921–929.
[6] J. P. Schnitzler, T. P. Jungblut, M. Köfferlein, C. Langebartels, W. Heller, H. Sandermann, Jr., *Plant Cell Environ.*, submitted.
[7] G. Seckmeyer, H. D. Payer, *J. Photochem. Photobiol. B: Biol.* **1993**, *21*, 175–181.
[8] S. Z. Imvanova, G. G. Zapesochnaya, N. A. Tyukavkina, S. A. Medvedeva, *Chem. Nat. Compd. (Engl. Trans.)* **1978**, *14*, 335–336.
[9] W. Szymczak, K. Wittmaack, *Nucl. Instrum. Methods Phys. Res. Sect. B* **1994**, *88*, 149–153.
[10] a) W. E. Gläßgen, H. U. Seitz, J. W. Metzger, *Biomed. Environ. Mass Spectrom.* **1992**, *21*, 271–277; b) W. E. Gläßgen, V. Wray, D. Strack, J. W. Metzger, H. U. Seitz, *Phytochemistry* **1992**, *31*, 1593–1601; c) W. E. Gläßgen, J. W. Metzger, S. Heuer, D. Strack, *ibid.* **1993**, *32*, 1525–1527; d) S. Heuer, V. Wray, J. W. Metzger, D. Strack, *ibid.* **1992**, *31*, 1801–1807; S. Heuer, S. Richter, J. W. Metzger, V. Wray, M. Nimtz, D. Strack, *ibid.*, **1994**, *37*, 761–767.
[11] K. J. Lendzian, A. Nakajiama, H. Ziegler, *Trees* **1986**, *1*, 47–53.
[12] J.-P. Schnitzler, T. P. Jungblut, W. Heller, P. Hutzler, U. Heinzmann, E. Schmelzer, D. Ernst, C. Langebartels, H. Sandermann, Jr., *Plant J.*, submitted.
[13] W. Szymczak (GSF-Forschungszentrum), DE-B 3904308, **1993**; US-A 4970390, **1990**.

Self-Assembled Helicates of Zinc and Cadmium Cyanides, $[M_x(CN)_{2x+1}]^-$, $x \leq 27$**

Ian Dance,* Phillip Dean, and Keith Fisher

Metal cyanide compounds, long known in the solid and solution phases, are virtually unknown in the pristine conditions of the gas phase.[1] We report here the formation of a series of gaseous zinc and cadmium cyanide anions of general formula $[M_x(CN)_{2x+1}]^-$ for x up to 27. Density functional (DF) theory and force-field (FF) calculations indicate that these ions have regular helical structures.

We recently found that solid CuCN and AgCN under laser ablation at 1064 nm form two series of ions, $[M_x(CN)_{x-1}]^+$ and $[M_x(CN)_{x+1}]^-$ ($x \leq 5$, M = Cu or Ag), with evidence for the formation of the neutral molecules $[M_x(CN)_{2x}]^0$, $x \leq 5$.[1a] We concluded that the ions $[M_x(CN)_{x-1}]^+$ and $[M_x(CN)_{x+1}]^-$ have completely linear structures with alternating M and CN groups on the basis of 1) the observed addition of two molecules of NH_3, H_2S, or CO to the cations $[M_x(CN)_{x-1}]^+$, 2) the observed association of the anions $[Ag_x(CN)_{x+1}]^-$ with one or two Na^+ ions, and 3) density functional optimizations of the molecular structures.

The negative ions formed by similar laser ablation of $Zn(CN)_2$ and $Cd(CN)_2$ have the compositions $[M_x(CN)_{2x+1}]^-$ for x up to 27 and possibly higher. In the mass spectrum for the product mixture from $Cd(CN)_2$ (Fig. 1) signals for members of the series for $x < 8$ are almost nonexistent, while the most abundant ions are in the region $15 \leq x \leq 23$. The spectrum of the $[Zn_x(CN)_{2x+1}]^-$ ions is similar, with more pronounced intensities at $x = 15$, 17, 19, and with the ions $3 \leq x \leq 8$ apparent.

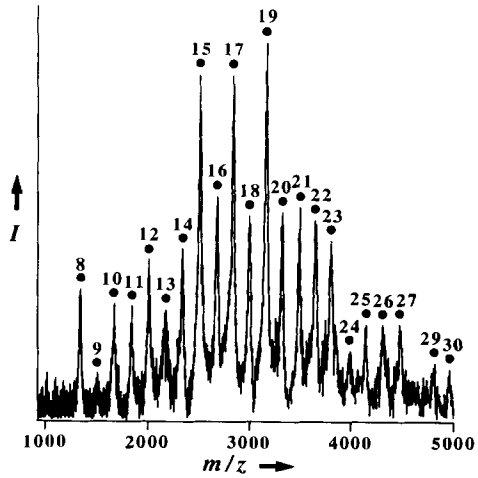


Fig. 1. Mass spectrum of ions $[Cd_x(CN)_{2x+1}]^-$ formed by laser ablation of solid $Cd(CN)_2$; laser power ca. 12000 MWcm^{-2}, $\lambda = 1064$ nm. Values of x are marked above the peaks.

What are the structures of these ions? We seek the structural principle for the continuous series $[M_x(CN)_{2x+1}]^-$, in which the zinc and cadmium cyanides are presumably isostructural. We expect that the structural motif should maximize the cluster density, as is achieved with anisotropic structures in the Cu/Ag series. There are two reasons why the $[M_x(CN)_{2x+1}]^-$ ions are unlikely to be fragments of the diamondoid crystal structures of $Zn(CN)_2$ and $Cd(CN)_2$. Firstly, the $M(CN)_2$ lattices have inherently low density, with long linear M-CN-M connections, compensated by the occurrence of interpenetrating unconnected diamondoid lattices,[2] or lattice filling with solvent.[3–5] Secondly, fragments excised to maintain consistent acceptable coordination at all metal atoms do not provide the observed continuous series of compositions.

In order to approach the structures of the observed ions, we first determined the relevant structural principles, using DF methods[7] to explore the structures of smaller members of the series (Fig. 2). For both $[Zn_2(CN)_5]^-$ and $[Zn_3(CN)_7]^-$ the isomer with the linear Zn-CN-Zn bridges, trigonal-planar coordination at Zn, and linear Zn-CN termini is clearly the most stable. The optimization sequence similarly indicates that CN bridges other than linear M-CN-M are less favorable, a conclusion consistent with the computational results for copper and silver cyanide complexes, and with the crystal structures of other $Zn(CN)_2$ and $Cd(CN)_2$ derivatives.[3–6, 8]

[*] Prof. I. Dance, Prof. P. A. W. Dean,[+] Dr. K. Fisher
School of Chemistry, University of New South Wales
Sydney 2052 (Australia)
Telefax: Int. code + (2)662-2835
e-mail: I. Dance@unsw.edu.au.

[+] Permanent address: Department of Chemistry,
University of Western Ontario, London, Ontario (Canada)

[**] We thank the Australian Research Council for financial support, and the Australian Numerical Simulation and Modelling Services for the generous provision of computing resources. P. A. W. D. is grateful to the University of Western Ontario for sabbatical leave, and to the National Sciences and Engineering Research Council of Canada for providing partial travel funds.

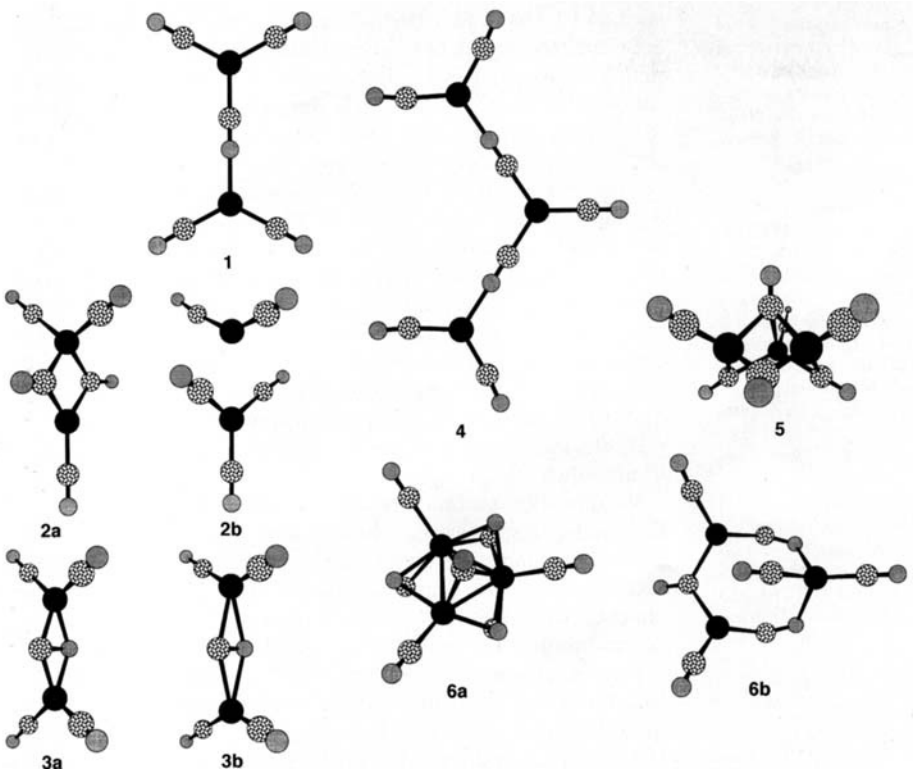


Fig. 2. Structures of zinc cyanides optimized by DF methods (● = Zn, ◎ = C, ○ = N). a) $[Zn_2(CN)_5]^-$: relative to the most stable structure **1**, the energies for **2b** and **3b** are + 80 and + 118 kJ mol^{-1}, respectively. The optimization of **2a** with (μ-CN)$_2$ to **2b** involved separation of the bridges and approach to a linear (140°) NC-Zn-CN arrangment and a trigonal-planar (116, 122°) [Zn(CN)$_3$] arrangement. The optimization of **3a** with (μ,η^2-CN) to **3b** involved elongation of the bridge and approach to two linear (140°) NC-Zn-CN units. b) $[Zn_3(CN)_7]^-$: relative to the most stable structure **4**, the energies for **5** and **6b** are + 110 and + 230 kJ mol^{-1}. The optimization of **6a**, with (μ,η^2-CN)$_3$(μ_3-CN), to **6b** involved substantial rearrangement of the bridges to more stable parallel arrays with secondary interactions.

Structure element **4** provides the clue to the structural principle that generates the series, namely the helical structure type illustrated in Figure 3 for $[Zn_{27}(CN)_{55}]^-$. In this structure the primary coordination of each zinc atom is nominally trigonal planar, the coordinated CN units are either linear bridging or linear terminal, and the helix is stabilized by secondary interactions between Zn atoms and bridging C and N atoms of the contiguous strand. These stabilizing interactions require a nonintegral number n of Zn(CN)$_2$ units per turn; reasonable geometries result from $n = 4.67$ and 5.67 (as in Fig. 3). The helical structure type maintains linear M-CN-M bridges, has the same coordination for all metal atoms, provides for a continuous series $[M_x(CN)_{2x+1}]^-$, and accounts for the enhanced stability for larger values of x through the increased opportunities for interstrand interactions.

We have evaluated the stabilities and geometries of the helical structures by DF and FF methods. The structures of $[Zn_9(CN)_{19}]^-$ with $n = 4.67$ and 5.67 optimized by DF[7] are stable helices with normal bond lengths; the secondary interactions between contiguous strands correspond to Zn–CN distances of 3.65 to 3.85 Å. These geometry optimizations also reveal that the terminal CN ligands peripheral to the helix are not perpendicular to the helix axis, but inclined slightly towards an adjacent strand of the helix as a consequence of coulombic attractions between $CN^{\delta-}$ and $Zn^{\delta+}$. The helical ions with $x > 9$ were modeled by FF methods, using bond lengths, bond angles, and atomic partial charges from the DF calculations.[9] These calculations confirm the stability of the helices with $n = 4.67$ and 5.67, reproduce the interstrand distances found in the DF calculations, and yield the characteristic inclinations of the terminal CN groups. The FF methods can be applied to all of the observed ions; the structure shown in Figure 3 was also optimized by this method.

All of these results support the stability of the helical structure type, which accounts for the continuous series of observed ions in the mass spectra, and for the lesser abundance of the zinc cyanide ions and absence of the cadmium cyanide ions with $x < 8$, which do not benefit from the stabilizing interstrand interactions. Alternative structural motifs such as graphitic arrays of M-CN-M linkages or M_x polyhedra with linear CN bridges along edges predict stoichiometries and mass spectra different from our observations. The helix is supramolecular and dependent on nonbonded interactions.

Finally, what are the prospects for crystallization of these structures, or, by extension, the infinite uncharged helix? Crystallization of zinc and cadmium cyanides from polar and protic noncoordinating solvents has always yielded inclusion lattices without helical motifs.[3–6] However, crystallization from nonpolar aprotic solvent systems (or cocrystallizing media) should enhance the influences of the intrahelix electrostatic interactions.

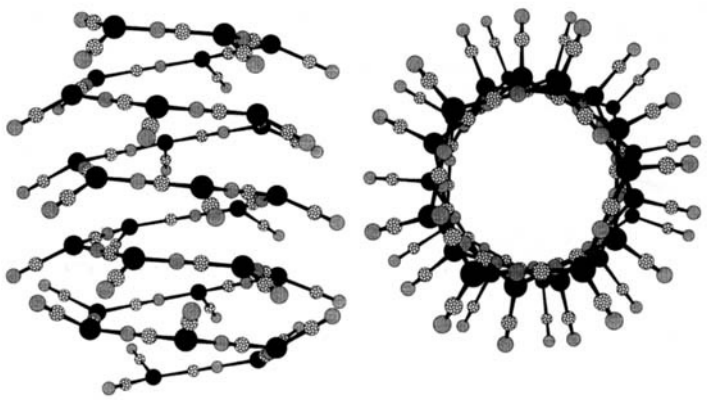


Fig. 3. Side view (left) and top view (right) of the optimized helical structure of $[Zn_{27}(CN)_{55}]^-$ with 5.67 Zn(CN)$_2$ units per turn.

Received: July 19, 1994
Revised version: September 26, 1994 [Z 7140 IE]
German version: *Angew. Chem.* **1995**, *107*, 366

Keywords: cadmium compounds · cyanides · density function methods · helices · zinc compounds

[1] a) I. G. Dance, P. A. W. Dean, K. J. Fisher, *Inorg. Chem.* **1994**, *33*, 6261; b) W. M. Mackenzie, A. H. Clyne, L. S. MacDonald, *J. Inst. Brew.* **1990**, *96*, 223-232.

[2] B. F. Hoskins, R. Robson, *J. Am. Chem. Soc.*, **1990**, *112*, 1546.

[3] a) T. Kitazawa, S. Nishikiori, R. Kuroda, T. Iwamoto, *Chem. Lett.* **1988**, 459; b) T. Kitazawa, S. Nishikiori, R. Kuroda, T. Iwamoto, *Chem. Lett.* **1988**, 1729; c) T. Kitazawa, S. Nishikiori, A. Yamagishi, R. Kuroda, T. Iwamoto *J. Chem.*

Soc. Chem. Commun. **1992**, 413; d) T. Iwamoto in *Inclusion Compounds, Vol. 5* (Eds.: J. L. Atwood, J. E. D. Davies, D. D. MacNicol), Oxford University Press, Oxford, **1991**, pp. 177–212.

[4] a) B. F. Abrahams, B. F. Hoskins, R. Robson *J. Chem. Soc. Chem. Commun.* **1990**, 60; b) B. F. Abrahams, B. F. Hoskins, J. Liu, R. Robson *J. Am. Chem. Soc.* **1991**, *113*, 3045; c) B. F. Abrahams, M. J. Hardie, B. F. Hoskins, R. Robson, G. A. Williams, *ibid.* **1992**, *114*, 10641.

[5] J. Kim, D. Whang, J. I. Lee, K. Kim, *J. Chem. Soc. Chem. Commun.* **1993**, 1400.

[6] J. A. Ripmeester, C. I. Ratcliffe in *Spectroscopic and Computational Studies of Supramolecular Systems* (Ed.: J. E. D. Davies), Kluwer, Dordrecht, **1992**, pp. 1–27.

[7] a) Program DMol v2.3, Biosym Technologies Inc. Double numerical basis sets with polarization functions were used, with core orbitals frozen. The Vosko–Wilk–Nusair [7b] correlation functional and the Becke [7c] exchange functional with nonlocal corrections were employed. The calculations were spin restricted, for the even-electron anions, and involved unconstrained optimization of geometry. Electronic structures and details of geometric structures will be presented in the full publication. b) S. J. Vosko, L. Wilk, M. Nusair, *Can. J. Phys.* **1980**, *58*, 1200. c) A. D. Becke, *J. Chem. Phys.* **1988**, *88*, 2547.

[8] T. Kitazawa, M. Akiyama, M. Takashi, M. Takeda *J. Chem. Soc. Chem. Commun.* **1993**, 1112.

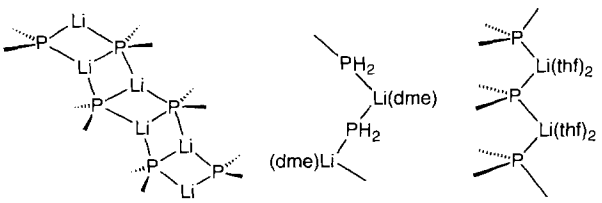
[9] Atomic partial charges (for $M_{27}(CN)_{55}]^-$): Zn + 0.59; Cd + 0.69; C_{term} −0.21 (Zn), −0.24 (Cd); N_{term} −0.14 (Zn), −0.15 (Cd); C_{br} −0.18 (Zn), −0.21 (Cd); N_{br} −0.10 (Zn), −0.11 (Cd); dielectric constant = *r*; angle quadratic constants [kJ rad^{-2} mol^{-1}] C-M-C 125, C-M-N 125, M-C-N 209, M-N-C 209; parameters for the potential well of nonbonding interactions *r** [Å], *ε** [kJ mol^{-1}] 2.03, 0.63 (C); 1.96, 0.71 (N); 1.90, 0.62 (Zn); 2.30, 0.96 (Cd); calculations with Discover v2.9, Biosym Technologies Inc.

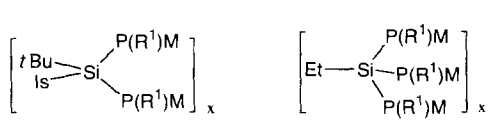
Novel Alkali Metal Phosphanide Aggregates**

Matthias Driess,* Gottfried Huttner, Norbert Knopf, Hans Pritzkow, and Laszlo Zsolnai

Dedicated to Professor Peter Paetzold on the occasion of his 60th birthday

Lithium phosphanides of the type $LiPR_2$ (R = H, alkyl, aryl, triorganosilyl) are key reagents in organophosphorus synthesis. They are capable of aggregation (cluster formation) and like the homologous amides often have two-dimensional, ladderlike structures **A**.[1] Nevertheless, polymeric chains **B**[2] and helical strands **C**[3] have also been observed. These structural differences and the degree of oligomerization *x* (x > 2) are based primarily on the spatial requirements of the substituents and the ratio of the number of lithium to donor solvent centers. This is, for example, confirmed very well by systematic investigations of the $LiP(SiMe_3)_2$/donor solvent system.[4]

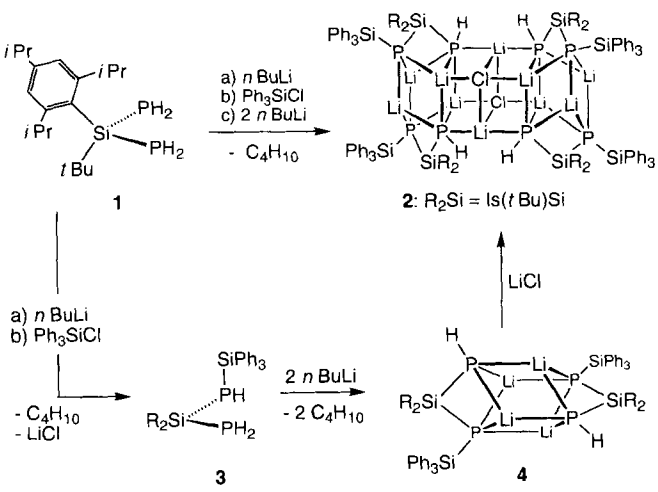




The aggregation of $(R_3Si)_2PM$ compounds (M = alkali metal) according to the "ladder structure" principle (**A**) led to the question of whether the highly functionalized molecular bis- and tris(alkali metal phosphanidyl)silanes of the type $[R_2Si(PR^1M)_2]$ (**D**) and $[RSi(PR^1M)_3]$ (**E**) organize according to the same building principle to give three-dimensional, closed aggregates. Furthermore, it should be studied whether mixed aggregates also exist and under which conditions (type of solvation, nature and number of metal centers) a closed arrangement of the cluster is possible; however, compounds of the type **D** and **E** were hitherto unknown.

We report here on the first lithium compounds of type **D** and **E** (**4** and **7**, respectively), which indeed have closed "dimeric" cluster structures; furthermore, we have isolated the mixed aggregate **2** from dimeric **D** and $(LiCl)_2$. In addition, we describe the dimeric sodium tris(phosphanide) **8** (type **E**), which is solvated by two molecules of toluene; **8** has an open polyhedron structure.

Colorless crystals of the dimeric bis(lithium phosphanidyl)silane **4** form in 87% yield in a one-pot reaction in toluene starting from the silylphosphane **3** with bulky substituents (prepared from **1**[5] by monosilylation with Ph_3SiCl) and two equivalents of *n*BuLi.



The composition of **4** is confirmed by correct C,H,P elemental analyses and cryoscopic measurements. The latter gave a degree of association *x* of about two for solutions in benzene (concentration range 0.018 to 0.033 M); because of the low solubility of **4**, *x* could not be measured at higher concentrations. It is not possible to determine the constitution of **4** based on its ^{31}P and ^{7}Li NMR spectra,[6] since only broad signals are observed at 25 °C, and below −35 °C the solubility is not sufficient to obtain high-resolution spectra. So far we have been unable to obtain single crystals of **4** or a derivative ($SiMe_3$ or $SiiPr_3$ groups on phosphorus)[7] for an X-ray crystal structure analysis. In an attempt to grow suitable crystals of **4** from the LiCl-containing crude product in hot toluene, we observed that **4** reacts with LiCl. This reaction leads to colorless rhombuses of the unusual, sparingly soluble aggregate **2** (55% yield), the structure of which was determined by X-ray diffraction[8] (Fig. 1).

[*] Priv.-Doz. Dr. M. Driess, Prof. Dr. G. Huttner, Dipl.-Chem. N. Knopf, Dr. H. Pritzkow, Dr. L. Zsolnai
Anorganisch-chemisches Institut der Universität
Im Neuenheimer Feld 270, D-69120 Heidelberg (Germany)
Telefax: Int. code + (6221)564197

[**] This work was supported by the Deutsche Forschungsgemeinschaft (DFG Schwerpunktprogramm "Polyeder") and the Fonds der Chemischen Industrie.

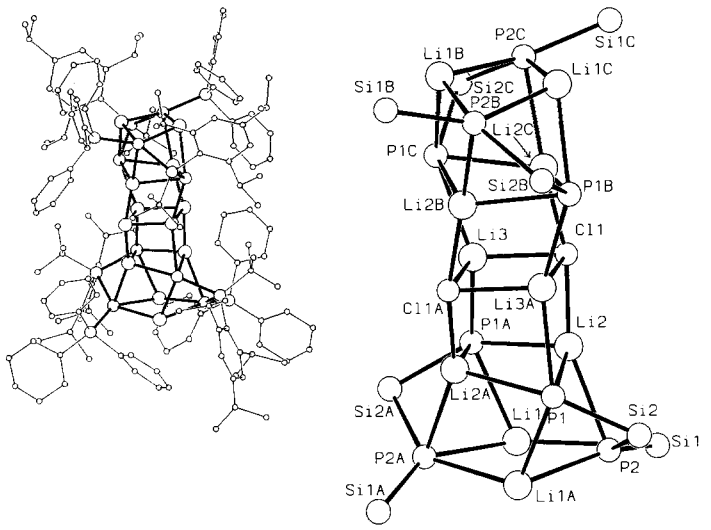
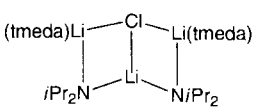


Fig. 1. Left: Crystal structure of **2**; right: framework of **2** shown without the organic groups. Selected distances [Å] and angles [°]: Cl1-Li3 2.20(3), Cl1-Li2 2.17(3), Li3-P1a 2.20(3), Li1-P 2.55–2.67(3), P1-Si2 2.237(6), P2-Si1 2.203(7), P2-Si2 2.252(6); Li2-Cl1-Li3 89.1(10), Li3-Cl1-Li3a 77(2), Cl1-Li3-Cl1a 103(2), Li1a-P1-Li2a 71.7(9), Li2-P1-Li2a 67.9(13), Si1-P2-Si2 129.0(3), Si1-P2-Li1a 146.9(7), Si2-P2-Li1a 83.1(6).

Compound **2** is a "dimer of dimers": two cluster molecules of **4** are linked to each other through a "middle deck" of $(LiCl)_2$. The phosphorus atoms are five- and six-coordinate, whereas the lithium centers have a distorted tetrahedral environment. The chlorine centers in the $(LiCl)_2$ middle deck are quasi-trigonal bipyramidally coordinated. Particularly noteworthy is the finding that the Li1 centers are each η^2 coordinated to a phenyl group of the $SiPh_3$ substituents. These interactions and the steric demand of the $SiPh_3$ group are probably responsible for the fact that no higher aggregation (attachment of LiCl and **4**) occurs. The Si–P (2.203(7)–2.252(6) Å) and Li–P distances (2.20(3) and 2.55–2.67(3) Å) lie in the normal range for lithium phosphanides. The Li–Cl distances are 2.20(3) (in the $(LiCl)_2$ ring) and 2.17(3) Å ("exocyclic" Li–Cl bonds) and are thus significantly shorter than in the lithium diisopropyllithium amide (LDA)–LiCl aggregate **5** (2.364–2.448(3) Å), in which the LiCl–"monomer" is complexed by two LDA units.[9]



5

The first lithium and sodium tris(phosphanides) **7** and **8**, respectively, form as colorless crystals by metalation of ethyl tris(triisopropylsilylphosphino)silane (**6**) with *n*BuLi and *n*BuNa, respectively, in toluene at −30 °C. Compound **6** is readily accessible from $EtSi(PH_2)_3$[10] in a one-pot reaction by lithiation with LDA in the mole ratio 1:3 in THF at −80 °C and subsequent reaction with three equivalents $iPr_3Si-OSO_2CF_3$. The trilithium derivative $EtSi(PHLi)_3$ decomposes above −30 °C, that is compounds of this type are stabilized substantially by the replacement of the H atoms at phosphorus by silyl groups.

Owing to the poor solubility of **7** and **8** in aliphatic and aromatic solvents it has so far not been possible to determine their structures in solution. Crystal structure analyses[8] revealed that in both cases dimeric aggregates with different topologies exist.

Whereas the donor-solvent-free **7** contains a $Si_2P_6Li_6$ framework in the form of a distorted rhombic dodecahedron (Fig. 2),

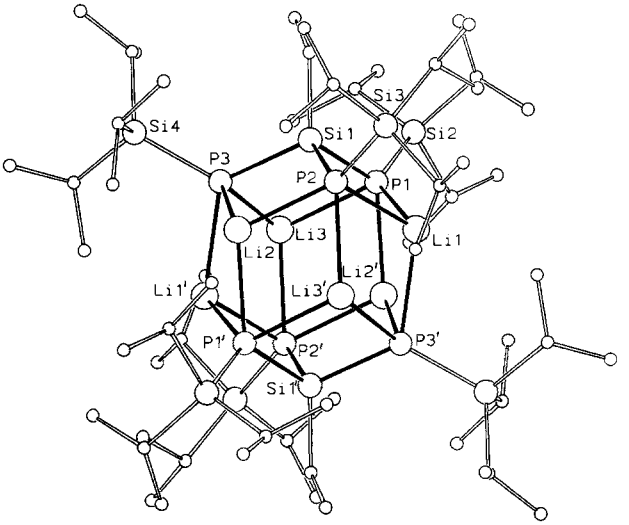


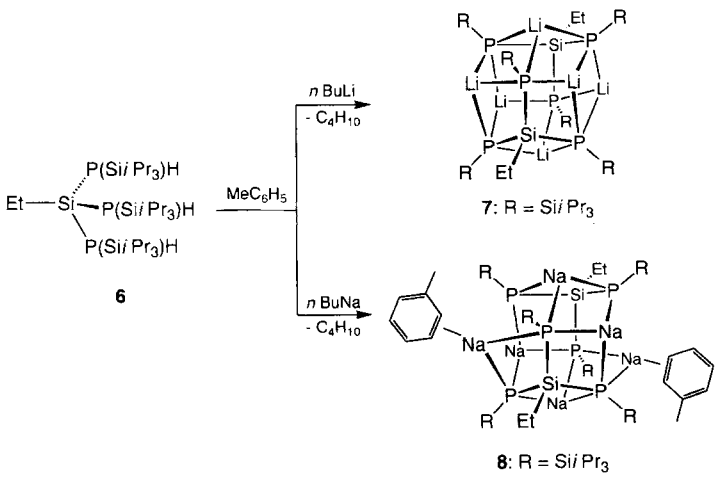
Fig. 2. Crystal structure of **7**. Selected distances [Å] and angles [°]: Li1-P1 2.464(5), Li1-P2 2.507(5), Li1-P3' 2.562(5), Li2-P2 2.449(5), Li2-P3 2.511(5), Li2-P1' 2.525(5), Li3-P3 2.452(5), Li3-P1 2.528(5), Li3-P2' 2.554(5), P1-Si2 2.236(1), P1-Si1 2.275(2), P2-Si1 2.271(2), P2-Si3 2.226(2); Si1-P1-Si2 123.89(6), Li1-P1-Si2 137.06(12), Li1-P1-Si1 81.71(13), Si1-P2-Si3 119.83(6), Li2-P2-Si3 140.38(13), Li2-P2-Si1 80.03(12), Si1-P3-Si4 120.95(6), Li3-P3-Si4 143.60(12), Li3-P3-Si1 83.48(13), P1-Si1-P3 103.36(7), P2-Si1-P3 106.66(5), P1-Si1-P2 104.62(6).

8, which is solvated with two molecules of toluene, has a $Si_2P_6Na_6$ framework with an open polyhedron structure (Fig. 3), although both compounds were prepared under the same reaction conditions. Compounds **7** and **8** have a center of symmetry. The structure of **8** can be described in a simplified way as a distorted drumlike $Si_2P_6Na_4$ framework, in which the atoms P1 and P3 (and P1′ and P3′) are bridged by the Na2 (Na2′) center. These Na bridging centers are each solvated with one molecule of toluene, which is surprisingly η^2 coordinated.

The structure of **7** is in accord with that of the homologous dimeric tris(lithioarsino)germane **9**[11] and that of the corresponding tris(lithioamino)silane.[12] The electronic saturation of the Li centers in **7** and **9** results from Li–P and Li–As multicenter bonding, respectively, as well as by Li-H-C interactions of adjacent methyl groups of the $SiiPr_3$ groups. The five-coordi-

$[\{t\text{BuGe}[\text{As}(\text{SiiPr}_3)\text{Li}]_3\}_2]$ **9**

nate P atoms reveal a distorted tetragonal-pyramidal coordination; the Li–P distances are 2.449–2.562(5) Å, that is they correspond with those in lithium disilylphosphanides.[3,4]



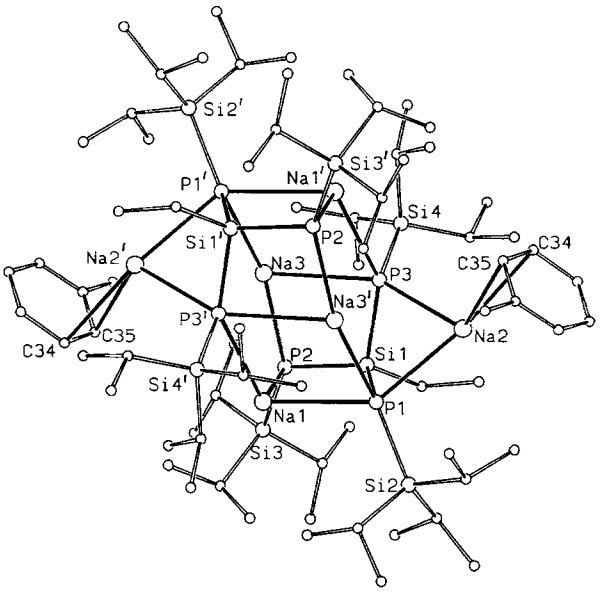


Fig. 3. Crystal structure of **8**. Selected distances [Å] and angles [°]: Na1-P1 2.878(2), Na1-P2 2.805(2), Na1-P3' 3.012(2), Na2-P1 2.858(2), Na2-P3 2.840(2), Na3-P1' 2.823(2), Na3-P2 2.778(2), Na3-P3 2.935(2), Na3-P3' 3.357(2), Si1-P 2.249–2.290(2), *i*PrSi-P 2.226–2.239(1), Na-Na 3.359–3.889(3); Si1-P1-Si2 122.48(5), Si1-P2-Si3 120.86(5), Si1-P3-Si4 113.87(5), P1-Si1-P2 116.20(5), P1-Si1-P3 95.04(6), P2-Si1-P3 105.69(6).

The structure of **8** results from the opening of two Na–P edges in the hypothetical $Si_2P_6Na_6$ rhombic dodecahedron by two molecules of toluene as donor. Toluene is known to be a relatively weak donor to alkali metal centers. Therefore why does **8** prefer an open polyhedron structure to the rhombic dodecahedral structure? The reason for this lies primarily in the differences in the sizes of lithium and sodium: the hypothetical $Si_2P_6Na_6$ rhombic dodecahedral framework has a pronounced ring strain, owing to the large differences between the Si1–P and Na–P distances (ca. 2.2 Å vs. 2.8 Å) and the restrictive, tripodal geometry of the SiP_3 increment, which is predestined to lead to an opening of the polyhedron. In contrast, the corresponding differences in the distances in **7** (2.236–2.275(2) Å vs. 2.449–2.562(5) Å) and in **9**[11] (Ge–As: 2.442–2.448(2) Å vs. Li–As: 2.52(2)–2.62(1) Å) are obviously such that these compounds are also generated in the donor-solvent-free form in ethereal solvents. The three unequivalent kinds of Na in **8** are coordinatively unsaturated because of the particularly bulky ligand spheres: With the exception of Na2, the Na centers are bound to three P atoms and have close contacts with H atoms of methine and methyl groups (Na-H-C interactions, Na–H distances: 2.44–2.54 Å) of adjacent $SiPr_3$ groups; in contrast, the Na2 center achieves its electronic stabilization primarily by bonding to two P and two toluene-C atoms. The Na–C distances are 2.882(5) and 2.968(5) Å. Similar Na–C distances were found in other complexes with π coordination of Na centers to arene ligands.[13]

At present we are testing whether molecular alkali metal oligophosphanides such as **4**, **7**, and **8** can be extended to give host lattices.

Experimental Procedure

2: **4** (780 mg, 0.65 mmol) in boiling toluene (ca. 50 mL) was treated with an excess of freshly prepared, anhydrous LiCl. After filtration (warm, GIV frit) to remove LiCl, the clear solution was concentrated to about 10 mL and crystallized at 0 °C. In this way **2** was isolated in a monocrystalline form. Yield: 430 mg (0.17 mmol, 55%)

4: A solution of **1** (2.33 g, 6.58 mmol) in toluene (50 mL) was lithiated with one equivalent *n*BuLi at −30 °C; the clear yellow solution was allowed to warm to room temperature and treated with a solution of Ph_3SiCl (1.93 g, 6.58 mmol) in toluene. The LiCl formed was filtered (GIV frit) off and the resulting clear solution was treated with two equivalents of *n*BuLi. Thereafter, the pale yellow solution was warmed to about 60 °C for 2 h to complete the conversion. Subsequently the solvent was removed in vacuum and the solid residue was washed with hexane (3 × 20 mL). Recrystallization afforded colorless, analytically pure **4**. Yield: 3.57 g (2.86 mmol, 87%).

6: $EtSi(PH_2)_3$ (0.51 g, 3.3 mmol) in THF (10 mL) was treated with LDA (10 mmol; freshly prepared from $HNiPr_2$ (1 g) and *n*BuLi (4 mL, 2.5 M solution in hexane) in THF (10 mL)) at −80 °C. After 1 h iPr_3SiOTf (3 g, 10 mmol) dissolved in THF (5 mL) was added to this solution and the mixture was allowed to warm to room temperature. The solvent was then removed under vacuum (10^{-2} Torr) and the residue was taken up in hexane (50 mL), filtered (to remove LiOTf), and the solvent was again removed. Yield: 1.8 g (2.8 mmol, 85%) of a colorless, viscous oil. ^{31}P NMR: $\delta = -236.0$ (d, $^1J(P,H) = 200$ Hz); ^{29}Si NMR: $\delta = 22.0$ (d, $SiPr_3$, $^1J(Si,P) = 42$ Hz), 9.5 (q, SiEt, $^1J(Si,P) = 66$ Hz); EI MS (70 eV): *m/z* (%): 624 (6) $[M^+]$, 581 (14) $[M^+ - iPr]$, 467 (34) $[M^+ - SiPr_3]$, 435 (100) $[M^+ - PHSiPr_3]$.

7: **6** (1 g, 1.6 mmol) was dissolved in toluene (50 mL) and treated with *n*BuLi (1.9 mL, 2.5 M solution in hexane) at −20 °C. After 8 h at room temperature the resulting suspension was heated (ca. 50 °C) until the solution cleared. Subsequent gradual cooling to room temperature afforded **7** as colorless crystals. Yield: 0.9 g (1.4 mmol, 88%).

8: **6** (1 g, 1.6 mmol) dissolved in toluene (10 mL) was added to a suspension of *n*BuNa (0.38 g, 4.8 mmol) in toluene (40 mL) at −20 °C and the mixture was stirred for 8 h at room temperature. The resulting suspension was heated until the solution cleared. Slow cooling to room temperature afforded colorless crystals. Yield 1 g (1.4 mmol, 88%).

Received: August 31, 1994
Revised version: October 12, 1994 [Z 7075/Z 7280 IE]
German version: *Angew. Chem.* **1995**, *107*, 354

Keywords: clusters · lithium compounds · phosphorus compounds

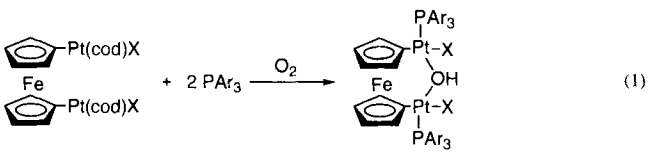
[1] Review: R. E. Mulvey, *Chem. Soc. Rev.* **1991**, *20*, 167.
[2] R. A. Jones, S. U. Koschmieder, C. M. Nunn, *Inorg. Chem.* **1987**, *26*, 3610; G. Becker, H. M. Hartmann, W. Schwarz, *Z. Anorg. Allg. Chem.* **1989**, *577*, 1.
[3] Review: G. Becker, B. Eschbach, D. Käshammer, O. Mundt, *Z. Anorg. Allg. Chem.* **1994**, *620*, 29, and references therein.
[4] G. Fritz, W. Hölderich, *Z. Anorg. Allg. Chem.* **1986**, *422*, 104; E. Hey, P. B. Hitchcock, M. F. Lappert, A. K. Rai, *J. Organomet. Chem.* **1987**, *325*, 1; E. Hey, C. L. Raston, B. W. Skelton, A. H. White, *ibid.* **1989**, *362*, 1; E. Hey-Hawkins, E. Sattler, *J. Chem. Soc. Chem. Commun.* **1992**, 775; F. Uhlig, S. Gremler, M. Dargatz, M. Scheer, E. Herrmann, *ibid.* **1991**, *606*, 105; M. Westerhausen, W. Schwarz, *J. Organomet. Chem.* **1993**, *463*, 51; see also ref. [2].
[5] M. Driess, M. Reisgys, H. Pritzkow, *Chem. Ber.* **1991**, *124*, 1931.
[6] ^{31}P NMR: $\delta = -163$ (br., PH, $^1J(P,H) = 170$ Hz), −182 (br., $PSiPh_3$); ^7Li NMR: $\delta = 0.60$ (br.), 0.45 (br.).
[7] M. Driess, unpublished.
[8] **2**: tetragonal, $P\bar{4}2c$, $a = 20.89(1)$, $c = 23.09(2)$ Å, $V = 10074$ Å^3, $Z = 2$, four-circle diffractometer (R3m/V, $Mo_{K\alpha}$ radiation, ω scan, $T = 200$ K), $2\theta_{max} = 47°$, 4512 reflections (2429 observed, $I > 2\sigma(I)$), refinement on F^2 (all data) [14], 433 parameters, $R1 = 0.129$, $wR2 = 0.423$ (all data). **7**: triclinic, $P\bar{1}$, $a = 13.314(7)$, $b = 14.101(7)$, $c = 14.162(7)$ Å, $\alpha = 99.73(3)$, $\beta = 114.86(3)$, $\gamma = 113.29(3)°$, $V = 2029$ Å^3, $Z = 1$, four-circle diffractometer ($Mo_{K\alpha}$ radiation, ω scan, room temperature), $2\theta_{max} = 50°$, 7136 reflections (5683 observed, $I > 2\sigma(I)$), refinement on F^2 (all data) [14], 414 parameters, $R1 = 0.046$, $wR2 = 0.132$. **8**: triclinic, $P\bar{1}$, $a = 13.182(7)$, $b = 14.512(7)$, $c = 14.788(8)$ Å, $\alpha = 62.75(4)$, $\beta = 69.95(4)$, $\gamma = 75.03(4)°$, $V = 2345$ Å^3, $Z = 1$, four-circle diffractometer ($Mo_{K\alpha}$ radiation, ω scan, $T = 218$ K), $2\theta_{max} = 55°$, 10085 reflections (8576 observed, $I > 2\sigma(I)$), refinement on F^2 (all data) [14], 440 parameters, $R1 = 0.044$, $wR2 = 0.121$. Further details of the crystal structure investigations may be obtained from the Fachinformationszentrum Karlsruhe, D-76344 Eggenstein-Leopoldshafen (Germany) on quoting the depository numbers CSD-401328 (**2**), 401329 (**7**), 401330 (**8**).
[9] F. S. Mair, W. Clegg, P. A. O'Neil, *J. Am. Chem. Soc.* **1993**, *115*, 3388.
[10] M. Baudler, G. Scholz, W. Oehlert, *Z. Naturforsch. B* **1989**, *44*, 627.
[11] M. Driess, L. Zsolnai, G. Huttner, *Angew. Chem.* **1993**, *105*, 1549; *Angew. Chem. Int. Ed. Engl.* **1993**, *32*, 1439.
[12] D. J. Brauer, H. Bürger, G. R. Liewald, J. Wilke, *J. Organomet. Chem.* **1985**, *287*, 305; *ibid.* **1986**, *308*, 119; M. Veith, A. Spaniol, J. Pöhlmann, F. Gross, V. Huch, *Chem. Ber.* **1993**, *126*, 2625.
[13] Review: E. Weiss, *Angew. Chem.* **1993**, *105*, 1565; *Angew. Chem. Int. Ed. Engl.* **1993**, *32*, 1501, and references therein; B. Köster, W. Schüssler, R. Boese, D. Bläser, *Chem. Ber.* **1991**, *124*, 2259.
[14] G. M. Sheldrick, SHELXL-93, Universität Göttingen 1993.

Reactions of 1,1′-Ferrocenediylbis{chloro-[(1,2,5,6-η)-1,5-cyclooctadiene]}diplatinum with Triarylphosphane and Molecular Oxygen**

Toshiya Yoshida, Shigeaki Tanaka, Tomohiro Adachi, Toshikatsu Yoshida, Kiyotaka Onitsuka, and Kenkichi Sonogashira*

In the chemistry of transition metal complexes containing metallocenes, intramolecular metal–metal interactions involving the metal atom of the metallocene have become one of the most interesting topics in recent years.[1] As part of our studies of ferrocenyl transition metal complexes[2] we have investigated the reactivities of the 1,1′-ferrocenediyldiplatinum complexes $[\{C_5H_4Pt(cod)X\}_2Fe]$ (X = Cl, Br; cod = cyclooctadiene) (**1**).[3] These complexes react with two mole equivalents of PAr_3 (Ar = Ph, p-$CH_3OC_6H_4$) and oxygen to give the novel paramagnetic μ-hydroxo complexes **2**. We wish to report here the chemistry of these and related complexes.

The μ-hydroxo-1,1′-ferrocenediyldiplatinum complexes **2** were prepared in yields of 46 to 62% as air-stable green crystals by ligand exchange reaction of the corresponding 1,1′-ferrocenediyldiplatinum complexes **1**, in which each Pt atom has a cyclooctadiene ligand, with two equivalents of PAr_3 in CH_2Cl_2 in the presence of molecular oxygen at room temperature for 6 h [Eq. (1)].[4]



(1)

1a X = Cl
1b X = Br

2a X = Cl, Ar = Ph
2b X = Br, Ar = Ph
2c X = Cl, Ar = p-$C_6H_4OCH_3$
2d X = Br, Ar = p-$C_6H_4OCH_3$

The IR spectrum of complex **2a** shows an absorption at 3440 cm^{-1} due to the stretching of the OH group.[5] In the ^1H NMR spectrum of **2a** the characteristic broad signal of the μ-OH unit appears at much higher field ($\delta = -23.5$) than those of other μ-hydroxo complexes,[6] and disappeared upon addition of a few drops of D_2O. The broad signals attributed to the cyclopentadienyl protons are observed at $\delta = 36.6$ and 26.6 owing to the paramagnetism of the ferrocenediyl group,[7] which was confirmed by the detection of a paramagnetic resonance in the ESR spectrum of **2a**. The cyclic voltammogram of **2a** in CH_2Cl_2 shows a reversible reduction peak ($E_{1/2} = -0.62$ V) ascribed to the reduction of Fe^{III} to Fe^{II} accompanied by decomposition to give an unknown product ($E_a = -0.37$ V) (Fig. 1). In an effort to obtain information about the origin of the μ-hydroxo group, we carried out several experiments. Treatment of **1a** with one equivalent of triphenylphosphane per platinum atom in thoroughly degassed and anhydrous solution did not

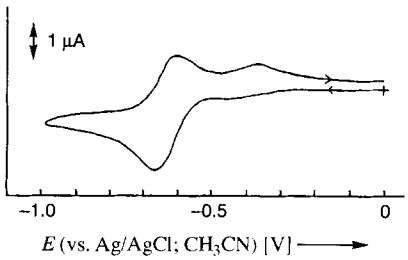
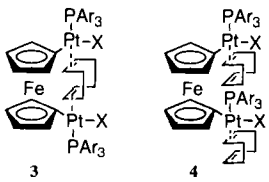


Fig. 1. Cyclic voltammogram of **2a** (10^{-3} M in CH_2Cl_2); scan rate 100 mVs^{-1}, supporting electrolyte tetrabutylammonium hexafluorophosphate (10^{-1} M), working electrode Pt disk (2 mm diameter).

lead the formation of **2a**. ^1H and ^{31}P NMR spectra of this reaction mixture indicated the presence of reactive diamagnetic intermediates such as **3** and **4**. Complex **2a** was not obtained when H_2O was added to this system, but it was generated by the introduction of dry air. These results suggest that the reactive intermediate is easily oxidized by molecular oxygen. Thus, we believe that the oxygen atom of complex **2** arises from O_2, though we have no indications of the origin of the hydrogen atom of the μ-hydroxo group.



A single-crystal X-ray structure analysis of **2c**[8] confirms the presence of an OH group bridging the two platinum atoms in a bent fashion. The unit cell contains two independent molecules with essentially the same structure, one of which is shown in Figure 2. The coordination around each platinum atom is square

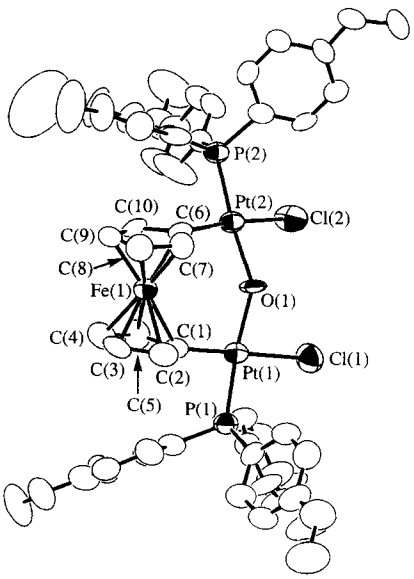


Fig. 2. Crystal structure of **2a**. Selected bond lengths [Å] and angles [°]: Pt(1)–Cl(1) 2.390(5), Pt(1)–P(1) 2.224(5), Pt(1)–O(1) 2.127(9), Pt(1)–C(1) 2.00(2), Pt(2)–Cl(2) 2.386(5), Pt(2)–P(2) 2.241(5), Pt(2)–O(1) 2.13(1), Pt(2)–C(6) 2.01(2); Cl(1)-Pt(1)-O(1) 83.5(3), P(1)-Pt(1)- O(1) 172.6(3), O(1)-Pt(1)-C(1) 93.0(5), Cl(2)-Pt(2)-O(1) 82.7(3), P(2)-Pt(2)-O(1) 177.3(3), O(1)-Pt(2)-C(6) 91.2(6), Pt(1)-O(1)- Pt(2) 138.9(5).

planar, and the dihedral angle between the two Pt coordination plane is 146.9°. These planes form dihedral angles of 87.1 and 63.8° with the adjacent cyclopentadienyl ligands. The roughly equal Pt–O bond lengths (2.127(9) and 2.13(1) Å) are longer

[*] Prof. Dr. K. Sonogashira, T. Yoshida, S. Tanaka, Dr. K. Onitsuka
Department of Applied Chemistry, Faculty of Engineering
Osaka City University, Sumiyoshi-ku, Osaka 558 (Japan)
Telefax: Int. code + (6)605-2769

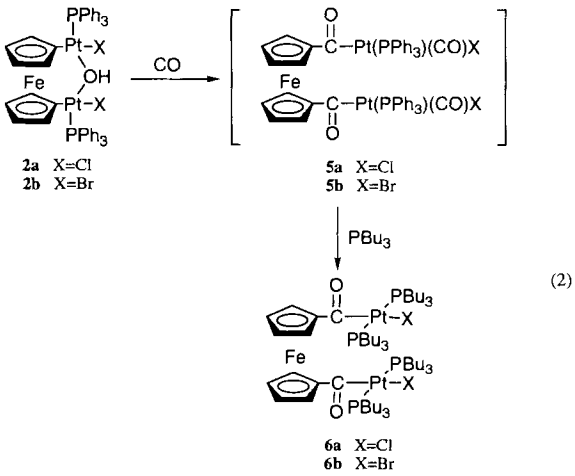
T. Adachi, Prof. Dr. T. Yoshida
Department of Chemistry, Faculty of Integrated Arts and Sciences
University of Osaka Prefecture (Japan)

[**] This work was supported by the the Ministry of Education, Science and Culture, Japan (Grant-in-Aid for Scientific Research no. 05236106 on Priority Area "Reactive Organometallics"). We thank Prof. A. Ichimura, Osaka City University, for helpful discussion and measurement of cyclic voltammogram.

 © VCH Verlagsgesellschaft mbH, D-69451 Weinheim, 1995 0570-0833/95/0303-0319 $ 10.00+.25/0

than that of $[NBu_4][\{Pt(C_6F_5)_2(\mu\text{-}OH)\}_2]$ (2.07(2) Å)[9] but agree with the average value found in $[\{Pt(PEt_3)_2(\mu\text{-}OH)\}_2]$ (2.130 Å).[10] The Pt-O-Pt angle of 138.9(5)° is significantly larger than those of the other μ-hydroxodiplatinum complexes (92(2)–101.4(6)°).[9, 10] The Pt–C bond lengths of 2.00(2) and 2.01(2) Å are within the range expected for a normal Pt–C bond in a σ-ferrocenylplatinum complex.[11] The Pt–Fe distances of 3.728(3) and 3.725(3) Å and the Pt–Pt distance of 3.990(2) Å indicate the absence of any direct M–M interaction. The separation of 3.49(1) Å between the oxygen atom and the iron atom does not reflect any bonding interaction. The ferrocenediyl group has a staggered conformation, and the dihedral angle between the two cyclopentadienyl ligands is 8.5°.

The reaction of **2a** with CO (30 kg cm^{-2}) in dichloromethane at room temperature gave the brown-red solid **5a**. Although we were not able to purify **5a**, its structure was assigned based on IR and ^{1}H NMR spectra. Subsequent treatment of **5a** with excess tri(*n*-butyl)phosphane led to the formation of stable orange crystals of **6a** [Eq. (2)]. In the IR spectrum of **6a** a CO stretching



2a X=Cl
2b X=Br

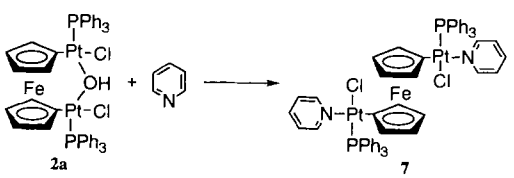
5a X=Cl
5b X=Br

6a X=Cl
6b X=Br

(2)

band at 1600 cm^{-1} indicates that CO inserted into the Pt–C bonds of **2a**. ^{1}H and ^{13}C NMR spectra reveal that the two cyclopentadienyl ligands are equivalent, and the *trans* arrangement of the Pt moieties is supported by a singlet in the ^{31}P NMR spectrum and the ^2J(P,C) coupling of the CO signal in the ^{13}C NMR spectrum. These data are consistent with the structure of **6a** which is produced by the insertion of one molecule of CO into each Pt–C bond of **2a**. The analogous reaction of **2b** gave insertion product **6b**.

When complex **2a** was treated with pyridine, the red complex **7** was isolated [Eq. (3)]. The structure of **7** determined by X-ray



2a **7**

(3)

crystallography is shown in Figure 3.[8] Apparently pyridine has cleaved the hydroxo bridge in **2a** following reduction of the complex; the pyridine ligand at each platinum atom is *trans* to the cyclopentadienyl ligand. The fate of the bridging hydroxo group is not known. The Pt atoms have the expected square-planar coordination with Pt–C σ bonds to the 1,1′-ferrocenediyl moieties and coordination to PPh_3, pyridine, and Cl ligands. The 1,1′-ferrocenediyl group adopts an eclipsed conformation with the Pt planes in a transoid orientation, which minimizes steric interaction across the ferrocene molecule. The tilt angle between the two cyclopentadienyl rings is 1.6°. The bond lengths and angles lie in the expected range.

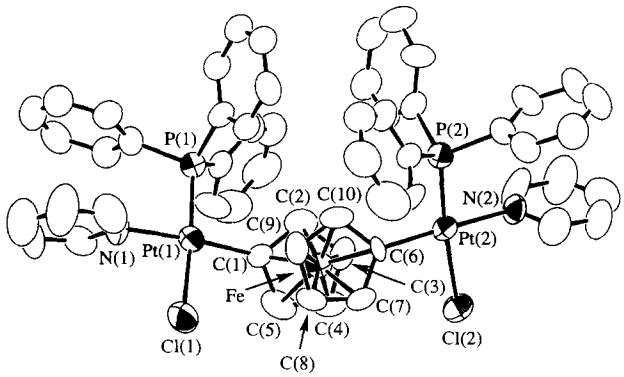


Fig. 3. Crystal structure of **7**. Selected bond lengths [Å]: Pt(1)–C(1) 2.02(1), Pt(1)–Cl(1) 2.362(4), Pt(1)–P(1) 2.216(4), Pt(1)–N(1) 2.15(1), Pt(2)–C(6) 2.03(1), Pt(2)–Cl(2) 2.361(4), Pt(2)–P(2) 2.208(4), Pt(2)–N(2) 2.15(1).

In conclusion, we have synthesized a novel paramagnetic μ-hydroxo 1,1′-ferrocenediyldiplatinum complex **2**, in which the 1,1′-ferrocenediyl group functions not only as a bridging ligand fixing the two platinum atoms at an appropriate distance but also as an electron pool. Complexes **2** are reduced by CO and pyridine to give diamagnetic complexes **6** and **7**, respectively. We are now exploring further reactions of these complexes.

Experimental Procedure

2a: To a solution of **1a** (101 mg, 0.117 mmol) in CH_2Cl_2 (20 mL) was added PPh_3 (63 mg, 0.240 mmol). The reaction mixture was stirred at room temperature for 6 h, during which time the color gradually turned from red to green. After removal of the solvent, the green residue was dissolved in 1,2-dichloroethane. Slow evaporation of this solution provided green crystals of complex **2a** (100 mg, 62%). M.p. 235–240 °C (decomp); IR (Nujol): $\tilde{\nu}$ = 3440 cm^{-1} (OH); ^{1}H NMR (CD_2Cl_2): δ = 36.56 (br, 4H; C_5H_4), 26.59 (br, 4H; C_5H_4), 12.80 (br, 12H; Ph), 10.89 (br, 12H; Ph), 10.15 (br, 6H; Ph), −23.49 (br, 1H; OH); ^{31}P NMR (CD_2Cl_2, PPh_3): δ = −84.88 (s); MS (FAB): *m/z*: 1168 $[M - OH]^+$; UV/Vis (CH_2Cl_2): λ_{max} ($\varepsilon \times 10^{-2}$) = 774 (6.05), 637 (4.03), 406 nm (27.0).

6a: A solution of **2a** (48 mg, 0.0347 mmol) in 10 mL of CH_2Cl_2 was placed in a 100 mL autoclave, which was then charged with CO (30 kg cm^{-2}). The reaction mixture was allowed to stand for 24 h at room temperature. Then tri(*n*-butyl)phosphane (70 mL, 0.281 mmol) was added and the solution stirred for 4 h at room temperature. The solvent was removed, and the residue was purified by column chromatography on silica gel (15 mm × 100 mm) with $CHCl_3$ as eluent. Recrystallization from hexane gave orange crystals of **6a** (19 mg, 37%). M.p. 131–132 °C; IR (KBr): $\tilde{\nu}$ = 1600 cm^{-1} (CO); ^{1}H NMR ($CDCl_3$): δ = 4.61 (s, 4H; C_5H_4), 4.23 (s, 4H; C_5H_4), 1.83 (br, 12H; CH_2), 1.67 (br, 12H; CH_2), 1.49–1.39 (m, 48H; CH_2), 0.92 (t, J = 7.3 Hz, 36H; CH_3). ^{13}C NMR ($CDCl_3$): δ = 213.62 (t, ^2J(P,C) = 5.3 Hz; CO); 97.92 (t, ^3J(P,C) = 4.2 Hz; C_5H_4 *ipso*), 70.54, 69.49 (C_5H_4), 25.97, 24.23, 21.72, 13.81 (PBu_3); ^{31}P NMR ($CDCl_3$, PPh_3): δ = 11.72 (J(Pt,P) = 3034 Hz).

7: A solution of **2a** (35 mg, 0.0295 mmol) in 10 mL of pyridine was stirred for 48 h at room temperature. The green solution gradually turned orange, and then a red orange precipitate (35 mg, 90%) was obtained. M.p. 237–241 °C (decomp).

Received: July 18, 1994
Revised version: October 18, 1994 [Z 7139 IE]
German version: *Angew. Chem.* **1995**, *107*, 351

Keywords: oxygen activation · phosphanes · platinum compounds · sandwich complexes

[1] D. Seyferth, B. W. Hames, T. G. Rucker, M. Cowie, R. S. Dickson, *Organometallics* **1983**, *2*, 472; S. Akabori, T. Kumagai, T. Shirashige, S. Sato, K. Kawazoe, C. Tamura, M. Sato, *ibid.* **1987**, *6*, 526; M. I. Bruce, P. A. Humphrey, O.bin Shawkataly, M. R. Snow, E. R. T. Tiekink, W. R. Cullen, *ibid.* **1990**, *9*, 2910; W. R. Cullen, S. J. Rettig, T.-C. Zheng, *ibid.* **1992**, *11*, 277; M. Sato, K. Suzuki, S. Akaori, *Chem. Lett.* **1987**, 2239; M. Sato, M. Sekino, S. Akabori, *J. Organomet. Chem.* **1988**, *344*, C31; M. Sato, M. Sekino, *ibid.* **1993**, *444*, 185; C. E. L. Headford, R. Mason, P. R. Ranatunge-Bandarage, B. H. Robinson, J. Simpson, *J. Chem. Soc. Chem. Commun.* **1990**, 601; H. Wadepohl, W. Galm, H. Pritzkow, A. Wolf, *ibid.* **1993**, 1459; H. Wadepohl, W. Galm, H. Pritzkow, A. Wolf, *Angew. Chem.* **1992**, *104*, 1050; *Angew. Chem. Int. Ed. Engl.* **1992**, *31*, 1058.

[2] S. Tanaka, T. Yoshida, T. Adachi, T. Yoshida, K. Onitsuka, K. Sonogashira, *Chem. Lett.* **1994**, 877.

[3] Z. Dawoodi, C. Eaborn, A. Pidcock, *J. Organomet. Chem.* **1979**, *170*, 95.

[4] J. W. Gilje, H. W. Roesky, *Chem. Rev.* **1994**, *94*, 895.

[5] G. W. Bushnell, K. R. Dixon, R. G. Hunter, J. J. McFarland, *Can. J. Chem.* **1972**, *50*, 3694; R. E. Fakley, A. Pidcock, *J. Chem. Soc. Dalton Trans.* **1977**, 1444; S. Wimmer, P. Castan, F. L. Wimmer, N. P. Johnson, *ibid.* **1989**, 403.

[6] G. López, J. Ruiz, G. García, J. M. Martí, G. Sánchez, J. García, *J. Organomet. Chem.* **1991**, *412*, 435; V. V. Grushin, H. Alper, *Organometallics* **1993**, *12*, 1890.

[7] U. Kölle, J. Kossakowski, N. Klaff, L. Wesemann, U. Englert, G. E. J. Herberich, *Angew. Chem.* **1991**, *103*, 732; *Angew. Chem. Int. Ed. Engl.* **1991**, *30*, 690; T.-Y. Dong, H.-M. Lin, M.-Y. Hwang, T.-Y. Lee, L.-H. Tseng, S.-M. Peng, G.-H. Lee, *J. Organomet. Chem.* **1991**, *414*, 227.

[8] Crystal data for **2c**: $0.80 \times 0.60 \times 0.10$ mm, monoclinic, space group $P2_1/a$, $a = 18.36(1)$, $b = 17.64(2)$, $c = 38.313(8)$ Å, $\beta = 97.04(3)^\circ$, $V = 12311(16)$ Å^3, $Z = 8$, $\rho_{calcd} = 1.608$ g cm^{-3}, $\mu(Mo_{K\alpha}) = 51.06$ cm^{-1}, ω-2θ scan, $6.0^\circ < 2\theta < 50.1^\circ$. All non-hydrogen atoms were refined anisotropically by full matrix least squares refinement against $|F|^2$; $R = 0.040$ and $Rw = 0.045$ for 8717 reflections with $I > 6.0\sigma(I)$ out of 17916 unique reflections (reflection/parameter ratio = 6.96), empirical absorption correction using DIFABS [12], GOF = 3.07, residual electron density = −0.89 to 1.04 e Å^{-3}. For **7**: $0.70 \times 0.30 \times 0.10$ mm, monoclinic, space group $P2_1/c$, $a = 10.22(2)$, $b = 24.907(7)$, $c = 22.175(9)$ Å, $\beta = 96.00(7)^\circ$, $V = 5614(11)$ Å^3, $Z = 4$, $\rho_{calcd} = 1.711$ g cm^{-3}, $\mu(Mo_{K\alpha}) = 54.73$ cm^{-1}, ω-2θ scan, $6.0^\circ < 2\theta < 45.1^\circ$. All non-hydrogen atoms were refined anisotropically by full matrix least squares refinement against $|F|^2$; $R = 0.038$ and $Rw = 0.041$ for 4449 reflections with $I > 9.0\sigma(I)$ out of 7564 unique reflections (reflection/parameter ratio = 7.10), empirical absorption correction using DIFABS [12], GOF = 3.17. Further details of the crystal structure may be obtained from the Director of the Cambridge Crystallographic Centre, 12 Union Road, GB-Cambridge CB2 1EZ (UK), on quoting the full journal citation.

[9] G. López, J. Ruiz, G. García, C. Vicente, J. M. Martí, J. A. Hermoso, A. Vegas, M. Martínez-Ripoll, *J. Chem. Soc. Dalton Trans.* **1992**, 53.

[10] G. W. Bushnell, *Can. J. Chem.* **1978**, *56*, 1773.

[11] R. E. Hollands, A. G. Osborne, R. H. Whiteley, C. J. Cardin, *J. Chem. Soc. Dalton Trans.* **1985**, 1527.

[12] N. Walker, D. Stuart, *Acta Crystallogr. Sect. A* **1983**, *39*, 158.

Complexes from Polyazacyclophanes, Fluorescence Indicators, and Metal Cations—An Example of Allosterism through Ring Contraction**

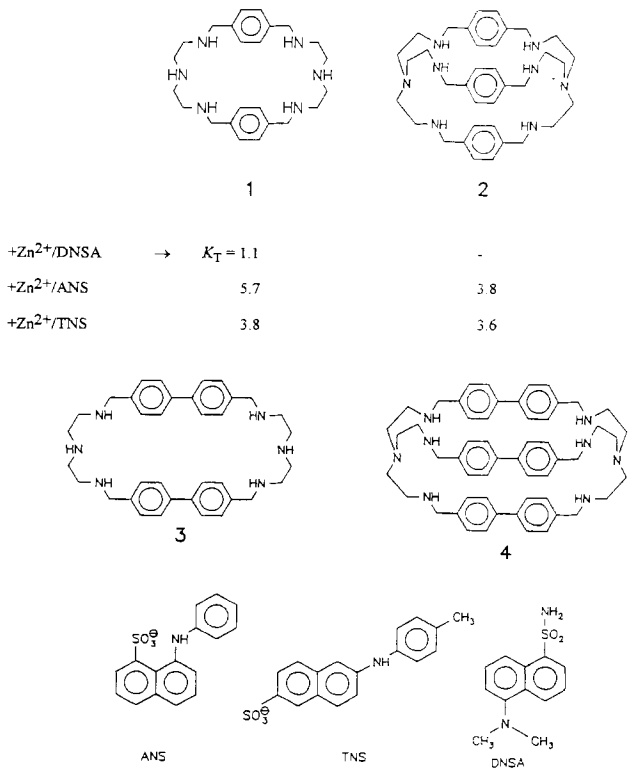
Ralf Baldes and Hans-Jörg Schneider*

Synthetic host–guest systems can be relatively easily designed to have a receptor containing several conformationally strongly coupled binding sites that may also bind organic substrates.[1] We report here on ternary complexes in which the cavity for a lipophilic guest molecule is fitted spacially by *contraction* of the hollow space, which is initiated by the binding of metal cations.

[*] Prof. Dr. H.-J. Schneider, Dipl.-Chem. R. Baldes
Fachrichtung Organische Chemie der Universität des Saarlandes
D-66144 Saarbrücken (Germany)
Telefax: Int. code + (681)4105

[**] Supramolecular Chemistry, Part 51. This work was supported by the Deutsche Forschungsgemeinschaft and the Fonds der Chemischen Industrie. We would like to thank the referees for their valuable suggestions regarding references. Part 50: H.-J. Schneider, M. Wang, *J. Org. Chem.* **1994**, *59*, 7473.

Molecular mechanics simulations (force-field CHARMm[3]) of polyazacyclophanes **1** and **2** (Scheme 1)—obtained by published procedures[2]—indicate an almost spherical shape with a wide cavity in the absence of complexing metal cations (Fig. 1a). When metal ions, for example zinc ions, are bound to the ethylene diamine moieties, the cavities become smaller and more strongly anisotropic (Fig. 1b), thus allowing an optimal enclosure of guest molecules of the naphthalene type (Scheme 2, Fig. 1c). The potential energy necessary for the formation of the smaller cavity is provided by the high stability constants[4] of metal complexes of the corresponding polyamine ligands. Unfortunately, the complexes of the new derivatives of **1** and **2** with biphenyl instead of benzene moieties (**3** and **4**, Scheme 1) are too insoluble in water, and we can only discuss here the allosteric properties of the well-known[2] polyazacyclophanes **1** and **2**. Because of the low solubility of these systems, the complexation reactions could not be monitered by NMR spectroscopy. However, using fluorescence spectroscopy and suitable indicators[5] (ANS (8-anilinonaphthalene-1-sulfonic acid), TNS (6-*p*-toluidino)-2-naphthalenesulfonic acid), DNSA (5-dimethylaminonaphthalene-2-sulfonic acid), Scheme 1), the expected cooperative effects could be quantified. At the same time this presented new possibilities for the detection of, for example, zinc ions in aqueous solution.



Scheme 1. Structures of the host ligands L and guest molecules G (fluorescence indicators) and their equilibrium constants (in units of 10^{-3} M^{-1}; water, 25 °C) for the ternary complex L·G·Zn^{2+}.

The addition of a solution of **1** (5×10^{-3} M, at pH 7.0 present as $\mathbf{1} \times 4H^+$) with $ZnCl_2$ (5×10^{-3} M) to a solution of the fluorescent dye DNSA (10^{-5} M) in water at pH 7.0 led to a considerable increase in the fluorescence emission F; from the saturation curve (Fig. 2) a constant $K_T = 1.1 \times 10^3$ M^{-1} with a scattering of about 8% could be calculated for the formation of the ternary complex L·G·M (**1**·DNSA·Zn^{2+}) from a nonlinear fitting

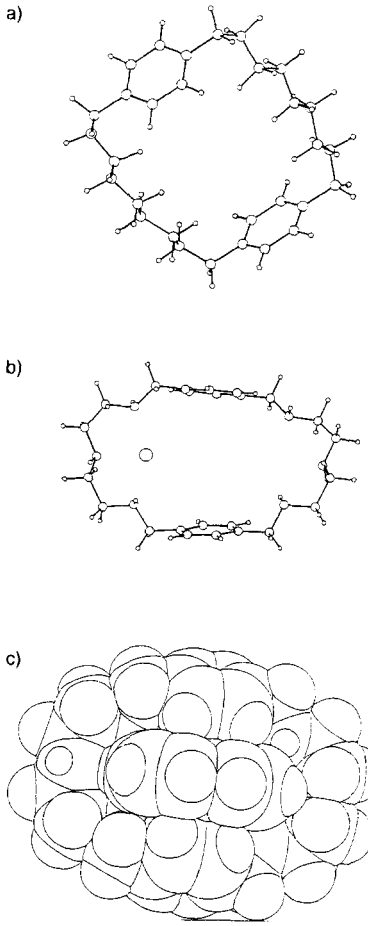


Fig. 1. Force-field-optimized (CHARMm [3]) structure of a) host **1** without a metal ion, b) **1** with a zinc ion, c) the complex of **1**·ANS·Zn^{2+} as space-filling model—the enclosed naphthalene ring is visible in the cavity.

on the basis of a 1:1 model. When only **1** was added, the increase of F was, at most, 4% compared to the effect obtained from the formation of the ternary complex; nevertheless, this was taken into account in the calculation on the basis of linear calibration curves ($r > 0.99$), along with the slight decrease in the concentration of DNSA during the titration. Control experiments showed that both Zn^{2+} and **1** alone have a negligible effect on the F values of DNSA, which implies that the complexation of DNSA in the absence of the metal ion acting as an allosteric effector is immeasurably small. On the basis of the increase in F from **1** and DNSA alone, which hardly exceeds the statistical error, the maximum value of the formation constant of the binary complex in the absence of metal ions can be estimated to be below $K_B = 5-10\,M^{-1}$. Thus, the value of the relative constant of the ternary complex of at least $K_{rel} = K_T/K_B = 10^2$ demonstrates a greater level of cooperation than in many other synthetic systems.[1] A distinctly smaller value is usually found for allosteric proteins.[6]

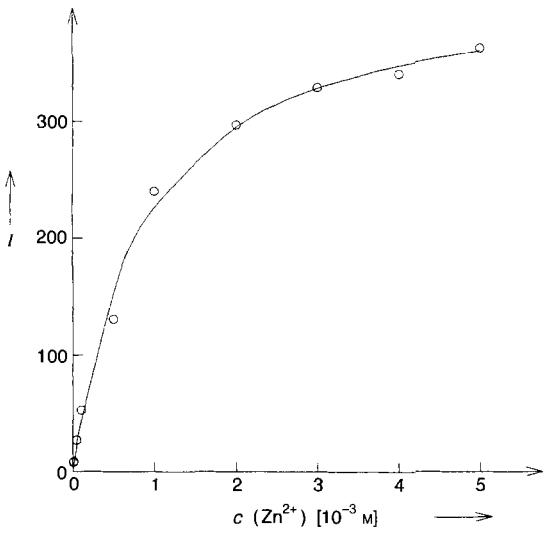
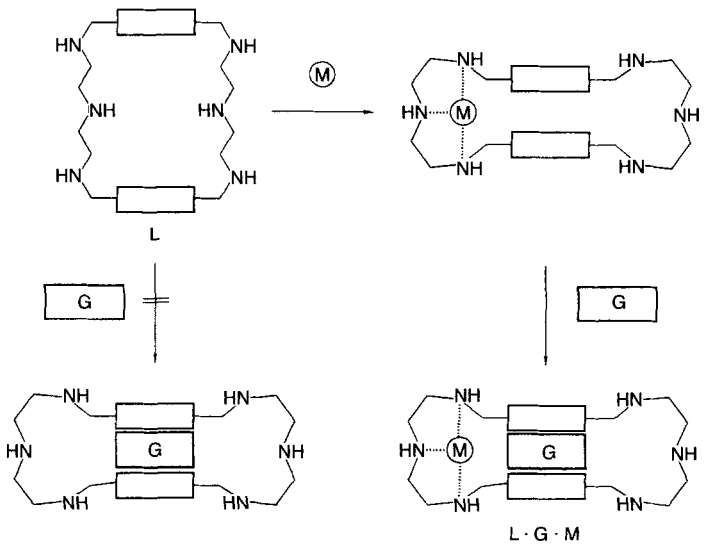


Fig. 2. Complex titration of DNSA (10^{-5} M) with a 1:1 mixture of **1** and $ZnCl_2$ (both 5×10^{-3} M; water, 25 °C, pH 7.0); fluorescence intensity in relative units; experimental values (corrected, see text) and nonlinear fitting for a 1:1 complex (continuous line).

All the host molecules L investigated have binding sites for two metal ions M. Indeed, a UV/vis titration with $CuSO_4$ indicates a composition M_2L, in particular for the more strongly binding tricyclic **2** (Fig. 3). However, not only the complex titration discussed above, but also a separate experiment (Fig. 4) indicated that a ternary complex with *one* metal ion is the dominant species. The simultaneous binding of an organic substrate in the ternary complex leading to a deformation of the second metal binding site is in agreement with molecular mechanics simulations, which indicate the instability of the corresponding



Scheme 2. Principle of the formation of ternary complexes through contraction of the metal-free macrocycle L after addition of metal cations M.

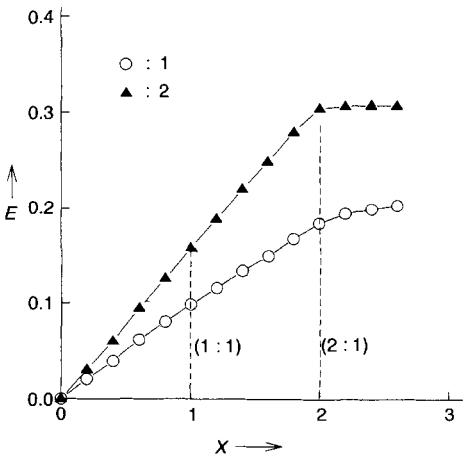


Fig. 3. Dependence of the UV/vis-extinction on the molar ratio X of Cu^{2+} to ligand; this shows a 2:1 (M_2L) stoichiometry for the complexes of Cu^{2+} with **1** and **2**; extinction at 620 nm (for **1**, $\varepsilon = 91.9\,L\,mol^{-1}\,cm^{-1}$) or at 860 nm (for **2**, $\varepsilon = 154\,mol^{-1}\,cm^{-1}$).

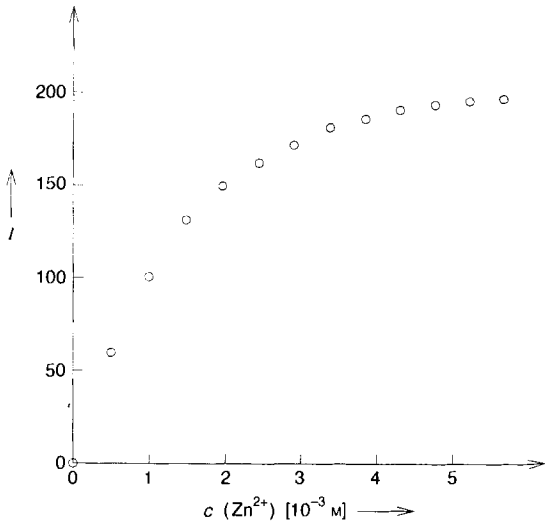


Fig. 4. Dependence of the fluorescence intensity of a mixture of DNSA (5×10^{-6} M) and **1** (5×10^{-3} M) on the $ZnCl_2$ concentration; shows the 1:1:1 (L · M · G) stoichiometry of the ternary complexes (for further information see the legend of Fig. 2).

L · G · 2 M (**1** · DNSA · $2Zn^{2+}$) complex. In this respect, the system described above is positively cooperative with regard to the ternary complex, but it is negatively cooperative with regard to a theoretical quaternary complex L · G · M_2 (**1** · DNSA · $2Zn^{2+}$).

The anionic substituents of the indicators ANS and TNS should lead to a further increase in the level of cooperation. Whilst the ternary complex with the electoneutral DNSA can only benefit from solvophobic and/or van der Waals binding forces in the allosteric closure of the lipophilic pocket, ionized substrates such as ANS and TNS can call on additional electrostatic energy in the sense of a cocomplexation. Indeed, the corresponding constants, which, as for DNSA, were obtained from the saturation curves after correction by linear calibration curves, show a four- to sixfold increase in the formation constants of the ternary complexes (Scheme 1); the cooperativities with ANS and TNS increase to at least $K_{rel} = 10^3$. (Problems of solubility limited the measurement to the determination of the constants for **3** and **4** shown in Scheme 1.)

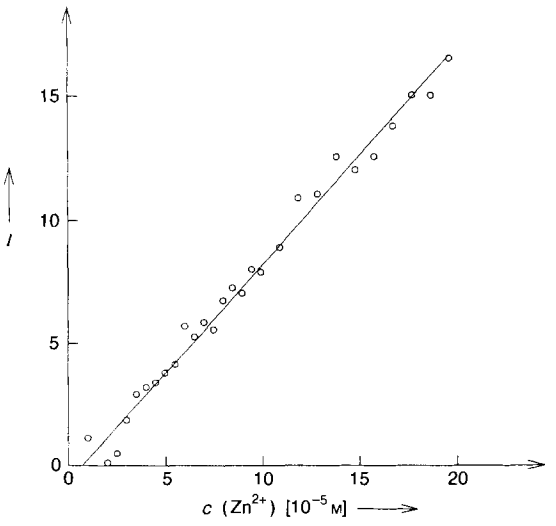


Fig. 5. Dependence of the fluorescence intensity of a mixture of $ZnCl_2$, DNSA (5×10^{-2} M) and **1** (5×10^{-3} M) on the $ZnCl_2$ concentration (maximum 2×10^{-4} M) (for further information see the legend of Fig. 2).

A possible application of the ternary complexes lies in the exploitation of the high sensitivity of fluoresence spectroscopic methods for the determination of the concentration of metal ions. Figure 5 shows that the concentration of Zn^{2+} in the region of 10^{-6} to 10^{-4} M is directly proportional to the fluorescence intensity.

Designed conformational coupling in synthetic complexes between heterotopic binding sites should allow the development of allosteric systems with potential technical and biological/medicinal applications. These systems can have considerably greater cooperativity than that possible in biopolymers.

Received: July 23, 1994
Revised version: October 25, 1994 [Z 7165 IE]
German version: *Angew. Chem.* **1995**, *107*, 380

Keywords: allosterism · azacyclophanes · fluorescent sensors · host–guest chemistry

[1] Previous work on allosteric host–guest complexes with organic substrates: a) F. Diederich, M. R. Heester, M. A. Uyeki, *Angew. Chem.* **1988**, *100*, 1775; *Angew. Chem. Int. Ed. Engl.* **1988**, *27*, 1705; b) H.-J. Schneider, D. Ruf, *ibid.* **1990**, *102*, 1192 and **1990**, *29*, 1159; c) P. Scrimin, P. Tecilla, U. Tonellato, N. Vignaga, *J. Chem. Soc. Chem. Commun.* **1991**, 449; d) R. B. Sijbesma, R. J. M. Nolte, *J. Am. Chem. Soc.* **1991**, *113*, 6695; e) M. T. Reetz, C. M. Niemeyer, K. Harms, *Angew. Chem.* **1991**, *103*, 1515; *Angew. Chem. Int. Ed. Engl.* **1991**, *30*, 1472; f) H.-J. Schneider, F. Werner, *J. Chem. Soc. Chem. Commun.* **1992**, 490; g) M. Inouye, T. Konishi, K. Isagawa, *J. Am. Chem. Soc.* **1993**, *115*, 8091; h) H.-J. Schneider, D. Güttes, U. Schneider, *ibid.* **1988**, *110*, 6449; i) J.-L. Pierre, G. Gagnaire, P. Chautemps, *Tetrahedron Lett.* **1992**, *33*, 217; G. Gagnaire, G. Gellon, J.-L. Pierre, *ibid.* **1988**, *29*, 933; j) P. Marsau, H. Andrianatoandro, T. Willms, J.-P. Desvergne, H. Bouas-Laurent, H. Hopf, R. Utermöhlen, *Chem. Ber.* **1993**, *126*, 1441; k) H. Bauer, J. Briaire, H. A. Staab, *Tetrahedron Lett.* **1985**, *26*, 6175; H. Bauer, V. Matz, M. Lang, C. Krieger, H. A. Staab, *Chem. Ber.* **1994**, *127*, 1993, and references therein.

[2] D. Chen, A. E. Martell, *Tetrahedron* **1991**, *47*, 6895, and references therein.

[3] A. T. Brünger, M. Karplus, *Acc. Chem. Res.* **1991**, *24*, 54.

[4] P. Paoletti, *Pure Appl. Chem.* **1984**, *56*, 492, and references therein.

[5] Application of fluorescent dyes for the investigation of cyclophane inclusion compounds: K. Odashima, K. Koga in *Cyclophanes*, *Vol. 2* (Eds.: P. N. Kuhn, S. M. Rosenfeld), Academic Press, New York, **1983**, pp. 629–677; I. Tabushi, K. Yamamura, *Top. Curr. Chem.* **1983**, *113*, 145; Y. Murakami, *ibid.* **1983**, *115*, 107, and references therein.

[6] In proteins a cooperativity of $K_{rel} > 10$ is regarded as strong: G. H. Czerlinski, *Biophys. Chem.* **1989**, *34*, 169, and references therein.

Preparation and Detection of Enantiomerically Enriched and Configurationally Stable α-Thioalkyllithium Compounds

Bernd Kaiser and Dieter Hoppe*

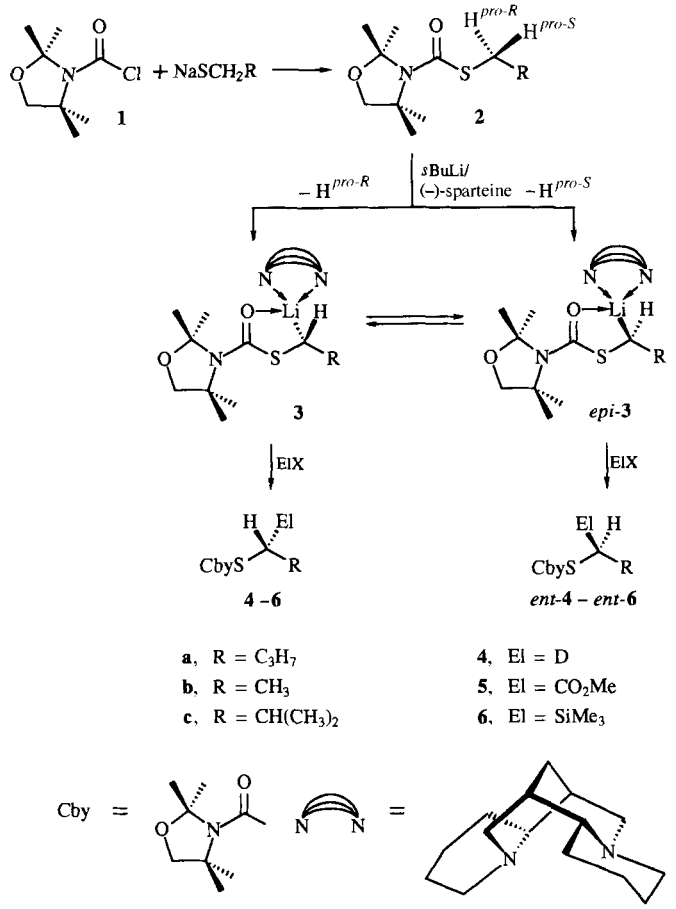
Dedicated to Professor Wolfgang Lüttke on the occasion of his 75th birthday

Chiral α-alkylthioalkyllithium compounds are, in contrast to their α-alkoxy analogues, configurationally instable even at −80 °C.[1] The causes and mechanisms of the configurational conversions have been thoroughly investigated.[2] For example, using racemic 1-arylthioalkyllithium compounds, Hoffmann et al.[1f] showed that sterically demanding aryl groups on the sulfur atom raise the barrier to configurational inversion and that the

[*] Prof. Dr. D. Hoppe, B. Kaiser
Organisch-Chemisches Institut der Universität
Correnstrasse 40, D-48149 Münster (Germany)
Telefax: Int. code + (251)83-9772

[**] This work was supported by the Fonds der Chemischen Industrie and the Deutsche Forschungsgemeinschaft.

torsion about the C–S bond is rate determining. Enantiomerically enriched α-thioalkyllithium compounds, whose chirality is determined solely by the stereogenic carbanionic center, have never been prepared to the best of our knowledge. We now report a method for forming enantiomerically enriched, configurationally labile ion pairs, and the synthesis of a configurationally stable α-thioalkyllithium compound. As we have shown,[3] several alkyl carbamates (**2** with O instead of S) can be lithiated under the influence of the chiral additive (−)-sparteine with effective differentiation between the enantiotopic protons *pro-S*-H and *pro-R*-H; the complexes (**3** with O instead of S) are configurationally stable, and electrophilic substitution leads to products (**4** with O instead of S) with retention of configuration



and enantiomeric excesses of ≥95% *ee*.[3e] The corresponding *S*-alkylthiocarbamates **2** formed from 1,3-oxazolidine-3-carbonyl chloride (**1**)[4] and sodium thiolates[5] were deprotonated under the same conditions in diethyl ether and trapped with various electrophiles to give the substitution products **4**–**6** (Table 1).[6, 7] The enantiomeric excesses were between 40 and 60% *ee* and are almost totally independent of the electrophile used.

Two explanations for the comparatively small enantiomeric excesses are possible: 1) The diastereomeric ion pairs **3** and *epi*-**3** are configurationally labile; they exist in equilibrium and their ratio is thermodynamically defined.[8] 2) **3** and *epi*-**3** are configurationally stable under the reaction conditions, but the chiral reagent cannot differentiate sufficiently between the enantiotopic protons of the starting compounds **2**.

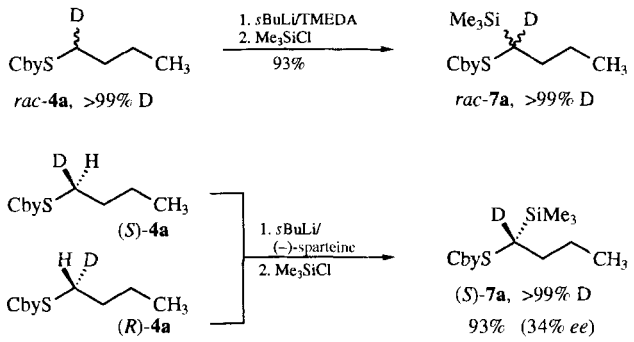
To investigate these possible explanations, we made use of the extremely high kinetic H/D isotope effect, which was recently

Table 1. Reaction conditions for the preparation of alkylthiocarbamates **4**–**6** and their properties.

Starting Cmpd.	Diamine	EIX	Product	Yield [%]	*ee* [%]	$[\alpha]_D^{20}$ [b] (*c*)
2a	TMEDA	MeOD	**4a**	91		
2a	TMEDA	CO_2 [a]	*rac*-**5a**	92		
2a	(−)-sparteine	CO_2 [a]	**5a**	91	47 [c]	−19.4 (1.33)
2a	TMEDA	Me_2SiCl	*rac*-**6a**	92		
2a	(−)-sparteine	Me_3SiCl	**6a**	91	46 [d]	+5.3 (1.26)
2b	TMEDA	CO_2 [a]	*rac*-**5b**	71		
2b	(−)-sparteine	CO_2 [a]	**5b**	89	40 [c]	−25.2 (1.64)
2b	TMEDA	Me_3SiCl	*rac*-**6b**	86		
2b	(−)-sparteine	Me_3SiCl	**6b**	95	40 [d]	+18.4 (1.71)
2c	TMEDA	CO_2 [a]	*rac*-**5c**	88		
2c	(−)-sparteine	CO_2 [a]	**5c**	77	60 [c]	−34.4 (1.87)
2c	TMEDA	Me_3SiCl	*rac*-**6c**	56		
2c	(−)-sparteine	Me_3SiCl	**6c**	– [e]		

[a] Only El; final esterification of the acid with diazomethane. [b] Specific rotation of the partially enantiomerically enriched sample in CH_2Cl_2. [c] 10 mg of tris[3-(heptafluoropropylhydroxymethylene)-(+)-camphorato]europium [Eu(hfc)$_3$]. [d] 10 mg of the compounds with 5 mg of [Pr(hfc)$_3$]. [e] No reaction.

demonstrated for the deprotonation of similar compounds.[9] In a control experiment, less than 1% D was lost during the deprotonation of *rac*-**4a** with *s*BuLi/*N*,*N*,*N*′,*N*′-tetramethylethane-1,2-diamine (TMEDA) under "achiral conditions" and subsequent silylation to give *rac*-**7a**;[10] this corresponds to an isotope effect $k_H/k_D \geq 100$. In an analogous experiment with the chiral complexing agent (−)-sparteine, (*S*)-**7a** was formed in 93% yield with a deuterium content of >99% of the theoretical

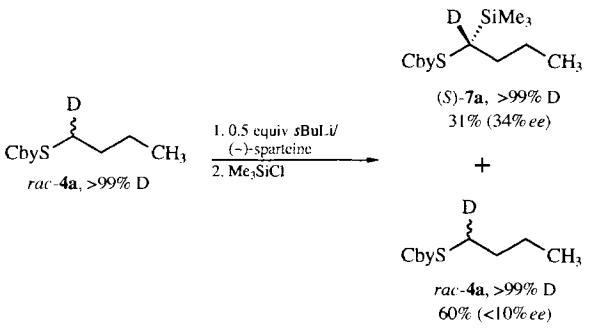


value, and in 34% *ee*. Because of the enantiomeric excess, the first explanation appears to be correct; that is, the reaction proceeds via an intermediate lithiated species that is configurationally labile even at −78 °C. Similar equilibrations have been confirmed for the lithium/(−)-sparteine complexes of primary allyl[8a, b] and benzyl anions.[8c] We attribute the reduced configurational stability of **3**, in comparison to its O analogues, to a reduced rigidity of the chelate complex, which in turn is due to a better stabilization of the negative charge by the sulfur atom,[11] as well as the longer bond length in the sulfur compound (C–S ca. 180 pm, C–O ca. 140 pm).[12] In addition, the good yield indicates that the enantiotopic differentiation in the deprotonation of carbamate **4a** is insufficient. If the chiral base could efficiently differentiate between the enantiotopic protons, (*R*)-**4a**, which contains a proton topologically equivalent to the *pro-S*-H in **2a**, would react more rapidly under kinetic racemic resolution.

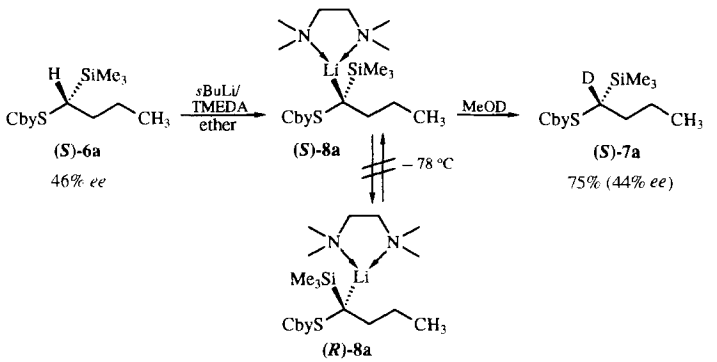
To estimate the relative rates of hydrogen abstraction from the enantiotopic positions, racemate **4a** was deprotonated in the

 © VCH Verlagsgesellschaft mbH, D-69451 Weinheim, 1995 0570-0833/95/0303-0324 $ 10.00+.25/0

presence of only 0.5 equivalents of chiral base, and the carbanions formed in this way were trapped with chlorotrimethylsilane. In the starting material isolated at the end of the experiment (60%) the enantiomer ratio (*R*)-**4a**:(*S*)-**4a** was determined to be 45:55 by ^{1}H NMR spectroscopy;[14] the removal of the *pro-S* proton in **2** is thus only slightly preferred.



Since the lithiated primary thiocarbamates of type **3** are not configurationally stable in ether at −78 °C, we thought that a more sterically demanding group at the carbanionic center might lead to higher configurational stability. Thus, (*S*)-**6a** (46% *ee*) was deprotonated with *s*BuLi/TMEDA under the conditions described above, left at −78 °C for 2.5 h, and the ion pair thus formed trapped with [D$_1$]methanol. The α-deuterated silane (*S*)-**7a** was obtained with 44% *ee*.[15] Even though the-



negative charge on the carbanion is stabilized by the trimethylsilyl group, synthetically useful configurational stability was observed. Thus, the formation of a configurationally stable, enantiomerically enriched α-thioalkyllithium compound has been achieved for the first time.

Experimental Procedure

To a solution of (−)-sparteine (352 mg, 1.5 mmol) or TMEDA (174 mg, 1.5 mmol) in 10 mL of ether cooled to −78 °C was added dropwise 1.25 mmol of an approximately 1.4 M solution of *sec*-butyllithium in isopentane/cyclohexane. The reaction mixture was stirred for 10 min at −78 °C, then 1.0 mmol of the carbamate (**2a-c**, **4a**, **6a**) was slowly added dropwise and the solution stirred for a further 2.5 h. Finally, 3.0 mmol of the desired electrophile was added by syringe and the mixture stirred a further 4 h at −78 °C. The workup consisted of pouring the solution into a mixture of 20 mL of 2 N HCl and 20 mL of ether. The product was purified in the usual fashion. The resulting carboxylic acids were treated with diazomethane to provide the methyl esters **5a-c**.

Received: August 22, 1994 [Z 7259 IE]
German version: *Angew. Chem.* **1995**, *107*, 344

Keywords: chirality · lithium compounds · thioethers

[1] H. J. Reich, M. D. Bowe, *J. Am. Chem. Soc.* **1990**, *112*, 8994; b) H. J. Reich, R. R. Dykstra, *ibid.* **1993**, *115*, 7041; c) T. Cohen, M. Bhupathy, *Acc. Chem. Res.* **1989**, *22*, 152; d) K. Brinckmann, R. Brückner, *Chem. Ber.* **1993**, *126*, 1227; e) P. G. McDougal, B. D. Condon, *Tetrahedron Lett.* **1989**, *30*, 789; f) T. Ruhland, R. Dress, R. W. Hoffmann, *Angew. Chem.* **1993**, *105*, 1487; *Angew. Chem. Int. Ed. Engl.* **1993**, *32*, 1467; R. W. Hoffmann, M. Julius, F. Chemla, T. Ruhland, G. Frenzen, *Tetrahedron* **1994**, *50* 6049; g) H. J. Reich, R. R. Dykstra, *Angew. Chem.* **1993**, *105*, 1489; *Angew. Chem. Int. Ed. Engl.* **1993**, *32*, 1469; H. J. Reich, J. B. Borst, R. R. Dykstra, *Tetrahedron* **1994**, *50*, 5869.

[2] For a short review see: V. K. Aggarwal, *Angew. Chem.* **1994**, *106*, 185; *Angew. Chem. Int. Ed. Engl.* **1994**, *33*, 175.

[3] a) D. Hoppe, F. Hintze, P. Tebben, *Angew. Chem.* **1990**, *102*, 5872; *Angew. Chem. Int. Ed. Engl.* **1990**, *29*, 1422; b) A. Carstens, *Tetrahedron* **1994**, *50*, 6097; c) for a short review see: P. Knochel, *Angew. Chem.* **1992**, *104*, 1486; *Angew. Chem. Int. Ed. Engl.* **1992**, *31*, 1459; d) D. Hoppe, F. Hintze, P. Tebben, M. Paetow, H. Ahrens, J. Schwerdtfeger, P. Sommerfeld, J. Haller, W. Guarnieri, S. Kolczewski, T. Hense, I. Hoppe, *Pure Appl. Chem.* **1994**, *66*, 1479; for applications of α-amino-substituted: e) S. T. Kerrick, P. Beak, *J. Am. Chem. Soc.* **1991**, *113*, 9708; D. J. Gallagher, S. T. Kerrick, P. Beak, *ibid.* **1992**, *114*, 5872.

[4] F. Hintze, D. Hoppe, *Synthesis* **1992**, 1216.

[5] Thiocarbamates **2a** (95%), **2b** (87%), and **2c** (88%) were prepared from the corresponding alkanethiols with 2,2,4,4-tetramethyl-1,3-oxazolidine-3-carbonyl chloride by the sodium hydride route [4].

[6] All the products were fully characterized spectroscopically. Correct elemental analyses were also obtained for each product.

[7] a) For stereochemical correlation methyl (*S*)-lactate was converted to methyl (*R*)-(2-acetylthio)propanoate by using a Mitsunobu reaction [7b], the *S*-acetyl group removed [7c], and the enantiomeric excess of the known [7d] (*R*)-2-sulfanylpropanoic acid measured using correlated specific rotation as >95% *ee*. Finally, the carbamate group was introduced (cesium carbonate/THF). The specific rotation $[\alpha]_D^{20} = +36.4$ ($c = 1.41$, CH_2Cl_2)) for *ent*-**5b** (85% *ee*) corresponds well to that of the sample **5b** obtained by deprotonation (47% *ee*): $[\alpha]_D^{20} = -19.4$ ($c = 1.33$, CH_2Cl_2); b) R. P. Vollante, *Tetrahedron Lett.* **1981**, *22*, 3119; c) L. N. Owen, M. B. Rahman, *J. Chem. Soc. C* **1971**, 2432; d) B. Strijtveen, R. M. Kellog, *J. Org. Chem.*, **1986**, *51*, 3664.

[9] D. Hoppe, M. Paetow, F. Hintze, *Angew. Chem.* **1993**, *105*, 430; *Angew. Chem. Int. Ed. Engl.* **1993**, *32*, 394.

[10] The extent of deuteration was determined by GC-MS using NH_3 for chemical ionization.

[11] a) J. M. Lehn, G. Wipff, J. Demuynck, *Helv. Chim. Acta* **1977**, *60*, 1239; b) F. Bernardi, A. Bottoni, A. Venturini, A. Mangini, *J. Am. Chem. Soc.* **1986**, *108*, 8171.

[12] J. March, *Advanced Organic Chemistry*, 4th ed., Wiley, New York, **1992**, Chapter 1.

[13] O. Zschage, J.-R. Schwark, T. Krämer, *Tetrahedron* **1992**, *48*, 8377.

[14] ^{1}H NMR conditions: 360 MHz, 10 mg of **4a** + 0.9 mg of tris[3-(heptafluoropropylhydroxymethylene)-(+)-camphorato]europium(III) [Eu(hfc)$_3$] in 0.6 mL of $CDCl_3$; the signal of the α proton at $\delta = 6.4$ is split by roughly 0.02 ppm.

[15] $[\alpha]_D^{20} = 5.3$ ($c = 1.90$ in CH_2Cl_2, 44% *ee*); ^{1}H NMR conditions: 10 mg of **6a** + 10 mg of [Pr(hfc)$_3$] in 0.6 mL of $CDCl_3$.

[Fe(2,4,6-*t*Bu$_3$C$_6$H$_2$)$_2$], a Monomeric Diaryl Complex with Two-Coordinate Iron(II)**

Hardy Müller, Wolfgang Seidel,* and Helmar Görls

Homoleptic organo transition metal compounds with low coordination numbers are rare. This is especially true for neutral complexes of the type [MR$_n$] ($n < 4$) which are expected to exhibit interesting chemical properties based on their coordinatively unsaturated character. To date tetramesityldiiron[1] serves as the only example of a structurally characterized neutral

[*] Prof. Dr. W. Seidel
Institut für Anorganische und Analytische Chemie der Universität
August-Bebel-Strasse 2, D-07743 Jena (Germany)
Telefax: Int. code + (3641)635538
Dr. H. Müller
LS Polymerchemie der Technischen Universität Chemnitz/Zwickau (Germany)
Dr. H. Görls
Max-Planck-Gesellschaft
Arbeitsgruppe CO_2-Chemie an der Universität Jena (Germany)

[**] This work was supported by the Fonds der Chemischen Industrie.

iron(II) complex with organic ligands. In this complex the metal atom is three-coordinate; the same coordination number is found in the analogous Co(II) complex[2a] and in $[\{Mn(mes)_2\}_3]$ (mes = 2,4,6-$Me_3C_6H_2$).[2b] Even though two-coordinate iron(II) species are rare, Power et al. were able to show that they can be prepared by employing bulky amido ligands such as $[N(SiMePh_2)_2]^-$, $[N(SiMe_2Ph)_2]^-$, and $(NmesBmes_2)^-$.[3] In the crystal, these compounds have a N-Fe-N bond angle of approximately 170°. For the vaporizable iron(II) amide $[Fe\{N(SiMe_3)_2\}_2]$ in the gas phase, the two-coordinate nature of the central metal and a N-Fe-N bond angle of 180° was confirmed by electron diffraction studies.[4] Furthermore, Power et al. recently also reported the synthesis and characterization of thiolato complexes with two-coordinate iron(II).[5]

We therefore decided to investigate whether monomeric two-coordinate iron complexes of type $[FeR_2]$ could be obtained by the use of aryl ligands with bulkier substituents than those found in the three-coordinate tetramesityldiiron $[\{Fe(mes)(\mu\text{-mes})\}_2]$. We applied 2,4,6-$iPr_3C_6H_2$ (trip), 2,4,6-$Ph_3C_6H_2$ (triph), and 2,4,6-$tBu_3C_6H_2$ (mes*) as aryl ligands.

The corresponding compounds were synthesized analogously to the preparation of tetramesityldiiron; stoichiometric amounts (1:2) of $[FeBr_2(thf)_2]$ (**1**) and Grignard reagent were allowed to react in tetrahydrofuran, after that the magnesium halides were precipitated by addition of dioxan. The reaction with (trip)MgBr afforded a brown, crystalline substance of composition **2**. This compound is a dimer and structurally similar to tetramesityldiiron.[6]

$[\{Fe(trip)(\mu\text{-trip})\}_2]$ **2**

In contrast, treatment of the iron halide with (triph)MgBr does not afford the corresponding diaryliron complex. Instead, a colorless precipitate forms which presumably is an adduct of the reactants. No change in the nature of this precipitate is observed upon treatment with dioxan.

A similar colorless, fine-crystalline precipitate of the composition **3** is initially obtained when **1** is treated with two equivalents of (mes*)MgBr in tetrahydrofuran [Eq. (a)]. Addition of dioxan, followed by removal of the solvent and extraction of the residue with *n*-pentane yielded an air- and moisture-sensitive yellow product **4** [Eq. (b)]. Its magnetic moment of 4.77 μ_B at room

$$2\,[FeBr_2(thf)_2] + 4\,(mes^*)MgBr \xrightarrow{THF} [Fe_2Mg_3Br_6(mes^*)_4(thf)_2] + MgBr_2 \quad (a)$$
(**1**) (**3**)

$$[Fe_2Mg_3Br_6(mes^*)_4(thf)_2] \xrightarrow{THF/dioxan} 2\,[Fe(mes^*)_2] + 3\,MgBr_2(dioxan)_2 \quad (b)$$
(**3**) (**4**)

temperature is appropriate for an iron(II) high-spin complex. Notably, $[\{Fe(mes)(\mu\text{-mes})\}_2]$ and **2** show a markedly smaller magnetic moment.

The homoleptic diaryliron(II) compounds prepared dissolve readily in apolar solvents. The increase in size of the substituents on the aryl ligands has a decisive influence on the reactivity. The adduct formation with nitrogen bases and concurrent cleavage of the respective dimer has been reported for **2**[6] and $[\{Fe(mes)(\mu\text{-mes})\}_2]$;[7] however, no such reaction is observed for **4**. Moreover, whereas tetramesityldiiron rapidly undergoes an insertion reaction with isocyanate or CO,[8] the same reaction occurs at a much slower rate with **4**. Complex **4** is thermally surprisingly stable (decomposition occurs at 179 °C); this is a result of the steric shielding of the central atom, which in turn kinetically disfavors the decomposition reaction.

Single crystals of **4** suitable for an X-ray structure analysis were obtained from *n*-heptane.[9] The crystal structure analysis of **4** shows the presence of two-coordinate iron(II) centers in the C_2-symmetric molecules (Fig. 1). The Fe–C1 distance (2.051(5) Å)

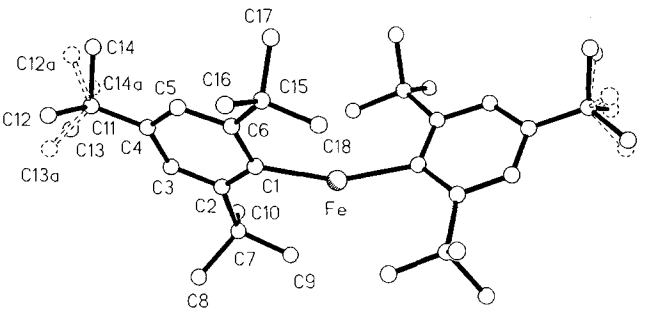


Fig. 1. Molecular structure of **4** in the crystal; selected bond lengths [Å] and angles [°]: Fe-C1 2.051(5), C1-C2 1.426(7), C1-C6 1.413(7), C2-C3 1.400(7), C3-C4 1.376(7), C4-C5 1.388(7), C5-C6 1.389(7), Fe···C18 2.822(8), Fe···C9 2.744(6), Fe···H9b 2.16#, Fe···H18c 2.33(1)#; C1-Fe-C1A 158.9(3), Fe-C1-C2 119.4(4), Fe-C1-C6 122.7(3), C1-C2-C7 124.3(4), C1-C6-C15 122.9(4), C1-C2-C3 120.2(5), C2-C3-C4 123.2(5), C3-C4-C5 116.2(5), C4-C5-C6 123.2(5), C1-C6-C5 120.8(4). Distances marked with a # were calculated based on the covalent radius of the hydrogen atom.

is comparable with the terminal Fe–C distances in tetramesityldiiron and those in **2**. The C1-Fe-C1A bond angle of 158.9(3)° is about 11° smaller than the corresponding angles in the aforementioned amides and about 17° smaller than that in $[Cu(mes^*)SMe_2]$[10] which serves as the only known compound of a 3d element with a (mes*) group. The neutral dialkylmanganese compound $[Mn\{C(SiMe_3)_3\}_2]$[11] in which the manganese(II) center is two-coordinate has a linear structure with an Mn–C bond length of 2.102 Å. The bent geometry at the iron center in **4** is most likely a result of packing effects; intermolecular interactions can be excluded. Larger deviations from a linear arrangement of ligands have also been reported for two-coordinate phosphane complexes of type $[M(PR_3)_2]$ (e.g. M = Pd, R = *c*-C_6H_{11}).[12]

An Fe···H distance of 2.1–2.3 Å can be calculated from the Fe···C9 and Fe···C18 distances of 2.744(6) Å and 2.822(8) Å, respectively. However, no evidence of agostic interactions in **4** was apparent from the IR spectrum (between 2700 and 2350 cm^{-1}) or from ^1H NMR investigations. The ^1H NMR spectrum in $[D_8]$toluene shows three paramagnetically shifted signals which are assigned to protons of the *para*- and *ortho*-*t*Bu groups and to aromatic protons. No splitting of these signals is observed even at temperatures as low as −80 °C; similar results have also been reported for thiolatoiron(II) complexes[5] and trimesitylrhodium.[13]

Experimental Procedure

All reactions were carried out under anaerobic and anhydrous conditions.

4: A solution of (mes*)MgBr (34.2 mmol, 103.5 mL) in THF was added dropwise over a period of 2.5 h to a stirred suspension of **1** (6.15 g, 17.08 mmol) in THF (30 mL). Stirring was continued for an additional 1.5 h, whereupon 1,4-dioxan (12 mL) in THF (15 mL) was slowly added to precipitate the $MgBr_2(dioxan)_2$. After 15 h the solution was evaporated to dryness and the residue was treated with *n*-pentane. After one hour the magnesium salts were collected on a filter and washed with the filtrate so to completely extract the products. The filtrate was then reduced in volume to about 30–40 mL. Crystallization was accomplished by cooling to −30 °C, and agitating the filtrate until the yellow compound started to crystallize. After 48 h the product was collected by filtration. Crystals suitable for a X-ray structure analysis were obtained upon cooling a saturated solution (*n*-heptane; 50 °C) to room temperature. Yield: 5.9 g (63%).

 © VCH Verlagsgesellschaft mbH, D-69451 Weinheim, 1995 0570-0833/95/0303-0326 $ 10.00+.25/0

$C_{36}H_{58}Fe$ (546.67 g mol^{-1}); elemental analysis: found C 80.51, H 10.12, Fe 10.16%; calcd C 79.09, H 10.69, Fe 10.22%; χ_{mol}(corr.) = 9.703×10^{-3} cm^3 mol^{-1} (291 K); $\mu_{eff} = 4.77\ \mu_B$; IR (Nujol): $\tilde{\nu} = 1590$ (m), 1522 (m), 1385 (s), 1362 (s), 1343 (s), 1247 (s), 1209 (m), 1168 (m), 1122 (m), 1023 (m), 934 (s), 899 (m), 879 (m), 743 (s), 715 (s), 646 (s), 569 (m), 471 (s) cm^{-1}; ^{1}H NMR ([D$_8$]toluene, 25 °C): $\delta = 18.6$ (s, 18H), 53 (s, 36H), 115 (s, 4H); m.p. 179 °C (exothermic).

Received: May 10, 1994
Revised: September 6, 1994 [Z69151E]
German version: *Angew. Chem.* **1995**, *107*, 386

Keywords: complexes with carbon ligands · iron compounds · structure elucidation

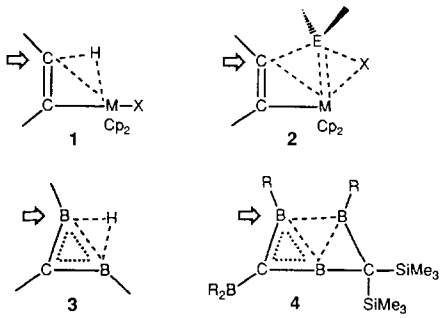
[1] H. Müller, W. Seidel, H. Görls, *J. Organomet. Chem.* **1993**, *445*, 133–136.
[2] a) K. H. Theopold, J. Silvestre, E. K. Byrne, D. S. Richeson, *Organometallics* **1989**, *8*, 2001–2009; b) S. Gambarotta, C. Floriani, A. Chiesi-Villa, C. Guastini, *J. Chem. Soc. Chem. Commun.* **1983**, 1128–1129.
[3] a) R. A. Bartlett, P. P. Power, *J. Am. Chem. Soc.* **1987**, *109*, 7563–7564; b) H. Chen, R. A. Bartlett, H. V. Rasika Dias, M. M. Olmstead, P. P. Power, *ibid.* **1989**, *111*, 4338–4345; c) H. Chen, R. A. Bartlett, M. M. Olmstead, P. P. Power, S. C. Shoner, *ibid.* **1990**, *112*, 1048–1055.
[4] R. A. Andersen, K. Faegri, J. C. Green, A. Haaland, M. F. Lappert, W.-P. Leung, K. Rypdal, *Inorg. Chem.* **1988**, *27*, 1782–1786.
[5] J. J. Ellison, K. Ruhlandt-Senge, P. P. Power, *Angew. Chem.* **1994**, *106*, 1248–1250; *Angew. Chem. Int. Ed. Engl.* **1994**, *33*, 1178–1180.
[6] a) H. Müller, Dissertion, Universität Jena, **1993**; b) The synthesis and structure of **2** has recently been reported: A. Klose, E. Solari, C. Floriani, A. Chiesi-Villa, C. Rizzoli, N. Re, *J. Am. Chem. Soc.* **1994**, *116*, 9123–9135.
[7] W. Seidel, K.-J. Lattermann, *Z. Chem.* **1983**, *23*, 31.
[8] H. Müller, W. Seidel, H. Görls, *J. Organomet. Chem.* **1994**, *472*, 215–220.
[9] Crystal data: $Mo_{K\alpha}$, $\lambda = 0.71069$ Å, θ-2ω scan, solution: heavy atom methods (SHELXS 86), refinement with MOLEN, hydrogen atoms calculated on ideal positions, $C_{36}H_{58}Fe$, $M = 546.7$ g mol^{-1}, $C2/c$, $a = 17.935(4)$, $b = 8.644(1)$, $c = 23.591(5)$ Å, $\beta = 109.89(1)°$, $V = 3439(1)$ Å^3, $Z = 4$, $\rho_{calcd} = 1.06$ g cm^{-3}, $\mu = 4.6$ cm^{-1}, $T = 293$ K, 6427 measured reflections, 5961 symmetry-independent reflections of which 1806 were observed ($I > 2\sigma(I)$), 165 refined parameters, $R = 0.073$, $R_w = 0.081$ ($w = 1/\sigma^2(F_0)$), residual electron density 0.58 e Å^{-3}. Further details of the crystal structure investigation may be obtained from the Fachinformationszentrum Karlsruhe, D-76344 Eggenstein-Leopoldshafen (Germany), on quoting the depository number CSD-58691.
[10] X. He, M. M. Olmstead, P. P. Power, *J. Am. Chem. Soc.* **1992**, *114*, 9668–9670.
[11] N. H. Buttrus, C. Eaborn, P. B. Hitchcock, J. D. Smith, A. C. Sullivan, *J. Chem. Soc. Chem. Commun.* **1985**, 1380–1381.
[12] A. Immirzi, A. Musco, *J. Chem. Soc. Chem. Commun.* **1974**, 400–401.
[13] R. S. Hay-Motherwell, B. Hussain-Bates, M. B. Hursthouse, G. Wilkinson, *J. Chem. Soc. Chem. Commun.* **1990**, 1242–1243.

Compounds with Planar Tetracoordinate Boron Atoms: Anti van't Hoff/Le Bel Geometries without Metal Centers**

Matthias Menzel, Dirk Steiner, Heinz-Jürgen Winkler, Dieter Schweikart, Sigrid Mehle, Stefan Fau, Gernot Frenking, Werner Massa, and Armin Berndt*

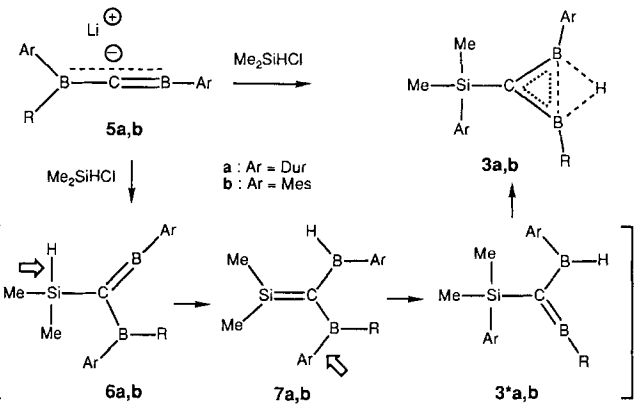
Dedicated to Prof. Paul von Ragué Schleyer on the occasion of his 65th birthday

Numerous compounds **1**[3, 4] and **2**[5] have anti van't Hoff/Le Bel geometries[1, 2] with planar tetracoordinate carbon atoms; all of them contain at least one metal atom (M = Ti, Zr, Hf...; E = H, B), and most contain even two (E = Al, Ga, Zr...) (Scheme 1). We show here by crystal structure analyses that compounds **3a** and **3c** contain planar tetracoordinate boron atoms. Compounds **3** and **4**[6] are examples of compounds having anti van't Hoff/Le Bel geometries *without* metal centers.



Scheme 1. **1**, **2**: M = Ti, Zr, Hf...; **1**: X = +, Cl, Br, CH_3; **2**: X = H, Cl, CH_3, C≡CR; E = B, Al, Ga, Zr...; **4**: R = 2,3,5,6-Me_4C_6H.

The H-bridged borylmethyleneboranes **3a, b** are obtained from the reaction of borylborataalkynes **5a, b**[6] with chlorodimethylsilane at 25 °C (Scheme 2). In these reactions a hydrogen atom is transferred from a silicon atom to a boron atom, and an



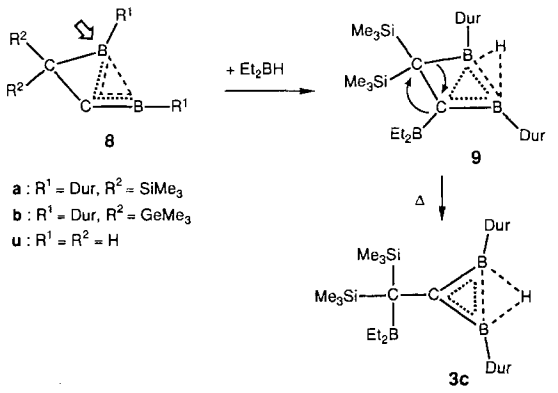
Scheme 2. R = $CH(SiMe_3)_2$; Dur = 2,3,5,6-Me_4C_6H; Mes = 2,4,6-$Me_3C_6H_2$.

aryl group from a boron atom to a silicon atom. Primary products are probably silylmethyleneboranes **6a, b**, which then give the diborylsilaethenes **7a, b** by means of a 1,3 shift of the hydrogen atom from the tetracoordinate silicon atom to the dicoordinate boron atom. The 1,3 shift of the aryl group from the boron atom with the bis(trimethylsilyl)methyl substituent R to the tricoordinate silicon atom formally leads to the classical borylmethyleneboranes **3*a, b**, which have the β-agostic[6] structure **3a, b**. Compound **3c** is formed by melting **9** (150 °C),[7] which in turn is accessible from **8a**[6] and diethylborane. In the reaction giving **3c** two boron atoms connected to the carbon atom framework change places—possibly by a double 1,2 rearrangement (Scheme 3). The respective substituents migrate together with the boron atoms.

Figure 1 shows the X-ray crystal structures of **3a** and **3c**;[8] the corresponding constitution of **3b** is deduced from the similarity of its NMR data to that of the framework atoms of **3a** and **3c** (Table 1).

[*] Prof. Dr. A. Berndt, Dipl.-Chem. M. Menzel, D. Steiner, H.-J. Winkler, D. Schweikart, Dr. S. Mehle, Dipl.-Chem. S. Fau, Prof. Dr. G. Frenking, Prof. Dr. W. Massa
Fachbereich Chemie der Universität
D-35032 Marburg (Germany)
Telefax: Int. code + (6421) 288917

[**] This work was supported by the Deutsche Forschungsgemeinschaft and the Fonds der Chemischen Industrie. In this paper the unsubstituted parent compounds are denoted with the letter u, all classical structures with a star, and all α- or β-agostic structures with the subscript α or β.



Scheme 3.

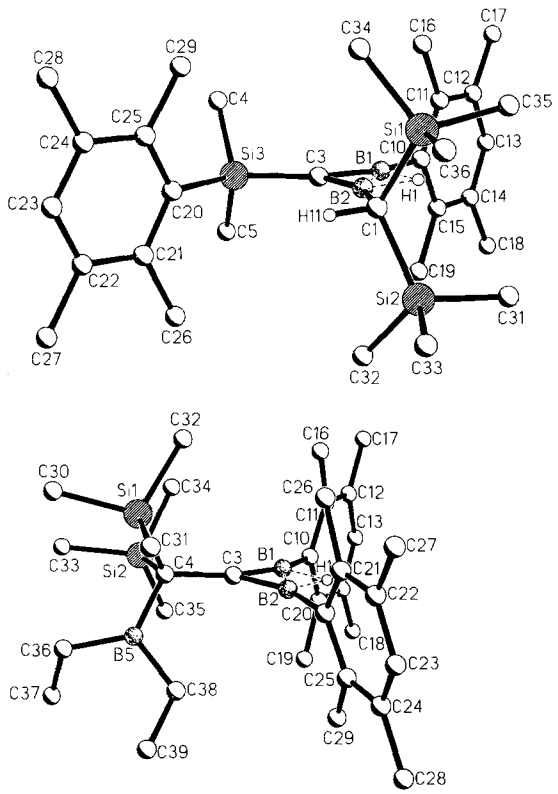


Fig. 1. Crystal structures of **3a** (top) and **3c** (bottom). Selected distances [pm] and angles [°] supplementary to the data in Table 2: **3a**: B1-C10 156.4(4), B2-C1 155.0(4), C3-Si3 183.5(2); B1-C3-B2 74.9(2), B1-B2-C3 52.3(2), C3-B1-C10 149.3(2), C3-B2-C1 150.4(2), B1-C3-Si3 142.1(2), B2-C3-Si3 142.8(2); C10-B1-B2-C1 −1.6(10), C10-B1-B2-C3 −178.1(6). **3c**: B1-C10 156.7(4), B2-C20 157.3(4), C3-C4 151.8(3); B1-C3-B2 73.1(2), B1-B2-C3 53.3(2), C3-B1-C10 154.3(2), C3-B2-C20 152.9(2), B1-C3-C4 143.2(2), B2-C3-C4 143.6(2); C10-B1-B2-C20 −2.9(8), C10-B1-C3-C4 1.4(7).

In Table 2 the distances in the CB_2H framework of **3a** and **3c** are compared with those calculated for the unsubstituted $\mathbf{3u}_\beta$.[2, 9, 10] The scattering of the B—H distances is within the bounds of the fundamentally low precision of H atom positions determined by X-ray diffraction. In **3a** and **3c** both boron atoms lie in the best fit plane of their four neighboring atoms with deviations of 0.6(3) and 2.8(3) pm for **3a** and 1.5(3) and 1.6(3) pm for **3c**. In **4**[6] this deviation is 0.4(3) pm for B2. The boron atoms in **3a** and **3c**, and the B2 atom in **4**, are thus planar tetracoordinate.

Table 1. Some physical data for compounds **3a–c** and **9**.

3a: colorless crystals, m.p. 174 °C, yield: 74%. – ^{1}H NMR (300 MHz, $CDCl_3$, 25 °C): $\delta = 0.09$ (s, 18H, $SiMe_3$), 0.52 (s, 6H, $SiMe_2$), 0.95 (d, $^3J(H,H) = 5.2$ Hz, 1H, CH(B)), 2.12, 2.18, 2.23, 2.29 (each s, 24H, *o*- and *m*-CH_3), 6.94, 6.97 (each s, each 1H, *p*-H), 7.36 (br. s, 1H, BHB); – ^{13}C NMR (125 MHz, $CDCl_3$, −40 °C): $\delta = 1.3$ (q, 6C, $SiMe_3$), 4.8 (q, 2C, $SiMe_2$), 9.0 (br. d, $^1J(C,H) = 107.9$ Hz, 1C, CH(B)), 20.0, 20.1, 20.7, 21.2 (each q, 8C, *o*- and *m*-CH_3), 130.4 (br. s, 1C, CB_2), 131.4, 132.1 (each d, each 1C, *p*-C), 134.4 (br. s, 1C, *i*-C(B)), 133.1, 133.3, 136.2, 140.0 (each s, 8C, *o*- and *m*-C), 137.8 (s, 1C, *i*-C(Si)); – ^{11}B NMR (96 MHz, $CDCl_3$, 25 °C): $\delta = 29$

3b: colorless oil, yield: 70%. – ^{1}H NMR (300 MHz, $CDCl_3$, 25 °C): $\delta = 0.33$ (s, 18H, $SiMe_3$), 0.77 (s, 6H, $SiMe_2$), 1.21 (d, $^3J(H,H) = 4.9$ Hz, 1H, CH(B)), 2.47, 2.52, 2.58, 2.65 (each s, 18H, *o*- and *p*-CH_3), 7.00, 7.07 (each s, each 2H, *m*-H), 7.53 (br. s, 1H, BHB); – ^{13}C NMR (75 MHz, $CDCl_3$, 25 °C): $\delta = 1.5$ (q, 6C, $SiMe_3$), 5.0 (q, 2C, $SiMe_2$), 9.6 (br. d, $^1J(C,H) = 105.7$ Hz, 1C, CH(B)), 20.9, 21.2, 23.1, 24.9 (each q, 6C, *o*- and *p*-CH_3), 127.4, 128.8 (each d, each 2C, *m*-C), 130.6 (br. s, 1C, *i*-C(B)), 133.3 (s, 1C, *i*-C(Si)) 138.0, 138.3 (each s, each 1C, *p*-C) 141.1, 143.9 (each s, each 2C, *o*-C); – ^{11}B NMR (96 MHz, $CDCl_3$, 25 °C): $\delta = 29$

3c: colorless crystals, m.p. 157 °C (decomp.), yield: 98%. – ^{1}H NMR (500 MHz, $CDCl_3$, −30 °C): $\delta = 0.03$ (s, 18H, $Si(CH_3)_3$), 0.95 (t, 6H, CH_2CH_3), 1.25 (q, 4H, CH_2CH_3), 2.20, 2.24 (each s, each 12H, *o*- and *m*-CH_3), 6.95 (s, 2H, *p*-H), 7.83 (br. s, 1H, BHB); – ^{13}C NMR (125 MHz, $CDCl_3$, −30 °C): $\delta = 2.4$ (q, 6C, $Si(CH_3)_3$), 9.1 (q, 2C, CH_2CH_3), 19.4 (br. t, 2C, CH_2CH_3), 20.0, 21.0 (each q, each 4C, *o*- and *m*-CH_3), 43.2 (s, 1C, CSi_2), 131.3 (d, 2C, *p*-C), 133.3, 136.1 (each s, each 4C, *o*- and *m*-C), 135.1 (br. s, 2C, *i*-C), 144.2 (br. s, 1C, CB_2); – ^{11}B NMR (96 MHz, $CDCl_3$, 25 °C): $\delta = 24, 82$

9: colorless solid, m.p. 148 °C (decomp.), yield: 81%. – ^{1}H NMR (300 MHz, $CDCl_3$, 25 °C): $\delta = -0.08, 0.26$ (each s, each 9H, $Si(CH_3)_3$), 1.14 (t, 6H, CH_2CH_3), 1.48 (q, 4H, CH_2CH_3), 1.96 (br.), 2.24, 2.29 (br.), 2.33, 2.45 (br.), 2.59 (each s, together 24H, *o*- and *m*-CH_3), 4.43 (br. s, 1H, BHB), 7.02, 7.12 (each s, each 1H, *p*-H); – ^{13}C NMR (75 MHz, $CDCl_3$, 25 °C): $\delta = 1.2$, 1.6 (each q, each 3C, $Si(CH_3)_3$), 9.5 (q, 2C, CH_2CH_3), 19.3 (br. t, 2C, CH_2CH_3), 20.2, 20.3, 21.1 (each q, together 8 °C, *o*- and *m*-CH_3), 28.8 (s, 1C, CSi_2), 86.2 (br. s, 1C, CB_2), 131.7, 134.7 (each d, each 1C, *p*-C), 132.6, 133.1, 137.0, 139.3, 140.0 (each s, together 8 °C, *o*- and *m*-C), 133.4, 133.6 (each br. s, each 1C, *i*-C); ^{11}B NMR (96 MHz, $CDCl_3$, 25 °C): $\delta = 5, 50, 80$

The three-center/two-electron (3c2e) bonds B—H—B in **3a–c** and B—B—B in **4** correspond to the 3c2e bonds M—H—C in **1** and M—E—C in **2**, respectively (Scheme 1). Planar tetracoordinate boron atoms are also present in the recently calculated structures $\mathbf{10}_\beta$ and $\mathbf{10}_\alpha$;[12] $\mathbf{10}_\beta$ is isoelectronic with $\mathbf{3u}_\beta$, and $\mathbf{10}_\alpha$ can be regarded as boryldiboranide(3) **10*** with a strong α-agostic[13, 14] interaction.

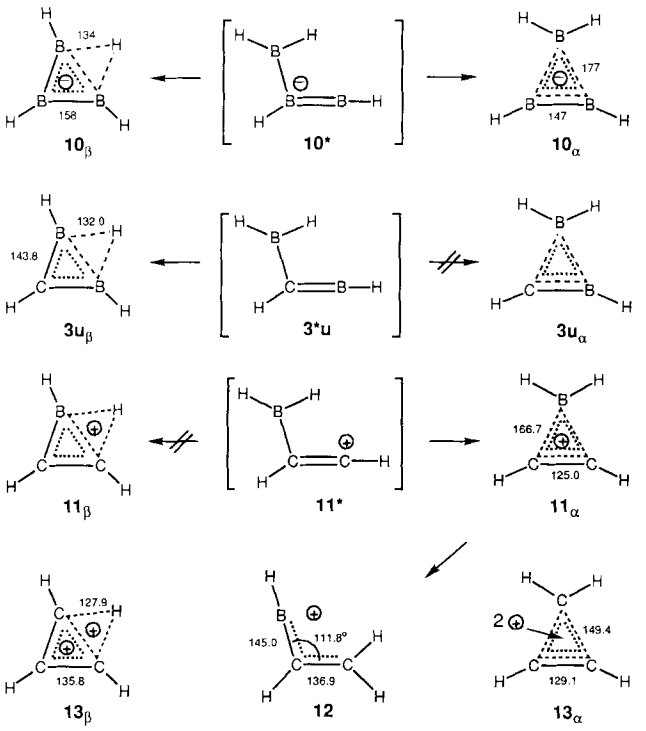
In order to determine the importance of the electronegativity for planar tetracoordinate boron atoms, we carried out MP2/6-31G* calculations on the β-borylvinyl cation **11***, which is isoelectronic with **3*u** and **10***.[15] Instead of finding the β-agostic bridged $\mathbf{11}_\beta$, which corresponds to $\mathbf{10}_\beta$ and $\mathbf{3u}_\beta$, $\mathbf{11}_\alpha$ corresponding to $\mathbf{10}_\alpha$ is found to be a minimum-energy structure; the boron atom of $\mathbf{11}_\alpha$ is planar tetracoordinate as a result of a strong α-agostic interaction. However, structure $\mathbf{11}_\alpha$ is 13.8 kcal mol^{-1} higher in energy than the classical 1-boraallyl cation **12**: the marked electron deficiency at the C^+ center in **11*** leads to the transfer of a hydride ion, that is, to a rearrangement—the extreme case[6] of an agostic interaction.[16]

Dications $\mathbf{13}_\alpha$ and $\mathbf{13}_\beta$ with planar tetracoordinate C atoms, isoelectronic with $\mathbf{3u}_\beta$, $\mathbf{10}_\beta$, and $\mathbf{11}_\beta$, and $\mathbf{10}_\alpha$ and $\mathbf{11}_\alpha$, respectively,

Table 2. Experimentally determined (**3a**, **3c**) and calculated [q][a] ($\mathbf{3u}_\beta$) distances in the CB_2H frameworks.

	3a	3c	$3u_\beta$
B1-B2	175.1(4)	173.5(4)	170.9
B1-C3	143.5(4)	145.4(4)	143.8
B2-C3	144.4(4)	146.2(4)	143.8
B1-H	128(2)	125(2)	132.0
B2-H	131(2)	124(2)	132.0

[a] MP2/6-31G* level.



are 14.4 and 14.6 kcal mol^{-1} higher in energy than the planar allene dication.[17]

The formation of compounds with anti van't Hoff/Le Bel geometries thus requires electropositive elements: in addition to metals, boron is also suitable.

Received: August 19, 1994 [Z 7249 IE]
German version: *Angew. Chem.* **1995**, *107*, 368

Keywords: ab initio calculations · anti van't Hoff/Le Bel geometries · boron compounds · borylmethyleneboranes

[1] R. Hofmann, W. Alder, C. F. Wilcox, Jr., *J. Am. Chem. Soc.* **1970**, *92*, 4992–4993; R. Hofmann, *Pure Appl. Chem.* **1971**, *28*, 181–194.

[2] J. B. Collins, J. D. Dill, E. D. Jemmis, Y. Apeloig, P. von R. Schleyer, R. Seeger, J. A. Pople, *J. Am. Chem. Soc.* **1976**, *98*, 5419–5427; K. Krogh-Jespersen, D. Cremer, D. Poppinger, J. A. Pople, P. von R. Schleyer, J. Chandrasekhar, *ibid.* **1979**, *101*, 4843–4851.

[3] a) G. Erker, W. Frömberg, K. Angermund, R. Schlund, C. Krüger, *J. Chem. Soc. Chem. Commun.* **1986**, 372–374; G. Erker, R. Schlund, C. Krüger, I. Hyla-Kryspin, R. Gleiter, *J. Organomet. Chem.* **1988**, *346*, C15–C18; G. G. Hlatky, H. W. Turner, R. R. Eckman, *J. Am. Chem. Soc.* **1989**, *111*, 2728–2729; I. Hyla, R. Gleiter, C. Krüger, R. Zwettler, G. Erker, *Organometallics* **1990**, *9*, 517–523; R. Gleiter, I. Hyla-Kryspin, S. Niu, G. Erker, *ibid.* **1993**, *12*, 3828–3836.

[4] In the literature compounds of type **1** are not explicitly included with those having planar tetracoordinate C atoms. However, their C–H β-agostic interaction corresponds to the C–E β-agostic interactions in **2**: the β-C–M distances—considered a criterion for the fourth coordination of the β-C atom—in **1** are only slightly longer than those in **2**.

[5] G. Erker, *Nachr. Chem. Tech. Lab.* **1992**, *40*, 1099–1104; M. Albrecht, G. Erker, C. Krüger, *Synlett* **1993**, 441–448, and references therein; G. Erker, M. Albrecht, C. Krüger, M. Nolte, S. Werner, *Organometallics* **1993**, *12*, 4979–4986; R. Gleiter, I. Hyla-Kryspin, S. Niu, G. Erker, *Angew. Chem.* **1993**, *105*, 753–755; *Angew. Chem. Int. Ed. Engl.* **1993**, *32*, 754; G. Erker, D. Röttger, *ibid.* **1993**, *105*, 1691–1693 and **1993**, *32*, 1623; P. Binger, F. Sandmeyer, C. Krüger, J. Kuhnigh, R. Goddard, G. Erker, *ibid.* **1994**, *106*, 213–215 and **1994**, *33*, 197.

[6] A. Berndt, *Angew. Chem.* **1993**, *105*, 1034–1058; *Angew. Chem. Int. Ed. Engl.* **1993**, *32*, 985–1009.

[7] The constitution of **9** ensues from the similarity of the chemical shifts of its framework atoms with those of known nonclassical 1,2-diboretanes: D. Steiner, C. Balzereit, H. J. Winkler, N. Stamatis, M. Hofmann, P. von R. Schleyer, W. Massa, A. Berndt, *Angew. Chem.* **1994**, *106*, 2391–2394; *Angew. Chem. Int. Ed. Engl.* **1994**, *33*, 2303–2306.

[8] Crystal structure determinations: Colorless crystals of **3a** and **3c** were examined on a four-circle diffractometer (CAD4, Enraf-Nonius) at −60 and 25 °C, respectively, with $Cu_{K\alpha}$ radiation ($\lambda = 154.178$ pm). **3a**: ($C_{30}H_{52}B_2Si_3$) crystal dimensions $0.4 \times 0.3 \times 0.3$ mm^3, monoclinic, space group $P2_1/n$, $Z = 4$, $a = 927.2(2)$, $b = 2792.9(6)$, $c = 1329.5(3)$ pm, $\beta = 105.16(3)°$, $V_{EZ} = 3323.0 \times 10^{-30}$ m^3, $\rho_{calcd} = 1.037$ g cm^{-3}; in total, 4370 reflections were measured with ω scans in the range up to $2\theta = 110°$; all 4162 independent reflections were used for the further calculation after LP correction (LP = Lorentz Polarization); no absorption correction ($\mu = 14.1$ cm^{-1}). The structure was solved by direct methods and refined against the F_o^2 data with full matrix. Most of the H atoms, in particular that bonded to the boron atoms, could be localized from difference Fourier syntheses, the positions of the rest were calculated. The H1 atom bonded to B1 and B2 could be freely refined with an isotropic temperature factor. The standard deviations of the site parameters of between 2.2 and 2.4 pm and the low temperature factor ($U = 0.046(6) \times 10^{-20}$ m^2 [= Å^2]) unequivocally indicate the good reliability of localization. All other H atoms were included riding on their bonding partners in groups with common isotropic temperature factors. Anisotropic temperature factors were used for all heavier atoms. The result was $wR_2 = 0.1112$, corresponding to $R = 0.0406$ for 3482 reflections $> 4\sigma(F_o)$, the maximum residual electron density was 0.29 e Å^{-3}. **3c**: ($C_{32}H_{56}B_2Si_2$) crystal dimensions $0.6 \times 0.3 \times 0.3$ mm^3, triclinic, space group $P\bar{1}$, $Z = 2$, $a = 885.3(2)$, $b = 1189.1(2)$, $c = 1605.4(3)$ pm, $\alpha = 93.41(3)°$, $\beta = 96.07(3)°$, $\gamma = 92.89(3)°$, $V_{EZ} = 1674.8 \times 10^{-30}$ m^3, $\rho_{calcd} = 1.048$ g cm^{-3}; in total, 4476 reflections were measured with ω scans in the range up to $2\theta = 110°$; all 4142 independent reflections were used for the further calculation after LP correction; no absorption correction ($\mu = 10.7$ cm^{-1}). The structure solution and refinement as carried out for **3a** led to $wR_2 = 0.1479$. $R = 0.049$ for 3686 reflections $> 4\sigma(F_o)$; the maximum residual electron density was 0.38 e Å^{-3}. Analogous to **3a**, the H1 atom in this case was also clearly localized (standard deviations of the site parameters 1.8–2.4 pm; $U = 0.040(6) \times 10^{-20}$ m^2 [= Å^2]). Further details of the crystal structure investigation may be obtained from the Fachinformationszentrum Karlsruhe, D-76344 Eggenstein-Leopoldshafen (Germany) on quoting the depository number CSD-58730.

[9] E. D. Jemmis, G. Subramanian, G. N. Srinivas, *J. Am. Chem. Soc.* **1992**, *114*, 7939–7941.

[10] Our own calculations for CB_2H_4 show [11] that **3u$_\beta$** is not only an energy minimum ($i = 0$), but also the global minimum on the potential energy surface. The energetically next highest lying isomer, the B-borylmethyleneborane $H_2C{=}B{-}BH_2$ (C_{2v}), is 30.6 kcal mol^{-1} (MP4/6-311G(2df,2pd)//MP2/6-31G(d)) less stable. The deep potential minimum of **3u$_\beta$** is also given by the calculated vibrational frequency for the out-of-plane mode of the bridging H atom, which is rather high at 504.7 cm^{-1} (MP2/6-31G(d)). The parent framework **3u$_\beta$** is thus energetically very stable according to the calculations.

[11] S. Fau, G. Frenking, *THEOCHEM* **1995**, in press.

[12] M. Krempp, R. Damrauer, C. H. DePuy, Y. Keheyan, *J. Am. Chem. Soc.* **1994**, *116*, 3629–3630.

[13] Bühl et al. recently recognized a planar tetracoordinate boron atom in the α-agostic distorted borylmethyleneborane **8u** (Scheme 3) [14]. In **8b** [6] the tetracoordinate boron atom lies 6.8 pm outside the plane of best fit of its four neighbors. Its bond to the duryl substituent is bent by 6.4° with respect to the plane of the framework atoms, probably owing to steric reasons.

[14] M. Bühl, J. Gauss, M. Hofmann, P. von R. Schleyer, *J. Am. Chem. Soc.* **1993**, *115*, 12385–12390.

[15] The geometries were optimized to the MP2/6-31G* level with the program GAUSSIAN 92: Gaussian 92, Revision A, M. J. Frisch, G. W. Trucks, H. Head-Gordon, P. M. W. Gill, M. W. Wond, J. B. Foresman, H. B. Schlegel, K. Raghavachari, M. A. Robb, J. S. Binkley, C. Gonzalez, R. Martin, D. J. Fox, D. J. DeFrees, J. Baker, J. J. P. Stewart, J. A. Pople, Gaussian, Inc. Pittsburgh, PA, **1992**.

[16] Structure **11$_\beta$**, in which the bridging H atom is 121.4 pm from the boron atom and 170.3 pm from the C atom (C–C 127.6, C–B 153.9 pm), is the transition state for the 1,2-H rearrangement **11$_\alpha$** → **12**. The activation barrier at the MP2/6-31G* + ZPE level is 3.7 kcal mol^{-1}.

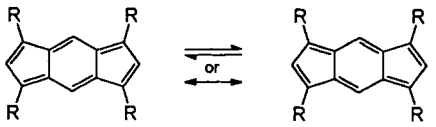
[17] K. Lammertsma, P. von R. Schleyer, *J. Am. Chem. Soc.* **1990**, *112*, 7935–7940, and references therein.

1,3,5,7-Tetra-*tert*-butyl-4-aza- and 1,3,5,7-Tetra-*tert*-butyl-4-phospha-*s*-indacene**

Teodor Silviu Balaban, Stefan Schardt, Volker Sturm, and Klaus Hafner*

Dedicated to Professor Wolfgang Lüttke on the occasion of his 75th birthday

s-Indacene (**1**),[1] a tricyclic, nonalternating [4n]π system, has been the subject of repeated theoretical and experimental investigations. Formally, **1** may be regarded as a [12]annulene perturbed by two σ bonds, and can therefore be considered as an antiaromatic compound. According to calculations carried out previously for **1**,[2-4] a ground state structure with localized double bonds and the C_{2h}-symmetrical π-bonding was suggested for isomers **1A** and **1B**.

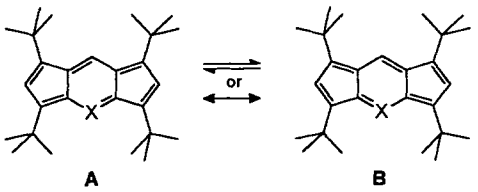


1: R=H
2: R=*t*Bu

In contrast to **1**, which could not be isolated, the kinetically stabilized 1,3,5,7-tetra-*tert*-butyl-*s*-indacene **2** has been found to be a stable compound. The D_{2h} structure with equidistant bond lengths established for **2** by an X-ray structure analysis[5,6] was attributed to an unusually strong electronic influence of the *tert*-butyl groups.[7] On the other hand, according to recent quantum chemical calculations by Koch et al.,[8] **1** is also expected to exist in the ground state as a delocalized π system with a D_{2h} structure. The limited stability of **1** is a consequence of the considerable singlet-diradical character of the *s*-indacene system.

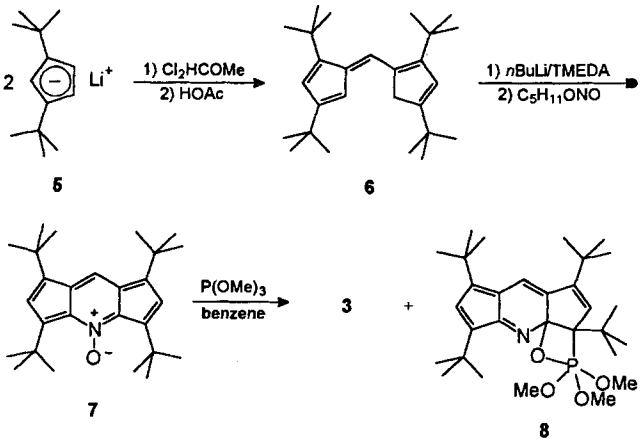
Only a few investigations of hetero-*s*-indacenes have been carried out so far. Owing to the electronically stabilizing substituents, the donor-substituted 1,3,5,7-tetrakis(diethylamino)-2,6-diaza-*s*-indacene synthesized by Gompper et al.[9] is not suitable for obtaining information about the influence of the nitrogen atoms on the π perimeter. The introduction of one nitrogen atom or a different heteroatom into the fully conjugated *s*-indacene system has not been described hitherto. Herein we report on the syntheses of 1,3,5,7-tetra-*tert*-butyl-4-aza-*s*-indacene (**3**) and its phospha-analogue (**4**) as well as on their bonding in comparison to that of the carbocycle **2**.

For the synthesis of **3**, (*E*)-1,3-di-*tert*-butyl-5-(2,4-di-*tert*-butylcyclopenta-1,3-dienylmethylidene)cyclopenta-1,3-diene (**6**) was prepared by reaction of lithium 1,3-di-*tert*-butylcyclopentadienide (**5**) with half an equivalent of 1,1-dichloromethyl methyl ether.[10-12] This could be transformed by deprotonation with

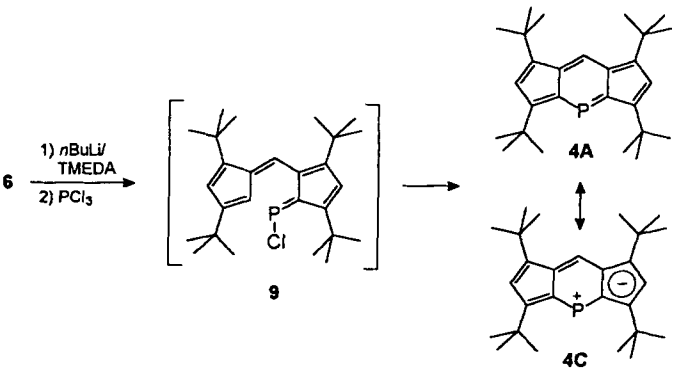


3: X=N
4: X=P

n-butyllithium in the presence of TMEDA and subsequent treatment with isoamyl nitrite into 1,3,5,7-tetra-*tert*-butyl-4-aza-*s*-indacene-*N*-oxide (**7**), which was obtained in 42% yield as a dark blue, fine crystalline powder (m.p. 261-263 °C (decomp.)).[13] Deoxygenation of **7** to give the 4-aza-*s*-indacene **3** was achieved with trimethyl phosphite in boiling benzene. This afforded the tricycle **3** in 75% yield as an extremely unstable, dark red solid (m.p. 136-138 °C (decomp.)). In addition to **3**, small amounts of the 1,2λ^5-oxaphosphetane **8** (bordeaux red plates, m.p. 181 °C, 17% yield) were isolated, whose structure was established by an X-ray structure analysis.[14]



In analogy to the synthesis of **7**, the pentafulvene **6** was deprotonated (*n*BuLi/TMEDA) and subsequently treated with phosphorus trichloride at −50 °C to give rise to the 1,3,5,7-tetra-*tert*-butyl-4-phospha-*s*-indacene **4**, which could be isolated as blue-black crystals with a metallic luster (m.p. 221-222 °C (decomp.), 75% yield). At room temperature **4** may be stored for several weeks under an inert atmosphere, and is only poorly soluble in organic solvents giving intense dark blue solutions. In the synthesis of **4**, the 6-phosphapentafulvene derivative **9**[15] may be



[*] Prof. Dr. K. Hafner, Dipl.-Ing. S. Schardt
Institut für Organische Chemie der Technischen Hochschule
Petersenstrasse 22, D-64827 Darmstadt (Germany)
Telefax: Int. code + (6151)16-3574
Dr. T. S. Balaban
C. D. Nenitzescu Institute of Organic Chemistry
Bucharest (Romania)
Dr. V. Sturm
Freudenberg, Weinheim (Germany)

[**] This work was supported by the Fonds der Chemischen Industrie and by the Dr. Otto-Röhm-Gedächtnisstiftung, Darmstadt. T. S. B. thanks the Alexander-von-Humboldt-Stiftung for a research stipendium.

an intermediate, whose 12π-electrocyclization and subsequent hydrogen chloride elimination generate the heterocycle **4**.

The spectroscopic data of the azaindacene **3** (see below) suggest only a slight perturbation of the electronic structure by the introduction of the nitrogen atom into the 4-position of the 12π perimeter of **2**. A potential loss of symmetry through localized double bonds is not observed. The 300 MHz ^{1}H NMR spectrum shows, in addition to two singlets for the *tert*-butyl groups, a common singlet for 2-H and 6-H, as well as one for 8-H. In the ^{1}H broadband decoupled ^{13}C NMR spectrum, six singlets are observed for the eleven ring carbon atoms. These data may be interpreted on the assumption of a C_{2v}-symmetric structure with π-electron delocalization and equivalent bond lengths, as well as a rapid bond shift of the localized π-bonding isomers **3A** and **3B**. A ^{13}C NMR spectrum in [D$_8$]THF recorded at 173 K shows no splitting of the signals by "freezing" a possible π-bond shift. The proton resonances of the azaindacene **3** experience a downfield shift of $\Delta\delta = 0.1$ for the 2-, 6-, and 8-H, compared with those of **2**. This small difference in chemical shift indicates the similarity between the electronic structures of both compounds.

The NMR spectra of the phosphaindacene **4** likewise show no signal splitting due to double bond localization, neither at room temperature nor at 173 K. The resonances in the ^{1}H NMR spectrum ($\Delta\delta = 0.25$ for 2-H and 6-H and 0.37 for 8-H) display a distinctly stronger downfield shift than those of **2**. The ^{1}H broadband decoupled ^{31}P NMR spectrum of **4** with a singlet at $\delta = 258.6$,[16] indicates a comparatively strong deshielded phosphorus nucleus. This could be attributed to an appreciable contribution of dipolar resonance structures with a formal positive charge at the phosphorus atom, for example **4C**. An X-ray structure analysis of **4** did not furnish any reliable data regarding bond lengths and angles owing to statistical disorder of the molecules in the crystal.[14]

The UV/Vis spectrum of **3** in dichloromethane shows an absorption maximum at $\lambda_{max} = 314$ nm with resolved vibrational fine structure and a further maximum at 564 nm (Fig. 1). In

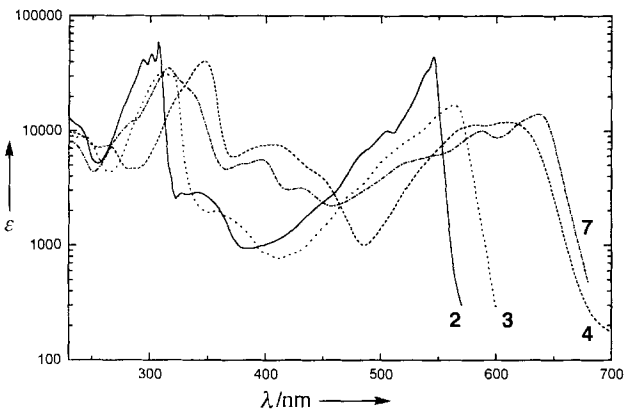
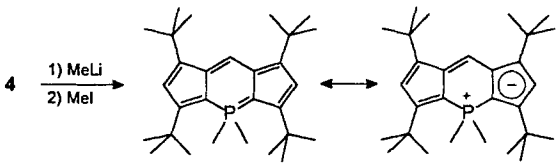


Fig. 1. UV/Vis spectra of the *s*-indacenes **2** and **3** in *n*-hexane, as well as those of **4** and **7** in CH_2Cl_2.

comparison with the carbocyclic *s*-indacene **2**, the absorption bands of the 4-aza-indacene **3** are shifted bathochromically by 10–15 nm with a very similar fine structure. However, the extinction coefficients of the heterocycle **3** are comparable to those of the parent system **2**. The UV/Vis absorptions of the phosphaindacene **4** ($\lambda_{max} = 346$, 582, and 610 nm) show a bathochromic shift of more than 30 nm relative to those of **2** (Fig. 1). The fact that these absorptions are shifted more bathochromically than those of the azaindacene **3** may be, presumably, attributed to a resonance structure of type **4C**.

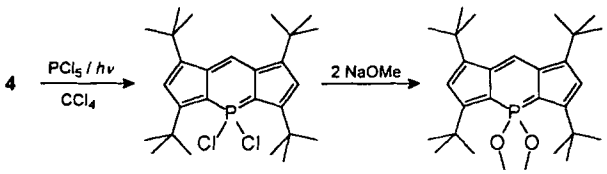
The reaction of the phosphaindacene **4** with methyllithium, followed by addition of methyl iodide led to 1,3,5,7-tetra-*tert*-butyl-4,4-dimethyl-4λ^5-phospha-*s*-indacene (**10**), which was obtained as stable red needles (58% yield, sublimes ≥ 310 °C).



10A **10C**

In an analogy to λ^5-phosphinines,[17] the cyclic π-conjugation is partially perturbed by the formally pentavalent phosphorus. The resulting decrease of the paramagnetic ring current effect leads to downfield shifts of $\Delta\delta = 0.59$ for 2-H and 6-H and 0.75 for 8-H in the ^{1}H NMR spectrum of **10**, relative to that of the λ^3-phosphaindacene **4**. The ^{31}P resonance of **10** at $\delta = -16.7$ is in the range of usual values as expected for cyclic conjugated phosphorus ylides and suggests a substantial contribution of the resonance stabilized betaine structure of type **10C** to the ground state of the λ^5-phospha-*s*-indacene **10**.

Upon irradiation (300 W, Osram Concentra), **4** reacts with phosphorus pentachloride under radical addition of one mole equivalent of chlorine at the phosphorus atom to give 1,3,5,7-tetra-*tert*-butyl-4,4-dichloro-4λ^5-phospha-*s*-indacene (**11**) (43% yield, pale green needles, sublimes ≥235 °C). Double nucleophilic substitution in the 4-position of **11** with sodium methoxide affords the 4,4-dimethoxy derivative **12** (48% yield, black



11 **12**

crystals, m.p. 228–229 °C, soluble in organic solvents leading to an emerald green coloration).

Some spectroscopic data for the compounds **2**–**4**, **7**, **8**, and **10**–**12** [18].

2 [5]: ^{1}H NMR (300 MHz, $CDCl_3$): $\delta = 1.18$ (s, 36 H; 1-, 3-, 5-, 7-*t*Bu), 5.29 (s, 2 H; 2-, 6-H), 6.90 (s, 2 H; 4-, 8-H); ^{13}C NMR (75.5 MHz, $CDCl_3$): $\delta = 31.2$ (C(CH_3)$_3$), 34.0 (*C*(CH_3)$_3$), 124.9 (C-2, C-6 or C-4, C-8), 129.1 (C-2, C-6 or C-4, C-8), 132.0 (C-3a, C-4a, C-7a, C-8a), 164.3 (C-1, C-3, C-5, C-7); UV/Vis (*n*-hexane): λ_{max} (lg ε) = 224 (4.10), 234 (4.03) (sh), 278 (4.23) (sh), 284 (4.37) (sh), 289 (4.48) (sh), 294 (4.61), 301 (4.66), 307 (4.77), 330 (3.45) (sh), 340 (3.48), 451 (3.41) (sh), 486 (3.83) (sh), 500 (3.96) (sh), 505 (4.01), 519 (4.11) (sh), 527 (4.26) (sh), 539 (4.51) (sh), 545 nm (4.64)

3: MS (70 eV): *m/z* (%): 377 (33) [M^+], 362 (100) [M^+ − Me], 332 (17) [M^+ − 3 Me], 320 (12) [M^+ − *t*Bu], 57 (34) [*t*Bu$^+$]; ^{1}H NMR (300 MHz, CD_2Cl_2): $\delta = 1.16$ (s, 18 H; 1-, 7-*t*Bu), 1.22 (s, 18 H; 3-, 5-*t*Bu), 5.41 (s, 2 H; 2-, 6-H), 6.81 (s, 1 H; 8-H); ^{13}C NMR (75.5 MHz, CD_2Cl_2): $\delta = 29.96$ (3-, 5-C(CH_3)$_3$), 30.50 (1-, 7-C(CH_3)$_3$), 33.85 (1-, 7- or 3-, 5-*C*(CH_3)$_3$), 34.49 (1-, 7- or 3-, 5-*C*(CH_3)$_3$), 126.58 (C-2, C-6), 126.96 (C-7a, C-8a), 128.71 (C-8), 153.44 (C-3a, C-4a), 163.21 (C-1, C-7 or C-3, C-5), 163.78 (C-1, C-7 or C-3, C-5); UV/Vis (CH_2Cl_2): λ_{max} (lg ε) = 236 (3.94), 301 (4.41) (sh), 307 (4.49), 314 (4.51), 320 (4.47), 355 (3.29) (sh), 505 (3.78) (sh), 527 (3.95) (sh), 564 nm (4.24)

4: MS (70 eV): *m/z* (%): 394 (47) [M^+], 379 (100) [M^+ − Me], 364 (25) [M^+ − 2 Me], 337 (28) [M^+ − *t*Bu], 57 (34) [*t*Bu$^+$]; ^{1}H NMR (300 MHz, CD_2Cl_2): $\delta = 1.24$ (s, 18 H; 1-, 7-*t*Bu), 1.34 (s, 18 H; 3-, 5-*t*Bu), 5.54 (d, ^4J(P,H) = 3.7 Hz, 2 H;

2-, 6-H), 7.27 (s, 1H; 8-H); ^{13}C NMR (75.5 MHz, CD_2Cl_2): δ = 31.70 (s, 1-, 7-C(CH_3)$_3$), 33.25 (d, ^4J(P,C) = 9.1 Hz, 3-, 5-C(CH_3)$_3$), 34.00 (s, 1-, 7- or 3-, 5-C(CH$_3$)$_3$), 35.49 (s, 1-, 7- or 3-, 5-C(CH$_3$)$_3$), 125.63 (d, ^3J(P,C) = 9.8 Hz, C-2, C-6), 131.50 (s, C-7a, C-8a), 132.15 (s, C-8), 149.19 (d, ^1J(P,C) = 47.4 Hz, C-3a, C-4a), 165.16 (d, ^XJ(P,C) = 9.9 Hz, C-1, C-7 or C-3, C-5), 173.18 (d, ^XJ(P,C) = 23.7 Hz, C-1, C-7 or C-3, C-5); ^{31}P NMR (121.5 MHz, $CDCl_3$): δ = 258.6; UV/Vis (CH_2Cl_2): λ_{max} (lgε) = 240 (3.96) (sh), 262 (3.87), 346 (4.61), 407 (3.88), 443 (3.64) (sh), 582 (4.06), 610 (4.08), 864 (2.30), 984 (2.23) (sh), 1120 nm (1.79) (sh)

7: MS (70 eV): m/z (%): 393 (42) [M^+], 378 (23) [M^+ − Me], 57 (36) [tBu$^+$]; ^{1}H NMR (300 MHz, $CDCl_3$): δ = 1.21 (s, 18H; 1-, 7-tBu), 1.27 (s, 18H; 3-, 5-tBu), 5.47 (s, 2H; 2-, 6-H), 6.98 (s, 1H; 8-H); ^{13}C NMR (75.5 MHz, $CDCl_3$): δ = 27.32 (3-, 5-C(CH_3)$_3$), 31.24 (1-, 7-C(CH_3)$_3$), 33.74 (1-, 7- or 3-, 5-C(CH_3)$_3$), 33.87 (1-, 7- or 3-, 5-C(CH$_3$)$_3$), 124.95 (C-2, C-6), 127.29 (C-8), 128.84 (C-7a, C-8a), 141.77 (C-3a, C-4a), 157.96 (C-1, C-7 or C-3, C-5), 158.99 (C-1, C-7 or C-3, C-5); UV/Vis (CH_2Cl_2): λ_{max} (lgε) = 239 (3.85) (sh), 288 (4.09) (sh), 316 (4.55), 334 (4.36) (sh), 380 (3.71), 396 (3.74), 432 (3.49), 528 (3.72) (sh), 547 (3.77), 587 (4.00), 627 (4.11) (sh), 637 nm (4.15)

8: MS (70 eV): m/z (%): 486 (6) [M^+ − OMe], 377 (42) [M^+ − OP(OMe)$_3$], 362 (100) [M^+ − OP(OMe)$_3$ − Me], 57 (34) [tBu$^+$]; ^{1}H NMR (300 MHz, $CDCl_3$): δ = 1.02 (br.s, 9H; 2a-tBu), 1.25 (s, 9H; tBu), 1.27 (s, 9H; tBu), 1.30 (s, 9H; tBu), 3.54 (d, ^3J(P,H) = 12.9 Hz, 9H; P(OCH$_3$)$_3$), 5.99 (d, ^3J(P,H) = 7.3 Hz, 1H; 3-H), 6.30 (s, 1H; 5-H or 7-H), 6.91 (s, 1H; 5-H or 7-H); ^{13}C NMR (75.5 MHz, $CDCl_3$): δ = 26.83 (br.s, 2a-C(CH_3)$_3$), 29.47 (s, C(CH_3)$_3$), 29.92 (s, C(CH_3)$_3$), 30.00 (s, C(CH_3)$_3$), 32.55 (s, C(CH$_3$)$_3$), 33.16 (d, ^XJ(P,C) = 2.0 Hz, C(CH$_3$)$_3$), 34.60 (s, C(CH$_3$)$_3$), 35.78 (d, ^2J(P,C) = 5.9 Hz, 2a-C(CH_3)$_3$), 53.50 (d, ^2J(P,C) = 10.7 Hz, OCH$_3$), 87.57 (d, ^1J(P,C) = 152.4 Hz, C-2a), 89.16 (d, ^2J(P,C) = 16.8 Hz, C-9a), 113.09 (s, C_{quat}), 117.10 (d, ^4J(P,C) = 4.3 Hz, C-5), 129.70 (d, ^2J(P,C) = 14.3 Hz, C-3), 135.26 (s, C-7), 143.99 (d, ^XJ(P,C) = 13.4 Hz, C_{quat}), 145.14 (s, C_{quat}), 150.04 (d, ^XJ(P,C) = 15.7 Hz, C_{quat}), 151.52 (s, C_{quat}), 175.45 (s, C-8a); ^{31}P NMR (121.5 MHz, $CDCl_3$): δ = − 29.4; UV/Vis (n-hexane): λ_{max} (lgε) = 250 (4.24), 303 (3.89), 493 nm (3.34)

10: MS (70 eV): m/z (%): 424 (93) [M^+], 409 (100) [M^+ − Me], 394 (4) [M^+ − 2Me], 379 (9) [M^+ − 3Me], 57 (13) [tBu$^+$]; ^{1}H NMR (300 MHz, $CDCl_3$): δ = 1.39 (s, 18H; 1-, 7- or 3-, 5-tBu), 1.40 (s, 18H; 1-, 7- or 3-, 5-tBu), 2.23 (d, ^2J(P,H) = 12.9 Hz, 6H; P(CH$_3$)$_2$), 6.13 (d, ^4J(P,H) = 6.9 Hz, 2H; 2-, 6-H), 8.02 (d, ^4J(P,H) = 2.8 Hz, 1H; 8-H); ^{13}C NMR (75.5 MHz, $CDCl_3$): δ = 22.04 (d, ^1J(P,C) = 58.1 Hz, P(CH$_3$)$_2$), 33.19 (s, 1-, 7- or 3-, 5-C(CH_3)$_3$), 33.25 (s, 1-, 7- or 3-, 5-C(CH_3)$_3$), 34.14 (s, 1-, 3-, 5- and 7-C(CH$_3$)$_3$), 91.00 (d, ^1J(P,C) = 100.0 Hz, C-3a, C-4a), 119.39 (d, ^3J(P,C) = 17.0 Hz, C-2, C-6), 124.27 (d, ^2J(P,C) = 12.1 Hz, C-7a, C-8a), 135.07 (s, C-8), 149.08 (d, ^XJ(P,C) = 9.3 Hz, C-1, C-7 or C-3, C-5), 154.13 (d, ^XJ(P,C) = 10.6 Hz, C-1, C-7 or C-3, C-5); ^{31}P NMR (121.5 MHz, $CDCl_3$): δ = − 16.7; UV/Vis (CH_2Cl_2): λ_{max} (lgε) = 234 (4.36), 303 (3.33), 318 (3.30), 457 (4.01), 575 nm (4.40)

11: MS (70 eV): m/z (%): 464, 466 (81, 55) [M^+], 449, 451 (100, 67) [M^+ − Me], 434, 436 (7, 6) [M^+ − 2Me], 394 (39) [M^+ − 2Cl], 379 (75) [M^+ − 2Cl − Me], 364 (25) [M^+ − 2Cl − 2Me], 337 (19) [M^+ − 2Cl − tBu], 57 (96) [tBu$^+$]; ^{1}H NMR (300 MHz, C_6D_6): δ = 1.36 (s, 18H; 1-, 7- or 3-, 5-tBu), 1.49 (s, 18H; 1-, 7- or 3-, 5-tBu), 6.30 (d, ^4J(P,H) = 9.1 Hz, 2H; 2-, 6-H), 8.03 (d, ^4J(P,H) = 2.4 Hz, 1H; 8-H); ^{13}C NMR (75.5 MHz, C_6D_6): δ = 32.43 (s, 1-, 7- or 3-, 5-C(CH_3)$_3$), 32.96 (s, 1-, 7- or 3-, 5-C(CH_3)$_3$), 33.77 (s, 1-, 7- or 3-, 5-C(CH$_3$)$_3$), 35.27 (s, 1-, 7- or 3-, 5-C(CH$_3$)$_3$), 96.88 (d, ^1J(P,C) = 119.9 Hz, C-3a, C-4a), 122.91 (d, ^3J(P,C) = 23.0 Hz, C-2, C-6), 129.61 (d, ^2J(P,C) = 18.9 Hz, C-7a, C-8a), 133.47 (s, C-8), 156.78 (d, ^XJ(P,C) = 17.3 Hz, C-1, C-7 or C-3, C-5), 164.10 (d, ^XJ(P,C) = 12.1 Hz, C-1, C-7 or C-3, C-5); ^{31}P NMR (121.5 MHz, C_6D_6): δ = 25.3; UV/Vis (CH_2Cl_2): λ_{max} (lgε) = 262 (4.55), 303 (3.74), 353 (3.48), 415 (3.68) (sh), 443 (3.93) (sh), 474 (4.24) (sh), 492 (4.40), 682 nm (3.85)

12: MS (70 eV): m/z (%): 456 (61) [M^+], 441 (100) [M^+ − Me], 426 (15) [M^+ − 2Me], 411 (7) [M^+ − 3Me], 57 (60) [tBu$^+$]; ^{1}H NMR (300 MHz, $CDCl_3$): δ = 1.32 (s, 18H; 1-, 7- or 3-, 5-tBu), 1.36 (s, 18H; 1-, 7- or 3-, 5-tBu), 3.58 (d, ^3J(P,H) = 13.8 Hz, 6H; P(OCH$_3$)$_2$), 5.95 (d, ^4J(P,H) = 6.7 Hz, 2H; 2-, 6-H), 7.68 (d, ^4J(P,H) = 3.2 Hz, 1H; 8-H); ^{13}C NMR (75.5 MHz, $CDCl_3$): δ = 31.82 (s, 1-, 7- or 3-, 5-C(CH_3)$_3$), 33.15 (s, 1-, 7- or 3-, 5-C(CH_3)$_3$), 33.50 (s, 1-, 7- or 3-, 5-C(CH$_3$)$_3$), 34.34 (s, 1-, 7- or 3-, 5-C(CH$_3$)$_3$), 52.43 (s, OCH$_3$), 88.81 (d, ^1J(P,C) = 140.6 Hz, C-3a, C-4a), 120.31 (d, ^3J(P,C) = 18.3 Hz, C-2, C-6), 130.51 (d, ^2J(P,C) = 17.9 Hz, C-7a, C-8a), 133.33 (s, C-8), 154.38 (d, ^XJ(P,C) = 13.5 Hz, C-1, C-7 or C-3, C-5), 161.46 (d, ^XJ(P,C) = 9.9 Hz, C-1, C-7 or C-3, C-5); ^{31}P NMR (121.5 MHz, $CDCl_3$): δ = 56.1; UV/Vis (CH_2Cl_2): λ_{max} (lgε) = 240 (4.47), 275 (3.75) (sh), 328 (3.26) (sh), 338 (3.39), 472 (4.22) (sh), 482 (4.32), 638 nm (4.00)

Received: August 17, 1994 [Z 7243 IE]
German version: *Angew. Chem.* **1995**, *107*, 360

Keywords: aromaticity · indacenes · Hückel rules

[1] K. Hafner, *Angew. Chem.* **1963**, *75*, 1041–1050; *Angew. Chem. Int. Ed. Engl.* **1964**, *3*, 165–173; K. Hafner, K. H. Häfner, C. König, M. Kreuder, G. Ploss, G. Schulz, E. Sturm, K. H. Vöpel, *ibid.* **1963**, *75*, 35–46 and **1963**, *2*, 123–134; E. Sturm, Dissertation, Universität München, **1963**.

[2] R. D. Brown, *J. Chem. Soc.* **1951**, 2391–2394; T. Nakajima, T. Saijo, H. Yamaguchi, *Tetrahedron* **1964**, *20*, 2119–2124.

[3] R. Klann, R. J. Bäuerle, F. Laermer, T. Elsaesser, M. Niemeyer, W. Lüttke, *Chem. Phys. Lett.* **1990**, *169*, 172–178.

[4] C. Gellini, G. Cardini, P. R. Salvi, G. Marconi, K. Hafner, *J. Phys. Chem.* **1993**, *97*, 1286–1293.

[5] K. Hafner, B. Stowasser, H.-P. Krimmer, S. Fischer, M. C. Böhm, H. J. Lindner, *Angew. Chem.* **1986**, *98*, 646–648; *Angew. Chem. Int. Ed. Engl.* **1986**, *25*, 630–632; K. Hafner, *Pure Appl. Chem.* **1982**, *54*, 939–956; *ibid.* **1990**, *62*, 531–540.

[6] J. D. Dunitz, C. Krüger, H. Irngartinger, E. F. Maverick, Y. Wang, M. Nixdorf, *Angew. Chem.* **1988**, *100*, 415–418; *Angew. Chem. Int. Ed. Engl.* **1988**, *27*, 387–389.

[7] E. Heilbronner, Z.-Z. Yang, *Angew. Chem.* **1987**, *99*, 369–371; *Angew. Chem. Int. Ed. Engl.* **1987**, *26*, 360–362.

[8] R. H. Hertwig, M. C. Holthausen, W. Koch, Z. B. Maksić, *Angew. Chem.* **1994**, *106*, 1252–1254; *Angew. Chem. Int. Ed. Engl.* **1994**, *33*, 1192–1194.

[9] F. Closs, R. Gompper, U. Nagel, H.-U. Wagner, *Angew. Chem.* **1987**, *99*, 1068–1070; *Angew. Chem. Int. Ed. Engl.* **1987**, *26*, 1037–1039.

[10] M. Eiermann, B. Stowasser, K. Hafner, K. Bierwirth, A. Frank, A. Lerch, J. Reußwig, *Chem. Ber.* **1990**, *123*, 1421–1431.

[11] S. Schardt, Diplomarbeit, Technische Hochschule Darmstadt, **1994**.

[12] Correct elemental analyses were obtained for all the compounds described.

[13] V. Sturm, Dissertation, Technische Hochschule Darmstadt, **1987**.

[14] H. J. Lindner, unpublished results.

[15] For synthesis of 6-phosphapentafulvenes see G. Märkl, K. M. Raab, *Tetrahedron Lett.* **1989**, *30*, 1077–1080.

[16] All ^{31}P NMR data are relative to 85% phosphoric acid as external standard.

[17] K. Dimroth, *Fortsch. Chem. Forsch.* **1973**, *38*, 1–147; *Acc. Chem. Res.* **1982**, *15*, 58–64.

[18] The NMR signals of **3**, **4**, and **7** could be assigned with the aid of ^{1}H,^{13}C-COSY spectra and NOE experiments.

Surprising Formation of a Carborane-Substituted Digallane**

Anil K. Saxena, Hongming Zhang, John A. Maguire, Narayan S. Hosmane,* and Alan H. Cowley*

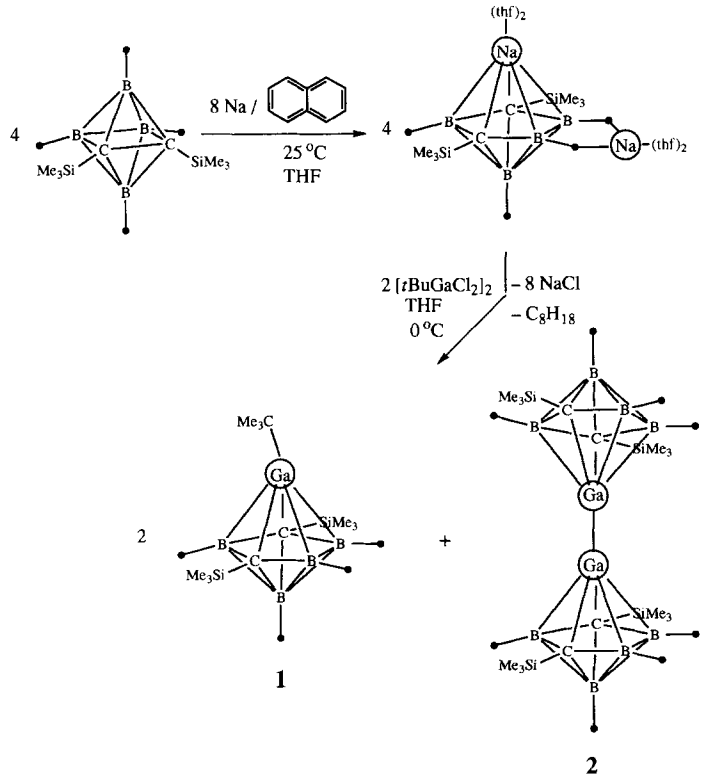
Dedicated to Professor M. Frederick Hawthorne on the occasion of his 65th birthday

Classical inorganic compounds with Ga–Ga bonds such as Ga_2Br_3[1] have been known for several years. However, organometallic derivatives with Ga–Ga bonds are of newer vintage,[2] and structurally characterized examples are restricted to the Ga^I and Ga^{II} compounds [GaC(SiMe$_3$)$_3$]$_4$[3] and Ga_2R_4 (R = (Me$_3$Si)$_2$CH,[4] 2,4,6-iPr$_3$C$_6$H$_2$,[5] and 2,4,6-(CF$_3$)$_3$C$_6$H$_2$[6]). We report a new class of compound in which the Ga–Ga bond is supported by 2,4-dicarba-*nido*-hexaborate(2$^-$) carborane ligands.

The reaction of one equivalent of [Ga(tBu)Cl$_2$]$_2$ with two equivalents of the disodium compound of *closo-exo*-5,6-Na(thf)$_2$-1-Na(thf)$_2$-2,4-(SiMe$_3$)$_2$-2,4-$C_2B_4H_4$[7] afforded a mixture of two products, **1** and **2** (Scheme 1), which were separated by fractional distillation and sublimation. Compound **1** is an air- and moisture-sensitive colorless oil for which the overall

[*] Prof. Dr. N. S. Hosmane, Dr. A. K. Saxena, Dr. H. Zhang, Prof. Dr. J. A. Maguire
Department of Chemistry, Southern Methodist University
Dallas, TX 75275 (USA)
Telefax: Int. code + (214) 768-4089
Prof. Dr. A. H. Cowley
Department of Chemistry and Biochemistry, The University of Texas at Austin
Austin, TX 78712 (USA)
Telefax: Int. code + (512) 471-6822

[**] This work was supported by grants from the National Science Foundation (CHE-91000672 to N. S. H. and CHE-9108228 to A. H. C.), the Robert A. Welch Foundation (N-1016 to N. S. H. and F-135 to A. H. C.), and the donors of the Petroleum Research Fund, administered by the American Chemical Society.



Scheme 1. • = H.

composition $C_{12}H_{31}B_4GaSi_2$ was established on the basis of elemental analysis and high-resolution mass spectrometry.[8] The ^{1}H, ^{13}C, and ^{11}B NMR spectra for **1** are very similar to those of the structurally characterized "carbons adjacent" isomer, *closo*-(*t*Bu)Ga-2,3-(SiMe$_3$)$_2$-2,3-$C_2B_4H_4$,[9] hence a *closo* structure with an η^5 attachment of the Ga*t*Bu moiety to the carborane cage can also be proposed in this case.

Compound **2** is an air- and moisture-sensitive solid with an empirical composition $(Me_3SiC)_2(BH)_4Ga$. The ^{11}B NMR spectrum of **2**[8] indicated the presence of three basal boron atoms and one apical boron atom. These observations, together with the detection of basal carbon atoms in the ^{13}C NMR spectrum and trimethylsilyl groups in the ^{1}H NMR spectrum, imply the presence of intact Me_3Si-substituted C_2B_3 moieties. It is significant that no peaks corresponding to *t*Bu groups were evident in either the ^{13}C or ^{1}H NMR spectra of **2**. In the EI high-resolution mass spectrum, the peak corresponding to the dimer at m/z = 574.1765 was accompanied by a cluster of other peaks with the appropriate isotopic intensities. Other prominent clusters of peaks corresponded to [dimer − Me]$^+$ and [monomer].$^+$ There was no mass spectrometric evidence for gallium hydride entities; moreover, no IR absorptions or Raman bands were detected in the Ga–H stretching region.

Confirmation of the structure of **2** was provided by X-ray crystallography.[10] The crystalline state comprises discrete dimeric molecules (Fig. 1) and there are no unusually short intermolecular contacts. In accord with the spectroscopic data, there are no indications of Ga–H bonds and the Ga–Ga distance in **2** (2.340(2) Å) is more than 0.2 Å shorter than the formally nonbonded Ga···Ga distances in the hydride-bridged species Ga_2H_6 (2.580(2) Å)[11] and $Me_2Ga(\mu\text{-}H)_2GaMe_2$ (2.610(5) Å).[12] The Ga–Ga distance in **2** is also shorter than those in the digallanes $Ga_2\{CH(SiMe_3)_2\}_4$ (2.541(1) Å),[4] Ga_2(2,4,6-*i*Pr$_3$C$_6$H$_2$)$_4$ (2.513(3) Å)[5] and Ga_2(2,4,6-(CF$_3$)$_3$C$_6$H$_2$)$_4$ (2.479(1) Å).[6] Interestingly, within experimental error, however, the Ga–Ga distance in **2** is equal to that in the anion radical $[Ga_2(2,4,6\text{-}iPr_3C_6H_2)_4]^{\cdot -}$ (2.343(2) Å)[5] and together they represent the shortest Ga–Ga distances known. Modeling studies[13] reveal that the steric protection of the Ga–Ga bond in **2** is significantly less than that in previous digallanes. It is therefore possible that the bond length in **2** corresponds to that of a "normal" Ga–Ga single bond in an organometallic compound.[14]

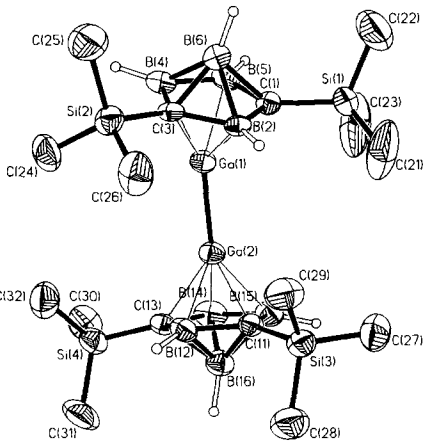


Fig. 1. Crystal structure of **2** showing the atom numbering scheme. The silyl-H atoms are omitted for clarity. Pertinent distances [Å] and angles [ ]: Ga(1)-Ga(2) 2.340(2), Ga(1)-Cnt(1) 1.679, Ga(1)-C(1) 2.164(8), Ga(1)-B(2) 2.232(11), Ga(1)-C(3) 2.146(10), Ga(1)-B(4) 2.145(11), Ga(1)-B(5) 2.125(10), Ga(2)-Cnt(2) 1.679, Ga(2)-C(11) 2.171(7), Ga(2)-B(12) 2.241(10), Ga(2)-C(13) 2.160(8), Ga(2)-B(14) 2.136(15), Ga(2)-B(15) 2.136(11); Cnt(1)-Ga(1)-Ga(2) 159.6, Cnt(2)-Ga(2)-Ga(1) 164.4. Cnt = center of the C_2B_3 ring.

When the disodium precursor was replaced by the corresponding dilithium species in Scheme 1, the *closo*-gallacarborane **1** was produced exclusively without the elimination of the *t*Bu group,[15] indicating that the reaction of the dilithium compound with $[Ga(t\text{Bu})Cl_2]_2$ involves a straightforward ligand replacement process to give **1**. While the mechanism for the formation of **2** is not known, the dependence of the reaction on the nature of the alkali metal in the carborane precursor indicates that **2** is probably not the result of a simple elimination of *t*Bu groups during the isolation of **1** by vacuum distillation. In principle, one would expect that such an elimination would favor the formation of a hydride-bridged species, such as $[(\text{carborane})Ga(\mu\text{-}H)]_2$, rather than **2**. However the absence of any evidence for Ga–H containing species with either the dilithium or the disodium compound tends to argue against extensive decomposition of **1** during the isolation process. Interestingly, we were not able to isolate **2** from the reaction of the dicarba-*nido*-hexaborate(2$^-$) ion with $Ga_2Cl_4 \cdot 2$dioxane or $GaCl_3$.

Finally, we note that the attachment of each Ga atom to the respective C_2B_3 carborane face is "slip distorted" in the sense that the Ga(1)–B(2) and Ga(2)–B(12) distances are about 0.1 Å longer than the other distances between the Ga atoms and the corresponding C_2B_3 moiety. The rotational orientation of the two C_2B_3 faces is such that the C(13)-Ga(2)-Ga(1)-C(3) dihedral angle is 58.3°.

Experimental Procedure

A sample of *closo-exo*-5,6-Na(thf)$_2$-1-Na(thf)$_2$-2,4-(SiMe$_3$)$_2$-2,4-$C_2B_4H_4$ (8.04 mmol) [7] was allowed to react for 4 h with anhydrous [*t*BuGaCl$_2$]$_2$ (1.59 g, 4.02 mmol) in dry THF (25 mL) at 0 °C, during which time the solution turned to pale yellow and some gray solid started to precipitate. At this point, the solvent and C_8H_{18} (spectroscopically identified but not measured) were removed from the heterogeneous product mixture resulting in a gray semi-solid. This residue was then subjected to a sequential fractional distillation/sublimation procedure. A colorless

oily liquid, later identified as **1**, was collected at 80–85 °C at 1.3 kPa pressure in a detachable U-trap held at 0 °C (1.02 g, 2.96 mmol, 37%). After further heating of the gray residue at 110–120 °C in vacuo, a colorless transparent crystalline solid, identified as **2**, sublimed out of the reaction flask and was collected in a second detachable U-trap at 0 °C (the side arms of both the reaction flask and the U-trap were maintained at about 100 °C with heating tape during the sublimation). The yield of highly air- and moisture-sensitive **2** was 13% (0.308 g, 0.536 mmol). Compound **2** (m.p. 48–49 °C) is soluble in both polar and nonpolar organic solvents. The gray residue that remained in the flask after the second sublimation was found to be insoluble in polar and nonpolar organic solvents and was discarded.

Received: August 3, 1994
Revised version: October 11, 1994 [Z7206IE]
German version: *Angew. Chem.* **1995**, *107*, 378

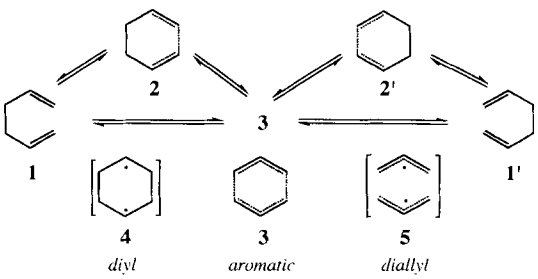
Keywords: carboranes · digallanes · gallium compounds

[1] W. Hönle, G. Gerlach, W. Weppner, A. Simon, *J. Solid State Chem.* **1986**, *61*, 171.
[2] For an excellent review, see W. Uhl, *Angew. Chem.* **1993**, *105*, 1449; *Angew. Chem. Int. Ed. Engl.* **1993**, *32*, 1386.
[3] W. Uhl, W. Hiller, M. Layh, W. Schwarz, *Angew. Chem.* **1992**, *104*, 1378; *Angew. Chem. Int. Ed. Engl.* **1992**, *31*, 1364.
[4] W. Uhl, M. Layh, T. Hildenbrand, *J. Organomet. Chem.* **1989**, *364*, 289.
[5] X. He, R. A. Bartlett, M. M. Olmstead, K. R. Senge, B. E. Sturgeon, P. P. Power, *Angew. Chem.* **1993**, *105*, 761; *Angew. Chem. Int. Ed. Engl.* **1993**, *32*, 717.
[6] R. D. Schluter, A. H. Cowley, D. A. Atwood, R. A. Jones, M. R. Bond, C. J. Carrano, *J. Am. Chem. Soc.* **1993**, *115*, 2070.
[7] N. S. Hosmane, L. Jia, H. Zhang, J. W. Bausch, G. K. S. Prakash, R. E. Williams, *Inorg. Chem.* **1991**, *30*, 3793.
[8] ^{1}H NMR (200 MHz, C_6D_6, 295 K, relative to external Me_4Si): **1**: δ = 5.0–3.8 (br, 3H; basal BH, $^1J(^1H,^{11}B)$: unresolved), 0.97 (s, 9H; CMe_3), 0.16 (s, 18 H; $SiMe_3$), signal due to apical BH could not be identified; **2**: δ = 4.8–3.6 (br, 3H; basal BH, $^1J(^1H,^{11}B)$: unresolved), 0.32 (s, 18 H; $SiMe_3$), signal due to apical BH could not be identified; ^{11}B NMR (64.2 MHz, C_6D_6, 295 K, relative to external $BF_3 \cdot OEt_2$): **1**: δ = 16.6 (d, 1B; basal BH, $^1J(^1H,^{11}B)$ = 164.8 Hz), 11.3 (d, 2B; basal BH, $^1J(^1H,^{11}B)$ = 146.5 Hz), −38.0 (d, 1B; apical BH, $^1J(^1H,^{11}B)$ = 174.0 Hz); **2**: δ = 11.1 (d, 3B; basal BH, $^1J(^1H,^{11}B)$: unresolved), −31.9 (d, 1B; apical BH, $^1J(^1H,^{11}B)$ = 156.3 Hz); ^{13}C NMR (50.3 MHz, C_6D_6, 295 K, relative to external Me_4Si): **1**: δ = 105.01 (s, br; cage carbons), 30.62 (q, Me, $^1J(^1H,^{13}C)$ = 121.09 Hz, $^3J(^1H,^{13}C)$ = 6.43 Hz), 29.68 (s, br; CMe_3), 0.81 (q, $SiMe_3$; $^1J(^1H,^{13}C)$ = 117.69 Hz]; **2**: δ 108.67 (s, br; cage carbons), 0.33 (q, $SiMe_3$, $^1J(^1H,^{13}C)$ = 121.27 Hz]; IR (cm^{-1}; $CDCl_3$ vs. $CDCl_3$): **1**: 2564.3 (s) [ν(B–H)] **2**: 2563.8 (s) [ν(B–H)]. Mass spectral analyses (high-resolution electron impact (HREI) peak match): theoretical mass for **1**: $^{12}C_{12}{}^1H_{31}{}^{11}B_4{}^{28}Si_2{}^{69}Ga$ *m/z* 344.1599; measured mass m/e 344.1593. **2**: $^{12}C_{16}{}^1H_{44}{}^{11}B_8{}^{28}Si_4{}^{69}Ga_2$, *m/z* 574.1779; measured mass m/e 574.1765. Anal. calcd for: $C_{12}H_{31}B_4Si_2Ga$ **1**: C 41.85, H 9.00. Found: C 41.38, H 9.28. Anal. calcd for $C_{16}H_{44}B_8Si_4Ga_2$ **2**: C 33.43; H 7.66. Found: C 33.42; H, 7.25.
[9] N. S. Hosmane, K. -J. Lu, H. Zang, L. Jia, A. H. Cowley, M. A. Mardones, *Organometallics*. **1991**, *10*, 963.
[10] Crystal data for **2**: $C_{16}H_{44}B_8Si_4Ga_2$, M = 574.8, triclinic, $P\bar{1}$, a = 10.986(4), b = 11.836(4), c = 14.616(5) Å, α = 92.16(3), β = 103.75(3), γ = 116.13(3) °; V = 1631(1) Å^3, Z = 2, ρ_{calcd} = 1.167 g cm^{-3}, μ = 1.798 mm^{-1}. Of 3706 data collected on a Siemens R3m/V diffractometer ($Mo_{K\alpha}$, 2θ = 3.5–40.0°, at −43 °C) 3477 reflections were unique and 2069 reflections were observed [$I > 6.0\,\sigma(I)$]. Data were corrected for Lorentz, polarization, and absorption effects. The structure was solved by heavy-atom methods on PC computers using SHELXTL-Plus (G. M. Sheldrick, Structure Determination Software Program Package, Siemens Analytical X-ray Instruments, Inc., Madison, WI, USA, **1990**). All non-H atoms were refined anisotropically. Carborane cage-H atoms were located on difference Fourier maps, while methyl H atoms on the "riding model". The final refinement of **2** converged at R = 0.0388, wR = 0.0468, and GOF = 1.03 for observed reflections. Further details of the crystal structure investigation may be obtained from the Fachinformationszentrum Karlsruhe, D-76344 Eggenstein-Leopoldshafen 2 (Germany), on quoting the depository number CSD-58695.
[11] C. R. Pulham, A. J. Downs, M. F. Goode, D. W. H. Rankin, H. E. Robertson, *J. Am. Chem. Soc.* **1991**, *113*, 5149.
[12] P. L. Baxter, A. J. Downs, D. W. H. Rankin, H. E. Robertson, *J. Chem. Soc., Dalton Trans.* **1985**, 807.
[13] A. Decken, University of Texas, Austin, personal communication.
[14] We thank a referee for this suggestion.
[15] A. K. Saxena, H. Zhang, J. A. Maguire, N. S. Hosmane, A. H. Cowley, unpublished results.

The Cope Rearrangement Transition Structure Is Not Diradicaloid, but Is It Aromatic?**

Haijun Jiao and Paul von Ragué Schleyer*

Any problem that has generated nearly a half century of controversy is not solved easily. What is the "precise mechanism" of the parent, degenerate Cope rearrangement of 1,5-hexadiene (**1**) (Scheme 1)?[1–4] Does the favored pathway with chairlike



Scheme 1. The stepwise and synchronous mechanisms of the Cope rearrangement. Transition structures with chair and boat conformations are possible.

transition structures follow a stepwise mechanism via a C_{2h}-symmetrical intermediate **3** (**3a**) and two equivalent C_2-symmetrical transition structures, **2** and **2'**, or is this a synchronous, fully concerted process in which the C_{2h}-symmetrical structure **3a** describes the only transition structure? What is the mechanism of the alternative route via boatlike transition structures, which are roughly 11 kcal mol^{-1} higher in energy?[4b] Do the transition states or intermediates have "diyl" character, in other words "diradicaloid" (singlet diradical) character, or are they better described as "delocalized" or "aromatic"?

Using experimental reference data which later proved to be inaccurate, Doering et al. estimated in 1971 that the hypothetical 1,4-cyclohexanediyl (**4**) was 33.7 kcal mol^{-1} higher in energy than 1,5-hexadiene (**1**).[4a] This value was essentially identical with the measured activation enthalpy of 33.5 ± 0.5 kcal mol^{-1} for the favored Cope pathway via chairlike transition structures.[4a] When the latest group enthalpy increments by Cohen and Benson are used,[4f] 1,4-cyclohexanediyl (**4**) appears to be 42 kcal mol^{-1} higher in energy than **1**. Hence, the likelihood of a diradicaloid mechanism is sharply diminished, and "the archetypal Cope rearrangement" is "restored securely to the land of concert."[4g] The dissociation of **1** into two allyl radicals (**5**) also is not competitive, since it is endothermic by 59.7 kcal mol^{-1}.[4c] Thus, our best estimates of the "energy of concert"[3c] are now 26.2 kcal mol^{-1} (based on **5**) and roughly 9 kcal mol^{-1} (based on **4**).

Likewise, the long-held assumption that only multireference ab initio treatments, which are capable of describing concerted and diradical transition states equally well, could provide unbiased calculations on the Cope rearrangement, was not confirmed.[2a–d] However, analysis of the CAS-MCSCF wavefunc-

[*] Prof. Dr. P. von R. Schleyer, Dipl.-Chem. H. Jiao
Computer-Chemie-Centrum
Institut für Organische Chemie I der Universität Erlangen-Nürnberg
Henkestrasse 42, D-91054 Erlangen (Germany)
Telefax: Int. code + (9131)85-9132

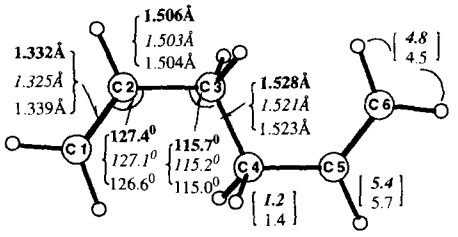
[**] This work was supported by the Fonds der Chemischen Industrie, the Convex Computer Corporation, the Deutsche Forschungsgemeinschaft, and the Volkswagen-Stiftung. We also thank Prof. W. Kutzelnigg and Prof. W. T. Borden for helpful suggestions, and the Shanxi Normal University (the People's Republic of China) for a scholarship (to H. J.).

tion revealed "that the chair transition structure has little diradical character."[2c, d] In their most recent CASPT2N study Borden et al. found the degenerate Cope rearrangement of 1,5-hexadiene (**1**) to be synchronous.[2f] A delocalized, rather than a diyl structure best describes transition structure **3**. Unlike earlier theoretical results (e.g. at CASSCF/6-31G*),[2d] the most recent computations, including our own, show that single-determinant theory with electron correlation (e.g. MP4SDTQ/6-31G*) yield results in excellent agreement with experiment, both in terms of the energies and the kinetic isotope effects.[2i]

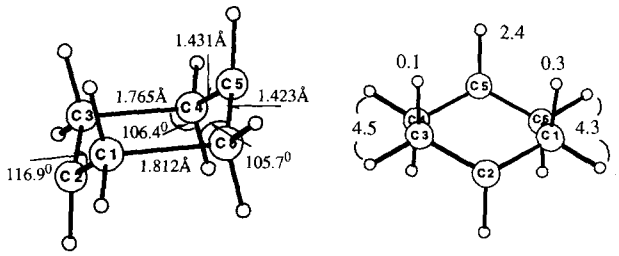
Hence, the mechanism of the parent Cope rearrangement is not "diradicaloid", but is it "aromatic"? To provide an answer, we have computed the magnetic properties of **1**–**4**. Several pericyclic reactions,[5] including the degenerate Cope rearrangement of semibullvalene,[5a,f] have already been examined in this manner. The shape of the potential energy surface (PES) around the C_{2h}-symmetrical structure **3a** varies with the theoretical level. Even though the PES is quite flat, we now find that this does not have any important consequence on the computed magnetic properties. Thus, there is no basic difference in the electronic structure of the transition structures for the synchronous (C_{2h}) and stepwise (C_2) mechanisms.

We employed frequency computations[6, 7] at three different *ab initio* levels with electron correlation (MP2(fc)/6-31G*, CID/6-31G*, and density functional theory (DFT)) to characterize the potential energy surfaces.[6b–d] DFT optimizations (Becke3LYP/6-311 + G*) employed Becke's three-parameter exchange functional with the correlation functional of Lee, Yang, and Parr, which includes both local and nonlocal DFT terms.[6b–d] While the "boat" pathway only has a single transition structure (**3a**) with one imaginary frequency (531 $i\,cm^{-1}$ (MP2), 809 $i\,cm^{-1}$ (CID), 499 $i\,cm^{-1}$ (Becke3LYP)), the nature of the "chair" pathway changed from level to level.

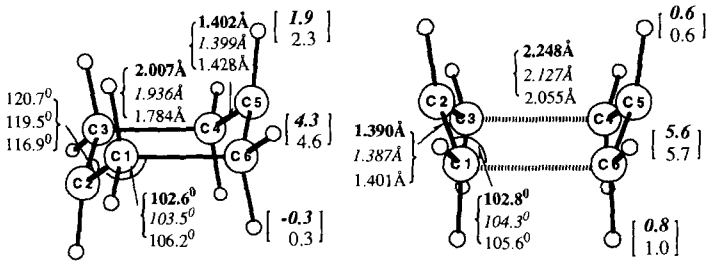
At MP2/6-31G* the C_{2h}-symmetrical form **3a** (Fig. 1, cf. Table 1) corresponds to a *minimum* (the lowest frequency was 109 cm^{-1}). The related transition structure **2** (C_2) (note the



1, C_{2h}



2, C_2



3a, C_{2h} **3b**, C_{2v}

Fig. 1. Optimized structures for **1**–**3** from Becke3LYP/6-311 + G* (in bold), CISD/6-31G* (in italics), and MP2/6-31G* calculations, along with calculated ^{1}H NMR shifts (in square brackets, IGLO/II//CISD/6-31G* (in bold) and IGLOII//MP2/6-31G* values).

Table 1. Comparison of important C–C distances [Å] of the chair (C_{2h}) and boat (C_{2v}) transition structures (TS) for the Cope rearrangement of **1** obtained at various levels of theory.

Level of theory	Chair TS		Boat TS		Ref.
	C1-C6	C1-C2	C1-C6	C1-C2	
MCSCF/3-21G	2.062	1.386	–	–	[2a]
CASSCF/3-21G	2.086	1.401	2.316	1.390	[2b]
RHF/3-21G	2.020	1.389	2.140 [a]	1.381 [a]	[2c]
RHF/6-31G*	2.046	1.390	2.203 [a]	1.383 [a]	[2g]
CASSCF/6-31G*	2.189	1.398	2.615	1.389	[2d]
CASPT2N/6-311G(2d,2p)	1.885	–	2.204	–	[2f]
MP4SDTQ/6-31G*	1.794	–	–	–	[2f] [b]
QCISD(T)/6-31G*	1.769	–	–	–	[2j]
MP2/6-31G*	1.784	1.428	2.055	1.401	[a]
CID/6-31G*	1.933	1.399	2.121	1.387	[a]
CISD/6-31G*	1.936	1.399	2.127	1.387	[a]
Becke3LYP/6-311 + G*	2.007	1.402	2.248	1.390	[a]

[a] This work. [b] In ref. 33 there.

closely related geometries of **2** and **3a**, Fig. 1) is characterized by one imaginary frequency (-143 cm^{-1}) but has almost exactly the same energy as **3a** (33.4 kcal mol^{-1}). The single-point energies at MP4SDTQ/6-31G* and at QCISD(T)/6-31G*, computed using the MP2/6-31G*-optimized geometries, also were nearly the same (within 0.2 kcal mol^{-1}, see Table 2). However, MP2 calculations tend to *overestimate* the effects of electron delocalization, for example the resonance energy of benzene.[7c] The same also may be true of CASPT2N calculations, which use second-order perturbation theory to obtain the dynamic correlation energy for all the electrons, starting from a CASSCF reference wave function.[2f]

Indeed, reoptimization at the levels CID/6-31G*, CISD/6-31G*, and Becke3LYP/6-311 + G* gave geometries for **3a** that were less compact than those at the MP2/6-31G* and CASPT2N levels (Table 1, Fig. 1). Moreover, **3a** was a *transition structure* with one large imaginary frequency both at CID/6-31G* (784 $i\,cm^{-1}$) and at Becke3LYP (579 $i\,cm^{-1}$).

Geometries: The starting compound 1,5-hexadiene (**1**) corresponds to a minimum (no imaginary frequencies at MP2, CID, and Becke3LYP) in the C_{2h}-symmetrical conformation; the geometries are all nearly the same (Fig. 1). Except for the value of 1.428 Å obtained with MP2, the C–C bond lengths of the allyl moieties in **3a** (C_{2h}) and in **3b** (C_{2v}) (Table 1) are all close to the allyl[5g] and benzene values (ca. 1.395 Å).[5a, b] The more critical C1 ··· C6 separations between the allyl units in **3b** (C_{2v}) and especially in **3a** (C_{2h}) are unusually sensitive to changes in the theoretical level (Table 1).[2j] The distances from MP2/6-31G*, MP4SDTQ/6-31G*, QCISD(T)/6-31G* calculations are shorter, but at the other levels the distances are more consistent with the approximately 2.08 Å separation in **3a** reported by Houk et al.[2i] in a recent theoretical analysis of the experimental kinetic isotope effects. The C1 ··· C6 separations in **3b** appear to

 © VCH Verlagsgesellschaft mbH, D-69451 Weinheim, 1995 0570-0833/95/0303-0335 $ 10.00+.25/0

be about 0.2 Å longer than in **3a**. These C–C distances are typical for bond formation or cleavage in many computed aromatic transition structures for pericyclic reactions.[2e]

Although useful for our analysis of the energies (see above) and magnetic properties, the MP2(fc)/6-31G* and CASPT2N geometries appear to be too compact. The chairlike MP2(fc)/6-31G* transition structure **2** with reduced C_2 symmetry (Fig. 1) may be an artifact. In **2**, the forming C1–C6 bond is 1.812 Å long, whereas the breaking C3–C4 bond is 1.765 Å long. The average value, 1.788 Å, is nearly the same as that in the symmetric intermediate **3a** at the same level of theory (1.784 Å).

Energies: The relative energies computed at various high theoretical levels are summarized in Table 2. These, along with the calculated thermal energies, give the activation enthalpies $\Delta H^{\neq}$ (500 K) which can be compared with the experimental data. Note that **2** and **3a** have nearly the same energy when the MP2(fc)/6-31G* geometries are employed (where the latter structure corresponds to a minimum).

Table 2. The calculated relative electronic energies E_{rel} and the activation enthalpies $\Delta H^{\neq}$ (both in kcal mol^{-1}, computed to 500 K) for the parent Cope rearrangement compared with the measured values.

Level of theory	Value	**1**, C_{2h}	**2**, C_2 chair	**3a**, C_{2h} chair	**3b**, C_{2v} boat	**5** allyl pair
MP4SDTQ/6-31G* //MP2(fc)/6-31G*	E_{rel}	0.0	32.5	32.7	44.9	–
QCISD(T))/6-31G* //MP2(fc)/6-31G*	E_{rel}	0.0	35.3	35.3	47.2	–
QCISD(T)/6-31G* //CISD/6-31G	E_{rel}	0.0	–	36.4	46.8	63.8
Becke3LYP/ 6-311+G*//Becke3LYP/ 6-311+G*	E_{rel}	0.0	–	33.7	41.5	54.0
MP4SDTQ/6-31G* //MP2(fc)/6-31G* [a]	$\Delta H^{\neq}$	0.0	31.1	32.1	43.1	–
QCISD(T)/6-31G* //MP2(fc)/6-31G* [a]	$\Delta H^{\neq}$	0.0	34.0	34.8	45.4	–
QCISD(T)/6-31G* //CISD/6-31G* [b]	$\Delta H^{\neq}$	0.0	–	34.8	45.0	57.9
Becke3LYP/ 6-311+G*//Becke3LYP/ 6-311+G* [b]	$\Delta H^{\neq}$	0.0	–	32.2	39.6	48.1
CASPT2N [c]	$\Delta H^{\neq}$	0.0	–	32.2	41.2	60.1
Experiment	$\Delta H^{\neq}$	0.0	33.3 ± 0.5 [4a]	33.3 ± 0.5 [4a]	44.7 ± 2.0 [9a]	59.7 [4c]

[a] MP2(fc)/6-31G* frequencies were employed. [b] CID/6-31G* frequencies were employed. [c] Ref. [2f]; CASSCF/6-31G* frequencies were employed.

The computed activation enthalpies for the chair pathway is nearly the same as that measured for 1,6-dideutero-1,5-hexadiene (33.3 ± 0.5 kcal mol^{-1})[4a] (Table 2). Moreover, the calculated activation entropies of −9.4 and −6.2 cal mol^{-1} K^{-1} for **3a** and **3b** are close to the measured values (−13.8 ± 1 and −3.0 ± 3.6 cal mol^{-1} K^{-1}, respectively, for the deuterated isomers).[4a, b, 9a, b] The calculated activation energy for the C_{2v}-symmetric transition structure **3b** is 7–12 kcal mol^{-1} higher in energy than that for the C_{2h}-symmetric structure **3a** (Table 2); the experimental estimate is 11 ± 3 kcal mol^{-1}. The energy difference between **1** and two allylic radicals **5** is 57.5 kcal mol^{-1} at QCISD(T)/6-31G*//CISD/6-31G* + E_{th} (CID/6-31G*, 500 K), which agrees well with experiment (59.7 kcal mol^{-1}),[4c] but the Becke3LYP value is too low. The CASPT2N level of Borden et al.[2f] (see Table 2) also performs well.

Magnetic Properties: Chemical shifts as well as magnetic susceptibilities and anisotropies were computed using the IGLO[8] method employing both the MP2/6-31G* and the CISD/6-31G* geometries. These calculated magnetic properties show pronounced ring current effects which characterize the aromaticity of pericyclic transition structures.[5] The ^{1}H nuclei are shielded (and deshielded), and the magnetic susceptibilities and anisotropies of the transition states are exalted, just as in benzenoid and other aromatic molecules (Table 3).[10–14]

The ^{1}H NMR shifts (Fig. 1) from IGLO/II calculations using both the MP2 and CISD geometries differ dramatically from values for normal polyenes such as compound **1**. In **3a** and **3b** the signals of the axial (inner) hydrogen atoms are all shifted upfield (δ = −0.3 to 2.4) relative to the corresponding signals of **1**, whereas the signals of the equatorial hydron atoms are shifted *downfield* (δ = 4.3–5.7). Note that the individual CH_2 hydrogens have the same chemical shifts in **1**, but show large differences ($\Delta\delta$ = 4.0 to 4.8) in **3a** and **3b**.

For **3a** the calculated magnetic susceptibility exaltations relative to that of 1,5-hexadiene (**1**) are −16.4 (MP2 geometry) and −19.9 (CISD geometry), and only a little less, −16.2 (MP2 geometry) for the asynchronous transition structure (**2**). The exaltation is −17.4 (CISD geometry) for the boat transition structure **3b**. Thus **2**, **3a**, and **3b** are aromatic, with larger exaltations than benzene (−13.7 experimentally,[11a] −13.4 based on IGLO/II calculations[14h]). Comparisons with values computed for other electrocyclic transition structures are summarized in Table 3, along with the measured and calculated activation energies and the energies of concert.

The calculated magnetic susceptibility anisotropies for **3a** (−55.0) and for **3b** (−56.6) are larger than that for **1** (−17.9) using the CISD geometries, and are comparable to that of benzene (−62.9). The value of the magnetic susceptibility an-

Table 3. Calculated (E_a) and measured activation energies (E_a, exp.), energies of concert (E_{con}) (all in kcal mol^{-1}) as well as the magnetic susceptibility exaltations (Λ/ 10^{-6} cm^3 mol^{-1}) for a selection of pericyclic reactions.

Reaction	E_a	Level	E_a, exp. [a]	E_{con}	Λ	Ref.
Cope: nonconcerted (**2**)	35.0	QCISD(T)	(34.4 ± 0.5)	22.9	−16.2	[b]
concerted (**3a**)	35.8	QCISD(T)	(34.4 ± 0.5)	22.1	−19.9 (−16.4) [c]	[b]
concerted (**3b**)	45.0	QCISD(T)	(44.7 ± 2)	12.9	−19.4	[b]
semibullvalene	4.1	MP2	(4.8 ± 0.2)	54	−21.8	[5a,f]
1,5-H Shift: cyclopentadiene	27.5	QCISD(T)	(24.3 ± 0.5)	50	−8.9	[5e]
1,3-pentadiene	36.9	QCISD(T)	(36.3 ± 0.5)	40	−9.9	[5e]
1,7-H Shift: 1,3,5-heptatriene	19.7	MP2	(20.8 ± 0.7)	60	−23.1	[5b]
Diels–Alder: C_2H_4 + butadiene	22.4	MP4SDTQ	(23.6)	5.7	−19.3	[5c]
C_2H_4 + cyclopentadiene	17.5	MP4SDTQ	(17.5)	13.7	−17.7	[5c]
Hexatriene → cyclohexadiene	30.4	MP4SDTQ	(29.9 ± 0.5)	15	−17.4	[5f]
Octatetraene → cyclooctatriene	15.0	MP4SDTQ	(17.0)	20	−12.6	[5d]
H_2 Elimination: 1,4-cyclohexadiene	44.9	MP4SDTQ	(43.8 ± 0.4)	30	−19.3	[5f]

[a] $E_a = \Delta H^{\neq} + RT$. [b] This work. [c] Based on MP2(fc)/6-31G* geometry.

isotropy of transition structure **2** for the stepwise reaction (− 47.8) is essentially identical with that of **3a** (− 47.9) when the MP2 geometries are used for both. Hence, all the magnetic criteria agree that **2** and **3a** do not differ significantly in their electronic character.

Conclusions: The geometries and energies determined by ab initio methods, as well as the IGLO analysis of the magnetic properties, show that the parent Cope rearrangement of 1,5-hexadiene occurs through a concerted, synchronous mechanism via an *aromatic* transition structure **3a**. This is a general feature of the pericyclic reactions we have studied in this context (Table 3). There appears to be no relationship between the energies of concert or the activation energies and the magnetic susceptibility exaltations (which are in the range of the benzene value, −13.7). The cyclic electron delocalization, which is responsible for the ring current effects, also stabilizes the transition structures, but is only one of the contributing factors governing the reactivity and mechanistic pathway.

Received: July 30, 1994 [Z 7192 IE]
German version: *Angew. Chem.* **1995**, *107*, 329

Keywords: ab initio calculations · Cope rearrangements · reaction mechanisms

[1] a) M. J. S. Dewar, C. Jie, *Tetrahedron* **1988**, *44*, 1358; b) *J. Am. Chem. Soc.* **1987**, *109*, 5893; c) *J. Chem. Soc. Chem. Commun.* **1987**, 1451; d) M. J. S. Dewar, G. P. Ford, M. L. McKee, M. L. Rzepa, L. E. Wade, *J. Am. Chem. Soc.* **1977**, *99*, 5069; e) M. J. S. Dewar, *ibid.* **1984**, *106*, 209; f) M. J. S. Dewar, E. F. Healy, *Chem. Phys. Lett.* **1987**, *141*, 521; g) T. E. Wessel, J. Berson, *J. Am. Chem. Soc.* **1994**, *116*, 459; h) A. C. Cope, E. M. Hardy, *ibid.* **1940**, *62*, 411; i) H. E. Zimmerman, *ibid.* **1966**, *88*, 1564; j) H. M. Frey, R. Walsh, *Chem. Rev.* **1969**, *69*, 103.

[2] a) Y. Osamura, S. Kato, K. Morokuma, D. Feller, E. R. Davidson, W. T. Borden, *J. Am. Chem. Soc.* **1984**, *106*, 3362; b) K. Morokuma, W. T. Borden, D. A. Hrovat, *ibid.* **1988**, *110*, 4474; c) D. A. Hrovat, W. T. Borden, R. L. Vance, N. G. Rondan, K. N. Houk, K. Morokuma, *ibid.* **1990**, *112*, 2018; d) M. Dupuis, C. Murray, E. R. Davidson, *ibid.* **1991**, *113*, 9756; e) K. N. Houk, Y. Li, J. D. Evanseck, *Angew. Chem.* **1992**, *104*, 711; *Angew. Chem. Int. Ed. Engl.* **1992**, *31*, 682; f) D. A. Hrovat, K. Morokuma, W. T. Borden, *J. Am. Chem. Soc.* **1994**, *116*, 1072; g) K. N. Houk, S. M. Gustafson, K. A. Black, *ibid.* **1992**, *114*, 8565; h) M. Bearpark, F. Bernardi, M. Olivucci, M. A. Robb, *ibid.* **1990**, *112*, 1732; i) O. Wiest, K. A. Black, K. N. Kouk, *ibid.* **1994**, *116*, in press; j) W. T. Borden, personal communication: The Cope potential energy surface is "pathologically flat" along the minimum-energy path passing through the C_{2h} minimum. Reasonable levels of theory can give C1–C6 distances that differ by as much as 0.3–0.4 Å (Table 1). The QCISD(T)/6-31G* single-point energies for CASSCF/6-31G* geometries, partially optimized at different R values, indicated $R = 1.769$ Å and $\Delta E = 35.9$ kcal mol^{-1}.

[3] a) W. T. Borden, R. J. Loncharich, K. N. Houk, *Annu. Rev. Phys. Chem.* **1988**, *39*, 213; b) M. J. S. Dewar, C. Jie, *Acc. Chem. Res.* **1992**, *25*, 537; c) W. von Doering, W. R. Roth, R. Breuckman, L. Figg, H. W. Lennartz, W. D. Fessner, H. Prinzbach, *Chem. Ber.* **1988**, *121*, 1.

[4] a) W. von E. Doering, V. G. Toscano, G. H. Beasley, *Tetrahedron* **1971**, *27*, 5299; b) J. J. Gajewski, *Org. Chem.* **1981**, *44*, 166; c) W. R. Roth, F. Bauer, A. Beitat, T. Ebbrecht, M. Wüstefeld, *Chem. Ber.* **1991**, *124*, 1453; d) J. A. Seetula, J. Russell, D. Gutman, *J. Am. Chem. Soc.* **1990**, *112*, 1347; e) E. Tschuikow-Roux, Y. Chen, *ibid.* **1989**, *111*, 9030; f) N. Cohen, S. W. Benson, *Chem. Rev.* **1993**, *93*, 2419; g) W. R. Roth, H.-W. Lennartz, V. von E. Doering, L. Birladeanu, C. A. Guyton, T. Kitagawa, *J. Am. Chem. Soc.* **1990**, *112*, 1722; h) K. J. Shea, G. J. Stoddard, W. P. England, C. D. Haffner, *ibid.* **1992**, *114*, 2635; i) K. J. Shea, R. B. Phillips, *ibid.* **1980**, *102*, 3156.

[5] a) H. Jiao, P. von R. Schleyer, *Angew. Chem.* **1993**, *105*, 1830; *Angew. Chem. Int. Ed. Engl.* **1993**, *32*, 1760; b) *ibid.* **1993**, *105*, 1833 and **1993**, *32*, 1763; c) R. Herges, H. Jiao, P. von R. Schleyer, *ibid.* **1994**, *106*, 1441 and **1994**, *33*, 1376; d) H. Jiao, P. von R. Schleyer, *J. Chem. Soc. Perkin Trans. 2* **1994**, 407; e) *J. Chem. Soc. Faraday Trans.* **1994**, 1559; f) *J. Am. Chem. Soc.*, submitted; g) P. von R. Schleyer, *ibid.* **1985**, *107*, 4793.

[6] a) Gaussian 92: M. J. Frisch, G. W. Trucks, M. Head-Gordon, P. M. W. Gill, M. W. Wong, J. B. Foresman, B. G. Johnson, H. B. Schlegel, M. A. Robb, E. S. Replogle, R. Gomperts, J. L. Andres, K. Raghavachari, J. S. Binkley, C. Gonzalez, R. L. Martin, D. J. Fox, D. J. DeFrees, J. Baker, J. J. P. Stewart, J. A. Pople, Gaussian Inc., Pittsburgh, PA, **1992**; b) *New Methods and Features in Gaussian 92/DFT* (adding density functional capabilities to Gaussian 92), Gaussian, Inc., Pittsburgh, PA, **1993**; c) J. W. Labanowski, J. Andzelm, *Density Functional Methods in Chemistry*, Springer, New York, **1991**; d) R. G. Parr, W. Yang, *Density Functional Theory of Atoms and Molecules*, Oxford University Press, New York, **1989**.

[7] a) W. J. Hehre, L. Radom, P. von R. Schleyer, J. A. Pople, *Ab Initio Molecular Orbital Theory*, Wiley, New York, **1986**; b) J. B. Foresman, Æ. Frisch, *Exploring Chemistry with Electronic Structure Methods: A Guide to Using Gaussian*, Gaussian, Inc., Pittsburgh, PA, **1993**; c) R. L. Disch, J. M. Schulman, *Chem. Phys. Lett.* **1988**, *152*, 402.

[8] W. Kutzelnigg, U. Fleischer, M. Schindler, *NMR Basic Princ. Prog.* **1990**, *23*, 165.

[9] a) M. J. Goldstein, M. S. Benzon, *J. Am. Chem. Soc.* **1972**, *94*, 5119; 7147; b) W. von E. Doering, W. Roth, *Tetrahedron* **1962**, *18*, 67.

[10] a) P. Pascal, *Ann. Chim. Phys.* **1910**, *19*, 5; b) L. Pauling, *J. Chem. Phys.* **1936**, *4*, 673; c) A. Pacault, *Ann. Chim.* **1946**, *1*, 567.

[11] For review of magnetic susceptibility exaltations see: a) H. J. Dauben, Jr., J. D. Wilson, J. L. Laity, *J. Am. Chem. Soc.* **1968**, *90*, 811; b) *ibid.* **1969**, *91*, 1991; c) *Nonbenzenoid Aromaticity, Vol. 2*, (Ed.: J. P. Synder). Academic Press, New York, **1971**, pp. 167–206; d) J.-F. Labarre, F. Crasnier, *Fortschr. Chem. Forsch.* **1971**, *24*, 33; e) . C. Haddon, V. R. Haddon, L. M. Jackman, *ibid.* **1971**, *16*, 112; f) C. K. Ingold, *Structures and Mechanisms of Organic Reactions*, Bell, London, **1953**, pp. 185–196.

[12] For magnetic susceptibility anisotropies see: a) R. C. Benson, W. H. Flygare, *J. Am. Chem. Soc.* **1970**, *92*, 7523; b) T. G. Schmalz, C. L. Norris, W. H. Flygare, *ibid.* **1973**, *95*, 7961; c) J. R. Davidson, A. K. Burnham, B. Siegel, P. Beak, W. H. Flygare, *ibid.* **1974**, *96*, 7394; d) T. G. Schmalz, T. D. Gierke, P. Beak, W. H. Flygare, *Tetrahedron Lett.* **1974**, 2885; e) M. H. Palmer, R. H. Findlay, *ibid.* **1974**, 253.

[13] Magnetic criteria were used in investigations of the homoaromaticity of carbocations in a) D. Cremer, F. Reichel, E. Kraka, *J. Am. Chem. Soc.* **1991**, *113*, 9459; b) D. Cremer, P. Svensson, E. Kraka, P. Ahlberg, *ibid.* **1993**, *115*, 7445; c) D. Cremer, P. Svensson, E. Kraka, E. Konkol, P. Ahlberg, *ibid.* **1993**, *115*, 7457.

[14] a) W. Kutzelnigg, U. Fleischer, P. Lazzeretti, V. Müllenkamp, *J. Am. Chem. Soc.* **1994**, *116*, 5298; b) H. Jiao, P. von R. Schleyer, *Proceedings of the First Conference on Computational Chemistry*, (Ed.: C. Troyanowsky), Ed. Amer. Inst. Physics, Jericho, New York, **1994**.

Aromaticity and Antiaromaticity in Five-Membered C_4H_4X Ring Systems: "Classical" and "Magnetic" Concepts May Not Be "Orthogonal"**

Paul von Ragué Schleyer,* Peter K. Freeman, Haijun Jiao, and Bernd Goldfuss

Despite the fundamental importance of aromaticity and antiaromaticity in chemistry,[1, 2] no generally acceptable definitions have been established.[1] Instead, aromaticity is discussed in terms of various criteria: energetic, structural, and magnetic. Aromatic stabilization energies (ASEs) have been deduced from experimental measurements, but as the needed reference thermochemical data often are not available, recourse has been made to theoretical data.[3, 4] Bond length analyses[5–7] are based on experimental (for example, from X-ray analyses) or

[*] Prof. Dr. P. von R. Schleyer, Dipl.-Chem. H. Jiao, Dipl.-Chem. B. Goldfuss
Computer-Chemie-Centrum
Institut für Organische Chemie der Universität Erlangen-Nürnberg
Henkestrasse 42, D-91054 Erlangen (Germany)
Telefax: Int. code +(9131)85-9132

Prof. P. K. Freeman
Department of Chemistry, Oregon State University
Corvallis, OR 97331 (USA)

[**] This work was supported by the Fonds der Chemischen Industrie (also through a scholarship to B. Goldfuss), the Convex Computer Corporation, the Deutsche Forschungsgemeinschaft, and the Stiftung Volkswagenwerk, as well as the National Institute of Environmental Health Sciences (Grant ES00040). We also thank Prof. Dr. W. Kutzelnigg for helpful suggestions, Prof. Dr. A. R. Katritzky for constructively critical discussions, and the Shanxi Normal University (the People's Republic of China) for a scholarship to H. Jiao.

theoretical[3, 4] structures. The C–C bond lengths in aromatic systems tend to be very similar, and the other bond lengths adjust accordingly. Aromatic compounds exhibit exalted diamagnetic susceptibilities[1, 8–11] as well as magnetic susceptibility anisotropies.[9] The external protons are deshielded (in the larger annulenes, internal protons are shielded),[1, 6c–h, 10] but not only ring currents cause these effects.

To what extent are these criteria related? Katritzky et al.'s[6a] "principle component analysis" of data sets for five- and six-membered heterocycles concluded that "the 'classical' and 'magnetic' concepts of aromaticity are almost completely orthogonal" and that "there are at least two types of aromaticity". Although Katritzky's analysis was based on a large number of common aromatic systems, the magnetic properties encompassed only a narrow range—in view of the likely experimental uncertainties, perhaps too limited a range for a definitive assessment. The present study helps dispel Katritzky's pessimistic conclusion by demonstrating that *linear relationships exist among the energetic, geometric, and magnetic criteria of aromaticity, and that these relationships even extend to antiaromatic systems.*

We have now examined a comprehensive set of five-membered C_4H_4X ring systems. Theoretical computations enable 4π electron antiaromatic (X = CH^+ (singlet), SiH^+, BH, and AlH) as well as 6π electron aromatic compounds (X = CH_2, PH, SiH^-, O, S, NH, and CH^-) to be included, so we employ a uniform set of good quality theoretical data to analyze systems with a much wider range of properties than Katritzky et al.[6a] As magnetic susceptibilities depend on ring size,[11] we have chosen the set of five-membered heterocycles because their shape is nearly uniform. The geometries (MP2(fc)/6-31G* level)[12, 13] and energies (with MP2(fc)/6-31G* zero point energy corrections) have been computed at reasonably high ab initio levels (with the GAUSSIAN 92 program[13]). For molecules of this type, MP2 geometries can be expected to be quite accurate.[14] Indeed, the optimized geometries for X = O, S, NH, and CH_2, as well as PH and AlH, are in excellent agreement with the experimental values (given in italics in parenthesis in Fig. 1).[15]

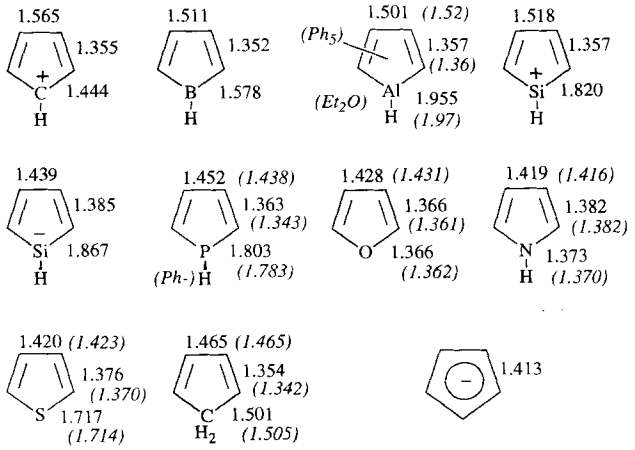
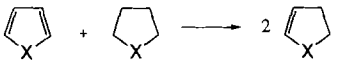


Fig. 1. The lengths of the C_4H_4X ring bonds at MP2(fc)/6-31G* level (experimental values are given in italics in parentheses).

IGLO calculations employing the MP2/6-31G* geometries and the basis set II (IGLO/II//MP2/6-31G*)[16] [9s5p(51111/2111) augmented by one set of d functions, $\eta = 1$, for carbon and 5s (311) augmented by one set of p functions, $\eta = 0.7$, for hydrogen; basis sets for other elements are given in Ref. [16] provided the magnetic susceptibilities and their anisotropies. These magnetic properties depend on the area of the ring,[11] but this should be nearly equal for the five-membered systems employed here. The homodesmotic reaction [Eq. (a)] was used to evaluate



(a)

the ASEs. Because the reference compounds all were computed in their most stable conformations, strain effects should be canceled to a large extent. Furthermore, the reference monoenes are conjugated, so Equation (a) gives the ASE associated with cyclic delocalization (positive energies denote the stabilization for aromatic compounds) or with cyclic localization (negative energies denote the destabilization of antiaromatic systems).

The magnetic susceptibility exaltation [Λ, Eq. (b)] is defined as the difference between the IGLO magnetic susceptibility for C_4H_4X (χ_M) and the value estimated for the hypothetical system without cyclic electron delocalization ($\chi_{M'}$). The latter is based

$$\Lambda = \chi_M - \chi_{M'} \quad \text{(b)}$$

on the group increments (for example, for CH and X) that we have determined by IGLO computations on appropriate model compounds. These magnetic susceptibility group increments (to be reported in a full paper) vary hardly at all with structure (that is, acyclic or cyclic). The exaltations Λ are negative (diamagnetic) for the aromatic compounds, but positive (paramagnetic) for the antiaromatic cases (Table 1).

Table 1. The calculated magnetic susceptibility exaltations Λ, magnetic susceptibility anisotropies χ_{anis} [10^{-6} cm^3 mol^{-1}], homodesmotic stabilization/destabilization energies ASE [kcal mol^{-1}], and the Julg parameters A for C_4H_4X rings.

X [a]	Symmetry	Λ [b]	χ_{anis}	ASE [b]	A
CH^+	C_{2v}	32.6	58.1	−56.7	−0.084
SiH^+	C_{2v}	13.2	−0.8	−24.1	0.346
BH	C_{2v}	12.8	−5.6	−19.3	0.354
AlH	C_{2v}	11.2	−11.4	−6.8	0.476
CH_2	C_{2v}	−2.4 (−6.5 [8b, c])	−31.0	3.7 (2.4 [10d])	0.684
PH	C_s	−3.3	−35.2	7.0	0.795
SiH^-	C_s	−7.7	−41.5	13.8	0.926
O	C_{2v}	−9.1 (−8.9 [6a])	−36.2	19.8	0.900
S	C_{2v}	−10.0 (−13.0 [6a])	−46.4	22.4	0.951
NH	C_{2v}	−12.1 (−10.4 [6a])	−41.8	25.5	0.967
CH^-	D_{5h}	−17.2	−45.8	28.8	1.000

[a] All species correspond to minima at MP2(fc)/6-31G* (no imaginary frequencies). [b] Experimental estimate in parentheses.

Table 1 also summarizes the aromatic stabilization energies [ASEs, Eq. (a)], the magnetic susceptibility exaltation Λ, the magnetic susceptibility anisotropies χ_{anis}, and the Julg parameter A [based on Eq. (c)],[5] a geometric criterion that has proved useful for quantitative comparisons of such heterocyclic molecules.[5] The χ_{anis} values do show a definite trend towards more negative values for the more aromatic systems, but may be less generally useful as a quantitative aromaticity criterion.

The Julg parameter A[5] defines the degree of aromaticity in terms of the deviations of the individual C–C bond lengths (r_i) from the mean carbon–carbon bond length (r). In Equation (c),

$$A = 1 - (225/n)\,\Sigma\,(1 - r_i/r)^2 \quad \text{(c)}$$

 © VCH Verlagsgesellschaft mbH, D-69451 Weinheim, 1995 0570-0833/95/0303-0338 $ 10.00+.25/0

n represents the number of C–C bonds (three in the C_4H_4X systems). $A = 1$ for benzene (D_{6h}) and the cyclopentadienyl ion (D_{5h}), that is, for the fully delocalized, highest symmetric systems. The empirical factor 225 provides an aromaticity scale in which $A = 0$ for the Kekulé form of benzene (assuming 1.33 and 1.52 Å C–C lengths).

A plot of the calculated magnetic susceptibility exaltations Λ versus ASE (Fig. 2) reveals a remarkable linear correlation that extends from the highly antiaromatic singlet cyclopentadienyl

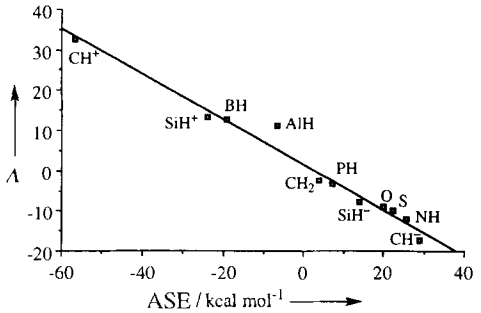


Fig. 2. Plot of the magnetic susceptibility exaltations Λ versus ASE for C_4H_4X rings. The correlation coefficient of the regression line ($y = 1.45 - 0.56\,x$) is $c = 0.99$.

cation to the highly aromatic cyclopentadienyl anion. The cyclopentadienyl anion (D_{5h}) contains π electrons that are fully delocalized ($A = 1$) and has the largest stabilization energy (ASE = +28.8 kcal mol^{-1}) as well as the most negative (diamagnetic) susceptibility exaltation ($\Lambda = -17.2$). In contrast, the singlet cyclopentadienyl cation (C_{2v}),[17] which is close in energy to the triplet ground state, has the largest destabilization energy (ASE = − 56.7 kcal mol^{-1}), the most positive (paramagnetic) exaltation ($\Lambda = +32.6$), and the smallest Julg parameter ($A = -0.084$).

The quantitative analysis of bond length is equally striking. The Julg parameter A correlates very well both with the stabilization/destabilization energy ASE (Fig. 3a, $c = 0.99$) and with

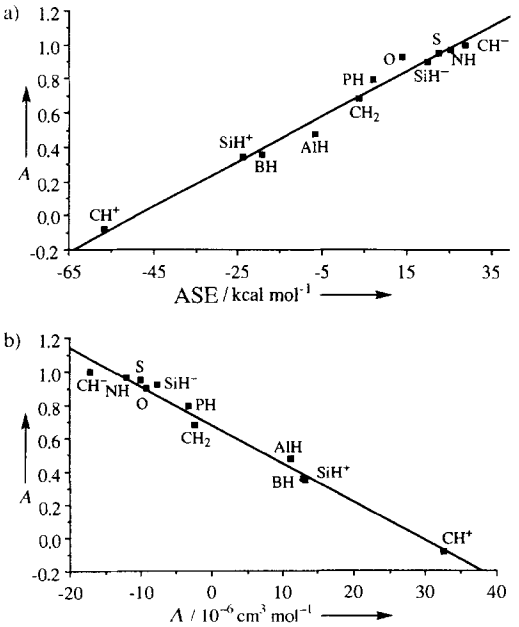


Fig. 3. Plot of Julg parameters A versus ASE (a) and versus magnetic susceptibility exaltations Λ (b). The correlation coefficients for the regression lines ($y = 0.65 + 0.01\,x$ (a); $y = 0.68 - 0.02\,x$ (b)) are both $c = 0.99$.

the magnetic susceptibility exaltation Λ (Fig. 3b, $c = 0.99$). Equal or nearly equal bond lengths in the ring (which are the average of typical single and double bond values) are an important characteristic of aromatic molecules.[1, 10] In contrast, antiaromatic molecules exhibit strong bond-length alternation.[1, 11b] Table 2 summarizes the typical single and double

Table 2. Typical lengths of C_{sp^2}–X single and double bonds and their average values in Å (at MP2(fc)/6-31G*).

C–X [a]		C=X		Average
C–C	1.504	C=C	1.339 [a]	1.421
C–C$^-$	1.418	C=C	1.375 [a]	1.396
C–C$^+$	1.422	C=C	1.367 [a]	1.394
C–C	1.450 [b]	C=C	1.350 [b]	1.400
C–O	1.375	C=O	1.228 [c]	1.301
C–S	1.762	C=S	1.629 [e]	1.695
C–N	1.385	C=N	1.280 [d]	1.332
C–Si$^+$	1.801	C=Si	1.724 [e]	1.762
C–Si$^-$	1.945	C=Si	1.724 [e]	1.834
C–B	1.559	C=B	1.390 [d]	1.424
C–P	1.380	C=P	1.681 [d]	1.755
C–Al	1.956	C=Al	1.808 [d]	1.882

[a] Based on divinyl derivatives X(HC=CH$_2$)$_2$. [b] Average values from open-chain polyenes, see Refs. [10b–e]. [c] Based on (H$_3$C)$_2$C=X. [d] From *trans*-H$_3$C–X=CH–CH$_3$ derivatives. [e] From *trans*-CH$_3$–SiH=CH–CH$_3$.

bond lengths as well as their average values, which may be compared with the optimized values for C_4H_4X given in Figure 1.

For the antiaromatic systems (X = CH$^+$ (singlet), BH, AlH, SiH$^+$) with C_{2v} symmetry, the C–C double bond lengths of 1.352–1.357 Å resemble those in polyenes (1.350 Å).[10b–e] On the other hand, the conjugated C–C single bond lengths are longer than those in polyenes (about 1.450 Å in *trans*-butadiene,[10e] 1,3-pentadiene,[10d] 1,3,5-heptatriene,[10b] and 1,3,5,7-octatetraene[10c]). In the singlet cyclopentadienyl cation (C_{2v} symmetry), the two C–C single bond lengths of 1.565 Å are 0.04 longer than those in cyclohexane (1.526 Å at MP2 level). Pronounced bond-length alternation is a typical antiaromatic feature. The C_{sp^2}–X bond lengths also are longer than the average values of typical single and double C_{sp^2}–X bonds, or may even be close to the single-bond lengths (Table 2). Thus, energetic, magnetic, and geometric criteria also characterize antiaromatic compounds.

Table 1 and Figure 2 show that the stabilization energies ASEs and the diamagnetic susceptibility exaltations of cyclopentadiene (X = CH$_2$) and phosphole (X = PH) are the smallest among the aromatic systems. In addition, The C=C and C–C bond lengths are rather normal. The possible aromaticity of cyclopentadiene (through the 2π hyperconjugative contribution of the CH$_2$ group)[9a, 10d, 11a] and especially of phosphole[18, 19] ("Despite their pyramidal structure, phospholes are 'aromatic' systems")[19b] have been debated. At best, these are "borderline" aromatics. This conclusion agrees with the results of other more recent analyses of the energy of phosphole,[18] which supersede earlier, low-level calculations.[19]

Like phosphole (X = PH), the isoelectronic silacyclopentadienyl anion (X = SiH$^-$) is another pyramidal five-membered ring heterocycle with (at least formally) 6π electrons. Our higher level results do not agree with the earlier theoretical conclusion[20] that the "silacyclopentadienyl anion has only weak aromatic character." "Moderate" would be a better description.[21] The Julg parameter is quite large ($A = 0.926$), and the ASE (13.8 kcal mol^{-1}) as well as the diamagnetic susceptibility exal-

 © VCH Verlagsgesellschaft mbH, D-69451 Weinheim, 1995 0570-0833/95/0303-0339 $ 10.00+.25/0

tation ($\Lambda = -7.7$) are about half the values for the cyclopentadienyl anion (Table 1).

The relative aromaticity of furan (X = O), thiophene (X = S), and pyrrole (X = NH) has been much discussed.[3] All have planar, C_{2v} symmetries, and their C–C "double" and "single" bond lengths are very similar and almost equal to the average distances given in Table 2. The C_{sp^2}–X bond lengths also are close to the average of single and double bond lengths. The diamagnetic exaltations, ASEs, and Λ values in Table 1 (plotted in Figures 2 and 3) give the same aromaticity order: pyrrole > thiophene > furan.

In conclusion, aromaticity and antiaromaticity are well characterized by a combination of geometric, energetic, and magnetic criteria. These criteria correlate quantitatively for the five-membered ring systems. Aromatic compounds are stabilized energetically and exhibit diamagnetic susceptibility exaltations Λ and negative anisotropies; bond-length equalization is apparent. In contrast, antiaromatic systems are destabilized; the single and double bonds are localized. The magnetic susceptibilities and anisotropies of antiaromatic systems are more positive due to paramagnetic ring-current effects. Cyclopentadiene is a borderline arene at best, but phosphole and the silacyclopentadienyl anion show increasing aromatic character. The pyrrole > thiophene > furan aromaticity order is established firmly, and the cyclopentadienyl anion is the "most aromatic" five-membered ring system.

Received: August 11, 1994 [Z 7231 IE]
German version: *Angew. Chem.* **1995**, *107*, 332

Keywords: ab initio calculations · aromaticity · heterocycles

[1] a) The literature is vast. Fortunately, an excellent new comprehensive review is available: V. I. Minkin, M. N. Glukhovtsev, B. Y. Simkin, *Aromaticity and Antiaromaticity; Electronic and Structural Aspects*, Wiley, New York, **1994**; b) P. J. Garratt, *Aromaticity*, Wiley, New York, **1986**, and references in both these sources.

[2] a) A. R. Katritzky, R. Taylor, *Adv. Heterocycl. Chem.* **1990**, *47*, 87; b) A. R. Katritzky, M. Karelson, N. Malhotra, *Heterocycles* **1991**, *32*, 127; c) A. R. Katritzky, C. W. Rees, *Comprehensive Heterocyclic Chemistry*, Pergamon, Elmsford, New York, **1984**; d) R. M. Acheson, *An Introduction to the Chemistry of Heterocyclic Compounds*, 3rd ed., Wiley, New York, **1976**; e) T. L. Gilchrist, *Heterocyclic Chemistry*, Pitman, Marshfield, MA, **1985**; f) *Heterocyclic Compounds, Vols. 1–9* (Ed.: R. C. Elderfield), Wiley, New York, **1950–1967**.

[3] F. Bernardi, A. Bottoni, A. Venturini, *J. Mol. Struct. (Theochem)* **1988**, *163*, 173, and references therein; more than 60 publications are listed there.

[4] a) K. F. Ferris, R. J. Bartlett, *J. Am. Chem. Soc.* **1992**, *114*, 8302; b) D. L. Cooper, S. C. Wright, J. Geratt, M. Raimondi, *J. Chem. Soc. Perkin Trans. 2* **1989**, 263; c) E. Uggerud, *ibid.* **1986**, 1857; d) M. N. Ramos, N. B. da Costa, Jr., B. B. Neto, *J. Mol. Struct.* **1993**, *294*, 29; e) P. Friedman, K. F. Ferris, *Int. J. Quantum Chem. Quantum Chem. Symp.* **1990**, *24*, 843.

[5] a) A. Julg, P. Francois, *Theor. Chim. Acta* **1967**, *7*, 249; b) S. M. van der Kerk, *J. Organomet. Chem.* **1981**, *215*, 315; c) *(Aromaticity, Pseudo-Aromaticity, Antiaromaticity) Jerusalem Symp. Quantum Chem. Biochem.* **1971**, *3*, 383.

[6] a) A. R. Katritzky, P. Barczynski, G. Musumarra, D. Pisano, M. Szafran, *J. Am. Chem. Soc.* **1989**, *111*, 7; b) *J. Prakt. Chem.* **1990**, *332*, 853, 870, 885; c) F. Fringuelle, G. Marino, A. Taticchi, *J. Chem. Soc. Perkin Trans. 2* **1974**, 332; d) S. S. Dharmatti, G. Govil, C. R. Kanekar, C. L. Khetrapal, M. Dhingra, *Proc. Indian Acad. Sci.* **1962**, *57*, 71; e) C. R. Kanekar, G. Govil, C. L. Khetrapal, M. Dhingra, *ibid.* **1966**, *64*, 315; f) M. Pasdeloup, J.-P. Laurent, G. Commenges, *J. Chim. Phys. Phys. Chim. Biol.* **1972**, *69*, 1022; g) D. J. Bertelli, C. Golino, *J. Org. Chem.* **1965**, *30*, 368; h) N. N. Magdesieva, *Adv. Heterocycl. Chem.* **1970**, *12*, 1; i) G. S. Reddy, J. H. Goldstein, *J. Am. Chem. Soc.* **1961**, *83*, 5020; j) K.-F. Wai, M. P. Sammes, *J. Chem. Soc. Perkin Trans. 1* **1992**, 2066.

[7] a) L. Nyulaszi, T. Veszpremi, J. Reffy, B. Burkhardt, M. Regitz, *J. Am. Chem. Soc.* **1992**, *114*, 9080; b) L. S. Khailkin, K. V. Vilkov, J. E. Boggs, *J. Mol. Struct.* **1988**, *172*, 241; c) E. J. P. Malar, *J. Org. Chem.* **1992**, *57*, 3694; d) K. Jug, *ibid.* **1983**, *48*, 1344; e) C. W. Bird, *Tetrahedron* **1993**, *49*, 8441; f) *ibid.* **1992**, *48*, 335, 1675; g) *ibid.* **1990**, *46*, 5697; h) *ibid.* **1985**, *41*, 1049; i) V. G. S. Box, *Heterocycles* **1991**, *10*, 2023.

[8] For magnetic susceptibility exaltation as an aromaticity criterion, see a) H. J. Dauben, Jr., J. D. Wilson, J. L. Laity, *J. Am. Chem. Soc.* **1968**, *90*, 811; b) *ibid.* **1969**, *91*, 1991. c) in *Nonbenzenoid Aromatics, Vol. II* (Ed.: J. P. Synder), Academic Press, New York, **1971**, p. 187, and references therein.

[9] For magnetic susceptibility anisotropy as an aromaticity criterion, see a) R. C. Benson, W. H. Flygare, *J. Am. Chem. Soc.* **1970**, *92*, 7523; b) T. G. Schmalz, C. L. Norris, W. H. Flygare, *ibid.* **1973**, *95*, 7961; c) J. R. Davidson, A. K. Burnham, B. Siegel, P. Beak, W. H. Flygare, *ibid.* **1974**, *96*, 7394; d) T. G. Schmalz, T. D. Gierke, P. Beak, W. H. Flygare, *Tetrahedron Lett.* **1974**, 2885; e) M. H. Palmer, R. H. Findlay, *ibid.* **1974**, 253.

[10] a) H. Jiao, P. von R. Schleyer, *Angew. Chem.* **1993**, *105*, 1830; *Angew. Chem. Int. Ed. Engl.* **1993**, *32*, 1760; b) *ibid.* **1993**, *105*, 1833 or **1993**, *32*, 1763; c) *J. Chem. Soc. Perkin Trans. 2* **1994**, 407; d) *J. Chem. Soc. Faraday Trans.* **1994**, *90*, 1559; e) R. Herges, H. Jiao, P. von R. Schleyer, *Angew. Chem.* **1994**, *106*, 1441; *Angew. Chem. Int. Ed. Engl.* **1994**, *33*, 1376; f) H. Jiao, P. von R. Schleyer, *ibid.* **1995**, *107*, 329 or **1995**, *34*, 334; g) M. Bühl, T. Walter, H. Jiao, P. von R. Schleyer, M. Saunders, F. A. L. Anet, *J. Am. Chem. Soc.* **1994**, *116*, 6005.

[11] a) U. Fleischer, W. Kutzelnigg, P. Lazzeretti, V. Mühlenkamp, *J. Am. Chem. Soc.* **1994**, *116*, 5298; b) H. Jiao, P. von R. Schleyer in *Proceedings of the First European Conference on Computational Chemistry* (Ed.: C. Troyanowsky), American Institute of Physics, Jericho, NY, **1994**; c) U. Fleischer, W. Kutzelnigg, P. Lazzeretti, personal communication.

[12] a) W. J. Hehre, L. Radom, P. von R. Schleyer, J. A. Pople, *Ab Initio Molecular Orbital Theory*, Wiley, New York, **1986**; b) J. B. Foresman, A. Frisch, *Exploring Chemistry with Electronic Structure Methods: A Guide to Using Gaussian*, Gaussian Inc., Pittsburgh, PA, **1993**.

[13] Gaussian 92, Revision B: M. J. Frisch, G. W. Trucks, M. Head-Gordon, P. M. W. Gill, M. W. Wong, J. B. Foresman, B. G. Johnson, H. B. Schlegel, M. A. Robb, E. S. Replogle, R. Gomperts, J. L. Andres, K. Raghavachari, J. S. Binkley, C. Gonzalez, R. L. Martin, D. J. Fox, D. J. Defrees, J. Baker, J. J. P. Stewart, J. A. Pople, Gaussian Inc., Pittsburgh, PA, **1992**.

[14] *Theoretical Structures of Molecules: Multiple Bonds (Landolt Börnstein, New Ser., Vol. II/22a–b* (Ed.: P. von R. Schleyer), Springer, Berlin, **1994**).

[15] a) D. Damiani, L. Ferretti, E. Gallinella, *Chem. Phys. Lett.* **1976**, *37*, 265, and references therein; b) on 1-phenylphosphole see P. Coggan, J. F. Engel, A. T. McPhail, L. D. Quin, *J. Am. Chem. Soc.* **1970**, *92*, 5779; c) on pentaphenylaluminol see C. Krüger, J. C. Sekutowski, H. Hoberg, R. Krause-Göing, *J. Organomet. Chem.* **1977**, *141*, 141.

[16] a) W. Kutzelnigg, U. Fleischer, M. Schindler, *NMR Basic Princ. Prog.* **1990**, *23*, 165; b) W. Kutzelnigg, *Isr. J. Chem.* **1980**, *19*, 193; c) M. Schindler, W. Kutzelnigg, *J. Chem. Phys.* **1982**, *76*, 1919.

[17] M. N. Glukhovtsev, B. Reindl, P. von R. Schleyer, *Mendeleev Commun.* **1993**, 100.

[18] a) K. K. Baldridge, M. S. Gordon, *J. Am. Chem. Soc.* **1988**, *110*, 4204; b) S. M. Bachrach, *J. Org. Chem.* **1993**, *58*, 5414; c) M. N. Glukhovtsev, P. von R. Schleyer, *J. Phys. Chem.*, submitted; d) S. M. Bachrach, L. Perriott, *J. Org. Chem.* **1994**, *59*, 3349.

[19] a) N. D. Epiotis, W. Cherry, *J. Am. Chem. Soc.* **1976**, *98*, 4365; b) W. Schäfer, A. Schweig, F. Mathey, *ibid.* **1976**, *98*, 407.

[20] a) M. S. Gordon, P. Boudjouk, F. Anwari, *J. Am. Chem. Soc.* **1983**, *105*, 4972; b) J. R. Damewood, Jr., *J. Org. Chem.* **1986**, *51*, 5028.

[21] B. Goldfuss, P. von R. Schleyer, *Organometallics* **1995**, in press.

Topochemical Aspects of the Formation of Networks in Layered Langmuir–Blodgett (LB) Assemblies**

Michael Seufert, Matthias Schaub, Gerhard Wenz, and Gerhard Wegner*

Reactions in layered assemblies of organic molecules as obtained by the Langmuir–Blodgett (LB) technique are frequently of topochemical nature,[1–6] that is the course of the reaction and the direction in which the product is formed are completely controlled by the packing of the starting material in the lattice.[3, 6] The monolayers of which LB assemblies are composed, extend in the x,y plane; the assembly direction defines the z axis

[*] Prof. Dr. G. Wegner, Dipl.-Chem. M. Seufert, Dr. M. Schaub
Max-Planck-Institut für Polymerforschung
Ackermannweg 10, D-55128 Mainz (Germany)
Telefax: Int. code + (6131)379-330
Prof. Dr. G. Wenz
Polymer-Institut der Universität Karlsruhe (Germany)

[**] This work was carried out as part of the project "Ultrathin Layers" supported by the MATFO-program of the German Ministry of Research and Technology (BMFT).

(Fig. 1a). All the reactions occurring in such systems can be characterized by a "dimensionality", where "dimensionality of the reaction" should be differentiated from "product dimensionality". The latter refers to the spatial structure of the product, that is for example whether a linear macromolecule or a two- or three-dimensional network is the reaction product. In contrast the dimensionality of the reaction describes the tensorial character of the reaction.

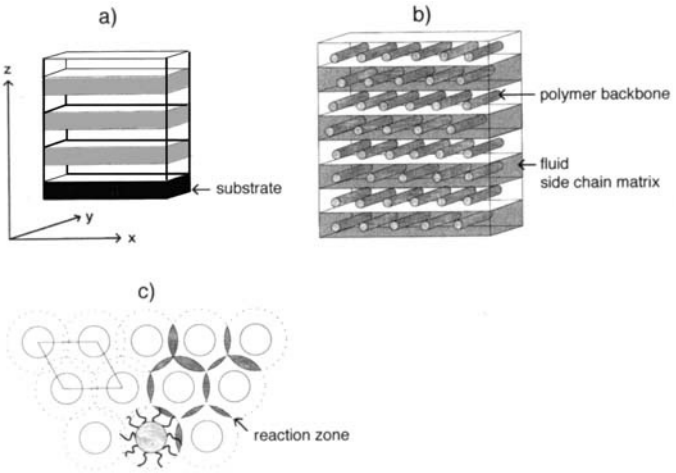
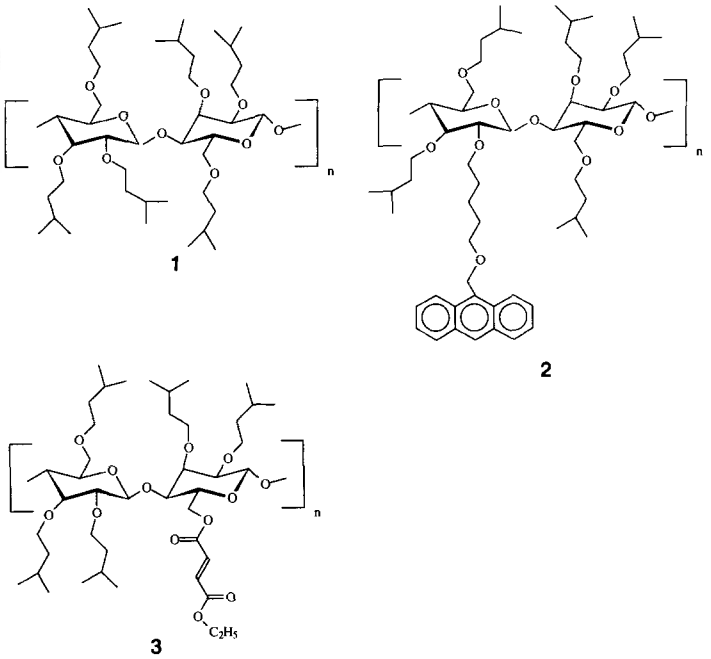


Fig. 1. a) General architecture of a LB layered assemblies. b) Layered assembly composed of "hairy rod" macromolecules [11–13]. c) Definition of the reaction zones relevant for intermolecular reactions. The schematic representation shows the hexagonally dense packing; other packing symmetries, for example a monoclinic packing of the macromolecules, would not affect the principal conclusions drawn from the model.

The polymerization of amphiphilic monomers within LB-layered assemblies is a reaction that proceeds in one direction and gives polymeric chains as one-dimensional products. The topochemical polymerization of amphiphilic dialkynes serves as an example.[6, 8] Other monomers, for example acrylates, give one-dimensional products as well, however, the polymerization within the layer plane does not occur with topochemical control of the chain direction. Thus, the reaction is pseudo one-dimensional. The lack of topochemical control leads to a decrease in "reaction-dimensionality" as compared to "product-dimensionality".[5]

Reactions with zero-dimensionality, that is a type of reaction which takes place at the site of individual molecules only, are exemplified by *cis-trans* isomerizations. The formation of a well-defined three-dimensional network starting from a LB-layered assembly has been described—to the best of our knowledge—only once, namely in the photochemical crosslinking of co-poly(glutamate)s which contained cinnamoyl groups in the side chains.[7] Work dedicated at the construction of purely two-dimensional networks[9] in LB-assemblies remained inconclusive, since additional reactions in the third dimension—the *z* direction—could not be excluded.[10] Two-dimensional networks should, however, be simply obtained by the same reactions as ordinarily used for formation of three-dimensional networks, if the reaction partners are kept far enough apart along the *z* direction that crosslinking remains limited to the *x,y* plane; thus, a matrix isolation of the reactive layers is attempted.

In the following, layered assemblies of cellulose derivatives are investigated, which may be regarded as copolymers composed of anhydroglucose units randomly substituted by ether and ester groups. They conform to the type of polymers characterized by a rigid backbone decorated by flexible side groups ("hairy rod macromolecules"). Layered LB assemblies obtainable from such molecules are well investigated.[11–13] We used isopentylcellulose (**1**) with a degree of substitution (DS) of 2.9, [5-(9-anthrylmethoxy)pentyl]isopentyl cellulose (**2**)(DS = 2.8 with respect to the isopentyl and 0.1 with respect to the anthryl residues) and a partially modified polymer containing fumarate residues (**3**) (DS = 2.5 with respect to the isopentyl and 0.25 with respect to fumarate residues). The average degree of polymerization P_n of the cellulose derivatives was 87.



The anthryl residues undergo a $4_\pi + 4_\pi$ cycloaddition[14] when irradiated which leads to a network. The reaction can be monitored by the decrease in the anthracene absorption at 250 nm. The reaction in the *z* direction is prevented by embedding single layers of **2** between layers of **1**. Figure 2a shows the

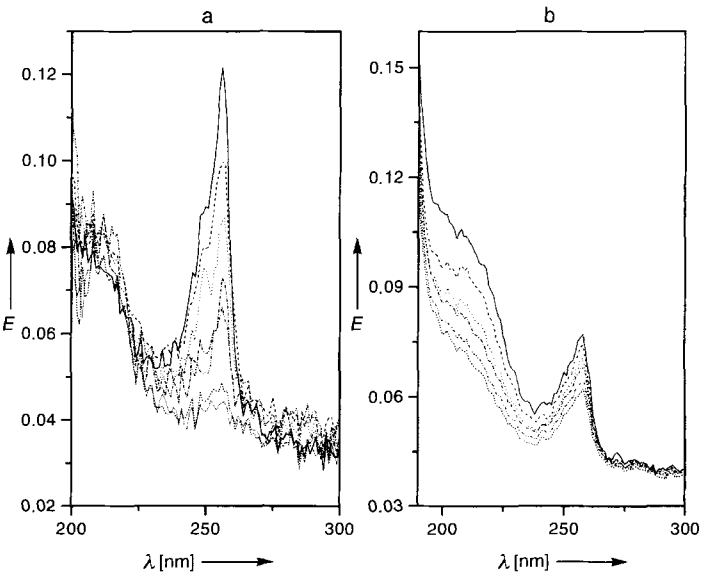


Fig. 2. a) UV spectra of a $(\mathbf{112})_{30}$ layered assembly depending on irradiation time: unirradiated, 30, 60, 120, 240, 480, 960s. b) UV spectra of a $(\mathbf{111123})_{15}$ layered assembly without annealing and after annealing for 10, 25, 50, 120, and 270 min.

 © VCH Verlagsgesellschaft mbH, D-69451 Weinheim, 1995 0570-0833/95/0303-0341 $ 10.00+.25/0

UV spectra of such a layered assembly consisting of 30 periodically repeated (**112**) layers as a function of the irradiation time. The intensity of the anthracene absorption decreases with increasing time of irradiation. The lack of reaction partners in the z direction restricts the reactivity of the anthryl groups to the x,y plane. This results in the formation of a two-dimensional network. Since the self-diffusion coefficient of the macromolecules is unmeasurably small in the layered assemblies,[11, 13] a photoreaction involving lateral diffusion of the macromolecules can be excluded. Annealing of the assembly (120 °C, 7 h in the dark) did not give rise to changes of the optical spectra.

A further strategy to create two-dimensional products involves selective cross-linking of adjacent layers. This reaction, which ought to proceed one-dimensionally in the z direction, nevertheless results in a two-dimensional network, as can be seen in Figure 1c. Reactions occurring in the x,y plane must be prevented here. This requires appropriate functionalization of adjacent layers as exemplified by a thermally induced $2_\pi + 4_\pi$ Diels–Alder reaction.[15] The reaction partners here are **2** and **3**. In order to demonstrate that a reaction in the x,y plane does not occur, single layers of **2** and **3** were each separated by two layers of **1**, that is a periodic structure of 11 such packages were assembled on a quartz substrate. If this $(\mathbf{112113})_{11}$ sample was annealed at 120–150 °C for more than five hours, no reaction occurred. If however, an analogous layered assembly was prepared in which, adjacent layers of **2** and **3** were each embedded between four layers of **1**, a substantial decrease of the intensity of the anthracene absorption band was observed when the sample was annealed at the same temperature (c.f. Fig. 2b). The only difference to the control experiment was the sequence of layers and, thus, the changes observed in the UV spectra can only be a consequence of a chemical reaction of **2** and **3** across the interface of adjacent layers.

X-ray reflectivity measurements[13, 16, 17] allow the monitoring of the overall thickness of the assembly described by $(\mathbf{111123})_{16}$ before and after the reaction. The "Kiessig-fringes" shown in Figure 3 that result from interference of X-rays reflected from the air/polymer and polymer/glass surface have been evaluated to give the data summarized in Table 1. The layered assembly exhibits a thickness of $D = 817$ Å immediately after preparation; it shrinks by about 3% to 790 Å in the course of the reaction. The periodic order of the single layers of the cellulose derivatives does not give rise to a Bragg reflection since the electron density fluctuation between backbone and side chain matrix is too small.[18] The double bonds of the fumarate residues in the freshly prepared sample, however, offer the possibility of achieving a contrast, by reaction with osmium tetraoxide. A Bragg reflection for a periodicity of 51.3 Å is observed in agreement with the sample architecture after it had been exposed to this reagent. Once the sample had been thermally crosslinked this Bragg reflection could not be produced because of the concentration of double bonds to be reacted with OsO_4 was too small.

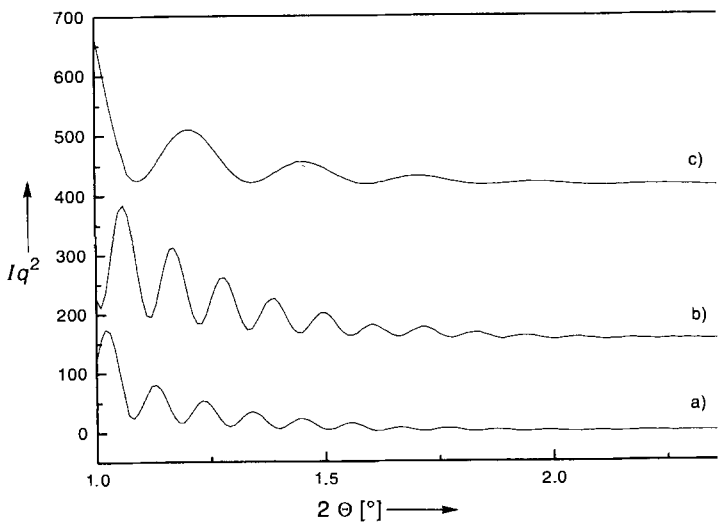


Fig. 3. X-ray reflection curve of a $(\mathbf{111123})_{16}$ layered assembly on glass: a) After preparation, b) after annealing (540 min, 150 °C), c) after extraction with toluene. I_{q^2} ($q = 2\theta/\lambda$) in arbitrary units.

Table 1. Dimensions of the layered assemblies $(\mathbf{111123})_N$ before and after thermally induced crosslinking.

Sample status	D [Å] [a]	d [Å] [b]	N [b]	d' [Å] [b]
as prepared	817	51.06	6	8.51
after annealing	790	49.38	6	8.23
after extraction	346.5	21.66	2	10.83

[a] Thickness of the layered assembly. [b] Thickness of periodic pattern of the assembly composed of N such repeat units; d' is the average thickness of a single monolayer.

The stability of the two-dimensional network obtained by Diels–Alder reaction was checked by washing the whole sample with chloroform or toluene, both good solvents for uncrosslinked cellulose derivatives. The UV transmission spectra of the layered assembly did not change, indicating that the number of chromophores per unit area remained constant. The corresponding X-ray reflectivity measurements showed, however, that the total thickness was drastically reduced to 346.5 Å, a reasonable value under the assumption that all layers consisting of **1** had been dissolved.

The thermally induced crosslinking of adjacent layers as a consequence of the chosen layer architecture is clearly a one-dimensional reaction proceeding along the z direction. However, the network obtained as the reaction product is two-dimensional. Since the dimensionality of product and reaction differ, the reaction may also be defined as pseudo two-dimensional. The dissolution of the interlayers composed of **1** serve as an additional means of manipulating the supramolecular architecture of the assembly along z. The formation of bonds between the reactive groups of adjacent macromolecules is restricted to the zones of overlap between the shells of the substituent groups surrounding each rodlike backbone. The situation is outlined in Figure 1c for a hexagonal dense packing of cylinders as the model of the architecture.

Although the reactions discussed here are not of topochemical nature in the strict sense of definition, they help to stabilize the periodic packing of the macromolecules. Futher work is necessary to establish the size of the zones of overlap and the restrictions in distance over which bimolecular reactions may occur within the limits of the architecture of such layered assemblies.

Experimental Procedure

1: Cellulose acetate (10 g) (DS = 2.34, $P_n = 150$) dissolved in dimethyl sulfoxide was treated with 3-methyl bromide (174 g) and NaOH (46 g) at room temperature for 8 days. The product was then poured into water (1.5 L) and extracted with CH_2Cl_2. The organic phase was concentrated and the residue precipitated from methanol. Yield (after drying in vacuo): 9.21 g (66%). $C_{20.5}H_{39}O_5$ (365.53). ^{1}H NMR (1,1,2,2-tetrachloro[D_2]ethane, 80 °C): $\delta = 4.3$ (d, 1H), 3.7–2.9 (m, 12H), 1.63 (s, 3H), 1.44 (m, 6H), 0.87 (s, 17H); DS (NMR) = 2.9. Membrane osmosis in toluene: $M_n = 32000\ \mathrm{g\,mol^{-1}}$.

5-(9-Anthrylmethoxy)1-bromopentane: NaH (3.6 g of an 80% suspension in mineral oil) was added to a solution of 9-anthrylmethanol (5 g) in anhydrous THF

(80 mL). The suspension was added dropwise to a mixture of 1,5-dibromopentane (55.2 g) in THF (80 mL) at 60 °C. The mixture was stirred under reflux for 20 h, it was then poured into water and the product was extracted with CH_2Cl_2. After workup and chromatographic purification (in toluene/ethyl acetate, 10/1, over silica) the yield was 6.7 g (78%). ^{1}H NMR ($CDCl_3$): δ = 8.31 (s, 1H), 8.22 (d, 2H), 7.88 (d, 2H), 7.35 (m, 4H), 5.31 (s, 2H), 3.5 (t, 2H), 3.19 (t, 2H), 1.64 (m, 2H), 1.49 (m, 2H), 1.31 (m, 2H).

2: Synthesis as described for **1**; the two bromides were added as a mixture. Components: cellulose acetate (0.5 g), NaOH (2.76 g), 3-methylbutyl bromide (10.1 g), 5-(9-anthrylmethoxy)1-bromopentane (0.715 g). Yield: 0.3 g (41.5%). ^{1}H NMR ([D_8]toluene, 100 °C) δ = 8.34 (d, 2H), 8.12 (s, 1H), 7.72 (d, 2H), 7.32 (m, 2H), 7.21 (m, 2H), 5.31 (d, 1H), 4.58 (d, 1H), 4.02 (m, 2H), 3.86–3.64 (m, 4H), 3.57 (m, 3H), 3.37 (m, 2H), 3.13 (t, 1H), 1.75 (m, 1H), 1.54 (m, 1H), 1.27 (m, 3H), 0.93 (m, 1H); $DS_{isopentyl}$ (NMR) = 2.8; $DS_{anthryl}$ (NMR) = 0.1.

3: **1** (0.91 g) (DS = 2.6) and monoethyl fumarate (0.15 g) were dissolved in THF (10 mL) (distilled over Na/K alloy). *para*-Dimethylaminopyridine (0.5 mg) and dicyclohexylcarbodiimide (0.21 g) dissolved in CH_2Cl_2 (5 mL) were added at 0 °C; the mixture was stirred at 0 °C for 4h and for an additional 12 h at 25 °C; workup procedure was as described for **1**. Yield: 0.761 g (71%). $C_{20.05}H_{36.6}O_{5.75}$ (369.71). ^{1}H NMR (1,1,2,2,-tetrachloro[D_2]ethane, 80 °C): δ = 6.85 (s, 0.5H), 4.5–2.9 (M, 12H), 1.8–1.1 (m, 9H), 0.9 (s, 15H); $DS_{isopentyl}$ (NMR) = 2.5; $DS_{fumarate}$ (NMR) = 0.25.

Preparation of the LB layers: for the quartz and glass substrates and for the characterization of the layered assemblies see ref. [19]. All substances were spread on the water surface (20 °C) as solutions of substance (5 mg) in chloroform (10 mL). With each down- and upstroke one monolayer of **1**, **2**, and **3** was transferred (dipping speed is 1 cm min^{-1}) and the transfer ratio was 1 ± 5%.—Transfer pressure: **1**: 14.5, **2**: 15.5, **3**: 16.5 m Nm^{-1}. Crosslinking: A Hg high-pressure lamp (Osram HBO 100W/2) was used for irradiation equipped with a quartz diffuser and an edge filter WG 360 at a sample distance of 30 cm.

Received: July 5, 1994
Revised version: August 27, 1994 [Z 7101 IE]
German version: *Angew. Chem.* **1995**, *107*, 363

Keywords: cellulose derivatives · Langmuir–Blodgett assemblies · supramolecular chemistry · topochemistry

[1] D. G. Whitten, *Angew. Chem.* **1979**, *91*, 472–483; *Angew. Chem. Int. Ed. Engl.* **1979**, *18*, 440–450.
[2] D. Möbius, *Mol. Cryst. Liq. Cryst.* **1983**, *96*, 319–334.
[3] C. Bubeck, *Thin Solid Films* **1988**, *160*, 1–14.
[4] H. Ringsdorf, B. Schlarb, J. Venzmer, *Angew. Chem.* **1988**, *100*, 117–162; *Angew. Chem. Int. Ed. Engl.* **1988**, *27*, 113–158.
[5] P. Eggl, D. Pink, B. Quinn, H. Ringsdorf, E. Sackmann, *Macromolecules* **1990**, *23*, 3472–3480.
[6] B. Tieke, *Adv. Polym. Sci.* **1985**, *71*, 79–152.
[7] S. Iida, M. Schaub, M. Schulze, G. Wegner, *Adv. Mater.* **1993**, *5*, 564–568.
[8] B. Tieke, H.-J. Graf, G. Wegner, B. Naegele, H. Ringsdorf, A. Banerjie, D. Day, J. B. Lando, *Colloid Polym. Sci.* **1977**, *255*, 521.
[9] H. Rehage, M. Veyssié, *Angew. Chem.* **1990**, *102*, 497–506; *Angew. Chem. Int. Ed. Engl.* **1990**, *29*, 439–448.
[10] B. J. Lee, T. Kunitake, *Langmuir* **1994**, *10*, 557–562.
[11] G. Wegner, *Mol. Cryst. Liq. Cryst.* **1993**, *235*, 1–34.
[12] S. Schwiegk, T. Vahlenkamp, Y. Xu, G. Wegner, *Macromolecules* **1992**, *25*, 2513–2525.
[13] M. Schaub, K. Mathauer, S. Schwiegk, P.-A. Albouy, G. Wenz, G. Wegner, *Thin Solid Films* **1992**, *210/211*, 397–400.
[14] K. Müllen, A. Böhm, G. Fiesser, R. O. Garay, H. Mauermann, S. Stein, *Polym. Prepr. (Am. Chem. Soc. Div. Polym. Chem.)* **1993**, *34*(1), 195.
[15] H. Wollweber, *Methoden Org. Chem. (Houben-Weyl) 4th ed. 1952*; *Bd. 5/1c*, **1970**, p. 977–1139.
[16] F. Rieutord, J. J. Benattar, L. Bosnio, *J. Phys.* **1986**, *47*, 1249–1256.
[17] F. Rieutord, J. J. Benattar, L. Bosio, P. Robin, C. Blot, R. de Kouchkovsky, *J. Phys.* **1987**, *48*, 679–687.
[18] M. Schaub, C. Fakirov, G. Lieser, G. Wenz, G. Wegner, P. A. Albouy, A. Schmidt, C. Majrkzak, S. Satija, H. Wu, M. D. Foster, *Macromolecules*, **1995**, *28*, in press.
[19] G. Wegner, *Ber. Bunsen-Ges. Phys. Chem.* **1991**, *95*, 1326, and references therein.

Characterization of an Oxo(porphyrinato)manganese(IV) Complex by X-ray Absorption Spectroscopy**

Khadija Ayougou, Eckard Bill, John M. Charnock, C. David Garner,* Dominique Mandon, Alfred X. Trautwein,* Raymond Weiss,* and Heiner Winkler

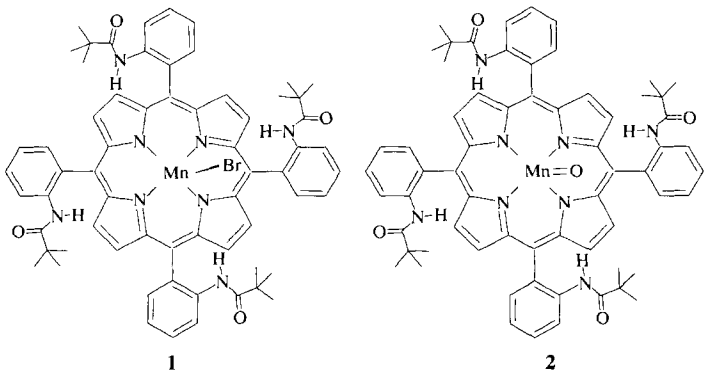
Two oxo(porphyrinato)manganese(IV) complexes generated by NaOCl or NaOBr oxidation of (porphyrinato)manganese(III) complexes have been isolated and shown to be capable of transferring an oxygen atom to styrene and triphenylphosphane.[1] Extended X-ray absorption fine structure (EXAFS) studies of these derivatives are compatible with a monomeric six-coordinate manganese(IV) porphyrin with a well defined Mn–O bond distance of 1.84 ± 0.02 Å and a water molecule as sixth ligand.[1] Formation of oxo(porphyrinato)manganese(IV) species by the reaction of (porphyrinato)manganese(III) complexes with potassium peroxycarbonate has also been reported.[2] Preliminary X-ray absorption spectroscopic (XAS) studies of the corresponding picket-fence porphyrin derivative have indicated a short Mn–X distance of 1.67 ± 0.03 Å, compatible with the presence of an Mn^{IV}=O group.[2]

Five- and six-coordinate, high-spin oxo(porphyrinato)manganese(IV) derivatives have also been obtained by peroxy acid or electrochemical oxidation of (porphyrinato)manganese(III) derivatives.[3–5] The presence of an Mn^{IV}=O moiety in these species was identified by assignment of the Mn–O stretching mode from a combination of FTIR and resonance Raman (rR) spectroscopy. However, EXAFS studies failed to demonstrate the presence of a short Mn–O bond distance.[3] To ascertain the presence of a Mn^{IV}=O moiety in the species obtained by reaction of picket-fence bromo(porphyrinato)manganese(III) with potassium peroxycarbonate and obtain more information on the Mn–O bond distance in this compound, we have reinvestigated this species by XAS. Herein we report the results of these studies.

The samples studied were prepared as 4 mM solutions by reaction at −70 °C of bromo-*meso*-tetra(α,α,α,α-pivalamidophenyl-porphyrinato)manganese(III) [$Mn^{III}Br(T_{piv}PP)$] (**1**; UV/VIS (THF): $\lambda_{max}(\varepsilon)$ = 361(66), 380(53), 475(117), 525(8), 581.5(13), 616.5(10) nm; Fig. 1) with a very large excess (10^3:1) of a THF/DMF solution of potassium superoxide KO_2 as 222-cryptate (222 = Kryptofix Hexaoxadiazabicyclohexacosane), saturated with carbon dioxide, as described previously.[12] At −70 °C the UV/Vis spectrum of the manganese species (**2**) in these samples showed bands at $\lambda_{max}(\varepsilon)$ = 436.5(196) and 555.0(20) nm (Fig. 1); monitoring of the reaction by UV/Vis spectroscopy indicated that a fast and complete conversion of the manganese(III) precursor into **2** requires the use of a large excess of $K(222)O_2/CO_2$.

[*] Prof. Dr. C. D. Garner, Dr. J. M. Charnock
Department of Chemistry, The University of Manchester
Manchester, M139PL (UK)
Telefax: Int. code + (161)275-4616
Prof. Dr. A. X. Trautwein, Dr. E. Bill, Dr. H. Winkler
Institut für Physik, Medizinische Universität zu Lübeck
Ratzeburger Allee 160, D-23538 Lübeck 1 (Germany)
Telefax: Int. code + (451)500-4214
Prof. Dr. R. Weiss, K. Ayougou, Dr. D. Mandon
Institut Le Bel (URA-CNRS 424), Université Louis Pasteur
4, Rue B. Pascal, F-67070 Strasbourg Cedex (France)
Telefax: Int. code + (88) 415363

[**] We gratefully acknowledge the support of the European HCM network "MASIMO" and the Director of the Daresbury Laboratory for provision of facilities. A.X.T. and R.W. also thank the Humboldt Foundation and the Max-Planck Gesellschaft for financial support.



1 2

This large excess prevented the observation of a clean EPR spectrum for **2**. Thus, the X-band EPR spectrum of such a sample at 4.2 K in frozen THF/DMF solution contained a very strong signal at a g value close to 2 and a very weak signal at a g value close to 4. The EPR spectrum of a THF/DMF solution

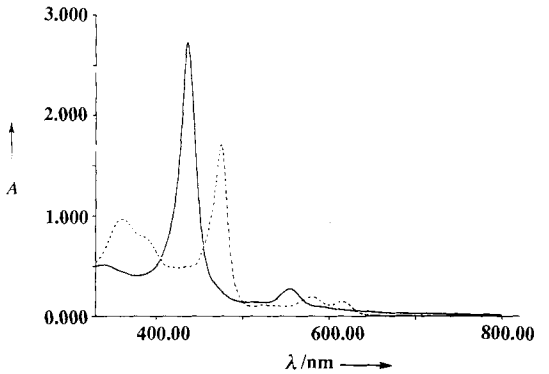


Fig. 1. UV/Vis spectra of **1** in THF (broken line) and **2** (solid line) in THF/DMF with a large excess (10^3:1) of $K(222)O_2/CO_2$.

containing only the oxidizing agent $K(222)O_2/CO_2$ demonstrated that the strong signal at $g \approx 2$ derives from this reagent. The weaker line at $g \approx 4$ is compatible with oxidation of the Mn^{III} complex **1** to a high-spin ($S = 3/2$) Mn^{IV} species, since high spin d^3 Mn^{IV} complexes in which the zero-field splitting parameter D is large exhibit EPR spectra with $g \approx 4$ and $g \approx 2$ signals.[6] These signals, which are masked by the intense signal of the oxidizing agent, can be made visible upon slow addition of only a small excess (5:1) of oxidizing reagent to **1**. Such a sample yields the spectrum depicted in Figure 2, leaving the majority of manganese in its EPR-silent trivalent state.

Samples of **2**, prepared with a large excess of the oxidizing agent (10^3:1), were transfered to aluminum cells with Mylar windows and frozen at 77 K. The manganese K-edge XAS was recorded at the SERC Daresbury Laboratory Synchroton Radiation Source, operating at 2 GeV with an average beam current of 150 mA. The sample cell was mounted on a liquid nitrogen cooled cold-finger cryostat. Data were collected in fluorescence mode on station 8.1 equipped with a double crystal Si(220) focusing monochromator and a prefocusing mirror. The second crystal was detuned to reject 30% of the beam to minimize harmonic contamination. Fluorescence was recorded with a 13-element Canberra solid-state detector. Two samples were measured; 16 scans were run for the first and 9 for the second. Individual scans showed no systematic variation, and each set of scans was summed and the two profiles compared; as the two

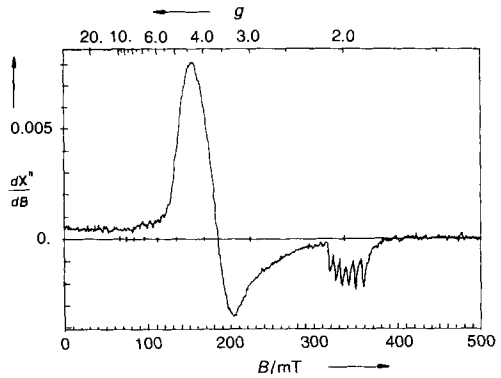


Fig. 2. EPR spectrum of the manganese compound obtained after reaction of **1** with a small excess (5:1) of $K(222)O_2/CO_2$. Microwave frequency 9.417 GHz, $T = 10$ K, microwave power 200 μW, modulation amplitude 1 mT.

spectra were identical in all features, all 25 scans were summed to give the final spectrum.

The background-substracted data (see Figure 3) showed a distinct pre-edge feature some 10 eV lower in energy than the edge. Transition metal–oxo and –nitrido complexes often exhibit an intense pre-edge transition.[7, 8] It is noted that the pre-edge peak of **2** is significantly weaker than the corresponding feature for $[Mn^{V}N(T(4\text{-}CH_3OP)P]$[8] (Fig. 3; T(4-$CH_3$OP)P = dianion of tetra(*p*-methoxyphenyl)porphyrin), $[Cr^{IV}O(TPP)]$, and $[Cr^{V}N(TPP)]$[9] (TPP = dianion of tetraphenylporphyrin). However, Fe^{IV}=O systems manifest a weak pre-edge transition, and this lack of intensity has been rationalized on the basis of a relatively long Fe–O bond (>1.6 Å).[9, 10] This argument is consistent with the data reported herein (vide infra).

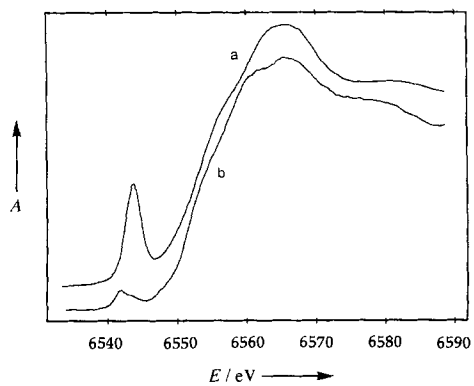


Fig. 3. Comparison of the manganese K pre-edge and edge peaks of $[Mn^{V}N(T(4\text{-}CH_3OP)P)]$ (a) and **2** (b).

The K-edge shift of manganese was measured relative to manganese metal foil. The edge position was selected as the maximum of the first derivative: +12.2 eV for **2**, +13.6 eV for $[Mn^{V}N(T(4\text{-}CH_3OP)P)]$,[8] +10.3 eV for β- and γ-$[Mn^{III}O(OH)]$,[11] and +8.3 eV for $[Mn^{II}SO_4]$. This is consistent with an oxidation state of IV for the manganese center present in **2**.

The isolated EXAFS was analyzed over the range $3 \leq k \leq 13$ Å^{-1} with EXCURV 90 and 92[12] by employing curved wave theory.[13–15] Phase shifts were calculated ab initio within these programs, from Xα-potentials and ground state, and their reliability checked by analysis of the manganese K-edge EXAFS recorded for $[Mn^{IV}(OCH_3)_2(TPP)]$,[6] and $[Mn^{V}N(T(4\text{-}CH_3OP)P)]$.[8] The metal–ligand distances of the

inner coordination spheres of these complexes were reproduced to within 0.03 Å of the corresponding crystallographic values. The EXAFS data were simulated by initially setting up a coordination environment comprising the axial ligands (or ligand) and a planar porphyrin ring with typical internal dimensions,[6, 8, 16–19] then varying the metal-backscatter distances (r), the Debye-Waller parameters ($2\sigma^2$), and E_0 until the best fit to the experimental EXAFS was achieved. The inclusion of multiple scattering from the atoms of the porphyrin ring was required to achieve a good fit at low k values. For $[Mn^{IV}(OCH_3)_2(TPP)]$ the metal was placed in the porphyrin plane,[6] but for $[Mn^{V}N(T(4\text{-}CH_3OP)P)]$ it was located 0.388 Å out of the plane.[8]

The number of independent parameters in these fits was reduced by fixing the coordination number and constraining the distances and Debye Waller factors for the pairs of pyrrole carbons at about 3 Å, and also for those at about 4.2 Å, to be the same. A similar approach was adopted in the simulations of the EXAFS of **2** (Fig. 4). In addition to the porphyrin ring, a

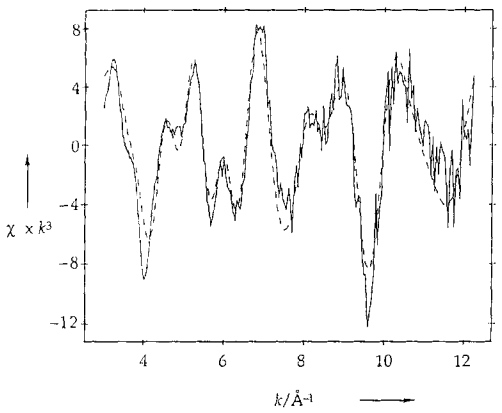


Fig. 4. EXAFS (solid line) and theoretical fit (broken line) of **2**.

light atom, assumed to be oxygen, at about 1.70 Å was required to reproduce the low r feature seen in the Fourier transform of the EXAFS (Fig. 5), and its inclusion improved the residual R factor[20] from 51.2 to 39.0. The number of independent parameters in the final fit was 14:6 pairs of r and $2\sigma^2$ (see Table 2), E_0, and the displacement of the manganese from the porphyrin plane. The possibility of a sixth ligand at the Mn^{IV} center in **2** at about 2.1 Å was investigated, but this was not

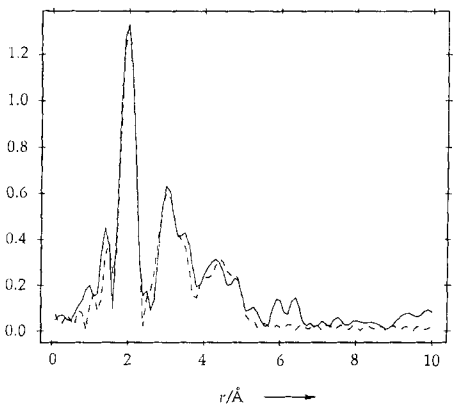


Fig. 5. Fourier transforms of the EXAFS of **2** (solid line) and theoretical fit (broken line).

justified by the improvement of the residual. Therefore, the Mn^{IV} center in **2** is considered to be five-coordinate (Table 1), and accordingly, the final simulations of the EXAFS data (Table 2 and Figs. 3 and 4) involved treatment of the multiple scattering of the porphyrin coordinated with the metal 0.5 Å out of the plane of this ligand.[16–18] The final metal–ligand distances obtained (Table 2) were Mn–O 1.69 ± 0.03 for Mn–O and 2.00 ± 0.03 Å for Mn–N.

Table 1. Coordination number (CN), spin state, and M–O bond lengths observed in oxometalloporphyrins [16–19, 22], dimethoxo(tetraphenylporphyrinato)-manganese(IV) [6], and in a macrocyclic tetraamidato-oxomanganese(V) complex. [21]

Porphyrin	CN	Spin S	M–O distance [Å]	Method	Ref.
$[Ti^{IV}O(OEP)]$	5	0	1.613(5)	X-ray	16
$[V^{IV}O(OEP)]$	5	1/2	1.620(2)	X-ray	17
$[Cr^{IV}O(TPP)]$	5	0	1.572(6)	X-ray	18
$[Mn^{IV}O(T_{piv}PP)]$	5	3/2	1.69 ± 0.03	EXAFS	this study
$[Fe^{IV}O(THF)(T_{piv}PP)]$	6	1	1.604(19)	X-ray	19
$[Fe^{IV}O(1\text{-}Melm)(TPP)]$	6	1	1.64 ± 0.03	EXAFS	22
$[Mn^{IV}(OCH_3)_2TPP]$	6	3/2	1.829(2)	X-ray	6
$[Mn^{V}O(\eta^4\text{-}L)][Et_4N]$	5	0	1.555(4)	X-ray	21

Table 2. Interpretation of EXAFS data (Mn K edge) for **2**.

Atom	CN [a]	r [Å] [b]	$2\sigma^2$ [Å^2]
O	1	1.69 [c]	0.005
N	4	2.00 [c]	0.003
C [d]	8	3.00	0.003
C [e]	4	3.35	0.011
C [d]	8	4.17	0.013
C [f]	4	4.82	0.026

[a] Coordination number, fixed at value shown. [b] Mn–atom distance. [c] Estimated uncertainty ±0.03 Å. [d] Pyrrole carbons. [e] *meso*-Carbon atoms. [f] α-Carbon atoms of pivalamidophenyl substituents.

Thus, the results of this XAS study are consistent with the postulated five-coordinate oxo-manganese(IV) derivative **2** produced by oxidation of $[Mn^{III}Br(T_{piv}PP)]$, in which the Mn–O bond lengths is 1.69 ± 0.03 Å. This value is in agreement with the results of the preliminary investigation,[2] and slightly shorter than the 1.84 ± 0.02 Å distance reported for the manganese porphyrin with a water molecule as a sixth ligand.[1] Furthermore, Table 1 compares the bond distances found in the oxo(porphyrinato)metal compounds that have been characterized to date with the Mn–O distances found in the non-oxo dimethoxo(porphyrinato)manganese(IV) complex.[6] The relatively weak pre-edge feature (Fig. 3) for the Mn^{IV}=O species **2** is consistent with a relatively long Mn–O bond, based on the arguments presented previously for Cr=O, Cr=N and Fe=O species.[9] The lengthening of the Mn^{IV}=O bond in **2** relative to the bond lengths in low-spin Cr^{IV}=O and Fe^{IV}=O porphyrin complexes is most probably related to the high-spin nature of this compound and, as shown by Spiro et al.,[4] to the special stability and low polarizability of the half-filled t_{2g}^3 subshell. Furthermore, an anionic macrocyclic tetraamidato–oxomanganese(V) complex has been characterized recently by X-ray crystallography.[21] The Mn=O length of 1.555(4) Å found in this five-coordinate, low-spin (S = 0), manganese(V) derivative is, as expected, shorter than the 1.69 Å found in **2**.

The high reactivity of the oxo(porphyrinato)manganese(IV) complexes towards olefins and saturated hydrocarbons is probably also related to the high-spin nature of these species.[2–4]

 © VCH Verlagsgesellschaft mbH, D-69451 Weinheim, 1995 0570-0833/95/0303-0345 $ 10.00+.25/0

The higher stability of the picket-fence porphyrin derivatives relative to those obtained with other porphyrins (H_2TPP, H_2TPFPP, H_2TMP[2, 3, 5]) indicates that the oxo group of the Mn=O moiety of **2** probably lies in the hydrophobic cavity formed by the four pivalamide pickets of this porphyrin.

Received: August 1, 1994 [Z 7198 IE]
German version: *Angew. Chem.* **1995**, *107*, 370

Keywords: EPR spectroscopy · EXAFS spectroscopy · manganese compounds · metalloporphyrins · porphyrinoids

[1] O. Bortolini, M. Ricci, B. Meunier, P. Friant, I. Ascone, J. Goulon, *Nouv. J. Chim.* **1986**, *10*, 39–49.
[2] M. Schappacher, R. Weiss, *Inorg. Chem.* **1987**, *26*, 1189–1190.
[3] J. T. Groves, M. K. Stern, *J. Am. Chem. Soc.* **1987**, *109*, 3812–3814.
[4] R. S. Czernuszewic, Y. O. Su, M. K. Stern, K. A. Macor, D. Kim, J. T. Groves, T. G. Spiro, *J. Am. Chem. Soc.* **1988**, *110*, 4158–4165.
[5] J. T. Groves, M. K. Stern, *J. Am. Chem. Soc.* **1988**, *110*, 8628–8638.
[6] M. J. Camenzind, F. J. Hollander, C. L. Hill, *Inorg. Chem.* **1982**, *21*, 4301–4308.
[7] T. D. Tullius, W. O. Gillum, R. M. K. Carlson, K. O. Hodgson, *J. Am. Chem. Soc.* **1980**, *102*, 5670–5676.
[8] This compound was prepared following the method outlined by C. L. Hill, F. J. Holländer, *J. Am. Chem. Soc.* **1982**, *104*, 7318–7319.
[9] J. E. Penner-Hahn, M. Benfatto, B. Hedman, T. Takahashi, S. Doniach, J. T. Groves, K. O. Hodgson, *Inorg. Chem.* **1986**, *25*, 2255–2259.
[10] J. E. Penner-Hahn, T. J. McMurry, M. Renner, L. Latos-Grazynsky, K. S. Eble, I. M. Davis, A. L. Balch, J. T. Groves, J. H. Dawson, K. O. Hodgson, *J. Biol. Chem.* **1983**, *258*, 12761–12764.
[11] P. Mackle, J. M. Charnock, C. D. Garner, F. C. Meldrum, S. Mann, *J. Am. Chem. Soc.* **1993**, *115*, 8471–8472.
[12] N. Binsted, J. W. Campbell, S. J. Gurman, P. C. Stepheson, *SERC Daresbury Laboratory, EXCURV 90 and 92 Programs* **1990**, **1992**.
[13] P. A. Lee, J. B. Pendry, *Phys. Rev. B: Solid State* **1975**, *11*, 2795–2811.
[14] S. J. Gurman, N. Binsted, I. Ross, *J. Phys. C* **1984**, *17*, 143–151.
[15] S. J. Gurman, N. Binsted, I. Ross, *J. Phys. C* **1986**, *19*, 1845–1861.
[16] R. Guilard, J. M. Latour, C. Lecompte, J. C. Marchon, J. Protas, D. Ripoll, *Inorg. Chem.* **1978**, *17*, 1228–1237.
[17] F. S. Molinaro, J. A. Ibers, *Inorg. Chem.* **1976**, *15*, 2278–2283.
[18] J. T. Groves, W. J. Kruper, Jr., R. C. Haushalter, W. M. Butler, *Inorg. Chem.* **1982**, *21*, 1363–1368.
[19] M. Schappacher, R. Weiss, R. Montiel-Montoya, A. X. Trautwein, A. Tabard, *J. Am. Chem. Soc.* **1985**, *107*, 3736–3838.
[20] N. Binsted, R. W. Strange, S. S. Hasnain, *Biochemistry* **1992**, *31*, 12117–12125.
[21] T. J. Collins, R. D. Powell, C. Slebodnick, E. S. Uffelman, *J. Am. Chem. Soc.* **1990**, *112*, 899–901.
[22] J. E. Penner-Hahn, K. S. Eble, T. J. McMurry, M. Renner, A. L. Balch, J. T. Groves, J. H. Dawson, K. O. Hodgson, *J. Am. Chem. Soc.* **1986**, *108*, 7819–7825.

Models for Bimetallic Catalysts: Multiple Oxidation States in Pt_3Re Cluster Cations**

Leijun Hao, Jianliang Xiao, Jagadese J. Vittal, and Richard J. Puddephatt*

Binding between oxo ligands and the small metal clusters present in the important oxide-supported bimetallic Pt–Re catalysts may occur at the metal-support interface and also during oxidation–reduction cycles.[1] However, knowledge of how oxygen interacts with the metal clusters is limited due to the difficulties in characterizing the heterogeneous materials. There are also few related metal oxo clusters to act as model compounds.[2, 3] The oxidation of **1** (dppm = $Ph_2PCH_2PPh_2$) with Me_3NO or oxygen to give the clusters **2** and **3**, respectively, was reported earlier.[4] Here we show that further oxidation of **3** to give the novel clusters **4**–**6** is possible (Scheme 1). The oxidation of **1** to **4**, **5**, or **6** leads to an increase in cluster electron count by

$[Pt_3\{Re(CO)_3\}(\mu\text{-dppm})_3]^+$ **1** $[Pt_3\{Re(CO)_3\}(\mu_3\text{-O})(\mu\text{-dppm})_3]^+$ **2**

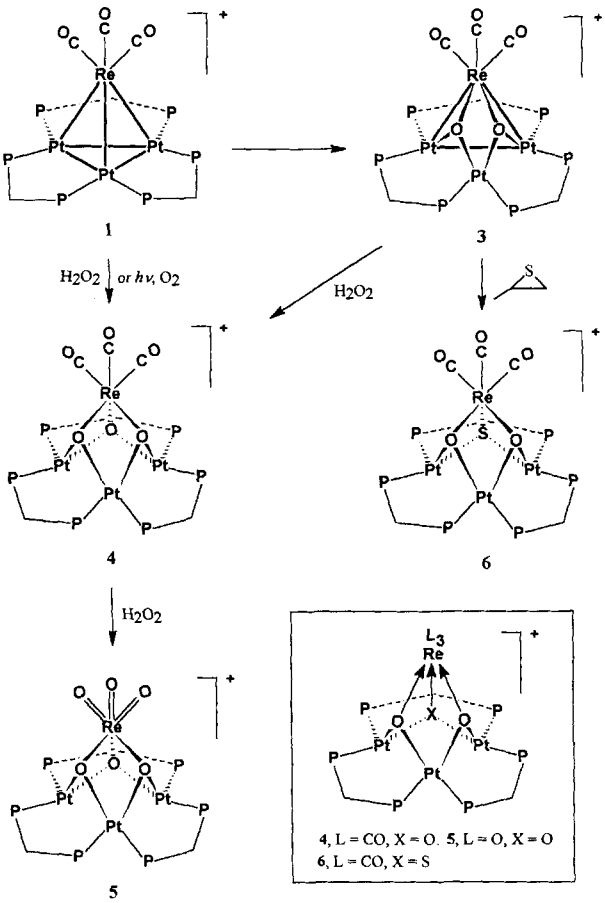
$[Pt_3\{Re(CO)_3\}(\mu_3\text{-O})_2(\mu\text{-dppm})_3]^+$ **3** $[Pt_3\{Re(CO)_3\}(\mu_3\text{-O})_3(\mu\text{-dppm})_3]^+$ **4**

$[Pt_3\{ReO_3\}(\mu_3\text{-O})_3(\mu\text{-dppm})_3]^+$ **5**

$[Pt_3\{Re(CO)_3\}(\mu_3\text{-O})_2(\mu_3\text{-S})(\mu\text{-dppm})_3]^+$ **6**

12 electrons (from 54 to 66 electrons) and the formation of **5** from **1** involves a 12-electron oxidation (from Pt_3Re^+ to Pt_3Re^{13+}) without cluster fragmentation. Such multielectron processes appear to be unprecedented in cluster chemistry.

The trioxo cluster **4** could be prepared either by the thermal reaction of **1** with hydrogen peroxide or the photochemical reaction of **1** with oxygen. In both cases, NMR monitoring showed that the reaction proceeded via the intermediacy of the dioxo cluster **3** (Scheme 1) and, as predicted on this basis, reaction of



Scheme 1.

cluster **3** with H_2O_2 led to addition of a third oxo ligand giving **4** in high yield. The analogous dioxo(thio) cluster **6** was obtained by sulfur atom addition in the reaction of cluster **3** with propene sulfide. Finally, the hexaoxo cluster **5** was obtained by further oxidation of **4** with H_2O_2; cluster **5** has low solubility in acetone and so precipitates as it is formed. The $Re(=O)_3$ frag-

[*] Prof. R. J. Puddephatt, L. Hao, Dr. J. Xiao, Dr. J. J. Vittal
Department of Chemistry, The University of Western Ontario
London, Ontario N6A 5B7 (Canada)
Telefax: Int. code + (519)661-3022

[**] This work was supported by the Natural Sciences and Engineering Research Council (Canada).

ment present in **5** is also present in $[Pt_3(ReO_3)(\mu\text{-dppm})_3]^+$, which was obtained by the high-temperature reaction of **1** or **3** with O_2.[5] The oxidation of Re–CO groups to Re=O groups finds precedent in the oxidation of $[(\eta^5\text{-}C_5Me_5)Re(CO)_3]$ to $[(\eta^5\text{-}C_5Me_5)ReO_3]$ in reaction with H_2O_2 or $O_2/h\nu$.[6] For the Pt_3Re clusters **1** and **3**, oxidation by oxygen atom addition evidently takes place first at the Pt–Re bonds; the $Re(CO)_3$ to $Re(=O)_3$ transformation has a higher activation energy.

Complexes **4** and **5** each give a single resonance in the ^{31}P NMR spectrum due to the phosphorus atoms and two resonances in the ^1H NMR spectrum due to the methylene protons of the dppm ligands, indicating a structure with C_{3v} symmetry. The magnitudes of the coupling constants $^1J(Pt,P)$ (3401 Hz for **4**, 3561 Hz for **5**) are greater than for the precursor **1** (2411 Hz), as expected since the phosphorus atoms are *trans* to the oxygen atoms rather than to the metal–metal bonds. The IR spectrum of **4** contains ν(CO) bands at 1987 and 1856 cm^{-1}, whose positions are close in energy to those in **1**–**3**;[4] the spectrum of **5** contains ν(Re=O) bands at 937 and 900 cm^{-1}, comparable to those observed in $[Pt_3(ReO_3)(\mu\text{-dppm})_3]^+$ (935 and 893 cm^{-1})[5] and $[(\eta^5\text{-}C_5Me_5)ReO_3]$ (909 and 878 cm^{-1}).[6]

The cluster **6** is C_2 symmetric and, as expected, the ^{31}P NMR spectrum exhibited three resonances due to the dppm ligands, with $^1J(Pt,P)$ values of 3388 and 3283 Hz (P atoms *trans* to oxygen atoms) and 3190 Hz (P atoms *trans* to the sulfur atom). The IR spectrum contains ν(CO) bands at 1989, 1865, and 1856 cm^{-1}. The structure of **6**, as the $[PF_6]^-$ salt, was confirmed crystallographically (Fig. 1).[7] Table 1 summarizes the changes

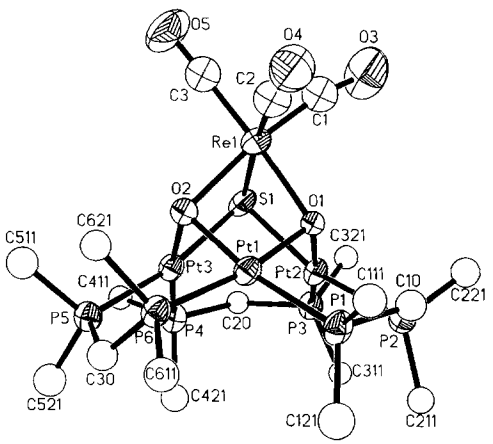


Fig. 1. A view of the structure of the cluster cation **6**. Only the *ipso* carbon atoms of the phenyl groups are shown for clarity.

in Pt–Pt and Pt–Re distances in **1**, **3**, and **6** as two oxo (**3**) and two oxo and one thio ligand (**6**), respectively, are added to cap the Pt_2Re faces of cluster **1**. It is immediately apparent that because of additional chalcogenido ligands all metal–metal separations increase in this series of clusters, and that complex **6** contains no metal–metal bonds.

Table 1. Comparison of the metal–metal distances in **1**, **3**, and **6**.

	1	**3**	**6**
Pt1-Pt2	2.611(1)	2.826(1)	3.254(2)
Pt1-Pt3	2.593(1)	3.094(1)	3.157(2)
Pt2-Pt3	2.608(1)	3.081(1)	3.143(2)
Pt1-Re	2.684(1)	2.843(1)	3.132(2)
Pt2-Re	2.649(1)	2.854(1)	3.378(2)
Pt3-Re	2.685(1)	3.228(1)	3.465(2)

Cluster **1** is intensely red-black and the color appears to be associated with the metal–metal bonds, while the clusters **4**–**6** are yellow or white, consistent with the absence of metal–metal bonds in all cases. The cluster electron count increases from 54 in **1** to 66 in each of **4**–**6** (each μ_3-O or μ_3-S ligand contributes four electrons, each terminal CO or O contributes two electrons). The additional 12 electrons in **4**–**6** cause the cleavage of all metal–metal bonds. Hence the $Pt_3Re(\mu_3\text{-}X)_3$ framework established for **6** is a model for the series **4**–**6** (X = O, S). A valence-bond representation of the bonding in **4**–**6** is shown in the inset in Scheme 1. Thus the metal centers in **4** and **6** are considered as octahedrally surrounded Re^I ions and square-planar surrounded Pt^{II} ions (PtP_2O_2 or PtP_2OS coordination); the sum of the oxidation states of the metal atoms increases from +1 in **1** to +7 in **4** and **6**. The platinum coordination is the same in **5**, but the rhenium is oxidized to Re^{VII} with octahedral ReO_6 coordination and the sum of oxidation states of the metal centers is now +13. We know of no cluster complexes containing this type of rhenium coordination but related mononuclear complexes are known.[8] For example, the complexes $[LReO_3]^+$ (L = 1,4,7-triazacyclononane, 1,4,7-trithiacyclononane) are related to **5** if the Pt_3O_3 ring is considered as a tridentate pseudo-crown ether ligand.[8] The high oxidation state of rhenium in **5** is shown by the Re ($4f_{7/2}$) binding energy of 45.6 eV in the X-ray photoelectron spectroscopy (XPS), only slightly lower than in Re_2O_7 (46.7 eV).[9]

The use of polyhedral skeletal electron theory to predict the extent of metal–metal bonding is central to the systematic study of cluster complexes. Previously, the effect of a 12-electron increase in cluster electron count could only be studied by using structurally similar clusters of different metals. A well-known example is found in the clusters $[Cp_4Fe_4(CO)_4]$ (60 electrons, six M–M bonds) and $[Cp_4Co_4S_4]$ (72 electrons, no M–M bonds).[10] The clusters **1** (54 electrons) and **4**–**6** (66 electrons) provide a particularly good example because all are based on the Pt_3Re core and because the intermediate 58- and 62-electron clusters are also known.[4] Similarly, the ability to increase the sum of the oxidation states of the metal atoms in the cluster **1** by six (**1** → **4**, **1** → **6**) or by 12 (**1** → **5**), while maintaining the cluster integrity is unprecedented.[11] There is a close analogy between the structure of the $Re(CO)_3(\mu\text{-}O)_3$ unit in **4** and that proposed for rhenium carbonyl complexes bound to oxide supports. The chemistry of **4** gives credence to the theory that oxophilic rhenium centers are present at the oxide support/bimetallic alloy interface in supported Pt–Re catalysts.[1, 12]

Received: August 24, 1994 [Z 7260 IE]
German version: *Angew. Chem.* **1995**, *107*, 349

Keywords: catalysis · clusters · complexes with chalcogen ligands · platinum compounds · rhenium compounds

[1] a) J. H. Sinfelt, *Bimetallic Catalysts. Discoveries, Concepts and Applications*, Wiley, New York, **1983**; b) *Metal Clusters in Catalysis* (Eds.: B. C. Gates, L. Guczi, H. Knozinger), Elsevier, New York, **1986**; c) J. H. Sinfelt, *Acc. Chem. Res.* **1987**, *20*, 134.

[2] a) S. L. Ingham, J. Lewis, P. R. Raithby, *J. Chem. Soc. Chem. Commun.* **1993**, 166; b) C. K. Schauer, E. J. Voss, M. Sabat, D. F. Shriver, *J. Am. Chem. Soc.* **1989**, *111*, 7662; c) Y. Chi, L. S. Hwang, G. H. Lee, S. M. Peng, *J. Chem. Soc. Chem. Commun.* **1988**, 1456; d) C. P. Gibson, A. D. Rae, D. R. Tomchick, L. F. Dahl, *J. Organomet. Chem.* **1988**, *340*, C23; e) F. A. Cotton, P. Lahuerta, M. Sanau, W. Schwotzer, *J. Am. Chem. Soc.* **1985**, *107*, 8284; f) C. K. Schauer, D. F. Shriver, *Angew. Chem.* **1987**, *99*, 275; *Angew. Chem. Int. Ed. Engl.* **1987**, *26*, 255; g) A. Colombie, J.-J. Bonnet, P. Fompeyrine, G. Lavigne, S. Sunshine, *Organometallics* **1986**, *5*, 2305; h) R. J. Goudsmit, B. F. G. Johnson, J. Lewis, P. R. Raithby, K. H. Whitmire, *J. Chem. Soc. Chem. Commun.* **1983**, 246; i) A. Ceriotti, L. Resconi, F. Demartin, G. Longoni, M. Manassero, M. Sansoni, *J. Organomet. Chem.* **1983**, *249*, C35; j) G. Lavigne, N. Lugan, J. J. Bonnet, *Nouv. J. Chim.* **1981**, *5*, 423.

 © *VCH Verlagsgesellschaft mbH, D-69451 Weinheim, 1995* *0570-0833/95/0303-0347 $ 10.00+.25/0*

[3] F. Bottomley, L. Sutin, *Adv. Organomet. Chem.* **1988**, *28*, 339.
[4] J. Xiao, J. J. Vittal, R. J. Puddephatt, L. Manojlović-Muir, K. W. Muir, *J. Am. Chem. Soc.* **1993**, *115*, 7882.
[5] J. Xiao, R. J. Puddephatt, L. Manojlović-Muir, K. W. Muir, *J. Am. Chem. Soc.* **1994**, *116*, 1129.
[6] a) W. A. Herrmann, *Angew. Chem.* **1988**, *100*, 1269; *Angew. Chem. Int. Ed. Engl.* **1988**, *27*, 1297; b) W. A. Herrmann, R. Serrano, H. Bock, *ibid.* **1984**, *96*, 364; and **1984**, *23*, 383.
[7] Crystallographic data for $[Pt_3\{Re(CO)_3\}(\mu_3\text{-}O)_2(\mu_3\text{-}S)(\mu\text{-dppm})_3][PF_6] \cdot Et_2O$, **6**$[PF_6] \cdot Et_2O$: Monoclinic, $P2_1/n$; $a = 17.133(3)$, $b = 23.494(4)$, $c = 19.976(4)$ Å, $\beta = 95.42(1)°$; $V = 8005(3)$ Å^3, $Z = 4$; Siemens P4 diffractometer with $Mo_{K\alpha}$ radiation, $\lambda = 0.71073$ Å, $T = 25°C$, $R = 0.0813$ for 446 parameters and 5725 reflections with $I \geq 2\sigma(I)$. Further details of the crystal structure investigation are available on request from the Director of the Cambridge Crystallographic Data Centre, 12 Union Road, GB-Cambridge CB2 1EW (UK), on quoting the full journal citation.
[8] W. A. Herrmann, P. W. Roesky, F. E. Kühn, W. Scherer, M. Kleine, *Angew. Chem.* **1993**, *105*, 1768; *Angew. Chem. Int. Ed. Engl.* **1993**, *32*, 1714.
[9] W. T. Tysoe, F. Zaera, G. A. Somorjai, *Surf. Sci.* **1988**, *200*, 1.
[10] H. Vahrenkamp, *Adv. Organomet. Chem.* **1983**, *22*, 169.
[11] P. Zanello, *Struct. Bonding (Berlin)* **1992**, *79*, 101.
[12] a) P. S. Kirlin, F. B. M. van Zon, D. C. Konigsberger, B. C. Gates, *J. Phys. Chem.* **1990**, *94*, 8439; b) S. K. Purnell, J.-R. Chang, B. C. Gates, *ibid.* **1993**, *97*, 4196; S. M. Augustine, W. M. H. Sachtler, *J. Catal.* **1989**, *116*, 184.

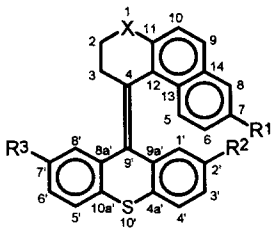
A Highly Stereoselective Optical Switching Process Based on Donor–Acceptor Substituted Dissymmetric Alkenes**

Wolter F. Jager, Johannes C. de Jong, Ben de Lange, Nina P. M. Huck, Auke Meetsma, and Ben L. Feringa*

The development of organic materials for optical data storage and molecular optical devices requires components whose physical properties can be modulated by light.[1] For a few bistable molecular systems based on photocyclization reactions impressive results have been obtained.[2] So far the bistable molecules are detected primarily by UV/Vis spectroscopy (photochromism),[1, 2] although detection based on changes in other properties such as refractive index[3] and conductivity[4] is also successfully employed.

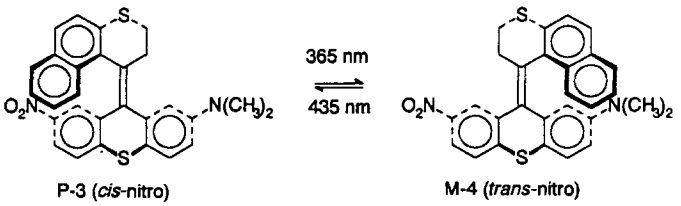
The first chiroptical molecular switch, based on the bistability of the helical *cis* and *trans* thioxanthenes **1** and **2**, was reported by our group.[5] These pseudoenantiomers[6] interconvert stereospecifically M-*cis* ⇌ P-*trans*; in other words the *cis*–*trans* isomerization of **1** and **2** is accompanied by a reversal of helicity. For these compounds a difference in the relative proportion of the two photostationary states of only 4% was reached (irradiation with $\lambda = 300$ nm: 64% M-*cis*, 36% P-*trans*; irradiation with $\lambda = 250$ nm: 68% M-*cis*, 32% P-*trans*), whereas 10% racemization (M-*cis* → P-*cis*; P-*trans* → M-*trans*) was observed after 20 switching cycles.[5]

We describe here a remarkably selective switching process based on the intrinsic chirality of donor–acceptor substituted



1 : X = CH_2, R^1 = CH_3, R^2 = OCH_3, R^3 = H
2 : X = CH_2, R^1 = CH_3, R^2 = H, R^3 = OCH_3
3 : X = S, R^1 = H, R^2 = NO_2, R^3 = N $(CH_3)_2$
4 : X = S, R^1 = H, R^2 = N $(CH_3)_2$, R^3 = NO_2

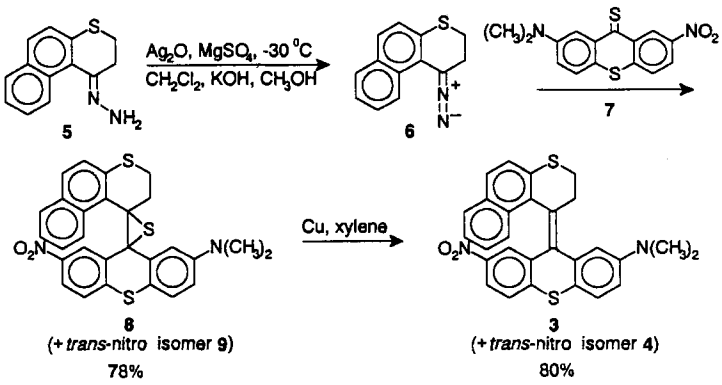
dissymmetric *cis* and *trans* **3** and **4**, respectively (Scheme 1). The absorption maxima of these compounds are red-shifted relative to those of **1** and **2**, allowing the switching process to take place in the visible. Moreover, increased thermal and photochemical stability towards racemization was obtained by the introduction of a sulfur atom at the 1-position.



Scheme 1. Chiroptical molecular switch based on the photoisomerization of P-**3** and M-**4**.

The photochemical isomerization P-**3** (*cis*-nitro) ⇌ M-**4** (*trans*-nitro) (Scheme 1) is detected by chiroptical techniques. Major advantages over other photochromic systems are: a) a more discriminative detection technique, since unlike UV spectra, circular dichroism (CD) and optical rotatory dispersion (ORD) spectra of both molecular forms P-**3** (*cis*-nitro) and M-**4** (*trans*-nitro) can reverse sign and are roughly mirror images; b) photochemical isomerization during readout[1] (fatigue) can be excluded by using ORD techniques employing a wavelength outside the absorption region.

The formation of the central double bond is the key step in the synthesis of **3** and **4** outlined in Scheme 2. Hydrazone **5** was



Scheme 2.

oxidized to the corresponding diazo compound **6** (Ag_2O, CH_2Cl_2, −30 °C), and subsequent 1,3-dipolar cycloaddition[7] with thioketone **7** was followed by extrusion of N_2 to provide the episulfides **8** (*cis*-nitro) and **9** (*trans*-nitro). The episulfides were desulfurized by reduction with copper powder to afford

[*] Prof. Dr. B. L. Feringa, Dr. W. F. Jager, Dr. J. C. de Jong, Dr. B. de Lange, Drs. N. P. M. Huck, Drs. A. Meetsma
Department of Organic and Molecular Inorganic Chemistry
Groningen Centre for Catalysis and Synthesis
University of Groningen
Nyenborgh 4, NL-9747 AG Groningen (The Netherlands)
Telefax: Int. code + (50)634296

[**] This investigation was financially supported by the Technology Foundation (STW) and the Dutch Foundation for Scientific Research (NWO), and was carried out in cooperation with Philips Research Laboratories (The Netherlands).

isomers **3** and **4** in a 60:40 ratio. The red *cis*-nitro isomer **3** (m.p. 212 °C) and the yellow *trans*-nitro isomer **4** (m.p. 206 °C) were separated chromatographically.[8]

Recrystallization of **3** from ethanol afforded crystals suitable for X-ray analysis. The molecular structure of **3** is depicted in Figure 1.[9] The arrangement about the central double bond is

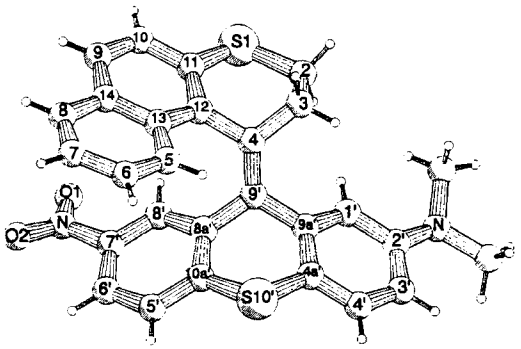


Fig. 1. X-ray crystal structure of **3** (PLUTO diagram).

nearly planar (dihedral angles 0.4–5.4°), and the bond length C4–C9′ has a normal value of 1.353 Å. The anti-folded helical structure, in which the top and bottom halves are tilted up and down, respectively, relative to the plane of the central double bond, and by which severe nonbonding interactions are avoided, is clearly shown. In **3** the nitroarene acceptor unit is located opposite the naphthalene moiety of the upper part of the molecule.

The enantiomers of **3** and **4** were resolved by chiral high-performance liquid chromatography (HPLC) with (+)-poly-(triphenylmethylmethacrylate) as a chiral stationary phase.[10] The configurations of all four stereoisomers M-**3**, P-**3**, M-**4**, and P-**4** were assigned by CD spectroscopy.[11] The enantiomers of **3** and **4** are perfectly stable under ambient conditions. The thermal racemization of P-**4** (*trans*-nitro) into M-**4** (*trans*-nitro), as determined by polarimetry at 85.0 and 90.0 °C, showed first-order kinetics with a barrier of 122.2 ± 0.5 kJ mol^{-1}. Introduction of a sulfur atom at the 1-position[12] increases the racemization barrier[13] by 12 kJ mol^{-1} relative to that of the carbon analogue **1**.[5] No thermal *cis*–*trans* isomerization (**3**⇌**4**) occurs. In contrast, a stereospecific photochemical *cis*–*trans* isomerization (P-**3**⇌M-**4**, λ = 300–435 nm, *n*-hexane) takes place readily and was monitored by CD, ^{1}H NMR spectroscopy, and HPLC analysis.

The UV/Vis spectra of **3** and **4** are clearly different (Fig. 2). Both compounds exhibit intense short-wavelength absorptions

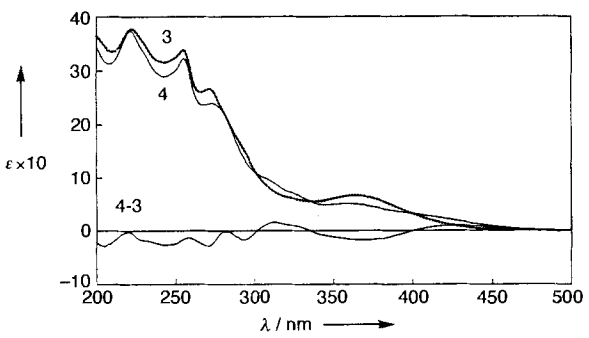


Fig. 2. UV spectra of **3** (dotted line) and **4** (solid line), and the difference spectrum (*n*-hexane).

at 220, 255, and 275 nm (ε = 25000–40000) and less intense long-wavelength absorptions. For **3** (*cis*-nitro) a well-defined absorption at 366 nm (ε = 7500) is observed, while **4** (*trans*-nitro) has a much broader, low-intensity absorption at 360 nm (ε = 5300). The CD spectra of P-**3** (*cis*-nitro) and M-**4** (*trans*-nitro) (Fig. 3) are roughly mirror images at most wavelengths. This is in accordance with the "pseudoenantiomeric nature"[6] of P-**3** and M-**4**, in which the chiral properties are mainly determined by the opposite helical structure.

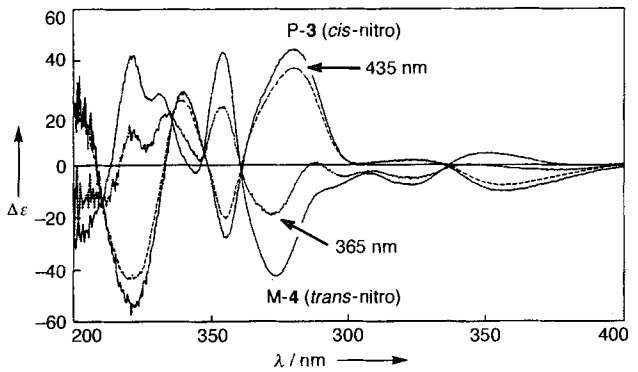


Fig. 3. CD spectra of M-**4**, P-**3**, and the photostationary states generated by irradiation at 365 and 435 nm (in *n*-hexane).

Irradiation of solutions of enantiomerically pure P-**3** (or M-**4**) in *n*-hexane at 300 and 350 nm for 10 s resulted in two distinct photostationary states. CD spectroscopy and chiral HPLC analysis revealed that at 300 nm the photostationary state was composed of 54% M-**4** (*trans*-nitro) and 46% P-**3** (*cis*-nitro), while the photostationary state at 350 nm was composed of 62% M-**4** (*trans*-nitro) and 38% P-**3** (*cis*-nitro). The P-**3**⇌M-**4** interconversion is perfectly reversible showing no trace of racemization after 60 switching cycles. The results of several irradiation experiments compiled in Table 1 show that the compositions of the photostationary states are strongly dependent on the solvents and wavelengths applied.[14]

Table 1. Composition of the mixture of diastereomers for the different photostationary states determined by irradiation of M-**4** in different solvents with light of different wavelengths.

Entry	Solvent	λ [nm]	Proportion of diastereomers [%]		(M-**4** vs P-**3**) [%]
1	*n*-hexane [a]	300	54 M-**4**	46 P-**3**	8
2	*n*-hexane [a, b]	350	62 M-**4**	38 P-**3**	24
3	cyclohexane [b]	350	62 M-**4**	38 P-**3**	24
4	toluene [b]	350	73 M-**4**	27 P-**3**	46
5	dioxane [b]	350	83 M-**4**	17 P-**3**	66
6	*n*-hexane [a]	313	50 M-**4**	50 P-**3**	0
7	*n*-hexane [a]	365	70 M-**4**	30 P-**3**	40
8	*n*-hexane [a]	405	53 M-**4**	47 P-**3**	6
9	*n*-hexane [a]	435	10 M-**4**	90 P-**3**	−80

[a] CD measurements. [b] HPLC analysis.

The extrema in the UV/Vis difference spectra of **3** and **4** (Fig. 2) at 314, 365, and 435 nm represent wavelengths at which after irradiation large differences in the composition of photostationary states can be expected.[15] Irradiation of either enantiomerically pure M-**4** (*trans*-nitro) or P-**3** (*cis*-nitro) at 365 nm results in a photostationary state composed of 70% M-**4** and 30% P-**3**. Alternating irradiation with 365 and 435 nm light results in a highly diastereoselective interconversion between

 © VCH Verlagsgesellschaft mbH, D-69451 Weinheim, 1995 0570-0833/95/0303-0349 $ 10.00+.25/0

photostationary states with ratios of M-**4** and P-**3** of 70:30 and 10:90, respectively (Table 1, Fig. 3). The results demonstrate that the photochemical isomerization of both P-**3** and M-**4** is stereospecific and also shows high wavelength-dependent diastereoselectivity. At the same time the photochemical and thermal stability of **3** and **4** towards racemization has greatly improved.

Unlike other known potential optical memory systems[1-4] the key feature of the bistable molecules described here is that switching is accompanied by inversion of the chirality. These chiral compounds are suited as optical write-read-erase information storage systems.[1, 16] Photochemical writing in the visible and reading by chiroptical means either in the visible (ORD) or in the UV (CD) may be possible. Furthermore an Erasable Direct Read After Write (EDRAW) process might be executed by using for instance 365 nm light for reading and erasing (P-**3** $\rightleftharpoons$ M-**4** isomerization). The fact that the switching process occurs between photostationary states in which either of the pseudoenantiomers P-**3** or M-**4** are present in large excess makes this switch relatively insensitive towards racemization or degradation processes, since these processes will lower the CD signals of these states but will not change their signs. Studies on incorporating the highly selective chiral switchable molecules in polymeric films or depositing them on surfaces to develop macroscopic information storage devices are currently in progress.

Experimental Procedure

8 and **9**: A stirred solution of hydrazone **5** (350 mg, 1.53 mmol) in anhydrous CH_2Cl_2 (40 mL) was cooled to $-30\,^{\circ}C$, whereupon $MgSO_4$ (approximately 1 g), Ag_2O (530 mg, 230 mmol, 1.5 equiv), and a saturated solution of KOH in methanol (1.2 mL) were successively added. After 30 min the deep red solution was filtered into another ice-cooled flask, and the remaining residue was washed with cold CH_2Cl_2 (15 mL). To this clear solution was added thioketone **7** in small portions. Evolution of nitrogen was observed, and the deep red color slowly disappeared. The thioketone was added until the evolution of nitrogen had ceased; a total of 200 mg (0.63 mmol) was necessary. After 3 h of stirring and a standard workup, the red residue was purified by flash column chromatography (SiO_2, CH_2Cl_2/pentane 1/1, $R_f = 0.30$). The orange crystalline product consisted of isomers **8** and **9** (60:40). Yield: 255 mg, 78% (based on the amount of **7** added). HRMS calcd. 514.084, found 514.084; Elemental analysis calcd for $C_{28}H_{22}N_2O_2S_3$: C 65.34, H 4.31, S 18.69; found C 65.00, H 4.27, S 18.51.

8 (*cis*-nitro): ^{1}H NMR (200 MHz, TMS): $\delta = 2.40-2.70$ (m, 4H), 3.10 (s, 6H), 6.76 (dd, $J = 8.55$, 2.56 Hz, 1H), 6.97 (d, $J = 7.54$ Hz, 1H), 7.07 (d, $J = 8.97$ Hz, 1H), 7.20-7.55 (m, 7H), 7.86 (d, $J = 2.56$ Hz, 1H), 9.03 (d, $J = 7.69$ Hz, 1H).

9 (*trans*-nitro): ^{1}H NMR (200 MHz, TMS): $\delta = 2.17$ (s, 6H), 2.40-2.80 (m, 4H), 6.27 (m, 2H), 6.90 (d, $J = 8.98$ Hz, 1H), 7.02 (d, $J = 8.65$ Hz, 1H), 7.23-7.68 (m, 6H), 8.13 (dd, $J = 8.55$, 2.56 Hz, 1H), 8.89 (d, $J = 8.97$ Hz, 1H).

3 and **4**: The mixture of episulfides **8** and **9** (95 mg, 0.18 mmol) was desulfurized as described in ref. [11b]. The red solid obtained (71 mg, 0.14 mmol, 80%) consisted of the two isomers **3** and **4**, which were readily separated by flash column chromatography (SiO_2, CH_2Cl_2/hexane 1/1, $R_f = 0.57$ and 0.67).

3 (*cis*-nitro): m.p. 212.2-212.6 °C; ^{1}H NMR (200 MHz, $CDCl_3$, TMS): $\delta = 3.07$ (s, 6H), 4.21 (dd, $J = 7.58$, 2.55 Hz, 4H), 6.76 (dd, $J = 8.55$, 2.57 Hz, 1H), 6.95-7.21 (m, 4H), 7.29 (d, $J = 2.57$ Hz, 1H), 7.36-7.76 (m, 6H); HRMS calcd 482.110, found 482.112; UV (*n*-hexane, λ_{max} (ε)): 220.8 (36700) 254.9 (34500) 272.0 (27700) 365.2 (7500); CD (P isomer, *n*-hexane, $\lambda_{max}(\Delta\varepsilon)$): 221 (-57) 240 (28.3) 255.2 (-28) 281.4 (44) 356 (-10).

4 (*trans*-nitro): m.p. 205.8-206.1 °C; ^{1}H NMR (200 MHz, $CDCl_3$, TMS): $\delta = 2.30$ (s, 6H), 3.45-3.72 (m, 4H), 5.93 (d, $J = 2.56$ Hz, 1H), 6.26 (dd, $J = 8.76$, 2.78 Hz, 1H), 7.01-7.19 (m, 3H), 7.39 (d, $J = 8.4$ Hz, 1H), 7.48-7.69 (m, 4H), 8.15 (dd, $J = 8.55$, 2.56 Hz, 1H), 8.43 (d, $J = 2.14$ Hz, 1H); UV (*n*-hexane, λ_{max} (ε)): 221.7 (37700) 252.2 (33900) 273.0 (25500) 360.0 (5300); CD (P isomer, *n*-hexane, λ_{max} ($\Delta\varepsilon$)): 221 (-42) 226.6 (-26) 244 (3.3) 254.2 (-43.3) 274.2 (42.4) 323.2 (7.7) 348 (-4.6).

Irradiations of 2×10^{-5} M solutions of enantiomerically pure **3** and **4** were performed in cylindrical quartz cells. Low-pressure mercury lamps (28 × 1 cm; 8 W) were used for irradiations at 300 and 350 nm, and the irradiation time was 10 s. For irradiations at 313, 365, 405, and 435 nm a 200 W high-pressure mercury lamp equipped with interference filters was employed. Typical irradiation times for this setup were 20 to 30 min.

Received: August 6, 1994 [Z 7215 IE]
German version: *Angew. Chem.* **1995**, *107*, 346

Keywords: helices · molecular switches · optical data storage · thioxanthenes

[1] a) B. L. Feringa, W. F. Jager, B. de Lange, *Tetrahedron* **1993**, *49*, 8267; b) M. Emmelius, G. Pawlowski, H. W. Vollmann, *Angew. Chem.* **1989**, *101*, 1475; *Angew. Chem. Int. Ed. Engl.* **1989**, *28*, 1445.
[2] a) Review: H. Dürr, *Angew. Chem.* **1989**, *101*, 427; *Angew. Chem. Int. Ed. Engl.* **1989**, *28*, 413; b) S. H. Kawai, S. L. Gilat, J. M. Lehn, *J. Chem. Soc. Chem. Commun.* **1994**, 1011; c) Y. Yokoyama, K. Sugiyama, S. Yamada, H. Takimoto, Y. Kurita, *Chem. Lett.* **1994**, 749; d) I. Cabrera, A. Dittrich, H. Ringsdorf, *Angew. Chem.* **1991**, *103*, 106; *Angew. Chem. Int. Ed. Engl.* **1991**, *30*, 76.
[3] J. H. Wendorff, M. Eich, B. Reck, H. Ringsdorf, *Makromol. Chem. Rapid Commun.* **1987**, *8*, 467.
[4] a) J. Achatz, C. Fischer, J. Salbeck, J. Daub, *J. Chem. Soc. Chem. Commun.* **1991**, 504; b) H. Tachibana, R. Azumi, Y. Kawabata, M. Matsumoto, T. Nakamura, *Chem. Lett.* **1992**, 173.
[5] B. L. Feringa, W. F. Jager, B. de Lange, E. W. Meijer, *J. Am. Chem. Soc.* **1991**, *113*, 5468.
[6] The term pseudoenantiomers is used in this context to indicate the opposite helicity of P-**3** and M-**4**.
[7] a) D. H. R. Barton, B. J. Willis, *J. Chem. Soc. Perkin Trans. 1* **1972**, 305; b) R. M. Kellogg, J. Buter, S. Wassenaar, *J. Org. Chem.* **1972**, *37*, 4045; c) A. Schönberg, B. König, E. Singer, *Chem. Ber.* **1967**, *100*, 767.
[8] Isomers **3** and **4** are readily distinguished by their ^{1}H NMR spectra, as the methyl singlet at $\delta = 3.07$ for **3** (dimethylamino group in the *trans* position) is shifted upfield to $\delta = 2.30$ for **4** (dimethylamino group in the *cis* position) owing to the shielding effect of the naphthalene moiety.
[9] Further details of the crystal structure investigation may be obtained from the Director of the Cambridge Crystallographic Data Centre, 12 Union Road, GB-Cambridge CB2 1EZ (UK), on quoting the full journal citation.
[10] Y. Okamoto, K. Hatada, *J. Liq. Chromatogr.* **1986**, *9*, 369.
[11] a) W. F. Jager, *Chiroptical Molecular Switches; Application of Inherently Dissymmetric Alkenes*, Dissertation, Groningen, **1994**; b) W. F. Jager, B. de Lange, A. M. Schoevaars, B. L. Feringa, *Tetrahedron: Asymmetry* **1993**, *4*, 1481.
[12] For the unsubstituted analogue of **4** (X = S, $R^1 = R^2 = R^3 = H$, Fig. 1) a racemization barrier of 120.9 ± 0.5 kJ mol^{-1} was determined, while for the unsubstituted analogue of **1** (X = CH_2, $R^1 = R^2 = R^3 = H$, Fig. 1) a racemization barrier of 110.7 ± 0.5 kJ mol^{-1} was determined (see ref. [11a]).
[13] B. L. Feringa, W. F. Jager, B. de Lange, *Tetrahedron Lett.* **1992**, *33*, 2887.
[14] In ethanol and chloroform no photostationary state was reached after 30 min irradiation at 300 nm, which implies that the quantum yields for the isomerization processes that occur in these solvents is at least a factor 100 lower than in *n*-hexane.
[15] The isomeric composition of the photostationary state upon irradiation at a wavelength λ is given by: [**3**]/[**4**] = $\varepsilon_4\Phi_{4\rightarrow3}/\varepsilon_3\Phi_{3\rightarrow4}$.
[16] E. W. Meijer, B. L. Feringa, *Mol. Cryst. Liq. Cryst.* **1993**, *235*, 169.

Asymmetric Syntheses of Stavudine (d4T) and Cordycepin by Cycloisomerization of Alkynyl Alcohols to Endocyclic Enol Ethers**

Frank E. McDonald* and Mark M. Gleason

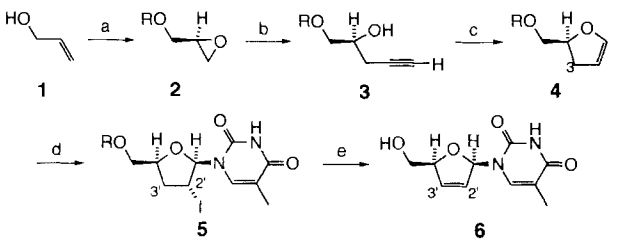
Various deoxynucleosides[1] show potent antiviral activity, particularly against the human immunodeficiency virus (HIV), which is the causative agent for acquired immunodeficiency syndrome (AIDS). Stavudine (2′,3′-didehydro-3′-deoxythymidine; d4T) retains the high antiviral activity of 3′-azido-3′-deoxythymidine (AZT) while exhibiting significantly lower bone marrow toxicity and reduced inhibition of mitochondrial DNA synthesis.[2] Cordycepin (3′-deoxyadenosine) has been widely

[*] Prof. F. E. McDonald, M. M. Gleason
Department of Chemistry, Northwestern University
2145 Sheridan Road, Evanston, IL 60208-3113 (USA)
Telefax: Int. code + (708)491-7713

[**] Acknowledgment is made to the donors of the Petroleum Research Fund, administered by the American Chemical Society, for partial support of this research. This work was also supported by Northwestern University and the Camille and Henry Dreyfus Foundation.

used as a probe for messenger RNA transcription and also exhibits antibiotic activity.[3] These compounds have been classically prepared by functional group manipulation of naturally occurring ribo- and 2'-deoxyribonucleosides or from carbohydrate precursors,[4] but more recently the synthesis of d4T has been reported from amino acid precursors.[5, 6] We envisioned that a shorter synthesis of deoxynucleosides might be obtained by molybdenum pentacarbonyl catalyzed cycloisomerization of acyclic alkynyl alcohols to endocyclic enol ethers.[7] Given the ready availability of chiral nonracemic alkynyl alcohols from achiral precursors[8, 9] as well as the demonstrated utility of endocyclic enol ethers in the synthesis of glycosides and nucleosides,[5, 10] we set out to establish the viability of the cycloisomerization strategy for asymmetric synthesis of deoxynucleosides.

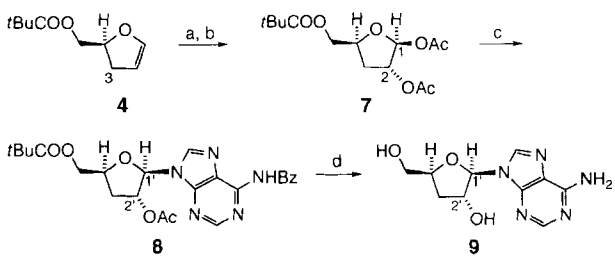
The asymmetric synthesis of an appropriate five-carbon alkynyl alcohol precursor begins with the preparation of (*S*)-glycidyl pivaloate (**2**) by utilizing asymmetric epoxidation of allyl alcohol followed by in situ derivatization[8, 11] (Scheme 1).



Scheme 1. Synthesis of stavudine (d4T) by $Mo(CO)_5$-mediated cycloisomerization. R = *t*BuCO. a) 5% $Ti(O{i}Pr)_4$, 6% D-diisopropyl tartrate, $Me_2C(Ph)OOH$, 3Å molecular sieves, CH_2Cl_2, −20 °C; *t*BuCOCl, Et_3N (37%); b) LiC≡CH, $BF_3{\cdot}OEt_2$, THF, −78 → −20 °C (70%); c) 50 mol% $Mo(CO)_6$, 50 mol% Me_3NO, Et_3N, Et_2O (80%); d) I_2, *N*,*N*-bis(trimethylsilyl)thymine, CH_2Cl_2 (94%, 7:1 mixture); e) 60 equiv. NaOMe, MeOH (80%).

Addition of lithium acetylide to **2** is regioselective for the unsubstituted epoxide terminus, but careful control of reaction temperature and use of boron trifluoride–etherate[12] is critical to avoid ester group migration. Mosher ester analysis of the alkynyl alcohol product **3** indicates an enantiomeric excess of 89% (±1%, ^{1}H NMR). Cyclization of **3** upon reaction with molybdenum hexacarbonyl/trimethylamine *N*-oxide in the presence of triethylamine provides the isomeric dihydrofuran **4** in 80% isolated yield. Iodine-mediated introduction of thymine to **4** gives a 7:1 ratio (in favor of the iodonucleoside **5**) of *anti*-addition products in excellent yield. Iodonucleoside **5** is unstable to silica gel chromatography, and best overall yields are obtained by treating the crude product with a large excess of freshly prepared sodium methoxide, which accomplishes pivaloate methanolysis as well as bimolecular elimination[5] of HI to afford stavudine (**6**). Thus the asymmetric synthesis of stavudine has been achieved in five steps (longest linear sequence) from achiral allyl alcohol, instead of the previous eight steps in the synthesis from L-glutamic acid.[5]

We have explored other functionalization routes to deoxynucleosides from dihydrofuran **4**. For instance, osmium tetraoxide catalyzed dihydroxylation[13] of **4** proceeds predominantly from the face opposite to the acyloxymethyl side chain, and acylation of the crude diol provides a 13:4:3:1 mixture of diacetylated products favoring **7** (Scheme 2, Table 1). This mixture is subjected to Lewis acid catalyzed adenine glycosylation[14] to give a 9:1 mixture of stereoisomers favoring **8**. Methanolysis of acyl groups followed by purification on silica



Scheme 2. Synthesis of cordycepin. a) 1% OsO_4, *N*-methylmorpholine oxide (NMO), THF/*t*BuOH/H_2O (67%); b) Ac_2O, Et_3N, CH_2Cl_2 (90%, 13:4:3:1 mixture); c) N^7-benzoyl-N^4,N^7-bis(trimethylsilyl)adenine, $Me_3SiOSO_2CF_3$, $ClCH_2CH_2Cl$, 83 °C (65%); d) NaOMe, MeOH (42%).

Table 1. Selected data for compounds **2**–**4**, **6**, **8**, and **9**.

2: $[\alpha]_D^{23} = +21.1$ ($c = 1.3$ in chloroform); ^{1}H NMR ($CDCl_3$): $\delta = 4.40$ (1H, dd, $J = 12.3, 2.9$ Hz), 3.91 (1H, dd, $J = 12.2, 6.1$ Hz), 3.22–3.17 (1H, m), 2.84 (1H, dd, $J = 4.5, 4.5$ Hz), 2.64 (1H, dd, $J = 4.9, 2.6$ Hz), 1.21 (9H, s); ^{13}C NMR ($CDCl_3$): $\delta = 178.1, 64.6, 49.4, 44.4, 38.7, 27.0$; IR (neat): $\tilde{\nu} = 2974, 2875, 1736, 1481, 1397, 1367, 1285, 1154, 1036, 991, 911, 858, 771\ cm^{-1}$.

3: $[\alpha]_D^{23} = +11.6$ ($c = 0.69$ in chloroform); ^{1}H NMR ($CDCl_3$): $\delta = 4.23–4.11$ (2H, m), 4.04–3.99 (1H, m), 2.46 (2H, dd, $J = 6.3, 2.7$ Hz), 2.35 (1H, br. d, $J = 4.5$ Hz), 2.06 (1H, dd, $J = 2.6, 2.6$ Hz), 1.21 (9H, s); ^{13}C NMR ($CDCl_3$): $\delta = 178.6, 79.5, 71.0, 68.0, 66.7, 38.7, 27.0, 23.6$; IR (neat): $\tilde{\nu} = 3462, 3293, 2966, 2875, 2122, 1727, 1481, 1399, 1286, 1161, 1103, 1037, 939\ cm^{-1}$; HR-MS (EI): calcd for $C_{10}H_{17}O_3$: *m/z*: 185.1177 [$M + H^+$], found 185.1165.

4: $[\alpha]_D^{23} = +85.4$ ($c = 1.46$ in chloroform); ^{1}H NMR ($CDCl_3$): $\delta = 6.28$ (1H, dd, $J = 2.3, 5.0$ Hz), 4.89 (1H, dd, $J = 2.6, 5.1$ Hz), 4.80–4.70 (1H, dddd, $J = 14.9, 7.3, 6.2, 4.3$ Hz), 4.19–4.09 (2H, m), 2.73 (1H, ddt, $J = 15.3, 10.6, 2.4$ Hz), 2.38 (1H, ddt, $J = 15.3, 7.3, 2.4$ Hz), 1.21 (9H, s); ^{13}C NMR ($CDCl_3$): $\delta = 178.4, 145.1, 98.9, 78.3, 65.8, 38.9, 31.4, 27.2$; IR (neat): $\tilde{\nu} = 2975, 2873, 1732, 1622, 1481, 1460, 1285, 1142, 1038, 951, 901, 706\ cm^{-1}$; HR-MS (EI): calcd for $C_{10}H_{16}O_3$: *m/z*: 184.1099 [M^+], found 184.1096.

6: m.p. 163–166 °C (164–166 °C [2b]); $[\alpha]_D^{23} = -42$ ($c = 0.52$ in water) ($[\alpha]_D^{20} = -46.1$ ($c = 0.7$ in water [2b]); ^{1}H NMR (D_2O): $\delta = 7.56$ (1H, s), 6.87 (1H, d, $J = 1.3$ Hz), 6.40 (1H, d, $J = 6.1$ Hz), 5.90 (1H, d, $J = 6.1$ Hz), 4.92 (1H, br. s), 3.72 (2H, d, $J = 3.0$ Hz), 1.78 (3H, s); ^{13}C NMR ([D_6]DMSO): $\delta = 164.1, 150.9, 136.9, 135.1, 126.0, 109.1, 89.0, 87.4, 62.4, 12.3$; IR (KBr): $\tilde{\nu} = 3472, 3176, 3035, 1672, 1465, 1256, 1095\ cm^{-1}$); HR-MS(EI): calcd for $C_{10}H_{12}N_2O_4$: *m/z*: 224.0797 [M^+], found 224.0805.

8: $[\alpha]_D^{23} = +5$ ($c = 1.02$ in chloroform); ^{1}H NMR ($CDCl_3$): $\delta = 9.28$ (1H, br. s), 8.74 (1H, s), 8.12 (1H, s), 8.03–7.96 (2H, m), 7.58–7.41 (3H, m), 6.09 (1H, d, $J = 1.5$ Hz), 5.74 (1H, d, $J = 6.0$ Hz), 4.66–4.57 (1H, m), 4.36 (1H, dd, $J = 12.3, 3.3$ Hz), 4.28 (1H, dd, $J = 12.3, 5.7$ Hz), 2.70–2.60 (1H, m), 2.22 (1H, dd, $J = 14.0, 4.4$ Hz), 2.12 (3H, s), 1.16 (9H, s); ^{13}C NMR ($CDCl_3$): $\delta = 178.2, 170.1, 164.6, 152.7, 151.1, 149.6, 141.6, 133.5, 132.7, 128.7, 127.8, 123.5, 90.0, 78.68, 77.7, 64.5, 38.8, 32.9, 27.1, 20.8$; IR (neat): $\tilde{\nu} = 3292, 2971, 1728, 1610, 1441, 1235, 1146, 1081\ cm^{-1}$; HR-MS (FAB): calcd for $C_{24}H_{28}N_5O_6$: *m/z*: 482.2040 [$M + H^+$], found 482.2072.

9: m.p. 205–206 °C (224–225 °C [3b]); $[\alpha]_D^{23} = -40$ ($c = 0.40$ in water) ($[\alpha]_D^{20} = -44$ ($c = 0.5$ in water [3b]); ^{1}H NMR ([D_6]DMSO): $\delta = 8.36$ (1H, s), 8.14 (1H, s), 7.30 (2H, br. s), 5.87 (1H, d, $J = 2.5$ Hz), 5.68 (1H, d, $J = 4.3$ Hz), 5.18 (1H, t, $J = 5.5$ Hz), 4.56 (1H, m), 4.35 (1H, ddd, $J = 8.3, 6.3$ Hz), 3.72–3.66 (1H, m), 3.55–3.47 (1H, m), 2.25 (1H, ddd, $J = 13.7, 8.7, 5.7$ Hz), 1.91 (1H, ddd, $J = 13.2, 6.6, 3.3$ Hz); ^{13}C NMR ([D_6]DMSO: $\delta = 156.0, 152.4, 148.8, 139.0, 119.1, 90.8, 80.7, 74.6, 62.6, 34.1$; IR (KBr): $\tilde{\nu} = 3329, 3129, 1677, 1609, 1481, 1422, 1384, 1341, 1298, 1206, 1092, 717\ cm^{-1}$; HR-MS (EI): calcd for $C_{10}H_{13}N_5O_3$: *m/z*: 251.1018 [M^+], found 251.1031.

[a] ^{1}H NMR spectra were recorded at 300 MHz and ^{13}C NMR spectra at 75 MHz.

gel affords complete separation of diastereomers to provide synthetic cordycepin (**9**).[3]

In conclusion, we have demonstrated an effective procedure for the preparation of the antiviral deoxynucleosides stavudine (**6**) and cordycepin (**9**), utilizing novel cyclization methodology as the missing link between readily available acyclic precursors and isomeric oxacyclic products. Since all the carbon atoms are derived from the simple achiral precursors allyl alcohol, acetylene, and the appropriate pyrimidine or purine bases, this methodology is well-suited for the preparation of enantiomeric

and diastereomeric analogs of these deoxynucleosides.[15] This synthetic route may also provide access to isotopically labeled nucleosides[16] for structural and pharmacological studies of nucleoside drugs as well as nucleotide polymers DNA and RNA.

Received: August 4, 1994 [Z 7208]
German version: *Angew. Chem.* **1995**, *107*, 356

Keywords: asymmetric syntheses · cyclizations · nucleosides

[1] a) H. Mitsuya, S. Broder, *Proc. Natl. Acad. Sci. USA* **1986**, *83*, 1911; b) D. M. Huryn, M. Okabe, *Chem. Rev.* **1992**, *92*, 1745; c. M. I. Johnston, D. F. Hoth, *Science* **1993**, *260*, 1286.

[2] a) J. Balzarini, G.-J. Kang, M. Dalal, P. Herdewijn, E. de Clercq, S. Broder, D. G. Johns, *Mol. Pharmacol.* **1987**, *32*, 162; b) M. M. Mansuri, J. E. Starrett, I. Ghazzouli, M. J. M. Hitchcock, R. Z. Sterzycki, V. Brankovan, T.-S. Lin, E. M. August, W. H. Prusoff, J.-P. Sommadossi, J. C. Martin, *J. Med. Chem.* **1989**, *32*, 461. c) Stavudine has recently been approved by the United States Food and Drug Administration for treatment of AIDS and HIV infection. *Chem. Eng. News.* **1994**, *72*(27), 22.

[3] a) E. A. Kaczka, E. L. Dulaney, C. O. Gitterman, H. B. Woodruff, K. Folkers, *Biochem. Biophys. Res. Commun.* **1964**, *14*, 452; b) E. Walton, F. W. Holly, G. E. Boxer, R. F. Nutt, S. R. Jenkins, *J. Med. Chem.* **1965**, *8*, 659; c) S. Penman, M. Rosbach, M. Penman, *Proc. Natl. Acad. Sci. USA* **1970**, *67*, 1878.

[4] a) A. Todd, T. L. V. Ulbricht, *J. Chem. Soc.* **1960**, 3275; b) W. W. Lee, A. Benitez, C. D. Anderson, L. Goodman, B. R. Baker, *J. Am. Chem. Soc.* **1961**, *83*, 1906; c) J. Horwitz, J. Chua, M. A. Da Rooge, M. Noel, I. L. Klundt, *J. Org. Chem.* **1966**, *31*, 205; d) C. J. Rizzo, J. P. Dougherty, R. Breslow, *Tetrahedron Lett.* **1992**, *33*, 4129.

[5] C. U. Kim, P. F. Misco, *Tetrahedron Lett.* **1992**, *33*, 5733.

[6] a) For syntheses of AZT from achiral precursors, see: M. W. Hager, D. C. Liotta, *J. Am. Chem. Soc.* **1991**, *113*, 5117; b) M. E. Jung, J. M. Gardiner, *J. Org. Chem.* **1991**, *56*, 2614.

[7] F. E. McDonald, C. B. Connolly, M. M. Gleason, T. B. Towne, K. D. Treiber, *J. Org. Chem.* **1993**, *58*, 6952.

[8] Y. Gao, J. M. Klunder, R. M. Hanson, H. Masamune, S. Y. Ko, K. B. Sharpless, *J. Am. Chem. Soc.* **1987**, *109*, 5765.

[9] a) N. Ikeda, I. Arai, H. Yamamoto, *J. Am. Chem. Soc.* **1986**, *108*, 483; b) E. J. Corey, C.-M. Yu, D.-H. Lee, *ibid.* **1990**, *112*, 878.

[10] a) H. Kawakami, T. Ebata, K. Koseki, K. Okano, K. Matsumoto, H. Matsushita, *Heterocycles* **1993**, *36*, 665; b) J. Wang, J. A. Wurster, L. J. Wilson, D. Liotta, *Tetrahedron Lett.* **1993**, *34*, 4881.

[11] Allyl alcohol is not completely consumed after 24 hours at −20 °C, but the expoxidation reaction is quenched at this point in order to ensure a high enantiomeric excess of glycidyl pivaloate **2**. The byproducts (allyl pivaloate and 2-phenyl-2-propanol) are removed by silica gel chromatography.

[12] M. Yamaguchi, I. Hirao, *Tetrahedron Lett.* **1983**, *24*, 391.

[13] M. Bednarski, S. Danishefsky, *J. Am. Chem. Soc.* **1986**, *108*, 7060.

[14] F. W. Lichtenthaler, P. Voss, A. Heerd, *Tetrahedron Lett.* **1974**, 2141.

[15] a) T.-S. Lin, M.-Z. Luo, M.-C. Liu, S. B. Pai, G. E. Dutschman, Y.-C. Cheng, *Biochem. Pharmacol.* **1994**, *47*, 171; b) T.-S. Lin, M.-Z. Luo, M.-C. Liu, *Tetrahedron Lett.* **1994**, *35*, 3477.

[16] a) P. C. Kline, A. S. Serianni, *J. Am. Chem. Soc.* **1990**, *112*, 7373; b) E. P. Nikonowicz, A. Pardi, *Nature (London)* **1992**, *355*, 184; c) R. T. Batey, M. Inada, E. Kujawinski, J. D. Puglisi, J. R. Williamson, *Nucleic Acids Res.* **1992**, *20*, 4515; d) M. J. Michnicka, J. W. Harper, G. C. King, *Biochemistry* **1993**, *32*, 395; e) S. Quant, R. W. Wechselberger, M. A. Wolter, K.-H. Wörner, P. Schell, J. W. Engels, C. Griesinger, H. Schwalbe, *Tetrahedron Lett.* **1994**, *35*, 6649.

Electron Transfer through DNA: Site-Specific Modification of Duplex DNA with Ruthenium Donors and Acceptors**

Thomas J. Meade* and Jon F. Kayyem

Long-range intramolecular electron transfer (ET) in protein–protein complexes and modified proteins takes place over appreciable distances at biologically significant rates.[1, 2] Experiments have confirmed its dependence on free energy and distance, as well as the importance of the reorganization of the ligand sphere and solvent environment.[3] Two factors that influence the rate of electron transfer that are far less understood in both inorganic and organic systems are the structure of the intervening medium and the orientation of the donor–acceptor unit.

A barrier to the further understanding of the factors that influence the mechanisms of long-range electron transfer is the development of an architecture capable of critically testing these properties. The unique ability of complementary single strands of DNA to hybridize into a rigid duplex of defined structure makes an oligonucleotide an attractive choice for use as a molecular template. This template can be modified with spectroscopically detectable and photochemically active redox centers at predetermined locations. Moreover, recent theoretical work suggests that the electronic coupling between donor and acceptor for modified DNA derivatives could display a remarkable dependence on nucleic acid sequence.[4]

In order to test these assumptions, we have devised a novel approach to prepare ruthenium-modified duplex DNA derivatives where the donor and acceptor are separated by any number of base pairs. The goal of this approach is to prepare a series of ruthenium-modified DNA derivatives in which 1) the ruthenium complexes are covalently and rigidly attached to a single site on the duplex, 2) the redox potential of each ruthenium complex can be varied independently, 3) the DNA duplex is unperturbed by the presence of the ruthenium complexes, and 4) the redox states of the donors and acceptors are spectroscopically distinguishable. This new synthetic procedure covalently attaches redox centers of varying potentials to a series of oligonucleotides each modified with a primary amino group at the 2′ position of the 5′-terminal ribose (Fig. 1). Intramolecular ET rates obtained from these rigidly attached redox centers should provide insight into the electronic coupling between donor and acceptor linked to DNA.

Our strategy for the preparation of these transition metal DNA derivatives involves a departure from previous work in which oligonucleotides have been modified with organic molecules and metal complexes at the terminal phosphates,[5–6] various heterocyclic bases,[7–11] and the ribose ring.[12–13] This new approach employs the synthesis of two sets of complementary strands (8–14 base pairs in length) of oligonucleotides modified with a terminal aminoribose[14] and subsequent covalent modification with redox-active ruthenium complexes. Unlike fluorescent DNA tags such as fluorescein isothiocyanate

[*] Dr. T. J. Meade, Dr. J. F. Kayyem
Division of Biology and The Beckman Institute
California Institute of Technology
Pasadena, CA 91125 (USA)
Telefax: Int. code + (818)449-5163

[**] This research was supported by the Donors of the Petroleum Research Fund, administered by the American Chemical Society, the Research Corporation, and the Biological Imaging Center of the Beckman Institute. The authors thank Harry Gray, Jay Winkler, I-Jy Chang, and Robert Kaiser for helpful discussions.

 © VCH Verlagsgesellschaft mbH, D-69451 Weinheim, 1995 0570-0833/95/0303-0352 $ 10.00+.25/0

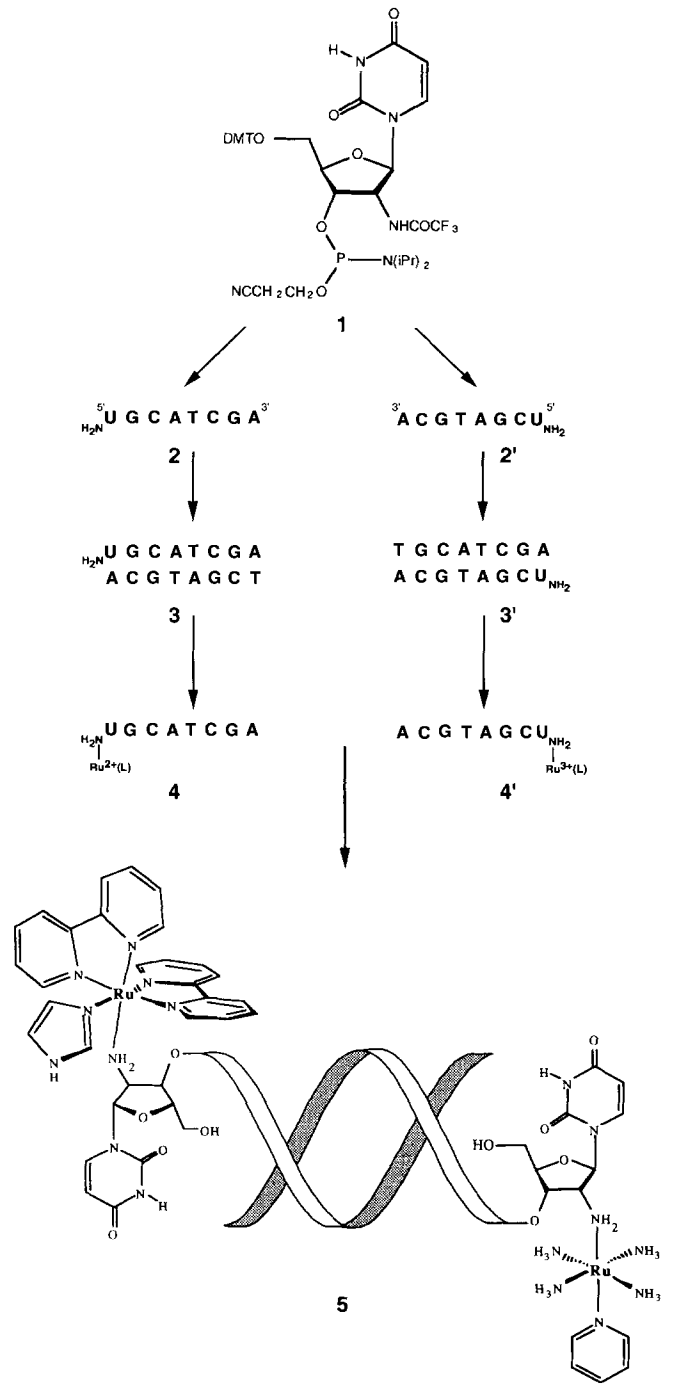


Fig. 1. Scheme for the preparation of duplex DNA labeled with donors and acceptors. The DMT-2′-*N*-trifluoroacetyl-protected phosphoroamidite (**1**) is incorporated into an oligodeoxyribonucleotide (**2**, **2′**) by automated solid-phase synthesis techniques and "protected" with a complementary strand (formation of **3**/**3′**). After reaction with a ruthenium complex, the complement is removed, and the modified oligonucleotide purified. The procedure is repeated and the strands annealed to yield **5**. Abbreviations U_{NH_2} = 2′-amino-2′-deoxyuridine; L = 2,2′-bipyridine, imidazole, pyridine, NH_3; DMT = dimethoxytrityl.

(FITC), the ruthenium complexes used in this work will react with the heterocyclic nitrogen atoms of the bases. Therefore, an unmodified complementary sequence is used as a large hydrogen-bonded blocking group to protect the sites on the bases that are susceptible to attack by the metal.[15] Under these conditions, the exposed primary 2′-amine at the 5′-terminal ribose position of the duplex DNA is readily modified with a variety of ruthenium complexes. In contrast, random ruthenium modification of the heterocyclic nitrogen centers is eliminated in some cases and substantially reduced in others.

A DMT-2′-*N*-trifluoroacetyl-protected phosphoroamidite (**1**) of 2′-amino-2′-deoxyuridine (U_{NH_2}) was prepared by variation of published procedures,[12] and oligodeoxyribonucleotides (**2**/**2′**) were assembled by standard solid-phase automated DNA synthesis techniques.[16] The 2′-amino-oligodeoxyribonucleotide **2** was annealed to the complementary sequence to form **3**. This U_{NH_2}-containing duplex was treated with $[Ru(bpy)_2CO_3]$, followed by imidazole in an inert atmosphere. The recovered duplex DNA was denatured in 7 M urea, and the ruthenium-modified oligonucleotide[17] was purified by using C-18 reversed-phase HPLC techniques (Fig. 2). This procedure was repeated with the complementary strand **2′** employing $[Ru(NH_3)_4(py)]^{2+}$ as the acceptor. Finally, the two ruthenium-modified oligonucleotides **4** and **4′** were annealed to give the desired duplex DNA **5** with a covalently bound donor and acceptor.

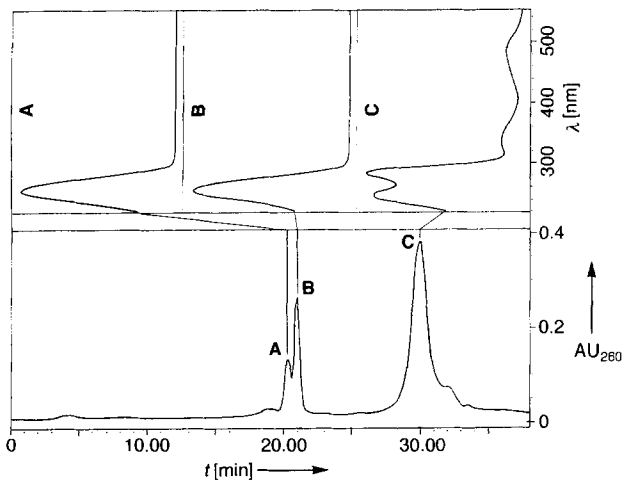


Fig. 2. HPLC analysis and UV/Vis spectra of duplex DNA following modification with ruthenium. Oligonucleotides were denatured in 7 M urea at 60 °C, injected onto a C-18 reversed-phase column, and eluted with a solvent mixture with a gradient of 2 to 40% CH_3CN in 7 M urea and 0.1 M triethylammonium acetate, pH 6.5. Peak A (25.4% CH_3CN) is unchanged amino-modified oligonucleotide (U_{NH_2}GCATCGA); peak B (27.7% CH_3CN) is the oligonucleotide complement of A (ACGTAGCT); peak C (38.8% CH_3CN) corresponds to Ru-modified A ($U_{NH_2Ru(bpy)_2}$(im)GCATCGA), where the absorption spectrum is consistent with the presence of a single $Ru(bpy)_2$(im)(U_{NH_2}) complex covalently bound to the oligonucleotide. Identities of peaks A, B, and C have been confirmed by coinjections of authentic samples and by enzymatic digestion (alkaline phosphatase, phosphodiesterase) followed by HPLC analysis of the nucleoside composition.

The new metal-modified oligonucleotides were characterized by fluorescent labeling, enzymatic digestion, and duplex-melting temperature studies. The aminoribose oligomers and their complements were treated with FITC under conditions that favor labeling of primary amines. As expected, only the 2′-amino-2′-deoxyribose site was labeled, which verified the presence of a primary amine on the DNA. Thermal denaturing and annealing experiments display similar melting temperatures for both ruthenium and aminoribose oligomers.[18] In addition, the amino-modified duplex DNA has been characterized by 2D NMR.[19] These data confirm that the donors and acceptors are covalently attached to the 2′-amino-2′-deoxyribose position and indicate that the DNA structure is unperturbed by the presence of the ruthenium complexes.

Kinetic measurements were performed by direct photoinduced and flash-quench techniques.[20] The rate of intramolecular electron transfer in the eight base-pair long duplex, modified with the acceptor $[Ru(bpy)_2(im)]^{3+}$ and the donor $[Ru(NH_3)_4(py)]^{2+}$, was determined to be $1.6(4) \times 10^6\ s^{-1}$ (metal–metal distance = 21 Å).[21] Since the driving force for this reaction ($-\Delta G^0 \approx 0.7$ eV) is well below the estimated reorganization energy ($\lambda \approx 0.9$ eV),[3, 20, 22] the activationless rate constant for electron transfer between ruthenium centers is expected to be roughly $2.5 \times 10^6\ s^{-1}$. Interestingly, this estimated k_{max} value is comparable to the k_{max} of one of the most efficient protein systems studied, His39-modified cytochrome c (Fe-to-Ru distance = 20.3 Å).[23]

Additional rates are required to determine the distance-dependent nature of this process, as well as to delineate the roles of base sequence and π-stacking in modulating the rates of long-range electron-transfer reactions through DNA.

Received: July 4, 1994
Supplemented: September 30, 1994 [Z 7094 IE]
German version: *Angew. Chem.* **1995**, *107*, 358

Keywords: bioinorganic chemistry · electron transfer · oligonucleotides · ruthenium compounds

[1] B. E. Bowler, A. L. Raphael, H. B. Gray, *Prog. Inorg. Chem.* **1990**, *38*, 259–323.
[2] *Met. Ions Biol. Syst.* **1991**, *27*.
[3] J. R. Winkler, H. B. Gray, *Chem. Rev.* **1992**, *92*, 369–379.
[4] S. M. Risser, D. N. Beratan, T. J. Meade, *J. Am. Chem. Soc.* **1993**, *115*, 2508–2510.
[5] N. T. Thuong, C. Hélène, *Angew. Chem.* **1993**, *105*, 697–723; *Angew. Chem. Int. Ed. Engl.* **1993**, *32*, 666–690.
[6] J. L. Mergny, S. Boutorine, T. Garestier, F. Belloc, M. Rougée, N. V. Bulychev, A. A. Koshkin, J. Bourson, A. V. Lebedev, B. Valeur, N. T. Thuong, C. Hélène, *Nucleic Acids Res.* **1994**, *22*, 920–928.
[7] U. Englisch, D. H. Gauss, *Angew. Chem.* **1991**, *103*, 629–646; *Angew. Chem. Int. Ed. Engl.* **1991**, *30*, 613–629.
[8] J. Tesler, K. A. Cruickshank, L. E. Morrison, T. L. Netzel, C. Chan, *J. Am. Chem. Soc.* **1989**, *111*, 7221–7226.
[9] J. Goodchild, *Bioconjugate Chem.* **1990**, *1*, 165–187.
[10] A. M. Brun, A. Harriman, *J. Am. Chem. Soc.* **1991**, *113*, 8153–8159.
[11] C. J. Murphy, M. R. Arkin, Y. Jenkins, N. D. Ghatlia, S. H. Bossmann, J. K. Barton, *Science* **1993**, *262*, 1025–1029.
[12] M. Imazawa, F. Eckstein, *J. Org. Chem.* **1979**, *44*, 2039–2041.
[13] P. S. Miller, P. Bhan, L. S. Kan, *Nucleosides Nucleotides* **1993**, *12*, 785–792.
[14] H. Aurup, T. Tuscgi, F. Benseler, J. Ludwig, F. Eckstein, *Nucleic Acids Res.* **1994**, *22*, 20–24.
[15] Unprotected oligonucleotides react with the ruthenium complexes very efficiently. Isolated products from these reactions show that several sites are labeled.
[16] *Oligonucleotides and Analogues: A Practical Approach* (Ed.: F. Eckstein), Oxford Univ. Press, Oxford, **1991**.
[17] The yield of ruthenium-modified aminoribose duplex is typically 25–50% (see Fig. 2, peak C).
[18] Temperatures at which 50% of the DNA strands are dissociated (T_m) were determined by thermal denaturation and annealing in 0.9 M NaCl and 0.1 M Na phosphate buffer (pH 7) by means of a Hewlett Packard 8452A diode-array spectrophotometer with HP 89090A Peltier temperature-control accessory. Unmodified octamers as controls revealed a single helix-to-coil transition point and a T_m of 45 °C. The aminoribose oligomers showed a lower T_m of 40 °C. The ruthenium-modified oligomers, when hybridized to their unmodified complements, showed broad helix-to-coil transitions between 36 °C and 42 °C. All kinetic measurements were performed in the presence of 1 M Na^+ to insure that the modified oligonucleotides were annealed at ambient temperature (22 °C).
[19] J. F. Kayyem, Y. Hi, S. L. Mayo, T. J. Meade, unpublished.
[20] I.-Jy Chang, H. B. Gray, J. R. Winkler, *J. Am. Chem. Soc.* **1991**, *113*, 7056–7057.
[21] The metal–metal distance was estimated from molecular graphics calculations.
[22] G. M. Brown, N. Sutin, *J. Am. Chem. Soc.* **1979**, *101*, 883–892.
[23] D. R. Casimiro, J. H. Richards, J. R. Winkler, H. B. Gray, *J. Phys. Chem.* **1993**, *97*, 13073–13077.

Structure and Bonding of Transition Metal Dihydrogen Complexes $[M(CO)_5(H_2)]$ (M = Cr, Mo, W)**

Stefan Dapprich and Gernot Frenking*

Dedicated to Professor Paul von Ragué Schleyer on the occasion of his 65th birthday

Since the first synthesis of a stable dihydrogen complex, $[W(CO)_3(PR_3)_2(\eta^2\text{-}H_2)]$ (R = *c*-C_6H_{11} (Cy), *i*Pr) was reported by Kubas et al.[1] in 1984,[1a] many theoretical and experimental studies on the structures and properties of transition metal dihydrogen complexes have been published.[2] Although metal dihydrogen complexes play an important role as intermediates in catalytic hydrogenation reactions, relatively little is known about their geometries and bond strengths. The exact experimental determination of the equilibrium geometry of the L_nM-H_2 moiety is difficult, because the very low barrier for rotation about the $M-H_2$ axis even at very low temperatures yields a high degree of librational motion, which artificially shortens the H–H bond.[2, 3] Neutron diffraction studies of several complexes showed surprisingly similar H–H distances of 0.82 Å,[2–4] but recent experimental investigations of dihydrogen complexes reported H–H distances of >1 Å.[5]

Even more difficult than the geometry is the experimental determination of the $M-H_2$ bond energy. Ishikawa et al.[6a] estimated from studies of the lifetimes of several $[W(CO)_5L]$ complexes a W–L binding energy of >16 kcal mol^{-1} for $L = H_2$. The metal–ligand binding enthalpy of H_2 in $[W(CO)_3(PCy_3)_2(H_2)]$ was determined by Gonzalez et al.[6b] by using solution calorimetry as $\Delta H = 9.9$ kcal mol^{-1}. A quantum mechanical study of $[Cr(CO)_5(H_2)]$ by Pacchioni[7] gave a dissociation energy of 9.6 kcal mol^{-1} for H_2 dissociation. However, this value was derived from calculations only at the Hartree–Fock level of theory with partially optimized geometries.

The parent carbonyl complexes $[M(CO)_5(H_2)]$ are important for the study of $M-H_2$ bonding, because the unsubstituted molecules make it possible to analyze the metal–dihydrogen interactions in detail. The chromium analogue $[Cr(CO)_5(H_2)]$ is of particular interest, as it is a postulated intermediate in the water gas shift reaction.[8] The complexes $[M(CO)_5(H_2)]$ (M = Cr, Mo, W) have been characterized in noble gas matrices by IR spectroscopy,[9] but the equilibrium geometries and bond energies are not known. We have recently shown that the metal–ligand bond lengths calculated at the MP2 level of theory and the theoretically predicted first dissociation energies at the CCSD(T) level of theory using effective core potentials for the metals in complexes $[M(CO)_5L]$ (M = Mo, W; L = CO, CS) are in excellent agreement with experimental values, while the calculated Cr–L interatomic distances of $[Cr(CO)_5L]$ are slightly too short and the first dissociation energies too high.[10] Similar results have been obtained for $[M(CO)_5]$ (M = Fe, Ru, Os) and $[M(CO)_4]$ (M = Ni, Pd, Pt).[11] In this paper we report the theoretically predicted equilibrium geometries, vibrational frequencies, and metal–dihydrogen bond energies of $[M(CO)_5(H_2)]$ (M = Cr, Mo, W) obtained at the same theoreti-

[*] Prof. Dr. G. Frenking, Dipl.-Chem. S. Dapprich
Fachbereich Chemie der Universität
Hans-Meerwein-Strasse, D-35032 Marburg (Germany)
Telefax: Int. code + (6421)282189
e-mail: frenking@ps1515.chemie.uni-marburg.de

[**] Theoretical Studies of Organometallic Compounds, Part 11. This work was supported by the Deutsche Forschungsgemeinschaft and the Fonds der Chemischen Industrie. Part 10: ref. [11].

cal level as in the previous studies.[10, 11] We also report a detailed analysis of the metal–dihydrogen bonding interactions.

Figure 1 shows the optimized geometries of the $[M(CO)_5(H_2)]$ molecules. The complexes are pseudo-octahedral (C_{2v}), and the *cis* (equatorial) carbonyl ligands are bent slightly away from the H_2 ligand. The theoretically predicted H–H distances are between 0.791 Å (M = Mo) and 0.814 Å (M = Cr). These values are in agreement with the results of neutron diffraction studies

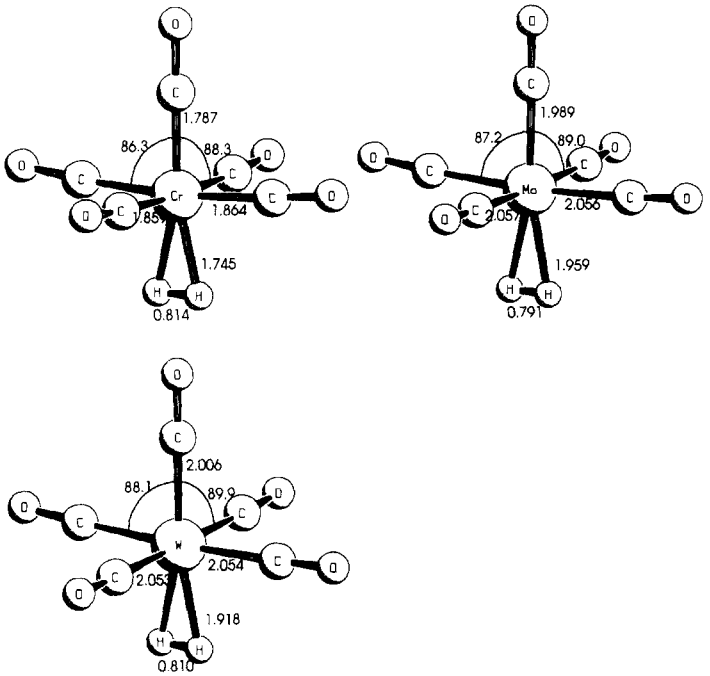


Fig. 1. Optimized geometries of $[M(CO)_5(H_2)]$ complexes at the MP2/II level. Bond lengths in Å, angles in degrees.

of several transition metal dihydrogen complexes, which show a H–H distance of roughly 0.82 Å despite widely varying ligand sets, central metal atoms, and charges.[3, 4] Also the predicted metal–hydrogen distances compare favorably with experimental results. The Mo–H bond length in $[Mo(CO)(H_2)(dppe)_2]$ (dppe = $Ph_2PCH_2CH_2PPh_2$) is reported as 1.92 Å.[3] Since the dppe ligand (π acceptor) enforces the L_nM-H_2 bonding, the calculated Mo–H distance of 1.959 Å in $[Mo(CO)_5(H_2)]$ appears reasonable. The calculated W–H distance in $[W(CO)_5(H_2)]$ (1.918 Å) is in good agreement with the experimental value of the original Kubas complex $[W(CO)_3(PiPr_3)_2(H_2)]$, which has ben reported as 1.95 Å (X-ray) and 1.89 Å (neutron diffration).[1, 20] The Cr–H bond length of the chromium analogue $[Cr(CO)_3(PiPr_3)_2(H_2)]$ has recently been determined by X-ray analysis (1.70–1.80 Å).[21] The calculated value for the Cr–H distances in $[Cr(CO)_5(H_2)]$ is 1.745 Å (Fig. 1). The comparison of the theoretical and experimental results for $[M(CO)_6]$ indicates that the H–H and M–H distances should be quite accurate.

Figure 1 shows that the theoretically predicted equilibrium geometries of the $[M(CO)_5(H_2)]$ complexes have the H_2 ligands eclipsing equatorial carbonyl groups that are *trans* to each other. An eclipsed conformation is also found in other dihydrogen complexes[2, 3] and has been rationalized by MO arguments.[3] The four equatorial carbonyl groups are bent away from the H_2 ligand, which leads to a hybridization of the metal d orbitals towards H_2. The carbonyl ligands eclipsing the H_2 ligand are more strongly bent out of the equatorial plane, which yields stronger sd hybridization at the metal and stronger $M-H_2$ interactions in this conformation.

Table 1 shows the theoretically predicted bond dissociation energies D_e and D_0 for the $(CO)_5M-H_2$ bonds. The theoretical

Table 1. Dissociation energies D_e and D_0 [kcal mol^{-1}] and ν_{H-H} vibrational frequencies $\tilde{\nu}$[cm^{-1}] of $[M(CO)_5(H_2)]$ calculated with basis set II [a].

	Method	$[Cr(CO)_5(H_2)]$	$[Mo(CO)_5(H_2)]$	$[W(CO)_5(H_2)]$
D_e	CCSD(T)	19.8	16.1	19.8
D_0	CCSD(T)	15.9	12.8	16.3
D_0	exp.	15.0 ± 1.3 [c]	–	> 16 [d]
$\tilde{\nu}$	MP2	3363	3612	3338
$\tilde{\nu}$	exp. [b]	3030	3080	2711

[a] See ref. [12]. [b] See ref. [9]. [c] Ref. [29]. [d] Ref. [6a].

value $D_0 = 16.3$ kcal mol^{-1} for $[W(CO)_5(H_2)]$ is in agreement with the experimental estimate of > 16 kcal mol^{-1}.[6a] The theoretically predicted value is also supported by the experimental values for the W–L binding enthalpies of $[W(CO)_3(PCy_3)_2L]$. The measured values are $\Delta H = 9.9$ kcal mol^{-1} (L = H_2) and $\Delta H = 30.4$ kcal mol^{-1} (L = CO).[6b] The first CO dissociation energy of $[W(CO)_6]$ is calculated as $D_0 = 45.7$ kcal mol^{-1},[10a] the experimental value is 46.0 ± 2 kcal mol^{-1}.[22] Thus, the W–CO bond strength of $[W(CO)_6]$ is stronger than in $[W(CO)_3(PCy_3)_2L]$ by a factor of 1.5. This factor gives an estimated bond strength of approximately 15 kcal mol^{-1} for the $W-H_2$ bond in $[W(CO)_5(H_2)]$, which is in good agreement with the calculated value of 16.3 kcal mol^{-1}.

The calculations suggest that the tungsten complex has the strongest $(CO)_5M-H_2$ bond, in the chromium complex it is only slightly weaker, and in the molybdenum complex it is the weakest of all. After we had completed our theoretical studies the experimentally determined $(CO)_5Cr-H_2$ binding enthalpy was published by Weitz et al.[29] By using transient IR spectroscopy, they determined a gas-phase value of 15.0 ± 1.3 kcal mol^{-1}, which is in excellent agreement with our calculated value of 15.9 kcal mol^{-1}. The calculated binding enthalpies correlate with the properties of Group 6 dihydrogen complexes, which shows the order W ≈ Cr > Mo for the $M-H_2$ bond strengths.[21] Also, the thermal stability of $[Mo(CO)_5H_2]$ in liquid Xe is clearly lower than that of the W and Cr analogues.[9b] However, the results of our previous study of $[M(CO)_6]$ and $[M(CO)_5(CS)]$ complexes indicate that the calculated $Cr-H_2$ dissociation energy may be slightly too high.[10] This reasoning is supported by comparison of the calculated and experimental IR spectra of the three complexes. Because the vibrational frequencies are the only observables for which theoretical and experimental values of the $[M(CO)_5H_2]$ complexes are available, the comparison of the results is very helpful for judging the accuracy of the theoretical results.

The theoretical H–H stretching frequencies were calculated by using the harmonic approximation. The resulting values may be too high; however, the frequency *shift* within a class of compounds should be calculated correctly. The theoretically predicted frequency for $[W(CO)_5H_2]$ ($\tilde{\nu} = 3338$ cm^{-1}) is significantly higher than the experimental value of 2711 cm^{-1}.[9] Experimental studies show a higher frequency for the molybdenum analogue (3080 cm^{-1}).[9] The calculated value for $[Mo(CO)_5H_2]$ is 3612 cm^{-1}. Thus, theory and experiment agree that the H–H stretching frequency of the molybdenum complex is roughly 300 cm^{-1} higher than that of the tungsten complex.

This corresponds to the calculated higher $(CO)_5M-H_2$ bond energy of the tungsten complex relative to that of the molybdenum complex. The experimentally observed H–H stretching frequency of $[Cr(CO)_5H_2]$ (3030 cm^{-1})[9] is only slightly lower than the value for the Mo complex. The calculations predict that the H–H stretching frequency of $[Cr(CO)_5H_2]$ (3363 cm^{-1}) is similar to that of the tungsten complex. This also indicates that the calculated $(CO)_2Cr-H_2$ bond strength may be too high.

A hotly debated question concerns the nature of $M-H_2$ bonding in transition metal dihydrogen complexes. The barrier to rotation around the metal–H_2 axis indicates that $d(\pi) \rightarrow \sigma^*$ backbonding is important in these compounds.[3] Based on an analysis of the IR spectra of $[W(CO)_5H_2]$, it was also concluded that the dihydrogen ligand is a relatively strong π acceptor.[9c] IR studies of metal carbonyl complexes containing a dinitrogen or dihydrogen ligand suggest that these two ligands have similar bonding properties.[23] Previous theoretical studies indicate that both $H_2 \rightarrow M$ σ-bonding and $M \rightarrow H_2$ π-backbonding are important in stable complexes.[4b, 24] Very recently, Morris and Schlaf used the Mössbauer spectra of several iron complexes to probe the π-bonding of various ligands.[25] From the plot of isomer shift versus quadrupole splitting they concluded that "π-bonding in transition metal dihydrogen complexes is very significant, more so than for N_2 or CO complexes".[25]

We used the recently introduced[26] charge decomposition analysis (CDA) to probe the nature of the metal–dihydrogen interactions in $[M(CO)_5H_2]$ complexes. In the CDA method the canonical (or natural) molecular orbitals of the complex are expressed in terms of the MOs of appropriately chosen fragments. In the present case, the MOs of $[M(CO)_5H_2]$ are formed by a linear combination of the MOs of $M(CO)_5$ and H_2 in the geometry of $[M(CO)_5H_2]$. Charge donation d_i from H_2 to $M(CO)_5$ for each orbital is then given by Equation (a). Similarly, the back donation b_i from $M(CO)_5$ to H_2 is given by Equation (b). Finally, the repulsive polarization r_i between the occupied orbitals of $M(CO)_5$ and H_2 is given by Equation (c). In

$$d_i = \sum_{k}^{\text{occ, A}} \sum_{n}^{\text{vac, B}} m_i c_{ki} c_{ni} \langle \varphi_k | \varphi_n \rangle \quad \text{(a)}$$

$$b_i = \sum_{l}^{\text{occ, B}} \sum_{m}^{\text{vac, A}} m_i c_{li} c_{mi} \langle \varphi_l | \varphi_m \rangle \quad \text{(b)}$$

$$r_i = \sum_{k}^{\text{occ, A}} \sum_{m}^{\text{occ, B}} m_i c_{ki} c_{mi} \langle \varphi_k | \varphi_m \rangle \quad \text{(c)}$$

these equations the following symbols are used: $A = H_2$, $B = M(CO)_5$, m = occupation number (2.0 in case of canonical orbitals), c = fragment orbital coefficient, φ = fragment MO.

The sum of the orbital contributions d_i, b_i, and r_i gives the total amount of donation, back donation, and charge repulsion, respectively. It has been shown for several complexes of main group and transition metal elements that the calculated values of d_i, b_i, and r_i correlate very nicely with qualitative models of donor–acceptor interactions.[26]

Table 2 shows the calculated contributions of the donation, back donation, and charge repulsion at the MP2/6-31G(d,p) level of theory for $[M(CO)_5H_2]$, $[W(CO)_6]$, and $[W(CO)_5N_2]$. CDA suggests that CO is a strong σ donor and a slightly weaker π acceptor. N_2 is predicted by CDA to be a very poor σ donor and a moderate π acceptor. This is in agreement with the analysis of the Mössbauer spectra of dinitrogen complexes by Bancroft et al.[27] CDA indicates that H_2 has similar π-acceptor properties as N_2 (Table 2). However, the values in Table 2 suggest clearly that, unlike N_2, H_2 is a strong σ donor! The σ donation of H_2 in $[W(CO)_5H_2]$ (0.349 e) is significantly greater than the contribution from π-backbonding (0.129 e). The values for the Cr and Mo analogues are very similar. The negative sign of the contributions by the repulsive polarization indicates that electronic charge is depleted from the overlapping area of the occupied orbitals of the fragments. The depletion is quite large for CO and N_2, but less so for H_2. It should be noted that there is no direct correlation between the calculated CDA values and the relative bond strength of the ligands.

Table 2. Results of charge decomposition analysis of $[M(CO)_5L]$ complexes; donation d, back donation b, and repulsive polarization r were calculated at the MP2/II level.

M	L	d	b	r	D_0
Cr	H_2	0.393	0.143	−0.147	15.9 [a]
Mo	H_2	0.315	0.105	−0.117	12.8 [a]
W	H_2	0.349	0.129	−0.105	16.3 [a]
W	CO	0.315	0.233	−0.278	45.7 [b]
W	N_2	0.027	0.107	−0.252	24.8 [c]

[a] See Table 1. [b] See ref. [10a]. [c] See ref. [10b].

To investigate the electronic structure of the dihydrogen complexes further, we used the topological analysis of the electronic structure and its associated gradients and Laplacian.[28] Figure 2 shows the Laplacian of the electron density distribution of

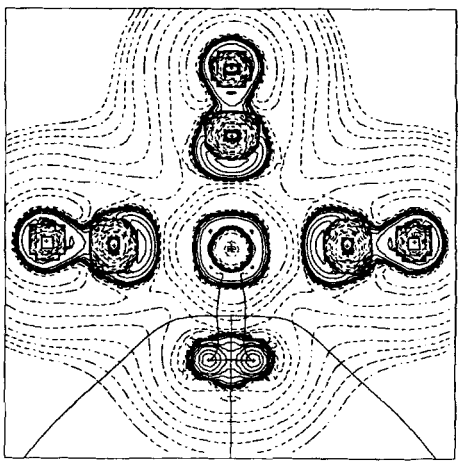


Fig. 2. Laplacian of the electron density distribution $\nabla^2\rho(r)$ of $[W(CO)_5(H_2)]$ at the MP2/II level. Dashed lines indicate charge depletion ($\nabla^2\rho(r) > 0$); solid lines indicate charge concentration ($\nabla^2\rho(r) < 0$). The solid lines connecting the atomic nuclei are the bond paths; the solid lines separating the atomic nuclei indicate the zero-flux surfaces in the molecular plane.

$[W(CO)_5(H_2)]$. Since the corresponding diagrams of the Cr and Mo analogues are very similar, they are not shown. The $M-H_2$ moiety has two distinct W–H bonds; there are two bond critical points for the W–H bonds, one for the H–H bond and one for the $M-H_2$ unit. The topology of the electronic structure of the $[M(CO)_5(H_2)]$ molecules indicates that the $M-H_2$ moiety has a cyclic structure and not a T-shaped form. The presence of a H–H bond critical point indicates that a true dihydrogen ligand exists, although there are two distinct metal–hydrogen bond paths.

Received: July 29, 1994
Revised version: September 29, 1994 [Z 7189 IE]
German version: *Angew. Chem.* **1995**, *107*, 383

Keywords: ab initio calculations · coordination · H_2 complexes

[1] a) G. J. Kubas, R. R. Ryan, B. I. Swanson, P. J. Vergamini, H. J. Wasserman, *J. Am. Chem. Soc.* **1984**, *106*, 451; b) G. J. Kubas, R. R. Ryan, D. J. Wroblewski, *ibid.* **1986**, *108*, 1229; c) G. J. Kubas, C. J. Unkefer, B. I. Swanson, E. Fukushima, *ibid.* **1986**, *108*, 7000.

[2] Reviews: a) D. M. Heinekey, W. J. Oldham, *Chem. Rev.* **1993**, *93*, 913; b) G. J. Kubas, *Acc. Chem. Res.* **1988**, *21*, 120; c) R. H. Crabtree, *ibid.* **1990**, *23*, 95; d) A. G. Ginsburg, A. A. Bagaturyants, *Metalloorg. Khim.* **1989**, *2*, 249; e) J. H. Morris, P. G. Jessop, *Coord. Chem. Rev.* **1992**, *121*, 155; f) R. H. Crabtree, D. G. Hamilton, *Adv. Organomet. Chem.* **1988**, *28*, 299; g) *Transition Metal Hydrides* (Ed.: A. Dedieu), VCH, Weinheim, **1991**.

[3] G. J. Kubas, C. J. Burns, J. Eckert, S. W. Johnson, A. C. Larson, P. J. Vergamini, C. J. Unkefer, G. R. K. Khalsa, S. A. Jackson, O. Eisenstein, *J. Am. Chem. Soc.* **1993**, *115*, 569.

[4] a) J. S. Ricci, T. F. Koetzle, M. T. Bautista, T. M. Hofstede, R. H. Morris, J. F. Sawyer, *J. Am. Chem. Soc.* **1989**, *111*, 8823; b) L. S. Van Der Sluys, J. Eckert, O. Eisenstein, J. H. Hall, J. C. Huffman, S. A. Jackson, T. F. Koetzle, G. J. Kubas, P. J. Vergamini, K. G. Caulton, *ibid.* **1990**, *112*, 4831.

[5] a) Y. Kim, H. Deng, D. W. Meek, A.Wojcicki, *J. Am. Chem. Soc.* **1990**, *112*, 2798; b) T. Hasegawa, Z. Li, S. Parkin, H. Hope, R. K. McMullan, T. F. Koetzle, H. Taube, *ibid.* **1994**, *116*, 4352; c) F. A. Cotton, R. L. Luck, *Inorg. Chem.* **1991**, *30*, 767; d) G. Jia, A. J. Lough, R. H. Morris, *Organometallics* **1992**, *11*, 161.

[6] a) Y.-I. Ishikawa, P. A. Hackett, D. M. Rayner, *J. Phys. Chem.* **1989**, *93*, 652; b) A. A. Gonzalez, K. Zhang, S. P. Nolan, R. Lopez de la Vega, S. L. Mukerjee, C. D. Hoff, G. J. Kubas, *Organometallics* **1988**, *7*, 2429.

[7] G. Pacchioni, *J. Am. Chem. Soc.* **1990**, *112*, 80.

[8] A. D. King, R. B. King, D. B. Yang, *J. Am. Chem. Soc.* **1981**, *103*, 2699.

[9] a) R. L. Sweany, *J. Am. Chem. Soc.* **1985**, *107*, 2374; b) R. K. Upmacis, M. Poliakoff, J. J. Turner, *ibid.* **1986**, *108*, 3645; c) R. R. Andrea, M. A. Vuurman, D. J. Stufkens, A. D. Oskam, *Recl. Trav. Chim. Pays-Bas* **1986**, *105*, 372.

[10] a) A. W. Ehlers, G. Frenking, *J. Am. Chem. Soc.* **1994**, *116*, 1514; b) *Organometallics*, submitted.

[11] A. W. Ehlers, G. Frenking, *Organometallics*, in press.

[12] The geometries and harmonic vibrational frequencies were calculated at the MP2 [13] level using effective core potentials (ECPs) and a (441/2111/*N*1) split-valence basis set for the metals, which is derived from the (55/5/*N* + 1) minimal basis set optimized by Hay and Wadt [14] (*N* = 4, 3, 2 for Cr, Mo, and W, respectively). The $(n-1)s^2$ and $(n-1)p^6$ electrons are treated explicitly as part of the valence electrons. The ECPs are optimized from nonrelativistic atom calculations of Cr and relativistic calculations of Mo and W. A 6-31G(d,p) all-electron basis set is used for C, O, H [15]. The dissociation energies were determined by using coupled-cluster theory with singles and doubles and a noniterative estimate of triple substitutions (CCSD(T)) [16]. The calculations were carried out using the program packages TURBOMOLE [17], ACES II [18], and Gaussian 92 [19].

[13] a) C. Møller, M. S. Plesset, *Phys. Rev.* **1934**, *46*, 618; b) J. S. Binkley, J. A. Pople, *Int. J. Quantum Chem.* **1975**, *9*, 229.

[14] P. J. Hay, W. R. Wadt, *J. Chem. Phys.* **1985**, *82*, 299.

[15] W. J. Hehre, R. Ditchfield, J. A. Pople, *J. Chem. Phys.* **1972**, *56*, 2257.

[16] a) J.Cizek, *J. Chem. Phys.* **1966**, *45*, 4256; b) J. A. Pople, R. Krishnan, H. B. Schlegel, J. S. Binkley, *Int. J. Quantum Chem.* **1978**, *14*, 545; c) R. J. Bartlett, G. D. Purvis, *ibid.* **1978**, *14*, 561; d) G. D. Purvis, R. J. Bartlett, *J. Chem. Phys.* **1982**, *76*, 1910; e) *ibid.* **1987**,*86*, 7041.

[17] a) M. Häser, R. Ahlrichs, *J. Comput. Chem.* **1989**, *10*, 104; b) R. Ahlrichs, M. Bär, M. Häser, H. Horn, C. Kölmel, *Chem. Phys. Lett.* **1989**, *162*, 165; c) H. Horn, H. Weiß, M. Häser, M. Ehrig, R. Ahlrichs, *J. Comput. Chem.* **1991**, *12*, 1058; d) M. Häser, J. Almlöf, M. W. Feyereisen, *Theor. Chim. Acta* **1991**, *79*, 115.

[18] ACES II: J. F. Stanton, J. Gauss, J. D. Watts, W. J. Lauderdale, R. J. Bartlett, University of Florida, Gainesville, FL, **1991**.

[19] Gaussian 92, Revision C: M. J. Frisch, G. W. Trucks, M. Head-Gordon, P. M. W. Gill, M. W. Wong, J. B. Foresman, H. B. Schlegel, K. Raghavachari, M. A. Robb, J. S. Binkley, C. Gonzalez, R. L. Martin, D. J. Fox, D. J. DeFrees, J. Baker, J. J. P. Stewart, J. A. Pople, Gaussian Inc., Pittsburg, PA, **1992**.

[20] R. L. Sweany, *J. Am. Chem. Soc.* **1986**, *108*, 6986.

[21] G. J. Kubas, J. E. Nelson, J. C. Bryan, J. Eckert, L. Wisniewski, K. Zilm, *Inorg. Chem.* **1994**, *33*, 2954.

[22] K. E. Lewis, D. M. Golden, G. P. Smith, *J. Am. Chem. Soc.* **1984**, *106*, 3905.

[23] a) R. H. Morris, K. A. Earl, R. L. Luck, N. J. Lazarowych, A. Sella, *Inorg. Chem.* **1987**, *26*, 2674; b) Y. F. Zheng, W. H. Wang, J. G. Lin, Y. B. She, K. J. Fu, *J. Phys. Chem.* **1992**, *96*, 9821; c) S. M. Howdle, M. A. Healy, M. Poliakoff, *J. Am. Chem. Soc.* **1990**, *112*, 4804.

[24] a) P. J. Hay, *J. Am. Chem. Soc.* **1987**, *109*, 705; b) Y. Jean, A. Lledos, B. Maouche, R. Aiad, *J. Chim. Phys. Phys. Chim. Biol.* **1987**, *84*, 805; c) F. Maseras, M. Duran, A. Lledos, J. Bertran, *J. Am. Chem. Soc.* **1991**, *113*, 2879; d) A. Albinati, V. I. Bakhmutov, K. G. Caulton, E. Clot, J. Eckert, O. Eisenstein, D. G. Gusev, V. V. Grushin, B. E. Hauger, W. T. Klooster, T. F. Koetzle, R. K. McMullan, T. J. O'Loughlin, M. Pelissier, R. S. Ricci, M. P. Sigalas, A. B. Vymenits, *ibid.* **1993**, *115*, 7300.

[25] R. H. Morris, M. Schlaf, *Inorg. Chem.* **1994**, *33*, 1725.

[26] S. Dapprich, G. Frenking, *J. Am. Chem. Soc.*, submitted.

[27] a) G. M. Bancroft, M. J. Mays, B. E. Prater, F. P. Stefanini, *J. Chem. Soc. A* **1970**, 2146; b) G. M. Bancroft, *Coord. Chem. Rev.* **1973**, *11*, 247.

[28] R. F. W. Bader, *Atoms in Molecules: A Quantum Theory*, Oxford University Press, Oxford, **1990**; see also R. F. W. Bader, P. L. A. Popelier, T. A. Keith, *Angew. Chem.* **1994**, *106*, 647; *Angew. Chem. Int. Ed. Engl.* **1994**, *33*, 620.

[29] J. R. Wells, P. G. House, E. Weitz, *J. Phys. Chem.* **1994**, *98*, 8343.

 © *VCH Verlagsgesellschaft mbH, D-69451 Weinheim, 1995* *0570-0833/95/0303-0357 $ 10.00+.25/0*

Searching Questions

Guardians of Science. Fairness and Reliability of Peer Review. By *H.-D. Daniel*. VCH Verlagsgesellschaft, Weinheim/VCH Publishers, New York, 1993. 118 pp., hardcover DM 78.00, $ 50.00.—ISBN 3-527-29041-9/1-56081-751-8

The subtitle "Fairness and Reliability of Peer Review" well describes what this book is about. The author, H.-D. Daniel, is one of Germany's leading experts in this area and is thus well qualified to examine this question. The data on which the study is based relate to the refereeing of one year's output of *Angewandte Chemie*. Manuscripts submitted for "Angewandte" are usually reviewed by two independent referees whose recommendations are then evaluated by the editor. To that extent the procedure is essentially the same as that normally applied to proposals submitted to the German Research Association (Deutsche Forschungsgemeinschaft, DFG), and thus the results are also relevant to the situation there. The author analyzes all the observations according to the rules of the art of statistics. He begins by trying to quantify the degree of agreement between the two specialist reviewers. If the recommendations are classified on a scale of 1 to 4, ranging from acceptance without change through two levels of revision to rejection, the statistical agreement seems surprisingly poor. However, if the recommendations are treated as being in agreement when they differ by only one point, the degree of consensus turns out to be satisfactory. To examine the "correctness" of decisions to reject, Daniel uses an interesting approach: he traces the fate of manuscripts that have been rejected and subsequently published elsewhere, and compares their frequency of citation with that of papers appearing in "Angewandte". As expected, the frequencies for the former are appreciably lower than those for the latter. Even Daniel does not know whether this might be simply because papers in "Angewandte" are generally cited more often (the journal has a high "impact factor"), and therefore one cannot conclude very much about the individual papers from this analysis. However, in the absence of any better approach this is certainly a useful piece of analysis. The book contains many other statistical analyses which are worth studying by everyone who is concerned with refereeing, either actively or passively, in other words every scientist engaged in research or university teaching.



There are two aspects to refereeing procedures. First there is the "correctness" of the decisions. As an insider I can confirm that, at least in the case of German referees, recommendations are made in good faith and to one's best ability. Secondly, however, there must be confidence within the scientific community that this is so. Since both the journals and the DFG preserve the anonymity of referees so far as possible (for very good reasons), great importance attaches to books and articles such as this which show, at least statistically, that the procedures are above reproach. However, I was somewhat surprised that Daniel gives no hint of recognition that, in the nature of things, every referee report must contain an element of subjectivity. All attempts to correct this by quantitative measures merely shift the problem to somewhere else. Daniel restricts himself to aspects that can be analyzed quantitatively. Thus he takes no account of the message that may be read "between the lines". We learn nothing here about the reviewer who writes a damning report but cannot bring himself to recommend rejection, nor about the one who gives a report that is intended to be favorable but qualifies it with sarcastic comments. In such cases the editor needs to be able to weigh up the situation and to know the peculiarities of his reviewers. I am disturbed by the many cases that are cited of manuscripts that were initially rejected (by a wide variety of journals, mostly well-known) but were later honored by Nobel prize awards. Unfortunately, refereeing systems probably suffer from a certain degree of conservatism, and have difficulty in dealing with anything which conflicts too much with current thinking—even when, as is usually the case, all those involved make great efforts to avoid this and value originality above all else.

In such an important matter as refereeing it is not surprising that there have already been many attempts at improving the system. One chapter lists every such proposal that I am aware of, and analyzes the experiences that have resulted from these in various places. For me personally this was the most interesting part of the book, showing as it does that there is probably no alternative to continuing with the present system. Here the ethical guidelines laid down by the American Chemical Society, which are reproduced in the book, deserve to be observed generally.

To complete this scholarly work Daniel includes a comprehensive bibliography of published work on the subject of refereeing together with extensive notes. The whole work is written in fluent English: 118 pages that are well worth reading.

Manfred Mahnig
Deutsche Forschungsgemeinschaft
Bonn (FRG)

Three-Dimensional Chemical Similarity Searching. By *C. Pepperrell*. Research Studies Press, Taunton, UK, 1994. XV, 304 pp., hardcover £ 57.50.—ISBN 0-86380-145-5

For well over a century chemists have relied on the two-dimensional structural formula for the display and communication of chemical information. This mode of representation of structure has certainly been the traditional mainstay for the

This section contains book reviews and a list of new books received by the editor. Book reviews are written by invitation from the editor. Suggestions for books to be reviewed and for book reviewers are welcome. Publishers should send brochures or (better) books to Dr. Ralf Baumann, Redaktion Angewandte Chemie, Postfach 101161, D-69451 Weinheim, Federal Republic of Germany. The editor reserves the right of selecting which books will be reviewed. Uninvited books not chosen for review will not be returned.

storage, manipulation, and retrieval of structural information in computerized systems. The *Chemical Abstracts* database alone comprises more than ten million such structures. The widespread and continuing use of the two-dimensional formula is, of course, a legacy of the past—it was bequeathed to us by pioneers such as Kekulé and Crum Brown who developed these formulas in the 1860s and then went on to show how they could be applied in the rationalization of chemical phenomena. Although this representation has served us well, the question now being raised is whether it has outlived its usefulness. Two-dimensional formulas are really quite unsuitable for computerized storage systems as the formulas need to be redrawn in the same format and orientation before structures can be compared. The comparing of structures and assessment of similarities has become very important during the past decade, following on from the realization that molecular similarity studies can be profitably exploited in the early stages of molecular design. The design of pharmaceutical drugs and agrochemicals in particular has benefited. In addition, a host of other modern chemical problems involve investigation of the stereochemistry or chirality of molecular species. It is thus hardly surprising that chemists are now beginning to take a serious look at the representation of chemical species by three-dimensional formulas.

The book reviewed here may be regarded as an important and innovative step in this direction. It comes from the information studies group at the University of Sheffield, arguably the world's leading group in the development of new approaches to the management of three-dimensional structural data. The author has chosen to focus on the techniques that may be used for searching three-dimensional structural databases, with special emphasis on similarity searching. After pointing out the limitations of two-dimensional searching, the author analyzes the role and effectiveness of four different three-dimensional similarity methods, namely the distance distribution method, the use of individual distances, atom mapping, and the maximal common substructure method. It is concluded that in overall terms the best of these is the atom mapping method, an approach based on a localized description of the three-dimensional environment of each atom in a molecule. When two molecules are to be compared, atoms with similar local environments are mapped on to each other, and the similarities between atoms so mapped are combined together to yield a global measure of the similarity of the two molecules. The rest of the book, including a 30-page appendix giving the results of sample calculations, is devoted to a discussion of the atom mapping method. Among other things, the author considers how the method may be optimized and made faster in practice, and describes a variety of elaborations that broaden its scope and applicability. In fact, with appropriate modifications, the method is applicable not only to relatively small molecules but also to the largest of macromolecules.

In presenting all this material in one volume the author has performed a very useful service to many different kinds of chemists. Structure-directed searching is now the most common type of query made to chemical structural databases and the demand is likely to grow considerably in the future. This work not only addresses the increasingly pressing problem of the storage and manipulation of three-dimensional data but also shows how similarity notions may be successfully incorporated into the searching of such data. Even though in its current form the method cannot cope with very large databases, it is certainly able to handle medium-sized databases containing up to 50000 structures. Moreover, research at present under way in several laboratories around the world will undoubtedly push up this limit substantially in the foreseeable future. The atom mapping method has many exciting potential applications and will feature in the design of molecular species for a variety of applications. The author is to be congratulated on bringing out such a useful and succinct guide to this rapidly evolving domain.

Dennis H. Rouvray
University of Georgia
Athens, GA (USA)

The World of Physical Chemistry. By *K. J. Laidler*. Oxford University Press, Oxford, 1993. 488 pp., hardcover £ 55.00.—ISBN 0-19-855597-0

The title of this book should really have been extended by adding the subtitle "A Historical Discourse". It contains a history of ideas in physical chemistry, from the beginnings when this classification did not yet exist, up to about the middle of the present century. To make for lighter reading the author intersperses the account with biographical notes about actors who have played important roles on this stage, although some of these have had little recognition. Some additional short biographies are collected together in an appendix, and there are plenty of literature references.

Three introductory chapters explain the background to the development of physical chemistry within the overall framework of the sciences, and discuss the nature of the problems that it addresses and the methods of working. The latter are illustrated by taking as examples two scientists with very different styles. H. Eyring and R. Norrish, and by outlining the development of the most important centers of physical chemistry research in England, Scotland, and North America. One chapter is concerned with the sources from which early physicochemical studies originated, and describes the beginnings of the journals that are now the leaders in this field. The heart of the book consists of the seven chapters outlining the development of the sub-disciplines of thermodynamics, the kinetic and statistical theory of matter, chemical spectroscopy, electrochemistry, chemical kinetics, colloid and interface chemistry, and quantum chemistry.

The author's treatment is firmly linked to the individual scientists and their contributions to the development of the subject. In the course of this he also mentions some little known facts. For example, I had not appreciated how wide-ranging was the work of D. L. Chapman, who not only contributed to the theory of the diffuse double layer by developing an early forerunner of the Debye-Hückel theory of electrolyte solutions, but also made important contributions to the understanding of reactions in the gas phase. Even more surprising is the reappraisal of the work of Agnes Pockel who, as a housewife in Braunschweig, carried out studies in her kitchen on the behavior of films of organic substances, the results of which were published thanks to the support of Lord Rayleigh. In her experiments she used an apparatus that already contained the essential elements of the Langmuir balance for measuring the surface tension of a film.

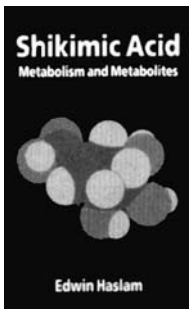
The reader will find that many recent developments are mentioned only very briefly or are even completely absent. However, to include all these would have made a larger book than was intended. The treatment is undoubtedly much colored by personal background, and an author from outside the English-speaking world would have given a different emphasis in many respects. However, that in itself adds to one's interest in reading this well-written book. In an age when the principles of physical chemistry are nearly always treated in a deductive way in textbooks, and the student is seldom told

 © VCH Verlagsgesellschaft mbH, D-69451 Weinheim, 1995 0570-0833/95/0303-0360 $ 10.00+.25/0

about the historical development of the subject, a book of this kind is especially welcome. Without a knowledge of the historical background one's understanding of the nature and purposes of the discipline can only be superficial. Also the motivation for research gains an extra dimension when one is aware of the paths and the false trails involved in arriving at the present state of knowledge. The book should be in the library of every physical chemistry department, and is also highly recommended for inclusion in scientists' personal collections.

Heinz Gerischer
Fritz-Haber-Institut
der Max-Planck-Gesellschaft
Berlin (FRG)

Shikimic Acid. By *E. Haslam*. Wiley, Chichester, 1993. 387 pp., hardcover, £ 75.00.—ISBN 0-471-93999-4



Shikimic acid is the key to one of nature's most astonishing and multifaceted pathways, namely the aromatic metabolism developed in various organisms, mostly in plants, but also in microorganisms and fungi. The fact that the shikimate pathway does not exist (any longer) in mammals is the reason for the worldwide intensive research, as it raises the possibility of developing selective inhibitors for use as herbicides, antifungalagents, or antibacterial agents. One already successful example is the herbicide glyphosate, which acts as an inhibitor of one of the enzymes of the shikimate pathway (5-enoylpyruvylshikimate-3-phosphate synthase). The above book by Haslam achieves considerably more than dealing with this important aspect of the application of biosynthetic studies and reviewing the progress made in research on the shikimate biosynthetic pathway during the past twenty years (since his first book, *The Shikimate Pathway*, was published). The new results of studies on the shikimate pathway offer insights into intriguing questions of molecular evolution, reveal a gold mine of unusual enzymology, and include examples of important applications of the latest advances in synthetic organic chemistry.

The book is divided into five chapters, allowing the reader easy access to the different interesting facets of the shikimate pathway. In Chapter 1 a short introduction and overview is given. This includes interesting views on evolutionary aspects (metabolic costs, multifunctional enzymes, possible reasons why the shikimate pathway to aromatic compounds no longer exists in mammals) and on the development of the methodologies (genetic engineering, organic synthesis) used in this research. Chapter 2 deals with the chemistry (isolation, derivatization, and synthesis) of the starting molecules and of all intermediates of the common shikimate pathway, i.e. up to chorismic acid, the major branch point. Several approaches to the synthesis of important intermediates such as the title compound shikimic acid or chorismic acid are compared and evaluated. Chapter 3 provides information about the unique enzymes and the enzymology involved in the common shikimate pathway (up to chorismic acid), reflecting the immense knowledge gained in this field during the past twenty years. A section within this chapter focuses on the above mentioned 5-enoylpyruvylshikimate-3-phosphate synthase and its inhibitor glyphosate, the herbicidal component of the commercially important weedkiller "Roundup". The following two chapters are the longest and deal with all aspects of the stages beyond chorismic acid, such as the various further biosynthetic pathways, the products, the enzymes involved, etc. Chapter 4 focuses on generally occurring, so-called primary metabolites and their enzymes, in particular the five key enzymes initiating the major metabolic branches from chorismic acid (chorismate mutase, anthranilate synthase, *p*-hydroxybenzoate synthase, isochorismate synthase, and *p*-aminobenzoate synthase). The products thereby formed (the "primary metabolites") are obviously essential for the producing organisms: the aromatic amino acids (e.g. phenylalanine, tryptophan), the benzo- and naphthoisoprene quinones (e.g. ubiquinone, vitamin K), and the folate coenzymes. Other enzymes that are involved, and the metabolism into and of aromatic products, such as the lignin metabolism in plants and the aromatic amino acid metabolism in mammals, are also discussed. Chapter 5 deals with the so-called secondary metabolites, the more or less individually produced "chemicals" of a particular organism. The chapter begins with a brief discussion of the term "secondary metabolism", which although historically based and often didactically useful, is imprecisely defined and misleading. The treatment is subdivided into natural products from microorganisms and those from plants. These special branches occurring mostly in the late but sometimes in the early shikimate pathway of certain organisms lead to important natural products such as antibiotics, mycotoxins, alkaloids, and flavonoids. There is also an addendum listing literature published after the manuscript was finished. This is divided into the main areas of chemistry/synthesis, enzymology, and biosynthesis, and covers the most recent literature (up to 1993!).

Shikimic Acid is written in an engaging and easily understandable style. Occasional quotations (e.g. from the Bible, from Oscar Wilde, and especially from important early researchers in the field) and excursions into the history of several of the intermediates or products of the shikimate pathway, together with the author's remarkably wide grasp of the broad field of natural products chemistry, make it a pleasure to read. The different facets of the rapidly advancing field of natural products chemistry are presented so elegantly and absorbingly that it would be small-minded to recount the few structural or printing errors. It is a pity that the high price will prevent many students from buying this excellent text, a rare example where a detailed overview of an important field of bioorganic chemistry is successfully embedded in a very entertaining story. As a source of motivation and a resource for preparing lectures as well as a reference book, *Shikimic Acid* is a must for everybody involved in teaching and research in the broad field of natural products and biochemistry.

Jürgen Rohr
Institut für Organische Chemie
der Universität Göttingen (FRG)

Shape in Chemistry. An Introduction to Molecular Shape and Topology. By *P. G. Mezey*. VCH Publishers, New York, 1993. XI, 224 pp., hardcover $ 75.00.—ISBN 0-89573-727-2

Shape is a concept of interest to a wide range of scientists. For instance, biologists map the shapes of microorganisms, geologists the shapes of rocks, and chemists the shapes of molecules. However, all use different measures, for there is no general agreement on how shape should be defined. Most chemists resort to the concept as and when it is needed, without ever trying to get to grips with it in any deep abstract sense. In this respect shape resembles a number of other chemical

 © VCH Verlagsgesellschaft mbH, D-69451 Weinheim, 1995 0570-0833/95/0303-0361 $ 10.00+.25/0

concepts—the examples of similarity and structure spring to mind—in that it is often used but never rigorously defined. This book focuses on molecular shape and in particular on measures to quantify it. In fact, over the past two centuries numerous contributions to the study of molecular shape have been made by a succession of distinguished scientists. Molecular shape first came of the fore when the founder of modern atomic theory, John Dalton, had a set of molecular models made for him in 1810. These were of the ball-and-stick variety still in use today, his idea being to display the shapes that simple molecules might assume. Other leading lights who worked on shape were Kekulé, who in the mid-1860s established the hexagonal shape of the benzene ring; van't Hoff and Le Bel, who in 1874 independently put forward the notion of the tetrahedral carbon atom; Fischer, who in 1894 proposed a lock and key model to illustrate the complementarity of a drug and its receptor; Pauling, who in the 1930s introduced the concept of hybridization to explain the shapes of many molecules; and Barton, who in 1950 coined the expression "conformational analysis" to describe his approach to the three-dimensional characterization of organic species. From about the 1950s a variety of shape descriptors began to appear: these ranged from the use of two-dimensional silhouettes by Amoore in the 1960s to the advocacy of shape topological indices by Kier in the 1980s. Over the past decade a plethora of exciting new ways of quantifying molecular shape—too numerous to go into here—have also been developed.

Unfortunately, precious little of this rich history of the evolution of shape concepts in chemistry is covered in Mezey's book. Indeed, this book contains only cursory references to some key problems that dominate the most recent work on molecular shape. A case in point is the controversy that has raged over the past dozen years on whether it is meaningful to assign shapes at all to objects that are as small and fuzzy as molecules. Quantum theoreticians such as Primas and Amann in Switzerland and Woolley in England have repeatedly pointed out that isolated molecules do not admit of a stable shape, and that the notion of shape can be introduced only via the Born–Oppenheimer approximation which effectively freezes the positions of the atomic nuclei. This fundamental question should surely have been addressed in this book, which claims that its principal objective is "to convince the reader that molecular shape is accessible to rigorous study". Another issue that I feel should have been explored is that of where to draw the line between micromolecular objects that clearly need to be discussed in terms of quantum theory and macromolecular objects such as large crystals that can be more conveniently discussed using classical mechanical language. Although Mezey emphasizes that molecular shape is a dynamic rather than a static property, and goes on to point out that much of our current thinking is based on the erroneous idea that the nuclei are fixed and so can be treated classically, he does not tell us when the classical approach might be valid, e.g. in the case of large molecules such as DNA. Nor does he discuss such novel topics as the treatment of crystals with oscillating shapes, the non-trivial problem of inferring three-dimensional structures from their two-dimensional projections, or the use of neural networks in the characterization of molecular shape.

Having outlined my criticisms of this book, I would now like to expand on its many virtues. First, a word or two about the author himself. Mezey is the most significant contributor to the discussion on molecular shape in the latter half of the twentieth century, and so it is appropriate and timely that he should write a book expaining his methods. He writes extremely well—even though English is not his mother tongue—and his ideas are always thought-provoking. Mezey has a tendency to clothe his ideas in mathematical language that is perhaps unfamiliar to many chemists. This sometimes makes his work rather challenging to the average chemist, though in the case of his book I feel he has risen to the occasion and produced a work of admirable clarity and one that is eminently readable. This book contains excellent accounts of the various methods he has developed for molecular shape analysis over the past two decades. Because Mezey believes that molecules are topological objects rather than geometric ones, he tends to make heavy use of algebraic topology. In his shape group methods for instance, which have been applied to molecular isodensity contours, electrostatic potentials, and van der Waals surfaces, the properties of the continuous functions characterizing the contours are captured by a family of algebraic shape groups. In an analogous fashion, his quantitative shape–activity relationships (QShAR) approach treats the geometric similarity of molecular species as a topological equivalence that can be quantified in terms of shape representations or shape descriptors. Both of these methods have the considerable advantages that they can be used on nonrigid molecules and that they lend themselves readily to computer processing. Moreover, it would appear that such methods are suited for molecular shape similarity and shape complementarity analysis in large families of molecules. As this will probably prove to be the case, Mezey's methods may well yield important and powerful new tools in the never-ending search for new drugs and in molecular design generally. It is this great promise of Mezey's work that makes the study of it so rewarding and this book so stimulating to read.

Dennis H. Rouvray
University of Georgia
Athens, GA (USA)

 © VCH Verlagsgesellschaft mbH, D-69451 Weinheim, 1995 0570-0833/95/0303-0362 $ 10.00+.25/0

New Books

Electron Microscopy and Analysis 1993. Edited by **A. J. Craven.** Institute of Physics, Bristol, **1993.** 538 pp., hardcover, £ 99.00. –ISBN 0-7503-0321-2

Recht für Chemiker. Einführung in das Chemikalien- und Grundstoffrecht. By **G. Borchert.** Hirzel, Stuttgart, **1994.** 346 pp., paperback, DM 48.00.—ISBN 3-7776-0567-0

Polymer Fractionation. By **F. Francuskiewicz.** Springer, Heidelberg, **1994.** 215 pp., hardcover, DM 98.00.—ISBN 3-540-57539-1

Farm-Hall-Berichte. Die abgehörten Gespräche der 1945/46 in England internierten deutschen Atomwissenschaftler. By **H. Rechenberg.** Wissenschaftliche Verlagsgesellschaft, Stuttgart, **1994.** 97 pp., softcover, DM 18.50.– ISBN 3-8047-1326-2

Wasseraufbereitung. By **K. Hancke.** VDI, Düsseldorf, **1994.** 308 pp., paperback, DM 78.00.—ISBN 3-18-401393-6

VDI-Lexikon Umwelttechnik. Edited by **F.-J. Dreyhaupt.** VDI, Düsseldorf, **1994.** 1361 pp., hardcover, DM 298.00.—ISBN 3-18-400891-6

Giftpflanzen - Pflanzengifte. Vorkommen, Wirkung, Therapie, allergische und phototoxische Reaktionen. 4th Ed. By **L. Roth et al.** Ecomed, Landsberg a. Lech, **1994.** 1100 pp., hardcover, DM 284.00 (subscription price DM 198.00).—ISBN 3-609-64810-4

Impinging-Stream Reactors. By **A. Tamir.** Elsevier, Amsterdam, **1994.** 780 pp., hardcover, $ 340.00.—ISBN 0-444-89400-4

Concepts in Protein Engineering and Design. Edited by **P. Wrede, G. Schneider.** De Gruyter, Berlin, **1994.** 378 pp., hardcover, DM 128.00.—ISBN 3-11-012975-2

Toxikologie für Chemiker und Biologen. By **W. Dekant, S. Vamvakas.** Spektrum, Heidelberg, **1994.** 405 pp., hardcover, DM 48.00.—ISBN 3-86025-218-6

Prinzipien der Biochemie. 2. Auflage. By **A. L. Lehninger, D. L. Nelson, M. M. Cox.** Spektrum, Heidelberg, **1994.** 1182 pp., hardcover, DM 128.00.—ISBN 3-86025-106-6

Ion Exchange: Theory and Practice. 2nd Ed. By **C. E. Harland.** Royal Society of Chemistry, London, **1994.** 285 pp., paperback, £ 16.95. –ISBN 0-85186-484-8

Animal Cells as Bioreactors. (Cambridge Studies in Biotechnology 11). By **T. Cartwright.** Cambridge University Press, Cambridge, **1994.** 184 pp., paperback, £ 30.00. ISBN 0-521-41258-7

Toxikologie chlororganischer Verbindungen. By **D. Henschler.** VCH, Weinheim, **1994.** 195 pp., hardcover, DM 68.00. –ISBN 3-527-29262-4

Schadstoffe im Grundwasser. 2nd Ed. Edited by **Deutsche Forschungsgemeinschaft.** VCH, Weinheim, **1994.** 737 pp., paperback, DM 168.00.—ISBN 3-527-27133-3

List of MAK and BAT Values 1994. Edited by **Deutsche Forschungsgemeinschaft.** VCH, Weinheim, **1994.** 165 pp., paperback, DM 54.00. –ISBN 3-527-27564-9

Stereoselective Synthesis. By **M. Nógrádi.** VCH, Weinheim/New York, **1994.** 368 pp., paperback, DM 68.00/ $ 45.00. –ISBN 3-527-29243-8/1-56081-895-6

Encyclopedia of Applied Physics. Vol. 10. Edited by **G. L. Trigg.** VCH, Weinheim/New York, **1994.** 590 pp., hardcover, DM 430.00/$ 295.00.—ISBN 3-527-28132-0

State-Selected and State-to-State/State Selected Ion Molecule Reaction Dynamics. Part 1: Experiment/Part 2: Theory. (Advances in Chemical Physics). Edited by **C.-Y. Ng and M. Baer.** Wiley, Chichester, Great Britain, **1994.** 686 pp./561pp., hardcover. £ 224.00 (set). ISBN 0-471-53258-4/0-471-53263-0

Chemical Speciation in the Environment. Edited by **A. M. Ure, C. M. Davidson.** Chapman & Hall, London, **1994.** 381 pp., hardcover, £ 79.00.—ISBN 0-7514-0021-1

Physical Chemistry of Macromolecules. Basic Principles and Issues. By **S. F. Sun.** Wiley, Chichester, Great Britain, **1994.** 453 pp., hardcover, £ 54.00.–ISBN 0-471-59788-0

Monoterpenoid Indole Alkaloids. Supplem. to Vol. 25, Part 4. By **J. E. Saxton.** Wiley, Chichester, Great Britain, **1994.** 860 pp., hardcover, £ 175.00.—ISBN 0-471-95112-9

PCR im medizinischen und biologischen Labor. Handbuch für den Praktiker. Edited by **M. Wink, H. Wehrle.** GIT Verlag, Darmstadt, **1994.** 237 pp., paperback, DM 64.00.—ISBN 3-928865-13-7

Analysis of Addictive and Misused Drugs. Edited by **J. A. Adamovics.** Marcel Dekker, New York, **1995.** 800 pp., hardcover, $ 195.00.—ISBN 0-8247-9238-6

Maillard Reactions in Chemistry, Food, and Health. Edited by **T. P. Labuza, G. A. Reieccius et al.** The Royal Society of Chemistry, Cambridge, **1994.** 440 pp., hardcover, £ 67.50.—ISBN 0-85186-802-9

Rheology. Principles, Measurements, and Applications. By **C. W. Macosko.** VCH, Weinheim, New York, **1994.** 533 pp., hardcover, $ 95.00.—ISBN 1-56081-579-5

Analytical Electrochemistry. By **J. Wang.** VCH, Weinheim, New York **1994.** 193 pp., hardcover, $ 59.95.—ISBN 1-56081-575-2

Electronic Processing in Catalysis. A Quantum Chemical Approach to Catalysis. By **S. Yoshida, S. Sakaki, H. Kobayashi.** VCH, Weinheim/ Kodansha, Tokyo, **1994.** 275 pp., hardcover, DM 168.00.—ISBN 3-527-29265-9 (VCH), 4-06-206499-5 (Kodansha)

Statistische Mechanik. Konzept der Theoretischen Physik. By **H. Römer, T. Filk.** VCH, Weinheim, **1994.** 280 pp., paperback, DM 58.00.—ISBN 3-527-29228-4

Luminescent Materials. By **G. Blasse, B. C. Grabmaier.** Springer, Heidelberg, **1994.** 232 pp., paperback, DM 78.00.—ISBN 3-540-58019-0

Advances in Polymer Science. Vol. 117. Edited by **A. Abe, H. Benoit, et al.** Springer, Heidelberg, **1994.** 337 pp., hardcover, DM 248.00.– ISBN 3-540-58238-8

Advances in Polymer Science. Vol. 118. Edited by **A. Abe, H. Benoit, et al.** Springer, Heidelberg, **1994.** 240 pp., hardcover, DM 208.00.– –ISBN 3-540-58340-8

Organische Chemie. By **H. R. Christen, F. Vögtle.** Salle/Sauerländer, Frankfurt, **1994.** 470 pp., hardcover, DM 148.00.—ISBN 3-425-05498-8

Wasser und Wasseruntersuchung. A6. By **L. A. Hütter.** Salle/Sauerländer, Frankfurt, **1994.** 528 pp., paperback, DM 79.80.– ISBN 3-7935-5075-3

Molecular and Biomolecular Electronics. (Advances in Chemistry Series No. 240). Edited by **R. R. Birge.** American Chemical Society, Washington, **1994.** 608 pp., hardcover, $ 139.95.—ISBN 0-8412-2698-9

Formulation and Delivery of Proteins and Peptides. (ACS Symposium Series No. 567). Edited by **J. L. Cleland, R. Langer.** American Chemical Society, Washington, **1994.** 376 pp., hardcover, $ 89.95.– –ISBN 0-8412-2959-7

Environmental Epidemiology. Effects of Environmental Chemicals on Human Health. (Advances in Chemistry Series No. 241). Edited by **W. M. Draper.** American Chemical Society, Washington, **1994.** 272 pp., hardcover/paperback, $79.95/49.95.–ISBN 0-8412-2517-6/0-8412-2933-3

Isopentenoids and Other Natural Products. Evolution and Function. (ACS Symposium Series No. 562). Edited by **W. D. Nes.** American Chemical Society, Washington, **1994.** 257 pp., hardcover, $ 69.95.– ISBN 0-8412-2934-1

Analytical Supercritical Fluid Extraction. Edited by **M. D. Luque de Castro et al.** Springer, Heidelberg, **1994.** 319 pp., hardcover, DM 148.00.– –ISBN 3-540-57495-6

NMR - Konzepte und Methoden. By **E. Krahe.** Springer, Heidelberg, **1994.** 245 pp., paperback, DM 48.00.— ISBN 3-540-58204-5

Modern Electroorganic Chemistry. By **D. Kyriacou.** Springer, Heidelberg, **1994.** 228 pp., hardcover, DM 98.00.—ISBN 3-540-57504-9

Advanced Computer-Assisted Techniques in Drug Discovery. Edited by **H. van de Waterbeemd.** VCH, Weinheim/New York, **1994.** 343 pp., hardcover, DM 168.00/ $ 100.00.—ISBN 3-527-29248-9

Ökotoxikologie von Pflanzenschutzmitteln. Edited by **Deutsche Forschungsgemeinschaft.** VCH, Weinheim, **1994.** 414 pp., paperback, DM 88.00.—ISBN 3-527-27565-7

Dictionary of Cytokines. By **H. Ibelgaufts.** VCH, Weinheim/New York. **1995.** 778 pp., hardcover, DM 184.00/ $ 110.00.– ISBN 3-527-30042-2

Detergents and Cleaners. A Handbook for Formulators. Edited by **K. R. Lange.** C. Hanser Verlag, München, **1994.** 296 pp., hardcover, DM 118.00.— ISBN 3-446-17307-2

Carbon Dioxide Chemistry: Environmental Issues. Edited by **J. Paul, C.-M. Pradier.** The Royal Society of Chemistry, Cambridge, **1994.** 405 pp., hardcover, £ 62.50.—ISBN 0-85186-634-4

The Chemistry of Organic Arsenic, Antimony and Bismuth Compounds. Edited by **S. Patai.** Wiley, Chichester, **1994.** 962 pp., hardcover, £ 250.00.–ISBN 0-471-93044-X

Chemie der Atmosphäre. Bedeutung für Klima und Umwelt. By **T. E. Graedel, P. J. Crutzen.** Spektrum Akademischer Verlag, Heidelberg. **1994.** 511 pp., hardcover, DM 78.00.—ISBN 3-86025-204-6

Solid State Electrochemistry. Edited by **P. G. Bruce.** Cambridge University Press, Cambridge, **1994.** 344 pp., hardcover, £ 60.00.—ISBN 0-521-40007-4

Heterocyclic Chemistry. 3rd Edition. By **J. A. Joule, K. Mills, G. F. Smith.** Chapman & Hall, London, **1994.** 516 pp., paperback, £ 19.99.–ISBN 0-412-41340-X

Kurze Einführung in die Chemie der Heterocyclen. By **K. Krohn, U. Wolf.** Teubner, Stuttgart, **1994.** 132 pp., paperback, DM 24.80.– ISBN 3-519-03532-4

PCR. Grundlagen und Anwendungen der Polymerase-Kettenreaktion. Edited by **H. G. Gassen, G. E. Sachse, A. Schulte.** G. Fischer Verlag, Stuttgart, **1994.** 123 pp., ring-bound, DM 38.00.—ISBN 3-437-20509-9

Catalysis of Organic Reactions. Edited by **M. G. Scaros, M. L. Prunier.** Marcel Dekker, New York, **1994.** 624 pp., hardcover, $ 195.00.–ISBN 0-8247-9364-1

Solid-State NMR III. Organic Matter. NMR Basic Principles and Progress, Vol. 32. Edited by **P. Diehl, E. Fluck, H. Günther, R. Kosfeld, J. Seelig.** Springer-Verlag, Heidelberg, **1994.** 213 pp., hardcover, DM 198.00.–ISBN 3-540-57399-2

Solid-State NMR IV. Methods and Applications of Solid-State NMR. NMR Basic Principles and Progress, Vol. 33. Edited by **P. Diehl, E. Fluck, H. Günther.** Springer-Verlag, Heidelberg, **1994.** 202 pp., hardcover, DM 198.00.–ISBN 3-540-58212-6

Vitamin B_{12}: How the Problem of Its Biosynthesis Was Solved

Francis Blanche, Beatrice Cameron, Joel Crouzet, Laurent Debussche, Denis Thibaut, Marc Vuilhorgne, Finian J. Leeper, and Alan R. Battersby*

Vitamin B_{12} is an essential vitamin for human health, and lack of it leads to pernicious anemia. This biological activity has attracted intense interest for some time; in addition, the complex architecture of the B_{12} molecule has fascinated chemists and biochemists since its discovery as the first natural organocobalt complex and the establishment of its structure by X-ray analysis. The organic ligand surrounding the cobalt displays many stereogenic centers along its periphery carrying reactive functional groups. This complexity led vitamin B_{12} to be rightly regarded as an extreme challenge to the synthetic chemist. Yet microorganisms achieve this synthesis in vivo with complete control of regio- and stereochemistry. How do they do it? This review tells the full remarkable story. Success in unraveling this biosynthetic puzzle resulted from a collaborative effort by biologists and chemists using the full range of methods available from their disciplines—from genetics at one end of the spectrum to synthesis and NMR spectroscopy at the other. This work can act as a guide for future research on the biosynthesis of yet more complex natural substances.

Keywords: bioorganic chemistry · biosynthesis · vitamin B_{12}

1. Introduction

1993 marked the end of an era for research on the biosynthesis of vitamin B_{12}, an essential vitamin that prevents pernicious anemia. Experiments carried out during roughly the previous 25 years had, by 1993, uncovered the complete pathway by which this remarkable cobalt-containing molecule is constructed in microorganisms. This is exciting because the problem of vitamin B_{12} biosynthesis had posed what is surely the greatest challenge in the biosynthetic arena. So much so, that it was known as the Mount Everest of biosynthetic problems. This mountain has now been climbed, fittingly on the 40th anniversary of Hillary and Tenzing's conquest of Everest itself. Progress up the mountain during the past 25 years initially showed steady progress during which critically important advances were made and solid bases were established. This phase was followed by a spectacular surge to the top during the past 10 years and especially during the last five.

The time is therefore ripe to write a review that sets a flag on the summit. Our aim is to relate how the latest surge was made by what was largely a European effort and to convey the excitement of a scientific chase full of surprises. We will emphasize at appropriate points in our account what in retrospect can be seen as the decisively important choices, techniques, and experimental approaches. Undoubtedly, the key choice was of the right B_{12}-producing organism for the experiments, and it will become clear why the one selected, *Pseudomonas denitrificans*, could not have been bettered. The decision to add the power of genetics and molecular biology to the array of approaches previously used for biosynthetic research was also of immense importance. But we must avoid giving the impression, which occasionally has currency, that when once the molecular biology is worked out, the rest is easy; far from it, as the reader will see. Huge difficulties still remained to be overcome at that stage, and the way through the maze depended heavily on the chromatographic techniques developed for the purification of proteins and water-soluble intermediates.

More details will be given of each of these key elements as the article unfolds, but the reader must be made aware at the outset of the scale of the B_{12} problem and what a broad sweep of interdisciplinary science was needed to solve it. That sweep extended from genetics and molecular biology, through protein chemistry and enzymology, and on to organic synthesis including radioactive and stable isotopic labeling with NMR spectroscopy as a marvellous final tool.

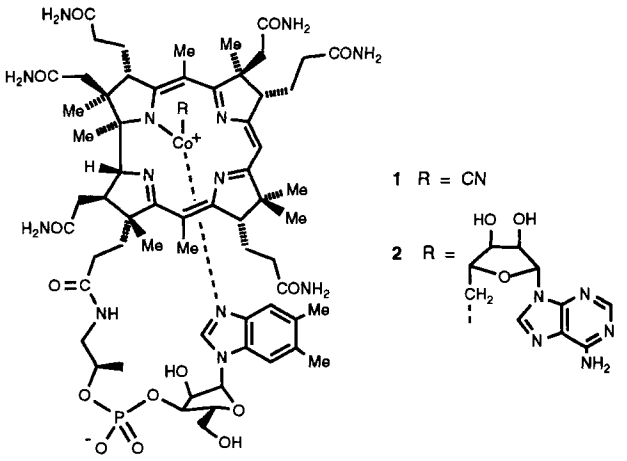
Before going further, it should be made clear that the B_{12} system, cyanocobalamin (**1**), is the form in which the vitamin is isolated for medicinal and commercial use; **1** and close derivatives with varying R groups are often called cobalamins. The

[*] Prof. Sir Alan Battersby, Dr. F. J. Leeper
University Chemical Laboratory
Lensfield Road, Cambridge CB2 1EW (UK)
Telefax: Int. code + (223)336362

F. Blanche, Dr. L. Debussche, D. Thibaut, Dr. M. Vuilhorgne (Département Analyse)

B. Cameron, Dr. J. Crouzet (Département des Biotechnologies)
Centre de Recherche de Vitry-Alfortville
Rhône-Poulenc Rorer S. A.
F-94403 Vitry-sur-Seine (France)

 © *VCH Verlagsgesellschaft mbH, D-69451 Weinheim, 1995* *0570-0833/95/0404-0383 $ 10.00+.25/0*



most important biologically active species is the coenzyme form, adenosylcobalamin (**2**) having an adenosyl residue in place of the cyano group of vitamin B_{12}. We will discuss later when and how this residue is added.

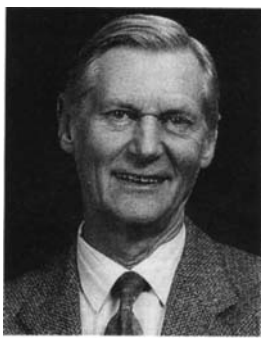
2. Laying the Foundations and Discovery of the First Three Unique B_{12} Intermediates

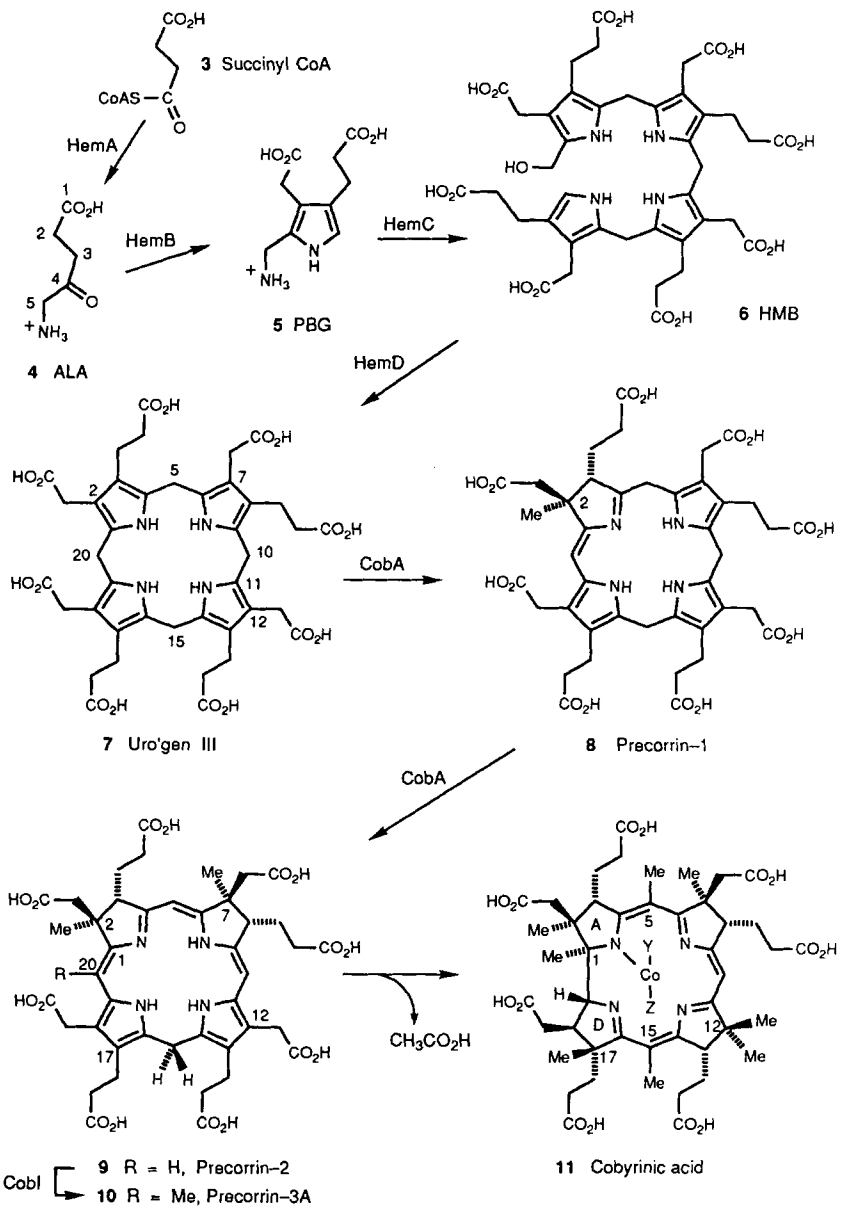
Vitamin B_{12} (**1**) belongs to a family of structurally related and biologically important pigments that also includes heme, the oxygen-carrying center of hemoglobin, and chlorophyll, which is responsible for photosynthesis. The biosynthetic pathway to all these "pigments of life" initially follows the same track starting from 5-aminolevulinic acid (ALA, **4**; Scheme 1) which, for *Pseudomonas*, is biosynthesized from succinyl CoA (**3**) and glycine[1] (as for animals, yeasts, and photosynthetic bacteria), whilst in plants and some other bacteria the starting material is glutamic acid. Two molecules of **4** are first condensed together to yield porphobilinogen (PBG, **5**), and then four molecules of PBG **5** are joined head-to-tail without rearrangement by the enzyme deaminase leading to hydroxymethylbilane (HMB, **6**).[2] Subsequently a fascinating ring closure and rearrangement process[2] catalyzed by cosynthetase generates uroporphyrinogen III (uro'gen III, **7**). This macrocycle is structurally modified in living systems to build heme and chlorophyll by a series of enzymic steps starting with decarboxylations and oxidation. This does not happen for B_{12} **1**; its pathway branches away from the others at uro'gen III **7**. In experiments with the bacterium *Propionibacterium shermanii* it was discovered that the diversion is initiated by C-methylation of **7** by methyl transfer from *S*-adenosylmethionine (SAM). These studies produced a rich harvest of biosynthetic information, but only those findings essential to understanding the main story of our article will be briefly given here. All the other results from this work are described in several reviews[3] which give complete literature references for this phase of the research.

Normally *Pr. shermanii* is grown on a medium containing cobalt. The cells can be disrupted to release a preparation of soluble proteins, which, together with the necessary cofactors, can be used to biosynthesize cobyrinic acid (**11**) from simpler precursors such as PBG **5** (Scheme 1). Notice the direct connection of ring A to ring D in **11**, a characteristic feature of the corrin ring system. Cobyrinic acid (**11**) is a late biosynthetic precursor of B_{12} **1** in *Pr. shermanii*, and it contains the fully constructed corrin macrocycle present in B_{12}. Presumably the biosynthesis does not go further in the broken-cell enzyme system, because the enzyme necessary for the next step beyond cobyrinic acid en route to B_{12} **1** is destroyed or lost from the soluble protein preparation or lacks its cofactor. It may be significant that the enzyme(s) responsible for the later amidations of carboxyl groups are reported to be unstable; also these enzymes in *Pr. shermanii* are known to transfer NH_2 from the amide group of glutamine.[4]

The discovery that the B_{12} biosynthetic pathway is diverted away from that for heme by C-methylation of uro'gen III **7** depended on an experiment that asked the question "What happens when *Pr. shermanii* cells are grown with strict exclusion of cobalt?" The striking answer was that now the cells did not biosynthesize cobyrinic acid (**11**), but three new substances appeared instead, which could be isolated either at their original oxidation level or as aromatic derivatives (by aerial dehydrogenation). A major effort was needed to establish the structures of all these compounds, and the findings allowed the next three intermediates beyond **7** to be set in place. Thus, uro'gen III **7** undergoes methylation first at C-2 to form precorrin-1[5] (**8**;

Alan R. Battersby is Emeritus Professor at the University of Cambridge (UK). He was born in 1925 in England and gained BSc and MSc degrees from the University of Manchester, a PhD from St. Andrews, and DSc and ScD degrees from Bristol and Cambridge, respectively. He has received many awards including the Karrer Medal (Switzerland), the Royal Medal (UK), the Roger Adams Medal (USA), the August-Wilhelm-von-Hofmann-Denkmünze (FRG), and the Wolf Prize (Israel). His interests are in the chemistry of living systems (especially vitamin B_{12} biosynthesis), music, camping, and fly fishing. – Dr. F. J. Leeper is a Lecturer at the University of Cambridge and Fellow of Emmanuel College; he has been a partner in the work on B_{12} since 1982. The research on vitamin B_{12} biosynthesis during the last ten years at the Rhone-Poulenc Rorer company has involved three groups. The group in biochemistry, led by Francis Blanche, with Laurent Debussche and Denis Thibaut, focuses on enzymology and purification of biosynthetic intermediates; Joel Crouzet, in collaboration with Beatrice Cameron, heads a group cloning bacterial targets and biosynthetic genes; Marc Vuilhorgne is in charge of structural analysis.





Scheme 1. Biosynthetic pathway from succinyl CoA (**3**) to precorrin-3A (**10**).

Scheme 1), which is further methylated at C-7 by the same methylase enzyme to form precorrin-2 (**9**). Then a second methylase introduces a third methyl group, and it was the first surprise of many to follow that the methylation site was C-20, leading to precorrin-3A (**10**). Importantly, precorrin-3A (**10**) was proved by unambiguous labeling experiments to be converted into cobyrinic acid (**11**) when it was incubated with the complete enzyme system prepared from normal *Pr. shermanii* cells grown on a cobalt-containing medium. So it is clear that exclusion of cobalt from growing *Pr. shermanii* cells interrupts the biosynthesis at precorrin-3A (**10**). A reasonable explanation is that in this organism, insertion of cobalt into the macrocycle occurs at or close to this stage. This hypothesis has been supported by recent studies based in one case on incorporation experiments with cobalt complexes of the aromatized derivatives of **9** and **10**,[6] and in the other by a novel application of triple isotopic pulse labeling (^{13}C, ^{14}C, ^{60}Co) using normal *Pr. shermanii* cells.[7]

Little is known at present about the enzymes of the B_{12} pathway in *Pr. shermanii*. Surely this will change over the coming years, for at present no enzyme has been purified and only the first methylase described above has even been enriched[8] (50-fold). More is known about the relevant enzymes in *Ps. denitrificans*, the organism on which we will focus in this review; for example, the two corresponding methylases responsible for converting uro'gen III **7** into precorrin-3A (**10**) are well characterized (see Section 11, Table 2).

Comparison of the structure of precorrin-3A (**10**) with that of cobyrinic acid (**11**) shows that, in addition to cobalt insertion, many more biosynthetic steps are needed before cobyrinic acid (**11**) is reached including a) ring contraction, b) more C-methylations, c) decarboxylation of the C-12 acetate residue, and d) possible redox changes. Before the final "surge to the summit," important knowledge had been gained concerning steps a) and b). Multiple labeling experiments on a microscale proved that C-20 and its attached methyl group are extruded as acetic acid (step a). For step b) the foregoing technique of pulse-labeling had been used earlier to find out the order of attachment of the additional five methyl groups needed to generate cobyrinic acid (**11**). The method was first developed to establish that the fourth methyl group is placed at C-17, and extension of the approach proved that the α methyl group at C-12 of **11** is the fifth one followed by that at C-1. Those at C-5 and C-15 were shown certainly to be the last ones added with roughly similar timing.

The reader now has a bird's-eye view of the start of the B_{12} biosynthetic pathway from succinyl CoA (**3**), available from primary metabolism, via ALA **4**, and running through to precorrin-3A (**10**) with every intermediate set in place (Scheme 1). Then there is a huge gap before cobyrinic acid (**11**) is reached. But acetic acid is extruded at some stage between **10** and **11**, and also the order of the last five methylations is established (17, 12α, 1, 5/15).

Naturally, great efforts were made over many years to isolate new intermediates from *Pr. shermanii* cells that follow precorrin-3A (**10**), but to no avail. Looking back from our present vantage point, one can see that *Pr. shermanii* was not the best organism for these studies, since the stages beyond precorrin-3A (**10**) involve cobalt complexes, and these may well be difficult to handle. A new way through the blockage was needed, and happily this came from research on a different organism, the aerobic bacterium *Pseudomonas denitrificans*. Fortunately, the strain SC510,[9] which is closely related to the strain used industrially and a high B_{12} producer, could be used. The productivity of this strain had been significantly improved relative to that of the

starting strain (MB580) by numerous chemical and physical steps of mutagenesis.[9] High production of vitamin B_{12} implies a high level of the relevant enzymic activities, obviously a great advantage for work on the isolation and characterization of the enzymes as well as for related biosynthetic studies. These enzymic levels are normally quite low in wild-type strains, resulting in production at best of only a few tens of milligrams of the vitamin per liter of culture. This switch to *Ps. denitrificans* with addition of the power of genetics and molecular biology proved decisive in moving the research forward again in a way beyond all our expectations.

3. Laying the Biological Foundations: Cloning of the *cob* Genes of *Ps. denitrificans*

3.1. Isolation of the Cob Mutants

When this work was initiated, no gene nor even a mutant deficient in cobalamin synthesis (a Cob mutant) in any bacterium had ever been isolated. Since, in addition, no enzyme of the pathway had been purified to homogeneity, no sequence data nor antibodies to any of the proteins were available. Therefore the plan was to clone the *cob* genes[10] by isolating mutants and performing genetic complementation. The biosynthetic pathway to vitamin B_{12} requires a large number of different enzymatic steps, and so the isolation of a very large number of mutants blocked in cobalamin synthesis was necessary to increase the likelihood that mutants deficient in most of the steps would be obtained. Two approaches were used to isolate Cob mutants[10] in *Pseudomonas putida* and *Agrobacterium tumefaciens*, both gram-negative bacteria that produce cobalamin under aerobic growth conditions.[9]

In *A. tumefaciens* the mutants were mostly obtained by chemical mutagenesis with *N*-methyl-*N'*-nitro-*N*-nitrosoguanidine. More than 22000 single colonies were analyzed individually for cobalamin synthesis by a microbiological assay.[9] This yielded 148 Cob mutants with reduced levels of cobalamin synthesis. In *Ps. putida* mutants were obtained by transposon Tn*5* mutagenesis. Transposon Tn*5* is a 5.7 kilobase (kb) segment of bacterial DNA that can insert with high frequency into the bacterial chromosome and contains a gene imparting resistance to the aminoglycoside antibiotic kanamycin. When the transposon is introduced into a recipient bacterium on a plasmid that is not maintained when the bacterium replicates, only those cells in which the transposon has inserted into the chromosome can survive in the presence of kanamycin. Selection of such kanamycin-resistant clones gives a series of mutants that carry a single copy of Tn*5* randomly inserted into the genome.[11] In this case, Cob mutants were identified as being those colonies unable to use ethanolamine as a source of nitrogen in the absence of added cobalamin. This selection depends on the fact that deamination of ethanolamine by ethanolamine ammonia-lyase requires coenzyme B_{12} as a cofactor. From 6400 mutant colonies, 26 were found to be unable to grow on the ethanolamine medium and were classed as Cob mutants.

3.2. Cloning 78 kb of DNA from *Ps. denitrificans* Carrying the *cob* Genes

The next step was to clone the *Ps. denitrificans cob* genes that "complemented" the foregoing mutations (i.e. they were able to restore cobalamin biosynthesis in the Cob mutants). For this purpose, a genomic library of the rifampin-resistant *Ps. denitrificans* strain SC510 Rif^r was constructed in *E. coli* on a plasmid (pXL59) which was capable of being transferred (or mobilized) into a wide range of other bacteria (including *Ps. denitrificans*) through a natural phenomenon called conjugation. This library consisted of approximately 3600 separate strains of *E. coli*, each with a plasmid carrying a different DNA insert from the *Ps. denitrificans* genome, with an average size of 13 kb. This library of plasmids should, statistically, represent more than 99% of the *Ps. denitrificans* genome.

This plasmid library was then mobilized in turn into each of Cob mutants prepared above. For each mutant, the 3600 different clones were assayed for their production of cobalamin by selecting colonies able to grow on the ethanolamine-containing medium or by looking directly for clones producing cobalamin at a level close to that of the parent strain. In such clones, the mutation was said to be complemented by the plasmid it harbored. Such a plasmid was therefore carrying at least one *Ps. denitrificans cob* gene responsible for the correction of the genetic defect of the mutant. In this way, 11 plasmids from the library were found to complement most of the mutants (17 out of 26 mutants in *Ps. putida* and 134 out of 148 mutants in *A. tumefaciens*). The inserts of the 11 plasmids were from four different genomic loci, referred to as complementation groups A to D, and they represent between them 78 kb of DNA. The loci are at least 10 kb apart, indicating that the genes are, to some extent, scattered over the chromosome of *Ps. denitrificans*.[12]

Smaller DNA fragments from this 78 kb of DNA were subcloned on the same mobilizable plasmid. By comparing which mutants each recombinant plasmid was able to complement, at least 14 different *cob* genes were identified within the 78 kb.

3.3. Genetic Analysis and Nucleotide Sequence Determination of the *cob* Genes

A genetic analysis was performed in order to identify all the genes carried by the cloned 78 kb of DNA. In essence, Tn5 transposon mutagenesis was used again to introduce further mutations into most parts of the 78 kb. This analysis revealed the presence of six more *cob* genes.[13–17] Altogether 22 *cob* genes were found and were named *cobA* to *cobQ* and *cobS* to *cobW*. Then the nucleotide sequence was determined for 35.9 kb out of the cloned 78 kb of DNA, including all 22 genes. In addition to the *cob* genes, eight other open reading frames (stretches of DNA that appear to code for proteins) were also found in the sequenced DNA. The organization of the genes in the four clusters (or complementation groups) is shown in Figure 1.

From the nucleotide sequence, the amino acid sequences of the Cob proteins could be predicted. This has proved extremely valuable since almost all the *Ps. denitrificans* genes required for

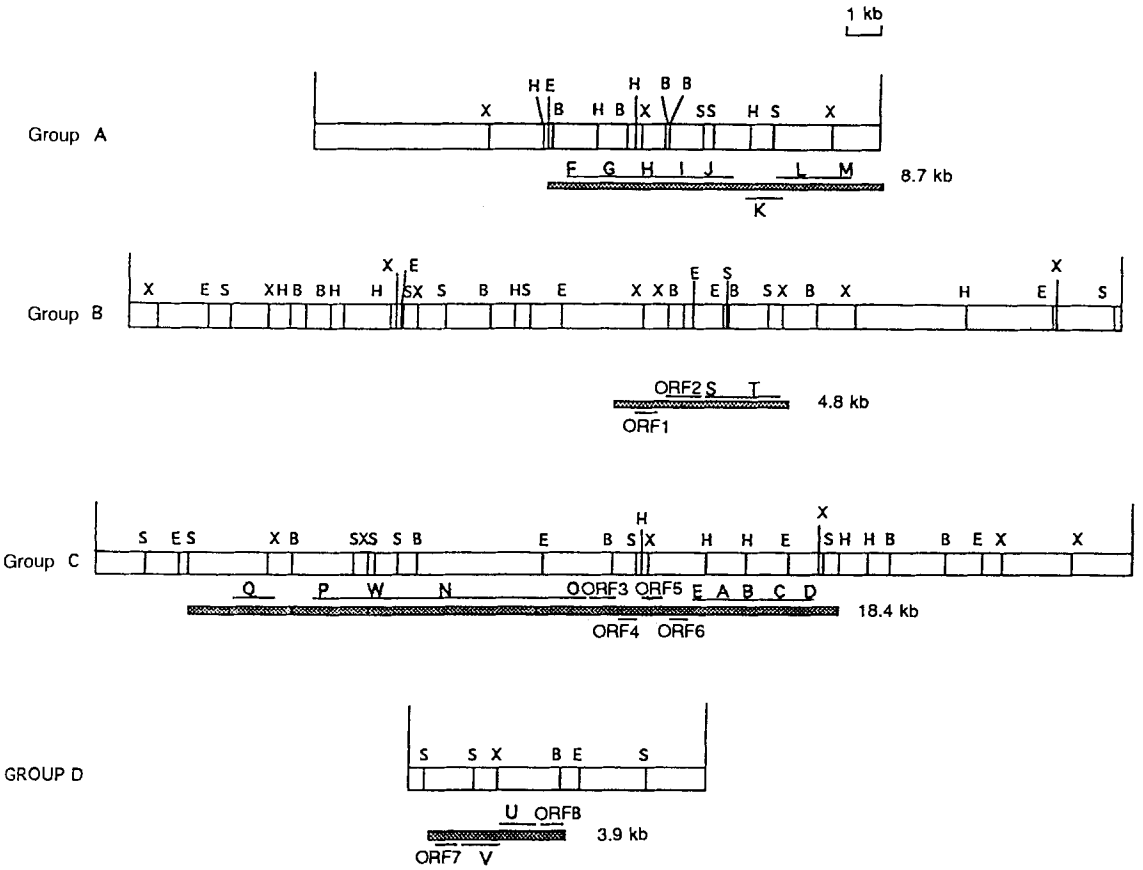


Fig. 1. Restriction map of the four complementation groups from *Ps. denitrificans*. Locations of the *cob* genes are shown by the corresponding letters below the DNA strand; open reading frames (ORFs) of unknown function are also shown. Sequenced fragments are indicated by hatched lines. A line above the hatched line indicates that the coding strand goes 5′ 3′ from left to right. Enzymes: B, *Bam* H1; E, *Eco* R1; H, *Hind* III; S, *Sst* 1; X, *Xho* 1.

coenzyme B_{12} synthesis were present among the 22 *cob* genes. Furthermore, the amino acid sequences of the Cob proteins could be compared with sequences in protein databases, and this allowed important deductions to be made about the probable functions of some proteins, particularly the methyltransferases. In addition, the *hemA* gene from *Ps. denitrificans*, encoding 5-aminolevulinic acid synthase, was also cloned and sequenced.[18] This gene was found not to be linked with any of the four complementation groups found for the *cob* genes.[12]

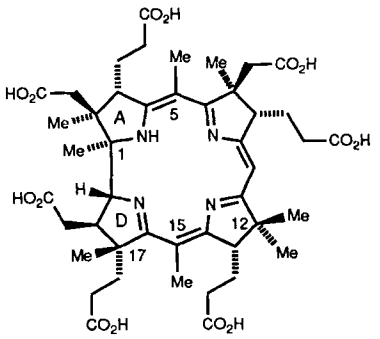
The foregoing work on gene cloning was of great importance for parallel research in enzymology and structural chemistry. The results from these two areas then provided positive feedback for the molecular biology. Thus, for many of the mutant strains, identification of the intermediate accumulated allowed the blocked step to be located and correlated with the gene that complemented the mutation.[13–16] Details of the mutants that accumulated the later, known intermediates on the B_{12} pathway are given in Table 1 towards the end of this review. Also, by inserting a particular gene into a multicopy plasmid, then production of the corresponding protein is enhanced, which greatly helps the enzymatic and chemical research. It would be invidious in an interdisciplinary effort to pick out any area as the most important, but the contribution from genetics and molecular biology was huge.

4. The Surge to the Summit

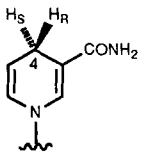
4.1. Isolation of Precorrin-6A and Proof of Its Surprising Structure

"Great oaks from little acorns grow." It was the crucial observation of a yellow fluorescence that corresponds to the acorn, and the whole story in the remaining part of this review is what grew from it. Cells of one recombinant strain of *Ps. denitrificans* [SC510(pXL253)], in which eight of the foregoing *cob* genes (*F*, *G*, *H*, *I*, *J*, *K*, *L*, and *M*) had been amplified, exhibited a strong yellow fluorescence under ultraviolet light. Fortunately, the substance responsible had recently been isolated and identified from *Ps. denitrificans* SC510 Rif^r;[19] it was hydrogenobyrinic acid (**12**), the cobalt-free analogue of cobyrinic acid (**11**). This was quite unexpected because although amidated derivatives of hydrogenobyrinic acid (**12**) had been found previously,[20] the parent had never been isolated and was thought not to occur in nature.[21] We will describe later how the intermediacy of hydrogenobyrinic acid (**12**) for the biosynthesis of vitamin B_{12} in *Ps. denitrificans* was clearly established. So this strain, producing considerable amounts of a late corrinoid precursor of vitamin B_{12}, was the ideal vehicle for biosynthetic experiments. A major effort then led to the development of a cell-free enzyme system from this strain which efficiently converted precorrin-3A (**10**)[22] through all the many steps into hydrogenobyrinic acid

(**12**). The latter could be detected on a minute scale by high-pressure liquid chromatography (HPLC)[23] with a fluorescence detector. The way was then open to a) optimize the incubation conditions and b) determine which cofactors are required for the conversion of precorrin-3A (**10**) into hydrogenobyrinic acid (**12**). It turned out that in addition to SAM, reduced nicotinamide adenine dinucleotide phosphate (NADPH) (**13** shows the relevant partial structure) was essential for this conversion.



12 Hydrogenobyrinic acid

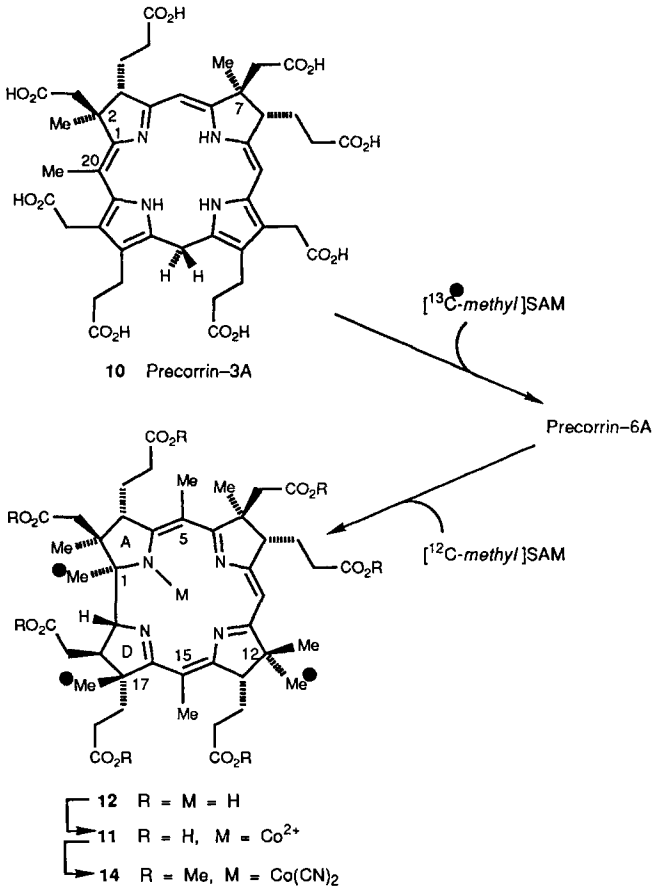


13
NADPH
partial structure

Research on vitamin B_{12} has been full of surprises, and the involvement of NADPH in the biosynthesis was one of them. Workers in the field had all thought it likely that B_{12} biosynthesis would not require external redox reagents. Thus, there was naturally intense interest in knowing what the NADPH does. To find out, the incubation was repeated with omission of NADPH; this experiment yielded a huge prize. Hydrogenobyrinic acid (**12**) was no longer produced and a new pale-yellow pigment accumulated in its place. When this new product, prepared enzymically in doubly labeled form (^3H, ^{14}C), was incubated with the above-mentioned enzyme system together with all the cofactors including NADPH, it was converted into hydrogenobyrinic acid (**12**) in high yield (50–90%) and without significant change in the ^3H:^{14}C ratio. This evidence left no doubt that after a long frustrating period, a new intermediate for B_{12} biosynthesis had at last been found.[24]

Preparation of the new product from [2,7,20-*methyl*-^{14}C]precorrin-3A **10** and [*methyl*-^{3}H]SAM established that three new methyl groups had been attached to precorrin-3A (**10**) during this conversion. Thus, the pale-yellow intermediate had been formed by hexamethylation of uro'gen III **7**, and hence it was named precorrin-6A.[5] The ^{14}C-labeling of the initial precorrin-3A (**10**) yielded another bonus in that the ^{14}C activity of precorrin-6A fitted with loss of its C-20 methyl group somewhere in the sequence leading to precorrin-6A. This result, combined with the earlier discovery with *Pr. shermanii* that ring contraction involved loss of C-20 and its attached methyl group (as acetic acid), gave strong indications that precorrin-6A was a contracted macrocycle.[24]

To which sites are the three new methyl groups attached in precorrin-6A? Initially this question was tackled indirectly by preparing precorrin-6A from unlabeled precorrin-3A (**10**) and using [*methyl*-^{13}C]SAM to label the three new methyl groups (Scheme 2). The product was then converted enzymically into hydrogenobyrinic acid (**12**), this time using unlabeled SAM. For



Scheme 2. Determining the position of the methyl groups in precorrin-6A.

analysis, **12** was transformed via cobyrinic acid (**11**) into heptamethyl cobyrinate (**14**, cobester) by nonenzymic cobalt insertion followed by esterification (Scheme 2). This approach was chosed because the ^{13}C NMR spectrum of cobester had been fully assigned.[25, 26] The ^{13}C NMR spectrum (Fig. 2) showed that the C-methyl groups appearing in cobester at C-17, C-12α,

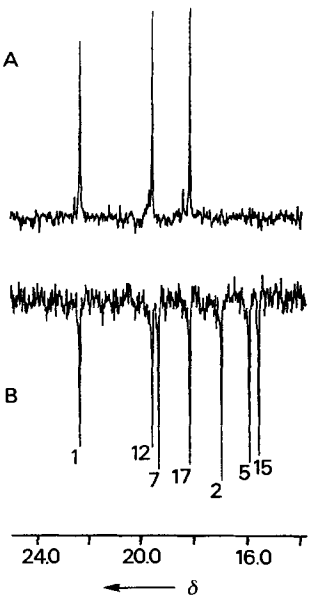
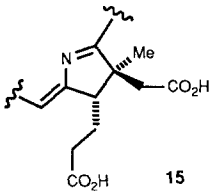


Fig. 2. Proton noise decoupled ^{13}C NMR spectrum (A) of labeled cobester (**14**) biosynthesized from precorrin-6A and (B) natural abundance ^{13}C-signals from all the C-methyl groups of unlabeled cobester (**14**).

and C-1 are present in precorrin-6A. These findings fit in well with the earlier results from pulse labeling, which showed the methyl groups at C-5 and C-15 of cobyrinic acid to be the ones added last. More recently, this has been shown to be true also for hydrogenobyrinic acid (**12**).[19]

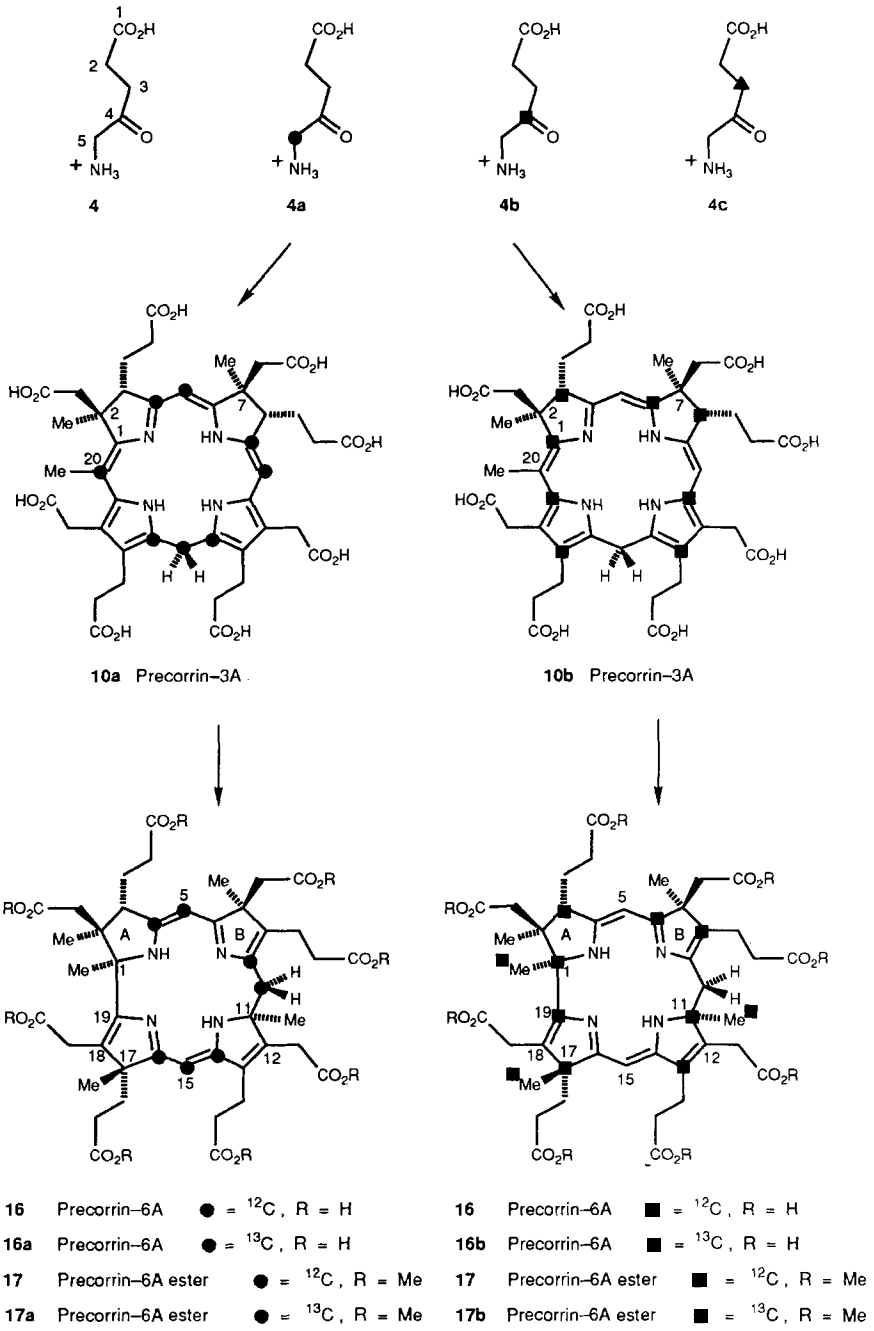
The mass spectrometric study of precorrin-6A methyl ester (molecular weight 1006) established, again surprisingly, that precorrin-6A itself is an octacarboxylic acid. So the acetate residue at C-12, which must undergo decarboxylation at some stage to generate the 12α-methyl group of hydrogenobyrinic acid (**12**), is still intact in precorrin-6A. This is odd because the decarboxylation will be blocked by methylation at C-12 (see **15**), yet it is certain that one of the C-methyl groups of precorrin-6A appears finally at C-12α in hydrogenobyrinic acid (**12**). The paradox will be resolved shortly. The final bonus from mass spectrometry was the evidence, from the molecular weight of 1006, that precorrin-6A stands at the oxidation level of a dehydrocorrin (seven double bonds) rather than a corrin (six double bonds).[24] So later reduction (by 2H) is needed to adjust the oxidation level of precorrin-6A to that of the final corrin **12**. This interlocks with the fact that precorrin-6A accumulates only in the absence of NADPH.



15

This structural information indicated unequivocally that precorrin-6A was a messenger carrying highly important information. It lay roughly at the center of that part of the pathway where nothing was known. Moreover, even the structural information gained by this stage did not fit at all with our previous speculations about what might happen in B_{12} biosynthesis. So it was with great excitement that an intensive effort was started to determine its complete structure. How could this be done? Since precorrin-6A has still not been crystallized, X-ray analysis was not an option. Also, although greatly increased amounts of precorrin-6A could be produced by using large quantities of overexpressed enzymes, these amounts were still rather small, generally in the range of 500 μg to 1 mg. But even the lower end of this range is enough to afford excellent ^{13}C NMR spectra, provided the molecule is produced in ^{13}C-labeled form; this then was the chosen approach.

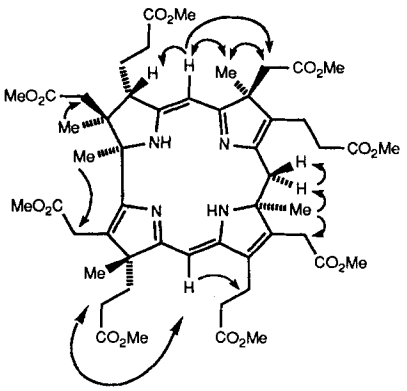
The appropriate combination of overproduced enzymes was used to convert [5-^{13}C]ALA **4a**, for example, into precorrin-3A **10a**[22] (Scheme 3). This labeling pattern follows unambiguously from rigorously established knowledge[2] of the biosynthetic steps from ALA **4** to uro'gen III **7**. The ^{13}C pattern is helpful, as the ^{13}C label at C-20 is the only one that stands alone. The set of three contiguous ^{13}C atoms around C-15 is also unique, whilst the remaining two pairs at C-4/C-5 and C-9/C-10 can be distinguished by suitable experiments. The labeled precorrin-3A **10a** was then converted into precorrin-6A **16a** by the correct set of overproduced enzymes, using unlabeled SAM, and the corresponding octamethyl ester **17a** was isolated for NMR study. Two further samples of precorrin-6A ester **17b** and **17c** (latter not illustrated) were prepared in the same way starting from [4-^{13}C]ALA **4b** and [3-^{13}C]ALA **4c**, respectively. Now



Scheme 3. ^{13}C-Labeling of precorrin-6A **16a** and **16b**.

[*methyl*-^{13}C]SAM was used as cofactor for the stages from precorrin-3A **10b** to precorrin-6A. In this way, every carbon atom of the macrocycle was ^{13}C-labeled in one or other of these three samples, as were the three C-methyl groups added during the stages after precorrin-3A.[27]

It is beyond the scope of this review to give a full account of the NMR analysis, but the key points should be highlighted to show its enormous power. The first sample, **17a**, from [5-^{13}C]ALA **4a**, showed that C-20 of precorrin-3A **10a** had been eliminated and that C-15 was an sp^2 carbon whereas C-10 was

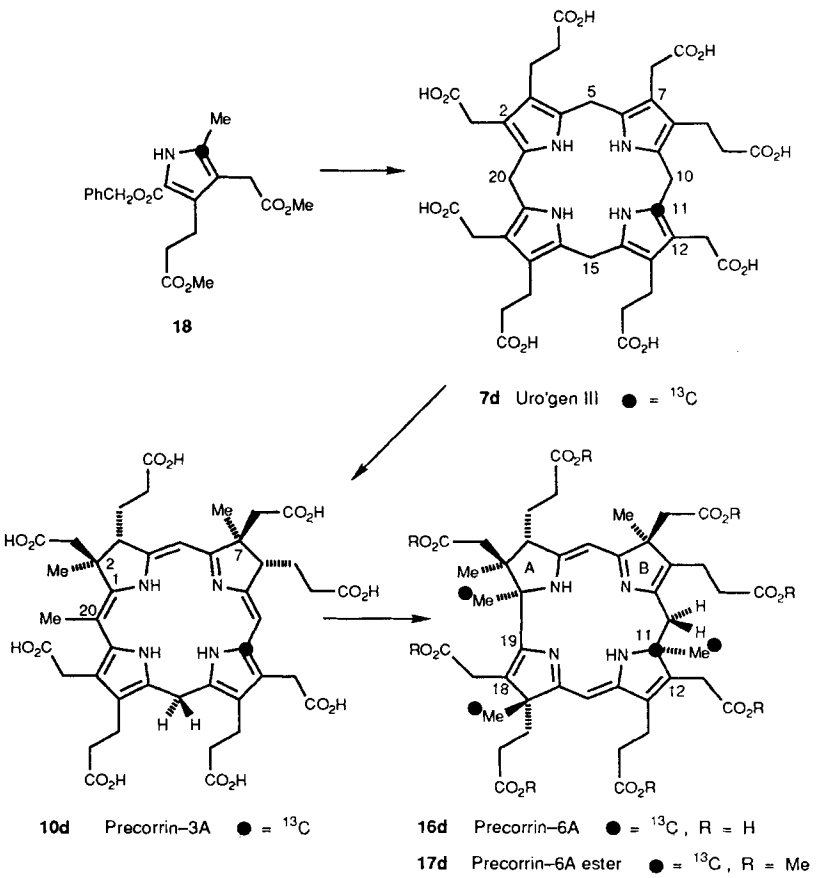


17-NOE

clearly sp^3 hybridized. However, it was the spectrum shown by precorrin-6A ester **17b** from [4-^{13}C]ALA **4b** that gave the shock. The signals from C-1 and C-19 firmly established that these atoms are directly bonded, confirming that ring contraction had occurred. Surprisingly, the three labeled methyl groups were all directly bonded to ^{13}C atoms. This was expected for the methyl groups at C-17 and C-1, but certainly not for the third one. Clearly this group could not be at C-12 (where it finally appears in hydrogenobyrinic acid (**12**)), because that is an unlabeled carbon. All the evidence pointed to methylation at the adjacent center, C-11. A separate study giving unambiguous proof will be described shortly. The spectrum of the sample of precorrin-6A from [3-^{13}C]ALA allowed further features of the illustrated structure to be set in place, as did the study of all three labeled samples **17a**, **17b**, and **17c**, for example by ^{1}H–^{13}C NMR correlation experiments to pick out ^{1}H–^{13}C couplings through up to three bonds. This approach allows a substantial region of the molecule around each ^{13}C-labeled center to be studied, and hence a connectivity pattern of ^{1}H and ^{13}C around the whole macrocycle can be established. An independent set of connections (see arrows on structure **17**-NOE) was gained by studying ^{1}H nuclear Overhauser effects by difference spectroscopy.

The sum of all this evidence led to the striking structure **17** for precorrin-6A ester and hence to structure **16** for precorrin-6A itself.[27,28] The illustrated configurations at C-2 and C-7 depend on the enzymic conversion of precorrin-6A (**16**) in high yield into hydrogenobyrinic acid (**12**), in which the configurations at these centers are beyond doubt. This direct relationship to **12** also sets the C-11 methyl group of precorrin-6A (**16**) in the α-position, because the C-11/C-12 migration of the CH_3 group will probably be suprafacial (see Section 4.4), and the 12α-methyl group of **12** is known to be derived from SAM.[3b] So surprising was this methylation of C-11 that we secured it with unimpeachable evidence (Scheme 4). This was done by unambiguous synthesis[29] of uroporphyrin III carrying a single ^{13}C label at C-11; just the starting material **18** for the synthesis is illustrated. The porphyrin was reduced to [11-^{13}C]uro'gen III **7d**, which was transformed by way of [11-^{13}C]precorrin-3A **10d** using [*methyl*-^{13}C]SAM into precorrin-6A **16d**, which was isolated as its ester **17d**. The ^{13}C NMR signal from C-11, the only label in the macrocycle, was a 38 Hz doublet, as was the signal from its attached methyl group.[29] Structure **16** for precorrin-6A was thus totally secure.

These striking discoveries changed our entire thinking about how vitamin B_{12} is biosynthesized; we had to abandon quite a number of our previously held views. The structure of precorrin-6A (**16**) revealed firstly that the ring-contraction step is not a late stage in the pathway, but has already happened at the hexamethylated stage. Secondly, the oxidation level does not stay constant throughout the biosynthesis. Since precorrin-6A (**16**) has two hydrogens less than either uro'gen III **7** or hydrogenobyrinic acid (**12**), an earlier oxidation and a later reduction step are needed. Thirdly, the 12-acetate residue is still



18 **7d** Uro'gen III ● = ^{13}C

10d Precorrin-3A ● = ^{13}C **16d** Precorrin-6A ● = ^{13}C, R = H **17d** Precorrin-6A ester ● = ^{13}C, R = Me

Scheme 4. Confirmation of methylation at C-11 of precorrin-6A **16d**.

intact, and decarboxylation of it does not have to occur before introduction of the fifth methyl group. Perhaps the most surprising realization was that the methyl group located at C-12 when the corrin macrocycle has been built is introduced initially at C-11. Notice that this C-11 methylation prevents the formation of a fully conjugated system, which accounts for the pale-yellow color of precorrin-6A (**16**).

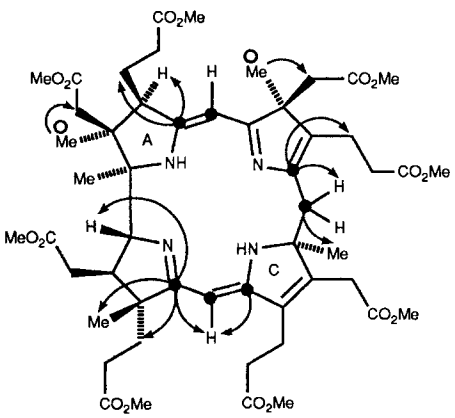
Precorrin-6A (**16**) serves as a crucial staging post on the B_{12} pathway; we can work forward from it towards B_{12} itself and also look backwards to fill in the gap between precorrin-3A (**10**) and precorrin-6A (**16**). Here we will first explore forward to complete the pathway as far as hydrogenobyrinic acid (**12**), which is how we proceeded experimentally.

4.2. Precorrin-6A Reductase and the Structure of Precorrin-6B

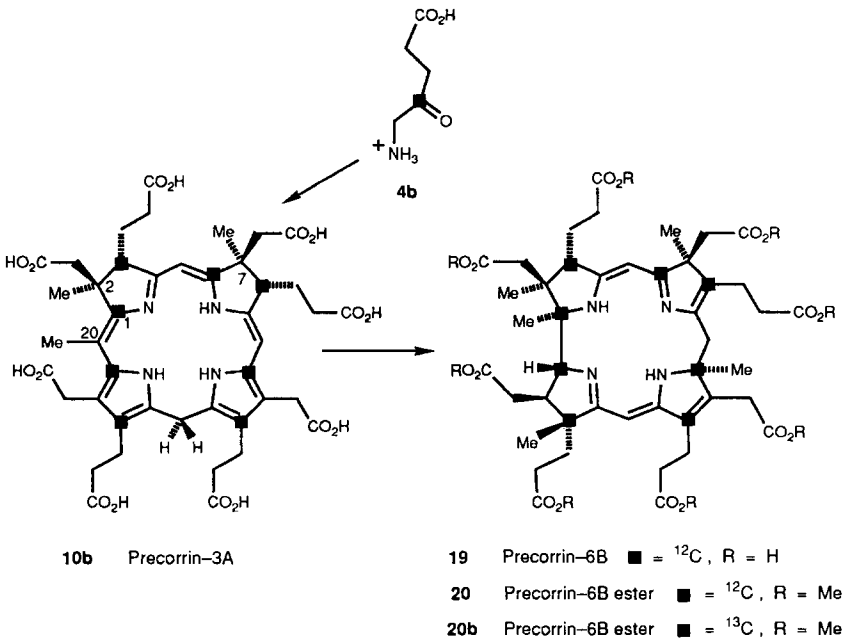
Logic tells us that since precorrin-6A (**16**) accumulated when a reduction step was blocked by exclusion of NADPH, it should be possible to isolate both the reductase enzyme and the normal reduction product, the next intermediate on the pathway. The way in which both were obtained illustrates perfectly how a complex biosynthetic sequence can be explored once the palette of the necessary enzymes is available. However, it should be remembered and emphasized that initially many proteins are known to be involved, but one does not know which enzyme does what!

The reduction product, precorrin-6B (Scheme 5), was first prepared by incubating precorrin-6A (**16**) with the complete set of overproduced enzymes encoded by the 8.7 kb fragment but *without* SAM.[30] This prevented the methylation of precorrin-6B, which, as will be seen, is involved in the next conversion step. So now precorrin-6B accumulated and could be isolated as such or, more conveniently, after esterification. The molecular weight of precorrin-6B was shown by fast-atom bombardment mass spectrometry (FAB-MS) to be 896, and the corresponding value for the methyl ester was 1008. Both values are two units higher than had been found for precorrin-6A (**16**) and its ester **17**, respectively, showing that only a single reduction step had occurred to form precorrin-6B. Moreover, the mass change from precorrin-6B to its methyl ester showed that *eight* carboxyl groups are present; in other words, decarboxylation of the 12-acetate had not occurred at this stage. The foregoing octamethyl ester turned out to be a mixture of the two C-3 epimers. Such ready formation of epimers was already a familiar feature of the chemistry[31] of many of the methylated macrocycles in Scheme 1. In this case it caused no problems, as the epimers were separable and their structures were determined[32] by the same approach developed for the work on precorrin-6A (**16**). Thus, they were biosynthesized from [4-^{13}C]ALA **4b** and, in a separate experiment, from [5-^{13}C]ALA **4a** by combining the actions of the necessary *ten* overproduced enzymes (Scheme 5). The isolated octamethyl ester of the resultant isotopomers of precorrin-6B and its epimer were then extensively studied by NMR; this phase of the work will be illustrated by just one example.

In the high-field ^{13}C NMR spectra of the labeled precorrin-6B ester **20b** and its epimer derived from [4-^{13}C]ALA **4b**, the ^{13}C signals from C-1 and C-19 stood out as being the only ones from directly coupled ^{13}C centers. The chemical shift showed C-19 to be an sp^3 carbon, whereas in precorrin-6A **16** C-19 is sp^2 hybridized. This indicated that the C-18/C-19 double bond of **16** had been reduced in precorrin-6B. As in precorrin-6A ester **17**,



C-8 is sp^2 hybridized and C-10 sp^3 hybridized. In addition, the spectra showed that the 3-*epi* isomer had been formed in slightly larger quantity (60% of total) than the normal isomer with unchanged C-3 configuration. So the former was used for ^{1}H–^{13}C long-range correlation experiments with the delay set to the optimum for couplings of 10 Hz to detect ^{13}C–^{1}H couplings through up to three bonds. This led to the connectivities illustrated by arrows for the 3-*epi*-precorrin-6B ester. The

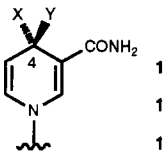


Scheme 5. ^{13}C-Labeling of precorrin-6B **20b**.

full set of results, together with those from the precorrin-6B ester **20a** (not shown) derived from [5-^{13}C]ALA **4a**, led unequivocally to structure **20** for precorrin-6B ester. It follows that precorrin-6B itself has structure[32] **19** or is a close tautomer.[28] Thus at this point on the pathway the oxidation level of precorrin-6B (**19**) has been neatly adjusted to match that of hydrogenobyrinic acid (**12**). The configuration at C-19 of **19** is assigned as illustrated, because precorrin-6B is converted in high yield into hydrogenobyrinic acid (**12**), in which the β configuration of H-19 is beyond doubt.

It was important for fuller understanding to study a) the regiospecificity and b) the stereospecificity of the foregoing reduction process. For a) the question is "To which end of the C-18/C-19 double bond does NADPH deliver the hydride equivalent?" and for b) "From which face of NADPH is it removed?" To answer the first question [4-$^2H_2$]NADPH **13a** was synthesized with 95% deuterium at C-4. It was used to reduce precorrin-6A (**16**) in combination with the greatly enriched reductase enzyme (Scheme 6). The precorrin-6B **19** thus formed was then converted into hydrogenobyrinic acid (**12**) with an enzyme system that was free from **12**. Subsequent nonenzymic insertion of cobalt yielded cobyrinic acid (**11**), which was esterified to give heptamethyl cobyrinate (cobester) **14**. The ^{1}H NMR spectrum of cobester had been fully assigned,[25, 26] and the spectrum of the biosynthetic product established that C-19 carried 25–30% deuterium. Careful study of the ^{2}H-labeled cobester by NMR spectroscopy and mass spectrometry showed that C-19 was the only deuteriated site.[33]

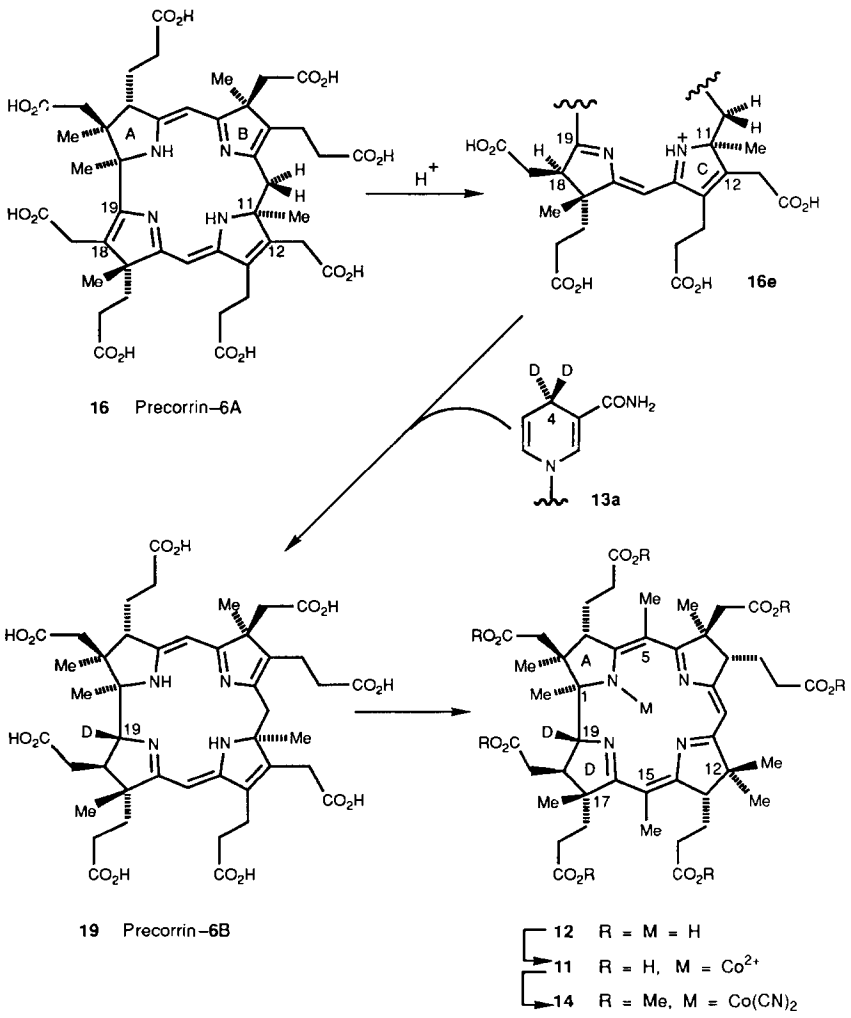
The reason for ^{2}H incorporation at C-19 being only 25–30% even though the NADPH is essentially fully deuteriated at C-4 is probably that the cofactor undergoes partial exchange of the deuterium at C-4 with the medium, a known process (via flavins?). Then the kinetic isotope effect favors transfer of ^{1}H rather than ^{2}H from the large excess of cofactor used. Nevertheless, these results establish that the reductase catalyzes hydride transfer specifically to C-19 of precorrin-6A (**16**). This makes sense mechanistically if precorrin-6A is protonated at C-18 to give **16e** (Scheme 6) before transfer of the hydride ion from NADPH.[33] The synthesis of [4*R*-^{2}H]NADPH **13b** and [4*S*-^{2}H]NADPH **13c** then allowed proof,[34] by exactly the same approach, that the reductase transfers specifically H_R of the cofactor **13**.



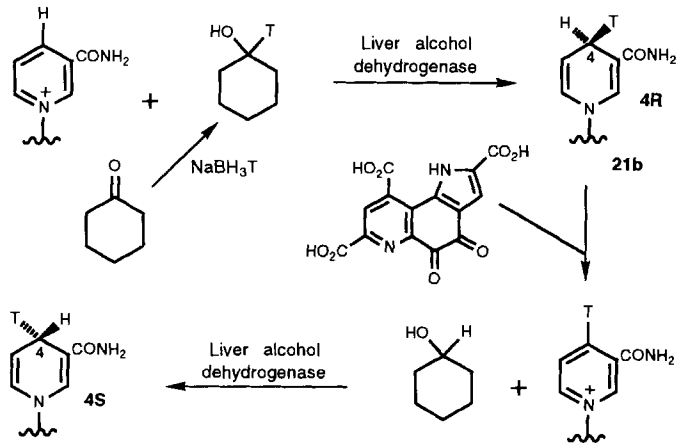
13a X = Y = ^{2}H
13b X = H, Y = ^{2}H
13c X = ^{2}H, Y = H

All these experiments proved beyond question that B_{12} biosynthesis in the aerobic *Ps. denitrificans* requires a reduction step. But does this hold true for *Pr. shermanii*, which is normally grown anaerobically or at most microaerophilically. This is a much more difficult problem, and it is helpful to outline how it was solved. The difficulties are that a) since only crude enzyme preparations are available (cf. the use of reasonably pure reductase above), exchange between the nicotinamide cofactors and the medium will be worse than in the foregoing work; b) the turnover to product will be low; and c) if reduction is indeed required in this organism, it is not known whether the cofactor is NADH or NADPH.

These problems were overcome by using the vastly greater sensitivity of tritium labeling. [4*R*-^{3}H]NADH **21b**, [4*S*-^{3}H]NADH **21c**, [4*R*-^{3}H]NADPH, and [4*S*-^{3}H]NADPH were synthesized;[35] the route to the first two compounds is outlined in Scheme 7. The last two were synthesized in a very similar way. The two 4*R* cofactors were combined in one incubation with the complete cell-free enzyme system[7, 36] prepared from *Pr. shermanii* cells with ^{14}C-labeled precorrin-2 (**9**) as the initial substrate. This cell-free system is able to carry out all the necessary biosynthetic steps to convert precorrin-2 (**9**) into cobyrinic acid (**11**). The important result was that tritium was incorporated into the cobyrinic acid (**11**) isolated from the experiment with the 4*R* cofactors but not from the parallel experiment in which the two 4*S* isomers were used. Interestingly, this is the same stereochemical selectivity found for the previous studies with *Ps. denitrificans*. Suitable degradation of the ^{3}H-labeled cobyrinic acid



Scheme 6. Proof of the site of hydride delivery in the reduction of precorrin-6A (**16**).



Scheme 7. Synthesis of [4*R*-^{3}H]NADH **21b** and [4*S*-^{3}H]NADH **21c**.

(**11**) proved that the tritium was located somewhere on rings A and D. Apart from the hydrogen atoms of methyl groups, which need not concern us, only H-18 and H-19 are introduced during the conversion of precorrin-2 (**9**) into **11**. Since H-18 is derived from the medium,[37] it follows that the tritium is at C-19.[38] Thus reduction was demonstrated to be a required step for B_{12} biosynthesis in both aerobic and anaerobic (microaerophilic) organisms.

As soon as it was clear that precorrin-6B (**19**) is the dihydro derivative of precorrin-6A (**16**), the chase was taken up to isolate the pure reductase enzyme. As always, the key was to develop a suitable assay, and here a coupled enzyme assay was used.[30] This depended on knowing that the next step beyond precorrin-6B (**19**) in the biosynthetic sequence is catalyzed by a methylase encoded by the *cobL* gene (more about this in Section 4.3). So precorrin-6B (**19**) generated by the reductase was methylated in situ by using a substantial excess of the CobL enzyme and [^{14}C-*methyl*]SAM. Since methylation can only occur after precorrin-6B (**19**) has been produced, determination of the radioactivity of the final product gave a measure of the reductase activity in the sample for assay. It was shown in this way that cell extracts from the recombinant strain in which the 8.7kb DNA fragment had been overexpressed exhibited ten times higher reductase activity than the parent strain without overexpression. The engineered strain was used for the isolation work, but even so, the amount of enzyme in the cells was surprisingly low. As a result, 14000-fold enrichment was needed to obtain precorrin-6A reductase in homogeneous state. It was shown to reduce precorrin-6A (**16**) to precorrin-6B (**19**) by an NADPH-dependent process.[30]

The N-terminal sequence of precorrin-6A reductase, together with three internal sequences obtained after tryptic digestion of the enzyme, showed that this protein is encoded by the *cobK* gene.[30] It is interesting that the *cobK* coding strand is the complementary one to that coding for the other seven *cob* genes carried by the 8.7kb DNA fragment. Also, the *cobK* coding sequence overlaps those for *cobJ* and *cobL* (Fig. 1); this arrangement may possibly control the relative level of expression of *cobK* and its neighbors. A further relationship that appears significant is that CobK shares 24.4% identity and 45% similarity with the CbiJ protein from *Salmonella typhimurium* (Table 2). The two proteins have similar molecular weights, and the regions of identity extend over their entire lengths. The CbiJ protein can therefore reasonably be considered as the homologue in *S. typhimurium* of precorrin-6A reductase in *Ps. denitrificans*. On this basis, it seems highly likely that a reduction step is required for B_{12} biosynthesis in anaerobic *S. typhimurium*.

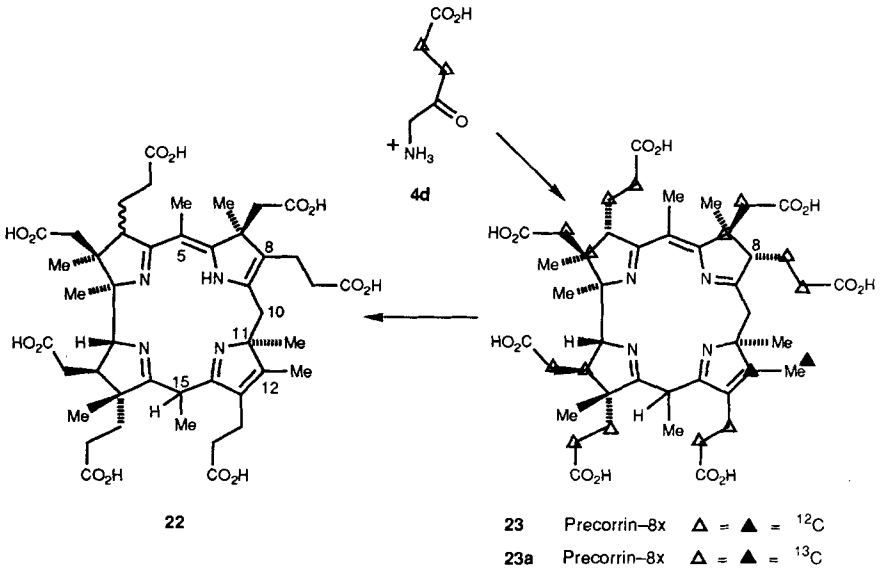
4.3. Isolation and Structure of Precorrin-8x

It is time to take stock of the changes needed for the conversion of precorrin-6B (**19**) into hydrogenobyrinic acid (**12**). They are, in unknown order at this stage, a) migration of the C-11 methyl group to C-12, b) decarboxylation of the C-12 acetate residue, and c) methylation at C-5 and C-15. The way forward was to screen the available enzymes for their ability to use precorrin-6B (**19**) as a substrate. Since it was certainly possible that methylation is involved in the next step, one study (it was the successful one) assayed for methyl transfer to precorrin-6B from [*methyl*-^{3}H]SAM. This led to the selection of the enzyme encoded by *cobL* which, after isolation on a preparative scale, smoothly converted precorrin-6B (**19**) into precorrin-8x.[39] We will return to this enzyme after describing the structural studies on precorrin-8x.[40]

A more convenient way to prepare precorrin-8x rather than by using the CobL enzyme was based on the observation that the final biosynthetic step which converts precorrin-8x into hydrogenobyrinic acid (**12**) is strongly affected by product inhibition.[39,41] Thus, ^{14}C-labeled precorrin-3A (as **10**), prepared from [4-^{14}C]ALA (as **4**), was incubated with the same collection of eight overproduced enzymes used earlier together with [*methyl*-^{3}H]SAM and a tenfold molar excess of unlabeled hydrogenobyrinic acid. Under these conditions the product was [^{3}H,^{14}C]precorrin-8x rather than labeled hydrogenobyrinic acid, and the ^{3}H:^{14}C ratio indicated that *five* methyl groups had been introduced.[42] Hence the new product is an octamethylated derivative of uro'gen III **7**, and it is therefore referred to as precorrin-8x.[40] Mass spectrometric measurements on precorrin-8x and on its methyl ester confirmed these findings and also showed that this product is an heptacarboxylic acid. Thus the remarkable conclusion was that the CobL enzyme catalyzes two very different types of reactions, decarboxylation and C-methylation. Methylation occurs presumably at C-5 and C-15, since these are the only methyl groups not in place for precorrin-6B (**19**). The doubly labeled precorrin-8x was converted very efficiently into hydrogenobyrinic acid (**12**) by incubation with the complete enzyme system, and there was no significant change in the ^{3}H:^{14}C ratio during this conversion. This is the evidence needed to establish precorrin-8x as a further new intermediate on the pathway to vitamin B_{12}.[42]

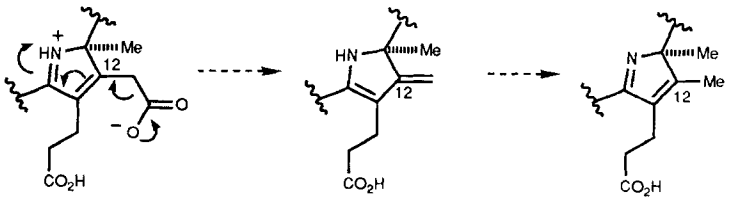
In contrast to the reasonably stable octamethyl esters of precorrin-6A (**16**) and precorrin-6B (**19**), the heptamethyl ester of precorrin-8x was so prone to oxidation that it was unsuitable for NMR work. Also, to our dismay, the ^{13}C NMR spectra from precorrin-8x as a solution in slightly acidic water showed a veritable forest of peaks. Eventually we discovered the reason: what must surely have been a single enzymic product initially changed under these very mild conditions into a mixture of at

least five closely related compounds. The impasse was overcome when it was observed that all five forms slowly changed to give the same final isomer, which was stable. Now that the target was stationary rather than moving, the multiple ^{13}C-labeling approach, so successful for precorrins-6A (**16**) and 6B (**19**), could be used to establish[43] the structure **22** for the stable form of precorrin-8x (Scheme 8). The two new C-methyl groups were indeed at C-5 and C-15; like C-10, C-15 was sp^3 hybridized, whilst C-8 was sp^2 hybridized. The assignment of the configurations at all the centers apart from C-3 and C-15 depends on the fact that precorrin-8x can be enzymically converted into hydrogenobyrinic acid (**12**). Since, however, hydrogenobyrinic acid is not formed when the stable form of precorrin-8x is incubated with the aforementioned enzyme system, the configurations at C-3 and C-15 (which might have changed) must be left unspecified at present.



Scheme 8. Determination of structure of precorrin-8x (**23**).

Interest now focused on finding out which of the five closely related forms of precorrin-8x was the true biosynthetic intermediate. HPLC separation of the five forms was the next step. One of these compounds was shown to be enzymically converted into hydrogenobyrinic acid (**12**) more rapidly and efficiently than any of the others. Still better, this form was reasonably stable at high pH. So this true intermediate was generated from precorrin-3A (as **10**), which in turn had been biosynthesized from [2,3-$^{13}C_2$]ALA **4d**. This experiment was designed to allow C-12 and its attached carbon to be studied in precorrin-8x; remember for work like this on a semi-micro scale, NMR information is available only at and around ^{13}C-labeled sites. The results showed that a methyl group is attached to C-12 which is itself an sp^2 center; these two carbon atoms are marked on structure **23a** as filled black triangles. This is important because the decarboxylation process initially generates a methylene group, which then tautomerizes into a methyl group (Scheme 9). All the foregoing results together with those from extensive ^1H NMR studies on the true precorrin-8x led to structure **23** for this intermediate.[43] That C-8 is sp^3 hybridized in precorrin-8x (**23**) was indicated by



Scheme 9. Mechanism of decarboxylation of 12-acetate group.

a ^{13}C NMR spectrum of the sample prepared from [4-^{13}C]ALA and [*methyl*-^{13}C]SAM taken quickly in the original weakly acid water before appreciable change to the stable form had occurred. This spectrum showed only a very weak signal around $\delta \approx 99$ where the C-8 signal of the stable form appears, and this signal increased in intensity as the change to **22** took place.

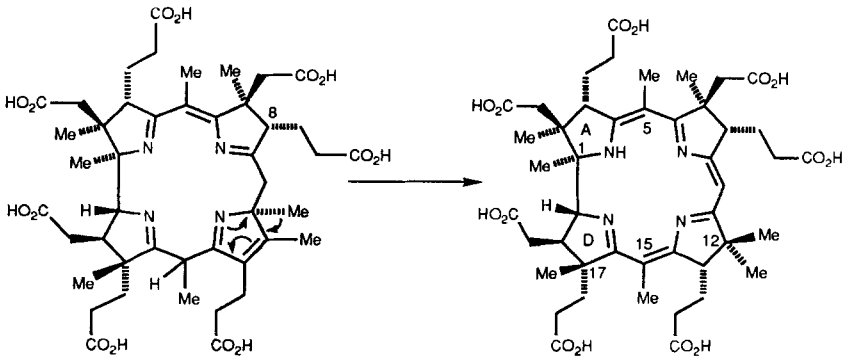
Comment is needed on the formation of at least four other forms from the true precorrin-8x (**23**). The latter can be expected to change to **22** thereby gaining stabilization[44] from the extended amidine system of rings A and B. The two separated chromophores can exist as other tautomers in addition to those shown in **22** and **23**, and epimerization is possible at C-3, C-8, and C-15. Different combinations of these regio- and stereoisomerizations can account for the generation of different forms, all of which eventually fall into the thermodynamic well represented by the stable form **22**. The stereochemical and other details will be addressed in future work when more important problems have been solved. This is the right priority, because the nature of precorrin-8x (**23**) has now been almost entirely revealed.

The enzyme responsible for the conversion of precorrin-6B (**19**) into precorrin-8x (**23**) has been purified to homogeneity[39] from an engineered strain [SC510(pXL253)] of *Ps. denitrificans* by using fast protein liquid chromatography (FPLC). This protein, encoded by the *cobL* gene, is a single polypeptide having M_r 43000 ± 1000, which matches the calculation of 42900 Daltons from the gene sequence. However, gel permeation studies point to strong association in the native state, possibly as an octamer. We have already commented on the remarkable ability of this enzyme to catalyze both C-methylation and decarboxylation. The sequence of the two methylations and decarboxylation is unknown at present. However, when precorrin-6A (**16**) is incubated without SAM with the standard preparation of eight enzymes (including CobL), the end product is precorrin-6B (**19**) and not its 12-decarboxylated form. So it is probable that at least one C-methylation precedes the decarboxylation step. When one compares the CobL sequence with the sequences of other methyltransferases of the B_{12} pathway (CobA, CobI and, as will be seen later, also CobF, CobJ, and CobM), part of the CobL protein can be assigned a methyltransferase function. There is also an additional carboxy-terminal domain of $M_r \approx 20000$ which probably carries the decar-

boxylase activity.[14, 39] This dual activity has been rationalized as resulting from the fusion of initially separate ancestral genes, one encoding for C-5/C-15 methylase activity, the other for acetate decarboxylase activity.[39] This interpretation has gained recent support by the description of two separate genes of the B_{12} pathway in *Salmonella typhimurium*, *cbiE* and *cbiT*.[45] These show strong homology with the amino-terminal and carboxy-terminal regions, respectively, of *cobL* (Table 2).

4.4. Final Rearrangement to Form the Corrin Macrocycle

Precorrin-8x (**23**) is isomeric with hydrogenobyrinic acid (**12**), and the conversion of the former into the latter is initiated by migration of the methyl group at C-11 over to C-12. This is a [1,5]sigmatropic rearrangement and will be suprafacial. In this way, the blockage to formation of a conjugated system is removed, and now the molecule can tautomerize and slide into the thermodynamic well represented by the extended conjugated system of hydrogenobyrinic acid (**12**) (Scheme 10). The rearrangement process was known to be catalyzed by an enzyme present in the mixture of overproduced proteins routinely used in many of the foregoing studies. It was first isolated[19] as a protein that specifically bound hydrogenobyrinic acid (**12**). Only later did it become clear that this protein was actually the enzyme catalyzing the formation of hydrogenobyrinic acid (**12**) from precorrin-8x (**23**), and the N-terminal sequence of this protein showed that its gene was *cobH*. Such are the twists and turns of scientific research! By then a strain of *Ps. denitrificans* [SC510 Rif^r(pXL1149)] had been constructed having *cobH* as the only amplified gene. The soluble protein from this strain gave pure CobH enzyme by repeated fractionation by FPLC on a series of different columns; hydrogenobyrinic acid synthase activity served as the assay.[42] Interlocking evidence that the correct enzyme and gene for the C-11/C-12 rearrangement had been located came from a further engineered strain of *Ps. denitrificans* in which *cobH* was not overexpressed. The forward transformation of precorrin-6A (**16**) by the soluble enzyme system from this strain stopped at the stage of precorrin-8x (**23**), which was isolated in 45% yield.[42]



23 Precorrin-8x **12** Hydrogenobyrinic acid

Scheme 10. Rearrangement of precorrin-8x (**23**) to hydrogenobyrinic acid (**12**).

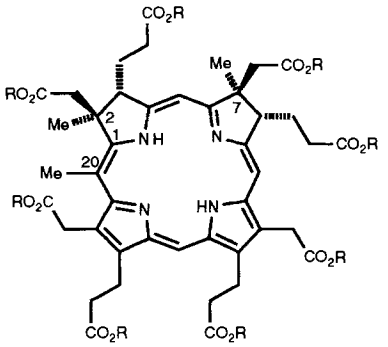
Under the usual denaturing conditions, the CobH enzyme has a relative molecular mass M_r of 22000 ± 1000, and gel permeation studies showed the protein to be monomeric.[42] Enzymes that catalyze rearrangement reactions are particularly interesting, and one wonders how CobH catalyzes the C-11/C-12 methyl migration. Ring-C of precorrin-8x (**23**) is a disubstituted pyrrolenine apparently capable of rearranging on its own[46] — but it does not. Possibly the enzymic trick is to change an unfavorable conformation of precorrin-8x (**23**) as it binds into a favorable one with the stereoelectronics appropriate for rearrangement. Since this enzyme can be obtained in larger quantities and is a relatively small monomeric protein, future research on it should be rewarding.

Our survey has now briefly described the early part of the B_{12} pathway, summarized in Scheme 1, leading from ALA **4** through to precorrin-3A (**10**). Then followed a fuller account of the discovery of precorrin-6A (**16**), which opened the way for the rest of the pathway to be elucidated through to hydrogenobyrinic acid (**12**), adding two further new intermediates, precorrin-6B (**19**) and precorrin-8x (**23**). Having worked forwards from precorrin-6A (**16**), we can now work backwards from it towards precorrin-3A (**10**) to fill the only remaining gap in the route to the first corrinoid intermediate **12**. However, a hidden thread needs first to be picked out.

5. Synthesis Using an Array of Overproduced Enzymes

Many times so far in this review, complex materials have, without further comment, been "synthesized enzymically" using a combination of enzymes available in quantity by overexpression of the corresponding genes. The opportunities opened up by this approach are far too important, especially for organic chemists, to let the topic be somewhat hidden. The in vitro synthesis of precorrin-6A (**16**) from ALA **4**, which was the basis of all the structural work, involved the combined use of nine overproduced enzymes.[24] The similar synthesis of hydrogenobyrinic acid (**12**) required twelve overproduced enzymes to work together in a sequential way.[24] In both cases, quite sufficient material was produced for further enzymic and spectroscopic experiments. As far as we know, these are the earliest examples (1990) in which large numbers of overproduced enzymes have been used for such syntheses, certainly in the tetrapyrrole field. But other groups have provided related examples in this and other fields,[3d, 47] although generally smaller numbers of enzymes are involved.

Comparison of the nonenzymic and enzymic synthetic approaches for the preparation of precorrin-3A (**10**) illustrates well the enormous power of the enzymic route. A stereocontrolled nonenzymic synthesis was developed[48] of the isobacteriochlorin octamethyl ester **30**; the corresponding octacarboxylic acid **29** is the didehydro form of precorrin-3A (**10**). Precorrin-3A (**10**) can readily be prepared from the ester **30**. The synthesis of **30** was the culmination of over ten years of research, which was necessary because initially no route was available for



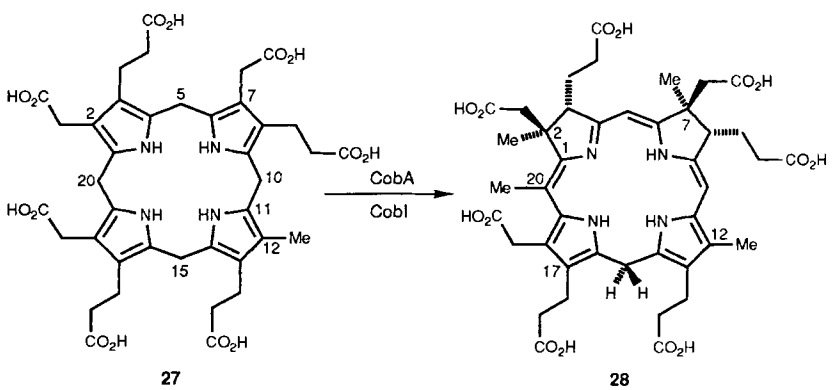
29 R = H
30 R = Me

synthesis of any isobacteriochlorin macrocycle, even those with simple substituents. This synthesis was a very satisfying one: it yielded a rich harvest of new chemistry, and many excellent chemists were trained during its development. But if one wishes to prepare precorrin-3A (**10**) or its relative **30** for further work, is such a nonenzymic synthesis the way to go? The answer has to be "no". To repeat the synthesis from the beginning would take two first-class chemists at least one year, and the final yield, assuming a reasonable scale at the start, would be 5 mg at best. How does this compare with enzymic synthesis?

Here the starting material, ALA **4**, can easily be synthesized on any desired scale. Scheme 1 shows that five enzymes are needed to transform ALA **4** into precorrin-3A (**10**), namely those encoded by *hemB*, *hemC*, *hemD*, *cobA*, and *cobI*. Strains that overexpress these genes are now available, so providing relatively large quantites of the corresponding enzymes.[49] It is true that many years of work were required to unravel the genetics and molecular biology to reach the present stage, but that is the completed foundation and we can now use these enzymes for synthesis. A standard laboratory-scale enzymic preparation[49] of precorrin-3A (**10**) yields 10–20 mg and, with the enzymes in hand, the whole synthesis from ALA **4** to precorrin-3A (**10**) takes about three days. Even taking into account growing the overproducing strains and isolating or enriching the enzymes, the time required is still just a few weeks. So more material is produced in far less time than for the nonenzymic approach.

It should be borne in mind that many enzymes are not totally substrate specific, and this can be used to advantage for the synthesis of analogues of a particular natural product. This involves the nonenzymic synthesis of a substrate having a structure somewhat different from the natural one. For example, if in Scheme 1, uro'gen III **7** is replaced by its 12-decarboxylated analogue **27** (Scheme 11), which can be synthesized by a straightforward nonenzymic route, the two methylase enzymes (from *cobA* and *cobI*) still function to produce the analogue **28** of precorrin-3A (**10**) having a methyl group at C-12 rather than an acetate residue.[50] Indeed, examples of such syntheses of analogues of natural products abound.[51]

In view of these huge developments in molecular biology and enzymology, how will natural products research look in ten years time? A substantial change seems inevitable, and it is most heartening to see the power of combined nonenzymic and enzymic synthesis. But this is still in the future; our survey can now return to the biosynthetic pathway and to filling the gap between precorrin-3A (**10**) and precorrin-6A (**16**).



27 **28**

Scheme 11. Enzymic synthesis of an analogue of a natural product.

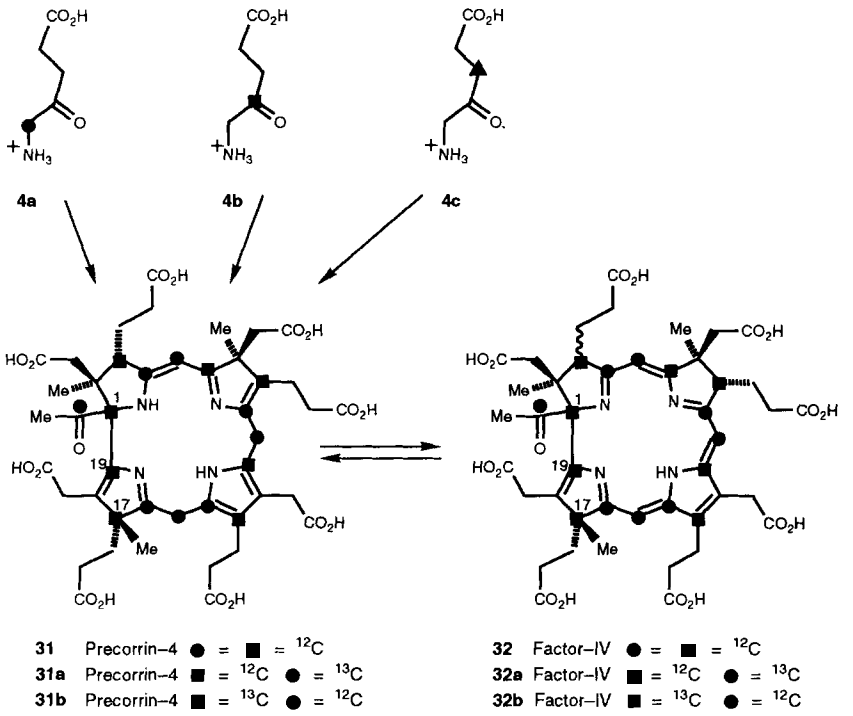
6. From Precorrin-3A to Precorrin-6A

6.1. Precorrin-4: Another Surprising Structure

The next step forward in the elucidation of the biosynthetic pathway showed the great value of preparing strains of the organism of interest in which specific genes have been eliminated. For *Ps. denitrificans*, deletion of the *cobM* gene from one strain led to an enzyme preparation that efficiently converted precorrin-3A (**10**) into a new tetramethylated intermediate shown to be precorrin-4.[52] For precorrin-2 (**9**) and precorrin-3A (**10**), the structural work had largely been carried out on the more stable conjugated derivatives (with two hydrogen atoms fewer), which were readily formed by aerial oxidation. The same held true for precorrin-4; it was smoothly converted in air into its didehydro derivative called Factor IV. This could be purified by chromatography which showed, in combination with mass spectrometry, the presence of two isomers having properties indicating that they were epimeric, probably at C-3.[52, 53] Since such epimerization has been observed for almost every intermediate isolated so far from the B_{12} pathway, it need not concern us further. The rest of the studies focused on the major epimer.

In the same way that precorrin-3A (**10**) had earlier been regenerated from its didehydro analogue **29** by enzymic reduction,[22] so Factor IV was reduced to reform precorrin-4 on incubation with the complete enzyme system including NADH but lacking NADPH. Then the forward biosynthetic steps continued from precorrin-4, but because NADPH was lacking, progress stopped at precorrin-6A (**16**), which was isolated. This result firmly places precorrin-4 on the biosynthetic track to vitamin B_{12}. It cannot be too strongly emphasized that it is essential to provide such clear evidence that a putative intermediate is biosynthetically converted into the final product or, as here, into another established intermediate.

The structural studies followed the approach, by now well established, of preparing three samples of Factor IV from [5-^{13}C]ALA **4a**, [4-^{13}C]ALA **4b**, and [3-^{13}C]ALA **4c**. The ^{13}C NMR and ^{1}H NMR results[52] from these three samples led to structure **32** for Factor IV; for clarity just the first two labeling patterns are shown in Scheme 12. Carbon atoms carry-



Scheme 12. ^{13}C-Labeling of precorrin-4 (**31**) and Factor IV (**32**).

ing the same symbol are ^{13}C-labeled in the same sample, whereas the ^{13}C-labels for carbon atoms marked with different symbols are in different samples. The key observations were that a) C-1 and C-19 are directly bonded, b) a low-field signal (δ = 210.8) shown by the sample **32a** from [5-^{13}C]ALA corresponds to the carbonyl group of the acetyl residue, and c) C-19 is an sp^2 center, thus placing the acetyl group at C-1. Since Factor IV (**32**) and precorrin-4 have a reversible redox relationship, structure **31** can be deduced for precorrin-4. Comparison of this structure with that of precorrin-3A (**10**) shows that both methylation at C-17 and oxidation have occurred (addition of one oxygen overall). This is the increase in oxidation state that is later reversed by the reductase CobK.

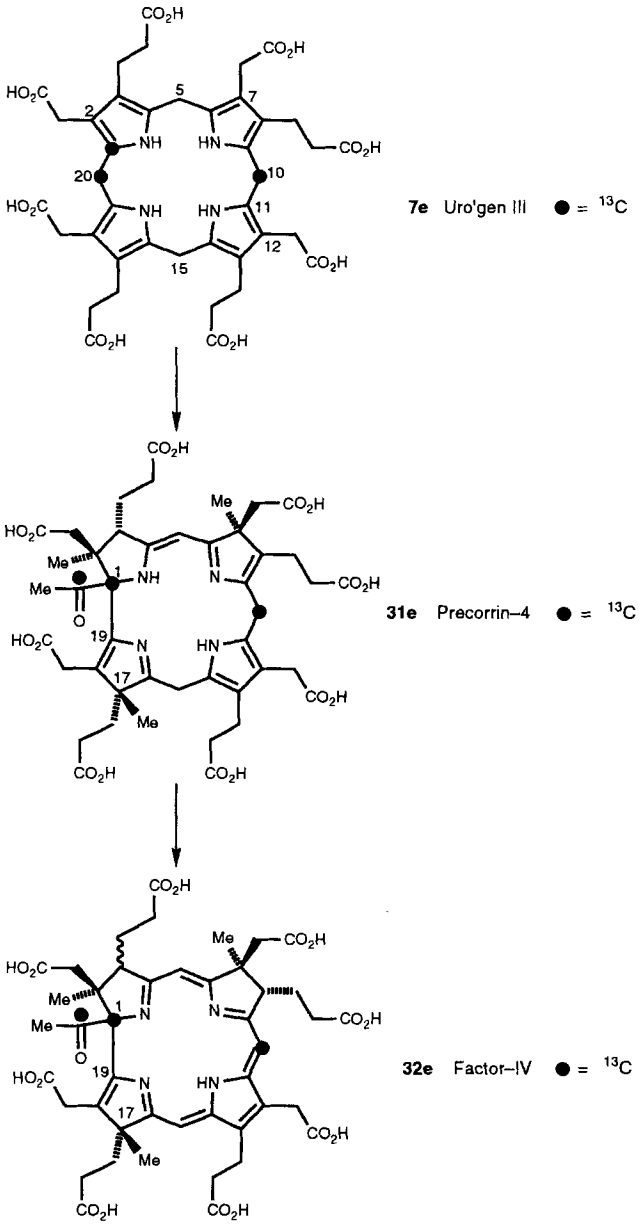
Once again, workers in the B_{12} field, and observers of it, were surprised by the structure of precorrin-4 (**31**). The very early ring contraction was one unexpected feature, but the greatest surprise was the appearance of the acetyl group at C-1; this shook our previous conceptions. That an acetyl group would be generated during the ring contraction followed from the likely mechanism.[44] The acetyl group would act as the source of acetic acid, the established extrusion product from ring contraction in *Pr. shemanii* (see Section 2). But everyone's speculations prior to the discovery of precorrin-4 (**31**) placed the acetyl group at C-19 rather than at C-1. This key element of structure **31** for precorrin-4 was supported by unimpeachable evidence derived from a combination of nonenzymic and enzymic synthesis together with NMR spectroscopic studies. [1,10,20-$^{13}C_3$]Uroporphyrin III ester was unambiguously synthesized from the starting material **18** illustrated in Scheme 4, and its ^{13}C NMR spectrum confirmed the direct linkage of the two important ^{13}C atoms C-1 and C-20. The product was hydrolyzed and reduced to yield [1,10,20-$^{13}C_3$]uro'gen III **7e** (Scheme 13), which was enzymically converted into precorrin-3A. After some purification steps, precorrin-3A was finally transformed into precorrin-4 **31e**, and hence into Factor IV **32e**, by incubation with the mixture of enzymes lacking CobM. The ^{13}C NMR spectrum of the labeled Factor IV showed that the signals from the acetyl carbonyl group (originally C-20) and from C-1 were doublets, in other words these carbons are directly bonded. The conclusion that the acetyl group of Factor IV (**32**), and so also of precorrin-4 (**31**), is attached at C-1 is thus a rigorous one.[53] In addition, Factor IV was biosynthesized from precorrin-3A **10b**, which had been prepared from [4-^{13}C]ALA **4b** and [*methyl*-^{13}C]SAM (Scheme 3). [*Methyl*-^{13}C]-SAM was also used in the final step as the source of the fourth methyl group. The doublets in the ^{13}C NMR spectrum of Factor IV from C-17 and the methyl group added last confirmed their direct connection. It was a valuable bonus to be able to observe the singlet from the methyl group of the acetyl residue.[53] Finally with regard to Factor IV, it is interesting that a close relative of the parent contracted macrocycle had been synthesized earlier for other studies.[54]

That the fourth methyl group to be attached to the macrocycle appears at C-17 in precorrin-4 (**31**) is in satisfying agreement with the the results of pulse-labeling studies, outlined earlier, on the order of the C-methylations after the third one. In both *Pr. shermanii* and *Ps. denitrificans* methylation occurred first at position 17, followed by 12, then 1, and finally at 5 and 15. The research already described on precorrin-6A (**16**) showed that the fifth methyl group, which resides in the corrins at C-12, is initially placed at C-11. As further transformation of precorrin-4 (**31**) is blocked by deletion of the *cobM* gene resulting in accumulation of precorrin-4 (**31**), and since the sequence of CobM shows it to be a methyltransferase, it follows that CobM is the 11-methyltransferase of *Ps. denitrificans*.[52]

Homogeneous CobM methyltransferase was isolated by a series of chromatographic steps from a strain of *Ps. denitrificans* in which only the *cobM* gene had been overexpressed. The molecular weight of CobM according to the usual SDS-PAGE (SDS-PAGE = sodium dodecylsulfate polyacrylamide gel electrophoresis) was 31 000 $\pm$ 2000. The sequence of the first fifteen residues at the N-terminus of CobM was in full agreement with expectation from the DNA sequence, although the N-terminal methionine had been processed off in the formation of the mature protein.[55]

6.2. A Pause to Catch Breath

The climb to the summit was now almost completed, and these last results are still fairly very recent. What remained to be done? Section 3 described how it was established that *nine* enzymes are required for the biosynthesis of hydrogenobyrinic acid (**12**) from uro'gen III **7**. These enzymes are encoded by the *cob* genes given letters *A*, *F*, *G*, *H*, *I*, *J*, *K*, *L*, *M*. Scheme 1



Scheme 13. Confirmation that the acetyl group of precorrin-4 (**31**) is at position 1.

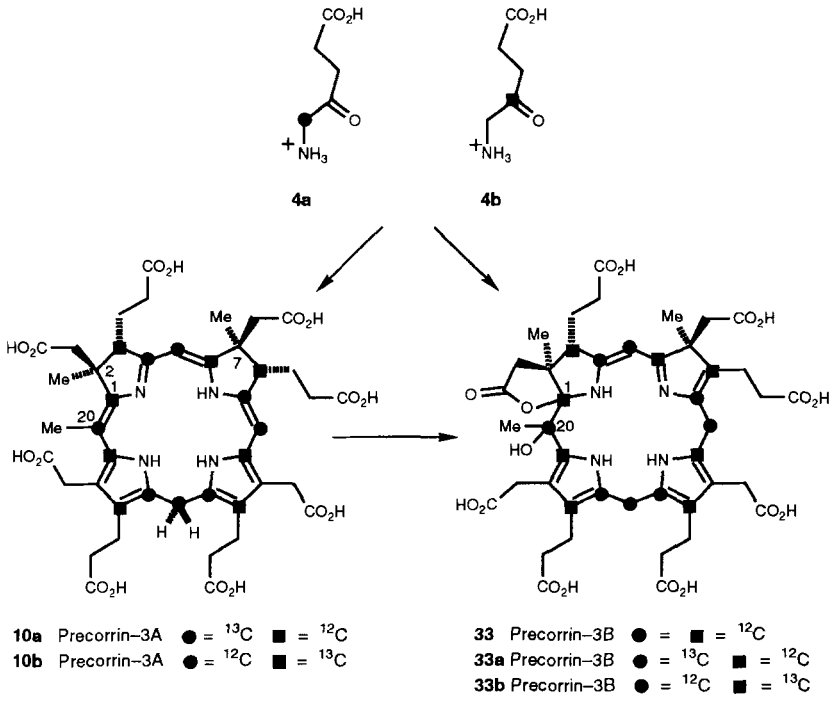
showed that *cobA* and *cobI* are needed to reach precorrin-3A (**10**). Then the main section of the review described how the functions of the enzymes encoded by *cobM*, *cobK*, *cobL*, and *cobH* were discovered. By this stage (March 1993) the remaining questions were apparent: What do the enzymes encoded by the remaining genes do? These genes are *cobG*, *cobF*, and *cobJ*. From what has been described already, the corresponding enzymes must convert precorrin-3A (**10**) into precorrin-6A (**16**) via the known precorrin-4 (**31**), which CobM must methylate at C-11 to form precorrin-5. Moreover, it was clear from comparisons of the sequences of CobF and CobJ with those of the known methyltransferases (CobA, I, M, and L) that these two enzymes are also methyltransferases. CobG, however, was quite different and seemed likely to catalyze the oxidative step which must occur before precorrin-4 (**31**). All this holds together perfectly since now only two C-methylations (at C-17 and C-1) have not been correlated with their enzymes, and CobJ and CobF are strong possibilities. The situation at this point was analogous to solving any multicomponent puzzle (such as a crossword or jigsaw puzzle): as more and more parts are put in place, the easier it is to solve the remainder. And by this stage, almost all the parts were in place.

6.3. Setting the Stage for the Ring Contraction: Precorrin-3B

These remaining problems were studied by testing the CobG, CobJ, and CobF enzymes alone and in combination for their ability to transform precorrin-3A (**10**). These experiments could only be done after construction of strains of *Ps. denitrificans* in which *cobG*, *cobJ*, and *cobF* had been separately amplified.[55] CobJ alone had no effect on precorrin-3A, whereas CobG and CobJ together yielded the known precorrin-4 (**31**). CobJ is a methyltransferase, and from the structure of precorrin-4 (**31**) one can conclude that CobJ must be the 17-methyltransferase. So CobG must act before CobJ. Pointers that CobG is the enzyme acting on precorrin-3A (**16**) had come earlier from eight engineered strains of *Ps. denitrificans* in which the genes *cobF* to *cobM* had been deleted one at a time. Only the strain lacking *cobG* accumulated precorrin-3A (**10**) intracellularly.[56] When tested, CobG alone converted precorrin-3A (**10**) into a new intermediate, which was not further methylated and so named precorrin-3B.[57] As for previous cases, two isomers were isolated and both were converted in high yield into precorrin-4 (**31**), the established B_{12} intermediate, when incubated with the CobJ enzyme and SAM.[55] These isomers are almost certainly epimeric at C-3; but this is a small point and the focus here will be on the major epimer. Mass spectrometry established its molecular weight as 894, which is 16 units higher that of precorrin-3A (**10**) and corresponds to the introduction of one oxygen atom into precorrin-3A (**10**) in forming precorrin-3B. Thus, CobG was confirmed as the oxidative enzyme.[57]

It is not necessary to give a full account of the structure determination of precorrin-3B, because exactly the same approach of multiple ^{13}C-labeling was used as for all the earlier new intermediates. But in addition, its Fourier transform infrared spectrum showed a strong band at 1799 cm^{-1} corresponding to the presence of a γ-lactone. The labeling patterns for two of the three differently ^{13}C-labeled samples of precorrin-3B are collected on structures **33a** and **33b** (Scheme 14). A thorough assignment was made of both the ^{13}C and ^{1}H NMR spectra, and $^{13}C-^{1}H$ short- and long-range connections were established around the macrocycle to add further strength to the assigned structure **33**.[57] In fact, the mass of evidence leaves no doubt that this structure is correct, although the configurations at C-20 and C-1 still need to be determined. The structure of precorrin-3B (**33**) was yet another surprise, since prior to 1990 the general expectation was that the next step beyond precorrin-3A (**10**) was probably C-17 methylation or decarboxylation of the 12-acetate. Also it is most interesting that the oxidative step leading to precorrin-3B (**33**) does not cause the ring contraction; the stage has been set for it to happen during the next conversion into precorrin-4 (**31**) catalyzed by CobJ when methylation of C-17 occurs.

Pure CobG enzyme is a brown-green protein isolated from a strain of *Ps. denitrificans* overexpressing *cobG* and *cobF*. The



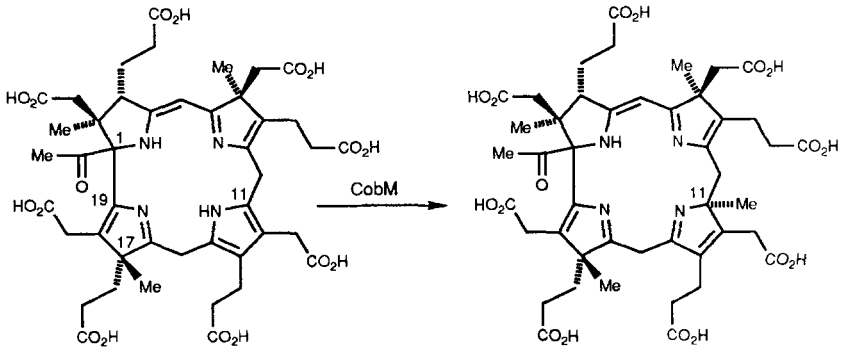
Scheme 14. ^{13}C-Labeling of precorrin-3B **33a** and **33b**.

molecular weight of CobG by SDS-PAGE is 46000 ± 2000. The assay was based on the production of precorrin-4 (**31**) from precorrin-3A (**10**) when the tested extracts were incubated with added CobJ. The properties of CobG and analyses for iron and sulfide all indicated that this enzyme is an iron–sulfur protein having one [4Fe-4S] cluster or two [2Fe-2S] clusters.[55] The C-terminal domain of CobG displays ≈25% identity to the corresponding domains of ferredoxin-sulfite reductase (EC 1.8.7.1), sulfite reductase hemoprotein CysI (EC 1.8.1.2), and ferredoxin-nitrite reductase (EC 1.7.7.1) (Table 2).[58, 59] Importantly, the four cysteine residues proposed to hold the [4Fe-4S] cluster in CysI and spinach nitrite reductase[58] lined up with positions 338, 344, 377, and 381 in the CobG sequence. The pure CobG enzyme catalyzed the conversion of precorrin-3A (**10**) into precorrin-3B (**33**) without added cofactors. Interestingly, under the anaerobic conditions used, this oxidation was roughly stoichiometric with respect to the enzyme. However, recently Scott's group reported the observation of ^{13}C NMR signals corresponding to the structure established above for precorrin-3B (**33**) when precorrin-3A (**10**) was incubated with CobG. The valuable observation was made that the CobG enzyme turns over in the presence of oxygen.[60]

6.4. Precorrin-5, a Structure this Time without Surprises

Already CobM had been pinpointed as the enzyme that methylates C-11 of precorrin-4 (31), and the product should be precorrin-5 (**34**). Also, CobF was the only enzyme left (and it is a methylase) to introduce the methyl group seen at C-1 of precorrin-6A (**16**). A priori, these two steps look reasonably straightforward, and it seemed very probable that this time there would not be surprise cards up the biosynthetic sleeve, and so it turned out. Precorrin-5 could be biosynthesized from precorrin-3A (**10**) by using CobG, CobJ, CobM, and SAM but without CobF[55] or alternatively, from precorrin-4 (**31**) by incubation with CobM and SAM.[61] Again multiply ^{13}C-labeled forms of precorrin-5 were generated as earlier to allow the structure **34** to be deduced by NMR spectroscopy.[61] As can be seen, **34** is the expected 11-methylated derivative of precorrin-4 (**31**) (Scheme 15). How the C-1 acetyl group of precorrin-5 (**34**) might be removed to allow C-methylation at this site will be considered later. The required reactivity is present, however, because the acetyl residue is intrinsically labile[55, 61] and is gradually lost almost certainly as acetic acid,[55] the elimination product found in earlier experiments with *Pr. shermanii*. This deacetylated product was isolated and called Factor V.[55]

The pathway from ALA **4** to hydrogenobyrinic acid (**12**) is now complete and will shortly be summarized with a mechanistic discussion. First, however, what has been discovered about *Ps. denitrificans* should be correlated with knowledge of the B_{12} pathway in *Pr. shermanii*.



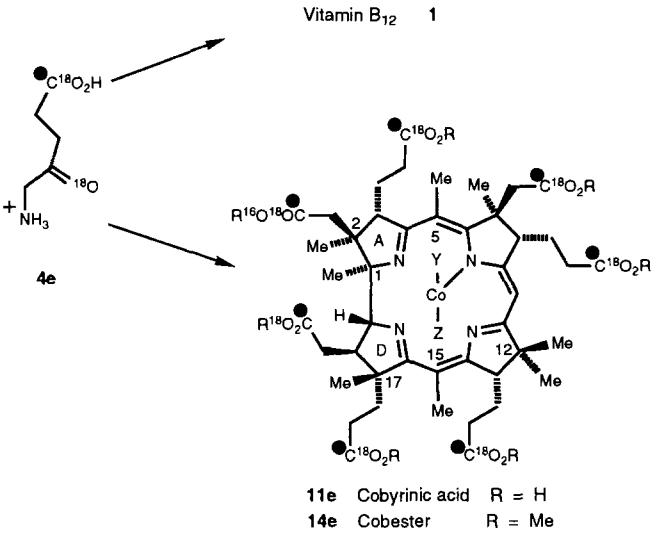
Scheme 15. Structure of precorrin-5 (**34**).

7. A Comparison of the B_{12} Pathways in *Ps. denitrificans* and *Pr. shermanii*

Ps. denitrificans is an aerobe and *Pr. shermanii* is grown microaerophilically, in other words almost anaerobically, for B_{12} production. Yet B_{12} pathways in these two organisms overlap to a large extent. The starting material, ALA **4**, and the product, coenzyme B_{12} (**2**), are the same for both, and all the steps as far as precorrin-3A (**10**) (or possibly precorrin-2 (**9**)) are held in

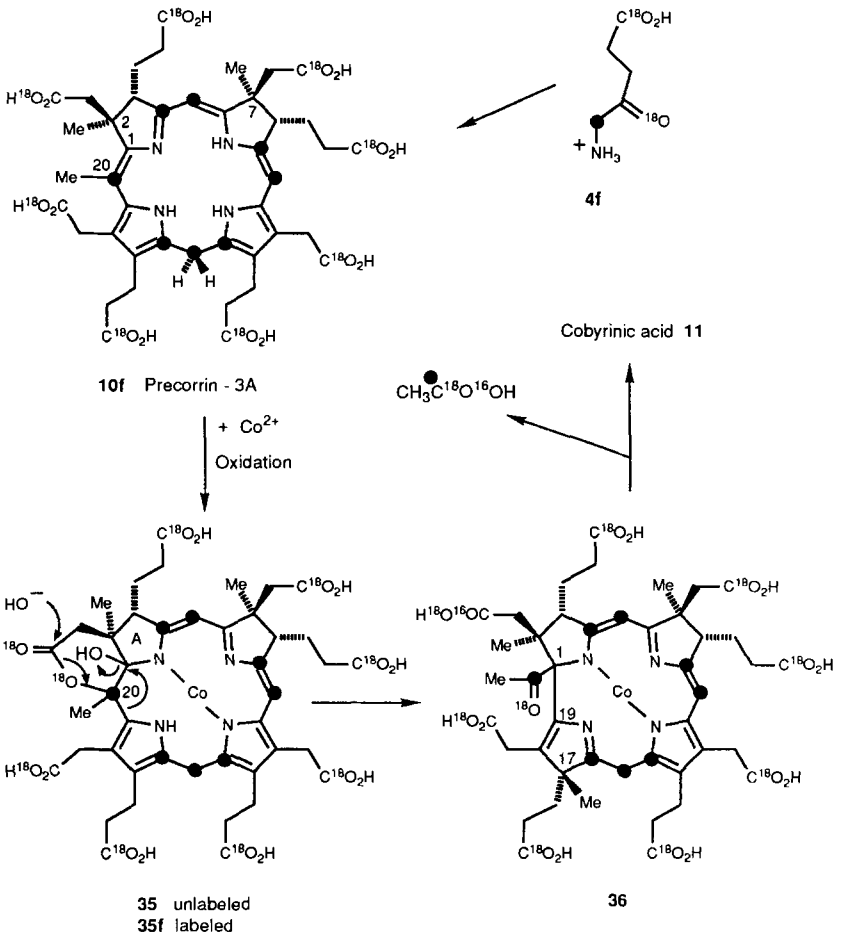
common. One clear difference is the timing of cobalt incorporation. For *Ps. denitrificans* the intermediates along the entire biosynthetic pathway to hydrogenobyrinic acid (**12**) are cobalt-free. Cobalt incorporation only occurs after the *a,c*-diamide **43** of hydrogenobyrinic acid has been formed; more details of this process will be discussed later. *Pr. shermanii* behaves differently and here, as described in Section 2, cobalt is probably inserted into precorrin-3A (**10**) or possibly into precorrin-2 (**9**). These studies showed that cobalt is inserted rapidly; in the incubation with $^{60}Co^{2+}$ and the complete enzyme system from the cells the incorporation is largely complete within ten minutes.[7] A key question then is, whether the rest of the pathway beyond precorrin-3A (**10**) in *Pr. shermanii* mirrors that in *Ps. denitrificans*; specifically, is the cobalt complex of precorrin-4 (**31**) converted into the cobalt derivatives of all the other precorrins described already, with the final direct rearrangement of cobalto-precorrin-8x into cobyrinic acid (**11**)? Experiments that gave the first indications that this route is indeed followed depended on incubating a set of ^{3}H,^{14}C doubly labeled metal-free precorrins with the enzyme system from *Pr. shermanii*. Small incorporations into cobyrinic acid (**11**), which had the expected ^{3}H:^{14}C ratio, were observed[62a] from precorrin-6A (**16**), precorrin-6B (**19**), and precorrin-8x (**23**). Taking into consideration that hydrogenobyrinic acid (**12**) is not incorporated into cobyrinic acid (**11**),[62b] this study indicated that cobalt complexes of **16**, **19**, and **23** formed spontaneously in the incubation mixtures are the likely intermediates of cobyrinic acid biosynthesis. In addition some hydrogenobyrinic acid (**12**) was synthesized from precorrin-8x (**23**), indicating the existence of enzymic activity in extracts of *Pr. shermanii* that can catalyze the [1,5]-methyl migration irrespective of the presence of the central cobalt ion. As for CobH,[42] this enzyme is likely to be the target of the inhibition by hydrogenobyrinic acid[62b] or by its own product cobyrinic acid.[41] So this is a start, and the way forward with *Pr. shermanii* undoubtedly is to carry out its genetic analysis so that the enzymes operating beyond precorrin-3A (**10**) will become available. This work should be enormously helped by the availability of the palette of enzymes from *Ps. denitrificans*.

Another interesting facet of B_{12} biosynthesis was brought to light by experiments on the side-chain carboxyl groups. When [1-^{13}C,1,4-$^{18}O_3$]ALA **4e** was incorporated into B_{12} **1** in *Pr. shermanii*, NMR studies proved that the C-2 acetamide group had undergone substantial loss of ^{18}O presumably by exchange with the medium,[63] and later this exchange was reported to be almost complete.[64] The presence of ^{18}O directly attached to ^{13}C can be detected by a characteristic upfield shift of the ^{13}C NMR signal relative to its normal position. To help locate where on the pathway this exchange occurs, [1-^{13}C,1,4-$^{18}O_3$]ALA **4e** was incorporated into the earlier intermediate, cobyrinic acid **11e** by using the same organism (Scheme 16). This intermediate has the advantage that both oxygen atoms of the carboxyl group can be examined. ^{13}C NMR spectra were recorded for the corresponding heptamethyl



Scheme 16. Study of oxygen exchange from side-chain carboxyl groups during the biosynthesis of cobyrinic acid **11e**.

ester, cobester **14e**. They showed that six of the seven carboxyl groups of cobyrinic acid **11e** had retained both oxygen atoms but that the C-2 acetate had lost one oxygen atom.[65] Whether a similar specific loss of one oxygen atom occurs in the biosynthesis of hydrogenobyrinic acid (**12**) by *Ps. denitrificans* is not yet known; the necessary experiments have not been carried out,



Scheme 17. Transfer of oxygen from a side-chain carboxyl group to the extruded acetic acid during biosynthesis in *Pr. shermanii*.

but they surely will be soon. A first clue as to how this specific loss of oxygen occurs came from examination of the acetic acid produced during the biosynthesis of cobyrinic acid (as **11**) in *Pr. shermanii* from [5-^{13}C,1,4-$^{18}O_3$]ALA **4f** (Scheme 17). This precursor places a ^{13}C atom at C-20 of precorrin-3A **10f**, and it is that carbon that appears finally as the carbonyl C atom of the carboxyl group of the acetic acid. A high-field ^{13}C NMR spectrum of a suitable ester of this acetic acid showed a ^{13}C signal shifted upfield by directly bonded ^{18}O. This result and those from control experiments checking possible exchange of oxygen from CO_2H with the medium indicated that transfer of one ^{18}O atom from a carboxyl side chain to the acetic acid had occurred to a high degree.[66] Presumably the transfer is from the C-2 acetate carboxyl group, since, as reported above, this group specifically loses one of its original oxygen atoms at some biosynthetic stage before formation of cobyrinic acid (**11**). This suggests that in *Pr. shermanii* a somewhat different lactonic intermediate **35** may be involved with δ-lactone formation onto C-20.[66] One can speculate that this occurs because the organism is growing without or at very low levels of oxygen. Also, the presence of cobalt will substantially affect the chemistry of the macrocycle. The δ-lactone **35** is just one possible candidate for the ring-contraction process. Others, for example one having an imine in ring-A, are essentially equivalent in a broad sense. However, structure **35** fits a plausible mechanism whereby ^{18}O could be transferred from the 2-acetate group to the extruded acetic acid.

8. Summary, Discussion, and Mechanisms of the Steps Leading up to Hydrogenobyrinic Acid (12)

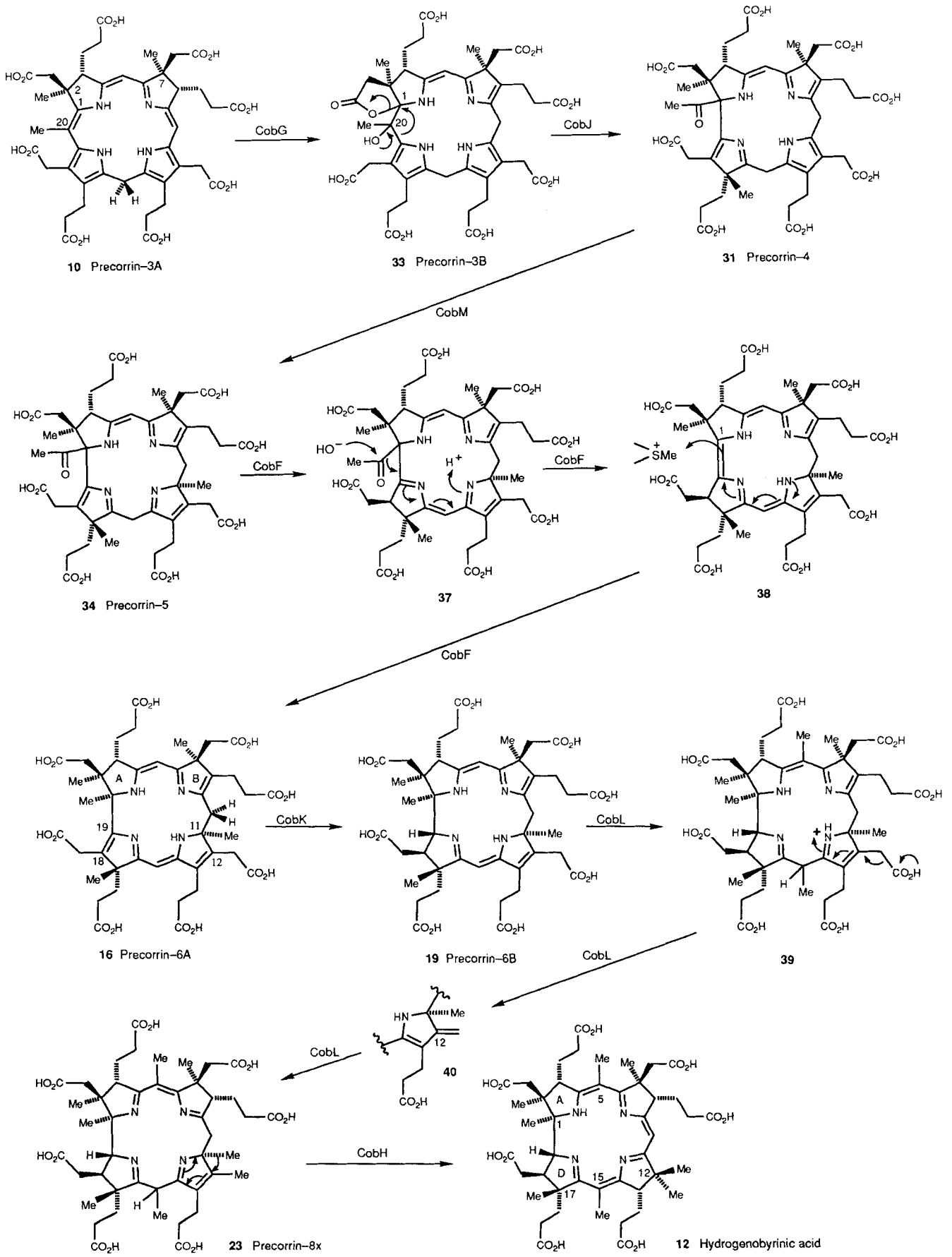
The time has come to assemble the entire biosynthetic pathway from uro'gen III **7** through to hydrogenobyrinic acid (**12**); the first section is given in Scheme 1 and the remainder in Scheme 18. It is certainly true that there have been more surprises and remarkable twists and turns along this sequence of steps than anyone had dreamed of. That has been the fascination of it. Equally appealing is the way the chemistry for each transformation prepares the way for the next one. Or is it more accurate to say as Eschenmoser has suggested[44] that as this amazing biosynthesis evolved, the intrinsic reactivity of each intermediate predetermined the nature of the next step?

Scheme 1 shows how the pathway from uro'gen III **7**, the parent of all the "pigments of life," branches off to vitamin B_{12} as a result of C-2 methylation. This step uses the available β-reactivity of pyrroles towards electrophiles (there is α-reactivity as well). An equivalent second methylation at C-7 by the same enzyme, CobA, then gives precorrin-2 (**9**). The third methyl group is inserted by the CobI enzyme at C-20 to form precorrin-3A (**10**). This was a surprising result at the time but can now be seen mechanistically as a β-methylation of an enamine. The story is continued in Scheme 18, which shows precorrin-3A (**10**) undergoing oxidation, catalyzed by CobG, to form the lactonic precorrin-3B (**33**). Looking at structure **33**, it should be recalled that the possible involvement of such lactones in B_{12} biosynthesis was first suggested and discussed by Eschenmoser.[44] CobG could be a monooxygenase or a dioxygenase, and it presumably needs a reducing cofactor; both aspects require further study. The C-1/C-20 double bond attacked is probably the most electron-rich in the molecule.

Precorrin-3B (**33**) is now perfectly set for a pinacol-type rearrangement[44] causing ring contraction. This is catalyzed by CobJ, which also carries out methylation at C-17. The contraction step is illustrated in Scheme 18 as occurring before C-17 methylation; this allows the electron-rich pyrrole ring to be the migrating group. Probably the methyl group at C-20 serves to block competing reactions; an example of such competition leading to a dead end in the absence of a methyl group has been provided by studies on related model systems.[44] The contraction step generates precorrin-4 (**31**) and places the acetyl residue at C-1; the ^{13}C NMR evidence provided by using ^{18}O labeling, as for earlier cases, indicated that the carbonyl oxygen of precorrin-4 is derived from molecular oxygen.[67] So this holds also for the C-20 hydroxyl group of precorrin-3B (**33**).

The chemistry carried out for the next two stages through to precorrin-6A (**16**) can only be described as exquisite. Mechanistic explanations were provided at a symposium in March 1993,[68] whereby one step establishes with perfection the reactivity required for the next one. Clearly the acetyl group at C-1 of precorrin-4 (**31**) must be removed to allow later methylation at that site. Arigoni pointed out[68] that the living system can achieve this objective by first methylating C-11, which is one of the α-positions of the only remaining pyrrole nucleus, to afford precorrin-5 (**34**). The C-11 methylation is carried out by the CobM enzyme which, as for CobI, is a straightforward methyltransferase carrying out one C-methylation. The other methyltransferases involved in the B_{12} pathway (CobA, J, F, and L) all achieve something more than just one methylation. Now only simple double-bond tautomerism within precorrin-5 (**34**) is necessary to reach structure **37**, which is the key to eliminating the acetyl group. As illustrated on that structure, the conjugated system across rings C and D allows ready hydrolytic removal of the acetyl group by a reverse Claisen condensation so releasing acetic acid. There is strong evidence to support the elimination of acetic acid in *Ps. denitrificans*[55] just as had earlier been rigorously proven for *Pr. shermanii*. Acetate elimination in this way, which is almost certainly enzyme-catalyzed in vivo, would generate the conjugated structure **38**. It was also highlighted by Battersby[68] that from ring C through to ring D and on to C-1, there is now an extended enamine to allow the C-1 methylation. The immediate product of "electron pushing" on structure **38** would be a tautomer of precorrin-6A (**16**). To reach the latter molecule, simple double-bond shifts are needed plausibly driven by the gain in stabilization by the extended amidine system[44] across rings C and D of precorrin-6A (**16**). Now we have reached the intermediate that started the exciting surge to the summit of Everest.

This is the point at which the oxidation level is adjusted to match that of hydrogenobyrinic acid (**12**). The necessary reduction is carried out by the NADPH-dependent enzyme CobK acting on the C-18 protonated form **16e** of precorrin-6A (**16**) (Scheme 6). Protonation allows delivery of the hydride to C-19; the electron acceptor is the imine of ring C in the protonated system **16e**. Now comes the transformation catalyzed by CobL,



Scheme 18. Biosynthetic pathway from precorrin-3A (**10**) to hydrogenobyrinic acid (**12**) in *Ps. denitrificans*.

the remarkable enzyme showing two very different activities, methyl transfer and decarboxylation. Good reasons were given in Section 4.3 why at least one methylation at C-5 or C-15 probably occurs before the decarboxylation. Note that as for every other C-methylation on this pathway the required reactivity is provided by an enamine. Scheme 18 shows both methyl groups in position before the 12-acetate is modified. It is plausible that the methylation at C-15 initiates the decarboxylation by completing the task, started by the crucial C-11 methylation step, of setting up a protonated pyrrolenine in ring C. Since it is well known that such systems undergo decarboxylation, one finally has a rational explanation of why specifically the 12-acetate group is decarboxylated. The fact that C-15 remains sp^3-hybridized in precorrin-8x (**23**) fits in with these ideas, and this outcome contrasts with the related events at C-5, where the methylation is followed by loss of a proton to regenerate the sp^2 state.

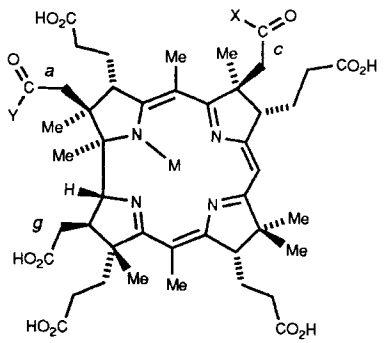
The keen observer will have noticed that the double bond in ring B of precorrin-8x (**23**) is located between N and C-9, whereas in many of the earlier intermediates, for example precorrin-6A (**10**), it appears between C-8 and C-9. The latter arrangement is proved for the isolated ester of precorrin-6A, but the double bond may or may not be in that position in the original enzymic product.[28] The possibility of double-bond migration during enzymic transformations was tested by preparing [^{3}H,^{14}C]precorrin-2 (as **9**) heavily labeled with ^{3}H at C-3 and C-8 (but not exclusively at these positions). The enzyme system from *Pr. shermanii* converted this precursor into cobyrinic acid (as **11**), which was shown by degradation of its ester, cobester (as **14**), to have lost the tritium from 8-H but retained the 3-H label.[69] So even under the enzymic conditions, a mechanism exists, such as the tautomerism discussed above, which exchanges specifically 8-H with the medium.

The decarboxylation step shown on structure **39** with the subsequent tautomerism of the product **40** regenerates the 5,5-disubstituted pyrrolenine system in ring C of precorrin-8x (**23**). This can now undergo a [1,5]sigmatropic suprafacial rearrangement, well-documented for such molecules,[70] which moves the C-11 methyl group to C-12. The blockage to conjugation is thus removed, and the characteristic conjugated chromophore of hydrogenobyrinic acid (**12**) can be established with consequent thermodynamic gain. Reaching hydrogenobyrinic acid (**12**) marked the end of an era; the mystery of how the corrin macrocycle of vitamin B_{12} (**1**) is biosynthesized had been solved. Further steps then lead to the is the construction of coenzyme B_{12} by a route described in the next section. It should be stressed that the research on the pathway beyond hydrogenobyrinic acid (**12**) was highly important in two ways: firstly, in its own right, to establish all the later steps up to coenzyme B_{12} in *Ps. denitrificans*, and secondly, to help solve the problem of how the corrin macrocycle is biosynthesized. Since at the outset 22 genes were known to be involved in the biosynthesis of coenzyme B_{12} (**2**), working out the function of those acting beyond hydrogenobyrinic acid (**12**) allowed crucial deductions about the earlier genes. This strategy was used to show that the products from the genes on the 8.7 kb fragment act in the pathway up to hydrogenobyrinic acid (**12**).

9. Building Coenzyme B_{12} from Hydrogenobyrinic Acid (12)

9.1. Cobalt-Free Corrinoids and the Insertion of Cobalt

The preceding sections have described the enzymes from *Ps. denitrificans* and the associated chemistry for the production of hydrogenobyrinic acid (**12**) in vitro. It has been shown that this organism also accumulates hydrogenobyrinic acid and its *a,c*-diamide **43** in vivo (even in the presence of cobalt ions) but not cobyrinic acid (**11**). This is in contrast to *Pr. shermanii*, which accumulates cobyrinic acid but not hydrogenobyrinic acid. This was the first suggestion that differences may exist in the timing of cobalt insertion in the two organisms; the early insertion process in *Pr. shermanii* was described in Section 2.



11 X = Y = OH, M = Co^{2+}
12 X = Y = OH, M = H
41 X = NH_2, Y = OH, M = H
42 X = NH_2, Y = OH, M = Co^{2+}
43 X = Y = NH_2, M = H
44 X = Y = NH_2, M = Co^{2+}

Several early observations pointed to hydrogenobyrinic acid *a,c*-diamide (**43**) as the substrate for chelation of cobalt in *Ps. denitrificans*. Firstly, in growing cultures of B_{12}-producing strains,[23, 71] as well as in Cob mutants (Table 1), the simplest cobalt-containing corrinoid detected was always cobyrinic acid *a,c*-diamide (**44**) and the most elaborate metal-free corrinoid was hydrogenobyrinic acid *a,c*-diamide (**43**). Secondly, metal-free corrinoids were shown to exhibit much higher affinities for the *a,c*-diamide synthase (CobB) than their cobalt-containing counterparts. Thirdly, CobB mutants accumulate not cobyrinic acid (**11**) but hydrogenobyrinic acid (**12**).[71] From this set of observations, it seemed highly probable that the pathway from hydrogenobyrinic acid (**12**) proceeds by amidation at positions *a* and *c*,[72] followed by cobalt chelation.

Table 1. Cob mutants blocked after completion of the macrocycle.

Mutant strain [a]	Pigment accumulated [d]	Complemented by
G 635, G 2636 [b], G 2638 [b]	hydrogenobyrinic acid **12**	*cobB*
G 622, G 623, G 630	hydrogenobyrinic acid **12** and diamide **43**	*cobN*
G 2035	hydrogenobyrinic acid **12** and -diamide **43**	*cobS*
G 2034, G 2037	none	*cobT*
G 631, G 632, G 633	cobyrinic acid diamide **44**	*cobO*
G 624, G 626	cobyrinic acid diamide **44**	*cobQ*
G 634	cobyric acid **48**	*cobD*
G 643, G 572 [c]	cobyric acid **48**	*cobC*
G 642, G 2043	cobinamide **49**	*cobP*
G 2038, G 2039, G 2040	GDP-cobinamide **51**	*cobV*

[a] Mutant of *A. tumefaciens* C58-C9 Rif^r unless otherwise mentioned [9]. [b] Mutant of *Ps. denitrificans* SC510 [13]. [c] Mutant of *Ps. putida* KT2440 Amp^r Rif^r [9]. [d] Pigments accumulated by mutants of *cobQ* onwards would initially be adenosylated, as shown in structures **47** - **49** and **51**, but were identified after loss of the adenosyl group.

9.2. Hydrogenobyrinic Acid *a,c*-Diamide Synthase

In order to develop an assay for the amidation activity, an HPLC method developed for the detection of cobalt corrinoids[23] was extended to metal-free corrinoids by using fluorescence detection.[71] This method provided proof that crude cell extracts from *Ps. denitrificans* transform hydrogenobyrinic acid (**12**) and cobyrinic acid (**11**) into their respective *c*-monoamide (**41** and **42**) and *a,c*-diamide derivatives (**43** and **44**) in presence of ATP/Mg^{2+} and glutamine.[71] The enzyme catalyzing the two amidation reactions was purified to homogeneity from a recombinant strain exhibiting 20 times the normal activity. This strain harbored a multicopy plasmid carrying five *cob* genes from complementation group C (*cobA* to *E*).[9, 13] N-Terminal amino acid sequencing and estimation of the molecular weight (45000) of the denatured enzyme by gel electrophoresis established that *cobB* is the gene coding for this enzyme.[71, 13] Under nondenaturing conditions an apparent molecular weight of 86000 was observed, indicating formation of a dimer.

Studies of the substrate specifities of this enzyme from *Ps. denitrificans* showed that the *c* side chain is amidated first followed by that at *a*. This sequence is the same as that deduced for *Pr. shermanii* and *Clostridium tetanomorphum* on the basis of isolation and incorporation of partially amidated intermediates using intact cells.[73] However, in these two organisms the substrates are the cobalt corrinoids, whereas for *Ps. denitrificans* the natural substrates are the metal-free corrinoids, which are much better substrates ($K_M < 1\,\mu M$) than the corresponding cobalt complexes ($K_M > 100\,\mu M$). Neither the acetate carboxyl group *g* nor any of the propionate carboxyl groups were amidated by the CobB enzyme. Comparison of the amino acid sequence of CobB with those of other amidotransferases suggested that the "glutamine amide transfer" domain[74] is located at the carboxy terminus of CobB, and allowed the prediction that the cysteine at position 326 is the active site residue involved in "covalent catalysis" of amide transfer.

9.3. Cobalt Insertion into Hydrogenobyrinic Acid *a,c*-Diamide (43)

Assaying for corrinoids by HPLC was again decisive in the detection of cobaltochelatase activity in *Ps. denitrificans*. In the presence of cobalt (Co^{2+}) and ATP/Mg^{2+}, hydrogenobyrinic acid *a,c*-diamide (**43**) was efficiently converted into its cobalt complex **45** (Scheme 19), whereas hydrogenobyrinic acid (**12**) was a much poorer substrate for cobalt insertion. Amplified chelatase activity was detected in strains harboring plasmids containing a 3.8 kb gene named *cobN*.[75]

During purification of cobaltochelatase, it emerged that in addition to the *cobN* gene product another protein component was also required. The two components were purified to homogeneity separately. CobN was shown to be a monomeric enzyme with a molecular weight of 140000, whereas its partner was an oligomer with a molecular weight of about 450000, consisting of two subunits with molecular weights of 38000 and 80000. After N-terminal amino acid sequencing, these subunits were shown to be encoded by *cobS* and *cobT*, respectively, the two *cob* genes from complementation group B.[16, 75] The oligomer component of cobaltochelatase was thus called CobST.

Although accumulation of metal-free corrinoids by strains mutated in the *cobN* and *cobS* genes had clearly indicated that these two genes were involved in cobalt insertion (Table 1), *cobT* had earlier been thought to have a different role. In addition, no homology between any of the three genes and the gene coding for ferrochelatase (the enzyme that inserts Fe^{2+} into protoporphyrin to make heme) could be found. Surprisingly, CobST activity was not significantly enhanced in extracts from strains in which *cobS* and *cobT* were amplified.[16, 75]

So far, the individual roles played by CobN and CobST in catalysis have not been elucidated. Binding studies indicated that CobN displays affinity for hydrogenobyrinic acid *a,c*-diamide and, to a lesser extent, for the cobalt ion, whilst CobST possesses one reactive SH group and an ATP-binding site.[75] This latter feature agrees well with the presence on the sequence of CobS of a phosphate-binding motif common to a number of ATP-binding proteins.[16, 76] Both ferrochelatase[77] and magnesium chelatase,[78] involved in heme and chlorophyll synthesis, respectively, are also reported to have a reactive SH group.

The strict dependence of cobaltochelatase activity on hydrolyzable ATP is interesting and magnesium chelatase is also apparently a complex ATP-dependent enzyme made up of two separable components.[78] Interestingly, CobN shows 28% and 22% identity (Table 2) with Oli and BchH, respectively, two proteins that could be involved in Mg^{2+} chelation during (bacterio)chlorophyll biosynthesis.[114, 115] In contrast to ferrochelatase, cobaltochelatase cannot use metals other than cobalt. Comparison of the affinities of the enzyme for hydrogenobyrinic acid (**12**) and its *a,c*-diamide **43** provided clear additional proof that the latter is the physiological substrate for the chelation step.[75] Finally, spectrophotometric monitoring of the reaction carried out under anaerobic conditions allowed identification of the Co^{II} complex, cob(II)yrinic acid *a,c*-diamide (**45**), rather than the Co^{III} complex **44**, as the reaction product, thus establishing that no overall redox change occurs during the cobalt insertion step.[75]

9.4. Reduction of Cob(II)yrinic acid *a,c*-diamide (45) to Co^{I} Complex 46 and Adenosylation

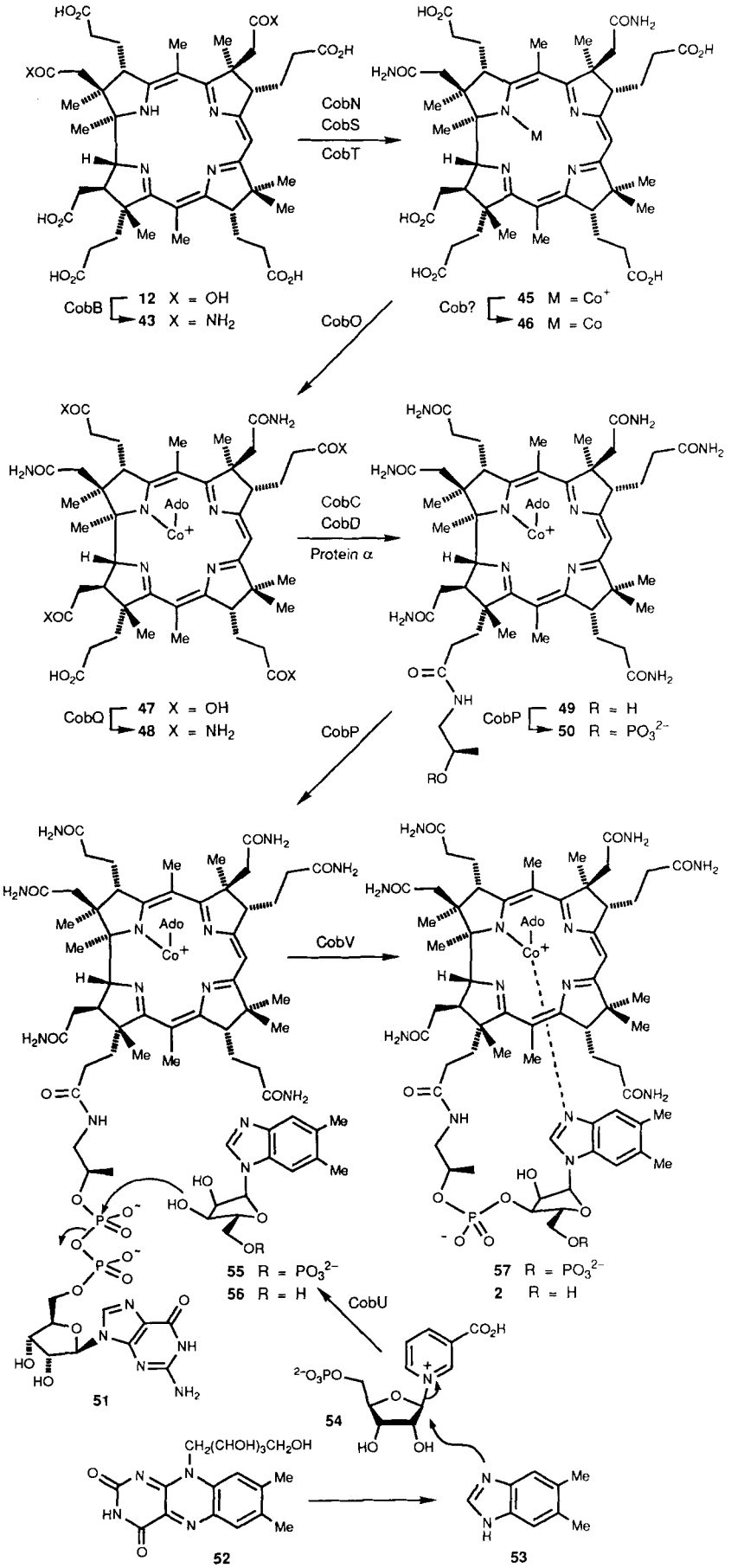
The pioneering work from Bernhauer's group[79] indicated early attachment of the adenosyl group as the upper ligand of cobalt during B_{12} biosynthesis in *Pr. shermanii*. Five partially amidated cobalt corrinoids (di- to hexaamides) can be isolated from cultures of *Ps. denitrificans*, and all are present in their adenosyl forms **47** to **48** (Scheme 19).[80] Thus it appears that the two organisms work in the same way.

It was known[81] that adenosylation of cobalamin in bacteria and eukaryotic cells involves the very nucleophilic Co^{I} corrinoid. Therefore, the next step after insertion of cobalt in *Ps. denitrificans* was expected to be reduction of cob(II)yrinic acid *a,c*-diamide (**45**) to the corresponding Co^{I} derivative **46** by a reductase enzyme. This activity was sought by using two complementary assays[82] differing in the way the extremely labile Co^{I} corrinoid **46** was trapped. In the first assay, the Co^{I} corrinoid was alkylated in situ by radioactive iodoacetic acid, and in

the second assay, the trapping was carried out enzymically by cob(I)alamin adenosyltransferase.[83] These assays allowed cob(II)yrinic acid *a,c*-diamide reductase to be purified 6300-fold to homogeneity. This enzyme is a dimer with a subunit molecular weight of roughly 16000 and was shown to be an NADH-dependent flavoprotein. Analysis of its N-terminal sequence revealed that the corresponding gene was not located on any of the four DNA fragments reported to encode cobalamin biosynthetic enzymes in *Ps. denitrificans*.

The purified enzyme catalyzes the reduction of Co^{II} to Co^{I} in all Co^{II} corrinoids from cob(II)yrinic acid *a,c*-diamide (**45**) to cob(II)alamin (as **1**). Its flavin cofactor is easily dissociable, and the enzyme is totally inactive without an added flavin; flavin mononucleotide (FMN) gives twice the activity that flavin adenine dinucleotide (FAD) does and is probably the preferred natural cofactor.[82] The cob(II)alamin reductase (EC 1.6.99.9), previously partially purified from *C. tetanomorphum*,[84] displayed a similar behavior, suggesting that it is identical in function to the cob(II)yrinic acid *a,c*-diamide reductase in *Ps. denitrificans*.

The adenosylating enzyme from *Ps. denitrificans* was also purified and characterized.[83] The procedures previously used for assaying cob(I)alamin adenosyltransferase activity (EC 2.5.1.17) from *Pr. shermanii* and *C. tetanomorphum*[81] were adapted to monitor adenosylation of any corrinoid by HPLC. A cell extract from a *Ps. denitrificans* strain in which the *cobO* gene was amplified was used as starting material for the purification because it had an elevated adenosylating activity. The purified enzyme, CobO, is a 27 kDa polypeptide encoded by *cobO*. It exists as a dimer and displays a substrate specificity similar to that of cob(II)yrinic acid *a,c*-diamide reductase, in other words, most Co^{I} corrinoids are adenosylated but not cob(I)yrinic acid. Apparently it only has an affinity for corrinoids with amidated *a* and/or *c* acetate side chains. In keeping with this, hydrogenobyrinic acid *a,c*-diamide strongly inhibited the enzyme and was found tightly bound to CobO in vivo.[85] The accumulation of cobyrinic acid *a,c*-diamide (**44**) by CobO mutants[83] (Table 1) supported the view that the main physiological function of CobO is adenosylation of cob(I)yrinic acid *a,c*-diamide (**46**) to give adenosylcobyrinic acid *a,c*-diamide (**47**).



Scheme 19. Biosynthetic pathway from hydrogenobyrinic acid (**12**) to coenzyme B_{12} (**2**).

9.5. From Adenosylcobyrinic Acid *a,c*-Diamide (47) to Adenosylcobinamide (49)

Early studies with *Pr. shermanii* led to ambiguous conclusions with regard to the sequence of amidations of peripheral carboxyl groups *b*, *d*, *e*, and *g*, and of attachment of (*R*)-1-amino-2-propanol.[73] Some authors concluded that the amidations follow a preferred but not strictly obligatory route and that the (*R*)-1-amino-2-propanol group is introduced at a stage that depends on cultivation conditions, whereas others suggested that (*R*)-1-amino-2-propanol is incorporated only after completion of the six other amidations and that the amidations follow one unique sequence. There is evidence that (*R*)-1-amino-2-propanol is derived from L-threonine,[73] but no threonine decarboxylase has been detected in vitamin B_{12} producing organisms.

In *Ps. denitrificans* the incompletely amidated cobalt corrinoids accumulated by growing cells have been purified and identified as adenosylcobyrinic acid *a,c*-diamide (**47**), triamide, tetraamide, and pentaamide as well as adenosylcobyric acid (**48**). The HPLC analyses were carried out after removal of the adenosyl group. Adenosylcobinamide (**49**) was also found in substantial amounts, whereas cobinic acids (which have the aminopropanol group attached but lack some or all of the primary amide groups) could not be detected, suggesting that the amidations precede insertion of (*R*)-1-amino-2-propanol.[80]

Meanwhile, it was found that extracts from strains of *Ps. denitrificans* with a plasmid containing the *cobQ* gene were capable of amidating adenosylcobyrinic acid *a,c*-diamide (**47**). As for the previous amidating enzyme, CobB, this activity required glutamine as the amino donor and ATP/Mg^{2+}. The enzyme responsible for the activity was purified to homogeneity and was indeed identified by its N-terminal sequence as the product of the *cobQ* gene.[80] This enzyme also is a homodimer, with a subunit molecular weight of around 57000. It was shown to catalyze all four amidations from adenosylcobyrinic acid *a,c*-diamide (**47**) to adenosylcobyric acid (**48**) via adenosylated cobyrinic acid triamide, tetraamide, and pentaamide intermediates. Corrinoids lacking the adenosyl group are not substrates.[80] HPLC separation of the intermediates (after replacement of the adenosyl group by cyanide) gave only one peak for each intermediate, suggesting that there is a single sequence of amidations performed by this enzyme.[80] It is perhaps not too surprising that a single enzyme is capable of amidating the three propionate carboxyl groups *b*, *d*, and *e*, but it is certainly interesting that it avoids amidating the fourth propionate group, *f*, whereas it does amidate the remaining acetate carboxyl group, *g*. Comparison of the CobB and CobQ sequences indicates 22% amino acid identity in the two enzymes. This finding leads to the prediction that the conserved cysteine at position 333 in CobQ is the active site residue involved in covalent catalysis.[74]

The enzymic system catalyzing the attachment of aminopropanol to adenosylcobyric acid (**48**) in *Ps. denitrificans* was found by ion-exchange HPLC to comprise two components designated α and β, both necessary for regaining overall activity.[85] The reaction was dependent on ATP/Mg^{2+} and (*R*)-1-amino-2-propanol (K_M 20 mM), and no activity was observed with (*S*)-1-amino-2-propanol or threonine. The enzyme was specific for adenosylcobyric acid (**48**) (K_M 1.6 μM), only weakly active on adenosylcobyrinic acid pentaamide (20% of the control), and inactive on the tetra-, tri-, and diamides. Protein α was purified 50000-fold to homogeneity; it is a 38 kDa polypeptide, the N-terminal sequence of which was not found on any of the four DNA fragments from *Ps. denitrificans* that encode B_{12} biosynthetic enzymes. Protein β was purified 1000-fold and was shown to be part of a large multiprotein complex of molecular mass >1 MDa which was not retained by any gel permeation FPLC column.

Cob mutants of *A. tumefaciens* and *Ps. putida* blocked in either *cobC* or *cobD* had been shown to accumulate adenosylcobyric acid (**48**) (Table 1), indicating that the products of the *cobC* and *cobD* genes are parts of the aminopropanol-attaching enzyme system.[13] To confirm this conclusion, two *E. coli* strains expressing either *cobC* alone or *cobC* and *D* together were constructed.[86] Extracts from the *cobCD* strain exhibited aminopropanol-attaching activity only when supplemented with protein α, indicating that protein β is probably made up of CobC and CobD. Extracts from the strain expressing CobC showed no activity when assayed under the same conditions.[85] In keeping with these results, cell extracts from a *Ps. denitrificans* strain overexpressing the *cobABCD* genes exhibited a tenfold higher level of protein β than the parent strain. Genetic studies have indicated that in *Salmonella typhimurium*[45] also, three genes are involved in the addition of the aminopropanol side chain.

10. From Adenosylcobinamide (49) to Coenzyme B_{12} (2): Building of the Nucleotide Loop

The assembly of the nucleotide loop is the final stage of the pathway to coenzyme B_{12}, and in *Pr. shermanii* this involves a four-step process.[87] It is probable that all the intermediates are adenosylated[79] in this organism also, but much of the early work only identified the compounds after removal of this labile group. However, the adenosylated form of cobyrinic acid *a,c*-diamide (**47**) has recently been isolated and identified from this source.[88] The first step is phosphorylation of the hydroxyl group of the (*R*)-1-amino-2-propanol residue of adenosylcobinamide (**49**) using ATP to yield adenosylcobinamide phosphate (**50**). Transfer of the guanosyl monophosphate (GMP) moiety from a molecule of the triphosphate (GTP) then gives adenosyl-GDP-cobinamide (**51**). Addition of α-ribazole 5′-phosphate (**55**) to the adenosyl-GDP-cobinamide, with loss of the GMP moiety again, yields adenosylcobalamin 5′-phosphate (**57**). Finally, dephosphorylation of this 5′-phosphate leads to adenosylcobalamin (**2**). Noteworthy is the need for a branch to the main pathway for the synthesis of α-ribazole 5′-phosphate (**55**), which is only required for the biosynthesis of coenzyme B_{12}. Methods for the synthesis of the cyano forms of these corrinoid intermediates have been described.[89]

Until our recent work, few studies on the enzymes involved in this part of the pathway had been reported, and the exact number of enzymes and genes necessary to reach coenzyme B_{12} from cobinamide was unknown. Our study began with the isolation and identification of the intermediates in their natural adenosylated forms.[90]

10.1. From Adenosylcobinamide (49) to Adenosyl-GDP-cobinamide (51)

The studies described in Section 9.5 provided adenosylcobinamide (**49**) and an HPLC system for assaying adenosylcorrinoids.[123] These were used in setting up an assay of ATP-dependent phosphorylation of **49**, and the range of strains overexpressing *cob* genes[9] was tested. It was found that genetic amplification of the *cobP* gene substantially increased the level of cobinamide kinase activity normally present in cell extracts.[90] This result was in agreement with the complementation studies, which showed that B_{12} production in strain G 642, a Cob mutant that accumulated adenosylcobinamide (**49**) (Table 1), was restored by introduction of a plasmid containing *cobP*.[9] Concurrently, cobinamide kinase was purified to homogeneity from a strain of *Ps. denitrificans* containing the same plasmid and was found to be a bifunctional enzyme catalyzing phosphorylation and also the next step, transfer of the GMP moiety from GTP to give adenosyl-GDP-cobinamide (**51**).[90] The N-terminal sequence of the purified enzyme identified it as the *cobP* gene product.[15]

This CobP enzyme was therefore a novel and interesting addition to the family of multifunctional Cob enzymes, which includes CobA, CobJ, CobF, CobL, CobB, and CobQ. It is surprisingly small for a bifunctional, homodimeric enzyme, with a subunit molecular weight of only 19442. In many proteins that bind ATP or GTP two consensus sequences make up the nucleotide triphosphate binding sites, but for CobP only one region matching these consensus sequences could be found for each of these substrates.[90] The most striking feature of the catalytic properties of CobP was that GTP is not only the substrate for the second reaction catalyzed by CobP, but it is also a regulator for the first step. It binds with high affinity (K_D 0.22 μM), causing the affinity of the enzyme for its initial substrate, adenosylcobinamide (**49**), to be lowered from 11.5 to 0.4 μM.[90]

In support of the above results, recent genetic studies have demonstrated that a gene[91] from *S. typhimurium*[45, 92] is homologous to *cobP*, and that the corresponding enzyme is responsible for the same two steps catalyzed by CobP; in addition the *S. typhimurium* enzyme seems to have a further function in the assimilation of nonadenosylated cobinamide.[93]

10.2. The α-Ribazole Branch of the Pathway

α-Ribazole (**56**) is an atypical nucleoside in which the unusual base 5,6-dimethylbenzimidazole (DMBI, **53**) is linked by an N-α-glycosidic bond to ribose. Nicotinate-nucleotide:dimethylbenzimidazole phosphoribosyltransferase, also called trans-*N*-glycosidase (EC 2.4.2.21), catalyzes the formation of α-ribazole 5′-phosphate (**55**) from DMBI **53** and β-nicotinate mononucleotide (**54**). This enzyme was partially purified from *Pr. shermanii* by Friedmann.[94] Recently, this enzyme has been purified to homogeneity from a recombinant strain of *Ps. denitrificans* which has the cobU gene amplified and shows an elevated trans-*N*-glycosidase activity.[17] Again the enzyme exists as a homodimer with a subunit molecular weight of 34640. The purified protein was confirmed as the product of the *cobU* gene by its N-terminal sequence. Hydrolysis of α-ribazole 5′-phosphate (**55**) to give α-ribazole (**56**) is carried out in *Pr. shermanii* by a 5′-phosphatase,[95] and this activity is also present in *Ps. denitrificans*.[17]

As DMBI **53** is a component of the standard medium used for growing *Ps. denitrificans* in all our studies,[9] its biosynthesis has not been studied in this organism. However, the conversion of riboflavin (**52**) into DMBI was demonstrated by Renz et al.[96] with crude cell extracts from *Pr. shermanii*, and mechanistic aspects of this transformation are still under investigation.[96b] The requirement for molecular oxygen makes this pathway unlikely in anaerobes, however, and an alternative pathway has recently been proposed for *Eubacterium limosum*.[97] Mutants blocked in the formation of DMBI **53** have been isolated in *S. typhimurium*.[98]

10.3. From Adenosyl-GDP-cobinamide (51) to Coenzyme B_{12} (2)

The last enzyme of the pathway was shown to transfer the adenosylcobinamide phosphate moiety of adenosyl-GDP-cobinamide (**51**) to either α-ribazole (**56**) or its 5′-phosphate **55** to yield adenosylcobalamin (**2**) or its 5′-phosphate **57**. The enzyme also accepted as substrate GDP-cobinamide lacking the adenosyl group[17] and was therefore named cobalamin (5′-phosphate) synthase. It was overexpressed by a factor of 90 in a *Ps. denitrificans* strain carrying a *cobV*-containing plasmid, from which it was purified 55-fold.[17] The most enriched preparations were not homogeneous but apparently consisted of a soluble high molecular weight protein complex made up of six separate proteins. Overexpression of a truncated *cobV* gene (20 codons missing) in *E. coli* also resulted in a significant increase of the cobalamin (5′-phosphate) synthase activity.[17] In addition, two Cob mutants that accumulated GDP-cobinamide (**51**) have their mutations complemented by a plasmid that carries the *cobV* gene[12] (Table 1). All these data provide evidence that *cobV* encodes cobalamin (5′-phosphate) synthase, although direct comparison of the amino acid sequence of the enzyme with that predicted from the gene sequence has not yet been possible.

11. Genetic Analysis of the Four *Ps. denitrificans* Genomic Loci Involved in Cobalamin Synthesis

There is a neat correlation between the genetic organization of the genes (Fig. 1) and the part of the pathway on which their products act. Complementation group C carries *cobA* encoding the first methyltransferase. Then complementation group A codes for all the enzymes involved in the conversion of precorrin-2 (**9**) into hydrogenobyrinic acid (**12**). The products of complementation group C allow the transformation of **12** into adenosyl-GDP-cobinamide (**51**) with CobS and CobT (the only two genes in complementation group B) necessary for cobalt insertion. The formation of α-ribazole phosphate (**55**) and the last step of the pathway require enzymes coded by complementation group D. *Bacillus megaterium* also has four different complementation groups,[99] but in *S. typhimurium* most of the genes are clustered at minute 41.[45] It is worthwhile noting that the genetic and molecular biology studies on these latter two

organisms alone did not lead to any major advances in the knowledge of the biosynthetic steps. Contributions from chemical and enzymological studies are essential, as we hope this review has made clear.

Since the sequences of the 22 Cob proteins in *Ps. denitrificans* were reported,[13-17] the sequences of *cob* genes from other bacteria have been described. The *Ps. denitrificans* Cob proteins have homologues involved in cobalamin synthesis in *S. typhimurium*, *B. megaterium*, *Rhodococcus sp*, *Rhizobium meliloti*, and *E. coli*; the relevant genes and the degree of identity of the proteins are shown in Table 2. In *S. typhimurium* a large number of genes involved in cobalamin synthesis have been cloned and identified.[45] By comparing the sequences of the proteins with those from *Ps. denitrificans*, whose functions are established, likely roles for the *S. typhimurium* proteins have been proposed.[45] However, no homologues have been found in *S. typhimurium* for CobC, E, F, G, N, S, T, and W produced by *Ps. denitrificans*. Conversely, no homologues are known in *Ps. denitrificans* for three genes in *S. typhimurium* (CbiN, CbiQ, and CbiO) which are thought to be involved in cobalt transport.

Escherichia coli has not been shown to synthesize cobalamin, but it does use exogenous cobinamide (**49** without the adenosyl group) to build coenzyme B_{12} (**2**). This organism does have homologues to four proteins of *Ps. denitrificans*, CobA, CobO, CobU, and CobV (see Table 2), and to the corresponding four proteins from *S. typhimurium* with a high degree of identity. The homologue of CobA, which is CysG in *E. coli*, catalyzes the methylation of uro'gen III **7** to give precorrin-2 (**9**), as well as the subsequent oxidation and insertion of iron required for the synthesis of siroheme,[100] whilst the homologues of the other three enzymes are involved in the assimilation of above non-adenosylated cobinamide. The fact should also be noted that the various methyltransferases (CobA, I, F, J, L, and M, and CysG) all share some homology with each other and with motifs found in most, if not all, SAM-dependent methyltransferases.[101]

Identification of the *cob* genes in *Ps. denitrificans* has allowed the effect of gene amplification on the level of synthesis of cobalamin to be studied. Amplification of a fragment carrying the *cobF* to *cobL* genes led to a 30% increase in cobalamin synthesis in a low cobalamin-producing strain, whereas amplification of *cobA* and *cobE* resulted in a twofold increase.[18] These results illustrate how effective genetic engineering can be for the improvement of strains used for the industrial production of compounds such as vitamin B_{12}.

Table 2. The genes of B_{12} biosynthesis in the order in which they are involved.

Enzyme	*Ps. denitrificans* Gene	Cluster	*S. typhimurium* Gene [45]	Ident. [a]	Other organisms Organism	Gene	Ident. [a]
C-2,C-7 methylase (SUMT) [105]	*cobA* [13]	C	*cysG* [107]	43.2	*Bacillus megaterium*	*cobA* [108]	43.5 [b]
					Escherichia coli	*cysG* [100]	41.6 [c]
					Methanobacterium ivanovii	*corA* [109]	40.4 [b]
C-20 methylase (SP_2MT) [106]	*cobI* [14]	A	*cbiL*	32.2			
precorrin-3B synthase [55]	*cobG* [14]	A	–		*S. typhimurium*	*cysI* [110]	24.1
					Anacystis nidulans	*sir* [111]	26.1
					Nicotiana tabacum	*nir-1* [112]	23.6
C-17 methylase [55]	*cobJ* [14]	A	*cbiH*	41.7			
C-11 methylase [55]	*cobM* [14]	A	*cbiF*	41.1	*Rhodococcus sp*	*cobM* [113]	56.9 [b]
C-1 methylase [55]	*cobF* [14]	A	–				
precorrin-6A reductase [30]	*cobK* [30]	A	*cbiJ*	24.4	*Rhodococcus sp*	*cobK* [113]	49.0 [b]
C-5,C-15 methylase/	*cobL* [14]	A	*cbiE*	31.9	*Rhodococcus sp*	*cobL* [113]	40.9 [b]
C-12 decarboxylase [39]			*cbiT*	30.9			
C-11 → C-12 mutase [42]	*cobH* [14]	A	*cbiC*	34.1			
Hby-*a,c*-diamide synthase [71]	*cobB* [13]	C	*cbiA*	32.0			
cobaltochelatase subunits [75]	*cobN* [15]	C	–		*Antirrhinum majus*	*oli* [114]	28.0
					Rhodobacter capsulatus	*bchH* [115]	21.7
	cobS [16]	B	–				
	cobT [16]	B	–				
cob(II)yrinic acid *a,c*-diamide reductase [82]	–	–	–				
cob(I)alamin adenosyl transferase [83]	*cobO* [15]	C	*cobA* [117]	41.4	*Escherichia coli*	*btuR* [116]	43.4 [c]
cobyric acid synthase [80]	*cobQ* [15]	C	*cbiP*	43.7	*Methanococcus voltae*	ORF230 [d] [118]	45.8 [b]
cobinamide synthase subunits [85]	*cobC* [13]	C	–		*S. typhimurium*	*hisC* [119]	24.9
	cobD [13]	C	*cbiB*	36.7			
	–	Protein α	–				
cobinamide kinase/cobinamide phosphate guanylyl transferase [90]	*cobP* [15]	C	*cobU*	40.6			
cobalamin(5'-phosphate) synthase [17]	*cobV* [17]	D	*cobS*	34.4	*Escherichia coli*	*cobS* [120]	32.1 [c]
nicotinate nucleotide: DMBI phosphoribosyltransferase [17]	*cobU* [17]	D	*cobT*	22.1	*Escherichia coli*	*cobT* [120]	27.5 [c]
					Rhizobium meliloti	ORF1-552 [d] [121]	96.2 [b]
	cobW [15]	C	–		*Pseudomonas chlororaphis*	ORFP47K [d] [122]	25.8
	cobE [13]	C	–				

[a] Percentage amino acid identity of the proteins from *S. typhimurium* or other organisms with the homologous protein in *Ps. denitrificans*. The protein sequences from this latter organism were compared with the following data banks: NBRF (release number 38), Swissprot (release number 27), PIR (release number 38), and EMBL (release number 37 plus the new entries until December 1993). The proteins with the highest identities were aligned by using the program developed by Kanehisa (*Nucleic Acids Res.* **1984**, *12*, 203) with the same parameters (minimum length of contiguous homologous amino acids = 2, maximum length for a deletion or insertion = 25, positive value for an insertion = 8, except = 7 for CobN and BchH). [b] Protein from an organism other than *Ps. denitrificans* or *S. typhimurium* proved or likely to be a Cob protein owing to the high level of identity to one of the *Ps. denitrificans* Cob proteins. [c] This *E. coli* protein catalyzes the same reaction as the *Ps. denitrificans* homologues but cannot be properly named a Cob protein since *E. coli* has not been described to synthesize cobalamin but can only synthesize precorrin-2 (for the production of sirohaem) and convert exogenous cobinamide into adenosylcobalamin. [d] ORF: open reading frame; a stretch of DNA at the position reported which probably codes for a protein but for which the corresponding protein has not been characterized.

12. Summary and Outlook

By the end of 1993, all the intermediates on the biosynthetic pathway between uro'gen III **7** and coenzyme B_{12} (**2**) in *Ps. denitrificans* had been isolated and their structures determined. The full sweep of the pathway can be viewed by joining together Schemes 1, 18 and 19. In addition, the enzymes catalyzing each step[102] had been characterized and in most cases, purified to homogeneity. The corresponding genes for all but two[103] of these enzymes had been identified, sequenced, and overexpressed. No one reading the literature on vitamin B_{12} five years ago could have possibly imagined that by 1993 the Everest of B_{12} would have been conquered.

Although the central problem has been solved, a few points need to be clarified:

A) There are two further *cob* genes, *cobE* and *cobW*,[104] essential for B_{12} production, whose functions are unknown.

B) Parts of the branch pathways providing (*R*)-1-amino-2-propanol and 5,6-dimethylbenzimidazole should still be studied. It may be relevant that eight other genes located within gene clusters B, C, and D have not been classified as *cob* genes, because mutations in them did not prevent coenzyme B_{12} synthesis. They may be involved in dimethylbenzimidazole biosynthesis or have roles related to B_{12} biosynthesis such as cobalt or B_{12} transport or formation of methyl cobalamin.

C) Experiments must be carried out to probe the mechanism of those biosynthetic transformations involving more than simple C-methylation (e.g. the ring contraction). In addition, some stereochemical details of a few intermediates are still lacking (e.g. for precorrin-8x).

D) Since there are differences between the pathways in *Ps. denitrificans* and other organisms such as *Pr. shermanii* and *S. typhimurium*, the relationship of the intermediates in the latter two organisms to the known ones in *Ps. denitrificans* should be worked out.

E) Lastly, knowledge of the chemistry and genes of the pathway opens the way to other more biological studies into areas such as the regulation of the pathway.

This work must pass to others since the Paris–Cambridge teams, having completed their major task as described in this review, are withdrawing from the field. Satisfyingly, the approach described for the study of B_{12} biosynthesis may serve as a model for solving other complex biosynthetic problems. Undoubtedly, an essential first step is to establish an interdisciplinary team skilled in genetics, molecular biology, enzymology, structural and synthetic chemistry, isotopic labeling, and NMR spectroscopy. We look forward to seeing the routes to other complex natural substances being revealed in this way.

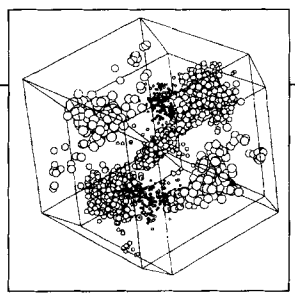
We wish warmly to thank all our colleagues for their many important contributions to the studies outlined in this review. In Paris these include L. Cauchois, S. Rigault, M.-C. Rouyez, C. Guilhot, C. Robin, M. Couder, A. Famechon, M. Chenu, J.-C. Muller, L. Maton, D. Bisch, M. Danzer, B. Monegier, D. Frechet, F. Herman, F. Debu, M.-H. Beydon, M. Rose, L. Naudin, and L. Louvel. In Cambridge they are A. I. D. Alanine, S. Balachandran, K. Ichinose, F. Kiuchi, M. Kodera, Y. Li, S. M. Monaghan, A. R. Pitt, A. Prelle, N. P. J. Stamford, R. A. Vishwakarma, and G. W. Weaver. We gratefully acknowledge financial support from the British Science and Engineering Research Council (SERC), Hoffmann La Roche, Roche Products, Zeneca, the Leverhulme Trust, and Rhône-Poulenc Rorer. We also extend thanks to J. Lunel, B. Brunie, A. Brun, M. Courtier, J.-F. Mayaux, P. E. Bost, J.-B. Le Pecq, and J.-C. Brunie for their constant support, to R. De Mot for providing results prior to publication, to Prof. G. Müller, Stuttgart, for his enthusiastic collaboration, and to him and Dr. C. Abell, Cambridge, for valuable discussions.

Received: April 27, 1994 [A64 IE]
German version: *Angew. Chem.* **1995**, *107*, 421

[1] J. P. Kusel, Y. H. Fa, A. L. Demain, *J. Gen. Microbiol.* **1984**, *130*, 835; F. Blanche, M. Couder, unpublished.
[2] Review: A. R. Battersby, F. J. Leeper, *Chem. Rev.* **1990**, *90*, 1261.
[3] a) A. R. Battersby, E. McDonald in B_{12}, *Vol. 1* (Ed.: D. Dolphin), Wiley, New York, **1982**, p. 107; b) A. R. Battersby, *Acc. Chem. Res.* **1986**, *19*, 147; c) *ibid.* **1993**, *26*, 15; d) A. I. Scott, *ibid.* **1990**, *23*, 308; *Angew. Chem.* **1993**, *105*, 1281; *Angew. Chem. Int. Ed. Engl.* **1993**, *32*, 1223.
[4] S. H. Ford, *Biochim. Biophys. Acta* **1985**, *841*, 306; A. A. Yeliseev, A. V. Pushkin, N. I. Zaitseva, Z. G. Evstigneeva, V. Ya. Bykhovsky, W. L. Kretovich, *ibid.* **1986**, *880*, 131.
[5] Biosynthetic intermediates that occur on the pathway before the first corrin macrocycle is generated are called precorrins. A number is attached corresponding to the number of C-methyl groups that have been introduced from *S*-adenosylmethionine (SAM) to produce that intermediate. Where two or more intermediates carry the same number of SAM-derived methyl groups, they are distinguished by adding letters to the number with A being added for the first such intermediate, B for the second, and so on. In some cases, temporary letters (x and y) have been used until the status of a particular intermediate became clear, so allowing the correct designation to be given later; for example, what was precorrin-6x is now precorrin-6A and precorrin-6y is precorrin-6B. For further details see H. C. Uzar, A. R. Battersby, T. A. Carpenter, F. J. Leeper, *J. Chem. Soc. Perkin Trans. 1* **1987**, 1689.
[6] G. Müller, K. Hlineny, E. Savvidis, F. Zipfel, J. Schmiedl, E. Schneider in *Chemical Aspects of Enzyme Biotechnology* (Eds.: T. B. Baldwin, F. M. Rushel, A. I. Scott), Plenum, New York, **1990**, p. 281; G. Müller, F. Zipfel, K. Hlineny, E. Savvidis, R. Hertle, U. Traub-Eberhard, A. I. Scott, H. J. Williams, N. J. Stolowich, P. J. Santander, M. J. Warren, F. Blanche, D. Thibaut, *J. Am. Chem. Soc.* **1991**, *113*, 9893.
[7] S. Balachandran, R. A. Vishwakarma, S. M. Monaghan, A. Prelle, N. P. J. Stamford, F. J. Leeper, A. R. Battersby, *J. Chem. Soc. Perkin Trans. 1* **1994**, 487.
[8] G. Müller, R. Deeg, K. D. Gneuss, G. Gunzer, H.-P. Kriemler in *Vitamin* B_{12} (Eds.: B. Zagalak, W. Friedrich), de Gruyter, Berlin, **1979**, p. 279.
[9] B. Cameron, K. Briggs, S. Pridmore, G. Brefort, J. Crouzet, *J. Bacteriol.* **1989**, *171*, 547.
[10] Names in italics beginning with a lowercase letter (e.g. *cobA*) refer to the genes, whereas those with a capital C in standard type (e.g. CobA) are for the proteins (enzymes).
[11] D. E. Berg, C. M. Berg, *Bio/Technology* **1983**, *1*, 417.
[12] J. Crouzet, unpublished.
[13] J. Crouzet, L. Cauchois, F. Blanche, L. Debussche, D. Thibaut, M.-C. Rouyez, S. Rigault, J.-F. Mayaux, B. Cameron, *J. Bacteriol.* **1990**, *172*, 5968.
[14] J. Crouzet, B. Cameron, L. Cauchois, S. Rigault, M.-C. Rouyez, F. Blanche, D. Thibaut, L. Debussche, *J. Bacteriol.* **1990**, *172*, 5980.
[15] J. Crouzet, S. Lévy-Schil, B. Cameron, L. Cauchois, S. Rigault, M.-C. Rouyez, F. Blanche, L. Debussche, D. Thibaut, *J. Bacteriol.* **1991**, *173*, 6074.
[16] B. Cameron, C. Guilhot, F. Blanche, L. Cauchois, M.-C. Rouyez, S. Rigault, S. Lévy-Schil, J. Crouzet, *J. Bacteriol.* **1991**, *173*, 6058.
[17] B. Cameron, F. Blanche, M.-C. Rouyez, D. Bisch, A. Famechon, M. Couder, L. Cauchois, D. Thibaut, L. Debussche, J. Crouzet, *J. Bacteriol.* **1991**, *173*, 6066.
[18] J. Crouzet, B. Cameron, F. Blanche, D. Thibaut, L. Debussche in *Industrial Microorganisms: Basic and Applied Molecular Genetics* (Eds.: R. H. Baltz, G. D. Hegeman, P. L. Skatrud), ASM, Washington, DC, **1993**, p. 195.
[19] F. Blanche, D. Thibaut, D. Frechet, M. Vuilhorgne, J. Crouzet, B. Cameron, K. Hlineny, U. Traub-Eberhard, M. Zboron, G. Müller, *Angew. Chem.* **1990**, *102*, 947; *Angew. Chem. Int. Ed. Engl.* **1990**, *29*, 884.
[20] B. Dresow, G. Schlingmann, L. Ernst, V. B. Koppenhagen, *J. Biol. Chem.* **1980**, *255*, 7637.
[21] V. B. Koppenhagen in B_{12}, *Vol. 2* (Ed.: D. Dolphin), Wiley, New York, **1982**, p. 105.
[22] If used as soon as it is formed, precorrin-3A (**10**) can be employed directly as the substrate for enzymic conversion into later intermediates on the pathway. However, since it undergoes ready oxidation in air, deliberate oxidation is often used to yield the didehydro derivative (an isobacteriochlorin), which is isolated and stored as its stable ester. Subsequent hydrolysis of the ester groups gives the acid, which conveniently undergoes enzymic reduction back to precorrin-3A on incubation with the complete enzyme system from *Ps. denitrificans* and either NADH or NADPH. The biosynthetic steps that follow precorrin-3A (**10**) then proceed normally.

[23] F. Blanche, D. Thibaut, M. Couder, J.-C. Muller, *Anal. Biochem.* **1990**, *189*, 24.
[24] D. Thibaut, L. Debussche, F. Blanche, *Proc. Natl. Acad. Sci. USA* **1990**, *87*, 8795.
[25] A. R. Battersby, C. Edington, C. J. R. Fookes, J. M. Hook, *J. Chem. Soc. Perkin Trans. 1* **1982**, 2265.
[26] L. Ernst, *Liebigs Ann. Chem.* **1981**, 376.
[27] D. Thibaut, F. Blanche, L. Debussche, F. J. Leeper, A. R. Battersby, *Proc. Natl. Acad. Sci. USA* **1990**, *87*, 8800.
[28] Ready conversion of one double-bond tautomer into another can occur in the macrocyclic B_{12} intermediates. Thus, precorrin-6A (**16**) may have a double bond from N to C-9 rather than at C-8/C-9, which is certainly its position in the isolated ester **17**. These close tautomers are included when one refers to precorrin-6A, and the same holds for all the other structures in this review.
[29] F. Blanche, M. Kodera, M. Couder, F. J. Leeper, D. Thibaut, A. R. Battersby, *J. Chem. Soc. Chem. Commun.* **1992**, 138.
[30] F. Blanche, D. Thibaut, A. Famechon, L. Debussche, B. Cameron, J. Crouzet, *J. Bacteriol.* **1992**, *174*, 1036.
[31] For example A. R. Battersby, E. McDonald, R. Neier, M. Thompson, *J. Chem. Soc. Chem. Commun.* **1979**, 960.
[32] D. Thibaut, F. Kiuchi, L. Debussche, F. J. Leeper, F. Blanche, A. R. Battersby, *J. Chem. Soc. Chem. Commun.* **1992**, 139.
[33] G. W. Weaver, F. J. Leeper, A. R. Battersby, F. Blanche, D. Thibaut, L. Debussche, *J. Chem. Soc. Chem. Commun.* **1991**, 976.
[34] F. Kiuchi, D. Thibaut, L. Debussche, F. J. Leeper, F. Blanche, A. R. Battersby, *J. Chem. Soc. Chem. Commun.* **1992**, 306.
[35] K. Ichinose, F. J. Leeper, A. R. Battersby, *J. Chem. Soc. Perkin Trans. 1* **1993**, 1213.
[36] A. R. Battersby, E. McDonald, R. Hollenstein, M. Ihara, F. Satoh, D. C. Williams, *J. Chem. Soc. Perkin Trans. 1* **1977**, 166.
[37] A. R. Battersby, C. Edington, C. J. R. Fookes, *J. Chem. Soc. Chem. Commun.* **1984**, 527; A. I. Scott, M. Kajiwara, P. J. Santander, *Proc. Natl. Acad. Sci. USA* **1987**, *84*, 6616.
[38] K. Ichinose, M. Kodera, F. J. Leeper, A. R. Battersby, *J. Chem. Soc. Chem. Commun.* **1993**, 515.
[39] F. Blanche, A. Famechon, D. Thibaut, L. Debussche, B. Cameron, J. Crouzet, *J. Bacteriol.* **1992**, *174*, 1050.
[40] Several well-defined events happen as precorrin-6B (**19**) is converted into precorrin-8x, but no intermediate has been detected. The present indications are that these events all occur in the active site of the single enzyme involved. However, evidence concerning their sequence may be gained in the future. For the time being, therefore, it is best to use the name of precorrin-8x and later either drop the x or replace it by the appropriate capital letter.
[41] Enzyme preparations from *Pr. shermanii* behave similarly; added cobyrinic acid (**11**) strongly inhibits its own formation: S. Monaghan, H. C. Uzar, A. R. Battersby, unpublished.
[42] D. Thibaut, M. Couder, A. Famechon, L. Debussche, B. Cameron, J. Crouzet, F. Blanche, *J. Bacteriol.* **1992**, *174*, 1043.
[43] D. Thibaut, F. Kiuchi, L. Debussche, F. Blanche, M. Kodera, F. J. Leeper, A. R. Battersby, *J. Chem. Soc. Chem. Commun.* **1992**, 982.
[44] A. Eschenmoser, *Angew. Chem.* **1988**, *100*, 5; *Angew. Chem. Int. Ed. Engl.* **1988**, *27*, 5.
[45] J. Roth, J. G. Lawrence, M. Rubenfield, S. Kieffer-Higgins, G. Church, *J. Bacteriol.* **1993**, *175*, 3303.
[46] A. R. Battersby, M. G. Baker, H. A. Broadbent, C. J. R. Fookes, F. J. Leeper, *J. Chem. Soc. Perkin Trans. 1* **1987**, 2027.
[47] S. Butt, S. M. Roberts, *Nat. Prod. Rep.* **1986**, *3*, 489.
[48] W. G. Whittingham, M. K. Ellis, P. Guerry, G. B. Henderson, B. Müller, D. A. Taylor, F. J. Leeper, A. R. Battersby, *J. Chem. Soc. Chem. Commun.* **1989**, 1116; B. Müller, A. N. Collins, M. K. Ellis, W. G. Whittingham, F. J. Leeper, A. R. Battersby *ibid.* **1989**, 1119.
[49] N. P. J. Stamford, A. I. D. Alanine, A. R. Pitt, B. Cameron, J. Crouzet, A. R. Battersby, unpublished.
[50] F. Blanche, S. Handa, D. Thibaut, C. L. Gibson, F. J. Leeper, A. R. Battersby, *J. Chem. Soc. Chem. Commun.* **1988**, 1117.
[51] For example A. I. Scott, H. J. Williams, N. J. Stolowich, P. Karuso, M. D. Gonzalez, F. Blanche, D. Thibaut, G. Müller, E. Savvidis, K. Hlineny, *J. Chem. Soc. Chem. Commun.* **1989**, 522.
[52] D. Thibaut, L. Debussche, D. Frechet, F. Herman, M. Vuilhorgne, F. Blanche, *J. Chem. Soc. Chem. Commun.* **1993**, 513.
[53] A. I. D. Alanine, K. Ichinose, D. Thibaut, L. Debussche, N. P. J. Stamford, F. J. Leeper, F. Blanche, A. R. Battersby, *J. Chem. Soc. Chem. Commun.* **1994**, 193.
[54] S. Ofner, V. Rasetti, B. Zehnder, A. Eschenmoser, *Helv. Chim. Acta* **1981**, *64*, 1431.
[55] L. Debussche, D. Thibaut, B. Cameron, J. Crouzet, F. Blanche, *J. Bacteriol.* **1993**, *175*, 7430.
[56] F. Blanche, J. Crouzet, B. Cameron, D. Thibaut, unpublished.
[57] L. Debussche, D. Thibaut, M. Danzer, F. Debu, D. Frechet, F. Herman, F. Blanche, M. Vuilhorgne, *J. Chem. Soc. Chem. Commun.* **1993**, 1100.
[58] J. Ostrowski, J.-Y. Wu, D. C. Rueger, B. E. Miller, L. M. Siegel, N. M. Kredich, *J. Biol. Chem.* **1989**, *264*, 15726.
[59] G. Gisselmann, A. Niehaus, J. D. Schwenn, *Bot. Acta* **1992**, *105*, 213.
[60] A. I. Scott, C. A. Roessner, N. J. Stolowich, J. B. Spencer, C. Min, S.-I. Ozaki, *FEBS Lett.* **1993**, *331*, 105.
[61] C. Min, B. P. Atshaves, C. A. Roessner, N. J. Stolowich, J. B. Spencer, A. I. Scott, *J. Am. Chem. Soc.* **1993**, *115*, 10380.
[62] a) F. Blanche, D. Thibaut, L. Debussche, R. Hertle, F. Zipfel, G. Müller, *Angew. Chem.* **1993**, *105*, 1704; *Angew. Chem. Int. Ed. Engl.* **1993**, *32*, 1651; b) T. E. Podschun, G. Müller, *ibid.* **1985**, *97*, 63 and **1985**, *24*, 46.
[63] K. Kurumaya, T. Okazaki, M. Kajiwara, *Chem. Pharm. Bull.* **1989**, *37*, 1151.
[64] A. I. Scott, N. J. Stolowich, B. P. Atshaves, P. Karuso, M. J. Warren, H. J. Williams, M. Kajiwara, K. Kurumaya, T. Okazaki, *J. Am. Chem. Soc.* **1991**, *113*, 9891.
[65] R. A. Vishwakarma, S. Balachandran, A. I. D. Alanine, N. P. J. Stamford, F. Kiuchi, F. J. Leeper, A. R. Battersby *J. Chem. Soc. Perkin Trans. 1* **1993**, 2893.
[66] S. Broers, A. Berry, D. Arigoni, unpublished; see also: *Ciba Found. Symp.* **1994**, *180*, 280.
[67] J. B. Spencer, N. J. Stolowich, C. A. Roessner, C. Min, A. I. Scott, *J. Am. Chem. Soc.* **1993**, *115*, 11610.
[68] *The Biosynthesis of Tetrapyrrole Pigments* (*Ciba Found. Symp.* **1994**, *180*).
[69] M. Kodera, F. J. Leeper, A. R. Battersby, *J. Chem. Soc. Chem. Commun.* **1992**, 435.
[70] A. R. Battersby, M. G. Baker, H. A. Broadbent, C. J. R. Fookes, F. J. Leeper, *J. Chem. Soc. Perkin Trans. 1* **1987**, 2027.
[71] L. Debussche, D. Thibaut, B. Cameron, J. Crouzet, F. Blanche, *J. Bacteriol.* **1990**, *172*, 6239.
[72] The seven carboxylic side chains of cobyrinic acid and related corrinoids are lettered *a* to *g* clockwise starting from the C-1 acetate side chain.
[73] H. C. Friedmann, L. M. Cagen, *Annu. Rev. Biochem.* **1970**, *24*, 159.
[74] H. Zalkin, *Adv. Enzymol. Relat. Areas Mol. Biol.* **1993**, *66*, 203.
[75] L. Debussche, M. Couder, D. Thibaut, B. Cameron, J. Crouzet, F. Blanche, *J. Bacteriol.* **1992**, *174*, 7445.
[76] J. E. Walker, M. Sarastre, M. J. Runswick, N. J. Gay, *EMBO J.* **1982**, *8*, 945.
[77] R. Labbe-Bois, *J. Biol. Chem.* **1990**, *265*, 7278.
[78] C. J. Walker, J. D. Weinstein, *Plant Physiol.* **1991**, *95*, 1189; *Proc. Natl. Acad. Sci. USA* **1991**, *88*, 5789.
[79] K. Bernhauer, F. Wagner, H. Michna, P. Rapp, H. Vogelmann, *Hoppe-Seyler's Z. Physiol. Chem.* **1968**, *349*, 1297.
[80] F. Blanche, M. Couder, L. Debussche, D. Thibaut, B. Cameron, J. Crouzet, *J. Bacteriol.* **1991**, *173*, 6046.
[81] R. O. Brady, E. G. Castanera, H. A. Barker, *J. Biol. Chem.* **1962**, *237*, 2325; E. Vitols, G. A. Walker, F. M. Huennekens, *ibid.* **1966**, *241*, 1455.
[82] F. Blanche, L. Maton, L. Debussche, D. Thibaut, *J. Bacteriol.* **1992**, *174*, 7452.
[83] L. Debussche, M. Couder, D. Thibaut, B. Cameron, J. Crouzet, F. Blanche, *J. Bacteriol.* **1991**, *173*, 6300.
[84] F. M. Huennekens, K. S. Vitols, K. Fujii, D. W. Jacobsen in B_{12}, *Vol. 1* (Ed.: D. Dolphin), Wiley, New York, **1982**, p. 145; G. A. Walker, S. Murphy, F. M. Huennekens, *Arch. Biochem. Biophys.* **1969**, *134*, 95.
[85] F. Blanche, L. Debussche, A. Famechon, D. Thibaut, unpublished.
[86] B. Cameron, J. Crouzet, unpublished.
[87] H. C. Friedmann in *Cobalamin* (Ed.: B. M. Babior), Wiley, New York, **1975**, p. 75.
[88] F. Kiuchi, F. J. Leeper, A. R. Battersby, unpublished.
[89] H. C. Friedmann, *J. Biol. Chem.* **1968**, *243*, 2065; R. A. Ronzio, H. A. Barker, *Biochemistry* **1967**, *6*, 2344.
[90] F. Blanche, L. Debussche, A. Famechon, D. Thibaut, B. Cameron, J. Crouzet, *J. Bacteriol.* **1991**, *173*, 6052.
[91] This gene in *S. typhimurium* has been named *cobU*; it is not the same as the *cobU* in *Ps. denitrificans*.
[92] G. A. O'Toole, M. R. Rondon, J. C. Escalante-Semerana, *J. Bacteriol.* **1993**, *175*, 3317.
[93] G. A. O'Toole, J. C. Escalante-Semerana, *J. Bacteriol.* **1993**, *175*, 6328.
[94] H. C. Friedmann, *J. Biol. Chem.* **1965**, *240*, 413.
[95] H. C. Friedmann, D. L. Harris, *J. Biol. Chem.* **1965**, *240*, 406.
[96] a) J. Horig, P. Renz in *Vitamin* B_{12} (Eds.: B. Zagalak, W. Friedrich), de Gruyter, New York, **1979**, p. 323; b) B. Lingens, T. A. Schild, B. Vogler, P. Renz, *Eur. J. Biochem.* **1992**, *207*, 981.
[97] J. R. A. Vogt, L. Lamm-Kolonko, P. Renz, *Eur. J. Biochem.* **1988**, *174*, 637; J. R. A. Vogt, P. Renz, *ibid.* **1988**, *171*, 655.
[98] J. C. Escalante-Semerana, M. G. Johnson, J. Roth, *J. Bacteriol.* **1992**, *174*, 24.
[99] R. N. Brey, C. D. B. Banner, J. B. Wolf, *J. Bacteriol.* **1986**, *167*, 623.
[100] T. Peakman, J. Crouzet, J.-F. Mayaux, S. Busby, S. Mohan, R. Nicholson, J. Cole, *Eur. J. Biochem.* **1990**, *191*, 315; J. B. Spencer, N. J. Stolowich, C. A. Roessner, A. I. Scott, *FEBS Lett.* **1993**, *335*, 57.
[101] D. Ingrosso, A. V. Fowler, J. Bleibaum, S. Clarke, *J. Biol. Chem.* **1989**, *264*, 20131.
[102] One more enzyme on the main pathway may exist that has not as yet been characterized—cobalamin 5'-phosphatase. This is not an essential part of the pathway, however, because CobV can catalyze the attachment of α-ribazole

(**56**) (as well as its 5′-phosphate **55**), thus avoiding the need for a subsequent phosphatase.
[103] The two characterized enzymes for which the genes have not been found are the cob(II)yrinic acid *a,c*-diamide reductase and protein z of the aminopropanol attachment system.
[104] CobW is homologous to the product of P47K from *Ps. chlororaphis* (Table 2; we thank A.-M. Crutz-Lecoq for pointing this out to us). The P47K protein seems to be important for the stabilization and/or maturation of nitrile hydratase and might be involved in binding the metal ion to the hydratase. Therefore it is possible that CobW has a role in binding cobalt to CobN.
[105] F. Blanche, L. Debussche, D. Thibaut, J. Crouzet, B. Cameron, *J. Bacteriol.* **1989**, *171*, 4222.
[106] D. Thibaut, M. Couder, J. Crouzet, L. Debussche, B. Cameron, F. Blanche, *J. Bacteriol.* **1990**, *172*, 6245.
[107] J. Wu, L. Siegel, N. Kredich, *J. Bacteriol.* **1991**, *173*, 325.
[108] C. Robin, F. Blanche, L. Cauchois, B. Cameron, M. Couder, J. Crouzet, *J. Bacteriol.* **1991**, *173*, 4893.
[109] F. Blanche, C. Robin, M. Couder, D. Faucher, L. Cauchois, B. Cameron, J. Crouzet, *J. Bacteriol.* **1991**, *173*, 4637.
[110] J. Ostrowski, N. Kredich, *J. Bacteriol.* **1989**, *171*, 130.
[111] G. Gisselmann, J. Schwenn, *NBRF database* **1992**, S19860.
[112] J. Kronenberg, A. Lepingle, M. Caboche, H. Vaucheret, *MGG Mol. Gen. Genet.* **1993**, *236*, 203.
[113] R. de Mot, I. Nagy, G. Schoofs, J. Vanderleyden, *EMBL database* **1993**, L21196.
[114] A. Hudson, R. Carpenter, S. Doyle, E. Coen, *EMBO J.* **1993**, *12*, 3711.
[115] D. Burke, M. Alberti, G. Armstrong, J. Hearst, *EMBL database* **1991**, Z11165.
[116] M. Lundrigan, R. Kadner, *J. Bacteriol.* **1989**, *171*, 154.
[117] J. Escalante-Semerena, S. Suh, J. Roth, *J. Bacteriol.* **1990**, *172*, 273.
[118] O. Possot, L. Sibold, J. P. Aubert, *Res. Microbiol.* **1989**, *140*, 355.
[119] M. Carlomagno, L. Chiariotti, P. Alifano, A. Nappo, C. Bruni, *J. Mol. Biol.* **1988**, *203*, 585.
[120] C. Collins, D. Gutman, J. Isaza, *EMBL database* **1993**, L25054.
[121] K. Miller, M. McKinstry, W. Hunt, B. Nixon, *Mol. Plant Microb. Interact.* **1992**, *5*, 363.
[122] M. Nishiyama, S. Horinouchi, M. Kobayashi, T. Nagasawa, H. Yamada, *J. Bacteriol.* **1991**, *173*, 2465.



Y. Ohashi (ed.)

Reactivity in Molecular Crystals

1993. XII, 348 pages. Hardcover. DM 198.00.
ISBN 3-527-29098-2

Do you need to design syntheses that are
- highly selective
- fast
- enantioselective with quantitative enantiomeric yield?

This book describes in detail how best to exploit the enormous synthetic potential of solid state reactions. Written by leading experts, it provides in depth information on
- the theoretical and physico-chemical approach to solid state reactions
- solid-to-solid organic reactions
- stereoselective solid state photoreactions
- reactivity and crystal structure

An ideal companion to Bürgi and Dunitz's *Structure Correlation*, this book will be highly useful to synthetic organic chemists, stereochemists, crystallographers, and solid-state chemists.

Enzymes in Organic Synthesis: Application to the Problems of Carbohydrate Recognition (Part 1)**

Chi-Huey Wong,* Randall L. Halcomb, Yoshitaka Ichikawa, and Tetsuya Kajimoto

Carbohydrates on cell surfaces are information molecules. Although only seven or eight monosaccharides are commonly used as building blocks in mammalian systems, the multifunctionality of these monomers can lead to the assembly of an immense variety of complex structures. Millions of different tetrasaccharide structures, for example, can be constructed from this small number of building blocks, if branching, the stereochemistry of glycosidic linkages, and the modification of hydroxyl and amino groups are taken into consideration. Oligosaccharides therefore represent an effective class of biomolecules that code for a vast amount of information required in various biological recognition processes, such as intercellular communication, signal transduction, cell adhesion, infection, cell differentiation, development, and metastasis. The pace of development of pharmaceuticals based on carbohydrates has, however, been slower than that based on other classes of biomolecules. Part of the reason is the lack of technologies for the study of complex carbohydrates. There is no method to amplify oligosaccharides for sequence analysis. There is no machine available for automated synthesis of oligosaccharides. In addition, the possibly poor bioavailability and difficulties in the large-scale synthesis of carbohydrates have undoubtedly contributed to this slow pace. The enzymatic and chemoenzymatic methods, especially those based on aldolases and glycosyltransferases, described here appear to be useful for the synthesis of mono- and oligosaccharides and related molecules. Further advances in glycobiology will probably lead to the development of new technologies for the study of carbohydrate recognition and for the synthesis of bioactive carbohydrates and mimetics to control the recognition processes.

Keywords: carbohydrates · enzymes · organic synthesis

Recent advances in synthetic organic chemistry have made possible the stereocontrolled synthesis of a large number of organic molecules. The field of synthetic organic chemistry now faces two very important issues: 1) the design of molecules with desirable properties for use in biological or material sciences and 2) the development of economical and environmentally acceptable processes for synthesis. Enzymes are able to contribute to the solution of both these issues and have increasingly been considered as a useful class of catalysts for organic synthesis. Numerous enzyme-catalyzed reactions (especially those based on hydrolytic enzymes such as lipases, esterases; and amidases) have been developed and become familiar to synthetic organic chemists. Recent advances have extended the field of enzymatic synthesis to many other complex types of reactions such as oxidoreductions, carbon–carbon bond–forming reactions, glycosylation reactions, and various group transfer reactions that are difficult or impossible to execute with conventional synthetic methods, thereby broadening the scope of its synthetic utility. One area which holds great promise for the use of enzymes is the synthesis of water-soluble, polyfunctional organic molecules, especially carbohydrate and carbohydrate-like molecules. Conventional synthesis of these molecules often requires multiple protections and deprotections and faces the problem of insufficient stereocontrol. The high regio- and stereoselectivity and mild reaction conditions in enzyme-catalyzed reactions provides a new opportunity to tackle many synthetic problems encountered in carbohydrate synthesis, particularly on a large scale. This review focuses on the use of enzymatic and chemoenzymatic methods for the synthesis of simple and complex carbohydrates and related substances, and their application to the problems associated with carbohydrate-mediated recognition in biological systems.

[*] Prof. Dr. C.-H. Wong, Dr. R. L. Halcomb
Department of Chemistry, The Scripps Research Institute
10666 North Torrey Pines Road, La Jolla, CA 92037 (USA)
Telefax: Int. code + (619)554-6731

Prof. Dr. Y. Ichikawa
Department of Pharmacology and Molecular Sciences
The Johns Hopkins University
Baltimore (USA)

Dr. T. Kajimoto
Frontier Research Program on Glycotechnology
The Institute of Physical and Chemical Research (RIKEN),
Wako City (Japan)

[**] Part 2: *Angew. Chem.* **1995**, *107*, Nr. 5; *Angew. Chem.* **1995**, *34*, No. 5.

 © VCH Verlagsgesellschaft mbH, D-69451 Weinheim, 1995 0570-0833/95/0404-0412 $ 10.00+.25/0

1. The Current Status of Enzymatic Organic Synthesis

The characteristics of instability, high cost, difficulty in handling, and narrow substrate specificity have been the drawbacks of enzymes as synthetic catalysts. As a result, application of enzymes has traditionally been limited to the analysis and small-scale synthesis of research biochemicals. This perception, however, has changed dramatically in the past ten years as a result of new developments in chemistry, biology, and in industry. Large numbers of known and new enzymes (Table 1) have been used in the transformation of natural or nonnatural substrates to synthetically useful intermediates or final products. Additionally, recombinant DNA technology had made possible the low-cost production of enzymes and the rational alteration of their properties. Perhaps the most useful application of enzyme catalysis is in the area of asymmetric synthesis, especially the synthesis of structurally well-defined molecules that are useful in medicine, agriculture, and biology.[1-5]

The biological activity of most drugs is due to their ability to interfere with receptor–ligand or enzyme–substrate interactions. A rational approach to drug development requires the design, synthesis, and study of a range of substrates, inhibitors, ligands, and derivatives that may be difficult to manipulate with classical synthetic methodology alone. With the potential advantages of enzyme catalysis as a practical route to carbohydrates, as well as the increasing environmental concerns and the regulatory constraints faced in the chemical and pharmaceutical industries, enzyme-based organic synthesis becomes an attractive option that may offer clean and mild processes for the production of materials with high optical purity.

A crucial question is whether an enzymatic approach to synthesis is practical. In many instances when enzymatic transformations are compared with the chemical methodology, they only represent an alternative or improved process, and whether replacement of an existing chemical process with an enzymatic method is beneficial remains an open question. In some cases, however, enyzmatic processes are more cost-effective and have clear advantages over chemical methods. For example, the use of DNA ligases and restriction enzymes to manipulate DNA has no competition from other techniques. Several large-scale enzymatic processes used in industry (resolution of amino acids with


C.-H. Wong


R. L. Halcomb


Y. Ichikawa


T. Kajimoto

Chi-Huey Wong received his B. S. and M. S. degrees from National Taiwan University, and a Ph.D. in chemistry from Massachusetts Institute of Technology under George M. Whitesides in 1982. After one year of postdoctoral research at Harvard University, he taught at texas A & M University for six years. Since 1989 he has been the Ernest W. Hahn Professor at The Scripps Research Institute. He is also Head of the Frontier Research Program on Glycotechnology at RIKEN, Japan. His current interests are in the area of bioorganic and synthetic chemistry, in particular the development of enzymes for organic synthesis, and the rational design and synthesis of inhibitors of enzymes and receptors. His honors include a Presidential Young Investigator Award in Chemistry, a Searle Scholar in Biomedical Sciences, and an A. C. Cope Scholar of the American Cancer Society. He received the International Carbohydrate Award. He is the author and coauthor of over 250 publications, one book, and 30 patents.

Randall L. Halcomb was born in 1965 and studied chemistry at the University of Alabama, completing his Ph.D. at Yale University under S. J. Danishefsky in 1992. He then spent two years as American Cancer Society Postdoctoral Fellow at The Scripps Research Institute. In June 1994 he joined the Department of Chemistry at the University of Colorado as Assistant Professor. His research interests include the synthesis and study of bioactive natural products and complex carbohydrates.

Yoshitaka Ichikawa was born in Tokyo in 1954. He received his Ph.D. in Agricultural Chemistry in 1986 from the University of Tokyo. He then worked at RIKEN and as postdoctoral associate at Johns Hopkins University and The Scripps Research Institute. He is currently Assistant Professor of Pharmacology and Molecular Sciences at the Johns Hopkins Medical School. His research interests include the synthesis and biological studies of complex carbohydrates.

Tetsuya Kajimoto was born in Osaka in 1960. He received his Ph.D. in Chemistry under K. Fuji in 1989 from Kyoto University. After one year of teaching and research as assistant professor at Kumamoto University, he did his postdoctoral work at The Scripps Research Institute. Since 1991 he has been Deputy Head of the Frontier Research Program on Glycotechnology at RIKEN. His research interests include the development of new technologies for the study of carbohydrate recognition in biological systems and the synthesis of inhibitors to control carbohydrate recognition processes.

Table 1. Enzymes commonly used for organic synthesis.

Enzymes not requiring cofactors	Enzymes not requiring stoichiometric cofactors	Enzymes requiring a cofactor [a]
1) Hydrolytic enzymes:	1) Flavoenzymes:	1) Kinases-ATP
esterases	glucose oxidase	2) Oxidoreductases-NAD(P)(H)
lipases	amino acid oxidases	
amidases	diaphorase	3) Methyl transferases-SAM
phospholipases	FMN reductase	
epoxide hydrolases		4) CoA-requiring enzymes
nucleoside phosphorylase	2) Pyridoxal phosphate enzymes:	
SAM synthetase		5) Sulfuryllyases-PAPS
2) Isomerases and lyases:	transaminases	
glucose isomerase	tyrosinase	
aspartase	δ-aminolevulinate dehydratase	
phenylalanine ammonia lyase	cystathionine synthetase	
fumarase	3) Metalloenzymes:	
cyanohydrin synthetase	galactose oxidase	
3) Aldolases	monooxygenases	
4) Glycosyl transferases	dioxygenases	
5) Glycosidases	hydrogenases	
	enoate reductases	
	aldolases	
	carboxylyases	
	nitrile hydrolases	
	4) Thiamine pyrophosphate enzymes:	
	decarboxylases	
	transaldolases	
	5) Others	
	SAH hydrolase	
	vitamin B_{12} dependent enzymes	
	PQQ (methoxatin)-enzymes	
	oxynitrilases	

[a] ATP = adenosine 5'-triphosphate; NAD(P) = nicotinamide adenine diphosphate (3'-phosphate); SAM = *S*-adenosylmethionine; PAPS = 3'-phosphoadenosyl-5'-phosphosulfate.

acylase, production of high-fructose corn syrup with glucoamylase and glucoisomerase, transformation of pig insulin to human insulin catalyzed by trypsin, preparation of penicillin analogs with penicillin acylase, synthesis of aspartame with thermolysin, and preparation of acrylamide from acrylonitrile catalyzed by nitrilehydrolase) have demonstrated that enzymatic catalysis can also provide a route to fine chemicals, medicinal agents, and commodity chemicals. In addition, synthesis and modification of mono-, oligo-, and polysaccharides and their conjugates and analogs, regioselective transformation of other complex molecules, and modification of recombinant DNA products such as glycoproteins may be best conducted enzymatically. It should be emphasized, however, that it is frequently less convenient in most circumstances to develop an enzymatic route to a substance required in milligram quantities than to carry through a classical chemical synthesis. When large quantities of that material are required, however, it will be worth the effort to develop appropriate enzymes for that synthesis.

Once a decision has been taken to attempt using enzymes for a given transformation, one or more enzymes capable of performing that type of transformation can be selected and the reaction conditions, such as temperature, pH, solvent, regulator, and protecting group, can be optimized. A number of enzymes are already commerically available, and many more can be easily isolated. The next step is to determine whether the enzyme possesses adequate activity for the desired transformation. Selectivity and specific activity are important factors at this stage. The specific activity of an enzyme is often presented in units (U): 1 U of enzyme will produce 1 μmol of product per minute at its maximum velocity, and the number of units per milligram of enzyme represents that enzyme's specific activity. If the specific activity is too low, the quantity of enzyme required for the synthesis is unrealistically large. In that event, it is necessary to use a more active enzyme, or to develop another enzyme by screening or by site-directed mutagenesis, or to abandon the project to chemical methodology. Similar considerations are also given to the evaluation of selectivity.

If the specific activity and selectivity are high enough to be practical, the remaining steps are relatively straightforward. Procedures can usually be found that will stabilize an enzyme adequately for bench-scale synthesis. Immobilization is usually straightforward, and when it is unsuccessful it may be perfectly practical to use the free enzyme in a homogeneous solution. The technique of site-directed or random mutagenesis can also be used to improve enzyme stability. Large-scale production of the enzyme can then be executed by using recombinant DNA technology. When all kinetic parameters (for example, k_{cat}, the Michaelis constant K_m, the rate of enzyme inactivation) for a desired transformation are available, one can, in principle, conduct a large-scale synthesis. In the case where no enzyme is known for the desired transformation, it is more laborious to find an appropriate enzyme, an chemical methodology may be the choice. The approaches based on screening and catalytic antibodies,[6] however, may be worth the effort if the desired transformation is important. Once a protein catalyst is found, its activity and stability can be improved as described previously. Proteins can also be attached to the surface of phage and screened for desired catalytic properties[7]. The catalytically active RNAs recently discovered have created a new dimension in biocatalysis, and nonprotein biocatalysts based on RNA are now also available to be exploited as synthetic catalysts.[8] Table 2 summarizes the current status of enzymatic catalysis, and Scheme 1 provides a strategic approach to the development of enzymatic catalysts. It is worth noting that although biocatalysts represent a new class of asymmetric catalysts that are useful for a variety of organic transformations, their improvement or alteration of specificity by site-directed mutagenesis remains a difficult task. Synthetic chemists capable of using and developing biocatalysts, however, will have a clear advantage in their ability to tackle the new generation of synthetic problems appearing at the interface between chemistry and biology.

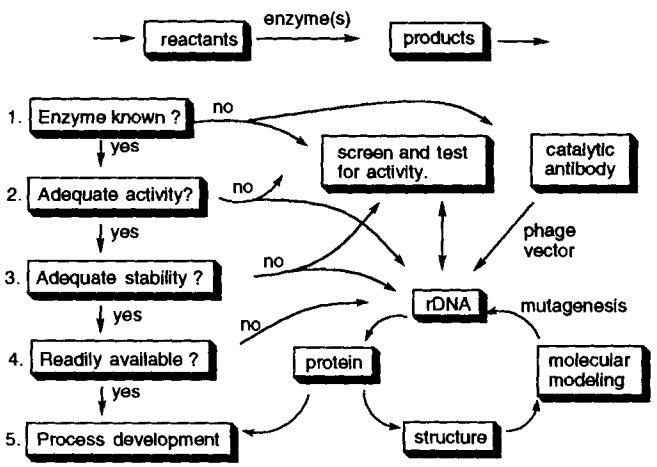
2. Enzymatic Catalysis in Glycobiology and Glycotechnology

Complex carbohydrates and their conjugates in biological systems are either structural or informational molecules. On the cell surface many carbohydrates of glycoconjugates are involved in various types of biochemical recognition processes,[9, 10] including growth, development, immune responses, infection, cell adhesion, metastasis, and numerous signal-transduction events. These compounds often exist in minute

Table 2. Status of certain generic problems in enzymatic catalysis.

Solved	*Current*	*Immediate Future*
immobilization	development of new laboratory-scale uses of enzymes	design and development of new enzymatic catalysts
cofactor regeneration (NAD(P), ATP, CoA, sugar nucleotides)	design of nonnatural substrates	chemoenzymatic synthesis of complex molecules
enzyme deactivation (thiol oxidation protease action)	use with organic cosolvents; one- and two-phase systems	multienzyme systems through metabolic pathway engineering
use of recombinant DNA for large-scale production of enzymes	enzyme stabilization	new catalysts from monoclonal Fab fragments
	overcoming product inhbition	
	cofactor regeneration (PAPS, SAM)	
	modification of enzyme activity and semi-synthetic enzymes	
	mutagenesis for changes in properties	
	exploration of enzymes from new species for synthetic utility	
	scale-up in pharmaceutical synthesis	
	multienzyme systems in synthesis	
	applications in synthesis of fine and specialty chemicals	
	antibody catalysts	

quantities and are difficult to isolate, characterize, and synthesize in quantities large enough for biological study and therapeutic evaluation. Although only seven or eight monosaccharides are commonly found as building blocks in mammalian systems,[11] the multifunctionality of these monomers enables an immense variety of complex structures to be assembled. Millions of tetrasaccharide structures, for example, can be constructed from this small number of building blocks, differing, for instance, in branching sites or the stereochemistry of glycosylation. Oligosaccharides therefore represent a class of molecules that can effectively code for vast amounts of information in various biological recognition process. The enzymes (for example glycosidases) involved in the biosynthesis and degradation of oligosaccharides have been valuable reagents for the determination of oligosaccharide structures,[12] and these enzymes and those involved in the formation of glycoside bonds (for example, glycosyltransferases) have proven to be useful catalysts for the synthesis of saccharides.[13, 14] These glycoenzymes are also interesting targets for inhibition, as they may be involved in metabolic disorders and diseases.[15, 16] Scheme 2 lists a number of naturally occurring carbohydrate structures and glycoconjugates that possess important biological activities.[17] Some of these compounds contain unusual glycosidic linkages or modifications (such as sulfation, methylation) for which an enzymatic synthesis has not been developed. Given the complexity and multifunctional nature of these structures, the synthesis of these and related compounds or designed mimetics in a practical manner remains a challening task. The following describes various types of enzymatic reactions which, when combined with simple chemical transformations, may provide a practical route to numerous sugar-like compounds.



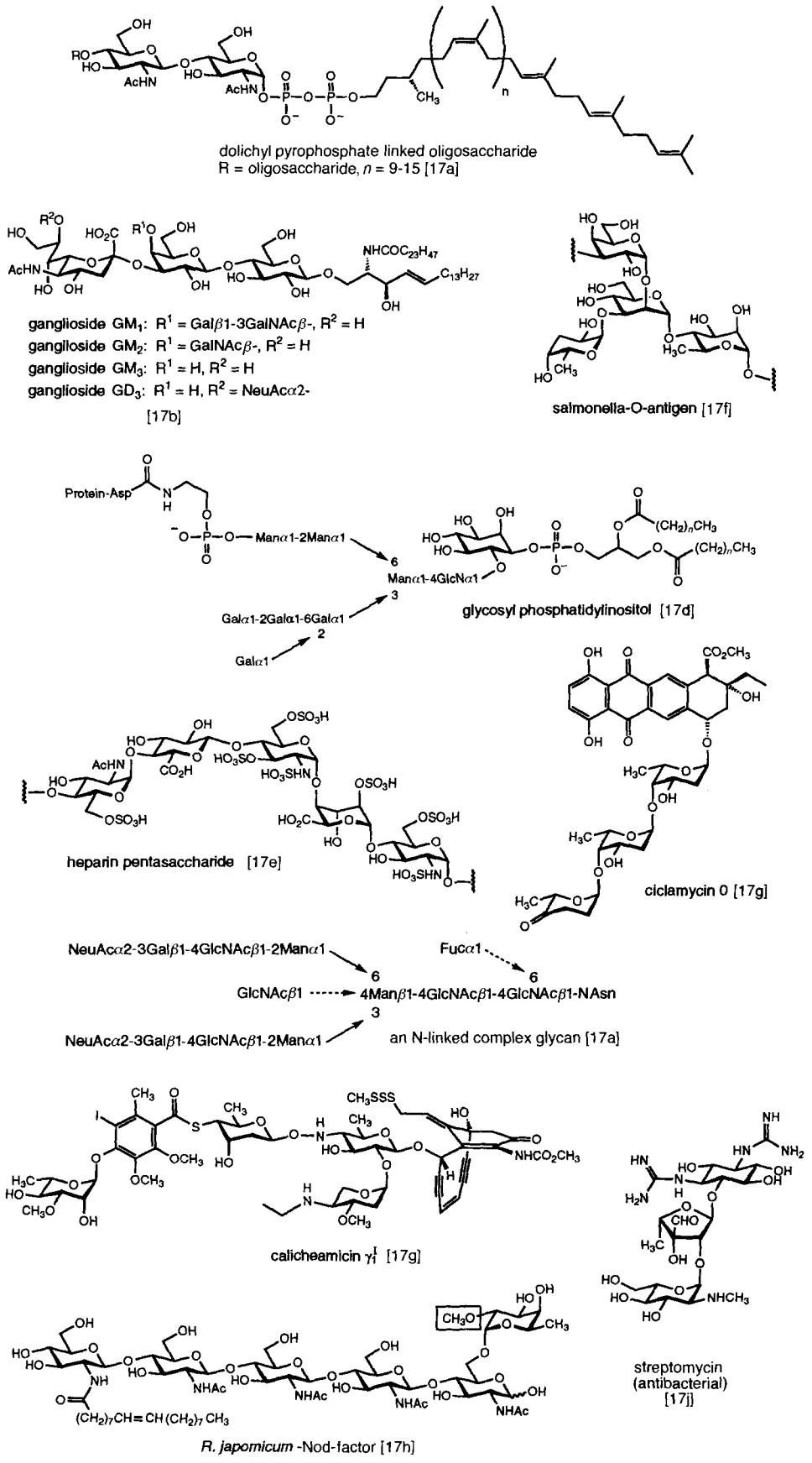
Scheme 1. Strategy for the development of enzymatic catalysts. If the enzyme for a specific reation is known, its specificity, specific activity, and stability may be further improved by protein engineering or screening. If the enzyme is unknown, it may be found by screening or designed by developing a catalytic antibody, and further improved by protein engineering (adapted from ref. [5]).

3. Synthesis of Monosaccharides and Related Structures Based on Aldolases

Aldolases, of which over twenty have been identified to date, usually catalyze the stereospecific aldol condensation of an aldehyde with a ketone donor. Two types of aldolases are known. Type I aldolases, which are primarily found in animals and higher plants, do not require a metal cofactor. In contrast, type II aldolases, found predominately in microorganisms, use a Zn^{2+} cofactor, which acts as a Lewis acid in the active site. In both cases, the aldolases accept a variety of nonnatural acceptor substrates, and in many cases, the stereoselectivity of the reaction is controlled by the enzyme and is highly predictable. Table 3 lists the aldolases which have been studied. The arrows indicate the C–C bond associated with aldol reactions. These enzymes have proven useful for the synthesis of both common and uncommon monosaccharides. Representative examples are the following.

3.1. Fructose-1,6-Diphosphate Aldolase [E.C. 4.1.2.13]

Fructose-1,6-diphosphate (FDP) aldolase catalyzes the reversible aldol addition of dihydroxyacetone phosphate (DHAP) and D-glyceraldehyde-3-phosphate (G3P) to form D-fructose-1,6-diphosphate (FDP), for which $K_{eq} \approx 10^4\ M^{-1}$ in favor of FDP formation (Scheme 3). Both type I and II enzymes have been isolated from a variety of eukaryotes and prokaryotes. Most of the mechanistic studies have been carried out with FDP aldolases from rabbit muscle[18] or yeast.[19] The X-ray structure (2.7 Å)[20] of the enzyme from rabbit muscle (RAMA = *r*abbit *m*uscle *a*ldolase) indicates that Lys-229 is responsible for Schiff-base formation with DHAP.[21] The distance between the Schiff-base nitrogen and the phosphate on G3P (glyceraldehyde-3-phosphate) in the active site of RAMA has been calculated to be 8.3 Å.[22] Another lysine residue in the active site (Lys_{107}), about 8.9 Å from the site of Schiff-base

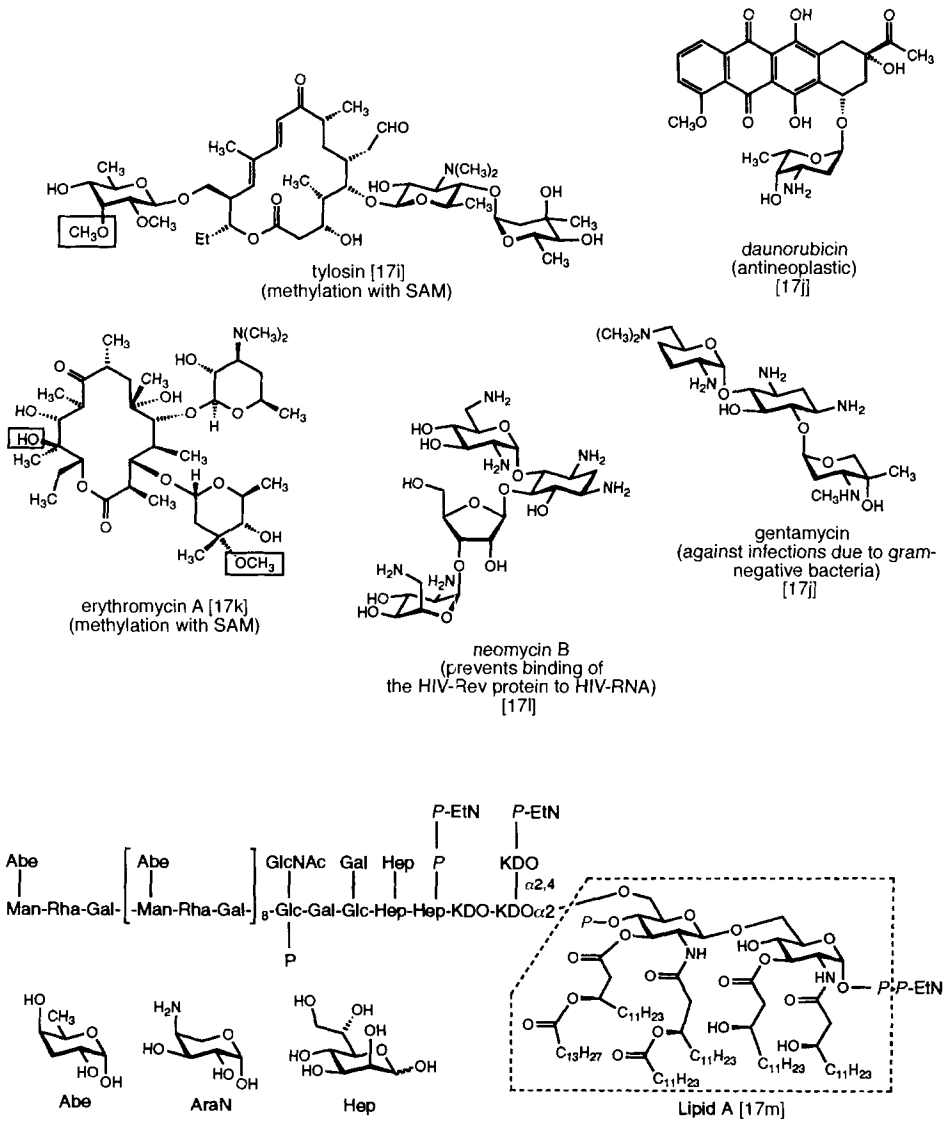


Scheme 2. Biologically active carbohydrates and glycoconjugates. SAM = *S*-adenosylmethionine. DAP = diaminopimelic acid.

formation,[20] is thought to stabilize the negatively charged phosphate of G3P (Scheme 3). The enzyme RAMA has been cloned and overexpressed, and site-directed mutagenesis studies have identified Asp-33 as another critical residue in catalysis.[23]

Generally, the type I FDP aldolases exist as tetramers ($M_r \approx 160$ KDa), while the type II enzymes are dimers ($M_r \approx 80$ KDa). The sequences of the type I enzymes have a high degree of homology (more than 50%), and the active site sequence is conserved throughout evolution.[20] However, significant differences in the C-terminal regions that may be important in mediating substrate specificity have been identified.[20] Some of the type I aldolases are commercially available and have useful specific activity (around 60 U mg^{-1}). These enzymes are not particularly air-sensitive, although there is an active site thiol group that may be susceptible to oxidation. The half-life of the free enzyme, which is about two days in aqueous solution at pH 7.0,[24] can be lengthened by immobilization or by enclosure in a dialysis membrane.[25] The type II aldolase from yeast is commercially available. Other microbial aldolases have recently been cloned and overexpressed.[24, 26-28] The enzyme from *E. coli* has no thiol group in the active site, and has a half life of approximately 60 days in 0.3 mM Zn^{2+} at pH 7.0.[24] Despite the small degree of homology in primary sequence between the enzymes from *E. coli* (type II) and rabbit muscle (type I), studies have shown they possess almost the same substrate specificity.

To date, FDP aldolase, especially RAMA, has been the most widely used aldolase in organic synthesis. This enzyme accepts a wide range of aldehyde acceptor substrates with DHAP as the donor to generate 3*S*, 4*R* vicinal diols, stereospecifically, with D-*threo* stereochemistry.[22, 24-25, 29-57] Suitable acceptors include unhindered aliphatic aldehydes,[25] and monosaccharides and their derivatives.[39] Phosphorylated aldehydes react more rapidly



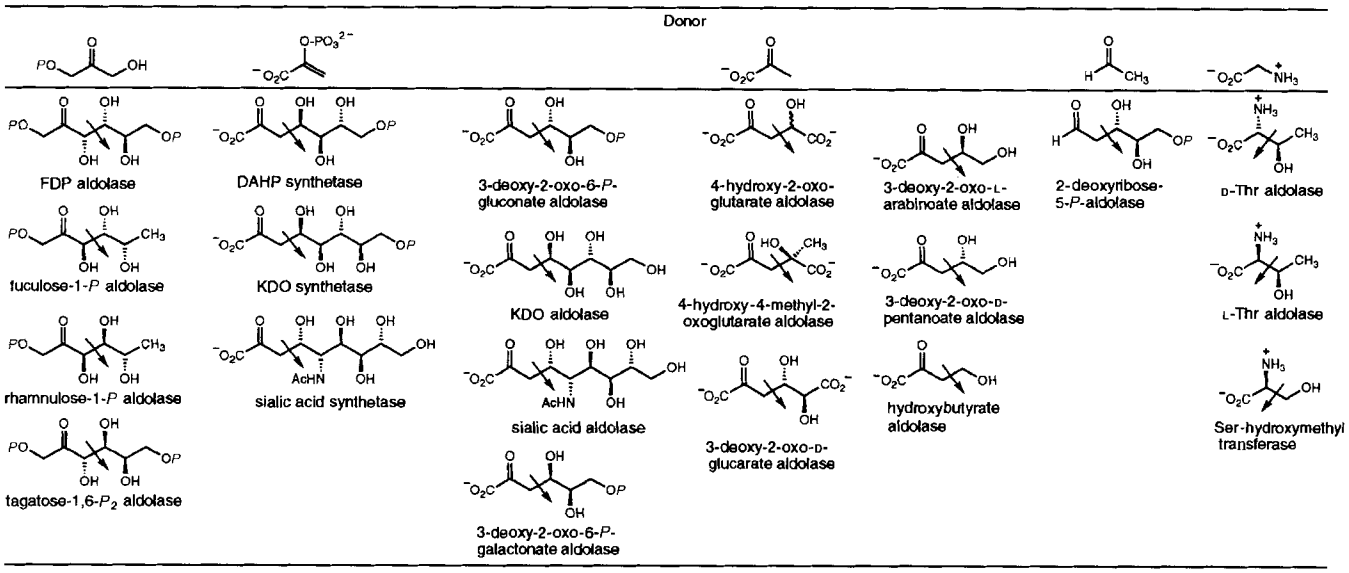
Scheme 2. (continued)

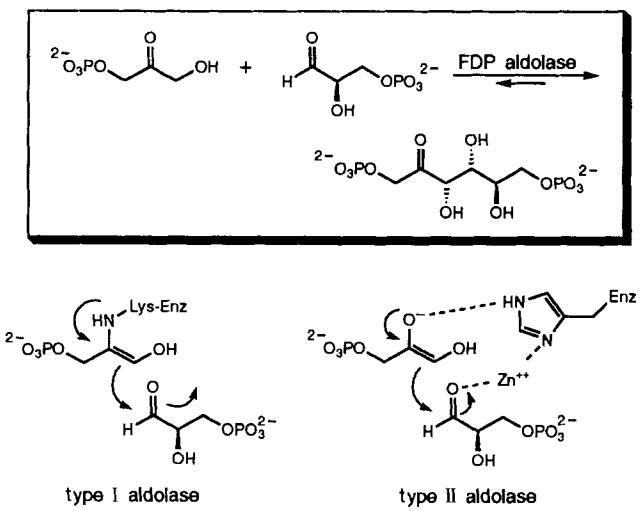
than their unphosphorylated analogs,[39] but aromatic, sterically hindered aliphatic, and α,β-unsaturated aldehydes are generally not substrates.[25] The specificity for the donor substrate is much more stringent. Six DHAP analogs have been found to be poor substrates for RAMA.[25, 40, 44b]

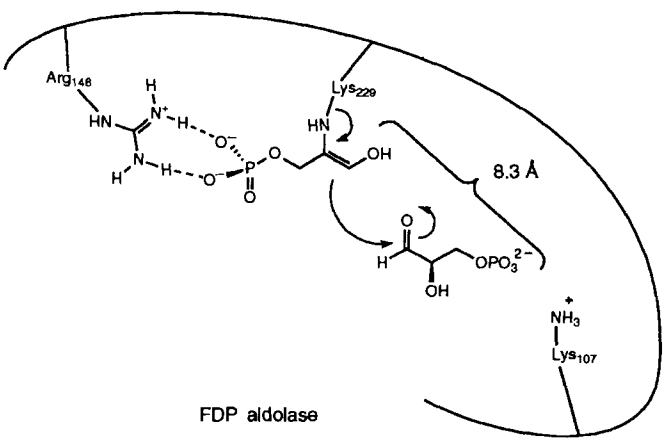
The diastereoselectivity exhibited by FDP aldolase was found to be dependent on the reaction conditions. In a kinetically controlled experiment, the D enantiomer of G3P was accepted by the enzyme with a 20:1 preference over the L enantiomer.[25] A lower enantioselectivity (about 5:1) was observed for the unphosphorylated aldehyde. Racemic mixtures of nonnatural aldehyde acceptors were also partially resolved in a kinetically controlled reaction. In RAMA, the kinetic selectivity is explained by the secondary binding of a charged group with the lysine residue that normally interacts with the phosphate on G3P.[22] When the substrate is constrained by two-point binding, nucleophilic *si* face attack onto the *R* aldehyde is faster, since the *S* aldehyde has a bulky group on the face that the nucleophilic approaches. A study with a series of carboxylated substrates supports this model.[22] When racemic ω-carboxylato-substituted α-hydroxyaldehydes ($^{-}OCO(CH_2)_nCH(OH)CHO$, $n = 1-3, 5$) were treated with DHAP and RAMA, the substrates which had carboxylates that could best overlap with the Lys-107 residue gave the highest enantiomeric excess.

In the cases where the product can cyclize to form a six-membered ring hemiacetal, a racemic mixture of aldehydes is resolved if the enzymatic reaction is under thermodynamical control. Since the reaction is reversible, the product with the fewest 1,3-diaxial interactions will predominate after equilibration. For example, with racemic β-hydroxybutyraldehyde[25, 32] or 2-hydroxymethyl-4-pentenal[32] as substrates, only a single diastereomer with the methyl or allyl group in the equatorial position was obtained (Scheme 4).

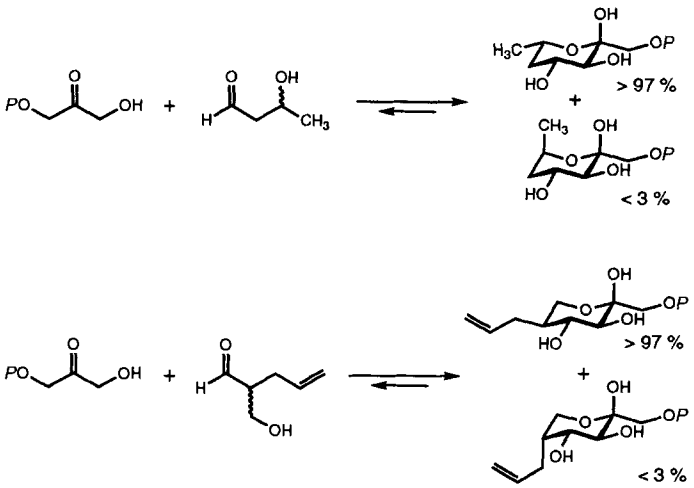
Table 3. Natural substrates for the most important aldolases. Underneath each compound that acts as aldol donor is the name of the relevant enzyme. Arrows indicate the bond formed or broken. FDP = Fructose-1,6-diphosphate, DAHP = dihydroxyacetone phosphate, KDO = 3-deoxy-D-*manno*-octulosonate.







Scheme 3. Mechanism of aldolase-catalyzed aldol reactions.

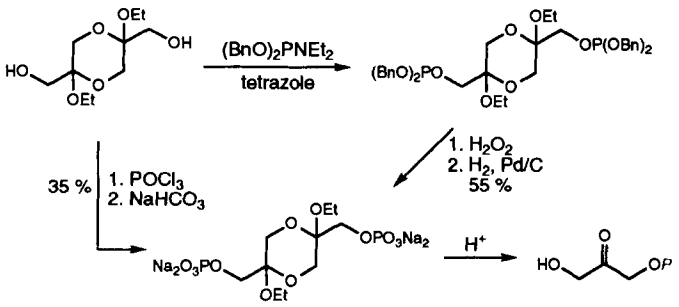


Scheme 4. Thermodynamically controlled resolution of racemic aldehydes with FDP aldolase from rabbit muscle (RAMA).

3.2. Synthesis of Dihydroxyacetone Phosphate

Most conveniently, dihydroxyacetone phosphate (DHAP) can be generated enzymatically in situ from FDP with FDP aldolase and triosephosphate isomerase (TPI).[29, 30] FDP aldolase catalyzes the retro-aldol reaction of FDP to give G3P and DHAP. G3P is rapidly isomerized to DHAP with TPI as the catalyst. One drawback to this method is that the thermodynamics of the reaction may favor the formation of FDP rather than the desired product. The overall reaction may not go to completion, and FDP may also inferfere with product isolation. Another enzymatic method for DHAP synthesis employs glycerol kinase to catalyze the phosphorylation of dihydroxyacetone (DHA) by ATP, with in situ regeneration at ATP.[29] Improved procedures for the synthesis of acetylphosphate and phosphoenolpyruvate (PEP) have been developed[41] in which DHAP is synthesized in 83% yield of approximately 87% puri-

ty with ATP regeneration. DHAP can also be synthesized nonenzymatically by phosphorylation of the ethyl acetal of dihydroxyacetone dimer with $(PhCH_2O)_2PNEt_2$ followed by subsequent oxidation to the phophate with H_2O_2 (Scheme 5),[42] or



Scheme 5. Chemical synthesis of DHAP. Bn = $PhCH_2$.

with either $POCl_3$ or $(PhO)_2POCl$.[43] Reductive cleavage of the aromatic rings, or hydrolysis of the chlorophosphate (for the $POCl_3$ example), yields a stable dimer precursor of DHAP, which can easily be converted into DHAP by acid-catalyzed hydrolysis. The overall procedure with $(PhO)_2POCl$ gives about 55% overall yield of DHAP, compared to 35% with $POCl_3$. A multienzyme system which converts sucrose into DHAP has also been utilized in aldolase reactions.[44a] Glycerophosphate oxidase coupled with peroxidase has also been used in the oxidation of glycerophosphate to DHAP. The enzyme also accepts the corresponding S- and N-phosphates.[44b]

Alternatively, DHAP can be replaced with a mixture of DHA and inorganic arsenate.[31, 45] When DHA reversibly reacts with inorganic arsenate ($k \approx 2.4 \times 10^{-3}\ M^{-1}s^{-1}$) dihydroxyacetone arsenate is formed, which is an analog of DHAP and is also a donor substrate for aldolases. In the presence of RAMA, TPI, and inorganic arsenate, DHA was converted to D-fructose in almost quantitative yield.[45] The arsenate ester of DHA acts as a substrate for the isomerase resulting in the formation of D-glyceraldehyde. D-Fructose is then generated when the remaining DHA arsenate reacts with D-glyceraldehyde in the aldol reaction. Generally, however, when DHA and inorganic arsenate replace DHAP in aldol additions, precautions should be taken, as arsenate is toxic. In addition, reaction rates are relatively small, and low yields of aldol products are often obtained.

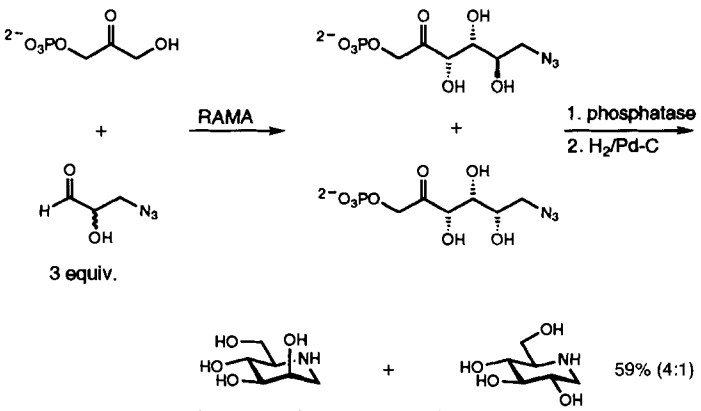
Inorganic vanadate also reacts with DHA to form the corresponding vanadate ester. However, this compound cannot be used as a DHAP analog, since inorganic vanadate also oxidizes DHA. In other organic phosphate-requiring enzymatic reactions where such oxidation does not occur, inorganic vanadate has been used to generate useful substrate analogs.[45]

Although several methods are available for DHAP synthesis and preference may be found in individual cases, that based on $(PhO)_2POCl$ appears to be the most practical. It avoids the problem arising with $POCl_3$ that phosphodiester by-products are formed. The phosphoramidite method does not have the problem of removing the aryl group. The reagent is, however, not commercially available, though it can be easily prepared in the laboratory (from PCl_3, benzyl alcohol, and diethylamine) and stored at room temperature for a long period of time.

3.3. Examples using FDP aldolase

Numerous examples that use FDP aldolase in organic synthesis have appeared recently. These include the production of ^{13}C-labeled sugars,[29, 46–47] nitrogen-containing sugars,[24, 33–35] deoxysugars,[30–32] fluorosugars,[31, 48] and sugars containing seven, eight, or nine carbon atoms[29–30, 32, 39] The aldehydes necessary for FDP aldolase are used in racemic form, but many nonnatural aldehydes prepared as one enantiomer, are employed as such. In general, two groups are used as "masked" aldehydes: a terminal olefin that can be cleaved by ozonolysis,[40] or an acetal that is deprotected through acid hydrolysis.[24] The α-chiral aldehydes can be prepared by nucleophilic ring opening of readily available (*R*)- and (*S*)-glycidaldehyde acetal, or the corresponding thiirane and aziridine.[49] Both enantiomers of glycidaldehyde acetal are prepared by lipase-catalyzed resolution of the diethyl acetal of 3-chloro-2-hydroxypropanal.[24, 49] Following resolution the epoxide is simply generated by treating the chloro alcohol with base. Enzymatic synthesis of novel bioactive sugars using some of these nonnatural aldehydes with FDP aldolase are represented by the examples discussed below.

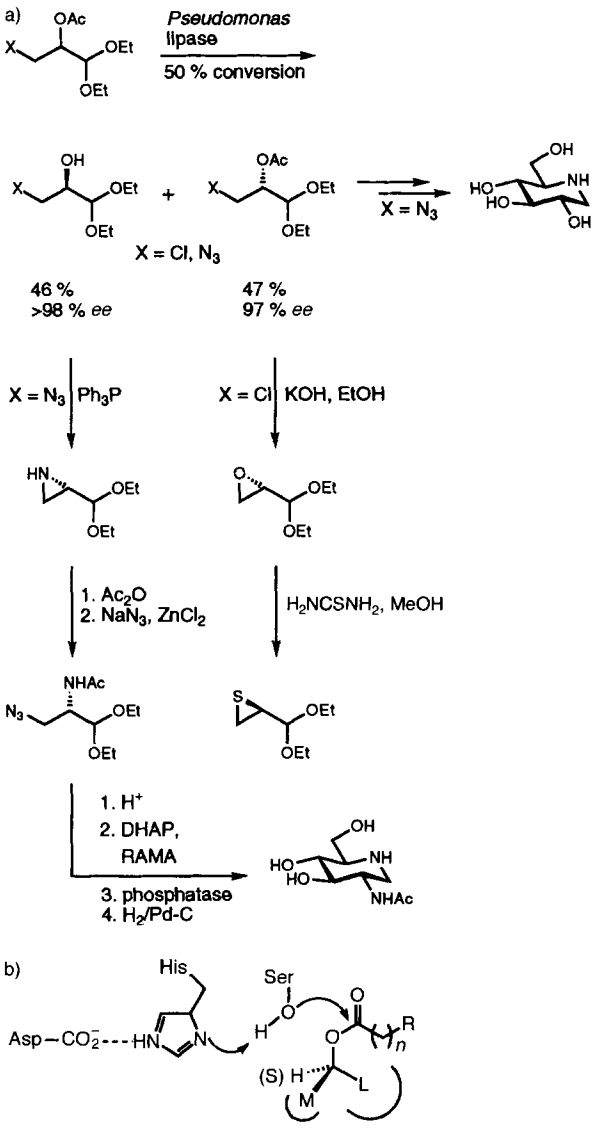
Aza sugars (polyhydroxy-N-heterocycles) have become increasingly important targets since they have been found to be inhibitors of glycoprocessing.[15, 50] Two potent glycosidase inhibitors, deoxynojirimycin and deoxymannojirimycin, were readily prepared in three steps in which RAMA was used in the key C–C bond-forming step.[33, 34] From racemic 3-azido-2-hydroxypropanal and DHAP, diastereomeric 6-azidoketones were formed. Following the acid phosphatase-catalyzed removal of phosphate and subsequent reductive amination (Scheme 6), the products were isolated in a 4:1 ratio favoring the *manno* derivative. A similar result was obtained with FDP aldolase from *E. coli*.[24] Deoxynojirimycin and deoxymannojirimycin can also be prepared exclusively by utilizing the respective optically pure azidoaldehydes.[24] Both (*R*)- and (*S*)-3-azido-2-hydroxy-



Scheme 6. Synthesis of aza sugars from racemic aldehydes with RAMA.

propanal were obtained in greater than 98% *ee* by resolution of the racemic acetal precursor catalyzed by LP-80 (Scheme 7).[24, 49] In a similar strategy several other 3-substituted 2-hydroxypropanal acetals were made as precursors to a variety of 6-substituted ketoses.[49] The analogous RAMA-catalyzed aldol reaction/reductive amination procedure has also been used in the synthesis of aza sugars derived from N-acetylglucosamine and N-acetylmannosamine, from (*S*)- and (*R*)-3-azido-2-acetamidopropanal, respectively (Scheme 7).[51]

When 2-azidoaldehydes were used as substrates for the RAMA-catalyzed aldol reaction/reductive amination, a number of polyhydroxylated pyrrolidines were synthesized (Scheme 8).[52, 53] 1,4-Dideoxy-1,4-imino-D-arabinitol was prepared from Cbz-protected (Cbz = benzyloxycarbonyl) α-aminoacetaldehyde[24] or azidoacetaldehyde.[52] Both (2*R*,5*R*)- and (2*S*,5*R*)-bis(hydroxymethyl)-(3*R*,4*R*)-dihydroxypyrrolidine were synthesized from racemic 2-azido-3-hydroxypropanal; the kinetic product of the aldol addition was converted into the (2*R*,5*R*) pyrrolidine,[52] while the thermodynamic product gave the (2*S*,5*R*) stereoisomer.[53] Similar transformations with 3-acetamido-2-azidopropanal gave aza sugars structurally related to *N*-acetylglucosamine.[58] A homo-aza sugar was prepared from a four-carbon azidoaldehyde (see Scheme 9).[59] An attempt to prepare seven-membered aza sugars by the same reductive amination process gave a six-membered amino sugar, however (see Scheme 10).[57] The Pd-catalyzed reductive amination of azidoketoses is stereoselective. The reduction presumably proceeds through an imine intermediate, which is further reduced to form a *trans* product. When an axial OH group is present in the imine intermediate, hydrogen is delivered to the face opposite to the axial OH group, presumably for steric reasons (see Scheme 11).



Scheme 7. Synthesis of aza sugars from enantiomerically pure aldehydes with RAMA. a) The chiral aldehydes can be resolved with lipase and converted into useful building blocks and substrates for aldolases. b) The mechanism and stereochemistry of the lipase-catalyzed nucleophilic ester cleavage. S, M, and L stand for the smallest, medium, and largest ligands, respectively.

6-Deoxy aza sugars and their analogs can also be prepared by direct reductive amination of the aldol products prior to removal of the phosphate group.[51] Reduction is thought to occur through the imine 6-phosphate intermediate (Scheme 11).

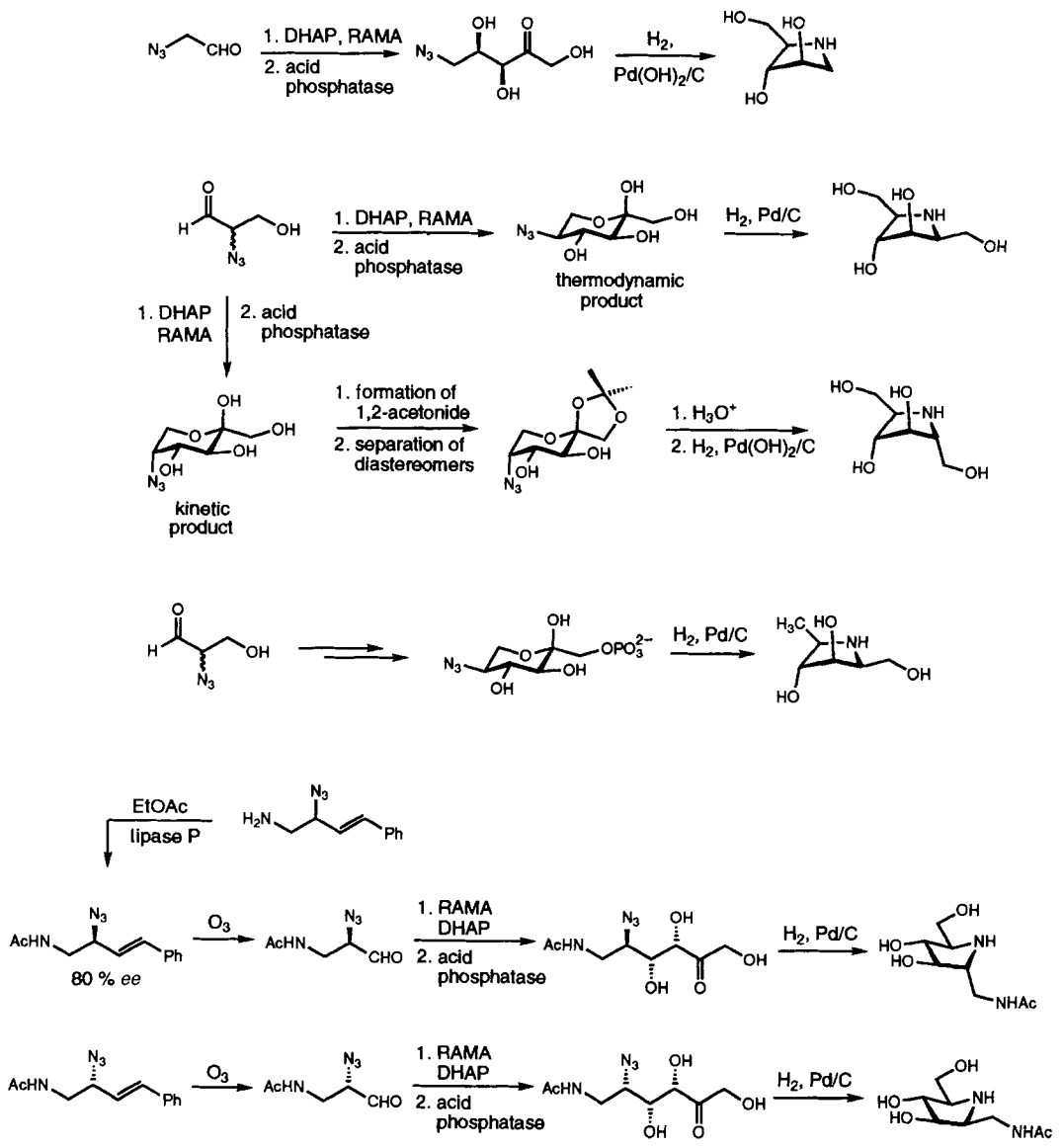
In addition to its application of aza sugars, RAMA catalyzes the synthesis of a variety of oxygen heterocycles. For example, 3-deoxy-D-*arabino*-heptulosonic acid 7-phosphate(DAHP), which is an important intermediate in the shikimate pathway for the biosynthesis of aromatic amino acids in plants, has been synthesized in this way (see Scheme 12)[36] from the substrate *N*-acetylaspartate β-semialdehyde in four steps in 13% overall yield. The enzymatic step produced the desired D-*threo* stereochemistry, and chemical reduction of the ketone gave the desired (6*R*) stereoisomer in 60% diastereomeric excess. Other analogs of DAHP are also potentially available by this route, since RAMA accommodates a number of aldehyde acceptors.

Products from the RAMA-catalyzed aldol reaction can be used to synthesize carbocycles.[38] The protected chloro sugar, generated from the aldolase reaction with chloroacetaldehyde, undergoes nucleophilic attack at the carbonyl carbon by allylmagnesium bromide. Under radical cyclization conditions, a cyclitol is produced (see Scheme 13). When the Grignard reagent is added in tetrahydrofuran, displacement of the chloride occurs to give the C-allyl-*threo*pentuloside as the major product. In principle, this technique can also be applied to the products of other aldolase-catalyzed reactions to provide stereoisomeric derivatives.

The discovery that RAMA also accepts pentose and hexose phosphates as viable substrates provided a new route to novel high-carbon sugars. Several of these compounds have been synthesized, including analogs of sialic acid and 3-deoxy-D-*manno*-octulosonate (KDO).[39] The reactions are, however, relatively slow.

Synthesis with RAMA is not limited to carbohydrate derivatives. In fact, during the synthesis of the naturally occurring beetle pheromone (+)-*exo*-brevicomin the aldolase reaction was used to establish the two chiral centers in the target molecule (see Scheme 14).[55] Another novel use of RAMA is the synthesis of homo-C-linked nucleosides (see Scheme 15).[60]

As shown in the many examples above, FDP aldolase generates several types of ketose monosaccharides. A number of the important naturally occurring carbohydrates are, however, aldoses. One way to generate aldoses from FDP-aldolase products is by using glucose isomerase (GI = xylose isomerase

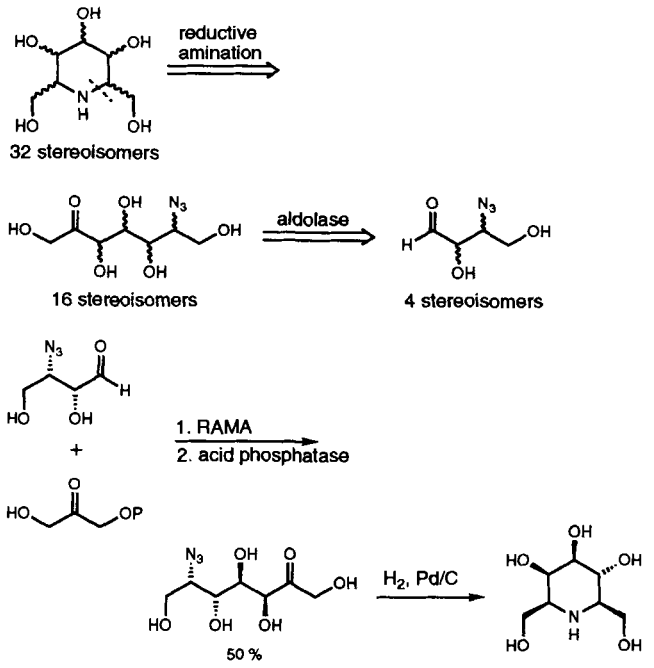


Scheme 8. Synthesis of polyhydroxylated pyrrolidines with RAMA.

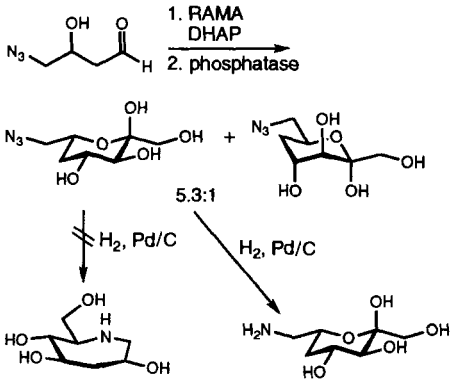
[EC 5.3.1.5]).[31, 61] This enzyme catalyzes the isomerization of fructose to glucose and is used in the food industry for the production of high-fructose corn syrup. GI also accepts fructose analogs that are modified at the 3, 5, or 6 positions (see Scheme 16).[31] Several FDP-aldolase products can be isomerized to a mixture of the ketose and aldose, and the two isomers can be subsequently separated using Ca^{2+}- or Ba^{2+}-treated cation exchange resins. Aldose analogs including 6-deoxy-, 6-fluoro-, 6-*O*-methyl-, and 6-azidoglucose have been synthesized with this FDP aldolase/GI methodology. Not all products from FDP aldolase reactions give the desired aldose when subjected to GI. In some cases (for instance, 5-deoxy-D-fructose) the equilibrium lies completely in favor of the ketose, while in others the products from the aldolase reaction are simply not substrates of GI.

An alternative method for aldose generation from the FDP aldolase products is through the "inversion strategy".[37] Here, monoprotected dialdehydes are used as substrates for FDP aldolase to generate protected aldehyde ketoses. The carbonyl group is then stereoselectively reduced, either chemically or enzymatically (with iditol dehydrogenase), and the aldehyde is subsequently deprotected to afford the aldose (see Scheme 17). The NADH-dependent iditol dehydrogenase (IDH) from *Candida utilis* (also known as sorbitol or polyol dehydrogenase [EC 1.1.14]) was used previously to reduce the carbonyl group of ketoses to give the *S* alcohol.[30] The corresponding *R* alcohol was obtained by nonstereoselective reduction of the ketone with $NaBH(OAc)_3$ from which the *S* epimer was selectively removed by oxidation catalyzed by IDH.[37]

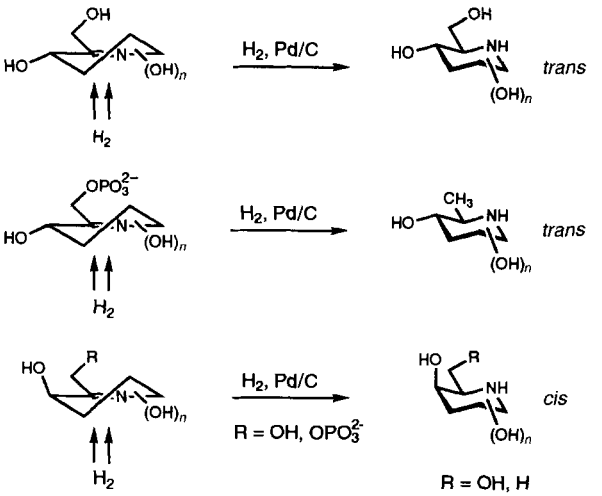
While most of the FDP-aldolase reactions use the commercially available aldolase from rabbit muscle, there is still considerable interest in determining the utility of FDP aldolase from other sources.[57] In fact, the type II aldolases from *E. coli*[24] and yeast,[27] which have been subcloned and overexpressed, have the potential to become useful synthetic catalysts, since they are more stable than RAMA and are available from a microbial as opposed to a mammalian source.



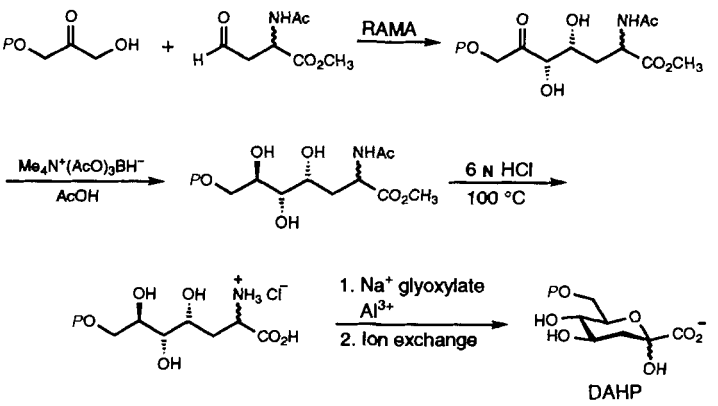
Scheme 9. Aldolase-mediated synthesis of six-membered homo-aza sugars.



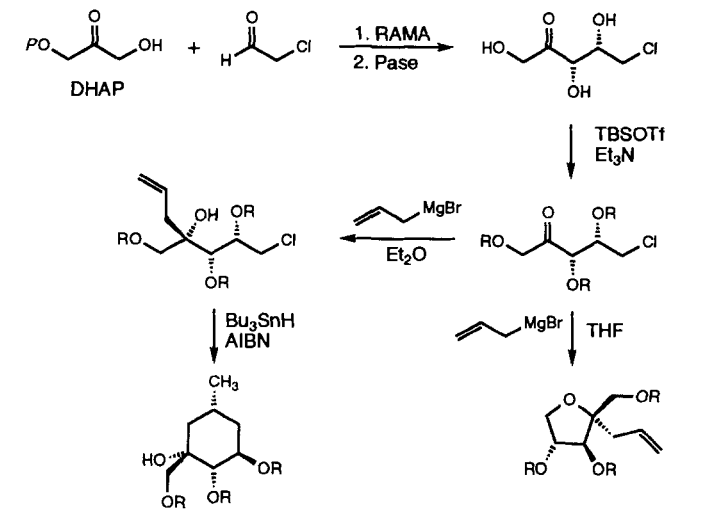
Scheme 10.



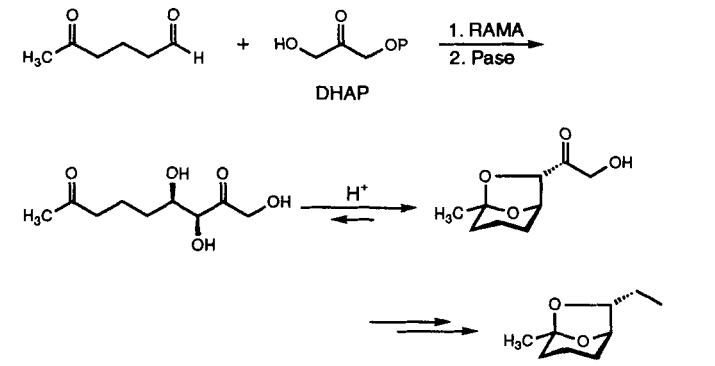
Scheme 11. Stereochemical course of intramolecular reductive amination. The *trans* products avoid torsional strain; the *cis* products minimize steric interactions.



Scheme 12. Synthesis of DAHP with RAMA.



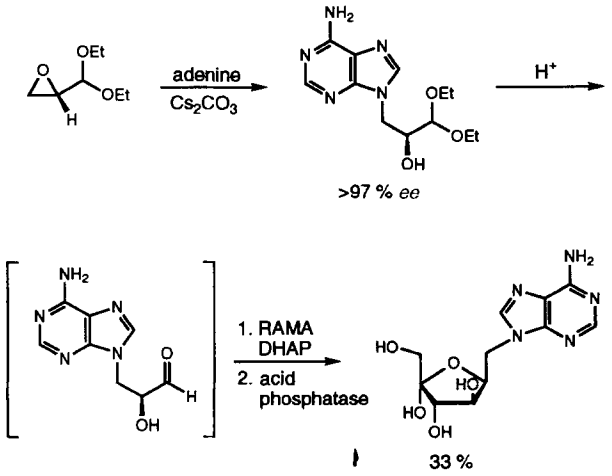
Scheme 13. Synthesis of a cyclitol and a C-glycoside with RAMA. AIBN = azoisobutyronitrile, TBS = *tert*-butyldimethylsilyl, Tf = SO_2CF_3 (triflate), R = TBS, Pase = phosphatase.



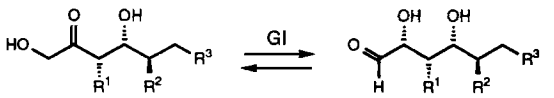
Scheme 14. Synthesis of (+)-*exo*-brevicomin with RAMA. Pase = phosphatase.

3.4. Fuculose-1-phosphate (Fuc-1-*P*) Aldolase [EC 4.1.2.17], Rhamnulose-1-phosphate (Rha-1-*P*) Aldolase [EC 4.1.2.19], and Tagatose-1,6-diphosphate (TDP) Aldolase

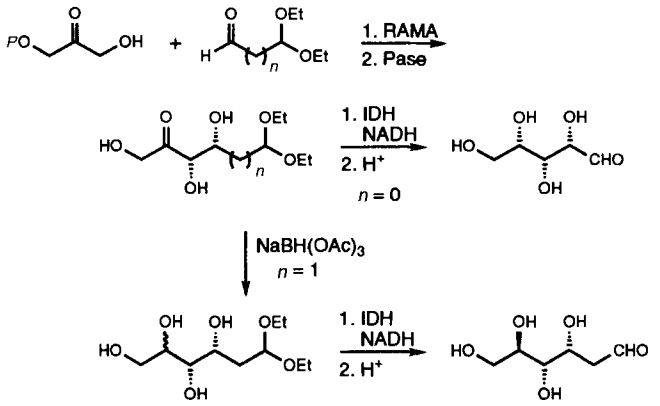
Besides FDP aldolase, there are three other known aldolases which use DHAP as the donor in the aldol reaction: Fuc-1-*P* aldolase, Rha-1-*P* aldolase, and TDP aldolase. Fuc-1-*P* aldo-



Scheme 15. Synthesis of homo-C-nucleosides.



Scheme 16. Substrate specificity of glucose isomerase (GI). R^1,R^2 = OH, H; R^3 = OH, H, F, OCH_3, N_3.



Scheme 17. Use of the "inversion strategy" to synthesize L-xylose ($n = 0$) and 2-deoxy-D-*arabino*-hexose ($n = 1$). Pase = phosphatase, IDH = iditol dehydrogenase.

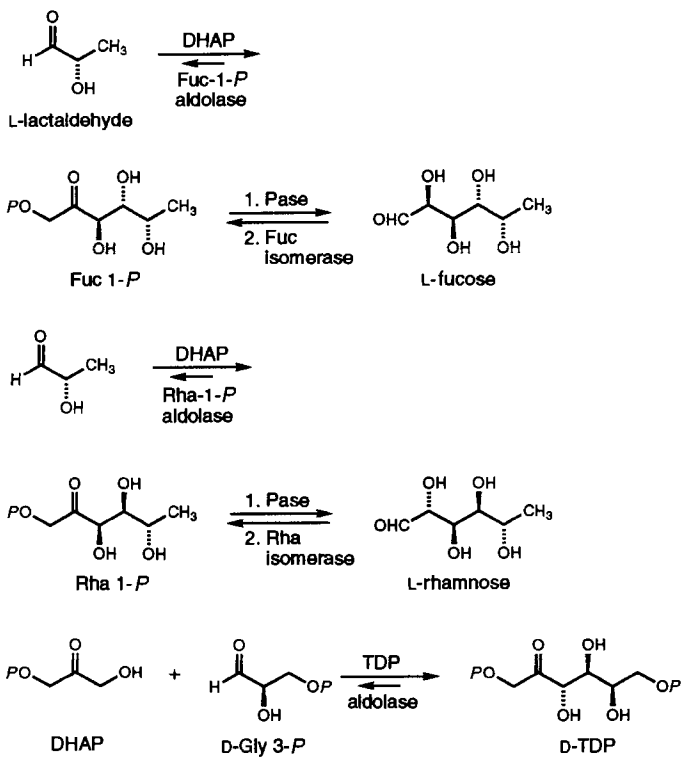
lase catalyzes the reversible condensation of DHAP and L-lactaldehyde to give L-Fuc-1-*P*, and with the same substrates, Rha-1-P aldolase produces L-Rha-1-*P* (Scheme 18). Both of these enzymes are type II aldolases and are found in several microorganisms.[62] Fuc-1-*P* aldolase[63-64] and Rha-1-*P* aldolase[64] have been cloned, overexpressed and subsequently purified. Tagatose-1,6-diphosphate (TDP) aldolase, a type I aldolase involved in the galactose metabolism of cocci, catalyzes the reversible condensation of G3P with DHAP to give D-TDP.

Both Fuc-1-*P* and Rha-1-*P* aldolase accept a variety of aldehydes to generate vicinal diols with D-*erythro* and L-*threo* configurations, respectively.[62-64] While the enzymes yield products with the (3*R*) configuration stereospecifically, the stereoselectivity at C-4 is somewhat diminished for a few substrates.[63] However, sterically unhindered 2-hydroxyaldehydes normally give very high diastereoselectivities.

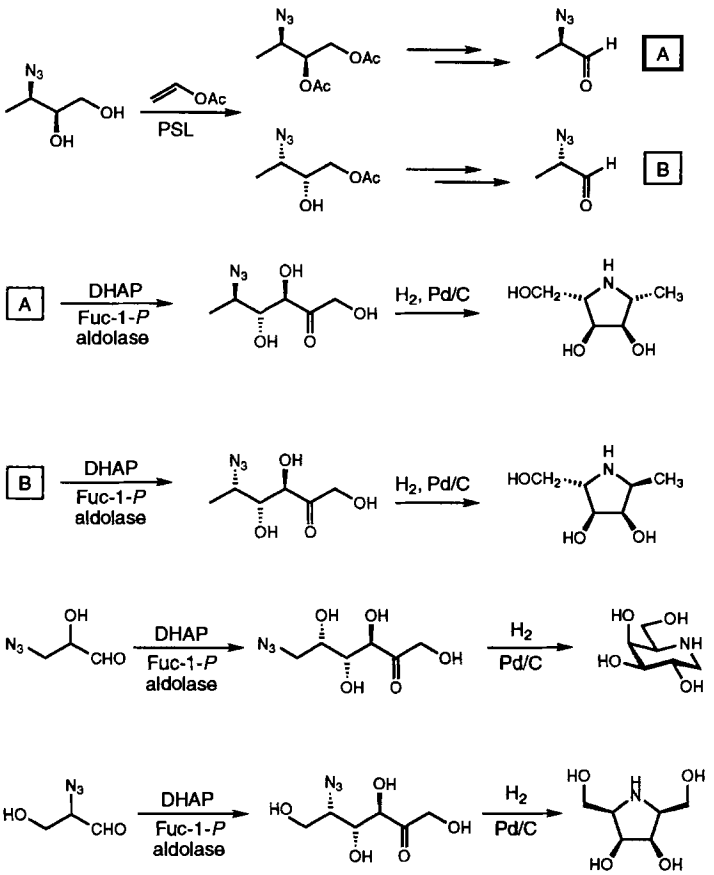
These two aldolases also show significant kinetic preference for the L-enantiomer of 2-hydroxyaldehydes (>95:5), so they facilitate the kinetic resolution of a racemic mixture of these compounds.[56] Both enzymes have been used in the synthesis of rare ketose-1-phosphates[56] and several aza and deoxyaza sugars.[53, 54, 65] Scheme 19 illustrates the use of Fuc-1-*P* aldolase in the synthesis of five-membered aza sugars, and Scheme 20 illustrates the enantiocomplementary nature of Rha-1-*P* aldolase and FDP aldolase.

Fuc-1-*P* and Rha-1-*P* aldolases have also been utilized in whole cell systems with DHA and catalytic inorganic arsenate.[45] With L-lactaldehyde and DHA/arsenate as the substrates in the Rha-1-*P* aldolase reaction, the aldol product L-rhamnulose was subsequently isomerized to L-rhamnose, catalyzed by rhamnose isomerase present in the cell. No such isomerization was observed with L-xylulose when the corresponding aldol product formed from glycoaldehyde was the substrate. Recent studies have since shown that both rhamnose and fucose isomerase only accept substrates with a paricular configuration, namely (2*R*,3*R*) and (2*S*,3*R*), respectively.[56]

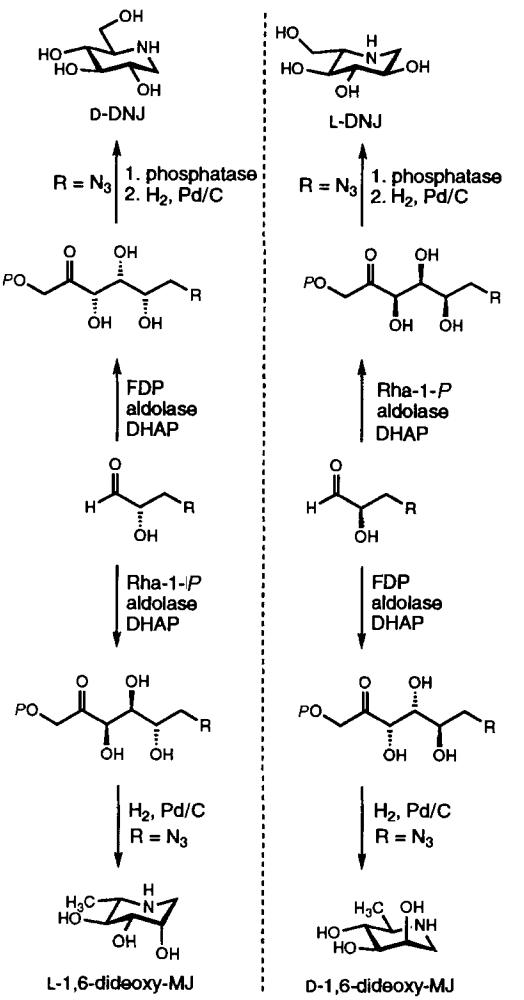
An alternative method for preparing the same ketose-1-phosphates available from the Rha-1-*P* and Fuc-1-*P* aldolases is to use the rhamnose and fucose isomerases.[56] The isomerase only partially converts the aldose into the ketose, so a second step in which the ketose is phosphorylated drives the reaction to completion. Several ketose-1-phosphates were prepared by using rhamnulose kinase in the second step to give overall yields of 72–90%.



Scheme 18. Aldol addition reaction catalyzed in vivo by fuculose-1-phosphate (Fuc-1-P) aldolase, rhamnulose 1-phosphate (Rha-1-P) aldolase, and tagatose-1,6-diphosphate (TDP) aldolase. Both fucose and rhamnose isomerases can be utilized to isomerize the corresponding ketose after dephosphorylation with phosphatase (Pase).



Scheme 19. Synthesis of aza sugars using fuculose-1-phosphate aldolase and *Pseudomonas* lipase (PSL).



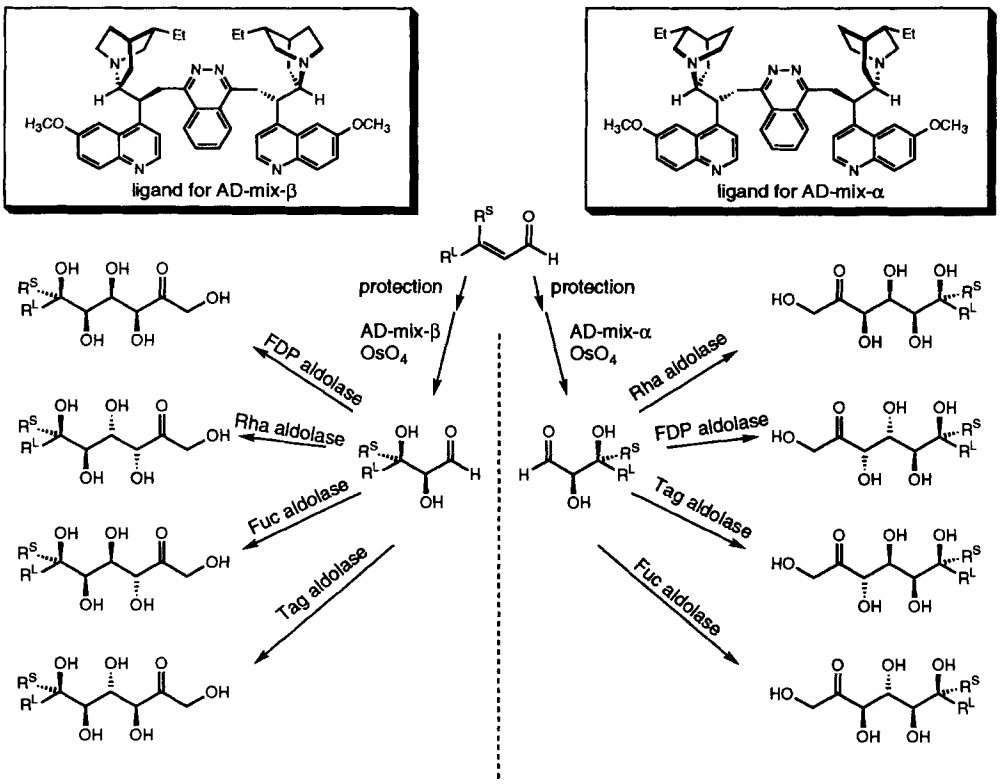
Scheme 20. Aldolase-mediated synthesis of each enantiomer of deoxynojirimycin (DNJ) and 1,6-dideoxymannojirimycin (1,6-dideoxy-MJ).

TDP aldolase has been isolated from several sources.[66] The enzym from *E. coli* has a narrow pH profile with an optimum at pH 7.5, but still displays acceptable activity within pH 6.5–7. Like the other DHAP aldolases, TDP aldolase accepts a variety of acceptor substrates for the aldol reaction, including glycoaldehyde, D- and L-glyceraldehyde, acetaldehyde, and *iso*-butyraldehyde.[67] However, in all cases investigated so far, a diastereomeric mixture of products is formed. Also, instead of exhibiting the expected *erythro* configuration as in D-tagatose, more than 90% of each product possessed the *threo* configuration similar to D-fructose. Only with the natural substrate D-glyceraldehyde does the major product (D-TDP) have the tagatose configuration. Due to this lack of stereoselectivity, TDP aldolase is not yet synthetically useful; however, with suitable protein engineering or screening, a highly stereoselective TDP may be created in the future.

From a synthetic point of view, each of the DHAP-dependent aldolases yields a product whose stereochemistry at C-3 and C-4 is complementary to the other products; that is, all four stereochemical permutations are provided by these aldolases. FDP, Rha-1-*P*, Tag-1-*P*, and Fuc-1-*P* aldolases provide four diastereomers from a variety of nonnatural aldehydes. In principle, either of the C-3/C-4 stereoisomeric ketoses is obtainable with these enzymes, which are now available from the American Type Culture Collection (ATCC) as recombinant *E. coli* strains. With a proper choise of aldehyde substrate, the enzymatic aldol reaction provides a new route to many common and uncommon sugars. Although several methods are available for the preparation of enantiomerically pure aldehydes as substrates for aldolases, the osmium-catalyzed dihydroxylation method developed by Sharpless[68] is perhaps the most useful, as it provides either enantiomer for use in enzymatic reactions (Scheme 21). Examples have been shown in the synthesis of enantiomeric D- and L-fructose and derivatives thereof (Scheme 22).[69] Other enzymatic routes to D and L sugars include lipase-catalyzed enantioselective acylation of glycals[70] and *meso* cyclic triols,[71] and alcohol dehydrogenase-catalyzed reductions (Scheme 23).[72]

3.5. *N*-Acetylneuraminic Acid (NeuAc) Aldolase [EC 4.1.3.3] and NeuAc Synthetase [EC 4.1.3.19]

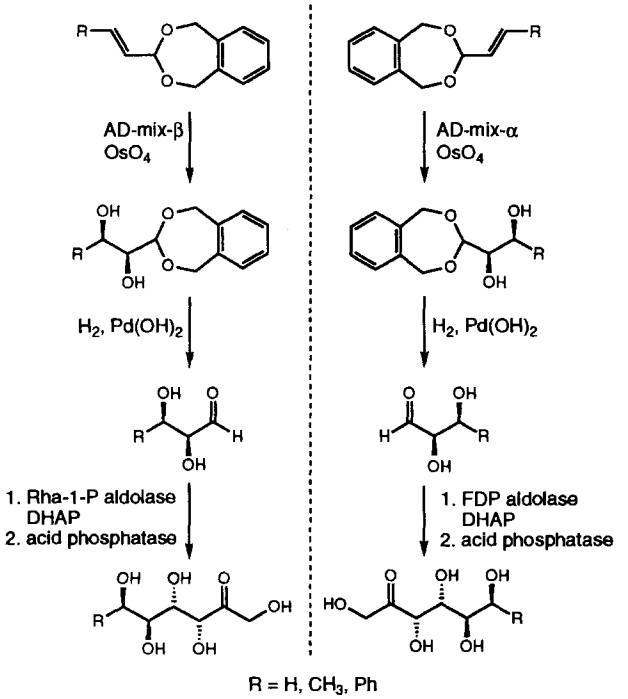
The enzyme NeuAc aldolase, also known as sialic acid aldolase, catalyzes the reversible condensation of pyruvate with D-*N*-acetylmannosamine (ManNAc) to form *N*-acetyl-5-amino-3,5-dideoxy-D-*galacto*-D-*glycero*-2-nonulosonic acid (NeuAc or sialic acid; see Scheme 24).[73, 74] Although the β anomer predominates in solution, the α anomer of NeuAc is the substrate for the enzyme, and the initial products of aldol cleavage are α-D-ManNAc and pyruvate.[75] The enzyme has a catabolic function in vivo, with an equilibrium constant for the retro-aldol reaction



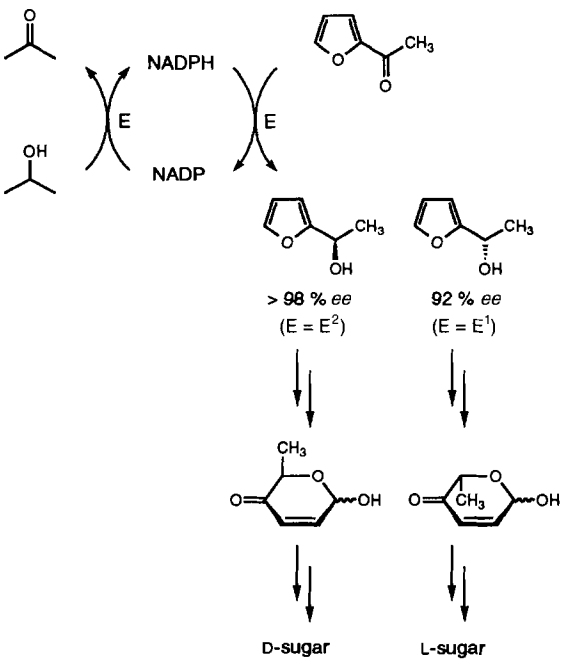
Scheme 21. Strategy for the enantioselective synthesis of all possible isomers of 2-ketohexose. (The larger substituent is indicated by R^L and the smaller by R^S.)

of 12.7 M^{-1}. However, for synthetic purposes, an equilibrium favoring the aldol product can be achieved by using excess pyruvate.[74] NeuAc aldolase has been isolated from both bacteria and animals, and in both cases it is a Schiff base-forming type I aldolase. The optimum pH for activity is 7.5, but it is still active between pH 6 and 9 and is stable to oxygen.[74, 76] The enzymes from *Clostridia* and *E. coli* are now commercially available (Toyobo), and the enzyme from *E. coli* has been cloned and overexpressed.[77] NeuAc aldolase has been used in both free and immobilized form,[78-82] and in some instances it has been enclosed in a dialysis membrane.[83]

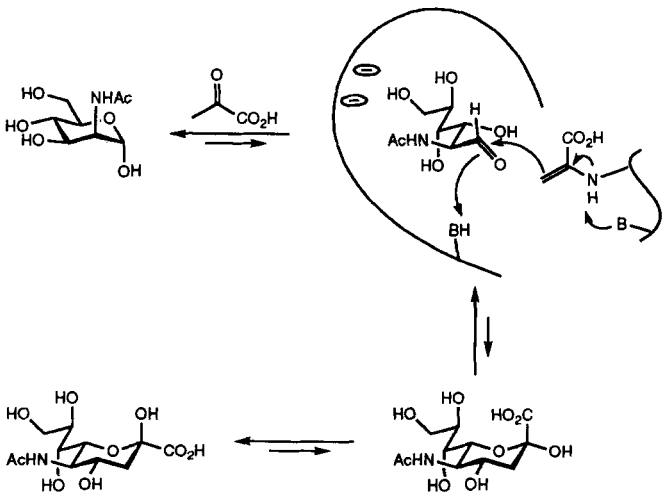
Synthetic studies have shown that a high conversion (about 90%) of ManNAc to NeuAc was achieved with the isolated enzyme, although seven equivalents of pyruvate were required. To eliminate the need for excess pyruvate and to aid in the isolation of products, the NeuAc synthesis can be coupled to a more thermodynamically favorable process. One example with ManNAc as the starting material involved the coupling of the NeuAc aldolase reaction with a subsequent sialyltransferase reaction to produce sialyl glycosides.[84] Another variant of this process uses a mixture of ManNAc and GlcNAc whereby the GlcNAc was epimerized to ManNAc chemically,[85] or enzymatically[86] with *N*-acetylglucosamine 2-epimerase. The excess pyruvate can also be decomposed by pruvate decarboxylase (see below).



Scheme 22. Tandem asymmetric dihydroxylation/asymmetric aldol reactions as a route to common and uncommon D and L sugars.



Scheme 23. Enantioselective route to L or D sugars with an enzyme-catalyzed asymmetric reduction. E^1 = alcohol dehydrogenase from *Thermoanaerobium brockii*, E^2 = alcohol dehydrogenase from *Lactobacillus*.

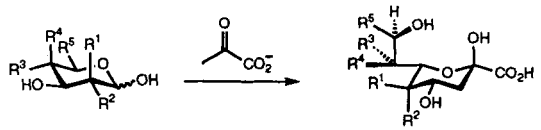


Scheme 24. Mechanism of the NeuAc aldolase catalyzed reaction.

Extensive substrate specificity studies were also carried out with NeuAc aldolase. Only pyruvate is acceptable as the donor; 3-fluoropyruvate, 3-bromopyruvate, 3-hydroxypyruvate, 2-oxobutyrate, and acetylphosphonate are not substrates.[81] In the case of the acceptor substrate the enzyme is more flexible. Substitutions at C-2, C-4, and C-6 of ManNAc are allowed with only a slight preference for the compounds having the same configuration at C-4, C-5, and C-6 as ManNAc.[81, 87–91] Some pentoses and their analogs are also substrates, but aldehydes with two or three carbon atoms are not accepted.

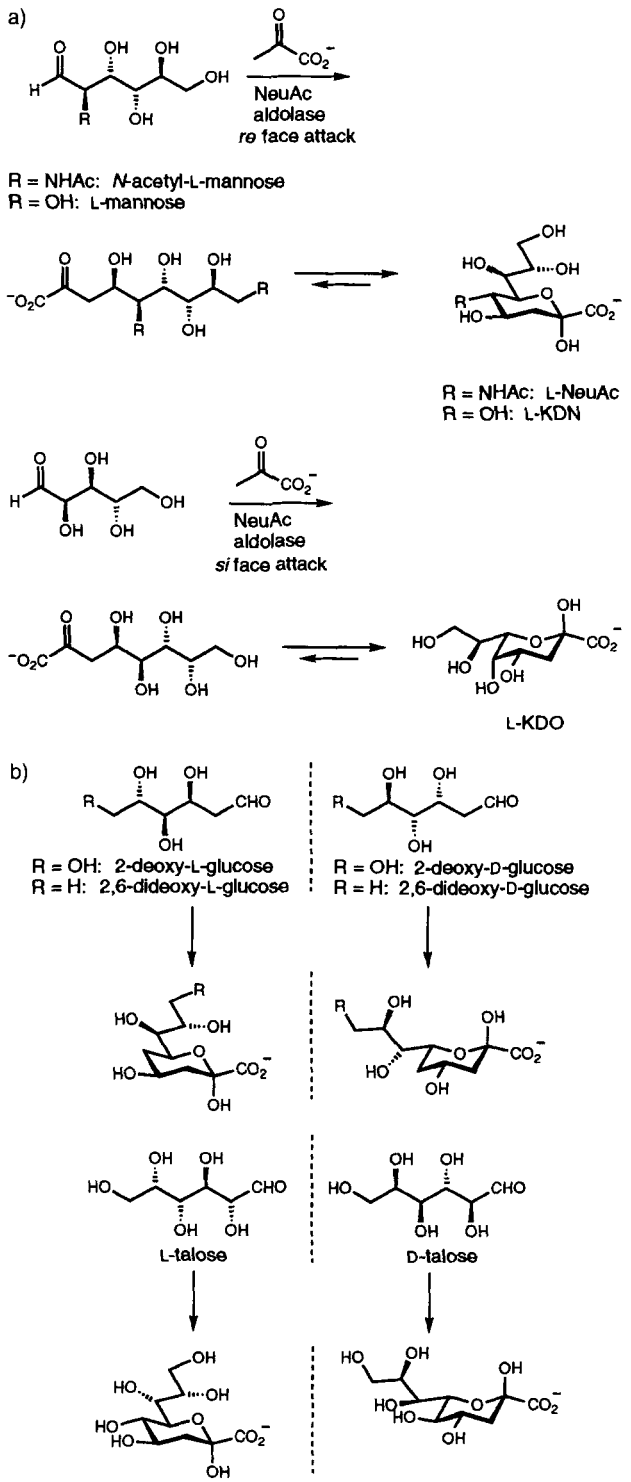
Recently much interest has been stimulated in NeuAc analogs by their role in cellular biology. NeuAc and derivatives are found at the termini of mammalian glycoconjugates and play an important role in biochemical recognition.[92] Polysialic acids are also found in bacteria and mammalian tissues, and may be involved in cell adhesion and cell–cell communication.[10] Because NeuAc aldolase accepts a wide variety of substrates and is readily available, many sialic acid derivatives have been prepared (Table 4) that may be used in biological studies.[93–97]

Table 4. Substrate specificity of NeuAc aldolases.



R^1	R^2	R^3	R^4	R^5	k_{rel}	Ref.
AcNH	H	OH	H	CH_2OH	1	78, 81, 83
AcNH	H	OH	H	CH_2OAc	0.2	78, 81
AcNH	H	OH	H	CH_2N_3	0.6	82, 91
AcNH	H	OH	H	CH_2F	0.6	82
OH	H	OH	H	CH_2OH	2	80
OH	H	H	H	CH_2OH	–	89
OH	H	H	F	CH_2F	–	82
OH	H	OH	H	H	0.1	90
H	H	OH	H	CH_2OH	1.3	90
H	OH	OH	H	CH_2OH	0.07	89
Ph	H	OH	H	CH_2OH	–	90
AcNH	H	OH	H	CH_2OCH_3	–	
AcNH	H	OH	H	$CH_2OCOCH(OH)CH_3$	–	
N_3	H	OH	H	CH_2OH	–	
AcNH	H	OH	H	$CH_2OP(O)Me_2$	–	82

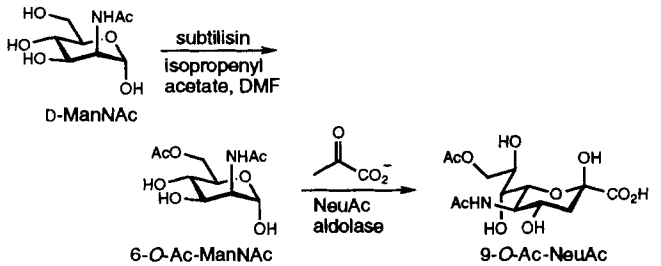
Of the many NeuAc derivatives synthesized so far, most give products with *S* configuration at C-4. Recent observations indicate, however, that under thermodynamically controlled conditions with certain sugars, the absolute configuration at C-4 can be reversed. For example, in the NeuAc aldolase-catalyzed synthesis of KDO a mixture of (*S*)-C-4 and (*R*)-C-4 products were



Scheme 25. a) Synthesis of L-NeuAc, L-KDN, and L-KDO with NeuAc aldolase. b) The substrate-controlled enantiocomplementary nature of NeuAc aldolase reactions with L and D sugars. Left: *re* face attack. Right: *si* face attack.

isolated when D-arabinose was the substrate.[90] NMR studies with several other sugars (for example L-mannose, D-gulose, 2-azido-2-deoxy-L-mannose) showed that over time, products with a C-4 equatorial group predominated, in some cases disregarding the normal stereochemical preference of the enzyme.[98] Apparently, pyruvate attacks the acceptor sugar to give the thermodynamically more stable product, and the facial selectivity is merely a consequence for the preference to form a C-4 equatorial product. Several biologically interesting L sugars were synthesized with this method, including N-LeuAc, L-KDO, and 3-deoxy-L-*galacto*-L-*glycero*-nonulosonic acid (L-KDN, Scheme 25). The excess pyruvate can be decomposed with pyruvate decarboxylase to simplify the product isolation.[98b]

A facile synthesis of 9-*O*-AcNeuAc[79] was improved by regioselective irreversible acetylation of ManNAc catalyzed by subtilisin, followed by a NeuAc aldolase-catalyzed condensation of the resulting 6-*O*-acetylManNAc with pyruvate (Scheme 26).[81] This two-step enzymatic synthesis provided

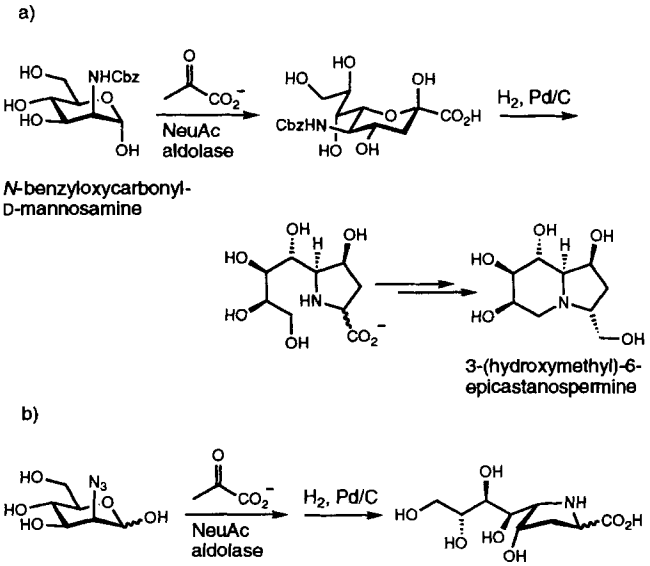


Scheme 26. Synthesis of 9-*O*-Ac-NeuAc by combined use of subtilisin and NeuAc aldolase.

9-*O*-acetyl-NeuAc in about 80% yield. Some other 9-O-acylated NeuAc derivatives may also be prepared in this fashion.[82]

Some other noteworthy examples include the synthesis of the α-methylketoside of an *N*-unprotected NeuAc for use in preparation of *N*-substituted NeuAc.[89] Also, polyacrylamides bearing pendant α-sialoside[95] groups and polymers of C-linked sialosides[96] were prepared and shown to strongly inhibit agglutination of erythrocytes by influence virus. Finally, a derivative of the potent glycosidase inhibitor castanospermine was synthesized starting from a NeuAc-catalyzed addition of pyruvate to *N*-Cbz-D-mannosamine. In this example, a reductive amination step of the aldolase product gives an aza sugar which is a precursor to 3-(hydroxymethyl)-6-epicastanospermine (Scheme 27a).[99] Another five-membered ring aza sugar has recently been prepared based on sialic acid aldolase (Scheme 27b).[100]

The synthesis of NeuAc in vivo is accomplished through NeuAc synthetase,[76] which catalyzes the irreversible condensation of PEP and *N*-acetylmannosamine. Although this enzyme has not yet been isolated and characterized, it may prove synthetically useful in the future, since the forward reaction is favored both kinetically and thermodynamically.

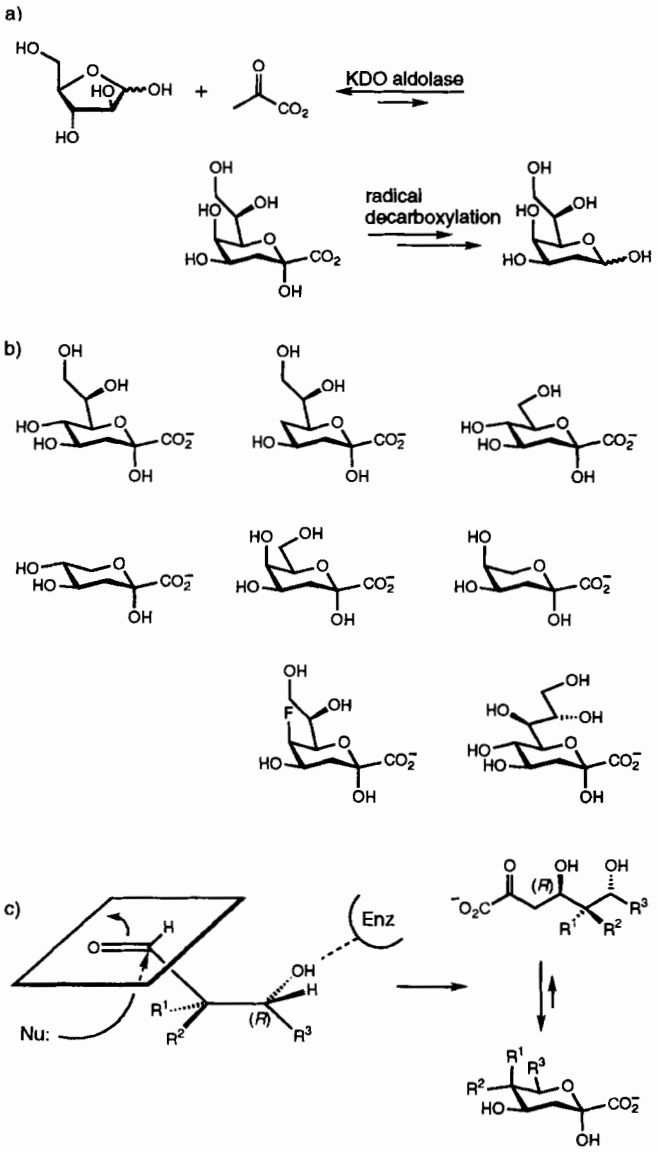


Scheme 27. Synthesis of aza sugars with NeuAc aldolase.

3.6. 3-Deoxy-D-*manno*-2-octulosonate Aldolase [E.C. 4.1.2.23] and 3-Deoxy-D-*manno*-2-octulosonate-8-phosphate Synthetase [E.C. 4.1.2.16]

3-Deoxy-D-*manno*-2-octulosonate aldolase, also known as 2-keto-3-deoxyoctanoate (KDO) aldolase, catalyzes the reversible condensation of pyruvate with D-arabinose to form KDO with an equilibrium constant for the cleavage of 0.77 M^{-1} (Scheme 28). KDO and its activated form CMP-KDO (CMP = cytidine monophosphate) are key intermediates in the synthesis of the outer membrane lipopolysaccharide (LPS) of gram-negative bacteria,[101] so analogs of KDO may inhibit LPS biosynthesis or LPS binding protein.[102–107] KDO aldolase has been isolated and purified from *E. coli*[108] and *Aerobacter cloacae*.[109] Preliminary investigations of this enzyme showed high specificity for KDO for the cleavage, whereas the condensation reaction proceeded with some flexibility; several nonnatural substrates, including D-ribose, D-xylose, D-lyxose, L-arabinose, D-arabinose-5-phosphate, and *N*-acetylmannosamine were reported to be weak substrates (relative rate less than 5% cf. D-arabinose).[108] More recent studies on the substrate specificity showed that the KDO aldolase from *Aureobacterium barkerei*, strain KDO-37-2, accepted an even wider variety of substrates that included trioses, tetroses, pentoses, and hexoses.[110] The enzymes is specific for substrates having *R* configuration at C-3, but the stereochemical requirements at C-2 are less stringent. The C-2 *S* configuration is favored under kinetic control, the C-2 *R* configuration under thermodynamic control. Several aldol addition reactions were conducted on a preparative scale including the synthesis of KDO itself which was obtained in a 67% yield. In each case, the pyruvate attacked from the *re* face of the carbonyl group of the acceptor substrate.

3-Deoxy-D-*manno*-2-octulosonate-8-phosphate synthetase, also known as 8-phospho-2-keto-3-deoxyoctanoate (KDO 8-P) synthetase, catalyzes the irreversible aldol reaction of PEP and D-arabinose 5-phosphate to give KDO 8-P.[111] The enzyme has been isolated from *E. coli*[112] and *Pseudomonas aeruginosa*,[113]

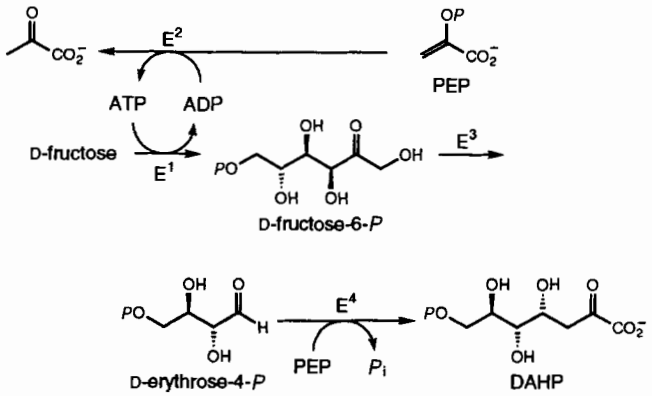


Scheme 28. a) Synthesis of longer chain 2-deoxy sugars with KDO aldolase; b) KDO derivatives synthesized with KDO aldolase; c) mechanism of the KDO aldolase catalyzed reaction: *re* face attack of the nucleophile Nu; the product formed by kinetic control has the *S* configuration (R^1 = OH, R^2 = H), while that favored thermodynamically has the *R* configuration (R^1 = H, R^2 = OH).

and the *E. coli* enzyme has been cloned and overexpressed in *E. coli* and *Salmonella typhimurium*.[114] KDO 8-P itself has been synthesized with KDO 8-P synthetase,[112] and the starting material, D-arabinose-5-phosphate, was generated either by hexokinase-catalyzed phosphorylation of arabinose[108] or by isomerase-catalyzed reaction of D-ribose-5-phosphate.[113] To date, the substrate specificity of KDO 8-P synthetase has not been well investigated, and initial studies indicate this enzyme is very specific for its natural substrates.

3.7. 3-Deoxy-D-*arabino*-2-heptulosonic Acid-7-Phosphate (DAHP) Synthetase [E.C. 4.1.2.15]

DAHP, also known as phospho-2-keto-3-deoxyheptanoate, is a key intermediate in the shikimate pathway for the biosynthesis of aromatic amino acids in plants.[115] In vivo, DAHP synthetase catalyzes the synthesis of DAHP from PEP and D-erythrose-4-phosphate.[116] The enzyme has been cloned and used to synthesize DAHP (Scheme 29).[117] The D-erythrose-4-phosphate necessary for the DAHP synthesis was generated in situ from Fru-6-*P* catalyzed by transketolase in the presence of D-ribose-5-phosphate. The Fru-6-*P* needed for this reaction was generated for D-fructose and ATP catalzyed by hexokinase in the presence of an ATP regeneration system. Further study on this particular enzyme system indicated that it is more efficient and economical to use whole cells containing a DAHP synthetase plasmid.[118] Such a system also provides the other necessary enzymes for the synthesis of DAHP. To date, little study has been conducted to determine the substrate specificity of this enzyme.

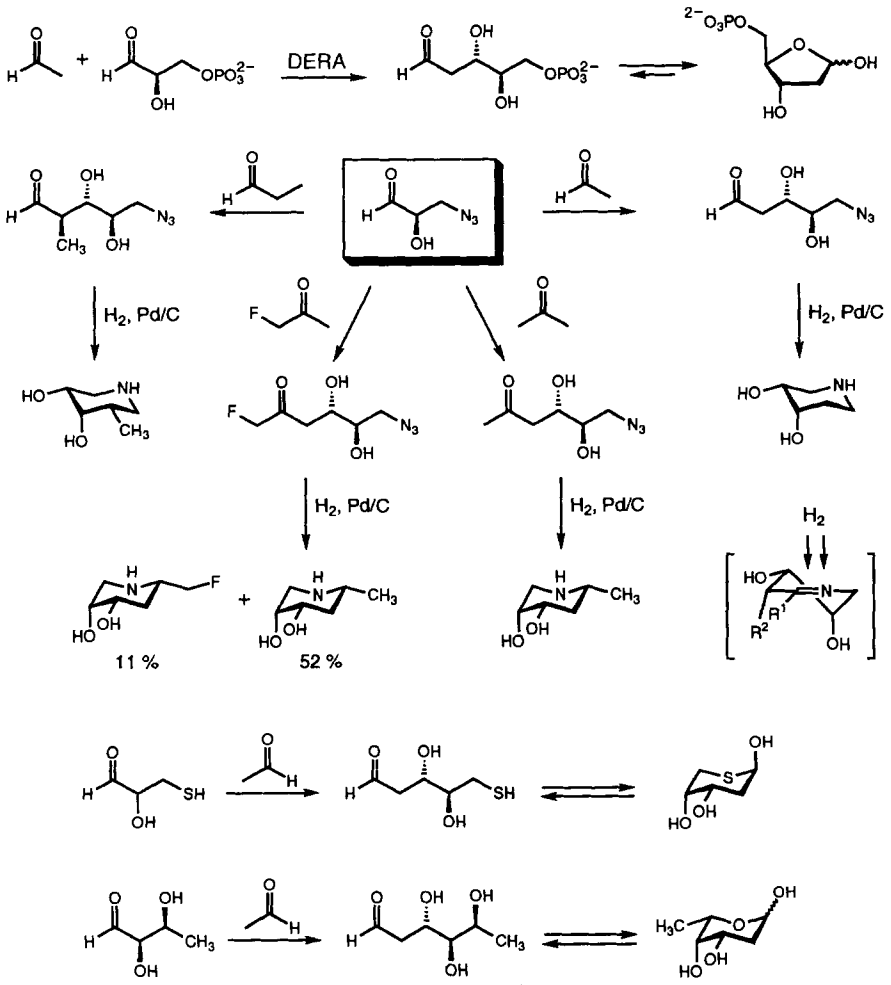


Scheme 29. Multienzyme synthesis of DAHP. E^1: hexokinase, E^2: pyruvate kinase, E^3: transketolase + D-ribose-5-P, E^4: DAHP synthetase.

3.8. 2-Deoxyribose-5-Phosphate Aldolase (DERA) [E.C. 4.1.2.4]

The enzyme DERA[119] is unique among the aldolases in that the donor of the aldol reaction is an aldehyde. In vivo, this enzyme catalyzes the reversible condensation of acetaldehyde and G3P to form D-2-deoxyribose-5-phosphate with an equilibrium constant for the condensation reaction of 2×10^{-4} M (Scheme 30). DERA is a type I aldolase and has been isolated from animal tissues[120] and several microorganisms.[121] The *E. coli* gene encoding the enzyme has been sequenced, subcloned,[122] and subsequently overexpressed in *E. coli*.[123] At 25 °C and pH 7.5 this enzyme is fairly stable and retains 70% of its activity after 10 days.

A number of nonnatural substrates are accepted by DERA, and the newly generated chiral center always has the *S* configuration. Specificity studies have been conducted with DERA from *Lactobacillus plantarum* (specific activity of about *6000* $U mg^{-1}$ for condensation)[124a] and *E. coli* (V_{max} = 21 $U mg^{-1}$ for aldol cleavage).[123] The enzyme from *L. plantarum* accepts various acceptor substrates including L-G3*P*, D-erythrose-4-phosphate, glycoaldehyde-phosphate, D-ribose-5-phosphate, D,L-glyceraldehyde, D-erythrose, and D-threose, but not D-ribose or glycoaldehyde.[124b] Only propionaldehyde could replace acetaldehyde as the donor but the rate of reaction



Scheme 30. Synthesis of N-, S-, and O-heterocycles with 2-deoxyribose-5-phosphate aldolase (DERA).

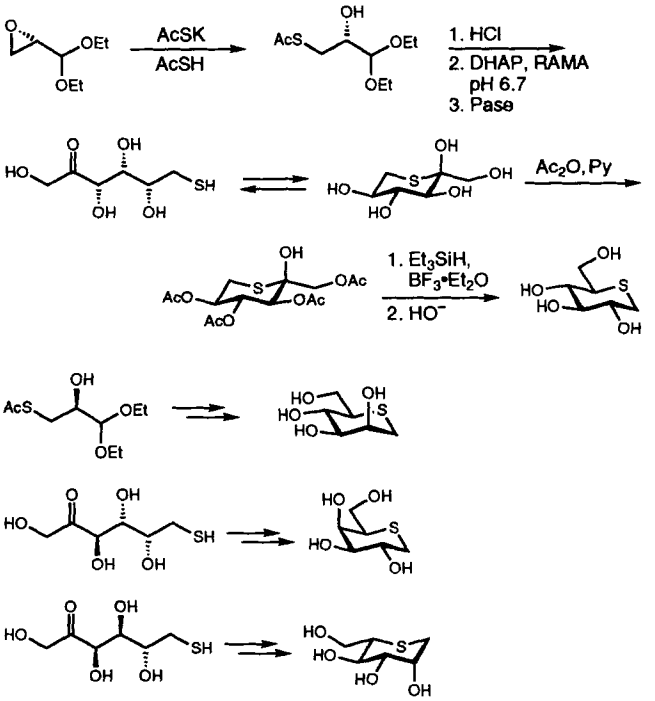
is low. The *E. coli* enzyme, on the other hand, is able to utilize several other donor substrates including acetaldehyde, propionaldehyde, acetone, and fluoroacetone.[123] A number of aliphatic aldehydes, sugars, and sugar phosphates are acceptor substrates. However, in some cases, the rates of the aldol reactions are very low (0.4–1% relative to the natural substrates). Among the several compounds synthesized from the *E. coli* enzymes are a fluoroketose and a trideoxyaza sugar (Scheme 30).

In addition to hydroxy- and azidoaldehydes, thioaldehydes can be used as acceptor substrates, which provides a new route to thiosugars (Scheme 31). Thioaldehydes are also acceptable by other aldolases such as the DHAP-dependent aldolases, and several thioketoses and deoxythiosugars have been prepared.[125] DERA also catalyzes sequential aldol reactions with three aldehyde substrates.[125]

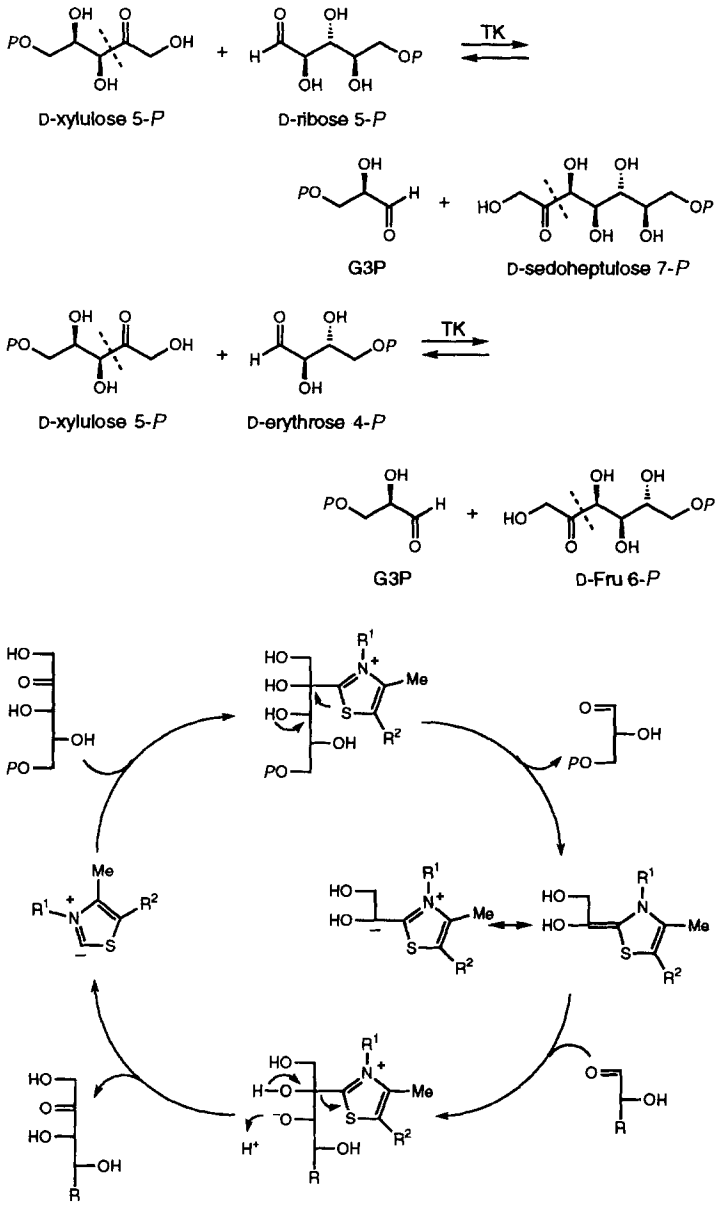
4. Ketol and Aldol Transfer Reactions

4.1. Transketolase [E.C. 2.2.1.1]

One of the enzymes in the pentose phoshphate pathway is transketolase (TK)[126] which reversibly transfers the C-1/C-2 ketol unit from D-xylulose-5-phosphate to D-ribose-5-phosphate to generate D-sedoheptulose-7-phosphate and G3P. The enzyme relies on two cofactors are activity: thiamine pyrophosphate (TPP) and Mg^{2+}. TK from baker's yeast is commercially available,[127] and the enzyme has also been isolated from spinach.[128–129] The enzyme isolated from yeast shows a slightly higher diastereoselectivity (about 100%)[129] than the enzyme from spinach (about 95%), and the newly formed hydroxymethine chiral center always possesses the *S* configuration. In addition to D-xylulose-5-phosphate, D-erythrose-4-phosphate acts as a ketol donor to produce D-Fru-6-*P* and G3P (Scheme 32). β-Hydroxypyruvic acid (HPA) also acts as a ketol donor[130] which is transferred to an aldose acceptor with an activity 4% that of the donor D-xylulose-5-phosphate.[128] One valuable feature of HPA is that once the ketol unit is transferred by TK, carbon dioxide is lost, rendering the overall reaction irreversible. Other analogs of HPA such as 2,3-dioxopropionic acid, 3-hydroxy-2-oxobutyric acid, 2-oxomalonic acid, and 2-oxogluconic acid, are not substrates,[131] but a wide range of aldehydes are ketol acceptors including aliphatic, α,β-unsaturated, aromatic, and heterocyclic alde-



Scheme 31. Synthesis of deoxythiosugars with aldolases. The ketoses in the penultimate and bottom lines are synthesized with Fuc-1-*P* and Rha-1-*P* aldolase as catalysts, respectively.



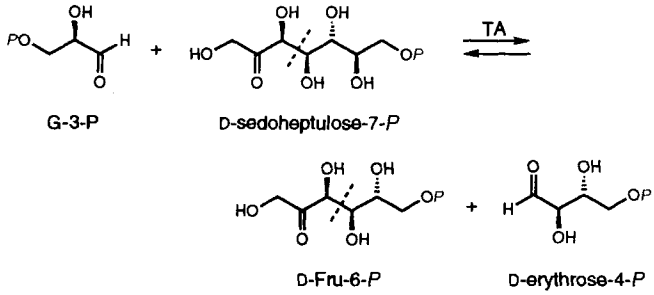
Scheme 32. Ketol transfer reactions in the oxidative pentose phosphate pathway catalyzed by transketolase (TK), and the mechanism of the catalysis.

hydes.[131-132] The presence of a hydroxy or an oxygen atom at C-2 and/or C-3 accelerates the reaction, while steric hindrance near the aldehyde decreases the rate. β-Hydroxyaldehydes epimeric at C-2 can be efficiently resolved by TK, since only the (2*R*) enantiomers are substrates giving 3,4-D-*threo* products.[131, 133] Beyond the C-2 configuration, the enzyme appears to have no preference for stereochemistry.

A few synthetic examples that employ TK are illustrated in the synthesis of (+)-*exo*-brevicomin[134] and the aza sugar 1,4-dideoxy-1,4-imino-D-arabinitol.[33] Both syntheses involve the condensation of HPA with racemic 2-hydroxyaldehydes in which the ketol units is diastereoselectively transferred to only the D-enantiomer of the aldehyde.

4.2. Transaldolase [E.C. 2.2.1.2]

Like transketolase, transaldolase (TA) is an enzyme in the oxidative pentose phosphate pathway.[126] TA, which operates through a Schiff base intermediate, catalyzes the transfer of the C-1/C-3 aldol unit from D-sedoheptulose-7-phosphate to G3P to produce D-Fru-6-*P* and D-erythrose-4-phosphate (Scheme 33). Although it is commercially available, TA has rarely been used in organic synthesis, and no detailed substrate specificity study has yet been performed. In one application TA was used in the synthesis of D-fructose from starch.[135] The aldol moiety was transferred from Fru-6-P to D-glyceraldehyde in the final step of this multienzyme synthesis of D-fructose.



Scheme 33. Aldol transfer reaction in the oxidative pentose phosphate pathway catalyzed by transaldolase (TA).

Conclusion

The enzymatic aldol addition reaction represents a new, useful method for the synthesis of various sugar and sugar-like structures, which themselves may find use in the study of carbohydrate-mediated recognition or as building blocks for the synthesis of complex carbohydrates. Although only a limited number of aldolases and their reactions are presented in this review, more than twenty different aldolases have been isolated, and several of these have been cloned and overexpressed. Because of the high stereoselectivity and flexibility of the acceptor in these enzymatic reactions, aldolases, and transaldolases are expected to be increasingly used, and the enzymatic aldol reactions will complement many other enzymatic (for example, those based on oxidoreductases and lipases) and nonenzymatic methods available for carbohydrate synthesis.

Received: January 31, 1993 [A 47 IE]
German version: *Angew. Chem.* **1995**, *107*, 453

[1] J. B. Jones, C. J. Sih, D. Perlman, *Application of Biochemical Systems in Organic Chemistry*, Wiley, New York, **1976**; C.-H. Wong, G. M. Whitesides, *Angew. Chem.* **1985**, *97*, 617; *Angew. Chem. Int. Ed. Engl.* **1985**, *24*, 617; H. Yamada, S. Shimizu, *ibid.* **1988**, *100*, 640 bzw. **1988**, *27*, 622; C.-S. Chen, C. J. Sih, *ibid.* **1989**, *101*, 711 bzw. **1989**, *28*, 695; C.-H. Wong, *Science* **1989**, *244*, 1145; A. M. Klibanov, *Acc. Chem. Res.* **1990**, *23*, 114; V. Schellenberger, H.-D. Jakubke, *Angew. Chem.* **1991**, *103*, 1440; *Angew. Chem. Int. Ed. Engl.* **1991**, *30*, 1437; H. Waldmann, *Kontakte* **1991** (2) 33; S. David, C. Auge, C. Gautheron, *Adv. Carbohydr. Chem. Biochem.* **1991**, *49*, 175; W. D. Fessner, *Kontakte* **1992** (3), 3; *ibid.* **1993** (1), 23; U. Korf, J. Thiem, *ibid.* **1992** (1), 3.
[2] H. G. Davies, R. H. Green, D. R. Kelly, S. M. Roberts, *Biotransformations in Preparative Organic Chemistry*, Academic Press, London, **1989**.
[3] K. Faber, *Biotransformations in Organic Chemistry*, Springer, Berlin, **1992**.
[4] S. M. Roberts, K. Wiggins, G. Casy, *Preparative Biotransformations*, Wiley, London, **1992**.

[5] C.-H. Wong, G. M. Whitesides, *Enzymes in Synthetic Organic Chemistry*, Pergamon, London, **1994**.
[6] R. A. Lerner, S. J. Benkovic, P. G. Schultz, *Science* **1991**, *252*, 659; P. G. Schultz, R. A. Lerner, *Acc. Chem. Res.* **1991**, *26*, 391.
[7] G. P. Smith, *Science* **1985**, *228*, 1315; J. McCafferty, A. D. Griffiths, G. Winter, D. J. Chiswell, *Nature (London)* **1990**, *348*, 552.
[8] T. R. Cech, *Science* **1987**, *236*, 1532; *Curr. Opin. Struct. Biol.* **1992**, *2*, 605.
[9] A. Varki, *Glycobiology* **1993**, *3*, 97; A. Kobata, *Acc. Chem. Res.* **1993**, *26*, 319; K. G. Rice, Y. C. Lee, *Adv. Enzymol.* **1993**, *66*, 41; S. Hakomori, *Cancer Res.* **1985**, *45*, 2405; N. Sharon, H. Lis, *Sci. Am.* **1993**, *268*, 82; W. I. Weiss, K. Drickamer, W. A. Hendrickson, *Nature (London)* **1992**, *360*, 127; J. P. Carver, *Pure Appl. Chem.* **1993**, *65*, 763; R. U. Lemieux, *Chem. Soc. Rev.* **1989**, *18*, 347.
[10] L. A. Lasky, *Science* **1992**, *258*, 964; J. C. Paulson in *Adhesion: Its Role in Inflammatory Disease* (Eds.: J. Harlan, D. Liu), Freeman, New York, **1992**, p. 19; T. Feizi, *Curr. Opin. Struct. Biol.* **1993**, *3*, 701.
[11] A. T. Beyer, J. E. Sadler, J. I. Rearick, J. C. Paulson, R. L. Hill, *Adv. Enzymol.* **1981**, *52*, 24.
[12] D. A. Ashford, *Curr. Opin. Biotechnol.* **1992**, *3*, 45; C. Edge, R. Parkh, T. Rademacher, M. Wormald, R. Dwek, *Nature (London)* **1992**, *358*, 693; A. Kobata, *Anal. Biochem.* **1979**, *100*, 1.
[13] K. G. I. Nilsson, *Trends Biotechnol.* **1988**, *6*, 256.
[14] Y. Ichikawa, G. C. Look, C.-H. Wong, *Anal. Biochem.* **1992**, *202*, 215.
[15] G. C. Look, C. H. Fotsch, C.-H. Wong, *Acc. Chem. Res.* **1993**, *26*, 182.
[16] Reviews on glycosidase inhibitors, see: A. D. Elbein, *Annu. Rev. Biochem.* **1987**, *56*, 497; L. E. Fellows, *Chem. Br.* **1987**, *23*, 842; B. Winchester, G. W. Fleet, *Glycobiology* **1992**, *2*, 199; for a bisubstrate analog inhibitors, see: M. M. Palcic, L. D. Heerze, O. P. Srivastava, O. Hindsgaul, *J. Biol. Chem.* **1989**, *264*, 17174.
[17] a) See ref. [11]; b) G. Schwarzmann, K. Sandhoff, *Biochemistry* **1990**, *29*, 10865; H. Wiegandt in *New Comprehensive Biochemistry* (Eds.: A. Neuberger, L. L. M. van Deenen), Elsevier, Amsterdam, **1985**, p. 199–260; c) see ref. [305]; d) M. G. Low, A. R. Saltiel, *Science* **1988**, *239*, 268; e) J. Choay, J.-C. Lormeau, M. Petitou, P. Sinay, J. Fareed, *Ann. N.Y. Acad. Sci.* **1981**, *370*, 664; f) M. Cygler, D. R. Rose, D. R. Bundle, *Science* **1991**, *253*, 442; g) review: K. C. Nicolaou, W.-M. Dai, *Angew. Chem.* **1991**, *103*, 1453; *Angew. Chem. Int. Ed. Engl.* **1991**, *30*, 1387; h) review: J. Denarie, J. Cullimore, *Cell* **1993**, *74*, 951; i) S. E. Fishman, K. Cox, J. L. Larson, P. A. Reynolds, E. T. Seno, W.-K. Yeh, R. van Frank, C. L. Hershberger, *Proc. Natl. Acad. Sci. USA* **1987**, *84*, 8248; j) review: C. A. A. van Boeckel, *Recl. Trav. Chim. Pays-Bas* **1986**, *105*, 35; k) Reviews: S. Masamune, G. S. Bates, J. W. Corcoran, *Angew. Chem.* **1977**, *89*, 602; *Angew. Chem. Int. Ed. Engl.* **1977**, *16*, 585; l) M. L. Zapp, S. Stern, M. R. Green, *Cell* **1993**, *74*, 969; m) L. Anderson, F. M. Unger, *Bacterial Lipopolysaccharides* (*ACS Symp. Ser.* **1983**, *231*); n) J. van Brunt, *Bio/Technology* **1986**, *4*, 780; o) H. Baumann, J.-R. Brisson, F. Michon, R. Pon, H. J. Jennings, *Biochemistry* **1993**, *32*, 4007; p) T. Boren, P. Falk, K. A. Roter, G. Larson, S. Normark, *Science* **1993**, *262*, 1892; q) see ref. [330] in C.-H. Wong, R. L. Halcomb, Y. Ichikawa, T. Kajimoto, *Angew. Chem.* **1995**, *107*, *No.* 5; *Angew. Chem. Int. Ed. Engl.* **1995**, *34*, No. 5.
[18] D. J. Kuo, I. A. Rose, *Biochemistry* **1985**, *24*, 3947; I. A. Rose, J. V. B. Warms, *ibid.* **1985**, *24*, 3952.
[19] J. T. Kadonaga, J. R. Knowles, *Biochemistry* **1983**, *22*, 130; J. G. Belasco, J. R. Knowles, *ibid.* **1983**, *22*, 122.
[20] J. Sygusch, D. Beaudy, M. Allaire, *Proc. Natl. Acad. Sci. USA* **1987**, *84*, 7846.
[21] D. G. E. Lubini, P. Christen Lubini, *Proc. Natl. Acad. Sci. USA* **1979**, *76*, 2527; C. Y. Lai, N. Nakai, D. Chang, *Science* **1974**, *183*, 1204.
[22] W. J. Lees, G. M. Whitesides, *J. Org. Chem.* **1983**, *58*, 1887.
[23] A. J. Morris, D. R. Tolan, *J. Biol. Chem.* **1993**, *268*, 1095.
[24] C. H. von der Osten, A. J. Sinskey, C. F. Barbas, Jr., R. L. Pederson, Y.-F. Wang, C.-H. Wong, *J. Am. Chem. Soc.* **1989**, *111*, 3924; I. Henderson, E. Garcia-Juneda, K. K.-C. Liu, Y.-L. Chen, G.-J. Shen, C.-H. Wong, *Bioorg. Med. Chem.* **1994**, *2*, 837.
[25] M. D. Bednarski, E. S. Simon, N. Bischofberger, W.-D. Fessner, M.-J. Kim, W. Lees, T. Saito, H. Waldmann, G. M. Whitesides, *J. Am. Chem. Soc.* **1989**, *111*, 627.
[26] C. H. von der Osten, C. F. Barbas III, C.-H. Wong, A. J. Sinskey, *Mol. Microbiol.* **1989**, *3*, 1625.
[27] P. R. Alefounder, S. A. Baldwin, R. N. Perham, N. Short, *Biochem. J.* **1989**, *257*, 529.
[28] H. G. Schwelberger, S. D. Kohlwein, F. Paltauf, *Eur. J. Biochem.* **1989**, *180*, 301.
[29] C.-H. Wong, G. M. Whitesides, *J. Org. Chem.* **1983**, *48*, 3199.
[30] C.-H. Wong, F. P. Mazenod, G. M. Whitesides, *J. Org. Chem.* **1983**, *48*, 3493.
[31] J. R. Durrwachter, D. G. Drueckhammer, K. Nozaki, H. M. Sweers, C.-H. Wong, *J. Am. Chem. Soc.* **1986**, *108*, 7812.
[32] J. R. Durrwachter, C.-H. Wong, *J. Org. Chem.* **1988**, *53*, 4175.
[33] T. Ziegler, A. Straub, F. Effenberger, *Angew. Chem.* **1988**, *100*, 737; *Angew. Chem. Int. Ed. Engl.* **1988**, *27*, 716.
[34] R. L. Pederson, M.-J. Kim, C.-H. Wong, *Tetrahedron Lett.* **1988**, *29*, 4645.
[35] A. Straub, F. Effenberger, P. Fischer, *J. Org. Chem.* **1990**, *55*, 3926.
[36] N. J. Turner, G. M. Whitesides, *J. Am. Chem. Soc.* **1989**, *111*, 624.
[37] C. W. Borysenko, A. Spaltenstein, J. A. Straub, G. M. Whitesides, *J. Am. Chem. Soc.* **1989**, *111*, 9275.
[38] W. Schmid, G. M. Whitesides, *J. Am. Chem. Soc.* **1990**, *112*, 9670.
[39] M. D. Bednarski, H. J. Waldmann, G. M. Whitesides, *Tetrahedron Lett.* **1986**, *27*, 5807. Fructose and sorbose diphosphate are better substrates than the corresponding 1-phosphates: O. C. Richards, W. J. Rutter, *J. Biol. Chem.* **1961**, *236*, 3185.
[40] N. Bischofberger, H. Waldmann, T. Saito, E. S. Simon, W. Lees, M. D. Bednarski, G. M. Whitesides, *J. Org. Chem.* **1988**, *53*, 3457.
[41] D. C. Crans, G. M. Whitesides, *J. Am. Chem. Soc.* **1985**, *107*, 7019; D. C. Crans, R. J. Kazlauskas, B. L. Hirschbein, C.-H. Wong, O. Abril, G. M. Whitesides, *Methods Enzymol.* **1987**, *136*, 263. For phosphoenolpyruvate synthesis see B. L. Hirschbein, F. P. Mazenod, G. M. Whitesides, *J. Org. Chem.* **1982**, *47*, 3765.
[42] R. L. Pederson, J. Esker, C.-H. Wong, *Tetrahedron* **1991**, *47*, 2643.
[43] $POCl_3$: F. Effenberger, A. Straub, *Tetrahedron Lett.* **1987**, *28*, 1641; $(PhO)_2POCl$: R. L. Colbran, J. K. N. Jones, N. K. Matheson, I. Rozema, *Carbohydr. Res.* **1967**, *4*, 355.
[44] a) W.-D. Fessner, C. Walter, *Angew. Chem.* **1992**, *104*, 643; *Angew. Chem. Int. Ed. Engl.* **1992**, *31*, 614; b) W.-D. Fessner, G. Sinerius, *ibid.* **1994**, *106*, 217 and **1994**, *33*, 209.
[45] D. G. Drueckhammer, J. R. Durrwachter, R. L. Pederson, D. C. Crans, L. Daniels, C.-H. Wong, *J. Org. Chem.* **1989**, *54*, 70; S.-H. Jung, J.-H. Geong, P. Miller, C.-H. Wong, *J. Org. Chem.* **1994**, *59*, 7182; T. J. Zamborelli, *Biochemistry* **1992**, *31*, 6812.
[46] A. S. Serianni, E. Cadman, J. Pierce, M. L. Hayes, R. Barker, *Methods Enzymol.* **1982**, *89*, 83.
[47] C.-H. Wong, G.-J. Shen, R. L. Pederson, Y.-F. Wang, W. J. Hennen, *Methods Enzymol.* **1991**, *202*, 591.
[48] C.-H. Wong, D. G. Drueckhammer, H. M. Sweers, *Fluorinated Carbohydrates: Chemical and Biochemical Aspects* (Ed.: N. F. Taylor) (*ACS Symp. Ser.* **1988**, *374*, 2942).
[49] R. L. Pederson, K. K.-C. Liu, J. F. Rutan, L. Chen, C.-H. Wong, *J. Org. Chem.* **1990**, *55*, 4897.
[50] A. D. Elbein, *Annu. Rev. Biochem.* **1987**, *56*, 497.
[51] T. Kajimoto, K. K.-C. Liu, R. L. Pederson, Z. Zhong, Y. Ichikawa, J. A. Porco, Jr., C.-H. Wong, *J. Am. Chem. Soc.* **1991**, *113*, 6187.
[52] R. R. Hung, J. A. Straub, G. M. Whitesides, *J. Org. Chem.* **1991**, *56*, 3849.
[53] a) K. K.-C. Liu, T. Kajimoto, L. Chen, Z. Zhong, Y. Ichikawa, C.-H. Wong, *J. Org. Chem.* **1991**, *56*, 6280; b) T. Kajimoto, L. Chen, K. K.-C. Liu, C.-H. Wong, *J. Am. Chem. Soc.* **1991**, *113*, 6678.
[54] Y.-F. Wang, D. P. Dumas, C.-H. Wong, *Tetrahedron Lett.* **1993**, *34*, 403.
[55] M. Schultz, H. Waldmann, W. Vogt, H. Kunz, *Tetrahedron Lett.* **1990**, *31*, 867.
[56] W.-D. Fessner, J. Badia, O. Eyrisch, A. Schneider, G. Sinerius, *Tetrahedron Lett.* **1992**, *33*, 5231.
[57] K. K.-C. Liu, R. L. Pederson, C.-H. Wong, *J. Chem. Soc. Perkin Trans. 1* **1991**, 2669.
[58] Y. Takaoka, T. Kajimoto, C.-H. Wong, *J. Org. Chem.* **1993**, *58*, 4809.
[59] I. Henderson, K. Laslo, C.-H. Wong, *Tetrahedron Lett.* **1994**, *35*, 359.
[60] K. K.-C. Liu, C.-H. Wong, *J. Org. Chem.* **1992**, *57*, 4789.
[61] C. A. Collyer, K. Henrick, D. M. Blow, *J. Mol. Biol.* **1990**, *212*, 211.
[62] T.-H. Chiu, D. S. Feingold, *Biochemistry* **1969**, *8*, 98; Y. Takagi, *Methods Enzymol.* **1966**, *9*, 542; T.-H. Chiu, R. Otto, J. Power, D. S. Feingold, *Biochim. Biophys. Acta* **1966**, *127*, 249.
[63] A. Ozaki, E. J. Toone, C. H. von der Osten, A. Sinskey, G. M. Whitesides, *J. Am. Chem. Soc.* **1990**, *112*, 4970.
[64] W.-D. Fessner, G. Sinerius, A. Schneider, M. Dreyer, G. E. Schulz, J. Badia, J. Aguilar, *Angew. Chem.* **1991**, *103*, 596; *Angew. Chem. Int. Ed. Engl.* **1991**, *30*, 555.
[65] W. J. Lees, G. M. Whitesides, *Bioorg. Chem.* **1992**, *20*, 173.
[66] V. L. Crow, T. D. Thomas, *J. Bacteriol.* **1982**, *151*, 600; D. L. Bissett, R. L. Anderson, *J. Biol. Chem.* **1980**, *255*, 8750; R. J. van Rooijen, S. van Schalkwijk, W. M. de Vos, *ibid.* **1991**, *266*, 7176.
[67] W.-D. Fessner, O. Eyrisch, *Angew. Chem.* **1992**, *104*, 76; *Angew. Chem. Int. Ed. Engl.* **1992**, *31*, 56.
[68] K. B. Sharpless, W. Amberg, Y. L. Bennani, G. A. Crispino, J. Hartung, K.-S. Jeong, H.-L. Kwong, K. Morikawa, Z.-M. Wang, D. Xu, X.-L. Zhang, *J. Org. Chem.* **1992**, *57*, 2768; and references therein.
[69] I. Henderson, K. B. Sharpless, C.-H. Wong, *J. Am. Chem. Soc.* **1994**, *116*, 558.
[70] D. B. Berkowitz, S. J. Danishefsky, *Tetrahedron Lett.* **1991**, *32*, 5497.
[71] C. R. Johnson, A. Golebiowski, D. H. Steensma, *J. Am. Chem. Soc.* **1992**, *114*, 9414.
[72] C. W. Bradshaw, W. Hummel, C.-H. Wong, *J. Org. Chem.* **1992**, *57*, 1532.
[73] D. G. Comb, S. Roseman, *J. Biol. Chem.* **1960**, *235*, 2529; P. Brunett, G. W. Jourdian, S. Roseman, *ibid.* **1962**, *237*, 2447; G. H. Devries, S. B. Binkley, *Arch. Biochem. Biophys.* **1972**, *151*, 234.
[74] Y. Uchida, Y. Tsukada, T. Sugimori, *J. Biochem. (Tokyo)* **1984**, *96*, 507; Y. Uchida, Y. Tsukada, T. Sugimori, *Agric. Biol. Chem.* **1985**, *49*, 181.
[75] C. M. Deijl, J. F. G. Vliegenthart, *Biochem. Biophys. Res. Commun.* **1983**, *111*, 668.

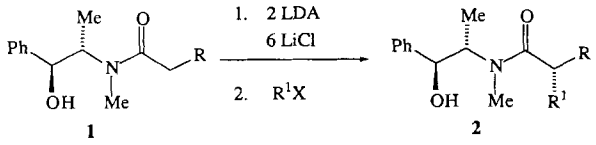
[76] R. S. Blacklow, L. Warren, *J. Biol. Chem.* **1962**, *237*, 3520; R. I. Merker, F. A. Troy, *Glycobiology* **1990**, *1*, 93; L. Warren, R. S. Blacklow, *Biochem. Biophys. Res. Commun.* **1962**, *7*, 433.
[77] K. Aisaka, S. Tamura, Y. Arai, T. Uwajima, *Biotechnol. Lett.* **1987**, *9*, 633; DNA sequence of the NeuAc aldolase gene: B. Kawakami, T. Kudo, Y. Narahashi, K. Horikoshi, *Agric. Biol. Chem.* **1986**, *50*, 2155.
[78] C. Auge, S. David, C. Gautheron, *Tetrahedron Lett.* **1985**, *25*, 4663.
[79] C. Auge, S. David, C. Gautheron, A. Veyrieres, *Tetrahedron Lett.* **1985**, *26*, 2439.
[80] C. Auge, C. Gautheron, *J. Chem. Soc. Chem. Commun.* **1987**, 859.
[81] W. M.-J. Kim, J. Hennen, H. M. Sweers, C.-H. Wong, *J. Am. Chem. Soc.* **1988**, *110*, 6481.
[82] J. L.-C. Liu, G.-J. Shen, Y. Ichikawa, J. R. Rutan, C. Zapata, W. F. Vann, C.-H. Wong, *J. Am. Chem. Soc.* **1992**, *114*, 3901.
[83] M. D. Bednarski, H. K. Chenault, E. S. Simon, G. M. Whitesides, *J. Am. Chem. Soc.* **1987**, *109*, 1283.
[84] Y. Ichikawa, J. L.-C. Liu, G.-J. Shen, C.-H. Wong, *J. Am. Chem. Soc.* **1991**, *113*, 6300.
[85] E. S. Simon, M. D. Bednarski, G. M. Whitesides, *J. Am. Chem. Soc.* **1988**, *110*, 7159.
[86] U. Kragl, D. Gygax, O. Ghisalba, C. Wandrey, *Angew. Chem.* **1991**, *103*, 854; *Angew. Chem. Int. Ed. Engl.* **1991**, *30*, 827.
[87] A. K. Shukla, R. Schauer, *Anal. Biochem.* **1986**, *158*, 158.
[88] C. Auge, S. David, C. Gautheron, A. Malleron, B. Cavaye, *New J. Chem.* **1988**, *12*, 733.
[89] A. Schrell, G. M. Whitesides, *Liebigs Ann. Chem.* **1990**, 1111.
[90] C. Auge, C. Gautheron, S. David, *Tetrahedron* **1990**, *46*, 201.
[91] R. Brossmer, U. Rose, D. Kasper, T. L. Smith, H. Grasmuk, F. M. Unger, *Biochem. Biophys. Res. Commun.* **1980**, *96*, 1282.
[92] R. Schauer, *Trends Biochem. Sci.* **1985**, *10*, 357; A. P. Corfield, R. Schauer in *Sialic Acids* (Ed.: R. Schauer), Springer, New York, **1982**, p. 195; J. C. Paulson, *Trends Biochem. Sci.* **1989**, *14*, 272.
[93] D. C. Drueckhammer, W. J. Hennen, R. L. Pederson, C. F. Barbas III, C. M. Gautheron,, T. Krach, C.-H. Wong, *Synthesis* **1991**, 499.
[94] S. David, C. Auge, C. Gautheron, *Adv. Carbohydr. Chem. Biochem.* **1991**, *49*, 175; R. L. Halcomb, W. Fitz, C.-H. Wong, *Tetrahedron: Asymmetry* **1994**, *5*, 2437.
[95] A. Spaltenstein, G. M. Whitesides, *J. Am. Chem. Soc.* **1991**, *113*, 686.
[96] J. O. Nagy, M. D. Bednarski, *Tetrahedron Lett.* **1991**, *32*, 3953; W. Spevak, J. O. Nagy, D. H. Charych, M. E. Schaefer, J. H. Gilbert, M. D. Bednarski, *J. Am. Chem. Soc.* **1993**, *115*, 1146.
[97] C. Auge, B. Bouxom, B. Cavaye, C. Gautheron, *Tetrahedron Lett.* **1989**, *30*, 2217.
[98] a) C. Gautheron-Le Narvor, Y. Ichikawa, C.-H. Wong, *J. Am. Chem. Soc.* **1991**, *113*, 7816; b) C.-H. Lin, T. Sugai, R. L. Halcomb, Y. Ichikawa, C.-H. Wong, *ibid.* **1992**, *114*, 10138.
[99] P. Zhou, H. M. Salleh, J. F. Honek, *J. Org. Chem.* **1993**, *58*, 264.
[100] R. L. Halcomb, C.-H. Wong, unpublished.
[101] C. R. H. Raetz, W. Dowhan, *J. Biol. Chem.* **1990**, *265*, 1235.
[102] R. R. Schumann, S. R. Leong, G. W. Flaggs, P. W. Gray, S. D. Wright, J. C. Mathison, P. S. Tobias, R. J. Ulevitch, *Science* **1990**, *249*, 1429.
[103] S. M. Hammond, A. Claesson, A. M. Jansson, L.-G. Pring, C. M. Town, B. Ekstrom, *Nature (London)* **1987**, *327*, 730; K. Luthman, M. Orbe, T. Waglund, A. Claesson, *J. Org. Chem.* **1987**, *52*, 3777.
[104] F. O. Andersson, B. Claesson, B. Samuelsson, *J. Org. Chem.* **1990**, *55*, 4699.
[105] D. W. Norbeck, J. B. Kramer, *Tetrahedron Lett.* **1987**, *28*, 773.
[106] P. H. Ray, J. E. Kelsey, E. C. Biogham, C. D. Benedict, T. A. Miller, *Bacterial Lipopolysaccharides* (*ACS Symp. Ser.* **1983**, *231*, 141).
[107] S. J. Danishefsky, M. P. Deninno, *Angew. Chem.* **1987**, *99*, 15; *Angew. Chem. Int. Ed. Engl.* **1987**, *26*, 15.
[108] M. A. Ghalambor, E. C. Heath, *J. Biol. Chem.* **1966**, *241*, 3222.
[109] M. A. Ghalambor, E. C. Heath, *Methods Enzymol.* **1966**, *9*, 534.
[110] T. Sugai, G.-J. Shen, Y. Ichikawa, C.-H. Wong, *J. Am. Chem. Soc.* **1993**, *115*, 413.
[111] P. H. Ray, *J. Bacteriol.* **1980**, *141*, 635; P. H. Ray, *Methods Enzymol.* **1982**, *83*, 525.
[112] M. D. Bednarski, D. C. Crans, R. DiCosimo, E. S. Simon, P. D. Stein, G. M. Whitesides, *Tetrahedron Lett.* **1988**, *29*, 427.
[113] D. H. Levin, E. Racker, *J. Biol. Chem.* **1959**, *234*, 2532.
[114] M. Woisetschlager, G. Hogenauer, *J. Bacteriol.* **1986**, *168*, 437.
[115] E. Haslam, *The Shikimate Pathway*, Butterworths, London, **1974**.
[116] D. B. Sprinson, P. R. Srinivasan, M. Katagiri, *Methods Enzymol.* **1962**, *5*, 394.
[117] L. M. Reimer, D. L. Conley, D. L. Pompliano, J. W. Frost, *J. Am. Chem. Soc.* **1986**, *108*, 8010.
[118] J. W. Frost, A. Berry, G. L. Disbrow, R. J. Staversky, J. C. Lievense, *J. Am. Chem. Soc.* **1992**, *114*, 3956.
[119] E. Racker, *J. Biol. Chem.* **1952**, *196*, 347.
[120] M. G. McGeown, F. H. Malpress, *Nature (London)* **1952**, *170*, 575.
[121] P. A. Hoffee, *Arch. Biochem. Biophys.* **1968**, *126*, 795.
[122] P. Valentin-Hansen, F Boetius, K. Hammer-Jespersen, I. Svendsen, *Eur. J. Biochem.* **1982**, *125*, 561.
[123] C. F. Barbas III, Y.-F. Wang, C.-H. Wong, *J. Am. Chem. Soc.* **1990**, *112*, 2013; L. Chen, D. P. Dumas, C.-H. Wong, *ibid.* **1992**, *114*, 741.
[124] a) W. E. Pricer, Jr., B. L. Horecker, *J. Biol. Chem.* **1960**, *235*, 1292; b) O. M. Rosen, P. Hoffee, B. L. Horecker, *J. Biol. Chem.* **1965**, *240*, 1517.
[125] F. Effenberger, A. Straub, V. Null, *Liebigs Ann. Chem.* **1992**, 1297. W.-C. Chou, L. Chen, J.-M. Fang, C.-H. Wong, *J. Am. Chem. Soc.*, **1994**, *16*, 6191; for sequential aldol reaction see H. J. M. Gigsen, C.-H. Wong, *ibid* **1994**, *116*, 8422.
[126] E. Racker in *The Enzymes, Vol. V* (Ed.: P. D. Boyer, H. Lardy, K. Myrback), Academic Press, New York, **1961**, p. 397; A. Mocali, D. Aldinucci, F. Paoletti, *Carbohydr. Res.* **1985**, *143*, 288.
[127] DNA sequence of the transketolase gene from yeast: T. S. Fletcher, I. L. Kwee, T. Nakada, C. Largman, B. M. Martin, *Biochemistry* **1992**, *31*, 1892.
[128] J. Bolte, C. Demuynck, H. Samaki, *Tetrahedron Lett.* **1987**, *28*, 5525; G. R. Hobbs, M. D. Lilly, N. J. Turner, J. M. Ward, A. J. Willets, J. M. Woodley, *J. Chem. Soc. Perkin Trans. 1* **1993**, 165.
[129] C. Demuynck, F. Fisson, I. Bennani-Baiti, H. Samaki, J.-C. Mani, *Agric. Biol. Chem.* **1990**, *54*, 3073.
[130] P. Srere, J. R. Cooper, M. Tabachnick, E. Racker, *Arch. Biochem. Biophys.* **1958**, *74*, 295.
[131] Y. Kobori, D. C. Myles, G. M. Whitesides, *J. Org. Chem.* **1992**, *57*, 5899.
[132] C. Demuynck, J. Bolte, L. Hecquet, V. Dalmas, *Tetrahedron Lett.* **1991**, *32*, 5085.
[133] F. Effenberger, V. Null, T. Ziegler, *Tetrahedron Lett.* **1992**, *33*, 5157.
[134] D. C. Myles, P. J. Andrulis III, G. M. Whitesides, *Tetrahedron Lett.* **1991**, *32*, 4835.
[135] A. Moradian, S. A. Benner, *J. Am. Chem. Soc.* **1992**, *114*, 6980.

Asymmetric Alkylation of Amide Enolates with Pseudoephedrine and Ephedrine as Chiral Auxiliaries—Unexpected Influence of Additives?**

Karola Rück*

Asymmetric alkylation of carboxylic acid derivatives has been studied intensively for about 15 years.[1] Numerous auxiliaries and tailor-made structures with high steric demands for effective *Re/Si* face differentiation have been synthesized and their efficiency tested.[1, 2] In recent years besides the preparative aspects of enolates, physico-chemical investigations into their structure–reactivity relationships have gained interest.[3] Crystal structure analyses, osmometric measurements, and NMR studies in solution are helpful in the investigation of the factors that may control enolate reactions.[3, 4]

In a recent publication[5] Myers at al. describe a method for alkylating amide enolates having pseudoephedrine as a chiral auxiliary. D-(+)-pseudoephedrine, an industrial product manufactured worldwide in ton quantities, has pharmaceutical applications because of its astringent effect. N-acylation with carboxylic acid chlorides and anhydrides provides crystalline products in high yields (90–95%). After deprotonation with LDA (2 equiv), *N*-acylpseudoephedrine derivatives **1** react with alkyl bromides or iodides efficiently and with high stereoselectivity in the presence of LiCl (6 equiv) in THF (Scheme 1). Even at 0 °C diastereoselectivities of >94% *de* were obtained.



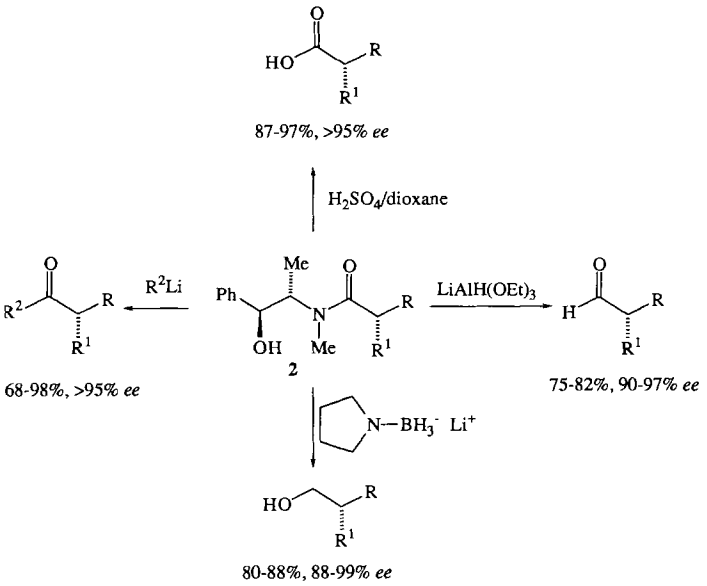
R = Me, Bn, Ph, Cl, *n*-Bu
R^1X = MeI, EtI, *n*-BuI, BnBr

80 - 99%, 94 - >99% *de*

Scheme 1. LDA = lithium diisopropylamide.

α-Alkyl-substituted carboxylic acid derivatives **2** can be isolated in 80–90% yield by simple recrystallization. A wide repertoire of cleavage reactions with recovery of the auxiliary demonstrates the synthetic potential of the pseudoephedrine amides (Scheme 2).

The authors note that the reaction time can be shortened and the conversion increased by addition of LiCl. The concentration



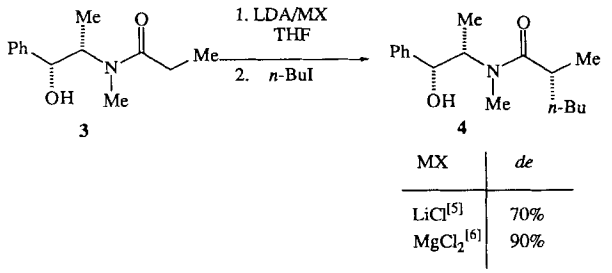
Scheme 2.

of LiCl did not seem to affect the diastereoselectivity of the reaction. Under the same reaction conditions the chiral auxiliary L-(−)-ephedrine led to markedly lower diastereoselectivities. Even in the presence of LiCl the alkylation product from *N*-propionylephedrine (**3**) and *n*-butyl iodide was formed with a diastereoselectivity of only 70% *de*. The work of Myers et al. extends the investigations of Larcheveque et al.,[6] who reported on the alkylation of amide enolates of ephedrine in 1978. Deprotonation of *N*-acylephedrines with LDA in the presence of hexamethylphosphoric acid triamide (HMPA) and subsequent reaction with alkyl halides provided products with diastereoselectivities of < 80:20. Only when $MgCl_2$ was added could diastereomeric ratios of > 95:5 be achieved (Scheme 3). Considering these results, one would not have predicted any great success for experiments with pseudoephedrine. How can the effects brought about by the addition of metal salts be explained?

Since the start of investigations into asymmetric reactions with enolates it has been known that the reactivity and selectivity is influenced not only by the base, but also by the use of cosolvents such as HMPA, and the addition of metal salts or Lewis acids.[1–3, 7] Lithium enolates, in particular, tend to form aggregates by self-assembly.[3] Decisive contributions to the ex-

[*] Dr. K. Rück
Institut für Organische Chemie der Universität
J.-J.-Becher-Weg 18–20, D-55099 Mainz (Germany)
Telefax: Int. code + (6131)39-4786

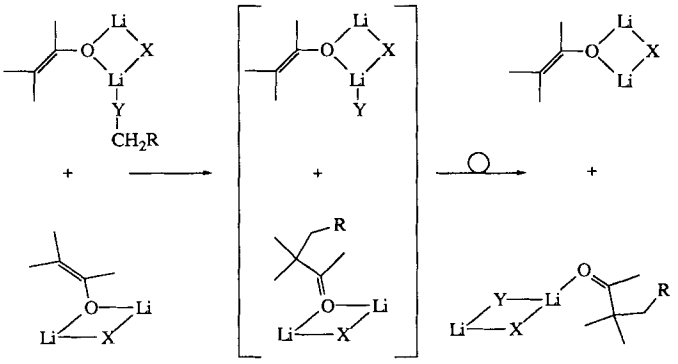
 © VCH Verlagsgesellschaft mbH, D-69451 Weinheim, 1995 0570-0833/95/0404-0433 $ 10.00+.25/0



MX	de
LiCl[5]	70%
$MgCl_2$[6]	90%

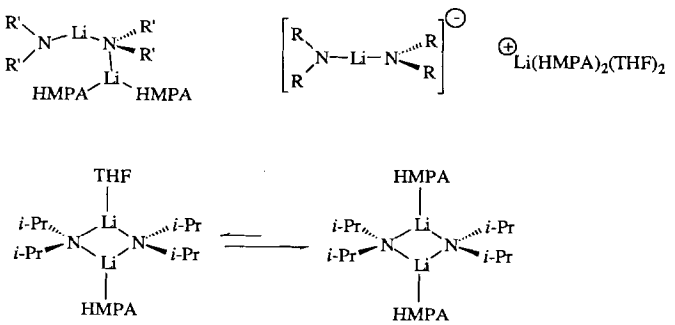
Scheme 3.

planation of this phenomenon have been made by Seebach et al. by crystal structure analyses of crystalline lithium enolates[8] as well as suggestions regarding the structure of the complexes in solution (Scheme 4).[3b]



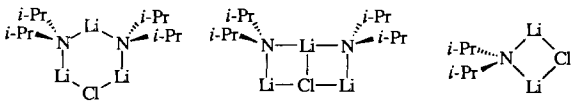
Scheme 4. RCH_2Y = alkyl halide.

The method of choice for structure determination in solution is NMR spectroscopy. New investigations based on ^6Li, ^{15}N, and ^{31}P measurements with isotopically labeled samples confirm earlier results and support conclusions about the solvent and concentration-dependent properties of lithium bases such as lithium hexamethyldisilazane (LiHMDS), LDA, and lithium tetramethylpiperidide (LiTMP).[9] Thus ^6Li-^{15}N coupling, for example, permits conclusions to be drawn about the degree of aggregation of $LiNR_2$ derivatives. Even now, despite its carcinogenicity, HMPA is often added to reaction mixtures to increase the reactivity of lithium compounds. Recently, mixed solvates/aggregates between HMPA and lithium bases (LiHMDS, LiTMP, LDA) were proved (Scheme 5).[10-12] The cosolvent does not break up the aggregates[10] but instead promotes formation of open dimers[11] and "triple ions".[12] Correspondingly, exact data



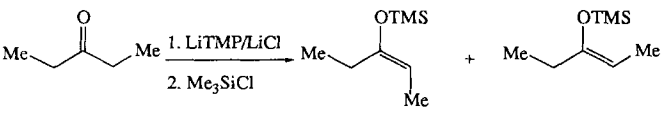
Scheme 5. R'_2N = TMP, R_2N = HMDS.

could be obtained for the structures of complexes of lithium bases and salts and their dependence on the concentration of the added salt (Scheme 6).[9, 10, 13]



Scheme 6.

A further problem in analyzing the reactions of enolates with electrophiles such as alkyl halides is the continually changing concentration of base, enolate, and metal salts during the course of the reaction. For example, stereochemical investigations and trapping experiments on the enolization of 3-pentanone (**5**) with LiTMP in THF demonstrate the consequences of the structural variety of the aggregates (Scheme 7).[10, 13] Whereas at 5% con-

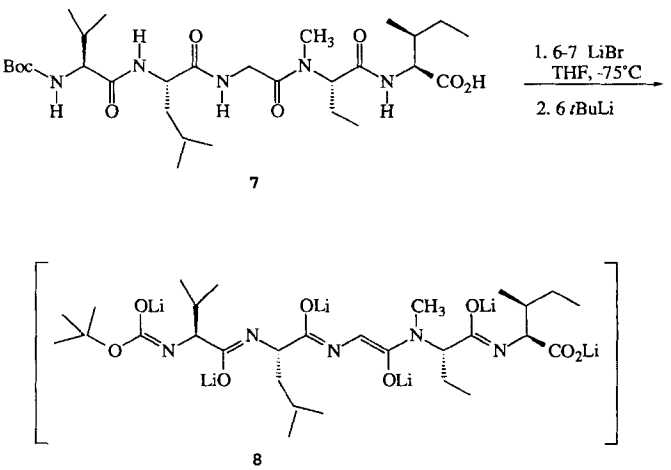


LiCl [equiv.]	E : Z
0.3-0.4	50-60 : 1
1-2	10-20 : 1

Scheme 7.

version the E/Z selectivity was 30:1, at greater than 80% conversion an E/Z selectivity of only >10:1 was observed. The addition of 0.3–0.4 equivalents of LiCl led to an E/Z ratio of 50:1; however, further increase in the amount of LiCl to >1.0 equivalents produced results identical to those obtained under salt-free conditions.

In the early 1980s Seebach et al. described similar "nonstoichiometric effects"[3a] for reactions with organolithium compounds.[3a, b, 14, 15] On the basis of these studies they have recently investigated the solubilization and diastereoselective alkylation of polylithiated open-chain and cyclic peptides in the presence of excess lithium salts and bases (Scheme 8).[3b, 16] Glycine and

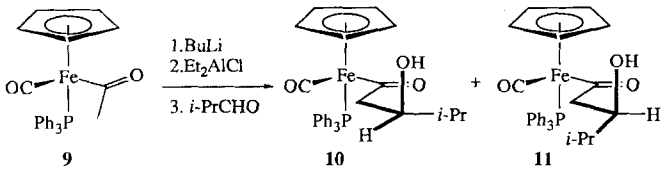


Scheme 8.

 © VCH Verlagsgesellschaft mbH, D-69451 Weinheim, 1995 0570-0833/95/0404-0434 $ 10.00+.25/0

sarcosine lithium enolates and dilithium azadienolates of peptide lithium salt complexes were alkylated in yields of up to 90% with diastereoselectivities ranging from 1:1 to 9:1.[16]

Davies et al.[17] and Liebeskind et al.[18] also reported on the unusual effect of metal salts[7] in studies on chiral transition metal enolates. In reactions of **9** with aldehydes the stoichiometry of the butyllithium and the added aluminum Lewis acid clearly influence stereoselection (Scheme 9).[18] van Koten et al. conduct-

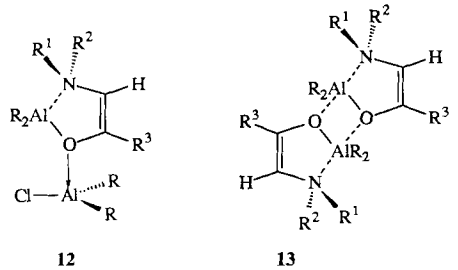


9 **10** **11**

BuLi [equiv.]	Et_2AlCl [equiv.]	**11 : 10**
1.1	4	1.5 : 1.0
2	5	36 : 1.0

Scheme 9.

ed mechanistic studies on the structure–reactivity relationships of zinc and aluminum enolates obtained by the transmetalation of lithium enolates.[19] The aluminum enolate aggregates **12** and **13** were isolated and characterized by crystal structure analysis and NMR spectroscopy (Scheme 10).



12 **13**

Scheme 10.

The work of Myers et al.[5] illustrates the synthetic potential of the use of metal salts (instead of HMPA!) in reactions of enolates. It is not surprising that the mechanism of chiral induction is not yet fully understood; further investigations are necessary.[5] Unanswered questions also remain even for tailor-made, well-established auxiliaries, whose asymmetric induction can be explained convincingly based on the monomer structures and consideration of chelation and steric factors. Thus, we await the results of systematic investigations on the influence of metal salts[7] and new applications of these supposedly well-known reactions.

German version: *Angew. Chem.* **1995**, *107*, 475

Keywords: alkylations · asymmetric syntheses · metalations · metal salt effect

[1] a) D. Caine in *Comprehensive Organic Synthesis, Vol. 3* (Eds.: B. M. Trost, I. Fleming, G. Pattenden), Pergamon Press, New York, **1991**, p. 1; b) D. A. Evans, J. M. Takacs, *Tetrahedron Lett.* **1980**, *21*, 4233; c) W. Oppolzer, R. Moretti, S. Thomi, *ibid.* **1989**, *30*, 5603; d) K.-S. Jeong, K. Parris, P. Ballester, J. Rebek Jr., *Angew. Chem.* **1990**, *102*, 550; *Angew. Chem. Int. Ed. Engl.* **1990**, *29*, 555.

[2] a) J. D. Morrison, *Asymmetric Synthesis*, Academic Press, New York, 1984; b) M. Nogradi, *Stereoselective Synthesis*, 2nd ed., VCH, Weinheim, **1995**.

[3] Reviews: a) D. Seebach, *Proc. Robert A. Welch Found. Conf. Chem. Res. 27: Stereospecificity in Chemistry and Biochemistry* (7.–9. Nov. 1983), Houston, TX, USA, **1984**, 93–145; b) D. Seebach, *Angew. Chem.* **1988**, *100*, 1685; *Angew. Chem. Int. Ed. Engl.* **1988**, *27*, 1624; c) G. Boche, *ibid.* **1989**, *101*, 286 and **1989**, *28*, 277.

[4] a) L. M. Jackman, T. S. Dunne, *J. Am. Chem. Soc.* **1985**, *107*, 2805, and references therein; b) P. G. Willard, M. J. Hintze, *J. Am. Chem. Soc.* **1987**, *109*, 5539; c) J. Corset, F. Froment, M.-F. Lautié, N. Ratovelomanana, J. Seyden-Penne, T. Strzalko, M.-C. Roux-Schmitt, *ibid.* **1993**, *115*, 1684.

[5] A. G. Myers, B. H. Yang, H. Chen, J. L. Gleason, *J. Am. Chem. Soc.* **1994**, *116*, 9361.

[6] a) M. Larcheveque, E. Ignatova, T. Cuvigny, *Tetrahedron Lett.* **1978**, *41*, 3961; b) M. Larcheveque, E. Ignatova, T. Cuvigny, *J. Organomet. Chem.* **1979**, *177*, 5.

[7] A. Loupy, B. Tchoubar, *Salt Effects in Organic and Organometallic Chemistry*, VCH, Weinheim, **1992**.

[8] a) R. Amstutz, W. B. Schweizer, D. Seebach, J. D. Dunitz, *Helv. Chim. Acta* **1981**, *64*, 2617; b) W. Bauer, T. Laube, D. Seebach, *Chem. Ber.* **1985**, *118*, 764.

[9] D. B. Collum, *Acc. Chem. Res.* **1993**, *26*, 227.

[10] a) A. S. Galiano-Roth, Y.-J. Kim, J. H. Gilchrist, A. T. Harrison, D. J. Fuller, D. B. Collum, *J. Am. Chem. Soc.* **1991**, *113*, 5053; b) Y.-J. Kim, M. P. Bernstein, A. S. Galiano-Roth, F. E. Romesberg, P. W. Williard, D. J. Fuller, A. T. Harrison, D. B. Collum, *J. Org. Chem.* **1991**, *56*, 4435.

[11] P. L. Hall, J. H. Gilchrist, A. T. Harrison, D. J. Fuller, D. B. Collum, *J. Am. Chem. Soc.* **1991**, *113*, 9575.

[12] F. E. Romesberg, M. P. Bernstein, J. H. Gilchrist, A. T. Harrison, D. J. Fuller, D. B. Collum, *J. Am. Chem. Soc.* **1993**, *115*, 3475.

[13] P. L. Hall, J. H. Gilchrist, D. B. Collum, *J. Am. Chem. Soc.* **1991**, *113*, 9571.

[14] H. Estermann, D. Seebach, *Helv. Chim. Acta* **1988**, *71*, 1824.

[15] Studies on the effect of magnesium salts [3a] on stereodifferentiation in nucleophilic additions: D. Seebach, I. M. P. Huber, M. A. Syfrig, *Helv. Chem. Acta* **1987**, *70*, 1357; *ibid.* **1987**, *70*, 1944.

[16] a) D. Seebach, H. Bossler, H. Gründler, S.-I. Shoda, *Helv. Chim. Acta* **1991**, *74*, 197; b) S. A. Miller, S. L. Griffiths, D. Seebach, *ibid.* **1993**, *76*, 563; c) H. G. Bossler, D. Seebach, *ibid.* **1994**, *77*, 1124.

[17] G. J. Baird, J. A. Vol.y, S. G. Davies, O. Watts, *J. Organomet. Chem.* **1985**, *285*, 213.

[18] L. S. Liebeskind, M. E. Welker, R. W. Fengl, *J. Am. Chem. Soc.* **1986**, *108*, 6328.

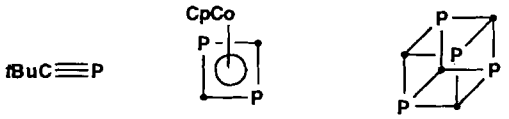
[19] a) F. H. van der Steen, G. P. M. van Mier, A. L. Spek, J. Kroon, G. van Koten, *J. Am. Chem. Soc.* **1991**, *113*, 5742; b) F. H. van der Steen, H. Kleijn, A. L. Spek, G. van Koten, *J. Org. Chem.* **1991**, *56*, 5868; c) F. H. van der Steen, H. Kleijn, J. T. B. H. Jastrezebski, G. van Koten, *ibid.* **1991**, *56*, 5147; d) F. H. van der Steen, J. Boersma, A. L. Spek, G. van Koten, *Organometallics* **1991**, *10*, 2467.

 © *VCH Verlagsgesellschaft mbH, D-69451 Weinheim, 1995* *0570-0833/95/0404-0435 $ 10.00+.25/0*

Phosphaalkyne Cyclooligomers: From Dimers to Hexamers—First Steps on the Way to Phosphorus–Carbon Cage Compounds

Rainer Streubel*

The synthesis of 2,2-dimethylpropylidynephosphane **1** (*tert*-butylphosphaacetylene), the first phosphaalkyne stable at room temperature, by Becker et al. in 1981[1] marked the start of a remarkable development of this compound as a synthetic building block in phosphorus heterocycle[2] and complex chemistry.[3] Initial milestones in the oligomerization of **1** were its cyclodimerization in the coordination sphere of cobalt to give the η^4-1,3-diphosphacyclobutadiene complex **2** reported by Nixon et al.[4] and Binger et al[5] in 1986, and the thermal cyclotetramerization of **1** to give the tetraphosphacubane **3** described by Regitz et al. in 1989[6] (Scheme 1). Except for these [2 + 2] cycloadditions of **1**, only reactions with heteroalkenes and higher alkene homologues are known to date.[2, 7]



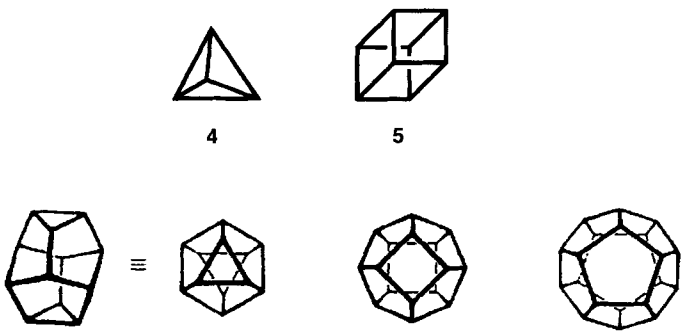
1 2 3

Scheme 1. The solid black dots here and in the subsequent formula represent *t*BuC groups. Cp = C_5H_5.

The most recent reports on the synthesis of novel *tert*-butylphosphaacetylene cyclooligomers are presented herein as a progress report in this still evolving field of research. Since parallels with the development of the synthetic chemistry of the acetylene cyclooligomers $(C_2H_2)_n$, from the errors at the outset to the later successes through metal catalysis, are both interesting and instructive, this chemistry will be reviewed briefly beforehand in as far as it concerns the synthesis of highly symmetrical cage molecules of the general formula $(CH)_{2n}$.[8]

The origin of the chemistry of acetylene cyclooligomers dates back to about 1870, to the benzene synthesis of Berthelot[9] and the work of Kekulé.[10] The next important advance was the successful, albeit very laborious, multistep synthesis of cyclooctatetraene (cot) by Willstätter et al. in 1913.[11] The first metal-catalyzed cyclooligomerization of wide-ranging preparative and also theoretical significance was accomplished by Reppe et al. in 1948[12] with the cyclotetramerization of acetylene to cot in the presence of nickel diacetylacetonate. In the following four decades, transition-metal catalyzed cyclizations[13] and cycloadditions[14] of alkynes developed into an extensive and fascinating research area. The homogeneously catalyzed pyridine synthesis[15] through the cyclocotrimerization of alkynes and nitriles is chosen here by way of example. The cyclobutadiene complex of Pettit[16] gave fresh impetus to the debate over the hitherto unsolved problem of "diacetylene" (cyclobutadiene).[17] This chapter was concluded with the matrix-isolation of cyclobutadiene (Chapman et al.[18] and Krantz et al.[19]) in 1973 and the synthesis of tetra-*tert*-butylcyclobutadiene and tetra-*tert*-butyltetrahedrane by Maier et al. in 1978.[20] The kinetic stabilization by the introduction of four *tert*-butyl groups ("corset effect") enabled the isolation and reactivity studies of these *tert*-butyl-substituted cyclobutadiene and tetrahedrane derivatives under standard conditions.[20] Thus, tetra-*tert*-butylcyclobutadiene does not undergo dimerization, unlike the mono-, di-, and tri-*tert*-butyl-substituted cyclobutadiene derivatives.[19, 20]

It is thus already established that tetra-*tert*-butyltetrahedrane, a derivative of the polycyclic hydrocarbon $(CH)_4$ **4**, cannot be obtained through cyclooligomerization; the construction of the hydrocarbon framework follows a multistep synthetic strategy to give the tetra-*tert*-butylcyclopentadienone,[20] from which the tetrahedrane derivative was generated upon irradiation. In the light of this example it is hardly surprising that in the synthetic design of highly symmetrical $(CH)_{2n}$ polycycles, the cyclooligomerization of acetylene derivatives merits a rather insignificant role, which becomes even less important with the complexity of the target molecule.[21] This is illustrated most impressively by the multistep syntheses of cubane $(CH)_8$ (**5**),[22] *p*-[3^2,5^6]octahedrane $(CH)_{12}$ (**6**),[23] *p*-[4^2,5^8]decahedrane $(CH)_{16}$ (**7**),[24] or even dodecahedrane $(CH)_{20}$ (**8**).[25, 26]



4 5

≡

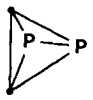
6 7 8

Interest in heteroacetylene cyclooligomers and cyclocooligomers was stimulated by the synthesis of the first azete derivative (azacyclobutadiene),[27] particularly since calculations had predicted a stabilization of the azacyclobutadiene system by the nitrogen atom (decrease in the negative resonance energy).[28] Questions about the possible existence of phosphete and diphosphete derivatives arose, if not earlier, with the syntheses of **2** and **3**. Preliminary ab initio calculations on the problem of phosphaacetylene cyclooligomerization were recently carried out on HC≡P oligomers (HCP → $1/n$ $(HCP)_n$; $n = 2-6$) as models for *t*BuC≡P oligomers. Despite the different theoretical levels,

[*] Dr. R. Streubel
Institut für Anorganische und Analytische Chemie der Technischen Universität
Postfach 3329, D-38023-Braunschweig (Germany)
Telefax: Int. code + (531)391-5387

 © VCH Verlagsgesellschaft mbH, D-69451 Weinheim, 1995 0570-0833/95/0404-0436 $ 10.00+.25/0

the following trends are emerge: 1) the dimerization of HCP proceeds preferentially in the manner of a head-to-head rather than a head-to-tail dimerization;[29] 2) the relative order of stability is **9** > **10** > **11**;[29-32] 3) energetically, dimerization is distinctly less favorable than tetramerization[31, 32] or even trimerization;[33] 4) the thermodynamic stability of the HCP cyclooligomers improves with an increasing degree of oligomerization *n*.



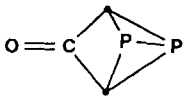
9



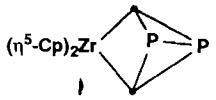
10



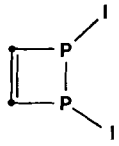
11



12

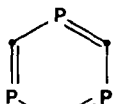


13

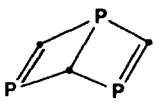


14

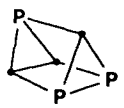
Against the background of these theoretical predictions on the dimerization of the phosphaalkyne HCP, the latest attempts at the synthesis of 1,2- and 1,3-diphosphetes **10** and **11** seem all the more intriguing. Starting from the tricyclic zirconium compound **13**, the synthesis of **10** was realized through a reaction sequence comprising exchange of metal complex fragment, valence isomerization, and reductive elimination; however, under these conditions, **10** dimerizes immediately to the *anti*-tricyclooctadiene **18**.[31] A structural peculiarity of compound **18** is its central, planar P_4 ring. The P–P bond lengths are 221.9 and 223.6 pm with inner ring angles of 89.9 and 90.1°. Further indication of the intermediacy of **10** was obtained by the same research group through the elimination of iodine from **14** with a Pt(0) complex; the end result of this reaction is once again the dimer **18**. Another windfall from the synthesis of tetraphosphacubane **3** was the discovery of compound **19**,[31] which is a new dimer of 1,3-diphosphete **11**. As is also the case for other tetramers,[33] the P=C bonds in **19** are still intact. These, and also the central 1,2-diphosphetane ring, do not, however, exhibit any structural peculiarities. Whereas the dimerization **11** → **20** proceeds analogously to that of 1,3-di-*tert*-butylcyclobutadiene—in terms of a Diels–Alder reaction—the dimerizations **10** → **18** and **11** → **19** observed here reveal an anomaly. Even though the reaction **10** → **18** was classified as a Diels–Alder reaction and **11** → **19** as a dimerization,[32] both recall the problem of the dimerization of tri-*tert*-butylcyclobutadiene on the basis of the stereochemistry of their end products; different radical mechanisms were suggested as an explanation of this two-step process.[20b] This should also be considered when discussing the reaction mechanism for diphosphetes **9** and **10**, since according to the theoretical predictions, the energy separation between the lowest energy singlet and triplet states is smaller for **9** and **10** than for cyclobutadiene.[30]



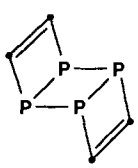
15



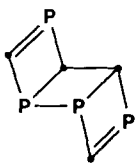
16



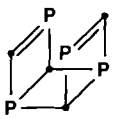
17



18

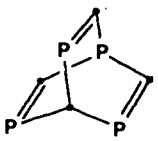


19

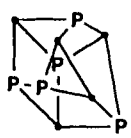


20

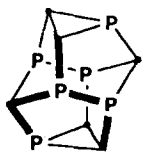
The high efficiency of the metal-controlled synthetic step was once again demonstrated with the synthesis of the 1,3,5,7-tetraphosphabarrelene derivative **21** by Binger et al.[34] Starting from bis(cyclooctatetraene)zirconium and *tert*-butylphosphaacetylene **1**, the zirconium precursor complex for **21** was obtained in 81% yield; mild oxidative decomplexation with hexachloroethane afforded **21** in 88% yield. A η^6-1,3,5-triphosphabenzenezirconium complex was postulated by the authors as a possible intermediate.[35] In this context it is astonishing that no "free" trimers of type **15**–**17** are known to date, although potential precursors such as complexes of **16**[36] have already been reported, and at least the HCP cyclotrimers are thermodynamically more stable than their tetrameric congeners. Possibly more than just a glimmer of hope in this field is the complex-driven 2:1 cyclotrimerization of *tert*-butylphosphaacetylene **1** and acetylene derivatives leading to $1\lambda^3,3\lambda^3$-diphosphabenzene complexes, from which the ligands could be oxidatively liberated.[37]



21



22



23

The synthesis of the first *t*BuCP hexamer **23** with a C_{2h}-symmetric *p*-[3^2,5^6]octahedrane cage is most encouraging and may provide further impetus to the synthesis of phosphorus–carbon cage compounds. In a similar synthesis to that of the known pentamer **22**,[38] compound **23** may, together with other species, be generated from a $[P_2C_3tBu_3]^-/[P_3C_2tBu_2]^-$ mixture by oxidative coupling with $[PtCl_2(cod)]$ (cod = 1,5-cyclooctadiene),[31] though the low yield (ca. 2%) is unsatisfactory and the mechanism has hitherto eluded clarification. The structural relationship between **23** and the cage hydrocarbon **6** is striking and once again demonstrates the potential for interchange between the isolobal fragments CR and P as building blocks in these systems.

As demonstrated by this spotlight on these three current research topics in the synthesis of *t*BuCP cyclooligomers, the oligomerization of pure **1** has advanced "only" as far as the tetramer, but has thrown up a series of highly interesting questions about potential synthetic routes to **9** (possibly from **12**, or perhaps from **18**?) and also the possibility, starting from the

 © VCH Verlagsgesellschaft mbH, D-69451 Weinheim, 1995 0570-0833/95/0404-0437 $ 10.00+.25/0

tricyclic compounds **18** and **19**, of striving towards valence isomerization mediated by a heavy metal cation (such as Ag^+) to form tetraphosphacyclooctatetraene (cf. ref. [39]). The synthesis of the first 1,3,5,7-tetraphosphabarrelene **21** ensures that the complex-driven synthesis will also remain an exciting prospect. In particular the synthesis of the *t*BuCP hexamer **23** has opened doors to the development of novel phosphorus–carbon cage compounds. For an understanding of this reaction—do template effects play a role?—as well as the development of any consistent synthetic strategies, a whole series of experiments are, however, still necessary.

German version: *Angew. Chem.* **1995**, *107*, 478

Keywords: tert-butylphosphaacetylene · phosphaalkynes · phosphorus heterocycles · phosphorus–carbon cage compounds

[1] G. Becker, G. Gresser, W. Uhl, *Z. Naturforsch. B* **1981**, *36*, 16–19.
[2] Review: M. Regitz, *Phosphaalkynes* in *Multiple Bonds and Low Coordination in Phosphorus Chemistry* (Eds.: M. Regitz, O. J. Scherer), Thieme, Stuttgart, **1990**, pp. 58–89.
[3] Review: a) P. Binger, *Phosphaalkynes* in *Multiple bonds and Low Coordination in Phosphorus Chemistry* (Eds.: M. Regitz, O. J. Scherer), Thieme, Stuttgart, **1990**, pp. 90–106; b) J. F. Nixon, *Endeavour* **1991**, *15*, 49–57.
[4] P. B. Hitchcock, M. J. Maah, J. F. Nixon, *J. Chem. Soc. Chem. Commun.* **1986**, 737–738.
[5] P. Binger, R. Milczarek, R. Mynott, M. Regitz, W. Rösch, *Angew. Chem.* **1986**, *98*, 645–646; *Angew. Chem. Int. Ed. Engl.* **1986**, *25*, 644–645.
[6] T. Wettling, J. Schneider, O. Wagner, C. Kreiter, M. Regitz, *Angew. Chem.* **1989**, *101*, 1035–1037; *Angew. Chem. Int. Ed. Engl.* **1989**, *28*, 1013–1015.
[7] a) G. Becker, W. Becker, R. Knebel, H. Schmidt, M. Mildenbrand, M. Westerhausen, *Phosphorus Sulfur Relat. Elem.* **1987**, *30*, 349–352;) R. Streubel, M. Frost, M. Nieger, E. Niecke, *Bull. Soc. Chim. Fr.* **1993**, *103*, 642–646.
[8] Review: a) *Cage Hydrocarbons* (Ed.: G. A. Olah), Wiley, New York, **1990**, and references therein.; *Carbocyclic Cage Compounds* (Eds.: E. Osawa, O. Yonemitsu), VCH, New York, **1992**, and references therein.
[9] M. Berthelot, *Justus Liebigs Ann. Chem.* **1867**, *141*, 173–184.
[10] A. Kekulé, *Justus Liebigs Ann. Chem.* **1872**, *162*, 77–174.
[11] a) R. Willstätter, E. Waser, *Ber. Deut. Chem. Ges.* **1911**, *44*, 3423–3445; b) R. Willstätter, M. Heidelberger, *ibid.* **1913**, *46*, 517–527.
[12] W. Reppe, O. Schlichting, K. Klager, T. Toeppel, *Justus Liebigs Ann. Chem.* **1948**, *560*, 1–92.
[13] Review: M. J. Winter, *Alkyne Oligomerization* in *The Chemistry of the Metal-Carbon Bond. Carbon-Carbon Bond Formation Using Organometallic Compounds, Vol. 3* (Eds.: F. R. Hartley, S. Patai), Wiley, Chichester, **1985**, chapter 5.
[14] Review: N. E. Shore, *Chem. Rev.* **1988**, *88*, 1081–1119.
[15] Review: H. Bönnemann, *Angew. Chem.* **1985**, *97*, 264–279; *Angew. Chem. Int. Ed. Engl.* **1985**, *24*, 248–263.
[16] G. F. Emerson, L. Watts, R. Pettit, *J. Am. Chem. Soc.* **1965**, *87*, 131–133.
[17] Review: a) M. R. Cava, M. J. Mitchell: *Cyclobutadiene and Related Compounds*, Academic Press, New York, **1967**; b) G. Maier, *Angew. Chem.* **1974**, *86*, 491–505; *Angew. Chem. Int. Ed. Engl.* **1974**, *13*, 425–439, and references therein.
[18] O. L. Chapman, C. L. McIntosh, J. Pacansky, *J. Am. Chem. Soc.* **1973**, *95*, 614–617; b) O. L. Chapman, D. De La Cruz, R. Roth, J. Pacansky, *J. Am. Chem. Soc.* **1973**, *95*, 1337–1338.
[19] A. Krantz, C. Y. Lin, M. D. Newton, *J. Am. Chem. Soc.* **1973**, *95*, 2744–2746.
[20] Review: a) N. S. Zefirov, A. S. Koz'min, A. V. Abramenkov, *Russ. Chem. Rev. (Engl. Transl.)* **1978**, *47*, 163–171; b) G. Maier, *Angew. Chem.* **1988**, *100*, 317–341; *Angew. Chem. Int. Ed. Engl.* **1988**, *27*, 295–319.
[21] There are, however, impressive individual examples of the application potential of acetylene derivatives. For examples, see the oxidative/photochemical dimerization of di-*tert*-butylacetylene to the tetra-*tert*-butyltetrahedrane radical cation (ref. [68] in ref.[20b]) or the cyclotetramerization of perfluoro-2-butyne to the corresponding cubane (ref. [4] in ref. [22]).
[22] Reviews: a) P. E. Eaton, *Tetrahedron* **1979**, *35*, 2189–2223; b) *Angew. Chem.* **1992**, *104*, 1447–1462; *Angew. Chem. Int. Ed. Engl.* **1992**, *31*, 1421–1456.
[23] C.-H. Lee, S. Liang, T. Haumann, R. Boesse, A. de Meijere, *Angew. Chem.* **1993**, *105*, 611–613; *Angew. Chem. Int. Ed. Engl.* **1993**, *32*, 559–601.
[24] All attempts at the synthesis of **7** have remained unsuccessful: see ref. [8] and references therein.
[25] Reviews: L. A. Paquette, *Chem. Rev.* **1989**, *89*, 1051–1065; H. Prinzbach, K. Weber, *Angew. Chem.* **1994**, *106*,2329–2348; *Angew. Chem. Int. Ed. Engl.* **1994**, *33*, 2239–2257.
[26] For problems in the nomenclature of **4**–**8**, see refs. [8, 20, 21–25] and references therein.
[27] a) G. Seybold, U. Jersak, R. Gompper, *Angew. Chem.* **1973**, *85*, 918–920; *Angew. Chem. Int. Ed. Engl.* **1973**, *12*, 847–849; b) U.-J. Vogelbacher, M. Regitz, R. Mynott, *Angew. Chem.* **1986**, *98*, 835–836; *Angew. Chem. Int. Ed. Engl.* **1986**, *24*, 842–843.
[28] M. J. S. Dewar, N. Trinajstić, *Theor. Chim. Acta* **1970**, *17*, 235–238.
[29] Relative energies were derived from MP4sdto/6-31G-energy calculations: M. T. Nguyen, L. Landuyt, L. G. Vanquickenborne, *J. Org. Chem.* **1993**, *58*, 2817–2821.
[30] Ab initio calculations at the MCSCF level: W. W. Schoeller, T. Busch, *Angew. Chem.* **1993**, *105*, 635–637; *Angew. Int. Chem. Ed. Engl.* **1993**, *32*, 617–619.
[31] Relative energies were derived from MP4sdto/6-31G-energy calculations: V. Caliman, P. B. Hitchcock, J. F. Nixon, M. Hofmann, P. von R. Schleyer, *Angew. Chem.* **1994**, *106*, 2284–2286; *Angew. Chem. Int. Ed. Engl.* **1994**, *33*, 2221–2223.
[32] Relative energies were derived from MP4sdto/6-31G-energy calculations: B. Geissler, S. Barth, U. Bergsträsser, M. Slany, J. Durkin, P. B. Hitchcock, M. Hofmann, P. Binger, J. F. Nixon, P. von R. Schleyer, M. Regitz, *Angew. Chem.* **1995**, *107*, 485–488; *Angew. Chem. Int. Ed. Engl.* **1995**, *34*, 484–487.
[33] See ref. [21] in ref. [31].
[34] P. Binger, G. Glaser, B. Gabor, R. Mynott, *Angew. Chem.* **1995**, *107*, 114–116; *Angew. Chem. Int. Ed. Engl.* **1995**, *34*, 81–83.
[35] A. R. Barron, A. H. Cowley, *Angew. Chem.* **1987**, *99*, 956–957; *Angew. Chem. Int. Ed. Engl.* **1987**, *26*, 907–908.
[36] a) R. Milczarek, W. Rüsseler, P. Binger, K. Jonas, K. Angermund, C. Krüger, M. Regitz, *Angew. Chem.* **1987**, *99*, 957–958; *Angew. Chem. Int. Ed. Engl.* **1987**, *26*, 908–909; b) B. Breit, U. Bergsträsser, G. Maas, M. Regitz, *ibid.* **1992**, *104*, 1043–1046 and **1992**, *31*, 1055–1058.
[37] D. Böhm, F. Knoch, S. Kummer, U. Schmidt, U. Zenneck, *Angew. Chem.* **1995**, *107*, 259–262; *Angew. Chem.* **1995**, *34*, 198–201.
[38] R. Bartsch, P. B. Hitchcock, J. F. Nixon, *J. Organomet. Chem.* **1989**, *375*, C31–C34.
[39] Review: K. Hasenrück, H.-D. Martin, R. Walsh, *Chem. Rev.* **1989**, *89*, 1125–1146.

 © *VCH Verlagsgesellschaft mbH, D-69451 Weinheim, 1995* *0570-0833/95/0404-0438 $ 10.00+.25/0*

The Consequences of an Electrostatic "Forced Marriage" between Two Electron-Rich Particles: Strained Ion Pairs**

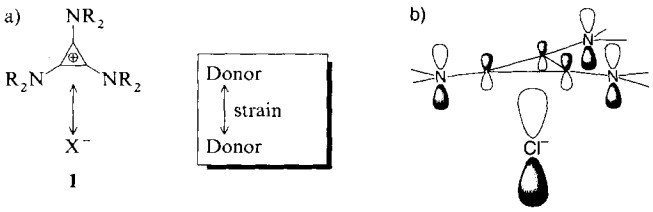
Robert Weiss,* Thomas Brenner, Frank Hampel, and Alexander Wolski

Dedicated to Prof. Paul von Ragué Schleyer on the occasion of his 65th birthday

Two translationally independent electron-rich particles would principally repel each other, unless they had opposing electrical charge and would thus form an ion pair in a suitable solvent. Under these conditions, a novel interionic strain could build up, which would result from the interionic orbital repulsion and should express itself in the increased reactivity of both ionic components towards other reagents. In order to confirm this, salts would have to be synthesized in which electron-rich cations are combined with electron-rich anions. Cations are generally, however, electron-deficient systems; the notable exception to this rule are the tris(dialkylamino)-substituted cyclopropenylium ions, which according to Gerson et al. can be considered as electron-excess systems.[1] These electronic properties are the cause of their unusual behavior in comparison to other carbenium ions: For example, the tris(dimethylamino)cyclopropenylium ion (TDA cation) functions as the donor component in deeply colored charge transfer (CT) salts with tetracyanoethylene (TCNE) or 2,3-dichloro-5,6-dicyano-*p*-benzoquinone (DDQ).[2, 3] The TDA cation also behaves as a donor with respect to electron-deficient anions of the type $ElCl_6^-$ (El = Sb, Nb, Ta); in these reactions deeply coloured "inverse CT salts" with one-dimensionally stacked structures result.[4–8] TDA salts can be readily oxidized to give stable isolable radical dicationic salts.[9–11]

If this cation is combined with donor anions (e.g. halide ions), ion pairs of the type **1** are obtained which contain—as required above—two oppositely charged electron-excess systems as electronic antagonists (Scheme 1 a). This is demonstrated in that the $E_{1/2}$ values of about 1.4 V (vs Ag/AgCl; 0.1 N NEt_4Cl/CH_3CN) for the oxidation of both the TDA cation and the chloride ion are almost the same, in spite of the opposing charges of these ions.[12, 13] At the point of maximum electrostatic attraction between the constituent ions of **1** (centrosymmetric arrangement), the orbital repulsion of the two would also have its maximum effect. The latter should be especially pronounced for the corresponding HOMO/HOMO interaction since the interacting orbitals have the same local symmetry (see Scheme 1 b).

We inferred from this, that TDA halides should exhibit a distinctly lower tendency to form inner ion pairs in dipolar aprotic solvents than other known saltlike halides. They are possibly, therefore, highly effective sources of naked halide ions. In order to check this hypothesis, we treated the readily accessible[9] tris(dimethylamino)cyclopropenylium chloride (TDACl) **1a** with acceptors and were thus able to establish a readiness to coordinate which far exceeded our expectations. In this paper, we report on novel compounds with hydrogen bonds whose formation can be interpreted as resulting because of the ion pair strain defined above.



1

Scheme 1. a) **1**: X^- = halide; **1a**: X^- = chloride, R = methyl (TDACl). b) Interacting orbitals involved in the HOMO/HOMO interaction between the ions in **1a**.

We were able to show that defined 1:1 adducts can be precipitated from solutions of carboxylic acids of very different structural types in CH_2Cl_2 in the presence of TDACl **1a**, by addition of nonpolar solvents such as Et_2O or CCl_4. A selection of the products obtained is shown in Table 1. It is noticeable that adduct formation in the homologous series of aliphatic carboxylic acids does not occur for homologues higher than propionic acid. In addition to the decreasing acid strengths of the organic acids, the reason for this can possibly be traced back to the lower lattice energies for increasingly bulky alkyl groups of the organic acid.

Table 1. Selection of TDACl adducts with organic acids and phenols.

Adduct component (AC)	TDACl : AC	Adduct component (AC)	TDACl : AC
benzoic acid	1:1 (**2**)	phenol	1:1
p-chlorobenzoic acid	1:1	*o*-nitrophenol	1:1
p-nitrobenzoic acid	1:1	*p*-cresol	1:1
toluenesulphonic acid	1:1	*o*-cresol	1:1
benzilic acid	1:1	2,4-dichlorophenol	1:1
cinnamic acid	1:1	2,4,6-trinitrophenol	1:1
formic acid	1:1	1-naphthol	1:1
acetic acid	1:1	2-naphthol	1:1
chloroacetic acid	1:1		
dichloroacetic acid	1:1		
trichloroacetic acid	1:1		
trifluoroacetic acid	1:1		
oxalic acid	2:1		
fumaric acid	2:1		
acetylenedicarboxylic acid	2:1		

An X-ray structure analysis was carried out for the benzoic acid adduct **2** (Fig. 1). This adduct was obtained in the form of colorless crystals by carefully layering an equimolar solution of the two components in CH_2Cl_2 with Et_2O and allowing the reaction mixture to stand at $-18\,^{\circ}C$.[14] The asymmetric unit of the structure of **2** contains, in addition to TDACl, one molecule of benzoic acid and one molecule of CH_2Cl_2 as solvent. The chloride ion from TDACl forms a strong hydrogen bond with the acidic proton of the benzoic acid (Cl···H 1.988, O–H 0.891, O···Cl 2.870 Å) and a second very weak one to a proton of the solvent molecule CH_2Cl_2 (Cl···H 2.554 Å). The angle of the Cl-H-O unit is 170°.

[*] Prof. Dr. R. Weiss, Dipl.-Chem. T. Brenner, Dr. F. Hampel, Dr. A. Wolski
Institut für Organische Chemie der Universität Erlangen-Nürnberg
Henkestrasse 42, D-91054 Erlangen (Germany)
Telefax: Int. code + (9131)85-9132

[**] This work was supported by the Fonds der Chemischen Industrie.

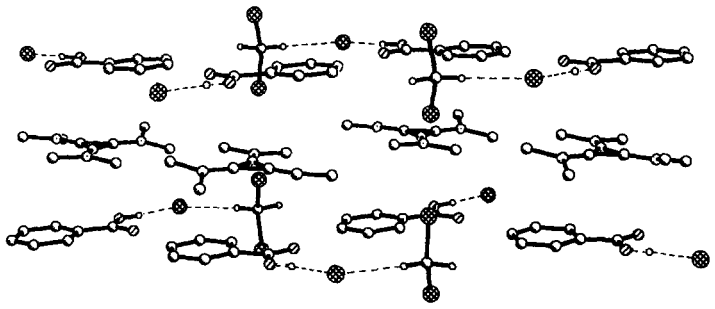


Fig. 1. Crystal structure of **2**. The spheres with lined hatching correspond to O atoms, those with crossed hatching to Cl atoms, those with spots to N atoms; large white spheres correspond to C atoms, small white spheres to H atoms.

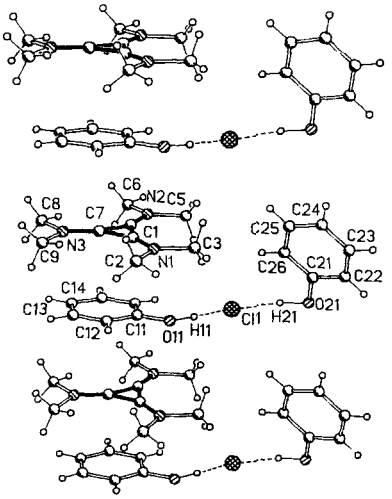


Fig. 2. Crystal structure of **7**. Important distances [Å] and angles [°]: Cl1–H11 2.003(3), Cl1–O11 3.034(9), O11–H11, 1.04(2), Cl1–H21 2.126(8), Cl1–O21 3.086(5), H21–O21 0.96(2); H21-Cl1-H11 120.94.

Although the cyclopropenylium ions and the benzoic acid molecules are stacked in an alternating fashion, the buildup of the structure shows that this is not attributed to π interactions. That the latter is not a prerequisite for the successful formation of adduct can be clearly seen from the tendency of formation of adducts with aliphatic carboxylic acids (Table 1). According to this, the strong hydrogen bond between the carboxylic acid and the Cl^- ion is the decisive energetic factor in the formation of this adduct.

Other excellent chloride donors, such as the salts **3**–**6**, cannot form comparable adducts. This is particularly remarkable in the

$[NEt_4]Cl$ **3** $[C(NMe_2)_3]Cl$ **4** $[N\{P(NMe_2)_3\}_2]Cl$ **5** $[P\{NP(NMe_2)_3\}_4]Cl$ **6**

case of the phosphonium salts **5** and **6**, which according to latest investigations[15] should contain naked chloride ions of high reactivity. The possible conclusion that voluminous spherical chloride salts are not capable of forming such adducts for steric reasons is not valid, because the guanidinium salt **4**, whose planar cation is very similar to that of TDACl as regards geometrical considerations, does not form adducts with hydrogen bonds of the type introduced above.

Analogously, when two molar equivalents of TDACl **1a** are treated with dicarboxylic acids, the corresponding 2:1 adducts are obtained. This adduct formation is accompanied by a break up of the polymeric hydrogen bonds of these carboxylic acids[16] and therefore leads to them dissolving in CH_2Cl_2. These 2:1 adducts can be obtained as stable compounds in a form pure enough for analytical purposes by precipitating with nonpolar solvents. To our knowledge, isolable adducts of carboxylic acids and Cl^- ions which are connected by hydrogen bonds were previously unknown. The driving force of their formation must be considerable, as it requires the annulment of the classical low-energy association patterns of organic acids.[16]

TDACl also forms novel adducts with phenol and phenol derivatives. Some of these adducts are listed in Table 1. The 2:1 phenol/TDACl adduct **7** was obtained in crystalline form by recrystallizing a primary 1:1 adduct of phenol with TDACl from CH_2Cl_2/Et_2O under the above conditions. The result of the X-ray structure analysis is shown in Figure 2.[17] The TDACl and phenol molecules form a stack in which the π-electron systems of the components lie almost parallel to one another. The Cl^- counterion is located in the spaces between the stacks and is involved in two hydrogen bonds which are significantly different as regards their strengths. Judging by the O–Cl distances, one strong hydrogen bond is formed between the chloride ion and the OH group of the phenol molecule sandwiched between two cyclopropenylium ions (O···Cl 3.034, Cl···H 2.003(3), O–H 1.04(2) Å), whereas the corresponding distance in the second hydrogen bond, in which a phenol molecule intercalated in the lattice spaces participates, is 3.086 Å (C···H 2.126(8), O–H 0.96(2) Å). This thus indicates a clearly weaker bonding system.[18] The phenol molecule built into the stack is obviously significantly more acidic than the "free" one. Since both aromatic stack components are classified as electron-excess compounds, a CT arising from the phenol and directed at the TDACl cannot be considered a possible reason for the acidification of the sandwiched phenol. The van der Waals attraction between the π-electron system of the components that would be expected at the interplanar distance of about 3.5 Å is also unable to explain the observed effect. One possible explanation, however, could be found in the assumption that the phenol molecules in the stack are acidified by the electrostatic field effect of the neighboring cyclopropenylium ions. The latter would have a considerably lesser effect on the "free" phenol molecules due to their significantly larger distance from the cationic components.

The coordination behavior of the Cl^- ions in TDACl was not observed until now. We assume that this unusual behavior is due to the release of the ion pair strain defined above which produces an additional thermodynamic driving force.[20]

In addition to the adducts of TDACl introduced in this paper, a whole range of other previously unknown hydrogen-bonded adducts with diverse OH-, NH-, and CH- components were obtained.[21] Related phenomena were also observed with other halide ions. The following publication should be consulted in order to compare the behavior of the analogous iodide salts.[22] Finally, other types of counterion such as N_3^-, OCN^-, or NO_2^-, can be activated in an analogous fashion.

Received: July 20, 1994
Revised version: October 15, 1994 [Z 7147 IE]
German version: *Angew. Chem.* **1995**, *107*, 481

Keywords: adducts · cyclopropenylium compounds · halogen compounds · hydrogen bonds · ion pairs

[1] F. Gerson, G. Plattner, Z. Yoshida, *Mol. Phys.* **1971**, *21*, 1027–1032.
[2] R. Weiss, unpublished results.
[3] V. Jesch, Dissertation, Universität Erlangen-Nürnberg, **1988**.
[4] H. N. Schäfer, H. Burzlaff, A. H. Grimmeiss, R. Weiss, *Acta Crystallogr. Sect. C* **1991**, *47*, 1808–1811.
[5] H. N. Schäfer, H. Burzlaff, A. H. Grimmeiss, R. Weiss, *Acta Crystallogr. Sect. C* **1992**, *48*, 795–798.

 © VCH Verlagsgesellschaft mbH, D-69451 Weinheim, 1995 0570-0833/95/0404-0440 $ 10.00+.25/0

[6] H. N. Schäfer, H. Burzlaff, A. H. Grimmeiss, R. Weiss, *Acta Crystallogr. Sect. C* **1992**, *48*, 912–913.
[7] A. H. Grimmeiss, Dissertation, Universität Erlangen-Nürnberg, **1991**.
[8] H. N. Schäfer, Dissertation, Universität Erlangen-Nürnberg, **1992**.
[9] R. Weiss, K. Schloter, *Tetrahedron Lett.* **1975**, 3491–3494.
[10] R. Weiss, A. H. Grimmeiss, *Z. Naturforsch. B* **1989**, *44*, 1447–1450.
[11] R. Weiss, A. H. Grimmeiss, *Z. Naturforsch. B* **1991**, *46*, 104–110.
[12] R. W. Johnson, *Tetrahedron Lett.* **1976**, 589–592.
[13] L. Eberson, *Acta Chem. Scand. Ser. B* **1984**, *38*, 439–459.
[14] a) Crystal structure analysis of **2** ($C_{17}H_{26}Cl_3N_3O_2$); $M = 410.76$, orthorhombic, space group *Pbcm*, $a = 11.544(4)$, $b = 13.206(8)$, $c = 13.784(3)$ Å, $\alpha = \beta = \gamma = 90°$, $V = 2101(2)$ Å^3, $Z = 4$, $\rho_{calcd} = 1.298$ Mgm^{-3}, data collection on a Nicolet R3mv four-circle diffractometer with monochromated $Mo_{K\alpha}$ radiation, ($\lambda = 0.71073$) in the range $4° < 2\theta < 57°$; 3505 reflections measured of which 2525 independent; structure solution with direct methods (SHELXTL Plus 4.11); data refinement using full matrix against F^2 using the least squares method (SHELXL 93, G. M. Sheldrick, Universität Göttingen, **1993**). All non-hydrogen atoms were refined anisotropically; all hydrogen atoms were localized using difference Fourier syntheses and independently refined isotropically; 191 refined parameters; R values for [$I > 2\sigma(I)$]: $R1 = 0.0594$; $wR2 = 0.1511$. b) Further details of the crystal structure investigations may be obtained from the Director of the Cambridge Crystallographic Data Centre, 12 Union Road, GB-Cambridge CB2 1EZ on quoting the full journal citation.
[15] R. Schwesinger, R. Link, G. Thiele, H. Rotter, D. Honert, H.-H. Limbach, F. Männle, *Angew. Chem.* **1991**, *103*, 1376–1378; *Angew. Chem. Int. Ed. Engl.* **1991**, *30*, 1372.
[16] J. Bernstein, M. C. Etter, L. Leiserowitz in *Structure Correlation, Vol. 2* (Eds.: H. B. Bürgi, J. D. Dunitz), VCH, Weinheim, **1994**, pp. 431–500.
[17] Crystal structure analysis of **7** ($C_{21}H_{30}ClN_3O_2$); $M = 391.9$, monoclinic, space group $P2_1/n$, $a = 7.1360(9)$, $b = 19.332(5)$, $c = 15.975(4)$ Å, $\beta = 94.45(2)°$, $V = 2197.2(8)$ Å^3, $Z = 4$, $\rho_{calcd} = 1.185$ Mgm^{-3}, data collected with a Huber four-circle diffractometer with monochromated $Mo_{K\alpha}$ radiation, ($\lambda = 0.71073$) in the range $6 < 2\theta < 50°$; 4611 reflections measured, of which 3889 independent ($R_{int} = 0.0103$); structure solution with direct methods (SHELXS86, G. M. Sheldrick, Universität Göttingen, **1986**); data refinement using full matrix against F^2 using the least squares method (SHELXS76, G. M. Sheldrick, Cambridge, **1976**). All non-hydrogen atoms were refined anisotropically; H 11 and H 12 were localized with difference Fourier syntheses and independently refined isotropically; all other hydrogen atoms were refined on geometrically calculated positions with common U values using a riding model. 259 refined parameters; R values for [$F > 3\sigma(F)$]: $R = 0.0571$; $wR = 0.0237$ [14b].
[18] We recently succeeded in determining the X-ray structure of the TDACl/phenol 1:1 adduct. In the previously unpublished structure, the O···Cl distance is 2.936 Å and thus considerably shorter than both the distances in the TDACl/bisphenol adduct. Only one example for a 1:1 H-bonding system is known in the literature between *p*-nitrophenol and the electron-rich methyltri(*p*-nitrophenoxy)phosphonium chloride [19]. The fact that, in spite of the significantly higher acidity of the phenol component ($\delta pK_a \approx 2.5$), an O–Cl distance of 3.015 Å is observed, about 0.08 Å longer than observed in the TDACl/phenol 1:1 adduct, underlines the greater readiness of the chloride ion in TDACl to coordinate.
[19] D. J. Schomburg, *J. Am. Chem. Soc.* **1980**, *102*, 1055–1058.
[20] Of special interest is the structure of TDACl itself. Typically enough, the halides cannot be obtained in solvent-free form. We interpret this as being an indirect indication of the unfavorable coordination relationships in an ionic lattice with electronically similar components, but of opposite charge.
[21] R. Weiss, T. Brenner, unpublished results.
[22] R. Weiss, M. Rechinger, F. Hampel, A. Wolski, *Angew. Chem.* **1995**, *107*, 483; *Angew. Chem. Int. Ed. Engl.* **1995**, *34*, 441.

Stable 1:1 Adducts from Iodoacetylenes and Iodide Ions: Ion Pair Strain as an Additional Driving Force?**

Robert Weiss,* Michael Rechinger, Frank Hampel, and Alexander Wolski

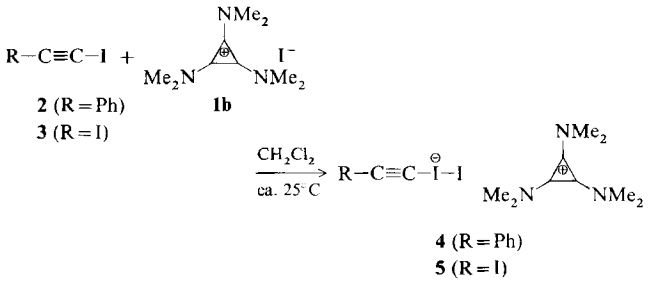
Dedicated to Professor Paul von Ragué Schleyer on the occasion of his 65th birthday

The chloride ions of the salt **1a** undergo coordination with unprecedented readiness even with weakly acidic compounds to form novel adducts with hydrogen bonds.[1a] In the case of this salt, there were strong indications that a new type of strain in the corresponding ion pair **1a** is responsible for the unusual reactivity of the chloride ion. In order to check whether this activation is also effective in the case of the "soft" iodide ions, we treated the salt **1b** with organic iodine compounds as soft σ* acceptors. This resulted in the formation of many novel hypervalent adducts.[1b]



1a: X = Cl
1b: X = I

We report here on the reactions of **1b** with 2-iodo-1-phenylacetylene (**2**) as a monofunctional σ* acceptor, and with diiodoacetylene (**3**) as a bifunctional σ* acceptor, in which stable n → σ* adducts between iodide ions and C_{sp}-bonded iodine centers were obtained for the first time.[2] The two 1:1 complexes **4** and **5** were prepared by simply adding tris(dimethylamino)cyclopropenylium iodide (TDAI) (**1b**) to the acetylene component in CH_2Cl_2. Compound **4** was precipitated from the reaction mixture by addition of Et_2O. Recrystallization from CH_2Cl_2/Et_2O delivered **4** in the form of colorless needles which were suitable for an X-ray crystal structure analysis.[4]



2 (R = Ph)
3 (R = I)
1b
4 (R = Ph)
5 (R = I)

The I–I distance of 3.44 Å in the anion of **4** is very long in comparison to that in molecular iodine (2.66 Å),[5] but considerably shorter than the I–I bond length of 4.35 Å which would be expected on consideration of the sum of the van der Waals radii.[5] Compared to the I–I distances of the adducts formed from iodide and neutral compounds with C_{sp^3}-bonded iodine centers (3.57–3.69 Å[6, 7]), the I–I bond in the anion of **4** is very short. It lies in the range of those I–I distances that we found in iodocarbenium iodides with C_{sp^2}-bonded iodine atoms (3.37 Å).[8] The C–I bond of 2.02 Å is longer than that of a noncoordinated iodoacetylene.[9]

One of the remarkable features of **4** is its extremely unusual highly symmetrical ionic lattice (space group *Pbam*), which is made up of an alternating series of purely anionic and purely

[*] Prof. Dr. R. Weiss, Dipl.-Chem. M. Rechinger, Dr. F. Hampel, Dr. A. Wolski
Institut für Organische Chemie der Universität Erlangen-Nürnberg
Henkestrasse 42, D-91054 Erlangen (Germany)
Telefax: Int. code + (9131)85-9132

[**] This work was supported by the Fonds der Chemischen Industrie.

cationic layers. Both dipole–dipole interactions and hydrogen bonds are determining factors for the buildup of the anionic lattice as a whole (Fig. 1a). In each case, two anions connect to form a head-to-tail adduct by dipole–dipole interactions. These pairs of anions are connected to one another through weak hydrogen bonds between the terminal iodine atom and an *ortho*-hydrogen atom of a neighboring phenyl ring (colored black in Fig. 1a) to give an absolutely planar layer with dense packing.[10]

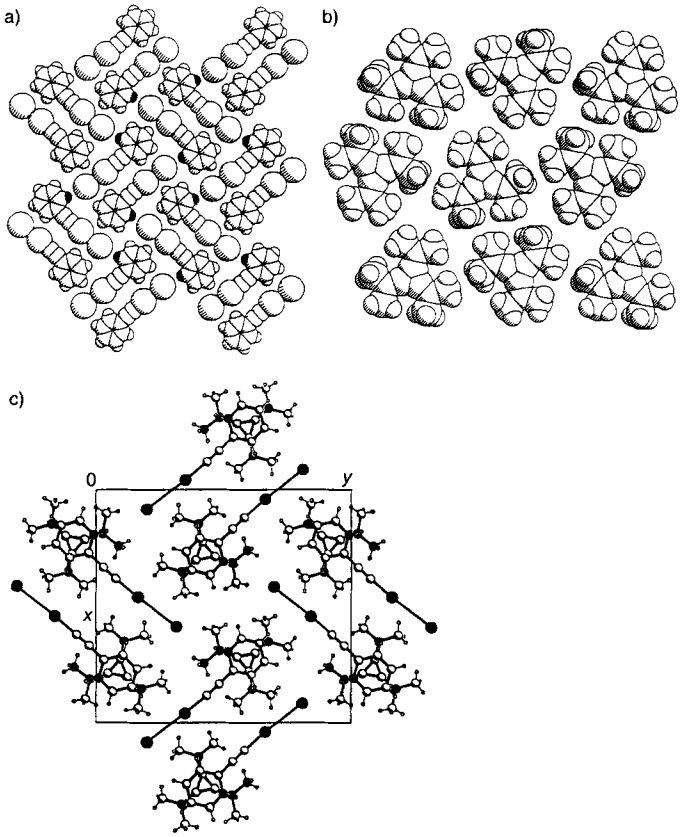


Fig. 1. a) Crystal structure of the anion in **4**. Selected distances [Å]: C–I 2.02, I–I 3.44. b) Crystal structure of the cation in **4**. c) Crystal structure of **4**.

Layers of likewise planar TDA cations lie between the individual anion layers, and are hexagonal closest packed in the lattice (Fig. 1b). Thus, each cyclopropenylium ion is placed directly above or below the phenyl ring of an anion. As in graphite, the distance between the two layers is 3.35 Å.[11] The cohesion of the layers in the lattice is brought about primarily by electrostatic interactions which are superimposed by van der Waals forces. The latter are probably responsible for the stacking of the aromatic components. The crystal structure of **4** is shown in Figure 1c.

In contrast to **2**, diiodoacetylene **3** can function as a bifunctional σ^* acceptor. With the intention of preparing the corresponding 2:1 adduct of TDAI and diiodoacetylene, **1b** and **3** were allowed to react (mole ratio 2:1) in CH_2Cl_2. A colorless precipitate was formed immediately; however, the analysis indicated only a 1:1 adduct of the two components. On cooling the filtrate to $-18\,^{\circ}C$, **5** precipitated with one equivalent of CH_2Cl_2 in the form of colorless needles which were suitable for an X-ray structure analysis.[12] The molecular structure of **5** is shown in Figure 2.

The system TDAI/diiodoacetylene **5** forms a novel hypervalent one-dimensional polymer. The bifunctional σ^*-acceptor centers of diiodoacetylene are each connected by an iodide ion

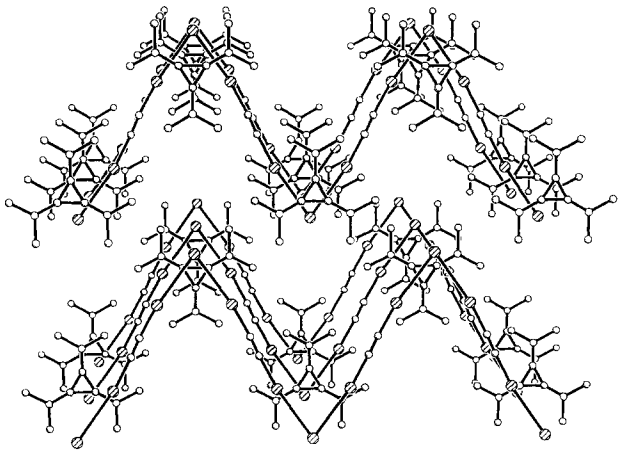


Fig. 2. Crystal structure of **5**. Selected distances [Å] and angle [°]: C–I 2.053, I–I 3.398, I-I-I 69.9; the CH_2Cl_2 molecules are not shown.

which functions as a bifunctional donor with orthogonal lone pairs.[13] The resulting polymeric zigzag chains lie exactly in a plane. Quite remarkable in this is the unusually small bond angle of 70° which occurs on the dicoordinate I^- ion; this value was also determined in $n \rightarrow \sigma^*$ adducts formed from iodide and iodoform;[6, 7] as yet this cannot be explained satisfactorily. Both the I–I bond length of 3.398 Å and the C–I bond length of 2.053 Å lie in the same range as those in the monomeric structure **4**. The TDA cations in **5** are arranged above the partially anionic iodine center at a distance of 3.36 Å and form a stacking structure running perpendicular to the anionic polymer. All cations within a stack are arranged in an eclipsed fashion. A structure that forms part of a "corrugated structure" thus ensues, in which neighboring zigzag chains interlock in the manner shown in Figure 2.

Whereas **4** forms a two-dimensional layer lattice, **5** has only a one-dimensional band structure. Only those TDA cations, which belong to one "anion wire", are found in the same plane. The cations of two neighboring polymeric wires are shifted by 1/2 in the *z* direction. In this way a molecular lattice results which is also found in other TDA salts.[15]

The question posed at the beginning concerning an increased readiness for coordination of the iodide ion in salts **1b**, based on the postulated ion strain, can only be partially answered at the moment. Whereas **2** only forms a hypervalent adduct with **1b**, but not with other iodide donors,[16] **3** can also be successfully treated with alternative sources of iodide.[17] A conceivable reason for this behavior is the known higher σ^* acidity of C_2I_2 compared with that of 2-iodo-1-phenylacetylene (**2**),[18] which could effect a leveling influence with respect to the iodide coordination.

Experimental Procedure

4: **2** (0.15 mL, 250 mg, 1.1 mmol) was dissolved in CH_2Cl_2 (20 mL) and a solution of **1b** (315 mg, 1.1 mmol) in CH_2Cl_2 (5 mL) was added dropwise at room temperature. After the mixture had been stirred for 18 h, the adduct was precipitated by addition of Et_2O, then filtered off and washed twice with Et_2O (10 mL), and dried under vacuum for 8 h. Yield: 520 mg (92%). Single crystals of **4** were obtained by recrystallization from CH_2Cl_2/Et_2O. C, H, N elemental analysis correct; ^{1}H-NMR (400 MHz; $CDCl_3$, 25 °C, TMS): δ = 3.21 (s, 18H, $N(CH_3)_2$), 7.32 (m, 3H, CH), 7.41 (m, 2H, CH); ^{13}C-NMR (100 MHz; $CDCl_3$, 25 °C, TMS): δ = 11.9 (CI), 42.9 ($N(CH_3)_2$), 92.9 (CCI), 117.9, 123.4, 128.1, 128.4, 132.0; IR (KBr): $\tilde{\nu}$[cm^{-1}] = 3050 (w), 1545 (ss), 1205 (m), 1070 (m), 1050 (m), 1010 (s), 790 (w), 770 (m), 760 (m), 750 (m), 700 (w), 680 (m); Raman: $\tilde{\nu}$[cm^{-1}] = 3037(w), 2919 (m), 2804 (w), 2147 (s), 2071 (w), 1590 (s), 1210 (s), 1179 (w), 995 (m), 802 (w), 563 (m), 526 (w), 331 (w), 214 (s), 132 (s); MS (70 eV): *m/z* (%): 228 (100) [$C_8H_5I^+$], 127 (8) [I^+], 101 (30) [$C_8H_5^+$].

 © VCH Verlagsgesellschaft mbH, D-69451 Weinheim, 1995 0570-0833/95/0404-0442 $ 10.00+.25/0

5: **3** (1.23 g, 4.44 mmol) was dissolved in CH_2Cl_2 (20 mL). A solution of **1b** (1.31 g, 4.44 mmol) in CH_2Cl_2 (10 mL) was added dropwise at room temperature. After the addition was complete, the product precipitated in the form of white needles. The reaction mixture was stirred for a further 5 h, the product filtered off and washed twice with CH_2Cl_2 (10 mL), and dried under vacuum for 8 h. Yield: 2.32 g (91.4%). Single crystals were obtained by allowing the filtrate to stand at $-20\,^{\circ}C$ for 24 h. C, H, N elemental analysis correct; IR (Nujol): $\tilde{\nu}$[cm^{-1}] = 1550 (ss), 1220 (ss), 1050 (m), 1020 (s), 785 (s), 720 (w), 630 (s); Raman: $\tilde{\nu}$[cm^{-1}] = 2078 (m), 1987 (w), 1406 (w), 1287 (w), 1228 (w), 1028 (w), 787 (w), 634 (m), 607 (w), 543 (w), 316 (m), 168 (ss); MS (70 eV): *m/z* (%): 278 (100) [$C_3I_2^+$], 254 (85) [I_2^+], 127 (65) [I^+].

Received: July 20, 1994 [Z 7148 IE]
German version: *Angew. Chem.* **1995**, *107*, 483

Keywords: adducts · cyclopropenylium compounds · halogen compounds · hypervalent compounds · solid-state structures

[1] a) R. Weiss, T. Brenner, F. Hampel, A. Wolski, *Angew. Chem.* **1995**, *107*, 481; *Angew. Chem. Int. Ed. Engl.* **1995**, *34*, 439; b) M. Rechinger, Dissertation, Universität Erlangen-Nürnberg, **1995**.

[2] Strong n → σ* contacts between iodide and C_{sp}-bonded iodine were postulated by us in explaining the reaction behavior and the extraordinary insolubility of *cyclo*-C_3I_4 [3].

[3] a) R. Weiss, H. Wolf, U. Schubert, T. Clark, *J. Am. Chem. Soc.* **1981**, *103*, 6142–6147; b) A. E. Reed, F. Weinhold, R. Weiss, J. Macheleid, *J. Phys. Chem.* **1985**, *89*, 2688–2694; c) R. Weiss, G.-E. Miess, A. Haller, W. Reinhardt, *Angew. Chem.* **1986**, *98*, 102–103; *Angew. Chem. Int. Ed. Engl.* **1986**, *25*, 103–104.

[4] a) Crystal structure analysis of **4** ($C_{17}H_{23}I_2N_3$): M = 523.18, orthorhombic, space group *Pbam*, a = 16.925(1), b = 18.254(1), c = 6.6976(8) Å, $\alpha = \beta = \gamma = 90^{\circ}$, V = 2069.2(3) Å^3, Z = 4, ρ_{calcd} = 1.679 Mg m^{-3}, 9084 reflections collected ($3.0 < 2\theta < 26.0^{\circ}$), 2222 independent and 1491 observed reflections [$F^2 > 2\sigma(F^2)$], 139 refined parameters, R = 0.0288, wR = 0.0719); all data were collected with a Huber four-circle diffractometer at 291 K with $Mo_{K\alpha}$ radiation (λ = 0.70993 Å). The structure was solved by direct methods (SHELXS86/SHELXL93). All non-hydrogen atoms were anisotropically refined, all hydrogen atoms isotropically. b) Further details of the crystal structure investigations may be obtained from the Fachinformationszentrum Karlsruhe, D-76344 Eggenstein-Leopoldshafen (Germany) on quoting the depository number CSD-58743.

[5] N. N. Greenwood, A. Earnshaw, *Chemistry of the Elements*, 1. ed., Pergamon, Oxford, **1984**, p. 934.

[6] R. Weiss, M. Rechinger, unpublished results.

[7] H.-G. Löhr, A. Engel, H.-P. Josel, F. Vögtle, W. Schuh, H. Puff, *J. Org. Chem.* **1984**, *49*, 1621–1627.

[8] R. Weiss, M. Rechinger, F. Hampel, *Angew. Chem.* **1994**, *106*, 901–903; *Angew. Chem. Int. Ed. Engl.* **1994**, *33*, 893–895.

[9] J. Sheridan, W. Gordy, *Phys. Rev.* **1952**, *20*, 735.

[10] A. I. Kitaigorodski, *Molekülkristalle*, Akademie-Verlag, Berlin, **1979**.

[11] A. F. Hollemann, E. Wieberg, *Lehrbuch der Anorganischen Chemie*, 91.–100. ed., de Gruyter, Berlin, **1985**, p. 702.

[12] Crystal structure analysis of **5** ($C_{12}H_{18}Cl_2I_3N_3$): M = 655.9, monoclinic, space group $C2/c$, a = 7.231(2), b = 22.916(8), c = 12.497(4) Å, α = 90, β = 89.98(3), γ = 90°, V = 2070.8(11) Å^3, Z = 4, ρ_{calcd} = 2.104 Mg m^{-3}, 4767 reflections collected ($3.0^{\circ} < 2\theta < 55.0^{\circ}$), 2442 independent and 1970 observed reflections [$F > 4.0\sigma(F)$], 92 refined parameters, R = 0.0427, wR = 0.0575); all data were collected with a Siemens R3m/V diffractometer at 200 K with $Mo_{K\alpha}$ radiation (λ = 0.71073 Å). The structure was solved by direct methods (SHELXTL-PLUS (VMS)). All non-hydrogen atoms were refined anisotropically, all hydrogen atoms isotropically in fixed ideal positions (riding model) [4b].

[13] In structural analogy to the bonding situation in the I_5^- ion [14].

[14] R. J. Hach, R. E. Rundle, *J. Am. Chem. Soc.* **1951**, *73*, 4321–4324.

[15] R. Weiss, M. Rechinger, F. Hampel, *Z. Kristallogr.*, in press.

[16] Tetrabutylammonium iodide and hexamethylguanidinium iodide were used as additional sources of iodide.

[17] 1:1 adducts of as yet undetermined structure were thus formed.

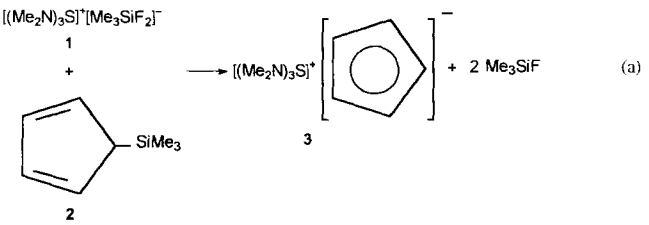
[18] C. Laurence, M. Queignec-Cabanetos, T. Dziembowska, R. Queignec, B. Wojtkowiak, *J. Am. Chem. Soc.* **1981**, *103*, 2567–2573.

Tris(dimethylamino)sulfoniumcyclopentadienide $[TAS]^+[C_5H_5]^-$ and Tris(dimethylamino)-sulfoniumpyrrolide $[TAS]^+[C_4H_4N]^-$: Two Isostructural Salts with "Naked" Anions A^- and the "Inverse" Sandwich-Cations $[\{(Me_2N)_3S\}_2A]^+$ ($A = C_5H_5^-$, $C_4H_4N^-$)**

Jens Wessel, Ulrich Behrens, Enno Lork, and Rüdiger Mews*

The cleavage of Si–C bonds by Bu_4NF or similar organic fluorides serves to remove Me_3Si protective groups with subsequent formation of C–H bonds.[1] Intermediates in these reactions are highly reactive carbanions, which, under the reaction conditions chosen, can abstract protons from neighboring molecules. Particularly suitable for the cleavage of Si–element bonds is "TAS-fluoride" (tris(dimethylamino)sulfonium difluorotrimethylsilicate) $[(Me_2N)_3S]^+[Me_3SiF_2]^-$ (**1**),[2, 3] which is readily available in HF-free form; the chemical behavior of the fluorosilicate ion corresponds to that of a "naked" fluoride ion.[4]

From the reaction of TAS-fluoride (**1**) with $C_5H_5SiMe_3$ (**2**) in CH_3CN at $-40\,^{\circ}C$, the TAS salt **3** can be isolated in high yield as a reddish solid [Eq. (a)].



The salt **3** is stable as a solid at room temperature. However, in CH_3CN and CH_2Cl_2, which are suitable solvents at low temperatures, **3** decomposes between $-40\,^{\circ}C$ and $-10\,^{\circ}C$ to give C_5H_6 among the products.

The aim of our investigations was the generation and the detection of "naked" Cp^- ions in the presence of base-free cations (that is, cations not complexed by auxiliary bases such as *N,N,N',N'*-tetramethylethylenediamine (TMEDA)); only two examples of "naked" Cp^- ions have been characterized by structural investigations in transition metal chemistry: $[[Re(NO)(CH_3)(PMe_3)_4]^+[C_5H_5]^-$[6] and $[Rh_2(dmpe)_4(\mu\text{-dmpe})]^{2+}[C_5H_5^-]_2$ (dmpe = 1,2-bis(dimethylphosphano)ethane).[7] In all of the other known structures of cyclopentadienide salts there are interactions between the anions and the cations.[8] This leads to the formation of polymeric structures ("supersandwich" compounds[9]) in alkali metal derivatives; these interactions are not terminated by the complexation of the cations by auxiliary bases.[10]

In TAS salts there are practically no cation–anion interactions in the solid state.[11] Therefore, the TAS^+ ion seemed particularly suitable for the generation of "naked" Cp^- ions. The crystal structure of **3** (Fig. 1) and the view of the crystal lattice (Fig. 2) show that the TAS cyclopentadienide can best be

[*] Prof. Dr. R. Mews, J. Wessel, Prof. Dr. U. Behrens, E. Lork
Institut für Anorganische und Physikalische Chemie der Universität Bremen
Leobener Strasse NW2, Postfach 330440, D-28334 Bremen (Germany)
Telefax: Int. code + (421) 218-4267

[**] This work was supported by the Fonds der Chemischen Industrie. We would like to thank one of the referees for the discerning examination of the manuscript.

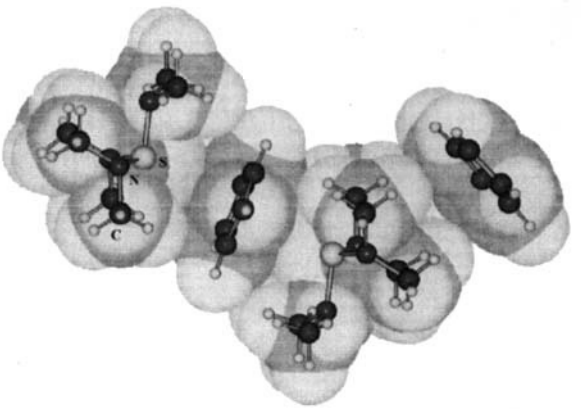


Fig. 1. Crystal structure of **3** (SCHAKAL drawing).

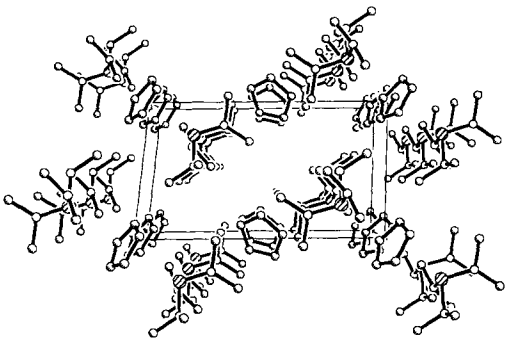


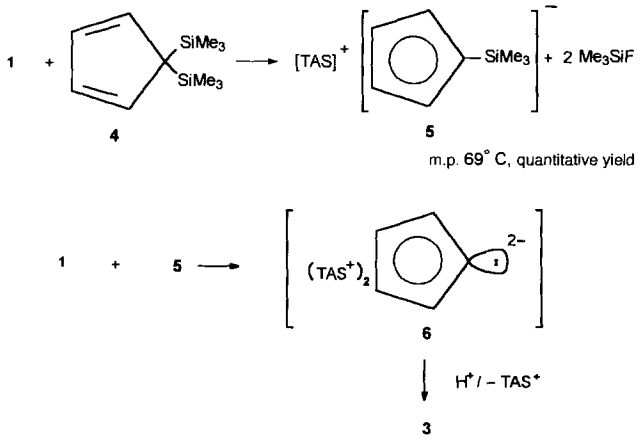
Fig. 2. View of the crystal lattice of **3**.

described as a $[(TAS)_2Cp]^+$ cation and a "naked" Cp^- anion.[12] The $[(TAS)Cp(TAS)]^+$ unit can be regarded as an "inverse sandwich". For this type of structure with a Cp unit in the center, there is only one example so far, a lithium compound.[13]

The solid-state structure of **3** can be understood from the anisotropy of the TAS^+ ions. As in the alkali metal cyclopentadienides,[14] the bonds in $[(TAS)_2Cp]^+$ can be regarded as anion–cation Coulomb interactions between the sulfonium centers and the central Cp^- ion, similar to the interactions in contact ion pairs (CIP). Because of the size of the sulfonium center these interactions are weak. The dimethylamino groups in the $(Me_2N)_3S^+$ ions can, again analogous to the chemistry of metal ions, be regarded as ligands or as solvating solvent molecules which separate the cation from the anion. The even weaker interaction between the $[(TAS)_2Cp]^+$ units and the "naked" Cp^- ion is similar to solvent-separated ion pairs (SSIP).[14]

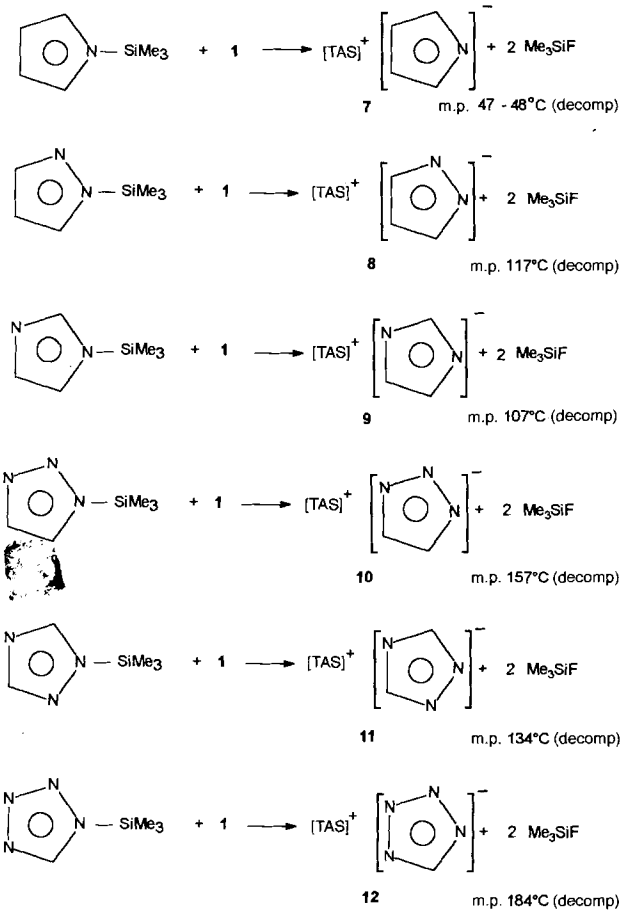
Not only the "naked" Cp^- anion, but also the $[(TAS)Cp(TAS)]^+$ cation lie on symmetry centers of the space group. This results in disorder of both Cp rings. The distances from the sulfonium centers to the middle of the enclosed Cp ring are 313.1(2) and 322.2(2) pm. These values differ somewhat because the mid-point of the Cp ring does not coincide exactly with the center of symmetry. The S–C distances vary between 330.0(4) and 341.0(4) pm, the sum of the van der Waals radii (of S and C) is 350 pm. The distance between the "naked" Cp ring and the sulfur atom of the cationic center is 512.9(2) pm. Both Cp rings were refined as perfect pentagons. The C–C distance of the enclosed Cp^- ring refined to 138.5(3) pm, and that of the "naked" Cp^- ring to 139.6(4) pm.[15] The C–C distances determined here for the C_5H_5 anion are in agreement with the results of ab initio calculations (d(C–C) = 139.3 pm).[16] Furthermore, these calculations indicate that the interactions with positive metal centers such as Li^+ lead to an increase in the C–C distance (141.7 pm); in transition metal derivatives the distances are of the order of 140–143 pm.[17]

The synthesis of $[TAS^+]_2[C_5H_4]^{2-}$ (**6**) via the stable intermediate $[TAS]^+[C_5H_4SiMe_3]^-$ (**5**) failed as a result of the high basicity of the anion of **5**. Thus, only **3** was isolated (Scheme 1).



Scheme 1.

However, $[TAS]^+[C_4H_4N]^-$ (**7**), which is isoelectronic to **6**, can, as for all the other azolide salts, be prepared by cleavage of the Si–N bonds from the corresponding silylated azoles in high yields (92–95%) (Scheme 2).



Scheme 2.

 © VCH Verlagsgesellschaft mbH, D-69451 Weinheim, 1995 0570-0833/95/0404-0444 $ 10.00+.25/0

The salts **7**–**12** were produced as pure compounds and unambiguously characterized by structural investigations. The pyrrole salt **7** crystallized in an analogous manner to **3** as $[(TAS)_2pyr]^+[pyr]^-$ (Figs. 3 and 4) in the space group $P\bar{1}$ with almost identical

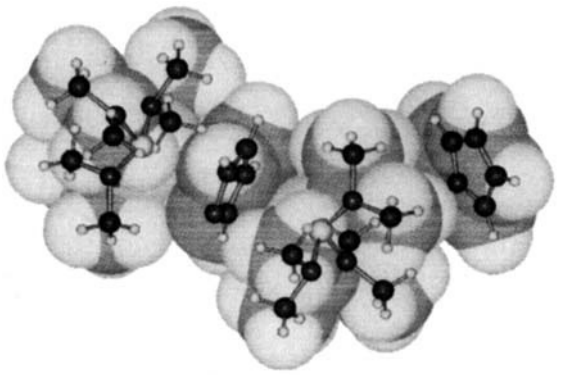


Fig. 3. Crystal structure of **7** (SCHAKAL drawing).

lattice constants.[21] Exact bond lengths for the $C_4H_4N^-$ ion cannot be given, since here, in addition to the disorder described for **3**, there is also a statistical distribution of CH/N. The distances of the sulfonium centers to the middle of the enclosed pyrrole ring are 314.1 and 319.5 pm; the shortest distance from the "naked" $C_4H_4N^-$ ring to the nearest sulfonium center is 508.5 pm.

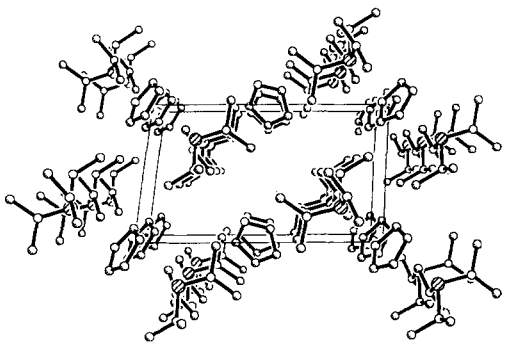


Fig. 4. View of the crystal lattice of **7**.

In **8** there are ion pairs with only weak interactions (distance sulfonium center–center of ring 315.4 pm), in **9**–**12** discrete anions and cations. Hitherto hardly any structural determinations of free azolide ions have been undertaken, and only the structure of the hydrate $Na(HCN_4)\cdot H_2O$[22] is described. In this salt the bond lengths are influenced by strong N···H···O hydrogen bonds. There seems to be very little disordering of the anions in the salts **8**–**12**: only for the imidazolide **9** (Fig. 5) are there larger standard deviations.[23]

As our investigations of **7** show, the TAS azolide salts seem to be considerably more stable than **3**. Elemental analysis and NMR spectra of the solutions indicate that after a day in CH_3CN or CH_2Cl_2 at room temperature there is no noticeable decomposition. Since the TAS azolides are readily soluble and have a relatively high stability they could be interesting as preparative reagents.

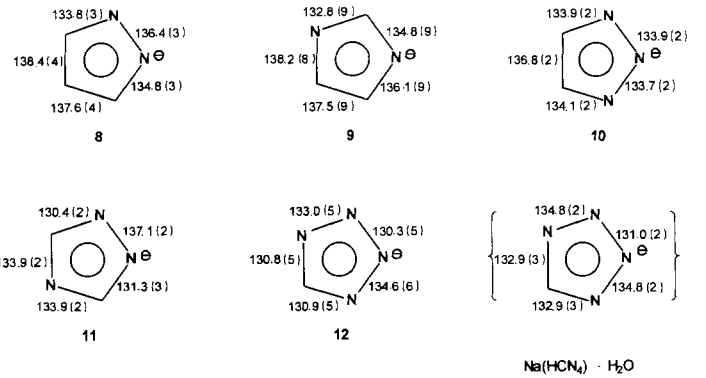


Fig. 5. Experimental bond lengths [pm] in the anions of the salts **8**–**12**. The structure of the anion in $Na(HCN_4)\cdot H_2O$ [21] is included for comparison.

Experimental Procedure

3: In a dry box, TAS-F (**1**; 1.30 g, 4.72 mmol) was placed into a double-tube vessel equipped with a Teflon tap, and $CpSiMe_3$ (**2**; 1.40 g, 10.0 mmol) [24] was introduced by syringe under N_2 into the second tube. CH_3CN (10 mL) was condensed as solvent into the tube containing the $CpSiMe_3$ at −196 °C under vacuum. The reaction vessel was warmed to −40 °C, and the solution of **2** in CH_3CN slowly poured onto **1**. To prevent decomposition reactions, the temperature of the reaction solution must not exceed −40 °C. After 1 h the Me_3SiF produced was removed under vacuum, the reaction solution carefully layered with diethyl ether (50 mL) and stored in a cryostat free from vibrations at −40 °C for two weeks. By decantation of the mother liquor from the crystals, the majority of the starting materials and decomposition products could be removed. After evaporation of the solvent, the crystals were washed with ether, and volatiles were quantatively removed under vacuum. Yield: 1.03 g (95%); m.p. 138 °C (dec.); ^1H NMR (CD_3CN, −40 °C): $\delta = 2.85$ (s, 18H; $[(CH_3)_2N]_3S^+$), 5.53 (s, 5H; C_5H_5).

7: Prepared in a similar manner to **3** from $C_4H_4NSiMe_3$ (1.80g (15.0mmol) [25] and **1** (1.50g, 5.45mmol). Yield: 1.10g **7** (93%, based on **1**); m.p. 47–48 °C (dec.); ^1H NMR (CD_3CN, 30 °C): $\delta = 2.85$ (s, 18H; $[(CH_3)_2N]_3S^+$), 6.08 ("t", 2H (3,4)), 6.76 ("t", 2H (2,5)); $^{13}C\{^1H\}$ NMR (CD_3CN, 30 °C): $\delta = 38.6$ ($[(CH_3)_2N]_3S^+$), 104.7 (C(3,4)), 126.8 (C(2,5)).

Received: February 5, 1994
Revised version: December 3, 1994 [Z 6673 IE]
German version: *Angew. Chem.* **1995**, *107*, 516

Keywords: azolides · cyclopentadienyl compounds · sandwich complexes · sulfonium salts

[1] For example G. L. Larson in *The Chemistry of Organosilicon Compounds* (Eds.: S. Patai, Z. Rappoport), Wiley, New York, **1989**, p. 789ff.
[2] W. J. Middleton, US-A 3940402, **1976**; *Org. Synth.* **1985**, *64*, 221–225.
[3] D. A. Dixon, W. B. Farnham, W. Heilemann, R. Mews, M. Noltemeyer, *Heteroat. Chem.* **1993**, *4*, 287–295.
[4] R. Mews, *Inorganic Fluorine Chemistry Toward the 21st Century* (Eds.: J. Thrasher, S. Strauss) (*ACS Symp. Ser.* **1994**, *555*, 148–166).
[5] The reddish color is possibly caused by small amounts of impurities that cannot be determined spectroscopically.
[6] C. P. Casey, J. M. O'Connor, K. J. Haller, *J. Am. Chem. Soc.* **1985**, *107*, 1241–1246.
[7] A. K. Kakkar, N. J. Taylor, T. B. Marder, *Organometallics* **1989**, *8*, 1765–1768.
[8] P. Jutzi, *J. Organomet. Chem.* **1990**, *400*, 1–17.
[9] For example P. Jutzi, W. Leffers, B. Hampel, S. Pohl, W. Saak, *Angew. Chem.* **1987**, *99*, 563–564; *Angew. Chem. Int. Ed. Engl.* **1987**, *26*, 584–585.
[10] For example T. Aoyagi, H. M. M. Shearer, K. Wade, *J. Organomet. Chem.* **1979**, *175*, 21–31.
[11] W. B. Farnham, R. L. Harlow, J. F. Whitney, G. A. Jones, L. J. Guggenberger, D. A. Dixon, W.-J. Middleton, J. C. Calabrese, *J. Am. Chem. Soc.* **1987**, *109*, 476–483.
[12] X-ray crystal structure analysis of **3** ($C_{11}H_{23}N_3S$), $M = 229.4$; crystal dimensions $1.0 \times 0.3 \times 0.1$ mm^3; triclinic, space group $P\bar{1}$ (No. 2), $a = 776.5(2)$, $b = 800.7(2)$, $c = 1218.9(2)$ pm, $\alpha = 88.69(3)$, $\beta = 85.22(3)$, $\gamma = 62.90(3)^\circ$, $V = 0.6722(3)$ nm^3, $Z = 2$, $\rho_{calcd} = 1.133$ Mg m^{-3}, $\mu = 0.218$ mm^{-1}. A suitable crystal for X-ray analysis was afixed to a glass fibre with Kel-F oil and measured on a Siemens P4 four-circle diffractometer at −100 °C (graphite monochromator, $Mo_{K\alpha}$ radiation, $\omega/2\theta$ scan). Of the 3369 measured reflections ($2.9^\circ < \theta < 27.5^\circ$), 3081 independent reflections remained after averaging. The structure was solved by direct methods. This indicated that the two symmetry-independent Cp units almost lie on the centers of symmetry in the space group; thus they are disordered. The Cp rings were therefore refined as perfect

 © VCH Verlagsgesellschaft mbH, D-69451 Weinheim, 1995 0570-0833/95/0404-0445 $ 10.00+.25/0

pentagons. The refinement calculations converged at $wR2 = 0.178$ (refined against F^2) for all 3081 reflections and 175 variables [$R_1 = 0.068$ for 2277 reflections with $I > 2\sigma(I)$; heavy atoms were assigned individual anisotropic deflection parameters, H atoms were calculated with a common isotropic temperature factor]. A difference Fourier synthesis indicated no residual electron density beyond + 0.74 and −0.92 e Å^{-3}. All the calculations (apart from the refinements) were carried out with the SHELXTL program system [18], refinements with the SHELXL program [19], and the drawings with SCHAKAL [20, 26].

[13] In[Li(Me$_2$NCH$_2$CH$_2$NMe$_2$)$_2$][Li$_2$(Me$_2$NCH$_2$CH$_2$NMe$_2$)$_2$(μ-η^5,η^5-MeC$_5$H$_4$)][(η^5-MeC$_5$H$_4$)$_6$ U$_2$ (μ-Me)]$_2$: S. D. Stults, R. A. Andersen, A. Zalkin, *J. Am. Chem. Soc.* **1989**, *111*, 4507–4508. Besides this only two examples from C$_9$H$_8$Sm chemistry (H. Schumann, J. Winterfeld, L. Esser, G. Kociok-Köhn, *Angew. Chem.* **1993**, *105*, 1212–1214; *Angew. Chem. Int. Ed. Engl.* **1993**, *32*, 1208–1210; H. Schumann, J. Winterfeld, F. H. Görliz, J. Pickardt, *J. Chem. Soc. Chem. Commun.* **1993**, 623) and from arene–Bi chemistry (A. Schier, J. M. Wallis, G. Müller, H. Schmidbaur, *Angew. Chem.* **1986**, *98*, 742; *Angew. Chem. Int. Ed. Engl.* **1986**, *25*, 757) are known.

[14] C. Lambert, P. von R. Schleyer, *Angew. Chem.* **1994**, *106*, 1187–1200; *Angew. Chem. Int. Ed. Engl.* **1994**, *33*, 1129–1140.

[15] Because of the disorder of both of the Cp rings in the crystal, the C–C bond lengths determined here may be subject to an additional systematic error.

[16] S. Alexandratos, A. Streitwieser, Jr., H. F. Schaefer III, *J. Am. Chem. Soc.* **1976**, *98*, 7959–7962.

[17] For example P. Seiler, J. D. Dunitz, *Acta Crystallogr. Sect B* **1979**, *35*, 2020–2032; P. J. Fitzpatrick, Y. Le Page, J. Sedman, I. S. Butler, *Inorg. Chem.* **1981**, *20*, 2852–2861.

[18] Siemens SHELXTL PLUS: Release for Siemens R3 Crystallographic Research systems, Siemens Analytical X-Ray Instruments Inc., Madison, WI, **1989**.

[19] G. M. Sheldrick, SHELXL-93, Universität Göttingen, **1993**.

[20] E. Keller, SCHAKAL-92, Universität Freiburg, **1992**.

[21] X-ray crystal structure analysis of **7** (C$_{10}$H$_{22}$N$_4$S), $M = 230.38$, crystal dimensions $0.7 \times 0.5 \times 0.4$ mm^3; triclinic, space group $P\bar{1}$ (No. 2), $a = 770.1(2)$, $b = 793.6(2)$, $c = 1197.2(3)$ pm, $\alpha = 87.07(2)$, $\beta = 84.11(2)$, $\gamma = 63.51(2)°$, $V = 0.6514(3)$ nm^3, $Z = 2$, $\rho_{calcd} = 1.175$ Mg m^{-3}, $\mu = 0.227$ mm^{-1}. Salt **7** was measured under the same conditions as **3**. In the $\omega/2\theta$ scan 5046 reflections were collected ($2.87° < \theta < 27.56°$). After averaging 3014 independent reflections remained. The structure was solved by direct methods. The refinement calculations converged at $wR2 = 0.1465$ (refined against F^2) for all 3014 reflections and 174 variables ($R_1 = 0.0517$ for reflections with $I > 2\theta(I)$). A difference Fourier synthesis showed no residual electron density beyond +0.58 and −0.61 e Å^{-3} [20,26].

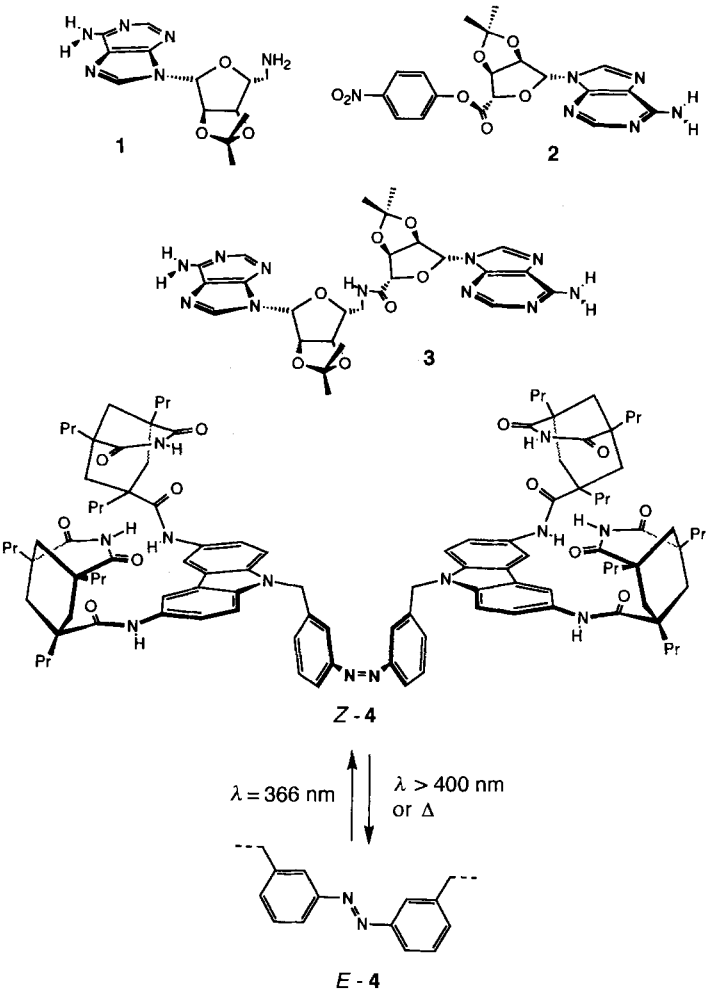
[22] G. J. Palenik, *Acta Crystallogr.* **1963**, *16*, 596–600.

[23] All the structural investigations were carried out at −110 °C.

[24] C. S. Kraihanzel, M. L. Losee, *J. Am. Chem. Soc.* **1986**, *90*, 4701–4705.

[25] L. Birkhofer, P. Richter, A. Ritter, *Chem. Ber.* **1960**, *93*, 2804–2809.

[26] Further details of the crystal structure investigations may be obtained from the Fachinformationszentrum Karlsruhe, D-76344 Eggenstein-Leopoldshafen (FRG) on quoting the depository number CSD-58690.



Light-Switchable Catalysis in Synthetic Receptors**

Frank Würthner and Julius Rebek, Jr.*

Controlling physical or chemical properties of molecules by external signals, for example light, is a popular subject of current research.[1–3] Much work is inspired by natural systems that use light as an energy source (e.g. in photosynthesis, in bacteria ion pumps) or as information to regulate biological processes (e.g. photomovement, photomorphogenesis).[2] Specifically, in the process of vision light-irradiation causes a *cis* → *trans* isomerization of retinal that induces a conformational change in the conjugated protein. The change of molecular shape initiates an enzymatic cascade that ultimately leads to a neural response.[4]

Recently, we have examined coupling reactions between aminoadenosine **1** and *p*-nitrophenyl ester **2** to give amide **3**. This reaction can be catalyzed by template molecules containing two adenine receptors linked by aliphatic or aromatic spacers.[5] The adenine receptor itself consists of two imides derived from Kemp's triacid attached to a carbazole moiety. These provide high binding affinities by chelating the purine nucleus ($K_a = 10^4$–10^5 M^{-1} in chloroform) and result in a predictable structure for the complex.[6]

Here we describe the properties of a new synthetic receptor **4** that mimics the first two steps of the vision process—the activation of a catalytic functionality by a light-induced change in molecular geometry (Fig. 1).[7]

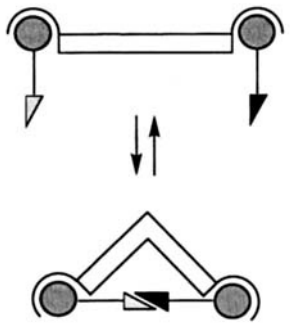
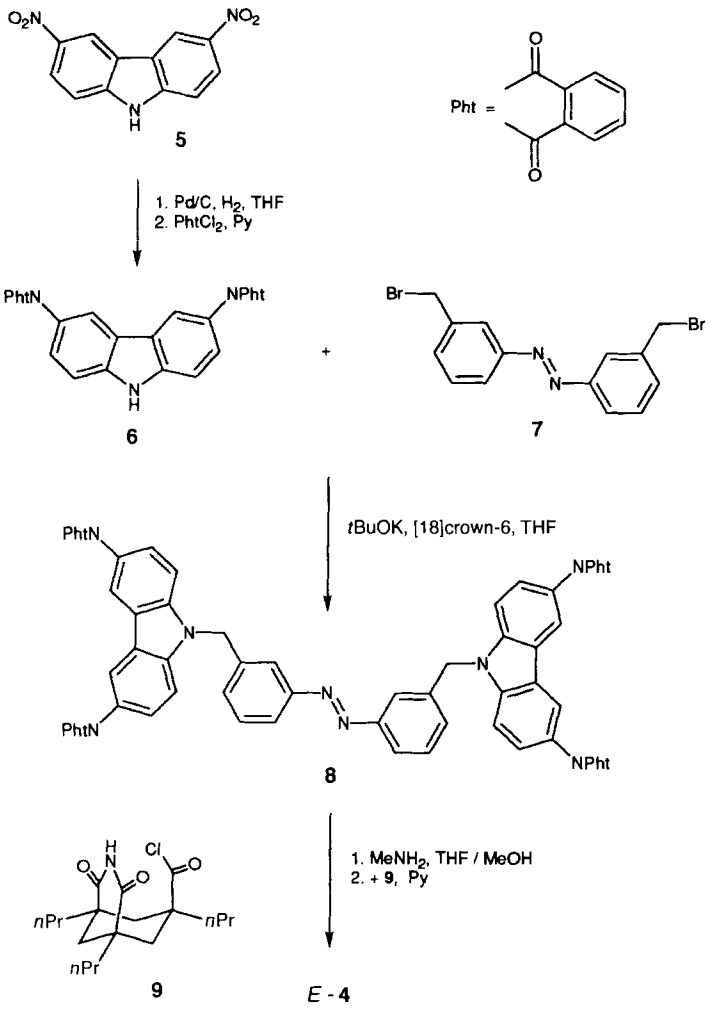


Fig. 1. Schematic representation of the switching by means of a structural change that brings the reactive groups (triangles) in close proximity.

The *trans*-azobenzene receptor **4** was prepared as shown in Scheme 1. Reduction of 3,6-dinitrocarbazole[8] with hydrogen on 10% Pd/C gave crude 3,6-diaminocarbazole, which was treated with phthaloyl dichloride to form the phthaloyl-protected diamine **6** in 80% yield. Two equivalents of **6** were treated with potassium *tert*-butoxide and alkylated with bis-3,3′-(bromomethyl)-azobenzene (**7**)[9] to give **8** in 40% yield. Deprotection of **8** with methylamine in THF/methanol and subsequent treatment of the resulting tetraamine with a slight excess of the tripropyl

[*] Prof. J. Rebek, Jr., Dr. F. Würthner
Department of Chemistry, Massachusetts Institute of Technology
Cambridge, MA 02139 (USA)
Telefax: Int. code + (617)253-7929

[**] This work was supported by the National Institutes of Health. F. W. thanks the Alexander von Humboldt Foundation for a Feodor Lynen Fellowship.



Scheme 1. Synthesis of **4**; Py = pyridine.

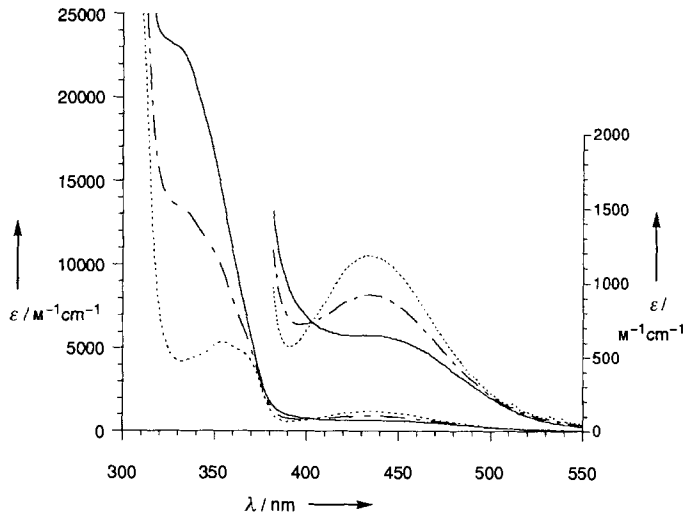


Fig. 2. UV/Vis spectra of receptor **4** in chloroform: *E*-**4** (——), *E*/*Z*-**4** in photostationary equilibrium at 366 nm (–·–·–), calculated spectrum of *Z*-**4** (·····).

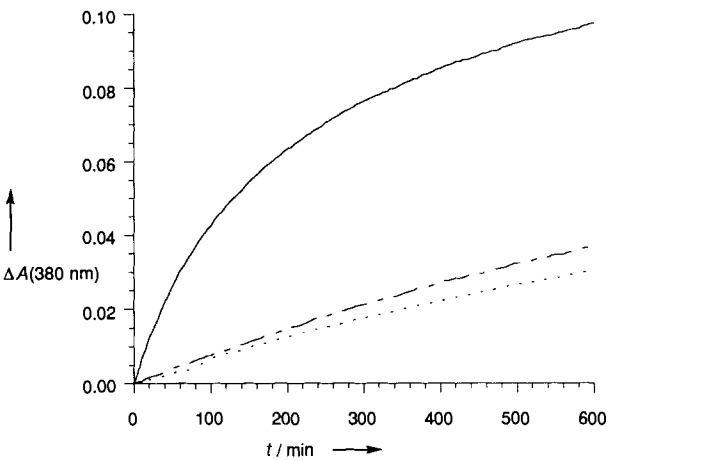


Fig. 3. Changes in absorption ΔA during the reaction of **1** and **2** in the absence of **4** (·····) and in the presence of one equivalent of *E*-**4** (–·–·–), and *E*/*Z*-**4** in its photostationary equilibrium at 366 nm (——).

imide acid chloride **9** in boiling pyridine gave receptor *E*-**4** in 55% yield.[10]

Receptor **4** showed the typical switching behavior of an azobenzene:[11] Depending on the wavelength chosen, different photostationary equilibria can be obtained which are interswitchable. Irradiation with light of wavelength of 366 nm yields a 1/1 mixture of *E* and *Z* isomer, whereas visible light causes conversion to an equilibrium with an *E*/*Z* ratio of 70/30.[12]

These mixtures exhibit high stability at room temperature in the dark, but may be converted to the pure *E* isomer at elevated temperature.[13] Compared to 3,3′-dimethylazobenzene, which exhibits a composition of 90% *Z* and 10% *E* isomer in its photostationary equilibrium at 366 nm, **4** shows a reduced range of interconversion. This may be attributed to absorption bands of the carbazole chromophore, which alter the ratio of excited *E* isomer to excited *Z* isomer by means of their absorption coefficients $\varepsilon(E)$ and $\varepsilon(Z)$. The remaining absorption band at 340–380 nm in the calculated spectrum of *Z*-**4** is characteristic for 3,6-bis(acylamino)-substituted carbazoles (Fig. 2).

The effect of receptor **4** on the rate of reaction between **1** and **2** is shown in Figure 3 and in Table 1.[14] The *E* isomer of **4** has a negligible effect on the reaction rate, but the *Z* isomer (in a 1/1 mixture with the *E* isomer) proved to be an efficient catalyst. Thus irradiation of **4** with light of wavelength 366 nm causes nearly a tenfold enhancement in the coupling rate. The addition of 9-ethyladenine or product **3** as competitive binders causes a drastic decrease of the catalytic activity of the template (Table 1).

These observations support the intermediacy of a termolecular complex composed of **1**, **2**, and **4** which is responsible for the catalytic effect. With adenine–receptor binding constants of 10^4–10^5 M^{-1}[5, 6] the amount of the reaction partners **1** and **2** in the termolecular complex [**1**·**2**·*Z*-**4**] at the beginning of the experiment is estimated to be in the range of 5–10%. These termolec-

Table 1. Effect of one equivalent of template **4** having different *E*/*Z* ratios on the initial rate of amide bond formation between **1** and **2** [14].

E/*Z* Ratio	Additives[a] (equiv)	Acceleration[b]
100/0	-	1.2
70/30	-	6.3
50/50	-	10.5
50/50	**3** (1)	1.7
50/50	9-EA (10)	1.9

[a] Competitive inhibitors; 9-EA = 9-ethyladenine. [b] Increase of the initial rate compared to that of the uncatalyzed reaction ($k = 1.5 \times 10^{-8}$ M min^{-1} [5]). All experiments were performed at lease twice. The statistical errors are <10%.

ular complexes produce high effective molarities which may result in fast reactions if the geometry of the supramolecular assembly is favorable and brings the two substrates close together. Both space-filling models and calculations (MacroModel) indicate several conformations for the termolecular complex [**1**·**2**·*Z*-**4**] in which the reactive groups of **1** and **2** are in close proximity, leading to a tetrahedral reaction intermediate that is tightly bound. For the more extended *E* isomer, however, reactive conformations are hardly accessible without energetically unfavorable distortions of the termolecular complex.[15] Hence, the geometrical isomerization of template **4** induced by light allows the control of its catalytic activity.

In summary, the system provides an example of photocontrolled template catalysis. The performance of this system mimics the integration of photoresponsive and catalytic functions in biological systems like rhodopsin, the natural phototrigger in the vision process.

Received: September 16, 1994 [Z 7323 IE]
German version: *Angew. Chem.* **1995**, *107*, 503

Keywords: isomerizations · photochemistry · template syntheses

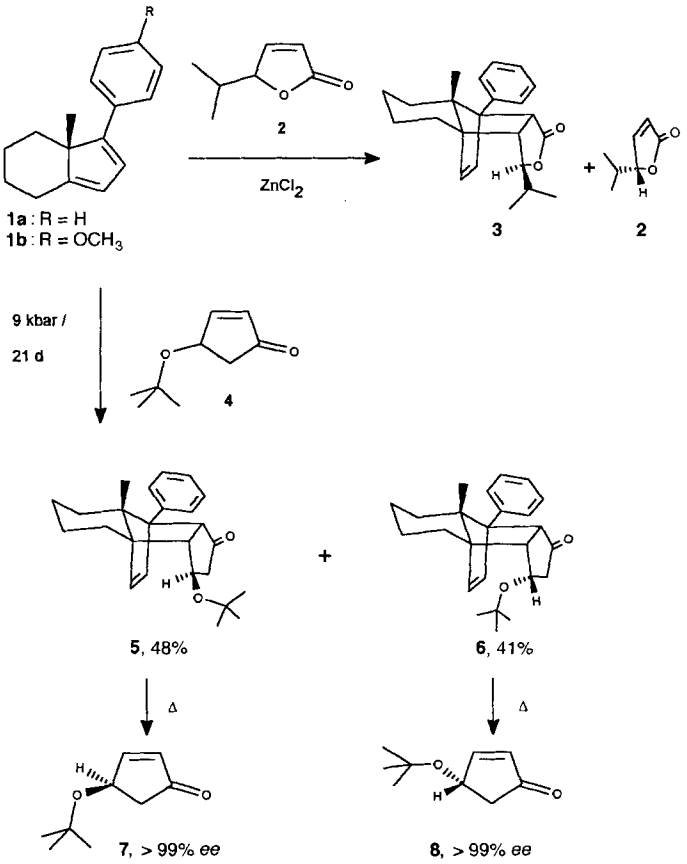
[1] *Photochromism, Molecules and Systems* (Eds.: H. Dürr, H. Bouas-Laurent), Elsevier, Amsterdam, **1990**.
[2] I. Willner, B. Willner in *Bioorganic Photochemistry, Vol. 2: Biological Applications of Photochemical Switches* (Ed.: H. Morrison), Wiley, New York, **1993**, pp. 1–110.
[3] a) S. Shinkai, O. Manabe, *Top. Curr. Chem.* **1984**, *121*, 67–104, and references therein; b) K. H. Neumann, F. Vögtle, *J. Chem. Soc. Chem. Commun.* **1988**, 520–522; c) H.-W. Losensky, H. Spelthann, A. Ehlen, F. Vögtle, J. Bargon, *Angew. Chem.* **1988**, *100*, 1225–1227; *Angew. Chem. Int. Ed. Engl.* **1988**, *31*, 1189–1191; d) I. Cabrera, A. Dittrich, H. Ringsdorf, *ibid.* **1991**, *103*, 106–108 and **1991**, *30*, 76–78; e) I. Willner, S. Marx, Y. Eichen, *ibid.* **1992**, *104*, 1255–1257 and **1992**, *31*, 1243–1244; f) I. Willner, S. Rubin, J. Wonner, F. Effenberger, P. Bäuerle, *J. Am. Chem. Soc.* **1992**, *114*, 3150–3151; g) S. L. Gilat, S. H. Kawai, J.-M. Lehn, *J. Chem. Soc. Chem. Commun.* **1993**, 1439–1442; h) T. Hohsaka, K. Kawashima, M. Sisido, *J. Am. Chem. Soc.* **1994**, *116*, 413–414; i) M. Lion-Dagan, E. Katz, I. Willner, *ibid.* **1994**, *116*, 7913–7914.
[4] a) L. Stryer, *Annu. Rev. Neurosci.* **1986**, *9*, 87–119; b) P. A. Liebman, K. R. Parker, E. A. Dratz, *Ann. Rev. Physiol.* **1987**, *49*, 765–791; c) F. Siebert in ref. [1], pp. 756–792.
[5] a) R. J. Pieters, I. Huc, J. Rebek, Jr., *Angew. Chem.* **1994**, *106*, 1667–1669; *Angew. Chem. Int. Ed. Engl.* **1994**, *33*, 1579–1581; b) *Tetrahedron*, in press; c) I. Huc, R. J. Pieters, J. Rebek, Jr., *J. Am. Chem. Soc.*, submitted.
[6] a) M. M. Conn, G. Deslongchamps, J. de Mendoza, J. Rebek, Jr., *J. Am. Chem. Soc.* **1993**, *115*, 3448–3557; b) R. J. Pieters, J. Rebek, Jr., *Recl. Trav. Chim. Pays-Bas*, **1993**, *112*, 330–334.
[7] Azobenzene was chosen as photoresponsive chromophore because of its pronounced geometrical change upon isomerization. For structural properties of *E* and *Z* azobenzenes see R. Allmann in *The Chemistry of the Hydrazo, Azo and Azoxy groups, Part 1* (Ed.: S. Patai), Wiley, New York, **1975**, pp. 23–52.
[8] H. M. Grotta, C. J. Riggle, A. E. Bearse, *J. Org. Chem.* **1964**, *29*, 2474–2476.
[9] E. Barles, N. H. Wassermann, B. F. Erlanger, *Proc. Nat. Acad. Sci. USA* **1971**, *68*, 1820–1823.
[10] To obtain pure *E*-**4**, the last step of the reaction and the chromatographic purification were performed under exclusion of light. All new compounds were characterized by ^{1}H NMR spectroscopy (300 MHz) and high-resolution mass spectrometry.
[11] a) H. Rau, *Angew. Chem.* **1973**, *85*, 248–258; *Angew. Chem. Int. Ed. Engl.* **1973**, *12*, 224–235; b) H. Rau in ref. [1], pp. 165–192; c) J. Griffiths, *Chem. Soc. Rev.* **1972**, *1*, 481–493.
[12] Irradiation at 366 nm was performed with a 4 W UV lamp. At a concentration of 0.05 mM **4**, the photostationary equilibrium was obtained after about 5 min. The *E*/*Z* ratio was determined by ^{1}H NMR spectroscopy (300 MHz).
[13] The rate constant of the thermal reisomerization at 25 °C in chloroform is less than 3×10^{-5} min^{-1}. Therefore absorption changes due to $Z \rightarrow E$ interconversion were negligible under the experimental conditions of our catalysis investigations.
[14] The experimental conditions are the same as those described in ref. [5]: c(**1**) = c(**2**) = 0.05 mM, c(Et_3N) = 4 mM at 25 °C in chloroform. Under these conditions hydrolysis of **2** is negligible and the reaction can be monitored spectrophotometrically at 380 or 390 nm following the release of *p*-nitrophenol.
[15] The slight accelerating factor may be due to a small catalytic effect of the template on the reactivity of the *p*-nitrophenyl ester **2**.

Discrimination between Enantiotopic Groups in a Diels–Alder Reaction**

Peter G. Jones, Hilmar Weinmann, Ekkehard Winterfeldt*

Dedicated to Professor H. M. R. Hoffmann on the occasion of his 60th birthday

While studying the totally regioselective cycloadditions of enantiomerically pure cyclopentadienes of type **1**,[1] we observed a marked degree of chiral recognition when alkyl-substituted 2π electron systems such as **2**, **4**, and **9** were used as dienophiles. In the case of **2** and **9**, only the (*R*) enantiomer was incorporated into the adduct (see **3** and **10**); the (*S*) enantiomer was recovered with high enantiomeric purity (>98% *ee*) (Schemes 1 and 2).[2, 3]

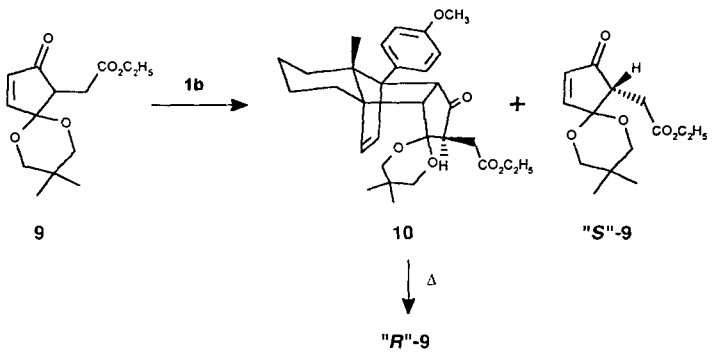


Scheme 1.

These results show clearly that the oxygen atom is less sterically demanding than a CH_2 group in the addition reaction (see **4**), although one would otherwise have expected electronic repulsion between the π electrons of the double bond and the lone

[*] Prof. Dr. E. Winterfeldt, Dipl.-Chem. H. Weinmann
Institut für Organische Chemie der Universität
Schneiderberg 1B, D-30167 Hannover (Germany)
Telefax: Int. code + (511)762-3011
Prof. Dr. P. G. Jones
Institut für Anorganische und Analytische Chemie
der Technischen Universität Braunschweig (Germany)

[**] This work was supported by the Fonds der Chemischen Industrie. H. W. thanks the Fonds der Chemischen Industrie for a Kekulé stipendium.



Scheme 2.

pairs of the oxygen. Following the assumption that the reaction represents a general and reliable technique for discriminating between the faces of a molecule, we chose the spirolactone **11** as a promising dienophile for the following reasons: firstly, it is easily prepared in large quantities;[4] secondly, based on the above considerations we expected regioselective and facially selective cycloadditions with differentiation between two enantiotopic groups, leading to the Diels–Alder adduct **12** (Scheme 3); finally, a diastereoselective epoxidation and subsequent retro-Diels–Alder reaction should afford the spirolactone **14**, which displays structural analogies to the manumycin antibiotics.[5]

At this point we should stress that this differentiation between enantiotopic groups allows the entire prochiral starting material to be converted to a single enantiomer in a predictable way. Additionally, since *ent*-**1** is also available, both enantiomers of spirolactone **14** and its derivatives are available for studying the relationship between absolute configuration and biological activity. It may be mentioned in passing that the current results also contribute to the discussion as to the "size" of a lone pair.[6] After much controversy it seems that arguments in favor of such steric requirements should be reinterpreted in terms of solvation effects, a phenomenon that may safely be excluded in our case.

We were indeed able to demonstrate that **11** reacts with **1b** to form a single cycloadduct in high yield (92%). If one is guided by a recent review article concerning the discrimination between enantiotopic groups,[7] this is the first such example from the area of cycloadditions.

Although the configuration of **12** had at this stage not been rigorously demonstrated despite complete spectroscopic data, we convinced ourselves of the perfect diastereoselectivity of the epoxidation providing **13** and of the release of the epoxylactone **14** (for which biological activity was unambiguously demonstrated[8]) by flash vacuum pyrolysis.

With respect to the question of electronic repulsion, we have also studied the cycloaddition of the spiroether **15**[4] (Scheme 3) and again obtained a single cycloadduct, although the electron density at the ether oxygen of this compound should be higher. The spectroscopic data, including nuclear Overhauser effect (NOE) measurements, again failed to provide completely unambiguous proof of the configurations, and although we were able to reduce selectively the double bond of the unsaturated ketone by using a variant of the ultrasound-promoted Luche reduction,[9] the spectroscopic data of compound **17** still left doubt as to the absolute configuration.

Since we were interested in configuration–activity studies, we had already prepared the adducts *ent*-**12** and *ent*-**17** from the (*R*)-**1**; this series provided crystals of compounds *ent*-**12** and *ent*-**17** suitable for X-ray structure analyses. The structure analyses were carried out at low temperature because of the conformational flexibility of the five-membered spiro rings,[10] and indeed provided the final structural proof (Fig. 1).

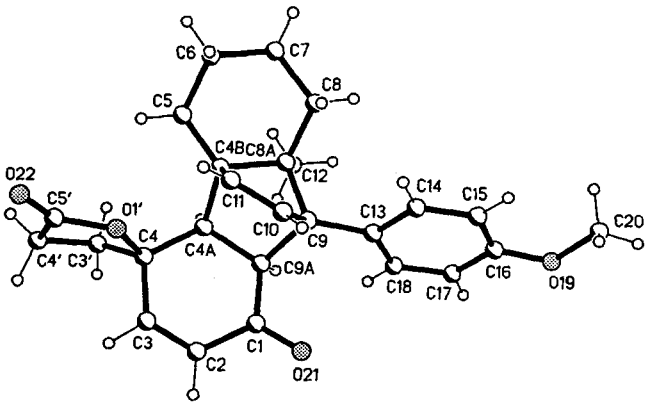
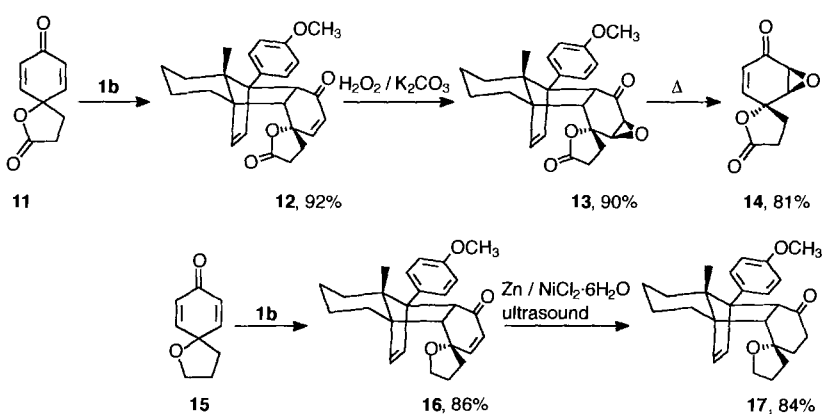


Fig. 1. Structure of the spirolactone adduct *ent*-**12** in the crystal.

Experimental Procedure

Spirolactone adduct **12**: A solution of 240 mg (1 mmol) of diene **1b** and 164 mg (1 mmol) of spirolactone **11** in 0.4 mL of freshly distilled dichlormethane was subjected to a pressure of 6.5 kbar in a Teflon tube for 14 d at 20 °C. After removal of solvent and purification by column chromatography on silica, 372 mg (0.92 mmol, 92%) of a white solid was obtained (m.p. 157 °C). $[\alpha]_D^{20} = -192.8°$ ($c = 1$ in $CHCl_3$); UV/Vis (CH_3OH): $\lambda_{max} = 225$ nm; IR (KBr): $\nu = 2925$ (m), 2862 (w), 1779 (vs), 1669 (s), 1516 (s), 1291 (m), 1177 (s), 1042 (w), 910 (w), 825 (w) cm^{-1}; ^1H NMR (200 MHz, $CDCl_3$): $\delta = 0.47$ (bd, $^3J(H,H) = 16$ Hz, 1H), 0.82 (s, 3H), 1.10–2.85 (m, 12H), 3.8 (s, 3H), 3.84 (d, $^3J(H,H) = 10$ Hz, 1H), 5.82 (d, $^3J(H,H) = 14$ Hz, 1H), 5.87 (d, $^3J(H,H) = 7.5$ Hz, 1H), 6.12 (d, $^3J(H,H) = 7.5$ Hz, 1H), 6.54 (dd, $^3J(H,H) = 14$ Hz, $^3J(H,H) = 1$ Hz, 1H), 6.88 (d, $^3J(H,H) = 11$ Hz, 2H), 7.31 (d, $^3J(H,H) = 11$ Hz, 2H); ^{13}C NMR (50 MHz, $CDCl_3$): $\delta = 15.2$, 21.0, 23.8, 27.16, 27.2, 22.8, 38.8, 49.4, 50.1, 55.1, 61.5, 62.3, 71.8, 84.2, 113.1, 128.4, 129.1, 130.8, 136.2, 138.4, 149.1, 158.4, 175.8, 198.1; MS (130 °C): *m/z* (%): 405 (1) $[M^+ + 1]$, 404 (3) $[M^+]$, 279 (1), 240 (30), 225 (11), 197 (9), 164 (39), 149 (9), 136 (17), 122 (34), 107 (21), 91 (100), 82 (23), 73 (37); High-resolution MS ($C_{26}H_{28}O_4$): calcd 404.1988, found 404.1999.

Spiroether adduct **16**: A solution of 240 mg (1 mmol) of diene **1b** and 150 mg (1 mmol) of spiroether **15** was treated as above, to yield 336 mg (0.86 mmol, 86%) of a white foam. $[\alpha]_D^{20} = -133.1°$ ($c = 1$ in $CHCl_3$); UV/Vis (CH_3OH): $\lambda_{max} = 226$ nm; IR (KBr): $\nu = 2920$ (m), 2861 (w), 1666 (s), 1515 (s), 1250 (s), 1181 (m), 1034 (m), 824 (w), 752 (w) cm^{-1}; ^1H NMR (200 MHz, $CDCl_3$): $\delta = 0.44$ (bd, $^3J(H,H) = 14$ Hz, 1H), 0.80 (s, 3H), 1.10–



Scheme 3.

 © VCH Verlagsgesellschaft mbH, D-69451 Weinheim, 1995 0570-0833/95/0404-0449 $ 10.00+.25/0

1.45 (m, 5H), 1.7–2.1 (m, 5H), 2.35 (dd, ^3J(H,H) = 9 Hz, ^3J(H,H) = 3 Hz, 1H), 2.52 (d, ^3J(H,H) = 9 Hz, 1H), 3.73 (d, ^3J(H,H) = 9 Hz, 1H), 3.8–3.9 (m, 4H), 4.0 (m, 1H), 5.72 (d, ^3J(H,H) = 10 Hz, 1H), 5.8 (d, ^3J(H,H) = 6 Hz, 1H), 6.06 (d, ^3J(H,H) = 6 Hz, 1H), 6.47 (dd, ^3J(H,H) = 10 Hz, ^3J(H,H) = 1 Hz, 1H), 6.88 (d, ^3J(H,H) = 9 Hz, 2H), 7.31 (d, ^3J(H,H) = 9 Hz, 2H); MS (120 °C): *m/z* (%): 391 (1) [$M^+ + 1$], 390 (3) [M^+], 241 (22), 240 (100), 225 (17), 197 (12), 165 (6), 150 (17), 121 (11), 90 (8), 83 (21), 66 (7); High-resolution MS ($C_{26}H_{30}O_3$): calcd 390.2195, found 390.2187.

Received: September 3, 1995 [Z 7289 IE]
German version: *Angew. Chem.* **1995**, *107*, 489

Keywords: asymmetric syntheses · Diels–Alder reactions

[1] E. Winterfeldt, *Chem. Rev.* **1993**, *93*, 827 - 843.
[2] M. Hansen, B. Wegener, E. Winterfeldt, *Tetrahedron: Asymmetry* **1993**, *4*, 345–350.
[3] M. Göres, E. Winterfeldt, *J. Chem. Soc. Perkin Trans. 1*, in press.
[4] Y. Tamura, T. Yakura, J. Haruta, Y. Kita, *J. Org. Chem.* **1987**, *52*, 3927–3930.
[5] F. Buzzetti, E. Gäumann, R. Hütter, W. Keller-Schierlein, L. Neipp, V. Prelog, H. Zähner, *Pharm. Acta Helv.* **1963**, *38*, 871; I. Sattler, C. Gröne, A. Zeeck, *J. Org. Chem.* **1993**, *58*, 6583–6587.
[6] E. L. Eliel, Sr. M. C. Knoeber, *J. Am. Chem. Soc.* **1966**, *88*, 5347–5349, and references therein; H. Förster, F. Vögtle, *Angew. Chem.* **1977**, *89*, 443–455; *Angew. Chem. Int. Ed. Engl.* **1977**, *16*, 429–441.
[7] M. E. Maier, *Nachr. Chem. Tech. Lab.* **1993**, *41*, 314.
[8] Dr. P. E. Hammann, Hoechst AG, Frankfurt am Main (FRG), personal communication.
[9] C. Petrier, J.-L. Luche, *Tetrahedron Lett.* **1987**, *28*, 2347–2350.
[10] X-ray structure analysis of *ent*-**12** (at −130 °C): orthorhombic, $P2_12_12_1$, a = 981.9(3), b = 1061.0(3), c = 1999.1(4) pm, Z = 4. Data collection: Stoe STADI-4 diffractometer, $Mo_{K\alpha}$ radiation, $2\theta_{max}$ = 50°, 2188 reflections. Structure solution: direct methods. Structure refinement: anisotropic on F^2 (program SHELXL-93, G. M. Sheldrick, Universität Göttingen), H Atoms with rigid methyl groups or riding model; $wR(F^2)$ = 0.145, conventional $R(F)$ = 0.061 for 273 parameters. In the five-membered spiro ring the C and O atoms could be unambiguously distinguished and all H atoms identified. The absolute configuration was *not* determined directly, but only from the known configuration of the starting material. X-ray structure analysis of *ent*-**17** (at −130 °C): isostructural to *ent*-**12**, a = 989.9(3), b = 1077.5(3), c = 1976.6(4) pm. Measurements as for *ent*-**12**. Refinement: in the spiro five-membered ring the atoms C4′, C5′ display high displacement parameters, but O1′ and C3′ could still be unambiguously distinguished. 2134 Reflections, $wR(F^2)$ = 0.131, conventional $R(F)$ = 0.052 for 264 parameters. Further details of the crystal structure investigations can be obtained from the Fachinformationszentrum Karlsruhe, D-76344 Eggenstein-Leopoldshafen (FRG), on quoting the depository numbers CSD-401277 (*ent*-**12**) and CSD-401278 (*ent*-**17**).

Discrete Crown-Shaped Te_8 Rings in Cs_3Te_{22}

William S. Sheldrick* and Michael Wachhold

The structural chemistry of the tellurium-rich tellurides has become a field of intensive research interest in recent years.[1] In analogy to the lighter Group 16 elements, sulfur and selenium, chainlike Te_n^{2-} [2] anions have been characterized, which may be considered to be derived from the infinite helices of the thermodynamically stable elemental modification.[3] However, most of the known telluride anions exhibit structures, which emphasize the propensity of the heavier element to increase its coordination number beyond two. Typical is the formation of T-shaped building units $TeTe_3^{n-}$ (e.g. in $NaTe_3$ [4] or $CsTe_4$ [5]) or square-planar building units $TeTe_4^{n-}$ (e.g. in Rb_2Te_5 [6] or Cs_2Te_5 [7]). Examples are known both for infinite one- to three-dimensional anionic structures as well as for anionic species composed only of discrete fragments.[1]

[*] Prof. Dr. W. S. Sheldrick, Dipl.-Chem. M. Wachhold
Lehrstuhl für Analytische Chemie der Universität
D-44780 Bochum (Germany)
Telefax: Int. code + (234)7094109

The synthesis of binary cesium tellurides has mainly been achieved from the elements themselves through use of high-temperature melts[5, 8] or ammonothermal reaction.[2, 6, 7] An alternative method is provided by the reduction of Cs_2TeO_3 (for Cs_2Te, Cs_2Te_3) or $Cs_2Te_2O_5$ (for Cs_2Te_2) with H_2 at temperatures between 663 and 703 K.[9]

We have recently reported the preparation of $RbTe_6$ by the reaction of Rb_2CO_3 with Te in overheated methanol at 190 °C, a reaction which is only successful in the presence of Ge.[10] $RbTe_6$ contains a higher metal-to-tellurium stoichiometric ratio than all other previously characterized alkali metal tellurides. It seems reasonable to assume that the formation of this rubidium telluride takes place by way of a surface reaction. In continuation of this previous work, we have now investigated the reaction of M_2CO_3 (M = K, Rb, Cs) with Te and As_2Te_3 under analogous conditions, which leads to the formation of tellurium-rich tellurides such as K_2Te_3 [2] and product mixtures of $RbTe_6$ [10] and Rb_2Te_5 [6] as well as Cs_3Te_{22} and $CsTe_4$ [5] in good yields (30–70%). The reaction of Cs_2CO_3 with As_2Te_3 alone in superheated methanol at 195 °C yields only the compound Cs_3Te_{22}, which exhibits a strikingly novel crystal structure.[11]

The crystal lattice of Cs_3Te_{22} (Fig. 1) contains both crown-shaped Te_8 rings and layer anions $^2_\infty[Te_4Te_{4/2}^{3-}]$. Comparison of

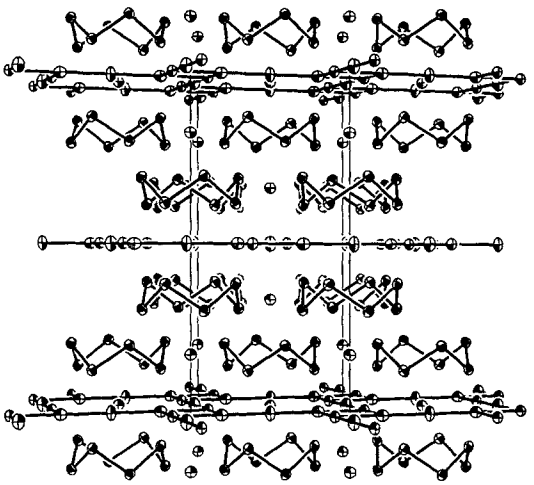


Fig. 1. Projection of the crystal structure of Cs_3Te_{22} perpendicular to [100].

the bond lengths and angles in the Te_8 rings with those of the element structures of S, Se, and Te allows the conclusion, in accordance with the Zintl–Klemm concept, that the negative charge in Cs_3Te_{22} has been fully transferred to the layer anions. For instance, the Te–Te distance of 2.8345(8) Å and the Te-Te-Te angle of 103.14(2)° in the helical chain of the thermodynamically stable elemental modification of tellurium[3] are only marginally larger than the average values of 2.80(2) Å and 100.0(16)° in the Te_8 rings of Cs_3Te_{22}. The Te_8 rings may be regarded as completing the series set up by the elemental structures X_8 of the lighter homologues S and Se.[12] Thus, the average X-X-X angle diminishes from 108.2(6)° in α-S_8 [13] through 105.7(16)° in α-Se_8 [14] to 100.0(16)° in Cs_3Te_{22}; at the same time the torsion angles X-X-X-X increase within the series, with their average values being 98.5(19)° in α-S_8, 101.3(32)° in α-Se_8 and 106.8(3)° in Cs_3Te_{22}. In contrast to the essentially undistorted crown conformation of the Te_8 rings in Cs_3Te_{22}, bicyclic structures have been observed for the known ionic species Te_8^{2-} and Te_8^{2+}. The Te_8^{2-} anions in $[K([15]crown\text{-}5)_2]_2Te_8$ contain both a four- and a five-membered ring, which are connected to one another by a

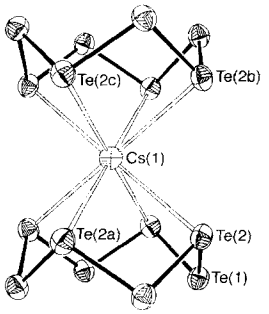


Fig. 2. Coordination of the cesium atom Cs(1) by two Te_8 rings. Bond length [Å] and angles [°]: Cs(1)-Te(2) 3.892(1); Te(2)-Cs(1)-Te(2a) 67.61(1), Te(2)-Cs(1)-Te(2b) 76.22(2), Te(1)-Cs(1)-Te(2c) 112.29(1).

central Te atom that is effectively square-planar coordinated.[15] In contrast, the structure of the Te_8^{2+} ion in $Te_8(WCl_6)_2$ is composed of two condensed five-membered rings, both of which exhibit an envelope conformation.[16] The stabilization of the neutral crown-shaped Te_8 rings[12] takes place in Cs_3Te_{22} in the coordination sphere of the cesium atom Cs(1), which is surrounded by what is effectively a cube of tellurium atoms Te(2) from two Te_8 rings (Fig. 2). It is interesting to note in this context, that Chivers et al. have recently very tentatively assigned a weak resonance at $\delta = 848$ in the ^{125}Te NMR spectrum of an S-Te melt to a Te_8 ring.[17]

The novel polyanion $^2_\infty[Te_4Te^{3-}_{4/2}]$ contains two crystallographically independent Te atoms, which exhibit different coordination geometries, namely linear and T-shaped (pseudo trigonal bipyramidal). Their mode of connection leads to the formation of Te_4 and Te_{12} squares (Fig. 3). An average Te–Te distance of 2.97 Å is observed in the comparable anion structure of $CsTe_4$,[5] which is composed of connected $TeTe_3^-$ building units. The increase in charge for the formally $TeTe_3^{2-}$ groups in Cs_3Te_{22} leads, as would be expected, to an increase in the average Te–Te bond length (3.03 Å). Derivation of the anion structure in Cs_3Te_{22} from a planar 4^4 net may be achieved by removal of 2/5 of all Te atoms.

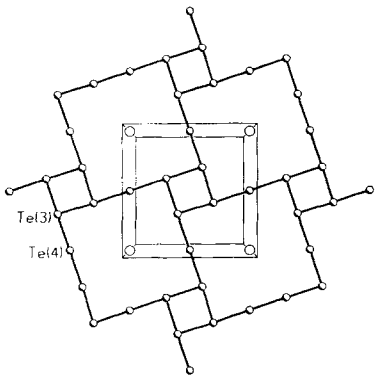


Fig. 3. Thinned 4^4 net of the layer anions $^2_\infty[Te_6^{3-}]$ with the unit cell. Bond lengths [Å] and angles [°]: Te(3)-Te(3) 3.003(2), Te(3)-Te(4) 3.077(1); Te(3)-Te(4)-Te(3) 180, Te(3)-Te(3)-Te(3) 90, Te(3)-Te(3)-Te(4) 88.53(4), 178.53(4).

The crystal structure of Cs_3Te_{22} exhibits two secondary Te(3)-Te(2) and four secondary Te(4)-Te(2) bonds of lengths 3.424(1) and 3.444(1) Å, respectively, between layer anions and Te_8 rings. In addition to the atom Te(3) of the Te layer ($4 \times 4.129(1)$ Å) both of the ring atoms Te(1) ($4 \times 4.096(1)$ Å, $4 \times 4.330(1)$ Å) and Te(2) ($4 \times 4.152(1)$ Å) are involved in the coordination of Cs(2) atom (see Fig. 1).

Two partial structures which embody contrasting aspects of tellurium chemistry are thus united by means of cationic stabilization in the crystal structure of Cs_3Te_{22}. Whereas the crown-shaped Te_8 rings are similar to the X_8 units of the lighter homologues S and Se, the layer anions $^2_\infty[Te_6^{3-}]$ may be derived from the α-Po structure of the heavier homologue.[1, 18]

Experimental Procedure

Cs_2CO_3 (0.157 g, 0.48 mmol) and As_2Te_3 (0.518 g, 0.97 mmol) in methanol (0.5 mL) were heated to 195 °C in a Carius tube under argon (heating rate 10 °C h^{-1}). After 2 d the tube was cooled to room temperature at a rate of 3 °C h^{-1} to afford gray crystals of Cs_3Te_{22} with metallic appearance (70% yield) as precipitate. The reflections of an X-ray powder diagram of the product could be indexed for Cs_3Te_{22}.

Received: September 20, 1994 [Z 7331 IE]
German version: *Angew. Chem.* **1995**, *107*, 490

Keywords: alkali metal compounds · solid-state structures · tellurium compounds

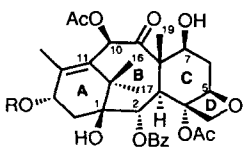
[1] P. Böttcher, *Angew. Chem.* **1988**, *100*, 781; *Angew. Chem. Int. Ed. Engl.* **1988**, *27*, 759.
[2] P. Böttcher, *J. Less-Common Met.* **1980**, *70*, 263; B. Eisenmann, H. Schäfer, *Angew. Chem.* **1978**, *90*, 731; *Angew. Chem. Int. Ed. Engl.* **1978**, *17*, 684; D. Fenske, G. Baum, H. Wolkers, B. Schreiner, F. Weller, K. Dehnicke, *Z. Anorg. Allg. Chem.* **1993**, *615*, 489.
[3] P. Cherin, P. Unger, *Acta Crystallogr.* **1967**, *23*, 670; C. Adenis, V. Langer, O. Lindqvist, *ibid. Sect. C* **1989**, *45*, 941.
[4] P. Böttcher, R. Keller, *Z. Anorg. Allg. Chem.* **1986**, *542*, 144.
[5] P. Böttcher, U. Kretschmann, *Z. Anorg. Allg. Chem.* **1985**, *523*, 145.
[6] P. Böttcher, U. Kretschmann, *J. Less-Common Met.* **1983**, *95*, 81.
[7] P. Böttcher, U. Kretschmann, *Z. Anorg. Allg. Chem.* **1982**, *491*, 39.
[8] K. A. Chuntonov, A. N. Kuznetsov, V. M. Federov, S. P. Yatsenko, *Izv. Akad. Nauk. SSSR. Neorg. Mater.* **1982**, *18*, 1108; M. G. Adamson, J. E. Leighty, *J. Nucl. Mater.* **1983**, *114*, 327; G. Prins, E. H. P. Cordfunke, *J. Less-Common Met.* **1984**, *104*, L1.
[9] J. W. Hobbs, R. J. Pulham, *J. Chem. Res. Synop.* **1994**, 68; *ibid.* **1994**, 156.
[10] W. S. Sheldrick, B. Schaaf, *Z. Naturforsch. B* **1994**, *49*, 993.
[11] Crystal structure analysis of Cs_3Te_{22}: tetragonal, $I4/m$, $a = b = 9.586(1)$, $c = 20.537(4)$ Å, $V = 1887.2(5)$ Å^3, $\rho_{calcd} = 5.64$ g cm^{-3}, $F(000) = 2618$. 1421 independent reflections were collected on a Siemens-P4-Diffractometer at $T = 295$ K using $Mo_{K\alpha}$ radiation (ω scan, $2\theta_{max} = 60°$, semiempirical absorption correction using ψ scans). After solution using direct methods [19] the structure was refined with SHELXL-93 [19] against $|F^2|$ to $R = 0.051$ [for 1146 reflections with $I \geq 2\sigma(I)$] and $wR2 = 0.128$ for 35 parameters. Further details of the crystal structure investigation may be obtained from Fachinformationszentrum Karlsruhe, D-76344 Eggenstein-Leopoldshafen (Germany), on quoting the depository number CSD-58655.
[12] R. S. Laitinen, P. Pekonen, R. J. Suontamo, *Coord. Chem. Rev.* **1994**, *130*, 1.
[13] S. J. Rettig, J. Trotter, *Acta Crystallogr. Sect. C* **1987**, 2260.
[14] P. Cherin, P. Unger, *Acta Crystallogr. Sect. B* **1972**, 313.
[15] B. Schreiner, K. Dehnicke, K. Maczek, D. Fenske, *Z. Anorg. Allg. Chem.* **1993**, 619, 1414.
[16] J. Beck, *Angew. Chem.* **1990**, *102*, 301; *Angew. Chem. Int. Ed. Engl.* **1990**, *29*, 293; *ibid.* **1994**, *106*, 172 and **1994**, *33*, 163.
[17] T. Chivers, R. S. Laitinen, K. J. Schmidt, J. Taavitsainen, *Inorg. Chem.* **1993**, *32*, 337.
[18] R. J. Desardo, R. C. Lange, *J. Inorg. Nucl. Chem.* **1966**, *28*, 1837.
[19] G. M. Sheldrick, SHELXS-86, A Program for StructureDetermination, Göttingen, **1986**; SHELXL-93, A Program for Structure Refinement, Göttingen, **1993**.

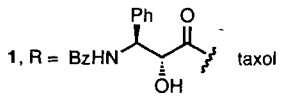
 © VCH Verlagsgesellschaft mbH, D-69451 Weinheim, 1995 0570-0833/95/0404-0451 $ 10.00+.25/0

A Novel Intramolecular Heck Reaction: Synthesis of a Cholesterol–Baccatin III Hybrid**

John J. Masters,* David K. Jung,
Samuel J. Danishefsky,* Lawrence B. Snyder,
Tae Kyo Park, Richard C. A. Isaacs, Cheryl A.
Alaimo, and Wendy B. Young

Taxol (**1**) is already playing a useful role in cancer chemotherapy.[1] While the ultimate limits of its applicability awaits precise definition, taxol or related compounds will clearly be part of the arsenal of clinically useful agents in the treatment of cancer. From the standpoint of chemistry, this series commands special attention.[2] It was never probable, nor is it now likely, that total synthesis would provide a useful route to the core structure, baccatin III (**2**) or to taxol (**1**) itself. Apparently no combination of starting materials is close enough in structure to baccatin III, in all its detail, to allow for formation of this natural product in anything but a multistep synthesis. Accordingly, total syntheses are not likely to be competitive with phytochemical routes.

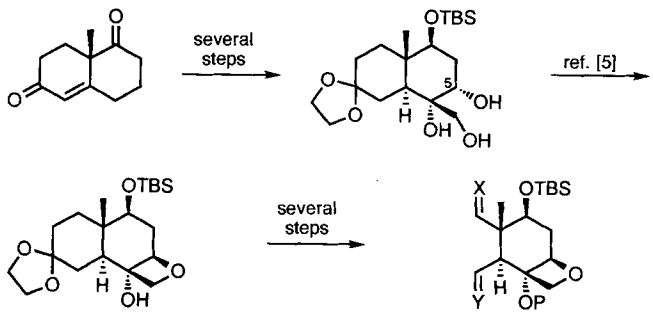




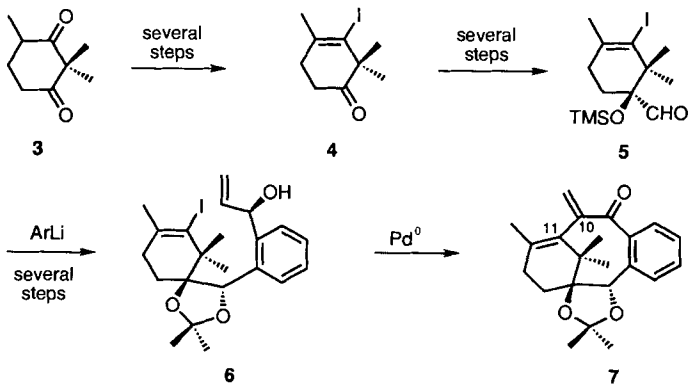
Nonetheless, the intellectual and experimental challenges associated with a total synthesis of baccatin III and taxol, only recently achieved in stunning and concurrent fashion by groups headed by Holton[3] and Nicolaou,[4] properly hold a special fascination for chemists. The baccatin III problem has already served to stimulate new conceptual and methodological advances in organic synthesis.[2] Moreover, continued interest in this field is fueled by the reasonable hope that synthetic mastery over the taxol problem will lead to simplified new structures which could not have been derived from baccatin III itself.

Our program in the taxol area has been directed along several lines. Our laboratory developed an enantiospecific route (by catalytic means) to the CD substructure of baccatin, with handles for attachment to ring A substructures.[5, 6] In these efforts, closure of the oxetane ring by inversion at C-5 in a fully functionalized system was demonstrated for the first time (Scheme 1). The total syntheses of Nicolaou et al. and Holton et al. both used this strategy.[7]

The starting material for A-ring constructs was the readily available 2,2,4-trimethylcyclohexane-1,3-dione (**3**).[8] Among the compounds obtained from **3** were the vinyl iodide **4**[9] and thence aldehyde **5**. Compound **6**, derived from **5**, was amenable to intramolecular Heck vinylation reactions thereby producing products of type **7** (Scheme 2).[10]



Scheme 1: TBS = *tert*-butyldimethylsilyl.



Scheme 2. Ar = aryl.

At this juncture, it was necessary to verify the applicability of the intramolecular Heck reaction to an aliphatic C ring based construct containing the C-19 methyl group. It is clear from the study of taxol literature[2] that methods successful in simpler structures may fail in more complex models in which closure triggers strong repulsion between the methyl groups at C-17 and C-19. In the research described here, we probed the applicability of a C-10/C-11 closure by an intramolecular Heck reaction, even in the context of such an abutment.

To answer this fascinating question, however, it was necessary to break new ground relative to the synthetic approach that led to substrates such as **6**. We focused on reaching a generic target of type **15**. It is instructive to consider the difficulties that had to be overcome in pursuing such a program (see Scheme 3).

The prospects of entering the required manifold by coupling a stereochemically defined secondary sp^3-type C-3 nucleophile such as **8** with an aldehyde of type **5** seemed particularly bleak. Alternatively, delivery of a sophisticated C-2 based nucleophile such as **9** to the hindered C-1 based ketone **4**, showed no promise based on early reconnaissance. Less forbidding was the possibility of adding a C-1 based vinyl nucleophile to a C-2 aldehyde. The feasibility, in principle, of such a C-1/C-2 coupling with a fully functionalized CD construct was in fact reported by our laboratory (**10** + **11** → **12**).[10] The use of a non-oxetane containing aldehyde in this context was a key element in Nicolaou's total synthesis of taxol by formation of the C-9/C-10 bond.[4, 11] Since we were now focusing on a C-10/C-11 bond closure, strict adaptation of our earlier route would require excision of the one carbon fragment mounted at C-11 (cf. $TBSOCH_2$ in **12**).

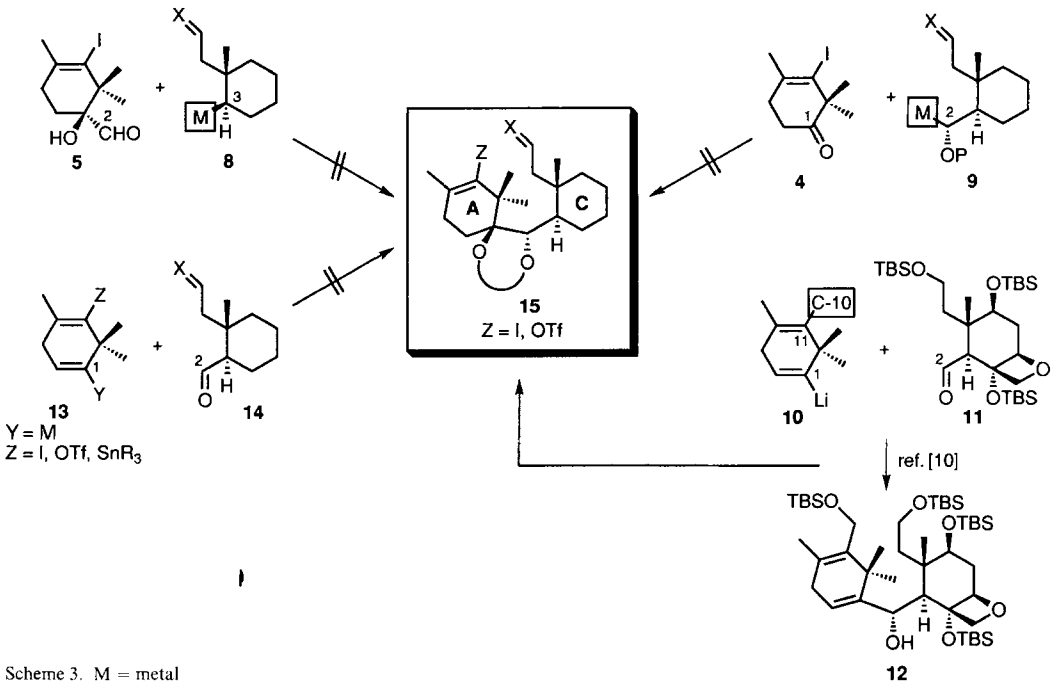
The use of A-ring constructs such as **13**, which simultaneously include the C-1 sp^2 nucleophile and the C-12/C-11 double bond with functionality suitable for a Heck reaction or a related closure, was a priori plausible. In fact, we explored several permutations summarized as **13** + **14**, wherein **14** was derived by

[*] Prof. S. J. Danishefsky,[+] Dr. J. J. Masters, Dr. D. K. Jung, Dr. L. B. Snyder, Dr. T. K. Park, Dr. R. C. A. Isaacs, Dr. C. A. Alaimo, Dr. W. B. Young
Memorial Sloan-Kettering Cancer Center
1275 York Avenue, New York, NY 10021 (USA)
Telefax: Int. code + (212)772-8691

[+] Alternative address:
Department of Chemistry, Havemeyer Hall
Columbia University, New York, NY 10027 (USA)
Telefax: Int. code + (212)854-7142

[**] This research was supported by National Institutes of Health (NIH, grant no. AI 16943). A Damon Runyon-Walter Winchell Cancer Fund Postdoctoral Fellowship to J. J. M. and an American Cancer Society Postdoctoral Fellowship to W. B. Y. are gratefully acknowledged. We thank Dr. G. Sukenick (Memorial Sloan-Kettering Cancer Center) for mass spectral analyses.

 © VCH Verlagsgesellschaft mbH, D-69451 Weinheim, 1995 0570-0833/95/0404-0452 $ 10.00+.25/0

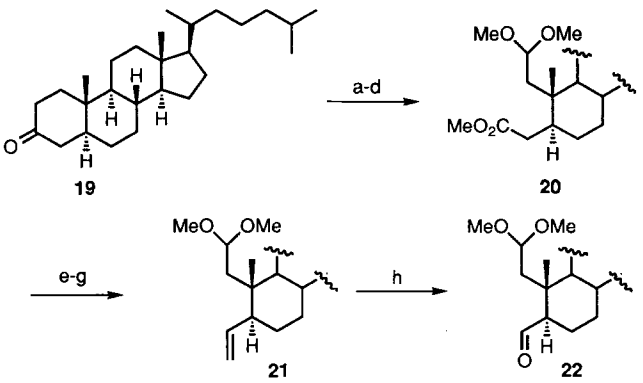


Scheme 3. M = metal

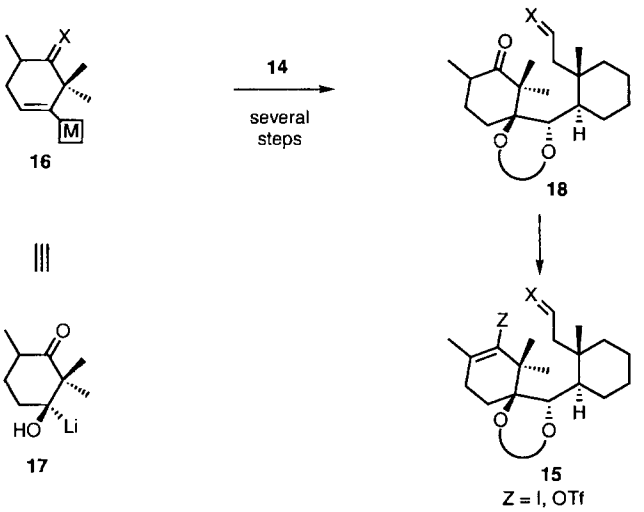
degradation of suitable cyclic precursors. This investigation was set aside when we were unable to generate a viable version of **13**.

Accordingly, we were obliged to examine the possibility of introducing the "pre-Heck functionality" at C-11 *after* the coupling of C-1 and C-2 had been achieved (cf. **15** in Scheme 4). Unveiling of the implement at C-11 for the Heck reaction would occur at a late stage, perhaps from a ketone such as **18**. Also, it would be necessary to achieve formal hydration of the C-14/C-1 double bond and, probably, to constrain the oxygen atoms at C-1 and C-2 in a cyclic arrangement, which would be conducive to a successful C-10/C-11 closure. Viewed in these terms, the desired A-ring unit would be based on the C-1 sp^2 nucleophile **16** (X unspecified), which would serve as a functional equivalent to the hypothetical nucleophile **17**.

5α-Cholestan-3-one (**19**) served as a suitable saturated C-ring substrate to test these issues (Scheme 5).[12] The commercially available steroid was degraded to acetal ester **20**. The C-2 ester was converted to the vinyl compound **21** by reduction followed by the standard Grieco-type protocol.[13] Ozonolysis of **21** afforded the desired C-2 aldehyde acetal **22**.



Scheme 5. a) $NaN(SiMe_3)_2$, THF, TBSCl, −78 °C, 92%; b) dimethyldioxirane, CH_2Cl_2, 0 °C, then Amberlyst 15, 88%; c) $Pb(OAc)_4$, 1/1 MeOH/C_6H_6, 0 °C, quant.; d) MeOH, pyridinium *p*-toluenesulfonate (PPTS), 70 °C, 89%; e) $LiAlH_4$, THF, 0 °C, quant.; f) *o*-$NO_2C_6H_4SeCN$, Bu_3P, THF, room temperature (RT), 86%; g) H_2O_2, THF, RT, 90%; h) O_3, CH_2Cl_2, −78 °C, then PPh_3, 91%.

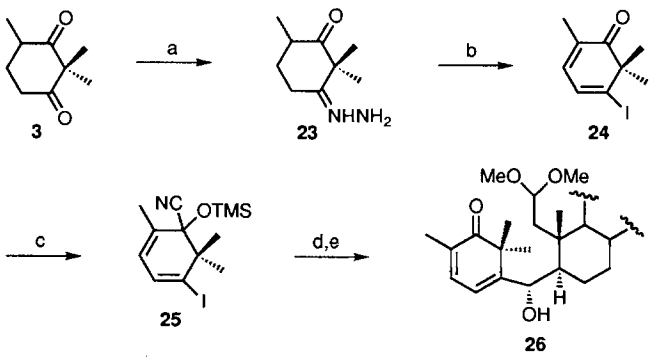


Scheme 4.

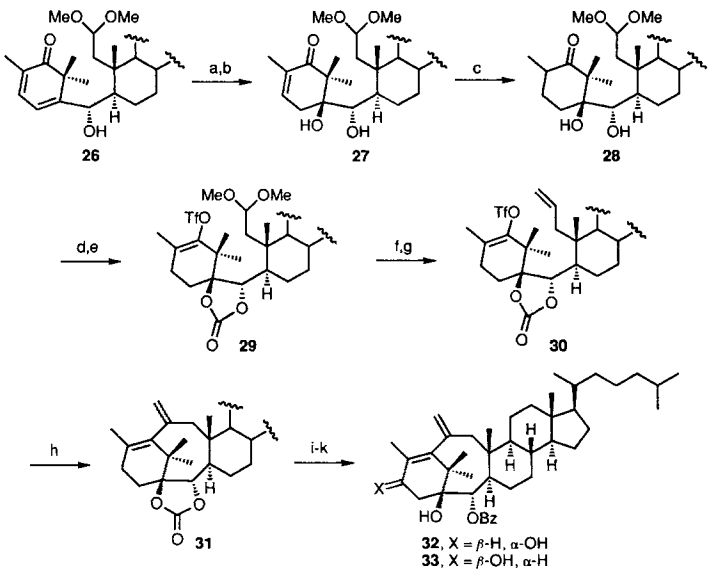
The starting material for a compound analogous to **16** was iododiene **25**, which was available from **3** by a three-step sequence (Scheme 6). The first step was formation of monohydrazone **23** at the less hindered C-1 position. Treatment of **23** with iodine and diazobicyclononane (DBN) in refluxing THF gave iododienone **24**, which was converted to **25** by cyanation. Remarkably, it was possible to lithiate vinyl iodide **25**. The lithium compound thus produced reacted with aldehyde **22** to afford, after decyanation, dienone **26** as a single stereoisomer at C-2.[14]

Compound **26** could be transformed into a desired masked precursor of type **15** for the Heck reaction (Scheme 7). A key reaction was the epoxidation of **26** mediated by vanadyl acetylacetonate to give a single β-epoxide.[11, 15] Exposure of this

 © VCH Verlagsgesellschaft mbH, D-69451 Weinheim, 1995 0570-0833/95/0404-0453 $ 10.00+.25/0



Scheme 6. a) H_2NNH_2, Et_3N, EtOH, RT, 71%; b) I_2, DBN, THF, reflux, 40%; c) TMSCN, KCN (cat), [18]crown-6 (cat), CH_2Cl_2, RT, 97%; d) *t*BuLi, THF, −78 °C, then **22**, 90%; e) nBu_4NF, THF, 0 °C, quant.



Scheme 7. a) $VO(acac)_2$, *t*BuOOH, CH_2Cl_2, 0 °C, 91%; b) H_2, 10% Pd/C, EtOH, 0 °C, 90%; c) b, then HOAc, 0 °C → RT, 56% (from epoxide); d) Cl_2CO, pyridine, CH_2Cl_2, 0 °C, quant; e) $KN(SiMe_3)_2$, $PhNTf_2$, THF, −78 °C, 90%; f) *p*TsOH, 4/1 acetone/H_2O, 75 °C, 80%; g) Ph_3PCH_3Br, *t*BuOK, THF, 0 °C, 95%; h) $[Pd(PPh_3)_4]$ (1.15 equiv), K_2CO_3, CH_3CN, 85 °C, 5 h, 50%; i) PhLi, THF, −78 °C, 75%; j) pyridinium dichromate (PDC), *t*BuOOH, C_6H_6, RT, 39%; k) $NaBH_4$, $CeCl_3$, $MeOH/CH_2Cl_2$, 0 °C, 52% **32** and 39% **33**.

enone epoxide to the action of hydrogen and 10% palladium on charcoal in ethanol led to the γ-hydroxyenone **27**. In this way the critical hydroxyl functions at C-1 and C-2 were introduced. Stabilization of the C-1 hydroxyl group was achieved by subsequent reduction of the enone. The hydroxyl groups at C-1 and C-2 in diol **28** were engaged as a cyclic carbonate.[16] The critical enol triflate linkage (see **29**) was introduced by deprotonation of the ketone by using potassium bis(trimethylsilyl)amide in the presence of *N*-phenyltrifluoromethanesulfonimide.[17] Cleavage of the acetal linkage gave rise to an aldehyde which upon methylenation gave the desired **30** in an overall yield of 16% from 5α-cholestan-3-one (**19**). The stage was now fully set for testing the intramolecular Heck reaction.

In the event, treatment of **30** with tetrakis(triphenylphosphane)palladium(0) and potassium carbonate in acetonitrile at 85 °C afforded the goal system **31** (50% yield), whose structure was verified crystallographically.[18] Opening of the carbonate linkage with phenyllithium[3, 4] afforded the C-2 benzoate which upon allylic oxidation and reduction produced the steroidal baccatin III construct **32** along with its C-13 epimer **33**.[19] The concise synthetic approach described here should allow access to other functionalized ABC baccatin III hybrid systems.

Experimental Procedure

All compounds reported displayed satisfactory ^1H NMR, IR, and mass spectra.

31: A 15 mL flask was charged with **30** (94.7 mg, 0.135 mmol), K_2CO_3 (37.0 mg, 0.270 mmol), and 4 Å molecular sieves. The mixture was taken up in 5 mL of CH_3CN and the flask placed in an 85 °C oil bath. $[(Ph_3P)_4Pd]$ (179 mg, 0.155 mmol) was added to the mixture in portions (5–10 mg) over 4.5 h, so as to maintain an ambered colored solution. Upon complete addition, the mixture was allowed to stir at 85 °C for an additional 0.5 h. The mixture was then cooled to ambient temperature, diluted with diethyl ether, filtered through a pad of Celite, and concentrated in vacuo. The residue was dissolved in diethyl ether, washed with saturated NH_4Cl (2×), and dried (K_2CO_3). Concentration in vacuo and purification of the residue by flash chromatography (SiO_2, 92/8 petroleum ether/diethyl ether) afforded 37.2 mg (50%) of **31** as a colorless solid. M.p. 204–205 °C; $[\alpha]_D = 34.0$ ($c = 0.47$; CH_2Cl_2); IR (film): $\nu = 2950, 2934, 2867, 1806, 1623, 1457, 1443, 1375, 1034\ cm^{-1}$; ^1H NMR (400 MHz, $CDCl_3$): $\delta = 5.10$ (s, 1H), 4.62 (s, 1H), 4.51 (d, 1H, $J = 5.6$ Hz), 2.81–2.70 (m, 1H), 2.45 (d, 1H, $J = 16.7$ Hz), 2.20–2.11 (m, 1H), 2.14 (d, 1H, $J = 16.5$ Hz), 2.06–1.87 (m, 4H), 1.85–1.70 (m, 3H), 1.78 (s, 3H), 1.68–1.60 (m, 1H), 1.57–1.45 (m, 3H), 1.40–0.70 (m, 16H), 1.32 (s, 3H), 1.23 (s, 3H), 0.89 (d, 3H, $J = 6.5$ Hz), 0.87 (d, 3H, $J = 6.6$ Hz), 0.86 (d, 3H, $J = 6.6$ Hz), 0.81 (s, 3H), 0.64 (s, 3H); ^{13}C NMR (75 MHz, $CDCl_3$): $\delta = 154.8, 143.6, 140.1, 134.4, 116.4, 93.6, 81.3, 56.8, 56.1, 49.4, 44.9, 43.3, 42.5, 41.5, 40.2, 39.9, 39.5, 36.1, 35.7, 35.6, 32.1, 30.1, 28.2, 28.0, 25.7, 24.1, 23.9, 23.7, 23.1, 23.0, 22.8, 22.5, 21.8, 20.5, 18.6, 18.2, 12.1$; MS ($NH_3$): calcd for $C_{37}H_{58}O_3$ (M^+) 550, found $(M+1)^+$ 551, $(M + NH_4)^+$ 568.

32-α-OH: Colorless solid; m.p. 101–102 °C; $[\alpha]_D = 8.5$ ($c = 0.20$; $CHCl_3$); IR (film): $\nu = 3662$ (br), 2931, 1711, 1277 cm^{-1}; ^1H NMR (400 MHz, $CDCl_3$): $\delta = 7.97$ (d, 2H, $J = 8.0$ Hz), 7.51–7.48 (m, 1H), 7.40–7.36 (m, 2H), 5.36 (d, 1H, $J = 5.4$ Hz), 5.04 (d, 1H, $J = 2.5$ Hz), 4.90–4.86 (m, 1H), 4.60 (d, 1H, $J = 2.6$ Hz), 2.60–2.58 (m, 1H), 2.41 (dd, 1H, $J = 10.0$, 15.1 Hz), 2.35 (s, 2H), 2.12 (dd, 1H, $J = 4.8$, 15.1 Hz), 1.98 (s, 1H), 1.93–1.90 (m, 1H), 1.88 (d, 3H, $J = 1.1$ Hz), 1.78–1.74 (m, 1H), 1.69–1.67 (m, 3H), 1.57–1.55 (m, 3H), 1.46–1.40 (m, 4H), 1.32 (s, 3H), 1.26–1.24 (m, 5H), 1.00–0.87 (m, 5H), 1.04 (s, 3H), 0.99–0.96 (m, 4H), 0.82 (d, 3H, $J = 6.2$ Hz), 0.79 (d, 3H, $J = 6.6$ Hz), 0.78 (d, 3H, $J = 6.6$ Hz), 0.76 (s, 3H), 0.53 (s, 3H). MS (NH_3) calcd for $C_{43}H_{64}O_4$ (M^+) 644, found $(M - H_2O + 1)^+$ 627.

33-β-OH: Colorless oil; $[\alpha]_D = 28.0$ ($c = 0.20$; $CHCl_3$); IR (film): $\nu = 3625$ (br), 2932, 1715, 1278 cm^{-1}; ^1H NMR (400 MHz, $CDCl_3$): $\delta = 7.97$ (d, 2H, $J = 8.0$ Hz), 7.52–7.49 (m, 1H), 7.40-7.37 (m, 2H), 5.37 (d, 1H, $J = 5.9$ Hz), 5.05 (s, 1H), 4.64 (s, 1H), 4.01–4.00 (m, 1H), 2.65 (dd, 1H, $J = 9.6$, 14.7 Hz), 2.41 (d, 1H, $J = 16.2$ Hz), 2.30 (d, 1H, $J = 16.2$ Hz), 2.10–1.98 (m, 1H), 2.01 (s, 1H), 1.95–1.91 (m, 5H), 1.72 (s, 3H), 1.64–1.21 (m, 3H), 1.47–1.43 (m, 5H), 1.31 (s, 3H), 1.28 (s, 3H), 1.24–1.22 (m, 2H), 1.10–0.89 (m, 8H), 0.89–0.82 (m, 3H) 0.82 (d, 3H, $J = 6.5$ Hz), 0.79 (d, 3H, $J = 6.5$ Hz), 0.78 (d, 3H, $J = 6.6$ Hz), 0.77 (s, 3H), 0.53 (s, 3H); MS (NH_3) calcd for $C_{43}H_{64}O_4$ (M)$^+$ 644, found $(M - H_2O + 1)^+$ 627.

Received: October 1, 1994 [Z 7372 IE]
German version: *Angew. Chem.* **1995**, *107*, 495

Keywords: baccatin III · Heck reactions · natural products synthesis · taxol

[1] For reviews, see: a) M. Rothenburg *Curr. Opin. Invest. Drugs.* **1993**, *2*, 1269; b) G. I. Georg, S. M. Ali, J. Zygmunt, L. R. Jayasinghe *Curr. Opin. Ther. Pat.* **1994**, *4*, 109; c) D. Guénard, F. Guéritte-Voegelein, P. Potier *Acc. Chem. Res.* **1993**, *26*, 160, see also ref. [2].

[2] For reviews, see: a) K. C. Nicolaou, W.-M. Dai, R. K. Guy *Angew. Chem.* **1994**, *106*, 38; *Angew. Chem. Int. Ed. Engl.* **1994**, *33*, 15; b) D. G. I. Kingston, A. A. Molinero, J. M. Rimoldi *Prog. Chem. Org. Nat. Prod.* **1993**, *61*, 1; c) C. S. Swindell *Org. Prep. Proc. Int.* **1991**, *23*, 465; d) D. G. I. Kingston *Pharmac. Ther.* **1991**, *52*, 1.

[3] R. A. Holton, C. Somoza, H.-B. Kim, F. Liang, R. J. Biediger, P. D. Boatman, M. Shindo, C. C. Smith, S. Kim, H. Nadizadeh, Y. Suzuki, C. Tao, P. Vu, S. Tang, P. Zhang, K. K. Murthi, L. N. Gentile, J. H. Liu *J. Am. Chem. Soc.* **1994**, *116*, 1597; R. A. Holton, H.-B. Kim, C. Somoza, F. Liang, R. J. Biediger, P. D. Boatman, M. Shindo, C. C. Smith, S. Kim, H. Nadizadeh, Y. Suzuki, C. Tao, P. Vu, S. Tang, P. Zhang, K. K. Murthi, L. N. Gentile, J. H. Liu *ibid.* **1994**, *116*, 1599.

[4] K. C. Nicolaou, Z. Yang, J. J. Liu, H. Ueno, P. G. Nantermet, R. K. Guy, C. F. Claiborne, J. Renaud, E. A. Couladouros, K. Paulvannan, E. J. Sorensen *Nature* **1994**, *367*, 630.

[5] T. V. Magee, W. G. Bornmann, R. C. A. Isaacs, S. J. Danishefsky *J. Org. Chem.* **1992**, *57*, 3274.

[6] M. J. Di Grandi, C. A. Coburn, R. C. A. Isaacs, S. J. Danishefsky *J. Org. Chem.* **1993**, *58*, 7728.
[7] For an oxetane synthesis on a taxicin substrate involving inversion at C-5 but without oxygenation at C-7, see: L. Ettouati, A. Ahond, C. Poupat, P. Potier *Tetrahedron* **1991**, *47*, 9823.
[8] Y. Queneau, W. J. Krol, W. G. Bornmann, S. J. Danishefsky *J. Org. Chem.* **1992**, *57*, 4043.
[9] M. J. Di Grandi, D. K. Jung, W. J. Krol, S. J. Danishefsky *J. Org. Chem.* **1993**, *58*, 4989.
[10] J. J. Masters, D. K. Jung, W. G. Bornmann, S. J. Danishefsky *Tetrahedron Lett.* **1993**, *34*, 7253.
[11] K. C. Nicolaou, Z. Yang, E. J. Sorensen, M. Nakada *J. Chem. Soc. Chem. Commun.* **1993**, 1024.
[12] For the use of 5α-cholestan-3-one as a C-ring construct in an intramolecular Diels–Alder approach to a baccatin III -steroid hybrid, see: C. A. Alaimo, C. A. Coburn, S. J. Danishefsky *Tetrahedron Lett.* **1994**, *35*, 6603.
[13] P. A. Grieco, S. Gilman, M. Nishizawa *J. Org. Chem.* **1976**, *41*, 1485.
[14] The stereochemistry of the C-2 carbinol center, originally formulated as having *S* configuration by analogy (see refs. [4, 11, 15]), has been verified by crystallographic means; see compound **31**.
[15] M. H. Kress, R. Ruel, W. H. Miller, Y. Kishi *Tetrahedron Lett.* **1993**, *34*, 5999, 6003.
[16] Reduction of the enone functionality in **27** was also required to achieve efficient protection of the C-1/C-2 diol.
[17] J. E. McMurray, W. J. Scott *Tetrahedron Lett.* **1983**, *24*, 979.
[18] The insertion step was particularly slow and resulted in precipitation of palladium(0). The use of stoichiometric $[Pd(PPh_3)_4]$ was required to obtain good yields of **31**.
[19] The stereochemistry of the C-13 carbinol center was determined from NOE experiments.

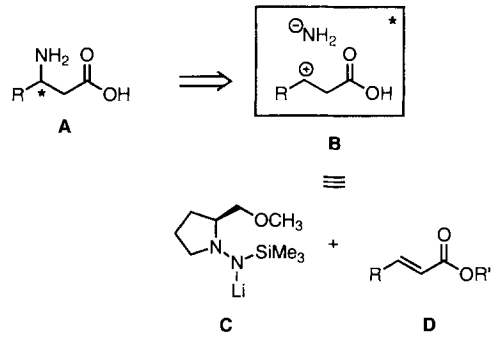
Enantioselective Synthesis of β-Amino Acids: TMS-SAMP as a Chiral Ammonia Equivalent for the Aza Analogous Michael Addition to α,β-Unsaturated Esters**

Dieter Enders,* Heiner Wahl, and Wolfgang Bettray

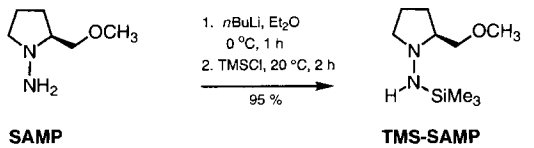
Dedicated to Professor Wilhelm Keim on the occasion of his 60th birthday

β-Amino acids **A** have achieved premier importance as substructures of numerous biologically active natural products[1] as well as building blocks for β-lactam antibiotics.[2] This is reflected by the ever increasing research activity in the field of their stereoselective synthesis.[3] One approach to this class of compounds makes use of enantiomerically pure building blocks provided by nature, for example aspartic acid.[4] On the other hand an increasing number of methods based on asymmetric synthesis can be applied.[5] Besides numerous methodologies for C–C bond formation some asymmetric approaches to C–N bond connections in accordance with the retrosynthetic analysis **A**⇒**B** have been developed in the recent past.[6–8] Using aza analogous Michael additions, achiral N-nucleophiles can be added to chiral Michael acceptors.[6] Alternatively chiral donors of amine functionality, especially N-silylated amides, have proven to be versatile soft nucleophiles,[8] for example **C** can be added to α,β-unsaturated ester **D** as achiral Michael acceptor.

We report here on a highly enantioselective synthesis of β-amino acids by hetero-Michael addition of (*S*)-2-methoxymethyl-1-trimethylsilylaminopyrrolidine (TMS-SAMP)[9] and its enantiomer TMS-RAMP, as chiral ammonia equivalents to (*E*)-configurated enoates.[10]

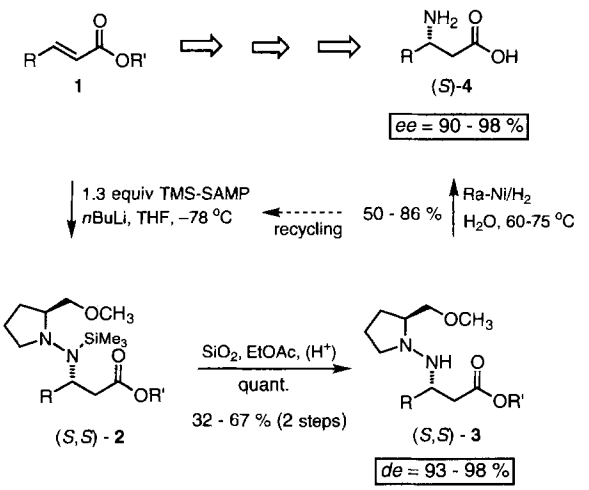


The new hydrazine auxiliary is prepared from SAMP and RAMP,[11] respectively, the well-established auxiliaries in asymmetric synthesis, by metalation with *n*-butyllithium in diethyl ether at 0 °C and subsequent silylation with chlorotrimethylsilane. TMS-SAMP and TMS-RAMP, respectively, are obtained by distillation in 95% yield as colorless liquids, which can be stored at −25 °C under argon (Scheme 1).[12]



Scheme 1. Synthesis of hetero-Michael donor TMS-SAMP.

In the synthesis of β-amino acids (Scheme 2), 1.3 equivalents of TMS-SAMP in tetrahydrofuran were metalated with *n*-butyllithium at −78 °C. The nucleophile **C** formed in this way was treated with the α,β-unsaturated esters **1** at −78 °C, affording the N-silylated β-hydrazinoesters (*S*,*S*)-**2** through conjugate addition. When simple methyl esters are used as Michael acceptors 1,2-addition occurs as a side reaction, leading to the formation of the corresponding α,β-unsaturated acyl hydrazides. The latter are formed exclusively if the unsilylated SAMP is used. The problem of 1,2-addition can be avoided by employing sterically



Scheme 2. Enantioselective synthesis of β-amino acids **4** by aza analogous Michael addition of TMS-SAMP to enoates.

[*] Prof. Dr. D. Enders, Dr. H. Wahl, Dr. W. Bettray
Institut für Organische Chemie der Technischen Hochschule
Professor-Pirlet-Strasse 1, D-52074 Aachen (Germany)
Telefax: Int. code + (241)8888 127

[**] This work was supported by the Fonds der Chemischen Industrie. We thank Degussa AG, BASF AG, Bayer AG, and Hoechst AG for the kind donation of chemicals.

demanding *tert*-butyl esters (R′ = *t*Bu). In addition better yields are obtained (see. **3b, i**, Table 1). Although the pure N-silylated β-hydrazinoesters **2** can be principally prepared by distillation [(*S,S*)-**2a** : 30% yield; *de* = 95%], it is recommendable to directly desilylate the crude products by stirring with a suspension of silica gel in ethyl acetate. The desilylation times are strongly dependent on the nature of the R group, ranging from 4 to 72 h (GC control). A significant reduction of the reaction time to 3 h is readily accomplished by the addition of a catalytic amount of

Table 1. Preparation of β-hydrazinoesters **3** by aza analogous Michael addition.

3	R	R′	Yield [%][a]	*de* [%][b]	$[\alpha]_D^{22}$ (*c*, $CHCl_3$)	Configuration
a	CH_3	CH_3	48	95	−97.6 (1.04)	(*S,S*)
a[c]	CH_3	CH_3	47	95	+96.4 (0.87)	(*R,R*)
b	C_2H_5	CH_3	37	95	−100.0 (1.02)	(*S,S*)
b	C_2H_5	*t*-C_4H_9	49	98	−93.2 (1.09)	(*S,S*)
c	*n*-C_3H_7	CH_3	40	95	−105.0 (1.00)	(*S,S*)
d	*i*-C_3H_7	*t*-C_4H_9	32	98	−69.4 (1.08)	(*S,R*)
e	*n*-C_4H_9	CH_3	39	≥94	−108.8 (0.98)	(*S,S*)
f	*i*-C_4H_9	CH_3	35	≥93	−113.8 (1.02)	(*S,S*)
g	*n*-C_5H_{11}	CH_3	39	≥94	−102.0 (1.05)	(*S,S*)
h	*n*-C_7H_{15}	CH_3	36	95	−87.9 (1.78)	(*S,S*)
i	*n*-$C_{11}H_{23}$	CH_3	35	95	−67.0 (1.10)	(*S,S*)
i	*n*-$C_{11}H_{23}$	*t*-C_4H_9	67	97	−98.5 (1.21)	(*S,S*)

[a] Total yield over two steps. [b] Determined by ^1H and ^{13}C spectroscopy. [c] TMS-RAMP was used as chiral auxiliary.

hydrochloric acid. Elution of the silica gel with methanol and subsequent chromatographic purification of the crude products (silica gel; petrol ether/ ethyl acetate 3/1) affords the β-hydrazinoesters (*S,S*)-**3** as pale yellow oils in 32–67% yield and with diastereomeric excesses of 93–98% *de* (determined by ^1H and ^{13}C NMR spectroscopy, Table 1). A conceivable diastereomeric enrichment by column chromatography can be ruled out due to the facile detection of both diastereoisomers by thin layer chromatography (molybdatophosphoric acid without heating). Furthermore, the correspondence of the *de* values of (*S,S*)-**2a, b** (determination by gas chromatography) and (*S,S*)-**3a, b** suggests that the acidic desilylation proceeds without epimerization.

Finally, the hydrazinoesters **3** are converted to the corresponding β-amino acids (*S*)-**4** by hydrogenolytic N–N cleavage with concomitant saponification of the ester function in an autoclave using Raney nickel and are obtained, after chromatographic purification (silica gel, ethanol/water 9/1), in 50–86% yield and with enantiomeric excesses of 90–98% *ee* (Table 2).

The determination of the enantiomeric excesses was carried out after derivatization of the corresponding methyl esters[13] with (*S*)-(+)-3,3,3-trifluoro-2-methoxy-2-phenylpropanoyl chloride (Mosher acid chloride) to the Mosher amides[14] by ^1H and ^{19}F NMR spectroscopy as well as gas chromatography. The comparison of the found *de* and *ee* values shows a slight divergence of 2–4%, which is in line with our experiences concerning N–N cleavage of similar hydrazines with Raney nickel.[15] The determination of the absolute configuration of the synthetic β-aminobutyric acid (*S*)-**4a** was carried out by comparison of the optical rotation with literature data ($[\alpha]_D^{18}$ = + 38.8 (*c* = 0.48, H_2O) for (*S*)-aminobutyric acid).[16] Under the assumption that all substrates react along the same reaction pathway, the β-amino acids **4b, c** and **4e–i** were also assigned the (*S*) configuration. Compound **4d** was assigned the (*R*) configuration because of the formal inversion of the substituent priorities in accordance with the CIP rules.

Table 2. Preparation of β-amino acids **4** by N–N bond cleavage of the hydrazinoesters **3**.

4	R	Yield [%]	*ee* [%] [a]	$[\alpha]_D^{22}$ (*c*,H_2O) [b]	M.p. [°C] [b,c]	Configuration
a	CH_3	86	93	+36.4 (1.04)	209	(S)
a[d]	CH_3	79	91	−35.7 (0.75)	205	(*R*)
b	C_2H_5	81	91[e]	+39.5 (0.97)	180	(*S*)
c	*n*-C_3H_7	85	92	+35.5 (1.01)	188	(*S*)
d	*i*-C_3H_7	60	98	+40.3 (1.02)	182	(*R*)
e	*n*-C_4H_9	80	≥90[f]	+33.3 (0.91)	202	(*S*)
f	*i*-C_4H_9	76	≥90[f]	+31.2 (0.76)	207	(*S*)
g	*n*-C_5H_{11}	85	≥90[f]	+31.1 (1.11)	201	(*S*)
h	*n*-C_7H_{15}	50	94	+26.6 (0.93)	199	(*S*)
i	*n*-$C_{11}H_{23}$	76	93[e]	+28.4 (0.90)	194	(*S*)

[a] The *ee* values of the β-amino acid methyl esters were determined as their corresponding Mosher's amides, prior to recrystallization [13]. [b] After one recrystallization from MeOH/EtOH [(*S*)-**4a**], MeOH/H_2O [(*R*)-**4a**], EtOH [(*S*)-**4b**·**c**·**f**–**i**, (*R*)-**4d**], MeOH/Et_2O [(*S*)-**4e**]. [c] With decomposition. [d] TMS-RAMP was used as chiral auxiliary. [e] Starting from the methyl esters (R′ = Me). [f] These results are based on the corresponding *de* values of the hydrazinoester **3** assuming a divergence of 2–4%.

The enantiomers (*R*)-**4**, as exemplified by (*R*)-**4a**, can be synthesized in an analogous fashion by the use of TMS-RAMP as N-Michael donor (Tables 1 and 2).[17]

The new variant of asymmetric hetero-Michael addition described herein, using TMS-SAMP as a chiral ammonia equivalent, opens a highly enantioselective pathway to β-amino acids and therefore to β-lactams.

Preliminary results show that the described methodology can be extended successfully to a Michael tandem process, that is an aza analogous 1,4-addition with subsequent α-alkylation of the intermediate ester enolate.[18]

Experimental Procedure

TMS-SAMP: To a stirred solution of SAMP (11.7 g, 90 mmol) in diethyl ether (100 mL) was added *n*-butyllithium (59.5 mL, 95 mmol, 1.6 M solution in hexane) at 0 °C under argon. After 1 h the reaction mixture was allowed to warm to room temperature and chlorotrimethylsilane (10.3 g, 95 mmol) was added. The solution was then heated to reflux for 1 h to complete the silylation. The solution was filtered to remove the precipitated LiCl, the ether was evaporated, and the residue was finally distilled to give 17.2 g (95%) TMS-SAMP as a colorless liquid [b.p. = 34–36 °C (0.2 Torr); $[\alpha]_D^{22}$ = − 99.3 (neat)].

4: *n*-Butyllithium (8.13 mL, 13 mmol, 1.6 M solution in hexane) was added dropwise to TMS-SAMP (2.63 g, 13 mmol) in THF (40 mL) at −78 °C. To complete metalation the solution was stirred for 30 min at −78 °C and then the enoate **1** (10 mmol) was added slowly at −78 °C and the mixture was stirred at this temperature for 3–18 h. The hydrolysis was carried out by pouring the reaction mixture into saturated $NaHCO_3$ solution (30 mL). The solution was extracted three times with dichloromethane, the combined extracts were dried over Na_2SO_4, and the solvent was removed in vacuo. The crude 1,4-adducts (*S,S*)-**2** were obtained as yellow oils. To achieve desilylation the adducts were dissolved, with a suspension of weakly acidic silica (40 g, type 60, 63-100 mesh, Merck), in ethyl acetate containing concentrated HCl (0.5 mL) and stirred at ambient temperature under an argon atmosphere. After complete removal of the silyl group (GC-control) the silica was washed with absolute methanol and then the solvent was removed in vacuo. The resulting brown oils were purified by flash column chromatography (silica gel, eluant: petrol ether/ethyl acetate 3/1), without diastereomeric enrichment, to give the pure β-hydrazinoesters (*S,S*)-**3** as pale yellow oils.

Preparation of Raney nickel for the N–N bond cleavage, (2–4 mmol per preparation): Ni-Al alloy (1 g per mmol of the β-hydrazinoester (*S,S*)-**3**) was suspended in H_2O (15 mL), then solid NaOH was added until no further evolution of hydrogen was observed. The suspension was heated to 70 °C for 30 min in a water bath, the solvent decanted, and the nickel sponge washed three times with water (10 mL). This yielded the catalyst with an estimated activity of W-9 [19].

N–N Bond cleavage: The N–N bond cleavage with concomitant ester hydrolysis was carried out in an autoclave with water (10 mL per mmol of β-hydrazinoester (*S,S*)-**3**) as solvent and Raney nickel as catalyst (reaction time: 17–20 h; temperature: 60–75 °C; H_2 pressure: 7.5–9.5 bar). After quantitative conversion (thin layer chromatographic control) the Ni-sponge was removed by filtration through celite, and the filtrate was concentrated in vacuo (water bath: 50–60 °C) to give a pale

solid. Upon flash column chromatography (silica, eluant: ethanol/water 9/1) and removal of traces of the solvent in vacuo the β-amino acids **4** were obtained as colorless, crystalline compounds after recrystallization from MeOH/EtOH [(*S*)-**4a**], MeOH/H_2O [(*R*)-**4a**], EtOH [(*S*)-**4b**, **c**, **f**–**i**, (*R*)-**4d**], MeOH/Et_2O [(*S*)-**4e**], respectively.

Received: September 3, 1994 [Z 7290 IE]
German version: *Angew. Chem.* **1995**, *107*, 527

Keywords: amino acids · asymmetric syntheses · chiral auxiliaries · Michael additions

[1] C. N. C. Drey in *Chemistry and Biochemistry of Amino Acids* (Eds.: G. C. Barret), Chapman and Hall, London, New York, **1985**. Examples: N. Otake, S. Takeuchi, T. Endo, H. Yonehara, *Tetrahedron Lett.* **1965**, *19*, 1411–1419; H. Allgaier, G. Winkelmann, G. Jung, *Liebigs Ann. Chem.* **1984**, 854–866; W. H. Pearson, J. V. Hines, *J. Org. Chem.* **1989**, *54*, 4235–4237; S.-K. Kang, D.-H. Lee, *Synlett* **1991**, 175–176; K. Hattori, H. Yamamoto, *Tetrahedron* **1994**, *50*, 2785–2792; M. E. Bunnage, S. G. Davies, C. J. Goodwin, *Synlett* **1993**, 731–732; *J. Chem. Soc. Perkin Trans. 1* **1993**, 1375–1376; M. E. Bunnage, A. J. Burke, S. G. Davies, C. J. Goodwin, *Tetrahedron: Asymmetry* **1994**, *5*, 203–206; M. E. Bunnage, S. G. Davies, C. J. Goodwin, O. Ichihara, *Tetrahedron* **1994**, *50*, 3975–3986.

[2] Review article: D. J. Hart, D.-C. Ha, *Chem. Rev.* **1989**, *89*, 1447–1465; M. J. Brown, *Heterocycles* **1989**, *29*, 2225–2244; G. Sedelmeier, *Nachr. Chem. Tech. Lab.* **1990**, *38*, 616–624; F. H. van der Steen, G. van Koten, *Tetrahedron* **1991**, *47*, 7503–7524. For an example see: L. S. Liebeskind, M. E. Welker, R. W. Fengl, *J. Am. Chem. Soc.* **1986**, *108*, 6328–6343; S. G. Davies, I. Dordor-Hedgecock, K. H. Sutton, J. C. Walker, R. H. Jones, K. Prout, *Tetrahedron* **1986**, *42*, 5123–5137; C. Gennari, I. Venturini, G. Gislon, G. Schimperna, *Tetrahedron Lett.* **1987**, *28*, 227–230; S. Kim, K. Y. Yi, J-Y. Namkung, *Heterocycles* **1989**, *29*, 1237–1240; P. A. Jacobi, W. Zheng, *Tetrahedron Lett.* **1993**, *34*, 2581–2584, 2585–2588; N. Asao, N. Tsukada, Y. Yamamoto, *J. Chem. Soc. Chem. Commun.* **1993**, 1660–1662.

[3] Review article: E. Juaristi, D. Quintana, J. Esclante, *Aldrichimica Acta*, **1994**, *27*, 3–11; D. C. Cole, *Tetrahedron* **1994**, *50*, 9517–9582.

[4] J. P. Konopelski, K. S. Chu, G. R. Negrete, *J. Org. Chem.* **1991**, *56*, 1355–1357; P. Gmeiner, *Liebigs Ann. Chem.* **1991**, 501–502; E. Juaristi, D. Quintana, *Tetrahedron: Asymmetry* **1992**, *3*, 723–726; K. S. Chu, G. R. Negrete, J. P. Konopelski, F. J. Lakner, N.-T. Woo, M. M. Olmstead, *J. Am. Chem. Soc.* **1992**, *114*, 1800–1812; C. W. Jefford, J. Wang, *Tetrahedron Lett.* **1993**, *34*, 1111–1114, 3119–3122.

[5] H. Kunz, D. Schanzenbach, *Angew. Chem.* **1989**, *101*, 1042–1043; *Angew. Chem. Int. Ed. Engl.* **1989**, *28*, 1068–1069; S. Laschat, H. Kunz, *Synlett* **1990**, 51–52; *J. Org. Chem.* **1991**, *56*, 5883–5889; D. Keirs, D. Moffat, K. Overton, T. Tomanek, *J. Chem. Soc. Perkin Trans. 1* **1991**, 1041–1051; D. H. Hua, S. W. Miao, J. S. Chen, S. Iguchi, *J. Org. Chem.* **1991**, *56*, 4–6; W. D. Lubell, M. Kitamura, R. Noyori, *Tetrahedron: Asymmetry* **1991**, *2*, 543–554; E. Juaristi, D. Quintana, B. Lamatsch, D. Seebach, *J. Org. Chem.* **1991**, *56*, 2553–2557; C. Andrés, A. Gonzáles, R. Pedrosa, A. Perez-Encabo, *Tetrahedron Lett.* **1992**, *33*, 2895–2898; E. Juaristi, J. Escalante, *J. Org. Chem.* **1993**, *58*, 2282–2285; M. K. Mokhallalati, M.-J. Wu, L. N. Pridgen, *Tetrahedron Lett.* **1993**, *34*, 47–50; D. Enders, M. Klatt, R. Funk, *Synlett* **1993**, 226–228; K. S. Chu, J. P. Konopelski, *Tetrahedron* **1993**, *49*, 9183–9190; K. Hattori, M. Miyata, H. Yamamoto, *J. Am. Chem. Soc.* **1993**, **115**, 1151–1152; M. Alcón, M. Canas, M. Poch, A. Moyano, M. A. Pericàs, A. Riera, *Tetrahedron Lett.* **1994**, *35*, 1589–1592; D. Enders, J. Schankat, M. Klatt, *Synlett* **1994**, 795–797; M. Shimano, A. I. Meyers, *J. Am. Chem. Soc.* **1994**, *116*, 6437–6438; V. A. Soloshonok, A. G. Kirilenko, N. A. Fokina, I. P. Shihkina, S. V. Galushko, V. P. Kukhar, V. K. Svedas, E. V. Kozlova, *Tetrahedron: Asymmetry*, **1994**, *5*, 1119–1126.

[6] J. d'Angelo, J. Maddaluno, *J. Am. Chem. Soc.* **1986**, *108*, 8112–8114; S. G. Davies, J. Dupont, R. J. C. Easton, *Tetrahedron: Asymmetry* **1990**, *1*, 279–280; D. Potin, F. Dumas, J. d'Angelo, *J. Am. Chem. Soc.* **1990**, *112*, 3483–3486; R. Amoroso, G. Cardillo, P. Sabatino, C. Tomasini, A. Trerè, *J. Org. Chem.* **1993**, *58*, 5615–5619; S. Matsubara, M. Yoshioka, K. Utimoto, *Chem. Lett.* **1994**, 827–830; G. Cardillo, A. de Simone, L. Gentilucci, P. Sabatino, C. Tomasini, *Tetrahedron Lett.* **1994**, *35*, 5051–5054; V. A. Soloshonok, A. G. Kirilenko, N. A. Fokina, V. P. Kukhar, S. V. Galushko, V. K. Svedas, G. Resnati *Tetrahedron: Asymmetry* **1994**, *5*, 1225–1228.

[7] J. M. Hawkins, G. C. Fu, *J. Org. Chem.* **1986**, *51*, 2820–2822; H. Estermann, D. Seebach, *Helv. Chim. Acta* **1988**, *71*, 1824–1839; K. Rudolf, J. M. Hawkins, R. J. Loncharich, K. N. Houk, *J. Org. Chem.* **1988**, *53*, 3879–3882; L. Wessjohann, G. McGaffin, A. de Meijere, *Synthesis* **1989**, 359–363; S. G. Davies, O. Ichihara, *Tetrahedron: Asymmetry* **1991**, *2*, 183–186; J. M. Hawkins, T. A. Lewis, *J. Org. Chem.* **1992**, *57*, 2114–2121; E. Juaristi, J. Escalante, B. Lamatsch, D. Seebach, *ibid.* **1992**, *57*, 2396–2398; M. Es-Sayed, C. Gratkowski, N. Krass, A. I. Meyers, A. de Meijere, *Tetrahedron Lett.* **1993**, *34*, 289–292; S. G. Davies, O. Ichihara, I. A. S. Walters, *Synlett* **1993**, 461–462; S. G. Davies, N. M. Garrido, O. Ichihara, I. A. S. Walters, *J. Chem. Soc. Chem. Commun.* **1993**, 1153–1155; J. G. Rico, R. J. Lindmark, T. E. Rogers, P. R. Bovy, *J. Org. Chem.* **1993**, *58*, 7948–7951; S. G. Davies, O. Ichihara, I. Lenoir, I. A. S. Walters, *J. Chem. Soc. Perkin Trans. 1* **1994**, 1411–1415; M. E. Bunnage, S. G. Davies, C. J. Goodwin, I. A. S. Walters, *Tetrahedron: Asymmetry* **1994**, *5*, 35–36; S. G. Davies, O. Ichihara, I. A. S. Walters, *Synlett* **1994**, 117–118; S. G. Davies, O. Ichihara, I. A. S. Walters, *J. Chem. Soc. Perkin Trans. 1* **1994**, 1141–1147.

[8] N. Asao, T. Uyehara, Y. Yamamoto, *Tetrahedron* **1988**, *44*, 4173–4180; T. Uyehara, N. Asao, Y. Yamamoto, *J. Chem. Soc. Chem. Commun.* **1989**, 753–754; N. Asao, T. Uyehara, Y. Yamamoto, *Tetrahedron* **1990**, *46*, 4563–4572; Y. Yamamoto, N. Asao, T. Uyehara, *J. Am. Chem. Soc.* **1992**, *114*, 5427–5429; T. Uyehara, N. Shida, Y. Yamamoto, *J. Org. Chem.* **1992**, *57*, 3139–3145, 5049–5051; I. Suzuki, H. Kin, Y. Yamamoto, *J. Am. Chem. Soc.* **1993**, *115*, 10139–10146; N. Shida; C. Kabuto, T. Niwa, T. Ebata, Y. Yamamoto, *J. Org. Chem.* **1994**, *59*, 4068–4075.

[9] A. S. Amaya, Dissertation, University of Bonn, **1985**.

[10] Dissertation, H. Wahl, Technical University of Aachen, **1990**.

[11] D. Enders in *Asymmetric Synthesis, Vol. 3* (Ed.: J. D. Morrison), Academic Press, Orlando, **1984**, p. 275; D. Enders, P. Fey, H. Kipphardt, *Org. Synth.* **1987**, *65*, 173–183.

[12] The new reagent TMS-SAMP is available on sale from November 1994.

[13] L.-F. Tietze, T. Eicher, *Reaktionen und Synthesen im organisch-chemischen Praktikum*, Thieme, Stuttgart, **1981**, p. 115.

[14] J. A. Dale, D. L. Dull, H. S. Mosher, *J. Org. Chem.* **1969**, *34*, 2543–2549; J. A. Dale, H. S. Mosher, *J. Am. Chem. Soc.* **1973**, *95*, 512–519.

[15] C. Nübling, Dissertation, Technical University of Aachen, **1987**; R. Funk, Dissertation, Technical University of Aachen, **1990**.

[16] K. Balenovic, C. Cesar, Z. Fuks, *J. Chem. Soc.* **1952**, 3316–3317; E. F. Paulus, D. Kobelt, H. Jensen, *Angew. Chem.* **1969**, 1048; *Angew. Chem. Int. Ed. Engl.* **1969**, *8*, 990–991.

[17] All new compounds gave satisfactory elemental analyses and spectral data (^1H, ^{13}C NMR, IR, MS).

[18] D. Enders, W. Bettray, unpublished results; W. Bettray, Dissertation, Technical University of Aachen, **1993**.

[19] Collective authors, *Organikum*, 15th ed., VEB Deutscher Verlag der Wissenschaften, Berlin, **1984**.

Sulfoxide-Stabilized Giant Palladium Clusters in Catalyzed Oxidations**

Rolf A. T. M. van Benthem, Henk Hiemstra,* Piet W. N. M. van Leeuwen, John W. Geus, and W. Nico Speckamp

Large transition metal clusters are gaining increasing attention as research targets for several reasons. Their existence on the borderline[1] between molecular states with discrete quantum energy levels and the actual metallic state with its typical bulk properties raises the interest of not only physicists and material scientists[1–3] but also of chemists working in the field of catalysis.[4–7] Since these species are also on the borderline between homogeneous and heterogeneous catalysts, they may perhaps have typical characteristics of both.

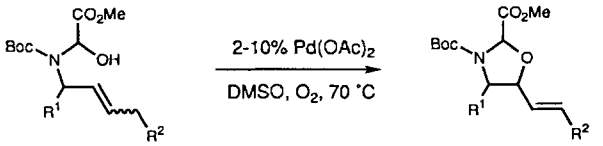
The feasibility of preparing platinum group transition metal clusters and colloids by reducing inorganic complexes in the presence of an appropiate stabilizing ligand such as phenanthroline has been demonstrated by Moiseev et al.[4] and Schmid et al.[1, 6] Phosphanes were also shown to be useful ligands for this pur-

[*] Dr. H. Hiemstra, R. A. T. M. van Benthem, Prof. Dr. W. N. Speckamp
Laboratory of Organic Chemistry, University of Amsterdam
Nieuwe Achtergracht 129, NL-1018 WS Amsterdam (The Netherlands)
Telefax: Int. code + (20) 5255670
Prof. Dr. P. W. N. M. van Leeuwen
Laboratory of Inorganic Chemistry,
University of Amsterdam (The Netherlands)
Prof. J. W. Geus
Laboratory of Inorganic Chemistry, University of Utrecht (The Netherlands)

[**] This investigation was supported by the Innovation Oriented Research Program on Catalysis of the Dutch Ministry of Economic Affairs.

pose.[7, 8] This communication describes the first example, to our knowledge, of sulfoxide-stabilized giant palladium clusters.[9]

Recently, we suggested[10] that large palladium clusters may be the catalytically active species in the oxidative cyclization of allylic *N*-hydroxymethyl carbamates (Scheme 1).[10, 11] It was



Scheme 1. Pd^{II}-catalyzed oxidative 5-*exo* cyclization of *N*-hydroxymethylamines. DMSO = Me_2SO.

shown that the solvent dimethyl sulfoxide (Me_2SO) plays an essential role in this process. Molecular oxygen could be employed as the stoichiometric oxidant in the absence of the common cocatalysts,[12] and Pd-black did not precipitate. Larock et al.[13] also observed that molecular oxygen alone is remarkably efficient in reoxidizing palladium in Me_2SO in the oxidative lactonization of unsaturated acids. Apparently, the catalytic system $Pd(OAc)_2/Me_2SO/O_2$ is quite versatile for oxidative reactions.[14] This prompted us to further explore the nature of this remarkable system.

We presumed that after initial reduction of $Pd(OAc)_2$ by the oxidative cyclization [Eq.(a)], the palladium(0) species formed is stabilized by Me_2SO as a ligand (L), and readily reoxidized by molecular oxygen [Eq.(b)] to catalyzed further cyclizations

$$Pd(OAc)_2 + \text{substrate} \rightarrow \text{product} + 2\,HOAc + Pd^0 \quad (a)$$

$$x\,Pd^0 + 2y\,HOAc + z\,L + 1/2y\,O_2 \rightarrow [Pd_x(OAc)_{2y}L_z] + y\,H_2O \quad (b)$$

[Eqs.(c), (d), and (a)]. Whether a polynuclear compound is the actual catalytically active species [Eq.(c)] or merely a precursor

$$[Pd_x(OAc)_{2y}L_z] + \text{substrate} \rightarrow \text{product} + 2\,HOAc + [Pd_x(OAc)_{2y-2}L_z] \quad (c)$$

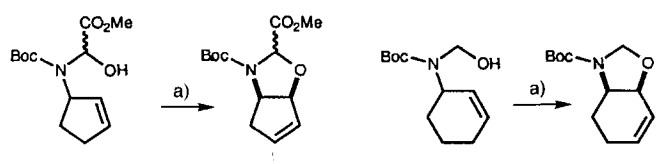
$$[Pd_x(OAc)_{2y}L_z] \rightarrow [Pd_{x-1}(OAc)_{2y-2}L_z] + Pd(OAc)_2 \quad (d)$$

of an active mononuclear species [Eq.(d)] remains to be established.[19] The unique role of Me_2SO in this process is most likely

$$[Pd_x(OAc)_{2y-2}L_z] + 2\,HOAc + 1/2\,O_2 \rightarrow [Pd_x(OAc)_{2y}L_z] + H_2O \quad (e)$$

linked to its two coordination modes. During the catalytic cycle the palladium catalyst can interact with either the "hard" oxygen lone pairs or the "soft" sulfur lone pair.[9, 15]

The substrates used for this investigation, the *N*-hydroxymethyl carbamates **1**[10, 11] and **3**, differ in reactivity towards $Pd(OAc)_2$. At room temperature cyclopentenylamine derivative **1** undergoes oxidative cyclization immediately upon addition of the catalyst to the reaction mixture, which then turns dark red-



Scheme 2. Reagents and conditions: a) 0.1 equiv $Pd(OAc)_2$, Me_2SO; $c = 0.2$–0.02 M; ca. 25–60 °C.

brown. According to TLC, this corresponds to about one turnover [Eq.(a)]. However, in the presence of molecular oxygen the subsequent reactions occur more slowly at this temperature.[16] When the first turnover is achieved under an argon atmosphere, the reaction stops at this point but the catalyst remains active. Thus, even after the reaction mixture is left for longer periods under argon at room temperature or 75 °C, purging the flask with molecular oxygen results in fast completion of the reaction. In contrast, cyclohexenylamine derivative **3** is virtually unreactive at room temperature. A comparable reaction rate for oxidative cyclization is reached at 60 °C. Again, the first turnover occurs much faster than the subsequent ones.

Typical reaction mixtures consisting of **1** or **3** and 0.10 equiv $Pd(OAc)_2$ under an atmosphere of molecular oxygen with concentrations between 0.2 and 0.02 M in Me_2SO were prepared for TEM imaging[18] according to published methods.[7, 17] Bright- and dark-field TEM images clearly showed the presence of large palladium clusters with more or less uniform size distribution in all samples. Figure 1 shows bright-field TEM images of a sample that was taken from a reaction mixture of **1** within seconds after the addition of $Pd(OAc)_2$ at room temperature, proving that the clusters are formed almost instantaneously. The particles are

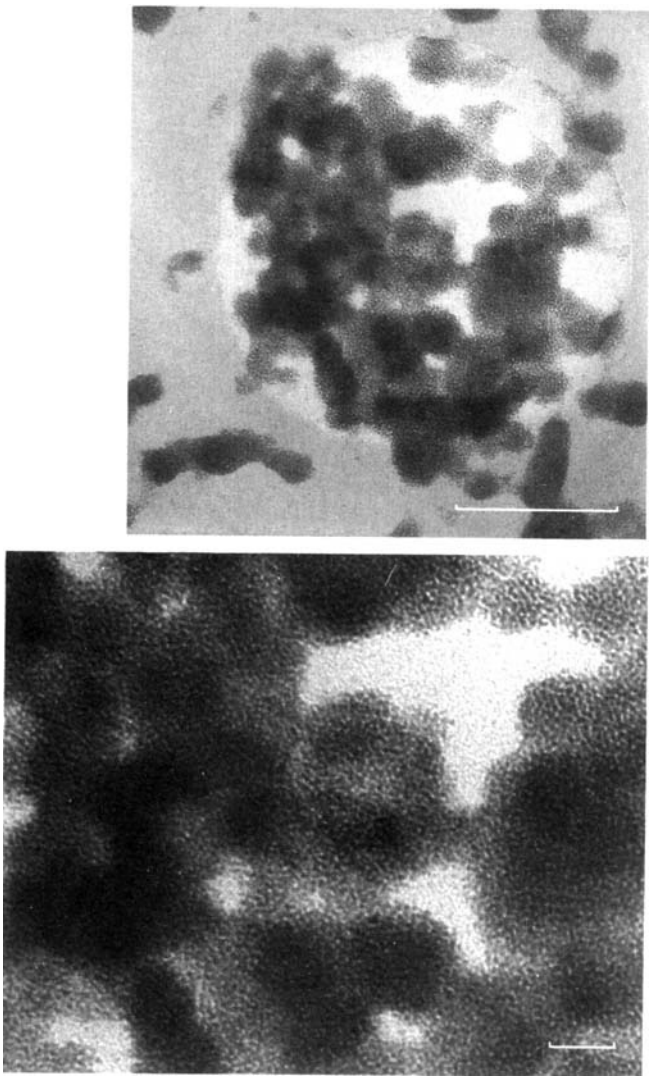


Fig. 1. Top: Typical TEM image of Me_2SO-stabilized palladium clusters (size 26 ± 4 Å). The bar corresponds to 100 nm. Bottom: Enlargement of a section of Fig. 1, top. The bar corresponds to 10 nm.

 © VCH Verlagsgesellschaft mbH, D-69451 Weinheim, 1995 0570-0833/95/0404-0458 $ 10.00+.25/0

26 ± 4 Å in size, corresponding to five- and six-shell clusters in the full-shell concept terminology.[1] TEM images from samples taken later in the course of the reaction did not differ substantially from the first one.

Hence, we must conclude that the clusters observed are involved in the reoxidation process [Eq.(e)] and in the catalytic process according to either Equation (c) or (d). The high affinity of the surfaces of large palladium clusters for molecular oxygen is known.[1, 4, 6, 7] The oxidative cyclization [Eq.(c)] is also believed to take place at the surface of the cluster.

As already mentioned, the reaction of **3** proceeded more slowly than that of **1**. Figure 2 shows TEM images of a sample taken after a reaction time of one minute at 60 °C. The size distribution is slightly less homogeneous and the particles are somewhat smaller as they vary in size from 15 to 27 Å, corresponding to three-, four- and five-shell clusters. As with carbamate **1**, the size distribution remains virtually unchanged during the course of the reaction.

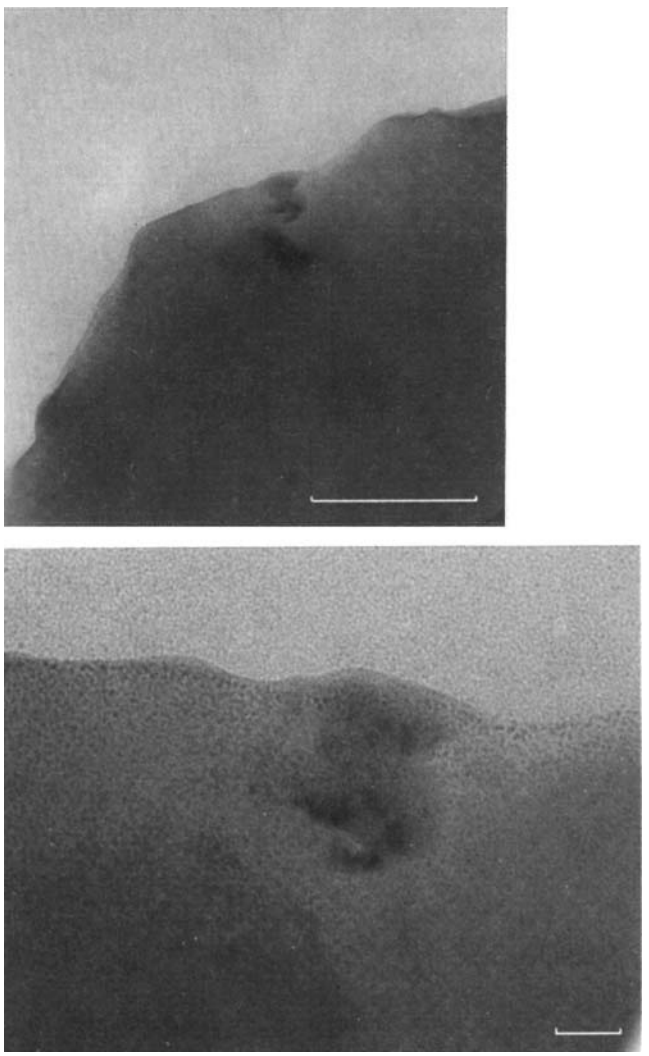


Fig. 2. Typical TEM image of Me_2SO-stabilized palladium clusters (size 21 ± 6 Å). The bar corresponds to 100 nm. Bottom: Enlargment of a section of Fig. 2, top. The bar corresponds to 10 nm.

The clusters formed with **1** after two turnovers at room temperature could be isolated as a black powder without loss of catalytic activity (Experimental Procedure). In elemental analyses of different batches the ratio of the number of Me_2SO molecules per Pd atom was found to range from 2.5–3.0/10. In the IR spectrum of these materials strong absorption bands at 1023 and 1127 cm^{-1} (S=O) indicated that Me_2SO is coordinated through both the O and S atoms (-32 cm^{-1} and $+72$ cm^{-1}, respectively, relative to the S=O absorption band of "free" Me_2SO at 1055 cm^{-1}).[9]

To the best of our knowledge, this is the first identification of isolated clusters *after* a *homogeneously* catalyzed reaction. The clusters reported by others[4] were characterized in stable form after preparation and *subsequently* shown to homogeneously catalyze oxidative reactions. It may well be that the clusters are modified under the reaction conditions (and remain or become catalytically active). For example, although these small metal particles in isolated form appear to be stable to molecular oxygen, oxidation to metal oxides by molecular oxygen in solution cannot be ruled out. Preliminary results of elemental analyses of our cluster material indeed suggest a PdO structure.

In conclusion, we have demonstrated 1) the feasibilty of preparing giant palladium clusters by reduction of $Pd(OAc)_2$ under an oxygen atmosphere with Me_2SO as both the solvent and the stabilizing ligand, and 2) the involvement of these Me_2SO-stabilized palladium clusters in a catalytic homogeneous oxidative reaction.

At present, we are working on further establishing the structure and nature of the clusters observed and determining whether they are the actual catalytically active species.[19]

Experimental Procedure

Palladium acetate (100 mg, 0.44 mmol) was dissolved in 2 mL of Me_2SO (previously dried and distilled from CaH_2). The flask was repeatedly evacuated and purged with molecular oxygen. Compound **1** [10] (240 mg, 0.88 mmol) was added at room temperature with vigorous stirring. The reaction mixture was heated at 40 °C for one minute and deemed complete by TLC and ^1H NMR spectroscopy. To the reaction mixture was added 100 mL of toluene (previously dried over sodium wire and distilled from P_2O_5). After 72 h at -20 °C a fluffy dark-brown solid had precipitated. The light brown toluene supernatant containing the oxazolidine product **2** and Me_2SO was decanted. The residue was washed by decantation with toluene (3×50 mL; the collected toluene layers yielded after aqueous workup 221 mg (93%) of crude **2**) and pentane (3×50 mL). A black powder (57 mg) was obtained after drying in vacuo. FTIR spectra were recorded (KBr disk) on a Nicolet 510 M FTIR spectrometer. The following procedure showed the material to be still highly catalytically active. In analogy to the published method [10], 4.2 mg of this material corresponding to an equal amount of $Pd(OAc)_2$ (0.02 mmol) was dissolved in 5 mL of dry Me_2SO. The flask was equipped with a septum and repeatedly evacuated and purged with molecular oxygen. An atmosphere of pure molecular oxygen was ensured throughout the procedure by means of a balloon. Under vigorous stirring **1** (271 mg, 1.00 mmol) was added at room temperature, and the clear dark brown mixture was heated to 70 °C. After 2 h of vigorous stirring the reaction was complete by TLC. The light yellow reaction mixture was poured into 50 mL of water and extracted with four 20 mL portions of a 1:1 mixture of diethyl ether and petroleum ether (b.p. 40–60 °C). The collected organic phases were dried over $MgSO_4$ and concentrated in vacuo. Purification (flash chromatography, ethyl acetate/hexanes 1:3, $R_f = 0.45$) provided **2** (242 mg, 0.90 mmol, 90%, 1:1 mixture of isomers) as a colorless oil.

Received: August 8, 1994 [Z 7218 IE]
German version: *Angew. Chem.* **1995**, *107*, 500

Keywords: catalysis · clusters · oxidations · palladium compounds · transmission electron microscopy

[1] G. Schmid, *Chem. Rev.* **1992**, *92*, 1709 and references therein.
[2] a) M. G. Bawendi, M. L. Steigerwald, L. E. Brus, *Annu. Rev. Phys. Chem* **1990**, *41*, 477; b) G. Schmid, *Mater. Chem. Phys.* **1991**, *29*, 133.
[3] S. Puvvada, S. Baral, G. M. Chow, S. B. Qadri, B. R. Ratna, *J. Am. Chem. Soc.* **1994**, *116*, 2135.
[4] a) M. N. Vargaftik, V. P. Zagorodnikov, I. P. Stolarov, I. I. Moiseev, D. I. Kochubey, V. A. Likholobov, A. L. Chuvilin, K. I. Zamaraev, *J. Mol. Catal.* **1989**, *53*, 315; b) I. I. Moiseev, T. A. Stromnova, M. N. Vargaftik, *ibid.* **1994**, *86*, 71.

 © VCH Verlagsgesellschaft mbH, D-69451 Weinheim, 1995 0570-0833/95/0404-0459 $ 10.00+.25/0

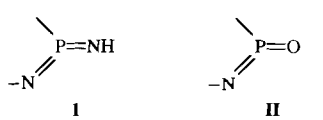
[5] a) L. N. Lewis, *J. Am. Chem. Soc.* **1992**, *92*, 5998; b) *Chem. Rev.* **1993**, *93*, 2693.
[6] G. Schmid, M. Harms, J.-O. Malm, J.-O. Bovin, J. Van Ruitenbeck, H. W. Zandbergen, W. T. Fu, *J. Am. Chem. Soc.* **1993**, *115*, 2046.
[7] C. Amiens, D. de Caro, B. Chaudret, J. S. Bradley, R. M. Mazel, C. Roucau, *J. Am. Chem. Soc.* **1993**, *115*, 11638.
[8] a) E. G. Mednikov, N. K. Eremenko, Y. L. Slovokinotov, Y. T. Struchov, G. P. Gubin, *J. Organomet. Chem.*, **1983**, *258*, 247; b) E. G. Mednikov, N. K. Eremenko, S. P. Gubin, *Koord. Khim.*, **1984**, *10*, 711.
[9] H. B. Kagan, B. Ronan in *Reviews on Heteroatom Chemistry, Vol. 7* (Eds.: S. Oae, A. Ohno, T. Okuyama), MYU, Tokyo, **1992**, pp. 92–116.
[10] R. A. T. M. Van Benthem, H. Hiemstra, J. J. Michels, W. N. Speckamp, *J. Chem. Soc. Chem. Commun.* **1994**, 357.
[11] R. A. T. M. Van Benthem, H. Hiemstra, W. N. Speckamp, *J. Org. Chem.* **1992**, *57*, 6083.
[12] Cocatalysts commonly used in Pd^{II}-catalyzed oxidations of organic compounds are for example: Cu^{II} salts: J. Smidt, W. Hafner, R. Jira, J. Sedlmeier, R. Sieber, R. Rüttinger, H. Kojer, *Angew. Chem.* **1959**, *71*, 176; J. Smidt,. W. Hafner, R. Jira, R. Sieber, J. Sedelmeier, A. Sabel, *Angew. Chem.* **1962**, *74*, *93; Angew. Chem. Int. Ed. Engl.* **1962**, *1*, 80; T. Hosokawa, T. Uno, S. Inui, S.-I. Murahashi, *J. Am. Chem. Soc.* **1981**, *103*, 2318; and benzoquinone combined with other redox couples: J.-E. Bäckvall, R. B. Hopkins, H. Grennberg, M. M. Mader, A. K. Awasthi, *J. Am. Chem. Soc.* **1990**, *112*, 5160.
[13] R. C. Larock, T. R. Hightower, *J. Org. Chem.* **1993**, *58*, 5298.
[14] R. A. T. M. Van Benthem, N. J. Newcombe, M. J. Moolenaar, H. Hiemstra, W. N. Speckamp, unpublished.
[15] X-ray structure analyses show that depending of the character of the complex, sulfoxides in Pt^{II} and Pd^{II} complexes are bound to the metal center through either the oxygen or sulfur atom: a) G. Annibale, L. Cattalini, V. Bertolasi, V. Ferretti, G. Gilli, M. L. Tobe, *J. Chem. Soc. Dalton Trans.* **1989**, 1265; b) D. P. Bancroft, F. A. Cotton, M. Verbruggen, *Acta Crystallogr. Sect. C* **1989**, *45*, 1289.
[16] With 0.1 equiv $Pd(OAc)_2$ this reaction reached completion after 20 h at room temperature.
[17] The samples were diluted 50-fold with 96% ethanol. A film of this solution was applied with a platinum wire eye onto a 2.3 mm copper grid previously covered with an amorphous carbon film. The sample was allowed to concentrate to dryness in air and was then ionized.
[18] TEM images were obtained on a Philips EM 420 electron microscope operating at 120 kV.
[19] Criteria for determining whether a reaction is catalyzed by a cluster or a mononuclear species are summarized in ref. [5b].

Synthesis, Structure, and Reactivity of an Imido- and an Oxo(imido)phosphorane R–P(=X)=NR (X = NH, O; R = $tBu_3C_6H_2$**

Martin Larbig, Martin Nieger, Volker von der Gönna, Alexander V. Ruban, and Edgar Niecke*

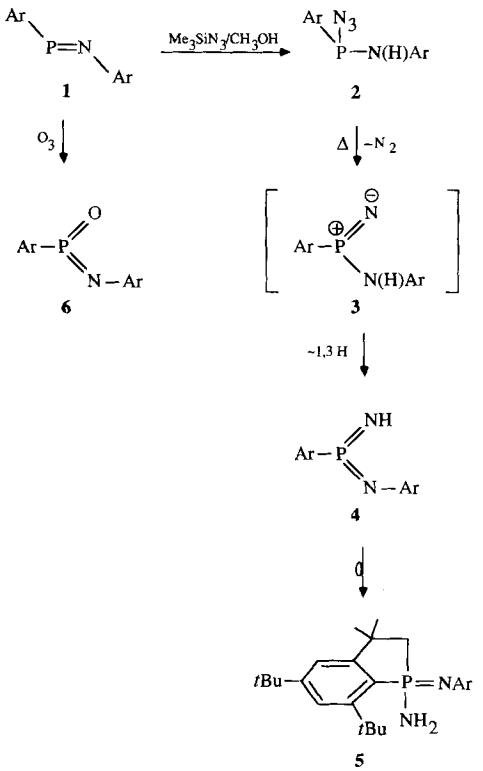
Dedicated to Professor Alfred Schmidpeter on the occasion of his 65th birthday

Bis(imino)phosphoranes are versatile synthetic building blocks for phosphorus–nitrogen heterocycles[1] and moreover have gained significance as ligands for homogeneous catalytic processes.[2] The possibility of extending the synthetic potential of these compounds by functionalization of an imine nitrogen atom[3] was the stimulus for the investigations described. We report here on the synthesis and structure of the first imido(imino)phosphorane (**I**) and on the structure of the oxygen derivative (**II**) isoelectronic to **I**. The existence of an oxo(imino)phosphorane had previously been based on NMR spectroscopic evidence only.[4]



I **II**

Treatment of the bisaryliminophosphane **1**[5] with trimethylsilylazide in the presence of one equivalent of methanol afforded the NH-functionalized amino(azido)phosphane **2** in a smooth reaction (Scheme 1). Compound **2** could be isolated as colorless



Scheme 1. Ar = 2,4,6-$tBu_3C_6H_2$.

thermally stable crystals. In solution, **2** decomposes above 40 °C with the elimination of nitrogen. The initially formed phosphinonitrene intermediate **3**[3] is stabilized by a 1,3-H shift[7] to give the imido(imino)phosphorane **4**. The iminophosphorane **5** isomeric to **4** is a by-product of the reaction, which can be obtained quantitatively by heating the reaction mixture for several days under reflux. The conversion **4** → **5** involves the CH activation of an *ortho*-positioned *tert*-butyl group on the phosphorus substituent by the highly electrophilic phosphorus center. One insertion reaction corresponding to this isomerization is also documented for the analogous aryldithioxophosphorane[8] and is thought to be responsible for the unsuccessful attempts at the synthesis of a kinetically stabilized aryldioxophosphorane.[9] The oxgen derivative **6** isoelectronic to **4** can be obtained by ozonization of **1** in CH_2Cl_2.

The composition and constitution of the compounds **2**, and **4**–**6** can deduced from the high-resolution mass spectra (molecular ion) and the results of NMR measurements. The constitution of **2** as that of an azidophosphorane and not that of a 4,5-dihydro-1*H*-tetraazaphosphole[10] is based on the presence of an intense absorption at 2105 cm^{-1} in the IR spectrum and the downfield position of the ^{31}P NMR signal ($\delta = 96.0$, $^2J(H,P) = 5.9$ Hz). The presence of an imido group in the vicinity of a coordinatively unsaturated phosphorus center in **4** is revealed by the structure of the doublet ($^2J(H,P) = 22.3$ Hz) and the typi-

[*] Prof. Dr. E. Niecke, Dipl.-Chem. M. Larbig, Dr. M. Nieger, Dr. V. von der Gönna, Dr. A. V. Ruban
Anorganisch-chemisches Institut der Universität
Gerhard-Domagk-Strasse 1, D-53121 Bonn (Germany)
Telefax: Int. code + (228)73-5327

[**] This work was supported by the Deutsche Forschungsgemeinschaft (SFB 334) and the Fonds der Chemischen Industrie.

cal position of the ^{1}H NMR (δ = 5.51) and ^{31}P NMR signals (δ = 45.8 Hz). The cyclic structure of **5** is indicated for example in the ^{13}C and ^{1}H NMR spectra by a methylene group linked with the phosphorus atom [$\delta(^{13}C)$ = 40.5 (J(P,C) = 76.3 Hz); $\delta(^1H)$ = 1.75 (J(H,P) = 11.0 Hz), 2.21 (J(H,P) = 12.0, J(H,H) = 15.1 Hz)].

The crystal structures of the compounds **2**, **4**, and **6** were confirmed by X-ray structure analyses. Figure 1 shows the molecular structure of the azidophosphane **2**. Like the azide groups in

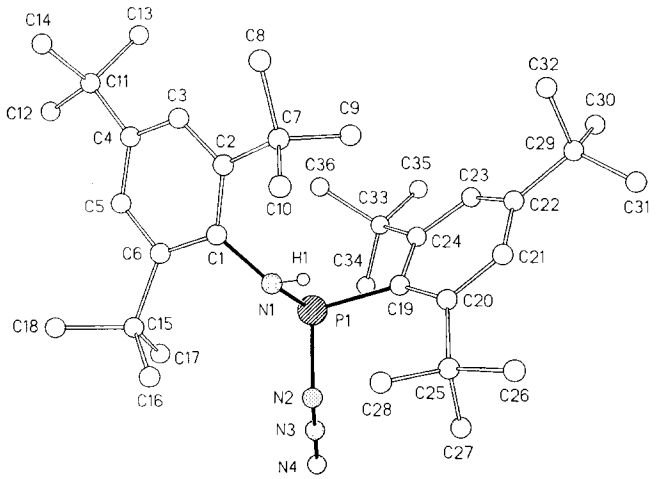


Fig. 1. Molecular structure of **2** in the crystal. Selected bond lengths [pm] and angles [°]: P1–N1 168.3(5), P1–N2 177.3(4), N2–N3 120.1(7), N3–N4 112.6(7), P1–C19 184.8(6); N1-P1-N2 100.8(2), N1-P1-C19 104.0(2), N2-P1-C19 104.2(2), P1-N1-C1 118.9(4), P1-N2-N3 118.4(4), N2-N3-N4 173.0(6).

the only structurally characterized azidophosphane, 2,4,6-tBu$_3$C$_6$H$_2$P(N$_3$)$_2$,[13] the N$_3$ substituent in **2** is almost linear (angle at N3: 173.0°); the N–N distances differ significantly (N2–N3 120.1 pm, N3–N4 112.6 pm) and the N2 atom is sp^2 hybridized (P1-N2-N3 118.4°). The relatively large P1–N2 distance (177.3 pm) possibly arises due to the repulsive interaction between the lone pairs on the N1 and P1 atoms. The distances P1–N1 (168.3 pm) and P1-C19 (184.8 pm) and the angles at the P atom (N2-P1-C19 104.2°, N1-P1-N2 100.8°, N1-P1-C19 104.0°) are not unusual.

The molecular structures of the phosphoranes **4** and **6** are shown in Figure 2 (the values in square brackets in the following refer to **6**). As in all structurally investigated imino(ylene)phosphoranes,[1] the central phosphorus atom is in a trigonal-planar environment (sum of the angles at P: 360.0° [360.0°]). The two ArP=NAr units adopt the thermodynamically favored E configuration,[14] just like the ArP=NH fragment in **4**. The aryl substituent at P1 is arranged approximately orthogonal to the central π-bond system (angle between the plane C19-P1-N1-N2 [C1-P1-N1-O1] and the aryl plane is 88.8° [89.1°]), in contrast the aryl group at N1 adopts an almost coplanar arrangement (angle between the plane C19-P1-N1-N2 [C1-P1-N1-O1] and the aryl plane is 8.3° [7.6°]). The angle at the imine nitrogen N1 (161.8° [160.0]), indicative of sp hybridization, is unusual. It explains the relatively short P–N1 distance (150.1 pm [148.9 pm]). The strengthening of the P–N1 bond in **4** is compensated by a weakening of the P–N2 bond (154.2 pm). Whether the P–O bond in **5** (146.6 pm) is also weakened cannot be verified due to the lack of data for comparison.[15]

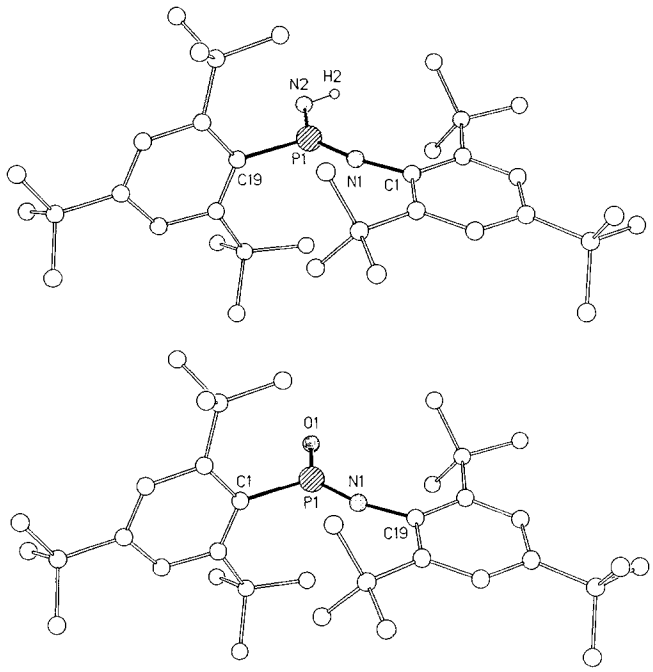


Fig. 2. Top: Molecular structure of **4** in the crystal. Selected bond lengths [pm] and angles [°]: P1–N1 150.1(2), P1–N2 154.2(2), P1–C19 180.1(2), N1–C1 140.8(3); N1-P1-N2 138.6(1), N1-P1-C19 114.1(1), N2-P1-C19 107.3(1), P1-N1-C1 161.8(1). Bottom: Molecular structure of **6** in the crystal. Selected bond lengths [pm] and angles [°]: P1–N1 148.9(2), P1–O1 146.6(2), P1–C1 179.6(2), N1–C19 140.7(2); O1-P1-N1 134.1(1), O1-P1-C1 112.1(1), N1-P1-C1 113.8(1), P1-N1-C19 160.0(1).

Experimental Procedure

2: A solution of the iminophosphorane **1** (5.34 g, 10 mmol), methanol (0.32 g, 10 mmol), and trimethylsilylazide (1.15 g, 15 mmol) in diethyl ether (30 mL) was stirred for about 12 h at room temperature. After the end of the reaction, which was apparent by a color change from deep violet to orange, all volatiles were removed in vacuum and the residue was taken up in hexane. The product was crystallized at 4 °C. Yield: 4.14 g (72%), m.p. 134–136 °C (decomp). ^{31}P NMR (C_6D_6): δ = 96.0 (d, ^2J(P,H) = 5.9 Hz); ^{1}H NMR (C_6D_6) (without aryl groups): δ = 4.86 (d, ^2J(H,P) = 5.9 Hz); MS (70 eV/200 °C) m/z (%): 578 [M^+] (2), 550 [$M^+ - N_2$] (28), 493 [$M^+ - N_2 - t$Bu] (100).

4, **5**: The azidophosphane **2** (1.47 g, 2.5 mmol) was dissolved in hexane (10 mL) and was heated with stirring at 60 °C for about 12 h until complete conversion (^{31}P NMR spectroscopic control). Subsequently, the solution was concentrated to about half and cooled to −30 °C. In this way the product precipitated as white crystals. Yield: 0.8 g (57%). M.p. 153–155 °C. ^{31}P NMR (C_6D_6): δ = 45.8 (d, ^2J(P,H) = 22.0 Hz); ^{1}H NMR (C_6D_6) (without aryl groups): δ = 5.51 (d, ^2J(H,P) = 22.3 Hz); MS (70 eV/190 °C) m/z (%): 550 [M^+] (5), 535 [M^+ – Me] (4), 493 [$M^+ - t$Bu] (100). When the reaction mixture was refluxed for 3d, **5** was formed quantitatively. M.p. 184–187 °C. ^{31}P NMR (C_6D_6): δ = 17.2; ^{1}H NMR (C_6D_6): δ 1.21 (s, 3H; Me), 1.23 (s, 3H; Me), 1.35, 1.48, 1.55, 1.86, 1.88 (all s, each 9H; tBu), 1.75 (dd, 1H, J(H,P) = 11.0, J(H,H) = 15.1 Hz; HCP) 2.21 (dd, J(H,P) = 12.0, J(H,H) = 15.1 Hz; HCP), 2.49 (d, 2H, J(H,P) = 1.3 Hz; H_2NP), 7.28 (dd, 1H, J(H,P) = 3.9, J(H,H) = 1.8 Hz; aryl-H), 7.58 (dd, 1H, J(H,P) = 2.2, J(H,H) = 2.4 Hz; aryl-H), 7.69 (dd, 1H, J(H,P) = 1.4, J(H,H) = 2.4 Hz; aryl-H), 7.72 (dd, 1H, J(H,P) = 5.1, J(H,H) = 1.8 Hz; aryl-H); ^{13}C NMR (C_6D_6) (selection): δ = 40.5 (d, J(C,P) = 76.3 Hz; CH_2P), 39.1 (d, J(C,P) = 7.6 Hz; Me_2CCP), 129.9 (d, J(C,P) = 126.7 Hz; *ipso*-CP); MS (70 eV/190 °C) m/z (%): 550 [M^+] (74), 535 [M^+ – Me] (73), 493 [$M^+ - t$Bu] (100).

6: An ozone-oxygen mixture was bubbled into a stirred solution of **1** (5.35 g, 10 mmol) in dichloromethane (150 mL) at −78 °C until a sudden change in color from violet to yellow took place. The solution was allowed to warm to room temperature and evaporated to dryness in vacuum. The residue was taken up in hexane (ca. 10 mL). The imino(oxo)phosphorane **6** crystallized from this solution at −30 °C. Yield: 4.8 g (87%), m.p. 120–122 °C. ^{31}P NMR (C_6D_6): δ = 34.2; MS (70 eV/180 °C) m/z (%) = 551 [M^+] (16), 494 [$M^+ - t$Bu] (100).

X-ray structure analysis for **2**: $C_{36}H_{59}N_4P$ [11]: colorless crystals, crystal dimensions 0.15 × 0.22 × 0.25 mm; M_r = 578.8; orthorhombic, space group *Pbca* (no. 61), a = 18.153(4), b = 17.684(4), c = 22.505(4) Å, V = 7.224(3) nm^3, Z = 8, $\mu(Cu_{K\alpha})$ = 0.87 mm^{-1}, T = 208 K, $F(000)$ = 2544. 9069 reflections up to $2\theta_{max}$ = 110° were measured on an Enraf-Nonius CAD4 diffractometer, of these 4546 were independent and were used for all calculations. The structure was solved by direct methods

 © VCH Verlagsgesellschaft mbH, D-69451 Weinheim, 1995 0570-0833/95/0404-0461 $ 10.00+.25/0

and refined anisotropically against F^2, the H atoms were refined with a riding model (HN free) (SHELXL-93 [12]). The final quality coefficient $wR2$ (F^2) was 0.214, with a conventional $R(F) = 0.065$ for 391 parameters. A semiempirical absorption correction based on ψ scans was carried out.

X-ray structure analysis for **6** [and **4**]: $C_{36}H_{58}NOP$ [$C_{36}H_{59}N_2P$] [11]: colorless crystals, crystal dimensions $0.40 \times 0.40 \times 0.50$ [$0.20 \times 0.40 \times 0.43$] mm; $M_r = 551.8$ [550.8]; monoclinic [monoclinic], space group $P2_1/c$ (no. 14) [$P2_1/c$ (no. 14)], $a = 18.660(1)$ [18.591(1)], $b = 9.999(1)$ [9.937(1)], $c = 21.138(1)$ [20.941(3)] Å, $\beta = 115.87(1)$ [115.73(1)]°, $V = 3.5487(4)$ [3.4849(7)] nm^3, $Z = 4$ [4], $\mu(Cu_{K\alpha}) = 0.86$ [0.86] mm^{-1}, $T = 293$ [200] K, $F(000) = 1216$ [1216]. 7468 [5412] reflections up to $2\theta_{max} = 148$ [120]° were measured on an Enraf-Nonius CAD4 diffractometer, of these 7239 [5155] were independent and were used for all calculations. The structure was solved by direct methods and refined anisotropically against F^2, the H atoms were refined with a riding model (SHELXL-93 [12]). The final quality coefficient $wR2$ (F^2) was 0.177 [0.171], with a conventional $R(F) = 0.052$ [0.057] for 353 [374] parameters [and 1 restraint]. A semiempirical absorption correction based on ψ scans and an extinction correction was carried out.

Received: September 14, 1994 [Z 7314 IE]
German version: *Angew. Chem.* **1995**, *107*, 505

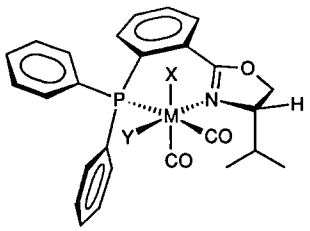
Keywords: nitrogen compounds · phosphoranes · phosphorus compounds

[1] Review: "Bis(imino)phosphoranes": E. Niecke, D. Gudat in *Multiple Bonds and Low Coordination in Phosphorus Chemistry* (Eds.: M. Regitz, O. J. Scherer), Thieme, Stuttgart, **1991**, pp. 392–404.
[2] W. Keim, R. Appel, A. Storeck, C. Krüger, R. Goddard, *Angew. Chem.* **1981**, *93*, 91–92; *Angew. Chem. Int. Ed. Engl.* **1981**, *20*, 116–117; G. Fink, V. Möhring, *Stud. Surf. Sci. Catal.* **1986**, *25*, 233–234.
[3] We have recently achieved the functionalization of the phosphorus atom in bis(imino)phosphoranes: A. Ruban, M. Nieger, E. Niecke, *Angew. Chem.* **1993**, *105*, 1544–1545; *Angew. Chem. Int. Ed. Engl.* **1993**, *32*, 1419–1420.
[4] L. N. Markovskii, V. D. Romanenko, A. V. Ruban, A. B. Drapailo, *J. Chem. Soc. Chem. Commun.* **1984**, 1692–1693.
[5] M. Lysek, Dissertation, Universität Bielefeld, **1987**.
[6] On the NMR spectroscopic detection of a phosphinonitrene see: A. Baceiredo, G. Bertrand, J. P. Majoral, G. Sicard, *J. Am. Chem. Soc.* **1984**, *106*, 6088–6089.
[7] The 1,3-silyl group shift is well documented for the decomposition of N-silylated amino(azido)phosphanes: J. Böske, E. Niecke, E. Ocando-Mavarez, J. P. Majoral, G. Bertrand, *Inorg. Chem.* **1986**, *25*, 2695–2698.
[8] A. H. Cowley, M. Pakulski, *Tetrahedron Lett.* **1984**, *25*, 2125–2126.
[9] J. I. Cadogan, S. Bracher, I. Gosney, S. Yaslak, *Phosphorus Sulfur* **1983**, *18*, 229–232; S. Bracher, J. I. Cadogan, I. Gosney, S. Yaslak, *J. Chem. Soc. Chem. Commun.* **1983**, 857–858.
[10] 4,5-Dihydro-1*H*-tetraazaphospholes are observed generally in the reaction of iminophosphanes with alkyl or aryl azides. Review: E. Niecke, D. Gudat, *Angew. Chem.* **1991**, *103*, 251–270; *Angew. Chem. Int. Ed. Engl.* **1991**, *30*, 217–236.
[11] Further details of the crystal structure investigations may be obtained from the Fachinformationszentrum Karlsruhe, D-76344 Eggenstein-Leopoldshafen (FRG) on quoting the depository number CSD-58656.
[12] G. M. Sheldrick, SHELXL-93, Universität Göttingen, **1993**.
[13] A. H. Cowley, F. Gabbai, R. Schluter, D. Atwood, *J. Am. Chem. Soc.* **1992**, *114*, 3142–3144.
[14] R. Ahlrichs, H. Schiffer, *J. Am. Chem. Soc.* **1985**, *107*, 6494–6498; W. W. Schoeller, C. Lerch, *Inorg. Chem.* **1986**, *25*, 576–580.
[15] In the only structurally investigated oxo(ylene)phosphorane, ArP(=O)=C(Ph)SiMe$_3$ (Ar = 2,4,6-tBu$_3$C$_6$H$_2$), the P–O distance was 145.8 pm: R. Appel, F. Knoch, H. Kunze, *Angew. Chem.* **1984**, *96*, 159; *Angew. Chem. Int. Ed. Engl.* **1984**, *23*, 157.

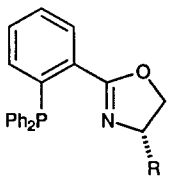
Chiral Phosphanodihydrooxazoles in Asymmetric Catalysis: Tungsten-Catalyzed Allylic Substitution**

Guy C. Lloyd-Jones and Andreas Pfaltz*

Recently, asymmetric Pd-catalyzed allylic substitution has received considerable attention and excellent enantioselectivities may now be achieved in certain cases.[1–3] Alternative transition metal catalysts for this reaction have been less actively researched. In the group VI series, Faller et al. have described stoichiometric stereospecific alkylations of allylmolybdenum complexes[4] and Trost et al. have done pioneering work on achiral molybdenum and tungsten catalysts with which the regioselectivity is often complementary to the Pd-catalyzed reaction.[5] Herein we report on the properties of tungsten complexes (**1**) of chiral phosphanodihydrooxazoles **2**[2c, d, 3b] as catalysts for enantioselective allylic substitution.[6]



1a M = W, X = Cl, Y = allyl
1b M = W, X = Br, Y = 1-phenylallyl
1c M = W, X = CH_3CN, Y = CO
1d M = W, X = CO, Y = CO
1e M = Mo, X = CH_3CN, Y = CO



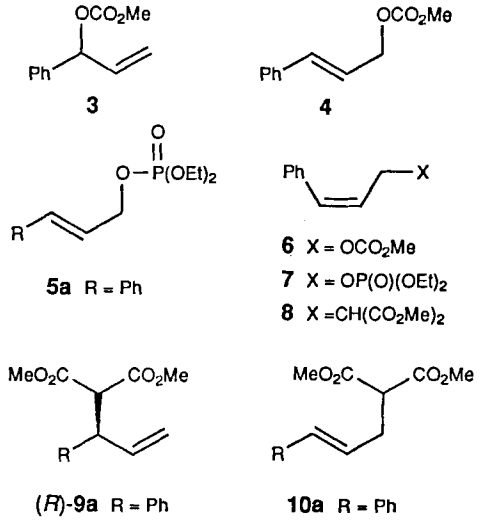
2a R = *i*Pr
2b R = Me
2c R = CH_2Ph
2d R = Ph
2e R = *t*Bu
2f R = *i*Bu

In initial experiments, racemic carbonate **3** was treated with $NaCH(CO_2Me)_2$ (2.6 equiv) in the presence of 9 mol% **1a** (THF, 60 °C) to afford (*S*)-**9a** and **10a** in 71% yield with encouraging regioselectivity (**9a**:**10a** = 78:22) but negligible enantioselectivity (5% *ee*). There was no reaction in the absence of catalyst. Primary carbonates **4** and **6** failed to react, however, the corresponding diethyl phosphate **5a** was smoothly converted to a 23:77 mixture of (*R*)-**9a** (82% *ee*) and **10a** in 75% yield, whilst the (*Z*) isomer **7** gave (*S*)-**9a** (17% *ee*) and **8** in 55% yield (**9a**:**8** = 18:82). Control experiments demonstrated that the regioselectivities, but not enantioselectivities were compromised by competing uncatalyzed reactions.[7] Interestingly, stoichiometric reactions of complexes **1a** or **1b** with excess $NaCH(CO_2Me)_2$ resulted in displacement of ligand **2a** and did not yield alkylation products. However, after addition of **5a** to the mixture, slow formation of **9a** and **10a** was observed.

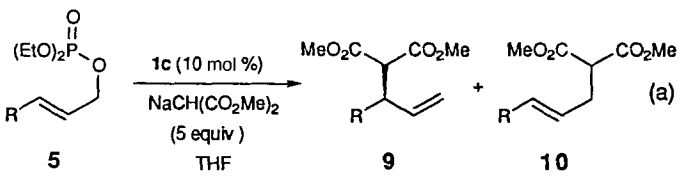
A more reactive as well as more selective catalyst was obtained by the following procedure: $[W(CO)_3(CH_3CN)_3]$ or [W(cycloheptatriene)$(CO)_3$] (10 mol%) was treated first with **2a** (60 °C, THF, 30 min), then $NaCH(CO_2Me)_2$ (2.6 equiv, THF,

[*] Prof. Dr. A. Pfaltz, Dr. G. C. Lloyd-Jones
Institut für Organische Chemie der Universität
St.-Johanns-Ring 19, CH-4056 Basel (Switzerland)
Telefax: Int. code + (61)322-6966

[**] Financial support of this work by the Swiss National Science Foundation and F. Hoffmann-La Roche, Basel, is gratefully acknowledged. G. C. L.-J. thanks the Royal Society (London) for a postdoctoral fellowship (1992–1994). We thank Mr Jürg Lehmann for preparing substrates **5a–e**.



60 °C, 2 h), and finally with the allylic phosphate at a range of temperatures (−30–+60 °C). The order of addition[8] and careful exclusion of oxygen were found to be crucial. Using this procedure, **5a** afforded (*R*)-**9a** as the major regioisomer in good yield and with high *ee* (at −10 °C: 95% yield of **9a** + **10a** (72:28), 96% *ee*; at 25 °C: 97% yield (69:31), 92% *ee*). Complex **1c** afforded an equally selective but more reactive catalyst than that generated in situ [Table 1, Eq. (a)].[9] Similarly high



enantio- and regioselectivities were also observed with other aromatic substrates **5b–e**.[10] (*E*)-2-Butenyl phosphate **5f**, on the other hand, reacted with reverse regioselectivity and moderate enantioselectivity. The isostructural Mo complex **1e** was not useful as a catalyst under these conditions (Table 1).

Table 1. Enantioselective allylic alkylation catalyzed by **1c** [Eq. (a)][a].

Substrate	R	*T* [°C]	*t* [h]	Yield [b] (**9** + **10**) [%]	**9**:**10**	*ee* of **9** [%] [c]
5a	Ph	−10	71	89	74:26	96 (*R*)
5b	4-MeC$_6$H$_4$	−13	208	92	80:20	95 (*R*)
		25	136	86	80:20	94 (*R*)
5c	4-ClC$_6$H$_4$	−13	214	95	80:20	89 (*R*)
		25	136	94	78:22	88 (*R*)
5d	4-PhC$_6$H$_4$	−13	228	98	79:21	90 (*R*)
		25	136	98	79:21	91 (*R*)
5e	1-naphthyl	−13	228	80	96:4	87 (*R*)
		25	136	93	95:5	86 (*R*)
5f	Me	25	19	77	27:73	65
5a	Ph[d]	25	71	28	12:78	61 (*R*)
7		25	84	84[e]	66:34[e]	30 (*S*)

[a] 10 mol% of **1c**; conditions: see Experimental Procedure. [b] Yields of **9** and **10** after chromatography. [c] Determined by HPLC (Chiralcel OJ). Configurational assignments: (*S*)-(−)-**9a** was converted to (*S*)-(+)-dimethyl phenylsuccinate. This confirms the previous mechanism-based assignment [4c]. (*R*)-(+)-**9b–d**: by CD comparison with (*R*)-(+)-**9a**. (*R*)-(+)-**9e**: by comparison of the CD spectrum of the corresponding 5,6,7,8-tetrahydronaphthyl-propyl derivative prepared by hydrogenation (Pt/Al_2O_3, 50 bar H_2, AcOH) with the spectrum of the phenylpropyl derivative obtained by hydrogenation of (*R*)-(+)-**9a**. [d] Using Mo complex **1e** generated in situ. [e] The products were (*S*)-**9a** and **8** (no (*E*) isomer **10a** detected).

Tungsten complexes of the phosphanodihydrooxazoles **2b, c** decomposed rapidly, whilst bulkier substituents at the stereogenic center (**2d–f**) resulted in dramatically lowered rates and selectivities. The rapid (*E*/*Z*) equilibration and epimerization processes that are prevalent under Pd catalysis[11] were not observed in any of the W-catalyzed reactions, consistent with previous observations by Trost et al.[5b] Hence compared to **5a**, the *Z* isomer **7** yields the opposite enantiomer of **9a** in 30% *ee* together with **8** but no detectable *E* isomer **10a**.

The active complex derived from **1c** is the first example of an enantioselective tungsten catalyst for allylic alkylation. The regio- and enantioselectivities with arylpropenyl phosphates **5a–e** are opposite to those obtained by using analogous Pd(phosphanodihydrooxazole) catalysts.[11] Our results further illustrate the utility of phosphanodihydrooxazole ligands[2c, d, 3b] in asymmetric catalysis.

Experimental Procedure

All manipulations were performed on a vacuum line under Ar with degassed solvents.

1c: A vigorously stirred suspension of [W(CO)$_3$(CH$_3$CN)$_3$] [12] (0.767 mmol) in THF (15 mL) and **2a** (1.34 mmol) was heated to 60 °C for 3 h, cooled to 25 °C, and filtered. The dark red filtrate was carefully layered with hexane (20 mL). After complete diffusion (9 days), the resultant dark red blocks were isolated by filtration, washed with 1:1 THF/hexane (2 × 20 mL) and dried in vacuo to afford **1c** (364 mg; 63%) as a 1:1 complex with THF [6]. Correct elemental analysis for $C_{33}H_{35}N_2O_5PW$. IR(KBr): $\tilde{\nu}_{CO}$ = 1907s, 1792s cm^{-1}.

Allylic substitution: In a glove box, **1c** (0.026 mmol) was transferred into an ampoule equipped with magnetic stirring bar and Young valve. On a vacuum line, THF (2 mL) was added and the mixture stirred at 25 °C for 2 h (deep purple-red solution), then treated with NaCH(CO$_2$Me)$_2$ (1.36 mmol in 1.4 mL of THF, 25 °C, 2 h). The red catalyst solution was frozen (liquid N_2) and combined with **5b** (0.26 mmol in 2 mL of THF). The ampoule was then sealed and warmed rapidly to −13 °C. After 208 h at −13 °C, the reaction mixture was treated with 2.8 M aqueous NH_4Cl (3 mL), extracted with CH_2Cl_2, dried over Na_2SO_4, and evaporated. The crude product (^{1}H NMR: **9b**:**10b** = 80:20) was purified by chromatography (silica gel, 2.5 × 25 cm; hexane/EtOAc 9:1) to afford (*R*)-**9b** (52 mg, 73%) as a colorless oil. $[\alpha]_D$ = +40.2 (*c* = 1.0, $CHCl_3$, 24 °C); HPLC (Chiralcel OJ; 0.46 × 25 cm, 0.5 mL min^{-1}, hexane/*i*PrOH 93:7, detection at 220 nm): t_R 42.8 min (*R*), 48.5 min (*S*). Tenfold scale-up with **5a** gave similar results.

Received: September 1, 1994 [Z 7284 IE]
German version: *Angew. Chem.* **1995**, *107*, 534

Keywords: alkylations · asymmetric syntheses · catalysis · dihydrooxazoles · tungsten compounds

[1] Reviews: G. Consiglio, R. M. Waymouth, *Chem. Rev.* **1989**, *89*, 257; C. G. Frost, J. Howarth, J. M. J. Williams, *Tetrahedron: Asymmetry* **1992**, *3*, 1089; T. Hayashi in *Catalytic Asymmetric Synthesis* (Ed.: I. Ojima), VCH, New York, **1993**, pp. 325–365.

[2] See for example a) T. Hayashi, *Pure Appl. Chem.* **1988**, *60*, 7; b) B. M. Trost, R. C. Bunt, *J. Am. Chem. Soc.* **1994**, *116*, 4089; c) J. Sprinz, M. Kiefer, G. Helmchen, M. Reggelin, G. Huttner, O. Walter, L. Zsolnai, *Tetrahedron Lett.* **1994**, *35*, 1523; d) G. J. Dawson, C. G. Frost, J. M. J. Williams, S. J. Coote, *ibid.* **1993**, *34*, 3149; e) J. M. Brown, D. I. Hulmes, P. J. Guiry, *Tetrahedron* **1994**, *50*, 4493; f) A. Togni, C. Breutel, A. Schnyder, F. Spindler, H. Landert, A. Tijani, *J. Am. Chem. Soc.* **1994**, *116*, 4062; g) D. Tanner, P. G. Andersson, A. Harden, P. Somfai, *Tetrahedron Lett.* **1994**, *35*, 4631.

[3] a) A. Pfaltz, *Acc. Chem. Res.* **1993**, *26*, 339; b) P. von Matt, A. Pfaltz, *Angew. Chem.* **1993**, *105*, 614; *Angew. Chem. Int. Ed. Engl.* **1993**, *32*, 566; P. von Matt, O. Loiseleur, G. Koch, A. Pfaltz, C. Lefeber, T. Feucht, G. Helmchen, *Tetrahedron: Asymmetry* **1994**, *5*, 573.

[4] a) J. W. Faller, M. R. Mazzieri, J. T. Nguyen, J. Parr, M. Tokunaga, *Pure Appl. Chem.* **1994**, *66*, 1463; b) J. W. Faller, K.-H. Chao, *J. Am. Chem. Soc.* **1983**, *105*, 3893; c) J. W. Faller, C. Lambert, M. R. Mazzieri, *J. Organomet. Chem.* **1990**, *383*, 161.

[5] a) Molybdenum: B. M. Trost, M. Lautens, *J. Am. Chem. Soc.* **1982**, *104*, 5543; *ibid.* **1983**, *105*, 3344; *ibid.* **1987**, *109*, 1469; *Tetrahedron* **1987**, *43*, 4817; B. M. Trost, C. A. Merlic, *J. Am. Chem. Soc.* **1990**, *112*, 9590; b) tunsten: B. M. Trost, M.-H. Hung, *ibid.* **1983**, *105*, 7757; *ibid.* **1984**, *106*, 6837; B. M. Trost, G. B. Tometzki, M.-H. Hung, *ibid.* **1987**, *109*, 2176.

[6] The synthesis and X-ray structures of complexes **1a–d** will be reported elsewhere: G. C. Lloyd-Jones, A. Pfaltz, *Z. Naturforsch. B*, in press.
[7] Uncatalyzed reactions (c(substrate) = 0.09 M in THF, 2.6 equiv of $NaCH(CO_2Me)_2$, 60 °C) gave exclusively the achiral regioisomers (81% **10a** from **5a** after 18 h; 58% **8** from **7** after 24 h). At −13 °C: ca. 1% conversion in two weeks (0.07 M **5a**, 5.5 equiv of $NaCH(CO_2Me)_2$).
[8] Reaction of $[W(CO)_3(CH_3CN)_3]$ with $NaCH(CO_2Me)_2$ in the presence of **2a** resulted in much lower activity. In the absence of $NaCH(CO_2Me)_2$, $[W(CO)_3(CH_3CN)_3]$ presumably reacts with **2a** and **5a** or **7** to generate analogues of **1b**, resulting in lower reactivity and poor regioselectivity. The importance of adding $NaCH(CO_2Me)_2$ before the substrate has also been noted with W(bpy) catalysts (ref. [5b]).
[9] $[W(CO)_3(CH_3CN)_3]$ reacts with **2a** (^1H, ^{31}P NMR, $[D_8]THF$) to yield a mixture including **1c**, **1d**, and $[(\mathbf{2a})_2W(CO)_3]$, the ratios of which depend on the relative amounts of the starting compounds (ref. [6]). Compound **1d** is inactive as a catalyst.
[10] Substrates **5a–e** were prepared from the corresponding aromatic aldehydes: (1) CH_2 = $CHMgCl$, THF, 25 °C, 60–83%; (2) Ac_2O, Et_3N, DMAP, CH_2Cl_2, 25 °C, 86–96%; (3) $[Pd(CH_3CN)_2Cl_2]$ (1 mol%), THF 25 °C, 68–97%; (4) MeOH, K_2CO_3 (cat), 25 °C, 47–81%; (5) $(EtO)_2POCl$, C_5H_5N, DMAP, CH_2Cl_2, 25 °C, 50–80%.
[11] P. von Matt, Dissertation, University of Basel, **1993**.
[12] D. P. Tate, W. R. Knipple, J. M. Augl, *Inorg. Chem.* **1962**, *1*, 433.

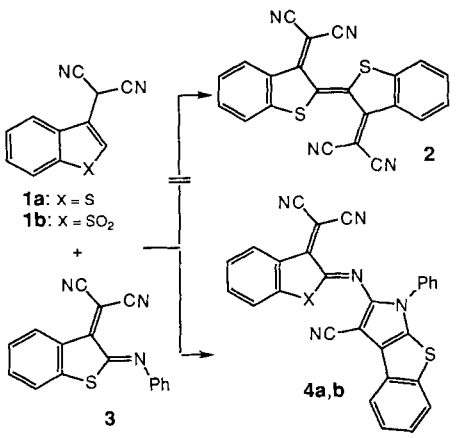
Bis(dicyanomethylene) and Bis(cyanoimino) Derivatives of Indigo and Thioindigo**

Rudolf Gompper,* Karsten Hartmann, Robert Kellner, and Kurt Polborn

Indigo and related compounds are of great technical importance owing to their properties as dyes. The indigo chromophore giving this class of relatively small and simple molecules their characteristic intense color has been the subject of numerous investigations.[1] Surprisingly, no indigo derivatives are known in which the O atoms of the carbonyl groups have been replaced by other electron-withdrawing groups. We report here on our successful synthesis of compounds of this type.

In our studies we focused on dicyanomethylene and cyanoimino groups, in particular, as acceptor groups. (The analogy between dicyanovinyl and carbonyl functions was discussed in detail previously.[2]) Since these groups extend the π-electron system, it was expected that the resulting chromogens would absorb at longer wavelengths, possibly even in the near-IR (> 700 nm). An additional bathochromic shift due to the twist of the compounds about the central double bond as a result of steric repulsion may also contribute (cf. ref. [3]).

A typical method for the synthesis of indigoid dyes is the condensation of compounds such as indolin-3-one ("indoxyl") or benzo[*b*]thiophen-3(2*H*)-one ("oxythionaphthene") with anils like 2-phenyliminoindolin-3-one ("isatin-2-anil").[4] However, the reaction of benzo[*b*]thien-3-ylmalodinitrile **1a**[5] with anil **3** in acetic anhydride/glacial acetic acid did not lead to the desired thioindigo derivative **2**. Instead an unusual reaction sequence produced a poorly soluble, dark blue compound (λ_{max} = 662 nm (DMSO)), which we assign structure **4a** based on its analytical and spectroscopic data (which are similar to those of the better characterized **4b**). To our knowledge, compounds of this type have not been described previously. The analogous compound **4b** (λ_{max} = 590 nm (DMSO)) was prepared from sulfone **1b**[5b, 6]



and **3**. The crystal structure analysis[7] of **4b** (Fig. 1) shows that the phenyl ring avoids interaction with the dicyanomethylene groups by twisting out of the plane of the tricyclic system. In contrast, the bond to the dicyanomethylene group (C2–C9) is only slightly twisted (8.3°).

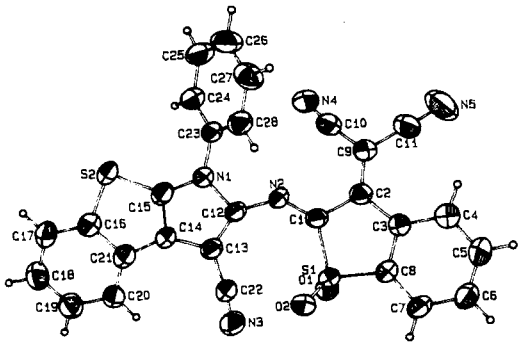
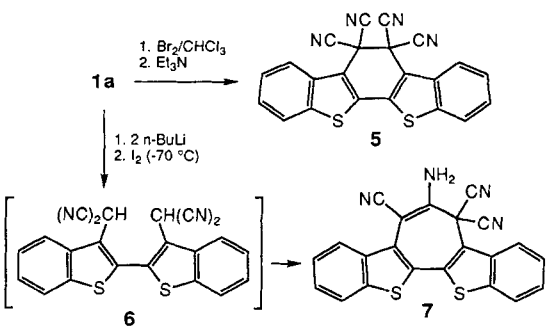


Fig. 1. Crystal structure of **4b** [7] (ORTEP plot). Selected bond lengths [Å] and angles [°]: C1-N 127.3(7), C1-C2 1461(8), C1-S1 180.1(4), C2-C9 136.1(6), C9-C10 144.3(8), C9-C11 142.5(9), C10-N4 141.1(8), C11-N5 113.1(8), C12-N1 142.0(7), C12-N2 133.6(8), C13-C22 142.7(7), C22-N3 112.9(7), C14-C15 138.6(6), C15-N1 134.3(8), C15-S2 171.9(6), C16-S2 177.0(5); C1-N2-C12 134.5(4), C1-S1-C8 92.8(2), C12-N1-C15 107.8(4), C15-S2-C16 89.5(3); C1-C2-C9-C10 6.39(0.87), C1-C2-C9-C11 1.61(0.55), C3-C2-C9-C11 6.22(0.91), C3-C2-C9-C10 10.99(0.53), C12-N1-C23-C24 46.87 (0.52), C15-N1-C23-C28 48.30(0.54).

Thioindigo can be obtained, for example, by treatment of 2-bromobenzo[*b*]thiophen-3(2*H*)-one with base or by reaction of its 2,2-dibromo derivative with benzo[*b*]thiophen-3(2*H*)-one.[8] Despite extensive efforts we were not able to prepare either the mono- or dibromo derivative of **1a** because of the instability of the products. However, treatment of a solution of **1a** in chloroform at room temperature with bromine, followed by addition of triethylamine gave the yellow bi(benzothiophene) derivative **5**



[*] Prof. Dr. R. Gompper, Dr. K. Hartmann, Dr. R. Kellner, Dr. K. Polborn
Institut für Organische Chemie der Universität
Karlstrasse 23, D-80333 München (Germany)
Telefax: Int. code + (89) 5902-420

[**] This work was supported by the Deutsche Forschungsgemeinschaft and the Fonds der Chemischen Industrie.

in addition to a small amount of an isomeric yellow compound. Electrocyclization of the *cis* derivative of **2** is presumed to provide **5**. The UV/VIS spectrum of the side product (λ_{max} = 425 nm (CH_2Cl_2)) indicates that it is not **2**, which like its *cis* isomer should absorb at much longer wavelengths.

In the crystal structure analysis[9] of **5** (Fig. 2) the twisted cyclohexadiene ring apparently prevents an eclipsed arrangement of the nitrile groups. As a result the planes of the two

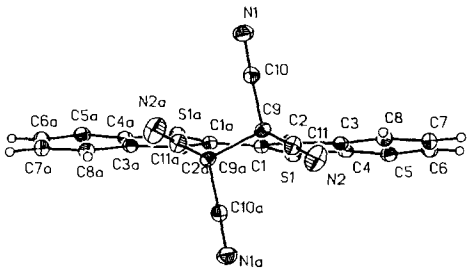


Fig. 2. Crystal structure of **5** [9] (ORTEP plot). Selected bond lengths [Å] and angles [°]: C1-C1a 145.1(6), C2-C9 152.4(4), C9-C9a 161.2(6), C2-C3 143.9(4), C1-S1 170.7(3), C9-C10 148.9(5), C9-C11 147.7(4); C2-C1-C1a 121.8(2), C2-C9-C9a 109.5(2), C1-C2-C3 113.3(3), C10-C9-C11 108.5(3), S1-C1-C2 113.4(2), C2-C3-C4 109.7(3), S1-C4-C3 112.5(2), C1-S1-C4 91.1(1).

benzo[*b*]thiophene units are tilted in opposite directions forming an angle of 17.8°. The extremely long single bond (C9–C9a; 161 pm) between the CN-substituted C atoms is especially noticeable. The conversion of **5** into **2** was not possible, even though similar reactions are known for related systems.[10]

The most common approach for the synthesis of indigoid compounds is the oxidative coupling of appropriate methylene-active "monomers" and dehydration of the resulting "dimers". Reaction of **1a** with oxidizing agents such as aerial oxygen and potassium dichromate, which are used to convert benzo[*b*]thiophene-3(2*H*)-one into thioindigo, did not lead to **2** or **5**. However, **1a** can be lithiated with butyllithium in THF at −70 °C and at the same temperature the lithium salt subsequently oxidized with iodine. The fleeting intermediate **6** undergoes ring closure to give the cycloheptatriene derivative, whose structure is similar to that of dimethylcycloheptadithiophenone.[11] We attempted to prepare the dianion of **6** by addition of two further equivalents of butyllithium and then oxidize it with iodine, but this did not succeed.

In the crystal structure analysis[12] of **7** (Fig. 3) the folding of the seven-membered ring and the slight tilt of the benzo[*b*]thiophene planes in opposite directions are evident.

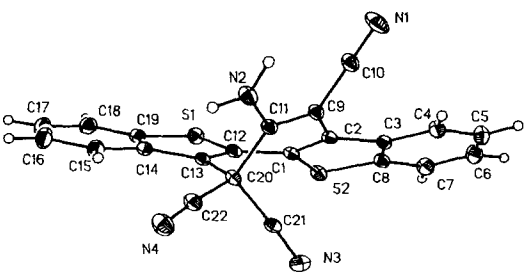
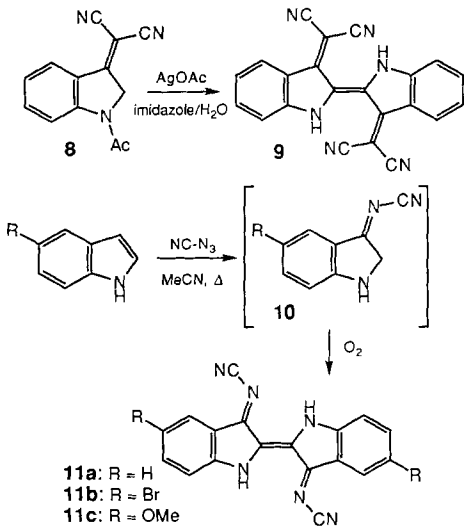


Fig. 3. Crystal structure of **7** [12] (ORTEP plot). Selected bond lengths [Å] and angles [°]: C1-C12 143.4(3), C1-C2 137.5(3), C2-C9 146.4(2), C9-C11 136.5(3), C11-C20 153.8(3), C13-C20 152.6(3), C12-C13 136.4(3), C1-S2 173.3(3), C8-S2 173.2(3), C3-C8 140.1(3), C2-C3 145.0(3); C1-C2-C9 123.9(2), C2-C9-C11 125.3(2), C11-C20-C13 107.4(1), C12-C13-C20 117.5(2), C1-C12-C13 126.1(2); C2-C1-C12-C13 −34.4(0.1), S2-C1-C12-S1 −34.0(0.2).

The conditions used for the conversion of **1a** into **5** or **7** did not convert indole derivative **8**[5b, 13] into **9**. However, oxidation of **8** to give **9** was possible with silver salts in the presence of organic bases. The best results were obtained with silver acetate in a mixture of two parts water and one part imidazole at 100 °C. Compound **9** forms as a dark green, poorly soluble powder and



can be purified by extractive recrystallization from chlorobenzene. The "medium effect" known for indigo is especially interesting here. A thin layer of solid **9** on a quartz plate absorbs at significantly longer wavelengths than in DMSO solution (λ_{max} = 778 vs 746 nm).

The bis(cyanoimino) derivatives **11** of indigo are formed by treatment of indoles with a solution of cyanogen azide in acetonitrile at reflux. In analogy to the conversion of olefins into *N*-cyanoimines by cyanogen azide[14] it can be assumed that indoline derivatives **10** form as intermediates, which are then oxidized by aerial oxygen to give **11**. The longest wavelength absorption of **11a** in DMSO lies at 751 nm (**11b**: 765; **11c**: 813 nm). Compounds **9** and **11** absorb at significantly longer wavelengths than indigo (λ_{max} (DMSO) = 621 nm), and are thus new near-IR dyes.

Like indigo, **9** and **11** can be converted to colorless, water-soluble forms by treatment with alkaline sodium dithionite solution. For **9** this process is irreversible; in the case of **11** the dye can be recovered by exposure to aerial oxygen or treatment with $K_3[Fe(CN)_6]$.

In conclusion the UV/VIS spectra of **9** and **11** display the anticipated strong bathochromic shift relative to that of indigo. Since crystal structure analyses of the new compounds are not available, the bonding relationships in **9** and **11** must be derived from AM1 calculations.[15] These indicate that in contrast to planar **11a**, **9** has a convex structure, in which the planes of the benzene rings are tilted towards each other forming an angle of 133°; the C atoms of the central C=C bond are only slightly *cis* pyramidalized (4°). The pronounced distortion of the entire chromophore explains why **9** absorbs at somewhat shorter wavelengths than **11a**, even though dicyanomethylene systems usually absorb at longer wavelengths than cyanoimine systems.[5b]

The fact that **9** could be prepared but **2** still remains elusive points out that the gain in energy upon formation of two benzothiophene systems is a key contribution to the stability of **5**. Consistent with this, the putative "dithio-thioindigo" is actually a 1,2-dithiine derivative[16] and structurally comparable to **5**.

Experimental Procedure

3: A solution of **1a** [5] (2.0 g, 10.09 mmol) in ethanol was treated with nitrosobenzene (1.18 g, 11.00 mmol). After addition of 0.2 mL of piperidine, the reaction mixture was stirred at room temperature for 30 min. The red precipitate was removed by vacuum filtration, washed with ethanol and ether, and recrystallized from ethanol. Yield 1.41 g (45%); dark red crystals, m.p. 165–166 °C. IR (KBr): ν = 3073, 2216, 1585, 1532, 1442, 1328, 1295, 1108, 771, 728, 685 cm^{-1}. – UV/VIS (DMSO): λ_{max} (ε) = 515 nm (22390). – ^1H NMR (400 MHz, [D$_6$]DMSO): δ = 7.31 (m, 4H), 7.41 (d, ^3J = 7.4 Hz, 1H), 7.47 (t, ^3J = 8.1 Hz, 2H), 7.57 (t, ^3J = 7.4 Hz, 1H), 8.60 (d, ^3J = 8.2 Hz, 1H). – ^{13}C NMR (400 MHz, [D$_6$]DMSO): δ = 79.04, 113.16, 114.00, 121.91, 124.02, 126.93, 127.52, 128.30, 128.60, 129.54, 135.86, 142.95, 147.49, 156.99. – MS (245 °C): *m/z* (%) = 287 (100, M^+), 261 (26, M^+ – CN), 184 (40, M^+ – CN – Ph), 157 (3, M^+ – HCN – CN – Ph), 77 (20, Ph^+).

4a: A mixture of **3** (0.17 g, 0.59 mmol), **1a** (0.14 g, 0.71 mmol), 5 g of acetic anhydride, and 1 g of glacial acetic acid was heated at reflux for 10 min. The reaction mixture was cooled, and the dark blue precipitate removed by vacuum filtration, washed with hot ethanol and ether, and recrystallized from a large volume of xylene. Yield 0.11 g (39%); fine, blue-violet, metallic needles, m.p. 358–359 °C. IR (KBr): ν = 3030, 2216, 1585, 1511, 1436, 1411, 1289, 1112, 1064, 770, 761, 739 cm^{-1}. – UV/VIS (DMSO): λ_{max} (ε) = 662 (15140), 319 nm (11750). – MS (250 °C): *m/z* (%) = 485 (26, $M^+ + H_2$), 483 (100, M^+), 458 (28, 485 – HCN), 432 (19, 458 – CN, 380 (9, M^+ – CN – Ph), 366 (7, M^+ – CN – NPh), 289 (9, $C_{17}H_{11}N_3S$), 274 (32, $C_{17}H_{10}N_2S$), 261 (4, $C_{16}H_9N_2S$), 246 (7). – High-resolution MS (250 °C, ref. = 480.9697): *m/z* = 483.0626 (calcd. 483.0621).

4b: Conditions analogous to those for **4a** were used but with **3** (0.65 g, 2.26 mmol) and 0.52 g of **1b** [5b,6]. Yield 0.21 g (39%); blue-violet crystals; m.p. >350 °C. IR (KBr): ν = 2223, 1595, 1539, 1436, 1383, 1322, 1227, 1170, 1052, 764, 745, 730 cm^{-1}. – UV/VIS (DMSO): λ_{max} (ε) = 590 (4470), 294 nm (10715). – MS (200 °C): *m/z* (%) = 515 (12, M^+), 451 (20, $M^+ - SO_2$), 424 (8, $M^+ - SO_2$ – HCN), 289 (100, $C_{17}H_{11}N_3S$), 261 (25, $C_{16}H_9N_2S$), 246 (17), 212 (51, $C_{11}H_4N_2OS$), 184 (19).

5: Compound **1a** (0.99 g, 5.00 mmol) was dissolved in 50 mL of anhydrous chloroform under nitrogen. A mixture of bromine (0.80 g, 5.00 mmol) and 10 mL of anhydrous chloroform was added dropwise to this solution. The reaction mixture was stirred at room temperature for ca. 12 h. Then a mixture of triethylamine (1.11 g, 11.0 mmol) and 7 mL of anhydrous chloroform was added dropwise. The reaction mixture was again stirred at room temperature for ca. 12 h before 500 mL of chloroform was added. The solution was washed successively with water, saturated sodium bicarbonate solution, saturated sodium thiosulfate solution, and water. The solution was dried over magnesium sulfate, filtered and concentrated to dryness. The residue was recrystallized from acetic anhydride. Yield 0.40 g (41%); pale yellowish platelets, m.p. 301 °C (decomp). The product was purified further by fractional crystallization from toluene, yielding in addition to **5** (pale yellow platelets, m.p. 311–312 °C (decomp)) a small amount of an isomer (fine yellow needles, m.p. >360 °C). **5**: IR (KBr): ν = 3060, 2255, 2248, 1510, 1461, 1436, 1322, 1315, 1242, 759, 727 cm^{-1}. – UV/VIS (CH_2Cl_2): λ_{max} (ε) = 386 (18620), 367 (23990), 350 (21380), 329 (sh, 14450), 257 (17380), 228 nm (30200). – ^1H NMR (400 MHz, $CDCl_3$): δ = 7.60 (ddd, ^3J = 8.1 Hz, ^3J = 7.2 Hz, ^4J = 1.2 Hz, 2H, H-3, H-8), 7.67 (ddd, ^3J = 8.4 Hz, ^3J = 7.2 Hz, ^4J = 1.2 Hz, 2H, H-2, H-9), 7.99 (mc, ^3J = 8.1 Hz, 2H, H-4, H-7), 8.46 (mc, ^3J = 8.4 Hz, 2H, H-1, H-10). – ^{13}C NMR (400 MHz, $CDCl_3$): δ = 43.41, 109.31, 112.42, 121.78, 123.63, 127.25, 127.51, 134.39, 134.67, 139.73. – MS (90 °C): *m/z* (%) = 392 (100, M^+), 366 (10, M^+ – CN), 340 (31, M^+ – 2CN), 334 (4, M^+ – SCN), 328 (2, $M^+ - C_3N_2$), 327 (3, $M^+ - C_3HN_2$), 313 (1, M^+ – HCN – 2CN), 308 (4, M^+ – 2CN – S), 302 (6, M^+ – CN – C_3N_2), 295 (4), 284 (2, $M^+ - C_6H_4S$), 196 (4, M^{2+}), 170 (4).

7: To a solution of **1a** (1.98 g, 10.0 mmol) in 75 mL of anhydrous THF at −70 °C under nitrogen was added dropwise a 15% solution of butyllithium in hexane (6.7 mL, 11.0 mmol). After 30 min at room temperature the reaction mixture was again cooled to −70 °C, and iodine (1.27 g, 5.00 mmol) was added. The reaction mixture was allowed to warm slowly to room temperature, stirred for ca. 12 h, and then poured into 400 mL of water with stirring. The initially formed oil crystallized after prolonged stirring. The crystals were removed by vacuum filtration and dried under vacuum. 1.46 g of the crude product was recrystallized from a large volume of ethanol. Yield 0.96 g (49%); pale pinkish platelets, m.p. 236–237 °C. IR (KBr): ν = 3433, 3360, 3205, 3056, 2205, 1636, 1569, 1317, 1227, 766, 753, 735 cm^{-1}. – UV/VIS (DMSO): λ_{max} (ε) = 377 (2455), 341 (sh, 15490), 293 (35480), 265 nm (22910). – ^1H NMR (400 MHz, [D$_6$]DMSO): δ = 7.58–7.71 (m, 4H, aryl-H), 8.15 (s, 2H, NH_2), 8.16 (mc, 1H, aryl-H), 8.19 (d, ^3J = 8 Hz, 1H, aryl-H), 8.40 (mc, 1H, aryl-H), 8.69 (d, ^3J = 8 Hz, 1H, aryl-H). – ^{13}C NMR (400 MHz, [D$_6$]DMSO): δ = 40.39, 73.29, 110.80, 115.28, 117.32, 121.77, 123.28, 123.6, 123.81, 125.48, 125.98, 126.40, 127.16, 127.71, 129.29, 133.36, 135.13, 136.07, 138.57, 140.03, 145.28. – MS (195 °C): *m/z* (%) = 394 (28, M^+), 368 (5, M^+ – CN), 340 (6, M^+ – 2HCN), 330 (100, $M^+ - C_3N_2$), 302 (8, M^+ – CN – $C_3H_2N_2$), 197 (4, M^{2+}), 165 (5).

9: To a solution of 5.0 g of imidazole in 10 mL of water at 100 °C was added **8** [5b,12] (0.75 g, 3.38 mmol). After 1 min silver acetate (1.50 g, 8.99 mmol) was added and the mixture stirred for 2 min. The mixture was vacuum-filtered while still hot and the residue washed with boiling dimethylformamide (2 × 20 mL). The dark green residue was extractively recrystallized from chlorobenzene. Yield 0.23 g (38%); dark green amorphous powder, m.p. >350 °C. IR (KBr): ν = 3292, 2206, 1605, 1590, 1406, 1310, 1221, 747 cm^{-1}. – UV/VIS (DMSO): λ_{max} = 746, 674, 435, 395 nm. – MS (245 °C): *m/z* (%) = 358 (100, M^+), 332 (13, M^+ – CN), 331 (18, M^+ – HCN), 305 (11, M^+ – HCN – CN), 278 (18, M^+ – 2HCN – CN), 180 (5, $C_{11}H_6N_3$).

11a: A solution of cyanogen bromide (3.70 g, 34.95 mmol) in 50 mL of anhydrous acetonitrile was treated with sodium azide (2.60 g, 39.92 mmol) and stirred at room temperature for 90 min. After the precipitate was filtered off, indole (4.0 g, 34.2 mmol) was added to the light yellow solution, which was then heated to reflux. After 1 h the resulting dark green precipitate was removed by vacuum filtration, washed with hot acetonitrile, and dried. Crude yield 1.50 g (28%); purification by recrystallization from xylene; fine blue-green needles, m.p. >350 °C. IR (KBr): ν = 3281, 2160, 1610, 1540, 1456, 1312, 1109, 763 cm^{-1}. – UV/VIS (DMSO): λ_{max} (ε) = 751 (28184), 558 (2240), 378 (11220), 306 nm (36310). – MS (245 °C): *m/z* (%) = 310 (76, M^+), 284 (14, M^+ – CN), 283 (25, M^+ – HCN), 269 (6, M^+ – HNCN), 257 (18, M^+ – HCN – NCN), 181 (10, $C_{10}H_5N_4$), 156 (6, $C_9H_6N_3$), 155 (6, $C_9H_5N_3$).

Correct elemental analyses were obtained for all compounds.

Received: September 8, 1994 [Z 7300 IE]
German version: *Angew. Chem.* **1995**, *107*, 531

Keywords: dyes · indigo derivatives · thioindigo derivatives

[1] a) J. Fabian, H. Hartmann, *Light Absorption of Organic Colorants*, Springer, Berlin, **1980**, p. 32, 115, 162; b) G. Miehe, P. Süsse, V. Kupcik, E. Egert, M. Nieger, G. Kunz, R. Gerke, B. Knieriem, M. Niemeyer, W. Lüttke, *Angew. Chem.* **1991**, *103*, 1008; *Angew. Chem. Int. Ed. Engl.* **1991**, *30*, 964.

[2] a) K. Wallenfels, K. Friedrich, J. Rieser, W. Ertel, K. Thieme, *Angew. Chem.* **1976**, *88*, 311; *Angew. Chem. Int. Ed. Engl.* **1976**, *15*, 261; b) W. J. Middleton, V. A. Engelhardt, *J. Am. Chem. Soc.* **1958**, *80*, 2788.

[3] A. Beck, R. Gompper, K. Polborn, H.-U. Wagner, *Angew. Chem.* **1993**, *105*, 1424; *Angew. Chem. Int. Ed. Engl.* **1993**, *32*, 1352.

[4] a) A. Bezdrik, P. Friedländer, *Ber. Dtsch. Chem. Ges.* **1908**, *41*, 375; b) R. Pummerer, *ibid.* **1911**, *44*, 338.

[5] a) K. Hashimoto, M. Nishikuri, A. Takeshita (Sumitomo Chemical), JP-B 60-220785, **1985** [*Chem. Abstr.* **1986**, *105*, 105845u]; b) R. Kellner, Dissertation, Universität München, **1991**.

[6] a) W. Baumann (Sandoz), GB-B 2,026,528, **1980** [*Chem. Abstr.* **1980**, *93*, 48539e]; b) W. Baumann (Sandoz), FR-B 2,438,045, **1980** [*Chem. Abstr.* **1981**, *94*, 4953b].

[7] Crystal structure analysis of **4b**: A suitable crystal was obtained by vapor diffusion of ether into a solution of **4b** in chloroform. $C_{28}H_{13}N_5O_2S_2 \cdot CH_3OH \cdot CH_3CN$, M = 588.67 g mol^{-1}, crystal dimensions 0.10 × 0.20 × 0.50 mm^3, triclinic, space group $P\bar{1}$ (no.2), a = 892.7(2), b = 1222.7(4), c = 1366.7(4) pm, α = 64.64(2), β = 76.83(2), γ = 80.35(2)°, V = 13.085 nm^3, Z = 2, ρ_{calcd} = 1.2273 g cm^{-3}. Enraf-Nonius CAD-4 diffractometer, $\mu(Mo_{K\alpha})$ = 2.400 cm^{-1}, T = 294 K, ω scan, 2θ range 4–46°, maximum measurement time 120 s, scan width (0.75 + 0.35 tanθ)°, 3805 reflections measured, of which 3625 were unique, and 2685 were classified as observed [$I > 3\sigma(I)$]. Structure refinement with the SIR program package, least squares refinement with the system MolEN, 376 parameters refined, R = 0.0559, R_w = 0.0925, maximum residual electron density 0.776/−0.237 10^{-6} e pm^{-3}. Further details of the crystal structure investigations may be obtained from the Fachinformationszentrum Karlsruhe, D-76344 Eggenstein-Leopoldshafen (FRG) on quoting the depository number CSD-58657.

[8] a) P. Friedländer, *Monatsh. Chem.* **1908**, *29*, 359; b) A. Bezdrik, P. Friedländer, P. Koeninger, *Ber. Dtsch. Chem. Ges.* **1908**, *41*, 227.

[9] Crystal structure analysis of **5**: A suitable crystal was obtained from a solution of **5** in toluene. $C_{22}H_8N_4S_2$, M = 392.4 g mol^{-1}, crystal dimensions 0.3 × 0.3 × 0.6 mm^3, monoclinic, space group $C2/c$ (no. 15), a = 1435.4(3), b = 942.6(2), c = 1311.4(4) pm, β = 93.61(2)°, V = 1.7707 nm^3, Z = 4, ρ_{calcd} = 1.472 g cm^{-3}. Enraf-Nonius CAD-4 diffractometer, $\mu(Mo_{K\alpha})$ = 3.02 cm^{-1}, T = 296 K, ω scan, 2θ range 4–46°, maximum measurement time 120 s, scan width (1.2 + 0.35 tanθ)°, 1356 reflections measured, of which 1183 were unique, and 1108 were classified as observed [$I > 3\sigma(I)$]. Structure solution with SHELX-86, refinement with SHELXTL-PLUS, R = 0.0392, R_w = 0.0413, maximum residual electron density 0.22/−0.27 10^{-6} e pm^{-3}.

[10] a) K. Uchida, Y. Nakayama, M. Irie, *Bull. Chem. Soc. Jpn.* **1990**, *63*, 1311; b) A. Pawlick, W. Grahn, A. Reisner, P. G. Jones, L. Ernst, *Angew. Chem.* **1994**, *106*, 2058; *Angew. Chem. Int. Ed. Engl.* **1994**, *33*, 1958.

[11] N. R. Krishnaswamy, C. S. S. R. Kumar, *Indian J. Chem. Sect. B* **1992**, *31*, 449.

[12] Crystal structure analysis of **7**: A suitable crystal was obtained by recrystallization from ethanol. $C_{22}H_{10}N_4S_2$, M = 394.48 g mol^{-1}, crystal dimensions 0.40 × 0.47 × 0.53 mm^3, monoclinic, space group $P2_1/c$ (no. 14), a = 1264.1(3), b = 908.3(2), c = 1621.5(4) pm, β = 98.33(2)°, V = 1.8421 nm^3, Z = 4, ρ_{calcd} = 1.422 g cm^{-3}. Enraf-Nonius CAD-4 diffractometer, $\mu(Mo_{K\alpha})$ = 2.909 cm^{-1},

$T = 294$ K, ω scan, 2θ range 4–46°, maximum measurement time 60 s, scan width $(0.9 + 0.35\tan\theta)°$, 2843 reflections measured, of which 2495 were unique, and 2368 were classified as observed $[I > 3\sigma(I)]$. Structure solution with SHELXS-86, refinement with SHELXTL-PLUS, $R = 0.0291$, $R_w = 0.0310$, maximum residual electron density $0.22/-0.19\ 10^{-6}$ e pm^{-3}.

[13] V. S. Velezheva, V. P. Sevodin, V. Y. Erofeev, N. K. Genkina, T. A. Kozik, V. V. Vampilova, N. N. Suvorov, *Khim. Geterosikl. Soedin.* **1977**, 360; *Chem. Abstr.* **1977**, *87*, 102257c.

[14] F. D. Marsh, M. E. Hermes, *J. Am. Chem. Soc.* **1964**, *86*, 4506.

[15] We thank Dr. U. Thibaut, Fa. Byk-Gulden, Konstanz (FRG), for conducting the AM1 calculations.

[16] W. Schroth, personal communication, **1990**; W. Schroth, E. Hintzsche, M. Felicetti, R. Spitzner, J. Sieler, R. Kempe, *Angew. Chem.* **1994**, *106*, 808; *Angew. Chem. Int. Ed. Engl.* **1994**, *33*, 739; W. Schroth, E. Hintzsche, H. Viola, R. Winkler, H. Klose, R. Boese, R. Kempe, J. Sieler, *Chem. Ber.* **1993**, *127*, 401; W. Schroth, M. Felicetti, E. Hintzsche, R. Spitzner, M. Pink, *Tetrahedron Lett.* **1994**, *35*, 1977.

A Cyclic Hexairon(III) Complex with an Octahedrally Coordinated Sodium Ion at the Center, an Example of the [12]Metallacrown-6 Structure Type**

Andrea Caneschi, Andrea Cornia, Stephen J. Lippard*

Over the past ten years, several studies have been carried out to investigate possible pathways for the hydrolytic aggregation of iron(III) in an aqueous environment.[1] One strategy has been to use suitably designed polydentate organic ligands to control the chemical routes leading ultimately to the deposition of solids containing a portion of the α-FeO(OH) (goethite) crystal lattice. In this manner, a variety of polynuclear iron-oxo aggregates has been isolated either from aqueous[2, 3] or nonaqueous[4, 5] solutions. In particular, new synthetic techniques have been developed that take advantage of hydrolytic polymerization processes involving iron(II)/iron(III) in nonaqueous solvents to build up polyiron-oxo aggregates, which may serve as models for the mineral core in ferritin.[5] Large polyiron complexes are also of interest for obtaining nanometer-size magnetic particles.[6] The possible use of hydrolytic processes in the deposition of thin layers of iron oxides[7] makes them attractive entities for materials science as well.

Solution studies have provided evidence for the existence of a cyclic hexanuclear iron(III) species, in which the metal ions are connected by two hydroxo ligands, tentatively formulated as **1**. Such a species may be responsible for the reversible gelation

$[Fe_6(OH)_{12}(sor)_6]^{6-}$ **1**, H_2sor = sorbitol

phenomena observed upon careful neutralization of concentrated alkaline aqueous solutions of iron(III) and sorbitol.[8] We report here on the preparation and characterization of the hexanuclear iron(III) compound **2**. A solid-state X-ray diffraction study reveals that **2** has precisely the same overall ring structure as that proposed for the $[Fe_6(OH)_{12}]^{6+}$ core in **1**, and surprisingly that this ring serves as a host for the sodium ion.[9] Compound **2** thus qualifies as an authentic example of the [12]metallacrown-6 structure type.[10]

$[NaFe_6(OCH_3)_{12}(dbm)_6]Cl \cdot 12\,CH_3OH \cdot CHCl_3$ **2**, Hdbm = dibenzoylmethane

The crystal lattice of **2**[11] comprises centrosymmetric $[NaFe_6(OCH_3)_{12}(dbm)_6]^+$ cations (Fig. 1), as well as disordered chloride anions, chloroform, and methanol molecules. The six iron atoms are located at the vertices of an almost regular hexagon, with Fe···Fe separations in the range 3.18–3.20 Å, vertex angles of 119.5–120.5°, and average deviations of ±0.024 Å from the best least-squares plane. The diameter of the ring, defined as the average distance between two opposing iron atoms, is 6.39(2) Å. Bis(methoxo) bridges connect adjacent iron atoms; the remaining two sites of the distorted octahedral coordination sphere of each iron(III) center are occupied by a chelating dibenzoylmethanido ligand. Adjacent Fe_2O_2 planes through each pair of methoxo ligands and their two bound iron atoms are twisted with respect to each other and form dihedral angles of 120–121° with the mean plane of the Fe_6 ring. As a consequence, within each layer of six oxygen atoms contributed by the methoxo bridges, one above and one below the plane through the iron(III) centers, three oxygen atoms lie closer to the virtual C_6 symmetry

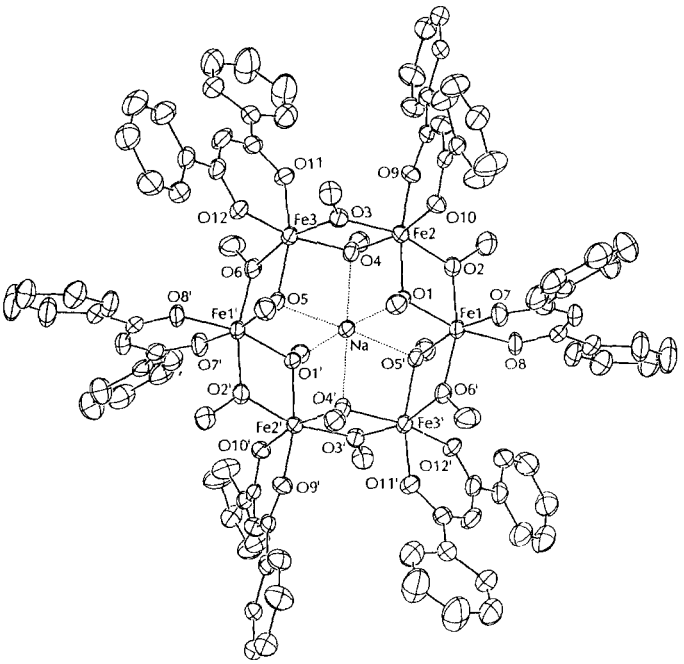


Fig. 1. ORTEP representation of the cation in **2** with atom labels. Hydrogen atoms have been omitted for clarity. An inversion center relates primed atoms to unprimed ones. Thermal ellipsoids enclose 50% probability. Relevant distances [Å] and angles [°]: Fe1-O1 2.022(3), Fe1-O2 2.005(5), Fe1-O5′ 2.019(3), Fe1-O6′ 2.003(5), Fe1-O7 1.983(3), Fe1-O8 1.975(4), Fe2-O1 2.029(5), Fe2-O2 2.001(3), Fe2-O3 2.016(4), Fe2-O4 2.025(3), Fe2-O9 1.998(5), Fe2-O10 1.977(3), Fe3-O3 2.003(3), Fe3-O4 2.027(4), Fe3-O5 2.032(5), Fe3-O6 2.007(3), Fe3-O11 1.979(5), Fe3-O12 1.996(4), Fe1-Fe2 3.184(1), Fe1′-Fe3 3.197(1), Fe2-Fe3 3.201(1), Na-O1 2.338(3), Na-O4 2.374(4), Na-O5 2.341(3); O1-Fe1-O2 75.5(2), O1-Fe1-O5′ 94.4(1), O2-Fe1-O5′ 93.1(2), O6′-Fe1-O1 94.7(2), O6′-Fe1-O5′ 75.1(2), O7-Fe1-O1 89.5(1), O7-Fe1-O2 99.8(2), O7-Fe1-O6′ 92.3(2), O8-Fe1-O2 92.5(2), O8-Fe1-O5′ 93.0(1), O8-Fe1-O6′ 98.4(2), O8-Fe1-O7 85.9(1), O4-Fe2-O3 74.9(1), O9-Fe2-O4 89.2(2), O9-Fe2-O3 99.6(2), O10-Fe2-O3 91.6(1), O10-Fe2-O9 86.9(2), O10-Fe2-O2 99.7(1), O10-Fe2-O1 92.5(2), O2-Fe2-O9 92.5(2), O2-Fe2-O4 94.8(1), O1-Fe2-O2 75.5(2), O3-Fe2-O1 92.7(2), O4-Fe2-O1 94.3(1), O4-Fe3-O3 75.1(1), O5-Fe3-O3 95.4(2), O5-Fe3-O4 95.0(2), O6-Fe3-O4 92.8(1), O6-Fe3-O5 74.7(2), O11-Fe3-O3 101.3(2), O11-Fe3-O4 92.6(2), O11-Fe3-O6 89.7(2), O12-Fe3-O3 89.9(1), O12-Fe3-O5 90.1(2), O12-Fe3-O6 102.6(1), O12-Fe3-O11 86.6(2), Fe1-Fe2-Fe3 119.51(3), Fe2-Fe3-Fe1′ 119.90(3), Fe3′-Fe1-Fe2 120.52(3), O4-Na-O1′ 101.8(1), O5-Na-O1′ 78.6(1), O5-Na-O4 78.8(1), O1-Na-O5 101.4(1), O1-Na-O4 78.2(1), O5-Na-O4′ 101.2(1).

[*] Prof. S. J. Lippard
Department of Chemistry, Massachusetts Institute of Technology
Cambridge, MA 02139 (USA)
Telefax: Int. code + (617)258-8150

Dr. A. Caneschi
Dipartimento di Chimica, Università degli Studi di Firenze (Italy)

A. Cornia
Dipartimento di Chimica, Università degli Studi di Modena (Italy)

[**] This work was supported by a grant from the National Science Foundation. A. Caneschi acknowledges the Consiglio Nazionale della Ricerche Comitato Nazionale Scienze Chimiche for funding his stay at MIT.

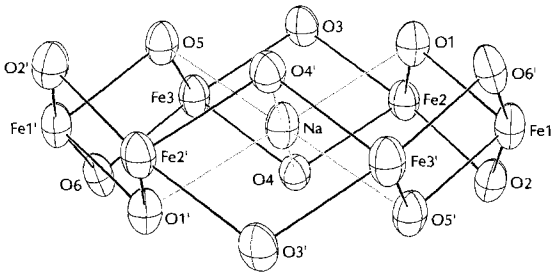


Fig. 2. ORTEP view of the iron–oxygen core of the cation in compound **2** with atom labels. An inversion center relates primed atoms to unprimed ones. Thermal ellipsoids enclose 50% probability.

axis of the hexamer than the other three. The corresponding O–C vectors are almost perpendicular to the mean plane of the ring, subtending angles of 86.0–87.6°. The remaining six methoxo ligands are directed outward from the center of the ring, and their O–C vectors form remarkably acute angles of 45.8–53.8° with the ring plane.

The sodium ion resides on a special position of $\bar{1}$ symmetry in the center of the ring, as unambiguously indicated by difference electron density maps. It is surrounded by a distorted octahedral cage of oxygen atoms (O1, O1′, O4, O4′, O5, and O5′) from the bridging methoxo ligands (Fig. 2). The Na–O distances (2.34–2.37 Å) reveal appreciable interactions of the sodium atom with the host cavity. As a consequence, average Fe–O(CH_3) distances for the methoxo ligands interacting with sodium are slightly longer than the remaining ones (Fig. 1). The O-Na-O and O-Fe-O angles in the four-membered rings are 78–79° and 94–95°, respectively.

Compound **2** is EPR silent at liquid-helium temperature, indicating a diamagnetic ($S = 0$) ground state. At higher temperatures, a broad signal appears at $g = 2$. Preliminary magnetic susceptibility measurements are consistent with these observations and reveal overall antiferromagnetic exchange coupling interactions between the paramagnetic iron(III) centers ($J = 20\ cm^{-1}$; $\mathcal{H} = J \sum_{i>j} (\boldsymbol{S}_i \cdot \boldsymbol{S}_j)$).

The ring structure of **2** is not unprecedented in transition metal chemistry[12, 13] and directly resembles some hexanuclear nickel(II) and palladium(II) alkanethioates.[13] Although polynuclear iron–sulfur complexes having a ring structure are well known,[14] the only cyclic oxygen-bridged iron complex reported so far is $[Fe(OCH_3)_2(O_2CCH_2Cl)]_{10}$.[15] In this respect, **2** is unique since it contains the $[Fe_6(OCH_3)_{12}]^{6+}$ core having only alkoxo bridges. This feature makes it an especially good structural model for cyclic intermediates proposed for the polyalcohol-promoted hydrolysis of iron(III) salts.[8] Moreover, because of its ability to harbor an alkali metal ion guest in a highly symmetric cavity comprising solely oxygen donors from monodentate bridges, the $[Fe_6(OCH_3)_{12}]^{6+}$ core of **2** can be considered a genuine inorganic analogue of [12]crown-6. An encapsulated sodium ion has similarly been found at the center of a cyclic hexacopper(II) complex,[16] but the structure is somewhat more complex owing to the present of bidentate bridging ligands, and its resemblance to [12]crown-6 is consequently less exact. Other inorganic systems described as metallacrowns have been reported in which additional bridging ligands are required to stabilize the host–guest complex.[10, 16, 17]

Finally, we note that the Anderson-type[18] topology of the iron(III) centers and sodium ion observed in **2** is reminiscent of the $[Fe_7(\mu_3\text{-}OH)_6(\mu_2\text{-}OH)_4\{(\mu_3\text{-}O)\text{-}Fe\}_2]^{13+}$ core found in complexes **3** and **4**.[3] This feature can be regarded as a fragment of a two dimensional AX_2 lattice such as found for CdI_2, which bears some resemblance to the structure of goethite. A similar

$[Fe_{17}(O)_4(OH)_{16}(heidi)_8(H_2O)_{12}]^{3+}$ **3** $[Fe_{19}(O)_6(OH)_{14}(heidi)_{10}(H_2O)_{12}]^{+}$ **4**

disposition of metal centers connected by μ_3-OCH_3 and μ_2-OPh ligands has been observed in an heptanuclear iron(II) aggregate.[19] Characteristic of these systems, and particularly evident from space-filling models of **2**, **3**, and **4**, is a flat, disklike structure with a peripheral hydrophobic shell afforded by the pendant organic ligands. The great tendency of the oxygen atoms to form hexagonal close-packed arrays is not altered by the presence of the organic moieties.

Received: September 20, 1994 [Z 7329 IE]
German version: *Angew. Chem.* **1995**, *107*, 511

Keywords: complexes with oxygen ligands · host–guest chemistry · iron compounds · magnetic properties

[1] K. S. Hagen, *Angew. Chem.* **1992**, *104*, 1036; *Angew. Chem. Int. Ed. Engl.* **1992**, *31*, 1010; S. J. Lippard, *ibid.* **1988**, *100*, 353 and **1988**, *27*, 344; S. J. Lippard, *Chem. Br.* **1986**, *22*, 222.

[2] K. Wieghardt, K. Pohl, I. Jibril, G. Huttner, *Angew. Chem.* **1984**, *96*, 66; *Angew. Chem. Int. Ed. Engl.* **1984**, *23*, 77; D. L. Jameson, C. L. Xie, D. N. Hendrickson, J. A. Potenza, H. J. Schugar, *J. Am. Chem. Soc.* **1987**, *109*, 740; C. J. Harding, R. K. Henderson, A. K. Powell, *Angew. Chem.* **1993**, *105*, 583; *Angew. Chem. Int. Ed. Engl.* **1993**, *32*, 570.

[3] S. L. Heath, A. N. Powell, *Angew. Chem.* **1992**, *104*, 191; *Angew. Chem. Int. Ed. Engl.* **1992**, *31*, 191.

[4] J. K. McCusker, C. A. Christmas, P. M. Hagen, R. K. Chadha, D. F. Harvey, D. N. Hendrickson, *J. Am. Chem. Soc.* **1991**, *113*, 6114; J. K. McCusker, J. B. Vincent, E. A. Schmitt, M. L. Mino, K. Shin, D. K. Coggin, P. M. Hagen, J. C. Huffman, G. Christou, D. N. Hendrickson, *ibid.* **1991**, *113*, 3012; K. Hegetschweiler, H. W. Schmalle, H. M. Streit, V. Gramlich, H.-U. Hund, I. Erni, *Inorg. Chem.* **1992**, *31*, 1299; K. Hegetschweiler, H. W. Schmalle, H. M. Streit, W. Schneider, *ibid.* **1990**, *29*, 3625; V. S. Nair, K. S. Hagen, *ibid.* **1992**, *31*, 4048; N. Kitajima, H. Amagai, N. Tamura, M. Ito, Y. Morooka, K. Heerwegh, A. Pénicaud, R. Mathur, C. A. Reed, P. D. W. Boyd, *ibid.* **1993**, *32*, 3583.

[5] K. L. Taft, G. C. Papaefthymiou, S. J. Lippard, *Inorg. Chem.* **1994**, *33*, 1510; *Science* **1993**, *259*, 1302; W. Micklitz, V. McKee, R. L. Rardin, L. E. Pence, G. C. Papaefthymiou, S. G. Bott, S. J. Lippard, *J. Am. Chem. Soc.* **1994**, *116*, 8061; W. Micklitz, S. J. Lippard, *ibid.* **1989**, *111*, 6856; W. A. Armstrong, M. E. Roth, S. J. Lippard, *ibid.* **1987**, *109*, 6318; S. M. Gorun, G. C. Papaefthymiou, R. B. Frankel, S. J. Lippard, *ibid.* **1987**, *109*, 3337; S. M. Gorun, S. J. Lippard, *Nature* **1986**, *319*, 666.

[6] G. C. Papefthymiou, *Phys. Rev. B* **1992**, *46*, 10366; C. D. Delfs, D. Gatteschi, L. Pardi, R. Sessoli, K. Wieghardt, D. Hanke, *Inorg. Chem.* **1993**, *32*, 3099.

[7] C. J. Brinkler, G. W. Scherer, *Sol-Gel Science: The Physics and Chemistry of Sol-Gel Processing*, Academic Press, New York, **1990**; M. Guglielmi, G. Principi, *J. Non-Cryst. Solids* **1982**, *48*, 161.

[8] W. Schneider, *Chimia* **1988**, *42*, 9; *Comments Inorg. Chem.* **1984**, *3*, 205.

[9] Reaction of $FeCl_3$ (1.622 g, 10 mmol) with 1 equiv of Hdbm (2.243 g, 10 mmol) and 4 equiv of sodium methoxide in 150 mL of anhydrous methanol results in the formation of a yellow precipitate which can be recrystallized in 30% yield by slow evaporation of methanol/chloroform solutions to yield large red-orange prisms of **2** which are suitable for X-ray diffraction experiments. After removal of the lattice methanol in vacuo, the compound analyzed (C, H, Fe, Na, Cl) satisfactorily as $[NaFe_6(OCH_3)_{12}(dbm)_6]Cl\cdot CHCl_3$. UV ($1.6 \times 10^{-5}$ M in $CHCl_3$): $\lambda = 255, 275, 308, 403, 482$ nm. IR (Nujol): $\tilde{\nu} = 3280$ (br), 1590 (s), 1530 (s), 1515 (s), 1305 (s), 1220 (m), 1065 (m), 1015 (s), 935 (w), 745 (s), 710 (m), 675 (m), 610 (w), 450 cm^{-1} (s).

[10] M. Lah, V. L. Pecoraro, *Comments Inorg. Chem.* **1990**, *11*, 59.

[11] Crystal data for **2**: $Fe_6Cl_4NaC_{115}H_{151}O_{36}$, $M_r = 2609.33$, crystal size $0.3 \times 0.5 \times 0.5$ mm, $Mo_{K\alpha}$ radiation $\lambda = 0.71069$ monoclinic, space group $C2/c$, $a = 28.812(4)$, $b = 17.158(3)$, $c = 28.368(5)$ Å, $\beta = 120.33(1)°$, $Z = 4$, $V = 12105(4)$ Å^3, $\rho_{calcd} = 1.431$ g cm^{-3}, $\rho_{exp} = 1.42(1)$ g cm^{-3}, $\mu = 8.1$ cm^{-1}. For 11190 reflections measured, 8891 unique observed reflections collected at 150 K with $F^2 > 3\sigma(F^2)$, $R = 0.071$ and $R_w = 0.082$. Several low intensity peaks outside the cluster were attributed to highly disordered methanol molecules and refined isotropically. All the remaining non-hydrogen atoms were treated anisotropically. The chloride ion and the chloroform molecule were not located. Hydrogen atoms were treated as fixed contributors in calculated positions with isotropic thermal parameters $B(H) = 1.2\,B_{eq}(C)$. Further details of the crystal structure determination are available from the Director of the Cambridge Crystallographic Data Centre, 12 Union Road, GB-Cambridge CB2 1EZ (UK) on quoting the full journal citation.

[12] R. N. Grimes, *Angew. Chem.* **1993**, *105*, 1350; *Angew. Chem. Int. Ed. Engl.* **1993**, *32*, 1289; J. R. Carruthers, K. Prout, F. J. C. Rossotti, *Acta Crystallogr. Sect. B* **1975**, *31*, 2044; J. Galy, A. Mosset, I. Grenthe, I. Puigdomènech, B. Sjöberg, F. Hultén, *J. Am. Chem. Soc.* **1987**, *109*, 380; G. A. Ardizzoia, M. A. Angaroni, G. La Monica, F. Cariati, M. Moret, N. Masciocchi, *J. Chem. Soc. Chem. Commun.* **1990**, 1021; U. Müller, *Angew. Chem.* **1981**, *93*, 697; *Angew.*

Chem. Int. Ed. Engl. **1981**, *20*, 692; O. I. Shchegolikhina, A. A. Zhdanov, V. A. Igonin, Yu. E. Ovchinnikov, V. E. Shklover, Yu. T. Struchkov, *Metalloorgan. Khim.* **1991**, *4*, 74; V. A. Igonin, O. I. Shchegolikhina, S. V. Lindeman, M. M. Levitsky, Yu. T. Struchkov, A. A. Zhdanov, *J. Organomet. Chem.* **1992**, *423*, 351.

[13] P. Woodward, L. F. Dahl, E. W. Abel, B. C. Crosse, *J. Am. Chem. Soc.* **1965**, *87*, 5251; R. O. Gould, M. M. Harding, *J. Chem. Soc. A* **1970**, 875; N. R. Kunchur, *Acta Crystallogr. Sect. B* **1968**, *24*, 1623; E. W. Abel, B. C. Crosse, *J. Chem. Soc. A* **1966**, 1377; I. G. Dance, M. L. Scudder, R. Secomb, *Inorg. Chem.* **1985**, *24*, 1201.

[14] J.-F. You, G. C. Papaefthymiou, R. H. Holm, *J. Am. Chem. Soc.* **1992**, *114*, 2697; J.-F. You, B. S. Snyder, G. C. Papaefthymiou, R. H. Holm, *ibid.* **1990**, *112*, 1067; W. Saak, G. Henkel, S. Pohl, *Angew. Chem.* **1984**, *96*, 153; *Angew. Chem. Int. Ed. Engl.* **1984**, *23*, 150.

[15] K. L. Taft, C. D. Delfs, G. C. Papaefthymiou, S. Foner, D. Gatteschi, S. J. Lippard, *J. Am. Chem. Soc.* **1994**, *116*, 821.

[16] A. J. Blake, R. O. Gould, P. E. Y. Milne, R. E. P. Winpenny, *J. Chem. Soc. Chem. Commun.* **1991**, 1453; A. J. Blake, R. O. Gould, C. M. Grant, P. E. Y. Milne, D. Reed, R. E. P. Winpenny, *Angew. Chem.* **1994**, *106*, 208; *Angew. Chem. Int. Ed. Engl.* **1994**, *33*, 195.

[17] M. S. Lah, M. L. Kirk, W. Hatfield, V. L. Pecoraro, *J. Chem. Soc. Chem. Commun.* **1989**, 1606; M. S. Lah, V. L. Pecoraro, *J. Am. Chem. Soc.* **1989**, *111*, 7258; B. R. Gibney, A. J. Stemmler, S. Pilotek, J. W. Kampf, V. L. Pecoraro, *Inorg. Chem.* **1993**, *32*, 6008.

[18] H. T. Evans, Jr., *Acta Crystallogr. Sect. B* **1974**, *30*, 2095.

[19] V. S. Nair, A. Kitaygorodskiy, K. S. Hagen, *Abstracts, 206th ACS National Meeting* (Chicago), **1993**.

Modified Triple Resonance NMR Experiments with Optimized Sensitivity for Rapidly Exchanging Protons**

Wolfgang Jahnke and Horst Kessler*

Multidimensional NMR spectroscopy has developed into the premier method for determining high-resolution structures of molecules in solution. A major concern in the development of pulse sequences is improving the sensitivity of the NMR experiments.[1] The weakest signals in NMR spectra often arise from amide protons that exchange rapidly with the solvent water, and these weak signals often constitute the limiting factor in signal assignment and structure determination of proteins. The intensity of these resonances can be enhanced when the water signal is not saturated during the pulse sequence.[2-4] We describe here modified triple resonance experiments in which the water signal is not saturated and composite pulse proton decoupling is used. The modified pulse sequences yield a sensitivity gain of up to 50% for rapidly exchanging amide protons, where enhanced sensitivity is of outstanding importance.

Biological macromolecules like proteins and nucleic acids are usually investigated in aqueous solution and under semiphysiological conditions, in other words at roughly neutral pH. Under these conditions chemical exchange takes place between protons of the molecule under investigation (e.g. a protein) and the solvent water. Besides protons of ionizable groups in the side chains, backbone amide protons exchange with the solvent protons at rates ranging from reciprocal milliseconds to reciprocal years. Hydrogen exchange has been the subject of several investigations,[5,6] and it can be expected that the dynamic feature of hydrogen exchange can enhance our understanding of structure and dynamics of proteins and nucleic acids. Hydrogen exchange, however, is not a pure blessing. Very rapidly exchanging protons such as hydroxyl groups of protein side chains or amide protons at the protein N-terminus are not found in the spectrum under normal conditions, and crucial amide proton signals are attenuated if presaturation is used.

It has recently been pointed out[2,3] that the signals of rapidly exchanging protons are attenuated not only by presaturation, but also by other methods used to suppress the water signal such as spinlock pulses[7] and gradients,[8] when the water signal is saturated prior to acquisition. This is due to the long T_1 relaxation time of water protons (4–5 s), which is much longer than the T_1 time of protein protons. The delay between successive scans is optimized for the relaxation of the protein protons and is too short for the magnetization of the water protons to relax back near thermal equilibrium. Instead, the water magnetization remains in a semisaturated state during the entire experiment, typically reaching less than 30% of its equilibrium value just before the next scan.

Several methods have been described for overcoming this problem by not saturating the water signal prior to acquisition, while still ensuring that water does not interfere with the detection of the desired protein signals. These methods include selective pulses on the water resonance,[2] improved phase cycling of proton pulses,[3,4] and the constructive use of radiation damping;[4] all of these methods result in alignment of water magnetization on the $+z$ axis before or shortly after acquisition. While selective pulses may be undesirable due to imperfect excitation profiles,[9] neither of the other two methods describes the possibility for proton decoupling by a composite pulse decoupling sequence. This type of decoupling is desirable when the desired coherence resides on nitrogen or carbon because of more favorable relaxation behavior.[10] It is not immediately obvious how composite pulse decoupling can be incorporated into pulse sequences where water magnetization must end up in a defined state (e.g. at the $+z$ axis) before acquisition. First, it seems that the decoupling time must be an integer multiple of the time required for one decoupling cycle, but this is hard to achieve if the decoupling time includes an incrementable delay such as the t_1 time. Second, B_0 field gradients applied during composite pulse decoupling interfere with the decoupling and should be avoided.

We propose here a modification of pulse sequences that allows the use of composite pulse decoupling for any desired time period, while improved sensitivity of rapidly exchanging amide protons is still achieved since water magnetization is realigned along the $+z$ axis prior to acquisition. The modification is illustrated with the constant time (CT) HNCA and HN(CO)CA experiment[11,12] in Figure 1, but can be applied to many NMR experiments.

The CT-HNCA sequence (Fig. 1a) starts with excitation of the amide protons, whose magnetization is subsequently transferred to ^{15}N by an INEPT transfer. During the delay needed to develop the ^{15}N-$^{13}C^{\alpha}$ coupling, ^{15}N coherence refocuses with respect to protons, and is completely refocused after $1/2\,^1J(N,H)$, approximately 5.5 ms. At this time composite pulse decoupling should start. The decoupling phase is irrelevant for protein protons, but is crucial to keep water magnetization in a defined state. The water magnetization has been aligned at the $-y$ axis by the first 90° proton pulse with phase x; it stays there since its resonance corresponds to the carrier frequency and is thus not affected by the following two proton pulses with phase $+/-y$. Proton decoupling is now possible if a sequence is selected that applies pulses only along one axis, and if this axis is chosen to be the y axis. The DIPSI-2 sequence,[13] for example, can be applied successfully along the y axis in this case. After $^{13}C^{\alpha}$ frequency

[*] Prof. Dr. H. Kessler, Dipl.-Chem. W. Jahnke
Institut für Organische Chemie und Biochemie
der Technischen Universität München
Lichtenbergstrasse 4, 85747 Garching (Germany)
Telefax: Int. code + (89)3209-3210

[**] This work was supported by the Deutsche Forschungsgemeinschaft and the Fonds der Chemischen Industrie (H. K.), and the Studienstiftung des deutschen Volkes (fellowship for W. J.). We thank Dr. Gerd Gemmecker for stimulating discussions.

 © VCH Verlagsgesellschaft mbH, D-69451 Weinheim, 1995 0570-0833/95/0404-0469 $ 10.00+.25/0

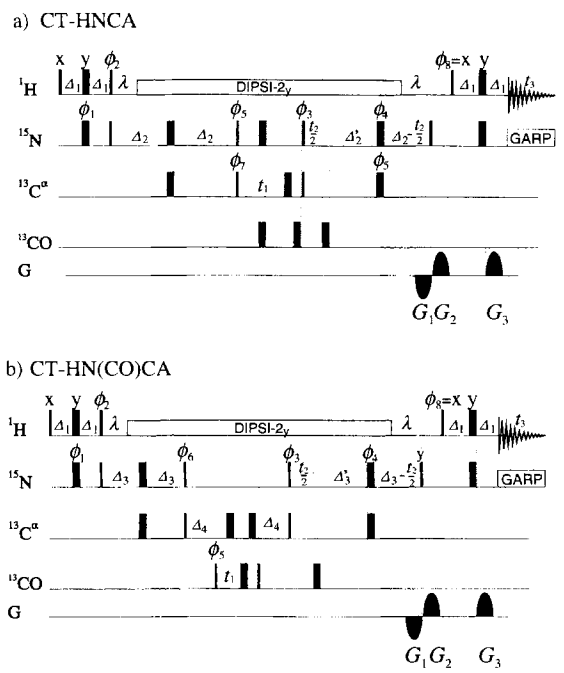


Fig. 1. Modified pulse sequences of a) CT-HNCA and b) CT-HN(CO)CA experiments. The strength of the B_1 decoupling field was 8.3 kHz. Thin and thick bars refer to 90° and 180° pulses, respectively. Pulses are applied along the x axis, unless otherwise indicated. Variable pulse phases are as follows: a) $\phi_1 = x, -x$; $\phi_2 = y, -y$; $\phi_3 = x$; $\phi_4 = 4(x), 4(y), 4(-x), 4(-y)$; $\phi_5 = 16(x), 16(-x)$; $\phi_7 = 2(x), 2(-x)$; receiver $= 2(x,-x,-x,x,-x,x,x,-x), 2(-x,x,x,-x,x,-x,-x,x)$. b) $\phi_1 = x, -x$; $\phi_2 = y, -y$; $\phi_3 = x$; $\phi_4 = 4(x), 4(y), 4(-x), 4(-y)$; $\phi_5 = 2(x), 2(-x)$; $\phi_6 = y, -y$; receiver $= 2(x), 4(-x), 2(x)$. Pulsed B_0 field gradients are sine-shaped and are applied for 1 ms, followed by a delay of 0.5 ms. Their relative strength is $G_1 = -39.6$, $G_2 = 39.6$ and $G_3 = 4$, with 100 being approximately 50 Gauss cm^{-1} at the center of the gradient. Gradient G_2 must be carefully optimized for maximum refocusing of water. Delays are as follows: $\Delta_1 = 2.25$ ms, $\lambda = 5.5$ ms, $\Delta_2 = 11$ ms, $\Delta'_2 = \Delta_2 - \tau_{180}(^{13}CO)$, $D_3 = 10$ ms, $\Delta'_3 = \Delta_3 - \tau_{180}(^{13}CO)$; $\Delta_4 = 6$ ms.

labeling in t_1 with decoupling of ^{15}N and ^{13}CO, a Bloch–Siegert shift compensating for the 180° pulse on ^{13}CO, and CT ^{15}N evolution in t_2, the coherence is transferred back to the amide protons, and is refocused and detected. Gradients G_1 and G_3 are included to select for the desired coherence pathway.

Water magnetization is spinlocked along the $-y$ axis by the DIPSI-2 decoupling sequence and is defocused by gradient G_1. It is not possible to refocus water magnetization by splitting G_1 into two gradients of the same strength but opposite sign on each side of a ^{15}N 180° pulse, since one of the gradients would have to be applied while composite pulse decoupling is active. Instead, the gradient for refocusing water magnetization is applied after the following ^{15}N 90° pulse, at a time when the protein magnetization is in an I_zS_z state but water magnetization is in the transverse plane. After the refocusing gradient G_2, the water magnetization is aligned along the $-y$ axis. It is then turned to the $-z$ axis by the 90° pulse with phase $\phi_8 = x$, and turned to the $+z$ axis by the following 180° proton pulse. A one-dimensional experiment shows that the longitudinal water magnetization reaches as much as 80% of its equilibrium value after this sequence. That means that exchanging amide protons obtain almost the full longitudinal magnetization from water protons and their signals are not a priori attenuated by the exchange process. Any water magnetization that is not realigned along the $+z$ axis (due to imperfect pulses or radiation damping) is defocused by gradient G_3, which supplies excellent suppression of the water signal.

The modified pulse sequence has been tested on a 2 mM sample of completely ^{15}N- and ^{13}C-labeled mannose permease domain IIA^{Man} at 310 K and pH 7.5.[14] This homodimer of 31 kDa contains a number of rapidly exchanging amide protons,[6] for which a considerable increase in sensitivity is expected when the water magnetization is flipped back to thermal equilibrium before acquisition. Figure 2 shows rows through the first 2D planes of

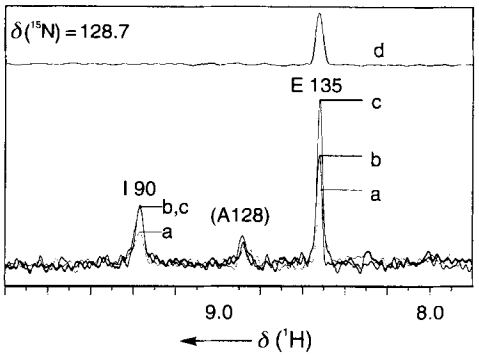


Fig. 2. ^1H rows from the first planes of CT-HNCA spectra taken at a ^{15}N frequency of 128.7. It can be seen that the proposed pulse sequence of Fig. 1a gives the best sensitivity for the rapidly exchanging amide proton. Residues A128 and E135 resonate at a slightly different ^{15}N frequencies. All experiments were recorded and processed under identical conditions on a Bruker AMX600 spectrometer with triple resonance equipment and self-shielded pulsed field gradients. 256 transients were accumulated for each of the 80 t_1 increments. The recycle time between successive scans including acquisition was 1.1 s.

spectra obtained with different versions of HNCA experiments: the CT experiment using 180° pulses for proton decoupling[11] (curve a), the CT experiment with composite pulse proton decoupling[11] and saturation of the water signal ($\phi_8 = y$ in Fig. 1a) by pulsed field gradients (curve b), and CT-HNCA (as described in Fig. 1a) using composite pulse proton decoupling and flipping water magnetization back to thermal equilibrium (curve c). In addition the corresponding row through a MEXICO spectrum is shown,[6] in which only rapidly exchanging protons give rise to cross peaks (curve d). It is obvious that proton decoupling by a composite pulse decoupling sequence (curve b) yields considerably higher sensitivity than decoupling by 180° pulses (curve a), as expected for a protein of this size.[10] An additional substantial increase in sensitivity is gained for rapidly exchanging amide protons if the water signal is not saturated prior to acquisition. This is seen in curve c for residue E135, which has a rapidly exchanging amide proton (curve d). The signal-to-noise ratio for this peak is about 50% higher when the water magnetization is flipped back to equilibrium before acquisition. Residue E135 is located near the C-terminus of the protein in a flexible part of the molecule that is not involved in regular secondary structure. Thus, E135 gives rise to a strong cross peak in spite of its rapidly exchanging amide proton. It is important to note, however, that since most other rapidly exchanging amide protons yield much weaker signals, the sensitivity enhancement obtained specifically for these signals is of outstanding importance.

In conjunction with the described possibility of using composite pulse proton decoupling, the technique of flipping water magnetization back to thermal equilibrium before acquisition can be applied without compromise to a wide variety of NMR experiments. Since the technique enhances the signal intensity predominantly for the weak resonances, for which enhanced sensitivity is most important, it can be expected that assignment of NMR spectra is greatly facilitated by this technique.

Received: August 12, 1994 [Z7235IE]
German version: *Angew. Chem.* **1995**, *107*, 536

Keywords: NMR spectroscopy · structure elucidation · proteins

 © VCH Verlagsgesellschaft mbH, D-69451 Weinheim, 1995 0570-0833/95/0404-0470 $ 10.00+.25/0

[1] A. G. Palmer, J. Cavanagh, P. E. Wright, M. Rance, *J. Magn. Reson.* **1991**, *93*, 151–170; J. Schleucher, M. Sattler, C. Griesinger, *Angew. Chem.* **1993**, *105*, 1518–1521; *Angew. Chem. Int. Ed. Engl.* **1993**, *32*, 1489–1492; L. E. Kay, P. Keifer, T. Saarinen, *J. Am. Chem. Soc.* **1992**, *114*, 10663–10665.
[2] S. Grzesiek, A. Bax, *J. Am. Chem. Soc.* **1993**, *115*, 12593–12594; N. A. Farrow, R. Muhandiram, A. U. Singer, S. M. Pascal, C. M. Kay, G. Gish, S. E. Shoelson, T. Pawson, J. D. Forman-Kay, L. E. Kay, *Biochemistry*, **1994**, *33*, 5984–6003.
[3] J. Stonehouse, G. L. Shaw, J. Keeler, E. D. Laue, *J. Magn. Reson. Ser. A* **1994**, *107*, 178–184.
[4] W. Jahnke, H. Kessler, *J. Biomol. NMR*, **1994**, *4*, 735–740.
[5] K. Wüthrich, *NMR of Proteins and Nucleic Acids*, Wiley-Interscience, New York, **1986**; E. Liepinsh, G. Otting, K. Wüthrich, *J. Biomol. NMR* **1992**, *2*, 447–465; R. Baldwin, *Curr. Opin. Struct. Biol.* **1993**, *3*, 84–91; C. K. Woodward, *ibid.* **1994**, *4*, 112–116; S. W. Englander, L. Mayne, *Annu. Rev. Biophys. Biomol. Struct.* **1992**, *21*, 243–265; C. Chyan, C. Wormald, C. Dobson, P. Evans, J. Baum, *Biochemistry* **1993**, *32*, 5681–5691; C. A. Rohl, R. L. Baldwin, *ibid.* **1994**, *33*, 7760–7767; N. J. Skelton, J. Kördel, M. Akke, W. J. Chazin, *J. Mol. Biol.* **1992**, *227*, 1100–1117; M. H. Werner, D. E. Wemmer, *J. ibid.* **1992**, *225*, 873–889; J. Czaplicki, C. Arrowsmith, O. Jardetzky, *J. Biomol. NMR* **1991**, *1*, 349–361; S. Spera, M. Ikura, A. Bax, *ibid.* **1991**, *1*, 155–165; S. Grzesiek, A. Bax, *ibid.* **1993**, *3*, 627–638.
[6] G. Gemmecker, W. Jahnke, H. Kessler, *J. Am. Chem. Soc.* **1993**, *115*, 11620–11621.
[7] B. A. Messerle, G. Wider, G. Otting, C. Weber, K. Wüthrich, *J. Magn. Reson.* **1989**, *85*, 608–613.
[8] A. Bax, P. G. De Jong, A. F. Mehlkopf, J. Smidt, *Chem. Phys. Lett.* **1980**, *69*, 567–570; R. E. Hurd, *J. Magn. Reson.* **1990**, *87*, 422–428.
[9] R. Freeman, *Chem. Rev.* **1991**, *91*, 1397–1412.; H. Kessler, S. Mronga, G. Gemmecker, *Magn. Reson. Chem.* **1991**, *29*, 527–557.
[10] A. Bax, M. Ikura, L. E. Kay, D. A. Torchia, R. Tschudin, *J. Magn. Reson.* **1990**, *86*, 304–318.
[11] S. Grzesiek, A. Bax, *J. Magn. Reson.* **1992**, *96*, 432–440.
[12] B. T. Farmer, R. A. Venters, L. D. Spicer, M. G. Wittekind, L. Müller, *J. Biomol. NMR* **1992**, *2*, 195–202.
[13] A. J. Shaka, C. J. Lee, A. Pines, *J. Magn. Reson.* **1988**, *77*, 274–293.
[14] S. Seip, J. Balbach, S. Behrens, H. Kessler, K. Flükiger, R. de Mayer, B. Erni, *Biochemistry* **1994**, *33*, 7174–7183.

The Arndt–Eistert Reaction in Peptide Chemistry: A Facile Access to Homopeptides**

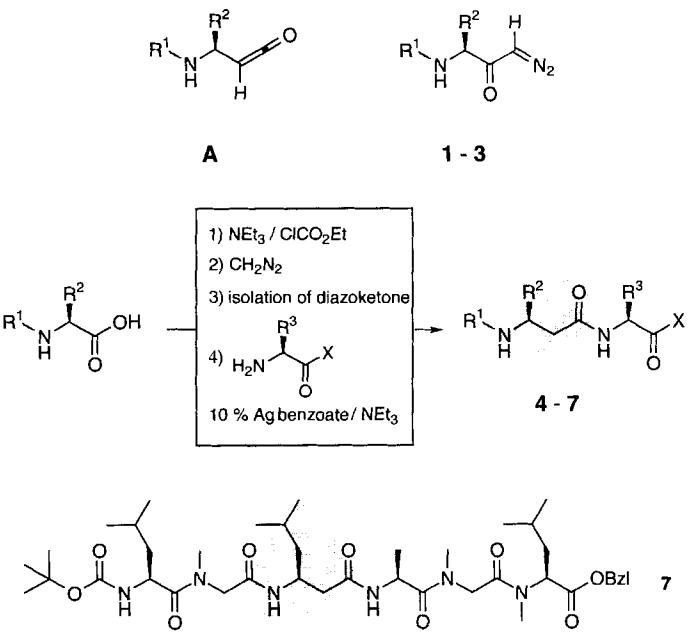
Joachim Podlech and Dieter Seebach*

β-Amino acids, though less abundant than α-amino acids, are components of natural peptides.[1] In recent years their importance for the preparation of modified peptides[2] and β-lactam antibiotics[3] has increased enormously. Quite a number of methods for the synthesis of enantiopure β-amino acids exists already.[4] Still it would be a conceptually new, simple approach for the construction of peptides containing β-amino acids, if the generation of the β-amino acid moiety could be combined with a peptide coupling step. To this end, we have now applied to peptides the chain extension of carboxylic acids developed by Arndt and Eistert.[5, 6]

When we started this work, it was not certain whether the peptidic ketenes **A** formed in this reaction could be trapped intermolecularly, and if so, whether they would couple selectively with the free amino function of a second peptide.

At first we simply coupled two amino acids following the sequence of steps outlined in Scheme 1. Activation of Z-protected alanine with ethyl chlorocarbonate to give the mixed anhydride and reaction with diazomethane in THF or Et_2O afforded the corresponding diazoketone **1** (R^1 = Z, R^2 = Me) in 80% yield. Like all compounds of this type obtained in the course of this investigation, the diazo compound **1** is a solid and could be purified by chromatography on silica gel or by recrystallization. A solution of **1** and 2–4 equivalents of valine benzyl ester[7] in THF was treated with Et_3N and a catalytic amount of silver benzoate at low temperature, yielding the homodipeptide **4**. In the same manner the protected di- and tripeptides Z-Ala-Ala-OH and Boc-Leu-Sar-Leu-OH were coupled via diazoketones **2** and **3**, respectively, with the tripeptides H-Ala-Sar-MeLeu-OBzl and H-Leu-Sar-Leu-OMe[8] (see Table 1). The formation of both the diazoketones and the homopeptides proceeds with good to very good yields. The products were characterized by mass spectrometry, elemental analysis, and by their optical rotation. Owing to the presence of rotamers, the NMR spectra are not informative, except for those of the protected dipeptides. All components of the peptide derivatives obtained are enantiopure, as proved by degradation to the free α- and β-amino acids and analysis by gas chromatography on chiral columns.[9]

To test whether the ketene of type **A** is actually the immediate precursor to the homopeptide derivatives, we decomposed (12% AgOCOPh, 6 h) the diazoketone **2** in THF in the absence of a nucleophile and then added MeOH. The methyl ester **9** was formed in virtually the same yield as when the reaction was



Scheme 1. Ketene **A** and diazoketones **1**–**3** generated as intermediates in the Arndt–Eistert reaction with amino acid and peptide derivatives, and coupling with homologation of two amino acids or two peptides to homopeptides (**4**–**7**). The formula of one of the synthesized homohexapeptides **7** is given. For R^1, R^2, R^3, and X see Table 1.

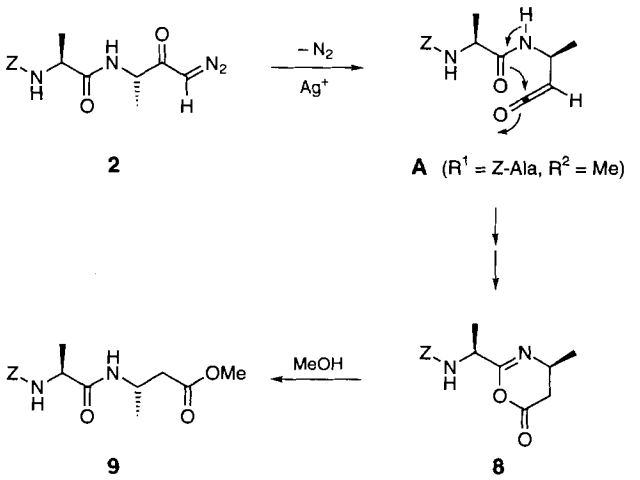
Table 1. Diazoketones **1**–**3** and homopeptide derivatives **4**–**7** synthesized according to Scheme 1. Abbreviations: Bzl = $PhCH_2$, Z = BzlOCO, Boc = *t*BuOCO, *i*Bu = CH_2CHMe_2. Optical rotations were measured in $CHCl_3$ with $c \approx 1$.

Cmpd.	R^1	R^2	R^3	X	Yield [%]	$[\alpha]_D$
1	Z	Me			80	
2	Z-Ala	Me			41	
3	Boc-Leu-Sar	*i*Bu			86	
4	Z	Me	*i*Pr	OBzl	81	−9.45
5	Z-Ala	Me	Me	Sar-MeLeu-OBzl	95	−48.6
6	Boc-Leu-Sar	*i*Bu	*i*Bu	Sar-Leu-OMe	60	−19.5
7	Boc-Leu-Sar	*i*Bu	Me	Sar-MeLeu-OBzl	61	−43.7

[*] Prof. Dr. D. Seebach, Dr. J. Podlech
Laboratorium für Organische Chemie
der Eidgenössischen Technischen Hochschule
ETH-Zentrum, Universitätstrasse 16, CH-8092 Zürich (Switzerland)
Telefax: Int. code + (1)632-1144

[**] We thank the Deutsche Forschungsgemeinschaft (fellowship for J. P.).

carried out in methanol as the solvent (Scheme 2). Since we did not consider it likely that the ketene was stable for 6 h, we examined a solution prepared in [D_6]THF by NMR spectroscopy. We found that not the ketene, but the dihydrooxazinone **8** is present in the solution,[10] and is stable for at least 12 h when air is excluded. This heterocycle is a cyclic imino anhydride, in other words an activated derivative, and reacts with nucleophiles to give the desired homopeptides.[11]



Scheme 2. Experiment used to identify the intermediate **8** formed from a peptidic ketene **A** and methanolysis product **9** (m.p. 111–113 °C, $[\alpha]_D = -46.9$ ($c = 1.06$, $CHCl_3$)).

The method for the synthesis of homopeptides presented here allows for an insertion of a β-amino acid at any stage of a peptide synthesis.[12] The active acyl derivative (**A** or dihydrooxazinone) involved reacts not only with amino acid esters and peptides with an unprotected N-terminus, but also with other nucleophiles. Experiments along these lines, for instance reactions with carbohydrates and 3-hydroxybutanoic acid oligomers[13] are in progress. The plethora of possibilities suggests that the method may be used for constructing new types of peptide-containing combinatorial libraries.[14]

Experimental Procedure

Diazoketone **3**: Et_3N (1.39 mL, 10.0 mmol) and $ClCO_2Et$ (953 μL, 10.0 mmol) were added to a solution of Boc-Leu-Sar-Leu-OH (4.16 g, 10.0 mmol) in THF (50 mL, distilled from Na/K) at −15 °C under argon. After 15 min the resulting solution was allowed to warm to −5 °C and then treated with a solution of CH_2N_2 [15] in ether, until the yellow color of CH_2N_2 persisted over a longer period of time. The mixture was allowed to warm to room temperature and stirred for an additional 3 h. Excess CH_2N_2 was destroyed by vigorous stirring or by addition of a small amount of HOAc. After aqueous workup by extraction with saturated $NaHCO_3$, NH_4Cl, and NaCl solutions, the organic solution was dried ($MgSO_4$) and concentrated to dryness. Chromatography on silica gel (ethyl acetate/hexane 2/1) gave diazoketone **3** in 86% yield (3.76 g, 8.60 mmol).

Protected homohexapeptide **7**: A solution of silver benzoate (16.0 mg, 70.0 μmol) in Et_3N (215 μL, 1.54 mmol) was added to a solution of **3** (238 mg, 541 μmol) and H-Ala-Sar-MeLeu-OBzl (528 mg, 1.40 mmol) in THF (10 mL) at −25 °C under argon with exclusion of light. The reaction mixture was warmed to room temperature over 3 h, and some Et_2O was added. After workup by extraction with HCl (0.2 N, 2 ×) and saturated NaCl, $NaHCO_3$, and NaCl solutions, the organic solution was dried ($MgSO_4$) and concentrated to dryness. The residue was purified by chromatography on silica gel (ethyl acetate) to give the protected homopeptide **7** (257 mg, 326 μmol, 60%).

Received: September 14, 1994 [Z 73121E]
German version: *Angew. Chem.* **1995**, *107*, 507

Keywords: β-amino acids · Arndt–Eistert reactions · dihydrooxazinones · homopeptides · peptide analogues

[1] C. N. C. Drey in *Chemistry and Biochemistry of Amino Acids*, (Ed.: G. C. Barrett), Chapman and Hall, London, **1985**, pp. 25–54.
[2] W. P. Frankmölle, G. Knübel, R. E. Moore, G. M. L. Patterson, *J. Antibiot.* **1992**, *45*, 1458–1466.
[3] *The Organic Chemistry of β-Lactams*, (Ed.: G. I. Georg), VCH, New York, **1993**.
[4] Recent comprehensive reviews: E. Juaristi, D. Quintana, J. Escalante, *Aldrichimica Acta* **1994**, *27*, 3–11; D. C. Cole, *Tetrahedron* **1994**, *50*, 9517–9582.
[5] a) F. Arndt, B. Eistert, W. Partale, *Ber. Dtsch. Chem. Ges.* **1927**, *60*, 1364–1370; b) T. Ye, M. A. McKervey, *Chem. Rev.* **1994**, *94*, 1091–1160.
[6] There are numerous reports about the application of this reaction for the homologation of α- to β-amino acids [4, 5b]. In almost all cases the enantiopurity of the products formed with retention of configuration was not determined by modern analytical techniques (NMR spectroscopy, gas chromatography) (K. Balenović, I. Jambrešić, B. Gašpert, D. Cerar, *Recl. Trav. Chim. Pays-Bas* **1956**, *75*, 1252–1258; K. Balenović, D. Fleš, I. Jambrešić, *Croat. Chem. Acta* **1956**, *28*, 303–305 and references therein). We used the following amino acid derivatives in the Arndt–Eistert reaction (activation via the mixed anhydrides): Z-Ala-OH, Z-Phe-OH, Boc-Phe-OH, Boc-*tert*-Leu-OH, Boc-Orn(Boc)-OH, Z-Phg-OH, Boc-Phg-OH. Analysis of the Mosher derivatives showed that all reactions, except for that of phenylglycine (Phg), occur with more than 98% retention of configuration. We tested milder activation methods with phenylglycine. Activation with isobutyl-2-isobutyloxy-1(2*H*)-quinolinecarboxylate (IIDQ) afforded diazoketone (10% racemization, as with $ClCO_2Et$), but reaction with *N*-hydroxysuccinimide/dicyclohexylcarbodiimide (HOSu/DCC) or benzotriazol-1-yl-oxytripyrrolidinophosphonium hexafluorophosphate (PyBOP) did not.
[7] The reaction could not be carried out with the hydrochloride of the amino acid ester.
[8] For the preparation of the di- and tripeptides used here, see: H. G. Bossler, D. Seebach, *Helv. Chim. Acta* **1994**, *77*, 1124–1165.
[9] S. Abdalla, E. Bayer, H. Frank, *Chromatographia* **1987**, *23*, 83–85; the enantiopurity of the β-amino acids could be determined by this method as well.
[10] Compound **8** was unambiguously identified by ^1H, ^{13}C, DEPT, COSY, and HETCOR NMR spectroscopy. In an analogous experiment the diazoketone from Z-alanine yielded Z-HomoAla-OMe when methanol was added after 6 h.
[11] Dihydrooxazinones of this type were generated from various β-amino acid derivatives by other methods and used as active esters (C. N. C. Drey, E. Mtetwa, *J. Chem. Soc. Perkin Trans. 1* **1982**, 1587–1592 and references therein).
[12] The method appears to be applicable to all appropriately protected amino acids except for tryptophane and histidine.
[13] H.-M. Müller, D. Seebach, *Angew. Chem.* **1993**, *105*, 483–509; *Angew. Chem. Int. Ed. Engl.* **1993**, *32*, 477–502.
[14] G. Jung, A. G. Beck-Sickinger, *Angew. Chem.* **1992**, *104*, 375–391; *Angew. Chem. Int. Ed. Engl.* **1992**, *31*, 367–383.
[15] **Caution:** The generation and the handling of diazomethane requires especial caution: P. Lombardi, *Chem. Ind. (London)* Nov. 5, 1990, 708. S. Moss, *ibid.* Feb. 21, 1994, 122.

Rapid Hydrolysis of RNA with a Cu^{II} Complex**

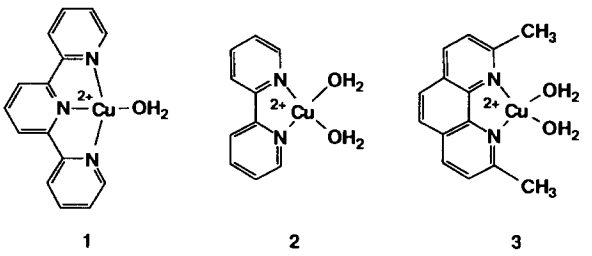
Barry Linkletter and Jik Chin*

Over the years, many interesting artificial enzymes that hydrolyze the phosphate diester bonds of RNA have been reported. They include nonmetallic compounds[1] as well as transition metal complexes[2] and lanthanide complexes.[3] Sequence-specific hydrolysis of RNA has recently been achieved by using various metal complexes covalently attached to deoxyoligoribonucleotides.[4, 5] Although these results are promising, the reactivities of artificial RNases fall far short of natural RNases. Typically, the half-life for artificial RNase-catalyzed hydrolysis

[*] Prof. J. Chin, B. Linkletter
Department of Chemistry, McGill University
801 Sherbrooke Street West, Montreal, Quebec H3A 2K6 (Canada)
Telefax: Int. code + (514)398-3797

[**] Financial support was provided by the National Science and Engineering Council of Canada and the U.S. Army Research Office.

of RNA at neutral pH and 50 °C ranges from hours to days. Hence there is much current interest in increasing the reactivity of artificial RNases as well as in understanding factors affecting the reactivity of such catalysts. $[Cu(terpy)(OH_2)]^{2+}$ (**1**) and $[Cu(bpy)(OH_2)_2]^{2+}$ (**2**) are two of the most reactive transition metal complexes reported to date for hydrolyzing the phosphate diester bonds of RNA (terpy: terpyridyl; bpy: 2,2'-bipyridyl).[2, 4] Here we compare the reactivity of [Cu(neocuproine)$(OH_2)_2$]$^{2+}$ (**3**) for hydrolyzing ApA to those of **1** and **2**.



1 **2** **3**

Copper complexes, **1**, **2**, and **3** were freshly generated in solution from the corresponding chlorides. Cleavage of ApA to A, Ap, and pA was monitored by high-pressure liquid chromatography (HPLC). Optimal reactivity of the copper complexes is reached at solution pH values close to the pK_a of the copper-coordinated water molecules. The pK_a values of the coordinated water molecules in **1**, **2**, and **3** are 8.2, 7.8, and 7.0, respectively, indicating that the copper center in **3** is the most Lewis acidic. The pseudo-first-order rate constants for **1**, **2**, and **3** (10 mM) promoted cleavage of ApA (0.5 mM) at the respective optimal pH values are $1.9\times10^{-5}\,s^{-1}$, $1.9\times10^{-7}\,s^{-1}$, and $3.9\times10^{-3}\,s^{-1}$. The half-lives for **1**, **2**, and **3** promoted cleavage of ApA are 10 hours, 42 days, and 3 minutes, respectively. All of the reaction solutions were buffered with *N*-(2-hydroxyethyl)piperazine-*N'*-2-ethanesulfonic acid (HEPES, 10 mM) and kept at 25 °C. A typical HPLC plot for **3** (10 mM) promoted cleavage of ApA (0.5 mM) at pH 7 and 20 °C is shown in Figure 1. The concentration of 2',3'-cAMP accumulates appreciably during the cleavage reaction, and it is subsequently converted to 3'-AMP and 2'-AMP in a ratio of about 6 to 1. It is evident from the HPLC plot that the cleavage reaction occurs hydrolytically at the phosphate rather than oxidatively at the ribose ring.

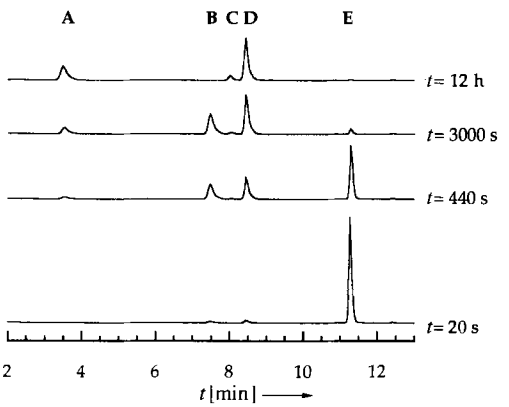


Fig. 1. Chromatograms for hydrolysis of ApA (0.1 mM) catalyzed by **3** (10 mM) in the presence of 10 mM HEPES buffer (pH 7) at 20 °C (after 20, 440, and 3000 s, and after 12 h). The traces shows disappearance of ApA (E) and appearance of adenosine (D) and 2',3'-cAMP (B), which opens to 3'-AMP (A) and 2'-AMP (C).

The rate of cleavage of ApA is first order (Fig. 2) with respect to the concentration of **3**, clearly indicating that the cleavage reaction is a mononuclear process (slope: 1.06; intercept: −0.56; correlation coefficient: 0.994). Interestingly, **3** is over 200 times more effective than **1** and over 20000 times more effective than **2** for catalyzing ApA cleavage. A phosphate diester coordinated to Co^{III} as a monodentate ligand hydrolyzes only about 10^2 times faster than the free phosphate diester.[6] Hence the dramatic difference in the reactivities of **1**, **2**, and **3** is unlikely to be solely due to the difference in the Lewis acidities of the metal complexes.

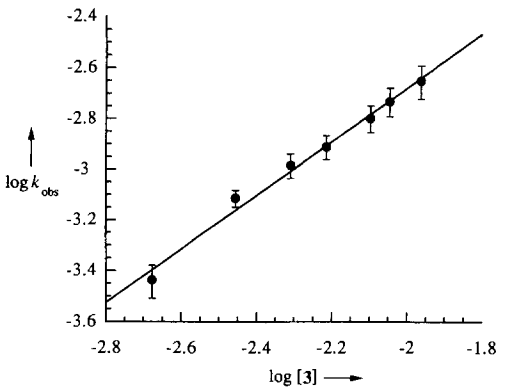
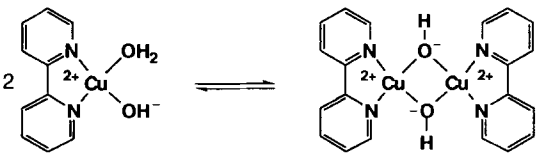


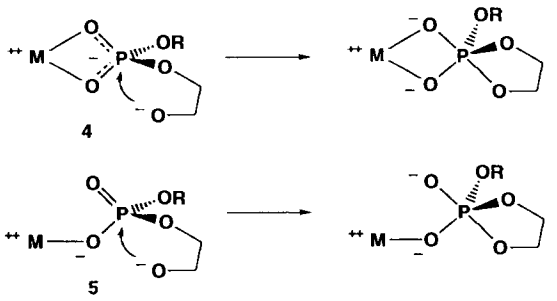
Fig. 2. Dependance of k_{obs} [s^{-1}] on the concentration of **3** [M] for hydrolysis of ApA (0.1 mM) in 10 mM HEPES buffer (pH 7) at 20 °C, as a log/log plot.

At neutral pH, **2** dimerizes[7] with an equilibrium constant of $1\times10^5\,M^{-1}$ [Eq. (a)], and the dimer is inactive for hydrolyzing ApA. At pH 7.8, only about 8% of **2** is in the monomeric form. In contrast, **3** does not dimerize appreciably under the reaction condition owing to the steric effect of the two methyl groups. When the dimerization of **2** is accounted for, **3** is still about 1000 times more reactive than **2** for hydrolyzing ApA.



(a)

One possible mechanism that can account for the high reactivity of **3** involves chelation of the phosphate diester to the copper complex resulting in double Lewis acid activation. In general, a phosphate diester that is chelated to a metal center (**4**) should hydrolyze more rapidly than a phosphate diester that is singly coordinated to a metal center (**5**). In the former case the



4 **5**

developing negative charge is stabilized by the cationic metal center, while in the latter case the developing negative charge is not stabilized by the metal. The metal center in **4** is providing double Lewis acid activation, while the metal center in **5** is providing single Lewis acid activation. We recently showed that a dinuclear metal complex can rapidly cleave an RNA model compound by providing double Lewis acid activation.[8] The two methyl groups in the neocuproine ligand should decrease the O-Cu-O bond angle in **3**, which should facilitate the chelation of phosphate diesters. In octahedral Co^{III} complexes, the O-Co-O bond angles in chelated phosphates are significantly smaller than the 90° angle found in regular octahedral complexes.[9]

Among simple compounds, lanthanides and their complexes are the most reactive for hydrolyzing nucleic acids.[10] However, enzymes use transition metals, Mg^{2+}, or Ca^{2+} to cleave phosphate esters. Consequently, there is considerable interest in developing simple transition metal, Mg^{2+}, or Ca^{2+} complexes that efficiently hydrolyze the phosphate diester bonds of RNA. Complex **3** represents by far the most reactive transition metal complex reported to date for hydrolyzing RNA.

Experimental Procedure

The copper chloride complexes [Cu(terpy)Cl]Cl, [Cu(bpy)Cl_2], and [Cu(neocuproine)Cl_2] were prepared by mixing the appropriate ligands with $CuCl_2$ in methanol. All of the ligands and $CuCl_2$ are soluble in methanol, whereas the complexes precipitate out of the solvent. Cleavage of ApA was monitored by HPLC (Hewlett-Packard 1090). In a typical kinetic experiment, a solution of ApA (0.5 mM), **3** (10 mM), and HEPES (10 mM) was allowed to react at pH 7.0 and 25 °C. Aliquots (50 μL) of the reaction mixture were quenched with 100 mM ethylenediaminetetraacetic acid (EDTA) (50 μL). The quenched solutions (10 μL) were injected onto a C-18 reversed-phase column (5 μm Hypersil maintained at 40 °C) and eluted for 5 min with $NH_4H_2PO_4$ (0.2 M at pH 5.5) followed by a 0–50% linear gradient of $NH_4H_2PO_4$ (0.2 M at pH 5.5) and methanol/water (3:2) solutions over 10 min with a flow rate of 0.5 mL min^{-1}.

Received: September 24, 1994 [Z 7351 IE]
German version: *Angew. Chem.* **1995**, *107*, 529

Keywords: bioinorganic chemistry · copper compounds · nucleic acids · RNA cleavage

[1] a) J. Smith, K. Ariga, E. V. Anslyn, *J. Am. Chem. Soc.* **1993**, *115*, 362; b) R. Breslow, M. Labelle, *ibid.* **1986**, *108*, 2655; c) B. Barbier, A. Brack, *ibid.* **1992**, *114*, 3511. For hydrolysis of RNA model compounds see: d) M. W. Göbel, J. W. Bats, G. Dürner, *Angew. Chem.* **1992**, *104*, 217; *Angew. Chem. Int. Ed. Engl.* **1992**, *31*, 207; e) V. Jubian, R. P. Dixon, A. Hamilton, *J. Am. Chem. Soc.* **1992**, *114*, 1120.

[2] a) M. K. Stern, J. K. Bashkin, E. D. Sall, *J. Am. Chem. Soc.* **1990**, *112*, 5357; b) Y. Matsumoto, M. Komiyama, *J. Chem. Soc. Chem. Commun.* **1990**, 1050; c) R. Breslow, D. L. Huang, E. Anslyn, *Proc. Natl. Acad. Sci. USA* **1989**, *86*, 1746.

[3] a) J. R. Morrow, L. A. Buttrey, V. M. Shelton, K. A. Berback, *J. Am. Chem. Soc.* **1992**, *114*, 1903; b) R. Breslow, D. L. Huang, *Proc. Natl. Acad. Sci. USA* **1991**, *88*, 4080; c) H.-J. Schneider, J. Rammo, R. Hettich, *Angew. Chem.* **1993**, *105*, 1773; *Angew. Chem. Int. Ed. Engl.* **1993**, *32*, 1716.

[4] J. K. Bashkin, E. I. Frolova, U. S. Sampath, *J. Am. Chem. Soc.* **1994**, *116*, 5981.

[5] D. Magda, R. A. Miller, J. L. Sessler, B. Iverson, *J. Am. Chem. Soc.* **1994**, *116*, 7439.

[6] P. Hendry, A. M. Sargeson, *Inorg. Chem.* **1990**, *29*, 92.

[7] R. L. Gustafson, A. E. Martell, *J. Am. Chem. Soc.* **1959**, *81*, 525.

[8] a) D. Wahnon, R. C. Hynes, J. Chin, *J. Chem. Soc. Chem. Commun.* **1994**, 1441; b) M. Wall, R. C. Hynes, J. Chin, *Angew. Chem.* **1993**, *105*, 1696; *Angew. Chem. Int. Ed. Engl.* **1993**, *32*, 1633.

[9] a) B. Anderson, R. M. Milburn, J. M. Harrowfield, G. B. Robertson, A. M. Sargeson, *J. Am. Chem. Soc.* **1977**, *99*, 2652; b) J. A. Connolly, M. Banaszczyk, R. C. Hynes, J. Chin, *Inorg. Chem.* **1994**, *33*, 665.

[10] a) B. K. Takasaki, J. Chin, *J. Am. Chem. Soc.* **1994**, *116*, 1121; b) B. K. Takasaki, J. Chin, *ibid.* **1993**, *115*, 9337; c) J. Sumaoka, S. Miyama, M. Komiyama, *J. Chem. Soc. Chem. Commun.* **1994**, 1755; d) M. Komiyama, K. Matsumura, Y. Matsumoto, *ibid.* **1992**, 640.

Photo Electron Transfer Induced Macrocyclization of *N*-Phthaloyl-ω-amino-carboxylic Acids**

Axel G. Griesbeck,* Andreas Henz, Karl Peters, Eva-Maria Peters, and Hans Georg von Schnering

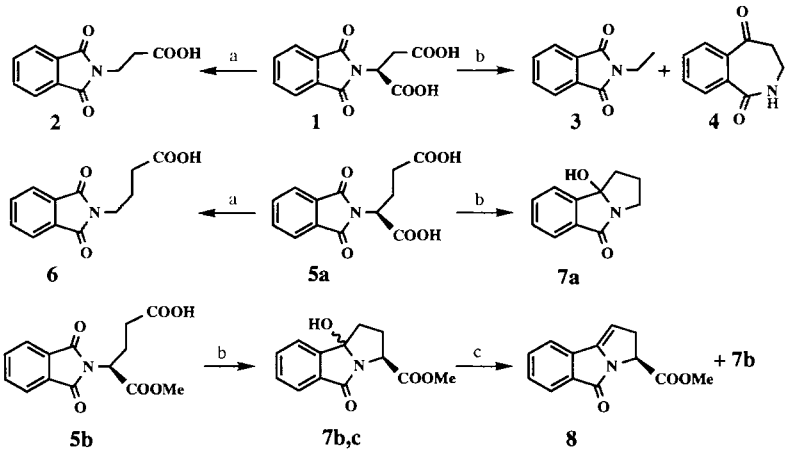
In the presence of strong electron donors such as arene carbonitriles,[1] heteroarenes,[2] and iminium cations,[3] aliphatic carboxylic acids and the respective anions can be photochemically decarboxylated. The carbon radicals produced undergo fragmentation or (re)combination. Intramolecular versions of these reactions yield complex products, for example spiroannulated heterocycles.[4] During our investigations on the photochemistry of *N*-phthaloylamino acids[5] we discovered a surprisingly efficient synthesis of systems containing medium-sized and large rings.

The photochemical approach to macrocycles requires a strong electron-donating substituent (e.g. thioether, enamine) in the side chain of the *N*-alkylphthalimide. The phthalimide chromophore behaves as an electron-accepting group ("remote photocyclization").[6] A disadvantage of this method is in all cases the incorporation of the electron donor into the ring system formed. An approach in which formation of the new O–C single bond is combined with extrusion of the electron donor would be promising.[7] ω-Aminocarboxylic acids could be suitable substrates; however, only the photochemical reactivity of α-amino acids has been reported up to now.[8] The corresponding *N*-phthaloyl derivatives are decarboxylated when irradiated at 300 nm. This reaction proceeds with high regioselectivity also in the presence of other carboxyl groups in β- or γ-position. Even prolonged photolysis does not cleave these remote substituents. We have used this principle for the synthesis of deuterium-labeled β- and γ-aminocarboxylic acids.[9] A decisive factor for the efficiency and regioselectivity might be formation of a intramolecular hydrogen bond. Presumably this reaction proceeds by a primary proton transfer[10] to the electronically excited phthalimide group (Excited State Proton Transfer, ESPT[11]) followed by an electron transfer step. Since remote carboxyl groups do not form this hydrogen bond, this initial proton transfer step cannot occur.

Electron transfer even from remote positions is possible for carboxylic acid anions when primary proton transfer is no longer necessary. Irradiation of *N*-Pht-aspartic acid **1** (Pht = phthaloyl) in acetone leads to *N*-Pht-β-amino-propionic acid **2** in quantitative yield. In the presence of ten equivalents of sodium carbonate, however, a 9:1 mixture of *N*-ethylphthalimide **3** and the cyclized compound **4** was isolated (Scheme 1). Still decarboxylation from the α-position is considerably faster, as was demonstrated for the glutamic acid derivative **5a**: irradiation under nonionic conditions leads to *N*-Pht-γ-aminobutyric acid **6** as the sole product. In the presence of sodium carbonate (ionic conditions) the benzopyrrolizidine **7a** is formed in 76% yield.

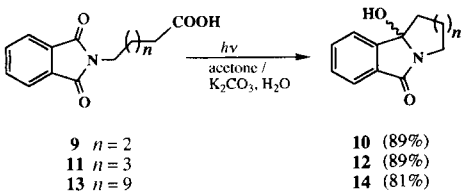
[*] Prof. Dr. A. G. Griesbeck,[+] Dipl.-Chem. A. Henz
Institut für Organische Chemie der Universität
Am Hubland, D-97074 Würzburg (Germany)
Dr. K. Peters, E.-M. Peters, Prof. Dr. H. G. von Schnering
Max-Planck-Institut für Festkörperforschung
Heisenbergstrasse 1, D-70569 Stuttgart (Germany)
[+] New address:
Institut für Organische Chemie der Universität
Greinstrasse 4, D-50939 Köln (Germany)
Telefax: Int. code + (221)470 5102

[**] This work was supported by the Deutsche Forschungsgemeinschaft (DFG Gr 881/7-1) and Degussa AG.



Scheme 1. a) 10 mM in acetone, 20 °C, *hv*, $\lambda = 300$ nm, N_2, 12 h; b) 10 mM in acetone, 10 equiv K_2CO_3, 2% H_2O, 20 °C, *hv*, $\lambda = 300$ nm, N_2, 12 h; c) 0.1 equiv CF_3COOH in CH_2Cl_2, 0 °C.

The UV absorption of the amide chromophore (e.g. in **7a**) is strongly blue-shifted relative to that of the substrate **5a**. Thus, **7a** is produced by a sequence of α- and γ-decarboxylation. Under identical conditions the corresponding C-protected glutamic acid derivative **5b**[12] provides a mixture of diastereomeric benzopyrrolizidines **7b** and **7c**, of which one isomer undergoes dehydration to form the enantiomerically pure enamide **8** when treated with trifluoroacetic acid. The other diastereomer (presumably the *cis* isomer) does not undergo dehydration.[13] After these "finger exercises" with short-chain amino acids (**5b**, **9**, **11**) we examined potential substrates for the synthesis of macrocycles. The 12-aminododecanoic acid derivative **13**[14] can be converted into azacyclotridecane **14** in 81% yield (Scheme 2, yields after recrystallization). Mass spectrometric analysis of compound **14** already indicated that no dimerization had occurred, a reaction that had to be expected because of the relatively high concentration (10 mM in acetone). The structure of **14** was additionally proven by X-ray analysis[15] (Fig. 1). In analogy to these results the spectroscopic data shows that dimers are not formed in any of the cases investigated. We assume therefore that already in the electronic ground state intramolecular complexation between the carboxylate anion and the phthalimido moiety makes intermolecular reactions unfavorable. The role of the countercation also accounts for this assumption: in the presence of ten equivalents of pyridine photodecarboxylation of **9** is drastically slower than the analogous reaction in the presence of sodium carbonate.



Scheme 2.

The synthesis of macrocyclic ring systems is unproblematic (Scheme 3): the 26-membered cyclic dipeptide **16** can be generated from the easiliy available substrate **15**[16] in 60% yield. Even substrates that are conformationally less flexible in the ground state can be efficiently converted under the photochemical conditions. For example, intramolecular (through-space) interactions between donor and acceptor groups cannot exist in the *trans*-cyclohexane derivative **17**. Still the tricyclic carbinol **18** is formed in 81% yield after relatively short irradiation time. Again no dimeric products are formed. After extrusion of CO_2 the C-radical centers combine with inversion at the α-C center to give **18** (Fig. 1).[15] 1,4-Donor–acceptor-substituted cyclohexanes have been widely studied as model systems for the investigation of electron transfer reactions ("superexchange mechanism" or "through-bond coupling ET").[17]

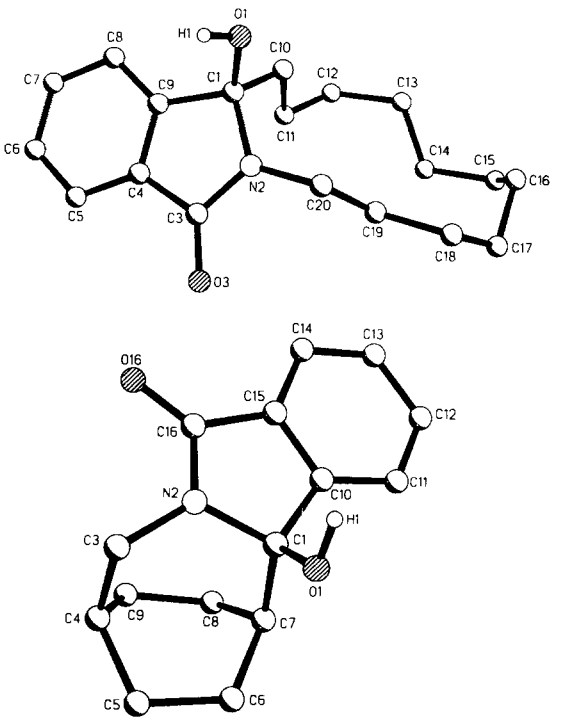
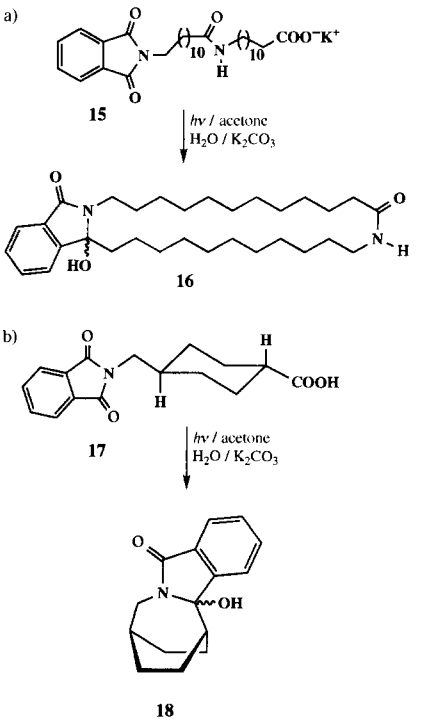


Fig. 1. Crystal structures of **14** (top) and **18** (bottom).



Scheme 3. a) Photocyclization of **15** to give **16**; b) photocyclization of **17** to give **18**.

This new synthesis of medium-sized ring systems and macrocycles may also be applied for the synthesis of cyclopeptides and macrocyclic crown ethers.

Experimental Procedure

A solution of 690 mg (2 mmol) of **13** in 200 mL of acetone was charged with 1.5 g of sodium carbonate in 3 mL of water and irradiated for 12 h at room temperature under a constant stream of nitrogen (Rayonet RPR-208 chamber reactor, eight RUL-3000 Å lamps, ca. 800 W). After evaporation of the solvent the residue was treated with 10 mL of ether, and the yellow precipitate was collected. Recrystallization from acetone gave 520 mg (81%) of **14** as colorless plates, m.p. 166–168 °C; ^{1}H NMR (250 MHz, $CDCl_3$): δ = 0.88–1.01 (m, 1H), 1.20–1.70 (m, 16H), 1.91–2.02 (m, 1H), 2.22–2.47 (m, 2H), 3.34–3.52 (m, 2H), 4.09 (s, 1H, OH), 7.57–7.63 (m, 1H), 7.68–7.80 (m, 3H); ^{13}C NMR (63 MHz, $CDCl_3$): δ = 21.3, 24.7, 24.8, 25.5, 26.0, 26.7, 26.8, 26.9, 28.4, 36.4, 38.5 (all CH_2), 91.6 (C_q), 121.5, 123.1, 129.2 (all CH), 131.0 (C_q), 132.1 (CH), 147.1, 168.3 (both C_q).

Received: September 8, 1994 [Z 7299 IE]
German version: *Angew. Chem.* **1995**, *107*, 498

Keywords: amino acids · cyclizations · macrocycles · photochemistry

[1] P. S. Mariano, *Acc. Chem. Res.* **1983**, *16*, 130–137.
[2] F.-T. Chiu, J. W. Ullrich, P. S. Mariano, *J. Org. Chem.* **1984**, *49*, 228–236.
[3] Y. Karauchi, H. Nobuhara, K. Ohga, *Bull. Chem. Soc. Jpn.* **1986**, *59*, 897–905.
[4] R. Noyori, M. Kato, M. Kawanishi, H. Nozaki, *Tetrahedron* **1969**, *25*, 1125–1136.
[5] a) A. G. Griesbeck, H. Mauder, *Angew. Chem.* **1992**, *103*, 97–99; *Angew. Chem. Int. Ed. Engl.* **1992**, *31*, 73–75; b) A. G. Griesbeck, H. Mauder, I. Müller, *Chem. Ber.* **1992**, *125*, 2467–2475; c) A. G. Griesbeck, H. Mauder, I. Müller, K. Peters, E.-M. Peters, H. G. von Schnering, *Tetrahedron Lett.* **1993**, *34*, 453–456; d) A. G. Griesbeck, A. Henz, J. Hirt, V. Ptatschek, T. Engel, D. Löffler, F. W. Schneider, *Tetrahedron* **1994**, *50*, 701–714.
[6] Recent publications: a) H. Takechi, M. Machida, N. Nishizono, Y. Kanaoka, *Chem. Pharm. Bull.* **1994**, *42*, 188–196; b) Y. Hatanaka, Y. Sato, H. Nakai, M. Wada, T. Mizoguchi, Y. Kanaoka, *Liebigs Ann. Chem.* **1992**, 1113–1123.
[7] A two-step application of this concept which uses 1,3-dithiolanoyl donor groups has been published: M. Wada, H. Nakai, Y. Sato, Y. Hatanaka, Y. Kanaoka, *Tetrahedron* **1983**, *39*, 2691–2698.
[8] Y. Sato, H. Nakai, T. Mizoguchi, M. Kawanishi, Y. Hatanaka, Y. Kanaoka, *Chem. Pharm. Bull.* **1982**, *30*, 1263–1265.
[9] A. G. Griesbeck, A. Henz, *Synlett*, **1994**, 931–932.
[10] The analogous migration of a trimethylsilyl group has been reported: U. C. Yoon, D. U. Kim, J. C. Kim, J. G. Lee, P. S. Mariano, Y. J. Lee, H. L. Ammon, *Tetrahedron Lett.* **1993**, *34*, 5859–5862.
[11] S. J. Formosinho, L. G. Arnaut, *J. Photochem. Photobiol. A* **1993**, *75*, 21–48.
[12] J. Hanus, V. Tolman, K. Veres, *Coll. Czech. Chem. Commun.* **1973**, *38*, 1212–1220.
[13] Spectroscopic data for **7b** und **8**: **7b**: ^{1}H NMR (250 MHz, $CDCl_3$): δ = 1.75 (ddd, J = 9.3, 11.2, 12.5 Hz, 1H), 2.53 (ddd, J = 2.3, 5.8, 12.5 Hz, 1H), 2.85 (mc, 2H), 3.91 (s, 3H), 4.73 (dd, J = 8.5, 8.6 Hz, 1H), 7.60–7.71 (m, 3H), 7.85 (d, J = 7.4 Hz, 1H); ^{13}C NMR (63 MHz, $CDCl_3$): δ = 33.0, 35.6 (both CH_2), 52.7 (CH_3), 55.5 (CH), 96.7 (C_q), 122.7, 124.1, 130.0 (all CH), 131.0 (C_q), 133.3 (CH), 146.8, 169.5, 173.1 (all C_q). – **8**: ^{1}H NMR (600 MHz, $CDCl_3$): δ = 2.24–2.32 (m, 1H), 3.15 (ddd, J = 3.3, 4.0, 10.2 Hz, 1H), 3.51 (ddd, J = 2.9, 4.0, 10.2 Hz, 1H), 3.68 (s, 3H), 4.70 (dd, J = 4.0, 10.4 Hz, 1H), 7.31–7.58 (m, 4H); ^{13}C NMR (63 MHz, $CDCl_3$): δ = 40.5 (CH_2), 52.3 (CH_3), 53.2 (C_q), 103.2, 120.7, 122.5, 128.4 (all CH), 130.0 (C_q), 131.2 (CH), 135.7, 141.4, 170.5, 173.8 (all C_q).
[14] E. J. Browne, J. B. Polya, *J. Chem. Soc. C* **1968**, 2904–2908.
[15] **14**: $C_{19}H_{27}NO_2$: M_r = 303.44, monoclinic ($P2_1/n$), a = 2018.4(8), b = 791.3(3), c = 1059.7(5) pm, β = 92.50(4)°, V = 1691(1) × 10^6 pm^3, Z = 4, $\rho_{calcd.}$ = 1.192 g cm^{-3}, crystal dimensions: 0.75 × 1.25 × 0.25 mm, total number of reflections: 4265; 3088 reflections for $F > 3\sigma(F)$, R = 0.055, R_w = 0.050. – **18**: $C_{15}H_{17}NO_2$: M_r = 243.31, orthorhombic (*Pbca*), a = 1411.2(6), b = 1881.8(4), c = 922.0(4) pm, V = 2449(2) × 10^6 pm^3, Z = 8, $\rho_{calcd.}$ = 1.320 g cm^{-3}, crystal dimensions: 0.4 × 1.1 × 0.15 mm, total number of reflections: 3204; 1798 reflections for $F > 3\sigma(F)$, R = 0.054, R_w = 0.046. For both structures: Siemens R3m/V Diffraktometer, $Mo_{K\alpha}$ radiation, graphite monochromator. Further details can be obtained from the Director of the Cambridge Crystallographic Data Centre, 12 Union Road, GB-Cambridge CB21EZ (UK), on quoting the full journal citation.
[16] Synthesis of **15** is analogous to: Y. Sato, H. Nakai, M. Wada, T. Mizoguchi, Y. Hatanaka, Y. Kanaoka, *Chem. Pharm. Bull.* **1992**, *40*, 3174–3180.
[17] a) G. L. Closs, L. T. Calcaterra, N. J. Green, K. W. Penfield, J. R. Miller, *J. Phys. Chem.* **1986**, *90*, 3673–3683. b) F. Lendzian, J. Schlüpmann, J. von Gersdorff, K. Möbius, H. Kurreck, *Angew. Chem.* **1991**, *103*, 1536–1539; *Angew. Chem. Int. Ed. Engl.* **1991**, *30*, 1461–1463.

Computational Evidence for the Existence of Cu^{III} Intermediates in Addition and Substitution Reactions with Dialkylcuprates**

Andrea E. Dorigo, Jutta Wanner, and Paul von Ragué Schleyer*

Dialkylcuprates are widely used nucleophilic agents in organic synthesis. Whether these species function as electron transfer[1] agents or react nucleophilically[2] has been debated at length, yet the mechanism remains unresolved. A potential problem with the nucleophilic mechanisms proposed by Corey[2] for additions to unsaturated bonds, and by Goering et al.[3] and Kreft[4] for substitution reactions, is that in both cases a Cu^{III} intermediate is involved.[5] To date, there is no direct experimental evidence for the existence of trialkylcopper structures. We now demonstrate computationally that trimethylcopper, $Cu(CH_3)_3$, indeed corresponds to an energy minimum when the copper center is stabilized by donors such as water or ammonia. Even in the absence of such electron donors, $Cu(CH_3)_3$ corresponds to a minimum at some of the levels of theory employed. These findings support the intermediacy of trialkylcopper species in the presence of ether solvents and/or nitrogen ligands, which are commonly used in dialkylcuprate reactions. We also show that $Cu(CH_3)_3$ and the inorganic CuF_3 molecule[6] have similar geometries; however, the copper center in the former has a much smaller natural charge than in the latter. The copper charge in $Cu(CH_3)_3$ is, in fact, similar to that in the Cu^{II} organocopper species $[CuCH_3]^+$ and $Cu(CH_3)_2$.

Ab initio calculations[7, 8] were performed on $Cu(CH_3)_3$ and its complexes with H_2O and NH_3. For comparison, CuH_3 and its complexes were investigated similarly. MP2 optimizations were performed first using a split-valence basis set[9] (basis set A) for structures **1**–**10** (Fig. 1). The second, larger basis set (designated APOL), employed for all structures except **7**, consisted of A augmented with polarization functions[10, 11] for copper and all atoms directly bonded to copper. Optimized geometries with the two basis sets are similar for all systems. Single-point energy calculations at the QCISD/APOL level were performed on the MP2/APOL geometries of structures **5**, **8**, and **9** (ethane). Analytical frequency analyses were performed both at MP2/A and MP2/APOL level to determined the nature of each stationary point (that is, whether it is a minimum, which is an intermediate, or a saddle point, which is a transition structure). Further geometry optimizations and frequency calculations on **5** were performed with density functional theory, using the non-local functional developed by Becke et al.[12] for the exchange terms and by Lee, Yang, and Parr[13] for the correlation; this formalism is denoted as BLYP in the following discussion. The APOL basis set was used for these calculations. The solvation of structure **5** was also investigated with the self-consistent reaction field (SCRF)[14] method to mimic the effect of an ether medium (the dielectric constant of ether, 4.197, was used). Table 1 lists the absolute energies, together with the number of negative eigenvalues of the Hessian matrix, of CuH_3 systems **1**–**3**, $Cu(CH_3)_3$[15] systems **4**–**6**, and of the transition structure (**7**) for the decomposition of **5** into $(H_2O)CuCH_3$[15]

[*] Prof. Dr. P. von R. Schleyer, Dr. A. E. Dorigo, Diplom-Chem. J. Wanner
Computer-Chemie-Centrum
Institut für Organische Chemie I der Universität Erlangen-Nürnberg
D-91054 Erlangen (Germany)
Telefax: Int. code + (9131)859-132

[**] This work was supported by the Volkswagen-Stiftung, by the Convex Computer Corporation, and by the Fonds der Chemischen Industrie. We are grateful to Professor Kisch (Universität Erlangen-Nürnberg) for useful discussions.

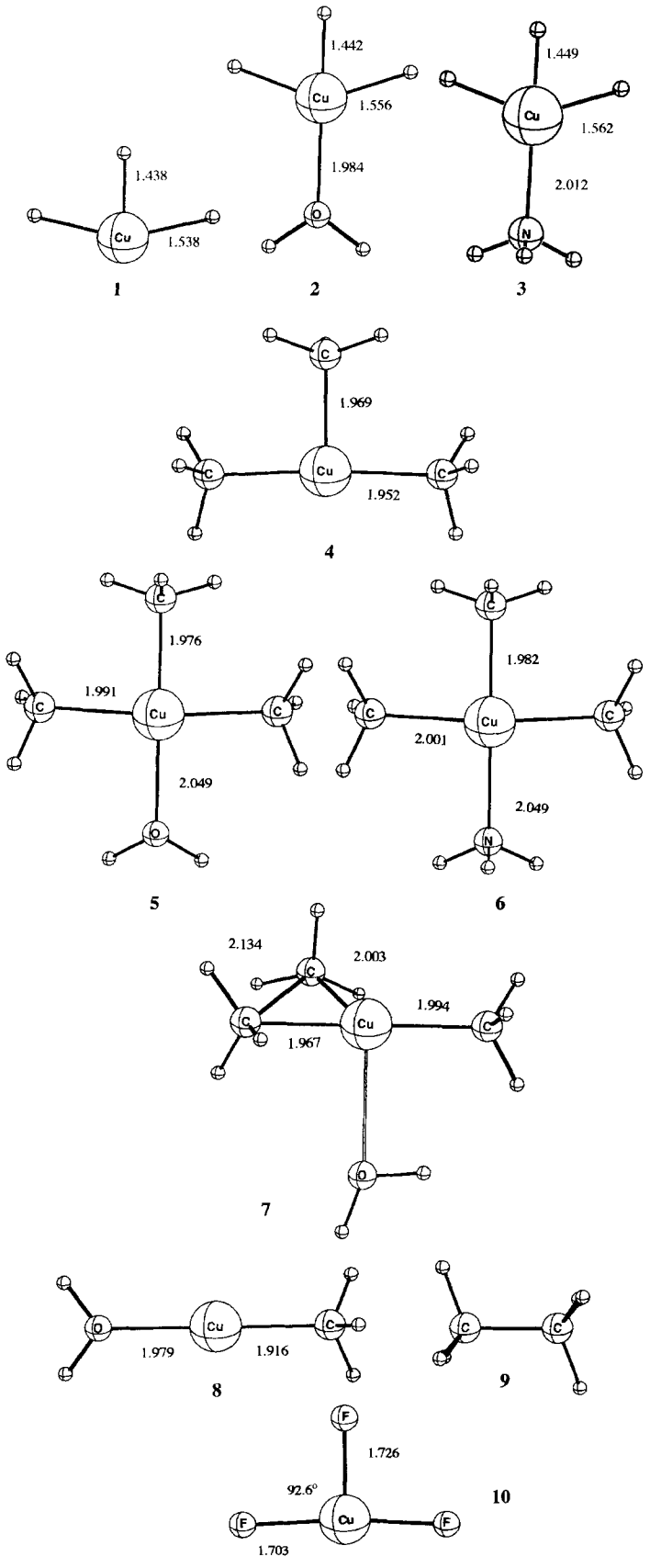


Fig. 1. Geometries of **1**–**6** and **8**–**10** optimized at the MP2/APOL level and of **7** optimized at the MP2/A level. Bond lengths are given in Å.

(**8**) and C_2H_6 (**9**). Figure 1 depicts the optimized geometries of **1**–**10**; selected parameters are given.

CuH_3 (**1**) was optimized in C_{2v} symmetry and its complexes with NH_3 and H_2O (**2** and **3**) in C_s symmetry. All three species are transition structures, both at MP2/A and MP2/APOL levels (Table 1). The MP2/APOL results are discussed here. The negative eigenvalue is large (ranging from $-791\ cm^{-1}$ to $-981\ cm^{-1}$) and corresponds to the formation of an H_2 molecule. The exothermicity of the reaction $\mathbf{1} \rightarrow CuH + H_2$ is 127.7 kcal mol^{-1}. $Cu(CH_3)_3$ (**4**; C_s) likewise is a transition structure (the negative eigenvalue of $-208\ cm^{-1}$ represents ethane formation). In contrast, both **5** and **6** lie at minima; however, since the frequency of the vibration that corresponds to ethane formation is small (99 cm^{-1} and 108 cm^{-1} for **5** and **6**, respectively), fragmentation should proceed readily. In all cases, the trialkylcopper fragment is T-shaped, as predicted theoretically by Hoffmann and Kochi.[16]

In order to assess the kinetic stability of **5** vis-à-vis loss of C_2H_6,[17] we calculated the transition structure **7**, which lies 13.9 kcal mol^{-1} above **5** at MP2/A. The energy of the products of the fragmentation of **5** (ethane (**9**) and the complex (**8**) between $CuCH_3$ and H_2O) lies 52.3 kcal mol^{-1} below that of **5** at QCISD/APOL//MP2/APOL. Structure **5** is thus kinetically stable though strongly disfavored thermodynamically relative to the reaction products. While we have not attempted to locate an analogous transition structure for the fragmentation of **6**, its kinetic stability can be expected to be similar to that of **5**, because the lowest calculated vibrational frequencies are similar (see Table 1).

Structure **5** corresponds to a minimum even at other levels of theory (see Table 1): SCRF optimization of **5** ($\varepsilon = 4.197$) gave a similar geometry to that already calculated in the absence of an electric field. Here the lowest vibrational frequency (84 cm^{-1}) is only slightly lower than the value calculated previously (99 cm^{-1}). Even BLYP/APOL geometry optimization and fre-

Table 1. Absolute energies (in −Hartree) calculated at the following levels: MP2/A (**1**–**10**), MP2/APOL (**1**–**6**, **8**–**10**), QCISD/APOL (**5**, **8**, **9**), SCRF/APOL (**5**), and BLYP/APOL (**4**, **5**). Values in parentheses (in cm^{-1}) refer to the number of negative eigenvalues of the Hessian matrix and the lowest positive vibrational frequency (for minima) or the negative vibrational frequency (for saddle points). Values in square brackets give the relative energies of **5**, **7**, and [8] and [9] (in kcal mol^{-1}).

Structure	MP2/A		MP2/APOL		QCISD/APOL //MP2/APOL [a]	
CuH_3 **1**	1640.48090 (1; −1004)		1640.62239 (1; −981)			
$(H_2O)CuH_3$ **2**	1716.67041 (1; −622)		1716.88432 (1; −812)			
$(H_3N)CuH_3$ **3**	1696.84017 (1; −555)		1697.04999 (1; −791)			
$Cu(CH_3)_3$ **4**	1758.05203 (1; −206)		1758.14294 (1; −208)		1759.95043 [b] (0; +59)	
$(H_2O)Cu(CH_3)_3$ **5**	1834.05801 (0; +99) [0.0]		1834.39035 (0; +99) [0.0]		1834.39567 [0.0]	
					1836.38907 [b] (0; +88)	
					1833.43853 [c] (0; +84)	
$(H_3N)Cu(CH_3)_3$ **6**	1814.22388 (0; +107)		1814.55204 (0; +108)			
7	1834.03589 [+13.9]					
$(H_2O)CuCH_3$ **8**	1754.73266	[−36.1]	1754.86429	[−21.1]	1754.95191	[−52.3]
C_2H_6 **9**	79.38289		79.49241		79.52715	
CuF_3 **10**	1937.39054		1937.66913 (0; +203)			

[a] Unless stated otherwise. [b] BLYP/APOL. [c] SCRF/APOL.

 © VCH Verlagsgesellschaft mbH, D-69451 Weinheim, 1995 0570-0833/95/0404-0477 $ 10.00+.25/0

quency calculation gave **5** to be a minimum (vibrational frequency = 88 cm^{-1}).

While trialkylcopper compounds have not been isolated experimentally, some inorganic Cu^{III} systems are known.[6] In all such systems, copper is bound to strongly electronegative atoms. As a model we chose CuF_3 (**10**) and calculated its structure to compare with the structural and electronic features of its organometallic counterparts **4**–**6**. The C_{2v}-symmetric structure for the CuF_3 minimum at MP2/APOL is T-shaped,[16] just like that of the trialkylcopper fragment in **4**–**6**. The occupied valence orbitals are similar in the two cases and corresponds to a d^8 electronic configuration at copper, as postulated by Hoffmann and Kochi.[16] However, natural population analyses reveal significant differences in the electronic charges on the copper centers in **4**–**6** and in **10**. Details of the structures for the minima **5** and **10** are important; all results refer to the APOL basis set. The natural population analysis[7] charge is 1.96 for copper in **10**. As expected, this is larger than that in CuF_2 (1.71). In contrast, the charge on copper in **5** is only 1.16 as a result of large back-donation from the methyl groups to the (formally) tripositive copper. Indeed, the charge of 1.16 is substantially smaller than that in $Cu(CH_3)_2$ (1.46), and only slightly larger than that in the $[CuCH_3]^+$ cation (1.05). Both of these molecules are Cu^{II} species. Thus, it is misleading to describe **5** as a Cu^{III} molecule, even though the copper is covalently bound to three centers. The charges on the CH_3 groups *trans* and *cis* to the water fragment in **5** are −0.12 and −0.52, respectively. Thus, **5** may be best viewed as a complex between $[CuCH_3]^+$ and the ethane radical anion.

Our calculations indicate that trialkylcopper intermediates stabilized by either nitrogen or oxygen nucleophiles correspond to local energy minima and are therefore viable reaction intermediates. It is known that, in contrast to copper, gold(III) compounds are fairly stable. The origins of this difference in stability are now being investigated.

Received: August 11, 1994 [Z 7230 IE]
German version: *Angew. Chem.* **1995**, *107*, 492

Keywords: ab initio calculations · copper compounds · cuprates

[1] H. O. House, *Acc. Chem. Res.* **1976**, *9*, 59; see also H. O. House, W. F. Fischer, *J. Org. Chem.* **1968**, *33*, 949.
[2] E. J. Corey, N. W. Boaz, *Tetrahedron Lett.* **1985**, *26*, 6015.
[3] H. L. Goering, S. S. Kantner, C. C. Tseng, *J. Org. Chem.* **1983**, *48*, 715; H. L. Goering, V. D. Singleton, Jr., *ibid.* **1983**, *48*, 1531; C. C. Tseng, S. D. Paisley, H. L. Goering, *ibid.* **1986**, *51*, 2884.
[4] A. Kreft, *Tetrahedron Lett.* **1977**, 1035.
[5] Evidence for the complexation of the cuprates through double bonds prior to nucleophilic addition has been obtained from ^{13}C NMR studies: S. H. Bertz, R. A. J. Smith, *J. Am. Chem. Soc.* **1989**, *111*, 8276. Even these authors suggest the intermediacy of a Cu^{III} species in the reaction. See also G. Hallnemo, T. Olsson, C. Ullenius, *J. Organomet. Chem.* **1985**, *282*, 133.
[6] For a discussion of inorganic Cu^{III} compounds, which, however, all contain tetracoordinate copper centers, see N. N. Greenwood, A. Earnshaw, *Chemistry of the Elements*, Pergamon, Oxford, **1984**, p. 1379.
[7] All calculations employed the Gaussian 92/DFT program: M. J. Frisch, G. W. Trucks, H. B. Schlegel, P. M. W. Gill, B. G. Johnson, M. W. Wong, J. B. Foresman, M. A. Robb, M. Head-Gordon, E. S. Replogle, R. Gomperts, J. L. Andres, K. Raghavachari, J. S. Binkley, C. Gonzalez, R. L. Martin, D. J. Fox, D. J. Defrees, J. Baker, J. J. P. Stewart, and J. A. Pople, Gaussian Inc., Pittsburgh, PA, **1993**. Natural charges were calculated according to the procedure of Reed and Weinhold: A. E. Reed, F. Weinhold, *J. Am. Chem. Soc.* **1985**, *107*, 1919.
[8] For all structures no open-shell (UHF) wavefunction exists that has a lower energy than the RHF wavefunctions computed here.
[9] The Ahlrichs basis set was used for copper: A. Schäfer, H. Horn, R. Ahlrichs, *J. Chem. Phys.* **1992**, *97*, 2571. The D95V basis set was used for the first row atoms and for hydrogen.
[10] Polarization functions used: one f function (exponent = 2.7 [11]) for Cu; one d function (exponent = 0.8) for F, O, N, and C; and one p function (exponent = 0.11) for the H atoms attached to copper in **1**–**3**.
[11] An exponent of 3.525 has been proposed for copper by Frenking et al.: A. W. Ehlers, M. Böhme, S. Dapprich, A. Gobbi, A. Höllwarth, V. Jonas, K. F. Köhler, R. Stegmann, A. Veldkamp, G. Frenking, *Chem. Phys. Lett.* **1993**, *208*, 111. Optimization of **4** with this exponent gave a similar geometry but a higher energy with both MP2 and BLYP.
[12] T. Ziegler, V. Tschinke, A. Becke, *Polyhedron* **1987**, *6*, 685.
[13] J. W. Labanowski, J. Andzelm, *Density Functional Methods in Chemistry*, Springer, New York, **1991**; R. G. Parr, W. Yang, *Density Functional Theory of Atoms and Molecules*, Oxford University Press, New York, **1992**; Gaussian 92/DF (New Methods and Features in Gaussian 92/DFT), Gaussian Inc., Pittsburgh, PA, **1993**. C. Lee, W. Yang, R. G. Parr, *Phys. Rev. B* **1988**, *37*, 785.
[14] M. W. Wong, M. J. Frisch, K. B. Wiberg, *J. Am. Chem. Soc.* **1991**, *113*, 4776.
[15] For related calculations on lithium dimethylcuprate, see A. E. Dorigo, K. Morokuma, *J. Chem. Soc. Chem. Commun.* **1989**, 1884; see also J. P. Snyder, G. E. Tipsword, D. P. Spangler, *J. Am. Chem. Soc.* **1992**, *114*, 1507; for related calculations on $[Cu(CF_3)_4]^-$ see: J. P. Snyder, *Angew. Chem.* **1995**, *107*, 112; *Angew. Chem. Int. Ed. Engl.* **1995**, *34*, 80; for high-level calculations on methylcopper, see M. Sodupe, C. W. Bauschlicher, T. J. Lee, *Chem. Phys. Lett.* **1992**, *189*, 266.
[16] The preference for a C_{2v}-symmetric (T-shaped) structure in CuX_3 systems is due to a first-order Jahn-Teller distortion of the trigonal planar D_{3h} structure; see S. Komiya, T. A. Albright, R. Hoffmann, J. K. Kochi, *J. Am. Chem. Soc.* **1977**, *99*, 8440; K. Tatsumi, R. Hoffmann, A. Yamamoto, J. K. Stille, *Bull. Chem. Soc. Jpn.* **1981**, *54*, 1857; P. Schwerdtfeger, P. D. W. Boyd, *Inorg. Chem.* **1992**, *31*, 327; S. Komiya, T. A. Albright, R. Hoffmann, J. K. Kochi, *J. Am. Chem. Soc.* **1976**, *98*, 7255. The authors of the last paper predict that the triplet states of CuX_3 species have D_{3h} symmetry. BLYP/APOL geometry optimization of the triplet state of **4**, $^3Cu(CH_3)_3$, indeed gives a structure with an essentially trigonal-planar coordination geometry for copper; however, this structure lies 13.9 kcal mol^{-1} above **4** in energy at this level.
[17] For other examples of a reductive elimination from a tetracoordinate d^8 system, see J. J. Low, W. A. Goodard, III, *J. Am. Chem. Soc.* **1984**, *106*, 6928, 8321; *ibid.* **1986**, *108*, 6115; *Organometallics* **1986**, *5*, 609.

The First Unambiguous Characterization of a Neutral Phosphorus Ylide–Lithium Complex: Isolation, Structure, and Ab Initio Investigations of $[(PhCH_2)_2NLi \cdot CH_2PPh_3]_2$**

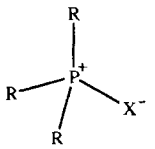
David R. Armstrong, Matthew G. Davidson,* and David Moncrieff

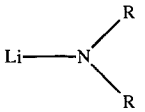
The Nobel Prize-winning discovery by Wittig of the reaction that bears his name[1] signaled the beginning of interest in phosphorus ylides. Though this interest was then in the realm of organic synthesis,[2] the mid-1960s saw the advent of the inorganic chemistry of these compounds. The isolation and characterization of (initially) silicon derivatives led rapidly to the development of an extensive literature of p-block and transition metal chemistry associated with both stabilized and nonstabi-

[*] Dr. M. G. Davidson
University Chemical Laboratory, Lensfield Road
GB-Cambridge CB2 1EW (UK)
Telefax: Int. code + (223)336362
Dr. D. R. Armstrong
Department of Pure and Applied Chemistry
University of Strathclyde, Glasgow G1 1XL (UK)
Dr. D. Moncrieff
Supercomputer Computations Research Institute
Florida State University
Tallahassee, FL 32306-4052 (USA)

[**] We would like to thank Dr. R. Snaith for helpful discussions and for the provision of laboratory facilities, and Dr. P. R. Raithby for the provision of X-ray facilities. We acknowledge the financial support of St John's College, Cambridge (Research Fellowshop for M.G.D.) and US Department of Energy (Contract No. DE-FC05-85ER2500000 for D.M.).

lized ylides.[3] However, the isolation and structural characterization of adducts of inorganic alkali metal salts and ylides, and of alkali metalated organic complexes with neutral phosphorus ylides has remained an unexplored area. This is surprising on two counts. Firstly, alkali metals are intimately associated with the generation of ylides from phosphonium halides.[4] Secondly, the use of phosphorus–carbon ylides (**1**, where X = CH_2) as neutral donors to early main group metals is only a small conceptual step from the use of isoelectronic phosphane oxide donors (**1**, where X = O) such as hexamethylphosphoramide [HMPA, **1a**]. This is a common Lewis base in the chemistry of





1a; R = Me_2N, X = O
1b; R = Ph, X = CH_2
1c; R = Ph, X = CH_2, NH, O
1d; R = H, X = CH_2, NH, O

2a; R = CH_2Ph
2b; R = H

alkali metal species,[5] and its phosphorus–oxygen bond has been shown by ab initio calculations to possess ylidic character.[6] We now report the crystal structure, solution behavior, and MO calculations for a simple, nonstabilized ylide complex of a lithium amide, the first neutral ylide complex of an alkali metal compound to be characterized in the solid state.

The well-characterized dibenzylamidolithium (**2a**) system[7] was chosen as a suitable metalated organic compound for complexation by a neutral ylide. Uncomplexed dibenzylamidolithium is trimeric in the solid state through formation of an Li_3N_3 ring, and with neutral Lewis base donors forms dimeric complexes containing Li_2N_2 rings.[7a] Triphenylphosphonium methylide (**1b**) was chosen as a suitable ylide, first since it is a readily isolable solid, second, any complexation to lithium through the ylidic carbon would be sterically unhindered, and third, its solid-state structure has been determined[8] thereby allowing structural and bonding effects within the ylide to be evaluated upon complexation to lithium.

Reaction of *n*BuLi with a chilled toluene/hexane solution of dibenzylamine and **1b** afforded a red precipitate, which dissolved on warming to give a deep red solution and on renewed cooling gave dichroic red/yellow crystals (see Experimental Procedure). ^{1}H NMR spectroscopy and elemental analysis suggested that the neutral complex **3** had indeed been isolated, and such

$[(PhCH_2)_2NLi \cdot CH_2PPh_3]_n$ **3**

was confirmed by a single-crystal X-ray diffraction study,[9] which revealed **3** to be dimeric ($n = 2$) in the solid state. The structure of **3** (Fig. 1) contains an unremarkable Li_2N_2 core [Li1–N1 2.013(4), Li1–N1a 2.000(4) Å; Li1-N1-Li1a 76.2(2), N1-Li1-N1a 103.8(2)°]. However, the coordination sphere of the three-coordinate lithium is completed by unprecedented terminal complexation of an ylidic carbon atom [C61-Li1 2.207(4) Å; P1-C61-Li1 130.8(2) Å]. This remarkably short C–Li distance falls within the lower end of the 2.1–2.4 Å range observed in the solid state for lithium alkyls.[5a] Not unexpectedly, coordination of the ylide to lithium in **3** renders the ylidic methylene group considerably more pyramidal within the complex than is observed in the crystal structure of **1b**[8] [in **3**, the sum of three angles (excluding those involving Li1) around C61 is 334°, compared to 353° in **1b**]. The P–C bond is, however, only slightly elongated by complexation [in **3**, P1–C61 = 1.702(2) Å; in **1b**, average P–C = 1.693 Å]. Complexation to lithium also effects little change in the geometry about phosphorus; distortions from ideal (localized C_{3v}) symmetry as have also been noted for **1b** are observed in **3** in that the C(phenyl)–P distance perpendicular to the methylene plane is elongated relative to the other two [P1–C31 = 1.835(2), P1–C41 = 1.811(2), P1–C51 = 1.813(2) Å], and the corresponding C(phenyl)-P1-C(methylene) angle is significantly larger than the other two [C31-P1-C61 = 118.08(10), C41-P1-C61 = 110.13(11), and C51-P1-C61 = 110.42(11)°].

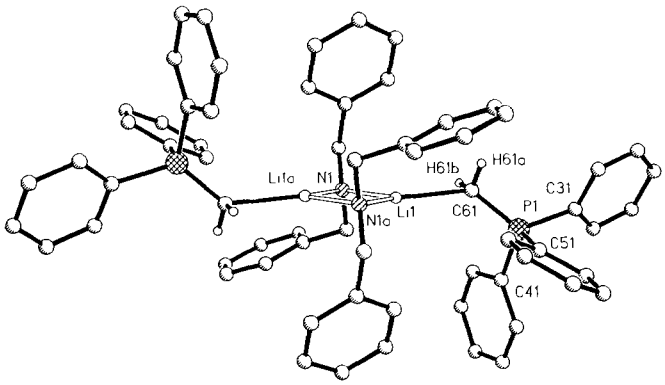


Fig. 1. Crystal structure of **3** (all hydrogen atoms except those of the ylidic carbon atoms are omitted for clarity). Selected bond lengths and angles: Li1–N1 2.013(4), Li1–N1a 2.000(4), Li1–C61 2.207(4) Å, C61–P1 1.702(2); Li1–N1–Li1a 76.2(2), N1–Li1–N1a 103.8(2), Li1–C61–P1 130.8(2).

To our knowledge, only two compounds with interactions between alkali metals and phosphorus ylides have previously been structurally characterized. Contrasting with **3** where the ylide acts only as a Lewis base donor, both are structures of metalated, anionic ylides. In both cases this results in delocalization of the negative charge over two or more carbanionoid centers: in $\{[Li(CH_2)P(C_6H_5)_2(CH_2)]_2(dioxane)_3\}_2 \cdot (dioxane)$[10] the molecular structure comprises an eight-membered ring in which two $[(CH_2)P(C_6H_5)_2(CH_2)]^-$ ligands bridge two lithium centers. In $[K(CHC_6H_5)P(CH_3)_2(CHC_6H_5)]_\infty$[11] the negative charge is further delocalized into the benzylic ring, which results in an interaction of the metal with *ortho* and *para* aromatic carbon atoms in addition to that with the two ylidic carbon atoms. The only other related crystal structure is that of a magnesium–uranium complex containing two neutral phosphorus ylide donors to magnesium. Here though, as the authors readily concede, only one crystal of the complex was serendipitously recovered from a NMR tube in which no magnesium compounds were thought to be present, and no rational synthesis could be developed.[12]

Though **3** is dimeric in the solid state, preliminary cryoscopic relative molecular mass (RMM) measurements suggest the presence of a monomer⇌oligomer equilibrium in benzene solution. At low concentration (0.0006 M, expressed in terms of monomer) the predominant species is monomeric (RMM = 464 ± 20, degree of association, $n = 0.97 \pm 0.04$), whereas at higher concentration (0.0010 M) RMM = 547 ± 25 ($n = 1.14 \pm 0.03$) indicating that some aggregation to higher oligomers takes place. Variable-concentration cryoscopic studies[13] are underway in order to quantify the nature of this oligomerization fully, though on the basis of the dimeric solid-state structure of **3**, it seems reasonable to propose that a monomer⇌dimer equilibrium operates. Although these data

alone do not preclude an alternative scenario of ligand dissociation taking place at low concentration (that is, $\mathbf{3}_n \rightleftharpoons \mathbf{2a}_n + n\,\mathbf{1b}$) this possibility may be discounted by variable-concentration ^{1}H NMR data. The signal due to the two protons of the ylidic carbon, which appears as a doublet due to $^2J_{PH}$ coupling, provides particularly useful information. At all concentrations of **3** in benzene this signal is shifted to higher frequency, and the coupling constant is reduced relative to that of the free ylide (see Experimental Procedure). In addition, the coupling constant is concentration-dependent for benzene solutions of **3**, whereas it is not for those of the free ylide. In dilute solution (0.0006 M) $^2J_{PH}$ = 3.3 Hz, whereas in more concentrated solution (0.044 M) $^2J_{PH}$ = 4.8 Hz ($^2J_{PH}$ = 7.2 Hz for the free ylide). Taking into account the cryoscopic results in the same solvent, the value observed for dilute solutions may be ascribed to the monomeric species, and that observed for higher concentrations to an oligomer (probably a dimer), or to an averaged value between that of the monomer and a higher oligomer. The fact that $^2J_{PH}$ *decreases* on dilution is consistent with an increase in the proportion of monomer present in solution. One would expect lithium to exert a greater influence over the electronic structure of the ylide (and therefore the observed coupling constants) in a monomer where the metal is only two-coordinate than it would in an oligomer where the lithium would be (at least) three-coordinate. If ligand dissociation from the dimer was taking place one would expect $^2J_{PH}$ to *increase* on dilution as a greater proportion of the free ylide becomes present in solution.

In addition to the solid-state and solution studies described above, features of phosphorus ylide complexation to lithium amides have come from theoretical calculations. Though many calculations have previously been performed on phosphorus ylides and related compounds,[14] none have dealt specifically with the coordination of neutral ylides to lithium compounds. Ab initio calculations have now been performed on a series of model compounds.[15] In addition to monomeric and dimeric models for **3**, isoelectronic iminophosphorane (**1**, where X = NH) and phosphane oxide (**1**, where X = O) complexes have also been studied. Optimization of monomeric adducts of the type **2a**·**1c** between lithium amide and a donor molecule gives complexation energies (the decrease in energy on bringing the two components together) of 25.5, 31.4, and 29.8 kcal mol^{-1} for X = CH_2, NH, and O, respectively. For dimeric adducts of the type $(\mathbf{2b}\cdot\mathbf{1d})_2$, complexation energies are, in all cases, less than for monomers (13.9, 19.3, and 20.5 kcal mol^{-1} for X = CH_2, NH, and O, respectively), though this reduction is more than compensated for by the stabilization gained by dimerization (20.6, 23.6, and 21.8 kcal mol^{-1} for X = CH_2, NH, and O, respectively). These results demonstrate that while the complexation energy of a phosphorus–carbon ylide to an alkali metal is less than that of the corresponding phosphane oxide or a iminophosphorane, it is of the same order of magnitude. That this is so is perhaps surprising and suggests that Lewis base donors containing ylidic carbon atoms may be used in alkali metal chemistry alongside more usual nitrogen- and oxygen-containing donors.

The synthesis of complex **3** is significant on several fronts. Firstly, it provides the first unambiguous structural characterization of such a complex. Secondly, lithium salts (invariably lithium bromide, present as a product from the generation of ylides from phosphonium bromide precursors) can have an effect on alkene stereochemistry in Wittig reactions,[2] and metalated (lithiated) ylides have also seen some synthetic utility, because they show enhanced reactivity over neutral ylides.[16] The effect of lithium amide–phosphorus ylide complexes on the course of Wittig reactions is currently being investigated. Thirdly, complexes like **3** may also find application as precursors for the preparation of ylide complexes with organometallic compounds of transition metals. Reactions of **3** and similar complexes with transition metal halides have been performed, and products are currently being characterized. Fourthly, the results of the calculations demonstrate the ability of ylidic carbon atoms to act as Lewis base donors to alkali metals. Systems containing ylidic carbon atoms stabilized by atoms other than phosphorus (S, N, As, and C) are, therefore, potential Lewis base donors to alkali metals. Lastly, the presence of hydrogen atoms on the donor atom of a complexant molecule, as in **1b**, provides reactivity at the point of complexation not available with common N- or O-containing donors. Potentially, this allows further metalation of a complex at this site, thereby providing a route to novel complexes containing different metals and different anions.

Experimental Procedure

1b was prepared and isolated according to ref. [17]. ^{1}H NMR (250 MHz, C_6D_6, TMS): δ = 0.80 (d, 2H, Ph_3PCH_2, $^2J_{PH}$ = 7.2 Hz), 7.00–7.07 (m, 9H, *m*- and *p*-Ph_3PCH_2), 7.72–7.78 (m, 6H, *o*-Ph_3PCH_2).

3: *n*-Butyllithium (1.6 mL of a 1.6 M solution in hexanes, 2.5 mmol) was added under nitrogen to a cooled (about 0 °C), stirred solution of **1b** (0.69 g, 2.5 mmol) and dibenzylamine (0.55 mL, 2.5 mmol) in hexane:toluene (1:1, 10 mL). The yellow solution immediately turned deep purple, and with further stirring a pink solid precipitated. Addition of toluene (30 mL) and heating (to about 70 °C) caused complete dissolution of the solid. After standing at room temperature for 3 h the solution yielded dichroic red/yellow crystals suitable for crystal structure analysis (0.72 g, 60%), m.p. 168–169 °C, satisfactory C, H, N, and P analysis. ^{1}H NMR (250 MHz, C_6D_6, TMS): 0.0006 M: δ = 0.73 (d, 2H, Ph_3PCH_2, $^2J_{PH}$ = 3.3 Hz), 4.00 (s, 4H, $(PhCH_2)_2N$), 7.00–7.47 (m, 19H, *m*- and *p*-Ph_3PCH_2 and $(PhCH_2)_2N$), 7.63–7.70 (m, 6H, *o*-Ph_3PCH_2); 0.042 M: δ = 0.52 (d, 2H, Ph_3PCH_2, $^2J_{PH}$ = 4.7 Hz), 4.06 (s, 4H, $(PhCH_2)_2N$), 6.97–7.38 (m, 19H, *m*- and *p*-Ph_3PCH_2 and $(PhCH_2)_2N$), 7.51–7.56 (m, 6H, *o*-Ph_3PCH_2).

Received: September 7, 1994 [Z 7296 IE]
German version: *Angew. Chem.* **1995**, *107*, 514

Keywords: ab initio calculations · alkali metal compounds · amides · phosphorus ylides

[1] Review of Wittig's work: E. Vedejs, *Science* **1980**, *207*, 42–44.
[2] Recent Review of organic aspects of phosphorus ylide chemistry: B. E. Maryanoff, A. B. Reitz, *Chem. Rev.* **1989**, *89*, 863.
[3] Reviews of the inorganic chemistry of phosphorus ylides: a) H. Schmidbaur, *Acc. Chem. Res.* **1975**, *8*, 62; b) H. Schmidbaur, *Angew. Chem.* **1983**, *95*, 980; *Angew. Chem. Int. Ed. Engl.* **1983**, *22*, 907; c) A. W. Johnson (with special contributions by W. C. Kaska, K. A. O. Starzewski and D. A. Dixon), *Ylides and Imines of Phosphorus*, Wiley, New York, **1993**.
[4] See ref. [3c], chapter 4.
[5] Reviews of the structural chemistry of alkali metals: a) W. Setzer, P. von R. Schleyer, *Adv. Organomet. Chem.* **1985**, *24*, 353; b) C. Schade, P. von R. Schleyer, *ibid.* **1987**, *27*, 169; c) K. Gregory, P. von R. Schleyer, R. Snaith, *Adv. Inorg. Chem.* **1991**, *37*, 47.
[6] D. R. Armstrong, S. Bennet, M. G. Davidson, R. Snaith, D. Stalke, D. S. Wright, *J. Chem. Soc. Chem. Commun.* **1992**, 262.
[7] a) D. Barr, W. Clegg, R. E. Mulvey, R. Snaith, *J. Chem. Soc. Chem. Commun.* **1984**, 285; b) *ibid.* **1984**, 287.
[8] a) J. C. J. Bart, *J. Chem. Soc. B* **1969**, 350; b) H. Schmidbaur, J. Jeong, A. Schier, W. Graf, D. L. Wilkinson, G. Müller, C. Krüger, *New J. Chem.* **1989**, *13*, 341.
[9] X-ray crystal data for **3**: $C_{33}H_{31}LiNP$, M_r = 479.50, triclinic, space group $P\bar{1}$, a = 9.689(2), b = 10.871(2), c = 12.731(3) Å, α = 92.17(3), β = 95.84(3), γ = 96.97(3)°, V = 1322.4(5) Å^3, Z = 2, $\rho_{calcd.}$ = 1.204 Mg m^3, $F(000)$ = 508, $\lambda(Mo_{K\alpha})$ = 0.71073 Å, $\mu(Mo_{K\alpha})$ = 0.126 mm^{-1}, T = 153(2) K. Data were collected on a Stoe four-circle diffractometer in the range $7° \le 2\theta \le 45°$ (4685 reflections were collected of which 3455 were independent, R_{int} = 0.0189). The structure was solved by direct methods [18] and refinement, based on F^2, was by full-matrix least-squares techniques [19] (all non-hydrogen atoms were refined anisotropically; H atoms, except H61a and H61b which were located and refined freely, were placed in calculated positions) to R_1 = 0.0367, wR_2 = 0.0964, for 3036 unique reflections for which $F > 4\sigma(F)$. Further details of the crystal structure are available on request from the Director of the Cambridge Crystallographic Data Centre, 12 Union Road, Cambridge, CB2 1EZ (UK) on quoting the full journal citation.

[10] R. E. Cramer, M. A. Bruck, J. W. Gilje, *Organometallics* **1986**, *5*, 1496.
[11] H. Schmidbaur, U. Deschler, B. Milewski-Mahrla, B. Zimmer-Gasser, *Chem. Ber.* **1981**, *114*, 612.
[12] R. E. Cramer, M. A. Bruck, J. W. Gilje, *Organometallics* **1988**, *7*, 1465.
[13] M. G. Davidson, R. Snaith, D. Stalke, D. S. Wright, *J. Org. Chem.* **1993**, *58*, 2810.
[14] a) H. J. Bestmann, A. J. Kos, K. Witzgall, P. v. R. Schleyer, *Chem. Ber.* **1986**, *119*, 1331; b) recent review of theoretical aspects of ylides and related posphorus-containing molecules: D. C. Gilheany, *Chem. Rev.* **1994**, *94*, 1339–1374.
[15] Ab initio MO calculations: 6-31G basis set [20a] with d orbitals on P atoms at the SCF level (monomeric complexes), 6-31G** basis set at the MP2 level [20b] (dimeric complexes) using the programs GAMESS [20c] and GAUSSIAN 92. [20d] All geometries were freely optimised. A manuscript for publication elsewhere is in preparation in which full details of all calculations performed will be given.
[16] H.-J. Cristau, *Chem. Rev.* **1994**, *94*, 1299–1313.
[17] H. Schmidbaur, H. Stühler, W. Vornberger, *Chem. Ber.* **1972**, *105*, 1084.
[18] G. M. Sheldrick, *Acta Crystallogr. Sect. A* **1990**, *46*, 467.
[19] G. M. Sheldrick, SHELXL-93, Program for crystal structure refinement, University of Göttingen, **1993**.
[20] a) W. J. Hehre, R. Ditchfield, J. A. Pople, *J. Chem. Phys.* **1972**, *56*, 2257; P. C. Hariharan, J. A. Pople, *Theor. Chim. Acta* **1973**, *28*, 213; M. J. Gordon, *Chem. Phys. Lett.* **1980**, *76*, 163; b) C. Moller, M. S. Plesset, *Phys. Rev.* **1934**, *46*, 618; c) M. Dupuis, D. Spangler, J. J. Wendoloski, NRCC Software Catalogue, Program No. QGZ1 (GAMESS); M. F. Guest, P. Fantucci, R. J. Harrison, J. Kendrick, J. H. van Lenthe, K. Schoeffel, P. Sherwood, GAMESS UK (CFS Ltd., *1993*); d) M. J. Frisch, G. W. Trucks, M. Head-Gordon, P. M. W. Gill, M. W. Wong, J. B. Foresman, B. G. Johnson, H. B. Schleger, M. A. Robb, E. S. Repogle, R. Gomperts, J. L. Andres, K. Raghavachari, J. S. Binkley, C. Gonzalez, R. L. Martin, D. Fox, D. L. Defrees, J. Baker, J. J. P. Stewart, J. A. Pople, Gaussian Inc., Pittsburgh PA, *1992*.

$C_{60}H_{60}$ and $C_{54}H_{48}$: Silver Ion Extraction with New Concave Hydrocarbons**

Jens Gross, Gabriele Harder, Fritz Vögtle,* Holger Stephan, and Karsten Gloe

Spherical hydrocarbons containing a cavity are of interest for both fullerene and host–guest chemistry. Three-dimensionally linked molecular structures made up of sixty carbon atoms may be possible precursors for the direct synthesis of fullerenes. On the other hand, the hydrophobic cavity of such spherical hydrocarbons, which is accessible through variable openings on the surface of the molecule, may host metal ions like Ag^{I}[1] and Ga^{I},[2] as well as charged[3] and uncharged[4] organic molecules. Some time ago we reported on a first spherical concave hydrocarbon **1** in which four benzene rings are linked by six ethano bridges.[5, 6] $C_{36}H_{36}$ represents the smallest member of a family of macropolycyclic hydrocarbons based on 1,3,5-trimethylenebenzene subunits. In Figure 1 (top) two further members of this series of homologues are depicted, which fit the formula $[C_9H_9]_{2n}$, in this case $n = 2$, 3, and 4.[7]

In the group of compounds with only 1,3,5-substituted benzene spacers no "spheriphanes" with 60 or 70 carbon atoms can be realized, yet these compounds are desirable in view of possible conversion to fullerenes. Compounds **4**–**6** (Fig. 1, bottom) indicate that other similar concave hydrocarbons are conceivable, which are constructed from benzene rings without exclusively 1,3,5-substitution or which contain other spacers. We report here on the syntheses of the previously unknown spherical hydrocarbons $C_{60}H_{60}$ **4** and $C_{54}H_{48}$ **5**, which affirm the universal applicability of the strategy of the synthesis of **1**.

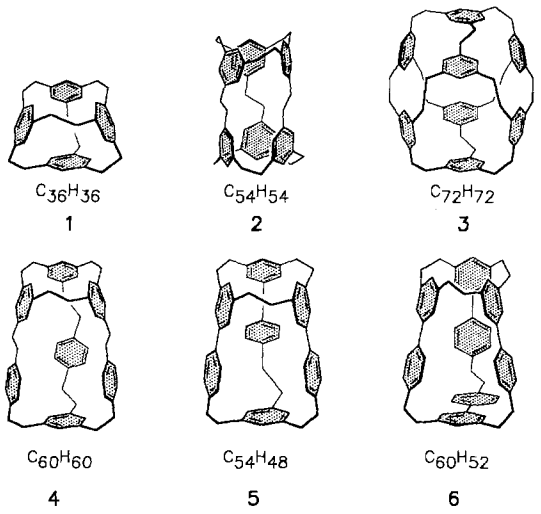


Fig. 1. Top: $C_{36}H_{36}$, $C_{54}H_{54}$, and $C_{72}H_{72}$ as members of the series of spherical hydrocarbons based on 1,3,5-trimethylenebenzene. Bottom: Some selected concave hydrocarbons linked by other than exclusive 1,3,5-connection of the benzene rings and different spacers.

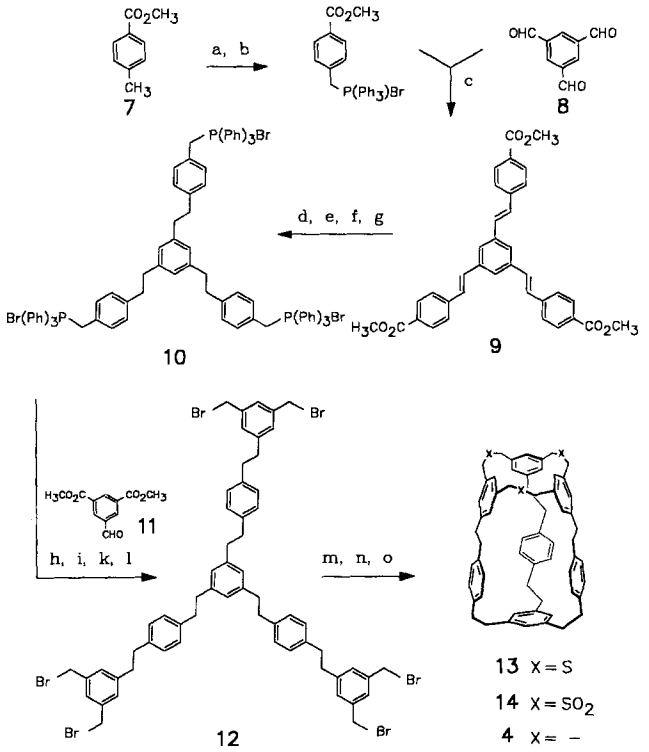
Synthesis of $C_{60}H_{60}$: The cyclization compound **12** was obtained from methyl *p*-toluenecarboxylate (**7**) in eleven synthetic steps. Bromination with *N*-bromosuccinimide (a in Scheme 1) phosphorylation, and threefold Wittig reaction with 1,3,5-benzenetrialdehyde **8**[8] yielded triene **9** as a mixture of isomers. Three-step refunctionalization (hydrogenation of the double bonds (d), reduction of the ester and subsequent acylation (e), and reaction with hydrobromic acid/glacial acetic acid (f)) gave the corresponding benzyl bromide, whose phosphorylation yielded in turn the Wittig compound **10**. Threefold olefination with dimethyl 5-formylisophthalate and application of the refunctionalization sequence (h, i, k, l) provided cyclization compound **12**. The macrotricyclic phane **13** was generated by a sulfide cyclization reaction[9] under dilution conditions[10] (m). Subsequent oxidation to **14** (n) followed by pyrolytic desulfurization[11, 12] (o) afforded the new decacyclic hydrocarbon **4**[13] (total yield from **12**: ≈5%). Direct cyclization of **12** with phenyllithium, which was a favorable alternative in the synthesis of $C_{36}H_{36}$, yielded only traces of polycycle **4**.

Synthesis of $C_{54}H_{48}$: Phosphonium bromide **17** was obtained by Suzuki coupling of dimethyl 5-iodoisophthalate with dihydroxy-*p*-tolylborane (**16**, *p*-tolylboronic acid)[14] (a in Scheme 2), followed by bromination with *N*-bromosuccinimide (NBS, b), and phosphorylation (c). Compound **17** was converted into triene **18** by a threefold Wittig reaction with 1,3,5-benzenetrialdehyde (d) analogous to the synthesis described before. Hydrogenation (e), reduction of the methyl ester and subsequent acetylation (f), and bromination (g) provided the cyclization compound **19**, which was converted into hydrocarbon **5**[15] through sulfide cyclization reaction (h), oxidation to the sulfone (i), and pyrolytic desulfurization reaction (k) (total yield from **12**: 3.5%).

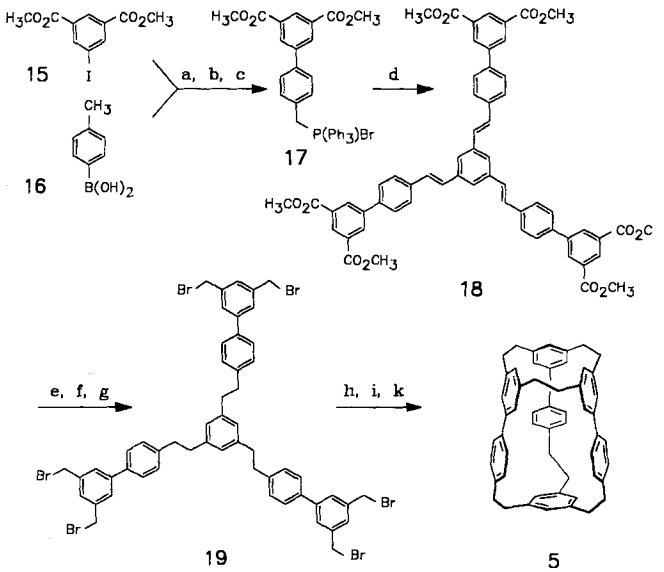
The two new macrotricycles **4** and **5** are high-melting compounds; their mass spectra display only the molecular ion peak

[*] Prof. Dr. F. Vögtle, Dr. J. Gross, Dipl.-Chem. G. Harder
Institut für Organische Chemie und Biochemie der Universität
Gerhard-Domagk-Strasse 1, D-53121 Bonn (Germany)
Telefax: Int. code + (228)73-5662
Prof. Dr. K. Gloe, Dr. H. Stephan
Institut für Anorganische Chemie der Technischen Universität Dresden

[**] This work was supported by the Bundesministerium für Forschung und Technologie (project no. 13N6070). We thank Prof. Dr. V. Boekelheide and Prof. Dr. J. E. McMurry for providing reference compounds, and Prof. Dr. F.-G. Klärner, Dipl.-Chem. J. Benkhoff, and Dipl.-Chem. V. Breitkopf for conducting the high-pressure experiments.



Scheme 1. a) NBS, azobisisobutyronitrile, CH_2Cl_2, *hv*, reflux, 79%; PPh_3, $CHCl_3$, 2 h reflux, 99%; c) Na/MeOH, *N*,*N*-dimethylformamide (DMF), argon, 4 h at 50 °C, 24%; d) 3 bar H_2, Pd/C (10%), toluene, 99%; e) $LiAlH_4$, THF, argon, 2 h reflux, then Ac_2O, 4 h reflux, 95%; f) HBr/glacial acetic acid (30%), 8 h at 60 °C, 88%; g) PPh_3, $CHCl_3$, 2 h reflux, 99%; h) Na/MeOH, DMF, argon, 4 h at 50 °C, 78%; i) 3 bar H_2, Pd/C (10%), toluene, 99%; k) $LiAlH_4$, THF, argon, 2 h reflux, then Ac_2O, 4 h reflux, 95%; l) HBr/glacial acetic acid (30%), 8 h at 60 °C, 93%; m) dilution conditions, 3 equiv $Na_2S \cdot 9H_2O$, 10 equiv Cs_2CO_3, benzene/EtOH (1:1), argon, 8 h reflux, 14%; n) 12 equiv *m*-chloroperoxybenzoic acid, $CHCl_3$, 24 h at room temperature, 96%; o) 10^{-6} Torr, 580 °C, 38%. Overall yield m–o: 5%.



Scheme 2. a) $[Pd(Ph_3)_4]$, 2 N Na_2CO_3, toluene argon, 95 °C, 8 h, 78%; b) NBS, azobisisobutyronitrile, CH_2Cl_2, *hv*, reflux, 73%; c) PPh_3, $CHCl_3$, 3 h reflux, 96%; d) Li/MeOH, THF, argon; 57%; e) 3 bar H_2, Pd/C (10%), toluene, 99%; f) $LiAlH_4$, THF, argon, 2 h reflux, then Ac_2O, 4 h reflux, 86%; g) HBr/glacial acetic acid (33%), 8 h at 60 °C, 73%; h) dilution conditions, 3 equiv $Na_2S \cdot 9H_2O$, 10 equiv Cs_2CO_3, benzene/EtOH (1:1), argon, 8 h reflux, 13%; i) 12 equiv *m*-chloroperoxybenzoic acid, $CHCl_3$, 24 h at room temperature, 71%; k) 10^{-2} Torr, 600 °C, 38%. Overall yield h–k: 3.5%.

and no fragmentation. While **5** shows only poor solubility in most organic solvents, **4** has good solubility properties because of the numerous ethano bridges and thus satisfies an important prerequisite for the investigation of host–guest interactions. The symmetry of the compounds is evident in their NMR spectra.[16, 17] Due to isochronism of protons in compound **5** only three ^1H NMR signals are observed for the aromatic protons, for **4** on the other hand, five.

By molecular modeling calculations[18] we determined the structures and dimensions of the cavities of the macrocycles (Fig. 2) in order to choose suitable guests for complexation

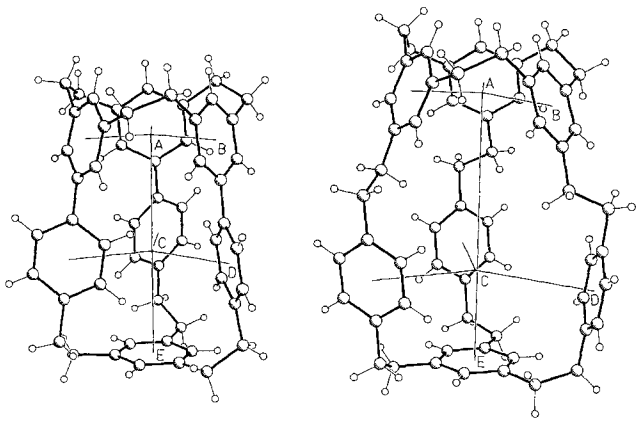


Fig. 2. The structures determined by molecular modeling [18] permit an estimation of the dimensions of the cavities [20]. Left: $C_{54}H_{48}$: A–B 250 pm, C–D 315 pm, A–E 800 pm. Right: $C_{60}H_{60}$: A–B 270 pm, C–D 415 pm, A–E 947 pm.

studies. Hydrocarbon **5**, for example, provides a tailored niche for an acetonitrile molecule, whereas **4** with its larger cavity could include molecules like adamantylamine or *tert*-butylamine.[3] While crystallization experiments for the preparation of the corresponding complexes have not been successful so far, preliminary tests show that the complexes may be obtained under extremely high pressures.[19]

In addition to small neutral molecules metal ions such as silver(I) are potential guests.[21] While the known π-prismands[1a, b, 2] and π-spherands[1c] form rings around Ag^I or Ga^I, the concave hydrocarbons could include ions within their three-dimensionally linked molecular frameworks. In extraction experiments of silver ions from aqueous solution[22] we determined the extraction efficiency of hydrocarbons **1**, **4**, and **5**, the well-known π-prismand **20**, and π-spherand **21**, as well as the reference compounds **22** and **23**[23] quantitatively.[24] Aqueous silver nitrate/picric acid solutions were extracted with a chloroform phase containing the hydrocarbon ligand in different concentrations (Fig. 3). The determination of the silver ion content in both phases with the radiotracer method[25] permits a comparison of the extraction efficiency and gives information about the stoichiometry of the complex.

As expected, reference compounds **22** and **23**, whose cavities are too small, do not extract Ag^I ions (Fig. 4). $C_{36}H_{36}$ **1** and tetraene **20** form 1:1 complexes in the organic phase, but show relatively poor extraction efficiency. $C_{54}H_{48}$ **5** extracts silver(I) in a comparable magnitude. The [2.2.2]paracyclophane **21** is able to extract efficiently over a wide range of concentrations because of its good solubility (at a ligand concentration of 5×10^{-2} M, 67% of the Ag^I is extracted) forming an 1:1 complex also. However, the best silver ion extraction is possible with

 © VCH Verlagsgesellschaft mbH, D-69451 Weinheim, 1995 0570-0833/95/0404-0482 $ 10.00+.25/0

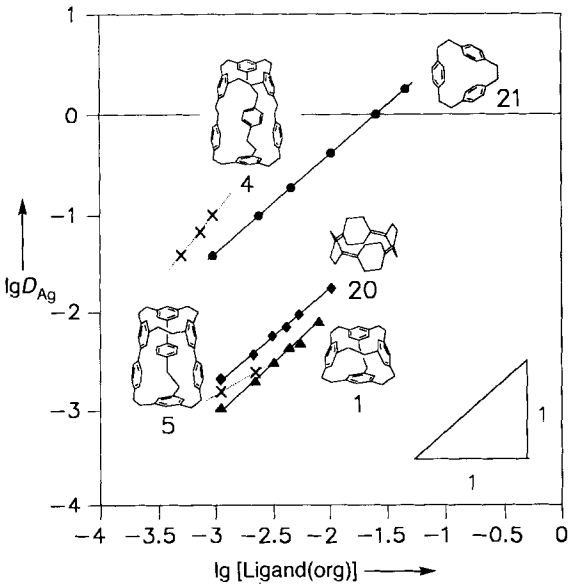


Fig. 3. The dependence of the distribution proportion D_{Ag} (D_{Ag} = [Ag] in chloroform)/[Ag] in water) on the concentration of the ligand in chloroform gives information about the extraction capacity and the composition of the complex. (Conditions: aqueous phase: $[AgNO_3] = 2.7 \times 10^{-4}$ M, [picric acid] $= 1 \times 10^{-2}$ M; organic phase: [ligand] $= 5 \times 10^{-4} - 5 \times 10^{-2}$ M in $CHCl_3$).

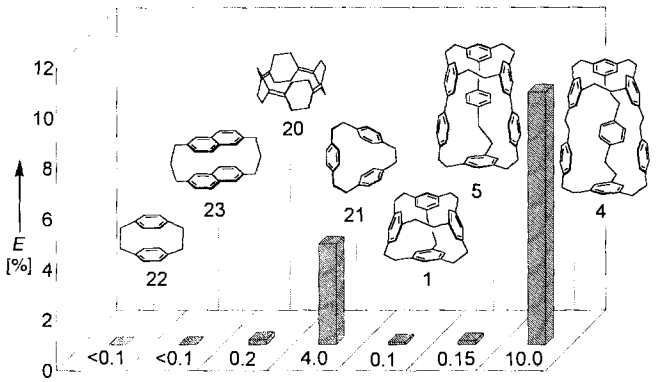


Fig. 4. Comparison of the extractabilities of Ag^{I} by selected hydrocarbons; [ligand] $= 1 \times 10^{-3}$ M in $CHCl_3$.

$C_{60}H_{60}$ **4**, which extracts more than twice as much Ag^{I} in comparison to **21** at low ligand concentrations (up to 1×10^{-3} M).[26] At higher concentrations the complex precipitates, and further investigations are not possible with this extraction system. Because of the few measured quantities, definite determination of the complex composition for both **4** and **5** is not possible.[27]

In comparison to complex ligands containing heteroatoms such as thiacrowns, which bind metal ions through their free electron pairs, we expect a more selective extraction of silver ions with the new concave hydrocarbons. Therefore, we investigated the extraction efficiency of the hydrocarbons **1**, **21**, and **4**, which were available in sufficient amounts, for different alkali, alkaline earth, and transition metal ions (Fig. 5). While **21** does not extract detectable amounts of either alkali metal ions or Tl^{I} and Hg^{II}, which have ionic radii comparable to that of Ag^{I}, an extractability of 0.1% for Tl^{I} is found with $C_{36}H_{36}$ (for Na^{I}, Ca^{II}, Zn^{II}, Hg^{II} < 0.1%). In the case of $C_{60}H_{60}$ the extractabilities for sodium, calcium, and zinc are also below 0.1%; for

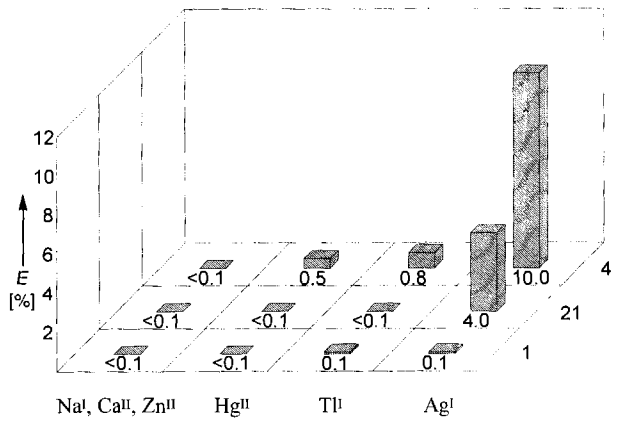


Fig. 5. Comparison of the extractabilities E of selected cations by the hydrocarbons **1**, **21**, **4** ([ligand] $= 1 \times 10^{-3}$ M in $CHCl_3$). The extractabilities of Na^{I}, Ca^{II} and Zn^{II} were investigated in separate experiments).

mercury and thallium the values are slightly higher with 0.5 and 0.8%, respectively (Fig. 5). Relative to other hydrocarbons $C_{60}H_{60}$ shows the highest extraction efficiency for silver observed to date and high selectivity. These results indicate that concave hydrocarbons not only form a new family of structurally appealing molecules but may also be of interest as selective host molecules.

Received: August 10, 1994 [Z 7226 IE]
German version: *Angew. Chem.* **1995**, *107*, 523

Keywords: host–guest chemistry · hydrocarbons · silver compounds · spherands

[1] Examples of silver π-prismands and π-spherands: a) H. C. Kang, A. W. Hanson, B. Eaton, V. Boekelheide, *J. Am. Chem. Soc.* **1985**, *107*, 1979–1985; b) J.-L. Pierre, P. Baret, P. Chautemps, M. Armand, *ibid.* **1981**, *103*, 2986–2988; C. Cohen-Addad, P. Baret, P. Chautemps, J.-L. Pierre, *Acta Crystallogr. Sect. C* **1983**, *39*, 1346–1349; c) J. E. McMurry, G. J. Harley, J. R. Matz, J. C. Clardy, J. Mitchell, *J. Am. Chem. Soc.* **1986**, *108*, 515–516; d) H. Schmidbaur, W. Bublak, B. Huber, G. Reber, G. Müller, *Angew. Chem.* **1986**, *98*, 1108–1109; *Angew. Chem. Int. Ed. Engl.* **1986**, *25*, 1089–1090; e) for further examples of π-donor contributions in the complexation of silver ions see: A. Ikeda, S. Shinkai, *J. Am. Chem. Soc.* **1994**, *116*, 3102–3110; R. Leppkes, F. Vögtle, *Chem. Ber.* **1983**, *116*, 215–219.

[2] a) H. Schmidbaur, R. Hager, B. Huber, G. Müller, *Angew. Chem.* **1987**, *99*, 354–356; *Angew. Chem. Int. Ed. Engl.* **1987**, *26*, 338–340; b) C. Elschenbroich, J. Schneider, M. Wünsch, J.-L. Pierre, P. Baret, P. Chautemps, *Chem. Ber.* **1988**, *121*, 177–183.

[3] For cation–π interactions of quaternary ammonia salts with electron-rich host compounds see P. C. Kearney, L. S. Mizoue, R. A. Kumpf, J. E. Forman, A. McCurdy, D. A. Dougherty, *J. Am. Chem. Soc.* **1993**, *115*, 9907–9919; M. A. Petti, T. J. Shepodd, R. E. Barrans, Jr., D. A. Dougherty, *ibid.* **1988**, *110*, 6825–6840.

[4] For the inclusion of uncharged molecules in cage compounds see: T. A. Robbins, C. B. Knobler, D. R. Bellew, D. J. Cram, *J. Am. Chem. Soc.* **1994**, *116*, 111–122; review: D. J. Cram, *Nature (London)* **1992**, *356*, 29–36.

[5] a) F. Vögtle, J. Gross, C. Seel, M. Nieger, *Angew. Chem.* **1992**, *104*, 1112–1113; *Angew. Chem. Int. Ed. Engl.* **1992**, *31*, 1069–1070; F. Vögtle, C. Seel, R. Berscheid, J. Groß, P.-M. Windscheif in *Computational Approaches in Supramolecular Chemistry* (Ed.: G. Wipff) (*NATO ASI Ser. Ser. C* **1994**, *426*, 311–317); b) L. F. Lindoy, *Nature (London)* **1992**, *359*, 778–779.

[6] The analogue of $C_{36}H_{36}$ with etheno bridges ($C_{36}H_{24}$) has been calculated with conjugation considerations: O. Wennerström, U. Noriander, *J. Phys. Chem.* **1985**, *89*, 3233–3237; electronic structures of conjugated "spheriphanes" have been discussed recently: P. W. Fowler, S. J. Austin, *J. Chem Inf. Comput. Sci.* **1994**, *34*, 264–269.

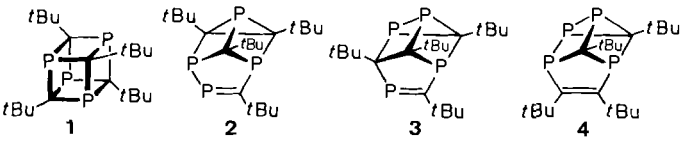
[7] If one considers the benzene spacers as corners and the ethano bridges as edges of polyhedra, $C_{36}H_{36}$ is a tetrahedron, $C_{54}H_{54}$ a prism, and $C_{72}H_{72}$ a cube. The faces of the polyhedra correspond to the openings on the surface of the molecule, an area surrounded by n corners corresponding to a $[2_n]$ metacyclophane window [7].
[8] W. Ried, F.-J. Königstein, *Chem. Ber.* **1959**, *92*, 2532–2545; H.-E. Högberg, O. Wennerström, *Acta Chem. Scand. Ser. B* **1982**, *36*, 661–667.
[9] F. Vögtle, *Cyclophan-Chemie*, Teubner, Stuttgart, **1990**; *Cyclophane Chemistry*, Wiley, Chichester, **1993**.
[10] P. Knops, N. Sendhoff, H.-B. Mekelburger, F. Vögtle, *Top. Curr. Chem.* **1992**, *161*, 1–36.
[11] A. Dohm, F. Vögtle, *Top. Curr. Chem.* **1991**, *161*, 69–106.
[12] We thank Prof. Dr. M. Jansen, Institut für Anorganische Chemie der Universität Bonn, for providing the high-vacuum pump and Dipl.-Chem. H. Seyeda for his help.
[13] $R_f = 0.48$ (petroleum ether 40–60/CH_2Cl_2 1:1); m.p. > 340 °C; IUPAC name: decacyclo[19.19.8.2.^{6,9}2.^{14,28}2.^{33,36}2.^{43,46}1.^{3,39}1.^{12,16}1.^{19,23}1.^{26,30}]hexaconta-1,3(57),6,8,12,14,16(58),19,21,23(59),26,28,30(60),33,35,39,43.45,49,53, 55-heneicosaene.
[14] Preparation analogous to that described by R. T. Hawkins, W. J. Lennarz, H. R. Snyder, *J. Am. Chem. Soc.* **1960**, *82*, 3053–3059.
[15] $R_f = 0.43$ (silica gel; eluent: petroleum ether 40–60/CH_2Cl_2 1:1); m.p. > 340 °C; IUPAC name: decacyclo[17.17.6.2^{6,9}.2^{12,26}.2^{39,42}.2^{29,32}.1^{3,35}.1^{10,14}.1.^{17,21}1.^{24,28}]tetrapentaconta-1,3(51),6,8,10,12,14(52),17,19,21-(53),24,26,28(54),29,31,35,39,41,43,47,49-heneicosaene.
[16] Spectroscopic data of **4**: ^{1}H NMR (400 MHz, $CDCl_3$): $\delta = 6.80$ (d, ^3J(H,H) = 8 Hz, 6H; ArH), 6.77 (t, ^3J(H,H) = 1.5 Hz, 3H; ArH), 6.67 (d, ^3J(H,H) = 8 Hz, 6H; ArH), 6.63 (d, ^3J(H,H) = 1.5 Hz, 6H; ArH), 6.42 (s, 3H; ArH), 3.0 (m, 12H; CH_2), 2.70 (m, 12H; CH_2), 2.61 (s, 12H; CH_2); ^{13}C NMR (100 MHz, $CDCl_3$): $\delta = 140.81$ (3C; C_q), 140.34 (3C; C_q), 139.60 (6C; C_q), 138.94 (3C; C_q), 138.25 (3C; C_q), 128.73 (6C; CH), 127.94 (6C; CH), 126.97 (3C; CH), 126.92 (3C; CH), 126.34 (6C; CH), 38.15 (3C; CH_2), 37.82 (3C; CH_2), 36.31 (3C; CH_2), 36.25 (3C; CH_2), 34.08 (3C; CH_2); MS (DEI): m/z (%): 780.4(100) [M^+].
[17] Spectroscopic data of **5**: ^{1}H NMR (250 MHz, $CDCl_3$): $\delta = 6.95$ (s, 3H; ArH), 6.73 (d, ^3J(H,H) = 1.5 Hz, 6H; ArH), 6.64 (s, 15H; ArH), 3.07 (m, 12H; CH_2), 3.04 (s, 12H); CH_2); ^{13}C NMR (62.89 MHz, $CDCl_3$): $\delta = 140.48$ (3C, C_q), 139.91 (3C, C_q), 139.36 (6C, C_q), 139.25 (3C, C_q), 139.07 (3C, C_q), 128.83 (6C, CH), 127.89 (3C, CH), 126.76 (6C, CH), 126.39 (6C, CH), 126.32 (3C, CH), 35.12 (3C, CH_2), 33.45 (6C, CH_2), 32.71 (3C, CH_2); MS (70 eV), m/z (%): 696.3770(100) [M^+], calcd: 696.3756.
[18] The geometries were fully optimized with PM3 (Mopac 6.0, QCPE 455) at the RHF SCF level.
[19] Solutions of hydrocarbon **5** in chloroform were treated with acetonitrile and warmed to 60 °C and 10 kbar for 24 h in a sealed Teflon tube in an autoclave. The samples were examined by NMR spectroscopy afterwards.
[20] Points B, D, and E mark the centers of the benzene rings, A and C the centers between these points.
[21] For ab initio calculations of endo- and exohedral complexation of alkali metal ions by **1** see: J. Cioslowski, Q. Lin, *J. Am. Chem. Soc.*, submitted.
[22] K. Gloe, P. Mühl, J. Beger, *Z. Chem.* **1988**, *28*, 1–14.
[23] The [3.3](2,6)naphthalenophane **23** was kindly supplied by Dipl.-Chem. F. Ott. Its preparation will be reported elsewhere.
[24] The silver complex of the deltaphane (cf. [1a]) is insoluble in chloroform, and therefore cannot be studied in more detail.
[25] K. Gloe, P. Mühl, *Isotopenpraxis* **1983**, *19*, 257–260.
[26] It is possible to recover silver as an amine complex without damaging the hydrocarbon ligand by washing with ammonia solution.
[27] If the straight line in Fig. 4 has a gradient of one, an 1:1 complex is present.

Tetraphosphatricyclo[4.2.0.0^{2,5}]octadienes; New Phosphaalkyne Cyclotetramers Derived from $\lambda^3\sigma^2$-Diphosphetes**

Bernhard Geissler, Stefan Barth, Uwe Bergsträsser, Michael Slany, Julie Durkin, Peter B. Hitchcock, Matthias Hofmann, Paul Binger,* John F. Nixon,* Paul von Ragué Schleyer,* and Manfred Regitz*

Dedicated to Professor Rolf Huisgen on the occasion of his 75th birthday

In the cyclooligomerization of alkynes there is a special interest in their cyclotetramers as also is the case in the series of phosphaalkynes (RC≡P). Following the original thermal cyclotetramerization of *t*BuC≡P with low selectivity to the tetraphosphacubane **1**,[1] specific high-yield syntheses[2] enable a detailed study to be made of the reactivity of this pentacycle.[3, 4]



Utilizing a stepwise route, the polycyclic isomers **2** and **3** containing phosphaalkene units are now accessible[5] which, on heating, quantitatively transform to the more thermodynamically stable compound **4**, which only contains $\lambda^3\sigma^3$-phosphorus atoms.[6, 7]

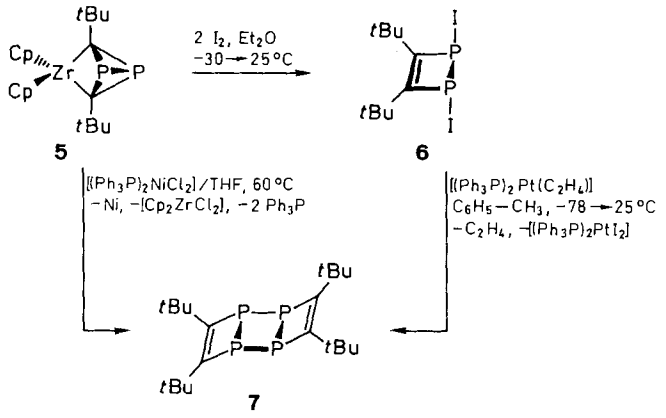
We now report the syntheses of the tetraphosphacyclooctadienes **7** and **13**, which represent a new type of phosphaalkyne cyclotetramer, and also present results of ab initio calculations on HC≡P cyclooligomers.

Treatment of the tricyclic zirconium compound **5**[2, 8] with $[(PPh_3)_2NiCl_2]$ leads to the removal of the $ZrCp_2$ fragment and to a dimerization resulting in the formation of the phosphaalkyne cyclotetramer **7** in 70% yield.

Treatment of the dihydrophosphete **6**, which is readily accessible from the reaction of **5** with iodine and whose structure has been established,[9] with $[(PPh_3)_2Pt(C_2H_4)]$ followed by iodine elimination and a further dimerization leads to the same product

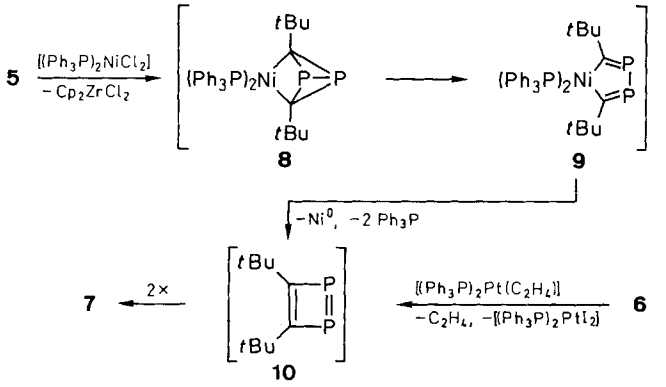
[*] Prof. Dr. M. Regitz, Dr. B. Geissler, Dr. S. Barth, Dr. U. Bergstrasser, Dr. M. Slany
Fachbereich Chemie der Universität
Erwin-Schrödinger-Strasse, D-67663 Kaiserslautern (Germany)
Telefax: Int. code + (631)205-3921
Prof. Dr. P. Binger
Max-Planck-Institut für Kohlenforschung
Kaiser-Wilhelm-Platz 1, D-45470 Mülheim an der Ruhr (Germany)
Telefax: Int. code + (208)1306-2980
Prof. Dr. J. F. Nixon, J. Durkin, Dr. P. B. Hitchcock
School of Chemistry and Molecular Sciences, University of Sussex
GB-Brighton BN1 9QJ (UK)
Telefax: Int. code + (273)677196
Prof. Dr. P. von R. Schleyer, Dipl.-Chem. M. Hofmann
Computer-Chemie-Centrum des Instituts für Organische Chemie
der Universität Erlangen-Nürnberg
Nägelsbachstrasse 25, D-91052 Erlangen (Germany)
Telefax: Int. code + (9131)85-9132

[**] Phosphorus Compounds Part 91. This work was supported by the Volkswagen Foundation, the Deutsche Forschungsgemeinschaft (Graduiertenkolleg, "Phosphor als Bindeglied verschiedener chemischer Disziplinen"), the Fonds der Chemischen Industrie and the Landesregierung von Rheinland-Pfalz. Part 90: K. K. Laali, B. Geissler, O. Wagner, J. Hoffmann, R. Armbrust, W. Eisfeld, M. Regitz, *J. Am. Chem. Soc.* **1994**, *116*, 9407–9408.



7 in 95% yield. Phosphaalkyne cyclotetramers of this structural type were previously unkown.

It seems likely that the tricyclic compound **7** results from the dimerization of the intermediate 1,2-diphosphete **10**.[10] The dehalogenation **6** → **10** appears very likely and the formation of **10** from **5** can also be readily rationalized. Thus, if one initially assumes that the transfer of the $P_2C_2tBu_2$ fragment from **5** to the $(Ph_3P)_2Ni$ group affords **8**,[11] the isomerization of **8** could result in diphosphanickelacyclopentadiene **9**. Elimination of the $(PPh_3)_2Ni$ fragment, which breaks up into Ni and PPh_3 (both isolated) under the reaction conditions (60 °C), is the final step leading to the formation of **10**. Similar types of C–C combinations are well known in synthetic organic chemistry.[12]



The elemental analysis and mass spectrometric data on **7** (see Table 1) confirm its cyclotetrameric composition. The NMR signals of the phosphorus atoms ($\delta = -23.4$), the sp^2-hybridized framework C atoms ($\delta = 172.4$), and the carbons and protons of the *t*Bu groups (see Table 1) are clearly indicative of the high symmetry of the cyclotetramer **7**.

The tricyclic structure of **7** has been fully established by a single crystal X-ray analysis[13, 14] and reveals an *anti*-arrangement of the two olefin units around a central cyclotetraphosphane unit. The presence of an inversion center in **7** is reflected by the identical pairwise sets of bond lengths and bond angles (Fig. 1).

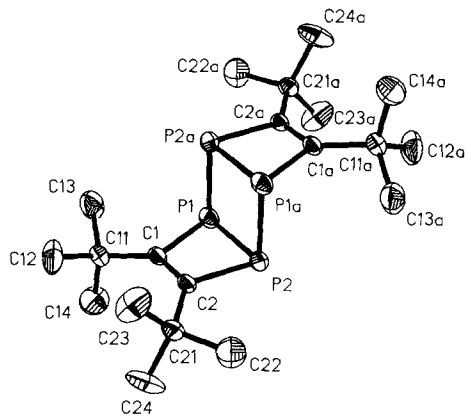


Fig. 1. Crystal structure of **7** (thermal elipsoid plot). Selected bond lengths and angles are listed in Table 2.

The four P atoms in **7** lie in a plane and form a rectangle whose edge lengths are 2.219 (calc. 2.283) and 2.236 (calc. 2.245) Å; the internal angles of 89.9 (calc. 90.0) and 90.1 (calc. 90.0)°, lie in the ideal range (see Table 2). Comparable structural data are already known for the related *trans*-1,2,4,5-tetraphosphatricyclo[3.1.0.0.^{2,4}]hexane system,[15] which also contains a planar P_4 unit. Monocyclic tetraphosphanes show comparable P–P distances but the P_4 unit is usually folded.[16] The atoms comprising the dihydrodiphosphete units C1, C2, P1, P2 and C1a, C2a, P1a, and P2a, respectively, lie in a plane and are arranged as a trapezium. The fold angle along the P1–P2 or P1a–P2a axis is 97.9 (calc. 96.5)°.

As previously mentioned, a high-yield synthesis of the tetraphosphacubane **1**, resulting from treatment of the zirconium

Table 2. Selected bond lengths [Å] and bond angles [°] for compounds **7** and **13** in comparison with the calculated values for the HCP cyclotetramers **7a** and **13a**, respectively (see Fig. 3).

	7 [a]	**7a** [b]		**13** [c]	**13a** [d]
P1-P2 [e]	2.219(1)	2.283	P1-P1a [f]	2.228(1)	2.284
P1-C1	1.837(3)	1.832	P1-C1	1.911(2)	1.904
P2-C2	1.834(2)	1.832	P1-C2	1.807(2)	1.809
C1-C2	1.348(5)	1.352	P2-C1	1.909(2)	1.875
P1-P2a	2.236(1)	2.245	P2-C2	1.672(2)	1.698
			C1-C1a	1.586(4)	1.539
P1-C1-C2	103.7(2)	104.7	P1a-P1-C1	79.41(5)	78.4
C1-C2-P2	103.7(2)	104.7	P1a-P1-C2	95.76(6)	95.8
C2-P2-P1	76.4(1)	75.3	C1-P1-C2	83.37(8)	80.3
P2-P1-C1	76.2(1)	75.3	C1-P2-C2	87.13(9)	84.1
C2-P2-P1a	97.3(1)	96.3	P1-C1-P2	88.96(8)	92.7
C1-P1-P2a	97.6(1)	96.3	P1-C1-C1a	98.36(6)	100.7
P1-P2-P1a	89.9(1)	90.0	P2-C1-C1a	114.2(2)	112.5
P2-P1-P2a	90.1(1)	90.0	P1-C2-P2	100.5(1)	102.4

[a] Crystal structure analysis, C_i. [b] //MP2(fu)/6-31G*, C_{2h}. [c] Crystal structure analysis, C_2. [d] //RMP2(fu)/6-31G*, C_2. [e] For numbering see Figure 1. [f] For numbering see Figure 2.

Table 1. Selected physical data of the tetraphosphatricyclo[4.2.0.0^{2,5}]octadienes **7** and **13** [a].

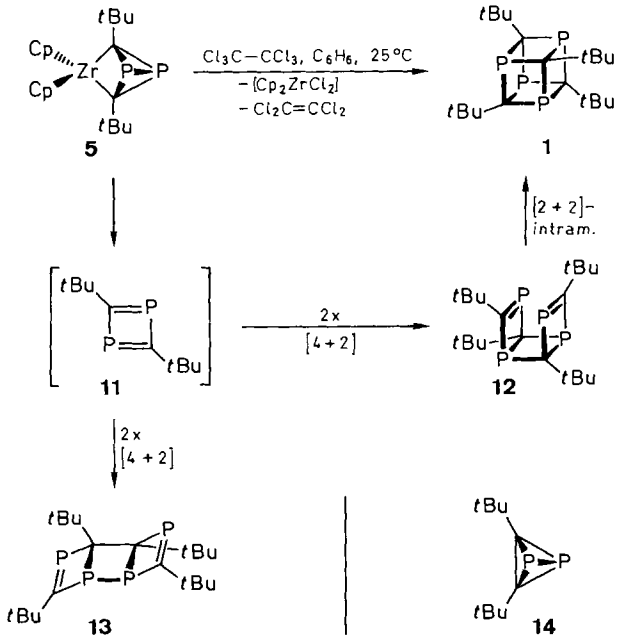
7: ^{1}H NMR: $\delta = 1.44$ (s, 36H, *t*Bu); ^{13}C NMR: $\delta = 31.6$ (pseudo-t, ^3J(P,C) = 2.7 Hz, $C(CH_3)_3$), 39.6 (pseudo-t, ^2J(P,C) = 2.3 Hz, $C(CH_3)_3$), 172.4 (m, framework-C); ^{31}P NMR: $\delta = -23.4$ (s); MS (70 eV): $m/z = 400$ (M^+, 26%), 262 ($M^+ - t$BuCC*t*Bu, 41%), 231 ($M^+ - t$BuCC*t*Bu, −P, 100%), 200 ($M^+/2$, 1%), 169 (*t*BuCC*t*BuP, 93%)

13: ^{1}H NMR: $\delta = 1.27, 1.52$ (each s, each 18H, *t*Bu); ^{31}P NMR: $\delta = 44.5$ (pseudo-t, ^2J(P,P) = 29.1 Hz, $\lambda^3\sigma^3$-P), 398.2 (pseudo-t, ^2J(P,P) = 29.1 Hz, $\lambda^3\sigma^2$-P); MS (70 eV): $m/z = 400$ (M^+, 45%), 262 ($M^+ - t$BuCC*t*Bu, 75%), 169 (*t*BuCC*t*BuP, 80%), 85 (*t*BuCP-CH_3, 100%), 69 (*t*BuC, 100%), 57 (*t*Bu, 90%)

[a] ^{1}H (90 or 400 MHz, TMS), ^{13}C (100.6 MHz, TMS) and ^{31}P NMR spectra (80.8 MHz, 85% H_3PO_4) in $CDCl_3$; **7**: C_6D_6; **13**: $CDCl_3$. MS: Finnigan MAT 90.

 © VCH Verlagsgesellschaft mbH, D-69451 Weinheim, 1995 0570-0833/95/0404-0485 $ 10.00+.25/0

compound **5** with C_2Cl_6, probably involves the intermediacy of the 1,3-diphosphete **11** and the tricyclic compound **12**.[2] We now report that under the same conditions a new cyclotetramer of *t*BuC≡P is also formed albeit in very low yield, which has not been previously observed and which has the structure **13**.



In the ^{31}P NMR spectrum of **13** there are two pseudo triplets of an A_2X_2 spin system (δ = 44.5, 398.2, ^2J(P,P) = 29.1 Hz) indicative of $\lambda^3\sigma^3$- and $\lambda^3\sigma^2$-phosphorus atoms. In contrast to the ^1H NMR spectrum of cyclotetramer **7**, that of **13** exhibits two signals (18H each). The mass spectrum provides confirmation of the cyclotetrameric structure (see Table 1).

This new cyclotetramer also has a tricyclic structure with a central 1,2-diphosphetane unit to which are attached two phosphaalkyne moeities with an *anti*-conformation, bonded as indicated by the crystal structure.[14, 17] The twofold rotation axis in **13** is reflected in the similar bond lengths and bond angles of the *trans*-dihydrodiphosphete rings (Fig. 2).

The bond length C2–P2 1.672 (calc. 1.698) Å lies in the expected range for phosphaalkenes.[18] Likewise the bond lengths within the diphosphetane unit (see Table 2) are in accord with the structural parameters found in monocyclic 1,2-diphosphetanes.[19, 20] The obvious explanation is that **13** is formed by a "head-to-head" dimerization of **11**, while the "head-to-tail" process (**11** → **12**) leads finally to the tetraphosphacubane **1**.

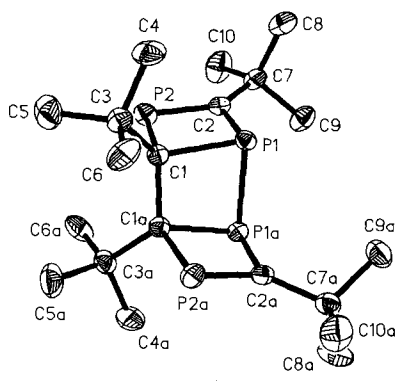


Fig. 2. Crystal structure of **13** (thermal elipsoid plot). Selected bond lengths and angles are listed in Table 2.

Model calculations, however, show that the postulated intermediate **12a** is 9.1 kcal mol^{-1} more stable than **1a** (see Fig. 3). For compound **12a**, the *cis* configuration is 0.9 kcal mol^{-1} more stable than the *trans* isomer. For compound **13a**, the *cis* configuration (1.4 kcal mol^{-1}) is also more favored. Probably, steric interactions in *cis*-**13** prevent its formation. The *trans*-configuration **7** is already preferred in the model (**7a**) (E_{rel} = – 3.6 kcal mol^{-1} relative to *cis*-). The domination of the dimerization **11** → **12** (product ratio **1** (via **12**):**13** ≈ 70:1) may be the result of kinetic factors; the unsubstituted tricycles **7a** and **13a** are energetically more favorable than the cubane **1a** (see Fig. 3).

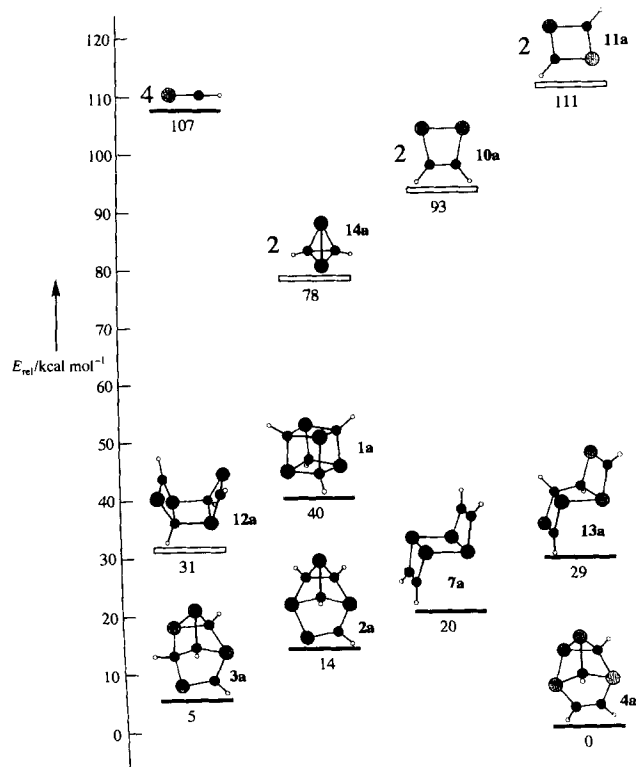


Fig. 3. Relative energies for HCP oligomers [23]. Hydrogen is white, carbon is black, and phosphorus is gray in the structures shown; black bars indicate where the *C*-alkyl derivatives are known experimentally, and white bars represent postulated structures.

Following our success in converting **5** with the P-coordinate [Fe(CO)$_4$] fragment into the η^4-ligated [Fe(CO)$_3$] complex **11**, by detaching the Cp_2Zr unit with C_2Cl_6,[2] we now provide further convincing evidence for the intermediacy of this 1,3-diphosphete in the conversion of the dimer complex **5** into the tetraphosphacubane **1**. In this connection it should be noted that the originally anticipated formation of the diphosphatetrahedrane **14** as an intermediate between **5** and **11** now seems unlikely. The unsubstituted 1,3-diphosphete **11a** has a considerably higher energy of formation than the isomeric tetrahedrane (see Fig. 3), which makes the isomerization of the initially generated diphosphatetrahedrane into the 1,3-diphosphete unlikely.[10, 21, 22]

For **2a** and **3a**, energies of 13.9 and 5.0 kcal mol^{-1}, respectively, relative to **4a** are calculated which is in good agreement with the observed thermal isomerizations **2** → **4** and **3** → **4**, respectively.[6, 7] The cubane **1a** is the most unfavorable of all the tetramers studied (see Fig. 3).

 © VCH Verlagsgesellschaft mbH, D-69451 Weinheim, 1995 0570-0833/95/0404-0486 $ 10.00+.25/0

The reaction energies for 2 **10a** → **7a** and 2 **11a** → **13a** are −72.8 and −82.0 kcal mol^{-1}, respectively. They are therefore considerably higher than the HCP dimerization energies to **10a** and **11a**.

Experimental Procedure

7 from **5**: To the suspension of bis(triphenylphosphane)nickel dichloride (1.27 g, 1.95 mmol) in tetrahydrofuran (50 mL) was added the zirconium complex **5** (0.82 g, 1.95 mmol) [2, 8], and after the solution had been heated for 4 h at 60 °C the solvent was removed at 30 °C/10^{-3} mbar. The residue was dissolved in *n*-pentane (50 mL) and elemental nickel and zirconium dichloride were filtered off with a frit filled with a 3 cm high layer of celite. Repeated removal of solvent afforded **7** which was still contaminated with triphenylphosphane, the latter could be removed by sublimation (70 °C/10^{-3} mbar)(^{31}P NMR monitored). Yield: 0.27 g (70%) colorless crystals; m.p. 240 °C (from ether at −78 °C).

7 from **6**: To a stirred solution of the dihydrodiphosphete **6** (0.91 g, 2.0 mmol) [9] in toluene (15 mL) was added at −78 °C η^2-ethene-bis(triphenylphosphane)platinum(0) (1.51 g, 2.02 mmol). After the reaction mixture had been warmed to room temperature, the insoluble residue was removed by filtration over celite and the filtrate evaporated to dryness. The residue was redissolved in *n*-pentane and a second filtration over celite resulted in a solution which was evaporated to dryness and purified as above. Yield: 0.38 g (95%) colorless crystals. These were identical with the product obtained from **5** (NMR spectroscopy).

13 from **5**: To a solution of **5** (1.4 g, 3.3 mmol) in benzene (10 mL) was added hexachloroethane (0.79 g, 3.3 mmol) and after the solution had been stirred for 5 d at room temperature it was evaporated to dryness at 25 °C/10^{-3} mbar. The resulting orange-yellow product was treated several times with petroleum ether (60–80 °C), the extracts collected and concentrated to about 5 mL in vacuo and then left to crystallize at 5 °C. After removal of the solvent with a syringe, **13** could be separated by hand as 2–3-mm-long small orange-red crystals from the tetraphosphacubane **1** [2]. Yield: 18 mg (1%). m.p. 135–136 °C.

Received: September 10, 1994 [Z 7303 IE]
German version: *Angew. Chem.* **1995**, *107*, 485

Keywords: ab initio calculations · cyclotetramers · diphosphete derivatives · polycycles

[1] T. Wettling, J. Schneider, O. Wagner, C. G. Kreiter, M. Regitz, *Angew. Chem.* **1989**, *101*, 1035–1037; *Angew. Chem. Int. Ed. Engl.* **1989**, *28*, 1013–1014.
[2] T. Wettling, B. Geissler, R. Schneider, S. Barth, P. Binger, M. Regitz, *Angew. Chem.* **1992**, *104*, 761–762; *Angew. Chem. Int. Ed. Engl.* **1992**, *31*, 758–759.
[3] M. Birkel, J. Schulz, U. Bergsträsser, M. Regitz, *Angew. Chem.* **1992**, *104*, 870–873; *Angew. Chem. Int. Ed. Engl.* **1992**, *31*, 879–882.
[4] K. K. Laali, M. Regitz, M. Birkel, P. J. Stang, C. M. Critell, *J. Org. Chem.* **1993**, *58*, 4105–4109.
[5] B. Breit, U. Bergsträsser, G. Maas, M. Regitz, *Angew. Chem.* **1992**, *104*, 1043–1046; *Angew. Chem. Int. Ed. Engl.* **1992**, *31*, 1055–1058.
[6] M. Regitz, T. Wettling, B. Breit, M. Birkel, B. Geissler, U. Bergsträsser, S. Barth, P. Binger, *Phosphorus Sulfur Silicon Relat. Elem.* **1993**, *76*, 261–264.
[7] M. Regitz in *Organic Synthesis via Organometallics* (Eds.: D. Enders, H.-J. Gais, W. Keim), Vieweg, Braunschweig, **1993**, pp. 93–113.
[8] P. Binger, B. Biedenbach, C. Krüger, M. Regitz, *Angew. Chem.* **1987**, *99*, 798–799; *Angew. Chem. Int. Ed. Engl.* **1987**, *26*, 764–765.
[9] P. Binger, T. Wettling, R. Schneider, F. Zurmühlen, U. Bergsträsser, J. Hoffmann, G. Maas, M. Regitz, *Angew. Chem.* **1991**, *103*, 208–211; *Angew. Chem. Int. Ed. Engl.* **1991**, *30*, 207–210.
[10] From the energy profile of the cyclodimerization of HC≡P it is known that head-to-head coupling to the 1,2-diphosphete is favored over the head-to-tail process. M. T. Nguyen, L. Landuyt, L. G. Vanquickenborne. *J. Org. Chem.* **1993**, *58*, 2817–2821.
[11] See for example the analogous exchange for RP, RB, or R_2Ge in ref. [9].
[12] J. P. Collmann, L. S. Hegedus, *Principles and Applications of Organotransition Metal Chemistry*, University Science Books, Mill Valley; **1980**. H. Alper in *Transition Metal Organometallics in Organic Synthesis* (Ed.: H. H. Wasserman), Academic Press, New York, **1978**.
[13] **7**: Data were collected with an Enraf-Nonius CAD4 diffractometer, $Mo_{K\alpha}$ radiation. $\lambda = 0.71073$ Å with a graphite monochromator; $C_{20}H_{36}P_4$, $M =$ 400.4 g mol^{-1}, triclinic, space group $P\bar{1}$ (no. 2). $a = 6.174(2)$, $b = 9.453(5)$, $c = 11.001(4)$ Å, $\alpha = 66.92(2)$, $\beta = 87.06(2)$, $\gamma = 79.57(2)°$; $Z = 1$; $V =$ 579.7(4) Å^3; $\rho_{calcd.} = 1.147$ g cm^{-3}; $\mu = 3.26$ cm^{-1}; $F(000) = 216$. 1945 reflections were measured and 1803 with $I > 3\sigma(I)$ were used in the structure refinement using 127 parameters. The resulting structure model converged at $R = 0.0593$ and $R_w = \Sigma(w\Delta^2 F/wF_o^2)^{1/2} = 0.0689$. The residuals in the difference Fourier analysis showed a maximum at 0.45 e Å^{-3} and a minimum at −0.46 e Å^{-3}. The molecule lies on a crystallographic inversion center [14].
[14] Further details of the structure analyses are available from the Fachinformationszentrum Karlsruhe D-76344, Eggenstein-Leopoldshafen (Germany), on quoting the depository number CSD-58099.
[15] E. Niecke, R. Streubel, M. Nieger, *Angew. Chem.* **1991**, *103*, 103–105; *Angew. Chem. Int. Ed. Engl.* **1991**, *30*, 90–91; For a further tricyclic polyphosphane with a central P_4 unit see: E. Niecke, O. Altmeyer, H. Nieger, F. Knoll, *ibid.* **1987**, *99*, 1299–1300 and **1987**, *26*, 1256–1257.
[16] M. Baudler, K. Glinka, *Chem. Rev.* **1993**, *93*, 1623–1667.
[17] **13**: Data were collected with an Enraf-Nonius CAD4 diffractometer, $Cu_{K\alpha}$ radiation $\lambda = 1.5418$ Å and a graphite monochromator; $C_{20}H_{36}P_4$, $M =$ 400.4 g mol^{-1} monoclinic, space group $C2/c$ (no 15). $a = 17.561(9)$, $b =$ 17.115(7), $c = 7.747(2)$ Å, $\beta = 95.54(3)°$; $Z = 4$; $V = 2317.6$ Å^3; $\rho_{calcd.} =$ 1.15 g cm^{-3}; $\mu = 30.4$ cm^{-1}; $F(000) = 864$; 2469 reflections were measured and 2125 $F^2 > 2\sigma(F^2)$ were used in the structure refinement using 181 parameters. The resulting structure model converged at $R = 0.039$ and $R_w = 0.051$. The residuals in the difference Fourier showed a maximum at 0.27 e Å and a minimum at −0.59 e Å. The molecule lies on a crystallographic twofold axis [14].
[18] R. Appel in *Multiple Bonds and Low Coordination in Phosphorus Chemistry* (Eds.: M. Regitz, O. J. Scherer), 1. edition, Thieme, Stuttgart, **1990**, p. 160.
[19] R. Appel, F. Koch, H. Kunz, *Chem. Ber.* **1984**, *117*, 3151–3159.
[20] G. Becker, W. Becker, O. Mundt, *Phosphorus Sulfur Silicon* **1983**, *14*, 267–283.
[21] W. W. Schoeller, T. Busch, *Angew. Chem.* **1993**, *105*, 635–637; *Angew. Chem. Int. Ed. Engl.* **1993**, *32*, 617–619.
[22] The related diphosphatetrahedrane **14a** is 16.2 kcal mol^{-1} more stable than the 1,3-diphosphete **13a**. For the C,C-dimethyl compound the energy difference is found to be 15.6 kcal mol^{-1}.
[23] The structure was optimized which HF/6-316*, and the nature of the stationary points established by means of an analytical frequency procedure. Optimization of the geometry was achieved by using MP2(fu)/6-31G* and relative energies by using MP4sdtq/6-316*. Refinement was by programs MP4sdtq/6-316*/MP2(fu)/6-316* + 0.89 ZPE (HF/6-316*). All results were processed with the Gaussian 92 program package. M. J. Frisch, G. W. Trucks, M. Head-Gordon, P. M. W. Gill, M. W. Wong, J. B. Foresman, B. G. Johnson, H. B. Schlegel, M. A. Robb, E. S. Replogle, R. Comperts, J. L. Andres, K. Raghavachari, J. S. Binkley, C. Gonzalez, R. L. Martin, D. J. Fox, D. J. Defrees, J. Baker, J. J. P. Stewart, J. A. Pople, *Gaussian 92, Gaussian Inc., Pittsburgh, PA*, **1992**. Zur Erklärung der Methoden siehe z.B. a) J. B. Foresman, A. E. Frisch, *Exploring Chemistry with Electronic Structure Methods: A Guide to Using Gaussian*, Gaussian Inc., Pittsburgh, PA, **1993**; b) W. J. Hehre, L. Radom, P. von R. Schleyer, J. A. Pople, *Ab initio Molecular Orbital Theory*, Wiley, New York, **1986**.

Crystal Structure of the Dimeric (4-*tert*-Butylthiazolato)(glyme)lithium: Carbene Character of a Formyl Anion Equivalent**

Gernot Boche,* Christof Hilf, Klaus Harms, Michael Marsch, and John C. W. Lohrenz

Dedicated to Professor Rolf Huisgen on the occasion of his 75th birthday

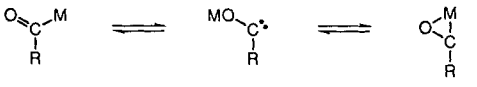
The question whether *nucleophilic acylations* with reagents of type **1** are possible has a long history.[1] Although compounds of type **1b** are comparatively easily accessible, the species **1** are only of limited use in synthesis. Not without reason was the concept of "Umpolung" created in the search for new methods of nucleophilic acylations.[2]

One of the problems is that the compounds **1** react like the isomeric alkoxycarbenes **1′**. Some dimerize rapidly even at −120 °C. This is in agreement with results of quantum-mechan-

[*] Prof. Dr. G. Boche, Dipl.-Chem. C. Hilf, Dr. K. Harms, M. Marsch, Dr. J. C. W. Lohrenz
Fachbereich Chemie der Universität
D-35032 Marburg (Germany)
Telefax: Int. code + (6421)28-8917

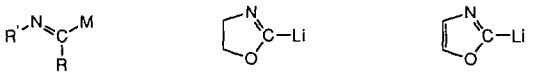
[**] This work was supported by the Deutsche Forschungsgemeinschaft (SFB 260 and the Graduiertenkolleg "Metallorganische Chemie") and the Fonds der Chemischen Industrie.

ical calculations for lithiated formaldehyde LiCH=O, which predict a C–O bridged structure **1"a** (R = H, M = Li) with a distinct carbene character.[3] Lithiated aldimines **2** seem to have a smaller propensity for dimerization, but this alternative has not gained any broader application.[4]



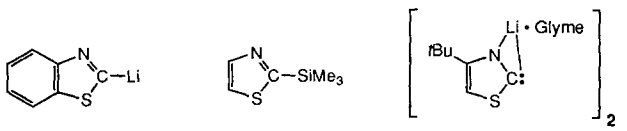
1 **1'** **1"**

a : R = H, Alkyl, Aryl
b : R = NR_2
M : Li, Na, K, MgHal, etc.



2 **3** **4**

Experiments with 2-lithio-4,5-dihydrooxazole (**3**) and 2-lithiooxazole (**4**) failed because of the easy ring-opening to the corresponding alkoxyisocyanide.[5] In contrast, lithiated benzothiazole **5**[6] and especially silylated thiazole **6**[7] have proven to be excellent formyl anion equivalents—one of the reasons is



5 **6** [**7** • Glyme]$_2$

the easily reducible C–S bond. In the following we report on the crystal structure analysis of the lithiated 4-*tert*-butylthiazole **7**, which crystallizes with glycol dimethyl ether (glyme) as [**7** · glyme]$_2$ (Fig. 1). Dimer [**7** · glyme]$_2$ proves, for the first time, the carbene character of a formyllithium equivalent.[8]

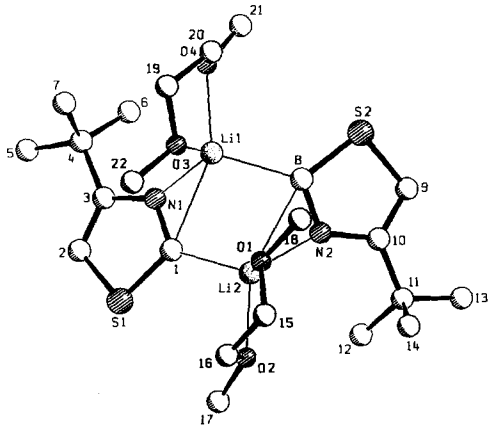
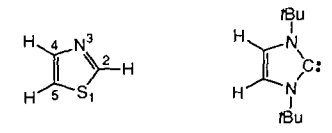


Fig. 1. Crystal structure of the dimeric (4-*tert*-butylthiazolato)(glyme)lithium [**7** · glyme]$_2$ [9].

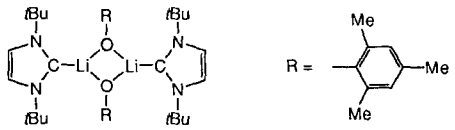
To this end we compare the structure of [**7** · glyme]$_2$ with that of thiazole **8**,[13] the recently characterized carbene **9**,[14] and with the calculated structure of the lithiated formaldehyde **1"a** (R = H, M = Li).[3]

In [**7** · glyme]$_2$ Li1 (Li2) is closely bound to N1(N2) [199.0(5) (201.1(5)) pm], but only loosely to C1(C8) [251.2(5)–(255.8(5)) pm].[16] The angle N1-C1-Li1 (N2-C8-Li2) amounts to 51.9(2) (51.1(2))°. Thus the distance between Li1(Li2) and the carbene C atom C1 (C8) is considerably larger than in **1"a** (R = H, M = Li), where Li–C = 189.1, Li–O = 183.5 pm and Li-C-O = 67.6° (MP2/6-31G*).[3] In the thiazole rings of [**7** · glyme]$_2$ the following distances were determined: C1–N1 (C8–N2) 133.2(4) (132.6(3)) pm; N1–C3 (N2–C10) 139.4(3) (139.2(3)) pm; C1–S1 (C8–S2) 176.3(3) (176.1(3)) pm; S1–C2(S2–C9) 170.8(3) (171.4(3)) pm; C2–C3 (C9–C10) 134.2(4) (134.8(4)) pm. In comparison with thiazole **8** the bond to the carbene-C1 atom are longer by 2.8 (2.2) pm (C1–N1 (C8–N2)) and by 3.9 (3.7) pm (C1–S1 (C8–S2)).[17] In the case of the carbene **9** a lengthening of the $C_{(carbene)}$–N bonds (by about 4 pm) is also observed on going from the corresponding imidazolium salt to **9**.[14] The small N-C-N angle is considered to be especially significant for the carbene structure of **9**: it decreases from 108.5–109.7° in imidazolium salts to 102.2° in **9**.[14] Similarly, the angle N-C-S of 115.1(8)° in thiazole **8** decreases in [**7** · glyme]$_2$ to N1-C1-S1 (N2-C8-S2) 107.9(2) (108.1(2))°. This is in line with calculations of structures of singlet carbenes, which yield R^1-C-R^2 angles of this order of magnitude.[18] Thus, the lithiated thiazole **7** has all the structural features of a lithiated formyllithium equivalent with distinct carbene character.[19, 20]



8 **9**

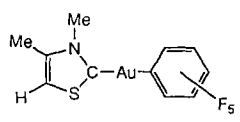
Soon after the discovery of stable nucleophilic carbenes, Lewis acid adducts of these compounds with various metals were characterized.[21] A carbene complex (**10**) from **9** with Li^+ as the Lewis acid has only recently been reported.[22]



10

Since the complexation of the carbene C-atom by Li^+ in [**7** · glyme]$_2$ is "inevitable" because of the dimerization, it is interesting to investigate the influence of the Lewis acid Li^+ on the carbene structure by comparing **10** with **9**. The $C_{(carbene)}$–N bonds in **10** (136.9 and 136.6 pm) are almost as long as those in **9** (136.7 and 137.3 pm); the N-C-N angles in **10** (102.8°) and **9** (102.2°) are also essentially the same. Hence, in this case Li^+ as the Lewis acid has not influence on the carbene structure. We conclude from these observations that this also applies to the carbene structure of the lithiated 4-*tert*-butylthiazole **7**. The $C_{(carbene)}$–Li distances in **10** (215.2 pm) and in [**7** · glyme]$_2$, (C1–Li2 = 217.7(5) and C8-Li1 = 217.5(5) pm) are nearly identical.[23, 24]

Similarly, a comparison of [**7** · glyme]$_2$ with the gold–carbene complex **11**[25] does not show any significant influence of the metal atom. The $C_{(carbene)}$–N distance in **11** (133.3 pm) is virtually the same as the one in [**7** · glyme]$_2$ (132.6 and 133.2 pm). The N-C-S angles are also comparable: they amount to 105.7° in **11**, and 107.9° and 108.1° in [**7** · glyme]$_2$. A slightly larger deviation is found only in



11

 © VCH Verlagsgesellschaft mbH, D-69451 Weinheim, 1995 0570-0833/95/0404-0488 $ 10.00+.25/0 Angew. Chem. Int. Ed. Engl. 1995, 34, No. 4

the $C_{(carbene)}$–S bonds, which are 172.1 pm in **11** and 176.3 (176.1 pm) in [**7** · glyme]$_2$.

In conclusion, the structure of the formyllithium equivalent [**7** · glyme]$_2$ corresponds to that of a nucleophilic carbene. The complexation with the Lewis acid Li^+ (dimerization) has essentially no influence on the structure.

Experimental Procedure

[**7** · glyme]$_2$: 4-*tert*-butylthiazole (141 mg, 1.00 mmol) in glycol dimethyl ether (2.7 mL) and *tert*-butyl methyl ether (0.1 mL) was deprotonated at −75 °C with 1.6 M methyllithium (0.7 mL, 1.12 mmol) in diethyl ether (30 min). After 5 days at −50 °C crystals of [**7** · glyme]$_2$ suitable for X-ray crystallography precipitated. Yield: 26 mg (18%). ^{1}H NMR ([D$_8$]THF, −50 °C): δ = 1.40 (s, 9H, C(CH_3)$_3$), 6.79 (s, 1H, H5). ^{13}C NMR ([D$_8$]THF, −50 °C): δ = 31.05 (C(CH_3)$_3$), 34.55 (*C*(CH_3)$_3$), 110.98 (C5), 166.24 (C4), 226.33 (C2). The ^{13}C resonance of the carbene C-atom in **9** is detected at δ = 213.2 [14a], the corresponding resonance of the gold complex **11** at δ = 214.5 pm [25]. The chemical shifts of the carbene-C signals in the ^{13}C NMR spectra of [**7** · glyme]$_2$, **9**, and **11** correspond to the results of quantum-mechanical calculations [14d].

Received: August 20, 1994 [Z 7256 IE]
German version: *Angew. Chem.* **1995**, *107*, 509

Keywords: acylation · carbenes · formyl anion equivalent

[1] a) H. Staudinger, *Chem. Ber.* **1908**, *41*, 2217–2219. Staudinger mentioned that the corresponding imino compounds (NR instead of O) should be more easily accessible: see ref. [2]; b) W. Schlenk, E. Bergmann, *Justus Liebigs Ann. Chem.* **1928**, *463*, 19–20; c) F. G. Fischer, O. Stoffers, *ibid.* **1933**, *500*, 253–270; d) G. Wittig, *Angew. Chem.* **1940**, *53*, 241–247, footnote 58; M. Ryang, S. H. Tsutsumi, *Bull. Chem. Soc. Jpn.* **1962**, *35*, 1121–1124; e) M. Schlosser, *Angew. Chem.* **1964**, *76*, 124–143; *Angew. Chem. Int. Ed. Engl.* **1964**, *3*, 287–306; f) G. Wittig, L. Gonsior, H. Vogel, *Justus Liebigs Ann. Chem.* **1965**, *688*, 1–13; g) K. V. Puzitskii, Y. T. Eiders, K. G. Ryabova, *Izv. Akad. Nauk SSSR Ser. Khim* **1966**, 1810; h) U. Wannagat, H. Seyffert, *Angew. Chem.* **1965**, *77*, 457–458; *Angew. Chem. Int. Ed. Engl.* **1965**, *4*, 438–439; i) U. Schöllkopf, F. Gerhart, *ibid.* **1967**, *79*, 819–820 and **1967**, *6*, 805; j) E. J. Corey, D. Seebach, R. Freedman, *J. Am. Chem. Soc.* **1967**, *89*, 434–436; k) P. Jutzi, F.-W. Schröder, *J. Organomet. Chem.* **1970**, *24*, 1–5; *Angew. Chem.* **1971**, *83*, 334; *Angew. Chem. Int. Ed. Engl.* **1971**, *10*, 339; l) U. S. Trzupek, T. L. Newirth, E. G. Kelly, N. E. Sbarbati, G. M. Whitesides, *J. Am. Chem. Soc.* **1973**, *95*, 8118–8133; m) V. Rautenstrauch, M. Joyeux, *Angew. Chem.* **1979**, *91*, 72–73; *Angew. Chem. Int. Ed. Engl.* **1979**, *18*, 83–85; n) T. Tsuda, M. Miwa, T. Saegusa, *J. Org. Chem.* **1979**, *44*, 3734–3736; o) N. S. Nudelman, A. A. Vitale, *J. Organomet. Chem.* **1983**, *241*, 143–156; N. S. Nudelman, T. O. Perez, *J. Org. Chem.* **1983**, *48*, 133–134; N. S. Nudelman, F. Doctorovich, *J. Chem. Soc. Perkin Trans. 2* **1994**, 1233–1238; P. Viruela-Martin, R. Viruela-Martin, F. Tomás, N. S. Nudelman, *J. Am. Chem. Soc.* **1994**, *116*, 10110–10116; p) D. Seyferth, R. M. Weinstein, R. C. Hui, W. L. Wang, C. M. Archer, *J. Org. Chem.* **1992**, *57*, 5620–5629; q) D. Seyferth, R. C. Hui, W. L. Wang, *ibid.* **1993**, *58*, 5843–5845 and papers of D. Seyferth et al. cited therein.

[2] D. Seebach, *Angew. Chem.* **1969**, *81*, 690–700; *Angew. Chem. Int. Ed. Engl.* **1969**, *8*, 639–649.

[3] E. Kaufmann, P. von R. Schleyer, S. Gronert, A. Streitwieser, Jr., M. Halpern, *J. Am. Chem. Soc.* **1987**, *109*, 2553–2559.

[4] a) H. M. Walborsky, G. E. Niznik, *J. Am. Chem. Soc.* **1969**, *91*, 778; b) H. M. Walborsky, W. H. Morrison III, G. E. Niznik, *ibid.* **1970**, *92*, 6675–6676; c) Y. Ito, T. Matsuura, M. Murakami, *ibid.* **1987**, *109*, 7888–7890; d) H. Watanabe, F. Yan, T. Sakai, K. Uneyama, *J. Org. Chem.* **1994**, *59*, 758–761.

[5] a) D. Hoppe, U. Schöllkopf, *Angew. Chem.* **1970**, *82*, 290–291; *Angew. Chem. Int. Ed. Engl.* **1970**, *9*, 300–301; b) B. E. Maryanoff, *Chem. Heterocycl. Compd.* **1986**, *45*; c) A. I. Meyers, *Heterocycles in Organic Synthesis*, Wiley, New York, **1974**.

[6] a)–c) E. J. Corey, D. Boger, *Tetrahedron Lett.* **1978**, 5–8, 9–12, 13–16; d) J. V. Metzger, *Chem. Heterocycl. Comp.* **1979**, *34*, Part 1–3.

[7] Recent reviews: A. Dondoni, *Synthesis* **1993**, 1162–1176, and references therein.

[8] η^1- and η^2-bound electrophile formyl complexes with transition metal compounds have been known for a long time: a) G. Fachinetti, C. Floriani, F. Macchetti, S. Merlino, *J. Chem. Soc. Chem. Commun.* **1976**, 522–523; b) Übersicht: J. A. Gladysz, *Adv. Organomet. Chem.* **1982**, *20*, 1–38; c) C. Elschenbroich, A. Salzer, *Organometallics*, 2. Aufl., VCH, Weinheim, **1992**.

[9] Crystal data of [**7** · Glyme]$_2$ ($C_{22}H_{40}Li_2N_2O_4S_2$, M = 474.56): orthorhombic, *Pbca*, a = 1226.5(1), b = 1454.4(2), c = 3244.4(6) pm, Z = 8, $\rho_{calcd.}$ = 1.089 g cm^{-3}, μ(Cu$_{K\alpha}$) = 18.69 cm^{-1}, crystal dimensions 0.6 × 0.4 × 0.2 mm, ENRAF-NONIUS CAD4 diffractometer (Cu$_{K\alpha}$ radiation, λ = 1.54178 Å, graphite monochromator, T 208 K); 3631 unique reflections collected. Solution by direct methods [10a], refinement with all data on F^2 [10b] to $wR2$ = 0.1654 ($w^{-1} = [\sigma^2(F_o^2) + (0.1145P)^2 + 2.0401P]$ with $P = (F_o^2 + 2F_c^2)/3$), all non-hydrogen atoms anisotropic, hydrogens (except those of the heterocyclic ring) at calculated positions with fixed isotropic temperature factors. The conventional R value $R1$ was 0.0598 for 3117 reflections with $I > 2\sigma(I)$. All calculations have been performed on a Micro-VAX II and a DEC AXP 3000-300 [11, 12]. Further details of the crystal structure determination may be obtained from the Fachinformationszentrum Karlsruhe, D-76344 Eggenstein-Leopoldshafen (Germany) on quoting the depository number CSD-380063.

[10] a) *SHELXTL-PLUS (VMS), Vers. 4.21*, Siemens Analytical X-Ray Instruments Inc., Madison, WI, **1990**; b) G. M. Sheldrick, *SHELXL-93*, Program for the Refinement of Crystal Structures, Göttingen, **1993**.

[11] A. L. Spek, *PLATON 94*, Program for Geometrical Analysis of Crystal Structures, Utrecht, **1994**.

[12] E. Keller, *SCHAKAL-88B*, A FORTRAN Program for the Graphic Representation of Molecular and Crystallographic Models, Freiburg, **1988**.

[13] L. Nygaard, E. Asmussen, J. H. Hog, R. C. Maheshwari, C. H. Nielsen, I. B. Petersen, *J. Mol. Struct.* **1971**, *8*, 225–233.

[14] a) A. J. Arduengo III, H. Bock, H. Chen, M. Denk, D. A. Dixon, J. C. Green, W. A. Herrmann, N. L. Jones, M. Wagner, R. J. West, *J. Am. Chem. Soc.* **1994**, *116*, 6641–6649; b) A. J. Arduengo III, R. L. Harlow, M. Kline, *ibid.* **1991**, *113*, 361–363; c) A. J. Arduengo III, H. V. R. Dias, R. L. Harlow, M. Kline, *ibid.* **1992**, *114*, 5530–5534; d) A. J. Arduengo III, D. A. Dixon, K. K. Kumashiro, C. Lee, W. P. Power, K. W. Zilm, *ibid.* **1994**, *116*, 6361–6367 (see also ref. [15]).

[15] a) Stable carbenes have also been isolated by A. Igau, H. Grützmacher, A. Baceiredo, G. Bertrand *J. Am. Chem. Soc.* **1988**, *110*, 6463–6466; b) see also M. Regitz, *Angew. Chem.* **1991**, *103*, 691–693; *Angew. Chem. Int. Ed. Engl.* **1991**, *30*, 674 and references therein.

[16] C-Li distances greater than 250 pm are generally not considered to be bonds: G. Boche, *Angew. Chem.* **1989**, *101*, 286–306; *Angew. Chem. Int. Ed. Engl.* **1989**, *28*, 277–297.

[17] Also N1–C3(N2–C10) is increased by 2.2(2.0) pm. S1–C2(S2–C9) remains essentially the same (± 0.5 pm), while C2–C3(C9–C10) is somewhat shortened (2.5(1.9) pm).

[18] a) C. W. Bauschlicher, Jr., H. F. Schaefer III, P. S. Bagus, *J. Am. Chem. Soc.* **1977**, *99*, 7106–7110; b) D. Feller, W. T. Borden, E. R. Davidson, *J. Chem. Phys.* **1979**, *71*, 4987–4992; c) D. A. Dixon, *ibid.* **1986**, *90*, 54–56; d) B. T. Luke, J. A. Pople, M.-B. Krogh-Jespersen, Y. Apeloig, M. Karni, J. Chandrasekhar, P. von R. Schleyer, *J. Am. Chem. Soc.* **1986**, *108*, 270–284.

[19] B. Lachmann, H. Steinmaus, H.-W. Wanzlick, *Tetrahedron* **1971**, *27*, 4085–4090, have been the first to study nucleophilic carbenes of the structural type **9**. See also references therein.

[20] The enormous importance of the analogous thiazol carbenes (general structure: Li in **7** is exchanged by a substituent R) in biochemical and other processes can only be mentioned here; see, for example, a) R. Breslow, *J. Am. Chem. Soc.* **1958**, *80*, 3719–3726; b) A. Schnellenberger, *Ann. N.Y. Acad. Sci.* **1982**, *378*, 51; c) C. J. Suckling, *Chem. Soc. Rev.* **1984**, *13*, 97–129; d) R. Kluger, *Chem. Rev.* **1987**, *87*, 863–876; e) H. Stetter, H. Kuhlmann, *Angew. Chem.* **1974**, *86*, 589; *Angew. Chem. Int. Ed. Engl.* **1974**, *13*, 539; f) P. Haake, *Tetrahedron Lett.* **1981**, *22*, 2939–2940; g) T. Matsumoto, M. Ohishi, S. Inoue, *J. Org. Chem.* **1985**, *50*, 603–606.

[21] a) A. J. Arduengo III, H. V. R. Dias, J. C. Calabrese, F. Davidson, *J. Am. Chem. Soc.* **1992**, *114*, 9724–9726; b) *Inorg. Chem.* **1993**, *32*, 1541–1542; c) *Organometallics* **1993**, *12*, 3405–3409; d) G. Alcaraz, R. Reed, A. Baceiredo, G. Bertrand, *J. Chem. Soc. Chem. Commun.* **1993**, 1354–1355; e) N. Kuhn, G. Henkel, T. Kratz, J. Kreutzberg, R. Boese, A. H. Maulitz, *Chem. Ber.* **1993**, *126*, 2041–2045; f) A. H. Cowley, F. P. Gabbai, C. J. Carrano, L. M. Mokry, M. R. Bond, G. Bertrand, *Angew. Chem.* **1994**, *106*, 584–586; *Angew. Chem. Int. Ed. Engl.* **1994**, *33*, 578–580; g) H. G. Raubenheimer, S. Cronje, P. H. van Rooyen, P. J. Olivier, J. G. Toerien, *ibid.* **1994**, *106*, 687–688 bzw. **1994**, *33*, 672–673, and references therein.

[22] A. J. Arduengo III, M. Tamm, personal communication, July 11, 1994. We thank A. J. Arduengo III for the data of **10**.

[23] MP2/6-31G* model calculations support the negligible influence of the complexation on the structure with Li^+ as Lewis acid. For example, the N-C-S angle in lithiothiazole (most stable singlet) is calculated to be 107.9°, while 108.6° results for a lithiothiazole · LiOH complex. For comparison: the calculated angle for the thiazole **8** is 115.4°.

[24] In an earlier paper we reported on the following four calculated structures of the Li/O carbenoid model, Li-CH_2-OH: 1. Li bridges C–O; 2. Li is bound only to C; the structure is 3. $H_2C\cdots OH(Li)$ and 4. $H_2C\cdots LiOH$. Experimental evidence has been found for the model cases 1–3. G. Boche, A. Opel, M. Marsch, K. Harms, F. Haller, J. C. W. Lohrenz, C. Thümmler, W. Koch, *Chem. Ber.* **1992**, *125*, 2265–2273. The structures of [**7** · glyme]$_2$ and **10** now experimentally verify the fourth (high-energy) model structure.

[25] H. G. Raubenheimer, F. Scott, M. Roos, R. Otte, *J. Chem. Soc. Chem. Commun.* **1990**, 1722; H. G. Raubenheimer, F. Scott, G. J. Krüger, J. G. Toerien, R. Otte, W. van Zyl, I. Taljaard, P. Oliver, L. Linford, *J. Chem. Soc. Dalton Trans.*, in press.

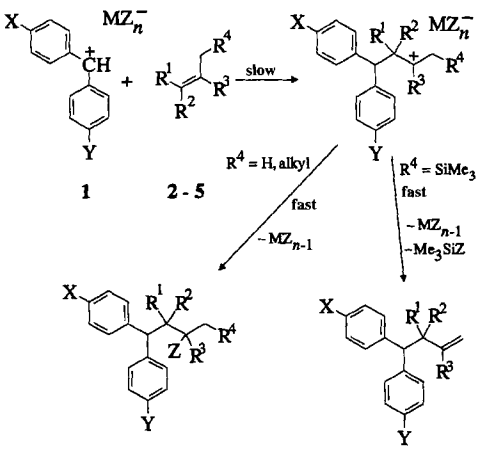
Common Origin of Enthalpic and Entropic Substituent Effects in Reactions of Benzhydryl Cations with Nucleophiles

Matthias Patz, Herbert Mayr*, Jörg Bartl, and Steen Steenken

Dedicated to Professor Christoph Rüchardt on the occasion of his 65th birthday

The investigation of substituent effects is one of the most important tools for the determination of reaction mechanisms. While effects of substituents on equilibria and rates of chemical reactions are usually attributable to differences in enthalpy, changes in the entropy of activation, particularly for reactions of reactive intermediates (fast reactions), have been recognized to be the origin of observed substituent effects.[1-3] For the reactions of *para*-substituted benzhydryl cations with π-nucleophiles, we now demonstrate that the change from enthalpic to entropic substituent effects occurs within these reaction series on going from slow to fast reactions. Consequently, the reactivity of the nucleophile determines whether changing substituents in the electrophile affects $\Delta H^{\neq}$ or $\Delta S^{\neq}$.

Detailed mechanistic investigations of the reactions of benzhydryl cations with alkenes[4] and other π-systems[5] have shown that generally the C–C bond formation is the rate-determining step of the reaction sequence depicted in Scheme 1, that



Scheme 1. The reaction of benzhydryl cations with compounds containing π-electron systems. **2**, $R^1 = R^3 = CH_3$, $R^2 = R^4 = H$; **3**, $R^1 = R^2 = H$, $R^3 = CH_3$, $R^4 = C_2H_5$; **4**, $R^1 = R^2 = R^3 = H$, $R^4 = Si(CH_3)_3$; **5**, $R^1 = R^2 = CH_3$, $R^3 = H$, $R^4 = Si(CH_3)_3$.

is, the measured rate constant represents the attack of the carbenium ion at the π-system. Reduction of the electron-donating ability of the substituents X and Y in the carbenium ion **1** gives rise to an acceleration of the reactions, which is caused entirely by the decrease of the enthalpy of activation while the entropy of activation remains constant within the accuracy of the measurements (Fig. 1). An analogous pattern has been observed for many reaction series with $k < 5 \times 10^4$ L mol^{-1}s^{-1}.[6]

For the reaction of the bis(*p*-tolyl)carbenium ion (**1**; X = Y = CH_3) with 2-methyl-2-butene (**2**) in CH_2Cl_2, rate constants k of $(6.9 \pm 0.3) \times 10^4$ L mol^{-1} s^{-1}, almost independent of temperature between -70 and -40 °C, have been observed, from which an activation energy E_a of (0.4 ± 0.6) kJ mol^{-1} and an enthalpy of activation $\Delta H^{\neq}$ of (-1.4 ± 0.6) kJ mol^{-1} (Fig. 1 top) can be calculated. Though no enthalpic barrier is present,

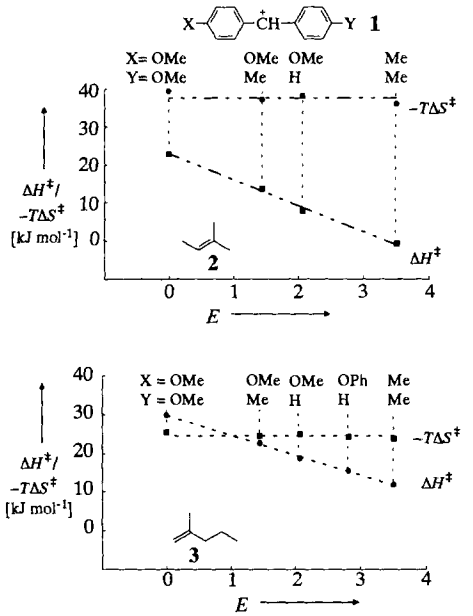


Figure. 1. Correlation between the activation parameters of the reactions of **2** (top), and **3** (bottom) with benzhydryl cations and their electrophilicities. $\Delta H^{\neq}$ and $\Delta S^{\neq}$ were calculated from rate measurements at -70 to -30 °C [6]; electrophilicity parameters E were obtained from ref. [7].

the observed rate constants are five orders of magnitude below the diffusion limit as a result of the large entropy term $-T\Delta S^{\neq}$. How do carbenium ions, which are less stabilized by substituents than **1** (X = Y = CH_3), behave?

To investigate the reactions of more electrophilic benzhydryl cations (**1**) with the same nucleophiles (**2**–**5**), we used the laser pulse method, employing acetonitrile as a solvent because photolysis of benzhydryl chlorides in dichloromethane almost entirely causes homolytic cleavage of the C–Cl bond.[8] As variation of the solvent has only a very small influence on the rates of the reactions of carbenium ions with neutral nucleophiles,[7,9] the rate constant measured for the reaction of the bis(*p*-chlorophenyl)carbenium ion (**1**, X = Y = Cl) with **2** ($k = 7.4 \times 10^7$ L mol^{-1} s^{-1}, CH_3CN, 20 °C) indicates that the replacement of X = Y = CH_3 by Cl in **1** causes an increase of reactivity by almost three orders of magnitude.[10] Since there was no enthalpic barrier even for the reaction of the considerably less reactive carbenium ion (**1**, X = Y = CH_3) with **2**, the further increase of reactivity must be due either to negative values of $\Delta H^{\neq}$ or to an increase of $\Delta S^{\neq}$. Two extreme cases are conceivable: The entropy of activation remains constant while $\Delta H^{\neq}$ becomes negative, or $\Delta H^{\neq}$ remains zero and the isentropic series (constancy of $\Delta S^{\neq}$ shown in Figure 1) does not include the reactions with more electrophilic carbenium ions. Within the Arrhenius formalism, the second possibility corresponds to an increase of the preexponential factor at constant activation

[*] Prof. Dr. H. Mayr, Dr. M. Patz, Dr. J. Bartl
Institut für Organische Chemie der Technischen Hochschule
Petersenstrasse 22, D-64287 Darmstadt (Germany)
Telefax: Int. code + (6151) 16-5591
Prof. Dr. S. Steenken
Max-Planck-Institut für Strahlenchemie
D-44780 Mühlheim (Germany)

[**] We thank the Deutsche Forschungsgemeinschaft for support of our work and are grateful to the Fonds der chemischen Industrie for the award of a Kekulé stipend (M. P.)

 © VCH Verlagsgesellschaft mbH, D-69451 Weinheim, 1995 0570-0833/95/0404-0490 $ 10.00+.25/0

energy. To differentiate these two possibilities, we studied the temperature dependence of the reaction of **2** with the benzhydryl cation **1** (X = Y = Cl) generated by laser flash photolysis in acetonitrile.[8] In eight experiments from −18 to +21 °C we observed temperature-independent rate constants of $(7.4 \pm 0.5) \times 10^7\,L\,mol^{-1}\,s^{-1}$ yielding the Arrhenius parameters $E_a = (-0.6 \pm 1.2)\,kJ\,mol^{-1}$ and $\lg A = 7.54 \pm 0.22$ and the Eyring parameters $\Delta H^{\neq} = (-2.9 \pm 1.1)\,kJ\,mol^{-1}$ and $\Delta S^{\neq} = (-104 \pm 4)\,J\,mol^{-1}\,K^{-1}$.

The thousandfold increase in reactivity on employing the dichloro- instead of the dimethyl-substituted benzhydryl cation is thus due to a change of the entropy term while $\Delta H^{\neq}$ remains close to zero. Though the initial question has thus been answered, the argument is weakened by the fact that a change of solvent could not be avoided for methodical reasons. We have, therefore, corroborated our conclusion by an additional experiment.

Like the alkenes **2** and **3**, the allylsilanes **4** and **5** also react with the *p*-methoxy- and phenoxy-substituted benzhydryl cations **1** at −70 °C in CH_2Cl_2 at rate constants from 10^{-1} to $10^4\,L\,mol^{-1}\,s^{-1}$. Again the change of reactivity is entirely due to a variation of $\Delta H^{\neq}$ while $\Delta S^{\neq}$ remains constant in both reaction series [for **4** $\Delta S^{\neq} = (-118.5 \pm 5.6)\,J\,mol^{-1}\,K^{-1}$; for **5** $\Delta S^{\neq} = (-163.9 \pm 2.8)\,J\,mol^{-1}\,K^{-1}$]. Extrapolation of the straight lines shown in Figure 2 yields a positive enthalpy of

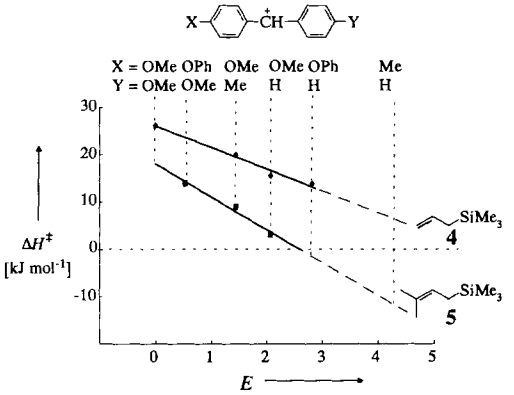
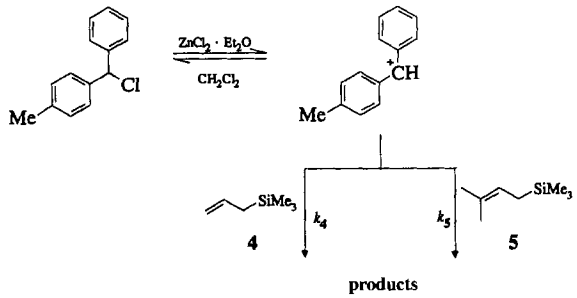


Figure 2. Correlation between the enthalpy of activation $\Delta H^{\neq}$ for the reactions of **4** [5a] and **5**[5a] with benzhydryl cations and their electrophilicity *E*.

activation for the reaction of the benzhydryl cation **1** (X = CH_3, Y = H) with **4** [$\Delta H^{\neq} = (6.2 \pm 2.9)\,kJ\,mol^{-1}$] and a negative value of $\Delta H^{\neq}$ [$(-12.0 \pm 1.7)\,kJ\,mol^{-1}$] for the corresponding reaction with **5**.

The relative reactivities of the two allylsilanes towards **1** (X = CH_3, Y = H) determined by competitive experiments show a strong dependence of the competition constant (k_5/k_4) on temperature (Scheme 2). By plotting $\lg(k_5/k_4)$ against $1/T$ the activation parameters $\Delta\Delta H^{\neq} = (11.7 \pm 0.6)\,kJ\,mol^{-1}$ and $\Delta\Delta S^{\neq} = (30.8 \pm 2.5)\,J\,mol^{-1}\,K^{-1}$ are obtained. Since a positive value of $\Delta H^{\neq}$ is extrapolated for the reaction of **1** (X = CH_3, Y = H) with **4** (Fig. 2), we can conclude that this reaction is part of the isentropic series [$\Delta S^{\neq} = (-118.5 \pm 5)\,J\,mol^{-1}\,K^{-1}$] in analogy to the situation for numerous related reaction series.[5, 6] The remarkable decrease of the difference of entropy from [$\Delta S_4^{\neq} - \Delta S_5^{\neq} = (45.4 \pm 6.4)\,J\,mol^{-1}\,K^{-1}$] for the less reactive benzhydryl cations of Figure 2 to $(30.8 \pm 2.5)\,J\,mol^{-1}\,K^{-1}$ for **1** (X = CH_3, Y = H) must therefore be due to the fact that the entropy of activation for the reaction of **5** with **1** (X = CH_3, Y = H) is less



T/°C	-68.5	-68.0	-30.5	0.0	20.0	20.0
k_5/k_4	23.5	21.2	9.5	4.4	2.6	3.0

Scheme 2. Competition experiments with **4** and **5**.

negative by $15\,J\,mol^{-1}\,K^{-1}$ compared to $\Delta S^{\neq}$ of the reactions of **5** with the methoxy- and phenoxy-substituted benzhydryl cations. As discussed above for the reactions with **2** and **3**, these reaction series also show that an increase of the electrophilicity of carbenium ions occurs with constant entropy of activation and a decrease of $\Delta H^{\neq}$ as long as there is an enthalpic barrier. When the enthalpic barrier has disappeared, the increase of electrophilicity is predominantly caused by an increase of $\Delta S^{\neq}$ which corresponds to an increase of the preexponential factor in the Arrhenius equation.

How can the discontinuous behavior of $\Delta S^{\neq}$ be explained? As $\Delta S^{\neq}$ represents a measure for the position of the transition state, we conclude that this remains unchanged within a reaction series,[11] as long as there is an enthalpic barrier. Only in the absence of an enthalpic barrier is an increase in the electrophilicity of the carbenium ions associated with a shift of the transition state (defined as the maximum of the Gibbs enthalpy[12]) towards the reactants. Assuming the same trajectory, the increase of $\Delta S^{\neq}$ can be rationalized, because at an earlier position of the reaction coordinate fewer degrees of freedom are restricted. As discussed for the additions of carbenes to alkenes by Houk et al.,[11] the large entropy contribution shifts the maximum of the Gibbs enthalpy (transition state) to a position of the reaction coordinate where the enthalpy of the activated complex is already lower than that of the reactants.

Alternatively, the increase of the entropy of activation can be explained by assuming that in cases without an enthalpy barrier activated complexes with different structures are involved, since lifting of the energy levels of the reactants now causes a broadening of the reaction channel and an increase in the number of only downhill trajectories.

The change from isentropic regions to regions with variable entropy, which has been demonstrated experimentally for two examples, might be a general phenomenon. Since bimolecular reactions typically have entropies of activation between −80 and $-180\,J\,mol^{-1}\,K^{-1}$, which contribute 23 to $53\,kJ\,mol^{-1}$ to $\Delta G^{\neq}$ at 20 °C, substituent effects should generally be observable as entropic effects when the rate constants *k* exceed values from 2×10^3 to $4 \times 10^8\,L\,mol^{-1}\,s^{-1}$ (from $\Delta H^{\neq} = 0$ and $\Delta S^{\neq} = -180$ and $-80\,J\,mol^{-1}\,K^{-1}$, respectively).

In agreement with this conclusion, Scaiano, Berson et al.[13] reported that the same order of reactivities of dienophiles that Sauer et al.[14] observed in reactions with 9,10-dimethylanthracene and cyclopentadiene (isentropic series) also holds for 3,4-dimethylenefuran, although the reactions with 9,10-dimethylanthracene and cyclopentadiene are characterized by variable values of $\Delta H^{\neq}$ and a constant $\Delta S^{\neq}$, whereas the reactions with the singlet diradical have almost equal (slightly nega-

tive) values of $\Delta H^{\neq}$, and the differences in reactivity are due to differences in the entropy of activation. Depending on the nature of the reaction partner, electronic substituent effects thus can affect either $\Delta H^{\neq}$ or $\Delta S^{\neq}$.

Received: August 27, 1994
Revised: October 12, 1994 [Z 7273IE]
German version: *Angew. Chem.* **1995**, *107*, 519

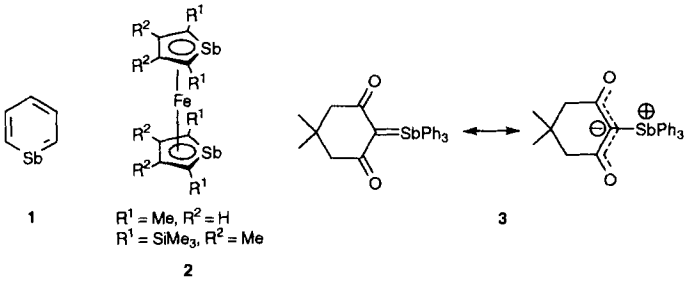
Keywords: carbocations · linear free energy relationships · reaction mechanisms · substituent effects

[1] General: a) B. Giese, *Angew. Chem.* **1977**, *89*, 162–173; *Angew. Chem. Int. Ed. Engl.* **1977**, *16*, 125–136; b) *Acc. Chem. Res.* **1984**, *17*, 438–442.
[2] Radicals: a) C. Rüchardt, H.-D. Beckhaus, *Top. Curr. Chem.* **1985**, *130*, 1–22; b) P. I. Abell in *Comprehensive Chemical Kinetics, Vol. 18* (Eds.: C. H. Bamford, C. F. H. Tipper, Elsevier, Amsterdam, **1976**, pp. 111–165; c) *Landoldt-Börnstein. Zahlenwerte und Funktionen aus Naturwissenschaft und Technik, Bd. 13* (Eds.: H. Fischer), Neue Serie, Gruppe II, **1984**.
[3] Carbenes: a) R. A. Moss, W. Lawrynowicz, N. J. Turro, I. R. Gould, Y. Cha, *J. Am. Chem. Soc.* **1986**, *108*, 7028–7032; b) N. Soundararajan, M. S. Platz, J. E. Jackson, M. P. Doyle, S.-M. Oon, M. T. H. Liu, S. M. Anand, *ibid.* **1988**, *110*, 7143–7152; c) J. E. Jackson, N. Soundararajan, M. S. Platz, M. P. Doyle, M. T. H. Liu, *Tetrahedron Lett.* **1989**, *30*, 1335–1338.
[4] a) H. Mayr, R. Schneider, C. Schade, J. Bartl, R. Bederke, *J. Am. Chem. Soc.* **1990**, *112*, 4446–4454; b) H. Mayr, *Angew. Chem.* **1990**, *102*, 1415–1428; *Angew. Chem. Int. Ed. Engl.* **1990**, *29*, 1371–1384.
[5] a) G. Hagen, H. Mayr, *J. Am. Chem. Soc.* **1991**, *113*, 4954–4961; b) H. Mayr, J. Bartl, G. Hagen, *Angew. Chem.* **1992**, *104*, 1689–1691; *Angew. Chem. Int. Ed. Engl.* **1992**, *31*, 1613–1615.
[6] H. Mayr, R. Schneider, U. Grabis, *J. Am. Chem. Soc.* **1990**, *112*, 4460–4467.
[7] H. Mayr, M. Patz, *Angew. Chem.* **1994**, *106*, 990–1010; *Angew. Chem. Int. Ed. Engl.* **1994**, *33*, 938–957.
[8] J. Bartl, S. Steenken, H. Mayr, R. A. McClelland, *J. Am. Chem. Soc.* **1990**, *112*, 6918–6928.
[9] For the reaction of bis(*p*-anisyl)methyl cation **1**, X = Y = OCH_3, with **3** a ratio of the reaction rates $k_{CH_3CN}/k_{CH_2Cl_2}$ of 3.2 was determined at −20 °C: M. Patz Dissertation, Technische Hochschule Darmstadt, **1994**.
[10] J. Bartl, S. Steenken, H. Mayr, *J. Am. Chem. Soc.* **1991**, *113*, 7710–7716.
[11] K. N. Houk, N. G. Rondan, J. Mareda, *Tetrahedron* **1985**, *41*, 1555–1563.
[12] a) D. G. Truhlar, W. L. Hase, J. T. Hynes, *J. Phys. Chem.* **1983**, *87*, 2664–2682; b) J. F. Blake, S. G. Wierschke, W. L. Jorgensen, *J. Am. Chem. Soc.* **1989**, *111*, 1919–1920 and references therein.
[13] J. C. Scaiano, V. Wintgens, K. Haider, J. A. Berson, *J. Am. Chem. Soc.* **1989**, *111*, 8732–8733.
[14] J. Sauer, H. Wiest, A. Mielert, *Z. Naturforsch. B* **1962**, *17*, 203–204.

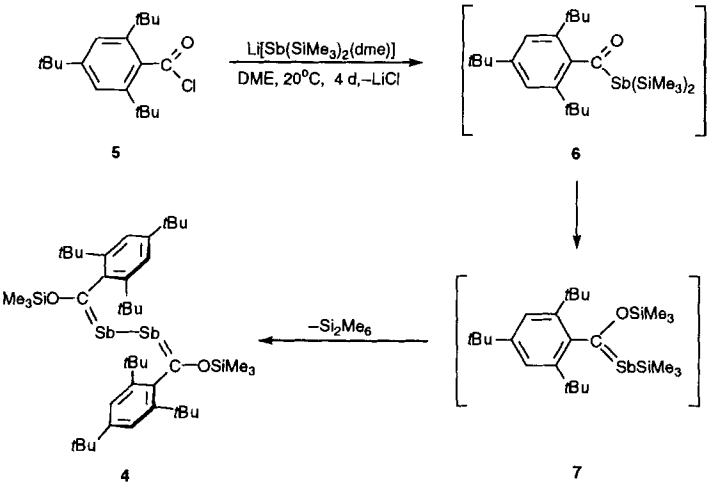
The First Distibabutadiene: Synthesis and Structure of *trans*-1,4-Bis(trimethylsiloxy)-1,4-bis(2,4,6-tri-*tert*-butylphenyl)-2,3-distibabutadiene**

Peter B. Hitchcock, Cameron Jones, and John F. Nixon*

Despite the considerable interest that has recently been shown in compounds containing phosphorus–carbon or arsenic–carbon multiple bonds,[1] the knowledge of analogous antimony compounds is sparse. In fact, structurally characterized examples of such compounds can be confined to a few cases where a λ^3,σ^2 Sb–C double bond is stabilized in an aromatic cyclic system, for example, **1**[2] and **2**.[3] Only in one of the canonical forms of resonance-stabilized λ^5,σ^4 stibonium ylides such as **3** have acyclic Sb–C double bonds been proposed.[4] As part of a continuing study of higher group 15 congeners with low coordination numbers,[5] we now report the synthesis and X-ray crystal structure of the first distibabutadiene **4**, which contains the first example of an acyclic λ^3,σ^2 Sb–C double bond.



Treatment of $Li[Sb(SiMe_3)_2(dme)]$[6] with the acid chloride **5** (Scheme 1) in dimethoxyethane (dme) afforded the deep red, mildly air-sensitive complex **4** (18% yield) after recrystallization from hexane. Although all manipulations were carried out in the



Scheme 1. Synthesis and proposed mechanism for the formation of **4**.

dark, considerable quantities of elemental antimony precipitated from solution during the course of the reaction (4 days), which seemingly accounts for the low yield of **4**. Moreover, when the less sterically hindered acid chloride *t*BuCOCl was employed in place of **5**, no 2,3-distibabutadiene formation was observed; instead high yields of the novel 2-stiba-1,3-dionate, $[\{[LiO(t\text{Bu})CSbC(t\text{Bu})O]_2(dme)\}_\infty]$ were obtained.[7] The phosphorus analogue of **4** has been reported in low yields as a product of the high temperature reaction of $P(SiMe_3)_3$ with **5**.[8] Similar attempts to form **4** by the reaction of $Sb(SiMe_3)_3$ with **5** led only to decomposition products. The heterobutadiene **4** was characterized by elemental analysis, mass spectrometry, ^1H NMR spectroscopy, and a single crystal X-ray structure determination.

From its molecular structure[9] (Fig. 1), compound **4** lies on an inversion center; atoms C1, Sb, Sb′, and C1′ are coplanar and adopt the sterically favourable *trans* configuration. The

[*] Prof. J. F. Nixon, Dr. P. B. Hitchcock, Dr. C. Jones[+]
School of Chemistry and Molecular Sciences
University of Sussex, GB-Brighton, BN1 9QJ (UK)
Telefax: Int. code + (273)677196
[+] Present address: Chemistry Department, University of Wales, Swansea, Singleton Park, GB-Swansea, SA2 8PP, UK.
[**] We acknowledge financial support from the Engineering and Physical Sciences Research Council (E.P.S.R.C.).

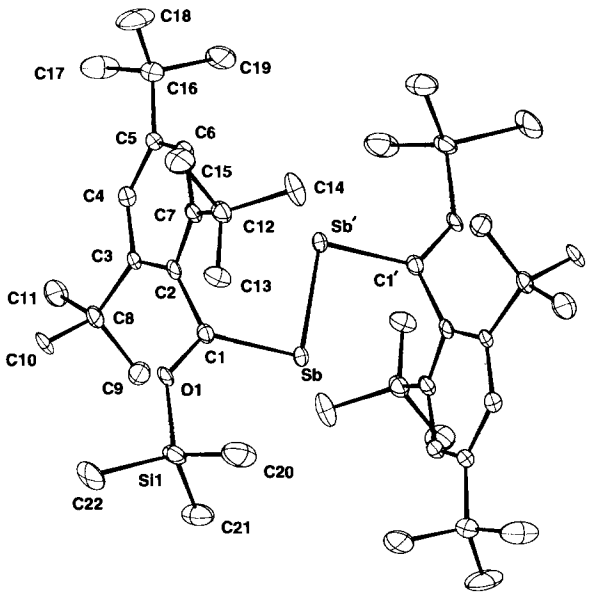


Fig. 1. Molecular structure (ORTEP, thermal ellipsoids represent 50% probability) of **4**. Important bond lengths [Å] and angles [°]: Sb–Sb' 2.774(1), Sb–C1 2.056(10), C1–O1 1.370(12), C1–C2 1.483(13), O1–Si1 1.676(7); Sb'-Sb-C1 94.7(3), Sb-C1-C2 123.0(7), Sb-C1-O1 122.2(7), C2-C1-O1 114.8(8), C1-O1-Si1 134.5(6).

coordination environment around the alkene carbon C1 is one of a trigonal plane (sum of the angles = 360.0°), which subtends a dihedral angle of 6(2)° with the plane of this butadiene backbone. The angle C1-Sb-Sb' [94.7(3)°] is considerably distorted from the 120° expected for an sp^2-hybridized Sb center and is significantly less than the corresponding C-P-P angle in related 2,3-diphosphabutadienes, for example $[P=C(OSiMe_3)(tBu)]_2$ [100.7(4)°].[10] To the best of our knowledge there are no known structurally characterized examples of 2,3-diarsabutadienes for comparison. This apparent trend to lower C-E-E angles for heavier elements E of group 15 can be explained by the inert s-pair effect and has been observed in the similar compound series RE=ER (E = N, P, As).[1]

It seems possible from the bond lengths within the molecule that a degree of double-bond delocalization is occurring. The distance Sb–C1 [2.056(10) Å] is longer than predicted in a high level (Hartree-Fock/3-21G* basis set) theoretical study on the stibaalkene $HSb=CH_2$ (2.01 Å),[11] and close to that seen in other delocalized systems [for example **1**, 2.050(5) Å],[2] or resonance-stabilized compounds [for example **3**, 2.049(4) Å].[4] Similarly, the Sb–Sb' distance [2.774(1) Å] is shorter than is normally found for Sb–Sb single bonds in distibanes, R_2SbSbR_2 (for example Ph_4Sb_2, 2.837(1) Å)[12] and is, in fact, close to that typically observed for Sb=Sb bonds η^2-coordinated to transition metal complex fragments, such as in $[Fe\{\eta^2\text{-}[(Me_3Si)_2CH]_2Sb_2\}(CO)_4]$ [2.774(1) Å].[13] However, the shortness of the Sb–Sb' bond in **4** relative to distibanes can also be explained by the smaller covalent radius of its sp^2-hybridized Sb center relative to that of the sp^3-hybridized center in distibanes. Similar shortenings have been observed for P–P bonds involving sp^2- and sp^3-hybridized phosphorus.[1] Therefore, it seems likely that the unusual stability of **4** is derived from a combination of partial double-bond delocalization in addition to the significant steric protection afforded to each antimony center. These factors also explain the apparent robustness of the Sb–Sb bond in **4** as evidenced by the absence of the monomeric fragment $[SbC(2,4,6\text{-}C_6H_2tBu_3)(OSiMe_3)]^+$ in its mass spectrum. In the mass spectra of corresponding 2,3-diphosphabutadiene systems P–P bond cleavage fragments are common.[8]

Considering the mechanism for the formation of **4**, a plausible initial step is a salt elimination reaction giving rise to **6** (Scheme 1). This then undergoes a 1,3-silyl shift yielding the unstable stibaalkene **7**, which then eliminates hexamethyldisilane in a coupling reaction to give the 2,3-distibabutadiene **4**. Similar coupling reactions involving the elimination of Si_2Me_6 have been reported in the formation of disilenes.[14] By contrast, the closely related reaction of **5** with $[Li\{As(SiMe_3)_2\}(thf)_2]$ leads to elimination of hexamethyldisiloxane from the arsenic analogue of **6**, thus affording the arsaalkyne $(2,4,6\text{-}C_6H_2tBu_3)C\equiv As$;[15] comparable stibaalkyne formation was not observed in the present work. We are currently pursuing a stable stibaalkyne by alternative routes in addition to examining the coordination chemistry of **4**.

Experimental Procedure

4: To a solution of $Li[Sb(SiMe_3)_2(dme)]$ (1.20 g, 3.3 mmol) in DME (20 mL) at −40 °C was added **5** (1.02 g, 3.3 mmol) in DME (15 mL). After 4 days (exclusion of light) at 20 °C, volatiles were removed from the resulting solution under vacuum (10^{-3} mbar). The residue was extracted with hexane (40 mL) and filtered, and the filtrate was concentrated under vacuum (10^{-3} mbar) to about 7 mL. Cooling to −30 °C for 12 h yielded **4** as deep red crystals. Yield 280 mg (18%); m.p. 213 °C (decomp.); ^{1}H NMR (250 MHz, C_6D_6, 25 °C, TMS) δ = 0.43 (s, 18H), $OSiMe_3$), 1.39 (s, 18H, *t*Bu), 1.65 (s, 36H, *t*Bu), 7.47 (s, 4H, Ar); MS (70 eV): *m/z* (%): 936(5) [M^+], 879(3) [$M^+ - tBu$], 345(45) [$tBu_3PhCOSiMe_3^+$], 273(100) [tBu_3PhCO^+], 73(60) [$SiMe_3^+$], 57(58) [tBu^+]. Satisfactory microanalytical data were obtained for **4**.

Received: September 12, 1994 [Z 7307 IE]
German version: *Angew. Chem.* **1995**, *107*, 522

Keywords: antimony compounds · heterobutadienes · multiple bonds

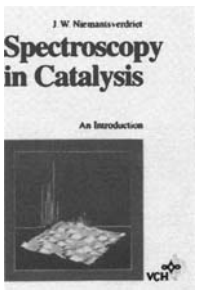
[1] N. C. Norman, *Polyhedron* **1993**, *12*, 2431, and references therein.
[2] G. D. Fong, R. L. Kuczkowski, A. J. Ashe III, *J. Mol. Spectrosc.* **1978**, *70*, 197.
[3] a) A. J. Ashe III, T. R. Diephouse, J. W. Kampf, S. M. Al-Taweel, *Organometallics* **1991**, *10*, 2068; b) A. J. Ashe III, J. W. Kampf, *ibid.* **1992**, *11*, 1491.
[4] G. Ferguson, C. Glidewell, I. Gosney, D. Lloyd, S. Metcalfe, H. Lumbroso, *J. Chem. Soc. Perkin Trans. II* **1988**, 1829.
[5] P. B. Hitchcock, C. Jones, J. F. Nixon, *J. Chem. Soc. Chem. Commun.* **1994**, 2601.
[6] G. Becker, A. Münch, C. Witthauer, *Z. Anorg. Allg. Chem.* **1982**, *492*, 15.
[7] J. Durkin, P. B. Hitchcock, C. Jones, J. F. Nixon, unpublished results.
[8] G. Märkl, H. Sejpka, *Tetrahedron Lett.* **1986**, *27*, 171.
[9] Crystal structure of **4**: T = 173 K; $C_{44}H_{76}O_2Si_2Sb_2$, triclinic, space group $P\bar{1}$ (No. 2), a = 9.894(4), b = 11.031(4), c = 12.215(4) Å, α = 101.58(3), β = 110.97(3), γ = 98.02(3)°, Z = 1, $\rho_{calcd.}$ = 1.31 g cm^{-3}, V = 1187(1) Å^3, $Mo_{K\alpha}$ (λ = 0.7107 Å), μ = 12.3 cm^{-1}, $F(000)$ = 486, crystal dimensions 0.2 × 0.15 × 0.1 mm, the structure was solved by heavy atom methods and refined to R = 0.074, R_w = 0.084 for 3200 observed reflections ($I > 2\sigma(I)$) (total unique reflections = 4156), number of parameters = 226, on an Enraf–Nonius CAD4 diffractometer. Max. residual electron density = 1.78(−0.33) e Å^{-3}, programs used: SHELXS-86, MolEN. Further details of the crystal structure investigations are available on request from the Director of the Cambridge Crystallographic Data Center, 12 Union Road, GB-Cambridge CB2 1EZ (UK), on quoting the full journal citation.
[10] R. Appel, V. Barth, F. Knoch, *Chem. Ber.* **1983**, *116*, 938.
[11] K. D. Dobbs, J. E. Boggs, A. H. Cowley, *Chem. Phys. Lett.* **1987**, *141*, 372.
[12] K. van Deuter, D. Rehder, *Cryst. Struct. Commun.* **1980**, *9*, 167.
[13] A. H. Cowley, N. C. Norman, M. Pakulski, D. L. Bricker, D. H. Russell, *J. Am. Chem. Soc.* **1985**, *107*, 8211.
[14] R. West, M. J. Fink, J. Michl, *Science* **1981**, *214*, 1343.
[15] G. Märkl, H. Sejpka, *Angew. Chem.* **1986**, *98*, 286; *Angew. Chem. Int. Ed. Engl.* **1986**, *25*, 264.

 © VCH Verlagsgesellschaft mbH, D-69451 Weinheim, 1995 0570-0833/95/0404-0493 $ 10.00+.25/0

A Wide Spectrum for Analysis

Spectroscopy in Catalysis. An Introduction. By *J. W. Niemantsverdriet*. VCH Verlagsgesellschaft, Weinheim/VCH Publishers, New York, 1993. 288 pp., hardcover DM 148.00, $ 95.00.—ISBN 3-527-28593-8/1-56081-792-5

Heterogeneous catalysis under real conditions is an extremely complicated process, not least due to the complex nature of the catalysts and the structural changes that they undergo as a result of variations in the reacting environment and other external conditions. Ultimately one would like to have experimental methods that could reveal in situ on an atomic scale the chemical processes occurring on catalyst surfaces. As these do not exist, systematic progress in understanding heterogeneous catalysis can only be achieved by the combined use of as many analytical techniques as possible in conjunction with model studies. The latter are important for two reasons. Firstly, they enable one to study systems under well-defined conditions with regard to surface structure, surface composition, and external reaction conditions, so that the dependence on individual variables can be investigated. Secondly, they can be carried out under conditions that are essential for many of the analytical methods; for example, ultra-high vacuum conditions are necessary for all types of electron spectroscopy.



This section contains book reviews and a list of new books received by the editor. Book reviews are written by invitation from the editor. Suggestions for books to be reviewed and for book reviewers are welcome. Publishers should send brochures or (better) books to Dr. Ralf Baumann, Redaktion Angewandte Chemie, Postfach 101161, D-69451 Weinheim, Federal Republic of Germany. The editor reserves the right of selecting which books will be reviewed. Uninvited books not chosen for review will not be returned.

Whereas on the one hand in-situ measurements under real conditions seldom lead to unambiguous conclusions about relationships, model studies on the other hand suffer from the inherent danger of oversimplification and the neglect of "synergistic effects". However, so far there has been no way out of this dilemma (the gap between surface science and catalysis) other than to approach the problem from the two sides simultaneously. With this in mind the book reviewed here makes a particularly useful contribution in describing as wide a range of complementary methods as possible.

The book begins with an introductory chapter outlining the basic features of heterogeneous catalysis, its enormous technological and economic importance, and the scientific problems that it poses. This is followed by seven chapters dealing with the most important methods used to study the physical properties of, and chemical processes occurring at, catalyst surfaces, as follows—Chapter 2: Temperature-programmed surface reaction and desorption techniques; Chapter 3: Photoelectron and Auger electron spectroscopies; Chapter 4: Ion scattering and ion spectroscopy techniques, including mass spectrometry of secondary ions and neutral particles; Chapter 5: Mössbauer spectroscopy; Chapter 6: X-Ray and electron diffraction methods; Chapter 7: Electron microscopy and scanning probe microscopy; Chapter 8: Vibrational spectroscopies with photon and electron excitation. Whereas those methods that depend on particles (electrons, ions, or atoms) for excitation or detection usually require vacuum conditions, the photon techniques can be used in situ. The methods described can provide answers to all the relevant questions, such as those relating to the atomic structure of surfaces, their qualitative and quantitative chemical composition and the distribution of the various surface constituents, the electronic structure of surfaces and adsorbed reacting species, and their vibrational properties as an indication of the nature of the chemical bonding.

The author is a physicist and an active researcher in an institute devoted to catalysis research. Through a good choice of subject matter and the way in which it is presented he makes a valuable contribution to bridging the gap between surface physics and catalyst research. The theoretical fundamentals of the individual methods are treated in a clear and easily understandable way, with just the right amount of detail for an initial assessment of the capabilities and limitations of the techniques for specific applications in catalysis research. Especially useful in this respect are the discussions that have been worked into the text in many places, comparing and evaluating the (mutually complementary) information given by the various methods when applied to a particular problem. Also of special value is Chapter 9, in which three case studies (supported rhodium catalysts, Co/Mo sulfide desulfuration catalysts, and alkali promotors on metal surfaces) are taken as examples, stretching each of the previously described methods to its full capabilities to yield the maximum information about the catalytic system.

The book can be recommended equally for the catalysis scientist, to extend his or her knowledge of the methods, to the surface physicist to stimulate interest in the analytical problems of heterogeneous catalysis, and for the student wishing to specialize in catalysis.

Klaus Wandelt
Institut für Physikalische Chemie
der Universität Bonn (FRG)

Fundamentals of Photoinduced Electron Transfer. By *G. J. Kavarnos*. VCH Verlagsgesellschaft, Weinheim/VCH Publishers, New York, 1993. 359 pp., hardcover DM 105.00, $ 75.00.—ISBN 3-527-27856-1/0-89573-751-5

This volume is intended to serve as an introduction and course book to accompany a lecture series on photochemistry for students of all branches of the natural sciences. Accordingly, special attention has been given to presenting the subject in a suitable form for teaching purposes. The text is divided into six chapters. The first two, "Introductory Concepts" and

 © VCH Verlagsgesellschaft mbH, D-69451 Weinheim, 1995 0570-0833/95/0404-0495 $ 10.00+.25/0

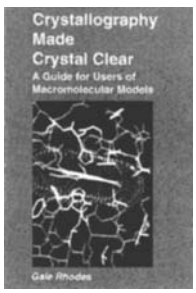
"Properties of Charge-Transfer Intermediates in Photoinduced Electron Transfer", give a general introduction to elementary theoretical models and the variables involved, and a survey of the most important experimental methods for studying electron transfer. The chapters on "Electron-Transfer Photochemistry", "Intramolecular Photoinduced Electron Transfer", and "Photoinduced Electron Transfer in Organized Assemblies and the Solid State" convey a comprehensive picture of the many different types of photoinduced electron transfer processes and the resulting chemical reactions, especially in organic molecules. The systems and reactions in which the initiating step is a photoinduced electron transfer range from isomerizations, cleavage of carbon–carbon bonds and other photochemical transformations, electron transfer processes in micelles, vesicles, and semiconductor surfaces, through to applications in photovoltaic cells and xerography. Lastly Chapter 6, "Theories of Photoinduced Electron Transfer", summarizes the main theoretical approaches to the interpretation and quantitative description of electron transfer rates. Each chapter begins with a useful introduction and ends with an extensive list of references, grouped under subject headings and partly annotated with comments, and a set of exercise problems (without answers).

To summarize the overall impression, the book serves its readers best when describing the many different phenomena, systems, and methods of investigation. Here the numerous figures and tables are a valuable aid to understanding. On the other hand, it is less convincing when dealing with the fundamentals of photoinduced electron transfer. Many of the important concepts involved in the description of these reactions, such as the through-bond and through-space couplings between electron donor and electron acceptor, the reorganization energy, and aspects of the thermodynamics, are treated in a misleading or even incorrect way. One glaring example is the relationship between the electronic coupling H_{el}, the donor–acceptor separation, and the validity of the "Golden Rule" for the rate of electron transfer. On page 308 the dependence of H_{el} on the separation is given as follows: "$H_{el} = H_{el}^0 \exp[-\beta(d - d^0)]$ where β is an orbital parameter, d is the actual separation distance ... Since β is a measure of the ability of an orbital to extend into space and interact with another orbital, the magnitude of interaction between donor and acceptor orbitals is inversely proportional to β." This statement does not make sense. Then, beginning in the second line of page 328: "Importantly, H_{el} is proportional to Δ_t, the distance separating two reactants (as well as their mutual stereoelectronic orientation), and thus by inference is also proportional to the probability that two states couple at a fixed nuclear configuration. The Golden Rule is valid for small Δ_t. If $\Delta_t \gg 0$, the rule breaks down." This is clearly wrong. Lastly, on page 329 we read the following statement about Δ_t: "The horizontal displacement between the minima of these potential energy curves ..." (i.e. the potential energy surfaces for reactants and products as functions of a nuclear coordinate) "... is given by Δ_t." This too is incorrect. Sadly, the list of such inconsistencies could be continued. Thus, the reader who wishes to learn not just about the phenomena but also about the mechanisms—in fact about the "fundamentals of photoinduced electron transfer"—would be better advised to go directly to the secondary literature that is plentifully cited in this book.

Hans Heitele
Institut für Physikalische und
Theoretische Chemie
der Technischen Universität München
Garching (FRG)

Crystallography made Crystal Clear. A Guide for Users of Macromolecular Models. By *G. Rhodes*. Academic Press, New York, 1993. 202 pp., paperback $ 34.95.—ISBN 0-12-587075-2

With the rapid development of molecular biology, and especially of genetic engineering, there is an increasing need for knowledge of the three-dimensional structures of biological macromolecules in full atomic detail. This information is essential in order to understand the mechanisms whereby they function and to achieve controlled biological action by the methods of protein design and drug design. The two methods currently used for structure determination are NMR spectroscopy and X-ray crystallography. NMR spectroscopy has the advantage that one can work with solutions, but difficulties arise with molecular masses above about 20000 u. Crystallography is not subject to this limitation, but suffers from notorious difficulties in obtaining single crystals, and from the necessity to prepare heavy atom derivatives to overcome the "phase problem".



Up to now the molecular biologist or biochemist wishing to learn about protein crystallography has needed to rely either on textbooks of biochemistry or biophysics which typically devote one or two chapters to crystallography, or on textbooks dealing specifically with protein crystallography, which are usually too detailed and contain too much mathematics for easy reading. The book by Gale Rhodes reviewed here exactly fills that gap. In just over 200 pages with many illustrations and without many mathematical formulas, the author explains how a crystal structure analysis is carried out—from the crystallization of the protein through to the final refinement of the structure. The book includes comments on the validity of models and, especially useful in my view, a guide to reading publications on crystallography.

Chapter 1 introduces electron density distributions in protein crystals with the help of colored illustrations and discusses their interpretation in terms of models, so as to kindle the reader's interest in discovering the results of crystallography. Chapter 2 gives a general survey of protein crystallography, and can be regarded as a summary of the chapters that follow. In Chapter 3 the reader learns about the methods used for crystallizing proteins and nucleic acids, and Chapter 4 explains in detail the diffraction of X-rays by the crystal lattice and the recording of the diffraction data using either cameras (film) or modern surface counters. Chapters 5 and 6 explain how the phase angles needed for calculating the electron density distribution in a novel structure are obtained through isomorphic substitution by heavy atoms using Patterson methods, and on the other hand how, in cases where similar related structures are known, the method of "molecular replacement" can be used. The author also describes how the electron density distribution can sometimes be modified (by "solvent flattening"), so as to obtain a significant improvement in signal-to-noise ratio. Chapter 7 is mainly concerned with estimating the quality of a claculated electron distribution, interpreting it in the form of a model displayed on a graphics screen, and refining such a model on the basis of the measured diffraction data. Chapter 8 discusses quality criteria for models, such as Ramanchandran plots, temperature factors, disordered regions in models, and unexpected electron density features which can be attributed to solvent molecules. The chapter ends by analyzing a publication con-

 © VCH Verlagsgesellschaft mbH, D-69451 Weinheim, 1995 0570-0833/95/0404-0496 $ 10.00+.25/0

cerned with a lipid-binding protein, which serves to illustrate and summarize the contents of the preceding seven chapters. Chapter 9 contains an excursion into software for displaying and manipulating molecular models.

The text is written in a fluent style and can be quickly understood even by nonspecialists. The few mathematical formulas included are essential for describing the relationships involved, and the figures are instructive and well chosen. The book entirely fulfills its aim of providing a bridge between molecular biologists and biochemists on the one hand and protein crystallographers on the other, and I recommend it to everyone who is concerned with molecular structures. The brevity of the text and the high standard of presentation ("crystal clear") make this a very suitable book to use as an accompaniment to practical sessions or as an introductory course in protein crystallography.

Wolfram Saenger
Institut für Kristallographie
der Freien Universität Berlin (FRG)

Applications of Mass Spectrometry to Organic Stereochemistry. (Series: Methods in Stereochemical Analysis.) Edited by *J. S. Splitter* and *F. Tureček*. VCH Verlagsgesellschaft, Weinheim/VCH Publishers, New York, 1994. 705 pp., hardcover DM 198.00, $ 125.00.—ISBN 3-527-26525-2/0-89573-303-X

Review articles on mass spectrometric studies of stereoisomeric compounds have appeared at irregular intervals over a period of many years, extending from Meyerson and Weitkamp (1968) through Green (1976, 1978) and Mandelbaum (1977, 1983) up to Tureček (1987). With the publication of this book we now have a comprehensive survey of the field. Twenty well-known authors have contributed articles on 22 topics, covering published work up to 1992. The ability to solve stereochemical problems is certainly not regarded as one of the particular strengths of mass spectrometry, but despite this there exists a surprising wealth of examples where stereochemical differences are clearly reflected in mass spectra. This applies even under the conditions of 70 eV electron impact ionization, which results in the transfer of a large amount of surplus energy, typically 2–10 eV. The likelihood of being able to distinguish between stereoisomers is intrinsically greater if the conversion to the gas phase and the subsequent ionization are carried out under conditions that minimize the excitation of the molecules. This can be achieved by suitable modifications to the instrumental conditions, such as cooling the ion source, the use of low voltage electron impact ionizaion, or substituting more gentle ionization processes such as photoionization, electric field ionization, or chemical ionization.

A short introductory chapter on the techniques of mass spectrometry (author: Falik) is followed by chapters dealing with the structures of ions and the influence of stereochemistry on the mass spectra of acyclic molecules (Splitter). Further chapters discuss the behavior of stereoisomeric cyclic compounds (Eadon, Valente, Tureček, Grützmacher, Vékey, Mandelbaum, Groenewold, Gross). In these compounds the ring structure limits the number of conformers that can exist, and there is then the possibility that this reduced mobility may result in stereospecific rearrangements causing differences in the mass spectra which can be interpreted. Using model compounds as examples, the authors describe in detail the most important types of phenomena, including enthalpy effects, "hidden" stereochemistry, effects of conformational changes, steric effects influencing the accessibility of hydrogen atoms for rearrangements, stabilization of carbocations by neighboring groups, retro-Diels–Alder fragmentations, and examples of the use of field ion kinetics (FIK) and mass-analyzed ion kinetic energy release (MIKE) measurement techniques.

A very informative chapter on the use of chemical ionization (Winkler, Splitter) describes results obtained with *E,Z*-isomeric olefins, and, in greater detail, cyclic compounds. By choosing appropriate reactant gases in the chemical ionization method it is possible to optimize specific fragmentation processes and/or adduct formation for the system under investigation. A separate chapter (Houriet, Tureček) is devoted to the study of stereochemical effects in an ion cyclotron resonance mass spectrometer, a type of instrument uniquely suited for investigating ion–molecule reactions. This technique yields information about the long-term behavior of ions. Next are several chapters on the behavior of stereoisomeric natural products, including terpenes and terpenoids (Enzell, Dahlmann, Bielawski), steroids (Tabet), quinolizidine and indole alkaloids (Tamás) and rotenoids (Kostova, Mollowa). The comprehensive article on the steroids also contains a substantial section on MS–MS "linked-scan" techniques. Other articles report on organometallic compounds (Nekrasov, Zagorewskii), measurements on labeled compounds (Tureček), and the estimation of enthalpies of formation (Splitter).

The material contained in the book is very comprehensive and well presented, although the style varies from one author to another. Often, however, the writers fail to distinguish clearly between textbook-style presentation and the mere cataloguing of facts. For example, the same basic phenomena are described several times over, especially in the early chapters. Few theoretical arguments are put forward to explain the different behavior of stereoisomers, and the structure of the book could have been tightened considerably by consistently separating the discussion of basic principles from the chapters that are more concerned with compound classes, with appropriate cross-references. The lack of sufficient coordination between the chapters is also evident in the dearth of cross-references and the fact that citations of key publications are often repeated.

From the user's point of view one would have preferred the chapter on mass-spectrometric methods to devote more attention to special measurement techniques and their relevance to distinguishing between stereoisomers. Here a critical evaluation of the procedures for determining relative peak heights and the reproducibility of such data with different types of instruments would have been very useful, as also would a discussion of the methods used for distinguishing between stereoisomers. The application of MS–MS techniques using the tandem mass spectrometers that are now becoming more widely available is only touched on briefly.

The book is well produced with a clear typeface, a considerable advantage in a book of this size. It is unfortunate, however, that the publishers have not redrawn the structural formulas, or at least insisted on a uniform style. Their quality varies greatly; often there are no compound numbers, and in some cases the relevant text is far removed from the illustration.

However, these criticisms do not alter the verdict that the comprehensiveness of the book and the overall high quality of presentation will ensure that it becomes a standard work in this field. It can therefore be recommended to all mass spectroscopists involved in the analysis of organic compounds, and to everyone else who wishes to learn about the capabilities of mass spectrometry for analyzing stereoisomeric compounds.

Heinrich Luftmann
Organisch-chemisches Institut
der Universität Münster (FRG)

 © VCH Verlagsgesellschaft mbH, D-69451 Weinheim, 1995 0570-0833/95/0404-0497 $ 10.00+.25/0

Covalent Inorganic Azides

Inis C. Tornieporth-Oetting* and Thomas M. Klapötke*

The chemistry of covalent inorganic azides originated with the synthesis of aqueous HN_3 solutions by Tony Curtis in 1890. A little later, in 1900, it proved possible to prepare iodine azide, IN_3, as the first member of the meanwhile complete series of halogen azides. Since then it has been possible to synthesize, in addition to HN_3 and the stable salt $H_2N_3^+SbF_6^-$, azide compounds of elements from Groups 13 to 17. In these compounds the N_3 moiety acts as a pseudohalogen and is primarily covalently coordinated to the nonmetal. Only a few organic azides, however, as well as HN_3, $H_2N_3^+$, and all halogen azides have been thoroughly studied with respect to structure and bonding. The combined application of diffraction methods (X-ray and electron diffraction) and microwave spectroscopy together with quantum chemical approaches such as ab initio SCF and density functional calculations have led in the last few years to an improved understanding of the molecular properties of numerous nonmetal azides, almost all of which are explosive. This interaction of theory and experiment has greatly enhanced the development of azide chemistry and has led to realistic expectations for the synthesis of as yet unknown nonmetal azides.

Keywords: ab initio calculations · azides · nitrogen compounds

1. Introduction

Covalent azides have been known for more than 100 years.[1] Table 1 contains a—by no means complete—list of main group azides in which the N_3 group acts as a pseudohalogen and is primarily covalently bound to the corresponding nonmetal. Until now, however, only very few of these compounds could be definitively structurally characterized. Examples include HN_3,[2] $H_2N_3^+$,[3] CF_3N_3,[4] $Te(N_3)_3^+$,[5] XN_3 (X = F,[6] Cl,[7] Br,[8] I[9, 10]), and $I(N_3)_2^-$.[11] If one considers the N_3 fragment as a pseudohalogen (absolute electronegativity according to Mulliken: Cl 8.3, Br 7.5, N_3 7.7 eV),[7b, 12] the hydrogen compound HN_3 and the pseudohalogen–halogen compounds XN_3 (X = F, Cl, Br, I) are the simplest members of this class of substances. This simplicity, combined with the strong tendency to detonate and the, in some cases, considerable toxicity, presents a significant challenge to the experimental chemist.[13] In this article, we wish to illuminate the interaction of experimental, preparative, structural, and theoretical studies in this area of chemistry, using examples of hydrogen and halogen azides with structures that, in most cases, have been definitively determined only over the last five years.[14, 15] Afterwards, the structure and bonding of species related to halogen azides, namely $I_2N_3^+$,[16] $I(N_3)_2^+$,[17] ONN_3,[18] and O_2NN_3,[19] will be discussed, and an outlook for future preparative studies in this field will be given.

[*] Dr. I. C. Tornieporth-Oetting
Institut für Anorganische und Analytische Chemie der Technischen Universität
Strasse des 17. Juni 135, D-10623 Berlin (Germany)
Telefax: Int. code + (30)314-26468
Prof. Dr. T. M. Klapötke
Chemistry Department, University of Glasgow
Glasgow G12 8QQ (UK)
Telefax: Int. code +(41)330 4888

2. Synthesis and Spectroscopic Properties

2.1. Synthesis

Covalent azides are highly explosive, especially in pure form. It is therefore imperative that work on a preparative scale is performed under appropriate safety precautions, such as face shields, protective leather clothing, gloves, and ear protection. Experiments should also be performed on as small a scale as feasible. As an example, the explosive decomposition of less than a gram of bromine azide kept in a glass flask which in turn was placed inside a metal-shielded glass Dewar, led to the complete pulverization of the glass and tearing of the metal shielding.[10, 30] All halogen azides are very sensitive in this respect. Chlorine azide and bromine azide are particularly sensitive to small pressure variations and regularly explode when $\Delta p \geq 0.05$ Torr.[8] Characteristic detonation data for some halogen azides and nitrosyl azide, N_4O, have been reported (Table 2).[10] These compounds are potentially better explosives than lead azide (see Table 2), which is used as a detonator. However, they are by far not kinetically stable enough to find use as detonators.[31–33]

Phosphorus nitrile azide, $[PN(N_3)_2]_3$, which can be isolated in pure form, is one of the most nitrogen-rich inorganic compounds (see Table 1).[22] This material is also very shock-sensitive in the solid state and detonates when mechanically stressed and upon exposure to an electric discharge. According to the results of ab initio calculations, the compound possesses approximate C_3 symmetry (Fig. 1),[32] its structure, however, has not yet been experimentally determined by diffraction methods. While the nitrogen-rich cation $As(N_3)_4^+$ is "stable" in SO_2

 © VCH Verlagsgesellschaft mbH, D-69451 Weinheim, 1995 0570-0833/95/0505-0511 $ 10.00+.25/0

Table 1. Selected covalent nonmetal azides and azide ions (the compounds marked by an asterisk have been structurally characterized).

Group 1	Group 13 [1]	Group 14 [1, 13]		Group 15 [1]			Group 16	Group 17 [10, 16, 17]
HN_3* [2]	$B(N_3)_3$	CF_3N_3* [4a]	H_3SiN_3*	Me_2NN_3 [20a, b]	$P(N_3)_5$ [24]	$Me_3P(N_3)^+$ [23]	$SO_2(N_3)_2$ [1]	FN_3*
$H_2N_3^+$* [3]	$B(N_3)_4^-$	$FC(O)N_3^*$ [4b]	$Si(N_3)_4$	ONN_3 [18] [c]	$OP(N_3)_3$ [24, 25]	$Me_2P(N_3)_2^+$ [23]	$MeSO_2N_3$ [1]	ClN_3*
	Ph_2BN_3	$C(N_3)^+{}_3$	Me_3SiN_3	O_2NN_3 [19] [c]	$O_2P(N_3)_2^-$ [25]	$MeP(N_3)_3^+$ [23]	$Te(N_3)_3^+$* [5]	BrN_3*
	$Ga(N_3)_3$	NCN_3* [21]	$PhSi(N_3)_3$	$(Me_3Si)_2NN_3$	$PX_{3-n}(N_3)_n$,	R_2AsN_3 [d], [27a]		IN_3*
		$(N_3CN)_3$*	$R'SnN_3$ [b]	$(FSO_2)_2NN_3$ [20c]	$n = 1,2$; X = Cl, Br	$RAs(N_3)_2$ [d], [27a]		$I_2N_3^+$
		$OC(N_3)_2$ [1d–g, 13]	$[Sn(N_3)_6]^{2-}$	$[PN(N_3)_2]_3$ [22]	$PCl_{6-n}(N_3)_n^-$,	$CF_3As(N_3)_2$ [27b]		$I(N_3)_2^+$
		$(CNN_3)_2$		$(CF_3)_2PN_3$	$n = 1$–6 [26]	$As(N_3)_4^+$ [e] [28]		$I(N_3)_2^-$*
		RN_3 [a]*		$P(N_3)_3$ [23]				
				$P(N_3)_4^+$ [23]				

[a] R = Me, Et, *i*Pr, *t*Bu, $CH_2{=}CH$, C_2H_4Cl, $CH_2{=}CHCH_2$, $NCCH_2$, F_2CH, CF_3. [b] R′ = nBu, 2,4,6-$(NO_2)_3C_6H_2$. [c] Cf. ref. [29]. [d] R = Me, Et, Ph. [e] AsF_6^- as counterion.

Table 2. Characteristic detonation data for IN_3, BrN_3, N_4O, and $Pb(N_3)_2$ [10].

	IN_3 (s)	BrN_3 (l)	N_4O (g)	$Pb(N_3)_2$ (s)
ΔH explosion [kcal kg^{-1}]	−571	−805	−1528	−367
standard gas volume [L kg^{-1}]	265	367	778	308
detonation temperature T_{ex} [K] [a]	6000	6000	4300	6000
moles of gas per kg (n)	11.8	16.4	34.7	13.7
specific energy f [m t kg^{-1}] [b]	60	83	177	50
lead block expansion per 10 g [cm^3]	140	230	>600	110
ΔH_f^0 [kcal mol^{-1}]	104 (s)	102 (l)	110 (g)	101 (s)

[a] T_{ex} estimated for the isochoric process [33]. [b] $f = nRT_{ex}$ ($R = 8.478 \times 10^{-4}$ m t K^{-1} mol^{-1}; 1 m t = 1000 kp m = 2.3423 kcal) [33].

solutions and has been characterized by multinuclear NMR (^{14}N, ^{75}As) and Raman spectroscopy, the compound $[As(N_3)_4]AsF_6$ is very explosive in the solid state.[28]

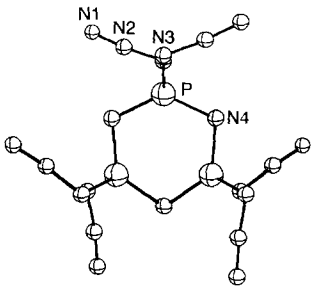


Fig. 1. Calculated molecular structure of $[PN(N_3)_2]_3$ (ab initio methods, RHF/6-31 + G*); d(N1–N2) = 1.16, d(N2–N3) = 1.32, d(N3–P) = 1.79, d(P-N4) = 1.73 Å.

Hydrazoic acid and many of its covalent inorganic (e.g., ClN_3, Me_3SiN_3) and organic derivatives (e.g., CH_3N_3) are also very toxic. HN_3 is as poisonous as hydrogen cyanide.[1a]

In spite of these difficulties (or maybe even because of them), several research groups did early work on the synthesis of hydrazoic acid,[34] its organic derivatives,[13, 35] and halogen azides.[14, 36] Even though HN_3 can be prepared by the action of dilute sulfuric acid on sodium azide or the reaction of nitrous acid and hydrazine, it is most readily synthesized on the preparative scale by the reaction of stearic acid with sodium azide at 100–130 °C in the melt [Eq. (a)].[3] The preparation of the halogen azides is best done according to the Equations (b)–(e).[14] We recently discovered an easy access to chlorine azide in a

$$CH_3(CH_2)_{16}COOH + NaN_3 \xrightarrow{\text{melt, } 110\text{–}130\,^\circ C} CH_3(CH_2)_{16}COONa + HN_3 \quad \text{(a)}$$

$$4\,HN_3 + 2\,F_2 \xrightarrow{\text{gas phase}} 3\,FN_3 + N_2 + NH_4F \quad \text{(b)}$$

$$NaN_3 + Cl_2 \xrightarrow{0\,^\circ C,\ H_2O} ClN_3 + NaCl \quad \text{(c)}$$

$$NaN_3 + Br_2 \xrightarrow{20\,^\circ C/0\,^\circ C,\ \text{pure}} BrN_3 + NaBr \quad \text{(d)}$$

$$AgN_3 + I_2 \xrightarrow{CFCl_3,\ 0\,^\circ C} IN_3 + AgI \quad \text{(e)}$$

Inis C. Tornieporth-Oetting was born on March 19, 1963 in Hamburg, Germany. She studied at the Universität Oldenburg and at the Technische Universität (TU) Berlin, where she also received her doctorate degree in 1992, working under the supervision of Thomas M. Klapötke. She is currently employed as a senior scientist at the TU Berlin. She is the author of more than forty publications and two chapters of books, and together with Klapötke is the coauthor of a textbook on nonmetal chemistry. Her research interests in the area of nitrogen chemistry stretch from the purely inorganic halogen chemistry of this element, including its fluorine chemistry, to the coordination chemistry of organic amino compounds and the study of biologically relevant amino acid model complexes.

Thomas M. Klapötke was born on February 24, 1961 in Göttingen, Germany. He studied at the Technische Universität Berlin and received his doctorate degree there in 1986, working under the supervision of Hartmut Köpf. After postdoctoral work with Jack Passmore at the University of New Brunswick, he completed his habilitation in 1990 at the TU Berlin. In 1995 he was appointed to the Ramsay Chair of Chemistry at the University of Glasgow. He is the holder of the Karl-Winnacker-Stipendium (1994) and has been awarded, amongst others, the Schering-Preis (1987) and the Maier-Leibnitz-Preis (1994). Furthermore, he is the author of more than 120 publications, six chapters of books, and with Tornieporth-Oetting is the coauthor of a textbook on nonmetal chemistry. His research interests encompass the preparative synthesis of unstable nonmetal compounds in the areas of nitrogen–halogen and nitrogen–chalcogen chemistry, including the chemistry of elemental fluorine, as well as the theoretical characterization of the bonding in these compounds.

solvent-free system by the reaction of trimethylsilyl azide and nitryl chloride [Eq. (f)]. After fractional condensation, it was possible to isolate pure liquid ClN_3.[19]

$$3\,Me_3SiN_3 + 3\,ClNO_2 \xrightarrow{-20\,^\circ C} 2\,ClN_3 + Me_3SiCl + Me_3SiOSiMe_3 + 2\,N_2O + N_2O_3 \quad (f)$$

2.2. ^{14}N NMR Spectroscopy

One of the most suitable methods for the characterization of covalent azides in solution is ^{14}N NMR spectroscopy, which has proven to be an invaluable tool for the study of small nitrogen-containing molecules.[37] In addition, during the last few years it was demonstrated that ^{14}N NMR spectroscopy could not only be utilized for the elucidation of structures in solution, but also for the determination of equilibrium constants and thermodynamic parameters.[38, 39] For many covalent azides, such as the halogen azides XN_3 (X = Cl, Br, I), covalent phosphorus and arsenic azides, as well as covalent azide ions such as $As(N_3)_4^+$, the ^{14}N NMR spectra show three well-resolved resonances, which have been assigned to the chemically inequivalent nitrogen atoms.[40–42, 79] Presumably owing to the large quadrupole moment of the nitrogen nucleus, there were no observable $^{14}N-^{14}N$ couplings. This is not surprising when considering the very small coupling constant, estimated at about 30 Hz. Using variable temperature and variable concentration ^{14}N NMR studies it was possible to demonstrate that iodine azide, which is monomeric in the gas phase but polymeric in the crystalline state, as well as alkylarsenic(III) azides, which are oligomeric as pure liquids, dissolve in $CDCl_3$ to give monomolecular solvates. In the temperature and concentration ranges studied, no azide exchange between the arsenic or iodine centers, respectively, was found. Figure 2 shows the ^{14}N NMR spectrum of Me_2AsN_3 as an example; the resonances were assigned according to the numbering shown in Figure 4.

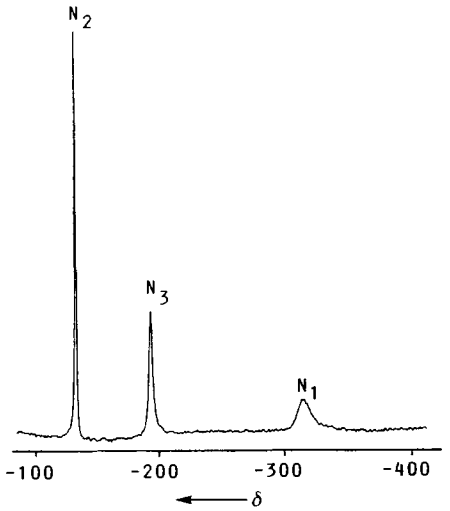


Fig. 2. ^{14}N NMR spectrum of Me_2AsN_3 (28.904 MHz, 1 mol L^{-1}, relative to $MeNO_2$, 22 °C, $CDCl_3$) [42].

3. Stability and Thermodynamics

Ab initio calculations have been used increasingly in recent years to extract bond energies and thermodynamic stabilities of covalent azides from calculated total energies.[18, 43] These data are, for obvious reasons, difficult to obtain experimentally.

The dissociation energies for HN_3 and the halogen azides have been calculated and appropriately corrected to yield dissociation enthalpies at room temperature ΔH [Eq. (g), X = H, F, Cl, Br, I; see also Table 3).[43, 44]

$$XN_3 \longrightarrow N_3 + X + \Delta H_g \quad (g)$$

Reaction (g) is strongly endothermic in all cases and the value calculated for HN_3 agrees well with the experimentally obtained data (85 kcal mol^{-1}).[45] According to Table 3, the $X-N_3$ bond

Table 3. Calculated reaction enthalpies ΔH [kcal mol^{-1}] and calculated standard enthalpies of formation ΔH_f^0 [kcal mol^{-1}] for the reactions (g)–(i) (MP2/6-31 G**) [43].

	ΔH_g	ΔH_h	ΔH_i	ΔH_f^0 (XN_3)
HN_3	96.9	14.9	−144.2	72.1
FN_3	57.8	−25.1	−164.4	82.2
ClN_3	48.5	−11.9	−185.6	92.8
BrN_3	46.9	−3.5	−193.2	102.1
IN_3	45.8	6.5	−191.4	103.6

energy decreases in the order H ≫ F > Cl > Br > I. This result should not be misinterpreted with respect to the stability of the halogen azides, however, since the thermal decomposition of XN_3 is not initiated by the breaking of the $X-N_3$ bond (X = H, F, Cl, Br, I), but, at least in the gas phase, by dissociation into $XN(^3\Sigma^-)$ and $N_2(^1\Sigma_g^+)$ [Eq. (h)]. The decomposition of solid

$$XN_3(^1A') \longrightarrow N_2(^1\Sigma_g^+) + XN(^3\Sigma^-) + \Delta H_h \quad (h)$$

IN_3 is much more complicated and not yet completely understood. Even though the gas phase decomposition reaction according to Equation (h) is spin-forbidden, pyrolysis experiments on HN_3 in the temperature range 285–470 °C have clearly shown that this species fragments into HN and N_2.[46] (See reference [13] regarding the gas phase pyrolysis of $NC-N_3$ and organic azides.) The occurrence of this singlet–triplet coupling during the HN_3 fragmentation has been the subject of extensive quantum chemical calculations at a very high level.[47]

The calculated values for ΔH_h (Table 3) of the halogen azides indicate that, in the gas phase, FN_3 should be least stable and IN_3 most stable. This is in agreement with experimental observations. In addition, the calculated dissociation enthalpy ΔH_h for HN_3 (Table 3) is in very good agreement with the experimental values of 15.0 kcal mol^{-1} [48] and 17.5 kcal mol^{-1}.[49] The dissociation according to Equation (h) is exothermic for FN_3, ClN_3, and BrN_3, and mildly endothermic for IN_3. However, the reaction enthalpies at room temperature ΔH_i, calculated for Equation (i), indicate that all halogen azides possess a large

$$2\,XN_3 \longrightarrow 3\,N_2 + X_2 + \Delta H_i \quad (i)$$

positive enthalpy of formation (Table 3). These two sets of data readily explain the extreme instability of all halogen azides on the one hand, and the slight, but clearly apparent kinetic stability of IN_3 on the other.[14] As was only recently shown experimentally, the dissociation barrier (to XN and N_2) is indeed larger for chlorine azide than for fluorine azide.[50]

The thermodynamic stability of the very labile *N*-oxides ON–N_3 (nitrosyl azide) and O_2N–N_3 (nitryl azide) [Eq. (j) and (k), respectively] has also been the subject of ab initio studies. The dissociation of N_4O into N_2O and N_2 was predicted to be very exothermic ($\Delta H_j^0 = -91$ kcal mol^{-1}).[18] N_4O_2, which so far has only been detected in solutions, also dissociates into the thermodynamically more stable N_2O ($\Delta H_k^0 = -57$ kcal mol^{-1}).[19]

$$ON-N_3 \longrightarrow N_2O + N_2 \quad (j)$$

$$O_2N-N_3 \longrightarrow 2\,N_2O \quad (k)$$

Experimentally it is possible to stabilize halogen azides, particularly iodine azide, through the formation of species that are more highly coordinated. The reaction of IN_3 with numerous nitrogen bases such as pyridine and α,α'-bipyridyl leads to the formation of stable donor–acceptor complexes, in which the nitrogen base is coordinated to the positively polarized iodine atom of IN_3.[51] This distinct polarization of the N–I bond also causes IN_3 to act as a Lewis acid towards halogenide or pseudohalogenide ions. IN_3 reacts with $NMe_4^+N_3^-$ to give the extremely explosive compound $NMe_4^+I(N_3)_2^-$.[52] The analogous species $PPh_4^+I(N_3)_2^-$, however, is not explosive.[52] Interestingly, in addition to the $I(N_3)_2^-$ anion, which, according to the pseudohalogen concept, corresponds to ICl_2^-, the ICl_2^+ analogue, namely the $I(N_3)_2^+$ cation has recently been prepared (see Section 4).[17]

Tetraazidoarsoniumhexafluoroarsenate, $As(N_3)_4^+AsF_6^-$, which can be handled well in SO_2 solutions, is very sensitive in the solid state and detonates upon exposure to mechanical stress or a high frequency discharge. Using a Born–Haber cycle, the reaction enthalpy of the decomposition according to Equation (l) was estimated to be $\Delta H_l = -406$ kcal mol^{-1}.[28]

$$[As(N_3)_4]AsF_6(s) \xrightarrow{\Delta H = -406\ \text{kcal mol}^{-1}} 2\,AsF_3(l) + 6\,N_2(g) \quad (l)$$

4. Structure and Bonding

In contrast to the ionic azides of the type $A^+N_3^-$ (A = metal, NH_4),[1a–i, 53] which all contain a linear N_3 unit of $D_{\infty h}$ symmetry, covalent azides present as discrete XN_3 species in the gas phase (X = H, halogen, etc.) display a bent *trans* C_s configuration with a N-N-N bond angle of approximately $172 \pm 3°$, and two significantly different N–N bond lengths (Fig. 3).[14]

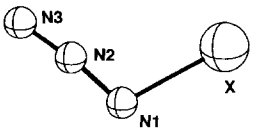


Fig. 3. Depiction of a covalent XN_3 azide in the bent *trans* C_s conformation.

Table 4 contains a summary of experimentally obtained and quantum mechanically calculated structural parameters for XN_3 azides. They show clearly the excellent agreement between the experimental data and those that were quantum mechanically calculated. It was necessary, however, to account for electron correlation (e.g., according to Møller-Plesset)[44] in order to obtain good correlation between the theoretical results and the experimental findings.[14] In addition, it proved to be very helpful to introduce quasirelativistic pseudopotentials for the heavy halogens bromine and iodine to account for relativistic effects. For instance, calculations utilizing an effective core potential often led to better results in less time than all-electron calculations.[54, 55]

What additional information can be gleaned from these MO calculations? The bent N_3 unit in covalent XN_3 azides and the different N–N bond lengths are particularly noteworthy. One of these bonds (N1–N2) is significantly shorter than a typical N–N single bond (1.44 Å), while the other (N2–N3) is slightly longer than the N≡N triple bond in N_2 (1.098 Å).[56] A localized orbital description[57] of the covalent XN_3 azides (X = H, F, Cl, Br, I, NO, NO_2) results in an NBO (natural bond orbital) analysis[57] that yields the configuration shown in Figure 4 as the energetically most favorable Lewis structure. According to this, there is a single bond between N1 and N2 and a triple bond between N2 and N3.

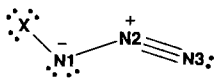


Fig. 4. Lewis structure of covalent XN_3 azides (NBO analysis).

The total energy $E = E(\text{Lewis}) + E(\text{non-Lewis})$ deviates in general only very little from E(Lewis) (most often E(non-Lewis) $< 1\%$ E(Lewis)). Therefore NBOs are well suited to describe the covalent effects in a molecule in accordance with its

Table 4. Structural parameters of covalent XN_3 azides (for atom numbering scheme see Fig. 3): experimental and ab initio data [10, 14, 43].

Compound	Experimental method [a]	Ab initio calculation	d(X-N1) [Å] exp./ab initio	d(N1–N2) [Å] exp./ab initio	d(N2–N3) [Å] exp./ab initio	∢(N1, N2, N3) [°] exp./ab initio	∢(X, N1, N2) [°] exp./ab initio
HN_3 [2]	MW (g)	[d]	1.015/1.018	1.243/1.250	1.134/1.158	171.3/171.2	108.8/109.7
FN_3 [6]	MW (g)	[d]	1.444/1.431	1.253/1.280	1.132/1.152	170.9/171.7	103.8/103.8
ClN_3 [7]	MW (g)	[d]	1.745/1.753	1.252/1.265	1.133/1.157	171.9/171.3	108.6/109.3
BrN_3 [8]	ED (g)	[d]	1.90/1.923	1.23/1.262	1.13/1.160	171/171.4	110/108.5
IN_3 [9, 10]	ED (g)	[d]	2.120/2.133	1.260/1.258	1.147/1.167	169.6/171.4	106.6/110.2
	X(s) [b]		2.30/–	1.28/–	1.09/–	174/–	114/–
$I(N_3)_2^+$ [17]	[c]	[e]	–/2.058	–/1.290	–/1.156	–/169.2	–/111.6
ONN_3 [18]	[c]	[e]	–/1.484	–/1.270	–/1.154	–/174.3	–/107.1
O_2NN_3 [19]	[c]	[e]	–/1.462	–/1.274	–/1.151	–/172.7	–/108.0

[a] MW: microwave data; ED: electron diffraction; X: X-ray diffraction. [b] The structure of solid, polymeric $(IN_3)_x$ has so far not been calculated. [c] No experimental structure data is known to date. [d] MP2/LANL1DZ + P. [e] MP2/6-31 + G*, iodine: ECP, basis set: [5s5p1d]/(3s3p1d)-(DZ + P).

"natural" Lewis structure. It is best to allow for the non-covalent effects which are ignored in the Lewis structure by a second-order perturbation calculation. The most important non-covalent contributions in the XN_3 system are the π-delocalization over the entire molecule (resonance) on the one hand and a strong intramolecular donor–acceptor interaction on the other. This interaction leads to the transfer of electron density from the filled (X–N1)-σ orbital into the unfilled, antibonding (N2–N3)-π^* orbital, which weakens the X–N1 and N2–N3 bonds, while it strengthens the N1–N2 bond. Table 5 lists linear NLMO (natural localized molecular orbital) bond orders for some XN_3 azides, which were obtained by allowing for noncovalent effects in the NBO analysis.[58] In addition, it is noteworthy that the total bond order (ΣBO) at the central N atom of the N_3 moiety is significantly greater than three in all cases.

Table 5. Linear NLMO bond orders (BO) and overall bond orders (ΣBO) in discrete covalent XN_3 azides (NBO analysis) [a].

	BO (X-N1)	BO (N1-N2)	BO (N2-N3)	ΣBO (N1)	ΣBO(N2)	ΣBO (N3)
HN_3	0.60	1.11	2.41	1.43	3.54	2.11
FN_3	0.67	1.06	2.30	1.52	3.34	2.08
ClN_3	0.90	1.09	2.38	1.76	3.47	2.12
BrN_3	0.79	1.10	2.38	1.65	3.50	2.10
IN_3	0.67	1.12	2.39	1.65	3.50	2.10
ONN_3	0.99	0.99	2.52	1.70	3.54	2.29
O_2NN_3	0.92	0.97	2.50	1.56	3.48	2.30
$I(N_3)_2^+$	0.80	0.98	2.45	1.57	3.47	2.20

[a] HF/6-31 + G*, for Cl, Br, I: ECP, basis set: [5s5p1d]/(3s3p1d) – (DZ + P) [59].

Among the halogen azides ClN_3 has by far the highest X–N1 bond order of 0.90 (Table 5). This is in agreement with the pseudohalogen concept, according to which the azide group has an electronegativity comparable to chlorine, which implies that the pseudohalogen-halogen compound ClN_3 is best compared to Cl_2.[7b] The fact that the stretching frequencies for both compounds are similar ($\tilde{\nu}$(Cl–Cl) = 546, $\tilde{\nu}$(Cl–N_3) = 542 cm^{-1})[7b] is also in agreement with the pseudohalogen theory. The rather high bond orders in the ON–N_3 and O_2N–N_3 bonds in the covalent nitrosyl and nitryl azides are also noteworthy,[18, 19, 29] and in order to take the covalent character of these compounds into account, it might be more useful to term them "tetranitrogen oxide" or "tetranitrogen dioxide".

A comparison of the linear X–N1 bond orders (Table 5) clearly shows the expected weak covalent bonds in the strongly polarized species HN_3, FN_3, and IN_3. A summary of calculated NPA (natural population analysis) charges is given in Table 6.

Table 6. NPA charges δ in covalent XN_3 azides [a].

	N1	N2	N3	X
HN_3	−0.67	+0.30	−0.03	+0.40
FN_3	−0.03	+0.23	+0.09	−0.29
ClN_3	−0.45	+0.29	+0.05	+0.12
BrN_3	−0.54	+0.29	+0.03	+0.21
IN_3	−0.62	+0.29	−0.00	+0.34
ONN_3 [b]	−0.35	+0.29	+0.12	+0.29
O_2NN_3 [c]	−0.32	+0.29	−0.17	+0.76
$I(N_3)_2^+$	−0.66	+0.26	+0.22	+1.37

[a] HF/6-31 + G*, for Cl, Br, I: ECP, basis set: [5s5p1d]/(3s3p1d) – (DZ + P) [59]. [b] δ at O = −0.34. [c] δ = −0.40 (at O_{trans}), −0.49 (at O_{cis}); *cis*/*trans* relative to the terminal N atom.

The experimentally observable weakness of the I–N bond in IN_3 [14, 36] and in inorganic N–I species in general[60] has been ascribed in early, more qualitative discussions to the strong polarity of this bond. The theoretical findings presented here confirm this view from a quantum mechanical basis.

The crystal structure analysis of IN_3 gave a surprising result that is so far unique among the halogen azides. Solid iodine azide is polymeric and present in the form of zigzag chains, with iodine atoms that are doubly coordinated in a linear fashion (Fig. 5).[9] It was also possible to synthesize the doubly coordinated ions $I(N_3)_2^+$[17] and $I(N_3)_2^-$[52] on a preparative scale. In agreement with the VSEPR theory, the coordination mode at the central iodine atom is bent (cation) and linear (anion, which is isoelectronic to the hypothetical $Xe(N_3)_2$), respectively.[61] It is noteworthy that the linear bond order of the I–N bond increases significantly from 0.67 for discrete IN_3 to 0.80 for the $I(N_3)_2^+$ cation (Table 5). Apparently iodine in binary N–I species favors higher coordination numbers, and forms more covalent N–I bonds. The structures of binary bromine–nitrogen compounds are unexplored with the exception of gaseous BrN_3.[8] The determination of the structure of solid bromine azide will be a substantial future challenge.

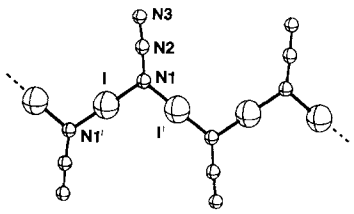


Fig. 5. Polymeric structure of iodine azide in the crystal (for structural parameters see Table 4) [9].

A comparison of the structures of the formally analogous cations $H_2N_3^+$[3] and $I_2N_3^+$[16] (Fig. 6) shows that according to

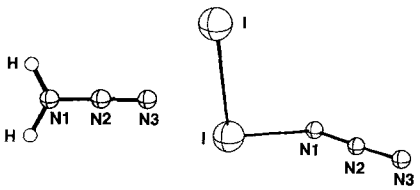


Fig. 6. Structures of the cations $H_2N_3^+$ (left, C_{2v}) and $I_2N_3^+$ (C_s).

the results of an X-ray crystal structure analysis, $H_2N_3^+$ displays C_{2v} symmetry in the crystal (SbF_6^- salt), while the $I_2N_3^+$ cation (in $I_2N_3^+EF_6^-$, E = As, Sb) has a chainlike planar C_s structure, as determined by Raman spectroscopy. This latter result is in agreement with ab inito calculations for which electron correlation was taken into account, which indicated that this C_s structure is only 2 kcal mol^{-1} lower in energy than the C_{2v} conformation, which was not observed experimentally. The two different structures for $H_2N_3^+$ and $I_2N_3^+$ are in accordance with the pseudohalogen concept, in which HN_3 is analogous to HCl, while IN_3 is more closely related to ICl. A comparison of the known structures of H_2Cl^+ (C_{2v}) and I_2Cl^+ (C_s) supports the analogy between $I_2N_3^+$ and I_2Cl^+. In both cases, like in all interhalogen species, the larger halogen occupies the central position.[62]

The structures discussed for the ions $I(N_3)_2^+$[17] and $I(N_3)_2^-$[52] also correspond with those expected by pseudo-

halogen theory and VSEPR theory:[61] $I(N_3)_2^+$ as AX_2E_2 type, bent at the central iodine; $I(N_3)_2^-$ as AX_2E_3 type, with linear coordination at the central iodine (Fig. 7).

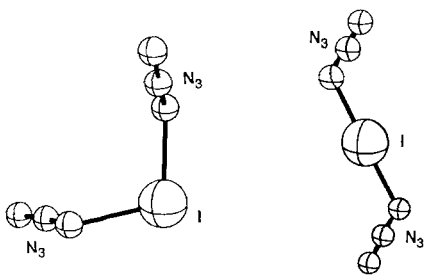


Fig. 7. Structures of the ions $I(N_3)_2^+$ (C_2) and $I(N_3)_2^-$ (C_2).

Even though the chemistry of the N_3 group can frequently be explained by using the pseudohalogen concept, it has not been possible to date to observe the species analogous to Cl_2, namely N_3-N_3. It is likely, however, that such a molecule would be in no way kinetically stabilized. High level quantum mechanical calculations have indicated that the most stable N_6 isomer should possess a twisted chainlike C_2 structure, which lies 188 kcal mol^{-1} above the energy of three N_2 molecules.[63] In contrast to benzene, cyclic hexazine, N_6, should assume a nonplanar twist-boat structure (D_2), which lies 26 kcal mol^{-1} above the energy of the C_2 chain structure.[63]

Suitable correlations of experimental and quantum mechanical molecular data together with calculations of energy hypersurfaces make it possible to estimate the structures of short-lived molecules that cannot be isolated on the preparative scale.[64] Every defined molecular state possesses a certain structure, and changes in its energy or charge distribution cause structural changes that occur through the molecule's specific molecular dynamics. The decomposition of the unstable nitrosyl azide, N_4O, will be used as an example.

N_4O was shown, on the basis of Raman spectroscopy, to have an open-chain C_s structure with a *trans-trans* arrangement at N1–N4 and N1–N2 (Fig. 8, left).[18] This compound has therefore two possible modes of unimolecular decay.[65] On the one hand, rotation around the N1–N4 axis can lead to the *cis-cis* isomer (Figs. 8 right, and 9), which then decomposes, according to the hypersurface shown in Figure 10, via cyclic N_4O into N_2O and N_2. On the other hand, the *trans-trans* isomer can also fragment directly by a change in the N1–N2 distance (Fig. 11). The rotation into the *cis-cis* isomer, however, has a calculated

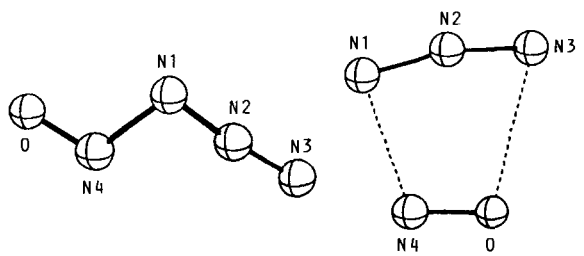


Fig. 8. Structures of nitrosyl azide, N_4O, in the *trans-trans* and *cis-cis* configurations, optimized at the MP2 level.

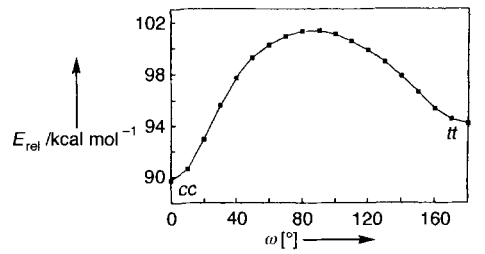


Fig. 9. Rotational barrier for the *cis-cis*/*trans-trans* isomerization of N_4O, calculated at the MP2 level. ω = O-N4-N1-N2 dihedral angle.

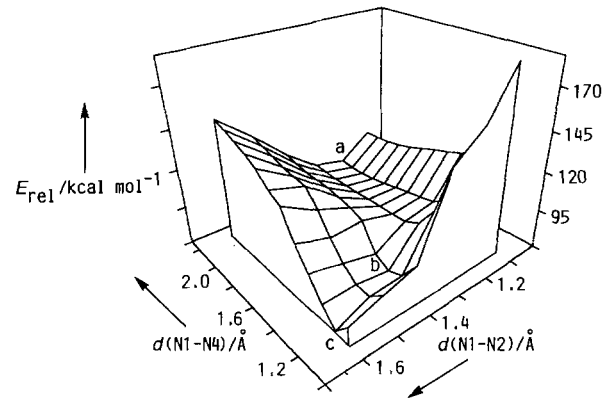


Fig. 10. Two-dimensional MP2 energy hypersurface for the decomposition of *cis-cis* N_4O; a: *cis-cis* N_4O, b: cyclic N_4O (C_{2v}), c: N_2O ($C_{\infty v}$) + N_2.

barrier of 7 kcal mol^{-1} (Fig. 9), while the transition state for the N1–N2 variation lies 24 kcal mol^{-1} in energy above the *trans-trans* isomer. This indicates that a unimolecular fragmentation into N_2O and N_2 is more likely to occur via *cis-cis* N_4O and cyclic N_4O. The calculated potential energy curve for the decomposition without the rotation (Fig. 11) shows that *trans-trans* N_4O does not lead to linear N_2O ($C_{\infty v}$), but rather to cyclic N_2O (C_{2v}). The hypersurface depicted in Figure 11 shows three minima: *trans-trans* N_4O, $C_{\infty v}$-N_2O + N_2, and C_{2v}-N_2O + N_2. Hence *trans-trans* N_4O can decompose not only by the pathway initiated by the rotation into the *cis-cis* isomer, but also by two additional pathways. Interestingly the transition

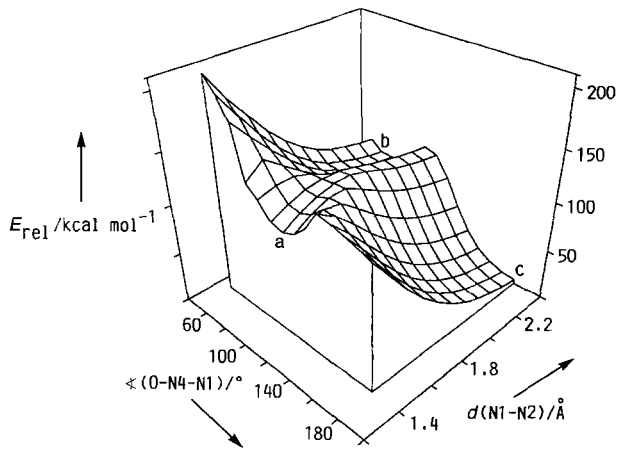


Fig. 11. Two-dimensional MP2 energy hypersurface for the decomposition of *trans-trans* N_4O; a: *trans-trans* N_4O, b: cyclic N_4O (C_{2v}) + N_2, c: N_2O ($C_{\infty v}$) + N_2.

state leading to cyclic N_2O (C_{2v}) is 2 kcal mol^{-1} lower in energy than that for the direct conversion into linear N_2O ($C_{\infty v}$) and N_2. (Quite recently the unimolecular decay of N_4O has been studied on the basis of qualitative increased valence bond representations[65b]).

At this point it appears appropriate to mention the results of pyrolysis experiments with azides in the gas phase.[13] These studies demonstrated that experimental investigations of reactive intermediates are not only of interest for the discovery of new compounds and the development of new synthetic methods. Moreover, it was possible to describe some aspects of the "microscopic" course of azide pyrolyses in a satisfactory way using calculated energy hypersurfaces, which allowed the first more detailed insight into the deceptively simple azide decomposition reaction.

The unimolecular decomposition of nitrosyl azide to N_2 and N_2O also appears to be very simple on the "macroscopic" level. Quantum chemical calculations of the energy hypersurfaces corresponding to the decomposition of N_4O (Figs. 10 and 11), however, do not only confirm the experimental finding of the formation of N_2 and N_2O, but also indicate that this fragmentation occurs in a much more complex manner. The formation of cyclic *N*-oxides as reactive intermediates appears certain. To our knowledge, such compounds have not yet been observed experimentally, therefore the results presented here might encourage more intensive efforts to prove the existence of these species experimentally by the methods of modern gas-phase analytical chemistry.

Furthermore, all molecular nitrogen oxides have a positive enthalpy of formation.[66] Consequently, N_2O_4 and mixtures of NO/N_2O_4 and NO_2/HNO_3 are already in use as environmentally safe (i.e., halogen-free) oxidizing agents in rocket engines, mostly in combination with methylhydrazine as fuel.[67a] There are extensive discussions about the use of extremely unstable *N*-oxides such as N_4O and N_4O_2 (which would be prepared in situ) as one-component fuels for the generation of hypersonic wind tunnels.[67b] Hence knowledge of the molecular decomposition of these unstable *N*-oxides (nitrosyl and nitryl azides) is not only of academic interest, but also of fundamental, if rather specific, interest to applied science.

5. Reactivity

It is not our intention to present a summary of the reactivity of covalent azides that could claim to be complete. This reactivity is extremely multifaceted, particularly in organic synthesis, but also in main group chemistry. Using a few selected examples from inorganic chemistry—with an emphasis on those that maintain the structural integrity of the azide moiety—we will present a glimpse of the chemistry of covalent azides.

The protonation of covalent azides is well known and much studied. The example of the protonated form of hydrazoic acid, $H_2N_3^+$, has already been discussed in Section 4.[13, 68] It can be prepared in superacidic media at low temperatures according to Equation (m). In contrast to many other compounds containing a covalent azide group, $H_2N_3^+SbF_6^-$ is not explosive.

$$HN_3 + SbF_5 + HF \longrightarrow H_2N_3^+SbF_6^- \quad \text{(m)}$$

It has already been discussed in Section 3 that IN_3 forms stable donor–acceptor complexes with many N-bases, including N_3^- [Eq. (n)]. This leads to a stabilization due to the higher

$$IN_3 + N_3^- \longrightarrow I(N_3)_2^- \quad \text{(n)}$$

coordination number (2) at the central iodine atom.[51, 52] During the formal addition of iodide to give $I_2N_3^-$, IN_3 also acts as a Lewis acid [Eq. (o)].[36c, 52a] Analogously, the reaction of IN_3

$$IN_3 + NMe_4^+ I^- \longrightarrow NMe_4^+ I_2N_3^- \quad \text{(o)}$$

with cyanide ions leads to the anion $[N_3I{-}C{\equiv}N{-}I{-}N_3]^-$. This species is assumed to contain a linear NICNIN unit with a bridging cyanide group.[36c, 52a]

Further anions of the type $[X{-}I{-}N_3]^-$ (X = F, Cl, Br, OCN, CN) have been described.[36b] Iodine azide can also react as a base, that is, it is amphoteric in the Lewis sense. This is best demonstrated by the reaction of IN_3 with "I^+" [Eq. (p)][16] and by the formation of the cation $I(N_3)_2^+$ [Eq. (q)][17] (for structures see Section 4).

$$IN_3 + \text{"}I^+\text{"} \xrightarrow{SO_2} I_2N_3^+ \quad \text{(p)}$$
$$(\text{"}I^+\text{"}: 1/2\, I_2 + 3/2\, AsF_5 \longrightarrow \text{"}I^+AsF_6^-\text{"} + 1/2\, AsF_3)$$

$$ICl_2^+ + 2\, AgN_3 \xrightarrow{SO_2} I(N_3)_2^+ + 2\, AgCl \quad \text{(q)}$$

In aqueous media, particularly in the presence of OH^- ions, halogen azides XN_3 (X = Cl, Br, I) hydrolyze in accordance to their bond polarity, that is, the halogen is positively polarized (see Section 4) [Eq. (r)].[36a] Iodine azide, in particular, owes its

$$XN_3 + 2\, OH^- \longrightarrow N_3^- + XO^- + H_2O \quad \text{(r)}$$

extreme reactivity in spite of the relatively high stability of the molecule (see Section 4) to the high polarity of the N–I bond. The iodine atom has acceptor as well as donor properties; the α-N atom (N1) of the N_3 group possesses primarily donor properties.[36c] Due to its significantly higher polarity and the resulting increased reactivity, IN_3 reacts much faster than ClN_3 with metal iodides and metal halogenides in general; an example is the substitution reaction of iodides of Group 13 elements [Eq. (s), E = B, Al, Ga].[36]

$$EI_3 + IN_3 \xrightarrow{\text{benzene}} I_2EN_3 + I_2 \quad \text{(s)}$$

IN_3 has proven useful in organic synthesis for the addition to olefinic double bonds. It was possible to demonstrate that the tendency to homolytic cleavage increases, as expected, in the order $IN_3 < BrN_3 < ClN_3$.[36c, 69] Equations (t) and (u) (R = Me, Ph) show examples of oxidative additions with iodine azide from the areas of purely inorganic chemistry and organometallic chemistry of the elements, respectively.[36]

$$2\, SnCl_2 + 2\, IN_3 \longrightarrow SnCl_2(N_3)_2 + \text{"}SnCl_2I_2\text{"} \quad \text{(t)}$$

$$R_3Sb + IN_3 \longrightarrow R_3SbI(N_3) \quad \text{(u)}$$

There are recent reports about the successful stepwise synthesis of di- and triphosphazenes using the Staudinger reaction and starting with $(CF_3)_2PN_3$ [Eqs. (v) and (w)].[70]

$$(CF_3)_2PI + NaN_3 \longrightarrow (CF_3)_2PN_3 + NaI \quad (v)$$

$$(CF_3)_2PN_3 \xrightarrow{PPh_3,\ -N_2} Ph_3P{=}N{-}P(CF_3)_2 \xrightarrow{(CF_3)_2PN_3,\ -N_2} Ph_3P{=}N{-}P(CF_3)_2{=}N{-}P(CF_3)_2 \quad (w)$$

Covalent triorgano-substituted azides of Group 14 elements have found the greatest preparative application [see also Eq. (f)]. Trimethylsilyl azide, Me_3SiN_3, for instance, has been successfully used by Kurt Dehnicke and others as nitrogen atom donor in the chemistry of sulfur and selenium.[71] In this way the preparation of many new Se–N compounds became possible, for example the neutral species Se_2NCl_3 as well as the cations $(SeCl)_2N^+$ and $(SeCl_2)_2N^+$. Recently, the synthesis of the novel compound $Se_3N_2Cl_2$ was performed, but this species has not yet been structurally characterized [Eq. (x)].[72] Certainly the most

$$3\,Se_2Cl_2 + 2\,Me_3SiN_3 \xrightarrow{CH_2Cl_2} 2\,Se_3N_2Cl_2 + 2\,Me_3SiCl + N_2 \quad (x)$$

spectacular success for the use of Me_3SiN_3 in the area of nonmetal chemistry has been the safe synthesis of polymeric sulfur nitride $(SN)_x$ [Eq. (y)], which up to now had been prepared by using the explosive compound S_4N_4.[73]

$$3\,Me_3SiN_3 + (NSCl)_3 \xrightarrow{MeCN,\ -15\,^\circ C} 3/x(SN)_x + 3\,Me_3SiCl + 9/2\,N_2 \quad (y)$$

The reaction of mesityl azide with bis[2,4,6-tris(trifluoromethyl)phenyl]stannylene, with subsequent elimination of N_2, permitted the preparation of azadistanniridines in good yields [Eq. (z), R* = 2,4,6-$(CF_3)_3C_6H_2$, Mes = mesityl].[74]

$$2\,R^*_2Sn + MesN_3 \longrightarrow R^*_2Sn\text{-}N(Mes)\text{-}SnR^*_2 + N_2 \quad (z)$$

The azide reaction known in organic chemistry can also be applied to the chemistry of phosphorus. For example, the reaction of cyclic alkyldithiophosphonic acid anhydrides with Me_3SiN_3 leads to quantitative yields of N-containing P–S heterocycles.[75] An example from organometallic chemistry is the reaction of Me_3SiN_3 with $R_2Al{-}AlR_2$, which leads to the formation of novel Al–N heterocycles. Depending on the reaction conditions, the azide moiety can be retained intact as a building block for the ring structure in these compounds.[76] In 1990 it was shown that sulfur azides such as $MeSO_2N_3$ can be successfully employed in the 1,3-dipolar cycloadditions of electrophilic azides to 5-alkylidenedihydrotetrazoles.[77] For some time, stannyl azides of the type R_3SnN_3 have found use in organic synthesis.[78]

6. Summary and Outlook

Covalent binary nonmetal azides, as we have exemplified with hydrazoic acid and the halogen azides, have been known for over 100 years, while the isolation on a preparative scale and the complete determination of the structures of these highly explosive species has only been feasible in the last few years. With the aid of high-level, ab initio calculations (taking into account electron correlation) it was possible for the first time to obtain theoretical insight into unusual, experimentally observable structural characteristics of covalent azides in general and halogen azides in particular. The excellent agreement between experiment (electron diffraction, microwave studies) and theory (ab initio) with respect to structural parameters gives credence to those calculated structures for which there are no experimental data due to the extreme lability of the compounds in question, for instance the novel *N*-oxides ONN_3 and O_2NN_3.

Why are we so strongly interested in the preparation of a class of compounds such as the covalent azides that need to be handled with such extreme care and precautions? We wish to demonstrate that even, and particularly, in the area of the main group chemistry of very simple binary compounds there are still many unanswered questions with regard to structure and bonding. There are also many new compounds in this area that are waiting to be synthesized on a preparative scale.

Now that questions about structure and bonding in covalent XN_3 azides appear to be answered to a certain extent, we wish to pay particular attention in the future to comparative discussions of gas-phase and solid-state structures and to the underlying questions of bonding. Until now the pair $IN_3(g)/[IN_3]_x(s)$ remains a singular result. Therefore the experimental determination of further structures of covalent azides, especially in the solid state, is necessary. In addition, the quantum mechanical description of the molecular structures of polymeric covalent species in the solid state, which up to now is unsatisfactory, must be improved. Many of the azides listed in Table 1 have been described in the literature, but in many cases the structural characterization has been incomplete or not performed at all. For instance, how does $tBu_2N{-}N_3$ crystallize? We will face up to these challenges in the future.

We thank our co-workers for their cooperation, especially Dr. Axel Schulz for performing numerous quantum chemical calculations. We are indebted to Prof. Dr. Paul von R. Schleyer, Dr. Peter Buzek, and Prof. Dr. Wolfram Koch, Erlangen, for intensive support which enabled us to perform independent calculations in our research group. Dr. Peter S. White is acknowledged for the collaboration in the area of X-ray crystal structure analyses (NATO, CRG 920034), Prof. Dr. István Hargittai and his co-workers are acknowledged for performing the electron diffraction experiments (partnership TU Berlin/TU Budapest). The experimental work in Berlin was generously supported by the Deutsche Forschungsgemeinschaft, the Fonds der Chemischen Industrie, and Bundesministerium für Bildung und Wissenschaft (Graduiertenkolleg). We thank both referees for many critical and stimulating comments.

Received: March 29, 1994
Revised version: August 30, 1994 [A 581E]
German version: *Angew. Chem.* **1995**, *107*, 559

[1] a) S. Patai, *The Chemistry of the Azido Group*, Wiley Interscience, London, **1971**; b) C. Grundmann, *Methoden Org. Chem. (Houben-Weyl) 4th ed. 1952–*, Vol. X/3, **1965**; c) G. Bertrand, J.-P. Majoral, A. Baceiredo, *Acc. Chem. Res.* **1986**, *19*, 17; d) A. D. Yoffe in *Developments in Inorganic Nitrogen Chemistry* (Ed.: C. B. Colburn), Elsevier, Amsterdam, **1966**, pp. 72ff; e) K. Jones in *Comprehensive Inorganic Chemistry, Vol. 2* (Eds.: J. C. Bailar, H. J. Emeléus, R. Nyholm, A. F. Trotman-Dickenson), Pergamon, Oxford, **1973**, pp. 276ff;

f) M. Green in *Developments in Inorganic Nitrogen Chemistry* (Ed.: C. B. Colburn), Elsevier, Amsterdam, **1966**, pp. 1 ff; g) P. Gray, *Q. Rev. Chem. Soc.* **1963**, *17*, 441; h) A. Hautzsch, M. Schümann, *Ber. Dtsch. Chem. Ges.* **1900**, *33*, 522; i) F. Raschig, *Ber. Dtsch. Chem. Ges.* **1908**, *41*, 4194..

[2] B. P. Winnewisser, *J. Mol. Spectrosc.* **1980**, *82*, 220.

[3] K. O. Christe, W. W. Wilson, D. A. Dixon, S. I. Khan, R. Bau, T. Metzenthin, R. Lu, *J. Am. Chem. Soc.* **1993**, *115*, 1836.

[4] a) K. O. Christe, D. Christen, H. Oberhammer, C. H. Schack, *Inorg. Chem.* **1984**, *23*, 4283; b) H. G. Mack, C. O. Della Védova, H. Willner, *J. Molec. Struct.* **1993**, *291*, 197.

[5] J. P. Johnson, G. K. MacLean, J. Passmore, P. S. White, *Can. J. Chem.* **1989**, *67*, 1687.

[6] D. Christen, H. G. Mack, G. Schatte, H. Willner, *J. Am. Chem. Soc.* **1988**, *110*, 707.

[7] a) R. L. Cook, M. C. L. Gerry, *J. Chem. Phys.* **1970**, *53*, 2525; b) A. Schulz, I. C. Tornieporth-Oetting, T. M. Klapötke, *Inorg. Chem.*, in press.

[8] M. Hargittai, I. C. Tornieporth-Oetting, T. M. Klapötke, M. Kolonits, I. Hargittai, *Angew. Chem.* **1993**, *105*, 773; *Angew. Chem. Int. Ed. Engl.* **1993**, *32*, 759. and references therein.

[9] a) P. Buzek, T. M. Klapötke, P. von R. Schleyer, I. C. Tornieporth-Oetting, P. S. White, *Angew. Chem.* **1993**, *105*, 289; *Angew. Chem. Int. Ed. Engl.* **1993**, *32*, 275; b) M. Hargittai, J. Molnár, T. M. Klapötke, I. C. Tornieporth-Oetting, M. Kolonits, I. Hargittai, *J. Phys. Chem.* **1994**, *98*, 10095.

[10] I. C. Tornieporth-Oetting, T. M. Klapötke in *Combustion Efficiency and Air Quality* (Eds.: I. Hargittai, T. Vidoczy), Plenum, New York, **1995**.

[11] U. Müller, R. Dübgen, K. Dehnicke, *Z. Anorg. Allg. Chem.* **1980**, *463*, 7.

[12] a) R. G. Parr, R. G. Pearson, *J. Am. Chem. Soc.* **1983**, *105*, 7512; b) R. G. Pearson, *Acc. Chem. Res.* **1990**, *23*, 1; c) *Chem. Br.* **1991**, 444; d) *Inorg. Chem.* **1988**, *27*, 734.

[13] H. Bock, R. Dammel, *Angew. Chem.* **1987**, *99*, 518; *Angew. Chem. Int. Ed. Engl.* **1987**, *26*, 504.

[14] I. C. Tornieporth-Oetting, T. M. Klapötke, *Comments Inorg. Chem.* **1993**, *15*, 137.

[15] W.-W. du Mont, *Nachr. Chem. Tech. Lab.* **1994**, *42*, 123.

[16] I. C. Tornieporth-Oetting, P. Buzek, P. von R. Schleyer, T. M. Klapötke, *Angew. Chem.* **1992**, *104*, 1391; *Angew. Chem. Int. Ed. Engl.* **1992**, *31*, 1338.

[17] I. C. Tornieporth-Oetting, T. M. Klapötke, A. Schulz, P. Buzek, P. von R. Schleyer, *Inorg. Chem.* **1993**, *32*, 5640.

[18] a) A. Schulz, I. C. Tornieporth-Oetting, T. M. Kapötke, *Angew. Chem.* **1993**, *105*, 1697; *Angew. Chem. Int. Ed. Engl.* **1993**, *32*, 1610; b) S. Stinson, *Chem. Eng. News* **1993**, *71* (*48*), 51.

[19] T. M. Klapötke, A. Schulz, I. C. Tornieporth-Oetting, *Chem. Ber.* **1994**, *127*, 2181.

[20] a) H. Bock, K. L. Kompa, *Angew. Chem.* **1962**, *74*, 327; *Angew. Chem. Int. Ed. Engl.* **1962**, *1*, 264; b) *Z. Anorg. Allg. Chem.* **1964**, *332*, 240; c) P. Geißler, H. Holfter, T. M. Klapötke, A. Schulz, *12th Winter Fluorine ACS Conference* **1995**, lecture 62, St. Petersburg, USA; d) *Chem. Eng. News* **1994**, *72* (45), 41.

[21] a) B. Bak, P. Jansen, H. Stafast, *Chem. Phys. Lett.* **1975**, *35*, 247; b) F. D. Marsh, M. E. Hermes, *J. Am. Chem. Soc.* **1964**, *86*, 4506; c) F. D. Marsh, *J. Org. Chem.* **1972**, *37*, 2966.

[22] a) C. Grundmann, R. Rätz, *Z. Naturforsch. B* **1955**, *10*, 116; b) R. A. Shaw, B. W. Fitzsimmons, B. C. Smith, *Chem. Rev.* **1962**, *62*, 247; c) M. S. Chang, A. J. Matuszko, *J. Am. Chem. Soc.* **1960**, *82*, 5756.

[23] a) A. Schmidt, *Chem. Ber.* **1970**, *103*, 3923; b) *ibid.* **1968**, *101*, 4015.

[24] W. Buder, A. Schmidt, *Z. Anorg. Allg. Chem.* **1975**, *415*, 263.

[25] K. B. Dillon, A. W. G. Platt, T. C. Waddington, *Inorg. Nucl. Chem. Lett.* **1978**, *14*, 511.

[26] K. B. Dillon, A. W. G. Platt, T. C. Waddington, *J. Chem. Soc. Dalton Trans.* **1980**, 1036.

[27] a) D. M. Revitt, D. B. Sowerby, *J. Chem. Soc. Dalton Trans.* **1972**, 847; b) H. G. Ang, W. L. Kwik, Y. W. Lee, H. Oberhammer, *Inorg. Chem.* **1994**, *33*, 4425.

[28] P. Geißler, Diplomarbeit, Technische Universität Berlin, **1994**.

[29] a) H. W. Lucien, *J. Am. Chem. Soc.* **1958**, *80*, 4458; b) M. P. Doyle, J. J. Maciejko, S. C. Busman, *ibid.* **1973**, *95*, 952.

[30] D. A. Spencer, *J. Chem. Soc.* **1925**, *127*, 216.

[31] E. A. Fletcher, *Chem. Eng. News* **1993**, *71* (*51*), 2.

[32] A. Schulz, T. M. Klapötke, unpublished results.

[33] a) J. Köhler, R. Meyer, *Explosivstoffe*, VCH, Weinheim, **1991**; b) H. D. Fair, R. F. Walker, *Physics and Chemistry of the Inorganic Azides*, Plenum, New York, **1977**.

[34] B. Krakow, R. C. Lord, G. O. Neely, *J. Mol. Spectrosc.* **1968**, *27*, 198.

[35] a) H. Bock, R. Dammel, L. Horner, *Chem. Ber.* **1981**, *114*, 220; b) H. Bock, B. Solouki, *Angew. Chem.* **1981**, *93*, 425; *Angew. Chem. Int. Ed. Engl.* **1981**, *20*, 427.

[36] a) K. Dehnicke, *Angew. Chem.* **1967**, *79*, 253; *Angew. Chem. Int. Ed. Engl.* **1967**, *6*, 240; b) *Adv. Inorg. Chem. Radiochem.* **1983**, *26*, 169; c) *Angew. Chem.* **1979**, *91*, 527; *Angew. Chem. Int. Ed. Engl.* **1979**, *18*, 507; d) *ibid.* **1976**, *88*, 612 and **1976**, *15*, 553.

[37] J. Mason, *Multinuclear NMR*, Plenum, New York, **1987**.

[38] P. S. Belton, J. D. Woollins, *Magn. Reson. Chem.* **1986**, *24*, 1080.

[39] J. Passmore, M. J. Schriver, *Inorg. Chem.* **1988**, *27*, 2749.

[40] N. Logan in *Nitrogen NMR* (Eds.: M. Witanowski, G. A. Webb), Plenum, London, **1973**, Chapter 6.

[41] W. Beck, W. Becker, K. F. Chew, W. Derbyshire, N. Logan, D. M. Revitt, D. B. Sowerby, *J. Chem. Soc. Dalton Trans.* **1972**, 245.

[42] P. Geissler, T. M. Klapötke, H.-J. Kroth, *Spectrochim. Acta Part A*, in press.

[43] M. Otto, S. D. Lotz, G. Frenking, *Inorg. Chem.* **1992**, *31*, 3647.

[44] W. J. Hehre, L. Radom, P. von R. Schleyer, J. Pople, *Ab Initio Molecular Orbital Theory*, Wiley, New York, **1986**.

[45] E. Illenberger, P. B. Comita, J. Brauman, H.-P. Fenzlaff, M. Heni, N. Heinrich, W. Koch, G. Frenking, *Ber. Bunsen-Ges. Phys. Chem.* **1985**, *89*, 1026.

[46] W. C. Richardson, D. W. Setser, *Can. J. Chem.* **1969**, *47*, 2725.

[47] M. H. Alexander, H.-J. Werner, P. J. Dagdigian, *J. Chem. Phys.* **1988**, *89*, 1388.

[48] B. R. Foy, M. P. Casassa, J. C. Stephenson, D. S. King, *J. Chem. Phys.* **1988**, *89*, 608.

[49] O. Kajimoto, T. Yamamoto, T. Fueno, *J. Phys. Chem.* **1979**, *83*, 429.

[50] D. J. Benard, M. A. Chowdhury, B. K. Winker, T. A. Seder, H. H. Michels, *J. Phys. Chem.* **1990**, *94*, 7507.

[51] H. Dörner, K. Dehnicke, W. Massa, R. Schmidt, *Z. Naturforsch. B* **1983**, *38*, 437.

[52] a) R. Dübgen, K. Dehnicke, *Naturwissenschaften* **1978**, *65*, 535; b) U. Müller, R. Dübgen, K. Dehnicke, *Z. Anorg. Allg. Chem.* **1980**, *463*, 7.

[53] K. O. Christe, W. W. Wilson, R. Bau, S. W. Bunte, *J. Am. Chem. Soc.* **1992**, *114*, 3411.

[54] Pseudopotentials: a) P. A. Christiansen, W. C. Ermler, K. S. Pitzer, *Annu. Rev. Phys. Chem.* **1985**, *36*, 407; b) K. Balasubramanian, K. S. Pitzer in *Ab Initio Methods in Quantum Chemistry* (Ed.: K. P. Lawley), Wiley, New York, **1987**, pp. 287 ff; c) P. Durand, J.-P. Malrieu, *ibid.*, pp. 321 ff; d) P. Fuentealba, O. Reyes, H. Stoll, H. Preuss, *J. Chem. Phys.* **1987**, *87*, 5338.

[55] Relativistic effects: a) K. S. Pitzer, *Acc. Chem. Res.* **1979**, *12*, 271; b) P. Pyykkö, J.-P. Deslaux, *ibid.* **1979**, *12*, 276; c) P. Pyykkö, *Chem. Rev.* **1988**, *88*, 563.

[56] C. F. Campana, F. Y.-K. Lo, L. F. Dahl, *Inorg. Chem.* **1979**, *18*, 3060.

[57] A. E. Reed, L. A. Curtiss, F. Weinhold, *Chem. Rev.* **1988**, *88*, 899.

[58] a) A. E. Reed, P. von R. Schleyer, *J. Am. Chem. Soc.* **1990**, *112*, 1434; b) *Inorg. Chem.* **1988**, *27*, 3969; c) A. E. Reed, F. Weinhold, *J. Chem. Phys.* **1985**, *83*, 1736.

[59] a) M. Kaupp, P. von R. Schleyer, H. Stoll, H. Preuss, *J. Am. Chem. Soc.* **1991**, *113*, 6012; b) A. Bergner, M. Dolg, W. Kuechle, H. Stoll, H. Preuss, *Mol. Phys.* **1993**, *80*, 1431.

[60] a) R. H. Davies, A. Finch, P. N. Gates, *J. Chem. Soc. Chem. Commun.* **1989**, 1461; b) I. C. Tornieporth-Oetting, T. M. Klapötke, *Angew. Chem.* **1990**, *102*, 726; *Angew. Chem. Int. Ed. Engl.* **1990**, *29*, 677.

[61] a) R. J. Gillespie, I. Hargittai, *The VSEPR Model of Molecular Geometry*, Allyn and Bacon, Boston, **1991**; b) R. F. W. Bader, R. J. Gillespie, P. J. MacDougall, *J. Am. Chem. Soc.* **1988**, *110*, 7329.

[62] I. C. Tornieporth-Oetting, T. M. Klapötke, *Heteroat. Chem.* **1993**, *4*, 543.

[63] a) M. N. Glukhovtsev, P. von R. Schleyer, *Chem. Phys. Lett.* **1992**, *198*, 547; b) R. D. Harcourt, *J. Mol. Struct.* **1993**, *300*, 245; c) *ibid.* **1972**, *12*, 351; d) *Lect. Notes Chem.* **1982**, *30*, 140.

[64] H. Bock, K. Ruppert, C. Näther, Z. Havlas, H.-F. Herrmann, C. Arad, I. Göbel, A. John, J. Meuret, S. Nick, A. Rauschenbach, W. Seitz, T. Vaupel, B. Solouki, *Angew. Chem.* **1992**, *104*, 564; *Angew. Chem. Int. Ed. Engl.* **1992**, *31*, 550.

[65] a) T. M. Klapötke, A. Schulz, *Chem. Ber.* in press; b) R. D. Harcourt, *J. Mol. Struct., Theochem.*, in press.

[66] T. M. Klapötke, I. C. Tornieporth-Oetting, *Nichtmetallchemie*, VCH, Weinheim, **1994**, p. 288.

[67] a) Rocketdyne Division, Rockwell International, Canoga Park, CA 91304, USA, Publication 571-N-2, 9-84; b) ref. [31].

[68] A. Schmidt, *Chem. Ber.* **1966**, *99*, 2976.

[69] G. L'abbé, A. Hassner, *Angew. Chem.* **1971**, *83*, 103; *Angew. Chem. Int. Ed. Engl.* **1971**, *10*, 98.

[70] H. G. Ang, Y. M. Cai, W. L. Kwik, *11th Winter Fluorine ACS Conference* **1993**, Lecture 35, St. Petersburg, USA.

[71] a) R. Wollert, A. Höllwarth, G. Frenking, D. Fenske, H. Goesmann, K. Dehnicke, *Angew. Chem.* **1992**, *104*, 1216; *Angew. Chem. Int. Ed. Engl.* **1992**, *31*, 1251; b) M. Broschag, T. M. Klapötke, I. C. Tornieporth-Oetting, *J. Chem. Soc. Chem. Commun.* **1992**, 1390.

[72] a) J. Siivari, T. Chivers, R. Laitinen, *Angew. Chem.* **1992**, *104*, 1539; *Angew. Chem. Int. Ed. Engl.* **1992**, *31*, 1518; b) T. Chivers, *Main Group Chem. News.* **1993**, *1*, 6, and references therein.

[73] a) F. A. Kennett, G. K. MacLean, J. Passmore, M. N. Sudheendra Rao, *J. Chem. Soc. Dalton Trans.* **1982**, 851; b) A. J. Banister, Z. V. Hauptman, J. Passmore, C.-M. Wong, P. S. White, *ibid.* **1986**, 2371; c) J. Passmore, M. N. Sudheendra Rao, *J. Chem. Soc. Chem. Commun.* **1980**, 1268.
[74] H. Grützmacher, H. Pritzkow, *Angew. Chem.* **1991**, *103*, 976; *Angew. Chem. Int. Ed. Engl.* **1991**, *30*, 1017.
[75] H. W. Roesky, M. Dietl, *Angew. Chem.* **1973**, *85*, 454; *Angew. Chem. Int. Ed. Engl.* **1973**, *12*, 425.
[76] a) W. Uhl, M. Koch, U. Schütz, *ADUC Chemiedozententagung* **1994**, Siegen, Vortrag A 37; b) W. Uhl, R. Gerding, S. Pohl, W. Saak, *Chem. Ber.* **1995**, *128*, 81.
[77] H. Quast, D. Regnat, E.-M. Peters, K. Peters, H. G. von Schnering, *Angew. Chem.* **1990**, *102*, 724; *Angew. Chem. Int. Ed. Engl.* **1990**, *29*, 695.
[78] a) G. Ossig, A. Meller, S. Freitag, R. Herbst-Irmer, G. Sheldrick, *Chem. Ber.* **1993**, *126*, 2247; b) H. R. Kricheldorf, G. Schwarz, J. Kaschig, *Angew. Chem.* **1977**, *89*, 570; *Angew. Chem. Int. Ed. Engl.* **1977**, *16*, 550.
[79] Below are the ^{14}N NMR chemical shifts and line widths ($\Delta\nu_{1/2}$ in Hz, in parentheses) of covalent azides ($R-N_a-N_b\equiv N_c$) and NaN_3 for comparison. [42].

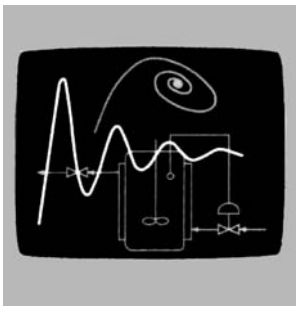
Compound	$\delta(N_a)$	$\delta(N_b)$	$\delta(N_c)$	Solvent
NaN_3		−128.1 (30)	−277.2 (65)	D_2O
$(CH_3)_3SiN_3$	−315.9 (200)	−141.5 (35)	−205.1 (35)	$CDCl_3$
ClN_3	−269.9 (240)	−119.2 (20)	−109.3 (50)	$CDCl_3$
BrN_3	−349.2 (475)	−122.0 (30)	−157.0 (90)	$CDCl_3$
IN_3	−351.2 (350)	−121.9 (20)	−156.6 (65)	$CDCl_3$
$(CH_3)_2AsN_3$	−312.5 (300)	−132.0 (50)	−191.9 (90)	$CDCl_3$
$CH_3As(N_3)_2$	−297.6 (200)	−129.3 (30)	−169.2 (70)	SO_2
$As(N_3)_3$	−318.0 (150)	−131.1 (15)	−165.2 (30)	$CDCl_3$
$[As(N_3)_4]^+$ [a]	−279.8 (375)	−135.4 (30)	−162.1 (125)	SO_2

[a] AsF_6^- salt.

Ingham, J. et al.

Chemical Engineering Dynamics

Modelling with PC Simulation



1994. XX, 701 pages with 430 figures.
Hardcover. DM 276.-/ öS 2153.-/ sFr. 256.-.
ISBN 3-527-28577-6

In this book, the reader is guided through the complex study of dynamic chemical engineering systems by the unique combination of a simplified presentation of the fundamental theory (Part 1) and direct hands-on computer experimentation with the provision of 85 accompanying computer-based simulation examples (Part 2) supplied on diskette.

The ISIM digital simulation language is very simple to use and its powerful interactive nature enables the readers to create their own simulations, based on their own specific problems. This powerful dynamic ISIM software is ready to run on any DOS personal computer.

The treatment employed in this book is well tried and tested, based on over 20 years experience in teaching an international post-experience course. Whether for the teacher, the student, the chemist or engineer, this book serves as the key to a greater understanding of chemical engineering dynamics through the fun and enjoyment of active learning.

To order please contact your bookseller or:

VCH, P.O. Box 10 11 61, D-69451 Weinheim. Telefax (0) 62 01 - 60 61 84

VCH, Hardstrasse 10, P.O. Box, CH-4020 Basel

VCH, 8 Wellington Court, Cambridge CB1 1HZ, UK

VCH, 220 East 23rd Street, New York, NY 10010-4606, USA (toll free: 1-800-367-8249)

VCH, Eikow Building, 10-9 Hongo 1-chome, Bunkyo-ku, Tokyo 113 Japan

VCH

Enzymes in Organic Synthesis: Application to the Problems of Carbohydrate Recognition (Part 2)**

Chi-Huey Wong,* Randall L. Halcomb, Yoshitaka Ichikawa, and Tetsuya Kajimoto

Recognition of carbohydrates by proteins and nucleic acids is highly specific, but the dissociation constants are relatively high (generally in the mM to high μM range) because of the lack of hydrophobic groups in the carbohydrates. The high specificity of this weak binding often comes from many hydrogen bonds and the coordination of metal ions as bridge between sugars and receptors. Though weak hydrophobic interactions between sugars and proteins have also been identified, the unique shape of a complex carbohydrate under the influence of anomeric and *exo* anomeric effects (the glycosidic torsion angles are therefore often not flexible but are typically somewhat restricted) and the topographic orientation of the hydroxyl and charged groups contribute most significantly to the recognition process. Studies on the structure–function relationship of a complex carbohydrate therefore require deliberate manipulation of its shape and functional groups, and synthesis of oligosaccharide analogs from modified monosaccharides is often useful to address the problem. The availability of various monosaccharides and their analogs for the synthesis of complex carbohydrates together with the information resulting from structural studies (such a NMR or X-ray studies on sugar–protein complexes) will certainly provide a basic understanding of complex carbohydrate recognition. An ultimate goal is to develop simple and easy-to-make non-carbohydrate molecules that resemble the active structure involved in carbohydrate–receptor interaction or the transition-state of an enzyme-catalyzed transformation (for example, glycosidase or glycosyltransferase reactions) and have the approprite bioavailability to be used to control the carbohydrate function in a specific manner. In part one of this review we described various enzymatic approaches to the synthesis of monosaccharides, analogs, and related structures. We describe in this part enzymatic and chemoenzymatic approaches to the synthesis of oligosaccarides and analogs, including those involved in E-selectin recognition, and strategies to inhibit glycosidases and glycosyltransferases.

Keywords: carbohydrates · enzymes · organic synthesis

5. Enzymatic Glycosidic Bond Formation

Nature employs two groups of enzymes in the biosynthesis of oligosaccharides: the enzymes of the Leloir pathway[136] and those of non-Leloir pathways. The Leloir pathway enzymes are responsible for the synthesis of most N- and O-linked glycoproteins and other glycoconjugates in mammalian systems. N-linked oligosaccharides are characterized by a β-glycosidic linkage between a GlcNAc residue and the δ-amide nitrogen atom of an asparagine residue. The less common O-linked glycoproteins contain an α-glycosidic linkage between a GalNAc (or xylose) and the hydroxyl group of a serine or threonine residue. Both O- and N-linked glycoproteins are cotranslationally glycosylated in the endoplasmic reticulum and the Golgi apparatus.[11, 137] The biosynthesis of the N-linked type involves an initial synthesis of a dolichyl pyrophosphoryl oligosaccharide intermediate in the endoplasmic reticulum by the action of GlcNAc-transferases and mannosyltransferases. This structure is further glucosylated, and then the entire oligosaccharide moiety is transferred to an ASn residue of the growing peptide chain by the enzyme oligosaccharyltransferase.[137] The Asn is typically part of the amino acid sequence Asn-X-Ser(Thr), where X is not Pro or Asp.[137–141] Before transport into the Golgi apparatus, the glucose residues and some mannose residues are removed in a process called trimming by the action of glucosidase I and II and a mannosidase to reveal a core pentasaccharide (peptide-Asn-$(GlcNAc)_2$-$(Man)_3$). The resulting core structure is further processed by mannosidases and glycosyltransferases present in the Golgi apparatus to produce either the high-mannose type, the complex type, or the hybrid type oligosaccharides. Mono-

[*] Prof. Dr. C.-H. Wong, Dr. R. L. Halcomb
Department of Chemistry, The Scripps Research Institute
10666 North Torrey Pines Road, La Jolla, CA 92037 (USA)
Telefax: Int. code + (619)554-6731
Prof. Dr. Y. Ichikawa
Department of Pharmacology and Molecular Sciences
The Johns Hopkins University, Baltimore (USA)
Dr. T. Kajimoto
Frontier Research Program on Glycotechnology
The Institute of Physical and Chemical Research (RIKEN), Wako City (Japan)

[**] Part 1: *Angew. Chem.* **1995**, *107*, 453; *Angew. Chem. Int. Ed. Engl.* **1995**, *34*, 412. The numbering of the sections, references, schemes, and Tables follows on from Part 1.

saccharides are then added sequentially to this core structure to provide the fully elaborated oligosaccharide chain.

In contrast to the dolichyl pyrophosphate mediated synthesis of N-linked oligosaccharides, the glycosyltransferases necessary for the synthesis of O-linked oligosaccharides are located in the Golgi apparatus.[137] The biosynthetic route to the O-linked type is also different. Monosaccharide residues are added sequentially to the growing oligosaccharide chain.

All mammalian cells, with the exception of erythrocytes, contain the necessary elements for glycosylation. In certain secretory cells, however, the preponderance of transferases is greater.[142]

As glycosyl donors, the glycosyltransferases of the Leloir pathway in mammalian systems utilize monosaccharides which are activated as glycosyl esters of nucleoside mono- or diphosphates.[137] Non-Leloir transferases typically utilize glycosyl phosphates as activated donors. The Leloir glycosyltransferases employ primarily eight nucleoside mono- or diphosphate sugars as monosaccharide donors for the synthesis of most oligosaccharides: UDP-Glc, UDP-GlcNAc, UDP-Gal, UDP-GalNAc, GDP-Man, GDP-Fuc, UDP-GlcUA, and CMP-NeuAc. Many other monosaccharides, such as the anionic or sulfated sugars of heparin and chondroitin sulfate, are also found in mammalian systems, but they usually are a result of modification of a particular sugar after it is incorporated into an oligosaccharide structure. A very diverse array of monosaccharides (for example, xylose, arabinose, 3-deoxy-*manno*-octulosonate (KDO), deoxysugars) and oligisaccharides is also resent in microorganisms, plants, and invertebrates.[143, 144] The enzymes responsible for their biosynthesis, however, have not been extensively exploited for synthesis, though they follow the same principles as those in mammalian systems.

The glycosyltransferases from the Leloir and non-Leloir pathways as well as glycosidases[13] have been exploited for the synthesis of oligosaccharides and glycoconjugates.[14, 145, 146] The function of glycosidases in vivo is to cleave glycosidic bonds; however, under appropriate conditions they can be useful synthetic catalysts. Each group of enzymes has certain advantages and disadvantages for synthesis. Glycosyltransferases are highly specific in the formation of glycosides; however, the availability of many of the necessary transferases is limited. Fortunately, the recent advances in genetic engineering and recombinant techniques are rapidly alleviating these drawbacks. Glycosidases have the advantage of wider availability and lower cost, but they are not as specific or high-yielding in synthetic reactions. Several other enzymatic methods have also been used to synthesize N-glycosides, such as nucleosides.

5.1. Donor Substrates for Glycosyltransferases

Most of the sugar nucleoside phosphates used as substrates for glycosyltransferases[137] are biosynthesized in vivo from the corresponding monosaccharides. The initial step is a kinase-mediated phosphorylation to produce a glycosyl phosphate. This glycosyl phosphate then reacts with a nucleoside triphosphate (NTP), catalyzed by sugar nucleoside diphosphate pyrophosphorylase, to afford an activated sugar nucleoside diphosphate [Eq. (a)]. Other sugar nucleoside phosphates, such as GDP-Fuc and UDP-GlcUA, are biosynthesized by further enzymatic modification of these existing key sugar nucleoside phosphates. Another exception is CMP-NeuAc, which is formed by the direct reaction of NeuAc with CTP [Eq. (b)]. Some of the enzymes involved in the biosynthesis of sugar nucleotides also accept nonnatural sugars as substrates. In general, however, the rates are quite slow, thus limiting the usefulness of this approach.

$$\text{Sugar-1-}P + \text{NTP} \longrightarrow \text{NDP-Sugar} + PP_i \quad \text{(a)}$$

$$\text{NeuAc} + \text{CTP} \longrightarrow \text{CMPNeuAc} + PP_i \quad \text{(b)}$$

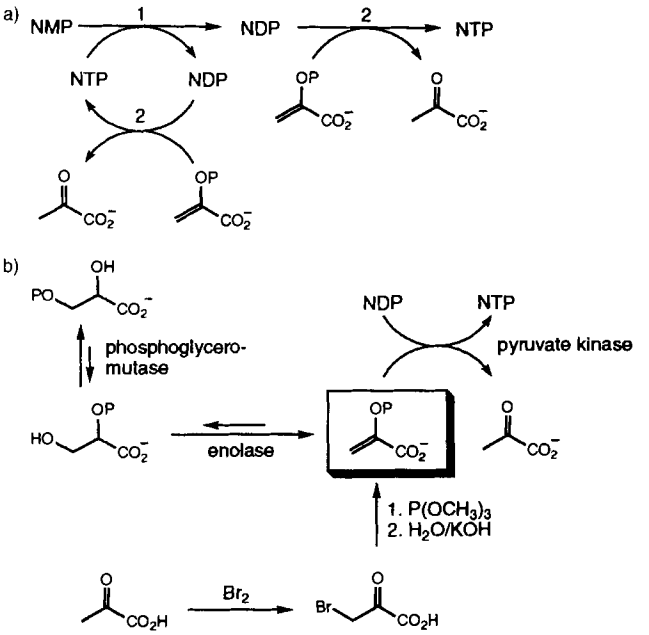
5.1.1. *Preparation of Nucleoside Triphosphates*

Chemical syntheses of some sugar nucleoside phosphates have been reported.[147] Most of these methods involve the reaction of an activated nucleoside monophosphate (NMP)[148–152] with a glycosyl phosphate to produce a sugar nucleoside diphosphate. Of the commonly used activated NMP derivatives, phosphoramidates such as phoshorimidazolidates[153–155] and phosphoromorpholidates[148–152] are considered the most effective. These activated NMPs may also be used to prepare NTPs by reaction with pyrophosphate.[155] A number of chemical methods are available for the synthesis of glycosyl phosphates. Reactions of phosphates with activated glycosyl donors[156] or chemical phosphorylation of anomeric hydroxyl groups[151–153, 157] have proven to be convenient. Additionally, routes via glycosyl phosphites are useful.[158] Enzymatic procedures are also available. Glycogen phosphorylase[159] and sucrose phosphorylase[160] were used to produce α-glucose-1-phosphate. Phosphoglucomutase can also be used to prepare glucose-1-phosphate from glucose-6-phosphate,[161] which is in turn synthesized from glucose by hexokinase.

The appropriate nucleoside triphosphates are utilized as substrates for the biosynthesis of sugar nucleoside phosphates. Biosynthesis-based enzymatic preparation of these donors for use in glycosylations therefore requires a synthesis of NTPs suitable for scale-up.

Most preparative-scale enzymatic syntheses of NTPs use commercially available NMPs as starting materials. Alternatively, all of the NMPs can be obtained from yeast RNA digests at low cost,[162] or can be easily prepared chemically. In general, these methods involve the sequential use of two kinases to transform NMPs to NTPs, via the corresponding nucleoside diphosphates (NDPs). Either of three kinases may be used to synthesize NTPs from the corresponding NDPs, each of which uses a different phosphoryl donor: pyruvate kinase [EC 2.7.1.40] uses phosphoenolpyruvate (PEP)[163, 164] as a phosphoryl donor, acetate kinase [EC 2.7.2.1] uses acetyl phosphate, and nucleoside-diphosphate kinase [EC 2.7.4.6] uses ATP. Pyruvate kinase is generally the enzyme of choice, because it is less expensive than nucleoside-diphosphate kinase,[155, 165] and because PEP is more stable and provides a more thermodynamically favorable driving force for phosphorylation than does acetyl phosphate (Scheme 34).

The preparation of NDPs from NMPs is more complicated and requires different enzymes for each NMP. Adenylate kinase [EC 2.7.4.3] phosphorylates AMP[155] and CMP,[166] and also slowly phosphorylates UMP. Guanylate kinase [EC 2.7.4.8] catalyzes the phosphorylation of GMP. Nucleoside-monophosphate



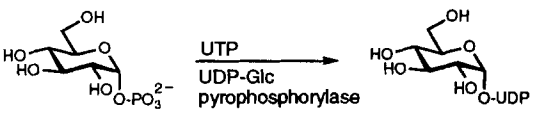
Scheme 34. a) Synthesis of nucleoside triphoshates (NTPs): 1. adenylate kinase ([EC 2.7.4.3], N = A, C, U), guanylate kinase ([EC 2.7.4.8], N = G), nucleoside monophosphate kinase ([EC 2.7.4.4], N = U); 2. pyruvate kinase [EC 2.7.1.40]. b) Synthesis of phosphoenol pyruvate (PEP).

kinase [EC 2.7.4.4] uses ATP to phosphorylate AMP, CMP, GMP, and UMP; however, the enzyme is relatively expensive and unstable.[155] Both CMP and UMP kinases exist but are not commercially available. If ATP is required as a phosphorylating agent, it is usually used in a catalytic amount and recycled from ADP with pyruvate kinase/PEP or acetate kinase/acetyl phosphate.[167] Phosphoenolpyruvate may be prepared chemically from pyruvate[163] or generated enzymatically from D-3-phosphoglyceric acid[164] (Scheme 34).

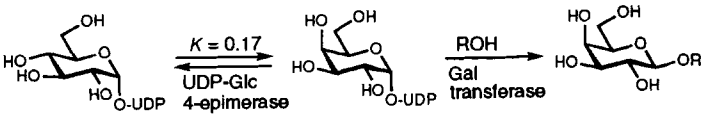
Comparisons of chemical and enzymatic methods for the synthesis of NTPs[155] lead to the conclusion that enzymatic methods provide the most convenient route to CTP and GTP. Chemical deamination of CTP is the best method for preparing UTP.[155] ATP is relatively inexpensive from commerical sources; nevertheless, it has also been synhesized enzymatically from AMP on a 50 mmol scale. Mixtures of NTPs can be prepared fromRNA by sequential reactions catalyzed by nuclease P1, polynucleotide phosphorylase, and pyruvate kinase.[168] This mixture can be selectively converted into a sugar nucleotide with a particular sugar nucleoside diphosphate pyrophosphorylase.[168]

5.1.2. UDP-Glucose (UDP-Glc) and UDP-Galactose (UDP-Gal)

UDP-Glucose has been prepared from UTP and glucose-1-phosphate under catalysis by UDP-glucose pyrophosphorylase (Scheme 35).[155, 161, 169] UDP-Gal can be synthesized in an analogous fashion with UDP-Gal pyrophosphorylase.[170] Additionally, UDP-Gal can be generated from UDP-Glc by epimerization of C-4 with UDP-glucose epimerase[161] (Scheme 36). Though the equilibrium for this reaction favors UD-Glc, it can be shifted by coupling the reaction to an in situ



Scheme 35. Synthesis of UDP-Glc.

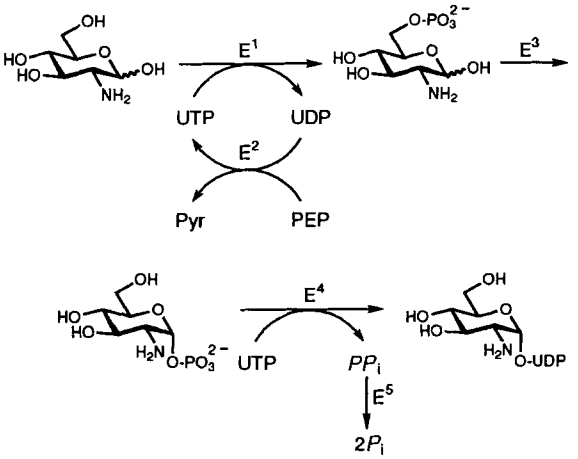


Scheme 36. Synthesis of UDP-Gal and its use in glycosylations.

glycosylation with galactosyltransferase. This concept has been applied to a large-scale synthesis of *N*-acetyllactosamine.[161] For gram amounts, UDP-Gal has been prepared from Gal-1-phosphate and UDP-Glc with UDP-Gal uridyltransferase,[172] followed *in situ* by glycosylation (see Section 5.2.8). Furthermore, UDP-Gal has been synthesized from UMP and Gal by means of dried cells of *Torulopsis candida*.[169] In this system, Gal-1-phosphate and UTP were generated *in situ* as substrates for UDP-Gal pyrophosphorylase. A recent chemical synthesis of UDP-2-deoxygalactose and its use in glycosylations has been recently reported.[173]

5.1.3. UDP-N-Acetylglucosamine (UDP-GlcNAc)

Two enzymatic methods have been developed for the synthesis of UDP-GlcNAc. The first involves a reaction between GlcNAc-1-phosphate and UTP, catalyzed by UDP-GlcNAc pyrophosphorylase.[169] UDP-GlcNAc pyrophosphorylase is currently not commercially available; to produce it, however, a whole-cell process using Baker's yeast can be employed. The enzyme from calf liver[170] can also be used in the synthesis. The second procedure exploits UDP-Glc pyrophosphorylase to catalyze a condensation between UTP and glucosamine-1-phosphate (GlcN-1-*P*) to afford UDP-glucosamine[172a] (Scheme 37). The product UDP-GlcN can then be selectively N-acetylated to provide UDP-

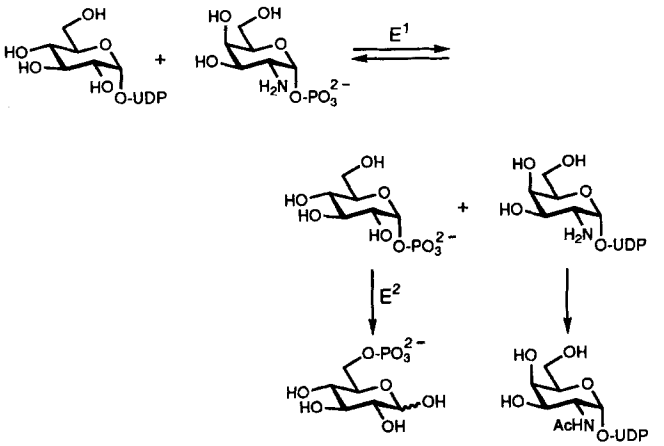


Scheme 37. Synthesis of UDP-GlcNAc. E^1 = hexokinase from yeast, E^2 = pyruvate kinase, E^3 = phosphoglucomutase, E^4 = UDP-Glc pyrophosphorylase, E^5 = inorganic pyrophosphatase, Pyr = pyruvate.

GlcNAc. GlcN-1-*P* was synthesized from GlcN by phosphorylation of the 6-position with hexokinase to give GlcN-6-*P*, followed by a phosphoglucomutase-catalyzed isomerization to provide GlcN-1-*P*. The second sequence can be performed in a hollow fiber reactor.[174]

5.1.4. UDP-N-Acetylgalactosamine (UDP-GalNAc)

UDP-GalNAc can be prepared from GalNAc-1-P and UTP with UDP-GalNAc pyrophosphorylase, or from UDP-GlcNAc with an epimerase; however, the necessary enzymes are not readily available. An alternative procedure has been reported that is based on a UMP exchange reaction between UDP-Glc and GalN-1-*P*, under catalysis by UDP-glucose: galactosylphosphate uridyltransferase [EC 2.7.7.12], which is commercially available (Scheme 38).[171, 175] Galactose-1-phosphate is



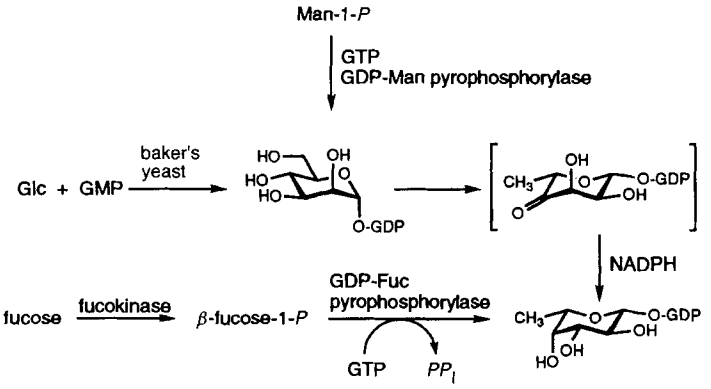
Scheme 38. Synthesis of UDP-GalNAc. E^1 = UDP-Glc: galactosylphosphate uridyltransferase, E^2: phosphoglucomutase.

the natural substrate for the enzyme, but 2-deoxygalactose-1-phosphate, 2-deoxyglucose-1-phosphate, and galactosamine-1-phosphate are also accepted. The equilibrium constant for the exchange reaction is about 1; phosphoglucomutase was therefore added to remove the product Glc-1-*P* and shift the equilibrium toward UDP-GalN. The UDP-GalN thus produced was acetylated with acetic anhydride in a subsequent step to give UDP-GalNAc.

A modification of the latter procedure has been adapted for a large-scale synthesis of UDP-GalNAc.[172b] In this procedure, galactosamine-1-phosphate was prepared with galactokinase coupled to an ATP regeneration system, and used as a substrate for the uridyltransferase. UDP-Glc was regenerated in situ from UTP and the product Glc-1-*P*, under catalysis by UDP-Glc pyrophosphorylase. This also shifts the equilibrium toward the formation of UDP-GalN. Finally, a chemical N-acetylation of the UDP-GalN thus produced with *N*-acetoxysuccinimide provides UDP-GalNAc. This procedure has also been adapted to an in situ synthesis of UDP-GalN for glycosylation, with cofactor regeneration, to provide β-glycosides of GalN (see Section 5.2.8).

5.1.5. GDP-Mannose (GDP-Man) and GDP-Fucose (GDP-Fuc)

GDP-Man has been prepared from Glc and GMP with dried Baker's yeast cells.[82] The procedure involves the biocatalytic conversion of glucose to Man-1-*P*, and a subsequent conversion to GDP-Man with GDP-Man pyrophosphorylase. A cell-free extract from Baker's yeast has also been used to synthesize GDP-Man from mannose.[176] A direct synthesis from chemically prepared Man-1-*P* and GTP, catalyzed by GDP-Man pyrophosphorylase [EC 2.7.7.13] is useful for a large scale (Scheme 39).[155]

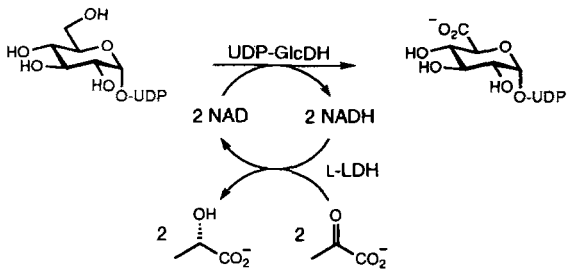


Scheme 39. Synthesis of GDP-Fuc.

GDP-fucose is biosynthesized in vivo from GDP-Man by an NADPH-dependent oxidoreductase enzyme system. Such systems have also been utilized for in vitro synthesis of GDP-Fuc. For example, the conversion of GDP-Man to GDP-Fuc was accomplished with a crude enzyme preparation from *Agrobacterium radiobacter*.[177] NADPH was regenerated in situ from NADP with glucose-6-phosphate dehydrogenase and Glc-6-*P*.[178] In a similar procedure, GDP-Fuc has been generated in situ for use in a glycosylation reaction with α1–3fucosyltransferase (see Section 5.2.3).[179] Enzymes from a minor biosynthetic pathway which synthesize GDP-Fuc from L-fucose-1-phosphate[179] or L-fucose[180] have also been exploited for synthesis.[179, 180] Fucose was phosphorylated by fucokinase [EC 2.7.1.52] to produce Fuc-1-*P*, which subsequently underwent a GDP-fucose pyrophosphorylase-catalyzed reaction with GTP to provide GDP-Fuc. Several practical chemical syntheses of GDP-Fuc have also been reported.[181]

5.1.6. UDP-Glucuronic Acid (UDP-GlcUA)

UDP-Glucuronic acid is biosynthesized by oxidation of UDP-Glc with UDP-Glc dehydrogenase, an NAD-dependent enzyme. Enzyme preparations from bovine liver have been employed for gram-scale syntheses of UDP-GlcUA (Scheme 40).[155, 182] The NAD cofactor was regenerated with lactate dehydrogenase in the presence of pyruvate. Additionally, extracts from guinea pig liver have been used to generate UDP-GlcUA in situ for use in enzymatic glycosylations with glucuronyltransferases.[138]

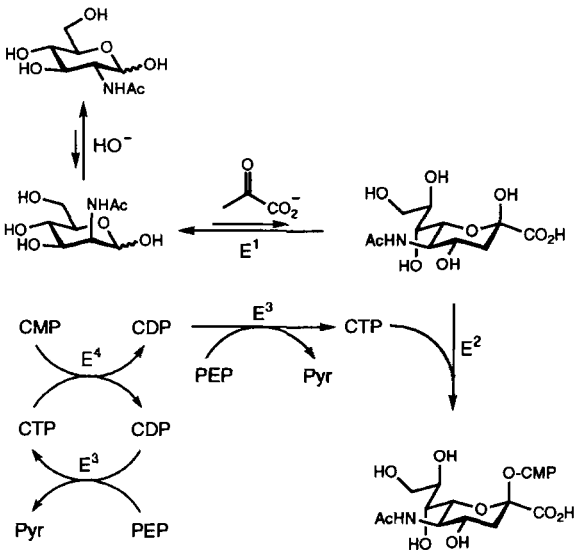


Scheme 40. Synthesis of UDP-GlcUA.

5.1.7. *CMP-N-Acetylneuraminic Acid (CMP-NeuAc)*

CMP-*N*-acetylneuraminic acid has been prepared enzymatically on small scales (less than 0.5 mmol) from CTP and NeuAc, under catalysis by CMP-NeuAc synthetase [EC 2.7.7.43].[184] An improvement in this procedure, which is suitable for multigram-scale synthesis,[185] has been developed: CTP is itself synthesized in situ from CMP with adenylate kinase and pyruvate kinase. Adenylate kinase catalyzes the equilibration of CTP and CMP to CDP, which is subsequently phosphorylated by pyruvate kinase to provide CTP. Another procedure has been employed in which the NeuAc used in the synthesis of CMP-NeuAc was prepared in a NeuAc aldolase-catalyzed reaction of pyruvate with *N*-acetylmannosamine, which was itself generated from *N*-acetylglucosamine by a base-catalyzed epimerization.[166] In a one-pot synthesis of CMP-NeuAc based on the latter procedure, NeuAc is prepared in situ from *N*-acetylmannosamine and pyruvate, catalyzed by sialic acid aldolase (Scheme 41).[186] Chemical syntheses of CMP-NeuAc have also been reported.[187–189]

The gene encoding *E. coli* CMP-NeuAc synthetase has been cloned[190, 191] and overexpressed in *E. coli* using λ-ZAP vector and the LacZ promotor[192, 193] or PKK223 vector-tac promotor.[194] The enzyme from calf brain has also been cloned and overexpressed. CMP-NeuAc synthetase was shown to accept



Scheme 41. Multienzymatic synthesis of CMP-NeuAc. E^1 = NeuAc aldolase, E^2: CMP-NeuAc synthetase, E^3: pyruvate kinase, E^4: adenylate kinase, Pyr = pyruvate.

several NeuAc derivatives as substrates. For example, 9-deoxy-7,9-dideoxy-, and 4,7,9-trideoxy-NeuAc are all converted into the corresponding CMP-NeuAc derivative.[195] On the other hand, neither the 4-oxo, 7-oxo, or 8-oxo derivatives of NeuAc, nor their dimethylacetals, are substrates for CMP-NeuAc synthetase.[196] The enzyme accepts a variety of modifications at the 9-position, and the hydroxyl group can be replaced with several different groups with little effect on the Michaelis constant K_m.[186, 197–199]

5.2. Substrate Specificity and Synthetic Applications of Glycosyltransferases

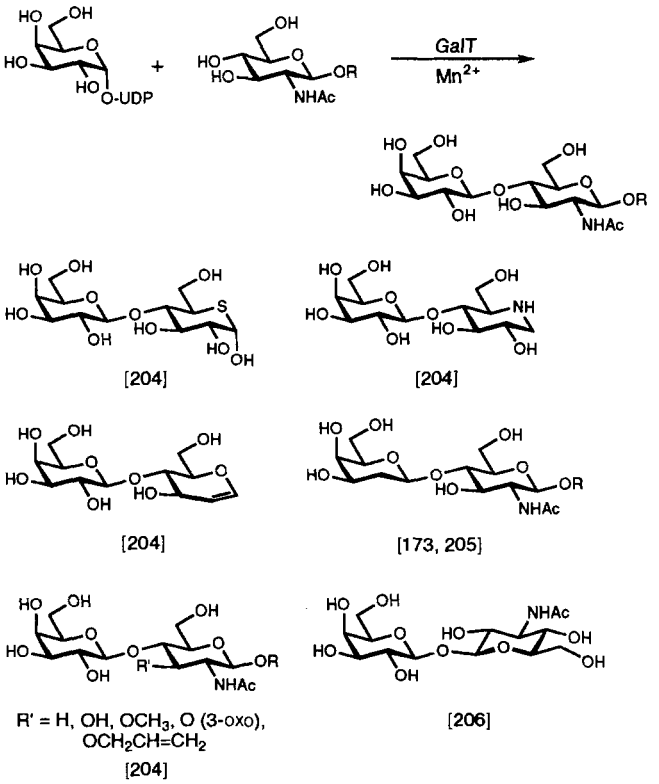
In general, for each sugar nucleotide glycosyl donor, many glycosyltransferases exist, each of which transfers the particular donor to different acceptors. These enzymes are generally considered to be specific for a given glycosyl donor and acceptor, as well as for the position and the configuration of the newly formed glycosidic bond. This specificity has led to the "one enzyme–one linkage" concept.[11] In other words, the specificity of the glycosyltransferases ensures fidelity in oligosaccharide sequences in vivo without the use of a template scheme. Though systematic investigations of the in vitro substrate specificity of most glycosyltransferases have not been carried out, some deviations from this picture of absolute specificity have been observed, both in the glycosyl donors and acceptors. Moreover, studies toward the design of inhibitors of glycoprotein biosynthesis[200] have also shown that the specificities of glycosyltransferases are not absolute.

5.2.1. *Galactosyltransferase (GalT)*

Because of its availability, β1–4-galactosyltransferase (UDP-Gal:N-acetylglucosamine β1–4-galactosyltransferase, [EC 2.4.1.22])[201, 202] is one of the most extensively studied mammalian glycosyltransferases with regard to synthesis and substrate specificity. This enzyme catalyzes the transfer of galactose from UDP-Gal to the 4-position of β-linked GlcNAc residues to produce the Galβ1–4GlcNAc substructure. In the presence of lactalbumin, however, glucose is the preferred acceptor, resulting in the formation of lactose, Galβ1–4Glc. The enzyme has been employed in the in vitro synthesis of *N*-acetyllactosamine and glycosides thereof, as well as other galactosides.

Galactosyltransferase utilizes as acceptor substrates *N*-acetylglucosamine and glucose and β-glycosides thereof, 2-deoxyglucose, D-xylose, 5-thioglucose, *N*-acetylmuramic acid, and *myo*-inositol.[201] Modifications at the 3- or 6-position of the acceptor GlcNAc are also tolerated. For example, Fucα1–6GlcNAc and NeuAcα2–6GlcNAc are substrates.[203] Acceptor substrates that are derivatized at the 3-position include 3-*O*-methyl-GlcNAc,[203] 3-deoxy-GlcNAc, 3-*O*-allyl-GlcNAcβOBu, and 3-oxo-GlcNAc.[204] All glycosides of GlcNAc that are substrates for the galactosyltransferase have β-glycosidic linkages. Both α- and β-glycosides of glucose are acceptable; however, the presence of lactalbumin is required for galactosyl transfer onto α-glcosides. Neither D-mannose, D-allose, D-galactose, D-ribose, nor D-xylose are substrates. Monosaccharides that have a negative charge, such as glucuronic acid and α-glucose-1-phosphate, are

also not accepted as substrates. Scheme 42 depicts several disaccharides that have been synthesized with galactosyltransferase.[173, 204–206] A particularly interesting example is the β,β-1,1-linked disaccharide, in which the anomeric hydroxyl of 3-acetamido-3-deoxyglucose serves as the acceptor moiety.[206b] The acetamido function apparently controls the position of glycosylation.



Scheme 42. Some disaccharides synthesized with β1–4galactosyltransferase.

β1–4Galactosyltransferase has also been employed in solid-phase oligosaccharide synthesis and has been used to galactosylate *gluco* or *cellobio* subunits of polymer-supported oligosaccharides and polysaccharides.[207] The resulting oligosaccharides can then be removed from the support by either a photochemical cleavage or a chymotrypsin-mediated hydrolysis. The types of polymer supports employed include polyacrylamide and a water-soluble poly(vinyl alcohol). *N*-Acetylglucosaminyl amino acids and peptides have also been used as substrates for galactosyltransferase to afford galactosylated glycopeptides.[205, 208] The carbohydrate chain can then be further extended with other transferases, such as sialyltransferase.[205, 208] Similarly, the synthesis of a ceramide glycoside, which was subsequently enzymatically sialylated, provided a G_{M_3} analog.[209]

As donor substrates, the β-galactosyltransferase also transfers glucose, 4- and 6-deoxygalactose, arabinose, glucosamine, galactosamine, *N*-acetylgalactosamine, 2-deoxygalactose, and 2-deoxyglucose from their UDP-derivatives to provide an enzymatic route to oligosaccharides that terminate in β-1,4-linked residues other than galactose (Table 5).[210–213] An example worthy of note is the transfer of 5-thiogalactose (entry 8).[212] Although the rate of the enzyme-catalyzed transfer of many of these nonnatural donor substrates is quite slow, this method is useful for milligram-scale synthesis. The α1–3-galactosyltransferase and α1–3GlcNAc transferase involved in the B and A blood-group antigens, respectively, have also been studied.[210b]

Table 5. Relative rates of β1–4galactosyltransferase-catalyzed transfer of donor substrates.

Donor substrates	k_{rel}	Ref.
UDP-Gal	100	[211a]
UDP-Glc	0.3	[210, 211a]
UDP-4-desoxy-Glc	5.5	[211a]
UDP-Ara	4.0, R = H 1.3, R = CH_3 0.2, R = CH_2F	[211a] [211b] [211b]
UDP-GalNAc	4.0	[210]
UDP-GlcNAc	0.00	[210]
UDP-GlcN	0.09	[210]
UDP-5-thio-Gal	5.0	[212]
UDP-2-desoxy-Gal	90	[173] [a], [205] [b]

[a] Generated in situ from 2-deoxygalactose with galactokinase/uridyltransferase [213]. [b] Generated in situ from 2-deoxyglucose with hexokinase/mutase/UDP-Glc pyrophosphatase/epimerase.

5.2.2. *Sialyltransferase (SiaT)*

Several α2–6- and α2–3 sialyltransferases have been used for oligosaccharide synthesis.[214–216] These sialyltransferases generally transfer *N*-acetylneuraminic acid to either the 6- or 3-position of terminal Gal or GalNAc residues. The α2–8-sialyltransferase is involved in the synthesis of α-2,8-linked polysialic acids.[217] Some sialyltransferases have been shown to accept CMP-NeuAc analogs that are derivatized at the 9-position of the sialic acid side chain,[197–199, 218] such as those in which the hydroxyl group at C-9 is replaced with an amino, fluoro, azido, acetamido, or benzamido group. Analogs of the acceptors

Galβ1-4GlcNAc and Galβ1-3GalNAc in which the acetamido function is replaced by an azide, phthalimide, carbamate, or pivaloyl functionality are also substrates for the enzymes.[219] A recent synthesis of a G_{M_3} analog started with a disaccharyl ceramide derivative in which the fatty acid amide group was replaced with an azide group.[220] To incorporate sialic acid analogs into sialosides is, however, problematic because sialyltransferases are very specific for CMP-sialic acid.

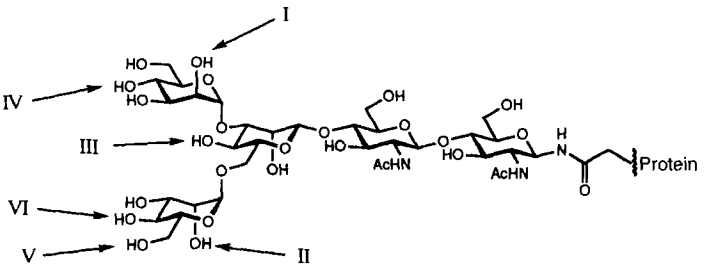
5.2.3. *Fucosyltransferase (FucT)*

Fucosyltransferases are involved in the biosynthesis of many oligosaccharide structures such as blood-group substances and antigens associated with the cell surface and tumors. Fucosylation is one of the last modifications of oligosaccharides in vivo. Several fucosyltransferases have been isolated and used for in vitro synthesis.[221-224] For example, α1-3fucosyltransferase has been used to L-fucosylate the 3-position of the GlcNAc of *N*-acetyllactosamine and of sialyl α2-3*N*-acetyllactosamine to provide the Lewis^x and sialyl Lewis^x structural motifs, respectively.[179, 221] Several other acceptor substrates with modifications in the GlcNAc residue can also be fucosylated (Scheme 43).[179] Galβ1-4Glc, Galβ1-4Glucal, and Galβ1-4(5-SGlc) are all substrates. A similar enzyme, α1-3(4fucosyltransferase, has also been used for synthesis. This enzyme fucosylates either the GlcNAc 3-position of Galβ1-4GlcNAc or the GlcNAc 4-position of Galβ1-3GlcNAc to afford Lewis^x or Lewis^a, respectively.[221, 222] The corresponding sialylated substrates have also been employed as acceptors.[221]

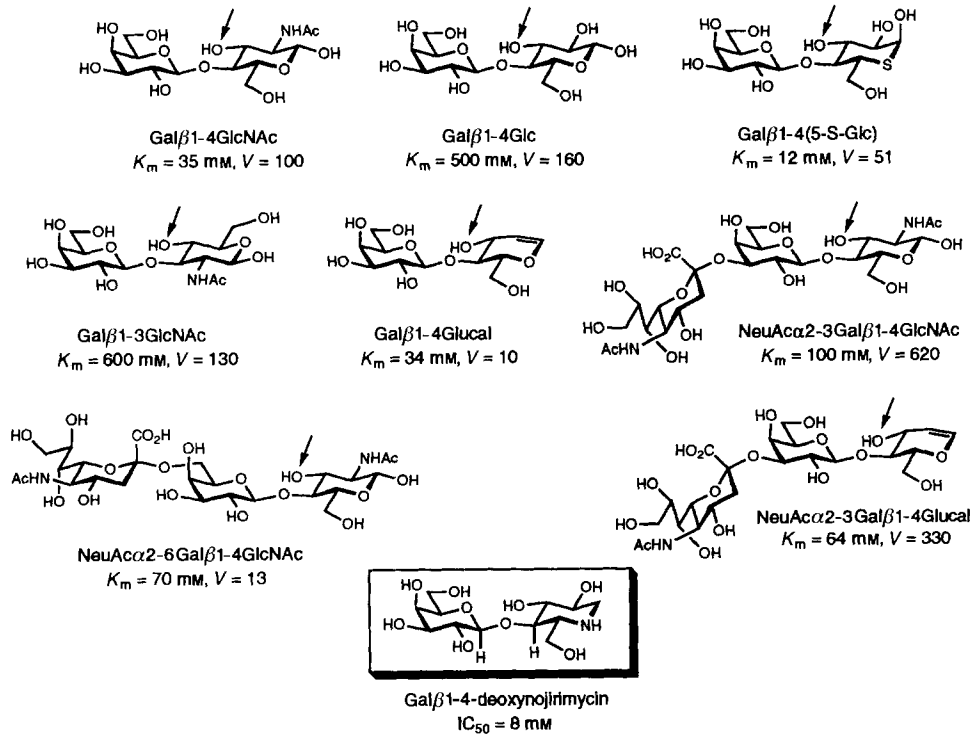
The Lewis^a α1-4fucosyltransferase has been shown to transfer nonnatural fucose derivatives from their GDP esters. 3-Deoxyfucose and L-arabinose are transferred to Galβ-1-4GlcNAcβO-$(CH_2)_8CO_2CH_3$ at a rate of 2.3% and 5.9%, respectively, relative to L-fucose.[224] Furthermore, this enzyme will transfer a fucose residue that is substituted at C-6 by a very large sterically demanding group. In particular, a synthetic blood-group antigen was attached, and the resulting „oligosacharide" was transferred to an acceptor from its GDP derivative by fucosyltransferase.[225] This approach has been used to alter the antigenic properties of cell-surface glycoproteins.

5.2.4. *N-Acetylglucosaminyltransferase*

In vivo, the *N*-acetylglucosaminyl transferases control the branching pattern of N-linked glycoproteins.[226, 227] Each of the enzymes transfers a βGlcNAc residue from the donor UDP-GlcNAc to a mannose or other acceptor. The GlcNAc transferases I-VI, which catalyze the addition of the GlcNAc residues to the core pentasaccharide of asparagine glycoproteins as outlined in Scheme 44, have been identified and character-



Scheme 44. Specificity of GlcNAc transferases I-VI.



Scheme 43. Substrates and inhibitors for fucosyltransferase. The reason that Galβ1-4deoxynojirimycin is an inhibitor may be due to a hydrogen bond between the NH group of the inhibitor and the base in the enzyme that abstracts the 3-OH proton of the acceptor (indicated by an arrow).

ized.[226-228] These, as well as other GlcNAc transferases, have been exploited for purposes of oligosaccharide synthesis.[229, 230]

GlcNAc transferases have also been utilized to transfer nonnatural residues to oligosaccharides. In addition to transferring GlcNAc, *N*-acetylglucosaminyl transferase I from human milk catalyzes the transfer of 3-, 4-, or 6-deoxy-GlcNAc from its UDP derivative to Manα1-3(Manα1-6)ManβO-$(CH_2)_8CO_2CH_3$.[229] The 4- and 6-deoxy-GlcNAc analogs can also be transferred by GlcNAc transferase II; however UDP-3-deoxy-GlcNAc is not a substrate for this enzyme.[229] One of the many synthetic applications of GlcNAc transferases is the attachment of the terminal GlcNAc of GlcNAcβ1-4GlcNAcα dolichyl pyrophosphate, a substance employed in the study of oligosaccharyl transferase.[231a] A murine kidney GlcNAc transferase was used

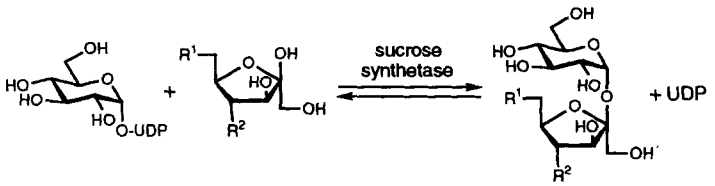
in the synthesis of a hexasaccharide containing sialyl Lewis^x. This enzyme catalyzes the transfer of GlcNAc to 6-OH of Galβ1-3GlcNAc.[231b]

5.2.5. *Mannosyltransferase*

Various mannosyltransferases have been shown to transfer mannose and 4-deoxymannose from their GDP adducts to acceptors.[232] The α1-2mannosyltransferase from yeast has been cloned and overexpressed in *E. coli* (about $1UL^{-1}$) and was employed to transfer mannose to the 2-position of various derivatized α-mannosides and α-mannosyl peptides to produce the Manα1-2Man structural unit.[233] A recent report indicates that mannosyltransferases from porcine liver accept GlcNAcβ1-4GlcNAc phytanyl pyrophosphate, an analog of the natural substrate in which the phytanyl moiety replaces dolichol.[234]

5.2.6. *Sucrose Synthetase*

The fructose derivatives 1-azido-1-deoxy-, 1-deoxy-1-fluoro-, 6-deoxy-, 6-deoxy-6-fluoro-, and 4-deoxy-4-fluorofructose have been used as glycosyl acceptors in the sucrose synthetase catalyzed synthesis of sucrose analogs (Scheme 45).[235] 6-Deoxy- and 6-deoxy-6-fluorofructose were generated in situ from the corresponding glucose derivatives under catalysis by glucose isomerase.[235] Because the reaction is reversible, the sucrose synthetase from rice was used for the preparation and regeneration of UDP-Glc. The enzyme also accepts TDP, ADP, and GDP.[236]



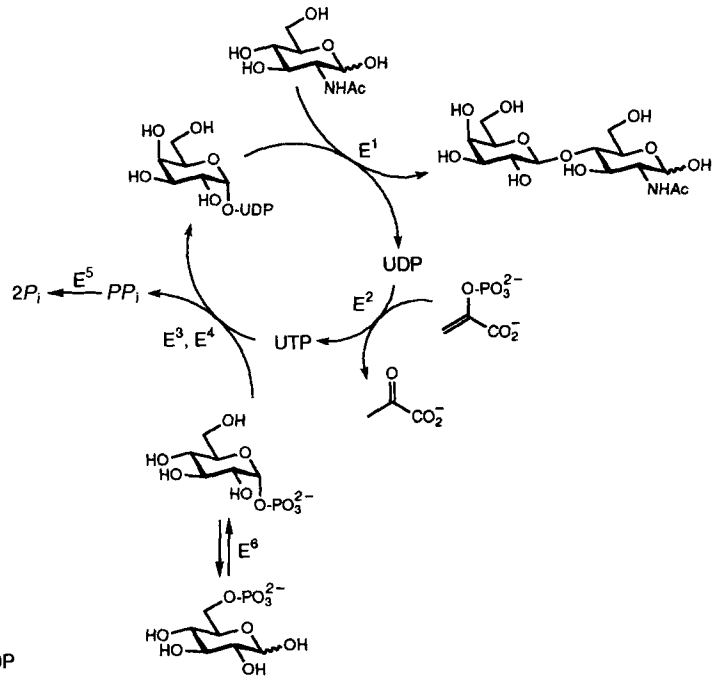
Scheme 45. Synthesis of sucrose analogs with sucrose synthetase. The system can also be used in the regeneration of UDP-Glc from sucrose and UDP. **a**: $R^1 = R^2 = OH$; **b**: $R^1 = F$, $R^2 = OH$; **c**: $R^1 = OH$, $R^2 = F$.

5.2.7. *Oligosaccharyltransferase*

As mentioned earlier, oligosaccharyltransferase catalyzes the transfer of an oligosaccharide consisting of two GlcNAc, nine mannose, and three glucose units from a dolichyl pyrophosphate intermediate to an Asn residue of a nascent peptide or protein.[137] The enzyme also transfers the minimal unit GlcNAcβ1-4GlcNAc from the corresponding dolichyl pyrophosphate donor or from a derivative in which the lipid component is truncated or simplified.[141] The minimal peptide that will serve as an acceptor is the tripeptide Asn-X-Ser/Thr. Oligosaccharyltransferase has been utilized for the in vitro synthesis of several peptides containing glycosylated Asn residues. The glycopeptides Bz-Asn(oligosaccharyl)-Leu-Thr-NH_2,[237] Bz-Asn-(GlcNAc$_2$)-Leu-Thr-NH_2,[238] and Ac-Asn(GlcNAc$_2$)-Leu-Thr-OCH_3/$NHCH_3$[140] were synthesized as well as glycosylated cyclic peptides such as Cys-Als-Asn(GlcNAc$_2$)-Cys-Thr-Ser-Ala.[140]

5.2.8. *In Situ Regeneration of the Cofactor*

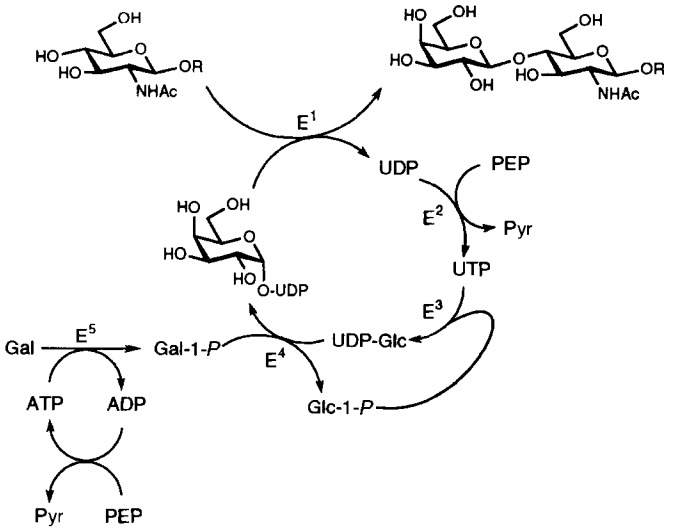
Though analytical- and small-scale synthesis with glycosyltransferases is extremely powerful, the high cost of sugar nucleotides and product inhibition caused by the released nucleoside mono- or diphosphates present major obstacles to large-scale synthesis. A simple solution to both of these problems is the regeneration of the sugar nucleotide in situ from the released nucleoside diphosphate. The first example of the use of such a strategy is the galactosyltransferase-catalyzed synthesis of *N*-acetyllactosamine.[161] (Scheme 46). A catalytic amount of UDP-Gal



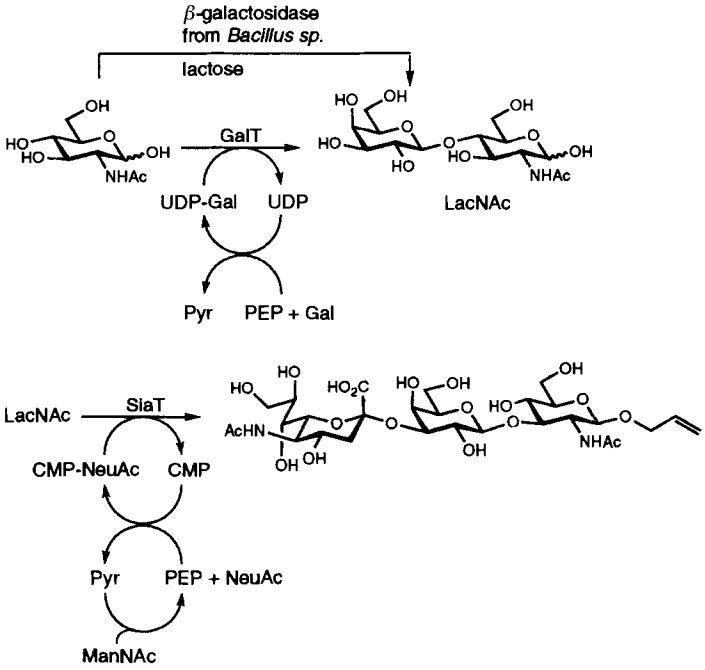
Scheme 46. Galactosyltransferase-catalyzed glycosylation involving UDP-glucose epimerase with in situ regeneration of UDP-Gal and UDP-Glc. E^1 = β1-4galactosyltransferase, E^2 = pyruvate kinase, E^3 = UDP-Glc pyrophosphorylase, E^4 = UDP-Glc epimerase, E^5 = inorganic pyrophosphorylase, E^6 = phosphoglucomutase.

is initially used to glycosylate GlcNAc; UDP-Gal is regenerated from the product UDP and galactose with an enzyme-catalyzed reaction sequence that requires stoichiometric amounts of a phosphorylating agent. Several oligosaccharides have been prepared with routes based on this concept.[203] A second regeneration system for UDP-Gal, which is based on the use of galactose-1-phosphate uridyltransferase, has also been developed[213] and has been used in the preparation of analogs such as 2'-deoxy-LacNAc and 2'-amino-2'-deoxy-LacNAc (Scheme 47). A third regeneration method for UDP-Gal is based on sucrose synthetase catalyzed formation of UDP-Glc from sucrose and UDP.[236]

In situ cofactor regeneration offers several advantages. First, a catalytic amount of nucleoside diphosphate and a stoichiometric amount of monosaccharide can be used as starting materials rather than a stoichiometric quantity of sugar nucleotide, thus reducing costs tremendously. Second, product inhibition by the released NDP is minimized due to its low concentration



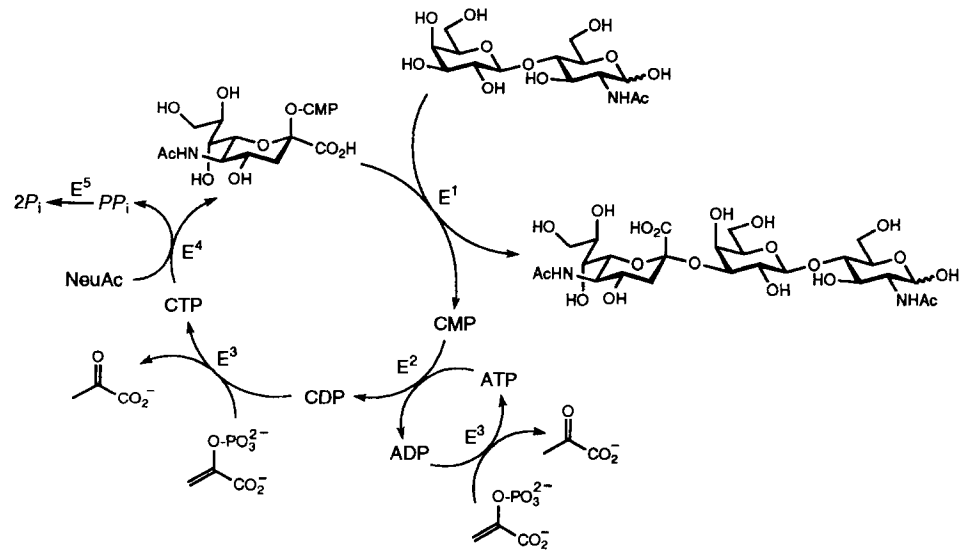
Scheme 47. Galactosyltransferase-catalyzed glycosylation involving galactose-1-phosphate uridyltransferase with in situ regeneration of UDP-Gal and UDP-Glc. E^1 = β1-4galactosyltransferase, E^2 = pyruvate kinase, E^3 = UDP-Glc pyrophosphorylase, E^4 = galactose-1-phosphate uridyltransferase, E^5 = galactokinase, Pyr = pyruvate.



Scheme 49. Synthesis of a trisaccharide with a galactosidase/sialyltransferase or galactosyltransferase/sialyltransferase enzyme system. Enzymatic sialylation of LacNAc in situ gave the trisaccharide that is no longer sensitive to galactosidase. Pyr = pyruvate.

in solution. And third, isolation of the product is greatly facilitated.

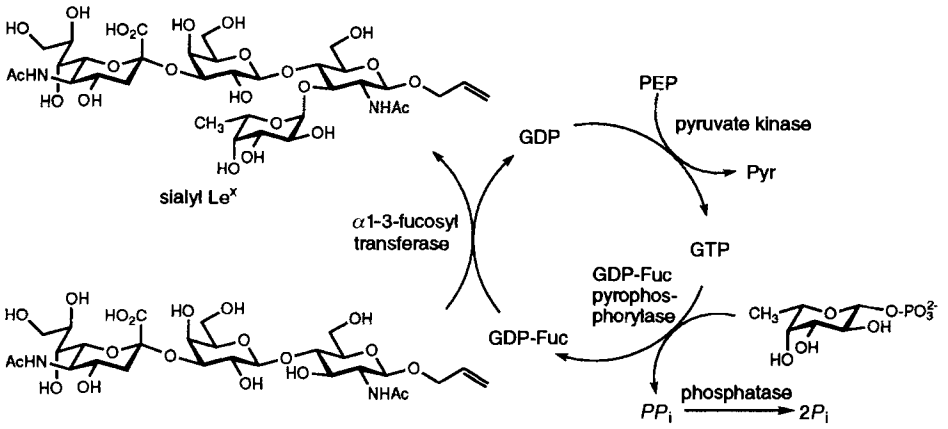
A regeneration system for CMP-NeuAc (Scheme 48) has also been developed.[192, 239] The UDP-Gal and CMP-NeuAc regeneration schemes can also be combined in a one-pot reaction (Scheme 49) and applied to the synthesis of sialyl oligosaccharides.[179] The development of these regeneration systems, as well as the more recent development of regeneration schemes or UDP-GlcNAc[240], GDP-Man,[233] and GDP-Fuc,[179] as well as UDP-GlcUA[183] should facilitate the more widespread use of glycosyltransferases for oligosaccharide synthesis. One example is the recent synthesis of sialyl Lewis^x (Scheme 50).[179]



Scheme 48. Enzymatic sialylation with in situ regeneration of CMP-NeuAc. E^1 = α2-3sialyltransferase, E^2 = nucleoside monophosphate kinase or adenylate kinase. E^3 = pyruvate kinase, E^4 = CMP-NeuAc synthetase. E^5 = pyrophosphate.

5.3. Cloning and Expression of Glycosyltransferases and Sugar Nucleotide Synthetases

Although many glycosyltransferases catalyze similar reactions and in many cases use the same donor substrate, there appears to be little sequence homology among the different transferases. There is, however, a significant homology between the same enzymes from different species. For instance, the protein sequence of β1-4galactosyltransferase from humans has an 86% identity with that of the enzyme from rat. The different glycosyltransferases do exhibit some similarity in that all the cDNA sequences determined to date encode regions consistent with a short N-terminal tail, a hydrophobic transmembrane sequence, a short stem sequence, and a large C-terminal catalytic domain.[244] In addition to the membrane-bound form of the glycosyltransferases, soluble forms of the enzymes have also been identified in various body fluids such as the blood, milk, and colostrum. Indeed, some of these enzymes have been isolated and purified from these fluids.[241-243] A comparison of the cDNA sequences of these soluble enzymes with the N-terminal protein sequence of the glycosyltransferases that have been sequenced suggests that the



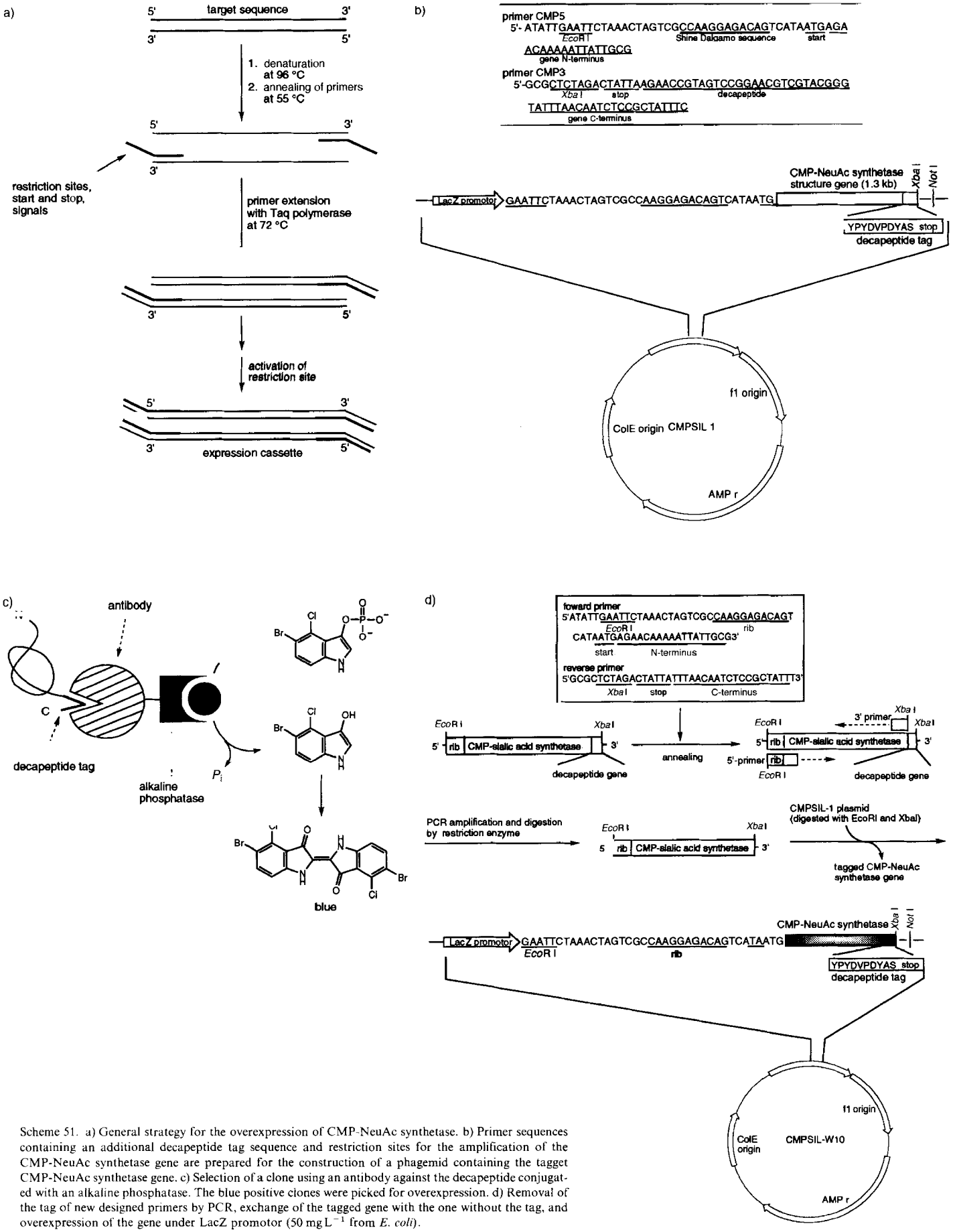
Scheme 50. Enzymatic fucosylation with in situregeneration of GDP-fucose.

stem region has been cleaved to release the large catalytic domain from the membrane. Presumably, this theme of signal sequence cleavage is typical for all the glycosyltransferases.[244]

The amount of the glycosyltransferase that can be isolated from a natural source is often limited by the low concentrations of these enzymes present in most tissues and body fluids. The purification of glycosyltransferases is further complicated by the relative instability of this group of enzymes.[11] For this reason, a great deal of interest has been directed toward the cloning of the glycosyltransferase genes into convenient expression systems. The general strategy involved in this procedure is outlined in Scheme 51a. The glycosyltransferase gene must first be identified and isolated from the mRNA pool by cloning of the cDNA to make a cDNA library. This library is then screened to identify the glycosyltransferase gene of interest among approximately 10^6 different sequences present in the library. Once identified, the gene is sequenced and a more complete cloning strategy is developed in order to incorporate the gene into an expression vector. This laborious path has successfully been practiced by several groups.[5, 244–253, 256–265] From various tissue sources cDNA is recovered, and, for example, the double stranded cDNA is ligated in λ phage through a convenient linker and packed into bacteriophages. The bacteriophages are then plated onto a lawn of *E. coli* and screened for the desired gene or gene product. The identification of the glycosyltransferase gene has most frequently been achieved by the hybridization of the gene to specific radiolabeled DNA probes.[245–248] Screening in this manner requires a previous knowledge of the gene sequence, information that in some cases may be obtained by extrapolation from a partial protein sequence or from the DNA sequence of the glycosyltransferase from a related source. Two other approaches have been used to screen glycosyltransferase cDNA libraries, both requiring successful transcription and translation of the gene product. In the cloning of the α2–6-sialyltransferase from rat liver, Weinstein et al. used polyclonal antibodies raised against the purified enzyme to screen the λ phages.[253] The other approach used by Larsen et al. alleviated the need for a previous knowledge of the sequence.[251] This method made use of the specificity of a lectin that recognizes the surface-expressed glycoconjugate product of the α1–3galactosyltransferase. The transfected cells were then panned in dishes coated with the lectin. The adherent cells were isolated and repanned for further purification. Each of these techniques makes use of libraries in which there are very few copies of the desired gene. A greater chance of success may be possible if the number of copies of the genes could be amplified. The introduction in 1985 of an in vitro amplification method based on the polymerase chain reaction (PCR) fulfilled this need.[254, 255] Of course, PCR (and Expression Cassette-PCR),[255] like the hybridization screening, requires a specific knowledge of the sequence.

Once identified, the genes are sequenced with standard procedures. An enlightened approach to the recloning of the gene into an expression vector is then used to develop an expression system. This recloning into expression systems has been performed with only a few of the glycosyltransferases. Toghrol et al. have inserted the mouse liver glucuronyltransferase gene into the yeast vector pEVP11 and expressed the enzyme in *Saccharomyces cerevisiae*.[245] The rat liver glucuronyltransferase, on the other hand, has been expressed in COS cells with the SV40 vector.[246] Bovine β1–4galactosyltransferase was cloned analogously.[247] A noteworthy approach toward the expression of the glycosyltransferase in *E. coli* has been developed to obtain human β1–4galactosyltransferase.[256] A unique *Rsr*II restriction site in the galactosyltransferase gene allowed the dissection of the sequence at the location of signal peptidase cleavage. The cohesive terminus was digested with Klenow fragment (the large subunit of the DNA polymerase I, which has a 3′ → 5′ exonuclease activity and cleaves the remaining bases at the restriction site), and the blunt end ligated to pIN-III-*omp*A_2[257] at *Eco*RI site that had also been treated with a Klenow fragment. Thus the code was generated for a fusion protein of the soluble form of galactosyltransferase with the *omp*A signal sequence (*omp*A = outer membrane protein A, an *E. coli* protein that controls secretion through its cleavable N-terminal signal sequence). Transcription and translation of this sequence in *E. coli* produced an active enzyme that was released into the periplasmic space. Purification and N-terminal sequencing of the enzyme verified the expresson of the soluble form of galactosyltransferase with an added N-terminal tail comprising three amino acids. The kinetic parameters of this enzyme appear to be identical to the isolated native enzyme. This system, however, only produced a very small amount of enzyme ($< 0.014\ U\ L^{-1}$). Though a 30-fold increase of productivity has been achieved with a modified *E. coli* host,[204] the level of productivity is still too low to be of practical synthetic value. More practical expression systems are perhaps those based on the baculo virus[179] and yeast.[258]

To date, very few glycosyltransferases have been cloned, expressed, and produced in quantities sufficient for enzymatic synthesis.[266] However, given the advantages of enzymatic synthesis of oligosaccharides over traditional schemes, research into the overexpression of glycosyltransferases will continue

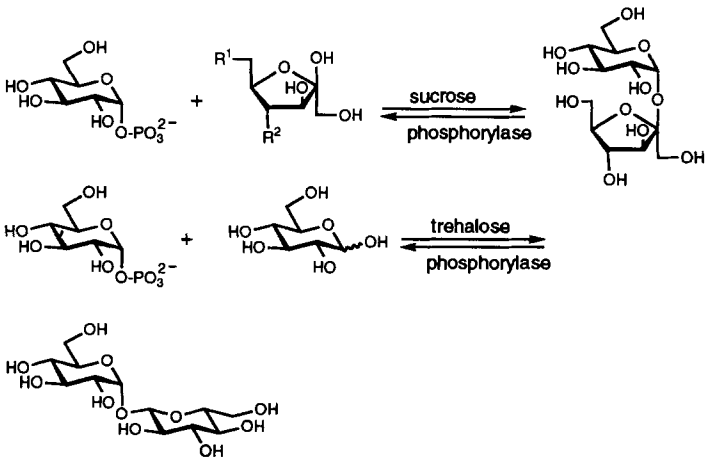


Scheme 51. a) General strategy for the overexpression of CMP-NeuAc synthetase. b) Primer sequences containing an additional decapeptide tag sequence and restriction sites for the amplification of the CMP-NeuAc synthetase gene are prepared for the construction of a phagemid containing the tagget CMP-NeuAc synthetase gene. c) Selection of a clone using an antibody against the decapeptide conjugated with an alkaline phosphatase. The blue positive clones were picked for overexpression. d) Removal of the tag of new designed primers by PCR, exchange of the tagged gene with the one without the tag, and overexpression of the gene under LacZ promotor (50 mg L^{-1} from *E. coli*).

to flourish. Schemes 51b–51d describe the procedures used in the overexpression of CMP-sialic acid synthetase in *E. coli* ($\sim 50\,mg\,L^{-1}$).

5.4. Non-Leloir Glycosyltransferases: Transfer of Glycosyl Donors from Glycosyl Phosphates and Glycosides

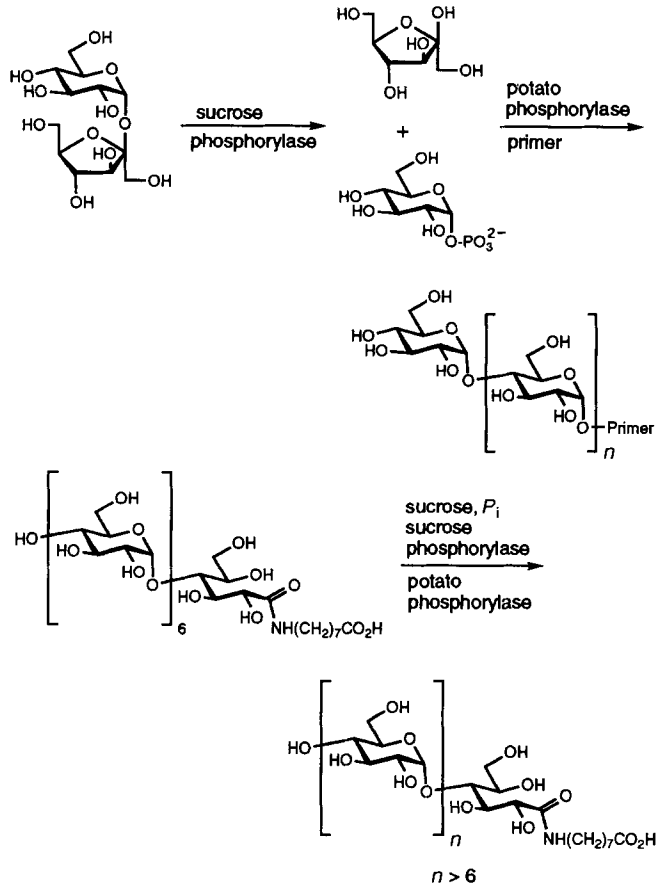
Oligosaccharides can also be prepared using non-Leloir glycosyltransferases. Phosphorolysis of polysaccharides is catalyzed by a group of these enzymes called glucan phosphorylases. The reaction is reversible and can be used in the synthesis of oligo- or polysaccharides. Two particularly important examples are the syntheses of sucrose and trehalose, catalyzed by sucrose phosphorylase[267] and trehalose phosphorylase[267] (Scheme 52). Examples of other enzymes of this class are those involved in synthesis of dextrans and levans.[268]



Scheme 52. Phosphorylase-catalyzed synthesis of sucrose and trehalose.

Non-Leloir transferases have also been used to synthesize a variety of polysaccharides. The synthesis of modified polysaccharides may provide materials with more desirable physical and biological properties than their natural counterparts. Approaches to influencing the characteristics of polymers include the control of genes encoding the enzymes responsible for their production, regulation of the activity of these enzymes, or the influence of their in vivo synthesis.[269] Potato phosphorylase [EC 2.4.1.1] has been used in vitro to prepare maltose oligomer,[159] and a family of linear and star- and comb-shaped polymers.[270]

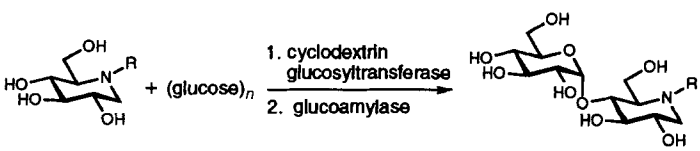
Improvement of this system has recently been accomplished with the use of a coupled enzyme system in which glucose-1-phosphate is generated in situ from sucrose and inorganic phosphate catalyzed by sucrose phosphorylase.[160] The inorganic phosphate liberated by potato phosphorylase is used by sucrose phosphorylase to drive the formation of polymer, thereby increasing the yield. This coupled enzyme system also allows for regulation of the molecular weight of the polysaccharide product by control of the concentration of the primer. Nonnatural primers bearing functional groups can also be used to prepare tailor-made polysaccharides for further manipulation, for example, for attachment to proteins or other compounds (Scheme 53).



Scheme 53. Phosphorylase-catalyzed polysaccharide synthesis.

Cyclodextrin α1–4glucosyltransferase [EC 2.4.1.19] from *Bacillus macerans* catalyzes the cyclization of oligomaltose to form α-, β-, and δ-cyclodextrin, as well as the transfer of sugars from cyclodextrin to an acceptor to form oligosaccharides.[271, 272] The enzyme can also transform α-glucosyl fluoride into a mixture of α- and β-cyclodextrins and maltooligomers in almost equal amounts.[273] When immobilized on a silica gel support that was functionalized with glutaraldehyde, the enzyme was very stable, and no loss of activity was observed after four weeks at 4 °C. With an appropriate choice of acceptor, this type of enzymatic catalysis may provide a new route to cyclodextrin analogs and novel oligosaccharides.

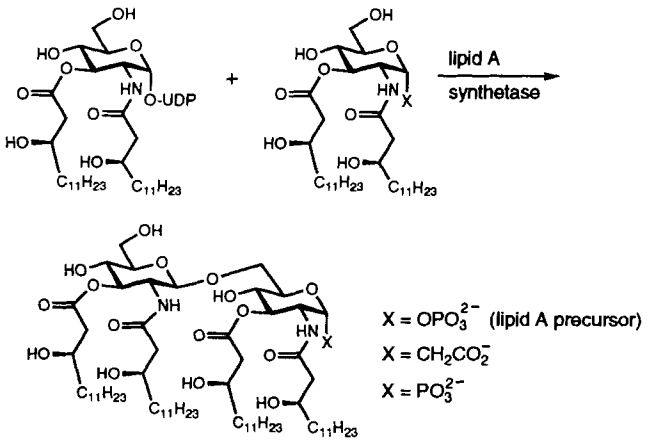
Nonnatural sugar acceptors that are structurally similar to glucose are also substrates for cyclodextrin glucosyl transferase. With deoxynojirimycin as acceptor and cyclodextrin as donor, an oligoglucosyl deoxynojirimycin was produced, which was subsequently hydrolyzed by glucoamylase to give 4-*O*-α-D-glucopyranosyl deoxynojirimycin in approximately 60% yield (Scheme 54).[274] A number of N-substituted derivatives of deoxynojirimycin were also good substrates for the transferase,



Scheme 54. Synthesis of glycosyl *N*-alkyldeoxynojirimycin derivatives.

and the products can be degraded with glucoamylase to glucosyl aza sugars. One of these glucosyl aza sugars, 4-*O*-α-D-glucopyranosyl-*N*-methyldeoxynojirimycin, was reported to be a potent inhibitor of glucosidase.

A key step in the biosynthesis of lipid A is the glycosylation of the 6-position of a 2,3-diacylglucosamine-1-phosphate by the donor UDP-2,3-diacylglucosamine to produce a lipid A precursor. This transformation is catalyzed by the enzyme lipid A synthetase, which has been cloned and overexpressed.[275] It has been used for the *in vitro* synthesis of the lipid A precursor and analogs thereof. Some examples include C-glycoside[276] and phosphate[277] analogs (Scheme 55).



Scheme 55. Synthesis of lipid A analogs with lipid A synthetase.

5.5. Glycosidases and Transglycosidases

Glycosides may be synthesized with glycosidase catalysts under either equilibrium or kinetically controlled conditions.[13] Though quite easy to perform, the equilibrium approach provides poor yields generally not exceeding 15%. Also, the low yield of the desired product and the formation of side products generally make purification difficult.

Kinetically controlled synthesis relies on the trapping of a reactive intermediate generated from an activated glycosyl donor with exogenous nucleophiles to form a new glycoside bond.[13] Suitable glycosyl donors for this transglycosylation reaction include di- or oligosaccharides, aryl glycosides, and glycosyl fluorides. This reaction must be carefully monitored, and stopped when the glycosyl donor is consumed in order to minimize glycoside hydrolysis.

Yields in kinetically controlled synthesis generally range from 20 to 40%. Although addition of organic solvent might be expected to increase product yields, as in the equilibrium controlled approach, this effect generally has not been observed.

The kinetically controlled approach has primarily been applied to the glycosidases that give products with retention of configuration. However, an inverting glycosidase has been used with glycosyl fluorides as glycosyl donors to afford products having the configuration at the anomeric position opposite to that of the donor.[278] For example, the α,α-linkage of α-D-glucopyranosyl-α-D-xylopyranoside has been prepared utilizing β-glucosylfluoride and α-trehalase.[279]

In general, the primary hydroxyl group of the acceptor reacts preferentially over secondary hydroxyl groups to give a 1,6-glycosidic linkage. Some control of selectivity has been demonstrated by the selection of an appropriate dono/acceptor combination.[280] For example, the reaction catalyzed by α-galactosidase of α-Gal-OPh-*p*-NO_2 with α-Gal-OMe (or allyl α-galactoside) and β-Gal-OMe forms predominantly α-1,3 and α-1,6 linkages, respectively.[280a, b] The configuration of the anomeric center of the acceptor controls, to some extent, the position of glycosylation. This situation was also observed in the β-*N*-acetylgalactosaminidase reactions.[280c] α-gal-OPh-*p*-NO_2 acting both as donor and acceptor, forms referentially the α-1,3 linkage whereas the *ortho* nitrophenyl glycoside reacts in a similar fashion to form predominantly the α-1,2-linkage.[280a, b] With β-galactosidase, mainly the β-1,3-linked disaccharides were formed when benzyl or allyl β-galactoside was used as acceptor.[13, 280a, b] The use of glycals as acceptors has also been employed as a means of controlling selectivity,[281] giving the 1,3-linked glycoside as the major product when the 6-position was free or blocked.

One can also use glycosidases from different species to control the regioselectivity. For example, the β-galactosidase from testes catalyzes the formation of Galβ1–3GlcNAc from lactose or Galβ1–3GlcNAcβSEt[282] from either GlcNAc or GlcNAcβSEt. Minor products were then hydrolyzed by *E. coli* β-galactosidase, which preferentially hydrolyzes β-1,6-linked galactosyl residue. The overall yield of the β-1,3-linked disaccharides was around 10–20%. Syntheses of polysaccharides based on kinetically controlled glycosidase reactions have been accomplished, as examplified by the cellulase-catalyzed polymerization of β-cellobiosyl fluoride to form cellulose, with a degree of polymerization of greater than 22.[283a] The β-galactosidase from *Bacillus circulans* was used in large-scale synthesis of *N*-acetyllactosamine[283b] from lactose and GlcNAc. When this reaction was coupled with the sialyltransferase reaction in situ, a sialyl lactosamine was prepared[283c] (see Scheme 49), thus preventing the secondary hydrolysis of the galactosidase product.

Glycosyl transfer to non-sugar acceptors has also been demonstrated. These reactions are especially interesting with chiral, racemic, or *meso* alcohols, as some degree of diastereoselectivity due to the asymmetric microenvironment of an enzyme active site might be expected. Indeed moderate to exceptional diastereoselectivities[14] have been observed.

Transglycosidases are related to glycosidases in that they cleave glycoside bonds, but they differ in that they usually transfer the glycosyl moiety to another acceptor with a minimal amount of hydrolysis. Transglycosidases are thus useful catalysts for glycosylation. For example, a β-fructofuranosidase from *Antherobacter sp.* K-1 transfers fructose from sucrose to the 6-position of the glucose residues of stevioside and rubusoside.[284] Also, a sucrase from *Bacillus subtilis* catalyzes the reversible transfer of fructose from sucrose to the 6-hydroxyl of a fructose unit at the nonreducing end of a levan chain.[285] Several nonnatural sucrose derivatives have been prepared by taking advantage of this process.[286]

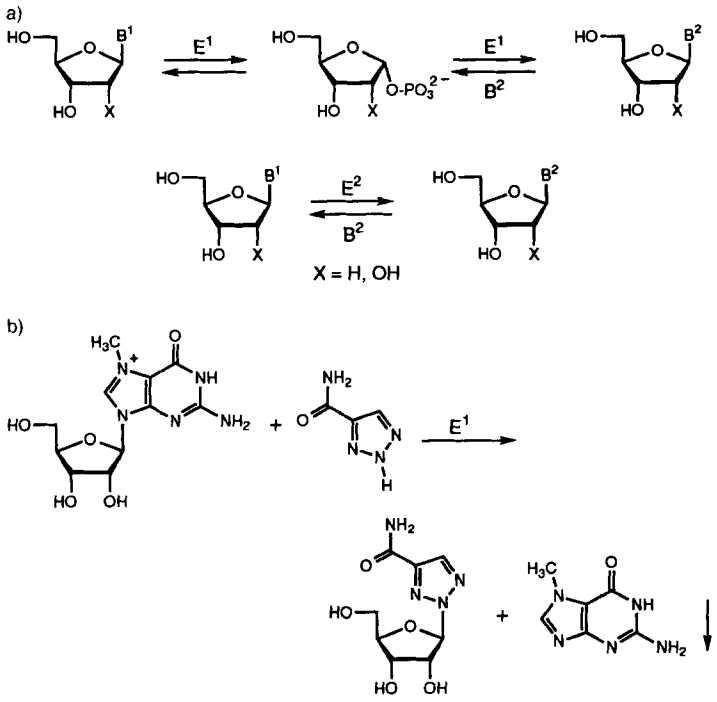
A transsialidase from *Trypanosoma cruzi* has been shown to transfer sialic acid reversibly to and from the 3-position of terminal β-Gal residues.[287] Chains terminating in α-linked galactose are not substrates. A number of oligosaccharides containing the

NeuAcα2-3Galβ substructure have been synthesized with this transsialidase.[288] Moreover, this enzyme has been shown to resialylate the terminal galactose units of the cell-surface glycoproteins and glycolipids of sialidase-treated erythrocytes.[289] and a galactoside.[290] Thus, the *T. cruzi* transsialidase potentially provides a useful alternative to α2-3sialytransferase.

5.6. Synthesis of Nucleosides

Nucleosides and their derivatives are ubiquitous in nature and are involved in a myriad of biochemical phenomena, most notably the storage and transfer of genetic information. Interest in this class of compounds has been stimulated by the efficacy of certain nucleosides as antiparasitic[291] (for example, 1-β-D-ribofuranosyl-1 *H*-pyrazolo[3,4-*d*]pyrimidin-4-one, allopurinol riboside) and antiviral (for example, 3'-azido-3'-deoxythymidine, azidovudine, AZT) agents.[292-293] Nucleosides have traditionally been prepared by various chemical methods.[294] These are multistep syntheses requiring protection and deprotection steps and glycosyl activation. Other problems include control of anomeric configuration, especially when preparing β-D-arabinofuranosyl- and 2'-deoxy-β-D-ribofuranosylnucleosides, and regiospecific C-N glycoside formation when there are several possible nucleophilic groups in the purine or pyrimidine base.

Two enzymatic methods have been used in the synthesis of nucleosides (Scheme 56a). Most enzymatic preparations of both natural and nonnatural nucleosides have been reported with nucleoside phosphorylases as catalysts.[295] These enzymes catalyze the reversible formation of a purine or pyrimidine nucleoside and inorganic phosphate from ribose-1-phosphate (R-1-P) and a purine or pyrimidine base. The equilibrium strongly favors nucleoside formation. Nucleoside synthesis has relied on the transfer of the ribose moiety of a readily available nucleoside to a different purine or pyrimidine base or analogs through the intermediacy of R-1-P. This work has been done primarily with isolated enzymes,[296] but whole cells have also been employed in a few cases.[297] The effects of deleterious hydrolases present in whole cells could be largely suppressed by conducting the reactions at 60 °C, a temperature at which the nucleoside phosphorylases maintain more than 70% of their original activity for three to five days.[297]



Scheme 56. a) Two strategies for enzyme-catalyzed nucleoside synthesis. E^1 = nucleoside phosphorylase, E^2 = transribosylase. Both E^1 and E^2 catalyze reversible reactions. b) When 7-*N*-methylguanosine is the donor, the reaction catalyzed by E^1 is irreversible.

Two basic strategies have generally been employed. The first involves isolation of R-1-P, which is prepared in good yield from a nucleoside in the presence of a high concentration of phosphate.[298] The isolated R-1-P is then used as the glycosyl donor in an enzymatic coupling reaction with added purine or pyrimidine bases or analogs. The second strategy involves a one-pot exchange of one nucleoside base for another in the presence of a catalytic amount of inorganic phosphate without isolation of R-1-P. The first strategy (isolation of R-1-P) is the most general, and almost any heterocycle that is a substrate for a nucleoside phosphorylase can be glycosylated by this method. The second strategy (in situ generation of R-1-P) is more limited. At best, it results in formation of an equilibium mixture of the substrate and the product nucleosides, from which the product must be isolated. In less favorable cases, the natural purine or pyrimidine base released from the glycosyl donor may be a potent competitive inhibitor with respect to the purine or pyrimidine analog, for which the enzyme has lower affinity. For example, because of competitive inhibition by hypoxanthine (K_m = 5.6 mM), 1,2,4-triazole-3-carboxamide (TCA, the aglycon component of virazole, K_m = 167 mM) cannot be glycosylated if inosine is the ribosyl donor and purine nucleoside phosphorylase (PNPase) the catalyst.[299] It was, however, possible to synthesize virazole by isolating of R-1-P and subsequently using it as the ribosyl donor.[299] An alternative way to circumvent the inhibition problems is to employ a pyrimidine nucleoside as the glycosyl donor and a purine (or purine analog) as the acceptor, since the released pyrimidine base does not inhibit the purine nucleoside phosphorylase.[300] By this method, both pyrimidine nucleoside phosphorylase and purine nucleoside phosphorylase are required.

Recently, direct purine-to-purine exchange reactions have been conducted without isolation of R-1-P with activated purine derivatives as the ribosyl donors.[301] The activated purine derivatives were prepared by 7-N-methylation of inosine and guanosine to provide derivatives that are excellent substrates for phosphorolytic cleavage by PNPase. The cleaved 7-*N*-methylpurines do not show any measurable product inhibition, and the equilibrium of the reaction greatly favors the product. The effectiveness of this approach was demonstrated by the one-pot synthesis of virazole from 1,2,4-triazole-3-carboxamide and 7-*N*-methyl guanosine (Scheme 56b).

The nucleoside phosphorylases accept a wide range of nucleoside analogs modified in both the base and glycosyl components, as substrates. Most of these reactions have been carried out in one step without isolation of the sugar phosphate, which has, however, been demonstrated to be an intermediate.

The use of nonnatural bases has met with much success with both natural and nonnatural glycosyl donors. However, a few limitations have been observed. For example, in the purine nucleoside phosphorylase catalyzed synthesis of certain imidazole[4,5-c]pyridine nucleosides (3-deazapurine nucleosides), the normally observed regiospecificity was lost, and a mixture of N-1 and N-3 glycosylated products was isolated. This problem was not encountered with purines, which retain the nitrogen at the 3-position: 2'-deoxyribosylation of unsubstituted purine gave only the N-9 glycosyl product.[300] Apparently either the N-3 nitrogen atom of the purine base or an appropriate substituent at C-6 is necessary for proper orientation of the base for regiospecific glycosylation.

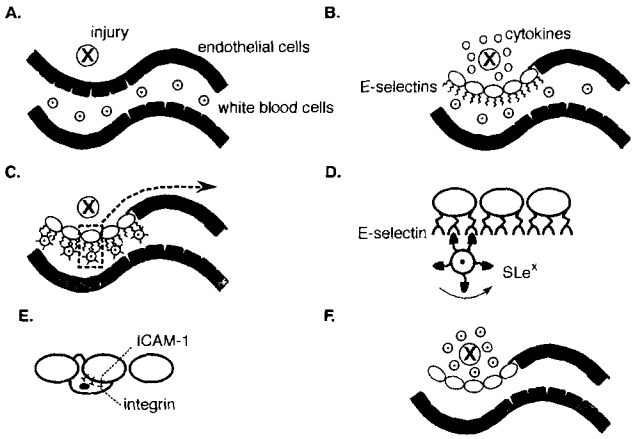
Sugar-modified nucleosides can be synthesized from glycosyl donors prepared by chemical modification of readily available nucleosides such as uridine and cytidine. Good yields of arabino-[297] and 2'-amino-2'-deoxyribonucleosides[293] have also been obtained enzymatically, although that of the enzymatic synthesis of 3'-amino-2',3'-dideoxyribonucleosides is low.[302] This low yield may be due to competition of the two pyrimidine heterocycles for enzyme binding or to an overall decreased reaction rate caused by alteration of the 3'-position, which may be important in substrate binding by the enzyme.[303]

N-Transribosylases have been employed in the synthesis of nucleoside analogs.[295, 304] Two classes of transribosylases have been identified: type I enzymes catalyze the transfer of the sugar moiety between two purine bases, and type II catalyze the transfer between any two bases. Like nucleoside phosphorylases, transribosylases are stereospecific for the β-anomer of the nucleoside product. Thymidine and 2'-deoxycytidine are the best glycosyl donors, and a reasonable amount of variation in the acceptor bases is tolerated. The transribosylase from *L. leichmanii* has been used to prepare 2-chloroadenosine, an antileukemic and immunosuppressive nucleoside.[304c]

5.7. Silyl Lewis^x and Related Structures

Carbohydrate-mediated cell adhesion is an important event, which can be initiated by tissue injury or infection and is involved in metastasis.[10] One such adhesion process that was recently discovered is the interaction between the glycoprotein E-selectin (formerly called *e*ndothelial *l*eukocyte *a*dhesion molecule or ELAM-1), which is expressed on the surface of endothelial cells during inflammation and an oligosaccharide structure displayed on the surface of neutrophils. The ligand recognized by E-selectin has been identified to be the tetrasaccharide sialyl Lewis^x (SLe^x), which is present at the terminus of glycolipids displayed on the surface of neutrophils.[305] The adhesion process[10] is stimulated by signaling molecules (cytokines) or other inflammatory factors (for example, toxins, lipopolysaccharides, leukotrienes) that induce the production of E-selectins. After binding to the endothelial cells, the white blood cells roll along the surface of the endothelium. Further adhesion occurs by protein–protein interactions, mediated by integrins on white blood cells and a protein ligand containing the RGD (Arg-Gly-Asp) sequence (called *i*ntercellular *a*dhesion molecule-1, ICAM-1) on endothelial cells. The white blood cells are then able to squeeze through gaps between endothelial cells and enter the adjacent tissue to help repair injury (Scheme 57).

If too many white blood cells are recruited to the site of injury, normal cells can also be destroyed. This can occur in the condition of septic shock, in chronic inflammatory diseases such as psoriasis and rheumatoid arthritis, and in the reperfusion tissue



Scheme 57. Inflammation of tissue involves E-selectin-mediated cell adhesion. When tissue injury occurs (A), cytokines are released to stimulate synthesis of E-selection (B). Adhesion then occurs through interaction of E-selectins and SLe^x on the surface of leukocytes (C, D). As leukocytes roll along the surface of endothelial cells, further adhesion occurs through interaction between integrins on leukocytes and the ligand on the endothelial cells that contain the sequence Arg-Gly-Asp (RGD) (called ICAM-1) (E). The leukocytes reach the injury site through small openings between the endothelial cells (F).

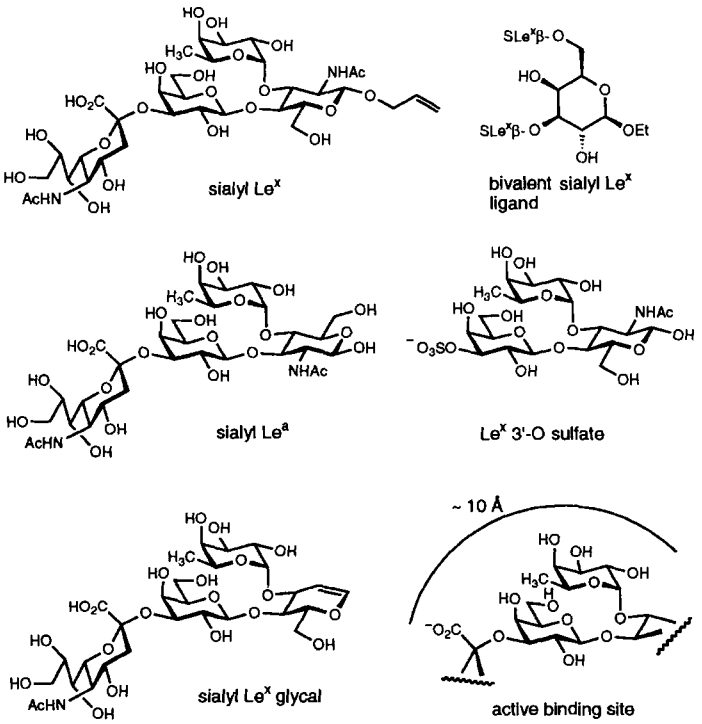
injury that occurs following heart attack, stroke, and organ transplant. High levels of sialyl Lewis^x have also been found on the surfaces of certain tumor and cancer cells (for instance, colon and lung cancer cells), which suggests that cancer cells may exploit this phenomenon of adhesion to metastasize after entering the blood stream.[10] In addition to E-selectin, two other carbohydrate-binding proteins, P- and L-selectin, also recognize sialylated ligands in cell-adhesion processes.

The discovery that the ligand for E-selectin is sialyl Lewis^x[305] provides new impetus for the development of therapeutic agents in the treatment of inflammation-related diseases and cancers. Since sialyl Lewis^x in solution competes with the white blood cells for binding to E-selectin, thus inhibiting the adhesion process, it may be useful as an anti-inflammatory to anticancer agent.[10] On the other hand, understanding the active conformation of sialyl Lewis^x recognized by E-selectin may also lead to the development of simple and easy-to-make inhibitors that are analogs or non-carbohydrate mimetics of sialyl Lewis^x with better bioavialability. Another approach is to inhibit the enzymes (such as the α1–3fucosyltransferase) associated with the biosynthesis of sialyl Lewis^x.

Considerable research has been directed toward the chemical synthesis of sialyl Lewis^x;[306–309] these syntheses tyically require multiple protection and deprotection steps, making large-scale production difficult. Enzymatic syntheses of sialyl Lewis^x based on glycosyltransferases proceed regio- and stereoselectively in aqueous solution, without the need for protecting groups.[179, 310–311] With the advances in recombinant DNA technology for the cloning and overproduction of enzymes and

the development of sugar nucleotide regeneration, sialyl Lewis^x can now be produced in large quantities. (Cytel Co., San Diego, California, is producing SLe^x in kg quantities as a drug candidate for the treatment of reperfusion tissue injury.)

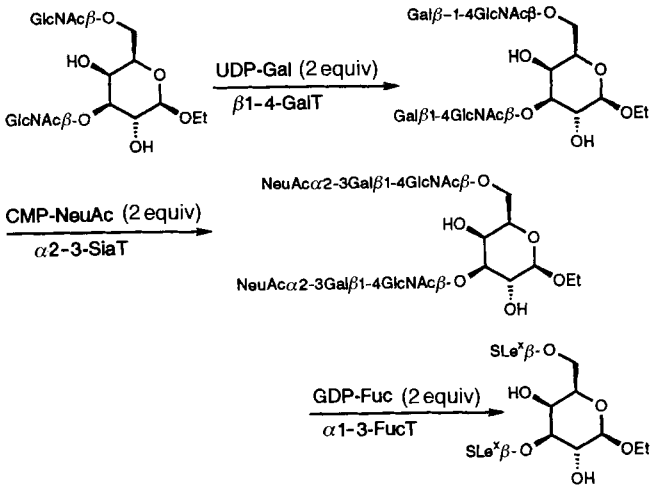
The enzymatic method has also been used for the synthesis of [^{13}C]Gal-1-labeled sialyl Lewis^x,[179] which was used for conformational analysis with NMR spectroscopy. In addition, sialyl Lewis^a (SLe^a),[179, 312] SLe^x glycal,[179] and Le^x-3′-sulfate[313] are also conformationally[179] similar to SLe^x and biologically as active (Scheme 58). The results of these studies indicate that the active binding domain of sialyl Lewis^x consists primarily of the galactose, fucose, and the carboxylate group of the sialic acid. The methyl group of the fucose is not essential, as the fucose residue can be replaced with arabinose.[314] The three hydroxyl groups of the fucose, however, are required.[314]



Scheme 58. Ligands for E-selectin and the minimum active binding site. Sialyl Lewis^a, sialyl Lewis^a, Le^x-3′-O-sulfate, and SLe^x glycal exhibit almost the same binding activity to E-selectin in vitro ($IC_{50} \approx 1-2$ mM). The three OH groups of Fuc are essential, while the CH_3 group is not required. Ion-spray mass analysis using the collision-induced decomposition technique indicated that the Ca^{2+} ions may be located in the Lewis^x moiety.

Further studies on the nature of ligand recognition by E-selectin revealed that a bivalent ligand consisting of two sialyl Lewis^x groups anchored onto ethyl β-galactoside by β-1,3- and β-1,6-linkages was five times better at blocking adhesion ($IC_{50} = 0.4$ mM) than monovalent SLe^x. This observation suggests the possibility of a multivalent ligand–receptor interaction.[314] All these activities were measured in vitro based on an enzyme-linked immunosorbant assay (ELISA). The level of in vivo activity of sialyl Lewis^x is, however, not very clear. The IC_{50} for protecting lung injury in rats appears to be, for example, about 1 μM.[315] While the structure of the E-selectin–ligand complex and the role of Ca^{2+} in the ligand binding are still not known, further experiments with defined multivalent ligands or mimetics with appropriate spacers should clarify the nature of E-selectin-mediated cell adhesion and may suggest new approaches to the discovery and development of antiadhesion molecules. Of particular interest is the development of non-carbohydrate molecules to mimic the topography of the sialyl Lewis^x binding region composed of carboxylate, galactose, and fucose.

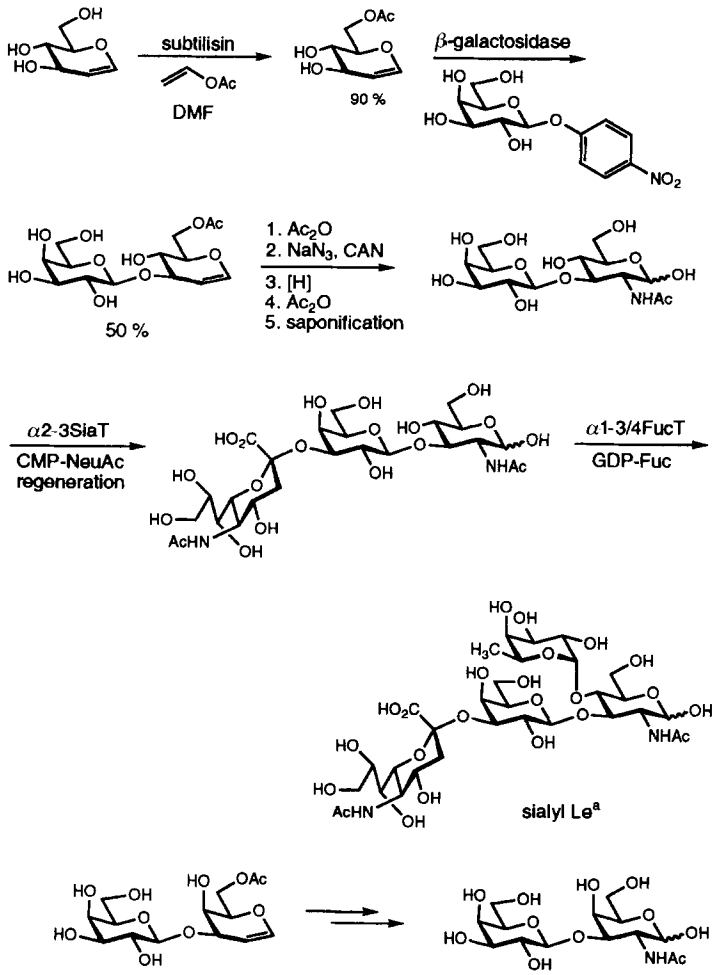
The glycosidic bonds in SLe^x, SLe^x glycal, and Le^x can be formed enzymatically with glycosyltransferases. Introduction of a sulfate group to the 3′-position of Le^x with a sulfate-transfer enzyme coupled with regeneration of PAPS for large-scale process, however, has not been developed. The synthesis of the bivalent oligosaccharide ligand containing two SLe^x groups was very straightforward, starting with a chemically prepared trisaccharide followed by three glycosyltransferase reactions (Scheme 59).[314] Since the glycosyltransferase required for the



Scheme 59. Synthesis of a bivalent ligand containing two SLe^x groups. Two sugar residues are are incorporated in each enzymatic step.

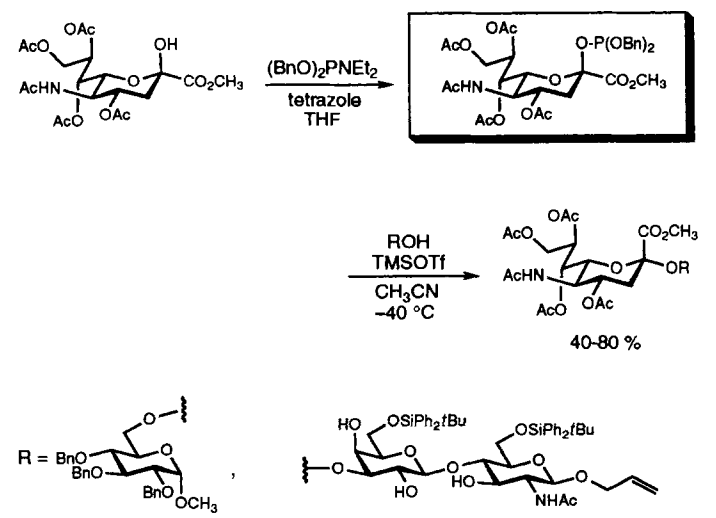
synthesis of the Galβ1–3GlcNAc core unit of SLe^a is not readily available, this disaccharide was prepared chemoenzymatically from glucal by subtilisin-catalyzed acetylation followed by β-galactosidase-catalyzed galactosylation and azidonitration (Scheme 60).[150] The remaining glycosidic bonds were then formed with appropriate glycosyltransferases. Another SLe^x analog derived from SLe^x glycal was prepared by chloroperoxidase-catalyzed halohydration (Scheme 61).[316] This halogenated SLe^x may have the same activity as SLe^x, since the active conformation should not change. Although the halohydration is, in general, not stereoselective, the enzymatic halohydration of sialic acid glycal is regio- and stereoselective, giving 3-bromosialic acid with the bromide in the axial position. Presumably a bound hypobromite intermediate is involved.

It is noteworthy that though enzymatic synthesis of oligosaccharides is potentially useful for large-scale processes, the method is quite limited, as many oligosaccharide analogs cannot be prepared enzymatically. Synthesis of modified oligosaccharides thus requires the use of chemical glycosylation.[317] The scope and mechanism of recently developed glycosyl phosphites in glycosylation[318] has been examined in detail,[319] and the

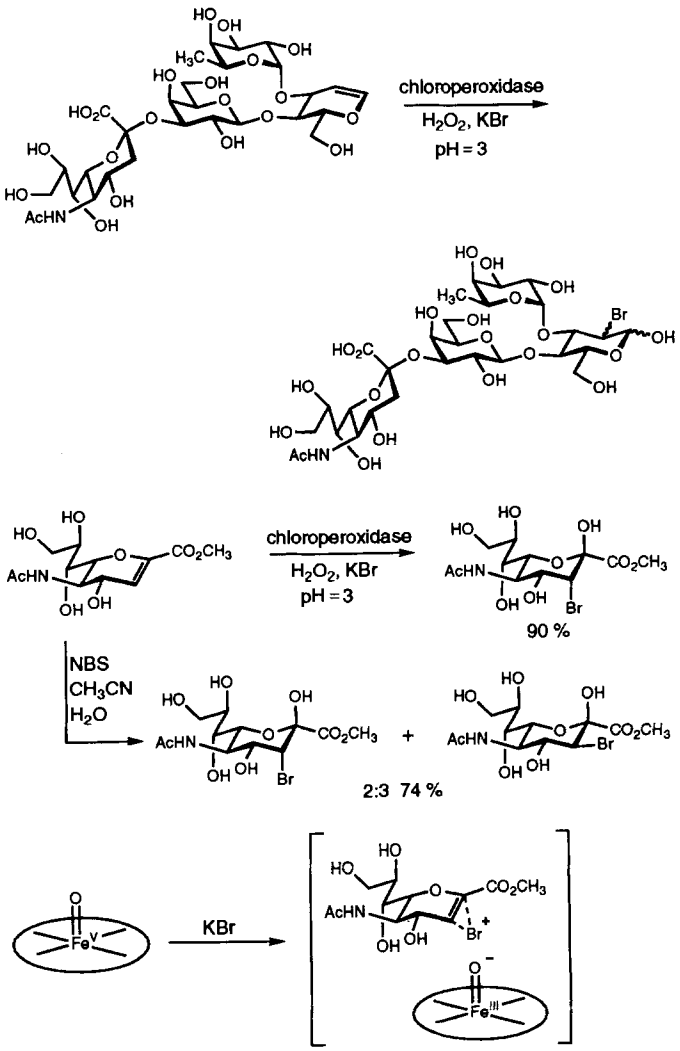


Scheme 60. Synthesis of sialyl Lewis^a with galactosidase/sialyltransferase/fucosyltransferase. Glucal was regioselectively acylated in DMF in the presence of 3% aqueous phosphate buffer. CAN = cerium ammonium nitrate.

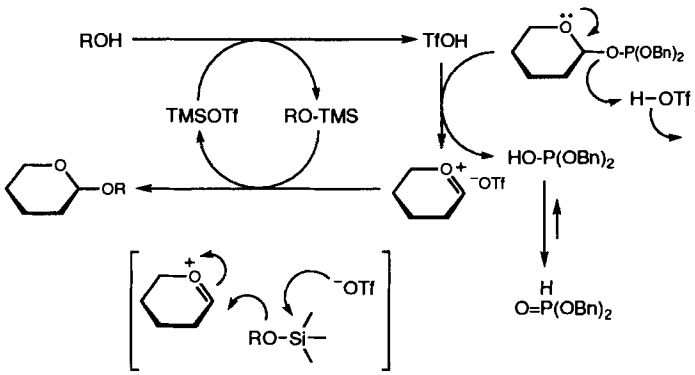
method appears to be particularly effective for sialylation (Scheme 62) and fucosylation. Mechanistic study of the glycosylation reactions indicates that triflic acid is involved in the activation when trimethylsilyl trifluoromethanesulfonate (TMSOTf) is used in catalytic amounts (Scheme 63).[319]



Scheme 62. Chemical sialylation with a sialyl phosphite.



Scheme 61. Chloroperoxidase-catalyzed bromination of glycals.



Scheme 63. Proposed mechanism of glycosylation with phosphites.

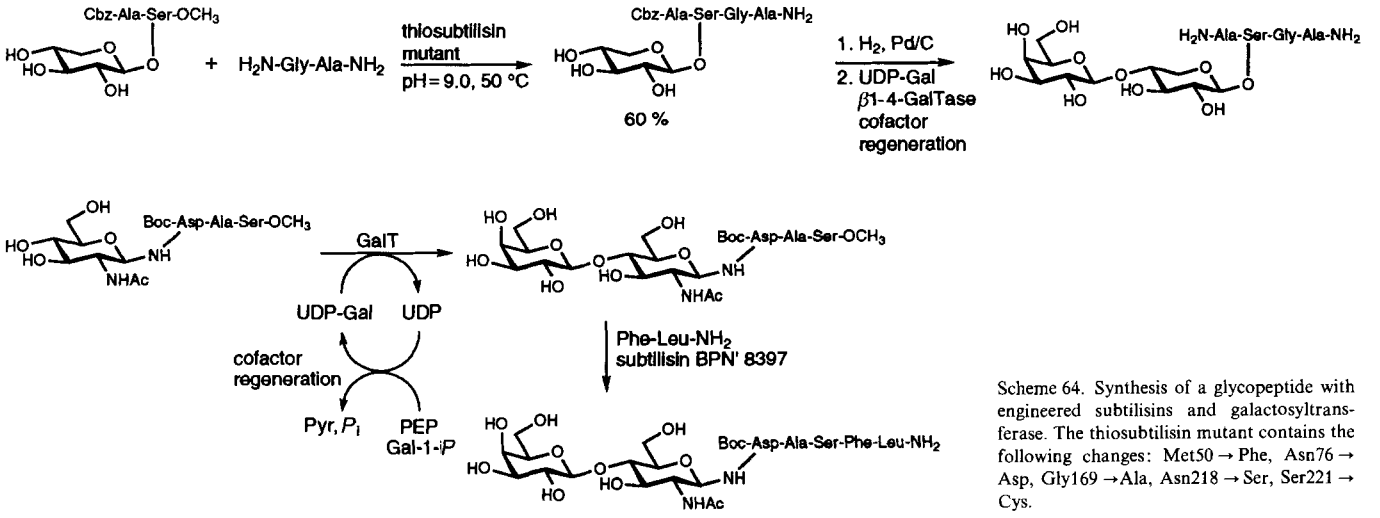
6. Glycopeptide Synthesis and Glycoprotein Remodeling

A number of the proteins of interest as human pharmaceuticals (tissue plasminogen activator, juvenile human growth hormone, CD4) are glycoproteins. There is substantial interest in developing methods that will permit modification of oligosaccharide

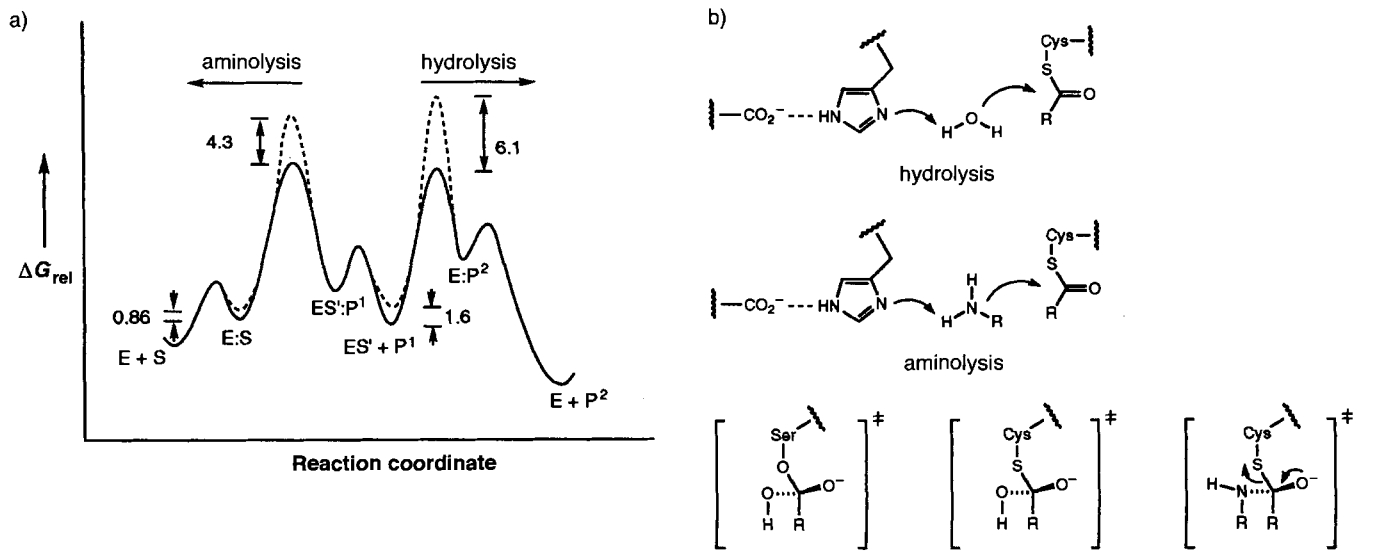
structures on these glycoproteins by removing and adding sugar units ("remodeling") and in making new types of protein-oligosaccharide conjugates.[320, 321] The motivation for these efforts is the hope and that modification of the sugar components of naturally occurring or nonnatural glycoproteins might increase serum lifetime and the solubility of the drug, decrease antigenicity, and promote uptake by target cells and tissues.

Enzymes are feasible catalysts for manipulating the oligosaccharide content and structure of glycoproteins. The delicacy and polyfunctional character of proteins and the requirement for high selectivity in their modification indicate that classical synthetic methods will be of limited use. The major obstacle to the widespread use of enzymes for glycoprotein remodeling and generation is the lack of availability of many of the glycosyl transferases that are plausible candidates and the uncertainty whether glycosyltransferases that probably act on unfolded or partially folded proteins in vivo will be active at the surface of a completely folded protein.

A useful method for glycopeptide synthesis incorporates glycosylamino acids into oligopeptides chemically[322] or enzymatically[323] and subsequently introduces additional sugars with glycosyltransferases. Enzymatic formation of peptide and glycoside bonds is quite effective, because both procedures can be carried out in aqueous solution, thus minimizing protection/deprotection steps in peptide synthesis. Glycosyl amino acids can be used as the P_2, P_3, P'_2, and P'_3 residue in subtilisin-catalyzed-glycopeptide segment condensation. Using a thermostable variant developed by site-directed mutagenesis in which the active-site Ser is converted to Cys, the enzymatic coupling of glycopeptide segments can be carried out efficiently at 60 °C in aqueous solution (Scheme 64).[323] The enzyme prefers aminolysis over hydrolysis by a factor about 10000, and kinetics studies indicate that the selectivity arises because the acyl–enzyme intermediate reacts more selectively with the amine nucleophile than the wild-type enzyme (Scheme 65).[323] Chemical synthesis of glycopeptides followed by enzymatic glycosylation, however,



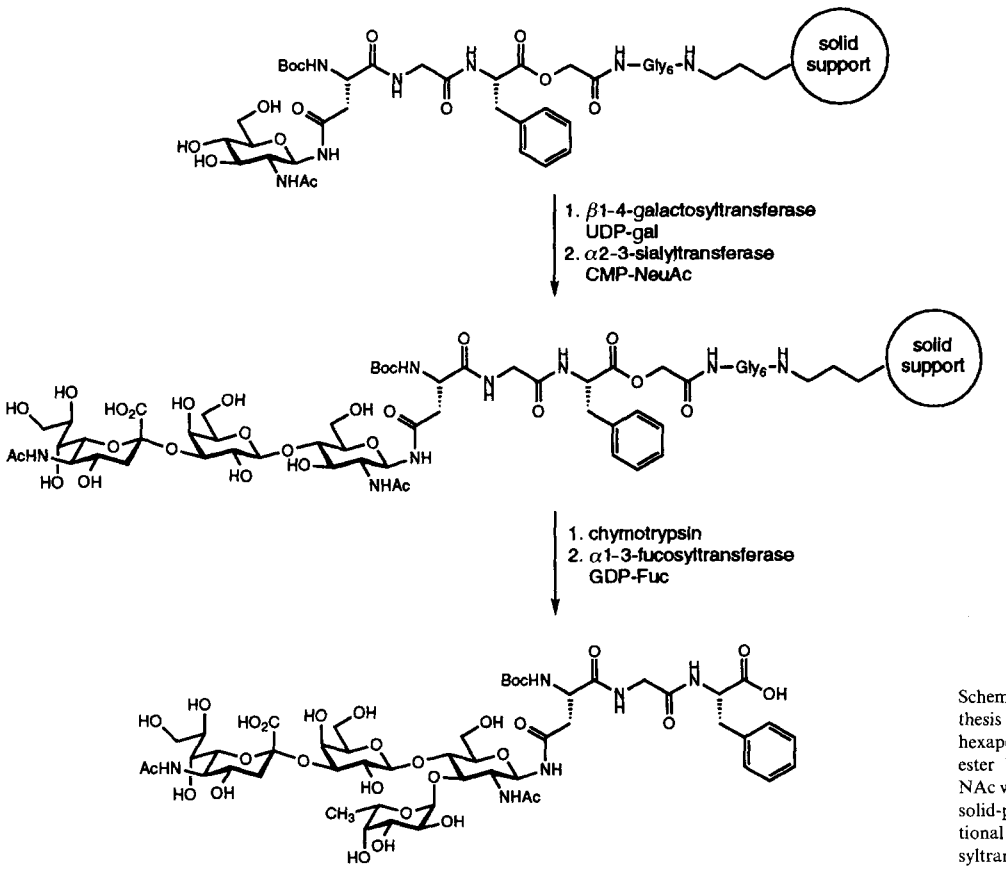
Scheme 64. Synthesis of a glycopeptide with engineered subtilisins and galactosyltransferase. The thiosubtilisin mutant contains the following changes: Met50 → Phe, Asn76 → Asp, Gly169 → Ala, Asn218 → Ser, Ser221 → Cys.



Scheme 65. a) Energy diagram for aminolysis/hydrolysis catalyzed by subtilisin (—) and thiosubilisin (····). ΔG_{rel} is in units of kcal mol^{-1}. E = enzyme, ES' = acylated enzyme, S = peptide, P_1 = amine nucleophile, P_2 = acid. b) Mechanism of thiosubtilisin-catalyzed hydrolysis and aminolysis. (For clarity the oxygen atom of serine and the sulfur atom of cysteine have been explicitly depicted.)

works very well on an aminopropylsilica support.[324] A key element in this strategy is the attachment of a proper acceptor–spacer group with a selectively cleavable bond. The method allows rapid iterative formation of peptide and glycosidic bonds in organic and aqueous solvents, respectively; the glycopeptides are released from the support enzymatically (Scheme 66).

charged transition-state structure is generated by general-acid- and general-base-catalysis, presumably from carboxylic acid and carboxylate residues in the active site of the enzyme. Compounds which resemble the transition-state structure of the glycosidic cleavage or glycosyltransfer reactions are therefore potent inhibitors of the enzyme. The aza sugars described previously seem to be inhibitors resembling the transition state, as they

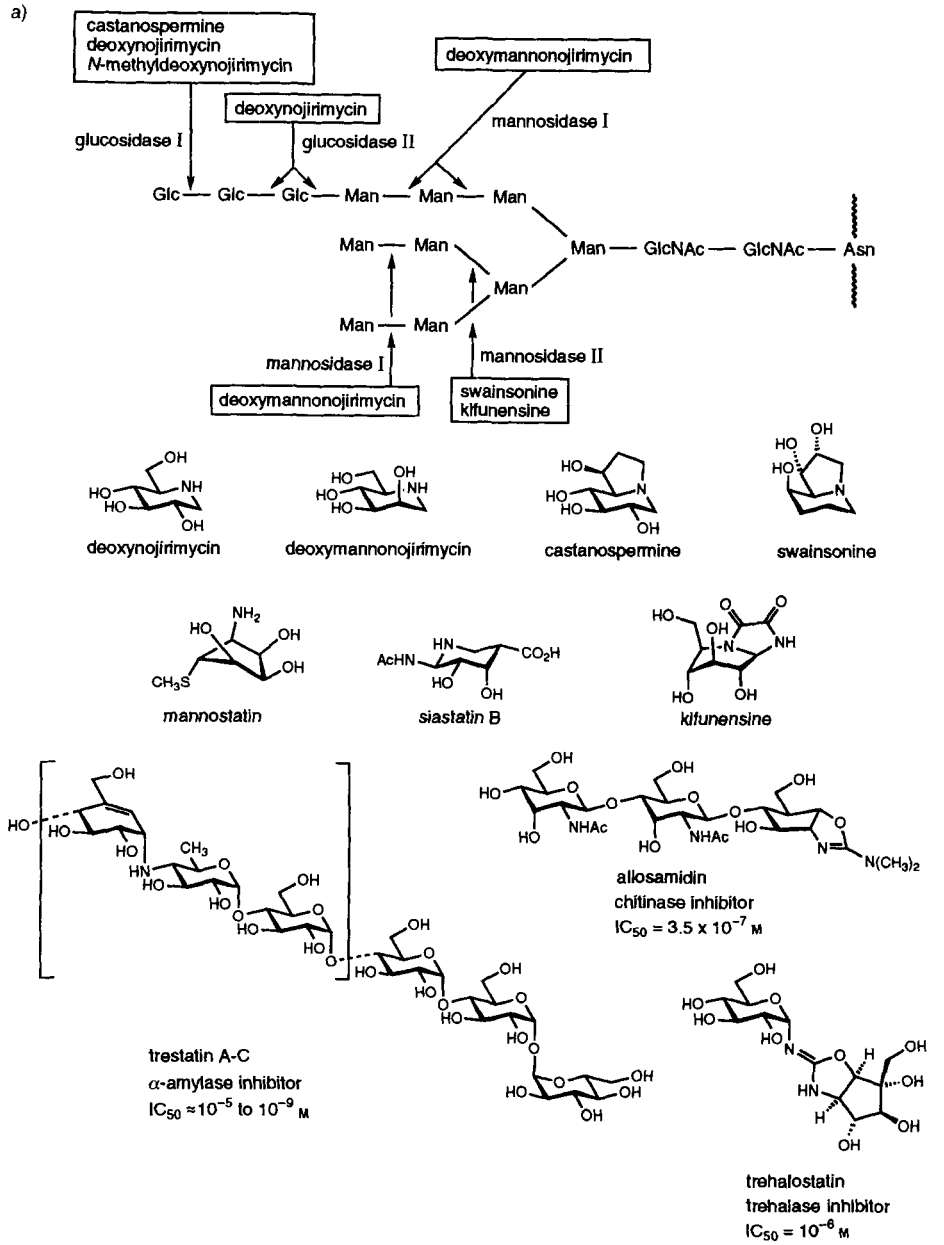


Scheme 66. Solid-supported chemoenzymatic synthesis of a glycopeptide containing SLe^x. The hexapeptide spacer (Gly_6), chymotrypsin-sensitive ester linkage, and oligopeptide-containing GlcNAc were attached to the support by conventional solid-phase synthesis (chemical coupling). Additional sugar residues were then added with glycosyltransferases.

7. Inhibition of Glycosidases and Glycosyltransferases

Glycosidases and glycosyltransferases are important enzymes for the processing of various oligosaccharide-containing glycoproteins and glycolipids. The profound impact of these enzymes on life processes has made them desirable targets for inhibition.[15, 16] Glycoprocessing inhibitors have been used to treat diabetes and other metabolic disorders, and have been implicated in the blocking of infection, inflammation, and metastasis. Some representative examples of naturally occurring and synthetic inhibitors of glycosidases and glycosyltransferases are presented in Schemes 67 and 68.[325] The mechanisms of the reactions with glycosidases and to some extent with glycosyltransferases have been studied.[326] It is generally postulated that the reactions proceed through a half-chair (or twist-boat) transition state with substanial sp^2 character at the anomeric carbon. This positively

show potent inhibition activities. Both five- and six-membered aza sugars can be easily prepared by the aldolase reactions, and they can be considered as building blocks for the development of sequence-specific glycosidase or glycosyltransferase inhibitors. The synergistic inhibition of α1–3fucosyltransferase with the fucosyl-like five-membered aza-sugars and GDP (Scheme 69, see p. 542)[179] is of particular interest, as it provides a new direction in the design of glycosyltransferase inhibitors. Another interesting observation is that most naturally occurring glycosyltransferase inhibitors do not have he pyrophosphate moiety. Perhaps sugars (for instance, in tunicamycin) or peptides can be used to mimic the pyrophosphate–Mn^{2+} component of the sugar nucleotide in glycosyltransferase reactions. Other mimics of pyrophosphate–Mn^{2+} complexes may be useful as a linker between aza sugars and nucleosides for the development of aza sugar nucleosides as synthetic glycosyl-



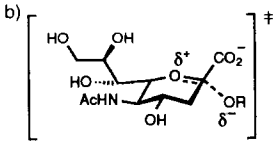
Scheme 67. a) Naturally occurring glycosidase inhibitors and their site of inhibition in the biosynthesis of glycoproteins [325a].

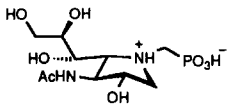
transferase inhibitors. The issue of stability and bioavailability associated with sugar-based inhibitors will have to be examined further if carbohydrates are to be drug candidates. The discovery that C-linked glycosides possess the same conformation as the parent O-linked glycosides[327, 328] is important, because C-linked glycosides may be metabolically stable. Similarly, C-linked aza glycosides, guanido-sugar-containing glycosides,[329] and O-linked carbocycles may have a desirable conformation and may be useful as sequence-specific endoglycosidase and glycosyltransferase inhibitors (Scheme 70, see p. 542). With regard to the preparation of inhibitors to block the multivalent interaction of receptors or enzymes with their ligands or inhibitors, the phospholipase D-catalyzed transphosphatidylation[330] may offer a new method for the preparation of multivalent inhibitors, as phospholipids tend to form a liposome by self-assembly (Scheme 71, see p. 543).

8. Future Opportunities

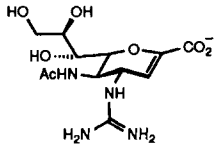
The pace of development of carbohydrate-derived pharmaceutical agents has, in general, been slower than that of more convenient classes of materials, undoubtedly partly because of the difficulties in the synthesis and analysis of carbohydrates. At least three areas of biology and medicinal chemistry have redi-

b)

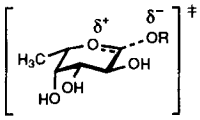


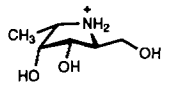


$K_i = 5.3 \times 10^{-5}$ M
sialidase (*V. cholae*)
[325b]

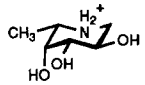


$K_i = 2 \times 10^{-10}$ M
influenza virus sialidase
[325c]

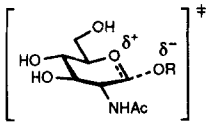


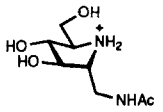


$K_i = 1.4 \times 10^{-6}$ M
α-fucosidase (bovine kidney)
[54]

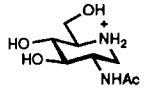


$K_i = 1 \times 10^{-8}$ M
α-fucosidase
(human liver) [325d]

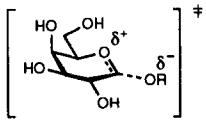


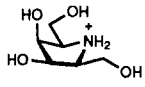


$K_i = 1.9 \times 10^{-6}$ M
β-*N*-acetylglucosaminidase
(Jack beans) [58]

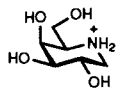


$K_i = 3.8 \times 10^{-7}$ M
β-*N*-acetylglucosaminidase
(bovine kidney) [51]

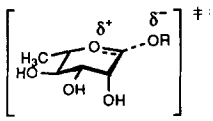


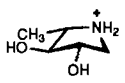


$K_i = 5.0 \times 10^{-8}$ M
α-galactosidase
(green coffee beans) [325e]

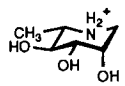


$K_i = 1.6 \times 10^{-9}$ M
α-galactosidase
(green coffee beans) [325f]

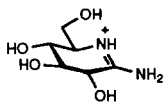




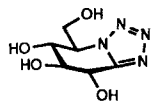
$K_i = 5 \times 10^{-6}$ M
α-rhamnosidase
[525g]



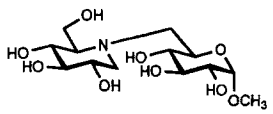
$K_i = 5 \times 10^{-5}$ M
α-rhamnosidase
[325g]



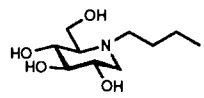
$K_i = 10^{-6}$ M [325g]
β-glucosidase
α-mannosidase
α-galactosidase



$K_i = 8 \times 10^{-5}$ M [325h]
β-glucosidase



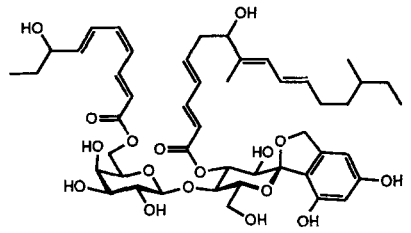
inhibitor of rat sucrase
$K_i = 2 \times 10^{-7}$ [325i]



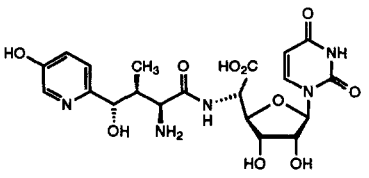
anti-HIV glucosidase I
[325j]

Scheme 67. b) Synthetic glycosidase inhibitors containing five- or six-membered sugar units.

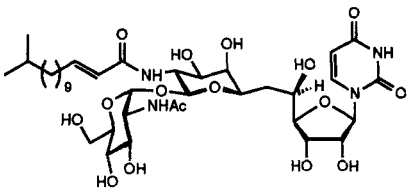
rected attention to carbohydrates. First, interfering with the assembly of bacterial cell walls[331] remains one of the most successful strategies for the development of antimicrobials. As bacterial resistance to the classical β-lactam antibiotics, the penams and cephams, becomes more widespread, there is increasing interest in disturbing with the biosynthesis of the characteristic carbohydrate components of the cell wall, especially KDO, heptulose, lipid A, peptidoglycans and related materials. Interest in cell-wall constituents is also heigtened by their relevance to vaccines and to starting point for the development of non-protein immunomodulating compounds. Second, cell-surface carbohydrates are central to cell–cell communication, cell adhesion, infection differentiation, and development. They may be relevant to abnormal states of differentiation, such as those



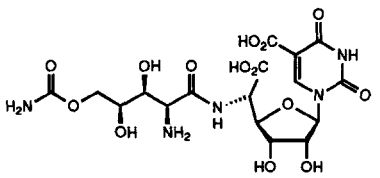
papulacandin B
glucan synthase inhibitor
$IC_{50} = 1.2 \times 10^{-6}$ M



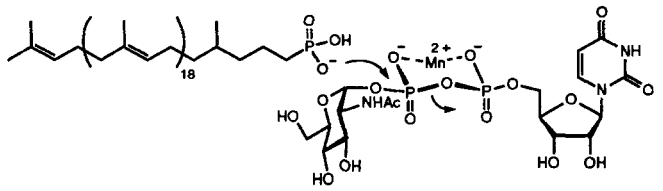
nikkomycin Z
chitin synthetase inhibitor
$K_i = 1.4 \times 10^{-7}$ M



tunicamycin
inhibitor of transfer of UDP-GlcNAc

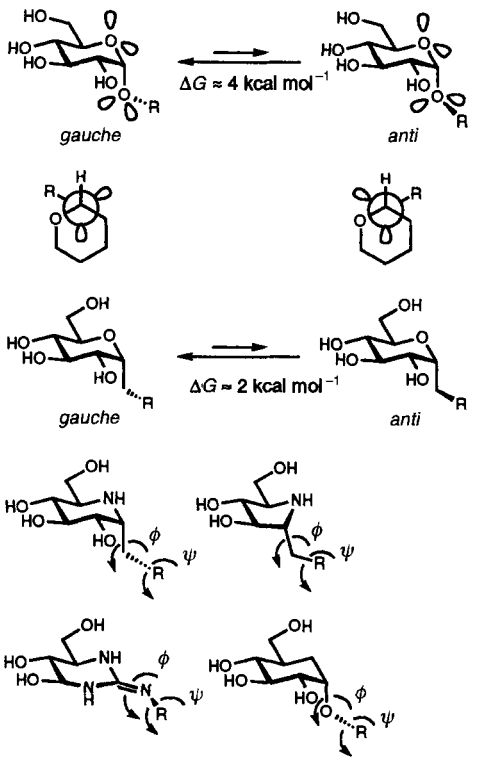


polyoxin D
chitin synthetase inhibitor
$K_i = 9.0 \times 10^{-7}$ M

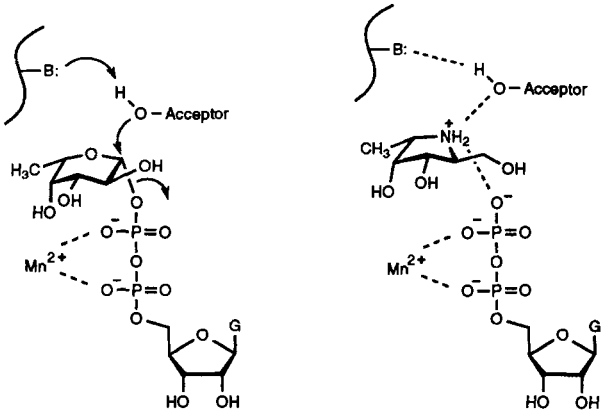


GlcNAc phosphotransferase reaction

Scheme 68. Naturally occurring glycosyltransferase inhibitors. Tunicamycin appears to mimic the transition state of the GlcNAc phosphotransferase reaction.

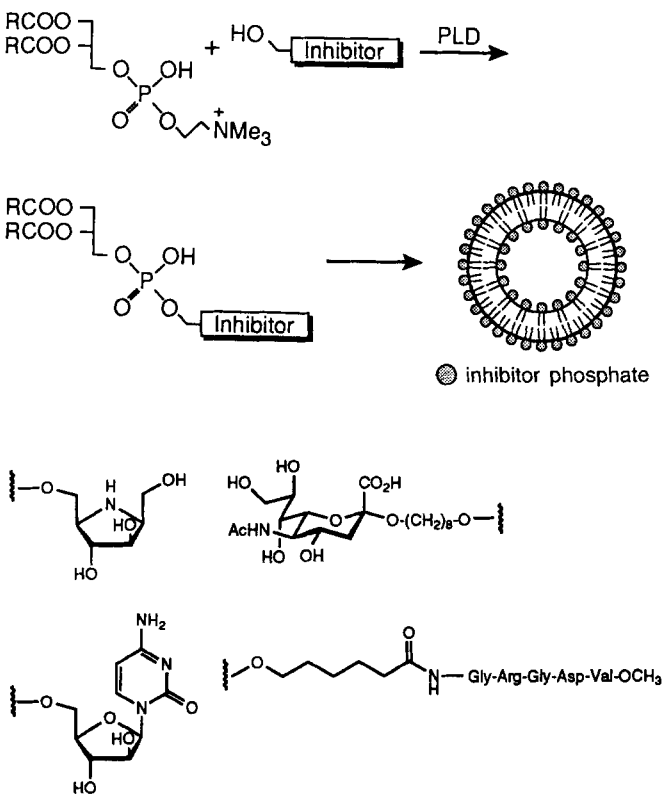


Scheme 70. *Exo* anomeric effect and the conformation of synthetic glycosidase inhibitors. α-Glycosides prefer the *gauche* conformation as a result of the anomeric and *exo* anomeric effects. The C-linked glycosides exhibit a similar conformation to the parent O-linked glycosides. The conformations of C-linked aza glycosides, N-linked guanidino sugars, and O-linked carbocycles (potential sequence-specific glycosidase and glycosyltransferase inhibitors) must still be established.



Scheme 69. Mechanism of fucosyltransferase-catalyzed reaction and synergistic inhibition of the enzyme by GDP and an aza sugar (a fucosidase inhibitor).

characterizing some malignancies. Synthesis of these cell-surface ligands on large scales by enzymatic or chemoenzymatic methods for therapeutic evaluation are beginning to be realized. The enzymes involved in the biosynthesis of these ligands also represent interesting targets for therapeutic development. Third, the broad interest in diagnostics has finally begun to generate interest in carbohydrates as markers of human health. In addition, there are a number of other possible applications of carbohydrates (for example, as dietary constituents, as antivirals, or as components of liposomes) that warrant attention. Enzymatic methods of synthesis will contribute to further research in all of these areas by rendering carbohydrates more accessible.



Scheme 71. Synthesis of phospholipid-inhibitor conjugates catalyzed by phospholipase D (PLD). They self-assemble into a liposome bilayer with numerous inhibitors on the surfaces (a simple system for the synthesis of polyvalent ligands and inhibitors). Examples shown are an azasugar, a nucleoside, RGD peptide (the ligand of integrin), and a sialic acid bound to a phospholipid (influenza hemagglutinin receptor).

Work at The Scripps Research Institute was supported by the National Institutes of Health, the National Science Foundation, and Cytel Corporation, San Diego, and at RIKEN by the Frontier Research Program sponsored by the Japanese Science and Technology Agency. R.L.H. acknowledges support from the American Cancer Society in the form of a postdoctoral fellowship.

Received: January 13, 1994 [A 47b]
German version: *Angew. Chem.* **1995**, *107*, 559

[136] L. F. Leloir, *Science* **1971**, *172*, 1299.
[137] R. Kornfeld, S. Kornfeld, *Annu. Rev. Biochem.* **1985**, *54*, 631.
[138] W. J. Lennarz, *Biochemistry* **1987**, *26*, 7205.
[139] S. C. Hubbard, *Annu. Rev. Biochem.* **1981**, *50*, 555.
[140] a) B. Imperiali, K. L. Shannon, K. W. Rickert, *J. Am. Chem. Soc.* **1992**, *114*, 7942; b) B. Imperiali, K. L. Shannon, M. Unno, K. W. Rickert, *ibid.* **1992**, *114*, 7944.
[141] a) H. A. Kaplan, J. K. Welply, W. J. Lennarz, *Biochim. Biophys. Acta* **1987**, *906*, 161; b) A. Abbadi, M. Mcharfi, A. Aubry, S. Promilat, G. Boussard, M. Marrand, *J. Am. Chem. Soc.* **1991**, *113*, 2729; c) B. Imperiali, K. L. Shannon, *Biochemistry* **1991**, *30*, 4374; d) C. B. Sharma, L. Lehle, W. Tanner, *Eur. J. Biochem.* **1981**, *116*, 101.
[142] J. Roth, *Biochim. Biophys. Acta* **1987**, *906*, 405.
[143] H. Grisebach, *Adv. Carbohydr. Chem. Biochem.* **1978**, *35*, 80.
[144] J. H. Hash, *Methods Enzymol.* **1975**, *43*; R. N. Russell, H.-W. Liu, *J. Am. Chem. Soc.* **1991**, *113*, 7777; J. A. Vara, C. R. Hutchinson, *J. Biol. Chem.* **1988**, *263*, 14992; P. J. Oths, R. M. Hayer, H. G. Floss, *Carbohydr. Res.* **1990**, *198*, 91.
[145] O. Hindsgaul, *Semin. Cell Biol.* **1991**, *2*, 319.
[146] D. G. Drueckhammer, W. J. Hennen, R. L. Pederson, C. F. Barbas III, C. M. Gautheron, T. Krach, C.-H. Wong, *Synthesis* **1991**, 499.
[147] a) J. E. Heidlas, K. W. Williams, G. M. Whitesides, *Acc. Chem. Res.* **1992**, *25*, 307; b) N. K. Kochetkov, V. N. Shibaev, *Adv. Carbohydr. Chem. Biochem.* **1973**, *28*, 307.
[148] H. G. Khorana, *Some Recent Developments in the Chemistry of Phosphate Esters of Biological Interests*, Wiley, New York, **1961**.
[149] A. M. Michelson, *The Chemistry of Nucleosides and Nucleotides*, Academic Press, New York, **1963**.
[150] V. M. Clark, D. W. Hutchinson, A. J. Kirby, S. G. Warren, *Angew. Chem.* **1964**, *76*, 704; *Angew. Chem. Int. Ed. Engl.* **1964**, *3*, 678.
[151] L. A. Slotin, *Synthesis* **1977**, 737.
[152] K. H. Scheit, *Nucleotides Analogs, Synthesis and Biological Function*, Wiley, New York, **1980**.
[153] F. Cramer, H. Neunhoeffer, *Chem. Ber.* **1962**, *95*, 1664.
[154] D. E. Hoard, D. G. Ott, *J. Am. Chem. Soc.* **1965**, *87*, 1785.
[155] E. S. Simon, S. Grabowski, G. M. Whitesides, *J. Org. Chem.* **1990**, *55*, 1834.
[156] a) R. R. Schmidt, *Angew. Chem.* **1986**, *98*, 213; *Angew. Chem. Int. Ed. Engl.* **1986**, *25*, 212; b) P. Pale, G. M. Whitesides, *J. Org. Chem.* **1991**, *56*, 4547.
[157] U. B. Gokhale, O. Hindsgaul, M. M. Palcic, *Can. J. Chem.* **1990**, *68*, 1063.
[158] M. M. Sim, H. Kondo, C.-H. Wong, *J. Am. Chem. Soc.* **1993**, *115*, 2260.
[159] a) B. Pfannemuller, *Staerke* **1968**, *11*, 341; b) W. Praznik, R. Ebermann, *Starch/Staerke* **1979**, *31*, 288.
[160] H. Waldmann, D. Gygax, M. D. Bednarski, W. R. Shangraw, G. M. Whitesides, *Carbohydr. Res.* **1986**, *157*, C4.
[161] C.-H. Wong, S. L. Haynie, G. M. Whitesides, *J. Org. Chem.* **1982**, *47*, 5416.
[162] H. J. Leucks, J. M. Lewis, V. M. Rios-Mercadillo, G. M. Whitesides, *J. Am. Chem. Soc.* **1979**, *101*, 5829.
[163] B. L. Hirschbein, F. P. Mazenod, G. M. Whitesides, *J. Org. Chem.* **1982**, *47*, 3765.
[164] E. S. Simon, S. Grabowski, G. M. Whitesides, *J. Am. Chem. Soc.* **1989**, *111*, 8920.
[165] M.-J. Kim, G. M. Whitesides, *Appl. Biochem. Biotechnol.* **1987**, *16*, 95.
[166] E. S. Simon, M. D. Bednarski, G. M. Whitesides, *J. Am. Chem. Soc.* **1988**, *110*, 7159.
[167] H. K. Chenault, E. S. Simon, G. M. Whitesides in *Biotechnology and Genetic Engineering Reviews, Vol. 6* (Ed.: G. E. Russell), Intercept, Wimborne, Dorset, **1988**, Chapter 6.
[168] C.-H. Wong, S. L. Haynie, G. M. Whitesides, *J. Am. Chem. Soc.* **1983**, *105*, 115.
[169] a) K. Kawaguchi, H. Kawai, T. Tochikura, *Methods Carbohydr. Chem.* **1980**, *8*, 261; b) T. Tochikura, K. Kawaguchi, H. Kawai, Y. Mugibayashi, K. Ogata, *Hakko Kogaku Zasshi* **1968**, *46*, 970; c) T. Tochikura, H. Kawai, S. Tobe, K. Kawaguchi, M. Osugi, K. Ogata, *ibid.* **1968**, *46*, 957.
[170] U. Korf, J. Thimm, J. Thiem, *Synlett* **1991**, 313.
[171] V. Ginsburg, *Adv. Enzymol.* **1964**, *26*, 35.
[172] a) J. E. Heidlas, W. J. Lees, P. Pale, G. M. Whitesides, *J. Org. Chem.* **1992**, *57*, 146; b) J. E. Heidlas, W. J. Lees, G. M. Whitesides, *ibid.* **1992**, *57*, 152.
[173] G. Srivastava, O. Hindsgaul, M. M. Palcic, *Carbohydr. Res.* **1993**, *245*, 137.
[174] P. A. Ropp, P.-W. Cheng, *Anal. Biochem.* **1990**, *187*, 104.
[175] F. Maley, *Methods Enzymol.* **1972**, *28*, 271.
[176] T. J. Grier, J. R. Rasmussen, *Anal. Biochem.* **1982**, *127*, 100.
[177] V. Ginsberg, *J. Biol. Chem.* **1960**, *235*, 2196.
[178] K. Yamamoto, T. Maruyama, H. Kumagai, T. Tochikura, T. Seno, H. Yamaguchi, *Agric. Biol. Chem.* **1984**, *48*, 823.
[179] Y. Ichikawa, Y.-C. Lin, D. P. Dumas, G.-J. Shen, E. Garcia-Junceda, M. A. Williams, R. Bayer, C. Ketcham, L. E. Walker, J. C. Paulson, C.-H. Wong, *J. Am. Chem. Soc.* **1992**, *114*, 9283.
[180] R. Stiller, J. Thiem, *Liebigs Ann. Chem.* **1992**, 467.
[181] a) H. A. Nunez, J. V. O'Connor, P. R. Rosevear, R. Barker, *Can. J. Chem.* **1981**, *59*, 2086; b) V. B. Gokhale, O. Hindsgaul, M. M. Palcic, *ibid.* **1990**, *68*, 1063; c) R. R. Schmidt, B. Wegmann, K.-H. Jung, *Liebigs Ann. Chem.* **1991**, *191*, 121; d) G. H. Veeneman, H. J. G. Broxterman, G. H. van der Marel, J. H. van Boom, *Tetrahedron Lett.* **1991**, *32*, 6175; e) Y. Ichikawa, M. M. Sim, C.-H. Wong, *J. Org. Chem.* **1992**, *57*, 2943.
[182] E. J. Toone, E. S. Simon, G. M. Whitesides, *J. Org. Chem.* **1991**, *56*, 5603.
[183] D. Gygax, P. Spies, T. Winkler, U. Pfarr, *Tetrahedron* **1991**, *28*, 5119.
[184] a) H. H. Higa, J. C. Paulson, *J. Biol. Chem.* **1985**, *260*, 8838; b) J. Thiem, W. Treder, *Angew. Chem.* **1986**, *98*, 1100; *Angew. Chem. Int. Ed. Engl.* **1986**, *25*, 1096; c) D. H. van den Eijnden, W. van Dijk, *Hoppe-Seyler's Z. Physiol. Chem.* **1972**, *353*, 1817; d) J. Haverkamp, J. M. Beau, R. Schauer, *ibid.* **1972**, *360*, 159; e) E. L. Kean, *J. Biol. Chem.* **1970**, *9*, 2391; f) C. Auge, C. Gautheron, *Tetrahedron Lett.* **1988**, *29*, 789.
[185] J. Thiem, P. Stangier, *Liebigs Ann. Chem.* **1990**, 1101.
[186] J. L.-C. Liu, G.-J. Shen, Y. Ichikawa, J. F. Rutan, G. Zapata, W. F. Vann, C.-H. Wong, *J. Am. Chem. Soc.* **1992**, *114*, 3901.

[187] T. J. Martin, R. R. Schmidt, *Tetrahedron Lett.* **1993**, *34*, 1765.
[188] H. Kondo, Y. Ichikawa, C.-H. Wong, *J. Am. Chem. Soc.* **1992**, *114*, 8748.
[189] S. Makino, Y. Ueno, M. Ishikawa, Y. Hayakawa, T. Hata, *Tetrahedron Lett.* **1993**, *34*, 2775.
[190] L. Warren, R. Blacklow, *J. Biol. Chem.* **1962**, *237*, 3527; W. F. Vann, R. P. Silver, C. Abeiyon, K. Chang, W. Aaronson, A. Sutton, C. W. Finn, W. Lindner, M. Kotsatos, *J. Biol. Chem.* **1987**, *262*, 17562.
[191] G. Zapata, W. F. Vann, W. Aaronson, M. S. Lewis, M. Moos, *J. Biol. Chem.* **1989**, *264*, 14769.
[192] Y. Ichikawa, G.-J. Shen, C.-H. Wong, *J. Am. Chem. Soc.* **1991**, *113*, 4698.
[193] G.-J. Shen, J. L.-C. Liu, C.-H. Wong, *Biocatalysis* **1992**, *6*, 31.
[194] S. L. Shames, E. S. Simon, C. W. Christopher, W. Schmid, G. M. Whitesides, L.-L. Yang, *Glycobiology* **1991**, *1*, 187.
[195] E. Schreiner, R. Christian, E. Zbiral, *Liebigs Ann. Chem.* **1990**, 93.
[196] M. Hartmann, R. Christian, E. Zbiral, *Liebigs Ann. Chem.* **1990**, 83.
[197] H. J. Gross, A. Buensch, J. C. Paulson, R. Brossmer, *Eur. J. Biochem.* **1987**, *168*, 595.
[198] H. J. Gross, R. Brossmer, *Eur. J. Biochem.* **1988**, *177*, 583.
[199] R. Schauer, M. Wember, C. F. do Amaral, *Hoppe-Seyler's Z. Physiol. Chem.* **1972**, *353*, 883.
[200] R.-T. Schwarz, R. Datema, *Adv. Carbohydr. Chem. Biochem.* **1982**, *40*, 287.
[201] a) F. L. Schanbacher, K. E. Ebner, *J. Biol. Chem.* **1970**, *245*, 5057; b) L. J. Berliner, M. E. Davis, K. E. Ebner, T. A. Beyer, J. E. Bell, *Mol. Cell. Biochem.* **1984**, *62*, 37; c) H. A. Nunez, R. Barker, *Biochemistry* **1980**, *19*, 489.
[202] a) I. P. Trayer, R. L. Hill, *J. Biol. Chem.* **1971**, *246*, 6666; b) P. Andrews, *FEBS Lett.* **1970**, *9*, 297; c) R. Barker, K. W. Olsen, J. H. Shaper, R. L. Hill, *J. Biol. Chem.* **1972**, *247*, 7135; d) A. K. Rao, F. Garver, J. Mendicino, *Biochemistry* **1976**, *15*, 5001.
[203] a) M. M. Palcic, O. P. Srivastava, O. Hindsgaul, *Carbohydr. Res.* **1987**, *159*, 315; b) C. Auge, S. David, C. Mathieu, C. Gautheron, *Tetrahedron Lett.* **1984**, *25*, 1467.
[204] C.-H. Wong, Y. Ichikawa, T. Krach, C. Gautheron-Le Narvor, D. P. Dumas, G. C. Look, *J. Am. Chem. Soc.* **1991**, *113*, 8137.
[205] J. Thiem, T. Wiemann, *Angew. Chem.* **1990**, *102*, 78; *Angew. Chem. Int. Ed. Engl.* **1990**, *29*, 80.
[206] a) Y. Nishida, T. Wiemann, J. Thiem, *Tetrahedron Lett.* **1992**, *33*, 8043; b) Y. Nishida, T. Wiemann, V. Sinwell, J. Thiem, *J. Am. Chem. Soc.* **1993**, *115*, 2536; c) Y. Nishida, T. Wiemann, J. Thiem, *Tetrahedron Lett.* **1993**, *34*, 2905.
[207] a) U. Zehavi, M. Herchman, *Carbohydr. Res.* **1984**, *133*, 339; b) U. Zehavi, S. Sadeh, M. Herchman, *ibid.* **1983**, *124*, 23.
[208] C. Unverzagt, H. Kunz, J. C. Paulson, *J. Am. Chem. Soc.* **1990**, *112*, 9308; C. Auge, C. Gautheron, H. Pora, *Carbohydr. Res.* **1989**, *193*, 288.
[209] B. Guilbert, T. H. Khan, S. L. Flitsch, *J. Chem. Soc. Chem. Commun.* **1992**, 1526.
[210] a) M. M. Palcic, O. Hindsgaul, *Glycobiology* **1991**, *1*, 205; b) T. L. Lowary, O. Hindsgaul, *Carbohydr. Res.* **1993**, *249*, 163.
[211] L. J. Berliner, R. D. Robinson, *Biochemistry* **1982**, *21*, 6340.
[212] a) H. Yuasa, O. Hindsgaul, M. M. Palcic, *J. Am. Chem. Soc.* **1992**, *114*, 5891; b) H. Kodama, Y. Kajihara, T. Endo, H. Hashimoto, *Tetrahedron Lett.* **1993**, *34*, 6419.
[213] C.-H. Wong, R. Wang, Y. Ichikawa, *J. Org. Chem.* **1992**, *57*, 4343.
[214] S. Sabesan, J. C. Paulson, *J. Am. Chem. Soc.* **1986**, *108*, 2068.
[215] J. Thiem, W. Treder, *Angew. Chem.* **1986**, *98*, 1100; *Angew. Chem. Int. Ed. Engl.* **1986**, *25*, 1096.
[216] C. Auge, C. Gautheron, *Tetrahedron Lett.* **1988**, *29*, 789.
[217] R. D. McCoy, E. R. Vimr, F. A. Troy, *J. Biol. Chem.* **1985**, *260*, 12695; F. A. Troy, M. A. McCloskey, *J. Biol. Chem.* **1979**, *2*, 7377; J. Finne, *Trends Biochem. Sci.* **1985**, 129.
[218] H. S. Condradt, A. Bunsch, R. Browwmer, *FEBS Lett.* **1984**, *170*, 295; C. R. Petrie, M. Sharma, O. D. Simmons, W. Korytnyk, *Carbohydr. Res.* **1989**, *186*, 326.
[219] Y. Ito, J. J. Gaudino, J. C. Paulson, *Pure Appl. Chem.* **1993**, *65*, 753.
[220] K. K.-C. Liu, S. J. Danishefsky, *J. Am. Chem. Soc.* **1993**, *115*, 4933.
[221] M. M. Palcic, A. P. Venot, R. M. Ratcliffe, O. Hindsgaul, *Carbohydr. Res.* **1989**, *190*, 1.
[222] D. P. Dumas, Y. Ichikawa, C.-H. Wong, J. B. Lowe, R. P. Nair, *Bioorg. Med. Chem. Lett.* **1991**, *1*, 425.
[223] P. R. Rosevear, H. A. Nunez, R. Barker, *Biochemistry* **1982**, *21*, 1421.
[224] U. B. Gokhale, O. Hindsgaul, M. M. Palcic, *Can. J. Chem.* **1990**, *68*, 1063.
[225] G. Srivastava, K. J. Kaur, O. Hindsgaul, M. M. Palcic, *J. Biol. Chem.* **1992**, *267*, 22356.
[226] H. Schachter, *Biochem. Cell Biol.* **1986**, *64*, 163.
[227] I. Brockhausen, E. Hull, O. Hindsgaul, H. Schachter, R. N. Shah, S. W. Michnick, J. P. Carver, *J. Biol. Chem.* **1989**, *264*, 11211.
[228] I. Brockhausen, J. Carver, H. Schachter, *Biochem. Cell Biol.* **1988**, *66*, 1134.
[229] G. Srivastava, G. Alton, O. Hindsgaul, *Carbohydr. Res.* **1990**, *207*, 259.
[230] a) K. J. Kaur, G. Alton, O. Hindsgaul, *Carbohydr. Res.* **1990**, *210*, 145; b) T. Linker, S. C. Crawley, O. Hindsgaul, *ibid.* **1993**, *245*, 323; c) I. Lindh, O. Hindsgaul, *J. Am. Chem. Soc.* **1991**, *113*, 216.
[231] a) B. Imperiali, J. W. Zimmerman, *Tetrahedron Lett.* **1990**, *31*, 6485; b) R. Oehrlein, O. Hindsgaul, M. M. Palcic, *Carbohydr. Res.* **1993**, *244*, 149.
[232] W. McDowell, T. J. Grier, J. R. Rasmussen, R. T. Schwarz, *Biochem. J.* **1987**, *248*, 523.
[233] P. Wang, G.-J. Shen, Y.-F. Wang, Y. Ichikawa, C.-H. Wong, *J. Org. Chem.* **1993**, *58*, 3985.
[234] a) S. L. Flitsch, J. P. Taylor, N. J. Turner, *J. Chem. Soc. Chem. Commun.* **1991**, *380*, 382; b) S. L. Flitsch, H. L. Pinches, J. P. Taylor, N. J. Turner, *J. Chem. Soc. Perkin Trans. 1* **1992**, 2087.
[235] a) P. J. Card, W. D. Hitz, *J. Am. Chem. Soc.* **1984**, *106*, 5348; b) P. J. Card, W. D. Hitz, K. G. Ripp, *J. Am. Chem. Soc.* **1986**, *108*, 158.
[236] L. Elling, M. Grothus, M.-R. Kula, *Glycobiology* **1993**, *3*, 349.
[237] R. S. Clark, S. Banerjee, J. K. Coward, *J. Org. Chem.* **1990**, *55*, 6275.
[238] J. Lee, J. K. Coward, *J. Org. Chem.* **1992**, *57*, 4126.
[239] Y. Ichikawa, J. J.-C. Liu, G.-J. Shen, C.-H. Wong, *J. Am. Chem. Soc.* **1991**, *113*, 6300.
[240] G. C. Look, Y. Ichikawa, G.-J. Shen, G.-J. Cheng, C.-H. Wong, *J. Org. Chem.* **1993**, *58*, 4326; J. C. Paulson, J. Weinstein, E. L. Ujita, K. J. Riggs, P.-H. Lai, *Biochem. Soc. Trans.* **1987**, *15*, 618.
[241] K. Brew, F. J. Castellino, J. C. Vanaman, R. L. Hill, *J. Biol. Chem.* **1970**, *245*, 4570.
[242] B. A. Bartholomew, G. W. Jourdian, S. Roseman, *J. Biol. Chem.* **1973**, *248*, 5751.
[243] M. Nagai, V. Dave, B. E. Kaplan, A. Yoshida, *J. Biol. Chem.* **1978**, *253*, 377.
[244] J. C. Paulson, K. J. Colley, *J. Biol. Chem.* **1989**, *264*, 17615.
[245] F. Toghrol, T. Kimura, I. S. Owens, *Biochemistry* **1990**, *29*, 2349.
[246] P. I. MacKenzie, *J. Biol. Chem.* **1986**, *261*, 6119.
[247] A. S. Masibay, P. K. Qasba, *Proc. Natl. Acad. Sci. USA* **1989**, *86*, 5733.
[248] H. Narimatsu, S. Sinha, K. Brew, H. Okayama, P. K. Qasba, *Proc. Natl. Acad. Sci. USA* **1986**, *83*, 4720.
[249] N. L. Shaper, W. W. Wright, J. H. Shaper, *Proc. Natl. Acad. Sci. USA* **1990**, *87*, 791.
[250] D. H. Joziasse, J. H. Shaper, D. H. van den Eijnden, A. J. Van Tunen, N. L. Shaper, *J. Biol. Chem.* **1989**, *264*, 14290.
[251] R. D. Larsen, V. P. Rajan, M. M. Ruff, J. Kukowska-Latallo, R. D. Cummings, J. B. Lowe, *Proc. Natl. Acad. Sci. USA* **1989**, *86*, 8227.
[252] R. D. Larsen, L. K. Ernst, R. P. Nair, J. B. Lowe, *Proc. Natl. Acad. Sci. USA* **1990**, *87*, 6674.
[253] J. Weinstein, E. U. Lee, K. McEntee, P.-H. Lai, J. C. Paulson, *J. Biol. Chem.* **1987**, *262*, 17735.
[254] a) R. K. Saiki, S. Scharf, F. Faloona, K. B. Mullis, G. T. Horn, H. A. Erlich, N. Arnheim, *Science* **1985**, *230*, 1350; b) N. Arnheim, C. H. Levenson, *Chem. Eng. News* **1990**, *68*(40), 36.
[255] K. D. MacFerrin, M. P. Terranova, S. L. Schreiber, G. L. Verdine, *Proc. Natl. Acad. Sci. USA* **1990**, *87*, 1937; K. Nakazawa, K. Furukawa, H. Narimatsu, A. Kobata, *J. Biochem.* **1993**, *113*, 747.
[256] D. Aoki, H. E. Appert, D. Johnson, S. S. Wong, M. N. Fukuda, *EMBO J.* **1990**, *9*, 3171.
[257] J. Ghrayab, H. Kimura, M. Takahara, H. Hsiung, Y. Masui, M. Inouye, *EMBO J.* **1984**, *3*, 2437.
[258] C. H. Krezdorn, G. Watsele, R. B. Kleene, S. X. Ivanov, E. G. Berger, *Eur. J. Biochem.* **1993**, *212*, 113.
[259] a) W. Gillespie, S. Kelm, J. C. Paulson, *J. Biol. Chem.* **1992**, *267*, 21004; b) D. X. Wen, B. D. Livingston, K. F. Medzihradszky, A. L. Burlingame, J. C. Paulson, *J. Biol. Chem.* **1992**, *267*, 21011.
[260] N. L. Shaper, G. F. Hollis, J. G. Douglas, I. R. Kirsch, J. H. Shaper, *J. Biol. Chem.* **1988**, *263*, 10420.
[261] G. D'Agostaro, B. Bendiak, M. Tropak, *Eur. J. Biochem.* **1989**, *183*, 211.
[262] K. Nakazawa, T. Ando, T. Kimura, H. Narimatsu, *J. Biochem.* **1988**, *104*, 165.
[263] N. L. Shaper, J. H. Shaper, J. L. Meuth, J. L. Fox, H. Chang, I. R. Kirsch, G. F. Hollis, *Proc. Natl. Acad. Sci. USA* **1986**, *83*, 1573.
[264] K. A. Masri, H. E. Appert, M. N. Fukuda, *Biochem. Biophys. Res. Commun.* **1988**, *157*, 657.
[265] a) FucT III: J. F. Kukowska-Latallo, R. D. Larsen, R. P. Nair, J. B. Lowe, *Genes Dev.* **1990**, *4*, 1288; b) FucT IV: R. Kumar, B. Potvin, W. A. Muller, P. Stanley, *J. Biol. Chem.* **1991**, *266*, 21777; c) FucT V: B. W. Weston, R. P. Nair, R. D. Larsen, J. B. Lowe, *ibid.* **1992**, *267*, 4152; d) FucT VI: B. W. Weston, P. L. Smith, R. J. Kelly, J. B. Lowe, *ibid.* **1992**, *267*, 24575.
[266] Review: J. B. Lowe, *Seminars in Cell Biology* **1991**, *2*, 289.
[267] S. L. Haynie, G. M. Whitesides, *Appl. Biochem. Biotechnol.* **1990**, *23*, 205.
[268] R. Dedonder, *Methods Enzymol.* **1966**, *8*, 500.
[269] a) D. Botstein, R. W. Davis in *Molecular Biology of the Yeast Saccharomyces; Metabolism and Gene Expression* (Eds.: J. N. Strathern, E. W. Jones, J. R. Broach), Cold Spring Harbor Laboratory, Plainview, NY, **1981**, p. 607; b) D. M. Carlson, *Pure Appl. Chem.* **1987**, *59*, 1489.
[270] G. Ziegast, B. Pfannemuller, *Carbohydr. Res.* **1987**, *160*, 185.
[271] a) D. French, *Adv. Carbohydr. Chem. Biochem.* **1957**, *12*, 189; b) W. Saenger, *Angew. Chem.* **1980**, *92*, 343; *Angew. Chem. Int. Ed. Engl.* **1980**, *19*, 344.

[272] a) H. Bender, *Carbohydr. Res.* **1980**, *78*, 133; b) K. Wallenfels, B. Foldi, H. Niermann, H. Bender, D. Linder, *ibid.* **1978**, *61*, 359.
[273] W. Treder, J. Thiem, M. Schlingmann, *Tetrahedron Lett.* **1986**, *27*, 5605.
[274] a) Y. Ezure, *Agric. Biol. Chem.* **1985**, *49*, 2159; b) Y. Ezure, S. Maruo, N. Ojima, K. Konno, H. Yamashita, K. Miyazaki, T. Seto, N. Yamada, M. Sugiyama, *ibid.* **1989**, *53*, 61.
[275] D. N. Crowell, M. S. Anderson, C. R. H. Raetz, *J. Bacteriol.* **1986**, *168*, 52.
[276] H. Vypel, D. Scholz, I. Macher, K. Schindlmaier, E. Schutze, *J. med. Chem.* **1991**, *34*, 2759.
[277] D. Scholz, K. Bednarik, G. Ehn, W. Neruda, E. Janzek, H. Loibner, K. Briner, A. Vasella, *J. Med. Chem.* **1992**, *35*, 2070.
[278] a) E. S. Hehre, T. Sawai, C. F. Brewer, M. Nakano, T. Kanda, *Biochemistry* **1982**, *21*, 3090; b) T. Kasumi, Y. Tsumuraya, C. F. Brewer, H. Kersters-Hilderson, M. Claeyssens, E. S. Hehre, *ibid.* **1987**, *26*, 3010.
[279] T. Kasumi, C. F. Brewer, E. T. Reese, E. S. Hehre, *Carbohydr. Res.* **1986**, *146*, 39.
[280] a) K. G. I. Nilsson, *Carbohydr. Res.* **1987**, *167*, 95; b) *ibid.* **1988**, *180*, 53; c) D. H. G. Crout, D. A. MacManus, J.-M. Ricca, S. Singh, P. Crithley, W. T. Gibson, *Pure Appl. Chem.* **1992**, *64*, 1079; d) J. Lehmann, E. Schroter, *Carbohydr. Res.* **1979**, *71*, 65.
[281] G. C. Look, C.-H. Wong, *Tetrahedron Lett.* **1992**, *33*, 4253.
[282] L. Hedbys, E. Johansson, K. Mosbach, P. O. Larsson, A. Gunnarsson, S. Svensson, H. Lonn, *Glycoconjugate J.* **1989**, *6*, 161.
[283] a) S. Kobayashi, K. Koshiwa, T. Kawasaki, S.-I. Shoda, *J. Am. Chem. Soc.* **1991**, *113*, 3079; b) G. F. Herrmann, U. Kragl, C. Wandrey, *Angew. Chem.* **1993**, *105*, 1399; *Angew. Chem. Int. Ed. Engl.* **1993**, *32*, 1342; c) G. F. Herrmann, Y. Ichikawa, C. Wandrey, F. C. A. Gaeta, J. C. Paulson, C.-H. Wong, *Tetrahedron Lett.* **1993**, *34*, 3091.
[284] H. Ishikawa, S. Kitahata, K. Ohtani, C. Ikuhara, O. Tanaka, *Agric. Biol. Chem.* **1990**, *54*, 3137.
[285] a) R. Dedonder, *Methods Enzymol.* **1964**, *8*, 500; b) F. Kunst, M. Pascal, J.-A. Lepesant, J. Walle, R. Dedonder, *Eur. J. Biochem.* **1974**, *42*, 611.
[286] E. B. Rathbone, A. J. Hacking, P. S. J. Cheetham, US-A 4617269, **1986**.
[287] S. Schenkman, J. Man-Shiow, G. W. Hart, V. Nussenzweig, *Cell* **1991**, *65*, 1117.
[288] F. Vanderkerckhove, S. Schenkman, L. P. de Carvalho, S. Tomlinson, M. Kiso, M. Yoshida, A. Hasegawa, V. Nussenzweig, *Glycobiology* **1992**, *3*, 541.
[289] S. Tomlinson, L. P. de Carvalho, F. Vanderkerckhove, V. Nussenzweig, *Glycobiology* **1991**, *2*, 549.
[290] Y. Ho, J. C. Paulson, *J. Am. Chem. Soc.* **1993**, *115*, 7862.
[291] D. J. Hupe, *Annu. Rep. Med. Chem.* **1986**, *21*, Chapter 23.
[292] M. M. Mansuri, J. C. Martin, *Annu. Rep. Med. Chem.* **1987**, *22*, Chapter 15.
[293] M. M. Mansuri, J. C. Martin, *Annu. Rep. Med. Chem.* **1988**, *23*, Chapter 17.
[294] a) *Nucleic Acid Chemistry, Part 3* (Eds.: L. B. Townsend, R. S. Tipson), Wiley, New York, **1986**; b) *Nucleoside Analogs; Chemistry, Biology and Medicinal Applications* (Eds.: R. T. Walker, E. Declerez, F. Eckstein), Plenum, New York, **1979**.
[295] D. W. Hutchinson, *Trends Biotechnol.* **1990**, *8*, 348.
[296] T. A. Krenitsky, G. W. Koszalka, J. V. Tuttle, J. L. Rideout, G. B. Elion, *Carbohydr. Res.* **1981**, *97*, 139.
[297] a) T. Utagawa, H. Morisawa, F. Yoshinaga, A. Yamazaki, K. Mitsugi, Y. Hirose, *Agric. Biol. Chem.* **1985**, *49*, 1053; b) T. Utagawa, H. Morisawa, S. Yamanaka, A. Yamazaki, F. Yoshinaga, Y. Hirose, *ibid.* **1985**, *49*, 2167.
[298] a) G. M. Tener, H. G. Khorana, *J. Chem. Soc.* **1957**, *79*, 437; b) Y. Inoue, F. Ling, A. Kimura, *Agric. Biol. Chem.* **1991**, *55*, 629.
[299] T. Utagawa, H. Morisasa, S. Yamanaka, A. Yamazaki, F. Yoshinaga, Y. Hirose, *Agric. Biol. Chem.* **1986**, *50*, 121.
[300] T. A. Krenitsky, J. L. Rideout, E. Y. Chao, G. W. Koszalka, F. Gurney, R. C. Crouch, N. K. Cohn, G. Wolberg, R. Vinegar, *J. Med. Chem.* **1986**, *29*, 138.
[301] W. J. Hennen, C.-H. Wong, *J. Org. Chem.* **1989**, *54*, 4692.
[302] T. A. Krenitsky, G. A. Freeman, S. R. Shaver, L. M. Beacham, S. Hurlbert, N. K. Cohn, L. P. Elwell, J. W. T. Selway, *J. Med. Chem.* **1983**, *26*, 891.
[303] J. D. Stoecker, S. E. Ealick, C. E. Bugg, R. E. Parks, Jr., *Proc. Fed. Am. Soc. Exp. Biol.* **1986**, *45*, 2773.
[304] a) J. Holguin, R. Cardinaud, *Eur. J. Biochem.* **1975**, *54*, 505; b) *ibid.* **1975**, *54*, 575; c) D. A. Carson, D. B. Wasson, E. Beutler, *Proc. Natl. Acad. Sci. USA* **1984**, *81*, 2232; d) D. A. Carson, D. B. Wasson, *Biochem. Biophys. Res. Commun.* **1988**, *155*, 829; e) D. Betbeder, D. W. Hutchinson, A. O. L. Richards, *Nucleic Acids Res.* **1989**, *17*, 4217.
[305] M. L. Phillips, E. Nudelman, F. C. A. Gaeta, M. Perez, A. K. Singhal, S. Hakomori, J. C. Paulson, *Science* **1990**, *250*, 1130; G. Waltz, A. Arufto, W. Kalanus, M. Bevilacqua, B. Seed, *ibid.* **1990**, *250*, 1132; J. B. Lowe, L. M. Stoolman, R. P. Nair, R. D. Larson, T. L. Berhend, R. M. Marks, *Cell* **1990**, *63*, 475. X-ray crystal structure analysis of E-selectin: B. J. Graves, R. L. Crowther, C. Chandran, J. M. Rumberger, S. Li, K.-S. Huang, D. M. Presky, P. C. Familletti, B. A. Wolitzky, D. K. Burns, *Nature (London)* **1994**, *367*, 532.
[306] A. Kameyama, H. Ishida, M. Kiso, A. Hasegawa, *Carbohydr. Res.* **1991**, *209*, C1.
[307] K. C. Nicolaou, C. W. Hummel, N. J. Bockovich, C.-H. Wong, *J. Chem. Soc. Chem. Commun.* **1991**, 870.
[308] H. Kondo, Y. Ichikawa, C.-H. Wong, *J. Am. Chem. Soc.* **1992**, *114*, 8748.
[309] S. J. Danishefsky, K. Koseki, D. A. Griffith, J. Gervay, J. M. Peterson, F. E. McDonald, T. Oriyama, *J. Am. Chem. Soc.* **1992**, *114*, 8331.
[310] M. M. Palcic, A. Venot, R. M. Ratcliffe, O. Hindsgaul, *Carbohydr. Res.* **1989**, *190*, 1.
[311] G. E. Ball, R. A. O'Neill, J. E. Schultz, J. B. Lowe, B. W. Weston, J. O. Nagy, E. G. Brown, C. J. Hobbs, M. D. Bednarski, *J. Am. Chem. Soc.* **1992**, *114*, 5449.
[312] D. Tyrrell, P. James, N. Rao, C. Foxall, S. Abbas, F. Dasgupta, M. Nashed, A. Hasegawa, M. Kiso, D. Asa, J. Kidd, B. K. Brandley, *Proc. Natl. Acad. Sci. USA* **1991**, *88*, 10372.
[313] C.-T. Yuen, A. M. Lawson, W. Chai, M. Larkin, M. S. Stoll, A. C. Stuart, F. X. Sullivan, T. J. Ahern, T. Feizi, *Biochemistry* **1992**, *31*, 9126.
[314] S. A. De Frees, F. C. A. Gaeta, Y.-C. Lin, Y. Ichikawa, C.-H. Wong, *J. Am. Chem. Soc.* **1993**, *115*, 7549.
[315] M. S. Mulligan, J. C. Paulson, S. A. DeFrees, Z.-L. Zheng, J. B. Lowe, P. A. Ward, *Nature (London)* **1993**, *364*, 149.
[316] H. Fu, H. Kondo, Y. Ichikawa, G. C. Look, C.-H. Wong, *J. Org. Chem.* **1992**, *57*, 7265.
[317] Representative chemical glycosylations: a) R. U. Lemieux, *Chem. Soc. Rev.* **1978**, *7*, 423; b) H. Paulsen, *Angew. Chem.* **1982**, *94*, 184; *Angew. Chem. Int. Ed. Engl.* **1982**, *21*, 155; c) Ref. [156a]; d) H. Kunz, *Angew. Chem.* **1987**, *99*, 297; *Angew. Chem. Int. Ed. Engl.* **1987**, *26*, 294; e) K. Okamoto, T. Goto, *Tetrahedron* **1989**, *45*, 5835; f) K. C. Nicolaou, T. Caulfield, H. Kataoka, P. Kumazawa, *J. Am. Chem. Soc.* **1988**, *110*, 7910; g) D. R. Mootoo, P. Konradsson, U. Udodong, B. Fraser-Reid, *ibid.* **1988**, *110*, 5583; R. L. Halcomb, S. J. Danishefsky, *ibid.* **1989**, *111*, 6661; i) R. W. Friesen, S. J. Danishefsky, *ibid.* **1989**, *111*, 6656; j) A. G. M. Barrett, B. C. B. Bezuidenhoudt, A. F. Gasiecki, A. R. Howell, M. A. Russell, *ibid.* **1989**, *111*, 1391; k) K. Briner, A. Vesella, *Helv. Chim. Acta* **1989**, *72*, 1371; l) D. Kahne, S. Walker, Y. Cheng, D. Van Engen, *J. Am. Chem. Soc.* **1989**, *111*, 6881; m) K. Suzuki, H. Maeta, T. Matsumoto, *Tetrahedron Lett.* **1989**, *30*, 4853; n) Y. Ito, T. Ogawa, *Tetrahedron* **1990**, *46*, 89; o) A. Hasegawa, T. Nagahama, H. Ohki, H. Hotta, M. Kiso, *J. Carbohydr. Chem.* **1991**, *10*, 493; p) A. Marra, P. Sinay, *Carbohydr. Res.* **1990**, *195*, 303; q) H. Lonn, K. Stenvall, *Tetrahedron Lett.* **1992**, *33*, 115; r) E. Kirchner, F. Thiem, R. Dernick, J. Heukeshoven, J. Thiem, *J. Carbohydr. Chem.* **1988**, *7*, 453; s) F. Barres, O. Hindsgaul, *J. Am. Chem. Soc.* **1991**, *113*, 9376; t) G. Stork, G. Kim, *ibid.* **1992**, *114*, 1087; u) P. J. Garegg, *Acc. Chem. Res.* **1992**, *25*, 575; v) K. Toshima, K. Tatsuta, *Chem. Rev.* **1993**, *93*, 1503.
[318] Sialylations with TMSOTf as catalyst: a) T. J. Martin, R. R. Schmidt, *Tetrahedron Lett.* **1992**, *33*, 6123; b) H. Kondo, Y. Ichikawa, C.-H. Wong, *J. Am. Chem. Soc.* **1992**, *114*, 8748; M. M. Sim, H. Kondo, C.-H. Wong, *ibid.* **1993**, *115*, 2260. With $ZnCl_2$ as Lewis acid: c) Y. Watanabe, C. Nakamoto, S. Ozaki, *Synlett* **1993**, *115*; E. J. Corey, Y.-J. Wu, *J. Am. Chem. Soc.* **1993**, *115*, 8871; d) Synthesis of CMP-NeuAc: T. J. Martin, R. R. Schmidt, *Tetrahedron Lett.* **1993**, *34*, 1765.
[319] H. Kondo, S. Aoki, Y. Ichikawa, R. L. Halcomb, H. Ritzen, C.-H. Wong, *J. Org. Chem.* **1994**, *59*, 864.
[320] a) H. S. Conradt, H. Egge, J. Peter-Katalinic, W. Reiser, T. Siklosi, K. Schaper, *J. Biol. Chem.* **1987**, *262*, 14600; b) S. P. Little, N. U. Bang, C. S. Harms, C. A. Marks, L. E. Mattler, *Biochemistry* **1984**, *23*, 6191.
[321] B. D. Livingston, E. M. D. Robertis, J. C. Paulson, *Glycobiology* **1990**, *1*, 39.
[322] H. Kunz, *Pure Appl. Chem.* **1993**, *65*, 1223; H. Garg, R. W. Jeanloz, *Adv. Carbohydr. Chem. Biochem.* **1985**, *43*, 135; T. Bielfeldt, S. Peters, M. Meldal, K. Bock, H. Paulsen, *Angew. Chem.* **1992**, *104*, 881; *Angew. Chem. Int. Ed. Engl.* **1992**, *31*, 857; F. E. McDonald, S. J. Danishefsky, *J. Org. Chem.* **1992**, *57*, 7001; S. T. Cohen-Anisfeld, P. T. Lansburg Jr., *J. Am. Chem. Soc.* **1993**, *115*, 10531; A. L. Handlon, B. Fraser-Reid, *ibid.* **1993**, *115*, 3796.
[323] C.-H. Wong, M. Schuster, P. Wang, P. Sears, *J. Am. Chem. Soc.* **1993**, *115*, 5893.
[324] M. Schuster, P. Wang, J. C. Paulson, C.-H. Wong, *J. Am. Chem. Soc.* **1994**, *116*, 1135.
[325] a) For a review see Ref. [15]; b) L. Czollnev, J. Kuszmann, A. Vasella, *Helv. Chim. Acta* **1990**, *73*, 1338; c) M. von Itzstein, W.-Y. Wu, G. B. Kok, M. S. Pegg, J. C. Dyason, D. Jin, T. van Phan, M. L. Smythe, H. F. White, S. W. Oliver, P. M. Colman, J. N. Varghese, D. M. Ryan, J. M. Woods, R. C. Bethell, V. J. Hotham, J. M. Cameron, C. R. Penn, *Nature (London)* **1993**, *363*, 418; d) B. Winchester, C. Barker, S. Baines, G. S. Jacob, S. K. Namgoong, G. Fleet, *Biochem. J.* **1990**, *265*, 277; e) Y.-F. Wang, Y. Takaoka, C.-H. Wong, *Angew. Chem.*, **1994**, *106*, 1343; *Angew. Chem. Int. Ed. Engl.* **1994**, *33*, 1242; f) R. C. Bernotas, M. A. Pezzone, B. Ganem, *Carbohydr. Res.* **1987**, *167*, 305; g) M. K. Tong, G. Papandreou, B. Ganem, *J. Am. Chem. Soc.* **1990**, *112*, 6137; h) P. Ermert, A. Vasella, *Helv. Chim. Acta* **1991**, *74*, 2043; i) K. M. Robinson, M. E. Begovic, B. L. Rhinehart, E. W. Heineke, J.-B. Ducep, P. R. Kastner, F. N. Marshall, C. Danzin, *Diabetes* **1991**, *40*, 825; j) G. B. Karlsson, T. D. Butters, R. A. Dwek, F. M. Platt, *J. Biol. Chem.* **1993**, *268*, 570; k) L. Provencher, D. H. Steensma, C.-H. Wong, *Bioorg. Med. Chem.*, in press.

[326] M. L. Sinnott, *Chem. Rev.* **1990**, *90*, 1171; M. Ashwell, X. Guo, M. L. Sinnott, *J. Am. Chem. Soc.* **1992**, *114*, 10158; P. Deslongchamps, *Pure Appl. Chem.* **1993**, *65*, 1161; R. Kuroki, L. H. Weaver, B. W. Matthews, *Science* **1993**, *262*, 2030; N. C. J. Strynadka, M. N. G. James, *J. Mol. Biol.* **1991**, *220*, 401; S. G. Withers, R. A. Warren, I. P. Street, K. Rupitz, J. B. Kempton, R. J. Aebersold, *J. Am. Chem. Soc.* **1990**, *112*, 5887; A. N. Singh, L. S. Hester, F. M. Raushel, *J. Biol. Chem.* **1987**, *262*, 2554.
[327] T.-C. Wu, P. G. Goekjian, Y. Kishi, *J. Org. Chem.* **1987**, *52*, 4819.
[328] K. N. Houk, J. E. Eksterowicz, Y.-D. Wu, C. D. Fuglesang, D. B. Mitchell, *J. Am. Chem. Soc.* **1993**, *115*, 4170.
[329] C. Fotsch, C.-H. Wong, *Tetrahedron Lett.*, in press.
[330] P. Wang, M. Schuster, Y.-F. Wang, C.-H. Wong, *J. Am. Chem. Soc.* **1993**, *115*, 10487.
[331] C. T. Walsh, *J. Biol. Chem.* **1989**, *264*, 2393; E. T. Rietschel, H. Brade, *Sci. Am.* **1992**, *267*, 54.

Direct Spectroscopic Evidence for a Hitherto Elusive "Zwitterionic" Excited State

Lutz H. Gade*

Direct experimental support for a theoretical concept in science is sometimes obtained in an area for which it was not originally proposed. The case we describe here is the simplest example of chemical bonding, the interaction of two electrons in weakly coupled orbitals on two atomic centers. As early as 1932 Mulliken analyzed the situation in the π-orbital domain of twisted ethylene[1] and a few years later the (related) electronic structure of the σ domain in "stretched" dihydrogen (i.e. an H_2 molecule in which the interatomic distance is increased well beyond its equilibrium value).[2] In both cases four electronic states are specified (Fig. 1): two low-energy "diradical" states

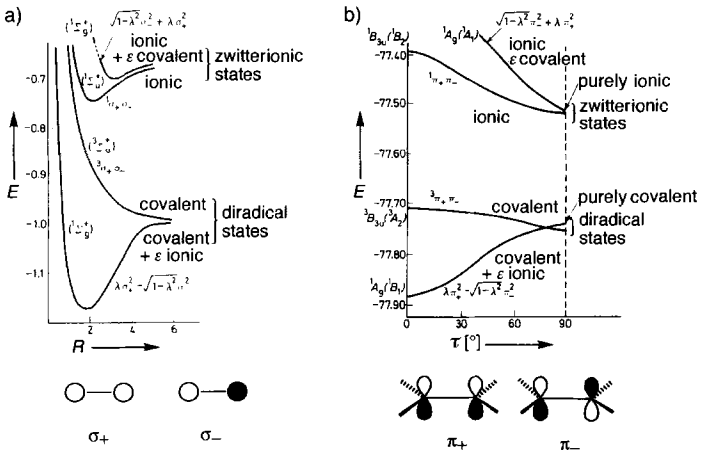
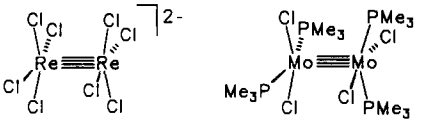


Fig. 1. The four electronic states of the $\sigma(1s)$- and $\pi(2p)$ manifolds in H_2 and ethylene, respectively. a) "Stretching" of H_2. VB description of the four states (atomic orbitals centerd on atoms A and B): $^1\Sigma_g^+ = {}^1[1s(A)1s(B)]$, $^3\Sigma_u^+ = {}^3[1s(A)1s(B)]$, $^1\Sigma_u^+ = {}^1[1s(A)1s(A) - 1s(B)1s(B)]$, $^1\Sigma_g^+ = {}^1[1s(A)1s(A) + 1s(B)1s(B)]$. b) "Twisting" of C_2H_4. In weakly coupled systems (H_2 at $R > 4a_0$; twist angle $\tau \approx 90°$) the four states may be clearly distinguished as either of diradical or zwitterionic nature (from ref. [3a]). E in Hartree, R in a_0.

(singlet and triplet) with the electrons in separate orbitals, and two higher energy "zwitterionic" singlet states.[3] The latter are derived from the symmetric and antisymmetric linear combination of wave functions representing the pairing of the two electrons in the two orbitals. It should be noted that these zwitterionic states do not have a net dipole moment in homosymmetric molecules. The fact that one of the states would represent the ground state in a real zwitterion is the reason for this potentially confusing terminology. However, in a polar environment (solution) these states may be subject to "sudden polarization" and display zwitterionic reactivity.[3]

Whereas the diradical states have been comprehensively studied over the past decades and provide the foundation for the description of the extensive organic chemistry of biradicals, the zwitterionic states have proved to be far more elusive (though invoked, for example, to explain the photoisomerization and cyclization of 1,3-dienes).[4] Recent studies of the solvent and substituent effects on the lifetime of the transient species generated by $\pi \rightarrow \pi^*$ excitation of alkenes have provided some indirect evidence for the existence of the postulated manifold of zwitterionic excited states.[5] However, its direct detection has to date not been achieved with these systems. The short lifetime and thus the transitory nature of the weak coupling, which is characteristic of the zwitterionic states during the stretching of bonds preceding dissociation or the twisting of bonds in isomerizations, is the main reason for this situation.

D. G. Nocera and co-workers have now reported the direct spectroscopic detection of the zwitterionic states in a weakly coupled two-electron two-orbital system.[6] As their object of study they chose the dinuclear complex **2** with a quadruple



1 **2**

metal–metal bond, which was first synthesized and characterized by F. A. Cotton et al.[7] What is it that almost predestines this particular compound for an investigation into the nature of the zwitterionic states? First of all, systems with a quadruple bond have a nontransitory weakly coupled set of orbitals virtually built into them: the δ and δ^* molecular orbitals derived from the d_{xy} metal orbitals. Their spatial arrangement is structurally reinforced by the σ and π bond framework which maintains their weak coupling. Secondly, the relatively bulky phosphane ligands sterically lock the system in its ground state conformation, and therefore the orientation of the d_{xy} orbital is

[*] Dr. L. H. Gade
Institut für Anorganische Chemie der Universität
Am Hubland, D-97074 Würzburg (Germany)
Telefax.: Int. code + (931)888-4605

 © VCH Verlagsgesellschaft mbH, D-69451 Weinheim, 1995 0570-0833/95/0505-0547 $ 10.00+.25/0

fixed. The choice of the PMe_3-substituted complex thus avoids complications arising from internal rotation about the metal–metal axis in an excited state of the molecule, as observed for instance for $[Re_2Cl_8]^{2-}$ (**1**) in solution. Finally, previous work performed in the groups of H. B. Gray,[8] F. A. Cotton,[9] and others[10, 11] has provided a reliable assignment of relevant bands in the UV/Vis absorption and emission spectra of several quadruply bonded compounds, which developed simultaneously with the theoretical understanding of the electronic structure[*] of these species.[12]

A qualitative energy level diagram showing the four-state δ manifold of M≡M complexes of D_{4h} symmetry (D_{2d} in the case of **2**) is displayed in Figure 2. The energy gap between the

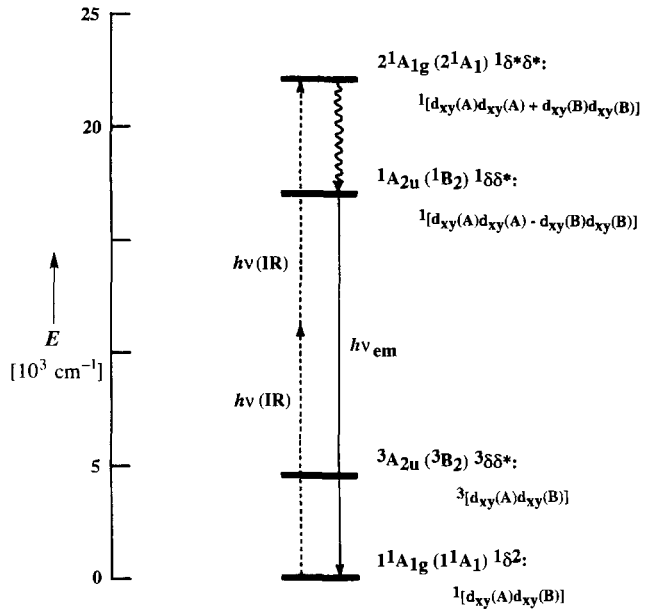
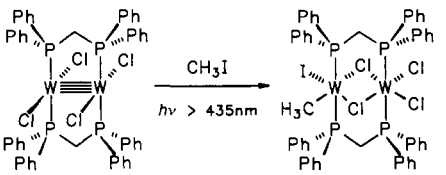


Fig. 2. A qualitative energy level diagram for the δ-δ* orbital manifold based on a valence bond model (orbitals centered on the two metal atoms A and B). The states are designated by their symmetry labels in D_{4h} and D_{2d} symmetries (the latter in brackets). The two-photon excitation (by absorption of two near-infrared photons) into the zwitterionic 2^1A_{1g} (2^1A_1) state is indicated, followed by internal conversion to the highly emissive $^1A_{2u}$ ($^1B_2$) state. The red fluorescence ($h\nu_{em}$) from this state was detected in the fluorescence experiment with two-photon excitation (adapted from ref. [6]).

ground state 1^1A_{1g} (1^1A_1) and the triplet state $^3A_{2u}$ ($^3B_2$) in **2** has been extrapolated recently from magnetic measurements[15] as well as from an elegant application of paramagnetic ^{31}P NMR spectroscopy to a series of related systems.[16] The low-frequency band in the UV/Vis spectra of the quadruply bonded dinuclear compounds corresponds to the excitation into the dipole-allowed zwitterionic $^1A_{2u}$ ($^1B_2$) state. In "sterically locked" complexes such as **2** relaxation into a twisted excited singlet state (as in **1**) is not feasible; the $^1A_{2u}$ ($^1B_2$) state therefore shows instantaneous and intense emission. The second zwitterionic excited singlet state corresponds approximately to a $(\delta^*)^2$ configuration (neglecting configuration interaction with the ground state 1^1A_{1g} (1^1A_1)) and is thus not allowed according to the selection rules for one-photon, electric-dipole transitions. Nocera and co-workers located this state in **2** by two-photon excitation fluorescence spectroscopy. Upon excitation into the 2^1A_1 state the system undergoes transition to $^1B_2$; the emission from the latter state is then detected. That the primary excited state is indeed populated by a two quantum transition was established by the dependence of the fluorescence intensity on the square of the incident excitation intensity.[17] The polarization ratio ($\Omega = I_{circ}/I_{lin} < 1$; circ, lin = circular and linear polarized irradiation) of the excitation fluorescence spectrum furthermore indicates that the excited state is indeed of $^1A_1$ symmetry,[18] as required for the second zwitterionic state of the investigated system. The small $2^1A_1 - {}^1B^2$ energy gap of 4800 cm^{-1} relative to the $^1B_2 - 1^1A_1$ gap of 17100 cm^{-1} indicates the very ionic nature of the doubly excited state 2^1A_1 (the authors give a preliminary estimate of 68%). With both zwitterionic states of the δ-δ* manifold now unambiguously located, the four-state structure of a weakly coupled two-electron two-orbital sytem has been established for the first time.

What is the significance of this study beyond the direct verification of an important model for chemical bonding dating back to the very beginning of quantum chemistry? For the inorganic photochemist it sheds new light on the potential photochemical reactivity of the metal–metal quadruple bond. The pairing of two electrons on one metal center and two "holes" on an adjacent one predisposes this type of system for multielectron reactivity. Recent investigations by the same group give first indications of such a reactive pattern, for instance, the two-electron photoreduction of CH_3I by $[W_2(dppm)_2Cl_4]$ [Eq.(a)].[19]



(a)

These recent developments have shown that the metal–metal quadruple bond continues to fascinate the chemical community even three decades after it was discovered by F. A. Cotton et al.[20]

German version: *Angew. Chem.* **1995**, *107*, 595

Keywords: fluorescence spectroscopy · metal–metal multiple bonds · photochemistry · zwitterionic states

[*] It should be mentioned in this context, however, that an "isolated δ-δ* manifold" model is entirely inadequate for a *quantitative* theoretical description of the δ-δ* photochemistry, as has been recently discussed by Bursten and Clayton [13] (and, previously, by others [14]). It should therefore be taken for what it is worth: a convenient approximation to the actual chemical bonding in dinuclear complexes with quadruple metal–metal bonds. The accurate calculations presented in ref. [12] include configuration interaction with states outside the δ-δ* manifold.

[1] R. S. Mulliken, *Phys. Rev.* **1932**, *41*, 751.
[2] R. S. Mulliken, *Phys. Rev.* **1936**, *50*, 1028.
[3] a) L. Salem, C. Rowland, *Angew. Chem.* **1972**, *84*, 86; *Angew. Chem. Int. Ed. Engl.* **1972**, *11*, 92; b) W. G. Dauben, L. Salem, N. J. Turro, *Acc. Chem. Res.* **1975**, *8*, 41; c) L. Salem, *Pure Appl. Chem* **1973**, *33*, 317 d) V. Bonačić-Koutecký, J. Koutecky, J. Michl, *Angew. Chem.* **1987**, *99*, 216; *Angew. Chem. Int. Ed. Engl.* **1987**, *26*, 170.
[4] W. G. Dauben, M. S. Kellogg, J. I. Seeman, N. D. Vietmeyer, P. H. Wendschuh, *Pure Appl. Chem* **1973**, *33*, 197 and references therein. See also: N. J. Turro, *Modern Molecular Photochemistry*, 2nd ed., University Science Books, Hill Valley, CA, USA, **1991**.

 © VCH Verlagsgesellschaft mbH, D-69451 Weinheim, 1995 0570-0833/95/0505-0548 $ 10.00+.25/0

[5] C. L. Schilling, E. F. Hilinski, *J. Am. Chem. Soc.* **1988**, *110*, 2296; J. Morais, J. Ma, M. B. Zimmt, *J. Phys. Chem.* **1991**, *95*, 3885; J. Ma, M. B. Zimmt, *J. Am. Chem. Soc.* **1992**, *114*, 9723.
[6] D. S. Engebretson, J. M. Zaleski, G. E. Leroi, D. G. Nocera, *Science* **1994**, *265*, 759.
[7] F. A. Cotton, M. W. Extine, T. R. Felthouse, B. W. S. Kolthammer, D. G. Lay, *J. Am. Chem. Soc.* **1981**, *103*, 4040.
[8] W. C. Trogler, H. B. Gray, *Acc. Chem. Res.* **1978**, *11*, 233; See for instance: C. D. Cowman, H. B. Gray, *J. Am. Chem. Soc.* **1973**, *95*, 8177; M. D. Hopkins, H. B. Gray, *ibid.* **1984**, *106*, 2468; M. D. Hopkins, H. B. Gray, V. M. Miskowski, *Polyhedron* **1987**, *4*, 705; V. M. Miskowski, H. B. Gray, M. D. Hopkins, *Inorg. Chem.* **1992**, *31*, 2085.
[9] F. A. Cotton, P. E. Fanwick, L. D. Gage, B. Kalbacher, D. S. Martin, *J. Am. Chem. Soc.* **1977**, *99*, 5642; P. E. Fanwick, D. S. Martin, F. A. Cotton, T. R. Webb, *Inorg. Chem.* **1977**, *16*, 2103.
[10] J. R. Winkler, D. G. Nocera, T. L. Netzel, *J. Am. Chem. Soc.* **1986**, *108*, 4451; H. W. Huang, D. S. Martin, *Inorg. Chem.* **1985**, *24*, 96.
[11] For a complete account, see: F. A. Cotton, R. A. Walton, *Multiple Bonds Between Metal Atoms*, 2nd ed., Clarendon Press, Oxford **1993**, Chapter 10.
[12] P. J. Hay, *J. Am. Chem. Soc.* **1982**, *104*, 7007; F. A. Cotton, X. Feng, *ibid.* **1993**, *115*, 1074.
[13] B. E. Bursten, T. W. Clayton, Jr., *J. Cluster Science* **1994**, *5*, 157.
[14] L. Noodleman, J. G. Norman, Jr., *J. Chem. Phys.* **1979**, *70*, 4903; W. C. Trogler, *J. Chem. Ed.* **1980**, *57*, 424; B. E. Bursten, D. L. Clark, *Polyhedron* **1987**, *6*, 695.
[15] M. D. Hopkins, T. C. Zietlow, V. M. Miskowski, H. B. Gray, *J. Am. Chem. Soc.* **1985**, *107*, 510.
[16] F. A. Cotton, J. L. Eglin, B. Hong, C. A. James, *J. Am. Chem. Soc.* **1992**, *114*, 4915; *Inorg. Chem.* **1993**, *32*, 2104.
[17] S. H. Lin, Y. Fujimura, H. J. Neusser, E. W. Schlag, *Multiphoton Spectroscopy of Molecules*, Academic Press, Orlando, FL, USA, **1984**, Chapter 4.
[18] P. R. Monson, W. M. McClain, *J. Chem. Phys.* **1970**, *53*, 29; W. M. McClain, *ibid.* **1971**, *55*, 2789; M. A. Nasciemento, *Chem. Phys.* **1983**, *74*, 51.
[19] C. M. Partigianoni, D. G. Nocera, *Inorg. Chem.* **1990**, *29*, 2033. See also: D. G. Nocera, *J. Cluster Sci.* **1994**, *5*, 185; C. M. Partigianoni, I.-J. Chang, D. G. Nocera, *Coord. Chem. Rev.* **1990**, *97*, 105.
[20] F. A. Cotton, N. F. Curtis, C. B. Harris, B. F. G. Johnson, S. J. Lippard, J. T. Mague, W. R. Robinson, J. S. Wood, *Science* **1964**, *145*, 1305.

Conical Intersections and the Mechanism of Singlet Photoreactions

Martin Klessinger*

The reaction pathway of a nonadiabatic photochemical reaction begins on the potential energy surface of the excited state (S_1) in the Franck–Condon region or at a spectroscopic minimum of the reactant and ends at the product minimum on the ground-state surface (S_0). The two stages on the S_1 and S_0 surface are separated by a funnel[1] at which radiationless decay from the excited state to the ground state becomes possible (Fig. 1). For a long time it was believed that the funnels mostly correspond to surface crossings (or touchings) that are at least weakly avoided, but recent work has shown that for a great number of inorganic[2] and organic[3] systems the crossings are actually unavoided and correspond to true conical intersections.[4] Nowadays it appears that conical intersections are a common feature in most nonadiabatic singlet photoreactions.

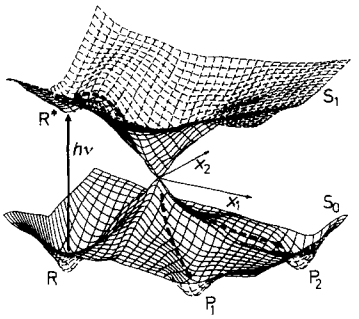


Fig. 1. Schematic representation of the potential energy surfaces of the ground state (S_0) and the excited state (S_1) of a nonadiabatic photoreaction of reactant R. Depending on the way the classical trajectories enter the conical intersection region, different ground-state valleys, which lead to products P_1 and P_2, can be reached.

A conical intersection is defined as follows: Two states, even if they have the same symmetry, intersect along an $(F-2)$-dimensional hyperline as the energy is plotted against the F nuclear coordinates ($F = 3N-6$).[5] While for any point of the $(F-2)$-dimensional intersection space the energies of the two states are the same, the degeneracy is lifted along the two remaining linearly independent coordinates $\boldsymbol{x}_1$ and $\boldsymbol{x}_2$. Thus, when the energy of the two states is plotted against these two geometrical variables (they are combinations of bond distances, angles, etc.), the corresponding energy surfaces have the shape of a double cone, as shown in Figure 1.

The gradient difference vector $\boldsymbol{x}_1$ is defined by Equation (a). In this direction the difference in the slopes of the upper and

$$\boldsymbol{x}_1 = \partial(E_0-E_1)/\partial\boldsymbol{q} \qquad \text{(a)}$$

the lower surface is largest. The nonadiabatic coupling vector $\boldsymbol{x}_2$ is given by Equation (b). This is the direction of nuclear dis-

$$\boldsymbol{x}_2 = \langle\Psi_0|\partial\Psi_1/\partial\boldsymbol{q}\rangle \qquad \text{(b)}$$

displacement that mixes the states two adiabatic wave functions at the cone point the best. If Ψ_0 and Ψ_1 are of different symmetries at the apex of the cone, $\boldsymbol{x}_2$ is the symmetry-lowering coordinate that permits them to mix. The vectors $\boldsymbol{x}_1$ and $\boldsymbol{x}_2$ are often nearly orthogonal. The gradient of neither of the touching surfaces is zero at the tip of the cones, as it would be for a true stationary point. Rather, it is the projection of the gradient onto the $(F-2)$-dimensional subspace orthogonal to $\boldsymbol{x}_1$ and $\boldsymbol{x}_2$ that goes to zero when the geometry of the conical intersection is optimized. Therefore, in the F-dimensional space, gradient-based search routines will not recognize the bottom of the funnel as a minimum, although it represents the lowest energy point on that surface (unless the funnel is strongly tilted).

From a mechanistic point of view a conical intersection funnel plays a similar role in a photochemical reaction as the transition state in a thermal reaction.[3] Both describe the geometry of the "reactive conformation" of the system. For a thermal reaction, the transition state corresponds to the point of the

[*] Prof. Dr. M. Klessinger
Organisch-Chemisches Institut der Universität
Corrensstrasse 40, D-48149 Münster (Germany)
Telefax: Int. code + (251)83-9772

 © VCH Verlagsgesellschaft mbH, D-69451 Weinheim, 1995 0570-0833/95/0505-0549 $ 10.00+.25/0

potential energy surface where the probability of passage from the reactant well to the product well is the largest. Similarly, in a photochemical reaction, a conical intersection represents the region of the excited-state surface where the probability of decay to the ground state is the largest. The initial motion after passage through a transition state is characterized by a single vector q_R (the normal coordinate of the imaginary vibrational frequency), that corresponds to the reaction path through the saddle point. In contrast, a conical intersection provides two linearly independent reaction-path directions x_1 and x_2. In the immediate vicinity of the apex of the cone the reaction path can follow any direction in the x_1, x_2 plane and may reach different reaction valleys that develop on the S_0 surface.

Thus, for a nonadiabatic photoreaction, the dynamics of nuclear motion can be described as shown schematically in Figure 1. After absorption of a photon, the system moves on the excited-state surface toward a funnel along classical trajectories following the bottom of valleys and possibly passing over barriers. In this region the energy separation between excited and ground state will be too large to allow a surface jump, until eventually the system enters the conical intersection region, where the energy gap is small and consequently the probability of a surface jump is large. The trajectories passing exactly through the tip of the cone proceed undisturbed. They follow the typically quite steep slope of the cone wall, thus converting electronic energy into energy of nuclear motion. The acceleration will often be in a direction close to the vector x_1. Trajectories that just miss the cone tip have some probability of staying on the upper surface, and some probability of jumping to the lower surface. In this latter case, an amount of energy equal to the height of the jump is converted into the component of motion in a direction given by the vector x_2 (nonadiabatic coupling). The determination of quantum yields of the various possible products requires the knowledge of the exact components of motion in the x_1 and x_2 directions. This, in turn, is available only from detailed dynamics calculations, which so far have been performed for simple model systems only.[6]

The most important consequence of the refinement of the original Oosterhoff model[7] is the fact that the $S_1 \rightarrow S_0$ decay does not occur at the "pericyclic minimum" (which, in fact, can be a transition state between two conical intersections, which might be equivalent by symmetry, cf. Fig. 2), but rather at geometries of lower symmetry.[3a] Efficient algorithms have been developed for locating the points of minimum energy within the $(F-2)$-dimensional intersection space and for determining the exact geometry at the conical intersections.[8] Geometries at which conical intersections are likely to occur may be predicted by means of simple models. From the two-electron—two-orbital model for biradicaloids,[9] for instance, it follows that certain perturbations δ that induce a splitting of those orbitals that are degenerate in the perfect biradical will lower the energy separation between the S_0 and S_1 states. For a value $\delta = \delta_0$ that is referred to as the critically heterosymmetric case this separation becomes zero, which results in a conical intersection.

Thus, for 90°-twisted ethylene the p orbitals are orthogonal and degenerate; the pericyclic geometry corresponds to a perfect biradical with a very large energy gap between S_1 and S_0. Replacement of one of the CH_2 groups by a more electronegative group transforms the perfect biradical into a heterosymmetric biradicaloid, and the 90°-twisted formaldiminium ion $CH_2{=}\overset{+}{N}H_2$ represents the critically heterosymmetric case. The energy gap is zero, and a conical intersection results.[10] In the case of the photochemical [2 + 2] cycloaddition, a rhomboidal distortion of the pericyclic geometry differentiates the otherwise degenerate energies of the localized nonbonding orbitals of the cyclobutadiene-like perfect biradical. This again decreases the energy gap, and eventually a conical intersection is reached (Fig. 2). The same conclusion is reached on the basis of a qualitative VB model that Bernardi, Olivucci, Robb and coworkers[11] developed for predicting and discussing the geometries of conical intersections and verified by ab initio calculations.[3a] For the photoreactions of butadiene[3j] they determined geometries of the conical intersection region that correspond to a distorted quasitetraradical, which is characterized by a combination of peripheral and diagonal interactions of the reactive orbitals (Fig. 3). The suggestion that the return to S_0 occurs through a conical intersection at a distorted pericyclic geometry involving diagonal interactions was first proposed on the basis of model calculations for H_4.[12] The various ways of recoupling the electrons of the tetraradical depicted in Scheme 1 demonstrate how different photoproducts may evolve from the same funnel.[3j,k]

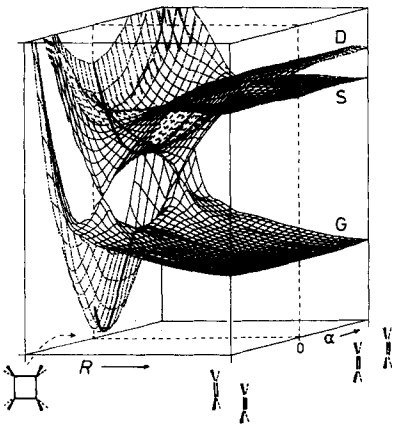


Fig. 2. Schematic representation of the potential energy surfaces of the singlet states for the photodimerization of ethylene, plotted as a function of the intermolecular distance R and the angle α that measures the deviation from the rectangular arrangement. G, S, and D label the surfaces described in the 2×2 CI model by the ground state, and the singly and the doubly excited configuration, respectively. The potential energy curves shown for $\alpha = 0$ correspond to the Oosterhoff model.

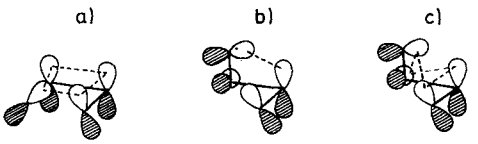
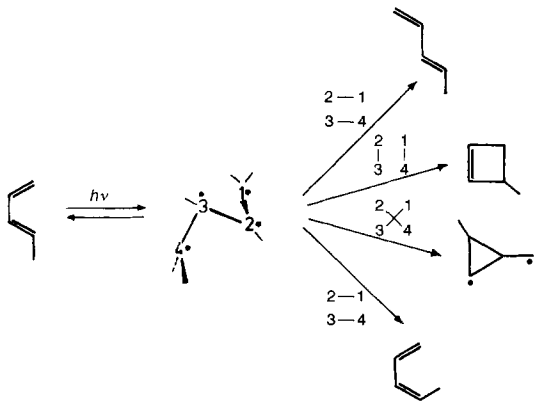


Fig. 3. π Orbital interactions in butadiene. a) Peripheral interactions along the perimeter at high-symmetry disrotatory pericyclic geometry; b) diagonal and c) peripheral interactions at the geometry of the conical intersection.

Recently, real conical intersections have been located by means of ab initio calculations for a large variety of photoreactions.[2,3] This demonstrates that the occurrence of this topological phenomenon, previously believed to be quite improbable, is

 © VCH Verlagsgesellschaft mbH, D-69451 Weinheim, 1995 0570-0833/95/0505-0550 $ 10.00+.25/0



Scheme 1. Possible courses for the photoreaction of pentadiene after formation of the tetraradical intermediate.

more likely to be the rule than an exception.[13] Substituents may affect 1) the excited-state reaction pathway toward the funnel, 2) the geometrical structure at the conical intersection, and 3) the dynamics of the decay and the ground-state reaction path. First studies of substituent effects in butadiene photochemistry[31] and in photochemical [2 + 2] cycloaddition[14] suggest that all three effects may be important.

German version: *Angew. Chem.* **1995**, *107*, 597

Keywords: ab initio calculations · conical intersection · diradicaloid · pericyclic reactions · photochemistry

[1] a) J. Michl, *Mol. Photochem.* **1972**, *4*, 243, 257, 287; b) J. Michl, V. Bonačić-Koutecký, *Electronic Aspects of Organic Photochemistry*, Wiley, New York, **1990**.

[2] O_3: a) G. J. Atchity, S. S. Xantheas, S. T. Elbert, K. Ruedenberg, *J. Chem. Phys.* **1991**, *94*, 8054. O_3^+: b) H. Müller, H. Köppel, L. S. Cederbaum, T. Schmelz, G. Chambaud, P. Rosmus, *Chem. Phys. Lett.* **1992**, *197*, 599. H_2 + He: c) M. R. Manaa, D. R. Yarkony, *J. Chem. Phys.* **1990**, *93*, 4473. H^+ + NO: d) *ibid.* **1992**, *97*, 715.

[3] Ethylene dimerization: a) F. Bernardi, S. De, M. Olivucci, M. A. Robb, *J. Am. Chem. Soc.* **1990**, *112*, 1737. Valence isomerizations of benzene and pyrazine: b) I. J. Palmer, M. Olivucci, F. Bernardi, M. A. Robb, *J. Org. Chem.* **1992**, *57*, 5081; c) I. J. Palmer, I. N. Ragazos, F. Bernardi, M. Olivucci, M. A. Robb, *J. Am. Chem. Soc.* **1993**, *115*, 673; d) A. L. Sobolewski, C. Woywod, W. Domcke, *J. Chem. Phys.* **1993**, *98*, 5627; e) W. Domcke, A. L. Sobolewski, C. Woywod, *Chem. Phys. Lett.* **1993**, *203*, 220. Ring opening of alkyl-substituted cyclobutenes: f) F. Bernardi, M. Olivucci, I. N. Ragazos, M. A. Robb, *J. Am. Chem. Soc.* **1992**, *114*, 2752. Sigmatropic rearrangements of but-1-ene: g) F. Bernardi, M. Olivucci, M. A. Robb, G. Tonachini, *ibid.* **1992**, *114*, 5805. Photochemical transformations of ergosterol: h) F. Bernardi, M. Olivucci, I. N. Ragazos, M. A. Robb, *ibid.* **1992**, *114*, 8211. Di-π-Methane rearrangement: i) M. Reguero, F. Bernardi, J. Jones, M. Olivucci, I. N. Ragazos, M. A. Robb, *ibid.* **1993**, *115*, 2073. Butadiene: j) M. Olivucci, I. N. Ragazos, F. Bernardi, M. A. Robb, *ibid.* **1993**, *115*, 3710. *cis–trans* Isomerization of hexatriene: k) M. Olivucci, F. Bernardi, P. Celani, I. N. Ragazos, M. A. Robb, *ibid.* **1994**, *116*, 1077. 2,3-Substituted butadienes: l) M. Olivucci, F. Bernardi, S. Ottani, M. A. Robb, *ibid.* **1994**, *116*, 2034. Carbene formation from diazirine and diazomethane: m) N. Yamamoto, F. Bernardi, A. Bottoni, M. Olivucci, M. A. Robb, S. Wilsey, *ibid.* **1994**, *116*, 2064. α,β-Enones: n) M. Reguero, M. Olivucci, F. Bernardi, M. A. Robb, *ibid.* **1994**, *116*, 2103. Paterno-Büchi reaction: o) I. J. Palmer, I. N. Ragazos, F. Bernardi, M. Olivucci, M. A. Robb, *ibid.* **1994**, *116*, 2121. Cyclohexadiene–hexatriene interconversion: p) P. Celani, S. Ottani, M. Olivucci, F. Bernardi, M. A. Robb, *ibid.* **1994**, *116*, 10141. Cyclopropylidene ring opening: q) G. J. Atchity, S. S. Xantheas, S. T. Elbert, K. Ruedenberg, *Theor. Chim. Acta* **1991**, *78*, 365. Photodissociations of methanethiol: r) D. R. Yarkony, *J. Chem. Phys.* **1994**, *100*, 3639.

[4] a) I. von Neumann, E. Wigner, *Z. Phys.* **1929**, *30*, 467; b) E. Teller, *J. Phys. Chem.* **1937**, *41*, 109; c) G. Herzberg, H. C. Longuet-Higgins, *Trans. Faraday Soc.* **1963**, *35*, 77; d) L. Salem, *Electrons in Chemical Reactions: First Principles*, Wiley, New York, **1982**; e) S. S. Xantheas, K. Ruedenberg, *J. Chem. Phys.* **1991**, *95*, 1862.

[5] The noncrossing rule, according to which potential energy curves of the same symmetry do not cross, is valid only for diatomics, cf. [4d].

[6] U. Manthe, H. Köppel, *J. Chem. Phys.* **1990**, *93*, 1669.

[7] W. T. A. M. van der Lugt, L. J. Oosterhoff, *J. Am. Chem. Soc.* **1969**, *91*, 6042.

[8] a) I. N. Ragazos, M. A. Robb, F. Bernardi, M. Olivucci, *Chem. Phys. Lett.* **1992**, *197*, 217; b) M. J. Bearpark, M. A. Robb, H. B. Schlegel, *ibid.* **1994**, *223*, 269; c) M. R. Mana, D. R. Yarkony, *J. Chem. Phys.* **1993**, *99*, 5251.

[9] V. Bonačić-Koutecký, J. Koutecký, J. Michl, *Angew. Chem.* **1987**, *99*,134; *Angew. Chem. Int. Ed. Engl.* **1987**, *26*, 170.

[10] V. Bonačić-Koutecký, J. Köhler, J. Michl, *Chem. Phys. Lett.* **1984**, *104*, 440.

[11] a) F. Bernardi, M. Olivucci, J. J. W. McDonall, M. A. Robb, *J. Chem. Phys.* **1988**, *89*, 6365; b) F. Bernardi, M. Olivucci, M. A. Robb, *J. Am. Chem. Soc.* **1992**, *114*, 1606.

[12] W. Gerhartz, R. D. Poshusta, J. Michl, *J. Am. Chem. Soc.* **1977**, *99*, 4263.

[13] M. Klessinger, J. Michl, *Excited States and Photochemistry of Organic Molecules*, VCH, New York, **1995**.

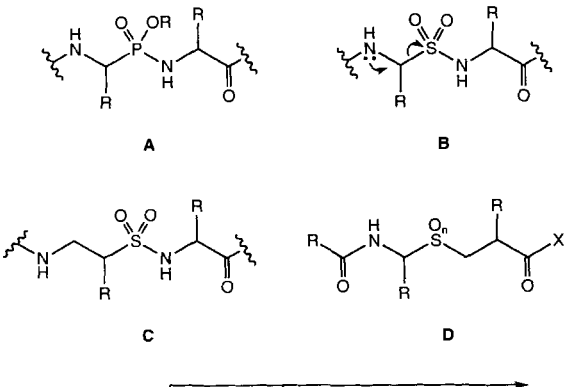
[14] J. Bentzien, M. Klessinger, *J. Org. Chem.* **1994**, *59*, 4887.

 © *VCH Verlagsgesellschaft mbH, D-69451 Weinheim, 1995* *0570-0833/95/0505-0551 $ 10.00+.25/0*

Synthesis of Ψ[SCH_2]-, Ψ[$SOCH_2$]-, and Ψ[SO_2CH_2]-Peptide Isosters*

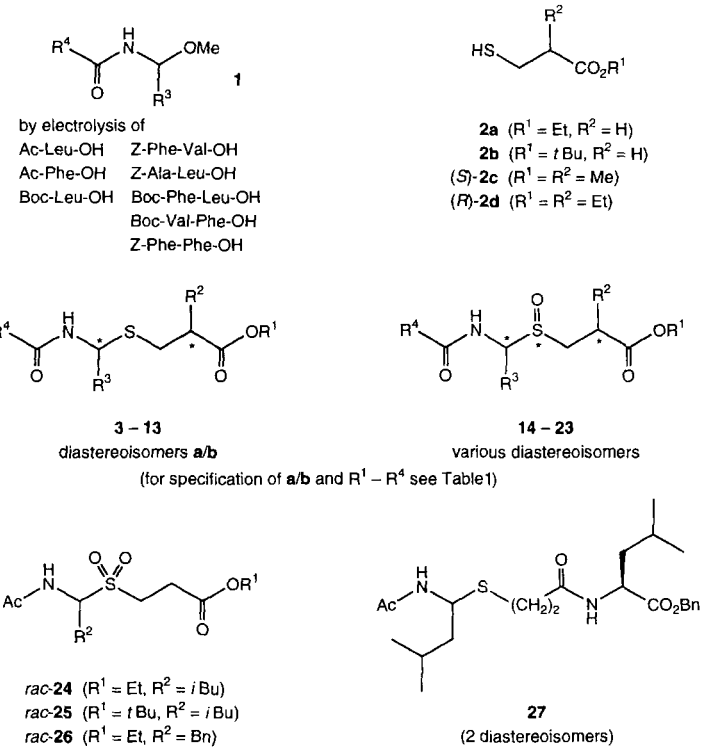
Thimo Sommerfeld and Dieter Seebach*

Though α-aminophosphonamides (**A**) are stable building blocks in peptides and serve as analogues of tetrahedral intermediates of peptide cleavage,[1a] the sulfur derivatives **B** could not be synthesized until now, despite many attempts. The instability of α-aminosulfonamides can be explained by an elimination, as indicated in Scheme 1[1b] (cf. formation and cleavage of hydrogensulfite adducts of aldehydes and ketones). Obviously, this complication is not present in the β-aminosulfonic acid derivatives **C**.[2] We have now prepared new types of sulfur-containing peptide isosteres[3] of type **D** ($n = 0, 1, 2$), in which a subtle interplay between the donor ability of the RCONH group and the nucleofugality of the SO_nCH_2 group determines the stability (see **D** and Table in Scheme 1).



Scheme 1. Peptide analogues **A**–**D**, bearing phosphorus- and sulfur-containing groups in the backbone. The stability of the sulfur derivative **D** described herein depends upon the oxidation state at sulfur and upon the nature of the acyl group at nitrogen. RCO-Xaa represents an N-protected amino acid moiety and ROCO a carbamate protecting group; for examples see Scheme 2, Table 1, and Experimental Procedure.

As starting materials we used the *N,O*-acetals **1**, which are easily accessible from amino acids or N-protected peptides by anodic oxidative decarboxylation.[4] Lewis acid mediated substitution of MeO for RS in the acetals **1** by methyl, ethyl, or *t*-butyl β-mercaptocarboxylates **2**[5] to yield the sulfides **3**–**13** (**D**, $n = 0$) and subsequent oxidation with tetrabutylammonium peroxomonosulfate (TBA oxone)[6] led to the sulfoxides **14**–**23** (**D**, $n = 1$) and sulfones **24**–**26** (**D**, $n = 2$) (see Table 1 and Experimental Procedure). In addition to the peptide analogues **3**–**26**, which bear the sulfur-containing δ-amino acid residue at the C-terminus, we also prepared **27** with this moiety at the N-terminus.



Scheme 2. Building blocks **1** and **2**, and products **3**–**13** with sulfide structure, **14**–**23** with sulfoxide structure, and **24**–**27** with sulfone structure ("*N,S*-, *N,SO*-, and *N,SO*$_2$-acetal structure"). The conditions for transacetalization (**1** → **3**–**13**) and oxidation (**3**–**13** → **14**–**26**) are given in the text, in the Experimental Procedure, and in Table 1. Bn = benzyl.

The reaction of **1** with **2**, which involves *N*-acyliminium ions as intermediates, is best performed in CH_2Cl_2 at −78 °C with $BF_3 \cdot OEt_2$ as the Lewis acid. As with other nucleophiles,[4] this reaction is not diastereoselective. The epimeric sulfides (*N,S*-acetals) **7a**–**13a** and **7b**–**13b** were formed in ratios ranging from 4:3 to 1:2 and in yields usually exceeding 90%. They could be separated and purified by chromatography (though with heavy losses) or by recrystallization. In the subsequent oxidation step, oxone proved to be superior to other reagents tested: the reaction in CH_2Cl_2 stops at low temperature (−75 °C, 30–60 min) after formation of the sulfoxide. The sulfones[7] are formed under more "drastic" conditions (excess oxone, 1–2 h, −30 to −20 °C); however, only the N-acetyl derivatives **24**–**26** could be isolated in pure form, albeit in poor yields.

[*] Prof. Dr. D. Seebach, Dr. T. L. Sommerfeld
Laboratorium für Organische Chemie
der Eidgenössischen Technischen Hochschule
ETH-Zentrum, Universitätstrasse 16, CH-8092 Zürich (Switzerland)
Telefax: Int. code + (1)632-1144

[**] Part of the Ph.D. thesis of T. L. Sommerfeld, Dissertation No. 10842, ETH Zürich, **1994**.

Table 1. Sulfides **3**–**13** prepared from *N,O*-acetals **1** and β-mercaptocarboxylates **2**. Sulfoxides **14**–**23** were prepared by subsequent oxidation with tetrabutylammonium peroxomonosulfate (TBA oxone). The diastereoisomers **7a**–**13a** move faster on silica gel than their epimers **7b**–**13b**. Bn = benzyl.

R^1	R^2 (Config. of **2**)	R^3	R^4CO	Sulfides no.	yield [%]	**a**:**b**	Sulfoxides no.	yield [%]	diastereoisomer ratio
Et	H	*i*Bu	Boc	**3**	33 [b]				
Et	H	*i*Bu	Ac	**4**	93 [a]		**14**	35 [b]	>20:1
*i*Bu	H	*i*Bu	Ac	**5**	82 [a]		**15**	86 [b]	4:1
Et	H	Bn	Ac	**6**	38 [b]		**16**	60 [b]	>20:1 [d]
Me	Me (*S*)	*i*Bu	Ac	**7**	38 [b]	4:3 [c]	**17**	70 [a]	1:1 [e] from **7a**
Me	Me (*S*)	Bn	Ac	**8**	52 [b]	1:1 [d]	**18**	92 [a]	>20:1 [d] from **8a** [f]
								99 [a]	9:1 [d] from **8b** [g]
Me	Me (*S*)	*i*Pr	Z-Phe	**9**	94 [a]	4:3 [d]	**19**	66 [b]	9:1 [e] from **9a**
								46 [b]	9:1 [e] from **9b**
Me	Me (*S*)	*i*Bu	Z-Ala	**10**	56 [b]	4:5 [c]	**20**	96 [a]	3:1 [e] from **10a**
								95 [a]	3:2 [e] from **10b**
Me	Me (*S*)	*i*Bu	Boc-Phe	**11**	94 [a]	1:1 [d]	**21**	86 [a]	2:1 [d] from **11a** [h]
								98 [a]	7:1 [e] from **11b**
Me	Me(*S*)	Bn	Z-Phe	**12**	81 [b]	1:1 [d]	**22**	99 [a]	4:1 [d] from **12a** [i]
								99 [a]	1:1 [e] from **12b**
Et	Et (*R*)	Bn	Boc-Val	**13**	51 [b]	1:2 [d]	**23**	50 [d]	>20:1 from **13b**

[a] Yield of crude product (by NMR spectroscopy). [b] Yield after chromatography. [c] Diastereoisomers separated by chromatography. [d] Separated by fractional crystallization. [e] Not separated, but pure according to elemental analysis after chromatography or precipitation. [f] M.p. 86 °C. [g] M.p. 88–89 °C. [h] Major product: m.p. 146–147 °C, $[\alpha]_D = +36.5$ ($c = 1$, MeOH). [i] For details see Experimental Procedure.

Often one of the two possible epimeric sulfoxides was formed very selectively (see last column in Table 1). The crude sulfides **3**–**13** (mostly oily products) were pure enough (**4**, **5**, **9**, and **11**) for the oxidizing step to the sulfoxides or were used after chromatography.[8] At least one of the stereoisomeric sulfoxides could be purified in each case and was characterized by elemental analysis, optical rotation, melting point, and IR, NMR, and mass spectra.[9] The access to *both* diasteroisomers could be advantageous for possible drug research with this novel type of peptide analogues. We have not yet been able to determine the configuration of the acetal and of the sulfoxide center in the products **7**–**23**. Since a chemical correlation is impossible, we are trying to grow single crystals of the solid compounds for X-ray analysis.

Experimental Procedure

12a, **12b**: To a solution of the *N,O*-acetal **1** (2.00 g, 4.62 mmol, from Z-Phe-Phe-OH, see Scheme 2) and the thiol **2c** (1.24 g, 9.24 mmol) in CH_2Cl_2 (40 mL) at −78 °C under argon was added $BF_3 \cdot OEt_2$ (0.580 mL, 4.62 mmol). After consumption of the starting material (about 30 min, monitoring with thin layer chromatography (tlc)) a saturated solution of $NaHCO_3$ (a few mL) was added. The solution was washed with saturated solutions of $NaHCO_3$ and NaCl, dried ($MgSO_4$), and the solvent was removed under reduced pressure. The sulfide (*N,S*-acetal) **12** (2.00 g, 81%) was isolated as a mixture of two epimers in a 1:1 ratio (**12a** and **12b**), which were separated by fractional crystallization (Et_2O/hexane).

22 (two diastereoisomers): A solution of 1.24 g (2.32 mmol) of the more readily crystallizing epimer **12a** (m.p. 131–132 °C, $[\alpha]_D = -47.6$ ($c = 0.9$, MeOH)) in CH_2Cl_2 (15 mL) at −78 °C was treated with a solution of tetrabutylammonium peroxomonosulfate (1.77 g, 2.55 mmol) in CH_2Cl_2 (10 mL). After about 30 min (tlc control), H_2O and EtOAc were added. The solution was extracted with H_2O (twice) and a saturated solution of NaCl, and dried with $MgSO_4$. After evaporation of the solvent, the sulfoxide **22** (epimer ratio 4:1) was isolated in quantitative yield. The epimers were separated by fractional crystallization. Major product: m.p. 124–125 °C, $[\alpha]_D = -83.6$ ($c = 1$, MeOH); minor product: m.p. 126–129 °C, $[\alpha]_D = +115.2$ ($c = 0.5$, MeOH).

Received: September 20, 1994 [Z 7333 IE]
German version: *Angew. Chem.* **1995**, *107*, 622

[1] a) P. A. Bartlett, C. K. Marlowe, *Science* **1987**, *235*, 569; b) T. Shiba, K. Miyoshi, S. Kusumoto, *Bull. Chem. Soc. Jpn.* **1977**, *50*, 254; W. F. Gilmore, H.-J. Lin, *J. Org. Chem.* **1978**, *43*, 4535; D. Merricks, P. G. Sammes, E. R. H. Walker, K. Henrick, M. M. McPartlin, *J. Chem. Soc. Perkin Trans. 1* **1991**, 2169.

[2] W. J. Moree, G. A. van der Marel, R. M. J. Liskamp, *Tetrahedron Lett.* **1991**, *32*, 409; *ibid.* **1992**, *33*, 6389; W. J. Moree, L. C. van Gent, L. C. van der Marel, R. M. J. Liskamp, *Tetrahedron* **1993**, *49*, 1133. Such an elimination can also not occur in the α,β-unsaturated γ-aminosulfonamides that have just been reported: C. Gennari, B. Salom, D. Potenza, A. Williams, *Angew. Chem.* **1994**, *106*, 2181; *Angew. Chem. Int. Ed. Engl.* **1994**, *33*, 2067.

[3] J. Gante, *Angew. Chem.* **1994**, *106*, 1780; *Angew. Chem. Int. Ed. Engl.* **1994**, *33*, 1699.

[4] P. Renaud, D. Seebach, *Angew. Chem.* **1986**, *98*, 836; *Angew. Chem. Int. Ed. Engl.* **1986**, *25*, 843; T. Shono, Y. Matsumura, K. Tsubata, K. Uchida, *J. Org. Chem.* **1986**, *51*, 2590; D. Seebach, R. Charczuk, C. Gerber, P. Renaud, *Helv. Chim. Acta* **1989**, *72*, 401; C. Gerber, D. Seebach, *ibid.* **1991**, *74*, 1373.

[5] M. Shimazaki, J. Hasegawa, K. Kan, K. Nomura, Y. Nose, H. Kondo, T. Ohashi, K. Watanabe, *Chem. Pharm. Bull.* **1982**, *30*, 3139. Instead of the Cl/SH substitution decribed herein, we used the Misunobu reaction with the commercially available hydroxy ester. For the synthesis of ethyl (*S*)-2-hydroxymethylbutanoate (the precursor for (*R*)-**2d**), see J. Ehrler, F. Giovannini, B. Lamatsch, D. Seebach, *Chimia* **1986**, *40*, 172; M. Sefkow, A. Neidlein, T. Sommerfeld, F. Sternfeld, M. A. Maestro, D. Seebach, *Liebigs Ann. Chem.* **1994**, 719.

[6] B. M. Trost, R. Braslau, *J. Org. Chem.* **1988**, *53*, 532.

[7] The substrates used by us were oxidized much faster than the sulfides tested by Trost et al. [6]. Since our products **14**–**26** are unstable under basic conditions, they must not be formed in the presence of hydrogencarbonate as recommended in [6].

[8] Compounds **3**–**13** are stable and easy to handle under neutral, weakly basic, or weakly acidic conditions; compounds **3**–**6**, **8a**, and **8b** were also characterized by elemental analysis.

[9] Compounds **24**–**27** were purified by chromatography and identified by NMR spectroscopy.

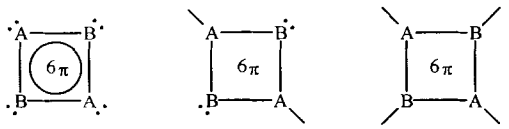
Keywords: peptide isosteres · sulfur compounds

A P_2C_2 Four-Membered Ring with Unusual Bonding—Synthesis, Structure, and Ring Opening of a 1,3-Diphosphacyclobutane-2,4-diyl**

Edgar Niecke,* Andre' Fuchs, Fred Baumeister, Martin Nieger, and Wolfgang W. Schoeller

Dedicated to Professor Peter Paetzold on the occasion of his 60th birthday

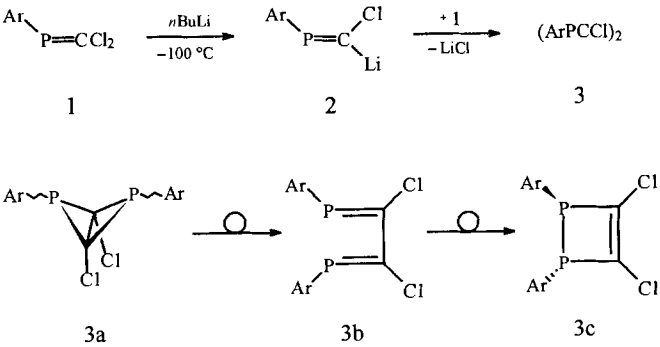
The delocalization of six π electrons in a four-membered ring heterocycle of type **I** has been well documented for disulfur dinitride (A = N, B = S).[1, 2] Likewise for isoelectronic compounds of the types **II** and **III** (e.g. A = C; B = O, S **II** and A = C; B = N, P **III**, respectively) structures have been discussed which appear to allow a π delocalization.[2d, e, 3] However, the spectroscopic identification or even the isolation of



I II III

such species has to date[4] not been achieved owing to the energetically favored valence isomerizations (ring closure to the bicycle or ring opening[2d, e, 3]). We report here on the synthesis and structure of the first stable P_2C_2 heterocycle **III** (A = C, B = P), which can be considered as an opened form (orbital isomer[5a]) of the corresponding bicyclic system.[5b] In the context of investigations on carbenoids with P–C pπ bonding[6] we were interested in the reaction of the phosphanylidene carbenoid[7] **2** with aryl(dichloromethylene)phosphane[8] **1**, which could possibly provide a route to the only still unknown 2,4 isomer[10] in the series of diphosphabicyclobutanes.[9]

The reaction of **1** (Ar = 2,4,6-$tBu_3C_6H_2$) with *n*-butyllithium in the mole ratio 2:1 led to the product **3** with the desired composition (elemental analysis), which was isolated in good yield (63%) in the form of deep red crystals (Scheme 1). The symmetrical structure of the compound was confirmed by the chemical equivalence of the two phosphorus nuclei in the ^{31}P NMR spectrum both in solution and in the solid state (δ = 26.5; δ_{iso} = 26.1). However, the strong deshielding of the ^{31}P nuclei as well as the chemical shift of the ring carbon atoms in the olefinic region (δ = 98.8 J(C,P) = 51.5 Hz) of the ^{13}C NMR spectrum are not consistent with a 2,4-diphosphabicyclobutane **3a**. These findings indicate rather the presence of a 1,2-dihydro-1,2-diphosphete[11] (**3c**), which should be derived from valence isomerization from **3a** via a 1,4-diphosphabuta-1,3-diene (**3b**).[12]



Scheme 1. Ar = 2,4,6-$tBu_3C_6H_2$.

Thus, the result of a single-crystal structure analysis was the more surprising;[13] it shows the P_2C_2 unit of **3** in the crystal as a planar four-membered ring (∢ CPC 87.8(1)°, ∢ PCP 92.2(1)°), in which the substituents at the carbon and the phosphorus atoms each adopt a *trans* configuration (Fig. 1). The

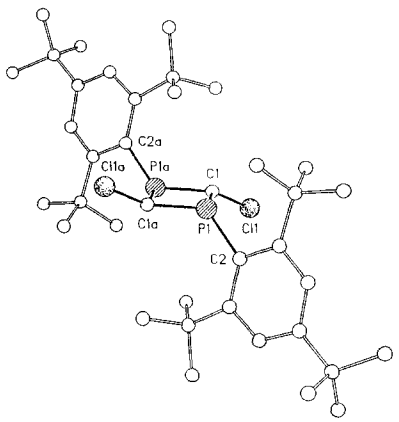


Fig. 1. Molecular structure of **3**. Selected bond lengths [pm] and angles [°]: C1–P1 174.9(3), P1-C1a 175.0(2), Cl1–C1 173.8(3), P1–C2 183.5(2); P1-C1-P1a 92.2(1), C1-P1-C1a 87.8(1), Cl1-C1-P1 127.6(2), Cl1-C1-P1a 127.5(2), C1-P1-C2 123.2(1), C1a-P1-C2 126.9(1).

pyramidalization at the phosphorus atoms (Σ 337.9°) is significantly more pronounced than at the carbon atoms (Σ 347.3°), however, small in comparison to 1,3-diphosphetanes (e.g. 293° in $(C_6H_5PCHNMe_2)_2$[15]). The P–C bonds, which are considerably shorter than a P–C single bond, are the same length within the error limits (174.9(3), 175.0(2) pm) and are similar to those in λ^3-phosphinines.[16] Longer P–C bonds occur in transition metal complexes of 1,3-diphosphacyclobutadienes,[17] for which likewise a delocalized π-electron structure is assumed. Furthermore, the different exocyclic bond angles at the phosphorus atoms (C1-P1-C2 123.2(1) and C1a-P1-C2 126.9(1)°) are worthy of note; they reveal the distortion of the molecular symmetry from C_{2h} to C_i. The exocyclic distances C–Cl 173.8(3), P-*ipso*-C 183.5(2) and also the bond angles and bond lengths in the aryl substituent show no peculiarities.

In order to determine the bonding in **3**, quantum chemical calculations on the parent structure, $(HP)_2(CH)_2$ **III**, were performed both at the MCSCF/DZP[19] and also at the MP2/6-31G(d,p) level[21] under complete geometry optimization. A MCSCF optimization of the geometry of **III** affords a singlet ground state with C_i symmetry. The singlet state with C_{2h} symmetry,[24] which lies higher in energy, is not a minimum on the

[*] Prof. Dr. E. Niecke, Dipl.-Chem. A. Fuchs, Dipl.-Chem. F. Baumeister, Dr. M. Nieger
Anorganisch-chemisches Institut der Universität
Gerhard-Domagk-Strasse 1, D-53121 Bonn (Germany)
Telefax: Int. code + (228)735327
Prof. Dr. W. W. Schoeller
Fakultät für Chemie der Universität
Postfach 8640, D-33615 Bielefeld (Germany)

[**] This work was supported by the Deutsche Forschungsgemeinschaft and the Fonds der Chemischen Industrie.

potential hypersurface. The corresponding structure can be considered as the transition state for a rearrangement of **III** into the 2,4-diphosphabicyclobutane system.[24] In contrast, ab initio calculations at the RHF level lead to ring-opened structures as energy minima.[2e]

The two dominant contributions to the CI wavefunction from the MCSCF calculation[19] for the ^1A_g state are found to be $\Phi(^1Ag) = 0.90|\pi_1^2\pi_2^2\pi_3^2\rangle - 0.40|\pi_1^2\pi_2^2\pi_4^2\rangle$. This corresponds to an occupation of the bonding π_3 orbital (HOMO) with 1.6 electrons. Thus, it follows that a considerable diradical contribution can be assigned to **III** (Fig. 2).[25]

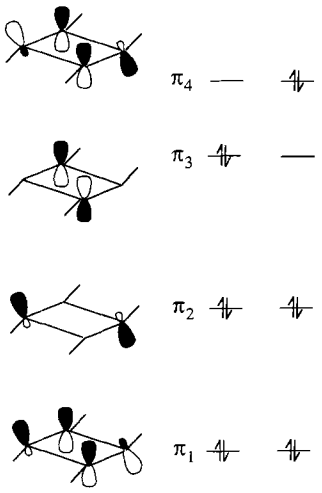


Fig. 2. Schematic representation of the π orbitals of **III**.

For the lowest lying triplet state (^3A_u), which according to a vibrational analysis[24] corresponds to an energy minimum, the geometry optimized MCSCF calculations give a structure with C_{2h} symmetry with only a small difference in energy of 5.5 kcal mol^{-1} to the ^1Ag state (after MRCI plus Davidson correction). A similar result is obtained from energy optimized MP2/6-31G(d,p) calculations, which afforded an energy difference (after MP4 correction[21]) between the ^1Ag and ^3A_u states of 7.4 kcal mol^{-1}. Figure 3 shows the geometries as well as the Mulliken populations for these two states. In contrast to the structure of the triplet state with mainly nonpolar P–C bonds, whose distances correspond approximately to those of normal P–C single bonds, the structure of the singlet state shows a stronger polar charge distribution in the ring. This leads, as is expected, to shorter P–C distances, which are in good agreement with the experimental values. The pyramidalization at the carbon atoms is likewise well reflected by the calculations, while the substituents at the phosphorus atoms as expected are more bent than those of the experimentally determined structure[26] (Fig 3).

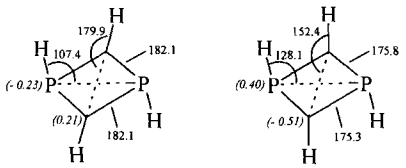
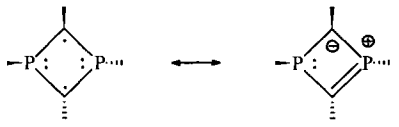


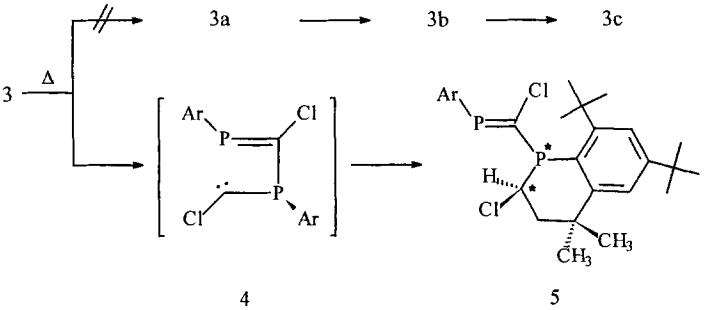
Fig. 3. Optimized geometries and Mulliken populations (left: ^3A_u state; right ^1A_g state).

The stabilization of the singlet state (^1Ag) can thus be explained by a conjugative interaction of the unpaired electrons at the carbon atoms with the nonbonding electron pairs of the phosphorus atoms. A planarization of all substituents, which would lead to perfect cyclic π conjugation as in the disulfur dinitride, however, is not achieved, above all because of the high inversion barrier at the phosphorus atom (42.7 kcal mol^{-1} in the phosphetane[27]). Therefore, **III** can on the one hand be considered as a delocalized π system and described by the diradical, **IIIa**, and dipolar limiting formula, **IIIb** (4 hybrids). On the other hand the heterocycle **III** can also be considered as an orbital isomer[5a] of the energetically poorer 2,4-diphosphabicyclobutane (– 36.9 kcal mol^{-1} relative to the *exo/endo* conformer of 2,4-diphosphabicyclobutane[28]).[29]



IIIa IIIb

In the case of compound **III**, a transannular C–C linkage leading to the formation of the bicycle is forbidden according to the Woodward–Hoffmann rules. In fact, on heating in toluene the thermally remarkably stable heterocycle **3** isomerizes not by ring closure to give the 2,4-diphosphabicyclobutane **3a** or to a thermodynamically more stable subsequent product (**3b**, **3c**), but by cleavage of the P–C bond to give the diphosphapropene **5**. A plausible intermediate of this reaction is the phosphanocarbene **4**,[31] which results from a ring opening and stabilizes by CH activation of an *ortho*-positioned *tert*-butyl group to give **5**. The carbene-analogous reaction behavior of such stabilized carbenes (λ^5-phosphaalkynes) is confirmed by a series of publications.[32]



4 5

We assume that the intramolecular ring closure **4** → **3** induced by the kinetically controlled reaction of the starting materials (**1**,**2**) is possibly the key for the successful verification of the P_2C_2 heterocycle **3**. Further investigations into the examination of this hypothesis and into the chemistry of this novel type of compound are in progress.[33]

Experimental Procedure

3: *n*BuLi (2.6 mL, 4.2 mmol of a 1.6 M solution in hexane) was added dropwise to a solution of 2,4,6-*t*Bu$_3$H$_2$C$_6$P=CCl$_2$ (3.0 g, 8.4 mmol) in THF (100 mL) at –100 °C. The resulting yellow reaction mixture was slowly warmed to room temperature, which caused a color change to dark red. Subsequently the solvent was removed in vacuum, the residue treated with pentane (ca. 50 mL), and the LiCl formed separated by filtration together with most of the product. The filter residue was extracted with pentane until it was colorless. Removal of the pentane in vacuum afforded 1.73 g (63%) **3** in the form of a dark red fine crystalline solid. M.p. 155–157 °C (decomp.). ^{31}P NMR (CH_2Cl_2, 303 K): $\delta = 26.5$. ^{31}P CP/MAS: NMR: $\delta_{iso} = 26.1$. ^{13}C NMR (CD_2Cl_2, 253 K): $\delta = 30.2$ (s, *o*-CC_3); 32.0 (s, *p*-CC_3); 33.7 (pseudo-t, $J(|C,P + C,P'|) = 9$ Hz, *o*-CC_3); 34.9 (s, *o*-CC_3); 38.0 (pseudo-*t*, $J(|C,P + C,P'|) = 4$ Hz, *o*-CC_3); 38.6 (s, *p*-CC_3); 98.8 (*t*, 51.5 Hz, CP_2); 122.5 (pseudo-t, $J(|C,P + C,P'|) = 13.8$ Hz, C3-aryl); 122.8 (s, C5-aryl); 124.1 (pseudo-t, $J(|C,P + C,P'|) = 34.4$ Hz, C1-aryl); 153.8 (s, C6-aryl); 157.4 (s, C4-aryl); 159.1 (pseudo-t, $J(|C,P + C,P'|) = 35.0$ Hz, C2-aryl). ^{1}H NMR (CD_2Cl_2, 253 K): $\delta = 1.26$ (s, 9H, *o*-*t*Bu-phenyl); 1.38, 1.77 (each s, 9H, *p*- and *o*-*t*Bu); 7.48, 7.51 (each s, br, *m*-H-phenyl). Rotation around the P–C(aryl) bond at about 303 K leads to an equivalence of the signals for the *o*-*t*Bu and *m*-phenyl protons. UV/Vis: $\lambda_{max}(\varepsilon) = 214$ (33000), 246 (26000), 356 (19000), 478 (900) nm. The mass spectrum of **3** is identical with that of the isomeric product **5**.

5: The heating of **3** (ca. 100 mg) in toluene to 100 °C led quantitatively to **5** in the form of two isomers **A** (70%) and **B** (30%) within 45 minutes. ^{31}P NMR (THF, 303 K): (A) $\delta = 306.4$, –3.1 (^2J(P,P) = 231 Hz, ^2J(P,H) = 22 Hz); [(B) $\delta = 281.2$, 4.5 (^2J(P,P) = 175.5 Hz]. ^{1}H NMR (C_6D_6, 303 K, selection: CH(Cl), CH_2): $\delta = 4.65$ (dddd, ^2J(P,H) = 22, ^3J(H,H) = 14, ^3J(H,H) = 3.5, ^4J(P,H) = 1.5 Hz, CHCl); [5.10 (dt, ^3J(H,H) = 9.5, ^2J(P,H) = ^3J(H,H) = 4 Hz, CHCl)]; 3.05 (td, ^2J(H,H) = ^3J(H,H) = 14, ^3J(P,H) = 5 Hz, CH_2); [2.55 (dddd, ^2J(H,H) = 14,

 © VCH Verlagsgesellschaft mbH, D-69451 Weinheim, 1995 0570-0833/95/0505-0556 $ 10.00+.25/0

$^3J(P,H) = 7.5$, $^3J(H,H) = 4$, $^5J(P,H) = 1$ Hz, CH_2)]; 2.21 (ddd, $^2J(H,H) = 14$, $^3J(P,H) = 5$, $^3J(H,H) = 3.5$ Hz, CH_2); [2.31 (ddd, $^2J(H,H) = 14$, $^3J(H,H) = 9.5$, $^3J(P,H) = 7.5$ Hz, CH_2)]. MS (70 eV): m/z (%) = 646 [M^+] (11), 611 [$M^+ - Cl$] (16), 589 [$M^+ - t$Bu] (19), 401 [$M^+ - t$Bu$_3$H$_2$C$_6$] (100) and other fragments: high resolution: found 646.3398, calcd. 646.3391.

Received: September 29, 1994 [Z 7367IE]
German version: *Angew. Chem.* **1995**, *107*, 640

Keywords: ab initio calculations · cyclizations · cyclobutadienes · electronic structure · phosphorus compounds

[1] a) M. J. Cohen, A. F. Saran, J. Kleppinger, *J. Am. Chem. Soc.* **1976**, *98*, 3844–3848; b) C. M. Mikulski, P. J. Russo, M. S. Saran, A. G. MacDiarmid, A. F. Garito, A. J. Heger, *ibid.* **1975**, *97*, 6358–6363.

[2] For the electronic structure of S_2N_2: a) J. Bragin, M. V. Evans, *J. Chem. Phys.* **1969**, *51*, 268–277; b) A. J. Banister, *Phosphorus Sulfur* **1979**, *6*, 421–428; c) A. A. Bhattacharyya, A. Bhattacharyya, R. R. Adkins, A. G. Turner, *J. Am. Chem. Soc.* **1981**, *103*, 7458–7465; d) G. van Zandwijk, R. A. J. Jansen, H. M. Buck, *ibid.* **1990**, *112*, 4155–4164; e) R. A. J. Janssen, *J. Phys. Chem.* **1993**, *97*, 6384–6397.

[3] P. H. M. Budzelaar, D. Cremer, M. Wallasch, E.-U. Würthwein, P. von R. Schleyer, *J. Am. Chem. Soc.* **1987**, *109*, 6290–6299.

[4] Cyclobutadiene dianions are known in the stable form. According to MNDO calculations on $(PhC)_4^{2-}$, the cyclic form is 11.2 kcal mol^{-1} more stable than the corresponding open butadiene valence isomer. G. Boche, H. Etzrodt, M. Marsch, W. Thiel, *Angew. Chem.* **1982**, *94*, 141–142; *Angew. Chem. Int. Ed. Engl.* **1982**, *21*, 133–134.

[5] a) M. J. S. Dewar, S. Kirschner, H. W. Kollmar, L. E. Wade, *J. Am. Chem. Soc.* **1974**, *96*, 5240–5242; b) A 1,3-diphosphacyclobutane-2,4-diyl intermediate is discussed in the reaction of $Cp_2Zr{-}C(t\text{Bu}){-}P{-}P{-}C(t\text{Bu})$ with Br_2/OEt_2 to give the 1,3-diphosphetane $(BrPC(H)t\text{Bu})_2$. M. Regitz, Universität Kaiserslautern, personal communication.

[6] a) W. Schilbach, V. von der Gönna, D. Gudat, M. Nieger, E. Niecke, *Angew. Chem.* **1994**, *106*, 1037–1039; *Angew. Chem. Int. Ed. Engl.* **1994**, *33*, 982–983; b) P. Becker, M. Nieger, E. Niecke, unpublished results.

[7] a) See [8]; b) R. Appel, M. Immenkeppel, *Z. Anorg. Allg. Chem.* **1987**, *553*, 7–14; c) M. Yoshifuji, T. Niitsu, N. Inamoto, *Chem. Lett.* **1988**, *10*, 1733–1734; d) S. J. Goede, F. Bickelhaupt, *Chem. Ber.* **1991**, *124*, 2677–2684.

[8] R. Appel, C. Casser, M. Immenkeppel, *Tetrahedron Lett.* **1985**, *26*, 3551–3554.

[9] For the synthesis of 1,2- and 1,3-diphosphabicyclobutanes: E. Niecke, H.-J. Metternich, R. Streubel, *Chem. Ber.* **1990**, *123*, 67–69.

[10] The 2,5-diphosphatricyclo[3.1.0.0^{2,6}]hex-3-ene contains a 2,4-diphosphabicyclobutane structural unit: Y. Kobayashi, S. Fujino, H. Hamana, I. Kumadaki, Y. Hanzawa, *J. Am. Chem. Soc.* **1977**, *99*, 8511.

[11] C. Charrier, M. Maigot, F. Mathey, F. Robert, Y. Jeanin, *Organometallics* **1986**, *5*, 623–630.

[12] On the electrocyclic ring closure of 1,4-diphosphabuta-1,3-dienes: a) R. Appel, V. Barth, *Tetrahedron Lett.* **1980**, *21*, 1923–1924; b) R. Appel, V. Barth, F. Knoch, *Chem. Ber.* **1983**, *116*, 938–950; c) A. M. Arif, A. R. Barron, A. H. Cowley, S. W. Hall, *J. Chem. Soc. Chem. Commun.* **1988**, *3*, 171–172.

[13] X-ray structure analysis of **3**: $C_{38}H_{58}Cl_2P_2$, red crystals, crystal dimensions $0.10 \times 0.25 \times 0.35$ mm; $M = 647.7$; triclinic, space group $P\bar{1}$ (no. 2), $a = 9.276(1)$, $b = 9.644(1)$, $c = 11.781(1)$ Å, $\alpha = 73.31(1)$, $\beta = 79.36(1)$, $\gamma = 0.78(1)°$, $V = 948.5(2)$ Å^3, $Z = 1$, $\mu(Cu_{K\alpha}) = 2.50$ mm^{-1}, $T = 200$ K, $F(000) = 350$. 3070 reflections up to $2\theta_{max} = 120°$ were measured on an Enraf-Nonius CAD4 diffractometer with $Cu_{K\alpha}$, of these 2819 were independent and were used for all calculations. The structure was solved by direct methods and refined anisotropically against F^2, the H atoms with a riding model (program SHELXL-93 [14]). The final quality coefficient $wR2(F^2)$ was 0.161, with a conventional $R(F) = 0.059$ for 200 parameters. A semiempirical absorption correction was carried out based on ψ scans and an extinction correction. Further details of the crystal structure investigation may be obtained from the Fachinformationszentrum Karlsruhe, D-76344 Eggenstein-Leopoldshafen (FRG) on quoting the depository number CSD-58731.

[14] G. Sheldrick, SHELXL-93, Universität Göttingen, **1993**.

[15] G. Becker, W. Massa, O. Mundt, R. Schmidt, *Z. Anorg. Allg. Chem.* **1982**, *485*, 23–35.

[16] G. Märkl, λ^3-Phosphinines, Aza-λ^3-phosphinines, and λ^3,λ^3-Diphosphinines in *Multiple Bonds and Low Coordination in Phosphorus Chemistry* (Hrsg.: M. Regitz, O. J. Scherer), Thieme, Stuttgart, **1990**, S. 220–254.

[17] a) B. Hitchcock, M. J. Maah, J. F. Nixon, *J. Chem. Soc. Chem. Commun.* **1986**, *10*, 737–738; b) J. F. Nixon, *Phosphorus Sulfur* **1987**, *30*, 471–474; c) P. Binger, R. Milcazarek, R. Mynott, C. Krüger, Y.-H. Tsai, E. Raabe, M. Regitz, *Chem. Ber.* **1988**, *121*, 637–645.

[18] E. D. Jemmis, P. von R. Schleyer, *J. Am. Chem. Soc.* **1982**, *104*, 4781–4788.

[19] MCSCF calculations: the DZP basis set was constructed from primitive Huzinaga functions: C(5,4X1/3,2X1), P(5,6X1/4,3X1), H(3,2X1); plus a set of polarization functions at all atoms ζ_d (C,P) = 0.8, 0.5; ζ_p(H) = 0.65; active space for the MCSCF geometry optimization $3a_g$ plus $3a_u$ orbitals; the multireference calculations were carried out in this space. All MCSCF and MRCI calculations were undertaken with the program system MOL-PRO [20].

[20] H.-J. Werner, W. Meyer, *J. Chem. Phys.* **1980**, *73*, 2342–2356; H. J. Werner, P. J. Knowles, *ibid.* **1985**, *82*, 5053–5063.

[21] Calculations at the MP2 and MP4 levels were carried out with the Gaussian-92/DTF program system, revision G.3 [22]. Both the singlet and the triplet states were geometry optimized at the MP2 level and subsequently calculated with regard to the electron correlation at the MP4SDTQ(fc)-level. The vibrational analyses (in harmonic approximation) show both states as minima on the energy hypersurface. For all triplet states the rule is $\langle s^2 \rangle = 2.07$, which shows a negligible spin contamination. The MP4 energies for the triplet sates were obtained by spin projection according to the PMP4 method [23].

[22] M. J. Frisch, G. W. Trucks, H. B. Schlegel, P. M. W. Gill, B. G. Johnson, M. W. Wong, J. B. Foresman, M. A. Robb, M. Head-Gordon, E. S. Replogle, R. Gomperts, J. L. Andres, K. Raghavachari, J. S. Binkley, C. Gonzalez, R. L. Martin, D. J. Fox, D. J. Defrees, J. Baker, J. J. P. Stewart, J. A. Pople, Gaussian Inc. Pittsburgh, PA, **1993**.

[23] H. B. Schlegel, *J. Chem. Phys.* **1986**, *84*, 4530–4534.

[24] W. W. Schoeller, unpublished results.

[25] Diradical structures are also derived for the compounds $(HA)_2B_2$ with A = P, N and B = N, P (type **II**), isoelectronic to $(HP)_2(CH)_2$. The results of detailed CI calculations will be reported elsewhere [24].

[26] Geometry optimizations for the ^1A_g and ^3A_u states at the MP2/6-31G* level on modellike substituted **3**, $(R^1P)_2(CR^2)_2$ (R^1 = H, Me; R^2 = H, Cl), show that Me substitution favors a planarization at the phosphorus atom. This leads to an increase of the difference in energies between these two states ($\Delta E = E(^3A_u) - E(^1A_g) = 10.6$ kcal mol^{-1}) in comparison to $(HP)_2(CH)_2$, whereas Cl substitution causes an opposite effect ($\Delta E = 4.0$ kcal mol^{-1}) [24].

[27] S. M. Bachrach, *J. Phys. Chem.* **1989**, *93*, 7780–7784.

[28] The calculations were carried out at the MP4SDTQ(fc)/6-31G(d,p)//6-31G(d,p) level.

[29] The 2,4-diphosphabicyclobutane is thermodynamically less stable than the 1,4-diphosphabuta-1,3-diene (−16.0 kcal mol^{-1} [24,28]), which can rearrange by way of a conrotatory ring closure into the 1,2-diphosphete [30].

[30] According to ab initio MP2/6-31G* calculations, the thermally allowed conrotatory ring closure of the *trans*-1,2-dihydro-1,2-diphosphete to the *cis*-1,4-diphosphabuta-1,3-diene is an endothermic reaction ($\Delta E = 8.7$ kcal mol^{-1}): S. M. Bachrach, M. Lui, *J. Org. Chem.* **1992**, *57*, 2040–2047.

[31] Phosphanocarbenes are known in stable form: A. Igau, H. Grützmacher, A. Baceiredo, G. Bertrand, *J. Am. Chem. Soc.* **1988**, *110*, 6463–6466.

[32] G. Bertrand, λ^5-Phosphaalkynes in *Multiple Bonds and Low Coordination in Phosphorus Chemistry* (Eds.: M. Regitz, O. J. Scherer), Thieme, Stuttgart, **1990**, pp. 443–454.

[33] A further example of this new structure type was made accessible with the compound $(RPCAr)_2$ (R = Ar–P=C(Cl), Ar = 2,4,6-tBu$_3$C$_6$H$_2$): F. Baumeister, M. Nieger, E. Niecke, unpublished results.

A New Method for the Synthesis of Amphipolar Phosphorus-Containing Heterocycles**

Hans H. Karsch,* Eva Witt, Arnold Schneider, Eberhardt Herdtweck, and Maximilian Heckel

Dedicated to Professor Alfred Schmidpeter on the occassion of his 65th birthday

Diphosphinomethanides show a rich and varied coordination behavior towards main group elements and transition metals.[1] Oxidative coupling of these ligands with transition metals results in the formation of C–C, C–P and P–P bonds, and reduced metal complexes comprising the rearranged organophosphorus ligands have been isolated as intermediates.[2] Analogous redox reactions have been reported for some main group elements[3] and their compounds [for example, Eq. (a)].[2] In these examples antimony and bismuth trichloride are reduced

[*] Prof. Dr. H. H. Karsch, Dipl.-Chem. E. Witt, Dr. A. Schneider, Dr. E. Herdtweck,[+] Dipl.-Chem. M. Heckel[+]
Anorganisch-Chemisches Institut der Technischen Universität München
Lichtenbergstrasse 4, D-85747 Garching (Germany)
Telefax: Int. code + (89)3209-3132

[+] X-ray structure analysis.

[**] We thank Mr. J. Riede for mounting the crystals and data collection.

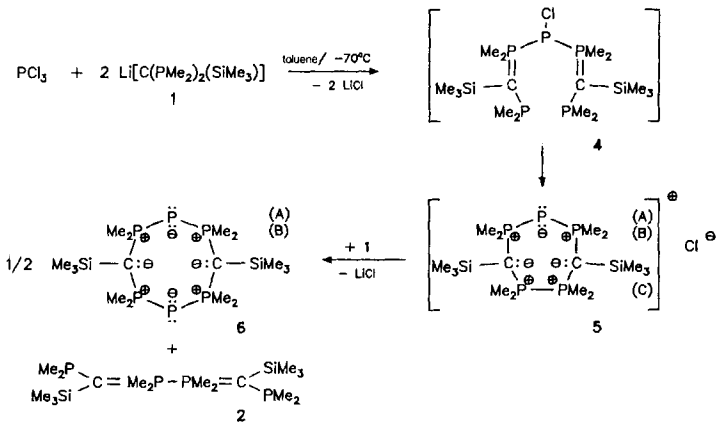
to afford the zerovalent metal and **2**, which contains two ylidic functions, whereas $AsCl_3$ yields compound **3** (arsenic bears an average oxidation state of + 0.5) in an analogous reaction. The latter compound is the first example of an intermediate containing a main group metal center in this type of reaction.[4]

$$MCl_3 + 3\ Li[C(PMe_2)_2(SiMe_3)] \xrightarrow[-3\ LiCl]{} M^0 + 1.5\ [(Me_2P)(SiMe_3)C{=}PMe_2{-}]_2 \quad (a)$$
M = Sb, Bi; 1; 2

$$4\ AsCl_3 + 12\ Li[C(PMe_2)_2(SiMe_3)] \xrightarrow[-12\ LiCl]{} \{\mu\text{-}[C(PMe_2)_2(SiMe_3)]As_2\}_2 + 5\ 2 \quad (b)$$
1; 3

As PCl_3 is even more difficult to reduce, we surmised that analogous reactions might provide a novel entry to reduced phosphorus compounds. Because both phosphino groups of the diphosphinomethanides can react, the formation of heterocyclic rings should be favored. Indeed, this concept can be applied in the synthesis of previously unknown heterocyclic rings that contain phosphorus as a ring member in the oxidation state +1 . However, the complicated course of reaction leads, in part, to completely unexpected results.

When PCl_3 reacts with **1** in toluene, the reaction sequence can be formulated as in Scheme 1. The crucial step in this sequence



Scheme 1. The course of the reaction of PCl_3 with **1** in toluene.

is the oxidative "outer-sphere coupling"[5] of the terminal PMe_2 groups. Ring formation and concurrent reduction of the central phosphorus atom yields **5**, which is a derivative of the "pentaphosphacycloheptatrienyl cation"[6] and is a new bisphosphane-stabilized phosphanylium ion.[7] Accordingly, upon further reaction of **5** with **1**, the anionic diphosphinomethanide displaces the "double" ylide **2**, and lithium chloride is eliminated. In analogy to other eight-membered rings which, however, have been prepared by a different route,[8] the product **6** is formulated as a dimer.[9]

The following findings provide support for the reaction mechanism depicted in Scheme 1: Replacing the chloride leaving group by a phenyl group prevents the redox reaction and P–P bond formation. Thus the reaction yields **7** according to Equation (c). To the best of our knowledge, **7** is the first 1,3-bis(alkylidene)-1λ^5,3λ^5-triphosphane (that is, a double ylide in which the two λ^5 phosphorus atoms are connected by a λ^3 phosphorus

$$PhPCl_2 + 2\ Li[C(PMe_2)_2(SiMe_3)] \xrightarrow[-2\ LiCl]{} PhP[PMe_2{=}C(PMe_2)(SiMe_3)]_2 \quad (c)$$
1; 7

atom) and represents a new type of ylide–phosphane chelating ligand. An X-ray structure analysis of the yellow crystals of **7**[10] confirms the phosphane/ phosphorane character (Fig. 1). The central P1 atom is in a pyramidal environment; however, the sum over all angles (316.5°) is slightly larger than the standard

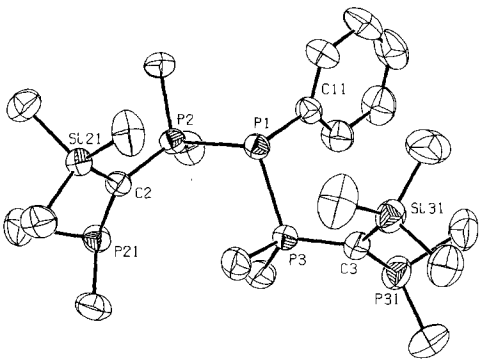
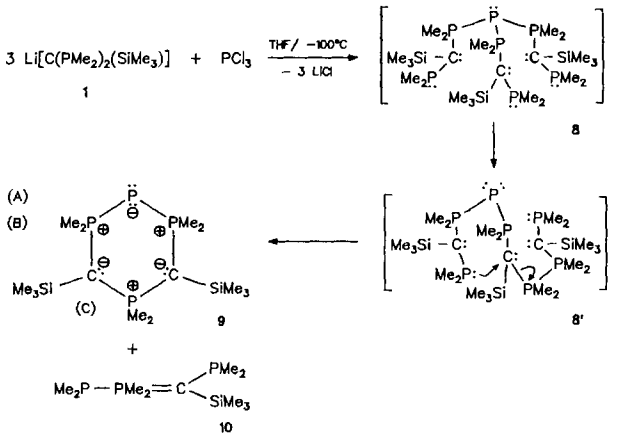


Fig. 1. Crystal structure of **7**. For clarity, hydrogen atoms were omitted. Selected distances [Å] and angles [°]: P1-P2 2.246(1), P1-P3 2.235(1), P1-C11 1.832(2), P2-C2 1.697(2), P3-C3 1.693(2), Si21-C2 1.855(2), P21-C2 1.793(2), Si31-C3 1.846(2), P31-C3 1.797(2); P2-P1-P3 107.9(1), C11-P1-P2 104.2(1), C11-P1-P3 104.4(1), P2-C2-P21 114.4(1), Si21-C2-P2 118.8(1), Si21-C2-P21 125.9(1), P3-C3-P31 112.7(1), Si31-C3-P3 121.7(1), Si31-C3-P31 124.6(1).

value. The distances for P1–P2 (2.246(1) Å) and P1–P3 (2.235(1) Å) are characteristic of single bonds, while the distances for P2–C2 (1.697(2) Å) and P3–C3 (1.693(2) Å) are typical of phosphorus ylides. The spatial arrangement of the P1 substituents is obviously dictated by their steric requirements.

The reaction between PCl_3 and **1** takes a completely different route when THF is used as solvent since, owing to the good solubility of **1** in THF, **1** is present in excess throughout the course of the reaction (Scheme 2). If one assumes that initially



Scheme 2. The course of the reaction of PCl_3 with **1** in THF.

the substituted phosphane **8** is formed, though it cannot be detected, a reaction sequence similar to the one depicted in Scheme 1 becomes feasible. This "outer-sphere coupling" reaction requires the assignment of ten electrons to the central phosphorus, an unfavorable situation which is alleviated by cleavage of a P–P bond of the initially formed—in this case seven-membered—ring. Another cycle of P–C bond forming and breaking steps that are in principal well-known[2] concludes the redox process. The six-membered heterocycle **9** is afforded as colorless

 © VCH Verlagsgesellschaft mbH, D-69451 Weinheim, 1995 0570-0833/95/0505-0558 $ 10.00+.25/0 Angew. Chem. Int. Ed. Engl. 1995, 34, No. 5

crystals. In addition, ylide **10** and varying amounts of **2**, **6**, and $HC(PMe_2)_2(SiMe_3)$ are also formed.[12]

Compound **9** can formally be classified as the first example of a tetraphosphabenzene; however, its description as a $1\lambda^5,3\lambda^5,5\lambda^5,2\lambda^3$-tetraphosphinine is more appropriate. It was anticipated that the molecular structure would reflect[15] the structural characteristics of planar λ^3-phosphinines[13] and various λ^5-di- and triphosphinines.[14] Surprisingly, this is not the case: the molecular structure of **9** (Fig. 2) is characterized by a

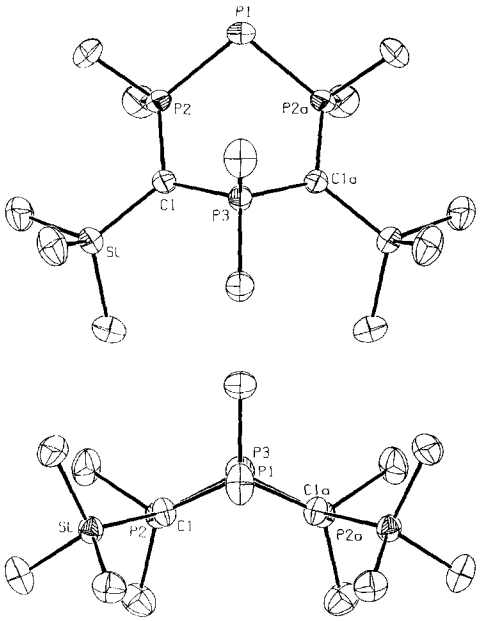
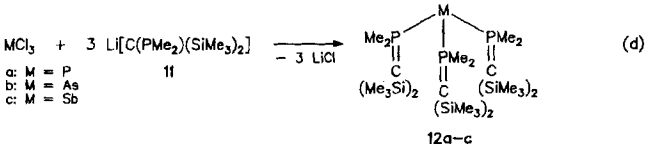


Fig. 2. Two views of the crystal structure of **9**. For clarity, hydrogen atoms were omitted. Selected distances [Å] and angles [°]: P1-P2 2.134(1), P2-C1 1.725(1), P3-C1 1.742(2), Si-C1 1.842(2); P2-P1-P2a 98.1(1), P1-P2-C1 116.4(1), P2-C1-P3 114.7(1), C1-P3-C1a 117.0(1), P2-C1-Si 122.0(4), P3-C1-Si 122.0(1).

pronounced folding (interplanar angle 127°) along the P1–P3 axis, which lies in a mirror plane. This structural feature supports the amphipolar (ylidic) principle.[17] As a result of its polar nature the P1–P2 bond (2.134(1) Å) is shortened, and the angle P2-P1-P2a is 98.08(3)°. All other distances and angles can also be interpreted in light of the aforementioned structural principle.

The successful isolation of analogs of the previously unknown isotetraphosphane/-phosphorane **8**[18] (that is, **12a–c**, which are $SiMe_3$-substituted instead of PMe_2-substituted [Eq. (d)][19, 20]) corroborates the earlier assumption (Scheme 2) that



8 is formed as an intermediate. At the same time it provides evidence for the decisive role of the terminal phosphino groups in the "outer-sphere coupling" process. These novel tris(P-ylide) derivatives (tris(alkylidenephosphoranyl)phosphane and its homologues)[21] **12a–c** form yellow crystals; **12b** is stable at room temperature.[22] The structure of **12b** (Fig. 3)[25] consists of an arsenic atom in a pyramidal environment surrounded by three phosphorus atoms (sum over all angles 316.8°). The As–P distances are in a range typical of single bonds. The ylidic nature of the P1–C1, P2–C2, and P3–C3 bonds is apparent from the characteristic shortening. The potential of **12a–c** as novel tripodal ligands is currently under investigation.

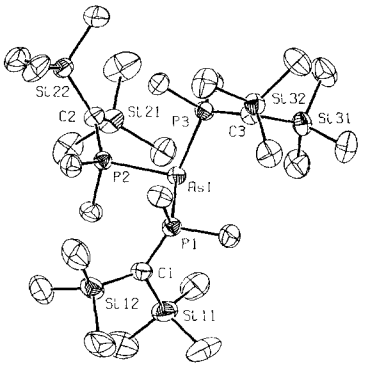


Fig. 3. Crystal structure of **12b**. For clarity, hydrogen atoms were omitted. Selected distances [Å] and angles [°]: As1-P1 2.383(1), As1-P2 2.386(1), As-P3 2.387(1), P1-C1 1.680(3), P2-C2 1.684(3), P3-C3 1.686(2), Si11-C1 1.858(3), Si12-C1 1.847(3), Si21-C2 1.849(2), Si22-C2 1.839(2), Si31-C3 1.860(3), Si32-C3 1.843(3); P1-As1-P2 104.8(2), P1-As1-P3 106.1(2), P2-As1-P3 105.9(2), As1-P1-C1 116.9(1), As1-P2-C2 117.0(1), As1-P3-C3 117.7(1), P1-C1-Si11 116.3(2), P1-C1-Si12 126.0(2), Si11-C1-Si12 117.1(1), P2-C2-Si21 116.4(1), P2-C2-Si22 126.8(1), Si21-C2-Si22 116.2(1), P3-C3-Si31 116.4(1), P3-C3-Si32 126.3(2), Si31-C3-Si32 116.9(1).

The unique cascade of bond forming and breaking reactions (P–P, P–C) described herein exemplifies how the properties of phosphinomethanides can be used for the directed synthesis of cyclic compounds with low-valent main group elements as constituents. During reaction design specific consideration has to be given to the following: The phosphinomethanide carbanion must be shielded by heteroelement substituents.[24] The cyclic redox reaction will only be initiated by a P–P bond formation involving terminal phosphino groups ("outer-sphere coupling") if good leaving groups are present that enable electrons to be transferred to the central atom. These conditions provide the framework for a broader application of this synthetic methodology.

Experimental Procedure

All reactions were conducted under anhydrous conditions in a nitrogen atmosphere. **7**: A solution of $PhPCl_2$ (0.3 mL, 2.23 mmol) in THF (8 mL) was slowly added dropwise at −78 °C to **1**[12] (1.05 g, 4.90 mmol) in THF (30 mL). The mixture was allowed to warm to room temperature and stirred for 3 h. The solvent was distilled off under vacuum, and the yellow residue was extracted twice with 35 mL portions of pentane. The pentane extracts were combined, and yellow crystals were afforded by slow evaporation of the solvent. The oily mother liquor was decanted, and the crystals were washed with a small amount of pentane. Yield: 0.41 g (35%). $^{31}P\{^1H\}$ NMR (C_6D_6, + 20 °C): ABB'CC' spin system, $\delta P_A = -27.59$, $\delta P_B = +16.28$, $\delta P_C = -38.76$, $J(P_AP_B) = 307.4$ Hz, $J(P_AP_C) = 15.0$ Hz, $J(P_BP_C) = 176.6$ Hz, $J(P_BP_{B'}) = 9$ Hz, $J(P_BP_{C'}) = 10$ Hz, $J(P_CP_{C'}) = 13$ Hz.

9: At −100 °C a solution of PCl_3 (0.168 mL, 1.93 mmol) in THF (20 mL) was slowly added to **1**[12] (1.24 g, 5.79 mmol) in THF (30 mL). The mixture was allowed to warm to room temperature and stirred for 12 h. Next, the solvent was removed under vacuum, and the residue extracted three times with 30 mL portions of pentane. The extracts were combined, and the pentane was removed under vacuum. On storage of the remaining yellow oil for 120 d at −10 °C colorless crystals of **9** precipitated. The oily supernatant was decanted, and the crystals were washed with a small amount of pentane. Yield: 0.24 g (32%). In addition to **9**, the supernatant contained **2**, **6**, and $HC(PMe_2)_2(SiMe_3)$, as shown by ^{31}P NMR spectroscopy. $^{31}P\{^1H\}$ NMR (C_6D_6, + 20 °C): AB_2C spin system, $\delta P_A = -140.36$ (m, $J(P_AP_B) = 348.3$ Hz, $J(P_AP_C) = 12.7$ Hz), $\delta P_B = +5.48$ (m, $J(P_BP_C) = 24.3$ Hz), $\delta P_C = +13.50$ (m).

12b: At −100 °C, $AsCl_3$ (0.21 mL, 2.53 mmol) was added by pipette to **11**·½ TMEDA [12] (2.38 g, 8.37 mmol) in THF (30 mL). The mixture was allowed to warm to room temperature and stirred for 2 h. The solvent was evaporated, and the residue was dried under vacuum and then extracted three times with 30 mL portions of pentane. The pentane extracts were combined, and the product precipitated as a yellow crystalline solid after concentration of the solution. Yield: 1.30 g (70.1%). $^{31}P\{^1H\}$ NMR (C_6D_6, + 20 °C): $\delta P = 13.51$ (s).

Received: September 28, 1994 [Z73641E]
German version: *Angew. Chem.* **1995**, *107*, 628

Keywords: heterocycles · low-valent compounds · phosphinomethanide · phosphorus ylides · oxidative coupling

[1] H. H. Karsch, *Russ. Chem. Bul.* **1993**, in press.
[2] H. H. Karsch, B. Deubelly, G. Grauvogl, G. Müller, *J. Organomet. Chem.* **1993**, *459*, 95.
[3] H. H. Karsch, unpublished.
[4] H. H. Karsch, A. Schier, *J. Chem. Soc. Chem. Commun.*, submitted.
[5] In contrast, coupling of atoms directly coordinated to the metal center is most commonly observed for transition metal complexes [2].
[6] $^{31}P\{^1H\}$ NMR von **5**: (C_6D_6, +20 °C): $\delta P_A = -119.26$ (t, 366.5 Hz), $\delta P_B = +19.45$ (m, 366.5/8.6 Hz), $\delta P_C = +23.24$ (m, 8.6 Hz).
[7] A. Schmidpeter, S. Lochschmidt, W. S. Sheldrick, *Angew. Chem.* **1985**, *97*, 214; *Angew. Chem. Int. Ed. Engl.* **1985**, *24*, 226.
[8] A. Schmidpeter, F. Steinmüller, W. S. Sheldrick, *Z. Anorg. Allg. Chem.* **1989**, *579*, 158.
[9] From the NMR spectroscopic data **6** cannot with certainty be dediced to be the dimer (eight-membered ring) or the monomer (four-membered ring). The mass spectrum (CI, + 30 °C) exhibits a peak at $m/z = 299$ ($[Me_2P-C(SiMe_3)-PMe_2-P-PMe_2]^+$), which is assigned to a fragment ion of the dimer. $^{31}P\{^1H\}$ NMR of **6** (C_6D_6, + 20 °C): $\delta P_A = -109.53$ (t, 250.7 Hz), $\delta P_B = +7.86$ (d, 250.7 Hz).
[10] a) **7**: Single crystals by recrystallization from pentane; $C_{22}H_{47}P_5Si_2$; Enraf-Nonius-CAD4 diffractometer; $Mo_{K\alpha}$ radiation; programs SHELXTL Plus Rel. 4.1, SHELXL-93, and DIFABS; structure solution by direct methods; triclinic; $P\bar{1}$; $a = 8.556(1)$, $b = 13.633(1)$, $c = 14.137(1)$ Å, $\alpha = 88.11(1)°$, $\beta = 89.60(1)°$, $\gamma = 72.20(1)°$, $V = 1569.2(2)$ Å^3, $Z = 2$, $\rho_{calcd} = 1.106$ g cm^{-3}, $\mu = 0.376$ mm^{-1}, $\theta-\theta$ scan, scan range $6° \le 2\theta \le 54°$, 6682 independent reflections, 5602 observed reflections with $F_0 > 4\sigma(F_0)$; 276 parameters; $R = 0.031$ and $wR^2 = 0.0784$ for $F_0 > 4\sigma(F_0)$, $R = 0.042$ and $wR^2 = 0.085$ for all data; maximum residual electron density 0.247 e Å^{-3}. (b) Further details of the crystal structure investigations may be obtained from the Fachinformationszentrum Karlsruhe, D-76344 Eggenstein-Leopoldshafen (FRG), on quoting the depository number CSD-58646.
[11] H. H. Karsch, R. Richter, A. Schier, *Z. Naturforsch. B* **1993**, *48*, 1533.
[12] H. H. Karsch, A. Appelt, B. Deubelly, K. Zellner, J. Riede, G. Müller, *Z. Naturforsch. B* **1988**, *43*, 1416.
[13] Pioneering papers: a) G. Märkl, *Angew. Chem.* **1966**, *78*, 907; *Angew. Chem. Int. Ed. Engl.* **1966**, *5*, 846; b) A. J. Ashe III, P. Shu, *J. Am. Chem. Soc.* **1971**, *93*, 1804.
[14] a) 1λ^5, 1λ^5-Diphosphinine: E. Fluck, W. Plass, G. Heckmann, *Z. Anorg. Allg. Chem.* **1990**, *588*, 181; b) 1λ^5, 3λ^5, 5λ^5-Triphosphinine: E. Fluck, G. Heckmann, W. Plass, M. Spahn, H. Borrmann, *J. Chem. Soc. Perkin Trans. 1* **1990**, 1223; c) 1λ^5, 3λ^5, 5λ^3-Triphosphinine: E. Fluck, G. Becker, B. Neumüller, R. Knebl, G. Heckmann, H. Riffel, *Z. Naturforsch. B* **1987**, *42*, 1213.
[15] For a structurally uncharacterized 1λ^5,3λ^5,2λ^3-triphosphinine, see S. F. Gamper, H. Schmidbaur, *Chem. Ber.* **1993**, *126*, 601.
[16] **9**: Single crystals from pentane; $C_{14}H_{36}P_4Si_2$; Enraf-Nonius-CAD4 diffractometer; $Mo_{K\alpha}$ radiation; programs Multan 11/82, Ortep-II, Platon-92, Pluton-92, Schakal, SDP; structure solution by direct methods; monoclinic; $P2_1/m$; $a = 6.551(2)$, $b = 20.221(2)$, $c = 8.681(2)$ Å, $\beta = 106.30(1)°$, $V = 1104$ Å^3, $Z = 2$, $\rho_{calcd} = 1.157$ g cm^{-3}, $\mu = 0.44$ mm^{-1}, ω scan, scan range $2° < 2\theta < 60°$, 3006 independent reflections, 171 parameters; $R = 0.037$; $R_w = 0.031$ (all data); maximum residual electron density 0.40 e Å^{-3} (cf. Ref. [10 b]).
[17] To distinguish clearly the underlying cyclic bonding interaction between alternately oppositely charged atoms (which is also conceivable for related species such as cyclotriphosphazenes) from aromatic bonding we suggest the term "amphipolar" [Gr. amphi = 1. change ("amphibian"), 2. round ("amphitheater")].
[18] Isotetraphosphanes have been studied intensively for some time now; see for example, M. Scheer, S. Gremler, E. Herrmann, U. Grünhagen, E. Kleinpeter, *Z. Anorg. Allg. Chem.* **1991**, *600*, 203, and references therein.
[19] $^{31}P\{^1H\}$ NMR for **12a**: (C_6D_6, + 20 °C), AB_3 spin system, $\delta P_A = -39.09$, $\delta P_B = 15.08$, $J(P_AP_B) = 360.8$ Hz.
[20] $^{31}P\{^1H\}$ NMR for **12c**: (C_6D_6, + 20 °C), $\delta P = -1.11$.
[21] Phosphorus-tris(*C*-ylide) derivatives $P(CH{=}PR_3)_3$ ("trisylenes") have been reported; however, recent findings cast some doubt on whether they were formulated correctly: a) K. Issleib, M. Lischewski, *J. Prakt. Chem.* **1969**, *311*, 857; b) *ibid.* **1970**, *312*, 135; see also: G. Jochum, Dissertation, Universität München, **1994**.
[22] Formally related are the recently synthesized tris(thiophosphinoyl)phosphanes $P[P(S)R_2]_3$: M. Scheer, F. Uhlig, T. T. Nam, M. Dargatz, H.-D. Schädler, E. Herrmann, *Z. Anorg. Allg. Chem.* **1990**, *585*, 177.
[23] **12b**: Single crystals by recrystallization from pentane; $C_{27}H_{72}AsP_3Si_6$; Enraf-Nonius-CAD4 diffractometer; $Mo_{K\alpha}$ radiation; programs SHELXR Plus Rel. 4.1; SHELXL-93, and DIFABS; structure solution by Patterson-method; triclinic; $P\bar{1}$; $a = 11.776(1)$, $b = 13.405(1)$, $c = 14.369(1)$ Å, $\alpha = 78.07°$, $\beta = 89.50(1)°$, $\gamma = 80.90(1)°$, $V = 2190.7(3)$ Å^3, $Z = 2$, $\rho_{calcd} = 1.112$ g cm^{-3}, $\mu = 1.065$ mm^{-1}, $\theta-\theta$ scan, scan range $6° \le 2\theta \le 52°$, 8529 independent reflections, 7281 observed reflections with $F_0 > 4\sigma(F_0)$; 358 parameters; $R = 0.033$ and $wR^2 = 0.085$ for $F_0 > 4\sigma(F_0)$; R = 0.046 and $wR^2 = 0.099$ (all data); maximum residual electron density 0.446 e Å^{-3} (cf. Ref. [10b]).
[24] The trihalogenides MCl_3 (M = P-Bi) react with the lithium phosphinomethanide $LiCH_2PMe_2$ that has only H substituents at the carbon atom to yield tris(phosphinomethyl) derivatives $M(CH_2PMe_2)_3$. For M = P: H. H. Karsch, H. Schmidbaur, *Z. Naturforsch. B* **1977**, 32, 762; for M = As, Sb: H. H. Karsch, E. Witt, unpublished results; for M = Bi: cf. Ref. [2].

Cobalt-Containing Molecular Sieves as Catalysts for the Low Conversion Autoxidation of Pure Cyclohexane**

Dominic L. Vanoppen, Dirk E. De Vos,*
Michel J. Genet, Paul G. Rouxhet and Peter A. Jacobs

CoAPO molecular sieves have already been studied as solid acid catalysts,[1] but the incorporation of cobalt into aluminophosphate [2] and aluminosilicate structures [3] could also open a route toward heterogenization of cobalt autoxidation catalysis. The autoxidation of cyclohexane is an important bulk process,[4] which is currently carried out in the presence of small amounts of dissolved cobalt salts. Reactions proceed by a free radical mechanism, yielding primarily cyclohexyl hydroperoxide (cHHP). Cobalt ions accelerate the overall reaction as new radicals are generated by cHHP decomposition in a Haber–Weiss cycle. As the primary oxidation products are more susceptible to oxidation than the substrate, conversion must be kept low to obtain reasonable selectivities for the products cyclohexanol and cyclohexanone. Precipitation deactivates the homogeneous catalysts.[4] Besides the technical advantages of catalyst heterogeneity, the catalyst activity, stability, and selectivity are thus important factors to be considered in developing new heterogeneous catalysts for this process. We studied the autoxidation of cyclohexane in the presence of CoAPO-5 and CoAPO-11 molecular sieves, monitoring activity and selectivity by product formation and oxygen consumption. Overall cobalt distribution and coordination were studied by elemental analysis, X-ray photoelectron spectroscopy (XPS), and UV-Vis reflectance spectroscopy (DRS) to evaluate heterogeneity and stability. Isolation of the cobalt sites by incorporation into the molecular sieve framework seems to be critical for obtaining active and truly heterogeneous autoxidation catalysts. These solid catalysts show an improved stability and selectivity over the classical cobalt naphthenate catalyst.

CoAPOs are aluminophosphate molecular sieves in which a few percent of Al^{3+} centers is substituted by Co^{2+} centers. CoAPO-5 has AFI-topology with channels with 12-membered rings, while CoAPO-11 has AEL-topology with only 10-membered rings forming the channels. Figure 1 shows formation of

[*] Dr. D. E. De Vos, D. L. Vanoppen, Prof. P. A. Jacobs
Centrum voor Oppervlaktechemie en Katalyse,
Katholieke Universiteit Leuven
Kardinaal Mercierlaan 92, B-3001 Leuven (Belgium)
Telefax: Int. code + (16) 321998
M. J. Genet, Prof. P. G. Rouxhet
Unité Chemie des Interfaces, Université Catholique de Louvain (Belgium)

[**] This work was supported by the Belgian Government (Interuniversitary Attraction Pole Interuniversitaire Attractiepool IUAP). We are indebted to N. F. W. O. (DEDV) and I. W. O. N. L. (DLV) for fellowships.

 © VCH Verlagsgesellschaft mbH, D-69451 Weinheim, 1995 0570-0833/95/0505-0560 $ 10.00+.25/0

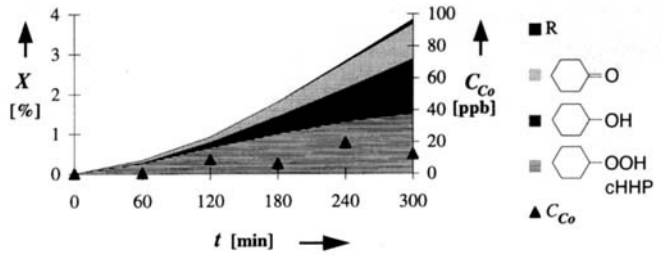


Fig. 1. Autoxidation of cyclohexane (75 mL) in the presence of 0.5 g CoAPO-5 (from gel with Co/(Co + Al) = 0.01) at 130 °C and 1 MPa O_2 initial pressure. Results were obtained in five independent reactions, by stopping reactions after 1, 2, 3, 4, and 5 h. Amount of products are expressed in % yield (X), calculated as (mmol product/mmol cyclohexane) × 100. R is the sum of caprolactone and acids detected. C_{Co} denotes concentration of dissolved cobalt.

products and evolution of free cobalt in a typical reaction. It is clear from Table 1 that the catalyst is truly heterogeneous, because the amount of dissolved cobalt is much lower than in homogeneous catalysis. Heterogenization of cobalt catalysis has

Table 1. Heterogeneity of autoxidation catalysis with CoAPO (75 mL cyclohexane, 1 MPa O_2 initial pressure, 5 h, 130 °C).

Catalyst	Conversion [%]	Dissolved [Co]
1) 0.5 g CoAPO-5 (0.01) [a]	3	12 ± 3 ppb
2) contribution from homogeneous catalysis [b]	–	7 ± 3 ppb
3) cobalt naphthenate	0.5	100 ppb
4) cobalt naphthenate	–	50 ppb

[a] The number in brackets denotes the Co/(Co + Al) ratio. [b] The reaction mixture is prepared by heating the mixture of 1) under N_2 for 5 h at 130 °C and filtering off the catalyst.

a dramatic effect on product distribution. With CoAPO-5, cHHP is a main product, whereas with a homogeneous catalyst it is only a minor one (Fig. 2). cHHP is an attractive primary

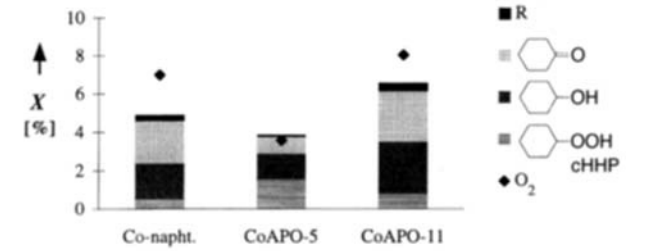


Fig. 2. Autoxidation of cyclohexane (75mL) in the presence of 0.5 g CoAPO-5, 0.5 g CoAPO-11 (from gels with Co/(Co + Al) = 0.01) or 33 ppm cobalt naphthenate (total amount of cobalt in all reactions is identical; 130 °C, 5 h, 1 MPa O_2 initial pressure). Products are expressed in % yield (X), as in Fig. 1. Oxygen consumption [(mmol O_2 consumed/mmol cyclohexane) × 100] was calculated from the difference in pressure at room temperature before and after reaction.

product, because ever more clean and convenient routes lead from it to cyclohexanol and cyclohexanone.[5] Furthermore CoAPOs yield higher selectivities for monofunctionalized products (Fig. 3).

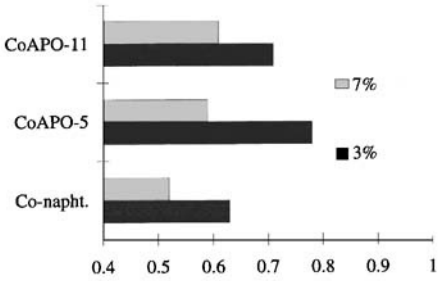


Fig. 3. Oxygen efficiency for monofunctionalization as a measure of the overall selectivity for monofunctionalization, calculated as (mmol cHHP + mmol cyclohexanone + 0.5x mmol cyclohexanol)/(mmol oxygen consumed). Reactions were stopped after consumption of 0.03 or 0.07 moles O_2 per mole cyclohexane (3 and 7% theoretical conversion to cyclohexanone or cHHP). Reaction mixtures and conditions were as in Fig. 2.

Quite unexpectedly since cyclohexane and its oxidation products are expected to diffuse only slowly into 10-membered ring channels,[6] CoAPO-11 molecular sieves exhibit higher catalytic activities than CoAPO-5. Lowering the cobalt content to zero (see Fig. 5) shows that in CoAPO-11, cobalt catalysis is superimposed on an effect of the molecular sieve itself, which promotes peroxide production. The mechanism behind this catalytic activity is still unclear, but may be related to enhanced hydroperoxide production observed in certain polar solvents[7] or in molecular sieve structures.[8]

The Co-naphthenate catalyst is deactivated by formation of precipitates, which seem to quench further reaction (Fig. 4). CoAPO catalysts are not deactivated, which we ascribe to immobilization of cobalt ions at framework positions. XPS and elementary analyses (Table 2) indeed indicate that the uniform

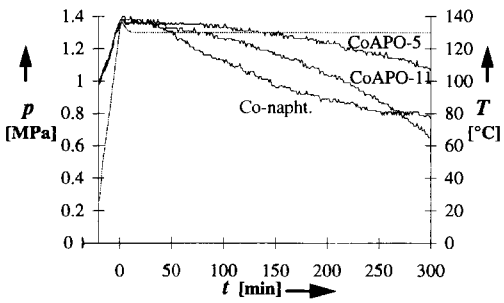


Fig. 4. Pressure decrease during autoxidation of cyclohexane in the presence of CoAPO-5, CoAPO-11, or cobalt naphthenate as a measure for oxygen consumption. Reaction mixtures as in Fig. 2. After reaction with cobalt naphthenate a purple precipitate could be filtered from the reaction mixture.

Table 2. Composition of catalysts from elemental analysis and XPS. XPS ratios were calculated from Al 2p and Co $2p_{3/2}$ lines.

Catalyst	Ratio Co/(Co + Al)					Co leached in reaction
	synthesis gel	bulk analysis	XPS			
			as synthesized	calcined + reduced with acetone	after reaction	
CoAPO-5	0.01	0.0096	0.008	0.006	0.008	0.07% [a]
CoAPO-11	0.01	0.0081	0.008	0.005	0.009	0.08% [a]
CoAPO-5	0.04	0.0363	0.016	0.016	0.014	0.15% [b]
CoAPO-5 0.04 with acetic acid as a promoter					0.129	0.08% [c]

[a] The reactions were stopped at 7% theoretical conversion (as in Fig. 3). [b], [c] The reactions were stopped after 5 h. [a], [b] DRS and XPS spectra gave no evidence for change in cobalt coordination.

 © VCH Verlagsgesellschaft mbH, D-69451 Weinheim, 1995 0570-0833/95/0505-0561 $ 10.00+.25/0

cobalt ion distribution is preserved during reaction in cyclohexane. These catalysts could be recalcined and reused at least four times without apparent loss of activity.

In contrast, a cobalt-exchanged zeolite Y in which the cobalt ions are highly mobile is catalytically inactive and even strongly inhibits reaction under conditions for spontaneous autoxidation (Table 3). The typical DRS features of exchanged cobalt ions disappear during reaction, which supports the hypothesis of quenching by cobalt clusters or precipitates.

Table 3. Inhibition of the autoxidation of cyclohexane (75 mL, 1 MPa O_2 initial pressure) by CoNaY.

Catalyst [a]	T [°C]	Conversion [%] (time)	Dissolved [Co]
0.5 g CoNaY (0.5)	130	– (5 h)	320 ppb
0.5 g CoNaY (1.5)	130	– (5 h)	260 ppb
–	145	3 (5 h)	–
0.5 g CoNaY (0.5)	145	– (5 h)	160 ppb

[a] The numbers in brackets denote the cobalt content in weight percent.

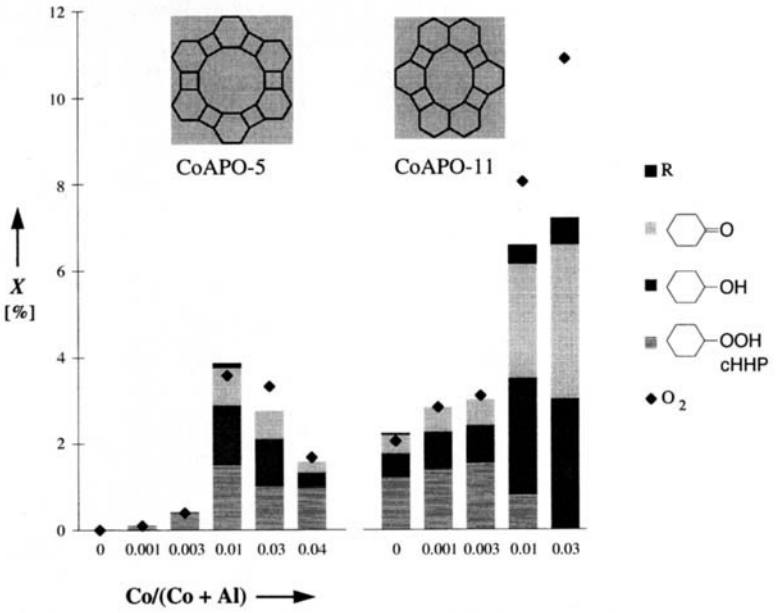


Fig. 5. Autoxidation of cyclohexane in the presence of CoAPO-5 or CoAPO-11 with different ratios of Co/(Co + Al). Reaction mixtures, conditions, notation, and calculation as in Fig. 2.

When acetic acid is used as a promoter,[9] the CoAPO molecular sieve seems to act as an inhibitor rather than as a catalyst (Table 4). XPS analysis after reaction in acetic acid indicates an eightfold increase of the cobalt signal (see Table 2) and splitting of the Co $2p_{3/2}$ line. Acid leaching of cobalt from its isolated sites and reprecipitation at the surface explains our observations. Clusters or precipitates again seem to quench the reaction.

Table 4. Autoxidation of cyclohexane (60 mL) with acetic acid (15 mL) as a promoter (1 MPa O_2 initial pressure).

Catalyst [a]	T [°C]	Reaction (time)	Dissolved [Co]
1) 0.5 g CoAPO-5 (0.04)	100	– (5 h)	820 ppb
2) –	130	all oxygen consumed (3.1 h)	–
3) 0.5 g CoAPO-5 (0.04)	130	all oxygen consumed (4.2 h)	110 ppb
4) test for contribution from homogeneous catalysis [b]	130	all oxygen consumed (1.1 h)	1700 ppb

[a] The numbers in brackets denote Co/(Co + Al) ratios. [b] The reaction mixture is prepared by heating the mixture of 3) under N_2 for 1 h at 130 °C and filtering off the catalyst.

Finally, a similar phenomenon is observed for CoAPO-5 in pure cyclohexane. Varying cobalt content (Fig. 5) shows that activity increases with increasing cobalt content at low loadings. Above a Co/(Co + Al) ratio of 0.01, higher leaching (up to 200 ppb) occurs, but no further increase in activity is observed. This can again be ascribed to a decrease in site isolation at higher cobalt content. Recent ^{31}P NMR studies indicate that CoAPO-11 displays a more uniform cobalt distribution than CoAPO-5 at high cobalt loadings.[10] This readily explains their different response toward increasing cobalt content (Fig. 5).

Therefore we conclude that site isolation is the key factor leading to active and truly heterogeneous catalysts. Adding acids or using catalysts with high cobalt content results in loss of this essential advantage.

Experimental

CoAPO molecular sieves were prepared by hydrothermal synthesis from gels with molar composition $2x\,Co(CH_3COO)_2 : 1\,P_2O_5 : (1-x)Al_2O_3 : 1.5\,Pr_3N : 40\,H_2O$ (CoAPO-5) or $2x\,Co(CH_3COO)_2 : 1\,P_2O_5 : (1-x)Al_2O_3 : 1\,Pr_2NH : 40\,H_2O$ (CoAPO-11) ($0 < x < 0.04$) in an autoclave under autogeneous pressure at 150 °C for 24 h (CoAPO-5) or 175 °C for 72 h (CoAPO-11). Gels were cooled during preparation. Crystallinity and cobalt incorporation were checked by X-ray diffraction and DRS (Varian Cary 5 with integration sphere). CoNaY was prepared by stirring NaY (PQ) in a dilute cobalt nitrate solution. All catalysts were calcined for about 12 h at 500 °C in a stream of oxygen prior to use. Autoxidation experiments were carried out in a 300 mL stainless steel Parr pressure reactor, passivated with a saturated sodium pyrophosphate solution [7].

Typical experiments used 0.5 g of catalyst and 75 mL of cyclohexane, and the headspace was filled with oxygen under a total pressure of 1 MPa, which allowed a conversion of approximately 10% [11]. The following products were detected by GC (CP-sil5 column, Chrompack): cyclohexanol, cyclohexanone, cHHP, caprolactone, and adipic, glutaric, succinic, caproic, valeric, and butyric acids. Deficiency in the oxygen mass balance can be ascribed to formation of esters that are invisible in GC. As cHHP partially decomposed upon injection, its concentration was estimated by double analysis, before and after reducing cHHP to cyclohexanol with Ph_3P [12]. For elemental analysis, reaction mixtures were extracted with 25 mL HNO_3 (1 N), and catalysts were dissolved in a HF solution. XPS studies were carried out on a SSX-100/206 Fisons spectrometer with a monochromatized Al X-ray source (analyzer pass energy 150 eV). Acquisition times of 3 h were needed to obtain acceptable signal-to-noise ratios. No charging effects were observed during accumulation.

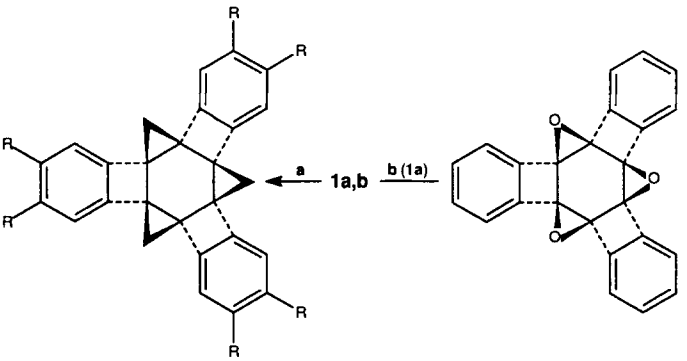
Received: August 30, 1994
Revised version: December 7, 1994 [Z 7278 IE]
German version: *Angew. Chem.* **1994**, *107*, 637

Keywords: aluminophosphate · autoxidation · catalysis · zeolites

[1] N. J. Tapp, N. B. Milestone, *J. Chem. Soc. Chem. Commun.* **1985**, 1801; J. Chen, J. M. Thomas, *ibid.* **1994**, 603; J. M. Thomas, *Angew. Chem.* **1994**, *106*, 963. *Angew. Chem. Int. Ed. Engl.* **1994**, *33*, 913.
[2] S. T. Wilson, E. M. Flanigen, UCC, US-A 4567029 567.029, **1986**; L. E. Iton, I. Choi, J. A. Desjardins, V. A. Maroni, *Zeolites* **1989**, *9*, 535; R. A. Schoonheydt, R. de Vos, J. Pelgrims, H. Leeman, *Stud. Surf. Sci. Catal.* **1989**, *49*, 559; C. Montes, M. E. Davis, B. Murray, M. Narayana, *J. Phys. Chem.* **1990**, *94*, 6425; B. Kraushaar-Czarnetzki, W. G. M. Hoogervorst, R. R. Andréa, C. A. Emeis, W. H. J. Stork, *J. Chem. Soc. Faraday Trans.* **1991**, *87*, 891.
[3] J. A. Rossin, C. Saldarriaga, M. E. Davis, *Zeolites* **1987**, *7*, 295.
[4] R. A. Sheldon, J. K. Kochi, *Metal-Catalyzed Oxidations of Organic Compounds*, Academic Press, New York, **1981**, Chapter 11; J. E. Lyons, *Appl. Ind. Catal. 1983–1984*, **1984**, *3*, 131, and references therein.
[5] J. D. Chen, J. Dakka, R. A. Sheldon, *Appl. Catal. A* **1994**, *108*, L1.

 © VCH Verlagsgesellschaft mbH, D-69451 Weinheim, 1995 0570-0833/95/0505-0562 $ 10.00+.25/0

[6] For diffusion of cyclohexane in ZSM-5 with comparable pore size see H. Chon, D. H. Park, *J. Catal.* **1988**, *114*, 1.
[7] K. Tanaka, J. Imamura, *Chem. Lett.* **1974**, 1347; U. Schuchardt, W. A. Carvalho, E. V. Spinacé, *Synlett* **1993**, 713.
[8] F. Blatter, H. Frei, *J. Am. Chem. Soc.* **1994**, *116*, 1812; D. E. Patton, R. S. Drago, *J. Chem. Soc. Perkin Trans. 1* **1993**, 1611.
[9] B. Kraushaar-Czarnetzki, W. G. M. Hoogervorst, *Eur. Pat. Appl.* 0519569A2, **1992**; S. S. Lin, H.-S. Weng, *Appl. Catal. A* **1993**, *105*, 289; B. Kraushaar-Czarnetzki, W. G. M. Hoogervorst, W. H. J. Stork, *Stud. Surf. Sci. Catal.* **1994**, *84*, 1869.
[10] M. P. J. Peeters, L. J. M. van de Ven, J. W. de Haan, J. H. C. van Hooff, *Coll. Surfaces* **1993**, *72*, 87.
[11] Mixtures of oxygen and organic vapors are potentially explosive, and care should be taken to protect personnel.
[12] G. B. Shul'pin, D. Attanasio, L. Suber, *J. Catal.* **1993**, *142*, 147.



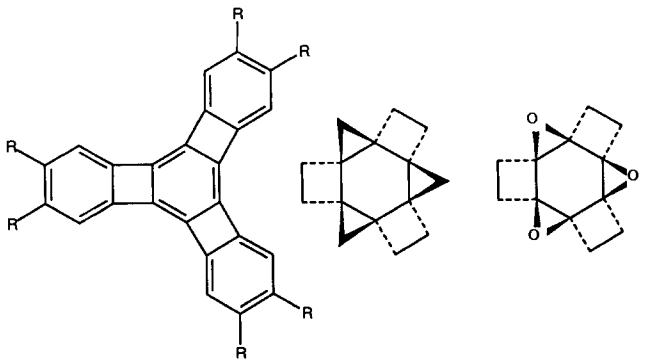
4a, R = H
4b, R = $Si(CH_3)_3$ **5**

Scheme 1. a) $(CH_3CH_2)_2Zn$, toluene, 60 °C, 97% of **4a**, 78% of **4b**; b) 3,3-dimethyl-1,2-dioxacyclopropane, acetone, 84%.

Novel Structures from Tris(benzocyclobutadieno)cyclohexatriene: Triscyclopropanation and Trisoxacyclopropanation to the First [2.1.2.1.2.1]Hexaannulanes**

Debra L. Mohler, K. Peter C. Vollhardt,* and Stefan Wolff

In the triangular [4]phenylene **1** ("tris(benzocyclobutadieno)-cyclohexatriene"),[1] σ-strain and antiaromatic π-effects[2] combine to impose a cyclohexatrienic structure on the central ring, which manifests itself chemically in its unprecedented ring-opening to the corresponding cyclic triyne[1] and facile all-*cis*-hydrogenation.[3] We now report the direct methylenation and oxidation of the cyclohexatriene unit in **1** to give the surprisingly stable novel compounds **4** and **5**, incorporating the unknown, highly strained[4] all-*cis*-[2.1.2.1.2.1]hexaannulane[5] frameworks **2** and **3**, respectively.



1a, R = H
1b, R = $Si(CH_3)_3$ **2** **3**

Cyclopropanation of **1a,b** to the *cis*-tris-σ-homobenzenes **4a,b** was achieved under modified Simmons–Smith conditions (Scheme 1).[6, 7] The products are remarkably thermally stable, surviving prolonged heating to 200 °C (**4a**, C_6D_6) or 340 °C (**4b**, neat). They are also inert to (at least relatively mild) hydrogenolysis conditions (H_2, 1 atm, Pd, THF, 20 °C). Their symmetry is apparent from the NMR spectral data,[7] and their chemical shift values are, perhaps surprisingly, not unexpected.[1, 3, 5, 8] The methylene hydrogens are relatively strongly[8] deshielded,[7] most likely due to the presence of the benzene rings, although we cannot rule out a contribution arising from the all-*cis* fusion of the cyclopropane rings.[8h] In the series of all-*cis*-σ-homobenzenes, **4** is unique for its lack of perturbing substituents on the methylene bridges. This feature allows a comparison of the two C–H coupling constants (*exo*, *endo*). Surprisingly, not only are their values essentially equal to those of model fused cyclopropanes and the parent ring itself,[9] but they are also identical ($J = 161.2$ Hz)!

The novelty of the framework **4** prompted the determination of the X-ray structural details of **4b** (Fig. 1).[10] Unlike hexamethyl-*trans*-σ-trishomobenzene,[11] but like several 3,5,9-trisubstituted *cis*-σ-trishomobenzenes and hexahydro-**1a**[3] (and several hetero-σ-trishomobenzenes),[12] the central cyclohexane unit is planar, but exhibits considerably less bond-length alternation (1.541, 1.510 Å), mainly because of a pronounced shortening of the bond of the four-membered rings (from 1.599 to 1.541 Å). While such bond shortening has been interpreted previously as indicating conjugation between the three-membered rings,[11, 12] rehybridization effects to accommodate ring strain are more likely the dominant cause of this phenomenon.[13] Otherwise, the benzocyclobutene units resemble those of **1b**,[1a] 1,2-dihydro-4,5-bis(trimethylsilyl)-,[14] and 1,2-dihydrobenzocyclobutene in geometry.[15] Finally, the average dihedral angle between the central cyclohexane and the benzocyclobutene moieties is 132.3°, noticeably expanded from hexahydro-**1a**,[3] while that to the cyclopropane planes is 121.3°. The latter value is in remarkable agreement with that calculated for the unknown parent *cis*-σ-trishomobenzene,[16] thought to be unstable at ambient temperatures with respect to electrocyclic ring opening.[8h, 17] In **4** such a retrocyclization could proceed with triscyclopropane participation to give a trisbenzocyclobutadiene structure, or by trisbenzocyclobutane opening[3] to result in three linked cyclopropene units. Both isomerizations are estimated to be endothermic,[18a, b] and no other facile (and detectable) pathways of rearrangement are open to the molecules, which provides a rationale for their baffling thermal robustness.

The trioxaannulane framework of **5** was prepared as shown in Scheme 1[7] with 3,3-dimethyl-1,2-dioxacyclopropane (dimethyldioxirane).[19] It is stable up to its melting point (180 °C),

[*] Prof. Dr. K. P. C. Vollhardt, Dr. D. L. Mohler, Dr. S. Wolff
Department of Chemistry, University of California at Berkeley
and
The Chemical Sciences Division, Lawrence Berkeley Laboratory
Berkeley, CA 94720 (USA)
Telefax: Int. code + (510) 643-5208

[**] This work was supported by the National Science Foundation (CHE-9202152). S. W. thanks the Deutsche Forschungsgemeinschaft for a postdoctoral fellowship (1989–1990).

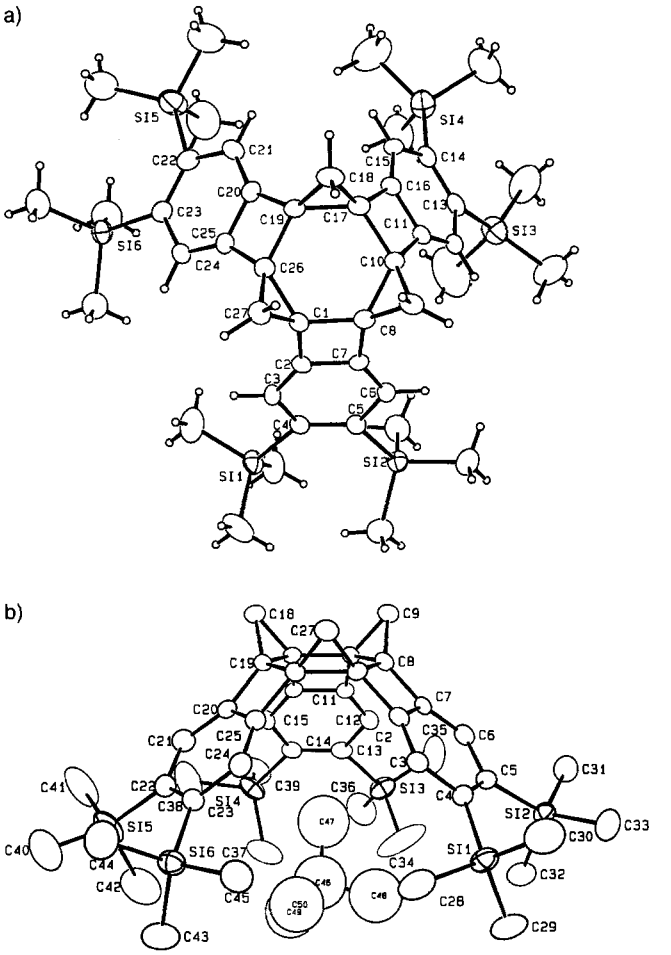


Fig. 1. Views from above (a) and the side (b) of the molecular structure of **4b**; Fig. 1b includes a solvent molecule, acetone. Ellipsoids are scaled to represent the 50% probability surface; hydrogen atoms are given as small spheres with arbitrary radius. Averaged selected distances [Å] and angles [°] (idealized C_{3v} symmetry): C1–C8 1.541, C8–C10 1.510, C8–C9 1.500, C1–C2 1.501, C2–C7 1.387, C2–C3 1.371, C3–C4 1.415, C4–C5 1.413; C2-C1-C8 87.2, C8-C1-C26 120.0, C26-C1-C27 59.7, C1-C2-C7 92.9, C3-C2-C7 122.4, C2-C3-C4 118.9, C3-C4-C5 119.6.

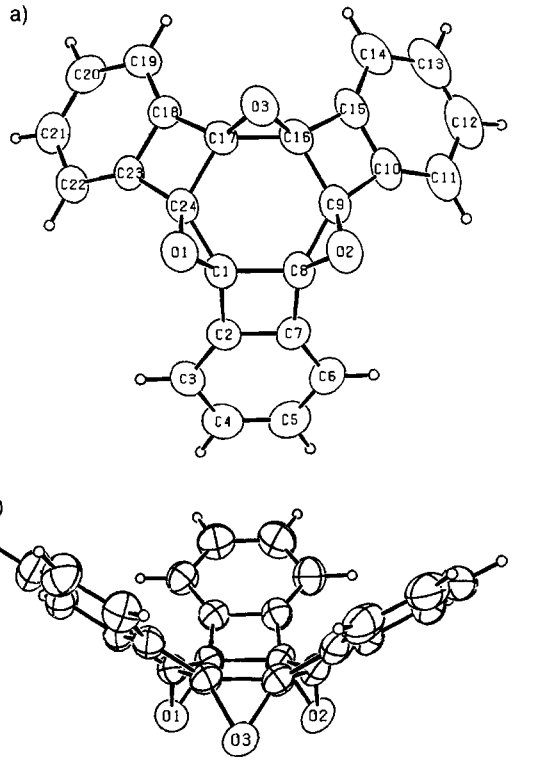


Fig. 2. View from above (a) and the side (b) of the molecular structure of **5**. Ellipsoids are scaled to represent the 50% probability surface; hydrogen atoms are given as small spheres with arbitrary radius. Averaged selected distances [Å] and angles [°] (for idealized C_{3v} symmetry): O1–C1 1.441, C1–C2 1.496, C1–C8 1.526, C1–C24 1.463, C2–C3 1.378, C2–C7 1.394, C3–C4 1.383, C4–C5 1.384; C1-O1-C24 61.0, C24-C1-O1 59.5, C2-C1-C8 87.5, C8-C1-C24 120.0., C1-C2-C7 92.5, C3-C2-C7 122.2, C2-C3-C4 115.6, C3-C4-C5 122.2.

when it slowly decomposes without a sign of internal ring opening, in this case not only for thermodynamic,[18a, c] but perhaps also kinetic reasons.[20] The ether bridges survived chromatography on silica gel, but not direct acid treatment (dilute aqueous CF_3CO_2H or HCl). Irradiation with a medium-pressure Hg lamp led to complete decomposition within minutes. Again, the symmetrical structure manifests itself in the simple signal pattern in the NMR spectrum,[7] in which the unusually large chemical shift of the central carbon atoms ($\delta = 76.3$) reflects the cumulative influence of the constituent parts of **5**.[20, 21]

The X-ray structural details of **5** are depicted in Figure 2.[22] The framework of **5** is similar to that of **4b** except that the bonds of the *cis*-trioxa-tris-σ-homobenzene unit are all shortened, while the bonds in the central, planar cyclohexane ring still alternate in length (1.526, 1.463 Å). The average dihedral angle between the cyclohexane ring and the benzocyclobutene planes is further expanded (relative to hexahydro-**1a** and **4b**) to 145.5°, while the three-membered rings point further inwards (114.5°). The structural changes on going from *cis*-benzenetrioxide[12b] to **5** are also instructive: the linkages between the oxacyclopropanes lengthen (1.488 to 1.526 Å) and the C–O bonds to the bridging oxygen atoms shorten (1.471 to 1.463 Å). The crown ether cavity is also clearly widened (dihedral angle change from 106.9° to 114.5°), thus lengthening the average O–O distance (2.82 Å to 3.15 Å) and providing new geometric constraints on the potential ability of the trisoxaface to function as a tridentate ligand for metals.[12d, e] This aspect is currently under investigation.

Received: September 20, 1994 [Z 7337 IE]
German version: *Angew. Chem.* **1995**, *107*, 601

Keywords: annulanes · cyclopropanations · epoxidations · homobenzenes · strained rings

[1] a) R. Diercks, K. P. C. Vollhardt, *J. Am. Chem. Soc.* **1986**, *108*, 3150; b) K. P. C. Vollhardt, *Pure Appl. Chem.* **1993**, *65*, 153.
[2] a) R. Faust, E. D. Glendening, A. Streitwieser, K. P. C. Vollhardt, *J. Am. Chem. Soc.* **1992**, *114*, 8263; b) E. D. Glendening, R. Faust, A. Streitwieser, K. P. C. Vollhardt, F. Weinhold, *ibid.* **1993**, *115*, 10952.
[3] D. L. Mohler, K. P. C. Vollhardt, S. Wolff, *Angew. Chem.* **1990**, *102*, 1200; *Angew. Chem. Int. Ed. Engl.* **1990**, *29*, 1151.
[4] H. Dodziuk, *Bull Chem. Soc. Jpn.* **1987**, *60*, 3775.
[5] a) J. A. Marshall, J. C. Peterson, L. Lebioda, *J. Am. Chem. Soc.* **1984**, *106*, 6006; b) D. Wehle, N. Schormann, L. Fitjer, *Chem. Ber.* **1988**, *121*, 2171.
[6] J. Furukawa, N. Kawabata, J. Nishimura, *Tetrahedron* **1968**, *24*, 53.
[7] All new compounds gave satisfactory analytical and spectral data: **4a**: colorless crystals, m.p. 280–286 °C (decomp.); UV/Vis (hexane): λ_{max} (log ε) = 239 (4.50), 281 (4.16), 288 (4.14) nm; IR (KBr): $\tilde{\nu}$ = 2932, 1456, 1437, 1212, 1122, 858, 646 cm^{-1}; MS (10 eV): *m/z* 342 (M^+, 39), 341 (65), 340 (61), 339 (100), 338 (27), 337 (41), 327 (32), 326 (66), 313 (20), 170 (16), 163 (23), 109 (19); ^1H NMR (300 MHz, C_6D_6): δ = 6.97 (AA'm, 6H), 6.82 (BB'm, 6H), 1.69 (d, J = 7 Hz, 3H), 1.14 (d, J = 7 Hz, 3H); $^{13}C\{^1H\}$ NMR (75 MHz, $CDCl_3$): δ = 147.74, 126.80, 118.48, 42.92, 16.55. **4b**: colorless crystals, m.p. > 360 °C; UV/Vis (hexane): λ_{max} (log ε) = 249 (4.70), 288 (3.91), 297 (3.76) nm; IR ($CHCl_3$): $\tilde{\nu}$ = 3056, 3001, 2961, 2934, 2905, 2874, 1450, 1256, 1083, 1012, 862, 840, 691, 647 cm^{-1}; MS (10 eV): *m/z* 774 (M^+, 7), 759 (4), 701 (6), 627 (5), 613 (7), 597 (7), 539 (5), 525 (8), 73 (100); ^1H NMR (300 MHz, $CDCl_3$): δ = 7.28 (s, 6H), 2.06 (d, J = 7 Hz, 3H), 1.44 (d, J = 7 Hz, 3H), 0.32 (s, 54 H); $^{13}C\{^1H\}$

NMR (75 MHz, $CDCl_3$): $\delta = 148.18$, 144.78, 124.81, 43.92, 16.97, 2.62. HR-MS Calcd for $C_{45}H_{66}Si_6$: 774.3780; found: 774.3779. **5**: colorless crystals, m.p. 180–182 °C (decomp.); IR (KBr): $\tilde{\nu} = 1613$, 1512, 1495, 1463, 1430, 1339, 1261, 1154, 1094, 1003, 918, 861, 802, 751 cm^{-1}; MS (70 eV): *m/z* 348 (M^+, 11), 316 (8), 261 (10), 248 (9), 176 (21), 175 (100), 174 (11), 156 (61), 135 (22), 127 (20), 123 (30), 121 (22), 107 (18), 85 (11), 73 (38); ^1H NMR (400 MHz, $CDCl_3$): $\delta = 7.46$ (AA'm, 6H), 7.38 (BB'm, 6H); $^{13}C\{^1H\}$ NMR (100 MHz, $CDCl_3$): $\delta = 143.71$, 131.50, 122.64, 76.25.

[8] a) A. de Meijere in *Cage Hydrocarbons* (Ed.: G. A. Olah), Wiley, New York, **1990**, p. 261; b) H. Prinzbach, D. Stusche, *Angew. Chem.* **1970**, *82*, 836; *Angew. Chem. Int. Ed. Engl.* **1970**, *9*, 799; c) M. Engelhard, W. Lüttke, *ibid.* **1972**, *84*, 346 and **1972**, *11*, 310; d) H. Prinzbach, R. Schwesinger, *ibid.* **1972**, *84*, 988 and **1972**, *11*, 940; e) P. Binger, G. Schroth, J. McMeeking, *ibid.* **1974**, *86*, 518 and **1974**, *13*, 465; f) A. de Meijere, D. Kaufmann, O. Schallner, *ibid.* **1971**, *83*, 404 and **1971**, *10*, 417; *Tetrahedron Lett.* **1973**, 553; g) P. Binger, J. McMeeking, U. Schuchardt, *Chem. Ber.* **1980**, *113*, 2372; h) D. Kaufmann, H.-H. Fick, O. Schallner, W. Spielmann, L.-U. Meyer, P. Gölitz, A. de Meijere, *ibid.* **1983**, *116*, 587; W. Spielmann, H.-H. Fick, L.-U. Meyer, A. de Meijere, *Tetrahedron Lett.* **1976**, 4057; i) C. Rücker, H. Prinzbach, *ibid.* **1983**, *24*, 4099; j) W.-D. Braschwitz, T. Otten, C. Rücker, H. Fritz, H. Prinzbach, *Angew. Chem.* **1989**, *101*, 1383; *Angew. Chem. Int. Ed. Engl.* **1989**, *28*, 1348.

[9] H.-O. Kalinowski, S. Berger, S. Braun, *^{13}C NMR Spektroskopie*, Thieme, Stuttgart, **1984**.

[10] Crystal size $0.21 \times 0.28 \times 0.50$ mm^3, space group $P2_1/n$, 2θ scan range 3–45°, $a = 11.6696(20)$ Å, $b = 21.345(7)$ Å, $c = 20.933$ (4) Å, $\alpha = 90.0$, $\beta = 93.132(13)$, $\gamma = 90.0°$, $V = 5206.4(36)$ $Å^3$, $Z = 4$, $\rho_{calcd} = 1.06$ g cm^{-3}, $\mu = 1.9$ cm^{-1}, 6784 unique reflections collected at 170 K, of which 4098 were taken as observed [$F^2 > 3\sigma(F^2)$], $R = 0.0514$, $R_w = 0.0580$. Hydrogen atoms were assigned idealized positions, adjusted based on residual peaks in the difference Fourier map during the last cycles of refinement [23].

[11] C. Krüger, P. J. Roberts, *Cryst. Struct. Commun.* **1974**, *3*, 459.

[12] a) C. Kabuto, M. Yagihara, T. Asao, Y. Kitahara, *Angew. Chem.* **1973**, *85*, 860; *Angew. Chem. Int. Ed. Engl.* **1973**, *12*, 836; b) W. Littke, U. Drück, *ibid.* **1974**, *86*, 557 and **1974**, *13*, 539; c) E. Vogel, A. Breuer, C.-D. Sommerfeld, R. E. Davis, L.-K. Liu, *ibid.* **1977**, *89*, 175 and **1977**, *16*, 169; d) I. Erden, P. Gölitz, R. Näder, A. de Meijere, *ibid.* **1981**, *93*, 605 and **1981**, 20, 583; e) R. Schwesinger, K. Piontek, W. Littke, O. Schweikert, H. Prinzbach, C. Krüger, Y.-H. Tsay, *Tetrahedron Lett.* **1982**, *23*, 2427; f) G. McMullen, M. Lutterbeck, H. Fritz, H. Prinzbach, C. Krüger, *Isr. J. Chem.* **1982**, *22*, 19; g) R. Schwesinger, K. Piontek, W. Littke, H. Prinzbach, *Angew. Chem.* **1985**, *97*, 344; *Angew. Chem. Int. Ed. Engl.* **1985**, *24*, 318.

[13] R. Boese, D. Bläser, W. E. Billups, M. M. Haley, A. H. Maulitz, D. L. Mohler, K. P. C. Vollhardt, *Angew. Chem.* **1994**, *106*, 321; *Angew. Chem. Int. Ed. Engl.* **1994**, *33*, 313.

[14] K. P. Moder, E. N. Duesler, N. J. Leonard, *Acta Crystallogr. Sect. B* **1981**, *37*, 289.

[15] R. Boese, D. Bläser, *Angew. Chem.* **1988**, *100*, 293; *Angew. Chem. Int. Ed. Engl.* **1988**, *27*, 304.

[16] J. Spanget-Larsen, R. Gleiter, *Angew. Chem.* **1978**, *90*, 471; *Angew. Chem. Int. Ed. Engl.* **1978**, *17*, 441.

[17] B. Zipperer, K.-H. Müller, B. Gallenkamp, R. Hildebrand, M. Fletschinger, D. Burger, M. Pillat, D. Hunkler, L. Knothe, H. Fritz, H. Prinzbach, *Chem. Ber.* **1988**, *121*, 757.

[18] a) S. W. Benson, *Thermochemical Kinetics*, 2nd ed., Wiley-Interscience, New York, **1976**; b) J. M. Schulman, R. L. Disch, *J. Am. Chem. Soc.* **1993**, *115*, 11153; c) O. V. Dorofeeva, *Thermochim. Acta* **1992**, *194*, 9.

[19] R. Jeyaraman, R. W. Murray, *J. Am. Chem. Soc.* **1984**, *106*, 2462; W. Adam, R. Curci, J. O. Edwards, *Acc. Chem. Res.* **1989**, *22*, 205.

[20] a) R. Schwesinger, H. Fritz, H. Prinzbach, *Chem. Ber.* **1979**, *112*, 3318; b) E. Vogel, H.-J. Altenbach, C.-D. Sommerfeld, *Angew. Chem.* **1972**, *84*, 986; *Angew. Chem. Int. Ed. Engl.* **1972**, *11*, 939; c) M. Stöbbe, U. Behrens, G. Adiwidjaja, P. Gölitz, A. de Meijere, *ibid.* **1983**, *95*, 904 and **1983**, *22*, 867; *Angew. Chem. Suppl.* **1983**, 1221.

[21] a) J. Kammerer, G. Rihs, H. Prinzbach, *Angew. Chem.* **1990**, *102*, 1087; *Angew. Chem. Int. Ed. Engl.* **1990**, *29*, 1038; b) N. R. Easton, Jr., F. A. L. Anet, P. A. Burns, C. S. Foote, *J. Am. Chem. Soc.* **1974**, *96*, 3945.

[22] Crystal size $0.18 \times 0.22 \times 0.38$ mm^3, space group $P2_1/n$, 2θ scan range 3–45°, $a = 7.9135(9)$ Å, $b = 17.8413(23)$ Å, $c = 12.4051(16)$ Å, $\alpha = 90.0$, $\beta = 102.593(10)$, $\gamma = 90.0°$, $V = 1709.3(7)$ $Å^3$, $Z = 4$, $\rho_{calcd} = 1.35$ g cm^{-3}, $\mu = 0.8$ cm^{-1}, 2229 unique reflections collected at room temperature, of which 1670 were taken as observed [$F^2 > 3\sigma(F^2)$], $R = 0.0292$, $R_w = 0.0374$. Hydrogen atoms were assigned idealized positions, adjusted based on residual peaks in the difference Fourier map during the last cycles of refinement [23].

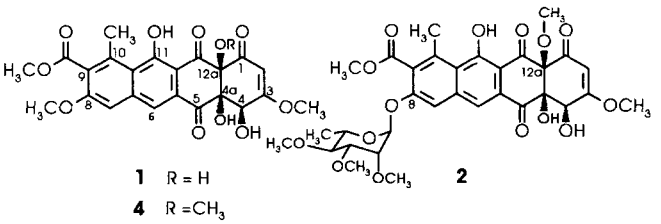
[23] Further details of the crystal structure analysis may be obtained from the Fachinformationszentrum Karlsruhe, D-76344 Eggenstein-Leopoldshafen (FRG) on quoting the depository number CSD-58663.

Biosynthetic Origin of the Oxygen Atoms of Tetracenomycin C**

György Udvarnoki, Christina Wagner, Reinhard Machinek, and Jürgen Rohr*

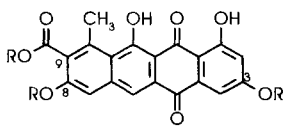
Dedicated to Professor Wolfgang Lüttke on the occasion of his 75th birthday

There is currently great interest in the details of the polyketide biosynthetic pathway, one of nature's most important routes for forming a diversity of bioactive compounds.[1] For the past few years we have focused our attention on polycyclic, aromatic polyketides,[2–4] so-called type II polyketides.[5] Recent investigations of the sources of oxygen in the metabolites have provided novel insights, for example, unexpected deoxygenation steps before aromatization during the general assembly of these polyketides.[4] The tetracenomycins (e.g. tetracenomycin C (**1**)) and elloramycins (e.g. elloramycin A (**2**)) form a small, distinct group of tetracyclic, aromatic polyketides whose biosyntheses have been extensively studied.[6–12] Nevertheless, the oxygenation reactions, the last steps of the biosynthesis of tetracenomycin C (**1**)[9–12] from its immediate precursor tetracenomycin A_2 (**3**), are not well understood and are still subjects of debate. We describe here the biosynthetic sources of all the oxygen atoms of tetracenomycin C (**1**) and, to our knowledge, the first experimental proof in biosynthetic studies of an oxygen atom deriving from H_2O.



1 R = H
4 R = CH_3

2



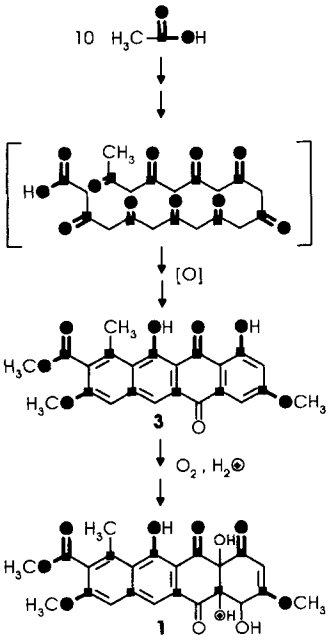
3 R = CH_3
5 R = H

In a study using an $^{18}O_2$-enriched atmosphere Rickards et al.[12] showed that only three oxygen atoms in tetracenomycin X (**4**), a close relative of **1** produced by *Nocardia mediterranea*, derive from molecular oxygen, namely O-4, O-5, and O-12a. These findings seemed to be in contradiction to the general biosynthetic pathway for the tetracenomycins outlined by Hutchinson et al.[9] (see also Scheme 1) and to the results of our studies with blocked mutants,[11] since the oxygen atom attached to C-4a did not derive from atmospheric oxygen. If this

[*] Priv.-Doz. Dr. J. Rohr, Dipl.-Ing. G. Udvarnoki, Dipl.-Chem. R. Machinek
Institut für Organische Chemie der Universität
Tammannstrasse 2, D-37077 Göttingen (Germany)
Telefax: Int. code + (551)39-9660

Dr. C. Wagner
Hans-Knöll-Institut für Naturstoff-Forschung e. V

[**] This work was supported by the Deutsche Forschungsgemeinschaft, the Bundesministerium für Forschung und Technologie, and the Fonds der Chemischen Industrie.



Scheme 1. Biosynthesis of tetracenomycin C (**1**).

oxygen atom is part of the acetate unit incorporated there, as one could assume from its position as well as from studies on related tetracycles bearing similar angular hydroxyl groups,[3, 13] then the biosynthesis of tetracenomycin C (**1**) does not proceed via aromatic intermediates such as tetracenomycin D_3 (**5**) and A_2 (**3**).[12, 14] Unfortunately, Rickards et al. did not resolve this ambiguity by carrying out additional feeding experiments, for example with ^{18}O-labeled acetate.

In a first series of experiments to find optimal incorporation conditions, we fed [1-^{13}C]acetate to a growing culture of *Streptomyces glaucescens* (strain Tü 49),[15] the producer of tetracenomycin C (**1**), and obtained sufficient incorporation rates (Table 1). The signal of the critical carbon atom C-4a, a broad singlet under standard NMR conditions, was not well enough resolved for possible detection of an ^{18}O upfield shift after labeling of 4a-OH. Systematic NMR studies with **1** finally yielded conditions under which C-4a gave rise to a sharp singlet (acetone as the solvent, $T = -30\,^{\circ}C$). After we completed the unambiguous assigment of the complete ^{13}C NMR spectrum of **1** (A in Table 1),[16] we approached the consequent feeding experiment with [1-^{13}C,$^{18}O_2$]acetate. The resulting samples of tetracenomycin C (**1**) showed ^{18}O upfield shifts of the expected magnitude for the signals of C-1, C-3, C-8, 9-C=O, 9-OCH_3, C-11, and C-12, but clearly not for C-4a (C in Table 1). Thus 4a-OH either derives from molecular oxygen, in contradiction to the earlier experiment,[12] or from water. Atmospheric oxygen has been proved to be the source for similar angular oxygen atoms in tetracyclines (tetracyclic aromatic polyketides structurally related to **1**).[17] Water has never been implicated as a source of oxygen atoms in studies on polycyclic, aromatic polyketides.

We examined this second, more attractive possibility by carrying out a fermentation of *Streptomyces glaucescens* (Tü 49) in 500 mL of $H_2{}^{18}O$ (10% ^{18}O). The resulting sample of **1**[18] showed an ^{18}O upfield shift for the signals of 3-OCH_3, C-4a, 8-OCH_3, and 9-OCH_3. The ^{18}O enrichments are about tenfold less than that obtained in the experiment with [1-^{13}C,$^{18}O_2$]acetate because of the tenfold lower ^{18}O enrichment of the labeled precursor (D in Table 1). The upfield shifts observed for the signals of the OCH_3 groups are surprising on first glance, but can be explained by partial ^{18}O exchange at the stage of the biosynthetic building blocks (acetate) and/or intermediates (e.g. tetracenomycin D_3 (**3**)). Nevertheless, this ^{18}O exchange is insignificant: the shifts are observable only for the signals of OCH_3 groups, which are much more intensive in the ^{13}C NMR spectrum than those of quarternary carbons. The oxygen atom linked at the quarternary C-4a, however, seems to stem directly from the ^{18}O-labeled water, because ^{18}O exchange is unlikely at this position. The ^{18}O enrichment of 4a-OH resulting from the experiment with the labeled water is by far the highest (D in Table 1).

Table 1. A: ^{13}C NMR data for tetracenomycin C (**1**); δ values relative to TMS in [D_6]acetone, −30 °C, 125.7 MHz, multiplicities from APT (*a*ttached *p*roton *t*est) and C,H-COSY experiments [a]. B: Specific incorporation rates [b] from the feeding experiment with [1-^{13}C]acetate. C: Upfield shifts ($\Delta\delta$ ^{13}C-^{18}O) in **1** obtained by feeding [1-^{13}C,$^{18}O_2$]acetate. D: Upfield shifts (ΔS ^{13}C-^{18}O) in **1** obtained from the fermentation in $H_2{}^{18}O$ (^{18}O enrichments in % [c]).

	A	B	C	D
C-1	190.8 s	10.5	0.05 (53)	–
C-2	99.7 d	–	–	–
C-3	175.3 s	8.5	0.02 (54)	–
3-OCH_3	57.2 q	–	–	0.02 (8)
C-4	70.3 d	–	–	–
C-4a	85.2 s	11.3	–	0.02 (15)
C-5	194.1 s	–	–	–
C-5a	141.2 s	5.5	–	–
C-6	120.7 d	–	–	–
C-6a	129.0 s	5.7	–	–
C-7	108.4 d	–	–	–
C-8	158.3 s	7.5	0.02 (53)	–
8-OCH_3	56.6 q	–	–	0.02 (8)
C-9	129.6 s	–	–	–
9-*C*=O	168.0 s	11.8	0.04 (32)	–
9-OCH_3	52.8q	–	0.01 (25)	0.02 (5)
C-10	137.9 s	5.2	–	–
10-CH_3	21.1 q	–	–	–
C-10a	121.0s	–	–	–
C-11	167.5 s	6.3	0.01 (47)	–
C-11a	109.8 s	–	–	–
C-12	197.9s	10.1	0.04 (50)	–
C-12a	83.6 s	–	–	–

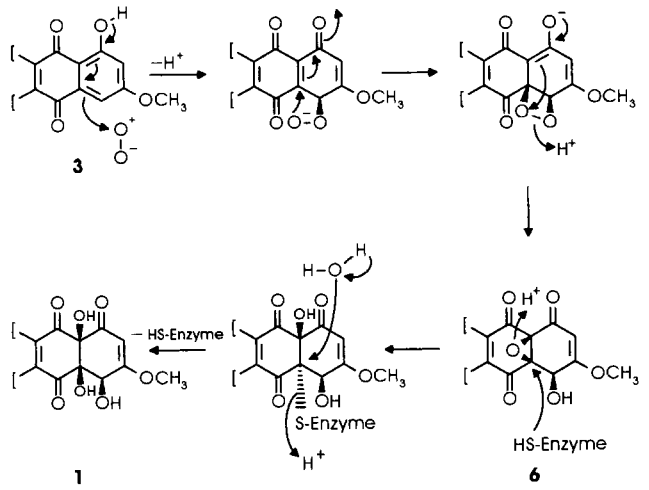
[a] The ^{13}C signals were further assigned through long-range C,H couplings (COLOC, HMBC) [25]. [b] Incorporation rates (± 1%) calculated according to Townsend, Scott, et al. [26]. [c] ^{18}O Enrichment = $[(I_{^{13}C-{}^{18}O}/I_{^{13}C-{}^{16}O} + I_{^{13}C-{}^{18}O})] \times 100\%$.

The findings described here (Scheme 1) are in agreement with all the results from earlier biosynthetic investigations on the tetracenomycins.[8–12] The studies were also aimed at comparing oxygenation steps in the biosynthesis of the tetracenomycins with those leading to other tetracyclic decaketides such as angucyclines and anthracyclines. Tetracenomycin C (**1**) is the first example among the polycyclic, aromatic polyketides requiring a molecule of H_2O to obtain its oxygen pattern. Thus, a novel enzymatic feature is implied, which is interesting for approaches to hybrid antibiotics through combination of the biosynthetic genes of the tetracenomycin producer *S. glaucescens* with related polyketide synthases of other producers of polycyclic, aromatic polyketides.[19, 20] For the oxygenation in the biosynthetic conversion of **3** into **1**, an epoxide intermediate such as **6** (Scheme 2) has to be assumed. It is unclear whether **6** is formed by two monooxygenases or only one dioxygenase; the latter possibility is in agreement with the suggested mechanisms found in oxygenation studies of aromatic compounds,[21a] as well as those proposed for the mode of action of vitamin K.[9c, 21b–e] This epoxide intermediate, however, would require an interesting, enzymatically controlled, but chemically unlikely "*cis* opening" to generate the stereocenters found in **1**.[6] Alternatively, the overall *cis* opening of the epoxide may result from an initial attack of an enzyme-bound SH group, which is then replaced by water in a S_N2-type reaction (Scheme 2).[22]

Experimental Procedure

Cultivation of the microorganism: *Streptomyces glaucescens* (Tü 49) was cultivated on slants (20% agar-agar, 10% malt extract, 4% glucose, 4% yeast extract, pH 7.0, adjusted before autoclaving) at 28 °C until sporulation occurred, then stored at 4 °C. The culture for the fermentations was innoculated directly from the slants and

 © VCH Verlagsgesellschaft mbH, D-69451 Weinheim, 1995 0570-0833/95/0505-0566 $ 10.00+.25/0



Scheme 2. Details of the oxygenation in the biosynthetic conversion of **3** into **1**.

shaken on a rotary shaker (type Multitron, Infors AG, Switzerland) in ten 250 mL, triply baffled Erlenmeyer flasks, each filled with 100 mL of R2YENG medium [23] for 96 h at 30 °C and 250 rpm.

Isolation of tetracenomycin C (**1**): The combined cultures were treated with 300 mL of MeOH and celite and filtered. The combined culture filtrates were extracted with 1 L of ethyl acetate and the extract concentrated to dryness. The residue was dissolved in MeOH and chromatographed on a Sephadex LH 20 column (2.5 × 100 cm, MeOH). Yield ca. 20 mg of **1**.

Feeding experiments with labeled precursors: a) Feeding of sodium [1-^{13}C]acetate: The labeled substrate (750 g L^{-1} culture) was dissolved in 75 mL of sterile water and neutralized with 0.1 M HCl. One-sixth (12.5 mL) of this solution was distributed every eight hours (36 h to 76 h after inoculation) among ten Erlenmeyer flasks each containing 100 mL of the growing culture of *S. glaucescens* Tü 49. b) Feeding of [1-^{13}C,$^{18}O_2$]acetate (1 g L^{-1}): As in a); to avoid ^{18}O exchange with the solvent, the labeled material was added in portions (6 × 166 mg); each portion was dissolved in 10 mL of sterile water directly before the feeding and neutralized immediately with 5 N NaOH. c) Feeding of $H_2{}^{18}O$: The cultivation (500 mL culture) was carried out as above using $H_2{}^{18}O$ (10% ^{18}O) for the preparation of the medium and as the cultivation solvent.

Labeled compounds: [1-^{13}C]Acetate (99% ^{13}C) was obtained from Cambridge Isotope Laboratories (Cambridge, MA, USA) and $H_2{}^{18}O$ (97.9% ^{18}O, 10% ^{18}O) from Isotec Inc. (Miamisburg, OH, USA). [1-^{13}C,$^{18}O_2$]Acetate was synthesized from [1-^{13}C]acetate and $H_2{}^{18}O$ (97% ^{18}O) [24].

Received: September 22, 1994 [Z 7342 IE]
German version: *Angew. Chem.* **1995**, *107*, 643

Keywords: biosynthesis · natural products · tetracenomycin C

[1] D. E. Cane, *Science* **1994**, *263*, 338–340, and references therein; D. O'Hagan, *The Polyketide Metabolites*, 1st ed. Horwood, Chichester, **1991**.
[2] J. Rohr, *J. Org. Chem.* **1992**, *57*, 5217–5223; J. Rohr, M. Schönewolf, G. Udvarnoki, K. Eckhardt, G. Schumann, C. Wagner, J. M. Beale, S. D. Sorey, *ibid.* **1993**, *58*, 2547–2551.
[3] G. Udvarnoki, T. Henkel, R. Machinek, J. Rohr, *J. Org. Chem.* **1992**, *57*, 1274–1276.
[4] H. Bockholt, G. Udvarnoki, J. Rohr, U. Mocek, J. M. Beale, H. G. Floss, *J. Org. Chem.* **1994**, *59*, 2064–2069; S. Weber, C. Zolke, J. Rohr, J. M. Beale, *ibid.* **1994**, *59*, 4211–4214, and references therein.
[5] D. A. Hopwood, D. A. Sherman, *Annu. Rev. Genet.* **1990**, *24*, 37–66.
[6] E. Egert, M. Noltemeyer, J. Siebers, J. Rohr, A. Zeeck, *J. Antibiot.* **1992**, *45*, 1190–1192, and references therein.
[7] J. Rohr, A. Zeeck, *J. Antibiot.* **1990**, *43*, 1169–1178, and references therein.
[8] B. Shen, H. Nakayama, C. R. Hutchinson, *J. Nat. Prod.* **1993**, *56*, 1288–1293.
[9] a) S. Yue, H. Motamedi, E. Wendt-Pienkowski, C. R. Hutchinson, *J. Bacteriol.* **1986**, *167*, 581–586; b) H. Motamedi, E. Wendt-Pienkowski, C. R. Hutchinson, *ibid.* **1986**, *167*, 575–580; c) H. Decker, H. Motamedi, C. R. Hutchinson, *ibid.* **1993**, *175*, 3876–3886.
[10] H. Decker, R. G. Summers, C. R. Hutchinson, *J. Antibiot.* **1994**, *47*, 54–63, and references therein.
[11] J. Rohr, S. Eick, A. Zeeck, P. Reuschenbach, H. Zähner, H. P. Fiedler, *J. Antibiot.* **1988**, *41*, 1066–1073.
[12] M. G. Anderson, C. L.-Y. Khoo, R. W. Rickards, *J. Antibiot.* **1989**, *42*, 640–643.
[13] A. E. de Jesus, W. E. Hull, P. S. Steyn, F. R. van Heerden, R. Vleggaar, *J. Chem. Soc. Chem. Commun.* **1982**, 902–904.
[14] These studies were based on sometimes ambiguous cosynthesis experiments with various blocked mutants of the tetracenomycin producer.
[15] We wish to thank Prof. Dr. H. Zähner, University of Tübingen, Germany, for providing us with the tetracenomycin producer *Streptomyces glaucescens* (strain Tü 49).
[16] A combination of homo- and heteronuclear (correlation) experiments (^{1}H NMR; ^{13}C NMR; C,H-COSY; COLOC [25a] = *co*rrelation spectroscopy via *lo*ng-range *co*uplings; HMBC [25b] = *h*etero *m*ultiple *b*ond *c*onnectivity spectroscopy) on **1** and its derivatives gave unambiguous results; earlier ^{13}C NMR assignments [6,7] are in part incorrect.
[17] L. A. Mitscher, J. K. Swayze, T. Högberg, I. Khanna, G. S. Raghav Rao, *J. Antibiot.* **1983**, *36*, 1405–1407; R. Thomas, D. J. Williams, *J. Chem. Soc. Chem. Commun.* **1985**, 802–803.
[18] Since the homogeneity of the magnetic field used in the NMR experiments was stable for only 1 h at −30 °C, five 1 h experiments were added to obtain a better signal-to-noise relationship.
[19] We are currently examining this in cooperation with Dr. H. Decker, University of Tübingen, Germany.
[20] a) L. Katz, S. Donadio, *Annu. Rev. Microbiol.* **1993**, *47*, 875–912, and references therein; b) R. McDaniel, S. Ebert-Khosla, D. A. Hopwood, C. Khosla, *Science* **1993**, *262*, 1546–1550; c) R. McDaniel, S. Ebert-Khosla, D. A. Hopwood, C. Khosla, *J. Am. Chem. Soc.* **1993**, *115*, 11671–11675; d) H. Fu, S. Ebert-Khosla, D. A. Hopwood, C. Khosla, *ibid.* **1994**, *116*, 4166–4170.
[21] a) H. Greenland, J. T. Pinhey, S. Sternhell, *Aust. J. Chem.* **1987**, *40*, 325–331; b) S. W. Ham, P. Dowd, *J. Am. Chem. Soc.* **1990**, *112*, 1660–1661; c) P. Dowd, S. W. Ham, S. J. Geib, *ibid.* **1991**, *113*, 7734–7743; d) P. Dowd, S. W. Ham, R. Hershline, *ibid.* **1992**, *114*, 7613–7617; e) P. Dowd, S. W. Ham, *J. Org. Chem.* **1992**, *57*, 3514–3516.
[22] a) R. B. Silverman, *J. Am. Chem. Soc.* **1981**, *103*, 5939–5941; b) P. C. Preusch, J. W. Suttie, *J. Org. Chem.* **1983**, *48*, 3301–3305.
[23] G. Hintermann, R. Crameri, M. Vogtli, R. Hütter, MGG *Mol. Gen. Genet.* **1984**, *196*, 513–520.
[24] P. D. Boyer, O. J. Koeppe, W. W. Luchsinger, *J. Am. Chem. Soc.* **1956**, *78*, 356–357.
[25] a) H. Kessler, C. Griesinger, J. Zarbock, H. R. Loosli, *J. Magn. Reson.* **1984**, *57*, 331–336; b) A. Bax, M. F. Summers, *J. Am. Chem. Soc.* **1986**, *108*, 2093–2094.
[26] A. I. Scott, C. A. Townsend, K. Okada, M. Kajiware, R. J. Cushley, P. J. Whitman, *J. Am. Chem. Soc.* **1974**, *96*, 8069–8080.

$ATh_{12}N_6X_{29}$ (A = Li... Rb; X = Cl, Br): A New Type of Thorium Cluster with a $Th_{12}N_6$ Core

Thomas P. Braun, Arndt Simon,* Fred Böttcher, and Fumio Ueno

The reduced halides of the rare earth elements exhibit a rich chemistry, in which discrete or condensed metal clusters play a major role.[1, 2] Primarily the 5d electrons are involved in metal–metal bonds in the clusters; the 4f electrons are much lower in energy. The possible participation of f electrons in the formation of metal–metal bonds is still in question. One prerequisite for this is significantly higher energies, as found in the 5f metals. We therefore started experiments to prepare reduced thorium halides as a "window towards the actinoids". Like the related element zirconium, thorium forms cluster compounds[3–5] if interstitial heteroatoms are allowed for stabilization. We have already reported on thorium cluster compounds with an octahedral Th_6Br_{15} unit,[6, 7] and we now describe compounds with the new cluster framework $Th_{12}Br_{29}$.

[*] Prof. Dr. A. Simon, Dr. T. P. Braun, Dr. F. Böttcher, Dr. F. Ueno
Max-Planck-Institut für Festkörperforschung
Heisenbergstrasse 1, D-70569 Stuttgart (Germany)
Telefax: Int. code + (711) 689-1642

 © VCH Verlagsgesellschaft mbH, D-69451 Weinheim, 1995 0570-0833/95/0505-0567 $ 10.00+.25/0

The phase $ATh_{12}N_6Br_{29}$ (A = Li... Rb) was first found for A = Li. However, complete structural characterization of the compound was not possible. The lithium atoms could not be localized by either X-ray crystallographic methods or by neutron diffraction on samples prepared with ^7Li. Later we found that these phases are also accessible with the heavier alkali metals sodium through rubidium as the A element. Even though these atoms could not be localized with X-ray methods either, they were essential in the preparations (introduced as bromides, azides, and also in elemental form). The presence of nitrogen was secured for single, selected crystals by using Nessler's reagent.[8] Whether nitrogen in these compounds can be replaced by neighboring elements was answered experimentally. Traces of oxygen (almost unavoidable) always lead to the formation of $ThOBr_2$ needles with an orange-red tinge caused by an excess of thorium. Apparently all of the oxygen present in the system is gettered by the formation of this compound. Use of carbon instead of nitrogen inhibits the formation of the cluster compound. These phases are also not formed when NH_4Br or ThH_2 are used as hydrogen sources, or when the reaction mixture is annealed in a H_2 atmosphere.

As the alkali metal atoms could not be localized in the bromides, we tried to prepare the chloride analogues with potassium and rubidium as the alkali metal. The desired compounds can indeed by synthesized, and the inclusion of the alkali metal atoms could be established by an X-ray structure analysis on a single crystal of $RbTh_{12}N_6Cl_{29}$.[9] Although the chlorides and the bromides belong to different crystal systems ($ATh_{12}N_6Cl_{29}$ are triclinic and $ATh_{12}N_6Br_{29}$ are orthorhombic), they are based on the same cluster units $Th_{12}N_6X_{41}$. The distances within the $Th_{12}N_6$ unit are also almost identical in both systems. Cyclic condensation of six nitrogen-centered thorium tetrahedra through common *cis* edges (i.e. every three tetrahedra share a common vertex) leads to formation of the new star-shaped cluster unit (Fig. 1). The thorium–thorium distances along the shared edges are shortened to 360 pm (as in thorium metal). As a consequence of the cyclic condensation, an octahedral void (compressed along the threefold axis) is formed inside the polyhedron. The $Th_{12}N_6$ unit is surrounded by a total of 41 halogen atoms divided into four groups:

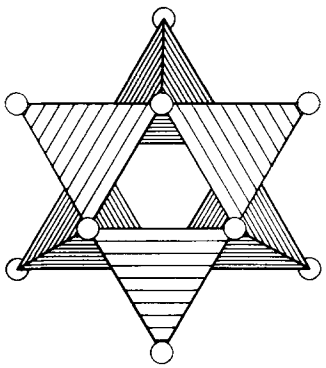


Fig. 1. Structure of the metal core of the $[Th_{12}N_6X_{41}]$ cluster: six nitrogen-centered thorium tetrahedra are joined though common *cis* edges.

1. One halogen atom is on either side of the basal plane of the central trigonal antiprism.
2. Another twelve halogen atoms surround these first halogen atoms in a close-packed fashion in the same planes.
3. A total of 18 halogen atoms are bound tripod-like in sets of three to the six peripheral thorium atoms.
4. The "waist" of the cluster contains nine additional halogen atoms, of which all nine are disordered in the case of the bromides, and three in the case of the chlorides.

Both the orthorhombic and the triclinic structure variant can formally be described by the connectivity scheme $ATh_{12}N_6X^i_{19}X^{i-a}_{4/2}X^{a-a}_{8/2}X^{a-a}_{6/3}X^{a-i}_{4/2}$. Following the treatment of octahedral cluster units by Schäfer and Schnering,[10] the outward singly bonded halogen atoms in the "tripod" positions are denoted as a, and all other halogen atoms bound to more than one thorium atom inside the cluster as i. With this formulation the two structure variants are differentiated only in the particular choice of the X^i positions used for the asymmetric $X^{i-a}_{4/2}$ link. The formation of the two structure variants in the solid can thus be attributed to subtle local variations in connectivity.

The arrangement of the metal and halogen atoms represents a section from the ZrCl-type structure.[11] If the interstitial nitrogen atoms in the tetrahedral voids are also considered, the arrangement is a section of the TbXH structure type.[12]

If we regard just the arrangement of the metal atoms, the new cluster type may be interpreted as a substitution variant of the octahedral M_6X_8 cluster type, in which some of the halogen atoms above the octahedral faces are replaced by additional metal atoms. Up to now only cluster compounds with one[13] or two faces[14–18] of more or less distorted octahedra capped by additional metal atoms were known. In comparison, six of these faces are capped in the star-shaped Th_{12} units.

If chemical bonds are considered in the simplest, purely ionic terms (i.e. $A^+(Th^{4+})_{12}(N^{3-})_6X^-_{29}$), two electrons (1 + 48 − 18 − 29 = 2) per cluster unit remain for occupying metal–metal bonding orbitals. According to Extended Hückel calculations[19] on the molecular unit $[Th_{12}N_6Cl_{41}]^{13-}$, the energetically distinct HOMO has symmetry class a_{1g} in the idealized point group $\bar{3}m$ (D_{3d}). Only the six inner thorium atoms contribute to this orbital with their 6d orbitals (Fig. 2). This six-center, two-electron bond stabilizes the entire cluster unit. The homonuclear bonds are thus confined to the central octahedron, whereas the nitrogen-centered tetrahedra best fit an ionic description. If one includes the Th 5f orbitals in the calculations, significant contribution of these orbitals to the metal–metal bonding HOMO results (at least on that level of the calculation). Hence these compounds are only obtained when the incorporation of the alkali metal atom provides an additional electron for the metal–metal bond. The structure analysis of $RbTh_{12}N_6Cl_{29}$ impressively demonstrates the inclusion of exactly one alkali metal atom. Even though the alkali metal atom is disordered over two positions, these positions can be localized easily. The occupation factors can be refined independently, and add up to a value of $x = 1.08(8)$ based on the formula unit $Rb_xTh_{12}N_6Cl_{29}$. In the final refinement these occupation factors were therefore constrained and refined together. The observed diamagnetism shows that these compounds are stoichiometric without a noticeable range homogeneity.

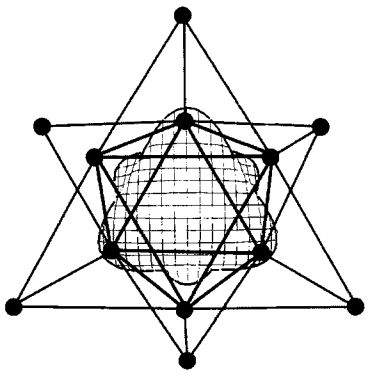


Fig. 2. Representation (ref. [20]) of the HOMO (a_{1g}) of the $[Th_{12}N_6X_{41}]$ cluster.

Experimental Procedure

The following preparation of $RbTh_{12}N_6Cl_{29}$ is representative for those of the other compounds: A Ta capsule containing 37.7 mg of Th (turnings), 700.1 mg of $ThBr_4$, 306.1 mg of Th_3N_4, and 30 mg of RbCl was sealed, protected from oxidation in a quartz ampule, annealed for 3 d at 680 °C, and then quenched. The samples obtained were single phase by X-ray crystallography (Guinier-Simon technique).

Received: October 8, 1994 [Z 7386IE]
German version: *Angew. Chem.* **1995**, *107*, 647

Keywords: clusters · solid-state chemistry · thorium compounds

[1] A. Simon, H. Mattausch, G. Miller, W. Bauhofer, R. K. Kremer in *Handbook On The Chemistry And Physics Of Rare Earth Elements - Structure, Bonding and Properties, Vol. 100*, (Ed.: K. A. J. Gschneidner, L. Eyring), North-Holland, Amsterdam, **1991**, p. 191.

[2] A. Simon, *Mater. Chem. Phys.* **1991**, *29*, 143.

[3] T. Hughbanks, G. Rosenthal, J. D. Corbett, *J. Am. Chem. Soc.* **1986**, *108*, 8289.

[4] R. P. Ziebarth, J. D. Corbett, *J. Less-Common Met.* **1988**, *137*, 21.

[5] J. Zhang, J. D. Corbett, *Inorg. Chem.* **1993**, *32*, 1566.

[6] A. Simon, F. Böttcher, J. K. Cockcroft, *Angew. Chem.* **1991**, *103*, 79; *Angew. Chem. Int. Ed. Engl.* **1991**, *30*, 101.

[7] F. Böttcher, A. Simon, R. K. Kremer, H. Buchkremer-Hermanns, J. K. Cockcroft, *Z. Anorg. Allg. Chem.* **1991**, *598/599*, 25.

[8] The sample was hydrolyzed, and the ammonia formed was precipitated with $Hg_2(NO_3)_2$ as $[HgNH_2]NO_3$.

[9] a) $RbTh_{12}N_6Cl_{29}$: space group $P\bar{1}$ (no. 2), $Z=1$; $P2_1$ diffractometer, $Mo_{K\alpha}$ radiation, $\lambda=71.073$ pm; $a=1071.95(10)$, $b=1198.44(11)$, $c=1210.12(11)$ pm, $\alpha=112.676(7)$, $\beta=102.443(7)$, $\gamma=104.952(7)°$; 4597 reflections, 4595 unique, 3899 with $F_0 \geq 3\sigma(F_0)$; $R=0.0416$, $R_w=0.0420$, $\rho_{calcd}=5.1\ g\,cm^{-3}$; b) $KTh_{12}N_6Br_{29}$: space group *Pnnm* (no. 58), $Z=2$; $P2_1$ diffractometer, $Mo_{K\alpha}$ radiation, $\lambda=71.073$ pm; $a=1752.4(4)$, $b=1194.3(2)$, $c=1403.1(3)$ pm; 9720 reflections, 2418 unique, 2172 with $F_0 \geq 3\sigma(F_0)$; $R=0.0589$. $R_w=0.0445$, $\rho_{calcd}=5.909\ g\,cm^{-3}$. Further details of the crystal structure investigation may be obtained from the Fachinformationszentrum Karlsruhe, D-76344 Eggenstein-Leopoldshafen (FRG), on quoting the depository number CSD-58681.

[10] H. Schäfer, H. G. Schnering, *Angew. Chem.* **1964**, *76*, 833.

[11] A. Cisar, J. D. Corbett, R. L. Daake, *Inorg. Chem.* **1979**, *18*, 836.

[12] F. Ueno, K. Ziebeck, H. Mattausch, A. Simon, *Rev. Chim. Miner.* **1984**, *21*, 804.

[13] C. E. Housecroft, A. L. Rheingold, X. Song, *Inorg. Chem.* **1992**, *31*, 4023.

[14] H. Leligny, M. Ledessert, T. Labbé, B. Raveau, W. H. McCarroll, *J. Solid State Chem.* **1990**, *87*, 35.

[15] P. F. Jackson, B. F. G. Johnson, J. Lewis, P. R. Raithby, *J. Chem. Soc. Chem. Commun.* **1980**, 60.

[16] M. Mc Partlin, D. M. P. Mingos, *Polyhedron* **1984**, *3*, 1321.

[17] P. Ciani, G. D'Alfonso, M. Freni, P. Romiti, A. Sironi, *J. Chem. Soc. Chem. Commun.* **1982**, 705.

[18] P. Gall, L. Toupet, P. Gongeon, *Acta Crystallogr. Sect. C* **1993**, *49*, 1580.

[19] M. H. Whangbo, M. Evain, T. Hughbanks, M. Kertesz, S. Wijeyesekera, C. Wilker, C. Zheng, R. Hoffmann: Programm EHMACC, QCPE 571 (1977). Parameters from J. P. Desclaux, *At. Data Nucl. Data Tables* **1973**, *12*, 311. (H_{ii} [eV], ζ_1, c_1, ζ_2, c_2): N(2s): −26.22, 1.885; N(2p): −13.84, 1.728; Cl(3s): −29.2, 2.25; Cl(3p): −13.8, 1.9; Th(7s): −5.31, 1.834; Th(6p): −27.75, 3.55; Th(6d): −10.048, 2.462, 0.76, 1.167, 0.408; Th(5f): −9.291, 4.48, 0.7677, 1.84, 0.4269.

[20] C. Mealli, D. Proserpio, *J. Chem. Educ.* **1990**, *67*, 399.

Polymers with Complexed Cyclobutadiene Units in the Main Chain: The First Example of a Thermotropic, Liquid Crystalline Organometallic Polymer**

Markus Altmann and Uwe H. F. Bunz*

Low molecular weight metallomesogens[1] were discovered some time ago and are now a topic of thorough investigation because of their optical and electronic properties.[2] In contrast, liquid crystalline, organometallic polymers have hardly been described. Among the few examples are the palladium/platinum alkyne polymers of Hagihara et al.[3] that have been known for several years and the more recent tricarbonylchromium-complexed polyaramides synthesized by Dembek et al.[4] In both cases the occurrence of lyotropic liquid crystalline phases is attributable to the rigid molecular structure (rigid rods) and thus to the shape anisotropism.[5]

In contrast to the conformationally flexible or bent diethynylated sandwich or half-sandwich complexes[6] the structure of the 1,3-diethynylcyclobutadiene metal complexes should make them suitable monomers for the construction of linear, stiff, organometallic polymers. Although in 1,3-diethynylcyclobutadiene(cyclopentadienyl)cobalt (**1**) a potential cyclobutadiene monomer is accessible on a gram scale,[7] no polymers with cyclobutadiene units in the main chain are yet known. In a preliminary experiment **1a** (R^1 = H) was stirred for 18 h with 1.0 equivalent of 1,4-dihexyl-2,5-diiodobenzene, 5 mol% of $[PdCl_2(PPh_3)_2]$, and CuI in diisopropylamine at room temperature.[8] Gel permeation chromatography (GPC) of the crude mixture, however, showed that a wide range of only low molecular weight products had been formed. On use of piperidine as base under otherwise identical conditions,[9] a yellow amorphous powder was obtained in 75% yield (see Table 1) after repeated precipitation of the dark reaction mixture into methanol and into pentane (see Experimental).

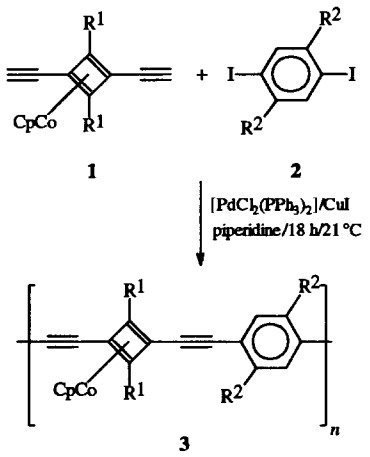


Table 1. Substitution patterns, yield, molecular weights, and average degree of polymerization $\bar{P}$ of the polymers **3a–e** after precipitation from methanol.

3	R^1	R^2	Yield [%]	M_n [10^3 gmol^{-1}]	M_w [10^3 gmol^{-1}]	$\bar{P}$
a	H	hexyl	75	3.66	19.4	18
b	$SiMe_3$	H	86	4.31	7.41	18
c	H	dodecyl	79	23.6	65.0	58
d	$SiMe_3$	hexyl	74	5.13	13.1	18
e	$SiMe_3$	dodecyl	79	4.91	20.1	12

Analytical GPC (chloroform) yielded a polydispersity of $M_w/M_n = 5.3$ (polystyrene as standard) for polymer **3a**; an M_n of 3660 gmol^{-1} was obtained. The ^{1}H NMR spectrum showed the expected resonances: Weak signals of end groups appear in the aromatic range at $\delta = 7.33$ and 7.64. The signal assigned to the ethynyl groups of the monomer has completely disappeared.

The polymers **3b** and **d** were prepared and purified in the same way as **3a** (for the synthesis of **3c** and **e**, see Experimental Procedure). The polymer **3c** has by far the highest molecular weight. After precipitation once from methanol and once from pentane, all the polymers form an intensely yellow amorphous powder, but take on an increasingly reddish tinge from **3a** through **3b** to **3d**. All polycondensates form strong, flexible and transparent films from solution. The physical data of **3a–e** are given in Table 2.

Rapid concentration of the solutions of **3a–e** in dichloromethane provides clear yellow films, which appear isotropic

[*] Dr. U. H. F. Bunz, M. Altmann
Max-Planck Institut für Polymerforschung
D-55021 Mainz (Germany)
Telefax: Int. code + (6131)379-100

[**] This work was supported by the BASF AG (gifts of chemicals) and the Volkswagen-Stiftung. U. H. F. B. thanks the Fonds der Chemischen Industrie for a Liebig Scholarship (1992–1994) and Prof. Dr. K. Müllen (Mainz) for support. We thank Dr. V. Enkelmann for discussions and Dr. B. Mohr for recording the powder diffractograms.

Table 2. Physical data of **3a–e** [a].

3a: IR (KBr): $\tilde{\nu}$[cm^{-1}] = 3105, 2955, 2925, 2856, 2190; ^{1}H NMR ($CDCl_3$): δ = 0.93 (t, ^3J(H,H) = 3.0 Hz), 1.36 (br. s), 1.61 (br. s), 2.64 (br. s), 4.66 (s), 5.06 (s), 7.18 (s); ^{13}C NMR (CD_2Cl_2): δ = 19.02 (q), 23.14, 29.63, 31.04, 32.11, 34.43, (5 t), 55.85 (d), 64.62 (s), 81.67 (d), 89.33, 91.50 (2 s), 128.32, 142.21 (2 s), 132.14 (d).

3b: IR (KBr): $\tilde{\nu}$[cm^{-1}] = 3104, 2953, 2923, 2853, 2188; ^{1}H NMR (CD_2Cl_2): δ = 0.88 (br. s), 1.29 (br. s), 1.55 (br. s), 2.65 (br. s), 4.67 (s), 5.06 (s 22.95, 142.20 (2), 7.17 (s); ^{13}C NMR (CD_2Cl_2): δ = 15.71 (q), 24.52, 31.19, 31.38, 31.50, 31.54, 32.48, 33.76, 35.82 (8 d), 55.78 (d), 64.61 (s), 81.58 (d), 89.29, 91.45 (2 s), 122.95, 142.20 (2 s), 132.05 (d).

3c: IR (KBr): $\tilde{\nu}$[cm^{-1}] = 3015, 2962, 2898, 2192, 2127; ^{1}H NMR (CD_2Cl_2): δ = 0.37 (s), 4.97 (s), 7.27 (s), 7.11, 7.64 (2 d, ^3J(H,H) = 8.5 Hz (terminal group)); ^{13}C NMR (CD_2Cl_2): δ = −0.31 (q), 65.39, 76.08 (2 s), 77.11, 91.08 (2s), 81.68 (d), 123.66 (s), 130.94 (d).

3d: IR (KBr): $\tilde{\nu}$[cm^{-1}] = 3105, 2956, 2927, 2869, 2190, 2132; ^{1}H NMR (CD_2Cl_2): δ = 0.39 (s), 0.92 (br. s), 1.35 (br. s), 1.60 (br. s), 2.67 (br. s), 5.00 (s), 7.14 (s); ^{13}C NMR (CD_2Cl_2): δ = 0.04 (q), 14.64 (q), 23.47, 29.87, 31.29, 32.63, 34.66 (5 t), 66.24, 76.28 (2 s), 81.96 (d), 90.84, 93.93 (2 s), 123.61, 141.83 (2 s), 132.53 (d).

3e: IR (KBr): $\tilde{\nu}$[cm^{-1}] = 3105, 2955, 2925, 2845, 2190, 2128; ^{1}H NMR (CD_2Cl_2): δ = 0.38 (s), 0.89 (t, ^3J(H,H) = 6 Hz), 1.29 (br. s), 1.61 (br. s), 2.66 (br. s), 4.99 (s, 5H;), 7.14 (s, 2H;), 14.63 (q, 2C), 23.45, 30.12, 30.26, 30.46, 31.53, 32.70, 34.69 (7 d), 66.25, 76.26 (2 s), 81.96 (5 d), 90.86, 93.92 (2 s), 123.63, 141.84 (2 s), 132.53 (d).

[a] The ^{13}C and ^{1}H NMR spectra were recorded at 200 and 500 MHz, respectively.

(black) under crossed polarizers and display no birefringence. If, however, the films are obtained by slow evaporation of the solvent (dichloromethane or -ethane), *schlieren* textures and/or Maltese crosses are observed under crossed polarizers; that is, **3a–e** form lyotropic liquid crystalline phases. Only in the case of **3c** was an isotropic film formed exclusively, and no lyotropic phase was detected. The *schlieren* textures and Maltese crosses of **3a**, **b**, **d**, and **e** do not disappear when the solvent has evaporated. This is a consequence of the restricted mobility of the polymer after removal of the solvent, which probably indicates that the polymer has a frozen liquid crystalline structure.

Thermogravimetric studies on **3d** as representative polymer showed that decomposition begins at about 250 °C and reaches a maximum at 450 °C. An investigation of the phase behavior of **3d** by differential thermal analysis revealed that in the first heating curve an endothermic monotropic phase transition (0.42 kcal mol^{-1}) occurs at about 115 °C, and at 155 °C a structural change was observed. In the cooling curve and in a second heating curve, transitions could no longer be observed. On heating a thin isotropic film obtained by evaporating a solution of **3d** in dichloromethane under the polarizing microscope (in a pure nitrogen atmosphere) to 160 °C, *schlieren* patterns (Fig. 1) were observed within a few minutes.[10] These showed no change whatever up to 250 °C and did not disappear on cooling. Liquid crystalline **3d** could, however, not be converted into the isotropic melt, because at about 300 °C the sample started to decompose, accompanied by considerable darkening. Differential thermal analysis of **3e** gave only two endothermic transitions at 55 and 80 °C, which are probably caused by melting of the side chains; for **3e** a mesophase was not found on heating to above 250 °C.

To understand the phase behavior of **3d** better, we performed X-ray diffraction experiments. The initially precipitated polymer is almost X-ray amorphous. A diffractogram recorded at 180 °C supports the disappearance of all *crystalline* order. In a sample of **3d** prepared by slow evaporation of a solution in dichloromethane, the polymer is (partially) crystalline.[11] If this material is heated to 180 °C and studied by diffractometry, the X-ray reflections also disappear to a large extent. This behavior is consistent with the occurrence of a nematic liquid crystal,

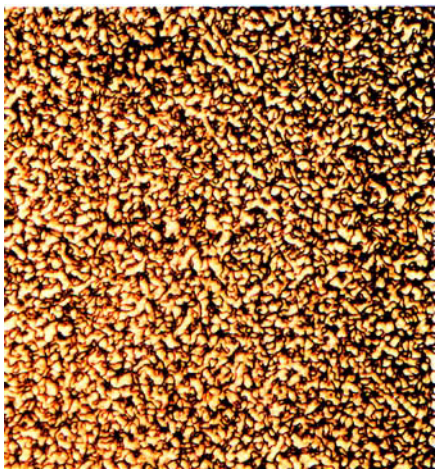


Fig. 1. Schlieren textures of **3d** in a film at 165 °C.

because the anticipated "nematic streak" is not always observable.[12]

We interpret the thermal behavior of **3d** in terms of melting of the side chains for the phase transition at 115 °C. The mobility of the main chain at this point does not appear large enough for the transition from the nonordered isotropic (or crystalline) phase to a liquid crystalline phase to take place. Only at about 160 °C, when the exothermic second phase transition takes place, does a pronounced *schlieren* texture form (Fig. 1).

Experimental Procedure

1 (0.60–1.0 mmol) was placed in a Schlenk tube with an equimolar amount of **2**, $[PdCl_2(PPh_3)_2]$ (5 mol%), and CuI. Under an inert atmosphere (N_2) dried piperidine (50 mL) was added. The initially clear yellow solution was stirred for 18 h at 21 °C, during which ammonium salts precipitated with concomitant darkening and increased viscosity. The mixture was worked up by filtering off the salts, removing the piperidine under reduced pressure, and dissolving the residue in chloroform. Methanol was then added till the polymer (yellow flakes) precipitated. By centrifugation and renewed dissolution and precipitation with pentane the polymers **3a**, **b**, and **d** can be isolated in pure state. Attempts to precipitate **3e** from pentane were unsuccessful. Instead **3e** was freed from low molecular impurities (M < 1000 g mol^{-1}) by GPC (chloroform). In the case of **3c** the precipitation from methanol yielded an insoluble product, and as for **3e** the purification had to be carried out by GPC (products with M < 1000 g mol^{-1} were discarded). The study of the phase transitions as well as the NMR spectroscopy was performed on the doubly precipitated polymers (**3a**, **b**, **d**).

Received: June 9, 1994
Revised: October 6, 1993 [Z 7020 IE]
German version: *Angew. Chem.* **1995**, *107*, 603

Keywords: cobalt compounds · complexes with cyclobutadiene · liquid crystalline polymers · organometallic polymers

[1] Review: S. A. Hudson, P. M. Maitlis, *Chem. Rev.* **1993**, *93*, 861; A.-M. Giroud-Godquin, P. Maitlis, *Angew. Chem.* **1991**, *103*, 370; *Angew. Chem. Int. Ed. Engl.* **1991**, *30*, 375.

[2] D. W. Bruce, X.-H. Liu, *J. Chem. Soc. Chem. Commun.* **1994**, 729; A. Werner, W. Friedrichsen, *ibid.* **1994**, 365; D. W. Bruce, *J. Chem. Soc. Dalton Trans.* **1993**, 2983; D. W. Bruce in *Inorganic Materials* (Eds.: D. W. Bruce, D. O'Hare), Wiley, Chichester, **1992**; P. Espinet, J. L. Serrano, L. A. Oro, M. A. Esteruelas, *Coord. Chem. Rev.* **1992**, *117*, 215.

[3] N. Hagihara, K. Sonoshigara, S. Takahashi, *Adv. Polym. Sci.* **1981**, *41*, 149, and references therein; S. J. Davies, B. F. G. Johnson, M. S. Kahn, J. Lewis, *J. Chem. Soc. Chem. Commun.* **1991**, 187, and references therein.

[4] A. A. Dembek, R. R. Burch, A. E. Feiring, *J. Am. Chem. Soc.* **1993**, *115*, 2087.

[5] H. Witteler, G. Lieser, G. Wegner, M. Schulze, *Makromol. Chem. Rapid. Commun.* **1993**, *14*, 471; J. Huber, U. Scherf, *ibid.* **1994**, *15*, 897.

[6] a) E. E. Bunel, L. Valle, N. L. Jones, P. J. Caroll, M. Gonzalez, N. Munoz, J. M. Manriquez, *Organometallics* **1988**, *7*, 789; b) J. E. C. Wiegelmann, U. H. F. Bunz, *ibid.* **1993**, *12*, 3792; c) M. D. Rausch, A. Siegel, L. P. Kleman,

J. Org. Chem. **1969**, *31*, 2703; d) M. Buchmeiser, H. Schottenberger, *J. Organomet. Chem.* **1992**, *441*, 457; *ibid.* **1992**, *436*, 223, and references therein; e) G. Doisneau, G. Balvoine, T. Fillebeen-Khan, *ibid.* **1992**, *425*, 113; f) K. Schlögl, W. Steyrer, *Monatsh. Chem.* **1965**, *96*, 1520.

[7] J. R. Fritch, K. P. C. Vollhardt, *J. Am. Chem. Soc.* **1979**, *100*, 1239; J. R. Fritch, K. P. C. Vollhardt, *Organometallics* **1982**, *1*, 580; U. H. F. Bunz, M. Altmann, *Makromol. Chem. Rapid Commun.* **1994**, *15*, 785.

[8] a) For the synthesis of arylalkynyl polymers through Pd coupling, see, for example, T. Yamamoto, M. Takagi, K. Kizu, T. Maruyama, K. Kubota, H. Kanbara, T. Kurihara, T. Kaino, *J. Chem. Soc. Chem. Commun.* **1993**, 797; D. L. Trumbo, C. S. Marvel, *J. Polym. Sci. Polym. Chem. Ed.* **1986**, 2411; T. X. Neenan, M. R. Callstrom, L. M. Scaramontzos, K. R. Stewart, G. M. Whitesides, *Macromolecules* **1988**, *21*, 3525; D. R. Rutherford, J. K. Stille, *ibid.* **1988**, *21*, 3530; b) Pd-catalyzed coupling of alkynes with alkylhalides: I. P. Beletskaya, *J. Organomet. Chem.* **1983**, *250*, 551; I. Cassar, *ibid.* **1975**, *93*, 253; H. A. Dieck, R. F. Heck, *ibid.* **1975**, *93*, 259; K. Sonoshigara, Y. Tohda, N. Hagihara, *Tetrahedron Lett.* **1975**, 4467.

[9] M. Alami, F. Ferri, G. Linstrumelle, *Tetrahedron Lett.* **1993**, *34*, 6403.

[10] D. Demus, L. Richter, *Textures of Liquid Crystals*, Verlag Chemie, Weinheim, **1978**.

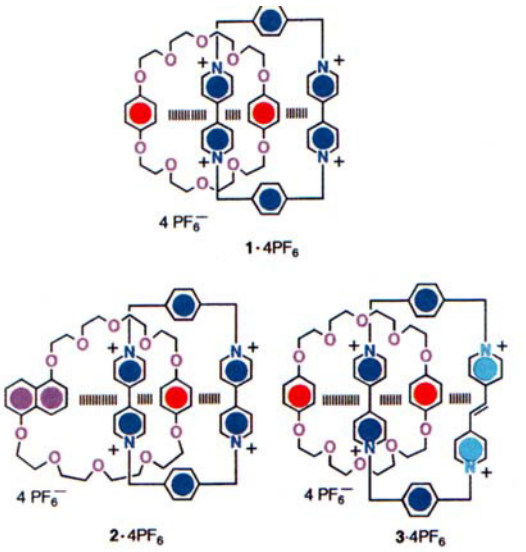
[11] Powder spectra: Siemens diffractometer D500, $Cu_{K\alpha}$ radiation; distances found 11.2, 7.1, 6.4, 5.1, 4.8, 4.3, and 3.7 Å. The reflection corresponding to the 11.2 distance is the most intense and probably represents the Co–Co distance in the chain. The 7.1 distance probably represents the interchain distance.

[12] A "streak" in the phase diagram is seen in the powder diffractogram as a pattern of unstructured scattering intensity with a sharp rise at small scattering angles. Although the integrated intensity of a streak can be very large, it is not necessarily observable on account of the large signal width.

Controlling Translational Isomerism in [2]Catenanes**

Peter R. Ashton, Lluïsa Pérez-García, J. Fraser Stoddart,* Andrew J. P. White, and David J. Williams

The recognition processes that lead to the self-assembly[1] of [2]catenanes[2] are controlled by the information stored in the molecular components which are constructed from "preprogramed" starting materials. This information[3] is trapped within the [2]catenanes molecules whose properties are quite different from those of their individual molecular components. The study of phenomena such as translational isomerism, a structural characteristic[4] of many of these intriguing molecules, may provide insight into the recognition processes that operate during their formation and subsequently in their molecular states. Furthermore, the control of the translational isomerism in catenanes is important in demonstrating their chemical properties and for predicting possible applications.[5] Some recent examples illustrate[6, 7] the progress that has been made already toward the construction of controllable catenanes and rotaxanes. In our own research laboratory, after the [2]catenane **1**-4PF_6 had been self-assembled,[2] the [2]catenane **2**-4PF_6 was also synthesized[8] by a template-directed approach in the belief that the different π-donating abilities of the 1,5-dioxynaphthalene unit and the hydroquinone ring would influence strongly the relative populations of the rapidly equilibrating translational isomers. In the event, the position of the equilibrium was found to be highly dependent on the dielectric constant of the medium in which the [2]catenane was dissolved.



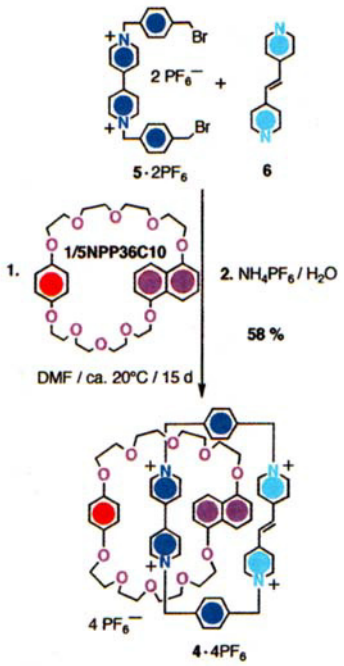
Another way to exercise control over the translational isomerism is by using π-extended viologen units as building blocks in the construction of interlocked molecular structures. We recently reported on the self-assembly, characterization, and electrochemical properties of the [2]catenane **3**-4PF_6,[9] in which the macrocyclic polyether, bis-*p*-phenylene[34]crown-10 (BPP34C10), is encircled by a tetracationic cyclophane containing one bipyridinium and one bis(pyridinium)ethylene unit.[9] In the case of **3**-4PF_6, the translational isomer, in which BPP34C10 encircles the bipyridinium rather than the bis(pyridinium)ethylene unit, is by far the more predominant one in CD_3COCD_3 solution at low temperature. This selectivity is a consequence of the lower π-accepting ability of the π-extended viologen unit relative to that of the parent viologen unit.

By combining both strategies, that is, by altering the different binding abilities of *both* the π-donor and π-acceptor units in these catenated structures, we should be able to exercise more control over their translational isomerism. Thus, we have designed and self-assembled a [2]catenane in which *all four* building blocks, the two π-donor and two π-acceptor units, are different. Here, we describe the synthesis of the [2]catenane **4**-4PF_6, which incorporates 1/5NPP36C10, a macrocyclic polyether containing *one* hydroquinone ring and *one* 1,5-dioxynaphthalene unit, as the π-electron rich macrocycle and a tetracationic cyclophane incorporating *one* bipyridinium and *one* bis(pyridinium)ethylene unit as the π-electron deficient components. We report on the characterization of **4**-4PF_6 by fast atom bombardment mass spectrometry (FABMS), X-ray crystallography, and dynamic ^{1}H NMR spectroscopy.

The [2]catenane **4**-4PF_6 was self-assembled using a template-directing methodology (Scheme 1).[10] The instantaneous formation of a complex between 1/5NPP36C10 and **5**-2PF_6 was followed by stepwise alkylation of **6** to form the [2]catenane **4**-4PF_6, which was isolated in 58% yield after counterion exchange and crystallization. The reaction was carried out in dimethylformamide (DMF) in the dark with an excess of the macrocyclic polyether. Positive-ion FABMS of this new compound revealed[11] peaks at $m/z = 1567$, 1422, and 1277 characteristic of the successive loss of one, two, and three PF_6^- counterions, respectively, from the molecular ion of **4**-4PF_6.

[*] Prof. J. F. Stoddart, Dr. L. Pérez-García, P. R. Ashton
School of Chemistry, The University of Birmingham
Edgbaston, Birmingham B15 2TT (UK)
Dr. D. J. Williams, Dr. A. J. P. White
Chemical Crystallography Laboratory
Department of Chemistry, Imperial College
South Kensington, London SW7 2AY (UK)

[**] This work was supported by the Engineering and Physical Sciences and Engineering Research Council (UK). We thank the Ministerio de Educación y Cienca (Spain) for a Fleming Postdoctoral Fellowship (to L. P.-G.).



Scheme 1. The template-directed synthesis of the [2]catenane **4**-4 PF_6.

The observation of peaks at $m/z = 836$ and 690, corresponding to the loss of one and two counterions, respectively, from the tetracationic cyclophane component of the [2]catenane, is characteristic[12] of the fragmentations of a [2]catenane by loss of one of its rings—in this case, the neutral crown ether.

The catenated structure of **4**-4PF_6 was confirmed by X-ray crystallography;[13, 14] suitable single crystals were grown by vapor diffusion of diisopropyl ether into an acetonitrile solution of the compound. The major point to note about the solid-state structure (Fig. 1) is that **4**-4PF_6 exists as only one isomer. The macrocyclic polyether is threaded through the center of the extended tetracationic cyclophane; the 1,5-dioxynaphthalene unit is positioned within the cavity of the tetracationic cyclophane, sandwiched between the π-electron deficient bipyridinium and bis(pyridinium)ethylene units;[15] the hydroquinone ring is located outside of the cavity alongside the bipyridinium component. The molecule has crystallographic C_2 symmetry about an axis passing through the centers of the ethylenic double bond, the 1,5-dioxynaphthalene ring, the bipyridinium unit, and the hydroquinone ring. The [2]catenane is stabilized further by a) T-type edge-to-face interactions between the 1,5-dioxynaphthalene and the *p*-xylyl spacers of the tetracationic cyclophane,[16] and b) weak C–H···O hydrogen bonding of the central oxygen atom in each polyether chain with both a *p*-xylyl hydrogen atom and one of the α-CH hydrogen atoms of the bipyridinium unit, at each "end" of the tetracation

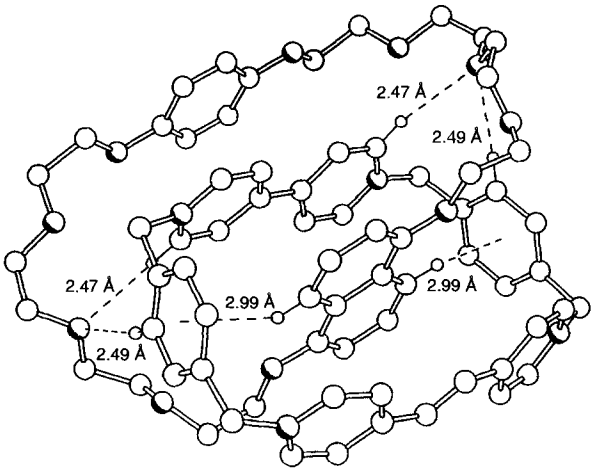


Fig. 1. The structure of the [2]catenane **4**-4PF_6 in the crystal; the additional stabilizing C–H···π and C–H···O interactions are shown.

ic cyclophane (Fig. 1).[16] The incorporation of one extended viologen in place of the bipyridinium unit into one of the sides of the tetracationic cyclophane increases significantly its overall dimensions and alters its recognition properties. The length increases from 10.3 to 11.2 Å and the width from 6.8 to 7.2 Å.[17] The center of the 1,5-dioxynaphthalene unit lies closer to the bipyridinium unit (3.50 Å) than to the double bond (3.72 Å) of the π-extended viologen component (Fig. 2). In common with **1**-4PF_6, the [2]catenane **4**-4PF_6 forms extended polar stacks in the crystals. An interesting feature of this stack is that the double bond of the extended viologen component lies appreciably closer (3.42 Å) to the hydroquinone ring of an adjacent [2]catenane than to the 1,5-dioxynaphthalene unit within the [2]catenane (3.72 Å); indeed the separation is less than the intramolecular distance (3.50 Å) between 1,5-dioxynaphthalene and the bipyridinium units.

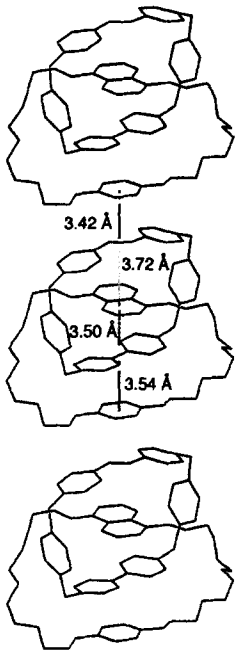
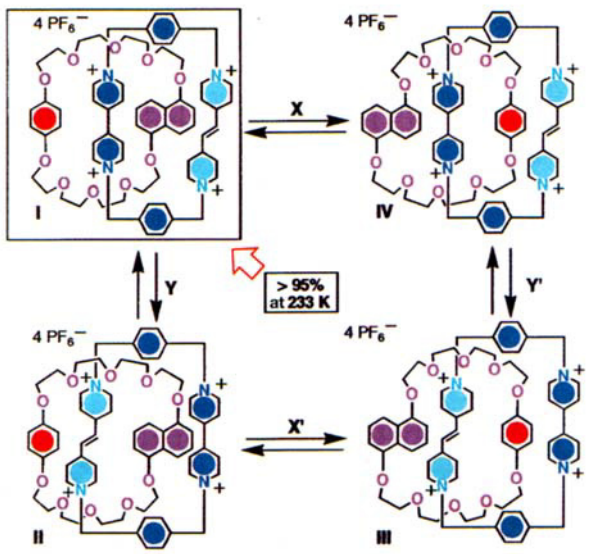


Fig. 2. Part of the extended polar stacks present in the crystals of the the [2]catenane **4**-4PF_6.

The [2]catenane **4**-4PF_6 consists of four different π systems, and therefore an equilibrium between four different translational isomers is possible (Scheme 2). Like [2]catenane **1**-4PF_6,[2] the new [2]catenane **4**-4PF_6 exhibits temperature-dependent ^{1}H NMR spectra.[18] However, the differences in the recognition processes between its components imbue the system with a high level of structural selectivity. One process (**X**/**X'**) is the equilibration of the π-electron rich hydroquinone ring and 1,5-dioxynaphthalene unit between positions either inside or alongside the tetracationic cyclophane. In the case of **4**-4PF_6, both in CD_3COCD_3 and CD_3CN solutions, ^{1}H NMR spectroscopic studies indicate that the circumrotation of 1/5NPP36C10 through the tetracationic cyclophane is already slow on the



Scheme 2. Equilibrium between the translational isomers (**I**–**IV**) of the [2]catenane **4**-4PF_6 in solution.

 © VCH Verlagsgesellschaft mbH, D-69451 Weinheim, 1995 0570-0833/95/0505-0572 $ 10.00+.25/0

^{1}H NMR timescale at room temperature, in other words, the process **X/X′** is "frozen out" and the aromatic π-electron donors (hydroquinone and 1,5-dioxynaphthalene) do not interchange their positions. The equilibrium (Scheme 2) is predominantly in favor of the translational isomers **I** and **II**, where the 1,5-dioxynaphthalane ring occupies the position inside the tetracationic cyclophane. This conclusion may be drawn from the fact that the ^{1}H NMR spectrum at room temperature in CD_3COCD_3 shows three well-resolved signals at $\delta = 3.77$, 5.71, and 6.37 corresponding to the H-4/8, H-3/7, and H-2/6 protons, respectively, of the 1,5-dioxynaphthalene unit, and one well-resolved singlet at $\delta = 6.08$ for the hydroquinone ring protons. None of the chemical shifts for these signals undergo any changes at lower temperatures, at least down to −40 °C, indicating that the two types of aromatic rings do not interchange on the ^{1}H NMR timescale. At + 40 °C, the four aromatic signals are slightly broadened, indicating that process **X/X′** is starting to occur on the ^{1}H NMR timescale. At this temperature, saturation transfer experiments led us to identify some low-intensity broad resonances present in the ^{1}H NMR spectrum, corresponding to the averaged signals resulting from protons in the rapidly equilibrating translational isomers **III** and **IV**, where the hydroquinone unit is located inside the tetracationic cyclophane. Thus, irradiation of these weak signals at $\delta = 7.13$ and 7.36, corresponding, respectively, to H-3/7 and H-4/8 on the "alongside" 1,5-dioxynaphthalene unit indicated that they are undergoing exchange with a triplet at $\delta = 5.73$ and a doublet at $\delta = 3.68$, corresponding to the same protons on the "inside" 1,5-dioxynaphthalene unit in the rapidly equilibrating translational isomers **I** and **II**. Direct integration of these signals in the ^{1}H NMR spectrum at room temperature, where process **X/X′** has already been frozen out, gave an equilibrium ratio of 88:12 for the translational isomers **I** and **II** versus **III** and **IV**. The second dynamic process (**Y/Y′** in Scheme 2) exhibited by **4**-4PF_6 involves pirouetting of 1/5NPP36C10 around the tetracationic cyclophane. At room temperature, this process is fast on the ^{1}H NMR timescale. However, below −40 °C, it is frozen out and the major isomer detected is the translational isomer **I**, where the π-electron deficient bipyridinium unit is located inside the tetracationic cyclophane. This is indicated by the relative simplicity of the ^{1}H NMR spectrum, in which only four major signals are observed for the α-bipyridinium protons, two doublets, corresponding to the bipyridinium unit, and two doublets, corresponding to the bis(pyridinium)ethylene unit. This temperature-dependent behavior associated with process **Y/Y′** was accompanied by changes in the ^{1}H NMR signals arising from all the protons in the tetracationic cyclophane component of the [2]catenane. Thus, at −40 °C, the signal corresponding to the olefinic protons of the bis(pyridinium)ethylene unit in translational isomer **I** appears at $\delta = 6.60$, only $\Delta\delta = 0.10$ downfield relative to the analogous signal in the room-temperature spectrum. This observation confirms that this signal corresponds to translational isomer **I**, where the π-extended viologen resides alongside the polyether cavity. Once again, a saturation transfer experiment at −20 °C showed the existence of site exchange between a high-intensity signal at $\delta = 6.56$ (**I**) and a low-intensity signal at $\delta = 6.15$ (**II**). These signals are associated with site exchange of the olefinic protons of a bis(pyridinium)ethylene unit, alongside and inside the macrocyclic polyether. This is evidence for the population of both translational isomers **I** and **II** (Scheme 2). Integration of the signals at −40 °C gave a ratio of 95:5 for isomers **I** and **II**. Neither of the other two possible isomers (**III** or **IV**) were detected at this temperature. In solution at low temperatures [2]catenane **4**-4PF_6 exists almost exclusively as one amongst four possible translational isomers. This one isomer is precisely the same as that observed in the solid by X-ray crystallography.

The [2]catenane **4**-4PF_6 shows how the recognition processes operating between the components of interlocked molecular systems express themselves in the properties of the molecules—in this case, by controlling translational isomerism. This finding demonstrates the progress that is being made toward the construction of controllable [2]catenanes.

Experimental Procedure

4-4PF_6: A solution of **5** (53 mg, 0.06 mmol) in dry DMF (5 mL) was added to a solution of 1/5NPP36C10 (77 mg, 0.13 mmol) in dry DMF (4 mL). A deep red color was formed immediately, and a solution of **6** (13 mg, 0.07 mmol) in dry DMF (1 mL) was added. After the reaction mixture had been stirred at room temperature for 15 d, the suspension was poured in Et_2O (50 mL). The red solid was filtered off, washed with Et_2O (10 mL) and CH_2Cl_2 (10 mL), and then dried before being dissolved in H_2O (15 mL) and Me_2CO (5 mL). Then, a saturated aqueous solution of NH_4PF_6 was added, and the solution was left to stand for ca. 15 h, during which time purple crystals formed. The suspension was filtered off, and the crystals were washed with H_2O (2 × 3 mL) and then dried to give **4**-4PF_6 as a purple solid (65 mg, 58%), m.p. >300 °C; positive-ion FABMS: *m/z*: 1567 $[M - PF_6]^+$, 1422 $[M - 2PF_6]^+$, 1277 $[M - 3PF_6]^+$; ^{1}H NMR (300 MHz, CD_3CN): $\delta = 3.20$–4.30 (m, 32H), 3.37 (d, $J = 8.0$ Hz, 2H), 5.57 (dd, $J = 7.5$, 8.0 Hz, 2H), 5.61 (d, $J = 13.5$ Hz, 2H), 5.68 (s, 4H), 5.80 (d, $J = 13.5$ Hz, 2H), 6.09 (s, 4H), 6.10 (s, 2H), 6.26 (d, $J = 7.5$ Hz, 2H), 7.06 (d, 4H), 7.27 (br s, 4H), 7.88 (d, $J = 8.5$ Hz, 4H), 7.98 (d, $J = 8.5$ Hz, 4H), 8.73 (br s, 8H).

Received: August 20, 1994 [Z 7253 IE]
German version: *Angew. Chem.* **1995**, *107*, 607

Keywords: catenanes · crown ethers · self-assembly · translational isomerism

[1] a) J. S. Lindsey, *New J. Chem.* **1991**, *15*, 153; b) D. Philp, J. F. Stoddart, *Synlett* **1991**, 445; c) G. M. Whitesides, J. P. Mathias, C. T. Seto, *Science* **1991**, *254*, 1312.

[2] a) P. R. Ashton, T. T. Goodnow, A. E. Kaifer, M. V. Reddington, A. M. Z. Slawin, N. Spencer, J. F. Stoddart, C. Vicent, D. J. Williams, *Angew. Chem.* **1989**, *101*, 1404; *Angew. Chem. Int. Ed. Engl.* **1989**, *28*, 1396; b) P. L. Anelli, P. R. Ashton, R. Ballardini, V. Balzani, M. Delgado, M. T. Gandolfi, T. T. Goodnow, A. E. Kaifer, D. Philp, M. Pietraszkiewicz, L. Prodi, M. V. Reddington, A. M. Z. Slawin, N. Spencer, J. F. Stoddart, C. Vicent, D. J. Williams, *J. Am. Chem. Soc.* **1992**, *114*, 193, and references therein.

[3] J.-M. Lehn, *Science* **1993**, *260*, 1762.

[4] G. Schill, K. Rissler, W. Vetter, *Angew. Chem.* **1981**, *93*, 197; *Angew. Chem. Int. Ed. Engl.* **1981**, *20*, 187.

[5] a) J. F. Stoddart, *Chem. Aust.* **1992**, *59*, 576; b) R. A. Bissell, J. F. Stoddart in *Computations for the Nano-Scale* (Eds.: P. E. Blöchl, A. J. Fisher, C. Joachim), Kluwer, Dordrecht, **1993**, p. 141; c) J. A. Preece, J. F. Stoddart in *The Ultimate Limits of Fabrication and Measurement* (Ed.: M. Welland), Kluwer, Dordrecht, **1994**, in press.

[6] a) P. R. Ashton, R. A. Bissell, N. Spencer, J. F. Stoddart, M. S. Tolley, *Synlett* **1992**, 914; b) P. R. Ashton, R. A. Bissell, R. Górski, D. Philp, N. Spencer, J. F. Stoddart, M. S. Tolley, *ibid.* **1992**, 919; c) P. R. Ashton, R. A. Bissell, N. Spencer, J. F. Stoddart, M. S. Tolley, *ibid.* **1992**, 923; d) E. Córdova, R. A. Bissell, N. Spencer, P. R. Ashton, J. F. Stoddart, A. E. Kaifer, *J. Org. Chem.* **1993**, *58*, 6550; e) R. A. Bissell, E. Córdova, A. E. Kaifer, J. F. Stoddart, *Nature* **1994**, *369*, 133.

[7] a) F. Vögtle, W. M. Müller, M. Bauer, K. Rissanen, *Angew. Chem.* **1993**, *105*, 1356; *Angew. Chem. Int. Ed. Engl.* **1993**, *32*, 1295; b) M. J. Gunter, M. R. Johnston, *J. Chem. Soc. Chem. Commun.* **1994**, 829; c) M. J. Gunter, D. C. R. Hockless, M. R. Johnston, B. W. Skelton, A. H. White, *J. Am. Chem. Soc.* **1994**, *116*, 4810; d) A. C. Benniston, A. Harriman, *Angew. Chem.* **1993**, *105*, 1553; *Angew. Chem. Int. Ed. Engl.* **1993**, *32*, 1459; e) A. C. Benniston, A. Harriman, V. M. Lynch, *Tetrahedron Lett.* **1994**, *35*, 1473.

[8] P. R. Ashton, R. Ballardini, V. Balzani, M. Blower, M. Ciano, M. T. Gandolfi, L. Prodi, C. H. McLean, D. Philp, N. Spencer, J. F. Stoddart, M. S. Tolley, *New J. Chem.* **1993**, *17*, 689.

[9] P. R. Ashton, R. Ballardini, V. Balzani, M. T. Gandolfi, D. J.-F. Marquis, L. Pérez-García, L. Prodi, J. F. Stoddart, M. Venturi, *J. Chem. Soc. Chem. Commun.* **1994**, 177.

[10] a) C. O. Dietrich-Buchecker, J.-P. Sauvage, *Chem. Rev.* **1987**, *87*, 795; b) J.-C. Chambron, C. Dietrich-Buchecker, J.-P. Sauvage, *Top. Curr. Chem.* **1993**, 165, 131; c) J. F. Stoddart, *An. Quim.* **1993**, *89*, 51; d) R. Hoss, F. Vögtle, *Angew. Chem.* **1994**, *106*, 389; *Angew. Chem. Int. Ed. Engl.* **1994**, *33*, 375; e) S. Anderson, H. L. Anderson, J. K. M. Sanders, *Acc. Chem. Res.* **1993**, *26*, 469;

f) H. L. Anderson, A. Bashall, K. Henrick, M. McPartlin, J. K. M. Sanders, *Angew. Chem.* **1994**, *106*, 445; *Angew. Chem. Int. Ed. Engl.* **1994**, *33*, 429.
[11] FAB mass spectra were obtained with a Kratos MS80RF mass spectrometer coupled to a DS90 system. The atom gun (Ion Tech Limited) was operated at 7 keV with a tube current of 2 mA. The primary beam of atoms was produced from research-grade krypton. Samples were dissolved in a small amount of 3-nitrobenzyl alcohol that had been coated onto a stainless steel probe. Spectra were recorded in the positive-ion mode at a scan speed of 30 s per decade.
[12] M. Vetter, G. Schill, *Tetrahedron* **1967**, *23*, 3079.
[13] Crystal data for **4**·4PF_6·4MeCN: monoclinic, $a = 35.075(10)$, $b = 14.171(3)$, $c = 20.020(6)$ Å, $\beta = 119.43(2)°$; $V = 8669$ Å^3, space group $C2/c$, $Z = 4$, $\rho = 1.44$ g cm^{-3}, $\mu(Cu_{K\alpha}) = 18$ cm^{-1}, 4063 independent observed reflections with $[|F_o| > 4\sigma(|F_o|), 2\theta < 116°]$ refined to $R = 0.116$, $Rw = 0.129$.
[14] Siemens P4/Ra diffractometer, ω scans, $Cu_{K\alpha}$ radiation (graphite monochromator). The structure was solved by direct methods and the major occupancy non-hydrogen atoms refined anisotropically. The minor occupancy atoms were refined isotropically. Further details of the crystal structure may be obtained from the Director of the Cambridge Crystallographic Data Centre, University Chemical Laboratory, Lensfield Road, Cambridge CB2 1EW (UK), on quoting the full journal citation.
[15] The $OC_{10}H_6O$ axis of the 1,5-dioxynaphthalene unit is inclined by 34° to the equatorial plane of the tetracationic cyclophane as defined by the mean plane of its four methylene carbon atoms.
[16] The distances between H-4 and H-8 on the naphthalene rings and the centers of their immediately adjacent *p*-xylyl rings are 2.99 Å and the C–H···centroid angles are 143°. In the case of the C–H···O interactions between one of the *p*-xylyl hydrogen atoms and the central oxygen atoms of the polyether chains, the H···O distances are 2.49 Å and the C–H···O angles are 167°. For the C–H···O interactions between the α-CH hydrogen atoms of the bipyridinium unit and the same oxygen atoms of the polyether chains, the H···O distances are 2.47 Å and the C–H···O angles are 169°.
[17] The length is defined as the distance between the centroids of the two *p*-xylyl rings, and the width as the distance between the centers of the bond(s) linking the pyridinium rings.
[18] The ^{1}H NMR spectra were recorded on a Bruker AMX400 spectrometer operating at 400.13 MHz. All chemical shifts are referenced via the residual $CHD_2COCHCD_2$ or CHD_2CN signals to Me_4Si.

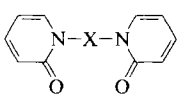
$[Mn(C_{18}H_{16}N_2O_2)_3](ClO_4)_2$: A Polymeric 34- and 68-Membered Metallacyclic Network Forming a Novel Woven Polycatenated Structure**

David M. L. Goodgame,* Stephan Menzer, Amanda M. Smith, and David J. Williams*

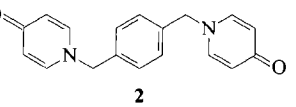
The past decade has seen the creation of many elegant interlocked molecular species, the most notable of which have been the catenanes, rotaxanes, and "knots" pioneered principally by Sauvage et al. and Stoddart et al.[1] Key factors in the development of this work have been the use of metal templating combined with appropriate ligand design, and the employment of noncovalent interactions as part of the synthetic strategy. An important feature of both these approaches has been the use of conformationally flexible components.

Concurrent with this has been the development of three-dimensional networks based primarily on linking metal centers with rodlike or other essentially rigid bridging components.[2] An occasional product of this latter work has been the formation of interpenetrating, adamantyl-like networks.[3] Interleaved, extended networks incorporating flexible bridging units are, however, rare.[4] We report here the discovery of an unusual, new, flexibly bridged, interpenetrating polycatenane.

We have recently been exploiting the conformational preferences of a series of extended-reach organic ligands of the general type **1** to create a range of two- and three-dimensional polymeric metallamacrocyclic networks.[5] Extending this work, we have



1



2

explored the effect of changing the position of the exocyclic O-donor group on the heterocyclic unit from *ortho* to the *para* position relative to the ring nitrogen, as in *N,N'-p*-phenylenedimethylenebis(pyridin-4-one) (**2**, *p*-XBP4). This has resulted in the formation, inter alia, of the polymer **3**.

$\{[Mn(p\text{-XBP4})_3](ClO_4)_2\}_n$ **3**

X-Ray analysis[6] of **3** shows that the crystal structure is based on a network of octahedrally coordinated Mn centers linked by *p*-XBP4 ligands (Fig. 1). There are two distinct ligand geometries (A and B) present in the structure in a 2:1 ratio. In A, one of the pyridone rings is essentially orthogonal to the central *p*-xylyl unit, whilst the other is in an "open book" conformation with respect to it. Bridges of this type link pairs of Mn centers, creating open 34-membered rings (Fig. 1). Within each 34-membered ring, adjacent pairs of *cis*-coordinated pyridone rings are held in a near coplanar arrangement by weak CH···O hydrogen bonds (H···O 2.33 and 2.48 Å) between the *ortho* CH group of one pyridone ring and the oxygen atom of its *cis*-coordinated neighbor.

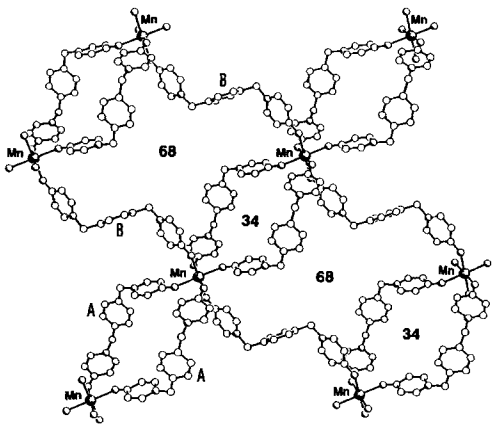


Fig. 1. Part of the network of 34- and 68-membered metallacycles, showing the ligand geometries A and B in **3**.

Ligands in arrangement B have the pyridone rings centrosymmetrically disposed but skewed to a position intermediate between an orthogonal orientation and an open-book conformation with respect to the *p*-xylyl spacer. These type B bridges serve to link pairs of the 34-membered rings, thus creating a set of 68-membered rings (Fig. 1). The manganese atoms within this network lie in the *ab* plane and are separated by two unit cell translations in both the *a* and *b* directions.

[*] Dr. D. M. L. Goodgame, Dr. D. J. Williams, Dr. S. Menzer, A. M. Smith
Chemistry Department
Imperical College of Science,
Technology and Medicine
London SW7 2AY (UK)
Telefax: Int. code +(171) 594-5804

[**] This work was supported by the Science and Engineering Research Council and the Commission of the European Communities.

The fascinating feature of the structure of **3** is that it comprises not one, but two such networks interwoven one with the other (Fig. 2). Each network is displaced by one unit cell translation in the *a* or *b* direction with respect to the other; thus, the manganese atoms in one network reside in the centers of the 68-membered rings of the other and vice versa. In addition, ligands of conformation B in one network are threaded through the centers of the 34-membered rings of the other, thus forming a polycatenated sheet structure.

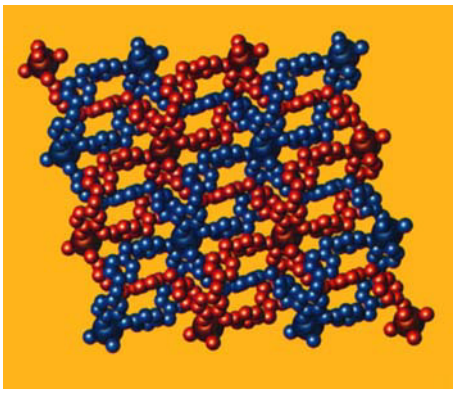


Fig. 2. Perspective view of the interwoven polycatenane structure of **3**. Manganese atoms are depicted as large spheres. The atoms of the individual networks are shown in red or blue.

The interpenetrating networks are stabilized by a combination of near parallel face-to-face and T-type edge-to-face $\pi-\pi$ interactions (Fig. 3). The face-to-face interactions are between the central *p*-xylyl ring (P) of the threading ligand (that is, type B) and one each (Q and Q′) of a pair of centrosymmetrically disposed pyridone rings of type A ligands, and also between the *p*-xylyl ring (T) of the type A ligand and the terminal pyridone ring (S′) of the thread.[7] The T-type interactions are between the pyridone ring (S) of the thread and the pyridone ring (R) of the type A ligand within the 34-membered ring.[7]

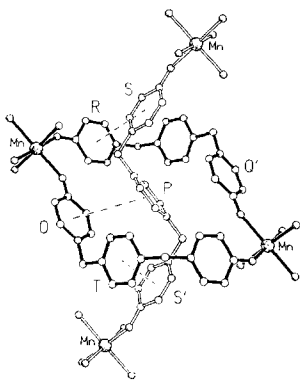


Fig. 3. The type B ligand is threaded through the center of one of the 34-membered rings. The face-to-face and edge-to-face interactions are indicated as broken lines. The ring P lies on a crystallographic center of symmetry.

The sheets have a pronounced corrugated cross section and adjacent sheets are positioned approximately ridge-to-ridge, creating channels within which the anions and acetonitrile solvate molecules are located. Studies by mass spectrometry (positive FAB to $m/z = 2500$) of solutions of **3** in water and in methanol showed that the polymer is broken up in these solvents. In each case the dominant species observed was (*p*-XBP4)H^+, and a much smaller peak assignable to (*p*-XBP4)$_2H^+$, but there was no conclusive evidence for oligomeric Mn-containing species under these conditions.

It is remarkable that such a complex, polycatenated structure is formed by **3** in preference to either the layered sheets of large ring metallacycles[8] or the three-dimensional networks of non-interpenetrating rings[9] we have observed previously with ligands of type **1**. The mechanism of the formation of the interpenetrating structure is manifestly complex, though it is possible that the aromatic–aromatic face-to-face and edge-to-face interactions may play an important templating role. Further studies are in progress to investigate the factors favoring the polycatenation process.

Experimental Procedure

Ligand **2**: Pyridin-4-one (0.02 mol) was treated with sodium butoxide (0.02 mol) in butan-1-ol (80 mL), α,α′-dibromo-*p*-xylene (0.01 mol) was added, and the mixture was heated at reflux for 6 h. After cooling, extraction with water (3 × 30 mL) gave the product as the crystalline tetrahydrate. Yield 45%: elemental analysis for $C_{18}H_{16}N_2O_2 \cdot 4H_2O$; found: C 59.39, H 6.43, N 7.77; calcd: C 59.33, H 6.64, N 7.69.

3: Dropwise addition of a solution of $Mn(ClO_4)_2 \cdot 6H_2O$ (0.033 mmol) in acetonitrile (4 mL) to a solution of **2** (0.1 mmol) in a mixture of acetonitrile (3 mL) and methanol (1 mL) yielded **3**. The precipitate that formed immediately was redissolved by addition of methanol (1 mL), and the resulting solution was allowed to evaporate slowly over concentrated sulfuric acid. Pale yellow crystals formed overnight and were collected by filtration, washed with cold acetonitrile, and air-dried. Yield 80%.

Received: August 10, 1994 [Z 7227 IE]
German version: *Angew. Chem.* **1995**, *107*, 605

Keywords: catenanes · complexes with oxygen ligands · manganese compounds · metallacycles · polymers

[1] See, for example, C. Dietrich-Buchecker, J.-P. Sauvage, *Bull. Soc. Chim. Fr.* **1992**, *129*, 113; J.-C. Chambron, C. Dietrich-Buchecker, J.-P. Sauvage, *Top. Curr. Chem.* **1993**, *165*, 131; P. L. Anelli, P. R. Ashton, R. Ballardini, V. Balzani, M. Delgado, M. T. Gandolfi, T. T. Goodnow, A. E. Kaifer, D. Philp, M. Pietraszkiewicz, L. Prodi, M. V. Reddington, A. M. Z. Slawin, N. Spencer, J. F. Stoddart, C. Vicent, D. J. Williams, *J. Am. Chem. Soc.* **1992**, *114*, 193, and references therein.

[2] For example: B. F. Abrahams, B. F. Hoskins, J. Liu, R. Robson, *J. Am. Chem. Soc.* **1991**, *113*, 3045, and references therein; H. O. Stumpf, L. Ouahab, Y. Pei, D. Grandjean, O. Kahn, *Science* **1993**, *261*, 447; H. O. Stumpf, L. Ouahab, Y. Pei, P. Bergerat, O. Kahn, *J. Am. Chem. Soc.* **1994**, *116*, 3866.

[3] L. R. MacGillivray, S. Subramanian, M. J. Zaworotko, *J. Chem. Soc. Chem. Commun.* **1994**, 1325, and references therein.

[4] D. J. Duchamp, R. E. Marsh, *Acta Crystallogr. Sect. B* **1969**, *25*, 5; K.-W. Kim, M. G. Kanatzidis, *J. Am. Chem. Soc.* **1992**, *114*, 4878.

[5] Z. Atherton, D. M. L. Goodgame, D. A. Katahira, S. Menzer, D. J. Williams, *J. Chem. Soc. Chem. Commun.* **1994**, 1423, and references therein.

[6] **3** · $2CH_3CN$: $a = 10.434(7)$, $b = 11.410(4)$, $c = 13.805(8)$ Å, $\alpha = 69.48(2)^\circ$, $\beta = 69.20(2)^\circ$, $\gamma = 77.62(2)^\circ$, $V = 1431.3(13)$ Å^3, $P\bar{1}$, $Z = 1$, $\mu(Cu_{K\alpha}) = 3.35$ mm^{-1}, $\rho_{calcd} = 1.407$ g cm^{-3}. Siemens P4/PC diffractometer, ω, graphite-monochromated $Cu_{K\alpha}$ radiation. The structure was solved by the heavy-atom method, corrected for absorption, and refined anisotropically to give $R = 0.062$ ($R_w = 0.069$) for 2408 independent observed reflections [$2\theta = 3-100$, $|F_o| > 4\sigma(|F_o|)$]. Further details of the crystal structure investigation can be obtained from the Director of the Cambridge Crystallographic Data Centre, 12 Union Road, GB-Cambridge CB2 1EZ (UK), by quoting the full literature citation.

[7] Ring P is inclined by 22° to rings Q and Q′, and the centroid–centroid separations are 4.32 Å. Rings T and S′ are inclined by 31° to each other and their centroid–centroid separation is 4.26 Å. Rings R and S are inclined by 86° and their centroid–centroid separation is 5.13 Å.

[8] For example: G. A. Doyle, D. M. L. Goodgame, S. P. W. Hill, D. J. Williams, *J. Chem. Soc. Chem. Commun.* **1993**, 207; S. P. W. Hill, PhD thesis, London University, **1993**.

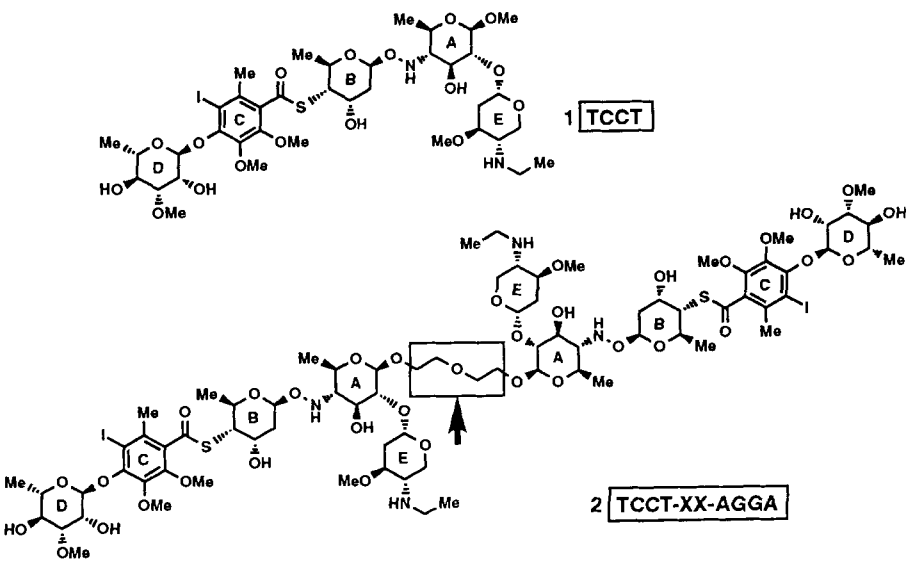
[9] For example: D. M. L. Goodgame, S. Menzer, A. M. Smith, D. J. Williams, *J. Chem. Soc. Chem. Commun.* **1994**, 1825.

 © VCH Verlagsgesellschaft mbH, D-69451 Weinheim, 1995 0570-0833/95/0505-0575 $ 10.00+.25/0

DNA–Carbohydrate Recognition: Design and Synthesis of an Eight-Base Sequence-Selective DNA-Binding Oligosaccharide**

K. C. Nicolaou,* Keiichi Ajito, Hironori Komatsu, Brian M. Smith, Tianhu Li, Miles G. Egan, and Luigi Gomez-Paloma

DNA-binding molecules, particularly those with sequence specificity, have considerable potential in chemistry, biology, and medicine.[1–7] Such molecules may provide the basis for further insights in the chemistry and structure of DNA, for the design and development of tools for molecular and cell biology, and for the development of antisense and gene therapies.[4–7] Following calicheamicin γ_1^I [8] as a lead, we have recently synthesized and studied the binding of a series of oligosaccharides to duplex DNA.[9–11] In these investigations[9, 10] oligosaccharide **1** (Scheme 1) emerged as the most potent and selective molecule, binding duplex DNA at TCCT sites with an affinity constant of $K_a \approx 10^6\ M^{-1}$. First synthesized in 1990 in our laboratory,[12] oligosaccharide **1** was recently shown by Crabtree et al.[13] to specifically inhibit transcription complexes. Appropriately designed oligomers of **1** should exhibit enhanced binding to duplex DNA in terms of potency and specificity. We now wish to report the design and chemical synthesis of the head-to-head dimer **2** (Scheme 1) of oligosaccharide **1**, which was designed to bind duplex DNA selectively at *TCCTXXAGGA* sequences.[14]



Scheme 1. Structures of calicheamicin γ_1^I oligosaccharides **1** (monomer, binds a TCCT site) and **2** (head-to-head dimer designed to bind a *TCCTXXAGGA* site). The tether is marked with an arrow.

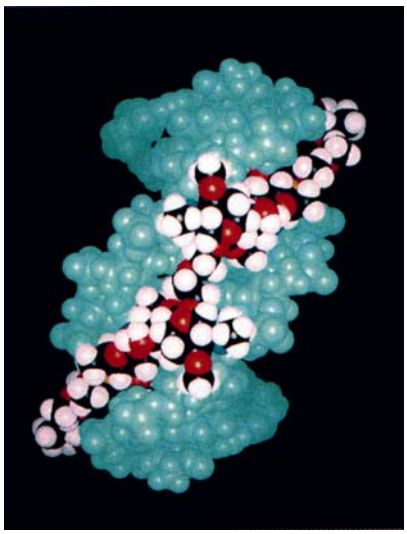


Fig. 1. Computer-generated model of dimer **2** bound to the minor groove of duplex DNA [GCA*TCCTATAGGA*TGC] along a *TCCTATAGGA* site.

Based on the detailed interactions of oligosaccharide **1** with a TCCT site of a duplex 10-mer DNA as determined by NMR spectroscopy,[11, 15] and footprinting experiments,[9, 10, 16] and by using computer modeling, the head-to-head dimer **2** was designed to dock properly into the minor groove of duplex DNA along a *TCCTXXAGGA* tract. The five-atom tether $-CH_2CH_2OCH_2CH_2-$ was found, by computer modeling, to allow optimum fit of the two oligosaccharide domains into their respective binding sites. Figure 1 depicts a computer-generated model of dimer **2** bound to duplex DNA along its target *TCCTXXAGGA* tract.

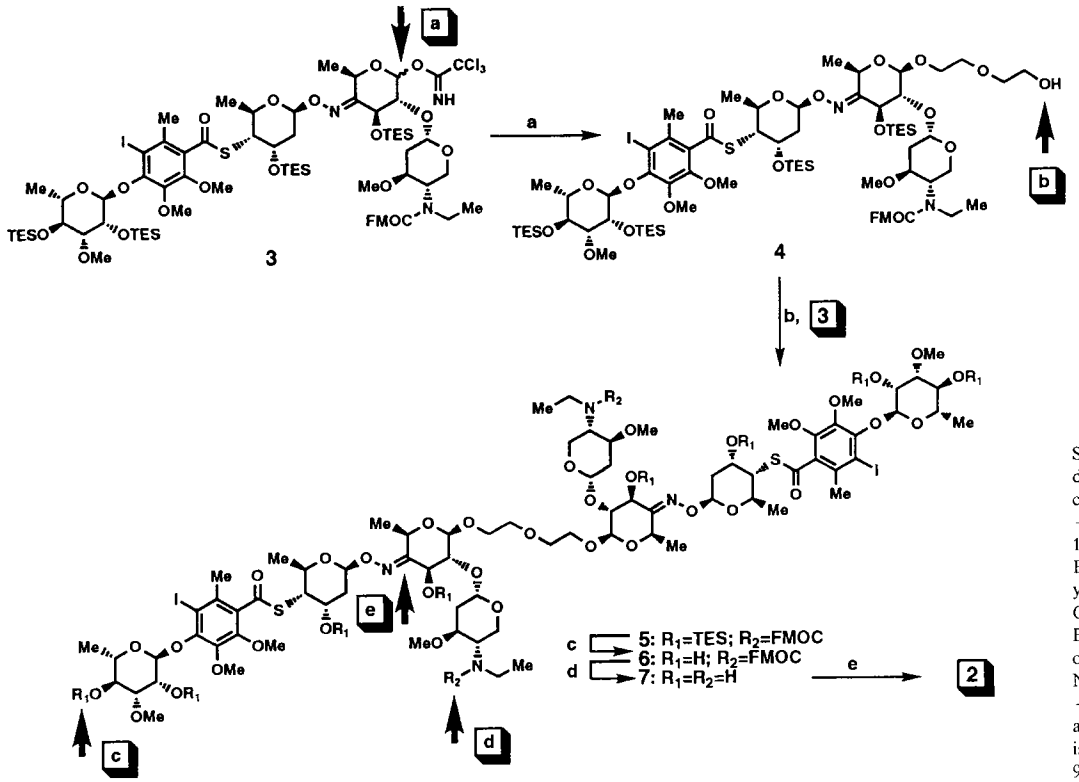
The synthesis of the designed decacyclic oligosaccharide **2** was carried out from the previously reported[17] key intermediate **3** as summarized in Scheme 2.[18] Coupling trichloroacetimidate **3** with excess diethylene glycol in CH_2Cl_2 at $-78 \rightarrow -40\,^\circ C$ in the presence of $BF_3 \cdot Et_2O$ provided compound **4** in 69% yield together with its α anomer (**4'**, 11% yield). The chromatographically separated **4**[19] was then coupled with a second molecule of **3** under similar conditions to afford the dimeric compound **5**[19] in 59% yield (plus 18% recovered starting material **4**). Desilylation of **5** with HF · pyridine followed by removal of the 9-fluorenylmethoxycarbonyl (FMOC) group led to the polyhydroxyl intermediate **7**, via compound **6**, in 76% overall yield. Finally, $NaCNBH_3$ reduction of **7** catalyzed by $BF_3 \cdot Et_2O$ resulted in the formation of the targeted compound **2**[19] in 46% yield. The structure of **2** was secured by spectroscopic means, particularly ^1H NMR spectroscopy which defined the stereochemistry at the newly generated anomeric and N-bearing centers.

Preliminary NMR studies (variable-temperature, NOESY, TOCSY) on a 1:1 complex of dimer **2** with ds[GCA*TCCTATAGGA*TGC] DNA revealed binding in the minor groove along the *TCCTATAGGA* tract. The data are consistent with a

[*] Prof. K. C. Nicolaou, K. Ajito, H. Komatsu, B. M. Smith, Dr. T. Li, M. G. Egan, Dr. L. Gomez-Paloma
Department of Chemistry, The Scripps Research Institute
10666 North Torrey Pines Road, La Jolla, CA 92037 (USA)
and
Department of Chemistry and Biochemistry, University of California, San Diego, 9500 Gilman Drive, La Jolla, CA 92093 (USA)
Telefax: Int. code +(619) 554-6738

[**] This work was financially supported by the National Institutes of Health (USA) and the University of California (Biotechnology Grant). Fellowship from Meiji Seika Kaisha, Ltd. (visiting scientist, K. A.), Mitsui Toatsu Chemicals, Inc. (visiting scientist, H. K.), and the Università Degli Studi Di Napoli "Frederico II" (visiting assistant professor, L. G. P.) are gratefully acknowledged.

 © VCH Verlagsgesellschaft mbH, D-69451 Weinheim, 1995 0570-0833/95/0505-0576 $ 10.00+.25/0



Scheme 2. Synthesis of head-to-head dimer **2**. a) 4.0 equiv diethylene glycol, 0.5 equiv $BF_3 \cdot Et_2O$, CH_2Cl_2, $-78 \rightarrow -40\,^{\circ}C$, 4 h, 69% yield plus 11% α anomer; b) 2.0 equiv **3**, 0.3 equiv $BF_3 \cdot Et_2O$, CH_2Cl_2, $-78\,^{\circ}C$, 5 h, 59% yield plus 18% recovered **4**; c) HF · py, CH_2Cl_2, py, $-40 \rightarrow 0\,^{\circ}C$, 20 h; d) Et_2NH/THF (1/1), 25 °C, 3 h, 76% overall yield from **5**; e) 60 equiv NaCNBH$_3$, 26 equiv $BF_3 \cdot Et_2O$, CH_2Cl_2, $-60 \rightarrow -40\,^{\circ}C$, 2.5 h, 46% yield plus a number of other, not characterized isomers. TES = triethylsilyl; FMOC = 9-fluorenylmethoxycarbonyl.

model in which two complexes are present at low temperature corresponding to one tightly bound pentasaccharide unit and one loosely bound unit; at higher temperatures the two states interconnect.[20]

Footprinting experiments with **2** were complicated, presumably owing to the interference of the molecule with the endonuclease used (deoxyribonuclease I) and the apparent multifaceted binding of the sugar to duplex DNA. Competition experiments with calicheamicin γ_1^I, however, revealed strong, concentration-dependent inhibition of DNA cleavage by the dimer **2** as expected (Fig. 2). In comparison with monomer **1** (lanes 8–10, Fig. 2), dimer **2** (lanes 5–7, Fig. 2) appears to exhibit considerably higher binding affinity to DNA.

Preliminary in vitro experiments[21] also indicated strong inhibiton of binding for certain transcription factors to DNA and interference with in vivo gene expression, suggesting potential application for molecules such as **2** to gene regulation and therapy.[13]

Further studies are needed to determine more precisely the interaction of dimer **2** with DNA and its potential in DNA recognition and gene regulation. The design, synthesis, and evaluation of higher oligomers of **1** and their corresponding enediyne-containing relatives are in progress.

Received: November 2, 1994 [Z 7449 IE]
German version: *Angew. Chem.* **1995**, *107*, 614

Keywords: DNA-binding molecules · DNA cleavage · molecular recognition · oligosaccharides

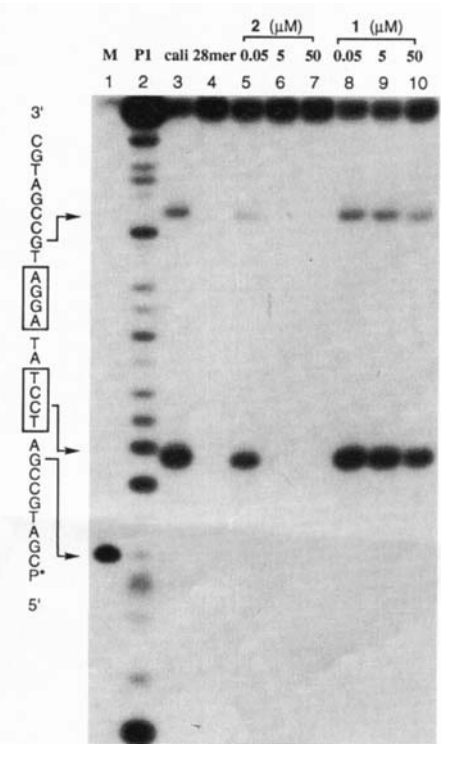


Fig. 2. Autoradiogram of denaturing polyacrylamide gel showing products of calicheamicin-induced DNA cleavage of [5'-^{32}P]-labeled, *TCCTATAGGA*-containing DNA duplex in the presence of oligosaccharides **1** and **2**. Lane 1: marker lane containing the products of DNA digestion with *Mbo* I restriction enzyme; lane 2: 28-mer ladder resulting from partial DNA digestion with nuclease P1; lane 4: [5'-^{32}P]-labeled 28-mer; lanes 3, 5–10: products of DNA cleavage with calicheamicin (250 nM) in the presence of varying concentrations of monomer **1** and dimer **2** (lane 3: no oligosaccharide, lane 5: 50 nM **2**, lane 6: 5 μM **2**, lane 7: 50 μM **2**, lane 8: 50 nM **1**, lane 9: 5 μM **1**, lane 10: 50 μM **1**). Methods: DNA cleavage by calicheamicin was performed as follows: The [5'-^{32}P]-labeled, *TCCTATAGGA*-containing DNA oligomer was incubated at 95 °C for 3 min and then cooled slowly to 25 °C over 1 h. An aliquot of the oligomer was added to a reaction mixture containing 20 mM NaCl, 30 mM Tris-HCl (pH 7.5), 10% DMSO (v/v), and varying concentrations of oligosaccharide **1** or **2** in a final volume of 40 μL, and the mixture was incubated at 37 °C for 20 min. Calicheamicin-dependent DNA cleavage was initiated by addition of 2 μL of 2-mercaptoethanol to attain a final concentration of 50 mM. Aliquots of 3 μL of reaction mixture were transferred to a dry, ice-cooled Eppendorf tube. An equal volume of gel loading buffer, containing 96% formamide, 7.5 mM Na_2EDTA 0.05% (w/v), bromophenol blue, and 0.05% (w/v) xylene cyanol, was added and the sample was stored at −70 °C until loading. Tris = tris(hydroxymethyl)aminoethane. DMSO = dimethyl sulfoxide, EDTA = ethylenediaminetetraacetic acid.

[1] K. C. Nicolaou, W.-M. Dai, *Angew. Chem.* **1991**, *103*, 1453; *Angew. Chem. Int. Ed. Engl.* **1991**, *30*, 1387.
[2] J. W. Lown, *Chemtracts* **1993**, *6*, 205.
[3] P. E. Nielsen, *Bioconjugate Chem.* **1991**, *2*, 1.
[4] E. Uhlmann, A. Peyman, *Chem. Rev.* **1990**, *90*, 543.
[5] P. B. Dervan in *Nucleic Acids and Molecular Biology, Vol. 2* (Ed.: F. Eckstein, D. M. J. Lilley), Springer, Heidelberg, **1988**, pp. 49–64.
[6] P. B. Dervan in *Oligodeoxynucleotides: Antisense of Gene Expression* (Ed.: J. S. Cohen), CRC Press, Boca Raton, FL, **1989**, pp. 197–210.
[7] C. Helene, J.-J. Toulme in *Oligodeoxynucleotides: Antisense of Gene Expression* (Ed.: J. S. Cohen), CRC Press, Boca Raton, FL, **1989**, pp. 137–172.
[8] M. D. Lee, K. M. Manning, D. R. Williams, N. A. Kuck, R. T. Testa, D. B. Borders, *J. Antibiot.* **1989**, *42*, 1070.
[9] T. Li, Z. Zeng, V. A. Estevez, K.-U. Baldenius, K. C. Nicolaou, G. F. Joyce, *J. Am. Chem. Soc.* **1994**, *116*, 3709.
[10] K. C. Nicolaou, S.-C. Tsay, T. Suzuki, G. F. Joyce, *J. Am. Chem. Soc.* **1992**, *114*, 7555.
[11] L. Gomez-Paloma, J. A. Smith, W. J. Chazin, K. C. Nicolaou, *J. Am. Chem. Soc.* **1994**, *116*, 3697.
[12] K. C. Nicolaou, R. D. Groneberg, T. Miyazaki, N. A. Stylianides, T. J. Schulze, W. Stahl, *J. Am. Chem. Soc.* **1990**, *112*, 8193. A second synthesis of **1** appeared later: R. L. Halcomb, S. H. Boyer, S. J. Danishefsky, *Angew. Chem.* **1992**, *104*, 314; *Angew. Chem. Int. Ed. Engl.* **1992**, *31*, 338.
[13] S. N. Ho, S. H. Boyer, S. L. Schreiber, S. J. Danishefsky, G. R. Crabtree, *Proc. Natl. Acad. Sci. USA*, **1994**, *91*, 9203.
[14] The TCCT site may be interchanged with a TCTC or a TTTT site, see refs. [9–11], and references therein.
[15] S. L. Walker, A. H. Andreotti, D. E. Kahne, *Tetrahedron* **1994**, *50*, 1351.
[16] J. Aiyar, S. J. Danishefsky, D. M. Crothers, *J. Am. Chem. Soc.* **1992**, *114*, 7552.
[17] K. C. Nicolaou, C. W. Hummel, M. Nakada, K. Shibayama, E. N. Pitsinos, H. Saimoto, Y. Mizuno, K.-U. Baldenius, A. L. Smith, *J. Am. Chem. Soc.* **1993**, *115*, 7625.
[18] All new compounds provided satisfactory spectroscopic and analytical data.
[19] Selected spectroscopic and physical properties of **2**, **4**, and **5**. **2**: Colorless solid: $R_f = 0.52$ (silica gel, MeOH/CH_2Cl_2 1/4); $[\alpha]_D^{23} = -41$ ($c = 0.50$, MeOH); IR (neat): $\tilde{\nu}_{max} = 3600-3200, 2973, 2933, 1673, 1455, 1416, 1392, 1319, 1239, 1100, 1066, 959\ cm^{-1}$; ^1H NMR (500 MHz, CD_3OD): $\delta = 5.62$ (br. s, 2H, D-1), 5.43 (br. s, 2H, E-1), 5.09 (br. d, $J = 10.0$ Hz, 2H, B-1), 4.49 (br. s, 2H, D-2), 4.38 (d, $J = 8.0$ Hz, 2H, A-1), 4.25 (br. s, 2H, B-3), 4.18 (dq, $J = 9.5$, 6.0 Hz, 2H, D-5), 4.06 (dq, $J = 10.5$, 6.5 Hz, 2H, B-5), 4.01–3.92 (m, 4H, E-5, C*H*HCH$_2$OCH$_2$C*H*H), 3.96 (dd, $J = 9.5$, 9.5 Hz, 2H, A-3), 3.92 (s, 6H, CH_3O), 3.87 (s, 6H, CH_3O), 3.84–3.71 (m, 12H, B-4, D-3, E-5′, CH*H*CH$_2$OC*H*$_2$CH*H*), 3.69 (dq, $J = 9.5$, 6.5 Hz, 2H, A-5), 3.61 (dd, $J = 9.5$, 9.5 Hz, 2H, D-4), 3.57 (s, 6H, CH_3O), 3.42 (s, 6H, CH_3O), 3.37 (dd, $J = 9.5$, 8.0 Hz, 2H, A-2), 2.89 (m, 2H, E-4), 2.80 (m, 4H, 2 × CH_3CH_2N), 2.47 (m, 2H, E-2$_{eq}$), 2.38 (s, 6H, ArCH_3), 2.28 (dd, $J = 9.5$, 9.5 Hz, 2H, A-4), 2.00 (m, 2H, B-2$_{eq}$), 1.79 (m, 2H, B-2$_{ax}$), 1.50 (m, 2H, E-2$_{ax}$), 1.41 (d, $J = 6.5$ Hz, 6H, B-6), 1.39 (d, $J = 6.5$ Hz, 6H, A-6), 1.28 (d, $J = 6.0$ Hz, 6H, D-6), 1.22 (br. t, $J = 6.8$ Hz, 6H, 2 × CH_3CH_2N); ^{13}C NMR (125 MHz, CD_3OD): $\delta = 194.1$, 153.2, 152.0, 144.6, 134.5, 132.5, 99.8, 94.2, 81.7, 80.6, 77.1, 72.6, 72.3, 72.1, 71.6, 71.3, 70.5, 69.4, 69.3, 69.3, 68.2, 62.3, 61.5, 59.9, 57.5, 56.2, 42.7, 41.6, 39.0, 35.2, 25.7, 19.4, 18.8, 14.7, 10.0; MS (positive ion ESI): m/z 1996; $[(M + H)^+]$, calcd for $C_{78}H_{124}I_2N_4O_{35}S_2$: 1996. – **4**: Colorless solid; $R_f = 0.15$ (silica gel, 2% MeOH in CH_2Cl_2); $[\alpha]_D^{23} = -21$ ($c = 1.7$, $CHCl_3$); IR (neat): $\tilde{\nu} = 2953, 2926, 2876, 1694, 1682, 1454, 1260, 1084, 1017\ cm^{-1}$; ^1H NMR (500 MHz, [D$_6$]DMSO, 80 °C): $\delta = 7.84$ (d, $J = 7.5$ Hz, 2H, FMOC), 7.63 (d, $J = 7.5$ Hz, 2H, FMOC), 7.39 (dd, $J = 7.5$, 7.5 Hz, 2H, FMOC), 7.31 (dd, $J = 7.5$, 7.5 Hz, 2H, FMOC), 5.42–5.37 (m, 2H, B-1, D-1), 5.08 (br. s, 1H, E-1), 4.75 (q, $J = 6.5$ Hz, 1H, A-5), 4.47–4.38 (m, 5H, A-1, B-3, D-2, CH_2-FMOC), 4.28 (t, $J = 6.0$ Hz, 1H, benzyl. FMOC), 4.22 (br. s, 1H, A-3), 4.05 (dq, $J = 9.0$, 6.5 Hz, 1H, D-5), 4.00 (dq, $J = 10.0$, 6.5 Hz, 1H, B-5), 3.84–3.72 (m, 5H, A-2, E-3, E-5, E-5′, C*H*HCH$_2$OCH$_2$CH$_2$OH), 3.82 (s, 3H, CH_3O), 3.78 (s, 3H, CH_3O), 3.70 (dd, $J = 9.0$, 9.0 Hz, 1H, D-4), 3.68 (dd, $J = 10.0$, 2.5 Hz, 1H, B-4), 3.66–3.42 (m, 8H, D-3, CH*H*CH$_2$OC*H*$_2$CH$_2$OH), 3.40 (s, 3H, CH_3O), 3.31 (m, 1H, E-4), 3.17 (s, 3H, CH_3O), 2.31 (s, 3H, ArCH_3), 2.24 (m, 1H, E-2$_{eq}$), 1.98 (m, 2H, B-2$_{eq,ax}$), 1.44 (d, $J = 6.5$ Hz, 3H, A-6), 1.29 (d, $J = 6.5$ Hz, 3H, B-6) 1.17 (d, $J = 6.5$ Hz, 3H, D-6), 0.99–0.91 (m, 36H, 4 × Si(CH$_2$C*H*$_3$)$_3$), 0.67–0.58 (m, 27H, 4 × Si(C*H*$_2$CH$_3$)$_3$, C*H*$_3$CH$_2$N); MS (positive ion ESI): m/z 1750; $[(M + Na)^+]$, calcd for $C_{80}H_{131}IN_2O_{21}SSi_4$: 1750. – **5**: Colorless solid; $R_f = 0.46$ (silica gel, ether/petroleum ether 1/1); $[\alpha]_D^{23} = -14$ ($c = 0.99$, $CHCl_3$); IR (neat): $\tilde{\nu} = 2954, 2936, 2876, 1700, 1456, 1417, 1239, 1140, 1085, 1016, 1004\ cm^{-1}$, ^1H NMR (500 MHz, [D$_6$]DMSO, 80 °C): $\delta = 7.83$ (d, $J = 7.5$ Hz, 4H, FMOC), 7.62 (d, $J = 7.0$ Hz, 4H, FMOC), 7.38 (dd, $J = 7.5$, 7.5 Hz, 4H, FMOC), 7.30 (dd, $J = 7.5$, 7.0 Hz, 4H, FMOC), 5.42–5.37 (m, 4H, B-1, D-1), 5.08 (br. s, 2H, E-1), 4.73 (q, $J = 7.0$ Hz, 2H, A-5), 4.45–4.37 (m, 10H, A-1, B-3, D-2, CH_2-FMOC), 4.26 (t, $J = 6.0$ Hz, 2H, benzyl. FMOC), 4.22 (br. s, 2H, A-3), 4.05 (dq, $J = 9.0$, 6.5 Hz, 2H, D-5), 3.99 (dq, $J = 10.5$, 6.5 Hz, 2H, B-5), 3.83–3.73 (m, 10H, A-2, E-3, E-5, E-5′, C*H*HCH$_2$OCH$_2$C*H*H), 3.81 (s, 6H, CH_3O), 3.77 (s, 6H, CH_3O), 3.70 (dd, $J = 9.0$, 9.0 Hz, 2H, D-4), 3.67 (dd, $J = 10.5$, 2.5 Hz, 2H, B-4), 3.63–3.52 (m, 8H, D-3, CH*H*CH$_2$OCH$_2$CH*H*), 3.39 (s, 6H, CH_3O), 3.32 (m, 2H, E-4), 3.16 (s, 6H, CH_3O), 2.31 (s, 6H, ArCH_3), 2.23 (m, 2H, E-2$_{eq}$), 1.95 (m, 4H, B-2$_{eq,ax}$), 1.43 (d, $J = 7.0$ Hz, 6H, A-6), 1.28 (d, $J = 6.5$ Hz, 6H, B-6), 1.16 (d, $J = 6.5$ Hz, 6H, D-6), 0.98–0.90 (m, 72H, 8 × Si(CH$_2$C*H*$_3$)$_3$); MS (positive ion ESI): m/z 3394; $[M_{AVE} - 2H^+ + 2Na^+]$, calcd for $C_{156}H_{252}I_2N_4O_{39}S_2Si_8$: 3394.
[20] The details of these NMR studies will be reported elsewhere in due course.
[21] We thank Drs. Peter Vogt and Chen Liu for their results. These and related studies will be reported in due course.

Spherical Cyclophosphazene Dendrimers to the Fifth Generation**

François Sournies, François Crasnier, Marcel Graffeuil, Jean-Paul Faucher, Roger Lahana, Marie-Christine Labarre, and Jean-François Labarre*

Dendrimers, that is, highly branched functionalized molecules formed by iterative reaction sequences, constitute a definite breakthrough into generations of new materials and are attracting considerable attention in organic, supramolecular, and polymer chemistry.[1] Only few of these macromolecules incorporate main group elements such as silicon,[2] germanium,[3] or phosphorus,[4] and only phosphorus dendrimers having charges within the cascade structure had been described[4] till very recently when two kinds of neutral phosphorus dendrimers were reported concomitantly by Majoral et al.[5] and by our group.[6, 7] Majoral's dendrimers have a structure resembling a cauliflower, with $SPCl_3$ as the core and possess 46 pentavalent phosphorus atoms and 48 terminal functions (aldehydic groups or phosphorus–chlorine bonds; molecular weight 11268 or 15381). His group is now synthesizing further generations having up to 384 functional groups (molecular weight 94146).[8]

Our dendrimers are spherical architectures which were designed from previously skillfully synthesized D_{3h} cyclophosphazene cores. Indeed, we recently reported[6, 7] pure cyclophosphazenic hexapodanes (termed sexapus because of the six tentacles, in analogy to an octopus) synthesized through a regiospecific peraminolysis of hexachlorocyclotriphosphazene ($N_3P_3Cl_6$) by long-chain diamines, $H_2N(CH_2)_nNH_2$ ($n \geq 6$), on ALPOT(50:11), that is, on alumina impregnated with a certain amount of potassium hydroxide.[9] These sexapus units are 3-dimensional polyfunctional cores suitable for generating spherical cyclophosphazene dendrimers (that is, resembling the structure of a dry dandelion flower and not of a cauliflower like Tomalia's dendrimers[1]). An attempt at the production of spheroid dendrimers belonging to carbon chemistry was recently made by

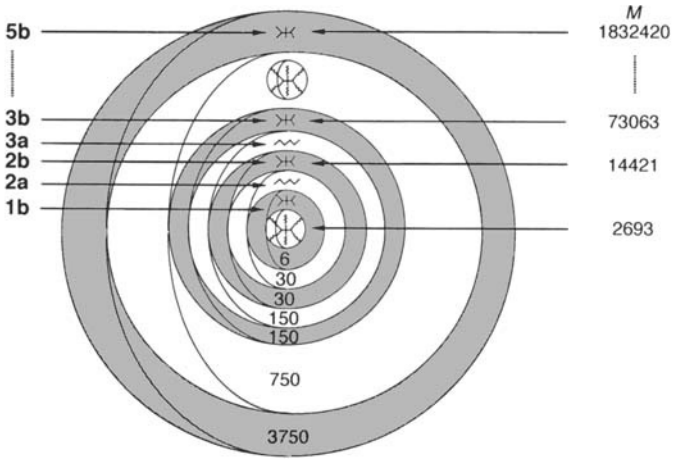
[*] Dr. J.-F. Labarre, Dr. F. Sournies, Dr. F. Crasnier, Dr. M. Graffeuil, Dr. J.-P. Faucher, Dr. M.-C. Labarre
Institut de Chimie Moléculaire Paul Sabatier, Laboratoire Structure & Vie
Université Paul Sabatier, 118 route de Narbonne
F-31062 Toulouse Cedex (France)
Telefax: Int. code + 61 251733
Dr. R. Lahana
Oxford Molecular SA, X-Pole, Ecole Polytechnique
F-91128 Palaiseau Cedex (France)

[**] On the Scent of Dandelion Dendrimers. Part 3. The authors are greatly indebted to the Université Paul Sabatier (ACRU 1993–1994) and the French Ministery of Education (66.71.50) for their generous financial support to this work. Sincere thanks are due to Dr. Suzanne Richelme who performed DCI/NH_3 and FAB measurements and to Dr. Alain Dall'Ava for ^{31}PNMR spectra. Part 2: [7].

Frechet[10] "through the linkage of two cauliflowers by their stumps", but such dendrimers are just spheroids and not, in a strict sense, spherical objects.

Scheme 1 shows that the amino end groups of tentacles in sexapus **1a** are accessible to further nucleophilic attacks. Our dendrimer design is based on a two-step process. In the first step $N_3P_3Cl_5$ flagstones (pentafunctional fans) are grafted at the end of each tentacle to give compounds **1b** (or generation 1) and in the second step the chlorine atoms of the $N_3P_3Cl_5$ flagstones are all substituted by a new set of long-chain diamines ($H_2N(CH_2)_n$-NH_2, $n \geq 6$) as linkers to give compounds **2a**. In other words, the linkage of such $N_3P_3Cl_5$ flagstones on sexapus cores leads to first-generation dendrimers, in which the number of linkers for further extension is multiplied by five with respect to the starting $N_3P_3Cl_6$ itself. Thus, every two-step procedure from **1b** yields a new generation. In this paper we report on the synthesis and structural characterization of such dendrimers from sexapus cores till the fifth generation (**5b**). Moreover, the chemical properties of dendrimers of the first (**1b**) and second (**2b**) generations were investigated to discover more about the point where steric congestion and/or loss of solubility will prevent further growth of the dendrimer.

The expected first-generation dendrimers **1b** are actually polybino structures,[11] and we demonstrated previously that the synthesis of such two-ring, bridged assemblies requires the use of polar solvents. In other words, toluene (which was used to obtain



Scheme 2. A general pattern for the step by step synthesis of dendrimers to the fifth generation. Left are the formula numbers, right the molecular weights M (for $n = 6$) of the first, second, third, and fifth generations, and in the middle the structural formulas of the added unit (top) and number of functionalities (bottom).

cores **1a**) is no longer the right solvent for reaction (a) and has to be replaced by diethyl ether. In addition, Et_3N was required

$$N_3P_3[HN(CH_2)_nNH_2]_6 + 6\,N_3P_3Cl_6 \longrightarrow N_3P_3[HN(CH_2)_nNH(N_3P_3Cl_5)]_6 + 6\,HCl \quad \text{(a)}$$

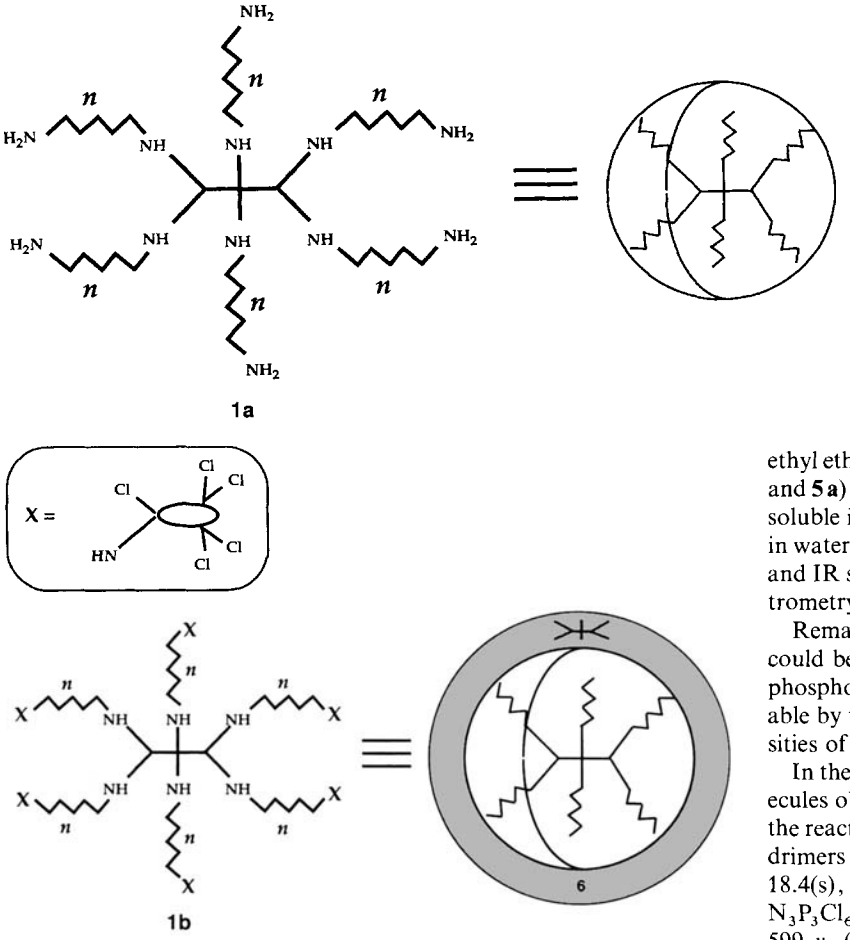
sexapus **1a** → **1b**

for scavenging hydrogen chloride. Incidentally, when ALPOT(50:11) is used, irrespective of the choice of solvent, no eluent can be found to remove the final products from the solid support.

Further elaboration to cascade molecules of the second (**2b**), third (**3b**), fourth (**4b**), and fifth generation (**5b**) is accomplished by repetition of the two-step procedure (Scheme 2). In each step, reactants are introduced in the correct stoichiometry. The only by-products are hydrogen chloride and the related hydrochlorides! All the compounds of the generations are stable and perfectly soluble in a wide variety of organic solvents (for example, chloroform, diethyl ether). All the intermediate compounds (**2a**, **3a**, **4a**, and **5a**) with amino groups at the periphery are no longer soluble in the organic solvents but are noticeably soluble in water. All the dendrimers were characterized by NMR and IR spectroscopy, and elemental analysis. Mass spectrometry (FAB or electron spray) was useful up to **2a**.

Remarkably, the construction of each generation could be easily followed by ^{31}P NMR spectroscopy: all phosphorus centers of each generation are distinguishable by their ^{31}P NMR chemical shifts and by the intensities of the different signals.

In the following we shall describe various cascade molecules obtained from sexapus **1a**, $n = 6$. Physical data of the reactants for the synthesis of the first-generation dendrimers **1b** are as follows: for the sexapus: $\delta(^{31}P) = 18.4$(s), m/z (MH^+) 826, $\nu(NH_2)$ 3410 cm^{-1} (br.); for $N_3P_3Cl_6$: $\delta(^{31}P) = 20.1$(s), m/z (MH^+) 345, ν_s (PCl) = 599, ν_{as} (PCl) = 520 cm^{-1}. Two days later both singlets at $\delta = 18.4$ and 20.1 had disappeared, and the signals of an A_2B system (peripheral PCl_2 and peripheral PClNH) to-



Scheme 1. Sexapus cores (**1a**), the precursors of dendrimers of the first generation (**1b**). Zigzag lines marked with n represent $(CH_2)_n$ chains within the -$HN(CH_2)_nNH_2$ tentacles. The central N_3P_3 ring has the bow-tie form proposed by R. A. Shaw.

 © VCH Verlagsgesellschaft mbH, D-69451 Weinheim, 1995 0570-0833/95/0505-0579 $ 10.00+.25/0

gether with the singlet of the phosphorus atoms from the core are revealed. Simultaneously, the symmetric and asymmetric PCl stretching modes from $N_3P_3Cl_6$ at 599 and 520 cm^{-1}, respectively, are replaced by modes at 589 and 513 cm^{-1}, which are characteristic for the first-generation dendrimers **1b**. Moreover, the NH_2 stretching frequency of the starting sexapus at 3410 cm^{-1} is no longer observed, but a unique N–H stretching frequency remains at 3234 cm^{-1}. In other words, ^{31}P NMR and FTIR spectroscopies are sufficient to characterize **1b**, $n = 6$.

The second-generation dendrimers **2b** are obtained through nucleophilic substitution of the 30 chlorine atoms of the first-generation **1b** by 30 diamino groups (leading to **2a**) and subsequent grafting of 30 $N_3P_3Cl_5$ moieties on the ends of the 30 new tentacles. Because this aminolysis on ALPOT(50:11) gave very poor yields ($\leq 25\%$), we chose Et_3N as scavenger for HCl and a polar solvent such as Et_2O. After 48 h the resulting light yellow syrupy oils, which are actually Et_2O-clathrates, are stirred (about 12 h) with large excess of *n*-heptane to afford the declathrated species as white powders.

The physical data for **2a** are as follows: $\delta(^{31}P) = 18.8$ (s, major signal), 19.3, 22.0 (each s, minor signals), $\nu_s(NH_2) = 3393\ cm^{-1}$, $\nu_{as}(NH_2) = 3333\ cm^{-1}$, $\delta(NH_2) = 1583\ cm^{-1}$.

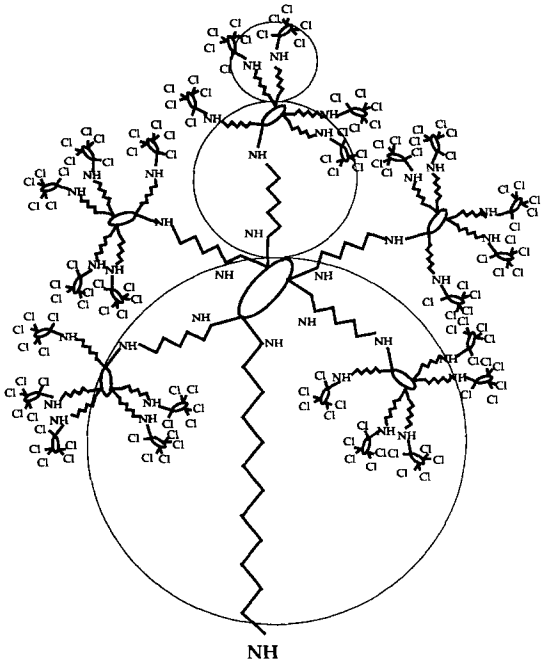
The transformation from **2a** to **2b** occurs upon grafting 30 $N_3P_3Cl_5$ moieties on the ends of the 30 tentacles. Modifications to ^{31}P NMR and FTIR data are strictly identical to the ones we described above when comparing the spectra from the sexapus **1a** and the first-generation dendrimers **1b**, that is, replacement of a ^{31}P NMR singlet by an A_2B system together with emergence of $\nu_s(PCl)$ and $\nu_{as}(PCl)$ stretching frequencies.

The purity of the products at each step was checked by thin layer chromatography with toluene/CCl_4 (3:1) as eluent. A unique spot was observed till the third-generation **3b**, where a minor side-spot appeared. Apparently this impurity corresponds to an incompletely substituted species in which some amino end groups of **3a** do not react with the $N_3P_3Cl_5$ moieties. This assumption is supported by the fact that final products **3b** are not fully soluble in organic solvents (as any compound of any generation of type **b** should be); a small amount (less than 10% in weight) is insoluble in organic solvents but soluble in water (like any precursor of type **a**).

In other words, at the level of third-generation dendrimers **3b**, about 10% excess $N_3P_3Cl_6$ rather than the strict 1:30 stoichiometry is required to obtain the compounds quantitatively. Nevertheless, further precursors and generations of dendrimers from sexapus cores may be synthesized till the fifth generation, but the amount of impurities (that is, species not completely substituted) increases slowly but steadily with the size of molecules. An efficient approach for circumventing this difficulty is based on the following consideration: the three steps consisting of the successive graft of *n* linkers, *n* $N_3P_3Cl_5$ fans, and another 5n linkers are strictly identical to the graft of *n* sexapus molecules! In Scheme 2, compounds **5a**, which are precursors of **5b**, were synthesized from compounds **3b** in this way. Such a procedure sharply decreases the risk of generating impurities.

In our opinion, cyclophosphazene dendrimers are Unusual Fascinating Objects (UFOs!) built from "fractal" structures (Scheme 3) where the chaining (one diamino tentacle plus one $N_3P_3Cl_5$ fan) can be repeated ad libitum. The upper limit to these constructions will be given by mathematics[12] or chemistry or both.

The structures of compounds **1b**, **2a**, **2b**, and **3a** were calculated with the molecular modeling package MAD[13] on an IBM RISC 6000 station. The units $H_2N(CH_2)_6NH_2$ and $H_2N(CH_2)_6NHN_3P_3Cl_5$ were constructed and their structures minimized; in the conformational analysis a tree-searching algorithm[14] with an extended MM2 force field[15] and a Newton–Raphson minimizer was used. The force field was tuned with results from X-ray structure and electron diffraction analyses. Five iterations were then used to build the full molecule in which steric contacts are avoided (Fig. 1). Careful checking of these structures shows that the limitation of the growth of the dendrimers within the cyclophosphazene series will be more probably due to the progressive filling of the "holes" around the primitive core than to a saturation of peripheral sites as predicted by de Gennes.[12] It seems to us that this important point will have to be given more weight than the "external saturation of active sites on the periphery of the dendrimer" in the design of future dendrimers. Most recently we succeeded in purifying fourth and fifth generations by single SiO_2 column chromatography with *n*-hexane/diethyl ether (2/1) as the eluent and are attempting to obtain crystals of these dendrimers.



Scheme 3. The "fractal" structure of the third-generation dendrimers.

Experimental Procedure

The ^{31}P NMR spectra were recorded on a Bruker AC 200 Spectrometer with H_3PO_4 (85%) as external reference. DCI and FAB mass spectra were recorded on a Ribermag R1010-H Quadrupole Mass Spectrometer. Hexachlorocyclotriphosphazene (degree of purity $\geq 99.8\%$) was generously donated by Shin Nisso Kako Co. Fluka supplied us with the primary diamines (degree of purity $\geq 98\%$).

Alumina-supported potassium hydroxide: Potassium hydroxide (Prolabo Rectapur, 11 g) in H_2O (250 mL) was mixed with neutral alumina for chromatography (Fluka, type 207 C, 90–110 mesh, 50 g). After stirring for 5 min, the water was removed under reduced pressure. The resulting powder was further dried at 70 °C for 24 h in an oven. This reagent [termed ALPOT(50:11)] may be kept in a desiccator without loss of activity for several months.

Synthesis of **1a**: ALPOT(50:11) (150 g) was first impregnated with a solution of $N_3P_3Cl_6$ in toluene (11.96 g in 400 mL) and the solvent was immediately removed in vacuo at 25 °C to fix $N_3P_3Cl_6$ to the alumina surface. Second, this system was impregnated with a solution of the 1,6-diaminohexane (6 equiv. 24.16 g) in toluene (200 mL), and the solvent was immediately removed in vacuo as before. Washing of the solid support twice with 200 mL portions of toluene gave **1a**, $n = 6$ (15.75 g, 55.5%). ^{31}P NMR (81.015 MHz): $\delta = 18.3$ (s); DCI/NH_3 MS: *m/z*: 826 (MH^+), 710 ($M^+ - HN(CH_2)_6NH_2$), 594 ($M^+ - 2(HN(CH_2)_6NH_2)$); FAB-MS (glycerol/thioglycerol (80/20) as matrix): *m/z* 826, 710, 594, 498 (M^+-3 ($HN(CH_2)_6NH_2$)). Thus, aminolysis of $N_3P_3Cl_6$ by 1,6-diaminohexane on ALPOT(50:11) yields instantaneously the pure hexadangling (or hexapodane) sexapus **1a**, $n = 6$ as a hygroscopic microcrystalline white powder (m.p. 39 °C). Moreover, the persubstitution of the 6 Cl atoms of $N_3P_3Cl_6$ by tentacles is accompanied by a vanishing of both strong

 © VCH Verlagsgesellschaft mbH, D-69451 Weinheim, 1995 0570-0833/95/0505-0580 $ 10.00+.25/0

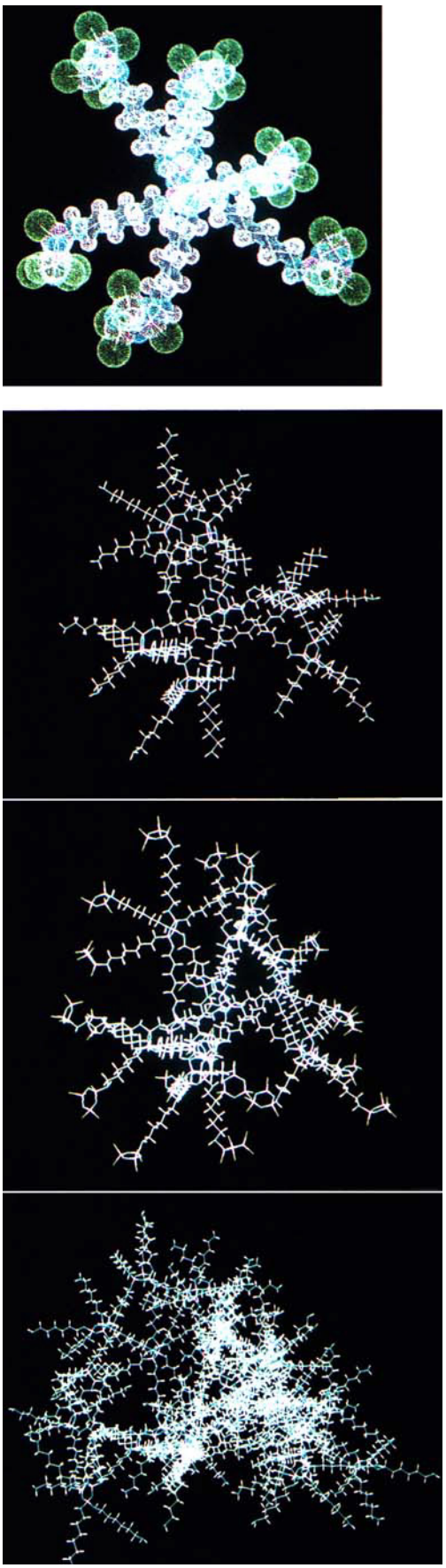


Fig. 1. From top to bottom: Structures of dendrimers **1b**, **2a**, **2b**, and **3a** from molecular modeling studies.

vibrational bands ν_s(PCl) and ν_{as}(PCl) of $N_3P_3Cl_6$ at 600 and 520 cm^{-1} and the emergence of ν(NH) bands at 3382 and 3319 cm^{-1}.

Synthesis of **1b**, $n = 6$: The reaction (a) was performed in Et_2O with Et_3N as HCl scavenger. The reaction was considered complete after 48 h when the singlet of **1a**, $n = 6$ in the ^{31}P NMR spectrum had disappeared. The product was soluble in $CDCl_3$. ^{31}P NMR (81.015 MHz): A_2B system (δ(PClNH) = 18.7 (t), $\delta(PCl_2)$ = 21.3 (d, ^2J(P,P) = 46.6 Hz), δ(P,core) = 22.0 (s). FAB-MS (*meta*-nitrobenzyl octyl ether (MNBE) as matrix): *m/z*: 2693 (M^+). We had to use MNBE instead of the more common glycerol/thioglycerol mixture as the matrix, because the 30 chlorine atoms of **1b**, $n = 6$ are substituted in situ by glyceryl and thioglyceryl groups, which led to molecules with masses much larger than 2000, beyond the threshold of response of the detector. The IR spectrum reveals an emergence of one ν(NH) band at 3234 cm^{-1} and no PCl band in the 400–600 cm^{-1} range.

Compounds **2a/2b**, **3a/3b**, **4a/4b**, and **5a/5b** with $n = 6$ were synthesized analogously to **1a** and **1b**, under the respective stoichiometric conditions. Average yields: **1a** → **1b** 90%, **1b** → **2a** 67%, **2a** → **2b** 75%, **2b** → **3a** 77%, **3a** → **3b** 80%, **3b** → **4a** 65%, **4a** → **4b** 92%, **4b** → **5a** 69%, and **5a** → **5b** 80%. The overall yield for the target molecule **5b** was thus 9%. However, in terms of molecular weights, 1 g of **1a** yields 199 g of **5b**.

Microanalytical data are not reported here, because the huge variations with respect to the carbon and chlorine content from one step to the next makes identification of each step unambiguous [6].

Received: October 10, 1994 [Z 7387 IE]
German version: *Angew. Chem.* **1995**, *107*, 610

Keywords: dendrimers · phosphorus compounds

[1] Reviews: D. A. Tomalia, A. M. Naylor, W. A. Goddard III, *Angew. Chem.* **1990**, *102*, 119; *Angew. Chem. Int. Ed. Engl.* **1990**, *29*, 138; H. B. Mekelburger, W. Jaworek, F. Vögtle, *ibid.* **1992**, *104*, 1609 and **1992**, *31*, 1571; M. F. Ottaviani, S. Bossmann, N. J. Turro, D. A. Tomalia, *J. Am. Chem. Soc.* **1994**, *116*, 661, and references therein.

[2] H. Uchida, Y. Kabe, K. Yoshino, A. Kawamata, T. Tsumuraya, S. Masamune, *J. Am. Chem. Soc.* **1990**, *112*, 7077; L. J. Mathias, T. W. Carothers, *ibid.* **1991**, *113*, 4043; E. A. Rebrov, A. M. Muzafarov, V. S. Papkov, A. A. Zhdanov, *Dokl. Akad. Nauk SSSR* **1989**, *309*, 376; A. W. van der Made, P. W. N. M. van Leeuwen, *J. Chem. Soc. Chem. Commun.* **1993**, 1400; D. Seyferth, D. Y. Son, A. L. Rheingold, R. L. Ostrander, *Organometallics* **1994**, *13*, 2682.

[3] P. Mazerolles, V. Huc, unpublished results.

[4] K. Rengan, R. Engel, *J. Chem. Soc. Chem. Commun.* **1990**, 1084; *J. Chem. Soc. Perkin Trans. 1* **1991**, 987; R. Engel, K. Rengan, C. S. Chan, *Phosphorus Sulfur Silicon Relat. Elem.* **1993**, *77*, 221.

[5] N. Launay, A.-M. Caminade, R. Lahana, J.-P. Majoral, *Angew. Chem.* **1994**, *106*, 1682; *Angew. Chem. Int. Ed. Engl.* **1994**, *33*, 1589.

[6] F. Sournies, L. Labrousse, M. Graffeuil, F. Crasnier, J.-P. Faucher, M.-C. Labarre, J.-F. Labarre, *Phosphorus Sulfur Silicon Relat. Elem.* **1994**, *89*, 47.

[7] F. Sournies, C. Fouga, M. Graffeuil, J.-P. Faucher, F. Crasnier, M.-C. Labarre, J.-F. Labarre, *Phosphorus Sulfur Silicon Relat. Elem.* **1994**, *90*, 159.

[8] N. Launay, A.-M. Caminade, J.-P. Majoral, *J. Am. Chem. Soc.*, in press.

[9] F. Sournies, M. Graffeuil, B. Séguès, F. Crasnier, D. Semenzin, G. Etemad-Moghadam, M. Koenig, J.-F. Labarre, *Phosphorus Sulfur Silicon Relat. Elem.* **1994**, *86*, 1; B. Séguès, F. Sournies, F. Crasnier, J.-F. Labarre, *ibid.* **1994**, *88*, 123.

[10] J. M. J. Fréchet, *Science* **1994**, *263*, 1710.

[11] Bino represents a unit comprising two N_3P_3 rings and one diamino bridge: G. Guerch, J.-F. Labarre, R. Lahana, R. Roques, F. Sournies, *J. Mol. Struct.* **1983**, *99*, 275; P. Castera, J.-P. Faucher, M. Granier, J.-F. Labarre, *Phosphorus Sulfur Relat. Elem.* **1987**, *32*, 37.

[12] P. G. de Gennes, H. Hervet, *J. Phys. Lett.* **1983**, *44*, L 351.

[13] The program MAD is available from Oxford Molecular Ltd., Oxford Science Park, The Magdalen Centre, GB-Sandford on Thames, OX44GA Oxford (UK).

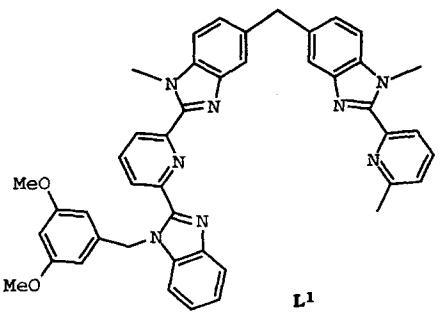
[14] M. Lipton, C. Still, *J. Comput. Chem.* **1988**, *9*, 343.

[15] N. L. Allinger, Y. H. Yuh, J.-H. Lii, *J. Am. Chem. Soc.* **1989**, *111*, 8551.

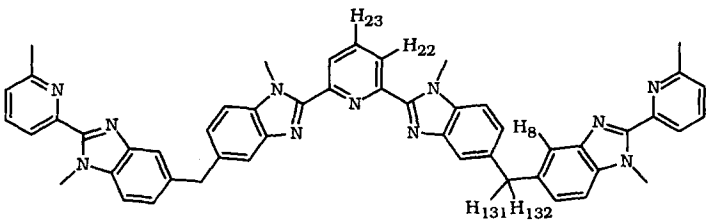
Formation of the First Isomeric [2]Catenates by Self-Assembly about Two Different Metal Ions**

Claude Piguet,* Gérald Bernardinelli, Alan F. Williams, and Bernard Bocquet

The control of molecular structures and topologies is a major goal in supramolecular chemistry,[1] and the self-assembly of tailored ligands with metal ions has been extensively used to produce organized architectures.[2-4] Double-helical,[2-5] triple-helical,[4, 6, 7] toroidal,[8] and cylindrical[9] homopolynuclear structures have been generated by the complexation of oligo(multidentate) ligands to two or more metal ions. The recent development of new segmental ligands with different binding units connected by suitable spacers[10] leads to programmed heteropolynuclear complexes where each metal ion occupies a coordination site corresponding to its stereochemical preferences.[11, 12] Thus, it was shown recently that ligand $\mathbf{L^1}$, containing both bi- and tridentate binding units (Scheme 1), reacts with a mixture of Fe^{II} and Ag^{I} ions to give the self-assembled heterodinuclear double-helical complex $[FeAg(\mathbf{L^1})_2]^{3+}$, where the Fe^{II} ion is pseudooctahedrally coordinated by the two tridentate units and the Ag^{I} center lies in the pseudotetrahedral site defined by the two remaining bidentate units.[11]



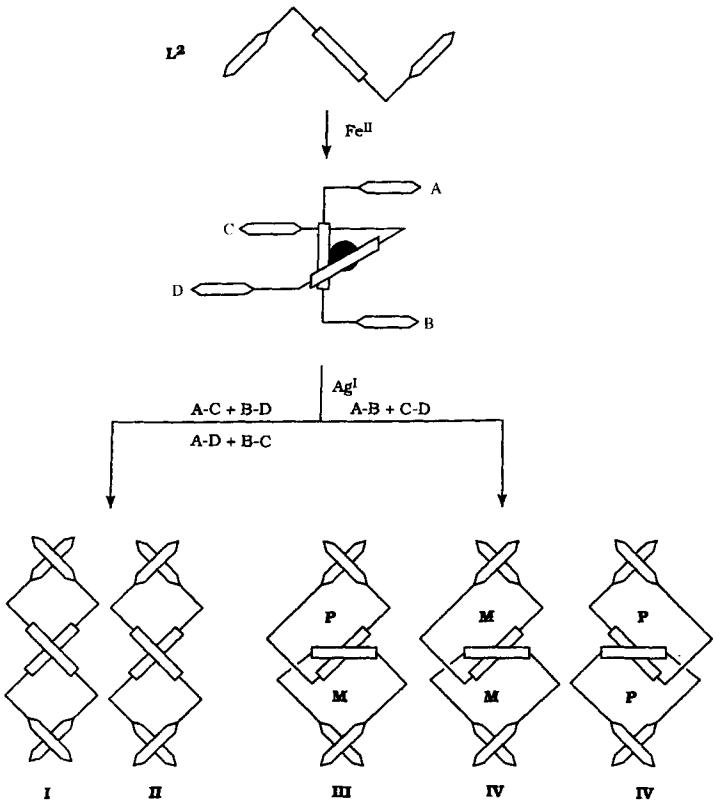
$\mathbf{L^1}$



$\mathbf{L^2}$

Scheme 1. Structures of the segmental ligands $\mathbf{L^1}$ and $\mathbf{L^2}$.

The ligand 1,1'-dimethyl-2,2'-bis(6-methylpyridin-2-yl)-5,5'-{pyridine-2,6-diylbis[(1-methyl-1*H*-benzimidazole-2,5-diyl)-methylene]}bis[1*H*-benzimidazole] ($\mathbf{L^2}$),[10] a logical extension of $\mathbf{L^1}$, similarly self-assembles with Fe^{II} and Ag^{I} ions in acetonitrile to give the heterotrinuclear complex $[FeAg_2(\mathbf{L^2})_2]^{4+}$, where the Fe^{II} center is pseudooctahedrally coordinated by the two tridentate binding units and each Ag^{I} ion is pseudotetrahedrally bound to two bidentate units.[11] Depending on which bidentate units bind to Ag^{I}, more than one organometallic macrocycle[13] may be envisaged leading to different topological isomers.[14] When the Ag^{I} ions are coordinated to bidentate units of different strands (A-D + B-C or A-C + B-D; Scheme 2), double-helical (**I**) or side-by-side (**II**) structures are expected; coordination of the Ag^{I} ions to the two bidentate units of the same strand (A-B + C-D) leads to the [2]catenates **III** and **IV**. In structures **III** and **IV** each organometallic macrocycle is itself helical and has either P or M helicity.[15] This leads to two isomers, the heterochiral, S_4-symmetric *meso* form **III** and the homochiral, D_2-symmetric **IV**, which exists as a pair of enantiomers (Scheme 2).



Scheme 2. Self-assembly of heterotrinuclear supramolecular complexes of $\mathbf{L^2}$ with Fe^{II} and Ag^{I} ions. ⬭ corresponds to a bidentate unit, ▭ a tridentate unit. **I** is a helical, D_2-symmetric structure, **II** a D_2-symmetric, side-by-side structure, **III** a S_4-symmetric (*P*,*M*)-[2]catenate, and **IV** D_2-symmetric (*M*,*M*)- and (*P*,*P*)-[2]catenates.

Crystallization of $[FeAg_2(\mathbf{L^2})_2](PF_6)_4$ gives dark violet crystals with two different morphologies, hexagonal prisms **A** and large pellets **B**, both of which were suitable for X-ray diffraction studies. The crystal structure of **A** corresponds to the formula $[FeAg_2(\mathbf{L^2})_2](PF_6)_4(CH_3OH)_{2.5}(H_2O)$ and shows it to be composed of the cation $[FeAg_2(\mathbf{L^2})_2]^{4+}$, four uncoordinated PF_6^- anions, and solvent molecules. The anions and solvent molecules are slightly disordered (see *Experimental Procedure*) but otherwise show no features of interest. The cation $[FeAg_2(\mathbf{L^2})_2]^{4+}$ adopts the [2]catenate structure and not the helix, and lies on a crystallographic C_2 axis passing through the three metal ions. The Fe^{II} center is coordinated by the two tridentate units of the two strands, while each Ag^{I} ion is pseudotetrahedrally bound to two bidentate units of one ligand, produc-

[*] Dr. C. Piguet, Dr. A. F. Williams, B. Bocquet
Département de Chimie Minérale, Analytique et Appliquée
Université de Genève
30 quai Ernest Ansermet, CH-1211 Genève 4 (Switzerland)
Telefax: Int. code +(22) 702 60 69
Dr. G. Bernardinelli
Laboratoire de Cristallographie aux Rayons-X, Université de Genève

[**] This work was supported by the Swiss National Foundation.

ing two helical interlocked organometallic macrocycles of opposite helicity (Figs. 1, 2) which correspond to the *meso*-(P,M) structure **III**. Figure 1 shows an ORTEP[16] stereoview of $[FeAg_2(\mathbf{L^2})_2]^{4+}$ perpendicular to the C_2 axis, and Figure 2 (left) gives a computer-generated representation[17] of the catenate structure in which the two macrocycles are shown in different colors. The intermetallic distances (Ag–Fe 8.156(3), 8.082(3) Å) are only slightly shorter than those reported for

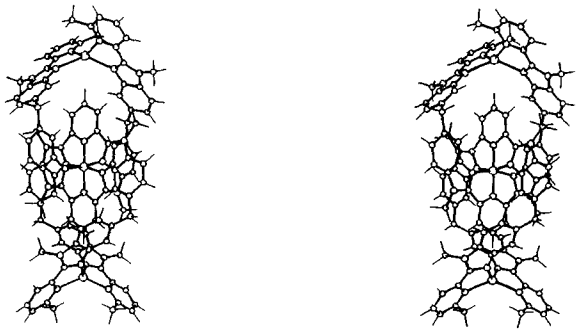


Fig. 1. ORTEP[16] stereoview of the heterochiral (*P*,*M*)-[2]catenate $[FeAg_2(\mathbf{L^2})_2]^{4+}$ perpendicular to the C_2 axis.

triple-helical complexes with similar ligands possessing the same diphenylmethane spacer (8.876(3) Å for a bis(tridentate) ligand[6] and 8.427(4) Å for a bis(bidentate) ligand[18]). This suggests that the catenate structure does not strongly constrain the spacers in $\mathbf{L^2}$. The meridionally coordinated tridentate units are roughly planar (see Table 2) and are maintained mutually perpendicular by pseudooctahedral coordination to the Fe^{II} center (dihedral angle between the mean planes of the aromatic tridentate units: 92.1(1)°). The Fe–N(py) bonds are slightly shorter than the Fe–N(bzim) bonds (py = pyridine, bzim = benzimidazole), but do not significantly deviate from the average value (1.918 Å) and are close to the reported values for $[Fe(\mathbf{L^3})_2]^{2+}$ ($\mathbf{L^3}$ = 2,6-bis(1*H*-benzimidazol-2′-yl)pyridine).[19]

As a result of the small average chelate angle of the bidentate units coordinated to the Ag^I ions (72.5°), the coordination spheres around the Ag^I centers may be best described as D_{2d}-distorted tetrahedrons.[20] However, a flattening along the C_2 axis of the molecule produces further distortions as exemplified by the large N(py)-Ag-N(py) and N(bzim)-Ag-N(bzim) angles (Table 1) and by the dihedral crossing angles between the planes defined by the two coordinated nitrogen atoms and the center Ag^I (81.3(3)° for strand a, 74.6(3)° for strand b; perfect tetrahedron: 90°). The Ag–N(py) bonds are slightly shorter than the Ag–N(bzim) bonds, as found for the Fe–N bonds, but the average value (2.311 Å) is close to the reported Ag–N bond length for the pseudotetrahedral complex $[Ag(tmbp)_2]^+$ (2.321 Å; tmbp = 4,4′,6,6′-tetramethyl-2,2′-bipyridine).[21] The twisting of the ligand required for the formation of the organometallic macrocycles is achieved by rotation about the C_{arom}-CH_2-C_{arom} bonds of the spacer, which places the aromatic benzimidazole planes connected to the methylene bridge in an approximately perpendicular arrangement (80.6(2) and 86.0(2)° for strands a and b, respectively; Table 2).

Table 1. Structural data for the *meso*-(P,M)-[2]catenate $[FeAg_2(\mathbf{L^2})_2]^{4+}$ **III**.

	Average	Minimum	Maximum
Bond length [Å]:			
Fe-N(py)	1.89(1)	1.88(1)	1.90(1)
Fe-N(bzim)	1.932(6)	1.928(6)	1.935(8)
Ag-N(py)	2.287(8)	2.281(8)	2.293(9)
Ag-N(bzim)	2.337(7)	2.331(9)	2.342(7)
Chelate angle [°]:			
N(bzim)-Fe-N(py)	81.3(3)	81.3(3)	81.4(4)
N(bzim)-Ag-N(py)	72.1(3)	71.7(3)	72.5(3)
Interligand angle [°]:			
N(py)-Fe-N(py)	180	180	180
N(bzim)-Fe-N(py)	98.7(2)	98.6(2)	98.7(2)
N(py)-Ag-N(py)	139(3)	135.3(3)	143.8(3)
N(bzim)-Ag-N(bzim)	133.7(4)	133.3(3)	134.1(3)
N(py)-Ag-N(bzim)	125(1)	126.7(3)	124.1(3)

Table 2. Selected interplane angles between aromatic rings of ligand $\mathbf{L^2}$.

Ring 1 [a]	Ring 2	Angle [°]	
		strand a	strand b
pAg	bAg	18.0(3)	8.1(3)
bAg	bFe	80.6(2)	86.0(2)
bFe	pFe	8.2(3)	5.2(3)

[a] The pyridine and benzimidazole rings bound to the Fe and Ag centers are denoted p and b, respectively. Thus, bAg is the benzimidazole ring bound to an Ag ion.

The X-ray diffraction data of the large pellets **B** also shows the cation $[FeAg_2(\mathbf{L^2})_2]^{4+}$ and four uncoordinated PF_6^- anions. But significant disorder in the crystal, arising from the lacunar occupation of the anionic sites, limits refinement of the data to $R = 0.14$ (see *Experimental Procedure*). Nevertheless, the resolution is sufficient to show that in **B** the cation $[FeAg_2(\mathbf{L^2})_2]^{4+}$ adopts the homochiral [2]catenate structure **IV** with two interlocked organometallic macrocycles of the same helicity leading to a racemic mixture of (*M*,*M*) and (*P*,*P*) enantiomers. Figure 2 gives a computer-generated representation[17] of the two structures of $[FeAg_2(\mathbf{L^2})_2]^{4+}$ in **A** (**III**, left) and in **B** (**IV**, right) showing the diastereomeric relationship between them.

^{1}H NMR studies have shown that **A** and **B** give the same spectrum in acetonitrile.[11] Detailed NOE measurements have established an almost perpendicular arrangement of the benzimidazole rings connected to the methylene bridge,[11] which preclude the formation of the side-by-side complex **II**, but do not

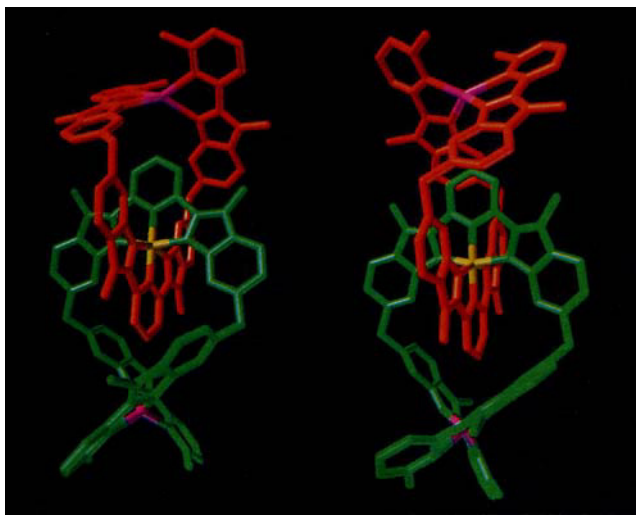


Fig. 2. VISP [17] representations of the two forms of $[FeAg_2(\mathbf{L^2})_2]^{4+}$, with the individual ligand strands of each complex in red or green. The heterochiral (*P*,*M*)-*meso* form **III** is shown on the left and the (*M*,*M*) enantiomer of the homochiral form **IV** on the right. Hydrogen atoms are omitted.

 © VCH Verlagsgesellschaft mbH, D-69451 Weinheim, 1995 0570-0833/95/0505-0583 $ 10.00+.25/0

allow the helicate (**I**) to be distinguished from the catenates (**III**, **IV**) in solution. However, the significant NOE effects observed between H_{23} and H_8, and H_{22} and H_8 (see Scheme 1) are only compatible with interstrand effects (H_{23a}–H_{8b}: 3.02–3.04 Å and H_{22a}–H_{8b}: 4.09–4.21 Å from the crystal structure of **III**) and demonstrate that the [2]catenate structure is maintained in acetonitrile for $[FeAg_2(\mathbf{L^2})_2]^{4+}$. The ^{1}H NMR spectrum at room temperature shows rapid exchange on the NMR timescale leading to an average D_{2d} symmetry for $[FeAg_2(\mathbf{L^2})_2]^{4+}$[11] and corresponding to a dynamic equilibrium between **III** and **IV**. This results from rapid interconversion of *P* and *M* helical enantiomers of each interlocked macrocycle on the NMR timescale ((*M*,*M*) ↔ (*M*,*P*) ↔ (*P*,*P*)). Cooling the sample to 240 K slows down the exchange processes, and the ^{1}H NMR spectrum shows the expected AB spin system for the diastereotopic protons H_{131} and H_{132}, in agreement with the catenate structures **III** and **IV**.[5]

In summary, the segmental ligand $\mathbf{L^2}$ reacts quantitatively with Fe^{II} and Ag^{I} in acetonitrile to give the first heteronuclear organometallic [2]catenate $[FeAg_2(\mathbf{L^2})_2]^{4+}$. As a result of the helicity of the organometallic macrocycles, both chiral (**IV**, (*P*,*P*) and (*M*,*M*)) and achiral (**III**, *meso* (*M*,*P*)) forms are found in the crystals, while rapid interconversion is observed in solution. This is, to our knowledge, the first self-assembly of a heterotrinuclear supramolecular complex. This new approach offers promising perspectives for the efficient synthesis of organized heteropolynuclear complexes with planned topologies and controlled physical properties.

Experimental Procedure

The ligand $\mathbf{L^2}$ [10] and the complex $[FeAg_2(\mathbf{L^2})_2](ClO_4)_4 \cdot 4H_2O$ [11] were obtained according to literature procedures. Crystals of $[FeAg_2(\mathbf{L^2})_2](PF_6)_4(CH_3OH)_{2.5}(H_2O)$ were obtained by vapor diffusion of methanol into a concentrated solution of $[FeAg_2(\mathbf{L^2})_2](ClO_4)_4 \cdot 4H_2O$ in acetonitrile containing a large excess of NBu_4PF_6. A dark violet hexagonal prism **A** ($0.15 \times 0.20 \times 0.26$ mm) was fixed on a quartz fiber with perfluoropolyether oil RS3000.

Crystal data for [2]catenate **III**: $FeAg_2C_{104.5}H_{108}N_{22}O_{3.5}P_4F_{24}$, $M = 2570.0$, monoclinic, $C2/c$, $a = 25.934(5)$, $b = 22.787(3)$, $c = 19.659(5)$ Å, $\beta = 107.79(1)°$, $V = 11\,062(4)$ Å^3 (by least-square refinement of 24 reflections ($35° \le 2\theta \le 50°$)), $Z = 4$, $\rho_{calcd} = 1.54$ g cm^{-3}, $F(000) = 5212$, $\mu(Cu_{K\alpha}) = 5.287$ mm^{-1}. Data collection and processing: Nonius CAD4 diffractometer, ω-2θ mode, scan width $= 1.2 + 0.15 \tan\theta$, scan speed 0.092° s^{-1}, $Cu_{K\alpha}$ radiation; $T = 200$ K; 5866 reflections measured ($4 \le 2\theta \le 100°$, $-25 < h < 25$, $0 < k < 22$, $0 < l < 19$), 5660 unique reflections (R_{int} for equivalent reflections = 0.043), of which 4174 were observable ($|F_o| > 4\sigma(F_o)$). Structure analysis and refinement: Data were corrected for Lorentz, polarization and absorption effects [22] (A^*min = 2.037, A^*max = 3.168). The structure was solved by direct methods using MULTAN 87 [23]; all other calculations used XTAL [24] system and ORTEP II [16] programs. Refinements (on *F*) were performed with full matrix, number of variables = 776. All non-hydrogen atoms were refined with anisotropic displacement parameters (89 atoms) except for one slightly disordered methanol molecule which was refined with isotropic displacement parameters. The cation $[FeAg_2(\mathbf{L^2})_2]^{4+}$ lies on a C_2 axis with Fe, Ag1, Ag2, N6a, N6b, C23a, C23b, H23a, and H23b in special positions 4e. Two hexafluorophosphate ions are found in special positions 4b and 4c (PF_6^- in position 4c is slightly disordered and refined with ten atomic positions for the fluorine atoms) and one in a general position. Final $R_w = 0.061$ ($\omega = 1$) for 776 variables and 4160 reflections. The mean shift/error on the last cycle was 0.003 and the maximum 0.14. Hydrogen atoms were placed in calculated positions and contributed to F_c calculations. The final Fourier difference synthesis showed a maximum of +0.83 and a minimum of −0.74 e Å^{-3}.

The crystal structure of the pellets **B** shows significant disorder and many attempts to solve it led to a final *R* factor of 0.14. At this level of resolution, solvent molecules are not observed. Four PF_6^- are in general positions with one anion showing a site occupancy of 0.5. The fifth hexafluorophosphate ion is in special position 2c. This statistical lacunar occupation of the anionic sites produces some disorder in the structure which explains the low ratio of observed reflections to number of variables.

Crystal data of [2]catenate **IV**: $FeAg_2C_{102}H_{86}N_{22}P_4F_{24}$, $M = 2471.4$, monoclinic, $P2_1/c$, $a = 13.1022(8)$, $b = 31.370(3)$, $c = 30.579(5)$ Å, $\beta = 95.976(5)°$, $V = 12\,500(2)$ Å^3 (by least-square refinement of 21 reflections ($33° \le 2\theta \le 47°$)), $Z = 4$, $\rho_{calcd} = 1.38$ g cm^{-3}, $\mu(Cu_{K\alpha}) = 4.68$ mm^{-1}. Violet pellets ($0.07 \times 0.30 \times 0.36$ mm) fixed on a quartz fiber with perfluoropolyether oil RS3000. Data collection and processing: Nonius CAD4 diffractometer, ω-2θ mode, ω scan width $= 1.2 + 0.15 \tan\theta$, scan speed 0.092° s^{-1}, $Cu_{K\alpha}$ radiation; $T = 200$ K; 13071 reflections measured ($4 \le 2\theta \le 100°$, $-12 < h < 12$, $0 < k < 31$, $0 < l < 30$), 12778 unique reflections (R_{int} for equivalent reflections = 0.14) of which 6500 were observable ($|F_o| > 4\sigma(F_o)$). Structure analysis and refinement: Data were corrected for Lorentz, polarization, and absorption effects [22] (A^*min = 1.412, A^*max = 4.610). The structure was solved by direct methods using MULTAN 87 [23]; all other calculations used the XTAL [24] system and ORTEP II [16] programs. Refinements (on *F*) were performed with two block matrices, maximum number of variables = 1431). Final $R_w = 0.14$ ($\omega = 1$) for 1431 variables and 6469 contributing reflections. Further details of the crystal structure investigation can be obtained from the Director of the Cambridge Crystallographic Data Centre, 12 Union Road, GB-Cambridge, CB2 1EZ (UK), on quoting the full journal citation.

Received: September 17, 1994 [Z 7324 IE]
German version: *Angew. Chem.* **1995**, *107*, ■

Keywords: catenates · helices · iron compounds · self-assembly · silver compounds

[1] J.-M. Lehn, *Angew. Chem.* **1990**, *102*, 1347–1362; *Angew. Chem. Int. Ed. Engl.* **1990**, *29*, 1304–1319; F. Vögtle, *Supramolecular Chemistry*, Wiley, Chichester, **1991**.
[2] J.-M. Lehn in *Perspectives in Coordination Chemistry* (Eds.: A. F. Williams, C. Floriani, A. E. Merbach), VCH, Weinheim, **1992**, pp. 447–462.
[3] E. C. Constable, *Tetrahedron* **1992**, *48*, 10013–10059.
[4] C. Piguet, G. Bernardinelli, B. Bocquet, A. Quattropanni, A. F. Williams, *J. Am. Chem. Soc.* **1992**, *114*, 7440–7451.
[5] J.-M. Lehn, A. Rigault, *Angew. Chem.* **1988**, *100*, 1121–1122; *Angew. Chem. Int. Ed. Engl.* **1988**, *27*, 1095–1097; K. T. Potts, M. Keshavarz-K, F. S. Tham, H. D. Abruna, C. Arana, *Inorg. Chem.* **1993**, *32*, 4422–4435; S. Rüttimann, C. Piguet, G. Bernardinelli, B. Bocquet, A. F. Williams, *J. Am. Chem. Soc.* **1992**, *114*, 4230–4237.
[6] C. Piguet, J. C. G. Bünzli, G. Bernardinelli, G. Hopfgartner, A. F. Williams, *J. Am. Chem. Soc.* **1993**, *115*, 8197–8206.
[7] R. Krämer, J.-M. Lehn, A. De Cian, J. Fischer, *Angew. Chem.* **1993**, *105*, 764–767; *Angew. Chem. Int. Ed. Engl.* **1993**, *32*, 703–706.
[8] S. Rüttimann, G. Bernardinelli, A. F. Williams, *Angew. Chem.* **1993**, *105*, 432–434; *Angew. Chem. Int. Ed. Engl.* **1993**, *32*, 392–394; G. Hopfgartner, C. Piguet, J. D. Henion, *J. Am. Soc. Mass. Spectrom.* **1994**, *5*, 748–756.
[9] P. Baxter, J.-M. Lehn, A. De Cian, J. Fischer, *Angew. Chem.* **1993**, *105*, 92–95; *Angew. Chem. Int. Ed. Engl.* **1993**, *32*, 69–72.
[10] C. Piguet, B. Bocquet, G. Hopfgartner, *Helv. Chim. Acta* **1994**, *77*, 931–942.
[11] C. Piguet, G. Hopfgartner, B. Bocquet, O. Schaad, A. F. Williams, *J. Am. Chem. Soc.* **1994**, *116*, 9092–9102.
[12] E. C. Constable, A. J. Edwards, P. R. Raithby, J. V. Walker, *Angew. Chem.* **1993**, *105*, 1486–1487; *Angew. Chem. Int. Ed. Engl.* **1993**, *32*, 1465–1467.
[13] G. J. Gruter, F. J. J. Kanter, P. R. Markies, T. Nomoto, O. S. Akkerman, F. Bickelhaupt, *J. Am. Chem. Soc.* **1993**, *115*, 12179–12180.
[14] J.-P. Sauvage, *Acc. Chem. Res.* **1990**, *23*, 319–327; N. van Gulick, *New J. Chem.* **1993**, *17*, 619–625.
[15] The helix is considered to wind starting from the viewer's eye to a point distant from the viewer. The screw sense is right- (*P*) or left-handed (*M*) corresponding to clockwise or counterclockwise; K. P. Meurer, F. Vögtle, *Top. Curr. Chem.* **1985**, *127*, 1–79. For **III** and **IV**, the helical axis of the macrocycles are perpendicular to the Ag-Fe-Ag axis.
[16] C. K. Johnson, ORTEP II, Report ORNL-5138, Oak Ridge National Laboratory, Oak Ridge, TN, **1976**.
[17] E. de Castro, S. Edelstein, VISP 1.0 Users Guide, University of Geneva, **1992**.
[18] A. F. Williams, C. Piguet, G. Bernardinelli, *Angew. Chem.* **1991**, *103*, 1530–1532; *Angew. Chem. Int. Ed. Engl.* **1991**, *30*, 1490–1492.
[19] S. Rüttimann, C. M. Moreau, A. F. Williams, G. Bernardinelli, A. W. Addison, *Polyhedron* **1992**, *11*, 635–646.
[20] J. F. Dobson, B. E. Green, P. C. Healy, C. H. L. Kennard, C. Pakwatchai, A. H. White, *Aust. J. Chem.* **1984**, *37*, 649–659.
[21] K. V. Goodwin, D. R. McMillin, W. R. Robinson, *Inorg. Chem.* **1986**, *25*, 2033–2036.
[22] E. Blanc, D. Schwarzenbach, H. D. Flack, *J. Appl. Crystallogr.* **1991**, *24*, 1035–1041.
[23] P. Main, S. J. Fiske, S. E. Hill, L. Lessinger, D. Germain, J. P. Declercq, M. M. Woolfson, *MULTAN 87*, Universities of York (England), and Louvaine-La-Neuve (Belgium), **1987**.
[24] S. R. Hall, H. D. Flack, J. M. Stewart, *XTAL 3.2 User's Manual*, Universities of Western Australia and Maryland, **1992**.

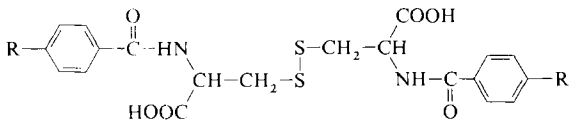
 © VCH Verlagsgesellschaft mbH, D-69451 Weinheim, 1995 0570-0833/95/0505-0584 $ 10.00+.25/0

X-Ray Structure of a Self-Assembled Gelating Fiber**

Fredric M. Menger,* Yasuhiro Yamasaki, Kelly K. Catlin, and Taisei Nishimi

Almost seventy years ago, chemist Dorothy Jordan noted that "gels are easier to recognize than to define".[1] We will attempt a definition nonetheless: Gels are semi-rigid colloidal systems rich in liquid. Protoplasm ranks as the most widespread example of this peculiar state of matter. A gel is formed by a molecular network, often fibrous in nature, that entrains the dispersing medium within its capillary spaces. Most organic gelators are polymeric (for example, gelatin,[2] poly(acrylic acid),[3] and hyaluronic acid[4]), but small molecules (for example, cholesteryl 4-(2-anthryloxy)butanoate,[5] 5-hexadecyl-2,4,6-triaminopyrimidine,[6] *N*-octylgluconamide,[7] and arborols[8]) can induce gelation as well.

We have long been interested in a little-known but remarkable gelator, dibenzoyl-L-cystine (DBC).[9] Although most gels require 1–10% gelator, DBC in water rigidifies at concentrations



DBC: R = H
DTC: R = Me

as low as 2 mM (0.1%). While attempting to learn how such miniscule quantities of DBC manage to self-assemble into a macroscopic network, we performed an X-ray analysis of a gel "fiber". Structural data at the atomic level is virtually unavailable for gel networks, and it is only through good fortune that these data became accessible. But before giving the details, let us summarize the properties of acylcystines in water.

DBC forms a firm, translucent gel in a thermally reversible process at a concentration of 4 mM in ethanol (5%)/water. Ethanol was used because the DBC tends to crystallize from pure water. There is, clearly, a delicate balance between gelation and crystallization. The gelating properties are destroyed when the S–S linkage is replaced by CH_2CH_2 or CH=CH groups.[10] This implies that the CH_2-S-S-CH_2 dihedral angle[11] of about 90 °C plays a key role in the formation of the molecular network. Gels do not form from esterified DBC or at basic pH values, which suggests the presence of either a favorable -COOH/-COOH attraction or a deleterious $-CO_2^-/-CO_2^-$ repulsion. Addition of NaCl (0.1 M) softens the gels, whereas more than 10% dioxane induces crystallization.

Diacetyl-L-cystine fails to gelate in ethanol (5%)/water. Di-*n*-octanoyl-L-cystine (4 mM) forms only a soft and cloudy gel. The superior quality of the DBC gel leads us to suspect that aromatic $\pi-\pi$ stacking stabilizes the creation of fibers. This conclusion is appealing, because intermolecular hydrogen bonding between DBC molecules in water would seem too unfavorable to serve as the sole adhesive force. Water, of course, normally dominates at the hydrogen-bonding sites of solutes dissolved within it.

[*] Prof. F. M. Menger, Y. Yamasaki, K. K. Catlin, T. Nishimi
Department of Chemistry, Emory University
Atlanta, GA 30322 (USA)
Telefax: Int. code +(404) 727-6586

[**] This work was supported by the National Institutes of Health.

Assembly of DBC molecules appears to be a cooperative event much like the micellization of surfactants. This was affirmed by a primitive yet informative experiment in which 2.0×2.0 cm^2 squares of Parafilm were placed on the surface of aged DBC gels. Known weights were then positioned carefully at the center of a film until the film submerged. A plot of "supportable weight" vs. DBC concentration (not shown) gave a sharp break at 1.6 mM, a value that might be qualitatively regarded as the "critical gelation concentration".

Spin-lattice relaxation studies with ^{13}C NMR spectroscopy on DBC have shown that gelation has no apparent effect on T_1 values.[9] We interpreted this result as proof for two distinct states: a monomeric species that possesses normal T_1 values and a self-assembled state whose ^{13}C resonances are broadened to the point of non-observability by long correlation times. This conclusion was affirmed by examining ^1H NMR line-widths of DBC's methylene signal. No line-broadening was observed from 0.5 mM to 10 mM DBC, a concentration range spanning the fluid-to-gel transformation. Quantitative comparison of NMR peak areas with those of an internal standard (2 mM DSS) showed conclusively that in ethanol (5%)/water 15% monomer (with normal line-widths) coexists with 85% gelated material (whose signals disappear into the baseline). In ethanol (25%)/water, DBC contains 40% monomer and 60% aggregate, while in ethanol (50%)/water only 20% of the DBC exists in the fibrous state. The sharp monomer peaks also prove that monomer does not exchange with fiber on the NMR time scale. Thus, the DBC fiber, unlike the micellar aggregate, is a fairly static entity.

Definitive structural information became available when, unexpectedly, crystalline di(*p*-toluoyl)-L-cystine (DTC) precipitated from solution before the gel had a chance to set. X-ray quality crystals (m.p. 194.5–196 °C) were obtained by recrystallizing the solid from methanol/ethyl acetate. The perennial question, namely, whether the solid-state structure reflects the solution properties, must be cautiously answered in the affirmative for several reasons: a) According to one theory,[10] gelation is a type of incomplete crystallization (the gel is considered to be microcrystalline forms surrounded by water). Small perturbations in conditions or structure (in our case, the addition of a methyl group to the aryl ring of DBC) can tip the scale in favor of the crystalline state. b) Throughout our work with acylcystine gels, it was obvious that the gels are poised to transform into the crystalline state. Thus, as mentioned, DBC will crystallize from gels if 5% ethanol is not present in the water or if more than 10% dioxane is added to the water. Crystallization seems too commonplace and too abrupt to postulate a molecular reorganization from a gel fiber into an entirely different solid-state structure. c) The X-ray structure in Figure 1 shows a linear association of DTC molecules, as one would expect for a fiber-forming system. To our knowledge, this is the first picture of a self-assembled gel fiber at the atomic level.

The crystal structure has a linear backbone containing disulfide linkages with CH_2-S-S-CH_2 dihedral angles alternating between 87° and 99°. Self-assembly is stabilized by long hydrogen bonds between amide-NH and carboxyl-CO functionalities (N···O distances range from 2.9 to 3.2 Å). Intrafiber association between the carboxyl groups appears to play little role, because they are stacked one upon another rather than held in a coplanar orientation. Ionization of the carboxyl groups apparently destroys the gel because of electrostatic repulsion. The aromatic rings extend to one side of the backbone, and every other ring is tilted by 22°. Toluoyl methyl groups are spaced in a repeating sequence of 6.66 Å, 4.12 Å, 7.36 Å, and 3.96 Å. The gel fiber is, therefore, held together by a favorable backbone

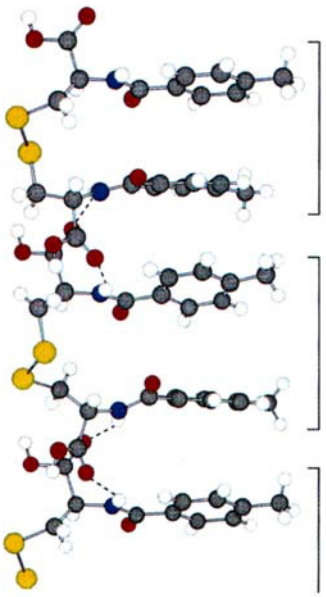


Fig. 1. X-ray crystal structure of di(*p*-toluoyl)-L-cystine (DTC). Red spheres represent oxygen, blue nitrogen, and yellow sulfur atoms. The dotted lines represent hydrogen bonds between amide-NH and carboxyl-CO functionalities. The N···O distances (and N-H-O angles) from bottom to top in the structure are 3.156 Å (130.4°), 3.172 Å (148.6°), 3.123 Å (148.0°), and 2.888 Å (135.2°).

orientation enhanced by hydrogen-bonding and $\pi-\pi$ stacking (or hydrophobic) interactions. This fortuitous blend of structural features accounts for the ability of acylcystines to gelate at remarkably low concentrations.

Figure 2 shows how two neighboring strands are held together by cooperative hydrogen bonding between carboxyl hydrogens and amide oxygens. The O···O distances are all about 2.6 Å in length. Single strands assemble into multi-filament fibers that we postulate can cause the gelation of aqueous solutions.[12]

The beautiful DNA-like structure of DTC in Figure 1 leads one to wonder whether acylcystines bearing nucleic acid bases instead of toluoyl groups would have self-replicative properties.[13]

Received: August 26, 1994 [Z 7270 IE]
German version: *Angew. Chem.* **1995**, *107*, 616

Keywords: cystine · gels · self-assembly · structure elucidation

[1] Y. Osada, S. B. Ross-Murphy, *Sci. Am.* **1993**, No. 5, 82.
[2] D. R. Eyre, *Science* **1980**, *207*, 1315.
[3] Y.-L. Yin, R. K. Prud'homme, F. Stanley in *Polyelectrolyte Gels* (Eds.: R. S. Harland, R. K. Prud'homme), American Chemical Society, Washington, **1992**, Chap. 6.
[4] D. A. Gibbs, E. W. Merril, K. A. Smith, E. A. Balazs, *Biopolymers* **1968**, *6*, 777.
[5] Y. Lin, B. Kachar, R. G. Weiss, *J. Am. Chem. Soc.* **1989**, *111*, 5542.
[6] K. Hanabusa, T. Miki, Y. Taguchi, T. Kogama, H. Shirai, *J. Chem. Soc. Chem. Commun.* **1993**, 1382.
[7] J.-H. Fuhrhop, S. Svenson, C. Boettcher, E. Rössler, H.-M. Vieth, *J. Am. Chem. Soc.* **1990**, *112*, 4307.
[8] G. R. Newkome, G. R. Baker, S. Arai, M. J. Saunders, P. S. Russo, K. J. Theriot, C. N. Moorefield, L. E. Rogers, J. E. Miller, T. R. Lieux, M. E. Murray, B. Phillips, L. Pascal, *J. Am. Chem. Soc.* **1990**, *112*, 8458.
[9] F. M. Menger, K. S. Venkatasubban, *J. Org. Chem.* **1978**, *43*, 3413.
[10] C. G. L. Wolf, E. K. Rideal, *Biochem. J.* **1922**, *16*, 548.
[11] B. Panijpan, *J. Chem. Educ.* **1977**, *54*, 670.
[12] For self-assembled fibers composed of entirely different compounds see J.-H. Fuhrhop, W. Helfrich, *Chem. Rev.* **1993**, *93*, 1565; F. Giulieri, M.-P. Krafft, J. G. Riess, *Angew. Chem.* **1994**, *106*, 1583; *Angew. Chem. Int. Ed. Engl.* **1994**, *33*, 1515; F. M. Menger, S. J. Lee, *J. Am. Chem. Soc.* **1994**, *116*, 5987.
[13] Single-crystal structure data for $C_{22}H_{24}N_2O_6S_2$: monoclinic space group $P2_1$ (no. 4), $a = 11.853(2)$, $b = 10.965(3)$, $c = 17.641(4)$, $\beta = 95.45(2)°$, $V = 2282.5(12)$ Å^3, $Z = 4$. Of 3946 measured reflections 3366 were symmetry-independent, of which 2957 ($I > 4\sigma(I)$) with $R = 0.0646$. Determination of the lattice parameters and measurement of the intensities were carried out with a Siemens P4RA diffractometer ($Cu_{K\alpha}$ radiations, $\mu = 2.472$, $2\theta_{max} = 109.0$). Empirical absorption correction and structure determination were carried out with SHELXS-86 and structure refinement with SHELXTL IRIS. Further details of the crystal structure determination are available on request from the Director of the Cambridge Crystallographic Data Centre, 12 Union Road, GB-Cambridge, CB2 1EZ (UK), on quoting the full journal citation.

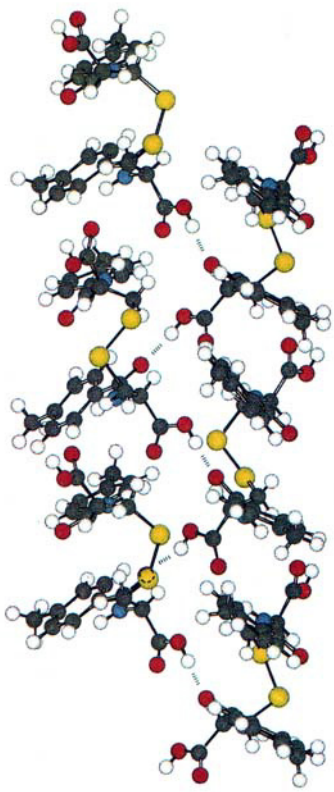


Fig. 2. X-ray crystal structure of two DTC strands held together by cooperative hydrogen bonds between carboxyl-hydrogen atoms and amide-CO groups (dotted lines). The O···O distances (and O-H-O angles) moving up the structure are 2.614 Å (172.4°), 2.653 Å (159.0°), 2.609 Å (157.6°), 2.624 Å (172.4°), and 2.614 Å (172.3°).

Hexakis(trifluoromethyl)tetrazane**

Burkhard Krumm, Ashwani Vij, Robert J. Kirchmeier,* Jean'ne M. Shreeve,* and Heinz Oberhammer*

While no element can compete with carbon in the number of contiguous atoms in saturated chemical compounds, stable straight-chain species composed of other elements are known, especially if fluorine atoms, fluorinated groups, or other electronegative species are present in the molecule, for example $CF_3(O)_nCF_3$ ($n = 1-3$) and O_nF_2 ($n = 1, 2, 4$). Fluorinated N_n compounds do exist and do exhibit surprising hydrolytic, thermal, and chemical stabilities. In contrast, the hydrogen-substituted analogues such as diazane, triazane, and tetrazane are increasingly unstable with increasing chain length. While tris(perfluoro-

[*] Prof. R. L. Kirchmeier, Prof. J. M. Shreeve, Dr. B. Krumm, Dr. A. Vij
Department of Chemistry, University of Idaho
Moscow, ID 83843 (USA)
Prof. Dr. H. Oberhammer
Institut für Physikalische und Theoretische Chemie der Universität
D-72076 Tübingen (Germany)
Telefax: Int. code + (7071)296910

[**] The work was supported by the U.S. National Science Foundation (CHE-9003509) and the Air Force Office of Scientific Research (91-0189).

 © VCH Verlagsgesellschaft mbH, D-69451 Weinheim, 1995 0570-0833/95/0505-0586 $ 10.00+.25/0

alkyl)amines $N(R_f)_3$[1-3] and tetrakis(perfluoroalkyl)diazanes $(R_f)_2NN(R_f)_2$[4,5] are well known, and their gas-phase structures determined, only recently have the synthesis and property characterization of per- and polyfluoroalkyl-substituted tetrazanes been reported.[5,6] All of the known fluorine-containing tetrazanes are relatively dense liquids of low volatility which solidify as glasses, precluding single-crystal X-ray structural analyses. As a consequence, the smallest, most symmetric perfluoroalkylated compound of this type, hexakis(trifluoromethyl)tetrazane (**4**), was selected for a structural study in the gas phase using electron diffraction (GED).[7]

Our synthesis of **4** differs from the one reported by Emeléus et al.[8] and provides a facile route to these N_4 compounds (Scheme 1). The conversion of the *N*-chloro-*N*-chlorodifluoro-

$$(CF_3)_2NN(Cl)CF_2Cl \xrightarrow[-Cl_2]{Me_3SnCl} (CF_3)_2NN{=}CF_2$$
1 **2**

$$\mathbf{2} + ClF \longrightarrow (CF_3)_2NN(Cl)CF_3$$
3

$$2\ \mathbf{3} \xrightarrow[-Cl_2]{h\nu} [(CF_3)_2N-N(CF_3)-N(CF_3)-N(CF_3)_2]$$
4

Scheme 1.

methyldiazane **1** to difluoromethylenediazane **2** is achieved by utilizing only a catalytic amount of chlorotrimethylstannane with benzonitrile as solvent. Chlorine is removed easily without the formation of side products. The intermediate trimethylstannyldiazane loses chlorotrimethylstannane at 25 °C and yields **2**. The chlorostannane again reacts with **1** with the evolution of Cl_2. The process continues until **1** is totally consumed. This is a convenient method for the preparation of perfluorinated difluoromethylenamines (or -azanes). The double bond can be chlorofluorinated with ClF to form *N*-chloro-*N*-trifluoro methyldiazane **3**. *N*-Chlorodiazanes are known to lose chlorine upon photolysis and dimerize to give tetrazanes.[9] In this way hexakis(trifluoromethyl)tetrazane (**4**) is obtained as a volatile, colorless liquid with considerable vapor pressure at 25 °C. Furthermore, this compound is air and water stable and does not decompose even at elevated temperatures. The ^{19}F NMR spectrum shows two broad signals for the terminal CF_3 groups, which are not equivalent at 25 °C. Another resonance at higher field for the CF_3 groups attached to the inner nitrogen atoms is split into a multiplet due to nonequivalent couplings to the outer CF_3 groups. In a variable-temperature NMR study the signals for the terminal CF_3 groups were found to coalesce at 58 °C. The features of the low-temperature NMR spectrum (−40 to −100 °C), which were reported earlier[10] for a solution of **4** in $CFCl_3$, could not be reproduced. Instead, we observed precipitation of the compound from solution upon cooling.

The radial distribution function (RDF) derived by Fourier transform of the experimental electron diffraction intensities is shown in Figure 1. A large number of molecular models with different torsional angles about the N–N bonds were tested. The models were evaluated according to two criteria: 1) no F···F contacts shorter than 2.5 Å (except within the CF_3 groups) and 2) agreement between calculated and experimental RDF. The RDF range 2.8–3.5 Å contains mainly C···F and F···F distances between adjacent CF_3 groups and N···F distances to CF_3 groups bonded to the neighboring nitrogen atom (e.g. from N1 to the CF_3 group of C2 or from N2 to the CF_3 groups of C1 and C1'). This RDF range can be reproduced only

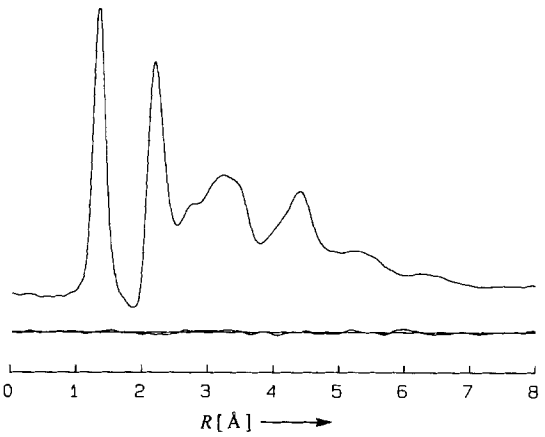


Fig. 1. Experimental radial distribution function for **4** and difference curve between experimental and calculated functions.

with models having planar or nearly planar coordination at all nitrogen atoms. The outer part of the RDF can be fitted satisfactorily only with models that have dihedral angles ϕ about the N–N bonds of close to 90° (for $\phi = 0°$ the lone pairs of electrons on adjacent nitrogen atoms are parallel).

The following constraints were applied in the least squares refinements: 1) local C_{3v} symmetry for the CF_3 groups, 2) local C_2 symmetry for the $(CF_3)_2N$ moieties, in other words the CF_3 groups are rotated about the N–C bonds in opposite directions, and 3) overall C_2 symmetry. The C_2 axis is perpendicular to the N2–N3 bond and bisects the dihedral angle ϕ(NNNN). Only mean values for the N–N and C–N bond lengths could be derived. The final results of the electron diffraction analysis are given in Table 1; the nitrogen-carbon skeleton of tetrazane **4** is

Table 1. Structure parameters of $[(CF_3)_2NN(CF_3)N(CF)_3N(CF_3)_2]$ (**4**) [a].

$(N-N)_{mean}$ [Å]	1.379 (11)	N1–N2–N3 [°]	116.4 (13)
$(N-C)_{mean}$ [Å]	1.438 (6)	N1–N2–C2 [°]	122.6 (15)
C–F [Å]	1.329 (3)	N3–N2–C2 [°]	120.4 (18)
F–C–F [°]	108.2 (2)	$\Sigma\alpha$(N2) [°] [b]	359.4 (27)
C1–N1–C1' [°]	120.3 (10)	ϕ(N1–N2–N3–N4) [°]	95.2 (11)
N2–N1–C1 [°]	117.6 (5)	ϕ(lp–N1–N2–lp) [°] [c]	90.1 (24)
$\Sigma\alpha$(N1) [°] [b]	355.5 (13)		

[a] Error limits are 3σ values. Atom numbering is given in Fig. 2. [b] Sum of bond angles around nitrogen atom. [c] Dihedral angle between lone pairs of electrons (lp) at N1 and N2.

shown in Figure 2. The coordination geometry at the inner nitrogen atoms N2 and N3 is planar (sum of bond angles $\Sigma\alpha$(N2) = 359.4(27)°) and that at the outer nitrogens N1 and N4 is nearly planar ($\Sigma\alpha$(N1) = 355.5(13)°). The NNNN chain has a skew conformation with ϕ(NNNN) = 95.2(11)°. The $(CF_3)_2N$ groups are rotated around the terminal N–N bonds by ϕ(lp-N-N-lp) = 90.1(24)°, such that the lone pairs (lp) at N1 and N2 (and those at N3 and N4) are perpendicular to each other. The structural features of the two $(CF_3)_2N-N(CF_3)$-halves are very similar to

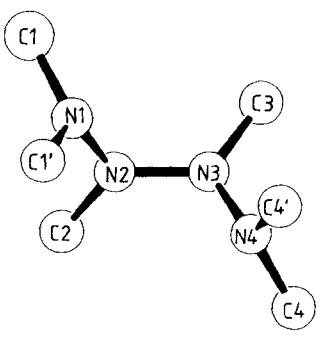


Fig. 2. Nitrogen-carbon skeleton of hexakis(trifluoromethyl)tetrazane (**4**).

 © VCH Verlagsgesellschaft mbH, D-69451 Weinheim, 1995 0570-0833/95/0505-0587 $ 10.00+.25/0

those of tetrakis(trifluoromethyl)diazane, which also has planar coordination at the nitrogen atoms ($\Sigma\alpha(N) = 359.5(26)°$), perpendicular nitrogen lone pairs ($\phi(lp-N-N-lp) = 88.4\ (40)°$), and an N–N bond length of 1.402(20) Å.[4] The unsaturated tetrazenes $R_2N-N=N-NR_2$ have planar nitrogen skeletons and *trans* configuration. The N–N single bonds are slightly longer (1.429(5) Å for R = H[11] and 1.394(5) Å for R = $SiMe_3$[12]) than those in the tetrazane **4** (1.379(11) Å).

Experimental Procedure

2: Diazane **1** (10 mmol) was condensed into 5 mL benzonitrile containing a catalytic amount of Me_3SnCl. The reaction mixture was stirred at 25 °C for 1 h before all volatile material was held over mercury for 5 h to remove chlorine. Distillation gave pure **2** as a colorless gas in quantitative yield, after passage through a trap at −90 °C. ^{19}F NMR ($CDCl_3$): $\delta = -65.2$ (d, $^5J(F,F) = 4.0$ Hz, 6F; $(CF_3)_2N$), −63.4 (d, $^2J(F,F) = 93.3$ Hz, 1F; N = C*F*F), −40.2 (d of sept, $^2J(F,F) = 93.3$ Hz, $^5J(F,F) = 4.0$ Hz, 1F; N = CF*F*); IR (gas): $\nu[cm^{-1}] = 1753$ (s, N=C), 1360 (s), 1326 (s), 1263 (s), 1220 (s), 982 (m), 959 (w), 734 (m); MS (EI): *m/z* (%): 216 (M^+, 7), 197 ($M^+ - F$, 6), 128 ($CF_3NN = CF^+$, 11), 109 (CF_3NNC^+, 2), 69 (CF_3^+, 100). Elemental analysis for $C_3F_8N_2$ (calcd/found): C 16.68/16.00, F 70.35/68.2.

3: Diazane **2** (5 mmol) and ClF (5.5 mmol) were condensed into a stainless steel reaction vessel and allowed to react for 12 h at 25 °C. Distillation through a −90 °C trap, in which $(CF_3)_2NN(Cl)CF_3$ condensed, gave the pure product as a colorless liquid in quantitative yield. ^{19}F NMR ($CDCl_3$): $\delta = -68.0$ (sept, $^5J(F,F) = 4.7$ Hz, 3F; $N(Cl)CF_3$), −61.4 (q, $^5J(F,F) = 4.7$ Hz, 6F; $(CF_3)_2N$); IR (gas): $\nu[cm^{-1}] =$ 1339(s), 1289 (s), 1265 (s), 1220 (s), 1178 (m), 1030 (w), 986 (m), 927 (w), 839 (w), 734 (m), 725 (m); MS (CI): *m/z* %: 270 (M^+, 1), 251 ($M^+ - F$, 15), 235 ($M^+ - Cl$, 16), 216 ($M^+ - ClF$, 50), 197 ($(CF_3)_2NN = CF^+$, 45), 148 ($CF_3NNCF_2H^+$, 38), 128 ($CF_3NN{=}CF^+$, 38), 109 (CF_3NNC^+, 11), 69 (CF_3^+, 100).

4: Diazane **3** (5 mmol) was condensed into a 100 mL quartz vessel and photolyzed for 5 h ($\lambda = 3000$ Å). Distillation of the contents gave tetrazane **4**, which was condensed in a trap at −80 °C, in 90% yield. ^{19}F NMR ($CDCl_3$): $\delta = 64.6$ (m, 6F; $NNCF_3$), −58.8, −60.3 (br., 12F; $(CF_3)_2N$); coalescence at 331 K, $\Delta G^* =$ 15.2 kcal mol^{-1}; IR (gas): $\nu[cm^{-1}] = 1347$ (m), 1312 (s), 1300 (s), 1284 (s), 1247 (m), 1201 (w), 1181 (w), 987 (m), 935 (w), 735 (m). IR- and mass spectral data were reported earlier [8].

Received: September, 13 1994 [Z 7311 IE]
German version: *Angew. Chem.* **1995**, *107*, 645

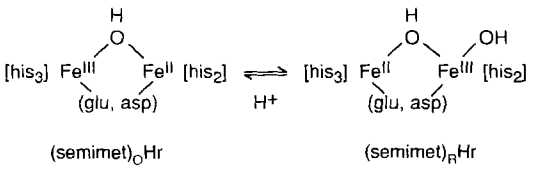
Keywords: electron diffraction analysis · hexakis(trifluoromethyl)tetrazane · nitrogen–fluorine compounds · tetrazanes

[1] H. Bock, I. Göbel, Z. Havlas, S. Liedle, H. Oberhammer, *Angew. Chem.* **1991**, *103*, 193; *Angew. Chem. Int. Ed. Engl.* **1991**, *30*, 187.
[2] H. Bürger, N. Niepel, G. Pawelke, H. Oberhammer, *J. Mol. Struct.* **1979**, *54*, 159.
[3] M. Gaensslen, U. Gross, H. Oberhammer, S. Rüdiger, *Angew. Chem.* **1992**, *104*, 1525; *Angew. Chem. Int. Ed. Engl.* **1992**, *31*, 1467.
[4] L. S. Bartell, H. K. Higginbotham, *Inorg. Chem.* **1965**, *9*, 1346.
[5] R. L. Kirchmeier, J. M. Shreeve, R. D. Verma, *Coord. Chem. Rev.* **1992**, *112*, 169, and references therein.
[6] G. Sarwar, N. R. Patel, Y. Y. Zheng, E. O. John, R. L. Kirchmeier, J. M. Shreeve, *Inorg. Chim. Acta* **1992**, *198–200*, 527.
[7] The GED intensities were recorded with a gas diffractograph KD-G2 at camera distances of 25 and 50 cm and with an accelerating voltage of about 60 kV. The temperature of the sample reservoir was −26 °C, that of the nozzle 15 °C. The photographic plates were evaluated according to standard methods (H. Oberhammer, W. Gombler, H. Willner, *J. Mol. Struct.* **1981**, *70*, 273). Molecular scattering intensities in the *s*-ranges 2–18 and 8–35 Å^{-1} ($s = (4\pi/\lambda)\sin\theta/2$, λ = electron wavelength, θ = scattering angle) were used for the structure determination.
[8] R. C. Dobbie, H. J. Emeléus, *J. Chem. Soc. A* **1966**, 933.
[9] G. Sarwar, R. L. Kirchmeier, J. M. Shreeve, *Inorg. Chem.* **1989**, *28*, 3345.
[10] M. G. Barlow, K. W. Cheung, *J. Fluorine Chem.* **1977**, *10*, 191.
[11] M. Veith, G. Schlemmer, *Z. Anorg. Allg. Chem.* **1982**, *494*, 7.
[12] M. Veith, *Acta Crystallogr. Sect. B* **1975**, *31*, 678.

A Model of Semimet Hemerythrin; NMR Spectroscopic Evidence of Valence Localization in Bis(μ-carboxylato)(μ-phenolato)diiron(II,III) Complexes in Solution**

Wakako Kanda, William Moneta, Michel Bardet, Elisabeth Bernard, Noële Debaecker, Jean Laugier, Azzedine Bousseksou, Sylvie Chardon-Noblat, and Jean-Marc Latour*

Hemerythrin (Hr), a dioxygen carrier found in sipunculid worms and other marine invertebrates, is considered the prototype of non-heme proteins with a diiron active site.[1] Since the early 1980s the structures of four distinct forms of the protein have been solved by X-ray crystallography.[2] In the deoxy form, the two Fe^{II} ions are bridged by one hydroxy and two carboxylate groups. The coordination spheres of the two iron ions are quite different. One is bound by three histidine residues and is thus hexacoordinate; the other is bound by only two histidines, thus leaving a coordination site accessible to dioxygen and other substrates. Oxygenation of Hr leads to deprotonation of the bridging hydroxo ligands, resulting in a (μ-oxo)diiron(III) unit with a terminal hydroperoxo ligand linked to the bridging oxo ligand through a hydrogen bond. The hydroperoxo ligand can be replaced by anions (e.g. azide) leading to the corresponding met forms, which have been structurally characterized.[2] Apart from the $[Fe^{II}Fe^{II}]$ and $[Fe^{III}Fe^{III}]$ states, two mixed-valence forms $[Fe^{II}Fe^{III}]$ have been detected. These semimet hemerythrins are obtained either by oxidation of the deoxy form ($(semimet)_OHr$) or by reduction of the met form ($(semimet)_RHr$). No X-ray structures are available for the semimet forms yet, but EXAFS[3] and other spectroscopic methods[4] have revealed a Fe^{II} (μ-OH)Fe^{III} unit. NMR experiments on $(semimet)_RHr$ derivatives in solution have shown that the valence of the two ions is localized.[5] Kurtz et al.[6] and Solomon et al.[7] have proposed that the two semimet forms differ in terms of the location of the valences of the iron atoms in the ligand environment as illustrated in Scheme 1.



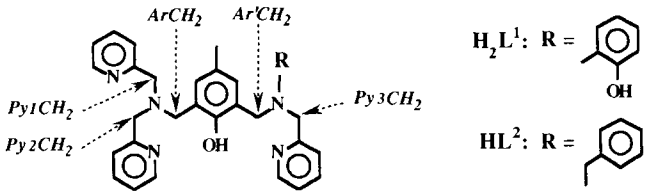
Scheme 1. Proposed structures of the semimet forms of hemerythrin. his = histidine, glu = L-glutamic acid, asp = L-aspartic acid.

[*] Dr. J.-M. Latour, Dr. W. Moneta, Dr. M. Bardet, E. Bernard, N. Debaecker
CEA/Département de Recherche Fondamentale sur la Matière Condensée
Laboratoire SESAM/CC, Centre d'Etudes de Grenoble
F-38054 Grenoble Cedex 9 (France)
Telefax: Int. code +76 88 50 90
Dr. W. Kanda
Department of Chemistry Wakayama University (Japan)
Dr. J. Laugier
Département de Recherche Fondamentale sur la Matière Condensée
Laboratoire SP2M/S, Centre d'Etudes de Grenoble (France)
Dr. A. Bousseksou
Laboratoire de Chimie de Coordination du CNRS, Toulouse Cedex (France)
Dr. S. Chardon-Noblat
Laboratoire d'Electrochimie Organique et de Photochimie Rédox
Université Joseph Fourier, Grenoble Cedex (France)

[**] This research was supported by the Centre National de la Recherche Scientifique (URA 1194). Support from the Japanese Ministry of Education, Science and Culture (grant to W. K.) is gratefully acknowledged.

Over the last decade, numerous μ-oxodiiron(III) complexes have been reported that mimic the physical properties of metHr.[8] However, in most cases the Fe^{III} ions are coordinatively saturated, and the compounds are not active catalysts. The one complex having the unsymmetrical structure of the Hr active site[9] exhibits some activity in hydrogen peroxide disproportionation. Fewer studies have focused on diiron(II)[10] and mixed-valence complexes.[11] Models of the semimet forms have been developed mostly by using ligands built on phenol-based ligands which mimic the hydroxo bridge of Hr. All the systems reported so far are coordinatively saturated and symmetrical. The latter feature results in delocalized valences for the two iron centers in solution at room temperature as shown by NMR experiments,[11] in contrast to the protein.

To model the structure and properties of hemerythrin and related proteins, we have synthesized new bridging ligands for diiron complexes (Scheme 2), which provide a phenolate and



Scheme 2. Structural formulas of ligands H_2L^1 (**1**) and HL^2 (**2**), and labeling of the methylene groups (see discussion of the NMR spectra).

other donor groups and mimic key features of the protein active sites. We recently reported on the structure of the $[Fe^{II}Fe^{III}]$ complex **1** with the ligand H_2L^1, which supplies one Fe ion with a terminal phenolate group (Scheme 2).[12] In this communication, we describe the synthesis and the structure of the first model of semimetHr that mimics the unsymmetrical histidine coordination of the protein active site, leaving a free coordination site on one iron center. In addition, variable-temperature NMR measurements show that the valences of the iron centers are localized in solution at room temperature as in $(semimet)_OHr$. Similar studies of complex **1** show that the valences are localized in the configuration found in $(semimet)_RHr$.

To mimic the active site of Hr we synthesized ligand HL^2, which provides three nitrogen donors to bind the first Fe center and only two for the second.[13] Reaction of HL^2 with two equivalents of $Fe(NO_3)_3 \cdot 9H_2O$ and one equivalent of disodium 1,3-benzenedipropionate (Na_2mpdp) affords a pale violet precipitate of **2** after addition of sodium tetraphenylborate. Recrystallization of the precipitate in acetonitrile/methanol furnishes dark purple crystals of **2** suitable for X-ray crystallography.[14] Elemental analysis and spectroscopic and magnetic studies show that **2** is a mixed-valence complex and support the proposed formulation.

$[Fe^{II}Fe^{III}L^2(H_2O)(mpdp)](BPh_4)_2 \cdot 2H_2O$ **2**

The structure of the cation of **2** is shown in Figure 1. The compound consists of discrete complex cations and tetraphenylborate counterions. The two iron ions are bridged by the phenolate oxygen atoms and two carboxylate groups from the mpdp ligand. The coordination sphere of Fe2 is completed by one tertiary and two pyridine nitrogen atoms, while that of Fe1 includes the oxygen atom of a water molecule in addition to one tertiary and one pyridine nitrogen atom. The Fe–Fe distance is 3.409 Å, which is close to that determined by EXAFS[3] for the

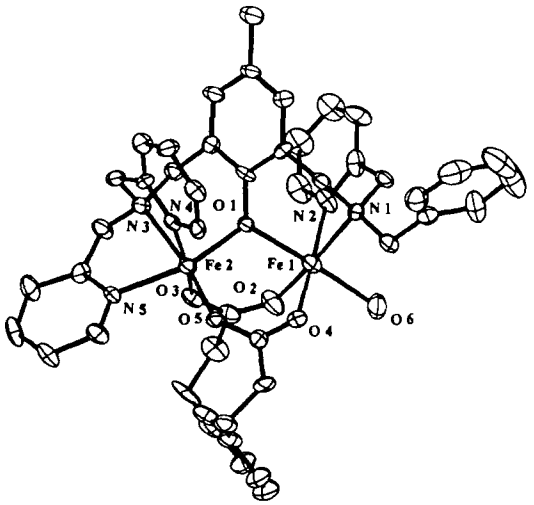


Fig. 1. Structure of the cation $[Fe_2L^2(mpdp)(H_2O)]^{2+}$ in the crystal of **2**. Important bond lengths [Å] and angle [°]: Fe1···Fe2 3.409(1), Fe1-O1 2.115(6), Fe1-O2 2.084(6), Fe1-O4 2.128(6), Fe1-O6 2.156(8), Fe1-N1 2.254(5), Fe1-N2 2.191(7), Fe2-O1 1.952(4), Fe2-O3 1.996(5), Fe2-O5 1.948(5), Fe2-N3 2.215(5), Fe2-N4 2.173(7), Fe2-N5 2.156(6); Fe1-O1-Fe2 113.9(2).

azide derivative of semimetHr (3.457 Å) and those found in other bis(μ-carboxylato)(μ-penolato)diiron(II,III) complexes.[11] The Fe-O-Fe unit is strongly asymmetric: the Fe2–O1 distance is 0.16 Å shorter than the Fe1–O1 separation. A similar trend is observed for the other metal–ligand distances and leads to the conclusion that the valences of the iron ions are localized. The Fe2 ion with the N_3O_3 coordination sphere, is in the +III oxidation state, while the Fe1 ion with the N_2O_4 coordination sphere is in the +II oxidation state. It is worth noting that this assignment is opposite to that for phenolate complex **1**, in which the terminal phenolate group stabilizes the Fe^{III} ion in the N_2O_4 site.

The valence localization of **2** in the solid state is supported by the Mössbauer spectra (80–300 K range). Two quadrupole split doublets are observed at 80 K with isomer shifts of 0.475(4) and 1.196(4) mm s^{-1} (relative to metallic iron at room temperature), splittings of 0.329(6) and 2.657(7) mm s^{-1}, and relative areas of 51(1) and 49(1)%, respectively. The first doublet is attributed unambiguously to the high-spin Fe^{III} center Fe2, while the second one corresponds to the high-spin Fe^{III} center Fe1. Similar Mössbauer parameters have been obtained for semimetHr.[1]

The electrochemical properties of **2** have been investigated in acetonitrile with 0.1 M tetrabutylammonium perchlorate. Cyclic voltammetry reveals a one-electron reduction at -0.36 V_{Ag/Ag^+} and an oxidation wave at about 0.5 V_{Ag/Ag^+}.[15] Since the latter wave overlaps with the oxidation wave of the tetraphenylborate anion, precise coulometric analysis is not possible. Spectroelectrochemical studies show that the reduction process is associated with the $[Fe^{II}Fe^{II}]/[Fe^{II}Fe^{III}]$ couple, and the oxidation with the formation of the Fe^{III}_2 derivative.

Both **1** and **2** have been characterized by ^{1}H NMR spectroscopy. Assignments of the signals were made by chemical substitution (replacement of mpdp by acetate), T_1 measurements, and COSY experiments, as well as by comparisons with spectra of related compounds.[10a, 11a, 16] Several features of **1** and **2** strongly suggest that the valences of the two Fe ions are also localized in solution on the NMR timescale and that the structure in solution is the same as that in the solid state.[17] These suppositions were established unambiguously through the use of variable-temperature NMR experiments. Figure 2a illustrates the dependence of the reduced chemical shift of the equatorial protons of the five methylene groups of complex **1**

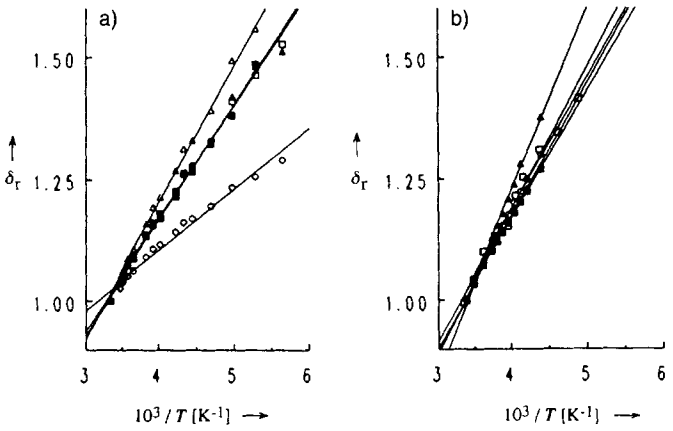


Fig. 2. Plot of the reduced chemical shift (δ_r is the ratio of the chemical shift at any temperature to the chemical shift at a reference temperature, here 293 K) versus the inverse of the temperature for the equatorial protons of complex **1** (a) and complex **2** (b); $ArCH_2$(eq) (□), Py1CH_2(eq) (△), Py2CH_2(eq) (○), Ar'CH_2(eq) (■), and Py3CH_2(eq) (▲).

with the inverse of temperature. (Equatorial protons are defined within the metallacycles by analogy with cyclohexane.) It is clearly seen that two protons, Ar'CH_2(eq) and Py3CH_2(eq), behave in the same manner, while the other three, $ArCH_2$(eq), Py1CH_2(eq), and Py2CH_2(eq), strongly differ. This behavior can be easily understood if the former protons are located in the vicinity of the magnetically isotropic Fe^{III} ion and the latter protons close to the magnetically anisotropic Fe^{II}. Examination of the corresponding plot for **2** (Fig. 2b) reveals that the same situation holds, but with opposite valences for the two Fe ions. These experiments demonstrate that the valences of the Fe centers in both complexes are localized in solution at room temperature and that in both cases the localization is the same as in the solid state: in **1** the Fe^{II} ion is in the N_3O_3 site, while in **2** it occupies the site accessible to the exogeneous ligand (a water molecule in the present case).

The similarity of the valence localization in **1** and **2** to that in $(semimet)_RHr$ and $(semimet)_OHr$, respectively, provides strong support for the Kurtz–Solomon hypothesis. Preliminary studies show that the terminal aqua ligand in **2** can be easily replaced, giving rise to very rich chemical behavior.

Experimental Procedure

To a solution of 0.2 g (0.38 mmol) of HL^2 in 6 mL of CH_3OH were added successively a solution of 0.31 g (0.76 mmol) of $Fe(NO_3)_3 \cdot 9H_2O$ in 3 mL of CH_3OH and a solution of 110 mg (0.38 mmol) of Na_2mpdp [18] in 5 mL of CH_3OH. The resulting violet solution was stirred for 4 h at room temperature. A solution of 0.53 g (1.52 mmol) of $NaBPh_4$ in 6 mL of CH_3OH was then added, and the mixture was stirred for roughly 15 h at room temperature. The pale purple precipitate that formed was filtered and recrystallized from acetonitrile/methanol to give dark purple crystals of **2** (0.32 g, yield 56%). The compound gave satisfactory elemental analysis and mass spectrum.

Received: August 15, 1994
Revised version: November 30, 1994 [Z 7237 IE]
German version: *Angew. Chem.* **1995**, *107*, 625

Keywords: complexes with nitrogen ligands · complexes with oxygen ligands · hemerythrin · iron compounds · protein mimics

[1] J. Sanders-Loehr in *Iron Carriers and Iron Proteins* (Ed.: T. M. Loehr), VCH, New York, **1989**, p. 373.
[2] M. A. Holmes, I. Le Trong, S. Turley, L. C. Sieker, R. E. Stenkamp, *J. Mol. Biol.* **1991**, *218*, 583, and references therein.
[3] R. C. Scarrow, M. J. Maroney, S. M. Palmer, L. Que, A. L. Roe, S. P. Salowe, J. Stubbe, *J. Am. Chem. Soc.* **1987**, *109*, 7857.
[4] H. Thomann, M. Bernardo, J. M. McCormick, S. Pulver, K. K. Andersson, J. D. Lipscomb, E. I. Solomon, *J. Am. Chem. Soc.* **1993**, *115*, 8881.
[5] M. J. Maroney, D. M. Kurtz, J. M. Nocek, L. L. Pearce, L. Que, *J. Am. Chem. Soc.* **1986**, *108*, 6871.
[6] L. L. Pearce, D. M. Kurtz, Y.-M. Xia, P. G. Debrunner, *J. Am. Chem. Soc.* **1987**, *109*, 7286.
[7] J. M. McCormick, E. I. Solomon, *J. Am. Chem. Soc.* **1990**, *112*, 2005.
[8] D. M. Kurtz, *Chem. Rev.* **1990**, *90*, 585.
[9] B. Mauerer, J. Crane, J. Schuler, K. Wieghardt, B. Nuber, *Angew. Chem.* **1993**, *105*, 306; *Angew. Chem. Int. Ed. Engl.* **1993**, *32*, 289.
[10] a) A. S. Borovik, M. P. Hendrich, T. R. Holman, E. Münck, V. Papaefthymiou, L. Que, *J. Am. Chem. Soc.* **1990**, *112*, 6031; b) K. S. Hagen, R. Lachicotte, *ibid.* **1992**, *114*, 8741, and references therein.
[11] a) A. S. Borovik, V. Papaefthymiou, L. F. Taylor, O. P. Anderson, L. Que, *J. Am. Chem. Soc.* **1989**, *111*, 6183; b) M. S. Mashuta, R. J. Webb, J. K. McCusker, E. A. Schmitt, K. J. Oberhausen, J. F. Richardson, R. M. Buchanan, D. N. Hendrickson, *ibid.* **1992**, *114*, 3815.
[12] E. Bernard, W. Moneta, J. Laugier, S. Chardon-Noblat, A. Deronzier, J.-P. Tuchagues, J.-M. Latour, *Angew. Chem.* **1994**, *106*, 914; *Angew. Chem. Int. Ed. Engl.* **1994**, *33*, 887.
[13] The ligand was obtained as described for H_2L^1 [12]; however, in the last step the amination reaction was performed with (2-pyridylmethyl)benzylamine (see ref. 9 in [12]). Mass spectrum of HL^2 (FAB^+, dichloromethane/nitrobenzyl alcohol): 530 [$M - H^+$].
[14] Crystal structure data of **2**: triclinic, space group $P\bar{1}$, $a = 13.208(5)$, $b = 13.700(6)$, $c = 23.88(1)$ Å, $Z = 2$, $V = 4163.5$ Å^3, measuring temperature 294 K, $Mo_{K\alpha}$ radiation, ($\lambda = 0.7107$ Å), 14538 symmetry-independent reflections, 4944 with $F > 4\sigma(F)$, $R = 0.077$, $R_w = 0.058$; structure solution by direct methods, H atoms at calculated positions. Further details of the crystal structure investigation may be obtained from the Director of the Cambridge Crystallographic Data Centre, 12 Union Road, GB-Cambridge CB2 1EZ (UK), on quoting the full journal citation.
[15] After electrochemical oxidation of the tetraphenylborate ion, the oxidative wave appears at a potential of $+0.48$ V_{Ag/Ag^+}. Coulometric and cyclic voltammetric analyses established that both waves correspond to reversible one-electron processes.
[16] a) L.-J. Ming, H. G. Jang, L. Que, *Inorg. Chem.* **1992**, *31*, 359; b) Z. Wang, T. R. Holman, L. Que, *Magn. Reson. Chem.* **1993**, *31*, 78.
[17] The smaller spectral range ($\Delta\delta = 400$) of the NMR signals of delocalized complexes compared to the present compounds is indicative of an averaging of the signals caused by delocalization. The occurrence of signals with negative chemical shifts is characteristic of Fe^{II} complexes [10a, 16a]. The presence of true Fe^{II} ions is further supported by comparison with the spectra of heterobimetallic complexes [16b].
[18] R. H. Beer, W. B. Tolman, S. G. Bott, S. J. Lippard, *Inorg. Chem.* **1989**, *28*, 557.

Synthesis of 1,2-Diphospholide Ions

Nicole Maigrot, Narcis Avarvari, Claude Charrier, and François Mathey*

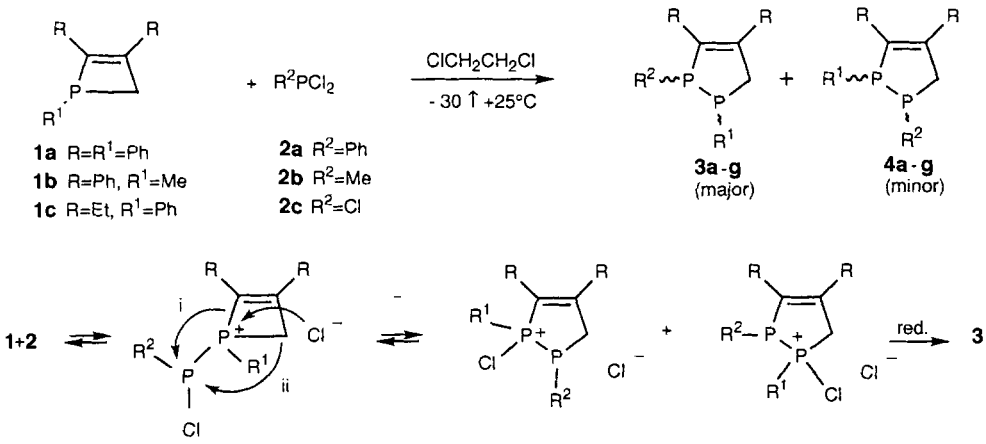
To date, the 1,2-diphospholide ions are the only members of the polyphosphacyclopentadienide family that have not yet been synthesized.[1] Their preparation would permit the completion of a series of aromatic species that results from the successive replacement of sp^2-CH units in an aromatic hydrocarbon by isolobal sp^2-P units. No such complete series exists for any heteroatom.

Several literature reports suggest that, were they made, 1,2-diphospholide ions would be stable: Padma Malar[2] has calculated similar aromaticity indexes for the hypothetical $[1,2\text{-}C_3H_3P_2]^-$ and the known $[1,2,3\text{-}C_2H_2P_3]^-$ anion.[3, 4] Furthermore, two groups have described ferrocene derivatives containing η^5-1,2-diphospholyl ligands,[5, 6] and more recently a zwitterionic phosphole derivative has been reported.[7]

Our approach relies on a transposition of our preceding work on 1,2,3-triphospholide ions.[4] As a first step, we devised a

[*] Prof. Dr. F. Mathey, N. Maigrot, N. Avarvari, Dr. C. Charrier
Laboratoire "Hétéroéléments et Coordination"
URA 1499 CNRS, DCPH, Ecole Polytechnique
F-91128 Palaiseau Cedex (France)
Telefax: Int. code +1 69 33 30 10

 © VCH Verlagsgesellschaft mbH, D-69451 Weinheim, 1995 0570-0833/95/0505-0590 $ 10.00+.25/0



Scheme 1. Synthetic route to 1,2-diphosphacyclopent-3-enes **3** and **4**, and the proposed reaction mechanism. For the ^{1}H NMR spectroscopic data see Table 2.

synthesis of the unknown 1,2-diphosphacyclopent-3-enes (Scheme 1). In essence, this comprised a formal insertion of phosphinidenes into 1,2-dihydrophosphetes (easily accessible from titanacyclobutenes and dihalophosphanes[8–10]), a process analogous to the reaction transforming phosphirenes into 1,2-dihydro-1,2-diphosphetes.[11] Our reasoning was that cyclic strain, which provides the driving force for the ring expansion of phosphirenes, is also significant in dihydrophosphetes. Our results are summarized in Tables 1 and 2.

Table 1. Synthesis of 1,2-diphosphacyclopent-3-enes **3** and **4**.

3/4	Substituents R	R¹	R²	Ratio 3:4	Yield 3 + 4 (%)
a	Ph	Ph	Ph	–	46
b	Ph	Ph	Me	75:25	40
c	Ph	Me	Ph	95:5	42
d	Ph	Me	Me	–	20
e	Ph	Ph	Cl	100:0	36
f	Et	Ph	Ph	–	22
g	Et	Ph	Cl	100:0	47

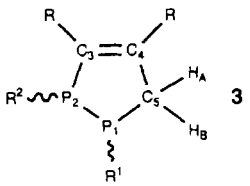
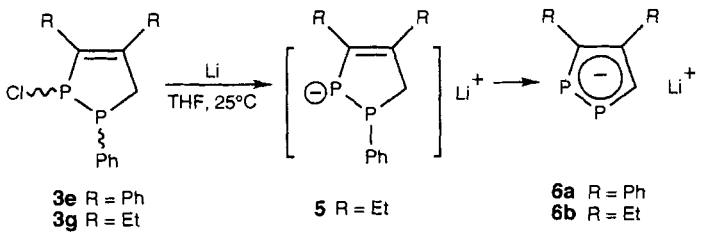


Table 2. Selected NMR data for compounds **3**.

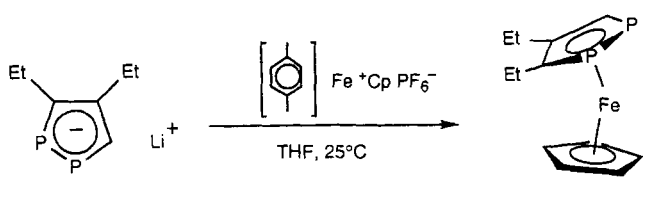
	^{1}H NMR $\delta(H_A)$ [2,3J(H,P)]	$\delta(H_B)$	^{31}P NMR δ(P1) [1J(P1,P2)]	δ(P2)	^{13}C NMR δ(C3) [1J(C3,P2)]	δ(C4) [2,3J(C4,P)]	δ(C5) [1J(C5,P1)]
3a (CD_2Cl_2)	3.76 [3.3,2.6]	4.35 [18.4,0]	–30.1 [226]	+30.9	138.76 [28.1]	150.4 [5.5]	44.47 [25.7]
3b (C_6D_6)	2.81 [3.1,2.1]	3.86 [16.2,0]	–48.9 [213]	+26.1	137.9 [28.5]	148.86 [7.0,4.5]	45.0 [26.1]
3c (C_6D_6)	3.56 [4.2,2.2]	4.10 [18.3,0]	–38.6 [211]	+13.9	142.44 [30.5]	144.8 [6.0,3.0]	43.06 [24.1]
3d (C_6D_6)	2.85 [3, 3]	3.88 [16.3,0]	–59.1 [201]	+11.5	142.1 [29.6]	144.3 [7, 3.5]	44.5 [24.2]
3e ($ClCH_2$)$_2$			+36.9 [262]	+96.7			
3f (CD_2Cl_2)	3.10 [3, 3]	3.46 [18, 1]	–29.8 [217]	+19.0	136.4 [24]	151.7 [6]	41.3 [23.2]
3g (C_6D_6)			+25.9 [262]	+101.6			

The proposed mechanism is outlined in Scheme 1. The compound serving as the reducing agent is, very probably, the starting material itself. Indeed, when a mixture containing equimolar quantities of **1** and **2** reacts to completion, **1** disappears completely whereas **2** is still present. Hence, the theoretical yield of the reaction is limited to 50%, as is observed. The two first steps are probably reversible, since when starting materials are used in which $R^1 \neq R^2$, R^1PCl_2 and the corresponding insertion products can be detected by ^{31}P NMR spectroscopy at the end of the reaction. As shown in Table 1, the insertion preferentially takes place into the P–C(sp^2) bond of **1**, probably because of a favorable two-electron interaction between the LUMO of the C=C bond and the lone pair of the exocyclic phosphorus atom in the intermediate dihydrophosphete quaternary salt. The structures of **3** and **4** are easily established through the large ^2J(H,P) coupling (16–18 Hz) between one of the CH_2 protons and P1.

The reduction of the chloro derivatives **3e** and **3g** by lithium in THF yields the expected 1,2-diphospholide anions **6a** and **6b**,



respectively. The reaction proceeds via an intermediate anion **5**, whose P–Ph bond is still intact and which can be detected when R = Et ($\delta(^{31}P) = -133.8, +20.6$, ^1J(P,P) = 339 Hz). The preliminary formation of this partly delocalized anion precludes the cleavage of the P–P bond in the second step leading to **6**. The anions **6** are characterized by the low-field shifts of their ^{31}P NMR signals (δ = 152–206), their huge ^1J(P,P) couplings of roughly 440 Hz, and their sizeable ^2J(P,H) couplings of about



 © VCH Verlagsgesellschaft mbH, D-69451 Weinheim, 1995 0570-0833/95/0505-0591 $ 10.00+.25/0

37 Hz. All these data are very characteristic of polyphospholide ions.[1] Further identification was achieved by the preparation of the 1,2-diphosphaferrocene **7** from **6b**.

Experimental Procedure

All the reactions were performed under argon, and the solvents were purified and dried by standard methods. For the synthesis of the initial titanacyclobutenes, see refs. [12, 13]. Dihydrophosphete **1a** was made as described in 65% yield [8–10]. **1b** appears to be unstable and has not been isolated: $\delta(^{31}P) = -19$. **1c** was recovered as a pale yellow oil in 20% yield: ^{31}P NMR (81.0 MHz, C_6D_6, H_3PO_4): $\delta = -10.6$; ^1H NMR (200 MHz, C_6D_6; TMS): $\delta = 0.92$ (t, $^3J(H,H) = 7.5$ Hz, 3H; Me), 0.98 (t, $^3J(H,H) = 7.5$ Hz, 3H; Me), 1.8–2.5 (m, 6H; $3CH_2$); ^{13}C NMR (50.0 MHz, C_6D_6, TMS): $\delta = 11.87$ (s, Me), 13.61 (d, $J(C,P) = 3.9$ Hz, Me), 21.73 (d, $^1J(C,P) = 10.8$ Hz, P-CH_2), 24.78 (d, $J(C,P) = 2.4$ Hz, C-CH_2), 27.52 (d, $J(C,P) = 7.5$ Hz, C-CH_2), 140.2 (d, $^1J(C,P) = 34.7$ Hz, sp^2-C), 145.85 (s, sp^2-C), 149.7 (d, $J(C,P) = 4.7$ Hz, sp^2-C).

3 (and **4**): $PhPCl_2$, $MePCl_2$, or PCl_3 (12×10^{-3} mol) was added dropwise to a solution of the corresponding dihydrophosphete **1** (12×10^{-3} mol) in 1,2-dichloroethane (25 mL) at $-30\,^\circ C$. The mixture was stirred and slowly warmed to room temperature. The reaction was stopped upon disappearance of **1** (^{31}P NMR). After evaporation of the solvent, the residue was chromatographed on silica gel (150 g, 60 mesh) with hexane/toluene (80/20) as the eluent. **3a**: pale yellow solid, m.p. 132 °C; **3b**: white solid, mixture of isomers; **3c**: white solid, m.p. 131 °C; **3d**: pale yellow oil; disulfide: m.p. 186 °C; **3e** and **3g** were not purified by chromatography but by thorough evaporation of the solvent and of the excess of PCl_3 under vacuum; **3f**: colorless oil. For ^1H NMR data see Table 2.

6: A solution of **3e** or **3g** (15×10^{-4} mol) in dry THF (5 mL) was stirred with lithium wire (5×10^{-2} g) at room temperature. For **6a**, the reaction was complete after 30 min. Dark brown solution: MS ($m/z = 253$ (M^-, 100%)); ^{31}P NMR: $\delta = 181.0$ (P1), 206.0 (P2), $^1J(P1,P2) = 444$ Hz, $^2J(P1,H) = 36.7$ Hz. For **6b**, the reaction required 4 d at 50 °C for completion. Brown solution: MS ($m/z = 157$ (M^-, 100%)); ^{31}P NMR: $\delta = 152.1$ (P1), 173.7 (P2), $^1J(P1,P2) = 436$ Hz, $^2J(P1,H) = 37$ Hz, $^3J(P2,CH_2) = 10.8$ Hz.

7: To the solution of **6b** was added solid NH_4Cl (8×10^{-2} g). The mixture was stirred for 1 h at room temperature, then $[Fe(\eta^6\text{-}1,4\text{-}Me_2C_6H_4)(\eta^5\text{-}C_5H_5)]^+PF_6^-$ [14] (0.56 g) was added. After additional stirring for 2 h, the solution was concentrated to 1.5 mL and chromatographed with hexane on silica gel. Compound **7** was recovered as a purple liquid in 25% yield. ^{31}P NMR (C_6D_6): $\delta = -34.5$ (P1), −9.9 (P2), $^1J(P1,P2) = 384$ Hz, $^2J(P1,H) = 36.5$ Hz, $^3J(P2,CH_2) = 10.6$ Hz; ^1H NMR (C_6D_6): $\delta = 1.03$ (t, $^3J(H,H) = 7$ Hz, 3H; Me); 1.17 (t, $^3J(H,H) = 7$ Hz, 3H; Me); 2.24 (m, 4H; $2CH_2$); 3.99 (s, 5H; Cp); 4.85 (d, $^2J(H,P) = 36.8$ Hz, 1H; P-CH); ^{13}C NMR (CD_2Cl_2): $\delta = 16.2$ (s, CH_3), 16.7 (s, CH_3), 23.0 (s, CH_2), 23.75 (d, $^2J(C,P) = 19$ Hz), 73.8 (s, Cp), 90.80 (d, $^1J(C,P) = 79$ Hz, P-CH), 99.7 (s, =C-CH), 101.3 (pt, P-C=).

Received: August 18, 1994 [Z 7245 IE]
German version: *Angew. Chem.* **1995**, *107*, 623

Keywords: diphosphacyclopentenes · diphospholides · phosphorus compounds · sandwich complexes

[1] For a recent review on phospholide ions, see: F. Mathey, *Coord. Chem. Rev.*, in press.
[2] E. J. Padma Malar, *J. Org. Chem.* **1992**, *57*, 3694.
[3] M. Baudler, J. Hahn, *Z. Naturforsch. B* **1990**, *45*, 1139.
[4] N. Maigrot, M. Sierra, C. Charrier, F. Mathey, *Bull. Soc. Chim. Fr.* **1994**, *131*, 397.
[5] L. Weber, R. Kirchhoff, R. Boese, H.-G. Stammler, *J. Chem. Soc. Chem. Commun.* **1991**, 1293.
[6] E. Niecke, D. Schmidt, *J. Chem. Soc. Chem. Commun.* **1991**, 1659.
[7] G. Jochem, A. Schmidpeter, M. Thomann, H. Nöth, *Angew. Chem.* **1994**, *106*, 708; *Angew. Chem. Int. Ed. Engl.* **1994**, *33*, 663.
[8] K. M. Doxsee, G. S. Chen, C. B. Knobler, *J. Am.Chem. Soc.* **1989**, *111*, 9129.
[9] W. Tumas, J. A. Suriano, R. L. Harlow, *Angew. Chem.* **1990**, *102*, 89; *Angew. Chem. Int. Ed. Engl.* **1990**, *29*, 75.
[10] K. M. Doxsee, E. M. Hanawalt, G. S. Chen, T. J. R. Weakley, H. Hope, C. B. Knobler, *Inorg. Chem.* **1991**, *30*, 3381.
[11] L. Ricard, N. Maigrot, C. Charrier, F. Mathey, *Angew. Chem.* **1987**, *99*, 590; *Angew. Chem. Int. Ed. Engl.* **1987**, *26*, 548.
[12] N. A. Petasis, D. K. Fu, *Organometallics* **1993**, *12*, 3776.
[13] K. M. Doxsee, J. J. J. Juliette, J. K. M. Mouser, K. Zientara, *Organometallics* **1993**, *12*, 4682.
[14] a) D. Astruc, *Tetrahedron* **1983**, *39*, 4027; b) R. M. G. Roberts, A. S. Wells, *Inorg. Chim. Acta* **1986**, *112*, 171.

[Bis{(η^5-pentamethylcyclopentadienyl)cobalt}-μ-(η^4:η^4-arene)]: Synthesis, Structure, and Unusual Reactivity of a New Type of Triple-Decker with Bridging Arene Ligands**

Jörg J. Schneider,* Uwe Denninger, Oliver Heinemann, and Carl Krüger

Dedicated to Professor Günther Wilke on the occasion of his 70th birthday

In organometallic triple-decker complexes with bridging carbacyclic π-perimeters, the bridging ligands are bonded to each transition metal with either maximum hapticity or lower.[1] In the mixed triple-decker **1**[2]—the first with a bridging η^6-coordinate arene ligand—the aromatic benzene "middle deck" can be exchanged with other arenes such as toluene or mesitylene at temperatures above 100 °C, and yet retain the original triple-decker structure. To our knowledge, this is the only compound known to date with an antifacial coordinated arene bridge with which this can be achieved.

$[\{(\eta^5\text{-Cp})V\}_2\text{-}\mu\text{-}(\eta^6\text{:}\eta^6\text{-}C_6H_6)]$ **1**

We report here on the synthesis and structural characterization of cobalt triple-decker complexes with μ-η^4:η^4-bonded arene ligands, as well as on their unusual reactivity with respect to ligand exchange. During the course of our investigations into the synthesis of nonbridged $[(\eta^5\text{-}C_5R_5)Co]$ dimers (R = alkyl), we studied the reductive ligand release occurring in the reaction of $[(\eta^5\text{-Cp*})(acac\text{-}O,O')Co]$[3] with alkali metal. If the reaction is performed in solvents such as diethyl ether or THF, **2** is formed along with other substances.[4] The additional hydrido ligands presumably originate from the solvent. If benzene or methyl-substituted arenes such as toluene or *o*-, *m*-, and *p*-xylene are used as solvent, the reaction with alkali metal—typically in a batch of about 10 mmol—requires 10–14 days to go to completion instead of just one day in ethers. The reaction times can, however, be considerably reduced by prior activation of the alkali metal with ultrasound. Admittedly, undesirable side products such as $[(\eta^5\text{-Cp*})(\eta^6\text{-arene})Co]$ and $[(\eta^5\text{-Cp*})_2Co]$ (identified in the crude product by means of mass spectrometry and ^1H NMR spectroscopy) are then also formed. If the ultrasonic activation is not used, compounds with the composition **3** can be isolated by crystallization in about 40–60% yield.

$[\{(\eta^5\text{-Cp*})Co\}_3H_4]$ **2**

[*] Priv.-Doz. Dr. J. J. Schneider,[+] Dr. U. Denninger,[++] Dipl.-Chem. O. Heinemann,[++] Prof. Dr. C. Krüger[++]
Max-Planck-Institut für Kohlenforschung
Kaiser-Wilhelm-Platz 1, D-45470 Mülheim an der Ruhr (FRG)
[+] New address:
Institut für Anorganische Chemie der Universität/Gesamthochschule
Universitätsstrasse 5–7, D-45117 Essen
Telefax: Int code + (201)183-2402

[++] Crystal structure analyses.

[**] We thank Dr. A. Rufinska for recording the solid state ^{13}C NMR spectra and Prof. Dr. P. Binger and Dr. F. Sandmeyer for a sample of the adamant-1-ylmethylidenephosphine. J. J. S. thanks the Deutsche Forschungsgemeinschaft for granting a Heisenberg Fellowship, and the Fonds der Chemischen Industrie for additional financial support. Abbreviations used: Cp = cyclopentadienyl, Cp* = pentamethylcyclopentadienyl, acac = acetylacetonate

 © VCH Verlagsgesellschaft mbH, D-69451 Weinheim, 1995 0570-0833/95/0505-0592 $ 10.00+.25/0

The compounds **3a–f** are brown solids, are stable for several months at 0 °C, and can be dissolved in aliphatic solvents and in diethyl ether without decomposition. The complexes react with aromatic solvents, however.

[{(η^5-Cp*)Co}$_2$-μ-(η^4:η^4-arene)] **3**

3a: arene = benzene
3b: arene = toluene
3c–e: arene = *o*-, m- bzw. *p*-xylene
3f: arene = cumene

The composition of the compounds of type **3** was confirmed by C, H, and Co elemental analyses, as well as by mass spectra in which the corresponding molecular ions were registered (admittedly only with low intensity). The most intensive signals in the mass spectra were attributed to the decomposition products of the complexes **3a–f**, such as the sandwich compound [(η^5-Cp*)$_2$Co] and the respective arene. The typical peak positions for the π-complexed arene were also found in the IR spectra. The positions of the resonance signals of the π-complexed arenes around δ = 3.19–2.70 in the ^{1}H NMR spectra of the compounds of type **3** identify them as diamagnetic complexes. With the exception of the signals of **3b**, all the signal groups in the ^{1}H NMR spectra of **3a** and **3c–f** are broadened. The temperature-dependence of the NMR spectra of **3b** as representative example was investigated: Down to 193 K both in the ^{1}H NMR and the ^{13}C NMR spectra, the typical splitting and coupling patterns that would be expected for a complex in solution with a time-averaged symmetrical μ-η^6:η^6-coordinate toluene ligand were observed. Neither the signals due to the arene and Cp* protons nor the signals due to the carbon atoms coalesce. This indicates a very low activation barrier to possible dynamic processes for **3b**. We first noticed the extraordinary behavior of the benzene derivative **3a** while taking a ^{13}C NMR spectrum at 27 °C. After several hours accumulation time of a spectrum of a freshly prepared sample of **3a**, signals from free benzene were observed, and the corresponding signals of the formally complexed benzene were missing. This indicated a ready exchange of the complexed benzene ligands with the deuterated [D$_6$]benzene used as solvent. In fact, if the NMR sample was worked up preparatively after two days, the corresponding [D$_6$]-**3a** was isolated quantitatively and characterized by NMR, IR, and mass spectroscopy. The signals from free arene were seen in the NMR spectra of the derivatives **3b–f** a short time after the samples had been prepared. This means that the aromatic middle-deck of these compounds is also as readily exchanged as that of **3a**. The arene ligand in compounds of type **3** is therefore apparently bonded in a labile fashion to both the {(η^5-Cp*)Co} units. Compound **3b** reacts with equimolar amounts of 1,3,5-cycloheptatriene or 1,3,5,7-cyclooctatetraene even at 20 °C within a short time to give the binuclear complexes **4**[5] and **5**.[6] The smooth exchange of the aromatic middle deck in **3b** under very mild reaction conditions is quite remarkable. The spectroscopic data and a crystal structure analysis[7] verified that the composition of compound **4** really does match that of the compound first prepared and characterized by Wadepohl. The smooth formation of **4** and **5** from **3b** without changing the binuclear structure, is observed even at room temperature; this argues against a dissociative mechanism for the ligand exchange in **3b**, that is, against the loss of a {(η^5-Cp*)Co} unit in the initial reaction step. Kinetic studies into the exchange process will be the subject of future investigations.

[{(η^5-Cp*)Co}$_2$-μ-(η^4:η^4-cycloheptatriene)] **4**

[{(η^5-CP*)Co}$_2$-μ-(η^4:η^4-cyclooctatetraene)] **5**

A conclusive decision in favor of one of the two conceivable structural variations of **3**, **A** and **B** (Fig. 1), was not possible from the existing preparative results and the spectroscopic data. Solid state CP/MAS ^{13}C NMR spectra of the arene derivatives **3b–f** also do not permit an unequivocal verdict on the structure, that is, on whether the {(η^5-Cp*)Co} units on the arene ligands are arranged synfacially or antifacially. In the case of **3b** for example, the signals in the arene region are broad at 83 K, but do correspond to those in the ^{13}C NMR spectrum of **3b** in solution as regards number and position. This would seem to indicate a distinct structural fluctuation—both in solution and in the solid. Such dynamic behavior in solids is not unusual and has already been confirmed for [Fe(CO)$_3$(η^4-C$_8$H$_8$)],[8] [Fe$_2$(CO)$_5$-μ-(η^8-C$_8$H$_8$)],[8] [Ru$_3$(CO)$_4$-μ-(η^8-C$_8$H$_8$)$_2$],[9, 10] and [Os$_3$(CO)$_8$(η^2-CH$_2$CH$_2$)-μ-(η^2:η^2:η^2-C$_6$H$_6$)],[11] by means of CP/MAS ^{13}C NMR experiments.

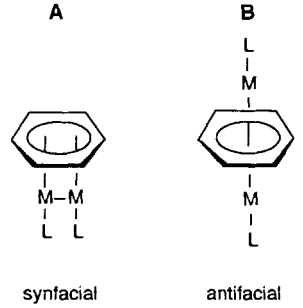


Fig. 1. Synfacial (**A**) and antifacial (**B**) coordination of two complex fragments to a bridging π-perimeter.

The molecular structure of **3f** in the crystal was determined by a single-crystal X-ray structure analysis (Fig. 2).[12] We assume that the derivatives **3a–e** have a similar structure. In **3f** the arene ligand bridges the two {(η^5-Cp*)Co} complex fragments in such a way that an antifacial arrangement of the two complex fragments results in a "slipped" triple-decker. Analogous structures can be found in the binuclear complexes of cyclooctatetraene (cot). An *anti*-μ-η^5:η^5 structure, comparable to that in **3f**, is present in [{(η^5-Cp)Rh}$_2$-μ-(cot)]$^{2+}$,[1d] [{(η^5-Cp)Fe}$_2$-μ-(cot)],[13] and [{(η^5-Cp)Ru}$_2$-μ-(cot)].[1e] Both the Co atoms in **3f** are η^4-bonded to the bridging arene ring. The C$_6$ arene system in **3f** is no longer planar, and a chair conformation results for the isopropylbenzene ligands. The bond angles C1-C6-C5 and C2-C3-C4 are 117.9(6) and 120.1(7)°, respectively. The atoms C2 and C3 of the isopropylbenzene ligand each bridge

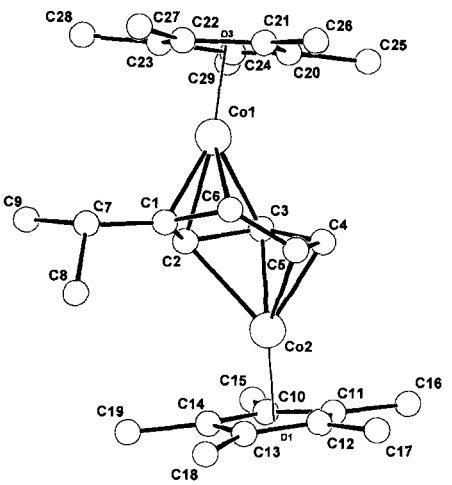
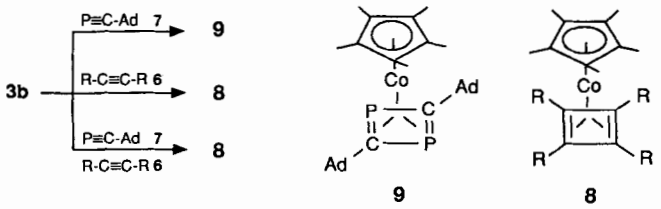


Fig. 2. Molecular structure of **3f** in the crystal. Hydrogen atoms not shown. Selected distances [Å] and angles [°]: Co1-C11.935(8), Co1-C3 2.1668(1), Co1-C2 2.062(7), Co1-C6 2.051(8), Co2-C2 2.255(8), Co2-C4 1.899(8), Co2-C3 2.053(8), Co2-C5 2.084(7), C1-C2 1.43(1), C3-C4 1.44(1), C5-C6 1.44(1), C1-C6 1.43(1), C2-C3 1.47(1), C4-C5 1.45(1), C7-C8 1.53(1), C7-C9 1.53(1); C6-C5-C4 116.3(7), C5-C4-C3 109.8(7) C6-C1-C2 110.0(7), C9-C7-C8 110.2(7).

 © VCH Verlagsgesellschaft mbH, D-69451 Weinheim, 1995 0570-0833/95/0505-0593 $ 10.00+.25/0

the metal atoms. The coordination of the arene ligand in **3f** thus corresponds to that of the cycloheptatriene in **4**[5, 7] and of the cot ligand in $[\{(\eta\text{-cot})Ti\}_2\text{-}\mu\text{-(cot)}]$.[1f, 1g] As is also the case in **4**, C2 and C3 are each bonded to both Co atoms through one longer and one shorter bond. In contrast to the corresponding bond in **4** (1.516(6)[5] and 1.492(9) Å[7]), however, the C2–C3 bond of 1.47(1) Å (in which both C atoms coordinate to both Co atoms) in **3f** is not significantly elongated. The antifacial μ-η^4:η^4 coordination, which was characterized here for the first time for arenes, is a novel mode of coordination for this important ligand type. Interestingly enough, for the heavier homologous element Rh, a closely related compound $[\{(\eta^5\text{-Cp})Rh\}_2\text{-}\mu\text{-}(\eta^3\text{:}\eta^3\text{-}C_6H_6)]$,[14] contains an arene that—in contrast to that in the Co complex **3f**—bridges the $\{(\eta^5\text{-Cp})Rh\}$ units in a synfacial fashion. The compound also contains a Rh–Rh bond.

We also investigated the reaction behavior of **3b** with respect to its participation in a possible dimerization or trimerization of alkyne **6** or λ^3-phosphaalkyne **7**[15] (Scheme 1). If solutions of



Scheme 1. Ad = adamantyl, R = phenyl.

3b in diethyl ether are treated with **6** or **7** at 20 °C (stoichiometry **3b**:**6**, **3b**:**7** 1:3) or 1:1 mixtures of the two alkynes (stoichiometry **3b**:**6,7** 1:1), the homo- and heteroalkyne components **6** and **7** are dimerized to form the corresponding cyclobutadiene complex **8** or diphosphacyclobutadiene complex **9**. The structure of **9** with a λ^3-1,3-diphosphete unit is confirmed by the crystal structure analysis[16] (Fig. 3). In the case of the reaction of mixtures of **6** and **7** with **3b**, only **8** is isolated. The product of a codimerization accompanied by the formation of a monophosphacyclobutadienecobalt(I) complex is not observed in this case. Nor is a cyclotrimerization of the λ^3-phosphaalkyne accompanied by the formation of triphosphinines observed.

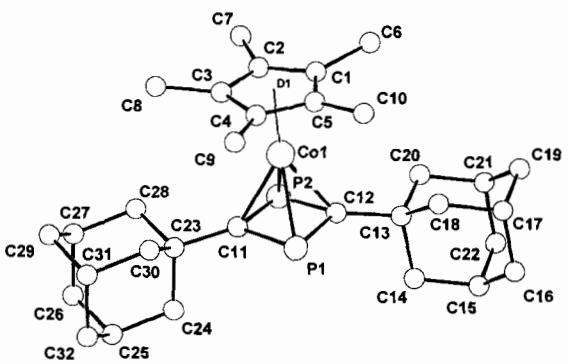


Fig. 3. Molecular structure of **9** in the crystal. Hydrogen atoms not shown. The asymmetric unit contains two independent molecules which do not differ significantly in their bonding parameters, however. For this reason, only molecule 1 is shown. Selected distances [Å] and angles [°]: Co1-C11 2.082(3), Co1-C12 2.082(3), Co1-P1 2.236(1), Co1-P2 2.253(1), C11-P1 1.795(3), C11-P2 1.792(3), C12-P1 1.787(3), C12-P2 1.789(3), C11-C23 1.505(4), C12-C13 1.509(4); P1-C11-C23 128.8(2), P1-C12-C13 128.9(2), P2-C12-C13 128.2(2), P2-C11-C23 128.8(2), P2-C12-P1 99.4(1), P2-C11-P1 99.0(1).

In conclusion, **3** demonstrates a remarkable reactivity with regard to ligand exchange and is also the first example for the exchange of the aromatic "middle deck" of a triple-decker at room temperature. Complex **3** thus seems to be a promising source of $[(\eta^5\text{-Cp*})Co]$ complex fragments and as a transfer reagent for these fragments in future studies.

Experimental Procedure

3a–f: $[(\eta^5\text{-Cp*})(\text{acac-}O,O')Co]$ (10 mmol) was dissolved in 100 mL of the particular arene concerned, and an equimolar amount of pieces of potassium metal were added. The surface of the potassium metal can be activated by ultrasound for a short period of time. The mixture was then stirred until the metal had dissolved completely (max. 2 weeks). During this time, the color of the reaction mixture changed from red to deep brown. A dirty-grey precipitate was also formed. Excess arene was then removed under vacuum, and the residue fully extracted with pentane. The extract was filtered, concentrated by removal of solvent under vacuum, and cooled to −78 °C to give the triple-decker complexes **3a–f** in crystalline form. Yield: 40–60%.

3a: MS (EI, 70 eV): *m/z* (%): 466 (5) [M^+], 386 (7), 329 (42), 192 (17), 78 (100), 51 (28); ^{1}H-NMR (200 MHz, 27 °C, [D$_6$]benzene): δ = 2.05 (s, 30H), 3.00 (s, 6H). – **3b**: MS (EI, 70 eV): *m/z* (%): 480 (30) [M^+], 386 (73), 329 (64), 92 (78), 91 (100); IR (KBr): $\tilde{\nu}$ = 730 (s, vw), 755 (vw), 775 (vw), 850 (vw), 990 (vw), 1020 (s), 1370 (vs), 1430–1470 (vs), 3020 cm^{-1} (vw); ^{1}H-NMR (300 MHz, 27 °C {−80 °C}, [D$_8$]THF): δ = 1.79 {1.77} (s, 30H), 1.57 {1.65} (s, 3H), 2.70 {2.21} (d, ^3J(H,H) = 4.6 Hz, 2H, 2.82 {2.36} (t, ^3J(H,H) = 4.6 Hz, 2H), 3.00 {3.32}(t, ^3J(H,H) = 4.6 Hz, 1H); ^{13}C-NMR (75.5 MHz, 32 °C {−80 °C}, [D$_8$]THF): δ = 10.9 {11.2} (q ^1J(C,H) = 126 Hz, 30H, Cp*), 20.6 {19.8} (q, ^1J(C,H) = 126 Hz, 3H, CH$_3$), 53.1 {50.5} (d, ^1J(C,H) = 167 Hz, *m*-C), 55.2 {51.3} (d, ^1J(C,H) = 166 Hz, *o*-C), 56.2 {60.8} (d, ^1J(C,H) = 172 Hz, *p*-C), 69.3 {74.3} (s, quart. C), 85.7 {86.3} (s, C_{Ring} on Cp*). – **3c**: MS (EI, 70 eV): *m/z* (%): 494 (34) [M^+], 386 (100) 329 (38), 300 (25), 192 (14), 133 (19), 106 (19), 91 (32); IR (KBr): $\tilde{\nu}$ = 770 (s), 795 (m), 860 cm^{-1} (vw); ^{1}H-NMR (200 MHz, 27 °C, [D$_6$]benzene): δ = 1.91 (s, 30H), 1.55 (s, 6H), 2.81 (s, 2H), 2.96 (s, 2H). – **3d**: MS (EI, 70 eV): *m/z* (%): 494 (33) [M^+], 386 (100), 329 (38), 300 (25), 192 (15), 133 (20), 106 (19), 91 (31); IR (KBr): $\tilde{\nu}$ = 840 (vw), 960 (vw), 1025 (s), 1375 (s), 1480 (s, br), 3020 cm^{-1} (vw); ^{1}H-NMR (200 MHz, 27 °C, [D$_6$]benzene): δ = 1.96 (s, 30H), 1.51 (s, 6H), 2.72 (s, 2H), 2.82 (s, 1H), 3.19 (s, 1H). – **3e**: MS (EI, 70 eV): *m/z* (%): 494 (4) [M^+], 386 (15), 329 (20), 106 (63), 91 (100); IR (KBr): $\tilde{\nu}$ = 680 (s), 850 (vw), 905 (vw), 1195 (vw), 3020 cm^{-1} (vw); ^{1}H-NMR (200 MHz, 27 °C, [D$_6$]benzene): δ = 1.97 (s, 30H), 1.63 (s, 6H), 2.71 (s, 4H). – **3f**: MS (EI, 70 eV): *m/z* (%): 508 (27) [M^+], 386 (88), 314 (100), 192 (41), 120 (25), 133 (28), 105 (93); IR (KBr): $\tilde{\nu}$ = 995 (s), 860 (m), 782 (m), 725 cm^{-1} (vw); ^{1}H-NMR (400 MHz, 27 °C, [D$_6$]benzene): δ = 1.02 (s, 1H), 1.32 (s, 6H), 1.98 (s, 30H), 3.0 (s, 2H), 3.05 (s, 1H), 3.20 (s, 2H). Single crystals of **3f** suitable for an X-ray structure analysis were obtained from a saturated diethyl ether solution of **3f** at −78 °C. Correct C, H, and Co elemental analyses were obtained for all the compounds **3a–f**.

[D$_6$]3a: **3a** (80 mg, 0.17 mmol) was dissolved in 5 mL [D$_6$]benzene and allowed to stand at room temperature for 2 days or at 0 °C for 1 week in a sealed NMR tube. The solvent was then fully removed and the residue analyzed. The yield was approximately quantitative. MS (EI, 70 eV): *m/z* (%): 472 (3) [M^+], 329 (6), 84 (100); ^{1}H-NMR (200 MHz, 27 °C, [D$_6$]benzene): δ = 2.01 (s, 30H); IR (KBr) $\tilde{\nu}$ = 2240 cm^{-1} (CD-Ring).

4: **3b** (120 mg, 0.25 mmol) was dissolved in 30 mL ether, and cycloheptatriene (0.026 mL, 0.25 mmol) added with continuous stirring. The mixture was stirred for 1 h, and all volatile components then removed under vacuum. The residue was taken up in pentane and filtered. Compound **4** crystallized at −30 °C in the form of brown crystals with a metallic luster. Yield : 84 mg (0.18 mmol, 72%). The C, H, and Co elemental analyses were correct. The spectroscopic data of **4** were identical with those in the literature [5].

5: **3b** (120 mg, 0.25 mmol) was dissolved in 30 mL ether, and cot (0.016 mL, 0.25 mmol) added while stirring. The mixture was stirred for 2 h, and the solution turned red. All volatile components were removed under vacuum, and the semicrystalline residue was dissolved in pentane and filtered. Compound **5**[16] crystallized at −30 °C in the form of red crystals. Yield: 82 mg (0.16 mmol, 64 %). The C, H, and Co elemental analyses were correct. MS (EI, 70 eV): *m/z* (%): 492 (100) [M^+], 386 (27), 329 (15), 297 (60), 243 (48), 133 (18); ^{1}H-NMR (200 MHz, 27 °C, [D$_8$]THF): δ = 3.0 (s, 8H), 1.42 (s, 30H); ^{13}C-NMR (50.32 MHz, 27 °C, [D$_8$]THF): δ = 91.45, 81.89, 9.13.

8, 9: **3b** (345 mg, 0.718 mmol) was dissolved in 50 mL ether and treated either with a) **6** (384 mg, 2.25 mmol), b) **7** (382 mg, 2.14 mmol), or c) **6** (122 mg, 0,68 mmol) and **7** (120 mg, 0.67 mmol) simultaneously. In each case the mixture was stirred for 12 h. In the case of a) and c), **8** precipitated as a yellow powder (230 mg, 0.42 mmol, 29%) as the reaction proceeded. The powder was purified sufficiently for analytical purposes by filtration and washing with pentane. In the case of b), the solvent was removed to give a viscous brown residue. This was dissolved in a small amount of ether, and **9** was obtained in the form of beige-brown crystals, which are suitable for

 © VCH Verlagsgesellschaft mbH, D-69451 Weinheim, 1995 0570-0833/95/0505-0594 $ 10.00+.25/0

X-ray structure analysis, by addition of CH_3CN and cooling to $-30\,^{\circ}C$. Yield: 189 mg (0.34 mmol, 24%).

8: **8**: MS (EI, 70 eV) m/z (%): 550 (100) $[M^+]$, 372 (26), 178 (54), 133 (39); ^{1}H-NMR (200 MHz, 27 °C, CD_2Cl_2): $\delta = 7.15-7.28$ (m, 20H), 1.42 (s, 15H); ^{13}C-NMR (50.3 MHz, 27 °C, CD_2Cl_2): $\delta = 8.86$ (q), 73.6 (s), 89.8 (s), 125.6 (d), 127.9 (d), 128.6 (d), 136.6 (s). – **9**: MS (EI, 70 eV): m/z (%): 550 (51) $[M^+]$, 488 (18), 256 (100); ^{1}H-NMR (400 MHz, 27 °C, CD_2Cl_2): $\delta = 1.27$ (s, 13H), 1.53 (m, 15H), 1.91 (s, 8H), 2.03 (s, 15H); ^{13}C-NMR (100.6 MHz, 27 °C, CD_2Cl_2): $\delta = 11.87$ (s), 28.18 (s), 35.84 (s), 35.97 (t), 41.99 (t), 91.91 (s), 109.13 (t); ^{31}P-NMR (81.02 MHz, 27 °C, CD_2Cl_2): $\delta = 24.86$. The C, H, P, and Co elemental analyses for **8** and **9** were correct.

Received: August 26, 1994
Revised version: October 26, 1994 [Z 72691E]
German version: *Angew. Chem.* **1995**, *107*, 631

Keywords: arene complexes · cobalt compounds · cyclobutadienes · sandwich complexes · triple-decker complexes

[1] Examples for C_6H_6 and derivatives: a) H. Wadepohl, *Angew. Chem.* **1992**, *104*, 253; *Angew. Chem. Int. Ed. Engl.* **1992**, *31*, 247; für C_8H_8: b) J. Edwin, W. E. Geiger, C. H. Bushweller, *Organometallics* **1988**, *7*, 1486; c) M. Moraczewski, W. E. Geiger, *J. Am. Chem. Soc.* **1978**, *100*, 7429; d) J. Edwin, W. E. Geiger, A. L. Rheingold, *ibid.* **1984**, *106*, 3052; e) W. E. Geiger, A. Salzer, J. Edwin, W. von Philipsborn, U. Piantini, A. L. Rheingold, *ibid.* **1990**, *112*, 7113; f) H. Breil, G. Wilke, *Angew. Chem.* **1966**, *78*, 942; *Angew. Chem. Int. Ed. Engl.* **1966**, *5*, 898; g) H. Dietrich, H. Dierks, *ibid.* **1966**, *78*, 943 or **1966**, *5*, 899; h) *Acta Crystallgr. Sect. B* **1986**, *24*, 58.

[2] A. W. Duff, K. Jonas, R. Goddard, H. J. Kraus, C. Krüger, *J. Am. Chem. Soc.* **1983**, *105*, 5479.

[3] J. M. Manriquez, L. Valle, E. E. Bunel, *Organometallics* **1985**, *4*, 1680.

[4] a) K. H. Theopold, J. L. Kersten, A. L. Rheingold, C. P. Casey, R. A. Wiedenhoefer, C. E. A. Hop, *Angew. Chem.* **1992**, *104*, 1364; *Angew. Chem. Int. Ed. Engl.* **1992**, *31*, 1341; b) J. J. Schneider, *ibid.* **1992**, *104*, 1422 or **1992**, *31*, 1392.

[5] H. Wadepohl, W. Galm, H. Pritzkow, *Angew. Chem.* **1990**, *102*, 701; *Angew. Chem. Int. Ed. Engl.* **1990**, *29*, 686.

[6] a) R. G. Beevor, S. A. Frith, J. L. Spencer, *J. Organomet. Chem.* **1981**, *221*, C25; b) S. A. Frith, J. L. Spencer, *Inorg. Synth.* **1985**, *23*, 15.

[7] R. Krömer, C. Krüger, Crystal structure analysis IO 1935, Max-Planck-Institut für Kohlenforschung, Mülheim an der Ruhr, unpublished.

[8] A. J. Campbell, C. E. Cottrell, C. A. Fyfe, K. R. Jeffrey, *Inorg. Chem.* **1976**, *15*, 1326.

[9] C. E. Cottrel, C. A. Fyfe, C. V. Senoff, *J. Organomet. Chem.* **1972**, *43*, 203.

[10] J. R. Lyerla, C. A. Fyfe, C. S. Yannoni, *J. Am. Chem. Soc.* **1979**, *101*, 1351.

[11] M. A. Gallop, B. F. G. Johnson, J. Keeler, J. Lewis, S. J. Heyes, C. M. Dobson, *J. Am. Chem. Soc.* **1992**, *114*, 2510.

[12] Crystal structure analysis of **3f**: Formula $C_{29}H_{42}Co_2$, $M = 508.5\,g\,mol^{-1}$, crystal size $0.28 \times 0.35 \times 0.39$ mm, triclinic, space group $P\bar{1}$ (No. 2), $a = 8.703(6)$, $b = 11.663(6)$, $c = 14.597(3)$ Å, $\alpha = 102.93(2)$, $\beta = 101.72(3)$, $\gamma = 111.70(5)$, $V = 1273.2$ Å^3, $\rho_{calcd} = 1.33\,g\,cm^{-3}$, $\mu = 13.14\,cm^{-1}$, $F(000) = 540$ e, $Z = 2$, Enraf-Nonius CAD4 diffractometer, $\lambda = 0.71069$ Å, measurement method ω-2θ, 6020 reflections measured ($\pm h, \pm k, +l$), $[(\sin\theta)/\lambda]_{max}$ 0.65 Å^{-1}, 5792 independent and 3653 observed reflections [$I > 2\sigma(I)$], 271 refined parameters, structure solved by heavy atom method, disorder in the C atomic positions of a Cp* ring, refinement using an occupation of 50:50 per C atom position, $R = 0.076$, $R_w = 0.074$ [$w = 1/\sigma^2(F_0)$], $R_{av} = 0.01$, maximum residual electron density = 1.05 e Å^{-3}. H atom positions were calculated and not used in the least-squares refinement; see [16b].

[13] C. Böhle, W. Siebert (Universität Heidelberg), X-ray structure analysis: C. Krüger, Mülheim an der Ruhr as cited in ref. [5].

[14] J. Müller, P. Escarpa Gaede, K. Qiao, *Angew. Chem.* **1993**, *105*, 1809; *Angew. Chem. Int. Ed. Engl.* **1993**, *32*, 1697.

[15] T. Allspach, M. Regitz, G. Becker, W. Becker, *Synthesis* **1986**, 31.

[16] a) Crystal structure analysis of **9**: Formula $C_{32}H_{45}CoP_2$, $M = 550.6\,g\,mol^{-1}$, crystal size $0.21 \times 0.28 \times 0.39$ mm, triclinic, space group $P\bar{1}$ (No. 2), $a = 12.692(2)$, $b = 15.071(3)$, $c = 17.795(3)$ Å, $\alpha = 111.21(1)$, $\beta = 97.45(1)$, $\gamma = 107.60(2)$, $V = 2899.0$ Å^3, $\rho_{calcd} = 1.26\,g\,cm^{-3}$, $\mu = 7.16\,cm^{-1}$, $F(000) = 1176$ e, $Z = 4$ (2 independent molecules in the asymmetric unit), Enraf-Nonius CAD4 diffractometer, $\lambda = 0.71069$ Å, measurement method ω-2θ, 13644 reflections measured ($\pm h, \pm k, +l$), $[(\sin\theta)/\lambda]_{max}$ 0.65 Å^{-1}, 13211 independent and 9642 observed reflections [$I > 2\sigma(I)$], 631 refined parameters, structure solved by heavy atom method, H atom positions were calculated and not used in the least-squares refinement, $R = 0.044$, $R_w = 0.046$ [$w = 1/\sigma^2(F_0)$], $R_{av} = 0.01$, maximum residual electron density = 0.36 e Å^{-3}. b) Further details of the crystal structure investigation may be obtained from the Fachinformationszentrum Karlsruhe, D-76344 Eggenstein-Leopoldshafen (FRG) on quoting the depository numbers CSD-58901.

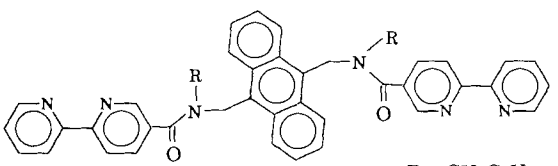
Electronic Energy Transfer in a Supramolecular Species Containing the $[Ru(bpy)_3]^{2+}$, $[Os(bpy)_3]^{2+}$, and Anthracene Chromophoric Units**

Peter Belser,* Roland Dux, Marcel Baak, Luisa De Cola,* and Vincenzo Balzani*

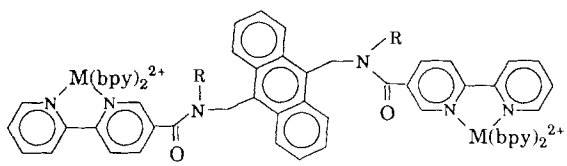
At the roots of supramolecular chemistry is the concept that supramolecular systems have the potential to achieve much more elaborate tasks than simple molecules:[1–6] while molecules can be involved in simple chemical *acts*, supramolecular systems can perform *functions*. In other words, supramolecular systems have the potential to behave as molecular devices. A particularly interesting class of molecular devices is that capable of using photons as energy or information inputs (photochemical molecular devices).[4, 7] An essential function in many photochemical molecular devices is electronic energy transfer.[4] The design of ordered supramolecular systems in which the path of electronic energy transfer can be synthetically predetermined and then switched by an external input is an important goal of current chemical research.[8]

Continuing our investigations on the study of energy transfer processes in supramolecular systems involving transition-metal complexes,[9, 10] we have designed and synthesized a three-component species in which i) energy transfer occurs in a predetermined direction and ii) its efficiency and rate can be strongly reduced as a consequence of a self-photosensitized reaction involving dioxygen.

The Ru-An-Os three-component system (Scheme 1) is made up of $[Ru(bpy)_3]^{2+}$- and $[Os(bpy)_3]^{2+}$-type units (indicated by



bpy-An-bpy



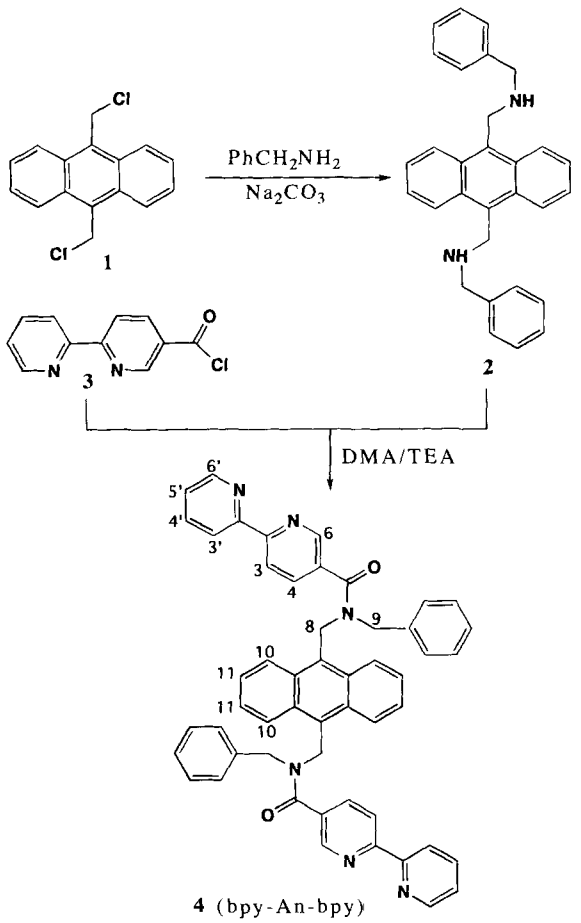
$[(bpy)_2Ru(bpy\text{-}An\text{-}bpy)Os(bpy)_2]^{4+}$	Ru-An-Os
$[(bpy)_2Ru(bpy\text{-}An\text{-}bpy)Ru(bpy)_2]^{4+}$	Ru-An-Ru
$[(bpy)_2Os(bpy\text{-}An\text{-}bpy)Os(bpy)_2]^{4+}$	Os-An-Os

Scheme 1. Structural formulas of the bpy-An-bpy bridging ligand and of its complexes. The abbreviations used to indicate the complexes are also shown.

[*] Prof. Dr. P. Belser, Dr. R. Dux, M. Baak
Institut für Anorganische und Analytische Chemie der Universität
Perolles, CH-1700 Fribourg (Switzerland)
Telefax: Int. code +(37) 299 738
Dr. L. De Cola, Prof. V. Balzani
Dipartimento di Chimica "G. Ciamician", Università di Bologna
via Selmi 2, I-40126 Bologna (Italy)
Telefax: Int. code +(51) 259 456

[**] This work was supported by the Swiss National Science Foundation, and Ministero della Università e della Ricerca Scientifica e Tecnologica (MURST) and Consiglio Nazionale delle Ricerche (Progetto Strategico CNR Tecnologie Chimiche Innovative) (Italy).

Ru and Os, respectively; bpy is 2,2′-bipyridine), linked to the 9,10 positions of an anthracene (An) ring. This arrangement has been chosen so as to have a gradient for energy transfer along the Ru-An-Os sequence (see below).[11] The analogous homometallic Ru-An-Ru and Os-An-Os species have also been prepared, and their properties will be mentioned when necessary for comparison. Very good model compounds for the isolated Ru-based and Os-based units of Ru-An-Os are the previously investigated[12] Ru and Os complexes with two bpy ligands and a bpy ligand which carries an amido-type substituent in a 5′ position. For the An-based unit of Ru-An-Os, the model compound is the bpy-An-bpy free ligand used to prepare the dinuclear complexes (Scheme 2). This compound shows, as expected, the same absorption spectrum (above 350 nm) and the same fluorescence spectrum and lifetime of anthracene.



Scheme 2. The synthesis of the bpy-An-bpy bridging ligand. See *Experimental Procedure* for details.

The absorption spectrum of Ru-An-Os (Fig. 1) is exactly that expected for a 1:1:1 mixture of the corresponding model compounds, indicating that the electronic interaction between the three components of the supramolecular system is very small. The structured absorption around 350–400 nm is due to the anthracene unit, the broad band with maximum at 451 nm receives contributions from spin-allowed metal-to-ligand charge-transfer (CT) transitions of the Ru-based and Os-based components, and the broad tail above 500 nm is due to spin-forbidden CT transitions of the Os-based component.

Luminescence experiments (inset in Fig. 1) were carried out with 464 nm excitation, corresponding to an isosbestic point of the $[Ru(bpy)_3]^{2+}$ and $[Os(bpy)_3]^{2+}$ moieties. In order to discuss

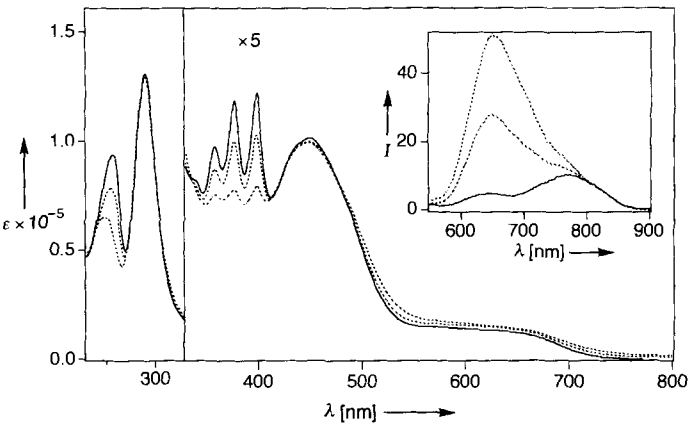


Fig. 1. Absorption and luminescence (inset) spectra in acetonitrile solution of Ru-An-Os (full line). The spectral changes caused by irradiation with visible light of aereated solution are also shown (dotted curves).

the results obtained (Table 1), reference will be made to the simplified energy level diagram of Figure 2. For deaerated acetonitrile solution, comparison with the behavior of the mononuclear model compound shows that the lifetime of the Ru-based emission of Ru-An-Os is extremely short. This indicates that in Ru-An-Os the ^{3}CT Ru-based excited state undergoes a quenching process. Quenching is confirmed by the fact that the intensity of the Ru-based luminescence band is extremely weak (about 0.5% that of the model compound). The quenching process involves energy transfer to the Os-based unit, as shown by a) the intensity of the Os-based 770 nm band, and b) the observation of a risetime, for the Os-based emission, which is close to the decay rate of the Ru-based luminescence. The rate constant for the quenching process can be calculated from the equation $k_{en} = 1/\tau - 1/\tau^{\circ}$, where τ and τ° are the luminescence lifetimes of the Ru-based moiety of Ru-An-Os and of the Ru model compound, respectively. From the values displayed in Table 1, k_{en} was calculated to be $4.7 \times 10^8\ s^{-1}$.

Table 1. Luminescence data [a].

	Deaerated solution [b]						Air-equilibrated solution			
	Ru-based			Os-based			Ru-based		Os-based	
	λ_{max} [nm]	τ [ns]	I_{rel} [c]	λ_{max} [nm]	τ [ns]	I_{rel} [c]	λ_{max} [nm]	τ [ns]	λ_{max} [nm]	τ [ns]
Ru model compound [d]	640	495	100	–	–	–	640	200	–	–
Os model compound [e]	–	–	–	770	18	100	–	–	780	14
Ru-An-Os	640	2.1	0.5	770	16	100 [f]	640	90 [g]	770	13

[a] In acetonitrile solution at room temperature. [b] After three freeze-pump-thaw cycles. [c] Excitation at 464 nm. [d] Ru-An-Ru and $1 \cdot Ru_3$ from ref. [12] for emission maximum; $1 \cdot Ru_3$ from ref. [12] for luminescence intensity and lifetime. [e] Os-An-Os; $1 \cdot Os_3$ from ref. [12] exhibits very similar properties. [f] The light absorbed by the Ru-based unit is as effective as that absorbed by the Os-based unit. [g] At the end of the photoreaction; the initial value was 1.7 ns.

 © VCH Verlagsgesellschaft mbH, D-69451 Weinheim, 1995 0570-0833/95/0505-0596 $ 10.00+.25/0

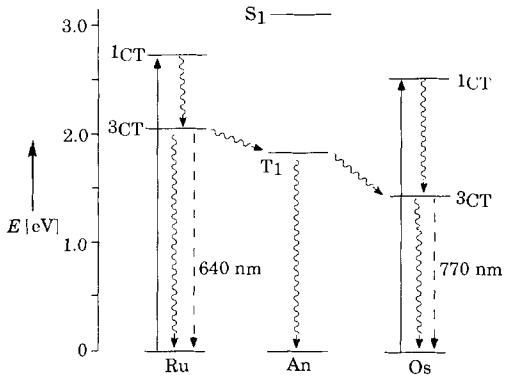


Fig. 2. Schematic diagram for the low-energy excited states of Ru-An-Os.

The occurrence of energy transfer from the Ru-based to the Os-based component of Ru-An-Os can be explained on the basis of the relative energy positions of the ^{3}CT levels of the two metal-containing units (Fig. 2). The structure of the supramolecular species, and the energy level diagram suggest that energy is first transferred from the ^{3}CT Ru-based excited state to the lowest triplet excited state of anthracene (T_1), which then transfers energy to the luminescent ^{3}CT excited state of the Os-based unit.[11] The experiments described below support this hypothesis. In air-equilibrated acetonitrile solutions the intensity of the luminescence of the Os-based unit is slightly weaker and the lifetime slightly shorter than in deaerated solutions. This is an expected result in view of the quenching effect of oxygen on the ^{3}MLCT excited state of Os^{II}-polypyridine compounds.[13]

Continuous irradiation with visible light of deaerated acetonitrile solutions of Ru-An-Os does not cause any change in the absorption and luminescence spectra. The energy absorbed by the Ru-based unit flows to the Os-based one, where it is dissipated by radiative and radiationless transitions. In air-equilibrated solutions, however, continuous irradiation causes a photoreaction, as shown by the progressive disappearance of the structured anthracene absorption in the 350–400 nm region (Fig. 1). A concomitant increase in the intensity of the Ru-based luminescence band at 640 nm is also observed (Fig. 1, inset). At the end of the photoreaction the lifetime of the recovered Ru-based emission is about 90 ns, that is much shorter than that of the model Ru compound (Table 1). These results indicate that in the photoreaction product the Ru-based luminescence is quenched with a rate constant of $0.6 \times 10^7\ s^{-1}$, a value about 80 times smaller than that found for Ru-An-Os. Although the experimental error is large because of the intense tail of the Ru-based luminescence, it is clear that the partial quenching of the Ru-based emission is still accompanied by sensitization of the Os-based luminescence (Fig. 1, inset). NMR measurements on the irradiated solutions indicate formation of an anthracene endoperoxide species as well as of other products where the anthracene aromaticity is no longer present.[14]

The results obtained in aerated solution can be interpreted by oxygen quenching of the Os-based ^{3}CT excited state of Ru-An-Os with formation of singlet oxygen [Eq. (a)], followed by attack of singlet oxygen on an anthracene ring to form an endoperoxide derivative [Eq. (b)],[15] which then may evolve[16] to give other products (indicated by Ru-X-Os) where the central ring of anthracene has lost its aromatic character [Eq. (c)].

$$Ru\text{-}An\text{-}(^3CT)Os + O_2 \longrightarrow Ru\text{-}An\text{-}Os + (^1\Delta)O_2 \quad (a)$$

$$Ru\text{-}An\text{-}Os + (^1\Delta)O_2 \longrightarrow Ru\text{-}An(O_2)\text{-}Os \quad (b)$$

$$Ru\text{-}An(O_2)\text{-}Os \longrightarrow Ru\text{-}X\text{-}Os \quad (c)$$

The very low quenching rate of the Ru-based excited state by the Os-based moiety in the photoproducts (where the anthracene aromaticity has been destroyed and, as a consequence, the T_1 level (Fig. 2) has been removed) indicates that the T_1 excited state of anthracene does play a role in the energy transfer process observed for Ru-An-Os.

In conclusion, electronic energy transfer from the Ru-based to the Os-based unit of Ru-An-Os takes place through the anthracene bridge with almost unitary efficiency and rate constant $4.7 \times 10^8\ s^{-1}$. When the aromaticity of the anthracene unit is destroyed by the self-photosensitized oxidation reaction, the rate constant and the efficiency of the energy transfer process from the Ru-based to the Os-based unit are strongly reduced.

Experimental Procedure

Benzyl[{10-(benzylaminomethyl)anthracen-9-yl}methyl]amine **2**: 9,10-Bis(chloromethyl)anthracene **1** [17] (4.21 g, 15.3 mmol) was added under stirring to anhydrous sodium carbonate (26 g, 0.245 mol) in benzylamine (250 mL, 2.29 mol). The mixture was stirred at room temperature for 8 h and the solid was filtered off. The excess of benzylamine was distilled from the filtrate. The remaining solid was dried in an oven at 80 °C for one day. For purification the residue was heated to reflux for 15 minutes in 6 M hydrochloric acid (75 mL) and the solid, which was formed after standing overnight, was filtered off. The solid was then stirred with sodium hydroxide (2 M solution, 200 mL) for 3 h. The clear solution was extracted with dichloromethane. The combined extracts were dried over magnesium sulfate. Evaporation of the solvent yielded **2** (5.93 g; 93%). ^{1}H NMR (300 MHz, [D$_6$]DMSO: δ = 2.5 (s, 2H, NH), 3.95 (s, 4H, CH_2), 4.53 (s, 4H, CH_2), 7.25–7.46 (m, 10H, CH_{ar}). FAB-MS: m/z = 416 (M^+), 310 (M^+ – benzylamine), 218 (M^+ – 2 benzylamine), 192 (anthracene–CH_2), 178 (anthracene). Satisfactory C, H, N, analysis for $C_{30}H_{28}N_2$.

9,10-Bis[2,2'-bipyridinyl-5-yl-carbonyl-(*N*-benzyl)aminomethyl]anthracene **4**: A mixture of amine **2** (1.62 g, 3.9 mmol) and triethylamine (TEA) (10 mL) in dimethylacetamide (DMA) (20 mL) was added to a stirred mixture of 2,2'-bipyridinyl-5-carbonyl chloride **3** [12] (2.18 g, 10 mmol) in DMA (50 mL). The mixture was stirred overnight and filtered. The organic layer was treated with 800 mL 5% $NaHCO_3$ solution. The precipitated solid was separated by centrifugation and dissolved in dichloromethane, washed with water, and dried over magnesium sulfate. Evaporation of the solvent yielded **4** (0.609 g; 20%). ^{1}H NMR (300 MHz, [D$_6$]DMSO, 100 °C): δ = 4.2 (s, 4H, CH_2(9)), 5.8 (s, 4H, CH_2(8)), 6.6–7.3 (m, 10H, benzyl), 7.42 (ddd, 2H, CH(5')), 7.64 (dd, 4H, CH(11)), 7.90 (ddd, 2H, CH(4')), 7.97 (dd, 2H, CH(4)), 8.17 (dd, 4H, CH(10)), 8.33 (ddd, 2H, CH(3')), 8.37 (dd, 2H, CH(3)), 8.66 (ddd, 2H, CH(6')), 8.73 (dd, 2H, CH(6)). FAB-MS: m/z = 803 ($M^+ + Na^+$), 597 (M – bpy–CO), 492 (M – bpy–CONH–benzyl), 391, 310, 218, 204 (CH_2–anthracenediyl–CH_2), 183 (bpy–CO), 156 (bpy), 149, 113, 71. Satisfactory C, H, N analysis for $C_{52}H_{40}N_6O_2$.

The metal complexes were prepared by using [M(bpy)$_2$Cl$_2$] (M = Ru, Os) and the bpy-An-bpy ligand in refluxing methoxyethanol. Upon addition of an excess of NH_4PF_6, the PF_6^- salts of the complexes were precipitated and purified as previously described [12].

Characterization of the metal complexes: Ru-An-Ru. ^{1}H NMR (300 MHz, [D$_6$]DMSO, 90 °C): δ = 3.85 (s, 4H, CH_2(9)), 5.67 (s, 4H, CH_2(8)), 6.49–6.55 (m, 4H, benzyl), 7.2–7.42 (m, 6H, benzyl), 7.3–7.8 (m, 26H, ar.), 7.9–8.2 (m, 16H, ar.), 8.5–8.8 (m, 12H, CH(3,3')). FAB-MS: m/z = 2074 ($M^+ - O_2 - PF_6$), 2042 ($M^+ - PF_6$), 1898 ($M^+ - 2PF_6$), 1754 ($M^+ - 3PF_6$), 1339, 1051. Satisfactory C, H, N, analysis for $C_{92}H_{72}F_{24}N_{14}O_2P_4Ru_2$.

Os-An-Os. ^{1}H NMR (300 MHz, [D$_6$]DMSO, 90 °C): δ = 3.85 (s, 4H, CH_2(9)), 5.67 (s, 4H, CH_2(8)), 6.4–6.55 (m, 4H, CH(benzyl)), 6.9–7.2 (m, 6H, CH(benzyl)), 7.3–7.8 (m, 26H, CH(5,5',6,6',11)), 7.7–8.0 (m, 16H, CH(4,4',10)), 8.5–8.8 (m, 12H, CH(3,3')). FAB-MS: m/z = 2386 (M^+ + Na), 2221 ($M^+ - PF_6$), 2073 ($M^+ - 2PF_6$), 1141, 1038, 750. Satisfactory C, H, N, analysis for $C_{92}H_{72}F_{24}N_{14}O_2Os_2P_4$.

Ru-An-Os. ^{1}H NMR (300 MHz, [D$_6$]DMSO, 100 °C): δ = 3.85 (s, 4H, CH_2(9)), 5.66 (s, 4H, CH_2(8)), 6.4–6.55 (m, 4H, CH(benzyl)), 6.9–7.2 (m, 6H, CH(benzyl)), 7.2–7.7 (m, 26H, CH_{ar}), 7.7–8.2 (m, 16H, CH(4,4',10)), 8.5–8.8 (m, 12H, CH(3,3')). FAB-MS: m/z = 2299 (M^+ + Na), 2133 ($M^+ - PF_6$), 1988 ($M^+ - 2PF_6$). Satisfactory C,H,N, analysis for $C_{92}H_{72}F_{24}N_{14}O_2OsP_4Ru$.

The equipment used to measure the absorption spectra, emission spectra, and luminescence lifetimes have been previously described [12].

Received: September 5, 1994 [Z 7291 IE]
German version: *Angew. Chem.* **1995**, *107*, 634

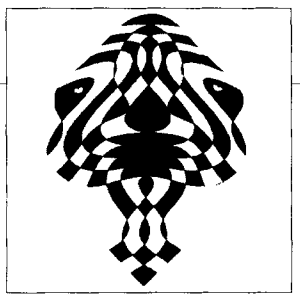
Keywords: charge transfer complexes · energy transfer · photochemistry · supramolecular chemistry · transition metal compounds

 © VCH Verlagsgesellschaft mbH, D-69451 Weinheim, 1995 0570-0833/95/0505-0597 $ 10.00+.25/0

[1] *Supramolecular Photochemistry* (Ed.: V. Balzani), Reidel, Dordrecht, **1987**.
[2] J.-M. Lehn, *Angew. Chem.* **1990**, *102*, 1347; *Angew. Chem. Int. Ed. Engl.* **1990**, *29*, 1304.
[3] F. Vögtle, *Supramolecular Chemistry*, Wiley, Chichester, **1991**.
[4] V. Balzani, F. Scandola, *Supramolecular Photochemistry*, Horwood, Chichester, **1991**.
[5] *Frontiers in Supramolecular Organic Chemistry and Photochemistry*, (Eds.: H. J. Schneider, H. Dürr), VCH, Weinheim, **1991**.
[6] *Supramolecular Chemistry* (Eds.: V. Balzani, L. De Cola), Kluwer, Dordrecht, **1992**.
[7] V. Balzani, L. Moggi, F. Scandola in ref. [1], p. 1.
[8] A very interesting three-component system where energy transfer can be switched on/off by a photochromic reaction of the central component has been recently reported: J. Walz, K. Ulrich, H. Port, H. C. Wolf, J. Wonner, F. Effenberger, *Chem. Phys. Lett.* **1993**, *213*, 321.
[9] a) F. Vögtle, M. Frank, M. Nieger, P. Belser, A. von Zelewsky, V. Balzani, F. Barigelletti, L. De Cola, L. Flamigni, *Angew. Chem.* **1993**, *105*, 1706; *Angew. Chem. Int. Ed. Engl.* **1993**, *32*, 1643; b) L. De Cola, V. Balzani, F. Barigelletti, L. Flamigni, P. Belser, A. von Zelewsky, M. Frank, F. Vögtle, *Inorg. Chem.* **1993**, *32*, 5228.
[10] a) F. Barigelletti, L. Flamigni, V. Balzani, J.-P. Collin, J.-P. Sauvage, A. Sour, E. C. Constable, A. M. W. Cargill Thompson, *J. Chem. Soc. Chem. Commun.* **1993**, 942; b) *J. Am. Chem. Soc.* **1994**, *116*, 7692.
[11] Energy transfer in soluble polymers containing appended $[Ru(bpy)_3]^{2+}$, $[Os(bpy)_3]^{2+}$, and anthracene units has been investigated by Meyer and coworkers: a) G. F. Strouse, L. A. Worl, J. N. Younathan, T. J. Meyer, *J. Am. Chem. Soc.* **1989**, *111*, 9101; b) W. E. Jones, S. M. Baxter, S. L. Mecklenburg, B. W. Erickson, B. M. Peek, T. J. Meyer in ref. [6], p. 249.
[12] P. Belser, A. von Zelewsky, M. Frank, C. Seel, F. Vögtle, L. de Cola, F. Barigelletti, V. Balzani, *J. Am. Chem. Soc.* **1993**, *115*, 4076.
[13] M. Z. Hoffman, F. Bolletta, L. Moggi, G. L. Hug, *J. Phys. Chem. Ref. Data* **1989**, *18*, 219.
[14] The two methylene groups of the Ru-An-Ru complex show chemical shifts of 5.67 and 3.85 ppm ([D_6]DMSO) respectively. In the case of the Ru-An-Ru μ-peroxo-compound, these resonances are replaced by a more complicated pattern in the region of 4.4–5.1 ppm ([D_6]DMSO). These -CH_2 signals comprise at least three different AB systems, because of restricted rotations induced by the μ-peroxo formation.
[15] A. Gilbert, J. Baggott, *Essentials of Molecular Photochemistry*, Blackwell, London, **1991**.
[16] R. Schmidt, H.-D. Bauer, *J. Photochem.* **1986**, *34*, 1.
[17] M. W. Miller, R. W. Amidon, P. O. Tawney, *J. Am. Chem. Soc.* **1955**, *77*, 2845.

Troubleshooting...

with VCH books!



Neuhoff, V.
Scientists in Conference
The Congress Organizer's Handbook
1987. X, 223 pages.
Hardcover. DM 68.00
ISBN 3-527-26579-1

Do you have to organize a conference? Well, sometimes, this can't be avoided. But you don't want to get crushed by the wheels of paperwork? And you want to stay in your budget? Then this handy little book is your survival kit!

Schoenfeld, R.
The Chemist's English
Third, revised edition with Say It in English, Please!
1990. XII, 195 pages with 9 figures.
Hardcover. DM 48.00
ISBN 3-527-28003-0

"Recommended without qualification; and a suitable gift for friends."
Chemical and Engineering News

"The book might well serve as a prescribed text for PhD students."
Nature

Ebel, H.F. /Bliefert, C. / Russey, W.
The Art of Scientific Writing
From Student Reports to Professional Publications in Chemistry and Related Fields
1990. XIX, 493 pages with 27 figures and 16 tables.
Softcover. DM 48.00
ISBN 3-527-26677-1

First of all, here we have a highly readable text on scientific communication - with all its ramifications from writing the most effective text to getting it published. Never before has so much information on scientific writing been assembled in a single book.

To order please contact your bookseller or:

VCH, P.O. Box 10 11 61, D-69451 Weinheim, Telefax (0) 62 01 - 60 61 84

VCH, Hardstrasse 10, P.O. Box, CH-4020 Basel

VCH, 8 Wellington Court, Cambridge CB1 1HZ, UK

VCH, 220 East 23rd Street, New York, NY 10010-4606, USA (toll free: 1-800-367-8249)

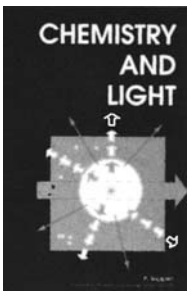
VCH, Eikow Building, 10-9 Hongo 1-chome, Bunkyo-ku, Tokyo 113 Japan

VCH

 © VCH Verlagsgesellschaft mbH, D-69451 Weinheim, 1995 0570-0833/95/0505-0598 $ 10.00+.25/0

World of Light

Chemistry and Light. By *P. Suppan.* Royal Society of Chemistry, Cambridge, 1994. 295 pp., paperback £ 19.50.—ISBN 0-85186-814-2



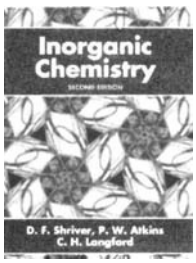
Anyone who maintains awareness of publications in the area of photochemistry knows that the subject is currently undergoing a renaissance in the form of monographs, reviews, and original papers (and thus also in research and development). However, in contrast to the wealth of publications on specific topic areas, there has up to now been a shortage of more comprehensive up-to-date general introductions to photochemistry. To help remedy that gap we now have this book by Suppan, which needs to be evaluated and compared with that edited by H. G. O. Becker: *Einführung in die Photochemie* (Deutscher Verlag der Wissenschaften, 1991).

Suppan's book begins with a short introduction (Chapter 1) in which photochemical reactions are compared with reactions in the absence of light and with thermal excitation. In Chapter 2 the author briefly discusses the various interactions between light and matter (photochemical, photoelectric, and electrooptical phenomena), then in Chapter 3 moves on to a more detailed treatment of excited states. Aspects covered here include absorption and emission spectra, potential diagrams and orbital diagrams, transitions from excited states, quenching, photophysical phenomena, and medium (solvent) effects. Chapter 4 deals at considerable length with the chemistry of excited states, covering not only "conventional" photoreactions but also inorganic photochemistry, chemiluminescence, and photochemistry in organized systems. In Chapter 5 ("Light and Life") the author discusses photosynthesis, phototaxis, photochemical damage to nucleic acids and proteins, and some examples from the photomedical field and bioluminescence. Chapter 6 ("Light in Industry") relates photochemistry to practical applications, discussing photographic processes, photopolymerizations, photochemical syntheses, photochromic phenomena, and the photochemistry of the atmosphere. Chapter 7 is of special importance for the experimentalist, with descriptions of laboratory techniques and equipment, including light sources, filters, lasers, and methods for studying luminescence and flash photolysis. Chapter 8 gives a brief survey of "Frontiers in Photochemistry", including time-resolved photolysis and spectroscopy, supramolecular photochemistry, and "hole-burning" experiments.

The book is clearly written, the figures are of high quality, and the text has been carefully checked and well printed. It is well suited for use as an introduction to the subject. A criticism is that some important topical aspects of the interactions between light and matter are omitted or only touched on briefly, including photovoltaic phenomena, photoelectrochemistry, sensitization of semiconductor electrodes and semiconducting colloids, solar photochemistry, renewable solar energy systems, photodynamic cancer therapy, and diagnostics. The Appendix explains band-gaps in semiconductors, but it is only with difficulty that one finds any reference to these in the main text. Also there are no tables listing photophysical properties of sensitizers. Not enough literature references are given, and no recent monographs on the subject are mentioned. However, despite these criticisms *Chemistry and Light* is a carefully written account of the fundamentals of photochemistry. If confronted with the choice between Suppan's book and that by Becker mentioned earlier, I would advise in favor of Becker, which contains more practical examples and data on compounds and reactions. It is more experimentally orientated and contains many more references to the primary literature.

Dieter Wöhrle
Institut für Organische und
Makromolekulare Chemie
der Universität Bremen (FRG)

Inorganic Chemistry. (Second edition). By *D. F. Shriver, P. W. Atkins* and *C. H. Langford.* Oxford University Press, Oxford, 1994. 819 pp., paperback £ 19.50.—ISBN 0-19-855396-X



The perennial questions when writing a textbook on inorganic chemistry are: what blend of theory and experimental facts to employ and, in a text of finite size, does one want an assemblage of basic knowledge or an emphasis on the latest developments? Further, from the user's point of view—how well is the theory applied to rationalize experimental knowledge? In this book the first two-fifths is devoted to theoretical principles and the remainder to mainly descriptive chemistry. The other questions are elaborated upon below.

In this second edition, apart from alterations to the text (expansion and refinement), there has been a reorganization of the material so that the book is now divided into three parts: "Foundations", "Systematic Chemistry of the Elements", and "Advanced Topics". New problems/exercises and more literature references have been added. Each chapter includes a summary of key points and ends with a list of further reading and a set of exercises (solutions in the Appendix) and advanced problems.

As an aid to learning, key concepts are in bold type when first introduced. Moreover, worked problems are included throughout the text, followed by a similar problem for the reader to consider. A rather wide left-hand margin is employed; this is filled with illustrations and annota-

This section contains book reviews and a list of new books received by the editor. Book reviews are written by invitation from the editor. Suggestions for books to be reviewed and for book reviewers are welcome. Publishers should send brochures or (better) books to Dr. Ralf Baumann, Redaktion Angewandte Chemie, Postfach 101161, D-69451 Weinheim, Federal Republic of Germany. The editor reserves the right of selecting which books will be reviewed. Uninvited books not chosen for review will not be returned.

 © *VCH Verlagsgesellschaft mbH, D-69451 Weinheim, 1995* *0570-0833/95/0505-0599 $ 10.00+.25/0*

tions to figures. This works well in most cases, although occasionally the figure is out of synchronization with the text. In fact the entire book is extremely well illustrated with a whole gamut of molecular orbital diagrams, figures, schemes, structures, spectra, and equations.

The "Foundations" section follows the traditional treatment: atomic and molecular structure, molecular shape and symmetry, structure of solids, acids and bases, metal complexes, redox. Part 2 ("Systematic Chemistry of the Elements") begins with a new chapter on the metals, followed by chapters on hydrogen and its compounds, main-group organometallic compounds, boron and carbon groups, nitrogen and oxygen groups, and halogens and the noble gases.

Part 3 ("Advanced Topics") covers effectively all aspects of transition metal chemistry, with chapters on electronic spectra of complexes, reaction mechanisms of d-block complexes, d- and f-block organometallic compounds, structures and properties of solids, and bioinorganic chemistry. The book ends with a series of appendices and a formula and subject index.

All the material that one would wish to cover in two years of undergraduate inorganic chemistry courses is contained in this one text. Part 2 is a balance of basic knowledge and the latest experimental results (e.g. buckminsterfullerene complexes, p. 482): the latter should serve to stimulate the enthusiasm of students. Excellent use is made of line drawings of molecular structures. A positive effort has been made to apply the theoretical principles (in particular molecular orbital theory) in the latter part of the book.

My negative comment is that on reading the book I experienced a sense of overcompression of the material in some sections, as if the authors have tried to reduce the text to a minimum number or words. The end result of being too brief is that these sections strike me as difficult for the student to assimilate. A slight amplification would greatly facilitate understanding. This runs contrary to the preface, which states that the writing and refinement of the text was undertaken with the advice of students and instructors.

Let me illustrate this with some selected examples, of which there are many. Chapter 1 on atomic structure is a brief summary with no more depth than a general chemistry text. It is too brief for anyone without knowledge of the subject to understand. Students reading a course on inorganic chemistry would already have had a general chemistry course and this material will be familiar. The aim is thus not clear. Is it to refresh the reader's memory or to provide a more detailed treatment than an introductory text? The former aim may be achieved, but not the latter. To cite two specific instances, the Uncertainty Principle (p. 12) merits only one-third of a page, and the radial distribution functions are shown only for hydrogen 1s, 2s, and 2p orbitals (the latter two in the form of a problem).

Similarly, the chapter on molecular structure describes UV photoelectron spectroscopy (PES) rather briefly (p. 65). A slight amplification would greatly enhance understanding; e.g. on page 67 it is stated that the "vibrational structure in the photoelectron spectrum can be very helpful in assigning the origin of the spectral line", but the authors fail to adequately explain how this can be used to make assignments. It is left for the reader to do this, and to relate the sample PES of dinitrogen (p. 66) to the molecular orbital energy level diagram three pages later.

Concerning the actual text, what is different is the rather frequent use of the first person plural (we, us), more than is generally found in chemistry books. There are several instances in the text of a loose colloquial style, e.g. on page 249: "and, although avoiding the pairing *penalty*, will have an energy higher by Δ_o"; page 240: "this *trick*, which is called the template effect".

In summary though, the positive aspects of the book far outweigh the foibles of style and layout. Students at all levels of inorganic chemistry will profit from a perusal of this text which describes the subject as it is in the 1990s.

Franz L. Wimmer
Department of Chemistry
Universiti Brunei
Darussalam (Brunei)

Structure and Properties of Polymers. (Series: Materials Science and Technology, Vol. 12.) Edited by *E. L. Thomas*. VCH Verlagsgesellschaft, Weinheim/VCH Publishers, New York, 1993. 786 pp., hardcover DM 430.00, $ 325.00.—ISBN 3-527-26825-1/0-89573-700-0

The series to which the volume *Structure and Properties of Polymers* belongs is intended to cover a wide range of topics in materials science and to serve both as a work of reference and for systematic study. Thus each chapter should treat its subject in greater detail than an encyclopedia but more concisely than a monograph. The series is intended for a broad readership, and is also suitable for the reader who wants a survey of recent developments in a related field.

The book covers a very wide range of subjects, giving an overview of all the topic areas in modern polymer physics. Polymer structure and elasticity, followed by viscoelastic, rheological, dielectric, and optical properties, are treated in 13 chapters. Three further chapters are devoted to high-strength polymer fibers, polymer surfaces and interfaces with other materials, and crazing and fracture.

The book begins with a chapter by L. J. Fetters and E. L. Thomas on the synthesis of model polymers, covering even very recent published work in this area. Chapter 2, by F. T. Gentile and U. W. Suter, deals with amorphous polymers and gives a good review of structural models (static atomistic modeling), including a detailed description of the model proposed by Theodoru and Suter. The diffusion of small molecules in glassy polymers is also treated. I particularly liked the chapter by B. Lotz and J. C. Wittmann on the structure of polymer single crystals, covering nearly every aspect of their formation, structure, properties, and deformational behavior. Experimental methods for studying polymer single crystals are only touched on briefly, but despite that the chapter is a mine of information for the interested reader. In contrast the following chapter by P. J. Barham on crystallization and morphology devotes much space to experimental methods (scattering techniques, microscopy, spectroscopy, calorimetry), while also not neglecting the fundamentals (nucleation and crystallization, structural types, models). Chapter 5, by M. Ballauff, is concerned with liquid crystal polymers, currently a topic of great interest. This is written in a clearly understandable way, and can be read as an introduction to the physics of liquid crystal polymers. Chapter 6 (T. Hashimoto) deals with the structure of polymer blends. Although one cannot expect an exhaustive coverage of this enormous field in a chapter of 41 pages, the treatment is far from superficial. Phase diagrams, the formation of microphases, and spinodal segregation in two-component systems are well described and discussed.

Next come several chapters that are mainly concerned with the mechanical properties of polymers: "Elastic Properties of Crystalline Polymers" (D. T. Grubb), "Rubber Elasticity" (R. Ullmann), "Viscoelastic Properties" and "Rheological Properties" (both by M. Doi), and "Elastic Deformation of Polymers" (B. Christ). Together with the later chapters "High-Strength Polymer Fibers" (H. Jiang, W. W. Adams, and R. K. Eby)

 © VCH Verlagsgesellschaft mbH, D-69451 Weinheim, 1995 0570-0833/95/0505-0600 $ 10.00+.25/0

and "Crazing and Fracture of Polymers" (I. Narisawa and A. F. Yee), these articles provide much more than a mere overview of these important areas of polymer physics. As well as the fundamentals they include details of methods of measurement and theoretical models, such as the Takayanagi model for mechanical behavior, the Mooney–Rivlin model for rubber elasticity, and the Rouse model.

The two chapters on dielectric properties (G. Williams) and optical properties (W. Knoll) contain a wealth of information, but this is presented in a readable style. The second of these also touches on the highly topical areas of optical fibers and optoelectronics. As the authors of the chapter on "Polymer Surfaces and Interfaces with Other Materials" (M. Tirrell and E. E. Parsonage) themselves point out, it was not possible here to cover all aspects of this broad field. The chapter concentrates on solid polymers and omits, for example, interactions with solvents, surfaces with adsorbates, and swelling phenomena.

On the whole the authors of this book seldom go into great detail. The reader who wishes to make a thorough study of a special area may regret this, but on the other hand those who wish to obtain an overview are spared the trouble of working through lengthy derivations. Despite being the work of 22 authors, the volume is surprisingly homogeneous; the unifying hand of the editor is evident throughout. It can be recommended not only for specialists but certainly also for students interested in this field, especially advanced and post-graduate students of polymer physics.

Structure–Property Relations in Polymers. Spectroscopy and Performance. (Series: Advances in Chemistry, Vol. 236.) Edited by *M. U. Urban* and *C. D. Craver*. American Chemical Society, Washington, D.C., 1993. 832 pp., hardcover $ 139.95.—ISBN 0-8412-2525-7

The book *Structure–Property Relations in Polymers* contains a selection of papers from the 200th National Meeting of the American Chemical Society (Washington, D.C., 1991), covering applications of Fourier transform (FT) infrared and Raman spectroscopy, fluorescence spectroscopy, and mass spectrometry in the polymer field. The preface announces the aim of bridging the gap between the molecular data yielded by these spectroscopic methods and specific macroscopic properties. It aims to serve the needs of both newcomers to polymer spectroscopy and experienced specialists. This is an ambitious objective, but in my view some of the contributions achieve it very well.

The 35 articles are arranged in six chapters; as well as bringing a degree of order to the topic areas, this in part gives the book some of the qualities of a monograph.

The first chapter, "Fundamental Aspects of the Spectroscopy of Polymers", is concerned with basic principles and recent developments in FT infrared and Raman spectroscopy, fluorescence spectroscopy, and mass spectrometry. Although intended as an introduction to the principles of these techniques, it also covers some recent developments, such as the use of multivariate data processing in polymer analysis.

The chapters that follow deal with the applications of the above methods to problems in polymer physics. Thus the second chapter is concerned with crystalline polymers and copolymers. Data from Raman spectra on the internal and longitudinal vibrational modes can be used in the structural analysis of crystalline polymers or in studying topotactic changes during solid-state polymerization. Interesting results from the application of FTIR spectroscopy to the analysis of phase behavior and the study of molecular interactions in polymer blends are also described. The use of near-IR spectroscopy for the quantitative analysis of a series of 25 thermoplastics is described in an interesting paper by H. F. Howell and J. K. Davis.

Chapter 3 deals with polymer surfaces and interfaces. The topics discussed include the role of surface-active agents in latex technology, and measurements on thick films. L. J. Fina contributes a very interesting article on the modeling of concentration gradients on polymer surfaces. Also worth special mention is an article by M. B. Mitchell on the technique of diffuse reflectance infrared Fourier transform (DRIFT) spectroscopy and its applications. Coatings are becoming ever more important in plastics technology, and the contribution by M. Claybourn and P. H. Turner describing FTIR and FT Raman measurements on coatings is therefore well worth reading. Other topics of special interest are FT Raman studies of dyes and the recording of Raman spectra during emulsion polymerization.

The chapter entitled "Spectroscopic Studies of Polymers in Solution and Polymer Networks" contains eight articles. Among the subjects discussed are metachromasy in dye–polyelectrolyte solutions, intermolecular association of polymers in water, photochemical and degradation reactions in polymers, and polymer–monomer interactions. Interesting applications of PALS (position annihilation lifetime spectroscopy) measurements for investigating changes of the in-situ free volume in polymer networks are described.

Chapter 4 consists of four contributions describing combinations of two or more techniques, such as FTIR with photoacoustic measurements, and differential thermoanalysis with thermogravimetric analysis.

The final chapter, "Polymer Analysis and Surface Modifications", is concerned with surface analytical methods such as SPI-SALI (single-photon ionization–surface analysis by laser ionization), SIRIS (sputter-initiated resonance ionization spectroscopy), SALISA (surface analysis by laser ionization of sputtered atoms), and pulsed radiofrequency plasma discharge spectroscopy. Applications of these techniques in areas such as inorganic polymer synthesis and polymer surface studies are described. Also interesting is the determination of the molecular mass of organic compounds by the K^+IDS (K^+ ionization of desorbed species) technique.

This volume is certainly a mine of information for the specialist, and can also be recommended for readers with interests in infrared spectroscopy.

Werner Wenig
Laboratorium für Angewandte Physik
der Universität-Gesamthochschule
Duisburg (FRG)

 © *VCH Verlagsgesellschaft mbH, D-69451 Weinheim, 1995* *0570-0833/95/0505-0601 $ 10.00+.25/0*

Probing Protein Structure and Function with an Expanded Genetic Code

Virginia W. Cornish, David Mendel, and Peter G. Schultz*

A general biosynthetic method has been developed which makes it possible to site-specifically incorporate unnatural amino acids with novel properties into proteins. In this approach the codon encoding the amino acid of interest is replaced with the "blank" nonsense codon UAG by oligonucleotide-directed mutagenesis. A suppressor tRNA that recognizes this codon is generated by run-off transcription and then chemically aminoacylated with the desired unnatural amino acid. Addition of the mutagenized gene and the aminoacylated suppressor tRNA to an in vitro extract capable of supporting protein biosynthesis generates a mutant protein containing the unnatural amino acid at the specified position. This methodology has recently been used to study the stability, specificity, and catalytic properties of a number of proteins. In these studies amino acids and analogues possessing altered hydrogen-bonding, electronic, and steric properties and unique backbone conformations have all been site-specifically incorporated into proteins. In addition, photoactivatable amino acids, isotopically labeled amino acids, and amino acids bearing biophysical probes have been inserted site-specifically. This chemistry increases our ability to carry out detailed physical organic studies on this important class of macromolecules.

Keywords: amino acids · mutagenesis · proteins

1. Introduction

Proteins are at the crossroads of virtually every biological process, including signal transduction, catalysis, gene regulation, and the immune response. Yet we still understand little about the mechanisms whereby these biopolymers, composed of twenty simple building blocks, carry out their remarkable range of functions. One important tool for probing the forces that govern protein structure and folding, biomolecular recognition, and catalysis is site-directed mutagenesis. This method makes it possible to substitute a specific amino acid in a protein with any of the other nineteen common amino acids.[1, 2] However, in contrast to studies of small molecules for which analogues with virtually any structural changes can be synthesized, changes in protein structure at a given site are limited to the common amino acids. Ideally, one would like to tailor the steric or electronic properties of an amino acid in a protein to address a specific structure–function question. Desired changes might include modifying the acidity, nucleophilicity, hydrogen-bonding, or hydrophobic properties of an amino acid side chain; altering or restricting the protein backbone conformation; or introducing biophysical probes such as spin labels or isotopic labels at a specific position within a protein. The possibility of substituting such unnatural amino acids, beyond those specified by the genetic code, would greatly expand our ability to manipulate and study protein structure and function and may allow for the generation of new proteins with novel properties.

A number of methods can be used to incorporate unnatural amino acids into proteins. Solid-phase peptide synthesis, particularly recent advances in the segment synthesis-condensation approach,[3] has allowed for the synthesis of small proteins ($\leq$12 kDa) containing novel amino acids in milligram quantities.[4–11] Protein semisynthesis, in which a synthetic peptide is ligated to a protein fragment to produce a full-length protein, has been used to incorporate unnatural amino acids into proteins.[12, 13] This approach is complicated by the need to cleave the protein specifically at the peptide ligation site and by difficulties in coupling the protein and peptide termini selectively. Chemical modification also has been used to introduce a variety of unnatural side chains into proteins including cofactors, spin labels, and oligonucleotides.[14–20] In this method, however, substitutions are largely restricted to simple derivatives of reactive amino acid side chains (e.g. lysine, cysteine, tyrosine) on the protein surface. Alternatively, biosynthetic methods that employ chemically modified aminoacyl-tRNAs have been used to incorporate a number of biophysical probes into proteins synthesized in vitro.[21, 22] This approach is limited, though, because mutations are restricted to derivatives of the natural amino acids and the modified amino acid is substituted at multiple sites. Furthermore, both the modified and natural amino acids are incorporated at the site of interest because of

[*] Prof. P. G. Schultz, V. W. Cornish
Department of Chemistry, University of California
Berkeley, CA 94720 (USA)
Telefax: Int. code +(510)643-6890
Dr. D. Mendel
Lilly Research Laboratories
Eli Lilly and Company
Indianapolis, IN 46285 (USA)

 © VCH Verlagsgesellschaft mbH, D-69451 Weinheim, 1995 0570-0833/95/0606-0621 $ 10.00+.25/0

difficulties in removing endogenous aminoacyl-tRNA from the in vitro extract.

Recently, a biosynthetic approach has been developed which for the first time makes possible the site-specific incorporation of a large variety of unnatural amino acids into proteins.[23-25] In this article we describe the methodology as well as its current scope and limitations. In addition, applications are described in which the substitution of unnatural amino acids with novel electronic, steric, and biophysical properties into proteins has provided new insights into the mechanisms of enzymatic catalysis, protein stability, and biomolecular recognition.

2. The Methodology

2.1. Design Considerations

The ability to incorporate unnatural amino acids site-specifically into proteins depends on the following observations: 1) Although three stop codons (UAA, UAG, and UGA) exist, only one is required for the termination of protein synthesis (Scheme 1), leaving two "blanks" in the genetic code (Scheme 2).[26,27] 2) Suppressor tRNAs, tRNAs that insert one of the common amino acids in response to a stop codon, function efficiently in vivo and in vitro.[28] 3) Anticodon–codon recognition is independent of the amino acid at the acceptor stem of the tRNA (the adaptor hypothesis).[29,30] 4) The translational machinery shows relatively broad substrate specificity.[31,32] In light of these facts, the following strategy was developed (Scheme 3). The codon for the amino acid of interest is replaced with the stop codon UAG through standard oligonucleotide-directed mutagenesis.[33] A suppressor tRNA that recognizes this codon is chemically acylated with the desired unnatural amino acid. Addition of the mutagenized gene or mRNA and the aminoacylated suppressor tRNA to an in vitro extract capable of supporting protein biosynthesis generates a mutant protein containing the unnatural amino acid at the desired position.[23,24] The development of this methodology requires the generation of the requisite suppressor tRNA, a general method for acylating the tRNA with unnatural amino acids, and the synthesis of sufficient protein in vitro for meaningful mechanistic or structural studies.

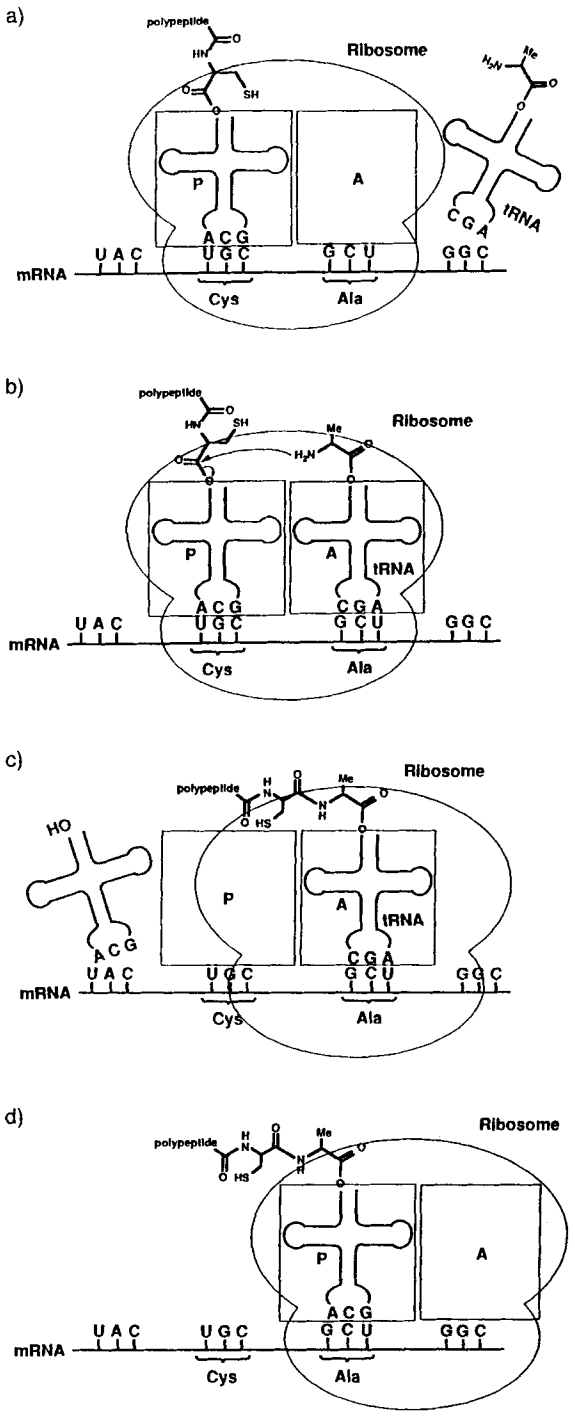
2.2. The Suppressor tRNA

The facile incorporation of an unnatural amino acid into a protein requires a tRNA that is recognized by the protein biosynthetic machinery sufficiently well to suppress a stop codon with high efficiency. This suppressor tRNA, however, cannot be a substrate for any of the aminoacyl-tRNA synthetases present in the in vitro protein synthesis extract. If the suppressor tRNA were recognized by any of the aminoacyl-tRNA synthetases, the tRNA could be subject to proofreading (deacylation of the noncognate amino acid) and/or aminoacylation with one of the common twenty amino acids. This recognition would result in either low suppression efficiencies or incorporation of a common amino acid, as well as the desired unnatural amino acid, in response to the stop codon.

We initially chose to construct an amber suppressor tRNA (a tRNA that recognizes the stop codon UAG) derived from yeast phenylalanyl-tRNA in which residues 34 to 37 have been replaced by 5′-CUAA-3′[34] (in accord with Yarus' rule).[35-37] This suppressor tRNA is known to function efficiently in vitro[34] and is likely to be a poor substrate for the *E. coli* aminoacyl-tRNA synthetases.[38] Alternatively, a suppressor tRNA derived from *E. coli* $tRNA^{Gly}$[39] has been used to suppress UAG codons in short peptides in a rabbit reticulocyte translation system.[25] Both suppressor tRNAs can be readily prepared in relatively large quantities by run-off transcription (Scheme 4).[40,41] Even though these tRNAs are produced in vitro and likely do not contain modified bases,[42] both incorporate unnatural amino acids efficiently and exhibit little readthrough (incorporation of any amino acid other than the desired unnatural amino acid in response to the UAG codon) at optimal Mg^{2+} concentrations.



Peter G. Schultz was born in 1956 in Cincinnati, Ohio, and did both his undergraduate and graduate work at the California Institute of Technology. His thesis work resulted in the design of the first synthetic sequence-selective DNA cleaving molecules. In 1985, after postdoctoral studies at the Massachusetts Institute of Technology, he joined the faculty of the University of California at Berkeley, where he is currently a Professor of Chemistry, a Principal Investigator at the Lawrence Berkeley Laboratory, and an Investigator of the Howard Hughes Medical Institute. His research interests span organic chemistry, molecular biology, and immunology. His research focuses on the study of mechanisms of molecular recognition and catalysis in biological systems and applications to the design of molecules with novel biological (and medicinal) function. His group has contributed to the development of catalytic antibodies, DNA binding proteins, peptides, and oligonucleotides, RNA compounds, and unnatural biopolymers such has oligourethanes and oligosulfones. He has developed methods for the incorporation of unnatural amino acids in proteins and for the manipulation of enzyme specifity through chemical and biological mutagenesis. Schultz has received many awards including the Waterman Award of the National Science Foundation, the Pure Chemistry Award of the American Chemical Society, the Young Investigator Award of the Protein Society, and the Wolf Prize in 1994.



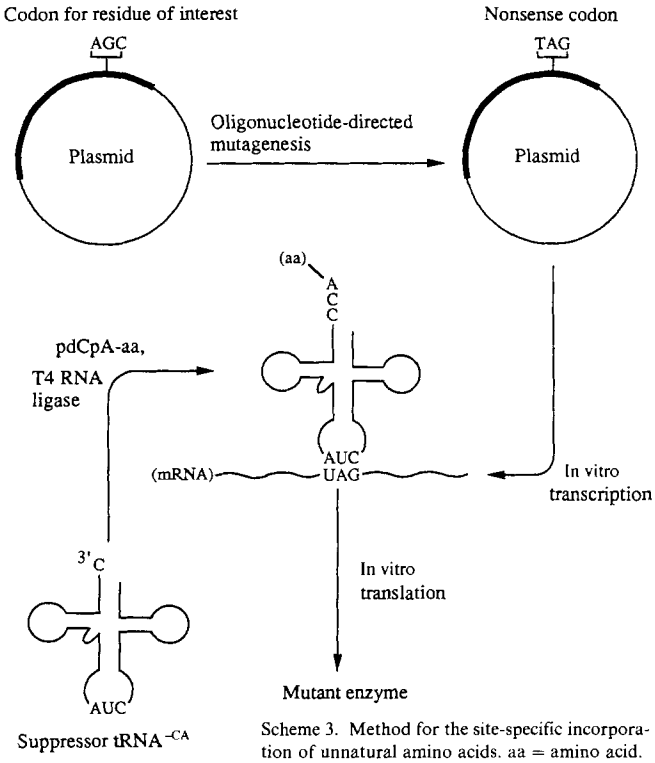
Scheme 1. Schematic representation of protein biosynthesis: a) binding of the aminoacyl-tRNA to the ribosomal complex; b) peptide bond formation; c) dissociation of the deacylated tRNA; d) ribosome translocation.

2.3. Aminoacylation of the tRNA

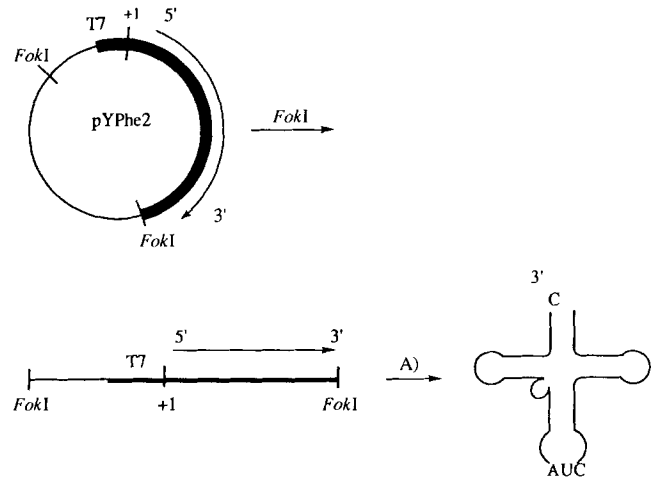
With the suppressor tRNA in hand, a general method for acylation of the tRNA with any unnatural amino acid had to be developed. Enzymatic aminoacylation of the tRNA with aminoacyl-tRNA synthetases is not general because of the high specificity of these enzymes.[43, 44] Direct chemical acylation is probably not practical owing to the large number of reactive sites in the tRNA. Consequently, a modification of a two-step

UUU, UUC: Phe	UCU, UCC, UCA, UCG: Ser	UAU, UAC: Tyr	UGU, UGC: Cys
UUA, UUG: Leu		UAA, UAG: TERM	UGA: TERM
			UGG: Trp
CUU, CUC, CUA, CUG: Leu	CCU, CCC, CCA, CCG: Pro	CAU, CAC: His	CGU, CGC, CGA, CGG: Arg
		CAA, CAG: Gln	
AUU, AUC: Ile	ACU, ACC, ACA, ACG: Thr	AAU, AAC: Asn	AGU, AGC: Ser
AUA: Met		AAA, AAG: Lys	AGA, AGG: Arg
GUU, GUC, GUA, GUG: Val	GCU, GCC, GCA, GCG: Ala	GAU, GAC: Asp	GGU, GGC, GGA, GGG: Gly
		GAA, GAG: Glu	

Scheme 2. The genetic code, TERM = termination codon.

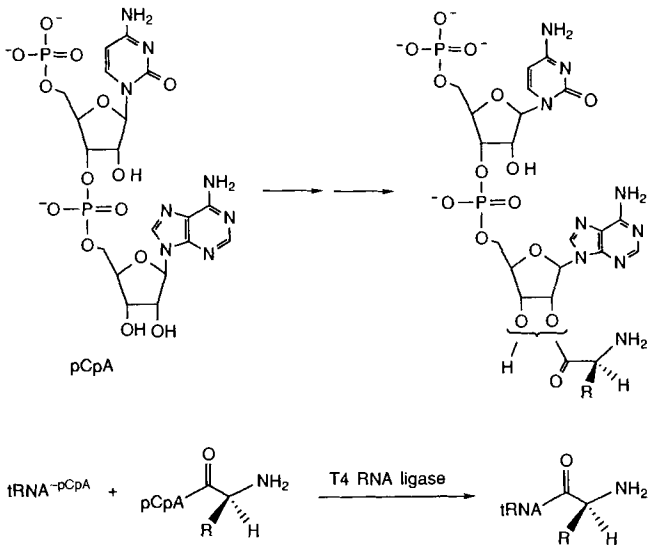


Scheme 3. Method for the site-specific incorporation of unnatural amino acids. aa = amino acid.



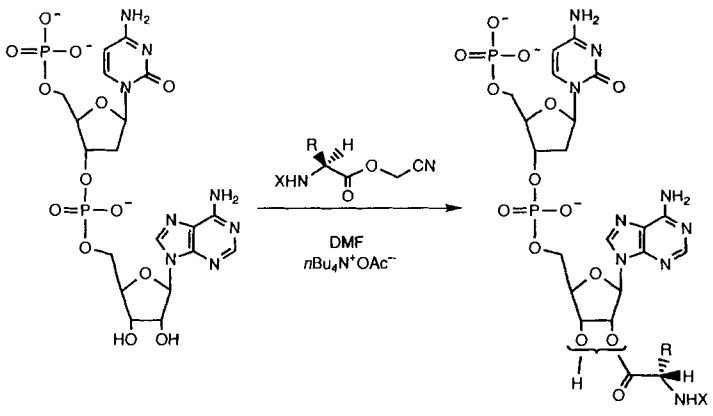
Scheme 4. Preparation of $tRNA^{Phe}_{CUA}$ by run-off transcription. The heavy line represents the DNA sequence coding $tRNA^{-CA}_{CUA}$. A) 1. T7 RNA polymerase, NTPs; 2. enzyme extraction, precipitation with EtOH. One thousand copies of tRNA are obtained per copy of DNA, in other words, roughly 1 mg tRNA per 30 μg digested template DNA.

method originally developed by Hecht et al.[45] was used in which the dinucleotide pCpA is chemically acylated with a N^{α}-protected amino acid and then enzymatically ligated to a truncated tRNA ($tRNA^{-CA}$ missing the terminal dinucleotide pCpA at the 3′-acceptor stem) (Scheme 5).[46] The truncated suppressor tRNA can be generated directly by run-off transcription of a *Fok*I linearized plasmid encoding the tRNA gene.[41]



Scheme 5. Strategy for the chemical aminoacylation of $tRNA^{Phe}_{CUA}$. R = amino acid side chain.

Acylation of the dinucleotide is complicated by side reactions including diacylation and acylation of the exocyclic amino groups of the bases which result in low yields of the desired product. Moreover, the aminoacyl tRNA linkage itself is relatively unstable in the pH range (7–8) required for efficient T4 RNA ligase function.[47, 48] We found that the cyanomethyl ester of an amino acid reacts selectively with the 2′,3′-hydroxyl groups of the ribose to give the monoacylated product, obviating the need to protect the dinucleotide prior to aminoacylation (Scheme 6).[49] In addition, deoxycytidine was substituted for cytidine in the dinucleotide, significantly simplifying the synthesis and eliminating another 2′-OH group without affecting biological activity. The α-amino group of the amino acid and any reactive side chains are protected as the nitroveratryloxy (NVOC) carbamate, ester, or ether[50, 51] prior to acylation of the dinucleotide. These protecting groups can be removed photochemically from the intact aminoacyl-tRNA (after ligation) in high yield under mildly acidic conditions which prevent deacylation of the aminoacyl-tRNA.[49] For light-sensitive amino acids the biphenylisopropyloxycarbonyl (BPOC) group can be used; the BPOC group is cleaved with mild acid from the aminoacyl-pdCpA prior to ligation to $tRNA^{-CA}$.[25, 49] This aminoacylation protocol is relatively straightforward, proceeds in high yield (both the aminoacylation and ligation reactions), and is applicable to amino acids with a wide variety of side chains.[48, 24] Nevertheless, the generation of a nonspecific "aminoacyl tRNA synthetase", either a lipase, mutagenized synthetase, or a catalytic antibody, could significantly simplify this step.[52–54]



Scheme 6. Simplified acylation of pdCpA using an amino acid cyanomethyl ester. R = amino acid side chain, X = protecting group.

2.4. In Vitro Protein Synthesis

Proteins are synthesized in vitro because no general methodology exists for introducing large quantities of the aminoacylated suppressor tRNA into intact, dividing cells.[55] We currently use an *E. coli* in vitro transcription/translation protein synthesis system.[56, 57, 24] This system consists of an *E. coli* S-30 extract which contains all of the proteins and RNAs required for transcription and translation. Nucleotide triphosphates, bacterial tRNAs, phosphoenolpyruvate, pyrophosphatase, a variety of salts (Mg^{2+} and Ca^{2+} concentration can significantly affect protein yields) and cofactors, and the DNA encoding the gene of interest are added to this S-30 extract to reconstitute protein synthesis in vitro. Typically the gene of interest is placed under a strong T7 or bacterial RNA polymerase promoter. The in vitro reaction can be carried out on scales ranging from 30 μL to 5 mL. The requisite S-30 can be prepared reasonably on a 2 L scale, the suppressor tRNA on a 30 mg scale, the aminoacyl-pdCpA on a 0.2 mmol scale, and the plasmid on a 12 mg scale. A major limitation of in vitro protein synthesis remains the relatively small quantities of protein that can be obtained. Regardless of whether the protein is synthesized from plasmid DNA using an *E. coli* transcription/translation system or from mRNA using a rabbit reticulocyte translation system, protein yields greater than $100\,\mu g\,mL^{-1}$ generally have not been achieved.[24] Many factors are known to affect protein expression levels in vivo, such as the strength of the RNA polymerase promoter, the particular ribosome-binding site, codon usage, and mRNA stability and secondary structure.[58, 59] Unfortunately, in vitro protein yields do not necessarily correlate with those obtained in vivo, and we have found no simple and general rules for ensuring high protein expression in vitro.

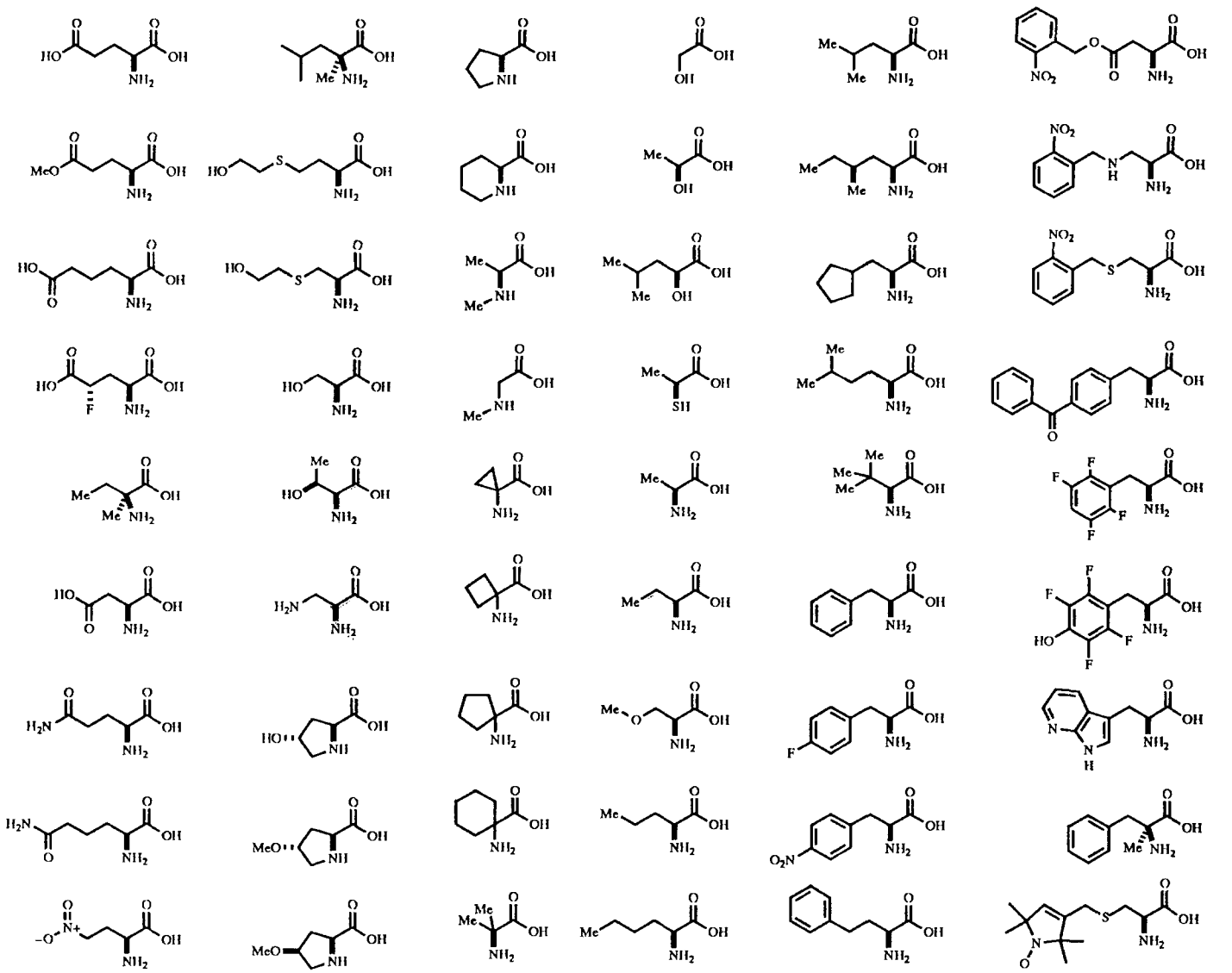
2.5. Scope of the Methodology

The relatively broad substrate specificity of the elongation factors and peptidyl transferase suggested that a wide variety of amino acids could be incorporated into proteins.[31, 32] This is in fact the case—over seventy amino acids have been incorporated at more than twenty sites in a variety of proteins by using the

above methodology (Scheme 7). Conformationally restricted amino acids (e.g. 2,4-methanoproline (not shown), cyclopropylglycine, and α-methyl-L-leucine), amino acids with spin labels and photoaffinity labels as side chains, amino acids with altered pK_A values and hydrogen-bonding properties, "caged" amino acids, α-hydroxy acids, and amino acids with unusual steric properties (e.g. *tert*-butylglycine) have all been incorporated into proteins. Suppression efficiencies can vary widely depending on the nature of the amino acid, ranging from 100% for substitution of L-norleucine for Gln 28 in 434 repressor[60] to 10% for incorporation of α-methyl-L-leucine in T4 lysozyme.[61] Although the suppression efficiency of a given amino acid cannot be predicted a priori, several trends emerge when the identities of the amino acids tested are correlated with their suppression efficiencies.[61, 62] In general, large hydrophobic amino acids such as *p*-benzoyl-L-phenylalanine are inserted with higher efficiency than small amino acids such as alanine and glycine, or charged amino acids such as homoglutamate or ornithine. This correlation is in agreement with reports that large, hydrophobic amino acids such as Trp and Phe bind more tightly to the *E. coli* elongation factor EF-Tu than do other natural amino acids such as Ala, Glu, and Lys.[63]

The stereochemistry of an amino acid also affects suppression efficiency. Although L-amino acids and some α,α-disubstituted amino acids such as α-aminoisobutyric acid (AIB) and cyclopentylglycine can be incorporated into proteins, D-amino acids do not seem to be accommodated by the translational machinery.[61] These stereochemical requirements are in agreement, for the most part, with previous studies on the affinity of a variety of unnatural aminoacyl-tRNAs for *E. coli* EF-Tu and the ribosome.[31] Interestingly, previous experiments, in which the ability of an aminoacyl-tRNA or aminoacyl-CpA to bind to the *E. coli* ribosomal A-site and participate in peptide elongation was studied, suggested that achiral amino acids like AIB could not be used as substrates by the *E. coli* protein biosynthetic machinery.[64–66]

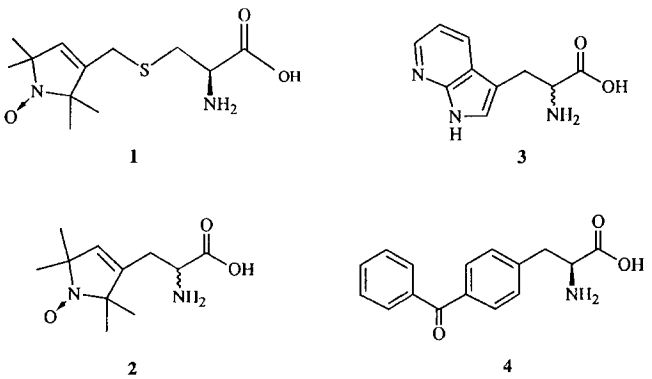
A variety of backbone mutations are accomodated by the translational machinery.[67] *N*-Methyl-L-phenylalanine (rabbit reticulocyte), *N*-methylglycine (*E. coli*) and *N*-methyl-L-alanine



Scheme 7. Examples of amino acids and analogues that have been successfully incorporated into proteins.

(*E. coli*) are site-specifically incorporated into proteins, whereas *N*-ethyl-L-alanine is not.[68] Pipecolinic acid, the six-membered version of proline, is accepted by the *E. coli* system, whereas the ring-contracted proline analogues aziridine-2-carboxylic acid and azetidine-2-carboxylic acid are not. (This may stem from chemical instability rather than from discrimination by the biosynthesis machinery.) However, Tirrell and others[69, 70] have reported the successful biosynthetic incorporation of L-azetidine-2-carboxylic acid into polypeptides. Other types of backbone replacements for α-amino acids that have been examined include β- and γ-amino acids such as β-alanine, γ-aminobutyric acid, and longer variants[71] as well as dipeptides and dipeptide mimetics.[72] To date, attempts to incorporate these amino acids using either *E. coli* or rabbit reticulocyte lysate systems have proven unsuccessful.

The precise structure of an amino acid also influences its suppression efficiency dramatically. For example, even though the spin-labeled amino acids **1** and **2** both contain the 1-oxyl-2,2,5,5-tetramethylpyrrolidine group (Scheme 8), only **1** could



Scheme 8. Structure of biophysical probes tested for incorporation into T4L.

be incorporated in vitro.[62] In addition, suppression efficiencies may vary with the nature of the in vitro protein synthesis system (prokaryotic vs. eukaryotic). While L-4′-(3-trifluoromethyl-3*H*-diazirin-3-yl)phenylalanine was incorporated poorly (<10% efficiency) when an *E. coli* in vitro transcription/translational system was used,[73] the same amino acid was inserted with higher efficiency (>40%) in a rabbit reticulocyte in vitro extract.[74] Finally, in contrast to in vivo results,[35–37] there appears to be little correlation between the codons adjacent to the UAG codon and suppression efficiencies.[62] As more unnatural amino acids are substituted into proteins, this methodology should provide additional insights into the specificity of the translational machinery and the factors governing in vitro suppression efficiency.

2.6. Future Work

Future work will focus on broadening the scope of the methodology by increasing protein yields, by minimizing the effect of the amino acid identity on suppression efficiency, and by developing ways to introduce more than one amino acid into a protein at a time. Efforts to improve protein yields will require improvements in in vitro protein synthesis. Higher protein yields may be achieved by using in vitro systems derived from other sources[55] or alternative approaches such as continuous flow in vitro systems.[75] Alternatively, since the *E. coli* transcription/translation system is active at 37 °C for about only one hour, protein expression levels may be increased by using other lysates such as lysed spheroplasts, capable of supporting protein synthesis for longer periods of time.[76, 77]

Suppression efficiencies may be improved by 1) altering nucleotides in the tRNA molecule involved in tRNA recognition by the elongation factors, the ribosome, or the aminoacyl-tRNA synthetases; 2) utilizing suppressor tRNAs from different species (here tRNA must be "engineered" to eliminate recognition by the corresponding aminoacyl-tRNA synthetase); 3) deleting release factor-1 (*E. coli*), which competes with the suppressor tRNA for recognition of the UAG codon, from the in vitro extract;[78] or 4) modifying the specificity of elongation factor EF-Tu. One would also like to be able to produce proteins containing several unnatural amino acids. A single unnatural amino acid can be incorporated at more than one position in a protein simply by introducing several UAG codons in the coding sequence.[79] Preliminary efforts to insert different amino acids into the same protein have focused on using the other nonsense codons,[80] infrequently occurring codons,[81] or a 65th codon composed of nonstandard nucleotides.[82]

3. Applications

In this section, several applications of the methodology are discussed to illustrate both the scope of the methodology and the kinds of questions that can be addressed when unnatural amino acids can be incorporated into proteins. These examples include the site-specific incorporation of biophysical probes into proteins, the construction of photocaged proteins, and studies of protein stability, enzyme mechanism, and signal transduction.

3.1. Biophysical Probes

Several amino acids that can serve as biophysical probes have been incorporated into proteins through unnatural amino acid mutagenesis (Scheme 8). A novel spin-labeled amino acid **1**, an unnatural fluorescent amino acid **3**, and an efficient cross-linking agent **4** were all introduced site-specifically at several external and internal positions in T4 lysozyme (T4L) with reasonable efficiency.[62] By taking advantage of recent loop-gap resonator technology, the ESR spectrum of approximately 10 μL of a 1 μM solution of purified T4L containing the spin-labeled amino acid **1** was measured. Replacement of one of the tryptophans in T4L by 7-azatryptophan (**3**) resulted in a red shift in the fluorescent emission maxima. In addition, amino acids that form active nitrene, carbene, and ketyl radicals have been successfully incorporated into *ras* p21 and T4L at specific positions.[62, 83] Photoaffinity probes can in principle be used to identify key components involved in complex biochemical processes, for example signal transduction and gene activation.

With considerably more effort, a sufficient quantity of purified T4L specifically labeled at site Ala82 with [^{13}C]Ala was produced. The proton resonances of the labeled residue were observed selectively, in both the native and denatured states, by using ^{13}C-decoupled ^{1}H NMR spectroscopy (Fig. 1).[84] Finally, enough staphylococcal nuclease (SNase) containing the unnatural amino acid homoglutamate at position Glu43 was obtained for determination of the mutant protein's structure by X-ray crystallography to a resolution of 2.4 Å.[85] The ability to incorporate probes capable of detecting local structure and dynamics into proteins site-specifically should allow for more precise studies of protein folding and stability, conformational changes in proteins, and the interaction of proteins with other proteins, small molecules, and membranes. For example, it should be possible to carry out site-specific spectroscopy on both the folded and unfolded states of proteins, compare denaturation curves for various regions of a protein, and probe local structural changes that occur during protein translocation.

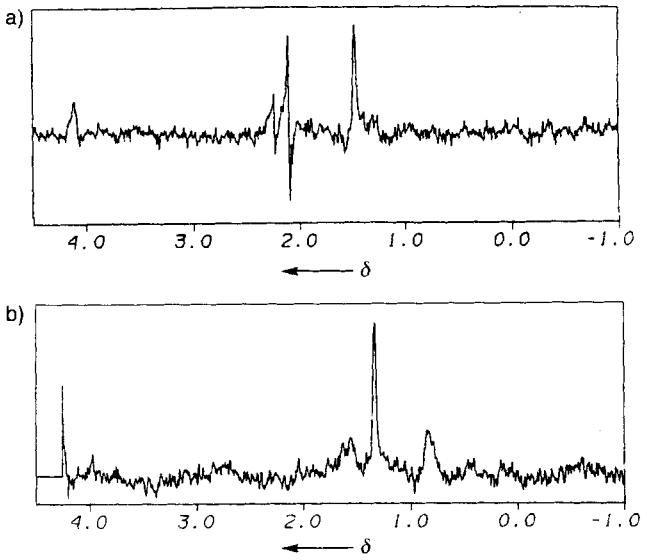
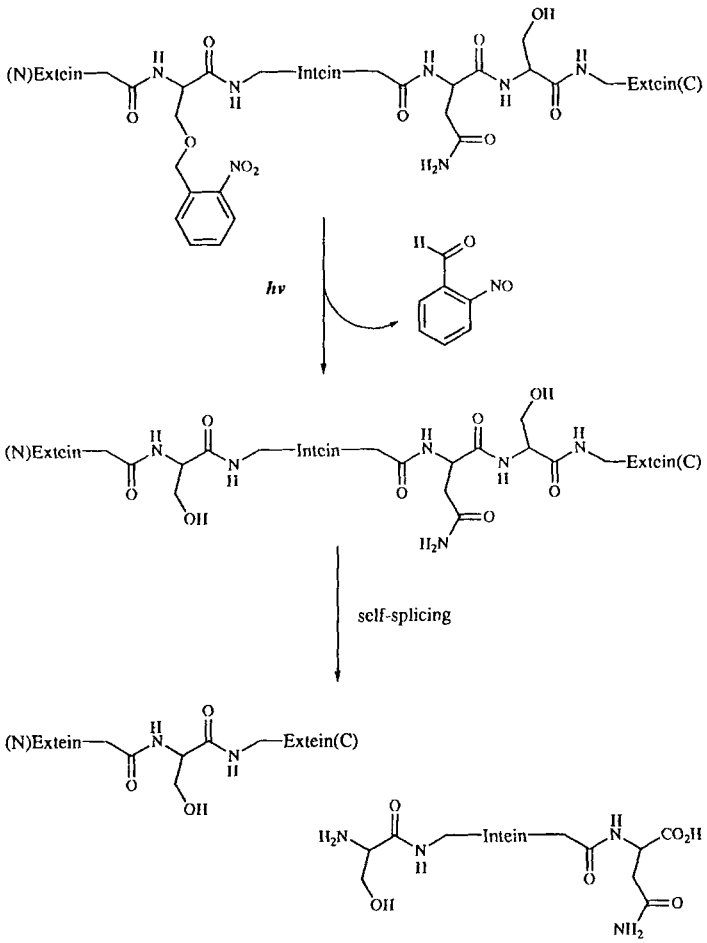


Fig. 1. a) ^{13}C-Decoupled ^{1}H NMR spectrum of the T4L variant Ala82 → [^{13}C]Ala; b) ^{13}C-decoupled ^{1}H NMR spectrum of the denatured form of the same sample.

3.2. "Caged" Proteins

Low molecular weight "caged" substances, inactive precursor molecules that can be rapidly activated by photolysis, are useful tools for biochemical studies.[86, 87] Mutagenesis with unnatural amino acids provides a unique approach to the construction of photocaged proteins. For example, the unnatural amino acid *ortho*-β-nitrobenzylaspartate was substituted for the active-site residue Asp20 in T4L.[88] Since Asp20 is essential for catalytic activity, the resulting protein was inactive. Removal of the protecting group by photolysis of the intact, modified protein restored full catalytic activity.

In a second example, a serine residue thought to be involved in the self-splicing reaction of the protein Vent DNA polymerase was replaced by *O*-nitrobenzylserine (Scheme 9).[89] The resulting caged polymerase did not undergo the self-splicing reaction, allowing the full-length protein to be isolated. Photolysis of the unspliced protein resulted in loss of the nitrobenzyl protecting group and subsequent protein splicing. This result demonstrates unequivocally that protein splicing occurs at the posttranslational level. The ability to construct caged proteins of this sort should make possible a broad range of time-resolved experiments relevant to catalytic mechanism, biomolecular recognition, and protein folding.



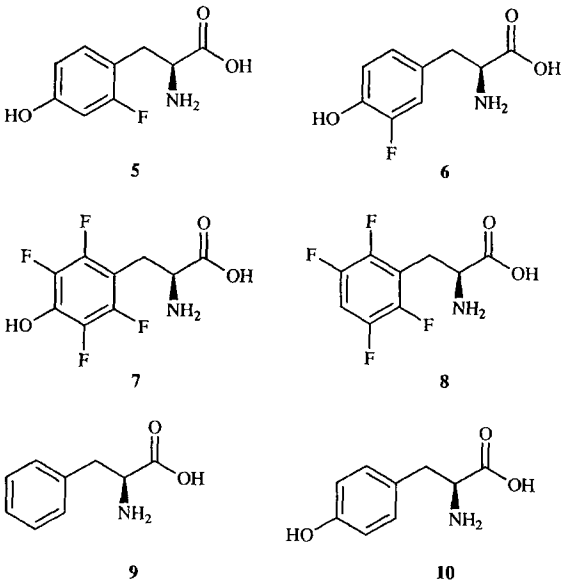
Scheme 9. Photoactivated self-splicing of Vent polymerase using a caged serine analogue. The mechanism of the protein self-splicing mechanism is not known.

3.3. Protein Stability

Mutagenesis with unnatural amino acids has been used to make defined mutations in proteins in the hope of gaining a more precise picture of the forces governing protein stability.[90, 91] An outstanding issue in the literature on protein stability and folding is the role of hydrogen bonding. Although hydrogen bonds are clearly important in determining the secondary and tertiary structure of proteins,[92, 93] the magnitude of their contribution to protein stability has been difficult to assess.[94, 95] Stabilization values for hydrogen bond formation determined from studies with mutants, in which one member of a hydrogen-bonded pair is deleted, vary considerably depending upon the nature and local environment of the hydro-

gen bond.[90, 96] Moreover, a concern in all such studies with mutants is the possibility of introducing additional destabilizing interactions by leaving an unpaired hydrogen bond donor or acceptor and/or altering local solvation and packing interactions (e.g. a Glu-Phe versus a Glu-Tyr pair).

In an effort to determine the degree to which side-chain hydrogen bonding stabilizes the folded state of proteins while minimizing the steric and electronic perturbations associated with deleting one member of a hydrogen-bonded pair, Tyr 27 in staphylococcal nuclease (SNase) was replaced with a number of isosteric, fluorinated tyrosine analogues, including 2-fluorotyrosine (**5**), 3-fluorotyrosine (**6**), and tetrafluorotyrosine (**7**) as well as 2,3,5,6-tetrafluorophenylalanine (**8**) and phenylalanine (**9**) (Scheme 10).[97] These mutants were designed to examine



Scheme 10. Structures of the amino acids with altered hydrogen-bonding properties substituted for Tyr 27 in SNase.

the effect of increasing the strength of the Tyr 27–Glu 10 hydrogen bond on protein stability. Denaturation studies of the corresponding mutants revealed a unique free energy correlation between stability constant K_{app} ($\alpha = 0.38$) and the pK_a of the hydroxyl group in the tyrosine analogue in position 27 (Fig. 2). Indeed, substitution of Tyr (pK_a ca. 10) with tetrafluoro-L-tyrosine (pK_a ca. 5) increased the stability of SNase by 2.3 kcal mol^{-1}. This experiment provides strong evidence that side-chain intramolecular hydrogen bonds can preferentially stabilize the folded state of a protein relative to the unfolded state in water. In addition this study effectively extends the use of substituent effects in physical organic chemistry from small molecules to proteins.

A series of mutations were also made in T4L to examine the role of backbone hydrogen bonding in determining protein stability.[68] The surface amino acid Ala 82 in T4L was replaced with its hydroxy isostere lactic acid (Fig. 11). Ala 82 is at a break between two helices with the NH group and side chain exposed to water. The Ala 82 → lactate mutation effectively substitutes a good hydrogen-bond acceptor, the amide carbonyl group, with

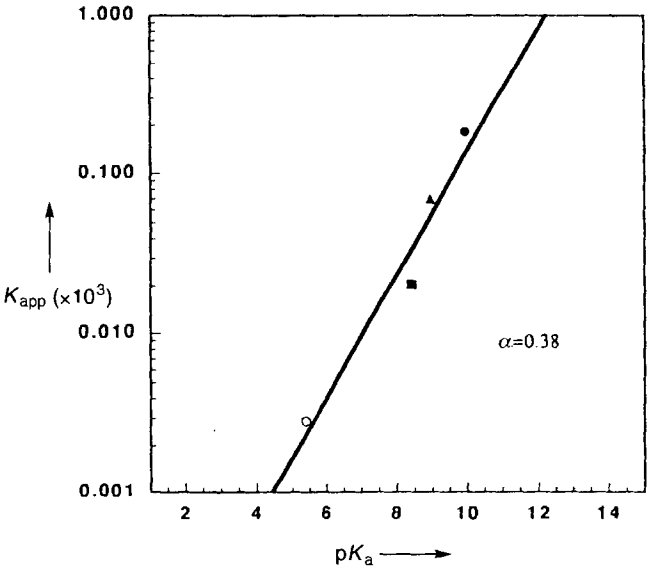
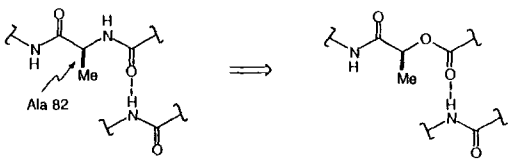


Fig. 2. The relation between the pK_a of the residue at position 27 (Tyr **10** and Tyr analogues **5**–**7**) and the stability (K_{app}) of the SNase. ● = **10**, ▲ = **5**, ■ = **6**, ○ = **7**.

a considerably weaker hydrogen-bond acceptor, the ester carbonyl group.[98] Because both esters and amides exist mainly in the *trans* conformation,[99] the destabilization caused by this substitution (decrease in the melting temperature T_m by 3.7 °C (1.0 kcal mol^{-1})) provides evidence that backbone amide hydrogen-bonding interactions do in fact help to stabilize proteins.



Scheme 11. Substitution of Ala 82 in T4L with lactic acid.

In an examination of the importance of packing interactions in the core of a protein,[100–103] replacements were made for Leu 133 which lies along the edge of the largest cavity in the interior of T4L (Fig. 3).[104] Previous attempts to stabilize T4L by increasing the packing density of the hydrophobic core by means of a Leu 133 → Phe or Ala 129 → Val mutation had been unsuccessful, as both mutations disrupt neighboring residues.[104] However, incorporation of the unnatural amino acid (*S,S*)-2-amino-4-methylhexanoic acid (**11**) and (*S*)-2-amino-3-cyclopentylpropanoic acid (**12**), both of which were designed to fill the cavity with minimal strain, stabilizes T4L, increasing the protein's melting temperature by 1.9 °C (0.6 kcal mol^{-1}) and 4.3 °C (1.24 kcal mol^{-1}), respectively.[105] This result demonstrates that amino acids that increase the bulk of buried hydrophobic residues without concomitant introduction of strain can increase protein stability significantly. As there is little difference in surface area between **12** and **11** (Δsurface area = 0.9 Å^2), the difference in stability between the two mutants likely reflects the fact that the cyclic amino acid **12** loses less conformational entropy upon folding than does the acyclic amino acid **11**. Consequently, side-chain conformational

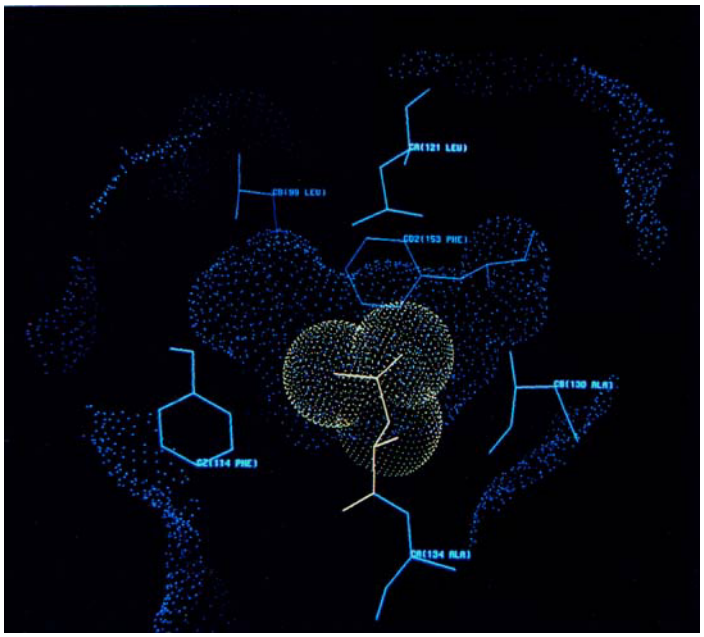
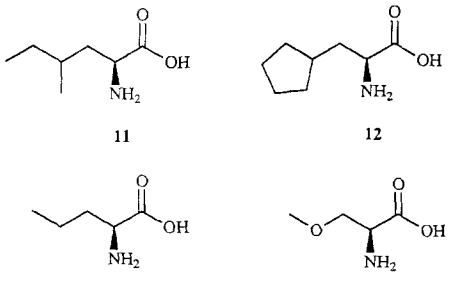


Fig. 3. Graphic representation of the van der Waals surfaces (yellow) of the side chains of Leu 133 in T4L.

entropy, as well as packing interactions, plays an important role in determining protein stability.

In a second example, substitution of norvaline (**13**) and *O*-methylserine (**14**) (Scheme 12) for Leu 133 allowed for a measurement of the effect of modifying side-chain hydrophobicity in the absence of changes in packing interactions or side-chain entropy.[105] In this case it was found that the difference in the stabilities of the two mutant enzymes relative to that of wild-type T4L corresponds to the difference in the partitioning ratios of the respective *N*-acetyl amide derivatives in octanol–water. This correlation provides further evidence that these partitioning ratios give an accurate measure of solvation effects.

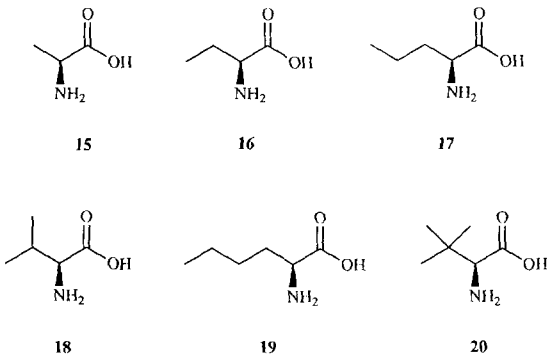


11 **12** **13** **14**

Scheme 12. Structures of the amino acids substituted for Leu 113 in T4L.

In another experiment, systematic removal of methyl and methylene groups from the Leu 133 side chain was found to lead to a stepwise decrease in protein stability.[105] However, the change was nonlinear; $\Delta\Delta G$ became increasingly large with decreasing side-chain surface area. This trend is reflected accurately in the semiquantitative estimates of the $\Delta\Delta G$ values and results from the net effect of changes in the hydrophobic, entropic, packing, and cavity energy terms.

The effects of incorporating β-branched amino acids were examined by comparing the stabilities of mutant proteins containing the series of branched and linear amino acids **15**–**20** (Scheme 13), at two surface-exposed sites in the middle of two



15 **16** **17** **18** **19** **20**

Scheme 13. β-Branched and linear amino acids incorporated at sites 44 and 68 in T4L.

α-helices in T4L.[106] The natural β-branched amino acids valine, isoleucine, and threonine are thought to destabilize α-helices. In known protein structures these amino acids occur infrequently in α-helices relative to amino acids such as leucine, and they destabilize α-helical peptides and protein α-helices.[107–113] For example, when a series of linear and branched amino acids were incorporated into an α-helical peptide, the β-branched amino acids were found to be destabilizing relative to the linear and γ-branched amino acids.[114] Substitution of *tert*-butylglycine (**20**) for *n*-butylglycine (**19**) or alanine (**15**) destabilizes the peptide by 0.9 kcal mol^{-1}; however, the same substitution either destabilizes T4L by 0.7 kcal mol^{-1} ($\Delta T_m = 2.6\,^{\circ}C$) (site 44) or stabilizes the protein by 0.3 kcal mol^{-1} ($\Delta T_m = 1.0\,^{\circ}C$) (site 68). This difference illustrates the difficulty in delineating simple rules as to which factors stabilize or destabilize proteins given the influence of context effects. In addition, the stabilities and simulated structures of the *tert*-butylglycine mutants have provided insight into the effects of β-branched side chains on α-helix stability in proteins.

The results described underscore the difficulty in interpreting mutagenesis data when more than one property of an amino acid is altered at once. The ability to precisely alter the structure of an amino acid should allow us to better dissect the individual contributions of hydrophobicity, packing, entropy, and cavity formation on protein stability. We are currently extending these studies to hydrogen bonding, and π–π and π–ion interactions in protein interiors.

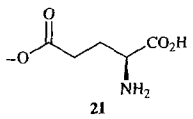
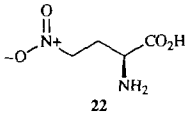
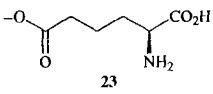
3.4. Enzyme Mechanisms

Mutagenesis with unnatural amino acids also is being used to probe the catalytic mechanisms of the enzymes staphylococcal nuclease, aspartate aminotransferase, methionine aminopeptidase, and ribonucleotide reductase. The enzyme staphylococcal nuclease (SNase) accelerates the hydrolysis of phosphodiester bonds in nucleic acids some 10^{16}-fold over the rate of the uncatalyzed reaction. This enzyme has been the subject of many struc-

tural, mechanistic, and mutagenesis studies aimed at understanding how enzymes can achieve such extraordinary rate enhancements.[115-119] Based on these studies it has been suggested that general base catalysis contributes significantly to the catalytic efficiency of this enzyme. Specifically, it is thought that Glu43 in SNase acts as a general base to activate a water molecule for attack on the phosphodiester backbone of DNA. Glu43 is known to be important for catalysis, because replacement by the natural amino acids Asp and Gln results in a significant loss in activity.[120]

Surprisingly, substitution of Glu43 with either homoglutamate **23** or the nitro analogue (*S*)-4-nitro-2-aminobutyric acid (**22**), which is both isoelectronic and isosteric to glutamate but a much poorer base, yielded mutant enzymes with kinetic constants similar to those of wild-type SNase under normal assay conditions (Table 1).[85] The pH dependence of the catalytic

Table 1. Catalytic efficiences of wild-type staphylococcal nuclease and mutants Glu43 → (*S*)-4-nitro-2-aminobutyric acid and Glu43 → homoglutamate. V_{max} = maximum reaction rate (measured based on the absorption at 260 nm, A_{260}), K_M = Michaelis constant.

Amino acid	V_{max} ($\mu g^{-1} min^{-1}$)	K_M(DNA) ($\mu g mL^{-1}$)	K_M(Ca^{2+}) (μM)
 **21**	6.7±0.7	8±3	320±30
 **22**	3.0±0.5	26±8	470±40
 **23**	5.2±0.2	10±2	290±30

efficiencies of these mutants (the pH profiles of the mutants with nitroglutamate **22** and homoglutamate **23** suggest that the nitronate anion is not formed) and the crystal structure of the homoglutamate43 mutant (Fig. 4) suggest that Glu43 may not be acting as a base, but rather may play a structural role, serving as a bidendate hydrogen-bond acceptor to fix the conformation of the neighboring loop. Independent studies by Gerlt et al., in which the loop adjacent to Glu43 was deleted from SNase, have led to the same conclusion.[121]

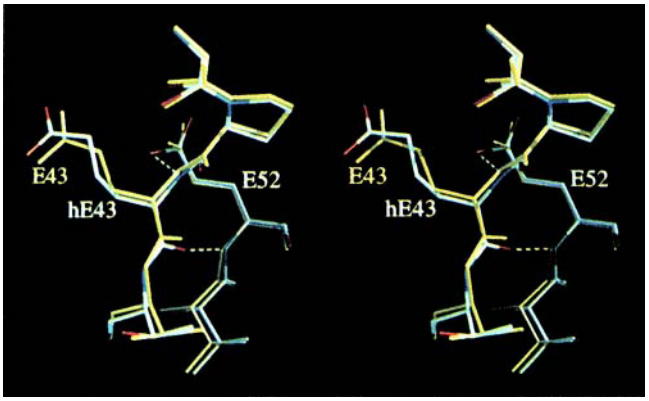


Fig. 4. Comparison of the positions of the side chains of Glu43 and homoglutamate43 as determined by X-ray crystallography for the apo wild-type and homoglutamate43 mutant proteins, respectively (stereoplot).

3.5. Cellular Signal Transduction

Mutagenesis with unnatural amino acids has been used to probe the role of *ras* p21 in cellular signal transduction pathways. Mammalian proteins encoded by the *ras* genes are thought to function as regulators of various signal transduction processes involved in cell growth and differentiation.[122-125] The chemical basis for signal regulation involves cycling of the protein between the inactive guanosine diphosphate (GDP) bound state and the active guanosine triphosphate (GTP) bound state (Fig. 5). Point mutations that result in a decrease in

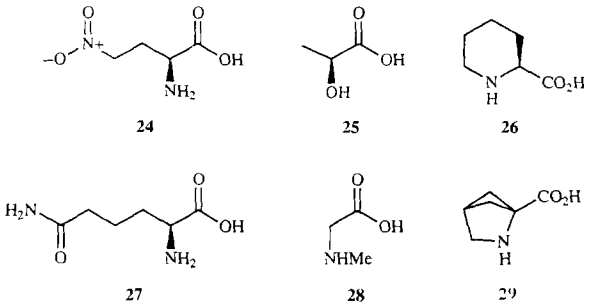


Fig. 5. Model of *ras* p21 with bound GTP [138].

the intrinsic GTPase activity of *ras* p21 or of the GTPase activity stimulated by GTPase activating protein (GAP) are associated with approximately 30% of human cancers.[123, 126-129] In order to better understand the molecular basis by which mutations in *ras* p21 lead to switch inactivation, we have substituted residues in loop L4 (the switch II region), loop L2 (the switch I region), and loop L1 (the phosphate binding loop) with a series of unnatural amino acids.[130-132]

Mutations at Gln61 are among the most common that lead to impaired intrinsic GTPase activity. This residue lies in loop L4 of *ras* p21, a region that undergoes conformational change upon GTP/GDP exchange.[133-140] On the basis of biochemical studies and the three-dimensional X-ray crystal structures of the GTP-, Gpp(CH_2)p-, and Gpp(NH)p-bound forms of *ras* p21, it has been proposed that Gln61 is critical for γ-phosphate binding

and catalysis.[133-141] Specifically, it has been proposed that the γ-carboxamide of Gln 61 either polarizes a water molecule (175) for attack on the γ-phosphate or stabilizes the incipient pentacoordinate transition state. In order to test these mechanistic hypotheses, we replaced Gln 61 with the isoelectronic, isosteric nitro analogue **24** and with homoglutamine **27** (Scheme 14).[130]



Scheme 14. Structures of some unnatural amino acids used to probe the switch function of *ras* p21.

Whereas seventeen natural mutants at position 61 have reduced GTPase activity and are not activated by GAP, both unnatural mutants had GTPase activity similar to that of the wild-type protein and were activated by GAP. The fact that these mutants retained activity suggests that residue 61 plays some other role in catalysis, perhaps serving to distort the bound GTP toward the transition state geometry.

Mutations at Gly 12 of *ras* p21 also result in impaired intrinsic GTPase activity and are commonly associated with oncogenic activation.[123, 142] Gly 12 occurs in a highly conserved type II β-turn, [Gly 11-X-X-X-Gly-Lys-(Ser or Thr)], a phosphate-binding loop found in many nucleotide-binding proteins.[143, 144] Mutation of Gly 12 to any common amino acid other than proline results in diminished GTPase activity.[142] To more fully understand the role of Gly 12 mutants in switch function, we inserted a number of unnatural amino acids and analogues at this site, including lactic acid (**25**, Lac), pipecolic acid (**26**, Pip), and *N*-methylglycine (**28**, MeGly) (Scheme 14).[130] The protein containing pipecolic acid (**26**) at position 12, which was expected to have a much more negative torsion angle ϕ than Gly 12, displayed GTPase activity similar to that of wild-type ras. The *N*-methylglycine (**28**) mutant also had comparable activity (N^{α}-methyl substitution also decreases ϕ values). Whereas the Ala 12 mutant had reduced GTPase activity, the variant with isosteric lactic acid (**25**), in which the backbone amide linkage is replaced by an ester linkage, had normal GTPase activity. The fact that only mutants that can adopt unusual backbone conformations are active suggests that a conformational change in loop L1 may relieve unfavorable side-chain interactions at position 12 in the transition state. However, even though the Pro 12, Pip 12, Lac 12, and MeGly 12 variants had intrinsic GTPase activity similar to that of wild-type *ras* p21, they were not activated by GAP. Moreover, the Gly 13 → Thr, Gly 13 → allothreonine, and Gly 13 → Ser proteins, which have intrinsic GTPase activity two to three times that of wild-type *ras* p21 (attributable to the β-hydroxyl group), were not activated by GAP and were not transforming in a germinal vesicle breakdown assay with *Xenopus laevis* oocytes. One interpretation of these results is that loop L1 can adopt two or more conformations in solution and that its positioning by one or more effector proteins modulates GTPase activity and onocogenic activation. The unusual backbone structures of the Gly 12 and Gly 13 mutants may prevent switch function.

In a third mutagenesis experiment the role of Pro 34 in loop L2 function was probed. The most significant difference between the GTP- and GDP-bound forms of *ras* p21 is in this region (residues 32–40).[133-140] It has been proposed that Pro 34, which is conserved in *ras* p21 and close to the active site, may play a role in controlling the conformation of loop L2, perhaps through a *cis–trans* isomerization of the Pro 34 amide bond.[137] In order to examine the structural and mechanistic role of this residue more precisely, Pro 34 was replaced with 2,4-methanoproline (**29**) (Scheme 14), which is strongly biased toward the *trans* configuration by virtue of the C_{α} substitution.[131] The fact that this mutant has intrinsic and GAP-activated GTPase activity comparable to that of the wild-type protein strongly suggests that the *cis–trans* isomerization of Pro 34 does not play a key role in signal transduction. Similar substitutions may be useful in probing the role of backbone isomerization in protein folding pathways.

4. Conclusion

The ability to incorporate unnatural amino acids into proteins site-specifically makes possible detailed physical studies on this important class of organic compounds. Mutations can be made to probe the precise nature of the contribution of an individual amino acid to protein structure or function, often without dramatic losses in activity. This methodology should provide new insights into and perhaps challenge assumptions about the nature of protein structure and function. In addition, it may be possible to generate mutant proteins with novel functions. The remaining goals are increasing the quantities of protein obtainable and finding ways to bypass the specificity of the protein biosynthetic machinery so that more diverse amino acid structures can be incorporated to further add to the power of this approach.

We are grateful for financial support for this work from the U. S. Office of Naval Research, National Institutes of Health, and the Department of Energy. V. W. C thanks the National Science Foundation for a Predoctoral Fellowship.

Received: April 6, 1994 [A 61 IE]
German version: *Angew. Chem.* **1995**, *107*, 677

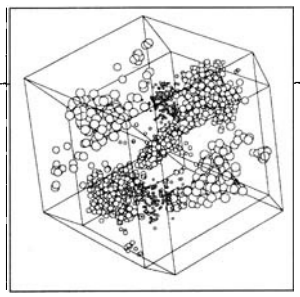
[1] M. J. Zoller, M. Smith, *Methods Enzymol.* **1983**, *100*, 468.
[2] J. R. Knowles, *Science* **1987**, *236*, 1252.
[3] D. Y. Jackson, J. Burnier, C. Quan, M. Stanley, J. Tom, J. A. Wells, *Science* **1994**, *266*, 243.
[4] E. Bayer, *Angew. Chem.* **1991**, *103*, 117; *Angew. Chem. Int. Ed. Engl.* **1991**, *30*, 113.
[5] T. Nakatsuka, T. Sasaki, E. T. Kaiser, *J. Am. Chem. Soc.* **1987**, *109*, 3808.
[6] F. M. Richards, H. W. Wyckoff in *The Enzymes, Vol. IV* (Ed.: P. D. Boyer), Academic Press, New York, **1971**.
[7] K. Hofmann, H. Bohn, *J. Am. Chem. Soc.* **1966**, *88*, 5914.
[8] E. T. Kaiser, D. S. Lawrence, *Science* **1984**, *226*, 505.
[9] E. T. Kaiser, *Acc. Chem. Res.* **1989**, *22*, 47.
[10] K. Rose, *J. Am. Chem. Soc.* **1994**, *116*, 30.

[11] M. Schnolzer, S. B. H. Kent, *Science* **1992**, *256*, 221; P. E. Dawson, T. W. Muir, I. Clark-Lewis, S. B. H. Kent, *ibid.*, **1994**, *266*, 776.
[12] R. E. Offord, *Protein Eng.* **1987**, *1*, 151.
[13] I. M. Chaiken, *Crit. Rev. Biochem.* **1981**, *11*, 255.
[14] E. T. Kaiser, D. S. Lawrence, S. E. Rokita, *Annu. Rev. Biochem.* **1985**, *54*, 565.
[15] D. S. Wuttke, H. B. Gray, S. L. Fisher, B. Imperiali, *J. Am. Chem. Soc.* **1993**, *115*, 8455.
[16] K. E. Neet, A. Nanci, D. E. Koshland, *J. Biol. Chem.* **1968**, *243*, 6392.
[17] L. Polgar, M. L. Bender, *J. Am. Chem. Soc.* **1966**, *88*, 3153.
[18] *Spin Labeling, Theory and Applications* (Ed.: L. Berliner), Academic Press, New York, **1976**.
[19] S. J. Pollack, G. Nakayama, P. G. Schultz, *Science* **1988**, *242*, 1038.
[20] D. R. Corey, P. G. Schultz, *Science* **1987**, *233*, 1401.
[21] U. C. Krieg, P. Walter, A. E. Johnson, *Proc. Natl. Acad. Sci. USA* **1986**, *83*, 8604.
[22] J. Brunner, *Annu. Rev. Biochem.* **1993**, *62*, 483.
[23] C. J. Noren, S. J. Anthony-Cahill, M. C. Griffith, P. G. Schultz, *Science* **1989**, *244*, 182.
[24] J. A. Ellman, D. Mendel, S. Anthony-Cahill, C. J. Noren, P. G. Schultz, *Methods Enzymol.* **1992**, *202*, 301.
[25] J. D. Bain, C. G. Glabe, T. A. Dix, A. R. Chamberlin, E. S. Diala, *J. Am. Chem. Soc.* **1989**, *111*, 8013.
[26] F. H. C. Crick, L. Barrett, S. Brenner, R. Watts-Tobin, *Nature (London)* **1961**, *192*, 1227.
[27] A. Brenner, A. O. W. Stretton, S. Kaplan, *Nature (London)* **1965**, *206*, 994.
[28] L. Bossi, J. R. Roth, *Nature (London)* **1980**, *286*, 123.
[29] F. H. C. Crick, *Symp. Soc. Exp. Biol.* **1958**, *12*, 138.
[30] F. Chapeville, F. Lipmann, G. von Ehrenstein, B. Weisblum, W. J. Ray, S. Benzer, *Proc. Natl. Acad. Sci. USA* **1962**, *48*, 1086.
[31] S. Chladek, M. Sprinzl, *Angew. Chem.* **1985**, *97*, 377; *Angew. Chem. Int. Ed. Engl.* **1985**, *24*, 371.
[32] S. M. Hecht, *Acc. Chem. Res.* **1992**, *25*, 545.
[33] J. R. Sayers, W. Schmidt, F. Eckstein, *Nucleic Acids Res.* **1988**, *16*, 791.
[34] A. Bruce, J. Atkins, N. Wills, O. Uhlenbeck, R. Gesteland, *Proc. Natl. Acad. Sci. USA* **1982**, *79*, 7127.
[35] D. Ayer, M. Yarus, *Science* **1986**, *231*, 393.
[36] L. Bossi, *J. Mol. Biol.* **1983**, *164*, 73.
[37] A. Miller, A. Albertini, *J. Mol. Biol.* **1983**, *164*, 59.
[38] Y. Kwok, J. T. Wong, *Can. J. Biochem.* **1980**, *58*, 213.
[39] J. W. Roberts, J. Carbon, *J. Biol. Chem.* **1975**, *250*, 5530.
[40] J. F. Milligan, D. R. Groebe, G. W. Witherell, O. C. Uhlenbeck, *Nucleic Acids Res.* **1987**, *15*, 8783.
[41] C. J. Noren, S. J. Anthony-Cahill, D. J. Suich, K. A. Noren, M. C. Griffith, P. G. Schultz, *Nucleic Acids Res.* **1990**, *18*, 83.
[42] K. M. Harrington, I. A. Nazarenko, D. B. Dix, R. C. Thompson, O. C. Uhlenbeck, *Biochemistry* **1993**, *32*, 7617.
[43] R. Giege, J. D. Puglisi, C. Florentz, *Progress Nucleic Acids Res. Mol. Biol.* **1993**, *45*, 129.
[44] P. Schimmel, *Annu. Rev. Biochem.* **1987**, *56*, 125.
[45] T. G. Heckler, L. H. Chang, Y. Zama, T. Naka, M. S. Chorghade, S. M. Hecht, *Biochemistry* **1984**, *23*, 1468.
[46] S. A. Robertson, C. J. Noren, S. J. Anthony-Cahill, M. C. Griffith, P. G. Schultz, *Nucleic Acids Res.* **1989**, *17*, 9649.
[47] D. Hentzen, P. Mandel, J. P. Garel, *Biochim. Biophys. Acta* **1972**, *281*, 228.
[48] M. C. Griffith, Ph.D. Thesis, University of California, Berkeley, **1990**.
[49] S. A. Robertson, J. A. Ellman, P. G. Schultz, *J. Am. Chem. Soc.* **1991**, *113*, 2722.
[50] A. Patchornik, B. Amit, R. B. Woodward, *J. Am. Chem. Soc.* **1970**, *92*, 6333.
[51] S. R. Adams, J. P. Y. Kao, R. Y. Tsien, *J. Am. Chem. Soc.* **1989**, *111*, 7957.
[52] D. Kern, R. Giege, J. P. Ebel, *Eur. J. Biochem.* **1972**, *31*, 148.
[53] N. Chinsky, A. L. Margolin, A. M. Klibanov, *J. Am. Chem. Soc.* **1989**, *111*, 386.
[54] P. Kast, H. Hennecke, *J. Mol. Biol.* **1991**, *222*, 99.
[55] *Transcription and Translation: A Practical Approach* (Eds.: B. D. Hames, S. J. Higgins), IRL Press, Oxford, **1984**.
[56] J. Pratt in ref. [55], p. 179.
[57] G. Zubay, *Annu. Rev. Genet.* **1973**, *7*, 267.
[58] D. V. Goeddel (Ed.:), *Methods Enzymol.* **1990**, *185*.
[59] *Maximizing Gene Expression* (Eds.: W. Rezenikoff, L. Gold), Buttersworth, Boston, **1986**.
[60] D. Suich, Ph.D. Thesis, University of California, Berkeley, **1993**.
[61] D. Mendel, J. Ellman, P. G. Schultz, *J. Am. Chem. Soc.* **1993**, *115*, 4359.
[62] V. W. Cornish, D. R. Benson, C. A. Altenbach, K. Hideg, W. L. Hubbell, P. G. Schultz, *Proc. Natl. Acad. Sci. USA* **1994**, *91*, 2910.
[63] A. Louie, F. Jurnak, *Biochemistry* **1985**, *24*, 6433.
[64] K. Quiggle, G. Kumar, T. W. Oh, E. K. Ryu, S. Chladek, *Biochemistry* **1981**, *20*, 3480.
[65] A. Bhuta, *Biochemistry* **1981**, *20*, 8.
[66] P. Bhuta, *Biochemistry* **1982**, *21*, 899.
[67] S. Fahnestock, H. Neumann, V. Shashoua, A. Rich, *Biochemistry* **1970**, *9*, 2477.
[68] J. A. Ellman, D. Mendel, P. G. Schultz, *Science* **1992**, *255*, 197.
[69] M. M. Grant, A. S. Brown, L. M. Corwin, R. F. Troxler, C. Franzblau, *Biochim. Biophys. Acta* **1975**, *404*, 180.
[70] D. A. Tirrell, T. J. Deming, personal communication.
[71] D. Mendel, J. A. Ellman, P. G. Schultz, unpublished.
[72] J. D. Bain, D. A. Wacker, E. E. Kuo, A. R. Chamberlin, *Tetrahedron* **1991**, *47*, 2389.
[73] D. Benson, J. A. Ellman, P. G. Schultz, unpublished.
[74] G. Baldwin, A. Martoglio, C. Zugliani, J. Brunner, *Biochemistry* **1988**, *27*, 7951.
[75] A. S. Spirin, V. I. Baranov, L. A. Ryabova, S. Y. Ovodov, Y. B. Alahhov, *Science* **1988**, *242*, 1162.
[76] O. Landman, S. Spiegelman, *Proc. Natl. Acad. Sci.* **1955**, *41*, 698.
[77] M. Nomura, J. Hosoda, S. Nishimura, *Biochim. Biophys. Acta* **1958**, *29*, 161.
[78] L. G. Kleina, J. M. Masson, J. Normanly, J. Abelson, J. H. Miller, *J. Mol. Biol.* **1990**, *213*, 705.
[79] V. W. Cornish, P. G. Schultz, unpublished.
[80] D. Mendel, P. G. Schultz, unpublished.
[81] M. Chunhua, W. Kudlicki, O. W. Odom, G. Kramer, B. Hardesty, *Biochemistry* **1993**, *32*, 7939.
[82] J. Bain, C. Switzer, A. Chamberlin, S. Benner, *Nature* **1992**, *356*, 537.
[83] J. A. Ellman, D. R. Benson, P. G. Schultz, unpublished.
[84] J. A. Ellman, B. F. Volkman, D. Mendel, P. G. Schultz, D. E. Wemmer, *J. Am. Chem. Soc.* **1992**, *114*, 7959.
[85] J. K. Judice, T. R. Gamble, E. C. Murphy, A. M. deVos, P. G. Schultz, *Science* **1993**, *261*, 1578.
[86] B. L. Stoddard, J. L. Bruhnke, D. Koenigs, N. Porter, D. Ringe, G. A. Petsko, *Biochemistry* **1990**, *29*, 8042.
[87] M. Wilcox, R. W. Viola, K. W. Johnson, A. P. Billington, B. C. Carpenter, J. A. McCray, A. P. Guzikowski, G. P. Hess, *J. Org. Chem.* **1990**, *55*, 1585.
[88] D. Mendel, J. A. Ellman, P. G. Schultz, *J. Am. Chem. Soc.* **1991**, *113*, 2758.
[89] X. Xiong, S. N. Cook, W. E. Jack, L. E. Danley, J. A. Ellman, P. G. Schultz, C. J. Noren, *Cell*, submitted.
[90] K. A. Dill, *Biochemistry* **1990**, *29*, 7133.
[91] B. W. Matthews, *Annu. Rev. Biochem.* **1993**, *62*, 139.
[92] L. Pauling, R. B. Corey, *Proc. Natl. Acad. Sci., USA* **1951**, *37*, 729.
[93] L. Pauling, R. B. Corey, H. R. Branson, *Proc. Natl. Acad. Sci., USA* **1951**, *37*, 205.
[94] G. A. Jeffrey, W. Saenger, *Hydrogen Bonding in Biological Molecules*, Springer, New York, **1991**.
[95] G. D. Rose, R. Wolfenden, *Annu. Rev. Biophys. Biomol. Struct.* **1993**, *22*, 381.
[96] A. R. Fersht, *Trends Biochem. Sci.* **1987**, *12*, 301.
[97] J. Thorson, E. Chapman, E. C. Murphy, P. G. Schultz, J. K. Judice, *J. Am. Chem. Soc.* **1995**, *117*, 1157.
[98] M. J. Kamlet, J. L. M. Abboud, M. H. Abraham, R. W. Taft, *J. Org. Chem.* **1983**, *48*, 2877.
[99] K. B. Wiberg, K. E. Laidig, *J. Am. Chem. Soc.* **1987**, *109*, 5935.
[100] K. Yutani, K. Ogasahara, T. Tsugita, Y. Sugino, *Proc. Natl. Acad. Sci. USA* **1987**, *84*, 4441.
[101] M. Matsumura, W. J. Becktel, B. W. Matthews, *Nature (London)* **1988**, *334*, 406.
[102] J. J. T. Kellis, K. Nyberg, D. Sali, A. R. Fersht, *Nature (London)* **1988**, *333*, 784.
[103] W. A. Lim, R. T. Sauer, *Nature (London)* **1989**, *339*, 31.
[104] M. Karpusas, W. A. Baase, M. Matsumura, B. W. Matthews, *Proc. Natl. Acad. Sci. USA* **1989**, *86*, 8237.
[105] D. Mendel, J. A. Ellman, Z. Chang, D. L. Veenstra, P. A. Kollman, P. G. Schultz, *Science* **1992**, *256*, 1798.
[106] V. W. Cornish, M. I. Kaplan, D. Veenstra, P. A. Kollman, P. G. Schultz, *Biochemistry* **1994**, *33*, 12022.
[107] P. Y. Chou, G. D. Fasman, *Annu. Rev. Biochem.* **1978**, *47*, 251.
[108] K. T. O'Neil, W. F. DeGrado, *Science* **1990**, *250*, 646.
[109] S. Padmanabhan, S. Marqusee, T. Ridgeway, T. M. Laue, R. L. Baldwin, *Nature (London)* **1990**, *344*, 268.
[110] P. C. Lyu, M. I. Liff, L. A. Marky, N. R. Kallenbach, *Science* **1990**, *250*, 669.
[111] M. Blaber, X.-J. Zhang, B. W. Matthews, *Science* **1993**, *260*, 1637.
[112] M. Blaber, X.-J. Zhang, J. D. Lindstrom, S. D. Deprot, W. A. Baase, B. W. Matthews, *J. Mol. Biol.* **1994**, *235*, 600.
[113] A. Horowitz, J. M. Matthews, A. R. Fersht, *J. Mol. Biol.* **1992**, *227*, 560.
[114] P. C. Lyu, J. C. Sherman, A. Chen, N. R. Kallenbach, *Proc. Natl. Acad. Sci. USA* **1991**, *88*, 5317.
[115] F. A. Cotton, E. E. J. Hazen, M. J. Legg, *Proc. Natl. Acad. Sci. USA* **1979**, *76*, 2551.
[116] P. J. Loll, E. E. Lattman, *Proteins* **1989**, *5*, 183.
[117] D. J. Weber, A. K. Meeker, A. S. Mildvan, *Biochemistry* **1991**, *30*, 6103.
[118] D. J. Weber, E. H. Serpersu, D. Shortle, A. S. Mildvan, *Biochemistry* **1990**, *29*, 8632.
[119] P. W. Tucker, J. E. E. Hazen, F. A. Cotton, *Mol. Cell. Biochem.* **1979**, *23*, 3.

[120] D. W. Hibler, N. J. Stolowich, M. A. Reynolds, J. A. Gerlt, J. A. Wilde, P. H. Bolton, *Biochemistry* **1987**, *26*, 6278.
[121] S. P. Hale, L. B. Poole, J. A. Gerlt, *Biochemistry* **1993**, *32*, 7479.
[122] M. Barbacid, *Annu. Rev. Biochem.* **1987**, *56*, 779.
[123] J. L. Bos, *Cancer Res.* **1989**, *49*, 4682.
[124] J. A. Glomset, M. H. Gelb, C. C. Fransworth, *Trends Biochem. Sci.* **1990**, *15*, 139.
[125] D. Spandidos, *Ras Oncogenes*, Plenum, New York, **1989**.
[126] M. Trahey, M. Trahey, G. Wong, R. Halenbeck, B. Rubinfield, G. A. Martin, M. Ladner, C. M. Long, W. J. Crosier, K. Watt, K. Koths, F. McCormick, *Science* **1988**, *242*, 1697.
[127] M. Trahey, F. McCormick, *Science* **1987**, *238*, 542.
[128] G. A. Martin, D. Viskochil, G. Bollag, P. C. McCabe, W. J. Crosier, H. Haubruck, L. Conroy, R. Clark, P. O'Connell, R. M. Cawthon, M. A. Innis, F. McCormick, *Cell* **1990**, *63*, 843.
[129] G. Xu, B. Lin, K. Tanaka, D. Dunn, D. Wood, R. Gesteland, R. White, R. Weiss, F. Tamanoi, *Cell* **1990**, *63*, 835.
[130] H. H. Chung, D. R. Benson, P. G. Schultz, *Science* **1993**, *259*, 806.
[131] H. H. Chung, D. R. Benson, V. W. Cornish, P. G. Schultz, *Proc. Natl. Acad. Sci. USA* **1993**, *90*, 10145.
[132] H. H. Chung, D. R. Benson, P. G. Schultz, *J. Am. Chem. Soc.* **1993**, *115*, 6414.
[133] A. M. d. Vos, L. Tong, M. Milgurn, P. Matias, J. Jancarik, S. Noguchi, S. Nishimura, K. Miura, E. Ohtsuka, S.-H. Kim, *Science* **1988**, *239*, 888.
[134] E. F. Pai, W. Kabsch, U. Krengel, K. C. Homes, J. John, A. Wittinghofer, *Nature (London)* **1989**, *341*, 209.
[135] L. Tong, M. V. Milburn, A. M. d. Vos, S.-H. Kim, *Science* **1989**, *245*, 244.
[136] M. V. Milburn, L. Tong, A. M. deVos, A. Brunger, Z. Yamaizumi, S. Nishimura, S.-H. Kim, *Science* **1990**, *247*, 939.
[137] E. F. Pai, U. Krengel, G. A. Petsko, R. S. Goody, W. Kabsch, A. Wittinghofer, *EMBO J.* **1990**, *9*, 2351.
[138] G. G. Prive, M. V. Milburn, L. Tong, A. M. deVos, Z. Yamaizumi, S. Nishimura, S.-H. Kim, *Proc. Natl. Acad. Sci. USA* **1992**, *89*, 3649.
[139] U. Krengel, I. Schilchting, A. Scherer, R. Schumann, M. Frech, J. John, W. Kabsch, E. F. Pal, A. Wittinghofer, *Cell* **1990**, *62*, 539.
[140] I. Schlichting, S. C. Almo, G. Rapp, K. Wilson, A. Petratos, A. Lentfer, A. Wittinghofer, W. Kabsch, E. F. Pai, G. A. Petsko, R. S. Goody, *Nature (London)* **1990**, *345*, 309.
[141] C. J. Der, T. Finkel, G. M. Cooper, *Cell* **1986**, *44*, 167.
[142] P. H. Seeburg, W. W. Colby, D. J. Capon, D. V. Goeddel, A. D. Levison, *Nature (London)* **1986**, *312*, 71.
[143] N. J. Gay, J. E. Walker, *Nature (London)* **1983**, *301*, 262.
[144] R. K. Wierenga, P. Terpstora, W. G. Hol, *J. Mol. Biol.* **1986**, *187*, 101.

Y. Ohashi (ed.)

Reactivity in Molecular Crystals



1993. XII, 348 pages. Hardcover. DM 198.00.
ISBN 3-527-29098-2

Do you need to design syntheses that are
- highly selective
- fast
- enantioselective with quantitative enantiomeric yield?

This book describes in detail how best to exploit the enormous synthetic potential of solid state reactions. Written by leading experts, it provides in depth information on
- the theoretical and physico-chemical approach to solid state reactions
- solid-to-solid organic reactions
- stereoselective solid state photoreactions
- reactivity and crystal structure

An ideal companion to Bürgi and Dunitz's *Structure Correlation*, this book will be highly useful to synthetic organic chemists, stereochemists, crystallographers, and solid-state chemists.

To order please contact your bookseller or:
VCH, P.O. Box 10 11 61,
D-69451 Weinheim,
Telefax (0) 62 01 - 60 61 84
VCH, Hardstrasse 10, P.O. Box,
CH-4020 Basel
VCH, 8 Wellington Court,
Cambridge CB1 1HZ, UK
VCH, 303 N.W. 12th Avenue,
Deerfield Beach, FL 33442-1788,
USA
toll-free: 1-800-367-8249 or
fax: 1-800-367-8247
VCH, Eikow Building,
10-9 Hongo 1-chome, Bunkyo-ku,
Tokyo 113

VCH

Preparative Solid-State Chemistry with High-Power CO_2 Lasers**

Sönke Möhr and Hanskarl Müller-Buschbaum*

The establishment of solid state chemistry as an independent field, which also has had a stimulating effect on material sciences, is a consequence of the experimental skill of chemists. The development of new methods led to an abundance of new compounds, the characteristic properties of which are linked with the solid state. The reaction temperature plays an important role in the synthesis of solid compounds; therefore, it is not surprising that a large number of the newly developed experimental techniques involve methods which can produce high temperatures on the open-ended temperature scale. Since the development of the CO_2 laser, the solid-state chemist has an excellent heat source available, and with the power available today the range of high temperatures possible has been extended considerably. A way is now open for producing metastable, "entropy-supported" high-temperature compounds and substances with anomalous oxidation states and with macroscopic defects.

Keywords: high-temperature reactions · laser chemistry · metastable compounds · solid-state chemistry

1. Introduction

In 1917, when Albert Einstein postulated the theoretical principles of the modern LASER (*L*ight *A*mplification by *S*timulated *E*mission of *R*adiation),[1] the interactions between light and material known at the time, that is, absorption and spontaneous emission, were supplemented by stimulated emission. Almost forty years later Gordon, Zeiger, and Townes[2] developed the first MASER (*M*icrowave *A*mplification by *S*timulated *E*mission of *R*adiation), taking into account the results of Basov and Prokhorov[3] on the amplification of electromagnetic radiation. From then on the development of the laser advanced more and more rapidly, culminating in the construction of the first flash-light pumped ruby laser by Maiman[4] in 1960. In the meantime, the number of types of laser has become so large that they are now divided into categories such as solid-state, liquid, and gas lasers. The original acronym LASER has now become the term "laser" which is used for the characterization and the use of a method, or, to refer to an apparatus which produces a characteristic radiation.

A broad spectrum of application arises from the large number of laser types, ranging from modulation techniques in information technology (glass fibers, scanners), metrology and surface testing (interferometry), and material processing, to coagulation of body tissues in medicine. The laser has also become important in chemistry. Numerous review articles[5–9] and monographs[10–12] have been published on the subject. It is, however, apparent that optical and spectroscopic applications of the laser for analytical purposes are of primary interest. There are only a few examples from the domain of molecular chemistry on the use of lasers in chemical synthesis, and in preparative solid-state chemistry they are also only used sporadically.

About 15 years ago we began our first experiments to introduce the CO_2 laser available then (with continuous-wave power up to about 500 Watt) into preparative solid-state chemistry.[13, 14] Since then articles have been published describing syntheses at normal pressure, under increased oxygen pressure, and under reducing conditions. Here we review applications of the CO_2 laser technique to date (lasers of medium power) and then report on new ways of using high-power lasers.

2. The Application of Medium-Power CO_2 Lasers for the Synthesis of New Solids

2.1. Synthesis at Normal Pressure in a Defined Gas Atmosphere

In a review article on the crystalline chemistry of lanthanoid oxides[15] published in 1981, methods of producing high temperatures in chemical laboratories were summarized. These differ not only in the method, but above all, in the efficiency of energy transfer to the solid substances. According to Reed,[16–18] hot flames and laminar argon plasmas transfer 0.2 $kWcm^{-2}$, direct current electric arcs transfer 16 $kWcm^{-2}$, but electron beams and lasers can transfer 10^3 $kWcm^{-2}$. Thus, it is evident that the CO_2 laser, developed by Patel,[19] and subsequently improved by admixture of nitrogen and helium,[20, 21] is

[*] Prof. Dr. H. Müller-Buschbaum, Dr. S. Möhr
Institut für Anorganische Chemie der Universität
Olshausenstrasse 40, D-24098 Kiel (FRG)
Telefax: Int. code + (431)880-1520)

 © VCH Verlagsgesellschaft mbH, D-69451 Weinheim, 1995 0570-0833/95/0606-0634 $ 10.00+.25/0

an unusually efficient source of radiation for heating solid materials.

The first reports on the use of CO_2 lasers for preparative purposes appeared in 1979.[13] The laser activity is based on the fact that the emission at 10.6 μm, which lies in the infra-red region, is absorbed by almost all substances, and by conversion of radiated energy into warmth they can be heated to high temperatures. This technique uses the same principle as that of a solar furnace, that is, the emitted radiation of a CO_2 laser is focused onto the sample, as shown in Figure 1. Here, the horizontally produced laser light is deflected into the vertical by a silicon mirror and then focused by KCl lenses of varying focal length. The sample can be heated simply in air or, as shown in Figure 1, in any chosen gas atmosphere. High-temperature reactions in a defined gas atmosphere are carried out in sealed quartz tubes, which, contrary to the principle of a Liebig condenser, are flushed with gas from top to bottom. This direction of flow hinders vapor deposition on the plane-parallel polished KCl window, which is connected to the quartz tube by O rings. The sample irradiated in this way (e.g. tablets of pressed oxide mixtures) absorbs the total energy in a relatively thin layer; this causes a steep temperature gradient from top to bottom because of the poor heat conduction in ceramic materials. The distribution of temperatures in the vertical direction depends on the radiation profile of the particular type of laser used.

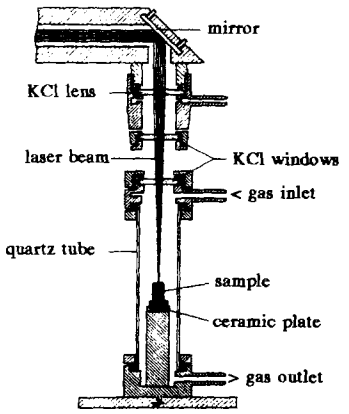


Fig. 1. Schematic representation of the method of working with medium-power CO_2 lasers under a defined gas atmosphere.

The first experiments using radiation energy from a CO_2 laser for the synthesis of new solids were carried out nearly twenty years ago. These involved, for example, the preparation of the following compounds: $La_2Ti_2O_7$,[22] $CaFe_6Al_6O_{19}$,[23] monoclinic $SrAl_2O_4$,[24] $Sr_6Nb_{34}O_{91}$,[25] $Ba_4FeTa_{10}O_{30}$,[26] $MBeLn_2O_5$ with M = Ca and Ln = La, Y;[27] Sr/La,[28] Sr/Sm; Ba/La,[29] Eu^{II}/Eu^{III}; Ca/Pr,[30] Ga/Gd; Ba/Nd,[31] Ca/Eu; Sr/Gd; Eu/Sm,[32] Eu/Gd; (Ca,Sr)/Sm; (Ba,Ca)/Nd; (Ba,Sr)/Nd,[33] $Ba_6Dy_2Al_4O_{15}$[34] and $Ba_6La_2Fe_4O_{15}$.[35] All substances were obtained as single crystals by recrystallization of molten oxide mixtures.

2.2. Synthesis Using High Oxygen Pressure

During a series of syntheses at high temperatures ($T > 1900\,°C$) the partial thermal decomposition of stable oxides was observed. Less stable oxides, for example those of transition metals in higher oxidation states, extensively decompose at high temperatures, so that chemical syntheses at high temperatures are not possible. For instance, Ag_2O, $Au_2O_3 \cdot xH_2O$, and HgO are particularly sensitive to heating, and therefore cannot be used in experiments with the CO_2 laser. In order to reduce the thermal decomposition of such substances or to shift the decomposition equilibrium towards the oxides, the work was carried out under high oxygen pressure. In this way the compounds given in Table 1 were successfully synthesized by conventional autoclave methods. The list shows that there is an upper temperature limit of around 700 °C for the stainless steel autoclaves used. At higher temperatures the oxy-

Table 1. Summary of the syntheses of oxometalates under increased oxygen pressure.

Compound	T [°C]	p [bar]	Ref.
$SrAg_6O_4$	650	3000	[36]
$BaAg_6O_4$	500	4500	[37]
$LaAuO_3$	600	2000	[38]
$La_4Au_2O_9$	600	700	[39]
$NaBi_2AuO_5$	300–600	3000–6000	[40]
$KBiO_3$	500–600	1000–2000	[42]
Sb_2O_5	600	2000	[43]
As_2O_5	500	1000	[44]
Ag_5GeO_4	320	500	[45, 46]
$BaHgO_2$	700	6000	[47]
$Ba_{0.75}Sr_{0.25}HgO_2$	610	6000	[48]
Ho_2HgO_4	620	6200	[49]
$SrHgO_2$	600–620	6000–6100	[50]
$BaAg_2Hg_{20}4$	630	6000	[51]
$Ba_2Hg_3Pd_7O_{14}$	630	3900	[52]
$CdHgO_2$	600	3900	[53]
$Ba_3Pt_4HgO_{11}$	620	3600–4200	[54]



Hanskarl Müller-Buschbaum was born in 1931 in Wallendorf in the Thüringer Wald. He studied chemistry and physics at the University of Grifswald, gaining his doctorate in 1960 under the supervision of H. Witzmann for research on UV-excited borate luminophores. He then joined the research staff at Siemens in Munich, where he carried out research work on hard superconductors. In 1962, he continued his academic career at the University of Münster with Wilhelm Klemm and in 1965 he joined Rudolf Hoppe at the University of Giessen where he gained his habilitation in 1966 for work on the generation of high temperatures with the low-pressure/high-frequency plasma burner and its application in high-temperature solid-state reactions. In 1969 he accepted the offer of a professorial chair for inorganic chemistry at the University of Kiel. His main research interests focus on solid-state chemical reactions at high temperatures using high frequency plasma discharges and the synthesis of metastable materials with the CO_2 laser technique.

gen-filled autoclaves themselves or their seals burn out from the inside. This problem led to the idea of heating the sample under increased oxygen pressure using laser irradiation, that is, the extent of the local heating is limited to exactly the size of the sample, which is, of course, small. For this purpose, autoclaves were constructed with KCl windows transparent to CO_2-laser radiation, which allowed the transfer of energy to the sample without the autoclave itself being heated to a considerable extent. Figure 2 shows the design of such an autoclave as used in combination with CO_2 laser techniques. The laser radiation is focused onto the sample through a KCl window sealed with indium and silver rings. The laser beam can be centered, and the course of the reaction can be monitored through a separate observation window. With this method it was possible to reduce the thermal decomposition of NiO at high temperatures to such an extent that single crystals of $SrNiO_2$[55] could be obtained from a reaction with SrO.

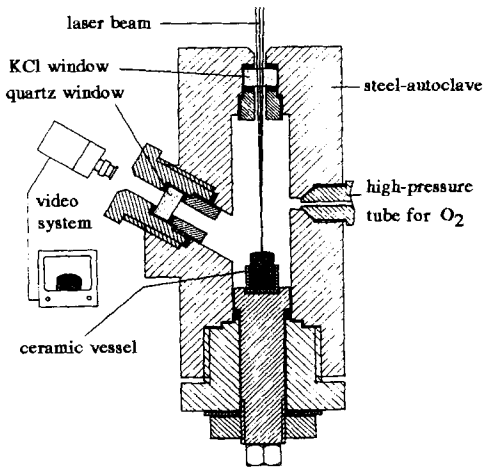


Fig. 2. Schematic representation of an autoclave for syntheses under oxygen pressure using CO_2 lasers.

However, this apparently simple method is restricted by the limited resistance to pressure of the KCl window, which, at pressures above 2000 bar and the simultaneous load of irradiation by the CO_2 laser, begins to deform so that the laser beam can no longer be focused. The energy density reaching the sample is then too low, and no high-temperature reactions under increased oxygen pressure can be carried out. A remedy for this problem is a cascade technique with several pressure stages so that each individual KCl window is only subjected to a maximum of 1000 bar. Unfortunately, this is experimentally very demanding, and the development had to be discontinued for financial reasons.

2.3. Synthesis of Metastable Compounds

In Section 2.1 it was mentioned that the energy irradiated onto the sample is absorbed in a thin layer. This causes the surface of the sample to heat up much more intensely than the deeper layers, and the resulting steep temperature gradient may lead to inhomogeneities in the composition of the reaction products and to demixing of the starting components. This effect is a limiting factor in the use of the CO_2 laser technique for preparative reactions under equilibrium conditions. However, the vertical and horizontal temperature gradient may also be an advantage for the synthesis of metastable compounds. The latter are only stable at high temperatures and are only formed in a relatively small range of temperatures which is very difficult to regulate precisely and is often even unknown. Within the temperature gradient of an irradiated tablet there exists an optimal range of temperatures for the synthesis of metastable compounds. When the sample is rapidly cooled from the high-temperature range after the reaction has taken place, the metastable compounds may be "frozen in" and can then be investigated at room temperature. The following compounds were synthesized in this way: $SrCr_2O_4$,[56] α-$CaCr_2O_4$,[57] $Ca_2Sc_6O_{12}$,[58] $SrCa_2Yb_{10}O_{18}$, $SrCa_2Lu_{10}O_{18}$,[59] $BaSrCaTm_{22}O_{36}$,[60] $Ba_2SrLu_{22}O_{36}$,[61] $Ba_2SrLn_6O_{12}$ (Ln = Yb, Tm),[62] $BaCa_2Ln_{10}O_{18}$ (Ln = Er, Yb;[63] Ln = Tm, (Tm,Sc)),[64] $BaSr_2Ln_6O_{12}$ (Ln = Y, Er, Tm),[65] $Sr_3Ln_4O_9$ (Ln = Nd,[66] La,[67] Pr, (La,Sm)[68]), $BaCa_2Y_6O_{12}$, $CaMg_3Y_8O_{16}$,[69] $BaNi_2M_8O_{15}$ (M = In,[70] (In,Sc)[71]) and $Mn_2Zn_3Ta_6O_{20}$.[72]

2.4. Synthesis of High-Temperature Modifications

In addition to pressure-stabilized and metastable compounds, high-temperature modifications of oxides have also been prepared. For example, it is interesting that the low-temperature modification of $Co_3(AsO_4)_2$[73, 74] is transformed on heating with a CO_2 laser to a high-temperature modification H-$Co_3(AsO_4)_2$,[75] the crystal structure of which is isotypic to that of $Cu_3(AsO_4)_2$.[76]

There were indications that a high-temperature modification existed of the low-temperature orthorhombic modification of $CaTa_2O_6$.[77] Preliminary experiments indicated a perovskite structure of the formula $CaTaO_3$,[78] containing tantalum in the unusual oxidation state IV. Later investigations revealed a small, cubic unit cell filled with one formula unit of $Ca_{0.5}TaO_3$.[79] Here, tantalum shows the expected oxidation number Ta^V, but the question of how $Ca_{0.5}$ can be interpreted in the small perovskite cell remained unanswered. Our experiments using the CO_2 laser technique produced larger single crystals, an X-ray analysis of which revealed a doubling of the lattice constants and a lowering of the symmetry. The elucidation of the structure gave a unit cell with eight times the volume in which only half of the calcium sites are occupied.[80] The unusual thermal ellipsoids of oxygen in the small unit cell disappear when these leave their special positions in the large unit cell.

Lanthanoid oxometalates of the composition Ln_2TiO_5 show a characteristic type of structure for compounds containing large lanthanoid ions, which was first found for La_2TiO_5[81] and then confirmed with Nd_2TiO_5[82] and Eu_2TiO_5.[83] High-temperature modifications were found for Ln_2TiO_5 with Ln = Gd, Dy, Er, Yb, and Lu,[84, 85] the structures of which remained, at first, unknown. Subsequently, the high-temperature modifica-

tion of Dy_2TiO_5[86] was synthesized by the CO_2 laser technique and its structure was elucidated by X-ray analysis. H-Dy_2TiO_5 crystallizes as a cubic pyrochlore ($Dy_2Ti_2O_7$) from which formally one TiO_2 unit has been removed, causing cation and anion defects to appear.

2.5. Syntheses of Low- and Mixed-Valent Oxometalates

2.5.1. Syntheses by Reduction with Hydrogen at High Temperatures

One advantage of the CO_2 laser technique (Fig. 1) is that it is possible to carry out reactions at high temperatures in a hydrogen atmosphere, that is, under reducing conditions. If the oxides are heated by CO_2 laser irradiation until the melting point is reached, on the upper surface of the tablet a liquid droplet is formed which is normally held together by surface tension. This droplet can be heated well above the melting point by further absorption of energy; thus, when this hot melt comes into contact with a hydrogen atmosphere, reduction reactions can occur which are not possible at lower temperatures for thermodynamic reasons ($\Delta G > 0$). At high temperatures (2000–3000 °C) the product $T\Delta S$ of the Gibbs–Helmholtz equation often reaches values which can compensate for a positive reaction enthalpy, thus reversing the sign of ΔG.

Reductions in superheated melts under these conditions are "self-crucible methods", that is the substrate is at the same time either the crucible material or the support for the superheated melt. Reductions with hydrogen at high temperatures led to a series of interesting compounds of the composition $MV_{10}O_{15}$ with M = Ba[87] and Sr[88] as well as $MCr_{10}O_{15}$ with M = Sr, Ba.[89] In these compounds vanadium and chromium are partially reduced to V^{III} and Cr^{II}, respectively. The low oxidation states of vanadium and chromium are indirectly confirmed in $SrNi_2Cr_8O_{15}$[90] and $BaNi_2Cr_8O_{15}$;[91] in $BaNi_2In_8O_{15}$[92] and $BaNi_2In_4Sc_4O_{15}$[93] Ni^{II} and In^{III} were assigned to face-sharing octahedra. $BaVO_{2.5}$[94] also belongs to the group of reduced high-temperature oxides containing vanadium in the oxidation state III.

2.5.2. Synthesis by Comproportionation

Metal oxides can also be reduced by metals. An elegant method is the comproportionation of oxides with metals as introduced by Ehrlich[95] with great success for the synthesis of low-valent titanium oxides. Experiments with medium-power CO_2 lasers only had a limited success in this area. For instance, in this way it was possible to heat SrO, Nb_2O_5, and Nb metal under the exclusion of oxygen and to synthesize $Sr_7Nb_2^{IV}Nb_4^{V}O_{21}$;[96] however, a considerable amount of the radiated energy was reflected by the niobium metal so that the desired high temperatures could not be reached. This provided the stimulus for the use of more powerful lasers and the development of a technique which is particularly suitable for reactions of oxides in the presence of metal melts.

3. Employment of High-Power CO_2 Lasers for Solid-State Synthesis

3.1. Apparatus for Solid-State Synthesis in a Defined Gas Atmosphere

The methods described in Section 2.5 for the reduction of oxides by hydrogen or by metals result in a high thermal load and destruction of the inert gas apparatus. A different design for the apparatus was required to cope with the radiated heat from the sample and the laser radiation reflected by metallic components. The primary objectives are the protection of the experimentalist from the invisible radiation, the protection of the radiation inlet port and the observation window from the high heat of radiation and finally, the handling of hot gases.

A new unit for the sample was constructed for solid-state reactions using high-power CO_2 lasers (power >1200 W; Fig. 3). The reaction chamber (I) made from an aluminum alloy

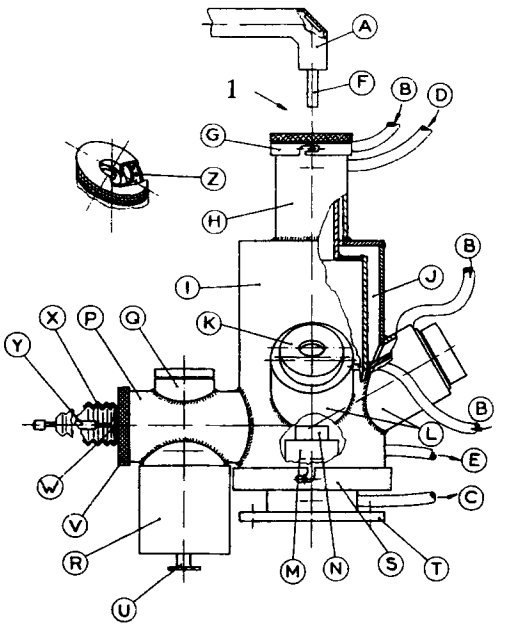


Fig. 3. Cross-section of the double-walled reaction chamber for high-temperature reactions with high-power CO_2 lasers. A = tilted mirror for deflecting the laser beam, B = gas inlet, C = gas outlet, D = cooling water inlet, E = cooling water outlet, F = protective tube against laser radiation, G = fastening device for the KCl window, H = upper part of the reaction chamber, I = reaction chamber, J = water cooling system, K = observation window, L = observation ports, M = sample holder, N = crucible, P = access port, Q = observation window, R = Dewar flask, S = base of the reaction chamber, T = cross-table, U = vacuum flange, V = holder for the manipulator, W = ball-and-socket joint, X = rubber sleeve, Y = manipulator, Z = partial view showing the tangential gas inlet at the windows.

(AlMg7) is double-walled. The inner and outer aluminum walls are kept at a uniform temperature by a water cooling system (J) (inlet at (D), outlet at (E)). The high thermal conductivity of the metal casing as well as the cooling system (J), which constantly removes the heat reaching the inner wall by heat radiation and convection, ensure that even for long reaction times the thermal load of all the components remains low. In order to allow the reaction to be monitored visually and the sample to be subjected to laser radiation, there are four ports in the reaction chamber (I). At three of these openings there are double-walled ports (L)

which are also joined to the cooling system (J). They are mounted in such a way that the reaction can be monitored under an observation angle of 60°. The tube (H) serves as an inlet for the radiation beam. The fourth opening in the the reaction chamber contains a separate quenching device (P). The first three ports mentioned have transparent windows.

The horizontal window is made of a plane-parallel ground KCl single crystal, and is connected by a bayonet joint (G) and O rings to the tube (H). To protect this KCl window against vaporized material, gas is allowed to flow (B) into the reaction chamber from twelve jets (Z) positioned tangentially to the laser axis. This gas flushes away vapors of oxides, suboxides, and metals from the window area. The turbulence of vaporized material observable in the larger chamber (I) is entrained by the spiraling flow of gas as it passes from (H) to (I). In this way the observation windows are also protected from condensing material.

The two observation windows are made of BK-7 (from Dr. Korth/Merck, Kiel-Altenholz), a special glass that has its absorption maximum at 10.6 μm which matches the radiation used here. This prevents the escape of scattered radiation. The spacing of 13 cm between the windows and the heated sample has been chosen so that the direct radiation does not lead to their destruction. The rotatable rings (K), each equipped with two filters (polarizer/analyzer), allow fine adjustment of the brightness during observation of the sample. As in the radiation inlet tube (H), each window is protected by a spiraling flow of gas into the reaction chamber by the pierced ring channels (Z) and gas supply lines (B), which also prevents condensation on the windows.

Finally, the sample can be moved through the port (P) by using the manipulator (Y) during the reaction, or, at the end of a high-temperature reaction, it can be thermally quenched by liquids in a Dewar flask (R). The quenching procedure can be monitored through the observation window (Q). The hot gases are removed from the reaction chamber through the gas outlet (C).

The whole apparatus can be lined up with the laser beam by a cross-table (T). The sample crucible (N) stands on a corundum block (M) and may also be observed on a monitor during the reaction. Figure 4 supplements the cross-section and shows the experimental setup with the beam entering vertically.

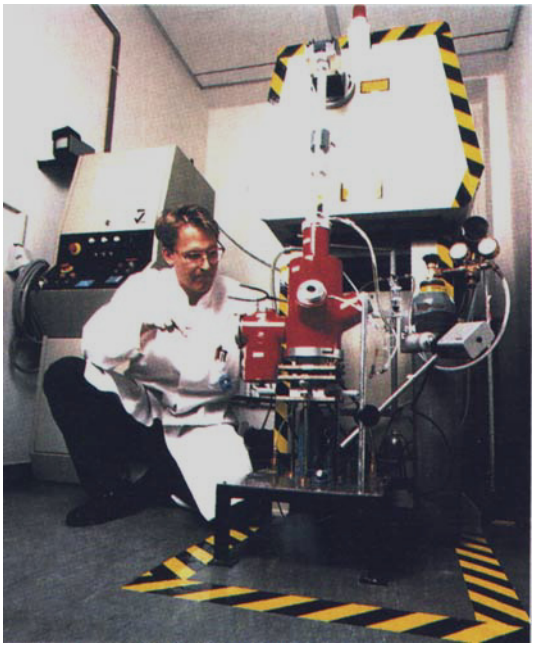


Fig. 4. View of the whole apparatus, with user terminal (left) and CO_2 laser (in the background).

3.2. Measurement of the Reaction Temperature

The sample temperature is measured pyrometrically and only refers to the surface temperature. Pyrometric measurement of temperature presupposes that the sample behaves as a black body. According to Kirchhoff's law the relationship between emitted and absorbed radiation at constant wavelength and constant temperature equals the intensity of the black body radiation [Eq. (a)].

$$I_{(\lambda,T)}A^{-1}_{(\lambda,T)} = I(\text{black body})_{(\lambda,T)} \quad \text{(a)}$$

According to the Stefan–Boltzmann law of radiation the intensity $I(\text{black body})_{(\lambda,T)}$ is proportional to T^4, and the wavelength of the maximum energy λ_m is inversely proportional to the temperature of the black body. This means that with monochromatic measurement of the sample temperature (red filter in the pyrometer), the errors in the measurement becoming increasingly large as the temperature rises. Deviations of a "gray body" from a black body can be corrected with an acceptable accuracy for "visible" wavelengths using Equation (b)[97] [T = temperature of the sample, T_S = temperature of the black body, A = absorption capacity of the sample, λ = wavelength at which the measurement is undertaken, C = constant from Planck's theory ($\equiv$ 1.439 cm K[98])].

$$1T^{-1} = 1T_S^{-1} + \lambda C^{-1} \ln A_{(\lambda,T)} \quad \text{(b)}$$

Figure 5 shows a series of curves calculated with this relationship for several values of the absorption coefficient A at wave-

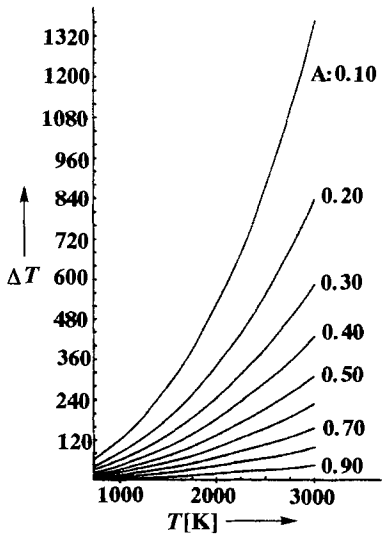


Fig. 5. Plot of the temperature difference as a function of the temperature to be measured for substances with different absorption coefficients (A); wavelength: 0.65 μm.

length $\lambda = 0.65$ μm. It is evident that measurement of the surface temperature for weakly absorbing substances at high temperatures is very inaccurate.

The situation is completely different when the CO_2 laser technique is used for measurement of temperature. Here, the irradiation energy is invisible to the visual pyrometric measurement; that is, each substance appears to have an absorption coefficient of $A = 1.0$, so that the temperature is read off along the abscissa of Figure 5. The inherent brightness observed for the sample is therefore characteristic of its surface temperature.

3.3. Examples of High-Temperature Reactions with High-Power CO_2 Lasers ($P > 1200$ W)

Within the framework of a dissertation[99] and using the apparatus described in Section 3.1, a hitherto unknown high-temperature modification of TiO[100] isotypic with tungsten carbide was synthesized at about 3000 °C.

Above 2600 °C an oxotitanate of the formula $Ba_2Ti^{III}_{12}Ti^{IV}O_{22}$[102] was obtained, which has a new type of structure with face-sharing $Ti^{III}_2O_9$ double-octahedra. Futhermore, for the first time it was possible to substitute Ti^{III} ions by other trivalent cations (here Cr^{III}) in $Ba_2Ti_6O_{12}$ at high temperatures;[103, 104] thus, single crystals of $Ba_2Ti_4CrO_{13}$[105] were investigated by X-ray structure analysis.

The oxides TiO_2 and Y_2O_3 reacted with titanium metal in an argon atmosphere above 2800 °C to give a $TiYO_{2.1}$ phase[101] containing Ti^{II}/Ti^{III} and Y^{II}. The X-ray structure analysis indicates the presence of a defect pyrochlore structure similar to that of the $Ti_{0.5}DyO_{2.5}$[86] phase. Finally, the oxoniobate $BaNb_3O_6$,[106] was synthesized at 2900 °C in the apparatus described. This mixed-valent compound shows open polyhedra not only for Nb^{II} and Nb^{IV} ions but also for Ba^{II} ions.

All the experiments were carried out in a borate-free $(BN)_x$ crucible. In order to avoid reactions with the walls of the crucible, it is important to have information on the vertical and horizontal temperature profiles in the sample. The thermal expansion has been measured for austenite heated up to 2000 °C.[107] However, the temperature profiles of oxides have not been determined, so the dimensions of the crucible must be chosen so that the maximum temperatures reached lie within the sample and do not reach the walls of the crucible.

The profile of the beam of the high-power laser used is also important (VFA 1200, BAASEL Lasertechnik GmbH, D-82319 Starnberg, Germany). The transverse electromagnetic ground mode (TEM_{00}) has an intensity profile which can be described by a Gaussian distribution curve. Since the peak sharpness is proportional to the width of the emitted beam of rays, it follows that for the beam diameter of 15 mm used, no thermal equipartition can exist horizontally in the reaction area. Samples of sufficient diameter and height lead to comparable results and avoid a reaction with the walls of the $(BN)_x$-crucible.

4. Summary and Outlook

High-temperature reactions with the CO_2 laser technique can be used to synthesize new solids, which seemed, until recently, to be inaccessible. This applies particularly to high-temperature reactions under defined gas atmospheres and to the combination of high pressures *and* high temperatures.

Kinetics no longer play a role in the formation of new compounds at high temperatures. Thermodynamics, in particular entropy, is the determining factor for the existence of new compounds and phases. The properties of all the metastable, "entropy-supported" substances described are largely unknown, because experimental techniques still have to be developed which can investigate these substances within the range of their thermodynamic stability.

In addition to the well-known methods for preparing and stabilizing compounds with metal ions in extremely low oxidation states, there is now this new method for syntheses at high temperatures, which has led to the formation of new high-temperature modifications and entropy-supported substances with low oxidation states. Compounds with disordered phases having deficits in subdomains or in the anionic and cationic part of the crystal structure are just beginning to be explored and will bring about a reconsideration of structures in terms of fragmented polyhedra instead of well-defined and complete coordination polyhedra. At present we can only speculate on the physical properties that may arise from such macroscopic defects.

The powerful CO_2 lasers can, with imaginative use of their high-power densities, extend the potential of known techniques—in particular high-pressure/high-temperature reactions between solids or recrystallization of compounds from melts unter extreme pressures. Interesting, partly because only very small amounts of substance are heated locally, are high-temperature syntheses in strong magnetic fields; these are already possible from the experimental point of view. One area still to be investigated is the interaction between strongly heated vapors of metals and compounds with melts or solids.

These few examples show that owing to the advantages associated with the production of high temperatures in a very small area, this method can expect a wide range of applications with interesting results.

We would like to thank the Deutsche Forschungsgemeinschaft and the Fonds der chemischen Industrie for their support with valuable materials. A special thanks is due to Herr Organista (Kiel) from the Deutscher Verband für Schweißtechnik for the complicated welding of the double-walled reaction chamber as well as to the workshops of the Institut für Anorganische Chemie for producing the component parts and the final processing.

Received: June 3, 1994 [A 68 IE]
German version: *Angew. Chem.* **1995**, *107*, 691
Translated by Gillian Scheibelein, Offenburg (FRG)

[1] A. Einstein, *Phys. Z.* **1917**, *18*, 121.
[2] J. Gordon, H. J. Zeiger, C. H. Townes, *Phys. Rev.* **1955**, *99*, 1264.
[3] N. G. Basov, A. M. Prokhorov, *Zh. Eksp. Teor. Fiz.* **1954**, *28*, 249.
[4] T. H. Maiman, *Nature* **1960**, *187*, 493.
[5] R. B. Hall, *Laser Focus* **1982**, *9*, 57.
[6] K. Kleinermann, J. Wolfrum, *Angew. Chem.* **1987**, *99*, 38; *Angew. Chem. Int. Ed. Engl.* **1987**, *26*, 38.
[7] F. P. Schäfer, *Appl. Phys.* **1988**, *B46*, 199.
[8] D. Bäuerle, *Appl. Phys.* **1988**, *B46*, 261.
[9] U. Schindewolf, *Chem. Unserer Zeit* **1972**, *6*, 17.
[10] W. W. Duley, *CO_2 Lasers, Effects and Applications*, Academic Press, London, **1976**.
[11] K. Tradowsky, *Laser: Grundlagen, Technik, Anwendung*, 3. Aufl., Vogel, Würzburg, **1977**.

[12] E. Grunwald, D. F. Dever, P. M. Keehn, *Megawatt Infrared Laser Chemistry*, Wiley, New York, **1976**.
[13] H. Müller-Buschbaum, H. Pausch, *Z. Naturforsch. B* **1979**, *34*, 371.
[14] H. Müller-Buschbaum, H. Pausch, *Z. Naturforsch. B* **1979**, *34*, 375.
[15] H. Müller-Buschbaum, *Angew. Chem.* **1981**, *93*, 1; *Angew. Chem. Int. Ed. Engl.* **1981**, *20*, 22.
[16] T. B. Reed, *Directed Heating with Atoms, Electrons and Photons*; ASM Tech. Dept., New York, **1962**.
[17] T. B. Reed, *Proc. XIX. Natl. Electron Conf.*, Chicago, **1963**, 645.
[18] T. B. Reed, *Sci. Ind.* **1965**, *12*, 1.
[19] C. K. N. Patel, *Phys. Rev.* **1964**, *136*, 1187.
[20] C. K. N. Patel, P. K. Tien, J. H. McFee, *Appl. Phys. Lett.* **1965**, *7*, 290.
[21] K. Gürs, *Z. Angew. Phys.* **1968**, *25*, 379.
[22] K. Scheunemann, H. Müller-Buschbaum, *J. Inorg. Nucl. Chem.* **1975**, *37*, 1879.
[23] M. Harder, H. Müller-Buschbaum, *Z. Naturforsch. B* **1977**, *32*, 833.
[24] A.-R. Schulze, H. Müller-Buschbaum, *Z. Anorg. Allg. Chem.* **1981**, *475*, 255.
[25] K. Schückel, H. Müller-Buschbaum, *Rev. Chim. Miner.* **1986**, *23*, 154.
[26] R. Brandt, H. Müller-Buschbaum, *Z. Anorg. Allg. Chem.* **1986**, *542*, 18.
[27] F. Schröder, H. Müller-Buschbaum, *J. Less-Common Met.* **1988**, *137*, 211.
[28] F. Schröder, H. Müller-Buschbaum, *Monatsh. Chem.* **1987**, *118*, 959.
[29] F. Schröder, H. Müller-Buschbaum, *Z. Anorg. Allg. Chem.* **1988**, *561*, 7.
[30] F. Schröder, H. Müller-Buschbaum, *Z. Anorg. Allg. Chem.* **1988**, *563*, 59.
[31] H. Müller-Buschbaum, S. Münchau, *J. Alloys Compd.* **1994**, *206*, 175.
[32] H. Müller-Buschbaum, M. Wolters, *J. Alloys Compd.* **1994**, *210*, L1.
[33] H. Müller-Buschbaum, S. Frenzen, *Z. Naturforsch. B* **1994**, *49*, 919.
[34] I. Rüter, H. Müller-Buschbaum, *Z. Anorg. Allg. Chem.* **1989**, *573*, 89.
[35] H. Mevs, H. Müller-Buschbaum, *J. Less-Common Met.* **1990**, *157*, 173.
[36] H.-L. Keller, H. Müller-Buschbaum, *Z. Anorg. Allg. Chem.* **1972**, *393*, 266.
[37] H.-L. Keller, H. Müller-Buschbaum, *Z. Naturforsch. B* **1973**, *28*, 263.
[38] M. Ralle, M. Jansen, *J. Solid State Chem.* **1993**, *105*, 378.
[39] M. Ralle, M. Jansen, *J. Alloys Compd.* **1994**, *203*, 7.
[40] J. Geb, M. Jansen, *Z. Anorg. Allg. Chem.* **1994**, *620*, 48.
[41] M. Bortz, M. Jansen, *Z. Anorg. Allg. Chem.* **1993**, *619*, 1446.
[42] M. Jansen, *Z. Naturforsch. B* **1977**, *32*, 1340.
[43] M. Jansen, *Acta Crystallogr. Sect. B* **1979**, *35*, 539.
[44] M. Jansen, *Z. Naturforsch. B* **1979**, *34*, 10.
[45] M. Jansen, C. Linke, *Z. Anorg. Allg. Chem.* **1992**, *616*, 95.
[46] M. Jansen, C. Linke, *Angew. Chem.* **1992**, *104*, 618; *Angew. Chem. Int. Ed. Engl.* **1992**, *31*, 653.
[47] M. Soll, H. Müller-Buschbaum, *J. Less-Common Met.* **1990**, *162*, 169.
[48] M. Soll, H. Müller-Buschbaum, *Monatsh. Chem.* **1990**, *121*, 787.
[49] M. Soll, H. Müller-Buschbaum, *J. Less-Common Met.* **1991**, *170*, 321.
[50] M. Soll, H. Müller-Buschbaum, *J. Less-Common Met.* **1991**, *175*, 295.
[51] M. Soll, H. Müller-Buschbaum, *Monatsh. Chem.* **1991**, *122*, 915.
[52] T. Hansen, H. Müller-Buschbaum, *Z. Anorg. Allg. Chem.* **1992**, *616*, 67.
[53] T. Hansen, H. Müller-Buschbaum, *Z. Anorg. Allg. Chem.* **1994**, *620*, 1137.
[54] T. Hansen, H. Müller-Buschbaum, *Z. Anorg. Allg. Chem.* **1994**, *620*, 1471.
[55] H. Pausch, H. Müller-Buschbaum, *Z. Anorg. Allg. Chem.* **1976**, *426*, 184.
[56] H. Pausch, H. Müller-Buschbaum, *Z. Anorg. Allg. Chem.* **1974**, *405*, 1.
[57] H. Pausch, H. Müller-Buschbaum, *Z. Anorg. Allg. Chem.* **1974**, *405*, 113.
[58] H. Müller-Buschbaum, W. Muschick, *Z. Anorg. Allg. Chem.* **1975**, *412*, 209.
[59] W. Muschik, H. Müller-Buschbaum, *Z. Naturforsch. B* **1976**, *31*, 1064.
[60] J. Krüger, H. Müller-Buschbaum, *Z. Anorg. Allg. Chem.* **1982**, *494*, 103.
[61] J. Krüger, H. Müller-Buschbaum, *Z. Anorg. Allg. Chem.* **1985**, *526*, 60.
[62] J. Krüger, H. Müller-Buschbaum, *J. Less-Common Met.* **1985**, *109*, 37.
[63] H. Müller-Buschbaum, H. Mevs, *J. Less-Common Met.* **1987**, *136*, 193.
[64] H. Müller-Buschbaum, A. Lenz, *J. Less. Common. Met.* **1989**, *156*, 173.
[65] A.-R. Schulze, H. Müller-Buschbaum, *Z. Naturforsch. B* **1981**, *36*, 837.
[66] A.-R. Schulze, H. Müller-Buschbaum, *Z. Anorg. Allg. Chem.* **1980**, *461*, 48.
[67] A.-R. Schulze, H. Müller-Buschbaum, *Z. Anorg. Allg. Chem.* **1980**, *471*, 59.
[68] H. Müller-Buschbaum, A. Boehlke, *Z. Anorg. Allg. Chem.* **1987**, *553*, 212.
[69] F. Schröder, H. Müller-Buschbaum, *J. Less-Common Met.* **1986**, *116*, 211.
[70] S. Schiffler, H. Müller-Buschbaum, *Z. Anorg. Allg. Chem.* **1986**, *542*, 25.
[71] H. Müller-Buschbaum, I. Rüter, *Z. Anorg. Allg. Chem.* **1989**, *572*, 109.
[72] U. Rohweder, H. Müller-Buschbaum, *J. Less-Common Met* **1989**, *152*, 7.
[73] N. Krishnamachari, C. Calvo, *Can. J. Chem.* **1970**, *48*, 881.
[74] R. Gopal, J. S. Rutherford, B. E. Robertson, *J. Solid State Chem.* **1980**, *32*, 29.
[75] B. Jasper-Tönnies, H. Müller-Buschbaum, *Z. Anorg. Allg. Chem.* **1984**, *517*, 161.
[76] S. J. Poulsen, C. Calvo, *Can. J. Chem.* **1968**, *46*, 917.
[77] L. Jahnberg, *Acta Chem. Scand.* **1963**, *17*, 2548.
[78] M. Gasperin, *Acta Crystallogr.* **1958**, *11*, 739.
[79] L. Jahnberg, S. Andersson, A. Magneli, *Acta Chem. Scand.* **1959**, *13*, 1248.
[80] P. Tiedemann, H. Müller-Buschbaum, *Z. Anorg. Allg. Chem.* **1984**, *516*, 201.
[81] E. F. Bertaut, M. Guillen, *Bull. Soc. Fr. Ceram.* **1966**, *72*, 57.
[82] H. Müller-Buschbaum, K. Scheunemann, *J. Inorg. Nucl. Chem.* **1973**, *35*, 1091.
[83] H. Müller-Buschbaum, J.-P. Werner, *J. Alloys Compd.* **1994**, *206*, L11.
[84] M. F. Queyroux, *C. R. Acad. Sci.*, Paris, **1965**, *259*, 1522.
[85] M. R. Collongues, M. F. Queyroux, M. Perez Y Jorba, M. J.-C. Gilles, *Bull. Soc. Chim. Fr.* **1965**, 1141.
[86] P. Tiedemann, H. Müller-Buschbaum, *Z. Anorg. Allg. Chem.* **1985**, *520*, 71.
[87] D. Chales de Beaulieu, H. Müller-Buschbaum, *Z. Naturforsch. B* **1980**, *35*, 669.
[88] D. Chales de Beaulieu, H. Müller-Buschbaum, *Z. Anorg. Allg. Chem.* **1981**, *472*, 33.
[89] E. Cuno, H. Müller-Buschbaum, *Z. Anorg. Allg. Chem.* **1989**, *572*, 89.
[90] E. Cuno, H. Müller-Buschbaum, *Monatsh. Chem.* **1989**, *120*, 1.
[91] E. Cuno, H. Müller-Buschbaum, *J. Less-Common Met.* **1989**, *146*, L11.
[92] S. Schiffler, H. Müller-Buschbaum, *Z. Anorg. Allg. Chem.* **1986**, *542*, 25.
[93] H. Müller-Buschbaum, I. Rüter, *Z. Anorg. Allg. Chem.* **1989**, *572*, 109.
[94] D. Chales de Beaulieu, H. Müller-Buschbaum, *Monatsh. Chem.* **1982**, *113*, 415.
[95] P. Ehrlich, *Z. Elektrochem.* **1939**, *45*, 362.
[96] K. Schückel, H. Müller-Buschbaum, *Z. Anorg. Allg. Chem.* **1985**, *523*, 69.
[97] F. X. Eder, *Moderne Meßmethoden der Physik II*, Deutscher Verlag der Wissenschaften, Berlin, **1956**.
[98] C. R. Barber, *Proc. Phys. Soc. London Sect. B* **1950**, *63*, 492.
[99] S. Möhr, *Dissertation*, Universität Kiel, **1994**.
[100] S. Möhr, H. Müller-Buschbaum, *Z. Anorg. Allg. Chem.* **1994**, *620*, 1175.
[101] S. Möhr, H. Müller-Buschbaum, *J. Alloys Compd.* **1994**, *210*, 115.
[102] S. Möhr, H. Müller-Buschbaum, *J. Alloys Compd.* **1993**, *199*, 203.
[103] J. Schmachtel, H. Müller-Buschbaum, *Z. Anorg. Allg. Chem.* **1977**, *435*, 243.
[104] B. H. Baur, E. Tillmanns, W. Hofmeister, *Cryst. Struct. Commun.* **1982**, *11*, 2021.
[105] S. Möhr, H. Müller-Buschbaum, *Z. Naturforsch. B* **1994**, *49*, 911.
[106] S. Möhr, H. Müller-Buschbaum, *Z. Naturforsch. B* **1994**, *49*, 915.
[107] G. Tsotridis, H. Rother, E. D. Hondros, *Naturwissenschaften* **1989**, *76*, 216.

Direct On-Line Coupling of Capillary Electrophoresis and ^{1}H NMR Spectroscopy

Klaus Albert*

Capillary electrophoresis[1, 2] (CE) as a new separation technique in addition to high-performance liquid chromatography (HPLC) is becoming more and more popular. In contrast to conventional electrophoresis techniques, capillary electrophoresis has the big advantage that due to the use of capillaries with internal diameters of 25–75 μm Joule heat occurring during an electrophoretic separation dissipates to the lattice. Separation in capillary electrophoresis is based on the different electrophoretic mobilities in an electric field of the charged molecules to be separated. At voltages ranging from 10–50 kV and currents ranging from 10–50 μA, a CE separation takes place within 5 to 30 minutes. The high efficiency of the separation has aroused a lot of interest in the CE separation technique for applications in the field of biopolymers (peptides, proteins, oligonucleotides) and in the field of naturally occurring compounds. One mode of CE is micellar electrokinetic capillary chromatography (MECC), in which charged micelle-inducing surfactants are added to the electrolyte creating a pseudo-stationary phase. In this way neutral molecules can also be separated.

CE separations are carried out in open- or gel-filled fused-silica capillaries (30–80 cm overall length) at flow rates in the nanoliter per second range. Both ends of the capillary are immersed in buffer reservoirs, the electric field is generated by a high-voltage power supply connected to two electrodes immersed in the buffer reservoirs (Fig. 1). The separation depends on the strength of the electric field, the temperature, the buffer composition, the pH value, the ionic strength, the viscosity, and the surface characteristics of the capillary used. The amount of compound required lies between the pg and ng range. The simplest way of injecting the probe is performed hydrostatically by raising the sample vial at the inlet end of the capillary.

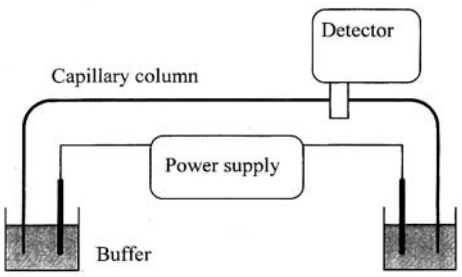


Fig. 1. Schematic diagram of a capillary electrophoresis instrument.

Detection using UV/Vis-photometers is performed in an on-column mode by directly using the capillary as detection cell. One of the most powerful methods for structure elucidation of separated compounds is on-line coupling of CE and electrospray mass spectrometry. For instance, this technique was used for characterization of peptides and proteins in the mass range of several kilodaltons[3] for characterization of oligonucleotides,[4] and for the analysis of plant pigments.[5, 6] An unequivocal structural assignment of separated compounds however can only be performed with the additional use of NMR spectroscopy.

NMR spectroscopy shows two severe disadvantages with respect to its practical application: The low sensitivity with respect to other investigation techniques neccessitates a large amount of sample, and the investigated samples should be pure otherwise the overlap of sample and impurity signals could lead to misinterpretations. Despite the insensitivity of NMR spectroscopy, first experiments to directly couple HPLC and NMR spectroscopy were already carried out in the 1980s.[7–9] However, HPLC–NMR coupling[10–12] as well as the coupling of supercritical fluid chromatography (SFC) with NMR spectroscopy[13] have only recently been applied more widely as labor- and time-saving methods.

In practice two different investigation techniques are performed. In the on-line continuous-flow mode the chromatographic separation is continuously monitored by recording ^{1}H NMR spectra with a minimal time resolution of eight s. The detection limit for a compound of low molecular weight (300 Dalton) is about 500 ng on a 600 MHz NMR instrument equipped with a 120 μL flow cell. In the stopped-flow mode two-dimensional assignment experiments can be performed with inverse ^{1}H{^{13}C}-continuous-flow probes. A big advantage of the coupling of separation techniques such as HPLC and SFC with ^{1}H NMR spectroscopy is the possibility of displaying the chromatogram as a contour plot. Here, ^{1}H NMR chemical shifts are plotted versus the retention times of the chromatographic separation. The introduction of a second dimension, the ^{1}H NMR chemical shift, enables a clear and accurate assignment of the signals even of overlapping peaks in contrast to conventional UV registration. Thus, the main disadvantages associated with chromatography, that is large amounts of substance and large detector volumes, are compensated.

[*] Priv.-Doz. Dr. K. Albert
Institut für Organische Chemie der Universität
Auf der Morgenstelle 18, D-72076 Tübingen (FRG)
Telefax: Int. code + (7071) 29-5246

 © VCH Verlagsgesellschaft mbH, D-69451 Weinheim, 1995 0570-0833/95/0606-0641 $ 10.00+.25/0

Special continuous-flow probes have been developed for HPLC–NMR and SFC–NMR coupling, which differ from conventional NMR probes mainly with respect to the arrangement of the NMR measuring coil (Fig. 2). In contrast to conventional NMR probes (Fig. 2a), the coil is directly fixed to the glass tube of the continuous-flow cell (Fig. 2b). Thus the ratio of coil

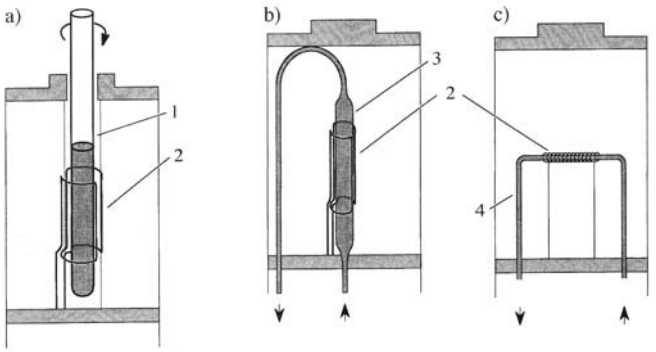


Fig. 2. Different arrangements of NMR probes. a) Conventional probe with rotation of the NMR tube. b) Continuous-flow probe for HPLC–NMR and SFC–NMR coupling. c) Probe for CE–NMR coupling. The arrows show the flow direction of the eluent. 1 = NMR tube (5 mm diameter); 2 = transmitter/receiver coils; 3 = flow cell; 4 = flow capillary.

volume to sample volume, the so-called filling factor, is improved resulting in an improved signal sensitivity. The disadvantage of this design lies in the fact that the NMR tube cannot be rotated. An alternative approach is shown in Figure 2c. Here, the NMR detection coil is positioned perpendicular to the magnetic field of the cryomagnet; this solenoid measuring coil assembly may lead to increased NMR signal sensitivity with respect to the double-saddle coil measuring assembly shown in Figure 2b. The disadvantage of the solenoid coil design is the difficulty of eliminating magnetic field inhomogenities, because the shim systems used for the homogenization in cryomagnets are optimized parallel to the rotation axis of the NMR tube (in z-direction parallel to magnetic field lines) and not in the perpendicular (x, y) direction. The volume required for measurement in a conventional NMR tube (5 mm diameter) is about 250 µL, the detection volumes employed in HPLC–NMR and SFC–NMR coupling are in the range of 40–120 µL.

The use of nanoliter volume sample cells to couple capillary electrophoresis with ^{1}H NMR spectroscopy was recently reported from Sweedler et al.[14, 15] for the first time. The NMR detection cell was built by wrapping a microcoil around a fused silica capillary (75 µm inside diameter) this creates a detection volume of 5 nL. With a capillary (outside diameter 350 µm), NMR signal line widths in the order of 7 to 11 Hz could be obtained. According to the authors the detection limit of 35 ng arginine can be reached within a measuring time of one minute. They report an on-line CE–NMR separation of arginine, glycine, and cysteine at an injection level of 20 nL and compound concentrations of 0.7–0.8 M. The absolute injected amount is in the 1–4 µg range.

The different parameters contributing to the NMR signal line width are discussed by the authors in detail. In addition to the effect of solution flow and the electrophoretic current-induced magnetic field, mainly susceptibility variations caused by the design of the microcoil used influence the resolution of the NMR signals. It is interesting to note that the authors observe a reduction in NMR signal line width as a function of current. With the 5 nL-measuring cell at a voltage of 6 kV and a current of 15 µA, a minimum in NMR signal line width of 12 Hz is found. Susceptibility variations of the measuring coil severely affect the NMR signal half width. By varying the coil diameter a reduction in NMR signal line width from 200 Hz to values lower than 20 Hz can be obtained. But a further increase of NMR resolution to values in the range of a few Hz for the observation of ^{1}H spin coupling constants is impossible. It is considered that a improved coil design will help to further reduce line widths.

Taking into account the NMR resolution and sensitivity values described by the authors, it is clear that the main development is due to the fact that NMR detection is performed in the nanoliter volume range. The practical benefit of the described CE–NMR coupling may be considered from different viewpoints. Due to the loss of stereochemical information one of the most important reasons to perform on-line coupling experiments using NMR spectroscopy as a detection technique is no longer applicable. A further argument is the application range of the described separation. CE is mainly used for the separation of biopolymers. NMR spectroscopic investigation of biopolymers is only possible in the stopped-flow mode. In analogy to HPLC–NMR and SFC–NMR coupling, a practicable CE–NMR on-line technique should enable the use of both techniques with a NMR resolution of 1–2 Hz comparable to routine acquisition conditions.

Sweedler et al. have shown that coupling of CE and NMR is possible using nanoliter-NMR detection cells. The described method of miniaturization must be continued to derive a NMR resolution under the described measuring conditions which is close to values attainable by conventional acquisition systems. When this goal is reached, further development of NMR instruments will take place with respect to the complete automation of NMR spectra acquisition.

German version: *Angew. Chem.* **1995**, *107*, 699

Keywords: analytical methods · capillary electrophoresis · NMR spectroscopy

[1] J. W. Jorgenson, K. D. Lukacs, *Anal. Chem.* **1981**, *53*, 1298–1302; *Science* **1983**, *222*, 266–272.
[2] J. A. Lux, U. Häusig, G. Schomburg, *J. High Resolut. Chromatogr.* **1990**, *13*, 373–374; H. Engelhardt, W. Beck, J. Kohr, T. Schmitt, *Angew. Chem.* **1993**, *105*, 659–680; *Angew. Chem. Int. Ed. Engl.* **1993**, *32*, 629–649; H. Engelhardt, W. Beck, T. Schmitt, *Kapillarelektrophorese*, Vieweg, Wiesbaden, **1995**.
[3] H.-J. Gaus, A. Beck-Sickinger, E. Bayer, *Anal. Chem.* **1993**, *65*, 1399–1405.
[4] E. Bayer, *Mod. Methods Protein Nucleic Acid Res.* **1990**, *3*, 133–148.
[5] W. E. Gläßgen, H. U. Seitz, J. W. Metzger, *Biol. Mass Spectrom.* **1992**, *21*, 271–277.
[6] S. Heuer, S. Richter, J. W. Metzger, V. Wray, M. Nimtz, D. Strack, *Phytochemistry* **1995**, *37*, 761–767.
[7] E. Bayer, K. Albert, M. Nieder, E. Grom, T. Keller, *J. Chromatogr.* **1979**, *186*, 497–507.
[8] H. C. Dorn, *Anal. Chem.* **1984**, *56*, 747A–758A.
[9] D. A. Laude, Jr., C. L. Wilkins, *Trends Anal. Chem.* **1986**, *5*, 230–235.
[10] K. Albert, E. Bayer in *HPLC Detection Newer Methods* (Ed.: G. Patonay), VCH, New York, **1992**, p. 197.
[11] M. Spraul, M. Hofmann, P. Dvortsak, J. K. Nicholson, I. D. Wilson, *Anal. Chem.* **1993**, *65*, 327–330.
[12] J. K. Roberts, R. J. Smith, *J. Chromatogr. A* **1995**, *677*, 385–389.
[13] K. Albert, U. Braumann, L.-H. Tseng, G. Nicholson, E. Bayer, M. Spraul, M. Hofmann, C. Dowle, M. Chippendale, *Anal. Chem.* **1995**, *66*, 3042–3046.
[14] N. Wu, T. L. Peck, A. G. Webb, R. L. Magin, J. V. Sweedler, *J. Am. Chem. Soc.* **1995**, *116*, 7929–7930.
[15] N. Wu, T. L. Peck, A. G. Webb, R. L. Magin, J. V. Sweedler, *Anal. Chem.* **1995**, *22*, 3849–3857.

 © VCH Verlagsgesellschaft mbH, D-69451 Weinheim, 1995 0570-0833/95/0606-0642 $ 10.00+.25/0

The Three-Dimensional Structure of Hammerhead Ribozymes**

Georg Sczakiel*

Ribonucleic acids (RNA) that can catalyze chemical reactions[1] have been the subject of intensive research ever since their discovery some thirteen years ago. Ribozymes—RNA molecules with a defined base sequence and three-dimensional structure—recognize certain RNA-sequences (substrates) in a base-specific manner and cleave a defined phosphoester bond of a defined base triplet. In naturally occurring ribozymes this step is essential, as for instance in the reproduction (replication) of certain satellite RNAs and viroids.[2] In these cases, the ribozyme and substrate sequences are found on the same RNA strand, leading to an intramolecular, in-*cis* cleavage. However, ribozymes can also act intermolecularly (in-*trans* cleavage),[3] with the result that they can be tailored to cleave any desired substrate RNA selectively, thereby inactivating it biologically. This explains the great importance that molecular biologists and biochemists attach to this class of substances today, and that in the long term makes therapeutic applications in vivo conceivable.[4]

One of the best studied ribozymes is the so-called hammerhead ribozyme,[5] which was first found in the avocado sunblotch viroid (ASBVd).[6] This natural system's genome is formed during replication as a covalently linked multimer, and the ribozyme activity serves to cleave it into unit lengths by an intramolecular reaction (in-*cis* cleavage). Recognition of the substrate RNA with the cleavable sequence motif (a base triplet) takes place by specific base interactions between the ribozyme and substrate strands (Fig. 1). Together with the complementary sequences of the substrate RNA, these 5′ and 3′ sequences of the ribozyme form Helices I and III of the hammerhead, and can therefore be understood as antisense sequences. The so-called catalytic domain formed between them consists of the structural components Helix II, the adjacent uridine turn, and the cleavable base triplet. These structural and functional domains together make up the catalytically active hammerhead, which can cleave the target domain only if metal ions such as Mg^{2+} ions are present. At least one Mg^{2+} ion is involved in the cleavage of the phosphodiester bridge between C17 and $A_{1.1}$ upstream of the cleavable base triplet ($G_{16.2}$, $U_{16.1}$ and C17; Fig. 1). This takes place by nucleophilic attack of the oxygen atom of the 2′-hydroxy group; release of the 5′-hydroxy group then proceeds via an intermediate with a trigonal–bipyramidal arrangement of the oxygen atoms around the central phosphorus atom, yielding a cyclic 2′,3′-phosphodiester and a free 5′-hydroxy group (Fig. 2). The crucial role of the 2′-hydroxy group is emphasized by the fact that a deoxyribose at the cleavage site prevents the cleavage reaction.[7]

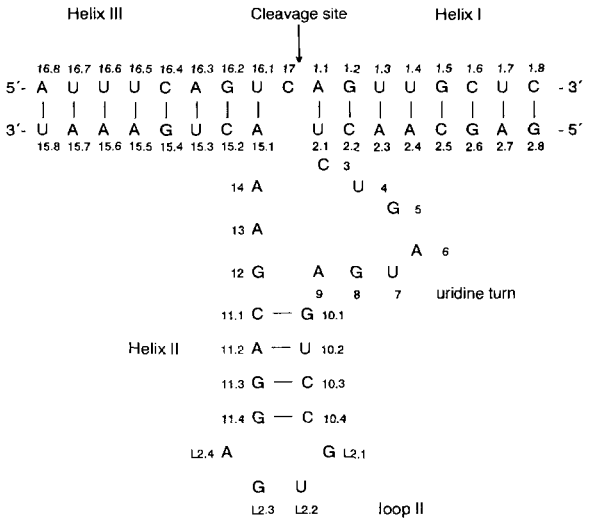


Fig. 1. Schematic diagram of the hammerhead with the nomenclature introduced by Hertel et al. [21].

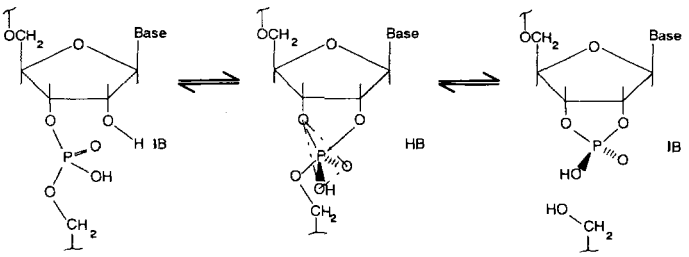


Fig. 2. Simplified reaction mechanism of the hammerhead ribozyme-mediated hydrolysis of the phosphodiester bond of RNA [5].

Recently, two independent groups have constructed three-dimensional structural models for the hammerhead ribozyme.[8, 9] The research group of F. Eckstein in Göttingen used chemical synthesis to produce ribozyme–substrate complexes, which were labeled on one of the three helices with a fluorescein group as fluorescence donor and on a second helix with a rhodamine group as acceptor. The ribozyme-mediated cleavage was prevented by introducing a 2′-deoxycytidine at the cleavage site. With this molecule fluorescence energy transfer (FRET) measurements could be made, and determination of energy transfer efficiencies permitted calculation of the distances between the donor and acceptor groups coupled to the helices. From these data, a structure proposal for the hammerhead ribozyme was worked out.[9] At the same time, the group of D. B. McKay in Boulder (USA) published the X-ray structure of a crystallized ribozyme–substrate complex.[8] In this study, the substrate strand consisted entirely of deoxyribonucleic acid (DNA) instead of RNA, so that the cleavage reaction could not take place. The structure determined in the crystal was remarkably consistent with the structural proposal of Eckstein et al., even though the latter was arrived at by a completely different method. The crystal

[*] Dr. G. Sczakiel
Forschungsschwerpunkt Angewandte Tumorvirologie
Deutsches Krebsforschungszentrum
Im Neuenheimer Feld 242, D-69120 Heidelberg (FRG)
Telefax: Int. code + (6221)424932
e-mail: vir037@atv-fs.inet.dkfz-heidelberg.de

[**] I thank Sigrid Eckardt, Matthias Homann, and Volker Patzel for critical reading of the manuscript.

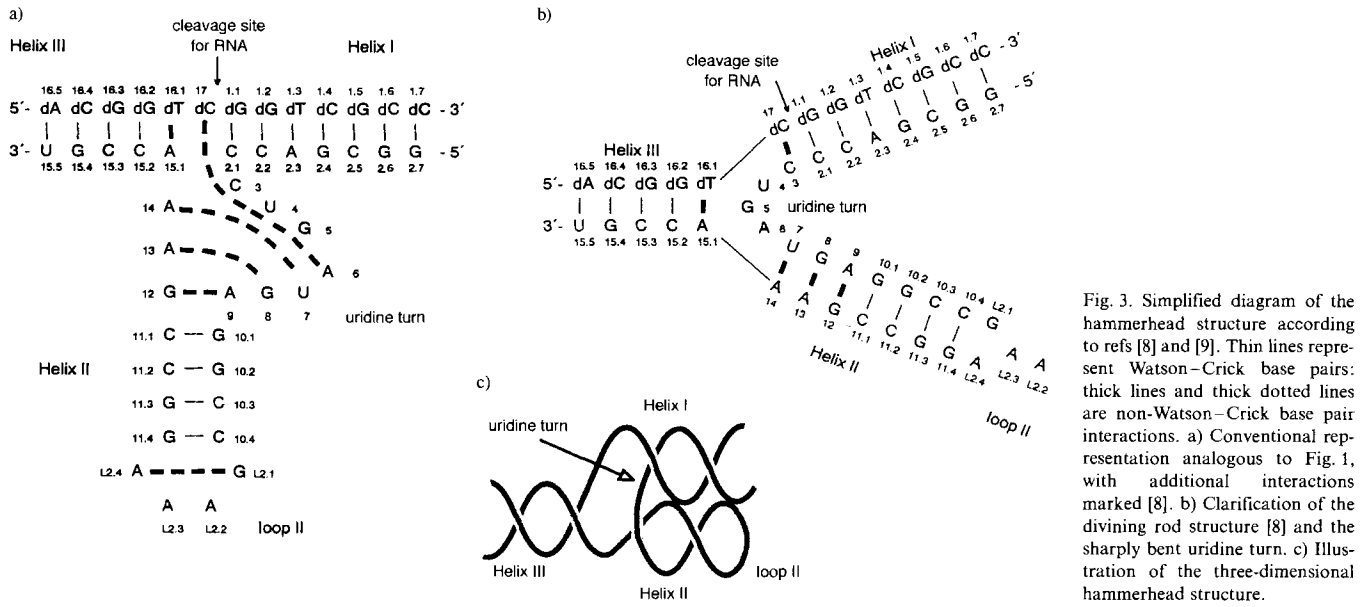


Fig. 3. Simplified diagram of the hammerhead structure according to refs [8] and [9]. Thin lines represent Watson–Crick base pairs: thick lines and thick dotted lines are non-Watson–Crick base pair interactions. a) Conventional representation analogous to Fig. 1, with additional interactions marked [8]. b) Clarification of the divining rod structure [8] and the sharply bent uridine turn. c) Illustration of the three-dimensional hammerhead structure.

structure also yields information about unexpected and nonconventional interactions between components of the hammerhead, which permit and explain the three-dimensional structure.

In previous structural models the three helices of the hammerhead were assumed to adopt a two-dimensional T-shaped structure (Fig. 3a). In the two new proposed structures the helices are almost collinear, leading to a sort of divining rod form (Fig. 3b). Helix III and Helix II are almost coaxial[8] or at a slight angle to each other,[9] whereas the axis of Helix I is collinear with that of Helix III but somewhat displaced from it (Fig. 3c). This implies that Helix II and Helix I are either arranged collinearly[8] or like a divining rod[9] (Fig. 3c). In addition to the Watson–Crick base pairs, several other interactions between the three helices (all of which are present in the A-form) are worth noting. The most remarkable of these is the extension of the otherwise short Helix II by three further base–base interactions close to the junction of the three helices (Fig. 3). Helix II is further stabilized by the interactions in loop II (5′-GAAA-3′), a so-called tetraloop.[10] A homopurine base pair (G–A) is formed in this loop, which allows stacking of the remaining two purines (A,A). A very similar loop structure is formed by the GAGA-loop (5′-GAGA-3′) of ricine-binding RNA, which was recently characterized by NMR studies.[11] The Helix II/loop II unit is therefore a significant component with regard to the structure and stability of the hammerhead. Compared to older structural models, helices I and III must be expanded by one base–base interaction in each case (C–C in helix I and A–U in helix III). The non-Watson–Crick pairing between A15.1 and dT16.1 is notable here. One marked result of the additional interaction and the configuration of all three helices is the very sharp angle of the uridine turn between helix I and helix II, whose structure corresponds almost exactly to that of the uridine turn in the anticodon loop and pseudouridine loop of yeast $tRNA^{Phe}$. This structural element receives additional stabilization from hydrogen bonds between the N3-atom of U4 and the *pro*-S_p-phosphate oxygen atom of U7, as well as between the 2′-OH group of U4 and the N7-atom of A_6. A further essential hydrogen bond is formed between the 2′-OH group of G5 in the uridine turn and the 2′-OH group of $C_{15.2}$ in Helix III. The importance of the 2′-OH group of G5 for the activity of the hammerhead ribozyme can also seen in the fact that exchange of arabinose for ribose in this position almost completely removes activity.[12]

Metal ions such as Mg^{2+}, Mn^{2+}, or Ca^{2+} are a necessary component of catalytically active hammerheads, though Mg^{2+} ions are usually used in vitro. The hammerhead ribozyme is therefore often regarded as a metalloenzyme.[13] When the oxygen atoms on the prochiral phosphodiester bridge which serves as substrate were exchanged for sulfur atoms, evidence was found that the *pro*-R_p-oxygen atom is coordinated to a Mg^{2+} ion (Fig. 4). No candidate for this coordination can be discerned in the crystal structure, though at another position in the structure a Mn^{2+} or Cd^{2+} ion is bound to the *pro*-R_p-phosphodiester oxygen atom of A9 as well as N7 of $G_{10.1}$ (presumably via an H_2O molecule). Pley et al. also discussed the possibility that a helix element at the end of Helix II (5′-$G_8A_9G_{10.1}$-3′) and 3′-$A_{14}A_{13}G_{12}$-5′) can bind an additional metal ion, a theory which is supported by activity studies with sulfur derivatives.[8] A simplified model for the participation of magnesium in ribozyme-mediated cleavage is illustrated in Figure 4 (from ref. [5]). Although a Mg^{2+} ion could be involved as magnesium hydroxide in the abstraction of the 2′-OH hydrogen atom, it is assumed that a second Mg^{2+} ion supports the cleavage of the P–O bond (Fig. 4). According to Sawata et al., the second Mg^{2+} ion could act directly as a Lewis acid at the leaving oxygen atom, and thereby play a role in the chemical step of the cleavage.[15] Independently of this, however, Mg^{2+} ions could have a structure-stabilizing function in the hammerhead. For example, it was recently shown with RNA-modifying reagents

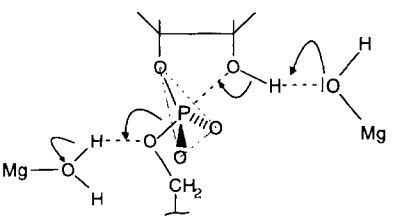


Fig. 4. Possible participation of Mg^{2+} ions in ribozyme-catalyzed cleavage.

 © VCH Verlagsgesellschaft mbH, D-69451 Weinheim, 1995 0570-0833/95/0606-0644 $ 10.00+.25/0

in solution that the three-dimensional structure of the hairpin ribozyme is clearly influenced and stabilized by the presence of Mg^{2+} ions.[16] Nonconventional base–base interactions also play a large role in substrate binding by the hairpin ribozyme.

Previous biochemical analyzes of the hammerhead ribozyme generally aimed to find correlations between directed chemical substitution of single functional groups or atoms and changes in cleavage activity by kinetic measurements. Conclusions were then drawn about the functional and to a lesser extent the structural significance of the changes made.[17] The effects of chemical and structural changes on measured kinetic parameters are largely due to changes in the transition state of the cleavage reaction, and cannot be accounted for in either X-ray analysis or during FRET measurements in solution. Packing effects in the crystal can also affect the RNA structure found and alter it compared to the solution structure. To a certain extent, therefore, deviations between biochemical data and the presented structures must be accepted, and do not detract from the quality of the structure determination. A more dependable structural model for the hammerhead will require the structural elucidation of further hammerhead ribozymes in the crystal and in solution. In this connection it seems relevant to ask why previous attempts to determine the hammerhead structure by NMR methods have obviously not been as successful. One conceivable cause for this is that the actual structure of the hammerhead in solution differs greatly from that assumed up till now. Thus, for example, in the highly concentrated solutions that are required for NMR studies not only 1:1 complexes of ribozyme and substrate might exist, but also multimers with higher mass and in addition a changed three-dimensional structure. This would not be surprising, if one remembers that during nondenaturing gel electrophoresis in the concentration range above 100 nM many RNA species produce several defined bands, which coalesce to a single band under denaturing conditions. However, the above, somewhat critical remarks should not detract from the fact that the majority of previous findings are in agreement with the two published three-dimensional structures, and may be explained with their assistance.

The three-dimensional hammerhead structure also affords a significantly better basis for discussions of previously unexplained observations. For example, the hydrolysis rate constants measured for catalytic antisense RNA (that is, hammerhead ribozymes with long-chain antisense flanks or long-chain substrate strands (more than 50 bases)) are a factor ≥ 100[18] smaller than those for short-chain ribozymes and substrates (less than 40 bases), which afford values for k_{obs} of around $1\,min^{-1}$. This value appears somewhat slow for an unhindered SN_2 reaction (see Fig. 2). This has encouraged speculation that the angle or flexibility between the three helices of the hammerhead or the configuration of the active site may have a decisive influence on the cleavage activity. One could thus imagine that an extreme extension of the ribozyme strand or the substrate strand (or both) could lead to negative effects on the exact configuration of the catalytic domain and the activity associated with it. The observation that a shortening of Helix III to the innermost Watson–Crick base pair ($N_{1.1}$–$N'_{2.1}$) does not affect the activity[19] is also in agreement with the structural model; the more distant base pairs are required neither for structural nor for functional reasons.

Our understanding of the structure and function of the hammerhead ribozyme has been clearly improved by the two studies presented, with their independent but concurring structure proposals. Numerous findings can be ordered and discussed on this basis. For chemists, the hammerhead ribozyme is now becoming ever more interesting. For application-oriented biochemists and molecular biologists, manageable models are emerging, with whose help medicinally relevant hammerhead ribozymes can be better designed and modified. In principle, it should be possible to produce just as broad a range of chemical modifications with synthetic ribozymes as in the area of antisense-oligonucleotides.[20] The structural elucidation of the hammerhead ribozyme certainly also contributes to our understanding of the biochemistry and biological importance of other active ribonucleic acids, which in the last few years have expanded the horizons of the conceivable and the feasible.

German version: *Angew. Chem.* **1995**, *107*, 701

Keywords: biochemistry · ribozymes · metalloenzymes · RNA · structural elucidation

[1] a) K. Kruger, P. J. Grabowski, A. J. Zaug, J. Sands, D. E. Gottschling, T. R. Cech, *Cell* **1982**, *31*, 147–157; b) C. K. Guerrier-Takada, K. Gardiner, T. Marsh, N. R. Pace, S. Altman, *ibid.* **1983**, *35*, 849–857; c) S. Altman, *Angew. Chem.* **1990**, *102*, 735–744; *Angew. Chem. Int. Ed. Engl.* **1990**, *29*, 749–758; d) T. R. Cech, *ibid.* **1990**, *102*, 745–755 bzw. **1990**, *29*, 759–768.

[2] a) T. R. Cech in *The RNA World* (Eds.: R. F. Gesteland, J. F. Atkins), Cold Spring Harbor Laboratory Press, **1993**, pp. 239–269; b) R. H. Symons, *Annu. Rev. Biochem.* **1992**, *61*, 641–671.

[3] a) O. C. Uhlenbeck, *Nature* **1987**, *328*, 4855–4861; b) J. Hasseloff, W. L. Gerlach, *ibid.* **1988**, *334*, 585–591; c) M. Koizumi, S. Iwai, S. Ohtsuka, *FEBS Lett.* **1988**, *239*, 285–288.

[4] a) J. J. Rossi, D. Elkins, J. A. Zaia, S. Sullivan, *AIDS Res. Hum. Retroviruses* **1992**, *8*, 183–189; b) S. Altman, *Proc. Natl. Acad. Sci. USA* **1993**, *90*, 10898; c) P. Marshall, J. B. Thompson, F. Eckstein, *Cell. Mol. Neurobiol.*, in press.

[5] J. Bratty, P. Chartrand, G. Ferbeyre, R. Cedergren, *Biochim. Biophys. Acta* **1993**, *1216*, 345–359.

[6] a) A. C. Forster, R. H. Symons, *Cell* **1987**, *49*, 211; b) A. C. Forster, R. H. Symons, *ibid.* **1987**, *50*, 9.

[7] J. Yang, J.-P. Perreault, D. Labuda, N. Usman, R. Cedergreen, *Biochemistry* **1990**, *29*, 11156–11160.

[8] H. W. Pley, K. M. Flaherty, D. B. McKay, *Nature* **1995**, *372*, 68–74.

[9] T. Tuschl, C. Gohlke, T. M. Jovin, E. Westhof, F. Eckstein, *Science* **1995**, *266*, 785–789.

[10] H. A. Heus, A. Pardi, *Science* **1991**, *253*, 191–194.

[11] M. Orita, F. Nishikawa, T. Shimayama, K. Taira, Y. Endo, S. Nishikawa, *Nucleic Acids Res.* **1993**, *21*, 5670–5678.

[12] D.-j. Fu, S. B. Rajur, L. W. McLaughlin, *Biochemistry* **1995**, *33*, 13903–13909.

[13] a) J. A. Piccirilli, J. S. Vyle, M. H. Caruthers, T. R. Cech, *Nature* **1993**, *361*, 85–88; b) M. Yarus, *FASEB J.* **1993**, *7*, 31–39; c) A. M. Pyle, *Science* **1993**, *261*, 709–714.

[14] D. E. Ruffner, O. C. Uhlenbeck, *Nucleic Acids Res.* **1990**, *18*, 6025–6029.

[15] S. Sawata, M. Komiyama, K. Taira, *J. Am. Chem. Soc.*, in press.

[16] S. E. Butcher, J. M. Burke, *J. Mol. Biol.* **1995**, *244*, 52–63.

[17] a) D. E. Ruffner, O. C. Uhlenbeck, *Nucleic Acids Res.* **1990**, *18*, 6025–6029; b) J. M. Buzayan, H. Van Tol, P. A. Feldstein, G. Bruening, *ibid.* **1990**, *18*, 4447–4451; c) O. Odai, H. Hiroaki, T. Sakata, T. Tanaka, S. Uesugi, *FEBS Lett.* **1990**, *267*, 150–152; d) W. A. Pieken, D. B. Olsen, F. Benseler, H. Aurup, F. Eckstein, *Science* **1991**, *253*, 314–317; e) D.-J. Fu, L. W. McLaughlin, *Proc. Natl. Acad. Sci. USA* **1992**, *89*, 3985–3989; f) G. Slim, M. Gait, *Biochem. Biophys. Res. Commun.* **1992**, *183*, 605–609.

[18] M. Homann, S. Tzortzakaki, M. Tabler, G. Sczakiel, *Nucleic Acids Res.* **1995**, *22*, 3951–3957.

[19] M. Homann, S. Tzortzakaki, K. Rittner, G. Sczakiel, M. Tabler, *Nucleic Acids Res.* **1993**, *21*, 2809–2814.

[20] C. Hélène, J. J. Toulmé, *Biochim. Biophys. Acta* **1990**, *1049*, 99–125; b) E. Uhlmann, A. Peymann, *Chem. Rev.* **1990**, *90*, 543–584; c) C. A. Stein, Y.-C. Cheng, *Science* **1993**, *261*, 1004–1012.

[21] K. J. Hertel, A. Pardi, O. C. Uhlenbeck, M. Koizumi, E. Ohtsuka, S. Uesugi, R. Cedergren, F. Eckstein, W. L. Gerlach, R. Hodgson, R. H. Symons, *Nucleic Acids Res.* **1992**, *20*, 3252.

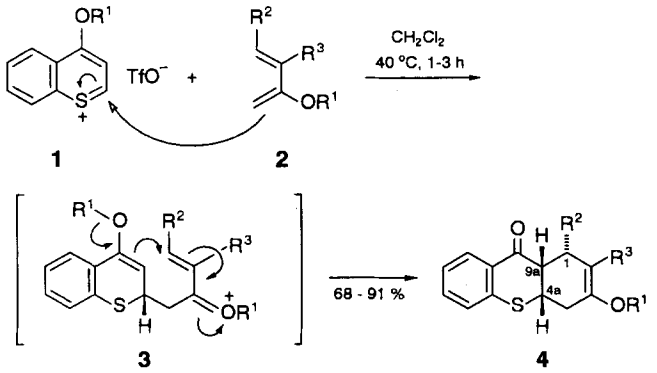
 © VCH Verlagsgesellschaft mbH, D-69451 Weinheim, 1995 0570-0833/95/0606-0645 $ 10.00+.25/0

Sequential Transformation of Benzothiopyrylium Salts to Diastereoselectively Annulated Benzothiopyranones**

Uwe Beifuss,* Henning Gehm, Mathias Noltemeyer, and Hans-Georg Schmidt

Dedicated to Professor Wolfgang Lüttke on the occasion of his 75th birthday

S-containing heterocycles are versatile synthetic building blocks that can be transformed by ring-contraction reactions, ring-opening reactions, or desulfurization.[1] Furthermore, S-heterocycles such as thioxanthenes are important both for pharmacological research[2a–c] and as dyes.[2d–j] In contrast to N- and O-containing heterocycles, only few methods are known for the stereoselective formation of S-containing heterocycles.[3] Whereas simple nucleophilic additions to C-2 and C-4 of 1-benzothiopyrylium salts have been described, stereoselective syntheses with 1-benzothiopyrylium salts have not been investigated to date.[4, 5] Using a novel method we were able to achieve the highly diastereoselective synthesis of annulated benzothiopyranones *rac*-**4** by the sequential reaction[6] of 4-silyloxy-1-benzothiopyrylium salts **1** with 2-silyloxy-1,3-butadienes **2** (Scheme 1).



Scheme 1. Diastereoselective sequential transformation of 4-silyloxy-1-benzothiopyrylium salts **1** with 2-silyloxy-1,3-butadienes **2** to diastereoselective annulated benzothiopyranones *rac*-**4** (R^1, R^2, R^3 see Table 1, only one enantiomer is shown).

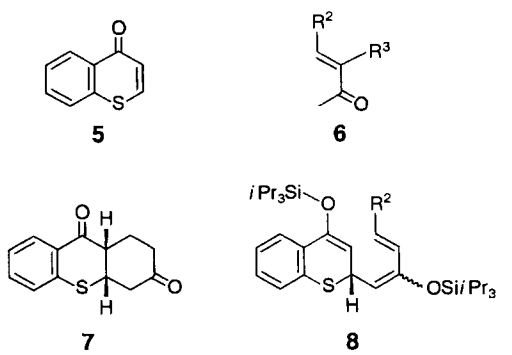
For this purpose, 4*H*-1-benzothiopyran-4-one (**5**)[7] is allowed to react with trialkylsilyl trifluoromethanesulfonates[9]—in analogy to the corresponding O-alkylation with methyl 2-nitrobenzenesulfonate[8]—to form **1** in situ and is then treated with **2** to obtain *rac*-**4** with formation of up to three stereogenic centers (Table 1). The 2-silyloxy-1,3-butadienes **2**[10] can either be used as such or can be prepared in situ by treating the respective methyl vinyl ketone **6** with a trialkylsilyl trifluoromethanesulfonate.[9]

Table 1. Results of the diastereoselective sequential transformations of 4-silyloxy-1-benzothiopyrylium salts **1** with 2-silyloxy-1,3-butadienes **2**.

1 [a]	R^1	**2** [b]	R^2	R^3	*t* [h] [c]	**4** [d] (Yield [%] [e])	**8** [f] (Yield [%])
a	$SiMe_3$	**a**	H	H	2.5	**a** (75 [g])	
b	$SitBuMe_2$	**b**	H	H	2.5	**b** (80)	
c	$SiiPr_3$	**c**	H	H	2.5	**c** (90)	
c	$SiiPr_3$	**d**	OMe	H	2.5	**d** (75)	
c	$SiiPr_3$	**e**	Ph	H	1.0	**e** (91)	
c	$SiiPr_3$	**f**	4-MeO-Ph	H	2.0	**f** (79)	**f** (14)
c	$SiiPr_3$	**g**	4-MeO_2C-Ph	H	2.0	**g** (91)	**g** (3)
c	$SiiPr_3$	**h**	4-NO_2-Ph	H	1.5	**h** (80)	**h** (15)
c	$SiiPr_3$	**i**	furyl	H	2.5	**i** (68)	**i** (12)
c	$SiiPr_3$	**j**	$-(CH_2)_4-$		3.0	**j** (87)	
c	$SiiPr_3$	**k**	$-(CH_2)_3-$		3.0	**k** (87)	

[a] Salts **1** were formed in situ from **5** and the appropriate trialkylsilyl trifluoromethanesulfonate. [b] Butadienes **2** were formed in situ from the required methyl vinyl ketone **6** and trialkylsilyl trifluoromethanesulfonate. [c] All transformations were performed at reflux in CH_2Cl_2. [d] All compounds were identified by their ^1H NMR, ^{13}C NMR, UV, and mass spectra. The elemental analyses are consistent with the calculated values (see also Table 2). [e] The yields are given for the analytically pure compounds. [f] The by-products **8f–i** were separated from **4f–i** by flash chromatography on silica gel (ether/petroleum ether $^1/_4$–$^1/_8$). [g] **4a** could not be isolated without decomposition upon chromatographic purification on silica gel (ether/petroleum ether 1/8). The yield is based on diketone **7**, which was obtained after acidic hydrolysis of **4a** (10% H_2SO_4, THF, 23 °C, 30 min) and subsequent flash chromatography on silica gel (ether/petroleum ether 1/1).

The transformation of **1a–c** with the unsubstituted 2-silyloxy-1,3-butadienes **2a–c** results exclusively in the highly diastereoselective formation of the *cis*-fused products *rac*-**4a**-*rac*-**4c**. The highest yield of the annulation product is obtained in the reaction of **1c** with **2c**. The trimethylsilyl enol ether *rac*-**4a** cannot be isolated without decomposition, but only as a mixture with its hydrolysis product, the diketone *rac*-**7**.



[*] Dr. U. Beifuss, Dipl.-Chem. H. Gehm
Institut für Organische Chemie der Universität
Tammannstrasse 2, D-37077 Göttingen (FRG)
Telefax: Int. code + (551)39-9660
Dr. M. Noltemeyer, H.-G. Schmidt
Institut für Anorganische Chemie der Universität Göttingen

[**] This work was supported by the Fonds der Chemischen Industrie and the Universität Göttingen. H. G. thanks the Fonds der Chemischen Industrie for a doctoral fellowship. We thank Professor Tietze for his generous support and continuous interest.

The transformations of **1c** with the 4-substituted and the 3,4-disubstituted 2-silyloxy-1,3-butadienes **2d**–**k** are specially noteworthy, since of the four possible diastereomers only the all-*cis* diastereomers *rac*-**4d**-*rac*-**4k** are formed with high diastereoselectivity in these reactions (Table 1). The 4-methoxy, 4-aryl, 4-heteroaryl, and 3,4-disubstituted cyclic compounds were converted into *rac*-**4d**-*rac*-**4k** in 68–91% yield. In the reactions of **2f**–**i**, by-products *rac*-**8f**-*rac*-**8i** were isolated in 3–15% yield.

The *cis*-configuration of the ring fusion in *rac*-**4a**-*rac*-**4k** is supported by the vicinal coupling between 4a-H and 9a-H in the ^{1}H NMR spectra, which is found to be J = 3.2 Hz for *rac*-**4c** (Table 2). The relative configuration at C-1 in *rac*-**4d**-*rac*-**4k** was determined by crystal structure analysis of *rac*-**4e**.[11] It is remarkable that the coupling constants ^3J (1-H, 9a-H) of up to J = 7.5 Hz in *rac*-**4d**-*rac*-**4k** are relatively high for the *cis* fusion between 1-H and 9a-H.

The formation of *rac*-**4** can be explained by a sequential 1,2- and 1,4-addition. We presume that the first step of this reaction sequence is an intermolecular 1,2-addition of the silyl enol ether functionality in **2** to the C=S$^+$ bond in **1**, forming the intermediate *rac*-**3**. The resultant Michael system subsequently undergoes an intramolecular 1,4-addition to the silyl enol ether functionality to give *rac*-**4**. The observed complete diastereoselectivity in the transformation of **1** and **2** to *rac*-**4** can be explained with the transition state structure depicted in Figure 1.

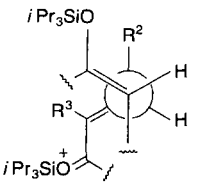


Fig. 1. Newman projection of the transition state structure for the reaction of **1** and **2** to *rac*-**4**.

An alternative to the proposed sequential mechanism is an intermolecular Diels–Alder reaction. The two-step mechanism of the reaction is supported by several experimental observations: In the transformation of **1c** with **2f**–**i**, products *rac*-**8f**-*rac*-**8i** that can be derived from the intermediates *rac*-**3f**-*rac*-**3i** are formed in yields of 3–15% (Table 1).

Furthermore we were able to obtain the 1,2-adduct *rac*-**9e** by treating **5** with **2e**.[12] This adduct reacts with 2,6-lutidinium triflate and triisopropylsilyl trifluoromethanesulfonate (TIPSOTf) to yield the all-*cis* product *rac*-**4e** in a highly diastereoselective intramolecular 1,4-addition, the same product that is formed in the one-pot synthesis of **1c** with **2e**. Regardless of the mechanism, the reactions of the 4-silyloxy-1-benzothiopyrylium salts and the 2-silyloxy-1,3-butadienes introduced herein provide a preparatively simple and highly diastereoselective access to annulated benzothiopyranones. Currently we are investigating whether the double activation of benzothiopyranones as 4-silyloxy-1-benzothiopyrylium salts can be applied in the synthesis of 2,3-*trans*-substituted 2,3-dihydro-4*H*-1-benzothiopyran-4-ones.

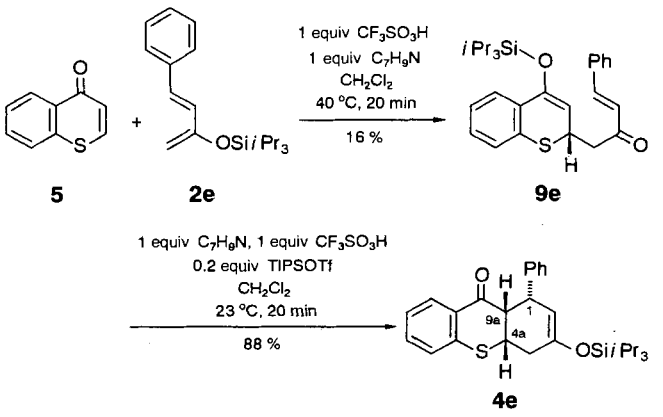


Table 2. Analytical and spectroscopic data of selected compounds [a].

4c: M.p. 60 °C; ^{1}H NMR (500 MHz, $CDCl_3$): δ = 1.00–1.05 (m, 18H; CH_3), 1.07–1.16 (m, 3H; $CH(CH_3)_2$), 2.16 (dddt, J = 2.2, 4.0, 5.5, 17.0 Hz, 1H; 1-H), 2.26 (m, 1H; 1-H), 2.57 (m, 1H; 4-H), 2.77 (m, 1H; 4-H), 3.00 (ddd, J = 3.2, 5.5, 7.0 Hz, 1H; 9a-H), 3.87 (td, J = 3.2, 5.5 Hz, 1H; 4a-H), 4.94 (tt, J = 1.4, 4.0 Hz, 1H; 2-H), 7.14 (ddd, J = 1.2, 7.0, 8.0 Hz, 1H; 7-H), 7.22 (ddd, J = 0.7, 1.2, 8.0 Hz, 1H; 5-H), 7.36 (ddd, J = 1.5, 7.0, 8.0 Hz, 1H; 6-H), 8.06 (ddd, J = 0.7, 1.5, 8.0 Hz, 1H; 8-H); ^{13}C NMR (50 MHz, $CDCl_3$): δ = 12.50 ($CH(CH_3)_2$), 17.92 (CH_3), 22.65 (C-1), 33.45 (C-4), 39.69 (C-4a), 45.79 (C-9a), 102.02 (C-2), 124.84 (C-7), 127.63 (C-5), 129.27 (C-8a), 129.40 (C-8), 133.34 (C-6), 140.87 (C-10a), 147.31 (C-3), 195.63 (C-9).

4e: M.p. 61 °C; ^{1}H NMR (500 MHz, $CDCl_3$): δ = 1.09–1.13 (m, 18H; $CH(CH_3)_2$), 1.18–1.26 (m, 3H; $CH(CH_3)_2$), 2.48 (dddd, J = 1.5, 2.5, 7.0, 18.0 Hz, 1H; 4-H), 2.67 (dddd, br, J = 1.5, 2.5, 6.5, 18.0 Hz, 1H; 4-H), 3.53 (dd, J = 3.5, 6.0 Hz, 1H; 9a-H), 3.97 (ddd, J = 3.5, 6.5, 7.0 Hz, 1H; 4a-H), 4.00 (m, 1H; 1-H), 5.30 (dt, J = 1.5, 3.5 Hz, 1H; 2-H), 6.92 (ddd, J = 1.0, 7.0, 8.0 Hz, 1H; 7-H), 6.98 (d, br, J = 8.0 Hz, 1H; 5-H), 7.03 (t, br, J = 7.5 Hz, 1H; 4′-H), 7.12 (t, J = 7.5 Hz, 2H; 3′-H, 5′-H), 7.20 (ddd, J = 1.5, 7.0, 8.0 Hz, 1H; 6-H), 7.37 (d, br, J = 7.5 Hz, 2H; 2′-H, 6′-H), 7.80 (ddd, J = 0.5, 1.5, 8.0 Hz, 1H; 8-H); ^{13}C NMR (50 MHz, $CDCl_3$): δ = 12.63 ($CH(CH_3)_2$), 18.04 ($CH(CH_3)_2$), 33.69 (C-4), 39.46 (C-4a), 42.67 (C-1), 50.20 (C-9a), 104.65 (C-2), 124.29 (C-7), 126.16 (C-4′), 126.75 (C-5), 127.21 (C-3′, C-5′), 128.95 (C-8), 129.45 (C-2′,C-6′), 130.33 (C-8a), 132.79 (C-6), 140.16 (C-10a), 141.22 (C-1′), 148.13 (C-3), 194.68 (C-9).

4j: M.p. 92 °C; ^{1}H NMR (500 MHz, $CDCl_3$): δ = 0.66–1.16 (m, 21H; $CH(CH_3)_2$), 1.18 (tq, J = 3.5, 13.0 Hz, 1H; 2-H_{ax}), 1.27 (tq, J = 3.5, 13.0 Hz, 1H; 3-H_{ax}), 1.35–1.41 (m, 1H; 1-H_{eq}), 1.50–1.58 (m, 1H; 4-H_{ax}), 1.62 (m, 1H; 2-H_{eq}), 1.68 (m, 1H; 3-H_{eq}), 1.96 (m, 1H; 1-H_{ax}), 2.23 (d, br, J = 17.5 Hz, 1H; 6-H), 2.51 (m, 1H; 12b-H), 2.76 (d, br, J = 17.5 Hz, 1H; 6-H), 3.00 (ddt, J = 2.5, 3.5, 13.5 Hz, 1H; 4-H_{eq}), 3.07 (dd, J = 3.5, 7.5 Hz; 12a-H), 4.06 (s, br, 1H; 6a-H), 7.14 (ddd, J = 1.0, 7.0, 8.0 Hz, 1H; 10-H), 7.21 (dd, J = 1.0, 8.0 Hz, 1H; 8-H), 7.34 (ddd, J = 1.5, 7.0, 8.0 Hz, 1H; 9-H), 8.10 (d, br, J = 8.0 Hz, 1H; 11-H); ^{13}C NMR (50 MHz, $CDCl_3$): δ = 13.24 ($CH(CH_3)_2$), 18.12 ($CH(CH_3)_2$), 26.68 (C-4), 27.23, 27.35 (C-2, C-3), 29.50 (C-1), 34.03 (C-6), 39.55 (C-6a), 39.80 (C-12b), 48.18 (C-12a), 117.29 (C-4a), 124.77 (C-10), 127.61 (C-8), 129.19 (C-11), 130.84 (C-11a), 133.07 (C-9), 137.07 (C-7a), 142.51 (C-5), 197.24 (C-12).

7: M.p. 124 °C; ^{1}H NMR (200 MHz, $CDCl_3$): δ = 1.83–1.99 (m, 1H; 1-H), 2.33–2.84 (m, 5H; 1-H, 2-H_2, 4-H_2), 3.26 (dt, J = 3.7, 7.5 Hz, 1H; 9a-H), 3.97 (dq, J = 0.5, 3.7 Hz, 1H; 4a-H), 7.17–7.27 (m, 2H; 5-H, 7-H), 7.38–7.48 (m, 1H; 7-H), 8.14 (m, 1H; 8-H); ^{13}C NMR (50 MHz, $CDCl_3$): δ = 24.18 (C-1), 38.85 (C-2), 42.05 (C-4a), 44.62 (C-4), 47.20 (C-9a), 125.37 (C-7), 125.45 (C-5), 129.03 (C-8a), 129.43 (C-8), 133.95 (C-6), 139.47 (C-10a), 194.65 (C-9), 206.83 (C-3).

8f: This compound was isolated as an E/Z mixture in a ratio of E/Z = 1.1:1.0 (^{1}H NMR, ^{13}C NMR).

^{1}H NMR (200 MHz, C_6D_6): δ = 1.00–1.30 (m, $CH(CH_3)_2$), 3.24 and 3.26 (s, OCH_3), 4.91 (dd, J = 5.5, 10.5 Hz, 2-H), 5.12 (dd, J = 6.5, 10.5 Hz, 2-H), 5.32–5.42 (m, 1′-H, 3-H), 5.56 (d, J = 10.5 Hz, 3-H), 6.25 (d, J = 15.5 Hz, 3′-H), 6.65–7.32 (m, 3′-H, 4′-H, arom. H), 7.37 (d, J = 15.5 Hz, 4′-H), 7.91 (dd, J = 1.5, 7.5 Hz, 5-H), 7.98 (dd, J = 1.5, 7.5 Hz, 5-H); ^{13}C NMR (50 MHz, C_6D_6): δ = 13.91 ($CH(CH_3)_2$), 19.04 ($CH(CH_3)_2$), 35.95 and 37.64 (C-2), 55.48 (OCH_3), 105.04 and 106.04 (C-3), 111.13 and 113.18 (C-1′), 125.19 and 125.26 (C-6), 125.75 and 125.99 (C-3′), 126.05 and 128.47 (C-8), 128.88 (C-3″, C-5″), 128.99 and 129.33 (C-7), 129.42 (C-2″, C-6″), 130.32 (C-5), 130.44 and 130.59 (C-1″), 132.02 and 132.68 C-4′), 132.09 and 132.74 (C-4a), 134.36 and 134.64 (C-8a), 149.51 and 150.33 (C-4), 150.51 and 150.56 (C-2′), 160.73 and 160.91 (C-4″).

9e: M.p. 65 °C; ^{1}H NMR (200 MHz, $CDCl_3$): δ = 1.05–1.20 (m, 21H; $CH(CH_3)_2$), 3.06 (dd, J = 2.5, 7.0 Hz, 2H; 1′-H_2), 4.06 (q, J = 7.0 Hz, 1H; 2-H), 5.39 (d, J = 7.0 Hz, 1H; 3-H), 6.64 (d, J = 16.0 Hz, 1H; 3′-H), 7.10–7.28 (m, 3H; 4′-H, 5-H, 7-H), 7.32–7.55 (m, 6H; 6-H, 6′-H, 7′-H, 8′-H, 9′-H, 10′-H), 7.62–7.72 (m, 1H; 8-H); ^{13}C NMR (50 MHz, $CDCl_3$): δ = 12.77 ($CH(CH_3)_2$), 18.05 ($CH(CH_3)_2$), 33.61 (C-2), 47.62 (C-1′), 103.92 (C-3), 124.24 (C-6), 125.22 (C-8), 126.24 (C-7), 127.53 (C-3′), 128.27 (C-5, C-6′, C-10′), 128.89 (C-7′, C-9′), 130.55 (C-8′), 131.22 (C-4a), 131.98 (C-8a), 134.29 (C-5′), 143.19 (C-4′), 149.08 (C-4), 197.38 (C-2′).

[a] All compounds gave correct elemental analyses or high-resolution mass spectrometric data (**8f**).

Experimental Procedure

Trialkylsilyl trifluoromethanesulfonate (1.5 mmol, 1.5 equiv) was added to 4*H*-1-benzothiopyran-4-one (**5**, 1.0 mmol) by syringe under argon, and the reaction mixture was heated at 70 °C for 1 h without stirring. Subsequently the mixture was allowed to cool, dichloromethane (2 mL), 2,6-lutidine (2.0 mmol), trialkylsilyl trifluoromethanesulfonate (0.6 mmol, 0.6 equiv), and a solution of the α,β-unsaturated ketone **6** (1.3–1.5 mmol) in dichloromethane (2 mL) were added consecutively, and the mixture was heated to reflux. After complete conversion (monitored by TLC), the reaction solution was allowed to cool, then 10 mL of an ice cold 5% sodium hydrogencarbonate solution was added, and the mixture quickly extracted with ice cold dichloromethane (three 10 mL portions). The complete workup must

 © VCH Verlagsgesellschaft mbH, D-69451 Weinheim, 1995 0570-0833/95/0606-0648 $ 10.00+.25/0

be performed under argon. After drying the combined organic layers over sodium sulfate and removing the solvent, the crude product was obtained, which was purified by flash chromatography on silica gel (50 g). Subsequent recrystallization provided compounds **4** in analytically pure form.

Received: July 22, 1995 [Z7153IE]
German version: *Angew. Chem.* **1995**, *107*, 705

Keywords: cascade reactions · sulfur compounds · annulation

[1] Review: a) L. I. Belen'kii in *Chemistry of Organosulfur Compounds* (Ed.: L. I. Belen'kii), Ellis Horwood, Chichester, **1990**, p. 193; b) T.-Y. Luh, Z.-J. Ni, *Synthesis* **1990**, 89; c) F. S. Guziec, Jr., L. J. Sanfilippo, *Tetrahedron* **1988**, *44*, 6241.

[2] a) Review: L. A. Damani, *Sulphur-Containing Drugs and Related Organic Compounds*, Ellis Horwood, Chichester, **1989**; b) A. Yoshida, K. Oda, T. Kassai, T. Koga, K. Hasegawa (Sankyo), *PCT Int. Appl.* WO 93/06096, **1993** [*Chem. Abstr.* **1993**, *119*, 180658c]; c) J. M. Ford, E. P. Bruggemann, I. Pastan, M. M. Gottesman, W. N. Hait, *Cancer Res.* **1990**, *50*, 1748; d) I. Okabayashi, N. Murakami, K. Sekiya, *J. Heterocyclic Chem.* **1989**, *26*, 635; e) B. L. Feringa, W. F. Jager, B. de Lange, *J. Chem. Soc. Chem. Commun.* **1993**, 288; f) K.-H. Pfoertner, M. Voelker, *J. Chem. Soc. Perkin Trans. 2* **1991**, 527; g) K.-H. Pfoertner, *ibid.* **1991**, 523; h) W. Fischer, *Helv. Chim. Acta* **1991**, *74*, 1119; i) C. H. Chen, J. L. Fox (Eastman Kodak), *Eur. Pat. Appl.* EP 330444, **1989** [*Chem. Abstr.* **1990**, *112*, 138909r]; j) S. Kimura, Y. Nakamura, S. Kurimoto, K. Motouchi (Sankyo Chemical), *Ger. Offen.* DE 2707784 A1, **1977** [*Chem. Abstr.* **1977**, *87*, 203075x].

[3] a) Review on the synthesis of six-membered S-containing heterocycles: J. Kuthan, P. Šebek, S. Böhm in *Advances in Heterocyclic Chemistry, Vol. 59* (Ed.: A. R. Katritzky), Academic Press, San Diego, **1995**, p. 179; R. Livingstone in *Rodd's Chemistry of Carbon Compounds, Vol. 4, Part E* (Ed.: M. F. Ansell), Elsevier, Amsterdam, **1990**, p. 398; A. H. Ingall in *Comprehensive Heterocyclic Chemistry, Vol. 3* (Eds.: A. R. Katritzky, C. W. Rees), Pergamon, Oxford, **1984**, p. 885; b) R. Armer, M. J. Begley, P. J. Cox, A. Persad, N. S. Simpkins, *J. Chem. Soc. Perkin Trans. 1* **1993**, 3099, 3105; c) C. W. Greengrass, J. A. Hughman, P. J. Parsons, *J. Chem. Soc. Chem. Commun.* **1985**, 889.

[4] Review on 1-benzothiopyrylium salts: a) I. Stahl, *Methoden Org. Chem. (Houben-Weyl) 4th ed. 1952 – Vol. E7a, Teil 1, Hetarene II*, p. 205; b) D. C. Dittmer, B. H. Patwardhan in *The Chemistry of the Sulphonium Group* (Eds.: C. J. M. Stirling, S. Patai), Wiley, Chichester, **1981**, p. 470.

[5] a) S. Watanabe, H. Nakazumi, S. Kado, K. Maeda, T. Kitao, *J. Chem. Res. Synop.* **1990**, 50; b) S. Watanabe, H. Nakazumi, K. Maeda, T. Kitao, *J. Chem. Soc. Chem. Commun.* **1990**, 421.

[6] a) L. F. Tietze, U. Beifuss, *Angew. Chem.* **1993**, *105*, 137; *Angew. Chem. Int. Ed. Engl.* **1993**, *32*, 131; b) H. M. R. Hoffmann, *ibid.* **1992**, *104*, 1361 and **1992**, *31*, 1332; c) T.-L. Ho, *Tandem Organic Reactions*, Wiley, New York, **1992**; d) H. Waldmann, *Nachr. Chem. Tech. Lab.* **1992**, *40*, 1133.

[7] a) F. Krollpfeiffer, H. Schultze, *Ber. Dtsch. Chem. Ges.* **1923**, *56*, 1819; b) P. R. Giles, C. M. Marson, *Aust. J. Chem.* **1992**, *45*, 439.

[8] A. I. Kiprianov, A. A. Tolmachev, *J. Gen. Chem. USSR (Engl. Transl.)* **1959**, *29*, 2828.

[9] Review on trialkylsilyl perfluoroalkanesulfonates: G. Simchen in *Advances in Silicon Chemistry, Vol. 1* (Eds.: G. L. Larson), JAI Press, Greenwich, **1991**, p. 189.

[10] Reviewsartikel: a) F. Fringuelli, A. Taticchi, *Dienes in the Diels-Alder Reaction*, Wiley, New York, **1990**; b) P. Brownbridge, *Synthesis* **1983**, 1, 85; c) E. W. Colvin, *Silicon in Organic Synthesis*, Butterworths, London, **1981**.

[11] Details of the crystal structure investigation may be obtained from the Fachinformationszentrum Karlsruhe, D-76344 Eggenstein-Leopoldshafen on quoting the depository number CSD-401508.

[12] The reaction was stopped after 50% conversion. After flash chromatography on silica gel (ether/petroleum ether 1/30), 50% of unreacted **2e**, 19% of all-*cis*-thioxanthon *rac*-**4e** and 16% of *rac*-**9e** were isolated.

Structure Determination in the Twilight Region Between Monolayers and 3-D Crystals; a Grazing Incidence X-Ray Diffraction Study of Nanocrystalline Aggregates of α,ω-Docosanediol at the Air–Water Interface**

Jaroslaw Majewski, Ron Edgar, Ronit Popovitz-Biro, Kristian Kjaer, Wim G. Bouwman, Jens Als-Nielsen, Meir Lahav, and Leslie Leiserowitz*

The understanding and control of three-dimensional (3D) crystal nucleation is of fundamental importance in pure and applied sciences. Direct observation of primarily formed, structured aggregates that may eventually lead to macroscopic crystals is therefore essential. From the crystallographic point of view, such nuclei present a challenge as a result of the complex diffraction patterns caused by limited repeat in certain directions and by imperfect order.

Previously certain amphiphiles and bolaamphiphiles[1] were shown to aggregate spontaneously into multilayered crystalline structures when spread at zero surface pressure on the water or formamide surface; their packing arrangements were not determined.[2–4] Here we report the application of grazing incidence synchrotron X-ray diffraction (GID) for the determination of the packing arrangements of crystalline aggregates of the bolaamphiphile α,ω-docosanediol ($HO(CH_2)_{22}OH$, C_{22} diol) which is spread more than one layer thick on the water surface.[3] This experimental approach has three unique virtues. Confining the layer to a water surface imposes physical boundary conditions to the molecules, which supports self-aggregation by reducing the number of degrees of freedom and allows formation of stable clusters. Moreover, in the GID experiment the penetration of X-ray beam is limited almost to the surface layer, which effectively eliminates background from the subphase.[5] Finally, it proved possible to examine by GID the effect of inhibition of growth of multilayer crystallites leading to a monolayer phase, which was achieved by the use of auxiliary molecules present in the spreading solution.

The long-chain diols $HO(CH_2)_nOH$ were chosen for study by GID in view of their ice-nucleating properties[6] and the possibility of elucidating the crystal structure if the interchain packing properties and hydrogen-bonding requirements were also taken into account. The GID data from the C_{22} diol were measured at 70, 100, 200% of the surface coverage necessary for a monolayer,[7, 8] with no detectable surface pressure. The Bragg reflections in the GID powder pattern of C_{22} diol are shown in Figure 1a. The q_z widths of the z component of the Bragg reflections, the Bragg rods, (shown in Fig. 1b) correspond to crystallites with an average thickness of two layers.[9] The positions of the two Bragg peaks at $q_{xy} = 1.52$ and $1.72\ \text{Å}^{-1}$ ($q_{xy} = 2\pi/d$, where d is the spacing between scattering planes) lead to a rectangular cell with $a = 5.04$ Å and $b = 7.30$ Å; thus the two reflections are indexed as {1,1} and {0,2} respectively. These cell dimensions are characteristic evidence of a herringbone

[*] Professor L. Leiserowitz, J. Majewski, R. Edgar, Dr. R. Popovitz-Biro, Prof. M. Lahav
Department of Materials and Interfaces
The Weizmann Institute of Science, 76100 Rehovot (Israel)
Telefax: Int. code + (8)34-4138
Dr. K. Kjaer, Dr. W. G. Bouwman, Prof. J. Als-Nielsen
Department of Physics
Risø National Laboratory, DK-4000 Roskilde (Denmark)

[**] We acknowledge financial support from the Minerva Foundation, Munich, Germany.

 © VCH Verlagsgesellschaft mbH, D-69451 Weinheim, 1995 0570-0833/95/0606-0649 $ 10.00+.25/0

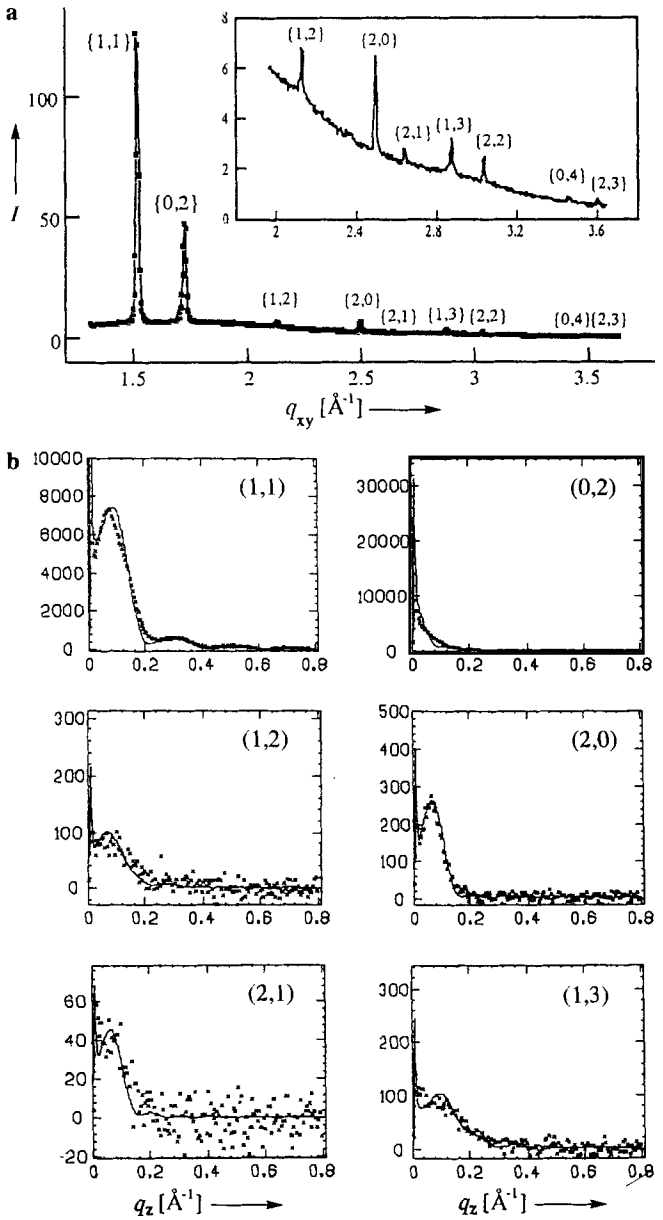
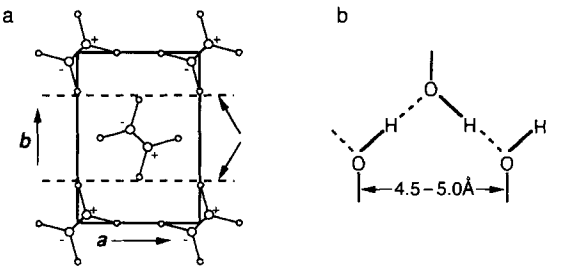


Fig. 1. a) The Bragg reflections in the GID powder pattern of the C_{22} diol on water, measured at 200% coverage (assuming monolayer formation). The inset shows an expanded view of the higher order reflections. The reflections were obtained by scanning along the horizontal scattering vector q_{xy} and integrating the intensity along the vertical scattering vector q_z. I in 1000 counts. b) Observed (×) and calculated (full line) intensity profiles of the z component of the Bragg reflections (Bragg rods) of the C_{22} diol (six of the nine Bragg rods are shown), obtained by recording the intensity distribution along q_z while integrating across the appropriate Bragg peak in q_{xy}. The fit was calculated for the molecular packing arrangement of the bilayer shown in Fig. 3 and described in the text. In each case the ordinate represents the relative intensity.

motif[10] of hydrocarbon chains in an all-*trans* conformation, generated by glide symmetry in the unit cell.

The intensity profiles of the Bragg rods show that the molecular chains are aligned almost perpendicular to the water surface, which is in agreement with the cell dimensions. The observation that the Bragg rod for the {0,2} reflection peaks at $q_z \approx 0$ Å^{-1} and that the {1,1} and {2,0} reflections both peak at $q_z \approx 0.08$ Å^{-1} indicate that the chains are slightly tilted along the a direction. Consequently the molecules within an ab layer must be related by an a glide[11] forming the herring-bone motif (Scheme 1a). In such an arrangement, the hydrocarbon chain



Scheme 1. a) Glide plane along a (dashed lines indicated by arrows) and the resulting herringbone pattern of the C_{22}-diol layers. For an explanation of the representation of the molecule, see legend of Figure 2 and the text. b) Definition of the repeat distance of hydrogen bonds.

axes must be parallel to one another and lie halfway between the neighboring glide planes to ensure good packing.[12] The molecular centers for the bottom layer are thus positioned at $x,y = (0,0)$ and $(1/2,1/2)$. A reasonable starting model of a second layer that would produce a strong {0,2} reflection would require the chain axes of the bottom and top layers to line up when viewed along the a axis. Consequently, the centers of the molecules of the second layer must also lie halfway between the neighboring a glide planes as for the first layer. Therefore the a glide planes coincide for the two layers as they would in a regular 3D crystal; the y coordinates of the centers of the two molecules in the top layer are 0 and 1/2. To fix the interlayer separation and the layer offset along the a direction we take advantage of the hydrogen bonding requirements. The repeat distance in an O–H···O chain motif involving OH groups varies from 4.5 to 5.0 Å (Scheme 1b); such an arrangement may be achieved by centers of inversion or twofold axes in space groups $P2_1/a$ and $A2/a$, respectively[13] (Fig. 2).

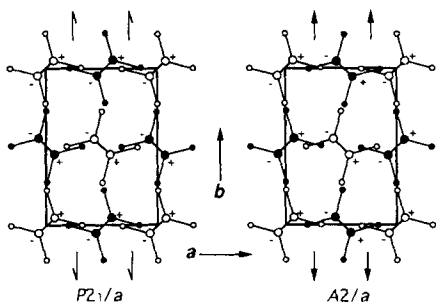


Fig. 2. Schematic views along the molecular axis showing the packing arrangements of two layers of the C_{22} diol in space groups $P2_1/a$ and $A2/a$. For convenience, only the hydrogen atoms of the chain and the two oxygen atoms are depicted. The open and filled circles represent the lower and upper layer respectively. The plus (+) and minus (−) signs at the oxygen atoms mark their difference in height within each layer. In space group $P2_1/a$ the a glide planes intersect the b axis at $y = 1/4$, 3/4 as shown in Scheme 1a. The crystallographic centers of inversion ($\bar{1}$) coincident with the molecular centers of inversion lie halfway between the glide planes. The twofold screw axes (2_1, →), which lie at $z = 0$, are generated by the combination of the a glide and $\bar{1}$ symmetry elements. The two neighboring molecular layers are related by translation along the c axis (which is not necessarily perpendicular to the ab plane in space group $P2_1/a$). In space group $A2/a$, the two neighboring molecular layers (each of which contains a 2_1 axis as in $P2_1/a$) are related by twofold axes (2, ⟶) at $z = 1/4$. Note that the space group symbol A specifies molecular translation of neighboring layers along the diagonal $1/2(b + c)$.

The corresponding molecular models for two layers were generated,[14] their X-ray structure factors calculated,[16] and the models refined by adjusting the relative positions of the layers along the a axis to fit the observed Bragg rod data[17] and best

 © VCH Verlagsgesellschaft mbH, D-69451 Weinheim, 1995 0570-0833/95/0606-0650 $ 10.00+.25/0

satisfy hydrogen-bonding geometry. The latter constraint also enabled us to fix the absolute orientation of the molecular chain about its long axis; only one of the two possible azimuthal angles gave reasonable interlayer O–H···O hydrogen bonding.[18] Furthermore, the intralayer *a* glide plane was allowed a minor relaxation by leaning the *a* glide planes by an angle δ away from the plane perpendicular to the water surface[19] to obtain the best fit of the Bragg rod profiles. The packing arrangement for this bilayer of symmetry slightly relaxed from $P2_1/a$ is shown in Figure 3, and the corresponding Bragg rod fit

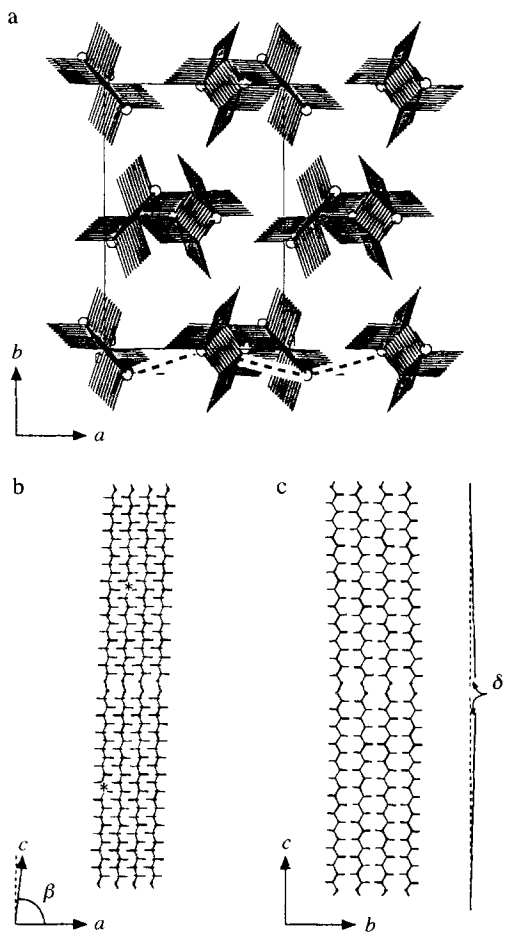


Fig. 3. Bilayer packing arrangement of the molecular model of C_{22} diol in a pseudo $P2_1/a$ space group. a) View perpendicular to the *ab* plane. Dashed lines show the hydrogen-bonding pattern along the *a* axis. The calculated distances between the hydrogen-bonded oxygen atoms are 2.5 and 3.4 Å. These two values can easily be brought to a satisfactory hydrogen-bonding mean of approximately 2.9 Å by minor adjustments in molecular tilt, rotation about the molecular axes, or conformation. b) View along the *b* axis. The length of the *c* "axis" is given by the distance separating the two asterisks placed on the molecular centers of two molecules in the top and bottom layers. c) View along the *a* axis. The layers were made to lean in opposite directions by an angle δ for the best fit to the Bragg rod data.

in Figure 1 b.[20, 21] In this model structure the two layers are related by a "pseudo-translation" axis *c*, with unit cell dimensions $a = 5.04$ Å, $b = 7.30$ Å, $c = 30.2$ Å, $\alpha = 90°$, $\beta = 84°$ and $\gamma = 90°$.

Inhibition of multilayer formation was accomplished by introducing 10% of the monoalcohol $C_{24}H_{49}OH$ into the initial solution and spreading the material for 100% monolayer coverage. The idea was to use an amphiphilic additive that might mix with the host matrix through favorable lateral interactions, but might hinder the interlayer interactions and thereby inhibit multilayer buildup (Fig. 4). Two major phases,[22] a mono- and a multilayer (α and β respectively), now appear in the X-ray scattering intensity map $I(q_{xy}, q_z)$. These two phases have overlapping {1,1} reflections but resolved {0,2} reflections that are easily assigned to their appropriate phase by the widths of their corresponding Bragg rods and q_{xy} positions. The calculated occupancy of the two phases indicates that only about 15% of the coverage is attributable to the double layer; the rest is occupied by monolayer.[23]

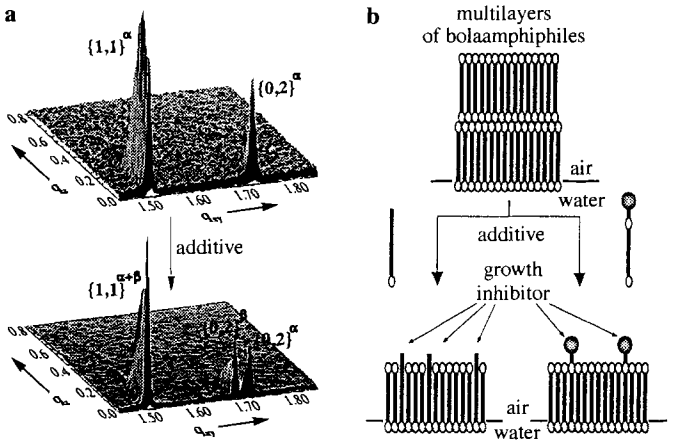


Fig. 4. a) Two-dimensional intensity distribution $I(q_{xy},q_z)$ of the diffraction pattern of 100% surface coverage of pure C_{22} diol (top) and C_{22} diol containing 10% of $C_{24}H_{49}OH$ (bottom) on the water subphase (also spread for 100% surface coverage), as a function of the horizontal (q_{xy}) and vertical (q_z) scattering vectors. Only the {1,1} and {0,2} Bragg rods are depicted. The α and β phases are bilayer and monolayer structures, respectively. b) Scheme showing inhibition by the two kinds of additive of bilayer formation (top) of C_{22} diol yielding monolayer (bottom).

The GID pattern of the C_{22} diol was also measured with $HO(CH_2)_{22}OCH_2C_6H_5$ as additive. This additive was far more effective than $C_{24}H_{49}OH$, by virtue of the bulky phenyl group: only 5% almost completely inhibited multilayer formation.

In this report we have demonstrated the use of GID, complemented by molecular packing and hydrogen-bonding considerations, for the determination of the probable "space groups" and molecular packing arrangement of the crystalline aggregates, only a few layers thick.[24] Clearly, the film formed comprises islands of bilayer in equilibrium, presumably with pure water surface, in the range of surface coverage from 70% to 200%. We cannot however, rule out the presence of minor amounts of multilayer and monolayer material. The bilayer islands have an average translational coherence length in the range of 400–1000 Å. A relaxation of crystal symmetry, commonly observed by means of GID in amphiphilic monolayers, is also found in the bilayer systems, although the extent and the causes thereof, in terms of possible influence of the water subphase, requires further investigation.

The analysis of this structure has also allowed a determination of the absolute orientation of the diol chains; such configurations for monolayers of simple chainlike molecules are almost impossible to ascertain from analysis of the GID data. In spite of the meager amount of diffraction data compared to that from 3D crystals, the derived models were based on very few assumptions. We may state that the layer structure is unambiguously determined by the unit cell dimensions and the interlayer hydrogen-bonding requirements. However, an ambiguity arose in fixing the interlayer structure, yielding two possible arrangements, both of which could be fitted to the *z* component of the Bragg data.

 © VCH Verlagsgesellschaft mbH, D-69451 Weinheim, 1995 0570-0833/95/0606-0651 $ 10.00+.25/0

The molecular packing characteristics in this class of bolaamphiphilic materials is currently under investigation for a wide range of chain lengths.[25]

Received: September 14, 1995 [Z 7313 IE]
German version: *Angew. Chem.* **1995**, *107*, 707

Keywords: bolaamphiphiles · structure elucidation · thin films

[1] A bolaamphiphile contains a hydrophobic chain with hydrophilic groups at both ends. See G. H. Escamilla, G. R. Newkome, *Angew. Chem.* **1995**, *106*, 2016; *Angew. Chem. Int. Ed. Engl.* **1995**, *33*, 1937.

[2] R. Popovitz-Biro, J. Majewski, L. Margulis, S. Cohen, L. Leiserowitz, M. Lahav, *J. Phys. Chem.* **1995**, *98*, 4970.

[3] R. Popovitz-Biro, J. Majewski, L. Margulis, S. Cohen, L. Leiserowitz, M. Lahav, *Adv. Mater.* **1995**, *6*, 956.

[4] a) S. Weinbach, K. Kjaer, W. G. Bouwman, G. Grübel, G. Legrand, J. Als-Nielsen, M. Lahav, L. Leiserowitz, *Science* **1995**, *264*, 1566; b) S. Weinbach, K. Kjaer, J. Als-Nielsen, M. Lahav, L. Leiserowitz, *J. Phys. Chem.* **1993**, *97*, 5200.

[5] J. Als-Nielsen, K. Kjaer in *Proceedings of the NATO Advanced Study Institute Phase Transition in Soft Condensed Matter* (Eds.: T. Riste, D. Sherrington), Plenum, New York, Geilo, Norway, **1989**, p. 113.

[6] R. Popovitz-Biro, unpublished results.

[7] The GID measurements were performed at the BW1 wiggler beamline at HASYLAB, DESY, Hamburg, Germany, on a liquid surface diffractometer. A beam of wavelength 1.35 Å was incident at a grazing angle slightly below the critical angle for total external reflection. This geometrical configuration enhances surface sensitivity. The footprint of the X-ray beam on the water surface was 5 × 50 mm. The backgound level of scattering was reduced by a He atmosphere inside the trough. Detection of both the horizontal (q_{xy}) and vertical (q_z) components of the diffracted beam was done by a vertical oriented position-sensitive detector (q_z resolution) mounted behind a Soller collimator giving q_{xy} resolution. The bolaamphiphiles were spread at room temperature from 5×10^{-4} M chloroform solution over the Millipore-filtered water contained in a Langmuir trough mounted on the diffractometer. GID measurements were performed after cooling of the subphase to 5 °C. More experimental details are given in Ref. [12].

[8] The GID pattern for 70, 100, and 200% surface coverage were essentially the same, differing only in intensity and thus in the number of observable peaks.

[9] Two layers are found by GID in contrast to the two to five layers of the C_{22} diol observed after deposition on mica, by atomic force microscopy [2]. We may reconcile this difference by bearing in mind that the multilayers are prepared under dynamic conditions away from equilibrium, and so slight changes in temperature, pressure, and support may lead to structural differences.

[10] D. M. Small in *Handbook of Lipid Research, Vol. 4*, Plenum, New York, **1986**.

[11] The *b* glide is ruled out since it would lead to a crisscrossed arrangement of chain axes and so to a poor packing, which has not yet been observed. Moreover, such a packing would not fit the Bragg rod profiles.

[12] F. Leveiller, D. Jacquemain, L. Leiserowitz, K. Kjaer, J. Als-Nielsen, *J. Phys. Chem.* **1992**, *96*, 10380.

[13] The inversion centers and twofold axes are crystallographically correct for the molecular chains, but only statistically correct for the hydroxyl hydrogen atoms in the hydrogen-bonding chain (Scheme 1b), which must be disordered as in the 3D crystal structures of hexagonal ice [15a], methanol [15b], $C_{16}H_{33}OH$ [15c], and $C_{24}H_{49}OH$ [15d]. A completely ordered O–H···O hydrogen-bonded system with identical O–H···O repeat along the hydrogen-bond chain axis *a* may be achieved with a twofold screw axis parallel to *a*. Such an arrangement would yield the commonly observed orthorhombic space group *Pcab*, but was found not to fit the GID data, which requires all the chains axes to be tilted in the same direction vis-a-vis the *a* axis.

[14] The best fit of the calculated Bragg rod intensity profiles to the observed data was obtained for an interlayer offset along the *a* axis of 3.3 Å and an interlayer separation of 30 Å. Furthermore, modeling with one or three layers yielded calculated Bragg rods with shapes distinctly different from those of the observed data.

[15] a) D. W. Peterson, H. A. Levy, *Acta Crystallogr.* **1957**, *10*, 70; K. Shimaoko, *J. Phys. Soc. Jpn.* **1960**, *15*, 106; b) K. J. Tauer, W. N. Lipscomb, *Acta Crystallogr.* **1952**, *5*, 606; c) S. Abrahamsson, G. Larsson, E. von Sydow, *ibid.* **1960**, *13*, 770; d) J.-L. Wang, F. Leveiller, D. Jacquemain, K. Kjaer, J. Als-Nielsen, M. Lahav, L. Leiserowitz, *J. Am. Chem. Soc.* **1995**, *116*, 1192.

[16] D. Jacquemain, S. Grayer Wolf, F. Leveiller, K. Kjaer, M. Deutsh, J. Als-Nielsen, M. Lahav, L. Leiserowitz, *Angew. Chem.* **1992**, *104*, 134; *Angew. Chem. Int. Ed. Engl.* **1992**, *31*, 130.

[17] Model structures made up of one or three layers did not fit the observed Bragg rod data satisfactorily. We also note that for the given grazing incidence geometry the intensity of the X-ray beam falls off exponentially with depth of penetration of a value I_0/e (where I_0 is the intensity of the incident beam) for the depth $\Lambda \approx 90$ Å. If the thickness of the multilayer crystallites is less than 2 Λ, the shape of the Bragg rod is barely affected by the limited penetration depth. Furthermore the shape of the two-dimensional contour of the diffracted intensity $I(q_{xy},q_z)$ of the various reflections (not presented here) show that the *ab* plane of the multilayer crystallites are primarily parallel to the water surface. There is, however, some tendency for deviation therefrom. If such a spread of crystalline misorientation from the plane of water surface is pronounced, it would give rise to an apparent broadening of the Bragg rods along q_z, which would have to be treated in a detailed analysis (K. Kjaer, W. G. Bouwman, unpublished work).

[18] For a chainlike hydrocarbon molecule the limited number of observable peaks in the GID data does not allow one to differentiate between two structures differing in orientation by 180° about the long molecular axis unless other criteria are introduced.

[19] This reduction in crystal symmetry was found to be necessary for a good fit to the GID data of monolayer structures of several amphiphilic molecules on water [12, 15d]. In the multilayer C_{22}-diol structure the lean angles for the first and second layers were in opposite directions. In the refined structure the molecular chains are tilted by 1.5° along the *a* axis and leaned by 1.5° along the *b* axis.

[20] In this packing the center of inversion and twofold axes relating the two layers in the two space group are lost. Moreover, the relaxation of the $P2_1/a$ (or $A2/a$) symmetry is also manifested by the presence of an observed but very weak symmetry-forbidden {1,0} reflection.

[21] The results for symmetry relaxed from $A2/a$ are very similar to that for $P2_1/a$ and so are not shown here.

[22] In addition to α and β phases a minor γ phase exhibiting two very weak Bragg rods was observed. Their intensities were approximately one hundredth those of the major phases. The q_{xy}, q_z positions of these two Bragg rods indicate a rectangular unit cell of dimensions $a = 5.08$ Å, $b = 8.73$ Å. Modeling yielded multilayer (trilayer) structure with the molecules tilted by about 30° from the vertical in the *b* direction.

[23] The intensity profiles of the {0,2} and {2,0} (not shown in Fig. 4a) reflections of monolayer phase α were used to derive a model of its structure. The calculated intensity contribution of this model structure was subtracted from the intensity profile of the unresolved {1,1} reflection. The remaining intensity profile together with the resolved {0,2} reflection of the β phase was well fitted to the calculated structure of the bilayer previously determined (Fig. 3). The unit cell of the monolayer was found to differ slightly from that of the double layer: $a = 5.0$, $b = 7.43$ Å.

[24] A detailed determination of the multilayer structure would also benefit from atom–atom potential energy calculations as carried out on the amphiphilic monolayer structures [12].

[25] The structures of the C_{16}, C_{23}, and C_{30} diols will be reported elsewhere.

On the Mechanism of Action of Urocanase: Observation of the Enzyme-Bound NAD^+–Inhibitor Adduct by ^{13}C NMR Spectroscopy**

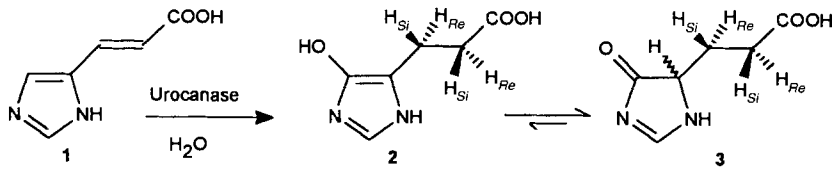
Carsten Schubert, Herbert Röttele, Manfred Spraul, and János Rétey*

Urocanase (E.C. 4.2.1.49) catalyzes the second step in the degradation of histidine in most cells (Scheme 1) and contains a tightly bound NAD^+ which is essential for catalytic activity.[1, 2] NAD^+ is supposed to function as an electrophilic catalyst and forms a transient covalent adduct with the imidazole ring of the substrate, urocanic acid (**1**).[3] According to the mechanism postulated by us,[3–5] the unusual addition of water leading to 5′-hydroxyimidazolepropionic acid **2** occurs in a chemically

[*] Prof. Dr. J. Rétey, Dr. C. Schubert, Dr. H. Röttele
Institut für Organische Chemie der Universität
Richard-Willstätter-Allee, D-76128 Karlsruhe (Germany)
Telefax: Int. code + (721)608-4823

Dr. M. Spraul
Bruker Analytische Meßtechnik GmbH
D-76287 Rheinstetten (Germany)

[**] Generous financial support by the Deutsche Forschungsgemeinschaft and the Fonds der Chemischen Industrie is acknowledged. We thank Ms. J. Herman for numerous enzyme isolations.



Scheme 1. Steric course of the urocanase reaction. The protons incorporated from the solvent are added to the *Re* face.

plausible manner. Intermediate **2** is in a spontaneous equilibrium with imidazolonepropionic acid **3**.[6]

Recently we determined the structure of an NAD^+–inhibitor adduct, which is formed on urocanase and is most likely analogous to the transient NAD^+–substrate adduct, by measuring the one-bond ^{13}C-^{13}C coupling constants.[5] Because of its instability the double ^{13}C-labeled adduct had to be stabilized by oxidation while still bound to the enzyme and was subsequently separated from the enzyme.[4, 7]

Here we report on our direct observation of the native adduct in the enzyme-bound state for which we used difference ^{13}C NMR spectroscopy. To enhance the relevant ^{13}C signals both position 4 of the prosthetic NAD^+ and position 5′ of the inhibitor were enriched with ^{13}C. In a first experiment we applied urocanase containing (4-^{13}C)NAD^+ (99% ^{13}C). In the 150 MHz ^{13}C NMR spectrum the enzyme-bound (4-^{13}C)-NAD^+ gives rise to a broad signal at $\delta = 146$ (Fig. 1). After

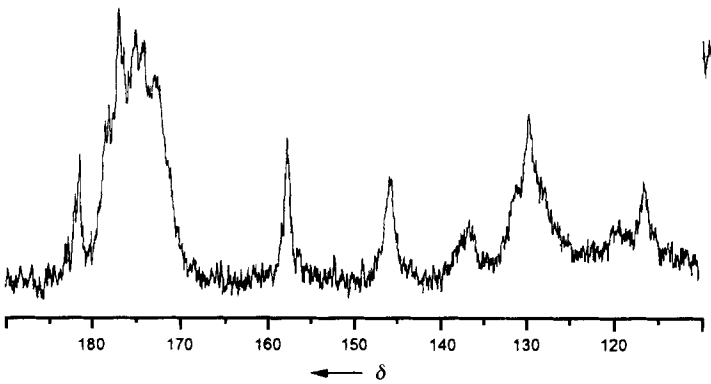


Fig. 1. Low-field portion of the 150 MHz ^{13}C NMR spectrum of the (4-^{13}C)NAD^+-containing urocanase. The broad signal at $\delta = 146$ stems from the C-4 atom of the nicotinamide moiety (99% ^{13}C). Approximately 120 mg (0.99 μmol) of urocanase in 2 mL of 50 mM K_2HPO_4 buffer, pH 7.5, H_2O/D_2O 8:1, 10 mm NMR tube, ^1H broadband decoupled, line broadening = 10 Hz, $T = 300$ K, 30 000 transients.

addition of unlabeled imidazolepropionic acid in tenfold excess (fivefold excess with respect to the active sites) the signal at $\delta = 146$ largely disappears, while at the same time a new, likewise broad signal at $\delta = 37.7$ arises. This indicates that practically all active sites are occupied by the inhibitor and is most clearly seen in the difference spectrum (Fig. 2). Besides the sharp ^{13}C NMR signals of the excess unbound imidazolepropionic acid, one observes the signal of the ^{13}C-4 atom of the enzyme-bound (4-^{13}C)NAD^+–imidazolepropionate adduct (**4** or **4a**; Scheme 2) at $\delta = 37.7$. For comparison: The C-4 atom of NADH **5** resonates at $\delta = 21.9$, whereas that of C-4 phosphorylated dihydropyridine derivative **6** appears at $\delta = 78.7$.[8]

In a further experiment, in which instead of NAD^+ now the inhibitor, imidazolepropionic acid, was labeled with ^{13}C in the 5′ position, the observation of the enzyme-bound adduct was confirmed, and the chemical shift of the C-5′ atom was determined. In the difference spectrum (Fig. 3) two ^{13}C NMR signals are observed in the region between $\delta = 80$ and $\delta = 120$, namely at $\delta = 117$ and at $\delta = 87.5$ for the free and the bound (5′-^{13}C) imidazolepropionic acid, respectively. The large highfield shift of the C-5′ signal indicates that the imidazole ring in the enzyme-bound adduct is not aromatic; in other words the adduct has structure **4a**.

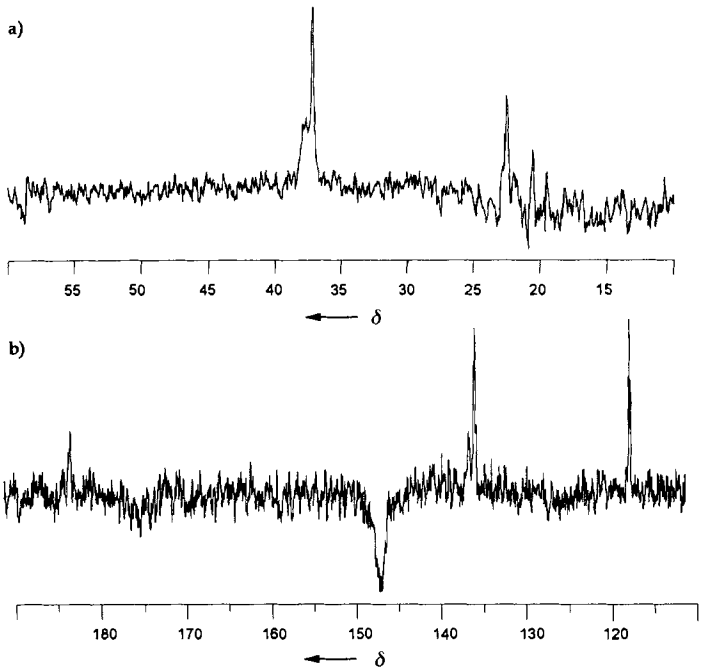
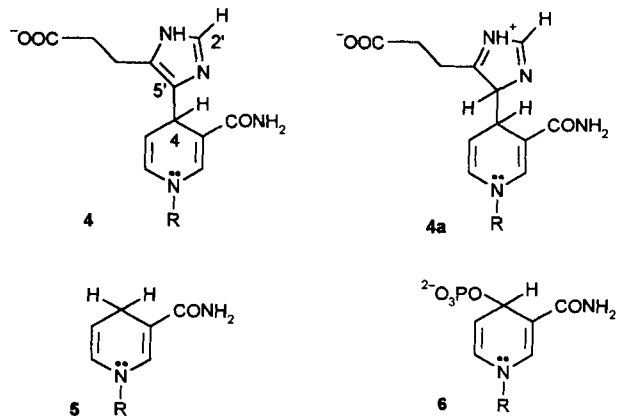


Fig. 2. ^{13}C NMR difference spectrum of (4-^{13}C)NAD^+-containing urocanase (after – before) addition of 9.9 μmol of imidazolepropionic acid. a) High-field portion, b) low-field portion. The broad signal at $\delta = 37.7$ arises from the enzyme-bound (4-^{13}C)NAD^+–imidazolepropionate adduct.



Scheme 2. Possible structures of the enzyme-bound NAD^+–imidazolepropionate adduct **4** and **4a** and structures of NADH **5** and of the NAD–4-phosphate adduct **6**. R = adenosine diphosphate ribosyl.

The preference of **4a** over **4** at the active site can be explained by an ionic interaction of a negatively charged group of the enzyme and the positively charged nitrogen atom of the imida-

 © VCH Verlagsgesellschaft mbH, D-69451 Weinheim, 1995 0570-0833/95/0606-0653 $ 10.00+.25/0

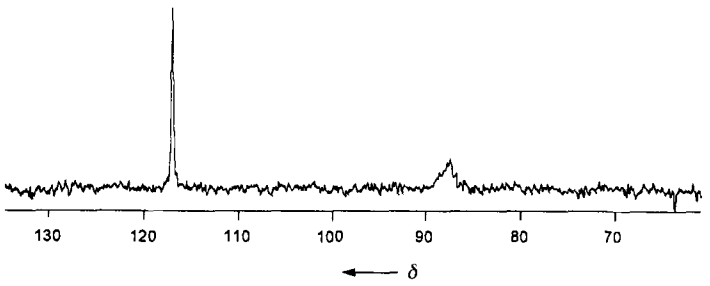


Fig. 3. 100 MHz ^{13}C NMR difference spectrum of unlabeled urocanase (after − before) addition of 2 μmol of (5′-^{13}C)imidazolepropionic acid. The broad signal at $\delta = 87.5$ arises from the NAD$^+$−(5′-^{13}C)imidazolepropionate adduct; the sharp signal at $\delta = 117$ corresponds to free (5′-^{13}C)imidazolepropionic acid. Approximately 150 mg (1.22 μmol) of urocanase in 2 mL of 50 mM K_2HPO_4 buffer, pH 7.5. H_2O/D_2O 8:1, 10 mm NMR tube, ^{1}H-broadband decoupled, NOE unsuppressed, line broadening = 10 Hz, $T = 297$ K, 52000 scans.

zole ring. Evidence for an equilibrium between **4a** and **4** is provided by the previously observed urocanase-catalyzed exchange of the H-5 atom of imidazole propionate with solvent protons.[6, 9, 10]

Received: November 4, 1995 [Z 7452 IE]
German version: *Angew. Chem.* **1995**, *107*, 719

Keywords: ^{13}C NMR spectroscopy · enzyme mechanisms · urocanase

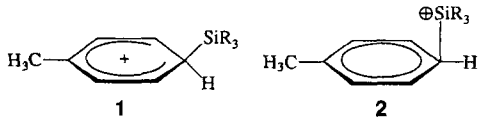
[1] R. M. Egan, A. T. Phillips, *J. Biol. Chem.* **1977**, *252*, 5701–5707.
[2] V. Keul, F. Kaeppeli, C. Ghosh, T. Krebs, J. A. Robinson, J. Rétey, *J. Biol. Chem.* **1979**, *254*, 843–851.
[3] J. Rétey, *Arch. Biochem. Biophys.* **1995**, *314*, 1–16.
[4] J. Klepp, A. Fallert-Müller, K. Grimm, W. E. Hull, J. Rétey, *Eur. J. Biochem.* **1990**, *192*, 669–676.
[5] C. Schubert, Y. Zhao, J.-H. Shin, J. Rétey, *Angew. Chem.* **1995**, *106*, 1331–1332; *Angew. Chem. Int. Ed. Engl.* **1995**, *33*, 1279–1280.
[6] E. Gerlinger, W. E. Hull, J. Rétey, *Eur. J. Biochem.* **1981**, *117*, 629–634.
[7] L. H. Matherly, C. W. De Brosse, A. T. Phillips, *Biochemistry* **1982**, *21*, 2789–2794.
[8] J.-F. Biellmann, C. Lapinte, E. Haid, G. Weimann, *Biochemistry* **1979**, *18*, 1212–1217.
[9] R. M. Egan, L. H. Matherly, A. T. Phillips, *Biochemistry* **1981**, *20*, 132–137.
[10] S. Sawada, K. Endo, M. Ushida, N. Esaki, K. Soda, *Bull. Kyoto Univ. Education Ser. B* **1981**, *51*, 11–17.

$[R_3Si-arene]^+$ σ Complexes in the Gas Phase**

Fulvio Cacace,* Marina Attinà, and Simonetta Fornarini

The report by Lambert et al.[1] that an R_3Si^+ ion that is not coordinated to the anion and only weakly to the solvent exists in the solid $[Et_3SiB(C_6F_5)_4 \cdot$ toluene$]$ has stirred a controversy, mainly focused on the role of toluene.

Schleyer et al.,[2] in agreement with Olah et al.,[3] argue that the compound is actually a salt of the arenium ion $[Et_3Si \cdot$ toluene$]^+$, that is, a σ complex of type **1**. According to Pauling,[4] in the compound studied by Lambert et al.[1] a covalent bond does exist between the Si atom and the *para* C atom of toluene molecule, despite their large separation (2.18 Å), and a significant fraction of the positive charge of Et_3Si^+ is transferred to the aromatic ring. Reed et al.[5] recognize the existence of a covalent interaction between the Et_3Si group and the toluene molecule and assign the adduct the structure of a π complex with an sp^2 carbon (**2**), rather than of the σ complex **1** with an sp^3 carbon.



Discrimination between the above structures is difficult, since it is necessarily based on certain critical parameters such as the Si-C-C_{para} angle, whose values deduced from crystal structure analysis happen to be intermediate between those expected for unperturbed ions **1** and **2**. Indeed, the intrinsic structural features of the ions in the crystal lattice are affected by interactions with neighboring molecules, which detracts from the generality of the conclusions and may account for their inconsistency with the results of theoretical calculations on free, unperturbed species found exclusively in the gas phase.[6]

We have addressed the problem by investigating in the gas phase the same $[R_3Si$-arene$]^+$ adducts studied in the solid state by the radiolytic technique[7] and by the FT-ICR (ICR = ion cyclotron resonance) mass spectrometry. The reaction sequence shown in Scheme 1 in which B denotes a gaseous base or nucleophile was used.

$$R_3Si^+ + C_6X_5R^1 \longrightarrow [R_3Si{-}C_6X_5R^1]^+ \quad (I)$$

$$[R_3Si{-}C_6X_5R^1]^+ + B \longrightarrow R_3SiB^+ + C_6X_5R^1 \quad (II)$$

$$[R_3Si{-}C_6X_5R^1]^+ + B \longrightarrow R_3SiC_6X_4R^1 + BX^+ \quad (III)$$

(R = Et, *i*Pr; R^1 = X, CX_3; X = H, D)

In the radiolytic experiments, the *i*-$C_3H_7^+$ ions from the γ irradiation of gaseous mixtures containing C_3H_8 as the bulk component react with R_3SiH to give R_3Si^+ ions, which react with toluene according to (I) to yield $[R_3Si{-}C_7H_8]^+$ adducts. The latter, efficiently deactivated by thermalization in the dense gas, undergo reactions (II) or (III) or both with the bases and nucleophiles present in the system, yielding neutral products that are analyzed by GC/MS.[7] The composition of typical systems and the yields of the products, expressed by their G_{+M} values (molecules formed per 100 eV), are reported in Table 1. In the absence of added bases, only cymenes are formed from

Table 1. Gas-phase trialkylsilylation of toluene [a].

Partial pressures/Torr [b]			R	Product yields (G_{+M}) [c]		
C_3H_8	Toluene	Additives		$MeC_6H_4SiR_3$	(*meta*:*para*)	MeC_6H_4*i*-Pr
615	1.70	pyridine: 0.85	*i*Pr	0.16	(20:80)	0.13
650	1.63	pyridine: 0.36	*i*Pr	0.12	(21:79)	0.13
620	1.80	pyridine: 1.75	*i*Pr	0.16	(20:80)	0.14
650	1.60	Et_3N: 0.78	*i*Pr	0.076	(24:76)	0.23
630	1.68	iPr_2EtN: 0.80	*i*Pr	0.038	(34:66)	0.21
620	1.87	–	*i*Pr	0.012	(31:63)	0.34
650	2.07	$(MeO)_3PO$: 1.01	*i*Pr	0.007	(25:75)	0.30
630	1.10	pyridine: 1.30	Et	0.07	(24:76)	0.15
650	1.40	–	Et	–	–	0.19
670	0.82	Et_3N: 0.79	Et	0.088	(24:76)	0.14

[a] All irradiations performed at 80 °C. [b] All systems contained R_3SiH (10 Torr) and O_2 (10 Torr). [c] Standard deviation: ±10%.

[*] Prof. F. Cacace, Prof. M. Attinà, Prof. S. Fornarini
Università di Roma "La Sapienza"
P. le Aldo Moro 5, 1-00185 Rome (Italy)
Telefax: Int. code + (6)49913-888

[**] This work was supported by Italian Ministero dell'Università e della Ricerca Scientifica e Tecnologica (MURST) and Consiglio Nazionale delle Ricerche (CNR). The experimental help of F. Angelelli and A. Ricci is gratefully acknowledged.

the direct alkylation of toluene by $i\text{-}C_3H_7^+$; the yields of silylated products are negligible. Formation of *m*- and *p*-trialkylsilyltoluenes can only be observed when nitrogen bases such as Et_3N or pyridine are added to the gas.

Such observations can be explained by the presence of oxygenated nucleophiles that are either invariably in the system as adventitious impurities (H_2O), or formed by the radiolysis (H_2O, CH_2O, CH_3OH, $(CH_3)_2CO$, etc.), or deliberately added ($(CH_3O)_3PO$). These nucleophiles exclusively promote desilylation (II),[8] thus preventing formation of neutral silylated products. The addition of strong bases such as Et_3N or pyridine has two opposite effects. On one hand it allows formation of silylated products by deprotonation (III). On the other, the base efficiently intercepts the charged electrophiles $i\text{-}C_3H_7^+$ and R_3Si^+ and depresses the yields. This accounts for the peculiar dependence of the silylation yields on base concentration, normally characterized by a maximum that is observed at pyridine pressures of 0.5–1.5 Torr under the experimental conditions typical for analogous radiolytic reactions.[8b, 8c, 8d] The ionic character of the silylation process is demonstrated, inter alia, by the negligible yields of products unless an appropriate base was deliberately added, which ruled out contributions from neutral, radiolytically formed reactive species, such as radicals and excited molecules. The radiolytic results indicate that at least a fraction of the $[R_3Si\text{–}C_6X_5R^1]^+$ adducts react with the base according to reaction (III), which is typical of ions having the σ complex structure **1**.

In the FT-ICR MS approach, a typical experiment involves formation of Et_3Si^+ ions by ionization of Et_3SiH and their reaction with C_6D_6, introduced by a pulse valve. In this way a benzene pressure of about 10^{-5} Torr is obtained, albeit for only 5×10^{-3} s, which allows partial collisional stabilization of the $[Et_3Si\text{–}C_6D_6]^+$ adducts from reaction (I).[9] Following removal of C_6D_6, all ions except the adduct are ejected by repeated, low-power radiofrequency pulses. This isolation procedure is designed to be as fast and mild as possible to minimize losses of $[Et_3Si\text{–}C_6D_6]^+$ ions and reduce their unintentional off-resonance excitation. In this way $[Et_3Si\text{–}C_6D_6]^+$ ions that are sufficiently thermalized to prevent extensive fragmentation are isolated. The reaction of the isolated $[Et_3Si\text{–}C_6D_6]^+$ cations with the neutral species present in the cell (Et_3SiH, Et_3N, and traces of adventitious water) gives a complex pattern of products (Fig. 1). Products $[Et_3SiNEt_3]^+$ and Et_3ND^+ of both processes (II) and (III) are detected. The other charged products have been shown by control experiments to arise from the reactions of Et_3Si^+, initially formed by the fragmentation of a minor fraction of excited $[Et_3Si\text{–}C_6D_6]^+$ adducts, or from the reactions of the latter with Et_3SiH.

The above FT-ICR MS results are significant, since in the first place they demonstrate directly the individual steps of the reaction sequence (I)–(III). Furthermore, insight into the structure of $[Et_3Si\text{–}C_6D_6]^+$ adducts is provided by applying a general criterion whose validity has been recently verified in the specific case of aromatic silylation:[8c] π complexes such as **2** react exclusively according to ligand exchange (II), whereas σ complexes such as **1** can undergo both reactions (II) and (III). According to this criterion, the FT-ICR MS experiments indicate that σ complex **1** must be formed from reaction (I), since D^+ transfer from $[Et_3Si\text{–}C_6D_6]^+$ to Et_3N does occur. The concurrent Et_3Si^+ transfer can be traced either to the presence of the π complex **2**, and/or to the fact that **1** not only reacts according to (III) but also according to (II).

In conclusion, the actual isolation of the silylated neutral products from radiolytic reactions and the mechanistic insight from FT-ICR mass spectrometry provide compelling evidence

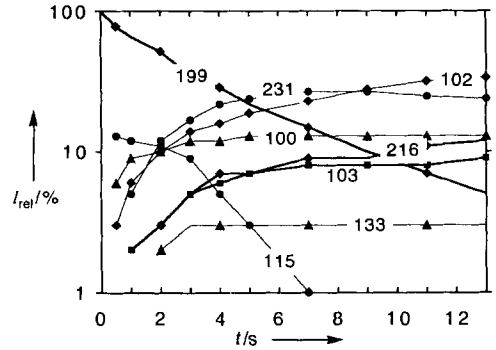


Fig. 1. Plot of the logarithm of the normalized intensities of the most intense peaks in the ICR mass spectrum as a function of the reaction time. Total pressure in the cell 1.5×10^{-8} Torr, Et_3N partial pressure 4×10^{-9} Torr, temperature 300 K. *m/z*: 199 $[Et_3SiC_6D_6^+]$, 100 $[Et_3N-H^+]$, 102 $[Et_3NH^+]$, 103 $[Et_3ND^+]$, 216 $[Et_3NSiEt_3^+]$, 133 $[Et_3SiOH_2^+]$, 231 $[Et_3SiEt_3SiH^+]$.

for the existence of σ complexes **1**. This is particularly relevant to the current debate on the structure of $[R_3Si\text{–arene}]^+$ adducts, since the gas phase is the only medium where free cations, unperturbed by environmental factors, can exist.[8, 10] Nevertheless, the present results do not rule out the existence of π complex **2**, for example, as species in equilibrium with the corresponding σ complex **1**.

Experimental Procedure

The gaseous samples for the radiolytic experiments were prepared in sealed glass vessels by described procedures[7] using commercial research grade products, Et_3SiH, iPr_3SiH, $(MeO)_3PO$, Et_3N, iPr_2NEt, pyridine, toluene, [D_8]toluene, benzene, and [D_6]benzene from Aldrich Chimica and CH_4, C_3H_8, and O_2 from Matheson Gas Products. The irradiations were carried out at 80 °C in a ^{60}Co 220 γ-cell from Nuclear Canada. The total dose was 1×10^4 Gy. The solution of the radiolytic products in cyclohexane was analyzed by GLC-MS on a fused silica column 50 m long with 0.2 mm inner diameter and coated with a 0.5 μm cross-linked methylsilicone film. A Hewlett Packard 5890 gas-chromatograph and a HP 5970B mass selective detector with internal standard ($PhSiMe_3$) calibration was used. The ICR MS experiments were performed with a Bruker Spectrospin Apex TM 47e FT-MS instrument equipped with an external ion source, a cylindrical (60 mm length, 60 mm diameter) "infinity" cell and a 4.7 T superconducting magnet. Duplicate experiments were performed with an EXTREL FTMS 2001 mass spectrometer, equipped with an Odissey Data Station and a FTMS autoprobe.

Received: May 9, 1995
Revised: November 24, 1995 [Z 6918 IE]
German version: *Angew. Chem.* **1995**, *107*, 754

Keywords: arene complexes · gas-phase chemistry · mass spectrometry · silyl cations

[1] a) J. B. Lambert, S. Zhang, C. L. Stern, J. C. Huffman, *Science* **1993**, *260*, 1917; b) J. B. Lambert, S. Zhang, *ibid.* **1995**, *263*, 984.
[2] P. von R. Schleyer, P. Buzek, T. Müller, Y. Apeloig, H.-U. Siehl, *Angew. Chem.* **1993**, *105*, 1558; *Angew. Chem. Int. Ed. Engl.* **1993**, *32*, 1471.
[3] G. A. Olah, G. Rasul, X.-Y. Li, H. A. Bucholz, G. Sandford, G. K. S. Prakash, *Science* **1995**, *263*, 983.
[4] L. Pauling, *Science* **1995**, *263*, 983.
[5] a) C. A. Reed, Z. Xie, R. Bau, A. Benesi, *Science* **1993**, *262*, 402; b) C. A. Reed, Z. Xie, *ibid.* **1995**, *263*, 986.
[6] For example, the C-Si-C angle in the Et_3Si group in **1**, R = Et, is not 120° as expected for a free Et_3Si^+ ion but an average of 114° according to the crystal structure analysis. This difference has been traced to the interaction of the ion with the "distant" toluene molecule; see ref. [1].
[7] For a review of the principles and applications of the radiolysis technique, see F. Cacace, *Acc. Chem. Res.* **1988**, *21*, 215.
[8] a) C. M. Wojtyniak, J. A. Stone, *Int. J. Mass Spectrom. Ion Processes* **1986**, *74*, 59; b) S. Fornarini, *J. Org. Chem.* **1988**, *53*, 1314; c) F. Cacace, M. E. Crestoni, S. Fornarini, R. Gabrielli, *Int. J. Mass Spectrom. Ion Processes* **1988**, *84*, 17; d) M. E. Crestoni, S. Fornarini, M. Speranza, *J. Am. Chem. Soc.* **1990**, *112*, 6929.
[9] Reaction (I) is appreciably exothermic: $\Delta H°$ is -23.9 and -26.6 kcal mol^{-1} for the addition of $(CH_3)_3Si^+$ to benzene and toluene, respectively; see ref. [8a].
[10] M. E. Crestoni, S. Fornarini, *Angew. Chem.* **1995**, *106*, 1157; *Angew. Chem. Int. Ed. Engl.* **1995**, *33*, 1094.

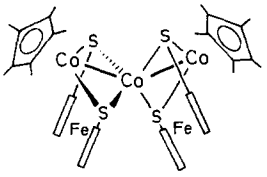
 © VCH Verlagsgesellschaft mbH, D-69451 Weinheim, 1995 0570-0833/95/0606-0655 $ 10.00+.25/0

A Co_3 Complex Containing a Bent Trimetal Chain, and Other 1,1′-Ferrocenedithiolato Complexes**

Max Herberhold,* Guo-Xin Jin, and Arnold L. Rheingold

Tricobalt complexes with either bridging sulfido or organothiolato ligands generally contain a closed Co_3 triangle;[1] well-known examples include $[\{Co(CO)_3\}_3(\mu_3\text{-}S)]$,[2] $[\{CpCo\}_3(\mu_3\text{-}S)(\mu_3\text{-}L)]$ (μ_3-L = S,[3,4] CO,[3,4] CS,[5] CNR (R = C_6H_{11}, C_6H_4Me-4)[6]), $[\{Co[\mu_2\text{-}(SCH_2)_2C_6H_4]\}_3(\mu_3\text{-}S)]^{2-}$,[7] and $[\{Co(CO)\}_3(\mu_2\text{-}SEt)_5(\mu_2\text{-}CO)]$.[8] We now report on the first complex of this kind in which an open tricobalt skeleton is present.

The binuclear, chloro-bridged complex $[(Cp^*CoCl_2)_2]$[9] reacts with the dilithium derivative of 1,1′-ferrocenedithiol, $[fc(SLi)_2]$, in tetrahydrofuran to give the violet, paramagnetic tricobalt compound **1**.



$[Co\{Cp^*Co(\mu_2\text{-}S_2fc)\}_2]$ **1**

The molecular structure of **1** has been established by a single-crystal X-ray structure analysis[10] (Fig. 1). Only the two terminal cobalt atoms of the Co_3 backbone in **1** have retained their Cp* ring. The two Co–Co bonds (2.584(1) Å) are each supported by a symmetrically bridging 1,1′-ferrocenedithiolate ligand. The four sulfur atoms surround the central cobalt atom Co(1) in a distorted tetrahedral arrangement; this coordination geometry is also observed in complexes such as $[Co_2(SiPr)_2(\mu_2\text{-}SiPr)_3]$.[11] The Co–S bond lengths in **1** are in the normal range: 2.275(2) Å (average) at the central Co(1) atom, 2.220(2) Å (average) at the terminal Co(2) atoms. Cobalt–iron interactions are clearly absent (Fe···Co(1) 3.893 Å, Fe···Co(2) 4.062 Å). The cyclopentadienyl rings of the 1,1′-ferrocenedithiolato ligands are arranged parallel and eclipsed with a ring–ring distance of 3.29 Å.

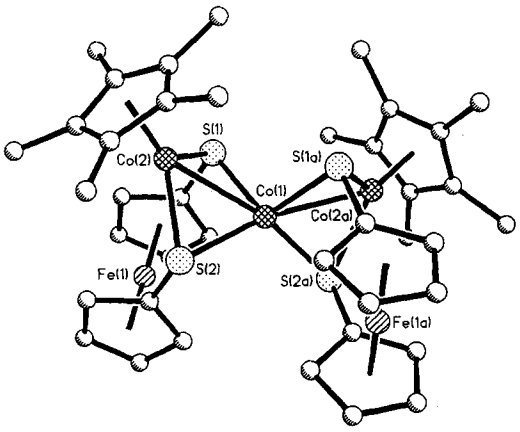
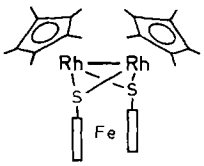


Fig. 1. Crystal structure of **1**. Selected distances [Å] and angles [°]: Co(1)-Co(2) 2.584(1), Co(2)-Cp*(center) 1.689, Co(1)-S(1) 2.278(2), Co(1)-S(2) 2.272(2), Co(2)-S(1) 2.213(2), Co(2)-S(2) 2.227(2), S(1)-S(1a) 3.780, S(2)-S(2a) 3.868, S(1)-S(2) 3.346; Co(2)-Co(1)-Co(2a) 137.9(1), Co(1)-Co(2)-Cp*(center) 149, S(1)-Co(1)-S(2) 94.7(1), S(1)-Co(2)-S(2) 97.8(1), S(1)-Co(1)-S(1a) 112.1(1), S(1)-Co(1)-S(2a) 120.2(1).

The Co–Co distances in **1** are found in the range expected for single bonds. Comparable Co–Co bond lengths were reported, for example, for $[\{CpCo(\mu\text{-}StBu)\}_2]$ (2.467(1) Å),[12] $[Co_2(CO)_6(\mu\text{-}S)_2]^{2+}$ (2.498(9) Å),[13] $[\{Cp'Co\}_3(\mu_3\text{-}S)_2]^{n+}$ (n = 0: two 2.48 Å (average), one 3.17 Å; n = 1: two 2.49 Å (average), one 2.87 Å; n = 2: three 2.52 Å (average)),[14] $[\{Co(CO)\}_3(\mu_2\text{-}SEt)_5(\mu_2\text{-}CO)]$ (2.552 Å (average)),[8] and $[\{Co(CO)_3\}_3(\mu_3\text{-}S)]$ (2.637 Å (average)).[2]

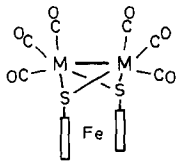
Surprisingly, the related reaction between $[(Cp^*RhCl_2)_2]$[15] and $[fc(SLi)_2]$ in THF [Eq. (a)] leads preferentially to a dirhodium complex **2**, which is similar to the known hexacarbonyl(1,1′-ferrocenedithiolato)diiron and -diruthenium compounds, **3**[16] and **4**,[17] respectively.

$$[(Cp^*RhCl_2)_2] + 2[fc(SLi)_2] \xrightarrow[-78\,^\circ C,\ -4\,LiCl]{THF} \underset{\mathbf{2}}{[Cp^*_2Rh_2(\mu_2\text{-}S_2fc)]} + [(fcS_2)_n] \quad (a)$$



$[Cp^*_2Rh_2(\mu_2\text{-}S_2fc)]$

2

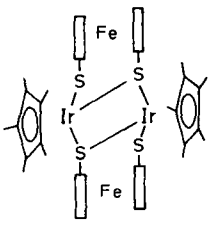


$[M_2(CO)_6(\mu_2\text{-}S_2fc)]$

3: M = Fe
4: M = Ru

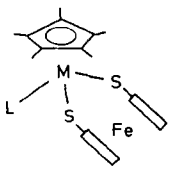
The formation of **1** and **2** from $[(Cp^*MCl_2)_2]$ (M = Co, Rh) involves redox processes during which the metal center is partially reduced by $[fc(SLi)_2]$. The 14-electron fragments $[Fe(CO)_3]$/$[Ru(CO)_3]$ and [Cp*Co]/[Cp*Rh] of **1**–**4** are isolobal.[18] Complexes **2**–**4** each contain a M_2S_2 tetrahedrane framework and obey the 18-electron rule.

If the metal atoms are formally assigned the oxidation state ±0 and the ligands are considered as neutral building blocks (e.g. Cp* as a five-electron ligand), the 1,1′-ferrocenedithiolato group, $[S_2fc]$, acts as a six-electron ligand in **1**–**4**. On the other hand, the iridium compound **5** contains two four-electron $[S_2fc]$ ligands, but no metal–metal bond.[19] Compound **5** is generated in low yield (2–5%) by the reaction of $[(Cp^*IrCl_2)_2]$[15] with $[fc(SLi)_2]$; a more attractive route (70–80%) to **5** is the sulfur-induced triphenylphosphane abstraction from the mononuclear



$[Cp^*_2Ir_2(\mu_2\text{-}S_2fc)_2]$

5



$[Cp^*M(L)(S_2fc)]$

6a: M = Rh (L = PMe_3)
6b: M = Ir (L = PPh_3)

[*] Prof. M. Herberhold, Dr. G.-X. Jin
Laboratorium für Anorganische Chemie der Universität
Postfach 101251, D-95440 Bayreuth (Germany)
Telefax: Int. code + (921)55-2157
Prof. A. L. Rheingold
Department of Chemistry, University of Delaware (USA)

[**] This work was supported by the Deutsche Forschungsgemeinschaft and the Fonds der Chemischen Industrie. We thank Prof. W. Bronger, Aachen, for the magnetic measurements. Abbreviations: Cp = η^5-C_5H_5; Cp′ = η^5-C_5H_4Me; Cp* = η^5-C_5Me_5; fc = 1,1′-ferrocenediyl ($[Fe(C_5H_4^-)_2]$); fcS_2 = 1,1′-ferrocenedithiolato, ($[Fe(C_5H_4S)_2]$).

precursor $[Cp^*Ir(PPh_3)(S_2fc)]$ (**6b**).[19] In the very stable 18-electron complexes **6a** and **6c** [S_2fc] functions as a two-electron ligand. The dimeric structure of **5** has been confirmed by an X-ray crystal structure analysis for the selenium analogue, $[Cp^*_2Ir_2(Se_2fc)_2]$.

In summary, the 1,1′-ferrocenedithiolato unit [S_2fc] is a versatile ligand system which may function as a two-electron (in **6a** and **6b**), four-electron (in **5**), or six-electron donor (in **1**–**4**) and which may act as either chelating or bridging ligand.

Experimental Procedure

1: A green solution of $[(Cp^*CoCl_2)_2]$ [9] (0.42 g, 0.80 mmol) in THF (20 mL) and an orange solution of $[fc(SLi)_2]$ (0.45 g, 1.1 mmol) in THF (100 mL) were combined at −78 °C. The color of the homogeneous mixture changed to violet. The solution was stirred for 3 h at room temperature. After removal of the solvent, the residue was separated by column chromatography on silica gel (Merck, Kieselgel 60). Elution with pentane/CH_2Cl_2 (1:2) gave **1**. Recrystallizion from $CHCl_3$/toluene/hexane mixtures at −25 °C gave violet microcrystals of **1** (0.15 g, 30.1%, m.p. 248 °C). EI-MS (70 eV): prominent peaks at *m/z* (%): 943 (100) [M^+], 808 (10) [$M^+ - Cp^*$], 636 (48) [$Cp^*_2Co_2(S_2fc)^+$], 501 (22) [$Cp^*Co_2(S_2fc)^+$], 442 (42) [$Cp^*Co(S_2fc)^+$]; strong peaks due to the ferrocene oligomers (*m/z* 370 [Fc_2^+], 554 [Fc(fc)Fc$^+$], 738 [$Fc(fc)_2Fc^+$]) were also observed. The effective magnetic moment was found to be 5.6 μ_B at room temperature; it decreases with decreasing temperature to reach 3.4 μ_B at 6 K [20].

2. The reaction of $[(Cp^*RhCl_2)_2]$ [15] (0.24 g, 0.38 mmol) with $[fc(SLi)_2]$ (0.31 g, 0.76 mmol) in THF (130 mL) was started at −78 °C and then continued for 4 h at room temperature. Chromatography over silica (with CH_2Cl_2/hexane mixtures for elution) gave several bands; isolation of the first (violet) zone which follows [FcH] and recrystallization from hexane or pentane gave violet crystals of (**2**) (0.12 g, 41%, m.p. 168 °C). ^{1}H NMR ($CDCl_3$): δ = 1.99 (s, C_5Me_5, 30H), 3.74, 4.39 (vt, fc, 4 + 4H); EI-MS (70 eV): *m/z* 723 (100%) [$M^+ - H$].

Received: December 29, 1993
Revised version: December 13, 1995 [Z 6592 IE]
German version: *Angew. Chem.* **1995**, *107*, 716

Keywords: cobalt compounds · complexes with sulfur ligands · iridium compounds · rhodium compounds · sandwich complexes

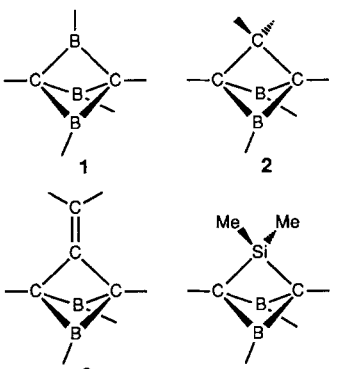
[1] Reviews: a) D. A. Buckingham, C. R. Clark in *Comprehensive Coordination Chemistry, Vol. 4* (Eds.: G. Wilkinson, R. D. Gillard, J. A. McCleverty), Pergamon, **1987**, p. 635–900; b) R. D. W. Kemmitt, D. R. Russell in *Comprehensive Organometallic Chemistry, Vol. 5* (Eds.: G. Wilkinson, F. G. A. Stone, E. W. Abel), Pergamon, **1982**, p. 1–276.
[2] C. H. Wei, L. F. Dahl, *Inorg. Chem.* **1967**, *6*, 1229–1236.
[3] P. D. Frisch, L. F. Dahl, *J. Am. Chem. Soc.* **1972**, *94*, 5082–5084.
[4] S. Otsuka, A. Nakamura, T. Yoshida, *Liebigs Ann. Chem.* **1968**, *719*, 54–60.
[5] a) H. Werner, K. Leonhard, *Angew. Chem.* **1979**, *91*, 663–664; *Angew. Chem. Int. Ed. Engl.* **1979**, *18*, 663; b) H. Werner, K. Leonhard, O. Kolb, E. Röttinger, H. Vahrenkamp, *Chem. Ber.* **1980**, *113*, 1654–1662.
[6] a) J. Fortune, A. R. Manning, F. S. Stephens, *J. Chem. Soc. Chem. Commun.* **1983**, 1071–1072; b) A. R. Manning, L. O'Dwyer, P. A. McArdle, D. Cunningham, *J. Organomet. Chem.* **1995**, *474*, 173–176.
[7] G. Henkel, W. Tremel, B. Krebs, *Angew. Chem.* **1983**, *95*, 314; *Angew. Chem. Int. Ed. Engl.* **1983**, *22*, 318; *Angew. Chem. Suppl.* **1983**, 307–322.
[8] C. H. Wei, L. F. Dahl, *J. Am. Chem. Soc.* **1968**, *90*, 3960–3969, 3977–3983.
[9] U. Kölle, B. Fuss, *Chem. Ber.* **1984**, *117*, 743–752.
[10] Data for the crystal structure analysis of $C_{40}H_{46}Co_3Fe_2S_4$ (**1**): diffractometer: Siemens P4 ($Mo_{K\alpha}$, λ = 0.71073 Å, graphite monochromator); monoclinic, *P2/n*, *a* = 12.558(3), *b* = 10.151(2), *c* = 15.792(3) Å, β = 107.54(2)°, *Z* = 2, violet-black platelet, dimensions 0.04 × 0.38 × 0.40 mm. Measured range: 4.0° ≤ 2θ ≤ 45.0°; measured octant *hkl*, *T* = 298 K; measured reflections: 5235; independent reflections: 2516 (R_{int} = 0.049); observed reflections: 1746 ($F > 4.0\,\sigma(F)$); structure solution with direct methods (SHELXTL PLUS (VMS)); number of refined parameters: 222; *R* = 0.0493; *wR* = 0.0599 ($w^{-1} = \sigma^2(F) + 0.0020\,F^2$); maximum/minimum residual electron density: 0.54/−0.49 e Å^{-3}. Further details of the crystal structure investigation may be obtained from the Fachinformationszentrum Karlsruhe, D-76344 Eggenstein-Leopoldshafen (Germany), on quoting the depository number CSD-58076.
[11] G. Henkel, S. Weissgräber, *Angew. Chem.* **1992**, *104*, 1382–1383; *Angew. Chem. Int. Ed. Engl.* **1992**, *31*, 1368–1369.
[12] A. Shaver, S. Morris, R. Turrin, V. W. Day, *Inorg. Chem.* **1990**, *29*, 3622–3623.
[13] R. Minkwitz, H. Borrmann, J. Nowicki, *Z. Naturforsch. B* **1992**, *47*, 915–918.
[14] C. R. Pulliam, J. B. Thoden, A. M. Stacy, B. Spencer, M. H. Englert, L. F. Dahl, *J. Am. Chem. Soc.* **1991**, *113*, 7398–7410.
[15] J. W. Kang, K. Moseley, P. M. Maitlis, *J. Am. Chem. Soc.* **1969**, *91*, 5970–5977.
[16] D. Seyferth, B. W. Hames, *Inorg. Chim. Acta* **1983**, *77*, L1–L2.
[17] W. R. Cullen, A. Talaba, S. J. Rettig, *Organometallics* **1992**, *11*, 3152–3156.
[18] a) R. Hoffmann, *Angew. Chem.* **1982**, *94*, 725–739; *Angew. Chem. Int. Ed. Engl.* **1982**, *21*, 711–724; b) F. G. A. Stone, *ibid.* **1984**, *96*, 85–96 and **1984**, *23*, 89–99.
[19] M. Herberhold, G.-X. Jin, A. L. Rheingold, G. F. Sheats, *Z. Naturforsch. B* **1992**, *47*, 1091–1098.
[20] W. Bronger, RWTH Aachen, personal communication, **1995**.

Heteroatom-Substituted Bicyclo[1.1.1]pentanes with Two Boron Atoms as Electron-Deficient Centers**

Matthias Menzel, Christine Wieczorek, Sigrid Mehle, Jürgen Allwohn, Heinz-Jürgen Winkler, Markus Unverzagt, Matthias Hofmann, Paul von Ragué Schleyer, Stefan Berger, Werner Massa, and Armin Berndt*

Dedicated to Professor Peter Paetzold on the occasion of his 60th birthday

The dicarbapentaboranes(5) (**1**)[2] are the only known bicyclo[1.1.1]pentane derivatives[1] with boron atoms as electron-deficient centers. Here we report on the synthesis, X-ray crystal structures, and NMR data of the 2-methylene (**3a**) and 2-sila (**4a**) derivatives of diborabicyclo[1.1.1]pentane **2**. In addition, we computed the geometries and the chemical shifts of the unsubstituted (u) parent compounds **2u**, **3u**, and **4u** by ab initio methods to rationalize the observed properties of **3a** and **4a**.

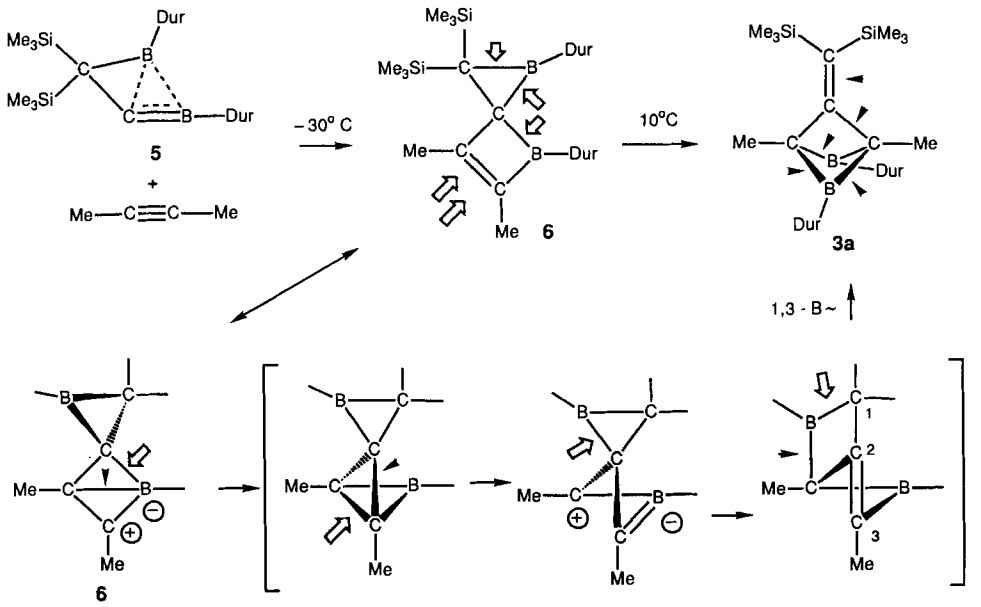


1,4-Diboraspiro[2.3]-hex-5-ene **6** can be obtained from methyleneborane **5**[3] and 2-butyne at −30 °C. It isomerizes to **3a** in less than one hour at 10 °C. A plausible[4] reaction mechanism involving low energy intermediates[5] is given. (The bonds marked in Scheme 1 with open arrows and black arrowheads are broken and formed, respectively).

The X-ray crystal structure[6] of **3a** (Fig. 1) shows a surprising feature: the C2–B4 distance (188.3 pm) is significantly shorter than the C2–B5 distance (197.7 pm) even though higher

[*] Prof. Dr. A. Berndt, Dr. M. Menzel, Dr. C. Wieczorek, Dr. S. Mehle, Dr. J. Allwohn, Dipl.-Chem. H.-J. Winkler, M. Unverzagt, Prof. Dr. S. Berger, Prof. Dr. W. Massa
Fachbereich Chemie der Universität
D-35032 Marburg (Germany)
Telefax: Int. code + (6421)28 89 17
Dipl.-Chem. M. Hofmann, Prof. Dr. P. von R. Schleyer
Computer-Chemie-Centrum der Universität
Nägelsbachstrasse 25, D-91052 Erlangen (Germany)

[**] This work was supported by the Deutsche Forschungsgemeinschaft, the Volkswagen-Stiftung, the Convex Computer Corporation, and the Fonds der Chemischen Industrie.



Scheme 1. Synthesis of **3a** starting from **5** and proposed mechanism for the isomerization **6** → **3a**. The open arrows mark the bonds to be broken in the next step, the black arrowheads the bonds that formed in the last step. Dur = 2,3,5,6-tetramethylphenyl.

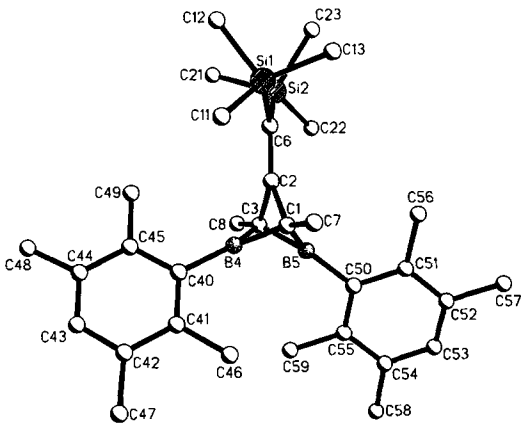
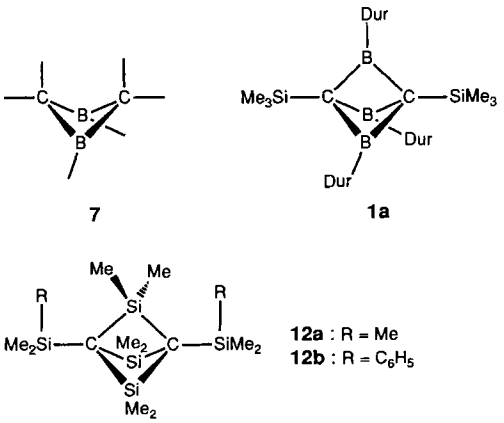


Fig. 1. Crystal structure of **3a**. Relevant distances [pm] and angles [°] (in addition to Table 1): C1-B4 153.9(3), C3-B4 160.9(4), C1-B5 157.5(3), C3-B5 154.1(4), C1-C2 156.4(4), C3-C2 152.9(3), C1 · · · C3 217.4(4), C2-C6 136.4(3); C1-B4-C3 87.3(2), C3-B5-C1 88.4(2), C1-C2-C3 89.2(2), B4-C1-C2 74.7(2), B4-C3-C2 73.7(2), B5-C1-C2 78.1(2), B5-C3-C2 80.1(2); C1-C2-C6-Si1 −23.6(3), C1-C2-C6-Si2 156.6(2)

symmetry is possible. In contrast, in the ^{13}C NMR spectrum of **3a** signals of only one kind of duryl group were observed even at −80 °C. Hence, the boron atoms are equivalent in solution according to NMR spectroscopy. The boron chemical shift for **3a** ($\delta(^{11}B) = 34$) is far from the usual range for 1,3-diboretanes **7** ($\delta(^{11}B) = 82 \pm 2$[7]) but close to that of dicarbapentaborane(5) **1a** ($\delta(^{11}B) = 21$).

The MP2(fc)/6-31G* geometry[8] **3u** (Fig. 2), like that of **3a**, exhibits a short (170.7 pm, C2–B4) and a long (208.1 pm, C2–B5) carbon–boron distance. The C_{2v} structure **3u*** with equal distances for C2–B4 and C2–B5 (188.4 pm) is 3.0 kcal mol^{-1} higher in energy than **3u** and is the transition structure for the rapid exchange of the chemical environments of the boron atoms in **3u**.[10] GIAO-MP2/tzpdz calculations[9] (Fig. 2) gave boron chemical shifts of $\delta(^{11}B) = 6.2$ (B4) and 34.9 (B5) for **3u**. The average value, 20.6, is in accord with the experimental value $\delta(^{11}B) = 34$, when the effects of the different substituents are taken into account (compare $\delta(^{11}B) = 1.9$ for **1u**[2] and 21 for **1a**). The C=C bond in **3u** hardly influences the strong shielding



12a : R = Me
12b : R = C_6H_5

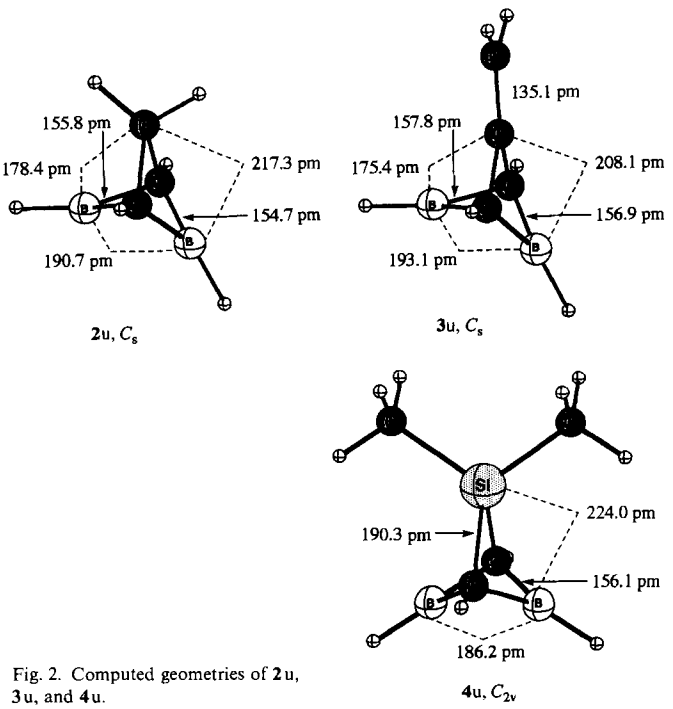


Fig. 2. Computed geometries of **2u**, **3u**, and **4u**.

 © VCH Verlagsgesellschaft mbH, D-69451 Weinheim, 1995 0570-0833/95/0606-0658 $ 10.00+.25/0

Table 1. Computed (**2u**, **3u**, **4u**) and experimental distances (**3a**, **4a**) [pm] and chemical shieldings of framework atoms.

	2u (X = C2)	**3u** (X = C2)	**3a** (X = C2)	**4u** (X = Si)	**4a** (X = Si)
X-B4	178.4	170.7	188.3(3)	224.0	223.2(6)
X-B5	217.3	208.1	197.7	224.0	225.2(6)
B4-B5	190.7	193.1	194.9(3)	186.2	187.6(6)
$\delta(^{13}C1,C3)$	72.0	76.8	91.7	82.2	98.6
$\delta(^{11}B4)$	10.9	6.2	34	39.2	46
$\delta(^{11}B5)$	40.0	34.9	34	39.1	46
δ(X)	−1.4	101.4	124.2	−140.4	−99.6
$\delta(^{13}C6)$	–	106.8	80.2	–	–

of the boron atoms.[11] The GIAO-MP2 $\delta(^{11}B)$ NMR shifts of **2u** (10.9 (B4) and 40.0 (B5)) are only about 5 ppm larger than those of **3u**. The lowest energy structure of **2u** (C_s), like **3u**, has a short C2–B4 distance (178.4 pm) and a long C2–B5 distance (217.3 pm). The C_{2v} symmetry form, **2u***, a transition structure with equal C2–B distances (201.1 pm), is 3.2 kcal mol^{-1} higher in energy than **2u**. Strong hyperconjugation between the strained C1–C2,C3 bonds and B4 and between the B4–C1,C3 bonds and B5 results in the strong boron shieldings in **3u** and **2u**. Analogous interactions of a boron atom with four neighboring strained C–B bonds give rise to the strong boron shielding in dicarbapentaborane **1** (see above). This was shown by means of an NBO analysis[12] involving a second-order perturbative estimation of donor–acceptor interactions. In addition, in **3u** π-electron density is transferred from the C2–C6 bond to B4, and there is back donation from the B4–C1,C3 bonds into the C2–C6 π^* orbital. Analogous but weaker interactions take place in **2u**, where C-H σ and σ^* orbitals act as donors and acceptors, respectively.

Hence, the nonclassical characteristics of **1** are not changed when one boron atom is replaced by an sp^2 (**3**) or an sp^3 (**2**) carbon atom. In the related 2-sila-4,5-diborabicyclo[1.1.1]-pentanes **4**, the nonclassical character of **1** is also conserved to a large extent. Borataalkyne **8**[13] reacts with chlorodimethylsilane to give **4a**, probably via intermediates **9**–**11** (Scheme 2). The crystal structure of **4a** is shown in Figure 3.[6] Important distances and the chemical shifts of the framework atoms are listed with those calculated for **4u** in Table 1. The experimental distances of **4a** differ little from those computed for **4u**. The chemical shift of the boron atoms in **4a** (δ = 46) lies *between* the values of classical 1,3-diboretanes **7** and the nonclassical dicarbapentaboranes **1**. The chemical shifts computed for **4u**, $\delta(^{11}B)$ = 39.1 and $\delta(^{29}Si)$ = −140.4, agree with the experimental values of **4a** (see Table 1), as long as the substituent effects are taken into account. Note the strong shielding of the bridging silicon atom in **4a**, $\delta(^{29}Si)$ = −99.6. The Si atoms in the $SiMe_2$ bridges in trisilabicyclo[1.1.1]pentanes **12a**, **b**[14] form C1-Si-C3 angles (79.5°) comparable to those in **4a** (75.4°), but the ^{29}Si chemical shifts of −4.9 (**12a**) and 31.9 (**12b**) differ. Therefore, the small angle at the Si2 atom of **4a** is not the source of the strong shielding.[15] No unusual chemical shifts are observed in bicyclo[1.1.1]pentanes, either.[17]

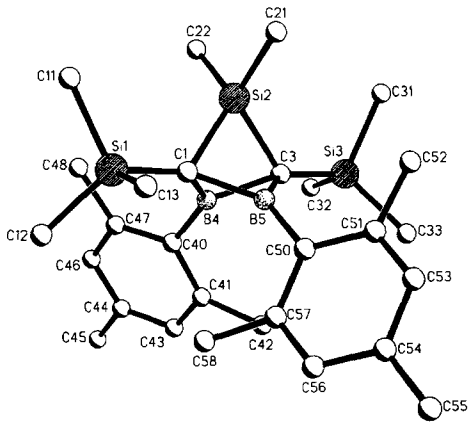
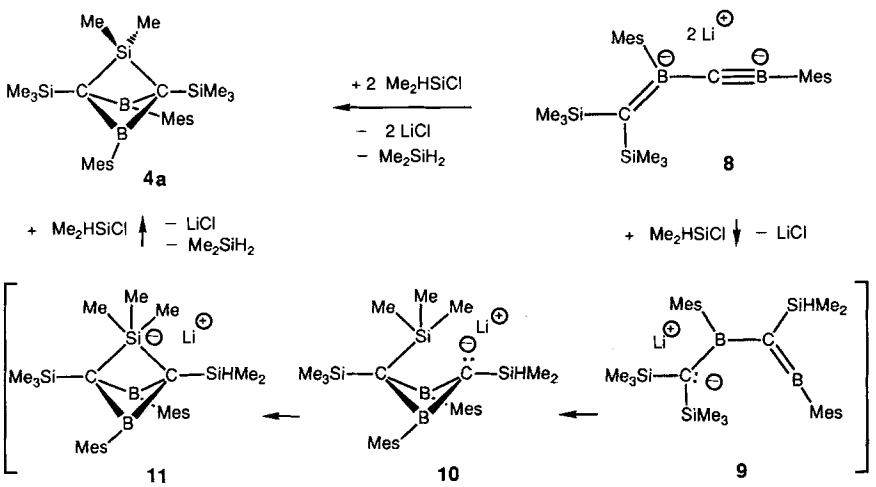


Fig. 3. Crystal structure of **4a**. Relevant distances [pm] and angles [°] (in addition to Table 1): C1-B4 158.3(6), C3-B4 159.9(6), C1-B5 159.2(6), C3-B5 156.9(7), C1-Si2 189.4(5), C3-Si2 189.3(4), C1···C3 231.7(6); C1-B4-C3 93.4(4), C3-B5-C1 94.4(4), C1-Si2-C3 75.4(2), B4-C1-Si2 78.6(3), B4-C3-Si2 79.2(3), B5-C1-Si2 80.6(3), B5-C3-Si2 80.1(3).

The strong shielding of framework atoms in heterobicyclo[1.1.1]pentanes is apparently due to the presence of electron-deficient centers. The second-order perturbative estimation of donor–acceptor interactions with NBO analysis[12] revealed that hyperconjugation of the C–B bonds in **4u** and in **1u** is equally strong. However, there are twice as many C–B bonds per boron atom in the latter. The hyperconjugation in **4u** is significantly weaker, because Si–C bonds are not as effective as C–B bonds as hyperconjugative donors. 2-Sila-4,5-diborabicyclo[1.1.1]pentanes **4** differ from dicarbapentaboranes(5) **1** only in the magnitude of the nonclassical interactions. These sila derivatives **4** are the simplest[18] examples of heterodicarboranes. Physical data for **1a**, **3a**, **4a**, and **6** are listed in Table 2.



Scheme 2. Synthesis of **4a**. Mes = 2,4,6-trimethylphenyl.

Experimental Procedure

6 and **3a**: 2-Butyne (0.18 g, 3.25 mmol) was added dropwise to a solution of **5** (1.49 g, 3.25 mmol) in 30 mL of pentane cooled to −78 °C. After the mixture had warmed to −30 °C, all volatile components were removed under high vacuum, and the pale yellow solid **6** was dissolved in 50 mL of pentane with cooling. The pale yellow suspension was warmed to 7 °C and stirred at this temperature until a clear red solution formed. The volatile material was removed under vacuum, the resulting yellow residue taken up in hexane at 0 °C, and the solid that precipitated removed by filtration through a D4 frit. **3a** crystallized from hexane at −30 °C as yellow cubes.

4a: Chlorodimethylsilane (2.0 g, 21.2 mmol) was added dropwise to a solution of **8** (4.19 g, 7.07 mmol) in 50 mL of diethyl ether cooled at −20 °C. The mixture was kept at −10 °C for 2 h and then stirred and

Table 2. Selected physical data for compounds **1a**, **3a**, **4a**, and **6**.

1a (colorless crystals): m.p. > 200 °C, yield: 69%. – ^{1}H NMR (500 MHz, $CDCl_3$, −30 °C): δ = −0.03 (s, 18H, $SiMe_3$), 2.15, 2.23 (each s, each 18H, *o*- and *m*-CH_3), 7.03 (s, 3H, *p*-H); ^{13}C NMR (125 MHz, $CDCl_3$, −30 °C): δ = −1.3 (6C, $SiMe_3$), 20.4, 20.9 (each 6C, *o*- and *m*-CH_3), 127.0 (2C, CB_2), 131.5, 133.5, 136.4 (total of 15C, *o*-, *m*-, *p*-C), 132.4 (br., 3C, *i*-C); ^{11}B NMR (96 MHz, $CDCl_3$, 25 °C): δ = 21

3a (yellow crystals): m.p. 62 °C, yield: 75%. – ^{1}H NMR (400 MHz, $CDCl_3$, −40 °C): δ = 0.24 (s, 18H, $SiMe_3$), 1.97 (s, 6H, CH_3), 2.20, 2.34 (each s, total of 24H, *o*- and *m*-CH_3), 7.15 (s, 2H, *p*-H); ^{13}C NMR (125 MHz, CD_2Cl_2, −60 °C): δ = 3.9 (q, 6C, $SiMe_3$), 12.6 (q, 2C, CH_3), 19.4, 19.9 (each q, 8C, *o*- and *m*-CH_3), 80.2 (s, 1C, ^1J(C, Si) = 58 Hz, CSi_2), 91.7 (s, 2C, CB_2), 124.2 (br.s, 1C, $=CC_2$), 132.6 (d, 2C, *p*-C), 133.8, 136.7 (each s, each 4C, *o*- and *m*-C), 142.5 (br.s, 2C, *i*-C); ^{11}B NMR (96 MHz, pentane, 10 °C): δ = 34

4a (colorless crystals): m.p. 165 °C, yield: 73%. – ^{1}H NMR (300 MHz, $CDCl_3$, 25 °C): δ = 0.01 (s, 18H, $SiMe_3$), 0.39 (s, 6H, $SiMe_2$), 2.22 (18H, *o*- and *p*-CH_3), 6.75 (s, 4H, *m*-H), ^{13}C NMR (100 MHz, $CDCl_3$, 25 °C): δ = 0.3 (q, 6C, $SiMe_3$), 5.0 (q, 2C, $SiMe_2$), 21.0 (q, 2C, *p*-CH_3), 23.4 (q, 4C, *o*-CH_3), 98.6 (s, 2C, CB_2), 128.0 (d, 4C, *m*-C), 133.9 (br.s, 2C, *i*-C), 137.6 (s, 2C, *p*-C), 140.1 (s, 4C, *o*-C); ^{11}B NMR (96 MHz, $CDCl_3$, 25 °C): δ = 46; ^{29}Si NMR (79 MHz, $CDCl_3$, 25 °C): δ = −11.0 (s, 2Si, $SiMe_3$), −99.6 (s, 1Si, $SiMe_2$)

6 (pale yellow solid): yield: quantitative by NMR spectroscopy. – ^{13}C NMR (125 MHz, $CDCl_3$, −30 °C): δ = 2.3, 2.9 (each q, each 3C, $SiMe_3$), 13.6, 15.8 (each q, each 1C, CH_3), 19.2 (br.), 19.3 (br.), 19.6 (br.), 19.8 (br.), 20.1 (br.), 20.3 (each q, 8C, *o*- and *m*-CH_3), 24.6 (s, 1C, CSi_2), 51.2 (br.s, 1C, CB_2), 130.3, 132.7 (each d, each 1C, *p*-C), 131.0, 133.0, 133.3, 136.3 (each s, 6C, *o*- and *m*-C), 138.1 (br.s, 1C, *i*-C), 144.0 (br.s, 2C, *o*-C of Dur on three-membered ring), 155.8 (s, 1C, $=CC_2$), 164.5 (br.s, 1C, =CB)

warmed to 25 °C for another 10 h. The volatile components were removed under vacuum, the residue was treated with pentane, and the the lithium chloride was removed with a D4 frit. The pentane soluton was concentrated and cooled to −20 °C to yield 2.5 g of **4a** as fine needles.

Received: June 22/July 22, 1995
Revised version: December 6, 1995 [Z 7065/7158 IE]
German version: *Angew. Chem.* **1995**, *107*, 728

Keywords: bicyclopentanes · boron compounds · hyperconjugation

[1] a) D. Bromm, U. Seebold, M. Noltemeyer, A. Meller, *Chem. Ber.* **1991**, *124*, 2645–2649; b) M. Bühl, J. Gauss, M. Hofmann, P. von R. Schleyer, *J. Am. Chem. Soc.* **1993**, *115*, 12385–12390, and references therein.

[2] R. Köster, M. A. Grassberger, *Angew. Chem.* **1967**, *79*, 197–219; *Angew. Chem. Int. Ed. Engl.* **1967**, *6*, 218–240; M. A. Grassberger, R. Köster in *Methoden Org. Chem. (Houben-Weyl) 4th ed. 1952* – Vol. XIII/3c, **1984**, pp. 156–214.

[3] A. Berndt, *Angew. Chem.* **1993**, *105*, 1034–1058; *Angew. Chem. Int. Ed. Engl.* **1993**, *32*, 985–1009, and references therein.

[4] For the small activation energy for allyl shifts in borylallyl compounds see M. Bühl, P. von R. Schleyer, M. A. Imbrahim, T. Clark, *J. Am. Chem. Soc.* **1991**, *113*, 2466–2471, and references therein.

[5] The triple bond of 2-butyne is cleaved during the reaction with **5** by insertion of two B-Dur fragments and one $C{=}C(SiMe_3)_2$ moiety. Similar insertions were reported for the reaction of alkynes with B_4H_{10}: M. A. Fox, R. Greatrex, M. Hofmann, P. von R. Schleyer, *Angew. Chem.* **1995**, *106*, 2384–2386; *Angew. Chem. Int. Ed. Engl.* **1995**, *33*, 2298–2300, and references therein.

[6] X-ray structure analyses were conducted with a four-circle diffractometer (CAD4, Enraf-Nonius) with $Cu_{K\alpha}$ radiation (λ = 154.178 ppm) at −80 °C. The structures were solved by direct methods and refined with full matrix against the F_o^2 data employing the SHELXL-93 system (**3a**) or against the F_o data with the SHELXTL-plus (**4a**) system. Anisotropic temperature factors were used for all non-hydrogen atoms. **3a**. $C_{32}H_{50}B_2Si_2$, crystal dimensions 0.5 × 0.3 × 0.3 mm^3, triclinic, space group $P\bar{1}$, Z = 2, a = 880.4(2), b = 1190.0(2), c = 1600.7(3) pm, α = 88.73(3), β = 88.97(3), γ = 79.88(3)°, V = 1650.3 × 10^{-30} m^3, ρ_{calcd} = 1.031 g cm^{-3}; total of 5259 reflections collected in ω-scan mode up to 2θ = 150°; 5120 out of 5123 independent reflections used in subsequent calculations after LP correction; no absorption correction (μ = 10.8 cm^{-1}). The hydrogen atoms were considered in the calculations to be „riding" on their bonding partners in groups with common isotropic temperature factors. Final wR_2 = 0.1622 and R = 0.050 for 3825 reflections with $F_o > 4\sigma(F_o)$. The maximum residual electron density was 0.27 e Å^{-3}. **4a**: $C_{28}H_{46}B_2Si_3$, crystal dimensions 0.5 × 0.3 × 0.6 mm^3, monoclinic, space group $P2_1/c$, Z = 4, a = 1337.6(5), b = 1347.9(2), c = 1779.2(7) pm, β = 106.81(2)°, V = 3070.6 × 10^{-30} m^3, ρ_{calcd} = 1.057 g cm^{-3}; total of 4544 reflections collected in ω-scan mode up to 2θ = 110°; 3256 (with $F_o > 3\sigma(F_o)$) out of 3849 independent reflections used in subsequent calculations after LP correction; no absorption correction (μ = 14.1 cm^{-1}). All hydrogen atoms could be localized by difference Fourier synthesis and were considered in the calculations as riding on their bonding partners in groups with common isotropic temperature factors. Employing weights of $w = 1/\sigma^2(F_o)$ resulted in R = 0.063 and wR = 0.058. The maximum residual electron density was 0.50 e Å^{-3}. Further details of the crystal structure investigation may be obtained from the Fachinformationszentrum Karlsruhe, D-76344 Eggenstein-Leopoldshafen (FRG), on quoting the depository number CSD-58797.

[7] G. Schmidt, G. Baum, A. Berndt, *Angew. Chem.* **1986**, *98*, 1123–1124; *Angew. Chem. Int. Ed. Engl.* **1986**, *25*, 1111–1112.

[8] Geometry optimizations and frequency calculations were performed with Gaussian 92 to determine the nature of the stationary points: M. J. Frisch, G. W. Trucks, M. Head-Gordon, P. M. W. Gill, M. W. Gomperts, J. L. Andres, K. Raghavachari, J. S. Binkley, C. Gonzalez, R. I. Martin, D. J. Fox, D. J. Defrees, J. Baker, J. J. P. Stewart, J. A. Pople, Gaussian 92, Gaussian, Inc., Pittsburgh, PA, USA, **1992**.

[9] For GIAO-MP2 see a) J. Gauss, *Chem. Phys. Lett.* **1992**, *191*, 614; b) J. Gauss, *J. Chem. Phys.* **1993**, *99*, 3629–3643. The method was implemented in ACESII: ACESII, an ab initio program system by J. F. Stanton, J. Gauss, J. D. Watts, W. J. Lauderdale, R. J. Bartlett, Quantum Theory Project, University of Florida, 1991 and 1992. tzpdz stands for "triple zeta plus polarization" basis sets for heavy atoms and "double zeta" basis sets for hydrogen atoms: A. Schäfer, H. Horn, R. Ahlrichs, *J. Chem. Phys.* **1992**, *97*, 2571–2577.

[10] The notably different NMR shifts of the C atoms in the C=C bonds in **3a** and **3u** are likely to be due to the trimethylsilyl substituents, which induce a negative partial charge at C6 (stabilized by the α-Si effect) and a positive partial charge at C2. IGLO(II′) computations for **3u′** (two SiH_3 substituents at C6) show significant shielding of C6 ($\delta(^{13}C)$ = 95.0) and deshielding of C2 ($\delta(^{13}C)$ = 142.2) relative to the data computed for **3u** at the same level ($\delta(^{13}C)$ = 112.5 (C6) and 118.0 (C2)). The difference $\Delta\delta(^{13}C)$ (C2,6) is 47 ppm for **3u′**, close to the experimental difference of 44 ppm. **3u′** was too large for GIAO-MP2/tzpdz computations.

[11] Siebert et al. reported strong shielding for the boron atom of a 3-methylenboretane derivative: M. Enders, H. Pritzkow, W. Siebert, *Angew. Chem.* **1992**, *104*, 628–629; *Angew. Chem. Int. Ed. Engl.* **1992**, *31*, 606–607.

[12] NBO = natural bond orbital: A. E. Reed, L. A. Curtiss, F. Weinhold, *Chem. Rev.* **1988**, *88*, 899–926.

[13] J. Allwohn, M. Pilz, R. Hunold, W. Massa, A. Berndt, *Angew. Chem.* **1990**, *102*, 1084–1085; *Angew. Chem. Int. Ed. Engl.* **1990**, *29*, 1032–1033.

[14] W. Ando, H. Yoshida, K. Kurishima, M. Sugiyama, *J. Am. Chem. Soc.* **1991**, *113*, 7790–7792.

[15] The Si atoms in siliranes are considerably shielded: $\delta(^{29}Si)$ = −49.3 to −58.8 [16].

[16] R. L. Lambert, D. Seyferth, *J. Am. Chem. Soc.* **1972**, *94*, 9246–9248; P. Boudjouk, E. Black, R. Kumarathasan, *Organometallics* **1991**, *10*, 2095–2096, and references therein.

[17] M. Barfield, *J. Am. Chem. Soc.* **1993**, *115*, 6916–6928, and references therein.

[18] Heterodicarbaboranes with four and more boron atoms: L. J. Todd in *Metal Interactions with Boron Clusters* (Ed.: R. N. Grimes), Plenum, New York, **1982**, pp. 145–171; J. Kim, S. Kim, Y. Do, *J. Chem. Soc. Chem. Commun.* **1992**, 938–939, and references therein; A. K. Saxena, N. S. Hosmane, *Chem. Rev.* **1993**, *93*, 1081–1124.

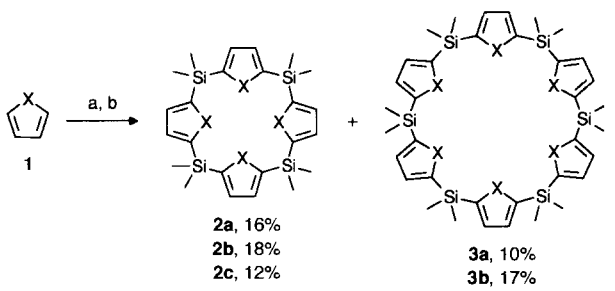
 © VCH Verlagsgesellschaft mbH, D-69451 Weinheim, 1995 0570-0833/95/0606-0660 $ 10.00+.25/0

Silicon-Bridged Macrocycles—Synthesis of Sila-calixarenes**

Burkhard König,* Martin Rödel, Peter Bubenitschek, and Peter G. Jones

Specific recognition on a molecular level requires close correspondence between the shape of the receptor and the substrate molecule, or between lock and key in the image of Emil Fischer.[1] Macrocyclic structures can provide the necessary preorganization of the host for the inclusion process, and therefore most artifical receptors are cyclic molecules.[2] Carbon is the common bridging element in natural and synthetic macrocycles, such as porphyrins or calixarenes. However, carbon does not contribute to the binding properties of these ligands, while elements such as silicon, tin, or phosphorus can serve as additional coordination sites.[3] We describe here the facile synthesis of silicon-bridged macrocycles, including the first silacalix[4]arene, from readily available starting materials.

Furan, thiophene, and *N*-methylpyrrole, **1a–c**, are deprotonated in the 2- and 5-position by treatment with two equivalents *n*BuLi/TMEDA/KO*t*Bu (1/1/1) (TMEDA = *N*,*N*,*N*′*N*′-tetramethyl-1,2-ethanediamine) in hexane.[4] Slow addition of a solution of Me_2SiCl_2 in hexane gave the macrocyclic tetramers **2a–c**[5] and hexamers **3a–b** in yields up to 35% (Scheme 1, Table 1). The fast reaction of the organolithium compounds with Me_2SiCl_2 enabled the synthesis of the cyclic structures at organolithium concentrations of 10^{-2} M.



Scheme 1. Macrocyclization of heterocyclic dianions with Me_2SiCl_2; **a**, X = O; **b**, X = S[4]; **c**, X = NMe. a) 2.1 equiv *n*BuLi/TMEDA/KO*t*Bu (1/1/1) hexane, 2 h, −90 to 25 °C; b) 1.0 equiv Me_2SiCl_2, slow addition. For **2b** see also ref.[5].

All macrocycles, with the exception of **3a**, are high melting, crystalline solids, readily soluble in nonpolar organic solvents. The X-ray structure analysis of **2b** (Fig. 1)[6] displays crystallographic inversion symmetry and a 1,3-*anti* arrangement of the thiophene units in the crystal, similar to its known carbocyclic analogue tetrathiaporphyrinogene.[7]

While the hexa- and tetrameric structures of thiophene and furan were obtained in nearly equal amounts, the silaporphyrinogene **2c** was the single isolated cyclic structure from *N*-methylpyrrole. Macrocycles with ring sizes other than four or six in the reaction mixtures could be detected only in traces by mass spectrometry.

Table 1. Selected spectroscopic data [a] of **2a,c**, **3a**, **3b**, **5**, **6**, **8**, and **9**.

2a: Colorless crystals, m.p. 115 °C; ^{1}H NMR: δ = 0.53 (s, 24H), 6.65 (s, 8H); ^{13}C NMR: δ = −3.18 (+), 120.38 (+), 161.83 (C_{quat}); MS (70 eV): *m/z* (%): 496 (100) [M^+].

2c: White solid, m.p. 295 °C; ^{1}H NMR: δ = 0.44 (s, 24H), 3.00 (s, 12H), 6.41 (s, 8H); ^{13}C NMR: δ = −1.93 (+), 35.53 (+), 119.69 (+), 136.40 (C_{quat}); MS (70 eV): *m/z* (%): 548 (20) [M^+], 492 (100).

3a: Oil; ^{1}H NMR: δ = 0.55 (s, 36H), 6.68 (s, 12H); ^{13}C NMR: δ = −3.08 (+), 121.03 (+), 161.85 (C_{quat}); MS (70 eV): *m/z* (%): 744 (10) [M^+], 207 (100).

3b: White solid, m.p. 290 °C; ^{1}H NMR: δ = 0.62 (s, 36H), 7.33 (s, 12H); ^{13}C NMR: δ = 0.00 (+), 136.54 (+), 143.81 (C_{quat}); MS (70 eV): *m/z* (%): 840 (100) [M^+].

5: Colorless crystals, m.p. 106 °C; ^{1}H NMR: δ = 0.52 (s, 6H), 1.20 (s, 18H), 3.65 (s, 6H), 6.70 (m, 2H), 7.30 (m, 4H); ^{13}C NMR: δ = −1.70 (+), 31.55 (+), 34.05 (C_{quat}), 55.05 (+), 108.95 (+), 125.72 (C_{quat}), 127.18 (+), 133.33 (+), 142.36 (C_{quat}), 162.28 (C_{quat}); MS (70 eV): *m/z* (%): 384 (40) [M^+], 369 (100) [M^+−Me].

6: White solid, m.p. 160 °C; ^{1}H NMR: δ = 0.46 (br. s, 24H), 1.12 (br. s, 36H), 3.00 (br. s, 12H), 7.36 (br. s, 8H); ^{13}C NMR: δ = 0.44 (+), 31.43 (+), 31.47 (+), 34.30 (C_{quat}), 130.24 (C_{quat}), 135.13 (+), 144.62 (C_{quat}), 169.16 (C_{quat}); MS (70 eV): *m/z* (%): 880 (20) [M^+], 865 (20) [M^+−Me], 57 (100).

8: Oil, ^{1}H NMR: δ = 0.59 (s, 6H), 3.52 (s, 6H), 3.83 (s, 6H), 7.00 (m, 6H); ^{13}C NMR: δ = −0.65 (+), 56.20 (+), 60.82 (+), 114.65 (+), 124.64 (+), 127.79 (+), 133.29 (C_{quat}), 152.60 (C_{quat}), 154.49 (C_{quat}); MS (70 eV): *m/z* (%): 332 (11) [M^+], 225 (100).

9: Colorless crystals, m.p. 280 °C; ^{1}H NMR: δ = 0.63 (s, 24H), 3.58 (s, 24H), 6.57 (s, 8H); ^{13}C NMR: δ = −1.22 (+), 59.43 (+), 130.45 (+), 135.15 (C_{quat}), 157.02 (C_{quat}); MS (70 eV): *m/z* (%): 776 (40) [M^+], 57 (100).

[a] ^{1}H NMR: 400 MHz, $CDCl_3$, TMS; ^{13}C NMR: 100 MHz, $CDCl_3$; the multiplicity of the ^{13}C NMR signals was determined by the DEPT technique and quoted as (+) for CH_3 and CH, and (−) for CH_2 and C_{quat} for quaternary carbon atoms.

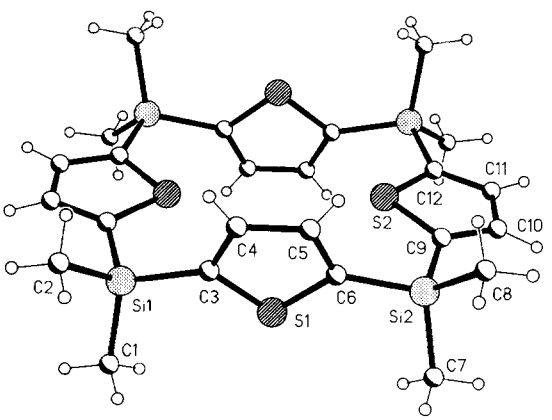
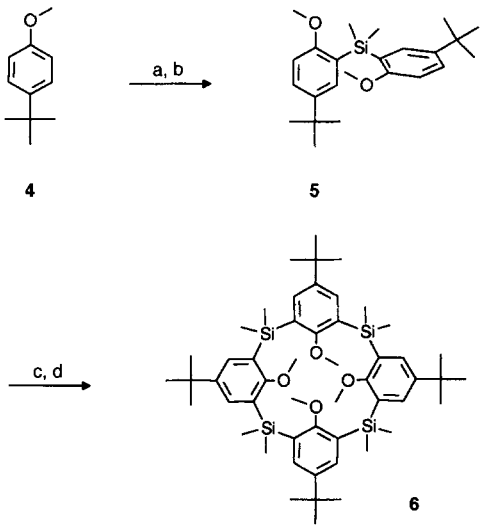


Fig. 1. Crystal structure of **2b**. Selected bond lengths [pm] and angles [°]: Si1–C3 185.7(2), S1–C3 172.5(2), C3–C4 136.8(2), C4–C5 141.8(2); C6-Si2-C9 107.56(7), (S1-C3-C6)-(S2-C9-C12) 98.7.

Methoxy groups have a strong *ortho* directing effect in the lithiation of aromatic rings.[8] However, the stabilization is insufficient to allow the formation of dianions. Therefore a stepwise procedure is necessary to obtain cyclic structures from *para-tert*-butylmethoxybenzene and Me_2SiCl_2 (Scheme 2). Monolithiation of **4** followed by reaction with Me_2SiCl_2 gave the crystalline dimer **5**, which was characterized by X-ray structure analysis.[6] Bislithiation of **5** was achieved with two equivalents *n*BuLi/TMEDA at room temperature and subsequent slow addition of one equivalent Me_2SiCl_2 yielded the *para-tert*-butylsilacalix[4]arene (**6**) in 16% isolated yield. The simple ^{1}H NMR spectrum of **6** indicates conformational mobility at room temperature in solution. At lower temperatures the signals significantly broaden, but defined conformers, as in the case of the carbocyclic

[*] Dr. B. König, M. Rödel, Dipl.-Chem. P. Bubenitschek
Institut für Organische Chemie der Technischen Universität
Hagenring 30, D-38106 Braunschweig (FRG)
Telefax: Int. code + (531)391-5388
Prof. Dr. P. G. Jones
Institut für Anorganische und Analytische Chemie der
Technischen Universität Braunschweig (FRG)

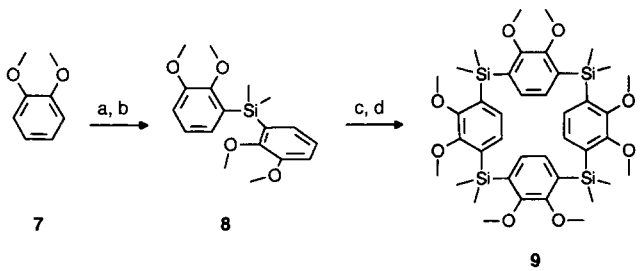
[**] This work was supported by the Fonds der Chemischen Industrie and the Deutsche Forschungsgemeinschaft. B. K. thanks the Fonds der Chemischen Industrie for a Liebig stipendium and Prof. Dr. H. Hopf for his support.



Scheme 2. Synthesis of the silacalix[4]arene **6**; a) 1.1 equiv *n*BuLi/TMEDA (1/1), 12 h, room temperature; b) 0.5 equiv Me_2SiCl_2; c) 2.1 equiv *n*BuLi/TMEDA (1/1), 12 h, room temperature; d) 1.0 equiv Me_2SiCl_2.

analogue *para-tert*-butylcalix[4]arene,[9] are not observed. The longer silicon–carbon bridges in **6** facilitate the rotation of the aromatic units.

1,2-Dimethoxybenzene (**7**) was converted to the dimer **8** and cyclized to macrocycle **9**[10] by the same procedure (Scheme 3, Table 1). Octa-methoxysila[1.1.1.1]paracyclophane (**9**) is, like **6**, a mobile compound at room temperature. A separation of the NMR signals is observed at $-90\,^{\circ}C$, indicating that the rotation of the aromatic rings or the *pseudo*-rotation of the *gem*-methyl groups becomes slow, on NMR time scale.[11]



Scheme 3. Synthesis of the sila[1.1.1.1]paracyclophane **9**; a)–d) see Scheme 2.

The reaction of bis-lithiated aromatic and heteroaromatic species with dichlorosilanes is a simple route to stable silicon-bridged macrocycles. Preliminary results with $PhPCl_2$ and Me_2SnCl_2 as electrophiles have also shown that other elements such as phosphorus or tin can substitute for silicon. The synthetic scope of the reaction and the good solubility of the silicon-bridged macrocycles in nonpolar organic solvents might lead to new synthetic receptors with additional coordination sites for the inclusion and the transport of ions or neutral guest molecules.

Experimental Procedure

2b, **3b**: *n*BuLi (1.26 mL, 10 M in hexane) was added to thiophene (504 mg, 6.0 mmol) and TMEDA (1.9 mL, 12.6 mmol) in dry hexane (300 mL) under nitrogen; the mixture was stirred for 30 min at room temperature and heated to reflux for an additional 30 min. Me_2SiCl_2 (730 µL, 6.0 mmol) in dry hexane (50 mL) was slowly added by syringe (5 mL h^{-1}), the mixture was stirred for an additional hour, poured into water (300 mL), the organic layer was washed with two portions of water, dried over $MgSO_4$, and evaporated in vacuo. The crude product was chromatographed on silica gel with CCl_4 (or petroleum ether:ether 8:1) as eluent to yield fraction I: 154 mg (18%) **2b**[5]; fraction II: 146 mg (17%) **3b**.

5: A mixture of *para-tert*-butylmethoxybenzene **4** (16.4 g, 100 mmol), TMEDA (16.4 mL, 110 mmol), and *n*BuLi (11 mL, 10 M) in ether (200 mL) was stirred at room temperature for 12 h, Me_2SiCl_2 (6 mL, 50 mmol) was added and the reaction mixture was stirred for additional 1 h. Usual workup, filtration through silica gel and recrystallization from *n*-heptane, yielded 16.15 g (84%) **5** as large crystals.

6: *n*BuLi (1.3 mL, 10 M in hexane) was added to a solution of **5** (2.3 g, 6.0 mmol) and TMEDA (2.0 mL, 13.4 mmol) in hexane (300 mL) under nitrogen and the mixture was strirred for 12 h at room temperature. Me_2SiCl_2 (0.73 mL, 6.0 mmol) in hexane (50 mL) was added over 7 h by syringe, the reaction mixture was poured into water (300 mL), and the organic layer was washed with water, dried, and evaporated in vacuo. Chromatography on silica gel (petroleum ether, 5% ether) gave 442 mg (16%) **6**.

Received: October 27, 1995 [Z7433IE]
German version: *Angew. Chem.* **1995**, *107*, 752

Keywords: calixarenes · macrocycles · silicon compounds · supramolecular chemistry

[1] E. Fischer, *Chem. Ber.* **1894**, *27*, 2985–2993; F. Vögtle, *Supramolecular Chemistry*, Wiley, New York 1991; F. W. Lichtenthaler, *Angew. Chem.* **1995**, *106*, 2456–2467; *Angew. Chem. Int. Ed. Engl.* **1995**, *33*, 2364–2374.

[2] B. Dietrich, P. Viout, J.-M. Lehn, *Macrocyclic Chemistry*, VCH, Weinheim, **1993**; for the synthesis of macrocycles from dilithio intermediates see J. Lin, Y. Pang, V. G. Young, T. J. Barton, *J. Am. Chem. Soc.* **1993**, *115*, 3794–3795; X. Yang, C. B. Knobler, Z. Zheng, M. F. Hawthorne, *ibid.* **1995**, *116*, 7142–7159.

[3] For the coordination properties of heteroelements in macrocycles see: tin: M. T. Blanda, J. H. Horner, M. Newcomb, *J. Org. Chem.* **1989**, *54*, 4626–4636; phosphorus: A.-M. Caminade, J. P. Majoral, *Chem. Rev.* **1995**, *94*, 1183–1213; silicon: M. E. Jung, H. Xia, *Tetrahedron Lett.* **1988**, *29*, 297–300; mercury: M. F. Hawthorne, X. Yang, Z. Zheng, *Pure Appl. Chem.* **1995**, *94*, 245–254.

[4] L. Brandsma, *Preparative Polar Organometallic Chemistry 1*, Springer, Berlin, **1990**; B. J. Wakefield, *Organolithium Methods*, Academic Press, London, **1988**; thiophene is sufficently acidic to be deprotonated in the 2,5-positions by *n*BuLi/TMEDA in hexane.

[5] Only the tetrameric structure **2b** was isolated in the previously reported reaction of a thiophene dimer with Me_2SiCl_2: T. Kauffmann, H.-H. Kniese, *Tetrahedron Lett.* **1973**, 4043–4046.

[6] X-ray crystal structure determination of **2b**: $C_{24}H_{32}S_4Si_4$, $M_r = 561.10$, triclinic, space group $P\bar{1}$, $a = 631.97(6)$, $b = 1017.05(10)$, $c = 1223.81(10)$ pm, $\alpha = 104.048(6)$, $\beta = 97.968(8)$, $\gamma = 96.465(8)^{\circ}$, $V = 0.74690(12)$ nm^3, $Z = 1$, $\lambda(Mo_{K\alpha}) = 71.073$ pm, $T = 173$ K. The final $wR(F^2)$ value was 0.072 for all 3394 reflections ($2\theta \leq 55^{\circ}$), with a conventional $R(F)$ value of 0.028 for 149 parameters. Siemens-P4 diffractometer with a Siemens-LT-2 low-temperature attachment. Program: SHELXL-93 (G. M. Sheldrick, Universität Göttingen). X-ray crystal structure determination of **5**: $C_{24}H_{36}O_2Si$, $M_r = 384.62$, triclinic, space group $P\bar{1}$, $a = 700.5(2)$, $b = 1040.1(2)$, $c = 1688.5(3)$ pm, $\alpha = 73.67(2)$, $\beta = 87.92(2)$, $\gamma = 82.27(14)^{\circ}$, $V = 1.1698(4)$ nm^3, $Z = 2$, $\lambda(Mo_{K\alpha}) = 71.073$ pm, $T = 143$ K. The final $wR(F^2)$ value was 0.156 for all 4277 reflections ($2\theta \leq 50^{\circ}$), with a conventional $R(F)$ value of 0.058 for 254 parameters. Stoe-STADI-4 diffractometer with a Siemens LT-2 low-temperature attachment. Further details of the structre invesigations can be obtained from the Fachinformationszentrum Karlsruhe, D-76344 Eggenstein-Leopoldshafen (FRG), on quoting the depository numbers CSD-401382 (**2b**) and CSD-401383 (**5**).

[7] E. Vogel, P. Röhrig, M. Sicken, B. Knipp, A. Herrmann, M. Pohl, H. Schmickler, J. Lex, *Angew. Chem.* **1989**, *101*, 1683–1686; *Angew. Chem. Int. Ed. Engl.* **1989**, *28*, 1651–1654.

[8] G. P. Crowther, R. J. Sundberg, A. M. Sarpeshkar, *J. Org. Chem.* **1984**, *49*, 4657–4663.

[9] L. C. Groenen, J.-D. van Loon, W. Verboom, S. Harkema, A. Casnati, R. Ungaro, A. Pochini, F. Ugozzoli, D. N. Reinholdt, *J. Am. Chem. Soc.* **1991**, *113*, 2385–2392; C. D. Gutsche, B. Dhawan, J. A. Levine, K. H. No, L. J. Bauer, *Tetrahedron* **1983**, *39*, 409–426.

[10] For a carbocyclic [1.1.1.1]paracyclophane see Y. Miyahara, T. Inazu, T. Yoshino, *Tetrahedron Lett.* **1983**, *24*, 5277–5280; analogous sulfur compound: M. L. Kaplan, W. D. Reents, Jr., *ibid.* **1982**, *23*, 373–374.

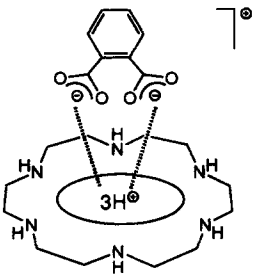
[11] The activation energy of this process could not be derived from the spectra due to the incomplete separation of the signals even at $-90\,^{\circ}C$.

 © VCH Verlagsgesellschaft mbH, D-69451 Weinheim, 1995 0570-0833/95/0606-0662 $ 10.00+.25/0

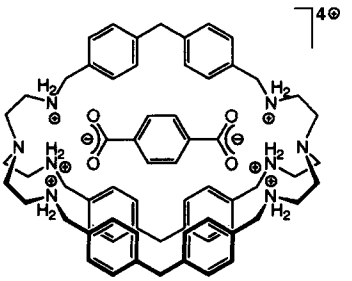
Molecular Recognition of Terephthalic Acid by Supramolecular Self-Assembly of an Acridine-Pendant Cyclen–Zn^{II} Complex**

Eiichi Kimura,* Takuya Ikeda, Mitsuhiko Shionoya, and Motoo Shiro

Selective molecular recognition of anionic substrates is of current interest. One classic example of a receptor is the cationic macrocyclic polyammonium compound that binds with phthalate (*o* isomer) to form complex **1** more strongly than with isophthalate (*m* isomer) or terephthalate (*p* isomer) due to more favorable electrostatic and hydrogen bonding interactions.[1] More recently, cryptate **2** was reported; here the substrate terephthalate dianion, which fits in the cavity, is bound by multiple hydrogen bonding, electrostatic, and hydrophobic interactions within a macrobicyclic polyammonium cryptand.[2]



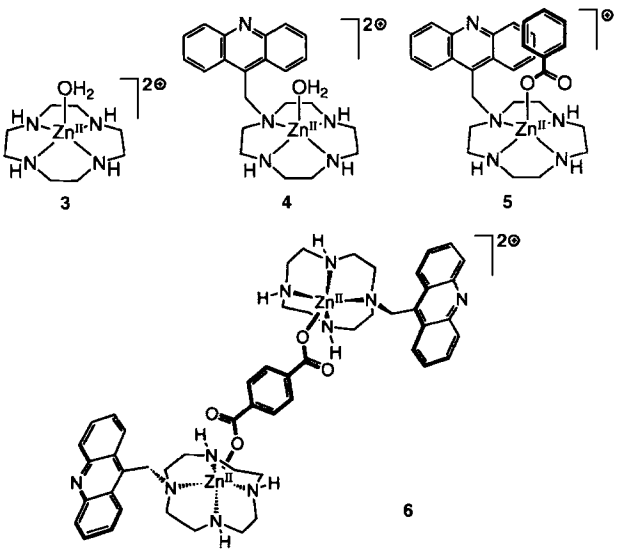
1



2

Another supramolecular approach to the selective molecular recognition of anions could involve the formation of aggregates by self-assembly of two or more molecular subunits through noncovalent interactions. If the binding partners are sufficiently complementary, the subunits might spontaneously build up an ordered aggregate.

In the context of our work on zinc(II) complexes of cyclen (**3**) and its acridine-pendant derivative **4**, which were initially designed for selective recognition of thymine and its derivatives,[3] we have found that **4** has a fairly strong affinity for the benzoate anion.[4] It yields a 1:1 complex **5** with a stability constant of log $K = 2.25 \pm 0.05$ in aqueous solution (K = [**5**]/([**4**][anion]) [M^{-1}], ionic strength $I = 0.10$ ($NaNO_3$), 25 °C). Complex **4** (10 mM) interacts with terephthalic acid (5 mM) in an aqueous solution containing ClO_4^- (25 mM) at pH 8.4 [25 mM TAPS buffer (TAPS = *N*-tris(hydroxymethyl)methyl-3-aminopropanesulfonic acid)] to form a crystalline precipitate of **6** immediately in high yield (90% based on terephthalic acid).



3 4 5

6

The isolated complex **6** comprises two Zn^{II} complexes **4** and one terephthalate dianion. It was characterized by ^1H NMR (in [D_6]DMSO) and IR spectroscopy ($\tilde{\nu} = 1599\ cm^{-1}$ (COO^-), 1360 (COO^-)) and elemental analysis.[5]

We initially suspected this 2:1 complex of having pronounced intramolecular π (guest)-π (host) stacking interactions. However, the X-ray crystal structure analysis of **6**·BF_4^-·ClO_4^-·$3H_2O$[6] (Fig. 1), showed more complex interactions. The zinc(II) ion

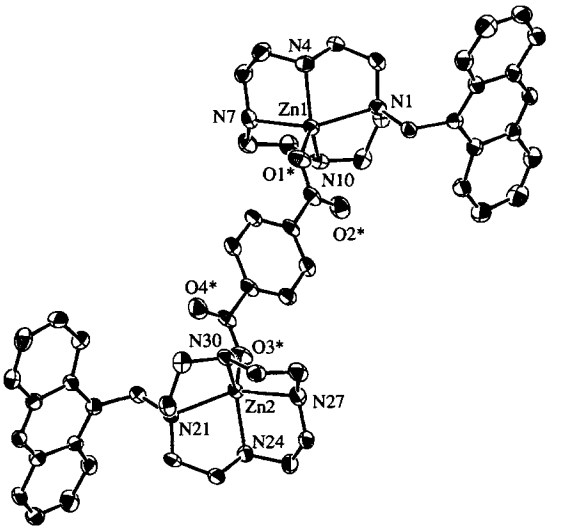


Fig. 1. An ORTEP plot (30 % probability ellipsoids) of **6**·BF_4^-·ClO_4^-·$3H_2O$. The perchlorate anion, the tetrafluoroborate anion, and the three water molecules are omitted for clarity. Selected bond lengths [Å] and angles [°]: Zn1–O1* 1.946(7), Zn2–O3*, 1.906(7), Zn1–N1 2.283(7), Zn1–N4 2.096(6), Zn1–N7 2.184(8), Zn1–N10 2.099(8), Zn2–N21 2.296(6), Zn2–N24 2.105(6), Zn2–N27 2.184(8), Zn2–N30 2.093(8); O1*-Zn1-N1 119.8(3), O1*-Zn1-N4 110.3(3), O1*-Zn1-N7 101.3(3), O1*-Zn1-N10 117.4(3), O3*-Zn2-N21 116.7(3), O3*-Zn2-N24 113.4(3), O3*-Zn2-N27 104.7(3), O3*-Zn2-N30 113.9(3).

resides in a distorted square-pyramidal environment, coordinated by four nitrogen atoms of the cyclen subunit and an oxygen atom of the terephthalate carboxylate anion (O1*–Zn1 1.946(7), O3*–Zn2 1.906(7) Å). In the crystal structure, the intercomplex array is more interesting (Fig. 2). The counterions (ClO_4^- and BF_4^-) lie in middle between two zinc(II) complexes,

[*] Prof. Dr. E. Kimura, T. Ikeda, Dr. M. Shionoya
Department of Medicinal Chemistry, School of Medicine
Hiroshima University, Kasumi 1-2-3, Minami-ku, Hiroshima 734 (Japan)
Telefax: Int. code + (82) 257-5324
Dr. M. Shiro
Rigaku Corporation, Matsubaracho 3-9-12, Akishima, Tokyo 196 (Japan)

[**] This work was supported by the Ministry of Education, Science and Culture in Japan, Grant-in-Aid (Scientific Research (A), No. 04403024 (E. K.) and Scientific Research (C) No.06807172 (M. S.)), the Kato Memorial Bioscience Foundation, the Tokyo Biochemical Research Foundation (M.S.), and The Japan Science Society (Sasagawa Scientific Research Grant (T. I.)). NMR instruments and a computer graphic system CAChe (Tetronix Co.) in the Medical Molecules Exploring Center of Hiroshima University were used. cyclen = 1,4,7,10-tetraazacyclododecane.

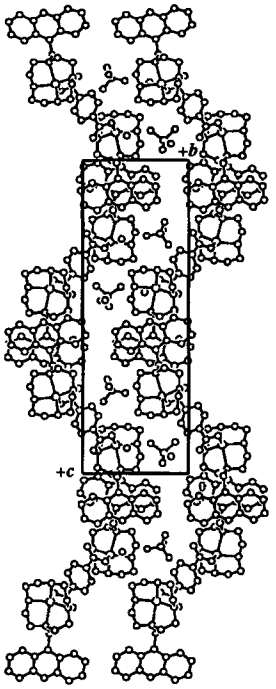
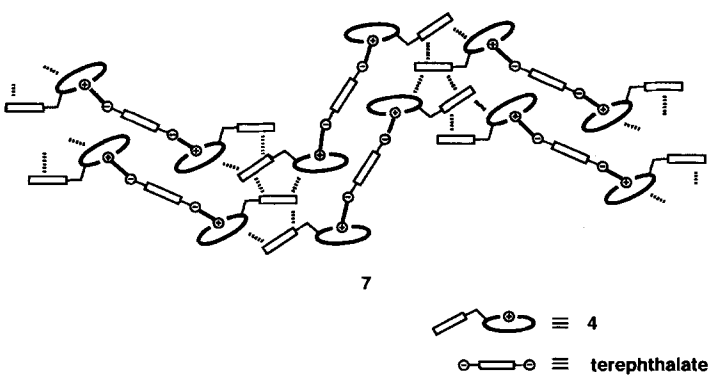


Fig. 2. Arrangement of the complex $6 \cdot BF_4^- \cdot ClO_4^- \cdot 3H_2O$ in the crystal along the crystallographic *a* axis.

and contribute greatly to the neutralization of the repulsive cationic charges. Two of the three water molecules lie in the vicinity of each zinc(II) ion and the third in that of a counterion. It is assumed that all molecules in a unit cell, that is two zinc(II) complexes, one terephthalate dianion, one ClO_4^- ion and one BF_4^-, and three water molecules, participate in the stabilization of this complex. Furthermore, the intermolecular interactions between the two acridine groups (at the closest interplane contact of 3.78 Å) and between an acridine group and the ethylene unit of a cyclen ring (closest contact 3.40 Å) form a well-organized chainlike aggregate **7** (Scheme 1). The pronounced stability of this supramolecular compound may be responsible for its extremely low solubility in water. Attempts to determine the stability constant of this 2:1 complex by potentiometric pH titration were unsuccessful, since the 2:1 complex precipitated immediately upon addition of the titrant.

It became apparent that the tendency of **6** to self-assemble into the supramolecule **7**, which is insoluble in water, may permit terephthalate to be separated efficiently from its isomers phthalate and isophthalate. The 2:1 complexes of phthalate and isophthalate with **4** were prepared as described for terephthalate. Both complexes remained in aqueous solution and scarcely precipitated out. We then tested the separation in the following way: 0.4 mL of an aqueous solution of $4 \cdot 2NO_3^-$ (20 mM)[8] was added to 0.4 mL of a solution containing the *o*, *m*, *p* isomers (each 10 mM) at pH 8.4 (25 mM TAPS buffer, 25 mM $NaClO_4$, 25 °C); immediate precipitation occurred. After 6 hours, the mixture was centrifuged and 0.54 mL of the upper solution layer was withdrawn and treated with D_2O (0.06 mL, 0.3% sodium [2,2,3,3-D_4]3-(trimethylsilyl)propionate). The ^1H NMR spectrum of this solution showed that the *p* isomer had almost completely disappeared, while most of the *o* (>95%) and *m* (>90%) isomers remained. According to the ^1H NMR spectrum in [D_6]DMSO of the collected precipitates, the major component (80%) was the *p* isomer **6**; a minor component (8%) comprising the 2:1 complex of **4** and isophthalate (*m* isomer) (the resulting composite; *p*:*m*:*o* = 10:1:0). The best separation of terephthalate from the *m* and *o* isomers with **4** (*p*:*m*:*o* = 15:1:0) was achieved when 5% CH_3CN was added to the above test solution.

We conclude that **4** selectively separates terephthalate as insoluble crystals from a mixture of terephthalate and its isomers phthalate and isophthalate, not because its 2:1 complex **6** has a particularly high stability constant, but because it is additionally stabilized by self-assembly into an ordered aggregate **7**. Metal complexes with aromatic pendants should also be useful for the molecular recognition of other anionic molecules in aqueous media.



Scheme 1. Schematic representation of the chainlike aggregate **7** formed from **6**.

Received: September 20, 1995 [Z 7334 IE]
German version: *Angew. Chem.* **1995**, *107*, 711

Keywords: complexes with nitrogen ligands · molecular recognition · supramolecular chemistry · zinc compounds

[1] a) E. Kimura, *Pure Appl. Chem.* **1993**, *65*, 355–359; b) *J. Inclusion Phenomena* **1989**, *7*, 183–191; c) *Pure Appl. Chem.* **1989**, *61*, 823–828; d) E. Kimura, A. Sakonaka, *J. Am. Chem. Soc.* **1982**, *104*, 4984–4985; e) E. Kimura, A. Sakonaka, T. Yatsunami, M. Kodama, *ibid.* **1981**, *103*, 3041–3045; d) E. Kimura, A. Watanabe, M. Kodama, *ibid.* **1983**, *105*, 2063–2066; e) E. Kimura, M. Kodama, T. Yatsunami, *ibid.* **1982**, *103*, 3041–3045.

[2] a) J.-M. Lehn, R. Méric, J.-P. Vigneron, I. Bkouche-Waksman, C. Pascard, *J. Chem. Soc. Chem. Commun.* **1991**, 62–64; b) J.-M. Lehn, *Angew. Chem.* **1988**, *100*, 91–116; *Angew. Chem. Int. Ed. Engl.* **1988**, *27*, 89–112.

[3] a) M. Shionoya, E. Kimura, M. Shiro, *J. Am. Chem. Soc.* **1993**, *115*, 6730–6737; b) M. Shionoya, T. Ikeda, E. Kimura, M. Shiro, *ibid.* **1995**, *116*, 3848–3859; c) M. Shionoya, M. Sugiyama, E. Kimura, *J. Chem. Soc. Chem. Commun.* **1995**, 1747–1748.

[4] Anion affinity for **3**, see E. Kimura, T. Shiota, T. Koike, M. Shiro, M. Kodama, *J. Am. Chem. Soc.* **1990**, *112*, 5805–5811.

[5] Synthesis of $6 \cdot BF_4^- \cdot ClO_4^- \cdot 3H_2O$: A solution of $4 \cdot 2ClO_4$ (32.3 mg, 0.050 mmol) in hot CH_3CN (3 mL) was added to a solution of diammonium terephthalate salts (5.0 mg, 0.025 mmol) in H_2O (3 mL). After cooling, $NaBF_4$ (0.5 mL, 1 M) was added to the mixture, which was dried a desiccator in the presence of KOH under reduced pressure. Orange prisms, suitable for X-ray analysis, were obtained (28 mg, 88%). IR (KBr): $\tilde{\nu}$ 1599 (COO^-), 1451, 1360 (COO^-), 1098, 1084, 974, 765, 714, 627 cm^{-1}. ^1H NMR (400 Hz, [D_6]DMSO, 20 mM at 30 °C, TMS): δ = 2.40–2.46 (4H, m, NCH_2), 2.65–2.90 (m, 24H; NCH_2), 3.05–3.15 (m, 4H; NCH_2), 4.1–4.2 (br, 2H; cyclen-NH), 4.5–4.6 (br, 4H; cyclen-NH), 5.11 (brs, 4H; $ArCH_2$), 7.59 (t, J = 7.56 Hz, 4H; ArH), 7.80 (pseudo-t, J = 7.80/6.84 Hz 4H; ArH), 8.10 (s, 4H; terephthalate), 8.16 (dd, J = 8.78, 0.98 Hz, 4H; ArH), 8.50 (d, J = 8.78 Hz, 4H; ArH). ^{13}C NMR ([D_6]DMSO, 20 mM at 30 °C, TMS): δ = 42.78, 43.55, 44.69, 45.32, 49.77, 125.08, 126.41, 126.43, 129.14, 129.84, 129.89, 137.38, 137.66, 148.12, 171.21. Anal. calcd for $C_{52}H_{62}N_{10}O_4Zn_2 \cdot BF_4 \cdot ClO_4 \cdot 3H_2O$: C 49.48; H 5.43; N 11.10. Found: C 49.43; H 5.49; N 11.03.

[6] Crystal data of $6 \cdot BF_4^- \cdot ClO_4^- \cdot 3H_2O$: yellow prismatic crystal ($0.2 \times 0.15 \times 0.05$ mm^3); the lattice parameters and intensity data were measured on a Rigaku AFC7R diffractometer with graphite-monochromated $Cu_{K\alpha}$ radiation and a 12 kW rotating anode generator. The structure was solved by direct methods and expanded Fourier techniques. Some non-hydrogen atoms were refined anisotropically, while the rest were refined isotropically. Hydrogen atoms were included but not refined. Empirical formula $C_{52}H_{68}N_{10}O_{11}BF_4ClZn_2$, monoclinic, space group $P2_1$ (no. 4), a = 9.406(2), b = 29.651(2), c = 10.766(2) Å, β = 111.7641°, V = 2788.6(4) Å^3, Z = 2, ρ_{calcd} = 1.503 g cm^3, $2\theta_{max}$ = 120.2°, radiation $Cu_{K\alpha}$ (λ = 1.54178 Å), μ = 21.99 cm^{-1}, graphite monochromated, temperature 20.0 °C, scan type ω-2θ, refinement full-matrix least-squares. The final cycle of the refinement was based on 3572 observed reflections to give R = 0.047 and R_w = 0.070. All calculations were performed using the teXsan [7] program. Further details of the crystal structure investigation can be obtained from the Director of the Cambridge Crystallographic Data centre, 12 Union Road, GB-Cambridge CB2 1EZ (UK), on quoting the full journal citation.

[7] teXsan: Crystal Structure Analysis Package, Molcular Structure Corporation (**1985**, **1992**).

[8] The compound was prepared by a modified procedure [3b], using $Zn(NO_3)_2 \cdot 6H_2O$ instead of $Zn(ClO_4)_2 \cdot 6H_2O$.

Coupling of Endothermic Thermal Cracking with Exothermic Oxidative Dehydrogenation of Ethane to Ethylene Using a Diluted SrO/La_2O_3 Catalyst

Vasant R. Choudhary,* Balu S. Uphade, and Shafeek A. R. Mulla

Presently ethylene is produced by the thermal cracking of ethane, ethane–propane mixtures, or naphtha.[1] This process is endothermic and hence energy intensive, and also produces large quantities of coke. Recently efforts have been made to convert ethane to ethylene by catalytic oxidative dehydrogenation of ethane.[2–8] Although the oxidative dehydrogenation [Eq. (a)] is moderately exothermic, it can become highly hazardous and difficult to control because the combustion of ethane [Eqs. (b) and (c)] is highly exothermic. A small increase

$$C_2H_6 + 0.5\,O_2 \longrightarrow C_2H_4 + H_2O + 25.1\ \text{kcal mol}^{-1} \quad \text{(a)}$$

$$C_2H_6 + 3.5\,O_2 \longrightarrow 2\,CO_2 + 3\,H_2O + 341.5\ \text{kcal mol}^{-1} \quad \text{(b)}$$

$$C_2H_6 + 2.5\,O_2 \longrightarrow 2\,CO + 3\,H_2O + 206.6\ \text{kcal mol}^{-1} \quad \text{(c)}$$

in the conversion of ethane to CO and CO_2 results in a large increase in the released reaction heat. Also, high ethane conversion coupled with high space velocity causes the release of a large amount of heat in a small catalyst zone. Because of these problems, the removal of heat from the reactor becomes very difficult, and the process can become uncontrolled owing to the formation of hot spots in the reactor. The conversion of ethane to ethylene in an energy-efficient (without applied energy) and safe manner is of great importance. In this communication we show that the endothermic cracking of ethane can be coupled with its oxidative dehydrogenation. The two reactions are carried out simultaneously in the presence of steam and limited O_2, by using a supported catalyst having high thermal/hydrothermal stability, SrO/La_2O_3/SA 5205, diluted with an inert solid. In this way ethane can be converted to ethylene efficiently and safely with high conversion and selectivity, and without coke formation. Our results reveal that by manipulating reaction conditions, particularly the temperature and the C_2H_6/O_2 ratio in the feed, this process can be made almost thermoneutral, mildly endothermic, or mildly exothermic, thus requiring little or no external energy.

Our results are summarized in Figures 1 and 2. The plots show the effects of the reaction temperature and the C_2H_6/O_2 mole ratio in the feed on conversion, selectivity, ratio of ethane conversion by cracking to ethane conversion by oxidation, net heat of reaction ΔH_r, and energy input to the reactor furnace. The coupled process is catalyzed by a supported catalyst with the composition SrO (17.3 wt%)/La_2O_3 (17.9 wt%)/SA 5205 diluted uniformly with the support SA 5205. This support is inert and porous (porosity: 50%), has a low surface area ($<0.01\ m^2 g^{-1}$), and consists of mainly Al_2O_3 (86.1 wt%) and SiO_2 (11.8 wt%). The net heat of the reaction is estimated by subtracting the heat of formation of the components in the feed (at the reaction temperature) from that of the components in the product stream.

The coupled process requires little or no external energy because the heat produced in the exothermic reactions is used instantly in the simultaneous endothermic reactions. Further,

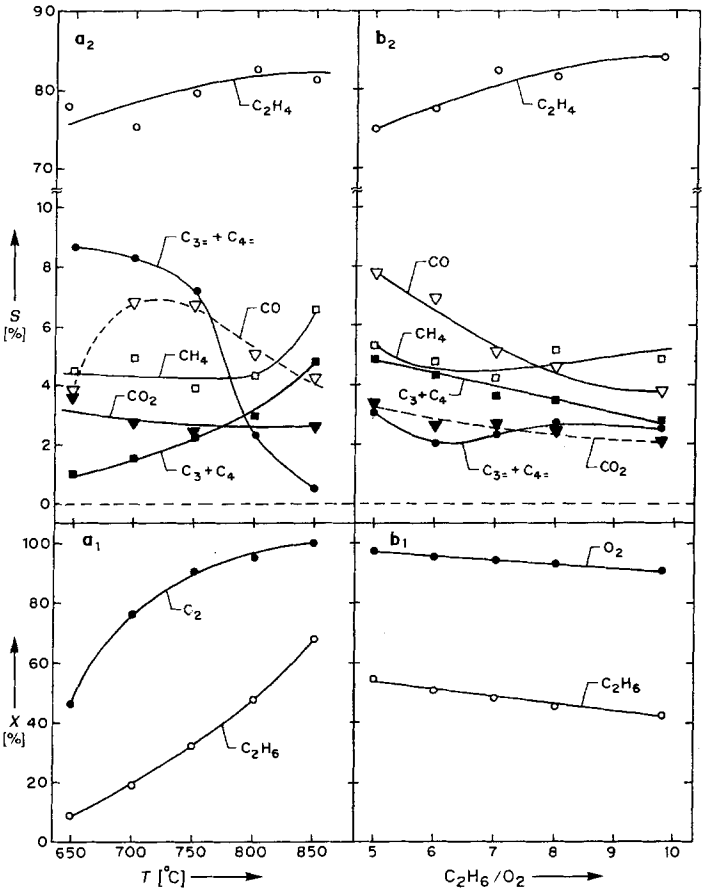


Fig. 1. Influence of a) reaction temperature and b) C_2H_6/O_2 mole ratio in feed on conversion and selectivity in the coupled process (T = reaction temperature, X = conversion, S = product selectivity). a) C_2H_6/O_2 mole ratio in feed = 7.0, b) T = 800 °C; C_2H_6/steam mole ratio = 1.0 and total space velocity = 35 100 cm^3 per g of diluted catalyst per h; ratio support/catalyst (wt/wt) = 2.0.

because the catalyst is dilute, longer residence times are possible for the slow noncatalytic reactions (particularly the thermal cracking of hydrocarbons). Heat removal from the reactor is also simplified since the heat transfer area of the reactor is increased.

The ratio of the conversion of ethane by endothermic cracking to that by exothermic oxidation (obtained from the feed and product compositions and reactions stoichiometry) increases with increasing reaction temperature and also with the C_2H_6/O_2 ratio. Consequently, the net heat of reaction (or the reaction endothermicity) also increases. The energy input to the reactor furnace for the coupled process (at different reaction conditions) relative to the energy input required in the absence of any reaction to maintain the same temperature is quite consistent with the net heat of reaction ΔH_r at the different reaction conditions. These observations clearly demonstrate the occurrence of simultaneous endothermic cracking and exothermic oxidative reactions and also the energy saving in the coupled process.

The overall process is thought to involve a complex series of catalytic surface reactions and noncatalytic reactions in the gas-phase. We suggest that the reaction is initiated on the catalyst (which also shows high activity/selectivity for the oxidative coupling of methane[9]) by formation of ethyl radicals from the surface reaction of ethane with adsorbed or lattice oxygen [Eq. (d)].

$$C_2H_6 + [O] \longrightarrow C_2H_5^{\cdot} + [OH] \quad \text{(d)}$$

[*] Dr. V. R. Choudhary, B. S. Uphade, S. A. R. Mulla
Chemical Engineering Division, National Chemical Laboratory
Pune 411008 (India)
Telefax: Int. code + (212)330233

 © VCH Verlagsgesellschaft mbH, D-69451 Weinheim, 1995 0570-0833/95/0606-0665 $ 10.00+.25/0

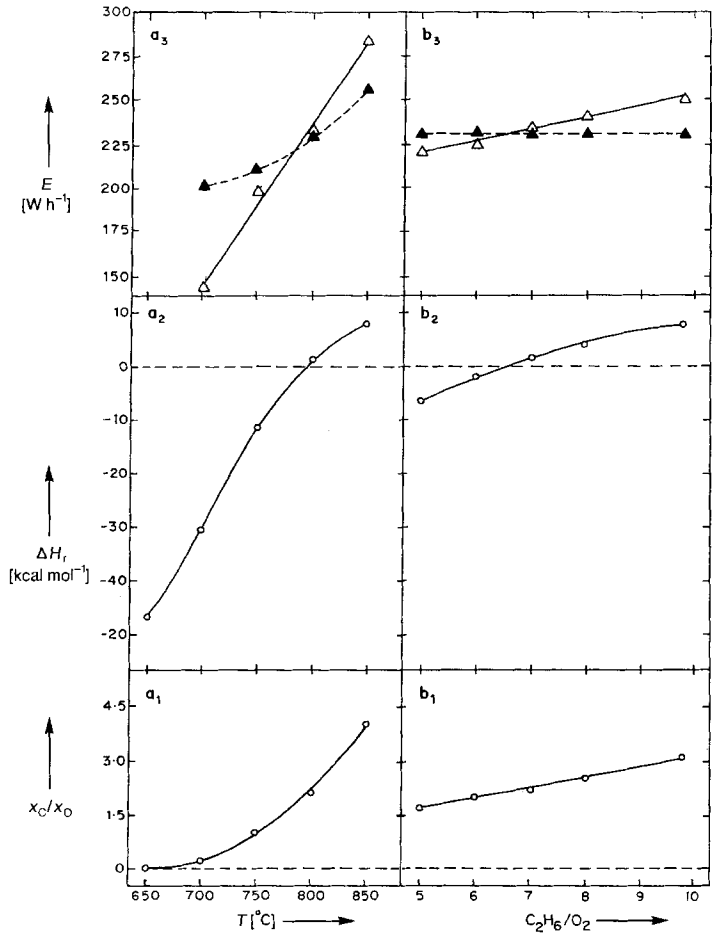


Fig. 2. Influence of a) reaction temperature and b) C_2H_6/O_6 mole ratio in feed on the relative conversion x_C/x_O of ethane by its cracking and oxidation reactions, on the net heat of reaction ΔH_r and energy input E to reactor furnace with (Δ) or without reaction (▲). T = reaction temperature. x_C = conversion of ethane by thermal cracking reactions, x_O = conversion of ethane by oxidation reactions.

(2 [OH] + 0.5 O_2 → H_2O + [O]; [OH] and [O] represent surface- or lattice-bound OH and O species, respectively.) The ethyl radicals desorb in the gas phase, and their subsequent homogeneous reactions lead to the formation of ethylene and longer chain hydrocarbons [Eqs. (e)–(h)].

$$C_2H_5^{\cdot} \longrightarrow C_2H_4 + H^{\cdot} \quad (e)$$

$$C_2H_6 + H^{\cdot} \longrightarrow C_2H_5^{\cdot} + H_2 \quad (f)$$

$$2\,C_2H_5^{\cdot} \longrightarrow C_4H_{10} \quad (g)$$

$$C_4H_{10} \longrightarrow \text{cracking products} \quad (h)$$

At higher temperatures the reaction should also be initiated by the formation of ethyl radicals from ethane [Eq. (i)]. The thermal decomposition of ethyl radicals [Eq. (e)] and ethane [Eq. (i)] is highly endothermic (ΔH_r = 36.4 and 100.6 kcal mol^{-1}, respectively). Since reaction (i) has a high activation energy (89.0 kcal mol^{-1})[10], it is predominant only at higher temperatures and lower concentrations of O_2. The thermal decomposition of ethyl radicals is also expected to be more predominant under these conditions. The results are quite consistent with these expectations. At higher oxygen concentrations ethyl radicals are also expected to be formed [Eq. (j)] and converted to ethylene [Eq. (k)] in the gas phase.

$$C_2H_6 \longrightarrow C_2H_5^{\cdot} + H^{\cdot} \quad (i)$$

$$C_2H_6 + O_2 \longrightarrow C_2H_5^{\cdot} + HO_2^{\cdot} \quad (j)$$

$$C_2H_5^{\cdot} + O_2 \longrightarrow C_2H_4 + HO_2^{\cdot} \quad (k)$$

Ethyl radicals may also undergo catalytic oxidative conversions [Eqs. (l) and (m)].

$$C_2H_5^{\cdot} + [O] \longrightarrow C_2H_4 + [O] \quad (l)$$

$$C_2H_4 + [O] \longrightarrow \text{combustion products (CO, } CO_2 \text{ and } CH_4) \quad (m)$$

The coupled process is thus very complex and involves a large number of homogeneous free radical reactions[10,11] in addition to catalytic reactions, depending upon the process conditions. Nevertheless, the process is very simple to conduct. The addition of steam in the feed is found to prevent formation of tarlike product and coke in the process.

The coupled process can be operated with a very low net heat produced or consumed and consequently with a low adiabatic increase or decrease in temperature. Thus further development may lead to a simple adiabatic reactor with very low capital and operating costs. Further work is required for understanding the nonisothermal behavior of such a reactor for the process and the complex reaction mechanism.

Experimental Procedure

The supported catalyst [SrO (17.3 wt%)/La_2O_3 (17.9 wt%)/SA 5205] was prepared by impregnating a commercial catalyst support SA 5205 (Norton Co., USA), crushed to 22–30 mesh size particles, first with lanthanum nitrate (GR LOBA) and then with strontium nitrate (extra pure, LOBA) by using the incipient wetness technique. After each impregnation the resulting particles were dried at 90 °C for 16 h and then calcined in static air at 900 °C for 4 h. The ethane conversions were conducted at atmospheric pressure in a continuous-flow tubular quartz reactor (i.d.: 5 mm) packed with 0.3 g of the diluted catalyst (catalyst diluted by uniformly mixing 0.1 g of the supported catalyst and 0.2 g of the support having the same particle size) and having a very low dead volume. The C_2H_6/steam mole ratio in the feed was 1.0 and total space velocity of the feed (measured at 0 °C and 1 atm) was 35100 cm^3 per gram of diluted catalyst per hour. The reactor was kept in a constant temperature zone of a tubular furnace (dia.: 2.0 cm). The energy input to the furnace, with and without reaction (at the same temperature and ambient conditions) was measued with an energy meter. The reaction temperature was measured with a Chromel-Alumel thermocouple in the diluted catalyst bed. The reactor effluent gases were cooled to 0 °C to remove water. The feed and products were analyzed by on-line gas chromatography. The error in C, H, O balances was less than 5%.

Received: July 7, 1995
Revised version: September 30, 1995 [Z 7107IE]
German version: *Angew. Chem.* **1995**, *107*, 721

Keywords: cracking · dehydrogenation · ethane · ethylene · heterogenous catalysis · oxidation

[1] L. Kniel, O. Winter, K. Stork, *Ethylene: Keystone to the Petrochemical Industry*, Marcel Dekker, New York, **1980**.
[2] A. Argent, P. Harris, *J. Chem. Soc. Chem. Commun.* **1986**, 1058–1059.
[3] E. Morales, J. H. Lunsford, *J. Catal.* **1989**, *118*, 255–265.
[4] S. J. Conway, J. H. Lunsford, *J. Catal.* **1991**, *131* 513–522.
[5] H. M. Swaan, A. Toebes, K. Seshan, J. G. Van Ommen, J. R. H. Ross, *Catal. Today* **1992**, *13*, 629–634.
[6] O. Desponds, R. L. Keiski, G. A. Somorjai, *Catal. Lett.* **1993**, *19*, 17–32.
[7] M. Huff, L. D. Schmidt, *J. Phys. Chem.* **1993**, *97*, 11815–11822.
[8] M. Zhang, J. Liu, R. Lan, L. Ji, X. Chen, *J. Chem. Soc. Chem. Commun.* **1993**, 1480–1481.
[9] V. R. Choudhary, B. S. Uphade, S. A. R. Mulla, unpublished results.
[10] Q. Chen, J. H. B. J. Hoebink, G. B. Marin, *Ind. Eng. Chem. Res.* **1991**, *30*, 2088–2097.
[11] R. A. Geisbrecht, M. E. Daubert, *Ind. Eng. Chem. Process Des. Dev.* **1975**, *14*, 159–166.

^{31}P CP/MAS NMR Spectroscopy of Transition Metal Phosphane Complexes: "*J*-Recoupling" between Chemically Equivalent ^{31}P Nuclei in Polycrystalline Compounds of the Type *trans*-[$(PR_3)_2MX_2$], M = Pd, Pt**

Elke Klaus and Angelika Sebald*

Spectroscopic properties of transition metal complexes are of fundamental interest in many branches of chemistry. In the case of Pd- and Pt-phosphane complexes, NMR spectroscopy in solution has for a long time been widely and successfully used for the investigation of structural and bonding properties.[1] The increasingly widespread availability of high-resolution solid-state NMR techniques, such as cross-polarization magic angle spinning[2] (CP/MAS) NMR provides an additional source of information, which may not be readily available from solution-state NMR or single-crystal X-ray studies. The ^{31}P nucleus, in particular, has become a popular CP/MAS target as it is usually straightforward to obtain ^{31}P MAS and CP/MAS NMR spectra of polycrystalline solids. This is also documented by a large, ever increasing number of publications dealing with CP/MAS NMR spectroscopy of this nucleus in transition metal phosphane complexes.[3] We report here on ^{31}P CP/MAS NMR spectra of square-planar Pd^{II} and Pt^{II} complexes of the type *trans*-[$(R_3P)_2MX_2$], M = Pd, Pt, in which the two phosphorus atoms are crystallographically equivalent. The two phosphane ligands R_3P in such complexes constitute a homonuclear ^{31}P spin pair. The solid-state NMR properties of homonuclear spin pairs under MAS conditions have recently been a major focus of much theoretical and experimental work.[4] We will show that for compounds of the type *trans*-[$(R_3P)_2MX_2$] seemingly minor, unimportant chemical modifications can completely alter the MAS NMR properties of the ^{31}P spin pair and that, therefore, reliable interpretation of such routinely available ^{31}P CP/MAS spectra must fully consider all orientation-dependent interactions within the ^{31}P spin pair.

Our ^{31}P CP/MAS NMR results on compounds *trans*-[$(R_3P)_2MX_2$] **1** (M = Pd) and **2** (M = Pt) are summarized in Table 1, in which the respective ^{31}P shielding tensor components are also listed. The general Hamiltonian operator for a homonuclear spin pair, such as the two ^{31}P nuclei in **1** and **2**, can be defined as in Equation (a), where $\mathcal{H}_Z$ is the Zeeman interaction,

$$\mathcal{H} = \mathcal{H}_Z + \mathcal{H}_{CS} + \mathcal{H}_J + \mathcal{H}_{DD} \qquad (a)$$

$\mathcal{H}_{CS}$ is the chemical shielding, $\mathcal{H}_{DD}$ is the homodipolar and $\mathcal{H}_J$ is the indirect homonuclear spin-spin coupling (*J* coupling). $\mathcal{H}_{CS}$, $\mathcal{H}_{DD}$, and $\mathcal{H}_J$ are orientation dependent with respect to the static magnetic field $\boldsymbol{B}_0$. If we refer to rapidly and isotropically reorienting molecules (as in non-viscous solutions), $\mathcal{H}_J$ and $\mathcal{H}_{CS}$ are averaged to their isotropic values J_{iso} and δ_{iso}, respectively, whereas $\mathcal{H}_{DD}$ is averaged to zero. In solution our pair of chemically equivalent ^{31}P nuclei in **1** and **2** is an A_2 spin system, giving rise to one single ^{31}P resonance: both ^{31}P nuclei have the same isotropic chemical shift $\delta(^{31}P)$; the isotropic *J*-coupling $^2J(^{31}P,^{31}P)$ is present but not observable since the intensity of the two outer transition lines is zero.[5] This "solution NMR" behavior is precisely what we find in the ^{31}P CP/MAS spectra of compounds **1a**, **2a**, **2c**, and **2d**: one sharp ^{31}P resonance flanked by ^{195}Pt satellites due to $^1J(^{195}Pt,^{31}P)$ for compounds **2** at all magnetic field strengths B_0 of 2.4–11.7 T and for MAS frequencies ranging from 0.8–12 kHz. A typical example, the ^{31}P CP/MAS spectrum of **2d** for two different MAS frequencies, is shown in Figure 1. It is extremely tempting to consider this ^{31}P CP/MAS behavior as typical for chemically equivalent ^{31}P spin pairs in crystalline solids, in analogy to the A_2 spin system in solution. In fact, the opposite is true: for a ^{31}P spin pair in solids very special circumstances are required to produce this appearance analogous to the A_2 spin system in solution.[4a] These special circumstances and the more general case of a chemically equivalent ^{31}P spin pair in the solid state will be discussed in the following.

Table 1. ^{31}P CP/MAS NMR results for the complexes **1** and **2** [a].

Komplex	δ_{iso} [b]	$^1J(^{195}Pt,^{31}P)$ [Hz]	$^2J(^{31}P,^{31}P)$ [Hz]	σ_{11}	σ_{22}	σ_{33}	η [c]
trans-[$(PEt_3)_2PdCl_2$] **1a**	18.3			16	5	−76	0.2
trans-[$(PnBu_3)_2PdCl_2$] **1b**	10.9		537	16	9	−57	0.2
trans-[$(PEt_3)_2PtCl_2$] **2a**	13.0	2393		60	−4	−95	0.8
trans-[$(PnBu_3)_2PtCl_2$] **2b**	5.6	2414	437	53	0	−70	0.8
trans-[$(PEt_3)_2PtHCl$] **2c**	26.1	2673		13	−18	−74	0.6
trans-[$(PEt_3)_2Pt(SC{\equiv}CtBu)_2$] **2d**	15.5	2537		52	−6	−92	0.6
trans-[$(PPh_3)_2Pt(SC{\equiv}CtBu)_2$] **2e**	30.0	2807	447				
	35.0	3112					

[a] All ^{31}P CP/MAS NMR spectra were obtained on Bruker MSL 100, MSL 300, or MSL 500 NMR spectrometers, using standard probes. Experimental parameters: recycle delays 2–10 s, contact times 0.3–1.5 ms, MAS frequencies 0.8–12 kHz. δ_{iso} and $^1J(^{195}Pt,^{31}P)$ were determined from fast spinning experiments. [b] Relative to external H_3PO_4 ($\delta = 0$). [c] Haeberlens notation [6] is used to report shielding tensor components: $\delta_{iso} = -\sigma_{iso}$; $|\sigma_{33} - \sigma_{iso}| \geq |\sigma_{11} - \sigma_{iso}| \geq |\sigma_{22} - \sigma_{iso}|$; $\eta = (\sigma_{22} - \sigma_{11})(\sigma_{33} - \sigma_{iso})^{-1}$.

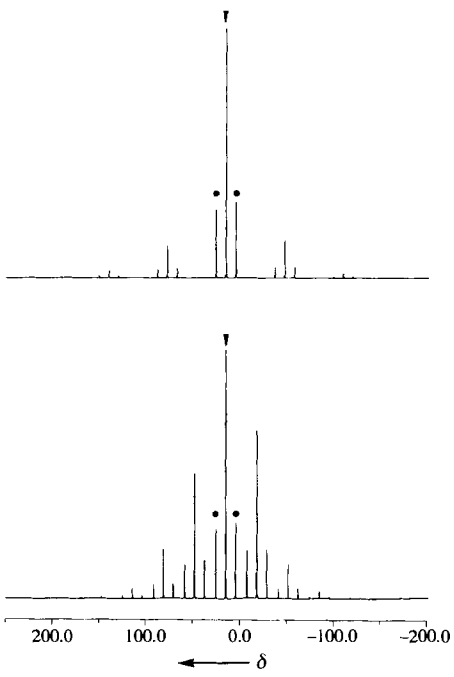


Fig. 1. 121.5 MHz ^{31}P CP/MAS NMR spectrum of **2d** at MAS frequencies of 7.6 kHz (top) and 4 kHz (bottom). The isotropic resonance is marked by an arrow, the ^{195}Pt satellites by a black dots.

[*] Priv.-Doz. Dr. A. Sebald, Dipl.-Chem. E. Klaus
Bayerisches Geoinstitut, Universität Bayreuth
D-95440 Bayreuth (FRG)
Telefax: Int. code + (921)553769

[**] This work was supported by the Deutsche Forschungsgemeinschaft and the Fonds der Chemischen Industrie. We thank Degussa AG, Hanau, for their loan of precious metal salts and Dr. W. Weigand, Universität München, for compounds **2d**, e. Prof. D. Michel, Leipzig, kindly provided access to the MSL 500 spectrometer.

 © VCH Verlagsgesellschaft mbH, D-69451 Weinheim, 1995 0570-0833/95/0606-0667 $ 10.00+.25/0

Let us consider a spin pair in one single crystallite in a rigid powder sample. Furthermore, let us ignore the influence of anisotropy in J and the dipole–dipole interaction DD in the following explanation. In solid-state NMR, every single spin in a different orientation with respect to $\boldsymbol{B}_0$ will give rise to a distinct resonance line. If two chemically equivalent nuclei in a spin pair lead to only one single resonance for *every* possible orientation of the crystallite with respect to $\boldsymbol{B}_0$, these two nuclei are said to be magnetically equivalent.[4f, 6] This is possible only if the symmetry element connecting the two chemical shielding tensors of the two nuclei happens to be an inversion center. Within this symmetry requirement, there is no crystallite orientation possible which would lead to an instantaneous chemical shift difference δ_{CSA} for the spin pair.[4c, f] Hence, the intensity of the outer transitions due to J-coupling is zero for all orientations, and we observe the same spectral features in the solid state (one sharp resonance) as for the A_2 spin system in solution. Apparently, this symmetry criterion, that is the presence of an inversion center, is fulfilled for our solid compounds **1a**, **2a**, **2c**, and **2d**. Note that in all four cases the magnetically equivalent ^{31}P spin pair is produced by a pair of Et_3P ligands.

Let us consider next the more general case of a pair of chemically equivalent nuclei where the two shielding tensors are connected by a symmetry operation other than a center of inversion. Now there will be orientations of the crystallite with respect to $\boldsymbol{B}_0$ for which the two nuclei will give rise to two distinct resonances; the two nuclei are no longer magnetically equivalent, but will still display an identical isotropic chemical shift. The difference in the instantaneous chemical shift δ_{CSA} for certain orientations is the reason why in the solid state it is possible to observe J-coupling between chemically equivalent nuclei.[4c] In practice we do not work with single crystals but with polycristalline powders under MAS conditions. We observe this "J-recoupling" phenomenon[4c, f] in the ^{31}P CP/MAS NMR spectra of compounds **1b** and **2b**. In both cases the pair of chemically equivalent, but magnetically nonequivalent ^{31}P nuclei is produced by a pair of nBu$_3$P ligands! The effects of different magnetic field strengths B_0 and MAS frequencies on the J-recoupling pattern in the ^{31}P CP/MAS NMR spectra of **1b** are illustrated in Figure 2.

MAS leads to the well-known high-resolution spinning sideband patterns where the anisotropic interactions are not completely averaged but scaled, depending on the MAS frequency. Under MAS the nuclear spin Hamiltonian becomes periodically time-dependent. At $t = Nt_R$ (where t_R is the rotor period and N an integer), it can be described by an effective Hamiltonian consisting of an average Hamiltonian operator plus higher order correction terms as developed by Maricq and Waugh [Eq. (b)–(d)].[7] Our discussion will only include the first order cor-

$$\mathcal{H}_{eff} = \mathcal{H}^{(0)} + \mathcal{H}^{(1)} + \mathcal{H}^{(2)} + \ldots . \qquad \text{(b)}$$

$$\mathcal{H}^{(0)} = \frac{1}{t_R}\int_0^{t_R} \mathcal{H}(t)\,dt \qquad \text{(c)}$$

$$\mathcal{H}^{(1)} = \frac{-i}{2t_R}\int_0^{t_R} dt_2 \int_0^{t_2} [\mathcal{H}(t_2), \mathcal{H}(t_1)]\,dt_1 \qquad \text{(d)}$$

rectionterm. After inserting the time-dependent terms $\mathcal{H}_{eff}$ can be described according to Equation (e),[7, 4f] where K is a complex expression depending on DD, δ_{CSA}, and the MAS frequency

$$\mathcal{H}_{eff} = \omega_{iso}(I_{1z} + I_{2z}) + \omega_J I_1 \cdot I_2 - iK\frac{I_{1+}I_{2-} - I_{1-}I_{2+}}{2} \qquad \text{(e)}$$

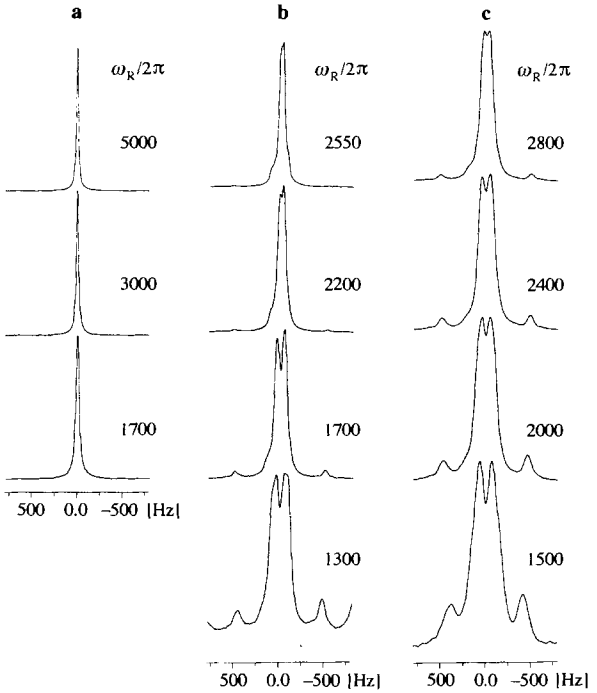


Fig. 2. ^{31}P CP/MAS NMR spectra of **1b** at different magnetic field strengths and different MAS frequencies. Only the isotropic region is shown. Note the interplay of B_0 (a) 40.5 MHz, b) 121.5 MHz, c) 202.5 MHz) and ω_R and the increasing intensity of the J-recoupling pattern with decreasing MAS frequencies. MAS frequencies $\omega_R/2\pi$ in Hz are given for each spectrum.

ω_R ($K \sim \omega_R^{-1}$, $\sim\delta_{CSA}$, $\sim$DD). The transition frequencies and their relative intensities are readily obtained from Equations (f)–(i),[7, 4c, f] where $D = [K^2 + \omega_J^2]^{1/2}$.

$$\omega_1 = \omega_{iso} + 1/2(D + \omega_J) \qquad P_1 = 1 - \frac{\omega_J}{D} \qquad \text{(f)}$$

$$\omega_2 = \omega_{iso} + 1/2(D - \omega_J) \qquad P_2 = 1 + \frac{\omega_J}{D} \qquad \text{(g)}$$

$$\omega_3 = \omega_{iso} - 1/2(D - \omega_J) \qquad P_3 = 1 + \frac{\omega_J}{D} \qquad \text{(h)}$$

$$\omega_4 = \omega_{iso} - 1/2(D + \omega_J) \qquad P_4 = 1 - \frac{\omega_J}{D} \qquad \text{(i)}$$

Here we only quote the final result; the full mathematical treatment can be found in the literature.[7, 4f] Equations (f–i) are identical with those for an AB spin system in solution, with two important exceptions: an AB spin pair in solution has two distinct chemical shifts ω_A, ω_B, and the corresponding mixing term has a different form ($D_{solution} = (1/2\,(\omega_B - \omega_A)^2 + w_J^2)^{1/2}$).[5] For an A_2 system in solution ($\omega_A = \omega_B$) it is obvious that P_1 and P_4 would be zero. In the solid state the mixing term D depends on K and, thus, on DD, δ_{CSA}, and ω_R. If δ_{CSA} or DD is zero, the mixing term D_{solid} takes the form of the mixing term $D_{solution}$ ($\delta_{CSA} = 0$ is what we observe in the ^{31}P CP/MAS spectra of **1a**, **2a**, **2c**, and **2d**). Figures 2 and 3 show how the anisotropic term K influences positions and intensities of the four transitions as a function of B_0 and ω_R for the case of magnetically nonequivalent spins (such as in **1b**, **2b**). The two internal parameters DD and δ_{CSA} are differently influenced by $\boldsymbol{B}_0$: δ_{CSA} is proportional to B_0, while DD is solely dependent on the internuclear distance between the two spins. Figure 3 also demonstates how $|^2J(^{31}P,^{31}P)|$ can be extracted from a series of ^{31}P CP/MAS NMR spectra. This procedure has also been used to determine

 © VCH Verlagsgesellschaft mbH, D-69451 Weinheim, 1995 0570-0833/95/0606-0668 $ 10.00+.25/0

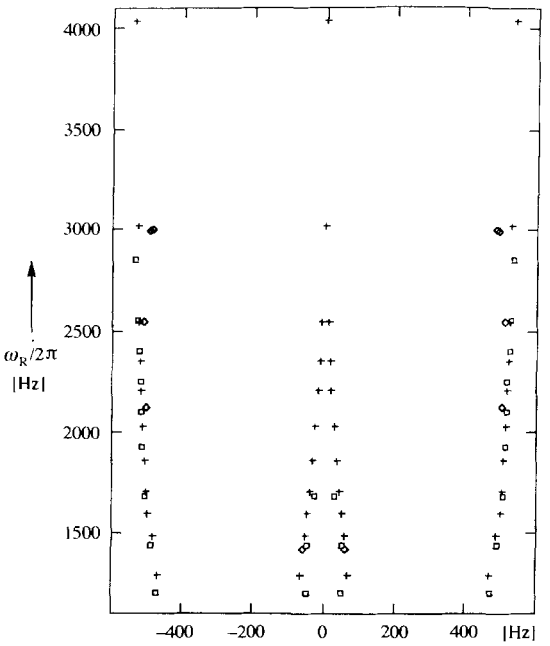


Fig. 3. Plot of relative positions of ^{31}P NMR resonances of **1b** versus $\omega_R/2\pi$ [Hz]. The symbols +, ◇, and □ refer to MSL 300, MSL 100, and MSL 500 data, respectively (for the latter two ω_R is scaled to allow for one common ω_R axis). Note that $|^2J(^{31}P,^{31}P)|$ in this case (and for **2b**) is given by alternate transitions 1,3 and 2,4, respectively, which is not possible for a solution-state AB spin system [4f,5].

$|^2J(^{31}P,^{31}P)|$ for solid $[(Ph_3P)_2Hg(NO_3)_2]$.[4f] Not only is it possible to obtain $|J_{iso}|$ for such pairs of chemically equivalent nuclei, the anisotropic perturbation term K also offers possibilities to determine relative chemical shielding tensor orientations from powder samples, a point which only recently has received attention.[8, 9]

The correct interpretation of routine ^{31}P CP/MAS NMR spectra of transition metal phosphane complexes generally requires careful consideration of the solid-state NMR properties of homonuclear spin pairs, including measurements over a wide range of ω_R and, if possible, at more than one B_0 strength. A, chemically speaking, minor modification such as replacing Et_3P by nBu_3P in otherwise homologous compounds can lead to expressedly different ^{31}P CP/MAS NMR properties (see also Table 1, compounds **2d, e**: the replacement of Et_3P for Ph_3P leads us from a magnetically equivalent pair to an even chemically inequivalent ^{31}P spin pair). Finally, it is well known from solution NMR spectroscopy that strongly coupled subsets of complex spin systems leave their complex footprints in the weakly coupled parts of such spectra.[5] The ^{195}Pt nucleus in compounds of the type *cis*- or *trans*-$[(R_3P)_2PtX_2]$ forms the X-part in a complex solid-state ABX spin system,[10] the homonuclear ^{31}P AB part and its complex ^{31}P CP/MAS behavior will also be mirrored in ^{195}Pt CP/MAS NMR spectra of such compounds.

Received: September 27, 1995 [Z 7360 IE]
German version: *Angew. Chem.* **1995**, *107*, 713

Keywords: complexes with phosphorus ligands · NMR spectroscopy · solid-state NMR spectroscopy

[1] P. S. Pregosin, R. W. Kunz, *^{31}P and ^{13}C NMR of Transition Metal Complexes (NMR Basic Princ. Prog.* **1979**, *16*).
[2] a) A. Pines, M. G. Gibby, J. S. Waugh, *J. Chem. Phys.* **1972**, *56*, 1776; b) *ibid.* **1973**, *59*, 569; c) J. Schaefer, E. O. Stejskal, *J. Am. Chem. Soc.* 1976, *98*, 1031
[3] See, for example: J. A. Davies, S. Dutremez, *Coord. Chem. Rev.* **1992**, *114*, 61 and references therein.
[4] a) A. Kubo, C. A. McDowell, *J. Chem. Phys.* **1990**, *92*, 7156; b) T. Nakai, C. A. McDowell, *ibid.* **1992**, *96*, 3452; c) R. Challoner, T. Nakai, C. A. McDowell, *ibid.* **1991**, *94*, 7038; d) D. P. Raleigh, G. S. Harbison, T. G. Neiss, J. E. Roberts, R. G. Griffin, *Chem. Phys. Lett.* **1987**, *138*, 285; e) M. H. Lewitt, D. P. Raleigh, F. Creuzet, R. G. Griffin, *J. Chem. Phys.* **1990**, *92*, 6347; f) G. Wu, R. E. Wasylishen, *ibid.* **1993**, *98*, 6138; g) *ibid.* **1993**, *99*, 6321.
[5] P. L. Corio, *Structure of High-Resolution NMR Spectra*, Academic Press, New York London, **1966**.
[6] U. Haeberlen, *High Resolution NMR in Solids. Selective Averaging. Supplement 1 (Adv. Magn. Reson.* **1976**).
[7] M. M. Maricq, J. S. Waugh, *J. Chem. Phys.* 1979, *70*, 3300.
[8] T. Nakai, C. A. McDowell, *J. Am. Chem. Soc.* **1995**, *116*, 6373.
[9] a) G. Wu, R. E. Wasylishen, *J. Chem. Phys.* **1995**, *100*, 4828, 5546.
[10] R. Challoner, C. A. McDowell, *J. Magn. Reson.* **1992**, *98*, 123.

μ-Nitridodiiron Complexes with Asymmetric $[Fe^{IV}\equiv N-Fe^{III}]^{4+}$ and Symmetric $[Fe^{IV}=N=Fe^{IV}]^{5+}$ Structural Elements**

Thomas Jüstel, Thomas Weyhermüller, Karl Wieghardt,* Eckhard Bill, Marek Lengen, Alfred X. Trautwein, and Peter Hildebrandt

Dinuclear μ-nitridodiiron complexes with porphyrin or phthalocyanine ligands can be prepared in good yields by the thermolysis[2] or photolysis[3] of the corresponding mononuclear azidoiron(III) complexes, with the concomitant loss of N_2.[1-11] The resulting compounds contain a symmetric, linear[4] $[Fe=N=Fe]^{4+}$ moiety, in which both Fe ions are formally in the oxidation state + 3.5.[5] These complexes exhibit an ESR-active, $S = 1/2$ ground state[6] that results from the intramolecular antiferromagnetic coupling of a low-spin $Fe^{III}(d^5)$ and a low-spin $Fe^{IV}(d^4)$ center. As the Mössbauer spectra, even at low temperatures, show only *one* quadrupole doublet with isomer shifts ranging from $\delta = 0.08-0.18$ mm s^{-1},[7] these complexes belong to class III in the Robin and Day classification scheme,[8] with complete delocalization of the excess electron.[5] These complexes can be electrochemically[9] as well as chemically[10] oxidized to yield compounds containing a $[Fe^{IV}=N=Fe^{IV}]^{5+}$ unit; these compounds, however, have not yet been structurally characterized. They exhibit a diamagnetic ground state ($S = 0$) due to the strong antiferromagnetic coupling of two Fe^{IV} ($S = 1$) ions. Further oxidation leads to coordinated porphyrin π-radical cations.[11] μ-oxo bridged porphyrin,[12] phthalocyanine,[12] and porphycene and corrole[13] complexes with $[Fe^{III}$-O-$Fe^{III}]^{4+}$, $[Fe^{3.5}$-O-$Fe^{3.5}]^{5+}$, and $[Fe^{IV}$-O-$Fe^{IV}]^{6+}$ structural units have also been reported, the latter group only recently.

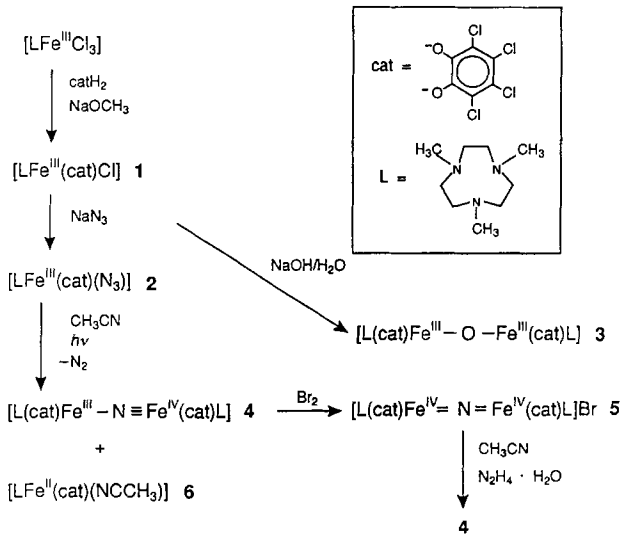
The planar, tetradentate dianions of porphyrins, phthalocyanines, and porphycenes, all of which have an N_4 donor set, enforce the low-spin configuration of the Fe^{III} and Fe^{IV} centers in complexes containing these ligands. We have examined, whether a similar chemistry, but with a high-spin configuration, can be developed by employing weaker, redox-inactive, neutral ligands containing O and N donor atoms. For this purpose, we

[*] Prof. Dr. K. Wieghardt, Dipl.-Chem. T. Jüstel, Dipl.-Chem. T. Weyhermüller, Dr. P. Hildebrandt
Max-Planck-Institut für Strahlenchemie
Stiftstrasse 34-36, D-45470 Mülheim an der Ruhr (FRG)
Telefax: Int. code + (208) 3063951
Dr. E. Bill, Dipl.-Phys. M. Lengen, Prof. Dr. A. X. Trautwein
Institut für Physik, Universität Lübeck (FRG)

[**] This work was supported by the Fonds der Chemischen Industrie and the Deutsche Forschungsgemeinschaft.

used 1,4,7-trimethyl-1,4,7-triazacyclononane, L, and tetrachlorocatechol, $catH_2$, as ligands.

The synthesis of the complexes **1**–**6** is summarized in Scheme 1. The reaction of $[LFe^{III}Cl_3]$ with tetrachlorocatecholate in anhydrous methanol yields dark green microcrystals of complex **1**.[14] Its chloro ligand can be replaced with an azido ligand by the reaction with NaN_3 in acetone, leading to the green compound **2**. The hydrolysis of **1** in acetone with $NaOH/H_2O$ leads to the dinuclear complex **3**, which contains a linear $[Fe^{III}$-O-$Fe^{III}]^{4+}$ unit. Photolysis of an ice-cooled solution of **2** in anhydrous, argon-purged acetonitrile, using a quartz Hg immersion



Scheme 1. Preparation of complexes **1**–**6**.

lamp, leads under loss of N_2 to black crystals of **4**, which can be recrystallized from dichloromethane. Workup of the reaction solution under an inert N_2 atmosphere yielded microcrystalline $\mathbf{6}\cdot 2H_2O$. Depending on the residual oxygen and moisture in the solvent employed, complex **4** is contaminated by small amounts of **3**.

The stoichiometry of the reaction $3\ \mathbf{2} \rightarrow \mathbf{4} + \mathbf{6} + 4N_2$ was verified by quantitative volumetric determinations of the N_2 formed during the reaction: per equivalent of **2**, 1.30 ± 0.2 equivalents of N_2 are formed (theoretical value: 1.33). The bromine oxidation of **4** in dichloromethane results in green-black crystals of the salt **5**. As **3**, present as a contaminant of **4**, cannot be oxidized by bromine, it remains in solution after the precipitation of **5**. Subsequent reduction of **5** with $N_2H_4\cdot H_2O$ in acetonitrile yields pure **4**.

The X-ray crystal structure analyses[15] of $\mathbf{3}\cdot 2$toluene, **4**, and $\mathbf{5}\cdot CH_3CN$ (Fig. 1 and Table 1) confirm the dinuclear nature of these species. All iron atoms are coordinated in a distorted octahedral fashion by a facially bound triamine and a didentate catecholato ligand; the sixth coordination site is occupied by the oxo bridge in **3** and the nitrido bridge in **4** and **5**, respectively. The dinuclear complexes display C_i symmetry, that is the bridging nitrogen atom in **4** and **5** and the bridging oxygen atom in **3** are located on a crystallographic center of symmetry.

Upon examination of the distribution of the total and residual electron density in the three Fe-X-Fe structural units (Fig. 2), it is apparent that only in **3** and **5** is the Fe-X-Fe unit indeed linear and symmetric. It was possible to calculate two statically disordered positions for the bridging nitrogen atom in **4**, using a split atom model (with occupancy factor of 0.5, on either side of

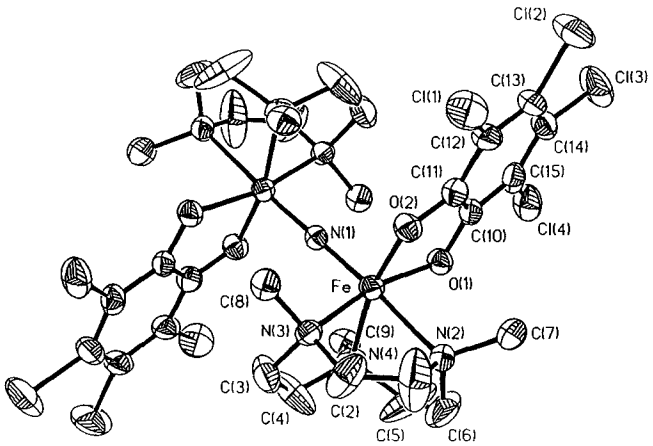


Fig. 1. Structure of the monocation of **5** in the crystal. The structures of the neutral complexes **3** and **4** are very similar and are not shown. In all cases, the oxygen and nitrogen atoms of the oxo or nitrido bridges, respectively, are situated on a crystallographic center of symmetry. Important structural parameters of **3**–**5** are given in Table 1.

Table 1. Comparison of the structural data of complexes **3**–**5**.

Complex	3	4	5
Fe-X/Å [a]	1.804(1)	1.495(7)	1.703(1)
		1.976(7)	
$Fe-O_{cat}$/Å	1.996(4)	1.960(3)	1.912(4)
	1.992(4)	1.978(3)	1.913(4)
$Fe-N_{trans}$/Å [b]	2.379(5)	2.356(4)	2.195(6)
$Fe-N_{cis}$/Å [b]	2.198(6)	2.129(3)	2.048(5)
	2.225(5)	2.137(3)	2.039(5)
O-C/Å	1.325(7)	1.329(5)	1.342(7)
	1.324(7)	1.323(4)	1.328(8)
Fe-X-Fe/°	180	180	180

[a] $X = O^{2-}$ in **3** and $X = N^{3-}$ in **4**, **5**. [b] $Fe-N_{amine}$ bond lengths in the *trans* or *cis* positions to the Fe–X bond.

the center of symmetry). This implies that the Fe-N-Fe unit in **4** is *asymmetric*, with a short Fe≡N bond of 1.50(1) and a long Fe–N distance of 1.98(1) Å.[16] Due to the disorder of the asymmetric $[Fe^{IV}\equiv N-Fe^{III}]^{4+}$ moiety in the unit cell, the $Fe-N_{amine}$ and $Fe-O_{cat}$ values for **4** given in Table 1 represent only the average values for the LFe^{III}(cat) and LFe^{IV}(cat) units. The crystal structure of **4** provides the first indication that in **4** the valencies are localized.

It is remarkable that the corresponding O–C and C–C bond lengths of the coordinated catecholato ligands are identical for all three structures within experimental error, indicating that they are independent of the formal oxidation state of the iron centers.

The cat^{2-} ligand is bound in all three complexes **3**, **4**, and **5** as catecholate dianion.[17] It is interesting to compare corresponding bond lengths in **3**, containing a $[Fe^{III}$-O-$Fe^{III}]^{4+}$ unit, and **5**, with a $[Fe^{IV}=N=Fe^{IV}]^{5+}$ moiety. The $Fe-O_{cat}$ distances in **3** are 0.082 Å longer than those found in **5**, while the $Fe-N_{amine}$ bonds *cis* to the bridging atom are even 0.168 Å longer in **3** than in **5**. The *trans* $Fe-N_{amine}$ bond in **3** is 0.184 Å longer than the one found in **5** (Table 1). These large differences in bond lengths can be understood when looking at the electronic configuration of the iron centers: in the LFe^{III}(cat) unit, a high-spin configuration is present ($S = 5/2$), with two half-filled e_g^* orbitals, while in the LFe^{IV}(cat) unit a low-spin configuration ($S = 1$) with *empty* e_g^* orbitals is present. It is remarkable that the apparent (i.e., averaged) $Fe-O_{cat}$ and *cis*-$Fe-N_{amine}$ distances in **4** correspond to the arithmetic mean of the equivalent

 © VCH Verlagsgesellschaft mbH, D-69451 Weinheim, 1995 0570-0833/95/0606-0670 $ 10.00+.25/0

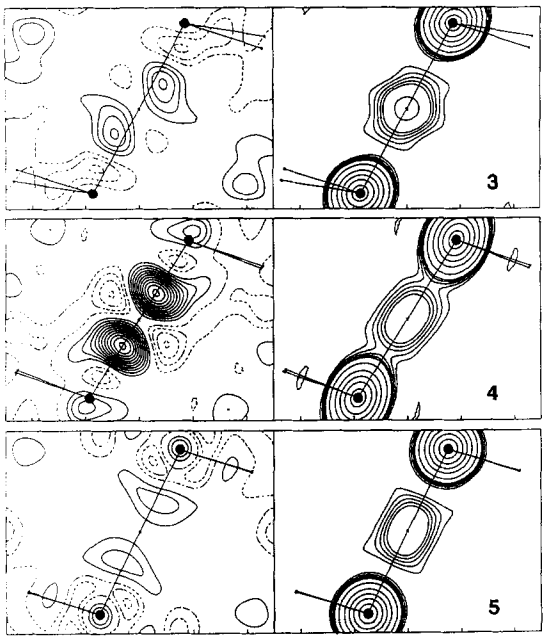


Fig. 2. Calculated contour maps of the residual electron density ($F_o - F_c$; left side) and the observed total electron density (F_o; right side) for the Fe-X-Fe moieties in the crystal structures of **3**–**5**. The plane shown is located between the catecholate oxygen atoms, it contains the iron atoms as well as the bridging oxygen and nitrogen atoms. The calculated values F_c were obtained after refinement for the structures had converged, using anisotropic temperature factors for the LFe(cat) units, while the bridging O atoms in **3** and the bridging N atoms in **4** and **5** were given isotropic temperature factors, as they are located on a crystallographic center of symmetry. The gradients for the electron density are as follows: left side: —— 0.1 e Å^{-3}; – – – −0.1 e Å^{-3}; right side: (going inward) 1, 2, ... 5 e Å^{-3}, going further inward 10, 20, ... 50 e Å^{-3}. (● = Fe atoms)

distances in **3** and **5**. The oxo bridge in **3** and the nitrido bridge in **5** exert a strong *trans* effect on the *trans*-Fe–N_{amine} bond ($\Delta[(Fe-N_{amine})_{trans}-(Fe-N_{amine})_{cis}]$: 0.17 Å in **3** and 0.22 Å in **5**).

Measurements of the molar magnetic susceptibilities (Faraday balance) yielded effective magnetic moments for the mononuclear complexes **1** and **2** that are characteristic for octahedral high-spin iron(III) complexes ($S = 5/2$) (Table 2), while the mononuclear species **6** was found to have a high-spin Fe^{II} configuration ($S = 2$). Complex **3** exhibited strongly temperature-dependent magnetic moments (4–298 K, SQUID magnetometer), which could be fitted without problems with the isotropic Heisenberg-Dirac-vanVleck model ($H = -2J\,\vec{S}_1 \cdot \vec{S}_2$, $S_1 = S_2 = 5/2$, $g = 2.0$ (fixed)), and a paramagnetic impurity of 2% ($S = 5/2$)), yielding $J = -90 \pm 4\ cm^{-1}$. Compound **3** therefore contains two high-spin Fe^{III} ions, which are antiferromagnetically coupled by a superexchange mechanism (oxo bridges), resulting in an $S = 0$ ground state.[12] Analogous measurements on **4** yielded a temperature-independent magnetic moment μ of 3.8 μ_B per dinuclear complex in the temperature range 50–300 K. Below 50 K, μ decreased to 2.8 μ_B at 3.0 K due to the zero-field splitting ($D_{3/2} = 13 \pm 4\ cm^{-1}$). Hence **4** has an $S = 3/2$ ground state resulting from strong antiferromagnetic coupling between a high-spin Fe^{III} ($S = 5/2$) and a low-spin Fe^{IV} ($S = 1$) center ($|J| > 150\ cm^{-1}$). The X-band ESR spectrum of **4** in dichloromethane at 10 K (Fig. 3) confirms the $S = 3/2$ ground state. The zero-field splitting was determined from the temperature dependence of the signal (3.0–40 K) to be $16 \pm 5\ cm^{-1}$, which is in good agreement with the value determined by susceptibility measurements. Complex **5** is diamagnetic even at 298 K ($S = 0$ ground state), indicating very strong

Table 2. Selected physical data for the complexes **1**–**6**.

1: IR: ν(Fe–O_{cat}) 564, ν(C–O_{cat}) 1250 cm^{-1}; UV/Vis (CH_3CN): λ_{max} (ε, M^{-1}cm^{-1}) = 304 (7800), 460 (1640), 704 nm (2400); magnetic moment (293 K): $\mu_{eff} = 5.8\ \mu_B$; ESR (X-band, DMSO, 10 K): rhombic signal $g_x = 5.7$, $g_y = 6.5$, $g_z = 2.0$; rhombicity $E/D = 0.017$.

2: IR: ν(Fe–O_{cat}) 563, $\delta(N_3)$ 640, $\nu_s(N_3)$ 1345, ν(C–O_{cat}) 1245, $\nu_{as}(N_3)$ 2069 cm^{-1}; UV/Vis (CH_3CN): λ_{max} (ε) = 306 (8600), 411 (3300), 680 nm (2500); magnetic moment (293 K): $\mu_{eff} = 5.7\ \mu_B$; ESR (X-band, acetone, 10 K): rhombic signal $g_x = 5.6$, $g_y = 6.5$, $g_z = 2.0$; rhombicity $E/D = 0.019$.

3: IR: ν_{as}(Fe-^{16}O-Fe) 817, ν_{as}(Fe-^{18}O-Fe) 777 cm^{-1}; resonance Raman (excitation at 407 and 483 nm; acetone): ν_s(Fe-^{16}O-Fe) 354, ν(Fe–O_{cat}) 544 cm^{-1} (both bands do not exhibit an isotope effect when the bridging O atom is labeled with ^{18}O); UV/Vis (CH_3CN): λ_{max} (ε) = 260 (16.3×10^3), 304 (14.3×10^3), 491 nm (5.0×10^3); cyclic voltammetry (0.10 *M* [N(*n*Bu)$_4$]PF_6, acetone): reversible one-electron oxidation at $E_{1/2} = +0.42$ V vs. Fc^+/Fc, irreversible reduction (1e) at −1.10 V.

4: MS (FAB): *m/z* (%): 960 (0.65) [M^+]; UV/Vis (CH_2Cl_2): λ_{max} (ε) = 328 (16.9×10^3), 423 (4900), 442 (sh), 876 nm (300); resonance Raman (excitation at 413 nm, CH_2Cl_2): strongest band at 911.3 cm^{-1} ν(Fe-^{14}N-Fe) or at 884.2 cm^{-1} for the ^{15}N-labeled complex; cyclic voltammetry (0.10 *M* [N(*n*Bu)$_4$]PF_6, CH_2Cl_2): reversible one-electron oxidation at $E_{1/2} = +0.55$ V vs. Fc^+/Fc, irreversible one-electron reduction at −0.61 V. The electronic spectrum of **4** exhibits an intervalence band at 876 nm ($\varepsilon = 300\ M^{-1}cm^{-1}$), which is not found in the spectra of **3** and **5**.

5·CH_3CN: MS (FAB): *m/z* (%): 960 (100) [M^+]; resonance Raman (acetone): excitation at 413 nm: strongest band at 407 cm^{-1} ν_s(Fe-N-Fe), which does not show an isotope effect upon ^{15}N labeling; excitation at 520 nm: strongest band at 568 cm^{-1} ν(Fe–O_{cat}) (IR: 570 cm^{-1}); UV/Vis (CH_3CN): λ_{max} (ε) = 228 (5.5×10^4), 267 (8.9×10^4), 316 (3.3×10^4), 523 (2.2×10^3), 617 (1.7×10^3), 770 nm (1.1×10^3); ^{1}H NMR (400 MHz, CD_3NO_2) of the PF_6^-·toluene salt of **5**: δ = 7.15 (m, aromatic toluene protons), 3.41 (s, 6H; CH_3), 2.4–3.2 (m, 12H; N-CH_2-CH_2-N), 2.25 (CH_3, toluene), 1.95 (s, 3H, CH_3).

6·$2H_2O$: MS (FAB): *m/z* (%): 473 (5) [M^+]; IR: ν(C≡N) 2197 cm^{-1}; UV/Vis (CH_3CN): λ_{max} (ε) = 520 (820); magnetic moment (293 K): $\mu_{eff} = 5.0\ \mu_B$.

intramolecular antiferromagnetic coupling ($|J| > 200\ cm^{-1}$) between two low-spin Fe^{IV} ($S = 1$) ions.

The Mössbauer spectrum of solid **4** at 77 K is composed of three subspectra (Table 3; Fig. 4). The weak doublet at $\delta = 0.48$ mm s^{-1} is identical to that found for **3** and can therefore by attributed to the contamination by the μ-oxodiiron(III) compound. The two other doublets are of equal intensity, but exhibit very different isomer shifts. The signal at $\delta = 0.52$ mm s^{-1} is typical for octahedrally coordinated high-spin Fe^{III}, while the doublet at $\delta = 0.09$ mm s^{-1} is characteristic for octahedrally coordinated low-spin Fe^{IV}—it is also found for complex **5** containing the $[Fe^{IV}=N=Fe^{IV}]^{5+}$ unit. The isomer shifts confirm the formulation of **4** as a mixed-valent $Fe^{III}Fe^{IV}$ complex, with localized valences on the time scale of Mössbauer spectroscopy (10^{-7} s).[19] These results contrast strongly to those obtained for the porphyrin and phthalocyanine complexes known so far, which contain a symmetric, electronically delocalized $[Fe^{3.5}=N=Fe^{3.5}]^{4+}$ structural unit and an $S = 1/2$ ground state.

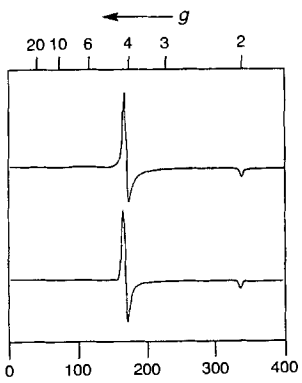


Fig. 3. X-band ESR spectra of **4** in CH_2Cl_2 at 10 K. Upper trace: experimentally obtained spectrum (9.4325 GHz; 20 μW/40 dB, modulation frequency: 100.0 kHz, modulation amplitude 1.00 mT); lower trace: simulated spectrum, having $g_x = 3.985$, $g_y = 4.140$, $g_z = 1.999$, rhombicity parameter $E/D = 0.013$. The ordinate axis is in arbitrary units of dX''/dB.

Complex **4** belongs therefore to class II (maybe even only to class I) in the Robin–Day scheme for mixed-valent compounds.[8] This stems presumably from the large Franck–Condon energy bar-

 © VCH Verlagsgesellschaft mbH, D-69451 Weinheim, 1995 0570-0833/95/0606-0671 $ 10.00+.25/0

Table 3. Mössbauer parameters for the complexes **2**–**6**.

Complex	T [K]	δ [mm s^{-1}] [a]	ΔE_Q [mm s^{-1}] [b]	Γ [mm s^{-1}] [c]	% [d]
2	3.7	0.43	0.98	0.40	100
3	4.2	0.46	1.41	0.29	100
4 [e]	77	0.09	0.81	0.22	45.2
		0.52	1.67	0.77	45.6
		0.48	1.41	0.26	9.1
5	77	0.04	1.55	0.26	100
6	77	1.06	1.54	0.74	100

[a] Isomer shift relative to α-Fe at 298 K. [b] Quadrupole splitting. [c] Line width. [d] % contribution to the subspectrum. [e] The Mössbauer parameters δ, ΔE_Q, and Γ were determined from field and temperature dependent measurements, using samples containing different amounts of **3**.

rier, which prevents an effective delocalization of the excess electron due to the significantly different Fe–N and Fe–O bond lengths in the LFe(cat) unit of the high-spin Fe^{III} ion on the one hand and the low-spin Fe^{IV} ion in **4** and the asymmetric $[Fe^{III}-N\equiv Fe^{IV}]^{4+}$ bridging moiety on the other.

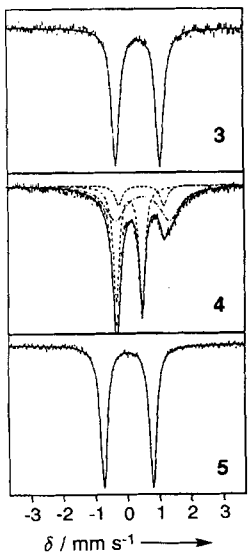


Fig. 4 Mössbauer spectra of **3** (4.2 K), **4** and **5** (77 K) (isomer shift relative to α-Fe (295 K)). The relative transmission is plotted on the ordinate axis.

Experimental Procedure

1: $catH_2$ (0.30 g) and sodium methanolate (0.13 g) was added to a suspension of $LFeCl_3$ (0.30 g) [18] in anhydrous methanol (30 mL). The mixture was heated to reflux for 4 h. Upon cooling to 20 °C, dark green microcrystals of **1** formed. Yield 0.43 g (94%).

2: A solution of **1** (0.30 g) and NaN_3 (0.40 g) in anhydrous acetone (150 mL) was heated to reflux for 6 h. Upon cooling to −25 °C, green crystals of **2** formed. Yield 0.27 g (90%).

3: An aqueous NaOH solution (6 mL, 0.10 M) was added with intense stirring to a suspension of **1** (0.30 g) in acetone (100 mL). The mixture was subsequently stirred for 3 h at 20 °C and filtered. The filtrate was placed in an open container and left undisturbed for 24 h. Red crystals of **3** formed during this period. Yield 0.26 g (93%). Recrystallization from acetone/toluene (1:1) led to single crystals of **3**·2toluene.

4: A solution of **2** (0.10 g) in anhydrous acetonitrile (200 mL) was irradiated for 5 h with a quartz Hg immersion lamp. The solution was kept at 0 °C and argon was bubbled through the mixture throughout the process. During the irradiation, black crystals of **4** precipitated, which were recrystallized from CH_2Cl_2. Yield 0.40 g (42%). This material is contaminated to varying degrees by **3**, depending on the residual water and oxygen contents.

5: Br_2 (0.50 mL) was added dropwise with stirring to a solution of **4** (0.10 g) in dry CH_2Cl_2 (50 mL). After the mixture had been stirred for 3 h at 20 °C, black-green crystals formed, which were recrystallized from acetonitrile/toluene (1:1): **5**·CH_3CN; yield 0.80 g (74%). The reduction of **5** (0.50 g) in acetonitrile (50 mL) using $N_2H_4\cdot H_2O$ yielded pure, crystalline **4**.

6: The photolysis of **2** led to the nearly quantitative precipitation of **4**, due to its extremely low solubility in CH_3CN. The resulting solution was subjected to filtration, after which the solvent was removed by rotary evaporation under an N_2 atmosphere. The gray-black residue was dissolved in a deoxygenated 1:1 mixture of acetone/toluene. Slow evaporation of this solution led to the precipitation of violet crystals of **6**·$2H_2O$. Yield 40% (based on **2**).

All compounds yielded satisfactory elemental analyses for C, H, N, Cl, and Fe.

Received: November 25, 1995 [Z 7504 IE]
German version: *Angew. Chem.* **1995**, *107*, 744

Keywords: complexes with nitrogen ligands · electron localization · iron compounds · Mössbauer spectroscopy

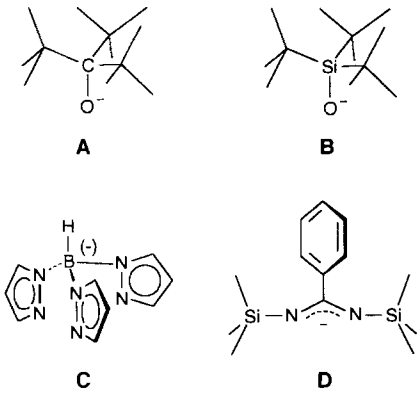
[1] K. Dehnicke, J. Strähle, *Angew. Chem.* **1992**, *104*, 978; *Angew. Chem. Int. Ed. Engl.* **1992**, *31*, 955.
[2] D. A. Summerville, I. A. Cohen, *J. Am. Chem. Soc.* **1976**, *98*, 1747.
[3] J. W. Buchler, C. Dreher, *Z. Naturforsch. B* **1984**, *39*, 222.
[4] W. R. Scheidt, D. A. Summerville, I. A. Cohen, *J. Am. Chem. Soc.* **1976**, *98*, 6623.
[5] a) K. Kadish, L. A. Bottomley, J. G. Brace, N. Winograd, *J. Am. Chem. Soc.* **1980**, *102*, 4341; b) K. Tatsumi, R. Hoffmann, M. H. Whangbo, *J. Chem. Soc. Chem. Commun.* **1980**, 509; c) K. Tatsumi, R. Hoffmann, *J. Am. Chem. Soc.* **1981**, *103*, 3328.
[6] L. A. Bottomley, B. B. Garrett, *Inorg. Chem.* **1982**, *21*, 1260.
[7] For an example, see Table 1 in C. Ercolani, S. Hewage, R. Heucher, G. Rossi, *Inorg. Chem.* **1993**, *32*, 2975.
[8] M. B. Robin, P. Day, *Adv. Inorg. Chem. Radiochem.* **1967**, *10*, 247.
[9] a) L. A. Bottomley, J.-N. Gorce, V. L. Goedken, C. Ercolani, *Inorg. Chem.* **1985**, *24*, 3733; b) K. M. Kadish, R. K. Rhodes, L. A. Bottomley, H. M. Goff, *ibid.* **1981**, *20*, 3195.
[10] C. Ercolani, M. Gardini, G. Pennesi, G. Rossi, U. Russo, *Inorg. Chem.* **1988**, *27*, 422.
[11] a) D. R. English, D. N. Hendrickson, K. S. Suslick, *Inorg. Chem.* **1985**, *24*, 122; b) B. Moubaraki, D. Benlian, A. Baldy, M. Pierrot, *Acta Crystallogr. Sect. C* **1989**, *45*, 393.
[12] D. M. Kurtz, Jr., *Chem. Rev.* **1990**, *90*, 585, and references cited therein.
[13] a) E. Vogel, S. Will, A. Schulze-Tilling, L. Neumann, J. Lex, E. Bill, A. X. Trautwein, K. Wieghardt, *Angew. Chem.* **1995**, *106*, 771; *Angew. Chem. Int. Ed. Engl.* **1995**, *33*, 731; b) M. Lausmann, I. Zimmer, J. Lex, H. Lueken, K. Wieghardt, E. Vogel, *ibid.* **1995**, *106*, 776; and **1995**, *33*, 736.
[14] An analogous complex, [Fe(tacn)(cat')Cl] (tacn = 1,4,7-triazacyclononane, cat' = 3,5-di-*tert*-butylcatecholate) has recently been reported: A. Dei, D. Gatteschi, L. Pardi, *Inorg. Chem.* **1993**, *32*, 1389.
[15] **3**·2toluene: $C_{44}H_{58}Cl_8Fe_2N_6O_5$, crystals grown from acetonitrile/toluene; monoclinic, space group $P2_1/m$, $a = 10.563(6)$, $b = 12.617(3)$, $c = 19.659(9)$ Å, $\beta = 100.31(9)°$, $Z = 2$; $\rho_{calcd} = 1.48$ g cm^{-3}; $\mu_{Mo} = 1.026$ mm^{-1}; 3297 observed reflections ($I \geq 2.0\sigma(I)$); empirical absorption correction, ψ scans; $2\theta_{max} = 55°$; $R = 0.065$; $wR = 0.066$; maximum residual electron density 0.67 e Å^{-3}. **4**: $C_{30}H_{42}Cl_8Fe_2N_7O_4$, crystals grown from dichloromethane; monoclinic, space group $P2_1/n$, $a = 8.807(1)$, $b = 17.024(2)$, $c = 13.011(2)$ Å, $\beta = 90.78(3)°$, $Z = 2$; $\rho_{calcd} = 1.63$ g cm^{-3}; $\mu_{Mo} = 1.337$ mm^{-1}; 2880 observed reflections ($I \geq 2.0\sigma(I)$); empirical absorption correction, ψ scans; $2\theta_{max} = 55°$; $R = 0.048$; $wR = 0.048$; maximum residual electron density 0.53 e Å^{-3}. **5**·CH_3CN: $C_{32}H_{45}BrCl_8Fe_2N_8O_4$, crystals grown from acetonitrile/toluene; monoclinic, space group $C2/c$, $a = 20.845(7)$, $b = 13.781(6)$, $c = 15.408(5)$ Å, $\beta = 99.80(2)°$, $Z = 4$; $\rho_{calcd} = 1.646$ g cm^{-3}; $\mu_{Mo} = 2.117$ mm^{-1}; 2586 observed reflections ($I \geq 2.0\sigma(I)$); empirical absorption correction, ψ scans; $2\theta_{max} = 55°$; $R = 0.060$; $wR = 0.058$; maximum residual electron density 0.96 e Å^{-3}, located in the vicinity of the disordered acetonitrile molecule, which was refined using a split-atom model. The data collection was performed at 293 K using a Siemens P4 diffractometer, employing monochromatic $Mo_{K\alpha}$ radiation. The structures were solved using Patterson and difference Fourier syntheses and were refined against F^2 for all observed, independent reflections. Heavy atoms were given anisotropic temperature factors. H atoms, which were placed in calculated positions, were given isotropic temperature factors; $wR = [\Sigma w(F_o^2 - F_c^2)^2/\Sigma w(F_o^2)^2]^{1/2}$. The Siemens-SHELXTL-PLUS program package (PC version) by G. M. Sheldrick (Universität Göttingen) was used for the structure solutions and refinements. Further details on the crystal structure investigations may be obtained from the Fachinformationszentrum Karlsruhe, D-76344 Eggenstein-Leopoldshafen, on quoting the depository number CSD-58767.
[16] The Fe–N distance of 1.50(1) Å is unrealistically short; a distance of about 1.60 Å is more likely to be correct.
[17] O. Carugo, C. B. Castellani, K. Djinovic, M. Rizzi, *J. Chem. Soc. Dalton Trans.* **1992**, 837.
[18] J. A. Hartmann, R. L. Rardin, P. Chaudhuri, K. Pohl, K. Wieghardt, B. Nuber, J. Weiss, G. C. Papaefthymiou, R. B. Frankel, S. J. Lippard, *J. Am. Chem. Soc.* **1987**, *109*, 7387.
[19] Whether the spin density of two unpaired electrons is localized on the Fe^{IV} ion or delocalized over the N≡Fe moiety can only be determined by magnetic Mössbauer measurements and MO calculations.

 © VCH Verlagsgesellschaft mbH, D-69451 Weinheim, 1995 0570-0833/95/0606-0672 $ 10.00+.25/0

Lanthanoid Complexes with [(dad)Li] Ligands—New Starting Materials for Organolanthanoid Chemistry**

Helmar Görls, Bernhard Neumüller, Annett Scholz, and Joachim Scholz*

In contrast to transition metal compounds, for which the 18-e$^-$ rule generally enables one to make a reliable statement about the relative stability, the steric saturation of the metal atom plays a decisive role for the stability of the organolanthanoid compounds. For this reason, pentamethylcyclopentadienyl (Cp*) and cyclopentadienyl ligands (RCp) with bulky substituents R[1] or other known Cp equivalents employed in transition metal chemistry such as tritox (**A**), silox (**B**), scorpionate (**C**), or benzamidinate ligands (**D**) are an essential prerequisite for the preparation of most organolanthanoid compounds.[2] These ligands are also advantageous from a preparative point of view since their use frequently leads to highly soluble compounds.

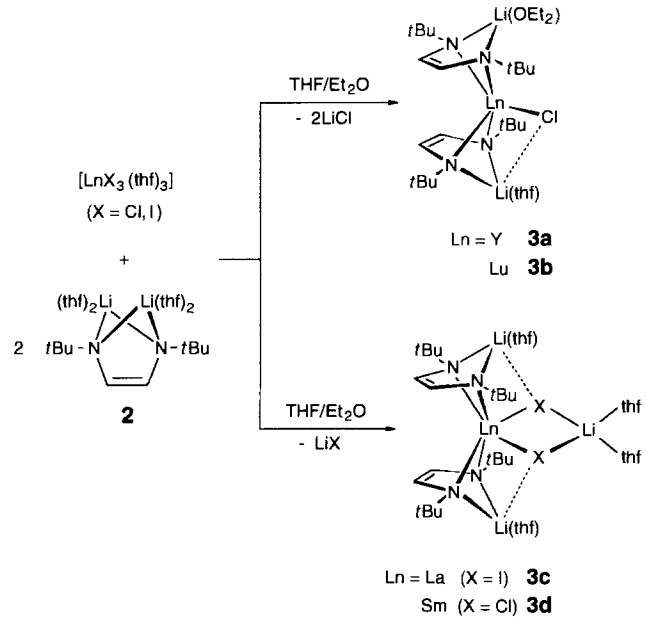


In connection with the application of 1,4-diaza-1,3-diene ligands in organometallic chemistry, it has been shown that the sterically very demanding *N,N'*-bis(*tert*-butyl)glyoxaldiimine **1** (dad) can also shield reactive centers of the molecule.[3] Furthermore, as the dianion (enediamide) it is capable of stabilizing transition metals in high oxidation states.[4] However, in lanthanoid chemistry little has been made of these useful properties: To date very few lanthanoid–dad complexes are known and in these **1** occurs almost exclusively as a radical anion.[5]

(*t*Bu)N=CHCH=N(*t*Bu) **1**

We report here on the synthesis and the structure of lanthanoid complexes in which **1** is bound as a dianion to lanthanoid ions and [(dad)Li]$^-$ units assume the function of Cp ligands. Furthermore, these novel lanthanoid–dad complexes offer an alternative to cyclopentadienyllanthanoid halides, the most commonly used starting materials in lanthanoid chemistry, because of their simple method of preparation and their good solubility.

The lithium–dad compound **2** is particularly suitable for the transfer of the dad dianion $\mathbf{1}^{2-}$ to the lanthanoid ion (Scheme 1). Compound **2** forms quantitatively in the reaction of **1**, which is readily accessible from *tert*-butylamine and glyoxal, with 2 molar equivalents of lithium in THF.[6] The subsequent reaction of



Scheme 1. Synthesis of the new complexes **3**.

2 with the lanthanoid halide–THF adducts $[YCl_3(thf)_3]$, $[LaI_3(thf)_3]$, $[SmCl_3(thf)_3]$, or $[LuCl_3(thf)_3]$, each in the mole ratio 2:1, leads to orange to red-brown solutions, from which the new lanthanoid complexes can be isolated as pale yellow (**3a** and **3b**), shiny yellow (**3c**), and black-red crystals (**3d**) in 75–95% yields after separation of the lithium halide and recrystallization from diethyl ether. As expected, the complexes **3a–d** decompose very rapidly in air; however, under an argon atmosphere they can be stored indefinitely and are thermally stable. Furthermore, it is remarkable that the new complexes are readily soluble in both diethyl ether and THF as well as in aromatic and aliphatic hydrocarbons.

Simple NMR spectra containing only one set of signals for the dad ligand indicate that **3a–d** are highly symmetrical. In the ^{13}C NMR spectra, the signal of the azomethine-C atom shifted to high field relative to that of the free ligand **1** confirms that the two heterodienes are bound as dianions to the lanthanoid ion (**1**: $\delta = 158.14$; **3a–d**: $\delta = 111.61-118.36$). Thus, the chemical shifts of the azomethine-C atoms of **3a–d** are remarkably very similar to those of the lithium–dad compound **2** ($\delta = 113.79$).[6b]

The results of the X-ray crystal structure analyses of **3b** and **3d** show that contrary to the NMR data, and evidently depending on the radius of the lanthanoid ion, two different types of complex exist.[7] Single crystals of **3b** form on cooling of a saturated solution of the compound in diethyl ether; Figure 1 shows the results of the structure analysis. The Lu atom forms the center of a coordination polyhedron generated by the Cl and the four N atoms of the two dad ligands. The four N atoms bridge the Lu with two Li atoms; the two (LuN_2Li) rings formed are twisted by 89.7(1)° with respect to each other and are linked to each other through the Lu center. The two dad ligands show

[*] Dr. J. Scholz, Dr. A. Scholz
Institut für Anorganische Chemie der Universität Halle-Wittenberg
Geusaer Strasse, D-06217 Merseburg (FRG)
Telefax: Int. code + (3461)46-2370
Dr. H. Görls
Max-Planck-Gruppe für "CO_2-Chemie" am Institut für Anorganische Chemie der Universität Jena (FRG)
Dr. B. Neumüller
Fachbereich Chemie der Universität Marburg (FRG)

[**] This work was supported by the Deutsche Forschungsgemeinschaft.

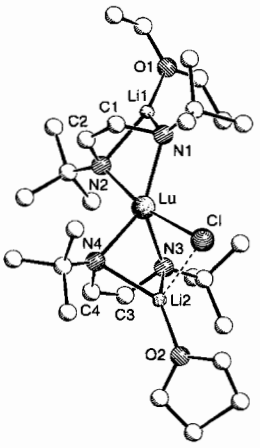
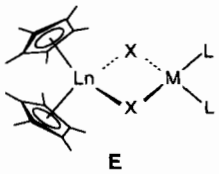


Fig. 1. Molecular structure of **3b** in the crystal. Selected bond lengths [Å], bond, torsion, and interplanar angles [°]: Lu-N1 2.282(3), Lu-N2 2.265(4), Lu-N3 2.212(3), Lu-N4 2.214(4), Lu-C1 2.659(4), Lu-C2 2.643(4), Lu-Cl 2.726(2), Lu-Li1 3.175(7), Lu-Li2 2.866(8), Li1-N1 2.078(8), Li1-N2 2.076(8), Li1-C1 2.239(9), Li1-C2 2.237(9), Li1-O1 1.940(8), Li2-N3 2.202(10), Li2-N4 2.176(10), Li2-C3 2.330(10), Li2-C4 2.323(10), Li2-O2 1.925(9), Li2-Cl 2.429(9), N1-C1 1.411(6), N2-C2 1.390(5), N3-C3 1.414(6), N4-C4 1.403(6), C1-C2 1.363(6), C3-C4 1.356(7); N1-Lu-N2 75.4(1), N3-Lu-N4 76.6(1), N1-Li1-N2 84.1(3), N3-Li2-N4 77.6(3), Lu-Cl-Li2 67.3(2), Li1-Lu-Li2 164.6(2); (N1,Lu,N2)(N3,Lu,N4) 89.7(1), (N1,Lu,N2)(N1,Li1,N2) 36.4(3), (N1,Lu,N2)(N1,C1,C2,N2) 64.5(2), (N3,Ln,N4)(N3,Li2,N4) 67.3(2), (N3,Lu,N4)(N3,C3,C4,N4) 30.2(2); N1-C1-C2-N2 −0.5(6), N3-C3-C4-N4 −1.2(6).

a "long-short-long" sequence of the N–C=C–N bond lengths typical for an enediamide structure. Short distances between the olefinic C atoms C1 and C2 and the metal centers Li1 and Lu, which are arranged on the opposite sides of the *cis*-configurated dad dianion (N1–C1=C2–N2), in particular, emphasize its bridging function. These distances lie in the range of usual Li–C and Lu–C bonds and indicate an intensive π interaction; thus, this dad dianion is formally coordinated η^4 to both metals.[9] Overall a structure motif results which was observed very recently for a Yb compound[5c] and is also comparable with that of the dilithium–dad compound [{Li(thf)$_2$}$_2${N(Me-4-C$_6$H$_4$)C(Ph)=C(Ph)N(Me-4-C$_6$H$_4$)}] reported by us a short while ago.[8] In the case of the second dad dianion a π interaction simply occurs between the C3–C4 double bond and Li2.

Remarkably, on recrystallization of **3b** from diethyl ether only the molecule of THF coordinated to the Li1 atom is substituted by diethyl ether. The reason for this is presumably the additional contact of the Cl atom with Li2 (Li2–Cl 2.429(9) Å), which leads to a tetrahedral coordination of Li2 and thus makes the replacement of THF at this Li atom kinetically more difficult.

The structure of **3d** differs from that of **3b** significantly in that the central Sm atom achieves the coordination number six by the addition of one molecule of LiCl; thus, overall the Sm atom is surrounded in a distorted octahedral fashion by four N and two Cl atoms (Fig. 2).[7] The two Cl atoms bridge the Sm atom with the Li2 atom, which is coordinatively saturated by two molecules of THF. Thus, overall, the molecular structure of **3d** is very similar to those of many bis(pentamethylcyclopentadienyl)lanthanoid halides [Cp$^*_2$Ln(μ-X)$_2$ML$_2$] **E** (Ln = lanthanoid; X = Cl, Br, I; M = Li, Na, K; L = Et$_2$O, THF, dme).[10] Evidently, the formation of this characteristic structure type for **3c** and **3d** is favored by the larger ionic radius of Sm^{3+} (0.964 Å) and La^{3+} (1.061 Å) relative to that of Y^{3+} (0.892 Å) and Lu^{3+} (0.848 Å).[11] Important structure elements of **3b**, however, are also present in **3d**; for example, the interaction of the Sm atom with the π-electron system C2=C3 of the dad ligand (Sm–C2 2.681(6), Sm–C3 2.654(6) Å) and the threefold coordination of the Li centers Li1 and Li1a. The latter is undoubtedly attributed to the spatial demand of the *tert*-butyl groups of the dad ligands, which prevents that more than one molecule of THF can be coordinated to these Li atoms.[12]



E

The low symmetry of the molecule structure of **3b** leads to the conclusion that the simple NMR spectra of this compound are simulated by a rapid molecular dynamic at room temperature. In fact the sharp singlets of the dad ligands in the ^{1}H NMR spectra ([D$_8$]THF) of **3a–d** coalesce on lowering the temperature at which the sample was measured and each singlet splits into two signals of equal intensity. An inversion of the folded metallacyclic five-membered ring M(NC=CN), like that which has been observed for many dad complexes of electron-deficient transition metals (Scheme 2, top[13]), can be ruled out as a reason for this dynamic behavior. First, the Li atoms block the swinging of the five-membered ring about the N,N′ axis, and second, even with a rapid inversion of both heterodiene ligands in **3a** and **3b**, the signals would be nonequivalent because of the differing influence of the Cl atom. Therefore, we assume that the [(dad)Li] units undergo a rotation or at least an oscillation at the complex core (Scheme 2, bottom). According to preliminary investigations, the energy barrier of this exchange process is 44.5(±1) kJ mol^{-1} for **3a** and 54.6(±) kJ mol^{-1} for **3b**.

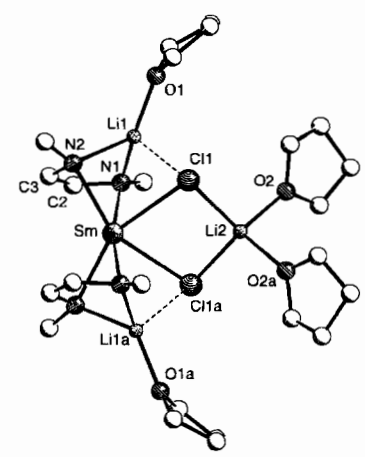
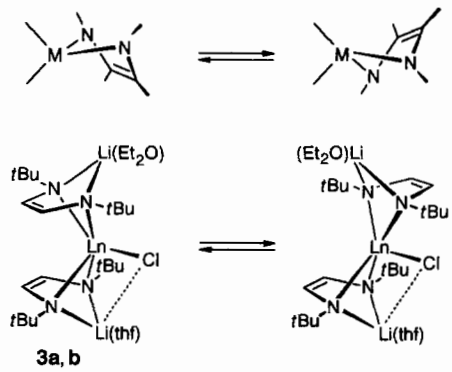


Fig. 2. Molecular structure of **3d** in the crystal. Only the quaternary C atoms of the *tert*-butyl groups are shown for clarity. Selected bond lengths [Å], bond, torsion, and interplanar angles [°]: Sm1-N1 2.482(4), Sm1-N2 2.420(5), Sm1-C2 2.681(6), Sm1-C3 2.654(6), Sm1-Cl1 2.878(2), Sm1-Li1 2.986(8), Li1-N1 2.08(1), Li1-N2 2.10(1), Li1-Cl1 2.50(1), Li2-Cl1 2.338(8), Li1-O1 1.93(1), Li2-O2 1.99(1), N1-C2 1.393(7), N2-C3 1.390(8), C2-C3 1.366(9); Cl1-Sm1-Cl1a 77.76(4), N1-Sm1-N2 68.2(2), N1-Sm1-N1a 169.7(1), N1-Sm-N2a 117.1(2), Cl1-Li2-Cl1a 101.2(5), Sm1-Cl1-Li2 90.5(2), O2-Li2-O2a 95.4(6), N1-C2-C3 120.2(6), N2-C3-C2 119.4(6), N1-Sm1-Cl1 81.7(1), N2-Sm1-Cl1 81.3(1); (Sm1,N1,N2)(Sm1,N1a,N2a) 67, (Sm1,N1,N2)(N1,N2,C2,C3) 77; N1-C2-C3-N2 0.0(1).

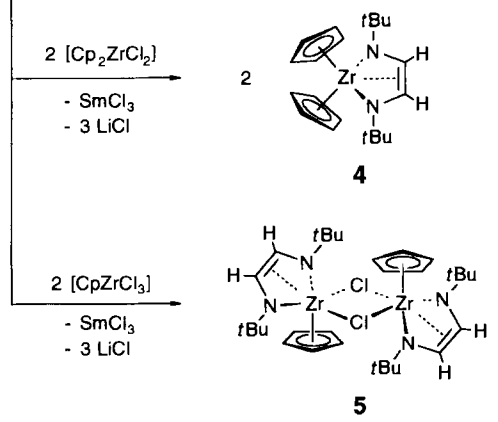


Scheme 2. Top: Inversion of the folded, five-membered metallacycle in dad complexes; bottom: postulated rotation or oscillation process in **3a, b**.

Owing to their structural relationship with the cyclopentadienyllanthanoid halides, the new lanthanoid–dad complexes **3a–d** are of interest as starting materials in organolanthanoid chemistry. Thus, not only can the halogen atoms be substituted by organic groups or other ligands, but also the Li atoms can be replaced by other metals. In this way **3a–d** open a route to new

 © VCH Verlagsgesellschaft mbH, D-69451 Weinheim, 1995 0570-0833/95/0606-0674 $ 10.00+.25/0

3d



lanthanoid multinuclear complexes. However, in these reactions it must be noted that the complexes **3** under certain conditions, like the lithium–dad compound **2** itself, act simply as a dad transferer: for example, the reaction of **3d** with $[Cp_2ZrCl_2]$ or $[CpZrCl_3]$ leads smoothly to the formation of the complexes **4** and **5**, respectively.[14]

Experimental Procedure

All reactions were carried out in thoroughly dried and degassed solvents under an argon atmosphere.

3a: $[YCl_3(thf)_3]$ (3.72 g, 9.04 mmol) was added to a solution of **2** [prepared from **1** (3.04 g, 18.08 mmol) and lithium (0.251 g, 36.16 mmol) in THF (100 mL)] at −78 °C and stirred. The reaction mixture was allowed to warm slowly to room temperature and stirred for a further 24 h. Subsequently the solvent was removed under vacuum, and the residue was extracted with diethyl ether (100 mL). Pale yellow crystals of **3a** precipitated from the extract at −20 °C (yield 5.16 g, 92% based on $[YCl_3(thf)_3]$, correct elemental analysis). ^{1}H NMR (300 MHz, [D$_8$]THF, 20 °C): δ = 5.50 (s, 4H; NCH=), 3.62 (m, 4H; OCH_2CH_2), 3.38 (q, 4H; OCH_2CH_3), 1.78 (m, 4H; OCH_2CH_2), 1.14 (s, 36H; CMe_3), 1.12 (t, 6H; OCH_2CH_3); ^{13}C NMR (75 MHz, [D$_8$]THF, 25 °C): δ = 113.02 (dd, ^1J(C,H) = 160.6 Hz, ^2J(C,H) = 8.4 Hz; NCH=), 66.25 (t, ^1J(C,H) = 139.1 Hz; OCH_2CH_3), 53.23 (s; CMe_3), 32.00 (q, ^1J(C,H) = 123.0 Hz; CMe_3), 15.62 (q, ^1J(C,H) = 125.5 Hz; OCH_2CH_3).

3b: $[LuCl_3(thf)_3]$ (3.25 g, 6.53 mmol) was added to a solution of **2** [prepared from **1** (2.20 g, 13.06 mmol) and lithium (0.181 g, 26.12 mmol) in THF (100 mL)] at −78 °C and stirred. The workup of the reaction mixture was carried out as for **3a**. Yield 3.60 g of pale yellow crystals of **3b**, 78% based on $[LuCl_3(thf)_3]$, correct elemental analysis. Crystals suitable for an X-ray crystal structure analysis were obtained by recrystallization from diethyl ether. ^{1}H NMR (300 MHz, [D$_8$]THF, 20 °C): δ = 5.55 (s, 4H; NCH=), 3.62 (m, 4H; OCH_2CH_2), 3.38 (q, 4H; OCH_2CH_3), 1.78 (m, 4H; OCH_2CH_2), 1.14 (s, 36H; CMe_3), 1.11 (t, 6H; OCH_2CH_3); ^{13}C NMR (75 MHz, [D$_8$]THF, 25 °C): δ = 111.61 (dd, ^1J(C,H) = 161.7 Hz, ^2J(C,H) = 8.3 Hz; NCH=), 66.18 (t, ^1J(C,H) = 139 Hz; OCH_2CH_3), 53.41 (s; CMe_3), 31.73 (q, ^1J(C,H) = 123.7 Hz; CMe_3), 15.72 (q, ^1J(C,H) = 125.5 Hz; OCH_2CH_3).

3c: $[LaI_3(thf)_3]$ (8.16 g, 11.09 mmol) was added in portions to a solution of **2** [prepared from **1** (3.73 g, 22.18 mmol) and lithium (0.308 g, 44.36 mmol) in THF (150 mL)] at −78 °C and stirred. The workup of the reaction mixture was carried out as for **3a**. Yield 8.34 g of bright yellow crystals of **3c**, 75% based on $[LaI_3(thf)_3]$, correct elemental analysis. ^{1}H NMR (300 MHz, [D$_8$]THF, 20 °C): δ = 5.40 (s, 4H; NCH=), 3.63 (m, 16H; OCH_2CH_2), 1.78 (m, 16H; OCH_2CH_2), 1.18 (s, 36H; CMe_3); ^{13}C NMR (75 MHz, [D$_8$]THF, 25 °C): δ = 115.88 (dd, ^1J(C,H) = 157.2 Hz, ^2J(C,H) = 9.4 Hz; NCH=), 68.21 (t, ^1J(C,H) = 144.6 Hz; OCH_2CH_2), 53.81 (s; CMe_3), 33.66 (q, ^1J(C,H) = 123.6 Hz; CMe_3), 26.29 (t, ^1J(C,H) = 132.1 Hz; OCH_2CH_2).

3d: $[SmCl_3(thf)_3]$ (12.00 g, 25.37 mmol) was added in portions to a solution of **2** [prepared from **1** (8.54 g, 50.74 mmol) and lithium (0.704 g, 101.48 mmol) in THF (200 mL)] at −78 °C and stirred. The workup of the reaction mixture was carried out as for **3a**. Yield 20.90 g of black-red crystals of **3d**, 95% based on $[SmCl_3(thf)_3]$, correct elemental analysis. Crystals suitable for an X-ray crystal structure analysis were obtained by recrystallization from diethyl ether. ^{1}H NMR (300 MHz, [D$_8$]THF, 20 °C): δ = 6.36 (br.s, 4H; NCH=), 3.61 (br.m, 16H; OCH_2CH_2), 1.76 (br.m, 16H; OCH_2CH_2), 1.18 (br.s, 36H; CMe_3); ^{13}C NMR (75 MHz, [D$_8$]THF, 25 °C): δ = 118.36 (NCH=), 68.21 (OCH_2CH_2), 57.67 (CMe_3), 29.92 (CMe_3), 26.31 (OCH_2CH_2); (−60 °C): δ = 121.56 (NCH=), 108.18 (NCH=), 67.42 (OCH_2CH_2), 57.48 (CMe_3), 56.02 (CMe_3), 31.24 (CMe_3), 30.07 (CMe_3), 16.30 (OCH_2CH_2).

Received: November 2, 1995 [Z 7444 IE]
German version: *Angew. Chem.* **1995**, *107*, 732

Keywords: cyclopentadiene analogues · complexes with nitrogen ligands · heterodiene complexes · lanthanoid compounds

[1] Reviews on organolanthanoid chemistry: a) H. Schumann, *Angew. Chem.* **1984**, *96*, 475–493; *Angew. Chem. Int. Ed. Engl.* **1984**, *23*, 474–493; b) W. J. Evans, *Adv. Organomet. Chem.* **1985**, *24*, 131–177; c) *Polyhedron* **1987**, *6*, 803–835.

[2] a) Tritox $[\{Me_3C\}_3CO]^-$: W. A. Herrmann, R. Anwander, W. Scherer, *Chem. Ber.* **1993**, *126*, 1533–1539; b) M. Wedler, J. W. Gilje, U. Pieper, D. Stalke, M. Noltemeyer, F. T. Edelmann, *ibid.* **1991**, *124*, 1163–1165; c) silox $[(Me_3C)_3SiO]^-$: W. A. Herrmann, R. Anwander, M. Kleine, W. Scherer, *ibid.* **1992**, *125*, 1971–1979; d) scorpionate $[HB(pz)_3]^-$: M. V. Steiner, J. Takats, *J. Am. Chem. Soc.* **1983**, *105*, 410–415; e) L. Hasinoff, J. Takats, X. W. Zhang, A. H. Bond, R. D. Rodgers, *ibid.* **1995**, *116*, 8833–8834; f) benzamidinate $[PhC(NSiMe_3)_2]^-$: M. Wedler, M. Noltemeyer, U. Pieper, H.-G. Schmidt, D. Stalke, F. T. Edelmann, *Angew. Chem.* **1990**, *102*, 941–943; *Angew. Chem. Int. Ed. Engl.* **1990**, *29*, 894–896; g) A. Recknagel, F. Knösel, H. Gornitzka, M. Noltemeyer, F. T. Edelmann, *J. Organomet. Chem.* **1991**, *417*, 363–375; h) M. Wedler, A. Recknagel, J. W. Gilje, M. Noltemeyer, F. T. Edelmann, *ibid.* **1992**, *426*, 295–306; i) M. Wedler, F. Knösel, U. Pieper, D. Stalke, F. T. Edelmann, H.-D. Amberger, *Chem. Ber.* **1992**, *125*, 2171–2181.

[3] (dad)E: a) E = C: A. J. Arduengo III, R. J. Harlow, M. Kline, *J. Am. Chem. Soc.* **1991**, *113*, 361–363; b) E = Si: M. Denk, R. K. Hayashi, R. West, *J. Chem. Soc. Chem. Commun.* **1995**, 33–34; c) E = Ge: W. A. Herrmann, M. Denk, J. Behm, W. Scherer, F.-J. Klingan, H. Bock, B. Solouki, M. Wagner, *Angew. Chem.* **1992**, *104*, 1489–1492; *Angew. Chem. Int. Ed. Engl.* **1992**, *31*, 1485–1488; $(dad)_2$M: d) M = Li, Mg, Zn: M. G. Gardiner, G. R. Hanson, M. J. Henderson, F. C. Lee, C. L. Raston, *Inorg. Chem.* **1995**, *33*, 2456–2461; e) M = Al: F. G. N. Cloke, C. I. Dalby, M. J. Henderson, P. B. Hitchcock, C. H. L. Kennard, R. N. Lamb, C. L. Raston, *J. Chem. Soc. Chem. Commun.* **1990**, 1394–1396; f) M = Ga: F. G. N. Cloke, G. R. Hanson, M. J. Henderson, P. B. Hitchcock, C. L. Raston, *ibid.* **1989**, 1002–1003.

[4] a) $(dad)_2$Ti: H. tom Dieck, J. Rieger, G. Fendesak, *Inorg. Chim. Acta* **1990**, *177*, 191–197; b) (dad)$_2$M (M = Zr, Hf): C. Trompke, Dissertation, Universität Hamburg, **1992**; c) (dad)M$(BH_4)_2$ (M = Ti, Zr): W. A. Herrmann, M. Denk, W. Scherer, F.-R. Klingan, *J. Organomet. Chem.* **1993**, *444*, C21–C24.

[5] a) $(dad)_3$Ln (Ln = Y, Nd, Sm, Yb): F. G. N. Cloke, H. C. de Lemos, A. A. Sameh, *J. Chem. Soc. Chem. Commun.* **1986**, 1344–1345; b) $(dad)_3$Sm: F. G. N. Cloke, *Chem. Soc. Rev.* **1993**, 17–24; c) $(dad)_2$Yb: A. A. Trifonov, A. V. Protchenko, V. K. Cherkasov, M. N. Bochkarev, *Metallorgan. Khim.* **1989**, *2*, 471; d) $[Cp_2^*Sm(dad)]$: A. Recknagel, M. Noltemeyer, F. T. Edelmann, *J. Organomet. Chem.* **1991**, *410*, 53–61. e) After the completion of our work the Yb complex $[Cp_2Yb(\mu\text{-dad})Li(dme)]$ was published; the central Yb(μ-dad)Li-structural unit is comparable with that of **3a**: A. A. Trifonov, L. N. Zakharov, M. M. Bochkarev, Yu. T. Struchkov, *Izv. Akad. Nauk SSSR Ser. Khim.* **1995**, 148–151.

[6] a) **1**: J. M. Kliegman, R. K. Barnes, *Tetrahedron* **1970**, *26*, 2555–2560; 1H NMR (300 MHz, [D$_8$]THF, 25 °C): δ = 7.83 (s, 2H; N=CH), 1.20 (s, 18H, CMe_3); ^{13}C NMR (75 MHz, [D$_8$]THF, 20 °C): δ = 158.14 (dd, ^1J(C,H) = 161.1 Hz, ^2J(C,H) = 10.6 Hz; N=CH), 58.40 (s; CMe_3), 29.72 (q, ^1J(C,H) = 125.8 Hz; CMe_3); b) **2**: **1** (5.20 g, 30.90 mmol) was dissolved in THF (100 mL) and treated with lithium sand (0.429 g, 61.80 mmol) at room temperature. The reaction mixture changed to orange red and was stirred for 24 h. Subsequently the solvent was removed under vacuum and the residue taken up in a mixture of diethyl ether/*n*-pentane (50 mL). Compound **2** crystallized at −20 °C as a THF adduct of the composition $[\{Li(thf)_2\}_2\{(tBu)NCH{=}CHN(tBu)\}]$. 1H NMR (300 MHz, [D$_8$]THF, −80 °C): δ = 5.16 (s, 2H; NCH=), 1.00 (s, 18H; CMe_3); (75 MHz, [D$_8$]THF, −80 °C): δ = 113.79 (dd, ^1J(C,H) = 154.8 Hz, ^2J(C,H) = 11.4 Hz; NCN=), 51.13 (s; CMe_3), 33.35 (q, ^1J(C,H) = 124.4 Hz; CMe_3).

[7] X-ray structure analysis of **3b**: $C_{28}H_{58}ClN_4O_2Li_2Lu$, M = 707.08 g mol^{-1}, crystal dimensions 0.40 × 0.40 × 0.38 mm^3, triclinic, space group $P\bar{1}$, a = 1063.1(2), b = 1202.8(2), c = 1422.4(3) pm, α = 81.40(3), β = 83.06(3), γ = 81.07(3)°, V = 1767.7(6) × 10^6 pm^3, Z = 2, ρ_{calcd} = 1.328 g cm^{-3}, Enraf-Nonius CAD-4 diffractometer, $Mo_{K\alpha}$ radiation, λ = 71.073 pm, graphite monochromator, T = 183(2) K, μ = 2.895 mm^{-1}, scan range $2.59 < \omega < 25.97°$, 7260 measured reflections, 6915 symmetry independent reflections, 6906 of which were observed ($I > 2\sigma(I)$), 343 refined parameters, R_1 = 0.0430, wR_2 = 0.0874. X-ray structure analysis of **3d**: $C_{36}H_{72}Cl_2N_4O_4Li_3Sm$, M = 867.08 g mol^{-1}, crystal dimensions 0.50 × 0.45 × 0.45 mm^3, monoclinic, space group $C2/c$, a = 1649.4(2), b = 1270.9(2), c = 2238.4(4) pm, β = 108.67(1)°, V = 4445(1) × 10^6 pm^3, Z = 4, ρ_{calcd} = 1.296 g cm^{-3}, Enraf-Nonius

 © VCH Verlagsgesellschaft mbH, D-69451 Weinheim, 1995 0570-0833/95/0606-0675 $ 10.00+.25/0

CAD-4 diffractometer, $Mo_{K\alpha}$ radiation, $\lambda = 71.071$ pm, graphite monochromator, $T = 193$ K, scan range $6.2 < 2\theta < 52.7°$, 4503 symmetry independent reflections, 3406 of which were observed ($|F_o| > 4\sigma|F_o|$), $R_1 = 0.0485$, $wR_2 = 0.1127$. The two split positions C611 (occupation factor 0.8, anisotropicic) and C612 (occupation factor 0.2, isotropic) were calculated for the disordered C atom C61. All H atoms except H2 and H3 were calculated for an ideal geometry and were refined with mutual deflection parameters. H2 and H3 were refined free. Structure representations with SCHAKAL 92 (E. Keller, Universität Freiburg, **1992**). Further details of the crystal structure investigations may be obtained from the Fachinformationszentrum Karlsruhe, D-76344 Eggenstein-Leopoldshafen (FRG) on quoting the depository number CSD-58697.

[8] J. Scholz, B. Richter, R. Goddard, C. Krüger, *Chem. Ber.* **1993**, *126*, 57–61.

[9] a) A distance of 2.50 Å has been discussed as an upper limit for a Li–C interaction: W. Zarges, M. Marsch, K. Harms, W. Koch, G. Frenking, G. Boche, *Chem. Ber.* **1991**, *124*, 543–549; b) The Ln–(C=C) distances in **3b** and **3d** are comparable with the average Ln–C_{Cp^*} distances of $Cp^*_2Ln^{III}$ complexes (Sm: 2.68(1)–2.80(1) Å; Lu 2.63(2)–2.66(2) Å [10]).

[10] W. J. Evans, S. E. Foster, *J. Organomet. Chem.* **1992**, *433*, 79–94. Whereas in the $[Cp^*_2Ln(\mu\text{-}X)_2ML_2]$ complexes the X-Ln-X′ planes are almost perpendicular to the Cp*-Ln-Cp* planes, in **3d** the Cl1-Sm-Cl1a plane is only tilted towards the center(**1**)-Ln-center(**1**)′ plane by 55° because of the short Li1–Cl1 and Li1a–Cl1a contacts, respectively.

[11] F. A. Cotton, G. Wilkinson, *Advanced Inorganic Chemistry*, 4. edition, Wiley, New York, **1980**.

[12] Likewise for steric reasons the Li is only three-coordinate in: a) $[\{(Me_3Si)_2NLi\}_2 \cdot 2Et_2O]$: M. F. Lappert, M. J. Slade, A. Singh, J. L. Atwood, R. D. Rogers, R. Shakir, *J. Am. Chem. Soc.* **1983**, *105*, 302–304; b) $[\{(Me_3Si)_2NLi\}_2 \cdot 2THF]$: L. M. Engelhardt, B. S. Jolly, P. C. Punk, C. L. Raston, B. W. Skelton, A. H. White, *Aust. J. Chem.* **1986**, *39*, 133; c) P. G. Willard, M. A. Nichols, *J. Am. Chem. Soc.* **1991**, *113*, 9671–9673.

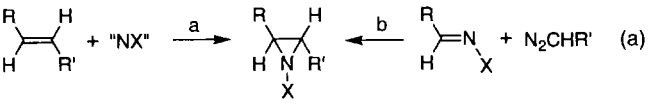
[13] a) J. Scholz, M. Dlikan, D. Ströhl, A. Dietrich, H. Schumann, K.-H. Thiele, *Chem. Ber.* **1990**, *123*, 2279–2285; b) R. Goddard, C. Krüger, G. A. Hadi, K.-H. Thiele, J. Scholz, *Z. Naturforsch. B* **1995**, *49*, 519–528; c) see also [4b, c].

[14] **4**: orange-yellow crystals; ^{1}H NMR (300 MHz, [D$_8$]THF, 25 °C): $\delta = 5.94$ (s, 5H; Cp), 5.52 (s, 2H; NCH=), 5.50 (s, 5H; Cp), 1.26 (s, 18H; CMe_3); ^{13}C NMR (75 MHz, [D$_8$]THF, 20 °C): $\delta = 108.74$ (d, ^1J(C,H) = 170.6 Hz; Cp), 107.86 (dd, ^1J(C,H) = 161.7 Hz, ^2J(C,H) = 9.7 Hz; NCH=), 101.64 (d, ^1J(C,H) = 169.9 Hz; Cp), 58.00 (s; CMe_3), 32.12 (q, ^1J(C,H) = 125.0 Hz; CMe_3). – **5**: pale yellow crystals; ^{1}H NMR (300 MHz, [D$_8$]THF, 20 °C): $\delta = 6.36$ (s, 5H; Cp), 5.87 (s, 2H; NCH=), 1.24 (s, 18H; CMe_3); ^{13}C NMR (75 MHz, [D$_8$]THF, 25 °C): $\delta = 111.54$ (d, ^1J(C,H) = 172.0 Hz; Cp), 105.31 (dd, ^1J(C,H) = 168.7 Hz, ^2J(C,H) = 10.2 Hz; NCH=), 59.46 (s; CMe_3), 31.56 (q, ^1J(C,H) = 125.4 Hz; CMe_3).

Carbenoid Transfer to Imines: A New Asymmetric Catalytic Synthesis of Aziridines**

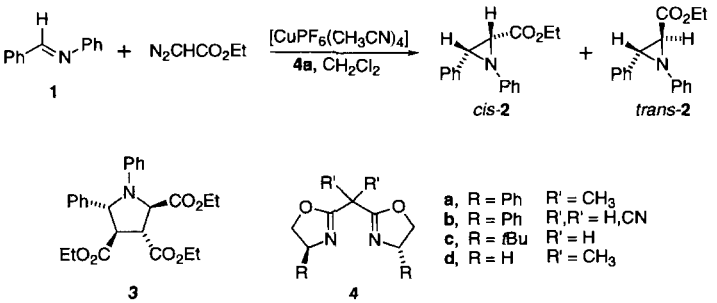
Karl B. Hansen, Nathaniel S. Finney, and Eric N. Jacobsen*

Aziridines are versatile precursors for the synthesis of unnatural amino acids and other nitrogen-containing compounds of biological importance.[1] However, the use of aziridines as chiral building blocks in synthesis has been somewhat restricted because their preparation in optically active form typically requires multiple-step transformation of available starting materials. Quite recently, asymmetric metal-catalyzed nitrene transfer to olefins has emerged as the first direct method for the enantioselective synthesis of aziridines from prochiral substrates [Eq. (a), path a).[2] In principle, the catalytic asymmetric transfer of carbenes to imines represents a complementary alternative for the preparation of these compounds [Eq. (a), path b).



Among the potential advantages of the latter approach are the synthetic accessibility of imines and diazocarbonyl compounds, the high reaction efficiency (the only by-product being nitrogen), and the inherent convergence associated with coupling two potentially complex fragments. Although the synthesis of aziridines by metal-mediated reaction of imines with carbenes has some limited precedent,[3] asymmetric variants have not been developed. We report herein the first successful application of this strategy to the catalytic synthesis of aziridines in optically active form.

The transition metal catalyzed transfer of diazocarbonyl-derived carbenes to imines was investigated by employing the readily prepared *N*-benzylidene aniline (**1**).[4] A range of established protocols for asymmetric catalytic carbene transfer was examined, including systems based on Cu, Rh, and Ru.[5] Of these, it was found that copper(I) salts, in association with bis(-dihydrooxazole) ligands, were most effective in catalyzing aziridination reactions.[6] Thus, treatment of **1** with ethyl diazoacetate in the presence of copper(I) hexafluorophosphate $[Cu(PF_6)(CH_3CN)_4)]$[7] and **4a–c** resulted in the formation of enantiomerically enriched aziridine **2** as a mixture of two diastereomers, and racemic pyrrolidine **3** (Scheme 1, Table 1).[8, 9]



Scheme 1. Synthesis of aziridines **2**; only one enantiomer of is shown.

Table 1. Spectroscopic data for *cis*-**2**, *trans*-**2**, and **3**.

cis-**2**: ^{1}H NMR ($CDCl_3$, 25 °C): $\delta = 7.40–7.60$ (m, 2H), 7.20–7.40 (m, 5H), 6.90–7.05 (m, 3H), 3.95–4.15 (m, 2H; CH_2), 3.57 (d, ^3J(H,H) = 6.8 Hz, 1H; CH), 3.19 (d, ^3J(H,H) = 6.8 Hz, 1H; CH), 0.98 (t, ^3J(H,H) = 7.1 Hz, 3H; CH_3); IR (neat): $\tilde{\nu} = 1748$ cm^{-1} (C=O), 1724 (C=O); MS (70 eV): *m/z* (%): 267 (22) [M^+], 222 (21) [M^+–OEt], 194 (100) [M^+–CO_2Et].

trans-**2**: ^{1}H NMR: $\delta = 7.10–7.35$ (m, 7H), 6.75–6.95 (m, 3H), 4.05–4.20 (m, 2H; CH_2), 3.82 (d, ^3J(H,H) = 2.5 Hz, 1H; CH), 3.24 (d, ^3J(H,H) = 2.5 Hz, 1H; CH), 1.17 (t, ^3J(H,H) = 7.2 Hz, 3H; CH_3); IR: $\tilde{\nu} = 1736$ cm^{-1} (C=O); MS: *m/z* (%): 267 (25) [M^+], 222 (22) [M^+–OEt], 194 (100) [M^+–CO_2Et].

3: ^{1}H NMR: $\delta = 7.15–7.30$ (m, 5H), 6.95–7.05 (m, 2H), 6.60–6.70 (m, 1H), 6.45–6.55 (m, 2H), 5.39 (d, ^3J(H,H) = 4.0 Hz, 1H; CH), 5.33 (d, ^3J(H,H) = 2.0 Hz, 1H; CH), 4.00–4.25 (m, 6H; 3 × CH_2), 3.84 (dd, ^3J(H,H) = 3.0, 2.0 Hz, 1H; CH), 3.58 (dd, ^3J(H,H) = 4.0, 3.0 Hz, 1H; CH), 1.30 (m, 3H; CH_3), 1.16 (t, ^3J(H,H) = 7.5 Hz, 1H; CH_3), 1.10 (t, ^3J(H,H) = 7.0 Hz, 1H; CH_3); IR: $\tilde{\nu} = 1738$ cm^{-1} (C=O); MS: *m/z* (%): 440 (65) [M^+ + H], 366 (100) [M^+–CO_2Et], 293 (52) [M^+–2 × CO_2Et].

The achiral bis(dihydrooxazole) **4d** provided the highest diastereoselectivity and chemical yield among the ligands tested;[11] the Evans bis(dihydrooxazole), **4a**,[5e] proved to be the most effective among chiral ligands in terms of yield and diastereo- and enantioselectivity (Table 2).

[*] Prof. E. N. Jacobsen, K. B. Hansen, N. S. Finney
Harvard University, Department of Chemistry
12 Oxford Street, Cambridge, MA 02138 (USA)
Telefax: Int. code + (617)496-1880

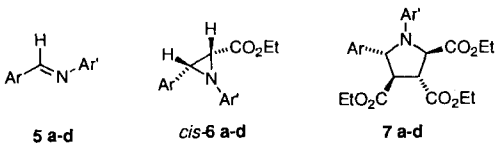
[**] This work was supported by an award to E. N. J. from the Packard Foundation, and through a postdoctoral fellowship to N. S. F. from the National Institutes of Health (GM16639).

Table 2. Aziridination in the presence of lignads **4a–d**.

Ligand	Yield[%] **2**[a]	*cis*/*trans*	*ee*(*cis*)[%]/*ee*(*trans*)[%][b]	Yield[%] **3**[a]
4a	37	4	44/35	10
4b	19	3	15/7	11
4c	10	2	11/2	5
4d	65	>10	–	<5

[a] Yield based on imine. [b] Absolute configuration not assinged; enantiomeric excess determined by HPLC.

The aziridination reaction proved to be quite sensitive to the electronic properties of the substrate imine (Scheme 2). The methyl-substituted imine **5a** underwent aziridination with increased diastereoselectivity but reduced yield, while reaction of chloro-substituted imine **5b** led to exclusive formation of the corresponding pyrrolidine in low yield (Table 3). Incorporation of an electron-donating group in the aniline-derived portion of the imine resulted in slightly lower aziridine yield but improved enantio- and diastereoselectivity. Efforts to extend this aziridination methodology to other classes of imines have not yet been fruitful.[12]



a, Ar = *p*-$H_3CC_6H_4$ Ar' = C_6H_5
b, Ar = *p*-ClC_6H_4 Ar' = C_6H_5
c, Ar = C_6H_5 Ar' = *p*-$H_3COC_6H_4$
d, Ar = C_6H_5 Ar' = *p*-ClC_6H_4

Scheme 2. Synthesis of azirines **6**; only one enantiomer is shown.

Table 3. Aziridination of **5a–d** in the presence of ligand **4a**.

Imine	Yield[%] **6**[a]	*cis*/*trans*	*ee*(*cis*)[%]/*ee*(*trans*)[%][b]	Yield[%] **7**[a]
5a	17	9	44/26	<5
5b	<5	–	–	10
5c	23	9	67/32	<5
5d	34	4	49/22	<5

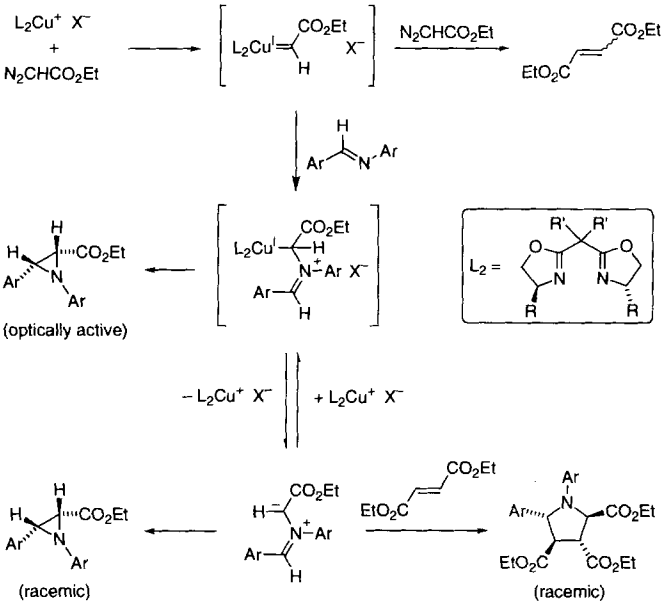
[a] Yield based on imine. [b] Absolute configuration not assigned; enantiomeric excess determined by HPLC.

The following observations, in conjunction with the formation of racemic pyrrolidine, allow the deduction of a plausible mechanism for this reaction. Treatment of **1** with excess ethyl diazoacetate led to increased yield of **3**, at the expense of aziridine formation. Treatment of **1** with a single equivalent of ethyl diazoacetate in the presence of two equivalents of diethyl fumarate similarly afforded **3** as the exclusive product. When dimethyl fumarate was employed instead, the corresponding 2-carboxyethyl-3,4-bis(carboxymethyl)pyrrolidine was formed. Thus, aziridine and pyrrolidine appear to arise from a common intermediate which is siphoned off to pyrrolidine in the presence of fumarate.[13] We propose that this intermediate is an azomethine ylide: azomethine ylides generated in the absence of transition metals and dipolarophiles are known to undergo intramolecular cyclization to form aziridines;[14] further, there is precedent for the formation of ylide intermediates by the attack of a heteroatom lone pair on a metallocarbene, and these ylides are known to react with dipolarophiles such as fumarates.[15, 16]

The generation of aziridine in optically active form indicates that its formation is mediated by the copper–bis(dihydrooxazole) complex. In contrast, the formation of racemic **3** suggests that pyrrolidine arises from the azomethine ylide by a path that is not metal mediated, and that the azomethine ylide thus exists as an equilibrating mixture of metal-complexed and uncomplexed forms. That the two forms equilibrate is evidenced by the suppression of aziridine formation accompanied by enhanced pyrrolidine formation in the presence of added dipolarophile. An important consequence of the generation of free azomethine ylide is that it can, in principle, form racemic aziridine as well as pyrrolidine. While there can be no direct observation of racemic aziridine formation under these conditions, we note the following. First, there is some variability (±5%) of the enantiomeric excesses of *cis*- and *trans*-**2** formed under the standard conditions. In general, lower enantiomeric excesses of **2** are accompanied by increased formation of pyrrolidine. Second, performing the reaction in a less polar solvent system (CH_2Cl_2:hexanes), which should suppress dissociation of the ylide from the copper–bis(dihydrooxazole) complex, results in an increase in the enantiomeric excess of isolated *cis*-**2** (53% *ee*).

The evidence outlined above is summarized by the mechanism depicted in Scheme 3. Thus, we propose that a transient bis(dihydrooxazole)copper carbene complex is generated and reacts either with diazoester to form a mixture of diethyl maleate and fumarate[13] or with the imine nitrogen lone pair to form a metal-complexed azomethine ylide. The complexed ylide may then undergo intramolecular ring closure to form aziridine enantioselectively, or it may reversibly dissociate from the metal–ligand complex. In its dissociated state, the free azomethine ylide can either undergo either dipolar cycloaddition with diethyl fumarate to generate racemic pyrrolidine or intramolecular cyclization to form racemic aziridine.

This work illustrates for the first time that the chemistry of azomethine ylides can be influenced by a transition metal complex; in the process, it outlines an extremely direct strategy for the synthesis of enantiomerically enriched *N*-aryl aziridines and, accordingly, of *N*-aryl amino acids. On the basis of the mechanistic analysis provided above, the development of a highly effective catalyst for enantioselective aziridination is predicted to



Scheme 3. Proposed reaction mechanism for the copper-catalyzed aziridination of imines with diazocarbonyl compounds; only one enantiomer is shown.

require a catalyst system for which azomethine ylide dissociation is completely suppressed. This may be attainable simply by judicious ligand design; however, it is possible that a fundamentally different metal–ligand system will be required. In this context, it is compelling to note the potential similarities between metal complexes of azomethine ylides and π-allyl ligands, especially in light of the recent marked advances in asymmetric catalysis with π-allyl complexes.[17]

Experimental Procedure

Representative procedure for the aziridination of **1**: A solution of **1** (0.113 g, 0.625 mmol, 1.000 equiv), **4a** (0.031 g, 0.094 mmol, 0.150 equiv, Aldrich), and $[CuPF_6(CH_3CN)_4]$ [7] (0.023 g, 0.063 mmol, 0.100 equiv) in CH_2Cl_2 (2.50 mL) containing 4 Å molecular sieves was stirred under nitrogen at room temperature for 10 min. Ethyl diazoacetate (2.50 mL, 0.25 M in CH_2Cl_2, 0.625 mmol, 1.000 equiv) was added by syringe pump over 12.5 h, and the solution was allowed to stir 1 h after the addition was complete. The crude reaction mixture was filtered through a plug of basic alumina (Brockmann, Activity I), eluting with CH_2Cl_2, and analyzed by GC and ^{1}H NMR after addition of a known quantity of internal standard (acetophenone). Alternatively, the reaction mixture could be purified directly by chromatography on silica gel (gradient elution, hexanes → 2% ethyl acetate in hexanes → 4% ethyl acetate in hexanes; R_f (10% ethyl acetate in hexanes): 0.50 (*cis*-**2**), 0.65 (*trans*-**2**).

Received: October 31, 1995 [Z 7438 IE]
German version: *Angew. Chem.* **1995**, *107*, 750

Keywords: asymmetric synthesis · aziridines · chiral ligands · copper complexes

[1] a) J. A. Deyrup in *Heterocycles, Vol. 4* (Ed.: A. Hassner), Wiley, New York, **1983**, p. 1; b) A. Padwa, A. D. Woolhouse in *Comprehensive Heterocyclic Chemistry, Vol. 7* (Ed.: W. Lwowski), Pergammon, Oxford, **1984**, p. 1; c) D. Tanner, *Angew. Chem.* **1995**, *106*, 625–643; *Angew. Chem. Int. Ed. Engl.* **1995**, *33*, 599–618.

[2] Z. Li, K. R. Conser, E. N. Jacobsen, *J. Am. Chem. Soc.* **1993**, *115*, 5326–5327; b) D. A. Evans, M. M. Faul, M. T. Bilodeau, B. A. Anderson, D. M. Barnes, *ibid.* **1993**, *115*, 5328–5329.

[3] a) P. Baret, H. Buffet, J.-L. Pierre, *Bull. Soc. Chim. Fr.* **1972**, 2493–2501; b) A. J. Hubert, A. Feron, R. Warin, P. Teyssie, *Tetrahedron Lett.* **1976**, 1317–1318; c) H. Sano, M. Takebayashi, *Kinki Daigaku Rikogakubu Kenkyu Hokoku* **1976**, *11*, 42–52 [*Chem. Abstr.* **1976**, *88*, 36836h]; d) M. Bartnik, G. Mloston, *Tetrahedron Lett.* **1984**, 2569–2576.

[4] R. W. Layer, *Chem. Rev.* **1963**, *63*, 489–510.

[5] Cu-mediated cyclopropanation: a) S. Nozaki, S. Moriuti, H. Takaya, R. Noyori, *Tetrahedron Lett.* **1966**, 5239–5244; b) T. Aratani, *Pure Appl. Chem.* **1985**, *57*, 1839–1844; c) H. Fritschi, U. Leutenegger, A. Pfaltz, *Helv. Chim. Acta* **1988**, *71*, 1553–1565; d) R. E. Lowenthal, A. Abiko, S. Masamune, *Tetrahedron Lett.* **1990**, *31*, 6005–6008; e) D. A. Evans, K. A. Woerpel, M. M. Hinman, M. M. Faul, *J. Am. Chem. Soc.* **1991**, *113*, 726–727. Rh-mediated cyclopropanation: f) M. P. Doyle in *Catalytic Asymmetric Synthesis* (Ed.: I. Ojima), VCH, New York, **1995**, p. 63. Ru-mediated cyclopropanation: g) H. Nishiyama, Y. Itoh, H. Matsumoto, S.-B. Park, K. Itoh, *J. Am. Chem. Soc.* **1995**, *116*, 2223–2224.

[6] For a discussion on the development and application of chiral bis(dihydrooxazole)s and related ligands in asymmetric catalysis, see: A. Pfaltz *Acc. Chem. Res.* **1993**, *26*, 339-345.

[7] G. J. Kubas, *Inorg. Synth.* **1979**, *19*, 90–92.

[8] *N*-Aryl aziridines undergo rapid inversion at nitrogen, and thus the configuration at nitrogen is not an issue in the present case. a) F. A. Anet, J. M. Osyany, *J. Am. Chem. Soc.* **1967**, *89*, 352–356; b) F. A. Anet, R. D. Trepka, D. J. Cram, *ibid.* **1967**, *89*, 357–363.

[9] The relative configuration of the aziridines was assigned on the basis of coupling constants; the absolute configuration was not assigned. The relative configuration of the pyrrolidine was assigned on the basis of coupling constants and nOe measurements. The enantiomeric excesses of the aziridines were determined by HPLC analysis of chromatographically purified material (Regis Whelk-O column; 1% isopropyl alcohol in hexane). The peaks of the enantiomers were assigned on the basis of their superimposable UV spectra as well as by comparison to racemic material (prepared by employing **4d**). Pyrrolidine **3** isolated from the reaction under standard conditions was determined to be racemic by ^{1}H NMR spectroscopic analysis of chromatographically purified material in the presence of $[Eu(hfc)_3]$ and (*R*)-2,2,2-trifluoro-1-(9-anthryl)-ethanol [10]. The peaks of the enantiomers were assigned by comparison to racemic material (prepared by employing racemic **4a**).

[10] W. H. Pirkle, J. R. Hauske, *J. Org. Chem.* **1977**, *42*, 2436–2439.

[11] Ligand **4d** was prepared from dimethyl malononitrile and ethanolamine according to H. Witte, W. Seeliger *Liebigs Ann. Chem.* **1974**, 996-1009.

[12] Other substrates screened include alkylimines, tosylimines, *O*-methyloximes, and *N*,*N*-dimethylhydrazones.

[13] The formation of fumarate and maleate by-products in copper-catalyzed reactions of diazoesters is a well-known and practically inevitable reaction [5f].

[14] a) E. K. Fields, S. M. Sandri, *Chem. Ind.* **1959**, 1216–1217; b) J. Graefe, *Z. Chem.* **1974**, *14*, 469; c) M. K. Meilahn, D. K. Olsen, W. J. Brittain, R. T. Anders, *J. Org. Chem.* **1978**, *43*, 1346–1350; d) J. R. McCarthy, C. L. Barney, M. J. O'Donnell, J. C. Huffman, *J. Chem. Soc. Chem. Comm.* **1987**, 469–470.

[15] For a review of the chemistry of ylides formed from the reaction of heteroatom nucleophiles with carbenes, see: a) A. Padwa, *Acc. Chem. Res.* **1991**, *24*, 22–28; b) A. Padwa, S. F. Hornbuckle, *Chem. Rev.* **1991**, *91*, 263–309.

[16] In this context, we have observed that while *N*-benzylidenebenzylamine is not an effective substrate for aziridination, it does react under the prescribed conditions to produce trace quantities of the adduct arising from dipolar cycloaddition of the corresponding azomethine ylide.

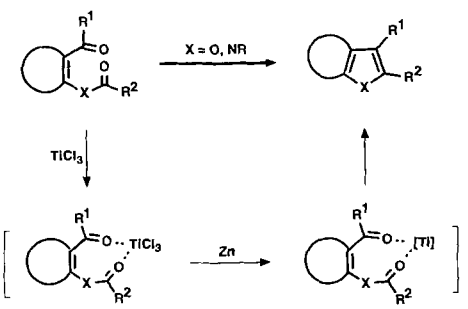
[17] a) T. Hayashi in *Catalytic Asymmetric Synthesis* (Ed.: I. Ojima), VCH, New York, **1995**, p. 325; b) P. Von Matt, A. Pfaltz, *Angew. Chem.* **1993**, *105*, 614–616; *Angew. Chem. Int. Ed. Engl.* **1993**, *32*, 566–568; c) J. Sprinz, G. Helmchen, *Tetrahedron Lett.* **1993**, *34*, 1769–1772; d) G. J. Dawson, C. G. Frost, J. M. J. Williams, S. J. Coote, *Tetrahedron Lett.* **1993**, *34*, 3149–3150. For a preliminary report on the chemistry of 2-aza-π-allyl Pd systems, see: M. J. O'Donnell, X. Yang, M. Li, *Tetrahedron Lett.* **1990**, *31*, 5135–5138.

Titanium-Induced Zipper Reactions**

Alois Fürstner,* Arne Ptock, Holger Weintritt, Richard Goddard, and Carl Krüger

The low-valent titanium-induced coupling of carbonyl compounds to alkenes, generally referred to as the McMurry reaction,[1] has recently found two important extensions. First, the restriction to aldehydes and ketones as the only starting materials has been overcome. Second, a new approach to aromatic heterocycles based upon the reductive cyclization of oxoesters or oxoamides has witnessed a substantially broader structural scope and made a realm of differently substituted furans, benzo[b]furans, pyrroles, and indoles readily accessible from simple precursors (Scheme 1).[2–5]

In addition to this new branch of applications, the experimental setup of McMurry reactions has been markedly simplified. In contrast to the established two-step procedure (i.e. preparation of the activated titanium prior to the addition of the carbonyl compound) we have been able to devise a substantially



Scheme 1. Low-valent titanium [Ti] induced reductive oxoester (X = O) or oxoamide (X = NR, R = H, alkyl, tosyl) cyclization reactions under "instant" conditions [3–5]. The rational for the site-selective preparation of [Ti] depicted in this Scheme does not imply an exclusive chelate formation. Other types of complexation between the substrate and the titanium species may also occur [5].

[*] Priv.-Doz. Dr. A. Fürstner, Dipl.-Chem. A. Ptock, H. Weintritt, Dr. R. Goddard, Prof. Dr. C. Krüger
Max-Planck-Institut für Kohlenforschung
Kaiser-Wilhelm-Platz 1, D-45470 Mülheim an der Ruhr (FRG)
Telefax: Int. code + (208)306 2980

[**] This work was supported by the Volkswagen Stiftung and the Fonds der Chemischen Industrie.

shorter one-step protocol. Although this "instant" method essentially comprises heating a mixture of the respective substrate, $TiCl_3$, and Zn in one pot, the complexation of the Lewis acidic $TiCl_3$ to the substrate ensures that the active titanium species is formed within the coordination sphere of those carbonyl groups to be coupled (Scheme 1). We now report that this "site-selective metal activation" results in an amazing and unprecedented chemo- and regioselectivity in the reductive cyclization of polycarbonyl compounds.

Substrate **1a** is readily prepared from commercially available 2-amino benzophenone and oxalyl chloride. If a mixture of **1a**, $TiCl_3$, and zinc dust in an inert solvent (DME or MeCN) is heated to refux until TLC shows complete conversion of the substrate, the 2,2'-biindolyl **2a** is formed exclusively (Table 1, entries 1,2).[7] Neither conventional McMurry coupling of both the ketone groups of **1a**, nor formation of 2-quinolones upon reaction of the ketones with the distal amides,[6] nor intermolecular coupling processes interfere with this domino two-by-two ketoamide cyclization. The X-ray structure of **2a** is shown in Figure 1.[8] Comparison with entry 3 in Table 1 proves that the "instant" protocol rivals the best of the conventional two-step procedures that use preformed titanium–graphite as coupling agent.[9]

From a previous investigation on the reductive indole synthesis we concluded that the electronic properties of the keto group in oxoamides of the constitution shown in Scheme 1 (X = NR) determine the rate of titanium-mediated cyclizations.[5] As a rule substrates with R^1 = aryl react faster than those with R^1 = alkyl. We prepared the unsymmetrical oxalic acid diamide **1b** in order to probe this conclusion. While it affords the respective 2,2'-biindole **2b** in high yield on prolonged heating with $TiCl_3$ and Zn in DME (entry 4), the monoindole derivative **3** is in fact obtained in 60% isolated yield if the instant coupling is stopped after a reaction time of 4 h (entry 5). This result not only nicely fits our anticipated mechanism, but is also one of the extremely rare examples in which an unprotected keto group survives the exposure to low-valent titanium.[10]

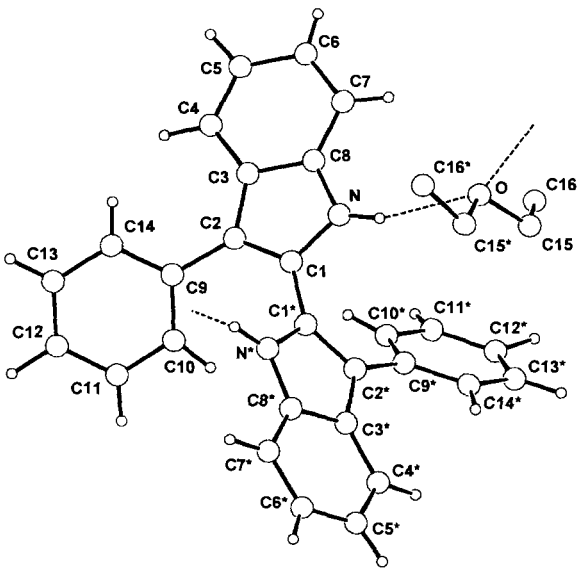


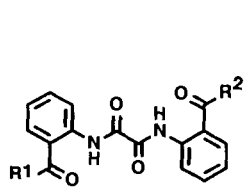
Fig. 1. Structure of the 2,2'-biindolyl derivative **2a**·Et_2O in the crystal. A twofold axis passes through the center of the C1–C1* bond. Selected bond lengths [Å], bond angles [°], and torsion angles [°]: C1–C1* 1.467(3), C1–N 1.377(3), C1–C2 1.382(3), C2–C3 1.433(3), C2–C9 1.476(3), C8–N 1.368(3), N–H···O(Et_2O) 3.173(2); C8-N-C1 108.9(2), C1*-C1-N 120.2(2), C1*-C1-C2 130.2(2), C2-C1-N 109.7(2), C9-C2-C1 126.4(2), C7-C8-N 129.7(2), C3-C8-N 108.1(2), N···O(Et_2O)···N** 127.9(1), N-C1-C1*-N* 125.3(4), C1-C2-C9-C10 −36.4(4).

Table 1. Titanium-induced "instant" coupling [5] of oxoamides to di- or oligoindoles. The cyclizations were carried out by refluxing a mixture of the substrate, $TiCl_3$ (4–10 equiv) and Zn dust (8–20 equiv) in the given solvent under Ar.

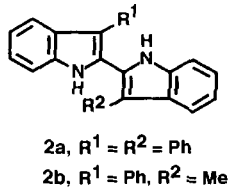
No.	Oxoamide	Solvent	t[h]	Product (Yield [%])
1	**1a**	DME	3	**2a** (81)
2	**1a**	MeCN	1	**2a** (61)
3	**1a**	THF	3.5	**2a** (65)[a]
4	**1b**	DME	20	**2b** (76)[b]
5	**1b**	DME	4	**3** (60)
6	**4a**	DME	2	**5a** (88)
7	**4b**	DME	23	**5b** (77)
8	**6**	DME	2	**7** (95)
9	**12**	DME	1.5	**13** (86)
10	**16**	DME	2.5	**17** (80)

[a] With preformed titanium–graphite ($C_8K/TiCl_3$ = 2/1) [9] as the reagent. [b] The product slowly decomposes when kept in solution.

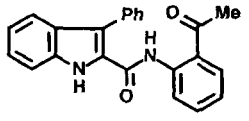
Using di- or triacid chlorides instead of oxalyl chloride for the N-acylation of the parent 2-acylaniline derivatives allows the incorporation of spacers between the indole rings. Compounds **4a**, **b** and **6** cyclized readily in a completely chemo- and regioselective way (entries 6–8 in Table 1). The stability of the products formed turned out to be dependent on the substituent R at C-3 of the indole units. Derivatives with R = Ph are completely stable, while those bearing a methyl group may suffer oxidative degradation.[11, 12] It is also worth mentioning that several of



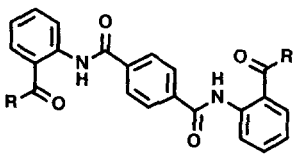
1a, $R^1 = R^2 = Ph$
1b, $R^1 = Ph$, $R^2 = Me$



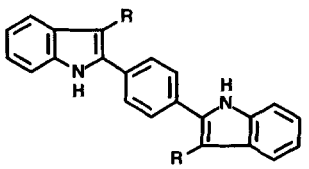
2a, $R^1 = R^2 = Ph$
2b, $R^1 = Ph$, $R^2 = Me$



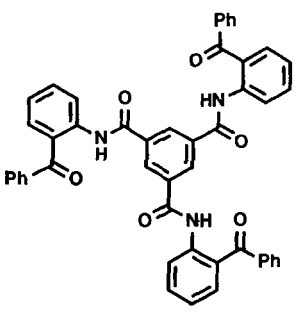
3



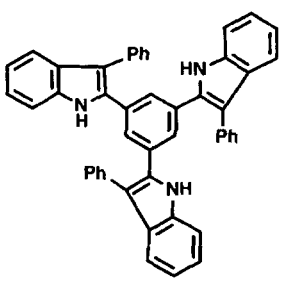
4a, R = Ph
4b, R = Me



5a, R = Ph
5b, R = Me



6

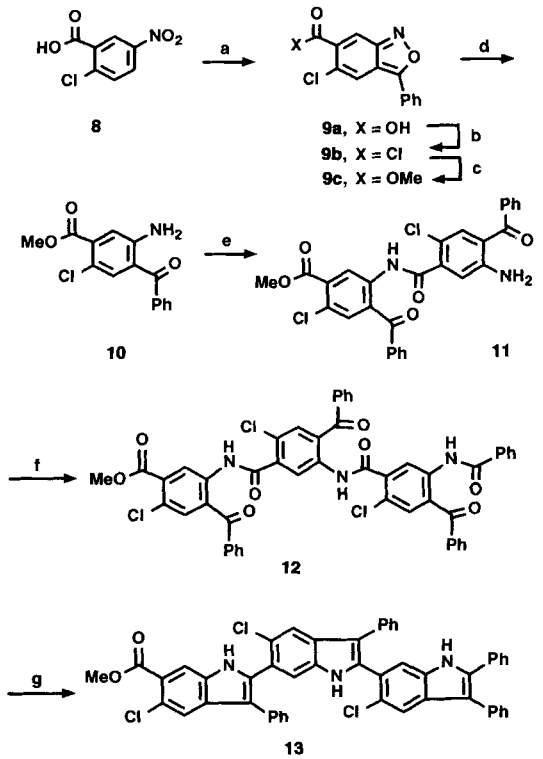


7

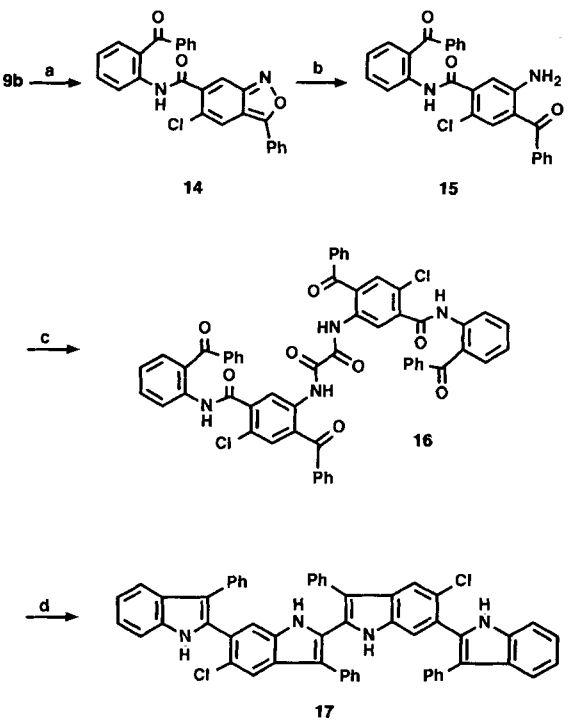
the starting materials used in this study are highly insoluble in all common (NMR) solvents. Although we could not obtain high-resolution ^{13}C NMR spectra of compounds **1a,b** and **4** and had to characterize them by magic angle spinning (MAS)-^{13}C NMR,[13] they nevertheless react rapidly to the di- or triindolyl compounds under "instant" conditions.

The results summarized above prompted further extensions. Benzisoxazole **9a** was chosen as an appropriate starting material for the formation of linear indole oligomers of defined length with head-to-tail linked heterocyclic units. Compound **9a** is obtained in multigram amounts by nucleophilic attack of benzyl cyanide anion on nitroarene **8**.[14] As its benzisoxazole entity is a 2-aminoketone surrogate, an iterative sequence of 1) reductive scission of the N–O bond followed by 2) acylation gives rise to oligooxoamides ready for titanium-induced ring closure. This is illustrated by compounds **12** and **16**, prepared as depicted in Schemes 2 and 3.

Upon heating a suspension of substrate **16**, $TiCl_3$, and Zn in DME (0.02 M), this polyfunctional compound undergoes a titanium-induced zipper reaction with the exclusive formation of quaterindole **17** in 80% isolated yield, despite its numerous options for other intra- as well as intermolecular coupling processes. Likewise, the carbonyl groups in substrate **12** reacted strictly pairwise, always a ketone with its proximate amide, to give product **13** in 86% isolated yield. Taking these results and the high functional group compatibility of the instant ring closure[5] into account, even longer, monodispere oligomers and other substitution patterns in the products should be accessible in a similar way.[15] We are presently pursuing this option.



Scheme 2. Synthesis of the terindole **13** with head-to-tail linkage. a) $C_6H_5CH_2CN$, NaOH, MeOH, 0 °C (3 h) → room temperature (16 h), 41–75% [15]; b) $SOCl_2$, toluene, reflux, 1 h, 84%; c) MeOH, pyridine, reflux, 3 h, 76%; d) Fe dust, HOAc/H_2O (100/1), 55–60 °C, 1 h, 88%; e) 1) **9b**, CH_2Cl_2, pyridine, DMAP cat., room temperature, 72%; 2) Fe dust, HOAc/H_2O (100/1), 55–60 °C, 2 h, 94%; f) 1) **9b**, CH_2Cl_2, pyridine, DMAP cat., 2 h, room temperature, 96%; 2) Fe dust, HOAc/H_2O (100/1), 55 → 110 °C, 5 h, 72%; 3) benzoyl chloride, pyridine, CH_2Cl_2, DMAP cat., 3 h, room temperature, 92%; g) $TiCl_3$ (8 equiv), Zn dust (16 equiv), DME, reflux, 86%.



Scheme 3. Synthesis of the quaterindole **17** with head-tail-tail-head linkage. a) 2-aminobenzophenone, CH_2Cl_2, pyridine, DMAP cat., room temperature, 24 h, 81%; b) Fe dust, HOAc/H_2O (100/1), 55–60 °C, 1 h, 93%; c) oxalyl chloride (0.5 equiv), CH_2Cl_2, pyridine, DMAP cat., 2 h, room temperature, 70%; d) $TiCl_3$ (10 equiv), Zn dust (20 equiv), DME, reflux, 2.5 h, 80%.

Experimental Procedure

A suspension of **1a** (200 mg, 0.45 mmol) [16], $TiCl_3$ (282 mg, 1.83 mmol), and zinc dust (239 mg, 3.66 mmol) in DME (30 mL) was heated to reflux under Ar for 3 h. The mixture was allowed to cool to ambient temperature, filtered through a short pad of silica, and the insoluble residues were washed with ethyl acetate (50 mL in several portions). The combined filtrates were evaporated and the residue chromatographed (SiO_2) with hexane/ethyl acetate (10/1) as eluent. Thus, product **2a** was obtained as pale yellow crystals (140 mg, 81%). M.p. 232–233 °C; ^1H NMR (200 MHz, $CDCl_3$): $\delta = 7.95$ (bs, 2H, NH), 7.64–7.30 (m, 12H), 7.21–7.04 (m, 6H); ^{13}C NMR (50 MHz, $CDCl_3$): $\delta = 135.86$ (s), 134.37 (s), 130.23 (d), 128.98 (d), 127.77 (s), 127.11 (d), 125.97 (s), 123.11 (d), 120.39 (d), 119.38 (d), 115.88 (s), 110.87 (d); MS (70 eV): *m/z* (%): 385 (35), 384 (100) [M^+], 192 (10).

Received: September 28 [Z7363IE]
German version: Angew. Chem. **1995**, *107*, 725

Keywords: indoles · McMurry reactions · titanium compounds

[1] a) J. E. McMurry, *Chem. Rev.* **1989**, *89*, 1513–1524; b) D. Lenoir, *Synthesis* **1989**, 883–897; c) C. Betschart, D. Seebach, *Chimia* **1989**, *43*, 39–49; d) A. Fürstner, *Angew. Chem.* **1993**, *105*, 171–197; *Angew. Chem. Int. Ed. Engl.* **1993**, *32*, 164–189.

[2] Amides have been considered inert towards low-valent titanium, see ref. [1a]. For an approach to carbocycles based upon oxoester cyclizations see: J. E. McMurry, D. D. Miller, *J. Am. Chem. Soc.* **1983**, *105*, 1660–1661.

[3] a) A. Fürstner, D. N. Jumbam, *Tetrahedron* **1992**, *48*, 5991–6010; b) A. Fürstner, D. N. Jumbam, H. Weidmann, *Tetrahedron Lett.* **1991**, *32*, 6695–6696; c) A. Fürstner, D. N. Jumbam, *J. Chem. Soc. Chem. Commun.* **1993**, 211–212; d) A. Banerji, S. K. Nayak, *J. Chem. Soc. Chem. Commun.* **1990**, 150–151; e) pyrrole synthesis: A. Hupperts, A. Fürstner, unpublished results.

[4] a) For an application to the synthesis of the tumor-inhibitor zindoxifene see: A. Fürstner, D. N. Jumbam, G. Seidel, *Chem. Ber.* **1994**, *127*, 1125–1130; b) alkaloid syntheses: A. Fürstner, A. Ernst, *Tetrahedron*, **1995**, *51*, 773–786.

[5] A. Fürstner, A. Hupperts, A. Ptock, E. Janssen, *J. Org. Chem.* **1994**, *59*, 5215–5229.

[6] For a titanium-mediated synthesis of 2-quinolones and coumarins see: A. Fürstner, D. N. Jumbam, N. Shi, *Z. Naturforsch. B*, in press.

[7] Classical approaches to this structural unit are scarce and hampered by low yields, see a) W. Madelung, *Liebigs Ann. Chem.* **1914**, *405*, 58–95; b) J. Bergman, N. Eklund, *Tetrahedron*, **1980**, *36*, 1439–1443; c) A. Kubo, K. Uchino, *Heterocycles*, **1981**, *16*, 1441–1443; d) L. Capuano, S. Drescher, V. Ham-

merer, M. Hanisch, *Chem. Ber.* **1988**, *121*, 2259–2261; e) K. Jesudoss, P. C. Srinivasan, *Synth. Commun.* **1994**, *24*, 1701–1708; f) D. S. C. Black, *Synlett* **1993**, 246–252 and references therein; g) for an improvement see: U. Pindar, Y. S. Kim, D. Schollmeyer, *J. Heterocycl. Chem.* **1994**, *31*, 377–386.

[8] Data on the crystal structure analysis of **2a**·Et_2O: formula $C_{28}H_{20}N_2 \cdot C_4H_{10}O$, $M_r = 458.6\ g\,mol^{-1}$, crystal dimensions: $0.32 \times 0.53 \times 0.56$ mm, $a = b = 13.506(1)$, $c = 14.206(1)$ Å, $V = 2591.3$ Å^3, $\rho_{calcd} = 1.18\ g\,cm^{-3}$, $\mu = 5.15\ cm^{-1}$, $Z = 4$, tetragonal, space group $P4_12_12$ (no. 92), Enraf-Nonius CAD4 diffractometer, $\lambda = 1.54178$ Å, ω-2θ scan, 11102 measured reflections ($+h, \pm k, \pm l$), $[(\sin\theta/\lambda)_{max}\ 0.63\ Å^{-1}]$, 2664 independent and 2446 observed reflections [$I > 2\sigma(I)$], direct methods, 189 refined parameters, $\Sigma w(\Delta F^2)^2$ minimized, $R = 0.054$, $R_w = 0.170$ [$w = 1/\sigma^2(F_o^2) + (0.100P)^2$, with $P = (F_o^2 + 2F_c^2)/3$], max. residual electron density 0.25 eÅ^{-3}, non-hydrogen atoms anisotropic (C15,C16 isotropic), H atoms found and refined, except H atoms of Et_2O, which have been calculated and fixed ($U_H = 0.1$ Å^2). Further details of the crystal structure investigation may be obtained from the Fachinformationszentrum Karlsruhe, D-76344 Eggenstein-Leopoldshafen, on quoting the depository number CSD-58763.

[9] a) A. Fürstner, H. Weidmann, *Synthesis* **1987**, 1071–1075; b) A. Fürstner, R. Csuk, C. Rohrer, H. Weidmann, *J. Chem. Soc. Perkin Trans. 1* **1988**, 1729–1734; c) D. L. J. Clive, C. Zhang, K. S. K. Murthy, W. D. Hayward, S. Daigneault, *J. Org. Chem.* **1991**, *56*, 6447–6458.

[10] A few other examples were reported in the literature: a) ref. [3c]; b) Y. J. Wu, D. J. Burnell, *Tetrahedron Lett.* **1988**, *29*, 4369–4372; c) W. G. Dauben, I. Farkas, D. P. Bridon, C. P. Chuang, K. E. Henegar, *J. Am. Chem. Soc.* **1991**, *113*, 5883–5884; d) F. E. Ziegler, H. Lim, *J. Org. Chem.* **1982**, *47*, 5229–5230.

[11] The parent 2,2'-biindolyl (**2**, $R^1 = R^2 = H$) cannot be readily obtained in this way, since the reductive indole cyclization is known to give low or variable yields when applied to 2-acylamido benzaldehyde derivatives, see ref. [5].

[12] This is well precedented in the literature, see: A. Z. Britton, G. F. Smith, *J. Chem. Soc. Perkin Trans. 1* **1972**, 418–420.

[13] We thank Dr. A. Rufinska, (Mülheim, Germany), for recording and interpreting the MAS-NMR spectra; details will be reported in a forthcoming paper.

[14] A. Jaszkowska, B. Serafinowa, *Rocz. Chem.* **1972**, *46*, 2051–2059 [*Chem. Abstr.* **1973**, *78*, 124215d].

[15] For leading references on di-, oligo-, and polyindoles in material science see: a) G. Zotti, S. Zecchin, G. Schiavon, R. Seraglia, A. Berlin, A. Canavesi, *Chem. Mat.* **1994**, *6*, 1742–1748; b) S. Hünig, H. C. Steinmetzer, *Liebigs Ann. Chem.* **1976**, 1090–1102; c) M. M. Murray, P. Kaszynski, D. A. Kaisaki, W. Chang, D. A. Dougherty, *J. Am. Chem. Soc.* **1994**, *116*, 8152–8161 and references therein.

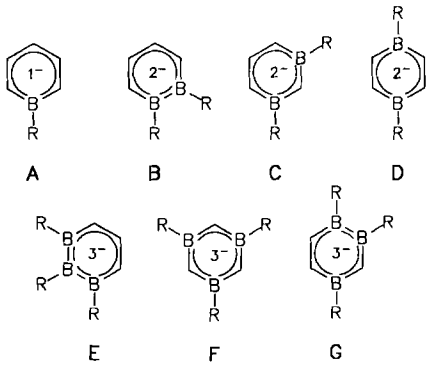
[16] D. S. C. Black, C. H. B. Vanderzalm, L. C. H. Wong, *Austr. J. Chem.* **1982**, *35*, 2435–2443.

A μ-η^6:η^6-1,3,5-Triboratabenzenebis(cyclopentadienylcobalt) Triple-Decker Complex**

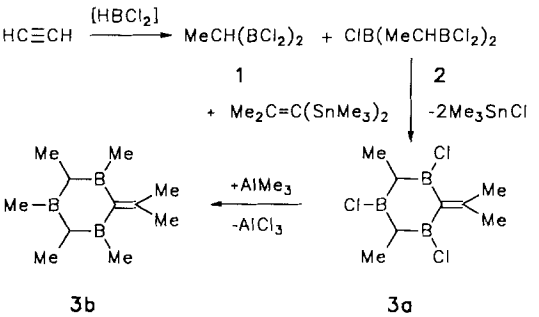
Thomas Deforth, Hans Pritzkow, and Walter Siebert*

Dedicated to Professor Peter Paetzold on the occasion of his 60th birthday

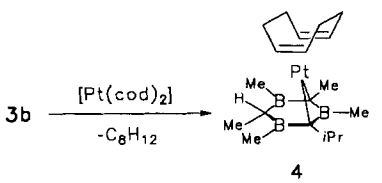
Derivatives of boratabenzene **A**[1] and diboratabenzenes **B**,[2] **C**,[3] and **D**[4] belong to a class of six-membered boron–carbon heterocycles. Neither metal complexes nor the free trianions of the possible triboratabenzene isomers **E**–**G** were yet known. The *arachno* framework of the trianions themselves could possibly undergo two-electron oxidation with formation of the anionic *nido* clusters 2,3,4- and 2,3,5-tricarbahexaborane.[5, 6] Deprotonation of 1,3,5-triethyl-2,4,6-trimethyl-1,3,5-triboracyclohexane[7] or 1,3,5-tris(dimethylamino)-1,3,5-triboracyclohexane[8] could be a suitable method to produce **F**. Here, we present another strategy for the formation of metal complexes of the triboratabenzene **F** via 2-isopropylidene-1,3,4,5,6-pentamethyl-1,3,5-triboracyclohexane (**3b**). An η^2 interaction of a CpCo complex fragment (Cp = C_5H_5) with the exocyclic double bond in **3b** results in a metal-induced hydrogen migration and an η^6 complexation of the ring. Addition of a further CpCo fragment provides the triple-decker **6**.



1,1-Bis(dichloroboryl)ethane (**1**),[10] and bis(1-dichloroborylethyl)chloroborane (**2**) as side product, are formed by the hydroboration of acetylene with $HBCl_2$[9] at -60 °C.[11] Ring closure of **2** through a tin–boron exchange reaction with 1,1-bis(trimethylstannyl)isobutene results in 1,3,5-trichloro-2-isopropylidene-4,6-dimethyl-1,3,5-triboracyclohexane (**3a**). Subsequent methylation with $AlMe_3$ provides **3b**. Compounds **1**–**3** are air-sensitive liquids. Compounds **2** and **3** each have two chiral centers and are found as a mixture of diastereomers. They are seen in the ^1H and ^{13}C NMR spectra as two sets of signals with the same coupling pattern. Since the isomers could not be separated, an unambiguous assignment was not possible.



In order to investigate the ligand characteristics of **3b**, it was first allowed to react with $Pt(cod)_2$ (cod = 1,5-cyclooctadiene). The spectroscopic data for the resulting yellow solid does not show η^2 complexation to the exocyclic double bond, but rather is consistent for the σ complex **4** with two Pt–C bonds. The ^1H NMR spectrum shows the corresponding coupling pattern for the transformation of the isopropylidene to the isopropyl group by 1,4-hydrogen migration from a MeCH unit to the exocyclic C atom. The small up-field shift of the ^{11}B NMR signals suggests a weak interaction between the platinum atom and the boryl groups; this is confirmed by a crystal structure analysis.[12]



[*] Prof. Dr. W. Siebert, T. Deforth, Dr. H. Pritzkow
Anorganisch-chemisches Institut der Universität
Im Neuenheimer Feld 270, D-69120 Heidelberg (Germany)
Telefax: Int. code + (6221)56-4197

[**] This work was supported by the Deutschen Forschungsgemeinschaft (Sonderforschungsbereich 247), the Fonds der Chemischen Industrie, and BASF AG.

Figure 1 shows the C_3B_3 heterocycle in a boat conformation with σ bonds Pt–C2 and Pt–C4, and long interatomic Pt–B distances. The coordination around platinum is approximately square planar. Also in solution there is no agostic Pt-H-C6 interaction resulting in the formation of an 18 VE complex.

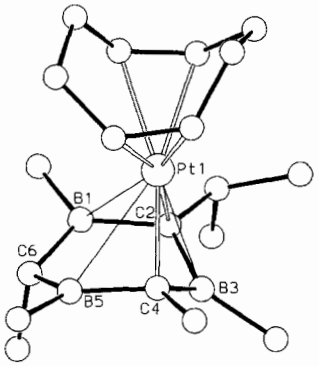
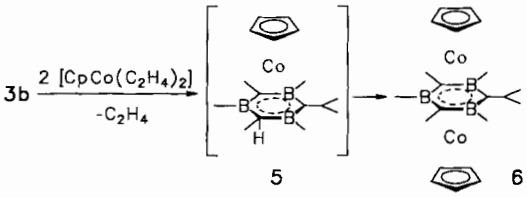


Fig. 1. Molecular structure of **4** in the crystal. Selected bond distances [Å] and angles [°]: Pt1-C2 2.163(6), Pt1-C4 2.111(6), Pt1-B1 2.593(7), Pt1-B3 2.449(7), Pt1-B5 2.658(7), B1-C2 1.563(9), C2-B3 1.556(9), B3-C4 1.551(9), C4-B5 1.542(9), B5-C6 1.590(9), C6-B1 1.572(8); C6-B1-C2 119.6(5), B1-C2-B3 116.5(5), C2-B3-C4 108.6(5), B3-C4-B5 116.4(5), C4-B5-C6 119.4(5), B5-C6-B1 110.3(5).

A 1,4-hydrogen migration in **3b** induced by a CpCo fragment is expected to produce the reactive 18 VE complex **5**. This analog of cyclopentadienylcobalt-2,3-dihydro-1,3-diborole complexes[14] could then be built up to a triple-decker complex with a CpCo unit. At room temperature the reaction with $[CpCo(C_2H_4)_2]$, accompanied by evolution of ethylene, provides the olive-green triple-decker complex **6** and a red compound **5′**, whose constitution is not yet clear.[15] The ^1H NMR spectrum of paramagnetic **6** shows broadened signals in the range



$\delta = +10 - -50$. Oxidation with $AgBF_4$ results in the diamagnetic 30 VE $\mathbf{6}^+$ BF_4^-, whose triple-decker structure is confirmed by NMR spectroscopy. Appearance of a septet and a doublet signalizes, as in the case of **4**, the transformation of the isopropylidene group in **3b** into the isopropyl substituent. The ^{11}B NMR shift of $\delta = 19$ indicates a bifacial coordination of the 1,3,5-triboratabenzene to the CpCo complex fragments.

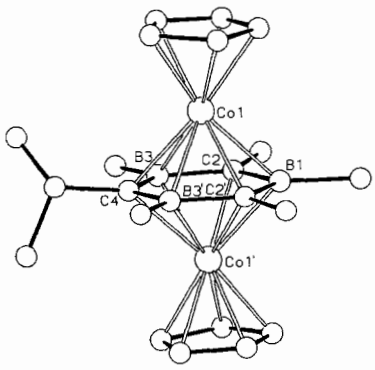


Fig. 2. Molecular structure of **6** in the crystal. Selected bond distances [Å] and angles [°]: Co1-B1 2.200(5), Co1-C2 2.129(5), Co1-C2′ 2.151(5), Co1-B3 2.229(6), Co1-B3′ 2.220(5), Co1-C4 2.217(5), B1-C2 1.519(8), C2-B3 1.545(9), B3-C4 1.521(7); C2′-B1-C2 113.4(6), B1-C2-B3 125.7(5), C2-B3-C4 116.2(3), B3-C4-B3′ 122.8(6).

The crystal structure analysis of **6** confirms that both Co atoms are η^6-bonded to the planar C_3B_3 ring (Fig. 2). As expected, the Co–Co distance of 3.14 Å is shorter than in the analogous 31 VE triple-decker complexes[16] (3.30 Å) with the smaller 2,3-dihydro-1,3-diborolyl bridging ligand (C_3B_2 ring). The B–C distances within the ring have approximately the same value (1.519(8)–1.545(9) Å).

Our results prove that the 3e-ligand C_3B_3 is incorporated into the triple-decker complexes **6** and $\mathbf{6}^+$, where this triboratabenzene **F** is stabilized by the cationic CpCo fragments. We postulate the intermediate **5** for the formation of **6**, which has not yet been detected.

Experimental Procedure

2: Trimethylsilane (0.4 mmol) in hexane (100 mL) was added dropwise to a solution of BCl_3 (0.4 mmol) in hexane (100 mL) at −78 °C under a continuous stream of acetylene (in situ synthesis of $HBCl_2$ [17]). After the solution had warmed to room temperature and the hexane solvent had been removed, **1** (23% yield, b.p. 65 °C/50 Torr) and **2** (10% yield, b.p. 100 °C/50 Torr) were isolated by distillation. **2**: ^1H NMR (200 MHz, C_6D_6): $\delta = 2.32$ (br. q, 2H, CH), 2.12 (br. q, 2H, CH), 1.07 (d, 6H, $^3J(H,H) = 6.33$ Hz, CH_3), 1.00 (d, 6H, $^3J(H,H) = 6.50$ Hz, CH_3); ^{13}C NMR (50 MHz, C_6D_6): $\delta = 42$ (br., CH), 13.66 (CH_3), 13.34 (CH_3); ^{11}B NMR (64.2 MHz, C_6D_6): $\delta = 74$ (1B), 61 (2B); EI-MS: *m/z* (%): 266 (0.5) [M^+], 231 (3.8) [$M^+ - Cl$].

3a: **2** (18 mmol) and $Me_2C{=}C(SnMe_3)_2$ [18] (19 mmol), each in toluene (25 mL), were simultaneously added with stirring to toluene (50 mL) within 2 hr at −50 °C. The solution was allowed to warm to room temperature overnight, and the solvent and Mg_3SnCl were removed (5 Torr) over one day. Subsequent distillation (36 °C/0.005 Torr) provided **3a** in 91% yield. ^1H NMR (200 MHz, C_6D_6): $\delta = 1.94$ (s, 6H, $C(CH_3)_2$)), 1.85 (s, 6H, $C(CH_3)_2$)), 1.36 (d, 6H, $^3J(H,H) = 6.06$ Hz, $CHCH_3$), 1.31 (d, 6H, $^3J(H,H) = 6.05$ Hz, $CHCH_3$), 1.10 (br. q, 2H, CH); ^{13}C NMR (50 MHz, C_6D_6): $\delta = 173.2$ ($C(CH_3)_2$), 165.9 ($C(CH_3)_2$), 44 (br., CH), 28.6 ($C(CH_3)_2$), 27.5 ($C(CH_3)_2$), 12.1 ($CHCH_3$), 11.9 ($CHCH_3$); ^{11}B NMR (64.2 MHz, C_6D_6): $\delta = 71$ (1B), 69 (2B); EI-MS: *m/z* (%): 248(51) [M^+], 219 (54) [$M^+ - Cl$].

3b: A solution of $AlMe_3$ (7.0 mmol) in pentane (20 mL) was added dropwise to **3a** (7.0 mmol) in pentane (20 mL) at −50 °C. Warming to room temperature, removing the solvent, and distillation provided **3b** (85% yield, b.p. 35 °C/0.1 Torr). ^1H NMR (200 MHz, C_6D_6). $\delta = 2.38$ (br. q, 2H, $CHCH_3$), 2.18 (br. q, 2H, $CHCH_3$), 1.78 (s, 6H, $C(CH_3)_2$), 1.75 (s, 6H, $C(CH_3)_2$), 1.33 (d, $^3J(H,H) = 6.0$ Hz, 6H, $CHCH_3$), 1.29 (d, $^3J(H,H) = 6.0$ Hz, 6H, $CHCH_3$), 0.95 (s, 6H, BCH_3), 0.91 (s, 6H, BCH_3), 0.72 (s, 3H, BCH_3), 0.61 (s, 3H, BCH_3); ^{13}C NMR (50 MHz, C_6D_6): $\delta = 144.9$ ($C(CH_3)_2$), 129.2 ($C(H_3)_2$), 50 (br., CH), 48 (br., CH), 26.9 ($C(CH_3)_2$), 26.5 ($C(CH_3)_2$), 13.8 ($CHCH_3$), 12.2 ($CHCH_3$), 8.3 (br., BCH_3); ^{11}B NMR (64.2 MHz, C_6D_6): $\delta = 82$ (1B), 80 (2B); EI-MS: *m/z* (%): 188 (6) [M^+], 173 (5) [$M^+ - CH_3$], 158 (3) [$M^+ - 2CH_3$].

4: A solution of **3b** (1.5 M) in benzene (0.8 mL) was added by a syringe to a solution of $Pt(cod)_2$ (1.0 mmol) in benzene (15 mL) and stirred for 12 h. After removal of the solvent, column chromatography (Al_2O_3, deactivated with 6% H_2O) of the yellow residue with hexane eluent provided **4** in 33% yield, m.p. 65 °C. ^1H NMR (200 MHz, C_6D_6): $\delta = 4.1-5.0$ (m, 4H, CH_{cod}), 2.99 (m, 1H, $CHCH_3$), 1.99 (s, $^3J(Pt,H) = 25.5$ Hz, 3H, CH_3), 1.7–1.15 (m, 8H, $CH_{2,cod}$), 1.47 (d, $^3J(H,H) = 6.77$ Hz, 3H, $CHCH_3$), 1.31 (d, $^3J(H,H) = 6.86$ Hz, 3H, $CHCH_3$), 1.11 (d, 3H, $CHCH_3$), 1.08 (s, 3H, BCH_3), 0.89 (s, 3H, BCH_3), 0.86 (s, 3H, BCH_3), 0.62 (q, $^3J(H,H) = 7.67$ Hz, $J(Pt,H) = 23.2$ Hz, 1H, $CHCH_3$); ^{13}C NMR (50 MHz, C_6D_6): $\delta = 100.54$ (CH_{cod}), 97.58 (CH_{cod}), 96.86 (CH_{cod}), 95.20 (CH_{cod}), 33.84, 30.80 ($CH_{2,cod}$), 29.93 ($CH_{2,cod}$), 29.23 ($CH_{2,cod}$), 27.72 ($CH_{2,cod}$), 26.33, 25.22, 18.97, 18.89, 7.5 (br.), 6.7 (br.); ^{11}B NMR (64.2 MHz, C_6D_6): $\delta = 62$ (2B), 52 (1B); EI-MS: *m/z* (%): 490 (100) [M^+].

6: A solution of **3b** (1.5 M) in benzene was added to $CpCo(C_2H_4)_2$ (1.8 mmol) in pentane (10 mL) by syringe and the mixture stirred for 12 hr. Removal of the solvent and subsequent chromatographic workup (Al_2O_3, deactivated with 6% H_2O) with hexane as eluant provided red **5′** (23% yield, b.p. 22 °C) and olive-green **6** (8% yield, m.p. 78 °C). **5′**: ^1H NMR (200 MHz, C_6D_6): $\delta = 4.44$ (s, 5H), 1.24 (br. s, 9H), 0.77 (br. s, 9H), −0.1 (br. s, 3H;); ^{13}C NMR (50 MHz, C_6D_6): $\delta = 83$ (br.), 80.8, 14.9, 0 bis −7 (several broad signals); ^{11}B NMR (64.2 MHz, C_6D_6): $\delta = 28.6$ (1B), 11.8 (2B); EI-MS: *m/z* (%): 311 (43) [$M^+ + 1$]. **6**: EI-MS: *m/z* (%): 435 (62) [M^+], 311 (100) [$M^+ - CpCo$],189 (36) [Cp_2Co^+], 124 (13) [$CpCo^+$]; CV (DME, $Bu_4N^+PF_6^-$): $E^0 = -0.22$ (rev. ox), −1.24 (rev. red.), −2.41 (irrev. red.).

$\mathbf{6}^+$: Oxidation of **6** with equimolar $AgBF_4$ in Et_2O produces dark green $\mathbf{6}^+BF_4^-$ (95% yield, m.p. >200 °C decomp.). ^1H NMR (200 MHz, CD_2Cl_2): $\delta = 4.69$ (s, 10H, C_5H_5), 3.67 (sept., 1H, $CHCH_3$), 2.67 (s, 6H, $CHCH_3$), 1.64 (d, $^3J(H,H) = 7.03$ Hz, 6H, $CH(CH_3)_2$), 1.43 (s, 3H, BCH_3), 1.31 (s, 6H, BCH_3); ^{13}C NMR (50 MHz, CD_2Cl_2): $\delta = 81.9$ (C_5H_5), 37.7 (CH), 26.6 (CH_3), 25.1 (CH_3), 3 (br. BCH_3); ^{11}B NMR (64.2 MHz, CD_2Cl_2): $\delta = 19.0$ (BF_4^-); FD^+-MS: *m/z* (%): 435 (100) [M^+].

Received: November 7, 1995 [Z 7456 IE]
German version: *Angew. Chem.* **1995**, *107*, 748

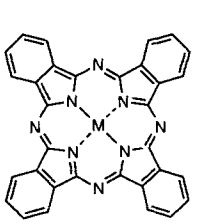
Keywords: boron compounds · cobalt compounds · heteroarenes · platinum compounds · triple-decker compounds

[1] G. R. Herberich, *Comprehensive Organometallic Chemistry* **1982**, *1*, 392–399, and references therein; A. J. Ashe III, P. Shu, *J. Am. Chem. Soc.* **1971**, *93*, 1804.
[2] G. E. Herberich, B. Heßner, M. Hostalek, *Angew. Chem.* **1986**, *98*, 637–638; *Angew. Chem. Int. Ed. Engl.* **1986**, *25*, 642.
[3] C. Balzereit, H.-J. Winkler, W. Massa, A. Berndt, *Angew. Chem.* **1995**, *106*, 2394–2396; *Angew. Chem. Int. Ed. Engl.* **1995**, *33*, 2306–2308.
[4] G. E. Herberich, B. Heßner, *Chem. Ber.* **1982**, *115*, 3115–3127.
[5] R. N. Grimes, C. L. Bramlett, R. L. Vance, *Inorg. Chem.* **1968**, *7*, 1066–1070.
[6] A. Feßenbecker, A. Hergel, R. Hettrich, V. Schäfer, W. Siebert, *Chem. Ber.* **1993**, *126*, 2205–2210.
[7] R. Köster, G. Benedikt, *Angew. Chem.* **1964**, *76*, 650; *Angew. Chem. Int. Ed. Engl.* **1964**, *3*, 515.
[8] H. Hess, *Acta Crystallogr. Sect. B* **1969**, *25*, 2334–2337; P. Krohmer, J. Goubeau, *Chem. Ber.* **1971**, *104*, 1347–1361.
[9] H. C. Brown, N. Ravindran, *J. Am. Chem. Soc.* **1973**, *95*, 2396.
[10] G. Knörzer, W. Siebert, *Z. Naturforsch. B* **1990**, *45*, 15–18.
[11] T. Deforth, planned Dissertation, Universität Heidelberg, **1995**.
[12] **4**: triclinic, space group $P\bar{1}$, $a = 8.293(12)$, $b = 9.772(18)$, $c = 13.410(18)$ Å, $\alpha = 91.39(9)$, $\beta = 97.00(9)$, $\gamma = 109.38(9)°$, $V = 1015$ Å^3, $Z = 2$; 5900 reflections (four-cycle diffractometer, $T = -55$ °C $Mo_{K\alpha}$, ω scan, $\theta_{max} = 30°$), structure solution with direct methods [13], refinement (Pt, C, B anisotropic, H atoms isotropically in calculated positions or as part of a rigid group, 227 parameters), with all reflections based on F^2 [13]: $wR2 = 0.091$, $R1 = 0.036$ (for 5242 observed reflections with $I > 2\sigma(I)$). **6**: tetragonal, space group $P4_12_12$, $a = b = 8.781(4)$, $c = 27.926(14)$ Å, $V = 2153$ Å, $Z = 4$; 3164 reflections (four-cycle diffractometer, $T = -55$ °C $Mo_{K\alpha}$, ω scan, $\theta_{max} = 30°$), structure solution with direct methods [13], refinements (Co, C, B anisotropic, H atoms in calculated positions or isotropically as part of a rigid group, 133 parameters) with all reflections based on F^2 [13]: $wR2 = 0.131$, $R1 = 0.047$ (for 1868 observed reflections with $I > 2\sigma(I)$). The molecule has a crystallographically imposed twofold axis through B1 and C4; the methyl group on B1 and the isopropyl group on C4 are disordered. Further details of the crystal structure investigation may be obtained from the Fachinformationszentrum Karlsruhe, D-76344 Eggenstein-Leopoldshafen (FRG) on quoting the depository number CSD-401420(**4**), 401419(**6**).
[13] G. M. Sheldrick, SHELXS86, Universität Göttingen, **1986**, SHELXL 93, Universität Göttingen, **1993**.
[14] J. Edwin, M. C. Böhm, N. Chester, D. H. Hoffman, R. Hoffmann, H. Pritzkow, W. Siebert, K. Stumpf, H. Wadepohl, *Organometallics* **1983**, *2*, 1666–1674.
[15] NMR and MS Data for red **5'** suggest the compound $[(MeC)_4(MeB)_3CoCp]$, which could have been formed by the transformation of the isopropylidene group into two MeC units.
[16] M. Enders, G. Gangnus, R. Hettrich, Z. Magos-Martin, M. Stephan, H. Pritzkow, W. Siebert, U. Zenneck, *Chem. Ber.* **1993**, 126, 2197–2203.
[17] R. Soundarajan, D. S. Matteson, *J. Org. Chem.* **1990**, *55*, 2274–2275.
[18] T. N. Mitchell, W. Reimann, *Organometallics* **1986**, *5*, 1991–1997.

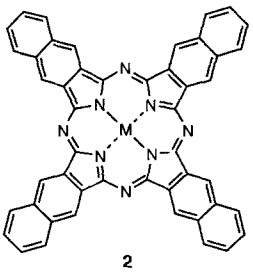
Tetraphenanthro[9,10-*b*:9,10-*g*:9,10-*l*:9,10-*q*]-porphyrin, a New Highly Conjugated Porphyrin System**

Timothy D. Lash* and Bennett H. Novak

Porphyrins have a remarkable number of important functions in nature (hemes, chlorophylls, etc.), and have many unusual structural and chemical properties. Although porphyrins have been extensively studied by organic chemists for well over a century, structural variants of porphyrins[2] such as porphycene[3] were only discovered relatively recently.[4] In addition, many symmetrically substituted porphyrin systems of theoretical and potentially practical significance have yet to be described.[5] In our recent work, we have been interested in developing synthetic routes to new highly conjugated porphyrin systems.[1, 6, 7] This has led to the first syntheses of mono-[1, 6] and dinaphthoporphyrins.[7] These studies were initially stimulated by our ongoing interests in porphyrin geochemistry,[8, 9] and by the suggestion that porphyrin structures embedded in graphite-like matrices were present in the kerogen fractions of mature organic-rich sediments.[10] These systems are structurally related to phthalocyanines (**1**) and naphthocyanines (**2**), and hence may have value in numerous material science applications.[11] In addition, red-shifted porphyrin-like chromophores are being investigated as photosensitizers in photodynamic therapy.[12]

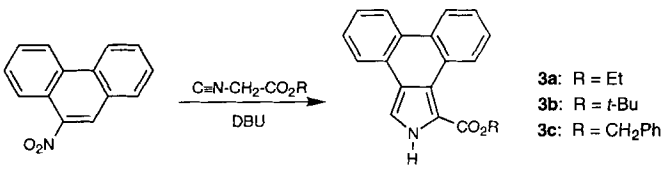


1



2

The synthesis of novel porphyrins bearing polycyclic arene units is dependent upon the availability of suitably substituted pyrrolic precursors. Recently, we reported that 9-nitrophenanthrene underwent a "Barton–Zard" type of pyrrole condensation[13] with isocyanoacetates to give the corresponding phenanthropyrroles **3a–c** in excellent yields (Scheme 1).[14, 15] The novel tetracyclic compound **3a** has now been utilized to prepare the first example of a tetraphenanthroporphyrin.

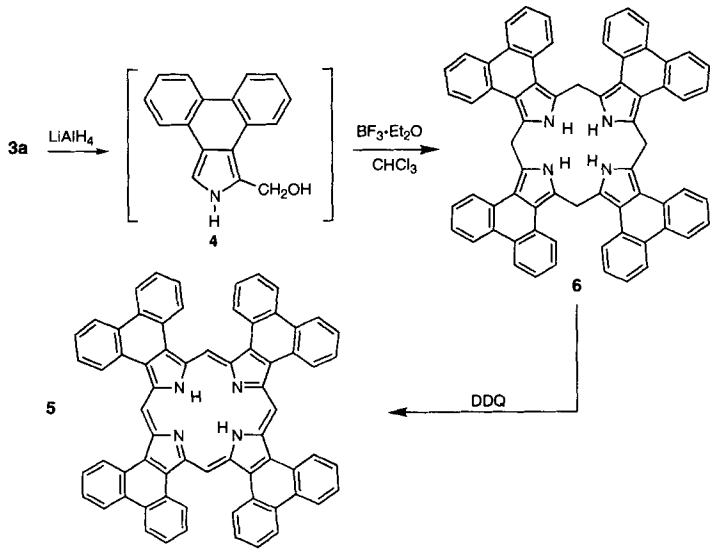


Scheme 1. Synthesis of phenanthropyrroles from 9-nitrophenanthrene. DBU = 1,8-diazabicyclo[5.4.0]undec-7-ene.

Reduction of **3a** with lithium aluminum hydride under mild conditions gave the corresponding alcohol **4** and subsequent treatment of **4** with boron trifluoride etherate in chloroform, followed by oxidation with 2,3-dichloro-5,6-dicyano-1,4-benzoquinone (DDQ), afforded tetraphenanthro[9,10-*b*:9,10-*g*:9,10-*l*:9,10-*q*]porphyrin (**5**) in 13% yield (Scheme 2). Initially, we attempted the cyclotetramerization of **4** in refluxing pyridine/acetic acid,[9b, 16] but this resulted in the formation of no detectable porphyrin product. This was attributed to the steric crowding in this unusual porphyrin system. Milder conditions have been successfully used to prepare crowded porphyrin structures,[17] and this suggested that the methodology developed by Lindsey et al. for the preparation of *meso*-tetrasubstituted porphyrins[18] might give reasonable results for our system. Reaction of **4** in dichloromethane with boron trifluoride etherate as the acid catalyst afforded, after dehydrogenation with DDQ, a rather impure sample of porphyrin **5**. However, when the solvent was switched to chloroform, as mentioned above, the required heptadecacyclic porphyrin was obtained in good yield. Commercially available chloroform contains approximately 0.8% ethanol and it is probable that this is largely

[*] Prof. T. D. Lash, B. H. Novak
Department of Chemistry, Illinois State University
Normal, Illinois 61790-4160 (USA)
Telefax: Int. code + (309) 438-5538

[**] Porphyrins with Exocyclic Rings. Part 6. This work was supported by the National Science Foundation under Grant No. CHE-9201149. MS data were obtained from the University of Illinois, Urbana-Champaign. Part 5: [1].



Scheme 2. Synthesis of tetraphenanthro[9,10-*b*:9,10-*g*:9,10-*l*:9,10-*q*]porphyrin **5**.

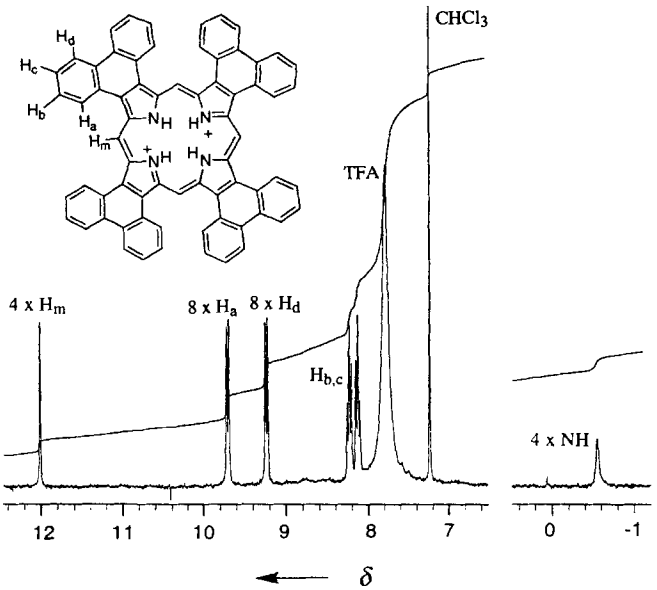


Fig. 2. 300 MHz ^{1}H NMR spectrum of **5** in trifluoroacetic acid/deuteriochloroform.

responsible for the improved results (see ref. [18b]). It seems likely that porphyrinogen **6** is the initially formed product and subsequent dehydrogenation with DDQ then led to **5**.

Porphyrin **5** was isolated as a dark green powder and was virtually insoluble in most organic solvents. In trifluoroacetic acid (TFA)/chloroform, the diprotonated form of **5** gave green solutions, and the electronic spectra showed dramatically red-shifted absorption bands compared to those of any previously reported porphyrin structure (Fig. 1). The Soret band was observed near 480 nm and two bathochromically shifted Q bands were observed at 615 and 668 nm. In neutral solvents, the electronic spectra for **5** showed very broad, ill-defined absorption bands. The ^{1}H NMR spectrum of **5** in trifluoroacetic acid/deuteriochloroform (Fig. 2) is consistent with the proposed structure of this highly symmetrical porphyrin dication and shows four separate sets of signals corresponding to the four distinct types of phenanthrene protons. These protons were only slightly deshielded relative to those of phenanthropyrrole **3a**, apart from the protons that protrude towards the *meso* bridges. This suggests that the major macrocyclic ring current involves the internal porphyrin 18 π-electron pathway. Although the phenanthrene protons labeled H_a in Figure 2 and the adjacent *meso* protons (H_m) are significantly deshielded, the signals of the latter appearing at $\delta = 12$, this appears to be primarily due to the steric congestion in this structure. The ^{13}C NMR spectrum for **5** in trifluoroacetic acid/deuteriochloroform showed only nine signals, which confirms the highly symmetrical nature of this 68 carbon system. Fast atom bombardment (FAB) mass spectrometry for **5** gave the expected $[M + H]^+$ peak at $m/z = 911$.

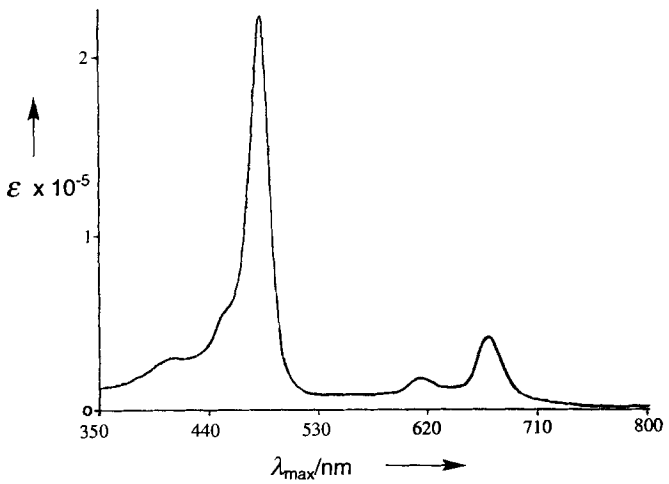


Fig. 1. Electronic absorption spectrum of **5** in 1% trifluoroacetic acid/chloroform.

Tetraphenanthroporphyrin **5** is one of the most highly conjugated porphyrin systems described to date and represents a potentially fascinating structure for further study. The results described here suggest that this methodology could make whole classes of new highly conjugated porphyrin systems available.

Experimental Procedure

5: A solution of phenanthropyrrole **3** (0.500 g, 1.73 mmol) in THF (50 mL) was added dropwise over a period of 20–30 min to a stirred mixture of lithium aluminum hydride (0.130 g, 3.425 mmol) in THF (50 mL), while the temperature of the mixture was maintained at 0 °C with the aid of a salt-ice bath. The mixture was stirred for an additional 1 h, water was added, and the organic phase separated. The aqueous layer was extracted with chloroform (2 × 50 mL), and the combined organic solutions were washed with water (50 mL) and dried over sodium sulfate. The solvent was evaporated on a rotary evaporator; the temperature of the water bath was maintained at 25–30 °C. The residual oil was taken up in chloroform (125 mL), the air was purged with nitrogen and boron trifluoride etherate solution in dichloromethane (68 µL, 2.5 M) was added. The resulting pale blue mixture was stirred in the dark at room temperature for 1 h. DDQ (0.290 g, 1.277 mmol) was added in a single portion, and stirring was continued for a further 1 h. The mixture was washed with water (50 mL), 5% sodium bicarbonate solution (50 mL), and water (50 mL), and the solvent evaporated under reduced pressure. The dark residue was recrystallized twice from chloroform/methanol to give the tetraphenanthroporphyrin **5** as a dark green powder. Selected physical and spectroscopic data for **5**: m.p. > 400 °C; UV/Vis (1% TFA/$CHCl_3$): λ_{max} [nm] (lgε) = 482 (5.35), 615 (4.26), 668 (4.63); UV/Vis (benzene): λ_{max} [nm] = 430, 650, 704; IR (KBr): ν = 3300, 3077, 3030, 1566, 1428, 1210, 1166, 967, 866, 812, 759, 714, 672, 616, 533 cm^{-1}; ^{1}H NMR (300 MHz, TFA/$CDCl_3$): δ = −0.55 (4H, br, 4 × NH), 8.13 (8H, t), 8.24 (8H, t), 9.24 (8H, d, 8.3 Hz), 9.71 (8H, d, J = 8.2 Hz) (32 × phenanthrene-H), 12.01 (4H, s, 4 × *meso*-H); ^{13}C NMR (TFA/$CDCl_3$): δ = 101.37 (*meso*-CH), 125.06, 126.90, 127.33, 129.56, 129.68, 129.75, 133.80, 139.55; HRMS (FAB): calculated for $C_{68}H_{38}N_4$ + H: m/z 911.3175; found: 911.3168. Correct C, H, N analysis for $C_{68}H_{38}N_4 \cdot 2H_2O$.

Received: October 10, 1995 [Z 7390 IE]
German version: *Angew. Chem.* **1995**, *107*, 723

Keywords: porphyrins · tetraphenanthroporphyrins

 © VCH Verlagsgesellschaft mbH, D-69451 Weinheim, 1995 0570-0833/95/0606-0684 $ 10.00+.25/0

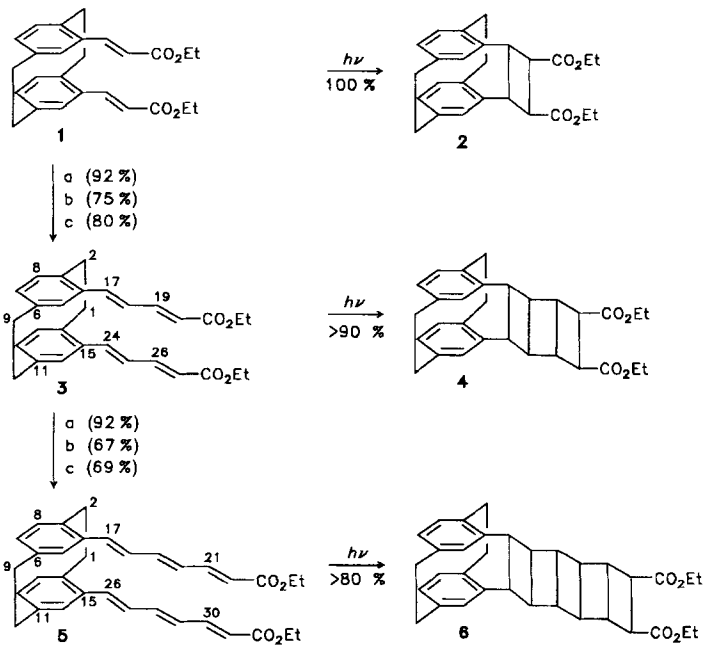
[1] T. D. Lash, C. P. Denny, *Tetrahedron*, **1995**, *51*, 59.
[2] J. L. Sessler, A. K. Burrell, *Top. Curr. Chem.* **1991**, *161*, 177–273.
[3] E. Vogel, M. Kocher, H. Schmickler, J. Lex, *Angew. Chem.* **1986**, *98*, 262; *Angew. Chem. Int. Ed. Engl.* **1986**, *25*, 257.
[4] P. J. Chmielewski, L. Latos-Grazynski, K. Rachlewicz, T. Glowiak, *Angew. Chem.* **1995**, *106*, 305; *Angew. Chem. Int. Ed. Engl.* **1995**, *33*, 779. H. Furuta, T. Asano, T. Ogawa, *J. Am. Chem. Soc.* **1995**, *116*, 767. J. L. Sessler, *Angew. Chem.* **1995**, *106*, 1410; *Angew. Chem. Int. Ed. Engl.* **1995**, *33*, 1348.
[5] For instance, 2,3,7,8,12,13,17,18-octamethoxyporphyrin was only reported very recently: A. Merz, R. Schropp, J. Lex, *Angew. Chem.* **1993**, *105*, 296; *Angew. Chem. Int. Ed. Engl.* **1993**, *32*, 291.
[6] T. D. Lash, *Energy Fuels* **1993**, *7*, 166.
[7] T. D. Lash, T. J. Roper, *Tetrahedron Lett.* **1995**, *35*, 7715.
[8] T. D. Lash, R. P. Balasubramaniam, J. J. Catarello, M. C. Johnson, D. A. May, Jr., K. A. Bladel, J. M. Feeley, M. C. Hoehner, T. G. Marron, T. H. Nguyen, T. J. Perun, Jr., D. M. Quizon, C. M. Shiner, A. Watson, *Energy Fuels* **1990**, *4*, 668.
[9] a) T. D. Lash, K. A. Bladel, C. M. Shiner, D. L. Zajeski, R. P. Balasubramaniam, *J. Org. Chem.* **1992**, *57*, 4809; b) D. A. May, Jr., T. D. Lash, *ibid.*, **1992**, *57*, 4820–4828. c) T. D. Lash, J. J. Catarello, *Tetrahedron* **1993**, *49*, 4159. d) D. M. Quizon-Colquitt, T. D. Lash, *J. Heterocycl. Chem.* **1993**, *30*, 477–482.
[10] T. F. Yen in *The Role of Trace Metals in Petroleum* (Ed.: T. F. Yen), Ann Arbor Science Publ., Ann Arbor, USA, **1975**, pp 1–30.
[11] *Phthalocyanines: Properties and Applications, Vol. 1–3*, (Ed.: C. C. Leznoff), VCH, **1990–1993**.
[12] S. B. Brown, T. G. Truscott, *Chem. Br.* **1993**, *29*, 955.
[13] D. H. R. Barton, J. Kervagoret, S. Z. Zard, *Tetrahedron* **1990**, *46*, 7587. T. D. Lash, J. R. Bellettini, J. A. Bastian, K. B. Couch, *Synthesis* **1995**, 170.
[14] T. D. Lash, B. H. Novak, Y. Lin, *Tetrahedron Lett.* **1995**, *35*, 2493.
[15] See also: N. Ono, H. Hironaga, K. Simizu, K. Ono, K. Kuwano, T. Ogawa, *J. Chem. Soc. Chem. Commun.* **1995**, 1019.
[16] A. Treibs, N. Haberle, *Justus Liebigs Ann. Chem.* **1968**, *450*, 164.
[17] See for example, C. J. Medforth, M. O. Senge, K. M. Smith, L. D. Sparks, J. A. Shelnutt, *J. Am. Chem. Soc.* **1992**, *114*, 9859.
[18] a) J. S. Lindsey, I. C. Schreiman, H. C. Hsu, P. C. Kearney, A. M. Marguerettaz, *J. Org. Chem.* **1987**, *52*, 827. b) J. S. Lindsey, R. W. Wagner, *ibid.* **1989**, *54*, 828.

Topochemical Reaction Control in Solution**

Henning Hopf,* Helmut Greiving, Peter G. Jones, and Peter Bubenitschek

Dedicated to Professor Wolfgang Lüttke on the occasion of his 75th birthday

The photodimerization of cinnamic acid in the solid state is a classic example of topochemical reaction control: the correlation of the product configuration with the packing of the starting material in the crystal lattice.[1, 2] Products can form only if a given distance between the reactants is not exceeded; for the [2 + 2] cycloaddition of cinnamic acids the reactants can be separated by at most 360–410 pm (α- and β-cinnamic acid). Greater intermolecular separations such as those in the so-called γ structures of the cinnamic acids (>470 nm) result in photostability.[2] For application of topochemical principles in solution—an attractive prospect, for example, for stereocontrolled synthesis—a stable structure in solution must be found to replace the crystal lattice as an ordering principle. In this context [m.n]cyclophanes are especially suitable, as we have shown recently in studies on cinnamophane **1**.[3] This bis(cinnamic acid) is sterically fixed because of the alkano bridges (distance between the olefinic double bonds 350 pm[3]) and on irradiation reacts quantitatively both in the solid state and in solution to give the cyclobutane **2**. The quantum yield of 0.84 (methanol, −90 °C) for this reaction is the highest ever measured for the dimerization of a cinnamic acid derivative.[3]



Scheme 1. Synthesis of [*n*]ladderanes from pseudo-geminal-substituted [2.2]paracyclophanepolyenes; a) DIBAL-H, Et_2O, N_2, $-80 \rightarrow 0$ °C; b) MnO_2, CH_2Cl_2, N_2, room temperature; c) NaH, $(EtO)_2P(O)CH_2COOEt$, THF, N_2, room temperature.

The controlling effect of the cyclophane framework is not so surprising, since the reacting groups of **1** are directly attached to the framework. We wondered therefore whether extension of the double bond system, which would necessarily increase its flexibility, would reduce the control exerted by the cyclophane spacer. For this purpose compound **1** was reduced with diisobutylaluminum hydride and the resulting diol oxidized with MnO_2 to afford the dialdehyde, which was treated with ethyl diethylphosphonoacetate in a Wittig–Horner chain extension. Diester **3**, obtained in an overall yield of 55%, has an all-*trans* structure based on spectroscopic data.[4] Irradiation of **3** (ethanol, 150 W Hg high-pressure lamp, 30 min, room temperature, Pyrex) afforded phane **4** in >90% yield. The structure of **4**, which contains three annelated cyclobutane rings, was confirmed by spectroscopic[5] and crystallographic data.[6] With even longer pseudogeminal substituents stereocontrol is still not lost, as proved by the photoreaction of the deep-yellow bis(triene)diester **5**, which was prepared from **3** by procedure described above.[7] Irradiation of **5** in methanol in a Pyrex apparatus with a 450 W Hg high-pressure lamp for 60 min at room temperature furnished the colorless [5]ladderane **6** (83% yield);[8] spectroscopic data unequivocally showed **6** to be a higher homologue of **4**.[9] The structure was confirmed by a crystal structure analysis (Fig. 1).[10].

The four-membered rings in **6** are planar to within 1 pm; the interplanar angles are between 112 and 114°. The absolute torsion angles about the six chain bondsC18-C19-C20-C21 and C27-C28-C29-C30 lie in the range from 178 and 180°. The first bond between the chains, C17–C26, is very long (162.6(3) pm);

[*] Prof. Dr. H. Hopf, Dipl.-Chem. H. Greiving, Dipl.-Chem. P. Bubenitschek
Institut für Organische Chemie der Technischen Universität
Hagenring 30, D-38106 Braunschweig (FRG)
Telefax: Int. code + (531) 391-5388
Prof. Dr. P. G. Jones
Institut für Anorganische und Analytische Chemie
der Technischen Universitat Braunschweig

[**] Topochemical Reaction Control in Solution, Part 2. This work was supported by the Deutsche Forschungsgemeinschaft and the Fonds der Chemischen Industrie. Part 1: ref. [3].

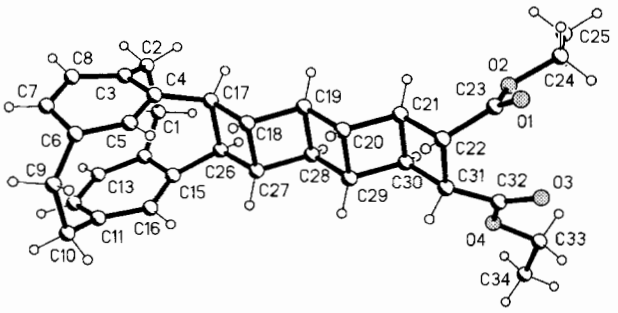
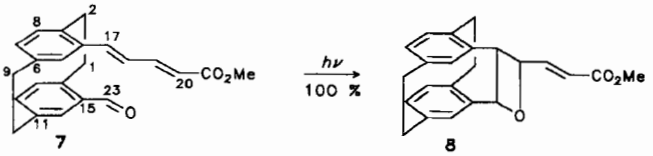


Fig. 1. Crystal structure of [5]ladderane **6**.

the others can be considered to be somewhat extended single bonds (156.4–157.7 pm). The corresponding distances in **4** are very similar.

The polycycloaddition of **5** is reversible. Ladderane **6** can be heated (180 °C) or irradiated (λ = 270 nm, methanol) to regenerate bis(triene) **5**; thus this pair of isomers is a new photochromic system.

The reaction of the phosphonate with an excess of the dialdehyde obtained from **1** affords monoester **7**. A methyl pentadienecarboxylate group is located directly above the formyl substituent in **7**, providing ideal conditions for an intramolecular Paterno–Büchi reaction. Indeed, irradiation of **7** (ethanol, 150 W Hg high-pressure lamp), room temperature, Pyrex) furnishes the expected oxetane **8** in quantitative yields.[11, 12]



The examples described here may usher in the use of [m.n]-phanes as spacer elements. Aside from the obvious potential of introducing other photo- and thermoactive substituents in the pseudo-geminal positions in [2.2]paracyclophanes, substituents can also be introduced in pseudo-*ortho* positions in these molecules, thus leading to a pseudo-dihedral angle of 60°. To what extent the reactivity would be reduced in this structural variation remains to be seen. Another open question is the effect of increasing the distance between the reacting substituents by extending the phane bridges.[13] It will never be possible to adjust the distance between the substituents or functional groups with infinite variability, but this ideal may be better approximated by using phanes as "set screws" rather than other rigid spacers. In addition, when other aromatic subunits are used in the cyclophanes in place of the benzene rings, other pseudo-dihedral angles besides 0 and 60° are possible. Thus, phane spacers should allow the deliberate positioning of substituents in three-dimensional space.

Received: October 14, 1995 [Z 7403 IE]
German version: *Angew. Chem.* **1995**, *107*, 742

Keywords: cyclophanes · phanes · photochemistry · topochemistry

[1] M. D. Cohen, G. M. J. Schmidt, F. I. Sonntag, *J. Chem. Soc.* **1964**, 200–2013.
[2] G. M. J. Schmidt, *Solid State Photochemistry*, Verlag Chemie, Weinheim, **1976**.
[3] H. Greiving, H. Hopf, P. G. Jones, P. Bubenitschek, J. P. Desvergne, H. Bouas-Laurent, *J. Chem. Soc. Chem. Commun.* **1995**, 1075–1076.
[4] NMR data of **3**: ^{1}H NMR (400.1 MHz, $CDCl_3$): δ = 7.34 (dd, J(19,18) = J(26,25) = 11.2 Hz, J(19,20) = J(26,27) = 15.2 Hz, 2H, 19-H, 26-H), 6.89 (d, J(17,18) = J(24,25) = 15.4 Hz, 2H, 17-H, 24-H), 6.70 (br. s, 2H, 5-H, 16-H), 6.52 (dd, J(18,19) = J(25,26) = 11.2 Hz, J(18,17) = J(25,24) = 15.4 Hz, 2H, 18-H, 25-H), 6.50 (br. s, 4H, 7-H, 8-H, 12-H, 13-H), 5.83 (d, J(20,19) = J(27,26) = 15.2 Hz, 2H, 20-H, 27-H), 4.19 (qd, J(22,23) = J(29,30) = 7.1 Hz, J = 1.8 Hz, 4H, 22-H, 29-H), 3.48–3.43 (m, 2H, 1a-H, 2a-H), 3.06–2.99 (m, 6H, 1b-H, 2b-H, 9-H, 10-H), 1.30 (t, J(23,22) = J(30,29) = 7.1 Hz, 6H, 23-H, 30-H); ^{13}C NMR (100.6 MHz, $CDCl_3$): δ = 166.77 (s, C-21, C-28), 144.70 (d, C-19, C-26), 139.71, 138.65, 136.09 (each s, C-3, C-4, C-6, C-11, C-14, C-15), 138.27 (d, C-17, C-24), 134.98, 133.53, 126.88 (each d, C-18, C-25, C-7, C-8, C-12, C-13), 129.49 (d, C-5, C-16), 120.83 (d, C-20, C-27); 60.12 (t, C-22, C-29), 34.92 (t, C-9, C-10), 32.62 (t, C-1, C-2), 14.26 (q, C-23, C-30).
[5] NMR data of **4**: ^{1}H NMR (250.1 MHz, $CDCl_3$): δ = 6.47 (dd, J(7,8) = J(12,13) = 7.8 Hz, J(7,5) = J(12,16) = 1.6 Hz, 2H, 7-H, 12-H), 6.20 (d, J(8,7) = J(13,12) = 7.8 Hz, 2H, 8-H, 13-H), 6.19 (d, J(5,7) = J(16,12) = 1.6 Hz, 2H, 5-H, 16-H), 4.36 (br. s, 2H, 17-H, 24-H), 4.19 (q, J(22,23) = J(29,30) = 7.1 Hz, 4H, 22-H, 29-H), 3.59 (br. s, 2H, 20-H, 27-H), 3.42 (br. s, 2H, 19-H, 26-H), 3.18 (br. s, 2H, 18-H, 25-H), 3.15–2.96 (m, 6H, 1a-H, 2a-H, 9-H, 10-H), 2.61–2.54 (m, 2H, 1b-H, 2b-H), 1.30 (t, J(23,22) = J(30,29) = 7.1 Hz, 6H, 23-H, 30-H); ^{13}C NMR (62.9 MHz, $CDCl_3$): δ = 172.73 (s, C-21, C-28), 140.35, 140.01, 139.33 (each s, C-3, C-4, C-6, C-11, C-14, C-15), 134.47, 133.01, 128.82 (each d, C-5, C-7, C-8, C-12, C-13, C-16), 60.85 (t, C-22, C-29), 51.49, 45.99, 43.03, 41.93 (each d, C-17, C-18, C-19, C-20, C-24, C-25, C-26, C-27), 36.21, 32.13 (each t, C-1, C-2, C-9, C-10), 14.27 (q, C-23, C-30).
[6] To save space the crystal structure of **4** is not shown. Crystal data for **4**: monoclinic, $P2_1/n$, a = 747.97(14), b = 1664.0(4), c = 1839.8(3) pm, β = 95.76(2)°, Z = 4, T = −130 °C. Crystal dimensions 0.2 × 0.2 × 0.15 mm. Stoe STADI-4 diffractometer, 5629 relections ($Mo_{K\alpha}$ radiation), $2\theta_{max}$ = 50°), of which 4028 were independent (R_{int} = 0.048). Structure solution by direct methods. Structure refinement anisotropicic on F^2 (program SHELXL-93), H atoms with a riding model. The final $wR(F^2)$ was 0.181, conventional $R(F)$ = 0.068 for 309 parameters. See ref. [10b].
[7] NMR data of **5**: ^{1}H NMR (400.1 MHz, $CDCl_3$): δ = 7.28 (dd, J(21,22) = J(30,31) = 15.1 Hz, J(21,20) = J(30,29) = 11.3 Hz, 2H, 21-H, 30-H), 6.72 (d, J(17,18) = J(26,27) = 14.9 Hz, 2H, 17-H, 26-H), 6.67 (br. s, 2H, 5-H, 16-H), 6.60 (dd, J(19,20) = J(28,29) = 14.3 Hz, J(18,19) = J(28,27) = 10.8 Hz, 2H, 19-H, 28-H), 6.52 (dd, J(18,17) = J(27,26) = 15.0 Hz, J(18,19) = J(27,28) = 10.8 Hz, 2H; 18-H, 27-H), 6.50 (d, J(8,7) = J(13,12) = 7.8 Hz, 2H, 8-H, 13-H), 6.48 (dd, J(7,8) = J(12,13) = 7.8 Hz, J(7,5) = J(12,16) = 1.5 Hz, 2H, 7-H, 12-H); 6.29 (dd, J(20,19) = J(29,28) = 14.2 Hz, J(20,21) = J(29,30) = 11.4 Hz, 2H, 20-H, 29-H), 5.80 (d, J(22,21) = J(31,30) = 15.2 Hz, 2H, 22-H, 31-H), 4.19 (dd, J(24,25) = J(33,34) = 7.1 Hz, J = 1.0 Hz, 4H, 24-H, 33-H); 3.50–3.45 (m, 2H, 1a-H, 2a-H), 3.09–3.02 (m, 4H, 9-H, 10-H), 3.03–2.99 (m, 2H, 1b-H, 2b-H), 1.29 (t, J(25,24) = J(34,33) = 7.1 Hz, 6H, 25-H, 34-H); ^{13}C NMR (100.6 MHz, $CDCl_3$): δ = 166.96 (s, C-23, C-32), 144.26 (d, C-21, C-30), 141.16 (d, C-19, D-28), 139.62, 138.26, 136.75 (each s, C-3, C-4, C-6, C-11, C-14, C-15), 134.95 (d, C-8, C-13), 134.92 (d, C-17, C-26), 132.98 (d, C-7, C-12), 130.04 (d, C-20, C-29), 129.41 (d, C-5, C-16), 128.85 (d, C-18, C-27), 120.69 (d, C-22), C-31), 60.19 (t, C-24, C-33), 35.04 (t, C-9, C-10), 32.72 (t, C-1, C-2), 14.30 (q, C-25, C-34).
[8] Linear oligo- and polymers consisting of annelated cyclobutadiene units are called [*n*]ladderanes. The known synthetic routes to these novel polycycles rely almost exclusively on multiple additions of cyclobutadienes: G. Mehta, M. B. Viswanath, A. C. Kunwar, K. R. Kumar, D. S. K. Reddy, *J. Chem. Soc. Chem. Commun.* **1995**, 739–740, and references therein; see also J. Meinwald, J. Mioduski, *Tetrahedron Lett.* **1974**, 3839–3842; H. D. Martin, B. Mayer, M. Pütter, H. Höchstetter, *Angew. Chem.* **1981**, *93*, 695–696; *Angew. Chem. Int. Ed. Engl.* **1981**, *20*, 677–678, and references therein.
[9] NMR data of **6**: ^{1}H NMR (200.1 MHz, $CDCl_3$): δ = 6.46 (dd, J(7,8) = J(12,13) = 7.7 Hz, J(7,5) = J(12,16) = 1.5 Hz, 2H, 7-H, 12-H), 6.23 (d, J(5,7) = J(16,12) = 1.5 Hz, 2H, 5-H, 16-H), 6.20 (d, J(8,7) = J(13,12) = 7.7 Hz, 2H, 8-H, 13-H), 4.40 (br. s, 2H, 17-H, 26-H), 4.17 (q, J(24,25) = J(33,34) = 7.1 Hz, 4H, 24-H, 33-H), 3.55 (br. s, 2H, 22-H, 31-H), 3.17–2.91 (m, 14H, 1a-H, 2a-H, 9-H, 10-H, 18-H, 19-H, 20-H, 21-H, 27-H, 28-H, 29-H, 30-H), 2.60–2.53 (m, 2H, 1b-H, 2b-H), 1.28 (t, J(25,24) = J(34,33) = 7.1 Hz, 6H, 25-H, 34-H); ^{13}C NMR (50.3 MHz, $CDCl_3$): δ = 172.73 (s, C-23, C-32), 140.66, 139.89, 139.23 (each s, C-3, C-4, C-6, C-11, C-14, C-15), 134.57, 132.87, 128.58 (each d, C-5, C-7, C-8, C-12, C-13, C-16), 60.66 (t, C-24, C-33), 52.15, 48.20, 47.76, 46.15, 42.29, 41.19 (each d, C-17, C-18, C-19, C-20, C-21, C-22, C-26, C-27, C-28, C-29, C-30, C-31), 36.15, 32.07 (each t, C-1, C-2, C-9, C-10), 14.16 (q, C-25, C-33).
[10] a) Crystal data for **6**: triclinic, $P\bar{1}$, a = 945.32(12), b = 1156.4(2), c = 1315.1(2) pm, α = 105.291(10), β = 98.518(10), γ = 105.642(10)°, Z = 2, T = −100 °C. Crystal dimensions 0.6 × 0.4 × 0.3 mm, Siemens P4 diffractometer, 4520 reflections, of which 4453 were independent (R_{int} = 0.15), $wR(R^2)$ = 0.129, $R(F)$ = 0.047, 345 parameters (otherwise as for **4**). b) Further details of the crystal structure investigations may be obtained from the Fachinformationszentrum Karlsruhe, D-76344 Eggenstein-Leopoldshafen (FRG) on quoting the depository numbers CSD-401446 (**4**) and 401447 (**6**).

[11] NMR data of **8**: ^{1}H NMR (400.1 MHz, $CDCl_3$): $\delta = 7.37$ (dd, $J(19,20) = 15.6$ Hz, $J(19,18) = 3.9$ Hz, 1H, 19-H), 6.77 (d, $J(16,12) = 1.7$ Hz, 1H, 16-H), 6.56–6.49 (m, 5H, 5-H, 7-H, 12-H, 20-H, 23-H), 6.25 (d, $J(8,7)$ or $J(13,12) = 7.7$ Hz, 1H, 8-H or 13-H), 6.18 (d, $J(8,7)$ or $J(13,12) = 7.8$ Hz, 1H, 8-H or 13-H), 5.59–5.57(m, 1H, 18-H), 4.40–4.37 (m, 1H, 17-H), 3.83 (s, 3H, 22-H), 3.28–2.96 (m, 5H, CH_2), 2.89–2.78 (m, 1H, CH_2), 2.65–2.52 (m, 2H, CH_2); ^{13}C NMR (100.6 MHz, $CDCl_3$): $\delta = 166.86$ (s, C-21), 140.61, 140.42, 139.48, 139.00, 135.97, 135.95 (each s, C-3, C-4, C-6, C-11, C-14, C-15), 147.64, 134.36, 133.61, 132.93, 129.96, 129.69, 120.35 (each d, C-5, C-7, C-8, C-12, C-13, C-16, C-19, C-20), 84.62, 77.66 (each d, C-18, C-23), 51.78, 51.56 (C-17, C-22), 36.31, 36.12, 32.26, 30.41, (each t, C-1, C-2, C-9, C-10).

[12] The parent system 4-formyl-15-vinyl[2.2]paracyclophane also reacts on irradiation to give the corresponding oxetane: S. Hentschel, Dissertation, Braunschweig, **1989**.

[13] For the synthesis and characteristic of psuedo-geminal [*m.n*]phanes with propano and butano bridges see Z. Pechlivanidis, Dissertation, Braunschweig, **1992**.

The Synthesis and Crystal Structures of $RbC(SiMe_3)_3$ and $CsC(SiMe_3)_3 \cdot 3.5C_6H_6$: A One-dimensional Ionic Solid and an Ionic Solid with a Molecular Structure**

Colin Eaborn, Peter B. Hitchcock, Keith Izod, and J. David Smith*

Little is known about the structures of alkylrubidium and -cesium derivatives.[1, 2] The unsolvated methyl compounds crystallize with ionic lattices comprising Rb^+ or Cs^+ ions and pyramidal Me^- ions.[1] Pentamethyldiethylenetriamine (pmdta) derivatives MR(pmdta) form linear polymers (R = CPh_3, M = Rb, Cs)[3] or dimers (R = $CH(SiMe_3)_2$, M = Rb),[4] and the yellow tris(trimethylsilyl)silyl compounds crystallize as dimeric toluene solvates.[5]

We have now shown that tris(trimethylsilyl)methylrubidium (**1**) and -cesium (**2**) may be obtained by metalation of $HC(SiMe_3)_3$ with the now readily available methylmetal derivatives[1] (prepared in situ in a slightly modified version of the original synthesis,[6] from methyllithium and the ether-soluble alkali metal 2-ethylhexoxides). Although both compounds are exceedingly air and moisture sensitive, crystals suitable for X-ray diffraction studies were obtained.

$RbC(SiMe_3)_3$ **1** $CsC(SiMe_3)_3$ **2**

We first determined the structure of the Cs derivative **2**, obtained as a yellow benzene solvate $\mathbf{2} \cdot 3.5(C_6H_6)$. The results[7] show that each Cs^+ ion is coordinated to the central carbon atom of the neighboring anion (Fig. 1) and to three benzene molecules η^6, leading to a quasi-tetrahedral arrangement. In addition, molecules of uncoordinated benzene are found in the lattice. The benzene is easily lost in vacuum, suggesting that it is weakly bound. The Cs–C1 bond length in $\mathbf{2} \cdot 3.5C_6H_6$ (332.5(12) pm) is very similar to that in the complex $CsCPh_3 \cdot$pmdta (334.8(4) pm)[3], and the distances from the Cs ion to the C atoms of the benzene rings (mean 381(2) pm) are similar to those in the toluene solvates $CsSi(SiMe_3)_3 \cdot 1.5$PhMe (mean 380(2) pm)[5] and $Cs[Al_7O_6Me_{16}] \cdot 3$PhMe (364–394 pm).[8]

[*] Dr. J. D. Smith, Prof C. Eaborn, Dr P. B. Hitchcock, Dr K. Izod
School of Chemistry and Molecular Sciences
University of Sussex
Brighton BN1 9QJ (UK)
Telefax: Int. code + (273) 677-196

[**] This work was supported by the Engineering and Physical Sciences Research Council.

The average distances of the Cs ion to the centers of the benzene rings of 358 pm are somewhat shorter. The mean Si-C1-Si angle (117.3(5)°) is much larger than the ideal value for a tetrahedron. This shows that the Cs–C1 bond is highly ionic,[9] with charge delocalized in such a way that the inner Si–C1 bonds are shortened. In contrast, the D-C-D angles in $NaCD_3$ and KCD_3, measured at 1.5 K, are 105–106°.[11]

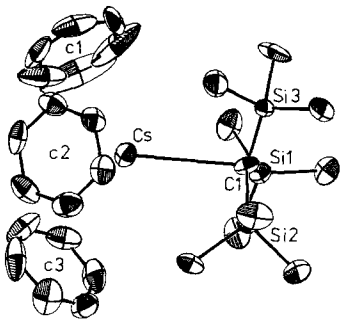


Fig. 1. Molecular structure of $\mathbf{2} \cdot 3.5C_6H_6$; 0.5 mol of lattice benzene omitted (50% vibrational ellipsoids). Significant bond lengths [pm] and angles[°]: Cs–C1 332.5(12), Cs-c_1 (c: centroid of benzene ring) 343.3, Cs-c_2 350.7, Cs-c_3 379.0, C–Si 181.7(11),* Si–Me 188.6(13);* c_1-Cs-c_2 99.4, c_1-Cs-c_3 107, c_2-Cs-c_3 93.0, Cs-C1-Si1 99.3(4), Cs-C1-Si2 97.0(4), Cs-C1-Si3 102.5(4), Si-C1-Si 117.3(5).* Me-Si-Me 103.0(3)*. The values marked with an * are mean values.

We had earlier found[10] that tris(trimethylsilyl)methylpotassium crystallized from benzene as a solvent-free one-dimensional ionic solid with chains of alternate K^+ ions and planar $[C(SiMe_3)_3]^-$ ions. It was thus of interest to determine whether the structure of the rubidium compound **1** was like that of the potassium or the cesium analogue. The structure of **1** was found to resemble that of the potassium derivative, but the planar anions are significantly distorted from C_3 symmetry (Fig. 2).[11] Whereas in the potassium compound each K^+ interacts with the central carbon atom and six methyl groups (three from the anion on the left and three from that on the right, thus preserving the threefold symmetry), the Rb^+ ion is apparently large enough to interact with eight methyl groups from the adjacent anions. Two methyl groups, one at C9, involved in the interaction with the cation, and one at C4, which is not, are forced into the space between Si1 and Si3, thus opening the Si-C-Si angle from the ideal value of 120° to 126°.

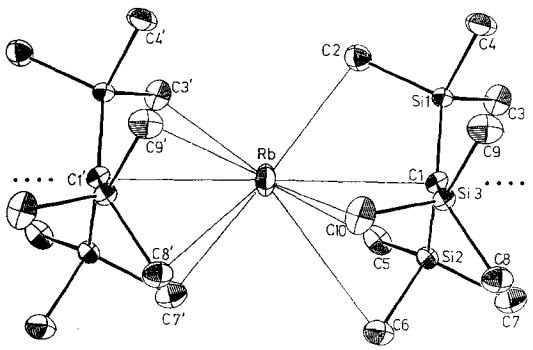


Fig. 2. The molecular structure of **1**. Selected bond lengths [pm] and angles [°]: Rb–C1 329.1(7),Rb–C1' 328.7(7), Rb–C2 327.8(9), Rb–C3' 358.6(6), Rb–C5 365.3(8), Rb–C6 364.3(8), Rb-C7' 342.8(8), Rb–C8' 355.1(9), Rb–C9 377.2(9'), Rb–C10 328.4(7), C–Si 181.5(7),* Si–Me 188.0(8);* C1-Rb-C1 177.7(2), Rb-C1 Rb''177.7(2), Si1-C1-Si2 116.5(4), Si1-C1-Si3 126.6(4), Si2-C1-Si3 116.8(4), Me-Si-Me 102.9(4),* C1-Si-Me 115.4(4). The values marked with an * are mean values.

In compounds $XC(SiMe_3)_3$, the Si-C-Si angles can be readily distorted from the ideal tetrahedral value in response to the steric and electronic requirements of the group X.[9] The significant distortion of the planar CSi_3 skeleton in **1** from C_3 symmetry is of a type not previously observed. The structures of **1** and **2** show that the more polarizable alkali metal ions interact with

 © VCH Verlagsgesellschaft mbH, D-69451 Weinheim, 1995 0570-0833/95/0606-0687 $ 10.00+.25/0

both methyl groups and benzene molecules. It would be of interest to know whether the M···Me interactions involve H or C atoms, but so far the X-ray data do not provide clear evidence on this point. Similar M···Me interactions are found in $[Yb\{C(SiMe_3)_3\}_2]$[12] and several related compounds. The $M^+\cdots(C_6H_6)$ interactions are strong enough when M = Cs to break the ionic $(M^+R^-)_n$ chains formed when M = K[10] or Rb; thus, individual ion pairs are separated by benzene solvate molecules, and the packing diagram looks like that for an organic compound in which interactions between molecules are weak.

Experimental Procedure

1: A solution of MeLi (13.6 mmol) in Et_2O (8 mL) was added to a cold (−10 °C) solution of 2-ethylhexoxyrubidium (2.92 g, 11.14 mmol) in Et_2O (30 mL). The solution was allowed to warm until the onset of effervescence (C_2H_4 evolution) showed that MeRb had begun to form. The solution was then cooled to −10 °C. $HC(SiMe_3)_3$ (14.8 mmol) was added and the mixture was stirred for 2 h at −10 °C and for a further 12 h during which time it slowly reached room temperature. The solvent was removed in vacuum and the residue was washed with light petroleum (3 × 30 mL) then extracted with benzene. The extract was evaporated and the residue was recrystallized from benzene/heptane to give colorless needles of **1** (2.26 g, 64%). The compound was too air and moisture sensitive for satisfactory C and H analysis; ^{1}H NMR (C_6D_6, chemical shifts relative to $SiMe_4$, 25 °C) δ = 0.32 (s, Me_3Si); ^{13}C NMR: δ = 6.89 (CSi_3), 8.36 (Me_3Si); ^{29}Si NMR: δ = −11.1.

2: CsR was made similarly from 2-ethylhexoxycesium (1.74 g, 6.38 mmol), MeLi (6.4 mmol) and $HC(SiMe_3)_3$ (6.0 mmol) in ether (30 mL) at −78 °C. The mixture was stirred for 0.5 h then allowed to warm slowly to room temperature during 1 h. The solvent was removed in vacuum, and the residue washed with light petroleum (3 × 30 mL) and then recrystallized from benzene to give extremely moisture-sensitive pyrophoric pale yellow plates of the benzene solvate $2\cdot 3.5C_6H_6$. ^{1}H NMR (C_6D_6, 25 °C): δ = 0.35 s, Me_3Si). ^{13}C NMR: δ = 8.22 (Me_3Si), 9.80 (CSi_3); ^{29}Si NMR: δ = −13.5.

Received: November 2, 1995 [Z 7448 IE]
German version: *Angew. Chem.* **1995**, *107*, 756

Keywords: alkali metal compounds · metalation · solid-state structures

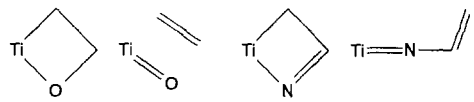
[1] E. Weiss, *Angew. Chem.* **1993**, *105*, 1565; *Angew. Chem. Int. Ed. Engl.* **1993**, *32*, 1501.
[2] C. Schade, P. von R. Schleyer, *Adv. Organometal. Chem.* **1987**, *27*, 169.
[3] D. Hoffmann, W. Bauer, P. von R. Schleyer, U. Pieper, D. Stalke, *Organometallics*, **1993**, *12*, 1193.
[4] P. B. Hitchcock, M. F. Lappert, W-P. Leung, L. Diansheng, T. Shun, *J. Chem. Soc. Chem. Commun.* **1993**, 1386.
[5] K. W. Klinkhammer, W. Schwarz, *Z. Anorg. Allg. Chem.* **1993**, *619*, 1777.
[6] E. Weiss, H. Köster, *Chem. Ber.* **1977**, *110*, 717.
[7] Crystal data for $C_{31}H_{48}CsSi_3$ $2\cdot 3.5C_6H_6$: M = 637.9, monoclinic, space group $C2/c$, a = 36.227 (17), b = 11.429(10), c = 17.903(8) Å, β = 112.19(4)°, V = 6863.5 Å^3, $Mo_{K\alpha}$ radiation, λ = 0.71069 Å, Z = 8, ρ = 1.24 g cm^{-3}, $F(000)$ = 2648, μ ($Mo_{K\alpha}$) = 11.9 cm^{-1}, T = 173 K, 3467 reflections measured and 2387 with $|F^2| > 2\sigma(F^2)$ used. No decay correction, absorption correction (DIFABS). Structure analysis by heavy atom methods using SHELXS-86. Full matrix least squares refinement using Enraf-Nonius MOLEN programmes with non-H atoms anisotropic and H atoms in fixed calculated positions with U_{iso} = 1.3 U_{eq} for parent atoms. Final R = 0.056, R' = 0.061, S = 1.5 [11b].
[8] J. L. Atwood, *J. Inclusion Phenom.* **1985**, *3*, 13.
[9] P. T. Brain, M. Mehta, D. W. H. Rankin, H. E. Robertson, C. Eaborn, J. D. Smith, A. D. Webb, *J. Chem. Soc. Dalton Trans.* **1995**, 349.
[10] C. Eaborn, P. B. Hitchcock, K. Izod, A. J. Jaggar, J. D. Smith, *Organometallics*, **1995**, *13*, 753.
[11] a) Crystal data for $C_{10}H_{27}RbSi_3$ **1**, M = 317.1, triclinic, space group $P\bar{1}$, a = 6.576(2), b = 9.022(3), c = 14.587(4) Å, α = 86.00(2), β = 81.59(2), γ = 70.91(2)°, V = 808.8(4) Å^3. $Mo_{K\alpha}$ radiation λ = 0.71069 Å, Z = 2, ρ = 1.30 g cm^{-3}, $F(000)$ = 332, $\mu(Mo_{K\alpha})$ = 31.7 cm^{-1}, T = 173 K. 3887 reflections measured and 2220 with $|F^2| > 2\sigma(F^2)$ used. No decay correction, empirical absorption correction. Structure analysis and refinement as for $2\cdot 3.5C_6H_6$. Final R = 0.069, R' = 0.064, S = 1.4. b) Further details of the crystal structure investigations may be obtained from the Director of the Cambridge Crystallographic Data Centre, 12 Union Road, GB-Cambridge CB2 1EZ (UK), on quoting the full journal citation.
[12] C. Eaborn, P. B. Hitchcock, K. Izod, J. D. Smith, *J. Am. Chem. Soc.* **1994**, *116*, 12071.

Synthesis and Structure of 1-Aza- and 1-Phospha-2-titanacyclobut-4-enes**

Rüdiger Beckhaus,* Isabelle Strauß, and Trixie Wagner

Dedicated to Professor Peter Paetzold on the occasion of his 60th birthday

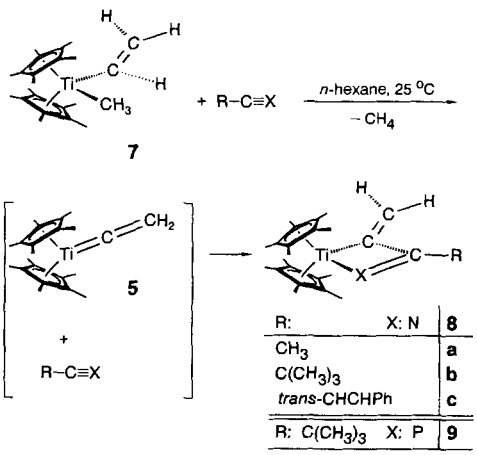
Oxatitanacyclobutanes[1] and azatitanacyclobutenes[2] are discussed as intermediates in reactions of carbenoid titanium compounds with carbonyl compounds or nitriles, respectively. The high electrophilicity of the metal center has to date prohibited the isolation and characterization of **1** and **3**; spontaneous ring opening affords either carbonyl olefination (**1** → **2**),[3] or products of intermediately formed vinylimido species **4** corresponding to the reaction of **3** → **4**.[2b, 4]



1 **2** **3** **4**

The first stable and structurally characterized 1-oxa-2-titanacyclobutanes with a planar four-membered ring [5] were isolated by reaction of the permethylated titanocene vinylidene fragment $[Cp^*_2Ti{=}C{=}CH_2]$ (**5**) with heterocumulenes;[6] compound **5** may be obtained from $[Cp^*_2TiC(=CH_2)CH_2CH_2]$ (**6**) or $[Cp^*_2Ti(CH_3)(CH{=}CH_2)]$ (**7**) after elimination of ethylene or methane, respectively. Subsequently we report on the advantages associated with the use of **5** instead of $[Cp_2Ti{=}CH_2]$ intermediates in the preparation of azatitanacyclobutenes **3**. Furthermore, encouraged by the synthesis of the first 1-phospha-2-rhodacyclobut-4-ene by Binger et al.[7] we studied the reactivity of **5** towards the phosphaalkyne *t*Bu–C≡P.

The reaction of solutions of **7** in *n*-hexane with acetonitrile, pivalonitrile, cinnamonitrile, or 2-*tert*-butyl-1-phosphaacetylene[8] at room temperature led almost quantitatively to the prod-



[*] Priv.-Doz. Dr. R. Beckhaus, Dipl.-Chem. I. Strauß, Dipl.-Chem. T. Wagner
Institut für Anorganische Chemie der Technische Hochschule
Professor-Pirlet-Strasse 1, D-52056 Aachen (FRG)
Telefax: Int. code + (241)8888 288

[**] This work was supported by the Deutschen Forschungsgemeinschaft and the Fonds der Chemischen Industrie. We thank Prof. Dr. G. E. Herberich for his continuing interest and Prof. Dr. P. Paetzold for a sample of *t*BuCP (Technische Hochschule Aachen). Stimulating discussions with Prof. Dr. R. H. Grubbs (California Institute of Technology) are gratefully acknowledged.

ucts **8a–c**, and **9**, respectively, (Table 1) and its isomer **9′**(NMR spectroscopic determination). The complexes **8b** and **8c** were isolated as red ashlars or needles in 53% and 38% yield, respectively. Purification of **8a** was prevented by its low tendency to crystallize. The isomer **9** was obtained as brown ashlars in 35% yield. The mass spectra of **8b**, **8c**, and **9** exhibit the peaks expected for the molecular ions.

The two different chemical shifts for the protons of the *exo*-methylene group in the ^{1}H NMR spectra appear to be a particularly characteristic feature of these new complexes and similar metallacycles (δ = 4.98, 6.04 (**8a**); 4.87, 6.25 (**8b**); 5.05, 6.36 (**8c**); 3.49, 5.45 (**9**)).[9] Moreover the chemical shifts of the ring carbon atoms in the ^{13}C NMR spectra are consistent with a σ-Ti-bonded sp^2 carbon atom and a C=N or C=P carbon atom not bonded to a metal (δ = 195.0, 146.9 (**8a**); 184.5, 157.4 (**8b**); 192.6, 146.0 (**8c**); 194.1, 195.8 (**9**)). A metal-bonded λ^3 phosphorus atom in **9**[7, 10] is indicated by its high downfield shift in the ^{31}P{^{1}H} NMR spectrum (δ = 549).

The structures of **8b** and **9** in solution determined by NMR spectroscopy have been confirmed by X-ray crystal structure analyses[11] (Fig. 1). The structures show planar heterotitanacyclobutenes. The alternating bond lengths of the sequences C1-C2-C3-X (X = N, P) are comparable to a conjugated π-bond system, similar to that of free butadiene.[12]

Furthermore the interatomic distances (Ti–X and C–X; X = N, P) and the small angles (Ti-X-C) prove the existence of an sp^2 hybridized X atom with a noncoordinated lone pair.[13]

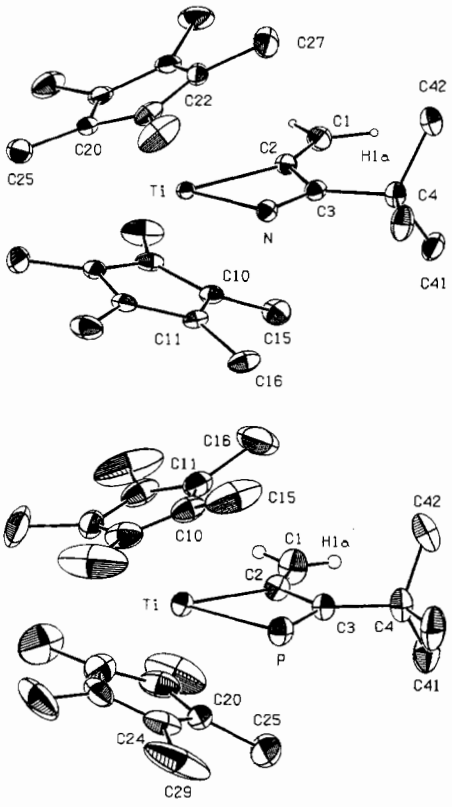
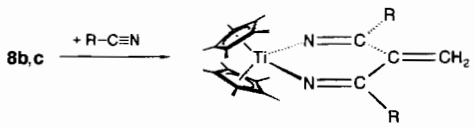


Fig. 1. Molecular structure of **8b** (top) and **9** (bottom) in the solid state. Selected bond lengths [Å] and angles [°] (Cp(1) and Cp(2) represent the centers of the Cp* ligands of the titanocene fragment; values in square brackets correspond to the parameters of **9**: X = N(**8b**), P (**9**)): Ti–Cp(1) 2.1055(5) [2.1053(9)], Ti–Cp(2) 2.1048(5) [2.1029(9)], Ti–X 2.017(2) [2.504(2)], Ti–C(2) 2.134(2) [2.161(5)], C(2)–C(1) 1.337(3) [1.326(8)], C(2)–C(3) 1.485(3) [1.473(7)], X–C(3) 1.290(3) [1.701(5)]; Cp(1)-Ti-Cp(2) 140.0(1) [139.4(2)], C(2)-Ti-X 67.85(8) [68.2(1)], Ti-X-C(3) 94.5(1) [81.1(2)], X-C(3)-C(2) 113.2(2) [111.6(3)], C(3)-C(2)-Ti 84.4(1) [99.1(3)], C(1)-C(2)-Ti 145.4(2) [133.1(4)].

Thus, the reactivity of [$Cp_2Ti{=}CH_2$]-based consecutive products observed by Doxsee et al. (that is the rearrangement (**3** → **4**)[2, 4]) can be regarded as a consequence of the participation of the nitrogen lone pair in the bonding to the titanium center, leading to the widening of the Ti-N-C angle and subsequent opening of the azatitanacyclobutene ring (→ **4**).[14] In contrast, because of the higher basicity of the permethylated cyclopentadienyl ligands, the electrophilicity at the titanium center is reduced in complexes **8** and **9**. An excess of nitrile and higher temperatures favor the insertion of another nitrile molecule into **8b** and **8c** to give **10a** and **10b**, respectively (**10a**: 64% yield).



10a : R = $C(CH_3)_3$
10b : R = CHCHPh

Whereas end-on coordination dominates in nitrile complexes,[15] phosphaalkyne ligands prefer side-on coordination due to the π character of their HOMO (i.e. the π-n separation is greater for phosphaalkynes than for nitriles).[16] After initial coordination of the nitrile (**A**), cycloaddition takes place via a suprafacial arrangement **B** to give **8**.

In the synthesis of **9**, an isomeric compound **9′** (corresponding to **C**) was detected in solution by NMR spectroscopy, but this has not yet been isolated (**9′**: ^{31}P{^{1}H} NMR: δ = 2.09 (s); ^{1}H NMR: δ = 6.66 (d, $^3J_{(H,P)}$ = 30 Hz, 1H, =CH_2), 5.80 (d, $^3J_{(H,P)}$ = 50 Hz, 1H, =CH_2), 1.60 (s, 30H)). The experimental

Table 1. Characteristic data of the compounds **8a–c**, **9**, and **10a** [a].

8a: ^{1}H NMR: δ = 6.04 (d, ^2J(H,H) = 1 Hz, 1H, =CH_2), 4.98 (d, ^2J(H,H) = 1 Hz, 1H, =CH_2), 2.13 (s, 3H, CH_3), 1.66 (s, 30 H, $C_5(CH_3)_5$); ^{13}C{^{1}H} NMR: δ = 195.0 (Ti–C), 146.9 (C=N), 120.1 ($C_5(CH_3)_5$), 110.0 (=CH_2), 18.6 (CH_3), 11.8 ($C_5(CH_3)_5$).

8b: M.p. 120 °C (decomp); ^{1}H NMR: δ = 6.25 (d, ^2J(H,H) = 1 Hz, 1H, =CH_2), 4.87 (d, ^2J(H,H) = 1 Hz, 1H, =CH_2), 1.67 (s, 30 H, $C_5(CH_3)_5$), 1.44 (s, 9H, *t*Bu); ^{13}C{^{1}H} NMR: δ = 184.5 (Ti–C), 157.4 (C=N), 120.3 ($C_5(CH_3)_5$), 109.6 (=CH_2), 39.2 ($C(CH_3)_3$), 30.4 ($C(CH_3)_3$), 11.8 ($C_5(CH_3)_5$); MS (70 eV) *m/z* (%): 427 (22) [M^+], 412 (17) [$M^+ - CH_3$], 400 (14), 370 (5) [$M^+ - C_4H_9$] 344 (31), 318 (100) [$M^+ - C_7H_{11}N$]; C, H analysis: C: calcd 75.86, found 75.91; H: calcd 9.67, found 9.84.

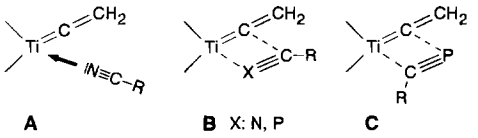
8c: M.p. 129 °C (decomp); ^{1}H NMR: δ = 7.66 (d, ^3J(H,H) = 16 Hz, 1H, CH=CH), 7.43–7.38 (m, 2H, *o*-H_{arom}), 7.41 (d, ^3J(H,H) = 16 Hz, 1H, CH=CH), 7.09–7.05 (m, 2H, *m*-H_{arom}), 7.01 (tt, ^3J(H,H) = 7 Hz, ^4J(H,H) = 2 Hz, 1H, *p*-H_{arom}), 6.36 (d, ^2J(H,H) = 1 Hz, 1H, =CH_2), 5.05 (d, ^2J(H,H) = 1 Hz, 1H, =CH_2), 1.69 (s, 30 H, $C_5(CH_3)_5$); ^{13}C{^{1}H} NMR: δ = 192.6 (Ti–C), 146.0 (C=N), 138.5 (*ipso*-C_{arom}), 131.6 (CH=CH), 128.7 (*o*-C_{arom}), 127.8 (*p*-C_{arom}), 127.4 (*m*-C_{arom}), 120.4 ($C_5(CH_3)_5$), 118.0 (CH=CH), 108.9 (=CH_2), 11.7 ($C_5(CH_3)_5$); MS (70 eV) *m/z* (%): 474 (31) [$M^+ + H$], 459 (14) [$M^+ - CH_2$], 447 (11), 344 (5), 318 (36) [$M^+ - C_{11}H_9N$]; C, H analysis: C: calcd 78.63, found 77.62; H: calcd 8.30, found 8.39.

9: ^{1}H NMR: δ = 5.45 (dd, ^2J(H,H) = 1 Hz, ^4J(P,H) = 4 Hz, 1H, =CH_2), 3.49 (dd, ^2J(H,H) = 1 Hz, ^4J(P,H) = 4 Hz, 1H, =CH_2), 1.65 (s, 30 H, $C_5(CH_3)_5$), 1.57 (s, 9H, *t*Bu); ^{13}C{^{1}H} NMR: δ = 195.8 (d, ^1J(P,C) = 66 Hz, P=C), 194.1 (s, Ti–C), 120.9 (s, $C_5(CH_3)_5$), 97.9 (d, ^3J(P,C) = 31 Hz, =CH_2), 40.7 (d, ^2J(P,C) = 6 Hz, $C(CH_3)_3$), 32.8 (d, ^3J(P,C) = 10 Hz, $C(CH_3)_3$), 12.2 (d, J(P,C) = 4 Hz, $C_5(CH_3)_5$); ^{31}P{^{1}H} NMR: δ = 549.0 (s); MS (70 eV) *m/z* (%): 444 (34) [M^+], 319 (100) [$M^+ - C_7H_{10}P$].

10a: M.p. 130 °C (decomp); ^{1}H NMR: δ = 5.97 (s, 2H, =CH_2), 1.72 (s, 30 H, $C_5(CH_3)_5$), 1.41 (s, 18H, *t*Bu); ^{13}C{^{1}H} NMR: δ = 163.9 (C=N), 140.8 (*C*=CH_2), 121.4 (=CH_2), 119.0 ($C_5(CH_3)_5$), 41.3 ($C(CH_3)_3$), 32.0 ($C(CH_3)_3$), 12.1 ($C_5(CH_3)_5$); MS (70 eV) *m/z* (%): 510 (10) [M^+] 318 (100) [$M - (C(=N)(tBu))_2(C=CH_2)$]; C, H analyis C: calcd 75.27, found 74.95; H: calcd 9.87, found 9.95.

[a] ^{1}H (500 MHz, ext. stand. TMS), ^{13}C (125MHz, ext. stand. TMS), ^{31}P (202.4 MHz, ext. stand. 85% H_3PO_4) NMR spectra were recorded in C_6D_6 at room temperature (**8a**: 300 MHz (^{1}H), 125 MHz (^{13}C)).

 © VCH Verlagsgesellschaft mbH, D-69451 Weinheim, 1995 0570-0833/95/0606-0689 $ 10.00+.25/0



A B X: N, P C

data for **9** are consistent with initial η^2 coordination, thus demonstrating the alkyne-like behavior of the phosphaacetylene. Further investigations will be necessary to establish whether higher regioselectivities can be achieved by the use of bulkier RCP derivatives.

Experimental Procedure

8b: Pivalonitrile (0.22 mL, 2 mmol) was added dropwise to a solution of **7** (0.72 g, 2 mmol) in *n*-hexane (50 mL) at −20 °C and the reaction mixture was stirred for two hours at room temperature. The solvent was removed at 0–10 °C and **8b** was obtained as crude product. Recrystallization from *n*-heptane yielded 0.42 g (53%) **8b** as red ashlars or needles.

Analogous procedures afforded the compounds **8a** and **8c**, as well as **9** by using 2-*tert*-butyl-1-phosphaacetylene (60% in hexamethyldisiloxane). Treatment of complex **7** with 10 equivalents of pivalonitrile for four days afforded complex **10a** in 44% yield as red ashlars or needles from a solution of **10a** and **8b**.

Received: November 2, 1995 [Z 7428 IE]
German version: *Angew. Chem.* **1995**, *107*, 738

Keywords: metallacycles · nitriles · phosphaalkynes · titanium compounds

[1] B. Schiott, K. A. Jorgensen, *J. Chem. Soc. Dalton Trans.* **1993**, 337–344, and references therein.

[2] a) K. M. Doxsee, J. K. M. Mouser, J. B. Farahi, *Synlett*, **1992**, 13–21; b) K. M. Doxsee, J. B. Farahi, H. Hope, *J. Am. Chem. Soc.* **1991**, *113*, 8889–8898; c) K. M. Doxsee, J. B. Farahi, *ibid.* **1988**, *110*, 7239–7240.

[3] a) S. H. Pine, G. S. Shen, H. Hoang, *Synthesis*, **1991**, 165–167; b) N. A. Petasis, E. I. Bzowej, *J. Am. Chem. Soc.* **1990**, *112*, 6392–6394; c) H. U. Reissig, *Nachr. Chem. Tech. Lab.* **1986**, *34*, 562–565; d) F. N. Tebbe, G. W. Parshall, G. S. Reddy, *J. Am. Chem. Soc.*, **1978**, *100*, 3611–3613.

[4] K. M. Doxsee, J. B. Farahi, *J. Chem. Soc. Chem. Commun.* **1990**, 1452–1454.

[5] R. H. Grubbs describes alternative syntheses of $L_nM\overline{OC(=CR_2)}CH_2$ derivatives attributing their stability to the puckering of the oxetane rings: S. C. Ho, S. Hentges, R. H. Grubbs, *Organometallics*, **1988**, *7*, 780–782.

[6] a) R. Beckhaus, J. Oster, T. Wagner, *Chem. Ber.* **1995**, *127*, 1003–1013; b) R. Beckhaus, I. Strauß, T. Wagner, P. Kiprof, *Angew. Chem.* **1993**, *105*, 281–283; *Angew. Chem. Int. Ed. Engl.* **1993**, *32*, 264–266; c) R. Beckhaus in *Organometallics in Organic Synthesis*, (Eds.: D. Enders, H.-J. Gais, W. Keim), Vieweg, Braunschweig, **1993**, p. 131.

[7] P. Binger, J. Haas, A. T. Herrmann, F. Langhauser, C. Krüger, *Angew. Chem.* **1991**, *103*, 316–318; *Angew. Chem. Int. Ed. Engl.* **1991**, *30*, 310–312.

[8] G. Becker, H. Schmidt, G. Uhl, W. Uhl, *Inorg. Synth.* **1990**, *27*, 249–253.

[9] Differences up to 2.5 ppm for the chemical shifts of the protons of the *exo* methylene group were observed for a lot of titanaoxetanes [6a, 6b].

[10] a) P. B. Hitchcock, C. Jones, J. F. Nixon, *Angew. Chem.* **1995**, *106*, 478–480; *Angew. Chem. Int. Ed. Engl.* **1995**, *33*, 463–465; b) D. Gudat, E. Niecke, W. Malisch, U. Hofmockel, S. Quashie, A. H. Cowley, A. M. Arif, B. Krebs, M. Dartmann, *J. Chem. Soc. Chem. Commun.* **1985**, 1687–1689.

[11] a) Crystal structure determinations: compounds **8b** and **9** are isotypic (**8b**): Enraf-Nonius CAD4 diffractometer, $Cu_{K\alpha}$ radiation ($\lambda = 1.5418$ Å), $T = -90$ °C; crystal dimensions $0.10 \times 0.15 \times 0.40$ mm^3, $C_{27}H_{41}NTi$; $M_r = 427.53$ g mol^{-1}; $a = 10.277(4)$, $b = 14.251(3)$, $c = 8.514(3)$ Å, $\alpha = 90.36(2)$, $\beta = 104.25(3)$, $\gamma = 91.89(3)$°; $V = 1208(1)$ Å^3; triclinic, space group $P\bar{1}$ (no. 2), $Z = 2$, $\rho_{calcd} = 1.176$ g cm^{-3}, $\mu = 30.74$ cm^{-1}, $F(000) = 464.0$; 6099 reflections were measured in the range $5 \le \theta \le 70$° (ω scan), 4795 of which with $I > 3\sigma(I)$, 3776 independent reflections with $I > 2\sigma(I)$ were used for 270 parameters; solution and refinement of the structure with SDP [11b]; $R = 0.052$, $R_w = 0.061$, GOF = 1.809; residual electron density 0.434 eÅ^{-3}. **9**: Enraf-Nonius CAD4 diffractometer, $Mo_{K\alpha}$ radiation ($\lambda = 0.7107$), $T = -15$°; crystal dimensions $0.20 \times 0.40 \times 0.85$ mm^3, $C_{27}H_{41}PTi$; $M_r = 444.50$ g mol^{-1}; $a = 10.183(4)$, $b = 14.678(4)$, $c = 8.610(4)$ Å, $\alpha = 94.55(3)$, $\beta = 100.87(4)$, $\gamma = 88.61(3)$°; $V = 1260(2)$ Å^3; triclinic, space group $P\bar{1}$ (no. 2), $Z = 2$, $\rho_{calcd} = 1.171$ g cm^{-3}, $\mu = 4.07$ cm^{-1}, $F(000) = 480.0$; 4650 reflections were measured in the range $3 \le \theta \le 25$° (ω scan), 3047 of which with $I > 3\sigma(I)$), 2855 independent reflections with $I > 3\sigma(I)$ were used for 270 parameters; solution and refinement of the structure with SDP [11b]; $R = 0.068$, $R_w = 0.076$, GOF = 2.570; residual electron density 0.524 eÅ^{-3}. In both structures all non-hydrogen atoms were refined anisotropically, hydrogen atoms H1a, H1b at the exocyclic methylene group were refined isotropically. All other hydrogen atoms were treated as riding atoms. Neither correction for absorption nor for extinction was applied. Further details of the crystal structure investigations are available on request from the Fachinformationszentrum Karlsruhe, D-76344 Eggenstein-Leopoldshafen (FRG), on quoting the depository numbers CSD-40448 (**8b**) and 40449 (**9**); b) B. A. Frenz, The Enraf-Nonius CAD4-SDP: A Real-Time System for Concurrent X-Ray Data Collection and Crystal Structure Determination in *Computing in Crystallography*, (Eds.: H. Schenk, R. Olthof-Hazekamp, H. van Koningsveld, G. C. Bassi), Delft University, SDP-PLUS, Version 1.1 (**1984**) and VAXSDP, Version 2.2 (**1985**).

[12] K. P. C. Vollhardt, *Organic Chemistry*, 1st ed., Freeman, New York, **1987**.

[13] X = N: [2b, 13a]; X = P: [7, 10a, 13b]; a) M. Bochmann, A. J. Jaggar, M. B. Hursthouse, M. Mazid, *Polyhedron*, **1990**, *9*, 2097–2100; b) P. Binger, B. Breitenbach, A. T. Herrmann, F. Langhauser, P. Betz, R. Goddard, C. Krüger, *Chem. Ber.* **1990**, *123*, 1617–1623.

[14] Ti-N-C angles [°] of imido derivatives 164.3(3) [14a]; 173.1(3) [14b]; a) C. H. Winter, P. H. Sheridan, T. S. Lewkebandara, M. J. Heeg, J. W. Proscia, *J. Am. Chem. Soc.* **1992**, *114*, 1095–1097; b) J. E. Hill, R. D. Profilet, P. E. Fanwick, I. P. Rothwell, *Angew. Chem.* **1990**, *102*, 713–714; *Angew. Chem. Int. Ed. Engl.* **1990**, *29*, 664–665.

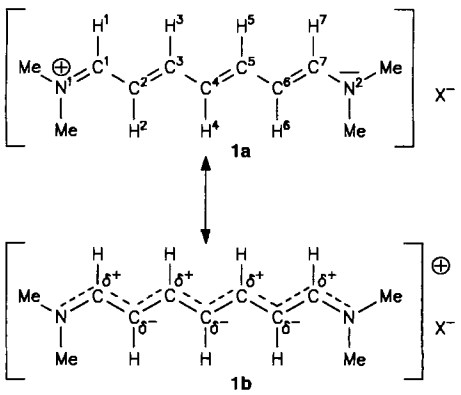
[15] a) J. E. Bercaw, D. L. Davies, P. T. Wolczanski, *Organometallics*, **1986**, *5*, 443–450; b) S. A. Cohen, J. E. Bercaw, *ibid.* **1985**, *4*, 1006–1014; c) J. R. Strickler, D. E. Wigley, *ibid.* **1990**, *9*, 1665–1669; d) B. N. Storhoff, H. C. Lewis Jr., *Coord. Chem. Rev.* **1977**, *23*, 1–29; e) T. Hirabayashi, K. Itoh, S. Sakai, Y. Ishii, *J. Organomet. Chem.* **1970**, *21*, 273–280.

[16] a) A. C. Gaumont, J. M. Denis, *Chem. Rev.* **1995**, *94*, 1413–1439; b) P. B. Hitchcock, M. J. Maah, J. F. Nixon, J. A. Zora, J. Leigh, M. A. Bakar, *Angew. Chem.* **1987**, *99*, 497–498; *Angew. Chem. Int. Ed. Engl.* **1987**, *26*, 474–475; c) J. F. Nixon, *Chem. Rev.* **1988**, *88*, 1327–1362; d) M. Regitz, P. Binger, *Angew. Chem.* **1988**, *100*, 1541–1565; *Angew. Chem. Int. Ed. Engl.* **1988**, *27*, 1484–1508.

Deformation of Polymethine Structures by Intermolecular Interactions**

Lars Dähne* and Günter Reck

Intermolecular interactions in polymethine dye systems have been the subject of great interest in recent years in the context of nonlinear optical processes,[1] energy transfer,[2] and conversion of solar into electrical energy.[3] Symmetrical polymethine dyes are characterized by maximal delocalization and therefore high polarizability of the linear π-electron system (Scheme 1, mesomer-



Scheme 1. Structural models of the 1,7-bis(dimethylamino)heptamethinium salts **1**-X.

[*] Dr. L. Dähne
Institut für Physikalische Chemie der Freien Universität
Takustrasse 3, D-14195 Berlin (FRG)
Telefax: Int. code + (30) 838-6612
Dr. G. Reck, Bundesanstalt für Materialforschung und -prüfung, Berlin (FRG)

[**] This work was supported by the Deutsche Forschungsgemeinschaft.

ic structure **1b**). The formal single and double bonds are of equal length in the frontier structure **1a**, whereas the π-electron density alternates on the C atoms of the chain.[4] The polarization of the π system in the direction of the frontier structure **1a** should feasible through intermolecular interactions with anions lying asymmetrical to the methine chain.[5]

A bond lengths alternation of 6 pm was calculated on the basis of Coulombic interactions for the 1,7-bis(dimethylamino)heptamethinium ion BDH^+ **1**, if the anion is removed to 400 pm away from one of the terminal nitrogen atoms.[5] The bond lengths alternation is defined as the difference between the single and double bond lengths [Eq. (a)] and could reach a maximum value of 10.5 pm in the case of localized bonds.

bond lengths alternation = (N1/C1 + C2/C3 + C4/C5 + C6/C7 − C1/C2 − C3/C4 − C5/C6 − C7/N2)/4 (a)

N/C = lengths of the bonds

The bonds of the methine chain of **1** are arranged symmetrically with respect to the C4 atom in solution and are not affected by counterions.[6] In contrast to pure inorganic anions[7] tetraarylborate ions form contact ion pairs with bis(indoleninyl) trimethinium cations in aqueous solution.[8] These ion pairs undergo electron transfer reactions on electronic excitation.[9] A new type of ion pairs called penetrated ion pairs forms, if the aryl groups are very large (e.g. 4-(1-triptycyl)phenyl-).[10]

We have examined the interactions between the BPh_4^- ion and the BDH^+ dye **1** which serves as a model compound of the class of cyanine dyes. ^1H NMR measurements on **1**-BPh_4 show that the signals of the methine-H atoms are shifted to higher fields in contrast to other BDH^+ salts (Table 1). The vicinal coupling constants remain the same however.

Table 1. Chemical shift of the ^1H NMR signals of BDH^+X^- (1-X); measured at acetone with 500 MHz.

	1/7-H	2/6-H	3/5-H	4-H	N-CH_3	N-CH_3
1-ClO_4	7.706	5.874	7.390	6.256	3.166	3.362
1-BF_4	7.702	5.874	7.390	6.256	3.166	3.362
1-BPh_4	7.514	5.815	7.279	6.224	3.089	3.262
difference	0.188 (0.192)	0.059	0.111	0.032	0.077	0.100

The shift of the signal of **1** to higher field is caused by the ring current effect of closely adjacent phenyl groups of BPh_4^- ions which are associated with the cation. The stronger interference at the H1/H7 and H3/H5 atoms suggests the fixation of counterions on the side of positivated methine-C atoms (Scheme 1). This association does not change the structure of the polymethine chain in the temporary average, since the bond order and the symmetry of **1** are conserved.

For a cation–anion association the optical spectra of the salts of **1** should differ in accordance with the dissociation properties of the solvent (Table 2). Similar to other cyanine dyes[8], 1-BPh_4 forms ion pairs in water. The π-π* transition energy of the ion pairs is shifted by $\Delta E = 2650\ cm^{-1}$ to the red relative to the free molecule. This value is significantly higher than the shift of the hitherto examined bis(indoleninyl)trimethincyanine dyes ($\Delta E = 1196\ cm^{-1}$).[8] In solvents with high dielectric constant, the light absorption of the dye is not affected by the anion; the ions are completely dissociated. Apparently no associates are present in acetone either. The reason may be the substantially lower concentration in the optical measurements compared to the NMR experiments. In solvents with lower dielectric constant, the transition energy depends on the anion and is for 1-BPh_4 slightly lower than for 1-ClO_4. Compared to the other spectra the long wave UV/Vis absorption band for both salts is strongly broadened.

Table 2. UV/Vis data of two 1-BPh_4 and 1-ClO_4 in solvents of different polarity [a].

Solvent	ε_0	1-BPh_4			1-ClO_4		
		λ_{max}	ε	$\omega_{1/2}$	λ_{max}	ε	$\omega_{1/2}$
H_2O	80.0	507/583	[b]	[b]	507.0	187500	1353
MeOH	32.7	508.8	181210	1324	507.2	188300	1324
acetone	20.7	510.4	178680	1360	510.4	179200	1360
$CHCl_3$	4.8	515.2	149500	1370	511.4	156200	1433
C_6H_6	2.3	514.8	130200	1446	508.4	117500	1608

[a] λ_{max} in nm; ε in L $mol^{-1}\,cm^{-1}$, half width $\omega_{1/2}$ in cm^{-1}. [b] Ion pair.

Also in the solid state the BPh_4^- anion influences the dye cation considerably. The higher melting point of 1-BPh_4 (197 °C) compared to other salts of this dye (162–178 °C), the low solubility in water as well as changes in the IR spectrum (KBr) point to special interactions.

The results of the X-ray structure analysis of 1-BPh_4 shows that the bond lengths of the polymethine chain alternate in these crystals (Table 3).[14] The bond lengths alternation was calculated to be 1.22 pm [Eq.(a)],[15] which corresponds to a shift of the symmetrical mesomeric structure **1b** in the direction of the frontier structure **1a** by 12%.

Table 3. Bond lengths in the polymethine chain in crystals of 1-BPh_4.

Bond	length [pm]	Bond	length [pm]
N1-C1	131.4 (short)	C4-C5	137.4 (short)
C1-C2	138.5 (long)	C5-C6	138.6 (long)
C2-C3	137.6 (short)	C6-C7	136.7 (short)
C2-C4	139.0 (long)	N2-C7	131.9 (long)

In the hitherto examined **1**-X crystals[7] (X = Cl^-, ClO_4^-, BF_4^-) no bond lengths alternation of **1b** was found. To determine the reason for this difference, the molecular environment of the polymethine chain in the **1**-X salts was examined on the basis of X-ray structural data.[7] In the chloride and perchlorate salts the anions are located symmetrically with respect to the polymethine chain. Hence a polarization of the π-electron system could not occur. In contrast, the anions are unsymmetrically oriented in the tetrafluoroborate and tetraphenylborate salts of **1**.

An estimate was made of the asymmetry of the Coulomb forces caused by anions acting on the π-electron system of the dye. Here it was assumed that the heptamethine chain is a rodlike dipole limited by nitrogen atoms, and the anions are point charges. Taking into consideration all anions within a distance of 1000 pm from the nitrogen atoms, the relative difference of the forces acting at the ends of the dipole amounts to $\Delta F_{Coul} = 4.9 \times 10^{-11}$ N and 14.8×10^{-11} N for the two different molecule sites in the 1-BF_4 crystal and to only $\Delta F_{Coul} = 1.6 \times 10^{-11}$ N in 1-BPh_4.

In spite of the conspicuously higher asymmetry of the force field at 1-BF_4, a polarization of the π-electron system does not exist. Therefore the Coulomb forces between anion and cation cannot be the deciding factor for the electron polarization. The BPh_4^- ion acts as a π ligand forming η^6-arene complexes with electron-rich fragments of metal complexes.[11] The association between uncharged merocyanine dyes and benzene is also based on interactions between the π-electron systems.[12]

 © VCH Verlagsgesellschaft mbH, D-69451 Weinheim, 1995 0570-0833/95/0606-0691 $ 10.00+.25/0

Figure 1 shows the phenyl rings of the BPh_4^-, which are in the vicinity of the polymethine chain. At the "left-hand" side of the molecule the influence of the anions is noticeably higher because of their larger number and the shorter distance of the phenyl rings from the methine chain. The polarization of the methine

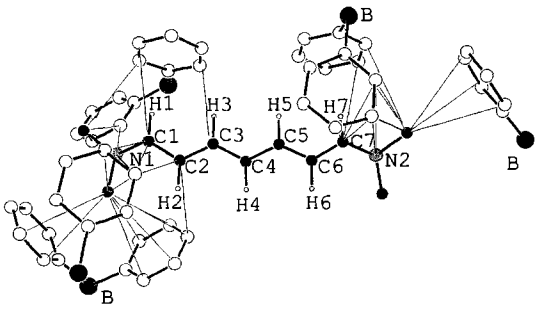


Fig. 1. Volume segment in crystals of the 1-BPh_4 (for simplification phenyl rings, whose carbon atoms are more than 400 pm away from the methine chain, have been omitted; thin lines denote intermolecular distances less than 380 pm)

π-electron system caused by electron-rich phenyl rings leads to a positivation of this side and therewith to the deformation of the molecular structure. Vice versa a polarization of the anions is also probable, in which the phenyl rings in the vicinity of the cation **1** should show a significantly higher electron density. We assume therefore, that inductive forces between the easily polarizable π-electron systems of the cations and anions dominate in the distortion of the polymethine structure.

The deformation of the polymethine chain is also conceivable as an effect of an aggregation of dye molecules. Such aggregates were observed in other crystals of **1** in which the distances between the cations amounted to only 348 pm.[7] In 1-BPh_4, the dye cations exist however as dimers (Fig. 2). A mutual polarization of the methine chains could be excluded, because of the comparatively large distance of 471 pm between the molecule plains and because of the head-to-head arrangement of the more positively charged ends of the polymethine chains.

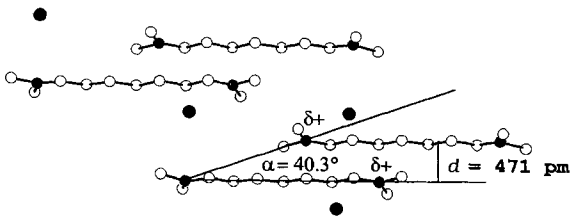


Fig. 2. Structure of the polymethine dimer in the crystal.

The bathochromic shifted UV/Vis absorption band found for ion pairs in aqueous solution cannot be explained by the observed distortion of the π-electron system, because a disturbance of the symmetrical polymethine system should shift the optical transition to higher energy. As for bis(indoleninyl)trimethine cyanine BPh_4 complexes,[8] it was concluded from optical data that the ion pairs should exist as dimers. This model is confirmed in an excellent manner by the crystal structure (Fig. 2). In agreement with the theory of molecular excitons of Kasha et al.[13] the dislocation angle of $\alpha = 40.3°$ between the dye molecules leads to the observed bathochromic shift of the transition energy.

A calculation of the ring current effect on the basis of the crystal structure results in graduations of the high-field shift of the methine protons qualitatively similar to those obtained in the ^1H NMR measurement in acetone (see Table 1). The calculated values are however two-to-three times larger and do not reflect the symmetry of **1** found in solution. In contrast to the aqueous solution, the anions are associated more weakly in organic solvents, because of the absent hydrophobic forces. Therefore, fluctuating motion of anions causes averaging of the NMR signals and broadening of the optical absorption band.

To summarize, the first experimental evidence has been obtained for the deformation of a symmetrical polymethine system caused by intermolecular interactions. The determining forces are not, as first assumed, Coulomb relations between anions and cation or dipole–dipole interactions between the cations, but an induction of charge shift in the easily polarizable π-electron systems of anion and cation by electrostatic interactions. All polymethine dyes possess as the principal structural element a π-electron system similar to that of the investigated model compound. Therefore it may be assumed that such polarization will also occur for other polymethine dyes with corresponding arrangement of tetraarylborate anions in the solid state. However the polarization should be less pronounced for polymethines with smaller π-electron systems (tri-, pentamethines) and with shielding end groups (e.g. indoleninyl).

Experimental Procedure

1-BPh_4: A solution of $NaBPh_4$ (2.32 g, 7.00 mmol) in water (400 mL) was added dropwise to a solution of 1-Cl (1.43 g, 5.00 mmol) in methanol (50 mL) at room temperature. The product which was sparingly soluble in water was filtered, washed, and recrystallized from dry acetone. This afforded 2.30 g (92%) of red prismatic crystals of 1-BPh_4. M.p. 196–197 °C; correct C,H,N analysis; MS: (FAB^+): *m/z* 179 (23)[M^+], (FAB^-): *m/z* 318, 319, 320 (5, 14, 5)[M^-]; UV/Vis data were obtained following dilution of a concentrated standard solution in acetone. Therefore, each stated solvent contains 0.1 vol.% acetone.

Received: September 17, 1995 [Z7326IE]
German version: *Angew. Chem.* **1995**, *107*, 735

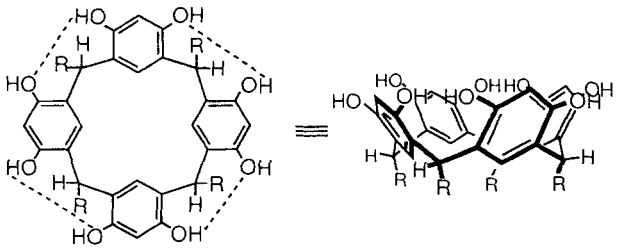
Keywords: dyes · electron polarization · ion pairs · polymethines

[1] S. Kobayashi, *Mol. Cryst. Liq. Cryst.* **1992**, *217*, 77–80.
[2] S. De Boer, K. J. Kink, D. A. Wiersma, *Chem. Phys. Lett.* **1987**, *137*, 99–106.
[3] A. J. McEvoy, *Sol. Energy Mater.* **1995**, *32*, 221–227.
[4] S. Dähne, *Chimia* **1991**, *45*, 288–294.
[5] C. B. Gorman, S. R. Marder, *Proc. Natl. Acad. Sci. USA* **1993**, *90*, 11297–11301.
[6] J. Dale, R. G. Lichtenthaler, *Acta Chem. Scand. Ser B* **1979**, *33*, 141–147.
[7] P. Groth, *Acta Chem. Scand. Ser B* **1987**, *41*, 547-552; L. Dähne, W. Grahn, P. G. Jones, A. Chrapkowsky, *Z. Kristallogr.* **1993**, *209*, 514–516; L. Dähne, G. Reck, *ibid.* **1995**, *210*, 40–43.
[8] B. Armitage, J. Retterer, D. F. O'Brien, *J. Am. Chem. Soc.* **1993**, *115*, 10786–10790.
[9] G. B. Schuster, *J. Am. Chem. Soc.* **1992**, *114*, 793-794.
[10] G. Boche, *Angew. Chem.* **1992**, *104*, 742–743; *Angew. Chem. Int. Ed. Engl.* **1992**, *31*, 731–732.
[11] M. Bochmann, *Ang. Chem.* **1992**, *104*, 1206–1207; *Angew. Chem. Int. Ed. Engl.* **1992**, *31*, 1181–1182.
[12] R. Radeglia, S. Dähne, *Ber. Bunsen-Ges. Phys. Chem.* **1966**, *70*, 745–750.
[13] E. G. McRae, M. Kasha, *J. Chem. Phys.* **1958**, *28*, 721–722.
[14] X-ray analysis of **$BDH^+BPh_4^-$**: triclinic, space group $P\bar{1}$ (no. 2); $a = 903.8(2)$, $b = 1169.3(3)$, $c = 1491.4(3)$ pm, $\alpha = 73.60(2)$, $\beta = 85.03(2)$, $\gamma = 81.35(2)°$; $V = 1493.3(5) \times 10^6$ pm^3; $Z = 2$; $\rho_{calcd} = 1.11$ gcm^{-3}; $Mo_{K\alpha}$ radiation ($\lambda = 71.07$ pm); $\mu = 0.059$ mm^{-1}; $F(000) = 536$; $T = 293 \pm 1$ K; crystal size: $0.5 \times 0.4 \times 0.35$ mm^3; $2\theta_{max} = 52°$; CAD4 diffractometer (Enraf-Nonius); 5884 independent reflexes, 5442 reflexes with $I_0 > 1/\sigma(I)$ were used; *hkl* regions: $h = 0–11$; $k = -13–14$, $l = -18–18$; solution of structure: direct methods (MULTAN 82); refinement: 500 parameters, full matrix, riding model; least squares against F; $R = 0.066$, $R_w = 0.075$; residual electron density 300–500 enm^{-3}; anisotropically refined for non-H atoms, H atoms were found. Further details of the crystal structure investigation may be obtained from the Fachinformationszentrum Karlsruhe, D-76344 Eggenstein-Leopoldhafen (FRG), on quoting the depository number CSD-401228.
[15] Recently the crystal structure of 1-BPh_4^- and the bond lengths alternation (1.18 pm) was verified by U. Schilde (University of Potsdam).

A Non-Peptidic Ion Channel with K^+ Selectivity

Yasutaka Tanaka, Yoshiaki Kobuke,* and Masahiro Sokabe

The sequence analyses of several channel proteins have defined the molecular basis of ion channels through the identification of several associated subunits in the biological membrane and a central ion-conducting pore.[1] Site-directed mutagenesis has further clarified the pore mechanism.[2] Stable and simple synthetic molecules that can transport ions across the membrane by means of a channel mechanism have also attracted much attention, and some non-peptidic channel mimics have been reported.[3] However, the detailed characterization of these molecules at the single-channel level as reported for natural channels is presently lacking. In principle measurement of the single ion channel current is required to establish the channel mechanism.[4] We have demonstrated that a chimeric pore of molecular aggregates with an oligoether ion pair showed a single ion channel current. A few kinds of channels having corresponding conductance levels seem to reflect different aggregation numbers.[5] Here we report on the structurally well-defined macrocyclic amphiphile **1a**, which forms channels having single ion channel currents and only one type of the channel conductance. This is the first example of an artificial ion channel that recognizes, monovalent cations and displays selectivity for K^+ ions.



1a : R= $CH_3(CH_2)_{16}$
1b : R = $CH_3(CH_2)_{10}$

Condensation of resorcinol with octadecanal under acidic conditions afforded the amphiphilic cyclic tetramer **1a** whose alkyl chains are similar in length to the lipid used in this study.[6] The ^1H NMR spectra of **1a** indicated that the molecule has fourfold symmetry; the alkyl chains are arranged in an all-axial, all-*cis* configuration (like **1b**).[7] After incorporation into planar soybean lecithin bilayers, **1a** exhibited the typical characteristics of a single ion channel: a stable and constant conductance (6.1 ± 0.8 pS) at various voltages with transitions between open and closed states in a membrane separating two 0.5 M KCl solutions (Fig. 1).[8] The symmetry in the channel current with respect to the voltage reversal across the membrane (Fig. 2) suggests the existence of a symmetric channel structure. Since a stable conductance was not observed in the absence of **1a**, neither leakage nor artifact currents can satisfactorily account for these observations. In contrast, use of **1b**, which has shorter

[*] Prof. Dr. Y. Kobuke, Dr. Y. Tanaka
Department of Materials Science, Faculty of Engineering
Shizuoka University
Hamamatsu, Shizuoka 432 (Japan)
Telefax: Int. code + (53)473-4170
Prof. Dr. M. Sokabe
Nagoya University (Japan)

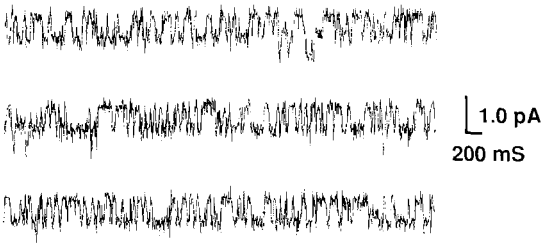


Fig. 1. Typical records of single-channel currents for soybean lecithin membranes containing **1a**; −74.4 mV in 0.5 M KCl solutions.

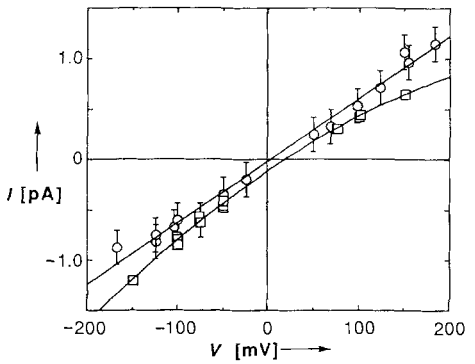


Fig. 2. Current-to-voltage relationship of membranes under the same conditions as in Figure 1 (○) and between two solutions (□) one containing 50 mM KCl and 450 mM NaCl, and the other 450 mM KCl and 50 mM NaCl.

alkyl chains, did not produce stable channel currents, showing that only when the amphiphile has alkyl tails capable of spanning half the membrane thickness can it form a stable channel structure. The conductance observed with **1a** remained constant during more than 90% of current records with variations in the molar ratio of **1a** to lipid between 1:200 and 1:3000. This is in marked contrast to the observation of several conductance levels for the molecular aggregate channels including synthetic peptides,[5, 9] where the different levels were assigned to the action of different sized aggregates. These results may also signify that monomeric **1a** penetrates nicely a single lipid layer of the bilayer. The cavity formed by the four resorcinol rings, which is extended by the four alkyl chains in **1a**, excludes the entry of lipid molecules and thus provides the channel pore for the passage of ions. Water molecules may also occupy the channel and coordinate to ions passing through the pore. On the assumption that the cavity formed by **1a** recognizes the positioning of another molecule of **1a** in the other half of the bilayer, a tail-to-tail dimer of **1a** forms (Fig. 3) and thus gives rise a symmetric transmembrane channel similar to the Gramicidin A channel.[10] In accordance with this dimer model, channel activities were not observed when **1a** was added to only one side of the lipid membrane, probably because such a bulky amphiphile does not flip-flop easily.

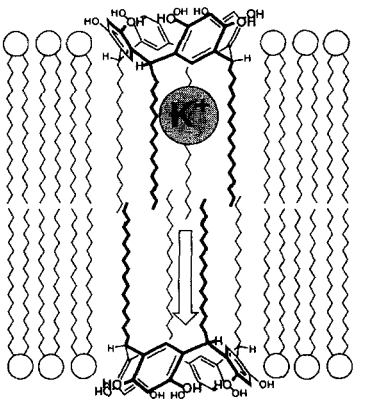


Fig. 3. Hypothetical structure of a channel formed by **1a** in lipid bilayers.

 © VCH Verlagsgesellschaft mbH, D-69451 Weinheim, 1995 0570-0833/95/0606-0693 $ 10.00+.25/0

Under the conditions of single-salt gradients (0.5 M KCl/0.1 M KCl), the channel formed by **1a** showed a reversal potential of 35.9 mV, indicating that it has a distinct selectivity for cations over anions. The permeability ratio P_{K^+}/P_{Cl^-} of 20, calculated with the Goldman–Hodgkin–Katz equation,[4] is comparable to those observed for natural cation channels. Similar reversal potential measurements under gradients of K^+ and Na^+ ions revealed that the channel discriminates K^+ from Na^+ ions with a permeability ratio P_{K^+}/P_{Na^+} of roughly 3 (Fig. 2). In contrast, Rb^+ ions blocked the K^+ ion current: the solution containing K^+ and Rb^+ ions (0.05 M KCl, 0.45 M RbCl/0.45 M KCl, 0.05 M RbCl) provided no stable channel currents in 20 independent measurements. When the biionic solution was exchanged for 0.5 M KCl solutions, K^+-driven currents appeared immediately. Thus, the channel formed by **1a** shows maximum selectivity for K^+ ions like naturally occurring K^+ channels, but behaves differently from the latter one with respect ot the passage of Rb^+ ions.

Selectivity of ion permeation through membrane channels is determined primarily by the narrowest region of the channel pore termed the selectivity filter. The relation between the electric field strength at the filter and the dehydration energy of the permeating ion determines the extent of dehydration.[4] The selectivity mechanism in voltage-gated K^+ channels has been discussed in detail. It is generally accepted that the K^+-selective filter consists of an "aromatic cage" formed by four tyrosine residues, which provides a weak electric field allowing complete dehydration of K^+ ions but not of Na^+ ions. Consequently, the K^+ ions can pass through the filter but not the Na^+ ions. The π electrons of the aryl groups probably contribute to the lowering of the potential barrier for passage of K^+ ions through attractive π–cation interactions.[11] This mechanism may also explain the selectivity observed in **1a** channels. The narrowest section of the ion conducting pore in **1a** comprises the four resorcinol rings with a weak electric field. The section is thought to be just large enough to allow naked K^+ ions ($r = 1.33$ Å) to pass but not the slightly larger Rb^+ ions ($r = 1.47$ Å). According to molecular dynamics simulations, the size of this opening in **1a** resembles that of the pore of *p-tert*-butyl-calix[4]arene-tetraamide, which permits the passage of K^+ ions but not Cs^+ ions ($r = 1.69$ Å).[12]

We have described here the first example of selective ion-transport through a membrane bilayer by means of a channel mechanism with a simple and stable synthetic molecule. In a membrane bilayer dimers of **1a** reproduce the essential biological properties of a single ion channel. This simplest model of a single ion channel may offer insight into the origins of ion selectivity in ion channels.

Received: August 30, 1995
Revised version: December 1, 1995 [Z 7277 IE]
German version: *Angew. Chem.* **1995**, *107*, 717

Keywords: ion channels · membrane models · resorcinol

[1] See for instance: M. Noda, S.Shimizu, T. Tanabe, T. Takai, T. Kayano, T. Ikeda, H. Takahashi, H. Nakayama, Y. Kanaoka, N. Minamino, K. Kangawa, H. Matsuo, M. A. Raftery, T. Hirose, S. Inayama, H. Hayashida, T. Miyata, S. Numa, *Nature* **1984**, *312*, 121.

[2] For voltage-gated K^+ channels see: a) C. Miller, *Science* **1991**, *252*, 1092, and references therein; b) G. A. Lopez, Y. N. Jan, L. Y. Jan, *Nature* **1995**, *367*, 179, and references therein.

[3] a) I. Tabushi, Y. Kuroda, K. Yokota, *Tetrahedron Lett.* **1982**, *23*, 4601; b) U. F. Kragten, M. F. M. Roks, R. J. M. Nolte, *J. Chem. Soc. Chem. Commun.* **1985**, 1275; c) J.-H. Fuhrhop, U. Liman, V. Koesling, *J. Am. Chem. Soc.* **1988**, *110*, 6840; d) A. Nakano, Q. Xie, J. V. Mallen, L. Echegoyen, G. W. Gokel, *ibid.* **1990**, *112*, 1287; e) F. M. Menger, D. S. Davis, R. A. Persichetti, J.-J. Lee, *ibid.* **1990**, *112*, 2451; f) M. J. Pregel, L. Jullien, J.-M. Lehn, *Angew. Chem.* **1992**, *104*, 1695; *Angew. Chem. Int. Ed. Engl.* **1992**, *31*, 1637; g) T. M. Fyles, T. D. James, K. C. Kaye, *J. Am. Chem. Soc.* **1993**, *115*, 12315; h) E. Stadler, P. Dedek, K. Yamashita, S. L. Regen, *ibid.* **1995**, *116*, 6677.

[4] B. Hille, *Ionic Channels of Excitable Membranes*, 2nd ed., Sinauer, Sunderland, MA, **1992**.

[5] Y. Kobuke, K. Ueda, M. Sokabe, *J. Am. Chem. Soc.* **1992**, *114*, 7618.

[6] **1a**: Yield 50%; m.p. >300 °C; ^{1}H NMR (90 MHz, $CDCl_3$): $\delta = 7.22$, 6.12 (each s, each 4H; aryl-H), 4.30 (t, 4H; CHR), 2.15, 1.26 (128H; CH_2), 0.88 (t, 12H; CH_3), 7.5–10.5 (br, 8H; Ar-OH), 3.8 (br, 2H; H_2O); MS (FAB): *m/z* 1441 ($M^+ + H$); correct C,H,O analysis.

[7] a) Y. Aoyama, Y. Tanaka, S. Sugahara, *J. Am. Chem. Soc.* **1989**, *111*, 5397; b) Y. Tanaka, Y. Aoyama, *Bull. Chem. Soc. Jpn.* **1990**, *63*, 3343.

[8] The experimental procedures were identical to those we used previously [5]. The gating kinetics is not discussed here, but the lifetimes of open and closed states are in the order of seconds to milliseconds.

[9] a) M. T. Tosteson, D. S. Auld, D. C. Tosteson, *Proc. Natl. Acad. Sci. U.S.A.* **1989**, *86*, 707; b) A. Grove, M. Mutter, J. E. Rivier, M. Montal, *J. Am. Chem. Soc.* **1993**, *115*, 5919, and references therein; c) K. S. Åkerfeldt, J. D. Lear, Z. R. Wasserman, L. A. Chung, W. F. DeGrado, *Acc. Chem. Res.* **1993**, *26*, 191. For peptide channels exhibiting one type of conductance see: d) M. Montal, M. S. Montal, J. M. Tomich, *Proc. Natl. Acad. Sci. U.S.A.* **1990**, *87*, 6929; e) A. Grove, J. M. Tomich, M. Montal, *ibid.* **1991**, *88*, 6418; f) M. R. Ghadiri, J. R. Granja, L. K. Buehler, *Nature* **1995**, *369*, 301.

[10] W. Veatch, L. Stryer, *J. Mol. Biol.* **1977**, *113*, 89.

[11] a) L. Heginbotham, R. MacKinnon, *Neuron* **1992**, *8*, 483; b) S. R. Durell, H. R. Guy, *Biophys. J.* **1992**, *62*, 238; c) S. Bogusz, A. Boxer, D. D. Busath, *Protein Eng.* **1992**, *5*, 285; d) R. A. Kumpf, D. A. Dougherty, *Science* **1993**, *261*, 1708.

[12] P. Guilbaud, A. Varnek, G. Wipff, *J. Am. Chem. Soc.* **1993**, *115*, 8298.

Triple-Helix Formation of Oligodeoxynucleotides Containing [(3′*S*,5′*R*)-2′-Deoxy-3′,5′-ethano-β-D-ribofuranosyl]nucleosides ("Bicyclo-deoxynucleosides")**

Martin Bolli and Christian Leumann*

In memory of Rolf Scheffold

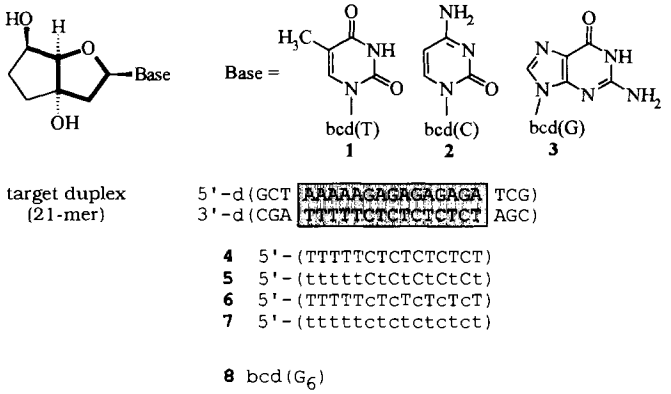
High-affinity, sequence-specific recognition of single- and double-stranded RNA and DNA by oligonucleotide analogues is important for the selective control of gene expression.[2] The formation of triple helices either from a DNA duplex or of double helices from an RNA single strand represents a way to interfere with transcription in DNA, and translation in RNA.[3] Two structural motifs in triple helices have been identified to date; they differ in the composition of the base triple and the strand polarity. In the py–pu:py motif the third strand consisting only of pyrimidine bases is paired to the Hoogsteen side of the purine strand in a parallel fashion, forming T–A:T and C^+–G:C base triples.[4] In the pu–pu:py motif the third strand is purine-rich and paired in an antiparallel orientation to the Hoogsteen side of the purine strand of the Watson–Crick duplex and exhibits G–G:C, A–A:T, and T–A:T base triples.[5] Both motifs require strandwise separation of purine and pyrimidine bases. Within the py–pu:py motif, stronger triplex formation with single-stranded nucleic acids was observed by reducing the molecularity of association with circular or hairpin-forming oligonucleotides.[6] DNA analogues that exhibit stronger binding to double-helical DNA comprise oligonucleotides with modi-

[*] Prof. Dr. C. Leumann, M. Bolli
Institut für Organische Chemie der Universität
Freiestrasse 3, CH-3012 Bern (Switzerland)
Telefax: Int. code + (31)631-8057

[**] Nucleic Acid Analogues with Restricted Conformational Flexibility in the Sugar–Phosphate Backbone, Part 4. This work was supported by the Swiss National Science foundation. Part 3: [1]

fied sugar and base moieties,[7] or phosphate replacements,[8] or both.[9] A remarkable increase in the binding efficiency of the third strand is observed with oligonucleotides containing dinucleoside units that are linked by a conformationally constrained acetal group.[10]

We recently described the design and the synthesis of novel nucleoside analogues ("bicyclonucleosides", Scheme 1).[1, 11] The main structural features of the bicyclonucleosides are a conformation of the furanose unit restricted to the 2'-*endo*/1'-*exo* range



Scheme 1. Top: Structures of the nucleoside analogues bicyclothymidine (bcd(T), **1**), bicyclodeoxycytosine (bcd(C), **2**), and bicyclodeoxyguanosine (bcd(G), **3**) and the duplex target sequences for T_m analysis of third-strand binding. Bottom: Sequences **4**–**7** for triple-helix formation (t = bcd(T) = **1**, c = bcd(C) = **2**, T and C = natural deoxynucleosides thymidine and 2'-deoxycytidine).

and a preferential equatorial orientation of the secondary hydroxyl group in the carbocyclic ring.[11a, c] Prominent properties of decanucleotides of bicyclodeoxyadenosine are strong duplex formation with the RNA complement poly(U) and about a 20-fold increase (relative to the natural equivalent) in third strand binding with the corresponding DNA complement.[1, 11b] We now report on the triple-helix-forming properties of mixed-sequence oligonucleotides (**4**–**7**) containing bicyclothymidine (**1**) and bicyclodeoxycytidine (**2**) with a natural 21-mer DNA target duplex, as well as the complex-forming properties of a hexanucleotide of bicyclodeoxyguanosine (**3**) with the RNA polymer poly(C) within the py–pu:py structural motif (Scheme 1).

The synthesis of bicyclonucleosides and the corresponding cyanoethylphosphoramidite building blocks for oligonucleotide chain extension has been reported earlier.[1, 11a] The assembly of the oligonucleotides **4**–**8** was performed by automated solid-phase synthesis in analogy to the procedure already developed for bicyclo-DNA on a 1 μmol scale. The synthesis is completely compatible with that of natural DNA and proceeded in average coupling efficiencies of 98% per elongation cycle.[12] After detachment from the solid support and removal of the base and phosphate protecting groups, the crude oligomers were purified by ion exchange HPLC. In representative cases further analysis was performed by mass spectrometry.[13]

Triple-helix formation of the oligomers **4**–**7** with the 21-mer DNA target duplex was monitored by recording UV-melting curves at pH 6.0 and 6.5 for 200 mM NaCl and 1 M NaCl, respectively. The corresponding T_m and hyperchromicity data are summarized in Table 1. Figure 1 shows the melting curves of the triplexes of **4**–**7** with the target duplex at pH 6.0 and 1 M NaCl.[15] In all cases two well-separated transitions are observed. Those at higher temperature correspond to dissociation of the target duplex 21-mer, and those at lower temperatures to the

Table 1. T_m values [°C] and hyperchromicity [%] (in parentheses) of the dissociation of the third strand **4**–**7** from UV-melting curves (260 nm). Triplex concentration 0.9–1.1 μM in 10 mM NaH_2PO_4.

Strand	pH 6.0		pH 6.5	
	200 mM NaCl	1 M NaCl	200 mM NaCl	1 M NaCl
4	40.8 (8)	42.8 (10)	30.9 (6)	32.1 (9)
5	47.5 (7)	52.2 (10)	40.8 (3)	40.9 (8)
6	24.3 (6)	29.2 (9)	15.4 (3)	17.9 (8)
7	27.4 (2)	31.0 (7)	18.0 (2)	20.3 (5)

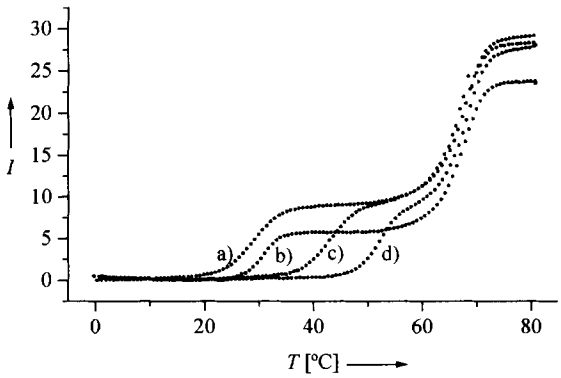


Fig. 1. UV-melting curves (λ = 260 nm) of **6** (a), **7** (b), **4** (c), and **5** (d) with the duplex target sequence (10 mM NaH_2PO_4, 1 M NaCl, pH 6.0. Triplex concentration 0.9–1.1 μM. T_m of target duplex 71 ± 1 °C.

melting of the triplex into single strands **4**–**7** and the target duplex. In all experiments the stability of the target duplex remained invariant as expected ($T_m \approx 71$ °C). However, large differences in the efficiency of triple-helix formation as a consequence of the nature of the bicyclic nucleosides were observed. By replacement of all 2'-deoxycytidine nucleosides in the third strand by bicyclodeoxycytidine **2**, a decrease in T_m of 2.7 °C per modification (mod.) occurs relative to the control sequence **4**. This contrasts with an increase in T_m of 1 °C/mod. when thymidine is replaced by the bicyclic analogue **1**. The completely bicyclic sequence **7** binds to the duplex with the same affinity as the sequence containing only bicyclodeoxycytidine (**6**). In this case the hyperchromicity is significantly lower than in the others, most probably due to incomplete base pairing with the target sequence over the whole oligonucleotide length.

The melting curves a) and c) in Figure 1 and the corresponding hybridization curves are superimposable at the applied temperature gradient (0.5 K min^{-1}) and therefore represent equilibrium binding. In the case of b) and d), melting and hybridization curves are different, the latter reflecting a broader transition with T_m at lower temperatures.[12] This behavior indicates slower triple-helix formation with increasing numbers of bicyclodeoxynucleosides. Kinetics of triple-helix formation is also dependent on the salt concentration.[17] Increasing the amount of NaCl in the buffer from 200 mM to 1 M (pH 6.0) reduces the extent of hysteresis of the melting and hybridization curves. A concomittant increase in triple-helix stability is observed in all cases investigated.[16a]

While negligible differences in pK_a between the nucleobase in **2** and 2'-deoxycytidine are expected, the decrease in binding efficiency observed with **6** relative to **4** is more likely to be due to differences in conformation of the two protonated cytosine nucleosides. NMR investigations on triple-helical natural DNA structures within the py–pu:py motif provided evidence for different conformational preferences of protonated cytidine and

thymidine residues in the Hoogsteen third strand, the former occurring preferentially in a 3′-*endo* and the latter in a 2′-*endo* conformation.[18] Bicyclonucleosides, however, show strong preference for the 1′-*exo*/2′-*endo* sugar conformation irrespective of the nature of the base.[11] The observation that the stability of oligonucleotides containing bicyclodeoxynucleosides is lower for bicyclodeoxycytidine containing **6** and higher for bicyclothymidine containing **5** is in agreement with the NMR data and provides additional evidence that the preferred conformation of the third strand backbone in DNA triplexes with the py–pu:py motif is heterogeneous.

To investigate the potential of duplex and triplex formation of oligomers of bicyclodeoxyguanosine we measured T_m data of mixtures of hexamer **8** with the RNA complement poly(C) (base stoichiometry C:G = 2:1) at different pH values between 5.5 and 8.3. In contrast to the analogous experiments in the bcd(A)/poly(U) series,[11b] the bcd(G)/poly(C) system allows easy differentiation of whether the pyrimidine strand pairs to the Watson–Crick or the Hoogsteen side of the purine strand simply by varying the pH. From the plot of T_m vs. pH in Figure 2 it becomes

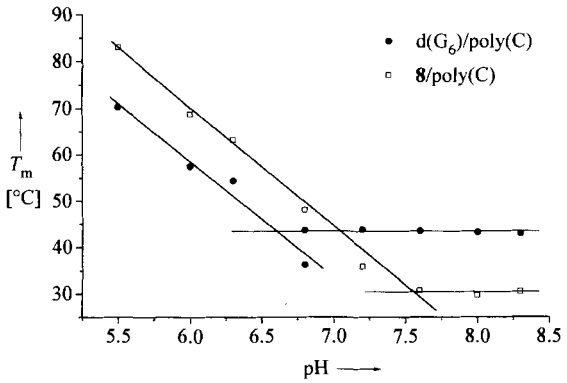


Fig. 2. T_m values from UV-melting curves (λ = 280 nm) of **8** and d(G_6) with poly(C) (ratio C:G = 2:1) in 150 mM NaCl/10 mM NaH_2PO_4 as function of pH. Overall base concentration 33.8–40 μM. Individual T_m values (λ = 250 nm) for triplex → duplex and duplex → single strand transitions were obtained at pH 6.8 in the case of d(G_6)/poly(C).

clear that the melting temperature is independent of proton concentration above pH 7.6 in both pairing systems d(G_6):poly(C) and **8**:poly(C), thus indicating only (charge-neutral) Watson–Crick base pairing. The corresponding T_m data (30 °C for **8**:poly(C) and 43 °C for d(G_6):poly(C)) clearly demonstrate an energetic advantage for the Watson–Crick duplex d(G_6):poly(C). Below pH 6.5 in both systems a linear increase in T_m as a function of pH is observed, which is due to triple-helix formation involving protonated cytosine bases. Comparison of the T_m data of d(G_6):poly(C) and **8**:poly(C) shows that at a given pH triplex formation is energetically favored in the latter case ($\Delta T_m \approx 12$ °C). This demonstrates that bicyclooligonucleotide **8** favors Hoogsteen binding and disfavors Watson–Crick binding of its RNA complement relative to its natural analogue. As a consequence, triplex formation of poly(C) with **8** is already observed about 0.5 pH units higher than in the reference system. This leads to higher overall complex stability for **8**:poly(C) than for the reference system below pH 7.1.

The results presented here clearly demonstrate that bicyclothymidine **1** can be used advantageously for the preparation of high-affinity, triple-helix-forming oligonucleotides within the py–pu:py motif. There is a considerable potential to increase triple-helix stability further by using oligonucleotides containing **1** in combination with nonnatural, base-modified deoxycytidine substitutes or with 2′-O-alkylated cytidine derivatives.[19] The fact that oligomers of bicyclodeoxyguanosine (and possibly also bicyclodeoxyadenosine) show increased acceptor properties at the Hoogsteen binding site is unprecedented for sugar-modified oligonucleotide analogues and might lead to analogues that form strong Hoogsteen base-paired duplexes or triplexes with pyrimidine-rich RNA.

Received: October 21, 1995 [Z 7417 IE]
German version: *Angew. Chem.* **1995**, *107*, 740

Keywords: bicyclonucleotides · double helix · DNA · oligonucleotides · RNA · triple helix

[1] M. Tarköy, C. Leumann, *Helv. Chim. Acta*, **1995**, *77*, 716–744.
[2] E. Uhlmann, A. Peyman, *Chem. Rev.* **1990**, *90*, 543–584; J. Goodchild, *Bioconjugate Chem.* **1990**, *1*, 165–187; J. Engels, *Nachr. Chem. Tech. Lab.* **1991**, *39*, 1250–1254; U. Englisch, D. Gauss, *Angew. Chem.* **1991**, *103*, 629–646; *Angew. Chem. Int. Ed. Engl.* **1991**, *30*, 613–629.
[3] N. T. Thuong, C. Hélène, *Angew. Chem.* **1993**, *105*, 697–723; *Angew. Chem. Int. Ed. Engl.* **1993**, *32*, 666–690.
[4] H. E. Moser, P. B. Dervan, *Science* **1987**, *238*, 645–650; J.-C. François, T. Saison-Behmoaras, C. Hélène, *Nucleic Acids Res.* **1988**, *16*, 11431–11440.
[5] M. Cooney, G. Czernuszewicz, E. H. Postel, S. J. Flint, M. E. Hogan, *Science* **1988**, *241*, 456–459; P. A. Beal, P. B. Dervan, *ibid.* **1991**, *251*, 1360–1363.
[6] G. Prakash, E. T. Kool, *J. Chem. Soc. Chem. Commun.* **1991**, 1161–1163; C. Giovannangeli, T. Montenay-Garestier, M. Rougée, M. Chassignol, N. T. Thuong, C. Hélène, *J. Am. Chem. Soc.* **1991**, *113*, 7775–7777; S. Wang, E. T. Kool, *ibid.* **1995**, *116*, 8857–8858.
[7] a) A. Ono, P. O. P. Ts'o, L.-S. Kan, *J. Am. Chem. Soc.* **1991**, *113*, 4032–4033; b) J. S. Koh, P. B. Dervan, *ibid.* **1992**, *114*, 1470–1478; c) B. C. Froehler, D. J. Ricca, *ibid.* **1992**, *114*, 8320–8322; d) B. C. Froehler, S. Wadwani, T. J. Terhorst, S. R. Gerrard, *Tetrahedron Lett.* **1992**, *33*, 5307–5310; e) S. H. Krawczyk, J. F. Milligan, S. Wadwani, C. Moulds, B. C. Froehler, M. D. Matteucci, *Proc. Natl. Acad. Sci. USA*, **1992**, *89*, 3761–3764.
[8] a) R. K. Jones, K.-Y. Lin, J. F. Milligan, S. Wadwani, M. D. Matteucci, *J. Org. Chem.* **1993**, *58*, 2983–2991; b) S. Gryaznov, J.-K. Chen, *J. Am. Chem. Soc.* **1995**, *116*, 3143–3144.
[9] K.-Y. Lin, J. S. Pudlo, R. J. Jones, N. Bischofberger, M. D. Matteucci, B. C. Froehler, *Bioorg. Med. Chem. Lett.* **1995**, *4*, 1061–1064.
[10] R. J. Jones, S. Swaminathan, J. F. Milligan, S. Wadwani, B. C. Froehler, M. D. Matteucci, *J. Am. Chem. Soc.* **1993**, *115*, 9816–9817.
[11] a) M. Tarköy, M. Bolli, B. Schweizer, C. Leumann, *Helv. Chim. Acta* **1993**, *76*, 481–510; b) M. Tarköy, C. Leumann, *Angew. Chem.* **1993**, *105*, 1516–1518, *Angew. Chem. Int. Ed. Engl.* **1993**, *32*, 1432–1434; c) M. Egli, P. Lubini, M. Bolli, M. Dobler, C. Leumann, *J. Am. Chem. Soc.* **1993**, *115*, 5855–5856.
[12] M. Bolli, "Nucleinsäure-Analoga mit konformationell eingeschränktem Zucker-Phosphat-Rückgrat: Synthese und Eigenschaften", Dissertation, University of Bern, **1995**.
[13] Crude oligomers **4**–**7** were purified by anion exchange (IE) HPLC (column: Nucleogen 60 DEAE, Macherey-Nagel; elution with a linear KCl gradient in 20 mM KH_2PO_4, pH 6.0 in H_2O:CH_3CN 4:1). Crude **8** was isolated in pure form by IE-HPLC (column: Mono-Q HR 5/5 , Pharmacia; elution with a linear gradient of NaCl in 0.01 M NaOH). Homogeneous fractions were collected and desalted by filtration over Sep-Pak (Waters). Oligonucleotides **6** and **7** were further analyzed by matrix-assisted laser-desorption time-of-flight mass spectrometry by using the method of Pieles et al. [14] (*m/z* 4554.1 (**6**), 4815.7 (**7**)).
[14] U. Pieles, W. Zürcher, M. Schär, H. E. Moser, *Nucleic Acids Res.* **1993**, *21*, 3191–3196.
[15] These sequences for the duplex target and third strand were chosen, because much data on thermodynamic properties of triple-helix formation is known for this particular sequence of natural DNA [16] and of DNA analogues (including reversed sequence orientation) [7b–d, 8a, 9, 10].
[16] a) G. E. Plum, Y.-W. Park, S. F. Singleton, P. B. Dervan, K. J. Breslauer, *Proc. Natl. Acad. Sci. USA*, **1990**, *87*, 9436–9440; b) S. F. Singleton, P. B. Dervan, *Biochemistry* **1992**, *31*, 10995–11003; c) *ibid.* **1993**, *32*, 13171–13179.
[17] L. J. Maher III, P. B. Dervan, B. J. Wold, *Biochemistry*, **1990**, *29*, 8820–8826.
[18] R. F. Macaya, P. Schultze, J. Feigon, *J. Am. Chem. Soc.* **1992**, *114*, 781–783; R. Macaya, E. Wang, P. Schultze, V. Sklenár, J. Feigon, *J. Mol. Biol.* **1992**, *225*, 755–773.
[19] M. Shimizu, A. Konishi, Y. Shimada, H. Inoue, E. Ohtsuka, *FEBS Lett.* **1992**, *302*, 155–158.

 © VCH Verlagsgesellschaft mbH, D-69451 Weinheim, 1995 0570-0833/95/0606-0696 $ 10.00+.25/0

Handy for Genetic Engineering

Introduction to Molecular Cloning Techniques. By *G. Lucotte* and *F. Baneyx*. VCH Verlagsgesellschaft, Weinheim/VCH Publishers, New York, 1993. 298 pp., hardcover DM 79.00, $ 49.00.—ISBN 3-527-89613-9/1-56081-613-9

For anyone who has even a passing acquaintance with the subject, the title of this book must inevitably provoke the reaction: "What? yet another book on molecular cloning techniques?" One thinks immediately of the existing standard works in this field: laboratory manuals such as "Maniatis" and *Current Protocols*, and reference sources such as the *Parat Encyclopedic Dictionary of Genetics*, to name only those that are probably most familiar. The book reviewed here does not fit into either of these categories. Instead, as explained on the dustcover, it is intended for students and laboratory technicians concerned with microbiology, molecular biology, genetics, biotechnology, and chemical engineering. Thus it aims to introduce the reader to selected problems of genetic engineering, and is a mixture of textbook and laboratory manual. In each of the 23 chapters a short theoretical introduction is followed by a series of simple experiments and exercise problems. Throughout the book these are concerned exclusively with the commonest host organism, the prokaryotic *Eschericia coli*, despite the fact that many other such "domesticated animals", such as baculoviruses and yeasts, are nowadays used as standard organisms in genetics laboratories. However, this restriction seems to me to be entirely in keeping with the declared aims of this little book, even though it was not strictly necessary. Compared with the usual works on the subject the book has the considerable advantage of being compact and convenient to handle.

It consists of six parts whose contents vary from one to seven chapters, together with several appendices, answers to the exercise problems, a bibliography arranged according to chapters, and an index. Part 1 describes the host organism *E. coli* and introduces the relevant nomenclature. Part 2 introduces restriction enzymes and the techniques of methylation and electrophoresis. Part 3 deals with cloning vectors such as phages and plasmids, including the isolation of plasmid-DNA, the transformation of *E. coli* by plasmid-DNA, and in-vitro DNA packaging. Part 4 is concerned with the preparation of DNA and RNA from tissues or gels, the isolation and characterization of mRNA, electrophoresis of RNA, in-vitro protein synthesis, tissue-specific concentration of mRNAs, and the preparation of cDNA by reverse transcription. Part 5 deals with cloning techniques such as ligation and the cloning of cDNA fragments by elongation with homopolymers or synthetic sequences. Part 6 is concerned with libraries of genomes, cDNAs, and cosmids. Throughout the book the literature of the 1970s and 1980s is covered.

The appendices are very useful and practically orientated, and can also be used in everyday laboratory work. They include tables of bacterial strains and restriction enzymes, examples of isoschizomers, methylation patterns, and descriptions of several enzymes and vectors which could otherwise only be found by laborious searching through catalogs or original publications. Unfortunately though, some of the tables are badly set out. For example, in the detailed table of restriction enzymes, instead of the entries being listed according to the enzyme abbreviations, as would have been logical, they are arranged alphabetically according to the host organisms from which they originate. Would a reader who is not a microbiologist know, for example, that the enzyme *Aor* I comes from the organism *Acetobacter aceti* sub. *orleansis*? Appendices 13 and 14 describe the enzymes RNase A and DNase I respectively, with RNase A being given, absurdly, a whole page with only two and a half lines. A similar situation occurs with DNase I and RNase H. Here more detail was needed if the descriptions were to be included at all; otherwise it would have been better to omit these appendices. The structure of the index is not always consistent. For example, under the entry "Vector" one reads "See bacteriophage cloning vectors; plasmid cloning vectors", but neither of these appears in the index. Is this meant to refer to Chapter 6 with the title "Bacteriophage cloning vectors"? If so, what about the second reference?—There is no chapter or section entitled "Plasmid cloning vectors". Instead of sending the reader on an odyssey in search of these, it would have been more helpful to give actual page-numbers. This applies especially to the vectors described in Appendices 8–10 (the base sequence and restriction map for the vector pBR322, and the structure of the pUC vectors).

Defects such as these do, of course, detract from the usefulness of the book as a quick reference source for use in the laboratory. However, it can be thoroughly recommended for the readership mentioned above and for interested non-specialists as a convenient and concise introduction to molecular cloning techniques.

Michael Famulok
Institut für Biochemie
der Universität München
Martinsried (FRG)

This section contains book reviews and a list of new books received by the editor. Book reviews are written by invitation from the editor. Suggestions for books to be reviewed and for book reviewers are welcome. Publishers should send brochures or (better) books to Dr. Ralf Baumann, Redaktion Angewandte Chemie, Postfach 101161, D-69451 Weinheim, Federal Republic of Germany. The editor reserves the right of selecting which books will be reviewed. Uninvited books not chosen for review will not be returned.

 © *VCH Verlagsgesellschaft mbH, D-69451 Weinheim, 1995* *0570-0833/95/0606-0697 $ 10.00+.25/0*

Calixarenes, Macrocycles with (Almost) Unlimited Possibilities

Volker Böhmer

The condensation reaction between *p-tert*-butylphenol and formaldehyde leads in a single step to good yields of cyclic oligomers in which, depending on the reaction conditions, either four, six, or eight phenol units are joined by methylene bridges. The beakerlike shape of the most stable conformation of the tetramer has led to their being given the name "calixarenes" (calix = chalice). Resorcinol can undergo condensation in a similar manner with a variety of aldehydes to afford cyclic tetramers with the same basic structure (the resorcarenes). In both cases the reaction does not require the use of dilution techniques, so that large quantities of product can be readily obtained. In addition, the parent compounds can be modified in various ways, in particular at the phenolic hydroxy groups or the phenyl residues; these approaches can be used separately or in combination. Calixarenes are thus ideal starting materials for the synthesis of various types of host molecules and can also act as building blocks for the construction of larger molecular systems with defined structures and functions. Their potential applications range from use as highly specific ligands for analytical chemistry, sensor techniques and medical diagnostics to their use in the decontamination of waste water and the construction of artificial enzymes and the synthesis of new materials for nonlinear optics or for ultrathin layers and sieve membranes with molecular pores.

Keywords: calixarenes · host-guest compounds · metacyclophanes · resorcarenes · supramolecular chemistry

1. Introduction

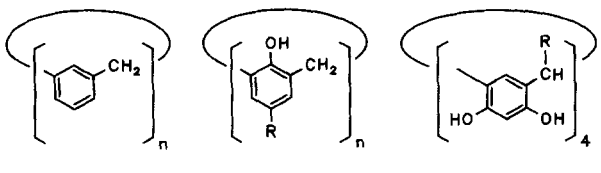
The name calixarenes was introduced by Gutsche[1] for the cyclic oligomers which are obtained from the condensation of formaldehyde with *p*-alkylphenols under alkaline conditions.[1, 2] The use of this word ("calix" means "beaker" in Latin and Greek) was suggested in particular by the shape of the tetramer, which can (and generally does) adopt a bowl- or beakerlike conformation which indicates the possibility of the inclusion of "guest" molecules.

Cyclic tetramers of this type had been described (or postulated[3a]) before and in some cases synthesized by defined reaction sequences.[3b] Most of these attempts were made with the goal of understanding the formation and properties of phenol-formaldehyde condensates on the basis of defined oligomeric model compounds. However, it required a point of view different from that of the polymer chemist to put this class of substances into the perspective of their present importance. Pedersen's discovery of the crown ethers stimulated the development of those areas of research known today as host–guest chemistry, inclusion compounds, or even supramolecular chemistry; the importance of the "cyclic oligonuclear phenolic compounds" was thus seen in a completely different light.

[*] Dr. V. Böhmer
Institut für Organische Chemie der Universität
Abteilung Lehramt Chemie
J.-J.-Becher-Weg 34, SB1, D-55099 Mainz (FRG)
Telefax: Int. code + (6131)39-5419

The condensation of resorcinol with aldehydes (but not with formaldehyde) under acidic conditions also leads to cyclic tetramers, and here again the initial structural postulates date back to the 1940s.[1] It is thus only logical to denote these compounds, which are also [1.1.1.1]metacyclophanes, as calixarenes, since nomenclature is normally based on the basic skeleton of a class of substances.

In what follows the name calix[*n*]arenes will generally be used for 1_n-metacyclophanes (general formula **I**), regardless of whether the phenolic hydroxy groups are intraannular (*endo*) or extraannular (*exo*) or whether individual units bear any phenolic OH groups at all. Although this review will deal primarily with calixarenes derived from phenol (calixarenes of type **II**), important results concerning calix[4]arenes derived from resorcinol (calixarenes of type **III**) will also be discussed. The term "resorcarenes" will be used to distinguish calixarenes of type **III**



I **II** **III**

Scheme 1. **I**: Calix[*n*]arenes or 1_n-metacyclophanes, **II**: Calix[*n*]arenes of phenol (or calixarenes in the narrow sense). The hydroxy groups are in the *endo* position. **III**: Calix[4]arenes derived from resorcinol or resorc[4]arenes. The hydroxy groups are in the *exo* position.

 © VCH Verlagsgesellschaft mbH, D-69451 Weinheim, 1995 0570-0833/95/0707-0713 $ 10.00+.25/0

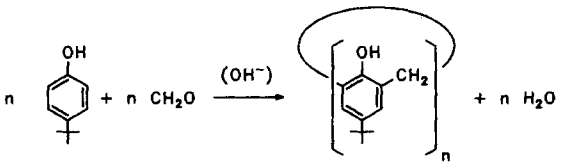
from those of type **II**. Compounds will also be referred to in which the methylene bridges or the phenol units are replaced by other related structural elements. However, orthocyclophanes such as the cyclotriveratrylenes or cryptophanes[4] and other macrocycles containing phenol building blocks will not be dealt with here.

2. Syntheses

2.1. One-Pot Procedures

The interest which calixarenes have aroused in the last ten years[5] is due in the main to their ready availability. Multigram amounts can be obtained on a laboratory scale in a relatively simple manner starting from cheap starting materials; in this calixarenes differ from many other synthetic macrocycles.

It is mainly thanks to the work of Gutsche that today the reaction conditions for the direct "one-pot synthesis" of calixarenes **1** with four, six, or eight *tert*-butylphenol units are known very exactly.[1, 6] Condensation of *tert*-butylphenol with formaldehyde under alkaline conditions (NaOH, KOH) leads in one step to the tetra-,[6a] hexa-,[6b] or octamer[6c] in yields (after recrystallization) of about 50, 85, and 63%, respectively.



1a–e (n = 4–8)

The reaction conditions determine which calixarene is formed.[7] The optimum amount of base for the formation of the tetramer and octamer appears to lie at about 0.03 mole NaOH per mole *tert*-butylphenol, the tetramer requiring higher temperatures (diphenyl ether, reflux) than the octamer (xylene, reflux). Considerably larger amounts of base (0.4 mole KOH per mole *tert*-butylphenol) favor the formation of the hexamer.

This ready availability of the calixarenes is quite amazing, since during this reaction either 8, 12, or 16 covalent bonds are newly formed in a defined manner. No other example is known in polymer chemistry in which four, six, or eight molecules of two different bifunctional starting materials form almost solely *one* cyclic tetra-, hexa-, and octamer, respectively. These cyclic compounds are in fact much more readily available than the corresponding linear oligomers.

Even though (at least in the case of *tert*-butylphenol) the synthetic conditions are known relatively exactly, many questions still remain with regard to the reaction mechanism. While various steps in the reaction between phenols and formaldehyde are well understood[1, 8] (and such steps must occur several times during the formation of the calixarenes), the reasons for the formation of particular calixarenes are virtually unknown. It is remarkable that macrocycles with an even number of phenol units are formed preferably[7] (cf. Table 1). There is a considerable amount of evidence that the calix[4]arene is the thermodynamically most stable product (it can for example be obtained from calix[6]- or calix[8]arene under basic conditions), while calix[8]arene is formed under kinetic control. In contrast, a template effect has been suggested as an explanation for the formation of calix[6]arene.[9a] Gutsche proposed an intramolecular reaction for the conversion of calix[8]arene into calix[4]arene.[1] However, experiments with a mixture of labeled and unlabeled calix[8]arene as the starting material show a rapid statistical distribution of the label in the tetramer.[9b] The conversion of calix[6]arene into calix[4]arene also argues against an intramolecular "constriction process".

More concisely, the ready availability of the calixarenes applies only when *p-tert*-butylphenol is used as the starting material. While the results for *p-tert*-pentylphenol are similar[10] (although the yields are somewhat lower), the formation of the hexamer starting from *p-tert*-octylphenol [*p*-(1,1,3,3-tetramethylbutyl)-phenol] has been mentioned,[11] but not yet described in detail. *p*-Adamantylphenol apparently yields only the octamer (71%). Calixarenes with an odd number of building blocks (5,[8] 7,[12] and even 9[11] and greater[9b]) have also been obtained from *p-tert*-butylphenol by direct condensation, but the yields are considerably lower. However, the formation of a tetramer has not yet been described starting from either *p*-phenylphenol or from *p-n*-alkylphenols (including *p*-cresol). Calix[7]arenes can



Volker Böhmer was born in 1941 in Rauscha near Görlitz and studied chemistry at the Universität Mainz. He received his doctorate in 1969 under the supervision of Prof. H. Kämmerer for work on phenolic multinuclear compounds as supports for synthetic matrix reactions. With the exception of a stay as a guest lecturer at the university in Le Mans (1976/77) he has remained loyal to the Universität Mainz. He has played a major role in the development of the Department for Teacher Trainees in Chemistry, where he is now Academic Director. His research interests are defined oligomers and particularly calixarenes. He is the author of approximately 130 publications, of which more than 50 have been concerned with calixarenes.

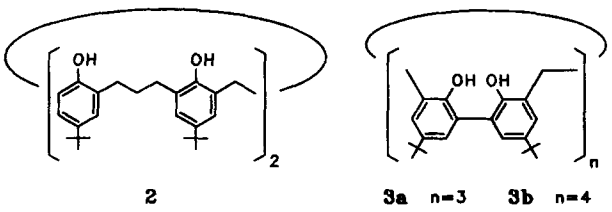
be obtained, however, from *p*-cresol and *p*-ethylphenol.[13] One reason for these confusing results certainly lies in the different solubilities of the various compounds which partly precipitate during the synthesis. Table 1 contains a survey of the "one-pot" syntheses presently known.

Table 1. Yield [%] of calix[*n*]arenes in one-pot syntheses starting from *p*-substituted (R) phenols. Values in parentheses refer to chromatographically isolated products. References are given in square brackets.

R	*n* = 4	5	6	7	8
Me				22 [13]	
Et				24 [13]	
*i*Pr	(10) [14]		26 [14]		? [14]
*t*Bu	49 [6a]	10–15 [7]	83–88 [6b]	(6) [12]	62–65 [6c]
t-pentyl [a]	6–7 [10]		30 [10]		37–41 [10]
t-octyl [b]	31 [15]				30 [16]
adamantyl				71 [11]	
n-alkyl			10 [17]		12 [17]
benzyl		33 [18]	16 [18]		12 [18]
Ph			(10) [19]	(41) [20]	7–14 [19]

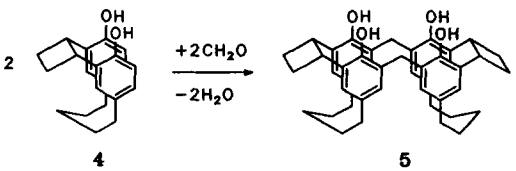
[a] *t*-Pentyl = 1,1-dimethylpropyl (-$C(CH_3)_2$-CH_2-CH_3). [b] *t*-Octyl = 1,1,3,3-tetramethylbutyl (-$C(CH_3)_2$-CH_2-$C(CH_3)_3$).

Results obtained in recent years suggest that the one-pot conditions (condensation with formaldehyde in the presence of alkali metal hydroxides in nonpolar solvents) are also applicable when diphenols are used as starting materials; this could open the way to a variety of interesting macrocycles. Thus, for example 1,3-bis(2-hydroxy-5-*tert*-butylphenyl)propane can undergo reaction with formaldehyde in the presence of NaOH to give the cyclic dimer **2** in 90% yield.[21] In contrast, the reactions of 2,2'-dihydroxy-5,5'-di-*tert*-butylbiphenyl lead to either the cyclic trimer (**3a**) or the tetramer (**3b**) in about 50% yield,



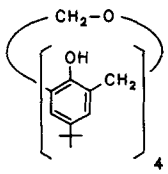
2 **3a** n=3 **3b** n=4

depending on the size of the alkali metal cation present,[22] while the relatively rigid macrocyclic diphenol **4** can be converted to the cyclic dimer **5**.[23]



4 **5**

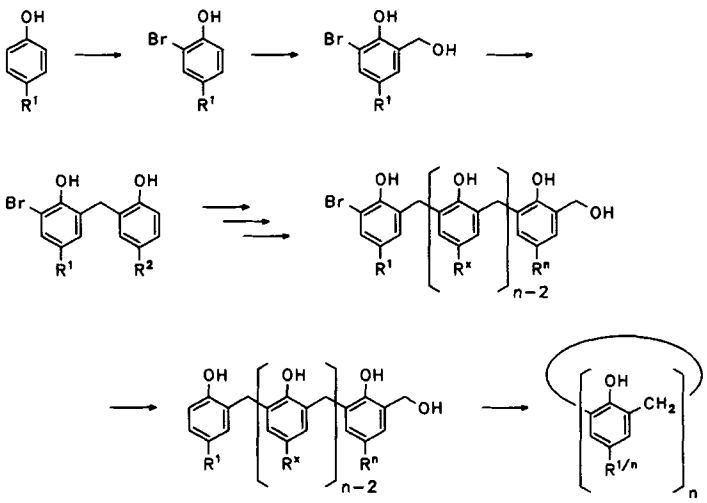
Condensation with formaldehyde under alkaline conditions can also lead to products with dimethylene ether bridges. The "dihomooxacalix[4]arene" **6** was identified at an early stage as one of the possible products of the one-pot reaction.[1] Macrocycles with several CH_2-O-CH_2 bridges can however be more readily prepared by the elimination of water from doubly hydroxymethylated phenols or from oligomers.[24a–c] Macrobi- and -tricyclic compounds with CH_2-O-CH_2 bridges have been obtained from the corresponding functionalized phenol ether derivatives by Williamson synthesis.[24d]



6

2.2. Stepwise Syntheses

The calixarenes obtained from a one-pot synthesis necessarily have the same substituent in all the *p*-positions. Calixarenes with different substituents can be obtained by the stepwise synthesis described by Hayes and Hunter[25] and further optimized by Kämmerer, Happel et al.[26] This stepwise synthesis starts from an *o*-bromo-*p*-alkylphenol and uses a series of alternating hydroxymethylation and condensation steps to build up a linear oligomer with a hydroxymethyl group at one end; this can then be cyclized under dilution conditions after the other *o*-position has been freed by dehalogenation (Scheme 2).



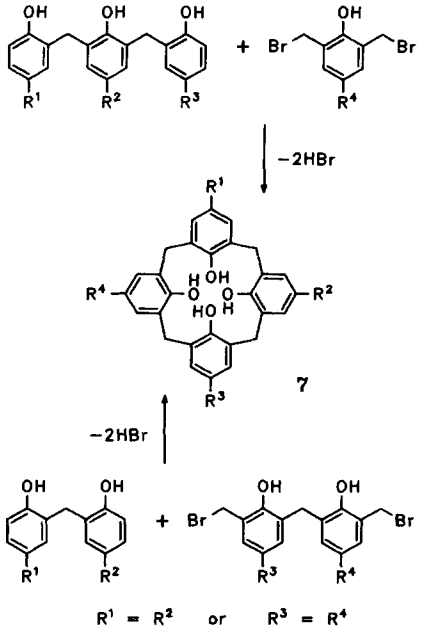
Scheme 2. Stepwise synthesis of calix[*n*]arenes (x = 2 to n–1).

The yields obtained in the cyclization step are generally very good, but because of the large number of steps the synthesis is complicated and the overall yield low. In addition the number of possible substituents in the *p*-position compatible with the synthetic steps involved is limited.

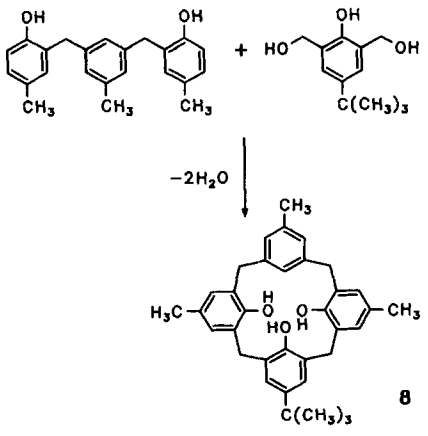
In special cases a shorter approach to linear, monohydroxymethylated tetramers has been described;[27] however, the stepwise synthesis[28] appears at present to be generally of only historical interest (see Section 2.6). But, even today it would probably be the primary choice for the synthesis of calixarenes which are built up from different alkylphenol units, and the calix[5]arenes prepared by this strategy are still the only known examples of this type.[26b,f]

2.3. Fragment Condensation

While the last step in the stepwise synthesis involves the cyclization of *one* linear starting molecule in *one intra*molecular reaction step, it is also possible to prepare (in particular) calix[4]arenes from two (or more) fragments, that is the cyclization step is preceded by (at least) one *inter*molecular condensation step. Condensations using the "3 + 1"[29] and "2 + 2"[30] principles have been used for the synthesis of a range of calix[4]arenes **7**; substituents such as COOR, NO_2, N=N-Ph, and halogen can be present in the *p*-position.[29c, 31]

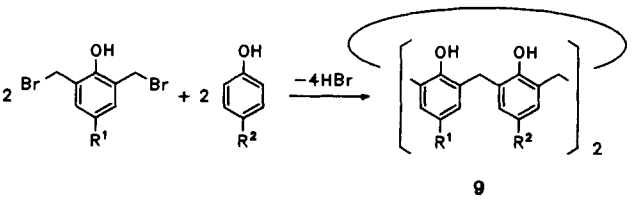


Compounds with substituted bridges (Ar-CHR-Ar; Ar denotes aryl throughout the text)[31] and those with *m*-substituted phenol units have also been prepared in this way.[32] The best yields (up to 35%) have so far been obtained in dioxane in the presence of $TiCl_4$; however, the optimum conditions for the reaction and the workup differ in each case. For example, the trihydroxycalixarene **8** was obtained in dioxane by using sulfuric acid as the catalyst.[33a]

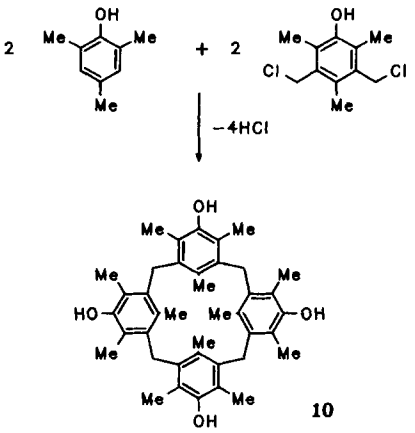


It also appears feasible to prepare calix[5]- and calix[6]arenes in this manner (i.e., according to the "3 + 2" or "3 + 3" principle); however, only one example of the synthesis of a calix[6]arene has so far been described.[29c, 34] Apparently the conditions for the synthesis ($TiCl_4$/dioxane) lead to the cleavage of Ar-CH_2-Ar bonds, since "3 + 3" experiments led among other products to calix[4]arenes, while a calix[5]arene was obtained as a by-product in the preparation of **8**.[33b]

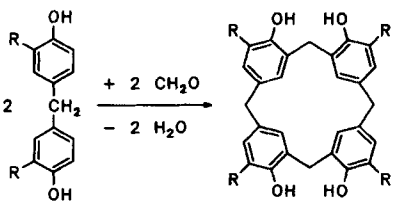
The tendency for the formation of calix[4]arenes observed in the presence of $TiCl_4$ can be applied in the "2 × 1 + 2 × 1" synthesis, which was used to obtain calix[4]arenes **9** with two alternating building units (including 4-chloro-3,5-dimethylphenol) in about 10% yield.[35]



The calix[4]arene **10** with extraannular hydroxy groups was formed in considerably better yield (60%) from the condensation of mesitol with chloromethylated mesitol in nitromethane using $SnCl_4$ as the catalyst.[36] Complications, which again appear to be due to the cleavage of Ar-CH_2-Ar bonds, are observed when other chloromethylated arenes are used.



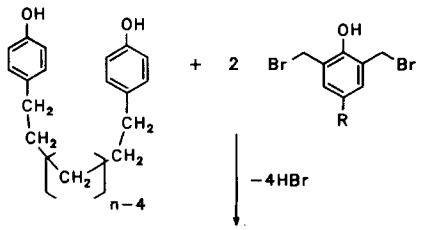
p-Linked dimers **11** can be treated with paraformaldehyde in xylene to give calix[4]arenes **12** with four *exo*-hydroxy groups[37] in yields upto 35% (**12a**).[37b] The possibility of forming a new intramolecular hydrogen bond between the OH groups appears to play an important role in the formation of the product, since **12** is for example not formed from the *o*-bridged dimer isomeric to **11**, in which such hydrogen bonds are already present.[38] In addition, the yield decreases to 5% in the case of **12b**.[38b] The stepwise synthesis can also be used to prepare calix[4]arenes of type **12** which contain different substituents in the *o*-positions.[38a]



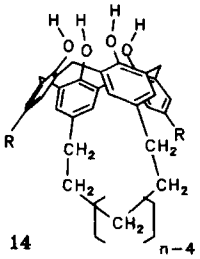
11 **a** R = $C(CH_3)_3$ **12**
b R = CH_3

2.4. Bridged, Double, and Annelated Calixarenes

When the phenol used in the "2 × 1 + 2 × 1" synthesis of **9** is replaced by a *p*-linked diphenol **13** (α,ω-bis(4-hydroxyphenyl)alkane), it is possible to prepare calix[4]arenes such as **14** in which two opposite *p*-positions are bridged by an aliphatic chain.[39]

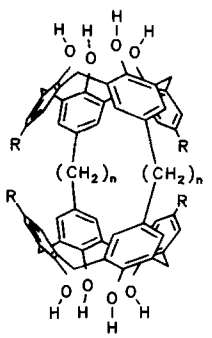


13



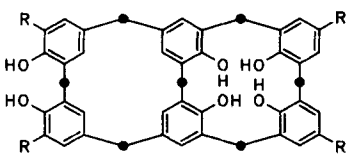
14

The synthesis of compounds **14**, with yields up to 34%,[40] has so far been realized for chain lengths $n = 5-16$ and the substituents R = Me, *t*Bu, alkyl, or cycloalkyl, phenyl, and chlorine. The byproducts can include double calix[4]arenes such as **15** in which two calix[4]arene units are linked by two aliphatic bridges.[41]



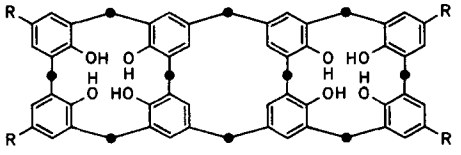
15

When a dimer is replaced in the "2 + 2" synthesis by a calix[4]arene of type **12** with two or four free *o*-positions, it is possible to obtain compounds in which either two (**16**) or three (**17**) calix[4]arene units are linked in a similar manner to the benzene rings in naphthalene or anthracene ("annelated calixarenes").[37b] A further extension of these annelated structures appears possible.



16

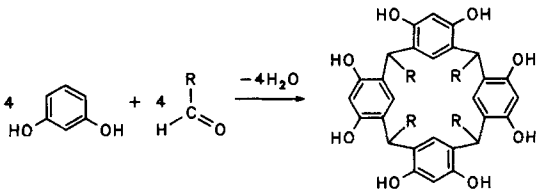
• = CH_2



17

2.5. Resorc[4]arenes

Because of its greater reactivity resorcinol affords no defined condensation products with formaldehyde. Cyclic tetramers can however be obtained by acid-catalyzed condensation with other less reactive aldehydes.[1] Larger cyclic oligomers have so far not been observed. The situation is complicated by the fact that for **18** because of the different relative configurations at the bridges (-CHR-) four diastereomers are possible which may be classified as *rccc*, *rcct*, *rctt*, and *rtct*.[42]

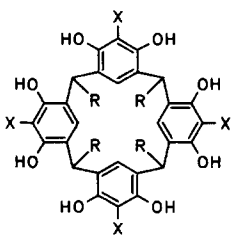


18

In 1980, Högberg[43] isolated the two isomers with the *rccc* and *rctt* configurations from the condensation between resorcinol and acetaldehyde or benzaldehyde; these are also formed with other aldehydes.[44] The *rcct* compound was later isolated in a few cases.[45] The fourth possible isomer (*rtct*) apparently occurs in very small amounts and has only been isolated by chromatography.[45c,d]

Conditions have however been found under which the all-*cis* isomer (*rccc*) can be obtained in good to excellent yields from a variety of aldehydes[45e] such as acetaldehyde,[43a] heptanal,[45a] dodecanal,[44a] dodecenal,[46] 3-oxopropanesulfonic acid (in the form of its cyclic acetal),[47] benzaldehyde[43b] (and substituted benzaldehydes including 4-formylbenzo[15]crown-5[48]), thiophene-,[44b] and ferrocenecarboxaldehyde.[49] The *rctt* isomer is often formed under kinetic control[43b] and is converted after longer reaction times into the thermodynamically more stable *rccc* isomer. The formation of Ar-CHR-Ar bonds must therefore be at least partially reversible. This isomerization, which is useful for preparative purposes, cannot always be realized, and the formation of the *rcct* and *rctt* isomers from pure *rccc* has also been observed.[45b]

It appears certain that the intramolecular hydrogen bonds between the OH groups of neighboring resorcinol units is the main cause of the preferred formation of the cyclic tetramer and, in combination with the preferred axial arrangement of the groups R (cf. Section 3.2.3), also for the preferred formation of the *rccc* isomer. Neither resorcinol monomethyl ether[45b] nor resorcinols which bear substituents such as NO_2 or COOH in 2-position afford the cyclic tetramer,[44a] since these (also generally deactivating) substituents are in competition with the OH–OH hydrogen bonds. On the other hand, compounds **19** were



19a X = OH
19b X = Alkyl
20 R = H, X = Alkyl

obtained with pyrogallol[50] and with 2-alkylresorcinols.[44a] Since 2-alkylresorcinols have only two reactive *ortho*- or *para*-positions (with respect to the hydroxy groups) they can also react with formaldehyde to give calix[4]arenes **20** with methylene bridges.[51]

It should be mentioned that cyclic tetramers have also been obtained (as their octamethyl ethers) from esters of 2,4-dimethoxycinnamic acid by treatment with BF_3,[52] a method which opens up a new and interesting route to resorcarenes.

2.6. Other Related Macrocycles

The descriptive quality of the name calixarene has been responsible for its recent use for other similar macrocycles. Some examples follow.

The closest relatives of the calixarenes derived from phenol are cyclic tetramers in which up to four methylene bridges are replaced by sulfur bridges.[53] With the exception of the tetrathio compound they were all obtained by stepwise syntheses from linear oligomers.[53b]

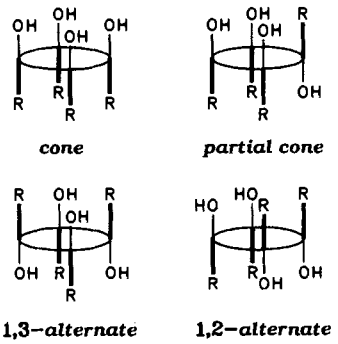
Macrocycles with $-CH_2-NR-CH_2-$ bridge(s) have been referred to as azacalixarenes (e.g. hexahomotriazacalix[3]arene) in analogy to the "dihomooxacalixarene" **6** and similar compounds.[24] "All-homocalixarenes", that is macrocycles in which all the methylene bridges are replaced by ethylene bridges,[55] have been obtained by Vögtle et al. from bisbromomethylated anisoles by Müller-Röscheisen cyclization,[55a, b] while Tashiro et al. have synthesized similar compounds via the corresponding CH_2-S-CH_2-bridged macrocycles by using "traditional" procedures known from cyclophane chemistry.[56] [3.3.3.3]Metacyclophanes with anisole building blocks were prepared in a similar manner.[57]

The phenol building blocks have also been exchanged for other structures.[55b, 58] Recent examples include calixarenes derived from furans,[59a,b] calix[3]indoles,[59c] and calix[4]naphthalenes.[59d, e] It is a moot point as to whether the names used are suitable in all cases, but further developments of this kind can be expected. Thus, for example, cyclic tetramers with Pt-bridged uracil units also show structural analogies to cali[4]arenes.[60]

3. The Conformations of the Parent Compounds

One of the most fascinating aspects of calixarenes lies in the variety of conformations which they can assume; these result from the (more or less) free rotation about the σ bonds of the Ar-CH_2-Ar groups.

In the case of calix[4]arenes, the relative orientations of the phenol units shown in Scheme 3 can in principle be assumed. Gutsche has introduced the terms "*cone*", "*partial cone*", "*1,2-alternate*", and "*1,3-alternate*", which are generally accepted today, to these basis conformations.[61a] They differ with respect to the position of the phenolic OH groups (and the *p*-positions) with respect to the molecular plane (here easily defined by the C atoms of the methylene bridges). A reference plane of this type is also clearly defined in the case of the calix[5]arenes, but not for larger oligomers: the conformations of the latter have been described in the literature in a correspondingly bewildering manner.[61b]



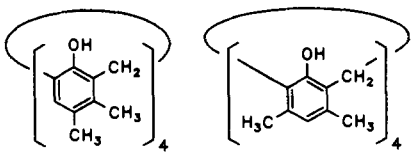
Scheme 3. The four basic conformations of a calix[4]arene; compare also Figs. 1 and 3.

3.1. Structures in the Crystal

3.1.1. *Calixarenes of Type II*

All crystal structures of calix[4]arenes with free OH groups so far reported,[62] including those of compounds containing different phenolic units,[63] have shown that the calixarene adopts the *cone* conformation, since the latter is stabilized by intramolecular hydrogen bonds between the hydroxy groups.[64] The arrangement of the molecules in the crystal lattice and the possible inclusion of guest molecules are not particularly important in this context (Fig. 1). This is the case even when a considerable deformation of the *cone* conformation is caused by the presence of one[65] or two[66] *m*-methyl groups per phenol unit and the resulting steric constraints.

However, while in the *p-tert*-butylcalix[4]arene **1a** (the toluene complex of which exhibits C_{4v} symmetry[67]) the four phenol units are twisted by an angle of 123° with respect to the reference plane, compounds **21** and **22** contain two phenol units which are nearly orthogonal to the reference plane while the two others are twisted out-



21 **22**

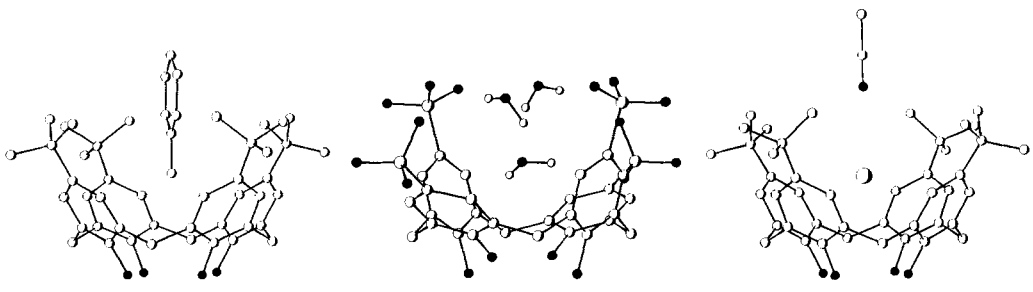


Fig. 1. Calix[4]arenes in the *cone* conformation (according to X-ray structure analyses). Oxygen and nitrogen atoms are black, hydrogen atoms in general not shown. Left: *tert*-butylcalix[4]arene **1a** with included toluene [67]; middle: *p*-sulfonic acid derivative with OH-π-bonded water as guest [68]; right: cesium salt of **1a** with the Cs^+ ion in the molecular cavity [69].

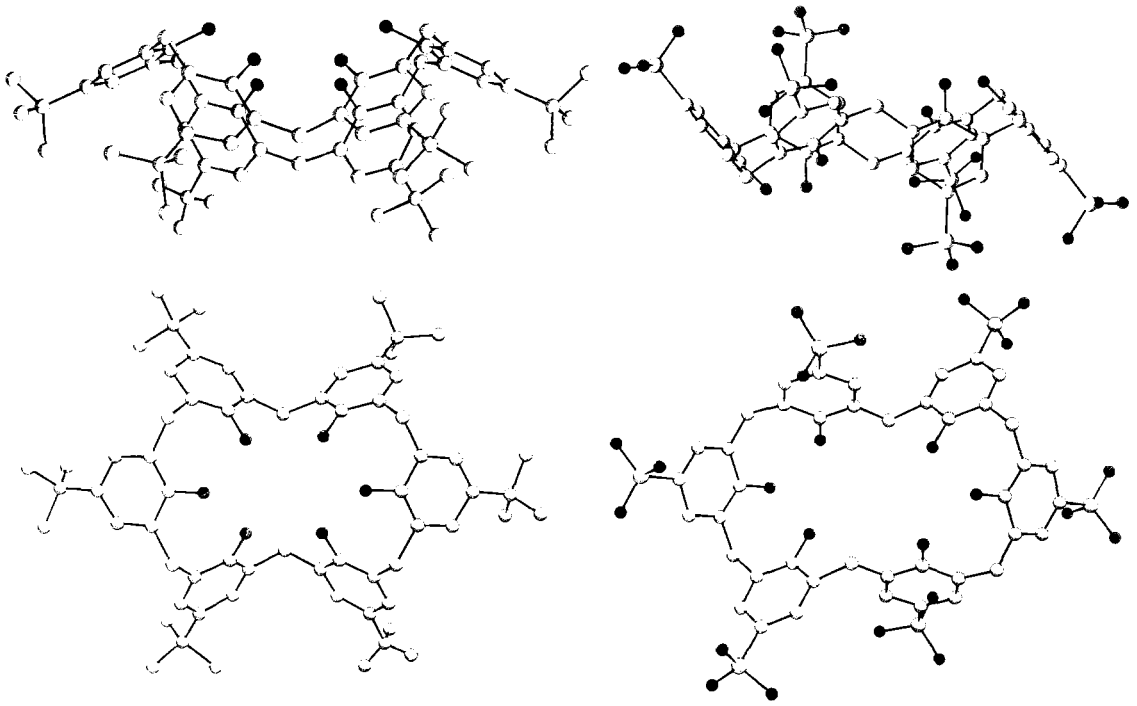


Fig. 2. Two typical conformations of calix[6]arenes in the crystal, seen from two different perspectives (oxygen atoms are black, hydrogen atoms not shown). Left: *tert*-butylcalix[6]arene [72b]; right: calix[6]arene-*p*-sulfonic acid (sodium salt) [72c].

wards. In other words, two opposite phenol units are almost parallel, while the other two are almost orthogonal to one another. A similar deformation of the *cone* conformation in the bridged calix[4]arenes **14** is caused by the aliphatic chain linking the opposite *p*-positions; this deformation increases with decreasing chain length.[39b, c, 70]

All the known crystal structures of calix[5]arenes[71] also show a *cone*-like molecular conformation, which is in turn determined by intramolecular hydrogen bonds between the phenolic OH groups. The distances between neighboring O atoms are however on average somewhat larger than in the calix[4]arenes.

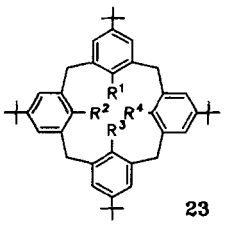
In calix[6]arenes[72] two completely different conformations have so far been observed in the crystalline state: a) all the OH groups are on one side of the molecule, the methylene bridges being arranged in a boat-shaped manner; b) groups of three neighboring OH functionalities are present on the opposing sides of the molecule (see Fig. 2). These two arrangements, each of which then contains the maximum number of intramolecular hydrogen bonds, can be visualized by joining together two three-quarter fragments of a calix[4]arene either in the same or in the opposite sense.

A simple visualization of this type is no longer possible for the calix[7]-[73] or calix[8]arenes.[74] An unequivocal description of their conformations makes use of the two torsional angles about the Ar-CH_2 bonds, which should always be reported.[75]

3.1.2. *Other Aspects*

The importance of the intramolecular hydrogen bonds for the conformation of calix[4]arenes with *endo*-OH groups becomes clear when **22** is compared with **10**, which exists in the 1,3-*alternate* conformation[36] (neighboring dipoles are arranged in an opposing manner). An additional methyl group in the *p*-position of each phenolic unit would certainly not play a decisive role in determining the conformation of **22** but would make the two compounds regioisomers which can formally be interconverted by the exchange of these *p*-methyl groups for the OH groups. In contrast, a *cone* conformation was found for **12a** with two intramolecular hydrogen bonds between the *exo*-OH groups, a stabilization, which would also be possible in the 1,2-*alternate* conformation.[38a]

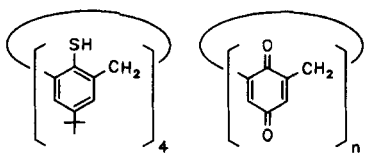
The influence of the hydrogen bonds also becomes clear when the structures of calix[4]arenes with less than four *endo*-OH groups are considered. While the aminodiphenol **23h**[76c] still exists in the *cone* conformation, the diphenol **23b** and the OH-



23

	R^1	R^2	R^3	R^4
a	OH	OH	OH	H
b	OH	H	OH	H
c	OH	OH	H	H
d	OH	H	H	H
e	H	H	H	H
f	NH_2	OH	OH	OH
g	NH_2	OH	NH_2	OH
h	H	OH	NH_2	OH

free compound **23e** take up the 1,3-*alternate* conformation.[76] Removal of the *tert*-butyl groups from **23e** leads to the parent compound, which exists in the crystalline state in a "chair" form in which opposing benzene rings are coplanar.[77] The tetrathiocalix[4]arene **24**,[78] analogous to **1a**, exists in the 1,3-*alternate* conformation, while the tetraquinone **25a** takes up a *partial cone* conformation.[79]



24 **25a–c** (n=4–6)

3.1.3. *Resorcarenes*

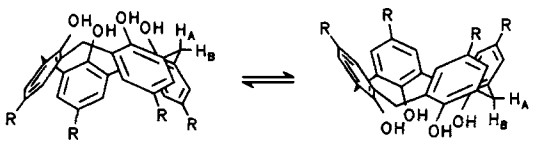
The few known crystal structures of the parent compounds with free OH groups are those of all-*cis* isomers,[80] the configuration of which is thus confirmed.[44a] The molecules always exist in the *cone* conformation in which the groups at the bridging C atoms are arranged in an axial manner. Intramolecular hydrogen bonds between the OH groups of neighboring resorcinol units also provide a stabilizing factor, although not all the intramolecular hydrogen bonds possible are formed, for example when hydrogen bonds to included solvent molecules exist.[44a] In the known examples the macrocycle does not have an exact fourfold symmetry, even in the recently described tetraanions of some ammonium salts;[81a] however, C_4 symmetry has been found for a tetra(di-*n*-propylaminomethyl) derivative.[81b]

3.2. The Structure in Solution

3.2.1. *Calix[4]arenes of Type II*

Calix[4]arenes always exist in the *cone* conformation also in solution.[1] This is clear from the ^{1}H NMR spectrum, which for example in the case of the *tert*-butylcalix[4]arene **1a** shows singlets for the hydroxy, the aromatic, and the *tert*-butyl protons. The four methylene groups are also equivalent, but the two protons of each CH_2 group are nonequivalent in the *cone* conformation. Thus, at low temperatures a pair of doublets is observed with a coupling constant of 12–14 Hz typical of geminal protons.

These signals become broader when the temperature is increased and eventually collapse to form a sharp singlet at higher temperatures. This can best be explained in terms of a rapid exchange between the two opposed (but identical) *cone* conformations, in which the OH groups pass through the interior of the macrocycle, the originally equatorial proton becoming axial and vice versa. Thus the NMR spectrum shows only an "averaged" signal.



Scheme 4. Ring inversion of *p*-substituted calix[4]arenes.

The energy barrier for the ring inversion can be derived from the temperature-dependence of the ^{1}H NMR spectra.[1, 26a, f, 82] Typical values are collected in Tables 2–4; they show that the substituent in *p*-position has almost no influence on the energy barrier. The latter, however, decreases when a nonpolar aprotic solvent such as $CDCl_3$ or benzene is replaced by a polar solvent such as pyridine. This is not surprising, since the inversion requires that the hydroxy groups pass through the ring, so that the cyclic arrangement of the hydrogen bonds is temporarily interrupted or at least loosened. Solvents which can break hydrogen bonds will thus lead to a decrease in the energy barrier.

Little is known about the mechanism of this *cone*-to-*cone* rearrangement. Two limiting cases appear possible:[1] a) a stepwise conversion through the sequence *cone* → *partial-cone* → 1,3-*alt*ernate/1,2-*alt*ernate → *partial-cone* → *cone*; b) a concerted conversion involving only one single transition state. Computer simulations (molecular dynamics) suggest the *partial cone* and *alternate* conformations as possible intermediates.[84]

While the ^{1}H NMR spectrum of **21** provides no evidence for deviation from fourfold symmetry (C_{4v}) even down to the lowest temperatures studied (−130 °C),[85] **22** (which has eight methyl groups in *m*-positions) exhibits two signals at −80 °C for both the

Table 2. Activation parameters for the ring inversion of calixarenes obtained from simulation of the ^{1}H NMR spectra as a function of temperature (lineshape analysis of the Ar-CH_2-Ar signals).

n/R (Cmpd.)	Solvent	ΔG^* (25 °C) [kcal mol^{-1}]	ΔH^* [kcal mol^{-1}]	ΔS^* [cal mol^{-1} K^{-1}]	Ref.
4/H	$CDCl_3$	15.7	14.2	−5.0	[82a]
4/*t*Bu (**1a**)	$CDCl_3$	16.4	15.9	−1.7	[82a]
	toluene	16.1	15.8	−1.0	[82a]
	benzene	15.8	14.6	−6.0	[82a]
	pyridine	14.3	11.3	−10	[82a]
4/SO_3Na	D_2O	14.1	10.4	−12	[82b]
8/*t*Bu (**1e**)	$CDCl_3$	16.8	17.4	2.0	[82a]
23g	$CDCl_3$	13.9	13.5	−1.4	[82c]
	pyridine	14.9	10.9	−13.9	[82c]
23b	CD_2Cl_2	8.9	10.7	5.9	[82d]
23d	CD_2Cl_2	10.1	9.0	−3.7	[82d]
20 (X = C_6H_{11})	$CDCl_3$	12.0	9.8	−7.5	[51]

Table 3. Energy barriers for the ring inversion of calixarenes obtained from the rate constant for the spin exchange of the methylene protons at the coalescence temperature T_c [a]. Comparison of ring size (*n*) and *p*-substituent (R) in two different solvents [b].

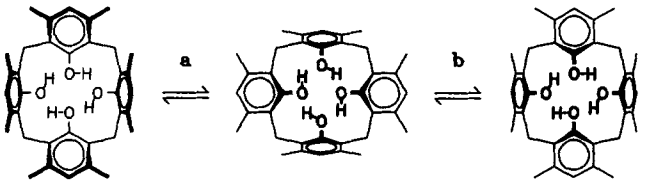
n/R (Cmpd.)	$CDCl_3$		[D_5]Pyridine	
	ΔG^* [kcal mol^{-1}]	T_c [K]	ΔG^* [kcal mol^{-1}]	T_c [K]
4/H	14.9	309	11.8	251
4/*t*Bu (**1a**)	15.7	325	13.7	288
4/C_6H_5	15.3	317	12.8	271
4/*t*-octyl	14.6	303	12.4	260
5/*t*Bu (**1b**)	13.2	271		
6/*t*Bu (**1c**)	13.3	284	9.0	219
7/*t*Bu (**1d**)	13.4	288 [c]		
8/*t*Bu (**1e**)	15.7	326	<9	<183
8/*t*-Octyl	15.2	316	<9	<183
9/*t*Bu (**1f**)	13.5	290 [c]		

[a] $k = \pi(\Delta\nu^2/2 + 3J^2)^{1/2}$. [b] Values for 100 MHz spectra, taken from ref. [1]; [c] 300 MHz spectra.

Table 4. Energy barriers for the ring inversion of calixarenes (analogous to Table 3). Comparison of particular calixarenes.

Compound or (*n*/R)	Solvent	ΔG^* [kcal mol^{-1}]	T_c [K]	Ref.
4/Me [a]	$CDCl_3$	14.6	323	[65]
21	$CDCl_3$	13.4	281	[65]
22	$CD_2Cl_2/CDCl_3$	10.9	214	
		10.7	224 [b]	[66]
23a	$CD_2Cl_2/CDCl_3$	9.6	213	[76a, c]
23b	$CDCl_2F$	9.6	202	[76b]
23c	$CDCl_2F$	10.6 [c]	221–239	[180]
23f	$CDCl_3$	14.8	312	[181]
23h	$CD_2Cl_2/CDCl_3$	11.6	246	[76a, c]
5/Me [a]	$CDCl_3$	12.7	281	[83]
55	$C_2D_2Cl_4$	17.3	355	[83]

[a] Calix[4]- or calix[5]arene derived from *p*-cresol. [b] Determined from the signal of the methylene protons. [c] Average value from three signals.



Scheme 5. Possibilities for conformational interconversion in the case of octamethylcalix[4]arene **22**: a) ring inversion, b) pseudorotation.

aromatic protons and the methyl groups.[66] Thus, as in the crystal, the conformation with the lowest energy has C_{2v} symmetry.

The conformational conversion from C_{2v} to C_{2v} occurs by ring inversion (route a) and not by pseudorotation (route b); this follows from the equal values of the energy barriers for the coalescence of the signals for CH_3 and ArH on the one side and the CH_2 groups on the other.[66] This energy barrier is however nearly 5 kcal mol^{-1} lower than that for example for **1a**. If the same energy level is assumed in all cases for the (energetically highest) transition state, this indicates a higher energy level (because of the "loosened" hydrogen bonds) for the C_{2v} conformation, which may generally be involved in the conformational interconversion.

3.2.2. *Larger Calixarenes of Type II*

As in the case of calix[4]arenes, the ^{1}H NMR spectra of all other calixarenes exhibit a singlet for the methylene protons in solution when the temperature is sufficiently high (e.g. 50 °C). At lower temperatures (e.g. −40 °C) this singlet splits into *one* pair of doublets for calix[5]arenes, while in the case of calix[6]- and calix[7]arenes *three* and *seven* pairs are observed, respectively.[86] Remarkably, calix[8]arenes also give rise to only *one* pair of doublets at low temperatures.[87] Apparently the intramolecular hydrogen bonds stabilize a highly symmetrical conformation with a regular "up and down" arrangement of the phenol units in which all the methylene bridges are equivalent, while the environment of the protons is similar to that in calix[4]arenes. The higher cyclic oligomers again adopt very unsymmetrical conformations.[9b]

The number of signals indicates that the calix[6]arenes have a conformation with a plane of symmetry, a center of symmetry, or a twofold axis. In the case of a calix[6]arene with two different phenol building blocks in an alternating arrangement, which from its molecular structure contains a threefold axis, the result is that at low temperatures a completely unsymmetrical conformation is observed.[88]

The lower barrier to the ring inversion for the calix[5]-, calix[6]-, and calix[7]arenes (see Table 3), as determined from dynamic NMR spectra, corresponds to the greater flexibility to be expected for the larger rings. Surprisingly the temperature dependence of the signals for the methylene protons of the calix[8]arenes in $CDCl_3$ corresponds very closely to that found for the calix[4]arenes.[82a, 87] The greater flexibility of the "eight-membered" ring is only noticeable in a solvent such as pyridine which breaks down the hydrogen bonds; here only a singlet is observed for the methylene protons at the lowest temperatures studied (−90 °C).

3.2.3. *Other Calix[4]arenes*

The calix[4]arenes **10** and **24** exhibit only a singlet for the methylene protons across a large temperature range. It is thus logical to assume a fixed 1,3-*alternate* conformation for these molecules, as is found in the crystalline state,[36, 78a] although this result could also be explained on the basis of a completely flexible molecule. In contrast, 1_4-metacyclophanes such as **23e** which bear no OH groups[1, 77] and calix[4]arenes of type **12** with *exo*-hydroxy groups are indeed flexible. Energy barriers for calix[4]arenes with only two or three *endo*-OH groups and for calix[4]arenes which contain NH_2 groups rather than OH groups can be found in Table 4.

There have been few studies on the conformations of resorcarenes in solution.[89] Because of their lower solubility their octaesters have normally been studied;[43b] however, these ester groups introduce additional steric effects.[90] The *rccc* isomer shows only one set of signals for all the protons of the resorcinol unit.[91] It apparently adopts a *cone* conformation with effective C_{4v} symmetry and an axial arrangement of the substituents R, which is in turn stabilized by intramolecular hydrogen bonds. There are no indications of the presence of a *cone* conformation with an equatorial arrangement of the groups R on the bridges, and even at lower temperatures no evidence for the formation of a conformation with C_{2v} symmetry (in which the octaesters occur[90]) as found for example for **22**. In the case of the *rcct* and *rctt* isomers there is an equilibrium between the "diamond" or "chair" conformation found for the octaesters and the *cone* conformation[89] in which one or two groups on the bridges are equatorial.

The resorcarene **20** with methylene bridges, derived from 2-hexylresorcinol, has a C_{4v} *cone* conformation at low temperature and undergoes a *cone* → *cone* inversion with $\Delta G^{\neq}$ = 12.0 kcal mol^{-1}, a value which is clearly lower than that observed for calix[4]arenes with *endo*-OH groups.[51] Although intraannular groups such as the OH groups can slow the ring inversion for steric reasons, the difference appears to be caused primarily by the weaker hydrogen bonds of the extraannular hydroxy groups (see also the spectroscopic data in Table 5).

4. Some Properties

Calixarenes generally have very high melting points (often above 300 °C, in some cases even above 400 °C) and a low solubility in all standard solvents.[1, 2, 92] (Their ready preparation by one-pot syntheses may be due in part to the fact that insoluble products precipitate out under the reaction conditions). The melting points can however be modified[93] and the solubility in organic solvents improved[92a, b] by the use of suitable derivatives (see Section 5). It is even possible to achieve solubility in water (up to 0.3 mol L^{-1}).[92c]

The physical behavior of calixarenes is mainly determined by the intramolecular hydrogen bonds between the phenolic OH groups. The strength of the latter can be established from IR and ^{1}H NMR spectra (Table 5). In general all calixarenes with *endo*-OH groups exhibit a considerable shift of the OH frequency to lower wavenumbers compared to the free phenols; this shift is much lower for compounds with *exo*-OH groups such as **12**. Here, as in the resorcarenes (**18**, **20**) only pairs of hydrogen-bond

Table 5. Spectroscopic characterization of the intramolecular hydrogen bonds in selected calixarenes; values taken from refs. [1,2,39c,51a,65,66,70,95,96]. Solvent for IR and ^{1}H NMR spectroscopy $CHCl_3$ or $CDCl_3$.

Compound	ν(OH) [cm^{-1}]	δ values
1a	3138	10.2
1b	3299	8.0
1c	3152	10.42
1d	3149	10.3
1e	3190	9.6
14 ($n = 5$)	3395	6.93/6.87 [b]
14 ($n = 7$)	3289	8.65/8.47 [b]
14 ($n = 9$)	3205	9.53
14 ($n = 16$)	3179	10.19
21	3230 [a]	10.61
22	3290 [a]	8.19
12a	3150 [a]	6.33
12 (R = H)	3250 [a]	8.50 [c]
18 (R = $C_{12}H_{23}$)	3250	9.60/9.28 [b]
20 (X = C_6H_{13})	3420	6.30

[a] KBr pellet. [b] Two different OH groups. [c] [D$_6$]Acetone.

ed OH groups are possible[91] but not a completely closed ring. In the ^{1}H NMR spectra there is a corresponding shift of the OH signals to lower field. Both effects are in general parallel (see Table 5), in particular for compounds with *endo*-hydroxy groups.

When the *cone* conformation of bridged calixarenes of type **14** is deformed by shorter chains (this deformation has been characterized quantitatively by a series of X-ray crystal structures[39b, c, 70]) there is a continuous weakening of the intramolecular hydrogen bonds.[70] This has also been confirmed by photo-CIDNP (CIDNP = chemically induced dynamic nuclear polarization) studies.[94]

The acidity of the phenolic OH groups, which is for example important for all selective substitution reactions, is also determined by the system of intramolecular hydrogen bonds. The pK_{a1} of calix[4]arenes is considerably reduced in comparison with the pK_a values of corresponding phenols, as semiempirical calculations suggest.[84] However, the pK_{a2} value lies considerably higher.[97]

An example is provided by the values for the dissociation of the first two phenolic OH groups in calix[4]arenetetrasulfonate, which have recently been determined by two groups to be 3.34 and 11.5[98] and 3.26 and 11.8.[99] The reduction in pK_{a1} is lower for corresponding calix[6]- and calix[8]arenes[100] and is comparable with that of the pK_{a1} value for linear oligomers.[101] The dependence reported earlier of the pK_{a1} value of calix[4]arenes containing a *p*-nitrophenol unit on the *p*-substituent of the opposing phenol unit[102] was not confirmed in later studies.

Very little is known about the acidity of resorcarenes.[103] In the case of the *rccc* isomer the first four protons can be readily removed to give a symmetrical tetraanion (which is stabilized by four intramolecular O$^-$ ··· HO bridges),[103] while even methoxide in methanol cannot remove any further protons. However, the different conformation of the *rctt* isomer permits the formation of the corresponding octaanion.

5. Fundamental Reactions of Calixarenes

Chemical modification of calixarenes does not only permit the synthesis of new host molecules by the introduction of additional functional groups, it also allows control of the conformation of calixarenes and hindrance of conformational inversion. In addition, larger molecules based on calixarene units are becoming increasingly available (see Section 6). In this respect calixarenes are greatly superior to other macrocyclic molecules such as crown ethers or cyclodextrins.[5b]

5.1. Calixarenes of Type II

Calixarenes derived from phenol can undergo modification in two main ways: 1) by the introduction of residues (functional groups) at the phenolic hydroxy groups; 2) by (electrophilic) substitution in the *p*-position with respect to the phenolic hydroxy group (subsequent to elimination of the *tert*-butyl group originally present).

5.1.1. Complete O-Alkylation and O-Acylation

The reaction of all the OH groups with monofunctional reagents to give ether or ester derivatives can generally be carried out without any problems.[1, 86] In the case of calix[4]arenes this has an additional interesting aspect: since larger substituents (acetyl, propyl, or larger[104]) cannot pass through the macrocycle, it is possible to fix all the conformations discussed above and to isolate them as stable conformers. In the meantime, not only have a large number of O-alkyl and O-acyl derivatives been obtained in defined conformations, but in some cases all four conformers have been obtained in a pure form.[105]

As Table 6 demonstrates for one example, these conformations can be readily distinguished from their ^{1}H NMR spectra

Table 6. Number and type of signals in the ^{1}H NMR spectra of tetraethers of *tert*-butylcalix[4]arene **26** ($n = 4$, Y = CH_2-R′ and O-CH_2-R′, R = $C(CH_3)_3$).

Conformation	ArH	O-CH_2-R′	Ar-CH_2-Ar	$C(CH_3)_3$
cone	1s	1s	2d	1s
partial cone	2s (2×2H) 2d (2×2H)	2s (2×2H) 2d (2×2H)	4d (4x2H)	3s (1:2:1)
1,2-*alternate*	2d (2×4H)	2d (2×4H)	1s (4H) 2d (2×2H)	1s
1,3-*alternate*	1s	1s	1s	1s

(and also determined in mixtures).[106] Furthermore, the conformations of such derivatives have often been confirmed by X-ray structural analysis. Figure 3 shows some examples.

It has often been possible to obtain tetraalkylated derivatives solely in the *cone* conformation. Apart from simple ethers with ethyleneglycol (**26a**)[108] or pyridylmethyl groups (**26b**),[109] the following are worthy of mention because of their importance as ionophores (see Section 8): ester (**27a**),[110] amide (**27b**),[111] and ketone derivatives (**27c**).[110a, 112] The latter can be readily obtained by reactions with reagents such as Br-CH_2-CO-OR, Cl-CH_2-CO-NR_2, and Cl-CH_2-CO-R, respectively. Sterically more demanding residues can also be introduced with retention of the *cone* conformation, as is shown by the synthesis of the phosphinate esters **26c**[113] and in particular the dendrimers **26e**.[114]

The formation of the *cone* conformation often appears to be favored by a template effect of the metal ions present (such as Na^+) (cf. the selectivity of ligands of this type). Thus the reac-

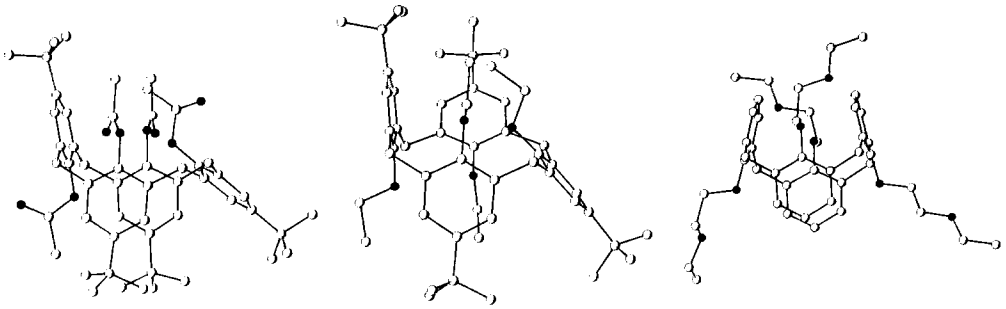
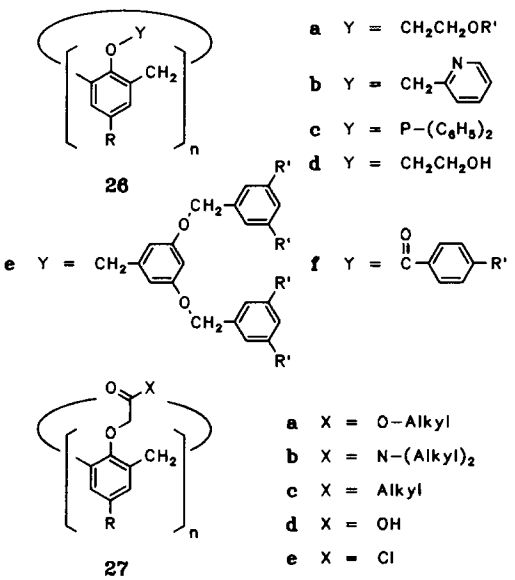


Fig. 3. Derivatives of calix[4]arenes with fixed conformations (oxygen atoms are black, hydrogen atoms not shown). Left: tetraacetate in the *partial cone* conformation [107a]; middle: tetraethyl ether in the 1,2-*alternate* conformation [107b]; right: tetraethoxyethyl ether in the 1,3-*alternate* conformation [107c].

tion of ethyl bromoacetate with **1a** in acetone in the presence of Na_2CO_3 affords 100% of the *cone* isomer, while in the presence of Cs_2CO_3 the *partial cone* isomer is formed quantitatively. This effect is not so apparent in the case of the calix[4]arene which is unsubstituted in *p*-position. The same is true for **1a** when acetone is replaced by dimethylformamide (DMF) as solvent; *alternate* conformations have not been observed in this case.[105b] In contrast, ethers of type **26a** were obtained by alkylation with



the corresponding tosylates in DMF with Cs_2CO_3 as the base in the 1,3-*alternate* conformation (selectivity up to 100%, isolated yield up to 75%),[107c] while in the presence of NaH the *cone* conformation was formed.[115] Studies on the formation of the *p*-substituted tetrabenzoates **26f** showed a clear dependence of the resulting conformation on both the *p*-substituent in the benzoyl group to be introduced and the *p*-substituent present in the calixarene.[116] Even these few examples show that a general concept for the synthesis of a particular O-acyl or O-alkyl derivative in a certain conformation is not in sight at present because of the many factors involved and may perhaps never be achieved.

The complete reaction of all hydroxy groups to give derivatives of types **26** and **27** has also been described for calix[5]-,[117] calix[6]-,[1, 108, 110b, 118, 119] and calix[8]arenes.[1, 11, 110b, 119b, 120a] Different conformations should be obtainable, at least in the case of the calix[5]arenes, since it is probable that O-alkyl groups larger than the propyl group cannot pass through the macrocycle.[117b] However, defined derivatives of calix[5]arene have so far only been obtained in the *cone* conformation. For larger macrocycles (calix[6]arene and above) the complete fixation of a certain conformation by means of large substituents on the phenolic oxygen atoms appears less probable, since there will be an increasing tendency for the *p*-substituents to swing through the ring.[1, 121]

Substituents at the oxygen atoms can in turn be modified by further reactions. As examples we can mention hydrolysis,[117a, 122] transesterification,[122b] aminolysis,[123] and reduction[124] of esters of type **27a**. Many such esters[123] and amides **27b**[111e] have been obtained in this manner from the acid **27d** and the acid chloride **27e**, and also the alcohol **26d** has served as a precursor for further derivatives.[124a] Homologous alcohols with 3-hydroxypropoxy groups were obtained recently by hydroboration of allyl ethers.[124b]

5.1.2. *Selective Reactions at the Hydroxy Groups*

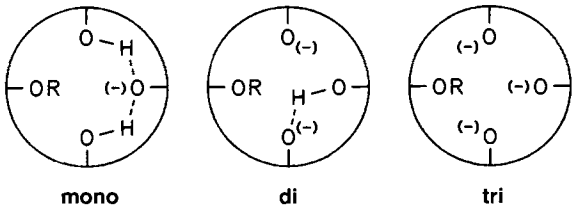
The regioselective reaction of single hydroxy groups in calixarenes is important for many purposes, in particular for the construction of larger molecules starting from several calixarene building units (see Section 6).[125] The possible regioisomers have been denoted in the case of calix[4]arenes by expressions such as *distal* or *proximal*; however, the numbering of the phenol units as used below (in analogy to the *alternate* conformations) is more readily applicable to higher oligomers.[126]

One of the first examples of selective functionalization to be described was that of the tribenzoate of the unsubstituted calix[4]arene.[127] (Other triesters were later obtained in acetonitrile by using 1-methylimidazole as the base[128]). The remaining OH group can undergo etherification; thus, monoethers are accessible after hydrolysis of the ester groups.[127, 129]

Direct monoalkylation has been carried out using an excess of the alkylating agent and K_2CO_3 (0.6 equiv in CH_3CN) or CsF (1.2 equiv in DMF) as a very weak base,[130] but also with NaH in toluene[105a, 131] or with $Ba(OH)_2$ in DMF.[105a] The controlled cleavage of 1,3-diethers[126] or tetraethers with either one or three equivalents of trimethylsilyl iodide offers another possible alternative.[132] Monoesters were also obtained in a similar manner from 1,3-diesters by reaction with imidazole.[128] The direct formation of triethers (in the *syn,syn* arrangment, see Section 5.1.3) was achieved by using $BaO/Ba(OH)_2$ in DMF.[105b, 117a, 133]

By far the best results in the selective O-alkylation (as in O-acylation[128, 134]) of calix[4]arenes were obtained by reaction of two equivalents of a relatively weak base (e.g. 1 mole K_2CO_3 per mole of calix[4]arene).[135] A variety of 1,3-diethers (includ-

ing the 2-pyridylmethyl ether,[109] see below) were thus obtained in yields (of the pure compound) which were often higher than those of the corresponding tetraethers. These results can also be readily understood on a theoretical basis,[125] since the most stable anion (stabilized by two intramolecular hydrogen bonds) of the monoether formed in the first step is obtained by deprotonation of the opposing hydroxy group (Scheme 6).



Scheme 6. Anions of a calix[4]arene monoether.

The formation of two isomeric (*syn,anti*) 1,3-dibenzoates, both in good yields, in the acylation with excess benzoyl chloride and NaH under very similar reaction conditions (THF, 0 °C, and toluene, reflux, respectively) is remarkable. [134b]

Dialkylation with a stoichiometric amount (in practice often 2.2 equivalents) of the alkylating agent in the presence of an excess of a strong base (e.g. NaH in DMF/THF) would on the other hand have to occur via the 2,4-dianion or via the trianion, from which the formation of the 1,2-diether should also be favored for statistical reasons. This has indeed been shown in a number of cases,[136] although the yields of 1,2-diethers (which are also sterically less favored than the 1,3-diethers) are in general lower.[136c]

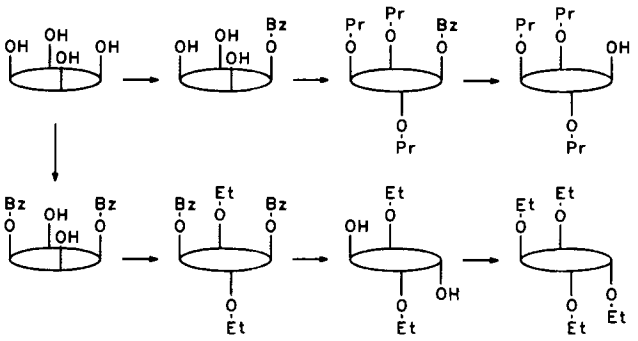
An alternative route to 1,2-diethers is the selective cleavage of neighboring ether groups by $TiBr_4$, as shown for example in the case of the tetramethyl ether of **1a**.[137] The synthesis of the 1,2-bis(3,5-dinitrobenzoate) of *tert*-butylcalix[4]arene has been carried out starting from the corresponding 1,3-diester in the presence of imidazole.[128]

While the regioselective derivatization of calix[5]arenes by O-alkylation or O-acylation with monofunctional reagents has not yet been described, an increasing number of partial esters or ethers of (mostly *tert*-butyl-substituted) calix[6]arenes has been obtained recently. Some preparatively useful examples include 1,4-diethers[138a, b] as well as 1,2,4,5-tetraethers[138a, b] and -esters.[138a, 139] Mono-[138a] and 1,2-diethers[138c] as well as 1,2-di- and pentaesters[139] have also been prepared. It has recently been possible to obtain all the methyl ethers of *tert*-butylcalix[6]arene **1c** (in some cases in very good yields)[140] as well as ten of the twelve possible pyridylmethyl ethers.[138b]

It is difficult (or at present not possible) to provide a rational explanation for the regioselective formation of certain O-alkyl or O-acyl products. Thus, for example the (unsubstituted) calix[6]arene affords the 1,2,3-trimethyl ether[141] under conditions which when applied to the *tert*-butylcalix[6]arene **1c** lead to the 1,3,5-trimethyl ether.[142] One of the products isolated from the phosphorylation of **1c** with $POCl(OEt)_2$ and $PSCl(OEt)_2$ was a 1,2,4-triester.[143]

Other more sophisticated selective functionalizations of the phenolic OH groups can however be expected in the near future, as exemplified by the 1,3,5,7-tetrabenzyl ether of calix[8]arene **1e** described recently.[144]

It is of course possible to obtain in a sequence of synthetic steps derivatives containing different O-acyl or O-alkyl residues;[118a, 135a, 136b, 142b, 145] in the case of calix[4]-arenes[105a, 107b, 145c] (and recently calix[6]arenes[138c]) different conformational isomers have also been described. The use of protecting groups for the preparation of particular conformers is demonstrated by the two examples[105a, 107b] shown in Scheme 7.



Scheme 7. Specific synthesis of calix[4]arene derivatives in a certain conformation using benzyl residues as protecting groups.

Subsequent reactions at the O-alkyl groups can also occur in a selective manner, as shown by the monohydrolysis of tetraethyl esters of type **27a** in nonpolar solvents.[146] Using the more reactive tetra-*tert*-butyl ester two opposing ester groups can be hydrolzed.[122c]

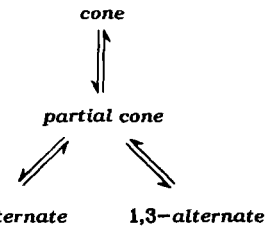
5.1.3. *Conformations of O-Alkyl Derivatives*

The residues present in partially O-alkylated (or O-acylated) products can also lie either on the same side (*syn*) or on opposite sides (*anti*) of the molecule. In contrast to the situation of the conformationally completely fixed tetra derivatives, it is *not appropriate* to use the terms *cone*, *partial cone*, etc. to describe such diastereomers (conformers) derived from calix[4]arenes, since free OH groups can still pass through the macrocycle, as is shown unequivocally by subsequent reactions in which derivatives with *different* conformations are obtained.[133c, 147] Thus, for example, a 1,3-diether in the *syn*-configuration can (at least in principle) assume a *cone*, *partial cone*, or 1,3-*alternate* conformation. Thus these terms should be used in such cases only for the characterization of *conformations*, while the relative orientation of the residues is described well by the terms *syn* and *anti*.[62]

In practice *syn*-1,3-diethers exist in the *cone* conformation, which is characterised by the presence of *one* pair of doublets (AX system) for the methylene protons ($\Delta\delta \approx 0.5-0.6$). *Anti*-1,3-diethers, also show only *one* pair of doublets (AB system) for the methylene protons; however, the difference in the chemical shift is smaller ($\Delta\delta \approx 0.2$). To explain this, a conformation has been proposed in which the opposite phenol units are coplanar;[107b, 131b] this may, however, be equivalent to a rapid interconversion of the two equivalent 1,2-*alternate* conformations.[148] In the case of 1,2-diethers the *syn* isomers adopt the *cone* and the *anti* isomers the *partial cone* conformation, respec-

tively. This can readily be explained by the formation of a maximum number of OH–OH hydrogen bonds.[149]

Interesting, and in the main still unsolved, questions are posed by the methyl ethers of calix[4]arenes. The tetramethyl ethers are surprisingly nearly as flexible as compounds with four free OH groups. However, a mixture of several conformations generally exists in solution because of the lack of intramolecular hydrogen bonds (Scheme 8);[107b, 150] the composition of such a mixture is determined among other factors by the solvent[150] and by the substituents in the *p*-positions.[151] Temperature-dependent measurements do not only provide the energy differences between the various conformations;[151b] two-dimensional exhange NMR spectroscopy can be used in special cases to determine the rate constants for their interconversion.[152]



Scheme 8. Conformational interconversion for tetramethyl ethers of calix[4]arenes.

Although in the case of calix[4]arenes methoxy groups can also pass through the ring, mono- and dimethyl ethers are fixed in the *cone* conformation (with respect to the NMR timescale) up to high temperatures (125 °C).[150] No information is yet available on the energy barrier for the *cone* → *cone* interconversion, although it is apparent that this stabilization is caused by a combination of steric effects *and* intramolecular hydrogen bonds.

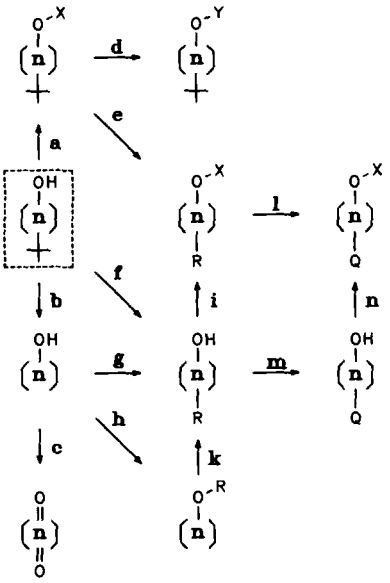
5.1.4. Substitution in p-Position

It is fortuitous that the calixarenes derived from *tert*-butylphenol are obtained particularly readily, since the *tert*-butyl group can easily be removed by $AlCl_3$-catalyzed transalkylation in the presence of a suitable acceptor such as toluene or phenol.[153] This reaction[154] plays a key role in calixarene chemistry, since a large variety of calixarenes with different substituents in the *p*-positions can be obtained by subsequent electrophilic substitution.

Virtually all the common substitutions which are possible for phenols (or phenol ethers) have been carried out on calixarenes or their alkyl ether derivatives: halogenation,[19, 155, 156] nitration,[157] sulfonation,[158] sulfochlorination,[159] chloromethylation,[160] aminomethylation,[161] acylation,[162] and coupling with diazonium salts.[163] Sulfonation[164] and nitration[165] products have also been obtained directly by *ipso*-substitution of the *tert*-butyl groups, and nitro compounds in addition via the sulfonic acids[158a] or the nitroso compounds.[157] Claisen rearrangements of allyl ethers[127, 153] and Fries rearrangements[166] have also been carried out.

The substituents thus introduced can undergo further reactions.[1, 86] Isomerization and/or ozonolysis of allyl groups,[153] haloform reactions of acetyl groups,[155a] aryl–aryl coupling by the Suzuki reaction,[167] reduction of nitro-,[115, 168] azo-,[79] or acyl groups,[162] or further substitution at chlorosulfone[159] and chloromethyl groups[151c, 160, 169] are just some important examples, in a by no means complete list, in which the "quinonemethide route" deserves special mention: aminomethylation with dimethylamine, quaternization ("complete methylation"), elimination of trimethylamine and addition of a nucleophile to the intermediately formed quinonemethide allows the introduction of very different residues.[170]

The number of possible derivatives can be imagined when one considers the combination of these reactions with suitable derivatizations at the phenolic OH groups (see Scheme 9).



Scheme 9. Summary of important chemical modifications which have been realized for calix[*n*]arenes of Type **II**: a, h, i, n: Formation of various ethers or esters, b: Transbutylation; c: Oxidation to quinones; d: Hydrolysis of ester groups, reduction of ester, amide, or nitrile groups; e: *ipso*-Nitration; f: Sulfonation; g: Electrophilic substitutions (halogenation, sulfonation, sulfochlorination, formylation, acylation, coupling with diazonium salts, chloromethylation, aminomethylation); k: Claisen rearrangement, Fries rearrangement; l: Reduction of nitro groups, aryl–aryl coupling, haloform oxidation, transformation of allyl groups; m: Nucleophilic substitution of quaternary ammonium groups.

Again it is very desirable not to substitute *all* the *p*-positions but only certain positions, if possible selectively.[125] Although partial substitutions such as nitration,[115, 165a] formylation,[171] iodination,[156c] aminomethylation[170] of calix[4]arenes (or their tetraethers) have been described, each carefully directed selective functionalization begins with the OH groups. The selectivity that can be achieved here can then be transferred to the *p*-positions, since (as a rule) phenol units are more reactive than phenol ether or ester units.

The most important strategies described are the following, which can be combined to effect the synthesis of "more ambitious" structures:

- the selective de- or better transbutylation of partially O-alkylated or O-acylated calixarenes under carefully controlled reaction conditions, which has been successful in the case of calix[4]-[128, 135c] and calix[6]arene derivatives;[138a]
- the selective substitution of partially O-alkylated or O-acylated calixarenes. In the case of the calix[4]arenes examples of bromination,[135c] formylation,[135c] acylation,[172] nitration[135c, 168] and aminomethylation[135c] are known;
- the selective Claisen rearrangement, which has been described for mono-[127] and 1,3-diallyl ethers[135c] of calix[4]arenes.

It can easily be predicted that these strategies will find further application in the future.

5.1.5. *Further Reactions*

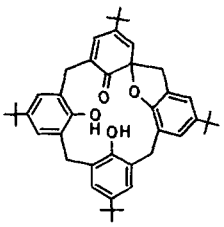
An important modification of the calixarene skeleton is the oxidation of phenol units to *p*-quinones. The first examples of calixquinones were obtained from multistep syntheses;[79] however, the direct oxidation of phenol units or even of *tert*-butylphenol units is also possible, $Tl(OOCCF_3)_3$ being the most important reagent for this purpose.[173] It is also possible to oxidize phenol units in the presence of phenol ether[174] or phenol ester units.[173] Mono-, di-, and triquinone derivatives of calix[4]arene and diquinones of calix[6]arene[173] have been prepared in this manner and in some cases characterized by X-ray crystal structure analysis.[174a]

Apart from reduction to give hydroquinone units,[173] various addition reactions to the quinone system have been described;[175] these can in principle be used for the introduction of substituents at the *m*-position with respect to the *endo*-hydroxy groups.[175b]

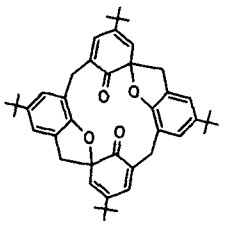
The complete oxidation of the methylene bridges to carboxyl groups and their subsequent reduction to hydroxy groups has also been reported;[176] the stereochemistry of the latter step is unclear.

Many studies have dealt with the elimination of the phenolic OH groups[76, 120, 177] (with the goal of carrying out further substitution reactions at the free *endo* positions) or their exchange for NH_2[178] or SH groups[78, 177a]. While the complete reductive cleavage of all the phosphate groups using potassium in liquid ammonia was carried out successfully for calix[4]-, calix[6]-, and calix[8]arenes,[120] the reaction with liquid ammonia led to the introduction of only two amino groups.[178] However, in the case of the *tert*-butylcalix[4]arene **1a** the complete "replacement" of all OH groups by SH was possible.[78a] The decisive step in the synthesis of **24** was the Newman–Kwart rearrangement of the thiocarbamates.

Biali et al. have introduced an interesting strategy for the modification of the calixarene skeleton. Mild oxidation of **1a** with phenyltrimethylammonium tribromide leads to spirodienones such as **28** or **29**;[179a, b] trispirodienones[179c] are formed from **1c**. Starting from **28** it was possible to phosphorylate and subsequently eliminate the two (neighboring) OH groups[180] as well as to introduce *one endo*-amino group.[181]



28

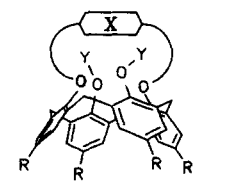


29

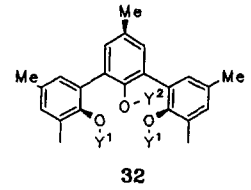
5.2. Resorcarenes

Exhaustive O-acylation and O-alkylation with monofunctional reagents is also no problem here. The corresponding octaesters have often been used for structural determinations or for isomer separation because of their better solubility.[43, 45, 89] Remarkable examples are provided by the introduction of eight ferrocene residues[48b] and the selective reaction of only one hydroxy group per resorcinol unit[182] (see Section 7.3).

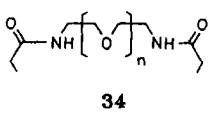
Electrophilic substitutions in the 2-position of the resorcinol units are also possible. These include bromination,[183] coupling with diazonium salts,[184] and aminomethylation.[81b, 185] However, the most "spectacular" compounds, which were prepared from the cyclic tetramer of resorcinol, will be described in the next section.



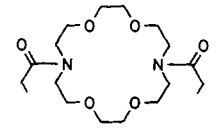
30



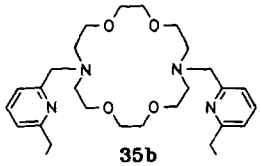
32



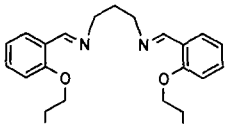
34



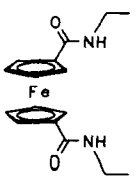
35a



35b



36



37

6. Macrobicyclic and Multimacrocyclic Compounds

The reactions between calixarenes and bifunctional reagents can lead, through bridging, to macrobicyclic molecules. In addition, more complex ("multimacrocyclic") structures such as double or triple calixarenes, cavitands, carcerands etc. have been prepared from calixarenes or resorcarenes.

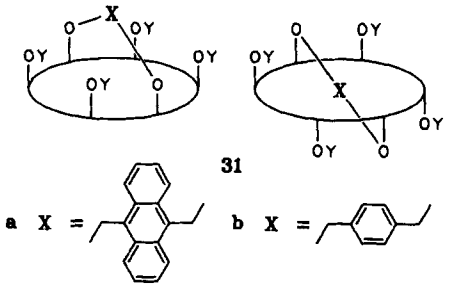
6.1. Derivatives of Calixarenes of Type II

The first crown ethers **30** derived from tert-butylcalix[4]arene were prepared as early as 1983[186] and at the same time they provided the first examples of selective alkylation in the 1,3-position. While these crown ethers assume a *cone* conformation,[187] the subsequent alkylation of the remaining OH groups leads to derivatives which can be fixed in the *cone*, *partial cone*, or 1,3-*alternate* conformation.[188a] Di-O-alkylation in the 1,3-position with a monofunctional reagent, followed by cyclization with the corresponding ditosylate (Cs_2CO_3/CH_3CN) is an alternative route, which, because of the template effect of the Cs^+ ions, leads to compounds in the 1,3-*alternate* conformation.[189a] Analogous reactions were used to prepare bis-crown ether derivatives in the 1,3-*alternate* conformation[188] as well as larger molecules consisting of two calix[4]arene units linked by polyether chains.[190]

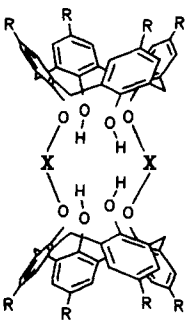
The accessibility of 1,2-dimethyl ethers also made possible the synthesis of mono- and bis-crown ethers of calix[4]arenes in which two neighboring phenol units are bridged.[137] While we were recently able to obtain 1,3-crown ethers in good

yield starting from *tert*-butylcalix[5]arene (including an example of a 1,2-crown),[191] crown ethers derived from larger calixarenes have not so far been described, although the first examples of 1,3- and 1,4-crowns of calix[6]arenes are known.[189b,c]

However, macrobicyclic derivatives of calix[6]arenes have been reported. The reactions of dicarboxylic acid dichlorides with 1,4-diethers of **1c** led to 2,5-bislactones.[138a,192] The bridging of opposite phenol units by reaction of **1c** with bishalomethylated arenes took place in the presence of $KOSiMe_3$ as the base. Exhaustive methylation of the remaining OH groups led to tetramethyl ethers which interestingly adopt different conformations.[192] While **31a** with its voluminous anthracene bridge apparently retains its conformation, the phenyl-bridged compound **31b** assumes a conformation in which this bridge is threaded through the macroring, thus motivating the authors to speak of a "self-anchored rotaxane".[192]



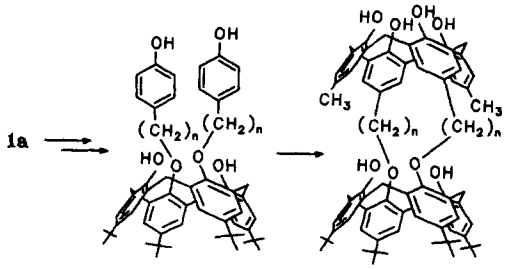
A structure which can be modified in a variety of ways and which has unique complex-forming properties (see Section 8.3.1) is generated by combining the rigid *m*-terphenyl skeleton with calix[4]arenes. In these calixspherands **32**,[193] which can be obtained from the free calix[4]arenes[193c] or from their 1,3-dimethyl ethers[193a,b] by reaction with bisbromomethylated *m*-terphenyls, the bridge again connects two opposite phenol units. In contrast, the intramolecular bridging reaction with phthalic acid dichloride involves neighboring phenol units,[194] so that the phthaloyl residue can in principle be used as a protecting group for neighboring OH groups.[195] Other bifunctional reagents, in particular those which do not tend to 1,3-bridging for steric reasons, have been used successfully for the synthesis of double (**33**) or even triple calixarenes.[196]



33

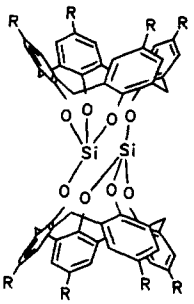
Starting from the readily available 1,3-diacid **27d** (in the form of its dichloride or dimethyl ester) and diamines or azacrowns, it was possible to obtain azacalix crown ethers **34**[123,197] or calixcryptands **35a**.[197] The calixcryptand **35b** was prepared in an analogous manner starting from the corresponding 1,3-diether.[198a] The Schiff bases **36**[199] and the ferrocene carbonamides **37**[198b] are also worthy of mention.

1,3-Diesters of 3,5-dinitrobenzoic acid lead after reduction of the nitro groups and subsequent double intramolecular bridging by amide bonds to "double-cavity calixarenes".[134] However, in this case the name promises more than the molecules in fact offer, because the tetralactam ring is collapsed and the host molecule is thus unable to take up a guest. The double calix[4]arenes **38** have been prepared starting from **1a**, the last step occurring in analogy to the synthesis of **14**. In contrast to **15** and **33**, the two calix[4]arene units (which exist in the *cone* conformation) in **38** are bridged in a head-to-tail manner.[200]



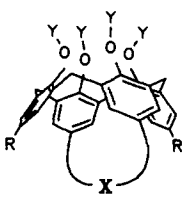
38

Derivatives in which the oxygen atoms of three neighboring phenol units are linked covalently by a single atom have also been prepared. The corresponding "multicyclic" phosphates can be obtained by heating "open-chain" diethyl phosphates with elimination of ethanol[201] or directly by reactions with phosphorus pentachloride.[202] Treatment of **1a** with silicon tetrachloride leads to the double calix[4]arene **39** bridged by two silicon atoms; in **39** the two cavities are oriented in opposite directions.[203] Similar structures containing aluminum[204a] or titanium[204b] are also known, and even the bridging of all four oxygen atoms of **1a** by a single atom (P, Mo, W)[205] has been described (see Section 9.2).

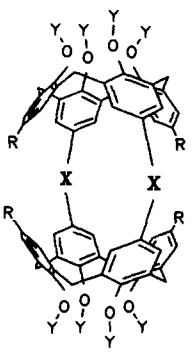


39

Starting from calix[4]arenes functionalized at opposing *p*-positions (at the "upper rim"), bridged calixarenes (**40**)[152,171,206] and double calixarenes (**41**)[156b,171,207] have been obtained in which the two cavities are oriented in opposing directions. Attempts to demethylate these "upper rim" calix crown ethers[152] (**40**, $X = CH_2\text{-}(O\text{-}CH_2\text{-}CH_2)_n\text{-}O\text{-}CH_2$, $Y = CH_3$), which resemble the bridged calix[4]arenes **14**, were not successful. However, the potential for the synthesis of molecules of the general type **40** and **41** is by no means exhausted.

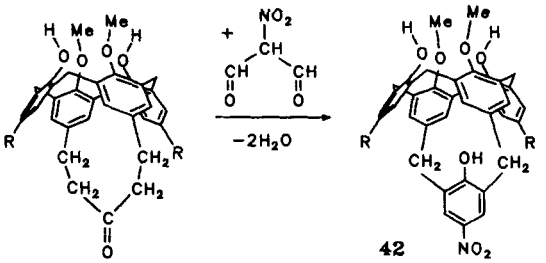


40



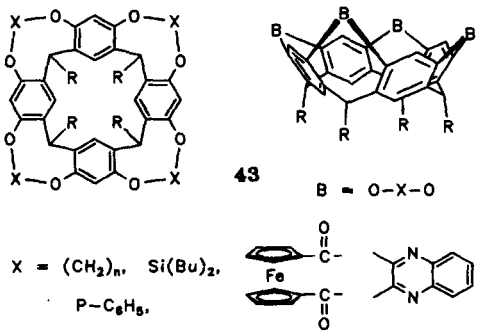
41

For example, one interesting aspect is bridging by the structural element CH_2-CH_2-CO-CH_2-CH_2, which can be converted by reaction with nitromalonaldehyde into a methylene-bridged *p*-nitrophenol unit, so that (formally) *two* new calix[4]arene systems are formed. Compounds of type **42** can thus be described as "bicyclocalix[4]arenes".[208]

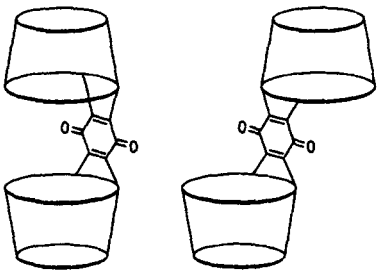


6.2. Derivatives of Resorcarenes

By far the most ambitious three-dimensional structures have been prepared starting from calixarenes based on resorcinol, in particular by Cram et al. Although these compounds will not be discussed in detail here, the general principles are presented. Intramolecular linkage of the oxygen functions of neighboring resorcinol units in the all-*cis* isomer leads to the (more or less) rigid structures **43** with a permanent cavity ("enforced cavity"); these have been given the general name cavitands by Cram.[209] A great variety of examples with X = CH_2, $(CH_2)_2$, and $(CH_2)_3$ have been synthesized from reactions of resorcarenes with $BrCH_2Cl$ or the corresponding ditosylates and in many cases these have been characterized by X-ray structural analysis.[183] Cyclization has also been achieved by using $Si(Bu)_2$,[210] PC_6H_5,[211a,b] or P(O)OR.[211c] Molecules with deeper cavities are obtained if larger units are used for intramolecular bridging, for example, by reaction with ferrocene dicarboxylic acid dichloride[49c] or dichloroquinoxaline.[212]

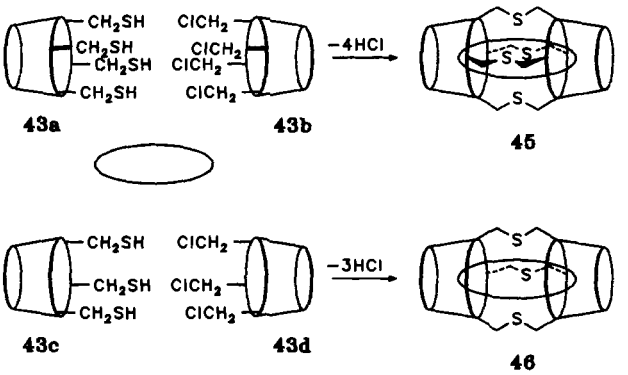


Apart from the completely bridged compounds, (nonspecific) incomplete reactions also afford singly, doubly, and triply bridged cavitands.[213a] The remaining six, four, or two hydroxy groups can then be used for further reactions, for example to introduce a different type of bridge (see Section 7.2). Two isomeric dimers **44a, b** ("ditopic cavitands") can be isolated if this additional bridging is carried out by using the tetrafunctional fluoranil; X-ray structural analysis has shown these to have the C and Z forms.[213a] The differing reactivity of the units with free hydroxy groups can also be used for further selective reactions (Claisen rearrangement,[213b] dehalogenation[213c]).



Cavitands of the type **43** can be functionalized in various ways in the 2-position of resorcinol, starting for example from 2-bromoresorcinol units, which can be obtained by bromination of the original calixarene prior to its conversion to the cavitand.[183] In this connection we should mention the remarkable quadruple sidechain bromination of cavitands of 2-methylresorcinol,[214] which proceeds in very good yields without any attack on the Ar-CHR-Ar structures. This is explained by the fact that the ring structure does not allow the formation of a planar benzyl radical.

Two of these functionalized cavitands **43a, b** can be connected through four bridges at the 2-positions in different ways,[215] as exemplified in Scheme 10.



Scheme 10. Synthesis of carcerands or hemicarcerands with the inclusion of a guest (prisoner) of suitable size (symbolized by the ellipse).

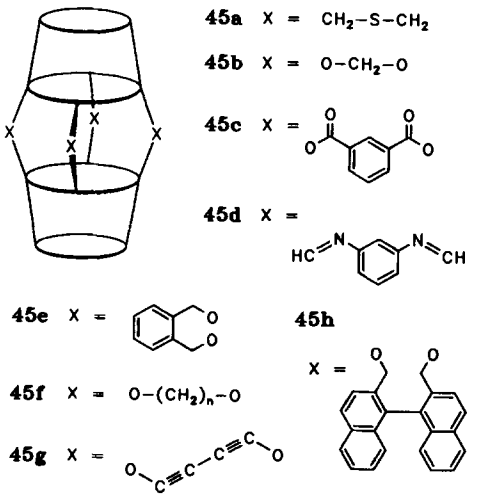
During this linkage reaction one (or even two) smaller molecules can be included in the new, completely closed cavity. Although these molecules are not held by covalent bonds, they can no longer escape from the cavity, since the openings available are too small. Cram has thus introduced the quite logical name "carcerand" for compounds of type **45** and "carceplex" for their inclusion complexes.

Several carcerands of this type (**45a, b**) have been described. They differ in the resorcarene **18** from which they are derived, and in particular in the structural elements which link two cavitands to form a carcerand. The presence of a molecule suitable for inclusion is necessary for the successful formation of a carcerand.[215d,e]

The linkage of two cavitands (**43c, d**) by only three bridges can also occur,[216] and this makes similar inclusions possible (Scheme 10). In compounds **46** one of the "doors" is large enough to permit the "imprisoned" molecule to "escape" under drastic conditions (heating for a longer period under high vacuum or in

suitable solvents). Compound **46** has thus been given the name "hemicarcerand".

Hemicarcerands have a stable cavity which cannot collapse, even when it is empty. Their openings are however large enough (at least in principle) to permit smaller molecules to pass through them. This goal can also be achieved when two cavitands are linked by four bridges when, as in the examples **45c–h**, these bridges are large enough.[217]



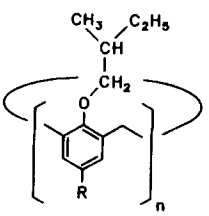
Such an "empty" hemicarcerand is now prepared to take up any suitable molecule or atom which is offered. Thus hemicarceplexes with a large variety of included molecules which do not need to be present during the synthesis are available (see Section 9.6). Remarkable "prisoners" include noble gases, but also larger molecules such as cyclophanes have undergone inclusion.[217]

7. Chiral Calixarenes

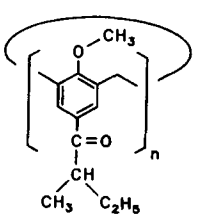
7.1. Derivatives with Chiral Substituents

Just like any other molecules calixarenes can be converted into chiral derivatives by the introduction of chiral substituents. In the case of calixarenes derived from phenols this can be done either at the phenolic OH groups or at the *p*-positions. Examples for this have been described mainly by Shinkai et al.[119]

The use of enantiomerically pure reagents leads directly to pure enantiomeric products (e.g. **47**, **48**), providing that the derivatization occurs without racemization. Thus, it is possible to obtain larger amounts of products, which is not yet the case in the examples to be discussed in Sections 7.2 and 7.3 below.



47



48

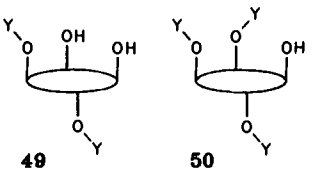
The chirality of compounds **47** and **48** is due solely to the chirality of the single units. However, calixarenes offer an additional possibility for the preparation of chiral host molecules because of their nonplanar molecular structure. Such inherently chiral calixarenes[218] have so far mainly been members of the calix[4]arene family.

7.2. Asymmetric Calixarenes

The first attempts involved the synthesis of calix[4]arenes with three (in the sequence AABC)[30a] or four[29b] different *p*-substituted phenol units (**7**) or the introduction of a single *m*-substituted phenol unit.[32a, 175]

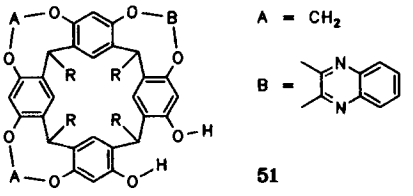
In order to obtain stable enantiomers the ring inversion, which in this case is equivalent to racemization, must be prevented, for example by the introduction of sufficiently large groups at the phenol oxygen atoms. Because of the asymmetry of such calixarenes it is necessary to achieve complete conversion of all the OH groups to a derivative in the *cone* conformation,[219a] and this can cause problems, which are probably also due to the asymmetry.[219] However, the tetrapropyl ether of a calix[4]arene containing *one* 3-methyl-4-isopropylphenol unit has been prepared in the *cone* conformation and separated into its enantiomers by chromatography using chiral stationary phases.[220]

The same asymmetric pattern can in principle be achieved by O-alkylation (or O-acylation) when different residues are bonded to the phenol oxygen atoms,[109, 131a] thus at the same time fixing the conformation. For this, at least two different groups are required for an all-*syn* arrangement of the O-alkyl groups. Additional possibilities arise when the O-alkyl groups are in an *anti*-arrangement; thus, for example, compounds of the type **49** or **50** are chiral. Such compounds[223] have been described mainly by Shinkai et al.[131a, 221] and Pappalardo et al.[109, 222]



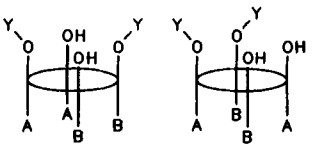
49 **50**

Chiral cavitands **51** have been obtained from resorcarenes using a similar principle by introducing two different bridges (A, B).[213a]



51

The 1,3-derivatives **52** of calix[4]arenes of the type AABB are readily prepared compounds with inherent chirality and are as usual obtained in very good yields.[224] Here the asymmetry is due to the fact that the plane of symmetry of the calixarene moiety differs from that of the oxygen substituent arrangement,[225] in



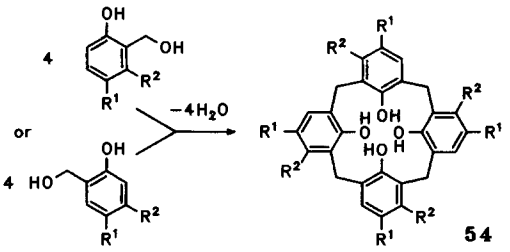
52 **53**

analogy, for example, to the atropisomers of biphenyls. Examples of 1,2-diether derivatives **53** of calix[4]arenes of the type ABAB can also be prepared;[226] this is however more difficult since 1,2-di-O-alkylation typically occurs less selectively than 1,3-di-O-alkylation.

Finally in this section we should mention the spirodienones **28**, which can be obtained from calix[4]arenes (and probably also from higher oligomers).[179] $Cr(CO)_3$ complexes of tetraethers of calix[4]arenes can also be asymmetrical.[227]

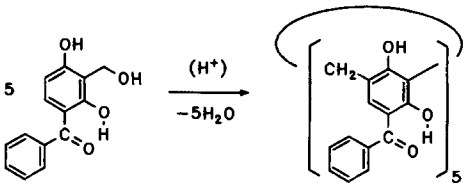
7.3. Dissymmetric Calixarenes

Dissymmetric calixarenes with an *n*-fold axis of symmetry are particularly attractive, not only from the aesthetic point of view. Calix[4]arenes **54** with C_4 symmetry have been obtained with yields in the cyclization step of up to 30%.[65, 228]

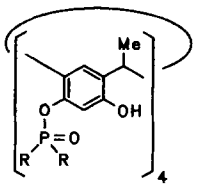


Because of the equivalence of their phenol units all the O-alkylation products (from mono- to tetraethers) are available in a defined manner. 1,3-Diether derivatives in particular (which have C_2 symmetry) have been prepared in good yields and separated into their enantiomers.[229]

The cyclocondensation of 2,4-dihydroxy-3-hydroxymethyl benzophenone leads surprisingly to the calix[5]arene **55** with C_5 symmetry, as has been shown unequivocally by NMR spectroscopy and mass spectrometry as well as by X-ray structural



analysis.[83] This is not only an unusual example of a molecule with inherent C_5 symmetry but also the first calix[5]arene derived from resorcinol in which in contrast to the resorcarenes *all* the resorcinol units are connected in the 2,6-position.[230]



56

C_4-symmetrical derivatives of the resorcarenes have recently been obtained by controlled esterification of only one OH group per resorcinol unit.[182] Compounds such as **56** could provide the starting point for many new attractive host molecules. The formation of the oxazine rings in the condensation of resorcarene with primary amines and formaldehyde occurs also regioselectively.[185b, c] In this case the C_4 symmetry was confirmed by an X-ray structural analysis.[185c]

While the calixarene-like macrocycles **3** with biphenyl units[22] are flexible (and thus achiral), their biphenyl units can be fixed in a particular conformation by etherification; this leads to chiral derivatives with atropisomeric units. Derivatives with overall C_2 symmetry have been obtained in excellent yields from the cyclic trimer **3a**,[231] while the isomer with D_3 symmetry is apparently less readily available.

8. Calixarenes as Host Molecules

One of the most important properties of calixarenes is without doubt their ability to include smaller molecules and ions reversibly. Although the parent compounds form inclusion compounds in the solid state with such different guests as arenes (benzene, anisole, pyridine, tetralin), acetone, chloroform, acetonitrile, methanol, and water[1, 2, 62] (see also Fig. 1), in solution their derivatives have become important as host molecules or ligands.

8.1. Complexation of Metal Ions: Calixarenes as Ionophores

8.1.1. Unmodified Calixarenes

Simple *tert*-butylcalixarenes are capable of (proton-coupled) transport of alkali metal ions (especially Cs^+) through an organic membrane (CH_2Cl_2/CCl_4); while the selectivity for Cs^+ was found to be highest for **1a**, the highest transport rate was found for **1e**.[10] The suggestion made by Izatt that Cs^+ ions could be complexed within the cavities of calixarene anions provided the best explanation so far for the high transport rate, which was observed under analogous conditions for the bridged calixarenes **14** when $n = 8$.[39] This is also supported by the structure of the Cs^+ salt[69] of **1a** (see Fig. 1c) and by the results of ^{131}Cs NMR measurements on the Cs complexes of **14**.[232]

Harrowfield et al. have described a number of other neutral complexes of Ca^{2+},[233] lanthanoides (La, Eu, Pr, Tm, Lu),[233, 234a–d] and actinoides(UO_2^{2+}, Th^{IV});[235] apart from **1a**, **1c**, and **1e** the bishomocalixarene **6** was also used as a ligand.[234c] Bimetallic complexes with **1e**[234a, b] are of interest because of their photophysical properties.[234d, e]

p-(Phenylazo)calixarenes bind silver and mercury ions selectively; this has been explained on the basis of metal ion induced azo-hydrazone tautomerism.[236] The tetramercaptocalixarene **24** in the 1,3-*alternate* conformation forms 1:2 complexes with mercury.[78b]

8.1.2. Neutral Ligands of the Podand Type

Complexation of Alkali Metal and Alkaline Earth Metal Ions

Derivatives with the structures **27a–c** have been studied in detail (extraction studies, complex formation constants in ho-

mogeneous solution, ion transport through liquid membranes),[110b, 111e, 117a, 122a] and several general rules can be formulated:

- Both esters and ketones prefer to complex alkali metal ions rather than alkaline earth metal ions.
- The ion selectivity depends on the ring size and in the case of calix[4]arenes also on the conformation.[105b]
- Tetraesters in the *cone* conformation are selective for Na^+ (e.g. $\beta(Na^+)/\beta(K^+) = 400$ in methanol[110b]), while the other conformations favor K^+.[105b]
- Pentaesters (*cone*) complex the larger cations preferably without making any particular distinction between K^+, Rb^+, and Cs^+.[117a]
- Hexaesters prefer Cs^+ (e.g. the hexaethyl ester of the calix[6]arene unsubstituted in the *p*-position shows a Cs^+/Na^+ selectivity of 230 in extraction experiments), while octaesters no longer exhibit any complexing abilities of note.[110b]
- "Fine tuning" of the selectivities is possible by varying the alkoxy groups.[135a]
- Tertiary amides bind alkali metal ions considerably more strongly than do the esters (lg β in MeOH is larger by almost 3), but at the cost of selectivity.[111c]
- In contrast to ester and ketone derivatives, amides are also stronger complexing agents for alkaline earth metal ions (high β values for Ca^{2+}, Sr^{2+}, and Ba^{2+} with respect to that for Mg^{2+}; the Ca^{2+}/Mg^{2+} selectivity of 7.8 (lg β in MeOH) is the largest observed for neutral ligands).[121]
- Derivatives with mixed functionalities[110b, 135d, 136b, 237] offer a further possibility for tailoring the complexing properties.

Structure of the Complexes

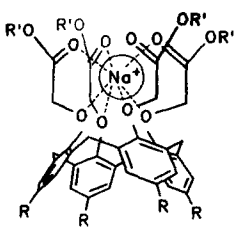
Complexes of **27a** ($n = 4$) with Na^+ or Li^+ in $CDCl_3$ are kinetically stable on the NMR timescale.[110a] Their ^1H NMR spectra are consistent with effective C_4 symmetry. This is also the case for the free ligands (see Table 7), although relaxation measurements show the latter to have a mobility greater than that of the complexes.[238] All known ligands of the type **27a–c** ($n = 4$) adopt a deformed *cone* conformation in the crystalline state in which two phenol units are almost parallel and the other two are "bent outwards".[2, 62b] The carbonyl oxygen atoms also point outwards.

Table 7. Comparison of the ^1H NMR spectra of **27a** and its kinetically stable Li^+ and Na^+ complexes in $CDCl_3$ (δ values, in parentheses the change in δ).

Proton	**27a**	+ LiSCN	+ NaSCN
Ar-H	6.75	7.04 (+0.29)	7.09 (+0.34)
O-CH_2-CO	4.78	4.81 (+0.03)	4.45 (−0.33)
Ar-CH_AH$_B$-Ar	4.83	4.61 (−0.22)	4.22 (−0.61)
Ar-CH$_A$-H_B-Ar	3.17	3.36 (+0.19)	3.37 (+0.20)
O-CH_2-CH_3	4.19	4.44 (+0.25)	4.35 (+0.16)
O-CH_2-CH_3	1.27	1.38 (+0.11)	1.39 (+0.12)
C(CH_3)$_3$	1.05	1.12 (+0.07)	1.11 (+0.06)

At present the only crystal structure known is that of the K^+ complex of the tetraamide,[111d] which shows "ideal" C_{4v}-symmetry.[239] The K^+ ion is embedded in a "sandwich-like" manner between the planes of the phenol and carbonyl oxygen atoms, which are slightly twisted about the common fourfold axis. It is assumed on the basis of NMR measurements that all analogous complexes have a similar type of structure in solution.

The fourfold symmetry, which follows from the spectrum of the free ligand in solution, thus apparently represents the time average of two (identical) conformations with twofold symmetry which are in equilibrium via a fourfold transition state. The complexation of a cation (see Scheme 11) causes the carbonyl groups to twist inwards and "forces" the ligand in the complex into a "true" fourfold symmetry.[219b, 240, 241]



Scheme 11. Na^+ complex of the tetraester derivative **27a**.

In the case of tetraester derivatives of the calix[4]arenes **54**, twofold symmetry is also observed in solution at low temperatures and the complex is kinetically (and probably thermodynamically) less stable.[65] This is in agreement with the considerable decrease in the complex formation constants (by more than five orders of magnitude for Na^+) for the tetraester derivatives of bridged calix[4]arenes (**14**) when the length of the bridge is reduced from eight to five carbon atoms.[40] The deformation thus caused can no longer be accomodated in the complex.

Little is known about the structure (and in some cases even about the composition) of corresponding derivatives of larger calixarenes. The hexaamide **27b** ($n = 6$) apparently forms a 1:2 complex with Na^+ which probably exists in a *cone*-like conformation.[118a] In contrast, guanidinium ions form 1:1 complexes, the corresponding trimethoxytriamide being clearly more selective. Hexaester or hexaamide derivatives of this type generally exist in solution as mixtures of conformers, while in the crystalline state a 1,2,3-*syn*-4,5,6-*anti*-conformation is often found.[2, 62b]

Other Cations

Tetraamides such as **27b** ($n = 4$) also form complexes with lanthanide ions,[242] which in contrast to the free ligands are often soluble in polar solvents (water, methanol).[243] The Tb^{III} complex exhibits luminescence in aqueous solution with a high quantum yield and long lifetime.[242] The luminescence properties can be further enhanced when one of the amide groups is replaced by a "sensitizer" group (e.g. phenacyl, 4-phenylphenacyl).[244]

Ester derivatives of type **27a** ($n = 5$) can also complex silver ions.[117a] The complexation of transition metals (heavy metals) is certainly favored by the incorporation of "softer" donor atoms such as nitrogen (as the amine),[198a, 245] sulfur,[198a, 246] or phosphorus.[247] Systematic, and in particular comparable, studies on the complexation of metal ions are scarce, so that general conclusions cannot yet be drawn. The examples in Table 8 indicate the possibilities available.[124] Simple ethers of the

Table 8. O-Alkyl derivatives of *tert*-butylcalix[4]arene in the *cone* conformation as an ionophore in CHEMFETs [124].

Detectable ion	O-Alkyl group
Ag^+	$Y^1 = Y^3 = OCH_2CH_2SCH_3$; $Y^2 = Y^4 = OH$
Cu^{2+}	$Y^1 - Y^4 = OCH_2CH_2SC(S)N(C_2H_5)_2$
Cd^{2+}	$Y^1 - Y^4 = OCH_2CH_2OCH_2C(S)N(CH_3)_2$
Pb^{2+}	$Y^1 - Y^4 = OCH_2C(S)N(CH_3)_2$

calix[4]arene can also complex silver ions; however, the arenes function as π-electron bases. NMR studies and X-ray crystal structure analyses of ethers in the *cone* and *partial cone* conformation show that the Ag^+ ion is bound in a sandwich-like manner between two opposite phenyl units.[248]

8.1.3. Calix Crowns, Calix Cryptands

Among the alkali metal ions K^+ is complexed selectively by crown ethers of the type **30** ($n = 3$), which can be used as carriers in liquid membranes.[249a, b] It is interesting that the free dimethyl ether apparently exists in the *cone* conformation, while the K^+ complex adopts a (flattened) *partial cone* conformation.[193b] Derivatives in the *cone*, *partial cone*, and 1,3-*alternate* conformations can be obtained when the methoxy groups are replaced by ethoxy groups; these are sufficiently stable for the necessary studies.[249c] Here, the *partial cone* conformation has shown the highest K^+/Na^+ selectivity (1.2×10^4) so far observed for a synthetic ionophore.[188]

Cs^+-selective ligands are obtained if the crown ether ring is enlarged ($n = 4$).[250a] The most active in this case are derivatives (Y = *n*Pr, *i*Pr, *n*-octyl) which are fixed in the 1,3-*alternate* conformation.[189a] The Cs^+/Na^+ selectivities of 3×10^4 and greater found for extraction (*o*-nitrophenyl hexyl ether) from acid solutions (1 M HNO_3) offer promising prospects for the enrichment of ^{137}Cs from radioactive waste. This high selectivity is due to interactions between the "soft" Cs^+ ion and the π electrons,[250b, c] which were confirmed by the X-ray structure analysis of a Cs^+ picrate complex.[189a] 1,3-Crown ethers derived from calix[5]arene also show Cs^+ selectivity,[251] while no particular complexing properties have been described for the 1,2-crowns based on calix[4]arene.

The calixspherands **32** form alkali metal ion complexes of unusual kinetic stability.[193, 252] The half-lives for the decomplexation of Na^+ and K^+ in $CDCl_3$ (saturated with D_2O), are 3.7 and 2.2 years (!), respectively, when $Y = Y^1 = Y^2 = CH_3$. In the crystalline state and also in solution the free ligand is present in the *cone* conformation[193c, 252a] (an earlier report[193b] suggested otherwise), while in the complex it adopts a flattened *partial cone* conformation. The complexed ion is thus extremely effectively shielded against attack by (for example) water molecules, so that its removal from the complex by stepwise solvation is hindered.

The substitution described above gives a half-life of only 2.8 h for the particularly interesting Rb^+ ion. The results of force field calculations[253] indicate that the larger cation causes a more pronounced bending of the *m*-terphenyl bridge and thus a decreased shielding. The increase in the kinetic stability with increasing size of the substituent Y^2 on the central ring of the *m*-terphenyl unit is in agreement with this explanation.[193c] The half-life for decomplexation increases to 139 h when $Y^2 = Et$, and to 180 days when $Y^2 = i$Pr, while the thermodynamic stability of the complexes remains the same. The half-lives for the exchange of Rb^+ for Na^+/K^+ in polar solvents such as acetone or DMSO[252b] are sufficiently large to enable practical applications in the area of medical diagnostics (the Rb/Kr method).[254a] Even for Ag^+ ions the kinetic stabilities achieved are considerable;[254b] these can certainly be increased by partial replacement of the donor oxygen atoms by sulfur.

8.1.4. Ligands with Additional Ionizable Groups

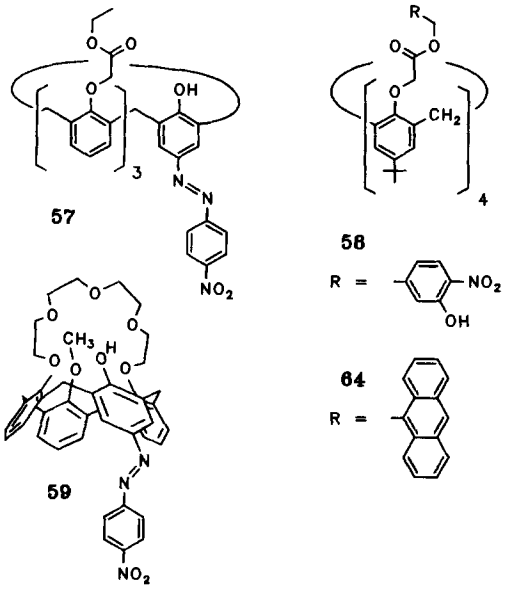
The introduction of additional ionizable groups makes it possible in principle to obtain neutral complexes with metal ions, which should for example make the transport of cations through liquid membranes independent of the anion. Under suitable conditions calixarene carboxylic acids of the type **27d** bind alkali metal ions, and in particular alkaline earth metal ions, much more strongly than do the corresponding esters, ketones, or amides,[122c] high Ca^{2+}/Mg^{2+} selectivities again being observed. Like similar siderophores, derivatives with hydroxamic acid residues show a great affinity for Fe^{3+} ions.[255a] If the number of carboxy groups in compounds of type **27** are matched with the charge of the cation, ligands are obtained which form neutral complexes. Very recent examples include Ca^{2+}-selective ligands[255b] and receptors for lanthanoides (Eu^{3+}, Tb^{3+}),[255c] which in addition to amide functions contain two and three $-OCH_2COOH$ groups, respectively. The combination of such ionizable groups with, for example, the structure of the calix crowns should open up further possibilities.

In contrast to many (in practice competing) heavy metal ions with an octahedral coordination sphere, uranyl ions (UO_2^{2+}) prefer to form complexes with hexagonal (or pentagonal) planar coordination; suitable derivatives of calix[6]arene (or calix[5]arene) readily make this possible. Shinkai et al. in particular have studied calix[5]- and calix[6]arenes with sulfonate[256a, d] or phosphonate groups[256e] in the *p*-position and/or O-alkyl groups such as $-CH_2COOH$[256a, b, f] or $-CH_2C(O)NHOH$[256c] as uranophiles in extraction and transport experiments.[256b] Under suitable conditions complex formation constants of up to $K_{uranyl} = 10^{18}-10^{19}$ (the values for the analogous calix[4]arenes are 15–16 powers of ten lower) and selectivities of $K_{uranyl}/K_{Me} = 10^{12}-10^{17}$ have been observed. The low rate of complexation and decomplexation, which is orders of magnitude lower than for the corresponding linear oligomers, seems to be a problem.[256d] The presence of only three carboxyl groups with C_3 symmetry affords selectivity advantages with respect to hexacarboxylic acids (**27d**).[256f] Molecular dynamics simulations on the complexation of UO_2^{2+} by calix[6]arenes were described recently.[256g]

8.1.5. Chromoionophores

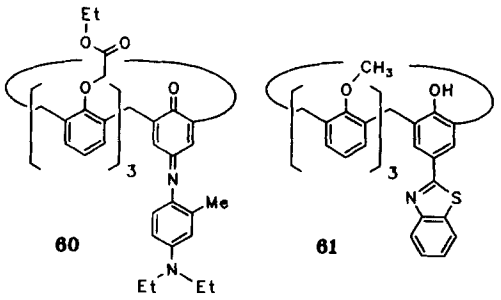
For sensor applications the generation of an optical signal as a direct result of the complexation of a metal ion is desirable. In recent years a series of calix[4]arene derivatives has been synthesized which exhibit a change in their absorption (UV/Vis) or fluoresecence spectra in the presence of metal ions and which thus have potential for applications in optical sensors.[257] The examples discussed below also show the wide range of possible variations in the calixarene skeleton.

The triester **57** (Li^+)[258a], the tetraester **58** (Li^+ better than Na^+),[258b, c] and the crown ether **59** (K^+)[129] exhibit considerable changes (bathochromic shifts) in their absorption spectra when the metal ions given in parentheses are added; these are due to the dissociation of the azophenol or nitrophenol units in the metal complex. While in the case of **57** and **58** the phenolate oxygen atom acts directly as a donor, the complexation of **58** probably occurs in the conventional manner (with phenol and

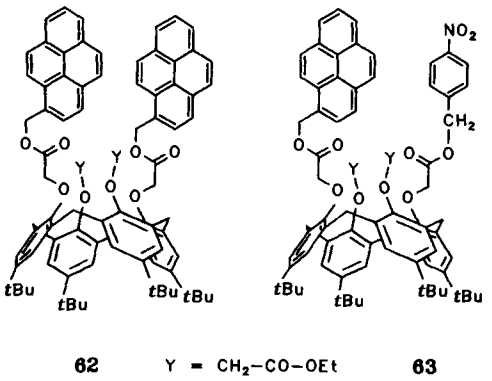


carbonyl oxygen atoms as the donors). The proximity of the positive charge of the metal cation will however favor the deprotonation of the nitrophenol in the presence of a suitable amine.

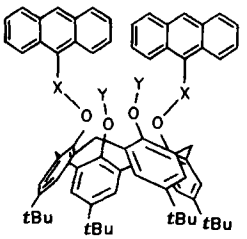
Large bathochromic shifts in the longer wavelength range are observed in the case of indophenol derivatives;[259] these result from the interaction between the metal ion and the carbonyl oxygen of the chromophoric system. Compound **60** shows Na^+-selectivity,[259a] while a corresponding derivative with two opposing indophenol units is Ca^{2+}-selective.[259b] The trimethyl ether **61**[260] is constructed on the same principle used in **57**: it contains a benzothiazole-substituted phenol unit, the fluorescence spectrum of which shows Li^+-selective changes.



The tetraesters **62** and **63**,[261] in which two pyrene residues or a pyrene and a *p*-nitrobenzyl residue, respectively, are attached to opposite phenol units, provide an impressive demonstration of the conformational change discussed in Section 8.1.2 which occurs on complexation of Na^+ ions in derivatives of type **27**. In the free ligands these two groups can come into contact, while they are spatially separated in the Na^+ complex. Thus **62** shows a strong (intramolecular) excimer emission for the pyrene residues which is reduced by Na^+ ions in favor of the monomer emission.[261a] In **63**, however, the fluorescence of the pyrene residue is quenched by the nitrobenzyl group.[261b] The complexation of Na^+ ions again separates the two groups and thus prevents the fluorescence quenching.[262]



The anthryl group can also act as a fluorophore, and the tetraesters **64**[263] undergo changes in their fluorescence spectra in the presence of Li^+, Na^+, and K^+ ions. The intramolecular photodimerization of anthryl residues has been made use of in the derivatives **65**,[264] the observed effects depending on the nature of the binding to the calixarene. In the case of **65a** the photodimer complexes Na^+ ions better than does the starting material,[264a] and the thermal back reaction is slowed down considerably by Na^+ ions; with **65b**, however, the extractability of the Na^+ ions is decreased considerably by the dimerization.[264b]



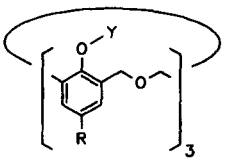
65a, X = CH_2CH_2O, Y = $CH_2CH_2OC_2H_5$

65b, X = $CH_2C(O)OCH_2CH_2O$, Y = $CH_2CH_2CH_3$

The following observation is also of interest in connection with light-switchable molecular systems.[264c] Ditopic receptors for metal ions are obtained when two molecules of type **27d** are joined by the ester residues.[265] ^1H NMR studies show that a metal ion can interchange in an intramolecular manner between the two binding sites. Similar ditopic receptors can be obtained when the linkage occurs by two bridges[265c] and certainly can also be equipped with chromophoric groups. An (intramolecular) exchange could then also be followed optically.

8.2. Complexation of Organic Cations

Water-soluble calixarene derivatives such as the *p*-sulfonic acids complex ammonium ions;[266] this is mainly due to the electrostatic interaction with the calixarene anion.[267] Depending on the pH value (and the variations in the charge distribution in the host induced thereby) the inclusion can occur in different orientations.[267b] The tetraanions of resorcarenes are also good receptors for quaternary ammonium ions such as choline, association constants of up to 10^5 L mol^{-1} being observed.[103] Cor-



Y = Alkyl

Y = CH_2–CO–OR

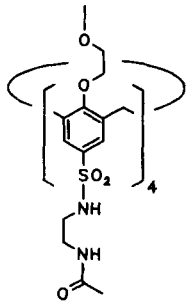
66

responding complexes have been detected in vacuum using a mass spectrometer.[81]

Neutral ligands such as the alkyl ethers (**26**, Y = *n*Pr) can function as π-bases and complex tetraalkylammonium ions in organic solvents.[268a] The triester and triether **66** of the trioxacalix[3]arene in the *cone* conformation exhibit high affinity for ammonium ions in extraction experiments because of their threefold symmetry.[268c, d]

8.3. Complexation of Anions

In comparison with the large variety of ligands which have been described for metal cations the development of selective host molecules for anions is still in its infancy. This is also true for receptors based on calixarenes. Thus calix[4]arenes with two opposite cobaltocene groups which in solution form 1:1 and 1:2 complexes unspecifically with mono- and dianions have only recently been synthesized.[269a] Selectivity for $H_2PO_4^-$ with respect to HSO_4^- and Cl^- (electrochemical detection by cyclovoltammetry in acetone) has been reported for the ferrocenamide-bridged calix[4]arene **37**.[189b, 269b] The sulfonamide **67** binds anions by hydrogen bonds; a remarkable selectivity (10^2) was found in $CDCl_3$ for HSO_4^- (with an association constant of 10^5 L mol^{-1}) with respect for example to Cl^- or NO_3^-.[159a] Calix[4]arenes with urea residues bound by spacers to the "lower rim" bind halide ions ($Cl^- > Br^- > I^-$, K_{ass} up to 7×10^3 L mol^{-1} in $CDCl_3$).[270] Consideration of the structures described in Section 8.1 indicates that the development of receptors which can bind cations *and* anions selectively at the same time can only be a question of time. Such ligands would be of considerable importance for transport across liquid membranes (see Addendum).



67

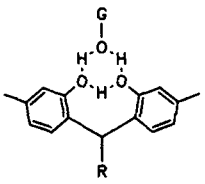
The selective inclusion of halide ions in the solid state by metal complexes of phosphonites derived from resorcarenes is mentioned for the sake of completeness.[211b]

8.4. Complexation of Neutral Molecules

The development of host molecules for neutral guests, a possibility which was indicated by the first X-ray structural analyses of calixarenes, is basically still in its infancy. Unspecific complexation of aromatic hydrocarbons (caused by hydrophobic interactions) has for example been described for various water-soluble calixarenes; a certain selectivity is derived from the ring size.[161] Measurements of association constants for a genuine molecular inclusion are made difficult by the fact that it is necessary to work below the critical micelle concentration, and it is in fact often the case that a suitable guest (e.g. a dye) is chosen according to the host available.[271]

The inclusion of organic guest molecules has also been observed for cavitands derived from resorcarenes.[212b] These compounds can in principle be used for the removal of organic impurities from water.[272]

Aoyama et al. have carried out detailed studies on the use of resorcarenes **18** (in particular with R = $C_{11}H_{23}$) as host molecules. In nonpolar solvents such as chloroform they bind a large number of guest molecules which contain hydroxy groups.[273]. The predominant interaction occurs through hydrogen bonds (Scheme 12),[274] which involve two neighboring OH groups of the host and one OH group of the guest.



Scheme 12. Interaction with the hydroxy groups of a guest G in resorcarenes.

Guests such as diols,[273a, b] sugars,[273b, c, d] or dicarboxylic acids[273e] are bound through (at least) two contacts of this type. In the case of simple alcohols CH-π interactions (which cannot be excluded in other cases) are also involved as a second contact.[273f] Considerable selectivities have been observed in spite of the relatively simple structure of the host. Thus dicarboxylic acids can be differentiated according to their length[273e] and diols with respect to the stereochemical arrangement of the hydroxy groups.[273a] In contrast to glucose, fructose can be solubilized in CCl_4 by complexation[273d] and the formation of glycosides from ribose occurs with high stereoselectivity.[273i] In the formation of complexes with glycosides there is an additional strong cooperative effect due to hydrogen bonds between the associated guest molecules.[273g, h] Water-soluble calixarenes (R = $CH_2CH_2SO_3H$) derived from resorcinol (**18**),[275] from pyrogallol (**19a**),[276a] and from 2-methylresorcinol (**19b**)[276b] can bind molecules such as hydrophobic sugars and nucleosides[275] as well as amino acids[276a] in solution, the host functioning as a π base. A resorcarene derivative obtained by aminomethylation with proline can serve as a chiral NMR shift reagent.[276c]

9. Supramolecular Structures

Self-assembly to give supramolecular structures: catch-phrases such as these (in some cases already overused) characterize recent developments which go beyond the narrow area of host–guest chemistry. In what follows we shall discuss (without making any claim to completeness) various relevant results in the calixarene area which reflect present trends and possible future developments.

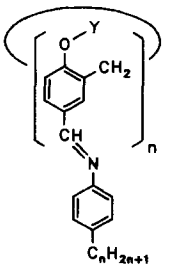
9.1. The Crystalline State

A variety of remarkable supramolecular arrangements have been described for calixarenes in the crystalline state. These are in some cases determined by weak forces,[277] interactions between methyl groups and π systems often playing a decisive role.[187] As well as the inclusion of *one* guest molecule in a single molecular cavity,[278a] it is also possible for *two* molecules of, for example, *tert*-butylcalix[4]arene to encapsulate one single

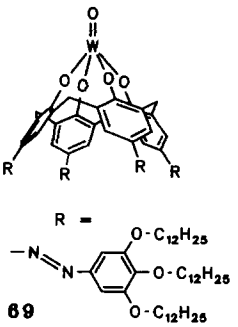
guest molecule (anisole).[279] The double[278b] or triple inclusion[234c] of guests has also been observed. Self-complexation can lead to chainlike molecular arrangements.[71c, 195] In the case of alkali metal salts of calix[4]arene sulfonates J. L. Atwood et al. have described layer-type structures, which they describe as "organic clay".[280] In the case of transition metals "second sphere" and with Eu^{3+} even "third sphere" coordination by calixarenes has been described.[281]

9.2. Liquid Crystalline Systems

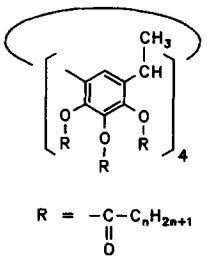
The calix[*n*]arenes **68** (Y = CH_3) can form liquid crystalline phases as is typical for azomethines of this type.[282a] Columnar mesophases are however obtained when Y = *n*Pr and $n = 4$, since the calixarene is now fixed in the *cone* conformation,[282b] so that the molecules have a "rigid" bowl-shaped mesogeneous center. Columnar mesophases are also observed for **69**, the center here being even more rigid because of the quadruple binding of a tungsten atom.[283] Similar examples (**70**) were described earlier starting from all-*cis* resorcarenes,[50, 284] in which the axial arrangement of the methyl groups at the bridges leads to the conformational fixation of the center.



68



69

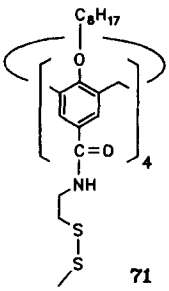


70

It should be mentioned in this connection that because of its permanent dipole moment the *cone* tetrapropyl ether of tetranitrocalix[4]arene can undergo orientation in thin polymethylmethacrylate (PMMA) films when strong electrical fields are applied;[285a] it was possible to increase the concentration of the "NLO-phore" to 100%(!) (NLO = nonlinear optic).[285b]

9.3. Mono- and Multilayers

Suitably substituted calixarenes can also be spread on aqueous subphases; depending on the derivative, the hydrophilic end can lie on the "upper rim" or the "lower rim".[108a, 165b, 286, 287] Monolayers of this type can be stabilized by cross-linking reactions.[286b] Mono- and multilayers have also been transferred to suitable carriers using the Langmuir–Blodgett technique.[165b, 286c, d] Thioether derivatives of cavitands form monolayers spontaneously on gold surfaces.[288, 317b] Such results may have considerable potential in sensor techniques or nonlinear optics. The affinity of various sugars for monolayers of **18** (R = $C_{11}H_{23}$) (and correspondingly modified electrodes) has already been demonstrated.[289]

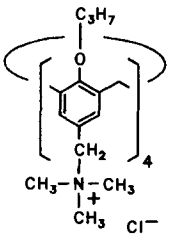


71

It is possible by transferring monolayers of the calix[6]arene **71** to polymeric carrier materials (poly[1-(trimethylsilyl)-1-propyne]) to obtain membranes whose permeability for gases can be regulated by their "molecular pore size".[286c–e] The permeability for SF_6 was already too small to be measured after only two layers had been transferred, whereas smaller molecules like nitrogen and helium still diffused through the membrane. The "perm selectivity" P(He)/P(N_2) was found to be 21 ± 4.

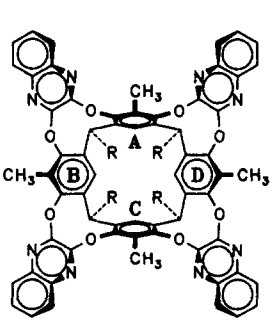
9.4. Aggregation in Solution

Long-chain *p*-acylcalixarenes, for example, *p*-dodecanoylcalix[8]arenes, and their linear analogues, form stable gels in a variety of organic solvents (including some alcohols).[290] Comparisons with the corresponding methyl ethers and *p*-alkylcalixarenes show that a three-dimensional network is built up, probably through hydrogen bonds between the hydroxy and carbonyl groups. Calix[4]arene ethers which bear a self-complementary α-pyridone residue at two opposite *p*-positions prefer to form linear aggregates linked by hydrogen bonds which can be "denatured" by urea derivatives.[291] The influence of the conformation is shown by the aggregation of the (moderately) water-soluble tetraammonium salt **72**; while the isomer with the *cone* conformation forms micelles, that with the 1,3-*alternate* conformation does not.[292]



72

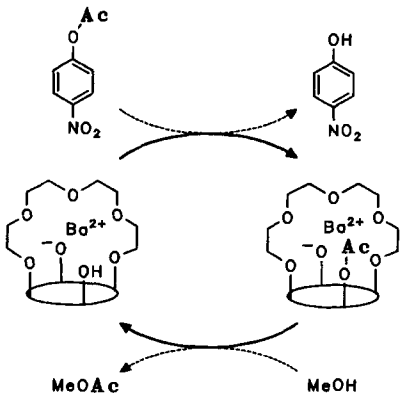
Compounds such as **73** with "rectangular surfaces" ("velcrands") form defined dimers ("velcraplexes") in solution and in the crystal by the "lock and key principle".[293] The 2-methyl groups of two opposing resorcinol units (A, C) are oriented upwards, the other two (B, D) outwards. The methyl groups A and C then act as "pegs" and fit into the "holes" formed by B and D. Both homo- and heterodimers are found in chloroform with association constants of up to 10^5 L mol^{-1}.[293c]



73

9.5. Calixarenes as Transacylase Models

Calixarenes and calixarene derivatives can be used as catalysts, for example for solvolysis reactions,[294] or as phase transfer catalysts.[108b, 118b, 295] A particularly interesting system which has been characterized in detail is the Ba^{2+} complex of the crown ether **30** ($n = 3$, R = *t*Bu).[296] It exhibits typical features of an enzyme catalysis, such as "burst kinetics" and steady state behavior for an intermediate product. Under certain conditions the methanolysis of *p*-nitrophenyl acetate is accelerated by a factor of 10; since this effect is not caused by either Ba^{2+} ions or the crown ether when used separately it appears justified to speak of a "supramolecular catalyst" (Scheme 13). The monoacetate of **30** was isolated and identified as an intermediate in the reaction; its alkaline methanolysis is accelerated by a factor of more than a million by Ba^{2+} and Sr^{2+} ions.[297] The catalytic cycle has a turnover number of 5.5×10^{-3} min^{-1} (i.e. eight cycles per day); while this is of course not comparable with those typical for enzymes, the model system is unique in type.



Scheme 13. The Ba^{2+} complex of calix[4]-crown-5 as a transacylase model.

While similar catalytic effects can be observed for crown ethers of *tert*-butylcalix[5]arene, crown ethers derived from bridged calixarenes and from C_4-calixarenes are inactive,[298] probably because they exist in a more rigid conformation with the hydroxy groups oriented inwards.

9.6. Reactions within the "Interior" of Molecules

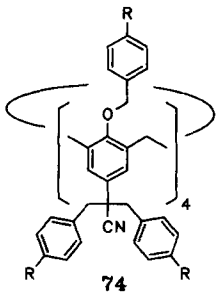
Completely new perspectives have been opened up by the inclusion of smaller molecules in carcerands and hemicarcerands, a process characterized by Cram as "constrictive bonding". It was possible using such a hemicarcerand as a "molecular reaction vessel" to produce the highly reactive cyclobutadiene from α-pyrone as the "prisoner" (in this instance the word guest is not really appropriate!). Cyclobutadiene normally reacts immediately, for example to yield cyclooctatetraene by dimerization. However, the perfect isolation of each single molecule prevents such intermolecular reactions: at normal temperatures cyclobutadiene is stable in the interior of the hemicarcerand. The controlled reaction with reactants which are small enough to pass through the "gate" of the hemicarcerand is however possible. Thus for example oxygen gives maleindialdehyde[299] by a synthetic route which, while certainly not cheap, is definitely unique. According to the authors the interior of carcerands or hemicarcerands must be considered as a "new state of matter".

9.7. Conclusions

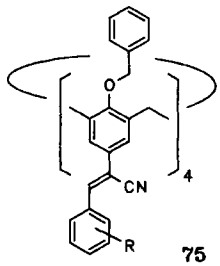
The few examples discussed here demonstrate that the title chosen for this report is certainly not an exaggeration. Many research groups are striving to synthesize even larger molecular systems with controlled functionalities. The calixarene structure, which behaves as a "molecular chameleon"[300] can be used in many ways as a building block. A final example which helps to make this clear is the molecule with a permanent cavity of about 1.5 to 2.0 nm in diameter[301], consisting of two subunits of types **I** and **II**, which are bridged by a total of eight relatively rigid bridges.

10. Addendum[302]

From the multitude of new derivatives of calix[4]arenes products derived from p-cyanomethylcalix[4]arene should be mentioned which can be converted in good yield to the dodecabenzyl derivative (**74** in the *cone* or 1,3-*alternate* conformation)[303] or by an aldol condensation with benzaldehydes to **75**. In these cases the cyano functionalities are still available, so that com-



74



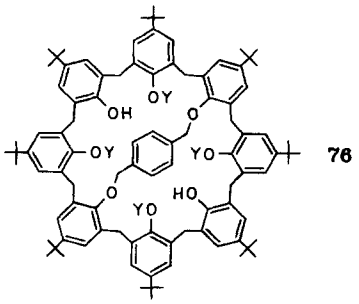
75

pounds such as **74** could serve as starting materials for novel dendrimers. The possibilities for incorporation of phosphorus are also apparently unlimited;[304] compounds containing phosphorus with coordination numbers from 3 to 6 have been described.[304a, b] Of particular interest are sandwich-like organometallic compounds which are formed in good yields by metalation of up to four of the "phenolic outer surfaces" by (for example) cyclopentadienyl derivatives of rhodium or iridium.[305] These compounds are stable, have been characterized by X-ray crystallography, and because of the presence of "positive" phenol building blocks they are suited for the inclusion of anions.

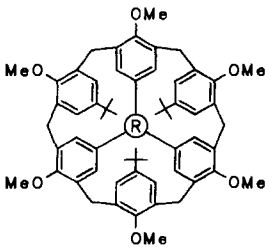
Further progress has been made in the selective derivatization (O-alkylation and acylation) of calix[6]arenes.[306] The effects of the dominant factors, such as relative acidity of the OH groups, conformation of the intermediates, size and reactivity of the reagent, are apparently slowly becoming much clearer. As in the case of calix[4]arenes the substitution pattern obtained can also be transferred to the *p*-positions, for example by selective trans-

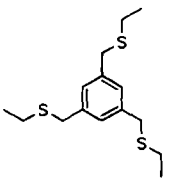
butylation (see below) or by *ipso*-nitration.[306b] In addition to numerous ethers, the first examples of "double" calix[6]arenes have also been obtained.[306c]

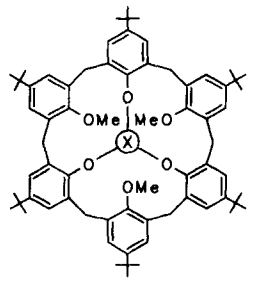
1,3,5,7-Tetra-O-alkyl derviatives of calix[8]arenes have also been obtained in yields of up to 50%.[307a] These have been converted by means of difunctional reagents to the first 1,5-O-bridged calix[8]arenes **76**.[307b] The isolation of the 1,2,4-tri- and 1,2,3,4-tetramethyl ethers of *t*-butylcalix[8]arene **1e** in yields of 68 and 21%, respectively, demonstrates that other substitution patterns are also possible.[307a]

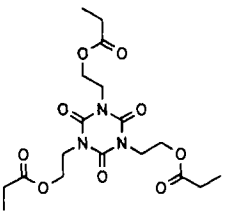


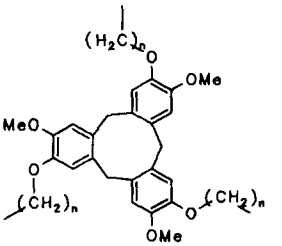
76



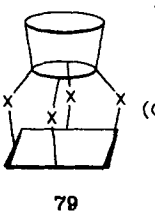
77, R = 



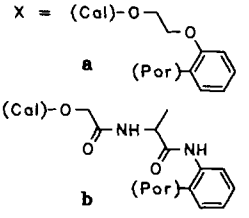
78a, X = 

78b, X = 

The combination of calix[6]arenes with building blocks that have threefold symmetry[308, 309] to afford larger host molecules such as **77** and **78** is remarkable: the coupling can take place either at the "upper rim"[308a] or the "lower rim".[308b, 309] In each case the starting material was the 1,3,5-trimethyl ether of **1c**. Initial derivatization of the hydroxyl groups or the *p*-positions was followed by reaction with trifunctional reagents[308] or in the case of the inherently chiral C_3-symmetrical cryptocalix[6]arenes **78b**[309] by the formation of the cyclotriveratrylene system in analogy to cryptophanes.[4]



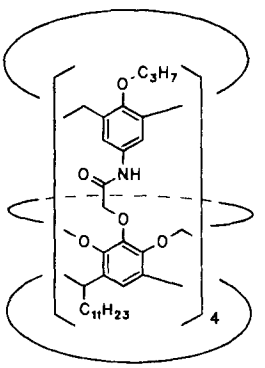
79



Compounds in which the porphyrin system is linked to one (**79**)[310] or two[311] calix[4]arene units to form larger structures have also been prepared for the first time in preparatively satisfactory yields. In this case it is possible to start from calix[4]arene derivatives with benzaldehyde side arms (on the upper or lower rim) and to build up the porphyrin system by condensation with pyrrole.[310a, 311] In the case of **79a** the calixarene even acts as a template.[311] The linkage of a correspondingly functionalized porphyrin with a calixarene derivative represents a second synthetic route;[310b] **79b** is chiral because of the alanine residues present. Further exciting developments in these directions can be expected.

Larger molecules with up to three calix[4]arene units have also been constructed for the first time from derivatives which exist in the 1,3-*alternate* conformation.[312a] Although the spacers so far used in the linkages (bisphenol A) are still too long (and thus too flexible) for the term "nanotubes" to be really valid, this goal now appears attainable in the short term. It has been shown for suitable derivatives in the 1,3-*alternate* conformation[312b] that Ag^+ ions can probably be transported through such "tubes". Double calix[4]arenes in which two units are linked by Cu^{II} complexes[313] or hydrogen bonds[314] are also of interest. It is remarkable that only the formation of dimers, and not of larger associates, is reported.

Cram et al. have synthesized new hemicarcerands of type **45** which contain other bridges.[315] Using the corresponding carceplexes it is possible to carry out either reactions of the included molecule (e.g. oxidation of divalent phenols to quinones without the observation of side reactions[315b]) or reactions at the bridges without loss of the included molecule.[315a] Photochemical reactions of included molecules are also possible.[316]

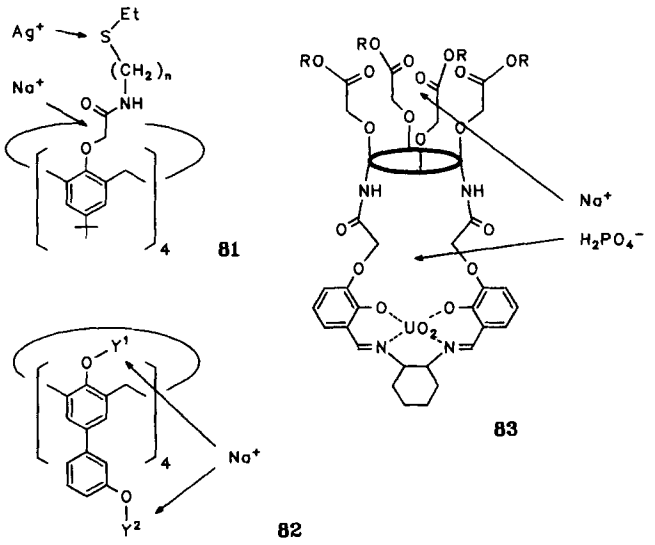


80

The carcerands **80** prepared by Reinhoudt et al. are particularly remarkable; these consist of a cavitand based on resorcarene and a calixarene.[317a] In contrast to compounds **45** they have *no* plane of symmetry orthogonal to the fourfold axis of the molecules and thus have a permanent dipole moment in the direction of this axis. Included molecules can thus take up two orientations, as has been shown in the case of dimethylacetamide and N-methylpyrrolidone. However, these rotate rapidly about the molecular axis, so that the carceplex as such has effective C_4 symmetry. The authors consider that they have discovered a new type of stereoisomerism, which they refer to as *carceroisomerism*. Carceplexes of this type could conceivably be used for information storage on a "molecular basis". Since resorcarenes containing long-chain thioether residues at the bridges can form

monolayers on gold surfaces,[288, 317b] such systems are in principle thus "manageable".

A large number of new chromo-[318] and fluorogenic[319] calixarene derivatives has been prepared. Of particular interest are: pyrene derivatives (cf. **62**, **63**) of type **66**[319a] for ammonium ions, guanidinium-sensitive pyrene derivatives of **1c**[319c] and chromogenic calix[6]arenes containing an indoaniline unit (cf. **60**), which are sensitive to uranyl ions.[318c] The capabilities of the basic calix[4]arene skeleton are particularly clear in the case of the ditopic receptors **81**–**83**. Compound **81** combines hard and soft donor groups on one side of the molecule,[320] while **82** exhibits "cooperation" in the bonding of metal ions by the ether amide ligand functions Y^1 and Y^2 on the both sides of the molecule.[321] The calix[4]arene-salen hybrid **83** is a bifunctional receptor for NaH_2PO_4.[322]



$Y^1 = Y^2 = CH_2-CO-N(Et)_2$

The multifarious possibilities available to calixarenes are demonstrated further by the use of specifically modified derivatives as phase transfer catalysts,[323] as pseudo-stationary phases in capillary electrophoresis[324] and as host components in sensors[325] (e.g. for organic molecules), though space does not permit a detailed discussion. Redox-active hosts such as calixarenes with *p*-quinone units may however provide new possibilities.[326]

Special mention should be made of the separation and purification of C_{60} with the help of calixarenes.[327] In contrast to C_{70}, C_{60} forms a relatively insoluble 1:1 complex with *tert*-butylcalix[8]arene in toluene; this can be purified by recrystallization and split into its components with $CHCl_3$, which can then readily be separated. The denser C_{60} sinks to the bottom of the vessel and can in this way be obtained in larger quantities with a degree of purity >99.5%.[327a] Enrichment of C_{70} is possible by complexation with *tert*-butylcalix[6]arene. Thus the authors suggest that the readily available calixarenes afford an inexpensive approach to the expensive fullerenes. The supramolecular interaction between fullerenes and calixarenes or similar host molecules[327d] also appears to be of fundamental interest.

Our own work in this area has been supported by the Deutsche Forschungsgemeinschaft and the European Community, and we thank both organizations for this support. I also wish to thank those many colleagues who have helped in the preparation of this manuscript both by critical discussion and constructive suggestions and by providing me with results, manuscripts, and figures. My thanks are due in particular to Dr. I. Thondorf for the figures based on X-ray structural analyses and to Dr. C. Grüttner and Dipl.-Chem. O. Mogck for their careful corrections.

Received: December 11, 1993
Addendum: November 29, 1994 [A431E]
German version: *Angew. Chem.* **1995**, *107*, 785
Translated by Dr. T. N. Mitchell, Dortmund (FRG)

[1] C. D. Gutsche, *Calixarenes*, The Royal Society of Chemistry, Cambridge, England, **1989**.
[2] *Calixarenes. A Versatile Class of Macrocyclic Compounds*, (Eds.: J. Vicens, V. Böhmer), Kluwer, Dordrecht, **1991**.
[3] a) An exact molecular weight determination was difficult and several "tetramers" were later shown to be octamers. b) An excellent description of the development of calixarene chemistry can be found in ref. [1]. Together with [2] this provides details of all the important developments up to the end of the 1980s. For a special acknowledgement of the earliest developments see: T. Kappe, *Oesterr. Chem. Ztg.* **1992**, *93*, 28-31.
[4] a) A. Collet, *Tetrahedron* **1987**, *43*, 5725–5759; b) A. Collet, J. P. Dutasta, B. Lozach, *Adv. Supramol. Chem.* **1993**, *3*, 1–35; c) A. Collet, J.-P. Dutasta, B. Lozach, J. Canceill, *Top. Curr. Chem.* **1993**, *165*, 103–129.
[5] a) See also the recent review of some aspects of the chemistry of calixarenes derived from phenol: S. Shinkai, *Tetrahedron*, **1993**, *49*, 8933-8968. b) Because of the variety of possibilities they offer, calixarenes are described there (in comparison with crown ethers and cryptands) as "supramolecules of the third generation"; see also S. Shinkai, *Adv. Supramol. Chem.* **1993**, *3*, 97–130. c) A review of calixarenes as enzyme models is provided by: J. L. Atwood, G. W. Orr, K. D. Robinson, F. Hamada, *Supramol. Chem.* **1993**, *2*, 309–317.
[6] a) C. D. Gutsche, M. Iqbal, *Org. Synth.* **1990**, *68*, 234–237; b) C. D. Gutsche, B. Dhawan, M. Leonis, D. Steward, *ibid.* **1990**, *68*, 238–242; c) J. H. Munch, C. D. Gutshe, *ibid.* **1990**, *68*, 243–246.
[7] Although the pentamer is obtained in considerably lower yield, it can be synthesized reproducibly when tetralin is used as the reaction medium: D. Stewart, C. D. Gutsche, *Org. Prep. Proc. Int.* **1993**, *25*, 137–139. b) In the meantime the yield has been increased to 16.1%: K. Iwamoto, K. Araki, S. Shinkai, *Bull. Chem. Soc. Jpn.* **1994**, *67*, 1499–1502.
[8] See for example: A. Knop, V. Böhmer, L. A. Pilato in *Comprehensive Polymer Science, Vol. 5* (Eds.: G. Allen, J. C. Bevington), Pergamon Press, Oxford **1989**, p. 611–647.
[9] a) For template syntheses in general see R. Hoss, F. Vögtle, *Angew. Chem.* **1994**, *106*, 389–398; *Angew. Chem. Int. Ed. Engl.* **1994**, *33*, 375–384; b) C. D. Gutsche, unpublished results, personal communication.
[10] S. R. Izatt, R. T. Hawkins, J. J. Christensen, R. M. Izatt, *J. Am. Chem. Soc.* **1985**, *107*, 63–66.
[11] I. E. Lubitov, E. A. Shokova, V. V. Kovalev, *Synlett.* **1993**, 647–648.
[12] Y. Nakamoto, S. Ishida, *Makromol. Chem. Rapid Commun.* **1982**, *3*, 705–707.
[13] Z. Asfari, J. Vicens, *Makromol. Chem. Rapid Commun.* **1989**, *10*, 181–183.
[14] B. Dhawan, S.-I. Chen, C. D. Gutsche, *Makromol. Chem.* **1987**, *188*, 921–950.
[15] K. Araki, A. Yanagi, S. Shinkai, *Tetrahedron* **1993**, *49*, 6763–6722.
[16] V. Bocchi, D. Foina, A. Pochini, R. Ungaro, G. D. Andreetti, *Tetahedron* **1982**, *38*, 373–378.
[17] Z. Asfari, J. Vicens, *Tetrahedron Lett.* **1988**, *29*, 2659–2660.
[18] a) B. Souley, Z. Asfari, J. Vicens, *Pol. J. Chem.* **1992**, *66*, 959–961; b) *p*-Cumylcalix[6]arene was obtained in 21% yield: A. Ettahiri, A. Thozet, M. Perrin, *Supramol. Chem.* **1994**, *3*, 191–196.
[19] C. D. Gutsche, P. F. Pagoria, *J. Org. Chem.* **1985**, *50*, 5795–5802.
[20] Y. Nakamoto, personal communication.
[21] a) T. Yamato, Y. Saruwatari, S. Nagayama, K. Maeda, M. Tashiro, *J. Chem. Soc. Chem. Commun.* **1992**, 861–862. b) Macrocycles with alternating methylene and ethylene bridges have also been obtained in this manner: T. Yamato, Y. Saruwatari, L. K. Doamekpor, K. Hasegawa, M. Koike, *Chem. Ber.* **1993**, *126*, 2501–2504.
[22] T. Yamato, K. Hasegawa, Y. Saruwatari, L. K. Doamekpor, *Chem. Ber.* **1993**, *126*, 1435–1439.
[23] a) Y. Okada, F. Ishii, Y. Kasai, J. Nishimura, *Chem. Lett.* **1992**, 755–758. b) Ionophores derived from **5**: Y. Okada, F. Ishii, Y. Kasai, J. Nishimura, *Tetrahedron Lett.* **1993**, *34*, 1971–1974. c) Reaction of **5** to give [1.4.1.4.]-metacyclophanes: Y. Okada, F. Ishii, Y. Kasai, J. Nishimura, *J. Chem. Soc. Chem. Commun.* **1993**, 976–978.

[24] a) B. Dhawan, C. D. Gutsche, *J. Org. Chem.* **1983**, *48*, 1536–1539; b) P. Zerr, M. Mussrabi, J. Vicens, *Tetrahedron Lett.* **1991**, *32*, 1879–1880; c) P. D. Hampton, Z. Bencze, W. Tong, C. E. Daitch, *J. Org. Chem.* **1994**, *59*, 4838–4843; d) B. Masci, S. Saccheo, *Tetrahedron* **1994**, *49*, 10739–10748.

[25] B. T. Hayes, R. F. Hunter, *J. Appl. Chem.* **1958**, *8*, 743–748.

[26] a) H. Kämmerer, G. Happel, F. Caesar, *Makromol. Chem.* **1972**, *162*, 179–197; b) G. Happel, B. Mathiasch, H. Kämmerer, *ibid.* **1975**, *176*, 3317–3334; c) H. Kämmerer, G. Happel, *ibid.* **1978**, *179*, 1199–1207; d) *ibid.* **1981**, *182*, 759–768; e) *ibid.* **1980**, *181*, 2049–2062; f) H. Kämmerer, G. Happel, B. Mathiasch, *ibid.* **1981**, *182*, 1685–1694.

[27] K. H. No, C. D. Gutsche, *J. Org. Chem.* **1982**, *47*, 2713–2719.

[28] Initially also compound **1a** obtained by the one-pot procedure was confirmed in this way: C. D. Gutsche, B. Dhawan, K. H. No, R. Muthukrishnan, *J. Am. Chem. Soc.* **1981**, *103*, 3782–3792.

[29] a) V. Böhmer, P. Chhim, H. Kämmerer, *Makromol. Chem.* **1979**, *180*, 2503–2506; b) V. Böhmer, F. Marschollek, L. Zetta, *J. Org. Chem.* **1987**, *52*, 3200–3205; c) J. de Mendoza, P. M. Nieto, P. Prados, C. Sanchez, *Tetrahedron* **1990**, *46*, 671–682; d) K. No, K. L. Hwang, *Bull. Korean Chem. Soc.* **1993**, *14*, 753–755.

[30] V. Böhmer, L. Merkel, U. Kunz, *J. Chem. Soc. Chem. Commun.* **1987**, 896–897. b) The azulene analogue of a calix[4]arene tetramethyl ether has also been obtained by 2 + 2 condensation, see ref. [58].

[31] a) C. Grüttner, V. Böhmer, W. Vogt, I. Thondorf, S. E. Biali, F. Grynszpan, *Tetahedron Lett.* **1994**, *35*, 6267–6270; b) see also: G. Sartori, R. Maggi, F. Bigi, A. Arduini, A. Pastorio, C. Porta, *J. Chem. Soc. Perkin Trans. 1* **1994**, 1657–1658.

[32] a) H. Casabianca, J. Royer, A. Satrallah, A. Taty-C, J. Vicens, *Tetrahedron. Lett.* **1987**, *28*, 6595–6596; b) M. Tabatabai, W. Vogt, V. Böhmer, *ibid.* **1990**, *31*, 3295–3298.

[33] a) Y. Fukazawa, K. Deyama, S. Usui, *Tetrahedron Lett.* **1992**, *33*, 5803–5806; b) for tetrahydroxycalix[5]arenes see: S. Usui, K. Deyama, R. Kinoshita, Y. Odagaki, Y. Fukazawa, *ibid.* **1993**, *34*, 8127–8130.

[34] We recently obtained calix[6]arenes, including examples with OH groups in *exo* position in a "4 + 2" condensation, cf. ref. [38].

[35] V. Böhmer, K. Jung, M. Schön, A. Wolff, *J. Org. Chem.* **1992**, *57*, 790–792.

[36] S. Pappalardo, G. Ferguson, J. F. Gallagher, *J. Org. Chem.* **1992**, *57*, 7102–7109.

[37] a) D.W. Chasar, *J. Org. Chem.* **1985**, *50*, 545–546. b) V. Böhmer, R. Dörrenbächer, W. Vogt, L. Zetta, *Tetrahedron Lett.* **1992**, *33*, 769–772.

[38] a) V. Böhmer, W. Vogt, R. Dörrenbächer, M. Frings, G. Ferguson, unpublished results. b) The sterically more demanding *tert*-butyl groups favor an intramolecular hydrogen bond more than do methyl groups.

[39] a) V. Böhmer, H. Goldmann, W. Vogt, *J. Chem. Soc. Chem. Commun.* **1985**, 667–668; b) E. Paulus, V. Böhmer, H. Goldmann, W. Vogt, *J. Chem. Soc. Perkin Trans. 2*, **1987**, 1609–1615; c) H. Goldmann, W. Vogt, E. Paulus, V. Böhmer, *J. Am. Chem. Soc.* **1988**, *110*, 6811–6817.

[40] F. Arnaud-Neu, V. Böhmer, L. Guerra, M. A. McKervey, E. F. Paulus, A. Rodriguez, M.-J. Schwing-Weill, M. Tabatabai, W. Vogt, *J. Phys. Org. Chem.* **1992**, *5*, 471–481.

[41] a) V. Böhmer, H. Goldmann, M. Tabatabai, unpublished results. b) Here we should also mention similar double calix[4]arenes with one or four bridges: V. Böhmer, H. Goldmann, W. Vogt, J. Vicens, Z. Asfari, *Tetrahedron Lett.* **1989**, *30*, 1391–1394.

[42] This defines the orientation of the group R with respect to one of the CHR bridges. If the macrocyclic system is viewed as being planar, these groups are either on the same side (c) or on the opposite side (t) to the group taken as a reference (r). However, this classification is not always used. Gutsche uses the *cis/trans* notation to denote the relative orientation of two neighboring bridges (cf. [1]). Thus he describes the *rtct* isomer as the *trans,trans,trans,trans* isomer. Further confusion is caused by the fact that these configurational isomers can (at least in principle) adopt different conformations, and that these two stereochemical aspects are not always clearly distinguished.

[43] a) A. G. S. Högberg, *J. Org. Chem.* **1980**, *45*, 4498–4500; b) A. G. S. Högberg, *J. Am. Chem. Soc.* **1980**, *102*, 6046–6050.

[44] a) L. M. Tunstadt, J. A. Tucker, E. Dalcanale, J. Weiser, J. A. Bryant, J. C. Sherman, R. C. Hegelson, C. B. Knobler, D. J. Cram, *J. Org. Chem.* **1989**, *54*, 1305–1312; b) R. J. M. Egberink, P. L. H. Cobben, W. Verboom, S. Harkema, D. N. Reinhoudt, *J. Incl. Phenom. Mol. Recogn.* **1992**, *12*, 151–158.

[45] a) L. Abis, E. Dalcanale, A. Du vosel, S. Spera, *J. Org. Chem.* **1988**, *53*, 5475–5479; b) F. Weinelt, H.-J. Schneider, *ibid.* **1991**, *56*, 5527–5535; c) G. Mann, F. Weinelt, S. Hauptmann, *J. Phys. Org. Chem.* **1989**, *2*, 531–539; d) G. Mann, V. Tittelbach-Helmrich, T. Lippmann, K. Müller, *Chromatographia* **1992**, *34*, 453–456; e) for the application of other aldehydes see ref. [185a].

[46] V. Böhmer, W. Vogt, R. Arnecke, unpublished results.

[47] K. Kobayashi, Y. Asakawa, Y. Kato, Y. Aoyama, *J. Am. Chem. Soc.* **1992**, *114*, 10307–10313.

[48] a) P. D. Beer, E. L. Tite, A. Ibbotson, *J. Chem. Soc. Chem. Commun.* **1989**, 1874–1876; b) P. D. Beer, E. L. Tite, A. Ibbotson, *J. Chem. Soc. Dalton Trans.* **1991**, 1691–1698.

[49] a) P. D. Beer, E. L. Tite, *Tetahedron Lett.* **1988**, *29*, 2349–2352; b) P. D. Beer, M. G. B. Drew, A. Ibbotson, E. L. Tite, *J. Chem. Soc. Chem. Commun.* **1988**, 1498–1500; c) P. D. Beer, E. L. Tite, M. G. B. Drew, A. Ibbotson, *J. Chem. Soc. Dalton Trans.* **1990**, 2543–2550.

[50] G. Cometti, E. Dalcanale, A. Du vosel, A.-M. Levelut, *J. Chem. Soc. Chem. Commun.* **1990**, 163–165.

[51] H. Konishi, O. Morikawa, *J. Chem. Soc. Chem. Commun.* **1993**, 34–35. b) The octamethyl ether of the methylene-bridged resorc[4]arene has been obtained by cyclization of 2,4-dimethoxybenzyl alcohol: O. M. Falama, E. Al-Farhan, P. M. Keehn, R. Stevenson, *Tetrahedron Lett.* **1994**, *35*, 65–68.

[52] a) B. Botta, P. Iacomacci, C. Di Giovanni, G. Delle Monache, E. Gacs-Baitz, M. Botta, A. Tafi, F. Corelli, D. Misiti, *J. Org. Chem.* **1992**, *57*, 3259–3261; b) B. Botta, M. C. Di Giovanni, G. Delle Monache, M. C. De Rosa, E. Gacs-Baitz, M. Botta, F. Corelli, A. Tafi, A. Santini, E. Benedetti, C. Pedone, D. Misiti, *ibid.* **1994**, *59*, 1532–1541.

[53] a) T. Sone, Y. Ohba, K. Moriya, H. Kumada, *Workshop on Calixarenes and Related Compounds*, 2.–4. June 1993, Kurume, Japan; b) Y. Ohba, K. Moriya, T. Sone, *Bull. Chem. Soc. Jpn.* **1991**, *64*, 576–582.

[54] a) H. Takemura, K. Yoshimura, I. U. Khan, T. Shinyozu, T. Inazu, *Tetrahedron Lett.* **1992**, *33*, 5775–5778; b) I. U. Khan, H. Takemura, M. Suenaga, T. Shinmyozu, T. Inazu, *J. Org. Chem.* **1993**, *58*, 3158–3161.

[55] F. Vögtle, J. Schmitz, M. Nieger, *Chem. Ber.* **1992**, *125*, 2523–2631; b) J. Schmitz, F. Vögtle, M. Nieger, K. Gloe, H. Stephan, O. Heitzsch, H.-J. Buschmann, K. Hasse, K. Cammann, *ibid.* **1993**, *126*, 2483–2491. c) Analogous macrocycles with pyridine building blocks can be obtained in the same manner: F. Vögtle, G. Brodesser, M. Nieger, K. Rissanen, *Recl. Trav. Chim. Pays-Bas* **1993**, *112*, 325–329. ; d) further examples: J. Schmitz, F. Vögtle, M. Nieger, K. Gloe, H. Stephan, O. Heitzsch, H.-J. Buschmann, *Supramol. Chem.* **1994**, *4*, 115–119.

[56] a) A. Tsuge, K. Tanaka, S. Sonda, S. Mataka, M. Tashiro, *J. Chem. Soc. Chem. Comm.* **1991**, 1329–1330, and references therein; b) M. Tashiro, A. Tsuge, T. Sawada, T. Makishima, S. Horie, T. Arimura, T. Yamato, *J. Org. Chem.* **1990**, *55*, 2404–2409.

[57] D. H. Burns, J. D. Miller, J. Santana, *J. Org. Chem.* **1993**, *58*, 6526–6528.

[58] A particularly ingenious example is the calix[4]arene derived from methoxyazulene: T. Asao, S. Ito, N. Morita, *Tetrahedron Lett.* **1988**, *29*, 2839–2842.

[59] a) R. M. Musau, A. Whiting, *J. Chem. Soc. Chem. Commun.* **1993**, 1029–1031; b) R. M. Musau, A. Whiting, *J. Chem. Soc. Perkin Trans 1*, **1994**, 2881–2888; c) D. S. C. Black, M. C. Bowyer, N. Kumar, P. S. R. Mitchell, *J. Chem. Soc. Chem. Commun.* **1993**, 819–821; d) P. E. Georghiou, Z. P. Li, *Tetrahedron Lett.* **1993**, *34*, 2887–2890. e) The structures of cyclic tetramers in which chromotropic acid units are linked by methylene bridges, appear, in view of the given data, not to be confirmed unequivocally: B.-P. Poh, C. M. Tan, C. L. Loh, *Tetrahedron* **1993**, *49*, 3489–3856, and references therein.

[60] a) H. Rauter, E. C. Hillgeris, B. Lippert, *J. Chem. Soc. Chem. Commun.* **1992**, 1385–1386; b) H. Rauter, E. C. Hillgeris, A. Erxleben, B. Lippert, *J. Am. Chem. Soc.* **1994**, *116*, 616–624.

[61] a) This has already been formulated in principle by Cornforth (cf. ref. [1]), although he considered these conformers to be separable isomers. b) A description suggested recently by Gutsche et al. for calix[6]arenes (cf. ref. [92]) could also be applied to other calixarenes.

[62] a) M. Perrin, D. Oehler, *Conformations of Calixarenes in the Crystalline State* in ref. [2], p. 65–85; b) G. D. Andreetti, F. Ugozzoli, *Inclusion Properties and Host-Guest Interactions of Calixarenes in the Solid State* in ref. [2], p. 87–123. For more recent examples see ref. [167a, 278a] and c) N. Ehlinger, S. Lecocq, R. Perrin, M. Perrin, *Supramol. Chem.* **1993**, *2*, 71–82.

[63] a) F. Gharnati, M. Perrin, S. Rantsordas, H. Goldmann, V. Böhmer, *J. Cryst. Spectr. Res.* **1991**, *21*, 69–74; b) S. Rantsordras, M. Perrin, F. Gharnati, S. Lecocq, W. Vogt, T. Fey, V. Böhmer, *J. Incl. Phenom. Mol. Recogn.* **1990**, *9*, 145–152; c) E. M. Georgiev, J. T. Mague, D. M. Roundhill, *Supramol. Chem.* **1993**, *2*, 53–60; d) Y. Ueda, T. Fujiwara, K. I. Tomita, Z. Asfari, J. Vicens, *J. Incl. Phenom. Mol. Recogn.* **1993**, *15*, 341–349.

[64] Shinkai et al. report that *p*-hexanoylcalix[4]arene crystallizes out in the *partial cone* conformation from the melt at higher temperatures (see ref. [162]).

[65] G. D. Andreetti, V. Böhmer, J. G. Jordan, M. Tabatabai, F. Ugozzoli, W. Vogt, A. Wolff, *Z. Org. Chem.* **1993**, *58*, 4023–4032.

[66] E. Dahan, S. E. Biali, *J. Org. Chem.* **1991**, *56*, 7269–7274.

[67] a) G. D. Andreetti, R. Ungaro, A. Pochini, *J. Chem. Soc. Chem. Commun.* **1979**, 1005–1007; b) For the reduced symmetry of the moleular complexes at low temperature see: G. A. Facey, R. H. Dubois, M. Zakrzewski, C. I. Ratcliffe, J. L. Atwood, J. A. Ripmeester, *Supramol. Chem.* **1993**, *1*, 199–200.

[68] J. L. Atwood, F. Hamada, K. D. Robinson, G. W. Orr, R. L. Vicent, *Nature* **1991**, *349*, 683–684.

[69] J. M. Harrowfield, M. I. Ogden, W. R. Richmond, A. H. White, *J. Chem. Soc. Chem. Commun.* **1991**, 1159–1161.

[70] V. Böhmer, H. Goldmann, W. Vogt, E. F. Paulus, F. L. Tobiason, M. J. Thielman, *J. Chem. Soc. Perkin Trans. 2* **1990**, 1769–1775.

[71] a) M. Coruzzi, G. D. Andreetti, V. Bocchi, A. Pochini, R. Ungaro, *J. Chem. Soc. Perkin Trans. 2* **1982**, 1133–1138; b) M. Perrin, S. Lecocq, *J. Incl. Phe-*

nom. Mol. Recogn. **1991**, *11*, 171–183; c) R. K. Juneja, K. D. Robinson, G. W. Orr, R. H. Dubois, K. A. Belmore, J. L. Atwood, J. M. Ripmeester, C. I. Ratcliffe, *ibid.* **1992**, *13*, 93–96; d) J. F. Gallagher, G. Ferguson, V. Böhmer, D. Kraft, *Acta Cryst. C*, **1994**, *50*, 73–77; e) for the crystal structure of a tetrahydroxycalix[5]arene see ref. [33b], for a calix[5]arene with C_s symmetry see ref. [83].

[72] a) M. Halit, D. Oehler, M. Perrin, A. Thozet, R. Perrin, J. Vicens, M. Bourakhouadar, *J. Incl. Phenom.* **1988**, *6*, 613–623; b) G. D. Andreetti, F. Ugozzoli, A. Casnati, E. Ghidini, A. Pochini, R. Ungaro, *Gazz. Chim. Ital.* **1989**, *119*, 47–50; c) J. L. Atwood, D. L. Clark, R. K. Juneja, G. W. Orr, K. D. Robinson, R. L. Vincent, *J. Am. Chem. Soc.* **1992**, *114*, 7558–7559; d) L. M. Engelhardt, B. M. Furphy, J. M. Harrowfield, D. L. Kepert, A. H. White, F. R. Wilner, *Aust. J. Chem.* **1988**, *41*, 1465–1476; e) see also ref. [18b].

[73] a) M. Perrin, S. Lecocq, *C. R. Acad. Sci. Paris* **1990**, *310*, 515–; b) G. D. Andreetti, F. Ugozzoli, Y. Nakamoto, S.-I. Ishida, *J. Incl. Phenom. Mol. Recogn.* **1991**, *10*, 241–253.

[74] a) C. D. Gutsche, A. E. Gutsche, A. I. Karaulov, *J. Incl. Phenom.* **1985**, *3*, 447–451; b) M. Czugler, S. Tisza, G. Speier, *J. Incl. Phenom. Mol. Recogn.* **1991**, *11*, 323–331.

[75] Since the aromatic systems (including the atoms bonded to them) can be considered to be planar even as a very good approximation, a calix[*n*]arene can in principle be described by $(n-1)$ pairs of such torsional angles. However, *n* pairs are given for the sake of clarity. The *cone* conformation (and any *cone*-like conformation) is characterized by a continual change of sign (+ −) within these pairs. The other conformations of calix[4]arenes are described as follows: *partial cone* + −, + −, + +, − ; 1,2-*alternate* + −, + −, + +, −, and 1,3-*alternate* + +, − , + +, −. The conformations of calix[6]arenes (Fig. 2) have torsional angles with the following sign sequences: left) + −, + −, − +, + −, + −, − + ; right) + −, + −, + , − +, − +, −. Compare: F. Ugozzoli, G. D. Andreetti, *J. Incl. Phenom. Mol. Recogn.* **1992**, *13*, 337–348.

[76] a) F. Grynszpan, Z. Goren, S. E. Biali, *J. Org. Chem.* **1991**, *56*, 532–536; b) F. Grynszpan, S. E. Biali, *Tetrahedron Lett.* **1991**, *32*, 5155–5158. c) The compound originally described in **23a** turned out to be **23h**: F. Grynszpan, O. Aleksiuk, S. E. Biali, *J. Org. Chem.* **1994**, *59*, 2070–2074.

[77] J. E. McMurry, J. C. Phelan, *Tetrahedron Lett.* **1991**, *32*, 5655–5658.

[78] a) C. G. Gibbs, C. D. Gutsche, *J. Am. Chem. Soc.* **1993**, *115*, 5338–5339; b) X. Delaigue, J. M. Harrowfield, M. W. Hosseini, A. De Cian, J. Fischer, N. Kyritsakas, *J. Chem. Soc. Chem. Commun.* **1994**, 1579–1580. c) Like **1a**, **10** has also been converted to the corresponding tetramercapto compound: X. Delaigue, M. W. Hosseini, *Tetrahedron Lett.* **1993**, *34*, 8111–8112.

[79] a) Y. Morita, T. Agawa, Y. Kai, N. Kanehisa, N. Kasai, E. Nomura, H. Taniguchi, *Chem. Lett.* **1989**, 1349–1352; b) Y. Morita, T. Agawa, E. Nomura, H. Taniguchi, *J. Org. Chem.* **1992**, *57*, 3658–3662.

[80] Most of the structures refer to derivatives such as the octaesters (Section 5.2), cavitands, carcerands etc. (Section 6.2) and thus also naturally prove the structure of the parent calix[4]arenes.

[81] a) T. Lippmann, H. Wilde, M. Pink, A. Schäfer, M. Hesse, G. Mann, *Angew. Chem.* **1993**, *105*, 1258–1260; *Angew. Chem. Int. Ed. Engl.* **1993**, *32*, 1195–; b) D. A. Leigh, P. Linnane, R. G. Pritchard, G. Jackson, *J. Chem. Soc. Chem. Commun.* **1994**, 389–390.

[82] a) K. Araki, S. Shinkai, T. Matsuda, *Chem. Lett.* **1989**, 581–584; b) S. Shinkai, K. Araki, T. Matsuda, O. Manabe, *Bull. Chem. Soc. Jpn.* **1989**, 3856–3862; c) K. Araki, H. Murakami, F. Ohseto, S. Shinkai, *Chem. Lett.* **1992**, 539–542; d) T. Harada, F. Ohseto, S. Shinkai, *Tetrahedron* **1994**, *50*, 13377–13394.

[83] M. Tabatabai, W. Vogt, V. Böhmer, G. Ferguson, E. F. Paulus, *Supramol. Chem.* **1994**, *4*, 147–152.

[84] P. D. J. Grootenhuis, P. A. Kollman, L. C. Groenen, D. N. Reinhoudt, G. J. van Hummel, F. Ugozzoli, G. D. Andreetti, *J. Am. Chem. Soc.* **1990**, *112*, 4165–4176.

[85] S. Biali, V. Böhmer et al. unpublished results.

[86] C. D. Gutsche, *Single Step Synthesis and Properties of Calixarenes*, in ref. [2], p. 3–37.

[87] C. D. Gutsche, L. J. Bauer, *Tetrahedron Lett.* **1981**, *22*, 4763–4766.

[88] M. A. Molins, P. M. Nieto, C. Sanchez, P. Prados, J. de Mendoza, M. Pons, *J. Org. Chem.* **1992**, *57*, 6924–6931.

[89] L. Abis, E. Dalcanale, A. Du Vosel, S. Spera, *J. Chem. Soc. Perkin Trans. 2* **1990**, 2075–2080.

[90] In these octaesters, which are derivatives of isomers with different configurations, the conformation with an axial arrangement of the groups at the carbon atoms of the bridges seems to be general (but see ref. [45c]). The *rccc* isomer has a flattened *cone* conformation with C_{2v} symmetry, often described as the boat conformation. The interconversion $C_{2v} \rightarrow C_{2v}$ occurs via a transition state with C_{4v} symmetry. The *rcct* isomer has a chair conformation with C_{2h} symmetry, which can be the time average of two *partial cone* or two 1,2-*alternate* conformations. The *rcci* isomer takes up a 1,2-*alternate* conformation with C_s symmetry, which has also been described as the diamond conformation (see ref. [45a]).

[91] The two signals, each for four OH protons, which are observed in $CDCl_3$ but not in [D_6]acetone or [D_6]dimethyl sulfoxide, are assigned to different OH groups in systems of cyclic hydrogen bonds, see ref. [274].

[92] Solubilities in benzonitrile (and several other solvents) have recently been reported: a) A. F. Danil de Namor, M. T. G. Pardo, D. A. P. Tanaka, F. S. S. Velarde, J. D. C. Garcia, M. C. Cabaleiro, J. M. A. Al-Rawi *J. Chem. Soc. Faraday Trans.* **1993**, *89*, 2727–2736; b) A. F. Danil de Namor, *Pure Appl. Chem.* **1993**, *65*, 193–202; c) M. H. B. Grote Gansey, W. Verboom, D. N. Reinhoudt, *Tetrahedron Lett.* **1994**, *35*, 7127–7130; d) Y. Shi, Z. Zhang, *J. Chem. Soc. Chem. Commun.* **1994**, 375–376.

[93] Melting point differences of up to 180 °C can be caused merely by different sequences of the phenol units in positional isomers of calix[4]arenes of the type ABCD, see ref. [29b].

[94] V. Böhmer, H. Goldmann, R. Kaptein, L. Zetta, *J. Chem. Soc. Chem. Commun.* **1987**, 1358–1360.

[95] S. W. Keller, G. M. Schuster, F. L. Tobiason, *Polym. Mater. Sci. Eng.* **1987**, *57*, 906–910.

[96] Y. Aoyama, Y. Tanaka, S. Sugahara, *J. Am. Chem. Soc.* **1989**, *111*, 5397–5404.

[97] S. Shinkai, K. Araki, P. D. J. Grootenhuis, D. N. Reinhoudt, *J. Chem. Soc. Perkin Trans. 2* **1991**, 1883–1886. Earlier measurements, in which in part considerably lower values for pK_{a2} were obtained, appear to be less reliable.

[98] G. Arenea, R. Cali, G. G. Lombardo, E. Rizzarelli, D. Sciotto, R. Ungaro, A. Casnati, *Supramol. Chem.* **1992**, *1*, 19–24.

[99] I. Yoshida, N. Yamamoto, F. Sagara, D. Ishii, K. Ueno, S. Shinkai, *Bull. Chem. Soc. Jpn.* **1992**, *65*, 1012–1015.

[100] J.-P. Scharff, M. Mahjoubi, R. Perrin, *New J. Chem.* **1992**, *15*, 883–887.

[101] V. Böhmer, E. Schade, C. Antes, J. Pachta, W. Vogt, H. Kämmerer, *Makromol. Chem.* **1983**, *184*, 2361–2376.

[102] V. Böhmer, E. Schade, W. Vogt, *Makromol. Chem. Rapid. Commun.*, **1984**, *5*, 221–224.

[103] See for example: H.-J. Schneider, D. Güttes, U. Schneider, *J. Am. Chem. Soc.* **1988**, *110*, 6449–6454.

[104] A slow isomerization of the tetra-O-alkyl derivatives has been observed for ethyl groups (K. Araki, K. Iwamoto, S. Shinkai, T. Matsuda, *Chem. Lett.* **1989**, 1747–1750) and even for β-hydroxyethyl groups (footnote in ref. [285a]).

[105] a) K. Iwamoto, K. Araki, S. Shinkai, *Tetrahedron* **1991**, *47*, 4325–4342; b) K. Iwamoto, S. Shinkai, *J. Org. Chem.* **1992**, *57*, 7066–7073.

[106] Conclusions as to the conformation can also be reached on the basis of the chemical shift of the methylene bridges in the ^{13}C NMR spectra: C. Jaime, J. de Mendoza, P. Prados, P. M. Nieto, C. Sanchez, *J. Org. Chem.* **1991**, *56*, 3372–3376.

[107] a) C. Rizzoli, G. D. Andreetti, R. Ungaro, A. Pochini, *J. Mol. Struct.* **1982**, *82*, 133–141; b) L. C. Groenen, J.-D. van Loon, W. Verboom, S. Harkema, A. Casnati, R. Ungaro, A. Pochini, F. Ugozzoli, D. N. Reinhoudt, *J. Am. Chem. Soc.* **1991**, *113*, 2385–2392; c) W. Verboom, S. Datta, Z. Asfari, S. Harkema, D. N. Reinhoudt, *J. Org. Chem.* **1992**, *57*, 5394–5398.

[108] a) M. Conner, I. Kudelka, S. L. Regen, *Langmuir* **1991**, *7*, 982–987; b) K. Araki, A. Yanagi, S. Shinkai, *Tetrahedron* **1993**, *49*, 6763–6772.

[109] S. Pappallardo, L. Giunta, M. Foti, G. Ferguson, J. F. Gallagher, B. Kaitner, *J. Org. Chem.* **1992**, *57*, 2611–2624.

[110] a) A. Arduini, A. Pochini, S. Reverberi, R. Ungaro, G. D. Andreetti, F. Ugozzoli, *Tetrahedron* **1986**, *42*, 2089–2100; b) F. Arnaud-Neu, E. M. Collins, M. Deasy, G. Ferguson, S. J. Harris, B. Kaitner, A. J. Lough, M. A. McKervey, E. Marques, B. L. Ruhl, M. J. Schwing-Weill, E. M. Seward, *J. Am. Chem. Soc.* **1989**, *111*, 8681–8691.

[111] a) S.-K. Chang, I. Cho, *J. Chem. Soc. Perkin Trans. 2* **1986**, 211–214; b) S.-K. Chang, S.-K. Kwon, I. Cho, *Chem. Lett.* **1987**, 947–948; c) G. Calestani, F. Ugozzoli, A. Arduini, E. Ghidini, R. Ungaro, *J. Chem. Soc. Chem. Commun.* **1987**, 344–346; d) A. Arduini, E. Ghidini, A. Pochini, R. Ungaro, G. D. Andreetti, G. Calestani, F. Ugozzoli, *J. Incl. Phenom.* **1988**, *6*, 119–134; e) F. Arnaud-Neu, M.-J. Schwing-Weill, K. Ziat, S. Cremin, S. J. Harris, M. A. McKervey, *New. J. Chem.* **1991**, *15*, 33–37.

[112] G. Ferguson, B. Kaitner, M. A. McKervey, E. M. Seward, *J. Chem. Soc. Chem. Commun.* **1987**, 584–585.

[113] C. Floriani, D. Jacoby, A. Chiesa-Villa, C. Gustini, *Angew. Chem.* **1989**, *101*, 1430–1431; *Angew. Chem. Int. Ed. Engl.* **1989**, *28*, 1376–1377.

[114] M. A. McKervey et al., unpublished results, personal communication.

[115] J.-D. van Loon, J. F. Heida, W. Verboom, D. N. Reinhoudt, *Recl. Trav. Chim. Pays-Bas* **1992**, *111*, 353–359.

[116] M. Iqbal, T. Mangiafico, C. D. Gutsche, *Tetrahedron* **1992**, *43*, 4917–4930.

[117] a) A. Barrett, M. A. McKervey, J. F. Malone, A. Walker, F. Arnaud-Neu, L. Guerra, M.-J. Schwing-Weill, C. D. Gutsche, D. R. Stewart, *J. Chem. Soc. Perkin Trans. 2* **1993**, 1475–1479; b) B. Souley, Z. Asfari, J. Vicens, *Pol. J. Chem.* **1993**, *67*, 763–767; c) careful investigations of the conformations of ether and ester derivatives the *t*-butylcalix[5]arene: D. R. Stewart, M. Krawiec, R. P. Kashyap, W. H. Watson, C. D. Gutsche, *J. Am. Chem. Soc.* **1995**, *117*, 586–601.

[118] a) A. Casnati, P. Minari, A. Pochini, R. Ungaro, W. F. Nijenhuis, F. de Jong, D. N. Reinhoudt, *Isr. J. Chem.* **1992**, *32*, 79–87; b) E. Nomura, H. Taniguchi, K. Kawaguchi, Y. Otsuji, *J. Org. Chem.* **1993**, *58*, 4709–4715.

[119] a) T. Arimura, H. Kawabata, T. Matsuda, T. Muramatsu, H. Satoh, K. Fujio, O. Manabe, S. Shinkai, *J. Org. Chem.* **1991**, *56*, 301–306; b) A. Ikeda, T. Nagasaki, S. Shinkai, *J. Phys. Org. Chem.* **1992**, 5, 699–710.

[120] a) Z. Goren, S. E. Biali, *J. Chem. Soc. Perkin Trans. 1* **1990**, 1484–1487; cf. also ref. [76]; b) J.-B. Regnouf de Vains, S. Pellet-Rostaing, R. Lamartine, *Tetahedron Lett.* **1994**, *35*, 8147–8150.

[121] a) C. D. Gutsche, L. J. Bauer, *J. Am. Chem. Soc.* **1985**, *107*, 6059–6063; b) H. Otsuka, K. Araki, T. Sakaki, K. Nakashima, S. Shinkai, *Tetrahedron Lett.* **1993**, *34*, 7275–7278.

[122] a) R. Ungaro, A. Pochini, G. D. Andreetti, *J. Incl. Phenom.* **1984**, *2*, 199–206; b) F. Arnaud-Neu, G. Barrett, S. Cremin, M. Deasy, G. Ferguson, S. J. Harris, A. J. Lough, L. Guerra, M. A. McKervey, M.-J. Schwing-Weill, P. Schwinté, *J. Chem. Soc. Perkin Trans. 2* **1992**, 1119–1125; c) F. Arnaud-Neu, G. Barrett, S. J. Harris, M. Owens, M. A. McKervey, M.-J. Schwing-Weill, P. Schwinté, *Inorg. Chem.* **1993**, *32*, 2644–2650.

[123] R. Ostaszewski, T. W. Stevens, W. Verboom, D. N. Reinhoudt, *Recl. Trav. Chim. Pays-Bas* **1991**, *110*, 294–298.

[124] a) P. L. H. M. Cobben, R. J. M. Egberink, J. G. Bomer, P. Bergveld, W. Verboom, D. N. Reinhoudt, *J. Am. Chem. Soc.* **1992**, *114*, 10573–10582; b) J. K. Moran, E. M. Georgiev, A. T. Yordanov, J. T. Mague, D. M. Roundhill, *J. Org. Chem.* **1994**, *59*, 5990–5998.

[125] J. D. van Loon, W. Verboom, D. N. Reinhoudt, *Org. Prep. Proced. Int.* **1992**, *24*, 437–462.

[126] While a numbering of all the C atoms based on the IUPAC name is also used, so that for example the 1,3-dimethyl ether of a calix[4]arene is to be named as 25,27-dihydroxy-26,28-dimethoxycalix[4]arene (see ref. [1]), this inconsequence appears to cause no confusion in practice.

[127] a) C. D. Gutsche, L.-G. Lin, *Tetrahedron* **1986**, *42*, 1633–1640; b) for a similar strategy see: S. Shang, D. V. Khasnis, J. M. Burton, C. J. Santini, M. M. Fan, A. C. Small, M. Lattman, *Organometallics* **1994**, *13*, 5157–5159.

[128] K. A. See, F. R. Fronczek, W. H. Watson, R. P. Kashyap, C. D. Gutsche, *J. Org. Chem.* **1991**, *56*, 7256–7268.

[129] A. M. King, C. P. Moore, K. R. A. Samankumara Sandanayake, I. O. Sutherland, *J. Chem. Soc. Chem. Commun.* **1992**, 582–584.

[130] L. C. Groenen, B. H. M. Ruel, A. Casnati, W. Verboom, A. Pochini, R. Ungaro, D. N. Reinhoudt, *Tetrahedron* **1991**, *47*, 8379–8384.

[131] a) K. Iwamoto, A. Yanagi, T. Arimura, T. Matsuda, S. Shinkai, *Chem. Lett.* **1990**, 1901–1904; b) K. Iwamoto, A. Yanagi, K. Araki, S. Shinkai, *ibid.* **1991**, 473–476.

[132] A. Casnati, A. Arduini, E. Ghidini, A. Pochini, R. Ungaro, *Tetrahedron* **1991**, *47*, 2221–2228.

[133] a) C. D. Gutsche, B. Dhawan, J. A. Levine, K. N. No, L. J. Bauer, *Tetrahedron* **1983**, *39*, 409–426; b) K. Iwamoto, K. Fujimoto, T. Matsuda, S. Shinkai, *Tetrahedron Lett.* **1990**, *31*, 7169–7172; c) K. Iwamoto, K. Araki, S. Shinkai, *J. Org. Chem.*, **1991**, *56*, 4955–4962.

[134] a) C. D. Gutsche, K. A. See, *J. Org. Chem.* **1992**, *57*, 4527–4539; b) C. Shu, W. Liu, M. Ku, F. Tang, M. Yeh, L. Lin, *ibid.* **1994**, *59*, 3730–3733.

[135] a) E. M. Collins, M. A. McKervey, S. J. Harris, *J. Chem. Soc. Perkin Trans. 1* **1989**, 372–374; b) J.-D. van Loon, A. Arduini, W. Verboom, R. Ungaro, G. J. van Hummel, S. Harkema, D. N. Reinhoudt, *Tetrahedron Lett.* **1989**, *30*, 2681–2684; c) J.-D. v. Loon, A. Arduini, L. Coppi, W. Verboom, A. Pochini, R. Ungaro, S. Harkema, D. N. Reinhoudt, *J. Org. Chem.* **1990**, *55*, 5639–5646; d) E. M. Collins, M. A. McKervey, E. Madigan, M. B. Moran, M. Owens, G. Ferguson, S. J. Harris, *J. Chem. Soc. Perkin Trans. 1* **1991**, 3137–3142.

[136] L. C. Groenen, B. H. M. Ruel, A. Casnati, P. Timmerman, W. Verboom, S. Harkema, A. Pochini, R. Ungaro, D. N. Reinhoudt, *Tetrahedron Lett.* **1991**, *32*, 2675–2678; b) J. A. J. Brunink, W. Verboom, J. F. J. Engbersen, S. Harkema, D. N. Reinhoudt, *Recl. Trav. Chim. Pays-Bas* **1992**, *111*, 511–516; c) in the case of 1,2-O-alkylation with 2-chloromethylpyridine a yield of 85% was recently reported [222b].

[137] a) A. Arduini, A. Casnati, L. Dodi, A. Pochini, R. Ungaro, *J. Chem. Soc. Chem. Commun.* **1990**, 1597–1598. b) For the synthesis of 1,2- and 1,3-crown ethers of calix[4]arenes cf. also: H. Yamamoto, T. Sakaki, S. Shinkai, *Chem. Lett.* **1994**, 469–472.

[138] a) S. Kanamathareddy, C. D. Gutsche, *J. Org. Chem.* **1992**, *57*, 3160–3166; b) P. Neri, S. Pappalardo, *ibid.* **1993**, *58*, 1048–1053; c) P. Neri, C. Rocco, G. M. L. Consoli, M. Piattelli, *ibid.* **1993**, *58*, 6535–6537.

[139] J. S. Rogers, C. D. Gutsche, *J. Org. Chem.* **1992**, *57*, 3152–3159.

[140] a) R. G. Janssen, W. Verboom, D. N. Reinhoudt, A. Casnati, M. Freriks, A. Pochini, F. Ugozzoli, R. Ungaro, P. M. Nieto, M. Carramolino, F. Cuevas, P. Prados, J. de Mendoza, *Synthesis* **1993**, 380–386. b) Other selective derivates of calix[6]arene see: J. de Mendoza, M. Carramolino, F. Cuevas, P. M. Nieto, P. Prados, D. N. Reinhoudt, W. Verboom, R. Ungaro, A. Casnati, *ibid.* **1994**, 47–50; c) H. Otsuka, K. Araki, S. Shinkai, *J. Org. Chem.* **1994**, *59*, 1542–1547.

[141] J. K. Moran, D. M. Roundhill, *Inorg. Chem.* **1992**, *31*, 4213–4215.

[142] A. Casnati, P. Minari, A. Pochini, R. Ungaro, *J. Chem. Soc. Chem. Commun.* **1991**, 1413–1414.

[143] R. G. Janssen, W. Verboom, S. Harkema, G. J. van Hummel, D. N. Reinhoudt, A. Pochini, R. Ungaro, P. Prados, J. de Mendoza, *J. Chem. Soc. Chem. Commun.* **1993**, 506–508.

[144] P. Neri, C. Geraci, M. Piattelli, *Tetrahedron Lett.* **1993**, *34*, 3319–3322; cf. also ref. [307].

[145] a) S. Shinkai, K. Fujimoto, T. Otsuka, H. L. Ammon, *J. Org. Chem.* **1992**, *57*, 1516–1523; b) K. Fujimoto, N. Nishiyama, H. Tsuzuki, S. Shinkai, *J. Chem. Soc. Perkin Trans. 2* **1992**, 643–648; c) A. Casnati, A. Pochini, R. Ungaro, R. Cacciapaglia, L. Mandolini, *J. Chem. Soc. Perkin Trans 1* **1991**, 2052–2054.

[146] G. Barrett, V. Böhmer, G. Ferguson, J. F. Gallagher, S. J. Harris, R. G. Leonard, M. A. McKervey, M. Owens, M. Tabatabai, A. Vierengel, W. Vogt, *J. Chem. Soc. Perkin Trans. 2* **1992**, 1595–1601.

[147] K. Iwamoto, K. Araki, S. Shinkai, *J. Chem. Soc. Perkin Trans. 1* **1991**, 1611–1613.

[148] A structure, in which the opposing phenol units are really coplanar, would lead on the basis of standard bond lengths to an unusually short O–O distance and should therefore not correspond to an energy minimum.

[149] J. A. Kanters, A. Schouten, E. Steinwender, J. H. van der Maas, L. C. Groenen, D. N. Reinhoudt, *J. Mol. Struct.* **1992**, *269*, 49–64.

[150] a) L. C. Groenen, E. Steinwender, B. T.G. Lutz, J. H. van der Maas, D. N. Reinhoudt, *J. Chem. Soc. Perkin Trans. 2*, **1992**, 1893–1898; b) K. Iwamoto, A. Ikeda, K. Araki, T. Harada, S. Shinkai, *Tetrahedron* **1993**, *49*, 9937–9946.

[151] a) T. Nagasaki, K. Sisido, T. Arimura, S. Shinkai, *Tetrahedron*, **1992**, *48*, 797–804. b) T. Harad, J. M. Rudzinski, S. Shinkai, *J. Chem. Soc. Perkin Trans. 2*, **1992**, 2109–2115.

[152] a) J.-D. van Loon, L. D. Groenen, S. S. Wijmenga, W. Verboom, D. N. Reinhoudt, *J. Am. Chem. Soc.* **1991**, *113*, 2378–2384; b) J. Blixt, C. Detellier, *J. Am. Chem. Soc.* **1994**, *116*, 11957–11960.

[153] C. D. Gutsche, J. A. Levine, P. K. Sujeeth, *J. Org. Chem.* **1985**, *50*, 5802–5806; for a particular example see ref. [260].

[154] The elimination of *tert*-butyl groups had already been carried out for calix[4]arenes before Gutsche coined this name: H. Kämmerer, G. Happel, V. Böhmer, D. Rathay, *Monatsh. Chem.* **1978**, *109*, 767–773.

[155] a) M. Conner, V. Janout, S. L. Regen, *J. Org. Chem.* **1992**, *57*, 3744–3746; b) see also: F. Hamada, S. G. Bott, G. W. Orr, A. W. Coleman, H. M. Zhang, J. L. Atwood, *J. Incl. Phenom. Mol. Recogn.* **1990**, *9*, 195–206.

[156] Iodine derivatives have been obtained indirectly: a) A. Arduini, A. Pochini, A. Rizzi, A. R. Sicuri, R. Ungaro, *Tetrahedron Lett.* **1990**, *31*, 4653–4656; b) A. Arduini, A. Pochini, A. R. Sicuri, A. Secchi, R. Ungaro, *Gazz. Chim. Ital.* **1994**, *124*, 129–132. c) For the direct iodination with $AgOOCCF_3/I_2$ and further reactions see: P. Timmerman, W. Verboom, D. N. Reinhoudt, A. Arduini, S. Grandi, A. R. Sicuri, A. Pochini, R. Ungaro, *Synthesis*, **1994**, 185–189.

[157] K. No, Y. Noh, *Bull. Korean Chem. Soc.* **1986**, *7*, 314–316.

[158] a) S. Shinkai, K. Araki, T. Tsubaki, T. Arimura, O. Manabe, *J. Chem. Soc. Perkin Trans. 1* **1987**, 2297–2299; b) A. Casnati, Y. Ting, D. Berti, M. Fabbi, A. Pochini, R. Ungaro, D. Sciotto, G. G. Lombardo, *Tetrahedron* **1993**, *49*, 9815–9822.

[159] a) Y. Morzherin, D. M. Rudkevich, W. Verboom, D. N. Reinhoudt, *J. Org. Chem.* **1993**, *58*, 7602–7605; b) calixarenes with chlorosulfone groups have also been obtained from the corresponding sulfonic acids: S. Shinkai, H. Kawabata, T. Matsuda, H. Kawaguchi, O. Manage, *Bull. Chem. Soc. Jpn.* **1990**, *63*, 1272–1274.

[160] M. Almi, A. Arduini, A. Casnati, A. Pochini, R. Ungaro, *Tetrahedron* **1989**, *45*, 2177–2182.

[161] a) C. D. Gutsche, K. C. Nam, *J. Am. Chem. Soc.* **1988**, *110*, 6153–6162; b) C. D. Gutsche, I. Alam, *Tetrahedron* **1988**, *44*, 4689–4694; c) for aminomethylation see also ref. [170].

[162] a) S. Shinkai, T. Nagasaki, K.Iwamoto, A. Ikeda, G.-X. He, T. Matsuda, M. Iwamoto, *Bull. Chem. Soc. Jpn.* **1991**, *64*, 381–386; b) Z.-T. Huang, G.-Q. Wang, *Chem. Ber.* **1994**, *127*, 519–523.

[163] a) S. Shinkai, K. Araki, J. Shibita, O. Manabe, *J. Chem. Soc. Perkin Trans. 1* **1989**, 195–196; b) M. Yeh, F. Tang, S. Chen, W. Liu, L. Lin, *J. Org. Chem.* **1994**, *59*, 754–757.

[164] J. L. Atwood, S. G. Bott, *Water Soluble Calixarene Salts. A Class of Compounds with Solid-State Structures Resembling Those of Clays.* in ref. [2], p. 199–210.

[165] a) W. Verboom, A. Durie, R. Egberink, Z. Asfari, D. N. Reinhoudt, *J. Org. Chem.* **1992**, *57*, 1313–1316; b) M. Brake, V. Böhmer, P. Krämer, W. Vogt, R. Wortmann, *Supramol. Chem.* **1993**, *2*, 65–70.

[166] a) K. No, Y. Noh, Y. Kim, *Bull. Korean Chem. Soc.* **1986**, *7*, 442; b) T. Arimura, S. Shinkai, T. Matsuda, Y. Hirata, H. Satoh, O. Manabe, *Bull. Chem. Soc. Jpn.* **1988**, *61*, 3733–3734.

[167] a) R. K. Juneja, K. D. Robinson, C. P. Johnson, J. L. Atwood, *J. Am. Chem. Soc.* **1993**, *115*, 3818–3819; b) M. S. Wong, J. F. Nicoud, *Tetrahedron Lett.* **1993**, *34*, 8237–8240; c) K. S. Paek, H. J. Ihm, K. H. No, *Bull. Korean Chem. Soc.* **1994**, *15*, p. 422–423.

[168] P. D. Beer, M. G. B. Drew, C. Hazlewood, D. Hesek, J. Hodacova, S. E. Stokes, *J. Chem. Soc. Chem. Commun.* **1993**, 229–231.

[169] A. Arduini, A. Pochini, A. Rizzi, A. R. Sicuri, F. Ugozzoli, R. Ungaro, *Tetrahedron* **1992**, *48*, 905–912.

[170] I. Alam, S. K. Sharma, C. D. Gutsche, *J. Org. Chem.* **1994**, *59*, 3716–3720.

[171] A. Arduini, G. Manfredi, A. Pochini, A. R. Sicuri, R. Ungaro, *J. Chem. Soc. Chem. Commun.* **1991**, 936–937.

[172] Z.-T. Huang, G.-Q. Wang, *J. Chem. Soc. Perkin Trans. 1* **1993**, 167–168; see also ref. [162b].

[173] P. A. Reddy, R. P. Kashyap, W. H. Watson, C. D. Gutsche, *Isr. J. Chem.* **1992**, *32*, 89–96.

[174] a) A. Casnati, E. Comelli, M. Fabbi, V. Bocchi, G. Mori, F. Ugozzoli, A. M. Manotti Lanfredi, A. Pochini, R. Ungaro, *Recl. Trav. Chim. Pays-Bas* **1993**, *112*, 384–392; b) P. D. Beer, Z. Chen, P. A. Gale, *Tetrahedron*, **1994**, *50*, 931–940; c) P. D. Beer, Z. Chen, M. G. B. Drew, P. A. Gale, *J. Chem. Soc. Chem. Commun.* **1994**, 2207–2208.

[175] a) P. A. Reddy, C. D. Gutsche, *J. Org. Chem.* **1993**, *58*, 3245–3251. b) Surprisingly also the bromination and nitration of *p*-acetamidophenol units leads to calix[4]arenes with *m*-substituted phenol units: W. Verboom, P. J. Bodewes, G. van Essen, P. Timmerman, G. J. van Hummel, S. Harkema, D. N. Reinhoudt, *Tetrahedron*, **1995**, *51*, 499–512.

[176] G. Görmar, K. Seiffarth, M. Schulz, J. Zimmermann, G. Flämig, *Makromol. Chem.* **1990**, *191*, 81–87.

[177] a) Y. Ting, W. Verboom, L. C. Groenen, J.-D. van Loon, D. N. Reinhoudt, *J. Chem. Soc. Chem. Commun.* **1990**, 1432–1433; b) F. Frynszpan, N. Dinoor, S. E. Biali, *Tetrahedron Lett.* **1991**, 1909–1912; c) F. Grynszpan, S. Biali, *J. Phys. Org. Chem.* **1992**, *5*, 155–159.

[178] F. Ohseto, H. Murkami, K. Araki, S. Shinkai, *Tetrahedron Lett.* **1992**, *33*, 1217–1220.

[179] a) A. M. Litwak, S. E. Biali, *J. Org. Chem.* **1992**, *57*, 1943–1945; b) A. M. Litwak, F. Grynszpan, O. Aleksiuk, S. Cohen, S. E. Biali, *ibid.* **1993**, *58*, 393–402; c) F. Grynszpan, S. E. Biali, *J. Chem. Soc. Chem. Commun.* **1994**, 2545–2546.

[180] O. Aleksiuk, F. Grynszpan, S. E. Biali, *J. Chem. Soc. Chem. Commun.* **1993**, 11–13.

[181] O. Aleksiuk, F. Grynszpan, S. E. Biali, *J. Org. Chem.* **1993**, *58*, 1994–1996.

[182] L. N. Markovsky, V. I. Kal'chenko, D. M. Rudkevich, A. N. Shivanyuk, *Mendeleev Commun.* **1992**, 106–108; the NMR data can however be explained better by a structure in which two opposite units are each doubly acylated.

[183] D. J. Cram, S. Karbach, H.-E. Kim, C. B. Knobler, E. F. Maverick, J. L. Ericson, R. C. Helgeson, *J. Am. Chem. Soc.* **1988**, *110*, 2229–2237.

[184] O. Manabe, K. Asakura, T. Nishi, S. Shinkai, *Chem. Lett.* **1990**, 1219–1222.

[185] a) U. Schneider, H. J. Schneider, *Chem. Ber.* **1994**, *127*, 2455–2469; b) Y. Matsushita, T. Matsui, *Tetrahedron Lett.* **1993**, *34*, 7433–7436; c) R. Arnecke, V. Böhmer, E. F. Paulus, W. Vogt, *J. Am. Chem. Soc.* **1995**, *117*, in press; for the X-ray structure analysis see ref. [81b]; d) H.-J. Schneider, U. Schneider, *J. Incl. Phenom. Mol. Recogn.* **1994**, in press.

[186] C. Alfieri, E. Dradi, A. Pochini, R. Ungaro, G. D. Andreetti, *J. Chem. Soc. Chem. Commun.* **1983**, 1075–1076.

[187] For the conformation in the crystalline state cf. also: G. D. Andreetti, O. Ori, F. Ugozzoli, C. Alfieri, A. Pochini, R. Ungaro, *J. Incl. Phenom.* **1988**, *6*, 523–536.

[188] a) E. Ghidini, F. Ugozzoli, R. Ungaro, S. Harkema, A. Abu El-Fadl, D. N. Reinhoudt, *J. Am. Chem. Soc.* **1990**, *112*, 6979–6985; b) Z. Asfari, J. M. Harrowfield, A. N. Sobolev, J. Vicens, *Aust. J. Chem.* **1994**, *47*, 757–762.

[189] a) R. Ungaro, A. Casnati, F. Ugozzoli, A. Pochini, J.-F. Dozol, C. Hill, H. Rouquette, *Angew. Chem.* **1994**, *106*, 1551–1553, *Angew. Chem. Int. Ed. Engl.* **1994**, *33*, 1506–1509; b) R. Ungaro, A. Pochini, personal communication; c) A. Casnati, P. Jacopozzi, A. Pochini, F. Ugozzoli, R. Cacciapaglia, L. Mandolini, R. Ungaro, *Tetrahedron* **1995**, *51*, 591–598.

[190] a) Z. Asfari, R. Abidi, F. Arnaud, J. Vicens, *J. Incl. Phenom. Mol. Recogn.* **1992**, *13*, 163–169; b) Z. Asfari, J. Weiss, J. Vicens, *Pol. J. Chem.* **1992**, *66*, 709–711; c) Z. Asfari, S. Pappalardo, J. Vicens, *J. Incl. Phenom. Mol. Recogn.* **1992**, *14*, 189–192.

[191] D. Kraft, R. Arnecke, V. Böhmer, W. Vogt, *Tetrahedron* **1993**, *27*, 6019–6024.

[192] S. Kanamathareddy, C. D. Gutsche, *J. Am. Chem. Soc.* **1993**, *115*, 6572–6579.

[193] a) D. N. Reinhoudt, P. J. Dijkstra, P. J. A. in't Veld, K. E. Bugge, S. Harkema, R. Ungaro, E. Ghidini, *J. Am. Chem. Soc.* **1987**, *109*, 4761–4762; b) P. J. Dijkstra, J. A. J. Brunink, K.-E. Bugge, D. N. Reinhoudt, S. Harkema, R. Ungaro, F. Ugozzoli, E. Ghidini, *ibid.* **1989**, *111*, 7567–7575; c) W. I. Iwema Bakker, M. Haas, C. Khoo-Beattie, R. Ostaszewski, S. M. Franken, H. J. den Hertog, Jr., W. Verboom, D. de Zeeuw, S. Harkema, D. N. Rheinhoudt, *ibid.* **1994**, *116*, 123–133.

[194] J.-D. van Loon, D. Kraft, M. J. K. Ankoné, W. Verboom, S. Harkema, W. Vogt, V. Böhmer, D. N. Reinhoudt, *J. Org. Chem.* **1990**, *55*, 5176–5179.

[195] D. Kraft, V. Böhmer, W. Vogt, G. Ferguson, J. F. Gallagher *J. Chem. Soc. Perkin Trans. 1* **1994**, 1221–1230.

[196] a) D. Kraft, J.-D. van Loon, M. Owens, W. Verboom, W. Vogt, M. A. McKervey, V. Böhmer, D. N. Reinhoudt, *Tetrahedron Lett.* **1990**, *31*, 4941–4944; b) P. D. Beer, A. D. Keefe, A. M. Z. Slawin, D. J. Williams, *J. Chem. Soc. Dalton Trans.* **1990**, 3675–3682; c) cf. also: G. Ulrich, R. Ziessel, *Tetrahedron Lett.* **1994**, *35*, 6299–6302.

[197] V. Böhmer, G. Ferguson, J. F. Gallagher, A. J. Lough, M. A. McKervey, E. Madigan, M. B. Moran, J. Philips, G. Williams, *J. Chem. Soc. Perkin Trans. 1* **1993**, 1521–1527.

[198] a) P. D. Beer, J. P. Martin, M. G. B. Drew, *Tetrahedron* **1992**, *48*, 9917–9928; b) P. D. Beer, Z. Chen, A. J. Goulden, A. Graydon, S. E. Stokes, T. Wear, *J. Chem. Soc. Chem. Commun.* **1993**, 1834–1836.

[199] a) R. Seangprasertkij, Z. Asfari, F. Arnaud, J. Weiss, J. Vicens, *J. Incl. Phenom. Mol. Recogn.* **1992**, *14*, 141–147; b) R. Seangprasertkij, Z. Asfari, F. Arnaud, J. Vicens, *J. Org. Chem.* **1994**, *59*, 1741–1744; c) cf. also the calix-salophene crowns in ref. [271].

[200] a) W. Wasikiewicz, G. Rokicki, J. Kielkiewicz, V. Böhmer, *Angew. Chem.* **1994**, *106*, 230–232; *Angew. Chem. Int. Ed. Engl.* **1994**, *33*, 214–216; b) for a similar example see: P. D. Beer, P. A. Gale, D. Hesek, *Tetrahedron Lett.* **1995**, *36*, 767–770.

[201] F. Grynszpan, O. Aleksiuk, S. E. Biali, *J. Chem. Soc. Chem. Commun.* **1993**, 13–16.

[202] J. Gloede, B. Costella, M. Ramm, R. Bienert, *Phosphorus, Sulfur, Silicon Relat. Elem.* **1993**, *84*, 217–222.

[203] a) X. Delaigue, M. W. Hosseini, A. De Cian, J. Fischer, E. Leize, S. Kieffer, A. Van Dorsselaer, *Tetrahedron Lett.* **1993**, *34*, 3285–3288; b) an Si/Ti bridged derivate: X. Delaigue, M. W. Hosseini, E. Leize, S. Kieffer, A. Van Dorsselaer, *ibid.* **1993**, *34*, 7561–7564; c) other similar derivatives: X. Delaigue, M. W. Hosseini, R. Graff, J.-P. Kintzinger, J. Raya, *ibid.* **1994**, *35*, 1711–1714.

[204] a) J. L. Atwood, S. G. Bott, C. Jones, C. L. Raston, *J. Chem. Soc. Chem. Commun.* **1992**, 1349–1351; b) M. M. Olmstead, G. Sigel, H. Hope, X. Xu, P. P. Power, *J. Am. Chem. Soc.* **1985**, *107*, 8087–8091.

[205] a) F. Corazza, C. Floriani, A. Chiesi-Villa, C. Guastini, *J. Chem. Soc. Chem. Commun.* **1990**, 640–641; b) D. V. Khasnis, M. Lattman, C. D. Gutsche, *J. Am. Chem. Soc.* **1990**, *112*, 9423–9425; c) see also ref. [283].

[206] Calixarenes in which two neighboring *p*-positions are bridged (compare ref. [37b]) have been described by A. Ikeda, S. Shinkai, *J. Chem. Soc. Perkin Trans. 1* **1993**, 2671–2673.

[207] a) A review of the synthesis of double calix[4]arenes has been given by Z. Asfari, J. Weiss, J. Vicens, *Synlett* **1993**, 719–725; b) for a particular example see: Z. Asfari, J. Vicens, J. Weiss, *Tetrahedron Lett.* **1993**, *34*, 627–628; c) compare also [156b]. For the linkage of two calix[4]arenes functionalized in *p*-position by four bridges (compare ref. [41b]) see: d) K. Araki, K. Sisido, K. Hisaichi, S. Shinkai, *ibid.* **1993**, *34*, 8297–8300; e) M. T. Blanda, K. E. Griswold, *J. Org. Chem.* **1994**, *59*, 3880–3889.

[208] B. Berger, V. Böhmer, E. Paulus, A. Rodriguez, W. Vogt, *Angew. Chem.* **1992**, *104*, 89–92; *Angew. Chem. Int. Ed. Engl.* **1992**, *31*, 96–99.

[209] D. J. Cram, *Science* **1983**, *219*, 1177–1183.

[210] J. A. Tucker, C. B. Knobler, K. N. Trueblood, D. J. Cram, *J. Am. Chem. Soc.* **1989**, *111*, 3688–3699.

[211] a) W. Xu, J. P. Rourke, J. J. Vittal, R. J. Puddephatt, *J. Chem. Soc. Chem. Commun.* **1993**, 145–147; b) W. Xu, J. J. Vittal, R. J. Puddephatt, *J. Am. Chem. Soc.* **1993**, *115*, 6456–6457; c) T. Lippmann, E. Dalcanale, G. Mann, *Tetrahedron Lett.* **1994**, *35*, 1685–1688; d) T. Lippmann, H. Wilde, E. Dalcanale, L. Mavilla, G. Mann, U. Heyer, S. Spera, *J. Org. Chem.* **1995**, *60*, 235–242.

[212] a) J. R. Moran, J. L. Ericson, E. Dalcanale, J. A. Bryant, C. B. Knobler, D. J. Cram, *J. Am. Chem. Soc.* **1991**, *113*, 5707–5714; b) P. Soncini, S. Bonsignore, E. Dalcanale, F. Ugozzoli, *J. Org. Chem.* **1992**, *57*, 4608–4612.

[213] a) D. J. Cram, L. M. Tunstad, C. B. Knobler, *J. Org. Chem.* **1992**, *57*, 528–535; b) T. N. Sorell, J. Richards, *Synlett*, **1992**, 155–156; c) P. Timmerman, M. G. A. van Mook, W. Verboom, G. J. van Hummel, S. Harkema, D. N. Reinhoudt, *Tetrahedron Lett.* **1992**, *33*, 3377–3380; d) the remaining OH groups could also participate in the complexation of metal ions: T. N. Sorrell, F. C. Pigge, P. S. White, *Inorg. Chem.* **1994**, *33*, 632–635.

[214] T. N. Sorrell, F. C. Pigge, *J. Org. Chem.* **1993**, *58*, 784–785.

[215] a) J. C. Sherman, D. J. Cram, *J. Am. Chem. Soc.* **1989**, *111*, 4527–4528; b) J. A. Bryant, M. T. Blanda, M. Vincenti, D. J. Cram, *J. Chem. Soc. Chem. Commun.* **1990**, 1403–1405; c) J. A. Bryant, M. T. Blanda, M. Vincenti, D. J. Cram, *J. Am. Chem. Soc.* **1991**, *113*, 2167–2172; d) J. C. Sherman, C. B. Knobler, D. J. Cram, *ibid.* **1991**, *113*, 2194–2204; e) R. G. Chapman, N. Chopra, E. D. Cochien, J. C. Sherman, *ibid.* **1994**, *116*, 369–370.

[216] a) M. E. Tanner, C. B. Knobler, D. J. Cram, *J. Am. Chem. Soc.* **1990**, *112*, 1659–1660; b) D. J. Cram, M. E. Tanner, C. B. Knobler, *ibid.* **1991**, *113*, 7717–7727.

[217] a) M. L. C. Quan, D. J. Cram, *J. Am. Chem. Soc.* **1991**, *13*, 2754–2755; b) J. K. Judice, D. J. Cram, *ibid.* **1991**, *113*, 2790–2791; c) M. L. C. Quan, C. B. Knobler, D. J. Cram, *J. Chem. Soc. Chem. Commun.* **1991**, 660–662; d) D. J. Cram, M. T. Blanda, K. Paek, C. B. Knobler, *J. Am. Chem. Soc.* **1992**, *114*, 7765–7773; e) D. J. Cram, R. Jaeger, K. Deshayes, *ibid.* **1993**, *115*, 10111–10116; e) T. A. Robbins, C. B. Knobler, D. R. Bellew, D. J. Cram, *ibid.* **1994**, *116*, 111–122; f) H.-J. Choi, M. L. C. Quan, C. B. Knobler, D. J. Cram, *J. Chem. Soc., Chem. Commun.* **1992**, 1733–1735.

[218] Comprehensive review: V. Böhmer, D. Kraft, M. Tabatabai, *J. Incl. Phenom. Mol. Recogn.*, in press.

[219] a) Otherwise a complex mixture of isomeric or similar derivatives would be formed. Thus for example four different mono- or trialkyl derivatives (with a *syn* arrangement) or four different tetraalkyl derivatives in the *cone* conformation are possible; b) L. Zetta, A. Wolff, W. Vogt, K.-L. Platt, V. Böhmer, *Tetrahedron* **1991**, *47*, 1911–1924.

[220] a) S. Shinkai, T. Arimura, H. Kawabata, H. Murakami, K. Araki, K. Iwamoto, T. Matsuda, *J. Chem. Soc. Chem. Commun.* **1990**, 1734–1736; b) S. Shinkai, T. Arimura, H. Kawabata, H. Murakami, K. Iwamoto, *J. Chem. Soc. Perkin Trans. 1* **1991**, 2429–2434.

[221] K. Iwamoto, H. Shimizu, K. Araki, S. Shinkai, *J. Am. Chem. Soc.* **1993**, *115*, 3997–4006.

[222] a) S. Pappalardo, S. Caccamese, L. Giunta, *Tetrahedron Lett.* **1991**, *32*, 7747–7750; b) G. Ferguson, J. F. Gallagher, L. Giunta, P. Neri, S. Pappalardo, M. Parisi, *J. Org. Chem.* **1994**, *59*, 42–53.

[223] Unfortunately a recent systematic classification (cf. ref. [221]) of all possibilities contains some mistakes and inconsistencies. The number of different O-alkylation products (in brackets the number of the chiral compounds) is as follows: 34 (17) tetra-, 13 (9) tri-, 8 (3) dialkyl ethers. Compare: V. Böhmer, D. Kraft, W. Vogt, *Supramol. Chem.* **1994**, *3*, 229–301.

[224] V. Böhmer, A. Wolff, W. Vogt, *J. Chem. Soc. Chem. Commun.* **1990**, 968–970.

[225] Mono- and tri-O-alkyl derivatives of calix[4]arenes of the type AABB have also no plane of symmetry, and analogous considerations apply to macrocycles such as **2** or **5** with a "non-quadratic" arrangement of the phenolic oxygen atoms; see ref. [23b].

[226] F. Marschollek, V. Böhmer, W. Vogt, unpublished results.

[227] a) H. Iki, T. Kikuchi, S. Shinkai, *J. Chem. Soc. Perkin Trans. 1* **1992**, 669–671; b) H. Iki, T. Kikuchi, S. Shinkai, *ibid.* **1993**, 205–210; c) for the conformation see H. Iki, T. Kikuchi, H. Tsuzuki, S. Shinkai, *Chem. Lett.* **1993**, 1735-1738; d) $Cr(CO)_3$ complexes can also be used for selective functionalization: T. Kikuchi, H. Iki, H. Tsuzuki, S. Shinkai, *Supramol. Chem.* **1993**, *1*, 103–106.

[228] A. Wolff, V. Böhmer, W. Vogt, F. Ugozzoli, G. D. Andreetti, *J. Org. Chem.* **1990**, *55*, 5665–5667.

[229] S. T. Pickard, W. H. Pirkle, M. Tabatabai, W. Vogt, V. Böhmer, *Chirality* **1993**, *5*, 310–314.

[230] This demonstrates best that the transitions between calixarenes in the narrow sense (Type **II**) and the resorcarenes (Type **III**) are gradual. For other calix[4]arenes with resorcinol units, which are bonded through the 2,6-positions, see ref. [32c].

[231] P. O'Sullivan, V. Böhmer, W. Vogt, E. F. Paulus, R. A. Jakobi, *Chem. Ber.* **1994**, *127*, 427–432.

[232] R. Assmus, V. Böhmer, J. M. Harrowfield, M. I. Ogden, W. R. Richmond, B. W. Skelton, A. H. White, *J. Chem. Soc. Dalton Trans.* **1993**, 2427–2433.

[233] J. M. Harrowfield, M. I. Ogden, W. R. Richmond, A. H. White, *J. Chem. Soc. Dalton Trans.* **1991**, 2153–2160.

[234] a) J. M. Harrowfield, M. I. Ogden, A. H. White, *Aust. J. Chem.* **1991**, *44*, 1237–1247; b) J. M. Harrowfield, M. I. Ogden, A. H. White, *ibid.* **1991**, *44*, 1249–1262; c) Z. Asfari, J. M. Harrowfield, M. I. Ogden, J. Vicens, A. H. White, *Angew. Chem.* **1991**, *103*, 887–889; *Angew. Chem. Int. Ed. Engl.* **1991**, *30*, 854–856; d) J.-C. G. Bünzli, P. Groidevaux, J. M. Harrowfield, *Inorg. Chem.* **1993**, *32*, 3306–3311; e) P. Froidevaux, J.-C. G. Bünzli, *J. Phys. Chem.* **1994**, *98*, 532–536; f) a Ce_2^{IV} complex was recently used as a catalyst for the hydroxylation of phenols with H_2O_2; see ref. [323c].

[235] a) J. M. Harrowfield, M. I. Ogden, A. H. White, *J. Chem. Soc. Dalton Trans.* **1991**, 979–985; b) J. M. Harrowfield, M. I. Ogden, A. H. White, *ibid.* **1991**, 2625–2632.

[236] E. Nomura, H. Taniguchi, Y. Otsuji, *Bull. Chem. Soc. Jpn.* **1993**,*66*, 3797–3801.

[237] K. Kimura, T. Matsuba, Y. Tsujimura, M. Yokoyama, *Anal. Chem.* **1992**, *64*, 2508–2511; see also ref. [255b,c].

[238] A. Yamada, T. Murase, K. Kikukawa, T. Arimura, S. Shinkai, *J. Chem. Soc. Perkin Trans. 2* **1991**, 793–797.

[239] Since this highly aesthetic structure is one of the most often reproduced representations of calixarenes we shall not include it here.

[240] The synergistic effect of acetonitrile on the complexation of alkali metal ions can also be understood on the basis that its inclusion in the hydrophobic cavity favors fourfold symmetry. a) A. F. Danil de Namor, N. Apaza de Sueros, M. A. McKervey, G. Barrett, F. Arnaud-Neu, M.-J. Schwing-Weill, *J. Chem. Soc. Chem. Commun.* **1991**, 1546–1548; b) A. F. Danil de Namor, M. C. Cabaleiro, B. M. Vuano, M. Salomon, O. I. Pieroni, D. A. P. Tanaka, C. Y. Ng, M. A. L. Tanco, N. M. Rodriguez, J. D. C. Garcia, A. R. Casal, *Pure Appl. Chem.* **1994**, *66*, 435–440; c) compare also the crystal structure of the calix[4]arene tetracarbonate: M. A. McKervey, E. M. Seward, G. Ferguson, B. L. Ruhl, *J. Org. Chem.* **1986**, *51*, 3581–3584.

[241] a) The conformational change of the O-alkyl groups can also be used in order to align them for an interaction with a further guest: H. Murakami, S. Shinkai, *J. Chem. Soc. Chem. Commun.* **1993**, 1533–1535; b) results of molecular dynamics calculations suggest, however, that this conformation of the complex can also not be regarded as "rigid": P. Guilbaud, A. Varnek, G. Wipff, *J. Am. Chem. Soc.* **1993**, *115*, 8298–8312.

[242] a) N. Sabbatini, M. Guardigli, A. Mecati, V. Balzani, R. Ungaro, E. Ghidini, A. Casnati, A. Pochini, *J. Chem. Soc. Chem. Commun.* **1990**, 878–879; b) Tb^{III} complexes of calixarene sulfonates also exhibit luminescence in aqueous solution: N. Sato, I. Yoshida, S. Shinkai, *Chem. Lett.* **1993**, 1261–1264.

[243] In contrast, Eu^{III} and Tb^{III} complexes of calix[4]arene ethers with pyridine N-oxide groups decompose in water: S. Pappalardo, F. Bottino, L. Giunta, M. Pietraszkiewicz, J. Karpiuk, *J. Incl. Phenom. Mol. Recogn.* **1991**, *10*, 387–392.

[244] N. Sato, S. Shinkai, *J. Chem. Soc. Perkin Trans. 2* **1993**, 621–624.

[245] T. Nagasaki, S. Shinkai, *Bull. Chem. Soc. Jpn.* **1992**, *65*, 471–475.

[246] See for example: K. M. O'Connor, G. Svehla, S. J. Harris, M. A. McKervey, *Anal. Proc.* **1993**, *30*, 137–139.

[247] See for example: D. Matt, C. Loeber, J. Vicens, Z. Asfari, *J. Chem. Soc. Chem. Commun.* **1993**, 604–606.

[248] A. Ikeda, H. Tsuzuki, S. Shinkai, *J. Chem. Soc. Perkin Trans. 2* **1994**, 2073–2080; cf. also ref. [250b].

[249] a) W. F. Nijenhuis, E. G. Buitenhuis, F. de Jong, E. J. R. Sudhölter, D. N. Reinhoudt, *J. Am. Chem. Soc.* **1991**, *113*, 7963–7968; b) with regard to the simultaneous transport of anions see: H. C. Visser, D. M. Rudkevich, W. Verboom, F. de Jong, D. N. Reinhoudt, *ibid*, **1994**, *116*, 11554–11555; c) in sensors (ion selective electrodes (ISE), CHEMFET) the slow isomerization leads to a continuous decrease in the selectivity: Z. Brzozka, B. Lammerink, D. N. Reinhoudt, E. Ghidini, R. Ungaro, *J. Chem. Soc. Perkin Trans. 2* **1993**, 1037–1040.

[250] a) In contrast, reduction of the size of the ring ($n = 2$) leads to the selectivity for Na^+, see ref. [325c]; b) similar observations have been made for tetra-O-alkyl derivatives in the 1,3-*alternate* conformation: A. Ikeda, S. Shinkai, *Tetrahedron Lett.* **1992**, 7385–7388 and *J. Am. Chem. Soc.* **1994**, *116*, 3102–3110; c) K^+ complexes in *1,3-alternate*-conformation: P. D. Beer, M. G. B. Drew, P. A. Gale, P. B. Leeson, M. I. Ogden, *J. Chem. Soc. Dalton Trans.* **1994**, 3479–3485.

[251] F. Arnaud-Neu, R. Arnecke, V. Böhmer, S. Fanni, J. Gordon, M.-J. Schwing, unpublished results.

[252] a) L. C. Groenen, J. A. J. Brunink, W. I. Iwema Bakker, S. Harkema, S. S. Wijmenga, D. N. Reinhoudt, *J. Chem. Soc. Perkin Trans. 2* **1992**, 1899–1906; b) For the determination of the kinetic stability see: W. I. Iwema Bakker, M. Haas, H. J. den Hertog, Jr., W. Verboom, D. de Zeeuw, D. Reinhoudt, *ibid.* **1994**, 11–14.

[253] For molecular dynamic calculations see: S. Miyamoto, P. A. Kollman, *J. Am. Chem. Soc.* **1992**, *114*, 3668–3674.

[254] a) For this purpose special calixspherands functionalized at the central ring of the terphenyl unit have been prepared and bound to organ-specific peptides: W. I. Iwema Bakker, M. Haas, H. J. den Hertog, Jr., W. Verboom, D. de Zeeuw, A. P. Bruins, D. N. Reinhoudt, *J. Org. Chem.* **1994**, *59*, 972–976 b) W. I. Iwema Bakker, W. Verboom, D. N. Reinhoudt, *J. Chem. Soc. Chem. Commun.* **1994**, 71–72.

[255] a) A. Arduini, A. Casnati, M. Fabbi, P. Minari, A. Pochini, A. R. Sicuri, R. Ungaro, *Supramol. Chem.* **1993**, *1*, 235–246; b) M. Ogata, K. Fujimoto, S. Shinkai, *J. Am. Chem. Soc.* **1994**, *116*, 4505–4506; c) D. M. Rudkevich, W. Verboom, E. van der Tool, C. J. van Staveren, F. M. Kaspersen, J. W. Verhoeven, D. N. Reinhoudt, *J. Chem. Soc. Perkin Trans. 2*, **1995**, 131–134.

[256] a) S. Shinkai, H. Koreishi, K. Ueda, T. Arimura, O. Manabe, *J. Am. Chem. Soc.* **1987**, *109*, 6371–6376; b) S. Shinkai, Y. Shiramama, H. Satoh, O. Manabe, T. Arimura, K. Fujimoto, T. Matsuda, *J. Chem. Soc. Perkin Trans. 2* **1989**, 1167–1171; c) T. Nagasaki, S. Shinkai, *ibid.* **1991**, 1063–1066; d) T. Nagasaki, K. Kawano, K. Araki, S. Shinkai, *ibid.* **1991**, 1325–1327; e) T. Nagasaki, T. Arimura, S. Shinkai, *Bull. Chem. Soc. Jpn.* **1991**, *64*, 2575–2577; f) K. Araki, N. Hashimoto, H. Otsuka, T. Nagasaki, S. Shinkai, *Chem. Lett.* **1993**, 829–832; g) P. Guilbaud, G. Wipff, *J. Incl. Phenom. Mol. Recogn.* **1993**, *16*, 169–188.

[257] See in this connection the combination of the trisbipyridyl-Ru^{II} complex with *tert*-butylcalix[4]arene to give a luminescence-pH sensor: R. Grigg, J. M. Holmes, S. K. Jones, W. D. J. A. Norbert, *J. Chem. Soc. Chem. Commun.* **1994**, 185–187.

[258] a) H. Shimizu, K. Iwamoto, K. Fujimoto, S. Shinkai, *Chem. Lett.* **1991**, 2147–2150; b) M. McCarrick, B. Wu, S. J. Harris, D. Diamond, G. Barrett, M. A. McKervey, *J. Chem. Soc. Chem. Commun.* **1992**, 1287–1289; c) M. McCarrick, B. Wu, S. J. Harris, D. Diamond, G. Barrett, M. A. McKervey, *J. Chem. Soc. Perkin Trans. 2* **1993**, 1963–1968.

[259] a) Y. Kubo, S. Hamaguchi, K. Kotani, K. Yoshida, *Tetrahedron Lett.* **1991**, *32*, 7419-7420; b) Y. Kubo, S. Hamaguchi, A. Niimi, K. Yoshida, S. Tokita, *J. Chem. Soc. Chem. Commun.* **1993**, 305-307; c) calix[4]arene derivatives with four indophenol units have also been described: Y. Kubo, Y. Endo, S. Tokita, *Workshop on Calixarenes and Related Compounds*, June 2–4, **1993**, Kurume, Japan.

[260] K. Iwamoto, K. Araki, H. Fujishima, S. Shinkai, *J. Chem. Soc. Perkin Trans. 1* **1992**, 1885–1887.

[261] a) T. Jin, K. Ichikawa, T. Koyama, *J. Chem. Soc. Chem. Commun.* **1992**, 499–501; b) I. Aoki, T. Sakaki, S. Shinkai, *J. Chem. Soc. Chem. Commun.* **1992**, 730–732.

[262] a) The replacement of the ethyl ester residues in **62** by methoxy groups leads to compounds whose fluorescence spectra depend on the polarity of the solvent: I. Aoki, H. Kawabata, K. Nakashima, S. Shinkai, *J. Chem. Soc. Chem.*

Commun. **1991** 1771–1773. b) The complexation of carboxylic acids can also be followed from the increase of the monomer emission in comparison with that of the excimer: I. Aoki, T. Sakaki, S. Tsutsui, S. Shinkai, *Tetrahedron Lett.* **1992**, *33*, 89–92.

[263] C. Pérez-Jiménez, S. J. Harris, D. Diamond, *J. Chem. Soc. Chem. Commun.* **1993**, 480–483.

[264] a) G. Deng, T. Sakaki, K. Nakashima, S. Shinkai, *Chem. Lett.* **1992**, 1287–1290; b) G. Deng, T. Sakaki, Y. Kawahara, S. Shinkai, *Tetrahedron Lett.* **1992**, *33*, 2163–2166; c) G. Deng, T. Sakaki, S. Shinkai, *J. Polym. Sci. A* **1993**, *31*, 1915–1919; d) G. Deng, T. Sakaki, Y. Kawahara, S. Shinkai, *Supramol. Chem.* **1993**, *2*, 71–76.

[265] a) M. A. McKervey, M. Owens, H.-R. Schulten, W. Vogt, V. Böhmer, *Angew. Chem.* **1990**, *102*, 326–328; *Angew. Chem. Int. Ed. Engl.* **1990**, *29*, 280–282; b) F. Ohseto, T. Sakaki, K. Araki, S. Shinkai, *Tetrahedron Lett.* **1993**, *34*, 2149–2152; c) F. Ohseto, S. Shinkai, *Chem. Lett.* **1993**, 2045–2048.

[266] For the crystal structure of ammonium salts of the calixarenes see: a) J. M. Harrowfield, M. I. Ogden, W. R. Richmond, B. W. Skelton, A. H. White, *J. Chem. Soc. Perkin Trans. 2*, **1993**, 2183–2190; b) J. M. Harrowfield, W. R. Richmond, A. Sobolev, A. H. White, *ibid.* **1994**, 5–9.

[267] a) S. Shinkai, K. Araki, T. Matsuda, O. Manabe, *Bull. Chem. Soc. Jpn.* **1989**, *62*, 3856–3862; b) S. Shinkai, K. Araki, T. Matsuda, N. Nishiyama, H. Ikeda, I. Takasu, M. Iwamoto, *J. Am. Chem. Soc.* **1990**, *112*, 9053–9058; c) S. Shinkai, K. Araki, M. Kubota, T. Arimura, T. Matsuda, *J. Org. Chem.* **1991**, *56*, 295–300; d) T. Morozumi, S. Shinkai, *J. Chem. Soc. Chem. Commun.* **1994**, 1219–1220; e) E. Morozumi, S. Shinkai, *Chem. Lett.* **1994**, 1515–1518.

[268] a) K. Araki, H. Shimizu, S. Shinkai, *Chem. Lett.* **1993**, 205–208; b) proof by mass spectrometry: F. Inokuchi, K. Araki, S. Shinkai, *ibid.* **1994**, 1383–1386; c) K. Araki, N. Hashimoto, H. Otsuka, S. Shinkai, *J. Org. Chem.* **1993**, *58*, 5958-5963; d) K. Araki, K. Inada, H. Otsuka, S. Shinkai, *Tetrahedron*, **1993**, *49*, 9465-9478; e) for the electrochemical detection of ammonium ions see ref. [174b].

[269] a) See ref. [168]; the effect can only with difficulty be reconciled with the calixarene structure, as podands with analogous ferrocenecarbonamide structures show even greater effects. b) bypyridyl-Ru^{II}-substituted calix[4]arenes as anion receptors: P. D. Beer, Z. Chen, A. J. Goulden, A. Grieve, D. Hesek, F. Szemes, T. Wear, *J. Chem. Soc. Chem. Commun.* **1994**, 1269–1271.

[270] J. Scheerder, M. Fochi, J. F. J. Engbersen, D. N. Reinhoudt, *J. Org. Chem.* **1994**, *59*, 7815–7820.

[271] The attempts to construct host molecules specifically for certain guest molecules include a barbiturate receptor (see ref. [115]) and carrier molecules for urea: W. F. Nijenhuis, A. R. van Doorn, A. M. Reichwein, F. de Jong, D. N. Reinhoudt, *J. Am. Chem. Soc.* **1991**, *113*, 3607–3608; A. M. Reichwein, W. Verboom, S. Harkema, A. L. Spek, D. N. Reinhoudt, *J. Chem. Soc. Perkin Trans. 2*, **1994**, 1167–1172; see in addition the reviews refs. [1], [2], and [5].

[272] E. Dalcanale, G. Costantini, P. Soncini, *J. Incl. Phenom. Mol. Recogn.* **1992**, *13*, 87–92; b) compare also the use of **Ic** for the removal of trihalogenomethanes: S. Barbara, R. L. Tamke, K. P. Wainright, *Chem. Ind.* **1990**, 804–805.

[273] a) Y. Kikuchi, Y. Kato, Y. Tanaka, H. Toi, Y. Aoyama, *J. Am. Chem. Soc.* **1991**, *113*, 1349–1354; b) Y. Kikuchi, K. Kobayashi, Y. Aoyama, *ibid.* **1992**, *114*, 1351–1358; c) Y. Aoyama, Y. Tanaka, S. Sugahara, *ibid.* **1989**, *111*, 5397–5404; d) Y. Tanaka, Y. Ubukata, Y. Aoyama, *Chem. Lett.* **1989**, 1905–1908; e) Y. Tanaka, Y. Kato, Y. Aoyama, *J. Am. Chem. Soc.* **1990**, *112*, 2807–2808; f) K. Kobayashi, Y. Asakawa, Y. Kikuchi, H. Toi, Y. Aoyama, *ibid.* **1993**, *115*, 2648–2654; g) K. Kikuchi, Y. Tanaka, S. Sutarto, K. Kobayashi, H. Toi, Y. Aoyama, *ibid.* **1992**, *114*, 10302–10306; h) Y. Kikuchi, H. Toi, Y. Aoyama, *Bull. Chem. Soc. Jpn.* **1993**, *66*, 1856–1858; i) Y. Tanaka, C. Khare, M. Yonezawa, Y. Aoyama, *Tetrahedron Lett.* **1990**, *31*, 6193–6196.

[274] Y. Tanaka, Y. Aoyama, *Bull. Chem. Soc. Jpn.* **1990**, *63*, 3343–3344.

[275] K. Kobayashi, Y. Asakawa, Y. Kato, Y. Aoyama, *J. Am. Chem. Soc.* **1992**, *114*, 10307–10313.

[276] a) K. Kobayashi, M. Tominaga, Y. Asakawa, Y. Aoyama, *Tetahedron Lett.* **1993**, *34*, 5121–5124; b) K. Kobayashi, Y. Asakawa, Y. Aoyama, *Supramol. Chem.* **1993**, *2*, 133–135; c) R. Yanagihara, M. Tominaga, Y. Aoyama, *J. Org. Chem.* **1994**, *59*, 6865–6867.

[277] a) J. L. Atwood, G. W. Orr, R. K. Juneja, S. G. Bott, F. Hamada, *Pure Appl. Chem.* **1993**, *65*, 1471–1476; b) J. L. Atwood, G. W. Orr, F. Hamada, S. G. Bott, K. D. Robinson, *Supramol. Chem.* **1992**, *1*, 15–17.

[278] a) For an example with a variable cavity ("molecular Venus flytrap") see: J. L. Atwood, G. W. Orr, S. G. Bott, K. D. Robinson, *Angew. Chem.* **1993**, *105*, 1114–1115; *Angew. Chem. Int. Ed. Engl.* **1993**, *32*, 1093–1094; b) for the simultaneous inclusion of Na^+ and toluene see: S. G. Bott, A. W. Coleman, J. L. Atwood, *J. Am. Chem. Soc.* **1986**, *108*, 1709–1710.

[279] R. Ungaro, A. Pochini, G. D. Andreetti, P. Domiano, *J. Chem. Soc. Perkin Trans. 2* **1985**, 197–201.

[280] a) A. W. Coleman, S. G. Bott, S. D. Morley, C. M. Means, K. D. Robinson, H. Zhang, J. L. Atwood, *Angew. Chem.* **1988**, *100*, 1412–1413; *Angew. Chem. Int. Ed. Engl.* **1988**, *27*, 1361–1362; b) J. L. Atwood, A. W. Coleman, H. Zhang, S. G. Bott, *J. Incl. Phenom. Mol. Recogn.* **1989**, *7*, 203–211.

[281] a) J. L. Atwood, G. W. Orr, F. Hamada, R. L. Vicent, S. G. Bott, K. D. Robinson, *J. Am. Chem. Soc.* **1991**, *113*, 2760–2761; b) J. L. Atwood, G. W. Orr, F. Hamada, R. L. Vicent, S. G. Bott, K. D. Robinson, *J. Incl. Phenom. Mol. Recogn.* **1992**, *14*, 37–46; c) J. L. Atwood, G. W. Orr, Kerry D. Robisnon, *Supramol. Chem.* **1994**, *3*, 89–91.

[282] a) T. Komori, S. Shinkai, *Chem. Lett.* **1992**, 901–904; b) T. Komori, S. Shinkai, *ibid.* **1993**, 1455–1458.

[283] B. Xu, T. M. Swager, *J. Am. Chem. Soc.* **1993**, *115*, 1159–1160.

[284] a) L. Abis, V. Arrighi, G. Cometti, E. Dalcanale, A. Du vosel, *Liq. Cryst.* **1991**, *9*, 277–284; b) see also: H. Budig, R. Paschke, S. Diele, I. Letko, G. Pelzl, *Ber. Bunsenges. Phys. Chem.* **1993**, *97*, 1355–1357.

[285] a) E. Kelderman, L. Derhaeg, G. J. T. Heesink, W. Verboom, J. F. J. Engbersen, N. F. van Hulst, A. Persoons, D. N. Reinhoudt, *Angew. Chem.* **1992**, *104*, 1107–1110; *Angew. Chem. Int. Ed. Engl.* **1992**, *31*, 1075–1077; b) G. J. T. Heesink, N. F. van Hulst, B. Bölger, E. Kelderman, J. F. J. Engbersen, W. Verboom, D. N. Reinhoudt, *Appl. Phys. Lett.* **1993**, *62*, 2015–2017; c) E. Kelderman, G. J. T. Heesink, L. Derhaeg, T. Verbiest, P. T. A. Klaase, W. Verboom, J. F. J. Engbersen, N. F. van Hulst, K. Clays, A. Persoons, D. N. Reinhoudt, *Adv. Mater.* **1993**, *5*, 925–930; d) for NLO-active calixarenes with more extensive π-electron systems see: E. Kelderman, L. Derhaeg, W. Verboom, J. F. J. Engbersen, S. Harkema, A. Persoons, D. N. Reinhoudt, *Supramol. Chem.* **1993**, *2*, 183–190.

[286] a) M. A. Markowitz, R. Bielski, S. L. Regen, *J. Am. Chem. Soc.* **1988**, *110*, 7545–7546; b) M. A. Markowitz, V. Janout, D. G. Castner, S. L. Regen, *ibid.* **1989**, *111*, 8192–8200; c) M. Conner, V. Janout, S. L. Regen, *ibid.* **1993**, *115*, 1178–1180; d) M. D. Conner, V. Janout, I. Kudelka, P. Dedek, J. Zhu, S. L. Regen, *Langmuir* **1993**, *9*, 2389–2397; e) P. Dedek, A. S. Webber, V. Janout, R. A. Hendel, S. L. Regen, *Langmuir* **1994**, *10*, 3943–3945.

[287] a) Y. Nakamoto, G. Kallinowski, V. Böhmer, W. Vogt, *Langmuir* **1989**, *5*, 1116–1117; b) W. C. Moreira, P. J. Dutton, R. Aroca, *Langmuir* **1994**, *10*, 4148–4152.

[288] D. N. Reinhoudt et al., *18. Int. Symp. Macrocycl. Chem.*, 27. June–2. July 1993, Enschede, The Netherlands.

[289] K. Kurihara, K. Ohta, Y. Tanaka, Y. Aoyama, T. Kunitake, *J. Am. Chem. Soc.* **1991**, *113*, 444–450.

[290] M. Aoki, K. Nakashima, H. Kawabata, S. Tsutsui, S. Shinkai, *J. Chem. Soc. Perkin Trans. 2* **1993**, 347–354.

[291] J.-D. van Loon, R. G. Janssen, W. Verboom, D. N. Reinhoudt, *Tetrahedron Lett.* **1992**, *33*, 5125–5128.

[292] S. Arimori, T. Nagasaki, S. Shinkai, *J. Chem. Soc. Perkin Trans. 1* **1993**, 887–889.

[293] a) J. A. Bryant, C. B. Knobler, D. J. Cram, *J. Am. Chem. Soc.* **1990**, *112*, 1254–1255; b) J. A. Bryant, J. L. Ericson, D. J. Cram, *ibid.* **1990**, *112*, 1255–1256; c) D. J. Cram, H.-J. Choi, J. A. Bryant, C. B. Knobler, *ibid.* **1992**, *114*, 7748–7765.

[295] a) S. Shinkai, Y. Shirahama, T. Tsubaki, O. Manabe, *J. Am. Chem. Soc.* **1989**, *111*, 5477–5478; b) S. Shinkai, Y. Shirahama, T. Tsubaki, O. Manabe, *J. Chem. Soc. Perkin Trans. 1* **1989**, 1859–1860.

[295] a) H. Taniguchi, E. Nomura, *Chem. Lett.* **1988**, 1773–1776; b) E. Nomura, H. Taniguchi, K. Kawaguchi, Y. Otsuji, *ibid.* **1991**, 2167–2170.

[296] R. Cacciapaglia, A. Casnati, L. Mandolini, R. Ungaro, *J. Am. Chem. Soc.* **1992**, *114*, 10956–10958.

[297] a) R. Cacciapaglia, A. Casnati, L. Mandolini, R. Ungaro, *J. Chem. Soc. Chem. Commun.* **1992**, 1291–1293. b) The alkaline hydrolysis of monobenzoates of *tert*-butylcalix[4]arene in ethanol/water is accelerated by a factor of up to 160 with respect to model compounds: K. B. Ray, R. H. Weatherhead, N. Pirincciogiu, A. Williams, *J. Chem. Soc. Perkin Trans. 2* **1994**, 83–88.

[298] R. Cacciapaglia, L. Mandolini, V. Böhmer et al., unpublished results.

[299] D. J. Cram, M. E. Tanner, R. Thomas, *Angew. Chem.* **1991**, *103*, 1048–1051; *Angew. Chem. Int. Ed. Engl.* **1991**, *30*, 1024–1026.

[300] E. van Dienst, W. I. Iwema Bakker, J. F. J. Engbersen, W. Verboom, D. N. Reinhoudt, *Pure Appl. Chem.* **1993**, *65*, 387–392.

[301] P. Timmerman, W. Verboom, F. C. J. M. van Veggel, W. P. van Hoorn, D. N. Reinhoudt, *Angew. Chem.* **1994**, *106*, 1313–1315; *Angew. Chem. Int. Ed. Engl.* **1994**, *33*, 1292–1295.

[302] In the period from December 1993 to November 1994 about 200 publications dealing with calixarenes and resorcarenes were published.

[303] a) S. K. Sharma, C. D. Gutsche, *Tetrahedron* **1994**, *50*, 4087–4104; b) *J. Org. Chem.* **1994**, *59*, 6030–6037; c) for the acylation of *p*-cyanomethylcalix[4]-arene see: S. K. Sharma, C. D. Gutsche, *Synthesis* **1994**, 813–822.

[304] a) D. V. Khasnis, J. M. Burton, J. D. McNeil, H. Zhang, M. Lattman, *Phosphorous, Sulfur, Silicon, Relat. Elem.* **1993**, *75*, 253–256; b) D. V. Khasnis, J. M. Burton, J. D. McNeil, C. J. Santini, H. Zhang, M. Lattman, *Inorg. Chem.* **1994**, *33*, 2657–2662. c) New phosphorus-containing ligands: C. Loeber, D. Matt, A. De Cian, J. Fischer, *J. Organomet. Chem.* **1994**, 297–305.

[305] J. W. Steed, R. K. Juneja, R. S. Burkhalter, J. L. Atwood, *J. Chem. Soc. Chem. Commun.* **1994**, 2205–2206.

[306] a) P. Neri, G. M. L. Consoli, F. Cunsolo, M. Piattelli, *Tetrahedron Lett.* **1994**, *35*, 2795–2798; b) J. P. M. van Duynhoven, R. G. Janssen, W. Verboom, S. M. Franken, A. Casnati, A. Pochini, R. Ungaro, J. de Mendoza, P. M. Nieto, P. Prados, D. N. Reinhoudt, *J. Am. Chem. Soc.* **1994**, *116*, 5814–5822; c) S. Kanamathareddy, C. D. Gutsche, *J. Org. Chem.* **1994**, *59*, 3871–3879.

[307] a) P. Neri, E. Battocolo, F. Cunsolo, C. Geraci, M. Piattelli, *J. Org. Chem.* **1994**, *59*, 3880–3889; b) F. Cunsolo, M. Piattelli, P. Neri, *J. Chem. Soc. Chem. Commun.* **1994**, 1917–1918.

[308] M. Takeshita, S. Nishio, S. Shinkai, *J. Org. Chem.* **1994**, *59*, 4032–4034, b) K. Araki, K. Akao, H. Otsuka, K. Nakashima, F. Inokuchi, S. Shinkai, *Chem. Lett.* **1994**, 1251–1254; however, these are not the first O-bridged calix[6]arene derivatives which show no ring inversion, compare ref. [201].

[309] R. G. Janssen, W. Verboom, J. P. M. Duynhoven, E. J. J. van Velzen, D. N. Reinhoudt, *Tetrahedron Lett.* **1994**, *35*, 6555–6558.

[310] a) N. Kobayashi, K. Mizuno, T. Osa, *Inorg. Chim. Acta* **1994**, *224*, 1–3; b) T. Nagasaki, H. Fujishima, S. Shinkai, *Chem. Lett.* **1994**, 989–992.

[311] D. M. Rudkevich, W. Verboom, D. N. Reinhoudt, *Tetrahedron Lett.* **1994**, *35*, 7131–7134.

[312] a) A. Ikeda, S. Shinkai, *J. Chem. Soc. Chem. Commun.* **1994**, 2375–2378; b) A. Ikeda, S. Shinkai, *J. Am. Chem. Soc.* **1994**, *116*, 3102–3310.

[313] K. Fujimoto,S. Shinkai, *Tetrahedron Lett.* **1994**, *35*, 2915–2918.

[314] K. Koh, K. Araki, S. Shinkai, *Tetrahedron Lett.* **1994**, *35*, 8255–8258.

[315] a) C. N. Eid Jr., C. B. Knobler, D. A. Gronbeck, D. J. Cram, *J. Am. Chem. Soc.* **1994**, *116*, 8506–8515; b) T. A. Robbins, D. J. Cram, *ibid.* **1993**, *115*, 12199.

[316] A. J. Parola, F. Pina, M. Maestri, N. Armaroli, V. Balzani, *New J. Chem.* **1994**, *18*, 659–661.

[317] a) P. Timmerman, W. Verboom, F. C. J. M. van Veggel, J. P. M. van Duynhoven, D. N. Reinhoudt, *Angew. Chem.* **1994**, *106*, 2437–2440; *Angew. Chem. Int. Ed. Engl.* **1994**, *33*, 2345–2348; b) cf. also: H. Adams, F. Davis, C. J. M. Stirling, *J. Chem. Soc. Chem. Commun.* **1994**, 2527–2529.

[318] a) M. McCarrick, S. J. Harris, D. Diamond, *J. Mater. Chem.* **1994**, *4*, 217–221; b) K. Toth, B. T. T. Lan, J. Jemey, M. Horvath, I. Bitter, A. Grün, B. Agai, L. Töke, *Talanta* **1994**, *41*, 1041–1049; c) Y. Kubo, S. Maeda, M. Nakamura, S. Tokita, *J. Chem. Soc. Chem. Commun.* **1994**, 1725–1726; d) for chromogenic calix[8]arenes see: H. M. Chawla, K. Srinivas, *Tetrahedron Lett.* **1994**, *35*, 2925–2928; the molecular structure reported is however unlikely for sterical reasons; e) the same authors propose a structure, which is sterically more probable, however the fourfold intramolecular bridging by bis-diazonium salts remains unlikely: H. M. Chawla, K. Srinivas, *J. Chem. Soc. Chem. Commun.* **1994**, 2593–2594.

[319] a) M. Takeshita, S. Shinkai, *Chem. Lett.* **1994**, 125–128; b) C. Perez-Jimenez, S. J. Harris, D. Diamond, *J. Mater. Chem.* **1994**, *4*, 145–151; c) M. Takeshita, S. Shinkai, *Chem. Lett.* **1994**, 1349–1352.

[320] K. N. Koh, T. Imada, T. Nagasaki, S. Shinkai, *Tetrahedron Lett.* **1994**, *35*, 4157–4160.

[321] C. A. Gleave, I. O. Sutherland, *J. Chem. Soc. Chem. Commun.* **1994**, 1873–1874.

[322] D. M. Rudkevich, W. Verboom, D. N. Reinhoudt, *J. Org. Chem.* **1994**, *59*, 3683–3686.

[323] a) E. Nomura, H. Taniguchi, Y. Otsuji, *Bull. Chem. Soc. Jpn.* **1994**, *67*, 309–311; b) Y. Okada, Y. Sugitani, Y. Kasai, J. Nishimura, *ibid.* **1994**, *67*, 586–588; c) H. M. Chawla, U. Hooda, V. Singh, *J. Chem. Soc. Chem. Commun.* **1994**, 617–618; d) E. Nomura, H. Taniguchi, Y. Otsuji, *Bull. Chem. Soc. Jpn.* **1994**, *67*, 792–799.

[324] a) D. Shohat, E. Grushka, *Anal. Chem.* **1994**, *66*, 747–750; b) K. Bächmann, A. Bazzanella, I. Haag, K.-Y. Han, R. Arnecke, V. Böhmer, W. Vogt, *Anal. Chem.*, in press.

[325] a) Sensors for neutral molecules, see: K.-D. Schierbaum, A. Gerlach, W. Göpel, W. M. Müller, F. Vögtle, A. Dominik, H. J. Roth, *Fresenius J. Anal. Chem.* **1994**, *349*, 372–379; b) for guanidinium CHEMFETS see F. J. B. Kremer, G. Chiosis, J. F. J. Engbersen, D. N. Reinhoudt, *J. Chem. Soc. Perkin Trans. 2* **1994**, 677–681; c) for new Na^+ electrodes with a high Na^+/K^+ selectivity based on calix[4]-crown-4 see: H. Yamamoto, S. Shinkai, *Chem. Lett.* **1994**, 1115–1118; d) amperometric detectors: J. Wang, J. Liu, *Anal. Chim. Acta* **1994**, *194*, 201–206; e) aldehyde-selective electrodes: W. H. Chan, P. X. Cai, X. H. Gu, *Analyst* **1994**, *119*, 1853–1857; f) Na^+-selective PVC membrane electrodes: K. M. O'Connor, M. Cherry, G. Svehla, S. J. Harris, M. A. McKervey, *Talanta* **1994**, *41*, 1207–1217.

[326] a) M. Gómez-Kaifer, P. Amruta Reddy, C. D. Gutsche, L. Echegoyen, *J. Am. Chem. Soc.* **1994**, *116*, 3580–3587; b) P. D. Beer, Z. Cheng, M. G. B. Drew, P. A. Gale, *J. Chem. Soc. Chem. Commun.* **1994**, 2207–2208; see also ref. [174b].

[327] a) J. L. Atwood, G. A. Koutsantonis, C. L. Raston, *Nature* **1994**, *368*, 229–231; b) a second slightly later publication reports the achievement of 99.8% purity using an amazingly identical procedure: T. Suzuki, K. Nakashima, S. Shinkai, *Chem. Lett.* **1994**, 699–702. For a highlight of these two papers see E. C. Constable, *Angew. Chem.* **1994**, *106*, 2359–2361; *Angew. Chem. Int. Ed. Engl.* **1994**, *33*, 2269–2271; c) for the interaction between fullerenes and calixarenes in the solid state see: R. M. Williams, J. M. Zwier, J. W. Verhoeven, G. H. Nachtegaal, A. P. M. Kentgens, *J. Am. Chem. Soc.* **1994**, *116*, 6965–6966; d) for the C_{60}/cycloveratrylene interaction see: J. W. Steed, P. C. Junk, J. L. Atwood, M. J. Barnes, C. L. Raston, R. S. Burkhalter, *ibid.* **1994**, *116*, 10346–10347; e) for C_{60} covalently linked to *tert*-butylcalix[8]arene see: M. Takeshita, T. Suzuki, S. Shinkai, *J. Chem. Soc. Chem. Commun.* **1994**, 2587–2588.

Carbon–Hydrogen Bonds of DNA Sugar Units as Targets for Chemical Nucleases and Drugs**

Geneviève Pratviel, Jean Bernadou,* and Bernard Meunier*

This review article focuses on the molecular aspects of DNA cleavage by synthetic chemical nucleases (transition metal complexes endowed with redox properties and DNA affinity) and natural drugs (cytotoxic agents such as bleomycins or enediynes). Unlike deoxyribonucleases, which catalyze the nucleophilic attack of water on the phosphorus atom of a particular phosphodiester entity, these nonhydrolytic DNA-cleavers are able to oxidize the sugar units, generally by hydrogen atom abstraction. Examples of oxidative attack on each of the five different C–H bonds of deoxyribose are known, depending on the nature, structure, type of activation, or mode of DNA interaction of the DNA-cleaver. Further evolution at the site of the initial lesion leads to the release of bases, oxidized deoxyribose units, or oxidized sugar fragments appended to the base or the terminal phosphate. In most cases the loss of a part (at least) of a nucleoside, with the concomitant loss of one base information, primarily induces the cleavage of the DNA strand. For both types of DNA cleavage reagents studied within the two last decades, the modes of activation and DNA binding are presented, as well as the details on the mechanism of deoxyribose oxidative degration. Because of the need for highly efficient and highly specific reagents, the development of new artificial and selective DNA cleavers, supported by an improved knowledge of these different mechanisms of DNA cleavage, is to-day a challenging area in the rational design of antitumoral or antiviral agents, as well as in the field of molecular biology.

Keywords: bleomycin · DNA cleavage · enediynes · transition metal complexes

1. Introduction

A large body of evidence has accumulated over the past three decades on the role of oxidative damage to biological macromolecules in ageing phenomena, chronic inflammation, ischemia, cancer, autoimmune diseases, transcription activation and, recently, in the induction of HIV expression.[1–2] Defenses against oxidative stress are organized in living organisms with nonenzymatic systems like vitamines [α-tocopherol (vitamin E), ascorbic acid (vitamin C), or β-carotene (vitamin A)], or with enzymes like superoxide dismutases, glutathione, peroxidase, and catalase.[2].

Within the two last decades, much data has been published on chemical and biochemical aspects of the structural damage generated by oxidative stress on cellular constituents (DNA, proteins, lipids, and carbohydrates). Aerobic life can be considered as a well-organized system against injury from oxidation by elimination of oxidants and reparation of damage to macromolecules. Repair of DNA is performed by DNA repair enzymes by several routes: nucleotide or base-excision repair, mismatch repair, and error-prone repair.[3] Oxidative damage to DNA can be initiated by ionizing radiation,[4] photooxidation (UV or visible light with or without photosentitizers),[5] hydroperoxides activated by traces of adventitious transition metals salts,[6] hydroxyl radicals,[7] or various other oxidizing agents (for a recent review article on the oxidative degradation of DNA, see ref. [8]). In this latter category, we find drugs like bleomycin, cytotoxic agents with an enediyne motif, and chemical nucleases mainly based on redox-active transition metal complexes (for recent review articles, see ref. [9]). DNA damage can be produced by oxidation of nucleobases or sugar units. More than 20 modified purines and pyrimidines resulting from oxidative damage have been identified.[10] This base damage threatens genomic integrity and is the origin of lethal effects or mutations in DNA. On the other hand, damage to deoxyribose leads to the loss of one base information and/or a break on a DNA strand, which might correspond to a lethal lesion, especially when an oxidation process produces a double-strand break (DSB), that is, two close single-strand breaks (SSBs) on opposite strands.

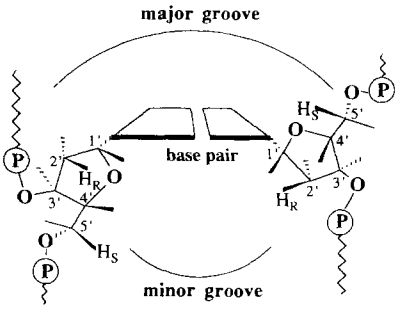
We will see in the present review that many highly cytotoxic drugs or chemical nucleases are able to generate double-strand breaks by oxidation of sugars on both strands of B-DNA (for a textbook on DNA structures, see ref. [11]). More precisely, all these sugar degradation processes are initiated by H abstrac-

[*] Dr. B. Meunier, Dr. G. Pratviel, Prof. Dr. J. Bernadou
Laboratoire de Chimie de Coordination du CNRS
205 route de Narbonne, F-31077 Toulouse cedex (France)
Telefax: Int. code +61 55 3003

[**] Abbreviations are listed in Section 5 at the end of the review.

tions, since the aliphatic nature of deoxyribose does not favor oxidation by electron abstraction. The C–H bonds of deoxyriboses have a well-defined arrangement, and their orientations with respect to drugs or chemical nuclease are also controlled by DNA itself by DNA–drug interactions. In addition, the homolysis of a C–H bond depends also on the substituents on the carbon: less energy is required to remove a H atom from a tertiary carbon than from a secondary carbon atom. But more important is the relative orientation of the drug to the sugar C–H bonds. For drugs interacting within the minor groove of B-DNA, two tertiary C–H bonds are easily accessible: C4′–H and C1′–H. The third tertiary C–H bond (C3′–H) is only accessible from the major groove. C2′ and C5′ are secondary carbon atoms. In both cases, one C–H bond is accessible from the minor groove the (*pro-R*) H atom at C2′ and the (*pro-S*) H atom at C5′; for assignments of prochiral hydrogen atoms at C5′ and C2′ see ref. [12]) and the other from the major groove. In Scheme 1 the different arrangement of deoxyribose C–H bonds with respect to the minor groove is depicted. It is essential for the rational drug design of antitumoral, antiviral agents, or other pharmaceuticals based on DNA cleavers to understand the way of these DNA sugar carbon–hydrogen bonds are activated at the molecular level.

Before the molecular aspects of deoxyribose C–H bond activation are analyzed (Section 3), the different modes of activation and DNA binding of chemical nucleases and drugs involved in this deoxyribose oxidative damage will be described (Section 2).



Scheme 1. Among seven C–H bonds of deoxyribose that are possible targets for oxidative activation, four point into the minor groove (indicated by wedge-shaped bonds), and three into the major groove (H_R and H_S refer to the absolute configuration (*pro-R* or *pro-S*) of hydrogen atoms at C2′ and C5′).

2. Chemical Nucleases and Drugs Able To Cleave DNA by Oxidation of a Sugar Unit

This section will be devoted to a survey of the nonhydrolytic chemical nucleases and drugs able to cleave the DNA phosphodiester backbone by sugar oxidation. These DNA cleavers differ completely from deoxyribonucleases that accomplish DNA scission by catalyzing the nucleophilic attack of a water molecule on the phosphorus atom of a particular phosphodiester bond.[13] In the past 15 years, several redox-active coordination complexes have been synthesized, and naturally occurring nucleolytic agents have been discovered that are able to cleave the phosphodiester backbone of nucleic acids under physiological conditions

Geneviève Pratviel was born in Toulouse (France) in 1959. She attended the University Paul Sabatier and received her degree in Biochemistry in 1983 and her PhD in Pharmacology in 1986 under the supervision of Bernard Meunier. After spending post-doctorate fellowship in the group of Prof. A. Sartorelli at Yale University she came back to the group of Bernard Meunier as a CNRS researcher in 1988 at the Laboratoire de Chimie de Coordination du CNRS. Her research interests are the mechanism of DNA cleavage applied to the development of biologically active compounds and genetic tools.


G. Pratviel


J. Bernadou


B. Meunier

Jean Bernadou was born in Villefranche-de-Rouergue (France) in 1947, studied Chemistry, Pharmacy (doctorate in Pharmaceutical Sciences in 1975) and Medicine (doctorate in 1985) at the University Paul Sabatier of Toulouse, where he was appointed Professor of Medicinal Chemistry in 1987. His collaboration with the group of Bernard Meunier started in 1980 with his research interests in the mechanisms of action of antitumor drugs. He is currently working on biological applications of metalloporphyrins, in particular on the topic discussed in the present review article.

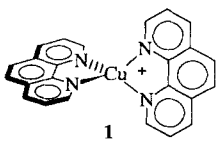
Bernard Meunier was born in Poitiers (France) in 1947 and obtained a first doctorate degree with Robert Corriu at the University of Montpellier in 1972. He joined Hugh Felkin at the Institut de Chimie des Substances Naturelles du CNRS of Natural Chemistry at Gif-sur-Yvette and obtained a second doctorate in 1977. After one year as post-doc at Oxford University with K. Prout, he moved to the Laboratoire de Chimie de Coordination du CNRS, where he is presently research director. His current research interests focus on metalloporphyrin-catalyzed oxidations, ligninase models, oxidations of pollutants, DNA cleavage by cationic manganese porphyrins, and anti-HIV molecules based on metalloporphyrin derivatives.

by oxidative attack on deoxyribose moieties. These synthetic nucleolytic agents are complexes of transition metals, $Cu(oP)_2$, Fe–EDTA,[*] or metalloporphyrins that perform DNA strand scission after activation 1) by reducing agents in the presence of molecular oxygen or hydrogen peroxide, or 2) by oxygen atom donors such as iodosylbenzene, magnesium monoperphthalate, or potassium monopersulfate. In some cases these DNA breaks are mediated by photoactivatable complexes (bipyridyl or phenanthroline complexes of rhodium, ruthenium, or cobalt). The most sophisticated nucleolytic agents are natural products isolated from strains of *Streptomyces* (bleomycin, neocarzinostatin), *Micromonospora echinospora* (calicheamicin), or *Actinomadura verrucospora* (esperamicin). All these chemical nucleases and drugs can be distinguished from other DNA-modifying compounds used in nucleic acid chemistry[14] by their preferential deoxyribose-directed reactivity. We have also included recent information on irradiation of 5-halouracil-containing DNAs and on photocleavage of DNA by rhodium complexes in order to illustrate the possibility of oxidative attacks on positions 2′ and 3′ of deoxyribose units. We propose an almost complete description of the different ways of activating five of the seven C–H bonds of deoxyribose: C1′–H, one (*pro-R*) hydrogen atom at C2′, C3′–H, C4′–H, and one (*pro-S*) hydrogen atom at C5′ (Scheme 1). Schemes 14 to 18 each summarize one of these five possibilities, and detail the subsequent potential reaction pathways. These schemes also display reaction products that have been isolated or chemically characterized and that can be used as reporters to identify at molecular level the attack sites on deoxyriboses by DNA cleavers. (For an excellent early review of the different routes for DNA cleavage, see ref. [9b].)

2.1. Bis(1,10-phenanthroline)copper, $Cu(oP)_2$

2.1.1. Mechanism of Potentiation

$Cu(oP)_2$ (**1**, Scheme 2) was the first chemical nuclease demonstrated to have an efficient nucleolytic activity on double-stranded DNA.[15,16] There are two essential coreactants, the Cu^I complex **1** and hydrogen peroxide.[15,17] Despite the frequent use of **1** as a cleaving agent, the exact nature of the reactive species involved in this DNA cleavage is still unknown. A popular view is that the hydrophobic cationic complex **1** binds to DNA and forms an intermediate that reacts with H_2O_2 to generate a hydroxyl radical ($HO^{\bullet}$). However, according to reports on the detailed chemistry of the cleavage reaction, freely diffusible hydroxyl radicals are not responsible for the strand scission.[17,18] Williams et al.[19] concluded that the DNA damaging species can diffuse over a limited range from the binding site of **1**, which suggests that it is also unlikely to be an oxo–copper complex. Whether this reactive species is a hydroxyl radical coordinated to a cupric ion (called crypto-OH[18]) is still an open question. The damage to DNA bases by activated **1** is typical of processes induced by hydroxyl radicals,[20] which suggests that at least a minor reaction pathway involves free hydroxyl radicals.



1

Scheme 2. Structure of bis(1,10-phenanthroline) copper **1**.

The one-electron reduction of the starting complex $Cu^{II}(oP)_2$ can be accomplished by adding exogeneous reducing agents (ascorbate,[21] thiols like mercaptopropionic acid,[17,21–23] 2-mercaptoethanol,[21] NADH[24]) or by using superoxide generators (xanthine/xanthine oxidase,[17] cobalt-60 γ-radiolysis). One-electron reductants such as the superoxide anion and thiol accomplish directly the reduction of the Cu^{II} complex, but two-electron reductants such as NADH are involved in a multistep reaction in which superoxide plays a central role.[24] H_2O_2 can be either added exogeneously, or generated in situ by spontaneous dismutation of the superoxide anion produced during oxidation of the Cu^I complex by molecular oxygen, by cobalt-60 γ-radiolysis of water, or from xanthine/xanthine oxidase.[17] In the presence of hydrogen peroxide, the DNA cleavage proceeds as rapidly under anaerobic conditions as under aerobic conditions.[17] In the absence of added hydrogen peroxide, oxygen is required, but its exclusive role is as a precursor for hydrogen peroxide in the oxidation of thiol catalyzed by $Cu(oP)_2$.[17]

As demonstrated by kinetic studies, the nuclease activity of $Cu(oP)_2$ proceeds by an ordered mechanism: the freely diffusing $Cu^{II}(oP)_2$ is first reduced to the Cu^I complex [Eq. (1) and (2)], which binds reversibly to DNA [Eq. (3)]. This noncovalently bound Cu^I complex is then oxidized by hydrogen peroxide to generate the reactive species responsible for DNA strand scission[25] [Eq. (4)]. The Cu^{II} complex also binds to DNA but the direct reduction of $Cu^{II}(oP)_2$–DNA by $O_2^{\bullet-}$ is very slow and can be neglected.[26]

$$2Cu^{II}(oP)_2 + 2RS^- \longrightarrow \underset{\mathbf{1}}{2Cu^{I}(oP)_2} + RSSR \quad (1)$$

$$Cu^{II}(oP)_2 + O_2^{\bullet-} \longrightarrow \underset{\mathbf{1}}{Cu^{I}(oP)_2} + O_2 \quad (2)$$

$$Cu^{I}(oP)_2 + DNA \longrightarrow Cu^{I}(oP)_2\text{-}DNA \quad (3)$$

$$Cu^{I}(oP)_2\text{-}DNA + H_2O_2 \longrightarrow [(oP)_2Cu^{III}\text{-}OH]DNA + OH^- \quad (4)$$

2.1.2. Interaction with Nucleic Acids

The pattern of DNA digestion in the presence of $Cu^I(oP)_2$ (**1**) is consistent with its binding in the minor groove of a right-handed double helix. The reactivity of **1** in the minor groove of DNA[27] is confirmed by "footprinting" studies on netropsin- and EcoRI-dodecamer complexes that are oxidatively degraded by $Cu^I(oP)_2$ (netropsin binds within the minor groove, and Eco RI within the major groove[15b,28]). The reaction mechanism involving the H atoms at C1′ and C4′ of the deoxyriboses (which are located within the minor groove) as the main targets of the oxidative attack are also in accord with this position for the cleaver.[15b] Initial observation of the inhibition of cleavage by intercalators implied that the cleavage reaction proceeded through an intercalative complex.[17] The nucleolytic activity $Cu^I(oP)_2$ is sequence-dependent but not nucleotide specific.[15c,29] The unsubstituted aromatic phenanthroline ligands of $Cu(oP)_2$ preclude hydrogen bonding interactions with bases as crucial factors for specificity.[15c] The only observed specificity is related to a predominant preference for binding at 5′-TAT triplets in the minor groove, which were cleaved most

[*] IUPAC nomenclature has not been used in this review.

strongly at the deoxyadenosine sugar ring. The related sequences TGT, TAAT, TAGpyr and CAGT were moderately preferred, while CAT and TAC triplets, and polypurine and polypyrimidine sequences were cleaved less often.[30, 31] The preference of Cu(*o*P)$_2$ for TAT may be related, in part, to sequence-dependent variations of the B conformation of DNA.[31] Stacking interactions are favored with a propeller-twisted base-pair. Changes in roll and twist angles open the minor groove of DNA at the TA step and facilitate penetration of the helix by an *o*P ring in either a partial intercalation or groove binding mode. Cu(*o*P)$_2$ is precluded by its tetrahedral geometry from full intercalation, but a model in which one phenanthroline ligand partially intercalates at a TA step is plausible.[32] Since Cu(*o*P)$_2$ attacks DNA from a binding site within the minor groove, the geometry of this structural domain must govern the cleavage specificity by the complex. Mutational changes can generate additional sites detectable by the complex, whereas DNase I, for example, did not detect substantial changes accompanying these base substitutions.[15b, 33] Single-stranded DNA is a poor substrate.[17, 22, 33a] Double-strand scission of DNA by Cu(*o*P)$_2$ is accomplished by two successive single-strand nicks. DSBs have been observed with a semisynthetic nuclease prepared by chemically linking Cu(*o*P)$_2$ to *E. coli* trp repressor.[34]

RNA is also a substrate for the nuclease activity of **1**. The copper complex shows a preference for single-stranded loops relative to double-stranded A structures present in RNA, but the detailed mechanism of cleavage is still unknown.[35]

The Cu(*o*P)$_2$/H_2O_2 system cleaves A, B, and Z forms of DNA at different rates: the B structure is the most easily cleaved; the A structure, formed by RNA–DNA hybrids, is cleaved on both strands at roughly one third the rate for B-DNA under comparable conditions; in contrast, the left-handed Z structure, with its deep narrow minor groove, is completely resistant to Cu(*o*P)$_2$ degradation.[15b, 22]

The nuclease activity of **1** can be aimed at specific DNA sequences by attachment of one *o*P ligand to the 5′ end of complementary oligodeoxynucleotides (ODNs). Although the *o*P–ODN does not permit attack at a unique site on the DNA like restriction enzymes, targeting of the nuclease activity by hybridization provides a method for analyzing single-stranded DNA[23, 36, 37] and RNA.[38] It is also possible to design an *o*P–ODN that can recognize and cleave specific sequences selectively on double-stranded DNA by the formation of a triple-helix.[37, 39] Sequence-targeted cleavage of nucleic acids by conjugates of phenanthroline complexes and oligo-α-deoxynucleotides, which are resistant to nucleases, could be used to regulate gene expression in vivo.[40]

The nucleolytic activity of **1** has also been directed at specific sites of attack with DNA-binding proteins as carriers, in order to study the interactions of DNA-binding proteins with DNA restriction fragments or to isolate long DNA fragments for sequencing, cloning, or chromosomal mapping.[34, 41] This strategy has been applied to the design of *tat*-based chemical nucleases useful for site-specific cleavage of HIV TAR RNA.[42] Sequence-specific scission of DNA by RNA-bound **1** has recently been described.[43] Conjugates prepared by tethering 1,10-phenanthroline to a dye binding in the minor groove like Hoechst 33258 have been used to increase the reactivity or to modify the selectivity.[44]

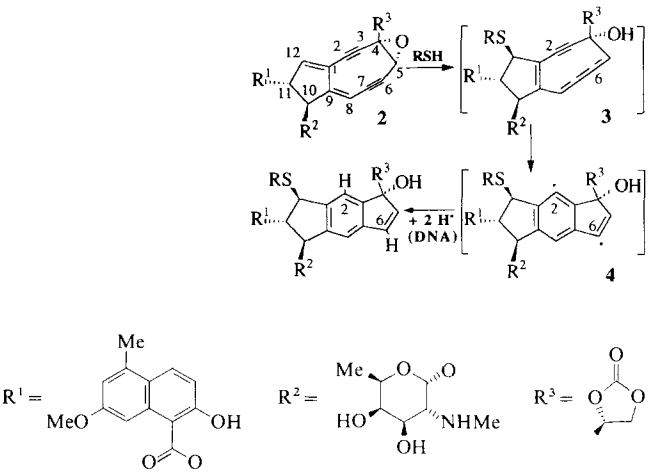
Extensive cleavage of DNA has been achieved with a chiral system related to **1** in which copper(II) is bound to one chelation site of a multifunctional ligand (4′,7′-phenanthrolino[5′,6′:5,6]pyrazine) while the second site is occupied by $Ru^{II}(bpy)_2$. Cleavage is almost exclusively limited to the *Λ* isomer of this chiral bimetallic complex.[45]

Mechanisms of DNA cleavage by **1** will be discussed in detail in Sections 3.1.1 and 3.4.1.

2.2. Enediyne Anticancer Antibiotics

2.2.1. Mechanism of Potentiation

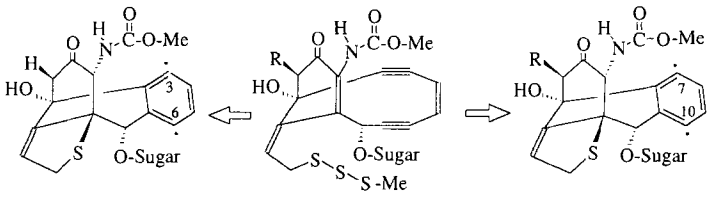
Naturally occurring enediyne anticancer antibiotics are prodrugs metabolized into active biradicals that can abstract hydrogen atoms from the sugar phosphate backbone of DNA in the presence of thiols.[9g] Among enediyne antibiotics, neocarzinostatin (NCS) has been extensively studied by Goldberg et al., and its mechanism of DNA cleavage is the best documented.[9d] Neocarzinostatin cleaves DNA through a nonprotein chromophore, NCS-chrom (**2**, Scheme 3). The nucleophilic addition



Scheme 3. Formation of a biradical **4** from **2** in the presence of a thiol, and abstraction of two hydrogen atoms from deoxyriboses of DNA.

of a thiol (or hydride) on the C12 position of **2** (→ **3**) gives rise to the rearrangement (cycloaromatization) to an indacene biradical (**4**) with C2 and C6 as radial centers. This biradical is able to abstract one or two hydrogen atoms from the DNA backbone, leading to SSBs or DSBs, respectively. The thiol necessary for the activation of **2** must have strong reducing properties, a good affinity for DNA, or a high nucleophilicity to ensure optimal activation.[46]

The other natural products presented in Schemes 4 and 5, calicheamicin γ_1^I (**5**, CAL; a total synthesis was recently described[47]), esperamicins **7**–**10** (ESP A, C, D, E), and dynemicin **12** (DYN), possess an enediyne unit as part of an overall structure that also contains a DNA-binding moiety (a glycosylated aminosugar or an intercalating structure) and a triggering



Scheme 4. Structures of CAL, ESP A, C, D, E, and their biradical species (for numbering rules see refs. [9f, 57].

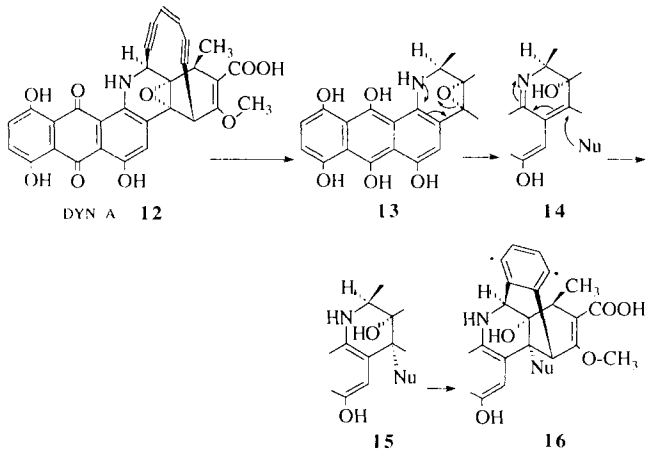
device (a methyltrisulfide group for CAL and ESP or a quinone for DYN). Reduction of these natural products with thiols initiates aromatization (Bergman type cycloaromatization,[48] see Schemes 3–5) of the enediyne moiety to a biradical species that is responsible for the DNA damaging properties[9g, 49] and the cytotoxicity of these drugs. In the case of activated CAL or ESP, the reducing thiol does not form a covalent adduct with the dye and gives rise to the 1,4-phenylene biradicals **6** and **11**.

DNA breaks mediated by enediyne compounds require oxygen, but neither reduced forms of dioxygen (such as the superoxide anion, hydrogen peroxide, or the free hydroxyl radical) nor transition metals are involved in the DNA damage (**2**,[50] **5**[51]). In the presence of DNA, sulfhydryls, and O_2, the enediyne compounds undergo a single oxidation–reduction cycle, which results in DNA cleavage and leaves an inactive form of the drug, devoid of further redox properties. The first step of the reaction, the generation of the biradical that abstracts H· from DNA, does not require O_2. In the next step with **2**, DNA cleavage is associated with the uptake of one equivalent of O_2 per mole of drug (DNA radical reacting with O_2) and is followed by the uptake of at least one equivalent of reducing agent. Under anaerobic conditions, misonidazole can replace dioxygen in the cleavage step (the DNA radical is quenched by misonidazole) and one equivalent of thiol is consumed per mole of **2**.[52] For other enediyne molecules the stoichiometry of O_2 and reductants has not been studied.

For **2** the C6 radical of the activated form **4** of the dye (Scheme 3) performs the predominant H abstraction (C5′ chemistry) from DNA.[53] The remaining C2 radical of the drug either reacts across the minor groove with the opposite strand of DNA in the case of suitable special DNA sequences (C1′, C4′, or C5′ chemistry) or degenerates and leaves the DNA at the level of a single-strand break. Selective quenching of the radical at C2 results in the conversion of **4** to a monofunctional reacting species[54] and is due to H· donation mainly from solvent or from the bound thiol. This could account for the predominance of SSBs (80%).

In the case of CAL (**5**, see Scheme 4), DDBs form 95% of DNA damage.[55] Both hydrogen atoms incorporated at the C3 and C6 positions of CAL biradical **6** originate solely from DNA.[12a, 56] For the esperamicin family **7**–**10** (see Scheme 4), the two radical centers on the reactive species **11** are C7 and C10.[9g, 57]

Dynemicin A (**12**, Scheme 5) can, for example, be activated through the reduction of the quinone unit to the compound **13**; opening of the adjacent epoxide provides **14** and attack by a nucleophile gives **15**. Then, in the absence of geometrical con-



Scheme 5. One proposition for the formation of the biradical **16** from DYN A (**12**) by bioreduction (Nu = nucleophile).

straints imposed by the epoxide ring, this activated intermediate undergoes a facile cycloaromatization to the biradical **16**, which causes the classical DNA H abstraction of this series of compounds.[9g, 58] So far, no detailed study of H abstraction from DNA by **12** has been reported.

Photochemical (for **2**, ESP **7**–**10**,[59] and **12**[60]), radiolytical (**2**),[61] or thermal activation (ESP[62]) are also possible and lead to DNA cleavage.

2.2.2. *Interaction with Nucleic Acids*

2.2.2.1. NCS-Chrom

Strong interaction of NCS-chrom (**2**) with DNA (affinity constant approximately $5 \times 10^6\ M^{-1}$), and proper positioning of the activated form of the drug provide clues to its DNA cleaving efficiency. NCS-chrom binds to DNA through intercalation of its naphthoate moiety and through external interaction of its protonated aminosugar residue with phosphate groups. The biradical part of the activated form is positioned in the minor groove of DNA,[63] and the intercalated part of the drug increases the distance between two base pairs within the interaction site. This detail is important when the site of the DSBs are compared with those for other enediyne drugs. Double-strand breaks of **2** are two base pairs (bp's) apart in the minor groove, compared to a 3 bp shift for other enediyne drugs. SSBs occur mostly at T residues (T ≫ A ≫ C > G) and show base specificity rather than sequence specificity.[9d] Double-strand breaks are sequence specific: 5′-AGC or 5′-AGT are the main DSB sites. They also involve different mechanisms on each strand: H5′ abstraction by the C6 radical of **2** occurs on one strand, and for some particular sequences, the C2 radical is properly located for the second H abstraction on the opposite strand, where it mediates mainly either C1′ or C4′ chemistry. All SSBs are due to C5′ chemistry, and for the DSBs studied so far, at least one strand is cleaved after H5′ abstraction.

Depending on the thiol used in DNA cleavage experiments with **2**, the amount and the nature of cleavage products are modified.[46, 64] The thiol is involved in the nucleophilic activation of the chromophore through a covalent bond, so it may

change the interaction of the activated drug with the minor groove of DNA and modify the C4′ to C5′ chemistry ratio, as well as the total amount of C4′ chemistry observed at some residues.[64] The nature of the thiol is also important for the DSB/SSB ratio.[46] One striking example is the generation of direct double-strand breaks by glutathione (GSH). GSH was shown to force the drug deeper into the minor groove of DNA at 5′-AGC/3′-TCG sequences, which increased drug activity at the C1′ sugar carbon.[46, 65]

The positioning of **2** in the minor groove of DNA is also dependant on the local microstructure at the interacting site. The introduction of mismatches in double-strand cleavage sites, or the replacement of guanine by inosine (without an NH_2 group pointing into the minor groove), changes the access of the biradical form of the drug to the C1′, C4′, or C5′ sugar carbons of DNA.[66]

Mechanisms of cleavage for **2** will be discussed in Section 3.1.2., 3.4.2.1 and 3.5.1.1 (C1′, C4′, and C5′ chemistries, respectively).

2.2.2.2. *Other Enediynes*

The other enediyne molecules mediate single- and a substantial number of double-strand breaks, because of the unique fit of the drugs in DNA. The generation of a phenylene biradical results in staggered double-strand cleavage sites through synchronous homolytic H abstractions from deoxyribose sites on opposing strands. This series of compounds also attacks DNA in the minor groove.

Calicheamicin γ_1^I: CAL **5** causes double-strand DNA lesions (more than 95%) in a plasmid or in a model of the cleavage site.[55] Each strand is cleaved by different mechanism. The preferred attack sites are the 5′ penultimate pyrimidine C of a 5′-TCCT sequence and the nucleotide N, three nucleotides toward the 3′ side of the paired G in the complementary sequence 3′-*N*NA*G*GA.[51].

In 1992 other sites of cleavage were reported: 5′-C*T*CT, 5′-ACCT, 5′-T*T*TT.[67a] CAL requires double-stranded helical DNA at the 5′ site of a 5′-TCCT sequence in order to anchor efficiently. This drug binds to the minor groove of B-DNA by orienting its oligosaccharide side chain toward the 3′ end of a 5′-TCCT sequence. For a review of CAL-DNA interactions, see ref. [9f]. The interaction of the drug with its recognition sequence is very sensitive to changes, and truncated or modified drugs show altered cleaving and recognition properties.[67] Variations of DNA sequence within the preferential binding site also affect the cleavage.[67b] There seems to be a real synergism of the two parts of the intact drug (carbohydrate domain and aglycone core) for the sequence-selective, double-strand cleaving efficiency of calicheamicin. CAL mediates C5′ chemistry on the T*C*CT strand (Section 3.5.1.2) and C4′ chemistry on the complementary strand (Section 3.4.2.2). Some C1′ chemistry may be involved in double-strand lesions,[55] but in the absence of any precise data will not be discussed further.

Esperamicins: Esperamicins **7**–**10** (Scheme 4) exhibit base selectivity (T > C > A > G), but less sequence selectivity than calicheamicin, in spite of their structural similarities. ESP A (**7**) is the only member of the ESP family to mediate SSBs. ESP C, D, and E (**8**–**10**) lack the fucosyl anthranilate moiety, and afford a substantial number of DSBs.[68] So, the presence of two side chains in ESP A might explain the production of SSBs, whereas a suitable single arm might confer the ability to generate DSBs (ESP C, D, and E). In the ESP family, the trisaccharide tail seems to be very important for the cleaving efficiency, since ESP D (**9**) or E (**10**), with one or two sugars missing) were considerably less efficient DNA cleavers while showing the same sequence selectivity.[57, 68a, 69]

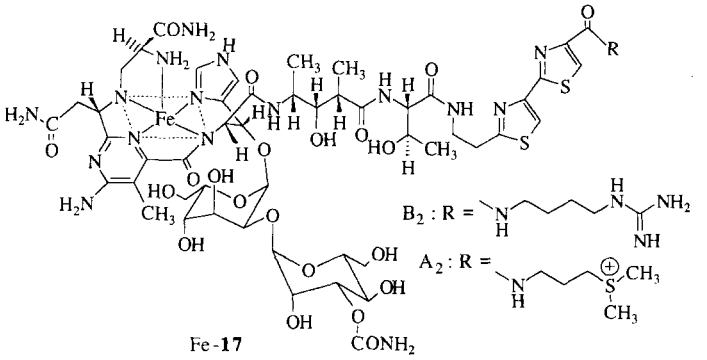
The binding of ESP to DNA is not as strict as for CAL (**5**) or for NCS-chrom (**2**). ESP may bind in the minor groove in two opposite orientations.[57] A 3′-staggered asymmetric cleavage pattern on the same sequences was reported for the double-strand cleaver ESP C **8** as well as for the single-strand cleaver ESP A **7**.[57, 68a] ESP A only mediates SSBs by targeting C5′ carbons on one or the other strand of the target DNA sequence, while ESP C, D, or E mediate DSBs with different mechanisms on each strand (two possible orientations of the drug in its target site). The authors propose that each radical position (C7 and C10) of the activated drug **11** has its own mechanism of deoxyribose-H abstraction: the radical at C7 would abstract a H4′ atom and that at C10 a H5′ atom. Because the activated entity **11** can bind in two orientations to DNA, a radical center can attack either the one or the other strand and so promote the corresponding chemistry on either strand. SSBs generated by ESP A can be explained by the loss of reactivity of the C7 radical center, probably due to congestion from the nearby fucosyl anthranilate group, and to the ability of the remaining C10 radical for H5′ abstraction. The mechanism of DNA cleavage for ESP involves both C4′ and C5′ chemistry (see Sections 3.4.2.3 and 3.5.1.3, respectively).

Dynemicins: Intercalation and minor groove binding have been proposed for the interaction of this type of drug with DNA.[58b] DYN A (**12**) causes single- and double-strand breaks, but is not base-specific. Dynemicins preferentially attack the base adjacent to the 3′ side of purine bases (5′-G*C*, 5′-G*T*, 5′-A*T*, and 5′-A*G*). They mediate strand breaks, three bp's apart (in the 3′ direction) in the two DNA strands.[70]

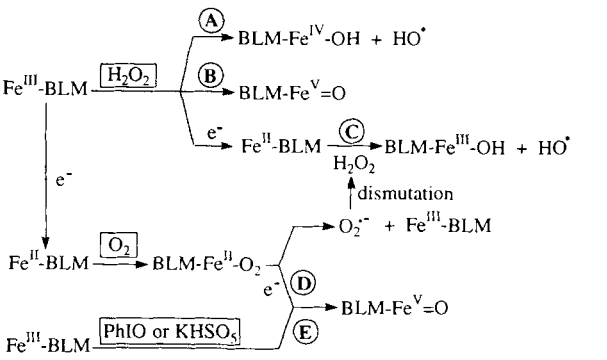
General remarks on enediyne drugs: The bifunctional nature of the enediyne biradicals make them potential double-strand cleavers. The degeneration of the biradical species to an entity with one active radical center may be due to altered positioning of the activated drug, or to steric hindrance or quenching of one of the radical centers by the fucosyl anthranilate moiety (for the ESP family) or by the thiol unit (for **2**). The optimal efficiency of enediyne drugs may thus not always be achieved, because of these surrounding tails.[55, 57] The radical center that is not influenced by a surrounding side chain will ordinarily mediate C5′ chemistry; the other one will react with the C4′ position of deoxyribose,[9d, 55, 57] and in some cases with C1′[66, 71] or C5′.[64]

2.3. Bleomycins

The bleomycins **17** (BLM, Scheme 6) are a family of glycopeptide-derived antibiotics, discovered by Umezawa and coworkers in 1966,[72] that have been used clinically against non-Hodgkin lymphomas, squamous cell carcinomas, and testicular tumors.[73] Their cytotoxic activity against mammalian cells is



Scheme 6. Structure of bleomycins A_2 and B_2 and proposed structure for their chelation of an iron atom.



Scheme 7. Potential pathways for activation of Fe–BLM complexes in the presence of O_2, H_2O_2, or oxygen atom donors (PhIO, $KHSO_5$).

generally assumed to correlate with their ability to bind to and cleave DNA.[74] More recently RNA has been reported as a possible target for BLM-mediated cleavage (see Section 3.4.3 for further details). Three domains can be distinguished in the structure of BLMs:[9a–b] the bithiazole and the positively charged chain contribute to specific binding to DNA; the pyrimidine, β-aminoalanine, and imidazole moieties are involved in dioxygen activation by chelating iron; finally, the gulose and carbamoylated mannose residues are perhaps responsible for the selective accumulation of BLM in some cancer cells, and might also participate in iron coordination and oxygen activation.[75] A large variety of analogues of BLM were snythesized to provide new insights into chemical or biochemical aspects of BLM activity. It has been possible, for example, to establish the coordination structures of metallobleomycins with more certainty,[76] to improve the dioxygen activating capability[77] or the DNA cleaving activity,[78] to carry out asymmetric epoxidation,[79] to modify the sequence specificity,[80] to better define the structural elements primarily responsible for controlling sequence-specific DNA cleavage,[81] and to develop chiral bleomycin models that discriminate according to chirality on cleaving DNA.[82]

2.3.1. *Mechanism of Potentiation*

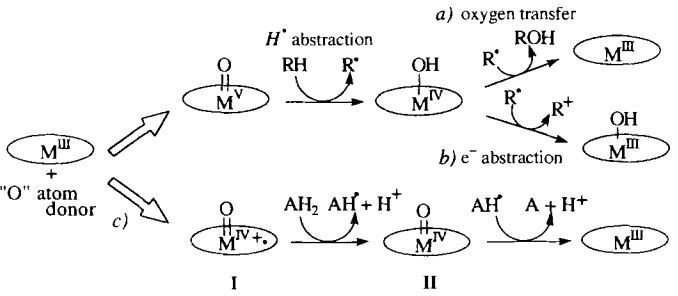
BLM-induced DNA breaks are mediated by several redox-active metals (iron, cobalt, copper) which are strongly chelated by nitrogen atoms of the peptide moiety of BLM and which react with molecular oxygen.[9a–b, 83] Oxygen activation by Fe^{II}–BLM requires an additional electron. This can be provided by disproportionation of two Fe^{II}–BLM molecules, by reductants such as ascorbic acid[84] or alkyl thiols,[84a, 84c] or by electrochemical reduction.[85] A key step in DNA lesions is the homolysis of the C4′–H bond of deoxyribose rings[86] by the "activated" bleomycin.[84a, 87] The exact nature of this activated BLM is still a matter of debate. All the hypotheses concerning the H4′-abstraction step can be classified in two categories (Scheme 7): a Fenton route (HO• as reactive species, routes Ⓐ and Ⓒ[84a]) or a P-450-like route (with BLM–Fe^{V}=O as hydroxylating agent, routes Ⓑ, Ⓓ, Ⓔ, first suggested by Burger et al.[87b]). Evidence to support a particular pathway can be obtained from the different ways of generating "activated BLM", from spectroscopic characteristics of intermediates, and from observed chemical reactivity.

Activated bleomycin can be generated by three different oxygen sources: molecular oxygen and electrons, hydrogen peroxide or alkyl hydroperoxides, and single oxygen atom donors. The usual methods for Fe–BLM activation (either Fe^{III}–BLM/O_2/$2e^-$ or Fe^{III}–BLM/H_2O_2) produce active species that behave similarly toward DNA.[88] Neither route distinguishes between the Fenton or the P-450 mechanism, since both are compatible with pathways Ⓒ and Ⓓ or Ⓐ and Ⓑ of Scheme 7. The formation of oxo–iron species has been well established for cytochrome P-450 itself with single oxygen atom donors like $NaIO_4$, H_2O_2, ROOH, or iodosylbenzene,[89] and for synthetic metalloporphyrins with peracids, iodosylbenzene, or NaOCl.[90] The association of iodosylbenzene with Fe^{III}–BLM strongly supports the formation of BLM–Fe^{V}=O[91] (route Ⓔ, Scheme 7); however, in this case possible Lewis acid catalysis which does not necessarily imply a FeV=O intermediate has been discussed.[92] Moreover, iodosylbenzene is not a benign oxygen surrogate in reactions with BLM, especially for the long incubation times generally used, and results should be viewed with caution.[93] With potassium monopersulfate ($KHSO_5$), a water-soluble oxygen atom donor at physiological pH (Scheme 7, route Ⓔ), activated Fe–BLM can give single- and double-strand breaks on DNA[94] or transfer oxygen to olefins.[95] When Fe^{III}–BLM is activated by particular alkylhydroperoxides that were shown to undergo homolytic scission of the O–O bond route Ⓐ in Scheme 7,[96a] the activated species is not capable of DNA cleavage.[96b] These data support the assignment of "activated BLM" to a high-valent bleomycin oxo–iron complex (the formation of such oxo–iron species from an alkylhydroperoxide requires a heterolytic splitting of the peroxidic O–O bond). The inefficiency of radical scavengers[97] in these reactions suggests that the active cleavage pathway goes predominantly through an oxo–iron route.

Consideration of the transformations of small molecules with activated Fe–BLM[9a, b] provides additional support for the existence of a BLM–Fe^{V}=O species. Also, the absence of similarities between the DNA cleavage pattern produced by Fe–MPE, a well-known producer of hydroxyl radicals and that produced by Fe–BLM (see Sections 3.4.2 and 3.4.4) indicates that Fe–MPE and Fe–BLM do not share a major common oxidative pathway for DNA cleavage, and that the free hydroxyl-

radical can be excluded as a major reactant for Fe–BLM-induced cleavage.[98a]

The nondiffusible activated BLM species, two redox equivalents above the nonactivated Fe^{III}–BLM, is formulated as BLM–Fe^{V}=O, and is capable of H abstraction from deoxyribose to give a carbon-centered radical. The resulting BLM complex, BLM–Fe^{IV}–OH, is still a strong oxidant (one redox state above that of the initial Fe^{III}–BLM) and may react with the generated carbon-centered radical to produce a hydroxylated derivative by a typical P-450 model route (oxygen-rebound mechanism[89a]) (Scheme 8, route a). But, as was recently



Scheme 8. Three possible oxidative pathways for BLM or Porph complexes (M = Fe or Mn): a) P-450 route; b) diverted P-450 route; c) peroxidase route. **I** is equivalent to the so-called "compound I"; **II** is equivalent to "compound II".

demonstrated on DNA,[99] the incorporated oxygen atom comes from the solvent. Thus this result points to an alternative possibility: activated BLM in the second step of the reaction can behave like a peroxidase (see classical mechanism in Scheme 8, route c), mediating an electron abstraction rather than transfer of an OH entity (diverted P-450 route, see Scheme 8, route b). Then, a water molecule can react with the generated carbocation and give the hydroxylated derivative.

Finally, little damage is detected on bases when DNA is incubated with Fe–BLM under conditions where DNA breaks are detected.[100] In 1993 it was reported that DNA can be cleaved by Ni^{III}–BLM if potassium monopersulfate is the oxidant.[101]

2.3.2. *Interaction with Nucleic Acids*

The association constant of Fe–BLM with duplex DNA is on the order of $10^5\ M^{-1}$.[102] BLM-mediated DNA cleavage is characterized by its sequence selectivity: most strand breaks occur at 5′-G-pyr sequences. In BLM, a small difference in the terminal amine chain and the absence of the gulose-mannose sugar moiety have a negligible effect on the sequence specificity of DNA cutting. Binding is mediated in part through electrostatic interactions, and probably also by intercalation or partial intercalation of the bithiazole moiety. Metallo–BLM probably binds in the minor groove of the B-DNA helix, where it covers 2 or 3 bp's on DNA. The 2-amino group of the guanine base adjacent to the 5′ side of the cleaved pyrimidine base is one key element of specific 5′-GC or GT recognition by the metallobleomycins; the bithiazole group probably plays an important role as an anchor on B-DNA.[103] Structurally altered DNA such as methylated DNA[104] or platinated DNA oligomers[105] may be relevant to changes in specificity or reactivity.

BLM produces double-strand breaks in DNA with a frequency far in excess of that expected from coincidence of single-strand breaks. The cleavage site on one strand is a pyrimidine in a 5′-G-pyr sequence, but in the complementary strand, the cleavage occurs at a site where single-strand cleavage is not common.[106] Both breaks result from specific attack on C4′.[107]

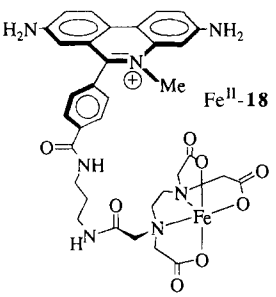
Attempts to modify the specificity of BLM have been undertaken by coupling BLM to oligonucleotides. The conjugates efficiently cleave the DNA at the GT sequence near the oligonucleotide binding site.[108]

Some studies have concluded that the cleavage of RNA is unlikely to be important for therapeutic action of BLM–Fe,[109] but other findings suggested the opposite.[81, 110] In spite of recent reports that RNA was not cleaved by BLM,[111] the three major classes of RNA have been shown to be degraded by BLM–Fe.[110, 112] RNA cleavage appears to be much more selective than DNA cleavage. While 5′-G-pyr-3′ sequences are also represented to a large extent among observed RNA cleavage sites, the cleavage seems to occur predominantly in single-stranded regions and at the junctions between single- and double-stranded regions. This suggests recognition of RNA tertiary structures, rather than recognition of specific sequences.

BLM has so far only been involved in C4′ deoxyribose oxidation (see Section 3.4.3 for details).

2.4. Fe–EDTA and Fe–MPE

Methidiumpropyl-EDTA (**18**, MPE, Scheme 9) is an early example of DNA-binding molecules able to target the redox activity of a metal ion like iron and to generate DNA breaks. It contains the DNA intercalator methidium, covalently bound by a short hydrocarbon tether to the metal chelator EDTA.[113, 114]



Fe^{II}-**18**

Scheme 9. Structure of the iron(II) complex of methidiumpropyl EDTA (**18**).

2.4.1. *Mechanism of Potentiation*

Both MPE and EDTA in the presence of iron(II) and molecular oxygen are able to break the backbone of DNA, probably by H abstraction from deoxyribose.[113, 115, 116] Fe–MPE cleaves plasmid DNA at a concentration two orders of magnitude lower (10^{-6} M) than Fe–EDTA (10^{-4} M). Addition of reducing agents such as dithiothreitol, sodium ascorbate, or NADH, which regenerate Fe^{II} from Fe^{III}, enables DNA cleavage at concentrations comparable to those used with bleomycin (10^{-8} M).[113]

Presumably in this mechanism, Fe^{II} reacts with O_2 to give Fe^{III} and $O_2^{\bullet-}$ [Eq. (5)]. The superoxide anion in protic media rapidly disproportionates to produce H_2O_2 [Eq. (6)]. Fe^{II} and H_2O_2 can then produce hydroxyl radicals by the known Fenton-type

$$Fe^{II}\text{–MPE} + O_2 \longrightarrow Fe^{III}\text{–MPE} + O_2^{\bullet-} \quad (5)$$

$$2O_2^{\bullet-} + 2H^+ \longrightarrow H_2O_2 + O_2 \quad (6)$$

chemistry [Eq. (7)].[113] When sodium ascorbate is used as reducing agent in the presence of dioxygen, a catalytic cycle is created, requiring lower concentrations of iron for DNA cleavage [Eqs. (5)–(8)].[115, 117]

$$Fe^{II}\text{-MPE} + H_2O_2 \longrightarrow Fe^{III}\text{-MPE} + HO^{\bullet} + OH^- \quad (7)$$

$$Fe^{III}\text{-MPE} + \text{reductant} \longrightarrow Fe^{II}\text{-MPE} \quad (8)$$

Superoxide dismutase, which depletes the system of free superoxide, and catalase, which disproportionates hydrogen peroxide into water and oxygen, are both able to inhibit the DNA cleavage mediated by Fe–MPE. This ability indicates the importance of free hydrogen peroxide as key intermediate in strand scission. Furthermore, in the absence of dioxygen no strand scission can be observed.[98, 113, 115] Because the concentration of the hydroxyl radical species decreases with distance from its point of formation, the decrease in the level of cleavage with distance from the position of the EDTA group is also consistent with a mechanism involving HO·.[118]

Fe^{III}–MPE was also examined for DNA-cleaving ability. Its direct oxidation with iodosylbenzene enhances cleavage of plasmid DNA. Whether this involves a perferryl species MPE–Fe^{V}=O or a coordinated hydroxyl species is still a matter of discussion.[9b, 98, 113]

2.4.2. *Interaction with Nucleic Acids*

Fe–EDTA is a negatively charged complex which does not associate electrostatically with DNA, so hydroxyl radicals cleave DNA with almost no sequence dependence.[98, 119, 120] This system is a useful reagent for footprints of proteins[117, 120, 121] or of small molecules (distamycin and actinomycin[122]), and can also provide information about DNA structures (unusual conformations adopted by the adenine tracts in DNA,[123] four-arm Holliday structures,[124] and bent DNA[116]).

Fe–MPE cleaves DNA in a relatively poor sequence-specific manner, which is not unexpected since the methidium unit is an intercalator of low overall base specificity. The only specificity known for this system is a slight preference for GC rich regions. Sequence specificity is significantly lower than that of DNase I, and the wide use of this reagent has proved to be very useful for many applications: for instance, the determination of the location, size, and relative importance of the binding sites of small molecules on native DNA[120, 125] or proteins on restriction fragments,[121, 126] and study of RNA[127] and chromatin[128] structures. For a discussion on the relative advantages of Fe–EDTA and Fe–MPE in footprinting experiments, see ref. [129]. The DNA-binding affinities of Ni^{II} and Mg^{II} complexes of MPE are similar to that of ethidium bromide (about $10^5\ M^{-1}$). The affinities of Fe^{II}–MPE or Fe^{III}–MPE cannot be determined, due to their efficiency as DNA cleavers. The binding site is probably a 2-bp site.[98]

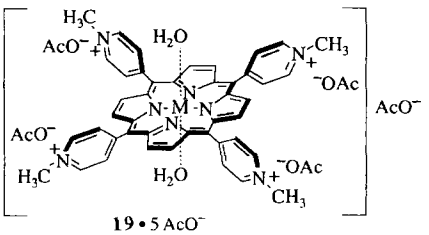
The attachment of Fe–EDTA to sequence-specific DNA binding molecules such as antibiotics, polypeptides, oligonucleotides, or proteins provide new classes of "DNA affinity cleaving molecules" and is the basis for the design and construction of artificial restriction endonucleases with defined target sequences and binding-site sizes.[98, 130] Accordingly, hybrid molecules have been synthesized by associating EDTA with distamycin,[9i, 98, 131] a chiral derivative of netropsin,[130, 132] oligopeptides,[119, 133] or oligonucleotides, in order to cleave single-stranded DNA (or RNA) under mild conditions[118, 134] or double-stranded DNA (by triple helix formation).[135]

The chemistry of Fe–EDTA complexes with DNA will be detailed in Section 3.4.4.

2.5. Cationic Metalloporphyrins

2.5.1. *Mechanism of Potentiation*

Synthetic metalloporphyrins are able to mimic oxygenation and oxidation reactions mediated by heme enzymes.[90a] Beside this mode of reactivity, iron or manganese porphyrins with peripheral positive charges, for example, Fe– or Mn–*meso*-tetra(4-*N*-methylpyridiniumyl)porphyrins **19** (Fe–TMPyP, Mn–TMPyP, Scheme 10; for crystallographic data on Mn–TMPyP see ref. [136]), exhibit strong interaction with DNA



19 • 5 AcO^-

Scheme 10. Structure of M–TMPyP pentaacetate (M = Fe^{III} or Mn^{III}) [136].

that brings a powerful oxidizing species into the vicinity of the target. The active oxidative species in the case of DNA cleavage is probably the same as that involved in catalytic oxygenation and oxidation reactions described for metalloporphyrins in general, namely, an oxoporphyrinato complex with the metal in a high oxidation state and able to hydroxylate a C–H bond or to epoxidize an olefin.[90a] This active species is generated in the presence of oxygen atom donor compounds like iodosylbenzene,[137] hydrogen peroxide,[138a] potassium monopersulfate,[138a–b, 138d] or magnesium monoperphthalate.[138c] Another way to generate oxo-metalloporphyrins is to use molecular oxygen associated with an electron source, as does cytochrome P-450.[89a, 137, 139] The most efficient method of oxidative cleavage of DNA is the oxidation of cationic Mn–porphyrins by $KHSO_5$.[138, 140] Data on DNA cleavage by Mn^{III}–TMPyP/$KHSO_5$ suggest that diffusible radical species are not involved in the reaction, because the breaks are well-defined and H_2O_2 is at least three orders of magnitude less efficient in generating the active species leading to cleavage.[138a] The high-valent TMPyP–Mn^{V}=O is a monoreacting DNA cleaver (unlike bireactive biradicals of enediyne drugs).[138a] Catalytic activity can be observed only if it is protected from self-oxidation (leading to the chromophore bleaching) by strong interaction with its target. For example when the DNA/Mn–porphyrin ratio was high (75 μM bp/5 nM Mn-porphyrin), up to five SSBs per Mn–TMPyP molecule were observed.[138a] A proposed activation/reaction cycle is presented in Scheme 8. The high-valent

TMPyP–Mn^{V}=O species that cleaves DNA is too reactive to be characterized. As discussed in Section 2.3.1 for high-valent BLM–Fe^{V}=O, neither P-450 (route a in Scheme 8) nor "diverted P-450" (route b) reactivity has been established for this compound. Whether the activated intermediate TMPyP–M^{IV}–OH oxygenates the DNA substrate directly by the rebound of the "HO equivalent" (route a) or by an electron transfer (route b) is still unknown. Studies of the source of O atom incorporated in DNA sugars would help answer this question (see Section 2.3.1).[99]

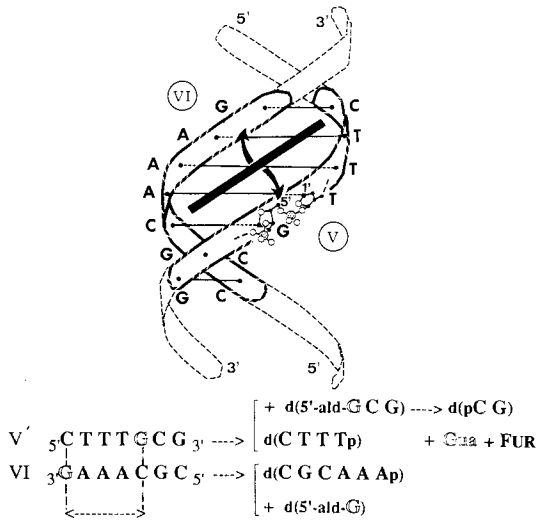
Electrochemically activated Mn^{III}–TMPyP and Fe^{III}–TMPyP have been used for DNA cleavage in the presence of O_2.[141] The mechanism of activation and cleavage in this case is potentially relevant to reports on chemical activation. Photochemically activated porphyrins are also able to cleave DNA,[142] probably by singlet oxygen production.

2.5.2. *Interaction with Nucleic Acids*

Mn–TMPyP belongs to a class of cationic metalloporphyrins that do not intercalate between DNA base-pairs but instead bind in the minor groove of AT-rich regions of DNA.[140, 141, 143] The Mn–porphyrin framework is devoid of any H-bonding donor/acceptor capacity and intercalation is precluded by the presence of an axial ligand on manganese.[136] Thus the ability of Mn–TMPyP to select AT-rich regions of DNA is apparently electrostatic or steric in origin. It has been proposed that this cationic metalloporphyrin is attracted by the high negative potential at the surface of the minor groove[144] of A · T-rich sequences. A close contact with the minor groove is necessary to improve the binding interaction and the cleaving efficiency of the metalloporphyrin, as deduced from studies on variations in total charge and in charge distribution at the macrocycle periphery.[143a–c, 145] At high ionic strength, the reagent is unable to bind or cleave DNA.[138a, 146]

Considering the size of Mn–TMPyP, it could span over five to six base-pairs in the minor groove of B-DNA, but the preferred cleaving site consists of three consecutive AT base-pairs creating a suitable "box" for highly selective DNA cleavage.[137, 138d, e, 143a, d] At this site Mn–TMPyP strictly mediates C5′ oxidation on nucleosides on both 3′ sides of the AT box:[147] one single-strand break on each strand leads to double-strand cleavage with a four base-pair shift to the 3′ end of the opposite DNA strand (Scheme 11). So far, there is no definite proof that such a cleavage pattern results from two SSBs by the same metalloporphyrin activated twice in the minor groove, or that it is effected by two different activated metalloporphyrins. On large DNA substrates, SSBs prevail[138a] and on oligonucleotides substrates (with one or two "AT boxes") DSBs are easily obtained.[147] Besides cleavage at $(A \cdot T)_3$ cleaving sites, some secondary reaction sequences are also noted, in which any one of the A · T pairs is replaced by a G · C base-pair.[143a] This secondary reactivity is particularly noticeable under drastic cleaving conditions[147] and is one order of magnitude less than that for $(A \cdot T)_3$ sites.

Mn–TMPyP is also able to degrade G · C-rich sequences with a reactivity two orders of magnitude weaker than the degradation of $(A \cdot T)_3$ sites. The mechanism of DNA lesions in these regions of DNA is not fully understood and may involve



Scheme 11. On using the Mn–TMPyP/$KHSO_5$ system the scission on the two strands of duplex V/VI shows a 4 bp shift (dashed double-headed arrow, bottom left) in direction of the 3′-ends. This is shown by analysis [147] of the cleavage products (bottom right).

sugar oxidation (C5′ or C1′) and/or base oxidations. Affinity constants of up to $10^7\ M^{-1}$ have been published for Mn–TMPyP at the $(A \cdot T)_3$ binding site.[138e] Other values ($10^5\ M^{-1}$ for A · T sequences and $10^3\ M^{-1}$ for G · C sequences) have also been reported.[148]

Hybrid molecules based on a metallotris(methylpyridinioyl)porphyrin moiety attached to oligonucleotides have been prepared, and were shown to selectively cleave a single-stranded 35-mer DNA corresponding to the initiation codon region of the *tat* gene of HIV-1.[149]

The mechanisms of DNA cleavage by Mn–TMPyP through C1′ and/or C5′ oxidation are described in Sections 3.1.3 and 3.5.2, respectively.

2.6. Photoactivated DNA Cleaving Agents: The Case of Phenanthrenequinonediiminerhodium(III) Complexes

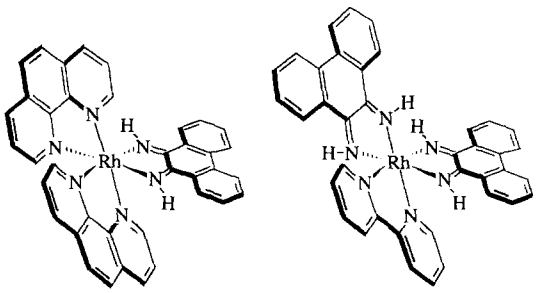
A number of studies have focused on the use of metal complexes or drugs to design spectroscopic DNA probes or photoactivated DNA cleaving agents.[150a–d] Photoactivation promotes strand cleavage only for some of these molecules.[150e] As well as metalloporphyrins or enediynes (Sections 2.5.1 and 2.2), a range of simple inorganic octahedral molecules are also capable of inducing single-strand scissions by photoexcitation of different absorption bands. This cleavage is induced by metal complexes known to bind to DNA principally in two noncovalent modes: 1) a groove-binding mode stabilized by hydrophobic interactions of the ligands with the major or the minor groove of DNA[150e, 151] and 2) intercalation.[152] For some of these photoactivatable complexes, the exact mode of DNA binding is still a matter of debate.[153] Rhodium,[154] ruthenium,[155] and cobalt[156] complexes have been used as cleaving agents for probing nucleic acid conformation and for the recognition of specific sites on a DNA strand.

Recently, a precise mechanism involving oxidative attack on the C3′–H bond of deoxyribose has been deduced for phenan-

threnequinonediiminerhodium(III) complexes and will be discussed in detail in this review.

2.6.1. *Mechanism of Potentiation*

The production of sharp and well-defined gel bands after the cleavage of restriction fragments or oligonucleotides suggest that DNA strand scission by photoactivated rhodium complexes is not mediated by a diffusible oxidant. The cleavage appears to involve a species that is generated precisely at the binding site and induces strand scission of DNA at that site. Irradiation of the rhodium complex at the wavelength of the ligand-to-metal charge transfer band (LMCT) leads to an excited state with a lifetime in the μs range. The active radical species from **20** and **21** (Scheme 12) that cleave DNA is likely to be the radical cation of the phi ligand that is intimately bound to DNA and is formed by the LMCT band irradiation. The position of the phi radical cation in the site enables a fast H abstraction from the deoxyribose ring, initiating the cleaving reaction.[157]



$Rh^{III}(phen)_2phi$ **20** $Rh^{III}(phi)_2bpy$ **21**

Scheme 12. Structures of the (9,10-phenanthrenequinonediimine)rhodium(III) complexes **20** and **21**.

2.6.2. *Interaction with Nucleic Acids*

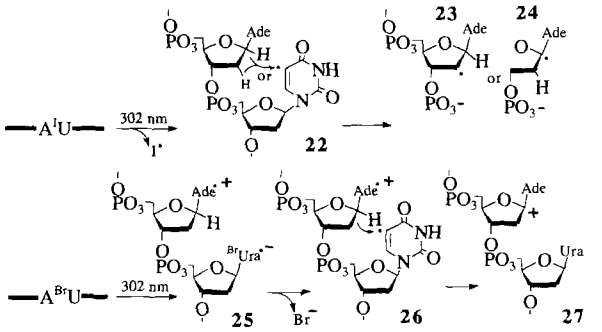
Upon photoactivation, the diphenanthroline complex **20** cleaves double-stranded DNA at 5′-pyrimidine–purine steps and in particular at the consensus sequence 5′-pyrimidine–purine, while **21**, despite containing ancillary imines for potential hydrogen bonding, cleaves DNA efficiently but in a generally sequence-neutral fashion. The asymmetry in the cleavage pattern to the 5′ side on each strand suggests that the rigid complex attacks B-DNA from the major groove of the helix. Given the propensity of the phi ligand for intercalation, **20** should contain the phenanthroline ligands in ancillary, nonintercalative positions along the groove, while for **21** one phi and one bpy should occupy the ancillary sites.[154a] NMR studies have recently provided direct structural evidence for specific intercalation of the octahedral chiral complex *Δ*-**20**, and indicate a preferential partial intercalation of the phi ligand whereas the phenanthroline ligands bind in ancillary positions.[158] Intercalation through the major groove is consistent with results of mechanistic studies on DNA cleavage by rhodium complexes, which demonstrate that H3′ abstraction is the initial step (see Scheme 16 and Section 3.3). Photocleavage experiments indicated enantioselective targeting of the 5′-CG step by *Δ*-**20**.

3. Hydrogen Abstraction from Different Positions of Deoxyribose, Leading to DNA Cleavage[159]

Each deoxyribose unit of DNA contains seven C–H bonds as possible targets for oxidative activation; four of them are located in the minor groove and three in the major groove (see Scheme 1). For all the chemical nucleases and drugs presented (in Section 2) a common initial step consists of one H abstraction, leaving the relevant carbon on the sugar as a radical species. We present here the manner in which this initial lesion leads to DNA cleavage under the different experimental conditions used in accord with the experimental evidence for the proposed mechanisms.

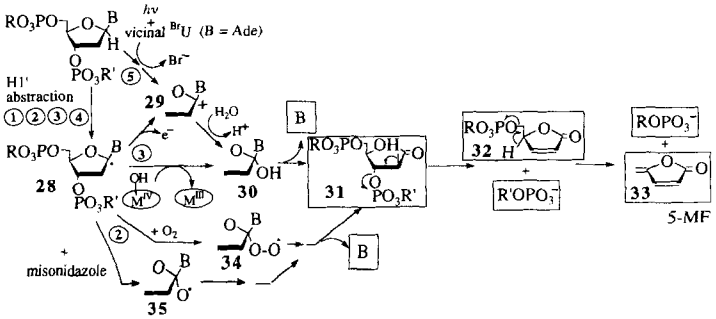
3.1. H1′ Abstraction: Cu(*o*P)$_2$, NCS-Chrom, Mn-TMPyP, and Halouracil-Containing Nucleotides

H1′ abstraction has been described for oxidative attack on DNA by Cu(*o*P)$_2$ (**1**), NCS-chrom (**2**), and Mn–TMPyP (**19**, M = Mn), producing a C1′-centered radical **28** (see Scheme 14). Photoreaction of 5-halouracil-containing oligonucleotides gives rise to C1′- or C2′-centered radicals (**23** or **24** in Scheme 13,



Scheme 13. Proposed reaction mechanisms for oxidative attack at C1′–H and C2′–H bonds in the case of halouracil-containing oligonucleotides [159].

respectively) via **22** or, alternatively, via **25** and **26** to the 1′ cation **27** (Scheme 13; see also **29** in Scheme 14). Usually, the next key steps of the DNA cleavage reaction (Scheme 14) are 1) the release of base associated with the formation of the oxidized abasic derivative **31**, 2) the first *β*-elimination inducing the



Scheme 14. Proposed reaction mechanisms when the initial site of attack by the oxidizing agent is at C1′ of the deoxyribose [159]. (①: **1**, ②: **2**, ③: **19**, ④: vicinal ^{I}U, ⑤: vicinal ^{Br}U)

strand break that leaves a 5′-phosphate end and a metastable α,β-unsaturated lactone (**32**) at the 3′ end, 3) the second and fast β-elimination allowing the recovery of the 3′-phosphorylated-ending DNA fragments and 5-methylene furanone (**33**) as the main sugar residue. Depending on the nature of the DNA cleaving agent, different aspects of this general cleavage pathway are more pronounced than others. C1′ chemistry for Fe^{II}–EDTA, Fe^{II}–MPE, and related compounds is considered to account for some experimental results; this point is briefly presented in Section 3.4.4.

3.1.1. $Cu(oP)_2$

Analysis of the products of DNA cleavage by $Cu(oP)_2$ (**1**) and hydrogen peroxide showed that phosphomonoesters are present at both the 5′ and 3′ termini (3′-phosphomonoester termini are the potent inhibitors of *E. coli* DNA polymerase activity, which provided the first evidence for the DNA scission reaction[15a, 15d]) and that bases are also released; the cleavage was proposed to occur by initial oxidation of the deoxyribose to a resonance-stabilized furan derivative.[29a] Later, under conditions where no reductant was used as coreactant, 5-methylene-2-furanone (**33**) was identified.[160] A possible reaction pathway that could accommodate the formation of these products from C1′ radical **28** is summarized in Scheme 14. The putative intermediate **32** at the 3′ terminus was observed by polyacrylamide gel electrophoresis (PAGE) during the cleavage reaction of a synthetic dodecamer and a restriction fragment containing the lactose control region.[28] No other information exists about intermediate steps except that the cleaving activity does not require the presence of molecular oxygen.[17]

The C1′ oxidation pathway accounts for 80–90% of the scission events induced by **1** (10–20% are related to cleavage chemistry at C4′, see Section 3.4.1).[15b] The relative importance of the two pathways, suggestive of a different rate of attack at two locations, depends on the DNA sequence,[28] as demonstrated by determination of the ratio of 3′-phosphoglycolate (attack at C4′) to 3′-phosphate (attack at C1′).

3.1.2. NCS-Chrom

C1′ chemistry occurs particularly at the *C* residue of double-strand lesion sites such as 5′-AG*C*/3′-TCG sequences,[9d, 71, 161] where it represents the major pathway of attack (72%), although some minor chemistry at C4′ or C5′ was also noted.[66a, 71] It is always accompanied by a strand break on the complementary 3′-*T*CG strand, where C5′ of the T residue is attacked. So, double-strand cleavage consists of a two-nucleotide 3′-stagger of the cleaved residues that represents the classic 3′-shift mediated by the NCS-chrom activated biradical **4** derived from **2** (see also Section 3.4.2). One important feature of this cleavage is the strong preference for glutathione (over neutral thiols, ME or DTT) in the C1′ chemistry induced by **2** (see Section 2.2.2.1).

Since the nucleolytic activity of **2** is dependent on the presence of molecular oxygen, a peroxy radical (**34**, Scheme 14) is probably involved initially with subsequent conversion into the oxidized intermediate **31** with concomitant release of base. Such oligonucleotides (**31**), observed on polyacrylamide gels,[161] migrated slightly faster than the full-length DNA and were transformed to the corresponding phosphate-ending fragments upon alkali treatment. DNA fragments carrying the α,β-unsaturated lactone **32** at their 3′ end (one β-elimination from **31**) were also seen on polyacrylamide gels of 5′-[^{32}P]-labeled oligonucleotides;[66a, 71] they migrated ahead of the corresponding 3′-phosphate-ending fragments. After enzymatic digestion of intermediate **31**, 2-deoxyribonolactone generated by the release of cytosine was isolated and characterized.[162] But 5-MF (**33**), the expected end-product of this reaction chain, was never observed because of the presence of reducing cofactors. When $NaBH_4$ was used as an activator for **2**, alkali-dependent breakage at the C residue was not prevented, which indicated that $NaBH_4$ is not able to reduce the oxidized intermediate **31**.[161] In addition, by careful examination of 5′-[^{32}P]-labeled DNA fragments through PAGE analyses, new bands could be observed with smaller mobility than that of the corresponding phosphate bands. These bands, which are converted into the 3′-phosphate-ending bands by piperidine treatment, were attributed to the adduct (Michael addition) between thiol and the 3′-terminal, α,β-unsaturated lactone **32**.[66b, 163] The mobility of this thiol adduct varies with the structure of the thiol.[66b] Such bands were also observed in the case of C4′ chemistry of **2** (see Section 3.4.2).

Under anaerobic conditions misonidazole can replace dioxygen for the production of the alkali-labile lesion at the C residue.[161] The mechanism is not fully understood: the question whether an oxy radical (**35**) or a peroxy radical (**34**) is involved as intermediate is still open (see Section 3.4.2).

Direct evidence for H1′ abstraction was also provided by experiments where H1′ was replaced by deuterium. Values of $k_H/k_D \approx 4$ for the deuterium isotope effect were determined from studies of alkali-induced cleavage of oxidized abasic derivatives (**31**).[71] Deuterium abstraction studies of the reacted chromophore (monitored by ^{1}H NMR spectroscopy) also indicate that the C2 of **2** is involved in the attack at the C residue of a 5′-AG*C* sequence.[54a]

3.1.3. Mn–TMPyP

The following stable reaction products were identified from several DNA and oligonucleotides cleavage reactions with Mn–TMPyP/$KHSO_5$: 5′- and 3′-phosphorylated termini, free bases, and 5-methylene furanone **33**.[164] The mechanism proposed to explain the formation of the product 5-methylene furanone is hydroxylation of C1′ as indicated in Scheme 14. The cleavage does not require the presence of molecular oxygen (M. Pitié et al., unpublished results). Two hypotheses (Schemes 8 and 14) may explain the evolution after the initial lesion: 1) the radical centered at C1′ (**28**) might be reoxidized by the Mn^{IV}(OH)-porphyrin by one-electron abstraction, giving the carbocation **29** that reacts with water and produces the 1′-hydroxylated derivative **30** ("diverted P-450 route" in Scheme 8, route b) or 2) the radical is directly hydroxylated by the Mn^{IV}(OH)porphyrin (cytochrome P-450 chemistry, see route a in Scheme 8 and Section 2.5.1). So far, neither the oxidized oligonucleotides **31** containing the abasic site nor oligonucleotides **32** bearing the α,β-unsaturated lactone have been observed except indirectly through their ultimate reaction product **33**.

With Mn–TMPyP/$KHSO_5$ as cleaving reagent, C1′ is the main oxidation target for single-stranded or GC-rich double-stranded DNA, but only a minor target for AT-rich sequences containing DNA (C5′ becomes then the main target, see Section 3.5.2).[164b]

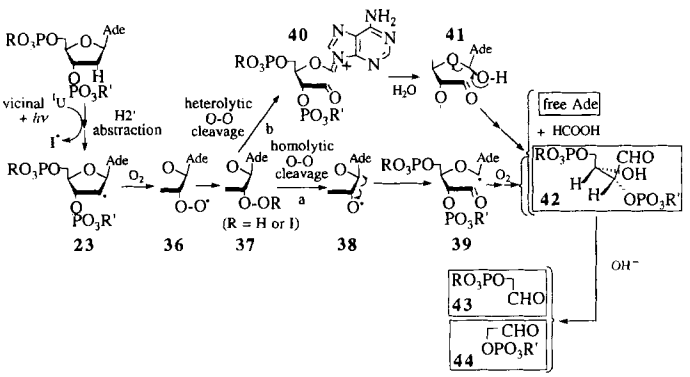
3.1.4. Halouracil-Containing Oligonucleotides

In an attractive hypothesis, formation of the 1′ cation **27** could occur in the UV-photoreaction of small oligonucleotides containing the 5′-A^{Br}U sequence (see Scheme 13). After an intramolecular electron transfer from adenine at the 5′ side to the adjacent ^{Br}U, the resulting ^{Br}U anion radical **25** would release a Br^- anion to produce a uracilyl radical **26**, which could then abstract the adjacent C1′ hydrogen atom of the deoxyadenosine radical cation to give rise to the 1′ cation **27**. Addition of another water molecule, loss of a proton, and release of the base (Scheme 14) would give the deoxyribonolactone derivative **31** (oxidized abasic site) which has been detected by HPLC and transformed to the corresponding phosphate-ending fragments upon treatment with hot NaOH. Without treatment with alkali and after enzymatic digestion of the oligonucleotide **31**, 2-deoxyribonolactone (with concomitant release of Ade) was isolated and characterized by spectroscopic and chemical methods.[165] The expected product 5-MF (**33**) coming from reaction of the oxidized abasic site of **31** was not observed, probably because of its instability under the experimental conditions (hot alkali treatment).

Photoreaction of 5-iodouracil-containing oligonucleotides[166] proceeds by an entirely different mechanism, which postulates competition between C1′ and C2′ oxidation products of the sugar residue at the 5′ side adjacent to the iodouracil residue. The sequence of events is indicated in Schemes 13 and 15. Photoreaction of ^{I}U proceeds by homolytic cleavage of the C5-I bond of uracil; the resulting uracilyl-5-yl radical (**22**, see Scheme 13) competitively abstracts the C2′ (→ **23**) or C1′ (→ **24**) hydrogen atoms of the deoxyribose at the 5′ side of ^{I}U. The C1′ and C2′ oxidation products **31** and **42** were observed (Schemes 14 and 15, respectively).

3.2. H2′ Abstraction: Iodouracil-Containing Nucleotides

While the chemistry of DNA damage resulting from H abstraction at C1′, C3′, C4′, and C5′ of the DNA deoxyribose is well documented, the DNA lesion resulting from H abstraction at C2′ has been scarcely studied. Characterization of erythrose-containing sites arising from H· abstraction at C2′ was only reported as one of the major types of damage induced by γ-radiolysis of DNA.[167] Very recently another example of deoxyribose C2′ oxidation in DNA was described during photoreaction of various 5-iodouracil containing oligonucleotides,[166] C2′ oxidation products were isolated directly for the first time. The proposed mechanism (Scheme 15) involves the peroxy radical **36**, which could be converted by homolytic cleavage of the O–O bond (via **37**, pathway a) into the oxy radical species **38**. β-Scission leads to **39**. The formation of the oxy radical from peroxy radical in double-stranded lesions of DNA by fragmentation of an O_4 bridge across the minor groove has been invoked

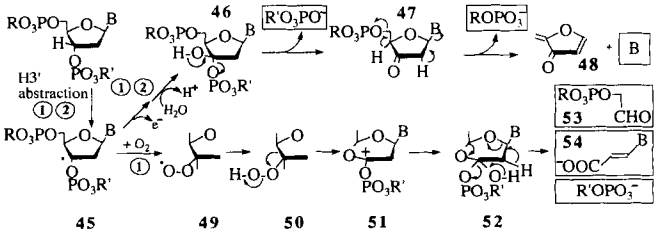


Scheme 15. Proposed reaction mechanisms when initial site of attack by the oxidizing agent is at C2′ of the deoxyribose [159].

for enediyne compounds (Sections 3.4.2, 3.5.1). But in the present case, combination of two C2′ peroxy radicals of A residues of 5′-A^{I}U/3′-A^{I}U does not seem sterically possible. Further reaction of **39** with molecular oxygen produces **42**, accompanied by the release of adenine. Alternatively, heterolytic cleavage of the O–O bond, perhaps favored by the formation of an R′OOI (pathway b), would also produce **42** via intermediates **40** and **41**. Under alkaline conditions the unstable compound **42** is cleaved and gives rise to fragments containing phosphoglycolaldehyde termini (**43** and **44**) by a retroaldol reaction. Compounds **42**, **43**, and **44** have been characterized, but the exact route of their formation remains to be elucidated.

3.3. H3′ Abstraction: Rhodium Complexes 20 and 21

Extensive studies have focused on DNA photocleavage by several photoactivated DNA cleaving agents. Among them, the phenanthrene-quinonediimine complexes of rhodium(III) (**20** and **21**) have received particular attention in terms of molecular mechanisms of DNA cleavage (Scheme 16).[154a, 157] While the complexes have similar photochemical properties, overall binding modes, and affinities, their cleavage patterns indicate different recognition characteristics (see Section 2.6.1.2), which may be understood based on the different molecular shapes of these two complexes. The shape of these compounds also governs the chemistry of strand scission. Because both complexes yield oligomers containing 3′- and 5′-phosphate termini and nucleic acid bases as primary products the sugar units seem to be reaction sites.[154a] For **21** these oligomeric products account for approximatively 70% of the reaction, but, in addition, base-



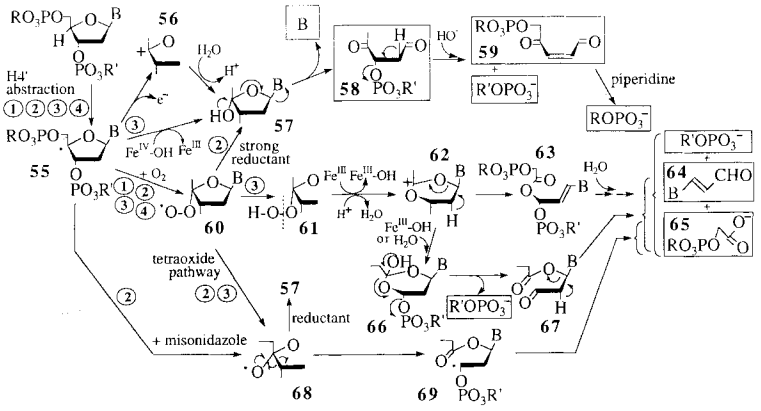
Scheme 16. Proposed reaction mechanisms when initial site of attack by the oxidizing agents (①: **21**, ②: **20**) is at C3′ of the deoxyribose [159].

substituted propenoic acids (**54**, so-called base propenoic acids) and oligomers **53** with a 3′-phosphoglycolaldehyde terminus are obtained (the remaining 30% of reaction).[157] The products obtained are consistent with photoreaction of rhodium complexes intercalated in the major groove of DNA, where the bound complex has a direct access to H3′. So the first step proposed is H3′ abstraction. This fact has been confirmed by using specifically tritiated DNA.[157] In an oxygen-independent pathway, C3′ radical **45** is converted into the 3′-hydroxylated compound **46**, probably by one electron abstraction by the rhodium complex (the excited state of this complex might be sufficiently oxidizing) and subsequent attack of a water molecule on the 3′ carbocation. Elimination of the 5′-phosphorylated end provides **47** (with ketone end group), which gives rise, by two successive β-eliminations, to the 3′-phosphorylated end, free base, and 2-methylene-3-furanone (**48**). In an oxygen-dependent pathway, the 3′ radical **45** gives, successively, peroxy radical (**49**) and a hydroperoxide derivative (**50**), which provides in several steps **51** and **52** (Criegee type rearrangement), the compound with 5′-phosphorylated terminus, a phosphoglycolaldehyde (**53**) and a base propenoic acid (**54**). So far, the search for any metastable intermediates, as have been seen for other carbon targets of deoxyribose, was unsuccessful.

C3′ chemistry might be invoked in DNA cleavage by Fe^{II}–EDTA and some related compounds to explain some experimental results; this point will be briefly presented in Section 3.4.4.

3.4. H4′ Abstraction: Cu(*o*P)$_2$, Enediynes, BLM, and Fe–EDTA/MPE

H4′ abstraction has been proposed as the common first step of the oxidative attack at C4′ by NCS-chrom (**2**), CAL (**5**), BLM (**17**), Cu(*o*P)$_2$ (**1**), and Fe–MPE (Fe–MPE) (Scheme 17). The resulting radical intermediate **55** can either be hydroxylated at C4′ (**57**) to yield, after cleavage, a 5′-phosphorylated terminus and a 3′-terminus bearing the sugar residue (**59**) or add an oxygen molecule to form a peroxy radical (**60**), which by different pathways can give rise to base propenal **64**, 3′-phosphoglycolate **65**, and compounds with 5′-phosphorylated termini. Partitioning between these two main pathways depends on the O_2 concentration and the nature of the cleaving DNA molecules and their activating cofactors.



Scheme 17. Proposed reaction mechanisms when initial site of attack by the oxidizing agent (①: **1**, ②: enediynes, ③: M-**17**, ④: Fe-**18**) is at C4′ of the deoxyribose. Final product **64** has never been observed for cleavages by **1** and Fe-**18** and could not be characterized for cleavages with enediynes [159]. The C4′-hydroxylated **58** is represented in its open-chain form.

3.4.1. Cu(*o*P)$_2$

Electrophoretic analyses of the scission of 5′- and 3′-[^{32}P]-labeled oligomers and large DNA fragments give important insights into the chemistry of the DNA strand scission by Cu(*o*P)$_2$ (**1**). The 3′- and 5′-phosphomonoesters are the main termini generated by this complex and are generated by C1′ oxidation chemistry (see Section 3.1.1 and Scheme 14). In addition, the 3′-phosphoglycolate products **65** are indicative of C4′ oxidative chemistry (Scheme 17).[15b, 28] Whereas ^{60}Co irradiation (another way for H1′ or H4′ abstraction) generates equivalent amounts of 3′-phosphomonoesters and 3′-phosphoglycolates,[28, 168] the amount of 3′-phosphoglycolate produced in cleavage mediated by **1** is substantially less than that of the 3′-phosphomonoester; C4′ chemistry is thus only a minor oxidation pathway. So far, no base propenal **64** or other fragments from sugars with three or five carbon atoms could be isolated, so the exact pathway from the C4′ radical **55** to the phosphoglycolate **65** is still unknown, and the mechanism remains to be proven (see also Sections 3.4.2 and 3.4.4).

3.4.2. Enediynes

3.4.2.1. NCS-Chrom

H4′ abstraction from deoxyriboses was mainly detected at T residues of 5′-G*T* steps on synthetic oligonucleotides.[64, 169, 170] Further studies revealed that this minor mechanism of DNA oxidation predominantly occurs in staggered double-strand lesions at the *T* residue of 5′-AG*T*/3′-TCA sequences.[46b, 171] But NCS-chrom (**2**) may shuttle between H4′ and H5′ abstraction at the same *T* residue, depending on the thiol,[64, 170] deuteriation,[64, 170] or the sequence of DNA.[66b] On the opposite strand at 5′-AGT/3′-*T*CA sites, the cleavage of *T* is due mainly to H5′ abstraction, but a shift to 4′ chemistry[66b] cannot be excluded.

The products from C4′ chemistry of **2** (Scheme 17) are the 4′-hydroxylated abasic derivative **58** (alkali-labile site) and the 3′-phosphoglycolate **65** (direct DNA break); both are derived from the common 4′-carbon-centered radical **55**. Unlike BLM complexes (see Section 3.4.3)[64] the base propenals **64**[9d, 66b] or malonaldehyde-like compounds containing C1′ and C2′ of deoxyribose[172] have been mentioned but have not yet been clearly described. Moreover, the fate of radical **55** does not depend on O_2 concentration (O_2 is involved in the production of both types of lesions) but is dependent on the nature of the **2**-activating thiol and on the type of lesion (SSB versus DSB). More phosphoglycolates occur at double-strand lesions sites.[46, 66b] Acidic or negatively charged thiols (that have low affinity for DNA, such as GSH and MPA) afford the greatest extent of phosphoglycolate production, but thiols with high reducing efficiency or ability to donate H· (which depends on the stability of the generated sulfanyl(thiyl) radical) did not induce 3′-phosphoglyco-

late production. So, the partitioning between the two routes involves a reduction-sensitive DNA intermediate. When this intermediate is reduced, the 4′-hydroxylated abasic **58** is formed; otherwise phosphoglycolates **65** are produced. The intermediate could be the peroxy radical **60** or the oxy radical **68**.

If the reduction-sensitive intermediate is the C4′-peroxy radical **60**, an easy reduction to the hydroperoxide **61** (by the reductant itself or by intramolecular H· donation[64]) would give the phosphoglycolate precursor (Criegee-type rearrangement) usually proposed.[57, 173] But, in the presence of a strongly reducing thiol, this peroxy radical intermediate may be preferentially converted into the 4′-hydroxylated precursor **57** of the 4′-hydroxylated abasic derivative **58**.

A second hypothesis, favored by Goldberg and co-workers, is that the reduction-sensitive intermediate is the C4′-oxy radical **68**. If this radical is reduced to the C4′-hydroxylated compound **57**, it gives rise to the 4′-hydroxylated abasic **58**. If not, it should rearrange to the phosphoglycolate[46b] by the classical β-scission of the oxygen radical mechanism (via **69**).[174] The same mechanism is also invoked in Sections 3.2 and 3.5.1.1 to explain experimental findings. Three features make the oxy radical the better candidate for phosphoglycolate production: 1) the predominance of phosphoglycolates at DSB sites could be explained by the formation and subsequent Russel fragmentation of a putative O_4 bridge across the minor groove [Eq. (9)];[46, 64, 174, 175] 2) in the case of cleavage by **2** of DNA,

$$2\,ROO^{\cdot} \longrightarrow ROOOOR \longrightarrow 2\,RO^{\cdot} + O_2 \qquad (9)$$

a Criegee-type rearrangement of the peroxide does not seem feasible (absence of metal, nonacidic conditions),[9d, 176] 3) when misonidazole replaces dioxygen to trap the carbon-centered radical **55**, the oxy radical **68** is formed directly, and the percentage of phosphoglycolate **65** increases.[46b, 64, 66]

Experimental evidence for C4′ oxidation on DNA cleavage by **2** is provided by the following experimental evidence: 1) HPLC monitoring of the oligonucleotide **58**, that has the full length but the 4′-hydroxylated abasic site.[169] The structure of this alkali-labile lesion was established by characterization of the pyridazine derivative that is formed by hydrazine treatment, and by comparison of the HPLC retention time of such oligonucleotides after their reduction to diols (two diastereoisomers) with that of a synthetic (*R*) isomer standard.[169] 2) PAGE analysis of 5′-[^{32}P]-labeled oligonucleotides ending with 3′-phosphate, 3′-phosphoglycolates (**65**), and intermediate **59**.[170] This latter intermediate is not usually observed directly on polyacrylamide gels because of its sensitivity to electrophoresis conditions.[170] If the loading buffer pH is above 8 a second β-elimination can occur (especially during the heat denaturation step before sample loading), transforming the band of **59** into the corresponding 3′-phosphate band. A nonambiguous quantification of 4′-alkali-labile oligonucleotides **58** can thus be done only after adding hydrazine to convert the **58** into a stable 3′-(3-pyridazinylmethyl)phosphate that will migrate slower than the corresponding Maxam–Gilbert sequencing marker[46b, 64] (see ref. [177] for details on this method). On the other hand, 3′-[^{32}P]-labeled substrates typically afford fragments ending with 5′-phosphate groups only after treatment with alkali.[46b] 3) Deuterium labeling at the 4′ position of deoxyriboses.[64, 170] The ratio of the kinetic isotope effect k_H/k_D was 4 for the glycolate formation and 3.7 for pyridazine formation (pathway via the 4′-hydroxylated abasic site).[64] When the kinetic isotope effect was analyzed at T sites of various G*T* steps, k_H/k_D ranged from 2.5 to 5.5.[170] 4) Gel chromatography. A minor band, slowly moving on polyacrylamide gels, was attributed to an adduct between the thiol used for the activation of **2** and the 3′-terminal unsaturated sugar **59** (Michael addition).[66b, 163]

3.4.2.2. CAL

H4′ abstraction from DNA sugars by CAL (**5**) was observed as part of a double-strand lesion at the frequent symmetric cleavage site 5′-GAT*C*CT/3′-*C*TAGGA. The oxidized bonds are the C5′–H bond of the *C* residue on the TCCT strand and the C4′–H bond of the *C* residue on the other strand.[12a, 55, 67b] The DNA cleavage products of the 5′-[^{32}P]-labeled AGGA strand consist of 3′-phosphoglycolates **65** (Scheme 17) and 4′-hydroxylated abasic derivatives **58**, which as pyridazine derivatives were resolved by PAGE analysis. No evidence for the production of base propenal has been reported. Interestingly, the formation of phosphoglycolate on one strand is always associated with C5′ chemistry on the complementary strand, supporting the involment of an O_4 bridge for glycolate production (Russel fragmentation, see Section 3.4.2.1).[46b, 55] Deuterium experiments followed by ^{1}H NMR spectroscopy showed that[12a] the deuterium atom on C4′ of the C residue in 3′-*C*TAGGA strand was transfered to the C3 position of the reduced CAL biradical **6** (see Scheme 4).

3.4.2.3. ESP

H4′ abstraction only occurs in double-strand lesions mediated by cleavers of the ESP family **8**–**10**. Phosphoglycolate **65**, the 4′-hydroxylated abasic derivative **59**, and the 3′-phosphate end have been identified on sequencing gels from 5′-[^{32}P]-labeled fragments of DNA.[57] In view of the structural similarity between ESP C (**8**) and CAL (**5**), the C7-centered radical of the activated drug **11** is assumed to abstract the H4′ atom (see Scheme 4). As was mentioned for C5′ chemistry (Section 3.5.1.3), no isotope effect was observed in this C4′ chemistry.[57]

3.4.3. Bleomycin

Two sets of products of DNA strand breaks by metallobleomycins (for example, **17**) have been identified, both of which involve oxidative destruction of the deoxyribose moiety. These products are now known in great detail: one set of products includes base propenals (**64**),[86, 178] 3′-phosphoglycolates (**65**),[179] and 5′-phosphate termini; the second set consists of free bases[180] and the evolution product from an alkali-labile lesion (4′-hydroxylated abasic derivative **58**).[177a] The proposed mechanistic pathway is outlined as ③ in Scheme 17.

As demonstrated by tritium and deuterium isotopic effects on H4′ abstraction,[9b, 181] the formation of both bases and base propenals is probably the consequence of a rate-determining C4′–H bond cleavage as the first step, followed by an oxygen-dependent partitioning of the intermediate **55**. The release of base requires no additional O_2 and is accompanied by the pro-

duction of an oxidatively damaged sugar **58**, which results in strand scission only in the presence of alkali (pH 12). The formation of base propenals **64** requires additional O_2 to that required to form "activated BLM", and is accompanied by spontaneous DNA strand scission and 3′-phosphoglycolate termini production. The magnitude of the 4′ isotope effect is not sensitive to changes in the partition ratio of the two proposed DNA cleavage pathways, but is sensitive ($k_H/k_D = 2-7$) to structural and electronic changes in the metal–BLM complex, underscoring the importance of favorable parameters in the orientation of the transition state.[182]

Results of cleavage of DNA deuteriated at other positions of the deoxyribose ring afford no isotope effect, suggesting high regiospecificity for the BLM-mediated C–H bond cleavage.[182]

Proposed mechanism for production of base propenals **64** *and 3′-terminal phosphoglycolate* **65**: Under aerobic conditions the 4′-radical **55** rapidly combines with O_2 to form a 4′-peroxy radical **60** at what is probably a diffusion-controlled rate.[183a] The fate of peroxy radical has been extensively studied.[9b, 183] It can undergo a wide variety of reactions including formation of O_4-containing compounds [Eq. (9)], H abstraction from reductants such as a thiol [Eq. (10)], and chain termination due to reduction by to low-valent transition metal ions [Eq. (11)].

$$ROO^{\cdot} + RSH \longrightarrow ROOH + RS^{\cdot} \quad (10)$$

$$ROO^{\cdot} + M^{II} \longrightarrow ROO^{-} + M^{III} \quad (11)$$

Thus the peroxy radical gives rise principally to the 4′-hydroperoxide **61**, and in some cases to the 4′-oxy radical **68**. The further conversion of 4′-hydroperoxide **61** has been proposed to occur by acid-catalyzed heterolytic cleavage of the peroxide O–O bond in a Criegee-type rearrangement. Instead of proton-catalysis, the Fe^{III}–BLM intermediate could act as a Lewis acid catalyst. A molecule of water or the putative iron-bound hydroxide could trap the carbocation intermediate **62** to give **66** and ultimately the dicarbonyl derivative **67** as a precursor to **64** and **65**.

Because of the stereospecific removal of the 2′-(*pro-R*) proton of deoxyribose and the fact that its release is kinetically more favorable than the release of base propenal from DNA,[178] an alternative pathway has been proposed: removal of the 2′-(*pro-R*) proton from the carbocation **62** and concomitant *anti*-elimination at O4′ would generate intermediate **63**. Further reaction yields propenal **64**, phosphoglycolate derivative **65**, and 5′-phosphate termini. This mechanism was confirmed by ^{18}O incorporation into the carbonyl group of **65** (in experiments carried out with $^{18}O_2$) and into the aldehyde group of **64** (in experiments carried out with $H_2{}^{18}O$).[173]

Proposed mechanism for release of nucleobases: The C4′ radical **55** may undergo a radical rebound mechanism analogous to that proposed by Groves and co-workers[89a] for P-450 systems (see also Scheme 8, pathway a) to produce the C4′-OH intermediate **57**. Alternatively, the radical **55** could be oxidized by BLM–Fe^{IV}–OH (electron transfer, see also Scheme 8 pathway b, and Section 2.3.1) to produce a C4′ carbenium ion **56**, which could then add water to give the C4′–OH intermediate **57**. This intermediate can collapse to produce free base and C4′-hydroxylated abasic **58**, represented here in its open form. In the presence of alkali, **58** could undergo a strand scission to afford 5′-phosphate termini and 3′ ends bearing an unsaturated oxidized sugar residue (**59**). A few years ago, oligonucleotides carrying this residue were observed in PAGE analyses of products from the BLM-mediated cleavage of a 5′-[^{32}P] DNA fragment.[170] Intermediate **59** was identified after 1) stabilization by $NaBH_4$ reduction, purification, and hydrolyses with P_1 nuclease and alkaline phosphatase to produce a mixture of *erythro*- and *threo*-2-deoxypentitols,[9b, 184] 2) reaction with NaOH to give a transient 2,4-dihydroxycyclopentenone,[177a, 185] and 3) treatment with aqueous alkylamines (for example, piperidine) to release 3′-phosphate termini.[177a] Reaction with hydrazine also allows quantitative detection of C4′-hydroxylated abasic **58** by transformation to 3′-(3-pyridazinylmethyl) phosphate termini.[177]

Attempts to define the source of oxygen in the oxygen carbohydrate moiety **58** (either molecular oxygen or water in the rebound or the electron transfer mechanisms) have been undertaken with ^{18}O labeled dioxygen or water.[9b, 99] The oxygen atom introduced in C4′ was derived almost exclusively from water, thus supporting the C4′-carbenium route.

The cleavage patterns observed during DNA strand scission mediated by photoactivated Co^{III}–BLM are dependent on the irradiation frequency but independent of O_2, and are very similar to those observed for Fe–BLM. They suggest that 3′-phosphoglycolate-modified ends,[186] free bases, and alkali-labile sites resulting in 3′-phosphate-modified ends [187] are produced. All the data are consistent with C4′ oxidation of deoxyribose, but the mechanism leading to the observed products has yet to be established unequivocally.

For the chemistry of RNA cleavage,[110–112] it has been suggested that Fe–BLM-mediated RNA degradation follows an oxidative pathway. Experimental data indicate release of bases concomitantly with RNA cleavage. In PAGE analysis, end-labeled RNAs give cleavage bands believed to have 3′-phosphoglycolate and 5′-phosphate termini. Due to the sensitivity of RNA to alkaline conditions (alkali-labile lesions cannot be detected easily) and to the difference in the sugar moiety of RNA and DNA (the postulated 2-hydroxylated base propenals are probably unstable if formed, and would hydrolyse fast to liberate bases), a molecular mechanism for RNA cleavage of the same type as for DNA cleavage has yet to be conclusively proven.

The question arises whether additional "minor" chemistry can occur in the degradation of DNA by BLM. H1′ abstraction analogous to that of H4′ has been postulated for DNA[188] and also for the DNA strand of an RNA–DNA heteroduplex.[189] While reasonable (in such a heteroduplex the opening of the minor groove leads to an enhanced accessibility of activated BLM to H1′ in addition to H4′), no evidence has been obtained for DNA degradation by a C1′ pathway.[190] Recently, modified self-complementary octadeoxyribonucleotides containing one ribo- or one arabino nucleoside at a position susceptible to oxidative degradation by Fe^{II}–BLM were found to afford products resulting from C1′ chemistry.[191]

It has also been demonstrated that activated BLM can induce damage to bases in a side reaction. The modified bases (such as 8-hydroxyguanine which was present in amounts about one-hundredth that of base propenal[85]) are identical with those

generated when hydroxyl radicals react with DNA. This finding suggests involvement of HO• in this reaction, probably through a partial decomposition of the oxo iron complex responsible for the main route of oxidative damage to C4′ of DNA.[100]

3.4.4. *Fe–EDTA, Fe–MPE, and Related Compounds*

The molecular mechanism of DNA cleavage by Fe–EDTA and derivatives in the presence of molecular oxygen or hydrogen peroxide has only been studied in detail for Fe–MPE. Little information on the mechanism of cleavage by Fe–EDTA itself is available;[98] generally it is assumed to be similar to that of Fe–MPE. Some particular aspects of the cleavage reaction have been described for hybrid molecules where Fe–EDTA is attached to sequence-specific DNA-binding molecules.

Although the mechanism of the DNA strand scission by Fe–MPE is still not understood in detail, some features have emerged.[98a] The products released from calf thymus DNA are the four nucleotide bases in a Ade + Thy/Gua + Cyt ratio in agreement with known DNA composition, which is consistent with the low specificity of Fe–MPE cleavage. Base release and strand scission are stoichiometric. The DNA termini at the cleavage sites are 5′-phosphates and roughly equal proportions of 3′-phosphates and 3′-phosphoglycolates. Few base propenals were detected: since β-mercaptoethanol (and probably also DTT) reacts with base propenals,[98a] these nucleoside residues would probably not be observed under these conditions even if they were formed.

All results are consistent with an oxidative degradation of deoxyribose rings of the DNA backbone, most likely by the hydroxyl radical which can abstract a hydrogen atom to initiate the DNA cleavage. C4′ chemistry as predominant route, C1′ chemistry in the minor groove, and C3′ chemistry in the major groove could account for the product distribution.

The main position of attack could be the 4′-hydrogen atom of the deoxyribose in the case of Fe–MPE, but this has not been clearly demonstrated for Fe–EDTA. H4′ abstraction as first step of the cleavage reaction may explain the release of nucleobases and the formation of 5′-phosphate and 3′-phosphoglycolate termini (**65**) by an O_2-dependent pathway (see Scheme 17). The absence of base propenals **64** (or unsuccessful efforts to characterize them) is reminiscent of observed results with Cu(*o*P)$_2$ (**1**) and enediynes, where, in the minor C4′ pathway of oxidative cleavage, the nature of monomeric species accompanying C3′–C4′ cleavage remains to be established (see Sections 3.4.1 and 3.4.2).

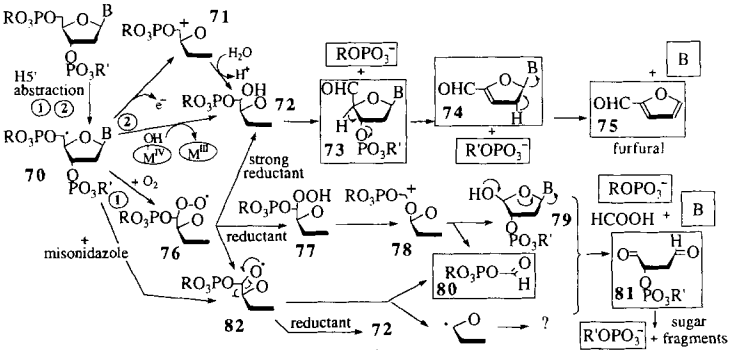
Chemistry at C1′ must be considered as a possible explanation for the presence of significant amounts of 3′-phosphate termini (see Scheme 14). However, due to the presence of reductants, 5-methylene-2-furanone (**33**), has not been characterized, so this proposed mechanism remains unconfirmed.[9b, 98a] Both the reactions outlined above should occur in the minor groove.

Chemistry occurring in the major groove has been also postulated.[9b] H3′ abstraction (see Scheme 1) produces the radical **45** (Scheme 16). Further reaction of this species in the absence of oxygen should give rise to free bases, 2-methylene-3-furanone (**48**), and 3′-phosphate and 5′-phosphate termini. In the presence of oxygen the production of 5′-phosphate termini, 3′-phosphoglycolaldehydes **53** (which would be oxidized to glycolic acid), and base propenoic acids **54** (which would not be expected to react with thiobarbituric acid, the usual reagent for base propenal characterization) may account for some results reported by Hertzberg and Dervan.[98a] This is not, however, likely to occur in the case of derivatives in which Fe–EDTA is attached to distamycin,[9i, 113, 131a] oligopeptides,[119, 131a, 133a] or proteins,[192] where, on the basis of PAGE analyses, the oxidative attack clearly occurs within the minor groove. On the other hand, when Fe–EDTA is attached to oligonucleotides[135] or some proteins,[193] the cleavage patterns support an oxidative attack from within the major groove, and so, in these cases, a mechanism involving H3′ abstraction has to be taken into consideration. In a similar manner the oxidative H5′(*pro-R*) abstraction (H5′ points towards the entrance of the major groove) has to be considered as another possible target (see Scheme 18).

An alternative mode to the direct HO•-mediated hydrogen abstraction from deoxyribose may involve an initial attack on the base moiety. This either gives a radical base species able to abstract a hydrogen atom from deoxyribose or creates an abasic site leading to strand break. This alternative pathway is based on the idea that base destruction accompanies the strand scission event.[9b]

3.5. H5′ Abstraction: Enediynes and Cationic Manganese Porphyrins

Until now, oxidative chemistry at C5′ of deoxyribose has been demonstrated only for enediynes and Mn–TMPyP. These compounds initiate the oxidation of the deoxyribose by H5′ abstraction, giving a C5′-centered radical **70** (Scheme 18).



Scheme 18. Proposed reaction mechanisms when initial site of attack by the oxidizing agent (①: enediynes **2**, **5**, **7**–**10**; ②: **19**) is at C5′ of the deoxyribose [159].

3.5.1. *Enediynes*

3.5.1.1. *NCS-Chrom*

C5′ chemistry represents the major mode of DNA cleavage by NCS-chrom (**2**): it causes all single-strand breaks and the cleavage of at least one strand for double-strand lesions.

Eighty percent of SSB lesions consist of breaks in which a 5′-aldehyde (**73**, Scheme 18) is facing a 3′-phosphate terminus, whereas in 20% one deoxyribose moiety is lost, and release of base accompanies 3′-phosphate and 5′-phosphate termini formation.

The C5′ radical **70** created by activated **2** combines with O_2 (as demonstrated by $^{18}O_2$ incorporation)[194] to give the 5′-peroxy radical **76**. The reduction of this radical by a excess of thiol (or other strong reductant) could result in the recovery of the 5′-hydroxy species **72** as proposed in the literature; alternatively **72** may come from **82**. Spontaneous cleavage of **72** affords fragment **73** with a 5′-aldehyde end. Nucleosides bearing the 5′-aldehyde group have been observed after enzymatic hydrolysis by HPLC.[195] When 3′-[^{32}P]-labeled fragments of DNA were analyzed on polyacrylamide gels, abnormal mobility of 5′-aldehydes **73** was also noted.[196] Aldehydes move about as fast as the markers produced by chemical treatment in the Maxam–Gilbert procedure, which have a 5′-phosphate end and two more nucleotides. Because of the presence of reducing agents, neither intermediate **74** nor end product **75** (Scheme 18) was observed. Some bands on polyacrylamide gels corresponded to fragments with a 5′-COOH end; their production was probably attributable to the presence of traces of metal.[9e, 196]

Some C5′ chemistry (10–20%) gives rise to gaps in a DNA strand with concomitant loss of a base. The fragments end with 5′-phosphate and 3′-phosphate.[196] To explain these lesions the following two mechanisms have been proposed: 1) The peroxy radical **76** is reduced to the hydroperoxide **77**. A Criegee-type rearrangement giving successively **78**, **79**, and **80**, could then account for the observed products **80** and **81**. This mechanism does not seem likely, because of the absence of any acid or metal catalysis.[9d, 64, 173] 2) The peroxy radical **76** is transformed to the oxy radical **82**, followed by a β-fragmentation with cleavage of the C4′–C5′ bond to generate an unstable 3′-formylphosphate-ending fragment **80**, which hydrolyzes into formic acid and a compound with 3′-phosphate terminus. In the case of double strand lesions the O_4 bridge may account for the formation of the oxy radical **82** [Eq. (9)].[46b] When misonidazole replaces O_2, these gaps constitute almost the only form of DNA lesions.[52, 197] In an ^{18}O-transfer experiment the carbonyl oxygen of the activated formyl moiety (trapped as formyl–Tris adduct) was derived from the nitro group oxygen of misonidazole.[198] The spontaneous transfer of formyl residues from **80** to nucleophiles (Tris or hydroxylamine)[197, 198] and a derivative of **81** stabilized by reduction with $NaBH_4$[199] were evident.

Because C5′ is located at the periphery of the DNA double strand, reduction of the sensitive intermediates **76** or **82** to the C5′-hydroxylated compound **72** may be readily achieved, which explains the predominance of 5′-aldehyde **73** and the lack of dependence on the reducing power of the thiol.

Small isotopes effects were observed in abstraction of deuterium from the 5′ position of T residues from a duplex oligonucleotide containing a TGTTTGA sequence ($k_H/k_D = 1.6$),[64] a 5′-AGC/3′-TCA sequence (1.25), or a restriction fragment of pBR322 plasmid (1.0–1.6 at T of 5′-GT steps; other T residues showed a variable sensitivity to 5′ deuteriation).[170] H5′ of deoxyribose is incorporated at the C6 radical of the activated NCS-chrom biradical **4** (see Scheme 3).[53]

3.5.1.2. CAL

CAL **5** mediates DSBs at preferred interaction sites: the H5′(*pro-S*) abstraction that occurs on the second nucleotide residue of the four-base-pair sequences 5′-TCCT or 5′-TTTT[51, 67a] involves the C6 radical of the activated CAL (**6**, see Scheme 4).[12a, 56] In PAGE analysis of cleavage products of the TCCT strand, the 5′-[^{32}P]-labeled fragments exhibited mobilities identical to the corresponding Maxam and Gilbert sequencing markers, thus suggesting the presence of 3′-phosphate ends.[51, 67b] Two major 3′-labeled fragments were resolved, one ending in a 5′-aldehyde (**73**, Scheme 18), and one ending in a 5′-carboxylic acid (dependent on metal traces, as described for NCS-chrom).[51]

3.5.1.3. ESP

Only C5′ chemistry is involved in SSBs mediated by ESP A (**7**), and this chemistry also occurs in DSBs for ESP C (**8**).[57] In the latter case, the activated drug mediates H5′ and H4′ abstraction on both strands of DNA. At some residues only 5′ chemistry is observed, at other ones both types of chemistry can take place. PAGE analysis of the cleavage of DNA substrates labeled with ^{32}P at the 5′ or 3′ ends showed 3′-phosphate termini and 5′-aldehyde-ended fragments **73**. The 5′-aldehyde terminus was characterized by its usual reduction to 5′-alcohol by NBH_4 treatment or by its conversion into a 5′-phosphate end upon piperidine treatment (this catalyzes two successive β-eliminations on **73** with the loss of deoxyribose moiety).

Sequence-specific isotope effect ratios for the cleavage of DNA were found to be very low (not significantly different from 1). In addition, contrary to what was observed for NCS-chrom, deuteration at either C5′ or C4′ had no effect on the relative partitioning of oxidative attack.[57] H5′ abstraction is due to the C10 radical of the activated biradical drug **11** (see Scheme 4).[57]

3.5.2. *Cationic Manganese Porphyrins*

Besides oxidative attack at C1′–H, (see Section 3.1.3), oxidative activation of C5′–H[147] constitutes the principal mechanism of activated Mn–TMPyP for cleavage of A · T-rich sequences of double-stranded DNA[137, 138d] (② in Scheme 18). In HPLC analysis of the products released in solution after a heating step, free bases, oxidized nucleosides (**74**),[200] and furfural (**75**) were observed and characterized.[164] Cleavage fragments from small oligonucleotides were analyzed by HPLC separation techniques or PAGE analyses,[137, 138e, 146, 147, 201] and their transformation by chemical and/or enzymatic treatment allowed their identification: 3′-phosphate-ending fragments were subjected to alkaline phosphatase to obtain the corresponding oligonucleotides with 3′-OH endings; 5′-CHO-ending fragments were either heated (inducing two successive β-eliminations, see below), oxidized by I_2 in an alkaline medium (5′-COOH end), or reduced by $NaBH_4$ (5′-CH_2OH end). Depending on the extent of cleavage and on the sequence at the 3′ side of $(A \cdot T)_3$ site, 5′-COOH-ending fragments could be observed immediately after cleavage of 3′-[^{32}P]-labeled oligonucleotides.[201, 202]

The proposed mechanism is indicated in Scheme 18. The activated cationic metalloporphyrin initiates the oxidation of the deoxyribose by H5′ abstraction to give a C5′ radical (**70**). Even in the absence of oxygen (the same cleaving reactivity was observed in absence or in presence of O_2: M. Pitié et al., unpublished data), **70** can be hydroxylated directly by

TMPyP–Mn^{IV}–OH, or in two steps by one-electron transfer followed by reaction of water with the carbocation **71**, to give the 5′-OH derivative **72**. Spontaneous cleavage follows, with formation of a 3′-phosphate end and 5′-aldehyde **73** (direct break of the DNA backbone). A first β-elimination then produces a second break on the DNA backbone with release of a 5′-phosphate end and the α,β-unsaturated aldehyde **74**. Finally a second β-elimination gives rise to free base and furfural (**75**) as sugar degradation product. The 5′-COOH ending fragments sometimes observed[201, 202] are probably due to a second oxidation by the recycled activated Mn–TMPyP at the same site.

The intermediate **74** was completely characterized by reduction with $NaBH_4$ (selective reduction of the aldehyde at C5′ to the alcohol without affecting the double bond) followed by hydrogenation with palladium on charcoal, to give 2′,3′-dideoxyribonucleosides having the natural β or the nonnatural α configuration at C4′.[200] The use of ^{31}P NMR spectroscopy has confirmed the formation of two 3′- and 5′-phosphate monoester ends in roughly equal proportions, which supports the mechanism described above.[164d]

It should be noted that selective C5′ chemistry can take place on both 3′ sides of the $(AT)_3$ double-strand cleavage site of the Mn–TMPyP/$KHSO_5$ system. This leads to direct strand breaks with a four base-pair, 3′-stagger of the cleaved residues,[147] which confirms that oxidative attack of the activated metalloporphyrin occurs from the minor groove of DNA (see Scheme 11).

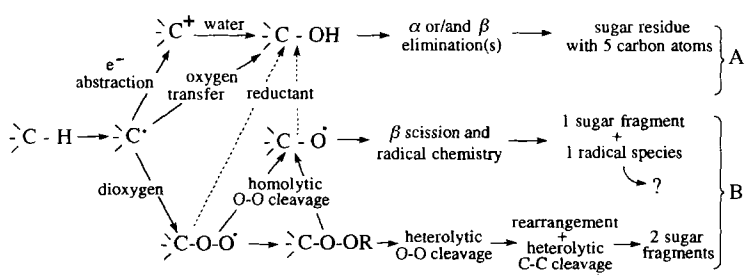
3.6. Concluding Remarks on Section 3

The oxidative attack on DNA by chemical nucleases and drugs described in the present section starts with the formation of a carbon-centered radical on positions 1′, 2′, 3′, 4′, or 5′ of deoxyribose (Scheme 19). This initial step corresponds formally to a one-electron oxidation ($H^{\cdot} = H^+ + e^-$). However, some DNA cleavers are capable of two-electron oxidations, and only in this case is direct hydroxylation of a carbon radical at the sugar possible, either by oxygen or electron transfer (Scheme 8, routes a and b). Further reaction of the unstable hydroxylated derivative could, without cleavage of any C–C bond, give rise to a sugar residue with five C atoms characteristic of each initial oxidative lesion (top of Scheme 19): 5-methylene-2-furanone (**33**, attack at C1′), 3-methylene-2-furanone (**48**, C3′), the C4′-hydroxylated abasic derivative (**58**, C4′), furfural (**75**, C5′).

If the rate of oxygen or electron transfer is too slow (as in the case of BLM), or if the DNA cleaver is only capable of one-electron oxidation (as in the case of enediynes and photoactivated halouracil oligonucleotides), the carbon radical reacts with molecular oxygen (for recent papers on the kinetics of oxygen rebound in hydroxylation reactions, see ref. [203]). The resulting unstable peroxy radical may be reduced to a hydroperoxide (R = H) by reductants [see Eqs. (10) and (11)] or by intramolecular H donation.[64] A heterolytic cleavage of the peroxide O–O bond may induce a rearrangement and the subsequent heterolytic cleavage of one adjacent C–C bond of the sugar (a Criegee-type rearrangement, for example). Two sugar fragments are usually (or might be) observed. Depending on the initially attacked carbon site and on which adjacent C–C bond is cleaved, two sets of two sugar fragments can be generated: one-carbon plus four-carbon fragments (C2′ chemistry: formic acid + **42**; C5′ chemistry: **80** + **81**) or two-carbon plus three-carbon fragments (C3′ chemistry: **53** + **54**; C4′ chemistry: **65** + **64**). Alternatively, for example when two peroxy radicals combine (O_4 route), a homolytic cleavage of the peroxide O–O bond giving an oxy radical may lead to a homolytic cleavage of the same adjacent C–C bond. The β-scission of the oxy radical would afford two kinds of fragments: one is the same as produced in the preceeding pathway: **42** (C2′), **54** (C3′), **65** (C4′), and **80** (C5′); the other one is a radical species whose fate is unknown and whose products have not yet been described.

In addition, the oxy and peroxy radicals can be considered reduction-sensitive intermediates, and their possible reduction can afford a hydroxylated sugar by competitive pathway.

All these reaction pathways are well illustrated and detailed in Schemes 17 and 18 for C4′ and C5′ chemistry. In Scheme 15, C2′ hydroxylation (that would lead to the ribo or arabino derivative) is not shown, since neither two-electron oxidation by halouracil derivatives nor reduction of a reduction-sensitive intermediate can be performed under the experimental conditions used. In addition no chemical agents able to hydroxylate C2′ directly have so far been reported. In Scheme 16, in the absence of O_2 the hydroxylated product **46** must be formed after a one-electron oxidation of the intermediate **45** (probably by the excited state of the rhodium complex); however, the exact nature of the species able to abstract H3′ is still unknown. Hydroxylation of C1′ can easily account for the observed products in Scheme 14. No other products of DNA degradation except oxidized abasic sites have been described, probably because the glycosidic bond is cleaved in preference to a sugar C–C bond.



Scheme 19. Two-electron (A) or one-electron (B) oxidation of deoxyribose mediated by drugs can lead to three main pathways for sugar evolution (R = H, OOR′).

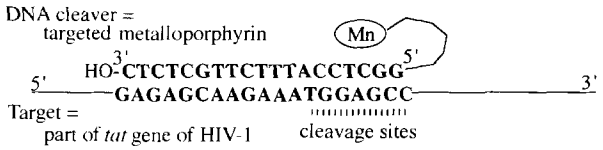
4. Concluding Remarks

Apart from nuclease enzymes, no naturally occurring, low molecular weight compounds have been discovered that can efficiently mediate hydrolysis of the phosphodiester bonds of the DNA backbone. The DNA-cleavage route selected by nature for cytotoxic drugs (bleomycin, enediyne) is a sugar oxidation and not a hydrolysis of phosphodiesters. So it is not surprising that synthetic transition metal complexes exhibiting redox properties and DNA affinity have been

developed as "chemical nucleases" (a misnomer—what about "chemical DNA sugar oxidases"?). Deoxyribose is a key target for DNA cleavers, and current knowledge of the different modes of oxidation of deoxyribose units leading to DNA breaks has been reviewed in the present article. Development of these artificial and selective DNA cleavers is a challenging area in the rational design of antitumoral and antiviral agents as well as in the field of molecular biology. The need for highly efficient (quantitative cleavage of the target must be reached) and highly specific (sequence specificity on large DNA fragments) cleaving reagents is obvious, and considerable progress has already been made. Improvements in several directions are still required:

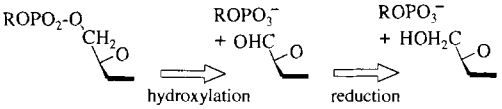
1) Cleaving efficiency: Discovery of truly double-strand and catalytic DNA cleavers (and also highly efficient RNA cleavers) is required in order to create new cytotoxic agents and tools for gene engineering. In the field of cancer chemotherapy, enediynes represent an example where an understanding of the chemistry and modes of action can help the design of highly efficient in vitro drugs, such as the synthetic dynemicins analogues described by Nicolaou and Smith.[9h] But the question whether in vitro efficiencies transferable to in vivo conditions still remains.

2) Specificity: A specific molecular site of attack without dispersion of lesions is also highly challenging, especially if genomic double-stranded DNA is the ultimate target. This property is not necessary in some cases: absence of selectivity allows use of some chemical nucleases as footprinting reagents for DNA or RNA, and they have some advantages over the DNase method. Sequence selectivity has been drastically increased by the covalent binding of DNA-cleaving moieties to oligonucleotides or to DNA-binding small molecules, peptides, or proteins. In particular, the attachment of an efficient DNA cleaver to a deoxyoligonucleotide should lead to a family of synthetic restriction enzymes with tailored specificity that might be useful in the analysis of complex genomes or could enhance the ability of an antisense deoxyoligonucleotides to block the expression of targeted gene. As an example of these last potential medical applications, we recently reported that the attachment of the cleaver motif {tris(methylpyridiniumyl)porphyrinato}-manganese(III), which is endowed with cytotoxic properties,[204] to a selected 19-mer vector allows selective recognition and cleavage of a 35-mer single-stranded DNA containing the initiation codon of the *tat* gene of HIV-1 (Scheme 20).[149]



Scheme 20. Selective cleavage by a tailored manganese porphyrin of a 35-mer single-stranded DNA containing the initiation codon of the *tat* gene of HIV-1 [149].

3) Selection of oxidizing agents able to leave DNA fragments ending with suitable termini for further enzymatic workup: Even though the cleavage of any selected DNA sequence is now possible, no efficient chemical models of a restriction enzyme that can hydrolyze a selected phosphodiester bond are yet available. However, in an alternative pathway, hydroxylation of C3′ or C5′ of deoxyribose immediately followed by reduction of the resulting 3′-ketone or 5′-aldehyde may enable this hydrolysis step to be mimicked (oxidation step + reduction step = "pseudo-hydrolysis"). This was recently demonstrated by using the Mn–TMPyP/$KHSO_5$ system and its specific hydroxylating activity at the C5′ position of deoxyribose [Eq. (12)]. The fragments may be coupled again by chemical methods, so this system might provide an alternative to the restriction endonuclease/ligase systems.[202]



(12)

Finally, even after a decade of fruitful research on chemical nucleases, the field is still open for discoveries of new efficient cleavers of RNA and double-stranded DNA in order to produce new selective cytotoxic agents and/or tools for genetic engineering.

5. Addendum

After submission of the original manuscript several articles have appeared in the literature. These papers are briefly mentioned below together with the appropriate sections where they should be inserted.

Section 2.1: Cleavage of megabase DNA substrates was performed with a DNA-binding protein modified by Cu(*o*P).[205] The structure of the *Escherichia coli* Fis–DNA complex was probed by a protein modified with a copper–phenanthroline cleaver.[206]

Section 2.2: The role of biradical species in DNA cleavage by neocarzinostatin chromophore (**2**) has been discussed recently.[207] Moreover, there is a critical role of the iodine substituent of the calicheamicin oligosaccharide and the guanine C2-NH_2 group within the minor groove of the target DNA.[208]

Section 2.3: The stability of the oxygenated form of Fe^{II}–BLM has been investigated.[209] A recent study by electrospray mass spectrometry of activated bleomycin suggested that the iron peroxide BLM–Fe^{III}–OOH is the active species.[210] The same iron peroxide was also proposed for bleomycin models.[211] A hybrid molecule containing bleomycin and the DNA-binding domain of Hin recombinase was used as DNA cleaver.[212] Both strands of a DNA–RNA heteroduplex were cleaved by Fe–BLM.[213]

Section 2.4: Fe–MPE and Fe–EDTA were used for mapping RNA regions in eukaryotic ribosomes. RNA fragments were analyzed by primer extension with reverse transcriptase using oligodeoxynucleotide primers.[214] The tertiary structure of $tRNA^{Phe}$ has been investigated by RNA–EDTA–Fe^{II} autocleavage.[215]

Section 2.5: The transfer in water of an oxygen atom from the high-valent TMPyP–Mn^{V}=O species to a water-soluble olefin was investigated. A "redox tautomerism" involving an axial water molecule was proposed to explain the incorporation of the oxygen atoms from water and from the peroxide in a 50:50 ratio.[216] The interaction of cationic porphyrin derivatives with calf thymus DNA was studied by linear dichroism and fluorescence energy transfer.[217]

Section 2.6: Binding of *Δ*- and *Λ*-$[Ru(phen)_3]^{2+}$ with a self-complementary decamer was investigated by NMR spec-

troscopy.[218] Enantioselective recognition of DNA by $Rh^{III}(phen)_2(phi)$ (**20**) was found to be controlled by the opening in the major groove that results from changes caused by propellerlike twisting of a base pair.[219]

Appendix: Important Abbreviations Used in the Text

A:	2′-deoxyadenosine
Ade:	adenine
bpy:	bipyridine
BLM:	bleomycin
bp:	base-pair
C:	2′-deoxycytidine
CAL:	calicheamicin
Cyt:	cytosine
DSB:	double-strand break
DTT:	dithiothreitol
DYN:	dynemicin
EDTA:	ethylenediaminetetraacetate
ESP:	esperamicin
G:	2′-deoxyguanosine
Gua:	guanine
GSH:	glutathione
ME:	mercaptoethanol
5-MF:	5-methylene-2-furanone
MPA:	3-mercaptoproprionic acid
MPE:	methidiumpropyl EDTA
N:	nucleotide
NADH:	nicotinamide adenine dinucleotide, reduced form
NCS:	neocarzinostatin
NCS-chrom:	neocarzinostatin chromophore
ODN:	oligodeoxynucleotide (The deoxyribo prefix was omitted in this review, since it focuses on DNA.)
*o*P:	*ortho*-phenanthroline = 1,10-phenanthroline (The classical abbreviation used is phen (see J. Reedijk, *Comprehensive Coordination Chemistry, Vol. 2* (Ed.: G. Wilkinson, Pergamon, **1987**, pp. 73–98); however we decided to keep the formulation $Cu(oP)_2$ for the bis(1,10-phenanthroline)copper complex popularized by D. Sigman in oxidative DNA cleavage research.)
PAGE:	polyacrylamide gel electrophoresis
phi:	phenanthrenequinonediimine
phen:	1,10-phenanthroline
Porph:	a porphyrinato ligand
pu:	purine
Py:	pyridine
pyr:	pyrimidine
TMPyP:	*meso*-tetrakis(*N*-methylpyridinio-4-yl)porphyrinato
SSB:	single-strand break
T:	thymidine
TAR:	trans-activation responsive region
tat:	trans-activator of transcription
Thy:	thymine
Tris:	tris(hydroxymethyl)aminomethane
Ura:	uracil

The authors are deeply indebted to the many co-workers and collaborators whose names are listed in the references. We are also grateful to the Centre National de la Recherche Scientifique (CNRS), the Association pour la Recherche contre le Cancer (ARC, Villejuif), the Agence Nationale de Recherches sur le Sida (ANRS, Paris), the Région Midi-Pyrénées and Genset (Paris) for financial support. We thank Lisa Rosenberg (University of British Columbia) for her assistance in preparing the manuscript.

Received: September 3, 1993
Revised version: February 12, 1994
Addendum: October 31, 1994 [A 211E]
German version: *Angew. Chem.* **1995**, *107*, 819

[1] B. N. Ames, *Science* **1983**, *221*, 1256–1264; W. Troll, R. Wiesner, *Annu. Rev. Pharmacol. Toxicol.* **1985**, *25*, 509–528; P. A. Cerutti, *Science* **1985**, *227*, 375–381; M. K. Shigenaga, C. J. Gimeno, B. N. Ames, *Proc. Natl. Acad. Sci. USA* **1989**, *86*, 9697–9701; *Methods Enzymol.* **1990**, *186* (A and B) (both volumes are dedicated to oxygen radicals in biological systems); T. Kalebic, A. Kinter, G. Poli, M. E. Anderson, A. Meister, A. Fauci, *Proc. Natl. Acad. Sci. USA* **1991**, *88*, 986–990; J. R. Wagner, C. C. Hu, B. N. Ames, *ibid.* **1992**, *89*, 3380–3384; and references therein; M. Becana, R. Klucas, *ibid.* **1992**, *89*, 8958–8962; A. W. Khan, Y. H. Mei, T. Wilson, *ibid.* **1992**, *89*, 11426–11427; S. Xanthondakis, G. Miao, F. Wang, Y. C. E. Pan, T. Curran, *EMBO J.* **1992**, *11*, 3323–3335; D. I. Feig, L. A. Loeb, *Biochemistry* **1993**, *32*, 4466–4473; S. Legrand-Poels, M. Hoebeke, D. Vaira, B. Rentier, J. Piette, *J. Photochem. Photobiol. B* **1993**, *17*, 229–237.

[2] H. Sies, *Angew. Chem.* **1986**, *98*, 1061–1075; *Angew. Chem. Int. Ed. Engl.* **1986**, *25*, 1058–1071; I. Fridovich, *Annu. Rev. Pharmacol. Toxicol.* **1983**, *23*, 239–257.

[3] E. C. Friedberg, *DNA Repair*, Freeman, New York, **1985**; M. M. Cox, I. R. Lehman, *Annu. Rev. Biochem.* **1987**, *56*, 229–262; A. Sancar, G. B. Sancar, *ibid.* **1988**, *57*, 29–67; R. M. Story, I. T. Weber, T. A. Steitz, *Nature (London)* **1992**, *355*, 318–325; S. Boiteux, E. Gajewski, J. Laval, M. Dizdaroglu, *Biochemistry* **1992**, *31*, 106–110.

[4] J. Cadet, M. Berger, C. Decarroz, J. R. Wagner, J. E. van Lier, Y. M. Ginot, P. Vigny, *Biochimie* **1986**, *68*, 813–834; C. von Sonntag, *The Chemical Basis of Radiation Biology*, Taylor and Francis, Philadelphia, **1987**; C. von Sonntag, H.-P. Schuchmann, *Methods Enzymol.* **1994**, *233*, 3–19.

[5] H. Urata, K. Yamamoto, M. Akagi, H. Hiroaki, S. Uesugi, *Biochemistry* **1989**, *28*, 9566–9569; J. Piette, *J. Photochem. Photobiol. B* **1991**, *11*, 241–260; H. Kasai, Z. Yamaizumi, M. Berger, J. Cadet, *J. Am. Chem. Soc.* **1992**, *114*, 9692–9694; L. P. Candeias, S. Steenken, *ibid.* **1993**, *115*, 2437–2440; N. Paillous, P. Vicendo, *J. Photochem. Photobiol. B* **1993**, *20*, 203–209.

[6] B. Demple, J. Halbrook, *Nature (London)* **1983**, *304*, 466–468; J. F. Mouret, F. Odin, M. Polverelli, J. Cadet, *Chem. Res. Toxicol.* **1990**, *3*, 102–110.

[7] S. Steenken, *Chem. Rev.* **1989**, *89*, 503–520; A. J. S. C. Vieira, S. Steenken, *J. Am. Chem. Soc.* **1990**, *112*, 6986–6994.

[8] D. G. Knorre, O. S. Federova, E. I. Frolova, *Russ. Chem. Rev. (Engl. Transl.)* **1993**, *62*, 65–86.

[9] a) S. M. Hecht, *Acc. Chem. Res.* **1986**, *19*, 383–391; b) J. Stubbe, J. W. Kozarich, *Chem. Rev.* **1987**, *87*, 1107–1136; c) D. H. Petering, R. W. Byrnes, W. E. Antholine, *Chem. Biol. Interact.* **1990**, *73*, 133–182; d) I. H. Goldberg, *Acc. Chem. Res.* **1991**, *24*, 191–198; e) *Free Radical Biol. Med.* **1987**, *3*, 41–54; f) M. D. Lee, G. A. Ellestad, D. B. Borders, *Acc. Chem. Res.* **1991**, *24*, 235–243; g) K. C. Nicolaou, W. M. Dai, *Angew. Chem.* **1991**, *103*, 1453–1481; *Angew. Chem. Int. Ed. Engl.* **1991**, *30*, 1387–1416; K. C. Nicolaou, A. L. Smith, E. W. Yue, *Proc. Natl. Acad. Sci. USA* **1993**, *90*, 5881–5888; h) K. C. Nicolaou, A. L. Smith, *Acc. Chem. Res.* **1992**, *25*, 497–503; i) J. S. Taylor, P. G. Schultz, P. B. Dervan, *Tetrahedron* **1984**, *40*, 457–465; j) I. Lee, J. K. Barton, *Biochemistry* **1993**, *32*, 6121–6127, and references therein; k) D. S. Sigman, T. W. Bruice, A. Mazumder, C. L. Sutton, *Acc. Chem. Res.* **1993**, *26*, 98–104; l) T. Tanaka, M. Hirama, K.-I. Fujita, M. Ishiguro, *J. Chem. Soc. Chem. Commun.* **1993**, 1205–1207.

[10] A. P. Grollman, M. Moriya, *Trends Genet.* **1993**, *9*, 246–249.

[11] W. Saenger, *Principles of Nucleic Acid Structure*, Springer, New York, **1984**.

[12] a) A. Mazumder, J. A. Gerlt, M. J. Absalon, J. Stubbe, R. P. Cunningham, J. Withka, P. H. Bolton, *Biochemistry* **1991**, *30*, 1119–1126; b) J. J. Hangeland, J. J. De Voss, J. A. Heath, C. A. Townsend, W. D. Ding, J. S. Ashcroft, G. A. Ellestad, *J. Am. Chem. Soc.* **1992**, *114*, 9200–9202.

[13] D. Suck, C. Oefner, *Nature (London)* **1986**, *321*, 620–625; J. A. McClarin, C. A. Frederick, B. C. Wang, P. Greene, H. W. Boyer, J. Grable, J. M. Rosenberg, *Science* **1986**, *234*, 1526–1541.

[14] A. M. Maxam, W. Gilbert, *Methods Enzymol.* **1980**, *65*, 499–560.

[15] a) D. S. Sigman, D. R. Graham, V. D'Aurora, A. M. Stern, *J. Biol. Chem.* **1979**, *254*, 12269–12272; b) D. S. Sigman, *Acc. Chem. Res.* **1986**, *19*, 180–186; c) C. Yoon, M. D. Kuwabara, R. Law, R. Wall, D. S. Sigman, *J. Biol. Chem.* **1988**, *263*, 8458–8463; d) D. S. Sigman, *Biochemistry* **1990**, *29*, 9097–9105; e) J. M. Veal, R. L. Hill, *ibid.* **1991**, *30*, 1132–1140; f) A. Spassky, *ibid.* **1992**, *31*, 10502–10509.

[16] V. M. Downey, B. G. Que, A. G. So, *Biochem. Biophys. Res. Commun.* **1980**, *93*, 264.

[17] L. E. Marshall, D. R. Graham, K. A. Reich, D. S. Sigman, *Biochemistry* **1981**, *20*, 244–250.

[18] G. R. Alastair Johnson, N. B. Nazhat, *J. Am. Chem. Soc.* **1987**, *109*, 1990–1994.
[19] L. D. Williams, J. Thivierge, I. H. Goldberg, *Nucleic Acids Res.* **1988**, *16*, 11607–11615.
[20] M. Dizdaroglu, O. I. Aruoma, B. Halliwell, *Biochemistry* **1990**, *29*, 8447–8451.
[21] J. M. Veal, K. Merchant, R. L. Rill, *Nucleic Acids Res.* **1991**, *19*, 3383–3388.
[22] L. E. Pope, D. S. Sigman, *Proc. Natl. Acad. Sci. USA* **1984**, *81*, 3–7
[23] J.-C. François, T. Saison-Behmoaras, M. Chassignol, N. T. Thuong, J.-S. Sun, C. Hélène, *Biochemistry* **1988**, *27*, 2272–2276.
[24] K. A. Reich, L. E. Marshall, D. R. Graham, D. S. Sigman, *J. Am. Chem. Soc.* **1981**, *103*, 3582–3584.
[25] T. B. Thederahn, M. D. Kuwabara, T. A. Larsen, D. S. Sigman, *J. Am. Chem. Soc.* **1989**, *111*, 4941–4946.
[26] S. Goldstein, G. Czapski, *J. Am. Chem. Soc.* **1986**, *108*, 2244–2250.

1986, *25*, 7401–7408.
[29] a) L. Marshal Pope, K. A. Reich, D. R. Graham, D. S. Sigman, *J. Biol. Chem.* **1982**, *257*, 12121–12128; b) D. S. Sigman, C. B. Chen, *Metal-DNA Chemistry* (Ed.: T. D. Tullius) (*ACS Symp. Ser.* **1989**, *402*, pp. 24–47).
[30] J. M. Veal, R. L. Rill, *Biochemistry* **1988**, *27*, 1822–1827.
[31] C. Yoon, M. D. Kuwabara, A. Spassky, D. S. Sigman, *Biochemistry* **1990**, *29*, 2116–2121.
[32] J. M. Veal, R. L. Rill, *Biochemistry* **1991**, *30*, 1132–1140.
[33] a) D. S. Sigman, A. Spassky, S. Rimsky, H. Buc, *Biopolymers* **1985**, *24*, 183–

Nucleic Acids Res. **1989**, *17*, 5361–5375.
[36] C. B. Chen, D. S. Sigman, *Proc. Natl. Acad. Sci. USA* **1986**, *83*, 7147–7151.
[37] J.-C. François, T. Saison-Behmoaras, M. Chassignol, N. T. Thuong, C. Hélène, *J. Biol. Chem.* **1989**, *264*, 5891–5898.
[38] C. B. Chen, D. S. Sigman, *J. Am. Chem. Soc.* **1988**, *110*, 6570–6572.
[39] J.-C. François, T. Saison-Behmoaras, C. Barbier, M. Chassignol, N. T. Thuong, C. Hélène, *Proc. Natl. Acad. Sci. USA* **1989**, *86*, 9702–9706.
[40] J.-S. Sun, J.-C. François, R. Lavery, T. Saison-Behmoaras, T. Montenay-Ga-

[42] S. D. Jayasena, B. H. Johnston, *Proc. Natl. Acad. Sci. USA* **1992**, *89*, 3526–3530.
[43] C. B. Chen, M. B. Gorin, D. S. Sigman, *Proc. Natl. Acad. Sci. USA* **1993**, *90*, 4206–4210.
[44] C. B. Chen, A. Mazumder, J.-F. Constant, D. S. Sigman, *Bioconjugate Chem.* **1993**, *4*, 69–77.
[45] A. D. Baker, R. J. Morgan, T. C. Strekas, *J. Chem. Soc. Chem. Commun.* **1992**, 1099–1100.
[46] a) P. C. Dedon, I. H. Goldberg, *Biochemistry* **1992**, *31*, 1909–1917; b) P. C. Dedon, Z.-W. Jiang, I. H. Goldberg, *ibid.* **1992**, *31*, 1917–1927.
[47] R. D. Groneberg, T. Miyazaki, N. A. Stylianides, T. J. Schulze, W. Stahl, E. P. Schreiner, T. Suzuki, Y. Iwabuchi, A. L. Smith, K. C. Nicolaou, *J. Am. Chem. Soc.* **1993**, *115*, 7593–7611; A. L. Smith, E. N. Pitsinos, C.-K. Hwang, Y. Mizuno, H. Saimoto, G. R. Scarlato, T. Suzuki, K. C. Nicolaou, *ibid.* **1993**, *115*, 7612–7624; K. C. Nicolaou, C. W. Hummel, M. Nakada, K. Shibayama, E. N. Pitsinos, H. Saimoto, Y. Mizuno, K.-U. Baldenius, A. L. Smith, *ibid.* **1993**, *115*, 7625–7635; see also K. C. Nicolaou, *Angew. Chem.* **1993**, *105*, 1462–1471; *Angew. Chem. Int. Ed. Engl.* **1993**, *32*, 1377–1385.
[48] R. G. Bergman, *Acc. Chem. Res.* **1973**, *6*, 25–31.
[49] N. Zein, W. J. McGahren, G. O. Morton, J. Ashcroft, G. A. Ellestad, *J. Am. Chem. Soc.* **1989**, *111*, 6888–6890.
[50] D.-H. Chin, I. H. Goldberg, *Biochemistry* **1986**, *25*, 1009–1015.
[51] N. Zein, A. M. Sinha, W. J. McGahren, G. A. Ellestad, *Science* **1988**, *240*, 1198–1201.
[52] L. S. Kappen, I. H. Goldberg, *Proc. Natl. Acad. Sci. USA* **1984**, *81*, 3312–3316.
[53] S. M. Meschwitz, I. H. Goldberg, *Proc. Natl. Acad. Sci. USA* **1991**, *88*, 3047–3051.

[56] J. J. De Voss, C. A. Townsend, W.-D. Ding, G. O. Morton, G. A. Ellestad, N. Zein, A. B. Tabor, S. L. Schreiber, *J. Am. Chem. Soc.* **1990**, *112*, 9669–9670.
[57] D. F. Christner, B. L. Frank, J. W. Kozarich, J. Stubbe, J. Golik, T. W. Doyle, I. E. Rosenberg, B. Krishnan, *J. Am. Chem. Soc.* **1992**, *114*, 8763–8767.
[58] a) M. F. Semmelhack, J. Gallagher, D. Cohen, *Tetrahedron Lett.* **1990**, *31*, 1521–1522; b) P. A. Wender, R. C. Kelly, S. Beckam, B. L. Miller, *Proc. Natl. Acad. Sci. USA* **1991**, *88*, 8835–8839; c) Y. Sugiura, T. Arakawa, M. Uesugi, T. Shiraki, H. Ohkuma, M. Konishi, *Biochemistry* **1991**, *30*, 2989–2992.

[62] Y. Uesawa, Y. Sugiura, *Biochemistry* **1991**, *30*, 9242–9246.
[63] D. Dasgupta, I. H. Goldberg, *Biochemistry* **1985**, *24*, 6913–6920.
[64] L. S. Kappen, I. H. Goldberg, B. L. Frank, L. Worth, Jr., D. F. Christner, J. W. Kozarich, J. Stubbe, *Biochemistry* **1991**, *30*, 2034–2042.
[65] A. Galat, I. H. Goldberg, *Nucleic Acids Res.* **1990**, *18*, 2093–2099.
[66] a) L. S. Kappen, I. H. Goldberg, *Proc. Natl. Acad. Sci. USA* **1992**, *89*, 6706–

[67] a) S. Walker, R. Landovitz, W. D. Ding, G. A. Ellestad, D. Kahne, *Proc. Natl. Acad. Sci. USA* **1992**, *89*, 4608–4612; b) N. Zein, M. Poncin, R. Nilakantan, G. A. Ellestad, *Science* **1989**, *244*, 697–699; c) J. Drak, N. Iwasawa, S. Danishefsky, D. M. Crothers, *Proc. Natl. Acad. Sci. USA* **1991**, *88*, 7464–7468; d) J. Aiyar, S. J. Danishefsky, D. M. Crothers, *J. Am. Chem. Soc.* **1992**, *114*, 7552–7554; e) K. C. Nicolaou, S.-C. Tsay, T. Suzuki, G. F. Joyce, *ibid.* **1992**, *114*, 7555–7557.
[68] a) Y. Sugiura, Y. Uesawa, Y. Takahashi, J. Kuwahara, J. Golik, T. W. Doyle, *Proc. Natl. Acad. Sci. USA* **1989**, *86*, 7672–7676; b) B. H. Long, J. Golik, S. Forenza, B. Ward, R. Rehfuss, J. C. Dabrowiak, J. J. Catino, S. T. Musial, K. W. Brookshire, T. W. Doyle, *ibid.* **1989**, *86*, 2–6; c) H. Kishikawa, Y.-P. Jiang, J. Goodisman, J. C. Dabrowiak, *J. Am. Chem. Soc.* **1991**, *113*, 5434–5440.
[69] M. Uesugi, Y. Sugiura, *Biochemistry* **1993**, *32*, 4622–4627.
[70] Y. Sugiura, T. Shiraki, M. Konishi, T. Oki, *Proc. Natl. Acad. Sci. USA* **1990**, *87*, 3831–3835.
[71] L. S. Kappen, I. H. Goldberg, S. H. Wu, J. Stubbe, L. Worth, Jr., J. W. Kozarich, *J. Am. Chem. Soc.* **1990**, *112*, 2797–2798.
[72] H. Umezawa, K. Maeda, T. Takeuchi, Y. Okami, *J. Antibiot. Ser. A.* **1966**, *19*, 200–209.
[73] H. Umezawa in *Bleomycin: Current Status and New Developments* (Eds.: S. K. Carter, S. T. Crooke, H. Umezawa), Academic Press, New York, **1978**, pp. 15–19.
[74] H. Suzuki, K. Nagai, H. Yakami, N. Tanaka, H. Umezawa, *J. Antibiot.* **1969**, *22*, 446–448; Y. Fujiwara, T. Kondo, *Biochem. Pharmacol.* **1973**, *22*, 323–333.

[79] Y. Kaku, M. Otsuka, M. Ohno, *Chem. Lett.* **1989**, 611–614; A. Suga, T. Sugiyama, M. Otsuka, M. Ohno, Y. Sugiura, K. Maeda, *Tetrahedron* **1991**, *47*, 1191–1204.
[80] M. Otsuka, T. Masuda, A. Haupt, M. Ohno, T. Shiraki, Y. Sugiura, K. Maeda, *J. Am. Chem. Soc.* **1990**, *112*, 838–845.
[81] B. J. Carter, K. S. Reddy, S. M. Hecht, *Tetrahedron* **1991**, *47*, 2463–2474.
[82] K. Shinozuka, H. Morishita, T. Yamazaki, Y. Sugiura, H. Sawai, *Tetrahedron Lett.* **1991**, *32*, 6869–6872.
[83] L. F. Povirk in *Molecular Aspects of Anti-Cancer Drug Action* (Eds.: S. Neidle, M. J. Waring), Verlag Chemie, Weinheim, **1983**, pp. 157–181.
[84] a) E. A. Sausville, J. Peisach, S. B. Horwitz, *Biochemistry* **1978**, *17*, 2740–2746; b) H. Sugiyama, R. E. Kilkuskie, L.-H. Chang, L.-T. Ma, S. M. Hecht, G. A. van der Marel, J. H. van Boom, *J. Am. Chem. Soc.* **1986**, *108*, 3852; c) G. R. Buettner, P. L. Moseley, *Biochemistry* **1992**, *31*, 9784–9788.
[85] a) R. B. Van Atta, E. C. Long, S. M. Hecht, G. A. van der Marel, J. H. van Boom, *J. Am. Chem. Soc.* **1989**, *111*, 2722–2724; b) K. Kohda, H. Kasai, T. Ogawa, T. Suzuki, Y. Kawazoe, *Chem. Pharm. Bull.* **1989**, *37*, 1028–1030.
[86] L. Giloni, M. Takeshita, F. Johnson, C. Iden, A. P. Grollman, *J. Biol. Chem.* **1981**, *256*, 8608–8615.
[87] a) Y. Sugiura, *J. Am. Chem. Soc.* **1980**, *102*, 5208–5215; b) R. M. Burger, J. Peisach, S. B. Horwitz, *J. Biol. Chem.* **1981**, *256*, 11636–11644; c) R. M. Burger, J. S. Blanchard, S. B. Horwitz, J. Peisach, *ibid.* **1985**, *260*, 15406–15409.
[88] A. Natrajan, S. M. Hecht, G. A. van der Marel, J. H. van Boom, *J. Am. Chem. Soc.* **1990**, *112*, 3997–4002.
[89] a) T. J. McMurry, J. T. Groves in [89d], pp. 1–28; b) V. Ullrich, *Top. Curr. Chem.* **1979**, *83*, 67–104; c) R. E. White, M. J. Coon, *Annu. Rev. Biochem.* **1980**, *49*, 315–356; d) *Cytochrome P-450: Structure, Mechanism and Biochemistry* (Ed.: P. Ortiz de Montellano), Plenum, New York, **1985**; e) A. Sorokin, A. Robert, B. Meunier, *J. Am. Chem. Soc.* **1993**, *115*, 7293–7299.
[90] a) B. Meunier, *Chem. Rev.* **1992**, *92*, 1411–1456; b) J. T. Groves, R. C. Haushalter, M. Nakamura, T. E. Nemo, B. J. Evans, *J. Am. Chem. Soc.* **1981**, *103*, 2884–2886; c) D. Mandon, R. Weiss, K. Jayaraj, A. Gold, J. Terner, E. Bill,

A. X. Trautwein, *Inorg. Chem.* **1992**, *31*, 4404–4409; d) O. Bortolini, B. Meunier, *J. Chem. Soc. Chem. Commun.* **1983**, 1364–1365; e) O. Bortolini, M. Ricci, B. Meunier, P. Friant, I. Ascone, J. Goulon, *Nouv. J. Chim.* **1986**, *10*, 39–49.

[91] a) N. Murugesan, G. M. Ehrenfeld, S. M. Hecht, *J. Biol. Chem.* **1982**, *257*, 8600–8603; b) N. Murugesan, S. M. Hecht, *J. Am. Chem. Soc.* **1985**, *107*, 493–500; c) *Inorg. Chem.* **1987**, *26*, 3835–3836.

[92] R. M. Moriarty, R. Penmasta, I. Prakash, *Tetrahedron Lett.* **1985**, *26*, 4699–4702; E. C. Long, S. A. Hecht, *ibid.* **1988**, *29*, 6413–6416.

[93] R. S. Magliozzo, J. Peisach, *Inorg. Chem.* **1989**, *28*, 608–611.

[94] G. Pratviel, J. Bernadou, B. Meunier, *Biochem. Biophys. Res. Commun.* **1986**, *136*, 1013–1020; *Biochem. Pharmacol.* **1989**, *38*, 133–140; B. Meunier, *New J. Chem.* **1992**, *16*, 203–211.

[95] M. Girardet, B. Meunier, *Tetrahedron Lett.* **1987**, *28*, 2955–2958.

[96] a) G. Padbury, S. G. Sligar, R. Labeque, L. J. Marnett, *Biochemistry* **1988**, *27*, 7846–7852; b) A. Natrajan, S. M. Hecht, G. A. van der Marel, J. H. van Boom, *J. Am. Chem. Soc.* **1990**, *112*, 4532–4538.

[97] R. E. Shepherd, T. J. Lomis, R. R. Koepsel, *J. Chem. Soc. Chem. Commun.* **1992**, 222–224.

[98] R. P. Hertzberg, P. B. Dervan, *Biochemistry* **1984**, *23*, 3934–3945; D. W. Celander, T. R. Cech, *ibid.* **1990**, *29*, 1355–1361; R. V. Prigodich, C. T. Martin, *ibid.* **1990**, *29*, 8017–8019.

[99] L. E. Rabow, G. H. McGall, J. Stubbe, J. W. Kozarich, *J. Am. Chem. Soc.* **1990**, *112*, 3203–3208.

[100] E. Gajewski, O. I. Aruoma, M. Dizdaroglu, B. Halliwell, *Biochemistry* **1991**, *30*, 2444–2448.

[101] L. L. Guan, J. Kuwahara, Y. Sugiura, *Biochemistry* **1993**, *32*, 6141–6145.

[102] J. C. Dabrowiak in *Advances in Inorganic Biochemistry* (Eds.: G. L. Eichhorn, L. G. Marzilli), Elsevier, New York, **1982**, pp. 69–113.

[103] J. Kuwahara, Y. Sugiura, *Proc. Natl. Acad. Sci. USA* **1988**, *85*, 2459–2463.

[104] R. P. Hertzberg, M. J. Caranfa, S. M. Hecht, *Biochemistry* **1988**, *27*, 3164–3174; E. C. Long, S. M. Hecht, G. A. van der Marel, J. H. van Boom, *J. Am. Chem. Soc.* **1990**, *112*, 5272–5276.

[105] B. Gold, V. Dange, M. A. Moore, A. Esastman, G. A. van der Marel, J. H. van Boom, S. M. Hecht, *J. Am. Chem. Soc.* **1988**, *110*, 2347–2349.

[106] L. F. Povirk, Y.-H. Han, R. J. Steighner, *Biochemistry* **1989**, *28*, 5808–5814.

[107] R. J. Steighner, L. F. Povirk, *Proc. Natl. Acad. Sci. USA* **1990**, *87*, 8350–8354.

[108] D. S. Sergeyev, V. F. Zarytova, S. V. Mamaev, T. S. Godovikova, V. V. Vlassov, *Antisense Res. Dev.* **1992**, *2*, 235–241; V. F. Zarytova, D. S. Sergeyev, T. S. Godovikova, *Bioconjugate Chem.* **1993**, *4*, 189–193.

[109] A. Hüttenhofer, S. Hudson, H. F. Noller, P. K. Mascharak, *J. Biol. Chem.* **1992**, *267*, 24471–24475.

[110] B. J. Carter, E. de Vroom, E. C. Long, G. A. van der Marel, J. H. van Boom, S. M. Hecht, *Proc. Natl. Acad. Sci. USA* **1990**, *87*, 9373–9377.

[111] C. E. Holmes, B. J. Carter, S. M. Hecht, *Biochemistry* **1993**, *32*, 4293–4307, and references therein.

[112] R. S. Magliozzo, J. Peisach, M. R. Ciriolo, *Mol. Pharmacol.* **1989**, *35*, 428–432.

[113] R. P. Hertzberg, P. B. Dervan, *J. Am. Chem. Soc.* **1982**, *104*, 313–315.

[114] C. H. L. Kennard, *Inorg. Chim. Acta* **1967**, *1*, 347–354.

[115] T. D. Tullius, B. A. Dombroski, *Science* **1985**, *230*, 679–681.

[116] T. D. Tullius, *Trends Biochem. Sci.* **1987**, 297–300.

[117] T. D. Tullius, *Nature (London)* **1988**, *332*, 663–664.

[118] S.-B. Lin, K. R. Blake, P. S. Miller, P. O. P. Ts'o, *Biochemistry* **1989**, *28*, 1054–1061.

[119] R. S. Youngquist, P. B. Dervan, *Proc. Natl. Acad. Sci. USA* **1985**, *82*, 2565–2569.

[120] R. P. Hertzberg, S. M. Hecht, V. L. Reynolds, I. J. Molineux, L. H. Hurley, *Biochemistry* **1986**, *25*, 1249–1258.

[121] S. I. Gunderson, K. A. Chapman, R. R. Burgess, *Biochemistry* **1987**, *26*, 1539–1546.

[122] M. E. A. Churchill, J. J. Hayes, T. D. Tullius, *Biochemistry* **1990**, *29*, 6043–6050.

[123] M. A. Price, T. D. Tullius, *Biochemistry* **1993**, *32*, 127–136; A. M. Burkhoff, T. D. Tullius, *Cell* **1987**, *48*, 935–943.

[124] M. E. A. Churchill, T. D. Tullius, N. R. Kallenbach, N. C. Seeman, *Proc. Natl. Acad. Sci. USA* **1988**, *85*, 4653–4656.

[125] M. W. Van Dyke, R. P. Hertzberg, P. B. Derwan, *Proc. Natl. Acad. Sci. USA* **1982**, *79*, 5470–5474; L. H. Hurley, C.-S. Lee, J. P. McGovren, M. A. Warpehoski, M. A. Mitchell, R. C. Kelly, P. A. Aristoff, *Biochemistry* **1988**, *27*, 3886–3892.

[126] M. Sawadogo, R. G. Roeder, *Cell* **1985**, *43*, 165–175; H.-M. Jantzen, U. Strähle, B. Gloss, F. Stewart, W. Schmid, M. Boshart, R. Miksicek, G. Schütz, *ibid.* **1987**, *49*, 29–38; N. F. Landolfi, X.-M. Yin, J. D. Capra, P. W. Tucker, *Biotechniques* **1989**, *7*, 500–504.

[127] C. P. H. Vary, J. N. Vournakis, *Proc. Natl. Acad. Sci. USA* **1984**, *81*, 6978–6982.

[128] I. L. Cartwright, R. P. Hertzberg, P. B. Dervan, S. C. Elgin, *Proc. Natl. Acad. Sci. USA* **1983**, *80*, 3213–3217; H. Richard-Foy, G. L. Hager, *EMBO J.* **1987**, *6*, 2321–2328.

[129] T. D. Tullius, B. A. Dombroski, M. E. A. Churchill, L. Kam, *Methods Enzymol.* **1987**, *155*, 537–558.

[130] P. B. Dervan, *Science* **1986**, *232*, 464–471.

[131] a) R. S. Youngquist, P. B. Dervan, *J. Am. Chem. Soc.* **1985**, *107*, 5528–5529; b) W. S. Wade, P. B. Dervan, *ibid.* **1987**, *109*, 1574–1575; c) P. G. Schultz, J. S. Taylor, P. B. Dervan, *ibid.* **1982**, *104*, 6861–6863.

[132] J. H. Griffin, P. B. Dervan, *J. Am. Chem. Soc.* **1986**, *108*, 5008–5009.

[133] a) J. P. Sluka, S. J. Horvath, M. F. Bruist, M. I. Simon, P. B. Dervan, *Science* **1987**, *238*, 1129–1132; b) R. S. Youngquist, P. B. Dervan, *J. Am. Chem. Soc.* **1987**, *109*, 7564–7566.

[134] a) A. S. Boutorin, V. V. Vlassov, S. A. Kazakov, I. V. Kutiavin, M. A. Podyminogin, *FEBS Lett.* **1984**, *172*, 43–46; b) B. C. F. Chu, L. E. Orgel, *Proc. Natl. Acad. Sci. USA* **1985**, *82*, 963–967; c) G. B. Dreyer, P. B. Dervan, *ibid.* **1985**, *82*, 968–972; d) M. Boidot-Forget, N. T. Thuong, M. Chassignol, C. Hélène, *C. R. Acad. Sci. Ser. 2* **1986**, *302*, 75–80.

[135] H. E. Moser, P. B. Dervan, *Science* **1987**, *238*, 645–650; S. A. Strobel, H. E. Moser, P. B. Dervan, *J. Am. Chem. Soc.* **1988**, *110*, 7927–7929; T. J. Povsic, P. B. Dervan, *ibid.* **1989**, *111*, 3059–3061; S. A. Strobel, P. B. Dervan, *ibid.* **1989**, *111*, 7286–7287; D. A. Horne, P. B. Dervan, *ibid.* **1990**, *112*, 2435–2437; S. A. Strobel, P. B. Dervan, *Science* **1990**, *249*, 73–75; L. C. Griffin, L. L. Kiessling, P. A. Beal, P. Gillespie, P. B. Dervan, *J. Am. Chem. Soc.* **1992**, *114*, 7976–7982; H. Han, P. B. Dervan, *Proc. Natl. Acad. Sci. USA* **1993**, *90*, 3806–3810.

[136] S. Prince, F. Körber, P. R. Cooke, J. R. Lindsay Smith, M. A. Mazid, *Acta Crystallogr. Sect. C* **1993**, *49*, 1158–1160.

[137] B. Ward, A. Skorobogaty, J. C. Dabrowiak, *Biochemistry* **1986**, *25*, 6875–6883.

[138] a) J. Bernadou, G. Pratviel, F. Bennis, M. Girardet, B. Meunier, *Biochemistry* **1989**, *28*, 7268–7275; b) E. Fouquet, G. Pratviel, J. Bernadou, B. Meunier, *J. Chem. Soc. Chem. Commun.* **1987**, 1169–1171; c) G. Pratviel, J. Bernadou, M. Ricci, B. Meunier, *Biochem. Biophys. Res. Commun.* **1989**, *160*, 1212–1218; d) B. Ward, R. Rehfuss, J. C. Dabrowiak, *J. Biomol. Struct. Dyn.* **1987**, *4*, 685–695; e) J. C. Dabrowiak, B. Ward, J. Goodisman, *Biochemistry* **1989**, *28*, 3314–3322.

[139] R. J. Fiel, T. A. Beerman, E. H. Mark, N. Datta-Gupta, *Biochem. Biophys. Res. Commun.* **1982**, *107*, 1067–1074.

[140] R. W. Byrnes, R. J. Fiel, N. Datta-Gupta, *Chem. Biol. Interact.* **1988**, *67*, 225–241.

[141] M. Rodriguez, T. Kodadek, M. Torres, A. J. Bard, *Bioconjugate Chem.* **1990**, *1*, 123–131.

[142] J. M. Kelly, M. J. Murphy, D. J. McConnell, C. OhUigin, *Nucleic Acids Res.* **1985**, *13*, 167–184; D. Praseuth, A. Gaudemer, J. B. Verlhac, I. Kraljic, I. Sissoeff, E. Guillé, *Photochem. Photobiol.* **1986**, *44*, 717–724; C. Sentagne, B. Meunier, N. Paillous, *J. Photochem. Photobiol.* **1992**, *16*, 47–59; D. T. Croke, L. Perrouault, M. A. Sari, J. P. Battioni, D. Mansuy, C. Hélène, T. Le Doan, *ibid.* **1993**, *18*, 41–50; T. Le Doan, L. Perrouault, M. Rougee, R. Bensasson, C. Hélène in *Photodynamic Therapy of Tumours and Other Diseases* (Eds: G. Jori, C. Perria), Libreria Progetto, Padova, Italy, **1985**, pp. 56–58.

[143] a) S. D. Bromley, B. Ward, J. C. Dabrowiak, *Nucleic Acids Res.* **1986**, *14*, 9133–9148; b) B. Ward, A. Skorobogaty, J. C. Dabrowiak, *Biochemistry* **1986**, *25*, 7827–7833; c) G. Raner, B. Ward, J. C. Dabrowiak, *J. Coord. Chem.* **1988**, *19*, 17–23; d) *Porphyrins as Probes of DNA Structure and Drug-DNA Interactions*: G. Raner, J. Goodisman, J. C. Dabrowiak, *ACS Symp. Ser.* **1989**, *402*, 74–89; e) R. F. Pasternack, E. J. Gibbs, *ibid.* **1989**, *402*, 59–73; f) R. F. Pasternack, E. J. Gibbs, J. J. Villafranca, *Biochemistry* **1983**, *22*, 5409–5417; g) J. A. Strickland, L. G. Marzilli, K. M. Gay, W. D. Wilson, *ibid.* **1988**, *27*, 8870–8878; h) R. J. Fiel, *J. Biomol. Struct. Dyn.* **1989**, *6*, 1259–1273; i) L. G. Marzilli, *New J. Chem.* **1990**, *14*, 409–420.

[144] X. Hui, N. Gresh, B. Pullman, *Nucleic Acids Res.* **1990**, *18*, 1109–1114; R. Lavery, B. Pullman, *J. Biomol. Struct. Dyn.* **1985**, *2*, 1021–1032; P. K. Weiner, R. Langeridge, J. M. Blaney, R. Schaefer, P. A. Kollman, *Proc. Natl. Acad. Sci. USA* **1982**, *79*, 3754–3758.

[145] L. G. Marzilli, G. Pethö, M. Lin, M. S. Kim, D. W. Dixon, *J. Am. Chem. Soc.* **1992**, *114*, 7575–7577; M. A. Sari, J. P. Battioni, D. Dupré, D. Mansuy, J. B. Le Pecq, *Biochemistry* **1990**, *29*, 4205–4215.

[146] R. B. Van Atta, J. Bernadou, B. Meunier, S. M. Hecht, *Biochemistry* **1990**, *29*, 4783–4789.

[147] M. Pitié, G. Pratviel, J. Bernadou, B. Meunier, *Proc. Natl. Acad. Sci. USA* **1992**, *89*, 3967–3971.

[148] L. Ding, J. Bernadou, B. Meunier, *Bioconjugate Chem.* **1991**, *2*, 201–206.

[149] C. Casas, C. J. Lacey, B. Meunier, *Bioconjugate Chem.* **1993**, *4*, 366–371; M. Pitié, C. Casas, C. J. Lacey, G. Pratviel, J. Bernadou, B. Meunier, *Angew. Chem.* **1993**, *105*, 607–609; *Angew. Chem. Int. Ed. Engl.* **1993**, *32*, 557–559.

[150] a) A. M. Pyle, J. K. Barton, *Prog. Inorg. Chem.* **1990**, *38*, 413–475; b) N. J. Turro, J. K. Barton, D. A. Tomalia, *Acc. Chem. Res.* **1991**, *24*, 332–340; c) J. K. Barton, *Science* **1986**, *233*, 727–734; d) C. V. Kumar, J. K. Barton, N. J. Turro, *J. Am. Chem. Soc.* **1985**, *107*, 5518–5523; e) M. B. Fleisher, K. C. Waterman, N. J. Turro, J. K. Barton, *Inorg. Chem.* **1986**, *25*, 3551–3552.

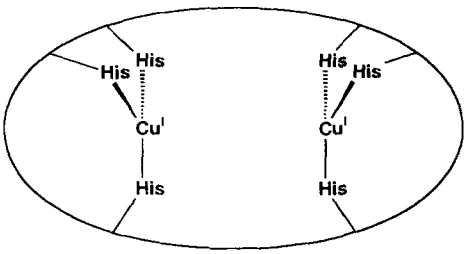
[151] E. C. Long, J. K. Barton, *Acc. Chem. Res.* **1990**, *23*, 273–279.

[152] J. P. Rehmann, J. K. Barton, *Biochemistry* **1990**, *29*, 1701–1709, 1710–1717.
[153] S. Satyanarayana, J. C. Dabrowiak, J. B. Chaires, *Biochemistry* **1993**, *32*, 2573–2584; S. Satyanarayana, J. C. Dabrowiak, J. B. Chaires, *ibid.* **1992**, *31*, 9319–9324; C. Hiort, B. Nordén, A. Rodger, *J. Am. Chem. Soc.* **1990**, *112*, 1971–1982; C. Hiort, P. Lincoln, B. Nordén, *ibid.* **1993**, *115*, 3448–3454; A. E. Friedman, C. V. Khumar, N. J. Turro, J. K. Barton, *Nucleic Acids Res.* **1991**, *19*, 2595–2602.
[154] a) A. M. Pyle, E. C. Long, J. K. Barton, *J. Am. Chem. Soc.* **1989**, *111*, 4520–4522; b) M. R. Kirshenbaum, R. Tribolet, J. K. Barton, *Nucleic Acids Res.* **1988**, *16*, 7943–7960.
[155] N. Grover, H. H. Thorp, *J. Am. Chem. Soc.* **1991**, *113*, 7030–7031; N. Grover, N. Gupta, P. Singh, H. H. Thorp, *Inorg. Chem.* **1992**, *31*, 2014–2020; H. Y. Mei, J. K. Barton, *Proc. Natl. Acad. Sci. USA* **1988**, *85*, 1339–1343; J. M. Kelly, D. J. McConnell, C. OhUigin, A. B. Tossi, A. Kirsch-De Mesmaeker, A. Masschelein, J. Nasielski, *J. Chem. Soc. Chem. Commun.* **1987**, 1821–1823; H. Y. Mei, J. K. Barton, *J. Am. Chem. Soc.* **1986**, *108*, 7414–7416.
[156] B. C. Müller, A. L. Raphael, J. K. Barton, *Proc. Natl. Acad. Sci. USA* **1987**, *84*, 1764–1768; R. J. Baseman, D. W. Pratt, M. Chow, P. Dowd, *J. Am. Chem. Soc.* **1976**, *98*, 5726.
[157] A. Sitlani, E. C. Long, A. M. Pyle, J. K. Barton, *J. Am. Chem. Soc.* **1992**, *114*, 2303–2312.
[158] S. S. David, J. K. Barton, *J. Am. Chem. Soc.* **1993**, *115*, 2984–2985.
[159] In Schemes 13 to 18 all products in frames have been detected and fully (or at least partially) characterized. A negative charge has been omitted for clarity on phosphodiesters and terminal phosphates.
[160] T. E. Goyne, D. S. Sigman, *J. Am. Chem. Soc.* **1987**, *109*, 2846–2848.
[161] L. S. Kappen, C. Chen, I. H. Goldberg, *Biochemistry* **1988**, *27*, 4331–4340.
[162] L. S. Kappen, I. H. Goldberg, *Biochemistry* **1989**, *28*, 1027–1032.
[163] M. Manoharan, A. Mazumder, S. C. Ransom, J. A. Gerlt, *J. Am. Chem. Soc.* **1988**, *110*, 2690–2691; V. Bailly, W. G. Verly, *Nucleic Acids Res.* **1988**, *16*, 9489–9496.
[164] a) J. Bernadou, B. Lauretta, G. Pratviel, B. Meunier, *C.R. Acad. Sci. Ser. 3* **1989**, *309*, 409–414; b) G. Pratviel, M. Pitié, J. Bernadou, B. Meunier, *Angew. Chem.* **1991**, *103*, 718–720; *Angew. Chem. Int. Ed. Engl.* **1991**, *30*, 702–704; c) G. Pratviel, M. Pitié, J. Bernadou, B. Meunier, *Nucleic Acids Res.* **1991**, *19*, 6283–6288; d) G. Gasmi, M. Pasdeloup, G. Pratviel, M. Pitié, J. Bernadou, B. Meunier, *ibid.* **1991**, *19*, 2835–2839.
[165] H. Sugiyama, Y. Tsutsumi, I. Saito, *J. Am. Chem. Soc.* **1990**, *112*, 6720–6721.
[166] H. Sugiyama, Y. Tsutsumi, K. Fujimoto, I. Saito, *J. Am. Chem. Soc.* **1993**, *115*, 4443–4448.
[167] M. Dizdaroglu, D. Schulte-Frohlinde, C. von Sonntag, *Z. Naturforsch. C* **1977**, *32*, 1021–1022.
[168] W. D. Hemmer, S. M. Grunberg, W. A. Haseltine, *J. Biol. Chem.* **1982**, *257*, 11750–11754; W. D. Henner, L. O. Rodriguez, S. M. Hecht, W. A. Haseltine, *ibid.* **1983**, *258*, 711–713.
[169] I. Saito, H. Kawabata, T. Fujiwara, H. Sugiyama, T. Matsuura, *J. Am. Chem. Soc.* **1989**, *111*, 8302–8303.
[170] B. L. Frank, L. Worth, Jr., D. F. Christner, J. W. Kozarich, J. Stubbe, L. S. Kappen, I. H. Goldberg, *J. Am. Chem. Soc.* **1991**, *113*, 2271–2275.
[171] P. C. Dedon, I. H. Goldberg, *J. Biol. Chem.* **1990**, *265*, 14713–14716.
[172] T. Hatayama, I. H. Goldberg, *Biochemistry* **1980**, *19*, 5890–5898.
[173] G. H. McGall, L. E. Rabow, G. W. Ashley, S. H. Wu, J. W. Kozarich, J. Stubbe, *J. Am. Chem. Soc.* **1992**, *114*, 4958–4967.
[174] D. Schulte-Frohlinde, C. von Sonntag in *Oxidative Stress* (Ed.: H. Sies), Academic Press, London, **1985**, pp. 11–40.
[175] C. von Sonntag, *Adv. Carbohydr. Chem. Biochem.* **1980**, *37*, 7–77.
[176] G. H. McGall, J. Stubbe, J. W. Kozarich, *J. Org. Chem.* **1991**, *56*, 48–55.
[177] a) H. Sugiyama, C. Xu, N. Murugesan, S. M. Hecht, G. A. van der Marel, J. H. van Boom, *Biochemistry* **1988**, *27*, 58–67; b) H. Sugiyama, H. Kawabata, T. Fujiwara, Y. Dannoue, I. Saito, *J. Am. Chem. Soc.* **1990**, *112*, 5252–5257.
[178] R. M. Burger, S. J. Projan, S. B. Horwitz, J. Peisach, *J. Biol. Chem.* **1986**, *261*, 15955–15959.
[179] N. Murugesan, C. Xu, G. M. Ehrenfeld, H. Sugiyama, R. E. Kilkuskie, L. O. Rodriguez, L. H. Chang, S. M. Hecht, *Biochemistry* **1985**, *24*, 5735–5744.
[180] J. C. Wu, J. W. Kozarich, J. Stubbe, *J. Biol. Chem.* **1983**, *258*, 4694–4697.
[181] J. W. Kozarich, L. Worth, Jr., B. L. Frank, D. F. Christner, D. E. Vanderwall, J. Stubbe, *Science* **1989**, *245*, 1396–1398.
[182] L. Worth, Jr., B. L. Frank, D. F. Christner, M. J. Absalon, J. Stubbe, J. W. Kozarich, *Biochemistry* **1993**, *32*, 2601–2609.
[183] a) K. U. Ingold, *Acc. Chem. Res.* **1969**, *2*, 1–9; b) C. von Sonntag, *Int. J. Radiat. Relat. Stud. Phys. Chem. Med.* **1984**, *46*, 507–518; c) E. Bothe, G. Behrens, E. Böhm, B. Sethuram, D. Schulte-Frohlinde, *ibid.* **1986**, *49*, 57–66.
[184] L. E. Rabow, J. Stubbe, J. W. Kozarich, *J. Am. Chem. Soc.* **1990**, *112*, 3169–3203.
[185] H. Sugiyama, C. Xu, N. Murugesan, S. Hecht, *J. Am. Chem. Soc.* **1985**, *107*, 4104–4105.
[186] T. G. Wenzel, C. H. Chang, C. F. Meares, *Biochemistry* **1985**, *24*, 3060–3069.
[187] I. Saito, T. Morii, H. Sugiyama, T. Matsuura, C. F. Meares, S. M. Hecht, *J. Am. Chem. Soc.* **1989**, *111*, 2307–2308.
[188] S. M. Hecht in *Bleomycin: Chemical, Biochemical and Biological Aspects* (Ed.: S. M. Hecht), Springer, New York, **1979**, pp. 1–23.
[189] C. R. Krishnamoorthy, D. E. Vanderwall, J. W. Kozarich, J. Stubbe, *J. Am. Chem. Soc.* **1988**, *110*, 2008–2009.
[190] M. J. Absalon, C. R. Krishnamoorthy, G. McGall, J. W. Kozarich, J. Stubbe, *Nucleic Acids Res.* **1992**, *20*, 4179–4185.
[191] R. J. Duff, E. de Vroom, A. Geluk, S. M. Hecht, *J. Am. Chem. Soc.* **1993**, *115*, 3350–3351.
[192] J. P. Sluka, S. J. Horvath, A. C. Glasgow, M. I. Simon, P. B. Dervan, *Biochemistry* **1990**, *29*, 6551–6561; D. P. Mack, J. P. Sluka, J. A. Shin, J. H. Griffin, M. I. Simon, P. B. Dervan, *ibid.* **1990**, *29*, 6561–6567.
[193] M. G. Oakley, P. B. Dervan, *Science* **1990**, *248*, 847–850; M. G. Oakley, M. Mrksich, P. B. Dervan, *Biochemistry* **1992**, *31*, 10969–10975.
[194] D.-H. Chin, S. A. Carr, I. H. Goldberg, *J. Biol. Chem.* **1984**, *259*, 9975–9978.
[195] L. S. Kappen, I. H. Goldberg, J. M. Liesch, *Proc. Natl. Acad. Sci. USA* **1982**, *79*, 744–748.
[196] L. S. Kappen, I. H. Goldberg, *Biochemistry* **1983**, *22*, 4872–4878.
[197] D.-H. Chin, L. S. Kappen, I. H. Goldberg, *Proc. Natl. Acad. Sci. USA* **1987**, *84*, 7070–7074.
[198] L. S. Kappen, T. R. Lee, C. Yang, I. H. Goldberg, *Biochemistry* **1989**, *28*, 4540–4542.
[199] H. Kawabata, H. Takeshita, T. Fujiwara, H. Sugiyama, T. Matsuura, I. Saito, *Tetrahedron Lett.* **1989**, *30*, 4263–4266.
[200] G. Pratviel, M. Pitié, C. Périgaud, G. Gosselin, J. Bernadou, B. Meunier, *J. Chem. Soc. Chem. Commun.* **1993**, 149–151.
[201] M. Pitié, G. Pratviel, J. Bernadou, B. Meunier in *The Activation of Dioxygen and Homogeneous Catalytic Oxidation* (Eds.: D. H. R. Barton, A. E. Martell, D. T. Sawyer), Plenum, New York, **1993**, pp. 333–346.
[202] G. Pratviel, V. Duarte, J. Bernadou, B. Meunier, *J. Am. Chem. Soc.* **1993**, *115*, 7939–7943.
[203] V. W. Bowry, K. U. Ingold, *J. Am. Chem. Soc.* **1991**, *113*, 5699–5707; J. K. Atkinson, K. U. Ingold, *Biochemistry* **1993**, *32*, 9209–9214.
[204] L. Ding, G. Etemad-Moghadam, B. Meunier, *Biochemistry* **1990**, *29*, 7868–7875; L. Ding, G. Etemad-Moghadam, S. Cros, C. Auclair, B. Meunier, *J. Med. Chem.* **1991**, *34*, 900–906.
[205] P. S. Pendergrast, Y. W. Ebright, R. H. Ebright, *Science* **1994**, *265*, 959–962.
[206] C. Q. Pan, J. A. Feng, S. E. Finkel, R. Landgraf, D. Sigman, *Proc. Natl. Acad. Sci. USA* **1994**, *91*, 1721–1725.
[207] O. D. Hensens, D.-H. Chin, A. Stassinopoulos, D. L. Zink, L. S. Kappen, I. H. Goldberg, *Proc. Natl. Acad. Sci. USA* **1994**, *91*, 4534–4538; A. G. Myers, S. B. Cohen, B. M. Kwon, *J. Am. Chem. Soc.* **1994**, *116*, 1670–1682.
[208] T. Li, Z. Zeng, V. A. Estevez, K. U. Baldenius, K. C. Nicolaou, G. F. Joyce, *J. Am. Chem. Soc.* **1994**, *116*, 3709–3715.
[209] P. Fulmer, D. H. Petering, *Biochemistry* **1994**, *33*, 5319–5327.
[210] J. W. Sam, X. J. Tang, J. Peisach, *J. Am. Chem. Soc.* **1994**, *116*, 5250–5256.
[211] R. J. Guajardo, S. E. Hudson, S. J. Brown, P. K. Mascharak, *J. Am. Chem. Soc.* **1993**, *115*, 7971–7977.
[212] M. G. Oakley, K. D. Turnbull, P. B. Dervan, *Bioconjugate Chem.* **1994**, *5*, 242–247.
[213] M. A. Morgan, S. M. Hecht, *Biochemistry* **1994**, *33*, 10286–10293.
[214] H. Han, A. Schepartz, M. Pellegrini, P. B. Dervan, *Biochemistry* **1994**, *33*, 9831–9844.
[215] H. Han, P. B. Dervan, *Proc. Natl. Acad. Sci. USA* **1994**, *91*, 4955–4959.
[216] J. Bernadou, A. S. Fabiano, A. Robert, B. Meunier, *J. Am. Chem. Soc.* **1994**, *116*, 9375–9376.
[217] U. Sehlstedt, S. K. Kim, P. Carter, J. Goodisman, J. F. Vallano, B. Nordén, J. C. Dabrowiak, *Biochemistry* **1994**, *33*, 417–426.
[218] M. Eriksson, M. Leijon, C. Hiort, B. Nordén, A. Gräslund, *Biochemistry* **1994**, *33*, 5031–5040.
[219] D. Campisi, T. Morii, J. K. Barton, *Biochemistry* **1994**, *33*, 4130–3139.

The Dinuclear Cu_A Center in Cytochrome *c* Oxidase and N_2O Reductase—A Metal–Metal Bond in Biology?

Helmut Bertagnolli* and Wolfgang Kaim*

Neighboring metal centers that cooperate functionally in proteins are bridged predominantly by O, N, or S donor ligands.[1] In special cases (such as in, for example, deoxyhemocyanin, an oxygen transport protein of molluscs and arthropods that can bind O_2 side-on), the metal centers (here Cu^I) can be held without additional bridging at a "nonbonding" distance of $d > 3.5$ Å by the protein framework.[2] Recently a *direct* metal–metal bond in biology was postulated for the first time for the dinuclear Cu_A center in a water-soluble protein domain of the cytochrome *c* oxidase of *Bacillus subtilis*;[3] this proposal was based on the results of new EXAFS measurements (EXAFS = extended X-ray absorption fine structure) and their interpretation in comparison with results from a model compound.



deoxyhemocyanin

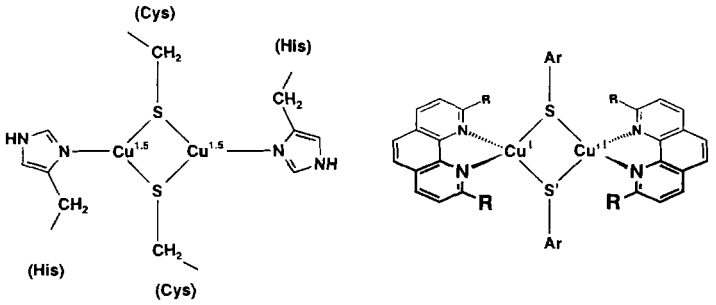
Although cytochrome *c* oxidase (COX) is one of the most important enzymes because of its role as terminal site for O_2-respiration,[4] there have been misconceptions concerning the metal content until very recently, as a glance at the latest editions of biochemistry textbooks shows.[5] They still assume the presence of two heme–iron centers (heme *a* and heme a_3) and only two copper ions (Cu_A and Cu_B). The heme a_3/Cu_B associate is presumed to be the catalytic center for O_2 binding and reduction that can be blocked by cyanide ions, whereas the isolated heme *a* and Cu_A centers have electron-transfer functions at relatively high potentials. The Cu_A center is characterized by absorption of light of long wavelengths (about 830 nm), small EPR hyperfine splitting, and unusually low *g* factor components, and has long been thought of as a mononuclear ion coordinated to two cysteine and two histidine residues.[1b, 5a, 6] In 1987, after a careful elemental analysis of the membrane protein COX (M_r 204 kDa), which comprises 13 very different subunits, Steffens, Bielwald, and Buse proposed that the enzyme indeed contained two heme groups, but a total of *three* copper ions.[7]

In the meantime a copper center detected in N_2O reductase (from the denitrifying bacterium *Pseudomonas stutzeri*) and characterized by Zumft et al. was found to have features that did not fit into the classical division of biological copper centers (types 1, 2, or 3).[1] However, it closely resembled the Cu_A center of cytochrome *c* oxidase.[8] Detailed EPR studies of the oxidized form by Kroneck et al.[9a] suggested a dinuclear, mixed-valent Cu^I/Cu^{II} system, in which *one* unpaired electron interacted with *two equivalent copper centers*. In such an electronically coupled dinuclear system, the oxidation states of both metal centers would be 1.5. Comparative EPR studies on N_2O reductase and cytochrome *c* oxidase at different microwave frequencies,[9b] taking into account the three different isotope combinations $^{63}Cu/^{63}Cu$, $^{63}Cu/^{65}Cu$, and $^{65}Cu/^{65}Cu$,[10] gave such a good agreement that there is no doubt about the existence of a dinuclear structure of the Cu_A center and the spin delocalization. In addition to the numerous mixed-valent Fe^{II}/Fe^{III} clusters in proteins[1, 11a] and the Mn^{III}/Mn^{IV} dimers with their characteristic EPR spectra in water oxidase and several other enzymes,[11b] the oxidized Cu_A centers are apparently another example of a biological, essentially mixed-valent, multinuclear arrangement.

Last year two concrete proposals were published for the detailed coordination of the two copper ions of Cu_A, based on unambiguously conserved amino acid residues (two Cys, two His, one Met). Lappalainen and Saraste suggested an arrangement in which the two metal ions are bridged by two cysteinate S centers (Scheme 1, left).[12] Low molecular weight models for this proposal exist in the form of neutral Cu^I/Cu^I dinuclear complexes (Scheme 1, right),[13] which have strongly differing geometries for the central CuSCu'S' four-membered ring, depending on the substitution in the 2,9 positions of the 1,10-phenanthroline ligands. Both structurally characterized Cu^I_2 model complexes (Scheme 1, right) are, however, only irreversibly oxidized.[13b]

An alternative structure (Scheme 2, left) for the Cu_A center of COX was put forward by Blackburn et al.,[3] based on EXAFS data for water-soluble Cu_A containing domains expressed from *Bacillus subtilis* and for a tricationic, sulfur-free Cu^I/Cu^{II} com-

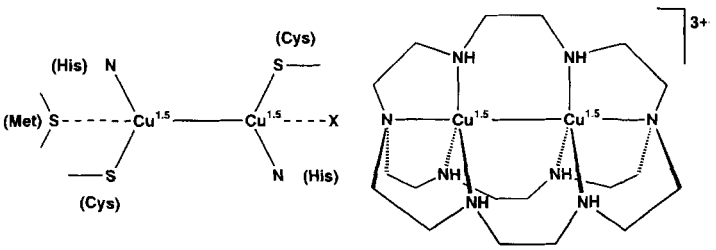
[*] Prof. Dr. H. Bertagnolli
Institut für Physikalische Chemie der Universität
D-70550 Stuttgart (Germany)
Telefax: Int. code + (711)685-4443
Prof. Dr. W. Kaim
Institut für Anorganische Chemie der Universität
D-70550 Stuttgart (Germany)
Telefax: Int. code + (711)685-4241



R	< CuSCu'	< SCuS'	d(CuCu')	ω(SCuS'/SCu'S')
H	68°	>105°	2.613 Å	149.9°
CH_3	81°	99°	3.019 Å	180.0°

Scheme 1. Ar = 2-tolyl, R = H, CH_3. Average values are given for the angles and distances in the models.

plex (Scheme 2, right). A distance of about 2.5 Å attributed to the Cu–Cu vector was interpreted as an indication of a first direct metal–metal bond in a biological system; the two histidine and cysteinate groups were assumed to be nonbridging ligands, and in addition, weak coordination to a methionine residue and a nonidentified group X was postulated.[3]



Scheme 2.

When such important conclusions are involved one question must be posed: Can EXAFS measurements[3] really provide unambiguous identification of a copper–copper bond in COX? The answer must be—and the authors concede this in several places in the text—no! Although these EXAFS measurements have the great advantage that a crystallographically characterized complex (Scheme 2, right) with a linear N-Cu-Cu-N arrangement and a Cu–Cu distance of 2.415 Å could be used as a model, two different EXAFS techniques were unfortunately applied. The model complex was studied in the solid phase where its transmission was measured; the COX domain, on the other hand, was examined in 20% glycerol solution, and the fluorescence radiation of a frozen solution was recorded. This means that the authors neglected to ensure that the concentration of copper ion absorbers in the two systems was as similar as possible. Still more important, however, is the application of two different principles of measurement. The type of background is different for measurements in transmission and fluorescence, and its determination is by no means trivial. Consequently, the extent to which the two measurements are comparable is limited.

The interpretation of EXAFS spectra is done by simulation. Such simulations require either a good model substance or theoretical back-scattering amplitudes and phases. The authors used the theoretical values of the program EXCURV 88 and are convinced that the multiple scattering in the simulation of the EXAFS spectrum of the model complex and COX can be neglected, although these effects can be substantial for a linear arrangement of atoms, which is the case in the model complex. The EXAFS spectrum of the model system was simulated with nine parameters. In the COX system the number is even higher since, in addition, the coordination number of at least two shells is varied and a fifth coordination shell is fitted. In the light of this number of parameters it must be asked, as indeed for almost all simulations of EXAFS spectra, whether a fit just as good can be achieved with other parameter values. The authors are very well aware of these problems and simulate the EXAFS spectra of the model system and COX domain with a set of parameters in which a Cu–S bond is assumed instead of a Cu–Cu bond. The fit index, a measure of the goodness of fit, changes by only 3% through this procedure.

Is that sufficient to postulate a Cu–Cu bond? No! And this is ultimately recognized by the authors, for they write "...the fit also converges to approximately the same value of the fit index." Then they continue "However, chemical considerations argue forcibly against the Cu–S interpretation. The Debye–Waller term ... is close to zero". However, merely a small value for the Debye–Waller factor is far from a definite indication of the existence of a metal–metal bond.

Let us gloss over the interpretation of the EXAFS measurements for the moment. Even if the copper–copper distance was indeed about 2.5 Å, doubt would remain about the presence of "true metal–metal bonding".[3] Surprisingly small copper–copper distances have been observed both in bridged Cu^{II}–Cu^{II} complexes (2.65 Å in dimeric copper(II) acetate with strong antiparallel spin–spin coupling) and multinuclear Cu^{I} compounds, yet it has not been found necessary to postulate a metal–metal bond, even for systems with d(Cu–Cu) = 2.35 Å.[14] In the mixed-valent model complex of Scheme 2, a model that is only of moderate value with respect to the electronic structure,[3] the crystallographically determined Cu–Cu distance of about 2.4 Å is comparable in size, and here too, the geometry is dictated by the ligands. The Cu–Cu distance in the doubly thiolato-bridged Cu^{I}_2 complex of Scheme 1 (R = H) is also just 2.61 Å, so neither the existence of a "biological metal–metal bond" nor the actual bridged or nonbridged structure of the dinuclear Cu_A center can be deduced from the available data. Nevertheless, as hypotheses, the structures in Schemes 2 and 3 provide an ideal field for modeling the composition, spectroscopy, and function of the Cu_A centers in proteins.

German version: *Angew. Chem.* **1995**, *107*, 847

Keywords: cytochrome *c* oxidase · EXAFS spectroscopy · metalloproteins · N_2O reductase

[1] a) W. Kaim, B. Schwederski, *Bioanorganische Chemie*, Teubner, Stuttgart **1992** (English edition: *Bioinorganic Chemistry*, Wiley, Chichester, **1994**); b) J. A. Cowan, *Inorganic Biochemistry*, VCH, New York, **1993**.
[2] K. A. Magnus, H. Ton-That, J. E. Carpenter, *Chem. Rev.* **1994**, *94*, 727.
[3] N. J. Blackburn, M. E. Barr, W. H. Woodruff, J. van der Oost, S. de Vries, *Biochemistry* **1994**, *33*, 10401.
[4] a) B. Kadenbach, *Angew. Chem.* **1983**, *95*, 273; *Angew. Chem. Int. Ed. Engl.* **1983**, *22*, 275; b) G. Buse, *Naturwiss. Rundsch.* **1986**, *39*, 518.

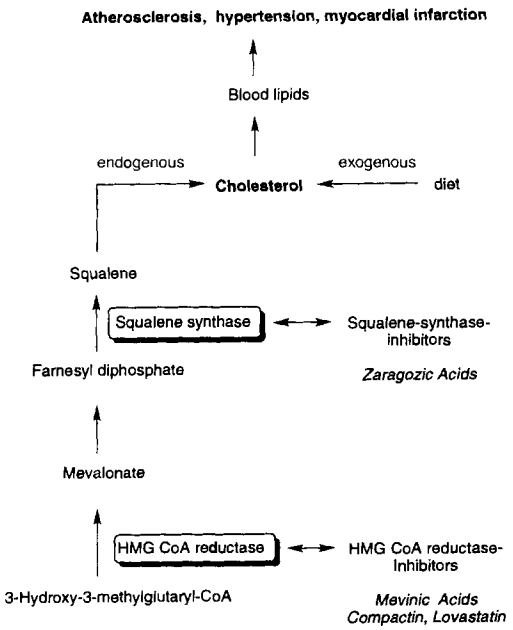
 © VCH Verlagsgesellschaft mbH, D-69451 Weinheim, 1995 0570-0833/95/0707-0772 $ 10.00+.25/0

[5] a) D. Voet, J. G. Voet, *Biochemistry*, Wiley, New York, **1990**; b) A. L. Lehninger, D. L. Nelson, M. M. Cox, *Principles of Biochemistry*, 2nd ed., Worth, New York, 1993, p. 554; c) L. Stryer, *Biochemistry*, Freeman, New York, **1988**, p. 406.
[6] T. H. Stevens, C. T. Martin, H. Wang, G. W. Brudvig, C. P. Scholes, S. I. Chan, *J. Biol. Chem.* **1982**, *257*, 12106.
[7] G. C. M. Steffens, R. Bielwald, G. Buse, *Eur. J. Biochem.* **1987**, *164*, 295.
[8] H. Jin, H. Thomann, C. L. Coyle, W. G. Zumft, *J. Am. Chem. Soc.* **1989**, *111*, 4262.
[9] a) P. M. H. Kroneck, W. E. Antholine, D. H. W. Kastrau, G. Buse, G. C. M. Steffens, W. G. Zumft, *FEBS Lett.* **1990**, *268*, 274; b) W. E. Antholine, D. H. W. Kastrau, G. C. M. Steffens, G. Buse, W. G. Zumft, P. M. H. Kroneck, *Eur. J. Biochem.* **1992**, *209*, 875.
[10] W. Kaim, M. Moscherosch, *J. Chem. Soc. Faraday Trans.* **1991**, *87*, 3185.
[11] a) S. J. Lippard, *Angew. Chem.* **1988**, *100*, 353; *Angew. Chem. Int. Ed. Engl.* **1988**, *27*, 344; b) K. Wieghardt, *ibid.* **1989**, *101*, 1179 and **1989**, *28*, 1153.
[12] P. Lappalainen, M. Saraste, *Biochim. Biophys. Acta* **1994**, *1187*, 222.
[13] a) R. K. Chadha, R. Kumar, D. G. Tuck, *Can. J. Chem.* **1987**, *65*, 1336; b) A. Stange, W. Kaim, *Z. Naturforsch. B* **1995**, *50*, 115.
[14] Review on the problem of $d^{10}\cdots d^{10}$ interactions in multinuclear complexes of the coinage metals: J. Strähle in *Unkonventionelle Wechselwirkungen in der Chemie metallischer Elemente* (Ed.: B. Krebs), VCH, Weinheim, **1992**, p. 357.

Total Syntheses of Zaragozic Acid

Ulrich Koert*

Who is nowadays not aware of the negative effects on health of high cholesterol levels in blood? Atherosclerosis, hypertension, and myocardiac infarction can be the consequences of this metabolic disturbance (Scheme 1).[1] On the one hand the



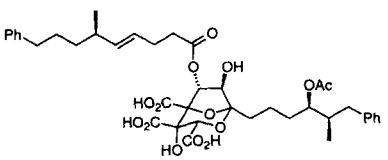
Scheme 1. Cholesterol in the human body: endogeneous build up, exogeneous introduction, and pathological consequences.

diet influences the cholesterol level exogenously, on the other hand the body builds up cholesterol endogenously. The biosynthetic pathway of cholesterol begins with a branching of the citric acid cycle. Starting from 3-hydroxy-3-methylglutaryl-(HMG)-CoA, farnesyldiphosphate is formed via mevalonate. The coupling of two molecules of farnesyldiphosphate yields squalene, which is then converted into cholesterol.

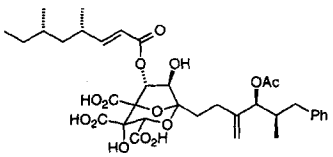
[*] Dr. U. Koert
Fachbereich Chemie der Universität
Hans-Meerwein-Strasse, D-35032 Marburg (Germany)
Telefax: Int. code + (6421)288917

If this endogenous production of cholesterol could be reduced, it would be of significant therapeutic use. With the discovery of the mevinic acids almost 15 years ago, an enzyme inhibitor for an enzyme participating in cholesterol biosynthesis, namely HMG-CoA reductase, was found for the first time. Today lovastatin, simvastatin, and pravastatin are standard components of the battery of pharmaceuticals.

Now a group of recently discovered natural products that inhibit another enzyme, squalene synthase, has become the focal point of attention: the zaragozic acids. In 1992 researchers at Merck, Sharp and Dohme,[2] and Glaxo[3] independently reported the discovery of a new family of natural products with squalene synthase inhibiting properties. The Merck group gave the new compounds the name zaragozic acids after the Spanish city of Zaragoza in which they had been found for the first time in fungal cultures. The Glaxo researchers named the new compounds squalestatins after their squalene synthase inhibiting effect.



Zaragozic Acid C 1



Zaragozic Acid A 2
(Squalestatin S1)

Representative compounds of this new group of natural products are zaragozic acid C (**1**) and zaragozic acid A (**2**) (= squalestatin S1). All zaragozic acids share a common 2,8-dioxabicyclo[3.2.1]octane skeleton (Fig. 1a), which is extremely polar as a result of three carboxyl groups in positions 3, 4, and 5 as well as three hydroxyl groups at C4, C6, and C7. An alkyl side chain (CH_2-C1-SK) is found at C1 and a fatty acid side chain at C6-O (C6-O-SK-CO). The spatial arrangement of the three COOH groups and the OH group at C4 is remarkable. This arrangement of functionalities corresponds to that of a citric acid molecule (Fig. 1b) in a frozen conformation. Thus, the binding site of squalene synthase for zaragozic acids could be one for citric acid.

 © VCH Verlagsgesellschaft mbH, D-69451 Weinheim, 1995 0570-0833/95/0707-0773 $ 10.00+.25/0

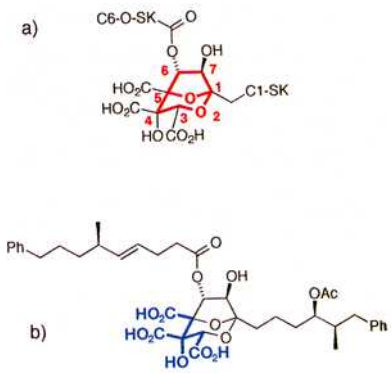


Fig. 1. a) Structure of the zaragozic acids with the 2,8-dioxabicyclo[3.2.1]octane skeleton (red); b) conformationally frozen citric acid partial structure (blue) in zaragozic acid C.

The biological activity of zaragozic acids and the complexity of their structures have attracted the attention of numerous synthetic chemists within a very short space of time.[4] At the end of 1994, three total syntheses were published: one by Carreira et al. (zaragozic acid C),[5] one by Nicolaou et al. (zaragozic acid A),[6] and one by Evans et al., which was carried out in collaboration with researchers at Merck, Sharp and Dohme (zaragozic acid C).[7] These three syntheses are compared in this highlight.

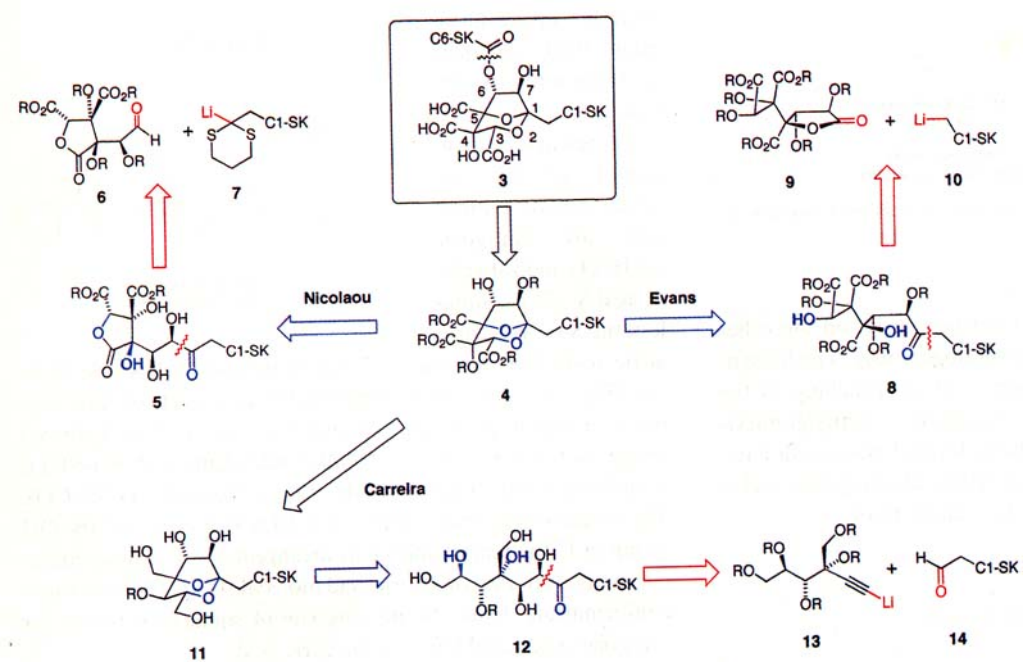
Scheme 2 shows the three retrosyntheses of zaragozic acids **3**. All three research groups introduce the acyl side chain at C6-O as the last step. Thus, the alcohol **4** is obtained as the precursor of the complete molecular skeleton **3**.

Apart from that, the synthetic pathways differ. Nicolaou derives the dioxabicyclo[3.2.1]octane skeleton from the ketone **5**, which can be split into the two building blocks **6** and **7** by cleavage of the C1–C7 bond. The synthetic strategy of Evans regards the ketone **8** as the precursor of the dioxabicyclo[3.2.1]octane **4**. The retrosynthetic cut between C1 and the adjacent C atom of the C1 side chain yields the building blocks **9** and **10**. These two syntheses have the common feature that the dioxabicyclo[3.2.1]octane is constructed inclusive of the carboxyl functions. A different route was followed by Carreira. In this the three carboxyl groups are introduced after the completion of the dioxabicyclo[3.2.1]octane. Thus, compound **4** is traced back to the tetraol **11**, which should be accessible from the acyclic precursor **12**. The cleavage of the C1–C7 bond leads to the building blocks **13** and **14**. Compared with the strategies of Nicolaou and Evans, Carreira thus has the chance to rapidly assemble the dioxabicyclo[3.2.1]octane. However, as it turned out the construction of the three carboxyl functions requires a considerable number of steps at the end of the synthesis. In all three syntheses, the dioxabicyclo[3.2.1]octane skeleton is obtained by acetal formation of a 4,6-dihydroxyketone by using standard procedures. The efficiency with which the acyclic precursors **5**, **8**, and **12** with their five stereogenic centers can be assembled will be important in the assessment of the syntheses.

The synthesis of zaragozic acid A[5] by Nicolaou is summarized in Schemes 3–7. Four of the five stereogenic centers are constructed by two stereoselective Sharpless dihydroxylations (Scheme 3). In the first, the diene **20**, which is synthesized in a few steps from the simple building blocks **15**–**18**, is converted enantioselectively to give the diol **21** (20% yield, 78% *ee*); in the second the olefin **23** is diastereoselectively dihydroxylated, and the product undergoes spontaneous lactonization to give **24** (83% yield, as a single diastereomer after crystallization).

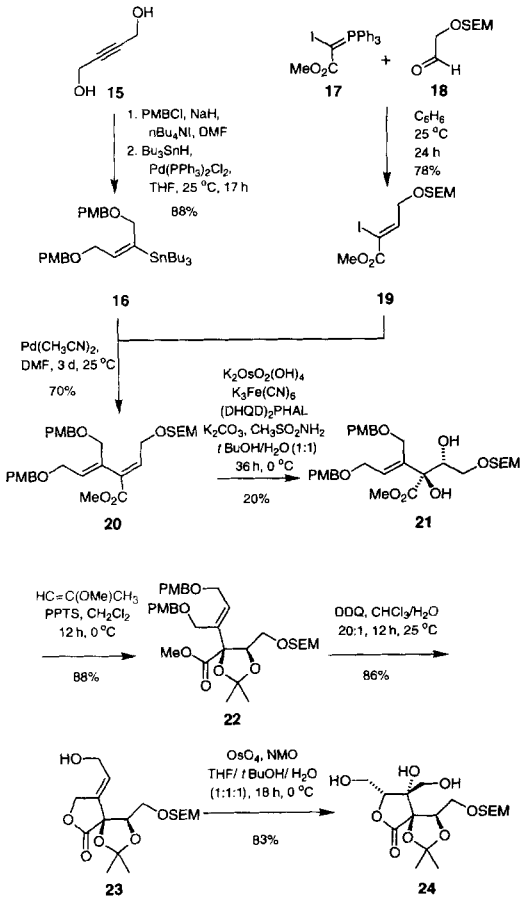
In the subsequent 12 steps (Scheme 4) the two primary alcohol functions in **24** are oxidized to carboxyl functions and protected as benzyl esters. After trimethylsilyl(TMS)-protection of the OH group at C4 Nicolaou then obtains the aldehyde **30**. Addition of the lithium compound prepared from the dithiane **31** to the C1 side chain (Scheme 5) of **30** delivers, with the formation of the alcohol **32**, the missing fifth stereogenic center. This addition is however unselective: two epimeric alcohols are formed (total yield 75% in a 1:1 ratio) and must be separated by chromatography. Removal of the thioacetal function in **33** leads to the hemiacetal **34**.

Under carefully worked out acidic conditions the lactone hemiacetal **34** rearranges into the dioxabicyclo[3.2.1]octane **35** (Scheme 6). By changing the alcohol protecting group and exchanging the methyl ester for a benzyl ester the diol **38a** is

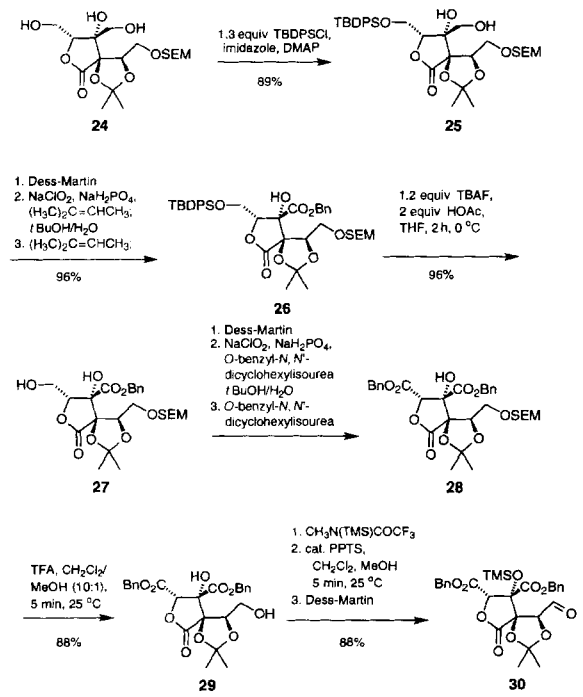


Scheme 2. Comparison of the retrosyntheses of zaragozic acids by Nicolaou, Carreira, and Evans.

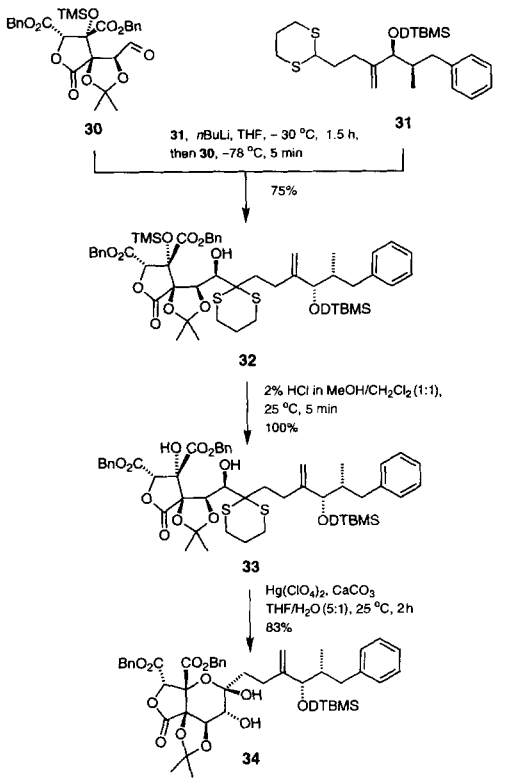
 © VCH Verlagsgesellschaft mbH, D-69451 Weinheim, 1995 0570-0833/95/0707-0774 $ 10.00+.25/0



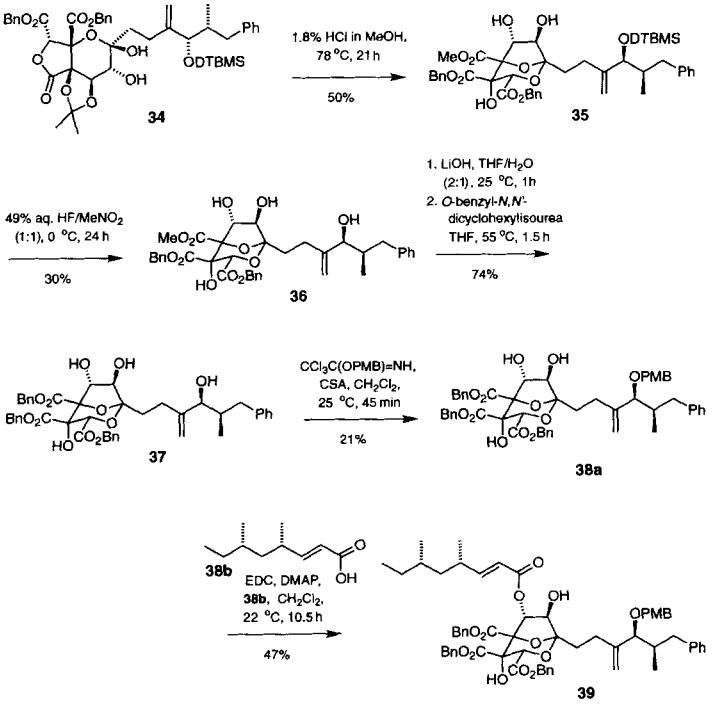
Scheme 3. Total synthesis of zaragozic acid A (**2**) by Nicolaou, part 1. PMB = *para*-methoxybenzyl, DMF = dimethylformamide, SEM = 2-(trimethylsilyl)ethoxymethyl, $(DHQD)_2PHAL$ = phthalazindiylbis(dihydroquinidine), PPTS = pyridinium *para*-toluenesulfonate, DDQ = 2,3-dichloro-5,6-dicyano-1,4-benzoquinone, NMO = *N*-methylmorpholinoxide.



Scheme 4. Total synthesis of zaragozic acid A (**2**) by Nicolaou, part 2. TBDPS = *tert*-butyldiphenylsilyl, DMAP = 4-dimethylaminopyridine, TBAF = tetra-*n*-butylammonium fluoride, TMS = trimethylsilyl.

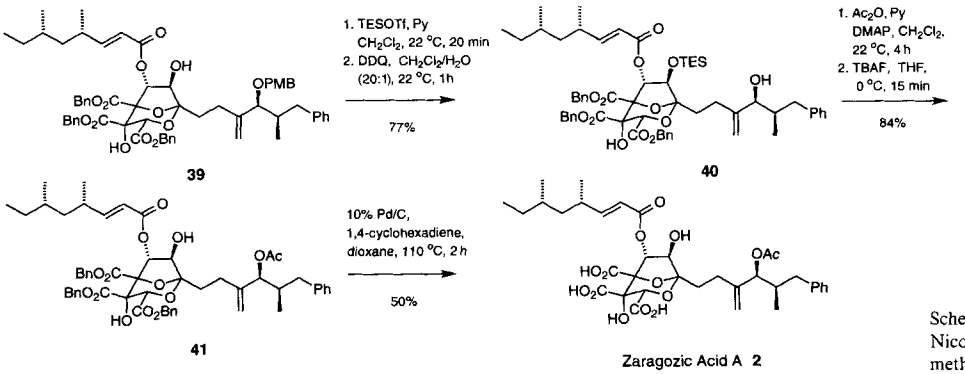


Scheme 5. Total synthesis of zaragozic acid A (**2**) by Nicolaou, part 3. DTBMS = di-*tert*-butylmethylsilyl.

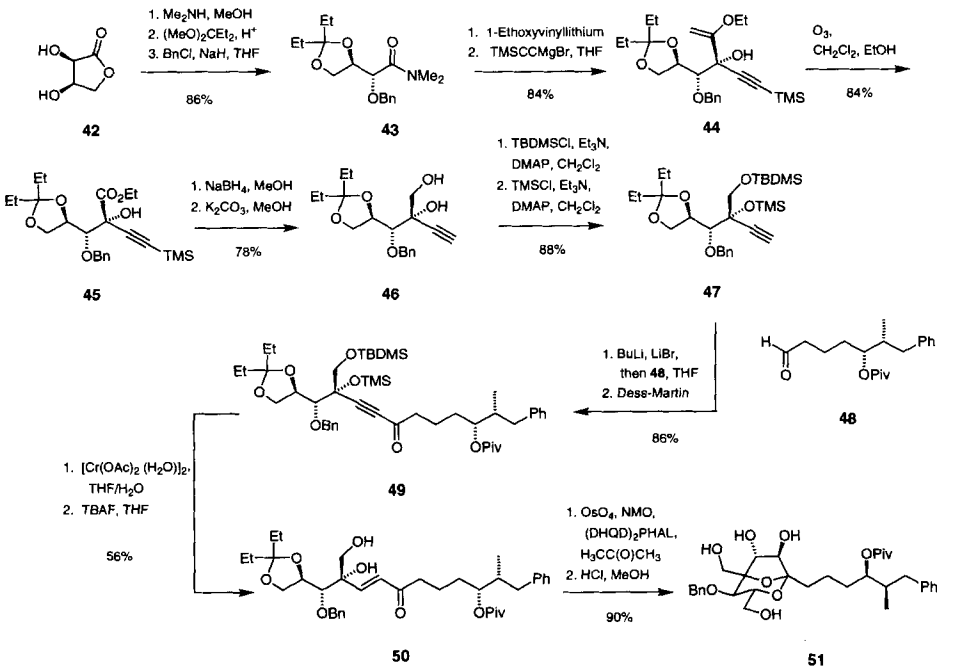


Scheme 6. Total synthesis of zaragozic acid A (**2**) by Nicolaou, part 4. CSA = camphorsulfonic acid, EDC = 1-ethyl-3-(3-dimethylaminopropyl)carbodiimide.

obtained, whose C6-OH function is esterified with the carboxylic acid **38b** leading to the formation of the tetraester **39**. The latter already contains the complete skeleton of zaragozic acid A. In this esterification the C6- and the C7-OH group can



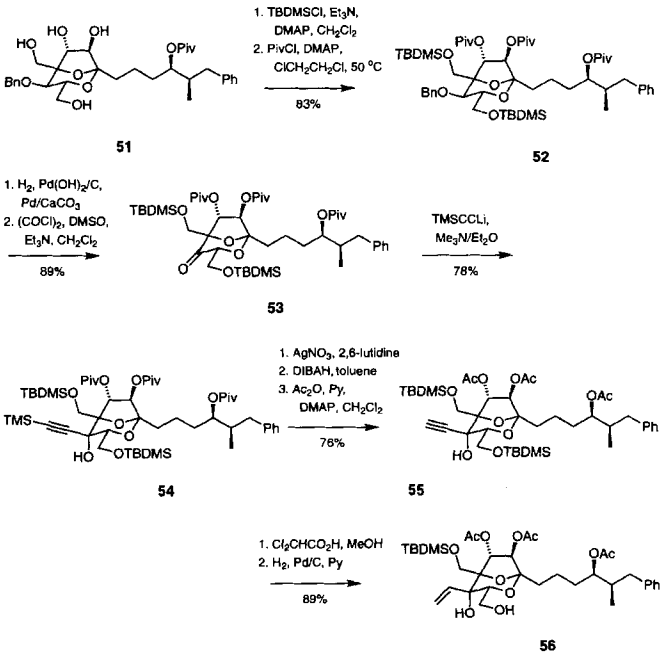
Scheme 7. Total synthesis of zaragozic acid A (**2**) by Nicolaou, part 5. TES = triethylsilyl, OTf = trifluoromethanesulfonate = triflate, Py = pyridine.



Scheme 8. Total synthesis of zaragozic acid C (**1**) by Carreira, part 1. TBDMS = *tert*-butyldimethylsilyl, Bn = $PhCH_2$.

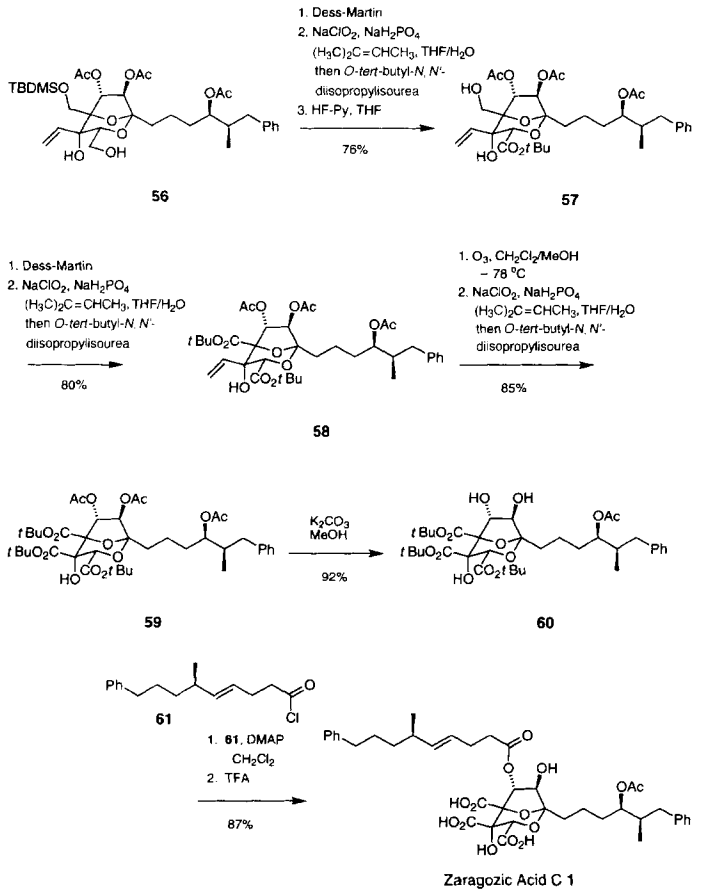
react. The selectivity of 3:2 in favor of the desired C6-OH group established by Nicolaou is rather low. Starting from **39** protecting group manipulations (5 steps, Scheme 7) gave the target compound zaragozic acid A (**2**).

The synthesis of zaragozic acid C (**1**) by Carreira[6] is given in Schemes 8–10. This synthesis starts from D-erythronic γ-lactone (**42**), a compound from the chiral pool.[8] An impressive feature of the synthesis is the conversion of the amide **43** into the alcohol **44** (Scheme 8): The reaction of ethoxyvinyllithium with the dimethylamide **43** can be stopped at the ketone intermediate. The subsequent reaction of the carbonyl function with the organomagnesium compound prepared from TMS–C≡CH proceeds stereoselectively (20:1). The vinyl ether group in **44** is a latent ester function: the ozonolysis of **44** in ethanol affords the ethyl ester **45**. Subsequently the terminal acetylene **47** is obtained via **46** by a standard sequence. The C1 side chain is attached through the coupling of **47** with the aldehyde **48** to give the ketone **49**. The two stereogenic centers still missing are produced by Sharpless dihydroxylation of the olefin **50** obtained after the oxidation and removal of the silyl protecting groups. Without a chiral ligand stereoselectivity cannot be achieved in this bishydroxylation step. With a chiral ligand, the diol is formed in a reagent-controlled reaction in the ratio 64:36 in



Scheme 9. Total synthesis of zaragozic acid C (**1**) by Carreira, part 2. Piv = pivaloyl, DMSO = dimethyl sulfoxide, DIBAH = diisobutylaluminum hydride.

 © VCH Verlagsgesellschaft mbH, D-69451 Weinheim, 1995 0570-0833/95/0707-0776 $ 10.00+.25/0



Scheme 10. Total synthesis of zaragozic acid C (1) by Carreira, part 3. TFA = trifluoroacetic acid.

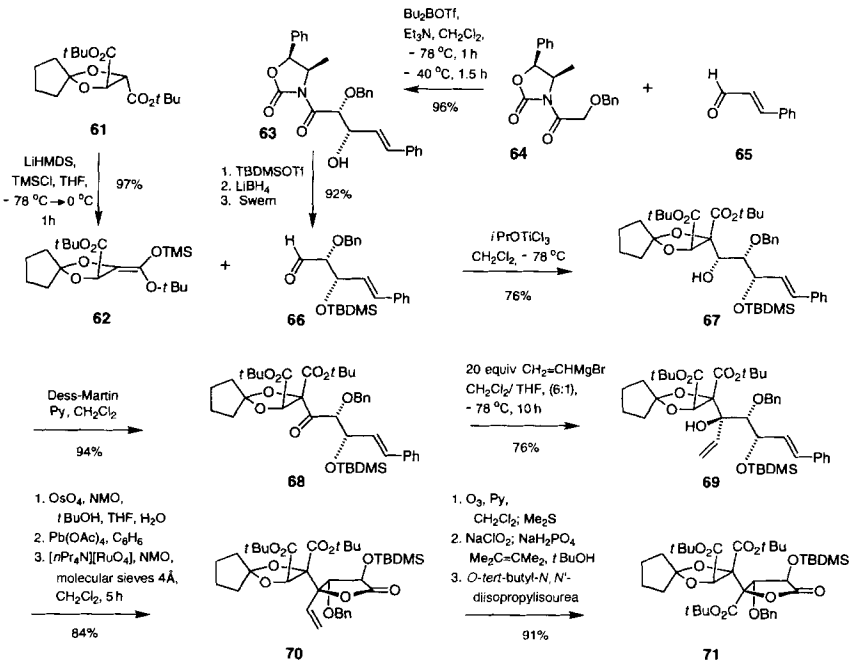
favor of the desired stereoisomer. In the subsequent synthetic step, the diol is cyclized under acidic conditions to give the dioxabicyclo[3.2.1]octane acetal (**51**).

To construct the missing quaternary center C4 Carreira transforms the compound **51** into the ketone **53** (Scheme 9). The addition of lithiated TMS–C≡CH to the carbonyl function of **53** to give the alcohol **54** is achieved with a stereoselectivity of 86:14. At this stage the pivaloyl protecting groups are replaced by acetyl protecting groups and the triple bond is reduced to a double bond to give compound **56**.

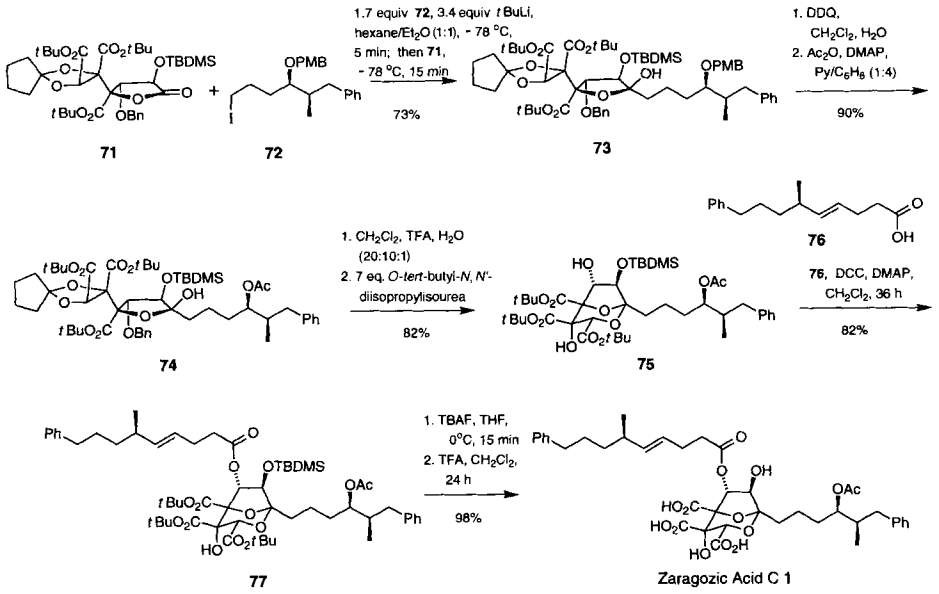
Carreira now oxidizes the two primary alcohol groups sequentially to give the carboxyl functions (**56** → **57** → **58**, Scheme 10). The third carboxyl function is formed by ozonolysis and subsequent oxidation of the aldehyde (**58** → **59**). This is followed by a remarkably selective hydrolysis of the triacetate **59** to give the monoacetate **60** in 92% yield(!). With regard to his final step, the introduction of the acyl side chain at C6-O, Carreira faces the same problem as Nicolaou: how can the C6-OH group be esterified selectively in the presence of the free C7-OH group? Carreira is unable to provide a satisfactory solution to the selectivity problem. From the reaction of the diol **60** with the acid chloride **61** he obtains the regioisomeric esters in the ratio 3:1 in favor of the undesired isomer. The desired isomer can be isolated by chromatography and after acidic hydrolysis of the *tert*-butyl esters the target compound zaragozic acid C (**1**) is obtained.

The total synthesis of zaragozic acid C (**1**) by Evans[7] is shown in Schemes 11 and 12. Evans identified a tartaric acid unit in the C3-C4 partial structure of zaragozic acid. Accordingly, his synthesis commences from a tartaric acid derivative (Scheme 11). The enantiomerically pure acetal **61** is readily accessible from di-*tert*-butyl D-tartrate. This is transformed into the silylketene acetal **62**, which reacts in a Lewis acid catalyzed aldol addition with the aldehyde **66** to give the adduct **67**. The aldehyde **66** was prepared stereoselectively with the oxazolidinone method developed by Evans (**64** + **65** → **63** → **66**). The Dess–Martin oxidation of **67** yields the ketone **68**. Addition of vinylmagnesium bromide to the keto-carbonyl function in **68** leads to the stereocontrolled construction of the quaternary center C5 with the formation of **69**. The stereochemical course of this addition can be explained with a chelate-controlled transition state controlled by the adjacent benzyl ether. Next, Evans transforms the styryl group in **69** oxidatively into a carboxyl function and closes the butyric lactone ring to give **70**. By the sequence **70** → **71** the vinyl group is transformed into the missing third carboxyl function of the zaragozic acid skeleton.

In the further course of the synthesis (Scheme 12) Evans attaches the side chain to C1 by the reaction of the organolithium compound accessible from the iodide **72** with the lactone **71** under the formation of **73**. The replacement of the *para*-methoxybenzyl(PMB) protecting group with an acetyl group yields the hemiacetal **74**. Subsequently, the hemiacetal **74** is converted under acidic conditions into the dioxabicyclo[3.2.1]octane **75**. With wise foresight the C7-OH group has been protected since



Scheme 11. Total synthesis of zaragozic acid C 1 by Evans, part 1. HMDS = 1,1,1,3,3,3-hexamethyldisilazanide.



Scheme 12. Total synthesis of zaragozic acid C (**1**) by Evans, part 2. DCC = dicyclohexylcarbodiimide, TFA = trifluoroacetic acid.

the beginning of the synthesis as a silyl ether with the result that the problem of selectivity between C6-OH and C7-OH does not arise in the following acylation step. The acyl side chain can thus be attached to C6-O without any problems: the reaction of the alcohol **75** with the carboxylic acid **76** affords the desired ester **77** in 82% yield. The deprotection of **77** to give the target compound zaragozic acid C (**1**) is almost quantitative.

A discussion of the preparation of the C1 side chains and the C6-O carboxylic acid, which was also effected by the three research groups by different methods, is not within the scope of this highlight. The interested reader should refer to the information in the original literature.[4d, 4e, 5–7]

All three total syntheses of zaragozic acid are examples of modern, efficient syntheses of natural products. The comparison of the number of steps and the overall yields of different synthetic routes always difficult and of only limited value. The longest linear sequence as a measure for the number of steps for the presented syntheses is 33 (Nicolaou), 36 (Carreira), and 21 steps (Evans). The overall yields are calculated to be 1 (Nicolaou), 1 (Carreira), and 15% (Evans). Noteworthy in the synthesis by Evans is the highly selective formation of each new stereogenic center. The stereo- and regioselectivities of some of the steps in the syntheses by Nicolaou and Carreira will surely be improved. The two research groups of Carreira and Nicolaou have been the first cross the finish line in the race for the total synthesis of zaragozic acids.

German version: *Angew. Chem.* **1995**, *107*, 849

Keywords: natural products · zaragozic acids · squalestatins · total syntheses

[1] M. S. Brown, J. L. Goldstein in *The Pharmacological Basis of Therapeutics*, 8th ed. (Eds.: A. Goodman Gilman, T. W. Rall, A. S. Nies, P. Taylor), McGraw-Hill, New York, **1993**, p. 874.

[2] K. E. Wilson, R. M. Burk, T. Biftu, R. G. Ball, K. Hoogsteen, *J. Org. Chem.* **1992**, *57*, 7151; J. D. Bergstrom, M. M. Kurtz, D. J. Rew, A. M. Amend, J. D. Karkas, R. G. Bosteor, V. S. Bansal, C. Dufresne, F. L. VanMiddlesworth, O. D. Hensens, J. M. Liesch, D. L. Zink, K. E. Wilson, J. Onishi, J. A. Milligan, G. Bills, L. Kaplan, M. Nallin Omstead, R. G. Jenkins, L. Huang, M. S. Meinz, L. Quinn, R. W. Burg, T. Biftu, R. G. Ball, K. Hoogsteen, *Proc. Natl. Acad. Sci. USA* **1993**, *90*, 80; C. Dufresne, K. E. Wilson, S. B. Singh, D. L. Zink, J. D. Bergstrom, D. Rew, J. D. Polishook, M. Meinz, L. Huang, K. C. Silverman, R. B. Lingham, M. Mojena, C. Cascales, F. Pelaez, J. B. Gibbs, *J. Nat. Prod.* **1993**, *56*, 1923.

[3] J. M. Dawson, J. E. Farthing, P. S. Marshall, R. F. Middleton, M. J. O'Neill, A. Shuttleworth, C. Stylli, R. M. Tait, P. M. Taylor, H. G. Wildman, A. D. Buss, D. Langley, M. V. Hayes, *J. Antibiot.* **1992**, *45*, 639; P. J. Sidebottom, R. M. Highcock, S. J. Lane, P. A. Procopiou, N. S. Watson, *ibid.* **1992**, *45*, 648; W. M. Blows, G. Foster, S. J. Lane, D. Noble, J. E. Piercey, P. J. Sidebottom, G. J. Webb, *ibid.* **1994**, *47*, 740.

[4] a) V. K. Aggarwal, M. F. Wang, A. Zaparucha, *J. Chem. Soc. Chem. Commun.* **1994**, 87; b) R. W. Gable, L. M. McVinish, M. A. Rizzacasa, *Aust. J. Chem.* **1994**, *47*, 1537; c) H. Abdel-Rahman, J. P. Adams, A. L. Boyes, M. J. Kelly, D. J. Mansfield, P. A. Procopiou, S. M. Roberts, D. H. Slee, N. S. Watson, *J. Chem. Soc. Chem. Commun.* **1993**, 1839; synthesis of the C1 side chains of zaragozic acids A and C: d) A. J. Robichaud, G. D. Berger, D. A. Evans, *Tetrahedron Lett.* **1993**, *34*, 8403; synthesis of the acyl side chain at C6-O of zaragozic acid C: e) C. Santini, R. G. Ball, G. D. Berger, *J. Org. Chem.* **1994**, *59*, 2261.

[5] E. M. Carreira, J. DuBois, *J. Am. Chem. Soc.* **1994**, *116*, 10825.

[6] a) K. C. Nicolaou, E. W. Yue, Y. Naniwa, F. De Riccardis, A. Nadin, J. E. Leresche, S. La Greca, Z. Yang, *Angew. Chem.* **1994**, *106*, 2306; *Angew. Chem. Int. Ed. Engl.* **1994**, *33*, 2184; b) K. C. Nicolaou, A. Nadin, J. E. Leresche, S. La Greca, T. Tsuri, E. W. Yue, Z. Yang, *ibid.* **1994**, *106*, 2309 and **1994**, *33*, 2187; c) K. C. Nicolaou, A. Nadin, J. E. Leresche, E. W. Yue , S. La Greca, *ibid.* **1994**, *106*, 2312 and **1994**, *33*, 2190.

[7] D. A. Evans, J. C. Barrow, J. L. Leighton, A. J. Robichaud, M. Sefkov, *J. Am. Chem. Soc.* **1994**, *116*, 12111.

[8] The authors indicate that the relatively expensive D-erythronic γ-lactone (**42**) (44.50 DM per gram (Aldrich)) can also be readily made from the less expensive D-isoascorbic acid.

Modeling the Remote-Controlled Organization of Particles in a Nanodimensional Cavity: Synthesis and Properties of $(Et_3NH)_3(tBuNH_3)_2Na_2[(H_2O)_2,N_3^- \subset V_{14}O_{22}(OH)_4(PhPO_3)_8]\cdot 6H_2O\cdot 2DMF$

Achim Müller,* Kai Hovemeier, Erich Krickemeyer, and Hartmut Bögge

Dedicated to Professor F. Albert Cotton on the occasion of his 65th birthday

One of the most important aspects for the future of chemical research is the examination of the experimental conditions under which it is possible to construct arrangements of higher complexity from simple building blocks, if possible, with tailor-made structural and functionality features. The aim of such experiments is not only to improve the understanding of the extreme complexity of natural processes, but also to synthesize molecular materials with desired properties. In this context, reactions in which the organization of weakly interacting species in an isolated system are influenced "from outside" are of interest, too. These problems are current topics in the field of supramolecular chemistry.[1-3]

The treatment of vanadium pentoxide with *tert*-butylamine, triethylamine (both as deprotonating agents), and hydrazine hydrate as reducing agent in the presence of sodium azide and phenylphosphonic acid produces the unusual host–guest compound **1** in a mixture (2.5:1) of water and *N*,*N*-dimethylformamide (DMF).

$(Et_3NH)_3(tBuNH_3)_2Na_2[(H_2O)_2, N_3^- \subset V_{14}O_{22}(OH)_4(PhPO_3)_8]\cdot 6H_2O\cdot 2DMF$

1

The compound has a closed, nanodimensional cavity and two external, open truncated cones or, in other words, ion channels formed by phenyl rings (Fig. 1a). The fundamental significance of the truncated cones is that the exchange of their contents enables a systematic study of the resulting influence on the organization of the guests in the cavity. Compound **1** was characterized by a single-crystal X-ray structure analysis,[4] bond valence sum calculations,[5] magnetochemical measurements, IR, Raman, and UV/Vis/NIR spectroscopy, elemental analysis, and manganometric titration of the V^{IV} centers.[4] Only the neutral molecules and anions occupying the central cavity of **1** are considered as included guests, and not those located in the truncated cones and coronands, that is, those on the outside wall of the host. (The nucleophilic [16]crown-8 type coronand is built from four $PhPO_2$ units and four vanadium atoms.[6, 7]) In the central cavity ten electron density maxima are found within the horizontal plane of symmetry, forming an approximate ellipse. Two H_2O molecules and an N_3^- ion lie disordered in these ten positions (Fig. 1a). The disordering is a consequence of the size of the cavity and the resulting weak interactions of the guests with the host (cf. the interpretation of the IR spectrum). In each truncated cone a Na^+ ion coordinated to two H_2O and one DMF molecules is located in such a way that the distorted octahedral coordination sphere of the Na^+ ion is completed by two O atoms of the coronand and the H_2O molecule in the center of the coronand (Fig. 2).

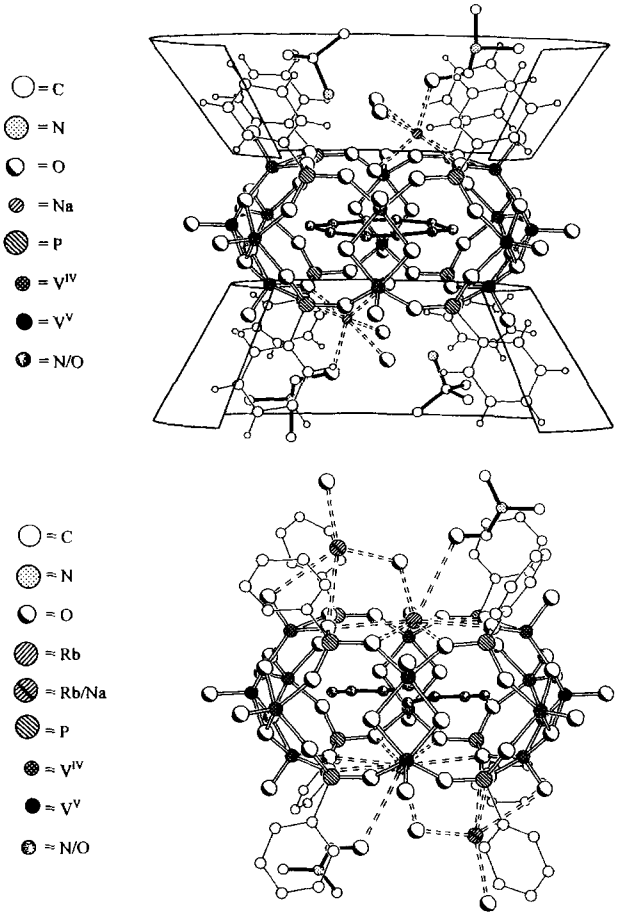


Fig. 1. a) Structure of the anion in crystals of **1** with two Na^+ and two $tBuNH_3^+$ ions, as well as six H_2O and two DMF molecules in the truncated cones (indicated schematically as cones from which a window has been cut out). b) Structure of the anion of **2** with one Na^+ and three Rb^+ ions as well as four H_2O and two DMF molecules in the truncated cones. The view in both cases is approximately along an idealized C_2 axis. Characteristic distances [pm]: **1**: Na-O(H_2O) 227.9–298.5, Na-O(DMF) 232.5, N($tBuNH_3$)-O(H_2O) 282.0, 285.9; **2**: Rb-O (coronand) 307.8–374.0, Rb-O(H_2O) 292.2, Rb-O(DMF) 357.5, Rb/Na-O(H_2O) 271.3, 287.8.

Treatment of **1** with about a thirteenfold excess of RbBr (the diameter of Rb^+ corresponds approximately to that of the coronand) in a 1:1.3 mixture of H_2O and DMF yields compound **2** (Fig. 1b). This shows that the exchange of the guests in the truncated cones of **1** has led to a reorganization and migration

$Et_3NH(tBuNH_3)_2(0.5\,Rb, 0.5\,Na)_2Rb_2[(H_2O)_2, N_3^- \subset V_{14}O_{22}(OH)_4(PhPO_3)_8]\cdot 10\,H_2O\cdot 2DMF$ **2**

[*] Prof. Dr. A. Müller, Dipl.-Chem. K. Hovemeier, E. Krickemeyer, Dr. H. Bögge
Fakultät für Chemie der Universität
Lehrstuhl für Anorganische Chemie I
Postfach 100131, D-33501 Bielefeld (Germany)
Telefax: Int. code + (521) 106-6003

 © VCH Verlagsgesellschaft mbH, D-69451 Weinheim, 1995 0570-0833/95/0707-0779 $ 10.00+.25/0

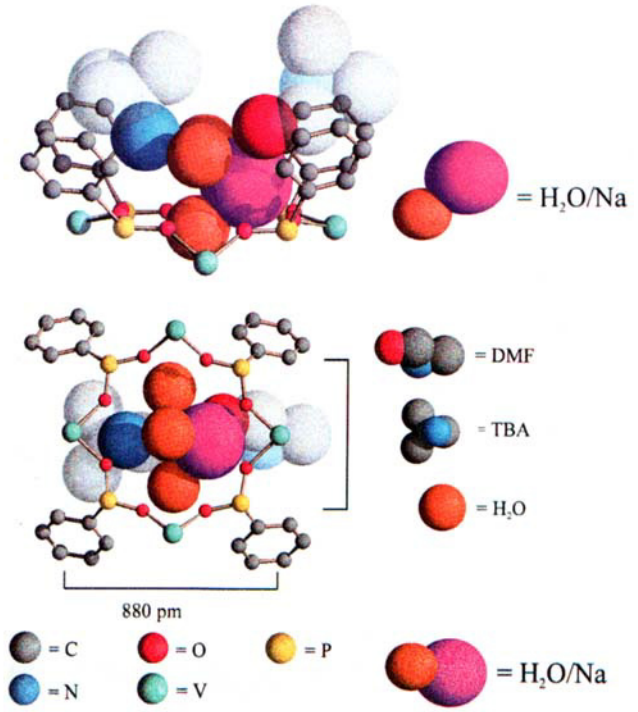


Fig. 2. Illustration of the arrangement of the particles in a truncated cone of **1**, in which the exchangeable particles that control the organization in the cavity (H_2O/Na^+; in **2** replaced by Rb^+) are emphasized. The view at the top is approximately parallel to the coronand plane, while that at the bottom is perpendicular to it, looking from the center of the cavity in the direction of the coronand.

of the particles in the cavity. In the horizontal plane of symmetry are now eight electron density maxima, which can be divided into two almost L-shaped groups (reproducible in several independent measurements with different single crystals! Fig. 1b).

A Rb^+ ion can now be found in the center of the coronand of **2**, as expected, instead of the H_2O molecule in **1**; this cation has an optimal "fit" because of its size. It is linked to a second Rb^+ ion by a bridging H_2O molecule. This ion takes the position of the tBuNH$_3^+$ ion of **1** (the position is occupied to about 50% by a Na^+ ion). The approximate square-pyramidal environment for the second Rb^+ ion is completed by two μ_2-O atoms of the coronand, a terminal O atom of the $\{V_5O_9\}^{3+}$ unit, and another H_2O molecule. The site of the DMF molecule remains almost the same as in **1**.

An important aspect is that the exchange of the content of the truncated cones and in particular of the H_2O molecule in the center of the coronand of **1** by a Rb^+ ion in **2** leads to a significant reorganization and migration of the particles in the central cavity that can be easily understood. During the reaction a H_2O molecule moves from its position in **1** to the bridging position between two V centers in **2**. Furthermore, the N_3^- ion "sets itself up" between the electrophilic centers (a V^V atom of the $\{V_5O_9\}^{3+}$ unit and a Rb^+ ion in the center of the coronand) (Fig. 1b).

The only weak interaction of the N_3^- ion with the host and its presence in the cavity is distinctly evident from the half width of the characteristic ν_{as}(NNN) band of compounds **1** and **2** at 2043 and 2044 cm^{-1}, respectively, which is only about a tenth of that in the corresponding alkali metal salts. In this context we must point out the possibility of using such compounds as ion cages, for example for spectroscopic studies.[8]

Compound **1**, whose anionic host part is soluble in organic solvents without decomposition, is apparently a suitable starting compound for further studies, because the contents of the truncated cone, and in particular the Na^+ ion that is slightly too small for the coronand, can easily be exchanged. The ambivalent cage system has an extremely high formation tendency, and on account of its size and the presence of a nucleophilic and an electrophilic component it can accommodate very different guests like NH_4^+, K^+, Rb^+, H_2O, MeCN, MeOH, Cl^-, Br^-, N_3^-, and even fragments of ion lattices.[6, 9] In our opinion these features enable further fundamental investigations into the influence of different "external fields" on the type of organization of diverse particles in the cavity of **1**, that is, the attempt to assess the extent of their control from the truncated cone. Controlled interactions of the type described here may be regarded as models for processes in ion channels in both the biological and the inanimate world. They might, however, also be relevant for the understanding of interactions between hydrophilic regions of proteins, their active metal cluster sites or their ligands, and substrates. Since, for instance, the N_3^- ion is a substrate of nitrogenase and some H_2O molecules fill the space between the homocitrate ligand of the FeMo cluster and the protein,[10] the relevance to this topical field is apparent. Of fundamental, general interest is certainly the fact that here the study of intermolecular interactions that are important, for instance, for molecular epigenesis is possible within smaller aggregates in a quasi-closed system.

Experimental Procedure

1: A mixture of V_2O_5 (1.10 g, 6.1 mmol), tBuNH$_2$ (1 mL), Et_3N (1 mL), H_2O (50 mL), and DMF (20 mL) was vigorously stirred in a 100 mL wide-necked Erlenmeyer flask at 60 °C until a grey-green solution formed. After addition of NaN_3 (1.00 g, 15.4 mmol), $PhPO_3H_2$ (2.00 g, 12.7 mmol), and N_2H_5OH (0.18 mL, 3.8 mmol), the volume of the then dark green solution was reduced to 50 mL under stirring at 60 °C, filtered, and cooled to room temperature. The resulting green crystals (which weathered slowly out of the mother liquor, but were soluble without decomposition in DMF and MeCN) were filtered off after 2–3 days (yield: 79% based on V).

2: A solution of **1** (520 mg, 162 μmol) and RbBr (340 mg, 2055 μmol) in a mixture of H_2O (4.5 mL) and DMF (6 mL) was heated at 80 °C with stirring for 10 min, filtered, cooled to room temperature, and allowed to stand in a closed vessel under an inert atmosphere to crystallize. The green crystals, which slowly weathered out of the mother liquor but were soluble without decomposition in DMF and MeCN, were filtered off after 3–4 days (yield: 53% based on V).

Received: October 7, 1994 [Z 73821E]
German version: *Angew. Chem.* **1995**, *107*, 857

Keywords: cage compounds · supramolecular chemistry · vanadium compounds

[1] J.-M. Lehn, *Angew. Chem.* **1988**, *100*, 91; *Angew. Chem. Int. Ed. Engl.* **1988**, *27*, 89; *ibid.* **1990**, *102*, 1347 and **1990**, *29*, 1304; J.-M. Lehn, *From Coordination Chemistry to Supramolecular Chemistry* in *Perspectives in Coordination Chemistry* (Eds.: A. F. Williams, C. Floriani, A. E. Merbach), VCH, Weinheim, **1992**, p. 447; R. Hoss, F. Vögtle, *Angew. Chem.* **1994**, *106*, 389; *Angew. Chem. Int. Ed. Engl.* **1994**, *33*, 375; F. Vögtle, *Supramolekulare Chemie*, 2nd ed., Teubner, Stuttgart, **1992**.

[2] J. S. Lindsey, *New J. Chem.* **1991**, *15*, 153.

[3] A. Müller, *Nature, (London)* **1991**, *352*, 115.

[4] **1**: Elemental analysis: $C_{80}H_{146}N_{10}Na_2O_{60}P_8V_{14}$, found (calcd): C 28.5 (29.9); H 4.8 (4.6); N 4.3 (4.4) (Kjehldahl); V^{IV} 19.6 (19.0); V 22.7 (22.2); Na 1.5 (1.4); H_2O 5.1 (4.5). Crystal structure analysis: $C2/c$, $a = 2697.9(5)$, $b = 2144.6(4)$, $c = 2292.4(5)$ pm, $\beta = 100.88(3)°$, $V = 13025(4) \times 10^6$ pm^3, $Z = 4$, $\varrho_{calcd} = 1.639$ g cm^{-3}; $2\theta_{max} = 54°$; solution with direct methods, $R = \sum \| F_0 | - | F_c \| / \sum | F_0 | = 0.081$ for 8809 independent reflections ($F_0 > 4\sigma(F_0)$). The compound $(Me_2NH_2)_5NH_4[2NH_4^+, 2Cl^- \subset V_{14}O_{22}(OH)_4(H_2O)_2(PhPO_3)_8] \cdot 5H_2O \cdot 4$ DMF [7] has a similar basic structure, but the contents of the truncated cone (or ion channel) is not exchangeable. **2**: Crystal structure analysis: $P2_1/n$, $a = 1703.5(3)$, $b = 2105.0(4)$, $c = 2032.2(4)$ pm, $\beta = 92.42(3)°$, $V = 7281(11) \times 10^6$ pm^3, $Z = 2$; $\rho_{calcd} = 1.489$ g cm^{-3}; $2\theta_{max} = 40°$; solution with direct methods, $R = \sum \| F_0 | - | F_c \| / \sum | F_0 | = 0.134$ for 2608 independent reflections ($F_0 > 4\sigma(F_0)$). The cationic lattice outside the host–guest construction has a large degree of disorder. On account of their sensitivity towards weathering, the crystals were embedded in silicon oil when removed from the mother liquor, and the measurements were performed at −80 °C (**1**) and −85 °C (**2**). Further details of the crystal structure investigation may be obtained from the Fach-

 © VCH Verlagsgesellschaft mbH, D-69451 Weinheim, 1995 0570-0833/95/0707-0780 $ 10.00+.25/0

informationszentrum Karlsruhe, D-76344 Eggenstein-Leopoldshafen (Germany) on quoting the depository number CSD-58689.

[5] Characterization of **1**: IR (KBr, some characteristic bands): $\tilde{\nu}$[cm^{-1}] = 2043 (m, ν_{as}, NNN), 1661 (m, δ, H_2O and ν, CO), 1474 (w, δ_{as}, CH_3), 1095 (vs, ν, PO_3), 998 (vs, ν, V = O_{term}). Characteristic bands in the Raman spectrum (solid, rotating pellet/λ_e = 488.0 nm): $\tilde{\nu}$[cm^{-1}] = 992 (w, ν, V = O_{term}). UV/Vis/NIR (in DMF): λ [10^{-3} cm^{-1}] = 33.0, 25.9 (π(O) → d(V) − CT), 14.3 (d(V) → d(V)). Magnetism (room temperature): μ_{eff}/anion = 5.19 μ_B and μ_{eff}/V^{IV} = 1.49 μ_B. The bond valence sum $\sum$ exp (−(R − R_0)/B) (R = V–O distance [pm], R_0 = 179 pm, B = 31.9 pm) is 4.9 for both V^V centers and 4.1 for the twelve V^{IV} centers (from I. D. Brown in *Structure and Bonding in Crystals, Vol. II* (Eds.: M. O'Keeffe, A. Navrotsky), Academic Press, New York, **1981**); see Fig. 1a. Characterization of **2**: IR (KBr, some characteristic bands): $\tilde{\nu}$[cm^{-1}] = 2044 (m, ν_{as}, NNN), 1661 (m, δ, H_2O and ν, CO), 1473 (w, δ_{as}, CH_3), 1094 (vs, ν, PO_3), 998 (vs, ν, V = O_{term}). Characteristic bands in the Raman spectrum (solid, rotating pellet/λ_e = 488.0 nm): $\tilde{\nu}$[cm^{-1}] = 992 (w, ν, V = O_{term}). UV/Vis/NIR (in DMF): λ[10^{-3} cm^{-1}] = 33.1, 25.9 (π(O) → d(V)-CT), 14.0 (d(V) → d(V)). The bond valence sum is 4.9 for both V^V centers and 4.1 for the twelve V^{IV} centers.

[6] A. Müller, K. Hovemeier, R. Rohlfing, *Angew. Chem.* **1992**, *104*, 1214; *Angew. Chem. Int. Ed. Engl.* **1992**, *31*, 1192.

[7] The compound $(Me_2NH_2)_5NH_4[2\,NH_4^+,\ 2\,Cl^- \subset V_{14}O_{22}(OH)_4(H_2O)_2(PhPO_3)_8] \cdot 5\,H_2O \cdot 4$ DMF encloses a fragment of the lattice of NH_4Cl in the central cavity and coronand; the truncated cone contains another three neutral molecules (two H_2O, one DMF).

[8] A. Müller, E. Diemann, E. Krickemeyer, S. Che, *Naturwissenschaften* **1993**, *80*, 77.

[9] M. I. Khan, J. Zubieta, *Angew. Chem.* **1994**, *106*, 784; *Angew. Chem. Int. Ed. Engl.* **1994**, *33*, 760. In the compound described here the $PhPO_3^{2-}$ ligands are replaced by $PhAsO_3^{2-}$ units and the $\{V_5O_9\}^{3+}$ unit by the $\{V_4O_5(PhAsO_3)\}^{4+}$ building block.

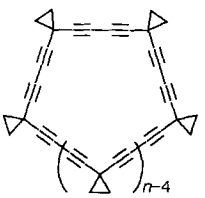
[10] J. B. Howard, D. C. Rees, *Annu. Rev. Biochem.* **1994**, *63*, 235; see also A. Müller, E. Krahn, *Angew. Chem.* **1995**, *107*, issue 10; *Angew. Chem. Int. Ed. Engl.* **1995**, *34*, issue 10; B. K. Burgess, *Nitrogenase Structure, Function and Genetics* in *Molybdenum Enzymes, Cofactors and Model systems* (*ACS Symp. Ser.* **1993**, *535*, 144).

The Reactivity of 1,3-Butadiyne Moieties in the "Exploding" [*n*]Rotanes—A Crown of Thiophenes**

Sergei Kozhushkov, Thomas Haumann, Roland Boese, Burkhardt Knieriem, Stefan Scheib, Peter Bäuerle, and Armin de Meijere*

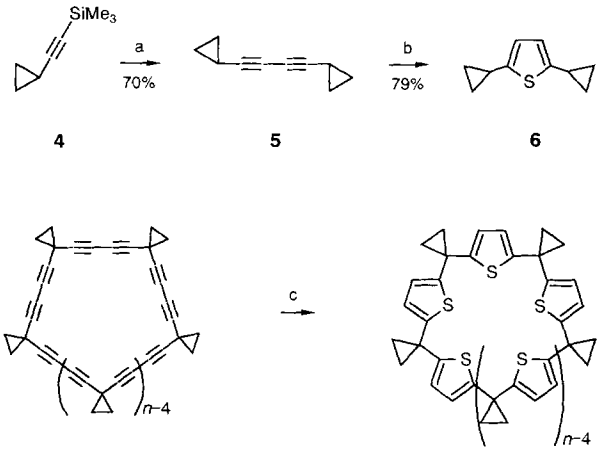
Dedicated to Professor Martin Klessinger on the occasion of his 60th birthday

In recent years, a variety of cyclic, macrocyclic, and oligocyclic polyacetylenes have been prepared.[1–5] On top of having interesting structural and physical properties, such compounds should show a rich chemistry due to the high reactivity of their acetylene moieties towards electrophiles, nucleophiles, and metal compounds.[4–6] In particular, molecules with 1,3-diyne units[7] should tend to give interesting new structures upon reaction with various reagents. Under this aspect the recently reported macrocyclic dehydrooligomers of 1,1-diethynylcyclopropane with spirocyclopropane rings between each two 1,3-diyne units such as **1**–**3**[8,9] are intriguing, as any clean transformation of all their diyne units would lead to novel cyclic structures with alternating spirocyclopropane and various other groups. In view of the known heterocyclization of 1,3-diynes to thiophenes,[10] we have probed the "exploding" [*n*]rotanes **1**–**3** for such transformations.



1, n = 5
2, n = 6
3, n = 8

To find the best suitable reaction conditions for substrates containing cyclopropane rings, the thiocyclization of dicyclopropyldiacetylene (**5**),[3] which was readily prepared from (trimethylsilylethynyl)cyclopropane (**4**)[11] by direct treatment with CuCl and $Cu(OAc)_2$[12] (Scheme 1), was tested. The best result was achieved with $Na_2S \cdot 9H_2O$ under strongly basic conditions (KOH/DMSO);[13] 2,5-dicyclopropylthiophene (**6**) was obtained from this reaction in 79% yield.[14]



1, n = 5
2, n = 6
3, n = 8

7, n = 5 (22%)
8, n = 6 (59%)
9, n = 8 (58%)

Scheme 1. a: 12 equiv CuCl, 16 equiv $Cu(OAc)_2$, 20 °C, 12 h. b: 2.2 equiv $Na_2S \cdot 9H_2O$, 2 equiv KOH, DMSO, 55 °C, 3 h. c: same as b, but 1 h.

Under the same conditions, the exploding [*n*]rotanes **1**–**3** react within 1 h to produce the corresponding macrocycles **7**–**9** with alternating thiophene and spirocyclopropane rings in surprisingly good yields (up to 59% for n = 6, Scheme 1). The relatively low yield of the [5.5]-macrocycle **7**[15] is caused by its instability, which led to partial decomposition upon attempted purification by column chromatography and recrystallization. The [6.6]-macrocycle **8** is significantly more stable and can be obtained in pure form by recrystallization from chloroform, but the [8.8]-macrocycle **9** is less stable again. At room temperature, **7** polymerizes rapidly in the solid state as well as in solution. Nevertheless, all three macrocycles **7**–**9** have been unequivocally identified and fully characterized by their mass spectra (EI ionization), in which the molecular ions appear as the parent peaks (100% relative intensity), and diagnostically simple ^{1}H and ^{13}C NMR spectra (Table 1). The exact molecular masses of compounds **7**–**9** have been determined as 610.0951, 732.1141, and 976.1522 g mol^{-1} by high-resolution mass spectrometry,[16] confirming their molecular formulas as $C_{35}H_{30}S_5$ for the cyclic dehydropentamer **7**, $C_{42}H_{36}S_6$ for the cyclic dehydrohexamer **8**, and $C_{56}H_{48}S_8$ for the cyclic dehydrooctamer **9** of 2-cyclopropylthiophene.

[*] Prof. Dr. A. de Meijere, Dr. B. Knieriem, Dr. S. Kozhushkov
Institut für Organische Chemie der Universität Göttingen
Tammannstrasse 2, D-37077 Göttingen (Germany)
Telefax: Int. code + (551) 39-9475
Prof. Dr. R. Boese, Dipl.-Chem. T. Haumann
Institut für Anorganische Chemie
der Universität-Gesamthochschule Essen (Germany)
Dipl.-Chem. S. Scheib, Prof. Dr. P. Bäuerle
Institut für Organische Chemie der Universität Würzburg (Germany)

[**] This work was supported by the Deutsche Forschungsgemeinschaft (Projekt Me 405/15-3) and the Fonds der Chemischen Industrie. We thank the companies BASF, Bayer, Degussa, Hoechst, and Hüls AG for generous gifts of chemicals.

Table 1. Physical and spectroscopic data of compounds **6**–**9**. NMR spectra: 250 MHz (^{1}H, $\delta(CHCl_3) = 7.26$), 62.9 MHz (^{13}C, additional DEPT, $\delta(CDCl_3) = 77.0$).

6: Colorless oil. ^{1}H NMR: $\delta = 0.65-0.85$ (m, 4H), 0.85–1.05 (m, 4H), 2.0–2.12 (m, 2H), 6.60 (s, 2H). ^{13}C NMR: $\delta = 9.12$ (CH_2), 10.99, 122.10 (CH), 145.0 (C) [14]

7: Yellow unstable powder. ^{1}H NMR: $\delta = 1.30$ (s, CH_2), 6.56 (s, CH). ^{13}C NMR: $\delta = 18.90$ (CH_2), 122.18 (CH), 21.58, 149.12 (C)

8: Colorless crystals, m.p. 248–250 °C (decomp.). ^{1}H NMR: $\delta = 1.33$ (s, CH_2), 6.57 (s, CH). ^{13}C NMR: $\delta = 19.88$ (CH_2), 123.84 (CH), 21.96, 148.22 (C)

9: White powder, decomp. > 100 °C. ^{1}H NMR: $\delta = 1.34$ (s, CH_2), 6.59 (s, CH). ^{13}C NMR: $\delta = 20.10$ (CH_2), 123.94 (CH), 21.98, 148.15 (C)

The ^{1}H NMR signals for compounds **7**–**9** show a weak downfield shift with increasing ring size, as was observed for **1**–**3**,[9] but in the ^{13}C NMR spectra only the signals of the methylene, methine, and cyclopropyl quaternary carbons are shifted downfield, whereas those of the thiophene quaternary carbons are shifted upfield with increasing ring size (Table 1).

The UV spectra of the macrocycles **7**–**9** in comparison to that for the basic chromophore 2,5-dicyclopropylthiophene (**6**) show a distinct bathochromic shift of the intense main absorption in the region 220–280 nm ($\varepsilon = 10200-21600$) and a distinct splitting into two bands (Fig. 1).[17]

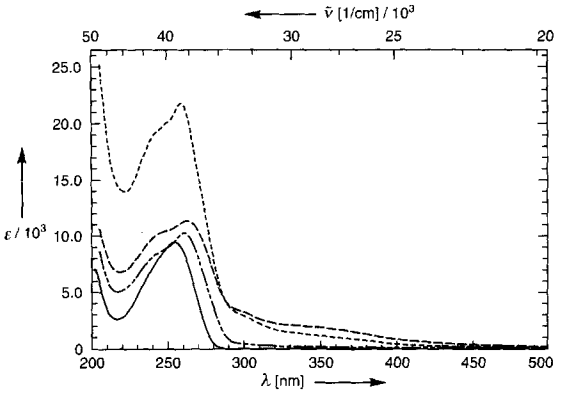
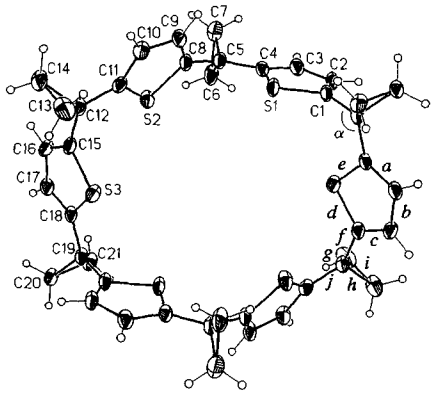


Fig. 1. UV spectra of 2,5-dicyclopropylthiophene (**6**) (—) and the "crowns of thiophenes" **7** (– – –), **8** (------) and **9** (– · – · –) in *t*-butyl methyl ether.

While attempts to grow good quality crystals of compounds **7** and **9** failed, [24](2,5)-cyclopropylthiophenocrown-6 (**8**) crystallized on slow concentration of a dilute solution in ethanol/dichloromethane in the form of needles, for which an X-ray structure analysis has been successfully performed. The macrocycle of **8** adopts a chairlike conformation (Fig. 2) with a center of inversion (overall S_6 symmetry). The two cyclopropyl groups on each thiophene unit are alternately almost bisected or perpendicular[18] to the planes of the adjacent thiophene groups (mean torsional angles S1-C4-C5-C8, S2-C11-C12-C15, and S3-C18-C19-C1′ = 8.6° and S1-C1-C19′-C18′, S2-C8-C5-C4, and S3-C15-C12-C11 = 98.8°). Accordingly, each cyclopropane ring has a close to optimal orientation for conjugation only with one of its neighboring thiophene moieties.

This unusual conformation with three sulfur atoms above and three below the equatorial plane probably results as an energetic compromise between the mutual repulsion of the sulfur atoms and a maximum conjugation between the cyclopropane and thiophene fragments. The diagonal interatomic distances between the sulfur atoms are far from being equal (S1–S3 = 6.523(2), S1–S1′ = 7.399(3), S1–S2′ = 6.090(2), S2–S3′ = 6.611(2), S2–S2′ = 7.406(3), S3–S3′ = 7.704(3) Å), and the whole assembly of



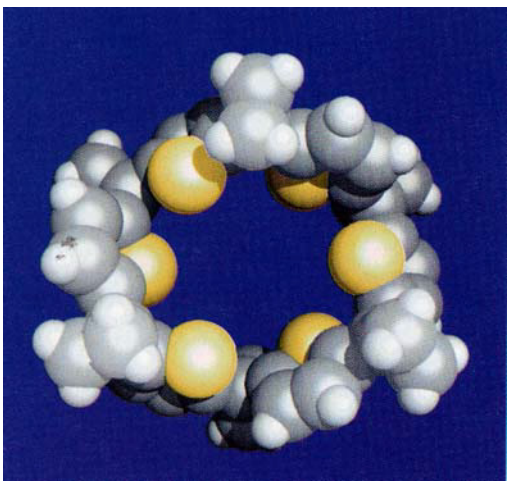


Fig. 2. Top: Crystal structure of [24](2,5)-cyclopropylthiophenocrown-6 $C_{42}H_{36}S_6$ (**8**) [19]. The numbering of atoms does not follow that recommended by IUPAC. Bond lengths [Å] and angles [°] (averaged over S_6 symmetry): $a = 1.353(4)$, $b = 1.405(3)$, $c = 1.365(5)$, $d = 1.719(2)$, $e = 1.723(4)$, $f = 1.489(4)$, $g = 1.515(3)$, $h = 1.509(9)$, $i = 1.486(6)$, $j = 1.488(6)$, $\alpha = 116.2(6)$. Bottom: The colored picture shows the three sulfur atoms each above and below the equatorial plane of the macrocycle **8**.

six sulfur atoms in one molecule corresponds to a large chair with a mean torsional angle of 56.0° and interatomic distances of S1–S2 = 4.208(2), S2–S3 = 3.659(2), S3–S1′ = 3.792(2) Å, two of which are a little smaller than the sum of van der Waals radii (3.90 Å[20]) of two sulfur atoms. In the cyclopropane rings the proximal bonds are longer than the distal ones (Fig. 2), which expresses an electron-withdrawing action of the thiophene moieties according to established theory.[21] The differences in the bond lengths ($\Delta = 0.029$ and 0.023 Å), however, are smaller than those in the exploding [6]rotane **2** ($\Delta = 0.055$ Å[8, 9]), but larger than those in vinylcyclopropane ($\Delta = 0.015$ Å[22]). It is probably the steric interaction of two neighboring sulfur atoms that causes the exocyclic angle on the spirocyclopropane rings ($\alpha = 116.2°$) to be a little larger than that in compound **2** ($\alpha = 115.5°$[8, 9]). The six thiophene units are undistorted with approximate local C_{2v} symmetry and bond lengths very close to those in thiophene[23a] and 2,5-disubstituted thiophenes.[23b]

In order to better understand the conformation of macrocycle **8**, its geometry was optimized both by molecular mechanics (MM2 + π-SCF[24]) and semiempirical calculations (AM1 and PM3[25]). These predict a conformation resembling a crown of thorns with three sulfur atoms pointing up and three down; in this conformation all the cyclopropane and neighboring thiophene rings are oriented perpendicular[18] with respect to each other.

 © VCH Verlagsgesellschaft mbH, D-69451 Weinheim, 1995 0570-0833/95/0707-0782 $ 10.00+.25/0

The crystal structure is not a minimum energy conformation according to these calculations, but a second minimum, slightly higher in energy than that for the crown, is found for a chair conformation close to that observed in the crystal. Apparently, the potential energy surface for conformational changes of this macrocycle is rather flat, and crystal lattice forces can easily change the adopted structure in the solid state. These macrocycles **7**–**9** all suffer from transannular strain, which may be the predominant reason for the observed instability of compound **7**.

The electrochemical behavior of the cyclopropyl-substituted thiophene model compound **6** and the [6.6]-macrocycle **8** were determined by cyclic voltammetry in methylene chloride with added tetrabutylammonium hexafluorophosphate. As expected for monomeric thiophenes, both oxidation potentials are irreversible indicating a quick follow-up reaction of the radical cations created. The peak potential found for 2,5-dicyclopropylthiophene (**6**) ($E_{pa} = 0.95$ V vs Fc/Fc^+) is distinctly lower than that of the cyclic compound **8** with $E_{pa} = 1.39$ V vs Fc/Fc^+.[26] These findings are in accord with the chairlike structure of **8** in which only one of the two cyclopropyl substituents on each thiophene moiety has the correct orientation for conjugative interaction. This decreased conjugation leads to an increased oxidation potential for **8**. The electrochemical measurements were hampered by the unusual fact that the oxidation of both compounds led to an immediate formation of an insulating film on the working electrode. Obviously, the first formed heterocyclic cation radicals undergo subsequent rearrangement (e. g. with ring opening of the cyclopropyl moieties) leading to highly reactive intermediates.[27]

The facile and high-yielding reaction of the exploding [*n*]rotanes with sodium sulfide to give structurally intriguing compounds suggests that other macrocyclic oligodiacetylenes should be capable of undergoing analogous transformations. Work along these lines is in progress.

Received: October 21, 1994 [Z 7418 IE]
German version: *Angew. Chem.* **1995**, *107*, 859

Keywords: alkynes · crown compounds · macrocycles · rotanes · thiophenes

[1] R. M. McQuilkin, P. J. Garratt, F. Sondheimer, *J. Am. Chem. Soc.* **1970**, *92*, 6682–6683.

[2] a) A. M. Boldi, F. Diederich, *Angew. Chem.* **1994**, *106*, 482–485; *Angew. Chem. Int. Ed. Engl.* **1994**, *33*, 468–471; b) L. Guo, J. D. Bradshaw, C. A. Tessier, W. J. Youngs, *J. Chem. Soc. Chem. Commun.* **1994**, 243–244, and references therein; c) F. Diederich, Y. Rubin, *Angew. Chem.* **1992**, *104*, 1123–1146; *Angew. Chem. Int. Ed. Engl.* **1992**, 31, 1101–1123.

[3] A. de Meijere, F. Jaekel, A. Simon, H. Borrmann, J. Köhler, D. Johnels, L. T. Scott, *J. Am. Chem. Soc.* **1991**, *113*, 3935–3941.

[4] a) L. T. Scott, M. J. Cooney, D. Johnels, *J. Am. Chem. Soc.* **1990**, *112*, 4054–4055; b) L. T. Scott, G. J. DeCicco, J. L. Hyun, G. Reinhardt, *ibid.* **1985**, *107*, 6546–6555.

[5] a) J. Anthony, C. B. Knobler, F. Diederich, *Angew. Chem.* **1993**, *105*, 437–440; *Angew. Chem. Int. Ed. Engl.* **1993**, *32*, 406–409; b) H. L. Anderson, R. Faust, Y. Rubin, F. Diederich, *ibid.* **1994**, *106*, 1427–1429 and **1994**, *33*, 1366–1368.

[6] F. Diederich, D. Philp, P. Seiler, *J. Chem. Soc. Chem. Commun.* **1994**, 205–208.

[7] Q. Zhou, P. J. Carroll, T. M. Swager, *J. Org. Chem.* **1994**, *59*, 1294–1301.

[8] A. de Meijere, S. Kozhushkov, C. Puls, T. Haumann, R. Boese, M. J. Cooney, L. T. Scott, *Angew. Chem.* **1994**, *106*, 934–936; *Angew. Chem. Int. Ed. Engl.* **1994**, *33*, 869–871.

[9] The "exploding" [5]- **1** and [8]rotane **3** were prepared according to a general strategy developed from the procedure used for compound **2** [8]: A. de Meijere, S. Kozhushkov, T. Haumann, R. Boese, C. Puls, M. J. Cooney, L. T. Scott, *Chem. Eur. J.* **1995**, *1*, in press.

[10] For reviews see: a) M. F. Shostakovskii, A. V. Bogdanova, *The Chemistry of Diacetylenes*, Wiley, New York, **1974**, p. 96 ff; b) J. Nakayama, T. Konishi, M. Hoshino, *Heterocycles* **1988**, *27*, 1731–1754; c) S. Gronowitz in *Heterocyclic Compounds, Vol. 44, Part 1* (Ed.: S. Gronowitz), Wiley, New York, **1985**, p. 11 ff.

[11] H.-C. Militzer, S. Schömenauer, C. Otte, C. Puls, J. Hain, S. Bräse, A. de Meijere, *Synthesis* **1993**, 998–1012.

[12] D. O'Krongly, S. R. Denmeade, M. Y. Chiang, R. Breslow, *J. Am. Chem. Soc.* **1985**, *107*, 5544–5545. Improved modified conditions for such oxidative acetylene couplings have been developed by: L. T. Scott, M. J. Cooney, C. Otte, C. Puls, T. Haumann, R. Boese, P. J. Caroll, A. B. Smith, III, A. de Meijere, *ibid.* **1994**, *116*, 10275–10283.

[13] M. G. Voronkov, B. A. Trofimov, V. V. Krjuchkov, S. V. Amosova, Y. M. Skvortsov, A. N. Volkov, A. G. Mal'kina, R. Y. Mushii, *Khim. Geterocykl. Soed.* **1981**, 1694; *Chem. Heterocycl. Comp.* **1981**, *17*, 1249.

[14] 2,5-Dicyclopropylthiophene (**6**) has previously been prepared in thirteen steps from thiophene-2-carbaldehyde: R. M. Kellogg, J. Buter, *J. Org. Chem.* **1971**, *36*, 2236–2244.

[15] For shortness, such compounds may be named [20](2,5)-cyclopropylthiophenocrown-5 (**7**), [24](2,5)-cyclopropylthiophenocrown-6 (**8**), and [32](2,5)-cyclopropylthiophenocrown-8 (**9**). According to the nomenclature rules for phanes (cf. F. Vögtle, P. Neumann, *Tetrahedron* **1970**, *26*, 5847–5873) **7** would be: 1,8,15,22,29-pentaethano-[1_5](2,5)thiophenophane.

[16] Molecular masses were confirmed by high-resolution mass spectrometry with preselected ion peak matching at R ≈ 10000 to be within ±2 ppm of the exact masses.

[17] As compounds **7** and **9** may have been contaminated with polymers, their UV data may be slightly adulterated.

[18] Cf. also: A. de Meijere, *Angew. Chem.* **1979**, *91*, 867–884; *Angew. Chem. Int. Ed. Engl.* **1979**, *18*, 809–825, and references therein.

[19] Structure determination of **8**: diffractometer Siemens P4V, $\lambda(Mo_{K\alpha})$, graphite monochromator, ω-scan, $3° \le 2\theta \le 50°$, direct methods [SHELXTL PLUS (UNIX)]. Crystal dimensions $0.6 \times 0.3 \times 0.1$ mm^3, space group *Pbca*, $Z = 4$, $T = 155$ K; cell dimensions: $a = 6.689(2)$, $b = 19.814(5)$, $c = 25.978(6)$ Å, orthorhombic, $\rho_{calcd} = 1.420$ g cm^{-3}. 3015 independent reflections, of which 2338 were considered observed ($F_0 \ge 4\sigma(F)$), 229 parameters for the structure refinement, all non-hydrogen atoms anisotropic, $R = 0.0573$, $R_w = 0.0585$. Further details of the crystal structure investigation may be obtained from the Fachinformationszentrum Karlsruhe, D-76344 Eggenstein-Leopoldshafen, on quoting the depository number CSD-401333.

[20] D. Brodalla, Dissertation, Universität Düsseldorf, **1983**.

[21] a) R. Hoffman, *Tetrahedron Lett.* **1970**, 2907–2909; b) H. Günther, *ibid.* **1970**, 5173–5177.

[22] D. Nijveld, A. Vos, *Acta Crystallogr. Sect. B* **1988**, *44*, 281, 289, 296.

[23] a) A. Henriksson-Enflo in *Heterocyclic Compounds, Vol. 44, Part 1* (Ed.: S. Gronowitz), Wiley, New York, **1985**, p. 245; b) Cambridge Crystallographic Data Base, Version 1994 (update 4.8.1994), 120481 entries.

[24] P. Aped, N. L. Allinger, *J. Am. Chem. Soc.* **1992**, *114*, 1–16, and references therein. The program PCM 89 by Serena software was used for the calculations.

[25] The program MOPAC by F. J. Seiler, Res. Lab., US Air Force Academy, Colorado Springs, CO. 80840, USA, was employed for the calculations.

[26] Experimental conditions: Pt wire, sealed in soft glass, 1 mm diameter. Reference electrode: Ag wire coated with AgCl, calibrated against the ferrocene/ferricenium couple. Counter electrode: Pt wire. **6**: $c = 6.7$ mmol L^{-1}, CH_2Cl_2, TBAHFP 0.1 M, 100 mV s^{-1}. **8**: $c = 2$ mmol L^{-1}, CH_2Cl_2, TBAHFP 0.1 M, 100 mV s^{-1}.

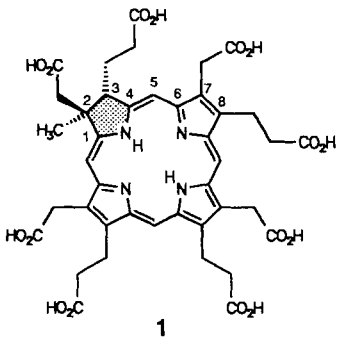
[27] In contrast, 2,5-diisopropylthiophene, prepared from diisopropyl-1,3-butadiyne in the same way as **6**, with $E_{pa} = 1.23$ V vs Fc/Fc^+ does not lead to an insulating film on the working electrode.

 © VCH Verlagsgesellschaft mbH, D-69451 Weinheim, 1995 0570-0833/95/0707-0783 $ 10.00+.25/0

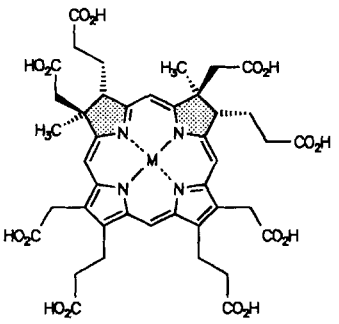
A Simple, Chirogenic, Enantioselective Synthesis of Chlorins and Isobacteriochlorins**

Dirk Kusch, Elke Töllner, Anngret Lincke, and Franz-Peter Montforts*

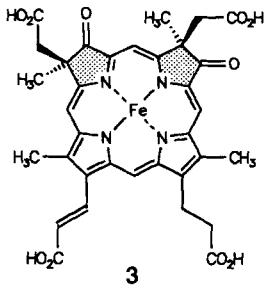
Factor I (**1**), sirohydrochlorin (**2a**), siroheme (**2b**), and heme d_1 (**3**) are naturally occurring porphyrinoids with the basic chlorin or isobacteriochlorin framework. Partially reduced derivatives of the metal-free macrocycles **1** and **2a** are important intermediates in the biosynthesis of vitamin B_{12};[1] the iron-containing isobacteriochlorins **2b** and **3** play a central role as cofactors for sulfite- or nitrite-reducing enzymes in bacteria and plants.[2]



1



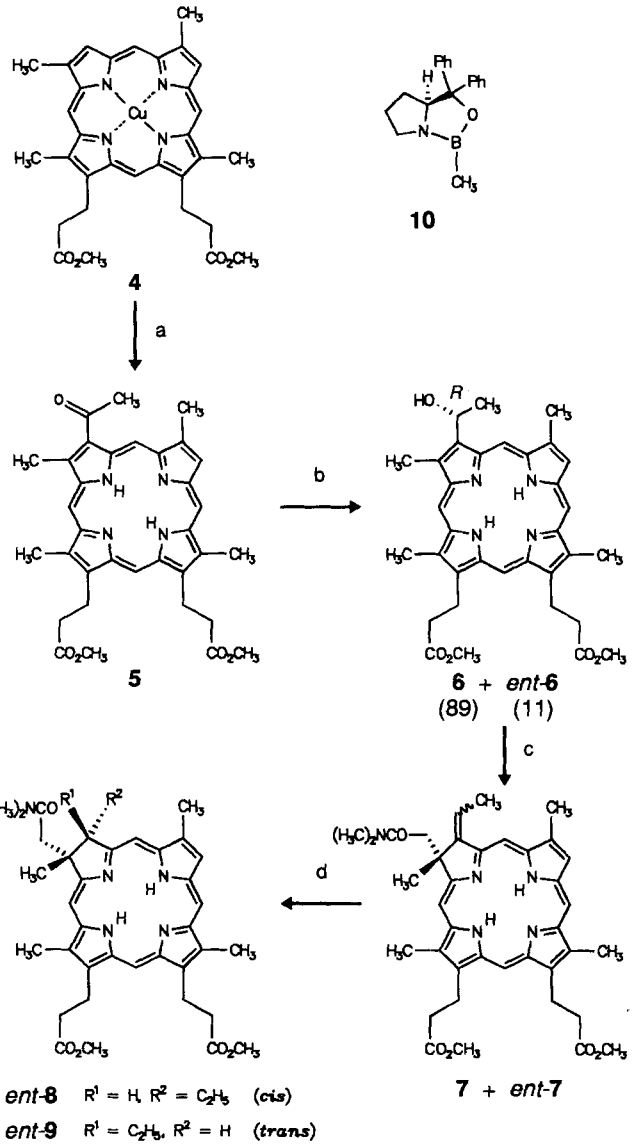
2a M = 2H
2b M = Fe



3

All but two syntheses of chlorins known to date[2] produce racemic mixtures; the exceptions are the syntheses of enantiomerically pure chlorophyll a, which was obtained by resolution of a racemate at the end of the synthesis,[2, 3] and factor I (**1**), which was synthesized from an optically active synthetic building block.[2, 4] Subsequent to the synthesis of the pure enantiomer sirohydrochlorin **2a**, [2, 5a] Battersby et al. were also able to synthesize the enantiomerically pure ligand of heme d_1 (**3**) in a total synthesis encompassing approximately 35 steps,[5b] and to establish the absolute configuration of **3**, since a glutamic acid derivative with a known configuration was used as a synthetic element. We recently determined the relative configuration of **3**.[2, 6] Here we describe a simple procedure for the synthesis of optically active chlorins and isobacteriochlorins with geminal dialkyl substituents, by chirogenic, enantioselective reduction and subsequent Claisen rearrangement with transfer of chirality.

The acylporphyrins **5** and **11**[7] form the starting point for our investigation. They have already been synthesized from the copper(II) complex **4** (Schemes 1 and 2). Under conditions which were carefully optimized with respect to concentrations of starting material and reagent, solvent, and temperature, and with rigorous exclusion of water, the prochiral ketones **5** and **11** can be reduced to give in high yield the alcohol **6** and hematoporphyrin dimethyl ester **12a** with borane dimethyl sulfide and the methyloxazaborolidine **10** as homochiral catalyst. The enantiomeric excess for **6** was 78%, determined by HPLC and ^{1}H NMR spectroscopy. The hematoporphyrin dimethyl ester **12a** was formed with an enantiomeric excess of 92%. The *R*



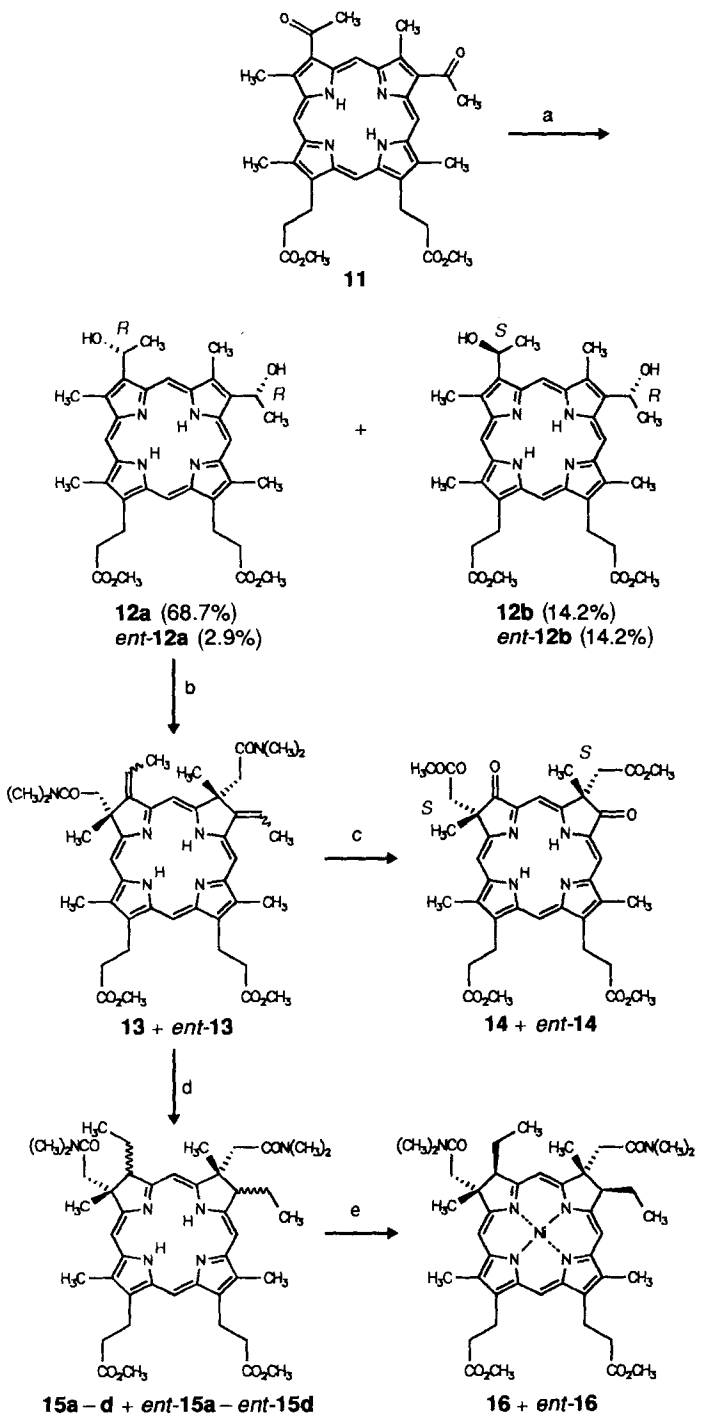
4 **10** **5** **6** + *ent*-**6** (89) (11) **7** + *ent*-**7**

8 + *ent*-**8** R^1 = H, R^2 = C_2H_5 (*cis*)
9 + *ent*-**9** R^1 = C_2H_5, R^2 = H (*trans*)

Scheme 1. Synthesis of chlorin **9**. a) 1. Ac_2O, $SnCl_4$, CH_2Cl_2, 0 °C, 20 s; 2. conc. H_2SO_4, 1 h; 3. CH_2N_2, Et_2O, separation of the structural isomers. b) 0.37 equiv. **10**, 0.88 equiv. $BH_3 \cdot SMe_2$, CH_2Cl_2, −12 °C, 5 h (91% **6**/*ent*-**6**, **6**:*ent*-**6** = 89:11); c) $CH_3C(OCH_3)_2N(CH_3)_2$, *o*-xylene, molecular sieve 3 Å, 155 °C, 2.5 h (82% **7**/*ent*-**7**); d) 1. $Pd(OAc)_2$, $HSi(OEt)_3$, THF/H_2O (4/1), room temperature, 15 min (**8**/*ent*-**8**:**9**/*ent*-**9** = 2.5:1); 2. *p*-TsOH, MeOH, reflux, 72 h (75% **8**/*ent*-**8**:**9**/*ent*-**9** = 1:2.5); 3. HPLC separation of the *cis*/*trans* isomer mixture: LiChrosorb RP-18 (16 × 250 mm), MeOH/water (90/10), 20 mL min^{-1}, λ = 393 nm; t_R (**8**) = 27.5, t_R (**9**) = 23 min. – All new compounds were characterized by elemental analysis, UV/Vis and ^{1}H NMR spectroscopy, and mass spectrometry. The scaled data agree with the corresponding data in the racemic series.

[*] Prof. Dr. F.-P. Montforts, Dr. D. Kusch, Dr. E. Töllner, A. Lincke
Institut für Organische Chemie, FB2 Biologie/Chemie der Universität
Postfach 330440, D-28334 Bremen (Germany)
Telefax: Int. code + (421)218-3720

[**] This work was supported by the Deutsche Forschungsgemeinschaft, the Fonds der Chemischen Industrie, and by the EU within the Human Capital and Mobility Program (PDT Euronet CHRX-CT93-0178). We thank Dr. H. Rosemeyer (Universität Osnabrück) for support during recording of CD spectra, and Prof. A. R. Battersby (Cambridge, UK) for supplying previously unpublished CD spectra for comparison.



a : ***trans, trans, trans***
b : ***cis, cis, cis***
c : ***cis, cis, trans***
d : ***trans, trans, cis***

Scheme 2. Synthesis of the isobacteriochlorins **14** and **16**. a) 0.65 equiv. **10**, 1.6 equiv. $BH_3 \cdot SMe_2$, CH_2Cl_2, −12 °C, 5 h (86.3% **12a**, **b** + *ent*-**12a**, **b**, **12a**:*ent*-**12a**:**12b**:*ent*-**12b** = 68.7:2.9:14.2:14.2); b) 1. $CH_3C(OCH_3)_2N(CH_3)_2$, *o*-xylene, molecular sieve 3 Å, 155 °C, 2.5 h; 2. flash chromatography, silica gel (ICN), CH_2Cl_2/ethyl acetate ester/MeOH (10/5/0.5); c) 1. $Zn(acac)_2$, $CHCl_3$, reflux, 3.5 h; 2. I_2, THF/H_2O (1/1), 25 °C, 5 h; $Na_2S_2O_3$, H_2O; 3. KOH, MeOH, 65 °C, 22 h; 4. aq. HCl, 65 °C, 30 min; 5. CH_2N_2, ether, MeOH, room temperature, 1 h (11.8% **14**/*ent*-**14** relative to **12a** + *ent*-**12a** in the reduction mixture); d) $Pd(OAc)_2$, THF/H_2O (4/1), $HSi(OEt)_3$, room temperature, 20 min (66.5% **15a–d** + *ent*-**15a–ent-15d**; e) 1. *p*-TsOH, MeOH, reflux, 50 h; 2. $Ni(acac)_2$, $CHCl_3$, MeOH, reflux, 8 h (59.9% **16a** + isomers; 36.8% **16a**/*ent*-**16a**). – All new compounds were characterized by elemental analysis, UV/Vis and ^1H NMR spectroscopy, and mass spectrometry. The scaled data agree with the corresponding data in the racemic series.

configuration of the stereogenic centers in **6** and **12a** can be concluded from the determination of the absolute configuration of **9** and **14**, which agrees with the transition state model for this type of reduction suggested by Corey.[8d]

The higher enantiomeric excess of **12a**, compared to the simple reduction of **5** to **6**, is only surprising at first glance. A closer observation shows that the fractions x of the resulting enantiomers **12a** and *ent*-**12a**, as well as those of the diastereomers **12b** and *ent*-**12b**, correspond in the product mixture to the terms of the binomial equation (a) [equations (b)–(d)], where W_{Si} and W_{Re} are the probabilities for attack from

$$W_{Si}^2 + 2\,W_{Si}W_{Re} + W_{Re}^2 = 1 \quad \text{(a)}$$

$$x(\mathbf{12a}) = W_{Si}^2 \quad \text{(b)}$$

$$x(\mathbf{12b}) + x(\textit{ent}\text{-}\mathbf{12b}) = 2\,W_{Si}W_{Re} \quad \text{(c)}$$

$$x(\textit{ent}\text{-}\mathbf{12a}) = W_{Re}^2 \quad \text{(d)}$$

the enantiotopic sides of the two keto groups.[11] Thus, it follows that the enantiomeric excess is significantly higher after two reductions than after the first reduction, since here the less probable (and undesirable) attack on the *Re* side mostly leads to formation of the unconvertable diastereomer, easily separable from the mixture, and the formation of *ent*-**12a** (W_{Re}^2) from it is secondary.[12] Analysis by HPLC of the hematoporphyrin ester in an achiral phase gives a diastereomer ratio of (**12a** + *ent*-**12a**)/(**12b** + *ent*-**12b**) of 2.53:1, from which an enantiomeric excess **12**/*ent*-**12** of 92% and a *Si*-selectivity (W_{Si}) of 83% can be calculated using equations (a)–(d). The fractions of the four stereoisomers were determined by HPLC of the corresponding dibenzoate in a homochiral phase (Fig. 1). Although the peaks for *ent*-**12a** and for one of the diastereomers **12b** and *ent*-**12b** coincide, an enantiomer excess of 88% and thus a *Si*-selectivity of 80% could be determined, since the signal for **12a** is completely separated. The selectivity thus corresponds to that determined for the reduction of **5**.

In the further course of the synthesis, the mixture of **6** and *ent*-**6**, as well as that of all the stereoisomers of **12**, underwent an amidoacetal Claisen rearrangement, in which the chirality of the hydroxy-substituted centers of the starting materials was completely transferred to the dialkylated centers of the products.[13, 15] The enantiomerically enriched chlorin **7** (**7**:*ent*-**7** = 89:11) is formed from **6**/*ent*-**6**, and the enantiomerically enriched isobacteriochlorin **13** (**13**:*ent*-**13** = 96:4) from **12a**/*ent*-**12a** (**12a**:*ent*-**12a** = 96:4). The undesired product of the rearrangement diastereomeric to **13**, formed from **12b**/*ent*-**12b**, is easily separated at this stage by flash chromatography. Thus the much more difficult separation of the hematoporphyrin ester stereoisomers can be avoided.

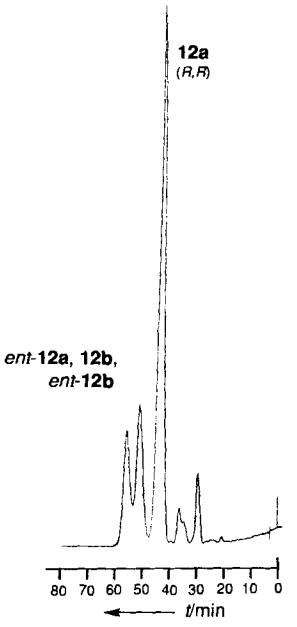


Fig. 1. Chromatogram from the HPLC of the dibenzoates of **12a**, *ent*-**12a**, **12b**, and *ent*-**12b** on a homochiral phase [Nucleosil Chiral 2, *n*-heptane/dioxane (77/23)].

Hydrogenation of the exocyclic double bonds in **7** and **13** is best performed with the method described by Tour.[16] Here the *cis* diastereomers **8** (from **7**) and **15a–d** of which the *cis,cis,cis* isomer **15b** dominates (from **13**) are kinetically preferred. The fraction of the thermodynamically more stable *trans* diastereomers **9** and **15a** formed as secondary products can be increased by subsequent acid-catalyzed equilibration. The enantiomerically enriched **9** was isolated by preparative HPLC (Table 1). The enantiomerically enriched *trans,trans,trans* isomer **15a** could be separated from its stereoisomers, which were only present in small amounts, by formation of **16** by complexation with nickel(II) (Table 1). The *trans*-ethylchlorin **9** can be clearly differentiated from *cis* isomer **8** by mass spectrometry or ^{1}H NMR spectroscopy. The absolute configuration of **9** is obtained by comparison of its CD spectrum with that for the octamethyl ester of Factor I, whose configuration is known. According to the mirrored courses of the CD curves (Fig. 2) for enantiomerically enriched **9** and for the octamethyl ester of Factor I,[18] **9** has the (*2R,3R*) configuration.[19]

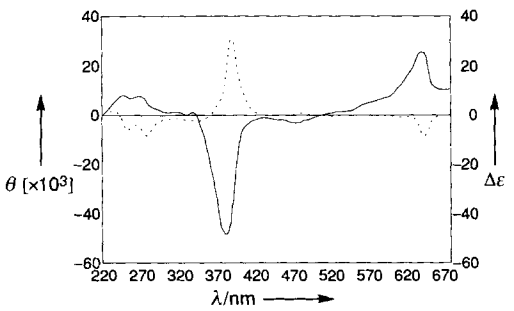


Fig. 2. CD spectra of the octamethyl ester of Factor I (·····) [18] and *trans*-chlorin **9** (**9**:*ent*-**9** = 89:11) (——) in MeOH. The $\Delta\varepsilon$ scale applies to the CD curve for the octamethyl ester of Factor I, and the θ scale for that from **9**.

The relative configuration of (isobacteriochlorinato)nickel(II) (**16**) follows from the typical fragmentation pattern of the mass spectrum,[17] whereas the absolute configuration is fixed by the enantioselective reduction, subsequent course of the synthesis, and comparison of its CD spectrum with that of the (sirohydrochlorinato octamethyl ester)nickel(II), whose configuration is known.[19]

Oxidative cleavage of the exocyclic double bond in **13**/*ent*-**13** (**13**:*ent*-**13** = 96:4) with simultaneous hydrolysis of the amide groups produces enantiomerically enriched dioxoisobacteriochlorin (**14**, Table 1). Compound **14** is an intermediate in all the previous syntheses[5, 6] of the metal-free ligand of heme d_1 (**3**) and, according to the comparison of the CD spectra, proves to be enantiomeric to the corresponding intermediate given in ref. [5b].

Table 1. Selected physical data for **9**, **14**, and **16**.

9: CD (MeOH, **9**:*ent*-**9** = 89:11): $\theta(\lambda)$ = +8020 (250 nm), +7700 (270), −48070 (383), −2950 (480), +25700 (640).

14: CD (MeOH, **14**:*ent*-**14** = 96:4): $\theta(\lambda)$ = −7750 (237 nm), −7600 (249), +7290 (288), +9150 (347), +9150 (366), −15550 (417), +3130 (440), −5810 (568), −2680 (642).

16: CD ($CHCl_3$, **16**:*ent*-**16** = 96:4): $\theta(\lambda)$ = −1610 (259 nm), +2980 (297), −7320 (374), +990 (405), +620 (415), +1240 (436), −370 (491), +4220 (554), +11540 (592); ^{1}H NMR (360 MHz, $CDCl_3$): δ = 3.76 (dd, $^3J_1$ = 9.2 Hz, $^3J_2$ = 3.9 Hz, 1H; 3-H), 3.83 (dd, $^3J_1$ = 8.9 Hz, $^3J_2$ = 5.3 Hz, 1H; 8-H), 6.48 (s, 1H; 5-H), 7.20 (s, 1H; 20-H), 7.42 (s, 1H; 10-H), 8.37 (s, 1H; 15-H); UV/Vis ($CHCl_3$): $\lambda_{max}(\varepsilon)$ = 594 (30700), 548 (7050), 524 (4550), 389 (32700), 280 nm (8300); MS (70 eV): *m/z* (%): 824 (28) [M^+ for ^{58}Ni], 737 (100) [$M^+ - C_4H_9NO$], 650 (50) [$M^+ - 2C_4H_9NO$].

The dependence of the catalytic functions and the redox properties of the isobacteriochlorins presented here and their metal complexes on their absolute and relative configurations is of interest for the understanding of many processes catalyzed in nature by hydroporphinoid compounds.[1d, 2] It should be mentioned that one of the hematoporphyrin stereoisomers **12b** and *ent*-**12b** is identical to porphyrin c, which was isolated from cytochrome c of various species.[20] Elsewhere we will give a full report of the first stereochemical assignment of porphyrin c to one of the synthesized hematoporphyrin stereoisomers, which is of importance for research into evolution.

Received: October 26, 1994
Revised: January 4, 1995 [Z7426/7427IE]
German version: *Angew. Chem.* **1995**, *107*, 874

Keywords: asymmetric syntheses · porphyrinoids

[1] a) A. I. Scott, *Angew. Chem.* **1993**, *105*, 1281; *Angew. Chem. Int. Ed. Engl.* **1993**, *32*, 1223; b) A. R. Battersby, *Acc. Chem. Res.* **1993**, *26*, 15; c) *Science* **1994**, *264*, 1551; d) A. Eschenmoser, *Angew. Chem.* **1988**, *100*, 5; *Angew. Chem. Int. Ed. Engl.* **1988**, *27*, 5; e) F. Blanche, B. Cameron, J. Crouzet, L. Debussche, D. Thibaut, M. Vuilhorgne, F. J. Leeper, A. R. Battersby, *Angew. Chem.* **1995**, *107*, 421; *Angew. Chem. Int. Ed. Engl.* **1995**, *34*, 383.

[2] Review on synthesis of natural substances with chlorin or isobacteriochlorin structures: F.-P. Montforts, B. Gerlach, F. Höper, *Chem. Rev.* **1994**, *94*, 327.

[3] R. B. Woodward, W. A. Ayer, J. M. Beaton, F. Bickelhaupt, R. Bonnett, P. Buchschacher, G. L. Closs, H. Dutler, J. Hannah, F. P. Hauck, S. Ito, A. Langemann, E. Le Goff, W. Leimgruber, W. Lwowski, J. Sauer, Z. Valenta, H. Volz, *J. Am. Chem. Soc.* **1960**, *82*, 3800.

[4] S. P. D. Turner, M. H. Block, Z. C. Sheng, S. C. Zimmermann, A. R. Battersby, *J. Chem. Soc. Chem. Commun.* **1985**, 583.

[5] a) M. H. Block, S. C. Zimmermann, G. B. Henderson, S. P. D. Turner, S. W. Westwood, F. J. Leeper, A. R. Battersby, *J. Chem. Soc. Chem. Commun.* **1985**, 1061; b) J. Micklefield, R. L. Mackman, C. J. Aucken, M. Beckmann, M. H. Block, F.-J. Leeper, A. R. Battersby, *ibid.* **1993**, 277.

[6] F.-P. Montforts, G. Mai, F. Romanowski, J. W. Bats, *Tetrahedron Lett.* **1992**, *33*, 765.

[7] H. Brockmann, Jr., K. M. Bliesener, H. H. Inhoffen, *Justus Liebigs Ann. Chem.* **1968**, 718.

[8] a) E. J. Corey, R. K. Bakshi, S. Shibata, C. P. Chen, V. K. Singh, *J. Am. Chem. Soc.* **1987**, *109*, 7925; b) E. J. Corey, *Pure Appl. Chem.* **1990**, *62*, 1209; c) D. J. Mathre, T. K. Jones, L. C. Xavier, T. J. Blacklock, R. A. Reamer, J. J. Mohan, E. T. T. Jones, K. Hoogsteen, M. W. Baum, E. J. J. Grabowsky, *J. Org. Chem.* **1991**, *56*, 751; T. K. Jones, J. J. Mohan, L. C. Xavier, T. J. Blacklock, R. A. Reamer, D. J. Mathre, P. Sohar, E. T. T. Jones, K. Hoogsteen, M. W. Baum, E. J. J. Grabowsky, *ibid.* **1991**, *56*, 763; d) E. J. Corey, M. Azimiora, S. Sarshar, *Tetrahedron Lett.* **1992**, *33*, 3429; D. K. Jones, D. C. Liotta, J. Shinhai, D. J. Mathre, *J. Org. Chem.* **1993**, *58*, 799.

[9] The enantiomeric excess of **6** was determined by HPLC, after conversion into the benzoate (benzoic acid anhydride, 4-dimethylaminopyridine, CH_2Cl_2, room temperature, 90 min) and chromatography on Nucleosil Chiral 2 (Macherey-Nagel) with *n*-heptane/dioxane 85/15 (1 mL min^{-1}) as solvent. t_R(benzoate of **6**) = 142 min, t_R(benzoate of *ent*-**6**) = 161 min.

[10] Lanthanoid shift experiments with tris[3-(heptafluoropropylhydroxymethylene)-(+)-camphorato]praseodymium(III) in $CDCl_3$ produced splitting of all signals in ^{1}H NMR spectra of **6**. The especially strong splitting of the signals of protons of pyrrole-fixed methyl groups and of some methine protons enabled the determination of the enantiomeric excess.

[11] The equations (b)–(d) are based on two assumptions: 1) that the reductions are independent of one another, which is valid because of the relatively large separation of the keto groups; and 2) that the selectivity is the same for both keto groups.

[12] The most prominent example of increased enantiomeric excess by multiple enantioselective chirogenic reactions is the perhydroxylation of squalene: G. A. Crispino, P. T. Ho, K. B. Sharpless, *Science* **1993**, *259*, 64-66.

[13] F.-P. Montforts, G. Zimmermann, *Angew. Chem.* **1986**, *98*, 451; *Angew. Chem. Int. Ed. Engl.* **1986**, *25*, 458; G. Haake, A. Meier, F.-P. Montforts, G. Scheurich, G. Zimmermann, *Liebigs Ann. Chem.* **1992**, 325.

[14] H. Meerwein, W. Florian, N. Schön, G. Stopp, *Justus Liebigs Ann. Chem.* **1961**, *641*, 1; D. Felix, K. Gschwend-Steen, A. E. Wick, A. Eschenmoser, *Helv. Chim. Acta* **1969**, *52*, 1030; A. E. Wick, D. Felix, K. Steen, A. Eschenmoser, *ibid.* **1964**, *47*, 2425; F. E. Ziegler, *Acc. Chem. Res.* **1977**, *10*, 227.

[15] The stereochemical result of the Claisen Rearrangement can be interpreted according to the 1,3 allyl strain concept (R. W. Hoffmann, *Chem. Rev.* **1989**, *89*, 1841).

 © VCH Verlagsgesellschaft mbH, D-69451 Weinheim, 1995 0570-0833/95/0707-0786 $ 10.00+.25/0

[16] J. M. Tour, J. P. Cooper, S. L. Pendalwar, *J. Org. Chem.* **1990**, *55*, 3452.
[17] P. Schulze, D. Kusch, A. Meier, F.-P. Montforts, *Org. Mass Spectrom.* **1994**, *29*, 496.
[18] A. R. Battersby, S. Seo, *J. Chem. Soc. Perkin Trans. 1* **1983**, 3049.
[19] This process for determination of the absolute configuration by comparison of CD spectra has been applied and tested by us in another case: F.-P. Montforts, C. Müller, A. Lincke, *Liebigs Ann. Chem.* **1990**, 415; see also A. Fässler, A. Kobelt, A. Pfaltz, A. Eschenmoser, C. Bladon, A. R. Battersby, R. K. Thauer, *Helv. Chim. Acta* **1985**, *68*, 2287.
[20] S. Kojo, K. Fukunishi, I. Tsukamato, *Angew. Chem.* **1989**, *101*, 64; *Angew. Chem. Int. Ed. Engl.* **1989**, *28*, 71.

Highly Stereoselective Allylation of Benzaldehyde: Generation of a Stereochemically Defined Allylzinc Species from a π-Allylpalladium Intermediate and Diethylzinc**

Yoshinao Tamaru,* Akihiro Tanaka, Kengo Yasui, Sachio Goto, and Shuji Tanaka

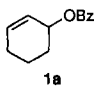
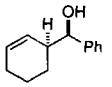
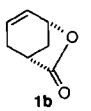
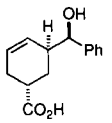
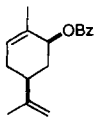
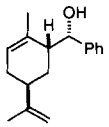
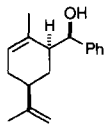
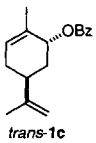
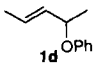
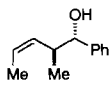
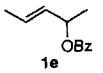
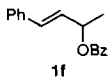
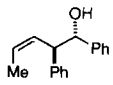
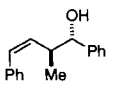
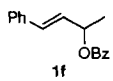
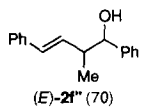
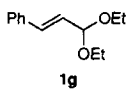
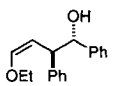
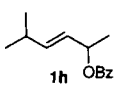
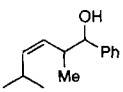
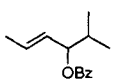
Generation of stereochemically defined organometallic reagents is important for efficient, stereoselective synthesis. Here we describe the stereoselective addition of 2-cyclohexenylzinc species, generated by the Pd^0-catalyzed reaction of 2-cyclohexenyl esters and diethylzinc, to benzaldehyde. We also report the analogous reaction of structurally fluxional acyclic 1,3-disubstituted allylzinc species generated in a similar way.

Recently we reported that diethylzinc can be used to promote the Pd^0-catalyzed allylation of carbonyl compounds (aldehydes, ketones, esters, lactones, acid anhydrides) with allylic substrates (allyl benzoates, acetates, phenyl ethers).[1] At that time, we proposed a reaction mechanism that involves the hitherto undefined equilibrium between a π-allylpalladium intermediate and diethylzinc, and diethylpalladium and an allylzinc species (umpolung of π-allylpalladium).

To obtain further information about the mechanistic details and also to test the synthetic scope of the umpolung technique, we examined the allylation of benzaldehyde with 2-cyclohexenyl substrates **1a–c** (Table 1, entries 1–4). The reactions proceeded smoothly under the conditions previously reported (**1** (1.2 mmol), benzaldehyde (1 mmol), diethylzinc (2.4 mmol), and tetrakis(triphenylphosphane)palladium (0.05 mmol) in THF (5 mL) at room temperature under nitrogen)[1] and provided homoallyl alcohols **2a–c** in good yields.

In sharp contrast to the moderate stereoselectivity for the allylation with 1- or 3-monosubstituted allylating agents (*syn*:*anti* ≈ 2:3),[1] all the reactions with 2-cyclohexenyl substrates provided the *syn* addition products exclusively. Furthermore, the reaction was stereoselective with respect to the configuration of allylic stereocenters. The reaction of **1b**[2] provided the inversion product *trans-syn*-**2b** as a single stereoisomer in quantitative yield (entry 2). A pair of stereoisomers *cis*- and *trans*-**1c**[3] showed similar selectivity: *cis*-**1c** furnished a mixture of an inversion (*trans-syn*-**2c**) and a retention product (*cis-syn*-**2c**) in a ratio of 87:13 (entry 3), and *trans*-**1c** afforded analogous products in a ratio of 82:18 (entry 4).

Table 1. Palladium(0)-catalyzed regio- and stereoselective allylation of benzaldehyde by umpolung of π-allylpalladium [a].

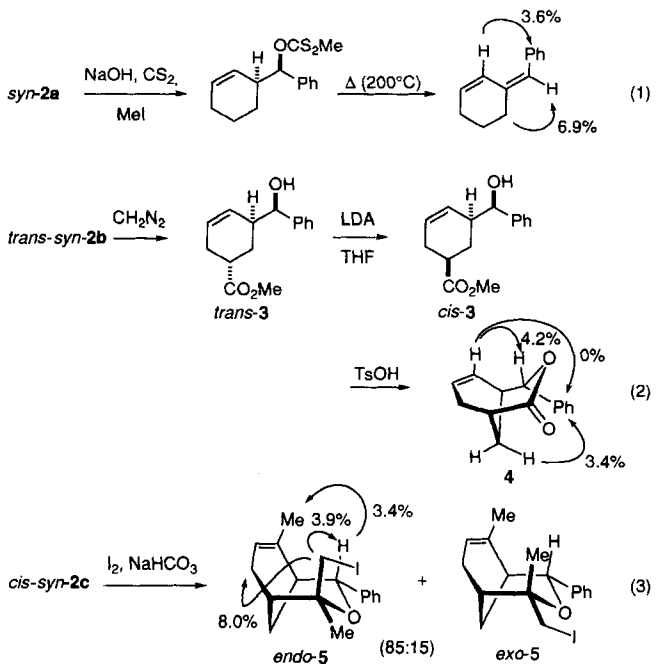
Entry	Allyl compound	Et_2Zn [mmol]	*t* [h]	Products (isolated yield [%])
1	 **1a**	2.4	7	 *syn*-**2a** (76)
2	 **1b**	2.4	5	 *trans-syn*-**2b** (95)[b]
3	 *cis*-**1c**[c]	2.4	46	 *trans-syn*-**2c** (80)  *cis-syn*-**2c** (12)
4	 *trans*-**1c**	2.4	45	*trans-syn*-**2c** (16) *cis-syn*-**2c** (72)
5	 **1d**	2.4	23	 (*Z*)-*anti*-**2d** (60)
6	 **1e**	2.4	26	(*Z*)-*anti*-**2d** (63)
7	 **1f**	2.4	24	 (*Z*)-*anti*-**2f** (71)  (*Z*)-*anti*-**2f'** (5)
8	 **1f**	2.4	24; 74, 65 °C	 (*E*)-**2f''** (70) (*Z*)-*anti*-**2f'** (5)
9	 **1g**	4.8	120	 (*Z*)-*anti*-**2g** (35)
10	 **1h**	2.4	48	 (*Z*)-**2h** (60) (*anti* : *syn* = 89:11)
11	 **1i**	2.4	65	(*Z*)-**2h** (62) (*anti* : *syn* = 86:14)

[a] Reaction conditions: benzaldehyde (1.0 mmol), allyl compound (1.2 mmol), Et_2Zn (indicated amount, 2 M in THF), and $[Pd(PPh_3)_4]$ (0.05 mmol) in THF (5 mL) under N_2, room temperature (unless otherwise specified). [b] Isolated as the methyl ester. [c] Contaminated with 2% of *trans*-**1c**.

[*] Prof. Y. Tamaru, A. Tanaka, K. Yasui, S. Goto, S. Tanaka
Department of Applied Chemistry,
Faculty of Engineering Nagasaki University
1-14 Bunkyo Machi, Nagasaki 852 (Japan)
Telefax: Int. code + (958)47-9008

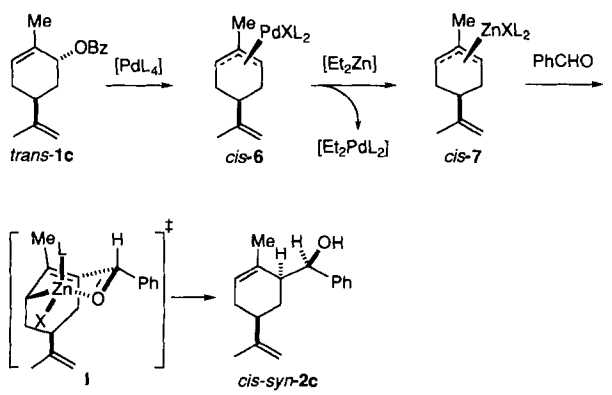
[**] Support from the Japanese Ministry of Education, Science and Culture is gratefully acknowledged. We thank Y. Ohhama for his splendid assistance with the NMR experiments.

The structures of products **2a–c** were determined unequivocally by NOE experiments[4] with the derivatives obtained through stereochemically well-defined transformations [Eqs. (1)–(3)].



Esterification of *trans-syn*-**2b**, followed by isomerization with LDA (4 equiv at −78 °C for 1 h in THF) provided a mixture of *trans*- and *cis*-**3** (43:57); only the *cis* isomer underwent lactonization (cat. toluenesulfonic acid in 1,2-dimethoxyethane at reflux for 8 h) to provide the bicyclic lactone **4** in 71% yield [Eq. (2)]. Iodoetherification[5] of the mixture of *cis-syn*- and *trans-syn*-**2c** (72:16, entry 4) provided bicyclic ethers *endo*- and *exo*-**5** (85:15, 80% yield based on *cis-syn*-**2c**); *trans-syn*-**2c** was recovered intact (80%).

A mechanistic rationale for the *syn*-selective addition with inversion of configuration at the allylic stereocenter is shown for *trans*-**1c** in Scheme 1. It is assumed that the cyclohexenylzinc species *cis*-**7** is formed selectively from *trans*-**1c** with inversion of the allylic stereocenter;[6] conversion of *trans*-**1c** into the π-allylpalladium complex *cis*-**6**[7] proceeds with inversion and subsequent transformation into *cis*-**7** with retention. The resulting *cis*-**7** is configurationally rather stable under the reaction conditions and adds to benzaldehyde via a six-membered chairlike transition state structure **I**.[8]

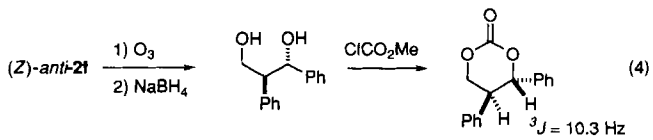


Scheme 1. Mechanistic rationale for inversion of configuration at the allylic center and *syn*-selective addition.

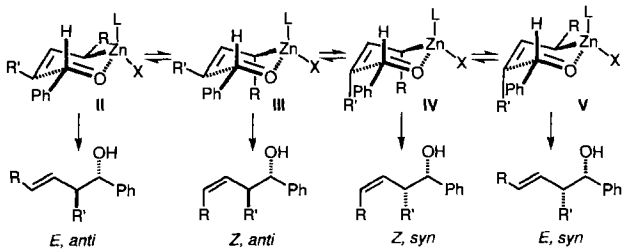
Stimulated by the excellent *syn* selectivity of the addition of cyclohexenylzinc, we examined acyclic 1,3-disubstituted allylic substrates and found that they also displayed pronounced selectivity, providing the *anti* products with (*Z*) configuration either exclusively (entries 5–7, 9) or selectively (entries 10, 11).[10] Despite the rather vigorous reaction conditions (room temperature, 1–3 d), the exclusive formation of (*Z*) isomers suggests that these reactions are controlled kinetically. Indeed, when the product mixture obtained from the reaction of **1f** was heated at 65 °C for a long period of time, (*Z*)-*anti*-**2f** disappeared completely and a diastereomeric mixture of (*E*)-**2f''** formed (3:2, entry 8).

Allylating agents with unsymmetrically substituted allyl groups showed interesting regioselectivity.[11] Allylic termini bearing phenyl groups are generally more reactive than the others (entries 7, 9). Whereas the reaction of **1g** and benzaldehyde yielded 1-ethoxy-3-phenylpropene **2g**, in the analogous reaction with 1,1-diethoxy-2-propene (4.8 equiv Et_2Zn, room temperature, 26 h) addition proceeded exclusively at the allylic terminus bearing the ethoxy groups[12] to furnish 3-ethoxy-4-hydroxy-4-phenyl-1-butene in 75% yield. When the steric bulk of the substituents in positions 1 and 3 differs substantially, the allylic terminus with the smaller substituent reacts preferentially (entries 10, 11).

The (*Z*) configuration of the products was determined from the coupling constants between the olefinic protons ($^3J = 10$–11 Hz). The *anti* configuration was deduced from the ^3J coupling constants of the *trans* protons of the cyclic carbonate derived from (*Z*)-*anti*-**2f** by ozonolysis, reductive workup, and esterification [Eq. (4)].[13]



Four plausible transition state structures are shown in Scheme 2. Structures **II** and **V** seem to be unfavorable because of the *gauche* interactions between the equatorial substituent R and both the ligand L and the counterion X[14] associated with the Zn^{2+} ion. Of the transition state structures with R in axial position, **III** is favored over **IV**, in which R and R′ have a 1,3-diaxial relationship.[16] Thus, addition may proceed selectively through **III** to give the (*Z*)-*anti* products. The preference of Ph as R′ might be due to resonance stabilization; the preference of Me over *i*Pr as R′ may be explained by the the smaller steric hindrance towards carbonyl carbon atom.



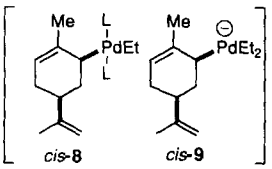
Scheme 2. Transition state structures for the addition of a π-allylzinc complex to benzaldehyde and the resulting products.

The advantages of the palladium-catalyzed allylation described here are the excellent stereoselectivity (*syn* addition with inversion of the allylic stereocenter for 2-cyclohexenyl substrates and (*Z*)-*anti* addition for acyclic 1,3-disubstituted allylic substrates) and the applicability to a range of allylic substrates[17] readily prepared from allylic alcohols and α,β-unsaturated aldehydes, as well as the ease with which the reaction can be performed.

Received: October 10, 1994 [Z 7389 IE]
German version: *Angew. Chem.* **1995**, *107*, 862

Keywords: allylation · π-allylpalladium compounds · umpolung · zinc compounds

[1] K. Yasui, Y. Goto, T. Yajima, Y. Taniseki, K. Fugami, A. Tanaka, Y. Tamaru, *Tetrahedron Lett.* **1993**, *34*, 7619–7622.
[2] M. Kato, M. Kageyama, R. Tanaka, K. Kuwahara, A. Yoshikoshi, *J. Org. Chem.* **1975**, *40*, 1932–1941.
[3] Preparation of *trans*- and *cis*-carveols (100 and 98% purity, respectively) will be reported elsewhere.
[4] E. Breitmaier, *Structure Elucidation by NMR in Organic Chemistry*, Wiley, New York, **1993**.
[5] Y. Tamaru, M. Hojo, S. Kawamura, S. Sawada, Z. Yoshida, *J. Org. Chem.* **1987**, *52*, 4062–4072.
[6] For attempts at stereoselective generation of C_{sp^3}–Zn bonds, see R. Duddu, M. Eckhardt, M. Furlong, H. P. Knoess, S. Berger, P. Knochel, *Tetrahedron* **1994**, *50*, 2415–2432; T. . Majid, M. C. P. Yeh, P. Knochel, *Tetrahedron Lett.* **1989**, *30*, 5069–5072.
[7] F. K. Sheffy, J. P. Godschalx, J. K. Stille, *J. Am. Chem. Soc.* **1984**, *106*, 4833–4840 and references therein.
[8] A σ-allylpalladium(II) species such as *cis*-**8** and *cis*-**9** may also be responsible for the allylation of aldehyde. However, *cis*-**8** is expected to be at best poorly nucleophilic, by analogy with the reaction behavior of related complexes [9], and *cis*-**9** is not capable of forming a cyclic transition state like **I**, since the palladium metal is negatively charged.



cis-**8** *cis*-**9**

[9] H. Kurosawa, A. Urabe, K. Miki, N. Kasai, *Organometallics* **1986**, *5*, 2002–2008.
[10] For the (*Z*)-*anti*-selective addition of allylboranes and -stannanes, see W. R. Roush in *Comprehensive Organic Synthesis*, Vol. 2 (Eds.: B. M. Trost, I. Fleming, C. H. Heathcock), Pergamon, Oxford, **1991**, p. 1.
[11] A. Yanagisawa, K. Yasue, H. Yamamoto, *Synlett* **1993**, 686–688.
[12] D. A. Evans, G. C. Andrews, B. Buckwalter, *J. Am. Chem. Soc.* **1974**, *96*, 5560–5561.
[13] T. Bando, H. Harayama, Y. Fukazawa, M. Shiro, K. Fugami, S. Tanaka, Y. Tamaru, *J. Org. Chem.* **1994**, *59*, 1465–1474.
[14] 1,3-Dimethylallylzinc bromide [15] reacted with benzaldehyde (−19 °C, 2 h, THF) to provide **2d** as a stereoisomeric mixture (62:21:17) with (*Z*)-*anti*-**2d** as the major product. The marked difference in stereoselectivity (cf. Table 1, entries 5, 6) may be attributed in part to the different counterion X ($PhCOO^-$, PhO^-, EtO^-, or Et^- vs. Br^-). Further studies to clarify mechanistic details are in progress.
[15] M. Bellassoued, Y. Frangin, M. Gaudemar, *Synthesis* **1977**, 205–208.
[16] R. W. Hoffmann, *Angew. Chem.* **1992**, *104*, 1147–1157; *Angew. Chem. Int. Ed. Engl.* **1992**, *31*, 1124–1134.
[17] Allylation under similar conditions is possible with allylic sulfides (Y. Tamaru, A. Tanaka, unpublished results). For allylation with allylic sulfones, see J. Clayden, M. Julia, *J. Chem. Soc. Chem. Commun.* **1994**, 1095–1096.

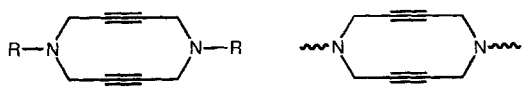
Novel "π-Boat" Cage Compounds as Potential Cryptands**

Rolf Gleiter,* Kirstin Hövermann, Joachim Ritter, and Bernhard Nuber

Dedicated to Professor Paul von Ragué Schleyer on the occasion of his 65th birthday

Since the discovery of the complexation properties of crown ethers, these species and their polycyclic congeners, the cryptands, have been studied in detail.[1] Because of their functional and geometrical properties azacryptands serve as excellent hosts for metal cations, organic cations, neutral organic molecules, and anions.[2]

Aliphatic and aromatic moieties have been used as bridging units. The aromatic units can serve as complexing functions for neutral organic molecules especially if π-π interactions between host and guest are possible. Thus numerous cryptands containing various π systems have been investigated.[3, 4] Nevertheless, there are only a few cryptands in which alkyne units combined with heteroatoms were used as building blocks.[5, 6] Our recent synthesis of *N,N'*-dialkyl-1,6-diazacyclodeca-3,8-diynes **1a–g**[7, 8] led to the idea of using the diazacyclodecadiynediyl unit **2** as a building block for new cryptands (Fig. 1). Each unit contains a pair of strongly interacting parallel triple bonds as a π system and two amine functions as linking elements.



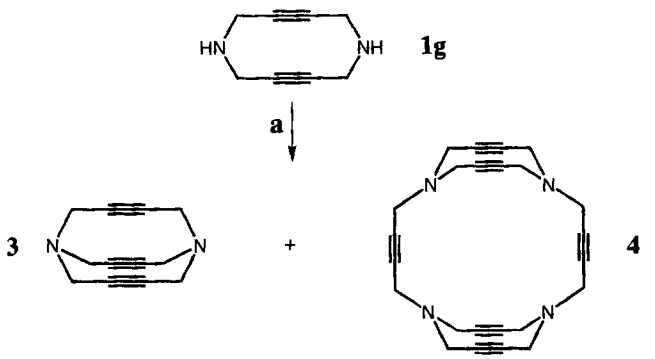
1a-g **2**

Fig. 1. **a**, R = Me; **b**, R = Et; **c**, R = *i*Pr; **d**, R = *t*Bu; **e**, R = *p*-tolyl; **f**, R = Ac; **g**, R = H.

Recent X-ray structure investigations[7, 8] have shown that **1a–g** can be considered as an elongated piperazine; however, they show more conformational flexibility than piperazine, since the triple bond units diminish the Pitzer strength between the methylene groups. As a result the boat conformation of **1a–g** is nearly as stable as the chair conformation, as indicated by dynamic NMR investigations and semiempirical calculations.[8, 9] This opens possibilities to use this unit for the construction of novel cagelike molecules by intra- and intermolecular bridging. We favored the 2-butyne-1,4-diyl unit as a linking bridge for geometrical and steric reasons. In fact we obtained the bicyclic triyne **3** by reacting **1g** with 1,4-dibromo-2-butyne as the main product in nearly 10% yield (Scheme 1). The bicyclic triyne **3** is the first example of a topological prismane-like preorganization of triple bonds. Compound **3** is stable in solution and at temperatures below −40 °C in the solid state (white crystals). In contrast, the dihydrochloride **3** · 2 HCl is stable at

[*] Prof. Dr. R. Gleiter, K. Hövermann, Dipl.-Chem. J. Ritter
Organisch-chemisches Institut der Universität
Im Neuenheimer Feld 270, D-69120 Heidelberg (Germany)
Telefax: Int. code +(6221) 56-4205
Dr. B. Nuber
Anorganisch-chemisches Institut der Universität Heidelberg (Germany)

[**] This work was supported by the Fonds der Chemischen Industrie, the Deutsche Forschungsgemeinschaft (SFB 247), and the BASF Aktiengesellschaft (Ludwigshafen). J. R. thanks the Studienstiftung des Deutschen Volkes for a Ph.D. grant. We thank Dr. M. Rentzea and Mrs. C. Berndt for FAB^+ spectrometric measurements.



Scheme 1. a) 1,4-Dibromo-2-butyne, K_2CO_3, THF, 66 °C, high dilution, **3**: 10%, **4**: 6%.

room temperature. The macrocyclic cage compound **4** was isolated as a side product.

This result encouraged us to study the reaction of **1g** with several α,α′-dihaloxylenes. However, to date these experiments have not led to bicyclic products; 1,4-bis(bromomethyl)benzene gave the "trimer" **5** and with the 1,3 isomer, the "dimer" **6** and "trimer" **7** were obtained. 2,6-Bis(bromo)methylpyridine afforded the "dimer" **8** (Scheme 2).

The most relevant NMR spectroscopic and mass spectrometric data of the new cage compounds are listed in Table 1. The structure of the bicyclic triyne **3** can be proved by NMR spectroscopic data since due to its D_{3h} symmetry it shows only one signal in the ^{1}H NMR spectrum and two signals in the ^{13}C NMR spectrum. To distinguish between possible dimeric and trimeric structures of **4**–**8** additional FAB$^+$ spectrometric data were necessary.

The X-ray structure investigations[10] on single crystals of the *meta*-cyclophane **6** show that the diyne ring moieties adopt a boat conformation[11, 12] (Fig. 2). The nitrogen lone pairs are

Table 1. Spectroscopic data of cage compounds **3**–**8**.

3: ^{1}H NMR (200 MHz, $CDCl_3$): δ = 3.72 (s); ^{13}C NMR (50.32 MHz, $CDCl_3$): δ = 86.6 (s, C≡C), 46.3 (t, CH_2N); HRMS ($C_{12}H_{12}N_2$): calcd.: 184.1000, found: 184.0990

4: ^{1}H NMR (200 MHz, $CDCl_3$): δ = 3.75 (s, 8H, CH_2N), 3.65 (s, 16H, CH_2N-Di-in); ^{13}C NMR (50.32 MHz, $CDCl_3$): δ = 83.4 (s, C≡C diyne), 81.7 (s, C≡C), 44.75 (t, CH_2N diyne), 43.92 (t, CH_2N); FAB$^+$-MS: m/z = 369.1 (M + 1), 368.0 (M), 367.1 (M − 1)

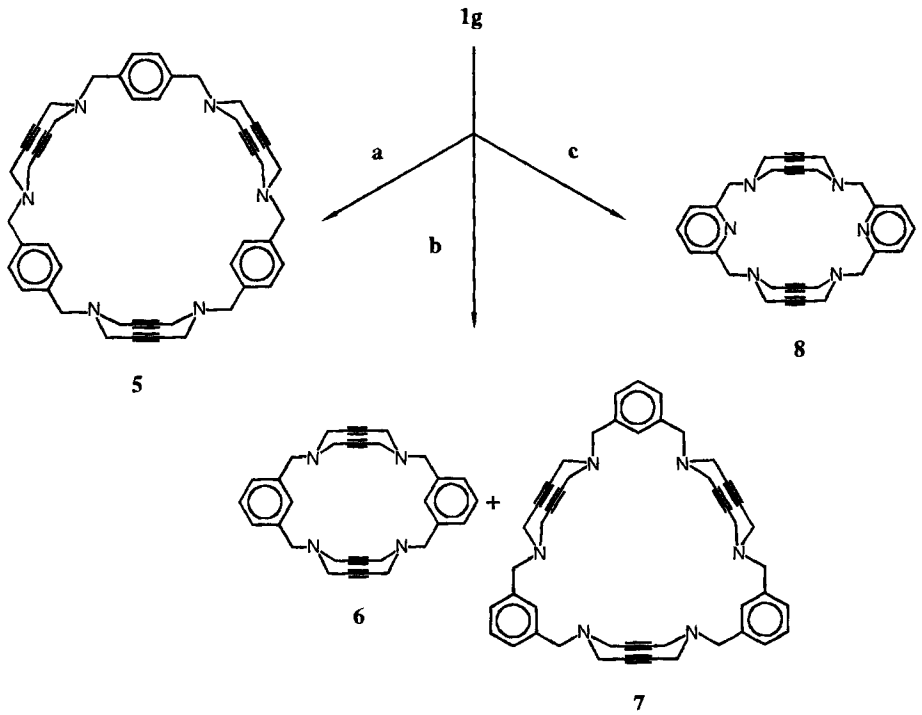
5: ^{1}H NMR (253 K) (200 MHz, $CDCl_3$): δ = 7.50 (s, 12H, arom. CH), 4.18 (s, 12H, benzyl. CH_2), 3.75–3.31 (AA′BB′, $^2J_{AB}$ = 16.2 Hz, 24H, CH_2N); ^{13}C NMR (75.46 MHz, $CDCl_3$): δ = 137.7 (s, arom. C-1, C-4), 129.6 (d, arom. CH), 83.0 (s, C≡C), 56.2 (t, benzyl. CH_2), 44.5 (t, CH_2N); FAB$^+$-MS: m/z = 711.3 (M + 3), 710.3 (M + 2), 709.3 (M + 1); 708.3 (M), 707.3 (M − 1)

6: ^{1}H NMR (300 MHz, $CDCl_3$): δ = 7.71 (s, 2H, arom. CH), 7.38 (m, 6H, arom. CH), 4.21 (s, 8H, benzyl. CH_2), 3.74–3.32 (AA′BB′, $^2J_{AB}$ = 15.8 Hz, 16H, CH_2N); ^{13}C NMR (75.46 MHz, $CDCl_3$): δ = 138.2 (s, arom. C-1, C-3), 131.2, 129.3, 129.0 (d, arom. CH), 82.8 (s, C≡C), 56.5 (t, benzyl. CH_2), 44.5 (t, CH_2N); FAB$^+$-MS: m/z = 475.3 (M + 3), 474.3 (M + 2), 472.2 (M + 1); 473.2 (M), 471.3 (M − 1)

7: ^{1}H NMR (300 MHz, $CDCl_3$): δ = 7.53 (s, 3H, arom. CH), 7.32 (m, 9H, arom. CH), 4.03 (s, 12H, benzyl. CH_2), 3.53 (s, 24H, CH_2N); ^{13}C NMR (75.46 MHz, $CDCl_3$): δ = 138.0 (s, arom. C-1, C-3), 130.6, 128.7, 128.4 (d, arom. CH), 82.8 (s, C≡C), 55.5 (t, benzyl. CH_2), 44.6 (t, CH_2N); FAB$^+$-MS: m/z = 711.4 (M + 3), 710.4 (M + 2), 709.4 (M + 1); 708.4 (M), 707.4 (M − 1)

8: ^{1}H NMR (300 MHz, $CDCl_3$): δ = 7.64 (t, ^3J = 7.7 Hz, 2H, arom. CH), 7.31 (d, ^3J = 7.7 Hz, 4H, arom. CH), 4.57 (s, 8H, py-CH_2), 3.77–3.40 (AA′BB′, $^2J_{AB}$ = 15.8 Hz, 16H, CH_2N); ^{13}C NMR (75.46 MHz, $CDCl_3$): δ = 158.3 (s, arom. C-2, C-6), 137.2, 120.3 (d, arom. CH), 82.9 (s, C≡C), 58.1 (t, py-CH_2), 45.0 (t, CH_2N); FAB$^+$-MS: m/z = 476.2 (M + 2), 475.2 (M + 1)

oriented equatorial outside, forcing the benzylic methylene groups into an axial inside position. The preference for axial oriented substituents in diazacyclodecadiynes has been shown in all known cases **1a**–**g**[13]. From the NMR spectroscopic data an equilibrium between an "outside" (**6a**) and an "inside" isomer (**6b**) cannot be excluded.[12, 13] This isomerization process could take place by nitrogen inversion and rotation of the benzylic methylene groups (Scheme 3).



Scheme 2. Reaction conditions: K_2CO_3, THF, reflux, high dilution; a) 1,4-bis(bromomethyl)benzene, **5**: 20%; b) 1,3-bis(bromomethyl)benzene, **6**: 27%, **7**: 15%; c) 2,6-bis(bromomethyl)pyridine, **8**: 25%.

Unlike in the *meta*-cyclophanes **6** and **8**, the diazacyclodecadiyne units in **4** show a fast ring inversion process at room temperature on the NMR time scale, indicated by two sharp ^{1}H NMR singlets in the ratio 2:1. The ^{1}H NMR signals of the NCH_2 groups of **6** and **8** are split into an AA′BB′ pattern owing to the inequivalency of the axial and equatorial hydrogen atoms of the cyclodecadiyne boat. The decreased rigidity of the "trimer" **5** is reflected by a broad signal for the NCH_2 groups in the ^{1}H NMR spectrum at room temperature. This signal is split into a sharp AA′BB′ pattern at 253 K (in $CDCl_3$, T_c = 295 K, $\Delta G^{\neq}$ = 14 kcal mol^{-1} (Table 1).

^{1}H NMR (300 MHz, $CDCl_3$) investigations reveal the complexation of one water molecule in **8** as evidenced by H/D exchange experiments [**8** · H_2O: δ = 3.57 (s, H_2O)]. Preliminary complexation experiments of **8** with Cu^+ ions revealed strong shifts and splitting of the aromatic and the benzylic hydrogen atoms in the ^{1}H NMR spec-

 © VCH Verlagsgesellschaft mbH, D-69451 Weinheim, 1995 0570-0833/95/0707-0790 $ 10.00+.25/0

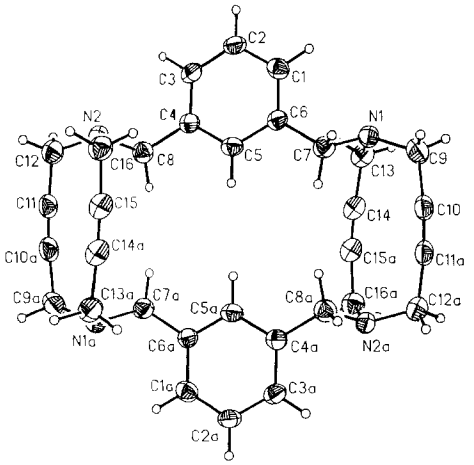
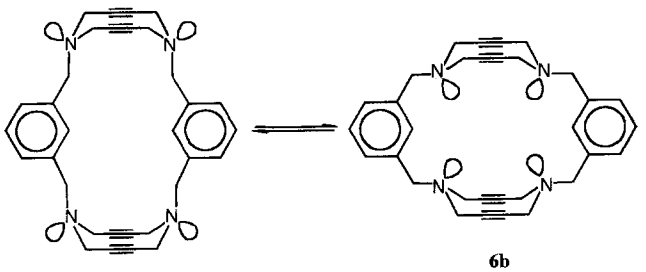


Fig. 2. Crystal structure of the *meta*-cyclophane **6** [10].



6a **6b**

Scheme 3. Possible equilibrium between the "outside" (**6a**) and "inside" isomer (**6b**) of **6** by nitrogen inversion and rotation of the benzylic methylene groups.

trum. Corresponding complexation reactions of **6** with Ag^+ ions have not been successful.

In light of the structures of the bicyclic triyne **3** and the cyclophane **6** we propose the name "π boat" cages for the bridged diazacyclodecadiynes.

Received: October 5, 1994
Revised version: December 29, 1994 [Z 7379 IE]
German version: *Angew. Chem.* **1995**, *107*, 867

Keywords: alkynes · cage compounds · phanes

[1] a) C. J. Pederson, *J. Am. Chem. Soc.* **1967**, *89*, 2495; b) C. J. Pederson, *Angew. Chem.* **1988**, *100*, 1053; *Angew. Chem. Int. Ed. Engl.* **1988**, *100*, 1021; c) J.-M. Lehn, *ibid.* **1988**, *100*, 91 and **1988**, *100*, 89; d) F. Vögtle, *Supramolekulare Chemie*, Teubner, Stuttgart, **1992**; e) *Crown Compounds, Towards Future Applications*, (Ed.: S. R. Cooper), VCH, Weinheim, **1992**; f) B. Dietrich, P. Viout, J.-M. Lehn, *Macrocyclic Chemistry*, VCH, Weinheim, **1993**.

[2] F. P. Schmidtchen, A. Gleich, A. Schummer, *Pure Appl. Chem.* **1989**, *61*, 1535.

[3] D. O'Krongly, S. R. Denmeade, M. Y. Chiang, R. Breslow, *J. Am. Chem. Soc.* **1985**, *107*, 5544; A. Bencini, V. Fusi, M. Micheloni, B. Valtancoli, *J. Chem. Soc. Chem. Commun.* **1994**, 1119.

[4] B. J. Whitlock, H. W. Whitlock, *J. Am. Chem. Soc.* **1994**, *116*, 2301; review: F. Diederich, *Cyclophanes*, Monographs in Supramolecular Chemistry 2; The Royal Society of Chemistry, London, **1991**.

[5] A. Nakano, Y. Li, P. Geoffroy, M. Kim, J. L. Atwood, S. Bott, H. Zhang, L. Echegoyen, G. W. Gokel, *Tetrahedron Lett.* **1989**, *30*, 5099.

[6] J. P. Sauvage, J. Weiss, *J. Am. Chem. Soc.* **1985**, *107*, 6108.

[7] R. Gleiter, J. Ritter, H. Irngartinger, J. Lichtenthäler, *Tetrahedron Lett.* **1991**, *32*, 2883; *ibid.* **1991**, *32*, 2887.

[8] J. Ritter, H. Irngartinger, R. Gleiter, unpublished.

[9] J.-J. Delpuech in *Cyclic Organonitrogen Stereodynamics* (Eds.: J. B. Lambert, Y. Takeuchi), VCH, Weinheim, **1992**.

[10] X-ray structure analysis of **6**: colorless crystals from $CHCl_3$, $C_{32}H_{32}N_4$, $M_r = 472.63$, monoclinic, space group C_{2h}^6, crystal size: $0.25 \times 0.50 \times 0.70$ mm, $a = 22.86(3)$, $b = 6.893(7)$, $c = 17.37(1)$ Å, $\beta = 155.39(5)^\circ$, $V = 2472.7$ Å^3, $F(000) = 1008$, $Z = 4$, $\rho_{calcd} = 1.27$ g cm^{-3}, $\mu = 0.07$ mm^{-1}, $Mo_{K\alpha}$ radiation, $\lambda = 0.7107$ Å. Intensity data were collected on a SYNTEX R3 diffractometer. 2740 measured reflections, 1402 independent reflections within $I > 2.5\sigma(I)$, number of reflections within $I > 2.0\sigma(I)$ not defined. The structure was solved with Patterson-Fourier methods carried out with SHELXTL PLUS. $R = 0.061$, $R_w = 0.051$. Further details of the crystal structure investigation may be obtained from the Fachinformationszentrum Karlsruhe, D-76344 Eggenstein-Leopoldshafen (Germany) on quoting the depository number CSD-58 843.

[11] Analogous compounds with piperazine instead of **1g**, in which the chair conformation is favored: K. Rissanen, J. Breitenbach, J. Huuskonen, *J. Chem. Soc. Chem. Commun.* **1994**, 1265.

[12] Piperazine macrocycles with chair conformation, which changes to boat conformation after metal complexation: P. W. Wade, R. D. Hancock, J. C. A. Boeyens, S. M. Dobson, *J. Chem. Soc. Dalton Trans.* **1990**, 483.

[13] R. W. Alder, *Acc. Chem. Res.* **1983**, *16*, 321.

Coordination of CO to the Alkaline Earth Metallocene $[(Me_5C_5)_2Ca]$**

Peter Selg, Hans H. Brintzinger,*
Richard A. Andersen,* and István T. Horváth*

Dedicated to Professor Richard R. Schmidt on the occasion of his 60th birthday

Compared to the countless transition metal carbonyl complexes, in which CO acts as a π acceptor for d electrons on the metal center, CO coordination to main group compounds has been observed in a few instances only. A gas-phase species HCO^+ has been found to have its ν(CO) absorption at 2184 cm^{-1}.[1] Diborane reacts with CO to give a volatile complex $[H_3B\text{-}CO]$ with $\nu(CO) = 2165$ cm^{-1}.[2] Microwave spectroscopy yields a dipole moment of 1.8 D for this molecule,[3] consistent with the charge distribution $[H_3B^-\text{-}C{\equiv}O^+]$.[4] Me_3Al was found to form a complex $[Me_3Al\text{-}CO]$ with $\nu(CO) = 2185$ cm^{-1} in a CO matrix at 15–35 K.[5] The increase of ν(CO) above that of free CO (2143 cm^{-1})[6] in all of these complexes indicates that CO is acting solely as a σ-donor ligand here. In $[Me_2Si\text{-}CO]$ and $[(Me_5C_5)_2Si\text{-}CO]$,[7, 8] on the other hand, ν(CO) is decreased to 1962 and 2065 cm^{-1}, respectively, consistent with a π-donor action of these divalent silicon species. Apart from low-temperature matrix studies,[9] CO coordination to alkaline earth compounds has not been reported so far. Here, we describe evidence

[*] Prof. Dr. H. H. Brintzinger, Dipl.-Chem. P. Selg
Fakultät für Chemie der Universität
D-78434 Konstanz (Germany)
Telefax: Int. code + (7531)883137

Prof. Dr. R. A. Andersen
Department of Chemistry and
Chemical Science Division of Lawrence Berkeley Laboratory
University of California
Berkeley, CA 94720 (USA)
Telefax: Int. code + (510)642-8369

Dr. I. T. Horváth
Corporate Research Science Laboratories
Exxon Research and Engineering Company
Annandale, NJ 08801 (USA)
Telefax: Int. code + (908)730-3042

[**] This work was supported by the Deutsche Forschungsgemeinschaft, by the Fonds der Chemische Industrie, and by the Director, Office of Energy Research, Office of Basic Energy Sciences, Chemical Sciences Division of the U. S. Department of Energy, under contract DE-AC03-76SF00098. R. A. A. thanks the Alexander-von-Humboldt Foundation for a Senior Scientist Award.

for the formation of the first carbonyl complex of an organo alkaline earth molecular compound, $[(Me_5C_5)_2Ca\text{-}CO]$.

When a solution of $[(Me_5C_5)_2Ca]$[11] in toluene is exposed to CO pressures of 2.5–70 bar in an elevated-pressure IR cell,[12] a new ν(CO) absorption appears at 2158 cm^{-1}. The appearance of this band, as well as its loss in intensity upon release of CO pressure, is practically instantaneous; repeated measurements at any given pressure show that these changes are reversible. Figure 1 shows the IR spectrum as a function of CO pressure at 10 °C. It is apparent that the change in absorbance at 2158 cm^{-1}, $\Delta E(2158)$, is a suitable measure for the extent of complex formation. A linear Hildebrand–Benesi plot[13] of $\Delta E(2158)^{-1}$ against

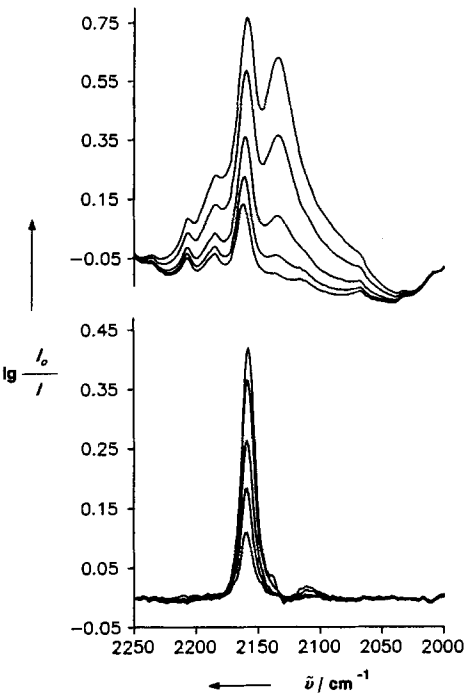


Fig. 1. IR spectra of a 4×10^{-2} M solution of $[(Me_5C_5)_2Ca]$ in toluene at 10 °C at CO pressures of 5, 10, 20, 40, and 60 bar; top: Base-line corrected spectra; bottom: Spectra corrected for the absorption of solvent and free CO in solution.

$p(CO)^{-1}$ indicates a stoichiometry $[(Me_5C_5)_2Ca\text{-}CO]$[14] and an equilibrium constant $K = 0.036$ bar^{-1} for the reaction between solvated decamethyl calcocene and gaseous CO [Eq. (a)]. Since

$$[(Me_5C_5)_2Ca](tol) + CO(gas) \rightleftharpoons [(Me_5C_5)_2Ca\text{-}CO](tol) \quad (a)$$

the concentration of dissolved CO is proportional to CO pressure, $c(CO) = p(CO) \times 7.1 \times 10^{-3}$ M bar^{-1}, throughout the temperature and pressure range considered here,[12] a value of $K = 5.1$ M^{-1} is obtained for the corresponding reaction involving dissolved CO [Eq. (b)]. IR spectroscopic measurements in the

$$[(Me_5C_5)_2Ca](tol) + CO(tol) \rightleftharpoons [(Me_5C_5)_2Ca\text{-}CO](tol) \quad (b)$$

temperature range of −27 to + 32 °C give values for the equilibrium constants as summarized in Table 1;[16] from these, thermodynamic values of $\Delta H_a^\circ = -25 \pm 5$ kJ mol^{-1} and $\Delta S_a^\circ = -110 \pm 10$ J $mol^{-1}K^{-1}$ are obtained for complex formation according to Equation (a), while values of $\Delta H_b^\circ = -25 \pm 5$ kJ mol^{-1} and $\Delta S_b^\circ = -70 \pm 10$ J $mol^{-1}K^{-1}$ are obtained for Equation (b).

Table 1. Temperature dependence of equilibrium constants K for reaction (a) and K for reaction (b) in toluene, as determined by IR spectroscopy (with e.s.d.).

T/°C	+32	+10	+3	−9	−18	−27
K/kbar^{-1}	15(3)	36(8)	51(3)	71(3)	115(14)	127(11)
K/M^{-1}	2.1	5.1	7.2	10.0	16.1	17.9

These data are confirmed by a ^{13}C NMR study at elevated CO pressures.[17] Solutions of $[(Me_5C_5)_2Ca]$ in $[D_8]$toluene under CO pressures up to 80 bar give only one ^{13}C NMR signal each for their C_5-ring, CH_3, and CO carbon atoms in the temperature range between + 30 and −70 °C,[18] indicating that the exchange of CO is rapid on the NMR time scale. The chemical shifts of these signals change with increasing CO pressure as indicated in Table 2. As changes in chemical shifts, $\Delta\delta$, are a

Table 2. ^{13}C NMR data for $[(Me_5C_5)_2Ca] + CO \rightleftharpoons [(Me_5C_5)_2Ca\text{-}CO]$ in $[D_8]$toluene at $T = 31.5$ °C [a].

p(CO)/bar	$\delta(CH_3)$	$\delta(C_5)$	δ(CO)
0	10.39	113.94	184.7 [b]
15	10.53	113.75	183.36
30	10.61	113.62	183.59
50	10.67	113.55	183.80
80	10.72	113.48	183.96
$[(C_5Me_5)_2Ca\text{-}CO]$	10.90(1) [b]	113.19(4) [b]	180.4 [b]

[a] Measured with a JEOL JMN GX 400 spectrometer operated at 96.4 MHz. chemical shifts relative to $\delta(C_6D_5CD_3) = 20.4$. [b] Obtained by least- square analysis from the values observed at p(CO) = 15–80 bar.

linear function of the mole fractions of free and complexed species, the equilibrium constant K, as well as the limiting values of $\Delta\delta$ for complete complex formation, can be obtained by a least-squares analysis of the essentially linear plots of $\Delta\delta^{-1}$ against $p(CO)^{-1}$. A value of $K = 0.024$ bar^{-1} at 31.5 °C, obtained in this manner, is in agreement with that derived from the IR data discussed above. A chemical shift of $\delta = 180.4$, determined for CO in $[(Me_5C_5)_2Ca\text{-}CO]$, places this CO resonance at higher fields than that of free CO in toluene solution ($\delta = 184.7$). $[(Me_5C_5)_2Ca\text{-}CO]$ differs in this regard from transition metal carbonyl complexes with partly filled *n*d subshells; in these, the CO ligands have their ^{13}C NMR signals at substantially lower fields than the signal of free CO.[19, 20]

With regard to both the ^{13}C chemical shift of its CO ligand to higher fields and the shift of ν(CO) to higher frequencies, compared to the respective values of free CO, $[(Me_5C_5)_2Ca\text{-}CO]$ resembles a number of recently reported noble metal CO complexes, mostly with *n*d^{10} electron configuration.[15] Our results show that d electrons are not essential for exothermic CO coordination. $[(Me_5C_5)_2Ca]$ appears to make up for its lack of d electrons by an unusual Lewis acidity, which is probably related to its bent structure.[21, 22] Metal–ligand bond formation can thus presumably occur with expenditures of reorganization energy much smaller than those required to bend typical transition metal sandwich compounds.[22, 23] In accord with this notion, no carbonyl complex formation is observed, up to CO pressures of 50 bar, in solutions of $[(Me_5C_5)_2Mg]$ in toluene, for which a strictly linear geometry has been established.[11] Preliminary experiments with the bent alkaline earth metallocene $[(Me_5C_5)_2Sr]$ [22, 24] indicate the formation of a carbonyl complex with $\nu(CO) = 2159$ cm^{-1}, similar to that observed for $[(Me_5C_5)_2Ca\text{-}CO]$.

 © VCH Verlagsgesellschaft mbH, D-69451 Weinheim, 1995 0570-0833/95/0707-0792 $ 10.00+.25/0

This is the first example of CO binding to a molecular alkaline earth metal compound. Previously described $[(Me_5C_5)_2Ca]$ complexes, such as $[(Me_5C_5)_2Ca(PEt_3)]$,[25] $[(Me_5C_5)_2Ca(Me-C\equiv C-Me)]$,[26] $[(Me_5C_5)_2Ca(Me_3Si-C\equiv C-C\equiv C-SiMe_3)]$,[27] and $[(Me_5C_5)_2Ca(CN\text{-}2,6\text{-}xylyl)_2]$ [25] show that one or two ligands can be coordinated at the Ca center. In the case of the carbonyl complex reported here, only one CO ligand appears to be taken up in the pressure range studied. The binding of CO to the Ca center is weaker than that of the diethyl ether ligand in $[(Me_5C_5)_2Ca(OEt_2)]$, as OEt_2 is not displaced by CO at pressures up to 120 bar. This observation and the similarity of ν(CO) frequencies in $[H_3B\text{-}CO]$ and $[(Me_5C_5)_2Ca\text{-}CO]$ are consistent with the view that CO acts solely as a σ-donor ligand towards $[(Me_5C_5)_2Ca]$ and that dipolar interactions are important for the Ca–CO bond.

Received: September 24, 1994
Revised version: December 23, 1994 [Z 7350IE]
German version: *Angew. Chem.* **1995**, *107*, 877

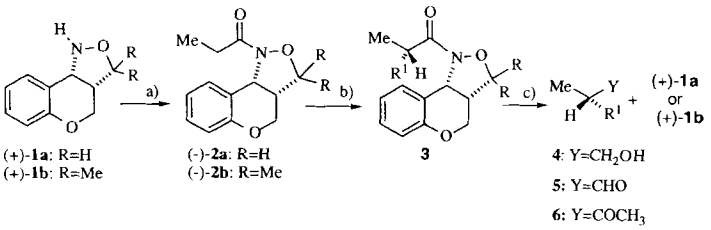
Keywords: alkaline earth metal compounds · carbonyl complexes · high-pressure chemistry · metallocenes

[1] S. C. Foster, A. R. W. McKellar, T. J. Sears, *J. Chem. Phys.* **1984**, *81*, 578; P. B. Davies, P. A. Hamilton, W. J. Rothwell, *ibid.* **1984**, *81*, 1598.
[2] A. B. Burg, H. I. Schlessinger, *J. Am. Chem. Soc.* **1937**, *59*, 780; A. B. Burg, *ibid.* **1952**, *74*, 3482; G. W. Bethke, M. K. Wilson, *J. Chem. Phys.* **1957**, *26*, 1118; R. C. Taylor, *ibid.* **1957**, *26*, 1131.
[3] W. Gordy, H. Ring, A. B. Burg, *Phys. Rev.* **1950**, *78*, 512.
[4] M. W. P. Strandberg, C. S. Pearsall, M. T. Weiss, *J. Chem. Phys.* **1949**, *17*, 429.
[5] R. Sanchez, C. Arrington, C. A. Arrington, Jr., *J. Am. Chem. Soc.* **1989**, *111*, 9110. At room temperature no indication of coordination was obtained up to a CO pressure of 10 bar.
[6] K. Nakamoto, *Infrared Spectra of Inorganic and Coordination Compounds*, 2nd. edition, Wiley, New York, **1970**, p. 78.
[7] C. A. Arrington, J. T. Petty, S. E. Payne, W. C. K. Haskins, *J. Am. Chem. Soc.* **1988**, *110*, 6240; M. Pearsall, R. West, *ibid.* **1988**, *110*, 7228.
[8] M. Tacke, C. Klein, D. J. Stufkens, A. Oskam, P. Jutzi, E. A. Bunte, *Z. Anorg. Allg. Chem.* **1993**, *619*, 865.
[9] Coordination of carbon monoxide to the alkaline earth fluorides MgF_2, CaF_2, SrF_2, and BaF_2 as well as to $CaCl_2$ in CO matrices at temperatures of about 10 K was deduced from the observation of one or several infrared absorption bands between 2160 and 2205 cm^{-1} [10a] and from changes in the Ca–Cl stretching frequency [10b].
[10] a) R. H. Hauge, S. E. Gransden, J. L. Margrave, *J. Chem. Soc. Dalton Trans.* **1979**, 745; b) I. R. Beattie, P. J. Jones, N. A. Young, *J. Am. Chem. Soc.* **1992**, *114*, 6146.
[11] R. A. Andersen, J. M. Boncella, C. J. Burns, R. Blom, A. Haaland, H. V. Volden, *J. Organomet. Chem.* **1986**, *312*, C49; R. A. Andersen, R. Blom, J. M. Boncella, C. J. Burns, H. V. Volden, *Acta Chem. Scand. Ser. A* **1987**, *41*, 24.
[12] E. U. van Raaij, C. D. Schmulbach, H. H. Brintzinger, *J. Organomet. Chem.* **1987**, *328*, 275. Blank experiments in the same cell without $[(Me_5C_5)_2Ca]$ give rise only to the absorption of free CO at 2134 cm^{-1}.
[13] H. A. Benesi, J. H. Hildebrand, *J. Am. Chem. Soc.* **1949**, *71*, 2703.
[14] A stoichiometry of $[(Me_5C_5)_2Ca(CO)_2]$ cannot be excluded on the basis of the observation of a single CO stretching absorption alone, since the symmetric and asymmetric stretching vibrations of such a dicarbonyl species could be unresolved (cf. ref. [15]); this stoichiometry is unlikely, however, since a plot of $\Delta E(2158)^{-1}$ vs. $p(CO)^{-2}$ deviates significantly from linearity.
[15] σ-Bonded carbonyl complexes of Pd^{2+}, Pt^{2+}, Ag^+, Au^+, Hg^{2+}, and Hg_2^{2+}: D. Belli Dell'Amico, F. Calderazzo, P. Robino, A. Segre, *J. Chem. Soc. Dalton Trans.* **1991**, 3017; J. J. Rack, B. Moasser, J. D. Gargulak, W. L. Gladfelter, H. D. Hochheimer, S. H. Strauss, *J. Chem. Soc. Chem. Commun.* **1994**, 685; H. Willner, M. Bodenbinder, C. Wang, F. Aubke, *ibid.*, **1994**, 1189; H. Willner, J. Schaebs, G. Hwang, F. Mistry, R. Jones, J. Trotter, F. Aubke, *J. Am. Chem. Soc.* **1992**, *114*, 8972; L. Weber, *Angew. Chem.* **1994**, *106*, 1131; *Angew. Chem. Int. Ed. Engl.* **1994**, *33*, 1077.
[16] An essentially unchanged value of ν(CO) $\approx$ 2159 cm^{-1} and similar absorbance changes in dependence on pressure and temperature are observed in methylcyclohexane solution and indicate that solvent effects are of minor importance for this equilibrium reaction.
[17] I. T. Horváth, J. M. Millar, *Chem. Rev.* **1991**, *91*, 1339.
[18] At lower temperatures, the solubility of $[(Me_5C_5)_2Ca]$ is insufficient for ^{13}C NMR measurements.
[19] B. E. Mann, B. F. Taylor, *^{13}C NMR Data for Organometallic Compounds*, Academic Press, New York **1981**.
[20] A ^{13}C NMR signal at $\delta = 158$ is observed for $[H_3B\text{-}CO]$: L. W. Hall, D. W. Lowman, P. D. Ellis, J. D. Odom, *Inorg. Chem.* **1975**, *14*, 580.
[21] R. A. Williams, T. P. Hanusa, J. C. Huffman, *Organometallics* **1990**, *9*, 1128.
[22] The energy required to change the centroid-calcium-centroid angle in the range of 180 to 150° has been estimated to be very small: R. Blom, K. Faegri, Jr., H. V. Volden, *Organometallics* **1990**, *9*, 372; M. Kaupp, P. von R. Schleyer, M. Dolg, H. Stoll, *J. Am. Chem. Soc.* **1992**, *114*, 8202; T. K. Hollis, J. K. Burdett, B. Bosnich, *Organometallics* **1993**, *12*, 3385.
[23] H. H. Brintzinger, L. L. Lohr, Jr., K. L. Tang Wong, *J. Am. Chem. Soc.* **1975**, *97*, 5146; K. M. Simpson, M. F. Rettig, R. M. Wing, *Organometallics* **1992**, *11*, 4363.
[24] R. A. Andersen, R. Blom, C. J. Burns, H. V. Volden, *J. Chem. Soc. Chem. Commun.* **1987**, 768.
[25] C. J. Burns, R. A. Andersen, *J. Organomet. Chem.* **1987**, *325*, 31.
[26] C. J. Burns, PhD Thesis, University of California Berkeley, **1987**.
[27] R. A. Williams, T. P. Hanusa, J. C. Huffman, *J. Am. Chem. Soc.* **1990**, *112*, 2454.

Benzopyranoisoxazolidines as Chiral Auxiliaries for Asymmetric Synthesis**

Atsushi Abiko, Osamu Moriya, Sandra A. Filla, and Satoru Masamune*

Highly stereoselective α-alkylation of carboxylic acid derivatives (RCH_2COX) can be performed with many known chiral auxiliaries such as oxazolidinone,[1] sultam heterocycles,[2] and others.[3] Here we report new chiral isoxazolidine auxiliaries (**1a** and **1b**), which not only effect equally high asymmetric induction but also offer the following distinct advantages: 1) acylation of the auxiliaries is achieved with an acid chloride and triethylamine, 2) alkylation with β-branched electrophiles can be performed by using their triflates, and 3) alkylated products can be converted directly into the corresponding alcohols, aldehydes, and ketones in one step with recovery of the auxiliary (see Scheme 1).[4]



Scheme 1. a) CH_3CH_2COCl, Et_3N/CH_2Cl_2. b) R^1X, KHMDS/THF. c) $LiBH_4$-EtOH/Et_2O or $LiAlH_4$/THF for **4**; DIBAL-H/THF for **5**; CH_3MgBr/THF for **6**.

Syntheses of **1a** and **1b** are very simple and readily applicable to a large-scale preparation (about 1 mol). The isoxazolidine skeleton was constructed by an intramolecular [3 + 2] cycloaddition involving a nitrone.[5] Thus, heating a mixture of *o*-allyl-

[*] Prof. S. Masamune, Dr. O. Moriya, Dr. S. A. Filla
Department of Chemistry
Massachusetts Institute of Technology
Cambridge, MA 02139 (USA)
Telefax: Int. code + (617)253-1340
Dr. A. Abiko
Institute for Fundamental Research, Kao Corporation
Ichikai-machi, Haga-gun, Tochigi, 321-34 (Japan)

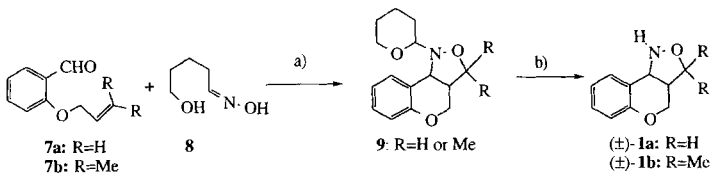
[**] S. M. gratefully acknowledges the National Institutes of Health, U. S. A. (CA48175) for financial support.

Table 1. Alkylation of (−)-**2** to produce **3** and its conversion into alcohol **4**.

Entry	2	R^1X (Procedure)	Product 3 Yield [%]	Diastereo-select.	M.p. [°C]	Alcohol 4 Yield [%]	$[\alpha]_D$ [a]	Ref.
1	(−)-**2a**	$PhCH_2Br$ (A)	94	98:2	oil	84	−11.1 (1.0)	[13a]
2	(−)-**2b**	$PhCH_2Br$ (A)	93	99:1	88–89	83	−10.9 (1.0)	
3	(−)-**2a**	$CH_2=CHCH_2Br$ (A)	80	95:5	48	71	−2.3 (2.0)	[13b]
4	(−)-**2b**	$CH_2=CHCH_2Br$ (A)	96	98:2	55–57	79	−2.2 (2.0)	
5	(−)-**2a**	$CH_2=C(CH_3)CH_2Br$ (A)	91	98:2	75–76	80	−3.8 (0.4)	[13c]
6	(−)-**2b**	$CH_2=C(CH_3)CH_2Br$ (A)	78	96:4	78–80	75	−3.7 (0.4)	
7	(−)-**2a**	n-$C_5H_{11}I$ (C)	72	98:2	oil	81	−13.2 (0.6)	[2]
8	(−)-**2a**	$C_6H_{11}CH_2OTf$ (B)	93	94:6	98–99	80	−18.1 (1.5)	[13d]
9	(−)-**2b**	$C_6H_{11}CH_2OTf$ (C)	90	98:2	81–82	64	−21.0 (1.7)	

[a] Measured at 20 °C in $CHCl_3$ as solvent except for entries 1 and 2 (benzene) and entries 5 and 6 (CH_2Cl_2). The concentration c is indicated in parenthesis. All of the major products **3** provided the corresponding (*S*)-alcohol **4** with >98 %*ee*.

oxybenzaldehyde (either **7a** or **7b**) and oxime **8**, in the presence of a catalytic amount of Bu_2SnO in toluene at reflux for 6 h in a Dean–Stark apparatus gave rise to the adduct **9**, which was subjected to acid hydrolysis (2 N HCl/EtOH = 1:1) at room temperature overnight to provide (±)-**1** [either (±)-**1a** in 80% yield or (±)-**1b** in 90% yield] (Scheme 2, Table 3). The use of Bu_2SnO



Scheme 2. a) **7a** or **7b** (0.17 mol), **8** (0.17 mol), Bu_2SnO (0.01 mol), reflux/toluene (200 mL). b) 2 N HCl/EtOH.

as a catalyst was essential for the cyclization. The resolution of both (±)-**1a** and (±)-**1b** was achieved with remarkable ease and efficiency.[6] Each enantiomer of the two racemates was obtained in about 80% yield and with >98% *ee*, and the absolute configurations of (+)-**1a** and (−)-**1b** were established by means of X-ray analysis of their derivatives.[7] Isoxazolidines are easily acylated with an acyl chloride in the presence of triethylamine, and the preparation of acyl derivatives of **1a** and **1b**, for example **2a,b** (Table 3), presented no problem.

Of the many bases examined for the deprotonation of (−)-**2**, potassium disilazide (KHMDS) was found to be the most satisfactory. The monoalkylated products were obtained in excellent yields under the following conditions: For most of the alkylations listed in Table 1, a cold solution of KHMDS (1.2 equiv, 0.2 M) in THF was transferred by cannula to a solution of (−)-**2** (1.0 equiv, 0.2–0.5 M) and an alkylating reagent (Table 1) in THF at −78 °C, and the resulting reaction mixture was stirred for 3 h at −78 °C (procedure A). In some cases, the procedure was slightly modified to enhance the yield of alkylated product; procedure B used the preformed enolate of **2**, and procedure C 3 equiv of hexamethylphosphoric triamide (HMPA) as an additive in ether. Sufficient care must be taken to keep the temperature low, because the enolate decomposed to some extent at higher temperature.[8] (The enolate of **2a** is less stable than that of **2b**.) The reaction mixture was worked up in the usual manner, and the diastereomeric ratio was determined by HPLC and/or ^1H NMR. It should be emphasized that **2** is not only alkylated with reactive electrophiles such as benzyl bromide, allyl bromide, and *n*-pentyl iodide, but also with cyclohexylmethyl triflate. This reaction with cyclohexylmethyl triflate serves as a model for an important transformation often encountered in natural product synthesis and usually cannot be achieved with conventional (oxazolidinone) auxiliaries.[9] Diastereomerically pure **3** could be isolated by crystallization and/or chromatography, the latter taking advantage of a large R_f difference between the diastereomers.

Efficient conversion of **3** into the corresponding alcohols **4**, aldehydes **5**, and ketones **6** with the concomitant recovery of **1a** or **1b** is a process just as important as diastereoselective alkylation. Treatment of **3** (1 equiv) with $LiBH_4$ (3 equiv) and ethanol (3 equiv), or with an excess of $LiAlH_4$, provided the alcohols **4**,[10] which were compared with the known enantiopure compounds to establish the absolute configuration of **4** (Table 1). It should be noted that separation of the alcohol **4** from the auxiliary **1** was effected by simple acid–base extraction. Conversion of **3** into **5** and **6** also proceeded smoothly with diisobutylaluminum hydride (DIBAL-H, 1.1 equiv) in THF (0 °C, 3 h) and Grignard reagents (3.0 equiv) in THF (−20 to 0 °C, 4–5 h), respectively (Table 2), without any loss of optical purity.

The utility of these chiral isoxazolidines is best illustrated by the successful transformations of **10** to **11a** and **11b**,[11] and of **12** to **14**, **15**, and **16** through **13**[12] (Scheme 3), which

Table 2. Conversion of the major diastereomer **3** into aldehyde **5** and ketone **6** with recovery of the auxiliary.

Entry	1	R^1	Aldehyde 5 Yield [%]	*ee* [%]	Config.	Recovered auxiliary [%]	Ketone 6 Yield [%]	*ee* [%]	Config.	Recovered auxiliary [%]
1	(+)-**1a**	$PhCH_2$	86	>98 [a]	(*S*) [b]	88	85	>98 [a]	(*S*) [b]	90
2	(+)-**1a**	n-C_5H_{11}	70	>94 [c]	(*S*)	70	70	>96 [d]	(*S*) [e]	73
3	(+)-**1b**	$PhCH_2$	84	>98 [a]	(*S*) [b]	80	86	>98 [a]	(*S*) [b]	91

[a] Measured by HPLC (Chiralcel OD, 4.6 × 250mm). [b] See ref. [14a]. [c] The aldehyde was reduced and the % *ee* of the resulting alcohol was measured by the Mosher method. [d] By means of ^1H NMR with $Eu(hfc)_3$. [e] See ref. [14b].

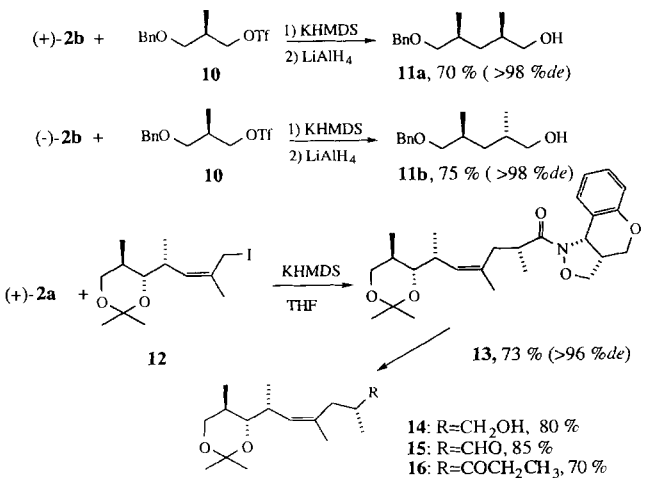
Table 3. Selected physical and spectroscopic data for **1a,b**, and **2a,b**.

(+)-**1a** and (−)-**1a**: ^{1}H NMR (300 MHz, $CDCl_3$, 20 °C, TMS): $\delta = 7.41$ (m, 1H), 7.23–7.39 (m, 1H), 7.00–7.21 (m, 2H), 5.00 (br, 1H), 4.30 (m, 2H), 4.22 (dd, $J = 5.0$, 11.4 Hz, 1H), 3.67–3.75 (m, 2H), 3.00 (m,1H); ^{13}C NMR (75.4 MHz, $CDCl_3$, 20 °C): $\delta = 155.5$, 131.3, 129.4, 121.6, 118.5, 117.3, 72.8, 65.2, 57.3, 40.7; HRMS (EI): *m/z* calcd for $C_{10}H_{11}NO_2$ (M^+) 177.0790, found 177.0787.

(+)-**1b** and (−)-**1b**: ^{1}H NMR ($CDCl_3$): $\delta = 7.38$ (m, 1H), 7.20 (m, 1H), 6.93 (m, 2H), 4.90 (br, 1H), 4.50 (d, $J = 6.6$ Hz, 1H), 4.20 (dd, $J = 5$, 9 Hz, 1H), 3.82 (dd, $J = 7.8$, 12 Hz, 1H), 2.52 (m, 1H), 1.44 (s, 3H), 1.29 (s, 3H); ^{13}C NMR ($CDCl_3$): $\delta = 155.1$, 131.0, 129.2, 121.4, 119.2, 117.1, 84.8, 63.5, 57.7, 48.1, 28.6, 21.3; HRMS (EI): *m/z* calcd for $C_{12}H_{15}NO_2$ 205.1103, found 205.1099.

(−)-**2a**, $[\alpha]_D^{20} = -293$ ($c = 1.40$ in $CHCl_3$) and (+)-**2a**, $[\alpha]_D^{20} = +294$ ($c = 1.06$ in $CHCl_3$); m.p. 76–77 °C; IR (Nujol): $\nu_{max} = 1660\ cm^{-1}$; ^{1}H NMR ($CDCl_3$): $\delta = 7.67$ (m, 1H), 7.18 (m, 1H), 7.00 (m, 1H), 6.86 (m, 1H), 5.44 (d, $J = 8.1$ Hz, 1H), 4.30 (dd, $J = 4.8$, 11.3 Hz, 1H), 4.00 (m, 2H), 3.86 (dd, $J = 9$, 11.3 Hz, 1H), 3.15 (m, 1H), 2.40-2.60 (m, 2H), 1.18 (t, $J = 7.5$ Hz, 3H); ^{13}C NMR ($CDCl_3$): $\delta = 177.5$, 154.9, 131.5, 128.9, 122.1, 121.8, 116.9, 71.4, 65.3, 52.3, 40.4, 26.1, 8.6; HRMS (EI) *m/z* calcd for $C_{13}H_{15}NO_3$ 233.1052, found 233.1052.

(−)-**2b**, $[\alpha]_D^{20} = -267$ ($c = 1.09$ in $CHCl_3$) and (+)-**2b**; $[\alpha]_D^{20} = +267$ ($c = 1.03$ in $CHCl_3$); m.p. 73–74 °C; IR (Nujol): $\nu_{max} = 1665$, 1580 cm^{-1}; ^{1}H NMR ($CDCl_3$): $\delta = 7.84$ (m, 1H), 7.17 (m, 1H), 6.97 (m, 1H), 6.86 (m, 1H), 5.42 (d, $J = 7.5$ Hz, 1H), 4.27 (dd, $J = 5$, 11.3 Hz, 1H), 3.81 (t, $J = 10.8$ Hz, 1H), 2.40–2.70 (m, 3H), 1.40 (s, 3H), 1.27 (s, 3H), 1.18 (t, $J = 7.2$ Hz, 3H); ^{13}C NMR ($CDCl_3$): $\delta = 177.7$, 154.6, 132.1, 128.8, 122.0, 121.9, 116.6, 84.3, 64.6, 53.6, 46.8, 26.6, 25.4, 19.7, 8.7; HRMS (EI) *m/z* calcd for $C_{15}H_{19}NO_3$ 261.1316, found 261.1316.



Scheme 3. Several examples to illustrate the use of isoxazolidine auxiliaries.

constitute important steps in our synthesis of polyketide natural products.

Received: October 25, 1994 [Z 7431 IE]
German version: *Angew. Chem.* **1995**, *107*, 869

Keywords: alkylation · asymmetric syntheses · chiral auxiliary · isoxazolidines

[1] D. A. Evans, M. D. Ennis, D. J. Marthre, *J. Am. Chem. Soc.* **1982**, *104*, 1737.
[2] W. Oppolzer, R. Moretti, S. Thomi, *Tetrahedron Lett.* **1989**, *30*, 5603.
[3] See for example S. E. Drewes, D. G. S. Malissar, G. H. O. Roos, *Chem. Ber.* **1993**, *126*, 2663, and references therein.
[4] a) M. Larcheveque, E. Ignatova, T. Luvigny, *J. Organomet. Chem.* **1979**, *177*, 5; b) A. G. Myers, B. H. Yang, H. Chen, J. L. Gleasen, *J. Am. Chem. Soc.* **1994**, *116*, 9361.
[5] Oppolzer et al. described a synthesis of (±)-**1a** (W. Oppolzer, K. Keller, *Tetrahedron Lett.* **1970**, 1117), which has been much improved in the present study. See also B. S. Orlek, P. G. Sammes, D. J. Walker, *J. Chem. Soc. Chem. Commun.* **1993**, 1412.
[6] A solution of (±)-**1a** (15 g) and (+)-10-camphorsulfonic acid (23 g) in acetone (200 mL) provided, upon six recrystallizations, (+)-salt, $[\alpha]_D^{20} = +61.5$ ($c = 1.10$ in MeOH) and (−)-salt, $[\alpha]_D^{20} = -13.6$ ($c = 1.15$ in MeOH) in 80% and 70% yields, respectively. It should be noted that the salts of (+)-**1a** and (−)-**1a** crystallized alternately from the same solution! From these salts, (+)-**1a**, $[\alpha]_D^{20} = +62.4$ (c = 1.11 in $CHCl_3$), m.p. 95–96 °C and (−)-**1a**, $[\alpha]_D^{20} = -62.4$ ($c = 1.11$ in $CHCl_3$) were recovered quantitatively. For the resolution of **1b**, (±)-**1b** was allowed to react with L-dibenzoyltartaric anhydride to give a diastereomeric mixture of amides, from which the (+)-amide was separated by crystallization from ethyl acetate and hexane. Simple alkaline hydrolysis afforded (−)-**1b**, m.p. 85–86 °C, $[\alpha]_D^{20} = -11.1$ ($c = 1.14$ in $CHCl_3$) in 80% overall yield. Optically pure (+)-**1b**, m.p. 85–86 °C, $[\alpha]_D^{20} = +11.1$ ($c = 1.33$ in $CHCl_3$) was obtained in 80% yield from the (+)-**1b**-rich mother liquor after removing (±)-**1b**, m.p. 120 °C, (20%) which first crystallized out from ether.
[7] The (+)-salt of **1a** with (+)-10-camphorsulfonic acid and an aldol adduct of (+)-**2b** were used for X-ray crystallographic analysis. The absolute configuration of the diol derived from the aldol is known. Detailed information will be published in a full paper.
[8] a) F. M. Cordero, A. Brandi, F. DeSarlo, G. Viti, *J. Chem. Soc. Chem. Commun.* **1994**, 1047; b) R. V. Hoffman, N. K. Nayyar, W. Chen, *J. Org. Chem.* **1993**, *58*, 2355.
[9] D. A. Evans, R. L. Dow, T. L. Shih, J. M. Takacs, R. J. Zahler, *J. Am. Chem. Soc.* **1990**, *112*, 5290.
[10] T. D. Penning, S. D. Djuric, R. A. Haack, V. J. Kalish, M. Miyashiro, B. Rowell, S. S. Yu, *Synth. Commun.* **1990**, *20*, 307.
[11] M. R. Hale, A. H. Hoveyda, *J. Org. Chem.* **1992**, *57*, 1643.
[12] S. A. Filla, Ph. D. thesis, Massachusetts Institute of Technology, Cambridge, MA, USA, **1994**.
[13] a) S. Terashima, S. Yamada, *Chem. Pharm. Bull.* **1968**, *16*,1953; b) L. E. Overman, L. A. Robinson, J. Zablocki, *J. Am. Chem. Soc.* **1992**, *114*, 368; c) M. A. Brimble, *Aust. J. Chem.* **1990**, *43*, 1035; d) P. A. Levene, R. E. Marker, *J. Biol. Chem.* **1935**, *110*, 299.
[14] a) M. V. Rangaishenvi, B. Singaram, H. C. Brown, *J. Org. Chem.* **1991**, *56*, 3286; b) T. Hayashi, Y. Matsumoto, Y. Ito, *Chem. Lett.* **1987**, 2037.

Formation of a Hexagonal Columnar Mesophase by N-Acylated Poly(ethylenimine)**

Hartmut Fischer, Surya S. Ghosh, Paul A. Heiney, Nicholas C. Maliszewskyj, Thomas Plesnivy, Helmut Ringsdorf,* and Markus Seitz

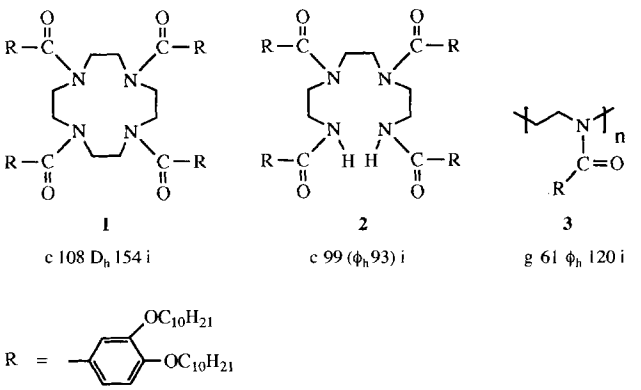
The macroscopic properties of self-organizing systems are strongly governed by the molecular structure of their constituent units. Nevertheless, in many cases the same supramolecular structures can be constructed with a wide variety of building blocks. In particular, hexagonal columnar mesophases (ϕ_h) are formed by various molecular structures.[1] The constituent unit of the liquid-crystalline phase may consist of relatively rigid macromolecules with flexible side chains, for example poly(dialkylsilane) or substituted poly(glutamate)s.[2–5] In addition, disk-shaped molecules exhibit predominantly this type of columnar arrangement (discotic hexagonal columnar mesophases, D_h).[6] Macrocyclic oligoamines (azacrowns) can also act as such central cores, provided that the conformational dynamics of the macrocycle is reduced by N-acylation with aromatic acids[7–11] or by complexation with transition metal ions.[12,13] In general, the

[*] Prof. H. Ringsdorf, T. Plesnivy, M. Seitz
Institut für Organische Chemie der Universität
J. J. Becher-Weg 18–22, D-55099 Mainz (Germany)
Telefax: Int. code + (6131) 393145
Dr. H. Fischer
University of Technology, Polymer Chemistry & Technology
Eindhoven (The Netherlands)
S. S. Ghosh, Prof. P. A. Heiney, N. C. Maliszewskyj
Department of Physics and Laboratory for Research on the Structure of Matter
University of Pennsylvania, Philadelphia, PA 19104 (USA)

[**] Work done at the University of Pennsylvania was supported by National Science Foundation grants DMR MRL 92-20668 and DMR 93-15341.

stability of the columnar mesophase formed by these molecules decreases with increasing ring size and thus increasing flexibility. Recently even open chain N-acylated oligoamines of comparable structure were found to exhibit liquid-crystalline phases.[14]

In this paper the scope of these systems containing N-acylated ethylenimine as the basic—in principal nonmesogenic—structural unit will be extended to a linear polymer, which will be compared to a macrocyclic and an open chain analogue (Fig. 1).



1 c 108 D_h 154 i

2 c 99 (ϕ_h 93) i

3 g 61 ϕ_h 120 i

Fig. 1. Structure and phase behavior of **1**, **2**, and **3**. The transition temperatures are given in °C (c: crystalline; D_h: discotic hexagonal columnar; i: isotropic; g: glassy; φ_h: hexagonal columnar; phase transition temperatures from the first cooling and second heating curves of the DSC measurements, scan rate 10 K min^{-1}).

For the macrocycle **1** the hexagonal columnar structure of the mesophase, which is still a matter of controversy for the cyclic, low molecular weight compounds,[14–17] is unambiguously demonstrated by the hexagonal X-ray diffraction pattern (Fig. 2).[18]

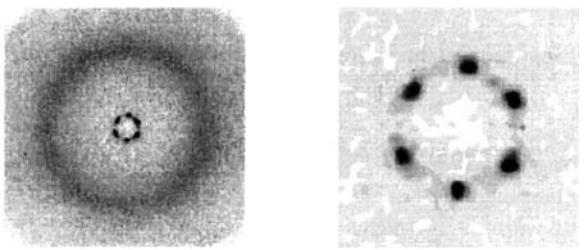


Fig. 2. X-ray picture (flat-plate camera) of a magnetically aligned monodomain of macrocycle **1** at 150 °C (cf. [18]). The low-angle region is shown magnified in the right picture.

In the oligoamide **2**, the open-chain analogue of **1**, the intrinsic discoid structure is lost. Nevertheless, a monotropic mesophase of presumably hexagonal columnar structure can be found as indicated by polarization microscopy and differential scanning calorimetry (DSC). This mesophase formation can, in principle, be explained by intramolecular hydrogen bonds between the terminal amide units which provide a disklike molecular conformation in the open-chain compound **2**, too.[14] The higher conformational flexibility of this system relative to that of macrocycle **1** is reflected by the monotropic nature of the mesophase.

The formation of hexagonal columnar mesophases by N-acylated oligoamines is therefore not restricted to macrocyclic, and thus intrinsic discoid, structures. In longer open-chain polymeric amides a discoid conformation by intramolecular hydrogen bonding is no longer favorable. Therefore, the N-acylated linear poly(ethylenimine) **3** was not expected to exhibit mesomorphic properties.

Nevertheless, an enantiotropic liquid-crystalline phase was detected for the polymer **3**. Slow cooling from the isotropic phase into the mesophase gave a texture characteristic for hexagonal mesophases with homeotropic regions. This texture is remarkably similar to those of the low molecular weight compounds **1** and **2**. In addition, preliminary studies on contact preparations show miscibility of **2** and **3** over the whole concentration range within the LC state, which indicates that both compounds have the same mesophase structure.

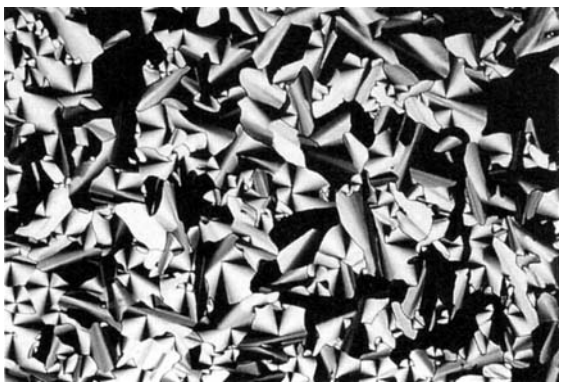


Fig. 3. Texture of the N-acylated linear poly(ethylenimine) **3** under the polarizing microscope at 116 °C, obtained after cooling from the isotropic phase to the given temperature (cooling rate: 0.2 K min^{-1}).

In accord with results from polarizing microscopy, the DSC heating trace (Fig. 4) shows a peak at 120 °C corresponding to the transition from a liquid-crystalline to an isotropic phase ($\Delta H_{\phi_h \rightarrow i}$ = 1.2 kJ mol^{-1} per repeating unit). In addition, one glass transition is found at 61 °C and another transition at about 80 °C.[19]

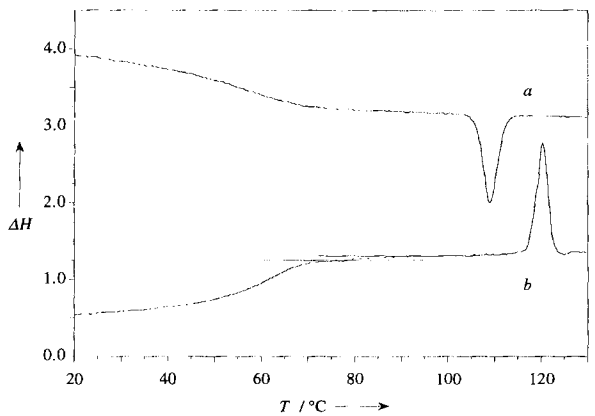


Fig. 4. DSC thermogram of the N-acylated poly(ethylenimine) **3**; a) first cooling b) second heating trace; scan rate: 10 K min^{-1}. As a guide for the eye, the second transition at about 80 °C is emphasized by two straight lines [19].

The X-ray diffraction pattern of the polymer **3** at 85 °C (Fig. 5) shows three reflections in the small-angle region with lattice spacings in the ratio of $1:1/\sqrt{3}:1/2$ characteristic of a hexagonal columnar arrangement. The hexagonal lattice parameter was determined to be 35.6 Å. In comparison, for the macrocyclic compound **1** the intercolumnar distance at 120 °C is 33.2 Å.

 © VCH Verlagsgesellschaft mbH, D-69451 Weinheim, 1995 0570-0833/95/0707-0796 $ 10.00+.25/0 Angew. Chem. Int. Ed. Engl. 1995, 34, No. 7

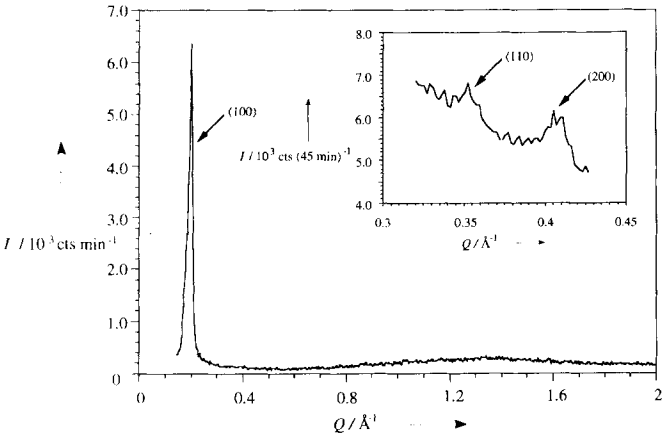


Fig. 5. X-ray diffraction pattern of **3** obtained at 85 °C after cooling from the isotropic state. Units are $Q = 4\pi\sin\theta/\lambda = 2\pi/d$. Inset shows scattering near the (110) and (200) peaks.

All investigated systems—macrocycle **1** and open-chain oligomer **2**, as well as the linear polymer **3**—exhibit the same supramolecular structure in the mesophase (Fig. 6). Whereas in the azacrown derivative **1** the discoid geometry is given by the

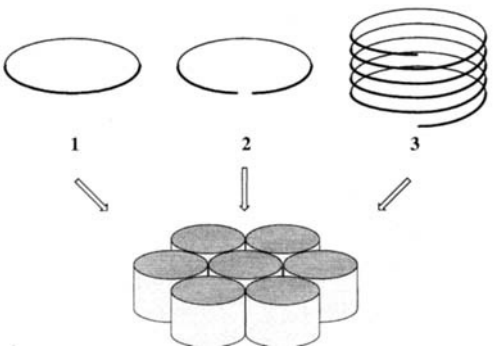


Fig. 6. Formation of hexagonal columnar phases by macrocyclic **1**, open-chain oligomeric **2**, and polymeric ethylenimine derivatives **3**. As a chiral center is lacking, both left- and right-handed helices are formed by the polymer.

molecular structure, in the open-chain oligoamide **2** this geometry can perhaps be achieved by means of hydrogen bonding. Conclusions about the molecular arrangement of the polymer **3** are speculative. However, based on the same mesophase behavior of the compounds under discussion, a possible molecular structure of the polymer could consist of a helical polymeric main chain (Fig. 6) radially surrounded by the side chains. This view is supported by the larger intercolumnar distance of the polymer **3** relative to that of the azacrown derivative **1**; for an extended polymer chain a smaller distance was expected.

Although the structure of **3** is not necessarily perfectly helical, the system may resemble that of poly-L-glutamates with long alkyl chain substituents, for which hexagonal columnar mesophases have indeed been observed.[20] However, whereas in the synthetic polypeptide the unsubstituted polymeric chain is helical, in the substituted poly(ethylenimine) **3** the formation of a helical structure of the main chain may be solely induced by the steric requirements of the 3,4-bisdecyloxybenzoyl substituents.[21] This side group has thus an important structural influence on the polymeric main chain, since the hexagonal columnar structure is in striking contrast to the lamellar structures that have been observed in linear poly(ethylenimines) acylated with benzoyl derivatives.[22, 23]

Finally, as the constituent unit is identical in the polymeric and the low molecular weight compounds, the described systems bridge the gap between classical discotic mesophases (that is, hexagonal columnar mesophases formed by disk-shaped molecules) and thermotropic liquid-crystalline columnar phases formed by linear polymers.

Experimental Procedure

The synthesis of the compound **1** (**2**) was performed by acylation of the commercially available 1,4,7,10-tetraazacyclododecane (triethylenetetramine tetrahydrochloride) with 3,4-bisdecyloxybenzoyl chloride according to known procedures [8, 9].

Synthesis of **3**: 3,4-bisdecanoxybenzoyl chloride (4.52 g, 10 mmol), linear poly(ethylenimine) (0.4 g, 9.3 mmol; prepared according to described procedures [24, 25]; degree of polymerization estimated to about 22) and *N*,*N*-dimethylaminopyridine (1.3 g, 11 mmol, DMAP) were stirred for 3 days at 70 °C in 150 mL of absolute *N*,*N*-dimethylformamide (DMF) under an argon atmosphere. The white precipitate was separated and dried for two days under high vacuum to remove the solvent. The crude product was suspended in dichloromethane and washed three times with water. After drying with anhydrous sodium sulfate the solution was concentrated, and the polymer precipitated in cold acetone. This procedure was repeated (purity of the product checked by TLC), and the polymer finally recrystallized from acetone to yield 1.4 g of a white powder. (Additional product was obtained by concentration of the filtrate of the reaction mixture. However, the product obtained in this way was rather impure and had to be extensively purified.)

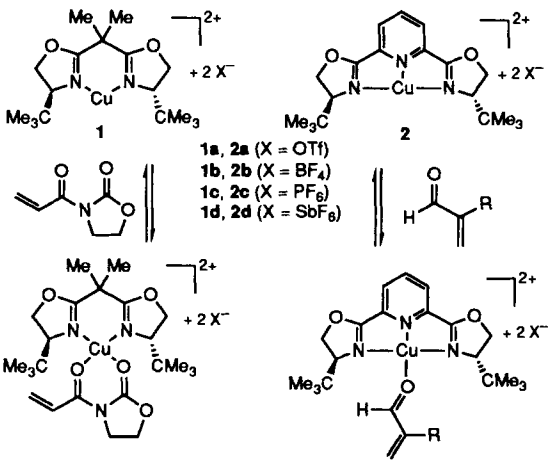
According to elemental analysis and ^{1}H NMR spectroscopy, the polymer is almost quantitatively acylated (>95%). ^{1}H NMR (200 MHz, $CDCl_3$): δ = 0.85 (t, 6H; $CH_3(CH_2)_9O$), 1.1–1.4, 1.5–1.9 (br., 32H; $CH_3(CH_2)_8CH_2O$), 3.3–3.6 (br., 4H; CH_2-N-CH_2), 3.8–4.0 (br., 4H; $CH_3(CH_2)_8CH_2O$), 6.6–6.8 (br., 4H; aromatic ring protons). Elemental analysis: calcd for $(C_{29}H_{49}NO_3)_n$ (corresponds to 100% substitution; M(repeat unit) = 459.72): C 75.77, H 10.74, N 3.05; found: C 75.40, H 10.63, N 2.94. GPC ($CHCl_3$; polystyrene standard): M_n = 10500 (calculated for P_n = 22: M_n = 10114).

Received: September 30, 1994 [Z 7368 IE]
German version: *Angew. Chem.* **1995**, *107*, 879

Keywords: liquid crystals · poly(ethylenimine)s · polymers

[1] G. Ungar, *Polymer* **1993**, *34*, 2050.
[2] A. J. Lovinger, F. C. Schilling, F. A. Bovey, J. M. Zeigler, *Macromolecules* **1986**, *19*, 2660.
[3] P. Weber, D. Guillon, A. Skoulios, R. D. Miller, *J. Phys.* **1989**, *50*, 793.
[4] P. Weber, D. Guillon, A. Skoulios, R. D. Miller, *Liq. Cryst.* **1990**, *8*, 825.
[5] Hexagonal columnar structures have even been observed for polymers without side branches. A comparative discussion of the formation of hexagonal phases by polymeric systems is provided by Ungar in [1].
[6] S. Chandrasekhar, *Liq. Cryst.* **1993**, *14*, 3.
[7] J.-M. Lehn, J. Malthete, A. M. Levelut, *J. Chem. Soc. Chem. Commun.* **1985**, 1794.
[8] C. Mertesdorf, H. Ringsdorf, *Liq. Cryst.* **1989**, *5*, 1757.
[9] G. Lattermann, *Liq. Cryst.* **1989**, *6*, 619.
[10] D. Tatarsky, K. Banerjee, W. T. Ford, *Chem. Mater.* **1990**, *2*, 138.
[11] C. Mertesdorf, H. Ringsdorf, *Molec. Eng.* **1992**, *2*, 189.
[12] A. Liebmann, C. Mertesdorf, T. Plesnivy, H. Ringsdorf, J. H. Wendorff, *Angew. Chem.* **1991**, *103*, 1358–1361; *Angew. Chem. Int. Ed. Engl.* **1991**, *30*, 1375–1377.
[13] G. Lattermann, S. Schmidt, R. Kleppinger, J. H. Wendorff, *Adv. Mater.* **1992**, *4*, 30.
[14] U. Stebani, G. Lattermann, M. Wittenberg, R. Festag, J. H. Wendorff, *Adv. Mater.* **1994**, *6*, 572.
[15] S. H. J. Idziak, N. C. Maliszewskyj, P. A. Heiney, J. P. McCauley, Jr., P. A. Sprengeler, A. B. Smith III, *J. Am. Chem. Soc.* **1991**, *113*, 7666.
[16] S. H. J. Idziak, N. C. Maliszewskyj, G. B. M. Vaughan, P. A. Heiney, C. Mertesdorf, H. Ringsdorf, J. P. McCauley, Jr., A. B. Smith III, *J. Chem. Soc. Chem. Commun.* **1992**, 98.
[17] J. Malthête, A.-M. Levelut, J.-M. Lehn, *J. Chem. Soc. Chem. Commun.* **1992**, 1434.
[18] Azacrown **1** has a high tendency to align on glass surfaces. In addition, a magnetic field of about 0.8 T has been applied perpendicular to the glass capillary. Goniometer scans confirm the hexagonal structure of the mesophase by the observance of (100) and (110) reflections, the corresponding distances of which are in the ratio of $1:1/\sqrt{3}$. However, the (110) reflection is weak and can only be observed by prolonged measuring times.
[19] Based on preliminary dielectric spectroscopy measurements the glass transition at 61 °C corresponds to mobility of the side groups. More extensive DSC studies on tempered samples showed that the second glass transition may arise from the melting of crystalline regions.

[20] J. Watanabe, Y. Takashina, *Macromolecules* **1991**, *24*, 3423.
[21] This kind of shape-induced formation of supramolecular structures is to some extent comparable with the results of Percec et al. on polymers with triangular structural units covalently attached to a polymeric chain which, with respect to the formation of a columnar structure, resemble the Tabacco Mosaic Virus: V. Percec, J. Heck, G. Johansson, D. Tomazos, M. Kawasumi, *J. Macromol. Sci. Pure Appl. Chem.* **1994**, *A31* (8), 1031.
[22] M. Litt, F. Rahl, L. G. Roldan, *J. Polym. Sci. A-2* **1969**, *7*, 463.
[23] For the sake of completeness, it should be noted that helical structures already have been found in anhydrous linear poly(ethylenimine), which according to X-ray studies exists as double-stranded helical chains. The unsubstituted linear polymer has hygroscopic properties and is readily transformed to the linear structure by absorption of water: Y. Chatani, T. Kobataka, H. Tadokoro, R. Tanaka, *Macromolecules* **1982**, *15*, 170. As a reference system for the described polyamide, however, the mentioned lamellar N-benzoylated poly(ethylenimine) [22] has to be considered.
[24] M. J. Han, J. Y. Chang, Y. Y. Lee, *Macromolecules* **1982**, *15*, 255.
[25] K. M. Kem, *J. Polym. Sci. Polym. Chem.* **1979**, *17*, 1977.



Scheme 1. Chiral Lewis acids derived from square-planar Cu^{II} complexes and their associated coordination complexes with complementary one- and two-point binding dienophiles.

C_2-Symmetric Cationic Copper(II) Complexes as Chiral Lewis Acids: Counterion Effects in the Enantioselective Diels–Alder Reaction**

David A. Evans,* Jerry A. Murry, Peter von Matt, Roger D. Norcross, and Scott J. Miller

We have recently documented the utility of chiral bis(oxazoline)copper(II) complexes **1** (oxazoline = dihydrooxazole) in the catalysis of asymmetric group transfer reactions such as cyclopropanation[1, 2] and aziridination.[3, 4] In addition, we have demonstrated that the C_2-symmetric bis(oxazoline)copper(II) triflate complex **1a** (triflate = trifluoromethanesulfonate = OTf) is also capable of functioning as an effective chiral Lewis acid in the Diels–Alder reaction with two-point binding *N*-acylimide dienophiles.[5] In an effort to broaden the utility of Lewis acidic chiral Cu^{II} complexes, we have prepared Cu^{II} complexes with tridentate bis(oxazolinyl)pyridine[6] (pybox) ligands, [Cu^{II}(pybox)X_2] (**2**) and probed their reactivity as chiral Lewis acids (Scheme 1). In conjunction with this investigation, we have uncovered dramatic counterion effects that strongly influence the reactivity of these Lewis acids. In this communication, we document the scope of these catalysts in enantioselective Diels–Alder reactions with unsaturated aldehyde and imide-derived dienophiles.

We began with an investigation of [Cu^{II}(pybox)] complexes which we anticipated would possess a preferred square-planar coordination geometry with a single accessible coordination site for carbonyl-derived dienophiles such as α,β-unsaturated aldehydes. Indeed, we have found that [Cu^{II}(pybox)] complexes **2** serve as effective chiral Lewis acids with aldehyde-derived dienophiles. For example, the cycloaddition of methacrolein with cyclopentadiene catalyzed by (pybox)Cu(OTf)$_2$ (**2a**) (5 mol%, CH_2Cl_2, −20 °C) afforded the desired cycloadducts with good *exo:endo* selectivity (96:4) and enantioselectivity (*exo* adduct: 85% ee).[7] However, extended reaction times (120 h) were required for complete conversion.

In an effort to increase catalyst reactivity, the cationic complexes **2b**–**2d** were prepared[6] and evaluated. As illustrated in Figure 1, a large counterion effect was observed in these reactions. For example, the cycloaddition of methacrolein with cyclopentadiene that required 120 hours for complete conversion with catalyst **2a** (X = OTf) was complete in 8 hours with catalyst **2d** (X = SbF_6). This comparison reveals that the counterion structure dramatically affects catalyst efficiency and that the "noncoordinating" counterions SbF_6^-, PF_6^-, and BF_4^-, strongly differ in degree of interaction with the Lewis acidic Cu^{II} center.[8]

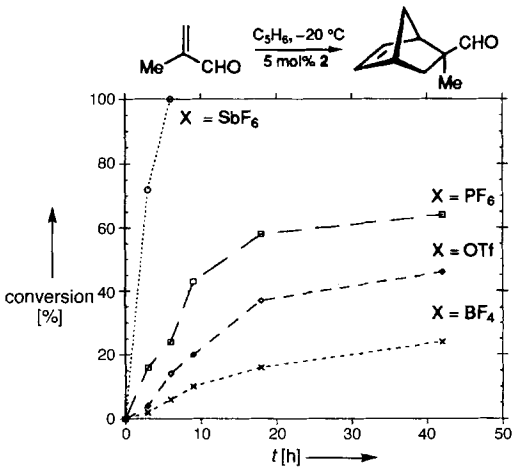


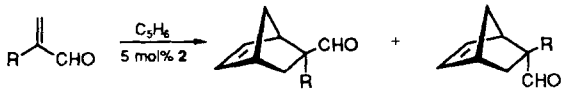
Fig. 1. Plot of the conversion [%] as a function of the reaction time [h] for the Diels–Alder reaction of methacrolein with cyclopentadiene catalyzed by **2** at −20 °C.

From the results of the preceding study, the cationic (pybox)Cu(SbF_6)$_2$ complex (**2d**) was determined to be the catalyst of choice, and its optimized performance in the Diels–Alder reactions of cyclopentadiene with representative aldehyde dienophiles is given in Table 1. The *tert*-butyl ligand **2** was originally chosen in analogy with the acrylimide results and provides enantioselectivities comparable to those reported in the literature.[9] Importantly, we have also found that the (*S*)-benzyl-pybox ligand, derived from L-phenylalanine, provides comparable

[*] Prof. D. A. Evans, J. A. Murry, P. von Matt, R. D. Norcross, S. J. Miller
Department of Chemistry, Harvard University
Cambridge, MA 02138 (USA)
Telefax: Int. code + (617)495-1460

[**] Financial support was provided by the National Science Foundation and the National Institutes of Health. Fellowships from the National Institutes of Health (J.A.M.), Swiss National Science Foundation, and Ciba-Geigy Jubiläumsstiftung (P. v. M.), NATO (R. D. N.), and the National Science Foundation (S.J.M.) are gratefully acknowledged. The NIH BRS Shared Instrument Grant Program 1 S10 RR01748-01A1 is acknowledged for providing NMR facilities.

Table 1. Enantioselective Diels–Alder reactions of α-substituted acroleins with cyclopentadiene catalyzed by Cu^{II} complexes **2a** and **2d** [a].

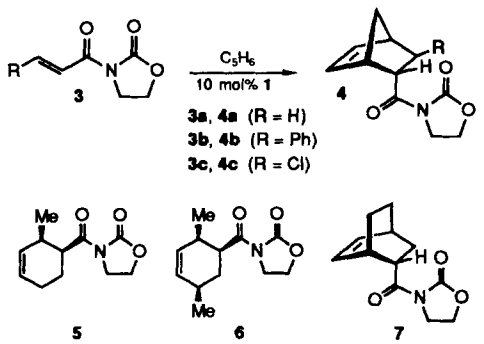


R	Catalyst	T[°C]	t[h]	*exo:endo*	*ee*[%]
H	**2d**	−20	18	6:94	85
Br	**2a**	−40	60	97:3	87
Br	**2d**	−78	12	98:2	96
Me	**2a**	−20	120	96:4	85
Me	**2d**	−40	8	97:3	92

[a] Reactions were performed in 4 mL CH_2Cl_2 with 2.0 mmol dienophile, 2.4 mmol cyclopentadiene, and 5 mol% catalyst. The *exo:endo* ratios determined by GLC. The enantiomeric excesses were determined by GLC after conversion of products to the (*R*,*R*)-pentanediol acetals (see ref. [10]).

enantioselectivities. For example, the Diels–Alder reaction of α-bromoacrolein with cyclopentadiene in the presence of the benzyl-pybox ligand provides the adduct in 95% enantiomeric excess. This readily available ligand is an attractive alternative to the more expensive *tert*-butylglycine derived variant.

The correlation of catalyst reactivity with the coordinating ability of the counterion for the [(pybox)Cu(X)$_2$] catalysts **2** led us to reinvestigate the bis(oxazoline)copper(II) catalyzed Diels–Alder reactions of acrylimides **3**. The bis(oxazoline)copper triflate complex **1a** was originally chosen with the expectation that the imide dienophile would successively displace both of the electronegative triflate ligands from the metal center in conjunction with the bidentate ligation of dienophile and Lewis acid.[5]



To the extent that the triflate counterion impairs the two-point dienophile binding motif, other coordination geometries could lead to diminished enantioselection. Accordingly, complexes **1b–d** were prepared and evaluated as catalysts in the Diels–Alder reaction of acrylimide **3a** (R = H) with cyclopentadiene (Table 2). As in the preceding study, catalysts **1a–1d** exhibited significantly different levels of activity in the Diels–Alder reaction. Again, the SbF_6-derived complex **1d** was found to be the catalyst of choice. For example, the rate of the Diels–Alder reaction of **3a** with cyclopentadiene catalyzed by **1d** (X = SbF_6) was approximately 20 times faster (−78 °C, 99% *ee*) than the rate of the analogous reaction promoted by the less efficient triflate complex **1a**. The cationic bis(oxazoline) complex **1d** was then probed for generality with a selection of cyclic and acyclic dienes.

Inspection of Table 2 reveals that the Diels–Alder reactions of these substrates are significantly improved with the more reactive cationic catalyst. The cycloadditions of the less reactive

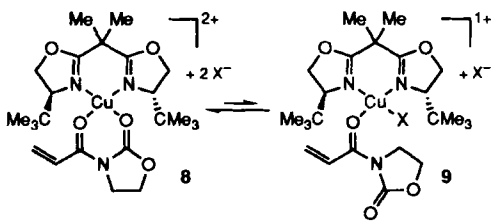
Table 2. Enantioselective Diels–Alder reactions of imide-derived dienophiles **3a–c** with dienes catalyzed by **1a** (X = OTf) and **1d** (X = SbF_6) at 25 °C [a].

Dienophile	R	Diene	Catalyst	t[h]	Yield [%] [b]	*endo:exo* [c]	*endo ee* [%] [d]	Product
3b	Ph		**1a**	24	85	90:10	99	**4b**
			1d	24	96	91:19	96	**4b**
3c	Cl		**1a**	24	<10	93:7	53	**4c**
			1d [e]	24	96	86:14	95	**4c**
3a	H		**1a**	12	72	75:25 [f]	86	**5**
			1d	12	70	91:9 [f]	94	**5**
3a	H		**1a**	36	66	78:22	84	**6**
			1d	12	59	77:23	93	**6**
3a	H		**1a**	48	90	98:2	82	**7**
			1d	5	90	95:5	93	**7**

[a] All reactions were carried out in CH_2Cl_2 (0.3 M in substrate) at 25 °C with 10 mol% catalyst. [b] Values refer to isolated yields. [c] Determined by ^1H NMR spectroscopy and/or GLC or HPLC. [d] Determined by chiral HPLC or GLC. [e] This reaction was performed on 11.0 g (62.4 mmol) of **3c** to give 14.5 g of **4c** (96% yield, 95% ee). [f] Ratio of **5** to all other isomers.

β-substituted dienophiles **3b** (R = Ph) and **3c** (R = Cl) with cyclopentadiene proceed with excellent selectivities (95–96% *ee*) at room temperature. In particular, the performance of the latter dienophile, a potentially useful acetylene surrogate, was significantly enhanced with the cationic catalyst. Complex **1d** (X = SbF_6) is also an excellent catalyst for less reactive dienes. For example, the two acyclic dienes and cyclohexadiene underwent catalyzed cycloadditions with the imide **3a** to afford the derived cycloadducts in good yields and enantioselectivities in the 93–94% range at room temperature.

In all instances, the cationic Cu^{II} complex **1d** (X = SbF_6) affords higher levels of asymmetric induction than the analogous triflate complex **1a**. The sense of asymmetric induction is fully consistent with the intervention of a square-planar catalyst-substrate complex **8**,[5] featuring the chelated dienophile in the s-*cis* conformation. We speculate that the moderately lower enantioselection exhibited by the triflate-based catalyst might be due to the intervention of a competing cycloaddition from a less highly organized one-point catalyst–dienophile complex such as **9**.



In summary, this study provides a rational basis for the design of Lewis acids based on the coordinating capacity of cationic Cu^{II} complexes which possess sufficient Lewis acidity to catalyze a range of synthetically useful Diels–Alder reactions. In particular, documentation of the importance of counterion structure in the use of cationic metal centers as Lewis acids has been made for the first time. Investigations on the scope of these complexes as chiral Lewis acids are ongoing.

Experimental Procedure

Diels–Alder reaction of methacrolein with cyclopentadiene catalyzed by **2d**: To a dry flask in an inert atmosphere dry box was added $CuBr_2$ (22 mg, 0.10 mmol), $AgSbF_6$ (69 mg, 0.20 mmol) and *tert*-butyl[pyridine-bis(oxazoline)] **2** (33 mg, 0.10 mmol). The flask was fitted with a serum cap, removed from the dry box and charged with 4 mL CH_2Cl_2. The resulting heterogenous mixture was allowed to stir for 6 h and then filtered through a plug of cotton to give a clear blue-green solution. This solution was then cooled to −40 °C and cyclopentadiene (2.4 mmol, 158 mg, 164 mL) was added followed by methacrolein (140 mg, 166 mL, 2.0 mmol). The reaction was monitored by taking a 100 μL aliquot and filtering through a small plug of silica gel eluting with 2 mL of diethyl ether. The solvent was removed in vacuo and the resulting oil dissolved in $CDCl_3$ and analyzed by ^1H NMR spectroscopy. The reaction mixture was monitored until the conversion was ≥95%. The crude reaction mixture was filtered through a plug of silica gel eluting with diethyl ether. The resulting solution was concentrated to give (1*R*,2*S*, 4*R*)-2-methylbicyclo-[2.2.1]hept-5-ene-2-carboxaldehyde as a clear colorless oil. $[\alpha]_D = +21.4$ ($c = 2.3$, EtOH); $R_f = 0.5$ (40% hexane/CH_2Cl_2); ^1H NMR (400 MHz, $CDCl_3$): $\delta = 9.69$ (s, 1H, CHO), 6.29 (dd, $J = 5.6$, 3.0 Hz, 1H, C(6)-H), 6.11 (dd, $J = 5.6$, 3.0 Hz, 1H C(5)-H), 2.89 (br s, 1H, C(1)-H), 2.82 (br s, 1H, C(4)-H), 2.25 (dd, $J = 11.9$, 3.8 Hz, 1H, C(3)HXH$_Y$), 1.39 (m, 2H, C(7)H$_2$), 1.01 (s, 3H, Me), 0.76 (d, $J = 11.9$ Hz, 1H, C(3)H$_X$HY); ^{13}C NMR (101 MHz, $CDCl_3$): $\delta = 205.8$, 139.5, 133.1, 53.9, 48.5, 47.6, 43.2, 34.6, 20.0; IR (neat): $\tilde{\nu} = 2973$, 2870, 2705, 1720, 1448, 1333, 1119 cm^{-1}; Exact mass calcd for $C_9H_{12}O$ 136.0893; found 136.0888 (EI). At this point the *exo*:*endo* product ratio was ascertained by GLC: DB-1701, 110 °C, 5 psi, t_r(*exo*) = 5.40, t_r(*endo*) = 6.01. This aliquot was then derivatized and used for determination of the enantioselectivity of the reaction. The cycloaddition product (14 mg, 0.10 mmol) was diluted with CH_2Cl_2 (0.5 mL) and (−)-(2*R*,4*R*)-pentanediol (20 mg, 0.20 mmol) and a few crystals of *p*-TsOH were added. After stirring for 6 h at room temperature, tlc analysis indicated that acetalization was complete. The reaction mixture was eluted through a short plug of silica with ether and analysed by capillary GLC. In this way the enantiomeric excess of the *exo* cycloaddition product was determined. Using the enantiomer of the diol, (+)-(2*S*,4*S*)-pentanediol, gave the same numeric value for the *exo* enantiomeric excess (within ±2% ee) indicating that there was negligible kinetic resolution during the acetalization reaction. Purification by flash chromatography gave the pure (2(1*R*,2*S*, 4*R*),9*R*,11*R*)-4,6-dimethyl-2-(2-methylbicyclo[2.2.1]hept-5-ene-2-yl)-1,3-dioxane. R_f 0.42 (20% EtOAc/hexanes); ^1H NMR (400 MHz, $CDCl_3$): $\delta = 6.13$–6.07 (m, 2H, C(5)-H, C(6)-H), 4.69 (s, 1H, C(8)-H), 4.32–4.28 (m, 1H, C(9)-H) 3.91–3.84 (m, 1H, C(11)-H) 2.73 (br s, 1H, C(1)-H), 2.65 (br s, 1H, C(4)-H), 1.76–1.55 (m, 3H, C(7)-CH$_2$, C(3)-H$_X$H$_Y$), 1.36 (d, $J = 7.0$ Hz, 3H, C(9)-CH$_3$), 1.28-1.33 (m, 2H, C(10)-CH$_2$), 1.20 (d, $J = 6.2$ Hz, 3H, C(11)-CH$_3$), 0.86 (s, 3H, C(2)-CH$_3$), 0.74 (dd, $J = 2.7$, 12.0 Hz, 1H, C(3)-H$_X$H$_Y$); ^{13}C NMR (101 MHz, $CDCl_3$): $\delta = 137.2$, 135.7, 99.5, 67.9, 67.7, 47.9, 47.4, 45.5, 37.2, 36.9, 21.9, 18.8, 17.3; IR (neat): $\tilde{\nu} = 3058$, 2969, 1449, 1375, 1334, 1240, 1136, 1058, 1004 cm^{-1}; Exact mass calcd for $C_{14}H_{22}O_2$ 222.1625; found 222.1620 (EI); GLC, DB-1701, 110 °C, 5 psi, t_r(minor product) = 29.89, t_r (major product) = 30.63 min.

Diels–Alder reaction of β-chloroimide **3c** with cyclopentadiene. A solution of catalyst **1d** (X = SbF_6) was prepared by mixing $CuCl_2$ (766 mg, 5.7 mmol), *tert*-butyl-bis(oxazoline) **1** (1.89 g, 6.3 mmol), and $AgSbF_6$ (3.92 g, 11.4 mmol) in CH_2Cl_2 (57 mL), stirring for 8 h at ambient temperature and filtering through celite. Imide **3c** (10.96 g, 62.4 mmol) was then added as a solution in CH_2Cl_2 (60 mL) by cannula (5 mL rinse of CH_2Cl_2). Immediately thereafter, cyclopentadiene (62 mL, 744 mmol) was added by syringe. The resulting solution was stirred at room temperature for 24 h. The reaction mixture was directly applied to a short column of silica gel (6 × 6 cm) and eluted with approximately 1 L of 1:1 ethyl acetate/hexane. Concentration afforded the unpurified product **4c** which was analyzed. ^1H NMR analysis indicated that the reaction had proceeded to >98% conversion. The unpurified reaction mixture was analyzed directly by chiral GLC, which showed the *endo*/*exo* ratio to be 87:13 (*endo* isomer 96% ee, chiraldex G-TA column; oven temperature = 150 °C, flow rate = 20 psi; t_r(*endo* major enantiomer) = 47.40, t_r (*endo* minor enantiomer) = 57.62, t_r(*exo* enantiomer 1) = 50.27, t_r(*exo* enantiomer 2) = 51.85). The product mixture was then purified by chromatography (8 × 32 cm silica gel, 30% ethyl acetate/hexane) to afford 14.45 g (59.8 mmol, 96%) of **4c** as a white solid. Recrystallization from ethyl acetate/hexane yielded enantiomerically pure **4c**: $[\alpha]_D = -113$ ($c = 1.10$, CH_2Cl_2); IR (CH_2Cl_2): $\tilde{\nu}$ 3000, 1781, 1699, 1480, 1387 cm^{-1}; ^1H NMR (400 MHz, $CDCl_3$): $\delta = 6.23$ (dd, 1H, $J = 5.6$, 3.3 Hz, C*H*=CH), 5.90 (dd, 1H, $J = 5.6$, 2.7 Hz, CH=C*H*), 4.41 (t, 2H, $J = 7.8$ Hz, OCH$_2$), 4.24 (m, 1H, -CH-), 4.13 (m, 1H, -CH-), 4.05–3.87 (m, 2H, -NCH$_2$), 3.39 (br d, 1H, $J = 1.4$ Hz, bridgehead H), 3.06 (br s, 1H, bridgehead H), 2.10 (br d, 1H, $J = 9.1$ Hz, one of -CH$_2$-), 1.72 (dd, 1H, $J = 9.0$, 1.7 Hz, one of -CH$_2$-); ^{13}C NMR (100 MHz, $CDCl_3$): $\delta = 172.0$, 153.2, 136.2, 134.4, 62.1, 58.8, 54.8, 52.4, 48.1, 46.9, 42.8; exact mass calcd for $C_{11}H_{12}N_1O_3Cl_1$ requires *m/z* 241.0506; found *m/z* 241.0494 (EI).

Received: November 25, 1994 [Z 7503 IE]
German version: *Angew. Chem.* **1995**, *107*, 864

Keywords: asymmetric syntheses · chelate ligands · copper compounds · Diels–Alder reactions · Lewis acids

[1] a) D. A Evans, K. A. Woerpel, M. M. Hinman, M. M. Faul, *J. Am. Chem. Soc.* **1991**, *113*, 726–728; b) D. A. Evans, K. A. Woerpel, M. J. Scott, *Angew. Chem. Int. Ed. Engl.* **1992**, *31*, 430–432.

[2] For related studies see: a) R. E. Lowenthal, S. Masamune, *Tetrahedron Lett.* **1990**, *31*, 6005–6008; b) D. Müller, G. Umbricht, B. Weber, A. Pfaltz, *Helv. Chim. Acta* **1991**, *74*, 232–240.

[3] D. A. Evans, M. M. Faul, M. T. Bilodeau, B. A. Anderson, D. M. Barnes, *J. Am. Chem. Soc.* **1993**, *115*, 5328–5329.

[4] Recently a second chiral Cu^{II} complex has also been reported to be an effective enantioselective aziridination catalyst: Z. Li, K. R. Conser, E. N. Jacobsen, *J. Am. Chem. Soc.* **1993**, *115*, 5326–5327.

[5] D. A. Evans, S. J. Miller, T. Lectka, *J. Am. Chem. Soc.* **1993**, *115*, 6460–6461.

[6] For the use of [(pybox)Rh] and [(pybox)Ru] complexes for ketone hydrosilylation and olefin cyclopropanation see: a) H. Nishyama, Y. Itoh, H. Matsumoto, S. Park, K. Itoh, *J. Am. Chem. Soc.* **1994**, *116*, 2223–2224 and references therein; b) H. Nishyama, M. Kondo, T. Nakamura, K. Itoh, *Organometallics* **1991**, *10*, 500–508. The experimental procedure for the synthesis of the pybox ligand may be found in this paper.

[7] The absolute stereochemical assignments for all compounds reported in this study have been made either by independent asymmetric synthesis (D. A. Evans, K. T. Chapman, J. Bisaha, *J. Am. Chem. Soc.* **1988**, *110*, 1238–1256) or by comparison of literature rotations.

[8] The fluoroborate counterion has been shown to strongly associate with Cu^{II}–amine complexes: D. S. Brown, J. D. Lee, B. G. A. Melsom, *Acta Crystallogr. Sect. B.* **1968**, *24*, 730–734.

[9] a) E. P. Kündig, B. Bourdin, G. Bernardinelli, *Angew. Chem.* **1994**, *106*, 1931–1934; *Angew. Chem. Int. Ed. Engl.* **1994**, *33*, 1856–1858; b) J. Bao, W. D. Wulff, *J. Am. Chem. Soc.* **1993**, *115*, 3814–3815; c) K. Maruoka, N. Murase, H. Yamamoto, *J. Org. Chem.* **1993**, *58*, 2938–2939; d) K. Ishihara, Q. Gao, H. Yamamoto, *J. Org. Chem.* **1993**, *58*, 6917–6919; e) E. J. Corey, T–P. Loh, *J. Am. Chem. Soc.* **1991**, *113*, 8966–8967; f) K. Furuta, S. Shimizu, Y. Miya, H. Yamamoto, *J. Org. Chem.* **1989**, *54*, 1481–1483.

[10] *exo*:*endo* Ratios determined by GLC analysis. (DB-1701, 110 °C, 5 psi) For acrolein: t_r(major product) = 5.32, t_r(minor product) = 5.92 min. For methacrolein: t_r(major product) = 5.40, t_r(minor product) = 6.01 min.; for bromoacrolein: t_r(starting aldehyde) = 2.33, t_r(major product) = 9.59, t_r(minor product) = 10.76 min. Enantiomeric excesses for acrolein and methacrolein adduct were determined by GLC analysis after conversion to the acetal of (*R*,*R*)-pentanediol (DB-1701, 110 °C, 5 psi) For the acrolein adduct-derived acetal: t_r(major product) = 28.15, t_r(minor product) = 28.91. For the methacrolein adduct-derived acetal: t_r(major product) = 29.89, t_r(minor product) = 30.55. For the bromoacrolein adduct, the enantiomeric excess was determined by GLC of the dimethyl acetal (GTA, 110 °C, 5 psi, t_r(minor product) = 62.95, t_r(major product) = 64.43 min and by ^{19}F NMR of the corresponding Mosher ester.

Aminocyclopentadienes, Aminoferrocenes, and Aminocobaltocenes**

Herbert Plenio* and Dirk Burth

More than forty years after the discovery of ferrocene, examples of aminocyclopentadienes and aminoferrocenes are still scarce.[1] Even what is probably the best synthesis (four steps starting from ferrocene) of the parent compound aminoferrocene $FcNH_2$ to date affords only small amounts;[2] alternate synthetic routes are equally demanding.[3] Several *N*,*N*-dialkylaminoferrocenes can, according to a paper by Boche et al., be prepared from *O*-tosylated *N*, *N*-dialkylhydroxylamines in good yields;[4] however, the number of hydroxyl derivatives[5] is limited and, in addition, the handling of these compounds poses certain risks,[6] which severely limits the possible applications of this reaction.

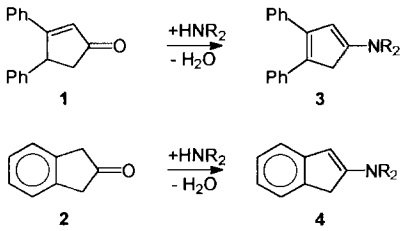
[*] Dr. H. Plenio, Dipl.-Chem. D. Burth
Institut für Anorganische und Analytische Chemie der Universität
Albertstrasse 21, D-79104 Freiburg (Germany)
Telefax: Int. code + (761)2035987
e-mail: plenio@sun8.ruf.uni-freiburg.de

[**] This work was supported by the Graduiertenkolleg "Ungepaarte Elektronen in Chemie und Biologie" and the Fonds der Chemischen Industrie. We wish to thank Prof. Dr. H. Vahrenkamp for his support as well as A. Warneke and T. Ludwig for their experimental assistance.

In the context of our own research in the area of redox-switchable ferrocene crown ethers,[7] we became interested in developing an efficient synthesis for aminocyclopentadienes, aminoferrocenes, and aminocobaltocenes.

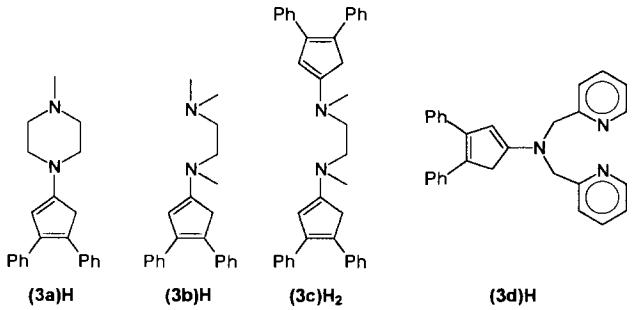
The reaction of ketones with secondary amines leads to enamines by the elimination of water.[8] Using cyclopentenones[9] as starting materials this reaction seemed ideally suited[7] for the preparation of *N,N*-dialkylaminocyclopentadienes, which could then be further reacted to yield the desired substituted ferrocenes and cobaltocenes.

Thus 3,4-diphenylcyclopent-2-enone (**1**)[10] and 2-indanone (**2**) were treated with secondary amines such as *N*-methylpiperazine (**a**), trimethylethylenediamine (**b**), *N,N'*-dimethylethylenediamine (**c**), and bis(2-picolyl)amine (**d**) (Scheme 1). In case of **1**, *N,N*-dialkylaminocyclopentadienes (**3a**)**H**, (**3b**)**H**, (**3c**)$\mathbf{H_2}$, and



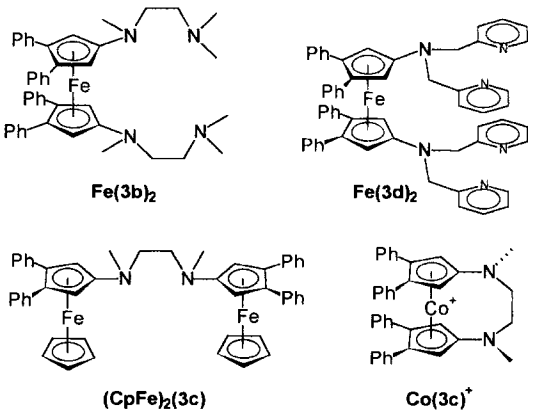
Scheme 1. Synthesis of *N,N*-dialkylaminocyclopentadienes **3** and -indenes **4**.

(**3d**)**H**, respectively, were afforded as pale yellow solids (Scheme 2) in yields ranging from 45–70%. The analogous indenes (**4a**)**H**, (**4b**)**H**, (**4c**)$\mathbf{H_2}$, and (**4d**)**H** were obtained in yields of >80%.[11] As a general observation, reactions involving 2-indanones (**2**) proceed at a faster rate and under milder conditions than the analogous reactions with 3,4-diphenylcyclopent-2-enone (**1**). An important characteristic of the secondary amines HNR_2 employed in this study is the presence of donor units in the R group. This allows the formation of σ donor metal complexes with the amine nitrogen as binding site.[12]



Scheme 2. A selection of the new *N,N*-dialkylaminocyclopentadienes **3** (the corresponding 2-(*N,N*-dialkylamino)indenes **4** are not shown).

The derivatives (**3a**)**H**, (**3b**)**H**, and (**3c**)$\mathbf{H_2}$, as well as (**4a**)**H**, (**4b**)**H**, and (**4c**)$\mathbf{H_2}$ (not shown) are readily deprotonated with *n*BuLi to give the corresponding lithium compounds, which were found to be stable in a moisture- and oxygen-free atmosphere. The *N,N*-dialkylaminoferrocenes **Fe**(**3a**)$_2$, **Fe**(**3b**)$_2$, and **Fe**(**3c**) were obtained in 30–50% yield by treating the lithium salts of **3** with $FeCl_2$. The corresponding cobaltocenes **Co**(**3a**)$_2$, **Co**(**3b**)$_2$, and **Co**(**3c**) can be synthesized in yields of 40–60% in an analogous fashion by reacting the lithium salts of **3** with $CoBr_2 \cdot 3THF$ (the products were isolated as their cobaltocinium salts following oxidation) (Scheme 3). The lithium salts of **4** react in the same way. The derivative (**3d**)**H** decomposed rapidly upon attempted deprotonation; however, the *N,N*-dialkylaminoferrocene **Fe**(**3d**)$_2$ could be prepared by treating (**3d**)**H** with $Fe(NiPr_2)_2$ which had been generated in situ. (**CpFe**)$_2$(**3c**) is readily accessible by irradiating a mixture of **Li**$_2$(**3c**) and $[CpFeL]^+[PF_6]^-$ with UV light (L = *p*-xylene).



Scheme 3. A selection of the new aminoferrocenes and aminocobaltocenes.

Oxidation of these new aminoferrocenes and aminocobaltocenes ($E_{1/2}$ **Fe**(**3c**) −0.01 V, **Fe**(**3d**)$_2$ 0.00 V, **Co**(**4b**)$_2$ −1.15 V, **Co**(**4c**) −1.08 V) occurs at significantly more negative potential than reported for ferrocene ($E_{1/2}$ = + 0.40 V in CH_3CN vs. Ag/AgCl) and cobaltocene ($E_{1/2}$ = − 0.94 V in CH_3CN vs. Ag/AgCl). As a result of the weakly electron-withdrawing nature of the aryl groups both the aminoferrocenes and aminocobaltocenes are less sensitive to oxidation than 1,1'-bis(dimethylamino)ferrocene ($E_{1/2}$ = − 0.23 V in CH_3CN vs. SCE) and 1,1'-bis(dimethylamino)cobaltocene ($E_{1/2}$ = −1.35 V in CH_3CN vs. SCE).[4, 13]

According to X-ray diffraction analyses[14] the structures of the aminoferrocenes **Fe**(**3a**)$_2$[15] and **Fe**(**3d**)$_2$[16] are very similar, despite the fact that the substituents at the amino groups vary considerably. Figure 1 depicts the structure of **Fe**(**3a**)$_2$ in the crystal as viewed along the axis centroid-Fe1-centroid. This projection shows that the six substituents of the ferrocene are arranged in such a manner that no unfavorable steric interactions result. The stacked phenyl rings are almost coplanar (12.4°); the distance between the two nitrogen atoms N1 and

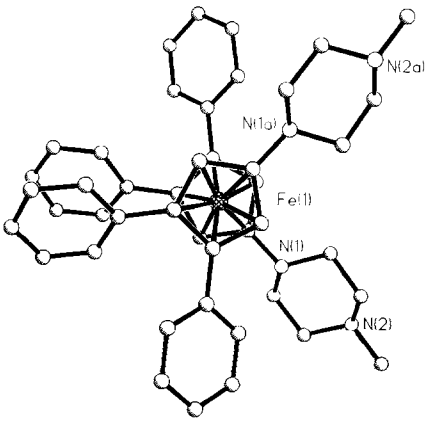


Fig. 1. Structure of **Fe**(**3a**)$_2$ in the crystal as viewed along the axis centroid-Fe1-centroid. For clarity, the hydrogen atoms have been omitted.

N1a is only 508.9 pm and thus they are already well preorganized for the chelating complexation of a metal ion. The substituents of the ferrocene are arranged in a similar way in the solid state for $\mathbf{Fe(3d)_2}$ (Fig. 2). The distance N1–N2 is also rather small (503.8 pm), and the planes of two stacked phenyl rings are only slightly tilted (24.1°). The bond lengths and angles in $\mathbf{Fe(3a)_2}$ and $\mathbf{Fe(3d)_2}$ are unremarkable.

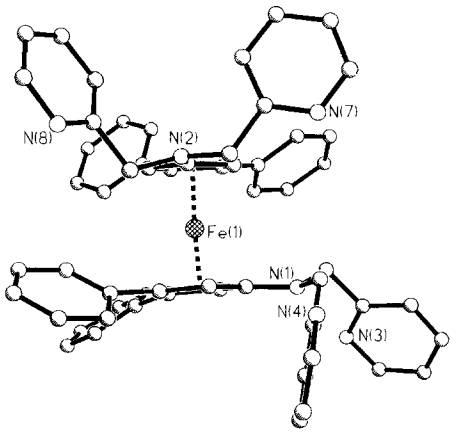


Fig. 2. Structure of $\mathbf{Fe(3d)_2}$ in the crystal as viewed along the plane of the cyclopentadienyl rings. For clarity, the hydrogen atoms have been omitted.

The nitrogen atoms contained in the side chains of the aminoferrocenes can be used for the formation of σ donor complexes. For instance, the isolation of a stable complex between two $LiClO_4$ and $\mathbf{Fe(3b)_2}$ demonstrates the relationship of the latter to TMEDA (tetramethylethylenediamine).

In summary, the reaction of 3,4-dimethylcyclopent-2-enone (**1**) and 2-indanone (**2**) with secondary amines provides a convenient entry to an almost unlimited number of *N,N*-dialkylaminocyclopentadienes **3** and -indenes **4**, respectively. Further reaction of compounds **3** and **4** has been shown to afford the corresponding aminoferrocenes and aminocobaltocenes. We are currently investigating the reactions of **3** and **4** with other metal salts and the complexation behavior of the donor atoms in the side chain.

Experimental Procedure

The following compounds were synthesized and fully characterized: *N,N*-dialkylaminocyclopentadienes, **(3a)H**, **(3b)H**, **(3c)H**, and **(3d)H**; 2-(*N,N*-dialkylamino)-indenes, **(4a)H**, **(4b)H**, **(4c)H**, and **(4d)H**; ferrocenes, $\mathbf{Fe(3a)_2}$, $\mathbf{Fe(3b)_2}$, **Fe(3c)**, $\mathbf{(CpFe)_2(3c)}$, $\mathbf{Fe(3d)_2}$; cobaltocenes, $\mathbf{Co(3a)_2}$, $\mathbf{Co(3b)_2}$, **Co(3c)**, $\mathbf{Co(4a)_2}$, $\mathbf{Co(4b)_2}$, **Co(4c)**, and $\mathbf{Co(4d)_2}$. Only a representative selection of experimental procedures and NMR data is given here.

(3d)H: A mixture of **1** (5.85 g, 25 mmol), bis(2-picolyl)amine (**d**) (5.0 g, 25 mmol), and *p*-toluenesulfonic acid (0.05 g) in benzene (100 mL) was heated to reflux for 48 h under N_2 in a water separator. After the solvent had been removed by vacuum destillation, the residue was recrystallized from toluene/hexane to afford **(3d)H** as a yellow powder. Yield: 6.0 g (58%). ^{1}H NMR ($CDCl_3$): δ = 3.64 (s, 2H, CpH), 4.66 (s, 4H, CH_2-Py), 5.26 (s, 1H, CpH), 6.97–7.34 (m, 14H, ArH + PyH), 7.63 (dt, J = 1.8, 7.7 Hz, 2H, PyH), 8.55 (d, J = 4.34 Hz, 2H, PyH).

$\mathbf{(3c)H_2}$: ^{1}H NMR ($CDCl_3$): δ = 2.92 (s, 6H, CH_3), 3.43 (s, 4H), 3.54 (s, 4H), 5.19 (s, 2H, CpH), 7.0–7.40 (m, 20H, ArH). ^{13}C NMR ($CDCl_3$): δ = 38.70, 42.66, 50.34, 102.20, 123.30, 124.52, 126.78, 126.84, 128.02, 128.31, 128.37, 137.64, 138.51, 143.58, 155.93.

(4b)H: Trimethylethylenediamine (**b**) (155 mg, 1.52 mmol) was added to a solution of **2** (200 mg, 1.52 mmol) in methanol (5 mL) and heated to reflux for 2 h. After the methanol had been removed by vacuum destillation, the product **(4b)H** was obtained as a brown oil. ^{1}H NMR ($CDCl_3$): δ = 2.25 (s, 6H, CH_3), 2.44 (t, J = 7.6 Hz, 2H, NCH_2), 2.86 (s, 3H, CH_3), 3.28 (t, J = 7.6 Hz, 2H, NCH_2), 3.36 (s, 2H, NC-CH_2), 5.29 (s, 1H, NC=CH), 6.77–7.18 (m, 4H, ArH). ^{13}C NMR ($CDCl_3$): δ = 36.75, 37.58, 45.21, 50.56, 55.77, 95.80, 116.02, 119.04, 122.02, 126.06, 136.00, 147.46, 156.29.

$\mathbf{Fe(3d)_2}$: **(3d)H** (414 mg, 1 mmol) was added to a solution of $FeCl_2$ (63.5 mg, 0.5 mmol) and $LiN(i\text{-}C_3H_7)_2$ (107 mg, 1 mmol) in THF (15 mL) at −78 °C. The reaction mixture was allowed to slowly warm to room temperature. After 2 h the solvent was removed by vacuum destillation and the residue was purified by chromatography using cyclohexane/ ethyl acetate/ Et_2NH (5:5:1) as eluant. Further purification was accomplished by recrystallization from toluene/hexane to give $\mathbf{Fe(3d)_2}$ as a deep red powder; yield: 154 mg (35%). ^{1}H NMR ($CDCl_3$): δ = 4.19 (s, 4H, CpH), 4.23 (s, 8H, CH_2-Py), 7.11 (ddd, J = 1.4, 4.8, 7.4 Hz, 4H, PyH), 6.59–6.79 (m, 20H, PyH + ArH), 7.17–7.23 (m, 8H, PyH + ArH), 8.10 (ddd, J = 0.9, 1.8, 4.8 Hz, 4H, PyH). ^{13}C NMR (C_6D_6): δ = 59.06, 60.81, 82.03, 116.61, 121.73, 122.40, 125.88, 127.90, 130.20, 135.92, 139.17, 149.51, 159.95. $C_{58}H_{48}FeN_6$ (884.9), calcd. (found): C 78.72 (78.25), H 5.47 (5.50), N 9.50 (9.78).

Fe(3c): ^{1}H NMR (C_6D_6): δ = 2.60 (s, 6H, CH_3), 2.95 (s, 4H, CH_2), 4.60 (s, 4H, FcH), 6.92–7.03 (m, 12H, ArH), 7.34–7.39 (m, 8H, ArH). ^{13}C NMR (C_6D_6): δ = 38.49, 48.86, 57.68, 82.99, 111.42, 125.96, 127.78, 129.71, 138.78.

$\mathbf{(CpFe)_2(3c)}$: ^{1}H NMR (C_6D_6): δ = 2.47 (s, 6H, CH_3), 3.01 (s, 4H, CH_2), 4.10 (s, 10H, C_5H_5), 7.06–7.10 (m, 12H, ArH), 7.50–7.55 (m, 8H, ArH). ^{13}C NMR ([D_6]acetone): δ = 39.84, 52.96, 57.50, 71.28, 81.85, 115.7, 126.57, 128.35, 130.40, 140.11. $C_{48}H_{22}Fe_2N_2$ (760.58), calcd. (found): C 75.80 (76.12), H 5.83 (5.58), N 3.68 (3.92).

$\mathbf{Co(4b)_2^+[CF_3SO_3]^-}$: ^{1}H NMR ($CD_3CN$): δ = 2.33 (s, 12H, CH_3), 2.49 (t, J = 6 Hz, 4H, NCH_2), 2.97 (s, 6H, CH_3), 3.31 (br, 4H, NCH_2), 5.72 (s, 4H, CpH), 7.08–7.12 (m, 4H, ArH), 7.28–7.33 (m, 4H, ArH). $C_{29}H_{38}CoF_3N_4O_3S \cdot CH_3OH$ (670.68), calcd. (found): C 53.73 (53.53), H 6.31 (6.21), N 8.35 (8.10).

Received: November 8, 1994 [Z 7458 IE]
German version: *Angew. Chem.* **1995**, *107*, 881

Keywords: aminocyclopentadienes · cyclopentadienylamines · ligands · sandwich complexes

[1] a) D. W. Macomber, W. P. Hart, M. D. Rausch, *Adv. Organomet. Chem.* **1982**, *21*, 1; b) R. Haltermann, *Chem. Rev.* **1992**, *92*, 965; c) J. Okuda, *Top. Curr. Chem.* **1991**, *160*, 97; d) N. J. Coville, K. E. duPlooy, W. Pickl, *Coord. Chem. Rev.* **1992**, *116*, 1; e) C. Janiak, H. Schumann, *Adv. Organomet. Chem.* **1991**, *33*, 291; f) P. Jutzi, *Chem. Rev.* **1986**, *86*, 983.

[2] M. Herberhold, M. Ellinger, L. Haumeier in *Organomet. Synth. Vol. 3* (Eds.: R. B. King, J. J. Eisch), Elsevier, Amsterdam, **1986**, p. 81.

[3] a) G. R. Knox, P. L. Pauson, D. Willison, E. Solcaniova, S. Toma, *Organometallics* **1990**, *9*, 301; b) G. R. Knox, P. Pauson, *J. Chem. Soc.* **1961**, 4615; c) M. Herberhold, M. Ellinger, W. Kremnitz, *J. Organomet. Chem.* **1983**, *241*, 227; d) F. S. Arimoto, A. C. Haven, *J. Am. Chem. Soc.* **1955**, *77*, 6295; e) A. M. Nesmeyanov, W. A. Ssasonowa, V. N. Drosd, *Chem. Ber.* **1960**, *93*, 2717; f) M. Herberhold in *Ferrocenes*, (Eds.: A. Togni, T. Hayashi), VCH, Weinheim, **1995**.

[4] a) M. Bernheim, G. Boche, *Angew. Chem.* **1980**, *92*, 1043; *Angew. Chem. Int. Ed. Engl.* **1980**, *19*, 1010; b) K. P. Stahl, G. Boche, W. Massa, *J. Organomet. Chem.* **1984**, *277*, 113.

[5] R. Stroh, *Methoden Org. Chem.* (*Houben-Weyl*), Vol. X/1, **1971**, p. 1091.

[6] $Me_2NO(SO_2CH_3)$ which is required in the synthesis of $[\eta^5\text{-}(C_5H_4NMe_2)Ir(CO)Cl]$ has been reported to have a tendency to decompose explosively: M. S. Blais, M. D. Rausch, *Organometallics* **1994**, *13*, 3557.

[7] a) H. Plenio, J. Yang, R. Diodone, J. Heinze, *Inorg. Chem.* **1994**, *33*, 4098; b) H. Plenio, H. El-Desoky, J. Heinze, *Chem. Ber.* **1993**, *126*, 2403; c) H. Plenio, R. Diodone, *J. Organomet. Chem.*, in press.

[8] *Enamines* (Ed.: A. G. Cook), Marcel Dekker, New York, **1988**.

[9] H. W. Thompson, B. S. Huegi, *J. Chem. Soc. Perkin Trans. 1* **1976**, 1603.

[10] a) T. A. Geissmann, C. F. Koelsch, *J. Org. Chem.* **1939**, *3*, 498; b) F. R. Japp, J. Knox, *J. Chem. Soc.* **1905**, *87*, 679.

[11] The aminocyclopentadienes **3** and -indenes **4** with varying amine groups are distinguished by adding small letters to the numbers; the free ligand is denoted by adding H to the symbol. The numbering scheme for the metallocenes is derived in the same way.

[12] a) H. Plenio, R. Diodone, *J. Org. Chem.* **1993**, *58*, 6650; b) P. Jutzi, M. O. Kristen, J. Dahlhaus, B. Neumann, H. G. Stammler, *Organometallics* **1993**, *12*, 2980.

[13] W. E. Geiger in *Organometallic Radical Processes* (Ed.: W. C. Trogler), Elsevier, Amsterdam, **1990**.

[14] G. M. Sheldrick, *SHELXS-86*, *SHELXL-93*, Universität Göttingen, **1986**, **1993**.

[15] a) X-ray structure analysis of $\mathbf{Fe(3a)_2} \cdot 0.5\,H_2O$ ($C_{44}H_{46}FeN_4 \cdot 0.5\,H_2O$): crystal dimensions: 0.5 × 0.4 × 0.4 mm^3, cubic, space group *Fd*-3, Z = 48, a = 36.905(4) Å, V = 50264(9) Å^3, ρ_{calcd} = 1.246 g cm^{-3}, θ = 2.4–23°, T = 293(2) K, 9144 reflections measured, 2953 of which are independent, empirical absorption correction, $\mu(Mo_{K\alpha})$ = 0.47 mm^{-1}, data/ parameters = 2003/ 231,

full-matrix least-squares refinement on F^2. H atom riding model, R values $[I > 4\sigma(I)]$: $R1 = 0.0635$, $wR2 = 0.171$. GOOF = 1.03, residual electron density = +0.41, −0.42 e Å^{-3}. The relatively poor quality of single crystals of **Fe(3a)$_2$** limited the data collection to $\theta = 23°$. This explains the large number of unobserved reflections and the moderate R values. b) Further details of the crystal structure investigations may be obtained from the Fachinformationszentrum Karlsruhe, D-76344 Eggenstein-Leopoldshafen (Germany), on quoting the depository numbers CSD-401290 (**Fe(3a)$_2$**·0.5 H$_2$O) and CSD-401324 **Fe(3d)$_2$**·H$_2$O.

[16] X-ray structure analysis of **Fe(3d)$_2$**·H$_2$O ($C_{58}H_{48}FeN_6$)·H$_2$O: crystal dimensions: 0.5 × 0.4 × 0.2 mm^3, triclinic, space group $P\bar{1}$, $Z = 2$, $a = 11.031(2)$, $b = 11.042(2)$, $c = 20.607(4)$ Å, $\alpha = 83.74(3)$, $\beta = 76.96$, $\delta = 79.47(3)°$, $V = 2398.1(8)$ Å^3, $\rho_{calcd} = 1.25$ g cm^{-3}, $\theta = 2.8$–$26°$, $T = 293(2)$ K, 9943 reflections measured, 9427 of which are independent reflections, empirical absorption correction, $\mu(Mo_{K\alpha}) = 0.36$ mm^{-1}, data/ parameters = 7209/ 588, full-matrix least-squares refinement on F^2, H atom riding model, R values $[I > 4\sigma(I)]$: $R1 = 0.0610$, $wR2 = 0.153$. GOOF = 1.09, residual electron density = +0.50, −0.40 e Å^{-3} [15b].

A Novel Allylic Anchor for Solid-Phase Synthesis—Synthesis of Protected and Unprotected O-Glycosylated Mucin-Type Glycopeptides**

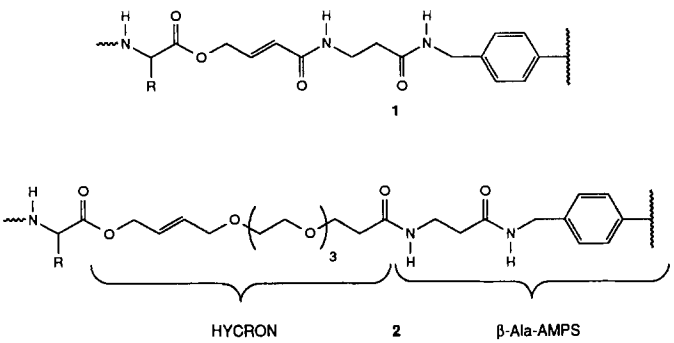
Oliver Seitz and Horst Kunz*

Dedicated to Professor Hans Jeschkeit on the occasion of his 65th birthday

Solid-phase synthesis provides rapid access to biologically relevant peptides.[1] The anchor group used between the target peptide and the polymeric support plays a very significant role. For glycopeptides as well as phosphopeptides or peptides containing acid- and base-sensitive protecting groups, which are to be employed in fragment condensations, the anchor group has to meet specific requirements. The same applies to the area of combinatorial chemistry for the preparation of peptide[2] and structure libraries.[3]

Anchoring through allyl esters[4] not only allows peptide derivatives to be detached without affecting acid- and base-labile structural elements, but also provides orthogonal stability relative to the temporary protecting groups commonly used in solid-phase peptide synthesis.[5] Thus, the *tert*-butyloxycarbonyl (Boc) group and the fluorenylmethoxycarbonyl (Fmoc) group can be used as N-terminal protecting groups. The cleavage of the allyl ester can be achieved by a palladium(0)-catalyzed transfer of the allyl group to a scavenger nucleophile like morpholine or *N*-methylaniline, which traps the allyl moiety irreversibly.[6] As a result, stabilized, long-lived cations are not generated as is the case with the frequently employed acid-labile anchors based on alkoxybenzyl, benzhydryl, or trityl esters.[7] This also avoids alkylation of nucleophilic structural elements[8] of the peptide and does not endanger acid-labile structural elements.

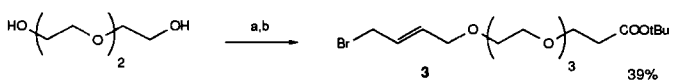
Derivatives of hydroxycrotonic acid were initially used to functionalize the polymeric support, aminomethylpolystyrene (AMPS), with allylic anchor groups.[5a] Insertion of a standard amino acid, for instance β-alanine, between the anchor and the polymer creates a spacer effect and allows the determination of the peptide loading independent of the degree of dryness.[9] Complex glycopeptides have been synthesized successfully according to this principle (β-HYCRAM **1**, Scheme 1).[10]



Scheme 1. Segments of peptide-loaded β-Ala-aminomethylpolystyrene (β-Ala-AMPS) with allylic anchor groups: β-HYCRAM **1** and novel anchor group HYCRON in **2**.

While the glycopeptides could be detached from the resin in high yields when the Boc strategy was used, reduced yields were observed when the Fmoc group was used as the temporary amino protection group. β-HYCRAM-bound glycine was used as a low molecular weight model. Upon exposure to morpholine/DMF (1:1) for 3 d, 12% of the allyl ester was aminolyzed.[11] As in many solid-phase syntheses, however, losses can occur at the dipeptide stage (formation of diketopiperazine) and, due to steric hindrance, during the cleavage process itself. Therefore a new anchor of the allyl ester type should incorporate a flexible, polar spacer in order to reduce steric hindrance and associations with the polystyrene matrix.[4] The achievements in solid-phase synthesis with graft copolymers made of polyethyleneglycol and polystyrene demonstrate the beneficial properties of polar spacers.[12] Moreover, the α,β-unsaturated carbonyl structure should be replaced to increase the stability against nucleophilic attack.

Structure **2** contains an allylic anchor (HYCRON) that meets the requirements outlined above. The precursor **3** of the allyl anchor, which allows the linkage to both the starting amino acid and the polymeric support, is synthesized by a sodium glycolate catalyzed Michael addition of triethgleneglycol to *tert*-butyl acrylate (Scheme 2) and subsequent reaction of the Michael adduct with 1,4-dibromo-2-butene under phase-transfer conditions.



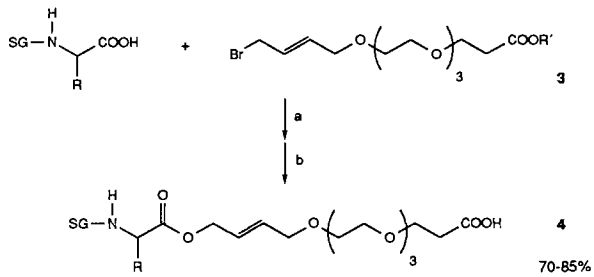
Scheme 2. a) H$_2$C=CH-COO*t*Bu, THF, sodium glycolate (1 mol%); b) BrCH$_2$-CH=CH-CH$_2$Br, NaOH, Bu$_4$NHSO$_4$, H$_2$O, CH$_2$Cl$_2$.

To load the polymer with the starting amino acid, the amino acid–anchor adduct **4** is prepared. Adduct **4** is obtained by reaction of the protected amino acid with allyl bromide **3** under phase-transfer conditions and subsequent cleavage of the carboxyl protecting group R′ (Scheme 3). The nucleophilic esterification avoids racemization of the starting amino acid, for example, the anchored threonine **5**.

The applicability of the new anchor (HYCRON) was tested in the solid-phase synthesis of the O-glycosylated tetrapeptide **6**. Peptide **6** is a partial structure of peptide T, a threonine-rich segment of the HIV-envelope protein gp 120.[13]

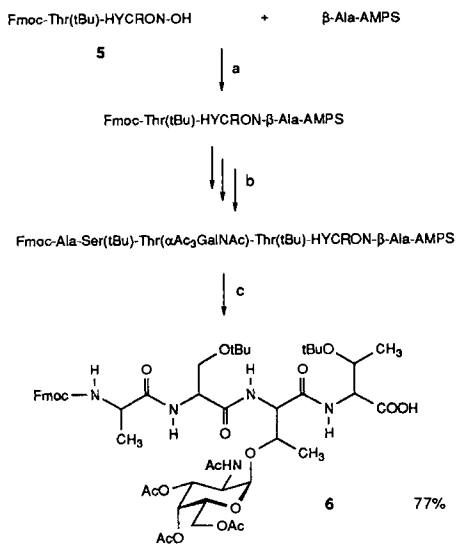
[*] Prof. Dr. H. Kunz, Dipl.-Chem. O. Seitz
Institut für Organische Chemie der Universität Mainz
J.-J. Becher-Weg 18-20, D-55099 Mainz (Germany)
Telefax: Int. code + (6131)39-4786

[**] This work was supported by the Deutsche Forschungsgemeinschaft, the Fonds der Chemischen Industrie, and the Boehringer-Ingelheim-Stiftung (stipend for O. S.). We are grateful to Professor C. Griesinger and Dr. R. Wechselberger, Universität Frankfurt/Main, for their help with multidimensional high-field NMR experiments.



Scheme 3. a) $NaHCO_3$, Bu_4NBr, H_2O, CH_2Cl_2; b) R' = *t*Bu: CF_3COOH; R' = CH_2COPh: Zn/AcOH.

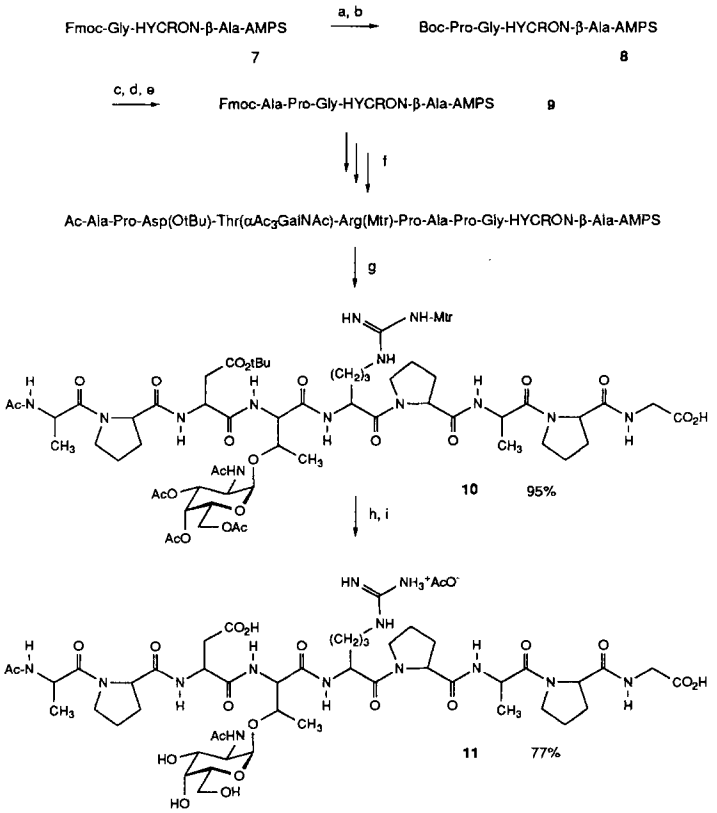
For the synthesis of **6**, aminomethylpolystyrene carrying β-alanine was loaded with the threonine anchor adduct **5** (Scheme 4). This as well as the following coupling reactions were accomplished with a three- to fourfold excess of diisopropylcarbodiimide (DIC)[14] and hydroxybenzotriazole (HOBt).[15] Any unchanged amino groups were capped after each coupling with



Scheme 4. a) DIC/HOBt, CH_2Cl_2; b) Fmoc detachment: DMF/morpholine (1:1); coupling: DIC/HOBt, CH_2Cl_2; capping: Ac_2O/pyridine (1:3); c) [$(PPh_3)_4Pd$], MeNHPh, DMF/DMSO (1:1) (see text).

The glycosylation pattern of the mucins and the balance of these phenomena appear to be closely related. It has been shown that T_N antigen structures (Ser/Thr(αGalNAc)) in breast tissue are tumor-associated, whereas T antigen structures (Ser/Thr(α-3-(βGal)-GalNAc)) are even tumor-specific.[19]

The Fmoc group of the glycine-loaded polymer **7** (Scheme 5), which was prepared from the adduct of the amino acid and the



Scheme 5. a) DMF/morpholine (1:1); b) Boc-Pro, DIC/HOBt; c) CH_2Cl_2/CF_3COOH (1:1); d) iPr_2NEt/CH_2Cl_2 (1:10); e) Fmoc-Ala, DIC/HOBt; f) see text; g) [$(PPh_3)_4Pd$], morpholine, DMF/DMSO (1:1); h) CF_3COOH/MeSEt/MeOPh (40:1:1); i) NaOMe/MeOH (pH = 8.5). Mtr = 4-methoxy-2,3,6-trimethylbenzenesulfonyl.

acetic anhydride/pyridine. The cleavage of the Fmoc group was achieved by exposure to DMF/morpholine (1:1) for 50 min. The carbohydrate building block was introduced as a preformed glycosyl amino acid (Fmoc-Thr(αAc_3GalNAc)). Detachment of the O-glycosylated tetrapeptide **6** was accomplished by a palladium(0)-catalyzed allyl transfer to *N*-methylaniline (96% yield).[16] The scavenger nucleophile *N*-methylaniline is not basic enough to cleave the Fmoc group. After twofold chromatography, the protected *O*-glycotetrapeptide **6** was obtained in a total yield of 77%[17] and was characterized by reversed-phase high-performance liquid chromatography (RP-HPLC), high-field NMR spectroscopy, and FAB-MS.

Glyconanapeptide **11** was prepared in another solid-phase synthesis using HYCRON-anchoring. Peptide **11** represents a partial sequence of the repeating unit of the MUC-1 mucin. Mucins are highly O-glycosylated proteins that are expressed in membranes of various epithelial cell types.[18] One phenomenon observed during tumor genesis is that the mucin-mediated adhesion and anti-adhesion processes are no longer under control.

anchor (**4**, SG = Fmoc, R = H), was detached with morpholine/DMF. The next amino acid to be coupled was *N-tert*-butyloxycarbonyl proline. The subsequent acidolysis of the Boc group from **8** prevents diketopiperazine formation during the cleavage of the protecting group. Subsequent couplings were performed exclusively with Fmoc-protected amino acids. All acylation reactions were performed in DMF. *O*-Glycosylthreonine and the following aspartic acid building block were coupled with *O*-(1*H*-benzotriazol-1-yl)-*N*,*N*,*N*',*N*'-tetramethyluronium tetrafluoroborate (TBTU)[20] and *N*-methylmorpholine. The other amino acids were activated with DIC and HOBt. In the case of the N-terminal amino acids proline and alanine, the coupling reactions were each repeated once. The terminal alanine was acetylated after Fmoc cleavage. The palladium(0)-catalyzed detachment of the polymer-bound glyconanapeptide was accomplished with the scavenger nucleophile morpholine in a yield of 93%.[16] After chromatography on silica gel, the glycopeptide **10** was isolated in a total yield of 95%.[21] Purity (>95% by HPLC) and structure of **10** were established by RP-HPLC, high-field NMR spectroscopy, and FAB-MS.

 © VCH Verlagsgesellschaft mbH, D-69451 Weinheim, 1995 0570-0833/95/0707-0804 $ 10.00+.25/0

To obtain the unprotected glycopeptide, the acid-labile protecting groups of **10** were cleaved with trifluoroacetic acid in the presence of ethyl methyl sulfide and anisole as cation scavengers.[22] The *O*-acetyl groups were removed by a sodium methoxide catalyzed transesterification in methanol.[7a] The *O*-glycopeptide **11** was purified by gel permeation chromatography on Sephadex G-15 and characterized by RP-HPLC, high-field NMR spectroscopy, and FAB-MS.[23]

These results show that allylic anchoring of the C-terminal amino acid to the HYCRON anchor provides the basis for an efficient solid-phase peptide synthesis. Without changing the allylic anchor, both Fmoc and Boc groups can be used as temporary protecting groups during the synthesis. Furthermore, both acid- and base-labile structural elements are maintained in the palladium(0)-catalyzed cleavage reaction, for example *tert*-butyl ester and *tert*-butyl ether groups, the Fmoc group, and the O-glycosidic bond in the synthesized glycopeptides **6** and **10**. With this method, glycopeptides can be obtained in high yields and in high purity directly after deblocking.

Received: December 7, 1994 [Z75291E]
German version: *Angew. Chem.* **1995**, *107*, 901

Keywords: solid-phase synthesis · glycopeptide · peptide

[1] a) R. B. Merrifield, *J. Am. Chem. Soc.* **1963**, *85*, 2149; b) G. B. Fields, R. L. Noble, *Int. J. Pept. Protein Res.* **1990**, *35*, 161; c) P. Lloyd-Williams, F. Albericio, E. Giralt, *Tetrahedron* **1993**, *49*, 11065.

[2] See, for example, G. Jung, A. G. Beck-Sickinger, *Angew. Chem.* **1992**, *104*, 357; *Angew. Chem. Int. Ed. Engl.* **1992**, *31*, 375.

[3] See, for example, W. H. Moos, G. D. Green, M. P. Pavia, *Annu. Rep. Med. Chem.* **1993**, *28*, 315.

[4] H. Kunz, B. Dombo (ORPEGEN GmbH), DE-A 3720269.3, **1987**; US-A 4929671, **1990**.

[5] a) H. Kunz, B. Dombo, *Angew. Chem.* **1988**, *100*, 732; *Angew. Chem. Int. Ed. Engl.* **1988**, *27*, 711; b) H. Kunz, B. Dombo, W. Kosch in *Peptides 1988* (Eds.: G. Jung, E. Bayer), de Gruyter, Berlin, **1989**, 154; c) B. Blankemeyer-Menge, R. Frank, *Tetrahedron Lett.* **1988**, *29*, 5871; d) F. Guibé, O. Dangles, G. Balavoine, A. Loffet, *ibid.* **1989**, *30*, 2641.

[6] a) H. Kunz, H. Waldmann, *Angew. Chem.* **1984**, *96*, 49; *Angew. Chem. Int. Ed. Engl.* **1984**, *23*, 71; b) M. Ciommer, H. Kunz, *Synlett* **1991**, 593.

[7] a) H. Paulsen, G. Merz, U. Weichert, *Angew. Chem.* **1988**, *100*, 1425; *Angew. Chem. Int. Ed. Engl.* **1988**, *27*, 1365; b) B. Lüning, T. Norberg, J. Tejbrant, *J. Chem. Soc. Chem. Commun.* **1987**, 1267; c) I. Laczko, M. Hollosi, L. Urge, K. E. Ugen, D. B. Weiner, H. H. Mautsch, J. Thurin, L. Otvos, *Biochemistry* **1990**, *29*, 4282; d) mucin-type glycopeptides: M. Meldal, S. Mouritsen, K. Bock, *Am. Chem. Soc. Symp. Ser.* **1993**, *519*, 19.

[8] a) E. Atherton, R. L. Cameron, R. C. Sheppard, *Tetrahedron* **1988**, *44*, 843; b) F. Albericio, N. Kneib-Cordonier, S. Biancalana, L. Geva, R. I. Masada, D. Hudsen, G. Barany, *J. Org. Chem.* **1990**, *55*, 3730.

[9] a) E. Atherton, D. L. J. Clive, R. C. Sheppard, *J. Am. Chem. Soc.* **1975**, *97*, 6584; b) F. Albericio, G. Barany, *Int. J. Pept. Protein Res.* **1985**, *26*, 92.

[10] W. Kosch, J. März, H. Kunz, *React. Polym.* **1994**, *22*, 181, and references therein.

[11] W. Kosch, Dissertation, Universität Mainz, **1992**.

[12] a) W. Rapp, L. Zhang, R. Häbich, E. Bayer in *Peptides* (Eds.: G. Jung, E. Bayer), de Gruyter, Berlin, **1988**, 199; b) E. Bayer, *Angew. Chem.* **1991**, *103*, 117; *Angew. Chem. Int. Ed. Engl.* **1991**, *30*, 113.

[13] a) M. Kowalski, J. Potz, L. Basiripour, T. Dorfman, W. C. Goh, E. Terwilliger, A. Dayton, G. Rosen, W. Haseltine, J. Sodroski, *Science* **1987**, *237*, 1351; b) C. B. Pert, J. M. Hill, M. R. Ruff, R. M. Berman, W. G. Robey, L. O. Arthur, F. W. Ruscetti, W. L. Farrar, *Proc. Natl. Acad. Sci. USA* **1986**, *83*, 9254.

[14] D. Sarantakis, J. Teichman, E. L. Lien, R. L. Fenichel, *Biochem. Biophys. Res. Commun.* **1976**, *73*, 336.

[15] W. König, R. Geiger, *Chem. Ber.* **1970**, *103*, 788.

[16] Detachment yield $= 100[1-(b_{pep}/b_{\beta\text{-Ala}})_n/(b_{pep}/b_{\beta\text{-Ala}})_v]$; b = loading, n = after detachment, v = before detachment.

[17] This yield is based on the original load of the polymer with β-alanine. Basing the yield on the initial amino acid load is not reasonable, because the amino acid analysis of hydroxyamino acids generally results in low values and thus in high yields.

[18] J. Hilkens, M. J. L. Ligtenberg, H. L. Vos, S. L. Litvinov, *TIBS* **1992**, *17*, 359.

[19] U. Karsten, G. Papsdorf, A. Pauly, B. Vojtesek, R. Moll, E. B. Lane, H. Clausen, P. Stosiek, M. Kasper, *Differentiation* (Berlin) **1993**, *54*, 55.

[20] R. Knorr, A. Trzeciak, W. Bannwarth, D. Gillessen, *Tetrahedron Lett.* **1989**, *30*, 1927.

[21] The total yield is based on the initial amino acid load. Obviously, it is impossible for the total yield to be higher than the detachment yield. This deviation, however, is within the experimental error of the amino acid analysis, which is the basis of all calculations of yields on the solid phase.

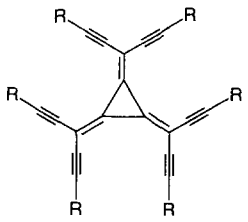
[22] E. Atherton, R. C. Sheppard, J. D. Wade, *J. Chem. Soc. Chem. Commun.* **1983**, 1060.

[23] R_f (Spherisorb ODSII C18/5μ, 250 × 4 mm, 1 mL min^{-1}) = 17.2 min (A: 0.1% TFA/MeCN, B: 0.1% TFA/H_2O; 0 to 2 min: 1% A in B, 2 to 24 min: 1% A in B to 30% A in B), $[\alpha]_D^{22} = -112.5$ °C ($c = 1$, H_2O); ^{1}H NMR (400 MHz, D_2O): $\delta = 4.82$ (H-1'), 4.75 (D^α), 4.48 (T^α), 4.33 (T^β); 2.75 (D^β); ^{13}C NMR (100.6 MHz, D_2O): $\delta = 98.6$ (C-1'), 75.2 (T^β), 50.8 (D^α), 29.4 (D^β); MS(FAB): $m/z = 1126.8$ ($M + H^+$).

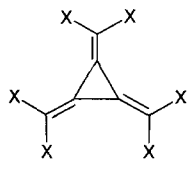
Hexakis(trimethylsilylethynyl)[3]radialene: A Carbon-Rich Chromophore with Unusual Electronic Properties**

Tim Lange, Volker Gramlich, Walter Amrein, François Diederich,* Maurice Gross, Corinne Boudon, and Jean-Paul Gisselbrecht

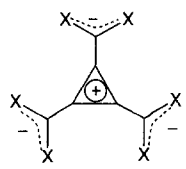
In our program targeting the construction of novel all-carbon molecules and polymeric networks,[1] we became interested in the synthesis of hexaethynyl[3]radialene (**1a**, $C_{18}H_6$), which had been independently identified both by Hopf and Maas[2] and by one of us[1a] as a suitable molecular precursor for a regular two-dimensional all-carbon network. A variety of [3]radialenes have been prepared, and their electronic and redox properties are strongly dependent on the nature of the substituents at the double bonds.[2] Derivatives with alkyl substituents generally are colorless and difficult to reduce, whereas those with electron-accepting groups, for example hexacyano[3]radialene (**2**) and hexakis(methoxycarbonyl)[3]radialene (**3**),[3] are colored and reducible to the corresponding radical anions and subsequently to the dianions. Radialene **2** is yellow and very unstable; it is readily reduced in two consecutive reversible one-electron steps to the stable dianion $\mathbf{2}^{2-}$ (see Table 1).[3] Radical anion $\mathbf{2}^{\bullet-}$



1a R = H
1b R = Me_3Si
1c R = $(i\text{-}Pr)_3Si$



2 X = CN
3 X = CO_2Me



4

[*] Prof. F. Diederich, Dr. W. Amrein, T. Lange
Laboratorium für Organische Chemie, ETH Zentrum
Universitätstrasse 16, CH-8092 Zürich (Switzerland)
Telefax: Int. code + (1)632-1109

Dr. V. Gramlich
Institut für Kristallographie und Petrographie, ETH-Zentrum
Sonneggstrasse 5, CH-8092 Zürich (Switzerland)

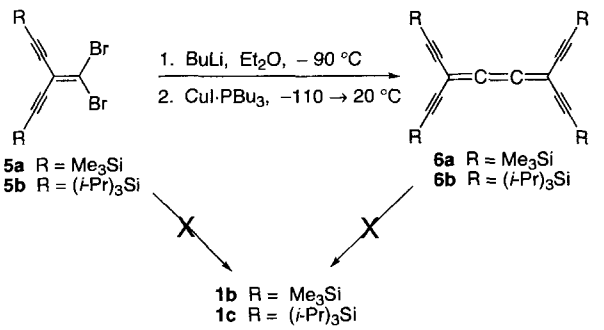
Prof. M. Gross, Dr. C. Boudon, Dr. J.-P. Gisselbrecht
Laboratoire d'Electrochimie et de Chimie Physique du Corps Solide
U. R. A. au C. N. R. S. n° 405, Faculté de Chimie, Université Louis Pasteur
1 et 4, rue Blaise Pascal, B. P. 296, F-67008 Strasbourg Cedex (France)

[**] This work was supported by the Schweizerische Nationalfonds zur Förderung der wissenschaftlichen Forschung.

acts as acceptor component in a variety of donor–acceptor complexes with both organic and organometallic donors, which had been prepared as potential organic ferromagnets.[4] In contrast, the yellow radialene **3** is a stable compound which can be reduced to the dianion $\mathbf{3}^{2-}$ via a short-lived radical anion $\mathbf{3}^{\bullet -}$.[3] MO calculations, ^{13}C NMR spectra, and X-ray structural data[4b] suggest that resonance structure **4** featuring an aromatic cyclopropenium cation and negative charges delocalized over the electron-withdrawing groups contributes significantly to the ground states of $\mathbf{2}^{2-}$ and $\mathbf{3}^{2-}$.

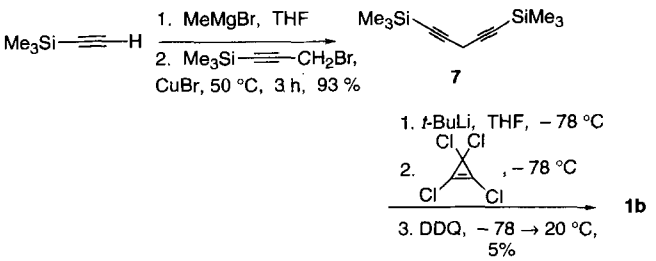
Hexaethynyl[3]radialene (**1a**) is isoelectronic and isosteric with the hexacyano derivative **2**, and it therefore was of interest to compare the structural and electronic properties of the two compounds. Since previous studies had shown that $(R_3Si\text{-}C{\equiv}C)_2C{=}$ fragments were electron accepting[5] and that dialkynylmethyl anions $(R_3Si\text{-}C{\equiv}C)_2CR'^-$ had significant stability,[6] we expected **1** to show the characteristic properties of an electron-accepting radialene. Additional incentive for the synthesis of **1** was provided by the computational prediction of its structure in high-level calculations by Schaefer and co-workers.[7] Here we describe the synthesis of hexakis(trimethylsilylethynyl)[3]radialene (**1b**) and report its low-temperature X-ray crystal structure and its unusual electronic and redox properties.

Initial attempts to prepare **1b** or the triisopropylsilyl-protected analogue **1c** from **5a**, **b** by the carbenoid cyclooligomerization method of Iyoda et al.[8] yielded the persilylethynylated butatrienes **6a**, **b** but no trace of radialene (Scheme 1).[5] Attempts to add carbenes or carbenoids, including those formed



Scheme 1. Unsuccessful attempts to prepare [3]radialene **1b**.

from **5a**, **b**, to the central double bond in **6a**, **b** also failed. The preparation of **1b** eventually succeeded starting from 1,5-bis(trimethylsilyl)-penta-1,4-diyne (**7**)[9] following, with modifications, the route employed by Fukunaga in the synthesis of **2** and **3** (Scheme 2).[3a] Addition of tetrachlorocyclopropene at –78 °C to the carbanion obtained by deprotonation of **6** with *t*BuLi, followed by oxidation with 2,3-dichloro-5,6-dicyano-*p*-benzoquinone (DDQ) of the presumably formed dianion $\mathbf{1b}^{2-}$



Scheme 2. Synthesis of [3]radialene **1b**.

yielded [3]radialene **1b** as a dark-red solid which melts under decomposition at 183 °C. DDQ was chosen as the oxidizing agent since it is sufficiently soluble in THF at the low temperatures required for the oxidation of $\mathbf{1b}^{2-}$ to **1b**. The new radialene is stable under laboratory conditions and dissolves in all common aprotic solvents. The low yield of 5% must be ascribed to side reactions, due in part to the instability of the intermediate dianion $\mathbf{1b}^{2-}$ and to decomposition of **1b** during chromatographic purification. The $i\text{Pr}_3\text{Si}$ derivative **1c** cannot be prepared by the same route, presumably because of the severe steric overcrowding of the six bulky $i\text{Pr}_3\text{Si}$ groups in the radialene product. Attempts to deprotect **1b** under mildest conditions with borax in solvents ranging from MeOH to THF and mixtures thereof converted **1b** to a new product as indicated by thin-layer chromatography; however, these solutions so far have been too unstable to allow spectral identification of this product as **1a**.

Radialene **1b** was characterized by matrix-assisted laser desorption ionization time-of-flight (MALDI-TOF) mass spectrometry. The spectrum obtained in the positive-ion mode with 2,5-dihydroxybenzoic acid (DHB) as matrix showed the molecular ion at m/z 654.4 as base peak in a highly resolved molecular ion cluster with an isotopic pattern in perfect agreement with that calculated (Fig. 1). Besides a complete absence of fragmentation,

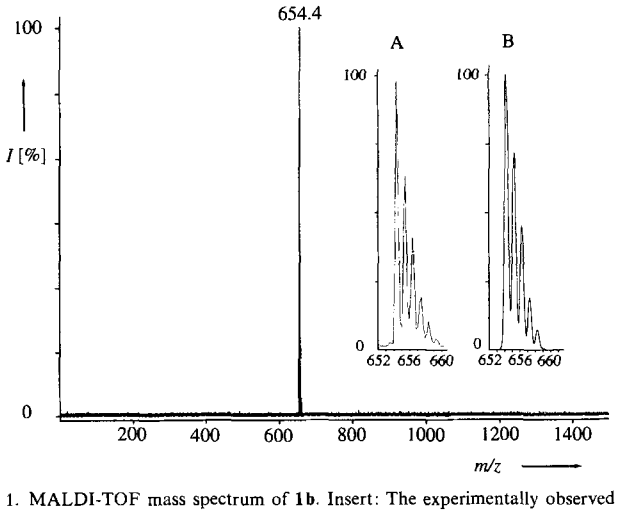


Fig. 1. MALDI-TOF mass spectrum of **1b**. Insert: The experimentally observed molecular ion cluster (A) is in excellent agreement with the calculated isotope pattern (B).

the reflectron spectrum also featured an unusually complete suppression of any matrix interference.[10] In contrast, electron impact mass spectrometry (70 eV) only gave a molecular ion with a relative intensity less than 0.05% besides a multitude of fragments due to extensive decay processes of the Me_3Si groups. This underscores once more the importance of LD-TOF mass spectrometry for the characterization of carbon-rich materials.[11]

In the IR spectrum (KBr) of **1b**, the C≡C stretches are observed at 2132 cm^{-1}, and the strong absorption at 1512 cm^{-1} is assigned to the double bonds. The ^1H NMR spectrum (500 MHz, $CDCl_3$) contains one singlet at $\delta = 0.23$, and the ^{13}C NMR spectrum (125.7 MHz, $CDCl_3$) displays the expected five peaks at $\delta = -0.2$, 92.5, 105.4, 106.0, and 126.7.

Radialene **1b** is highly colored; solutions in hexane are, quite unexpectedly, intensely purple-red and crystals are deep red. The electronic absorption spectrum in hexane (Fig. 2) extends to an end absorption around $\lambda = 620$ nm with the strong longest

 © VCH Verlagsgesellschaft mbH, D-69451 Weinheim, 1995 0570-0833/95/0707-0806 $ 10.00+.25/0

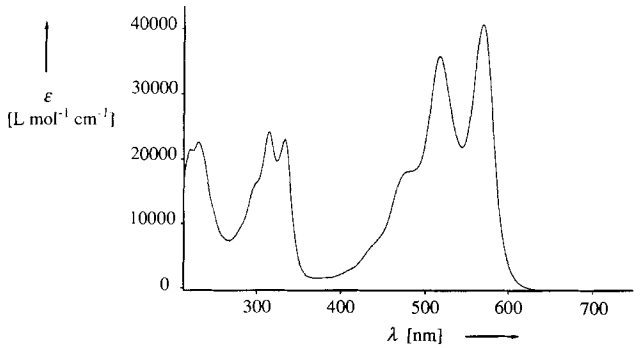
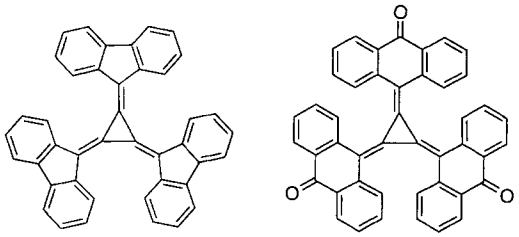


Fig. 2. Electronic absorption spectrum of **1b** in hexane, $T = 298$ K, $d = 1$ cm, $c = 2.37 \times 10^{-5}$ M.

wavelength band at $\lambda_{max} = 567$ nm ($\varepsilon = 41\,000$). These optical properties contrast those of yellow **2** and **3**, and rather resemble those of the highly colored tris(fluoren-9-ylidene)cyclopropane (**8**)[8b] and tris(9-anthron-10-ylidene)cyclopropane **9**,[12] π-acceptor radialenes (Table 1) with much larger π-electron chromophores.[13]



8 **9**

Unambiguous structural proof for **1b** was obtained by low-temperature (143 K) X-ray analysis of red platelets grown by slowly evaporating a solution of CH_3CN and CH_2Cl_2 (Fig. 3).[14] The carbon chromophore is nearly planar with a maximum deviation of 0.046 Å out of the best plane. The ideal D_{3h} symmetry of **1b** is reduced in the crystal presumably because of crystal packing effects. Significant distortions are seen owing to the steric compression between pairs of $Me_3Si-C\equiv C$ groups attached to neighboring exocyclic double bonds. The angles at the acetylenic C atoms deviate from linearity; the strongest angle reduction is observed for the bond angle C(44)-C(45)-Si(46) (165.9(2)°). In addition, the three ≡C−C−C≡ angles are reduced to an average value of 114.3°. Crystal packing effects rather than the steric compression of the Me_3Si groups seem to determine the extent (between 0.04 and 0.44 Å) to which the six Si atoms are turned out of the best plane of the carbon chromophore.

The C−C bond lengths in the three-membered ring adopt values between 1.420(5) and 1.431(3) Å, which is in the range of the endocyclic bonds observed in the parent [3]radialene and its hexamethyl derivative.[15] At values between 1.350(4) and 1.358(3) Å, the exocyclic C−C bonds adopt values typical for C=C bonds; Schaefer and co-workers had calculated by DZP SCF ab initio methods a value of 1.338 Å for **1a**.

The redox properties of **1b** were examined by stationary voltammetry on a platinum rotating disk electrode (RDE) and by cyclic voltammetry (CV) in either THF or CH_2Cl_2 containing Bu_4NPF_6 as supporting electrolyte. The radialene was readily reduced in two reversible one-electron charge transfers; the

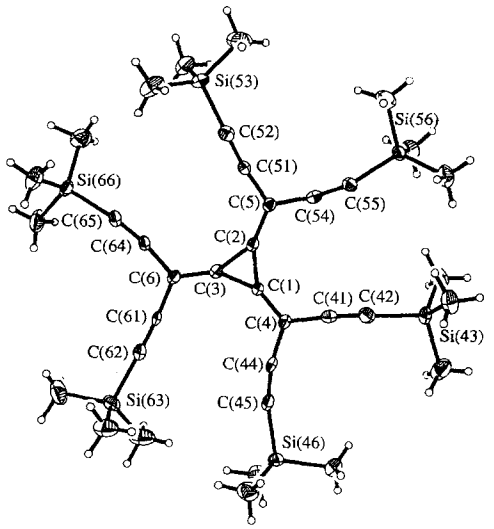


Fig. 3. Molecular structure of **1b** in the crystal. Selected bond lengths [Å] and bond angles [°]: C(1)-C(2) 1.429(4), C(1)-C(3) 1.420(5), C(1)-C(4) 1.355(4), C(2)-C(3) 1.431(3), C(2)-C(5) 1.358(3), C(3)-C(6) 1.350(4), C(4)-C(41) 1.429(4), C(4)-C(44) 1.436(3), C(5)-C(51) 1.431(4), C(5)-C(54) 1.430(4), C(6)-C(61) 1.439(4), C(6)-C(64) 1.428(4), all C≡C bonds are between 1.204(4) and 1.211(5); C(1)-C(2)-C(3) 59.5(2), C(1)-C(2)-C(5) 150.1(3), C(1)-C(3)-C(2) 60.2(2), C(1)-C(3)-C(6) 149.4(2), C(2)-C(1)-C(3) 60.3(2), C(2)-C(3)-C(6) 150.4(3), C(2)-C(1)-C(4) 148.2(3), C(3)-C(1)-C(4) 151.5(2), C(3)-C(2)-C(5) 150.4(3), C(41)-C(4)-C(44) 113.3(2), C(51)-C(5)-C(54) 114.4(2), C(61)-C(6)-C(64) 115.5(2), C(4)-C(44)-C(45) 169.6(3), C(44)-C(45)-Si(46) 165.9(2), C(5)-C(54)-C(55) 171.3(3), C(54)-C(55)-Si(56) 165.7(2), C(6)-C(64)-C(65) 172.0(3), C(64)-C(65)-Si(66) 169.8(2), all other C−C≡C and C≡C−Si angles between 171.3(3) and 177.8(2).

reductions occurred at −0.40 and −0.95 V, respectively, in THF (Fig. 4) and at −0.52 and −1.09 V in CH_2Cl_2 (vs. Ag/AgCl, see Table 1). The slopes of the waves obtained on the platinum RDE were close to the 58 mV expected for a one-electron

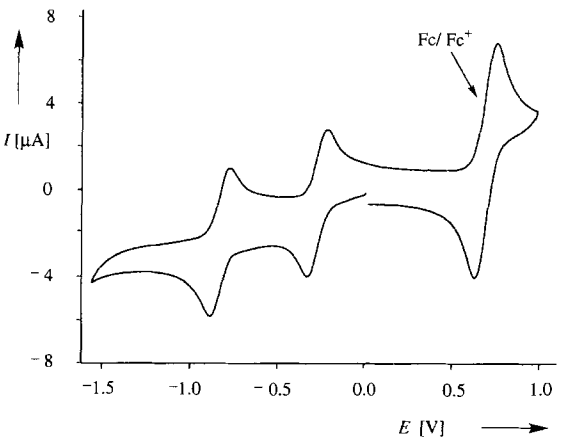


Fig. 4. Cyclic voltammogram of **1b** in THF (0.1 M Bu_4NPF_6) recorded with a Pt electrode at a sweep rate of 0.1 Vs^{-1}; Ag/AgCl reference electrode.

Nernstian charge transfer. In cyclic voltammetry the two reductions had the characteristics of a reversible one-electron charge transfer for scan rates ≥ 0.1 Vs^{-1}, whereas for lower sweep rates the second charge transfer became slightly "irreversible", characteristic of a subsequent chemical step associated with the second charge transfer under the experimental conditions.[16]

Thin-layer spectroelectrochemical measurements were carried out on an optically transparent thin-layer electrode. The conversion of **1b** to $\mathbf{1b}^{\bullet -}$ in THF showed well-defined isosbestic points at $\lambda = 306$, 345, 432, and 608 nm (Fig. 5). The radical

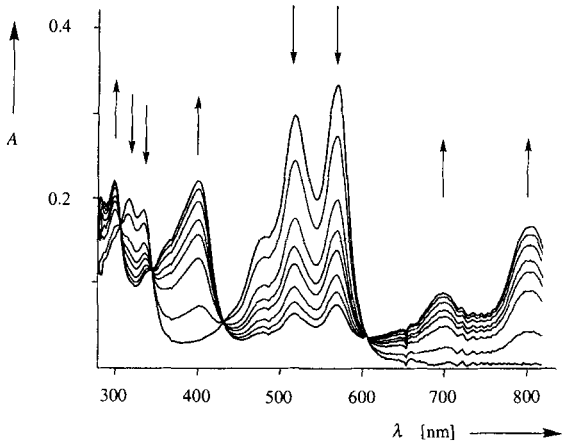


Fig. 5. Time-resolved UV/Vis spectra for the reduction of **1b** in THF (0.1 M Bu_4NPF_6) on an optically transparent thin-layer electrode; first reduction step at a controlled potential of −1.2 V vs. ferrocene.

anion $\mathbf{1b}^{\bullet -}$ could be quantitatively oxidized back to the neutral radialene only for short electrolysis times (less than 120 s); for longer reduction times, only a 90% recovery of **1b** was possible.

Further reduction of $\mathbf{1b}^{\bullet -}$ resulted in a decrease of the bands at around 700–800 nm, and the generated species were no longer oxidizable back to $\mathbf{1b}^{\bullet -}$ nor to the initial neutral species **1b**, probably as a result of chemical reactions of the strongly basic dianion. Large-scale electrolysis in CH_2Cl_2 in a classical three-electrode cell showed for the first reduction step a color change from purple-red to violet and for the second reduction step a color change from violet to light green.

Table 1. Redox potentials of electron-accepting [3]radialenes.

Radialene	$E^{1/2}_{red}$ (I)	$E^{1/2}_{red}$ (II)	Solvent	Reference electrode	Ref.
1b	−0.40	−0.95	THF	Ag/AgCl [a]	–
	−0.52	−1.09	CH_2Cl_2	Ag/AgCl [a]	–
2	+1.13	+0.34	CH_3CN	SCE	[3a]
3	+0.16	−0.07	CH_3CN	SCE	[3a]
8	−0.27	−0.75	DMF	Ag/AgCl	[8b]
9	+0.02	−0.28	CH_3CN	SCE	[12b]

[a] The redox potentials of **1b** were measured against ferrocene as internal standard as −0.96 and −1.51 V (in THF) and −0.94 and −1.51 V (in CH_2Cl_2). Ferrocene was oxidized in THF at +0.56 V and in CH_2Cl_2 at +0.42 V vs. Ag/AgCl.

With its six electron-withdrawing alkyne substituents at the double bonds, radialene **1b** exhibits redox properties similar to those of other derivatives with electron-accepting substituents and can be reduced stepwise and, under CV conditions, reversibly to the radical anion $\mathbf{1b}^{\bullet -}$ and subsequently to dianion $\mathbf{1b}^{2-}$. The cyclopropenium resonance structure **4** should contribute less to the stabilization of the ground state in $\mathbf{1b}^{2-}$ than in $\mathbf{2}^{2-}$ and $\mathbf{3}^{2-}$, since C≡C bonds stabilize negative charges in α position less effectively than cyano and methoxycarbonyl groups. The different stabilization of negative charges by the six substituents in the radical anion and dianion explains why **1b** is reduced at much more negative potentials than **2** and **3** (Table 1). No good explanation is currently available for the unexpectedly strong bathochromic shift of the electronic absorption spectrum of purple-red-colored **1b** compared to the spectra of yellow-colored **2** and **3**; further clarification of the electronic properties of **1b** and its reduced forms awaits high-level computational studies.

Experimental Procedure

To a solution of **7** (0.8 g, 3.84 mmol) in dry THF (25 mL) at −78 °C was added dropwise under Ar 1.7 M *t*BuLi (2.2 mL, 3.84 mmol) in pentane. The mixture was stirred for 1 h at −78 °C, then tetrachlorocyclopropene (114 mg, 0.64 mmol) in THF (1 mL) was added dropwise, and the red solution was stirred a further 10 min. At −78 °C, DDQ (0.22 g, 0.96 mmol) in THF (2 mL) was added, and the solution was allowed to warm to 20 °C. Pentane was added, and the organic phase was washed with 0.5 N HCl (1 ×) and saturated aqueous NH_4Cl (2 ×), dried ($MgSO_4$), and concentrated to dryness. The reaction mixture was dry-loaded on a plug of SiO_2, the plug eluted with hexane, and the filtrate, after concentration, chromatographed (80 g SiO_2, hexane/CH_2Cl_2 8:1) to afford **1b** (21 mg, 5%) as a red solid; m.p. 183 °C (decomp). IR (KBr): ν [cm^{-1}] = 2958 s, 2896 m, 2132 m, 1512 s, 1405 w, 1248 s, 1089 w, 851 s, 757 s, 699 m, 661 w, 628 m; ^1H NMR (500 MHz, $CDCl_3$): δ = 0.23 (s); ^{13}C NMR (125.7 MHz, $CDCl_3$): δ = 126.7, 106.0, 105.4, 92.5, −0.2; UV/Vis (hexane): λ_{max} (ε) = 567 (41 000), 516 (36 100), 479 (sh, 18 400), 333 (23 200), 314 (24 400), 298 (sh, 16 400), 230 (22 600), 221 (21 500); MALDI-TOF-MS: *m/z* 654 (M^+).

Received: November 9, 1994 [Z 7464 IE]
German version: *Angew. Chem.* **1995**, *107*, 898

Keywords: hydrocarbons · radialenes · spectroelectrochemistry

[1] a) F. Diederich, Y. Rubin, *Angew. Chem.* **1992**, *104*, 1123–1146; *Angew. Chem. Int. Ed. Engl.* **1992**, *31*, 1101–1123; b) F. Diederich, *Nature (London)* **1994**, *369*, 199–207.

[2] H. Hopf, G. Maas, *Angew. Chem.* **1992**, *104*, 953–977; *Angew. Chem. Int. Ed. Engl.* **1992**, *31*, 931–954.

[3] a) T. Fukunaga, *J. Am. Chem. Soc.* **1976**, *98*, 610–611; b) T. Fukunaga, M. D. Gordon, P. J. Krusic, *ibid.* **1976**, *98*, 611–613.

[4] a) J. S. Miller, A. J. Epstein, *Angew. Chem.* **1994**, *106*, 399–432; *Angew. Chem. Int. Ed. Engl.* **1994**, *33*, 385–415; b) M. D. Ward, *Organometallics* **1987**, *6*, 754–762; c) J. S. Miller, D. T. Glatzhofer, D. M. O'Hare, W. M. Reiff, A. Chakraborty, A. J. Epstein, *Inorg. Chem.* **1989**, *28*, 2930–2939; d) T. Sugimoto, Y. Misaki, Z.-I. Yoshida, J. Yamauchi, *Mol. Cryst. Liq. Cryst.* **1989**, *176*, 259–270; e) R. Breslow, *ibid.* **1985**, *125*, 261–267; f) T. J. LePage, R. Breslow, *J. Am. Chem. Soc.* **1987**, *109*, 6412–6421.

[5] J.-D. van Loon, P. Seiler, F. Diederich, *Angew. Chem.* **1993**, *105*, 1235–1238; *Angew. Chem. Int. Ed. Engl.* **1993**, *32*, 1187–1190.

[6] a) H. Hauptmann, *Tetrahedron Lett.* **1974**, 3593–3596; b) J. Anthony, C. Boudon, F. Diederich, J.-P. Gisselbrecht, V. Gramlich, M. Gross, M. Hobi, P. Seiler, *Angew. Chem.* **1994**, *106*, 794–798; *Angew. Chem. Int. Ed. Engl.* **1994**, *33*, 763–766.

[7] B. Ma, H. M. Sulzbach, Y. Xie, H. F. Schaefer III, *J. Am. Chem. Soc.* **1994**, *116*, 3529–3538.

[8] a) M. Iyoda, H. Otani, M. Oda, *J. Am. Chem. Soc.* **1986**, *108*, 5371–5372; b) M. Iyoda, H. Otani, M. Oda, *Angew. Chem.* **1988**, *100*, 1131–1132; *Angew. Chem. Int. Ed. Engl.* **1988**, *27*, 1080–1081; c) M. Iyoda, H. Kurata, M. Oda, C. Okubo, K. Nishimoto, *Angew. Chem.* **1993**, *105*, 97–98; *Angew. Chem. Int. Ed. Engl.* **1993**, *32*, 89–90.

[9] Compound **7** was prepared according to general procedures for the synthesis of 1,4-pentadiynes in: L. Brandsma, *Preparative Acetylenic Chemistry*, 2nd ed., Elsevier, Amsterdam, **1988**.

[10] The complete suppression of matrix interference suggests that the ionization of **1b** in the DHB matrix must proceed by a pure charge transfer (CT) process at a laser fluence well below the normal threshold of proton transfer in MALDI. This is consistent with recent results from Ledingham and co-workers. (C. T. J. Scott, C. Kosmidis, W. J. Jia, K. W. D. Ledingham, R. P. Singhal, *Rap. Commun. Mass Spectrom.* **1994**, *8*, 829–832), who report extensive subthreshold photoactivity of DHB. Alternatively, CT ionization of **1b** can be viewed as a matrix-assisted resonance two-photon ionization process, because the radialene absorbs strongly at the laser wavelength of 337 nm (3.67 eV).

[11] A. M. Boldi, F. Diederich, *Angew. Chem.* **1994**, *106*, 482–485; *Angew. Chem. Int. Ed. Engl.* **1994**, *33*, 482–485.

[12] a) J. L. Benham, R. West, J. A. T. Norman, *J. Am. Chem. Soc.* **1980**, *102*, 5047–5053; b) J. L. Benham, R. West, *ibid.* **1980**, *102*, 5054–5058.

[13] Longest absorption wavelength maxima of **3** [3b]: λ_{max} = 400 nm (ε 16 300, CH_3CN), of **8** [8b]: λ_{max} = 675 nm (ε 52 500, CH_2Cl_2), and of **9** [12a]: λ_{max} = 850 nm (ε 15 100, $CHCl_3$).

[14] Crystals of **1b** grown at room temperature crystallized in the triclinic space group $P\bar{1}$. On cooling to 143 K, a phase transition to the monoclinic space group $P2_1/n$ took place with doubling of the cell volume and without destruction of the crystal. X-ray crystal data for **1b** ($C_{36}H_{54}Si_6$, M_r = 655.3): Monoclinic space group $P2_1/n$, ρ_{calcd} = 1.020 gcm^{-3}, Z = 4, a = 15.909(5), b = 9.440(3), c = 28.410(11) Å, β = 90.39(3)°, V = 4267(3) Å^3, $Mo_{K\alpha}$ radiation, $2\theta \leq 50°$, 5322 unique reflections, T = 143 K. The structure was solved by direct methods (SHELXTL PLUS) and refined by full-matrix least squares

analysis using unit weights (heavy atoms anisotropic, H atoms fixed, whereby H positions are based on stereochemical considerations). Final $R(F) = 0.0368$, $wR(F) = 0.058$ for 596 variables and 4864 observed reflections with $F > 5\sigma(F)$. Further details of the crystal structure investigations may be obtained from the Director of the Cambridge Crystallographic Data Centre, University Chemical Laboratory, 12 Union Road, GB-Cambridge CB2 1EZ (UK), on quoting the full journal citation.

[15] a) J. D. Dunitz, A. Magnoli, *Helv. Chim. Acta* **1966**, *49*, 1680–1681; b) E. A. Dorko, J. L. Hencher, S. H. Bauer, *Tetrahedron* **1968**, *24*, 2425–2434; c) H. Dietrich, H. Dierks, *Angew. Chem.* **1968**, *80*, 487–488; *Angew. Chem. Int. Ed. Engl.* **1968**, *7*, 465.

[16] Although the solvents were dried, traces of moisture in the electrochemical cells cannot be excluded. Therefore, the chemical step mentioned could be the protonation of the dianion $\mathbf{1b}^{2-}$.

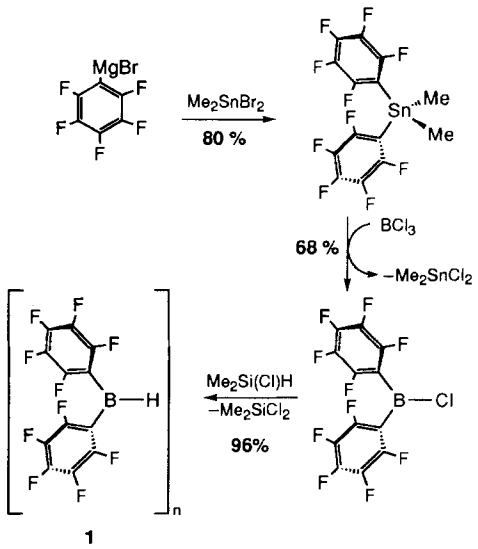
Bis(pentafluorophenyl)borane: Synthesis, Properties, and Hydroboration Chemistry of a Highly Electrophilic Borane Reagent**

Daniel J. Parks, Rupert E. von H. Spence, and Warren E. Piers*

Hydroboration is one of the most widely used reactions in organic synthesis.[1] A wide variety of borane reagents have been reported such that a library of reagents exists tailored to many different chemical situations. We were interested in the electrophilic and potentially very reactive borane $HB(C_6F_5)_2$ for possible applications in generation of soluble Ziegler–Natta-type olefin polymerization catalysts. These studies revealed this borane to be an exceptionally active hydroboration reagent. In this communication we describe its synthesis, characterization, and a preliminary survey of its activity towards alkenes and alkynes.

Bis(pentafluorophenyl)borane (**1**) was prepared from the known chloroborane $(C_6F_5)_2BCl$[2] in the absence of Lewis bases by reaction with hydride sources such as $[Cp_2Zr(Cl)H]_n$, Bu_3SnH, and $Me_2Si(Cl)H$ (Scheme 1). Traditional metathetical methods for transformations of this type[3] were not advisable because they necessitated the use of donor solvents which were difficult to remove completely (if at all) owing to the high Lewis acidity[4] of **1**.[5] The most convenient hydride transfer agent proved to be $Me_2Si(Cl)H$ since it also served as solvent for the reaction and the by-product Me_2SiCl_2 was easily removed; **1** was observed to precipitate over the course of one hour and was isolated in high yield by filtration. The overall yield of **1** from bromopentafluorobenzene was 52%.

Borane **1** is a white, microcrystalline, oxygen- and moisture-sensitive solid which was found to be to stable (i.e. it retained 100% of its activity) for at least three months when stored under an inert atmosphere at room temperature. Spectroscopic evidence indicated that the solid material is dimeric in structure. The infrared spectrum of the solid showed a strong band at 1550 cm^{-1} characteristic[6] of the ν_{asym} in-phase mode for a B-(μ-H)$_2$-B unit, and no bands corresponding to stretching vibrations of terminal B–H bonds were evident.[7] Solution NMR data were, however, consistent with the presence of monomeric



1

Scheme 1. Synthesis of $(C_6F_5)_2BH$ (**1**). In the last step the reagent $Me_2Si(Cl)H$ also serves as the solvent.

$(C_6F_5)_2BH$. Most convincingly, the ^{11}B NMR spectrum revealed the presence of a minor species ($\approx 10\%$) with a signal at $\delta = 60.1$ ppm in addition to a major species giving rise to a signal at $\delta = 18.0$. The downfield resonance appears in the region associated with monomeric dialkylboranes,[8] while the signal due to the major species is more typical of a dimeric borane.[9] Thus, although borane **1** is a dimer in the solid state, dissociation into a monomeric borane is facile in aromatic solvents.

Bis(pentafluorophenyl)borane is a highly active hydroboration reagent towards a range of simple alkenes and alkynes (Table 1). Addition of the olefin or alkyne to a suspension of the borane in benzene led to the rapid dissolution of the solid, and the reaction was complete *within two minutes*.[10] Even sterically demanding olefins (Table 1, entry 1) were hydroborated very rapidly, and the rates of hydroboration of methylcyclohexene and methylcyclopentene were almost identical.[11, 12] These observations are in contrast with those seen in reactions employing the common hydroboration reagent 9-borabicyclo[3.3.1]nonane (9-BBN) which, under identical conditions, required several hours to go to completion with these substrates. The only substrates that do not react rapidly with **1** are those having a $B(C_6F_5)_2$ functionality attached, in other words those formed upon monohydroboration of alkynes (entries 6–8). Not only are these alkenes more sterically encumbered, the electron-withdrawing effect of the $B(C_6F_5)_2$ substituent likely deactivates the double bond towards subsequent hydroboration. By comparison, hydroborations of alkynes with 9-BBN generally proceed more rapidly for the second hydroboration, often precluding isolation of the singly hydroborated product unless excess substrate is employed.[13]

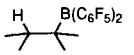
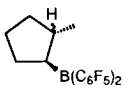
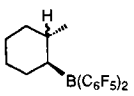
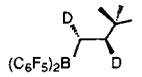
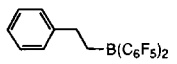
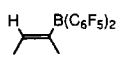
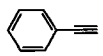
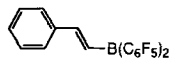
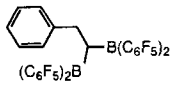
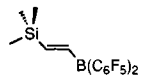
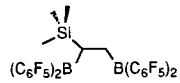
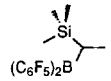
Entries 2–4 in Table 1 demonstrate that **1** hydroborates the substrates by the commonly accepted *cis* addition mechanism.[14] Regioselectivity was found to be excellent for substrates for which multiple products were possible. For example, styrene was hydroborated to give the isomer shown with >98% selectivity (as shown by ^1H NMR spectroscopy and oxidation to 2-phenylethanol, vide infra). In some instances (entries 1–3) facile isomerization by means of a retrohydroboration–rehydroboration sequence was observed over the course of a few hours at room temperature. This behavior is typical for substrates with thexyl substituents,[15] but for other substrates elevated temperatures are usually required to induce these rearrangements.[16] Fortu-

[*] Prof. W. E. Piers, D. J. Parks, Dr. R. E. von H. Spence
Guelph-Waterloo Centre for Graduate Work in Chemistry
Guelph Campus, Department of Chemistry and Biochemistry
University of Guelph
Guelph, Ontario N1G 2W1 (Canada)
Telefax: Int. code + (519)766-1499

[**] Financial support for this work was provided by the Novacor Research and Technology Corporation of Calgary, Alberta, and by the Natural Sciences and Engineering Council of Canada (postgraduate scholarship for D. J. P.).

 © VCH Verlagsgesellschaft mbH, D-69451 Weinheim, 1995 0570-0833/95/0707-0809 $ 10.00+.25/0

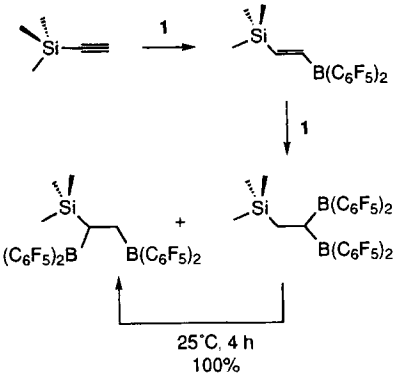
Table 1. Hydroboration of simple alkenes and alkynes with bis(pentafluorophenyl)borane (**1**) [a].

Entry	Substrate	Product (1 equiv. **1**)	Product (2 equiv. **1**)
1			
2[b]			
3[b]			
4[c]			
5[d]			
6			no reaction
7[b]			
8[b,e]			
9[f]			

[a] 100% yield by ^{1}H NMR (see ref. [10]). [b] Regioselectivity >98%. [c] [D_1]-**1** was used. [d] Small amounts (≈4%) of the other regioisomer were also detected. [e] The second hydroboration initially produced a mixture of regioisomers which converted quantitatively into the thermodynamic product shown (see text). [f] A thermodynamic mixture of isomers was observed (85:15); the major isomer is shown (see text).

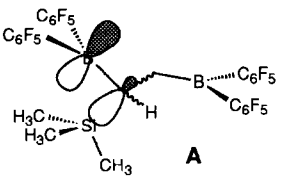
nately, the difference in the rates of initial hydroboration and rearrangement in these systems allows for good control in obtaining either the kinetic or thermodynamic products.

Selective monohydroboration of terminal alkynes was effected by reaction of substrates with a single equivalent of **1** (entries 7, 8). Although slower, double hydroboration occurred upon addition of a second equivalent of the borane. In the reaction of **1** with phenylacetylene, the product was the 1,1 isomer in accord with the normal selectivity observed with other borane reagents.[10] In contrast, the thermodynamic product for trimethylsilylacetylene was the 1,2 isomer. Initially, a mixture of the two possible products of double hydroboration was observed (ratio of 1,1:1,2 = 2.5:1, Scheme 2), which converted to the 1,2 regioisomer quantitatively. A similar phenomenon was observed for trimethyl(vinyl)silane (entry 9). The kinetic product in this reaction was that with the expected selectivity, 1-trimethylsilyl-2-bis(pentafluorophenyl)borylethane. Upon heating to 100 °C this compound isomerized to a mixture (ratio = 85:15) of the two possible regioisomers; the primary isomer was that with



Scheme 2. Hydroboration of trimethylsilylacetylene using 1.

boron attached to the α-carbon atom (see structural formula in Table 1). In the products arising from reaction of silylated substrates with BH_3 boron has been observed to occupy the α-position for electronic reasons, when steric repulsions between the Me_3Si group and boron substituents are at a minimum. Similarly, hydroboration of substrates with the general formula $RC{\equiv}CSiMe_3$ is selective: in the products boron is attached to the carbon atom α to silicon in the monohydroborated product.[17] These observations suggest that there is a thermodynamic preference for silicon to occupy a position β to a boron center in analogy to the well-known "β-silicon effect"[18] in the stabilization of carbocations. Instead of stabilizing a carbocation-like transition state structure, the boron migrates to form a more stable ground state structure **A**.



The generality of this phenomenon and its possible applications are being explored further.

Oxidation of the hydroborated products $RB(C_6F_5)_2$ could not be effected cleanly with aqueous methods or with *meta*-chloroperbenzoic acid (MCPBA) owing to the proteolytic instability of the $B(C_6F_5)_2$ group (loss of HC_6F_5). We have found that anhydrous Me_3NO[19] is a mild and efficient reagent for oxidizing alkylboranes to provide alcohols in good yields. For example 3,3-dimethyl-1-butanol was isolated in 58% yield (unoptimized) from the hydroboration of *tert*-butylethylene. We are exploring other methods for functionalizing these boranes. We are also interested in the properties of the boranes, particularly the dihydroborated products shown in entries 7 and 8, which should be excellent chelating Lewis acid activators for a variety of organic reactions and Ziegler–Natta olefin polymerization systems.[20]

Experimental Procedure

1: Into an evacuated flask containing $(C_6F_5)_2BCl$ (7.00 g, 18.4 mmol) at −78 °C was condensed $Me_2Si(Cl)H$ (10.2 g, 108 mmol). The flask was warmed to room temperature, upon which the chloroborane dissolved and a new white precipitate formed. The reaction mixture was stirred for 1 h and then filtered to give 6.14 g (17.7 mmol, 96%) of the borane as a white crystalline powder. ^{1}H NMR (C_6D_6): δ = 4.2 (br, full width at half maximum ≈25 Hz); ^{11}B NMR (C_6D_6, 25 °C): major component δ = 18.0; minor component δ = 60.1; ^{19}F{^{1}H} NMR (C_6D_6, 10 mM, 25 °C): major component (90%) δ = −134.8 (2F), −148.0 (1F), −160.7 (2F); minor component (10%) δ = −130.5 (2F), −143.4 (1F), −161.7 (2F); IR (Nujol, NaCl): ν = 1652 s, 1550 m (B-H), 1521 m, 1406 w, 1395 w, 1315 s, 1307 w, 1149 s, 1111 s, 1050 w, 1018 m, 975 s, 949 m, 937 w, 767 m, 661 m, 634 w, 624 w; MS (CI$^-$, 70 eV): *m/z* = 346 (M^+); anal. calcd for $C_{12}F_{10}BH$: C 41.67, H 0.29; found: C 41.87, H 0.33.

Deuteriobis(pentafluorophenyl)borane [D_1]-**1**: To a solution of $(C_6F_5)_2BCl$ (1.45 g, 3.8 mmol) in hexane (6 mL) was added a solution of tributyltin deuteride (1.11 g, 3.8 mmol) in hexane (2 mL) over 5 min. This led to the immediate precipitation of a white solid. After 1 h the reaction mixture was filtered; the solid was washed with

 © VCH Verlagsgesellschaft mbH, D-69451 Weinheim, 1995 0570-0833/95/0707-0810 $ 10.00+.25/0

a little cold hexane to give [D_1]-**1** (1.07 g, 3.1 mmol, 81%). $^2H\{^1H\}$ NMR (C_6H_6): $\delta = 4.2$ (br, full width at half maximum = 6 Hz).

General hydroboration procedure: To a suspension of $HB(C_6F_5)_2$ (0.1 mmol) in dry benzene (0.6 mL) under an argon atmosphere was added the dried alkene or alkyne substrate (1 equiv) by syringe. The mixture was sonicated for 30–60 s and then shaken. The reaction progress was monitored by ^1H NMR spectroscopy.

Received: October 11, 1994 [Z 7393 IE]
German version: *Angew. Chem.* **1995**, *107*, 895

Keywords: boranes · hydroborations

[1] a) H. C. Brown, *Hydroboration*, Benjamin, New York, **1962**; b) A. Pelter, K. Smith, H. C. Brown, *Borane Reagents*, Academic Press, London, **1988**; c) K. Smith, A. Pelter in *Comprehensive Organic Synthesis, Vol. 8* (Eds.: B. M. Trost, I. Fleming), Pergamon, New York, **1991**, p. 703.
[2] R. D. Chambers, T. Chivers, *J. Chem. Soc.* **1965**, 3933.
[3] K. Smith, A. Pelter, Z. Jin, *Angew. Chem.* **1994**, *106*, 913; *Angew. Chem. Int. Ed. Engl.* **1994**, *33*, 851.
[4] K. Ishihara, N. Hananki, H. Yamamoto, *Synlett* **1993**, 577.
[5] THF, for example, could not be removed, and at elevated temperatures (80 °C) **1** was observed to react with THF to yield $(C_6F_5)_2BO(CH_2)_3CH_3$.
[6] G. Socrates, *Infrared Characteristic Group Frequencies*, Wiley, New York, **1980**, p. 130.
[7] A. Pelter, K. Smith, D. Buss, A. Norbury, *Tetrahedron Lett.* **1991**, *32*, 6239.
[8] E. Negishi, J.-J. Katz, H. C. Brown, *J. Am. Chem. Soc.* **1972**, *94*, 4025.
[9] J. A. Soderquist, H. C. Brown, *J. Org. Chem.* **1980**, *45*, 3571.
[10] The reactions were all quantitative by NMR, and the products were characterized by ^1H and ^{13}C NMR spectroscopy or by further derivitization of the alkylborane products.
[11] H. C. Brown, R. Liotta, C. G. Scouten, *J. Am. Chem. Soc.* **1976**, *98*, 5297.
[12] Although relative rates of hydroboration for these two substrates may still be quite different, in practical terms the rate difference is not important owing to the high activity of **1**.
[13] H. C. Brown, C. G. Scouten, R. Liaotta, *J. Am. Chem. Soc.* **1979**, *101*, 96.
[14] H. C. Brown, B. C. Subba Rao, *J. Am. Chem. Soc.* **1959**, *81*, 6428.
[15] E. Negishi, H. C. Brown, *Synthesis* **1980**, 153.
[16] L. D. Field, S. P. Gallagher, *Tetrahedron Lett.* **1985**, *26*, 6125.
[17] a) J. A. Soderquist, J. C. Colberg, L. Del Valle, *J. Am. Chem. Soc.* **1989**, *111*, 4873; b) M. Hoshi, Y. Masuda, A. Arase, *J. Chem. Soc. Perkin Trans. 1* **1990**, 3237.
[18] J. B. Lambert, *Tetrahedron* **1990**, *46*, 2677.
[19] J. A. Soderquist, M. R. Najafi, *J. Org. Chem.* **1986**, *51*, 1330.
[20] L. Jia, X. Yang, C. Stern, T. J. Marks, *Organometallics* **1994**, *13*, 3755.

New Process for the Sulfonation of Phosphane Ligands for Catalysts**

Wolfgang A. Herrmann,* Guido P. Albanese, Rainer B. Manetsberger, Peter Lappe, and Helmut Bahrmann

Two-phase procedures have opened a new perspective for organometallic homogeneous catalysis as exemplified in hydroformylation.[1] Sulfonated phosphane ligands have proved themselves in the Ruhrchemie/Rhône–Poulenc process[1, 2] and suggest that a large potential may be anticipated for other C–C coupling reactions, too.[3] Fuming sulfuric acid (oleum), often the only effective sulfonating agent for arylphosphanes is not always satisfactory as a reagent for synthesis:[3d] parallel to the sulfonation of the aryl groups it also causes the formation of undesirable phosphane oxides, which, according to our present understanding, are useless for catalytic purposes and, in addition, are laborious to separate.[4]

These side reactions can be suppressed with low concentrations of SO_3 and short reaction times, but then mixtures of products with different degrees of sulfonation are formed. Phosphanes with a low degree of sulfonation, on the other hand, lead to an increased loss of the catalytically active (noble metal) complexes through extraction into the organic phase because of their poor water-solubility.[1a] Both disadvantages—phosphane formation and low, nonuniform degree of sulfonation—frequently militate against the industrial use of sulfonated phosphanes. In the following we show how these problems can be avoided.

Treating the standard ligand triphenylphosphane (TPP) according to the previous standard procedure at 20 °C with 30% oleum (30 wt% SO_3) under laboratory conditions yields, after 24 hours, a mixture of sulfonated products containing 12.4 mol% of phosphane oxides (Fig. 1a; ^{31}P NMR: $\delta = 36.45$), which must be separated from the sulfonated derivatives by a multistage extraction.[4]

We have now discovered that the addition of orthoboric acid to the sulfonation charges lessens the phosphane oxidation or suppresses it completely. The boric acid is initially dissolved in

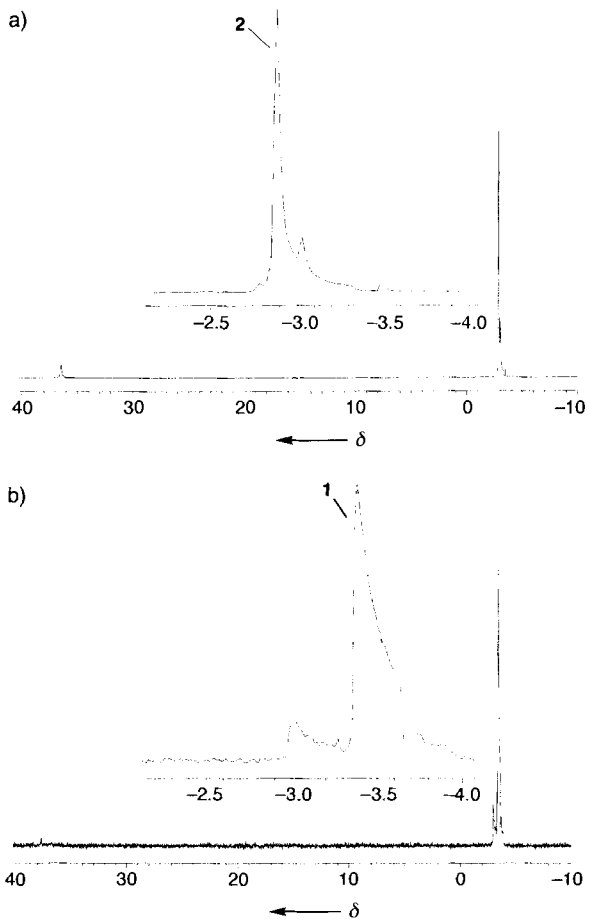


Fig. 1. a) ^{31}P NMR spectrum of triply sulfonated triphenylphosphane **2** (TPPTS; $\delta = 2.88$, 53.8 mol%), prepared according to the conventional procedures of ref. [4], crude hydrolysis mixture with 33.8 mol% of **1**. b) ^{31}P NMR spectrum of doubly sulfonated triphenylphosphane **1** (TPPDS), prepared with $H_2SO_4/B(OH)_3$/oleum; see text. The spectrum shows a very small amount of phosphane oxide ($\delta = 37.68$).

[*] Prof. Dr. W. A. Herrmann, G. P. Albanese, Dr. R. B. Manetsberger
Anorganisch-chemisches Institut der Technischen Universität München
Lichtenbergstrasse 4, D-85747 Garching (Germany)
Telefax: Int. code + (89) 3209-3473

Dr. P. Lappe, Dr. H. Bahrmann
Hoechst AG, Werk Ruhrchemie, D-46128 Oberhausen (Germany)

[**] Water-Soluble Metal Complexes and Catalysts, Part 8. This work was supported by the Bundesministerium für Forschung und Technologie. Part 7: W. A. Herrmann, C. W. Kohlpaintner, R. B. Manetsberger, H. Bahrmann, H. Kottmann, *J. Mol. Catal.*, in press.

96% sulfuric acid. The water that forms in the process [Eq. (a)] is then quantitatively "titrated" by oleum to H_2SO_4 [Eq. (b)],

$$B(OH)_3 + 5H_2SO_4 \rightleftharpoons [H_3SO_4]^+ + [B(OSO_3H)_4]^- + 3H_2O \quad (a)$$

$$3H_2O + 3SO_3 \rightleftharpoons 3H_2SO_4 \quad (b)$$

which removes the sulfur trioxide and simultaneously generates a superacidic medium [Eq. (a)],[5a] which apparently shows no significant oxidizing power. According to Gillespie et al., the Hammett acidity H_0 of the system $H_2SO_4/B(OH)_3/SO_3$ at low SO_3 concentrations increases substantially faster than that of the H_2SO_4/SO_3 system at the same SO_3 concentration. In the ^{11}B NMR spectrum apart from the signal of a three-coordinate boron species ($h_{1/2}$ = 425 Hz, $\delta = -0.11$), a signal of a highly symmetrical four-coordinate species ($h_{1/2}$ = 61 Hz, $\delta = -3.21$) is observed on addition of $B(OH)_3$ to 96% H_2SO_4. This resonance is likely to correspond to the borate $[B(OSO_3H)_4]^-$, an assignment supported by the values for the comparable systems $B(OSO_2CF_3)_3$ and $[B(OSO_2CF_3)_4]^-$, which have signal widths at half height of 198 and 53 Hz, respectively (CH_2Cl_2; ^{11}B NMR: $\delta = -1.11$ and -3.53, respectively).[6] As shown by ^{11}B NMR spectroscopy (Fig. 2), the equilibrium (a) is shifted completely to the right when the water produced by the reaction is removed by oleum [Eq. (b)]. These reactions may be followed easily through the electric conductivity of the solutions.[5b]

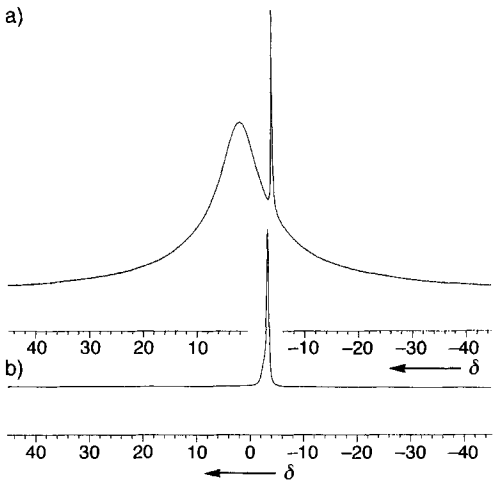


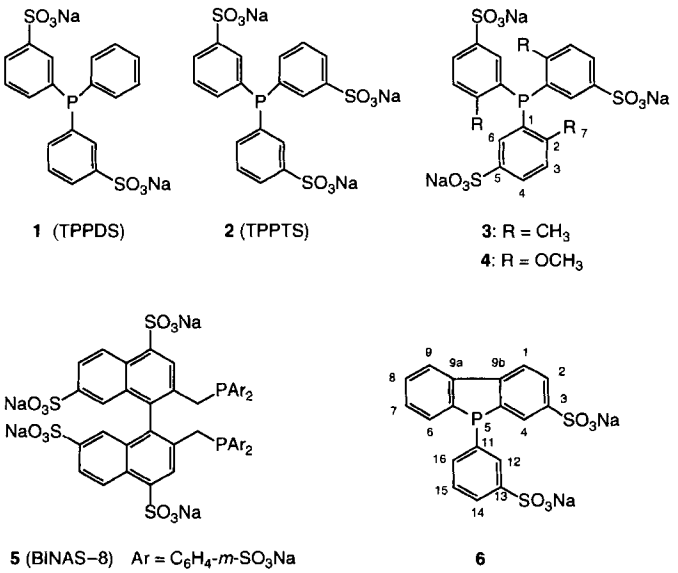
Fig. 2. a) ^{11}B NMR spectrum of boric acid in concentrated sulfuric acid. b) ^{11}B NMR spectrum of a) after addition of oleum; see text.

The boric acid effect stems from cooperation of two favorable circumstances: 1) The phosphanes to be sulfonated are quantitatively quaternized [Eq. (c)], which provides stability against oxidation. 2) Sulfonating species that are far weaker in oxidizing power than SO_3 are formed, for example $[H_3SO_4]^+$.

$$PR_3 + [H_3SO_4]^+ \longrightarrow [HPR_3]^+ + H_2SO_4 \quad (c)$$

The new process is advantageous for the following reasons:

1) For the first time a controlled sulfonation is possible: For example, we obtain selectively the disulfonated derivative TPPDS (**1**, Fig. 1b; ^{31}P NMR: $\delta = -3.38$) from TPP if the temperature of the sulfonation is 58 °C, whereas it is otherwise only accessible in a mixture. This conversion is virtually quantitative after three days. Interestingly even at 120 °C no further sulfonation to the triply sulfonated TPPTS (**2**) takes place, although noticeable phosphane oxidation occurs. TPPTS forms readily, however, if **1** is sulfonated with an excess of 30 wt% SO_3 at room temperature for three days. TPPTS already has industrial application.[1-3, 7]



2) The common ligands in homogeneous catalysis can now be exhaustively sulfonated without side products. Thus, within three days at 95 °C, tris(2-methylphenyl)phosphane affords the triply sulfonated phosphane **3**, a new ligand that enables comparative kinetic studies because of its *ortho* substitution. The deactivated tris(2-methoxyphenyl)phosphane can be converted into the new triply *meta*-sulfonated phosphane **4** with $H_2SO_4/B(OH)_3/SO_3$ [Eq. (a) and (b)] at room temperature within four days.

3) Highly sulfonated and therefore sufficiently water-soluble phosphanes can often be prepared only by this procedure. Thus with 1,1'-binaphthalene-2,2'-diylbis(methylene)bis(diphenylphosphane) (NAPHOS) only a mixture of four- to eightfold sulfonated species is achieved by conventional sulfonation with oleum (65% SO_3) (Fig. 3a), whereas now the product BINAS-8 (**5**, n = 8) can be prepared selectively without phosphane oxidation for the first time (Fig. 3b; ^{31}P NMR: $\delta = -10.44$).[8] However, an excess of SO_3 is required in this case. The

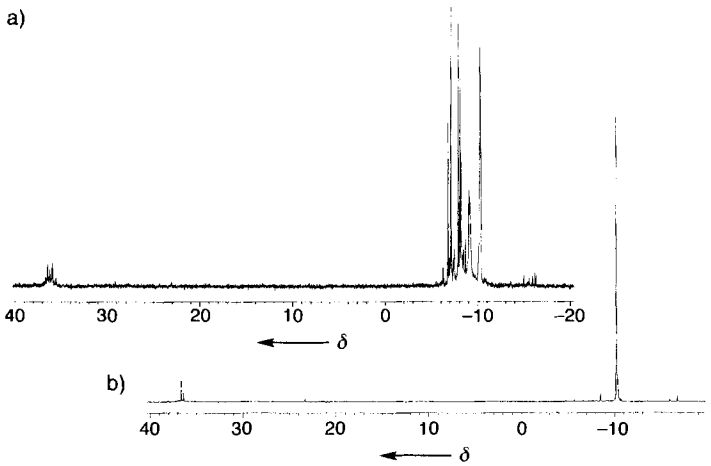


Fig. 3. a) Sulfonation of NAPHOS with oleum (65% SO_3). The actual SO_3 concentration is only 40% as a result of dilution with 96% H_2SO_4 (used to predissolve NAPHOS). The ^{31}P NMR spectrum shows the formation of phosphane oxides (δ = 35–37) and a mixture of many different sulfonated derivatives ($\delta = -6$ to 11). b) Sulfonation of NAPHOS with $H_2SO_4/B(OH)_3$/oleum (with the same SO_3 concentration as in a)); see text. The ^{31}P NMR spectrum confirms the uniformity of the product BINAS-8 (**5**). The amount of phosphane oxides (δ = 36–37) is about 3 mol%.

 © VCH Verlagsgesellschaft mbH, D-69451 Weinheim, 1995 0570-0833/95/0707-0812 $ 10.00+.25/0

catalyst formed by this ligand with rhodium(I) is the most efficient to date for propene hydroformylation with respect to activity, productivity, and *n*/*iso* selectivity.[9]

4) A sulfonation of the phospholes, in particular, failed previously because of the pronounced sensitivity to oxidation of this class of compounds. Now from 5-phenyl-5*H*-dibenzophosphole at 145° the selectively sulfonated product **6** can be obtained after 15 h in almost 90% yield as the first known water-soluble phosphole.[8] Phospholes are very promising ligands, inter alia for the hydroformylation of higher (and also functionalized) olefins.[10]

5) The excess boric acid is virtually completely removed in the hydrolytic product workup.

Studies into the kinetics of the sulfonation of triphenylphosphane point to different sulfonation species in the H_2SO_4/$B(OH)_3$/SO_3 system: Under identical conditions, in particular the same SO_3 concentration, highly sulfonated derivatives are formed more quickly than with the conventional H_2SO_4/SO_3 system. Probably the active electrophilic species in addition to SO_3 is essentially $[H_3SO_4]^+$,[11] which according to Equation (a) is present in higher concentrations.

In the light of the rapid development of two-phase catalysis, in particular with water as catalyst medium, the process described here for the direct sulfonation should represent an important breakthrough in catalyst development mainly as a consequence of its efficiency.

Experimental Procedure

Disodium *P*-phenyl-3,3′-phosphanediylbis(benzenesulfonate) **1**: Orthoboric acid (4.80 g, 77.8 mmol) was dissolved in concentrated sulfuric acid (96%, 20 mL). Oleum (20 mL, 65 wt% SO_3) was added dropwise so that in the sulfonation mixture a SO_3 concentration of about 0.9 wt% resulted. This excess SO_3 was removed under high vacuum at 60 °C within 45 min. Then triphenylphosphane (3.00 g, 11.4 mmol) was added (boric acid/phosphane = 6.8/1). The mixture was stirred until all solids were completely dissolved, heated to 58 °C for 4 days, and after cooling hydrolyzed with 50 mL degassed water. The extraction was performed with triisooctylamine (16 mL) in toluene (49 mL). The organic phase was washed with H_2O (3 × 20 mL) to remove the boric acid completely. After reextraction with NaOH (7.5 M) to pH = 11.8, the aqueous phase was neutralized with 3 M H_2SO_4, evaporated to dryness under vacuum, and the solid residue extracted with CH_3OH (40 mL). After removal of the solvent from the extract, **1** was recovered as a white glassy solid. Yield 4.69 g (94%), correct elemental analysis for C, H, Na, P, S, O.

Trisodium 3,3′,3″-phosphanetriyltris(4-methylbenzenesulfonate) **3**: Orthoboric acid (0.40 g, 6.6 mmol) was dissolved in concentrated sulfuric acid (96%, 3.75 mL), after which tris(2-methylphenyl)phosphane (0.50 g, 1.4 mmol) was dissolved in the mixture. Oleum (6.75 mL, 65 wt% SO_3) was added dropwise to the N_2-saturated solution, which had been cooled to 0 °C. After stirring for 3 days at 25 °C, the mixture was hydrolyzed on ice and extracted with triisooctylamine (2 mL) in toluene (20 mL) and worked up further as for **1** [12]. Yield 95%, correct elemental analysis for C, H, Na, P, S, O.

Trisodium 3,3′,3″-phosphanetriyltris(4-methoxybenzenesulfonate) **4** was prepared analogously to **3**.

Disodium 5-(3-sulfonatophenyl)-5*H*-dibenzophosphole-3-sulfonate **6**: Orthoboric acid (2.40 g, 38.4 mmol) was dissolved in concentrated sulfuric acid (96%, 8 mL). Oleum (10 mL, 65 wt% SO_3) was added dropwise so that in the sulfonation mixture a SO_3 concentration of about 5.6 wt% resulted. This excess SO_3 was removed under high vacuum at 60 °C within 45 min. Finally 5-phenyl-5*H*-dibenzophosphole (500 mg, 1.9 mmol) was added (boric acid/phosphane = 20/1), and the mixture was stirred until all solids had dissolved. The charge was heated for 15 h at 145 °C and after cooling hydrolyzed with degassed water (20 mL). The extraction was achieved with triisooctylamine (4 mL) in toluene (30 mL). The further workup of the product was as for **1** [12]. Yield: 852 mg (89%).

Received: August 9, 1994 [Z 7220 IE]
Publication delayed at the authors' request
German version: *Angew. Chem.* **1995**, *107*, 893

Keywords: catalysis · phosphane ligands · sulfonation

[1] a) W. A. Herrmann, C. W. Kohlpaintner, *Angew. Chem.* **1993**, *105*, 1588–1609; *Angew. Chem. Int. Ed. Engl.* **1993**, *32*, 1524–1544; b) P. Kalck, F. Monteil, *Adv. Organomet. Chem.* **1992**, *34*, 219–284; c) E. G. Kuntz, *CHEMTECH* **1987**, *17*, 570–575.

[2] a) B. Cornils, E. Wiebus, *Chem. Ing. Techn.* **1994**, *66*, 916–923; b) B. Cornils, J. Hibbel, W. Konkol, B. Lieder, J. Much, V. Schmid, E. Wiebus (Ruhrchemie AG), DE-B 3234701, **1982** [*Chem. Abstr.* **1984**, *100*, 194022k].

[3] a) Y. Tokitoh, N. Yoshimura (Kuraray Co.) EP-A 287066, **1988** [*Chem. Abstr.* **1989**, *110*, 78070g]; b) N. Yoshimura, M. Tamura, T. Higashi, K. Hino, M. Murasawa (Kuraray Co.), EP-B 04362226, **1991** [*Chem. Abstr.* **1991**, *115*, 158508z]; c) C. Mercier, P. Chabardes, *Pure Appl. Chem.* **1994**, *66*, 1509–1515; d) Alternative methods (indirect sulfonation): O. Herd, K. Langhans, O. Stelzer, N. Weferling, W. Sheldrick, *Angew. Chem.* **1993**, *105*, 1097–1099; *Angew. Chem. Int. Ed. Engl.* **1993**, *32*, 1058–1059; H. Herd, A. Kessler, K. P. Langhaus, O. Stelzer, W. Sheldrick, N. Weferling, *J. Organomet. Chem.* **1994**, *475*, 99–111.

[4] B. Cornils, P. Lappe, R. Gärtner, H. Springer (Ruhrchemie AG), EP-A 0107006, **1983** [*Chem. Abstr.* **1984**, *101*, 55331t].

[5] a) R. J. Gillespie, T. E. Peel, E. A. Robinson, *J. Am. Chem. Soc.* **1971**, *93*, 5083–5087; b) S. J. Bass, R. H. Flowers, R. J. Gillespie, E. A. Robinson, C. Solomons, *J. Chem. Soc.* **1960**, 4315–4339.

[6] G. A. Olah, K. Laali, O. Farooq, *J. Org. Chem.* **1984**, *49*, 4591–4494.

[7] a) E. G. Kuntz (Rhône-Poulenc S. A.), FR-B 2366237, **1976** [*Chem. Abstr.* **1977**, *87*, 101944n]; b) E. G. Kuntz (Rhône-Poulenc S. A.), FR-B 2733516, **1978** [*Chem. Abstr.* **1978**, *88*, 152026t].

[8] Assignment of constitution by 2D NMR spectroscopy; W. A. Herrmann, G. P. Albanese, R. B. Manetsberger, R. Schmid, W. R. Thiel, unpublished results. Characterization of **5**: ^{1}H-^{1}H-COSY NMR (D_2O): δ = 3.62 (d, $^2J_{HH'}$ = 13.8 Hz, 2H, HH′), 3.66 (d, $^2J_{HH'}$ = 13.8 Hz, 2H, HH′), 7.20 (d, $^2J_{HH}$ = 6.9 Hz, $^3J_{PH}$ = 6.8 Hz, 1H, H16′), 7.21 (d, $^2J_{HH}$ = 6.9 Hz, $^3J_{PH}$ = 6.8 Hz, 1H, H16′), 7.52 (tr, $^3J_{HH}$ = 7.7 Hz, 2H, H15′), 7.66 (tr, $^3J_{HH}$ = 7.6 Hz, 2H, H15), 7.71 (d, $^3J_{HH}$ = 7.5 Hz, $^3J_{PH}$ = 7.2 Hz, 1H, H16), 7.73 (d, $^3J_{HH}$ = 7.5 Hz, $^3J_{PH}$ = 7.2 Hz, 1H, H16), 7.77 (d, $^3J_{HH}$ = 9.0 Hz, 2H, H5), 7.90 (d, $^3J_{PH}$ = 5.4 Hz, 2H, H12′), 7.97(s, 2H, H3), 7.98 (d, $^3J_{HH}$ = 7.53 Hz, 2H, H14′), 8.05 (d, $^3J_{PH}$ = 5.8 Hz, 2H, H12), 8.10 (d, $^3J_{HH}$ = 7.71 Hz, 2H, H14), 8.70 (s, 2H, H8), 8.98 (d, $^3J_{HH}$ = 9.0 Hz, 2H, H6).

[9] W. A. Herrmann, C. W. Kohlpaintner, R. B. Manetsberger, H. Bahrmann, H. Kottmann, *J. Mol. Catal.*, in press.

[10] D. Neibecker, R. Reau, *J. Mol. Catal.* **1989**, *57*, 153–163.

[11] a) H. Cerfontain, *Mechanistic Aspects in Aromatic Sulfonation and Desulfonation*, Interscience, New York, **1968**; b) H. Cerfontein, C. W. F. Kort, *Int. J. Sulfur Chem. Part C* **1971**, *6*, 123–136.

[12] Characterization of **3**: ^{31}P{^{1}H} NMR (D_2O): δ = −22.8; ^{1}H NMR (D_2O): δ = 2.27 (s, 9H; CH_3), 7.17 (dd, $^3J_{HP}$ = 4.0 Hz, $^4J_{HH}$ = 1.8 Hz, 3H; H6), 7.35 (dd, $^3J_{HH}$ = 8.1 Hz, $^4J_{HP}$ = 4.7 Hz, 3H; H3), 7.79 (dd, $^4J_{HH}$ = 1.5 Hz, $^3J_{HP}$ = 7.9 Hz, 3H, H4); ^{13}C-{^{1}H} NMR (D_2O): δ = 146.5 (d, $^3J_{CP}$ = 25.8 Hz, C5), 141.41 (s, C1), 133.57 (d, $^2J_{CP}$ = 11.0 Hz, C2), 131.3 (d, $^3J_{CP}$ = 4.8 Hz, C3), 129.78 (s, C6), 126.88 (s, C4), 20.65 (d, $^3J_{CP}$ = 20.5 Hz, CH_3). – Characterization of **4**: ^{31}P{^{1}H} NMR (D_2O): δ = −31.99 (s); ^{1}H NMR (D_2O): δ = 3.78 (s, 9H; OCH_3), 7.20 (dd, $^4J_{HP}$ = 8.9 Hz, $^3J_{HH}$ = 4.6 Hz, 3H; H3), 7.24 (dd, $^4J_{HH}$ = 2.1 Hz, $^3J_{HH}$ = 4.6 Hz, 3H; H4), 7.93 (dd, $^4J_{HH}$ = 2.1 Hz, $^3J_{PH}$ = 9.6 Hz, 3H; H6); ^{13}C{^{1}H} NMR (D_2O): δ = 56.24 (s, OCH_3), 111.41 (s, C4), 122.17 (d, $^3J_{CP}$ = 11.5 Hz, C5), 129.31 (s, C6), 131.05 (d, $^3J_{CP}$ = 2.9 Hz, C3), 136.78 (d, $^2J_{CP}$ = 1.0 Hz, C1), 163.12 (d, $^2J_{CP}$ = 14.8 Hz, C2). – Characterization of **6**: ^{31}P{^{1}H} NMR (D_2O): δ = 17.42; ^{1}H-^{1}H-COSY NMR (D_2O): δ = 6.90 (dt, $^3J_{HH}$ = 7.3 Hz, $^4J_{HH}$ = 1.9 Hz, 2H; H8, H9), 7.01 (tt, $^3J_{HH}$ = 7.7 Hz, $^4J_{HP}$ = 12.0 Hz, $^4J_{HH}$ = 1.2 Hz, 1H; H16), 7.06 (td, $^3J_{HH}$ = 7.7 Hz, $^4J_{HP}$ = 3.2 Hz, 1H; H15), 7.20 (dd, $^3J_{HH}$ = 8.0 Hz, $^4J_{HP}$ = 4.4 Hz, 1H; H1), 7.32 (dt, $^3J_{HH}$ = 7.3 Hz, $^4J_{HH}$ = 1.9 Hz, 2H; H6, H7), 7.43 (dt, $^3J_{HP}$ = 14.0 Hz, $^4J_{HH}$ = 1.2 Hz, 1H; H12), 7.55 (ddd, $^3J_{HH}$ = 7.7 Hz, $^4J_{HH14}$ = 1.8 Hz, $^4J_{HH15}$ = 1.3 Hz, 1H; H14), 7.81 (dd, $^3J_{HH}$ = 8.0 Hz, $^4J_{HH}$ = 2.0 Hz, 1H, H2), 8.41 (dd, $^3J_{HP}$ = 14.0 Hz, $^4J_{HH}$ = 2.0 Hz, 1H; H4). The numbering of the atoms in **3**, **4**, and **6** is arbitrary.

 © VCH Verlagsgesellschaft mbH, D-69451 Weinheim, 1995 0570-0833/95/0707-0813 $ 10.00+.25/0

First Determination of the Ionization Potential of Americium and Curium**

Rüdiger Deissenberger, Stefan Köhler, Friedhelm Ames, Klaus Eberhardt, Nicole Erdmann, Heike Funk, Günter Herrmann, Heinz-Jürgen Kluge, Martin Nunnemann, Gerd Passler, Joachim Riegel, Franz Scheerer, Norbert Trautmann,* and Franz-Josef Urban

Investigations of chemical and physical properties of very heavy elements have, among other goals, the aim of determining whether the regularities of the Periodic Table of Elements are maintained up through the heaviest elements or whether they are disturbed by relativistic effects, that is, by changes of the electronic structure due to the relativistic mass increase of inner electrons. The first ionization potential of neutral atoms is one of the properties which sensitively depends on these relativistic effects.

Plutonium is the heaviest element whose first ionization potential has been determined experimentally. For the elements located at the beginning of the actinide series, ionization potentials have been measured by techniques such as surface ionization, electron impact, and laser spectroscopy.[1-6] Their ionization potentials have also been derived from thermochemical data by means of the Born–Haber cycle,[7] by calculations,[8] and by extrapolation from the spectral properties of the atoms.[9, 10] The most accurate ionization potentials have been obtained from the convergence of long series of highly excited Rydberg states;[4, 6] however, this required a large amount of data.

For elements beyond plutonium, ionization potentials have been derived only by extrapolation[10] based on the systematics of excited electron states. The reasons why experimental data cease in this region are illustrated by a precision measurement of the ionization potential of plutonium by using Rydberg series, which was published recently,[6] although performed some time ago: To produce an atomic beam of sufficient density, up to 2 g of radioactive plutonium-239 had to be used.

We present a method requiring much less material, only about 10^{12} atoms (≈ 0.4 ng). This method opens the possibility for determining ionization potentials of the heavier actinide elements. Because of their strong radioactivity, these elements can be conveniently handled only in very small quantities or are available only in extremely limited amounts. We have used this new approach to determine the ionization potential of the elements americium and curium for the first time. In order to test the method and its precision, the ionization potentials of thorium, neptunium, and plutonium were also measured, for which precise values are known. As an additional test, the ionization potential of americium was also determined by convergence of Rydberg series.

The new method is based on a technique developed for the determination of ultratrace quantities of actinide nuclides by resonance ionization mass spectrometry.[11] Americium may serve as an example, with the excitation scheme used shown in Figure 1. An atomic beam of the element is excited in two steps by intersection of two laser beams exactly tuned to the resonance energies (wavelengths $\lambda_1 = 640.52$ nm and $\lambda_2 = 654.42$ nm). A third laser beam ($\lambda_3 \approx 578$ nm) then scans the region of the ionization threshold by further excitation after the second resonance excitation step. The threshold appears as a sudden increase of the photoion count rate recorded with a channel plate detector after time-of-flight mass analysis. In the interaction zone of the atomic beam and the laser beams, an electric field is applied whose strength is varied from measurement to measurement. With increasing field strength E, the ionization threshold W_{th} is shifted to lower values, as Figure 2a,b shows for field strengths of

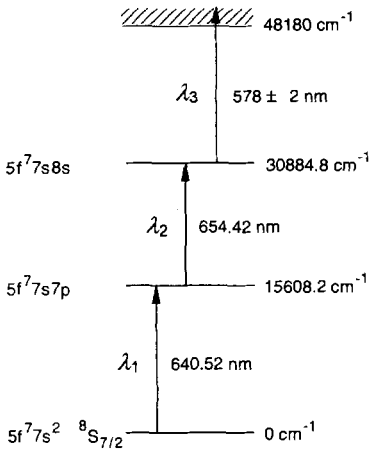


Fig. 1. Excitation scheme for americium as used in the determination of the first ionization potential by resonance ionization mass spectrometry. The two lower excitation steps λ_1 and λ_2 are kept in resonance, whereas the upper step λ_3 is tuned over the ionization threshold.

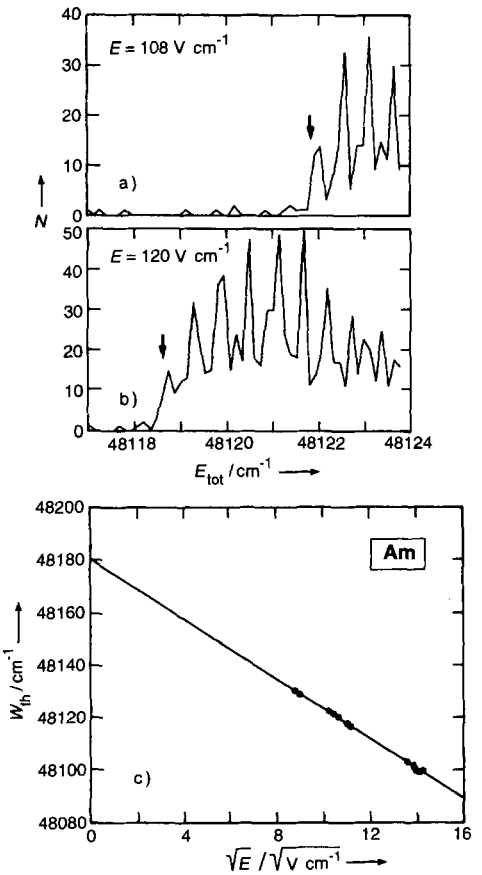


Fig. 2. Ionization threshold (arrows) of americium when applying an electric field of a) $E = 108$ Vcm^{-1} and b) $E = 120$ Vcm^{-1} to the zone of interaction between atomic beam and laser beams. Recorded is the number of ions N as function of the tuned wavelength λ_3 of the third laser; N is plotted versus the total photon energy E_{tot} of the three laser beams. In c) the resulting ionization thresholds W_{th} are plotted versus the square root of the field strength E. A straight line is obtained, as is expected according to Equation (a). Extrapolation to $E = 0$ gives the first ionization potential I_{Am} of americium.

[*] Dr. N. Trautmann, Dipl.-Chem. R. Deissenberger, Dipl.-Phys. S. Köhler, Dr. K. Eberhardt, Dipl.-Phys. N. Erdmann, Dipl.-Chem. H. Funk, Prof. Dr. G. Herrmann, Dr. J. Riegel
Institut für Kernchemie der Universität
Fritz-Strassmann-Weg 2, D-55099 Mainz (Germany)
Telefax: Int. code + (6131)39-4488
Dr. F. Ames, Prof. Dr. H.-J. Kluge, Dipl.-Phys. M. Nunnemann, Dr. G. Passler, Dr. F. Scheerer, Dr. F.-J. Urban
Institut für Physik der Universität Mainz (Germany)

[**] This work was supported by the Bundesministerium für Umwelt, Naturschutz und Reaktorsicherheit, by the Bundesministerium für Forschung und Technologie, and by the Deutsche Forschungsgemeinschaft.

 © VCH Verlagsgesellschaft mbH, D-69451 Weinheim, 1995 0570-0833/95/0707-0814 $ 10.00+.25/0

108 Vcm^{-1} and 120 Vcm^{-1}. The arrows mark the respective ionization thresholds. The peak structure seen beyond the thresholds is due to the Stark effect.

The quantities W_{th} and E are related to the first ionization potential I of the neutral atom as given in Equation (a).[12]

$$W_{th} = I - const\sqrt{E} \quad (a)$$

Figure 2c shows this for americium. By extrapolation to $E = 0$, the ionization potential $I_{Am} = 48180(3)\ cm^{-1} = 5.9736(3)$ eV is obtained. In the literature, only an extrapolated value $I_{Am} = 5.993(10)$ eV is reported,[10] deduced from the systematics of $5f^7 7s^2$ and $5f^7 7s8s$ states in the lighter actinide elements. Our additional determination by the convergence of three Rydberg series[14] gives $I_{Am} = 5.9739(2)$ eV, thus confirming the result obtained by resonance ionization mass spectrometry in electric fields. All these data were measured with 10^{12} atoms of americium-243; with a 7370 year half-life, it is the longest-lived americium isotope. Typical in such an experiment are count rates of a few Hertz and counting times of 10 to 30 minutes per field strength setting.

In Table 1 the ionization potentials measured by us are given and are compared with the most accurate values previously reported. The agreement is excellent. From this, we conclude that there is also high reliability for those ionization potentials that have been determined for the first time.

Table 1. First ionization potential I of actinide elements, determined by photoionization in an electric field (PIE), by convergence of Rydberg series (RSC), by life-time measurements of Rydberg and autoionizing states (LTM) as well as values extrapolated from level systematics (Ext).

Element	This work		Literature		
	I [eV]	method	I [eV]	method	ref.
Thorium	6.3067(2)	PIE	6.310(2)	LTM	[5]
Neptunium	6.2655(2)	PIE	6.2657(5)	RSC	[4]
Plutonium	6.0257(2)	PIE	6.0262(1)	RSC	[6]
Americium	5.9736(3)	PIE	5.993(10)	Ext	[10]
	5.9739(2)	RSC			
Curium	5.9914(2)	PIE	6.021(25)	Ext	[10]

Experimental Procedure[11]

The elements were electrochemically deposited as hydroxides on thin metal foils and covered with a layer of a reducing metal, for example, on rhenium foils with coating layers of rhenium or lead-doped platinum [16] or on tantalum with titanium coating. Thorium was used directly as a thin metal foil. By heating such filaments in the time-of-flight mass spectrometer, atomic beams were produced.

Laser beams with wavelengths from 520 to 850 nm (260 to 425 nm by frequency doubling) and bandwidths of several Gigahertz ($\approx$1 GHz with an intracavity etalon) were obtained from dye lasers pumped by two pulsed copper vapor lasers (repetition rate 6.5 kHz, power 30 W, pulse length 30 ns, wavelengths 510.6 and 578.2 nm with an intensity ratio of 2:1). The wavelengths were determined by a wavelength meter, occasionally also from absorption bands of molecular iodine. The laser beams were coupled into the apparatus either by quartz fibers or by prisms. The ions produced by intersection with the atomic beam were accelerated to an energy of 2.9 keV. After a drift length of 2.0 m the ions were detected with a channel plate detector.

Thorium was excited and ionized in three steps ($\lambda_1 = 580.42$ nm, $\lambda_2 = 622.90$ nm, $\lambda_3 \approx 568$ nm), neptunium in two steps [17] ($\lambda_1 = 311.82$ nm, $\lambda_2 \approx 544$ nm), plutonium in three steps ($\lambda_1 = 649.07$ nm, $\lambda_2 = 629.75$ nm, $\lambda_3 \approx 579$ nm), and curium in three steps ($\lambda_1 = 655.64$ nm, $\lambda_2 = 640.74$ nm, $\lambda_3 \approx 573$ nm).

Received: November 10, 1994 [Z 7467 IE]
German version: *Angew. Chem.* **1995**, *107*, 891

Keywords: actinides · americium · curium · ionization potentials

[1] D. H. Smith, G. R. Hertel, *J. Chem. Phys.* **1969**, *51*, 3105–3107.
[2] D. L. Hildenbrand, E. Murad, *J. Chem. Phys.* **1974**, *61*, 5466–5467.
[3] R. W. Solarz, C. A. May, L. R. Carlson, E. F. Worden, S. A. Johnson, J. A. Paisner, L. J. Radziemski, *Phys. Rev. A* **1976**, *14*, 1129–1136.
[4] E. F. Worden, J. C. Conway, *J. Opt. Soc. Am.* **1979**, *69*, 733–738.
[5] S. G. Johnson, B. L. Fearey, C. M. Miller, N. S. Nogar, *Spectrochim. Acta B* **1992**, *47*, 633–643.
[6] E. F. Worden, L. R. Carlson, S. A. Johnson, J. A. Paisner, R. W. Solarz, *J. Opt. Soc. Am. B* **1993**, *10*, 1998–2005.
[7] L. R. Morss, *J. Phys. Chem.* **1971**, *75*, 392–399.
[8] T. A. Carlson, C. W. Nestor, N. Wasserman, J. D. McDowell, **1970**, *Oak Ridge Nat. Lab. Rep. ORNL-4562.*
[9] J. Sugar, *J. Chem. Phys.* **1973**, *59*, 788–791.
[10] J. Sugar, *J. Chem. Phys.* **1974**, *60*, 4103.
[11] W. Ruster, F. Ames, H.-J. Kluge, E.-W. Otten, D. Rehklau, F. Scheerer, G. Herrmann, C. Mühleck, J. Riegel, H. Rimke, P. Sattelberger, N. Trautmann, *Nucl. Instrum. Methods Phys. Res. Sect. A* **1989**, *281*, 547–558.
[12] Equation (a) results as follows. According to the saddle point model [13], the excitation energy $W_{(r)}$ of an atom with a highly excited electron is given, relative to its electronic ground state, by 1) its Coulomb-energy in the nuclear field with an effective nuclear charge Z_{eff}, 2) by its potential energy in the applied external field of strength E, and 3) by the first ionization potential I. In the one-dimensional approximation [Eq. (b)]:

$$W_{(r)} = -\frac{Z_{eff}\, e^2}{4\pi\, \varepsilon_0\, r} - e\,E\,r + I \quad (b)$$

where r is the distance of the excited electron from the nucleus, e the electron charge, and ε_0 the dielectric constant of vacuum. For the ionization threshold W_{th}, which is the maximum value of $W_{(r)}$, Equation (c) results.

$$W_{th} = I - 2\sqrt{\frac{Z_{eff}\, e^3}{4\pi\, \varepsilon_0}}\sqrt{E} = I - const\sqrt{E} \quad (c)$$

[13] B. H. Bransden, C. J. Joachain, *Physics of Atoms and Molecules*, Longman, London, **1984**, p. 227.
[14] The energies of the levels E_n of Rydberg states of the principal quantum number n can be fitted [15] by Equation (d), to obtain the first ionization potential I. Here, R_{El} is the Rydberg constant of the respective element, and a, b are constants resulting from the fit. In our measurements of Rydberg series of americium, these states were populated by tuning the third laser. For ionization of the Rydberg states, an electric field of 100 Vcm^{-1} was applied 10 μs after the laser pulse.

$$E_n = I - \frac{R_{El}}{\{n - [a + b(I - E_n)]\}^2} \quad (d)$$

[15] A. N. Zherikin, V. I. Mishin, V. N. Fedoseev, *Opt. Spectrosc.* **1984**, *57*, 476–479.
[16] H. Wendeler, R. Deissenberger, F.-J. Urban, N. Trautmann, G. Herrmann, *Nucl. Instrum. Methods Phys. Res. Sect. A* **1993**, *334*, 93–95.
[17] J. Riegel, R. Deissenberger, G. Herrmann, S. Köhler, P. Sattelberger, N. Trautmann, H. Wendeler, F. Ames, H.-J. Kluge, F. Scheerer, F.-J. Urban, *Appl. Phys. Sect. B* **1993**, *56*, 275–280.

 © *VCH Verlagsgesellschaft mbH, D-69451 Weinheim, 1995* *0570-0833/95/0707-0815 $ 10.00+.25/0*

Self-Diffusion of Charged Polycyclic Systems and Their Parent Compounds: A PGSE NMR Study**

Yoram Cohen* and Ari Ayalon

Polycyclic anions with conjugated π electron systems have been investigated extensively in the last decades as test cases for Hückel theory.[1] These systems have also been used to study ion-pairing phenomena.[2] Although aggregation of organometallic compounds was predicted by theory and detected by experiment,[3] polycyclic dianions with π-conjugation in which the charge is thought to be delocalized over a relatively large organic skeleton have been treated in most studies as isolated species. Streitwieser has shown that lithium salts of conjugated hydrocarbon dianions may exist as "ion triplets" in which the lithium cations are located on opposite faces of the dianion.[4] It is therefore important to gain better insight into the actual species that prevail in the solution after metal reduction of polycyclic systems.

Diffusion measurements with the pulsed gradient spin echo (PGSE) NMR technique[5] has been used extensively to study chemical and biological systems.[6-8] Recently, the PGSE NMR technique was used to study aggregation of nucleotides[9a] and complexation of macrocycles[9b] as well as hydration of macromolecules.[10] Nevertheless, to the best of our knowledge, such measurements have never been performed on charged polycyclic systems.

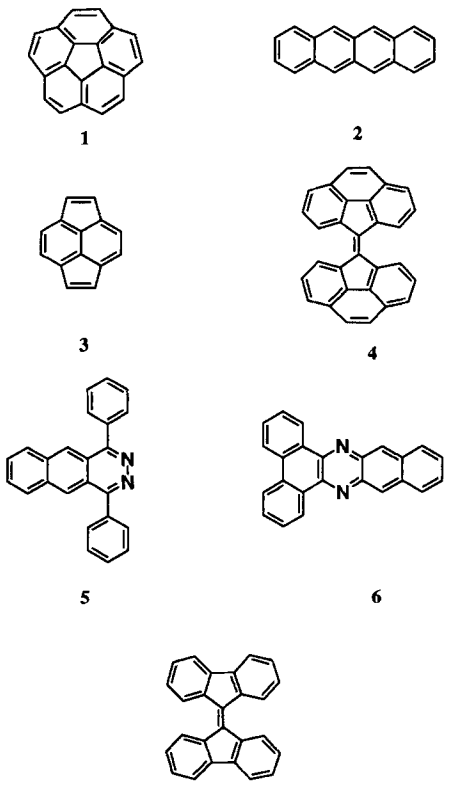
Here we report the self-diffusion coefficients of several polycyclic anions and their parent compounds as obtained by the PGSE NMR technique. Interestingly, the self-diffusion coefficients of the dianions were smaller than the self-diffusion coefficients of the parent compounds in all cases. Surprisingly, in some systems the decrease in the self-diffusion coefficient upon charging is much more pronounced than for other systems, thus suggesting that some of these species may exist preferentially as dimeric sandwich aggregates.

The self-diffusion coefficients were measured by the PGSE NMR technique (Fig. 1),[5] according to which the ratio between the echo intensity (at $t = \tau$) in the absence and in the presence of rectangular pulsed gradients G, ($A_{\tau,0}$ and $A_{\tau,G}$ respectively) is given by Equation (1)[5] where G is the gradient strength of the pulsed gradients [G cm^{-1}], γ the gyromagnetic

$$\ln(A_{\tau,G}/A_{\tau,0}) = -\gamma^2 G^2 \delta^2 (\Delta - \delta/3) D \quad (1)$$

ratio [rad s^{-1}], δ the length of the diffusion gradients [s], Δ the time separation between the edge of the first gradient and the second pulsed gradients [s], and D the self-diffusion coefficient of the observed spins [cm^2 s^{-1}].

The diffusion coefficients of the tetraanion of corannulene (**1**) and the dianions of tetracene (**2**), pyracylene (**3**), bi-(4*H*-cyclopenta[*def*]phenanthren-4-ylidene) (**4**), 1,4-diphenylbenzo[*h*]phthalazine (**5**), tribenzo[*aci*]phenazine (**6**) (Scheme 1), and their parent compounds were determined in [D$_8$]THF by the PGSE NMR technique in the presence of benzene and dichloromethane as internal and external standard, respectively.[11]



Scheme 1.

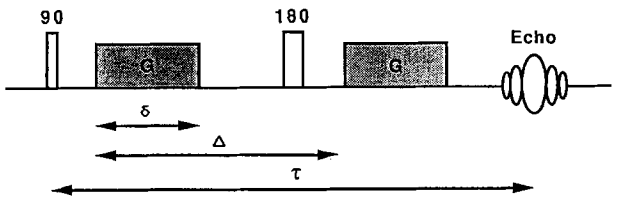


Fig. 1. The Stejskal–Tanner pulse sequence [5].

The data (see Fig. 2 and Table 1) show clearly that the self-diffusion coefficients of the ions are smaller than those of their neutral parent polycycles. From the data of Table 1 it is clear that the investigated systems can be divided into two groups on the basis of the relative changes in the diffusion coefficients upon reduction. In the first group (systems **1** to **3**) the self-diffusion coefficient of the ion is nearly half that of the parent compound. In the second group (systems **4**–**6**) there is only a 20–30% decrease in the self-diffusion coefficient upon formation of the anion. We found that $\mathbf{2}^{2-}/2\,Li^+$, $\mathbf{2}^{2-}/2\,Na^+$, and $\mathbf{2}^{2-}/2\,K^+$ have similar diffusion coefficients. Changing the concentration of $\mathbf{2}^{2-}/2\,Li^+$ by a factor of 10 had only little effect on the self-diffusion coefficient of the dianion after correcting for the changes in the viscosity of the solutions. The fact that no significant changes have been observed in the diffusion coefficient of

[*] Dr. Y. Cohen
School of Chemistry, The Sackler Faculty of Exact Sciences
Tel Aviv University, Ramat Aviv, Tel Aviv 69978 (Israel)
Telefax: Int. code +(3) 640-9293
Dr. A. Ayalon
Department of Organic Chemistry
The Hebrew University of Jerusalem (Israel)

[**] Diffusion in Physical Organic Chemistry, Part 2. This research was supported in part by the Wolfson Research Award administered by The Israel Academy of Sciences and Humanities. We thank Professor M. Rabinovitz, Hebrew University, Israel and Professor L. T. Scott, Boston College, USA for providing us with samples of corannulene. Part 1: [9b].

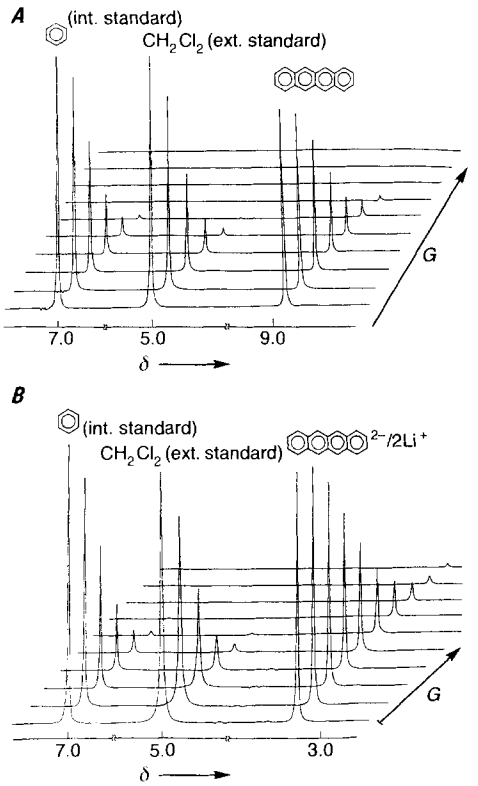


Fig. 2. The 500 MHz ^{1}H NMR ([D$_8$]THF, 298 K) spectra of the Stejskal–Tanner experiments [5] performed on A) a solution of **2** and B) a solution of $\mathbf{2}^{2-}$/2Li$^+$. For clarity only the singlet of the polycyclic systems are shown.

the benzene, which served as an internal standard proves that the observed changes in the diffusion coefficients are not due to change in the sample viscosity following the reduction.

The decrease in the self-diffusion coefficient upon reduction may arise from several factors, including ion-pair formation, aggregation of the ions, or increased solvation of the ions by the THF molecules. It appears that, at least in the case of the reduction of **2** to $\mathbf{2}^{2-}$, the nature of the alkali metal cation has only a relatively small effect on the diffusion coefficient of the dianions formed. This can be concluded from the similar diffusion coefficients of $\mathbf{2}^{2-}$/2Li^{2+}, $\mathbf{2}^{2-}$/2Na$^+$, and $\mathbf{2}^{2-}$/2K$^+$ (see Table 1).

Table 1. Diffusion coefficients D of polycyclic systems and their anions in [D$_8$]THF at 298 K.

System	D (CH_2Cl_2) (ext. stand.) [10^{-5} cm^2 s^{-1}]	D (benzene) (int. stand.) [10^{-5} cm^2 s^{-1}]	D (polycyclic system) [10^{-5} cm^2 s^{-1}]
1	3.73 ± 0.002	2.87 ± 0.017	1.57 ± 0.017
$\mathbf{1}^{4-}$/4Li$^+$	3.73 ± 0.002	2.90 ± 0.041	0.84 ± 0.017
2	3.83 ± 0.031	2.96 ± 0.027	1.83 ± 0.032
$\mathbf{2}^{2-}$/2Li$^+$ (2 mg)	3.79 ± 0.006	2.86 ± 0.039	0.96 ± 0.038
$\mathbf{2}^{2-}$/2Li$^+$ (20 mg)	3.78 ± 0.000	2.39 ± 0.043	0.71 ± 0.020
		2.86 ± 0.039	0.86 ± 0.017 [a]
$\mathbf{2}^{2-}$/2Na$^+$	3.80 ± 0.003	2.74 ± 0.014	0.94 ± 0.015
$\mathbf{2}^{2-}$/2K$^+$	3.79 ± 0.004	[b]	0.94 ± 0.014
3	3.82 ± 0.017	2.86 ± 0.025	1.90 ± 0.011
$\mathbf{3}^{2-}$/2Li$^+$	3.78 ± 0.015	2.82 ± 0.048	1.06 ± 0.057
4	3.80 ± 0.002	2.97 ± 0.014	1.38 ± 0.021
$\mathbf{4}^{2-}$/2Na$^+$	3.82 ± 0.002	2.99 ± 0.003	1.05 ± 0.014
5	3.79 ± 0.000	2.85 ± 0.041	1.17 ± 0.008
$\mathbf{5}^{2-}$/2Na$^+$	3.72 ± 0.030	2.84 ± 0.003	0.93 ± 0.030
6	3.79 ± 0.002	2.90 ± 0.015	1.38 ± 0.010
$\mathbf{6}^{2-}$/2Na$^+$	3.80 ± 0.002	2.97 ± 0.032	1.10 ± 0.026

[a] After correcting for viscosity changes. [b] Very broad signal for benzene, undetectable in the spin echo.

A plausible explanation for the above observations is that the reduction of **1**, **2**, and **3** (first group) affords charged systems in which, in addition to the decrease in the diffusion coefficient caused by increased solvation of the anions and association of the cations, an additional decrease in the diffusion coefficient is caused by a self-aggregation process. The corannulene tetraanion ($\mathbf{1}^{4-}$/4Li$^+$),[12a] which has been prepared recently, was subjected to an extensive study that demonstrated that $\mathbf{1}^{4-}$/4Li$^+$ forms a stable dimer with sandwich structure in THF solution.[12b] The similarity in the changes in the diffusion coefficients observed upon reduction of **1**, **2**, and **3** suggests that **2** and **3** may also form dimeric sandwich aggregates in which the alkali cations connect the two hydrocarbon dianion moieties.[13] In the reduction of systems **4**–**6** the main factors responsible for the decrease in the diffusion coefficients upon reduction seem to be solvation and ion-pair formation. In principle, the dimeric aggregates should be more stable in charged systems that have a rigid skeleton that can deviates only slightly from planarity. Interestingly, systems **1**–**3** are all such systems. System **4** is the only carbocyclic system we tested in which there is merely a 20–30% decrease in the self-diffusion coefficient following dianion formation. Dianion $\mathbf{4}^{2-}$, which was shown to be closely related to bifluoren-9-ylidene dianion ($\mathbf{7}^{2-}$)[14], probably adopts a nonplanar conformation similar to that of $\mathbf{7}^{2-}$, for which solution and crystal structures show a marked deviation from planarity.[15] This deviation from planarity in $\mathbf{4}^{2-}$ will cause severe steric interactions that will tend to reduce the stability of the dimeric sandwich aggregates. The ion $\mathbf{6}^{2-}$ might be an exception, as it is not clear whether this dianion can adopt a nonplanar structure. However, it has been pointed out that this dianion can be described as a superposition of virtually an "uncharged phenanthrene" molecule and a "benzo[*g*]quinoxaline dianion" moiety, which may suggest that these two π subunits are not coplanar.[1d, 16]

In principle several methods such as colligative methods, NMR relaxation time measurements, or even NMR chemical shifts may provide information about the aggregation state of a chemical species. However, since the polycyclic charged systems investigated here are prepared via radical anions, measurements of relaxation time will provide no insight into the actual species prevailing in solution. Arguments based on chemical shifts are difficult to apply to charged systems, since their chemical shifts are also affected by the ion-pairing equilibrium. Doubly and multiply charged polycycles are extremely reactive intermediates and are also more difficult to study by colligative methods.

In conclusion, we measured the changes in the self-diffusion coefficients of several polycyclic systems after their reduction by metal. There is a marked decrease in the self-diffusion coefficients upon reduction. The systems investigated may be divided to two groups: systems **1**–**3**, in which the diffusion coefficient of the charged system is nearly half that of the neutral parent compound and systems **4**–**6** in which the diffusion coefficient is decreased by only 20–30% upon reduction. In systems **4**–**6** the reduced self-diffusion coefficient of the charged system is attributed to ion-pair formation and more importantly to the excessive solvation of the dianions by the THF molecules. Dianions $\mathbf{2}^{2-}$ and $\mathbf{3}^{2-}$ show a more pronounced decrease in the diffusion coefficient, resembling the one observed for $\mathbf{1}^{4-}$/4Li$^+$, which is known to exist as a sandwiched dimer. This similarity suggests that dianions $\mathbf{2}^{2-}$ and $\mathbf{3}^{2-}$ may also exist, at least

partially, as dimeric sandwich aggregates. Dimerization of charged polycycles may be more important than previously thought.

Received: September 8, 1994
Revised version: December 19, 1994 [Z 7297 IE]
German version: *Angew. Chem.* **1995**, *107*, 888

Keywords: arene anions · arenes · diffusion · NMR spectroscopy

[1] Selected examples: a) T. J. Katz, *J. Am. Chem. Soc.* **1960**, *82*, 3784; b) J. F. M. Oth, K. Müllen, H. Konigshofen, M. Mann, Y. Sakata, E. Vogel, *Angew. Chem.* **1974**, *86*, 232; *Angew. Chem. Int. Ed. Engl.* **1974**, *13*, 284; c) K. Müllen, *Chem. Rev.* **1984**, *84*, 603; d) M. Rabinovitz, Y. Cohen, *Tetrahedron* **1988**, *44*, 6957.

[2] a) U. Edlund, *Org. Magn. Reson.* **1979**, *17*, 661; b) B. Eliasson, U. Edlund, *ibid.* **1983**, *21*, 322; c) K. Müllen, W. Huber, T. Meul, M. Nakagawa, M. Iyoda, *Tetrahedron* **1983**, *39*, 1595.

[3] See, for example, W. N. Setzer, P. von R. Schleyer, *Adv. Organomet. Chem.* **1985**, *24*, 353; D. B. Collum, *Acc. Chem. Res.* **1993**, *26*, 227.

[4] a) A. Streitwieser, J. T. Swanson, *J. Am. Chem. Soc.* **1983**, *105*, 2502; b) A. Streitwieser, *Acc. Chem. Res.* **1984**, *17*, 353.

[5] E. O. Stejskal, J. E. Tanner, *J. Chem. Phys.* **1965**, *42*, 288.

[6] a) P. Stilbs, *Prog. Nucl. Magn. Reson. Spectrosc.* **1987**, *19*, 1; b) E. W. Lang, H.-D. Ludemann, *ibid.* **1993**, *25*, 507.

[7] a) D. Le Bihan, E. Breron, D. Lallemand, P. Grenier, E. Cabanis, M. Laval-Jeantet, *Radiology* **1986**, *161*, 401; b) M. E. Moseley, Y. Cohen, J. Mintorovitch, L. Chileuitt, H. Shimizu, J. Kucharczyk, M. F. Wendland, P. R. Weinstein, *Magn. Reson. Med.* **1990**, *14*, 330.

[8] P. C. M. van Zijl, C. T. W. Moonen, *J. Magn. Reson.* **1990**, *87*, 18.

[9] a) R. Rymden, P. Stilbs, *Biophys. Chem.* **1985**, *21*, 145; b) O. Mayzel, Y. Cohen, *J. Chem. Soc. Chem. Commun.* **1994**, 1901.

[10] R. W. Kriwacki, R. Blake Hill, J. M. Flanagan, J. P. Caradonna, J. H. Prestegard, *J. Am. Chem. Soc.* **1993**, *115*, 8907.

[11] Measurements were carried out on sealed extended 5 mm NMR tubes containing a solution of the polycyclic compound in [D_8]THF, a small amount of benzene as internal reference, and a capillary of methylene chloride as an external reference. After the diffusion coefficients of the neutral sample had been determined, the tube was inverted to allow contact between the solution and the metal (lithium or sodium wire, or potassium minor) which reduced the polycyclic system. All ions gave their known ^{1}H NMR spectrum. All diffusion measurements were performed on a Bruker 500 MHz ARX NMR spectrometer equipped with a Z-gradient unit in an inverse probe for 5 mm NMR tubes. The pulsed gradients used were in the range from 0 to 41.57 cm^{-1}. The total echo time was typically 124 ms while δ and Δ were 2 ms and 62 ms, respectively. All diffusion coefficients are averages of at least 3 experiments, only data having a correlation coefficient (R^2) of more than 0.998 were included.

[12] a) A. Ayalon, M. Rabinovitz, P.-C. Cheng, L. T. Scott, *Angew. Chem.* **1992**, *104*, 1691; *Angew. Chem. Int. Ed. Engl.* **1992**, *31*, 1636; b) A. Ayalon, A. Sygula, P.-C. Cheng, M. Rabinovitz, P. W. Rabideau, L. T. Scott, *Science* **1994**, *265*, 1065.

[13] A few other dimers have recently been proposed: a) L. O. Paquette, W. Bauer, M. Sivik, M. Buhl, M. Feigel, P. von R. Schleyer, *J. Am. Chem. Soc.* **1990**, *112*, 8776; b) A. Sekiguchi, K. Ebata, C. Kabuto, H. Sakurai, *ibid.* **1991**, *113*, 7081.

[14] Y. Cohen, J. Klein, M. Rabinovitz, *J. Chem. Soc. Chem. Commun.* **1986**, 1071.

[15] a) M. Walzat, G. D. Stucky, *J. Organomet. Chem.* **1975**, *97*, 313; b) A. Ayalon, Ph.D. Thesis, The Hebrew University of Jerusalem, **1993**.

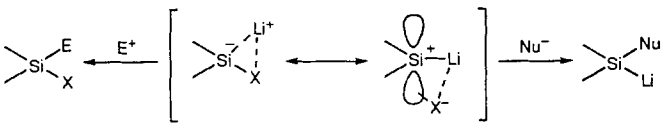
[16] Y. Cohen, A. Y. Meyer, M. Rabinovitz, *J. Am. Chem. Soc.* **1986**, *108*, 7039.

The Chemistry of Silylenoids: Preparation and Reactivity of (Alkoxysilyl)lithium Compounds**

Kohei Tamao* and Atsushi Kawachi

Over the past few decades a considerable number of studies have been made on carbenoids,[1] namely α-heteroatom-substituted organometallic compounds with nucleophilic and electrophilic properties. In contrast to this, the silicon analogues, namely the silylenoids,[2] have been much less extensively studied. To date only one theoretical study has been performed on SiH_2LiF.[3] The result of this study suggests that the Si–F bond is weakened when lithium is attached to the silicon atom, resulting in the appearance of a positive charge on silicon. Some experimental reports have postulated silylenoids $R_2Si(X)M$ as intermediates in the reduction of dihalosilanes R_2SiX_2 with alkali metals M, especially in polysilane synthesis.[4] The reactivities of silylenoids, however, have never been investigated. Such a study may thus shed new light on the mechanism of polysilane synthesis.

We now report the first experimental aspects of silylenoid chemistry (Scheme 1) in (alkoxysilyl)lithium compounds.[5] The



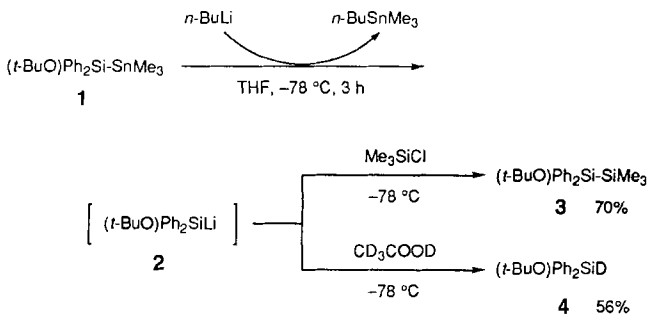
Scheme 1. Nucleophilic and electrophilic nature of silylenoids.

previously reported (aminosilyl)lithium compounds were stable functionalized silyl anions[6] and did not exhibit silylenoid character.[7] In view of the thermodynamic stability and kinetic lability of their substituents, (alkoxysilyl)lithium compounds[8] are expected to behave as silylenoids. Our particular interest has focused on the electrophilic nature of the (alkoxysilyl)lithium compounds as the most diagnostic indication of the silylenoid character, in agreement with the theoretical prediction. The results described herein may be regarded as the silicon version of the chemistry of lithium (alkoxy)carbenoids reported by Wittig et al. in 1957.[1g]

A tin–lithium exchange reaction[6, 9] at low temperature is the key step for the preparation of [(*tert*-butoxy)diphenylsilyl]lithium (**2**) (Scheme 2).[10] The (*tert*-butoxysilyl)stannane[11] **1** was allowed to react with two equivalents of *n*BuLi in THF at −78 °C for 3 h to give **2** as a yellow solution; **2** was trapped with Me_3SiCl to give the corresponding disilane **3** in 70% yield and with [D_4]acetic acid to give the deuterated silane **4** in 56% yield. Compound **2** was stable at −78 °C for at least 6 h (as the trapped product **3**, 66% yield) but it underwent self-condensation almost completely at 0 °C within 2 h (see Scheme 3). This finding markedly contrasts the high stability of the (aminosilyl)lithium compounds, which are stable at 0 °C for several days.[6]

[*] Prof. Dr. K. Tamao, A. Kawachi
Institute for Chemical Research, Kyoto University
Uji, Kyoto 611 (Japan)
Telefax: Int. code +(774) 33-7688

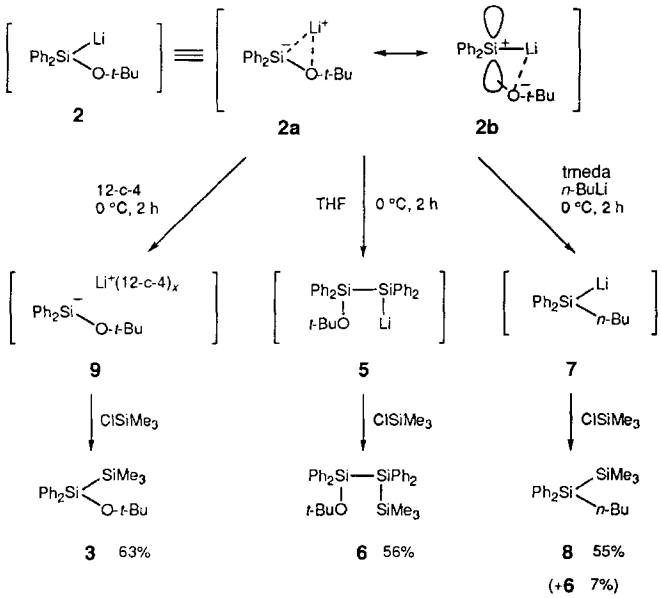
[**] We thank Prof. Y. Ito, Kyoto University, for useful discussions and support of this work. We are also grateful to Prof. P. von R. Schleyer (Erlangen) for fruitful discussion. A. K. thanks the Japan Society for the Promotion of Science (Fellowship for Japanese Junior Scientists). Thanks are also due to the Shin-etsu Chemical Co. and the Nitto Kasei Co. for gifts of chlorophenylsilanes and dichlorodimethylstannane, respectively.



Scheme 2. Preparation of **2**.

The ^{29}Si NMR chemical shift of **2** was observed at $\delta = 11.3$ (-80 °C, THF). This is a large downfield shift compared to the corresponding chlorosilane (tBuO)Ph_2SiCl ($\delta = -23.3$ ($\Delta\delta = +34.6$) and exhibits a remarkable contrast to the upfield shift of ordinary triorganosilyllithium compounds compared to chlorosilanes, for example $\delta(Ph_2MeSiLi) = -20.5$ and $\delta(Ph_2MeSiCl) = 10.0$ ($\Delta\delta = -30.5$).[12] It is noteworthy that the large downfield shifts for **2** is reminiscent of the well-known ^{13}C NMR behavior of carbenoids.[1d, e, h]

The ambiphilic reactivity of **2** was confirmed by the reactions summarized in Scheme 3. At 0 °C, **2** underwent bimolecular self-condensation smoothly, by nucleophilic substitution of the *tert*-butoxy group by another molecule of silyllithium, to give the



Scheme 3. Reactions of **2**. 12-C-4 = [12]crown-4.

disilanyl **5**, which afforded **6** in 56% yield after trapping with Me_3SiCl. In this self-condensation one molecule of **2** behaves as a nucleophile and the other as an electrophile. The generation of **5** was confirmed by the ^{29}Si NMR spectrum at 0 °C, which showed signals at $\delta = -43.7$ (Li–Si) and -2.3 (O–Si).[13]

The nucleophilic butylation of **2** with excess nBuLi (5 equiv based on **1**) in the presence of TMEDA (7 equiv based on **1**) afforded butyldiphenylsilyllithium (**7**). Upon trapping with Me_3SiCl, **7** gave the corresponding disilane **8**, in addition to the self-condensation product **6**.[14] The ratio **8**/**6** was 89/11 (62% total yield).[15] In the presence of TMEDA but in the absence of nBuLi, **2** undergoes self-condensation mainly at 0 °C for 2 h to form **6** in 51% yield, together with a small amount of **3** (7%), indicative of the preservation of the ambiphilic character of **2**.

The ambiphilic reactivity of **2** disappears completely by addition of a crown ether which is expected to form a "solvent-separated ion pair" **9**[1f] (Scheme 3). Thus, in the presence of two equivalents of [12]crown-4,[16] **9** was stable even at 0 °C for 2 h, giving the trapped product **3** in 63% yield, and underwent neither self-condensation nor butylation.[17]

The ambiphilic reactivity of **2** could, in analogy with carbenoid chemistry,[1] be accounted for by contribution from two limiting electronic structures, that is, a nucleophilic silylenoid structure **2a** and an electrophilic silylenoid structure **2b**[3] (Scheme 3). In **2b**, the electropositive lithium atom bound to silicon ionizes and activates the silicon–oxygen bond,[18] so that the silicon center becomes more susceptible to the nucleophilic attack than that in the ordinary neutral alkoxysilanes. The low-field ^{29}Si NMR signal for **2** supports the contribution of the electrophilic structure **2b**.

Some control experiments offered supporting evidence for the activation of the silicon–oxygen bond in **2**. A counter model, (tBuO)Ph_2SiMe, containing a neutral methyl group instead of a cationic lithium atom,[19] was hardly butylated with nBuLi (5 equiv) to form nBuPh$_2$SiMe (4% yield at 0 °C after 10 min in THF in the presence of TMEDA (5 equiv)). Under the same conditions, **2** was butylated to give **8** in 24% yield, together with 9% of **6**. Furthermore, (tBuO)Ph_2SiMe hardly reacted with **2** (1 equiv) or with $PhMe_2SiLi$ (10 equiv) at 0 °C for 2 h and gave essentially no silylated product (tBuO)$Ph_2SiSiMePh_2$ or $PhMe_2SiSiMePh_2$, whereas under these conditions **2** underwent self-condensation exclusively. The tBuO–Si bond in **2** is thus much more reactive than that in the model compound towards the nucleophiles.

No free silylene[2] appears to be generated under the present conditions, since in the presence of various trapping agents such as diethylmethylsilane, diphenylacetylene, and 2,3-dimethylbutadiene, no silylene-trapped products were obtained.[8, 20]

Two further points deserve comment. First, the ambiphilicity of the silylenoid allows the successive introduction of a nucleophile and of an electrophile to a silylene moiety.[21] The important point to be noted is that a nucleophile is introduced first with ease because of the high electrophilicity of silylenoid. This contrasts sharply with the conventional transformations involving simple silyl anions in which only an electrophile is introduced. This new reaction pattern may thus suggest potential synthetic utility of silylenoids.

Second, the reactivity of the silylenoid may be of use in terms of the elucidation of the mechanism of silicon chain elongation reactions in polysilane synthesis by reductive coupling of dihalosilanes R_2SiX_2 with alkali metals M.[4, 22] Our results thus strongly suggest a possibility for the direct conversion of the initially formed silylenoid species $R_2Si(X)M$ into a β-halodisilanyl metal species XR_2SiSiR_2M by self-condensation: This step has not previously been proposed for the mechanism of polysilane synthesis.[4, 22, 23]

Further studies are directed toward the development of various silylenoid species such as (halogenosilyl)lithium compounds, as well as the elucidation of the mechanism of polysilane synthesis.[24]

Experimental Procedure

2: To a solution of **1** (312 mg, 0.74 mmol) in THF (3.0 mL) was added dropwise over 1 min a hexane solution of nBuLi (0.91 mL, 1.5 mmol, 1.64 M) at -78 °C. The solution was stirred for 3 h to give a yellow solution of **2**.

3: To a solution of **2** in THF [prepared from **1** (0.74 mmol) and nBuLi (1.5 mmol) in THF (3.0 mL)] was added chlorotrimethylsilane (0.21 mL, 1.6 mmol) at -78 °C.

After stirring for 30 min, the solution was allowed to warm to room temperature. The solution was analyzed directly by GLC and the yield of **3** was estimated (70%) by using *n*-docosane as internal standard. A pure sample of **3** was obtained as a colorless oil by preparative GLC. ^{1}H NMR (200 MHz, C_6D_6, $\delta(C_6D_6) = 7.20$): $\delta = 0.28$ (s, 9H), 1.26 (s, 9H), 7.24–7.28 (m, 6H), 7.76–7.81 (m, 4H); ^{13}C NMR (50 MHz, C_6D_6): $\delta \approx -1.21$, 32.3, 73.3, 128.3, 129.5, 135.3, 139.2; MS (70 eV): m/z(%): 328 (1) [M^+], 313 (1) [$M^+ - Me$], 255 (7) [$M^+ - SiMe_3$], 199 (100); elemental analysis for $C_{19}H_{28}Si_2$: calcd: C 69.45; H 8.59; found: C 69.55; H 8.59.

6: A solution of **2** [prepared from **1** (0.800 mmol) with *n*BuLi (1.6 mmol) in THF (2.0 mL)] was allowed to warm to 0 °C and stirred for 2 h, followed by addition of chlorotrimethylsilane (0.22 mL, 1.76 mmol). The solution was stirred at 0 °C for 2 h and then allowed to warm to room temperature. A 5% aqueous solution of NH_4Cl (5 mL) was poured into the mixture. The mixture was extracted with Et_2O (3 × 10 mL). The combined organic layers were washed with H_2O (10 mL) and brine (10 mL), and dried over $MgSO_4$. The solution was concentrated to yield crude **6**. The yield of **6** was estimated by ^{1}H NMR spectroscopy (56%); mesitylene was used as internal standard. Pure **6** was obtained as a colorless oil by column chromatography on silica gel (hexane/CH_2Cl_2 = 10/1, $R_f = 0.46$). ^{1}H NMR (200 MHz, C_6D_6, $\delta(C_6D_6) = 7.20$): $\delta \approx 0.24$ (s, 9H), 1.28 (2, 9H), 7.14–7.20 (m, 12H), 7.76–7.83 (m, 8H); ^{13}C NMR (50 MHz, C_6D_6): $\delta = -0.51$, 32.24, 75.39, 128.00, 128.12, 128.77, 129.78, 135.90, 136.97, 138.54; MS (70 eV): m/z(%): 510 (1) [M^+], 453 (37) [$M^+ - t$Bu], 437 (1) [$M^+ - SiMe_3$], 255 (8), 240 (9), 199 (100); elemental analysis for $C_{31}H_{38}Si_3$: calcd: C 72.88; H 7.50; found: C 72.63; H 7.48.

Received: September 24, 1994
Revised version: December 5, 1994 [Z 7352 IE]
German version: *Angew. Chem.* **1995**, *107*, 886

Keywords: silicon compounds · silylenoids

[1] Pertinent reviews: a) G. Köbrich, *Angew. Chem.* **1972**, *84*, 557–569; *Angew. Chem. Int. Ed. Engl.* **1972**, *11*, 473–485; b) H. Nozaki, *Synlett* **1990**, 441–444; c) A. Maercker, *Angew. Chem.* **1993**, *105*, 1072–1074; *Angew. Chem. Int. Ed. Engl.* **1993**, *32*, 1023–1025. Some leading references: ^{13}C NMR: d) D. Seebach, H. Siegel, K. Müllen, K. Hiltbrunner, *Angew. Chem.* **1979**, *91*, 845–847; *Angew. Chem. Int. Ed. Engl.* **1979**, *18*, 784–786; e) D. Seebach, H. Siegel, J. Gabriel, R. Hässig, *Helv. Chim. Acta* **1980**, *63*, 2046–2053. Theoretical studies: f) P. von R. Schleyer, T. Clark, A. J. Kos, G. W. Spitznagel, C. Rohde, D. Arad, K. N. Houk, N. G. Rondan, *J. Am. Chem. Soc.* **1984**, *106*, 6467–6475. Alkoxycarbenoids: g) G. Wittig, E. Stahnnecker, *Justus Liebigs Ann. Chem.* **1957**, *605*, 69–93; h) G. Boche, F. Bosold, J. C. W. Lohrenz, A. Opel, P. Zulauf, *Chem. Ber.* **1993**, *126*, 1873–1885. Stereochemistry: i) M. Topolski, M. Duraisamy, J. Rachon, J. Gawronski, K. Gawronska, V. Goedken, H. M. Walborsky, *J. Org. Chem.* **1993**, *58*, 546–555. Synthetic applications: j) T. Harada, Y. Kotani, T. Katsuhira, A. Oku, *Tetrahedron Lett.* **1991**, *32*, 1573–1576.

[2] In analogy with the conventions applied for carbenoids, we will use the term "silylenoid" for a compound in which a metal atom and a leaving group are bound to the same silicon atom. The term "silylenoid character or nature" on the other hand will be used in more mechanistic sense for a species that reacts electrophilically.

[3] T. Clark, P. von R. Schleyer, *J. Organomet. Chem.* **1980**, *191*, 347–353.

[4] a) R. West, *J. Organomet. Chem.* **1986**, *300*, 327–346; b) C. L. Smith, R. Gooden, *ibid.* **1974**, *81*, 33–40; c) P. Boudjouk, U. Samaraweera, R. Sooriyakumaran, J. Chrusciel, K. R. Anderson, *Angew. Chem.* **1988**, *100*, 1406; *Angew. Chem. Int. Ed. Engl.* **1988**, *27*, 1355–1356; d) T. Tsumuraya, S. A. Batcheller, S. Masamune, *ibid.* **1991**, *103*, 916–944 or **1991**, *30*, 902–930; e) R. Corriu, G. Lanneau, C. Priou, F. Soulairol, N. Auner, R. Probst, R. Conlin, C. J. Tan, *J. Organomet. Chem.* **1994**, *466*, 55–68.

[5] Certain transition metal silylene complexes have been prepared successfully from metal $SiR_2(OTf)$ systems by Tilley et al., see for example): a) D. A. Straus, C. Zhang, G. E. Quimbita, S. D. Grumbine, R. H. Heyn, T. D. Tilley, A. L. Rheingold, S. J. Geib, *J. Am. Chem. Soc.* **1990**, *112*, 2673–2681; b) S. D. Grumbine, T. D. Tilley, *ibid.* **1993**, *115*, 7884–7885; c) reviews: P. D. Lickiss, *Chem. Soc. Rev.* **1992**, *21*, 272–279.

[6] K. Tamao, A. Kawachi, Y. Ito, *J. Am. Chem. Soc.* **1992**, *114*, 3989–3990.

[7] G. Boche, M. Marsch, J. Harbach, K. Harms, B. Ledig, F. Schubert, J. C. W. Lohrenz, H. Ahlbrecht, *Chem. Ber.* **1993**, *126*, 1887–1894.

[8] For previous work on transient alkoxy silyl anions: a) H. Watanabe, K. Higuchi, M. Kobayashi, M. Hara, Y. Koike, T. Kitahara, Y. Nagai, *J. Chem. Soc. Chem. Commun.* **1977**, 534–535; b) H. Watanabe, K. Higuchi, T. Goto, T. Muraoka, J. Inose, M. Kageyama, Y. Iizuka, M. Nozaki, Y. Nagai, *J. Organomet. Chem.* **1981**, *218*, 27–39.

[9] B. H. Lipshutz, D. C. Reuter, E. L. Ellsworth, *J. Org. Chem.* **1989**, *54*, 4975–4977.

[10] Wurtz-type reaction of (*tert*-butoxy)diphenylsilyl chloride with lithium in THF at 0 °C gave no detectable amounts of **2**.

[11] Compound **1** was prepared by the reaction of (*t*BuO)Ph_2SiCl with Me_3SnLi, and isolated by vacuum distillation in 79% yield.

[12] G. A. Olah, R. J. Hunadi, *J. Am. Chem. Soc.* **1980**, *102*, 6989.

[13] For the ^{29}Si NMR spectrum of a disilanyllithium see: K. E. Ruehl, M. E. Davis, K. Matyjaszewski, *Organometallics*, **1992**, *11*, 788.

[14] An enhanced facile substitution of a negative leaving group in the presence of an alkyllithium compound known as the most typical hint of carbenoid nature [1].

[15] In the absence of TMEDA, the ratio of **8**/**6** was 13/87 (54% total yield). The effect of TMEDA, however, is not clear and is now under study.

[16] For a recent example for inclusion of lithium cation by [12]crown-4, see: A. Heine, D. Stalke, *Angew. Chem.* **1994**, *106*, 121–123; *Angew. Chem. Int. Ed. Engl.* **1994**, *33*, 113–115.

[17] The attempted observation of ^{29}Si NMR spectra for **9** was unsuccessful owing to the formation of a white precipitate which was insoluble even at 0 °C.

[18] In carbenoid chemistry, ionization of this type is sometimes called "metal-assisted ionization" which involves a definite heteroatom–metal interaction, according to Walborsky et al. [1i].

[19] The methyl group in this model compound may not necessarily be bulkier than the lithium atom in **2**, since the lithium atom must be solvated.

[20] G. Raabe, J. Michl, in *The Chemistry of Organic Silicon Compounds* (Eds.: S. Patai, Z. Rappoport), Wiley, Chichester, England, **1989**, pp. 1015–1142.

[21] For an example of successive introduction of a nucleophile and an electrophile to carbenoids in organic synthesis, see: P. Knochel, N. Jeong, M. J. Rozema, M. C. P. Yeh, *J. Am. Chem. Soc.* **1989**, *111*, 6474–6476.

[22] a) D. J. Worsfold, in *Inorganic and Organometallic Polymers* (*ACS Symp. Ser.* **1988**, *360*), Chapter 8; b) R. D. Miller, J. Michl, *Chem. Rev.* **1989**, *89*, 1359–1410; c) R. D. Miller, D. Thompson, R. Sooriyakumaran, G. N. Fickes, *J. Polym. Sci. Part A* **1991**, *29*, 813–824; d) R. D. Miller, E. J. Ginsburg, D. Thompson, *Polym. J.* **1993**, *25*, 807–823; e) R. G. Jones, R. E. Benfield, R. H. Cragg, A. C. Swain, S. J. Webb, *Macromolecules* **1993**, *26*, 4878–4887, and references therein.

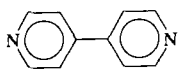
[23] Our proposal is based on the reasonable assumption that the silylenoid character of lithium(alkoxy)silylenoids can be applied to the reactivity of metal(halo)silylenoids.

[24] The sila-Wittig rearrangement of (alkoxysilyl)lithium compounds, that is the organic group migration from oxygen to silicon, analogous to the Wittig rearrangement, has also been observed and will be reported in due course.

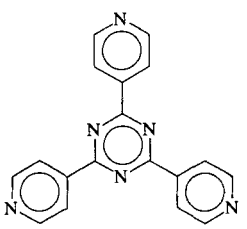
2,4,6-Tri(4-pyridyl)-1,3,5-triazine as a 3-Connecting Building Block for Infinite Nets**

Stuart R. Batten, Bernard F. Hoskins, and Richard Robson*

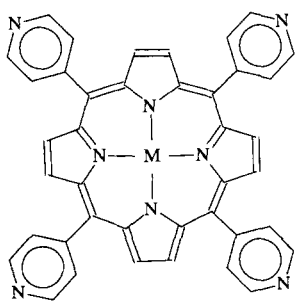
The results presented here form part of a study of the infinite two- (2D) and three-dimensional (3D) coordination networks derived from a family of 4-pyridyl-containing building blocks such as **1**,[1, 2] **2** (hereafter tpt), and **3**[3] amongst others.[4] This



1



2



3

[*] Dr. R. Robson, S. R. Batten, Dr. B. F. Hoskins
School of Chemistry
University of Melbourne
Parkville 3052, Victoria (Australia)
Telefax: Int. code +347-5180

[**] This work was supported by the Australian Research Council.

sort of investigation may lay the foundations for much more rational crystal engineering than is presently possible, allowing the future design and construction of solids with tailor-made properties (e.g. catalytic or electronic). Fujita et al. have recently made the very significant observation[5] that a cadmium-containing 2D square grid network derived from **1** that we originally reported[2] has catalytic properties, whilst PtS-related networks obtained, by design, from **3** generate very large channels with obvious implications for catalysis.[3]

We describe below the first crystallographically characterized 3D framework involving tpt (**2**), the trigonal member of the family. Some transition metal derivatives of this ligand have been previously isolated,[6] and molecular species in which three Zn centers are bonded to a single tpt ligand have been described.[7]

Infinite frameworks based on the simpler trigonal building block $C(CN)_3^-$ have been previously reported.[8, 9] This ligand with several divalent hexacoordinating metal ions affords derivatives of composition $[M\{C(CN)_3\}_2]$ containing two identical and independent but interpenetrating 3D (6,3)-connected nets with the same topology as the rutile prototype.[2, 9]

Mixtures of tpt-**2** in 1,1,2,2-tetrachloroethane and mercuric perchlorate in methanol produce brilliant, highly solvated crystals of composition **4** whose structure has been determined by

$[Hg(tpt)_2](ClO_4)_2 \cdot 6C_2H_2Cl_4$ **4**

single-crystal X-ray diffraction. A view of the Hg ions and tpt components of the cubic unit cell is shown in Figure 1. All metal centers are equivalent as are all tpt units, all ClO_4^- ions, and all $C_2H_2Cl_4$ molecules. The Hg centers and the tpt units form an infinite (6,3)-connected 3D network which we estimate to account for only approximately half the volume of the crystals; the spacious intraframework regions are occupied by well-ordered $C_2H_2Cl_4$ molecules and ClO_4^- ions.

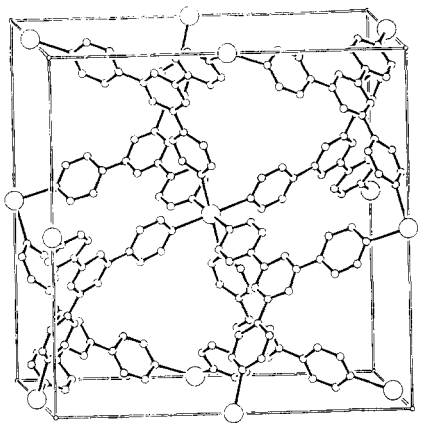


Fig. 1. The cubic unit cell of **4** showing only the Hg ions and tpt components. Large circles represent Hg atoms and small circles either C or N atoms. For clarity the C_5N and C_3N_3 rings are represented so as to obscure any structural features directly behind them. The Hg centers have an N_6 environment only slightly distorted from regular octahedral (Hg–N, 2.443(8) Å, N–Hg–N, 88.8(4)° and 91.2(4)°) provided by six tpt molecules each of which is coordinated to three metal centers at the corners of an equilateral triangle (Hg···Hg edge, 13.760(2) Å).

The three-dimensional disposition of these intraframework species is most simply represented in terms of the contents of a unit cell octant, as in Figure 2, all of which are equivalent. Each octant has a metal center at alternate corners, three of them being connected together by a tpt unit which is distorted from

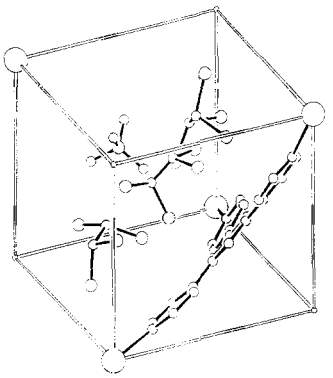


Fig. 2. An octant of the unit cell. Large circles represent Hg atoms, intermediate circles Cl atoms, and small circles either C, N, or O atoms. The angle between the planes of the triazine and pyridine rings is 9.5°. Three equivalent $C_2H_2Cl_4$ molecules are found within each octant arranged around the threefold axis. Within each $C_2H_2Cl_4$ molecule the torsional angle H-C-C-H is 60.5°.

internal coplanarity to become slightly domed; the displacement of the center of the triazine unit from the midpoint of the associated triangle of Hg centers is 0.86 Å. The fourth metal ion in the octant lies on a threefold axis perpendicular to the average tpt plane. Each octant contains one ClO_4^- ion with one of its Cl–O bonds coincident with the threefold axis and the oxygen pointing towards the tpt unit.

The large intraframework spaces are best described, in the absence of discernible linear channels, as consisting entirely of cavities between face-to-face tpt units of the type shown in Figure 3, each one merging into twelve others with which it shares large connecting "windows". The extensive solvation ($6C_2H_2Cl_4$ per Hg) reflects the spaciousness of these interconnected cavities.

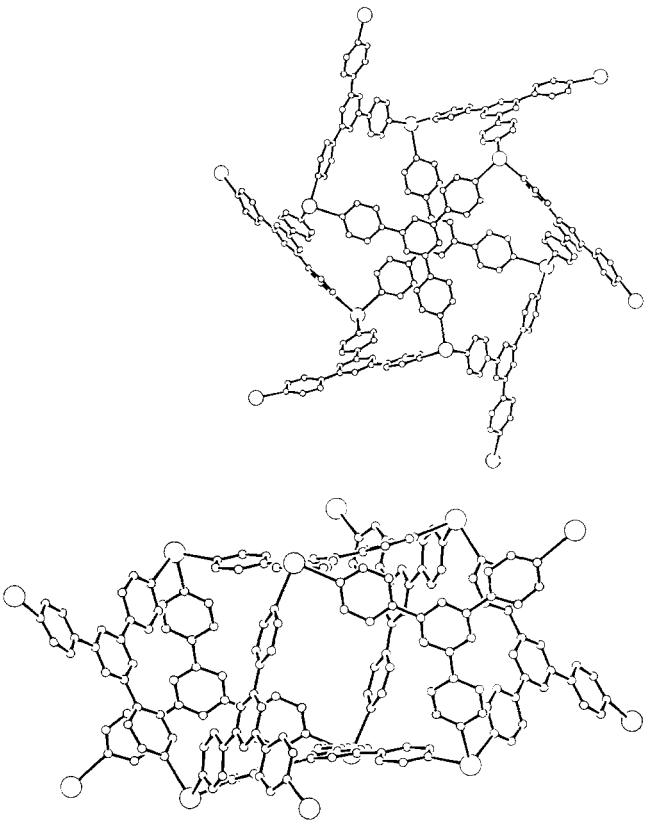


Fig. 3. A cavity formed between face-to-face tpt units. Top: Viewed slightly displaced from the threefold axis; bottom: viewed approximately edge-on to the face-to-face tpt units. For clarity C_5N and C_3N_3 rings are represented so as to obscure any structural features directly behind them. The separation between the triazines of the two face-to-face tpt units is 9.5 Å.

 © VCH Verlagsgesellschaft mbH, D-69451 Weinheim, 1995 0570-0833/95/0707-0821 $ 10.00+.25/0

The high degree of solvent and anion ordering in the structure of **4** is in marked contrast to the pronounced, liquidlike disorder which has been an outstanding feature of the highly solvated infinite framework solids constructed from other large molecular building blocks.[3, 10] However, the intraframework spaces in **4** admittedly represent a significantly smaller fraction of the crystal volume than in the others.

To the best of our knowledge the (6,3)-connected net of **4** has not been described before but, by sheer coincidence, an identical topology had been seen in our laboratory in crystals of $Cd(CN)_2 \cdot 2/3\,Et_3N$ only a short time before the present example was discovered.[11]

Well-characterized hexapyridinate complexes are rare, undoubtedly because of steric interference involving pyridine α-hydrogen atoms. (Of course, octahedral tris-2,2′-bipyridine (bpy) complexes in which this steric clash does not arise are stable and common.) To the best of our knowledge only three examples of crystallographically characterized metal hexapyridinates have been reported. In $[Fe(py)_6][Fe_4(CO)_{13}]$ (py = pyridine) the Fe–N bonds are distinctly elongated (2.25–2.29 Å) and the cation has a high-spin electronic configuration in contrast to the low-spin $[Fe(bpy)_3]^{2+}$.[12] $[Ru(py)_6](BF_4)_2$ with slightly shorter coordinate bonds (2.10–2.14 Å) is spin-paired.[13] The third example is $[Hg(py)_6](CF_3SO_3)_2$ in which the Hg–N distances of 2.42–2.48 Å are very similar to those in **4** (2.443(8) Å).[14]

The net underlying the structure of **4** can be related to the cubic pyrites net by the following imaginary transformation. The trigonal centers in a face-to-face pair (see pair in Fig. 3) are first deformed to become more pyramidal such that their separation decreases. The two approching centers are then bonded together, their connectivities increasing from three to four, to form a new net with the same topology as pyrites.

The (6,3)-connected topology adopted by the $[Hg(tpt)_2]^{2+}$ framework is to be contrasted with the rutile-related connectivity adopted by many divalent derivatives of the trigonal building block $C(CN)_3^-$.[2, 9] An essential feature of the rutile net is the presence of "four-membered" circuits (two octahedral centers and two trigonal centers). If the $[Hg(tpt)_2]^{2+}$ framework were to adopt the rutile connectivity, the analogous "four-membered" rings involving two octahedral metal centers and two planar tpt units, which would have to be coplanar or close to it, would lead to pronounced clashing between α-hydrogens of separate tpt units. Tpt, if it remains planar or close to it, would therefore seem innately unsuited to form a rutile-like net.

We estimate that for a given octahedral-to-trigonal distance, the (6,3) net of **4** is approximately 10% more dense than the rutile net, which is somewhat surprising since the shortest circuits in **4** are "six-membered" (three octahedral and three trigonal centers) in contrast to the "four-membered" shortest circuits in the rutile net. It is interesting to speculate why the net in **4** appears not to be adopted by AX_2 solids. We are presently exploring other three-dimensional nets formed by tpt, several of which generate large intraframework cavities and channels.

Experimental Procedure

Mixing $Hg(ClO_4)_2 \cdot 3H_2O$ (14 mg, 0.031 mmol) in methanol (10 mL) and tpt (25 mg, 0.080 mmol) in $C_2H_2Cl_4$ (10 mL) initially gave a small amount of very fine, cloudy white precipitate. After three days, however, large colorless crystals of $[Hg(tpt)_2](ClO_4)_2(C_2H_2Cl_4)_6$ grew (45 mg, 70%). The crystals were sensitive to loss of solvent.

Elemental analysis for $Hg(tpt)_2(ClO_4)_2 \cdot$ ca. $5C_2H_2Cl_4$: calcd: C 29.6, H 1.8, N 9.0, Cl 41.8; found: C 29.2, H 1.5, N 9.2, Cl 41.0. A crystal was sealed in a Lindemann glass capillary for crystallographic analysis. Crystal data of **4**: $M = 2031.25$, cubic, space group $Pa\bar{3}$ (no. 205), $a = 19.460(3)$ Å, $V = 7369(2)$ Å^3, $Z = 4$, crystal dimensions $0.29 \times 0.23 \times 0.14$ mm, $\rho_{calcd} = 1.830$, $\rho_{(meas.)} = 1.85(1)$ g cm^{-3}, $F(000) = 3976$, 5382 reflections measured, 3580 unique reflections, $2\theta_{max} = 60°$. Intensity data were measured at 295(1) K with $Mo_{K\alpha}$ radiation (graphite monochromator) using an Enraf-Nonius CAD-4MachS diffractometer and employing the $\omega/2\theta$ scan method; corrections for Lorentz, polarization, and absorption effects were applied ($\mu(Mo_{K\alpha}) = 30.1$ cm^{-1}, min./max. transmission = 0.5505/0.6878). The structure was solved using direct methods (SHELXS-86). A full-matrix least-squares refinement (SHELX-76) was then employed with anisotropic thermal parameters applied to all non-hydrogen atoms; pyridine hydrogens were assigned to calculated positions and refined with a common isotropic thermal parameter; no tetrachloroethane hydrogens were observed or included in the refinement; however their positions were calculated to allow the torsional H-C-C-H angle to be calculated. At convergence $R = 0.0442$ and $R_w = 0.0395$ for the 1149 observed reflections [$I \geq 3\sigma(I)$] with 146 parameters; max. residual electron density = 0.91 e Å^{-3}. Further details of the crystal structure investigation may be obtained from the Director of the Cambridge Crystallographic Data Centre, 12 Union Road, GB-Cambridge CB2 1EZ (UK), on quoting the full journal citation.

Received: October 8, 1994 [Z 7383 IE]
German version: *Angew. Chem.* **1995**, *107*, 884

Keywords: complexes with nitrogen ligands · mercury compounds · networks · triazines

[1] R. W. Gable, B. F. Hoskins, R. Robson, *J. Chem. Soc. Chem. Commun.* **1990**, 1677.
[2] R. Robson, B. F. Abrahams, S. R. Batten, R. W. Gable, B. F. Hoskins, J. Liu in *Supramolecular Architecture* (Ed.: T. Bein), ACS, Washington, DC, **1992**, p. 261.
[3] B. F. Abrahams, B. F. Hoskins, D. M. Michail, R. Robson, *Nature* **1994**, *369*, 727.
[4] B. F. Abrahams, M. J. Hardie, B. F. Hoskins, R. Robson, E. E. Sutherland, *J. Chem. Soc. Chem. Commun.* **1994**, 1049.
[5] M. Fujita, Y. J. Kwon, S. Washizu, K. Ogura, *J. Am. Chem. Soc.* **1994**, *116*, 1151.
[6] H. Biedermann, K. Wichmann, *Z. Naturforsch. B* **1974**, *29*, 360.
[7] H. L. Anderson, J. K. M. Sanders, *J. Chem. Soc. Chem. Commun.* **1989**, 1714.
[8] J. Konnert, D. Britton, *Inorg. Chem.* **1966**, *5*, 1193.
[9] S. R. Batten, B. F. Hoskins, R. Robson, *J. Chem. Soc. Chem. Commun.* **1991**, 445.
[10] B. F. Hoskins, R. Robson, *J. Am. Chem. Soc.* **1990**, *112*, 1546.
[11] B. F. Hoskins, R. Robson, N. V. Y. Scarlett, unpublished results.
[12] R. J. Doedens, L. F. Dahl, *J. Am. Chem. Soc.* **1966**, *88*, 4847.
[13] J. L. Templeton, *J. Am. Chem. Soc.* **1979**, *101*, 4906.
[14] R. Akesson, M. Sandstrom, C. Stalhandske, I. Persson, *Acta Chem. Scand.* **1991**, *45*, 16.

Reaction of a Vanadium(III) Amide with H_2: Isolation and Characterization of a Polynuclear Mixed-Valence Polyhydrido–Nitrido Complex**

Pietro Berno and Sandro Gambarotta*

The hydrogenolysis of a M–C bond by molecular hydrogen to form a metal hydride and a hydrocarbon is a key transformation in the organometallic chemistry of transition metals[1] and a fundamental step in both catalysis[2] and metal-promoted organic synthesis.[3] In contrast, only very little is known about the reaction of H_2 with M–X bonds (X = heteroatom)[4] in spite of the great possibilities that can be envisioned for catalysis. This challenging new aspect of molecular catalysis is now the target of active research, though almost exclusively with the late transition metals. Since early transition metals have been successfully used for promoting a very large number of organic transformations (insertion,[5] reductive coupling,[6] hydroamination,[7]

[*] Prof. Dr. S. Gambarotta, P. Berno
Department of Chemistry, University of Ottawa
Ottawa, Ontario K1N 6N5 (Canada)
Telefax: Int. code +(613) 562-5170

[**] This work was supported by the Natural Science and Engineering Research Council of Canada.

cyclization,[8] hydrosilation reactions,[9] etc.), cleavage of bonds between early transition metals and heteroatoms such as phosphorus, nitrogen, sulfur, or oxygen by molecular hydrogen would certainly open new and interesting perspectives.

Complexes with low-valent vanadium centers are particularly appealing, because vanadium is an important component of some metalloenzymes and proteins[10] and is involved in some promising transformations such as the catalytic hydrogenation of N_2.[11] Even more interesting is the fact that this reaction is promoted by in-situ-generated V^{II} hydroxide or V^{II} catecholate in conjunction with protic cocatalysts. These observations, together with the discovery that anionic, organic supporting ligands containing amide groups are able to transfer H_2 from the alkylamide to a substrate, and form metallacyclobutane rings and olefinic functions in the process,[12] prompted us to study the reactivity of the V–N bond of a novel series of V^{III} amides towards H_2.

In this paper we describe the hydrogenolysis of an amide-stabilized vanadacyclobutane to form an unprecedented mixed-valent complex **1** from trihydridodivanadium and nitrido divanadium complex fragments.

$[\{(Me_3P)_3V\}_2(\mu\text{-}H)_3]^+[\{[(Me_3Si)_2N]_2V\}_2(\mu\text{-}N)_2]^-$ **1**

The reaction of the dinuclear complex **2**[13] with either pyridine or PMe_3 cleaved the dinuclear structure to form the corresponding monomers **3a**[14] or **3b**. Although the cleavage of the

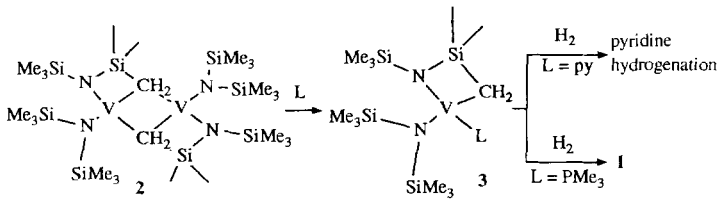
$[\{[(Me_3Si)_2N]V[CH_2(SiMe_2)N(SiMe_3)]\}_2]$ **2**

$[\{(Me_3Si)_2N\}V\{CH_2(SiMe_2)_2N(SiMe_3)\}(L)]$

3a: L = pyridine

3b: L = PMe_3

dinuclear structure did not affect the stability of the four-membered metallacyclobutane moiety, it has profound repercussions on its reactivity.[15] While the reaction of **1** with H_2 gave only intractable materials, the reaction of **3a** with H_2 (60 atm) in an autoclave at room temperature gave the expected hydrogenolysis of the V–C bond and, in addition, the stereoselective hydrogenation of the pyridine ring.[14] The same reaction carried out under identical reaction conditions with the PMe_3 complex yielded the novel complex **1** in moderate but reproducible yield (45%) (Scheme 1). The complex was isolated as deep-brown, very air-sensitive crystals from hexane. The formula had to be inferred from microanalytical data, since the ^1H NMR spectrum could not be interpreted because of the paramagnetism (μ_{eff} = 3.27 μ_B per formula unit). The presence of three hydrides in the complex was also supported by the formation of three equivalents of H_2 during a degradation experiment with seven equivalents of HCl in a closed vessel connected to a Toepler pump; the resulting gaseous mixture was analyzed by gas chromatography. The presence of the two nitrido moieties in the anionic units was indicated by the formation of NH_3 during the



Scheme 1.

hydrolysis. The absence of IR absorptions in the region 4000–2900 cm^{-1} ruled out the possibility that the nitrido ligands might actually be NH or NH_2 groups.

The molecular structure of **1** was elucidated by an X-ray crystal structure analysis (Fig. 1).[16] The molecule is composed of two separate $[\{(Me_3P)_3V\}_2(\mu\text{-}H)_3]^+$ and $[\{[Me_3Si)_2N]_2V\}_2(\mu\text{-}N)_2]^-$ fragments. The first unit is dinuclear with the two octahedrally coordinated vanadium atoms bridged by three hydrides [V3–H116 = 1.77(7) Å, V3–H64 = 1.88(2) Å, V3–H148 = 1.79(2) Å, V4–H64 = 1.87 Å, V4–H116 = 1.90(2) Å, V4–H148 = 1.78(2) Å] and arranged in the same face-sharing bioctahedral structure previously observed for the $[\{(thf)_3V\}_2(\mu\text{-}Cl)_3]^+$ cation.[17] The V–V distance [V3–V4 = 2.399(1) Å] suggests direct metal–metal interaction (either partial V–V bond or magnetic exchange). The second unit is also dinuclear

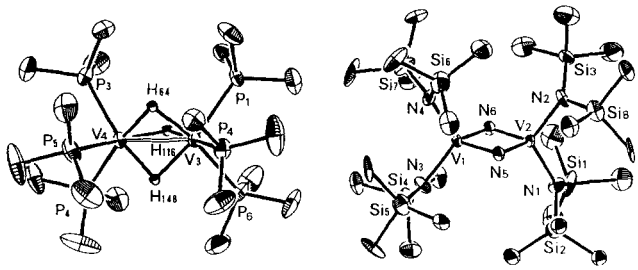


Fig. 1. Structure of **1** in the crystal (ORTEP diagram). The cation is depicted on the left, the anion on the right. Selected bond lengths [Å] and angles [°]: V1-V2 2.583(1), V1-N5 1.769(5), V1-N6 1.776(4), V2-N5 1.771(4), V2-N6 1.776(4), N5···N6 2.420(3), V2-N1 1.965(5), V2-N2 1.958(5), N1-V2-N2 114.1(2); N1-V2-N5 112.6(2), N1-V2-N6 112.5(2), V2-N1-Si1 118.5(3), V2-N1-Si2 121.2(3), V3-V4 2.399(1), V3-P1 2.514(2), V3-P4 2.505(2), V3-P6 2.498(2), V3-H64 1.88(2), V3-H116 1.77(7), V3-H148 1.79(2); P1-V3-P4 96.68(6), P1-V3-P6 96.48(7), P4-V3-P6 98.13(7), P1-V3-H116 87.0(2), P4-V3-H116 170.0(2), P6-V3-H116 91.0(2).

and is formed by two vanadium atoms linked together through a shared edge of their distorted coordination tetrahedra. The V–N distance, which is considerably shorter than usual for a bridging nitrogen atom is consistent with the presence of some V–N multiple-bond character.[18] The V_2N_2 core is planar with a rather short V···V distance [V1···V2 = 2.583(1) Å] and with structural parameters very similar to those of the recently reported $[\{Cp^*V(N)Cl\}_2]$ ($Cp^* = \eta^5\text{-}C_5Me_5$).[19] The long N···N distance [N···N = 2.420(3) Å] rules out the possibility that this unit might actually be a mixed-valence vanadium complex with a dinitrogen ligand bound side-on.[20] The cationic unit provides a rare example of a polyhydridovanadium structure.[21]

The oxidation states of the four vanadium atoms could not be conclusively assigned on the basis of the magnetic susceptibility measurements. Furthermore, attempts to isolate new species by both cation and anion exchange were unsuccessful yielding only extremely intractable air-sensitive oils. However, the structural similarity of the hydrido moiety with that of $[\{(thf)_3V\}_2(\mu\text{-}Cl)_3]^+$,[17] and of the recently crystallographically characterized $[\{(Me_3P)_3V\}_2(\mu\text{-}Cl)_3]^+Cl^-$,[22] makes very plausible the proposal that the unit $[\{(Me_3P)_3V\}_2(\mu\text{-}H)_3]$ contains vanadium in the divalent state and is cationic. The fairly high magnetic moment indicates that this unit is probably paramagnetic, in spite of the short V–V distance. The hydride moiety is undoubtedly formed by the hydrogenolysis of both the $V\text{–}CH_2$ and $V\text{–}N(SiMe_3)_2$ bonds since large amounts of $(Me_3Si)_2NH$ were identified in the GC-MS of the reaction mixture. The fact that no traces of methane or silanes (Me_3SiH, Me_2SiH_2, SiH_4) were detected in the reaction mixture discourages the idea that the

 © VCH Verlagsgesellschaft mbH, D-69451 Weinheim, 1995 0570-0833/95/0707-0823 $ 10.00+.25/0

two bridging nitrides arise from the hydrogenolysis of the N–Si bond. This result suggests that these groups are formed by reduction of dinitrogen, either present in the autoclave or during the workup of the reaction mixture. In agreement with these observations, reactions carried out on exclusion of N_2 yielded only intractable and pyrophoric oils.

The transformation of four molecules of **2** (containing V^{III}) into one molecule of **3** (containing two V^{II}, one V^{IV} and one V^{V}) implies a disproportionation with concomitant loss of one electron. The remaining five electrons necessary for the six-electron reduction of dinitrogen are provided by the oxidation of two and a half molecules of H_2. This also produces five of the eight hydrogen atoms necessary to protonate the four CH_2 moieties and the four NR_2 groups during the formation of four molecules of free amine. The remaining three protons are provided by three additional molecules of H_2 which simultaneously generate the three hydrides necessary for the cationic moiety of **3**. The overall stoichiometry is therefore as formulated in Equation (a).

$$4\,\mathbf{3b} + 5.5\,H_2 + N_2 \longrightarrow \mathbf{1} + 4\,(Me_3Si)_2NH \qquad (a)$$

Further work to clarify the reaction mechanism is presently in progress.

Experimental Procedure

PMe_3 (14.2 mmol) was added to a purple-blue solution of **1** (3.5 g, 4.74 mmol). The resulting burgundy red solution was transferred to an autoclave, pressurized with H_2 (60 atm), and allowed to stand at room temperature for 36 h. After venting, the autoclave was opened, and the clear brown solution was transferred to a Schlenck tube. After 2 days of stirring unter N_2 a brown crystalline solid started to separate. When the toluene was removed under vacuum and replaced by hexane, dark brown crystals of **1** precipitated immediately (1.5 g, 45%). Crystals suitable for X-ray diffraction were grown at room temperature in concentrated toluene solution. Elemental analysis: calcd (found) for $C_{42}H_{129}N_6Si_8P_6V_4 \cdot 1/2$ toluene: C 39.37 (39.31), H 9.77 (9.69), N 6.12 (6.09). IR (Nujol, KBr): $\tilde{\nu}$ [cm^{-1}] = 1421 (sh), 1030 (m), 1282 (m), 1241 (vs), 1173 (w), 1081 (w), 1019 (w), 951 (vs), 848 (vs), 786 (s), 754 (m), 724 (m), 700 (sh), 665 (s), 627 (m), 559 (vw). μ_{eff} = 2.73 μ_B per formula unit.

Received: September 24, 1994
Revised: November 18, 1994 [Z 7349 IE]
German version: *Angew. Chem.* **1995**, *107*, 871

Keywords: complexes with hydrido ligands · complexes with nitrido ligands · vanadium compounds

[1] See for example, *Comprehensive Organometallic Chemistry* (Ed.: G. Wilkinson), Pergamon, Oxford, **1982**.

[2] a) F. A. Cotton, G. Wilkinson, *Advanced Inorganic Chemistry*, 5th ed., Wiley Interscience, New York, **1988**; b) F. P. Pruchnik, *Organometallic Chemistry of the Transition Elements*, Plenum, New York, **1990**.

[3] *Transition Metal Organometallics in Organic Synthesis Vol. 33-1/2* (Ed.: H. Alper), Academic Press, New York, **1976**.

[4] a) P. G. Jessop, R. H. Morris, *Coord. Chem. Rev.* **1992**, *121*, 155; b) V. V. Grushin, *Acc. Chem. Res.* **1993**, *26*, 279; c) J. T. Poulton, K. Folting, W. E. Streib, K. G. Caulton, *Inorg. Chem.* **1992**, *31*, 3190; d) E. P. Capellani, P. A. Maltby, R. H. Morris, C. T. Schweitzer, M. R. Steele, *ibid.* **1989**, *28*, 4437; e) P. C. Scheller, J. B. Bonanno, P. T. Wolczanski, *J. Am. Chem. Soc.* **1994**, *116*, 4133.

[5] a) E. B. Coughlin, J. E. Bercaw, *J. Am. Chem. Soc.* **1992**, *114*, 7606; b) L. L. Whinnery, L. M. Henling, J. E. Bercaw, *ibid.* **1991**, *113*, 7575; c) W. E. Piers, J. E. Bercaw, *ibid.* **1990**, *112*, 9402; d) G. Parkin, J. E. Bercaw, *ibid.* **1989**, *111*, 391; e) F. J. Berg, J. L. Petersen, *Organometallics* **1993**, *12*, 3890; f) G. C. Bazan, W. P. Schaefer, J. E. Bercaw, *ibid.* **1993**, *12*, 2126; g) D. M. Amorose, R. A. Lee, J. L. Petersen, *ibid.* **1991**, *10*, 2191; h) G. Erker, F. Sogna, J. L. Petersen, R. Benn, H. Grandey, *ibid.* **1990**, *9*, 2462.

[6] a) L. D. Durfee, A. K. McMullen, I. P. Rothwell, *J. Am. Chem. Soc.* **1988**, *110*, 1463; b) J. E. Hill, G. J. Balaich, P. E. Fanwick, I. P. Rothwell, *Organometallics* **1991**, *10*, 3428; c) J. E. Hill, P. E. Fanwick, I. P. Rothwell, *ibid.* **1991**, *10*, 15; d) J. E. Hill, G. Balaich, P. E. Fanwick, I. P. Rothwell, *ibid.* **1993**, *12*, 2911.

[7] a) T. Marks, *J. Am. Chem. Soc.* **1989**, *111*, 4108; b) P. J. Walsh, A. M. Baranger, R. G. Bergmann, *ibid.* **1992**, *114*, 1708.

[8] a) S. L. Buchwald, S. M. King, *J. Am. Chem. Soc.* **1991**, *113*, 258; b) R. B. Grossman, W. M. Davis, S. L. Buchwald, *ibid.* **1991**, *113*, 2321; c) P. Rigollier, J. R. Young, L. A. Fowley, J. R. Stille, *ibid.* **1990**, *112*, 9441; d) G. J. Balaich, I. P. Rothwell, *ibid.* **1993**, *115*, 1582.

[9] For example, a) F. Gauvin, J. Britten, E. Samuel, J. F. Harrod, *J. Am. Chem. Soc.* **1992**, *114*, 1489; b) H. G. Woo, R. H. Heyn, D. T. Tilley, *ibid.* **1992**, *114*, 5698; c) H. G. Woo, J. F. Walzer, D. T. Tilley, *ibid.* **1992**, *114*, 7047.

[10] a) B. J. Hales, E. E. Case, J. E. Morningstar, M. F. Dzeba, M. A. Mauterer, *Biochemistry* **1986**, *25*, 7521; b) R. R. Eady, *Biofactors* **1988**, *1*, 111; c) G. N. George, C. L. Coyle, B. J. Hales, S. P. Cramer, *J. Am. Chem. Soc.* **1988**, *110*, 4057; d) J. E. Morningstar, B. J. Hales, *ibid.* **1987**, *109*, 6854.

[11] N. P. Luneva, S. A. Mironova, A. E. Shilov, M. Yu. Antipin, Y. T. Struchkov, *Angew. Chem.* **1993**, *105*, 1240; *Angew. Chem. Int. Ed. Engl.* **1993**, *32*, 1178; and references therein.

[12] J. Song, P. Berno, S. Gambarotta, *J. Am. Chem. Soc.* **1994**, *116*, 6927.

[13] P. Berno, S. Hao, R. Minhas, S. Gambarotta, *Organometallics* **1994**, *13*, 1052.

[14] P. Berno, S. Gambarotta, *Organometallics* **1994**, *13*, 2569.

[15] P. Berno, S. Gambarotta, *J. Chem. Soc. Chem. Commun.*, **1994**, 2419.

[16] Crystal data of **1**: $C_{42}H_{129}N_6Si_8P_6V_4 \cdot 1/2$ toluene, M_r = 1378.88, triclinic, $P\bar{1}$, a = 18.033(3), b = 19.693 (2), c = 12.464(3) Å, α = 102.75(1), β = 106.58(1), γ = 80.82(1)°, V = 4115(3) Å^3, Z = 2, ρ_{calcd} = 1.113 g cm^{-1}, μ = 6.84 cm^{-1}, $F(000)$ = 1484, R = 0.066 (R_w = 0.085) for 675 parameters and 9097 unique reflections. Non-hydrogen atom position were refined anisotropically. All the hydrogen atom positions were located and refined in the case of the bridging hydrides. Half a molecule of toluene was found in the lattice and was disordered over two positions. Some of the carbon atoms of the trimethylsilyl groups were also disordered over four positions. The disorder was modeled by splitting the occupancies of the carbon atoms over the two positions. Further details of the crystal structure investigations are available on request from the Director of the Cambridge Crystallographic Data Centre, University Chemical Laboratory, 12 Union Road, GB-Cambridge CB2 1EZ (UK), on quoting the full journal citation.

[17] a) F. A. Cotton, S. A. Duraj, M. W. Extine, G. E. Lewis, W. J. Roth, C. D. Schmulbach, W. Schwotzer, *J. Chem. Soc. Chem. Commun.* **1983**, 1377; b) F. A. Cotton, S. A. Duraj, L. R. Falvello, W. J. Roth, *Inorg. Chem.* **1985**, *24*, 4389; c) R. J. Bouma, J. H. Teuben, W. R. Beukema, R. L. Bansemer, J. C. Huffman, K. G. Caulton, *ibid.* **1984**, *23*, 2715; K. Folting, J. C. Huffman, R. L. Bansemer, K. G. Caulton, D. L. Martin, P. D. Smith, *ibid.* **1984**, *23*, 4589.

[18] K. Dehnicke, J. Strähle, *Angew. Chem.* **1992**, *104*, 978; *Angew. Chem. Int. Ed. Engl.* **1992**, *31*, 955.

[19] T. S. Haddad, A. Aistars, J. W. Ziller, N. M. Doherty, *Organometallics* **1993**, *12*, 2420.

[20] a) M. D. Fryzuk, T. S. Haddad, M. Mylvaganam, D. H. McConville, S. J. Rettig, *J. Am. Chem. Soc.* **1993**, *115*, 2782; b) K. Jonas, *Angew. Chem.* **1973**, *85*, 1050; *Angew. Chem. Int. Ed. Engl.* **1973**, *12*, 997; c) C. Krüger, Y.-H. Tsay, *ibid.* **1973**, *85*, 1051 and **1973**, *12*, 998; d) K. Jonas, D. J. Brauer, C. Kruger, P. J. Roberts, Y. Tasy, *J. Am. Chem. Soc.* **1976**, *98*, 74; e) G. P. Pez, P. Apgar, R. K. Crissey, *ibid.* **1982**, *104*, 482; f) R. Duchateau, S. Gambarotta, N. Beydoun, C. Bensimon, *ibid.* **1991**, *113*, 8986.

[21] a) R. L. Bansemer, J. C. Huffman, K. G. Caulton, *J. Am. Chem. Soc.* **1983**, *105*, 6163; b) B. Hessen, F. van Bolhuis, J. H. Teuben, J. L. Petersen, *ibid.* **1988**, *110*, 295; c) K. Jonas, V. Wieskamp, H. Y. Tsay, C. Kruger, *ibid.* **1983**, *103*, 5480.

[22] P. Berno, S. Gambarotta, unpublished results.

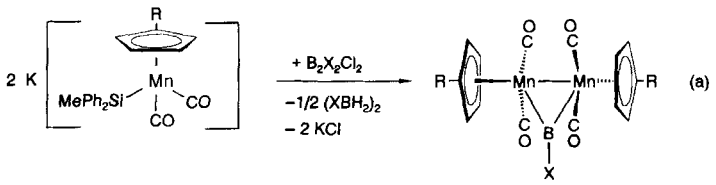
 © VCH Verlagsgesellschaft mbH, D-69451 Weinheim, 1995 0570-0833/95/0707-0824 $ 10.00+.25/0

Synthesis and Structure of the First Transition Metal Borylene Complexes

Holger Braunschweig* and Trixie Wagner

Dedicated to Professor Peter Paetzold on the occasion of his 60th birthday

Transition metal compounds with terminal[1] or bridging[2–4] carbene, nitrene, or oxo ligands are known; however, the analogous borylene complexes have not yet been described. With $[\mu\text{-BX}\{(\eta^5\text{-}C_5H_4R)Mn(CO)_2\}_2]$ **1**, **2**, we were able to synthesize [Eq. (a)], and in the case of **1a**, structurally characterize the first dinuclear complexes with a bridging borylene ligand.



1a R = H, X = NMe_2
1b R = Me, X = NMe_2
2 R = Me, X = *t*Bu

All three compounds can be isolated in the form of red crystals and are characterized by their high stability. For example, in the solid state they can be handled in air for long periods and melt without decomposition between 100 °C and 110 °C. The constitution in solution is derived from the NMR spectra. Despite the BN π-bonding component that is expected for products **1a** and **1b**, the ^{11}B NMR signal at $\delta = 103$ indicates little shielding. In the case of compound **2**, in which the *t*Bu group prevents π saturation of the boron atom, there is an extremely low-field shifted ^{11}B NMR signal at $\delta = 170$. The ^1H and ^{13}C NMR spectra prove that both C_5H_4R groups and the nitrogen-bound methyl groups in **1a**, **b** are equivalent. This, along with the nonequivalence of the four ring protons in C_5H_4Me (**1b**, **2**), supports the presence of a C_2-symmetrical molecule whose C_2 axis passes through the B–X bond.

The results of the X-ray structure analysis[5] of **1a** show that the molecule has approximate C_2 symmetry (Fig. 1) also in the crystalline state. The two manganese atoms and the boron atom form an isosceles triangle, in which the distance between the boron atom and each manganese atom is 203(1) pm and the distance between the two manganese atoms is 279.0(2) pm. The nitrogen atom bound to boron is trigonal-planar coordinated. The plane formed by C_2N (passing through the nitrogen atom) is only slightly rotated (8(3)°) with respect to the Mn_2B plane. The length of the boron–nitrogen bond is 139(1) pm and lies in the expected region for a boron–nitrogen double bond. The molecular structure is essentially analogous to that of the known methylene- and vinylidene-bridged complexes $[\mu\text{-}CH_2\{(\eta^5\text{-}C_5H_4Me)Mn(CO)_2\}_2]$[6] and $[\mu\text{-}CCH_2\{(\eta^5\text{-}C_5H_5)Mn(CO)_2\}_2]$,[7] respectively. These can be considered as dimetallacyclopropane derivatives. The agreement of the structural data and the CO stretching frequency supports the description of compounds **1** and **2** as dimetallaboriranes.

[*] Dr. H. Braunschweig, T. Wagner
Institut für Anorganische Chemie der Technischen Hochschule
D-52056 Aachen (Germany)
Telefax: Int. code + (241)8888-288

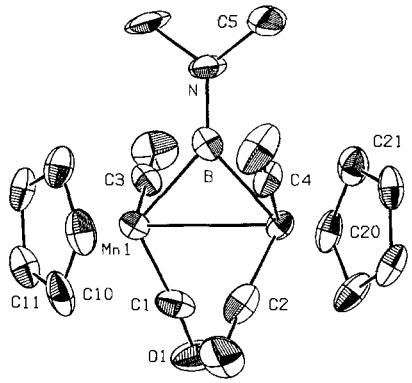


Fig. 1. Crystal structure of **1a**. Selected bond lengths [Å] and angles [°]: B-Mn1 2.03(1), B-Mn2 2.03(1), Mn1-Mn2 2.790(2), B-N 1.39(1), Mn1-Lp1 1.783(1), Mn2-Lp2 1.782(1); Mn1-B-Mn2 86.8(4), Mn1-Mn2-B 46.6(3), Mn2-Mn1-B 46.6(3); Lp1 is the point crossed by the plumbline from Mn1 through the plane formed by the atoms C10 to C14.

The formation of compounds **1a**, **b** and **2** is evidently the result of a complex reaction. In order to gain some insight into the course of the reaction, it was monitored by ^1H, ^{11}B, and ^{29}Si NMR spectroscopy. In addition to the borylene complexes, the only other boron-containing compound which is stoichiometrically formed is the corresponding diborane(6) derivative $(XBH_2)_2$ (X = NMe_2, *t*Bu). The boranes can be isolated from the reaction mixture by condensation in vacuum and unambiguously characterized by their ^1H and ^{11}B NMR spectra. The analogous reaction in [D$_6$]benzene yields the same product. Therefore, the solvent can be eliminated as the source of the boron-bound hydrogen atom in the diborane(6). The cleavage of the boron–boron bond in the starting diborane(4) decisively contributes to the formation of the borylene complex. This is demonstrated by the unsuccessful reaction of $K[(\eta^5\text{-}C_5H_4R)Mn(SiMePh_2)(CO)_2]$ with the boranes $XBCl_2$ [X = NMe_2, *t*Bu]. In addition to the above-mentioned diborane(6), the only characterizable side-product is a small amount of $[(\eta^5\text{-}C_5H_4R)Mn(CO)_3]$. The ^1H and ^{29}Si NMR spectra of the reaction solution as well as the THF-soluble reaction residue show that no soluble silicon-containing compound is formed during the reaction. Investigations of all the reaction components by gas chromatography and mass spectrometry provide no evidence of other products. The Ph_2MeSi group remains in the insoluble residue, in which silicon can be qualitatively analyzed by suitable methods. A chlorosilane elimination, as known for the reaction of $K[(\eta^5\text{-}C_5H_4Me)Mn(SiMePh_2)(CO)_2]$ with numerous chloride compounds,[8] does not take place; however, the Ph_2MeSi group is decisive for the occurrence of the reaction as is shown by the unsuccessful reaction of the diborane(4) with $K[(\eta^5\text{-}C_5H_4Me)Mn(H)(CO)_2]$.

Experimental Procedure

1a: A suspension of $K[(\eta^5\text{-}C_5H_5)Mn(SiMePh_2)(CO)_2]$ [9] (1.34 g, 3.3 mmol) in benzene (15 mL) was treated at room temperature with $B_2(NMe_2)_2Cl_2$ (0.18 g, 1.2 mmol) [10]. After stirring for 24 h all volatile components were removed in high vacuum (25 °C/0.001 Torr), and the residue was taken up in hexane (20 mL). After filtration, 0.62 g (46%) [μ-(dimethylamino)boryl-bis{dicarbonyl)η^5-cyclopentadienyl)manganese}(*Mn–Mn*)] **1a** was obtained at −40 °C as red crystals. NMR spectra in [D$_6$]benzene at 25 °C; ^1H NMR (500 MHz, TMS): $\delta = 2.85$ (s, 6H, NMe_2), 4.20 (s, 10H, $2C_5H_5$); ^{11}B NMR (160 MHz, $Et_2O \cdot BF_3$): $\delta = 103.0$; ^{13}C NMR (126 MHz, TMS): $\delta = 44.24$ (NMe_2), 84.85 (C_5H_5); IR (KBr): $\tilde{\nu} = 1960$ (m), 1917 (s), 1883 (s) cm^{-1} (C=O); correct elemental analysis.

1b: As described for **1a**, $K[(\eta^5\text{-}C_5H_4Me)Mn(SiMePh_2)(CO)_2]$ (2.00 g, 4.8 mmol) in benzene (20 mL) was treated with $B_2(NMe_2)_2Cl_2$ (0.36 g, 2.4 mmol) and 0.41 g (40%) red, crystalline **1b** was obtained. NMR spectra (same conditions as for **1a**): ^1H NMR: $\delta = 1.86$ (s, 6H, $2MeC_5H_4$), 2.93 (s, 6H, NMe_2), 3.99, 4.05, 4.10, 4.22 (4s

 © VCH Verlagsgesellschaft mbH, D-69451 Weinheim, 1995 0570-0833/95/0707-0825 $ 10.00+.25/0

br., 8H, $2MeC_5H_4$); ^{11}B NMR: $\delta = 102.8$; ^{13}C NMR: $\delta = 13.48$ (MeC_5H_4), 44.53 (NMe_2), 82.10, 84.18, 85.83, 87.56 (MeC_5H_4), 101.05 (MeC_5H_4); IR (KBr): $\tilde{\nu} = 1956$ (m), 1916 (s), 1883 (s) cm^{-1} (C=O); correct elemental analysis.

2: As described for **1a**, $K[(\eta^5\text{-}C_5H_4Me)Mn(SiMePh_2)(CO)_2]$ (2.44 g, 5.8 mmol) in benzene (20 mL) was treated with $B_2tBu_2Cl_2$ [11] (0.60 g, 2.9 mmol) and 0.42 g (32%) red, crystalline **2** was obtained. NMR spectra (same conditions as for **1a**); ^1H NMR: $\delta = 1.38$ (s, 9H, *t*Bu), 1.85 (s, 6H, $2MeC_5H_4$), 4.03, 4.10, 4.25, 4.30 (4s br., 8H, $2MeC_5H_4$); ^{11}B NMR: $\delta = 170.0$; ^{13}C NMR: $\delta = 13.31$ (MeC_5H_4), 31.97 (*t*Bu), 81.44, 83.01, 84.86, 89.98 (MeC_5H_4), 103.37 (MeC_5H_4); IR (KBr): $\tilde{\nu} = 1951$ (m), 1922 (s), 1878 (s) cm^{-1} (C=O); correct elemental analysis.

Received: November 9, 1994 [Z 7460 IE]
German version: *Angew. Chem.* **1995**, *107*, 904

Keywords: boron compounds · complexes with boron ligands · manganese compounds

[1] W. A. Nugent, J. M. Mayer, *Metal-Ligand Multiple Bonds*, Wiley, New York, **1988**.
[2] W. A. Herrmann, *J. Organomet. Chem.* **1983**, *250*, 319–343.
[3] M. H. Chisholm in *Comprehensive Coordination Chemistry, Vol. 2* (Eds.: G. Wilkinson, R. D. Gillard, J. A. McCleverty), Pergamon, Oxford, **1983**, p. 161.
[4] M. T. Pope, *Heteropoly and Isopoly Oxometallates*, Springer, New York, **1983**.
[5] Crystal data: crystal dimensions $0.10 \times 0.35 \times 0.60$ mm^3; $a = 7.938(2)$, $b = 15.035(4)$, $c = 28.854(5)$ Å; $V = 3444(2)$ $Å^3$; $Z = 8$; $\rho_{calcd} = 1.570$ $g cm^{-3}$; $\mu = 14.262$ cm^{-1}; orthorhombic space group, *Pbca* (no. 61); Enraf-Nonius CAD4 diffractometer; $Mo_{K\alpha}$ irradiation ($\lambda = 0.7107$ Å); measurement temperature −15 °C; 3549 measured reflections $3 \leq \theta \leq 28°$ (ω scan), from which 1190 with $I > 3\sigma(I)$, 1576 independent reflections with $I > 1\sigma(I)$ for 217 parameters; structure solution and refinement with SDP [12]; all non-hydrogen atoms were anisotropically refined, all hydrogen atoms were included for the refinement. Empirical absorptions correction with PSI-scans (max. transmission 99.80%, min. 75.45%) [13], no extinction correction, $R = 0.081$, $R_w = 0.069$, GOF = 1.529; residual electron density 0.947 $eÅ^{-3}$ 1.02 Å away from Mn1. Further details on crystal structure investigations can be obtained from the Fachinformationszentrum Karlsruhe, D-76344 Eggenstein-Leopoldshafen, on quoting the depository number CSD-401509.
[6] M. Creswick, I. Bernal, W. A. Herrmann, *J. Organomet. Chem.* **1979**, *172*, C39–42.
[7] K. Folting, J. C. Huffman, L. N. Lewis, K. G. Caulton, *Inorg. Chem.* **1979**, *18*, 3483–3486.
[8] U. Schubert, U. Kirchgässner, J. Grönen, H. Piana, *Polyhedron* **1989**, *8*, 1589–1593.
[9] E. Colomer, R. P. Corriu, C. Marzin, A. Vioux, *Inorg. Chem.* **1982**, *21*, 368–373.
[10] H. Nöth, H. Schick, W. Meister, *J. Organomet. Chem.* **1964**, *1*, 401–410.
[11] W. Biffar, H. Nöth, H. Pommerening, *Angew. Chem.* **1980**, *92*, 63–64; *Angew. Chem. Int. Ed. Engl.* **1980**, *19*, 56–57.
[12] B. A. Frenz, The ENRAF-NONIUS CAD4-SDP – a Real-Time System for Concurrent X-Ray Data Collection and Crystal Structure Determination (*Computing in Crystallography* (Eds.: H. Schenk, R. Olthof-Hazekamp, H. van Koningsveld, G. C. Bassi), Delft University), SDP-PLUS, Version 1.1, **1984** and VAXSDP, Version 2.2, **1985**.
[13] A. C. T. North, D. C. Phillips, F. S. Mathews, *Acta Crystallogr. Sect. A* **1968**, *24*, 351–359.

Corrigenda

The original title of the communication by G. Pampaloni et al., *Angew. Chem. Int. Ed. Engl.* **1994**, *33*, 1188, was shortened by the editorial office; it should read: $[Zr_3Cp_2(O_2CNiPr_2)_6(\mu_3\text{-}O)(\mu_2\text{-}CCO)]$, the First Crystallographically Established Ketenylidene Complex Obtained by a Metal-Assisted Deoxygenation of Carbon Monoxide; A Model for CO Reductive Cleavage on Metal Surfaces.

In the review article "Organometallic Compounds for Nonlinear Optics—The Search for En-light-enment!" by N. J. Long (*Angew. Chem. Int. Ed. Engl.* **1995**, *34*, 21–38) the β values for two compounds should be replaced by more recently published values. While the review was in press an article appeared in *SPIE*, Vol. 2143, pp. 14–19, in which the values quoted in the review from ref. [55] were corrected by the original authors. The β values of the complex ions $[(CN)_5Ru(\mu\text{-}CN)Ru(NH_3)_5]^-$ and $[(C_5H_5)Ru(PPh_3)(\mu\text{-}CN)Ru(NH_3)_5]^{3+}$ originally reported were found to be too large by a factor of six.

 © VCH Verlagsgesellschaft mbH, D-69451 Weinheim, 1995

For the practical application of molecules in nonlinear optics the reader can turn to Zyss and Chemla: *Nonlinear Optical Properties of Molecules and Crystals*, to Prasad and Williams: *Introduction to Nonlinear Optical Effects in Molecules and Polymers*, or to the many review articles on the subject—but read Wagnière's book first. Similarly, the *Introduction to Nonlinear Laser Spectroscopy* by Levinson and Kano would be a good port of call for the molecular spectroscopist.

Linear and Nonlinear Optical Properties of Molecules is competitively priced and should find its way onto the bookshelf of everyone working in molecular nonlinear optics or molecular spectroscopy in condensed phases. It is perhaps not the first book to turn to for a student entering the field, but will be invaluable when the time comes to construct a systematic framework for rationalizing and understanding the optical effects observable in molecular systems. The appendices contain a wealth of useful formulas and relationships and will be of use even to experienced practitioners in the field.

Colin D. Bain
Physical Chemistry Laboratory
University of Oxford
Oxford (United Kingdom)

Modern Medicinal Chemistry. (Ellis Horwood Series in Pharmaceutical Technology.) By *J. B. Taylor* and *P. D. Kennewell*. Ellis Horwood, New York, 1993. 290 pp., paperback $ 42.50.—ISBN 0-13-590399-8

Developments in medicinal chemistry have proceeded very rapidly in recent years as a result of the enormous advances in organic chemistry, biochemistry, molecular biology, physiology, and computer technology. It is doubtless for this reason that the authors of the book *Introductory Medicinal Chemistry*, which appeared 13 years ago, have now produced an updated version.

The present book contains five chapters: 1. Introduction; 2. The Pharmaceutical Phase; 3. The Pharmacokinetic Phase; 4. The Pharmacodynamic Phase; 5. Drug Discovery Processes. Chapter 1 contains a brief outline of the historical development of medicinal chemistry, illustrated by some examples of pharmacologically active agents. The authors discuss industrial and commercial aspects of the development of pharmaceutical products, and the relationship between the pharmaceutical industry and the legislators. Chapter 2 describes in detail the various forms in which pharmaceutical preparations are administered and the different types of applications. Chapter 3 then deals with the processes whereby active substances are absorbed and distributed, and their clearance, biotransformation, and metabolization, including the physicochemical and biochemical principles involved. The simple diagrams that are provided here as an aid to readers unfamiliar with anatomical terms are especially useful. Chapter 4 begins with an introduction to cell and membrane structure, then discusses receptor theories and kinetic and thermodynamic aspects of the interaction between ligands and receptors. Throughout the discussions much space is devoted to the relevant enzymes and their different types of inhibitors. Examples of particular enzyme inhibitors and the mechanisms whereby they function are briefly described. In Chapter 5 the authors describe the process of drug discovery, the basic principles of drug design, and some representative methods. Lastly they discuss the process of optimization starting from lead structures.

The book is mainly intended for undergraduate students of chemistry and pharmacology. On the whole it is well written and illustrated, and contains a good presentation of the general principles of pharmacology. However, there are some weaknesses. For example, not enough emphasis is given to the role of organic chemistry. The representation of chemical structures is not clear and consistent, and stereochemical details are often ignored or shown wrongly [e.g., compare the formulas of vitamin C (p. 13), tetramisol (p. 18), and L-dopa (p. 19)]. The definition of a non-competitive antagonist on page 126 is incorrect. The development of ligands for membrane receptors is scarcely mentioned. The description of the development of enzyme inhibitors is difficult to understand without previous specialist knowledge. Instead of the large number of examples given here, with the inevitable consequence that the principles involved are treated only superficially, it would have been better to discuss fewer examples in greater detail.

Athanassios Giannis
Institut für Organische Chemie
und Biochemie
der Universität Bonn (FRG)

 © VCH Verlagsgesellschaft mbH, D-69451 Weinheim, 1995 0570-0833/95/0707-0828 $ 10.00+.25/0

New Books

Nucleophilic Aromatic Substitution of Hydrogen. By **O. N. Chupakhin et al.** Academic Press, San Diego, **1994.** 367 pp., hardcover, $ 95.00.—ISBN 0-12-174640-2

Aufgaben zur Bioreaktionstechnik. By **K.-H. Wolf.** Springer, Heidelberg, **1994.** 302 pp., paperback, DM 49.80.—ISBN 3-540-57876-5

Lecture Notes in Quantum Chemistry II. Edited by **B. O. Ross.** Springer, Heidelberg, **1994.** 340 pp., paperback, DM 90.00.—ISBN 3-540-58620-2

Resorcinol. Its Uses and Derivatives. (Topics in Applied Chemistry). By **H. Dressler.** Plenum Press, New York, **1994.** 500 pp., hardcover, $ 115.00.—ISBN 0-306-44850-5

Photoelectron Spectroscopy. (Springer Series in Solid State Sciences 82). By **S. Hüfner.** Springer, Heidelberg, **1994.** 511 pp., hardcover, DM 168.00.—ISBN 3-540-19108-9

From the Lab into the World. A Pill for People, Pets and Bugs. By **C. Djerassi.** American Chemical Society, Washington, **1994.** 230 pp., hardcover, $ 24.95.—ISBN 0-8412-2808-6

Chemistry - An Experimental Science 2/e. Edited by **G. M Bodner/H. L. Pardue.** Wiley, Chichester, Great Britain, **1994.** 983 pp., paperback, £ 24.95.—ISBN 0-471-30571-5

Inorganic Experiments. Edited by **J. D. Woollins.** VCH, Weinheim, **1994.** 286 pp., hardcover, DM 148.00/$ 90.00. ISBN 3-527-29235-7

Spreadsheets for Chemists. By **G. Filby.** VCH, Weinheim/New York, **1994.** 408 pp., hardcover, DM 98.00/$ 60.00. ISBN 3-527-28570-9

Ion Chromatography. 2nd Ed. By **J. Weiss.** VCH, Weinheim/New York, **1994.** 464 pp., hardcover, DM 164.00/95.00. ISBN 3-527-28698-5

Dictionary of Gene Technology. By **G. Kahl.** VCH, Weinheim/New York, **1994.** 550 pp., hardcover, DM 184.00/90.00. ISBN 3-527-30005-8

Medizinische Chemie. By **R. B. Silverman.** VCH, Weinheim, **1994.** 440 pp., paperback, DM 68.00.—ISBN 3-527-29092-3

Density-Functional Theory of Atoms and Molecules. (International Series of Monographs on Chemistry, Vol. 16). By **R. G. Parr, W. Yang.** Oxford University Press, Oxford, **1995.** 333 pp., paperback, £ 25.00.—ISBN 0-19-509276-7

Analytiker Taschenbuch, Vol. 12. By **H. Günzler et al.** Springer, Heidelberg, **1994.** 332 pp., hardcover, DM 148.00. ISBN 3-540-57754-8

Radical Chemistry. (Ellis Horwood Series in Organic Chemistry). By **M. J. Perkins.** Ellis Horwood, New York, **1994.** 182 pp., paperback, $ 18.00.—ISBN 0-13-320920-2

Analytical Chemistry of Synthetic Colorants, Vol. 2. Edited by **A. T. Peters, H. S. Freeman.** Chapman & Hall, London, **1994.** 224 pp., hardcover, £ 75.00.—ISBN 0-7514-0208-7

Electrophoresis of Enzymes. By **G. M. Rothe.** Springer, Heidelberg, **1994.** 307 pp., hardcover, DM 98.00.—ISBN 3-540-58114-6

Advanced Composite Materials. By **L. A. Pilato.** Springer, Heidelberg, **1994.** 208 pp., hardcover, DM 138.00. ISBN 3-540-57563-4

Glass Chemistry. 2nd Ed. By **W. Vogel.** Springer, Heidelberg, **1994.** 464 pp., hardcover, DM 148.00.—ISBN 3-540-57572-3

Inorganic Chemistry of Main Group Elements. By **B. King.** VCH, New York, **1995.** 326 pp., hardcover, DM 115.00, $ 75.00.—ISBN 1-56081-679-1

Biological Exposure Values for Occupational Toxicants and Carcinogens. Critical Data Evaluation for BAT and EKA Values. Ed. by **D. Henschler, G. Lehnert.** VCH, Weinheim/New York, **1994.** 235 pp., hardcover, DM 158.00, $ 95.00 (subscription price: DM 115.00/$ 70.00).—ISBN 3-527-27032-9

Odors and Deodorization in the Environment. Edited by **G. Martin, P. Laffort.** VCH Weinheim/New York, **1994.** 486 pp., hardcover, DM 235.00, $ 145.00.—ISBN 1-56081-666-X

Vom Wasser. Edited by **Gesellschaft Deutscher Chemiker.** VCH, Weinheim/New York, **1994.** 459 pp., hardcover, DM 278.00.—ISBN 3-527-28651-9

Progress in Heterocyclic Chemistry, Vol. 6. Edited by **H. Suschitzky, E. F. V. Scriven.** Elsevier, Oxford, **1994.** 352 pp., hardcover, £ 95.00.—ISBN 0-08-042086-9

Binuclear Compounds 1, 8th Ed. Edited by **GMELIN Institute for Inorganic Chemistry.** Springer, Berlin, **1994.** 542 pp., hardcover, DM 3200.00.—ISBN 3-540-93695-5

Compounds with Germanium-Hydrogen Bonds, 8th Ed. Edited by **U. Krüerke, C. Siebert, B. Wöbke.** Springer, Berlin, **1994.** 364 pp., hardcover, DM 2200.00.—ISBN 3-540-93696-3

Non-Electronic Applications of Silicon Nitride. SiNx. SiNx:H, 8th Ed. Edited by **F. Schröder, W. Kurtz.** Springer, Berlin, **1994.** 386 pp., hardcover, DM 2375.00.—ISBN 3-540-93693-9

Compounds with Br, I, the Chalcogens (S, Se, Te, Po), B, and C, 8th Ed. Edited by **R. Keim, B. Schwager.** Springer, Berlin, **1994.** 367 pp., hardcover, DM 2290.00.—ISBN 3-540-93694-7

Ferrocenes. Homogeneous Catalysis. Organic Synthesis. Materials Science. Edited by **A. Togni, T. Hayashi.** VCH, Weinheim/New York, **1995.** 540 pp., hardcover, DM 248.00, $ 145.00. ISBN 3-527-29048-6

Industrial Color Testing. Fundamentals and Techniques. By **H. G. Völz.** VCH, Weinheim/New York, **1995.** 377 pp., hardcover, DM 198.00, $ 115.00.—ISBN 3-527-28643-8

Spectroscopy in Catalysis. By **J. W. Niemantsverdriet.** VCH, Weinheim/New York, **1995.** 288 pp., paperback, DM 78.00, $ 45.00.—ISBN 3-527-28726-4

Process Scale Liquid Chromatography. Edited by **G. Subramanian.** VCH, Weinheim/New York, **1995.** 225 pp., hardcover, DM 178.00, $ 105.00.—ISBN 3-527-28672-1

Automotive Paints and Coatings. Edited by **G. Fettis.** VCH, Weinheim/New York, **1995.** 240 pp., hardcover, DM 220.00, $ 130.00.—ISBN 3-527-28637-3.

GC für Anwender. By **W. Gottwald.** VCH, Weinheim, **1995.** 284 pp., paperback, DM 58.00. ISBN 3-527-28681-0

NMR-Spektroskopie für Anwender. By **W.-D. Herzog, M. Messerschmidt.** VCH, Weinheim, **1995.** 194 pp., paperback, DM 58.00.—ISBN 3-527-28690-X

Qualität im analytischen Labor. Qualitätssicherungssysteme. Maßnahmen zur Qualitätssicherung. Der ganzheitliche Qualitätsgedanke. Edited by **S. Kromidas.** VCH, Weinheim, **1995.** 392 pp., DM 118.00.—ISBN 3-527-28683-7

Safety in the Chemistry and Biochemistry Laboratory. By **A. Picot, P. Grenouillet.** VCH, Weinheim/New York, **1995.** 318 pp., hardcover, DM 98.00, $ 60.00.—ISBN 1-56081-040-8

Computational Chemistry Using the PC. Second Edition. By **D. W. Rogers.** VCH, Weinheim/New York, **1994.** 247 pp., hardcover, DM 98.00, $ 65.00. ISBN 1-56081-672-4

Diplom- und Doktorarbeit. 2nd Ed. Anleitungen für den naturwissenschaftlich-technischen Nachwuchs. By **H. F. Ebel, C. Bliefert.** VCH, Weinheim, **1994.** 227 pp., paperback, DM 41.00, $ 25.00.—ISBN 3-527-30060-0

Phosphorus-31 NMR Spectral Properties in Compound Characterization and Structural Analysis. Edited by **L. D. Quin, J. G. Verkade.** VCH, Weinheim, New York, **1994.** 450 pp., hardcover, DM 260.00, $ 150.00.—ISBN 1-56081-637-6

PCR. By **C. R. Newton, A. Graham.** Spektrum Akademischer Verlag, Heidelberg, **1994.** 206 pp., paperback, DM 39.80.—ISBN 3-86025-236-4

Gas Extraction. An Introduction to Fundamentals of Supercritical Fluids and the Application to Separation Processes. By **G. Brunner** (Topics in Physical Chemistry. Vol. 4). Steinkopff, Darmstadt, **1994.** 387 pp., hardcover, DM 44.80.—ISBN 3-7985-0944-1

Opportunities for Innovation: Biotechnology. Edited by **R. M. Busche et al.** Technomic Publishing AG, Basel, **1994.** 273 pp., paperback, SFr 67.00. ISBN 1-56676-253-7

Cyclophanes. By **E. Weber** (Topics in Current Chemistry. Vol. 172), Springer, Heidelberg, **1994.** 98 pp., hardcover, DM 178.00.—ISBN 3-540-58257-6

Multivariate Datenanalyse. Methodik und Anwendung in der Chemie und verwandten Gebieten. By **R + G. Henrion.** Springer, Heidelberg, **1994.** 261 pp. hardcover, DM 128.00. ISBN 3-540-58188-X

Free Radicals in Organic Chemistry. By **J. Fossey, D. Lefort, J. Sorba.** Wiley, Chichester, **1994.** 350 pp., hardcover, £ 45.00/paperback, £ 19.95.—ISBN 0-471-95495-0/0-471-95496-9

Organic Reactions. Logic and Simplicity. By **P. Laszlo.** Wiley, Chichester, **1995.** 736 pp., hardcover, £ 60.00/paperback, £ 24.95.—ISBN 0-471-93933-1/0-471-95278-8

Fluorine-Containing Amino Acids. Synthesis and Properties. Edited by **V. P. Kukhar, V. A. Soloshonok.** Wiley, Chichester, **1994.** 400 pp., hardcover, £ 90.00. ISBN 0-471-95203-6

Stereoselective Synthesis. By **R. S. Atkinson.** Wiley, Chichester, **1995.** 550 pp., hardcover, £ 85.00/paperback, £ 29.95.—ISBN 0-471-95250-8/0-471-95419-5

Monosaccharides. Their Chemistry and Their Roles in Natural Products. By **P. M. Collins, R. J. Ferrier.** Wiley, Chichester, **1995.** 400 pp., hardcover, £ 50.00/paperback, £ 18.95. ISBN 0-471-95342-3/0-471-95343-1

Monoterpenoid Indole Alkaloids. Supplement to Vol. 25, Part 4. By **J. E. Saxton.** Wiley, Chichester, **1994.** 860 pp., hardcover, £ 175.00.—ISBN 0-471-95112-9

Text and Graphics in the Electronic Age. Desktop Publishing for Scientists. By **W. E. Russey, C. Bliefert, C. Villain.** VCH, Weinheim/New York, **1995.** 359 pp., paperback, DM 84.00/$ 50.00.—ISBN 3-527-28519-9

Molecular Crystals. 2nd Ed. By **J. D. Wright.** Cambridge University Press, Cambridge **1995.** 221 pp., paperback, £13.95. ISBN 0-521-47730-1

Reviews on Analytical Chemistry - Euroanalysis VIII. Edited by **D. Littlejohn, D. Thorburn Burns.** Royal Society of Chemistry, Cambridge. **1994.** 366 pp., hardcover, £ 75.00.—ISBN 0-85186-982-3

Advanced Practical Organic Chemistry. 2nd Ed. By **J. Leonard, B. Lygo, G. Procter.** Chapman & Hall, Glasgow, **1995.** 298 pp., paperback, £ 19.99. ISBN 0-7514-0200-1

Model Reactions for Photosynthesis—Photoinduced Charge and Energy Transfer between Covalently Linked Porphyrin and Quinone Units

Harry Kurreck* and Martina Huber

Dedicated to Professor Fabian Gerson

Photosynthesis is one of the fascinating fields of current interdisciplinary research. It seems miraculous that nature, in the process of evolution, has managed to bring about the process of photosynthesis. The first step involves a charge separation at the reaction centers, which proceeds with 100% quantum yield from the photoexcited singlet state of the bacteriochlorophyll donor, despite the fact that the wasteful deactivation of the electron into the ground state should be highly favored. Biomimetic model compounds (that is, those which resemble the pigments nature has developed) have been constructed from porphyrins and quinones. These model systems have allowed the study of the factors contributing to the highly efficient charge separation. This report focuses on recent developments in the study of electron transfer in porphyrinoquinones. Some of the results of these investigations may not be not fully understood and are often the subject of controversial discussions.

Keywords: electron transfer · energy transfer · photosynthesis · porphyrins · quinones

1. Introduction

Life has been present on earth for over three billion years. In the process of evolution the development of photosynthesizing organisms (bacteria) represented an enormous step.[1, 2] A billion years later the development of plant photosynthesis with the two photosystems I and II provided the means by which a large part of the biosphere was created and maintained. Fundamental to photosynthesis is the reduction of CO_2 with the "weak", but abundant, reducing agent water, with concomitant formation of oxygen. However, even now, important new insights can be obtained by the study of photosynthetic bacteria that contain only one photosystem and therefore cannot split water, but require H_2S or inorganic acids as reducing agents.

From a chemical point of view life can be described as the ongoing interplay between animals and plants in terms of the Krebs and Calvin cycles, the most important cycles in the biosphere. The overall energy balance of these processes, which are driven by the literally life-giving sun, is endergonic.

The conversion of light energy into chemical energy, which has been optimized in the process of evolution, is a subject of interest not only in the area of basic research. The development of efficient, artificial photosynthetic systems for the conversion and storage of solar energy also requires a fundamental understanding of the processes that take place in natural photosynthesis. Such knowledge is also needed in herbicide research.[3]

A large number of coupled redox systems are involved in photosynthesis, in which the relationship between the various redox potentials plays a vital role. In order to understand the significance of sunlight to photosynthesis in this context, one must bear in mind that the ground and excited states of molecules can have drastically different redox potentials. In photosynthesis, the primary donor must first be photochemically promoted to an electronically excited state, which has appropriate electron-transfer (ET) characteristics. Porphyrins and their derivatives (chlorophyll, bacteriochlorophyll) with large π-electron systems are particularly well suited for this task, firstly because their molar extinction coefficient[*] is high, and secondly, because they absorb light over a wide spectral range. When one also takes into consideration other photosynthetically significant pigments (antenna systems), about 50% of the range of wavelengths of the radiation incident on the earth can be used photosynthetically. From a chemical point of view it is also important that the frequency range between UV and IR radiation is utilized, thus avoiding the possibility of photochemical bond cleavage by UV light on the one hand, and taking into account that IR radiation lacks the energy required to be photochemically significant.

In the photosynthetic reaction centers (RCs) the choice and arrangement of the participating pigments ensures a "down-

[*] Prof. Dr. H. Kurreck, Dr. M. Huber
Institut für Organische Chemie der Freien Universität
Takustrasse 3, D-14195 Berlin (Germany)
Telefax: Int. code + (30) 838-4248

[*] According to the most recent IUPAC recommendations the term molar absorption coefficient should be used.

 © VCH Verlagsgesellschaft mbH, D-69451 Weinheim, 1995 0570-0833/95/0808-0849 $ 10.00+.25/0

hill" ET. After excitation (by light) of the donor (the "special pair"—a dimer of bacteriochlorophyll (BChl) molecules, see Fig. 1), an electron is transferred stepwise via the intermediate bacteriopheophytin acceptor (BPh) to the primary and secondary quinone acceptors. In the first charge-separation step the electron is rapidly (in about 3 ps) transferred a large distance (17 Å) from the singlet photoexcited state of the special pair to the pheophytin. The role of the additional BChl molecule (the "extra-bacteriochlorophyll") in this transfer (that is, whether there is a short-lived intermediate state ($BChl_2^{+}BChl^{\bullet -}$), or whether the BChl contributes as a superexchange mediator[4]) is currently the subject of controversial discussions.[5] The results of a recent study favor the former interpretation, namely that the extra-bacteriochlorophyll in fact serves as an intermediate in the ET, that is, as a transient radical anion.[6] Investigation of the RCs of *Rhodobacter sphaeroides* with polarized light using sub-picosecond absorption spectroscopy revealed the existence of the extra-bacteriochlorophyll anion with a half-life of 0.9 ps. This species exhibited a marked dichroism. The stepwise ET via extra-bacteriochlorophyll appears therefore to be confirmed.

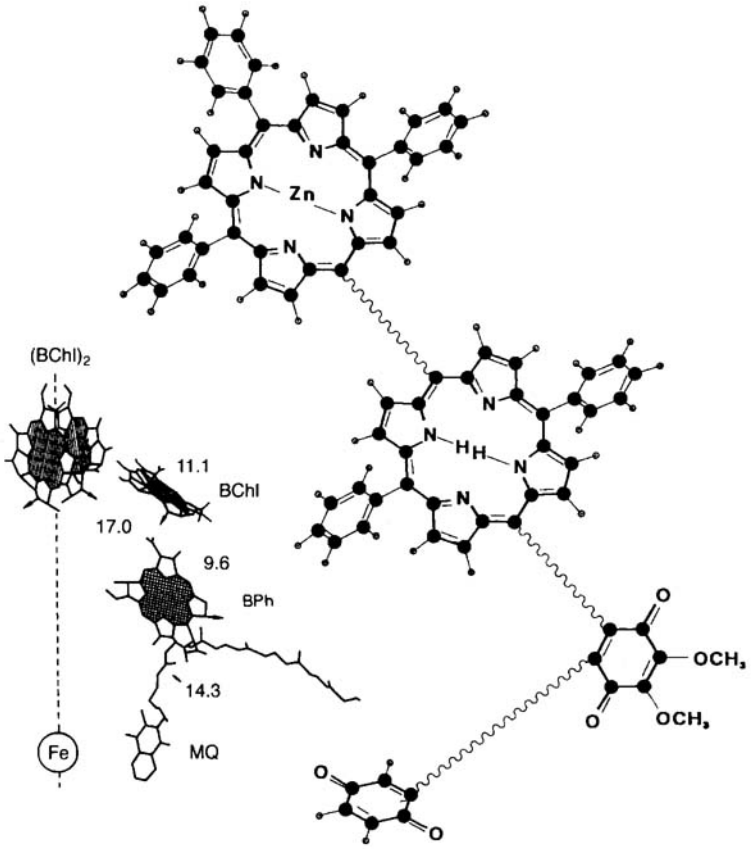


Fig. 1. Idealized model tetrad, consisting of a Zn-containing porphyrin and a free-base porphyrin, a ubiquinone(0) derivative, and a quinone. The redox potentials of the individual redox-active components provide a "downhill" cascade for the ET. On the left the arrangement of the pigments in a natural reaction center (only the photosynthetically active L or A branch of *Rhodopseudomonas viridis*) is depicted for comparison (cf. [8]); $(BChl)_2$: bacteriochlorophyll dimer ("special pair"); BChl: extra-bacteriochlorophyll; BPh: bacteriopheophytin; MQ: menaquinone. The numbers give the center-to-center distance of the pigments in Å.

Quinones appear to be predestined to be electron acceptors in nature for a variety of reasons: a) they possess suitable redox potentials, b) they can be converted stepwise into stable reduction products (hydroquinones) via the semiquinones, c) they can form hydrogen bonds, and undergo protonation/deprotonation reactions with ease, and finally, d) they are relatively small mobile molecules that can shuttle redox equivalents to the quinone pool.

Current research into the primary reactions of photosynthesis can be divided into two areas: on the one hand, the cultivation, isolation and, where possible, crystallization of natural plant or bacterial photosynthetic systems (for example, the reaction centers), and on the other, the development (that is, synthesis) of biomimetic model compounds. Model compounds have the advantage that specific properties of the complex ET reactions can be tuned by designing and preparing suitable organic molecules consisting of donor(s), bridge(s), and accep-

Harry Kurreck, born in 1932 in Halle/Saale, obtained his doctorate at the Freie Universität (FU) Berlin. He completed his habilitation in 1970 on the subject of triplet ground states and excited states in the cyclopentadienyl system. Since 1970 he has been Professor at the Institut für Organische Chemie der FU Berlin. His priority research topic is EPR/ENDOR studies on paramagnetic organic and bioorganic systems. In recent years he has concentrated in particular on the synthesis of model compounds for photosynthesis with the aim of making a contribution to the understanding of the primary step in photosynthesis by applying stationary and time-resolved optical spectroscopy and magnetic resonance methods.



H. Kurreck



M. Huber

Martina Huber, born in 1961 in Heidelberg, studied chemistry in Berlin, completing her doctorate there in 1989 with a thesis on electron transfer in biomimetic model compounds. During the two years of her subsequent postdoctorate period with Professor G. Feher (University of California San Diego, USA) she studied the electronic structure of primary electron donors of photosynthesizing bacteria. In addition she was involved in the X-ray structure analysis of modified reaction centers. Since 1991 she has worked on her habilitation at the FU Berlin on a thesis on magnetic resonance spectroscopy of single-crystal reaction centers of photosynthesizing bacteria.

tor(s). The synthesis of such model compounds should stimulate new insights into the ET mechanism, the final goal being the synthesis of compounds in which a rapid and highly efficient forward reaction (charge separation) can take place, which, combined with a slow back reaction, results in a long-lived, charge-separated state.

Our report focuses on model compounds that closely resemble the natural pigments of the reaction centers. Covalently linked porphyrin dimers and oligomers model the special pair of the reaction center and the light-collecting function of the antennae. Porphyrins and quinones have likewise proved to be particularly attractive in the study of ET phenomena. Figure 1 compares an idealized model compound, a "tetrad",[10] with the arrangement of pigments in a bacterial reaction center, as deduced from X-ray crystal structure analysis.[7-9]

Static and time-resolved optical and magnetic resonance spectroscopic methods have been applied to the identification and characterization of these systems. For the study of ET processes, time-resolved spectroscopy is indispensable. Since there are already several pertinent reviews on this subject,[11-14] we will focus on the current problems and trends in this area of research, using selected examples. For a better understanding of the ET process, a general outline of the ET theory will be presented in a phenomenological form, with particular emphasis on the Marcus theory,[15-22] the significance of which was underlined by the award of the Nobel Prize to R. A. Marcus in 1992.[23]

2. Theory of Electron Transfer

The following is a short synopsis of the theoretical basis of the rate of ET processes, insofar as it is necessary for the understanding of the experimental observations (for the presentation of fundamental theory and advanced methods of approximation, see refs. [19, 24-28]). Firstly, the case of diabatic[29] ET, characterized by a weak electronic coupling between donor and acceptor, will be discussed to introduce the relevant parameters, and secondly, the limits of the diabatic approximation and the formulation of adiabatic ET will be considered.

For diabatic ET, Fermi's golden rule applies, which describes the probability of radiationless transitions [Eq. (a)].[30] V_{DA} is

$$k_{ET} = \frac{2\pi}{\hbar} V_{DA}^2 F_{FC} \qquad (a)$$

the electronic matrix element, F_{FC} the Franck–Condon factor (more precisely, the squared overlap integral of the vibrational wave functions weighted by the Boltzmann distribution).

Franck–Condon Factor F_{FC}

Marcus provided an expression on the basis of a classical approximation, which according to modern quantum mechanical interpretation, can be identified with one part of the Franck–Condon term.[15-18] In the Marcus approximation the electronic states of the system consisting of donor and acceptor are represented by parabolic functions both before (D–A) and after (D^+–A^-) the ET (Fig. 2, D–A corresponds to ^{S*}P-S-Q, D^+–A^- to $P^{\bullet+}$-S-$Q^{\bullet-}$).[31] The position of the two parabolas relative to each other is completely described by two parameters: the standard free energy of reaction ΔG^0,[*] and the reorganization energy λ. Since allowed transitions between the electronic states can only occur where the parabolas cross, the free energy of activation $\Delta G^{\ddagger}$ can be calculated from ΔG^0 and λ (see Fig. 2). From this, the expression (b) for ET rates, given by

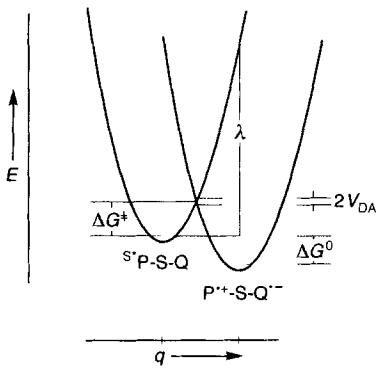


Fig. 2. Representation of the energy hypersurfaces for ET reactions in the context of the Marcus approximation. The potential energy of ^{S*}P-S-Q (porphyrin P in the singlet excited state, quinone Q in the ground state) and $P^{\bullet+}$-S-$Q^{\bullet-}$ (state after ET from P to Q) is shown as a function of the nuclear coordinate q. ΔG^0 is the standard free energy of reaction, $\Delta G^{\ddagger}$ is the free energy of activation, which can be calculated from ΔG^0 and λ (the reorganization energy). V_{DA}: electronic matrix element; V_{DA} is related to the splitting of the energy hypersurfaces in the transition region. For large values of V_{DA} the energy levels are split in such a way that the limiting case of adiabatic ET can be reached (modified from J. Schlüpmann, *Dissertation*, Freie Universität Berlin, **1992**).

$$k_{ET} = \kappa\, e^{-\frac{(\Delta G^0 + \lambda)^2}{4\lambda k_B T}} \qquad (b)$$

Marcus, is obtained. k_B is the Boltzmann constant, T the absolute temperature and κ a proportionality constant. The exponential dependence of the rate k_{ET} on $\Delta G^{\ddagger}$ corresponds to the approach of Eyring; the interpretation of κ will be considered in greater detail below [see Eq. (c)].

For exergonic reactions, that is, those where $\Delta G^0 < 0$, the ET rate increases with increasing exergonicity, reaches a maximum at $-\Delta G^0 = \lambda$, and decreases again for very negative ΔG^0 ("energy gap law"; this is the inverted region). It took approximately twenty years to verify this prediction of Marcus by experiment[32] (see also ref. [22]). Subsequently, the inverted region was also detected in ET studies of porphyrin–quinone model compounds.[33, 34]

Interestingly, the quantum mechanical derivation of the rates of ET reactions leads to an expression [Eq. (c)] that is very similar to that derived from Marcus Theory,[35] (see, for example, ref. [36]). Thus, κ in Equation (b) can be interpreted as a combination of the prefactor of the Franck–Condon factor [penultimate term in (c)] and V_{DA}, the electronic matrix element.

$$k_{ET} = \frac{2\pi}{\hbar} V_{DA}^2 \frac{1}{\sqrt{4\pi\lambda k_B T}} e^{-\frac{(\Delta G^0 + \lambda)^2}{4\lambda k_B T}} \qquad (c)$$

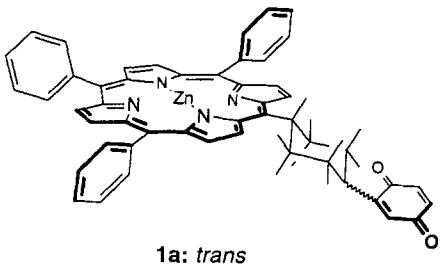
[*] The term Gibbs energy has been suggested for G.

Electronic Matrix Element V_{DA}

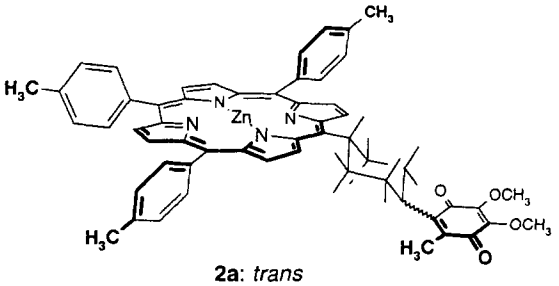
The electronic matrix element describes the probability of electronic transition between the energy hypersurfaces of reactant and product (Fig. 2). A commonly used approximation is Equation (d),[37, 38] where S_{DA} is the overlap integral of the elec-

$$V_{DA} = KS_{DA} \quad \text{(d)}$$

tronic wave functions (in general, molecular orbitals) and K is a proportionality factor whose magnitude depends on the system investigated. To a first approximation S_{DA} is calculated as the overlap integral between the molecular orbital occupied by the electron to be transferred and the molecular orbital of the acceptor into which it is transferred. Such an approach was used for a porphyrin–quinone model compound (**1a**).[39, 40] The exponential decay of the wave function with increasing internuclear distance leads to an exponential decrease in rate with increasing distance between D and A. V_{DA}, however, also depends on the relative orientation of D and A.[39, 41] Compounds like **1a, b** with a cyclohexanediyl bridge and diffferent acceptors, as in **2a, b**, were studied thoroughly by spectroscopic methods (see Section 4).



1a: *trans*
1b: *cis*



2a: *trans*
2b: *cis*

The "medium" between D and A can similarly contribute to the magnitude of V_{DA}. Of particular significance for model compounds are the bridge and possibly also solvent molecules. In bacterial reaction centers, for example, aromatic amino acid residues of the protein and the monomeric bacteriochlorophyll (BChl, Fig. 1) that lies between the primary electron donor $(BChl)_2$ and BPh, have been discussed as possible mediators in the ET process (cf. Section 1). One possible way in which the medium can participate in the ET process is provided by the superexchange mechanism. According to this mechanism, the MOs of the medium participate in the ET, thus facilitating it, although the state in which the electron (or the hole) is situated on the bridge is not considered an intermediate state (in the sense of a kinetic intermediate). Quantum mechanically, this participation can be described by an equation of the form (e),

$$V_{DA} = V^0_{DA} + (V_{DS}V_{SA})/\Delta E_{DS} \quad \text{(e)}$$

which can be derived from perturbation theory.[28] In this equation V^0_{DA} is the electronic matrix element corresponding to the direct interaction of D and A and V_{DS} and V_{SA} are the matrix elements of the interaction of the donor (D) or the acceptor (A) with the bridge orbitals (S). ΔE_{DS} is the difference in energy between the orbitals of D and S which take part in the ET. The influence of the bridge orbitals on V_{DA} thus depends not only on their electronic interaction (that is, in particular on whether their orientation to the relevant orbitals on D and A is favorable) but also whether they lie energetically close to the orbital on D. Also, the possibility of hole transfer must be considered as well as electron transfer. In other words both the LUMO and the HOMO of the bridge must be taken into account. Several quantum mechanical methods have been employed for the calculation of V_{DA} in this mechanism.[42, 43] In Section 4.1 an example of a possible superexchange mechanism in a model compound will be discussed.[44]

Diabatic and Adiabatic Electron Transfer

The use of Equation (a) assumes that the electronic matrix element is small (weak electronic interaction, corresponding, for example, to a large distance between D and A, a condition often fulfilled in biologically relevant ET processes) or that the probability of electronic transition is small compared to the rate of motion of the nuclei. This condition is not fulfilled in a couple of cases. 1) For strong electronic interactions the splitting of the energy levels is so large that each time the system reaches the transition region, ET takes place. Consequently, the reaction rate should be independent of V_{DA} and Equation (a) cannot be valid. 2) If the motion along a reaction coordinate (for example, a nuclear motion that is required for the ET, or solvent relaxation) is slow in comparison with the motion of the electron, it can control the rate of the whole process. For more detailed discussion of this area see, for example ref. [21] and particularly ref. [45].

To classify ET reactions, an adiabaticity parameter g has been defined [Equation (f)],[46, 47] where ω_C is the vibrational frequency characteristic of the slowest nuclear motion.[48] For $g \ll 1$, the reaction is considered to be diabatic, and when $g \gg 1$, the reaction is adiabatic. For adiabatic ET the rate constant is given by Equation (g) as quoted by Heitele.[21] The only new

$$g = 2\pi V^2_{DA}/\omega_C \hbar \lambda \quad \text{(f)}$$

$$k_{ET} = \frac{1}{\tau_L}\sqrt{\frac{\lambda}{16\pi k_B T}}\, e^{-\frac{(\Delta G^\circ + \lambda)^2}{4\lambda k_B T}} \quad \text{(g)}$$

parameter introduced here is τ_L, which is given by the equation $\tau_L = 1/\omega_C$.[48] As expected, the rate is independent of V_{DA}. Recently, however, Bixon and Jortner have discussed why this approximation may not hold for reactions in the inverted region and for $\Delta G^\ddagger = 0$.[49]

An example in which a transition from diabatic to adiabatic has been postulated is the reduction in rate of ET reactions of porphyrin–quinone model compounds in alcoholic solution, upon lowering the temperature (see Section 4.3).[50, 51] In this case the occurrence of the porphyrin triplet state and the observation of triplet products from the ET reaction at low temperatures has been interpreted as being due to a reduction in the ET rate from the singlet state, the dominant route of the reaction at room temperature. A slowing down of the reorientation of solvent molecules at or near the glass point of the alcohol, causing a transition from diabatic ET to adiabatic ET, has been postulated as the mechanism of the rate reduction. The relevant rate constant for this process, ω_C in Equation (f), is the longitudinal dielectric relaxation time τ_L of the solvent at a given temperature. As has been thoroughly discussed in [21], this relaxation time can be correlated with the Debye relaxation time of the solvent (τ_D), a parameter which is more easily determined experimentally (see, however, ref. [45]).

To illustrate the theoretically, and also practically, important interplay of the various parameters, their effect on k_{ET} will be discussed below.

Temperature Dependence of Rate of ET

The exponential term in Equations (b), (c), and (g) indicates that the temperature dependence of the rates should follow, to a first approximation, the Arrhenius equation. However, discrepancies can arise through, for example, a temperature dependence of the activation entropy ($\Delta S^{\neq}$). A special situation occurs for the case where $-\Delta G^0 = \lambda$, in which case $\Delta G^{\neq} = 0$ (Fig. 2), and the rate of ET is, according to the exponential term, independent of temperature. The proportionality of k_{ET} to $1/\sqrt{T}$, derived from the preexponential factor in Equation (c), would lead to a slight rate increase at lower temperatures.[52] For ET reactions in which $\Delta G^{\neq} \neq 0$, the $1/\sqrt{T}$ rate dependence should be less important than the exponential temperature dependence.

Besides these temperature dependencies, which are explicitly expressed in the equations, other implicit factors must be considered, in which the temperature influences one or other of the factors present in Equations (c) and (g). For example, a temperature-related change in the standard free enthalpy of reaction ΔG^0 can be caused by a change in the *static* dielectric constant of the solvent if the solvation of the charge-separated state changes as the temperature is varied. Temperature-dependent conformational changes in the D–A compound can also modulate V_{DA} and thereby k_{ET}. Naturally, the transition from diabatic to adiabatic ET described above is another consequence of change in temperature, which, in this case, has such a drastic influence that the ET rate has to be determined by a different set of molecular and/or local properties in different temperature ranges (cf. (c) and (g)). Further effects of temperature on solvent relaxation are discussed in refs. [45] and [53]. The possibilities mentioned here are expected to have widely varying effects depending on the model compound and the experimental conditions. A quantitative analysis of the temperature dependence, therefore, requires a consideration of all the possible factors involved.

Dependence of the Rate of ET on Distance

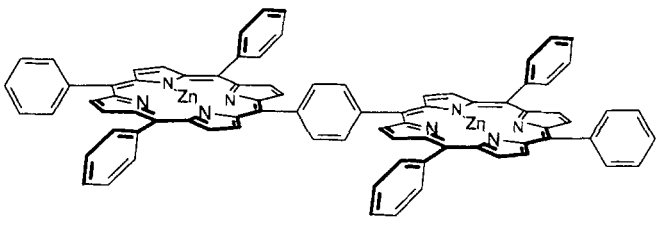
By far the largest influence of the donor–acceptor distance on k_{ET} comes from the exponential distance dependence of V_{DA}. Additionally, the donor–acceptor distance affects λ and ΔG^0.[54] A change in the distance dependence in this context is also expected from the superexchange mechanism, as discussed before.

Influence of the Solvent

The different means by which the solvent can influence k_{ET} have already been reported in detail.[21, 45, 53] One example that has already been treated here is the influence of the dielectric relaxation time (τ_L) on k_{ET}. The static dielectric constant of the solvent influences ΔG^0, particularly with respect to the solvation of the charge separated state $D^+ - A^-$. Finally, the high frequency dielectric constant (expressed by the refractive index n) affects the reorganization energy (more exactly, the external reorganization energy λ_0).[23]

3. Model Compounds, Syntheses, and Structures

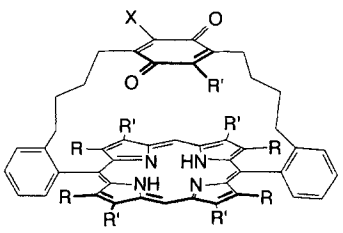
The design and synthesis of the porphyrin, and in particular the porphyrin–quinone system, is one of the more difficult tasks of synthetic organic chemistry. The preparation of model compounds of the type porphyrin–bridge–quinone (P-S-Q), can be carried out by the building block principle—for example, the retrosynthetic strategies P-S-Q⇒S-Q⇒Q or P-S-Q⇒P-S⇒S. Of these two possibilities, the first has been preferred by most workers. One can distinguish between targeted syntheses, where the alkylated porphyrins are generally constructed from dipyrromethanes and *a,c*-biladiene derivatives,[55, 56] and "one-pot" reactions in which, for symmetrically substituted, *meso*-arylated porphyrins, the appropriate aldehyde is treated with pyrrole; for the synthesis of unsymmetrical porphyrin derivatives (such as the "hybrid porphyrins"[57]) different aldehydes are treated with pyrrole. The very nature of the latter variant leads to a multitude of products that can be very difficult to separate. This results in yields as low as a few percent. Porphyrin dimers such as **3** can be synthesized from bisaldehydes; if the



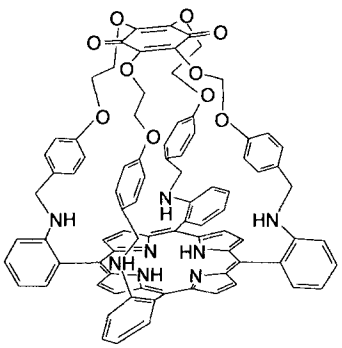
3

aldehyde contains the quinone component, or its (protected) precursor, P-S-Qs (or their precursors) can be formed.[58, 59] Particularly troublesome are those syntheses in which the molecule needs to display the characteristics that are especially desired for an investigation of the ET process—a rigid structure with defined geometry (in particular distance between, and rela-

tive orientation of donor and acceptor). Such properties are almost always achieved by the introduction of severe steric hindrance. Good examples of this type are the porphyrin–cyclophanes[60–63] such as **4** (with various substituents and substituent patterns)[64, 65] and **5**,[66, 67] in which the structural parameters can be varied in a specific manner by the use of different bridges. Recently reports have appeared on the synthesis of vertically stacked porphyrin–quinone–quinone and porphyrin–porphyrin–quinone cyclophanes. Such rigid molecules are suitable for the study of sequential electron transfers.[68]

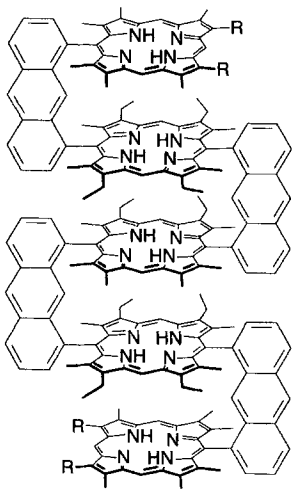


4



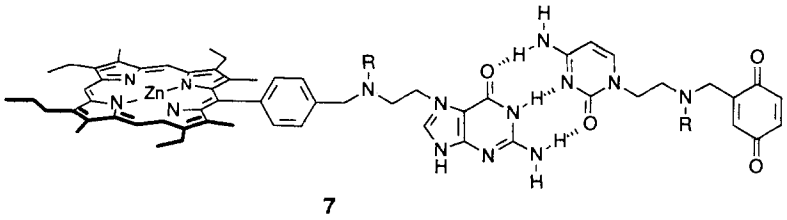
5

To simulate the stepwise ET pertinent to natural photosynthesis, model systems have been constructed that contain three or more covalently linked redox-active components.[11–14, 69] Vertically stacked porphyrins—structurally related to the porphyrinophanes mentioned above—such as **6** (R = $(CH_2)_5CH_3$) have also been synthesized, in which the porphyrin components are bonded in a *syn-peri* configuration by anthracene bridges.[70]



6

New, promising routes to the generation of well-defined model structures have recently been tested. Such methods had already been proposed, in particular by Rebek et al.,[71, 72] in connection with enantioselective complexation and for the modeling of synthetic receptors, and are based on the principle of molecular recognition. In this concept, covalent bond formation is replaced by noncovalent interactions such as, for example, H bonding.[73–75] Thus, an example of this approach would be first of all to link nucleobases, such as guanine and cytosine, covalently with porphyrins. Self-organization, as a consequence of Watson–Crick base pairing, allows the formation of defined porphyrin dimers or P-S-Qs. This principle was employed to prepare **7**, which contains stable hydrogen bonds analogous to the binding between complementary nucleic acid strands as in DNA and RNA. A related approach is the preparation of porphyrin dimers by self-organization of porphyrins with oppositely charged, peripheral substituents. These dimers are held together by electrostatic forces.[76, 77] Similarly, the use of crown ethers linked to quinone acceptors aims at the defined modification of model compounds without the use of covalent bonds.[78] The acceptor strength can be varied by complexation of the crown with different counterions. To investigate the influence of the extra-bacteriochlorophyll (cf. Fig. 1) on the ET between the special pair and the bacteriopheophytin, a rotaxane was synthesized that contained a crown-ether-like phenanthroline macrocycle sandwiched between two porphyrin units, each of which contained a different metal.[79]



7

Despite the impressive successes of preparative chemistry in synthesizing model compounds comprising multiple donors and acceptors, there still remains the challenging task of modifying the (seemingly more easily synthesized) diads in a specific way. The spectroscopic results obtained for diads can generally be more easily and clearly interpreted than those of triads, tetrads etc. Diad systems are, therefore, particularly well suited for the extension of our knowledge of the mechanism of the ET reactions.

4. Spectroscopic Investigations

An electron can be excited from the HOMO of the (porphyrin) donor into an antibonding MO by absorption of light of the appropriate frequency. The fate of the excited electron (until its eventual return to the ground state) is determined by the competition between internal conversion (IC), fluorescence, and spin–orbit-induced intersystem crossing (ISC). Furthermore, the charge- and energy-transfer processes of the specific chromophore and the properties of the quinone acceptor also have a role to play (cf. Fig. 3).[80] The relative contribution of each individual mode of decay is determined by the relative rates of each process. Spectroscopic methods enable the participating donors and acceptors to be studied in their ground and excited states, along with their spin states, spin dynamics, and the lifetimes of the transients. Extensively treated in the literature are optical methods such as fluorescence spectroscopy, transient absorption spectroscopy, resonance Raman spectroscopy, and magnetic resonance spectroscopy such as EPR spectroscopy and its extension to electron nuclear double resonance (ENDOR) and electron nuclear nuclear triple resonance (TRIPLE) spectroscopy. Pulsed EPR methods such as, for example, Fourier-transform (FT) and electron spin echo envelope modulation (ESEEM) are of increasing interest.[81] A review of the successfully applied new methods has appeared.[82]

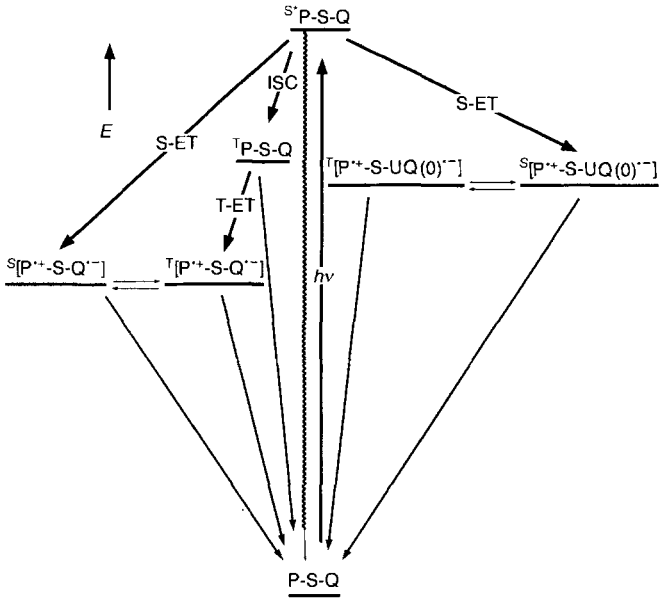


Fig. 3. Energy level diagram and reaction scheme for the photoexcitation of the *cyclohexanediyne-linked porphyrinquinones* **1** (P-S-Q) and **2** (P-S-UQ(0)) (that is, with a ubiquinone derivative as acceptor—the zero indicates that the oligoisoprenyl side chain is completely missing). The following symbols are used: ^{S*}P-S-Q and ^{S*}P-S-UQ(0) indicate the first singlet excited states of the porphyrin donor, ^{T}P-S-Q the triplet state of the porphyrin donor; singlet and triplet states of the charge-separated diradicals are labeled analogously. S-ET, T-ET symbolize singlet or triplet electron transfer, ISC selective spin–orbit intersystem crossing (the triplet ET path on the right hand side is not drawn). The wavy line represents the fluorescence decay of the singlet excited state. For estimates of the relative energy states, see [50, 51, 123]. P-S-UQ(0) and ^{S*}P-S-UQ(0) are not shown but assumed to be isoenergetic with the corresponding P-S-Q states.

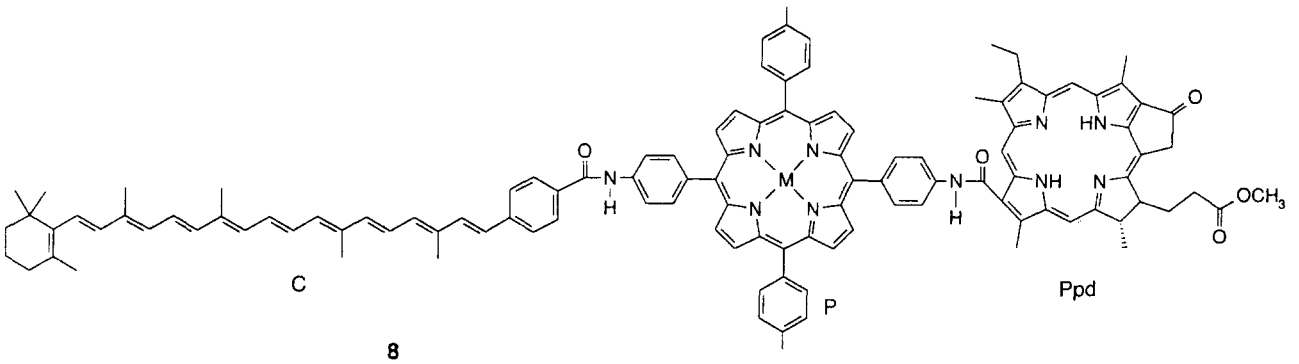
4.1 Optical Spectroscopy

As biologically active and extremely photoactive macrocycles with extended π-electron systems, the porphyrins display intense absorption bands in the visible and UV spectrum. For example, the Soret band has a molar extinction of about 100000. The four-orbital model, developed by Gouterman, has been extremely useful in the understanding of the optical properties of porphyrins .[83] Porphyrins and metalloporphyrins have relatively long-lived excited states, which makes them ideal precursors for subsequent reactions—for example ET. Additionally, porphyrins display a very effective ISC, which renders them capable of reactions arising from the triplet state.[84] It has been mentioned that the pigments relevant to photosynthesis are the partially hydrogenated porphyrins. These pigments, the chlorins and bacteriochlorins, are green rather than red, which is typical of the porphyrins. The origin of this difference in color is a destabilization of the π-electrons in the chlorins that raises the energy of the HOMO, but leaves the energy of one of the LUMOs practically unaltered.[85–87]

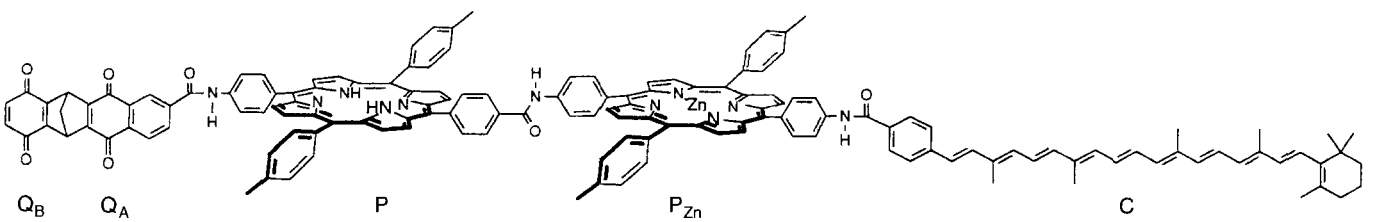
The potential of optical methods will now be demonstrated for the example of covalently linked porphyrins and later for porphyrins covalently bound to quinones (P-S-Qs).[88] Investigations into the possible participation of the bridge in the ET processes, for example within the framework of the superexchange mechanism (cf. Sections 1 and 2) will be discussed. This question is of interest in connection with the primary ET step in bacterial reaction centers, which involves the extra-bacteriochlorophyll (see Section 2). A possible function of the extra-bacteriochlorophyll in the other (inactive) pigment branch in the photosynthetic reaction centers is triplet energy transfer. The triad **8** has been chosen as representative example. Finally, the multistep energy and electron transfer of the complex pentad **9**, built up from a carotenoid (C), two porphyrins (P and P_{Zn}), and two quinones (Q_A and Q_B), will be described.

Covalently Linked Porphyrins

In photosynthetic organisms, light energy is first absorbed by a network of pigments—amongst others, (bacterio)chlorophylls in the light-collecting or antenna complexes. The light energy is then passed on further in rapid and vectorial energy transfer processes to the reaction center, where it initiates the

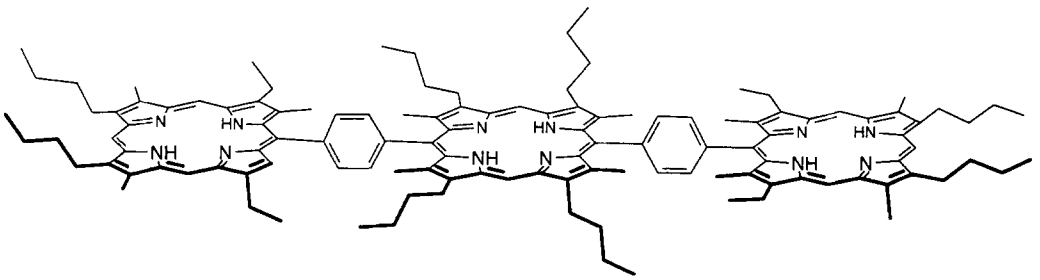


8



9

electron-transfer processes discussed in Section 2. In order to study the energy-transfer processes, porphyrins have been covalently linked in various ways, for instance as in the synthesis of complex systems such as **6**.[70] Sessler et al. have recently performed optical investigations on the porphyrin trimer **10**.[89] The absorption spectrum of **10** reveals that the absorption



10

bands in the visible range are broader than those of the corresponding monomer. This points to an excitonic interaction between the porphyrin units. The fluorescence quantum yield and lifetime of the excited singlet state are clearly reduced relative to those of the monomer. The radiationless quenching process responsible for this reduction cannot be explained by an increased ISC rate to the triplet state (which would also result in fluorescence quenching, see Fig. 3); rather it is attributed to an increase in the rate of IC. The lifetime of the triplet state is also substantially reduced. Obviously, the excitonic coupling favors the radiationless deactivation processes that couple the ground and excited states. In addition, through the coupling of **10** with quinone acceptors, the interplay of energy transfer within the trimer and electron transfer to the quinone could be studied.[89] The photophysical properties of sandwich-type porphyrin dimers, coupled through a lanthanide ion, were studied by very fast (on the femtosecond time scale) spectroscopy.[90] In these systems rapid radiationless deactivation processes were also observed. Of further interest is the observed wavelength-dependent variation in kinetics, which can be related to vibrational relaxation in the ps range.

Porphyrinquinones

When photoexcited into the S_1 state, porphyrin becomes a strong reducing agent, which has, for example, the ability to reduce quinones (compounds **1** and **2**) to semiquinones (cf. the energy level diagram in Figure 3). The effect of this ET can be observed with the naked eye, since solutions of these compounds do not visibly fluoresce at room temperature in contrast to solutions of tetraphenylporphyrinatozinc (ZnTPP) or the hydroquinoid forms of **1** and **2**. The fluorescence quenching results from intramolecular singlet-ET from the porphyrin to the quinone, which causes fast decay of the S_1 excited state of the former. This effectively reduces the lifetime of S_1.[40, 91]

The rate constant for the charge separation can be determined by picosecond fluorescence spectroscopy. The fluorescence decay can be measured by time-resolved single-photon counting[92] or with a synchroscan-streak-camera.[40, 93] In the case of **1**, the fluorescence decays monoexponentially over several lifetimes. The fluorescence decay curves for the metal-free P-S-Qs **1a** and **2a**, as well as those for their hydroquinoid derivatives, are shown in Figure 4. The difference between compounds with a hydroquinoid and a quinoid fragment can be clearly seen. Additionally, the more rapid decay of the excited state of **1a** relative to that of **2a** is recognizable. This difference is due to the smaller driving force of **2a** (that is, the less negative ΔG^0; ΔG^0 is related to the free energy of activation $\Delta G^{\neq}$, see Section 2)—cf. Figure 3. The more strongly negative reduction potential (by about 200–300 mV; measured by cyclic voltammetry[94]) makes the substituted quinones in **2a,b** poorer oxidants than the unsubstituted analogs **1a,b**. The incorporation of zinc into the porphyrin derivatives causes a drastic reduction in the lifetime of the singlet state of the porphyrin, which is partially brought about by an increase in the ET rate. This acceleration is to be expected, since the ET reaction is more strongly exergonic than for metal-free P-S-Q, and the reaction should lie in the "normal region", according to the nomenclature of Marcus.[40]

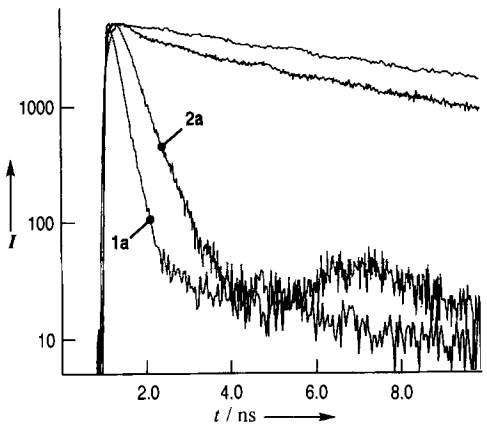


Fig. 4. Logarithmic representation of the fluorescence decay curve for the Zn-free P-S-Qs **1a** and **2a** (lower curves) and their hydroquinoid forms in CH_2Cl_2 at 295 K (upper trace: hydroquinone of **1a**). The more rapid fluorescence decay of **1a** is obvious. Simulations yield lifetimes for the excited states of 225 ps for **1a** and 360 ps for **2a** (ordinate: fluorescence intensity I in arbitrary units; abscissa: time t after the laser pulse) [91].

In a systematic study of a P-S-Q diad system, which strikingly illustrates the value of model studies, the dependence of the ET rates on the exergonicity ΔG^0 of charge separation and recombination was studied. This was achieved by variation of the solvent and the substituents (and thus the redox potential) of the quinone in such a way as to probe the normal and the inverted region of the Marcus curve (see Section 2).[95] According to this study, the rates of ET for charge separation and for charge recombination behave very differently with respect to variation in temperature or solvent polarity. In the systems investigated, the forward reaction should take place in the normal region of

the Marcus curve, whereas the back reaction (charge recombination) should lie in the inverted region. As expected, the value of k_{ET} for charge recombination becomes smaller with increasing exergonicity. Nevertheless, the temperature dependence of the rates in this range does not correspond to that predicted by Marcus theory. The temperature dependence of recombination in the range investigated (295 K to 193 K) is, in fact, distinctly less pronounced than that for charge separation, which lies in the normal region. It was thus suggested that charge separation and charge recombination have different mechanisms. The previously mentioned results of Bixon and Jortner (Section 2) are possibly of interest in this context.[49]

Staab et al. have studied the fluorescence behavior of porphyrinquinone–cyclophanes of the type **4**. They described the dependence of k_{ET} on the reduction potential of the acceptor components—varied by changes in substitution—and the solvent polarity.[96] If the quinone component contains methyl substituents, no fluorescence quenching is observed in apolar solvents, and therefore no ET. Obviously, the ET to the high-energy, charge-separated state is too slow relative to the lifetime of the excited singlet state of the porphyrin chromophore under normal fluorescence decay conditions, and thus is not competitive. On the other hand, in polar solvents, the charge-separated state is stabilized, and ET competes with normal fluorescence. Quinones with chloro substituents are stronger electron acceptors, and in these model compounds the increased driving force ΔG^0 for the ET is reflected by an effective fluorescence quenching.

The investigations of ET reactions from a donor to an acceptor connected to it by a bridge stimulate the question whether the unpaired electron is transferred through space or through the bonds of the bridge. In particular, the contribution of the molecules lying between the donor and the acceptor can be of great significance in the case of weak electronic coupling. The π-electron systems of the donor and acceptor need not be conjugated through the bridge; even aliphatic bridges can, for example, contribute to k_{ET} by the superexchange mechanism (see Section 2). Wasielewski et al. have studied the influence of the energy of the bridge orbitals. They compared the compounds **11a** and **12a** (unsubstituted bridges) with **11b** and **12b** (electron-donating methoxy substituents on the bridges) by means of absorption, fluorescence, and transients absorption spectroscopy.[44] Relevant configurations for a possible contribution of the bridge in forward and back ET reactions can be represented as in Scheme 1.

Forward reaction:

$$P\text{-}S\text{-}Q \longrightarrow P^{\bullet+}\text{-}S^{\bullet-}\text{-}Q \longrightarrow P^{\bullet+}\text{-}S\text{-}Q^{\bullet-}$$

Reverse reaction:

$$P^{\bullet+}\text{-}S\text{-}Q^{\bullet-} \longrightarrow P^{\bullet+}\text{-}S^{\bullet-}\text{-}Q \longrightarrow P\text{-}S\text{-}Q$$

or

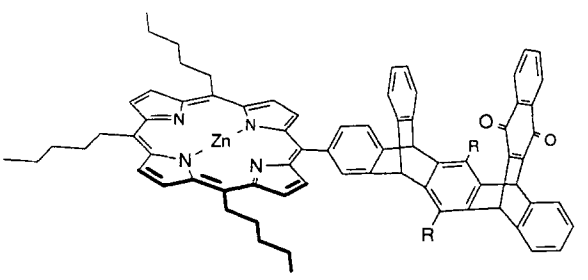
$$P^{\bullet+}\text{-}S\text{-}Q^{\bullet-} \longrightarrow P\text{-}S^{\bullet-}\text{-}Q^{\bullet-} \longrightarrow P\text{-}S\text{-}Q$$

Scheme 1.

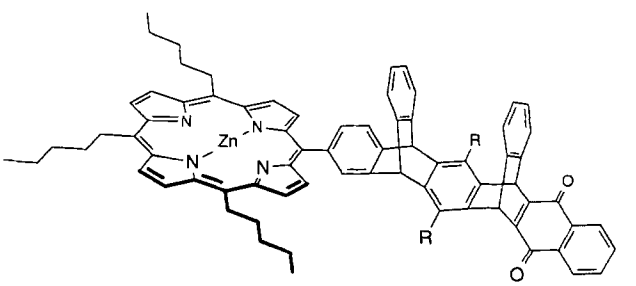
In the forward reaction the superexchange can contribute by means of the participation of the LUMOs of the bridge. Since the reduction potential of the bridge is not substantially altered by the methoxy substituents, it is to be expected that **11a/12a** and **11b/12b** should display similar rates of ET even if superexchange was relevant. Of the two configurations which are possible for the reverse reaction, a contribution to the superexchange by the second possibility would be favored on energy grounds. The oxidation potential of the bridge is altered by the substituents in such a way that the contribution to superexchange should be larger for **11b/12b** than for **11a/12a**. The experiment did indeed show that the forward reaction is hardly affected by the substituents, whereas the reverse reaction is markedly influenced. The rate of recombination from the charge-separated state is a factor of 3 to 4 larger for **11b/12b** than for **11a/12a**. The influence exerted by the substituents indicates that the bridge takes part in the ET reaction.[97]

A contribution from superexchange to the ET rate is also discussed in an investigation of free-base porphyrin/Zn-porphyrin/quinone triads with transient absorption spectroscopy in the femtosecond range; in these compounds the quinone is directly covalently linked to a porphyrin in the *meso* position.[98] From a comparison of the kinetics, it was concluded that the participation of the (central) Zn-porphyrin in the ET process along the lines of the superexchange mechanism was very likely. Furthermore, the role of vibronic relaxation was discussed, which could also cause similar time-dependent shifts on the picosecond and subpicosecond time scale.

Johnson et al.[99] and Wasielewski et al.[100] have investigated a covalently linked triad, constructed from a chlorophyll donor connected to a quinone acceptor through a porphyrin bridge; the distance between porphyrin and quinone is larger than in the previously described compounds[98] in which the redox-active components are directly coupled. Comparison of the optical properties of the monometalated with the doubly metalated and the free-base derivatives led to the conclusion that, upon charge separation, a charge-transfer state between the porphyrin and quinone can be assumed to exist, in which the porphyrin bridge is oxidized and the quinone reduced. Finally, the system relaxes into a charge-separated state, in which the chlorophyll is



11a, R = H
11b, R = OCH_3



12a, R = H
12b, R = OCH_3

oxidized and the quinone reduced. At 77 K, the recombination to the ground state is so slow that lifetimes of the order of milliseconds were observed for the charge-separated state. A superexchange mechanism in which the porphyrin LUMO takes part appeared to be incompatible with the kinetic data. In this respect the behavior of the model compound differs from the superexchange mechanism postulated for the first charge-transfer step in bacterial photosynthesis.[101]

A potential function of the extra-bacteriochlorophyll on the inactive pigment branch has been addressed in a different type of model compound. In the primary reactions of photosynthesis, light-induced charge separation results from singlet-ET. Triplet states occur only as by-products, for instance, as a result of too intense light irradiation through reverse-ET from the charge-separated transient. Possible triplet states of chlorophyll are dangerous, since they function as effective singlet oxygen generators; in nature they are, therefore, quenched by carotenoids. However, in bacterial reaction centers the carotene lies a considerable distance away from the bacteriochlorophyll dimer (the special pair). The possibility has therefore been mooted that the extra-bacteriochlorophyll in the inactive pigment branch, which lies between the dimer and the carotene, could serve as a triplet relay to the carotene where the triplet state is quenched. Gust et al. have recently investigated the triad **8**, consisting of a carotenoid (C), a porphyrin (P), and a pyropheophorbid (Ppd), by time-resolved optical spectroscopy and obtained the following results:[102] The Ppd excited singlet state is accesible either by direct excitation or by energy transfer from the neighboring excited porphyrin. The excited state of Ppd can undergo intersystem crossing to the triplet state. In oxygen-free solution this triplet state decays by triplet energy transfer to the carotene via the triplet state of the porphyrin (Scheme 2).

$$\text{C-P-Ppd} \xrightarrow{h\nu} \text{C-P-}^1\text{Ppd} \xrightarrow{\text{ISC}} \text{C-P-}^3\text{Ppd} \longrightarrow \text{C-}^3\text{P-Ppd} \longrightarrow {}^3\text{C-P-Ppd}$$

Scheme 2.

If oxygen is present in the solution, this quenching process competes effectively with the formation of singlet oxygen; consequently, the carotene actually does perform a protective function, at least to some extent. If the triad contains a zinc porphyrin instead of the free base, the triplet energy transfer is very ineffective, since the energy of the triplet state of porphyrinatozinc is too high. In this system no protection against photogenerated singlet oxygen is observed from the porphyrin triplet relay. The triplet relay ceases to be effective at lower temperatures, because the first energy transfer step is endergonic. Such behavior is also observed in natural systems.

The pentad **9** exemplifies the energy transfer and ET processes of photoexcited states (Fig. 5).[11, 103] The studies on **9** include stationary and time-resolved fluorescence methods (single-photon counting) as well as transients absorption spectroscopy. Both porphyrins can be photoexcited to their first excited singlet state S_1 by laser with light at 590 nm . Since the Zn-containing porphyrin fragment does not display strong fluorescence, one can assume that $^1P_{Zn}$ transfers the energy to the free base P with formation of ^1P (step 1, Fig. 5). ^1P can be directly generated by

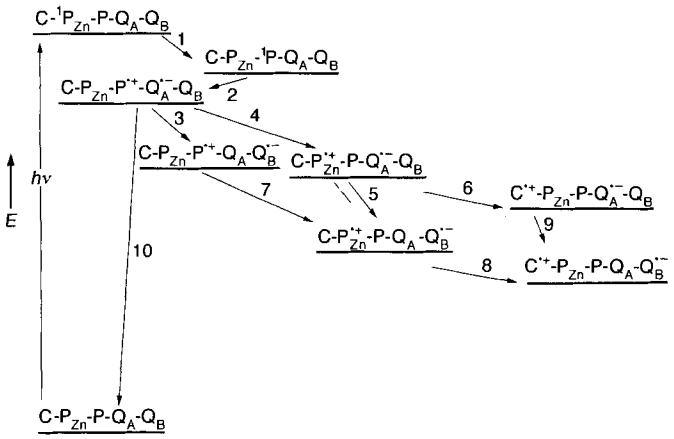


Fig. 5. Energy level diagram for the pentad **9** (C-P_{Zn}-P-Q_A-Q_B). The figure shows the various energy-transfer and electron-transfer steps and the transients involved; see text as well [11, 103].

excitation at 650 nm. Emission from ^1P is known to be substantially weaker than in the corresponding monomer. Obviously, therefore, fluorescence quenching by ET to the neighboring quinone Q_A is taking place (step 2, Fig. 5). The charge-separated states $P^{\bullet+}$, $Q_B^{\bullet-}$ or $P_{Zn}^{\bullet+}$, $Q_A^{\bullet-}$ are produced by the competing ET steps 3 and 4. After further branching ET steps, the charge-separated state $C^{\bullet+}$-P_{Zn}-P-Q_A-$Q_B^{\bullet-}$ is formed. This state has a relatively long lifetime of about 200 μs, brought about by the stepwise separation of charge and the concomitant increase in the distance between positive and negative charge. It can be detected by transient absorption spectroscopy on the nanosecond time scale. It has also been stated that the lifetime of the final charge-separated state of the corresponding completely metal-free pentad is even longer, namely 340 μs. However, the quantum yield is, in this case, lower than in the former pentad because of competing back reactions.

4.2. (Stationary) EPR and ENDOR Investigations

It has already been shown that the electronic interaction between donor and acceptor and thus their electronic wave functions are of significance for the understanding of the properties of ET. Also, since a (porphyrin) radical cation and a (semiquinone) radical anion are formed upon transfer of an electron, the exact determination of the spin density distribution in the corresponding radical fragments is of interest. Furthermore, since the spin density distribution is related to the structure (relative spatial configuration, twist angles), additional information about the preferred conformation of the P-S-Qs can be obtained. Because the large π-electron system provides many magnetic nuclei that contribute to the hyperfine structure, the higher resolution of ENDOR spectroscopy relative to EPR can be exploited to particular advantage.[104–106] When there are several radical species in solution or when there are different conformers present, ENDOR-induced EPR (EIE) spectroscopy is the technique of choice to record the spectra of individual components of the mixture.[105, 106] In Figure 6 the separation of the spectra of two species is presented for the semiquinone anion of **2b** (EIE spectra I and II). It should be noted that the

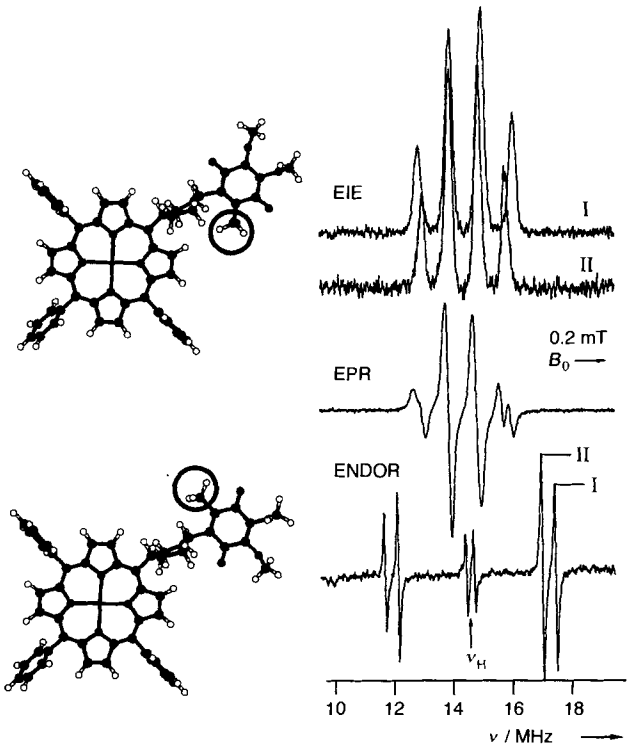


Fig. 6. EPR (290 K), ENDOR (290 K), and EIE spectra (270 K) of the chemically generated semiquinone radical anion of **2b**. The energetically favored conformations (derived from Alchemy III and MNDO calculations) are depicted. (The circles highlight the different positions of the CH_3 groups adjacent to the bridge). It can be seen that the spectra, in particular the EIE spectra, indicate two species with different *g*-factors. The Roman numerals in the ENDOR spectrum characterize the field positioning used in measuring the spectra I and II, respectively (in the Alchemy formulas the *p*-CH_3 groups on the phenyl rings of the porphyrin are omitted) [59, 91].

orientation of the quinone components relative to the cyclohexanediyl bridge in these confomers differs by 180°.[59, 91]

As already mentioned, the special pair in bacterial reaction centers consists of a bacteriochlorophyll dimer. In the radical cation, the unpaired electron is delocalized over both bacteriochlorophyll units. EPR and particularly ENDOR investigations have revealed that the ^1H and ^{14}N hyperfine coupling constants are smaller than those of the corresponding monomers.[107–110] It should be reasonable to model the special pair by using covalently bound porphyrin dimers. Many examples of such compounds have already been prepared (see Section 4.1).[111–113] EPR and ENDOR studies of radical derivatives of the porphyrin dimer **3** and modified compounds with *meta*-phenylene or diphenylmethano bridges have been carried out. A comparison of the hyperfine coupling constants with those of the monomeric analog, the ZnTPP radical cation,[114, 115] indicates that the unpaired electron in the former compounds is almost completely delocalized over both porphyrins, whereas in the compound with the methano bridge, the electron is localized on only one porphyrin unit. The CH_2 group behaves as an isolator between the two π-electron systems. Thus, only the first two compounds with delocalization of the unpaired electron over both porphyrin units exhibit a sufficiently large π–π overlap to cause delocalization and thus to mimic the electron distribution in the special pair in the bacterial reaction center.

4.3. Time-Resolved EPR Investigations in Isotropic Liquids

For the detection and investigation of paramagnetic, transient species, time-resolved EPR spectroscopy, be it the continuous wave (cw) or Fourier Transform method, is the technique of choice. Compared to optical spectroscopic methods like time-resolved fluorescence spectroscopy and absorption spectroscopy, EPR methods have the disadvantages of poorer time-resolution and more complicated data analysis (for example, the signal intensity in optical methods is directly proportional to the number of molecules in the observed state); nevertheless, short-lived intermediates can be more accurately—and often unambiguously—identified through their magnetic properties. In ET processes paramagnetic species can be generated not only by spin selective ISC, but also through the radical-pair mechanism. Shortly after their formation, the population of their spin systems created in this manner deviates from the thermal Boltzmann distribution. Fast spectroscopic techniques reveal ESP (electron spin polarization) effects, which are reflected by enhanced absorption or emission signals in the EPR spectra.[116] The polarization pattern of the EPR spectra often contains detailed information about the spin dynamics of the system under consideration. Time-resolved EPR investigations into the transient paramagnetic states of the reaction centers of bacteria and also of plants (photosystem I) have played an important role in the understanding of light-driven primary processes in photosynthesis.[117–121]

The processes induced by light excitation of the porphyrin chromophore (sketched in Figure 3) as exemplified by two selected model compounds, the cyclohexylene-connected P-S-Qs **1** and **2**, will now be described. After light excitation of the singlet ground state S_0 of the porphyrin to the first excited singlet state S_1 (any higher singlet states will deactivate to S_1 in less than 12 ps), deactivation to the ground state can occur by IC, fluorescence, or via the triplet state T_1, which is populated by ISC (^{T}P-S-Q, Fig. 3). In the presence of a quinone acceptor, another decay channel is opened through which singlet ET from S_1 or triplet ET from the ISC-derived triplet state T_1 of the porphyrin fragment can take place. The corresponding transient diradical ^{S,T}[P$^{\cdot+}$-S-Q$^{\cdot-}$] is formed, either in the triplet or singlet state. In principle, these two spin states can coherently mix in the sense of a radical-pair mechanism, or interconvert by ISC. The deactivation to the ground state by ET takes place from diradicals with singlet character.

In isotropic liquid solutions at room temperature **1** and **2** display rapid ET (in the picosecond range) from the optically excited S_1 state of the porphyrin to the quinone[40, 91] (see also the discussion of optical measurements of ET in **1** and **2** in Section 4.1). However, at lower temperatures in alcohols, (for example, ethanol, 150 K) EPR signals appear (Fig. 7); they can be attributed to a superposition of the signals of the triplet states of the porphyrin (^{T}P-S-Q) and of the radical pair (^{T}[P$^{\cdot+}$-S-Q$^{\cdot-}$]). The detection of ^{T}P-S-Q implies that the singlet ET (S-ET in Fig. 3), which dominates at room temperature, must be slowed down enough that the ISC to the porphyrin triplet state can successfully compete. The decrease in k_{ET} on cooling is explained by the transition from the diabatic ET to the solvent-controlled adiabatic ET (see Section 2).[50, 51, 122, 123] An estimation of k_{ET} from the relaxation time τ_L of ethanol in the

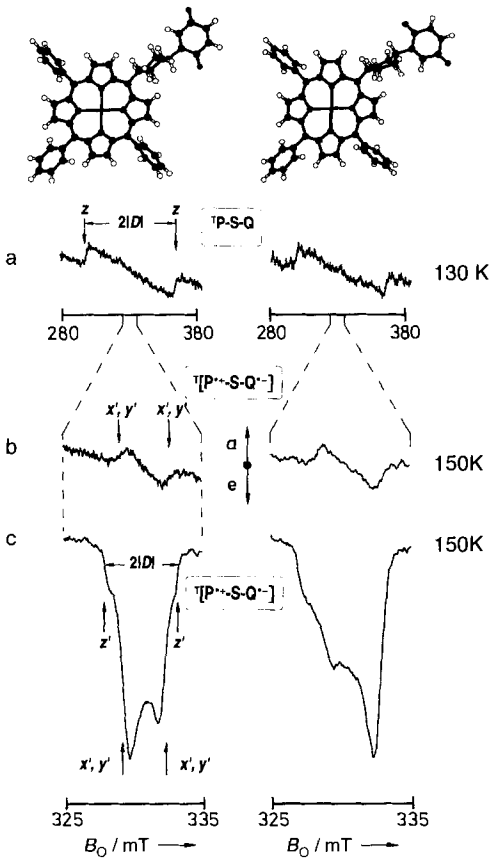


Fig. 7. Spin-polarized transient EPR spectra of P-S-Qs **1a** (left) and **1b** (right) after pulsed laser excitation of the porphyrin segment (10 ns, 584 nm, 8 mJ, pulse frequency 20 Hz). a) Spectra of ^{T}P-S-Q: delay time for **1a** 0.2 μs (polarization pattern (aaa eee), direct detection), for **1b** 0.4 μs (integration time 0.5 μs); b) early spectrum of ^{T}[P$^{\cdot+}$-S-Q$^{\cdot-}$], delay time 0.5 μs, integration time 0.5 μs, (aa ee); late spectrum of ^{T}[P$^{\cdot+}$-S-Q$^{\cdot-}$], delay time: 5 μs, integration time 0.5 μs. For interpretation see text. The structures were obtained from MNDO calculations and Alchemy III. Zero field splitting parameter D: a) 32.6 (**1a**), 32.8 (**1b**); b,c) 2.65 (**1a**), 3.75 mT (**1b**) [50, 91].

temperature range employed agrees roughly with the rate of ET obtained from experiment. In view of the problems connected with a quantitative analysis of the influence of solvent on the rate of ET,[21] this level of agreement can be considered to be satisfactory.[124] (However, it must be explicitly pointed out that according to newer theoretical and experimental investigations, fundamentally more complex relationships for solvent mobility and their influence on ET rates must be taken into account; see, for example, ref. [45, 53].)

The results of the time-resolved EPR investigations have already been thoroughly described.[50, 122] The essential results are summarized below. About 0.3 ps after the laser pulse, both compounds **1a** and **1b** display EPR spectra that extend over about 60 mT and consist essentially of three groups of signals, whose signal rise times are different (Fig. 7).[50, 91] While the intensity of the outer groups of signals decreases with time, the inner group becomes more intense. The polarization pattern of the outer groups is (aa ee) at low field (a = absorption, e = emission), whereas that of the middle group changes with time from (aa ee) to complete emission (ee ee). The outer signals in Figure 7a coincide well with those expected from a porphyrin in the triplet state; they represent the typical z turning points of an EPR powder pattern (xyz molecular coordinate system; principal axis z, perpendicular to the porphyrin plane). More exactly, they are the accidentally coincident z and y components, while the x components, which are superimposed at the center of the spectrum, cancel out because of their opposite phase; cf. also ref. [50].

The central group of signals, detectable after a delay of 0.5 μs, can be similarly assigned to a triplet species (expanded scale, Fig. 7b), namely the diradical ^{T}[P$^{\cdot+}$-S-Q$^{\cdot-}$]. The zero field splitting parameters D of 3.75 mT and 2.65 mT yield electron separations of 8.8 Å and 10.7 Å for the *cis* and *trans* compounds, respectively, according to the point–dipole model.[125] The point–dipole model is applicable in this case, since the distance between the unpaired electrons in the diradical is large relative to the extent of the π-electron systems of the porphyrin and quinone. Figure 7 shows the preferred conformations of the P-S-Qs **1a** and **1b**, as derived from the molecular modeling program Alchemy III. The separation of the two unpaired electrons in the diradical, obtained from the zero field splitting should correspond to the center-to-center distance of porphyrin and quinone, assuming that the spin densities are localized at the respective centers of gravity. As expected, one finds a smaller separation for *cis*-^{T}[P$^{\cdot+}$-S-Q$^{\cdot-}$] (righthand structure in Fig. 7) than for the *trans* compound.

Apart from the detection of the triplet state and the direct identification of the transient triplet species, the aforementioned polarization patterns are of particular interest, since they give information about the spin dynamics of the ET (Fig. 8). For the

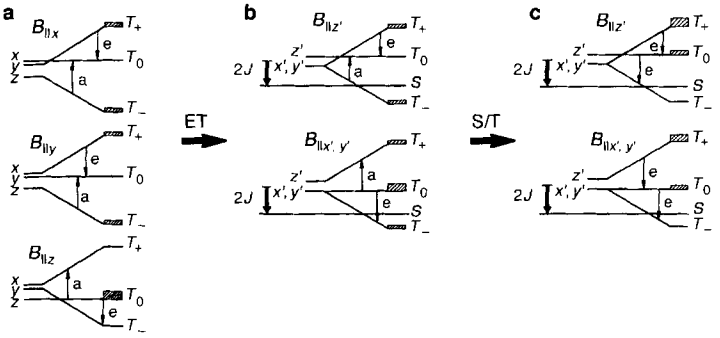


Fig. 8. Zeeman energy levels and excess spin populations for the three canonical orientations (B_0 field in each case parallel to one of the three major axes x, y, z of the zero field splitting tensor) of the triplet states ^{T}P-S-Q ($D>0$, $E\neq0$) and ^{T}[P$^{\cdot+}$-S-Q$^{\cdot-}$], (principal axes: x', y', z'; $D<0$, $E=0$). a) High field population of ^{T}P-S-Q as a result of spin selective ISC [126, 127]; b) initial population of the radical pair ^{T}[P$^{\cdot+}$-S-Q$^{\cdot-}$], J: exchange interactions; c) later population, arising from different recombination rates into the ground state P-S-Q (see text) [50].

Zn-containing P-S-Q **1**, the polarization pattern (aa ee) (actually (aaa eee)) of the signal assigned to the triplet state of the porphyrin corresponds to that reported in the literature for ZnTPP.[126, 127] The polarization is due to an anisotropic ISC, in which the T_z level is exclusively populated. In the high field approximation, T_0 for $B\|x$ and $B\|y$ are then "empty" with respect to the radiative part, whereas this level for $B\|z$ is overpopulated.

The polarization pattern assigned to the diradical, which appears after a delay of about 1 μs (aa ee), can be explained when the following assumptions are made: 1) The spin polarization of the porphyrin is carried over to the diradical during the ET.

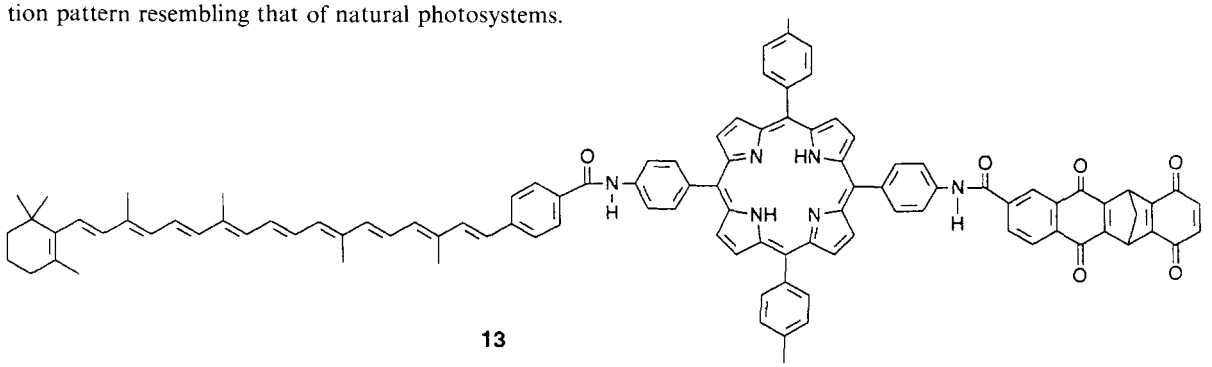
2) The z' principal axis is rotated by about 90° to the z axis and connects the centers of the porphyrin and quinone, with the result that T_0 for $B \| z'$ is empty and that for $B \| x'y'$ is overpopulated. 3) D of the diradical has the opposite sign to that of the triplet porphyrin.[128]

The development, over time, of the polarization pattern of the radical pairs' EPR spectra, which after a few microseconds change from (aa ee) to purely emissive spectra, can be explained by S/T mixing. The admixture of singlet character to T_0 and T_- levels causes a greater rate of depopulation from these levels by recombination into the ground state; thus the spectra turn completely into emission. The behavior is particularly complex, because, simultaneously with the decay of ET-induced polarization (due to spin–lattice relaxation), a new electron spin polarization is developed by S/T mixing. This temporal change of signal phase for both P-S-Qs can be seen clearly in Figure 7b and c. In both compounds the low-field z' and $x'y'$ transitions change from absorption to emission.[50]

The spin dynamics in the P-S-Qs are sensitive to structural variations in the molecular systems, as discussed in the following example: Compound **2** (already discussed in terms of its optical properties), in which the only difference to **1** is the replacement of the quinone fragment by ubiquinone, displays a completely different EPR polarization pattern to **1** for the corresponding charge-separated state $^{T}[P^{\bullet+}\text{-S-UQ}(0)^{\bullet-}]$. Instead of the early polarization pattern (aa ee), the pattern of **2** is, surprisingly, (ee aa).[129] Amongst other things, this difference in spin dynamics can be caused by the slower charge recombination from $^{S}[P^{\bullet+}\text{-S-UQ}(0)^{\bullet-}]$. This is to be expected for **2**, since ΔG^0 for charge recombination should be more negative than for **1**, and therefore should lie further in the inverted region.

Time-resolved FT- and cw-EPR experiments were also carried out on tetrad **13**, built up from a carotenoid, a porphyrin, and two quinones.[130] A long-lived (about 1 ms), charge-separated state in which the charges were localized on the ends of the tetrad (that is, on the carotenoid and on the terminal quinone) was photochemically generated. The transient radical species could, therefore, be very accurately characterized. It was assumed from analysis of the spin-polarized EPR spectra that the singlet ET probably occurred from the excited singlet state of the porphyrin.

Time-resolved EPR spectra could also be obtained from the already mentioned chlorophyll-porphyrin-quinone triads,[98] for which the lifetime of the charge-separated state is of the order of milliseconds. These spectra displayed a spin polarization pattern resembling that of natural photosystems.

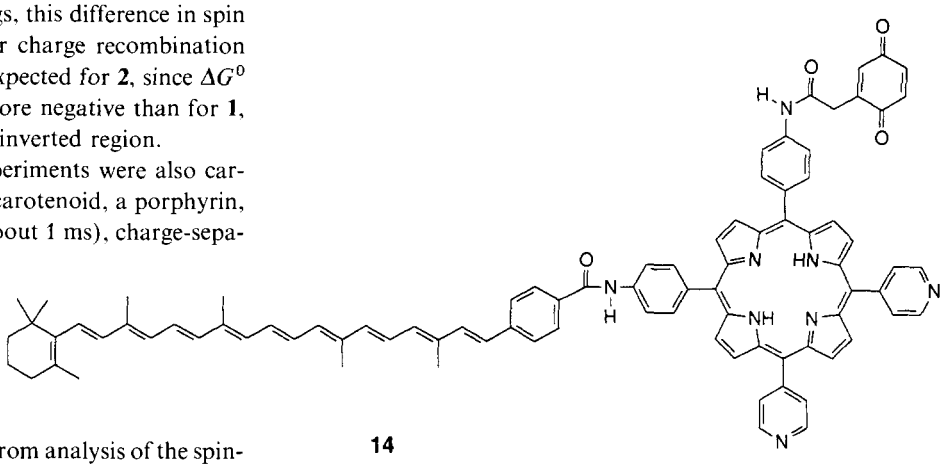


13

4.4. EPR Investigations in Anisotropic Liquids

The primary processes in natural photosynthetic reaction centers take place in membrane-bound protein complexes. The protein may have an influence on the unidirectionality of the ET, due to the spatial fixation of the redox-active pigments, and may contribute to the high efficiency of the charge separation. The central event of photosynthesis can be described as a light-driven cyclic flow of electrons, whose net effect is the generation of a proton gradient over the membrane[8, 9, 131] (see also the "chemiosmotic hypothesis"[132]). Any modeling of photosynthetic processes with the P-S-Qs in isotropic media, as discussed so far, thus lacks important contributions. It would, therefore, be challenging to model the photosynthetic membrane on, for example, micelles, vesicles, lipid membranes, or liquid crystals. Even though it is quite unlikely that the topological parameters of photosynthesis could be exactly mimicked by using such media, valuable information might still be obtained about the behavior of redox-active components in anisotropic surroundings.

Moore et al. have synthesized the amphiphilic triad **14** with the hydrophilic pyridinoporphyrin and the hydrophobic carotenoid fragments and studied it in various media including liposomes (phosphatidylcholine), that is, in closed, liquid-filled vesicles. They showed by measurement of the fluorescence



14

quenching with ascorbic acid/cytochrome c that the triad actually spanned the membrane of the liposome.[133] The carotenoid radical cation, formed through light-induced charge separation, oxidized cytochrome c (II) to cytochrome c (III), which then brought about oxidation of the ascorbic acid.

Liquid Crystalline Solutions

When liquid crystals are host media, they allow the individual anisotropic hyperfine components of paramagnetic derivatives of the P-S-Q guest molecules to be studied by EPR spectroscopy. Thus, quinones were chemically reduced to semiquinones, and the degree of ordering and the orientation of the guest molecules could be determined by static EPR or ENDOR spectroscopy from the anisotropic hyperfine shifts in nematic or smectic phases.[134]

The triplet state of ZnTPP, obtained photochemically by ISC in a liquid-crystalline matrix, has been investigated by means of time-resolved EPR spectroscopy.[126, 135, 136] As a result of the nematic ordering of the host molecules in an external magnetic field, the guest molecules also adopted a preferred orientation. In the nematic phase the preferred orientation of the porphyrin molecule aligns the line joining two opposite pyrrole nitrogen atoms parallel to the field axis. If the solution is frozen, the reorientation of the nematic molecules is hindered, which allows the angular dependence of the triplet spectrum to be studied by turning the sample tube in the magnetic field. By incorporation of mesogenic substituents in the porphyrin system, a different orientation can be forced upon the molecules, since the mesogenic substituents dictate the favored orientation.[137]

Recently the light-induced, intramolecular ET of the P-S-Qs **1a** and **1b** was studied in liquid crystals with time-resolved EPR spectroscopy.[138] Transient, paramagnetic species could be detected in the nematic phase over a wide range of temperatures (210–320 K). In isotropic (ethanol) solution this range is limited to 30 K (130–160 K). Whereas the EPR spectra of the charge-separated state in isotropic solution display an (aa ee) polarization pattern (Fig. 7[50]), in liquid-crystalline solution an (ee aa) pattern is observed. The definitive interpretation of these results is currently under intense debate. It has been postulated, for example, that the very bulky porphyrin donor is oriented in exactly the same way as ZnTPP, and therefore dictates the orientation of the P-S-Q. Accordingly, the dipolar axis of the diradical is tilted away from the field axis, since the bridge is bonded to the porphyrin framework in the *meso* position. This geometry could significantly influence the polarization pattern. The marked temperature dependence of the polarization is explained by competing triplet and singlet ET processes.

Micelles and Inverse Micelles

Micellar aggregates have proved their worth in modeling the photochemical ET processes in photosynthetic membranes.[139, 140] Thus, for example, mixtures of porphyrins or chlorophylls and quinones have been irradiated, and the interaction of the resulting ions with the interface of charged micelles has been studied with optical spectroscopy[141] and magnetic resonance methods.[142–145] The behavior of these mixtures was compared with that of the corresponding mixtures in isotropic solutions.[146] The semiquinone radical anion is destabilized by Coulombic interaction with the negatively charged micelles and expelled from the micelle. Remarkably, in micelles with a positively charged head group, an accelerated back-ET to the ground state was observed.[144] This is presumably due to the Coulombic attraction between the head group and the negative semiquinone radical anion.

Recently the first tentative experiments on light-induced ET of P-S-Qs in inverse micelles[147] were reported.[148, 149] Upon irradiation of a solution of **1a** in inverse micelles of cetyltrimethylammonium bromide (CTAB) (pH about 7) with light of high intensity, signals from radical species were observed in cw-EPR experiments (see below). The radicals observed here must have a distinctly longer lifetime than the signals described in Section 4.3, which were detected with time-resolved EPR spectroscopy.[150] Also missing is the characteristic dipole–dipole interaction described in Section 4.3. The following observations were made: Shortly after irradiation, the EPR spectrum of the doublet semiquinone fragment was obtained (Fig. 9a), which could be identified by comparison

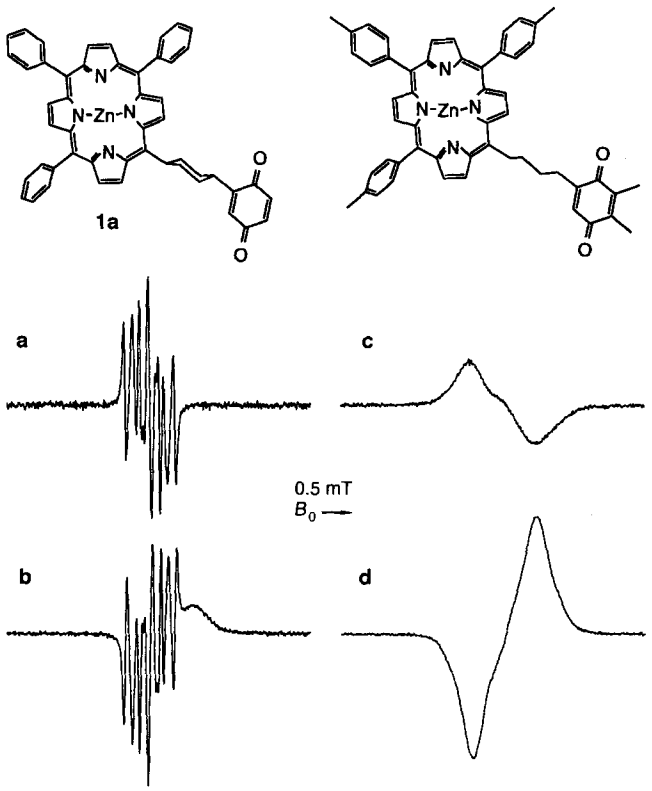


Fig. 9. EPR spectra of radicals produced by illumination in situ (in the resonator) in inverse micelles as solvent from the P-S-Q depicted (structures calculated by Alchemy III). Starting concentration 5×10^{-4} M; light source: 1000 W Hg-Xe lamp (Oriel), 395 nm cut-off filter. a) **1a**. b) Hydroquinone form of **1a** in inverse CTAB micelles. c) EPR dark spectrum of the P-S-Q (shown on the right) in inverse TX-100 micelles after irradiation and switching off the light. d) Emission EPR spectrum observed during irradiation [152].

with the spectrum of the identical chemically produced radical. The EPR signals disappear on extinguishing the light, and reappear on renewed exposure.[151] This result suggests that spin-polarized radical ions are formed in a rapid cyclic ET process. Upon extended irradiation these EPR signals become emission signals. Interestingly, if the hydroquinone derivative of **1a** is used instead of the quinone **1a** itself under otherwise equivalent reaction conditions, the EPR spectrum is entirely an emission spectrum immediately after the irradiation is started (Fig. 9b).[152] In addition, a second emission signal is observed, which can be assigned to the porphyrin radical. The spectral features therefore represent a superposition of both species.

Whereas the light-induced process in the P-S-Q system undoubtedly begins with an ET from porphyrin to quinone (the porphyrin hydroquinone derivative is formed to some extent in a photochemical side reaction), other processes must be considered in the hydroquinone system, since the hydroquinone cannot function as an electron acceptor. An ET from the hydroquinone to the porphyrin unit, with formation of the porphyrin radical anion, is conceivable.

It is remarkable that upon irradiation of the P-S-Q depicted in Figure 9 (right) in neutral inverse TX-100 micelles, a radical is formed that is also stable in the dark (Fig. 9c); its EPR spectrum appears, of course, in absorption.[153] Irradiation causes the phase of these absorption signals to turn into emission (Fig. 9d), which also brings about an increase in signal intensity (probably by spin polarization). Apparently, shortly after the photochemically induced ET, pronounced ESP processes take place creating the spin-polarized products that have sufficiently long lifetimes to be detected by cw-EPR spectroscopy. One can speculate whether, besides the triplet and radical-pair mechanisms, the recently developed radical-triplet-pair mechanism[154, 155] plays a role in this case. As a result of this mechanism, emission EPR spectra of doublet radicals appear, whose spin polarization is caused by interaction with triplet states (see also ref. [156]).

In this context, an extremely interesting experiment must be mentioned in which the quinone of a bacterial reaction center was pre-reduced to the Q_A semiquinone anion radical, which gave an EPR doublet signal in the dark.[157, 158] After photoexcitation of the bacteriochlorophyll dimer, ET proceeds only to the bacteriopheophytin. Because of the longer lifetime of this charge-separated state, an effective radical pair interaction between the radical cation of the bacteriochlorophyll dimer and the bacteriopheophytin radical anion takes place. The spin polarization caused by this process is transferred to the semiquinone doublet radical, whose signal is completely converted into emission. The differences in the interactions relevant to the spin-polarized states in the reaction center (spatially fixed redox components) and in (micellar) solution have already been discussed.[118, 119]

This report should be wound up with a curious experiment concerning ET between porphyrin and quinone: If one grinds up a mixture of crystals of a donor (ZnTPP) and an acceptor (substituted quinones) in an agate mortar, one observes an intense EPR powder spectrum typical of a triplet ground state (Fig. 10), which is assumed by the authors to be generated from a mechanochemically induced electron transfer leading to the formation of the stable diradical ZnTPP radical cation/semiquinone radical anion.[159, 160] The triplet state was unambiguously identified by EPR high field/low temperature polarization experiments (2 mm, F-band; 4.2 K) and also by the detection of the $\Delta m_s = 2$ ("half field") transition (see Fig. 10).

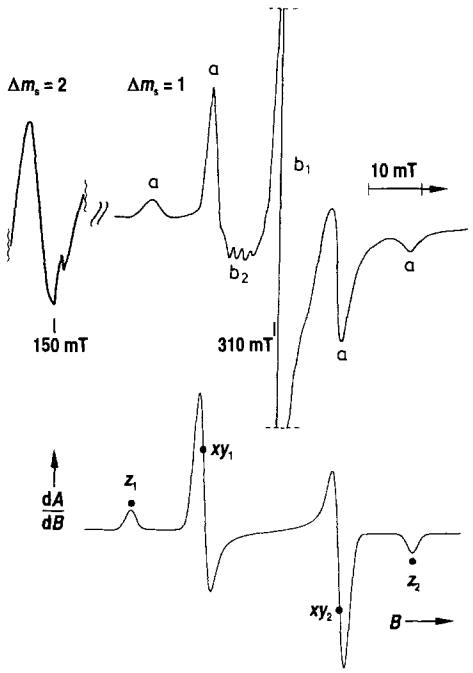


Fig. 10. Solid state EPR triplet spectrum (top, X band, 3 cm) of the diradical produced mechanochemically from a mixture of ZnTPP and 3,5-di-*tert*-butyl-*o*-quinone (see text). The signals a represent the ($\Delta m_s = 1$) *z* and *xy* components of the triplet molecule's spectrum, whereas the signals b belong to doublet radical impurities; the (split) signal at 150 mT corresponds to the $\Delta m_s = 2$ "half-field transition" [159]. For comparison, the first derivative of the $\Delta m_s = 1$ high-field part of an idealized EPR triplet spectrum is shown (bottom).

5. Summary and Outlook

The optical and magnetic properties of the photoexcited states of covalently linked porphyrins and porphyrinquinones can be modified substantially by tailor-made structural variations. These biomimetic model systems are suitable for experimental verification of ET theories and for the study of the photophysical processes that take place in the primary reactions of photosynthesis. However, the limitation remains that, for example, the spin dynamics observed in the ET processes of these artificial porphyrinquinone cascades[98, 119, 161] very rarely reproduce the polarization patterns found in natural systems successfully.[118] The synthesis of tailor-made P-S-Qs for the study of current problems and questions, including that of noncovalently bound redox-active systems and anisotropic media (micelles, vesicle membranes) is a challenge for the preparative chemist. Future work will, fundamentally, be coupled to the studies of natural photosynthesis; here, model compounds can make valuable contributions. In future work, the following questions will have to be addressed:

- what is the source of the unidirectionality (why is only one branch of the reaction center photosynthetically active?)[162]
- does the superexchange mechanism contribute significantly to ET or are other mechanisms more important
- how do the complex redox and protonation/deprotonation steps take place in both quinone acceptors
- what is the role of the amino acid residues of the protein in which the pigments are embedded (do they determine the unidirectionality?)

and finally

- what is the role of the very specific incorporation of the protein in the membrane in the early photosynthetic processes.

It certainly cannot be expected that the artificial photosynthetic devices presented in this article will address all the features of the native energy and ET processes. Nevertheless, despite the

preparative difficulties associated with the porphyrinquinones, their structural, chemical, and physical similarities to the natural pigments make them very attractive models. On the other hand, a great deal of information about fundamental questions of charge and energy transfer has also been obtained from less complex (nonbiomimetic) models.

Finally, if the concept is correct that the extra-bacteriochlorophyll plays a crucial role—be it as mediator or as a kinetic intermediate—in the efficiency of light-induced charge separation, the construction of the ultimate biomimetic model compound that exactly mimics the primary step of photosynthesis remains conceptually and preparatively a difficult challenge to meet.[163]

Our thanks are due to the co-workers named in the references and also to the many members of the group not mentioned, who have been involved in the difficult syntheses of the model compounds. We would also like to thank our friends and colleagues from the Department of Physics (the Möbius group) for constant, patient discussion of the results of our collaborative research. In particular we should mention Prof. Dr. K. Möbius, Dr. M. Plato, Dr. F. Lendzian, and Dr. J. Schlüpmann. M. H. thanks Prof. G. Feher for the very informative and fruitful postdoctoral work in his group and Prof. J. Fajer for fascinating discussions during his stay in Berlin. This work was supported by the Fonds der Chemischen Industrie and by the Deutsche Forschungsgemeinschaft (normal funding and SFB project 337 "Energy and Charge Transfer in Molecular Aggregates").

Addendum

The model compound mentioned in Section 3, in which a crown ether linked with a quinone acts as acceptor and which has a flexible butanediyl bridge to the porphyrin[78] was recently studied in the nematic phase of a liquid crystal by means of time-resolved EPR spectroscopy.[164] After a short period of irradiation with laser light, the transient diradical in the triplet state, formed by ET, proved to have an extended structure; from the changes in the EPR spectra after longer irradiation, a (photoinduced) refolding of the quinone over the porphyrin plane was deduced. In isotropic, moderately polar solvents, such a refolding can also be detected by NMR spectroscopy in the ground state of the analogous Zn complex.[78]

As could have been predicted, the fascinating, redox-active fullerenes have also joined the family of model compounds. "Buckyballs" have been covalently linked to porphyrins[165] and quinones.[166] These systems are very attractive for investigations with time-resolved spectroscopy.

Received: March 21, 1994 [A 55 IE]
Addendum: March 6, 1995
German version: *Angew. Chem.* **1995**, *107*, 929
Translated by Dr. D. J. Macquarrie, Naters, Switzerland

[1] R. K. Clayton, *Photosynthesis: Physical Mechanisms and Chemical Patterns*, IUPAB Biophysics Series, Cambridge University Press, London, **1980**, p. 31 ff., and references therein.
[2] H. J. van Gorhom in *Photosynthesis* (Ed.: J. Amesz), Elsevier, Amsterdam, **1987**, p. 343 ff.
[3] W. Draber, J. F. Kluth, K. Tietjen, A. Trebst, *Angew. Chem.* **1991**, *103*, 1650; *Angew. Chem. Int. Ed. Engl.* **1991**, *30*, 1621.
[4] The superexchange mechanism was developed during the discussion on whether the ET takes place through the bonds of the bridge ("through bond") or through space. According to this mechanism, the ET from donor to acceptor proceeds without a multistep process in which the electron is transferred initially to the bridge. The mixing of orbitals from the bridge increases the electronic interaction through "virtual" states; see text for further explanation. Cf., for example, V. Balzani, F. Scandola, *Supermolecular Photochemistry*, Ellis Horwood, New York, **1991**, p. 94.
[5] M. Bixon, J. Fajer, G. Feher, J. H. Freed, D. Gamliel, A. J. Hoff, H. Levanon, K. Möbius, R. Nechushtai, J. R. Norris, A. Scherz, J. L. Sessler, D. Stehlik, *Isr. J. Chem.* **1992**, *32*, 418, 497.
[6] T. Arlt, S. Schmidt, W. Kaiser, C. Lauterwasser, M. Meyer, H. Scheer, W. Zinth, *Proc. Natl. Acad. Sci. USA* **1993**, *90*, 11757.
[7] J. Deisenhofer, O. Epp, K. Miki, R. Huber, H. Michel, *J. Mol. Biol.* **1984**, 385; W. Zinth, M. Sander, J. Dobler, W. Kaiser, H. Michel, in *Antennas and Reaction Centers of Photosynthetic Bacteria* (Ed.: M. E. Michel-Beyerle) (*Springer Ser. Chem. Phys.* **1985**, *42*), p. 97 f.
[8] Nobel review: R. Huber, *Angew. Chem.* **1989**, *101*, 849; *Angew. Chem. Int. Ed. Engl.* **1989**, *28*, 848.
[9] Nobel review: J. Deisenhofer, H. Michel, *Angew. Chem.* **1989**, *101*, 872; *Angew. Chem. Int. Ed. Engl.* **1989**, *28*, 829; *EMBO J.* **1989**, *8*, 2149.
[10] The terminology *diad* (e.g. compounds **1**, **2**, **3**), *triad*, *tetrad*, and *pentad* indicates the number of redox-active components contained in the molecule.
[11] D. Gust, T. A. Moore, *Adv. Photochem.* **1991**, *16*, 1, and references therein.
[12] D. Gust, T. A. Moore, *Top. Curr. Chem.* **1991**, *159*, 103, and references therein.
[13] M. R. Wasielewski, *Chem. Rev.* **1992**, *92*, 435, and references therein.
[14] M. Bixon, J. Fajer, G. Feher, J. H. Freed, D. Gamliel, A. J. Hoff, H. Levanon, K. Möbius, R. Nechushtai, J. R. Norris, A. Scherz, J. L. Sessler, D. Stehlik, *Isr. J. Chem.* **1992**, *32*, 363, and references therein; *The Photosynthetic Reaction Center, Vol. I-II* (Eds.: J. Deisenhofer, J. R. Norris), Academic Press, New York, **1993**.
[15] R. A. Marcus, *J. Chem. Phys.* **1956**, *24*, 966, 979.
[16] R. A. Marcus, *Discuss. Faraday Soc.* **1960**, *29*, 21.
[17] R. A. Marcus, *J. Chem. Phys.* **1965**, *43*, 679.
[18] R. A. Marcus, *J. Phys. Chem.* **1968**, *72*, 891.
[19] R. A. Marcus, N. Sutin, *Biochim. Biophys. Acta* **1985**, *811*, 265.
[20] R. A. Marcus, *Isr. J. Chem.* **1988**, *28*, 205.
[21] H. Heitele, *Angew. Chem.* **1993**, *105*, 378; *Angew. Chem. Int. Ed. Engl.* **1993**, *32*, 359, and references therein.
[22] G. Grampp, *Angew. Chem.* **1993**, *105*, 724; *Angew. Chem. Int. Ed. Engl.* **1993**, *32*, 691.
[23] Nobel-review: R. A. Marcus, *Angew. Chem.* **1993**, *105*, 1161; *Angew. Chem. Int. Ed. Engl.* **1993**, *32*, 1111.
[24] J. R. Bolton, M. D. Archer in *Electron Transfer in Inorganic, Organic and Biological systems* (Eds.: J. R. Bolton, N. Mataga, G. McLendon) (*Adv. Chem. Ser.* **1991**, *228*), p. 7 f.
[25] D. De Vault, *Quantum Mechanical Tunneling in Biological systems*, Cambridge University Press, Cambridge, **1984**.
[26] M. D. Newton, N. Sutin, *Annu. Rev. Phys. Chem.* **1984**, *35*, 437.
[27] M. D. Newton, *Chem. Rev.* **1991**, *91*, 767.
[28] S. Larsson, *J. Am. Chem. Soc.* **1981**, *103*, 4043, and references therein.
[29] Although, in particular in Anglo-Saxon usage, the term "nonadiabatic" has persevered for such cases, we find the implicit double negative unattractive. We use therefore the term diabatic instead.
[30] See for example, P. W. Atkins, *Molecular Quantum Mechanics*, Oxford University Press, Oxford, **1984**, p. 198 ff.
[31] Actually, the parabolas represent sections through the multidimensional energy hypersurfaces of the reactants and the products. These sections are to be understood as trajectories along the nuclear coordinates relevant for the reaction. The representation of the potentials as parabolas is analogous to the description of vibrations according to the model of a harmonic oscillator where both electronic states are described with the same (averaged) force constant. One advantage of this description is that the theoretically predicted rate of ET depends on only a few parameters, which can be determined independently by experiments. Thus the theory is experimentally verifiable.
[32] G. L. Closs, L. T. Calcaterra, N. J. Green, K. W. Penfield, J. R. Miller, *J. Phys. Chem.* **1986**, *90*, 3673.
[33] M. R. Wasielewski, M. P. Niemczyk, W. A. Svec, E. B. Pewitt, *J. Am. Chem. Soc.* **1985**, *107*, 5562.
[34] It is amazing that for all solvents used in ref. [33], the same reorganization energy was found (the ET rates measured in the different solvents are plotted in one diagram, in which the rate constants of the model compounds are represented as a function of $-\Delta G^0$), even though the magnitude of λ, which determines the position of the curve maximum, should, in fact, depend strongly on the dielectric constant of the medium (see, for example, the cited publications of Marcus and refs. [21, 95]).
[35] The semiclassical approximation is given, which holds for the limiting case of high temperature in which the vibrational states can be treated as a continuum. On the basis of this formulation, the parallels to Marcus theory are most easily visualized.

[36] J. Ulstrup, J. Jortner, *J. Chem. Phys.* **1975**, *63*, 4358.
[37] R. Silbey, J. Jortner, S. A. Rice, M. T. Vala, *J. Chem. Phys.* **1965**, *42*, 733.
[38] R. Silbey, J. Jortner, S. A. Rice, M. T. Vala, *J. Chem. Phys.* **1965**, *43*, 2925.
[39] M. Huber, Dissertation, Freie Universität Berlin, **1989**.
[40] J. von Gersdorff, M. Huber, H. Schubert, D. Niethammer, B. Kirste, M. Plato, K. Möbius, H. Kurreck, R. Eichberger, R. Kietzmann, F. Willig, *Angew. Chem.* **1990**, *102*, 690; *Angew. Chem. Int. Ed. Engl.* **1990**, *29*, 670.
[41] R. J. Cave, S. J. Klippenstein, R. A. Marcus, *J. Chem. Phys.* **1986**, *84*, 3089.
[42] H. Heitele, M. E. Michel-Beyerle, P. Finckh, *Chem. Phys. Lett.* **1987**, *134*, 273.
[43] K. D. Jordan, M. Paddon-Row, *Chem. Rev.* **1992**, *92*, 395.
[44] M. R. Wasielewski, M. P. Niemczyk, D. G. Johnson, W. A. Svec, D. W. Minsek, *Tetrahedron* **1989**, *45*, 4785.
[45] P. F. Barbara, G. C. Walker, T. P. Smith, *Science* **1992**, *256*, 975, and references therein.
[46] J. N. Onuchic, D. A. Beratan, J. J. Hopfield, *J. Phys. Chem.* **1986**, *90*, 3707.
[47] I. Rips, J. Jortner, *J. Chem. Phys.* **1987**, *87*, 2090.
[48] In the formulation of Rips and Jortner [47], τ_L is used instead of ω_C ($\tau_L = 1/\omega_C$). Otherwise, the adiabaticity parameter differs by a factor of 2, which, for the purposes of the qualitative discussion presented here, is irrelevant.
[49] M. Bixon, J. Jortner, *Chem. Phys.* **1993**, *176*, 467.
[50] F. Lendzian, J. Schlüpmann, J. von Gersdorff, K. Möbius, H. Kurreck, *Angew. Chem.* **1991**, *103*, 1536; *Angew. Chem. Int. Ed. Engl.* **1991**, *30*, 1461.
[51] F. Lendzian, B. von Maltzan, *Chem. Phys. Lett.* **1991**, *180*, 191.
[52] At low temperatures, quantum mechanical tunneling processes and the quantization of the vibrational states will, nevertheless, be of increasing importance. The approximation given above for k_{ET} [Eq. (c)] must then be abandoned in favor of an explicit calculation of the Franck–Condon term.
[53] X. Song, R. A. Marcus, *J. Chem. Phys.* **1993**, *99*, 7768, and references therein.
[54] N. Sutin in *Electron Transfer in Inorganic, Organic and Biological systems* (Eds.: J. R. Bolton, N. Mataga, G. McLendon) (*Adv. Chem. Ser.* **1991**, *228*), p. 25f.
[55] See significant examples on synthesis in the series *The Porphyrins, Vol. I–VII* (Ed.: D. Dolphin), Academic Press, New York, **1978–1979**, and references therein.
[56] K. M. Smith, *Porphyrins and Metalloporphyrins*, Elsevier, Amsterdam, **1975**, and references therein.
[57] J. S. Lindsey, I. C. Schreimann, H. C. Hsu, P. C. Kearney, A. M. Marguerettaz, *J. Org. Chem.* **1987**, *52*, 827.
[58] J. von Gersdorff, B. Kirste, H. Kurreck, *Liebigs Ann. Chem.* **1993**, 897.
[59] H. Dieks, J. Sobek, P. Tian, H. Kurreck, *Tetrahedron Lett.* **1992**, *33*, 5951.
[60] J. Weiser, H. A. Staab, *Angew. Chem.* **1984**, *96*, 602; *Angew. Chem. Int. Ed. Engl.* **1984**, *23*, 623.
[61] J. Weiser, H. A. Staab, *Tetrahedron Lett.* **1985**, *26*, 6055.
[62] H. A. Staab, T. Carell, A. Döhling, *Chem. Ber.* **1994**, *127*, 223.
[63] H. A. Staab, C. Krieger, C. Anders, A. Rückemann, *Chem. Ber.* **1994**, *127*, 231.
[64] H. A. Staab, J. Weiser, E. Baumann, *Chem. Ber.* **1992**, *125*, 2275.
[65] C. Krieger, M. Dernbach, G. Voit, T. Carell, H. A. Staab, *Chem. Ber.* **1993**, *126*, 811.
[66] J. S. Lindsey, J. K. Delaney, D. C. Mauzerall, H. Linschitz, *J. Am. Chem. Soc.* **1988**, *110*, 3610.
[67] J. K. Delaney, D. C. Mauzerall, J. S. Lindsey, *J. Am. Chem. Soc.* **1990**, *112*, 957.
[68] H. A. Staab, M. Tercel, R. Fischer, C. Krieger, *Angew. Chem.* **1994**, *106*, 1531; *Angew. Chem. Int. Ed. Engl.* **1994**, *33*, 1463; H. A. Staab, T. Carell, *ibid.* **1994**, *106*, 1534 and **1994**, *33*, 1466.
[69] S.-C. Hung, S. Lin, A. N. Macpherson, J. M. DeGraziano, P. K. Kerrigan, P. A. Liddell, A. L. Moore, T. A. Moore, D. Gust, *J. Photochem. Photobiol. A* **1994**, *77*, 207.
[70] T. Nagata, A. Osuka, K. Maruyama, *J. Am. Chem. Soc.* **1990**, *112*, 3054.
[71] M. Famulok, K.-S. Jeong, G. Deslongchamps, J. Rebek, Jr., *Angew. Chem.* **1991**, *103*, 880; *Angew. Chem. Int. Ed. Engl.* **1991**, *30*, 858.
[72] G. Deslongchamps, A. Galan, J. de Mendoza, J. Rebek, Jr., *Angew. Chem.* **1992**, *104*, 58; *Angew. Chem. Int. Ed. Engl.* **1992**, *31*, 61.
[73] A. Harriman, D. Magda, J. L. Sessler, *J. Phys. Chem.* **1991**, *95*, 1530.
[74] A. Harriman, Y. Kubo, J. L. Sessler, *J. Am. Chem. Soc.* **1992**, *114*, 388.
[75] J. L. Sessler, B. Wang, A. Harriman, *J. Am. Chem. Soc.* **1993**, *115*, 10418.
[76] M. Hugerat, H. Levanon, E. Ojadi, L. Biczok, H. Linschitz, *Chem. Phys. Lett.* **1991**, *181*, 400.
[77] U. Hofstra, R. B. M. Koehorst, T. J. Schaafsma, *Chem. Phys. Lett.* **1986**, *130*, 555.
[78] L. Sun, J. von Gersdorff, D. Niethammer, P. Tian, H. Kurreck, *Angew. Chem.* **1994**, *106*, 2396; *Angew. Chem. Int. Ed. Engl.* **1994**, *33*, 2318. L. Sun, J. von Gersdorff, J. Sobek, H. Kurreck, *Tetrahedron* **1995**, *51*, 3535.
[79] J.-C. Chambron, S. Chardon-Noblat, A. Harriman, V. Heitz, J.-P. Sauvage, *Pure Appl. Chem.* **1993**, *65*, 2343.
[80] This is a typical representation of the state diagram in which the energy levels of the individual states are determined from both optical data (absorption spectrum) and electrochemical data (redox potentials). If the optically determined energy separation S_0–S_1 is identified with the sum of the oxidation and reduction potentials, a common zero point is obtained.
[81] L. Kevan in *Photoinduced Electron Transfer, Teil B* (Eds.: M. A. Fox, M. Chanon), Elsevier, Amsterdam, **1988**, p. 329f.
[82] M. Bixon, J. Fajer, G. Feher, J. H. Freed, D. Gamliel, A. J. Hoff, H. Levanon, K. Möbius, R. Nechushtai, J. R. Norris, A. Scherz, J. L. Sessler, D. Stehlik, *Isr. J. Chem.* **1992**, *32*, 469.
[83] M. Gouterman in *The Porphyrins, Vol. III* (Ed.: D. Dolphin), Academic Press, New York, **1978**, p. 1f.
[84] Actually, it was initially (and wrongly) assumed that charge separation in natural photosynthesis proceeded via the triplet state: R. E. Blankenship, A. McGuire, K. Sauer, *Proc. Natl. Acad. Sci. USA* **1975**, *72*, 4943; A. R. McIntosh, J. R. Bolton, *Nature* **1976**, *263*, 443.
[85] J. Fajer, D. C. Borg, A. Forman, R. H. Felton, D. Dolphin, L. Vegh, *Proc. Natl. Acad. Sci. USA* **1974**, *71*, 994; *ibid.* **1981**, *78*, 2652.
[86] M. Bixon, J. Fajer, G. Feher, J. H. Freed, D. Gamliel, A. J. Hoff, H. Levanon, K. Möbius, R. Nechushtai, J. R. Norris, A. Scherz, J. L. Sessler, D. Stehlik, *Isr. J. Chem.* **1992**, *32*, 449.
[87] Herein lies the answer to the centuries old question—more poetical than scientific—as posed by John Donne, a poet, or Sir Walter Raleigh: *Why is blood red and grass green?* The answer is an anticlimax, because there is no poetry in it: The HOMO in chlorin lies at higher energy.
[88] Details of the instrumentation and the experimental conditions are not discussed in this review; they are available in the cited literature.
[89] J. L. Sessler, V. L. Capuano, A. Harriman, *J. Am. Chem. Soc.* **1993**, *115*, 4618.
[90] O. Bilsel, J. Rodriguez, D. Holton, *J. Phys. Chem.* **1990**, *94*, 3508.
[91] H. Kurreck, H. Dieks, J. von Gersdorff, J. Sobek, P. Tian, M. Ebersole, K. Möbius, F. Willig, K. Schwarzburg, H. Levanon, K. Hasharoni in *Photochemical Conversion and Storage of Solar Energy* (Ed.: Zhao Wu Tian), International Academic Publishers, Peking, **1993**, p. 159f.
[92] T. Murao, I. Yamazaki, K. Yoshihara, *Appl. Opt.* **1982**, *21*, 2297.
[93] R. Eichberger, F. Willig, W. Storck, *Mol. Cryst. Liq. Cryst.* **1989**, *175*, 19.
[94] J. Sobek, H. Kurreck, unpublished.
[95] T. Asahi, M. Ohkohchi, R. Matsusaka, N. Mataga, R. P. Zhang, A. Osuka, K. Maruyama, *J. Am. Chem. Soc.* **1993**, *115*, 5665.
[96] H. A. Staab, G. Voit, J. Weiser, M. Futscher, *Chem. Ber.* **1992**, *125*, 2303; H. Heitele, F. Pöllinger, K. Kremer, M. E. Michel-Beyerle, M. Futscher, G. Foit, J. Weiser, H. A. Staab, *Chem. Phys. Lett.* **1992**, *188*, 270; F. Pöllinger, H. Heitele, M. E. Michel-Beyerle, C. Anders, M. Futscher, H. A. Staab, *ibid.* **1992**, *198*, 645.
[97] It should be mentioned that, as regards effective charge separation with acceleration of the back-reaction, the substitution of the bridge yielded the wrong effect. The desired lengthening of the lifetime of the charge-separated state should be able to be achieved by incorporating electron acceptors in the bridge since a retardation of the back-reaction is required.
[98] J. Rodriguez, C. Kirmaier, M. R. Johnson, R. A. Friesner, D. Holten, J. L. Sessler, *J. Am. Chem. Soc.* **1991**, *113*, 1652.
[99] D. G. Johnson, M. P. Niemczyk, D. W. Minsek, G. P. Wiederrecht, W. A. Svec, G. L. Gaines III, M. R. Wasielewski, *J. Am. Chem. Soc.* **1993**, *115*, 5692.
[100] M. R. Wasielewski, G. L. Gaines III, G. P. Wiederrecht, W. A. Svec, M. P. Niemczyk, *J. Am. Chem. Soc.* **1993**, *115*, 10442.
[101] M. Plato, K. Möbius, M. E. Michel-Beyerle, M. Bixon, J. Jortner, *J. Am. Chem. Soc.* **1988**, *110*, 7279.
[102] D. Gust, T. A. Moore, A. L. Moore, A. A. Krasnovsky, Jr., P. A. Liddell, D. Nicodem, J. M. DeGraziano, P. Kerrigan, L. R. Makings, P. J. Pessiki, *J. Am. Chem. Soc.* **1993**, *115*, 5684.
[103] D. Gust, T. A. Moore, A. L. Moore, S.-J. Lee, E. Bittersmann, D. K. Luttrull, A. A. Rehms, J. M. DeGraziano, X. C. Ma, F. Gao, R. E. Belfored, T. T. Trier, *Science* **1990**, *248*, 199.
[104] K. Möbius, M. Plato, W. Lubitz, *Phys. Rep.* **1982**, *87*, 171.
[105] H. Kurreck, B. Kirste, W. Lubitz, *Angew. Chem.* **1984**, *96*, 171; *Angew. Chem. Int. Ed. Engl.* **1984**, *23*, 173.
[106] H. Kurreck, B. Kirste, W. Lubitz, *Electron Nuclear Double Resonance Spectroscopy of Radicals in Solution* (*Methods Stereochem. Anal.* **1988**).
[107] J. R. Norris, R. A. Uphaus, H. L. Crespi, J. J. Katz, *Proc. Natl. Acad. Sci. USA* **1971**, *68*, 625.
[108] W. Lubitz, F. Lendzian, M. Plato, K. Möbius, E. Tränkle in *Antennas and Reaction Centres of Photosynthetic Bacteria* (Ed.: M. E. Michel-Beyerle) (*Springer Ser. Chem. Phys.* **1985**, *42*), p. 164.
[109] F. Lendzian, W. Lubitz, H. Scheer, A. J. Hoff, M. Plato, E. Tränkle, K. Möbius, *Chem. Phys. Lett.* **1988**, *148*, 377.
[110] F. Lendzian, M. Huber, R. A. Isaacson, B. Endeward, M. Plato, B. Bönigk, K. Möbius, W. Lubitz, G. Feher, *Biochim. Biophys. Acta* **1993**, *1183*, 139.
[111] D. Dolphin, J. Hiom, J. B. Paine, *J. Chem. Soc. Faraday Trans.* **1981**, *16*, 417.
[112] M. Huber, T. Galili, K. Möbius, H. Levanon, *Isr. J. Chem.* **1989**, *29*, 65.
[113] M. Huber, H. Kurreck, B. von Maltzan, M. Plato, K. Möbius, *J. Chem. Soc. Faraday Trans.* **1990**, *86*, 1087.
[114] J. Fajer, D. C. Borg, A. Forman, D. Dolphin, R. H. Felton, *J. Am. Chem. Soc.* **1970**, *92*, 3451.
[115] J. Fajer, M. S. Davis in *The Porphyrins, Vol. IV* (Ed.: D. Dolphin), Academic Press, New York, **1978**, p. 197f.

[116] See, for example: *Chemically Induced Magnetic Polarization* (Eds.: L. T. Muus, P. W. Atkins, K. A. McLachlan, J. B. Pedersen) (*NATO ASI Ser. Ser. C*, **1977**, *34*).
[117] a) *Proceedings of the International Workshop of Disordered Systems*, EMARDIS-1991 (Ed.: N. D. Yordanov), World Scientific, London, **1991**; b) A. J. Hoff in ref. [117a], p. 192f.
[118] P. J. Hore in *Advanced EPR, Applications in Biology and Biochemistry* (Ed.: A. J. Hoff), Elsevier, Amsterdam, **1989**, Kap. 12.
[119] M. Bixon, J. Fajer, G. Feher, J. H. Freed, D. Gamliel, A. J. Hoff, H. Levanon, K. Möbius, R. Nechushtai, J. R. Norris, A. Scherz, J. L. Sessler, D. Stehlik, *Isr. J. Chem.* **1992**, *32*, p. 387.
[120] G. Füchsle, R. Bittl, A. van der Est, W. Lubitz, D. Stehlik, *Biochim. Biophys. Acta* **1993**, *1142*, 23.
[121] A. van der Est, R. Bittl, E. C. Abresch, W. Lubitz, D. Stehlik, *Chem. Phys. Lett.* **1993**, *212*, 561.
[122] Detailed analysis of the spin dynamics of this system: J. Schlüpmann, F. Lendzian, M. Plato, K. Möbius, *J. Chem. Soc. Faraday Trans.* **1993**, *89*, 2853.
[123] H. Kurreck, J. von Gersdorff, B. Kirste, F. Lendzian, J. Schlüpmann, K. Möbius, F. Willig, R. Kietzmann in ref. [117a], p. 158f.
[124] Considering the many other temperature-dependent parameters (Section 2), one cannot exclude the possibility that other factors could contribute to the reduction in the rate of ET at lower temperatures, for example, variations in ΔG^0 and λ caused by different solvation, or changes in the conformation of the P-S-Q.
[125] E. Wasserman, L. C. Snyder, W. A. Yager, *J. Chem. Phys.* **1964**, *41*, 1763.
[126] H. Levanon, *Rev. Chem. Intermed.* **1987**, *8*, 287.
[127] J. H. van der Waals, W. G. van Dorp, T. J. Schaafsma in *The Porphyrins, Vol. IV* (Ed.: D. Dolphin), Academic Press, New York, **1979**, p. 257f.
[128] The zero field splitting D in the triplet state of the porphyrin is positive [127], whereas that for the diradical is negative. In the latter case, the dipole–dipole interaction of the unpaired electrons can be calculated classically, because the distance between the electrons is sufficiently large.
[129] G. Elger, J. Schlüpmann, K. Möbius, H. Dieks, H. Kurreck, unpublished.
[130] K. Hasharoni, H. Levanon, J. Tang, M. K. Bowman, J. R. Norris, D. Gust, T. A. Moore, A. L. Moore, *J. Am. Chem. Soc.* **1990**, *112*, 6477.
[131] M. Y. Okamura, G. Feher, N. Nelson in *Photosynthesis: Energy Conversion by Plants and Bacteria* (Ed.: Govindjee), Academic Press, New York, **1982**, p. 195f.
[132] Nobel-review: P. Mitchell, *Angew. Chem.* **1979**, *91*, 718.
[133] T. A. Moore, D. Gust, A. L. Moore, R. V. Bensasson, P. Seta, E. Bienvenue in *Supramolecular Photochemistry* (Ed.: V. Balzani) (*NATO ASI Ser. Ser. C*, **1987**, 214), p. 283f.
[134] B. Kirste, *Magn. Reson. Chem.* **1987**, *25*, 166.
[135] O. Gonen, H. Levanon, *J. Phys. Chem.* **1985**, *89*, 1637.
[136] A. Regev, T. Galili, H. Levanon, *J. Chem. Phys.* **1991**, *95*, 7907.
[137] S. Michaeli, M. Hugerat, H. Levanon, M. Bernitz, A. Natt, R. Neumann, *J. Am. Chem. Soc.* **1992**, *114*, 3612.
[138] **K. Hasharoni, H. Levanon, J. von** Gersdorff, H. Kurreck, K. Möbius, *J. Chem. Phys.* **1993**, *98*, **2916.**
[139] **N. J. Turro, M. Grätzel, A. M. Bra**un, *Angew. Chem.* **1980**, *92*, 712; *Angew. Chem. Int. Ed. Engl.* **1980**, *19*, **675.**
[140] M. Grätzel, *Pure Appl. Chem.* **1982**, *54*, 2369.
[141] C. Wolff, M. Grätzel, *Chem. Phys. Lett.* **1977**, *52*, 542.
[142] J. Schlüpmann, K. M. Salikhov, M. Plato, P. Jaegermann, F. Lendzian, K. **Möbius.** *Appl. Magn. Reson.* **1991**, *2*, **117.**
[143] **P. R. Levstein, H. van Willigen, M. Ebers**ole, F. W. Pijpers, *Mol. Cryst. Liq. Cryst.* **1991**, *194*, **123.**
[144] P. R. Levstein, H. van Willigen, *Chem. Phys. Lett.* **1991**, *187*, 415.
[145] P. Jaegermann, K. Möbius, P. Tian, *Res. Chem. Intermed.* **1993**, *19*, 355.
[146] H. van Willigen, M. Vuolle, K. P. Dinse, *J. Phys. Chem.* **1989**, *93*, 2441.
[147] In contrast to normal micelles in which the bulk water surrounds the micelle, whose interior is hydrophobic, in inverse micelles the hydrocarbon is outside, and the interior ("water pool") consists of water droplets. Inverse micelles are particularly suitable for EPR and ENDOR investigations, because these samples have lower dielectric losses in comparison to normal micelles: N. Bretz, I. Mastalsky, M. Elsner, H. Kurreck, *Angew. Chem.* **1987**, *99*, 357; *Angew. Chem. Int. Ed. Engl.* **1987**, *26*, 345; D. Niethammer, B. Kirste, H. Kurreck, *J. Chem. Soc. Faraday Trans.* **1990**, 3191; B. Kirste, D. Niethammer, P. Tian, H. Kurreck, *Appl. Magn. Reson.* **1992**, *3*, 1.
[148] H. Kurreck, P. Tian, H. Dieks, J. von Gersdorff, H. Newman, H. Schubert, T. Stabingis, A. Wiehe, J. Sobek, *Appl. Magn. Reson.* **1994**, *6*, 17.
[149] H. Kurreck, S. Aguirre, H. Dieks, J. Gätschmann, J. von Gersdorff, H. Newman, H. Schubert, M. Speck, T. Stabingis, J. Sobek, P. Tian, A. Wiehe, *Radiat. Phys. Chem.* **1995**, in press.
[150] The minimum lifetime of a light-induced, paramagnetic state must be of the order of several milliseconds in order to have a sufficiently large stationary lifetime, and thus a stationary radical concentration, for a cw-EPR experiment. For the spin-polarized radicals observed here, the signal intensity for a given radical concentration can be larger; this increase in sensitivity enables paramagnetic states of shorter lifetimes to be detected. In any case, the time constant of the apparatus (which is set by the detection system's electronics) fixes the lower limit for the lifetime at about 200 μs; cf. A. R. McIntosh, J. R. Bolton, *J. Magn. Reson.* **1978**, *32*, 167. In time-resolved cw-EPR the time-resolution is of the order of 100 ns.
[151] As is to be expected for a porphyrin system, the EPR signals disappear on prolonged irradiation, because irreversible, photoinduced decomposition takes place, or are part of the processes leading to radical products. The photostability of the P-S-Qs ranges between a few minutes and a few hours and depends on the nature of the bridge between porphyrin and quinone.
[152] C. W. M. Kay, H. Kurreck, S. N. Batchelor, P. Tian, J. Schlüpmann, K. Möbius, unpublished.
[153] On irradiation of mixtures of ZnTPP and halogenated quinones in dipalmitoylphosphatidinylcholine vesicles, EPR spectra were obtained that had a similar structure to the spectrum shown in Figure 9c. These EPR spectra were interpreted as a superposition of the spectrum of the ZnTPP cation and that of the semiquinone anion: M.-P. Lanot, L. Kevan, *J. Phys. Chem.* **1989**, *93*, 5280.
[154] C. Blättler, F. Jent, H. Paul, *Chem. Phys. Lett.* **1990**, *166*, 375; C. Blättler, H. Paul, *Res. Chem. Intermed.* **1991**, *16*, 201.
[155] G.-H. Goudsmit, H. Paul, A. I. Shushin, *J. Phys. Chem.* **1993**, *97*, 13243.
[156] N. J. Turro, I. V. Khudyakov, D. W. Dwyer, *J. Phys. Chem.* **1993**, *97*, 10530.
[157] P. Gast, A. J. Hoff, *Biochim. Biophys. Acta* **1979**, *548*, 520.
[158] A. J. Hoff in ref. [117a], p. 192f.
[159] S. D. Chemerisov, O. Ya. Grinberg, D. S. Tipikin, Ya. S. Lebedev, H. Kurreck, K. Möbius, *Chem. Phys. Lett.* **1994**, *218*, 353.
[160] See, in this context, H. Kurreck, *Angew. Chem.* **1993**, *105*, 1472; *Angew. Chem. Int. Ed. Engl.* **1993**, *32*, 1409.
[161] A. Angerhofer, M. R. Wasielewski, G. L. Gaines III, M. P. O'Neil, W. A. Svec, M. P. Niemczyk, *Z. Phys. Chem.* **1991**, *172*, 17, and references therein.
[162] Recently a study of the dielectric asymmetry in both ET branches of bacterial reaction centers was reported in which the electric field dependence of the absorption spectra of the chromophores (Stark effect) was determined. It was discussed whether this property could also be partly responsible for the asymmetric function in the reaction center: M. A. Steffen, K. Lao, S. G. Boxer, *Science* **1994**, *264*, 810.
[163] J. R. Norris in *Photochemical Conversion and Storage of Solar Energy* (Eds.: E. Pelizetti, M. Schiavello), Kluver, Dortrecht, **1991**, p. 141f.
[164] S. N. Batchelor, L. Sun, K. Möbius, H. Kurreck, *Magn. Reson. Chem.*, in press.
[165] P. A. Liddell, J. P. Sumida, A. N. MacPherson, L. Noss, G. R. Seely, K. N. Clark, A. L. Moore, T. A. Moore, D. Gust, *Photochem. Photobiol.* **1994**, *60*, 537.
[166] M. Iyoda, F. Sultana, S. Sasaki, M. Yoshida, *J. Chem. Soc. Chem. Commun.* **1994**, 1929.

Anticoagulatory Substances of Bloodsucking Animals: From Hirudin to Hirudin Mimetics

Johannes Dodt*

Bloodsucking animals contain substances in their saliva that specifically interfere with the blood clotting system. These substances are mainly low molecular weight proteins with a molecular mass of between 4 and 50 kDa. Some have become accessible in large quantities with the help of genetic engineering, and as a result their structures and structure–activity relationships have been studied and clinically tested. In the light of what is known about the mode of action of these natural products at the molecular level, new compounds with possible therapeutic effect can be derived. In the last ten years this approach has been tested with the proteinase inhibitor hirudin, obtained from medicinal leeches, and with the thrombin/hirudin complex. The serine protease thrombin plays a central role in the complex pathway of the blood clotting process and its pathophysiological effect finally results in thrombosis. The selectivity of the formation of complexes from hirudin and thrombin lies in the bivalent interaction of the inhibitor with the active site of the enzyme as well as with a substrate recognition site outside of the active site, the so-called fibrin(ogen) binding site (FBS). The knowledge of this mode of action enabled the synthesis of bifunctional thrombin inhibitors based on hirudin peptides. Hirudin and hirudin mimetics in vivo have been shown to be highly potent anticoagulants for the treatment of arterial and venous thrombosis.

Keywords: blood clotting · hirudin · pharmaceuticals · thrombin

1. Antithrombotic and Fibrinolytic Substances of Bloodsucking Parasites

The use of leeches as a remedy was recommended as early as the Sanscrit writings in India. Leech therapies were first described by the physician Nicandros of Colophon (200–130 B.C.) in Asia minor, but the real founder of this healing method was Themison of Laodicea in the first century B.C..[1] Ancyllus mentioned the bdellotomy or leech cut in 140 A.D., as a method to increase the withdrawal of blood. At the beginning of the nineteenth century leeching was widespread in Europe. In particular, the napoleonic army surgeon Broissais and his pupil Bouillaud regarded almost every illness as being due to excess irritation. Thus, leeches were not only employed for the withdrawal of blood, thereby, providing general relief for the patient, but also to cure widely differing illnesses such as the accumulation of blood, inflammations, infectious diseases, glandular function disturbances, and mental illnesses.[1, 2] The anticoagulatory effect of the salivary gland secretions of the leech Hirudo medicinalis (genus Hirudinidae) was first described by Haycraft in 1884.[3] In 1957 Markwardt managed to isolate a pure protein with inhibitory effect against thrombin,[4] which was named hirudin. Alongside this inhibitor a series of low molecular weight proteins have been isolated from bloodsucking parasites in past years, which specifically interfere in the reactions of blood clotting. As a result of their potential therapeutic use this field of anticoagulants is still being intensively researched today.

This article will initially provide a review of the reactions involved in blood clotting and subsequently present the mode of action of antithrombotic and fibrinolytic substances of bloodsucking parasites, as well as discuss the advantages and disadvantages of the underlying therapeutic concepts. The thrombin-specific inhibitor hirudin is a worthwhile example for investigating structure–activity relationships, not only because of its potential pharmaceutical use as an antithrombotic, but also because of its novel reaction mechanism.[5] The mode of action of hirudin was determined by X-ray crystallography of thrombin/r-hirudin complexes and from protein chemical and enzyme kinetic studies with recombinant hirudin (r-hirudin) and mutants of hirudin. These results gave impetus to the synthesis of low molecular weight peptide-based thrombin inhibitors. The development of these hirudin derivatives to obtain new anticoagulants will be shown with examples and their possible therapeutic application discussed.

1.1. The Physiology of Blood Clotting

Blood clotting (coagulation) must protect the vascular system of the body from life-threatening loss of blood when the vascu-

[*] Priv.-Doz. Dr. J. Dodt
Liebfrauenstrasse 16
D-45665 Recklinghausen (Germany)

 © VCH Verlagsgesellschaft mbH, D-69451 Weinheim, 1995 0570-0833/95/0808-0867 $ 10.00+.25/0

lar system is damaged. On the one hand mechanisms are present which concentrate and limit this coagulation process to the site of injury.[6-8] On the other hand, the fibrinolytic system takes care of the degradation of blood clots (thrombuses) and ensures that they do not lead to life-threatening occurrences such as lung embolism, stroke, and or cardiac infarction.[9]

Blood clotting is a complex system consisting of a) cellular and humoral components of the flowing blood, b) components of the vessel wall, and c) vasomotoric reactions, which interfere in the dynamic of blood flow. The cellular components are thrombocytes (blood platelets) and leucocytes, and the humoral components comprise clotting and fibrinolytic factors. Disturbances in the interplay of components can lead to complications, in which the equilibrium can be shifted either to favor bleeding or thrombosis.

Thrombocytes circulate passively through blood vessels, which are lined with a layer of endothelial cells (Fig. 1). As a primary response to a blood vessel injury the thrombocytes adhere to the site of injury, change their shape, secrete their granular contents, and aggregate. The status of blood platelet activation is modulated through a series of stimulating and inhibiting mediators.[10, 11] The blood platelets have specific receptors on their plasma membrane that pick up these stimuli and translate them into a physiological response.[12] During adhesion the thrombocytes bind through surface receptors to proteins of the extracellular matrix, which are exposed on damage of the endothelial cell layer.[13] This leads to activation of the blood platelets, amplification of the signal produced, and to the completion of platelet occlusion. The signal is enhanced either through the release of already formed components in the granular contents or by the synthesis of new substances. The granular contents, which enhance the signal, are serotonin and adenosinediphosphate (ADP) and the von Willebrand factor (vWF), fibrinogen and thrombospondin. The vWF supports adhesion of platelets to the subendothelial through the membrane glycoproteins Ib (GPIb) and, thus, effects their activation. A change in the conformation of the glycoprotein IIb-IIIa (GPIIb-IIIa; a member of the integrin family) as a consequence of this activation is an important prerequisite for the aggregation, in which the blood platelets bridge together directly across the fibrinogen molecules of the plasma.

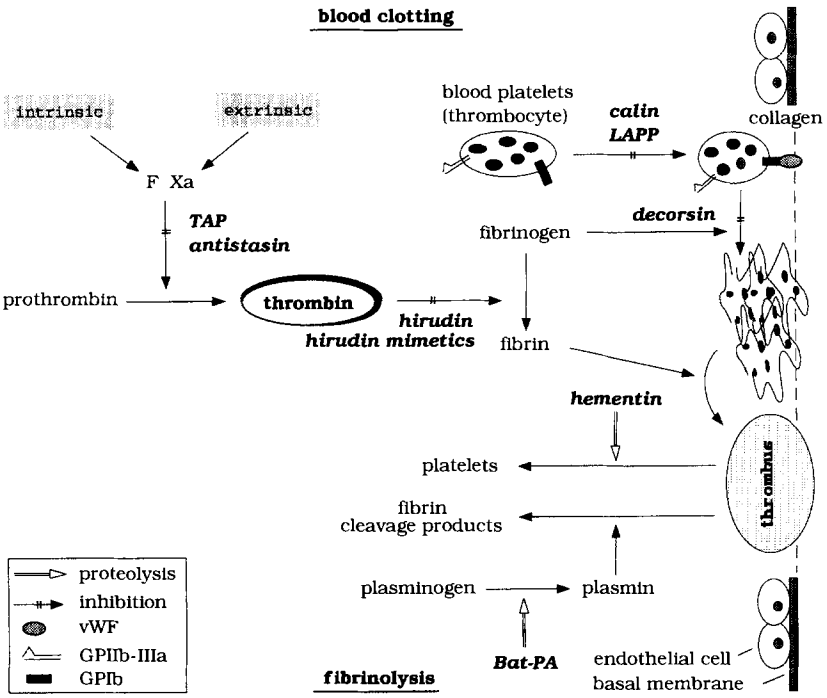
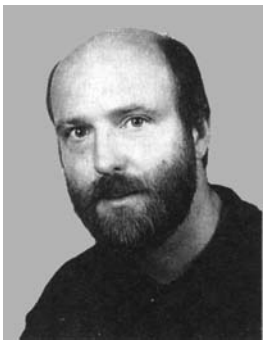


Fig. 1. Schematic representation of clotting and fibrinolysis processes with particular attention to the points of attack by the proteins of bloodsucking parasites; modified from ref. [140].

At the same time as the conglomeration of the platelets, the soluble components of the blood clotting pathway are activated, which leads to the formation of a fibrin net with trapping of platelets and other plasma cells at the site of injury. Blood clotting appears to be a succession of zymogen activations (substrate activations), in which the activated form of one factor catalyzes the activation of the next factor. A central feature of the blood clotting cascade is the formation of complexes between proteases and regulatory proteins (cofactors) and their substrates (zymogens) on membrane surfaces, for example on the surfaces of platelets.[6-8, 14] The course of the activation processes on the membrane surface restricts the



Johannes Dodt, born in 1954 in Recklinghausen, studied chemistry at the Universities of Münster and Munich. In 1985 he was awarded his doctorate under the supervision of Prof. Dr. H. Fritz for work which was undertaken at the Department of Clinical Chemistry and Clinical Biochemistry in the Surgical Clinic and Outpatient Clinic of the Ludwig-Maximilians-Universität in Munich. After a period of postdoctoral study under Prof. Dr. H. G. Gassen at the Institute for Biochemistry at the Technische Hochschule Darmstadt, from 1988 he was employed as a researcher and in 1993 he became a lecturer (Privatdozent) at the same institute. In 1994 he worked at Georgetown University in Washington D. C. The emphasis of his research work is in the area of proteases and protease inhibitors.

formation of thrombin at the site of injury. The series of events are, depending on the stimulus, formally divided into the reactions of the intrinsic or extrinsic pathways, which via a common pathway lead to the activation of the blood clotting factor α-thrombin. The key event for the initiation of blood clotting is the exposure of thromboplastin (a component of the extrinsic pathway), which is the cofactor for the factor VIIa-mediated activation of factor IX and factor X.[15-17] In the common pathway prothrombin is activated to thrombin by the prothrombinase complex (factor Xa, factor Va, phospholipids, Ca^{2+} ions) on the surface of activated blood platelets.[14]

Thrombin plays a central role in blood clotting and exerts an enzymatic as well as a hormone-like function, which either enhances or minimizes the blood clotting process.[18, 19] Fibrin results from the cleavage of fibrinogen by thrombin,[20] which polymerizes and forms the basis of the blood clot (thrombus). Factor XIIIa, which covalently meshes fibrin molecules together, is activated by thrombin[21] just like the cofactor proteins V[22] and VIII[23] in a positive feed-back reaction. In addition, thrombin is able to activate factor XI (intrinsic pathway) in the presence of negatively charged phospholipids (activated blood platelets).[24] Thrombin is the strongest stimulator of platelet aggregation, which is triggered by thrombin-mediated cleavage of the thrombin receptor.[25, 26] However, thrombin is also involved in the regulation of antithrombotic mechanisms. During binding to the endothelial cell receptor thrombomodulin the proteolytic activity is altered and thrombin becomes a potent activator of protein C.[27, 28] This protease inactivates the cofactor proteins Va and VIIIa, through which thrombin formation is halted. The interaction of thrombin with endothelial cells leads to the increased release of the tissue plasminogen activator (tPA), which induces fibrinolysis, or liberates, for example, prostaglandin I_2 (PGI_2) or nitrogen monoxide (NO), which exerts an influence on platelet aggregation.[29] The enzymatic activity of thrombin is regulated by endogenous inhibitors. α_2-Macroglobulin[30] as well as the serpins AT III[31] and heparin cofactor II[32] belong to this group of inhibitors.

In the fibrinolytic system the inactive zymogen plasminogen is converted into plasmin by plasminogen activators. The activated protease dissolves the blood clots, and the fibrin is degraded into soluble fibrin products. In this process the plasminogen activator and plasminogen bind together to the fibrin surface in order to ensure an optimal activation of plasminogen and the necessary contact with the fibrin substrate.[9] The fibrin surface also protects plasmin against inactivation by α_2-antiplasmin,[33] whilst the plasmin transported through the bloodstream is quickly inhibited by this inhibitor. Excessive reactions of plasmin in the blood leads to the consumption of the α_2-antiplasmin and degradation of the clotting factors V and VIII as well as of fibrinogen which results in a tendency towards bleeding.[34]

1.2. Leech Components: A Specific Intervention in the Blood Clotting Cascade

The adhesion and aggregation reactions of blood platelets are important targets for the development of effective antithrombotic substances.[35, 36] The active components of the leech intervene in different reaction steps in which blood platelets participate. The leech antiplatelet protein (LAPP) of the leech *Haementeria officinalis* (Table 1) inhibits the adhesion of platelets to collagen as well as the collagen-mediated aggregation.[37, 38] On the other hand, the protein calin of the leech *Hirudo medicinalis* inhibits, the adhesion of blood platelets to subendothelial structures,[39] whilst moubatin from the tick *Ornithodoros moubata* specifically inhibits the collagen-mediated aggregation reaction.[40, 41] The significant role of the glycoprotein GPIIb-IIIa for the aggregation reaction is apparent in patients with the Glanzmann syndrome.[42] As a consequence of a congenital defect or a deficiency of functioning GPIIb-IIIa, the platelets do not bind fibrinogen and do not aggregate. As this reaction is the common pathway of the platelet reaction for all stimuli, antagonists of GPIIb-IIIa can be seen as promising antithrombotic substances.[44] Decorsin obtained from the Mexican leech *Macrobdella decora* inhibits the platelet reaction since it is an antagonist of GPIIb-IIIa.[45] The antagonistic effect of this protein is mediated by the Arg-Gly-Asp (RGD-) sequence motif, as is also known for disintegrins from snake venoms.[46] The RGD sequence was originally discovered as the adhesion motif of fibronectin[47] and is also present in fibrinogen, vWF, and vitronectin circulating in the plasma. Therapeutic application in the treatment of unstable angina, acute cardiac

Table 1. Review of the anticoagulatory and fibrinolytic proteins of bloodsucking parasites.

Protein	Origin	M/kDa	Activity	Activity	Ref
hirudin	*Hirudo medicinalis*	7	thrombin inhibitor	K_i = 27 fM	[61, 88]
hemadin	*Haemadipsa sylvestris*	5.2	thrombin inhibitor	K_i = 100 fM	[72]
rhodniin	*Rhodnius prolixus*	11.1	thrombin inhibitor	K_i = 203 fM	[73]
antistasin	*Haementeria officinalis*	15	factor-Xa inhibitor	K_i = 0.4 nM	[135]
tick anticoagulant peptide (TAP)	*Ornithodoros moubata*	6.8	factor-Xa inhibitor	K_i = 0.5 nM	[136]
decorsin	*Macrobdella decora*	4.4	inhibition of ADP-induced platelet aggregation	IC_{50} = 500 nM	[20]
leech antiplatelet protein (LAPP)	*Haementeria officinalis*	16	inhibition of adhesion of platelets to collagen as well as collagen-induced platelet aggregation	IC_{50} = 60 nM	[12, 13]
calin	*Hirudo medicinalis*	55	inhibition of platelet adhesion	[a]	[14]
moubatin	*Ornithodoros moubata*	17	inhibition of collagen-induced platelet aggregation	IC_{50} = 50 nM	[15, 16]
hementin	*Haementeria ghilianii*	120	cleavage of fibrogen/dissolation of platelet-rich clots	K_m = 1 μM	[54, 55]
plaminogen activator of the vampire bat (Bat-PA)	*Desmodus rotundus*	49	activation of plasminogen/induction of fibrinolysis	k_{cat}/K_m = 4 or 174000 $M^{-1}s^{-1}$ in the presence and absence of fibrin	[49, 51]

[a] No information.

infarction, stroke, and as a supportive measure in thrombolytic therapy could be achieved with the above mentioned substances, which interfere in the platelet reactions.[44,48] As regards to the therapeutic use of such proteins and peptides, the question, however, remains open as to how the early stages of the platelet reaction, which are not inhibited by GPIIa–IIIA antagonists, affect the clotting.

The aim of the therapeutic application of plasminogen activators is the recanalization of thrombosed vessels, for example after cardiac infarction. A problem of this therapy with plasminogen activators available today (tissue plasminogen activator, single-chain plasminogen activator of the urokinase type, streptokinase, antistreplase) is in the simultaneous systemic activation of the fibrinolytic system, which results in a consumption of α_2-antiplasmin and the undesired plasmin reactions. Although the activity of tPA is fibrin-dependent, in this case it is not only the necessary therapeutic dosage, but also the additional stimulation of tPA activity through fibrin cleavage products which is responsible for these effects.[49] The vampire bat *Desmodus rotundus* possesses a plasminogen activator (Bat-PA) (see Table 1), which in vitro exhibits activity selectively in the presence of fibrin.[50,51] Therefore it is to be expected that the up to 600-fold fibrin selectivity of Bat-PA as compared to human tPA is advantageous for its pharmacological properties in thrombolytic therapies.[52] The advantage of the higher fibrin selectivity could, however, be reduced by the nonhuman origin of this proteinase and the associated danger of immune reactions. In a thrombosis model, experimentally occluded femoral arteries in rabbits were quickly recanalized by Bat-PA without triggering systemic effects such as fibrinogenolysis or plasminogen deficiency.[53] Bat-PA could, therefore, enhance the safety and effectiveness of a thrombolytic therapy, since the negative side effects of the thrombolytic therapies used up until now in the animal model were not observed. These results should at present, however, not be overestimated, since the fibrin selectivity attained in animal experiments with tPA was not confirmed in humans.[54] Moreover, the high fibrin selectivity of bat-PA in no way signifies a guarantee for a reduced risk of bleeding, since the converse is conceivable, that is the selectivity aimed exclusively at clots might dissolve the necessary hemostatic occlusion. Fundamentally, there is the danger in the application of plasminogen activators that thrombus-bound thrombin is released, which can lead to renewed clotting and especially the activation of platelets through cleavage of the thrombin receptor.[25,26] Accompanying antithrombotic measures certainly have a positive effect on the thrombolysis.[55]

Depending on the origin of a clot, platelet-rich or erythrocyte-rich clots can form. The hementin enzyme,[56] present in the leech *Haementeria ghilianii* (see Table 1) in the Amazon region, effects a specific and effective dissolution of platelet-rich thrombuses.[57] As tPA is relatively ineffective against platelet-rich clots in therapeutic doses,[58] hementin could as a result of its property, complement the thrombolytic therapeutic agents employed today.

The formation of thrombin in the blood clotting cascade causes the formation of all clots. A series of leeches and ticks have highly potent inhibitors (see Table 1) to control this key enzyme (hirudin, hemadin, rhodniin) or the thrombin activator factor Xa (antistasin, tick anticoagulant peptide (TAP)). These inhibitors have already proved themselves in vivo in a series of arterial as well as venous thrombosis models.[59–62] After a detailed presentation of the thrombin/hirudin complex formation and the development of hirudin mimetics the pharmacological aspects of these inhibitors will be discussed (see Section 4).

2. Thrombin/Hirudin Complexes: Hirudin, the Basic Structure of a New Class of Serine Protease Inhibitors

Based on the primary structure of hirudin,[63–65] consisting of 65 amino acid residues, the hirudin molecule can be divided into two regions: an N-terminal domain held together by three disulfide bridges and a C-terminal region, which shows a high content of acidic amino acid residues (Fig. 2A). An additional

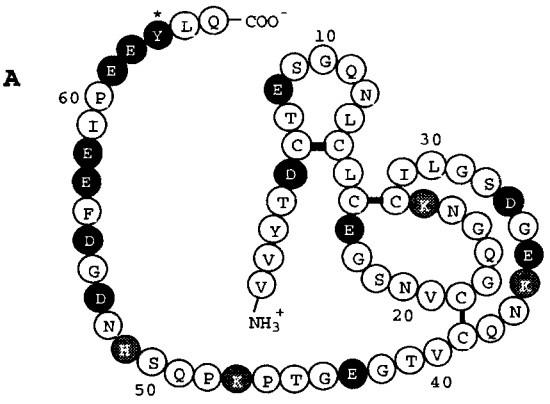


Fig. 2. Primary structures of hirudin-type thrombin inhibitors from leeches. A) Complete covalent structrure of hirudin[65]; *: the amino acid residue Tyr63 in naturally occurring hirudin is posttranslationally esterified with a sulfate. B) Comparison of the sequences of the isoforms 1–5 of hirudin from *Hirudo medicinalis*(1,2) [64,67]; *Hirudinaria manillensis*(3,4) [71,72]; *Haemadipsa sylvestris* (5) [73] (y: tyrosine sulfate ester; t: O-glycosylation of threonine). Hemadin (5) shows little sequence identity to the other inhibitors. It can, however, on the grounds of common structural characteristics be classed with the hirudin-type inhibitors [73].

acidic residue is produced by posttranslational modification of the tyrosine residue at position 63 into a sulfate ester *y*.[63,66,67] Up until now more than 20 primary structures of different forms of hirudin have been elucidated,[64,67–70] which partly differ only by few residues and show a minimal identity of 65% (Fig. 2B). In the *Hirudinidae* family, hirudin-type inhibitors, also from the leech *Hirudinaria* manillensis, were isolated and cloned.[71,72] The thrombin inhibitor hemadin from *Hemadipsa sylvestris* (family *Haemadipsidae*) is up until now the smallest naturally occurring thrombin inhibitor with 57 amino acid residues. It has, indeed, very little sequence identity to hirudin

(Fig. 2B), but based on common structural features, can be classed as the same type of inhibitor.[73]

The elucidation of the primary structure of hirudin forms made possible the cloning of a cDNA of hirudin[74] as well as the chemical synthesis of the corresponding genes.[75, 76] Production of the protein by genetic engineering methods facilitated structural investigations of the inhibitor in solution, the structural elucidation of the complex formed between thrombin and hirudin by X-ray structural analysis of protein crystals, and kinetic studies of the thrombin/hirudin complex formation using mutants of hirudin. In the following, hirudin mutants are designated as XnY-hirudin, where the amino acid residue X (single letter nomenclature) is replaced by the amino acid residue Y at position n.

2.1. The Three-Dimensional Structure of the Thrombin/r-Hirudin Complex

Based on its homology to trypsin and chymotrypsin, thrombin belongs to the class of the trypsin-like serine proteases. Like trypsin, thrombin has a specificity for basic amino acid residues in the P1 position of substrates. It is capable of cleaving a series of small peptide substrates but shows a marked specificity over macromolecular substrates. The structural basis for its substrate specificity was apparent from the three-dimensional structure of thrombin in the complex with the inhibitor D-Phe-Pro-Arg-chloromethyl ketone (PPACK-thrombin) (Fig. 3).[77] The active site with its catalytically active amino acid residues proceeded (see Figs. 3 and 4) from west to east with the binding of substrates from the N to the C terminus. Towards the "east rim", the active site forms a groove, the fibrin(ogen) binding site (FBS). The catalytic triad Ser195-His57-Asp102 does not differ from the other trypsin-like serine proteases; however, insertions as regards to trypsin lead to a deepening and narrowing of the structure of the active site. This is limited towards the "north rim" by the (Tyr-Pro-Pro-Trp)-loop and towards the "south

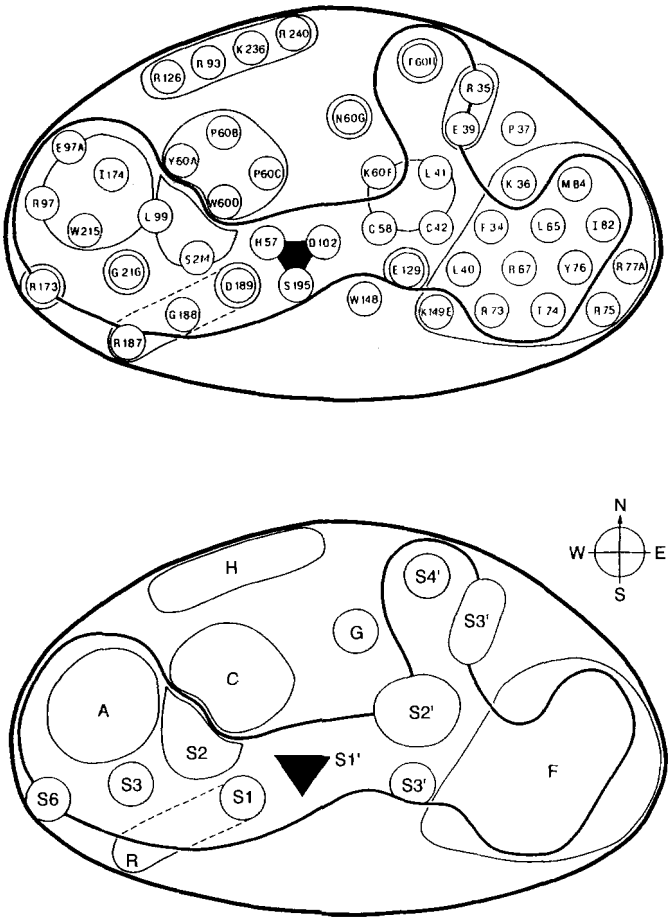


Fig. 4. Schematic representation of binding sites on the thrombin surface, from ref.[106]. Top: Representation of amino acid residues that are involved in the formation of the binding site; bottom: division of the surface into functional areas. ▼ = active site; S1–S6 = N-terminal specificity pockets to the cleavage site; A = aryl binding site; F = fibrin(ogen) binding site; H = assumed heparin binding site; G = glycosylation; S1′–S4′ = assumed C-terminal specificity pockets to the cleavage site; C = chemotactically acting region; R = Arg-Gly-Asp sequence. The compass defines the orientation relative to the active site.

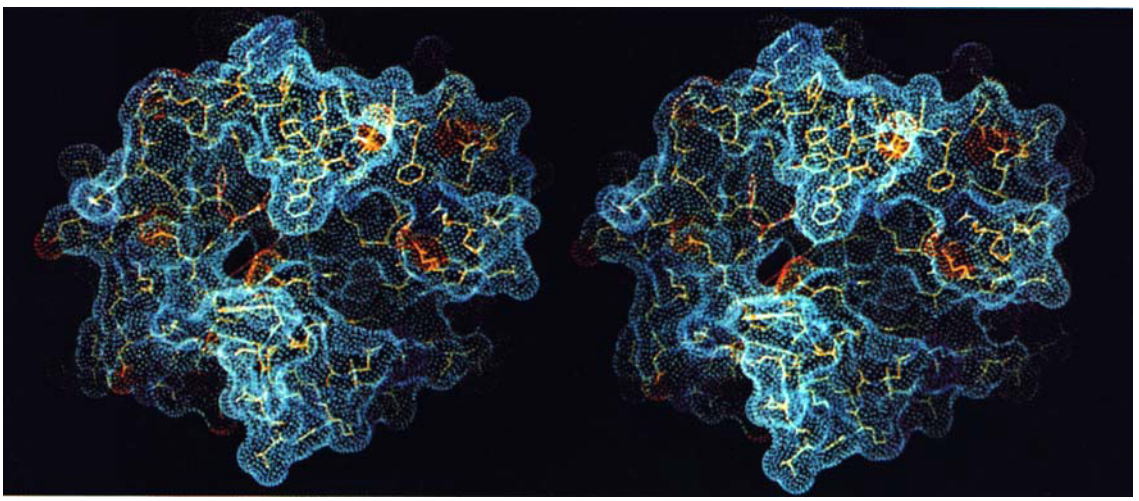


Fig. 3. View into the active site of human thrombin; stereorepresentation from ref.[77]. The molecular surface, represented by points (dot surface), corresponds to the portion of van der Waals radii of surface atoms, which is able to come into contact with solvent molecules (Connolly surface) [141]. The dark blue, orange-red, or light blue surfaces represent basic, acidic, or other amino acid residues, respectively. The peptide-based irreversible inhibitor D-Phe-Pro-Arg-chloromethylketone (orange-red) is bound in the active site. The side chain of the arginine residue of this inhibitor penetrates the specificity pocket S1. The recognition of macromolecular substrates occurs in the fibrin(ogen) binding sites, a groove running along the thrombin surface, which extends along the active site from west to east.

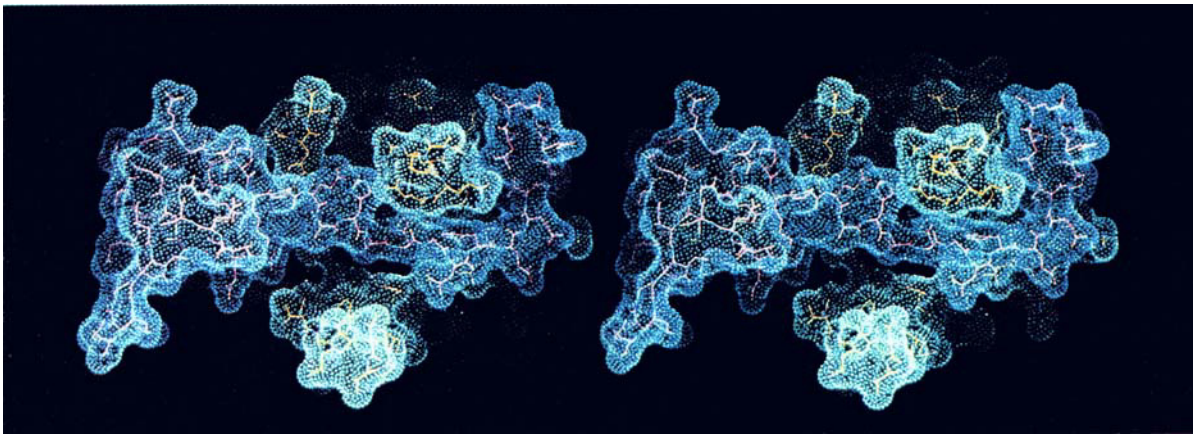


Fig. 5. Stereorepresentation of the structure of the thrombin/r-hirudin complex. A section of the thrombin structure is green, the hirudin structure is shown blue. The N-terminal region of the inhibitor (h-Tyr3 to h-Lys47) folds into a globular domain (left), whilst the C-terminus of the hirudin proceeds into a stretched out form along the FBS of thrombin and ends in a short 3_{10} helix. The orientation of thrombin corresponds to that shown in Figs. 3 and 4.

rim" by the Trp148-loop (Glu146 to Gly149D,[*] also called γ-loop) (Fig. 4). These additional structural elements determine in part the specificity of thrombin through steric exclusion of protein substrates. It was apparent from molecular modeling studies that "canonical protease inhibitors" would collide especially with the rigid (Trp-Pro-Pro-Trp)-loop, giving rise to a weak interaction with thrombin.[78] The primary specificity pocket S1 has an aspartic acid residue (t-Asp189),[**] which forms salt bridges with positively charged side chains of basic P1 residues. The hydrophobic S2 pocket is suitable for accommodating nonpolar residues of intermediate size (Pro, Ile, Ala, Val) and forms another hydrophobic pocket (aryl binding pocket A), which can interact especially with aromatic residues (Fig. 4). In the cleavage of macromolecular substrates such as fibrinogen, interactions with the active site of thrombin are not sufficient; in addition the recognition of the FBS is required.[79–81] These binding sites are formed from an accumulation of positively charged amino acid residues from the peptide chains t-Phe34 to t-Leu41 and t-Lys70 to t-Glu80 (Fig. 4).

In the complexes between serine proteases and inhibitors, which react with each other according to a "canonical pattern", an antiparallel β-sheet forms between the amino acid residues of a peptide loop situated on the surface of the inhibitor (reactive site loop) and the active site of the enzyme. The tertiary structure of this peptide loop is conserved in a family of inhibitors (e.g. Kazal, Kunitz, etc.). The conformation of the "reactive site loop" is practically identical in the free and in the bound form, and it is assumed that stabilization of the conformation by interactions with the core region of the inhibitor leads to stable enzyme/inhibitor complexes.[82] The "reactive site loop" is coordinated like a substrate by the target enzyme. It contains a hydrolyzable peptide bond (P1–P1′), whose P1 amino acid side chain determines the primary specificity of an inhibitor for a protease,[83] since the side chain of the P1 amino acid residue in this case binds in the specificity pocket (S1) of the target protease.[82]

The structure of the thrombin/r-hirudin complex in the crystal shows that from its mode of action, hirudin, in contrast to the canonical inhibitors, is a bivalent inhibitor.[84, 85] Hirudin is in contact with the active site at one end and with the FBS of thrombin at the other end (Fig. 5). In the complex the disulfide-bridged N-terminal domain (residues 1–48) lies above the active site of the thrombin molecule and, thus, prevents substrates gaining access to the active site. The C-terminal chain of the r-hirudin, which is completely disordered in solution,[86,87] adopts a stretched conformation and lies in the long groove on the thrombin surface which forms the FBS.

The N terminus of the inhibitor has essentially the same structure in the complex as in solution (determined by NMR studies).[86, 87] The N-terminal residues h-Ile1[***] to h-Thr4 penetrate the active site of thrombin (Fig. 6), in which the residues from h-Ile1 to h-Tyr3 form a parallel β-sheet with the thrombin residues t-Ser214 to t-Gly219. The free α-amino group of the N terminus of r-hirudin forms hydrogen bonds with the hydroxyl oxygen atom of the t-S195 residue participating in the catalysis and further with the carbonyl oxygen atom of the t-Ser214 residue. The side chain of h-Ile occupies the hydrophobic S2 pocket and the phenyl ring of h-Tyr3 residue fits into the aryl binding site (Fig. 6). Remarkably, the specificity pocket S1 remains unoccupied. Although h-Thr2 is situated at the entrance to this pocket, the side chain is too small to penetrate this pocket significantly. Intramolecular hydrogen bonds between the ε-amino group of the h-Lys47 residue and h-Thr4 or h-Asp5 could restrict the degrees of freedom of the five N-terminal residues. The N-terminal tripeptide is orientated in its position in the complex by a salt bridge between h-Asp5 and t-Arg221-A. A large proportion of the N-terminal domain does not interact with α-thrombin. Of the 48 N-terminal residues 15 are directly involved in 103 interactions of less than 4 Å; 41 of these intermolecular contacts[78] are attributed to the N-terminal tripeptide of the hirudin.

[*] The nomenclature of the amino acid residues is given according to ref.[77]. The numbering refers to the topologically equivalent residues of chymotrypsin. With insertions as regards to chymotrypsin one starts with the corresponding position (e.g. Thr149), assigning this number to the corresponding residue (here Gly) and add A, B, C, and so on (according to the position within the inserted amino acid residues, here D).

[**] The prefix t- denotes the amino acid residues of thrombin.

[***] The prefix h- denotes amino acid residues of hirudin.

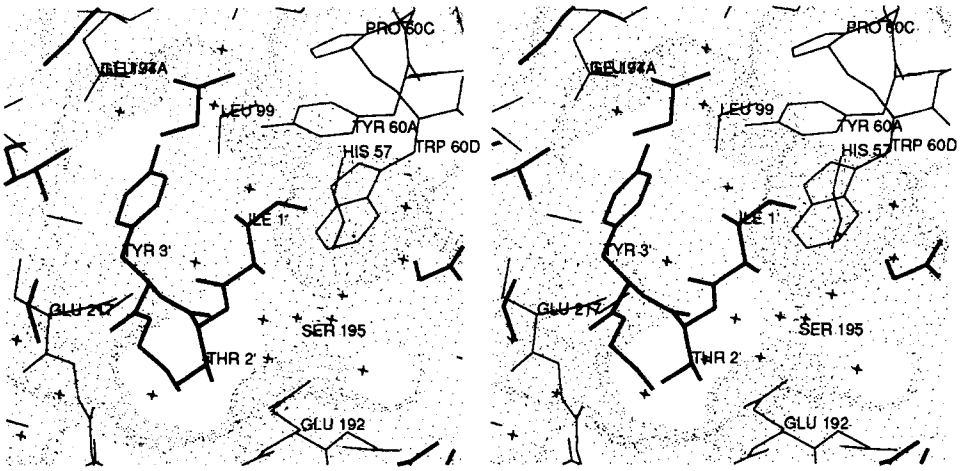


Fig. 6. The hirudin region h-Ile1–h-Thr4 (thick lines; nomenclature of the hirudin residue see Fig. 4) surrounded by amino acid residues of thrombin (thin lines), which are shown with the Connolly surface (see Fig. 3) and water molecules (crosses). The white area around h-Thr2 marks the entrance to the S1 pocket, which in the thrombin/r-hirudin complex is not occupied by an amino acid side chain of the inhibitor. The amino acid residue h-Ile1 occupies the hydrophobic S2 pocket of thrombin, its α-amino group is in hydrogen bonding distance to t-His57 Nε and t-Ser195 Oγ. Stereorepresentation from ref.[82]

The C-terminal region of the r-hirudin present in a stretched conformation (3.7 nm) with the positions 48–65 occupies the FBS (Figs. 5 and 7). A knick in the peptide chain at h-Asp55 causes a division into two regions of 1.8 nm and 1.9 nm in length. The C-terminal peptide chain begins with a polyproline-II helix of h-Pro46 to h-Pro48 followed by the residues h-Glu49 to h-His51, which form salt bridges and hydrogen bonds with thrombin. The following three residues cannot be described in more detail due to the difficulty in interpreting the electron density map. In this peptide segment there are 33 intermolecular contacts of less than 4 Å with thrombin. The conformation of the residues h-Asp55 to h-Pro60 is likewise stretched (1.5 nm long). The C terminus ends with a 3_{10} helix, which is formed from the amino acid residues h-Glu61 to h-Leu64. The contacts with the enzyme stem partly from ionic interactions between the acidic (h-Asp55, h-Glu57, h-Glu58, h-Gln65) and the basic residues of the FBS, and partly from nonionic interactions (h-Phe56, h-Ile59, h-Pro60, h-Tyr63, h-leu640). Of the 11 amino acid residues of the C terminus, eight residues form 81 contacts of less than 4 Å with thrombin.

The structure of the thrombin/r-hirudin complex is assigned to a completely novel bivalent type of inhibitor. Hence, it was also of biochemical interest to investigate more closely the complex formation.

2.2. The Formation of the Thrombin/Hirudin Complex

Studies to determine the role of individual amino acid residues or of structural areas of the molecule for the complex formation were partly carried out prior to X-ray structural analysis with r-hirudin mutants and hirudin fragments, chemically or enzymatically modified forms of thrombin, peptide antibodies against parts of the thrombin and chemical modifications of the amino acid residues of enzyme/inhibitor complexes. The studies provided a schematic picture of the formation of thrombin/hirudin complexes. In the following, studies shall be discussed in the context of the structure of the complex that are a prerequisite for an understanding of the formation mechanism.

Natural hirudin reacts quickly with α-thrombin ($k_{on} = 4 \times 10^8\ M^{-1}s^{-1}$) with the formation of 1:1 equimolar complexes ($K_i = 2.7 \times 10^{-14}$ M).[88] Hirudin can be regarded as a thrombin-specific inhibitor, even if recently the inhibition of the clotting enzyme factor Xa was determined to have an inhibition constant K_i of approximately 3×10^{-3} M.[89]

Studies of the kinetics of the thrombin/hirudin complex formation show that hirudin is a competitive inhibitor.[88] This is in agreement with the crystal structure of the complex, which excludes a simultaneous binding of the substrate and the three N-terminal residues of hirudin (see Fig. 5).[84] Since the apparent association rate constant, k_{on}, is dependent on the ionic strength and not, however, on the substrate concentration, a mechanism with at least two reaction steps was postulated.[88, 90] The elucidation of the reaction steps was achieved by stopped-flow measurements with r-hirudin.[91] The first and rate-determing step involves the binding of the C terminus of hirudin to thrombin. A rate constant of $2.9 \times 10^8\ M^{-1}s^{-1}$ was determined for this bimolecular step. After a change in conformation the N terminus reacts with the active site in the third step. For the

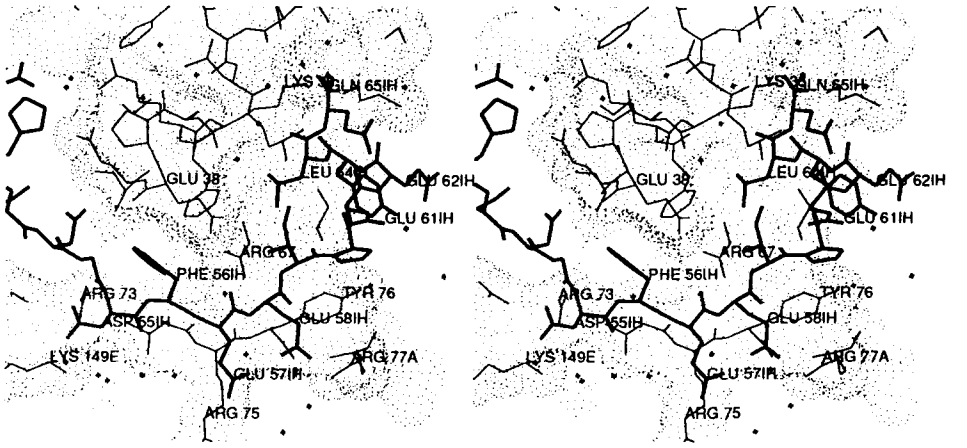


Fig. 7. Fibrin(ogen) binding sites of thrombin (thin lines) and C-terminal region of hirudin (thick lines) in the thrombin/r-hirudin complex, stereorepresentation from ref.[82]. The structure of thrombin is shown together with the Connolly surface.

decomposition of the complex the dissociation of the N terminus is rate-determining.

The free energy of binding of the reaction between r-hirudin and α-thrombin ($\Delta G_B = -75$ kJ mol^{-1}) virutally consists of the sum of the free energy of binding of the N terminal ($\Delta G_B = -42$ kJ mol^{-1}) and C terminal ($\Delta G_B = -32.6$ kJ mol^{-1}) hirudin fragments hirudin(1–51) and hirudin(52–65).[79, 81] That is, the binding of one fragment does not exert a large cooperative effect on the binding of the other fragment.[79, 81] However, C-terminal peptides modulate the amidolytic activity of the thrombin against tripeptidyl substrates.[79–81, 92] The peptides, depending on length and substrate, act as hyperbolic inhibitors or activators, that is catalytically active ternary enzyme/substrate/peptide complexes are formed. In the presence of the C-terminal peptide hirudin(52–65), the Michaelis constant for the tripeptidyl substrate is two to fourfold lower, and interaction with the N-terminal fragment is favorable by 2–3 kJ mol^{-1}.[79] The binding of C-terminal hirudin peptides leads to conformational changes in the γ-loop of thrombin, just as does the binding of "active site"-directed inhibitors.[93] The communication between the FBS and the active site by conformational changes in the γ-loop has, however, yet to be proven.[93] In the cleavage of fibrinogen, the C-terminal peptides behave as competitive inhibitors, which points to a mutually exclusive interaction with the FBS.[80, 81] N-terminal fragments of hirudin behave, as would be expected, as competitive inhibitors of fibrinogen cleavage and of tripeptidyl substrates.[79, 81]

Studies with shortened forms of hirudin already indicated the significance of an intact N terminus for the complex formation.[94] The contribution of the N terminal three amino acid residues for the complex formation were investigated by site-directed mutagenesis.[95–97] The two N-terminal positions, which in all forms of natural hirudin have branched hydrophobic amino acid residues, tolerate the exchange of amino acid residues to varying degrees. A comparison of the free energies of binding of the natural hirudins with those of the corresponding double mutants indicated that there was no cooperative effect in the binding of both the residues,[97] which would have been expected in the case of an interaction among the residues, or if the reaction mechanism had altered. Substituting the two N-terminal valine residues with glycine causes the free energy of binding to be lowered by 20.6 kJ mol^{-1} and may be considered to represent the maximal contribution to the complex formation (Table 2). Remarkably, the V2R mutant, which as a result of the lowering of the dissociation rate constant, has a K_i value one order of magnitude lower than that of r-hirudin. Based on molecular modeling studies one can assume that the arginine residue penetrates the specificity pocket and forms a salt bridge with t-Asp189.[97] One should, on the grounds of homology, postulate this interaction for the naturally occurring thrombin inhibitors from *Hirudinaria manillensis* and *Haemadipsa sylvestris* [73] (Fig. 2B). The h-Tyr3 residue forms a contact with the aryl binding pocket, which is formed from the t-Tyr60-A, t-Ile174, t-Trp60-D, and t-Leu99 residues. Furthermore, an interaction is observed with the aromatic system of t-Trp215, which is arranged perpendicular to the h-Tyr3 residue. The free energy of binding of the Y3A mutant, reduced by 12.6 kJ mol^{-2} (Table 2), underlines the significance of this aromatic residue,

Table 2. Kinetic parameters for the inhibition of α-thrombin with mutants of r-hirudin substituted at the N-terminus [a].

Inhibitor	$10^{-8} \times k_{on}$/ M^{-1} s^{-1}	$10^{5} \times k_{off}$/ s^{-1}	$10^{12} \times K_i$/ M	$-\Delta G_B$/ kJ mol^{-1}	$\Delta\Delta G_B$/ kJ mol^{-1}	Ref.
hirudin	4.7	0.98	0.021	81.0		[90]
r-hirudin	1.37	3.17	0.237	75.0		[90]
V1G	1.43	38.2	2.67	68.8	6.2	[97]
V2G			141.0	58.5	16.5	[97]
V1, 2G			694.0	54.4	20.6	[95]
V2R	1.15	0.31	0.027	80.6	−5.6	[97]
Y3A			30.9	62.4	12.6	[97]
Y3F			0.03	76.9	−4.1	[96]
			(0.18) [b]	(72.8) [b]		

[a] The change in the free energy of binding for complexes between thrombin and hirudin (designated here as the free energy of binding ΔG_B) was calculated according to the Equation $\Delta G_B = RT\ln K_i$. We have defined the change of in the free energy of binding for a particular mutant ($\Delta\Delta G_B$) relative to the free energy of binding for r-hirudin. The difference in the free energy of binding for a double mutant at positions x and y can be correlated by the Equation $\Delta\Delta G_{B(x,y)} = \Delta\Delta G_{B(x)} + \Delta\Delta G_{B(y)} + \Delta\Delta G_I$ with those of the corresponding single mutants [142]. $\Delta\Delta G_I$ is a measure of the extent of cooperation between the two sites and can be either positive or negative. [b] The values for r-hirudin from ref.[96] are given in parentheses.

which is conserved in almost every known form of hirudin up until now. Y3W- and Y3F-hirudin even show an improved affinity for thrombin (Table 2).[96]

The role of acidic amino acid residues of the C terminus of hirudin was elucidated by enzyme kinetic studies with hirudin mutants. Recombinant hirudins lack a sulfate ester at the h-Tyr63 position, which is manifest in a tenfold reduction of the equilibrium dissociation constants (see Table 2).[88, 98] Enzymatic phosphorylation[99] or sulfation[100] of h-Tyr63 restores the inhibitory properties. The negative charges of the h-Glu57, h-Glu58, h-Glu61, and h-Glu62 residues were substituted in turn with glutamine residues by site-directed mutagenesis. The contribution of the ionic and nonionic interactions to the free energy of binding was determined from the dependence of the equilibrium dissociation constants of the ionic strength for each of the mutants. The nonionic contribution is practically identical for every mutant (62.2–64.1 kJ mol^{-1}), whereas the ionic contribution decreases linearly with the decrease in the number of charges (29.6–8.9 kJ mol^{-1}). At zero ionic strength the ionic contribution constitutes approximately a third of the free energy of binding and approximately a fifth under physiological conditions.[101] The association rate constants for conditions, under which only nonionic interactions should result in a contribution, is expressed by the value $k_{on\infty}$. This value is virtually constant for all of the hirudin mutants and, thus, suggests that through the mutations no great changes in the tertiary structure of the inhibitor, which influence the interaction with thrombin, should have occurred (Table 3).[101] The contribution of the ionic interactions to the total free energy of binding is presumably, however, of secondary importance. Kinetic studies with mutants of hirudin, whose acidic amino acid residues between positions 55 to 65 were substituted, verify the dependence of the rate constant, k_{on}, on the number of charges in the molecule, which is expected for ionic interactions (Table 4).[90, 102] The decrease in the free energy of binding for each negatively charged group lies between 2.3 and 5.9 kJ mol^{-1}. Mutations at position 61 and 62 result in additive effects and do not indicate any interaction between these two residues. However, mutations at positions 57

Table 3. Effect of the ionic strength on the free energy of binding [a] and the rate constants of association [b] of the thrombin/hirudin complex formation.

Inhibitor	ΔG_{bio}/ kJ mol^{-1}	ΔG_{bio0}/ kJ mol^{-1}	$10^{-6} \times k_{on}$/ M^{-1} s^{-1}	ΔG_{io}/ kJ mol^{-1}
n-hirudin	63.3	29.6	–	–
r-hirudin	62.2	25.0	1.1	25.2
E62Q-hirudin	65.7	22.8	2.3	20.5
E57,58Q-hirudin	64.1	17.1	1.4	17.4
E57,58,62Q-hirudin	63.6	10.9	2.3	13.4
E57,58,61,62Q-hirudin	63.6	8.9	1.0	9.2

[a] The free energy of binding (ΔG_B) is calculated from the sum of the free energy of binding for nonionic ($\Delta G_{B(nio)}$) and ionic ($\Delta G_{B(io)}$) interactions. Equilibrium dissociation constants of the inhibitors were determined at ionic strengths (I) between 0.05 and 0.65. For an evaluation of the data see ref.[101]. [b] In the case of ionic interactions the rate constants of association (k_{on}) are also dependent on ionic strength. For an evaluation of the data see ref.[101].

Table 4. Influence of the charge of the C-terminal hirudin tail on parameters of thrombin/hirudin complex formation.

Inhibitor	$10^{-8} \times k_{on}$/ M^{-1} s^{-1}	$10^{5} \times k_{off}$/ s^{-1}	$10^{12} \times K_i$/ M	$-\Delta G_B$/ kJ mol^{-1}	$\Delta\Delta G_B$/ kJ mol^{-1}	Ref.
r-hirudin	1.37	3.2	0.24	75.0		[90]
E57Q	0.22	5.2	2.3	69.1	5.9	[102]
E58Q	1.1	19.9	1.8	69.7	5.3	[102]
E61Q	0.96	3.6	0.37	73.7	1.3	[90]
E62Q	0.67	3.7	0.55	72.2	2.8	[90]
E57,58Q	0.22	5.2	2.36	69.0	6.0	[90]
E61,62Q	0.45	3.9	0.87	71.5	3.5	[102]
E57,58,62Q	0.07	6.4	8.6	65.6	9.4	[90]
E57,58,61,62Q	0.04	6.3	14.1	64.4	10.6	[90]

and 58 yield a nonadditive effect, which can be accounted for by a change in the reaction mechanism or by large conformational changes of approximately 0.7 Å, which are necessary for the formation of the ion pair between h-Glu57 and t-Arg77A.[102] These results appear initially not to be in agreement with the X-ray structure, from which only intermolecular interactions between h-Asp55, h-Glu57, and h-Glu58 are apparent.[78, 84, 85, 103] Calculations of electrostatic field strengths clarify, however, that the C terminus of the hirudin and the FBS of the thrombin forms complementary electrostatic fields, whose interaction contributes to the binding energy without necessarily having to form direct ionic contacts.[82, 104] In this case the negatively charged amino acid residues of the C terminus could exert a kind of docking function, through which the number of collisions that do not lead to the product are reduced and the almost diffusion-controlled rate of complex formation is facilitated.[101] Despite the dominant function of the acidic residues of the C terminus for the thrombin/hirudin complex formation, the lowering of the free energy of binding by (in total) approximately 10 kJ mol^{-1}, when mutating h-Phe56, h-Pro60, and h-Tyr63 to alanine (see Table 4), shows clearly the contribution of nonpolar interactions of the C terminus to the total free energy of binding.[105]

Based on the described and until now unique pathway of the complex formation between an inhibitor and a serine protease, and the fact that hirudin shows neither a sequence nor a topological homology to the other inhibitors of the serine proteases, this inhibitor is to be regarded as having the basic structure for a new family of serine protease inhibitors.[65]

3. The Development of Hirudin Mimetics

Since the three-dimensional structures of α-thrombin and of complexes of α-thrombin and inhibitors are available, and the enzyme plays the central role in the clotting process, this proteinase is a suitable candidate for the development of antithrombotic active substances. Inhibitors of thrombin can be divided into peptide-based and nonpeptide-based compounds as well as those which are directed against the active site and/or the fibrin(ogen) binding sites.[106] Investigations on C-terminal peptides of hirudin that react with FBS have led to the synthesis of potent antithrombotic peptides and prompted the development of bivalent peptides, which react with both the active site and the FBS.

3.1. C-Terminal Peptides of Hirudin

The participation of the C-terminal amino acid residues of hirudin in the thrombin/hirudin interaction could already be deduced from the complete loss of the inhibitory activity (under the conditions of measurement) in the proteolytic decomposition of up to 22 of the C-terminal amino acid residues.[66, 94] The synthetic peptide N^{α}-acetylhirudin(46–65) (**3**; Table 5), 21 amino acids in length, is capable of inhibiting the cleavage of fibrinogen in a clotting test, without blocking the active site.[107]

Table 5. Inhibition of human thrombin by hirudin and C-terminal hirudin peptides.

Inhibitor		IC_{50} [a]	Ref.	K_i	Ref.
hirudin					
1	n-hirudin	2.3 nM	[134]	27 fM	[88]
2	r-hirudin	2.4 nM	[134]	237 fM	[90]
C-terminal peptides					
3	N^{α}-Ac-hirudin(45–65)	1.6 μM [b]	[107]	760 nM	[81]
		0.06 μM	[92]		
4	NH_2-hirudin(45–64)	1.09 μM	[110]		
5a	NH_2-hirudin(55–65)	7.1 μM [b]	[108]		
		0.35 μM	[92]		
5b	N^{α}-Ac-hirudin(55–65)	3.5 μM [b]	[92]		
6	NH_2-hirudin(53–64)	0.77 μM	[110]		
7	hirugen (= NH_2-hirudin(53–64), sulfated at Y63)	0.08 μM	[110]	560 nM	[80]

[a] IC_{50} values give the concentrations of inhibitor which double the clotting time. [b] Values for bovine α-thrombin.

This peptide was shortened to a length of eleven amino acid residues (hirudin(55–65) **5a**) or twelve amino acid residues (hirudin(53–64) **6**), whilst retaining the anticoagulatory activity (Table 5).[108–110] In the case of peptide **5a** the aromatic amino acid residue Phe56 is particularly important for the activity,[108] although this amino acid residue in hirudin only contributes 1.9 kJ mol^{-1} to the free energy of binding.[105] Sulfation of the tyrosine residue of **6** (the sulfated peptide is designated as hirugen **7**) enhances the anticoagulatory effect by a factor of 12.[110] With the aid of hirugen the interaction of the tyrosine sulfate ester with thrombin was elucidated for the first time.[111] The oxygen atoms of the sulfate group surprisingly do not form an ion pair with the charged groups, but either form a hydrogen bond directly to the t-Tyr76 or t-Ile81 residue or indirectly

through water molecules. Otherwise, the structure of the hirugen is almost identical to that of the hirudin(53–64) (**6**) in the thrombin/r-hirudin complex.

Conformational restriction of peptides through cyclization can, on the grounds of entropy, lead to the increase of its biological activity and to protection from proteolytic cleavage. Structure–activity studies on the peptide **5a** did not indicate any critical role of the amino acid residues Asp55, Glu58, Glu61, Glu62, Tyr63, Leu64, and Gln65 for the activity of this peptide.[108] The residues 58 and 61 were, based on molecular modeling studies, selected for the cyclization with formation of a lactam ring.[112] The amino acid residue Glu61 was replaced by either lysine or ornithine, and the residue 58 was replaced by glutamic acid or aspartic acid. This approach enabled the investigation of the ring-size dependence (16- to 18-membered lactam rings) of the antithrombotic activity of cyclized peptides. Amongst these peptides the *cyclo*-(Glu58, Lys61)-[hirudin(55–65)] with an 18-membered lactam ring is the most active. These results confirmed calculations, according to which the 18-membered ring preferentially adopts one conformation, which is similar to that in the bound state.[112] The biological activity of this peptide is, however, only higher by a factor of 2–4 than that of the corresponding linear peptide. One possible explanation might be found in the observation that C-terminal peptides already adopt an ordered structure in solution, which is similar to that in the bound state.[113] The stability of the cyclized peptides to proteolytic decomposition by plasma proteases as well as by pepsin, trypsin, and chymotrypsin is considerably enhanced. This protection is also partly manifest in the exocyclic peptide bonds of the inhibitors.[112]

3.2. Bivalent Thrombin Inhibitors Based on Hirudin Peptides

The C-terminal hirudin peptides indeed, possess structural elements for the specific recognition of thrombin; however, they cannot interact with the active site. Inhibitors, which utilize additional binding sites outside of or in conjunction with the active site, should have enhanced specificity and activity. Therefore the aim was to synthesize potent bivalent thrombin inhibitors by coupling peptides, which show a) a thrombin-specific recognition sequence and b) an inhibition of the active site of thrombin.

The similarity of the hirudin sequence Thr(45)-Pro-Lys-Pro(48) to the thrombin cleavage site Thr(154)-Pro-Arg-Ser(157) in the prothrombin molecule,[63] and the occurrence of the sequence D-Phe-Pro-Arg-X in thrombin inhibitors, which interact with the active site (X represents a non-cleavable bond), prompted the idea to substitute the amino acid residues Thr45 with D-Phe and Lys45 with Arg in the peptide **3**.[92] The residues 55–65 should facilitate the first interaction of this inhibitor with the FBS and support the intramolecular reaction with the active site. The two separate binding sites are separated by four amino acid residues in the substituted peptide. Whilst N^{α}-acetylhirudin(55–65) (**5b**) and D-Phe-Pro-Arg-Pro show IC_{50} values of 3.5 (see Table 5) and 250 μM, respectively, in the clotting test with bovine α-thrombin, coupling of the two binding sites across a spacer (peptide **8**, Table 6) effects a lowering of the IC_{50} values to 70 nM (4.1 nM for the human enzyme).[92] The free energy of binding of the two inhibitors behaves additively in the coupling as has already been described for the hirudin amino and carboxy terminal fragments (see Section 2.2). Peptide **8** is a competitive inhibitor of thrombin-mediated cleavage of tripeptidyl substrates with K_i values of 31 nM and 2.8 nM for bovine and human α-thrombin, respectively (Table 6).[92] Peptides of the general formula D-Phe-Pro-Arg-Pro-$(Gly)_n$-[hirudin(53–64)] (hirulog **9**) exhibit a comparable inhibitory activity with K_i values in the nM region.[114] The inhibitory effect is dependent on the number of glycine residues n (n = 2, 4, 6, 8). Hirulog compounds with n = 4–8 glycine units have K_i values of 2.3–3 nM, whilst a shorter spacer (n = 2) effects an increase in the K_i value of up to 64 nM. The specificity of hirulog-1 (n = 4) for thrombin was confirmed by studies on the inhibition of the enzyme factor Xa, plasmin, and trypsin; their amidolytic activity is scarcely influenced by hirolog-1, even with a 1000-fold molar excess. The X-ray structure analysis of the thrombin/hirulog-1 complex[111] showed that the interactions of individual functional regions of the bivalent inhibitor corrrespond to those of the individual components in the complex.

Table 6. Inhibition of human thrombin by peptides, which mimic the reaction mechanism of hirudin. The bivalent peptides deactivate the enzyme by interactions of the N-terminal amino acid residues (shown in three letter code) with the active site and blocking the FBS by the acidic C-terminal amino acid residues (the positions on the hirudin are given). These regions are coupled together by a suitable spacer (the amino acid residues are given in single letter code).

Inhibitor		IC_{50}/nM [a]	Ref.	K_i/nM	Ref.
bivalent peptides					
8	N^{α}-Ac-(D-Phe)-Pro-Arg-Pro-Q-S-H-N-D-G-[hirudin(55–65)]	70 [b]	[92]	31	[92]
		4.1	[92]	2.8	[92]
9	NH_2-(D-Phe)-Pro-Arg-Pro-G-G-G-G-[hirudin(53–64)]	3.9	[115]	2.3	[110]
bivalent peptides with more stable Arg-X bond					
10	N^{α}-Ac-(D-Phe)-Pro-Arg$\Psi(COCH_2)$-Gly-Q-S-H-N-D-G-[hirudin(55–65)]			0.37	[92]
11	NH_2-(D-Phe)-Pro-(β-homo-Arg)-G-G-G-G-G-[hirudin(53–64)]			7.4	[117]

[a], [b] see Table 5.

Although the P1′ amino acid residue constitutes an imino amino acid, peptides **8** and **9** are slowly hydrolyzed by thrombin.[92, 115] The reversal of the configuration at the proline residue 48, indeed, leads to proteolytic resistance of the Arg–D-Pro peptide bond; however, the K_i value (46 nM) and the IC_{50} value (45 nM) are enhanced.[92] Consequently, inhibitors with a noncleavable Arg–X bond were, thus, developed. Peptide **10** (see Table 6) was synthesized based on peptide **8**;[116] formally in this compound the peptide link of the Arg–X bond was replaced with a noncleavable ketomethylene functionality. The P1′ residue is isosteric with a glycine residue. Peptide **10** is a competitive thrombin inhibitor as regards to the cleavage of tripeptidyl substrates with a K_i value of 370 pM (see Table 6).

A similar procedure was selected in the preparation of hirulog-3 (**11**) starting from **9**: here a β-homoarginine residue, in which the peptide bond is displaced by a methylene group, was incorporated.[117] The three-dimensional structure of the thrombin/hirulog-3 complex [118] shows that the interactions of the D-Phe-Pro-(β-homoArg) portion of the hirulog-3 ressembled those of the D-Phe-Pro-Arg sequence of the PPACK

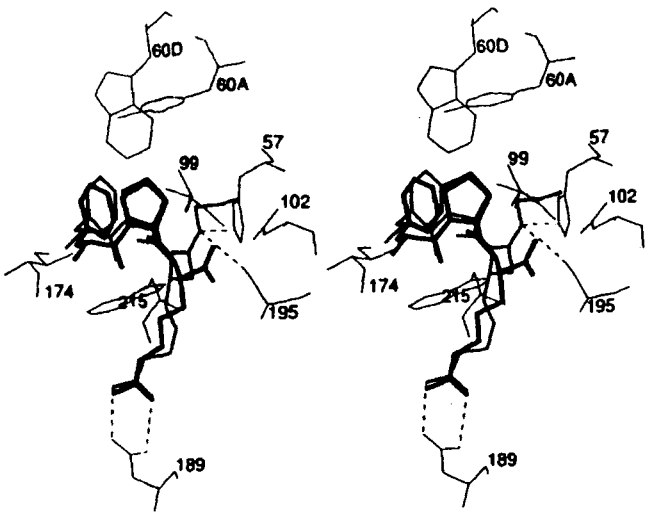


Fig. 8. Comparison of the interactions at the active site of thrombin (thin lines) between D-Phe-Pro-(β-homoArg)-Gly sequence in the thrombin/hirolog-3-complex (medium thickness) and the D-Phe-Pro-Arg sequence in the PPACK-thrombin and the thrombin/hirulog-1 complex (thick lines); stereorepresentation from ref.[118]. Hydrogen bonds are represented as dashed lines. The numbering of the amino acid residues of thrombin is given in accordance with [*] on page 872.

thrombin structure (Fig. 8). The guanidinyl group of the β-homoarginine residue forms a hydrogen bond-mediated ion pair with the t-Asp189 residue of the S1 pocket of thrombin comparable with that of the corresponding arginine residue. The methylene group of the β-homoarginine residue effects a displacement of the peptide chain by approximately one C–C bond length and thereby protects the peptide bond from nucleophilic attack by the t-Ser195 residue. The C terminii of hirulog-3 (**11**) and of r-hirudin are practically identical in structure in terms of their complexes with thrombin, whereas there is a mean structural deviation of 6 Å for the linker sequence (Fig. 9). The chain of the pentaglycine linker sequence of hirulog-3 is in much closer contact with thrombin than the corresponding r-hirudin unit. The S1′–S4′ binding sites of thrombin were identified for the first time from this structure: The P1′ amino acid side chain is restricted to small residues. The replacement of the P1′ amino acid Gly in hirulog-3 by the much larger Val residue reduces the free energy of binding by 8.6 kJ mol^{-1}, and supports this finding.[117] Alanine, serine, and threonine residues could presumably interact better than glycine, and small hydrophobic residues such as valine, leucine, and isoleucine could fill the S2′ pocket very well. The S3′ and S4′ pockets cannot be clearly described. Protein substrates of thrombin have either an arginine residue, or an amino acid with an amide functionality in the side chain or with a small side chain (e.g. Ser, Ala, Gly) at the P3′ position. However, the question still remains open whether natural substrates of thrombin are similarly in very close contact with thrombin in the P1′–P2′ region as the pentaglycine linker sequence of **11**. Since the P1′–P4′ residues in hirulog-3 are all glycine residues which can only undergo very weak interactions with thrombin, again from the thrombin/hirulog-3 structure new aspects for optimizing the antithrombotic activity of bivalent peptide inhibitors came to light.

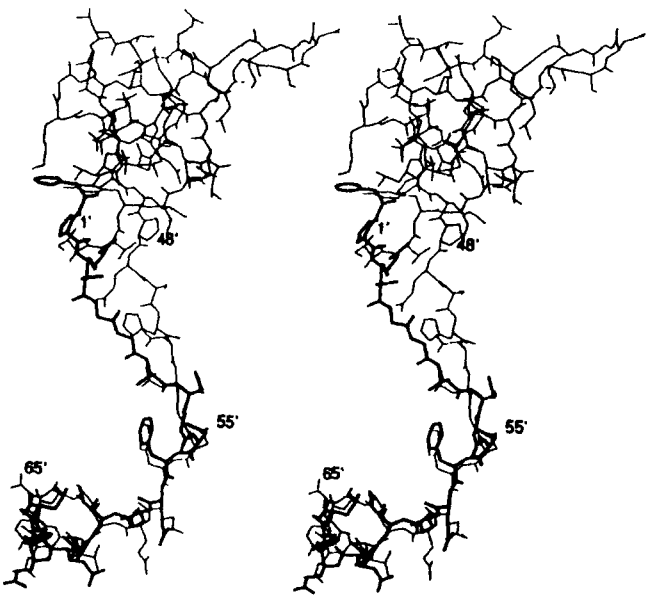


Fig. 9. Comparison of the structures of r-hirudin [84] (thin lines) and hirulog-3 [118] (thick lines) in their complexes with thrombin (stereorepresentation). Only the structures of the inhibitors are shown.

In this section the development of selective bivalent thrombin inhibitors based on hirudin has been described. In vitro hirudin and the thrombin-specific bivalent hirudin analogues of the compound types **9** to **12** possess similar anticoagulatory properties (see Table 6). Since these peptides, like hirudin, inhibit the activity of the protease thrombin and are presumably less antigenic than hirudin, they have aroused great interest in the last two to three years due to their clinical relevance and have led to the development and investigation of pharmacological properties of hirudin mimetics.[61]

4. Pharmacological Properties of Direct-Acting Thrombin Inhibitors

Experimentally produced thrombuses are prevented with hirudin (natural and recombinant) and hirudin analogues. This is applicable in vivo for venous thrombuses as well as for arterial occlusions.[60, 61, 119] What are the differences that make hirudin and hirudin mimetics (i.e. direct-acting thrombin inhibitors) particularly advantageous anticoagulants compared to heparin, which is currently the most important class of compound in the area of anticoagulants?

As has already been described in detail in this review hirudin and hiruidin mimetics react directly with thrombin. In contrast to this the effect of heparin is to interact with the plasma proteinase inhibitor antithrombin III (AT III). Heparin acts here as a cofactor and merely accelerates the complex formation of AT III with the clotting factors IXa, Xa, XIa (a = activated factor) or thrombin by several orders of magnitude.[120–123] Direct-acting inhibitors have the following advantages. 1) As the use of anticoagulants principally interferes in the clotting process, there is also the risk of bleeding. In studies on humans and animals an increase in the bleeding time was not observed in therapeutic applications of hirudin and hirudin mimetics;[59–61] in addition the direct-acting thrombin inhibitors have no effect on the blood platelets. During the application of

heparin, on the other hand, bleeding and a reduction in the number of thrombocytes presented the most important and most common complications.[124, 125] 2) Heparin is a heterogeneous preparation of glucosaminoglycans (a review is given in ref. [126]). As a result of its indirect mode of action heparin activity is coupled to the availability of the plasma protease inhibitors AT III or heparin cofactor II. Hirudin and hirudin mimetics, on the other hand, directly inhibit thrombin activity. They can, thus, be employed as effective anticoagulants even with a deficiency of AT III (e.g. disseminated intravascular coagulation) and their application does not lead to the consumption of endogenous inhibitors. 3) During the formation of a clot, a part of the α-thrombin binds to the fibrin and is trapped by the clot.[127] This thrombin is not accessible to heparin/AT III complexes and after being released from the clot has further proteolytic activity against low molecular weight and macromolecular substrates (e.g. fibrinogen).[128, 129] The direct-acting thrombin inhibitors hirudin and hirulog, however, inactivate the thrombin bound up by the clot.[127, 129, 130] 4) Neutralization of heparin by platelet factor 4, histidin-rich glycoprotein, or vitronectin as a result of an increased plasma level, or increased concentration at the site of the clotting process, could explain the limited effect of heparin.[131] The effect of direct-acting thrombin inhibitors is, on the other hand, not influenced by these proteins.

Although hirudin and r-hirudin are foreign proteins for humans and animals, they are tolerated well and do not lead to any detectable antibody formation.[132] Hirudins have a high bioavailability with simple pharmacokinetics. After a bolus injection the distribution phase lasts between 10 to 15 minutes, and a half-life of 0.5 to 1.5 hours was determined for the elimination.[60, 119, 133] Hirudins are distributed in the extracellular space and are excreted by the kidneys. 75–95% of the inhibitor is found in the urine in an unchanged and non-metabolized form.[134] Hirudins lead to a dose-dependent prolongation of the clotting parameters with intravenous as well as subcutaneous application.[59, 60, 119] The pharmacokinetic properties of hirulog-1[61] are similar. Hirulog-1 likewise effects a dose-dependent prolongation of the clotting parameters after intravenous or subcutaneous application and is eliminated by the kidneys after a half-life of approximately 0.6 hours. Hirulog is tolerated well and no antihirulog antibody formation is observed.[61]

The employment of direct-acting thrombin inhibitors is intended for the following clinical situations which have been proven in studies with animals: 1) prophylaxis and postoperative treatment of venous thrombosis and diffuse microthrombosis; 2) prevention of arterial thrombosis especially in heart surgery; 3) protection from reocclusion in fibrinolysis therapy and angioplasty; 4) protection from thrombotic occlusions in microsurgery; 5) avoidance of proliferation of smooth muscle cells of damaged vessel walls (restenosis prophylaxis) and 6) thrombosis prophylaxis during hemodialysis and other extracorporeal blood circulation (e.g. heart–lung machines).

Problems in connection with the clinical use of hirudin and hirudin mimetics can be seen in the choice of tests for monitoring the status of clotting and the availability of a hirudin antagonist. It must be determined whether measurement of the activated partial thromboplastin time (APPT), the activated clotting time (ACT), the thrombin time (TT), or thrombin inhibition in a chromogenic test give a correlation to the hirudin concentration or to the clotting status. These methods must be validated for this purpose. As antagonists of thrombin inhibitors, prothrombin complexes, monoclonal antibodies, factor VIIa, or VIIIa will be discussed, whose application remains to be assessed against the fast normalization of the clotting parameters when the inhibitor dose is stopped. To emphasize the possible advantages of the clinical application of direct-acting thrombin inhibitors, the results of some thrombosis models are presented.

Successful coronary thrombolysis depends on a fast recovery and maintenance of the blood flow in the region affected by the infarct. In tPA-induced thrombolysis in an experiment with rats the influence of thrombin inhibitors on the time until lysis of the clot and on the number of reocclusions during infusion of the inhibitor was determined.[135] Clot formation was caused by stenosis in the distal aorta after removal of the endothelial. After inducing thrombolysis with r-tPA (1 $mg\,kg^{-1}$ as a bolus injection) followed by r-tPA infusion (1 $mg\,kg^{-1}h^{-1}$ for 30 minutes) isotonic sodium chloride solution or a solution of the inhibitor (heparin, r-hirudin, or hirulog-1) were administered to the animals, in concentrations which led to a three- to fourfold enhancement of the activated partial thromboplastin time (APTT). Whereas the direct inhibitors significantly reduced the time for the lysis, heparin has no effect on the number of reocclusions during the time of observation. In the case of r-hirudin and hirulog no reocclusions occurred. It is assumed that the superior effect of direct-acting thrombin inhibitors stems from the inhibition of clot-bound thrombin, whilst in the case of heparin the thrombin released from the clots causes both the activation of blood platelets and the plasma clotting systems. In a thrombolysis model with streptokinase in dogs the influence of heparin and r-hirudin on reperfusion and reocclusion and remaining clot material was examined.[136] Whilst no recanalization was observed in the control animals, r-hirudin and heparin dose-dependently support the action of streptokinase. In the administration of r-hirudin or heparin in concentrations, which lead to a twofold prolongation of the APTT, r-hirudin shows, in contrast to heparin, a significantly higher occurrence of reperfusion (in eight out of eight animals (100%) in contrast to one out of eight animals (12%)), a shorter time up to reperfusion (33 min as opposed to 59 min), a longer lasting effect of reperfusion (106 to 10 min), and less remaining clot material. These studies were undertaken under conditions which only slightly influenced the clotting time, but did not influence the bleeding time.[136] However, the clinical relevance of these findings will only become apparent after the application of direct-acting thrombin inhibitors in humans.

The increase in the size of thrombuses in patients with venous thrombosis is as a result of the adhesion of fibrin onto already existing clots. The expansion of clots is supported by circulating and clot-bound thrombin. The development of such thrombuses can be completely inhibited by r-hirudin.[137] In a study on rabbits it was shown that r-hirudin not only effectively inhibited the enlargement of thrombuses, but this effect lasted for nine hours after infusion of r-hirudin, whilst the clotting parameters (APTT, TT) reach normal levels already 1.5 hours after infusion of the inhibitor.[138] In addition, experiments carried out in vitro

can only be interpreted by the fact that the far reaching and long lasting effect through plasma elimination again stems from the inhibition of clot-bound thrombin.

Clinical studies support the finding obtained from the animal experiments that direct-acting thrombin inhibitors have a better antithrombotic effect than heparin.[48] Advantageous application and dosage in humans and careful analysis of the data is to be determined in future studies.

5. Summary and Outlook

In the present review highly specific substances of bloodsucking parasites have been described, which specifically interfere in the complex clotting and fibrinolytic processes. The selective thrombin inhibitor hirudin from the leech *Hirudo medicinalis* belongs to this group of natural products. The structural data and structure–activity relationships of the thrombin/hirudin complex formation have been summarized, which has allowed the design and synthesis of novel hirudin derivatives.

These substances of bloodsucking parasites can also help to deepen our knowledge about the significance of individual reaction steps in blood clotting and fibrinolysis for hemostasis and thrombosis. Thus, for example, by employing hirudin or hirulog-1 for deep arterial injuries the thrombin dependency of arterial thrombotic occlusions was documented.[61] The employment of hirudin and of the specific factor Xa-inhibitor r-TAP in a thrombolysis model with r-tPA revealed that both clot-bound thrombin and active prothrombinase complexes contribute to the thrombogenicity of platelet-rich clots.[62]

The knowledge of the mode of action of the specific components of bloodsucking animals can, moreover, be useful when making specific changes to endogenous proteins. The thrombin-specific inhibitor rhodniin from the bug *Rhodnius prolixus* (see Table 1), based on its primary structure, belongs to the class of canonical proteinase inhibitors.[139] If this hypothesis should be confirmed, the results from structure–activity relationships of this leech protein could possibly be used for implementing specific changes to endogenous canonical inhibitors.

The successes outlined in the description of the hirudin mechanism, the resulting development of hirudin mimetics, and the obvious therapeutic advantages of direct-acting thrombin inhibitors should encourage us to intensify research in the area of natural products from bloodsucking parasites. A possible application of this research lies in the discovery of new proteins and the elucidation of unexpected mechanisms. Such molecules could serve as new lead structures and, as in the case of hirudin and hirudin mimetics, stimulate the specific development of better and safer anticoagulants.

I am very grateful to Priv.-Doz. Dr. W. Bode (Max-Planck Institut für Biochemie, Martinsried) for the preparation of the color illustrations.

Received: December 9, 1993 [A 41 IE]
German version: *Angew. Chem.* **1995**, *107*, 948
Translated by Dr. S. P. Auguste, Herlev (Denmark)

[1] K. Herter, *Der medizinische Blutegel und seine Verwandten*, Ziemsen, Wittenberg Lutherstadt, **1968**, p. 164–190.
[2] S. L. Adams, *Semin. Thromb. Hemostasis* **1989**, *15*, 261–268.
[3] J. B. Haycraft, *Arch. Exp. Pathol. Pharmakol.* **1884**, *18*, 209–217.
[4] F. Markwardt, *Hoppe-Seyler's Z. Physiol. Chem.* **1957**, *312*, 85–89.
[5] P. Walsmann, F. Markwardt, *Pharmazie* **1981**, *36*, 653–660.
[6] E. W. Davie, K. Fujikawa, *Annu. Rev. Biochem.* **1975**, *44*, 799–829.
[7] C. M. Jackson in *Methods of Enzymatic Analysis, Vol. V* (Ed.: H. U. Bergmeyer), 3rd ed., VCH, Weinheim, **1984**, pp. 316–351.
[8] P. B. Tracy, *Semin. Thromb. Hemostasis* **1988**, *14*, 227–233.
[9] D. Collen, *Thromb. Haemostasis* **1980**, *43*, 77–89.
[10] M. H. Kroll, A. I. Schafer, *Blood* **1989**, *74*, 1181–1195.
[11] L. F. Brass, J. A. Hoxie, D. R. Manning, *Thromb. Haemostasis* **1993**, *70*, 217–223.
[12] R. O. Hynes, *Cell* **1992**, *69*, 11–25.
[13] R. O. Hynes, *Thromb. Haemostasis* **1991**, *66*, 40–43.
[14] K. G. Mann, *Trends Biochem. Sci.* **1987**, *12*, 229–233.
[15] G. J. Broze, Jr., *Trends Cardiovasc. Med.* **1992**, *2*, 72–77.
[16] G. J. Broze, Jr., T. J. Girard, W. F. Novotny, *Biochemistry* **1990**, *29*, 7539–7546.
[17] S. I. Rapaport, *Thromb. Haemostasis* **1991**, *66*, 6–15.
[18] J. W. Fenton II, D. H. Bing, *Semin. Thromb. Hemostasis* **1986**, *12*, 200–208.
[19] J. W. Fenton II, *Semin. Thromb. Hemostasis* **1988**, *14*, 234–240.
[20] B. Blomback, M. Blomback, *Ann. N.Y. Acad. Sci.* **1972**, *202*, 77–97.
[21] L. Lorand, R. B. Credo, K. J. M. Miloszewski, *Prog. Hemostasis Thromb.* **1980**, *5*, 245–290.
[22] M. E. Nesheim, K. G. Mann, *J. Biol. Chem.* **1979**, *254*, 1326–1334.
[23] J. J. Toole, J. L. Knopf, J. M. Wozney, L. A. Sultzman, J. L. Buecker, D. D. Pittman, R. J. Kaufman, E. Brown, C. Shoemaker, E. C. Orr, G. W. Amphlett, W. B. Foster, M. L. Coe, G. J. Knutson, D. N. Fass, R. M. Hewick, *Nature (London)* **1984**, *312*, 342–347.
[24] K. Naito, K. Fujikawa, *J. Biol. Chem.* **1991**, *266*, 7353–7358.
[25] T.-K. H. Vu, D. T. Hung, V. I. Wheaton, S. R. Coughlin, *Cell* **1991**, *64*, 1057–1068.
[26] T.-K. H. Vu, V. I. Wheaton, D. T. Hung, I. Charo, S. R. Coughlin, *Nature (London)* **1991**, *353*, 674–677.
[27] N. L. Esmon, C. T. Esmon, *Semin. Thromb. Hemostasis* **1988**, *14*, 210–215.
[28] C. T. Esmon, *J. Biol. Chem.* **1989**, *264*, 4743–4746.
[29] A. J. Marcus in *Thrombosis and Hemorrhage* (Eds.: J. Loscalzo, A. I. Schafer), Blackwell, Boston, **1994**, pp. 279–289.
[30] L. Sottrup-Jensen in *The Plasma Proteins, Vol. 5* (Ed.: F. W. Putnam), Academic Press, New York, **1987**, pp. 191–291.
[31] R. D. Rosenberg, P. S. Damus, *J. Biol. Chem.* **1973**, *248*, 6490–6505.
[32] D. M. Tollefsen, P. W. Majerus, M. K. Blank, *J. Biol. Chem.* **1982**, *257*, 2162–2169.
[33] B. Wiman, D. Collen, *Nature (London)* **1978**, *272*, 549–550.
[34] H. R. Lijnen, D. Collen, *Thromb. Haemostasis* **1991**, *66*, 88–110.
[35] N. Kieffer, D. R. Phillips, *Annu. Rev. Cell Biol.* **1990**, *6*, 329–357.
[36] D. R. Phillips, I. F. Charo, R. M. Scarborough, *Cell* **1991**, *65*, 359–362.
[37] T. M. Connolly, J. W. Jacobs, C. Condra, *J. Biol. Chem.* **1992**, *267*, 6893–6898.
[38] P. M. Keller, L. D. Schultz, C. Condra, J. Karczewski, T. M. Connolly, *J. Biol. Chem.* **1992**, *267*, 6899–6904.
[39] R. Munro, C. P. Jones, R. T. Sawyer, *Blood Coagulation Fibrinolysis* **1991**, *2*, 179–184.
[40] L. Waxman, T. M. Connolly, *J. Biol. Chem.* **1993**, *268*, 5445–5449.
[41] P. M. Keller, L. Waxman, B. A. Arnold, L. D. Schultz, C. Condra, T. M. Connolly, *J. Biol. Chem.* **1993**, *268*, 5450–5456.
[42] J. Mustard, R. L. Kinlough-Rathbone, M. A. Packham, D. W. Perry, K. R. M. Pai, *Blood* **1979**, *54*, 987–993.
[43] M. L. Bajt, M. H. Ginsberg, A. L. Frelinger, M. C. Berndt, J. C. Loftus, *J. Biol. Chem.* **1992**, *267*, 3789–3794.
[44] A. J. Nichols, R. R. Ruffolo, Jr., W. F. Huffman, G. Poste, J. Samanen, *Trends Pharmacol. Sci.* **1992**, *13*, 413–414.
[45] J. L. Seymour, W. J. Henzel, B. Nevins, J. T. Stults, R. A. Lazarus, *J. Biol. Chem.* **1990**, *265*, 10143–10147.
[46] M. S. Dennis, W. J. Henzel, R. M. Pitti, M. T. Lipari, M. A. Napier, T. A. Deisher, S. Bunting, R. A. Lazarus, *Proc. Natl. Acad. Sci. USA* **1990**, *87*, 2471–2475.
[47] M. D. Pierschbacher, E. Ruoslathi, *Nature (London)* **1984**, *309*, 30–33.
[48] E. J. Topol, E. F. Plow, *Thromb. Haemostasis* **1993**, *70*, 94–98.
[49] J. I. Weitz, B. Leslie, J. Ginsberg, *J. Clin. Invest.* **1991**, *87*, 1082–1090.
[50] S. J. Gardell, L. T. Duong, R. E. Diehl, J. D. York, T. R. Hare, R. B. Register, J. W. Jacobs, R. A. F. Dixon, P. A. Friedman, *J. Biol. Chem.* **1989**, *264*, 17947–17952.
[51] T. R. Hare, S. J. Gardell, *Thromb. Haemostasis* **1992**, *68*, 165–169.
[52] P. W. Bergum, S. J. Gardell, *J. Biol. Chem.* **1992**, *267*, 17726–17731.
[53] S. J. Gardell, T. R. Hare, P. W. Bergum, G. C. Cuca, L. O'Neill-Palladino, S. M. Zavodny, *Blood* **1990**, *76*, 2560–2564.
[54] D. Collen, H. K. Gold in *Thrombolysis in Cardivascular Disease* (Eds.: D. Julian, W. Kübler, R. M. Norris, H. J. C. Swan, D. Collen, M. Verstraete), Dekker, New York, **1990**, pp. 45–67.

[55] I. Jang, H. Gold, R. C. Leinbach, J. T. Fallon, D. Collen, *Circ. Res.* **1990**, *67*, 1552–1561.
[56] S. M. Malinconico, J. B. Katz, A. Z. Budzynski, *J. Lab. Clin. Med.* **1984**, *103*, 44–58.
[57] R. Munro, *Platelets* **1991**, *2*, 55–56.
[58] I. K. Jang, H. K. Gold, A. A. Ziskind, J. T. Fallon, R. E. Holt, R. C. Leinbach, D. Collen, *Circulation* **1989**, *79*, 920–928.
[59] F. Markwardt, G. Nowack, J. Stürzebecher, *Haemostasis* **1991**, *21*, 133–136.
[60] F. Markwardt, *Semin. Thromb. Hemostasis* **1989**, *15*, 269–282.
[61] J. M. Maraganore, *Thromb. Haemostasis* **1993**, *70*, 208–211.
[62] G. P. Vlasuk, *Thromb. Haemostasis* **1993**, *70*, 212–216.
[63] T. E. Petersen, H. R. Roberts, L. Sottrup-Jensen, S. Magnusson, *Protides Biol. Fluids* **1978**, 145–149.
[64] J. Dodt, H. P. Müller, U. Seemüller, J.-Y. Chang, *FEBS Lett.* **1984**, *165*, 180–184.
[65] J. Dodt, U. Seemüller, R. Maschler, H. Fritz, *Biol. Chem. Hoppe-Seyler* **1985**, *366*, 379–385.
[66] J.-Y. Chang, *FEBS Lett.* **1983**, *164*, 307–313.
[67] J. Dodt, W. Machleidt, U. Seemüller, R. Maschler, H. Fritz, *Biol. Chem. Hoppe-Seyler* **1986**, *367*, 803–811.
[68] S. J. T. Mao, M. T. Yates, D. T. Blankenship, A. D. Cardin, J. L. Krstenansky, W. Lovenberg, R. L. Jackson, *Anal. Biochem.* **1987**, *161*, 514.
[69] D. Tripier, *Folia Haematol. (Leipzig)* **1988**, *115*, 30–35.
[70] M. Scharf, J. Engels, D. Tripier, *FEBS Lett.* **1989**, *255*, 105–110.
[71] V. Steiner, R. Knecht, K. O. Börnsen, E. Gassmann, S. R. Stone, F. Raschdorf, J.-M. Schlaeppi, R. Maschler, *Biochemistry* **1992**, *31*, 2294–2298.
[72] E. Scacheri, G. Nitti, B. Valsasina, G. Orsini, C. Visco, M. Ferrera, *Eur. J. Biochem.* **1993**, *214*, 295–304.
[73] K.-H. Strube, B. Kröger, S. Bialojan, M. Otte, J. Dodt, *J. Biol. Chem.* **1993**, *268*, 8590–8595.
[74] R. P. Harvey, E. Degryse, L. Stefani, F. Schamber, J.-P. Cazenave, M. Courtney, P. Tolstoshev, J.-P. Lecoq, *Proc. Natl. Acad. Sci. USA* **1986**, *83*, 1084–1088.
[75] C. Bergmann, J. Dodt, S. Köhler, E. Fink, H. G. Gassen, *Biol. Chem. Hoppe-Seyler* **1986**, *367*, 731–740.
[76] E. Fortkamp, M. Rieger, G. Heisterberg-Moutses, S. Schweitzer, R. Sommer, *DNA* **1986**, *5*, 511–516.
[77] W. Bode, I. Mayr, U. Baumann, R. Huber, S. R. Stone, J. Hofsteenge, *EMBO J.* **1989**, *8*, 3467–3475.
[78] W. Bode, D. Turk, A. Karshikov, *Protein Sci.* **1992**, *1*, 426–471.
[79] S. Dennis, A. Wallace, J. Hofsteenge, S. R. Stone, *Eur. J. Biochem.* **1990**, *188*, 61–66.
[80] M. C. Naski, J. W. Fenton II, J. M. Maraganore, S. T. Olson, J. A. Shafer, *J. Biol. Chem.* **1990**, *265*, 13484–13489.
[81] T. Schmitz, M. Rothe, J. Dodt, *Eur. J. Biochem.* **1991**, *195*, 251–256.
[82] W. Bode, R. Huber, *Eur. J. Biochem.* **1992**, *204*, 433–451.
[83] M. Laskowski, Jr., I. Kato, *Annu. Rev. Biochem.* **1980**, *49*, 593–626.
[84] T. J. Rydel, K. G. Ravichandran, A. Tulinsky, W. Bode, R. Huber, C. Roitsch, J. W. Fenton II, *Science* **1990**, *249*, 277–280.
[85] M. G. Grütter, J. P. Priestle, J. Rahuel, H. Grossenbacher, W. Bode, J. Hofsteenge, S. R. Stone, *EMBO J.* **1990**, *9*, 2361–2365.
[86] P. J. M. Folkers, G. M. Clore, P. C. Driscoll, J. Dodt, S. Köhler, A. M. Gronenborn, *Biochemistry* **1989**, *28*, 2601–2617.
[87] H. Haruyama, K. Wüthrich, *Biochemistry* **1989**, *28*, 4301–4312.
[88] S. R. Stone, J. Hofsteenge, *Biochemistry* **1986**, *25*, 4622–4628.
[89] S. P. Jordan, S.-S. Mao, S. D. Lewis, J. A. Shafer, *Biochemistry* **1992**, *31*, 5374–5380.
[90] P. Braun, S. Dennis, J. Hofsteenge, S. R. Stone, *Biochemistry* **1988**, *27*, 6517–6522.
[91] M. P. Jackman, M. A. A. Parry, J. Hofsteenge, S. R. Stone, *J. Biol. Chem.* **1992**, *267*, 15375–15383.
[92] J. DiMaio, B. Gibbs, D. Munn, J. Lefebvre, F. Ni, Y. Konishi, *J. Biol. Chem.* **1990**, *265*, 21698–21703.
[93] M. A. A. Parry, S. R. Stone, J. Hofsteenge, P. Jackman, *Biochem. J.* **1993**, *290*, 665–670.
[94] J. Dodt, U. Seemüller, H. Fritz, *Biol. Chem. Hoppe-Seyler* **1987**, *368*, 1447–1453.
[95] A. Wallace, S. Dennis, J. Hofsteenge, S. R. Stone, *Biochemistry* **1989**, *28*, 10079–10084.
[96] J. B. Lazar, R. C. Winant, P. H. Johnson, *J. Biol. Chem.* **1991**, *266*, 685–688.
[97] A. Betz, J. Hofsteenge, S. R. Stone, *Biochemistry* **1992**, *31*, 4557–4562.
[98] U. Seemüller, J. Dodt, E. Fink, H. Fritz in *Proteinase Inhibitors* (Eds.: A. Barrett, G. Salvesen), Elsevier, Amsterdam, **1986**, pp. 337–359.
[99] J. Hofsteenge, S. R. Stone, A. Donella-Deana, L. Pinna, *Eur. J. Biochem.* **1990**, *188*, 55–59.
[100] C. Niehrs, W. B. Huttner, D. Carvallos, E. Degryse, *J. Biol. Chem.* **1990**, *265*, 9314–9318.
[101] S. R. Stone, S. Dennis, J. Hofsteenge, *Biochemistry* **1989**, *28*, 6857–6863.
[102] A. Betz, J. Hofsteenge, S. R. Stone, *Biochem. J.* **1991**, *275*, 801–803.
[103] T. J. Rydel, A. Tulinsky, W. Bode, R. Huber, *J. Mol. Biol.* **1991**, *221*, 583–601.
[104] A. Karshikov, W. Bode, A. Tulinsky, S. R. Stone, *Protein Sci.* **1992**, *1*, 727–735.
[105] A. Betz, J. Hofsteenge, S. R. Stone, *Biochemistry* **1991**, *30*, 9848–9853.
[106] M. T. Stubbs, W. Bode, *Thromb. Res.* **1993**, *69*, 1–58.
[107] J. L. Krstenansky, S. J. T. Mao, *FEBS Lett.* **1987**, *211*, 10–16.
[108] J. L. Krstenansky, T. J. Owen, M. T. Yates, S. J. T. Mao, *J. Med. Chem.* **1987**, *30*, 1688–1691.
[109] S. J. T. Mao, M. T. Yates, T. J. Owen, J. L. Krstenansky, *Biochemistry* **1988**, *27*, 8170–8173.
[110] J. M. Maraganore, B. Chao, M. L. Joseph, J. Jablonski, K. L. Ramachandran, *J. Biol. Chem.* **1989**, *264*, 8692–8698.
[111] E. Skrzypczak-Jankun, V. E. Carperos, K. G. Ravichandran, A. Tulinsky, M. Westbrook, J. M. Maraganore, *J. Mol. Biol.* **1991**, *221*, 1379–1393.
[112] Z. Szewczuk, B. F. Gibbs, S. Y. Yue, E. O. Purisima, Y. Konishi, *Biochemistry* **1992**, *31*, 9132–9140.
[113] F. Ni, Y. Konishi, H. A. Scheraga, *Biochemistry* **1990**, *29*, 4479–4489.
[114] J. M. Maraganore, P. Bourdon, J. Jablonski, K. L. Ramachandran, J. W. Fenton II, *Biochemistry* **1990**, *29*, 7095–7101.
[115] J. I. Witting, P. Bourdon, D. V. Brezniak, J. M. Maraganore, J. W. Fenton II, *Biochem. J.* **1992**, *283*, 737–743.
[116] J. DiMaio, F. Ni, B. Gibbs, Y. Konishi, *FEBS Lett.* **1991**, *282*, 47–52.
[117] T. Kline, C. Hammond, P. Bourdon, J. M. Maraganore, *Biochem. Biophys. Res. Commun.* **1991**, *177*, 1049–1055.
[118] X. Qiu, K. P. Padmanabhan, V. E. Carperos, A. Tulinsky, T. Kline, J. M. Maraganore, J. W. Fenton II, *Biochemistry* **1992**, *31*, 11689–11697.
[119] F. Markwardt, G. Fink, B. Kaiser, H.-P. Klöcking, G. Nowack, M. Richter, J. Stürzebecher, *Pharmazie* **1988**, *43*, 202–207.
[120] F. Markwardt, P. Walsmann, *Hoppe-Seyler's Z. Physiol. Chem.* **1959**, *317*, 64–77.
[121] I. Björk, B. Nordenman, *Eur. J. Biochem.* **1976**, *68*, 507–511.
[122] P. L. Lane, J. Denton, A. Flynn, L. Thunberg, U. Lindahl, *Biochem. J.* **1984**, *218*, 732–735.
[123] S. T. Olson, I. Björk, *J. Biol. Chem.* **1991**, *266*, 6353–6364.
[124] J. Hirsh, *N. Engl. J. Med.* **1991**, *324*, 1565–1574.
[125] B. P. Schmitt, B. Adelmann, *Am. J. Med. Sci.* **1993**, *305*, 208–215.
[126] C. A. A. van Bockel, M. Petitou, *Angew. Chem.* **1993**, *105*, 1741–1761; *Angew. Chem. Int. Ed. Engl.* **1993**, *32*, 1671–1690.
[127] C. Y. Liu, H. L. Nossel, K. L. Kaplan, *J. Biol. Chem.* **1979**, *254*, 10421–10425.
[128] P. J. Hogg, P. M. Jackson, *Proc. Natl. Acad. Sci. USA* **1989**, *86*, 3619–3623.
[129] J. I. Weitz, M. Hudoba, D. Massel, J. M. Maraganore, J. Hirsh, *J. Clin. Invest.* **1990**, *86*, 385–391.
[130] R. Bar-Shavit, A. Eldor, I. Vlodavsky, *J. Clin. Invest.* **1989**, *84*, 1096–1104.
[131] D. A. Lane, J. Denton, L. Flynn, L. Thunberg, U. Lindahl, *Biochem. J.* **1984**, *218*, 725–732.
[132] J. Bichler, R. Gemmerli, H. Fritz, *Thromb. Res.* **1991**, *61*, 39–51.
[133] F. Markwardt, J. Hauptmann, G. Nowak, C. Kleßen, P. Walsmann, *Thromb. Haemostasis* **1982**, *47*, 226–229.
[134] A. Henschen, F. Markwardt, P. Walsmann, *Folia Haematol.* **1988**, *115*, 59–63.
[135] P. Klement, A. Borm, J. Hirsh, J. Maraganore, G. Wilson, J. Weitz, *Thromb. Haemostasis* **1992**, *68*, 64–68.
[136] D. F. Rigel, R. W. Olson, R. W. Lappe, *Circ. Res.* **1993**, *72*, 1091–1102.
[137] H.-P. Klöcking, F. Markwardt, *Pharmazie* **1989**, *44*, 341–342.
[138] G. Agnelli, C. Renga, J. I. Weitz, G. Nenci, J. Hirsh, *Blood* **1992**, *80*, 960–965.
[139] T. Friedrich, B. Kröger, S. Bialojan, H. G. Lemaire, H. W. Höffgen, P. Reuschenbach, M. Otte, J. Dodt, *J. Biol. Chem.* **1993**, *268*, 16216–16222.
[140] R. T. Sawyer, *Bio/Technology* **1991**, *9*, 513–518.
[141] M. L. Connolly, *Science* **1983**, *221*, 709–713.
[142] J. A. Wells, *Biochemistry* **1990**, *29*, 8511–8517.

Combinatorial Biosynthesis—An Approach in the Near Future?

Jürgen Rohr*

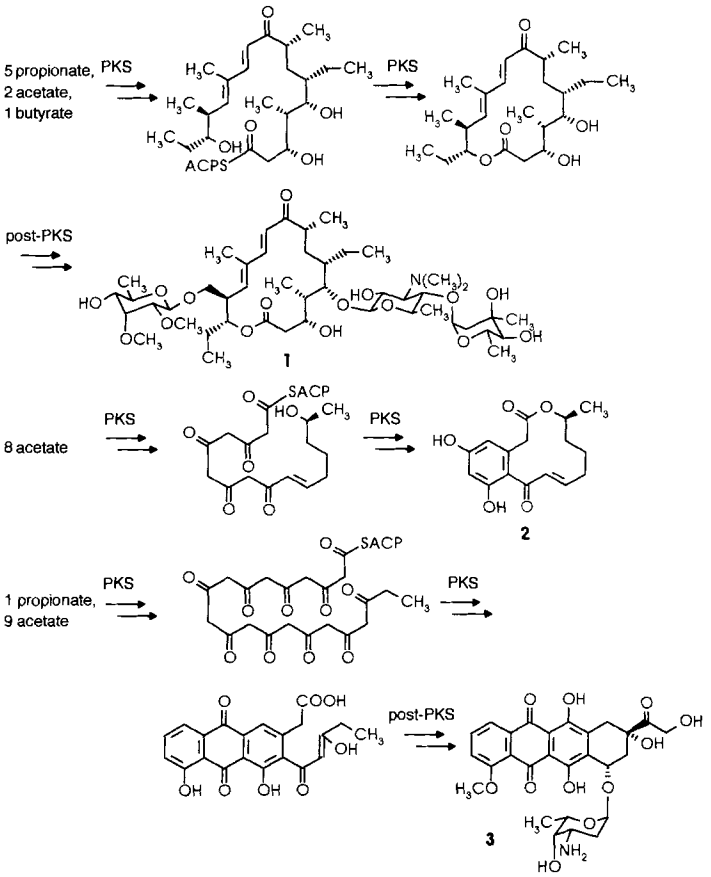
The search for new drugs requires the testing of tens of thousands of samples, whether pure compounds or natural products containing crude extracts, before a novel, promising lead structure is identified. As the chances of empirical screening assays and drug development procedures based on the natural product pool decline, it will be increasingly difficult to provide the existing screening assays with sufficient material. In this era of gene technology, an alternative strategy to the currently much discussed combinatorial chemistry approach for the generation of compound libraries[1] may be combining biosynthetic genes or changing them. Arbitrary or selective mutation may yield a whole palette of novel molecules and their variants, or specially tailored potential drugs. Recent developments in the polyketide area provide an optimistic outlook for restructuring and recombining building blocks and building principles of natural products.

The polyketide biosynthetic pathway is of the utmost relevance to combinatorial biosynthetic approaches, as this pathway, which is utilized by vastly different living organisms such as microorganisms, fungi, and plants, is naturally diverse. It also produces important pharmaceuticals, for example antibiotics, cytostatics, and immunosuppressants.[2] In this context, years of extensive biosynthetic investigations on the polyketide pathway, on the molecular biological level in particular, are beginning to bear fruit. An application of the knowledge gained, namely the targeted combination of polyketide synthase genes, succeeded recently, and an extension of this strategy is in sight. Simultaneously, further general information on polyketide biosynthesis was gained.

Polyketides are constructed by multifunctional enzymes, the polyketide synthases (PKSs), from short carboxylic acid units (primarily acetate, propionate, butyrate) which are activated as coemzyme A thioesters and by carboxylation (e.g., as malonyl CoA and methylmalonyl CoA) for the decarboxylative (Claisen) polycondensations. The β-oxo ester intermediates can be reduced during this assembly process (or afterwards, see below), further dehydrated, and hydrogenated, as in the related fatty acid biosynthesis.[2d]

Variation possibilities that finally result in the immense repertoire of polyketides arise from the degree of reduction of the β-keto function during the assembly process (→ carbonyl, hydroxymethylene, olefin, or methylene group), the stereochemical information introduced thereby (R/S alcohols, E/Z alkenes), and the type of building blocks used (acetate, propionate, butyrate, amino acid starter units etc.) and the number used (→ type of side chains, chain length). In addition, the folding of the growing polyketide chain, which may be stabilized by subsequent intramolecular ring-closing reactions (aldol condensations, Diels–Alder reactions etc.) results in various molecular frameworks. Finally a myriad of "post-polyketide" modifications (oxidations, reductions, alkylations, acylations, glycosylation reactions, introduction of further heteroatoms, etc.) may convert the biosynthesized molecular frameworks into highly specific bioactive drugs (Scheme 1).

Genetic studies have defined two classes of polyketide synthases—"modular", complex PKSs (type I) and those that



Scheme 1. Three typical examples of the variety of polyketide biosyntheses. Assembly of the primary polyketide through polyketide synthase (PKS), cyclizations (mainly also by PKS), and subsequent functionalizations (post-PKS) to give the macrolide antibiotic tylosin (**1**) [5a], the phytotoxin dehydrocurvularin (**2**) [5b], and the cytostatic adriamycin (**3**) [5c].

[*] Priv.-Doz. Dr. J. Rohr
Institut für Organische Chemie der Universität
Tammannstrasse 2, D-37077 Göttingen (Germany)
Telefax: Int. code + (551) 39-9660

 © VCH Verlagsgesellschaft mbH, D-69451 Weinheim, 1995 0570-0833/95/0808-0881 $ 10.00+.25/0

synthesize polycyclic aromatic polyketides (type II),[2b, 3] although it is likely that the transition between these two types is rather blurred.[4] Typical products of type I PKS are macrolides (e.g. tylosin (**1**),[5a] dehydrocurvularin (**2**)[5b]) and polyethers; type II PKS produce mostly aromatic polycycles such as anthracyclines[5c] (e.g., adriamycin (**3**)), tetracyclines, and angucyclines[5d] assembled from several, usually six-membered rings. Type II PKSs are assemblies of multifunctional proteins, which is reflected in their genetic pendant (Fig. 1, **B**). The first open

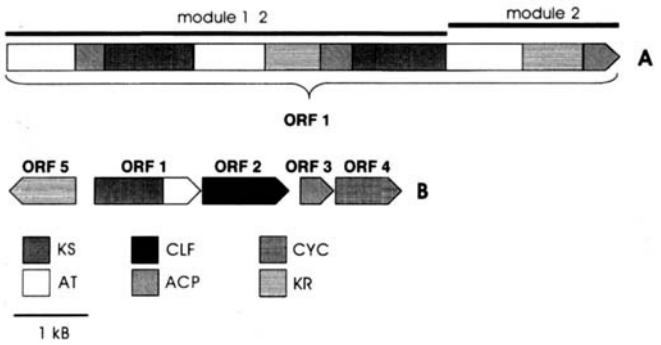
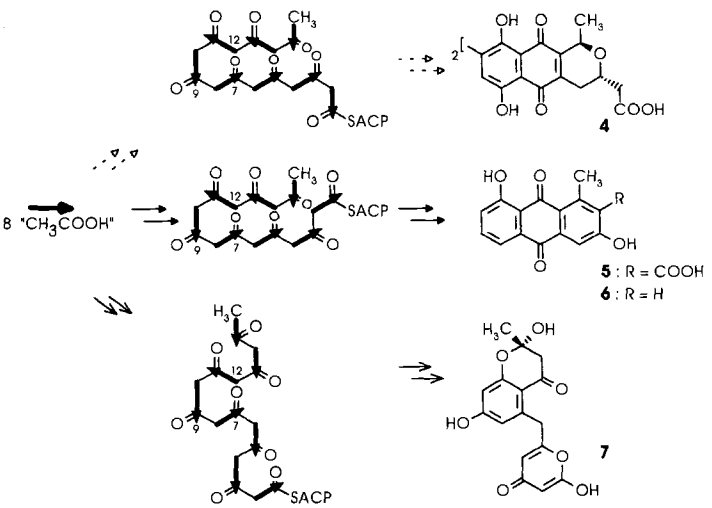


Fig. 1. Genetic analysis of polyketide synthases. **A:** Part of a type I PKS from the erythromycin biosynthesis [11a]; **B:** type II PKS from the actinorhodin biosynthesis [3,6a]. KS = ketosynthase, AT = acyltransferase, CLF = chain length determining factor, ACP = acyl carrier protein, CYC = cyclase, KR = ketoreductase.

reading frame (ORF1) codes for the β-ketosynthase/acyltransferase subunit (KS/AT), which catalyzes Claisen condensations, among other reactions. The second reading frame (ORF2) codes for a yet unidentified subfunctionality, which is currently thought inter alia to control the length of the growing polyketide chain (chain length determining factor, CLF). ORF3 codes for the acyl carrier protein (ACP), which binds the growing polyketide chain, while ORF4 encodes a cyclase and ORF5 a ketoreductase, which is not always present. These principles were defined through intensive genetic studies on streptomycetes, mainly on *S. coelicolor* and *S. glaucescens*, which produce actinorhodin (**4**) and tetracenomycin C (**8**), respectively.[3, 6]

That an intercombination of similar polyketide synthase genes can generate so-called hybrid antibiotics was shown by Hopwood et al. ten years ago. In sensational experiments they succeeded in (arbitrarily) mixing genes for the biosynthesis of actinorhodin with those for granaticin and for medermycin.[6d, e] After these initial successes, in which, however, only marginal changes in the biosynthetic products could be achieved (other configurations, an additional OH group), the excitement surrounding hybrid organisms and hybrid antibiotics died down.

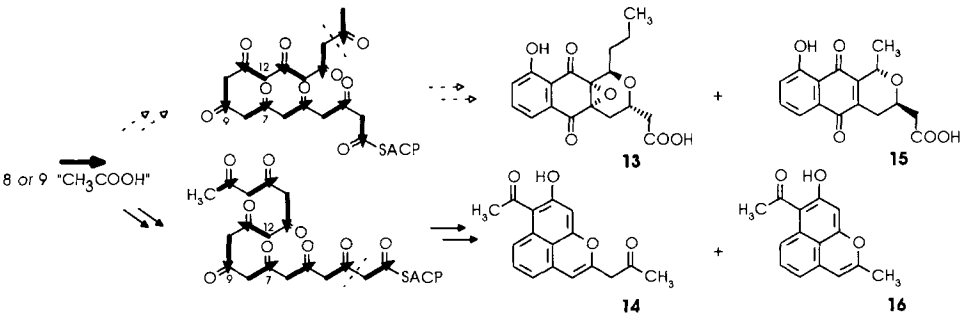
At the end of 1993 Khosla et al. described a host–vector system that allowed the specific exchange of polyketide synthase genes for the first time.[7] The system was originally designed for the modification of the more thoroughly investigated type II polyketide synthases, but it turned out to be suitable for type I PKSs as well.[8] The systematic exchange of type II PKS subunits on the genetic level not only further defined their functions, but also indicated the possible degrees of combinatorial freedom and thus opened up routes to completely novel molecules. In Khosla's *Streptomyces* host–vector system, a PKS gene acceptor–donor system, the specially designed organism (*Streptomyces coelicolor* CH999) that serves as a gene acceptor was constructed from the wild-type organism, the actinorhodin-producer *S. coelicolor*, through precise removal of the genes for actinorhodin biosynthesis. A low-copy plasmid tailored exactly to this host organism functions as the vector, that is, the gene donor system, permitting sections of the removed genes coding polyketide synthase to be reintroduced (control experiment) or analogous foreign PKS genes to be introduced (actual experiment). The following flexible, exchangeable gene cassettes were constructed: the poly-β-ketosynthase/acyltransferase genes (ORF1), the still unspecified ORF2 genes, and the acyl carrier protein genes (ORF3). Some components of the actinorhodin polyketide synthase gene cluster were established as constant domains, among others the activating genes for polyketide biosynthesis, which guarantee that the polyketide biosynthesis begins at its "natural" starting point (during the logarithmic growth phase of the streptomycetes). Initially the shuttle plasmid contained actinorhodin ketoreductase (ORF5), which reduces the 9-C=O group of the polyketide to the corresponding secondary alcohol. This reaction may be followed by elimination of water, resulting in removal of the oxygen atom at C-9. The plasmid also contains the cyclase (ORF4) responsible for the closure of the second ring. All these genes combined represent a minimal PKS, in other words, construction of a functional PKS would be impossible with fewer genes.[7a] For the control experiment, receptor organism CH999 was transformed with a plasmid containing the "standard" actinorhodin ORF1/ORF2/ORF3 genes, designated plasmid pRM5. The host–vector system was shown to function. The major product was 3,8-dihydroxy-1-methylanthraquinone-2-carboxylic acid (DMAC, **5**); the only minor product was its presumably nonenzymatically decarboxylated analogue aloesaponarin II (**6**) (Scheme 2). These results fulfill the expectations for the utilized gene set: the C_{16} polyketide is formed through correct first (cf. **4**) and second ring closures and one 9-C=O reduction (and subsequent dehydra-



Scheme 2. The natural biosynthesis of the octaketide actinorhodin (*act*, **4**) (top) in comparison with the control experiments with Khosla's host–vector system. Middle: Minimal *act*-PKS with functional ketoreductase (KR) yields the anthraquinones **5** (major product) and **6**; these products are also formed when the octaketide PKS of the granaticin producer (all possible combinations of ORF1, ORF2, and ORF3) or when only ORF1 of the tetracenomycin (a decaketide) producer is combined with *act*-PKS. Bottom: Minimal *act*-PKS without KR yields SEK4 **7**.

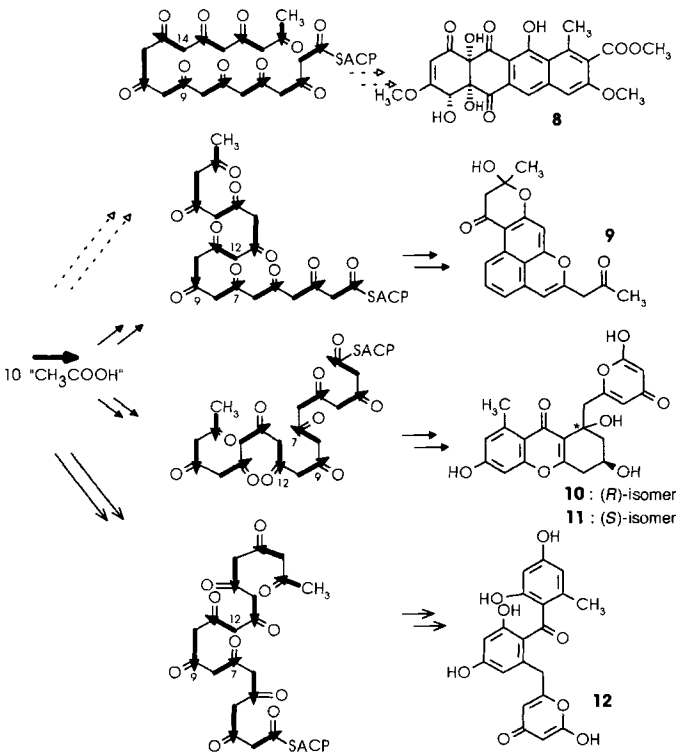
 © VCH Verlagsgesellschaft mbH, D-69451 Weinheim, 1995 0570-0833/95/0808-0882 $ 10.00+.25/0

tion). Thus DMAC **5** is the product of the "normal" minimal actinorhodin (*act*) polyketide synthase. Consequently, all possible ORF1/ORF2/ORF3 variants of control plasmid pRM5 were systematically constructed by using hetero PKS genes of the well-studied producers of tetracenomycin C (*S. glaucescens*) and granaticin (*S. violaceoruber*). In addition, partially characterized polyketide synthase genes, for example from the frenolicin/nanaomycin producer *S. roseofulvus* and the oxytetracyclin producer *S. rimosus*, were used. In two more cases, analogous plasmids were constructed with deactivated ketoreductase (KR) genes (ORF5).



Scheme 4. Combinations with nonaketide PKS. Top: Natural biosynthesis of frenolicin B (**13**) and nanaomycin (**15**). Below: Minimal frenolicin PKS/actinorhodin PKS with *act*-KR yields the hybrid products RM18 **14** and RM18b **16**.

It could be demonstrated that the control products **5** and **6** were always obtained whenever any KS/AT gene (ORF1) had been combined with an actinorhodin (*act*; C_{16}) ORF2 gene. The acyl carrier protein gene (ORF3) could be varied without visible consequences. In contrast, when both ORF1 and ORF2 genes of a foreign PKS were unified with the actinorhodin PKS genes, novel polycyclic compounds with completely different frameworks were produced (RM20 **9**, RM20b **10**, RM20c **11**, RM18 **14**, RM18b **16**; Schemes 3, 4). As in the natural actinorhodin biosynthesis, the 9-C=O group in these compounds is reduced to a secondary alcohol. Generally, the foreign organisms had to be producers of longer (nona-, deca-) polyketides (C_{18}, C_{20}).[9a] Dehydration usually took place after reduction of 9-C=O (→ **9**, **14**, and **16**), but not always (→ **10** and **11**[9b]). In the latter case a different, novel ring skeleton was formed. To explain the results it was proposed that actinorhodin cyclase, the enzyme responsible for the closure of the second ring, operates "chain length specifically" and is unable to convert polyketides with chain lengths differing from that specified in the natural biosynthesis, which yields an octaketide. The novel ring systems presumably result from spontaneous reactions.



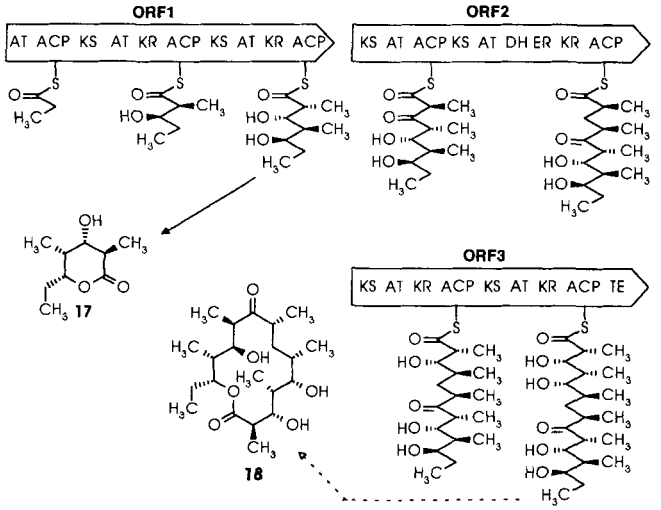
Scheme 3. Natural biosynthesis of tetracenomycin C (*tcm*, **8**) (top) and PKS combination products of the decaketide *tcm*-PKS (ORF1/ORF2) and octaketide *act*-PKS. Middle: The minimal *tcm*-PKS/*act*-KR hybrid yields the major product RM20 **9** and minor products RM20b **10** and RM20c **11**. The latter are also produced from tetracyclin/actinorhodin hybrid organisms. Bottom: Minimal *tcm*-PKS without *act*-KR yields SEK15 **12**.

The transformant organisms, which are completely identical to those described above except for the lack of functional ketoreductase (KR), assembled further types of molecular frameworks, namely the octaketide SEK4 **7** (Scheme 2, bottom) and the decaketide SEK15 **12** (Scheme 3, bottom). As expected, these molecules are constructed without reduction of CO groups and are therefore characterized by further types of folding and intramolecular cyclizations. The regioselectivities of these reactions are again presumably the result of nonenzymatic reactions, that is, with thermodynamic control. Retention or removal of the ketoreductase is therefore another degree of freedom for gene combinatorial polyketide constructions.

New information about the functions of the type II PKS subunits was gained. Since the length of the polyketide formed always coincides with that of the natural molecule, from the biosynthesis of which the ORF2 genes are derived, it could be concluded that ORF2 contains a chain length determining factor (CLF).[7a] The reduction of the CO groups occurs at this point (in contrast to with the type I polyketides) after the biosynthesis of the entire polyketide chain, possibly even after the first cyclization,[10] since hybrid organisms without functional KR still promote cyclization between C-7 and C-12 of the original polyketide chain.

In comparison with type II PKSs, type I PKSs are considerably larger and more complex (**A** in Fig. 1, Scheme 5). They catalyze a stepwise assembly of molecules such as macrolides which is analogous to the fatty acid biosynthesis. But the β-keto group resulting from each condensation step may either remain unchanged or is reduced to some degree.[2d] The modular open reading frames of gene clusters of type II PKSs can contain the necessary gene fragments for all possible variants in 1:1 correspondence to the programmed biosynthetic step. Thus there are ketoreductases (KR), dehydratases (DH), and enoyl reductases (ER) located after the β-ketosynthase/acyltransferase (KS/AT) genes necessary for the polyketide chain assembly. A number of

 © VCH Verlagsgesellschaft mbH, D-69451 Weinheim, 1995 0570-0833/95/0808-0883 $ 10.00+.25/0



Scheme 5. Biosynthesis of 6-deoxyerythronolide B (**18**) with modular type I PKS. The complete biosynthesis (including the lactonization) also functions in the *S. coelicolor* host–vector system after transformation of the ORF1/ORF2/ORF3 genes shown here. Lactone **17** is produced when only the ORF1 genes are transformed into the host organism. AT = acyltransferase, ACP = acyl carrier protein, KS = β-keto ACP synthase, KR = β-keto ACP reductase, DH = dehydratase, ER = enoyl reductase, TE = thioesterase/cyclase).

acyl carrier proteins (corresponding to the number of the building blocks) successively bear the growing polyketide chain until it is finally cleaved by a thioesterase (TE) (Scheme 5).[11a,b] Through selective inactivation of individual subactivities of this type of PKS, specifically modified macrolide analogues have already been obtained.[11a,c–e] Recently, Khosla et al. successfully performed the heterologous expression of type I PKS genes, for instance the entire gene cluster of 6-deoxyerythronolide B (**18**) synthase, into the *S. coelicolor* CH999 host organism described above, and thus could direct the production of macrolides.[8a] In addition, it was possible to express only the genes of the first open reading frame (ORF1), resulting in the production of δ-lactone **17**, if only in low yields.[8b] **17** contains exactly the expected functionalities programmed by the two modules of ORF1 (Fig. 1, Scheme 5). These results pave the way for the combination of macrolide-PKS with other PKS (type I or II). Surprisingly, the cyclic lactone is formed rather than the expected open-chain molecules. Whereas deoxyerythronolide B (**18**) is apparently cyclized directly by the thioesterase, a nonenzymatic reaction has to be considered for the formation of **17**. Alternatively, the intermediates are activated as lactones, which are passed on from subunit to subunit of the PKS. Analogous lactones were previously identified as shunt products of other macrolide producers.[12]

The results are encouraging, although the number of different ring systems obtained—in principle three novel carbon frameworks—is less than one would expect if nonenzymatic reactions were responsible for their formation. The resulting type of molecular framework seems to be chiefly dependent on the degree of reduction of the 9-C=O group (and the possible consequent dehydration). Clearly, all of the controlling factors of this gene combinatorial approach are not yet understood. For instance, what is the controlling factor for the first cyclization of type II polyketides? Why do the novel hybrid molecules often undergo decarboxylation (at C-1 of the polyketide chain)? This occurs rarely in the natural biosyntheses and only to a small extent in the control experiment. Model calculations might be useful in this context.[6a] All gene sets (ORFs) of different organisms could not be intercombined at random successfully, but there are many more examples of positive than of negative intercombinations, in which no polyketides were produced. There is already evidence that it will be possible in future to combine polyketide biosynthesis genes with various "post-polyketide" biosynthetic genes such as oxygenases or glycosyltransferases from foreign organisms.[13] In such an approach the formation of novel molecules depends on the substrate tolerance of the post-polyketide enzymes, and an even greater palette of genetically engineered hybrid products may be produced. The vision of constructing hybrid organisms in which only desired biosynthetic genes are combined, permitting a direct access of certain structural moieties, may become reality in the near future. The work described here paves the way for such a prospect, showing that many more combinations of biosynthetic genes are possible than one could have expected. This flexibility may be extended by using organisms with genetically modified primary metabolism capacities,[14] such that a broader range of building blocks can be used in natural product biosyntheses.

German version: *Angew. Chem.* **1995**, *107*, 963

Keywords: biosyntheses · gene technology · polyketides

[1] See a) R. M. J. Liskamp, *Angew. Chem.* **1994**, *106*, 661–664; *Angew. Chem. Int. Ed. Engl.* **1994**, *33*, 633–636, and references therein; b) P. Eckes, *ibid.* **1994**, *106*, 1649–1651 and **1994**, *33*, 1573–1575, and references therein; c) R. M. Baum, *Chem. Eng. News* **1994**, *72*(6), 20–26; d) T. Carell, E. A. Wintner, A. Bashir-Hashemi, J. Rebek, Jr., *Angew. Chem.* **1994**, *106*, 2159–2162; *Angew. Chem. Int. Ed. Engl.* **1994**, *33*, 2059–2061.

[2] a) D. O'Hagan, *The Polyketide Metabolites*, 1st ed., Ellis Horwood, Chichester, **1991**; b) L. Katz, S. Donadio, *Annu. Rev. Microbiol.* **1993**, *47*, 875–912; c) D. E. Cane, *Science* **1994**, *263*, 338–340, and references therein; d) J. Staunton, *Angew. Chem.* **1991**, *103*, 1331–1335; *Angew. Chem. Int. Ed. Engl.* **1991**, *30*, 1302–1306.

[3] D. H. Hopwood, D. A. Sherman, *Annu. Rev. Gen.* **1990**, *24*, 37–66.

[4] a) H. Bockholt, G. Udvarnoki, J. Rohr, U. Mocek, J. M. Beale, H. G. Floss, *J. Org. Chem.* **1994**, *59*, 2064–2069; b) S. Weber, C. Zolke, J. Rohr, J. M. Beale, *ibid.* **1994**, *59*, 4211–4214, and references therein; c) S. J. Gould, X.-C. Cheng, K. A. Halley, *J. Am. Chem. Soc.* **1992**, *114*, 10066–10068.

[5] a) S. Yue, J. S. Duncan, Y. Yamamoto, C. R. Hutchinson, *J. Am. Chem. Soc.* **1987**, *109*, 1253–1255, and references therein; b) Z. Li, F. M. Martin, J. C. Vederas, *ibid.* **1992**, *114*, 1531–1533, and references therein; c) C. Wagner, K. Eckardt, W. Ihn, G. Schumann, C. Stengel, W. F. Fleck, D. Tresselt, *J. Basic Microbiol.* **1991**, *35*, 223–240, and references therein; J. Rohr, R. Thiericke, *Nat. Prod. Rep.* **1992**, *9*, 103–137, and references therein.

[6] a) D. H. Sherman, M. J. Bibb, T. J. Simpson, D. Johnson, F. Malpartida, M. Fernandez-Moreno, E. Martinez, C. R. Hutchinson, D. A. Hopwood, *Tetrahedron* **1991**, *47*, 6029–6043; b) C. R Hutchinson, H. Decker, H. Motamedi, B. Shen, R. G. Summers, E. Wendt-Pienkowsky, W. Wessel in *Genetics and Molecular Biology of Industrial Microorganims* (Eds.: R. H. Baltz, T. Ingolia, G. Hegeman), American Society for Microbiology, Washington, D. C., **1993**, pp. 203–216, and references therein; c) H. Decker, H. Motamedi, C. R. Hutchinson, *J. Bacteriol.* **1993**, *175*, 3876–3886; d) H. Decker, R. G. Summers, C. R. Hutchinson, *J. Antibiot.* **1994**, *47*, 54–63, and references therein; e) D. A. Hopwood, F. Malpartida, H. M. Kieser, H. Ikeda, J. Duncan, I. Fujii, B. A. Rudd, H. G. Floss, S. Ōmura, *Nature (London)* **1985**, *314*, 642–644; b) S. Ōmura, H. Ikeda, F. Malpartida, H. M. Kieser, D. A. Hopwood, *Antimicrob. Agents Chemother.* **1986**, *29*, 13–19.

[7] a) R. McDaniel, S. Ebert-Khosla, D. A. Hopwood, C. Khosla, *Science* **1993**, *262*, 1546–1550; b) *J. Am. Chem. Soc.* **1993**, *115*, 11671–11675. c) H. Fu, S. Ebert-Khosla, D. A. Hopwood, C. Khosla, *ibid.* **1994**, *116*, 6443–6444; d) H. Fu, R. McDaniel, D. A. Hopwood, C. Khosla, *Biochemistry* **1994**, *33*, 9321–9326.

[8] a) C. M. Kao, L. Katz, C. Khosla, *Science* **1994**, *265*, 509–512; b) C. M. Kao, G. Luo, L. Katz, D. E. Cane, C. Khosla, *J. Am. Chem. Soc.* **1994**, *116*, 11612–11613.

 © VCH Verlagsgesellschaft mbH, D-69451 Weinheim, 1995 0570-0833/95/0808-0884 $ 10.00+.25/0

[9] a) In one case [7b] an octaketide (C_{16}) was converted into a novel molecule, which was explained by the "slippage" of the polyketide chain in the PKS. Alternatively, it is possible that a nonaketide is processed initially and later deacetylated (Scheme 4). b) RM20b **10** and RM20c **11** are (side) products when either tetracenomycin (*tcm*) or oxytetracyclin (*oct*) biosynthetic genes are used.
[10] H. Fu, S. Ebert-Khosla, D. A. Hopwood, C. Khosla, *J. Am. Chem. Soc.* **1994**, *116*, 4166–4170.
[11] a) S. Donadio, M. J. Staver, J. B. McAlpine, S. J. Swanson, L. Katz, *Science* **1991**, *252*, 675–679; b) P. F. Leadlay, J. Staunton, J. F. Aparicio, D. J. Bevitt, P. Caffrey, J. Cortes, A. Marsden, G. A. Roberts, *Biochem. Soc. Trans.* **1993**, *21*, 218–222; c) J. M. Weber, J. O. Leung, S. J. Swanson, K. B. Idler, J. B. McAlpine, *Science* **1991**, *252*, 114–117; d) D. Stassi, S. Donadio, M. J. Staver, L. Katz, *J. Bacteriol.* **1993**, *175*, 182–189; e) S. Donadio, J. B. McAlpine, P. J. Sheldon, M. Jackson, L. Katz, *Proc. Natl. Acad. Sci. USA* **1993**, *90*, 7119–7123.
[12] K. U. Bindseil, A. Zeeck, *Helv. Chim. Acta* **1993**, *76*, 150–157.
[13] a) H. Decker, S. Haag, G. Udvarnoki, J. Rohr, *Angew. Chem.* **1995**, *107*, in press; *Angew. Chem. Int. Ed. Engl.* **1995**, *34*, in press; b) C. R. Hutchinson, *Med. Res. Rev.* **1988**, *8*, 557–567, and references therein.
[14] M. Zhang, C. Eddy, K. Deanda, M. Finkelstein, S. Picataggio, *Science* **1995**, *267*, 240–243.

Control of Ion–Molecule Reactions in the Gas Phase

Karl-Heinz Gericke*

Chemists dream of selecting reaction channels by manipulating starting materials. Simply heating the reaction system will, in general, increase the rate of all reactions and side reactions, and may even open new channels, but real control of the outcome of a reactive encounter is not obtained. Most chemical reactions are statistical in nature, and heat is thus, in general, the only (and appropriate) way to influence the formation of products. However, there are outstanding exceptions to this general rule. For example, studies of the reaction of hydrogen or chlorine atoms with HOD confirm our expectations that the products formed depend on the bond that is vibronically excited: the stretched bond reacts. Therefore, we can control the product ratio OH + HD vs. OD + H_2 in the reaction H + HOD (or OH + DCl vs. OD + HCl in the reaction Cl + HOD) by activating different sides of the HOD reactant.[1, 2] Thus, motio along the reaction coordinate promotes the reaction.

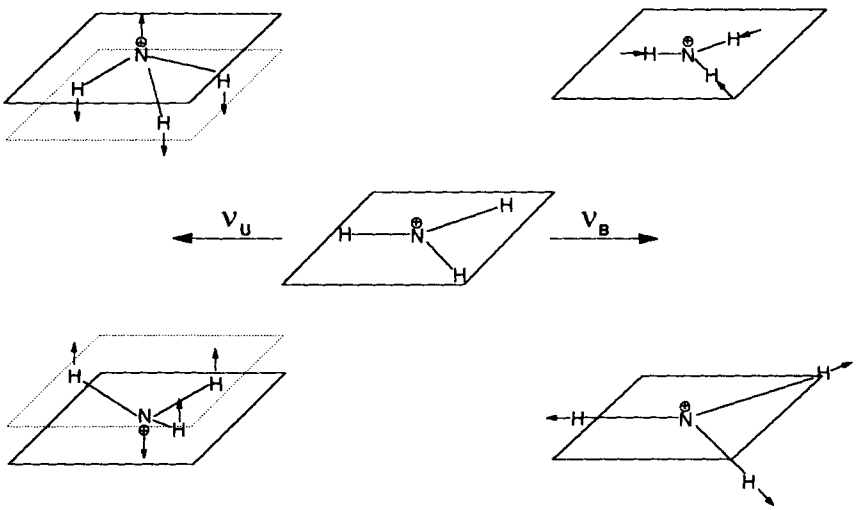


Fig. 1. Illustration of the ν_U umbrella mode (left) and the ν_B breathing mode (right) of the planar NH_3^+ ion (center). These modes have a strong influence on the branching ratio of the $NH_3^+ + ND_2$ reaction.

Unfortunately our experimental knowledge is very limited (the scientific way of saying we know almost nothing) in the case of more complex reactions: Does the reagent's type of internal motion still direct the outcome of the reactive encounter or does everything become statistical when larger reaction systems are involved?

The research group of Zare has recently demonstrated that in case of the reaction of NH_3 with ND_3, the branching ratio for these three different product channels (a)–(c) can be influenced

$$NH_3^+(v_R v_S) + ND_3 \xrightarrow{\text{charge transfer}} NH_3 + ND_3^+ \quad \text{(a)}$$

$$NH_3^+(v_R v_S) + ND_3 \xrightarrow{\text{proton transfer}} NH_2 + ND_3H^+ \quad \text{(b)}$$

$$NH_3^+(v_R v_S) + ND_3 \xrightarrow{\text{deuterium abstraction}} NH_3D^+ + ND_2 \quad \text{(c)}$$

by the choice of the internal NH_3^+ motion, although the energy of the different type of motions, that is, different ν_U or ν_B vibrational modes, is approximately the same.[3]

Two of the six vibrational modes of NH_3^+ are important for the course of the reaction (Fig. 1). In contrast to neutral NH_3, the positive ion is planar, and the so-called umbrella mode (ν_U) corresponds to an out-of-plane, totally symmetric, bending mode, while the breathing mode (ν_B) corresponds to an in-plane, totally symmetric, stretching mode of the hydrogen atoms.

With multiphoton ionization of NH_3 the NH_3^+ reactant is prepared in two nearly isoenergetic states, either with two quanta of the umbrella mode and one quantum of the breathing mode ($2\nu_U 1\nu_B$) or with five quanta of umbrella motion and no breathing excitation ($5\nu_U 0\nu_B$). A strong dependence of the product branching ratio is observed. For example, if two quanta of the umbrella mode (and one quantum of the breathing mode) are excited, roughly 47% of the total amount of products are generated by the proton transfer channel and 47% by the charge transfer channel. Roughly 6% of the products are generated by the deuterium abstraction channel. If five quanta of umbrella mode are excited, the contribution of the charge transfer chan-

[*] Dr. K.-H. Gericke
Institut für Physikalische und Theoretische Chemie der Universität
Marie-Curie-Strasse 11, D-60439 Frankfurt am Main (FRG)
Telefax: Int. code + (69)7982-9445

 © VCH Verlagsgesellschaft mbH, D-69451 Weinheim, 1995 0570-0833/95/0808-0885 $ 10.00+.25/0

nel increases to 56%, while the contribution from the proton transfer channel decreases to 36%. The deuterium abstraction channel is enhanced to 8%. The branching ratio also depends on the collision energy. In any case, the importance of the charge transfer and the deuterium channels is enhanced at the expense of the proton transfer channel when the umbrella motion is more strongly activated.[4, 5] However, it is still possible that the breathing motion influences the branching ratio, because the experimental runs also differ by one quantum of the v_B mode.

In another experiment Zare and co-workers compared identical amounts of umbrella mode excitation ($2v_U$) with ($1v_B$) and without ($0v_B$) breathing mode excitation. The important result is that breathing motion does not influence the branching ratio for the $NH_3^+ + ND_3$ reaction, whereas umbrella motion plays a large role in this polyatomic ion–molecule reaction over the studied collision energy range (1 eV to 5 eV).

The good news is that the reagent's type of internal motion can direct the outcome of a reactive encounter, which confirms the assumption that all three product channels are a result of a direct and fast reaction in which there is not enough time for complete energy redistribution. The bad news is that such polyatomic systems are so complicated that simple models that successfully treat the mode selectivity in small systems like H/Cl + HOD cannot completely explain the outcome of this ion–molecule reaction. Small systems told us that vibrational motion along the reaction coordinate enhances reactivity, whereas motion perpendicular to the reaction coordinate hinders reactivity or is ineffective. For example, the reaction rate of $H_2 + OH \rightarrow H_2O + H$ hardly changes if OH is vibrationally excited, whereas vibrational excitation of H_2 increases the reaction rate by almost two orders of magnitude. This model explains why deuterium abstraction in the $NH_3^+ + ND_3$ reaction is promoted but proton transfer is hindered by umbrella motion. However, we do not understand why the breathing motion does not favor the proton transfer channel, although this type of motion is directed along the reaction coordinate. Obviously a more detailed theoretical treatment than the simple reduction to a three particle model system is necessary.

German version: *Angew. Chem.* **1995**, *107*, 967

Keywords: ion–molecule reactions · kinetics · product selectivity

[1] A. Sinha, M. C. Hsiao, F. F. Crim, *J. Chem. Phys.* **1990**, *92*, 6333; *ibid.* **1991**, *94*, 4928.
[2] A. Sinha, J. D. Thoemke, F. F. Crim, *J. Chem. Phys.* **1992**, *96*, 6333.
[3] R. D. Guettler, G. C. Jones, Jr., A. Lynmarie, L. A. Posey, R. N. Zare, *Science* **1994**, *266*, 259.
[4] L. A. Posey, R. D. Guettler, N. J. Kirchner, R. N. Zare, *J. Chem. Phys.* **1994**, *101*, 3772.
[5] S. Tomoda, S. Suzuki, I. Koyano, *J. Chem. Phys.* **1988**, *89*, 7268.

 © VCH Verlagsgesellschaft mbH, D-69451 Weinheim, 1995 0570-0833/95/0808-0886 $ 10.00+.25/0

Octadecanuclearity in Manganese Carboxylate Chemistry: $K_4[Mn_{18}O_{16}(O_2CPh)_{22}(phth)_2(H_2O)_4]$ ($phthH_2$ = phthalic acid)**

Rachel C. Squire, Sheila M. J. Aubin, Kirsten Folting, William E. Streib, David N. Hendrickson,* and George Christou*

Our efforts in manganese carboxylate chemistry over the last several years have been stimulated by 1) the desire to prepare models of the Mn_4 aggregate responsible for photosynthetic water oxidation,[1] and 2) the search for molecular species with large values of spin S in the ground state to provide information on the factors responsible for the photosynthetic water oxidation and to find potential precursors to molecular ferromagnets.[2] Our results to date have been most gratifying, because we have come across both a wide variety of high nuclearity carboxylatomanganese aggregates with aesthetically pleasing structures and complexes with large values of S and other highly unusual magnetic properties.[3] For example, $[Mn_8O_6Cl_6(O_2CPh)_{12}(H_2O)_2]$ has an $S = 11$ ground state,[3e,f] whereas the $[Mn_{12}O_{12}(O_2CR)_{16}(H_2O)_4]^z$ complexes have $S = 9$ or 10 ($z = 0$) or $S = 19/2$ ($z = -1$) *and* exhibit superparamagnet-like behavior when examined by AC susceptometry—the only *molecular* species to do so.[3c,d,f] The latter complexes are also the highest nuclearity carboxylatomanganese species observed to date. However, we herein report a remarkable octadecanuclear Mn carboxylate aggregate, and describe its structure and magnetic properties.

The synthesis involved the reaction of **1**,[3e] which contains a $[Mn_4(\mu_3\text{-}O)_2]^{8+}$ butterfly-like core, with the monopotassium salt of phthalic acid ($phthH_2$; benzene-1,2-dicarboxylic acid). A dark red-brown MeCN solution of complex **1** was stirred for five days with one equivalent of potassium hydrogen phthalate and yielded a similarly colored solution and an off-white precipitate of KO_2CPh. The solution was filtered, and the filtrate allowed to concentrate at ambient temperature over 10 days to give essentially black crystals of **2**·10MeCN in about 30% yield.[4] Increase of the storage time by a factor of 2 leads to further product crystallization (total yield about 40%).

$(NnBu_4)[Mn_4O_2(O_2CPh)_9(H_2O)]$ **1**

$K_4[Mn_{18}O_{16}(O_2CPh)_{22}(phth)_2(H_2O)_4]\cdot 10MeCN$ **2**·10MeCN

The structure of **2** (Fig. 1)[4] has crystallographically imposed C_2 symmetry and idealized D_2 symmetry. Charge considerations indicate that the Mn centers are all in the Mn^{III} oxidation state. There is a central, almost linear Mn_4 unit (Mn1, Mn1′, Mn2, Mn2′) and seven Mn atoms above and below this unit, all held together by 16 μ_3-O^{2-} ions. The peripheral ligation is provided by 22 $PhCO_2^-$ groups in their familiar *syn,syn*-bridging mode, two terminal H_2O groups on each of two Mn atoms (Mn4 and Mn8), and two μ_4-$phth^{2-}$ groups whose O atoms each coordinate to different Mn atoms; the latter represents an unprecedented binding mode for this group. The two $phth^{2-}$ groups ligate to a total of six Mn atoms. The 16 μ_3-O^{2-} ions can be divided into four types: 1) O15, O15′, O20, and O20′ have distinctly pyramidal geometry with a sum-of-angles (SOA) of about 316°; 2) O11, O11′, O16, and O16′ (SOA ca. 345.5°) and O13, O13′, O18, O18′ (SOA ca. 355°) are also pyramidal, but

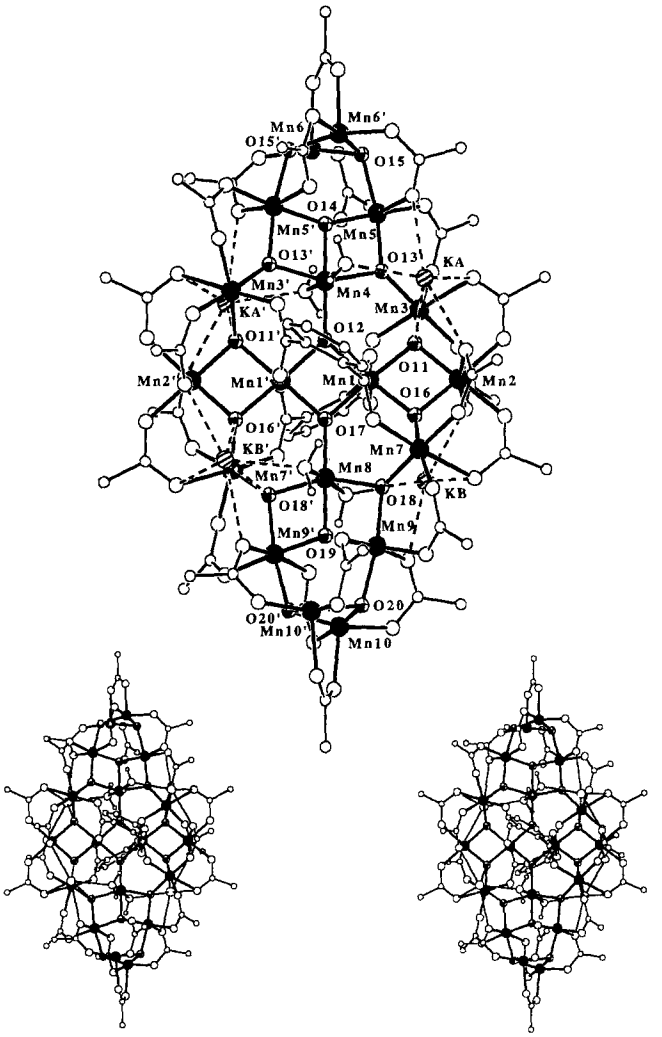


Fig. 1. ORTEP representation and stereoview of the structure of **2**; all but one of the benzoate-phenyl C atoms have been omitted for clarity. The terminal MeCN groups on the K^+ ions (KA and KB, diagonally shaded) are also omitted.

[*] Prof. Dr. D. N. Hendrickson, S. M. J. Aubin
Department of Chemistry, University of California at San Diego
La Jolla, CA 92093-0358 (USA)
Telefax: Int. code + (619) 534-5383
e-mail: dhendrickson@ucsd.edu
Prof. Dr. G. Christou, R. C. Squire, Dr. K. Folting, Dr. W. E. Streib
Department of Chemistry and the Molecular Structure Center
Indiana University, Bloomington, IN 47405-4001 (USA)
Telefax: Int. code + (812) 855-2399
e-mail: christou@indiana.edu

[**] This work was supported by the U.S. National Science Foundation (Grant CHE 9115286) and National Institutes of Health (Grant GM 39083).

with a more flattened geometry as indicated by the SOA; 3) O12 and O17 are planar (SOA about 360°) and very approximately trigonal; and 4) O14 and O19 are planar (SOA 360°) but with an almost T-shaped geometry (Mn5-O14-Mn5′ and Mn9-O19-Mn9′ are 151.5(3)° and 150.9(4)°, respectively). The Mn atoms are either five-coordinate, square-pyramidal (Mn6, Mn6′, Mn10, Mn10′), or distorted octahedral displaying the Jahn–Teller axial distortion (elongation) expected for a high-spin d^4 ion in near-octahedral geometry. The $[Mn_{18}O_{16}]$ core has a somewhat sheet-like appearance and is twisted slightly about the real C_2 (vertical) axis; these points are emphasized by the stereoview in Figure 2. The K^+ ions are tightly ion-paired with the tetraanion, and their positions are indicated in Figure 1; each also has a terminal MeCN ligand (not shown).

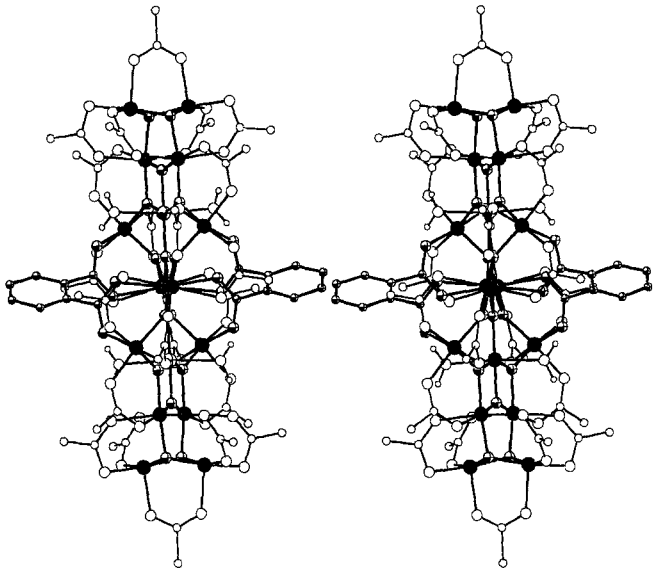
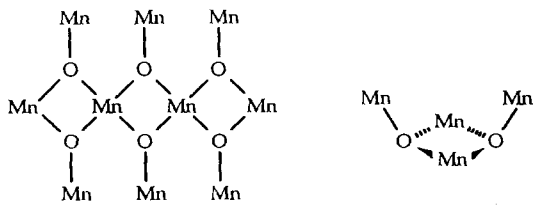


Fig. 2. ORTEP stereoview of complex **2** (without the K^+ ions) from a viewpoint essentially perpendicular to that in Figure 1 and approximately along the almost linear Mn_4 central unit. This view emphasizes the twist of the almost planar $[Mn_{18}O_{16}]$ core along the C_2 (vertical) axis.

An alternate and convenient description of **2** is as the result of fusing five $[Mn_4(\mu_3\text{-}O)_2]^{8+}$ units with either a planar or bent ("butterfly") Mn_4 unit (the latter as found in **1**).[3e, 5] The central $[Mn_{10}O_{16}]$ unit (**A**) represents the fusion of three such units



by sharing of "hinge" Mn atoms (Mn1 and Mn1′). Two additional $[Mn_4O_2]$ units (**B**) are then attached to the "wing-tip" positions of the central unit by atoms O13, O13′, O14 and O18, O18′, O19.

Variable-temperature, solid-state magnetic susceptibility studies were performed on powdered samples of complex **2** in the temperature range 2.00–320 K and in an applied magnetic field of 10 kG (1 T). The $\xi_M T$ value (ξ_M is the molar DC magnetic susceptibility per Mn_{18} complex) slowly decreases from 28.67 $cm^3 K mol^{-1}$ (15.14 μ_B per molecule) at 320.0 K to 0.376 $cm^3 K mol^{-1}$ (1.73 μ_B) at 2.00 K (Fig. 3). The spin-only value for an aggregate of eighteen noninteracting Mn^{III} ($S = 2$) ions is 54.00 cm^3 $K mol^{-1}$ (20.78 μ_B). Thus, there are appreciable antiferromagnetic exchange interactions within **2**.

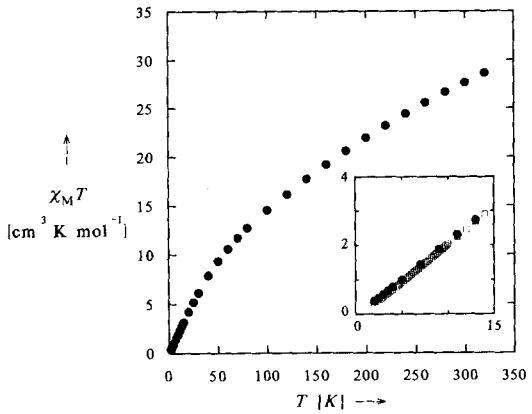


Fig. 3. Plot of $\xi_M T$ vs T data for complex **2** collected in an applied magnetic field of 10 kG. Corresponding μ_{eff} values are given in the text. The inset shows the $\xi_M T$ data in the 2–15 K range; DC data (•) measured at 10 kG and AC data (□) measured in zero DC field and 1.0 G AC field (500 Hz frequency) are shown.

AC magnetic susceptibility data were also collected for a polycrystalline sample of **2** in the 2.00–60.0 K range. These data were run in zero DC field with a 1.0 G AC field oscillating at 500 Hz. The AC susceptibility data nearly superimpose on the DC data. At the lowest temperatures (see inset in Figure 3) both $\xi_M T$ vs T plots extrapolate to $\xi_M T = 0$ at $T = 0$. Clearly, complex **2** has a $S = 0$ ground state.

Interestingly, Mn_x ($x > 3$) carboxylate complexes with ground states $S = 0$ are the exception rather than the rule. As stated earlier, one of the objectives of our program is to elucidate the various factors that lead to large S values in the ground state, and it is becoming apparent that one of these is spin frustration within certain topological arrangements.[6] That complex **2** with its large ensemble of paramagnetic ions should have an $S = 0$ ground state is thus somewhat surprising and of importance to this continuing search for an understanding of what is beneficial to obtaining large values of S and what is detrimental. A more detailed discussion will be presented in a full paper. From a synthetic inorganic viewpoint, the preparation of **2** shows that it is possible to generate Mn aggregates with nuclearities significantly greater than those known to date by relatively minor perturbations to the reaction system, in this case, the introduction of a dicarboxylate ligand. Further work along these lines is in progress, with the objective of increasing even further the number of high nuclearity Mn carboxylate aggregates available for study.

Received: October 27, 1994 [Z 7432 IE]
German version: *Angew. Chem.* **1995**, *107*, 969

Keywords: bioinorganic chemistry · complexes with carboxylato ligands · magnetic properties · manganese compounds

[1] a) G. W. Brudvig, R. H. Crabtree, *Prog. Inorg. Chem.* **1989**, *37*, 99; b) D. Ghanotakis, C. F. Yocum, *Annu. Rev. Plant Physiol. Plant Mol. Biol.*, **1990**, *41*, 255; c) *Manganese Redox Enzymes* (Ed.: V. L. Pecoraro), VCH, Weinheim, **1992**; d) R. J. Debus, *Biochim. Biophys. Acta* **1992**, *1102*, 269; e) Ö. Hansson, T. Wydrzynski, *Photosynth. Res.* **1990**, *23*, 131; f) G. Christou, *Acc. Chem. Res.* **1989**, *22*, 328.

[2] a) J. S. Miller, A. J. Epstein, *Angew. Chem.* **1994**, *106*, 399; *Angew. Chem. Int. Ed. Engl.* **1994**, *33*, 385; b) *Magnetic Molecular Materials* (Eds.: D. Gatteschi, O. Kahn, J. S. Miller, F. Palacio) (NATO ASI Ser. Ser. E **1991**, *198*); c) H. Iwamura, *Pure Appl. Chem.* **1986**, *58*, 187; *ibid.* **1987**, *59*, 1595; d) J. S. Miller, A. J. Epstein, W. M. Reiff, *Chem. Rev.* **1988**, *88*, 201; e) D. P. Goldberg, A. Caneschi, S. J. Lippard, *J. Am. Chem. Soc.* **1993**, *115*, 9299; f) A. Caneschi, D. Gatteschi, J. Laugier, P. Ray, R. Sessoli, C. Zanchini, *ibid.* **1988**, *110*, 2795; g) A. Caneschi, D. Gatteschi, R. Sessoli, A. L. Barra, L. C. Brunel, M. Guillat, *ibid.* **1991**, *113*, 5873.

[3] a) E. Libby, K. Folting, C. J. Huffman, J. C. Huffman, G. Christou, *Inorg. Chem.* **1993**, *32*, 2549, and references therein; b) M. W. Wemple, H.-L. Tsai, W. E. Streib, D. N. Hendrickson, G. Christou, *J. Chem. Soc. Chem. Commun.* **1994**, 1031; c) R. Sessoli, H.-L. Tsai, A. R. Schake, S. Wang, J. B. Vincent, K. Folting, D. Gatteschi, G. Christou, D. N. Hendrickson, *J. Am. Chem. Soc.* **1993**, *115*, 1804; d) H.-L. Tsai, H. Eppley, N. de Vries, K. Folting, G. Christou, D. N. Hendrickson, *J. Chem. Soc. Chem. Commun.* **1994**, 1745; e) S. Wang, J. C. Huffman, K. Folting, W. E. Streib, E. B. Lobkovsky, G. Christou, *Angew. Chem. Int. Ed. Engl.* **1991**, *30*, 1672; *Angew. Chem.* **1991**, *103*, 1681; f) H.-L. Tsai, S. Wang, K. Folting, W. E. Streib, D. N. Hendrickson, G. Christou, *J. Am. Chem. Soc.*, in press; g) H. J. Eppley, H.-L. Tsai, N. de Vries, K. Folting, G. Christou, D. N. Hendrickson, *ibid.* **1994**, *116*, 301.

[4] Solid dried under vacuum has lost all MeCN groups. Elemental analysis: calcd (found) for $C_{170}H_{126}O_{72}K_4Mn_{18}$: C 45.72 (45.50), H 2.84 (2.80), N 0.00 (0.00), Mn 22.14 (21.98), K 3.49 (3.50)%. Crystal data: $C_{190}H_{156}N_{10}O_{72}K_4Mn_{18}$, monoclinic, $C2/c$, $T = -167\,^{\circ}C$, $a = 22.673(5)$, $b = 33.426(7)$, $c = 27.991(8)$ Å, $\beta = 105.06(1)^{\circ}$, $V = 20484\,Å^3$, $Z = 4$, $\rho_{calcd} = 1.57\,g\,cm^{-3}$, $6^{\circ} \le 2\theta \le 45^{\circ}$, 10441 unique reflections with $F > 3\sigma(F)$. All non-hydrogen toms were refined anisotropically; hydrogen atoms were included in fixed, calculated positions. Final $R(R_w) = 0.00607\,(0.00606)\%$. Further details are available on request from the Director of the Cambridge Crystallographic Data Centre, 12 Union Road, Cambridge CB2, 1EZ (UK), on quoting the complete journal citation.

[5] a) J. B. Vincent, C. Christmas, H.-R. Chang, Q. Li, P. D. W. Boyd, J. C. Huffman, D. N. Hendrickson, G. Christou, *J. Am. Chem. Soc.* **1989**, *111*, 2086; b) E. Libby, J. K. McCusker, E. A. Schmitt, K. Folting, J. C. Huffman, D. N. Hendrickson, G. Christou, *Inorg. Chem.* **1991**, *30*, 3486; c) E. Bouwman, M. A. Bolcar, E. Libby, J. C. Huffman, K. Folting, G. Christou, *ibid.* **1992**, *31*, 5185.

[6] a) D. N. Hendrickson, G. Christou, E. A. Schmitt, E. Libby, J. S. Bashkin, S. Wang, H.-L. Tsai, J. B. Vincent, P. D. W. Boyd, J. C. Huffman, K. Folting, Q. Li, W. E. Streib, *J. Am. Chem. Soc.* **1992**, *114*, 2455; b) J. K. McCusker, J. B. Vincent, E. A. Schmitt, M. L. Mino, K. Shin, D. K. Coggin, P. M. Hagen, J. C. Huffman, G. Christou, D. N. Hendrickson, *J. Am. Chem. Soc.* **1991**, *113*, 3012; c) E. Libby, J. K. McCusker, E. A. Schmitt, K. Folting, D. N. Hendrickson, G. Christou, *Inorg. Chem.* **1991**, *30*, 3486; d) J. K. McCusker, H. G. Jang, S. Wang, G. Christou, D. N. Hendrickson, *ibid.* **1992**, *31*, 1874; e) S. Wang, H.-L. Tsai, W. E. Streib, G. Christou, D. N. Hendrickson, *J. Chem. Soc. Chem. Comm.* **1992**, 677; f) D. N. Hendrickson in *Research Frontiers in Magnetochemistry* (Ed.: C. J. O' Connor) World Scientific, Singapore, **1993**.

A Nickel(II) Azide Cubane: Characterization of the Magnetic Exchange Interactions Mediated by a Triply Bridging Azide Group Bound End-On**

Malcolm A. Halcrow, John C. Huffman, and George Christou*

We have a long-standing interest in manganese carboxylate aggregates as models for the Mn_4 cluster in the active center of green plants and cyanobacteria for photosynthetic water oxidation.[1] We prepared several $Mn^{III}_3Mn^{IV}$ complexes containing the distorted cubane $[Mn_4O_3X]^{6+}$ core (X = halide, carboxylate),[2] and also the cubane $[Co_4O_4]^{4+}$ core, together with protonated versions of the latter.[3] As an extension to this work, we recently turned our attention to cubane complexes containing other metal ions, to investigate the electronic and magnetic properties of this interesting class of compound further. We report here the cubane complex **1**; this is the first paramagnetic

$[Ni_4(\mu_3\text{-}N_3)_4(dbm)_4(EtOH)_4]$ **1** dbmH = dibenzoylmethane

molecule to contain end-on-coordinated, triply bridging azide ligands,[4-6] and thus provides an opportunity to characterize the magnetic exchange interactions mediated by azide in this rare bridging mode. The structure of one other $[M_4(N_3)_4]^{n+}$ cubane species is known, namely diamagnetic $[Pt_4(N_3)_4(CH_3)_{12}]$.[5]

A one-pot reaction of $Ni(ClO_4)_2 \cdot 6H_2O$, NaN_3, and Na(dbm) (in a 1:1:1 molar ratio) in EtOH at room temperature yields a bright green precipitate containing **1** and a little $NaClO_4$. Recrystallization from CH_2Cl_2/EtOH affords large green crystals of pure **1** in 78% overall yield. The IR spectrum of **1** as a Nujol mull shows, in addition to bands arising from dbm^- and coordinated EtOH, a very strong absorption at 2087 cm^{-1} attributable to the ν_{asym}(N-N-N) stretching vibration of coordinated azide;[7] this band appears at 2089 cm^{-1} in $CHCl_3$ solution. The ν_{sym}(N-N-N) and δ(N-N-N) vibrations also expected from a metal-bound azide[7] were masked by absorptions from the dbm^- ligand and could not be positively identified. The UV/Vis spectrum of **1** in $CHCl_3$ is typical of an octahedral Ni^{II} complex,[8] while the ^1H NMR spectrum of **1** in $CDCl_3$ shows the paramagnetically shifted resonances of only a single environment for dbm^- and EtOH.

The structure of the bis(toluene) solvate of **1** (Fig. 1)[9] contains a tetranuclear $[Ni_4(\mu_3\text{-}N_3)_4]^{4+}$ cubane core; the molecule has virtual C_2 symmetry and lies on a general position within the unit cell. Each Ni ion is octahedrally coordinated by three end-on-coordinated, triply bridging azide ligands, one chelating dbm^- ligand, and one ethanol ligand. Each ethanol ligand is intramolecularly hydrogen-bonded to an O atom in a dbm^- ligand that is

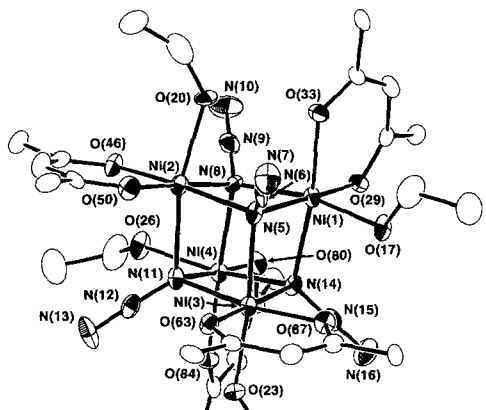


Fig. 1. ORTEP representation of complex **1** (ellipsoids at the 50% probability level). For clarity, only the *ipso* carbon atoms of the dbm^- phenyl rings are shown. Selected distances [Å] and angles [°]: Ni(1)···Ni(2) 3.168(1), Ni(1)···Ni(3) 3.146(1), Ni(1)···Ni(4) 3.231(1), Ni(2)···Ni(3) 3.239(1), Ni(2)···Ni(4) 3.177(1), Ni(3)···Ni(4) 3.156(1), Ni(1)–N(5) 2.141(5), Ni(1)–N(8) 2.136(6), Ni(1)–N(14) 2.094(5), Ni(2)–N(5) 2.117(5), Ni(2)–N(8) 2.111(5), Ni(2)–N(11) 2.138(6), Ni(3)–N(5) 2.132(6), Ni(3)–N(11) 2.100(5), Ni(3)–N(14) 2.132(5), Ni(4)–N(8) 2.109(6), Ni(4)–N(11) 2.150(5), Ni(4)–N(14) 2.113(6), Ni(1)-N(5)-Ni(2) 96.1(2), Ni(1)-N(5)-N(3) 94.8(2), Ni(2)-N(5)-Ni(3) 99.4(2), Ni(1)-N(8)-Ni(2) 96.5(2), Ni(1)-N(8)-Ni(4) 99.1(2), Ni(2)-N(8)-Ni(4) 97.7(2), Ni(2)-N(11)-Ni(3) 99.7(2), Ni(2)-N(11)-Ni(4) 95.6(2), Ni(3)-N(11)-Ni(4) 95.9(2), Ni(1)-N(14)-Ni(3) 96.2(2), Ni(1)-N(14)-Ni(4) 100.4(2), Ni(3)-N(14)-Ni(4) 96.1(2).

[*] Prof. Dr. G. Christou, Dr. M. A. Halcrow, Dr. J. C. Huffman
Department of Chemistry and Molecular Structure Center
Indiana University, Bloomington, IN 47405-4001 (USA)
Telefax: Int. code + (812)855-2399
e-mail: christou@indiana.edu

[**] This work was supported by the U.S. National Science Foundation (CHE 9311904). We thank Prof. K. R. Dunbar and J.-S. Sun (Michigan State University) for collection of magnetic susceptibility data, and Prof. J. Ribas (University of Barcelona) for a preprint of ref. [18].

bound to a neighboring Ni atom (averaged $O\cdots O = 2.703$ Å); this results in a distortion of the $[Ni_4(N_3)_4]^{4+}$ core from T_d to D_{2d} symmetry which results in the four faces of the cubane spanned by hydrogen bonds having shorter Ni–Ni distances and more acute Ni-N-Ni angles and Ni-N-N-Ni dihedral angles than the two faces not bridged in this fashion (average values for Ni1-N5-N8-Ni2, Ni1-N5-N14-Ni3, Ni2-N8-N11-Ni4, and Ni3-N11-N14-Ni4: $Ni\cdots Ni = 3.162$ Å, Ni-N-Ni = 96.1°, Ni-N-N-Ni = 167.1°; for Ni1-N8-N14-Ni4 and Ni2-N5-N11-Ni3: $Ni\cdots Ni = 3.235$ Å, Ni-N-Ni = 99.6°, Ni-N-N-Ni = 175.5°). This feature is also exhibited by several $[Ni_4(OR)_4]^{4+}$ cubanes that contain coordinated alcohol ligands intramolecularly hydrogen bonded in this manner.[10, 11] The azide ligands are each symmetrically coordinated to three Ni ions, and the Ni–N distances and Ni-N-N angles about each azide show only small differences with no discernable pattern. The Ni–N and Ni–O bond lengths for **1** are unremarkable, while the N–N distances within the azide ligands display the same "long–short" pattern shown by Ni^{II} complexes containing end-on-coordinated, doubly bridging azides.

Variable-temperature magnetic susceptibility measurements were performed on a powder sample of **1** between 320 and 5.00 K. The observed effective magnetic moment μ_{eff} for **1** rises from a value of 6.46 μ_B at 320 K to a maximum of 9.66 μ_B at 20 K, before slightly decreasing below 9.00 K (Fig. 2); the value at 20 K may

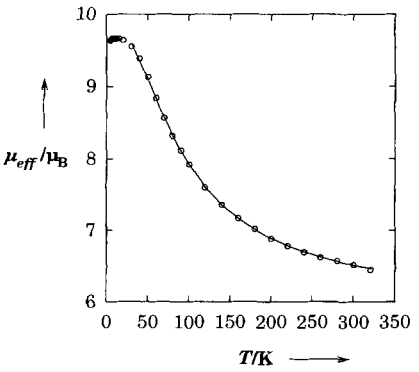


Fig. 2. A plot of effective magnetic moment μ_{eff} per Ni_4 unit vs. temperature T for complex **1**. The solid line represents the least-squares fit to a one-J (T_d symmetry) model; see the text for the fitting parameters. Only data for $T \geq 30$ K were employed to avoid problems at lower temperature arising from zero-field splitting of the $S = 4$ ground state.

be compared with the spin-only ($g = 2$) value of 8.94 μ_B calculated for an $S = 4$ ground state expected for four ferromagnetically coupled high-spin Ni^{II} ions. The data for temperatures ≥30 K were fit according to a one-J model (T_d symmetry) incorporating a Weiss constant θ to account for intermolecular interactions in the solid state[11] (fitting parameters $J = +11.9 \pm 0.5$ cm^{-1}, $g = 2.05$, $\theta = +3.0$ K; $\mathcal{H} = -2JS_1 \cdot S_2$; Fig. 2); utilization of a two-J model (D_{2d} symmetry) did not result in improved fits or in significant splitting (<0.1 cm^{-1}) of the two J parameters.

It is interesting that the distortions within the cubane core noted above are not reflected in the magnetic properties of **1**; this contrasts with the behavior of alkoxide-bridged cubanes, which show J values that are very sensitive to the Ni-O-Ni bridging angles within the faces of the cubane structure.[11–13] Specifically, the complex $[Ni_4(OMe)_4(dbm)_4(MeOH)_4]$, which exhibits similar patterns of MeOH···dbm hydrogen bonding and structural distortions within the $[Ni_4(\mu_3\text{-}OMe)_4]^{4+}$ unit, is best described by a two-J model incorporating both ferromagnetic and antiferromagnetic contributions.[12] The observed J value for **1** is weaker than any reported for coupling across a $[Ni_2(\eta^1,\mu\text{-}N_3)_2]$ bridge, consistent with the presence of triply, as opposed to doubly bridging azides in **1**.[14]

Two mechanisms for the transmission of superexchange interactions through azide ligands bridging end-on have been proposed, which involve accidental orthogonality[15] or spin polarization[16] as the dominant factor determining the sign of the observed coupling; both of these models predict ferromagnetic coupling between metal ions bridged by azide in end-on fashion in most (accidental orthogonality) or all (spin polarization) cases. In particular, a theoretical study of accidental orthogonality in Cu^{II} complexes containing a planar $[Cu_2(\eta^1,\mu\text{-}N_3)_2]^{2+}$ bridge predicted a switch from ferromagnetic to antiferromagnetic coupling for Cu-N-Cu angles greater than 103°.[15] In this regard, it is noteworthy that the average Ni-N-Ni bridge angle in **1** is 97.3°, which is unusually small for an azide bridging end-on in a dinuclear metal complex and is substantially below the predicted crossover value. While the use of Ni^{II} rather than Cu^{II} as metal center and the nonplanarity of the $[Ni_2(\mu\text{-}N_3)_2]$ bridges in **1** might be expected to cause small deviations from the published model,[17] the nature of the magnetic interactions present should be similar in the two types of compound, since both Ni^{II} and Cu^{II} only possess magnetic orbitals of σ symmetry. The lack of dependence of the coupling constant J on the Ni-N-Ni angle in **1** is difficult to reconcile on the basis of the accidental orthogonality model, but is consistent with the spin polarization model.[16] However, *antiferromagnetic* coupling mediated by end-on-coordinated, doubly bridging azide groups with an even more acute Ni-N-Ni angle of 84° was reported.[18] Clearly, the mechanism of superexchange coupling through end-on azide bridging ligands deserves further study, and the present work has provided an additional bridging mode for inclusion in these considerations.

Experimental Procedure

Solid NaN_3 (0.30 g, 4.9 mmol) and Na(dbm) (1.2 g, 4.9 mmol) were added to a solution of $Ni(ClO_4)_2 \cdot 6H_2O$ (1.8 g, 4.9 mmol) in EtOH (100 mL), and the mixture was stirred at room temperature for 4 h. The resultant green precipitate was filtered off, washed with EtOH, and dried in air. Recrystallization from CH_2Cl_2/EtOH afforded deep green blocks, which were not of X-ray quality (1.4 g, 78%); crystallization from toluene/EtOH gave a lower yield of crystals suitable for an X-ray diffraction study. Correct C,H,N,Ni analysis for $C_{68}H_{68}N_{12}O_{12}Ni_4$. IR (Nujol): $\tilde{\nu}$ = 3586 (w), 3270 (br), 3061 (w), 2087 (vs), 1618 (w), 1595 (s), 1554 (s), 1516 (s), 1454 (m), 1442 (w), 1402 (m), 1383 (s), 1312 (s), 1292 (m), 1267 (w), 1242 (m), 1229 (w), 1183 (w), 1157 (w), 1129 (w), 1086 (w), 1073 (w), 1057 (m), 1047 (m), 1024 (m), 1001 (w), 941 (m), 882 (w), 785 (w), 754 (m), 725 (s), 691 (m), 637 (m), 530 (m) cm^{-1}. IR ($CHCl_3$) $\tilde{\nu}$ = 2089 cm^{-1}. UV/Vis ($CHCl_3$; λ_{max} (ε_{max})): 246 (sh), 258 (85,520), 280 (sh), 364 (77,610), 412 (sh), 652 nm (41 dm^3 mol^{-1} cm^{-1}). ^{1}H NMR (300 MHz, $CDCl_3$): δ = 57.2, 50.4 (CH_3CH_2OH), 12.8, 11.7, 10.2, 9.3 (dbm *o*-, *m*- and *p*-phenyl, CH_3CH_2OH), −17.3 (dbm *meso*-CH).

Received: November 23, 1994 [Z 7492 IE]
German version: *Angew. Chem.* **1995**, *107*, 971

Keywords: complexes with nitrogen ligands · complexes with oxygen ligands · cubanes · magnetic properties · nickel compounds

[1] G. Christou, *Acc. Chem. Res.* **1989**, *22*, 328.
[2] a) D. N. Hendrickson, G. Christou, E. A. Schmitt, E. Libby, J. S. Bashkin, S. Wang, H.-L. Tsai, J. B. Vincent, P. D. W. Boyd, J. C. Huffman, K. Folting, Q. Li, W. E. Streib, *J. Am. Chem. Soc.* **1992**, *114*, 2455; b) S. Wang, H.-L. Tsai, W. E. Streib, G. Christou, D. N. Hendrickson, *J. Chem. Soc. Chem. Commun.* **1992**, 1427; c) S. Wang, H.-L. Tsai, K. S. Hagen, D. N. Hendrickson, G. Christou, *J. Am. Chem. Soc.* **1994**, *116*, 8376.
[3] a) K. Dimitrou, K. Folting, W. E. Streib, G. Christou, *J. Am. Chem. Soc.* **1993**, *115*, 6432; b) *J. Chem. Soc. Chem. Commun.* **1994**, 1385.
[4] a) Z. Dori, R. F. Ziolo, *Chem. Rev.* **1973**, *73*, 247; b) U. Müller, *Struct. Bonding (Berlin)* **1973**, *14*, 141; c) K. Vrieze, G. van Koten in *Comprehensive Coordination Chemistry, Vol. 2* (Eds.: G. Wilkinson, R. D. Gillard, J. A. McCleverty), Pergamon, Oxford, **1987**, Ch. 13.5, pp 225–236.

 © VCH Verlagsgesellschaft mbH, D-69451 Weinheim, 1995 0570-0833/95/0808-0890 $ 10.00+.25/0

[5] a) K.-H. von Dahlen, J. Lorberth, *J. Organomet. Chem.* **1974**, *65*, 267; b) M. Atam, U. Müller, *ibid.* **1974**, *71*, 435.

[6] a) M. A. S. Goher, T. C. W. Mak, *Inorg. Chim. Acta* **1985**, *99*, 223; b) F. A. Mautner, H. Krischner, C. Kratky, *Z. Kristallogr.* **1985**, *172*, 291; c) M. E. Gross, T. Siegrist, *Inorg. Chem.* **1992**, *31*, 4898.

[7] K. Nakamoto, *Infra-red and Raman spectra of Inorganic and Coordination Compounds*, 4th ed., Wiley, New York, **1986**.

[8] L. Sacconi, F. Mani, A. Bencini in *Comprehensive Coordination Chemistry, Vol. 5* (Eds.: G. Wilkinson, R. D. Gillard, J. A. McCleverty), Pergamon, Oxford, **1987**, Ch. 50, pp 45–68.

[9] Crystal data for **1**: $C_{68}H_{68}N_{12}O_{12}Ni_4 \cdot 2C_7H_8$, monoclinic, $P2_1/n$, $T = -174\,^{\circ}C$, $a = 14.295(2)$, $b = 23.203(4)$, $c = 24.542(4)$ Å, $\beta = 100.49(1)^{\circ}$, $V = 8004.2$ Å^3, $Z = 4$, $6^{\circ} < 2\theta < 45^{\circ}$, 991 refined parameters, 6163 unique reflections with $F > 2.33\sigma(F)$; $R = 0.0512$, $R_w = 0.0444$. Further details of the crystal structure investigation are available on request from the Director of the Cambridge Crystallographic Data Centre, 12 Union Road, GB-Cambridge CB2 1EZ (UK), on quoting the full journal citation.

[10] a) J. A. Bertrand, C. Marabella, D. G. Vanderveer, *Inorg. Chim. Acta* **1978**, *26*, 113; b) F. Paap, E. Bouwman, W. L. Driessen, R. A. G. de Graaf, J. Reedijk, *J. Chem. Soc. Dalton Trans.* **1985**, 737.

[11] a) J. E. Andrew, A. B. Blake, *J. Chem. Soc. (A)* **1969**, 1456; b) J. A. Bertrand, A. P. Ginsberg, R. I. Kaplan, C. E. Kirkwood, R. L. Martin, R. C. Sherwood, *Inorg. Chem.* **1971**, *10*, 240.

[12] M. A. Halcrow, J. C. Huffman, G. Christou, unpublished.

[13] a) J. A. Barnes, W. E. Hatfield, *Inorg. Chem.* **1971**, *10*, 2355; b) W. L. Gladfelter, M. W. Lynch, W. P. Schaefer, D. N. Hendrickson, H. B. Gray, *ibid.* **1981**, *20*, 2390; c) L. Ballester, E. Coronado, A. Gutièrrez, A. Monge, M. F. Perpiñan, E. Pinilla, T. Rico, *ibid.* **1992**, *31*, 2053.

[14] a) M. I. Arriortua, A. R. Cortès, L. Lezam, T. Rojo, X. Solans, M. Font-Bardia, *Inorg. Chim. Acta* **1990**, *174*, 263; b) A. Escuer, R. Vicente, J. Ribas, *J. Magn. Magn. Mater.* **1992**, *110*, 181; c) R. Cortès, J. I. Ruis de Larramendi, L. Lezama, T. Rojo, K. Urtiaga, M. Arriortua, *J. Chem. Soc., Dalton Trans.* **1992**, 2723; d) J. Ribas, M. Monfort, R. Costa, X. Solans, *Inorg. Chem.* **1993**, *32*, 695; e) R. Vicente, A. Escuer, J. Ribas, M. S. el Fallah, X. Solans, M. Font-Bardia, *ibid.* **1993**, *32*, 1920; f) J. Ribas, M. Monfort, C. Diaz, C. Bastos, X. Solans, *ibid.* **1994**, *33*, 484.

[15] J. Comarmond, P. Plumerè, J.-M. Lehn, Y. Agnus, R. Louis, R. Weiss, O. Kahn, I. Morgenstern-Badarau, *J. Am. Chem. Soc.* **1982**, *104*, 6330.

[16] M.-F. Charlot, O. Kahn, M. Chaillet, C. Larrieu, *J. Am. Chem. Soc.* **1986**, *108*, 2574.

[17] a) M.-F. Charlot, S. Jeannin, Y. Jeannin, O. Kahn, J. Lucrece-Abaul, J. Martin-Frère, *Inorg. Chem.* **1979**, *18*, 1675; b) M.-F. Charlot, O. Kahn, S. Jeannin, Y. Jeannin, *ibid.* **1980**, *19*, 1410.

[18] J. Ribas, M. Monfort, B. K. Ghosh, X. Solans, *Angew. Chem.* **1994**, *106*, 2177; *Angew. Chem. Int. Ed. Eng.* **1994**, *33*, 2087.

Complexes with Polar W–W Multiple Bonds: $[W_2(O\mathit{i}Pr)_4L(dmpe)_2]$ (L = $(H)_2$, CO) and $[W_2(O)_4(\mu\text{-}O)\{W(CO)(dmpe)_2\}_2]$**

Malcolm H. Chisholm,* Keith S. Kramer, and William E. Streib

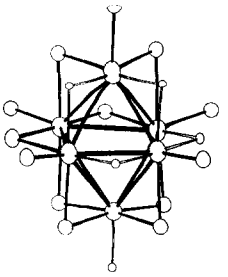
Dedicated to Professor F. A. Cotton on the occasion of his 65th birthday

The recent highlight by Herberhold and Jin[1] focused attention on heterometallic complexes with unbridged, polar metal–metal bonds. We describe here reactions in which a symmetric homonuclear complex containing a W–W triple bond yields asymmetric complexes with polar W–W bonds. One of the products described is a novel water-soluble tetranuclear complex involving nonbridged W–W bonds between tungsten atoms in oxidation states + 5 and 0.

[*] Prof. M. H. Chisholm, Dr. K. S. Kramer, Dr. W. E. Streib
Department of Chemistry and Molecular Structure Center
Indiana University
Bloomington, IN 47405 (USA)
Telefax: Int. code + (812)855-7148
e-mail: Chisholm@UCS. Indiana. Edu

[**] This work was supported by the Department of Energy, Office of Basic Sciences, Chemistry Division. dmpe = bis(dimethylphosphano)ethane.

The compound $[W_2(i\mathrm{Bu})_2(O\mathit{i}Pr)_4]$ and dihydrogen react in hydrocarbon solvents to give the hexanuclear hydridotungsten cluster $[W_6(H)_5(O\mathit{i}Pr)_{13}]$,[2] whose $W_6H_5O_{13}$ core is shown pictorially by **A** in Scheme 1. We reasoned that $[W_6(H)_5(O\mathit{i}Pr)_{13}]$ was formed stepwise from the coupling of reactive $[W_2(H)_2(O\mathit{i}Pr)_4]$ fragments. Ligand scrambling may account for the odd number of hydrido and alkoxido ligands in the product, and the formal oxidation state of each tungsten atom is maintained at + 3.



A

Scheme 1. The $W_6H_5O_{13}$ core **A** in $[W_6(H)_5(O\mathit{i}Pr)_{13}]$.

Consequently in an attempt to trap $[W_2(H)_2(O\mathit{i}Pr)_4]$ we have carried out the hydrogenation of $[W_2(i\mathrm{Bu})_2(O\mathit{i}Pr)_4]$ in the presence of chelating diphosphanes.[3] In the presence of bis(dimethylphosphano)ethane (dmpe), the dinuclear complex **1**

$[W_2(\mu\text{-}H)_2(O\mathit{i}Pr)_4(dmpe)_2]$ **1**

was obtained as a dark brown crystalline solid. The solid-state structure of **1** (Fig. 1) reveals that one W atom is coordinated to four O*i*Pr ligands and the other to two dmpe ligands. The structure is superficially similar to that of $[Mo_2(O\mathit{i}Pr)_4(dmpe)_2]$,[4] but the M–M distance in **1** (M = metal) is notably longer and

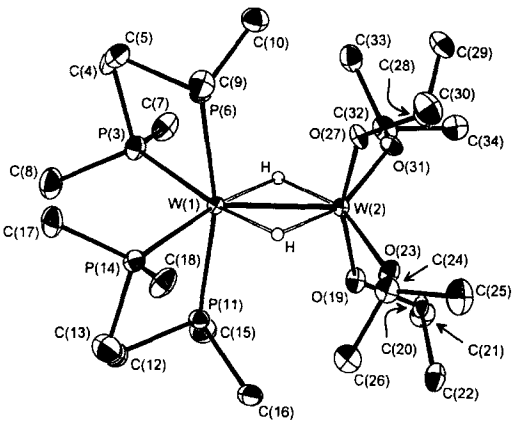


Fig. 1. ORTEP drawing showing the crystal structure of **1** (50% probability ellipsoids). Pertinent bond lengths [Å] and angles [°], averaged where appropriate: W-W 2.496(1), W-O 1.96(1), W-P(6,11) 2.424(2), W(1)-P(3,14) 2.486(2), W-W-P(6,11) 97.5(1), W-W-P(3,14) 130.3(1), W-W-O(23,31) 120.3(2), W-W-O(19,27) 99.4(2).

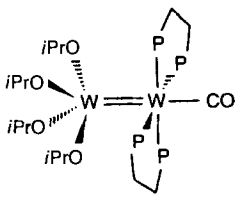
The coordination of the $M(dmpe)_2$ units is different. In $[Mo_2(O\mathit{i}Pr)_4(dmpe)_2]$ all the Mo-Mo-P bond angles range from 98.0(1) to 100.8(1)°, and the Mo–Mo bond length of 2.236(1) Å is typical for a Mo–Mo triple bond. In compound **1**, however, the W–W bond length of 2.496(1) Å is in the range expected for a W–W double bond, and two sets of W-W-P bond angles 97.5(1) and 130.3(1)°] define four positions of the octahedral coordination about W(2). In the structure shown in Figure 1 the two μ-H ligands are placed in proposed positions (hydride locating program XHYDEX),[5] and compound **1** is therefore formulated as $[W_2(\mu\text{-}H)_2(O\mathit{i}Pr)_4(dmpe)_2]$. In solution compound **1** is fluxional; at low temperatures at least two isomers are present, as is evident from the hydride and phosphorus signals. Owing to the broadness of the ^{31}P NMR signals at −80 °C, the

^{1}H-coupled ^{31}P spectrum did not provide any useful information. However, the presence of two hydrido ligands is further supported by the overall 1:2 ratio of hydride to methine resonances observed at $-60\,^{\circ}C$ in the ^{1}H NMR spectrum.

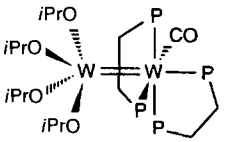
Compound **1** reacts in hydrocarbon solvents with carbon monoxide to evolve H_2 and form complex **2**. The reaction

$[W_2(O\mathit{i}Pr)_4(CO)(dmpe)_2]$ **2**

proceeds in two stages as monitored by ^{1}H NMR spectroscopy in [D$_6$]benzene. In the first step H_2 is liberated ($\delta = 4.5$), and the NMR spectra indicate the formation of a complex with the proposed structure **B** [^{31}P{^{1}H} NMR: $\delta = 26.2$, s, $J_{W\text{-}P} = 272$ Hz, intensity of the satellites corresponds to 14% of the peak intensity; ^{1}H NMR: $\delta = 2.1$ and 1.6, one set of proximal and distal methyl resonances for the dmpe ligands]. With time the kinetic product **B** slowly isomerizes to form **C** which has been crystallographically characterized.



B



C

The structure of the thermodynamically stable form of **2** is given in Figure 2. The CO ligand is *cis* to the W–W bond, which with a length of 2.524(1) Å is in the expected range for a

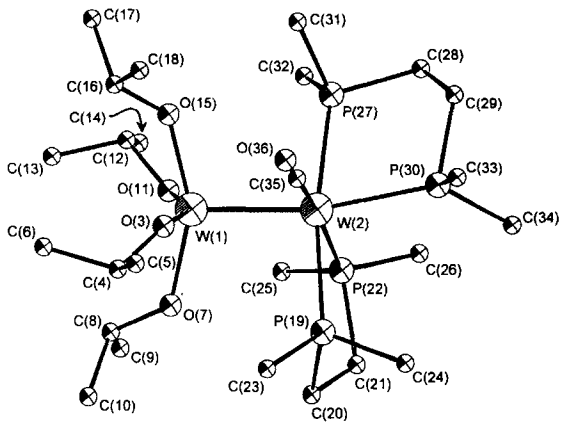


Fig. 2. Ball-and-stick drawing showing the crystal structure of **2** (enantiomer A in the asymmetric unit). Atoms C(21), P(22), C(29), and P(30) are unique to enantiomer A and were weighted only half. All other atoms are common to both enantiomers. Pertinent bond lengths [Å] and angles [°], averaged where appropriate: W-W 2.524(1), W-O 1.93(1), W-P 2.43(1), W-C 1.96(1), W-W-O 104.0(3), W-W-P(30) 166.0(4), W-W-P 95.4(1), W-W-C 94.4(4).

W–W double bond. The tungsten atoms are assigned oxidation states of +4 and 0. The arrangement of ligands about the W(CO)(dmpe)$_2$ unit leads to an ABMX spin system for the P nuclei in the ^{31}P NMR spectrum. It can also be seen that a d^6-W^0 center with one CO ligand [ν(CO) = 1827 cm^{-1}] has two electrons available for forming a W–W double bond with the d^2-W(OR)$_4$ center.

Compound **2** reacts with water to give the novel tetranuclear, water-soluble tungsten complex **3**, whose solid-state structure

$[W_2O_4(\mu\text{-}O)\{W(CO)(dmpe)_2\}_2]$ **3**

is given in Figure 3. The tungsten atoms in the central linear W-O-W moiety are each in a pseudotetrahedral environment with bonds to two terminal oxo groups and a further tungsten

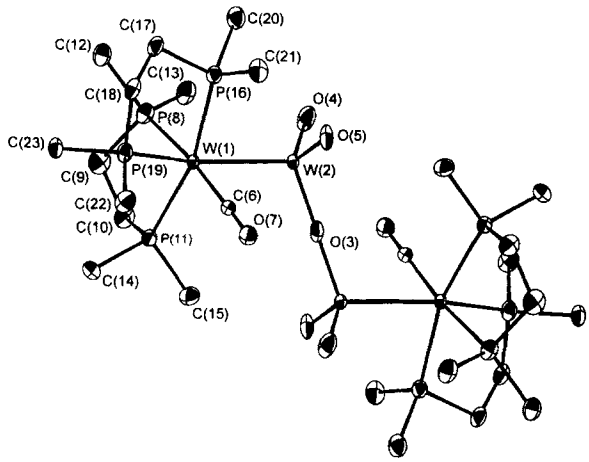


Fig. 3. ORTEP drawing showing the crystal structure of **3** (50% probability ellipsoids). Pertinent bond lengths [Å] and bond angles [°], averaged where appropriate: W-W 2.648(1), W- O(3) 1.88(1), W-O(4)(5) 1.73(1), W-C 1.95(1), W-P 2.490(1), W-W-O(3) 110.7(2), W-W-O(4,5) 109.8(2), W-W-C 72.8(2), W-W-P(19) 147.5(1), W-W-P 89.1(1).

atom. The two W(dmpe)$_2$(CO) units are mutually *anti* in what is an essentially ethane-like X$_2$(Y)W–O–W(Y)X$_2$ core. Since we can find no evidence for the existence of hydrido ligands in compound **3**, we propose that it contains unsupported metal–metal bonds between metal atoms having oxidation states of 0 and +5. Compound **3** is diamagnetic and in solution shows a complex ^{31}P NMR spectrum consistent with the presence of more than one rotamer in solution. The diamagnetism of compound **3** presumably arises from spin pairing of the oxo-bridged d^1-d^1 tungsten centers. The asymmetry of the complex removes the degeneracy of the d_{xz} and d_{yz} orbitals (the W-O-W axis is defined as the z axis), thus allowing spin pairing by occupation of a nonbonding three-center molecular orbital of π symmetry. The W–W single bond (2.648 Å) would then be the result of a dative interaction between the W^0 and the W^V centers.

In summary compounds **1**, **2**, and **3** reveal the remarkable ability of tungsten to form M–M bonds between metal atoms in very different oxidation states. This is in marked contrast to all of the chemistry that we have previously seen for so-called d^3-d^3 tungsten dimers.[6] We believe that the present compounds with W–W bonds between tungsten atoms in different oxidation states arise because the metal shows both class a and b character in liking both hard and soft ligands. Thus in each of the complexes **1**–**3** one tungsten atom coordinates all of the oxo substituents, while the other binds four P atoms as well as an additional carbonyl ligand in **2** and **3**. It may well therefore be possible that the results anticipated for early–late transition metal complexes can also be achieved with homometallic com-

 © VCH Verlagsgesellschaft mbH, D-69451 Weinheim, 1995 0570-0833/95/0808-0892 $ 10.00+.25/0

plexes with polar M–M bonds involving disparately hard and soft ligands. Clearly there is a need to explore this area of chemistry further.

Experimental Procedure

All reactions were carried out under N_2 using standard glovebox and Schlenk-line techniques. ^{1}H NMR spectra were recorded on a Varian XL-300 spectrometer at 300 MHz, and ^{31}P NMR spectra were recorded on a Nicolet NT-360 spectrometer at 146 MHz. NMR solvents were dried and deoxygenated prior to use.

1: In a 30 mL capacity Kontes brand solvent seal flask $[W_2(i\mathrm{Bu})_2(O i\mathrm{Pr})_4]$ (0.900 g, 1.25 mmol) was dissolved in roughly 15 mL of toluene, and dmpe (0.376 g, 2.51 mmol) was then added from a µL syringe. The mixture was frozen in liquid nitrogen and the flask evacuated and closed. Next, the flask was transferred to a gas-addition manifold where it was immersed in liquid nitrogen, and hydrogen (600 Torr, ca. 3 atm at 22 °C) was added. The Kontes tap was closed and the contents warmed to room temperature with stirring. After 24 h the excess hydrogen was released and the reaction mixture transferred to a standard Schlenk flask. The solvent volume was reduced in vacuo until crystallization began, and the mixture was warmed to regain homogeneity. The flask was left standing at room temperature for several hours and then cooled to −20 °C for another 24 h. Two crops of crystals were isolated in this manner; the mother liquor was removed and the crystals washed with cold hexane (yield: 0.985 g, 87%); Anal. calcd (found) for $C_{24}H_{62}O_4P_4W_2$: C 31.81 (31.94), H 6.89 (6.95); ^{1}H NMR (+ 60 °C, [D$_8$]toluene): δ = 4.65 (m, 4H, OC(*H*)(CH$_3$)$_2$), 1.41 (d, 24H, OC(H)(C*H*$_3$)$_2$), 1.62 (br. s, 32H, (CH$_3$)$_2$PCH$_2$CH$_2$P(CH$_3$)$_2$); ^{1}H NMR (− 60 °C, [D$_8$]toluene, W-H): δ = −12.4 (m), −1.60 (m), −1.04 (m); ^{31}P{^{1}H} NMR (+ 60 °C, [D$_8$]toluene): δ = 14.9 (br. s, dmpe); ^{31}P{^{1}H} NMR (− 80 °C, [D$_8$]toluene): δ = 18.12 (br. s, $J_{^{183}W-^{31}P}$ = 224.8 Hz), 14.02 (br. s, $J_{^{183}W-^{31}P}$ = 275.5 Hz), 5.37 (br. s, $J_{^{183}W-^{31}P}$ = 167.0 Hz); IR (KBr): ν_{H} = 1755, ν_{D} = 1250 cm^{-1}; crystal data for **1**: T = −160 °C; a = 9.841(1), b = 20.478(3), c = 17.280(3) Å, β = 95.70(1)°, Z = 4, ρ_{calcd} = 1.734 g cm^{-3}, space group $P2_1/n$; R(F) = 0.033, Rw(F) = 0.035 [7].

2: In a 20 mL capacity Kontes brand solvent seal flask $[W_2(H)_2(O i\mathrm{Pr})_4(\mathrm{dmpe})_2]$ (0.200 g, 0.221 mmol) was dissolved in roughly 10 mL of hexane. The solution was then frozen in liquid nitrogen and the flask evacuated. One atm of CO was added by way of a gas-transfer manifold, the flask closed. The reaction mixture was warmed to room temperature and stirred for 24 h. The reaction mixture was filter transferred to a standard Schlenk flask where the volume of solvent was then reduced to about 1 mL. After 3 to 4 d at −20 °C, brown crystals were isolated by cannulating off the mother liquor (yield: 0.190 g, 92%). Anal. calcd. (found) for $W_2P_4O_5C_{25}H_{60}$: C 32.21 (31.88), H 6.49 (6.27); ^{1}H NMR (22 °C, C_6D_6): δ = 4.63 (sept, 4H, OC(*H*)(CH$_3$)$_2$), 1.56 (d, 12H, OC(H)(C*H*$_3$)$_2$, 1.41 (d, 12H, OC(H)(C*H*$_3$)$_2$), 2.24, 2.14, 2.05, 1.86, 1.29, 1.26, 0.801, 0.468 (8d, 24H, (C*H*$_3$)$_2$PCH$_2$CH$_2$P(C*H*$_3$)$_2$); ^{13}C{^{1}H} NMR (22 °C, C_6D_6): δ = 224.0 (m, 1C, CO, $J_{^{183}W-^{13}C}$ = 158.6 Hz, $J_{^{13}C-^{31}P(trans)}$ = 27.3 Hz, $J_{^{13}C-^{31}P(cis)}$ = 4.8 Hz); ^{31}P{^{1}H} NMR (22 °C, C_6D_6): δ = 15.7 (AB quartet, 2P, dmpe), 6.8 (dd, 1P,dmpe), −3.0 (dd, 1P, dmpe); simulated coupling constants (Hz) for the ABMX system: J_{AB} = 85, J_{AM} = 16, J_{AX} = 0, J_{BM} = 0, J_{BX} = 13, J_{MX} = 23.5, $J_{\mathrm{W\text{-}P(A)}}$ = 370, $J_{\mathrm{W\text{-}P(B)}}$ = 260, $J_{\mathrm{W\text{-}P(M)}}$ = 190.5, $J_{\mathrm{W\text{-}P(X)}}$ = 130; IR (Nujol): ν_{CO} = 1827, $\nu_{^{13}\mathrm{CO}}$ = 1784 cm^{-1}; crystal data for **2**·0.5 toluene: T = −170 °C; a = 19.546(3), b = 21.745(4), c = 18.114(3) Å, Z = 8, ρ_{calcd} = 1.688 g cm^{-3}, space group *Pbca*; R(F) = 0.051, Rw(F) = 0.046 [7].

3: In a Kontes brand solvent seal flask complex **1** (0.200 g, 0.221 mmol) was dissolved in roughly 10 mL of toluene. One atm of CO was added to generate **2** as described previously. The solution of **2** was then transferred to a standard Schlenk flask, and a 1.11 M solution of H_2O in THF (600 µL, 0.662 mmol) was added by µL syringe. The reaction mixture was left at room temperature without stirring for 24 h, whereupon orange needles deposited on the sides of the flask. The mother liquor was removed by cannula and the orange solid washed twice with 5 mL of hexane and dried in vacuo (yield: 0.148 g, 97%). Compound **3** can also be generated directly from crystalline **2** in comparable yield. X-ray quality crystals were grown from CH_2Cl_2. Anal. calcd (found) for $W_4P_8O_7C_{26}H_{64}$: C 21.21 (20.83), H 4.38 (4.43); ^{1}H NMR (22 °C, [D$_5$]pyridine): δ = 0.900–2.23 (16 doublets consistent with the presence of two rotamers in a ratio of ca. 1.0–1.2); ^{31}P{^{1}H} NMR (22 °C, D_2O): δ = 13.9 (m, 1P), 8.5 (m, 1P), 0.767 (m, 2P); IR (KBr): ν_{CO} = 1800, $\nu_{^{13}\mathrm{CO}}$ = 1755 cm^{-1}; crystal data for **3**·4CH$_2$Cl$_2$: T = −169 °C; a = 13.282(2), b = 14.308(3), c = 15.319(3) Å, β = 97.88(1)°, Z = 4, ρ_{calcd} = 2.105 g cm^{-3}, space group $P2_1/n$; R(F) = 0.0245, Rw(F) = 0.027 [7].

Received: September 28, 1994 [Z 7365 IE]
German version: *Angew. Chem.* **1995**, *107*, 977

Keywords: complexes with oxygen ligands · complexes with phosphorus ligands · metal–metal bonds · tungsten compounds

[1] M. Herberhold, G. Jin, *Angew. Chem.* **1994**, *106*, 1016; *Angew. Chem. Int. Ed. Engl.* **1994**, *33*, 964.
[2] M. H. Chisholm, K. S. Kramer, W. E. Streib, *J. Am. Chem. Soc.* **1992**, 114, 3571.
[3] M. H. Chisholm, K. S. Kramer, unpublished.
[4] M. H. Chisholm, J. C. Huffman, W. G. Van Der Sluys, *J. Am. Chem. Soc.* **1987**, *109*, 2514.
[5] G. A. Orpen, *J. Chem. Soc. Dalton Trans.* **1980**, 2509, and references therein.
[6] M. H. Chisholm, *Accts. Chem. Res.*, **1990**, *23*, 419.
[7] Further details of the crystal structure investigations may be obtained from the Fachinformationszentrum Karlsruhe, D-76344 Eggenstein-Leopoldshafen (Germany), on quoting the depository number CSD-58696.

A Multienzyme System for a One-Pot Synthesis of Sialyl T-Antigen**

Vladimír Křen* and Joachim Thiem

The diverse roles of carbohydrates in biological recognition are increasingly a topic of research.[1] Sialic acid, a common structure in glycoconjugates, is particularly important because sialylated structures are involved in a variety of biological processes,[2] for example, cell surface communication,[3] immunogenicity, and circulation half-life of glycoproteins;[4] moreover, they are recognized as crucial structural elements of some antigenic determinants in tumors.[5]

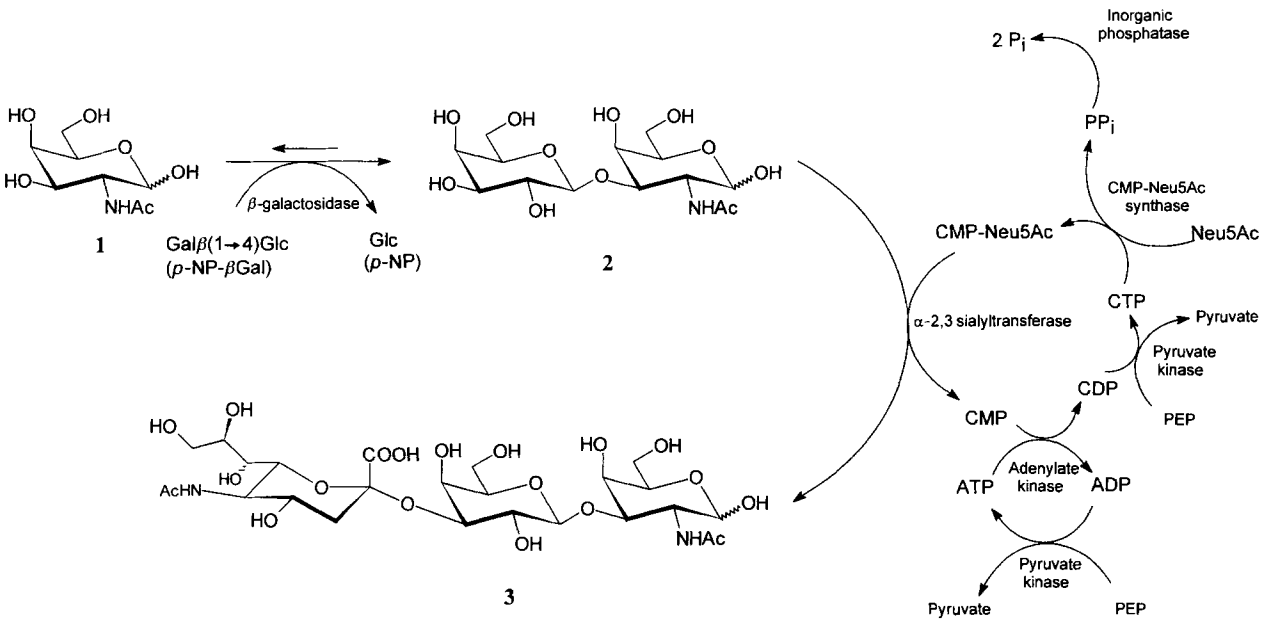
Thomsen–Friedenreich antigen (T-antigen), (Galβ(1 → 3)-GalNAcα-O-Ser), belongs to the antigens that are related to blood group determinants and is expressed in epithelial cancers.[6] A sialylated epitope, Neu5Acα(2 → 3)Galβ(1 → 3)GalNAc (**3**, Scheme 1) can be found in GM_1 glycolipids, human erythrocytes,[5, 7] and a bone marrow macrophage lectin.[7] The synthesis of this epitope is of considerable importance for immunological studies and for the preparation of, for example, synthetic antitumor vaccines.[8]

Enzymatic approaches to the synthesis of these epitope structures and their derivatives proved to be useful,[9, 10] in particular, those based on glycosyltransferases coupled with in situ regeneration of sugar nucleosides.[11, 12] The starting material for the preparation of **3**, Galβ(1 → 3)GalNAc (**2**), could be obtained either by a complicated multistep synthesis[13] or by an enzymatic transglycosylation employing β-galactosidases from bovine testes and *E. coli*, which, however, gave only 21% yield.[14] Both methods are rather complicated, and this is reflected in the extremely high price of the commercial product (approximately DM 100 per mg).

A combined sequential use of glycosyltransferases,[12] or glycosidase together with glycosyltransferase and a cofactor regeneration,[16] transforms the complicated multistep reactions into a one-pot reaction, thus avoiding laborious purification of the intermediates. Reverse hydrolysis of the disaccharide intermedi-

[*] Dr. V. Křen,[+] Prof. Dr. J. Thiem
Institut für Organische Chemie der Universität
Martin-Luther-King-Platz 6, D-20146 Hamburg (Germany)
Telefax: Int. code + (40)4123-4325
[+] Permanent address:
Institute of Microbiology, Academy of Sciences of the Czech Republic
Laboratory of Biotransformations
Vídeňská 1083, CZ-142 20 Prague 4 (Czech Republic)
Telefax: Int. code + (2)471-5743
e-mail: Křen@biomed.cas.cz

[**] Support of this work by a research fellowship from the Alexander-von-Humboldt Foundation to V. K. and by the Fonds der Chemischen Industrie is gratefully acknowledged.



Scheme 1.

ate is blocked by its glycosyltransferase-mediated conversion into an oligosaccharide, which is no longer a substrate for the glycosidase. An analogous approach has been employed recently for a chemoenzymatic synthesis of Neu5Acα(2 → 6)-LacNAc using commercial β-galactosidase from *Bacillus circulans* and α-2,6-sialyltransferase from rat liver.[16] We have now developed a sequential multienzyme one-pot system (Scheme 1) with cofactor regeneration for the preparation of the sialylated antigen T-epitope.

In the case of the above model compound[16] the optimal pH of the enzymes used lie in a narrow range, which substantially facilitated the operation as a multienzyme system. The optimal pH of CMP-Neu5Ac synthase (CMP = cytosine monophosphate) from calf brain is 9.0,[17, 18] that of α-2,3-sialyltransferase (ST) from porcine liver 6.5, and that of β-galactosidase from bovine testes (BTG) 4.3.[15] Although the optimal pH of α-2,3-ST is 6.5, it is usually synthesized at pH 7.5 to prevent decomposition of CMP-Neu5Ac at lower pH. This pH is still suitable for CMP-Neu5Ac synthase and for most of other enzymes required for CTP regeneration. The crucial question was whether BTG would be able to operate at a pH quite far from its optimal value to synthesize the intermediate disaccharide.

According to Distler and Jourdian[15] the activity of BTG at pH 7.5 for the substrate lactose is about 19% of its maximum activity. When *p*-nitrophenyl β-D-galactopyranoside (*p*-NP-Gal) is used, the rate of galactose release can be raised to about 30%. The transglycosylation activity of glycosidases in synthesis is quite often pronounced at more basic conditions than at the pH optimum.[19] Therefore, such a shift should support the transglycosylation reaction. Furthermore, the activity of BTG is about twice as high in the presence of *N*-acetylgalactosamine,[15] which most plausibly serves as an acceptor for galactose released, thus shifting the equilibrium of the reaction.

These phenomena should both be of advantage. The hypotheses were tested under real conditions (Na-cacodylate 25 mM, $MnCl_2$ 20 mM, NaCl 75 mM, Triton X-100 1.4% w/v) and *p*-NP-Gal as a substrate. At pH 6.5, 7.0, and 7.5 the BTG activity was 42%, 30%, and 26% of that at pH 4.3, respectively. GalNAc in the final concentration of 250 mM at pH 7.5 elevated the activity 3.6-fold. TLC (*n*-propanol: 1 M NH_3:H_2O = 6:2:1) confirmed the fast formation of the desired disaccharide component **2** in the reaction mixture.

To investigate the course of the ST reaction in the presence of *p*-nitrophenol released from *p*-NP-Gal, and the coupling of transgalactosylation of GalNAc with the transfer of Neu5Ac to the acceptor disaccharide, we used radioactively labeled CMP-Neu5Ac. When lactose was the Gal-donor instead of *p*-NP-Gal, the (analytical) yield of **3** was 20% higher. However, we decided to use *p*-NP-Gal for preparative purposes to simplify the purification procedure. This part of reaction sequence without CMP-Neu5Ac regeneration was optimized with the radioactively labeled substrate. It was shown that CMP-Neu5Ac is not hydrolyzed in the BTG preparation used.[14]

This part of the reaction sequence was then coupled to a modified multienzymatic system that regenerates CMP-Neu5Ac[12] (Scheme 1). The final composition of the reaction mixture for a semipreparative scale is given in the experimental section. The analytical yield of the trisaccharide **3** based on Neu5Ac was 45%, the isolated yield 36%.

The reaction was followed by a new colorimetric system that enabled the determination of the proportion of free Neu5Ac, CMP-Neu5Ac, and the product (**3**) at any time. The course of reaction and reactant additions could therefore be optimized (Fig. 1).

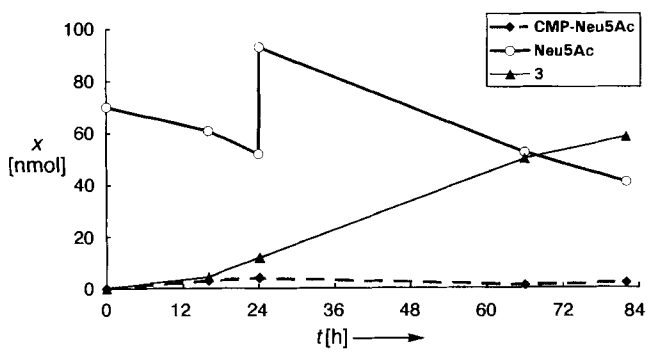


Fig. 1. Synthesis of **3** by incorporation of Neu5Ac into **2** (see Scheme 1) during the multienzyme one-pot reaction (*x* is the amount of substance, *t* the reaction time).

Neu5Ac is present in the reaction mixture in three forms: free, as CMP-Neu5Ac, and incorporated into the trisaccharide **3**. Total Neu5Ac can be determined after hydrolysis of the sample (pH 1, 80 °C, 1 h) by the thiobarbituric acid method.[21] The amount of Neu5Ac incorporated into the product **3**, that is, the analytical yield of the reaction, can be determined after passing the sample, diluted in phosphate buffer (5 mM, pH 6.9), through a Pasteur pipette filled with Dowex 1 × 8, 200–400/(PO_4^{3-}). The ion exchange resin retains both Neu5Ac and CMP-Neu5Ac so that the amount of the product can be assayed by the thiobarbituric acid method after acid hydrolysis. The sum of the Neu5Ac incorporated into the product **3** and into the CMP-Neu5Ac can be determined after treatment of the reaction mixture with $NaBH_4$, followed by acid hydrolysis and the thiobarbituric acid assay. Free Neu5Ac is reduced to the Neu5Ac-alditol that does not give a color reaction with thiobarbituric acid. This system is applicable to the optimization of the course of the reaction and the determination of the analytical yield of any other transsialylation reactions employing both sialyltransferases and sialidases.

In summary, the concept of multienzyme reactions with integrated cofactor regeneration was shown to be useful for sequential synthesis of rather complicated heterooligoglycosides. Furthermore, enzymes with rather widely separated optimal pH values can be employed when the reaction conditions carefully rationalized and optimized. These results open new perspectives for one-pot syntheses of glycosides having as many as three to four different glycosyl units.

Experimental Procedure

Enzymatic synthesis of **3**: Neu5Ac (70 μmol; 0.7 mL of 0.1 M solution neutralized to pH 7.5 by $NaHCO_3$), CMP (50 mg, 100 μmol), ATP (5 μmol), CTP (0.5 μmol), phosphoenolpyruvate (K salt, 300 mg, 200 μmol), **1** (150 mg, 0.7 mmol), *p*-nitrophenyl β-D-galactopyranoside (300 mg, 1 mmol), $MnCl_2$ (60 μmol; 60 μL of 1 M solution), $MgCl_2$ (0.12 mmol; 120 μL of 1 M solution), KCl (0.2 mmol; 200 μL of 1 M solution), and Na-cacodylate buffer (1 mL; 0.25 M, pH 7.5 containing 2% of Triton X-100) were mixed and adjusted to approximately 5 mL with H_2O. The pH was adjusted to 7.5 (NaOH). The enzymes myokinase from porcine muscle ([EC 2.7.4.3], 600 U), pyruvate kinase ([EC 2.7.1.40], 1200 U), inorganic phosphatase ([EC 3.6.1.1], 5 U), CMP-Neu5Ac synthase from calf brain immobilized on the CNBr Sepharose [20] ([EC 2.7.7.43], 1 U), β-galactosidase from bovine testes [14] ([EC 3.2.1.23], 1.5 U), α-2,3-sialyltransferase (porcine liver) ([EC 2.4.99], 0.1 U)[9, 17, 22] were added, and the mixture was made up to 10 mL. After 16 h of incubation at 37 °C more *p*-NP-Gal (300 mg, 200 μmol) and β-galactosidase (0.7 U) were added (pH was adjusted to 7.5), and after another 24 h Neu5Ac (40 μmol), CMP-Neu5Ac synthase (0.2 U), and sialyltransferase (0.07 U). After a further 24 h, sialyltransferase (0.07 U) was again added, and the reaction was terminated after a total of 82 h. The reaction mixture was diluted with water to twice its volume, and approximately 7 mL of Dowex 1 × 2 (200–400 mesh)/PO_4^{3-}, equilibrated in 5 mM NaP_i buffer, pH 6.9) were added. After 20 min the supernatant was collected, and the ion exchange resin was washed with 15 mL of the equilibration buffer. This treatment removes all free Neu5Ac, CMP-Neu5Ac, and *p*-nitrophenol. The pooled elutes were concentrated by lyophilization to approximately 2 mL and applied to the column (4 × 100 cm) of BioGel P2 (200–400 mesh) with water as eluent. The fractions containing the trisaccharide (refractometric detection, thiobarbiturate assay[21]) were pooled and lyophilized to give 27 mg of the product **3** (isolated yield 26 mg, 36%; analytical yield determined at the end of the reaction 45% based on Neu5Ac).

3: ^{1}H NMR (400 MHz, D_2O; equilibrium in water: α:β ratio 5:4): $\delta = 1.72$ (t, 0.56 H, $J_{3'''a,4'''} = J_{3'''a,3'''e} = 12.2$ Hz, H-3‴*a* β-anomer), 1.73 (t, 0.44 H, $J_{3'''a,4'''} = J_{3'''a,3'''e} = 12.2$ Hz, H-3‴*a* α-anomer), 1.97 (s, 3 H, 5′-NAc), 1.99 (s, 1.7 H, 2-NAc β-anomer), 1.99 (s, 1.3 H, 2-NAc α-anomer), 2.69 (dd, 1 H, $J_{3'''e,4'''} = 4.1$ Hz, H-3‴*e*), 4.44 (d, 0.44 H, $J_{1',2'} = 7.6$ Hz, H-1′ β-anomer), 4.51 (d, 0.56 H, $J_{1',2'} = 7.6$ Hz, H-1′ α-anomer), 4.63 (d, 0.44 H, $J_{1,2} = 9.2$ Hz, H-1 β-anomer), 5.17 (d, 0.56 H, $J_{1,2} = 4.1$ Hz, H-1 α-anomer). The data are in agreement with the previously published spectrum (250 MHz) [9] of **3**.

Received: November 15, 1994 [Z 7479 IE]
German version: *Angew. Chem.* **1995**, *107*, 979

Keywords: enzyme catalysis · β-galactosidase · oligosaccharide synthesis · sialyltransferase · T-antigen

[1] J. B. Lowe, L. M. Stolman, R. P. Nair, T. L. Berhend, R. M. Marks, *Cell* **1990**, *63*, 475–484; T. Feizi, *Trends Biochem. Sci.* **1991**, *16*, 84–86.
[2] R. Schauer, *Sialic Acid Chemistry, Metabolism and Function*, Springer, Vienna **1982**, and references therein; *Adv. Carbohydr. Chem. Biochem.* **1982**, *40*, 131–234; *Methods Enzymol.* **1987**, *138*, 132–161.
[3] G. Ashwell, J. Hartfort, *Annu. Rev. Biochem.* **1982**, *51*, 531–554.
[4] T. A. Springer, L. A. Lasky, *Nature* **1991** *349*, 196–197; C. Foxal, S. R. Watson, B. Dowbenko, C. Fennie, L. A. Lasky, M. Kiso, A. Hasagawa, D. Asa, B. K. Brandley, *J. Cell Biol.* **1992**, *117*, 895–902.
[5] S. Hakomori, *Annu. Rev. Immunol.* **1984**, *2*, 103–126; A. M. Cohen, A. Allaouf, M. Djaldetti, K. Weigl, N. Lehrer, H. Levinski, *Eur. J. Haematol.* **1989**, *43*, 191–194; F. Dall'Olio, N. Mallagoli, G. DeStefan, F. Minni, D. Marrano, F. Serafini, *Int. J. Cancer* **1989**, *44*, 434–439; J. C. Jamieson, G. McCaffrey, P. G. Harder, *Comp. Biochem. Physiol.B* **1993**, *105*, 29–33.
[6] G. F. Springer, *Science* **1984**, *224*, 1198–1206.
[7] O. Prokop, G. Uhlenbruck, *The Thomsen Phenomenon in Human Blood and Serum Groups*, MacLaren, London, **1969**, pp. 102–110; G. Uhlenbruck, G. I. Pardoe, G. W. G. Bird, *Z. Immunitätsforsch. Allg. Klin. Immunol.* 1969, *38*, 423–433; Y. Ito, J. J. Gaudino, J. C. Paulson, *Pure Appl. Chem.* **1993**, *65*, 753–762.
[8] P. O. Livingston, *Curr. Opinion Immunol.* **1992**, *4*, 624–629; J. Cohen, *Science*, **1993**, *262*, 841–843.
[9] A. Lubineau, C. Augé, P. Francois, *Carbohydr. Res.* **1992**, *228*, 137–144.
[10] J. Thiem, W. Treder, *Angew. Chem.* **1986**, *98*, 1100; *Angew. Chem Int. Ed. Engl.* **1986**, *25*, 1096–1097; S. Sabesan, J. C. Paulson, *J. Am. Chem. Soc.* **1986**, *108*, 2068–2080.
[11] C. Augé, C. Mathieu, C. Merienne, *Carbohydr. Res.* **1986**, *151*, 147–156; J. Thiem, T. Wiemann, *Angew. Chem.* **1991**, *103*, 1184–1185; *Angew. Chem. Int. Ed. Engl.* **1991**, *30*, 1163–1164; Y. Ichikawa, G.-J. Shen, C.-H. Wong, *J. Am. Chem. Soc.* **1991**, *113*, 4698–4700.
[12] P. Stangier, W. Treder, J. Thiem, *Glycoconjugate J.* **1993**, *10*, 26–33.
[13] A. Lubineau, H. Bienaymé, *Carbohydr. Res.* **1991**, *212*, 267–271.
[14] L. Hedbys, E. Johansson, K. Mosbach, P.-O. Larsson, *Carbohydr. Res.* **1989**, *186*, 217–223.
[15] J. J. Distler, G. W. Jourdian, *J. Biol. Chem.* **1973**, *248*, 6772–6780.
[16] G. F. Herrmann, Y. Ichikawa, C. Wandrey, F. C. A. Gaeta, J. C. Paulson, C.-H. Wong, *Tetrahedron Lett.* **1993**, *34*, 3091–3094.
[17] C. Augé, R. Fernandez-Fernandez, C. Gautheron, *Carbohydr. Res.* **1990**, *200*, 257–268.
[18] R. Schauer, M. Wember, C. Ferreira do Amaral, *Hoppe-Seyler's Z. Physiol. Chem.* **1972**, *353*, 883–886.
[19] V. Křen, *Biotechnol. Lett.* **1992**, *14*, 769–772; V. Křen, M. Flieger, P. Sajdl, *Appl. Microbiol. Biotechnol.* **1990**, *32*, 645–650.
[20] S. David, C. Augé, C. Gautheron, *Adv. Carbohydr. Chem. Biochem.* **1991**, *49*, 175–237.
[21] L. Warren, *J. Biol. Chem.* **1959**, *234*, 1971–1975.
[22] W. Gillespie, S. Kelm, J. C. Paulson, *J. Biol. Chem.* 1992, *267*, 21004–21010.

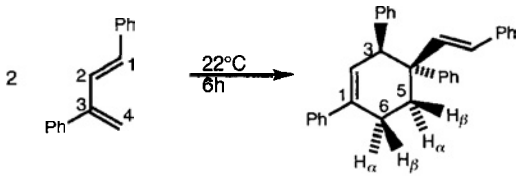
The Dimerization of (*E*)-1,3-Diphenyl-1,3-butadiene Proceeds Suprafacially with Respect to Both Components: Evidence for a Concerted [4 + 2] Cycloaddition

Johann Mulzer* and Katja Melzer

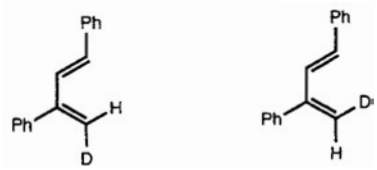
The stereochemistry of the dimerization of 1,3-butadiene and its derivatives has been studied intensively over the past two decades, with contradictory results. For instance, Stephenson et. al.[1] found that the stereochemical purity of the product was reduced by 10%. They interpreted this as the result of competing pathways, the allowed [$4_s + 2_s$] and forbidden [$4_s + 2_a$] pathways in a ratio of 9:1. According to a recent analysis by Klärner et. al.,[2, 3] the reaction actually proceeds with 97% stereoselectivity! An analogous result was obtained by Berson and Malherbe for the dimerization of piperylene.[4] Based on these findings a concerted mechanism was postulated as the dominant path-

[*] Prof. Dr. J. Mulzer, Dipl.-Chem. K. Melzer
Institut für Organische Chemie der Freien Universität
Takustrasse 3, D-14195 Berlin (Germany)
Telefax: Int. code + (30)838-5163

way for the dimerization of butadiene in competition with the stepwise mechanism. In the dimerization of 2,3-dimethyl-1,3-butadiene a two-step mechanism with a diradical intermediate competes with a concerted mechanism in a similiar way,[5] and a diradical mechanism was proved for one of the [4 + 2] dimers of chloroprene.[3] Ab initio calculations for 1,3-butadiene by Li and Houk showed a preference for the stepwise mechanism over the concerted one by 1.3 kcal mol^{-1}.[6] We found previously[7] that the dimerization of (*E*)-1,3-diphenyl-1,3-butadiene (**1**) significantly differs from the butadiene dimerizations studied to



1 **2**

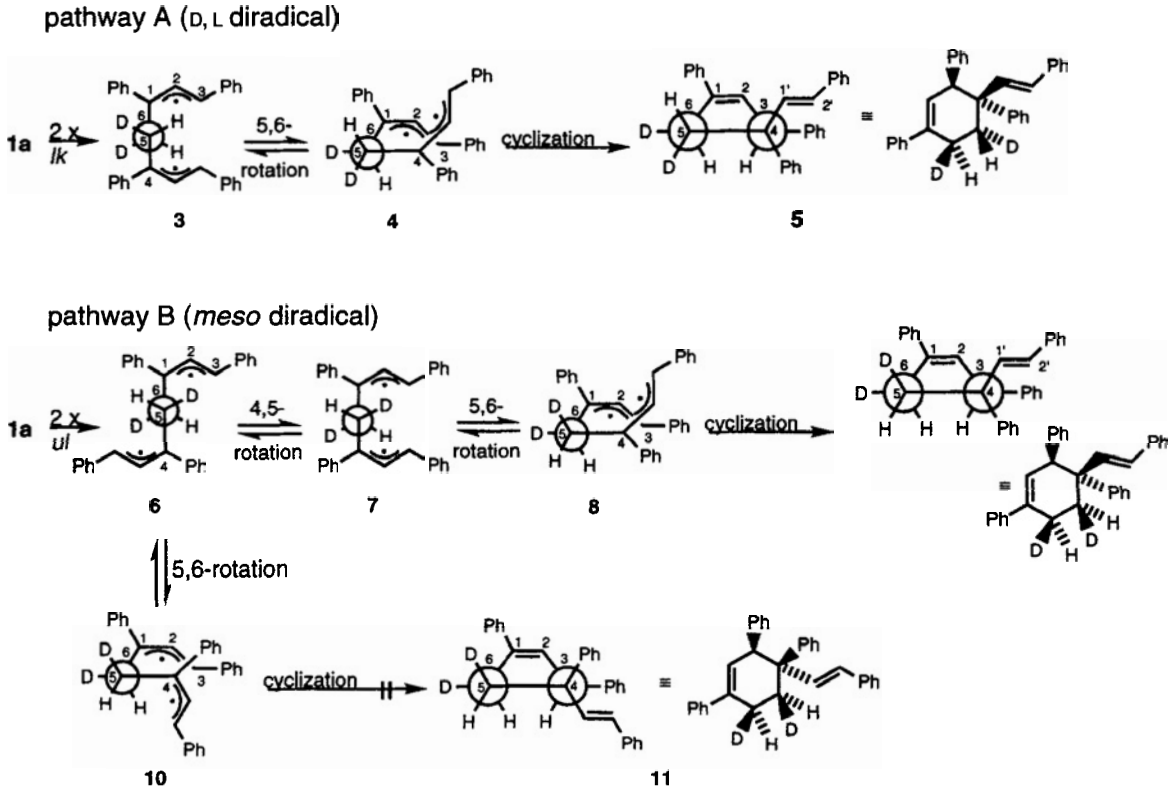


1a **1b**

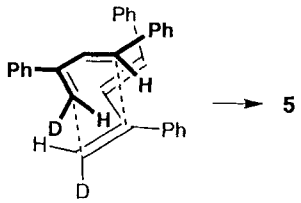
date. The reaction proceeds at 22 °C in condensed media and provides exclusively the [4 + 2] *endo* dimer **2** with high regio- and stereocontrol (both >97%). The reaction shows an significant substituent effect; for instance (*E*)-1,3-diphenyl-1,3-butadiene (**1**) dimerizes 10^6 times faster than 1,3-butadiene or its alkyl derivatives. For this reason and because of the low solvent effect the dimerization of **1** was regarded as a clearcut example of a diradical Diels–Alder-type cycloaddition.[7, 8]

To further support or disprove the diradical mechanism we decided to study the faciality of the reaction with respect to both the diene and the dienophile by using the monodeuterated butadienes **1a** and **1b**. In the diradical dimerization of **1a** (Scheme 1) the first bond forms between the terminal C atoms in 4-position. Bond formation proceeds with about equal rates by either pathway because of the low difference in energy between the diastereomeric diradicals **3** and **6**.[9] In pathway A the terminal C atoms are joined in a *Re–Re* or *Si–Si* fashion (*lk* arrangement) to give the D,L diradical **3**, which after rotation about the C5–C6 bond cyclizes to dimer **5** (*3r,4t,5t,6c* configuration). On the other hand, the initiating step in pathway B proceeds through a *ul* arrangement to give the *meso* diradical **6**. Rotation about the C5–C6 bond then leads to **10**, which obviously cannot cyclize owing to steric repulsion between the phenyl substituents, and the corresponding dimer **11** is not formed in the reaction. Cyclization is possible only after rotation about the C4–C5 bond giving **7**, followed by rotation about the C5–C6 bond yielding **8**. Cyclization then leads to dimer **9** (*3r,4t,5c,6c* configuration). Since no change in the deuterium distribution of the starting material was detected during the reaction, formation of both C–C bonds must be irreversible. Cyclization of the diradical intermediate proceeds equally well regardless of whether one (pathway A) or two rotations (pathway B) occur. Therefore if a diradical mechanism is involved, dimers **5** and **9** should be formed in equal amounts, whereas a concerted mechanism would lead to dimer **5** as the only product (Scheme 2).

For the synthesis of **1a** (Scheme 3) phenyl(trimethylsilyl)acetylene (**12**) was submitted to a *cis*-selective hydromagnesation.[10]

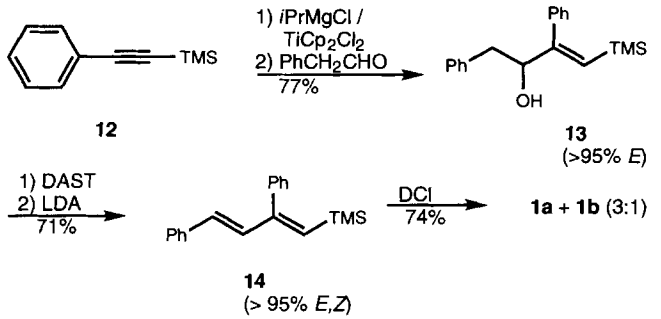


Scheme 1. Conceivable mechanisms for the diradical dimerization of **1**. The numbering of the C atoms corresponds to that of the product



Scheme 2. Concerted dimerization of **1**.

The resulting Grignard species was immediately quenched with phenylacetaldehyde to give alcohol **13** with (*E*) configuration. Treatment of **13** with *N*,*N*-diethylaminosulfur-trifluoride (DAST) and subsequently with LDA furnished the stereochemically pure (*E*,*Z*) silyldiene **14**. Deuteriolysis of **14** with DCl[11] led to a 3:1 mixture of the monodeuteriobutadienes **1a** and **1b**.[12] The dimerization of the **1a**/**b** mixture was performed without a solvent as described[7] to give the

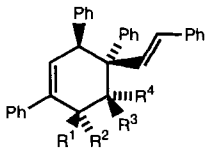


Scheme 3. Synthesis of **1a**, **b**.

crystalline dimers (see Table 1) in quantitative yield. NOE measurements (500 MHz) of undeuteriated **2** allowed the unambiguous assignment of the ^{1}H NMR signals of the protons in 5- and 6-position (Fig. 1). The intensities of these signals relative to that of the signal of 3-H were determined with a maximum error of $< 5\%$, and the ratio of 5-H_α:5-H_β:6-H_α:6-H_β was found to be 0.26:0.74:0.72:0.26.

On calculating the expected distribution of the deuterium label at the four positions, it must be considered that **1a** and **1b** (ratio 3:1) dimerize statistically. Table 1 shows how the expected relative intensities of the 5-H and 6-H signals for the products

Table 1. Calculated and experimental relative intensities for the ^{1}H NMR signals of the protons at C5 and C6 in the products arising from pathways A and B (e.g. rel. probability for **1a** + **1a** → **5** is $0.75 \times 0.75 = 0.56$; for **1a** + **1b** → **9**, $0.75 \times 0.25 = 0.19$ and so on).



	R^1	R^2	R^3	R^4
5	D	H	H	D
9	D	H	D	H
15	H	D	H	D
16	H	D	D	H

[4+2] Dimerization (rel. yield)	Relative intensity of signals 5-H_α	5-H_β	6-H_α	6-H_β
pathway A				
1a+**1a**→**5** (0.56)	0	0.56	0.56	0
1a+**1b**→**9** (0.19)	0.19	0	0.19	0
1b+**1a**→**15** (0.19)	0	0.19	0	0.19
1b+**1b**→**16** (0.06)	0.06	0	0	0.06
sum (pathway A)	0.25	0.75	0.75	0.25
pathway B				
1a+**1a**→**9** (0.56)	0.56	0	0.56	0
1a+**1b**→**5** (0.19)	0	0.19	0.19	0
1b+**1a**→**16** (0.19)	0.19	0	0	0.19
1b+**1b**→**15** (0.06)	0	0.06	0	0.06
sum (pathway B)	0.75	0.25	0.75	0.25
diradical [(A+B)2]	0.50	0.50	0.75	0.25
concerted	0.25	0.75	0.75	0.25
found	0.26	0.74	0.72	0.26

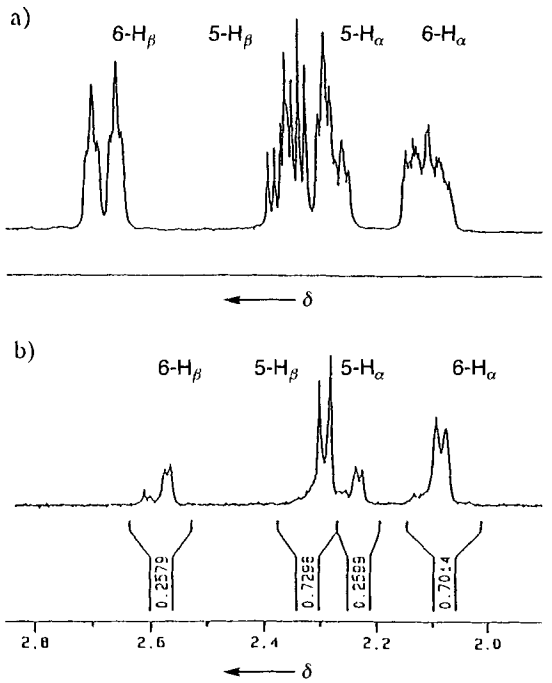
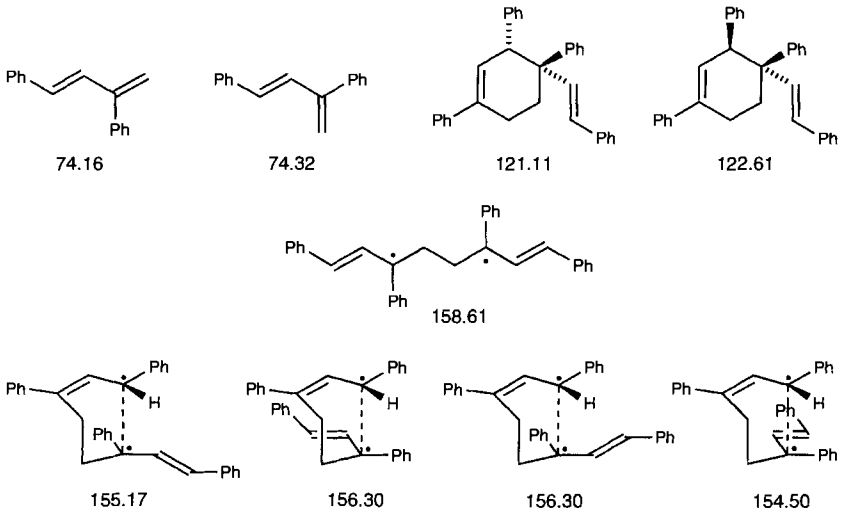


Fig. 1. a) Section of the ^{1}H NMR spectrum of **2**; b) section of the ^{1}H NMR spectrum of the mixture of deuterated regioisomers **5**, **9**, **15**, and **16** obtained from dimerization of **1a**,**b**.

of pathways A and B are calculated from the relative probabilities of the four combinations (**1a** + **1a**, **1a** + **1b**, **1b** + **1a**, **1b** + **1b**). The ratio of the signal intensities 5-H_α:5-H_β:6-H_α:6-H_β is 2:2:3:1 for the diradical mechanism and 1:3:3:1 for the concerted mechanism. The difference in the two mechanisms is reflected in the ratio of the relative intensities of the 5-H_α and 5-H_β signals, which is 1:1 for the diradical mechanism and 1:3 for the concerted mechanism. The experimentally determined ratio (Table 1, Fig. 1) indicates unequivocally that only the concerted mechanism is in effect in the dimerization. These conclusions are confirmed by force field calculations (MMEVBH).[13] The energy level diagram for the dimerization shows that the transition state in the diradical mechanism is 10 kcal mol^{-1} higher in energy than that in the concerted one (Fig. 2). The energies given in Figure 2 are mean values; the exact values are listed in Scheme 4. The high barrier for 1,6-cyclization with formation of the C3–C4 bond (13.4 kcal mol^{-1}) is remarkable. A comparable barrier for redissociation must be assumed to explain the irreversibility of the formation of the first C–C bond (between C1 and C6). This may be rationalized by a *cisoid* comformation of the diradical in the ground state (e.g. **4** and **8**) stabilized by π–π interactions between the allyl units, but this might be farfetched. In calculations on the dimerization of 1,3-butadiene Li and Houk found formation of the first C–C bond to be irreversible.[6]

We have shown that the dimerization of (*E*)-1,3-diphenylbutadiene follows a concerted mechanism, even though a diradical



Scheme 4. Energies of the starting materials, intermediates, transition states, and products for the [4 + 2] dimerization calculated with the force field MMEVBH [13].

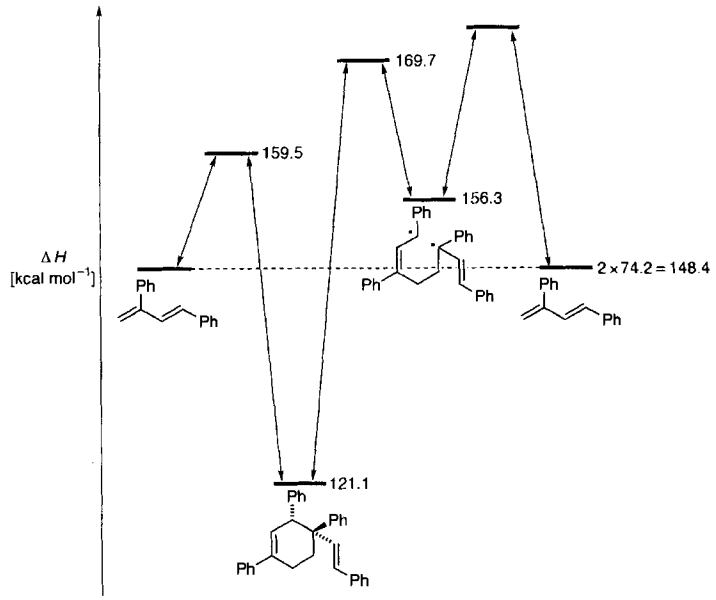


Fig. 2. Calculated energy profile for the dimerization of 1 [13].

intermediate would be stabilized. Doering et al. reached similar conclusions in studies of the Cope rearrangement: phenyl substituents facilitated the concerted mechanism.[14]

Received: September 15, 1994 [Z 7318 IE]
German version: *Angew. Chem.* **1995**, *107*, 981

Keywords: cycloadditions · dimerizations · diradicals

[1] L. M. Stephenson, R. V. Gemmer, S. Current, *J. Am. Chem. Soc.* **1975**, *107*, 5909–5910.
[2] F. G. Klärner, *Chem. Z.* **1989**, *23*, 53–63.
[3] F. G. Klärner, B. Krawczyk, V. Ruster, U. K. Deiters, *J. Am. Chem. Soc.* **1994**, *116*, 7646–7657.
[4] J. A. Berson, R. Malherbe, *J. Am. Chem. Soc.* **1975**, *107*, 5910–5912.
[5] G. Jenner, J. Rimmelin, *Tetrahedron Lett.* **1980**, *21*, 3039–3042.
[6] Y. Li, K. N. Houk, *J. Am. Chem. Soc.* **1993**, *115*, 7478–7485.
[7] J. Mulzer, U. Kühl, G. Huttner, K. Evertz, *Chem. Ber.* **1988**, *121*, 2231–2238.
[8] J. Sauer, R. Sustmann, *Angew. Chem.* **1980**, *92*, 773; *Angew. Chem. Int. Ed. Engl.* **1980**, *19*, 779–807.
[9] In a [4 + 2] dimerization one butadiene moiety must be in *s-cis* conformation; the second may be either *s-cis* or *s-trans*. If both partners are in *s-trans* conformation, only [2 + 2] cycloaddition can occur. Since we did not detect the corresponding product, we assume that **1** adopts mainly the *s-cis* conformation in the ground state. For simplicity we will consider this the sole conformation, although this point is not essential for our discussion.
[10] a) F. Sato, H. Ishikawa, and M. Sato, *Tetrahedron Lett.* **1981**, *22*, 85–88. b) F. Sato, *J. Organomet. Chem.* **1985**, *285*, 53–64.
[11] K. E. Koenig, W. P. Weber, *J. Am. Chem. Soc.* **1973**, *95*, 3416–3418.
[12] The incorporation of exactly one deuterium atom was proven by HRMS. The assignments of the (*E*) and (*Z*) configurations to **1a** and **b**, respectively, are based on the corresponding chemical shifts of the ^{1}H NMR signals of undeuteriated **1**. (δ((*E*)-4-H) = 5.52, δ((*Z*)-4-H) = 5.26).
[13] We thank Prof. Dr. W. R. Roth, Ruhr-Universität Bochum, for performing the calculations.
[14] W. von E. Doering, K. D. Belfield, J. He, *J. Am. Chem. Soc.* **1993**, *115*, 5414–5421.

$Li_5Pt_2H_9$, a Complex Hydride Containing Isolated $[Pt_2H_9]^{5-}$ Ions**

Welf Bronger* and Lothar à Brassard

In the area of alkali-metal platinum hydrides, we have previously reported the syntheses and the determination of the crystal structures of the compounds A_2PtH_4 (A = Na, K, Rb, or Cs)[1–3] and A_3PtH_5 (A = K, Rb, or Cs).[4] The structures of these ternary hydrides are all characterized by square-planar $[PtH_4]^{2-}$ ions. Because of the high thermal mobility of the hydrogen atoms, in each high-temperature modification of these compounds the averaged structure shows an octahedral coordination of each platinum atom with an occupation factor of 2/3.

The synthesis of these ternary hydrides entailed the conversion of the binary alkali-metal hydrides with platinum sponge in an atmosphere of highly pure hydrogen gas. The required reaction temperatures lay between 580 and 700 K while the hydrogen pressures varied between 1 and 10 bar.

Recently we have shown that it is possible, using high pressures of hydrogen, to oxidize platinum beyond the + II oxidation state and up to the + IV oxidation state, so obtaining hydrides of the composition A_2PtH_6 (A = Na, K, Rb, or Cs).[5–7] The determination of the structures of these compounds revealed that they are isotypic with that of K_2PtCl_6.

[*] Prof. Dr. W. Bronger, Dipl.-Chem. L. à Brassard
Institut für Anorganische Chemie der Technische Hochschule
Prof.-Pirlet-Str. 1, D-52056 Aachen (Germany)
Telefax: Int. code + (241) 888-8288

[**] This work was supported by the Bundesministerium für Forschung und Technologie, the Deutsche Forschungsgemeinschaft, the Fonds der Chemischen Industrie, the ICDD Grant-in-Aid Programme, and by the Large Installation Plan of the European Community Commission. We would like to thank Dr. Gudrun Auffermann and Dr. Paul Müller for carrying out the neutron diffraction experiments. Grateful thanks are also extended to the Hahn Meitner Institute (HMI) in Berlin and the Risø National Laboratory for allocating measurement time to us.

In the lithium/platinum/hydrogen system, only the compound $LiPtH_{0.66}$ has been hitherto synthesized and structurally characterized.[8] The structure of this compound corresponds to that of a metallic hydride in which lithium and platinum form alternate layers of hexagonal closest packed atoms. Dependent upon the temperature, the hydrogen atoms can reversibly occupy the available tetrahedral holes in this structure. The possibility remained that, under high hydrogen pressures, platinum could be oxidized further to yield saltlike, ternary lithium platinum hydrides. Our experiments now show that this is indeed possible. With a reaction pressure of 1250 bar of hydrogen at a temperature of 820 K and a reaction duration of one hour, a hitherto unknown hydride results, structural analysis of which yielded the composition $Li_5Pt_2H_9$. In this experiment a mixture of LiH (Alfa Products; stated purity 98%) and platinum (Degussa; stated purity 99.9%) in the respective molar ratio of 2.8:1 were employed, and the ternary hydride resulted as a finely crystalline, anthracite-colored caked solid, which was very air- and moisture-sensitive.

X-ray investigations using the Guinier method (Huber diffractometer G644) revealed a tetragonal unit cell in which the positions of the platinum atoms could be determined. In order to facilitate a complete structural elucidation, the corresponding deuteride, which could be synthesized by an analogous method to that used for the hydride, was subjected to elastic neutron diffraction studies. The first experiment was carried out at the reactor of the HMI in Berlin and yielded the complete structural determination. Further confirmation was provided by the data from a later experiment on the TAS III site of the DR3 reactor in the Risø National Laboratory (Denmark), which uses neutrons associated with a shorter wavelength than those generated at the HMI. An aluminum tube (diameter 10 mm, length 40 mm, wall thickness 0.05 mm) into which a second thin-walled aluminum tube (diameter 4.5 mm) was fitted to reduce the absorption effects further, served as the sample container for these studies. The substance was added to this hollow cylinder under argon, and the vessel sealed with a Viton gasket. The resulting data were analyzed with the program Fullprof (Rietfeld method).[9]

The lattice constants for the hydride and deuteride, determined from the Guinier diagrams, are reproduced in Table 1. The neutron diffraction diagram obtained on TAS III and that calculated for the refined structure are shown in Figure 1. The data are also collated in Table 1. When the refinement was complete, the occupation parameters of the atoms were allowed to vary. However, deviations from the $Li_5Pt_2H_9$ composition were not observed. The structure of the ternary hydride is depicted in Figure 2, but only half of the unit cell ($c/2$) is shown to retain clarity.

Table 1. Lattice constants of $Li_5Pt_2H_9$ and $Li_5Pt_2D_9$ (Guinier process, $Cu_{K\alpha_1}$ radiation) and the results of the elastic neutron diffraction experiments on workstation TAS III at room temperature (space group $I4/mcm$, $Z = 4$).

$Li_5Pt_2H_9$: $a = 8.376(1)$, $c = 8.556(1)$ Å
$Li_5Pt_2D_9$: $a = 8.347(1)$, $c = 8.524(1)$ Å
Measurement range: $14.0° < 2\theta < 120°$
Wavelength: 1.47321 Å
No. of reflections considered in the refinement: 142

Atom sites	x	y	z	B_{iso} [Å^2]
Pt in (8h)	0.157(1)	$x + 0.5$	0	0.14(6)
D1 in (32m)	0.075(1)	0.772(1)	0.134(1)	1.87(6)
D2 in (4d)	0	0.5	0	3.0(2)
Li1 in (16l)	0.349(3)	$x + 0.5$	0.159(3)	1.0(2)
Li2 in (4c)	0	0	0	2.3(7)

R-values: $R_{Bragg} = 0.090$, $R_{profile} = 0.092$

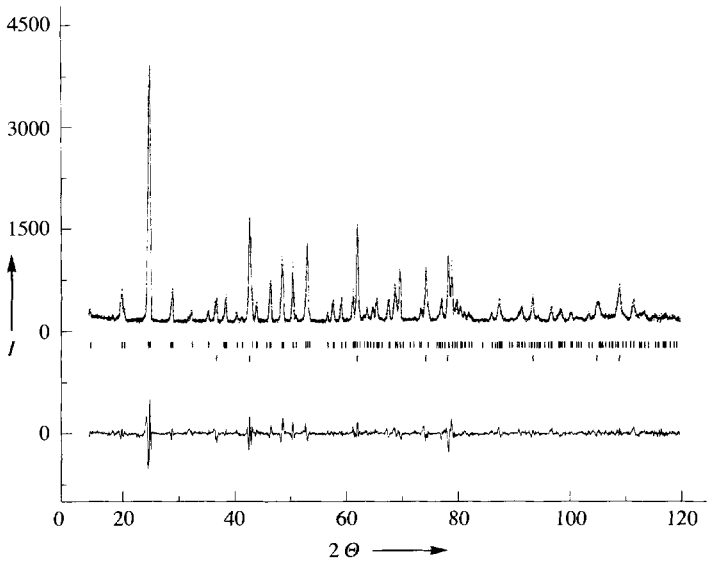


Fig. 1. The neutron diffraction diagram of $Li_5Pt_2D_9$, the measured (·), calculated (—), and difference profiles are depicted. In addition, the line diagrams of the reflections of $Li_5Pt_2D_9$ and of the aluminum tube, which was also refined, are shown.

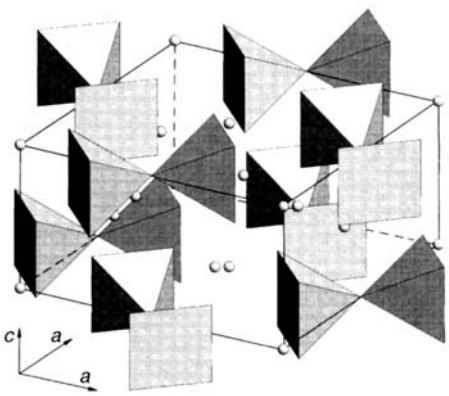


Fig. 2. The structure of $Li_5Pt_2D_9$. The square double pyramids formed by the deuterium atoms and centered by the platinum atoms are shown as well as the positions of the lithium atoms. The half unit cell ($c/2$) is indicated.

The atomic arrangement of $Li_5Pt_2D_9$ contains the surprisingly novel anionic complex $[Pt_2D_9]^{5-}$ (Fig. 3), in which the platinum atoms are each coordinated by five deuterium ligands. Four of these ligands form, within the experimental accuracy, a square plane. The platinum atom is displaced 0.196 Å from the center of the plane in the direction of the fifth, apical deuterium atom. The fifth deuterium atom acts simultaneously as the bridge to the second, identical coordination polyhedron such that the two planar pyramids are connected to each other through a common vertex. The Pt-D-Pt bridge is linear and the two square planes of deuterium ligands per anion are arranged in an eclipsed conformation with respect to one another. To our knowledge, an analogous structure has not hitherto been reported. Selected distances are compiled in Table 2. The Li2 atoms

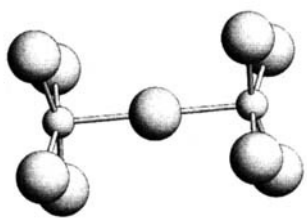


Fig. 3. The $[Pt_2D_9]^{5-}$ ion.

 © VCH Verlagsgesellschaft mbH, D-69451 Weinheim, 1995 0570-0833/95/0808-0899 $ 10.00+.25/0

Table 2. Selected distances [Å] in $Li_5Pt_2D_6$ [a].

Pt-D1 1.641(8) 4×	Li1-D1 2.152(23) 2×	D1-D1 2.324(14) 1×
Pt-D2 1.852(6) 1×	Li1-D1 2.131(25) 2×	D1-D1 2.283(12) 1×
Pt-Pt 3.704(12) 1×	Li1-D1 2.381(23) 2×	
Pt-Pt 4.453(8) 4×	Li1-D2 2.241(23) 1×	
	Li2-D1 2.306(7) 8×	

[a] For atomic numbering see Table 1.

are cubically coordinated by eight deuterium ligands while the Li1 atoms are sevenfold coordinated. The coordination polyhedron may be described as an extended, simple capped trigonal prism.

In order to obtain more information about the properties of this compound, its magnetic susceptibility was measured between 4 and 298 K by the Faraday method. A weak, virtually temperature-independent diamagnetism of $-90(10)\times 10^6\,cm^{-3}mol^{-1}$ was observed. The value calculated per formula unit from the diamagnetic increments is $-94\times 10^6\,cm^{-3}mol^{-1}$ when one substitutes the values -40 for Pt^{2+}, -0.6 for Li^+, and $-1.2\times 10^6\,cm^{-3}mol^{-1}$ for H^-.

Received: December 14, 1994 [Z75501E]
German version: *Angew. Chem.* **1995**, *107*, 984

Keywords: hydrides · lithium compounds · neutron diffraction · platinum compounds

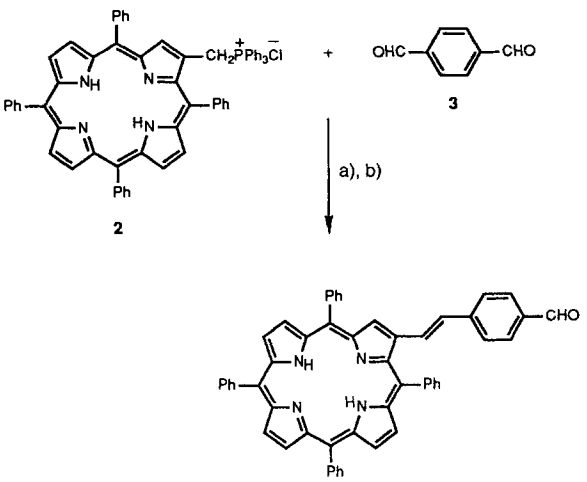
[1] W. Bronger, P. Müller, D. Schmitz, H. Spittank, *Z. Anorg. Allg. Chem.* **1984**, *516*, 35–41.
[2] W. Bronger, G. Auffermann, P. Müller, *J. Less-Common Met.* **1986**, *116*, 9–15.
[3] W. Bronger, G. Auffermann, P. Müller, *J. Less-Common Met.* **1988**, *142*, 243–252.
[4] W. Bronger, G. Auffermann, P. Müller, *Z. Anorg. Allg. Chem.* **1988**, *566*, 31–38.
[5] W. Bronger, G. Auffermann, *J. Alloys Comp.* **1995**, *219*, 45–47.
[6] W. Bronger, G. Auffermann, *Angew. Chem.* **1994**, *106*, 1144–1146; *Angew. Chem. Int. Ed. Engl.* **1994**, *33*, 1112–1114.
[7] W. Bronger, G. Auffermann, *Z. Anorg. Allg. Chem.*, in press.
[8] B. Nacken, W. Bronger, *J. Less-Common Met.* **1977**, *52*, 323–325.
[9] Program Fullprof (Version 2.4.2., December, 1993), J. Rodriguez-Carvagal, Institut Max von Laue-Paul Langevin, Grenoble.

Aldehyde-Appended Tetraphenylporphyrin: A New Building Block for Porphyrin Arrays**

Anthony K. Burrell, David L. Officer,* and David C. W. Reid

Photosynthesis is a marvelous but highly complex process that has intrigued researchers for many years.[1] It has been studied extensively by scientists from a variety of disciplines, with a view to increasing the understanding of the photosynthetic mechanism and utilizing this inexhaustible supply of energy. In the main, studies of the conversion of light to chemical energy have focused on the latter stages of the process, modeling the electron transfer processes involved with donor–acceptor molecules as models.[2] Much less attention has been paid to the mechanism of photon capture and the construction of the required light-harvesting porphyrin arrays. Viable syntheses of suitably large arrays have only recently become available with the development of "building block" methodologies as exemplified by the work of Anderson et al.,[3] Lin et al.,[1] and Lindsey et al.[4]. The building block approach is quick and inherently flexible since only small changes in the conditions give access to a variety of arrays. Herein we describe the synthesis and structure of a substituted tetraphenylporphyrin (TPP) **1** that has been used successfully in a building block approach to array construction.

Porphyrin **1** has a number of features that make it appealing as a building block. It is simple to prepare in high yield. The porphine ring can be metalated to alter the properties of the putative arrays. Aldehyde functionalities are well established in the syntheses of porphyrin systems. The synthesis of **1** relies on a Wittig reaction and is based on methodology developed by Bonfantini and Officer.[5] Reaction of phosphonium salt **2** and dialdehyde **3** under Wittig conditions gives a *cis*/*trans* mixture of **1** which is easily isomerized to *trans*-**1** in 80% overall yield (Scheme 1). Porphyrin **1** can be metalated[6] to give metalloporphyrins **1**-Cu, **1**-Ni, and **1**-Pd.[7]



Scheme 1. a) DBU, CH_2Cl_2, room temperature, 1 min; b) I_2, CH_2Cl_2, room temperature, 16 h.

Single crystals of **1**-Cu suitable for X-ray diffraction were obtained by slow diffusion of ethanol into a solution of **1**-Cu in chloroform, and the structural data were collected and refined by standard techniques.[8] We believe this to be the first 2-vinyl-substituted tetraphenylporphyrin to be characterized by X-ray crystallography. The crystal structure of **1**-Cu is shown in Figure 1, and several interesting features should be noted. The olefin unit and aldehyde are coplanar, while the torsion angle between the olefin and porphine ring[9] is small ($\approx 17°$). The overall planarity of this molecule (excluding the *meso*-phenyl substituents) and the fact that the solution UV/Vis spectra of **1** and **1**-Cu show red-shifted Soret bands (relative to TPP and CuTPP) lead us to believe that there is nothing preventing conjugation between the porphine and aldehyde moieties of **1**. This is contrary to previous postulations that conjugation of this kind is unlikely.[10] The existence of conjugation between porphine and aromatic aldehyde has important implications for the rate of electron transfer in oligomers and arrays containing this structural unit.

[*] Dr. D. L. Officer, Dr. A. K. Burrell, D. C. W. Reid
Department of Chemistry and Biochemistry
Massey University
Private Bag 11222, Palmerston North (New Zealand)
Telefax: Int. code + (6)3505682
e-mail: D. Officer@massey.ac.nz

[**] The authors gratefully acknowledge funding from the Massey University Postgraduate Scholarship and Graduate Research Fund, the William Georgetti Scholarship, and the Young Scientists' Fund, Royal Society of New Zealand (D. C. W. R).

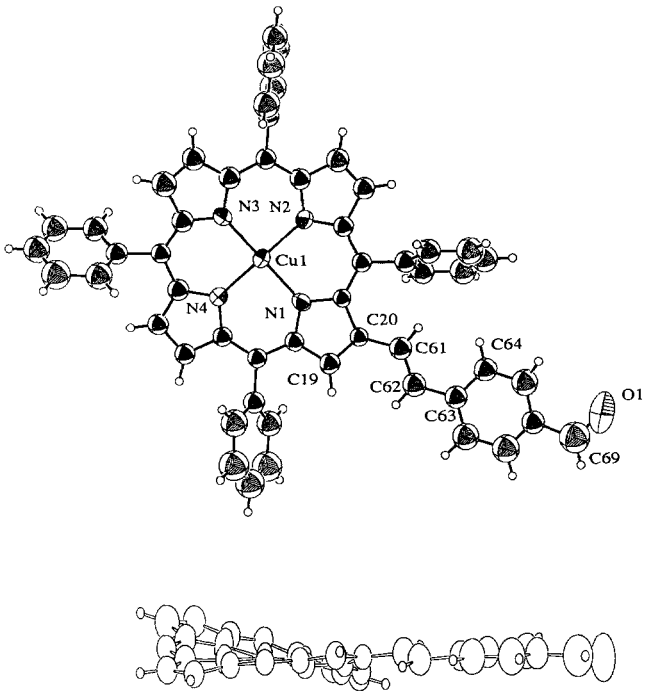


Fig. 1. Crystal structure of **1**-Cu. Top: Top view (torsion angle C19-C20-C61-C62 17(2)); bottom: side view (*meso*-phenyl rings omitted for clarity).

The stacking of the porphyrins in the crystal lattice (Fig. 2) is interesting. The $\pi-\pi$ interactions clearly present are typical of the kind predicted by Hunter and Sanders.[11] It should be noted, however, that they excluded tetraarylporphyrins from their calculations of porphyrin–porphyrin interactions in the solid state on the grounds that steric and electrostatic effects could disrupt these interactions. Figure 2 also shows a notable $\pi-\pi$ interaction between one porphine ring and the formyl-substituted aromatic ring of an adjacent molecule.

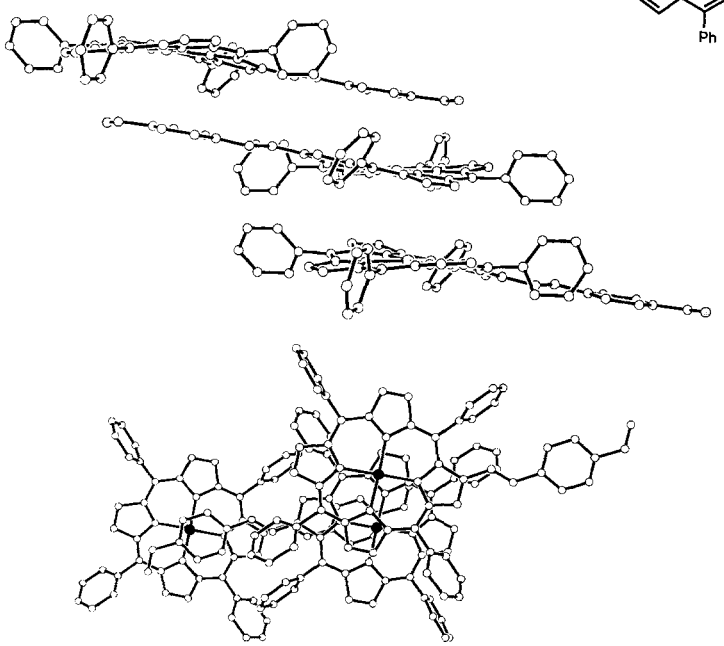
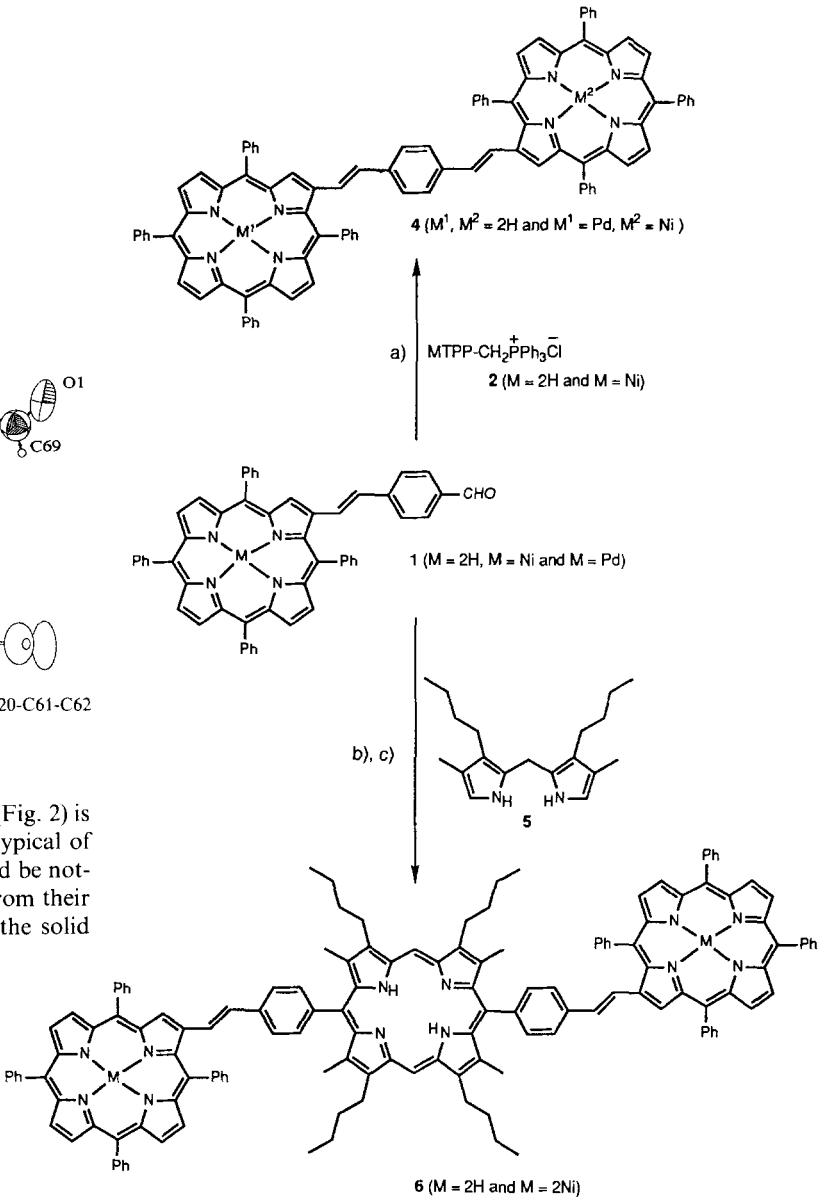


Fig. 2. An illustration of the π-stacking between molecules in crystals of **1**-Cu. Top: Side view; bottom: top view.



Scheme 2. a) Aqueous NaOH, CH_2Cl_2, room temperature, 1 h; b) CF_3COOH, CH_2Cl_2, room temperature, 4 h; c) *o*-chloranil, reflux, 8 h.

The utility of **1** as a building block for porphyrin arrays is demonstrated by the formation of dimeric and trimeric porphyrin systems. Thus, building block **1** undergoes a Wittig reaction with phosphonium salt **2** to give dimer **4** (Scheme 2). Given that the crystal structure and UV-Vis spectra of **1**-Cu imply conjugation between the porphine ring and the aldehyde group, dimer **4** is of interest because it has the potential to be fully conjugated across both porphine rings. Unfortunately the characterization of **4** is severely limited by poor solubility,[12] and therefore this issue remains unresolved until a more soluble analogue is available.[13] A similar Wittig reaction using **1**-Pd and **2**-Ni[14] gives the novel heterodimetallic complex **4**-PdNi. This illustrates the flexibility of this approach as well as the ease with which a variety of metals can be selectively incorporated into dimeric porphyrins by this methodology.

Facile condensation of **1** and dipyrrylmethane **5** gives the trimeric array **6** (Scheme 2).[15] Trimer **6** has better solubility than dimer **4** in organic solvents. If the condensation is repeated

with **1**-Ni, the trimer **6**-Ni_2 is obtained. Thus not only does this building block approach give access to arrays of different sizes but also systematic and controlled metalation is easily achieved.

Porphyrin **1** is an ideal building block for the synthesis porphyrin arrays. It is easily prepared on a large scale and in high yield, and can be metalated as required. The array-forming reactions (to form dimeric and trimeric porphyrins) are higher yielding than for comparable molecules prepared by linear synthetic strategies. Overall we believe that this building block approach has great promise, and our current research is directed towards using **1** and similar building blocks to construct larger arrays.

Experimental Procedure

1: Phosphonium salt **2** (113 mg, 0.12 mmol) and dialdehyde **3** (18 mg, 0.13 mmol) were dissolved in CH_2Cl_2 (20 mL) and stirred at room temperature before 1,8-diazabicyclo[5.4.0]undec-7-ene (DBU) (0.5 mL) was added. After 1 min, the reaction mixture was chromatographed (silica gel, 1:1 CH_2Cl_2:hexane) to give a purple solid. The solid, a *cis/trans* mixture of products, was dissolved in CH_2Cl_2 (40 mL). I_2 (22 mg, 87 mmol) was added and the reaction mixture stirred at room temperature for 16 h. The reaction mixture was diluted with CH_2Cl_2 (20 mL), washed with aqueous $Na_2S_2O_3$ (1 M; 2 × 20 mL) and H_2O (2 × 20 mL), and dried ($MgSO_4$), and the solvent was removed under reduced pressure. Flash chromatography as described above yielded *trans*-**1** as a purple solid (80 mg, 88%). ^1H NMR (270 MHz, $CDCl_3$, TMS): $\delta = -2.59$ (br. s, 2H; NH), 7.13 (d, $^3J = 16.2$ Hz, 1H; $H_{ethenyl}$), 7.31 (d, $^3J = 16.2$ Hz, 1H; $H_{ethenyl}$), 7.37 (d, 2H; H_{Ar}), 7.71–7.83 (m, 14H; $H_{m,pPh}$ and H_{Ar}), 8.18–8.27 (m, 8H; H_{oPh}), 8.72-8.83 (m, 6H; $H_{pyrrole}$), 9.02 (s, 1H; $H_{pyrrole}$), 9.99 (s, 1H; CHO); UV/Vis (CH_2Cl_2): λ_{max} (log ε) = 428 (5.31), 525 (4.32), 566 (4.13), 600 (3.95), 658 (3.69); FAB MS: *m/z*: 744 (M^+).

4: Aldehyde **1** (12 mg, 16 mmol) and phosphonium salt **2** (15 mg, 16 mmol) were dissolved in CH_2Cl_2 (3 mL), and a solution of NaOH (0.4 g) in H_2O (0.6 mL) was added. After 1 h of stirring at room temperature the reaction mixture was washed with H_2O (2 × 20 mL) and dried ($MgSO_4$), and the solvent removed under reduced pressure to give a purple solid [12]. FAB MS: *m/z*: 1356 (MH^+).

4-PdNi: This dimetalloporphyrin was prepared as for **4** with **1**-Pd as aldehyde and **2**-Ni as phosphonium salt [12]. FAB MS: *m/z*: 1517 (MH^+)

6: Dipyrrylmethane **5** (14 mg, 49 mmol) and aldehyde **1** (37 mg, 50 mmol) were dissolved in CH_2Cl_2 (5 mL) and the mixture bubbled with N_2 for 5 min. Trifluoroacetic acid (3.9 mL, 51 mmol) was added by syringe and the reaction stirred for 4 h at room temperature. *o*-Chloranil (19 mg, 77 mmol) was added and the reaction mixture heated to reflux for 8 h. The solvent was removed under reduced pressure and the resulting solid purified by column chromatography (silica gel, 5:1 CH_2Cl_2:hexane with 2% methanol). Trimer **6** was obtained as a purple solid (33 mg, 69%). ^1H NMR (270 MHz, $CDCl_3$, TMS): $\delta = -2.51$ (br. s, 4H; NH), −2.31 (br. s, 2H; NH), 1.15 (t, $^3J = 7.3$ Hz, 12H; $-CH_2CH_2CH_2CH_3$), 2.00–2.05 (m, 8H; $-CH_2CH_2CH_2CH_3$), 2.22–2.30 (m, 8H; $-CH_2CH_2CH_2CH_3$), 2.65 (s, 12H; $-CH_3$), 4.00–4.11 (m, 8H; $-CH_2CH_2CH_2CH_3$), 7.30 (d, $^3J = 16.2$ Hz, 2H; $H_{ethenyl}$), 7.64 (d, $^3J = 16.2$ Hz, 2H; $H_{ethenyl}$), 7.68 (d, $^3J = 7.9$ Hz, 4H; H_{Ar}), 7.79–7.88 (m, 24H; $H_{m,pPh}$), 8.06 (d, $^3J = 7.9$ Hz, 4H; H_{Ar}), 8.24–8.36 (m, 16H; H_{oPh}), 8.82–8.87 (m, 12H; $H_{pyrrole}$), 9.18 (s, 2H; $H_{pyrrole}$), 10.31 (s, 2H; *meso*-H); UV/Vis (CH_2Cl_2): λ_{max} (logε) = 426 (5.63), 518 (4.70), 566 (4.47), 598 (4.23), 654 (3.68); FAB MS: *m/z*: 2020 (MH^+).

6-Ni_2: This dimetalloporphyrin was prepared as for **6** with **1**-Ni as the aldehyde. Spectroscopic data for **6**-Ni_2 was consistent with the proposed structure.

Received: December 2, 1995 [Z 7517 IE]
German version: *Angew. Chem.* **1995**, *107*, 986

Keywords: photosynthesis · porphyrins · porphyrinoids

[1] V. S.-Y. Lin, S. G. DiMagno, M. J. Therien, *Science* **1994**, *264*, 1105–1111, and references therein.
[2] M. R. Wasielewski, *Chem. Rev.* **1992**, *92*, 435–461, and references therein.
[3] H. L. Anderson, S. J. Martin, D. D. C. Bradley, *Angew. Chem.* **1994**, *106*, 711–713; *Angew. Chem. Int. Ed. Engl.* **1994**, *33*, 655–657; H. L. Anderson, *Inorg. Chem.* **1994**, *33*, 972–981.
[4] S. Prathapan, T. E. Johnson, J. S. Lindsey, *J. Am. Chem. Soc.* **1993**, *115*, 7519–7520; J. Seth, V. Palaniappan, T. E. Johnson, S. Prathapan, J. S. Lindsey, D. F. Bocian, *ibid.* **1994**, *116*, 10578–10592; R. W. Wagner, J. S. Lindsey, *ibid.* **1994**, *116*, 9759–9760
[5] E. E. Bonfantini, D. L. Officer, *Tetrahedron Lett.* **1993**, *34*, 8531–8534.
[6] J. E. Falk in *Porphyrins and Metalloporphyrins* (Ed.: K. M. Smith), Elsevier, Amsterdam, **1975**.
[7] **1**-Cu: UV/Vis (CH_2Cl_2): λ_{max} (logε) = 428 (5.35), 549 (4.36), 586 (4.12); FAB MS: *m/z*: 806 (MH^+). **1**-Ni: UV/Vis (CH_2Cl_2): λ_{max} (logε) = 430 (5.24), 541 (4.22), 579 (4.10); FAB MS: *m/z*: 801 (MH^+). **1**-Pd: UV/Vis (CH_2Cl_2): λ_{max} (logε) = 426 (5.36), 533 (4.45), 569 (4.27).
[8] Crystal data for **1**-Cu·1.75$CHCl_3$: $C_{53}H_{34}CuN_4O \cdot 1.75CHCl_3$, dark purple rod, 0.15 × 0.21 × 0.13 mm; triclinic, space group $P\bar{1}$, $a = 13.778(6)$, $b = 13.845(3)$, $c = 14.676(5)$ Å, $\alpha = 104.68(2)$, $\beta = 116.44(3)$, $\gamma = 90.52(3)°$, $V = 2400.7(14)$ Å^3, $Z = 2$, $\rho_{calcd} = 1.402$ g cm^{-3}, $\mu = 0.792$ mm^{-1}, $T = 293$ K; Enraf-Nonius CAD4 diffractometer; $Mo_{K\alpha}$ radiation ($\lambda = 0.71073$ Å); scan method 2θ-θ; 5775 independent reflections with $4° < 2\theta < 44°$ were collected, of which 2307 with $F_0 > 4\sigma(F_0)$ were used in the refinement. The structure was solved by direct methods and refined by a full-matrix least-squares procedure using SHELXL-93 to give the final residuals of $R = 0.0883$, $wR^2 = 0.2107$, GOF = 0.908, refined against $|F^2|$. From the final difference Fourier maps the residual electron densities of 0.454 and −0.298 e Å^{-3} were present. Further details of the crystal structure investigation may be obtained from the Director of the Cambridge Crystallographic Data Centre, 12 Union Road, GB-Cambridge CB2 1EZ (UK), on quoting the full journal citation.
[9] The Cu(TPP) ring is slightly ruffled but not unusually so for porphine rings containing first-row transition elements [6].
[10] D. P. Arnold, L. J. Nitschinsk, *Tetrahedron* **1992**, *48*, 8781–8792; *Tetrahedron Lett.* **1993**, *34*, 693–696; D. P. Arnold, D. A. James, C. H. L. Kennard, G. Smith, *J. Chem. Soc. Chem. Commun.* **1994**, 2131–2132.
[11] C. A. Hunter, J. K. M. Sanders, *J. Am. Chem. Soc.* **1990**, *112*, 5525–5534.
[12] The solubility of **4** and metalated derivatives is poor, making purification difficult. Thus only mass spectrometry was available for characterization. The *ortho* and *meta* isomers of **1** have been prepared, as have the dimers. These dimers, particularly the *meta* dimer, are more soluble than the *para* dimer and thus have been fully characterized. This work will be reported elsewhere.
[13] The synthesis of functionalized tetraphenylporphyrin derivatives with increased solubility is currently underway in our laboratory.
[14] The preparation and characterization of **2**-Ni will be reported elsewhere.
[15] J. L. Sessler, V. L. Capuano, A. Harriman, *J. Am. Chem. Soc.* **1993**, *115*, 4618–4628.

Radical Additions of Activated Haloalkanes to Alkenes Initiated by Electron Transfer from Copper in Solvent-Free Systems**

Jürgen O. Metzger* and Ralf Mahler

Dedicated to Professor Hansjörg Sinn on the occasion of his 65th birthday

The need to reduce the amount of toxic waste and by-products arising from chemical processes requires increasing emphasis on the use of less toxic and environmentally compatible materials in the design of new synthetic methods.[1] The time has now come for ecological factors to be considered in the development of synthetic procedures and for them to play an important role in the assessment of the quality of any new synthesis. Within this context, the reduced use of ecologically suspect solvents is of considerable significance. Thus the radical bromination of alkylarenes in supercritical carbon dioxide has been reported recently.[2] The polymerization of neat methacrylate is an important example of a solvent-free industrial process.[3]

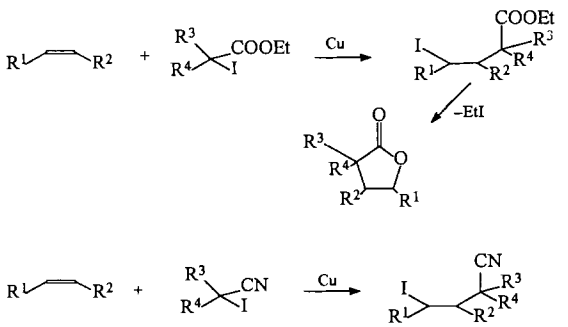
For some time now intermolecular radical addition reactions have been powerful tools in preparative organic chemistry,[4] but the most widely used methods have a number of ecological disadvantages for widespread industrial use. This applies particularly to the frequently used organotin compounds.[5, 6] Transi-

[*] Prof. Dr. J. O. Metzger, Dr. R. Mahler
Fachbereich Chemie der Universität
Carl-von-Ossietzky-Strasse 9-11, D-26111 Oldenburg (Germany)
Telefax: Int. code + (441)798-3329

[**] This work was supported by the Bundesministerium für Forschung und Technologie (0319450 D) and the Bundesministerium für Ernährung, Landwirtschaft und Forsten (93NR066-F-A).

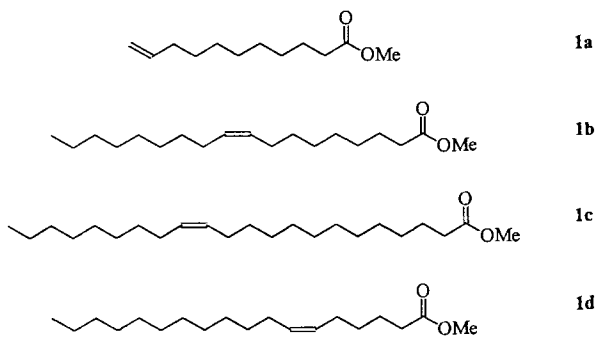
tion metal complexes and salts that initiate radical reactions by electron transfer processes[7] offer a viable alternative. Thus ethyl trichloroacetate and other compounds similarly activated by electron-withdrawing substituents may be induced to undergo radical addition to alkenes by copper(I) chloride[8] in acetonitrile, $[RuCl_2(PPh_3)_3]$,[9] $[CpMo(CO)_3]_2$,[10] $[CpFe(CO)_2]_2$,[10] and $[Co_2(CO)_8]$[10] in benzene and, in the latter example, without solvent.[10] These initiators,[11] as well as $[Pd(PPh_3)_4]$[12] in benzene and [Cu(bpy)Cl] in dichloromethane or 1,2-dichloroethane,[13] have been used successfully for the radical cyclization of esters of a number of suitable unsaturated α-halocarboxylic acids. Methyl α-iodo-(*Z*)-6-octadecenoate has been cyclized to cyclopentanecarboxylic acids by metallic silver in methanol.[14] Metallic copper has been used in the Ullmann reaction for the synthesis of diaryls from aryl halides,[15] and bromomalonodinitrile[16] and 2,2-dibromo-1,3-diones[17] have undergone addition to alkenes in benzene in the presence of copper as an initiator.

We now report the first radical addition of alkyl α-iodocarboxylates and α-iodoalkanenitriles to alkenes in the absence of solvent initiated by electron transfer from copper metal (Scheme 1). The alkenes most frequently used were the esters of



Scheme 1. Cu-catalyzed addition of alkyl α-iodocarboxylates and α-iodoalkanenitriles to alkenes. R^1, R^2, R^3, R^4 = H, alkyl, $(CH_2)_nCOOMe$.

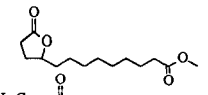
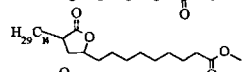
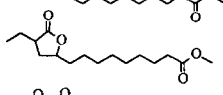
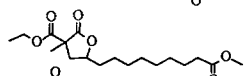
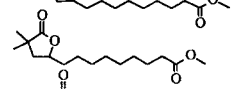
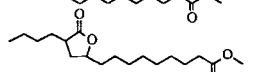
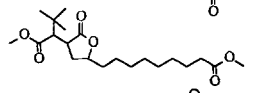
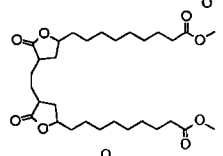
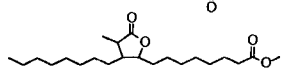
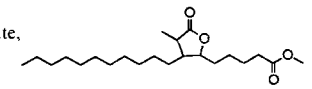
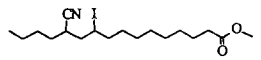
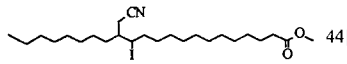
unsaturated carboxylic acids such as methyl 10-undecenoate (**1a**), methyl (*Z*)-9-octadecenoate (**1b**), methyl (*Z*)-13-docosenoate (**1c**), and methyl (*Z*)-6-octadecenoate (**1d**), which are of considerable interest as renewable raw materials.[18]



The reaction procedure is very simple: the alkene, iodo compound, and commercial copper powder are mixed without any pretreatment and heated at 100–130 °C in an inert atmosphere. After a simple workup procedure, the products are obtained analytically pure in satisfactory yields (Table 1).

The addition of alkyl 2-iodocarboxylates to 1-alkenes affords γ-lactones in high yields (entries 1, 2, 3b). The more readily

Table 1. Results of the copper-initiated addition of alkyl 2-halocarboxylates and 2-haloalkanenitriles to alkenes **1a–d**.

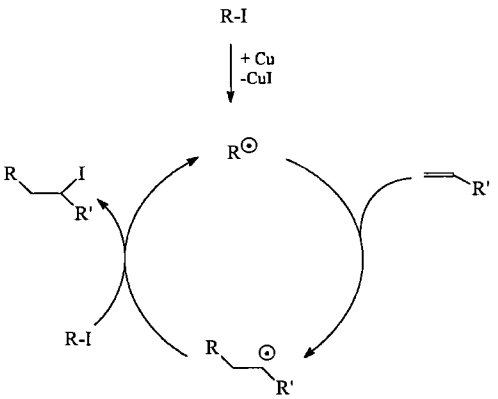
Entry	Alkene	Haloalkane	Product[a]	Yield [%]
1	**1a**	ethyl iodoacetate		70[b]
2	**1a**	methyl 2-iodopalmitate		79[b]
3a	**1a**	ethyl 2-bromobutyrate		41[b]
3b	**1a**	ethyl 2-iodobutyrate		80[b]
3c	**1a**	ethyl 2-bromobutyrate, NaI		72[b]
4	**1a**	diethyl 2-bromo-2-methylmalonate		87[b]
5	**1a**	ethyl 2-bromo-2-methylpropionate, NaI		54[b]
6	**1a**	methyl 2-bromohexanoate, NaI		70[b]
7	**1a**	dimethyl 2-bromo-3-*tert*-butylsuccinate, NaI		73[c]
8	**1a**	diethyl 2,5-diiodoadipate		60[c, e]
9	**1b**	ethyl 2-iodopropionate		51[b, d]
10	**1d**	ethyl 2-bromopropionate, NaI		60[b, d, f]
11	**1a**	2-bromohexanenitrile, NaI		55[b]
12	**1c**	iodoacetonitrile		44[b, d]

[a] All products were fully characterized by ^1H NMR and ^{13}C NMR spectroscopy and by mass spectrometry. [b] Isolated yield relative to starting alkene. [c] Isolated yield relative to starting haloalkane. [d] Regioisomeric mixture, ca. 1:1. [e] *c*(**1a**):*c*(iodoalkane) = 6:1. [f] The analogous additions of **1b** and **1c** gave the corresponding products in 58 and 59% yield, respectively.

available alkyl 2-bromocarboxylates also undergo copper-initiated addition to alkenes (entries 3a, 4). High yields are achieved with the more strongly activated alkyl bromomalonates (entry 4), however, yields from reaction with alkyl 2-bromomonocarboxylates (entry 3a) are much lower than with the corresponding iodo compounds (entry 3b). If the iodo derivative is formed from the corresponding bromo compound in situ by the addition of a stoichiometric amount of sodium iodide to the reaction mixture (entries 3c, 5–7), the products are obtained in high yields, similar to those obtained by direct use of the iodo derivatives. In this way primary, secondary, and tertiary alkyl 2-halocarboxylates were added to 1-alkenes. Of particular interest is the example of diethyl 2,5-diiodoadipate, which adds to two equivalents of **1a** to form a di-γ-lactone (entry 8). Radical addition to 1,2-dialkylethenes with extended alkyl groups such as methyl (*Z*)-9-octadecenoate (**1b**) using traditional methods frequently provides the products in only poor yields.[4] Thus in the benzoyl peroxide initiated addition of ethyl bromoacetate (in a tenfold excess) to methyl (*Z*)-9-octadecenoate the product is obtained in only 10% yield.[19] Moreover, using several variants of the tin procedure we were still unable to achieve satisfactory additions.[20] In contrast, with

copper initiation we were able to achieve yields in excess of 50% without any difficulty (entries 9, 10), which could be improved by very slow addition of the halo compound. 2-Iodo- and 2-bromoalkanenitriles add to 1-alkenes such as **1a** and to 1,2-dialkylethenes such as **1c** in an analogous manner (entries 11, 12). In these cases, the iodo functionality is retained, offering interesting possibilities for further transformations.

The reaction is initiated by electron transfer from copper to the activated haloalkane (Scheme 2). The electrophilic radical



Scheme 2. Mechanism for the Cu-initiated addition of iodoalkanes to alkenes. RI = alkyl 2-iodocarboxylates, 2-iodoalkanenitriles, R' = alkyl, $(CH_2)_nCOOMe$.

formed after cleavage of the halide adds to the electron-rich double bond of the alkene, and subsequent halogen abstraction affords the product, which in the case of alkyl 2-halocarboxylates cyclizes to a γ-lactone. About 30% of the copper is oxidized to copper(I) iodide during the reaction and about 20% of the haloalkane is reduced by halogen–hydrogen exchange. It is thus a radical chain reaction with a relatively short chain length. The C–I bond must be activated by an electron-withdrawing substituent. Iodine transfer onto the adduct radical by 1,3-induction is only slightly diastereoselective; the ratio of diastereoisomers is typically *cis*/*trans* = 1.5/1 (entry 2). The same stereoisomeric ratio was also obtained in the corresponding benzoyl peroxide initiated addition[22] and in Curran's iodine transfer method.[23] This confirms that like in these two reactions, the iodoalkane is also the iodine donor in the copper-initiated addition (Scheme 2). When the reaction is carried out with a bromoalkane and sodium iodide, the corresponding iodoalkane is formed as the intermediate, which was confirmed by gas chromatography. Key features of the reaction described here: no solvent is used, the workup procedure is simple in comparison to other methods since the copper powder initiator is unproblematic for workup and separation,[24] the reagents are used in essentially stoichiometric quantities, the yields are comparably high, even with 1,2-dialkylethenes, and the initiator can be reused (after total oxidation of the copper it is readily recovered by reduction).

Experimental Procedure

General method: A 50 mL, two-necked flask equipped with a magnetic stirrer, reflux condenser, and a gas inlet tube was charged with 1.3 equiv of iodoalkane, 1 equiv of alkene, and 1.3 equiv of copper powder (purum, Merck). The mixture was heated with constant stirring at 130 °C in an inert atmosphere [28]. The reaction was monitored by thin-layer chromatography and was usually complete within 3–7 h. The product was isolated by distillation; alternatively, the reaction mixture was taken up into diethyl ether and after removal of the copper salts by filtration and evaporation of the solvent on a rotary evaporator, the product was isolated by Kugelrohr distillation and recrystallization or flash chromatography.

Received: July 21, 1994
Revised version: November 21, 1994 [Z 7151 IE]
German version: *Angew. Chem.* **1995**, *107*, 1012

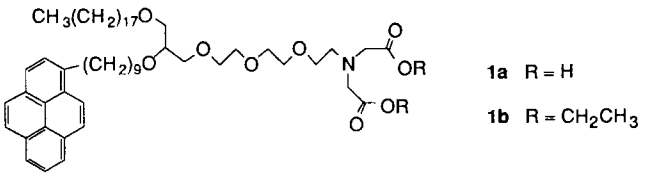
Keywords: electron transfer reactions · solvent-free conversions · radical additions

[1] J. Amato, Science **1993**, *259*, 1538–1541; D. L. Illman, *Chem. Eng. News* **1993**, *71*, (13), 5–6; **1994**, *72* (36), 22–27.
[2] J. M. Tanko, J. F. Blackert, *Science* **1994**, *263*, 203–205; G. Kaupp, *Angew. Chem.* **1994**, *106*, 1519–1522; *Angew. Chem. Int. Ed. Engl.* **1994**, *33*, 1452–1455.
[3] *Ullmann's Encyclopedia of Industrial Chemistry*, *Vol. A 22*, 5th ed. VCH, Weinheim, **1993**, pp. 4 ff.
[4] *C-Radikale* (Eds.: M. Regitz, B. Giese), *Methoden Org. Chem. (Houben-Weyl) 4th ed. 1952–*, Bd. E 19a, **1989**; W. B. Motherwell, D. Crich, *Free Radical Chain Reactions in Organic Synthesis*, Academic Press, London, **1992**.
[5] C. Chatgilialoglu, *Acc. Chem. Res.* **1992**, *25*, 188–194.
[6] B. Giese, *Angew. Chem.* **1989**, *101*, 993–1004; *Angew. Chem. Int. Ed. Engl.* **1989**, *28*, 969–980.
[7] J. K. Kochi, *Organometallic Mechanisms and Catalysis*, Academic Press, New York, **1978**, pp. 127–137.
[8] D. Belluš, *Pure Appl. Chem.* **1985**, *57*, 1827–1838.
[9] T. Nakano, M. Kayama, Y. Nagai, *Bull. Chem. Soc. Jpn.* **1987**, *60*, 1049–1052.
[10] Y. Mori, J. Tsuji, *Tetrahedron* **1972**, *28*, 29–35.
[11] S. Takano, S. Nishizawa, M. Akiyama, K. Ogasawara, *Synthesis* **1984**, 949–953; H. Nagashima, H. Wakamutsu, K. Itoh, *J. Chem. Soc. Chem. Commun.* **1984**, 652–655, T. K. Hayes, A. J. Freyer, M. Parvez, S. M. Weinreb, *J. Org. Chem.* **1986**, *51*, 5501–5503.
[12] D. P. Curran, C.-T. Chang, *Tetrahedron Lett.* **1990**, *31*, 933–936.
[13] J. H. Udding, C. J. M. Tujip, M. N. A. van Zandern, H. Hienstra, W. N. Speckamp, *J. Org. Chem.* **1994**, *59*, 1993–2003; H. Nagashima, N. Ozaki, M. Ishii, K. Seki, M. Washiyama, K. Itoh, *ibid.* **1993**, *58*, 464–470.
[14] J. O. Metzger, R. Mahler, *Liebigs Ann. Chem.* **1993**, 203–205.
[15] F. Ullmann, J. Bielecki, *Ber. Dtsch. Chem. Ges.* **1901**, *34*, 2174–2185.
[16] K. Torsell, E. Ruusa, *Ark. Kemi* **1964**, *23*, 479–483 [*Chem. Abstr.* **1965**, *63*, 5556]. J. R. Roland, E. L. Little, Jr., H. E. Winberg, *J. Org. Chem.* **1963**, *28*, 2809–2811.
[17] I. Yoshida, S. Jani, T. Ozawa, N. Kawabata, *J. Org. Chem.* **1985**, *50*, 3467–3473.
[18] H. Baumann, M. Bühler, H. Fochem, F. Hirsinger, H. Zoebelein, J. Falbe, *Angew. Chem.* **1988**, *100*, 42–62; *Angew. Chem. Int. Ed. Engl.* **1988**, *27*, 42–62.
[19] D. Lefort, G. Nikishin, G. Nee, J. Sorba, *Bull. Soc. Chim. France* **1968**, 4613–4621.
[20] Acceptable yields for additions to 1,2-dialkylethenes were obtained only by using a large excess of alkene, even with the highly activated iodomalonodinitrile [21].
[21] G. Thoma, D. P. Curran, S. V. Geib, B. Giese, W. Damm, F. Wetterich, *J. Am. Chem. Soc.* **1993**, *115*, 8585–8591.
[22] M. S. Kharash, P. S. Skell, P. Fisher, *J. Am. Chem. Soc.* **1948**, *70*, 1055–1059.
[23] D. P. Curran, C.-T. Chang, *J. Org. Chem.* **1989**, *54*, 3140–3157.
[24] The copper content of the products is about 1 ppm [25], in other words, of the same order of magnitude as the copper content of foodstuffs [26]. Copper is an essential trace element for humans and within certain limits is regarded as being physiologically safe. The method should therefore be suitable for the synthesis of pharmaceuticals.
[25] We thank Dr. I. Block, Staatliches Untersuchungsamt, Oldenburg, for determination of the copper content of our samples by atom absorption spectroscopy.
[26] M. C. Linder, *Biochemistry of Copper*, Plenum, New York, **1991**, pp. 5–6.
[27] M. Daunderer, *Klinische Toxikologie*, *Bd. 8*, *III-9.3*, ecomed, Landsberg, **1981**.
[28] We used a small excess of copper, whereby the reaction rate is increased. About 30% of the copper is oxidized during the reaction. The copper/copper iodide mixture can be reused twice as an initiator. The use of 1.3 equivalents of copper appears high from an ecological viewpoint, even though one batch can be used three times. With respect to both price and weight, however, the amount of copper used is low in comparison to that of the metal complexes mentioned in the text [9–13] such as $[Pd(PPh_3)_4]$. Furthermore, while the separation and recovery of homogeneous catalysts is often difficult if not impossible, that of the copper in our reactions is straightforward. Even the reaction temperature of 130 °C is ecologically acceptable when one considers that foods are cooked at about this temperature.

Metal-Induced Dispersion of Lipid Aggregates: A Simple, Selective, and Sensitive Fluorescent Metal Ion Sensor**

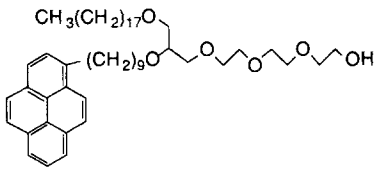
Darryl Y. Sasaki, Deborah R. Shnek, Daniel W. Pack, and Frances H. Arnold*

Lipid reorganization induced by specific ligand binding is a feature intrinsic to biological processes such as signaling,[1] membrane fusion,[2] cell docking,[3] and endocytosis.[4] Often the ligand is a protein, which generates lipid reorganization through multiple lipid–ligand interactions.[5] Lipid reorganization, however, can also be driven with small ions.[6] For example, calcium can induce phase separation of phosphatidylserine lipids in vesicles of phosphatidylcholine lipids[7] or alter the packing phase of cardiolipin from bilayer to inverted hexagonal.[8] In the course of studying substrate binding to metal-complexing lipids and their subsequent reorganization in membrane assemblies,[9] we discovered that metal ions can strongly affect the distribution of the metal-chelating lipid. Lipid **1a**, a pyrene-labeled lipid functionalized with iminodiacetic acid (IDA), forms aggregates when placed in vesicles of distearoyl phosphatidylcholine (DSPC), as evidenced by pyrene excimer formation in steady-state fluorescence measurements. Addition of divalent metal ions essentially instantaneously results in a dramatic reversal of the ratio of emission intensities of excimer and monomer, which is believed to coincide with dispersion of the pyrene-lipid into the gel phase of the matrix DSPC lipid. This process, which is highly sensitive and selective for Cu^{2+}, offers a particularly simple approach to Cu^{2+} detection and quantification.



1a R = H

1b R = CH_2CH_3



2

Lipids **1** and **2** can be co-sonicated in aqueous solution with various phosphatidylcholine lipids to prepare stable mixed bilayer vesicles. The steady-state fluorescence spectrum of 5 mol% lipid **1a** in vesicles of DSPC shown in Figure 1 (curve a) includes

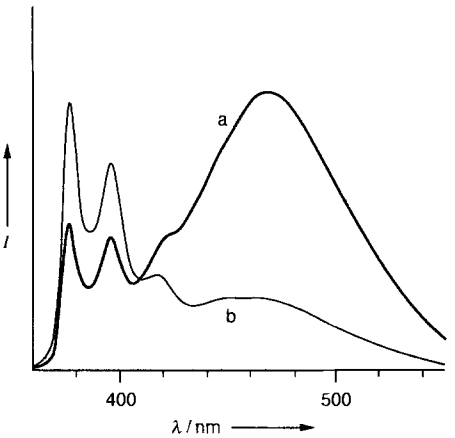


Fig. 1. Fluorescence emission spectra of a) 5% lipid **1a**/95% DSPC and b) 5% lipid **1a**/95% SOPC in a MOPS buffer at 25 °C. MOPS = 3-(4-morpholinyl)-1-propanesulfonic acid.

the monomer emission (maximum at 377 nm) and a broad featureless band with emission maximum at 470 nm, which is attributed to pyrene excimer. The large ratio of the fluorescence intensities of excimer and monomer (E/M) reflects a high local pyrene concentration in the bilayer assembly.[10] The E/M value of vesicles containing 5% lipid **1a** and 95% DSPC is 1.8 (curve a), but drops to only ≈ 0.2 or less in vesicles composed of 5% lipid **1a** in 1:1 DSPC–cholesterol (data not shown) or SOPC (2-oleoyl-1-stearoyl-*sn*-glycero-3-phosphocholine) (curve b). At 25 °C SOPC and DSPC–cholesterol matrix bilayers exist in the fluid phase, while DSPC is in the solid gel phase. The markedly different E/M values suggest that lipid **1a** aggregates or phase separates from the gel matrix of DSPC, but is dispersed in the two fluid bilayers.

The pronounced effect of divalent metal ions on the E/M value of lipid **1a** in DSPC vesicles is illustrated in Figure 2. With increasing metal ion (Mn^{2+}) concentration, the excimer emis-

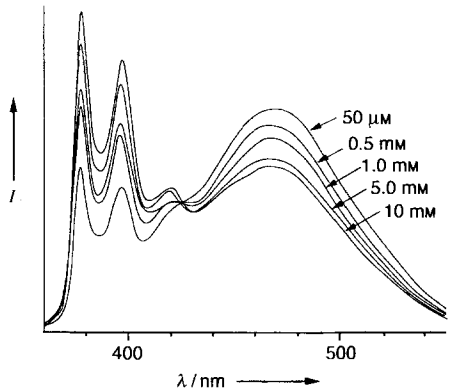


Fig. 2. Fluorescence emission spectra of 5% lipid **1a**/95% DSPC vesicles in a MOPS buffer at 25 °C with increasing concentrations of $MnCl_2$.

sion intensity decreases while the monomer emission increases. Other metal ions have a similar effect, but at different concentrations, as shown in Figure 3. The E/M curves generally parallel the metal ion binding constants to IDA, with the exception that Co^{2+} has a stronger affect than Ni^{2+}.[11] If the observed changes in the E/M values correspond to metal complexation by IDA, however, the metal binding affinity of the IDA headgroup appears to be attenuated by a factor of 100–1000 when incorpo-

[*] Prof. F. H. Arnold, D. R. Shnek, D. W. Pack
Division of Chemistry and Chemical Engineering 210-41
California Institute of Technology
Pasadena, CA 91125 (USA)
Telefax: Int. code + (818) 568-8743
D. Y. Sasaki
Sandia National Laboratory
Albuquerque, NM 87185-0368 (USA)

[**] This research was supported by the Office of Naval Research (N00014-92-J-1178) and the National Science Foundation (BCS-9108502). F. H. A. acknowledges an NSF PYI Award and a David and Lucile Packard Fellowship. D. R. S. is supported by a predoctoral training fellowship from the National Institute of General Medical Sciences, Pharmacology Sciences Program. D. W. P. is a Landau Fellow.

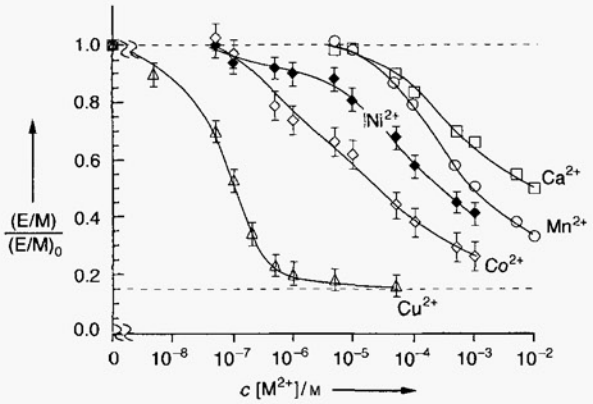


Fig. 3. E/M values (normalized by E/M values without added metal) for 5% lipid **1a**/95% DSPC vesicles, 0.11 mM total lipid, in the presence of various metal ions at 25 °C. The metals were added as the chloride salts in 0.1 M NaCl. Solid curves are drawn in for clarity.

rated into vesicles, relative to that of free *N*-(2-methoxyethyl)-iminodiacetate in solution.[12]

Sensitivity to lower concentrations of metal ions can be obtained by using more dilute vesicles (lower lipid concentrations). Figure 4 shows how titration with Cu^{2+} affects the E/M value of 5% lipid **1a**/95% DSPC vesicle solutions at three lipid concentrations, the lowest of which is 650 nM total phospholipid

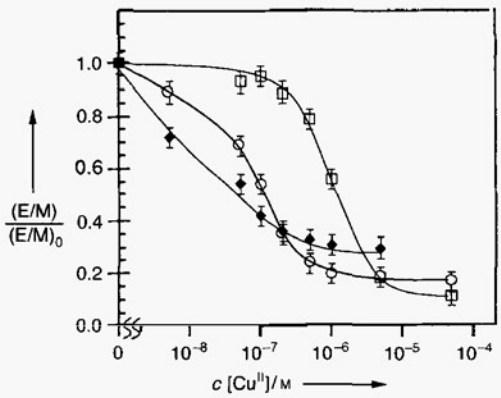


Fig. 4. E/M values (normalized by E/M values without added metal) for 5% lipid **1a**/95% DSPC vesicles in the presence of Cu^{2+} at 25 °C: Total phospholipid 65 μM (□), 6.5 mM (○), and 650 nM (●). The metal was added as the chloride salt in 0.1 M NaCl. Solid curves are drawn in for clarity.

(35 nM lipid **1a**). This system is sensitive to Cu^{2+} at concentrations of 5 nM (less than 1 ppb) in 0.1 M NaCl. It is conceivable that even greater sensitivity can be achieved by using even lower lipid concentrations and a pyrene-labeled lipid with a chelating headgroup with a higher affinity for the metal ion than IDA (e.g., nitrilotriacetate). The changes in E/M values shown in Figures 2–4 occur within seconds of metal ion addition and are completely reversible with the addition of excess ethylenediaminetetraacetate (EDTA).

Owing to the strong affinity of IDA for Cu^{2+}, this bilayer system is highly sensitive and selective for Cu^{2+}. Thus micromolar concentrations of Cu^{2+} ions can be detected in a 0.1 M NaCl solution containing millimolar concentrations of Ca^{2+}. Moreover, the fluorescence effects of submicromolar Cu^{2+} concentrations can be detected by the naked eye in black light (365 nm).

Metal titration studies performed with the non-metal-chelating pyrene lipids **1b** and **2** in DSPC vesicles confirm that the observed E/M change is a consequence of metal chelation by the IDA headgroup, rather than fluorescence quenching or a metal-induced perturbation of the membrane. The fluorescence E/M values of 5% lipid **1** and **2** in DSPC vesicles are shown in the form of a bar graph in Figure 5. While Cu^{2+} at 5 mM concentration induces a large change in the E/M value of the lipid **1a**/DSPC vesicles, it has very little effect on the E/M values of vesicles prepared with the nonchelating pyrene lipids. Even at Cu^{2+} concentrations 1000 times higher (mM), no significant change in fluorescence intensity or E/M value was observed for vesicles containing **1b** and **2**. Furthermore, metal ion addition to vesicles containing lipid **1a** in a fluid matrix (50% DSPC/50% cholesterol or SOPC) also induces only very small changes in the fluorescence E/M value (although quenching is observed for the more fluid SOPC matrix).

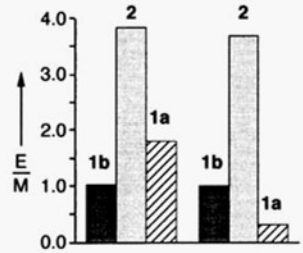


Fig. 5. Bar graph shows E/M values of DSPC vesicles containing 5 mol% lipid **1b**, **2**, or **1a** before (left) and after addition of $CuCl_2$ (5 mM) (right). All measurements done in a MOPS buffer at 25 °C.

It appears that complexation of the metal ion by the IDA headgroup induces the dispersal of lipid **1a** in the DSPC gel matrix, which results in the dramatic reduction in the rate of pyrene collisions, and therefore reduction of the E/M value. This process is illustrated in Figure 6.

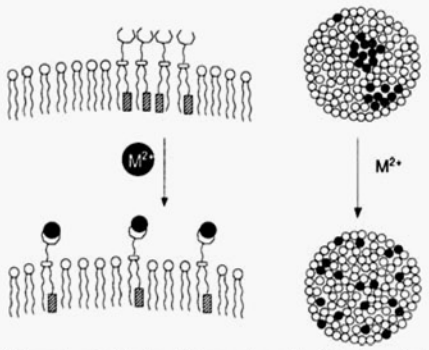


Fig. 6. Schematic representation of metal-induced dispersion of lipid **1a** in vesicles of 5% lipid **1a**/95% DSPC, as observed through fluorescence measurements at 25 °C. Lipid **1a** is believed to assemble into pyrene-rich aggregates which are dispersed upon chelation of a divalent metal ion by the lipid headgroup.

The reorganization of a lipid labeled with a light-emitting group induced by specific substrate binding provides a powerful method for detection of substrates in solution. As a sensing device, this extremely simple, two-component system offers some attractive features: its sensitivity for Cu^{2+} (nM) compares favorably to that of ion-selective electrodes[13] and other synthetic lipid-based sensors;[14] it is relatively insensitive to high concentrations of weakly binding metal ions such as Ca^{2+}; it can be regenerated by washing with a strong chelating agent (edta); and it has a rapid response time (seconds). Owing to its simplicity and essentially instantaneous signal transduction, this system could be readily adapted to continuous copper ion monitoring in a continuous flow fluorescence spectrometer. Studies

 © VCH Verlagsgesellschaft mbH, D-69451 Weinheim, 1995 0570-0833/95/0808-0906 $ 10.00+.25/0

to understand the mechanism by which metal binding induces dispersion of the lipid aggregates and investigations of the generality of this type of sensor are underway.

Experimental Procedure

Stock lipid solutions were made by dissolving lipids and cholesterol (Sigma) in $CHCl_3$ (HPLC grade). Lipid **1** or **2** and a matrix lipid (DSPC, SOPC, or 1:1 DSPC:cholesterol) were combined (5 mol% lipid **1** or **2**, 95 mol% matrix lipid) to give 10 μmol total lipid in 12 mL volumetric centrifuge tubes. The lipid mixture was concentrated under aspirator vacuum, and 3 mL of MOPS buffer (20 mM MOPS, 0.1 M NaCl, pH 7.5) was added to the tubes. The tubes were heated above 55 °C and sonicated with a probe tip (Heat Systems model 375) for 15 min at 25–35% power under argon atmosphere in an ice bath. The vesicles were centrifuged at 11000 rpm for 20 min to remove titanium particles. The phosphate concentration was determined for selected samples [15]. Vesicle sizes were measured by quasi-elastic light scattering by using a Microtrac Ultrafine Particle Analyzer (Leeds & Northrop) at 25 °C in phosphate buffer. The mean diameter was 49 nm (59 nm distribution width) for unmetalated vesicles. Vesicles were diluted 167-fold in MOPS buffer for metal-binding studies. Steady-state fluorescence measurements were performed at 25 °C on a temperature-controlled Shimadzu RF-450 spectrofluorimeter, excitation at 346 nm, 5 nm excitation and emission slit width.

Received: October 13, 1994
Revised version: December 6, 1994 [Z 7397 IE]
German version: *Angew. Chem.* **1995**, *107*, 994

Keywords: fluorescent sensors · lipids · metal ion analysis · vesicles

[1] a) K. Eichmann, *Angew. Chem.* **1993**, *105*, 56; *Angew. Chem. Int. Ed. Engl.* **1993**, *32*, 54; b) W. J. Fantl, D. E. Johnson, L. T. Williams, *Annu. Rev. Biochem.* **1993**, *62*, 453.

[2] a) J. Zimmerberg, S. S. Vogel, L. V. Chernomordik, *Annu. Rev. Biophys. Biomol. Struct.* **1993**, *22*, 433; b) D. Papahadjopoulos, G. Poste, B. E. Schaeffer, W. J. Vail, *Biochim. Biophys. Acta* **1974**, *352*, 10.

[3] R. B. Kelly, *Curr. Biol.* **1993**, *3*, 474.

[4] S. C. Silverstein, R. M. Steinman, Z. A. Cohn, *Annu. Rev. Biochem.* **1977**, *46*, 669.

[5] a) M. Ahlers, W. Muller, A. Reichert, H. Ringsdorf, J. Venzmer, *Angew. Chem.* **1990**, *102*, 1310; *Angew. Chem. Int. Ed. Engl.* **1990**, *29*, 1269; b) D. M. Haverstick, M. Glaser, *Biophys. J.* **1989**, *55*, 677; c) P. Antes, G. Schwarzmann, K. Sanhoff, *Chem. Phys. Lipids* **1992**, *62*, 269; d) J. R. Wiener, R. Pal, Y. Barenholz, R. R. Wagner, *Biochemistry* **1985**, *24*, 7651; e) G. B. Birrell, O. H. Griffith, *ibid.* **1976**, *15*, 2925.

[6] a) H. Hauser, *Chem. Phys. Lipids* **1991**, *57*, 309; b) K. Jacobson, D. Papahadjopoulos, *Biochemistry* **1975**, *14*, 152.

[7] S. Ohnishi, T. Ito, *Biochemistry* **1974**, *13*, 881.

[8] R. P. Rand, S. Sengupta, *Biochim. Biophys. Acta* **1972**, *255*, 484–492; b) B. deKruijff, A. J. Verkleij, J. Leunissen-Bijvelt, C. J. A. van Echteld, J. Hille, H. Rijnbout, *ibid.* **1982**, *693*, 1.

[9] D. R. Shnek, D. W. Pack, D. Y. Sasaki, F. H. Arnold, *Langmuir* **1994**, *10*, 2382.

[10] a) H.-J. Galla, W. Hartmann, *Chem. Phys. Lipids* **1980**, *27*, 199; b) H.-J. Galla, E. Sackmann, *Biochim. Biophys. Acta* **1974**, *339*, 103.

[11] The order of metal ion binding for *N*-(2-methoxyethyl)iminodiacetic acid in solution is Cu ≫ Ni > Co > Mn > Ca: A. E. Martell, P. M. Smith, *Critical Stability Constants, Vol. 6*, Plenum, New York, **1974**.

[12] The K_d, for example, of methoxyethyl iminodiacetate is 3×10^{-6} M for Mn^{2+}, whereas the E/M value of the vesicles begins to change at 10^{-5} M and shows a midpoint at ca. 3×10^{-4} M Mn^{2+} (Fig. 3).

[13] a) S. S. Kuan, G. G. Guilbault, *Biosensors: Fundamentals and Applications* (Eds.: A. P. F. Turner, I. Karube, G. S. Wilson), Oxford University Press, Oxford, **1987**, p. 135; b) S. L. Belli, A. Zirino, *Anal. Chem.* **1993**, 65, 2583; c) E. K. Quagraine, V. P. Y. Gadzekpo, *Analyst* **1992**, *117*, 1899; d) R. A. Durst, *Ion Selective Electrodes* (Ed.: E. A. Durst), National Bureau of Standards Publication, Washington, D. C., **1969**, p. 375.

[14] a) M. Lerchi, E. Bakker, B. Rusterholz, W. Simon, *Anal. Chem.* **1992**, *664*, 1534; b) M. Shimomura, T. Kunitake, *J. Am. Chem. Soc.* **1982**, *104*, 1757; c) A. Singh, L.-I. Tsao, M. Markowitz, B. P. Gaber, *Langmuir* **1992**, *8*, 1570; d) S. Terrettaz, H. Vogel, M. Grätzel, *J. Electroanal. Chem.* **1992**, *326*, 161; e) S. Steinberg, I. Rubinstein, *Langmuir* **1992**, *8*, 1183.

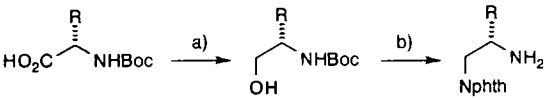
[15] W. R. Morrison, *Anal. Biochem* **1964**, *7*, 218.

Solid-Phase Syntheses of Unnatural Biopolymers Containing Repeating Urea Units**

Kevin Burgess,* D. Scott Linthicum, and Hunwoo Shin

In medicinal chemistry, urea bonds have been used as critical structural elements in enzyme inhibitors[1] and as switching points in retro-inverso peptidomimetics.[2] The advent of "split syntheses"[3] in combinatorial methodology,[4, 5] however, opens an avenue for identification of many other urea-based compounds with potentially useful pharmaceutical properties. Consequently, there is a need for preparations of urea precursors, and for solid-phase syntheses of compounds with several urea functionalities incorporated in systematic fashion. This communication describes solid-phase syntheses of the two oligourea compounds CH_2G^u. CH_2F^u. CH_2F^u. CH_2A^u. A-amide (**8**) and YG. CH_2G^u. CH_2F^u. L-amide (**9**). These labels are based on the one letter codes for the amino acids from which the urea units are derived (vide infra).

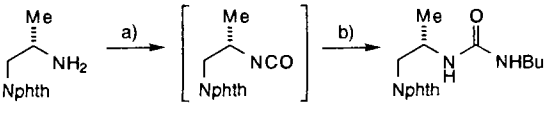
Monomers for the oligourea syntheses were prepared by reducing the *N*-Boc protected amino acids to the corresponding amino alcohols **1**, which were then used as electrophiles in Mitsunobu displacements with phthalimide. Formation of regioisomeric products via undesired *N*-Boc aziridine intermediates is known,[6] and might have been problematic, but it was not. Removal of the *N*-Boc group gave the required monoprotected diamines **2**.



1 *ca.* 80 % **2** *ca.* 70 %

Scheme 1. R = Me, CH_2Ph, H. a) 1) ClCOO*i*Bu, NEt_3, 0 °C, THF; 2) $NaBH_4$, H_2O. b) 1) Phthalimide (HNphth), PPh_3, EtOCON=NCOOEt, THF, 25 °C, 3 h; 2) $HCl_{(aq)}$, THF.

Trial reactions in solution were performed to determine whether urea derivatives like **4** arise from isocyanate intermediates of type **3** formed in situ. To do this, the monoprotected diamine from alanine (**2a**, R = Me) was treated with "triphosgene" (bis(trichloromethyl)carbonate)[7] and then with 1-aminobutane. NMR analysis of the crude material indicated that the only detectable product was the anticipated urea **4a**.



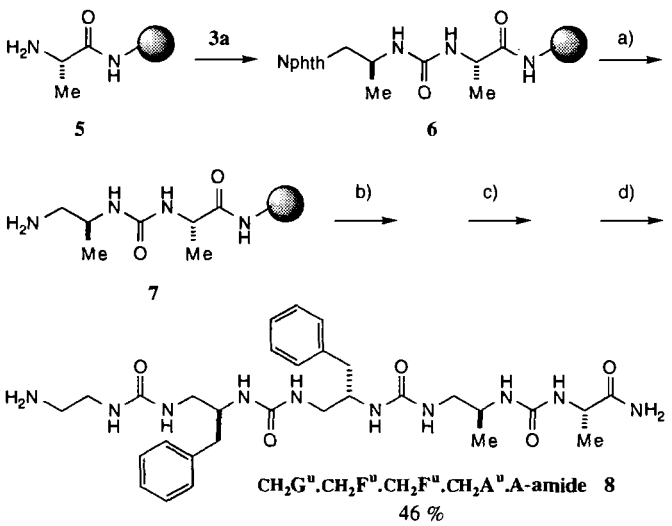
2a **3a** **4a**

Scheme 2. a) 0.33 equiv $(CCl_3O)_2CO$, NEt_3, CH_2Cl_2, 45 min, from 0–25 °C. b) $BuNH_2$, 12 h.

[*] Prof. K. Burgess, H. Shin
Department of Chemistry
Texas A & M University, College Station, TX 77843-3255 (USA)
Telefax: Int. code + (409) 845-8839
Dr. D. S. Linthicum
College of Veterinary Medicine, Texas A & M University (USA)

[**] Financial support for this work was obtained from the National Institutes of Health and The Robert A. Welch Foundation. K.B. is a NIH Research Career Development Awardee and an Alfred P. Sloan Scholar.

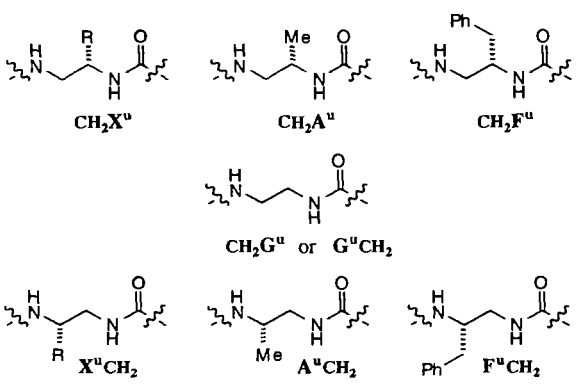
The next step was to extend the urea formation reactions to the solid phase. Fmoc-Ala was coupled to Rink's amide resin[8] (represented as a sphere in the following diagram) and deprotected[9] to give resin **5** with approximately 0.44 mmol of amino acid per gram of support. This was then treated with five equivalents of isocyanate **3a** generated in situ. Kaiser's ninhydrin test



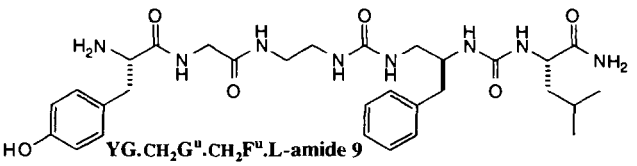
Scheme 3. Treatment with 5 equiv of **3a**, CH_2Cl_2, 1.5 h. a) 60% $N_2H_4 \cdot H_2O$/DMF, 15 h, 25 °C. b) Repeated addition and removal of protecting groups. c) Cleavage from the resin with TFA (see text). d) Purification with RP-HPLC.

showed the coupling to be complete after 1.5 h.[10] Removal of the phthaloyl group with 60% hydrazine hydrate in DMF was slow; HPLC studies indicated that the reaction was essentially complete only after approximately 10 h. Consequently, overnight deprotection steps were used in this synthesis, and modifications of the deprotection conditions are currently being investigated to improve the time efficiency. Four repetitions of the isocyanate addition/deprotection cycle gave a product which was then cleaved from the resin with a mixture of phenol, 1,2-ethanethiol, thioanisole, water, and trifluoroacetic acid (TFA) [3:1:2:2:40 (w/v/v/v/v)] for 12 h at 25 °C. Cation scavengers may be unnecessary in this particular cleavage reaction, but they were included as a precaution in this preliminary study. Purification of the crude product by RP-HPLC gave the product **8** as a colorless hygroscopic solid in 46% yield,[11] which corresponds to an average yield of 86% in each coupling step.

We abbreviate the structure of urea analogs using nomenclature of the type "CH_2X^u", where the superscript u denotes a urea-derived fragment, the one letter code X identifies the amino acid from which the isocyanate reagent was prepared, and the "CH_2" label precedes the chiral center. Alternative structures in which the chiral center precedes the CH_2 group are being investigated in our laboratories; following the nomenclature described above, these are denoted as "X^uCH_2". In this system the urea side chains correspond to those of the parent amino acid from which the urea is derived.[12]



A solid-phase approach almost identical to that described above also was used to prepare the Leu-enkephalin analog **9** (YG. CH_2G^u. CH_2F^u. L-amide).[13] In this case the isolated yield of product was only 17%, but this procedure has not yet been optimized.



As far as we are aware, this work constitutes the first solid-phase syntheses of oligourea derivatives, but indications in the recent literature suggest increasing interest in unnatural biopolymers containing ureas. Nowick et al. are investigating systems they call "molecular scaffolds", in which urea functionalities link side chains to polyamine backbones.[14] Simultaneously, Hutchins and Chapman demonstrated that simple isocyanates (for example, PhNCO) could be added to solid-supported amino acids, then cleaved to give compounds with one urea group per molecule.[15] The "capping" of solid-supported peptides with aryl and alkyl isocyanates is also known and has been applied in Kent's ladder sequencing method.[16]

Oligoureas have several attractive features with respect to potential roles in biological systems. They are structurally similar to polyamides, yet they should not be as vulnerable to proteolytic cleavage as peptides. Ureas tend to be water soluble, but the physical (and chemical) properties of oligoureas can be modified by appending different side chains. With suitable protection, all the side chains found in the protein amino acids could be incorporated into oligoureas of the type illustrated in this paper, and some unnatural side chains as well. The focus of our future research will be on preparing encoded combinatorial libraries based upon oligoureas of the type described in this paper.

Received: December 12, 1994 [Z 7542 IE]
German version: *Angew. Chem.* **1995**, *107*, 975

Keywords: solid-phase syntheses · urea

[1] P. Y. S. Lam, P. K. Jadhav, C. J. Eyermann, C. N. Hodge, Y. Ru, L. T. Bacheler, J. L. Meek, M. J. Otto, M. M. Rayner, Y. N. Wong, C.-H. Chang, P. C. Weber, D. A. Jackson, T. R. Sharpe, S. Erickson-Viitanen, *Science* **1994**, *263*, 380–4.
[2] M. Chorev, M. Goodman, *Acc. Chem. Res.* **1993**, *26*, 266–273.
[3] A. Furka, F. Sevestyen, M. Asgedom, G. Dibo, *Int. J. Peptide Res.* **1991**, *37*, 487–493.
[4] M. A. Gallop, R. W. Barrett, W. J. Dower, S. P. A. Fodor, E. M. Gordon, *J. Med. Chem.* **1994**, *37*, 1233–1251.
[5] E. M. Gordon, R. W. Barrett, W. J. Dower, S. P. A. Fodor, M. A. Gallop, *J. Med. Chem.* **1994**, *37*, 1385–1401.
[6] M. Ho, J. K. K. Chung, N. Tang, *Tetrahedron Lett.* **1993**, *34*, 6513–6516.
[7] P. Majer, R. S. Randad, *J. Org. Chem.* **1994**, *59*, 1937–1938.
[8] H. Rink, *Tetrahedron Lett.* **1987**, *28*, 3787–3790.
[9] E. Atherton, R. C. Sheppard, *Solid Phase Peptide Synthesis, A Practical Approach*, IRL, Oxford, **1989**.
[10] E. Kaiser, R. L. Colescott, C. D. Bossinger, P. I. Cook, *Anal. Biochem.* **1970**, *34*, 595–598.

 © VCH Verlagsgesellschaft mbH, D-69451 Weinheim, 1995 0570-0833/95/0808-0908 $ 10.00+.25/0

[11] CH_2G^u, CH_2I^{Cm}, CH_2F^u, CH_2A^u. A-amide (**8**) was purified using a C18 reverse phase column to a afford the product as a colorless, hygroscopic solid (46%). Retention time: 21.6 min (from 20% CH_3CN to 80% CH_3CN in 35 min). ^1H NMR (400 MHz, [D$_6$]DMSO): δ = 7.78 (s, br., 3H), 7.40 (s, 1H), 7.29–7.23 (m, 4H), 7.20–7.16 (m, 6H), 7.00 (s, 1H), 6.28 (m, 2H), 6.27–6.08 (m, 4H), 6.04 (m, 2H), 4.09 (J = 7.1 Hz, 1H), 3.93 (m, 1H), 3.84 (m, 1H), 3.58 (J = 6.1 Hz, 1H), 3.44 (m, 2H), 3.28 (m, 2H), 3.07 (m, 2H), 2.89 (m, 1H), 2.67 (m, 4H), 2.54 (m, 3H), 1.19 (d, J = 7.0, 3H), 0.91 (d, J = 6.7, 3H). ^{13}C NMR (50 MHz, [D$_6$]DMSO): δ = 175.17, 159.07, 158.73, 158.54, 158.39, 157.89, 157.53, 138.77, 129.09, 128.17, 125.99, 50.54, 49.91, 48.49, 45.83, 45.25, 44.54, 44.32, 37.01, 19.76, 18.70; MS: expected: 626.37 found: 626.82[M^+], 649.20[M^+ + Na], 664.99 [M^+ + K]; IR (KBr): $\tilde{\nu}$ = 1458, 1498, 1505, 1562, 1567, 1644, 2921, 3450. M.p.: 125–127 °C

[12] Consistent with the accepted use of amino acid one letter coding, the additional hydrogen at the *N*-terminus is not specifically identified. This convention avoids ambiguities, because H represents histidine in the one letter code.

[13] YG. CH_2G^u, CH_2F^u. L-amide (**9**) was purified by HPLC. Retention time: 20.1 min. (from 20% CH_3CN to 80% CH_3CN in 35 min.). ^1H NMR (400 MHz, $CDCl_3$): δ = 9.37(s, 1H), 8.71 (t, J = 5.6 Hz, 1H), 8.07 (d, br, J = 1.5 Hz, 1H), 7.96 (m, 1H), 7.28–7.24 (m, 2H), 7.19 (d, J = 7.3, 3H), 7.09 (d, J = 22.1 Hz, 1H), 7.01 (d, J = 20.5 Hz, 1H), 6.91 (s, 1H), 6.70 (d, J = 8.9 Hz, 2H), 6.12 (s, 1H), 6.05–6.01 (m, 2H), 5.95 (d, J = 8.2 Hz, 1H), 4.05 (m, 1H), 3.97 (m, 1H), 3.79 (dd, J = 16.5, 5.8 Hz, 1H), 3.73–3.69 (m, 2H), 3.10–2.92 (m, 7H), 2.82 (dd, J = 14.2, 8.1 Hz, 1H), 2.70 (dd, J = 13.7, 5.7 Hz, 1H), 2.59 (dd, J = 13.6, 7.4 Hz, 1H), 1.60–1.51 (m, 1H), 1.42–1.28 (m, 3H); ^{13}C NMR (50 MHz, [D$_6$]DMSO): δ = 165.37, 156.08, 155.99, 147.16, 143.90, 140.72, 137.59, 134.11, 132.19, 131.43, 129.81, 129.33, 127.56, 127.02, 125.35, 125.13, 120.09, 114.68, 66.30, 65.11, 46.74, 41.96, 34.42; IR (KBr): $\tilde{\nu}$ = 1438, 1455, 1517, 1559, 1671, 2934, 3380. MS: calcd for $C_{30}H_{45}N_8O_6$ [M + H]: 613.3462, found: 613.3481.

[14] J. S. Nowick, N. A. Powell, E. J. Martinez, E. M. Smith, G. Noronha, *J. Org. Chem.* **1992**, *57*, 3763–3765.

[15] S. M. Hutchins, K. T. Chapman, *Tetrahedron Lett.* **1994**, *35*, 4055–4058.

[16] B. T. Chait, R. Wang, R. C. Beavis, S. B. H. Kent, *Science* **1993**, *262*, 89–92.

A Highly Stereoselective Synthesis of 1,2-*trans*-C-Glycosides via Glycosyl Samarium(III) Compounds

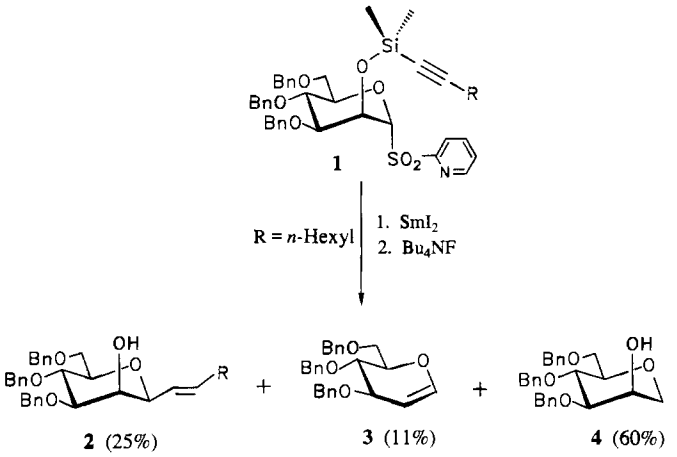
Daniel Mazéas, Troels Skrydstrup,* and Jean-Marie Beau*

C-Glycosides[1] are an important class of hydrolytically stable mimics of O- and N-glycosides usable as biological tools, particularly as potential artificial ligands for carbohydrate receptors in biological systems[2] as well as glycoenzyme regulators.[3] The interest in their construction was further intensified by the important discovery by Kishi et al.[4] that simple and complex C-glycosides adopt exoanomeric conformations similar to those of the parent O-glycosides.

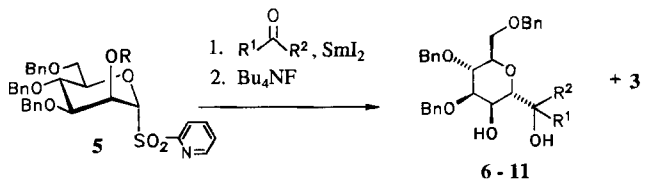
There are many possible approaches to the direct carbon–carbon bond formation at the anomeric center of carbohydrates, including the use of anomeric carbocations, radicals and carbenes.[1] The utility of anionic anomeric species, however, has been chiefly confined, until recently, to 2-deoxysugars[5, 6] or glycals,[1] since β-eliminations of the C-2-functionality[5a] occur even when a stabilizing substituent[7] is present at the anomeric center.[8] Exceptions have been provided with the α- and β-lithio reagents derived from D-glucopyranosyl units only when the unprotected C-2-hydroxyl group is lithiated before C-1[9] and the reactions are performed at low temperature[10] (≤ -78 °C) to prevent elimination of Li_2O, conditions under which these tetrahedral anionic species are configurationally stable.[11] Similar transformations using anomeric anionic species derived from α-D-mannopyranosyl units were never attempted, based on the assumption that *anti*-elimination of the axially disposed oxy function at C-2 would be an easy process. This is indeed what happened with a presumed α-lithio reagent of a 2-*O*-trimethylsilyl derivative of mannopyranose.[12]

In this work we report our findings of an extremely mild method for the stereoselective preparation of 1,2-*trans*-C-glycosides by reductive samariation of mannosyl and glucosyl 2-pyridyl sulfones and the coupling of the correspondingly formed glycosyl samarium(III) reagent under Barbier conditions with carbonyl compounds.[13] This coupling at room temperature obliterates the prior alkoxide formation at C-2.

We were led to this method while attempting the SmI_2-induced free radical cyclization of **1**.[14] Instead of forming the anticipated β-C-mannoside **2** and glucal **3** (the latter resulting



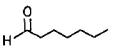
from a two-electron reduction process and elimination) as major products, the 1,5-anhydro derivative **4** was surprisingly isolated in 60% yield. This implied that the intermediate organosamarium(III) species displayed exceptional stability towards β-elimination and suggested further the possibility of a condensation of the 2-pyridyl sulfone **5** protected at O-2 (R = $SiMe_3$) with a



carbonyl compound. When a solution of **5** and cyclohexanone (1.5 equiv) in THF at 20 °C was treated with slightly more than two equivalents of SmI_2, an almost instantaneous reaction ensued leading to the α-C-mannoside **6** in 86% overall yield after desilylation[15] and only 1% of glucal **3** (Table 1, entry 1); the β-C-mannoside was not detected. Entries 2–4 in Table 1, exemplify that the reaction appears general with both alkyl ketones and aldehydes.[16]

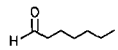
[*] Dr. T. Skrydstrup, Prof. Dr. J.-M. Beau, D. Mazéas
Université d'Orléans
Laboratoire de Biochimie Structurale, URA CNRS 499
F-Orléans Cédex 2 BP 6759 (France)
Present address: Université Paris-Sud
Laboratoire de Synthèse de Biomolécules, URA CNRS 462
Institut de Chimie Moléculaire d'Orsay
F-91405 Orsay Cédex (France)
Telefax: Int. code + (1)69853715

Table 1. Synthesis of the α-C mannosides **6**–**11**.

Entry	R [a]	Carbonyl compound [b]	Yield [%] C-glycoside [c]	Yield [%] **3**
1	$SiMe_3$		**6** 86	1
2	$SiMe_3$		**7** 80	3
3	$SiMe_3$		**8** 82 (9:2)	9
4	$SiMe_3$		**9** 77 (13:2)	7
5	$SiMe_3$		**10** 10 (2:1)	32
6	$SiMe_3$	—	[**4**] 91	9
7	Me		**11** 78 [d]	9
8	Ac		–	94

[a] The sulfones were prepared as described in ref. [14]. [b] For the reaction conditions see Experimental Procedure; 1.5 equiv of the carbonyl compound was used in each case. [c] Isolated yields after chromatography on silica gel; figures in brackets refer to the diastereomeric ratio as determined by ^1H NMR. [d] C-2-OH = C-2-OMe.

Table 2. Synthesis of the β-C glucosides **13**–**15**.

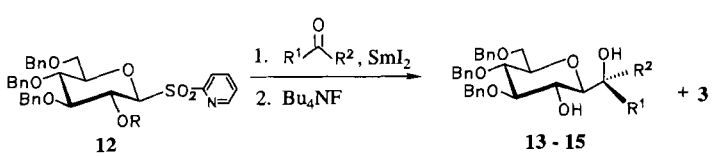
Entry	R [a]	Carbonyl compound [b]	Yield [%] C-glycoside [c]	Yield [%] **3**
1	$SiMe_3$ [d]		**13** 44	37
2	$SiMe_3$		**14** 43 (7:2)	36
3	$SiMe_3$	—	[e] 23	60
4	$SiMe_2tBu$		**13** 57	21
5	$SiMe_2tBu$		**15** 55 (3:2) [f]	22

[a], [b], and [c], see Table 1. [d] Isomeric α-2-pyridyl sulfone gave the same stereochemical results. [e] The yield corresponds to 1,5-anhydro-3,4,6-tri-*O*-benzyl-D-glucitol. [f] Known compound, see ref. [9b].

These results are remarkable for two reasons. First, the bimolecular organosamarium–carbonyl condensation is favored over the unimolecular elimination process, even though a favorable *trans*-diaxial relationship exists between the C-1–Sm and C-2–$OSiMe_3$ units. Second, although the α-tetrahydropyranyl anionic species are kinetically formed from a stepwise one-electron reduction pathway and exhibit substantial stereochemical stability at low temperature (−78 °C), the presumably thermodynamically more stable β-glycosyl samarium(III) species would be expected to dominate at higher temperatures providing the corresponding β-C-mannosides.[11]

These reactions must be performed under Barbier conditions, since addition of the carbonyl compound, even 20 s after SmI_2, did not lead to any condensation products. Again, it was surprising to observe the organosamarium reagent's preference for protonation from THF rather than elimination (Table 1 entry 6). The coupling reaction proceeded well (78%, entry 7) even when MeO group (instead of the $OSiMe_3$ group) is bound to the C-2 atom of the sulfone **5** (R = Me). With a C-2-acetoxy group, elimination finally took over (entry 8). Competitive reduction of benzaldehyde by SmI_2 explains the low yield for entry 5, although we have no explanation for the increased yield of the glucal formation.

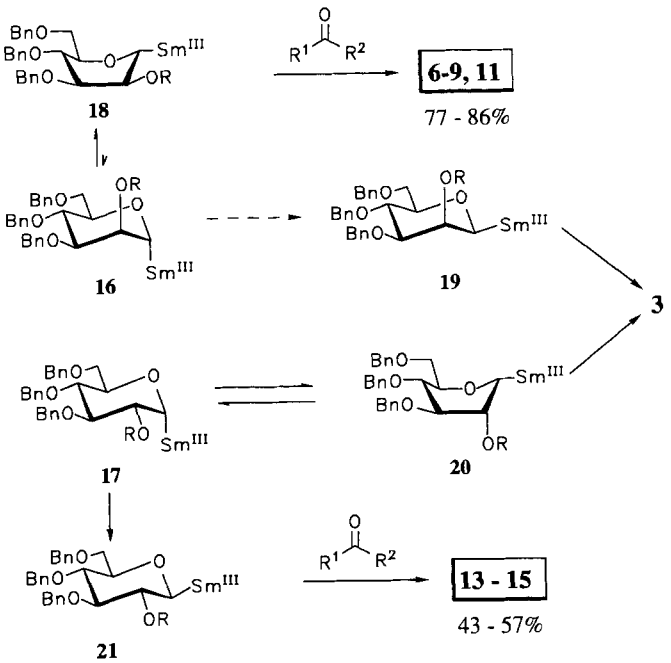
In contrast, β-C-glucosides **13**–**15** were formed exclusively from the corresponding glucosyl sulfones **12** giving moderate yields due to the competing elimination process (Table 2, entries 1 and 2). Acceptable yields were produced, however, when the trimethylsilyl group was substituted by a $SiMe_2tBu$ group; the yields of glycal decreased accordingly (entries 4 and 5).



12 **13 - 15**

Noteworthy is the dominance of glucal **3** in the absence of a carbonyl substrate (entry 3), in contrast to that observed for **5** (R = $SiMe_3$).[16]

This stereochemical discrepancy between the *manno* and the *gluco* series is tentatively explained in Scheme 1. Upon sulfone reduction, the kinetic α-oriented organosamarium species **16** or



Scheme 1.

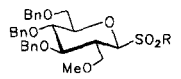
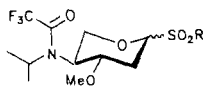
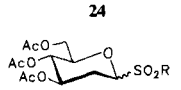
17 are produced by the reductive samariation of the corresponding anomeric radicals. In the *manno* series, rather than anomerization to **19**, **16** can undergo a facile conformational change to a possible boat or skew-boat conformer **18**, placing the C-1 and C-2 substituents in the sterically and energetically more favored equatorial positions, hence leading to the α-C-mannosides **6** to **11**. In the *gluco* series, this is probably a higher energetic process for **17**, since the already equatorially oriented C-2–O-2 bond must go through an eclipsed conformer with the C-1–Sm bond, hence anomerization to the β-species **21** may dominate. The

 © VCH Verlagsgesellschaft mbH, D-69451 Weinheim, 1995 0570-0833/95/0808-0910 $ 10.00+.25/0 Angew. Chem. Int. Ed. Engl. 1995, 34, No. 8

high 1,2-*trans* selectivity of the coupling process is therefore tentatively explained by a strong preference for a hitherto unknown *syn*-elimination mechanism operating with a β-heteroatom substituted organosamarium compound at room temperature which can only occur with **20** or possibly **19**. As observed experimentally, only the 1,2-*trans* species (e.g., **18** and **21**) would then give a productive C–C bond formation under the conditions used. In the *gluco* series, the higher yields obtained for the sterically more demanding $SiMe_2tBu$ (in place of the $SiMe_3$) C-2-protected sulfone **12** lend evidence for this hypothesis, although further confirmation is required. The behavior of these organosamarium(III) species is in high contrast to that of their lithium counterparts since, at −78 °C, the latter undergo either fast β-elimination (*manno* series) or 1,3-O-2 to C-1 silyl migration (*gluco* series).[12]

These assumptions were further supported by complementary experiments conducted on 2-deoxyglycosyl sulfones **22**–**25** (Table 3). The coupling products were obtained in good yields;

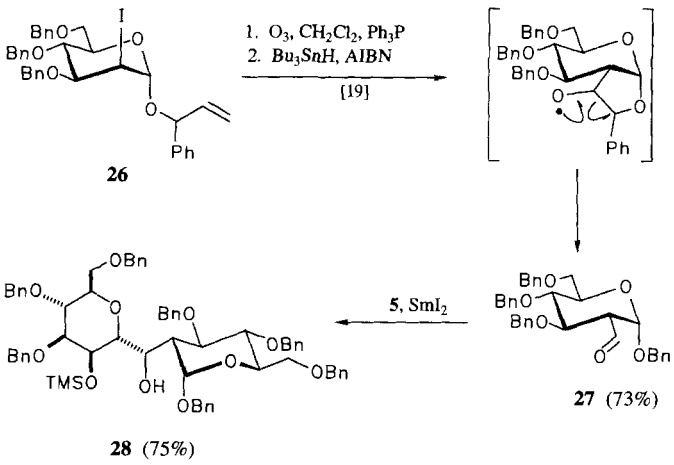
Table 3. Synthesis of the 2-deoxy-C-glucoside **22**–**25**.

Entry	Sulfone (R = 2-pyridyl)	Carbonyl compound [a]	Yield [%] C-glycoside (α:β) [b]
1	 **22**		82 (1:1)
2	 **23**		73 (1:4)
3	 **24**		80 (1:1.3) [17]
4	 **25**		88 (1:1)

[a] See [b], Table 1. [b] Isolated yields after chromatography on silica gel, α:β ratio was determined by ^1H NMR spectroscopy.

however no stereochemical preferences were displayed at the anomeric center for all 2-deoxyglycosides except for sulfone **23** (entry 2) with a carbon substituent at C-2. Placing a bulky substituent at position 2 (CH_2OCH_3 in **23** versus H in **22**) would disfavor a conformational change (as for **17** to **20**), thus decreasing the relative amount of the α-product. This suggests that the energy barrier for anomerization is close to that for a conformational change placing the C-1–Sm bond in an equatorial position. Noteworthy are the good yields obtained with the sulfone possessing trifluoroacetamide (**24**, entry 3) or even acetyl groups (**25**, entry 4).[17]

Finally, a carbon-linked disaccharide of a protected form of an α-D-mannopyranosyl(1 → 2)-D-glucopyranose was assembled efficiently by using the above procedure. Aldehyde **27** was prepared from the iodoglycoside **26**[18, 19] using a stereoselective transfer of a formyl group by a 5-*exo*cyclization-fragmentation procedure recently reported by Jung and Choe.[19] Reductive samariation of sulfone **5** (R = $SiMe_3$) in the presence of **27** gave the expected α-C-disaccharide **28** in 75% yield (isomeric ratio of 2:1 at the *exo*cyclic asymmetric center).



The preliminary results discussed herein suggest a viable and convenient way to 1,2-*trans*-C-glycosides which complements our recently reported SmI_2-induced 1,2-*cis*-C-glycoside methodology.[14] Further studies are currently underway concerning the mechanistic aspects of these reactions.

Experimental Procedure

C-Mannoside formation **6**: A 0.1 M solution of SmI_2 in THF (2.7 mL, 0.27 mmol) was added to a stirred solution of sulfone **5** (R = $SiMe_3$; 85 mg, 0.13 mmol) and cyclohexanone (20 μL, 0.19 mmol) at 20 °C. After stirring for 10 min, saturated aq. NH_4Cl was added to the reaction mixture which was then extracted twice with CH_2Cl_2. The combined organic phases were washed twice with water, dried with Na_2SO_4, and evaporated to dryness. The residue was redissolved in THF (5 mL), cooled to 0 °C, and 1.0 M Bu_4NF in THF (135 μL, 0.135 mmol) was added. After stirring for 5 min, water and CH_2Cl_2 were added, and the organic phase was washed twice with water, dried (Na_2SO_4) and evaporated to dryness. Flash chromatography (heptane: EtOAc, 7:1 → 3:1) gave first tribenzyl-D-glucal **3** (0.4 mg, 1%) and then **6** (60.5 mg, 86%); $[\alpha]_D^{20} = 8.0$ ($c = 0.80$, $CHCl_3$). ^1H NMR ($CDCl_3$, 300 MHz) (numbering of atoms is that of carbohydrate numbering): $\delta = 1.47-1.71$ (m, 10H, 5 CH_2), 2.50 (s, 1H, OH), 2.73 (d, 1H, $J = 5.2$ Hz, OH-2), 3.48 (d, 1H, $J = 7.7$ Hz, H-1), 3.62 (dd, 1H, $J = 10.2$, 5.0 Hz, H-6), 3.71 (dd, 1H, $J = 10.2$, 5.9 Hz, H-6'), 3.72 (dd, 1H, $J = 5.7$, 4.1 Hz, H-4), 3.87 (dd, 1H, J 5.7, 3.9 Hz, H-3), 4.11 (ddd, 1H, $J = 5.9$, 5.0, 4.1 Hz, H-5), 4.16 (ddd, 1H, $J = 7.7$, 5.2, 3.9 Hz, H-2), 4.49 (s, 2H, CH_2Ph), 4.51, 4.56, 4.60, 4.61 (4 d, 4H, $J = 12.0$ Hz, 4 CHPh), 7.32–7.38 (m, 15H, 3 Ph).

Received: September 28, 1994
Revised version: December 12, 1994 [Z 7362 IE]
German version: *Angew. Chem.* **1995**, *107*, 990

Keywords: aldehydes · asymmetric syntheses · C-glycosides · ketones · samarium compounds

[1] Recent reviews: M. H. D. Postema, *Tetrahedron* **1992**, *48*, 8545–8599; J. Herscovici, K. Antonakis in *Studies in Natural Products Chemistry, Vol. 10* (Ed.: Atta-ur-Rahman), Elsevier, Amsterdam, **1992**, pp. 337–403.

[2] C. R. Bertozzi, M. D. Bednarski, *Carbohydr. Res.* **1992**, *223*, 243–253; *J. Am. Chem. Soc.* **1992**, *114*, 5543–5546; C. R. Bertozzi, D. G. Cook, W. R. Kobertz, F. Gonzalez-Scarano, M. D. Bednarski, *ibid.* **114**, 10639–10641, and references therein.

[3] M. L. Sinnott, P. J. Smith, *J. Chem. Soc. Chem. Commun.* **1976**, 223–224; J.-C. Tang, B. E. Tropp, R. Engel, *Tetrahedron Lett.* **1978**, 723–726; D. W. Norbeck, J. B. Kramer, P. A. Lartey, *J. Org. Chem.* **1987**, *52*, 2174–2179; J. N. BeMiller, M. P. Yadar, V. N. Kalabokis, R. W. Myers, *Carbohydr. Res.* **1990**, *200*, 111–126; R. R. Schmidt, H. Dietrich, *Angew. Chem.* **1991**, *103*, 1348–1350; *Angew. Chem. Int. Ed. Engl.* **1991**, *30*, 1328–1329.

[4] T.-C. Wu, P. G. Goekjian, Y. Kishi, *J. Org. Chem.* **1987**, *52*, 4819–4823; P. G. Goekjian, T.-C. Wu, H.-Y. Kang, Y. Kishi, *ibid.* **1987**, *52*, 4823–4825; S. A. Babirad, Y. Wang, P. G. Goekjian, Y. Kishi, *ibid.* **1987**, *52*, 4825–4827; A. Wei, Y. Kishi, *ibid.* **1994**, *59*, 88–96 and previous work; see also: O. R. Martin, W. Lai, *ibid.* **1993**, *58*, 176–185; K. N. Houk, J. E. Eksterowicz, Y.-D. Wu, C. D. Fuglesang, D. B. Mitchell, *J. Am. Chem. Soc.* **1993**, *115*, 4170–4177.

[5] a) J.-M. Lancelin, L. Morin-Allory, P. Sinaÿ, *J. Chem. Soc. Chem. Commun.* **1984**, 355–356; b) P. Lesimple, J.-M. Beau, P. Sinaÿ, *ibid.* **1985**, 894–895; c) J.-M. Beau, P. Sinaÿ, *Tetrahedron Lett.* **1985**, *26*, 6185–6188; d) *ibid.* **1985**, *26*, 6189–6192, 6193–6196; f) D. K. Hutchinson, P. L. Fuchs, *J. Am. Chem. Soc.*

1987, *109*, 4930–4939; g) J. Prandi, C. Audin, J.-M. Beau, *Tetrahedron Lett.* **1991**, *32*, 769–772; h) M. S. Ermolenko, A. Olesker, G. Lukas, *ibid.* **1994**, *35*, 715–718.

[6] J. B. Ousset, C. Mioskowski, Y.-L. Yang, J. R. Falk, *Tetrahedron Lett.* **1984**, *25*, 5903–5906; S. V. Ley, B. Lygo, *ibid.* **1984**, *25*, 113–116.

[7] P. Lesimple, J.-M. Beau, G. Jaurand, P. Sinaÿ, *Tetrahedron Lett.* **1986**, *27*, 6201–6204; R. R. Schmidt, J. Kast, *ibid.* **1986**, *27*, 4007–4010; E. Dubois, J.-M. Beau, *J. Chem. Soc. Chem. Commun.* **1990**, 1191–1192.

[8] Exceptions: B. Aebisher, J. H. Bieri, P. Prewo, A. Vasella, *Helv. Chim. Acta* **1982**, *65*, 2251–2272; K. Mahmood, A. Vasella, B. Bernet, *ibid.* **1991**, *74*, 1555–1583 and previous work (anomeric nitrosugar); P. DeShong, G. A. Slough, V. Elango, G. L. Trainor, *J. Am. Chem. Soc.* **1985**, *107*, 7788–7790 (anomeric manganese complex); H. Chatani, T. Ikeda, T. Sano, N. Sonoda, H. Kurosawa, Y. Kawasaki, S. Murai, *J. Org. Chem.* **1988**, *53*, 3387–3389 (anomeric cobalt complex).

[9] a) V. Wittmann, H. Kessler, *Angew. Chem.* **1993**, *105*, 1138–1140; *Angew. Chem. Int. Ed. Engl.* **1993**, *32*, 1091–1093; b) P. Lesimple, J.-M. Beau, *Bioorg. Med. Chem.* **1994**, *2*, 1319–1330; c) O. Frey, M. Hoffmann, V. Wittmann, H. Kessler, P. Uhlmann, A. Vasella, *Helv. Chim. Acta* **1994**, *77*, 2060–2069. Similar syntheses of α- and β-acetamido-2-deoxy-C-glucosides: M. Hoffmann, H. Kessler, *Tetrahedron Lett.* **1994**, *35*, 6067–6070.

[10] A notable exception, which constitutes a precedent to this work, was recently provided by Sinaÿ et al. who showed that reductive samariation of 2,3,4,6-tetra-*O*-benzyl-β-D-glucopyranosyl phenyl sulfone by the SmI_2-HMPA system in the presence of simple carbonyl compounds provided the corresponding β-C-glucosides in low yields (18–24%): P. de Pouilly, A. Chénedé, J.-M. Mallet, P. Sinaÿ, *Bull. Soc. Chim. Fr.* **1993**, 130, 256–265.

[11] a) T. Cohen, M. Bhupathy, *Acc. Chem. Res.* **1989**, *22*, 152–161; b) S. D. Rychnovsky, D. E. Mickus, *Tetrahedron Lett.* **1989**, *30*, 3011–3014.

[12] V. Pedretti, A. Veyrières, P. Sinaÿ, *Tetrahedron* **1990**, *46*, 77–88.

[13] Mechanistic discussion of the Barbier reaction with samarium compounds: J. L. Namy, J. Collin, C. Bied, H. B. Kagan, *Synlett* **1992**, 733–734; D. P. Curran, T. L. Fevig, C. P. Jasperse, M. L. Totleben, *ibid.* **1992**, 943–961; G. A. Molander, J. A. McKie, *J. Org. Chem.* **1991**, *56*, 4112–4120. Recent review on the application of SmI_2: G. A. Molander, *Chem. Rev.* **1992**, *92*, 29–68.

[14] D. Mazéas, T. Skrydstrup, O. Doumeix, J.-M. Beau, *Angew. Chem.* **1994**, *106*, 1457–1459; *Angew. Chem. Int. Ed. Engl.* **1994**, *33*, 1383–1386.

[15] All α-C-mannosides **6** to **11** described in this study adopt a conformation close to that of $^{O}S_2$, e.g., $J_{1,2} = 7.4–7.8$, $J_{2,3} = 3.1–3.9$, $J_{3,4} = 5.3–5.7$, and $J_{4,5} = 3.2–4.1$ Hz. That these products are indeed the α-anomers was confirmed by a nuclear Overhauser effect between the C-1 and C-6 hydrogens in **6**. The 2-deoxy-C-glycosides display the following coupling constants: β-anomers, $J_{1,2} = 9.6–12.0$, $J_{1,2'} = 2.1–2.2$, $J_{3,4} = 8.2–9.3$ Hz; α-anomers, $J_{1,2} = 2.6–3.4$, $J_{1,2'} = 10.3–11.5$, $J_{3,4} = 2.8–4.0$ Hz.

[16] Reactions of **5** and **12** with aldehydes led to some selectivity (up to 6.5:1) at the newly created stereogenic center C-7 (compounds **8**–**10**, **14**, **15**). Although the major isomer in the *gluco* series was identified possessing the C-7 (*R*) configuration [9b], we have not yet determined the C-7 configuration in compounds **8**–**10**. Significant ^{1}H NMR data for the major isomers of these compounds are as follows: **8** (diacetate): $\delta = 3.79$ (H-1), 5.24 (H-2), 5.13 (H-7), $J_{1,2} = 2.6$, $J_{1,7} = 5.4$ Hz; **9** (diacetate): $\delta = 3.80$ (H-1), 5.20 (H-2), 4.95 (H-7), $J_{1,2} = 2.8$, $J_{1,7} = 6.1$ Hz; **10**: $\delta = 3.89$ (H-1), 3.83 (H-2), 4.81 (H-7), $J_{1,2} = 3.7$, $J_{1,7} = 7.8$ Hz.

[17] The anomeric composition of the C-glycosides derived from sulfone **24** was determined by derivatization to their corresponding imidazole thiocarbamates and chromatographic separation. Unfortunately, the composition of the C-7 diastereomers could not be determined due to the trifluoroacetamido group giving rise to rotameric mixtures.

[18] Compound **26** was obtained by NIS-assisted iodoglycosylation (J. Thiem, H. Karl, J. Schwenter, *Synthesis* **1978**, 696–698) of tri-*O*-benzyl-D-glucal with racemic 1-phenyl-3-propenol [19].

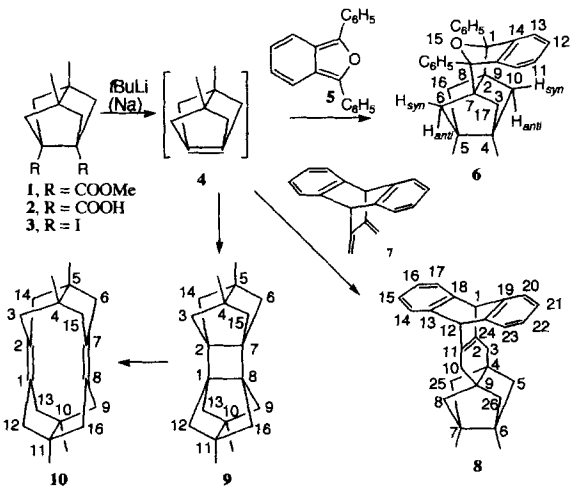
[19] M. E. Jung, S. W. T. Choe, *Tetrahedron Lett.* **1993**, *34*, 6247–6250.

Synthesis, Chemical Trapping, and Dimerization of 3,7-Dimethyltricyclo[3.3.0.0^{3,7}]oct-1(5)-ene: [2 + 2] Retrocycloaddition of the Cyclobutane Dimer**

Pelayo Camps,* Mercè Font-Bardia, Francesc Pérez, Xavier Solans, and Santiago Vázquez

"Pyramidalized" alkenes have attracted much attention since Weinshenker and Greene[1] published the synthesis of the first alkene of this kind. Szeimies published a review[2] on this topic in 1981, which was updated by Borden[3] in 1989 and by Luef and Keese[4] in 1991. Pyramidalized alkenes containing cubane,[5] homocubane,[6] dodecahedrane,[7] and other cage structures[8] have been recently described. Pyramidalized bridged cyclopropenes[9] and tribenzodihydroacepentalene[10] have also been prepared.

In particular, Borden at al.[8] synthesized several members of a series of tricyclo[3.3.*n*.0^{3,7}]alk-3(7)-enes and some derivatives for $n = 3, 2, 1$. The most pyramidalized member of this series[11] with $n = 0$ (tricyclo[3.3.0.0^{3,7}]oct-1(5)-ene) is as yet unkown, but a bis(ethano) derivative has been recently described.[8b] In this communication we describe the synthesis of 3,7-dimethyltricyclo[3.3.0.0^{3,7}]oct-1(5)-ene (**4**), its trapping with 1,3-diphenylisobenzofuran (**5**) and 11,12-dimethylene-9,10-dihydro-9,10-ethanoanthracene[12] (**7**), and its dimerization to the cyclobutane derivative **9**, which undergoes thermal conversion to diene **10** (Scheme 1).



Scheme 1. Synthesis, trapping, and dimerization of **4** and [2 + 2] retrocycloaddition of the cyclobutane dimer.

Our synthesis started with diester **1**[13] which on saponification gave the corresponding dicarboxylic acid **2**. Diodo compound **3** was obtained in 65% yield by iododecarboxylation of **2** with

[*] Prof. Dr. P. Camps, Dr. F. Pérez, Dipl.-Pharm. S. Vázquez
Laboratori de Química Farmacèutica, Facultat de Farmàcia
Universitat de Barcelona
Av. Diagonal s/n, E-08028 Barcelona (Spain)
Telefax: Int. code + (3)402-1886
Dr. M. Font-Bardia, Prof. Dr. X. Solans
Serveis Científico-Tècnics, Universitat de Barcelona (Spain)

[**] We thank Dr. C. Rücker (Institut für Organische Chemie und Biochemie, Universität Freiburg) for a copy of the POLCYC program used for naming the adducts and dimers derived from **4**. We thank Dr. M. Feliz and Dr. A. Linares for NMR analyses, Dr. A. Marín for mass spectra, and Dipl.-Chem. P. Domenech for elemental analyses.

iodosobenzene diacetate, following the Moriarty[14] modification of the Suárez[15] procedure. Reaction of **3** with *tert*-butyllithium in THF at −78 °C in the presence of diene **5** allowed us to isolate the corresponding Diels–Alder adduct **6** in 75% yield. Similarly, when the reaction was carried out in the presence of diene **7**, adduct **8** was obtained in 67% yield. The structure of these adducts was established by spectroscopic means, and in the case of **8** by X-ray diffraction analysis[16] (Fig. 1).

Table 1. Selected physical data for **2**, **3**, **6**, **8**, **9**, and **10** [20]: ^{1}H NMR and ^{13}C NMR spectra measured in $CDCl_3$; assignments given in the NMR spectra are based on DEPT, ^{1}H/^{1}H, and ^{1}H/^{13}C COSY experiments (HMQC and HMBC sequences); for the numbering of the atoms see Scheme 1. The elemental analyses (C, H, and I) of compounds **2**, **3**, **6**, **8**, and **10** agreed with calculated values within ±0.3.

2 (3,7-Dimethyltricyclo[3.3.0.0^{3,7}]octane-1,5-dicarboxylic acid): M.p. 166–168 °C; IR (KBr): $\tilde{\nu}$ = 3500–2500 (OH), 1700 (CO) cm^{-1}; ^{1}H NMR (200 MHz): δ = 1.19 (s, CH_3), 1.72 (d, J = 7.7 Hz), 1.95 (d, J = 7.7 Hz, CH_2), 8.5–9.5 (br., COOH); ^{13}C NMR (50.3 MHz): δ = 16.0 (CH_3), 48.0 (C, C3(7)), 55.9 (CH_2), 58.5 (C, C1(5)), 179.8 (C, COOH).

3 (1,5-Diiodo-3,7-dimethyltricyclo[3.3.0.0^{3,7}]octane): M.p. 95–97 °C (sublimed at 70 °C / 0.5 Torr); MS (70 eV): *m/z* (%): 388 (3) $[M]^{+}$, 261 (33) $[M-I]^{+}$, 135 (10), 134 (100) $[M-2I]^{+}$, 119 (30), 105 (12), 92 (16), 91 (24), 77 (12); ^{1}H NMR (200 MHz): δ = 1.19 (s, CH_3), 1.94 (d, J = 7.5 Hz), 2.19 (d, J = 7.5 Hz, CH_2); ^{13}C NMR (50.3 MHz): δ = 14.9 (CH_3), 45.0 (C, C1(5)), 48.8 (C, C3(7)), 65.6 (CH_2).

6 (4,5-Dimethyl-1,8-diphenyl-15-oxahexacyclo[6.6.1.1^{2,5}.1^{4,7}.0^{2,7}. 0^{9,14}]heptadeca-9,11,13-triene): M.p. 188–189 °C; MS (70 eV): *m/z* (%): 404 (8) $[M]^{+}$, 361 (10), 349 (25), 331 (13), 271 (38), 270 (85) $[C_{20}H_{14}O]^{+}$, 269 (11), 252 (10), 243 (17), 241 (25), 239 (19), 228 (10), 215 (15), 205 (11), 202 (12), 193 (23), 165 (31), 133 (22), 119 (18), 115 (12), 105 (100), 91 (42), 79 (11), 77 (69), 69 (12), 57 (21), 55 (22), 51 (14); ^{1}H NMR (500 MHz): δ = 1.02 (dd, J = 8.0 Hz, J' = 3.5 Hz, 3(17)-H*syn*), 1.09 (s, 4-CH_3), 1.12 (s, 5-CH_3), 1.52 (d, J = 8.0 Hz, 6(16)-H*anti*), 1.62 (dd, J = 8.0 Hz, J' = 3.5 Hz, 6(16)-H*syn*), 1.66 (d, J = 8.0 Hz, 3(17)-H*anti*), 6.99 (dd, J = 5.5 Hz, J' = 3.0 Hz, 11(12)-H), 7.13 (dd, J = 5.5 Hz, J' = 3.0 Hz, 10(13)-H), 7.38 (tt, J = 7.5 Hz, J' = 1.0 Hz, Ar-H*para*), 7.47 (t, J = 7.5 Hz, Ar-H*meta*), 7.65 (dd, J = 7.5 Hz, J' = 1.0 Hz, Ar-H*ortho*); ^{13}C NMR (50.3 MHz): Δ = 16.9 (CH_3, 4- and 5-CH_3), 51.0 (C, C5), 51.8 (C, C4), 53.8 (CH_2, C6(16)), 53.9 (CH_2, C3(17)), 66.3 (C, C2(7)), 87.9 (C, C1(8)), 119.9 (CH, C11(12)), 125.7 (CH, Ar-C*ortho*), 126.3 (CH, C10(13)), 127.3 (CH, Ar-C*para*), 128.2 (CH, Ar-C*meta*), 138.3 (C, Ar-C*ipso*), 148.1 (C, C9(14)).

8 (6,7-Dimethyloctacyclo[10.6.6.1^{4,7}.1^{6,9}.0^{2,11}.0^{4,9}.0^{13,18}.0^{19,24}]hexacosa-2(11), 13,15,17,19,21,23-heptaene): M.p. 195–196 °C; MS (70 eV): *m/z* (%): 364 (11) $[M]^{+}$, 215 (16), 178 (29), 135 (11), 134 (100) $[C_{10}H_{14}]^{+}$, 119 (19), 92 (12), 91 (13); ^{1}H NMR (500 MHz): δ = 0.98 (s, 6(7)-CH_3), 1.06 (d, J = 6.5 Hz), 1.26 (d, J = 6.5 Hz, 5(8,25,26)-H_2), 2.39 (s, 3(10)-H_2), 4.70 (s, 1(12)-H), 6.89 (dd, J = 5.2 Hz, J' = 3.2 Hz, 15(16,21,22)-H), 7.21 (dd, J = 5.2 Hz, J' = 3.2 Hz, 14(17,20,23)-H); ^{13}C NMR (50.3 MHz): δ = 16.9 (CH_3, 6(7)-CH_3), 32.6 (CH_2, C3(10)), 47.6 (C, C6(7)), 49.9 (C, C4(9)), 56.6 (CH, C1(12)), 59.3 (CH_2, C5(8,25,26)), 122.4 (CH, C14(17,20,23)), 124.1 (CH, C15(16,21,22)), 142.9 (C, C2(11)), 146.6 (C, C13(18,19,24)).

9 (4,5,10,11-Tetramethylheptacyclo[8.2.1.1^{2,5}.1^{4,7}.1^{8,11}.0^{1,8}.0^{2,7}]hexadecane): ^{1}H NMR (200 MHz): δ = 1.09 (s, CH_3), 1.35 (d, J = 6.9 Hz), 1.70 (d, J = 6.9 Hz, CH_2); ^{13}C NMR (50.3 MHz): δ = 16.5 (CH_3), 54.9 (CH_2), 50.9(C), the signal of the other quaternary carbon atom was not observed.

10 (4,5,10,11-Tetramethylpentacyclo[8.2.1.1^{2,5}.1^{4,7}.1^{8,11}]hexadeca-1,7-diene): M.p. 156–157 °C; MS (70 eV): *m/z* (%): 269 (15), 268 (68) $[M]^{+}$, 253 (12), 199 (39), 187 (28), 186 (34), 185 (33), 171 (20), 159 (18), 157 (17), 155 (11), 145 (11), 143 (15), 142 (10), 141 (14), 135 (29), 134 (54) $[C_{10}H_{14}]^{+}$, 133 (19), 131 (18), 129 (18), 128 (21), 120 (12), 119 (51), 117 (21), 115 (23), 107 (28), 106 (14), 105 (46), 103 (12), 95 (26), 94 (21), 93 (35), 92 (17), 91 (100), 81 (11), 79 (61), 78 (18), 77 (68), 69 (32), 67 (24), 65 (34), 57 (12), 55 (54), 53 (38), 52 (10), 51 (18); ^{1}H NMR (200 MHz): δ = 1.09 (s, CH_3), 2.00 (d, J = 12.0 Hz), 2.50 (d, J = 12.0 Hz, CH_2); ^{13}C NMR (50.3 MHz): δ = 24.9 (CH_3), 42.1 (C), 48.4 (CH_2), 130.4 (C).

The reaction of **3** with *tert*-butyllithium in THF at −78 °C, in the absence of a trapping agent, gave a complex mixture. The presence of a cyclobutane dimer (**9**) and products derived from the addition of *tert*-butyllithium to **4** was established by coupled gas–liquid chromatography and mass spectrometry (GLC/MS), and by ^{1}H and ^{13}C NMR spectroscopy. Attempts to isolate **9** by column chromatography or crystallization provided the diene dimer **10** in low yield.

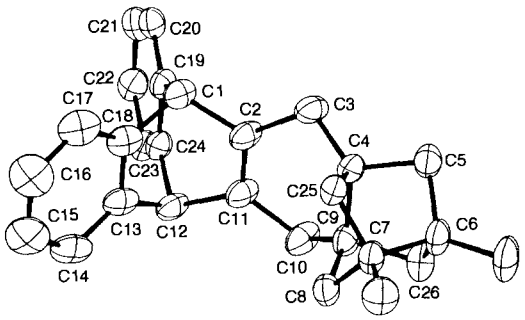


Fig. 1. Crystal structure (ORTEP) of adduct **8**. Selected distances [Å] and angles [°]: C4-C5 1.532(3), C4-C9 1.626(4), C5-C6 1.535(3), C6-C7 1.617(4); C3-C4-C5 119.7(2), C3-C4-C9 115.54(11), C4-C5-C6 95.0(2), C5-C4-C9 102.79(12), C5-C4-C25 95.9(2), C5-C6-C7 102.1(2), C5-C6-C26 96.2(2), C5-C6-CH_3 117.2(2), C6-C7-CH_3 116.5(3).

Reaction of **3** with a large excess of sodium (10 equiv) in dioxane at reflux for 4 h gave diene **10** as the only detectable product, which was isolated in 77% yield in crystalline form. Probably the initially formed cyclobutane dimer **9** is completely transformed into **10** under the reaction conditions. The formation of cyclobutane dimers from highly pyramidalized alkenes has been previouly observed,[10, 17] but a bis(ethano) derivative of tricyclo[3.3.0.0^{3,7}]oct-1(5)-ene[8b] failed to dimerize, probably because of steric hindrance. Cubene[5] and homocub-1(7)-ene[6a, b] also failed to dimerize. In addition, the opening of cyclobutane derivatives to dienes in very strained compounds has been described,[18] but such a reaction has never been reported for a cyclobutane dimer derived from a tricyclo[3.3.n.0^{3,7}]alk-3(7)-ene derivative with $1 \leq n \leq 3$.

Work is in progress to fully characterize the cyclobutane dimer **9** and apply this methodology to dimethyl tetracyclo[5.2.1.0^{2,6}.0^{3,8}]decane-7,8-dicarboxylate[19] in order to develop a convergent synthesis of dodecahedrane.

Experimental Procedure

Generation and trapping of **4**: To a solution of diiodide **3** (388 mg, 1.0 mmol) and the trapping agent (1.1–1.2 mmol) in anhydrous THF (15 mL) at −78 °C was added dropwise a 1.7 M solution of *tert*-butyllithium in pentane (1.0 mL, 1.7 mmol) under argon. The mixture was stirred for 0.5 h at −78 °C, quenched with methanol (5 mL), and allowed to warm to room temperature. Water (30 mL) was added, the mixture was extracted with diethyl ether (2 × 50 mL), and the combined organic extracts were dried with Na_2SO_4 and concentrated in vacuo. Column chromatography of the residue (silica gel, hexane/ethyl acetate) and crystallization from 2-propanol afforded the corresponding Diels–Alder adduct. Yields: **6**, 74%; **8**, 67%.

10: A mixture of freshly cut sodium (230 mg, 10 mmol) and anhydrous dioxane (10 mL) was heated under reflux until the sodium melted. Diiodide **3** (388 mg, 1.0 mmol) was added, and reflux was maintained for 4 h. The resulting suspension was allowed to warm to room temperature and filtered through Celite. The filtrate was concentrated in vacuo and the residue was crystallized from pentane to give **10** in 77% yield.

Received: October 28, 1994 [Z 7435 IE]
German version: *Angew. Chem.* **1995**, *107*, 1011

Keywords: alkenes · cage compounds · Diels–Alder reactions · hydrocarbons

[1] N. M. Weinshenker, F. D. Greene, *J. Am. Chem. Soc.* **1968**, *90*, 506.
[2] G. Szeimies, *Chimia* **1981**, *35*, 243–248.
[3] W. T. Borden, *Chem. Rev.* **1989**, *89*, 1095–1109.
[4] W. Luef, R. Keese, *Top. Stereochem.* **1991**, *20*, 231–318.
[5] P. E. Eaton, *Angew. Chem.* **1992**, *104*, 1447–1462; *Angew. Chem. Int. Ed. Engl.* **1992**, *31*, 1421–1436.
[6] a) D. A. Hrovat, W. T. Borden, *J. Am. Chem. Soc.* **1988**, *110*, 7229–7230; b) J. Schäfer, G. Szeimies, *Tetrahedron Lett.* **1988**, *29*, 5253–5254; c) M. C. Holthausen, W. Koch, *Angew. Chem.* **1994**, *106*, 682–684; *Angew. Chem. Int. Ed. Engl.* **1994**, *33*, 668–670.
[7] a) J. P. Kiplinger, F. R. Tollens, A. G. Marshall, T. Kobayashi, D. R. Lagerwall, L. A. Paquette, J. E. Bartmess, *J. Am. Chem. Soc.* **1989**, *111*, 6914–6919; b) J.-P. Melder, R. Pinkos, H. Fritz, H. Prinzbach, *Angew. Chem.* **1990**, *102*,

105–109; *Angew. Chem. Int. Ed. Engl.* **1990**, *29*, 95–99; c) L. A. Paquette, D. R. Lagerwall, J. L. King, S. Niwayama, R. Skerlj, *Tetrahedron Lett.* **1991**, *32*, 5259–5262; d) J.-P. Melder, R. Pinkos, H. Fritz, J. Wörth, H. Prinzbach, *J. Am. Chem. Soc.* **1992**, *114*, 10213–10231; e) R. Pinkos, J.-P. Melder, K. Weber, D. Hunkler, H. Prinzbach, *ibid.* **1993**, *115*, 7173–7191.

[8] a) A. Kumar, J. D. Lichtenhan, S. C. Critchlow, B. E. Eichinger, W. T. Borden, *J. Am. Chem. Soc.* **1990**, *112*, 5633–5634; b) B. M. Branan, L. A. Paquette, D. A. Hrovat, W. T. Borden, *ibid.* **1992**, *114*, 774–776; c) J. M. Smith, D. A. Hrovat, W. T. Borden, M. Allan, K. R. Asmis, C. Bulliard, E. Haselbach, U. C. Meier, *ibid.* **1993**, *115*, 3816–3817; d) J. G. Radziszewski, T.-K. Yin, G. E. Renzoni, D. A. Hrovat, W. T. Borden, J. Michl, *ibid.* **1993**, *115*, 1454–1456; e) J. Podlech, K. Polborn, G. Szeimies, *J. Org. Chem.* **1993**, *58*, 4113–4117.

[9] a) P. J. Chenier, D. A. Southard, Jr., *J. Org. Chem.* **1990**, *55*, 4333–4337; b) K. B. Wiberg, D. R. Artis, G. Bonneville, *J. Am. Chem. Soc.* **1991**, *113*, 7969–7979; c) P. J. Chenier, M. J. Bauer, C. L. Hodge, *J. Org. Chem.* **1992**, *57*, 5959–5962.

[10] a) R. Haag, B. Ohlhorst, M. Noltemeyer, A. Schuster, D. Kuck, A. de Meijere, *J. Chem. Soc. Chem. Commun.* **1993**, 1727–1729; b) R. Haag, D. Kuck, X.-Y. Fu, J. M. Cook, A. de Meijere, *Synlett* **1994**, 340–342.

[11] D. A. Hrovat, W. T. Borden, *J. Am. Chem. Soc.* **1988**, *110*, 4710–4718.

[12] H. Hart, A. Bashir-Hamedi, J. Luo, M. A. Meador, *Tetrahedron* **1986**, *42*, 1641–1654.

[13] P. Camps, C. Iglesias, M. J. Rodríguez, M. D. Grancha, M. E. Gregori, R. Lozano, M. A. Miranda, M. Figueredo, A. Linares, *Chem. Ber.* **1988**, *121*, 647–654.

[14] R. M. Moriarty, J. S. Khosrowshahi, T. M. Dalecki, *J. Chem. Soc. Chem. Commun.* **1987**, 675–676.

[15] J. I. Concepción, C. G. Francisco, R. Freire, R. Hernández, J. A. Salazar, E. Suárez, *J. Org. Chem.* **1986**, *51*, 402–404.

[16] Crystal data for **8**: orthorhombic, *Pnma*, $a = 2058.6(4)$, $b = 1143.5(3)$, $c = 900.6(2)$ pm ($\alpha = \beta = \gamma = 90°$); 3250 measured reflections all of them independent, of which 3200 with $I > 2\sigma(I)$ were used for the refinement; $R = 0.0325$, $wR = 0.751$. Further details of the crystal structure investigation may be obtained from the Fachinformationszentrum Karlsruhe, D-76344 Eggenstein-Leopoldshafen (Germany), on quoting the depository number CSD-58766.

[17] a) R. Greenhouse, W. T. Borden, K. Hirotsu, J. Clardy, *J. Am. Chem. Soc.* **1977**, *99*, 1664–1666; b) G. E. Renzoni, T.-K. Yin, W. T. Borden, *ibid.* **1986**, *108*, 7121–7122.

[18] a) K. B. Wiberg, M. G. Matturro, P. J. Okarma, M. E. Jason, *J. Am. Chem. Soc.* **1984**, *106*, 2194–2200; b) K. Kimura, H. Ohno, K. Morikawa, Y. Tobe, Y. Odaira, *J. Chem. Soc. Chem. Commun.* **1982**, 82–83.

[19] P. Camps, J. Castañé, M. T. Santos, *Chem. Lett.* **1984**, 1367–1370.

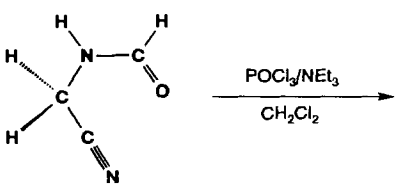
[20] The systematic names for **6**, **8**, **9**, and **10** were obtained with the POLCYC program: G. Rücker, C. Rücker, *Chimia*, **1990**, *44*, 116–120.

Synthesis, Structural Investigation, and Ligand Properties of Isocyanoacetonitrile**

Jürgen Buschmann, Dieter Lentz,* Peter Luger, Genivaldo Perpetuo, Dirk Scharn, Stefan Willemsen

Small molecules are favorite subjects for spectroscopic and structural investigations, because comparisons with theoretical calculations may contribute to a better understanding of the bonding. Malononitrile is the only well characterized and stable compound of the three isomeric compounds $CH_2(CN)_2$,[1] $CH_2(CN)(NC)$,[2, 3] (**1**) and $CH_2(NC)_2$.[4] Isocyanoacetonitrile, which is especially favorable for comparative investigations of the structural characteristics and ligand properties of the nitrile group and the isocyanide group, is insufficiently characterized, although it is mentioned in some patents and appears in a publication as a intermediate that was not isolated. The same is true for diisocyanomethane[4], the only known but poorly characterized geminal diisocyanide.

Here we present the synthesis of pure isocyanoacetonitrile (**1**), its spectroscopic characterization, its crystal structure analysis, and the first investigations of its complex chemistry. Starting with (formylamino)acetonitrile, which is prepared in good yields from aminoacetonitrile and acetylformate, an Ugi-reaction in dichloromethane gives a solution of isocyanoacetonitrile (**1**). [Eq. (a)]. Fractional condensation under high vacuum yields the colorless **1**, which is crystalline at $-30\,°C$ and melts at $-15\,°C$ to give a colorless liquid. Above $-10\,°C$ this liquid turns brown and decomposes rapidly.



1 (a)

The ^{14}N NMR spectrum [$\delta = -122$ ($\nu_{1/2} \approx 400$ Hz, $-CN$), -255 ($\nu_{1/2} \approx 18$ Hz, $-NC$)] and the ^{13}C NMR spectrum [$\delta = 29.9$ $\{^1J(^{14}N,^{13}C) \approx 7$ Hz; $CH_2\}$, 110.9 ($-CN$), 162.9 ($-NC$)] show the characteristic resonances for the isocyano group and the nitrile group in confirmation of the structure. Despite its instability we were able to grow a single crystal of **1** by zone melting and to determine the crystal structure by X-ray diffraction. Compound **1** crystallizes in the monoclinic space group *Pn* with two crystallographically independent molecules in the asymmetric unit. The unit cell (Fig. 1) also shows that the nitrile group and the isocyano group should be disordered if the centrosymmetric space group $P2_1/n$ is assumed.

Fig. 1. Unit cell (ORTEP plot [7]) of **1**.

In Table 1 the most important geometric parameters are summarized and compared with the results of an ab initio calculation.[6] The CN triple bond is significantly longer for the isocyano group than for the nitrile group, and both the nitrile group and the isocyano group are linear. According to ab initio calculations (HF/3-21G) the isocyano acetonitrile is less stable than malononitrile by 19.8 kcal mol^{-1}.

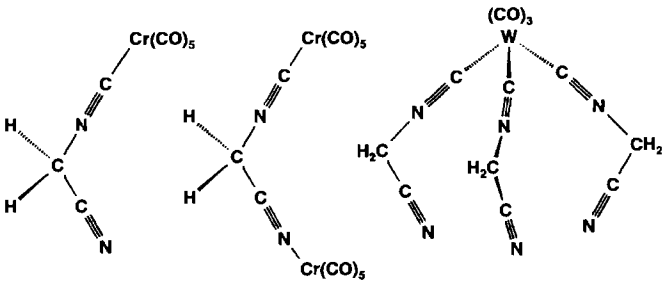
Pentacarbonyl(η^2-*cis*-cyclooctene)chromium or tricarbonyl(η^6-cycloheptatriene)tungsten both react with an excess of isocyanide **1** cleanly to give the complexes **2** and **4**, respectively (Scheme 1). The exclusive coordination of the metals to the isocyanide group is evident from the spectroscopic data, especially the $^1J(^{183}W,^{13}C)$ coupling constant of 116 Hz for the isocyanide carbon atom of the tungsten complex **4**, and from the

[*] Priv.-Doz. Dr. D. Lentz, D. Scharn, S. Willemsen
Institut für Anorganische und Analytische Chemie der Freien Universität
Fabeckstrasse 34–36, D-14195 Berlin (Germany)
Telefax: Int. code + (30)838-2424
Dr. J. Buschmann, Prof. Dr. P. Luger, G. Perpetuo
Institut für Kristallographie der Freien Universität Berlin (Germany)

[**] This work was supported by the Fonds der Chemischen Industrie and the Graduiertenkolleg "Synthese und Strukturuntersuchung niedermolekularer Verbindungen" of the Freie Universität und the Technische Universität Berlin.

Table 1. Bond lengths [pm] and bond angles [°] in **1** and the values from ab initio calculations for comparison.

	Molecule 1	Molecule 2	HF/3-21G
C-C	145(2)	145(2)	146.4
C-N	143(2)	140(2)	142.6
C≡N	113.8(14)	112(2)	113.7
N≡C	116(2)	117.8(14)	116.2
N-C-C	111.0(11)	110.1(10)	111.0
C≡N-C	177.1(12)	177.1(11)	179.3
N≡C-C	174.1(11)	173(2)	179.5



Scheme 1. Products of the reaction of **1** with $[(CO)_5Cr(\eta^2\text{-}C_8H_{14})]$ in CH_2Cl_2 (**2**), with $[(CO)_5Cr(thf)]$ in THF (**3**), and with $[(CO)_5W(\eta^2\text{-}C_7H_8)]$ in CH_2Cl_2 (**4**).

crystal structure analysis of **2** (Fig. 2). In **2** the chromium atom is almost octahedrally coordinated by five carbonyl ligands and the isocyanide ligand. A short Cr–C bond to the carbonyl ligand in *trans* position and a long bond to the isocyanide ligand demonstrate that this isocyanide ligand acts as a good σ-donor ligand. This finding is also reflected in the IR spectrum of **2**. The tungsten complex **4** exihibits only one set of signals in the ^1H and the ^{13}C NMR spectra as anticipated for a facial arrangement of the ligands.

Although the nitrile group can also be coordinated to a metal center in the reaction of **1** with excess of pentacarbonyl(tetrahydrofuran)chromium, **3** is so unstable that its formation was only proven by its mass spectrum.

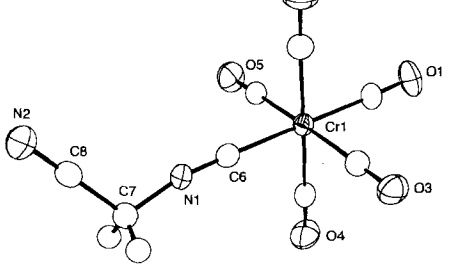


Fig. 2. Molecular structure (ORTEP plot [7]) of **2**. Important bond lengths [pm] and bond angles [°]. Cr1–C1 187.6(2), Cr–CO_{cis} 189.9(2)–191.1(2), Cr–C6 198.2(2), C6–N1 115.1(3), N1–C7 142.6(3), C7–C8 145.7(3), C8–N2 113.3(3), C6-N1-C7 168.9(2), N1-C7-C8 112.1(2), C7-C8-N2 178.0(3).

Experimental Procedure

1: (Formylamino)acetonitrile (6.93 g, 90 mmol) and triethylamine (45.81 g, 454 mmol) were dissolved in dichloromethane (250 mL) and cooled to 0 °C under steady stirring. During the next 75 min phosphoryl chloride (14.13 g, 92 mmol) was added to the well-cooled mixture. After 5 min of additional stirring the solution was washed once with a 30% sodium carbonate solution (250 mL) and twice with distilled water (200 mL). The yellow solution was stirred with sodium sulfate for 15 min. The by-products of the reaction and the solvent were removed from the organic phase by fractional condensation at room temperature. In the trap, which is cooled to −30 °C, **1** separates as a colorless crystalline solid. Yield: 1.45 g (24%). ^1H NMR: = 4.49; ^{13}C NMR: δ = 29.9 (t, CH_2, $^1J(^{14}N,^{13}C) \approx 7$ Hz), 110.9 (–CN), 162.9 (br, -NC); ^{14}N NMR (NO_3^-, ext. standard): $\delta = -122$ (-CN, $\nu_{1/2} \approx 400$ Hz), −225 (–NC, $\nu_{1/2} \approx 18$ Hz); IR (film): $\tilde{\nu}$ = 2975 s, 2943 m, 2160 vs, 1613 s, 1418 s, 1348 m, 982 s, 900 s, 800 w cm^{-1}; MS: *m/z*: 66 $[M^+]$, 40 $[NC_2H_2^+]$, 39 $[NC_2H^+]$, 38 $[NC_2^+]$, 28 $[NCH_2^+]$.

2: **1** (0.125 g, 2 mmol) was dissolved in dichloromethane under an argon atmosphere, and pentacarbonyl(*cis*-cyclooctene)chromium (0.462 g, 1.5 mmol) was added. The solution was stirred at room temperature for 45 min and then concentrated. The reaction products were separated by preparative TLC (eluent: dichloromethane/pentane 1:1). Complex **2** is eluted from the stationary phase by dichloromethane, and the solution crystallized at −20 °C; pale yellow crystals, m.p. 143 °C. Yield: 0.078 g (20%). ^1H NMR: δ = 4.65; ^{13}C NMR: δ = 110.0 (–CN), 32.8 (CH_2), 215.8 (s, CO_{trans}), 214.3 (s, CO_{cis}); IR (KBr): $\tilde{\nu}$ = 2983 vw, 2950 vw, 2174 m, 2067 m, 1986 s, 1974 s, 1926 vs, 1411 w, 1347 w, 1020 vw, 901 w, 653 s, 533 vw, 482 w, 447 w, 303 vw cm^{-1}; IR (CH_2Cl_2): $\tilde{\nu}$ = 2157 m, 2063 s, 1957 vs cm^{-1}; Raman: $\tilde{\nu}$ = 2989 vw, 2957 vw, 2272 vw, 2175 m, 2068 m, 1996 w, 1985 s, 1947 w, 1926 w, 1416 vw, 1351 vw, 958 vw, 904 vw, 677 vw, 651,vw, 541 vw, 462 w, 393 s, 361 vw, 227 vw, 117 vs cm^{-1}; MS: *m/z*: 258 $[M^+]$, 230 $[M^+-CO]$, 202 $[M^+-2CO]$, 174 $[M^+-3CO]$, 146 $[M^+-4CO]$, 118 $[M^+-5CO]$, 78 $[CrCN^+]$, 52 $[Cr^+]$.

4: Tricarbonyl(η^6-cycloheptatriene)tungsten (0.36 g, 1 mmol) in dichloromethane (5 mL) was added to a solution of **1** (0.3 g, 5 mmol) in dichloromethane (5 mL) at −20 °C. On warming to room temperature a yellow-brown precipitate formed, and the solution turned brown by the part decomposition of the isocyanide. The precipitate was recrystallized from dichloromethane/pentane. Yield: 0.126 g (27%), pale yellow crystals, m.p. 173 °C. ^1H NMR: δ = 4.90; ^{13}C NMR: δ = 32.3 [CH_2], 113.4 [–CN], 159.3 [–NC, $^1J(^{183}W,^{13}C)$ = 116 Hz], 201.5 [CO, $^1J(^{183}W,^{13}C)$ = 134 Hz]; IR (THF): $\tilde{\nu}$ = 2160 (NC), 2100 (NC), 1945 (CO), 1893 (CO) cm^{-1}; MS: *m/z*: 466 $[M^+]$, 428 $[M^+-CO]$, 382 $[M^+-3CO]$, 372 $(W(CO)_2(CNCH_2CN)_2^+]$, 316 $[W(CNCH_2CN)_2^+]$, 249 $[W(CNCH_2CN)^+]$.

Received: October 20, 1994 [Z 7415 IE]
German version: *Angew. Chem.* **1995**, *107*, 988

Keywords: chromium compounds · complexes with carbon ligands · isocyanides · nitriles · tungsten compounds

[1] *Beilsteins Handbuch der Organischen Chemie*, **1920**, *Bd. 2*, S. 589; **1929**, I. Erg.-Werk, *Bd. 2*, S. 256; **1942**, II. Erg.-Werk, *Bd. 2*, S. 535; **1961**, III. Erg.-Werk, *Bd. 2*, S. 1634; **1976**, IV. Erg.-Werk, *Bd. 2*, S. 1892.

[2] G. D. Hartmann (Merck), US-A 4 021 438 [*Chem. Abstr.* **1977**, *87*, 53264s]; W. Liebenow, K. Mannhardt, H. Engler (Ludwig Heumann), DE-A 3 107 599 [*Chem. Abstr.* **1982**, *97*, 198204p].

[3] G. D. Hartmann, L. M. Weinstock, *Synthesis* **1976**, 681.

[4] R. Neidlein, *Angew. Chem.* **1964**, *76*, 440; *Angew. Chem. Int. Ed. Engl.* **1964**, *3*, 382.

[5] Structure analyses: **1**: Single crystals of **1** were obtained by zone melting in a 0.5 mm capillary. The data were collected at −120 °C. Monoclinic, *Pn* (no. 7), a = 614.9(2), b = 756.3(1), c = 786.4(3) pm, β = 98.99(4)°, $V = 3.612(2) \times 10^8$ pm^3, $Z = 4$, $\rho_{calcd} = 1.22$ $g\,cm^{-3}$, $R = 0.054$ for 672 reflexes with $F_0 > 4\sigma(F_0)$, $wR_{2obs}/wR_{2all} = 0.106/0.132$, $w = [\sigma^2(F_o^2) + (0.0P)^2 + 0.42P]^{-1}$ with $P = [\mathrm{Max}(F_o^2,0) + 2F_c^2]/3$, $GoF = 1.049$, $Mo_{K\alpha}$, λ = 71.069 pm, 1148 crystallographically independent reflections $4° \le 2\theta \le 50°$ (Friedel pairs not merged), anisotropic temperature factors for C and N. H atoms refined with common isotropic temperature factors on calculated positions with C–H = 99 pm. Starting coordinates with direct methods (SHELXS-86 [8]), full-matrix least-squares refinement on F^2 (SHELXL-93 [9]), 91 refined parameters, residual electron density (max./min. = 0.179/−0.161 $e\,Å^{-3}$). **4**: Monoclinic, *C2/c* (no. 15), a = 2481.4(7), b = 582.2(2), c = 2053.3(6) pm, β = 134.57 °, $V = 2.113 \times 10^9$ pm^3, $Z = 8$, $\rho_{calcd} = 1.623$ $g\,cm^{-3}$, $R = 0.037$ for 2279 reflections with $F_0 > 4\sigma(F_0)$, $R = 0.050$ for all data, $wR_2 = 0.100$ for all data, $w = [\sigma^2(F_o^2) + (0.0572P)^2 + 0.50P]^{-1}$ with $P = [\mathrm{Max}(F_o^2, 0) + 2F_c^2]/3$, $Mo_{K\alpha}$, λ = 71.069 pm, 2817 crystallographically independent reflections $4° \le 2\theta \le 58.1°$, anisotropic temperature factors for Cr, C, N and O. H atoms refined on calculated positions (C–H 97 pm) with one isotropic temperature factor ($U_H = 0.062$). Starting coordinates by direct methods (SHELXS-86 [8]), full-matrix least-squares refinement on F_o^2 (SHELXL-93 [9]), 145 refined parameters. Residual electron density (max./min. 0.40/−0.22 $e\,Å^{-3}$). Further details of the crystal structure analyses may be obtained from the Fachinformationszentrum Karlsruhe, D-76344 Eggenstein-Leopoldshafen, on quoting the depository number CSD-58732.

[6] Gaussian 92, Revision C: M. J. Frisch, G. W. Trucks, M. Head-Gordon, P. M. W. Gill, M. W. Wong, J. B. Foresman, B. G. Johnson, H. B. Schlegel, M. A. Robb, E. S. Replogle, R. Gomperts, J. L. Andres, K. Raghavachari, J. S. Binkley, C. Gonzalez, R. L. Martin, D. J. Fox, D. J. Defrees, J. Baker, J. J. P. Stewart, J. A. Pople, Gaussian Inc., Pittsburgh, PA, **1992**.

[7] C. K. Johnson, ORTEP, A FORTRAN Thermal Ellipsoid Plot Program for Crystal Structure Illustrations, Report ORNL-3794. Oak Ridge National Laboratories, Oak Ridge Tennessee, **1970**.

[8] G. M. Sheldrick, SHELXS-86, A Program for Crystal Structure Solution, *Acta Crystallogr. Sect. A* **1990**, *46*, 467.

[9] G. M. Sheldrick, SHELXL-93, A Program for Crystal Structure Determination, Göttingen, **1993**.

Unprecedented Mode of Bonding for Olefins on Bimetallic Complexes: An Agostic Interaction of a sp^2 C–H Bond with a Ruthenium Center in Addition to a π bond to a Rhenium Center

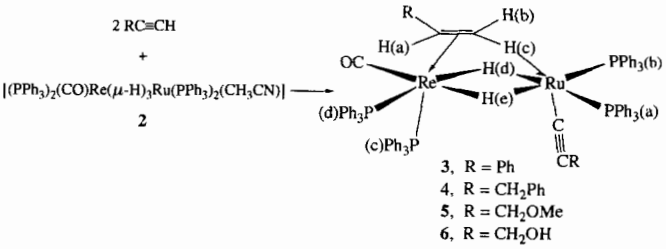
Zhongli He, Laurent Plasseraud, Isabel Moldes, Françoise Dahan, Denis Neibecker, Michel Etienne, and René Mathieu*

The study of the reactivity of bi- or polymetallic complexes toward unsaturated organic molecules has led to numerous examples of unusual modes of bonding and activation due to the proximity of the metal centers.[1] Here we report a new example of the synergy exerted by two different metal centers leading to an unprecedented mode of bonding for a monosubstituted alkene. In addition to a classical π bonding of the carbon–carbon double bond with one metal center, one of the sp^2 C–H bonds of the alkene experiences a static agostic interaction[2] with the second adjacent metal center.

This novel bonding situation was discovered during the course of the study of the reactivity of bimetallic polyhydride rhenium–ruthenium complexes[3] toward terminal alkynes. No reaction occurs between **1** and the terminal alkynes HC≡CR (R = Ph, CH_2Ph, CH_2OMe, CH_2OH, *t*Bu). Thus, we examined the reactivity of **2**, which was expected to be more reactive since it contains a labile nitrile ligand.[3b]

$[(PPh_3)_2(CO)HRe(\mu\text{-}H)_3RuH(PPh_3)_2]$ **1**

Except for the case of R = *t*Bu, **2** reacts at room temperature with an excess of each alkyne, leading to the formation of the complexes (**3** (R = Ph), **4** (R = CH_2Ph), **5** (R = CH_2OMe), and **6** (R = CH_2OH) in low to reasonable yields (Scheme 1).



Scheme 1.

The structure of these compounds was inferred by spectroscopic data (Table 1) and then confirmed by an X-ray study on a crystal of complex **5** (see Fig. 1).

Complex **3** can also be obtained in similar yield from the reaction of **1** and phenylacetylene at 50 °C in the presence of *tert*-butylethylene as a hydrogen acceptor. The lower thermal stability of the other complexes (**4**–**6**) prevents the extension of this method to the other alkynes used.

The IR spectra of the complexes (**3**–**6**) show characteristic absorptions for a σ-bound acetylide ligand,[4] (between 2103 and 2080 cm^{-1}), and for a terminal CO ligand (between 1830 and 1820 cm^{-1}); however the most informative data about their structure comes from a complete NMR analysis using homo- and heteronuclear decoupling experiments.

[*] Dr. R. Mathieu, Dr. Z. He, L. Plasseraud, Dr. I. Moldes, Dr. F. Dahan, Dr. D. Neibecker, Dr. M. Etienne,
Laboratoire de Chimie de Coordination du CNRS, UPR 8241, 205 Route de Narbonne, F-31077 Toulouse Cedex (France)
Telefax: Int. code + 61 55 30 03

Table 1. Selected IR and NMR spectroscopic data of the complexes **3**–**6**.

3: IR (CH_2Cl_2): $\tilde{\nu}$ = 2080 cm^{-1} (m) (C≡C), 1830 cm^{-1} (CO) (s); ^1H NMR (250 MHz, $CDCl_3$, TMS): δ = 4.59 (ddd, *J*(H(a), H(b)) = *J*(P(c), H(a)) = 9.8 Hz, *J*(H(a), H(c)) = 8.4 Hz; H(a)), 3.38 (broad d, *J*(H(a), H(b)) = 9.8 Hz; H(b)), −1.8 (broad d, *J*(H(a), H(c)) = 8.4 Hz; H(c)), −8.40 (ddd, *J*(H(d), P(a) or P(b)) = *J*(H(d), P(d)) = 32.5 Hz, *J*(H(d), P(c)) = 14 Hz; H(d)), −10.0 ((dd), *J*(H(e), P(b) or P(a)) = 17 Hz, *J*(H(e), P(a) or P(b)) = 65.9 Hz; H(e)); $^{31}P\{^1H\}$ NMR (101 MHz, $CDCl_3$, H_3PO_4 85%): δ = 53.9 (P(a) + P(b)), 33.5 (dd, *J*(P(c), P(d)) = 33.3 Hz, *J*(P(a) or P(b), P(c)) = 5.4 Hz), 29.3 (d, *J*(P(d), P(c)) = 33.0 Hz; P(d)); ^{13}C NMR (50 MHz, $CDCl_3$, TMS): δ = 201.4 (m) (CO), 149.2 (*C*≡CPh), 116.6 (C≡*C*Ph), 68.1 (d, *J*(C,H) = 153 Hz; CHPh), 39.8 (dd, *J*(C,H) = 112 Hz, 160 Hz; CH_2).

4: IR (CH_2Cl_2): $\tilde{\nu}$ = 2103 cm^{-1} (m) (C≡C), 1820 cm^{-1} (CO) (s); ^1H NMR (400 MHz, C_6D_6, TMS): δ = 3.23 (H(a) + C≡CC*H*$_2$R), 2.67 (broad d, *J*(H(a), H(b)) = 9 Hz; H(b)), −2.74 (broad d, *J*(H(a), H(c)) = 6 Hz; H(c)), −8.28 (ddd, *J*(H(d), P(d)) = 30 Hz, *J*(H(d), P(c)) = 15 Hz, *J*(H(d), P(a)) = 41 Hz; H(d)), −10.38 (dd, *J*(H(e), P(a)) = 13 Hz, *J*(H(e), P(b)) = 61 Hz; H(e)); $^{31}P\{^1H\}$ NMR (162 MHz, C_6D_6, H_3PO_4 85%): δ = 50.5 (dd, *J*(P(a), P(b)) = 22 Hz, *J*(P(a), P(c)) = 8 Hz; P(a)), 48 (d, *J*(P(a), P(b)) = 22 Hz; P(b)), 28.7 (dd, *J*(P(c), P(d)) = 33 Hz, *J*(P(a), P(c)) = 8 Hz; P(c)), 25.4 (d, *J*(P(d), P(c)) = 33 Hz; P(d)); ^{13}C-NMR (50 MHz, C_6D_6, TMS): δ = 203.4 (CO), 148.6 (*C*≡CR), 111.7 (C≡*C*R), 74.1 (d, *J*(C,H) = 136 Hz; CHR), 39 (dd, *J*(C,H) = 113 Hz, 164 Hz; CH_2).

5: IR (CH_2Cl_2): $\tilde{\nu}$ = 2095 cm^{-1} (m) (C≡C), 1820 cm^{-1} (CO) (s); ^1H NMR (400 MHz, C_6D_6, TMS): δ = 3.15 (dd, *J*(H(a), H(b)) = 8 Hz, *J*(H(a), H(c)) = 5.6 Hz; H(a)), 2.57 (broad d, *J*(H(a), H(b)) = 8 Hz; H(b)), −2.35 (broad d, *J*(H(a), H(c)) = 5.6 Hz; H(c)), −8.48 (dddd, *J*(H(d), P(d)) = 30 Hz, *J*(H(d), P(c)) = 14 Hz, *J*(H(d), P(b)) = 7 Hz, *J*(H(d), P(a)) = 39 Hz; H(d)), −10.46 (dd, *J*(H(e), P(a)) = 13 Hz, *J*(H(e), P(b)) = 60 Hz; H(e)); $^{31}P\{^1H\}$ NMR (162 MHz, C_6D_6, H_3PO_4 85%): δ = 50.5 (dd, *J*(P(a), P(b)) = 23 Hz, *J*(P(a), P(c)) = 8 Hz; P(a)), 48.6 (d, *J*(P(a), P(b)) = 23 Hz; P(b)), 28.8 (dd, *J*(P(c), P(d)) = 35 Hz, *J*(P(a), P(c)) = 8 Hz; P(c)), 25.4 (d, *J*(P(d), P(c)) = 35 Hz; P(d)); ^{13}C NMR (50 MHz, C_6D_6, TMS): δ = 201.9 (CO), 138.6 (*C*≡CR), 112 (C≡*C*R), 66.6 (d, *J*(C,H) = 153 Hz, CHR), 39.2 (dd, *J*(C,H) = 108 Hz, 166 Hz; CH_2).

6 [a]: IR (CH_2Cl_2): $\tilde{\nu}$ = 2097 cm^{-1} (m) (C≡C), 1827 cm^{-1} (CO) (s); ^1H NMR (200 MHz, C_6D_6, TMS): δ = 3.00 (m; H(a)), 2.40 (m; H(b)), −2.47 (m; H(c)), −8.80 (m; H(d)), −10.50 (bd, *J* = 61 Hz; H(e)); $^{31}P\{^1H\}$ NMR (81 MHz, C_6D_6, H_3PO_4 85%): δ = 50.5 (dd, *J*(P(a), P(b)) = 22 Hz; *J*(P(a), P(c)) = 8 Hz; P(a)), 49.9 (d, *J*(P(a), P(b)) = 22 Hz; P(b)), 27.9 (dd, *J*(P(c), P(d)) = 35 Hz, *J*(P(a), P(c)) = 8 Hz; P(c)), 24.5 (d, *J*(P(d), P(c)) = 35 Hz; P(d)); ^{13}C NMR (50 MHz, C_6D_6, TMS): δ = 202.4 (CO), 140.4 (*C*≡CR), 114.4 (C≡*C*R), 54.6 (d, *J*(C,H) = 160 Hz; CHR), 37.2 (dd, *J*(C,H) = 107 Hz, 166 Hz; CH_2).

[a] Heteronuclear decoupling experiments have not been performed on this complex.

In the ^1H NMR spectra we observe, apart from the R and Ph resonances, five multiplets, each of which is for a single hydrogen, two at low field (H(a) and H(b)) and three (H(c), H(d) and H(e)) upfield from the TMS resonance (see Scheme 1).

The ^{13}C NMR spectra exhibit among other signals, one doublet at $\delta \approx 70$ (^1J(C–H) = 153–160 Hz) and a doublet of doublets at $\delta \approx 39$ (^1J(C–H) = 107–113 Hz and 160–166 Hz), attributable to the coordinated carbon atoms of an alkene. Moreover, $^{13}C\{^1H\}$ selective decoupling experiments show that the smaller coupling constant of the high-field signal is associated with H(c). These two observations, namely a reduced ^1J(C–H) and a high-field resonance for the corresponding hydrogen atom, are fully consistent with an agostic interaction of the sp^2 C–H(c) bond with one metallic center.[2, 5] Furthermore, $^{13}C\{^{31}P\}$ selective decoupling experiments in the case of **3** indicate that the coordinated carbon atoms of the styrene molecule exhibit a small, unresolved coupling with the phosphorus atoms attached to rhenium only. A similar narrowing of the H(c) resonance in the ^1H NMR spectrum is evident when the ruthenium-bound phosphanes are irradiated in selective ^{31}P decoupling experiments. These spectroscopic data are consistent with π coordination of the alkene on the rhenium center and a C–H agostic interaction with the adjacent ruthenium atom.

Definitive proof for the proposed structure comes from an X-ray study[6] on crystals of the complex **5** (R = CH_2OMe; Fig. 1). As expected, it consists of a bimetallic complex; the two

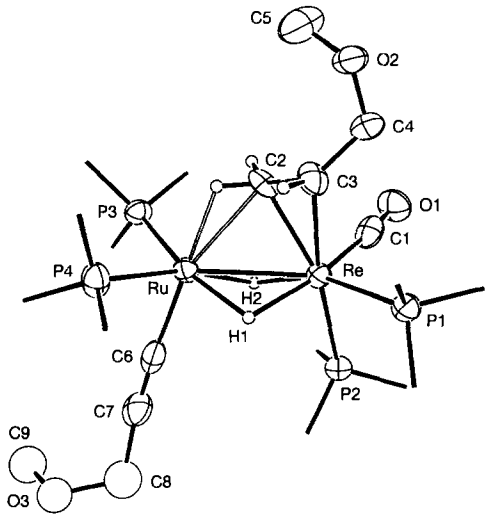


Fig. 1. Crystal structure of **5** (phenyl groups omitted). Selected distances [Å] and angles [°]: Re-Ru 2.7084(8), Re-C2 2.168(8), Re-C3 2.261(9), Ru-C2 2.357(7), Ru-H1(C2) 1.86(9). C2-C3 1.399(12), Ru-C6 1.985(11), C6-C7 1.179(15); P3-Ru-H1(C2) 84(2), P4-Ru-H1(C2) 96(2), C6-Ru-H1(C2) 177(2), Re-Ru-H1(C2) 72(2), Re-Ru-C2 50.1(2), P1-Re-C2 117.4(2), P1-Re-C3 81.1(2), C1-Re-C2 88.5(4), C1-Re-C3 90.0(4), P2-Re-C2 148.4(2), P2-Re-C3 173.1(2), Ru-Re-C2 56.4(2), Ru-Re-C3 84.3(2).

metal centers are bridged by two hydrido ligands, and the alkene is π bound to the rhenium atom. One hydrogen of the alkene methylene group is at bonding distance from the ruthenium atom. This hydrogen atom is *trans* to the acetylide ligand. In this way a potentially free apical coordination site at ruthenium is filled. The Ru–C2 distance is also consistent with a ruthenium–carbon interaction and compares well with the distance found (2.38(2) Å) for the carbon of the methylene group in agostic interaction in $[Ru(\eta^3\text{-butenyl})(PMe_2Ph)_3][PF_6]$.[7] The C–C double bond of the alkene is nearly parallel to the H2-Re-P1 axis, and the Re–C2 bond is significantly shorter than the Re–C3 bond. This situation is strongly reminiscent of the mode of bonding involving bridging, η^1,η^2-bound alkenyl groups.[8]

Hence, this bonding situation may be viewed as an arrested migration of a hydrido ligand from one metal center (ruthenium here) onto a bridging η^1,η^2-bound alkenyl group. This actually represents the last step of the hydrogenation of an alkyne leading to alkene formation at a heterobimetallic center. Considering the agostic interaction, the complex is formally a 32-electron bimetallic complex, that is two electrons short of saturation. This coordinative unsaturation certainly explains the stabilization of the unusual mode of bonding of the alkene in the complexes **3**–**6**.

To gain some insight into the mechanism of this reaction and to determine the origin of the hydrogen atoms transferred to the alkynes we have treated **2** with PhC≡CD. In the final product $[D_2]$-**3**, the H(b) and H(d) resonances represent less than 10% of the intensity of H(a) and H(c) resonances, which demonstrates that styrene formation occurs by hydride transfer from complex **2** and that one of the bridging hydrides in **3** originates from the oxidative addition of a second molecule in phenylacetylene, leading to the formation of the acetylide ligand.

Experimental Procedure

All manipulations were performed under argon. Complexes **1** and **2** were prepared according to published procedures [3]. General procedure: To **2** (0.2 g, 0.14 mmol) in CH_2Cl_2 (10 mL) was added 0.8 mmol of the alkyne and the solution was stirred at room temperature for 3 h. The solution was then evaporated to dryness under reduced pressure and the residue dissolved in CH_2Cl_2 (4 mL). Addition of methanol (4 mL) and cooling at −20 °C allowed the isolation of **3** (65%), **4** (26%), **5** (36%), and **6** (19%). Alternative procedure for **3**: To **1** (0.2 g) dissolved in THF (20 mL) was added phenylacetylene (0.1 mL) and *tert*-butylethylene (0.3 mL) and the mixture was heated at 50 °C for 5 h. The same purification procedure as above allowed the isolation of **3** in 75% yield.

Received: October 25, 1994 [Z 7424 IE]
German version: *Angew. Chem.* **1995**, *107*, 1005

Keywords: agostic interactions · C–H activation · binuclear complexes · rhenium compounds · ruthenium compounds

[1] See for instance: E. L. Muetterties, T. N. Rhodin, E. Band, C. F. Brucker, W. R. Pretzer, *Chem. Rev.* **1979**, *79*, 91; E. Sappa, A. Tiripicchio, P. Braunstein, *Coord. Chem. Rev.* **1985**, *65*, 219.

[2] M. Brookhart, M. L. H. Green, L. L. Wong, *Prog. Inorg. Chem.* **1988**, *36*, 1.

[3] a) M. Cazanoue, Z. He, D. Neibecker, R. Mathieu, *J. Chem. Soc. Chem. Commun.* **1991**, 307; b) Z. He, D. Neibecker, N. Lugan, R. Mathieu, *Organometallics* **1992**, *11*, 817; c) Z. He, S. Nefedov, N. Lugan, D. Neibecker, R. Mathieu, *ibid.* **1993**, *12*, 3837.

[4] K. W. Lee, W. T. Pennington, A. W. Cordes, T. L. Brown, *J. Am. Chem. Soc.* **1985**, *107*, 631.

[5] A similar value, 110 Hz, has been found for a sp^2 CH group in agostic interaction with a circonium center, see: F. R. Lemke, D. J. Szalda, R. M. Bullock, *J. Am. Chem. Soc.* **1991**, *113*, 8466.

[6] X-ray structure analysis of **5**, CH_2Cl_2: $C_{82}H_{77}O_3Cl_2P_4RuRe$; crystal size $0.40 \times 0.20 \times 0.10$ mm; monoclinic; space group $C2/c$; $Z = 8$; $a = 25.119(2)$, $b = 14.637(2)$, $c = 38.971(3)$ Å, $\beta = 94.40(1)°$; $V = 14286(3)$ Å^3; $\rho_{calcd} = 1.481$ g cm^{-3}; $2\theta_{max} = 44°$; $Mo_{K\alpha}$: $\lambda = 0.71073$ Å; graphite monochromator; ω-2θ scan; $T = 293$ K; 8978 measured reflections, 8755 independent reflections, 5147 observed ($F_o^2 > 3\sigma(F_o^2)$); Lp correction, Gaussian absorption correction $\mu = 2.04$ mm^{-1} ($T_{min} = 0.637$, $T_{max} = 0.800$); direct methods (SHELXS-86); full-matrix least-squares refinement (SHELX76), non H atoms anisotropic, except those of phenyl rings refined as isotropic rigid groups (C–C = 1.395 Å), those of the CH_2OCH_3 chain (oxygen O3 and methyl C9 are disordered), and the two disordered C atoms of the dichloromethane solvate, H atoms bonded to disordered atoms were not calculated, other H atoms were found on a difference Fourier map, those bound to C4 and C5 and to the phenyl rings where introduced in calculations in constrained geometry (C–H = 0.97 Å), those bound to C2 and C3 were refined, the two bridging hydrides were calculated by molecular mechanics methods (Orpen) and allowed to vary, variable parameters = 341, $R(F_o) = 0.037$, $R_w = 0.048$, $w = [\sigma^2(F_o) + 0.0011\,F_o^2]$, $S = 1.097$. Further details of the crystal structure investigation are available on request from the Director of the Cambridge Crystallographic Data Centre, 12 Union Road, GB-Cambridge CB2 1EZ (UK), on quoting the full journal citation.

[7] T. V. Ashworth, A. A. Chalmer, E. Meintjies, H. Oosthuizen, E. Singleton, *J. Organomet. Chem.* **1985**, *286*, 237.

[8] See for instance the case of a Re_2 complex: K. W. Lee, W. T. Pennington, A. W. Cordes, T. L. Brown, *J. Am. Chem. Soc.* **1985**, *107*, 631.

A Chiral Cyanohydrin Phosphate for Carbonyl Umpolung—Stereoselective Synthesis of Tertiary Cyanohydrins**

Thomas Schrader*

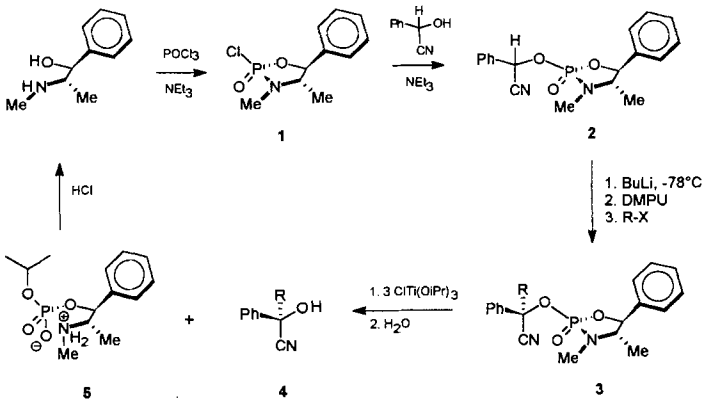
Cyanohydrins have been used for many years as umpoled carbonyl compounds.[1a] Their importance in organic synthesis as nucleophilic acyl anion equivalents increased significantly in the 1970s when Stork et al. introduced *O*-alkoxyalkylcyanohydrins[1b] and shortly afterwards Hünig et al. reported on *O*-silylcyanohydrins.[1c] These derivatives can be employed in the transformation of aldehydes into ketones,[2a] α-hydroxyketones,[2b] γ-oxoesters,[2c] and 1,4-diketones.[2d] Surprisingly, no enantio- and diastereoselective syntheses have been reported making use of cyanohydrins as umpoled carbonyl compounds.

[*] Dr. T. Schrader
Institut für Organische Chemie und Makromolekulare Chemie der Universität
Universitätsstrasse 1, D-40225 Düsseldorf (Germany)
Telefax: Int. code + (211) 311-4788

[**] I thank Prof. Mootz, Düsseldorf, for the X-ray structure analysis.

In the related field of aminonitrile chemistry efficient asymmetric procedures are also very rare; the Michael addition of chiral aminonitriles developed by Enders et al. represents a milestone in this area.[3]

During the past few years several enantioselective syntheses have been reported that focus on the use of cyclic phosphonates or phosphonamides with a stereogenic phosphorus atom.[4] Although high inductions are achieved, the stable P–C bond restricts the final products of these reactions to almost exclusively phosphonic acid derivatives.[5] This paper describes the new chiral cyanohydrin phosphate, **2**, in which the OH group of the benzaldehyde cyanohydrin is linked to a chiral phosphate. The latter can be removed hydrolytically after metalation and diastereoselective alkylation of **2** (Scheme 1).



Scheme 1.

Precursor **1** is easily obtained from (+)-pseudoephedrine and phosphoryl chloride. Exocyclic substitution of chloride by the free racemic cyanohydrin proceeds smoothly with complete retention of configuration at phosphorus.[6] Thus, **2** can be prepared from (+)-pseudoephedrine in a one-pot procedure with 45% overall yield (Scheme 1). Deprotonation with butyllithium followed by addition of an electrophile affords the alkylated products **3** with high diastereomeric excesses (*de* = 82–94%) (Table 1).

Table 1. Diastereoselectively alkylated cyanohydrin phosphates (*R*)-**3** and resulting tertiary cyanohydrins (*R*)-**4**.

3	R	Yield [%]	*de* [%]	4	R	Yield [%]	*ee*[a] [%]
a	allyl	47	90	**a**	allyl	79	
b	methyl	69	83	**b**	methyl	66	>96
c	*n*-propyl	58	82	**c**	*n*-propyl	92	
d	propargyl	65	82	**d**	propargyl	72	
e	benzyl	58	82	**e**	benzyl	85	>96
f	3,3-dimethylallyl	40	94				
g	cinnamyl	45	90				

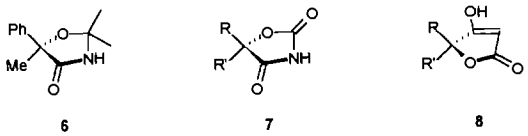
[a] Determined by cleavage of recrystallized, enantiomerically pure cyanohydrin phosphates **3**; in the case of **4b** and **4e** determined by NMR shift experiments.

The relative configuration of the cyanohydrin phosphates **3** was determined by X-ray structure analysis[7] of the benzylated product **3e**. (1*S*,2*S*)-(+)-Pseudoephedrine yields cyanohydrin phosphate **3e** with *R* configuration at the α-C atom, confirming that the metalated cyanohydrin phosphate **2** is preferentially attacked on its *Si* face. We developed a mild Lewis acid assisted method for selective removal of the auxiliary. Reaction of **3** with titanium chloride triisopropoxide and subsequent hydrolysis furnishes pure free cyanohydrin in the organic phase. (+)-Pseudoephedrine may be recovered in 68% yield from the aqueous phase after hydrolysis of intermediate **5**.

Cleavage of the phosphate proceeds with retention at the cyanohydrin, such that tertiary (*R*) cyanohydrins **4** are formed. This could be demonstrated with the methylated product **3b**, which was hydrolyzed to give atrolactamide and then cyclized with acetone to yield oxazolidinone **6**. The optical rotation of **6** after recrystallization was in agreement with the literature value for the (*R*) compound.[8]

The enantiomeric purity of the free tertiary cyanohydrins **4** was also determined by NMR spectroscopic analysis of their complexes with TADDOL (molar ratio 1:1 for TADDOL: cyanohydrin; TADDOL = (4*R*,5*R*)-α,α,α′,α′-tetraphenyl-1,3-dioxolane-4,5-dimethanol).[9] Hydrolysis of diastereomerically pure **3b** and **3e** leads in both cases to optically pure cyanohydrins with a signal ratio of >98:2.

The final products are key intermediates in the synthesis of pharmaceuticals such as 2,4-oxazolidinediones **7** (anticonvulsants, drugs for treatment of *diabetes mellitus*)[10a] and tetronic acids **8** (antibiotics, antitumor agents).[10b]



While numerous asymmetric syntheses[11] and enzymatic methods[11] have been developed for secondary cyanohydrins, a general approach to optically pure tertiary cyanohydrins has not been reported to date.[12] Preliminary experiments with aliphatic cyanohydrins and reactions of the new chiral acyl-anion equivalent **2** with other electrophiles such as Michael acceptors and acid chlorides show promising results.

Experimental Procedure

A solution of cyanohydrin phosphate **2** (5 g, 14.6 mmol) in 100 mL of dry THF was cooled to −78 °C, *n*-butyllithium (1.6 N solution in hexane, 11 mL, 17 mmol, 1.2 equiv) was added, and the reaction mixture was stirred for 20 min. *N*,*N*′-Dimethyl-*N*,*N*′-propylene urea (DMPU, 0.9 mL, 15 mmol, 1 equiv) [13] was added, and stirring was continued for another 20 min at −78 °C. The desired electrophile (1.3 equiv) was added and the resulting solution stirred for 3–6 h at −78 °C. After quenching with 50 mL of aqueous ammonium chloride, the organic phase was removed, the aqueous phase extracted with 50 mL of THF, and the combined organic phases dried over magnesium sulfate. The solvent was evaporated and the crude product purified either by recrystallization from toluene/acetone (10:1) or by chromatography over silica gel (0.04–0.063 mm). A solution of 10 mmol of the cyanohydrin phosphate **3** in 100 mL of dry THF was treated with titanium chloride triisopropoxide (1.0 M solution in hexane, 30 mmol, 3 equiv). The reaction mixture was stirred for 3 h at room temperature and subsequently quenched with 100 mL of water. The resulting two-phase system was stirred vigorously for another 3 h at room temperature. After the organic phase was removed and dried, the free cyanohydrin was obtained by simple concentration in vacuo and filtration through silica gel (toluene/acetone 10:1) [14]. From the aqueous phase the titanium salts were precipitated with NaOH, and the filtrate was hydrolyzed with 5 N HCl for 8 h at 80 °C. Neutralization and extraction with dichloromethane yielded free (+)-pseudoephedrine, which was extracted with the fourfold amount of water for 3 h to remove small amounts of (−)-ephedrine (68%, starting from **3**).

Received: October 31, 1994 [Z 7442 IE]
German version: *Angew. Chem.* **1995**, *107*, 1001

Keywords: asymmetric syntheses · cyanohydrins · drugs · umpolung

[1] a) D. Seebach, *Angew. Chem.* **1979**, *91*, 259; *Angew. Chem. Int. Ed. Engl.* **1979**, *18*, 239; J. D. Albright, *Tetrahedron* **1983**, *39*, 3207; b) G. Stork, L. Maldonado, *J. Am. Chem. Soc.* **1971**, *93*, 5286; c) K. Deuchert, U. Hertenstein, S. Hünig, *Synthesis* **1973**, 777.
[2] a) K. Deuchert, V. Hertenstein, S. Hünig, *Chem. Ber.* **1979**, *112*, 2045; b) S. Hünig, G. Wehner, *Synthesis* **1975**, 391; c) J. J. Gajewski, N. D. Conrad, *J. Am. Chem. Soc.* **1979**, *101*, 6693; d) G. Stork, L. Maldonado, *ibid.* **1974**, *96*, 5272.
[3] D. Enders, P. Gerdes, H. Kipphardt, *Angew. Chem.* **1990**, *102*, 226; *Angew. Chem. Int. Ed. Engl.* **1990**, *29*, 179.
[4] a) S. Denmark, J. E. Marlin, *J. Org. Chem.* **1987**, *52*, 5742; b) P. A. Bartlett, K. L. McLaren, *Phosphorus Sulfur* **1987**, *33*, 1; c) D. H. Hua, R. Chan-Yu-King, J. A. McKie, L. Myer, *J. Am. Chem. Soc.* **1987**, *109*, 5026; d) M. Sting, W. Steglich, *Synthesis* **1990**, 132; e) S. Hanessian, Y. L. Bennani, D. Delorme, *Tetrahedron Lett.* **1990**, *31*, 6461, 6465.
[5] Exception: G. Boche, W. Schrott, *Tetrahedron Lett.* **1982**, *23*, 5403.
[6] For reaction of **1** with simple alcohols see: D. B. Cooper, C. R. Hall, J. M. Morrison, T. D. Inch, *J. Chem. Soc. Perkin Trans. 1* **1977**, 1969.
[7] D. Mootz, H. Rütter, W. Poll, T. Schrader. Further details of the X-ray structural analysis may be obtained from the Fachinformationszentrum Karlsruhe, D-76344 Eggenstein-Leopoldshafen (Germany), by quoting the depository number CSD-401365.
[8] K. Freudenberg, J. Todd, R. Seidler, *Justus Liebigs Ann. Chem.* **1933**, *501*, 199.
[9] D. Seebach, C. von dem Bussche-Hünnefeld, A. K. Beck, U. Lengweiler, *Helv. Chim. Acta* **1992**, *75*, 438.
[10] a) A. C. Veronese, R. Callegari, A. Bertazzo, *Heterocycles* **1991**, *32*, 2205; b) M. V. Garcia, J. C. Menendez, M. Villacampa, M. M. Söllhuber, *Synthesis* **1991**, 697.
[11] F. Effenberger, *Angew. Chem.* **1994**, *106*, 1609; *Angew. Chem. Int. Ed. Engl.* **1994**, *33*, 1555.
[12] a) F. Effenberger, B. Hörsch, F. Weingart, T. Ziegler, S. Kühner, *Tetrahedron Lett.* **1991**, 2605, and references therein; D. M. Dalton, C. M. Garner, J. M. Fernandez, J. A. Gladysz, *J. Org. Chem.* **1991**, *56*, 6823. b) For the synthesis of α-branched α-hydroxycarboxylic acid derivatives see: D. Seebach, R. Naef, G. Calderari, *Tetrahedron* **1984**, *40*, 1313; T. Sugai, H. Kakeya, H. Ohta, *J. Org. Chem.* **1990**, *55*, 4643.
[13] T. Mukhopadhyay, D. Seebach, *Helv. Chim. Acta* **1982**, *65*, 385; D. Seebach, R. Hennig, T. Mukhopadhyay, *Chem. Ber.* **1982**, *115*, 1705.
[14] Often cleavage of a small amount (ca. 5%) of the labile tertiary cyanohydrin to the ketone is observed, but racemization of the cyanohydrin never occurs.

Synthesis and Structure of Organometallic Compounds with $(Al_2Si)_2$ and Al_3Sb_2 Frameworks**

Stephan Schulz, Torsten Schoop, Herbert W. Roesky,* Ludger Häming, Alexander Steiner, and Regine Herbst-Irmer

Dedicated to Professor Dr. Peter Paetzold on the occasion of his 60th birthday

Little is known about the reactivity of organometallic compounds containing Group 13 elements in the oxidation state I. In the case of indium and thallium, this can be explained by the stability of the compounds containing monovalent metal atoms. As far as aluminum and gallium are concerned, monovalent compounds recently became preparatively accessible.[1-3] Since finding a straightforward synthetic route to $[(Cp^*Al)_4]$ ($Cp^* = C_5Me_5$), we have been involved in the thorough investigation of the reactivity of this compound.[3] As demonstrated by a few examples,[3, 4, 5] aluminum(I) compounds mostly react to give compounds with the metal in the oxidation state III. The next question is: how does $[(Cp^*Al)_4]$ behave towards compounds that contain thermodynamically very stable Si–F bonds (Si–F bond energy = 543 kJ mol^{-1} (exp.))?[6] In the course of such reactions, both the tendency of aluminum(I) to oxidize to aluminum(III) and the formation of the thermodynamically very stable Al–F bond (Al–F bond energy = 659–672 kJ mol^{-1} (exp.))[6] are decisive. We chose Ph_2SiF_2 as the reaction partner.

$[(Cp^*Al)_4]$ was treated with an excess of Ph_2SiF_2 under reflux for three days to give almost colorless solution. The colorless complex **1** [Eq. (a)] was obtained as a solid on cooling the solution and redissolved on warming.

$$[(Cp^*Al)_4] + 2\,Ph_2SiF_2 \longrightarrow \underset{\mathbf{1}}{[\{(Cp^*AlF)_2SiPh_2\}_2]} \qquad (a)$$

The ^1H and ^{13}C NMR spectra confirm conclusively that the Cp* ligands were not eliminated in this reaction ($\delta = 1.83$, and $\delta = 11.4$ and 115.5, respectively). Cp* was, however, eliminated in the reaction of $[(Cp^*Al)_4]$ with $[(MeC_5H_4)_2TiF_2]$, which results in the formation of $[\{(MeC_5H_4)_2TiF_2\}_3Al]$.[7] The mass spectrum of **1** shows the heaviest ion to be the fragment $[M-Cp^*]$ (m/z 953); the signal has a relative intensity of 10% and the expected isotopic pattern.

Single crystals suitable for X-ray structure analysis (Fig. 1) were obtained by slowly cooling a solution of **1** in toluene over a period of 20 h. Crystals with the space group $P\bar{4}2_1c$ were formed.[8] The silicon atoms lie on the crystallographic $\bar{4}$ axis; the molecule thus belongs to the point group S_4. Compound **1** contains an eight-membered Al_4F_4 ring. This means that fluorine atoms were inserted into four of the original six Al–Al bonds of the Al_4 tetrahedron. Two aluminum atoms are each connected by a Ph_2Si bridge. This indicates that both tetracoordinate aluminum and silicon atoms are present in **1**. This type of bridging silicon atom between two aluminum atoms has not previously been observed; there are only a few examples of compounds containing Al–Si bonds in which the silicon atom is part of a terminal $SiMe_3$ group.[9] The average Al–F bond length is 184.6 pm and lies within the range observed for the few structurally characterized covalent aluminum fluorides[10-12]

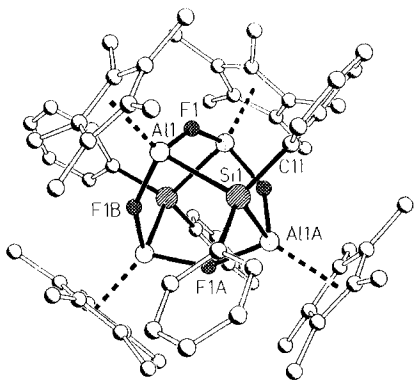


Fig. 1. Crystal structure of **1**. Selected distances [pm] and angles [°]: Al1-F1 184.3(1), Al1-F1B 184.8(1), Al1-C1 218.1(2), Al1-C2 217.2(2), Al1-C3 247.8(2), Al1-C4 267.2(3), Al1-C5 249.0(2), Al1-Cp*(center) 208.6(2), Al1-Si1 245.1(1); Al1-F1-Al1C 149.0(1), F1-Al1-F1B 88.3(1), F1-Al1-Si1 99.9(1), F1B-Al1-Si1 99.9(1), Al1-Si1-Al1A 99.7(1), C11-Si1-C11A 110.5(1), Al1-Si1-C11 110.7(1), Al1A-Si1-C11 112.5(1).

[*] Prof. Dr. H. W. Roesky, Dr. S. Schulz, Dipl.-Chem. T. Schoop, Dipl.-Chem. L. Häming, Dr. A. Steiner, Dr. R. Herbst-Irmer
Institut für Anorganische Chemie der Universität
Tammannstrasse 4, D-37077 Göttingen (Germany)
Telefax: Int. code + (551) 39-3373

[**] This work was supported by the Fonds der Chemischen Industrie, the Bundesministerium für Forschung und Technologie, the Volkswagen-Stiftung, and the Deutsche Forschungsgemeinschaft. T. S. thanks the Fonds der Chemischen Industrie for a doctoral grant.

(190 pm). The good agreement of the Al–F bond length and the Al–F–Al angle (149°) of **1** with the corresponding values in tetrameric Me_2AlF (181.0 pm and 146°), which also contains an eight-membered Al_4F_4 ring,[13] is very striking. This structural type is obviously a stable form of organometallic aluminum fluorides. The Al–Si bond lengths (245.1 pm) lie in the range of those reported in the literature.[9]

The [Cp*Al] monomer can be regarded as a carbene analogue. This simplifies our understanding of the formation of **1**, in which the aluminum atom of the [Cp*Al] is inserted in the Si–F bond. We then asked ourselves whether coupling reactions with other carbene analogues are possible and whether novel aluminum–element compounds can be built up from these. We chose $(t\mathrm{BuSb})_4$ as the reaction partner.[14]

The reaction of $[(Cp^*Al)_4]$ with $(t\mathrm{BuSb})_4$ was carried out in toluene in a molar ratio of 1:1 (60 °C). The solvent was slowly removed under vacuum, and from the orange-brown solution crystals of the composition $[(Cp^*Al)_3Sb_2]$ (**2**) [Eq. (b)] were

$$[(Cp^*Al)_4] + (t\mathrm{BuSb})_4 \longrightarrow Cp^*Al\begin{array}{c}Sb\\ \diagdown\\ Cp^*Al\\ \diagup\\ Sb\end{array}AlCp^* + \ldots \qquad (b)$$

2

formed as orange-brown hexagonal needles. The reaction did not proceed stoichiometrically with respect to **2** and $t\mathrm{Bu_3Sb}$; elemental antimony and other decomposition products were formed as well.[15] $(t\mathrm{BuSb})_4$ decomposes by eliminating *t*Bu groups. This reaction has been observed during the preparation of this compound as well as on warming $(t\mathrm{BuSb})_5$.[16]

The ^{1}H and ^{13}C NMR spectra of **2** show only signals of the Cp* ligand. The heaviest ion in the mass spectrum is the molecular ion with the correct isotopic pattern and 20% relative intensity. In addition, fragmentation also occurred. The elemental analysis confirms the composition of **2**. An X-ray diffraction experiment yields a model for **2** in which positions of the heavy atoms are consistent with the atomic arrangement given in Equation (b).[17]

The reaction of $[(Cp^*Al)_4]$ with elemental phosphorus leads to the formation of $[P_4(Cp^*Al)_6]$.[4] In the formation of **2**, $(t\mathrm{BuSb})_4$ functions as a source of antimony. No reaction was observed between $[(Cp^*Al)_4]$ and elemental antimony.

Experimental Procedure

1: A solution of $[(Cp^*Al)_4]$ (0.16 g, 0.25 mmol) and Ph_2SiF_2 (0.66 g, 3 mmol) in toluene (60 mL) was heated under reflux for three days and then allowed to cool slowly to room temperature. Colorless triangular crystals of **1** (0.21 g, 0.22 mmol, 88%) were obtained. M.p. 292 °C; ^{1}H NMR (400 MHz, C_6D_6, 25 °C, TMS): $\delta = 1.83$ (s, C_5Me_5, 60 H), 7.02–7.95 (m, C_6H_5, 20 H); ^{13}C NMR (100 MHz, C_6D_6, 25 °C, TMS): $\delta = 11.4$ (s, $C_5\mathit{Me}_5$), 115.5 (s, C_5Me_5), 131.4 (s, *ortho*-arene-C), 132.1 (s, *para*-arene-C), 134.7 (s, *meta*-arene-C), 136.3 (s, Si-C); IR (CsI): $\tilde{\nu}$[cm^{-1}] = 1261 s, 1152 s, 1094 vs, 1028 s, 998 s, 799 vs, 729 vs, 700 vs, 636 s, 599 s, 465 vs, 370 vs, 310 vs, 273 s; MS (EI, *m/z* (%)): 953 (10) [$M^+ - Cp^*$], 525 (100) [$M^+/2 - F$], 181 (15) [Cp*AlF], 162 (80) [Cp*Al]. Correct elemental analysis.

2: $[(Cp^*Al)_4]$ (0.16 g, 0.25 mmol) was dissolved in toluene (40 mL). A solution of $(t\mathrm{BuSb})_4$ (0.18 g, 0.25 mmol) in toluene (20 mL) was added dropwise. The mixture was heated to 60 °C for 6 h, which caused the solution to turn orange-brown. The solvent was then slowly removed under reduced pressure. Orange-brown crystals of **2** (0.16 g, 0.22 mmol, 65% with respect to $[(Cp^*Al)_4]$) were obtained. M.p. 199 °C (decomp.); ^{1}H NMR (250 MHz, C_6D_6, 25 °C, TMS): $\delta = 2.07$ (s, C_5Me_5); ^{13}C NMR (63 MHz, C_6D_6, 25 °C, TMS): $\delta = 11.9$ (s, $C_5\mathit{Me}_5$), 116.1 (s, C_5Me_5); IR (CsI): $\tilde{\nu}$[cm^{-1}] = 1261 s, 1146 s, 1098 vs, 1022 vs, 800 vs, 751 w, 726 w, 697 w, 588 w, 447 vs, 405 s; MS (EI, *m/z* (%)): 730 (20) [M^+], 568 (20) [$M^+ - Cp^*Al$], 406 (25) [$M^+ - 2Cp^*Al$], 162 (100) [Cp*Al]. Correct elemental analysis.

Received: December 2, 1994 [Z 7519 IE]
German version: *Angew. Chem.* **1995**, *107*, 1015

Keywords: aluminum compounds · antimony compounds · main group elements · silicon compounds

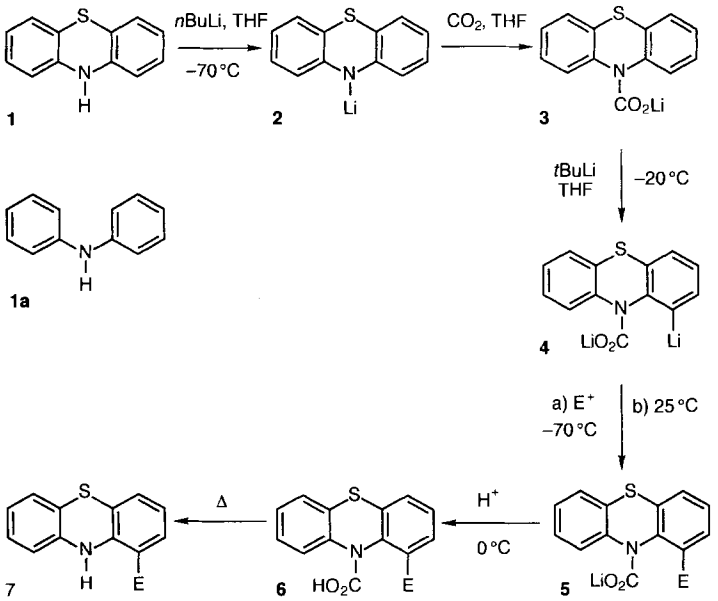
[1] C. Dohmeier, C. Robl, M. Tacke, H. Schnöckel, *Angew. Chem.* **1991**, *103*, 594; *Angew. Chem. Int. Ed. Engl.* **1991**, *30*, 564.
[2] D. Loos, H. Schnöckel, J. Gauss, U. Schneider, *Angew. Chem.* **1992**, *104*, 1376; *Angew. Chem. Int. Ed. Engl.* **1992**, *31*, 1362; W. Uhl, W. Hiller, M. Layh, W. Schwarz, *ibid.* **1992**, *104*, 1378 and **1992**, *31*, 1364.
[3] S. Schulz, H. W. Roesky, H.-J. Koch, G. M. Sheldrick, D. Stalke, A. Kuhn, *Angew. Chem.* **1993**, *105*, 1828; *Angew. Chem. Int. Ed. Engl.* **1993**, *32*, 1729.
[4] C. Dohmeier, H. Schnöckel, C. Robl, U. Schneider, R. Ahlrichs, *Angew. Chem.* **1994**, *106*, 225; *Angew. Chem. Int. Ed. Engl.* **1994**, *33*, 199.
[5] S. Schulz, H. W. Roesky, G. M. Sheldrick, L. Häming, R. Herbst-Irmer, *Angew. Chem.* **1994**, *105*, 1052; *Angew. Chem. Int. Ed. Engl.* **1994**, *33*, 969.
[6] R. T. Sanderson, *Polar Covalence*, Academic Press, New York, **1983**, p. 155; L. Pauling, *The Nature Of The Chemical Bond*, Cornell University Press, Ithaca, New York, **1960**, p. 85.
[7] H.-J. Koch, Dissertation, Göttingen, **1992**.
[8] Crystal structure data of **1**: $C_{64}H_{80}Al_4F_4Si_2 \cdot 2C_7H_8$, $M_r = 1273.65$, space group $P\bar{4}2_1c$, $a = b = 1586.7(2)$, $c = 1418.8(2)$ pm, $V = 3.5720(8)$ nm^3, $\rho_{calcd} = 1.184$ Mg m^{-3}, $F(000) = 1360$, $\lambda = 71.073$ pm, $\mu(Mo_{K\alpha}) = 0.151$ mm^{-1}. Intensities were determined at 193 K with a shock-cooled crystal in an oil drop [18] according to the $2\theta/\omega$ method in the range $8 \le 2\theta \le 50°$ on a STOE-Siemens-AED diffractometer. The colorless octahedral crystal measured $0.8 \times 0.6 \times 0.6$ mm. 10773 reflections were measured, 3122 independent ($R_{int} = 0.03$). A semiempirical absorption correction was carried out on 208 ψ-scanned reflections. The structure was solved by direct methods (SHELXS-90) [19] and refined using the least-squares method on F^2 (SHELXL-93) [20]. Hydrogen atoms were calculated on their ideal geometrical positions and refined according to a riding model in which the methyl groups were able to rotate around their local axes. The phenyl group was refined on two slightly twisted positions with respect to the position of C11 with occupation factors of 0.64/0.36 to account for its disorder. The disordered toluene molecule on the twofold axis was refined on two positions with occupation factors of 0.29/0.21. 545 restraints were used for the final refinement of the 346 parameters. The Flack parameter refined to 0.1(2) [21]. A minimum of -237 e nm^{-3} and a maximum of 209 e nm^{-3} were obtained for the last difference Fourier synthesis. $R1 = 0.0343$ ($F > 4\sigma(F)$), $wR2 = 0.0954$ (all data). $R1$ and $wR2$ are defined as follows: $R1 = \sum||F_o| - |F_c||/\sum|F_o|$ and $wR2 = \{[\sum w(F_o^2 - F_c^2)^2]/[\sum w(F_o^2)^2]\}^{1/2}$. Further details of the crystal structure investigation may be obtained from the Director of the Cambridge Crystallographic Data Centre, 12 Union Road, GB-Cambridge CB2 1EZ (UK), on quoting the full journal citation.
[9] J. F. Janik, E. N. Duesler, R. T. Paine, *Inorg. Chem.* **1987**, *26*, 4341; *ibid.* **1988**, *27*, 4335; J. F. Janik, E. N. Duesler, W. F. McNamara, M. Westerhausen, R. T. Paine, *Organometallics* **1989**, *8*, 506; M. L. Sierra, V. S. J. de Mel, J. P. Oliver, *ibid.* **1989**, *8*, 2312; L. Rösch, *Angew. Chem.* **1977**, *89*, 497; *Angew. Chem. Int. Ed. Engl.* **1977**, *16*, 480.
[10] W. Clegg, U. Klingebiel, J. Neemann, G. M. Sheldrick, *J. Organomet. Chem.* **1983**, *249*, 47.
[11] G. Allegra, G. Perego, *Acta Crystallogr.* **1963**, *16*, 185.
[12] J. L. Atwood, W. R. Newberry III, *J. Organomet. Chem.* **1974**, *66*, 15.
[13] G. Gundersen, T. Haugen, A. Haaland, *J. Organomet. Chem.* **1973**, *54*, 77.
[14] H. J. Breunig, W. Kanig, *Chem.-Ztg.* **1978**, *102*, 263; K. Issleib, B. Hamann, L. Schmidt, *Z. Anorg. Allg. Chem.* **1965**, *339*, 298.
[15] $[(Cp^*Al)_4]$ does not react with $(t\mathrm{BuSb})_4$ at room temperature. The reaction conditions have been chosen so as to provide optimum conditions between no reaction and a high rate of decomposition.
[16] H. J. Breunig, H. Kischkel, *Z. Anorg. Allg. Chem.* **1983**, *502*, 175.
[17] Due to problems, which possibly arise because of a superlattice, it has not yet been possible to obtain a final structural model.
[18] T. Kottke, D. Stalke, *J. Appl. Crystallogr.* **1993**, *26*, 615.
[19] G. M. Sheldrick, *Acta Crystallogr. Sect. A* **1990**, *46*, 467.
[20] G. M. Sheldrick, SHELXL-93, Universität Göttingen, **1993**.
[21] H. D. Flack, *Acta Crystallogr. Sect. A* **1983**, *39*, 876.

 © VCH Verlagsgesellschaft mbH, D-69451 Weinheim, 1995 0570-0833/95/0808-0920 $ 10.00+.25/0

Lithium Intermediates during the α-Lithiation and Subsequent α-Substitution of Heterocyclic Amines in the Presence of CO_2**

Sarah C. Ball, Ian Cragg-Hine,*
Matthew G. Davidson, Robert P. Davies,
Andrew J. Edwards, Isabel Lopez-Solera,
Paul R. Raithby, and Ronald Snaith

Lithium alkyls and amides are used to effect key deprotonation steps in numerous organic syntheses.[1] In this they are often so specific that subsequent electrophilic substitution of Li^+ gives a particular derivative of the organic precursor. Much is known about the structures of these lithium reagents,[2] but far less about how they operate, the origin of their selectivity, and the natures of lithiated organic compounds produced prior to work-up. We are therefore studying some well-established specific organic syntheses that use lithium reagents. Here we report preliminary results on the protocol established by Katritzky for specific α-substitution of NH-containing heterocycles in which the NH group is protected by carbon dioxide.[3] The Katritzky method has been applied to indoles,[3a] isoquinolines,[3b] phenothiazines,[3c] and related compounds. The one-pot method is illustrated for phenothiazine (**1**, Scheme 1). The amine **1** is converted first into the lithium amide **2**, which gives the lithium carbamate **3** on treatment with CO_2. Further lithiation is then held to afford specifically the α-lithio derivative **4**, whose treatment with an electrophile gives **5**. Acidification and decarboxylation give **6** and then the final α-substituted product **7**. Two key points are relevant to the mechanism of this synthetic strategy: 1) as well as preventing substitution at the nitrogen atom, it has been suggested that the CO_2 acts also as a directing group, possibly by "chelating" with the added *t*BuLi in the conversion of **3** to **4**; 2) to our knowledge, the lithium species of types **2**, **3**, **4**, **5** have not been isolated, identified, and structurally examined. To explore these points we have studied some of the key steps and intermediates along the conversion of **1** (Scheme 1)[3c] into its α-substituted derivatives. We have also examined the lithiation of a model system, diphenylamine (**1a**).



Scheme 1. The Katritzky method for the conversion of phenothiazine (**1**) into an α-substituted product (**7**).

Treatment of **1** in THF with *n*BuLi affords an amber-orange solution from which orange crystals of **2** · 3 thf were isolated (see Experimental Procedure). X-ray crystallography[4] shows that **2** · 3 thf is monomeric in the solid (Fig. 1), with Li–N and mean Li–O distances of 2.011(9) and 1.972(9) Å, respectively. There is nothing unusual about such a structure (five $R_2NLi \cdot 3$ thf monomers are in the Cambridge Crystallographic Data Base), although it is interesting that the phenothiazine anion is nonplanar. If CO_2 is bubbled through a chilled THF solution of **2** · 3 thf, its color lightens to pale yellow. Removal of solvent and recrystallization of the residue from toluene gives a microcrystalline material, identified as $(\mathbf{3} \cdot \text{thf})_n$ by elemental analysis and NMR and IR spectroscopy (in particular, a strong carboxylate stretch is seen at 1670 cm^{-1}). In addition, cryoscopic relative molecular mass (CRMM) measurements on solutions of $(\mathbf{3} \cdot \text{thf})_n$ in benzene give association state (n) values of 2.01 ± 0.09; the dominant species in solution is thus the dimer. Unfortunately, it proved impossible to get X-ray quality crystals of this complex, so we cannot confirm its suspected dimeric nature in the solid also. This failure made us switch our attention to systems based on diphenylamine (**1a**, Scheme 1); it contains all the essential features (NH unit, several aromatic CH units) of **1** and similar heterocycles.

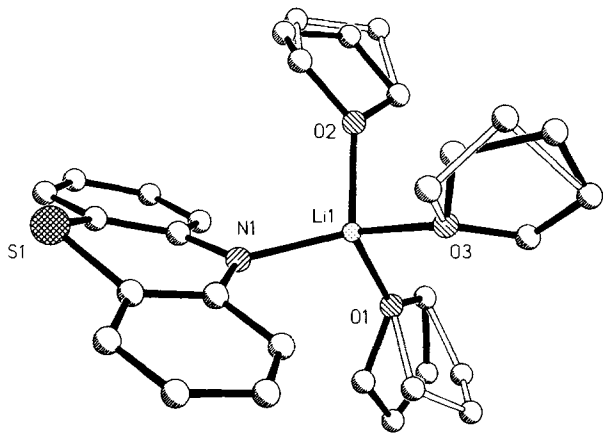


Fig. 1. The molecular structure of **2** · 3 thf (hydrogen atoms omitted for clarity). The disordered THF molecules are pictured in the two most highly refined positions.

Reaction of **1a** with *n*BuLi and then CO_2 in THF, followed by solvent removal and recrystallization of the residue from toluene/TMEDA (TMEDA = *N,N,N',N'*-tetramethylethylenediamine) afforded crystals of $(Ph_2NCO_2Li \cdot \text{tmeda})_n$, $(\mathbf{3a} \cdot \text{tmeda})_n$ (see Experimental Procedure). This is dimeric ($n = 2$) in the solid state.[5] The main structural feature (Fig. 2a) is the central, eight-membered $(LiOCO)_2$ ring [Li–O distances in Å range from 1.862(10) to 1.914(10); mean 1.886(10)]. Such a feature has been observed before in three dimeric lithium carboxylate structures,[6] but never for a lithium carbamate. The ring itself is formed from two near-planar monomeric units (Li1O3C2O4 and

[*] I. Cragg-Hine, S. C. Ball, Dr. M. G. Davidson, R. P. Davies, Dr. A. J. Edwards, Dr. I. Lopez-Solera, Dr. P. R. Raithby, Dr. R. Snaith
University Chemical Laboratory
Lensfield Road, Cambridge CB21EW (UK)
Telefax: Int. code + (223)336-362

[**] This work was supported by the SERC/EPSRC (R.P.D.) and The Associated Octel Company Ltd. (CASE Studentships for S.C.B. and I. C-H.), St. John's College, Cambridge (Research Fellowship for M.G.D.), The Royal Society (low-temperature X-ray diffraction apparatus, P.R.R.) and the Dirección General de Investigación Cientifica y Técnica (I. L-S.). We thank also Dr. D. Reed (University of Edinburgh), and Dr. J. Barker and Dr. D. Barr (Associated Octel Co. Ltd) for assistance with NMR spectroscopic and synthetic aspects of the work.

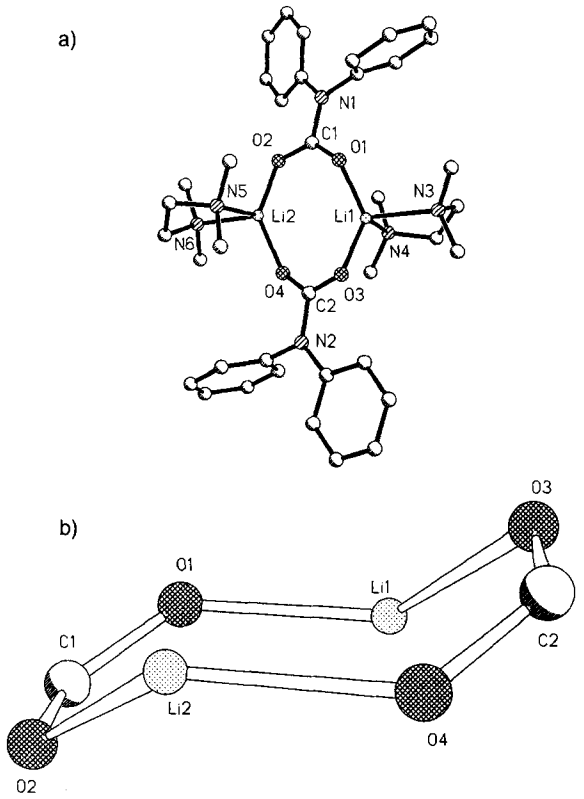


Fig. 2. a) The molecular structure of $(\mathbf{3a} \cdot \text{tmeda})_2$. b) The chair-shaped central $(LiOCO)_2$ ring of $(\mathbf{3a} \cdot \text{tmeda})_2$.

Li2O2C1O1), which link to give a chair-shaped dimer (Fig. 2b). Coordination around each Li^+ ion is completed by a TMEDA molecule [mean Li–N distance, 2.156(10) Å].

In $(\mathbf{3a} \cdot \text{tmeda})_2$, therefore, dimerization occurs even though each Li^+ ion is coordinated to two centers (from one TMEDA ligand). This supports our assertion that $(\mathbf{3} \cdot \text{thf})_n$ will be a dimer also. Since two THF molecules are (roughly) electronically equivalent to one TMEDA molecule, but are more demanding sterically, the implication is that incorporation of two THF complexants per Li^+ ion might lead to a monomeric structure. To probe this point, we treated **1a** in THF with *n*BuLi and the resulting solution with CS_2; this has also been used as a protecting group in the specific α-substitution of amines.[7] The crystalline product isolated from such a system is $Ph_2NCS_2Li \cdot 2\,thf$ (see Experimental Procedure), and it is indeed a monomer in the solid state (Fig. 3).[8] In this structure—the first of a lithium dithiacarbamate—the CS_2 unit chelates the Li^+ ion [mean Li–S 2.469(5) Å], whose tetrahedral coordination is completed by two THF molecules [mean Li–O 1.936(5) Å]. Surprisingly, this is the first example of definite CS_2–Li^+ chelation: in the only other related structure, that of the lithium trithiocarbonate complex $[Li(dme)_2]_2 \cdot (S_2CSCH_2CH_2SCS_2)$,[9] dme = $MeOCH_2CH_2OMe$, the Li–S contacts are understandably very long [mean 2.747(6) Å], since the complexed Li^+ ion is already four-coordinate.

Presumably, in $Ph_2NCS_2Li \cdot 2\,thf$ the larger S atoms allow the space for each Li^+ ion to accommodate two THF complexants, so dictating retention of a monomer, whereas in $(\mathbf{3} \cdot \text{thf})_n$ the smaller O atoms prevent incorporation of more than one THF molecule per Li^+ ion, and dimerization is then preferred. The balance between monomers and dimers is a fine one, as re-emphasized by studies on benzene solutions of $(\mathbf{3a} \cdot \text{tmeda})_n$. CRMM measurements give *n* values of 1.02 ± 0.04 in dilute solution

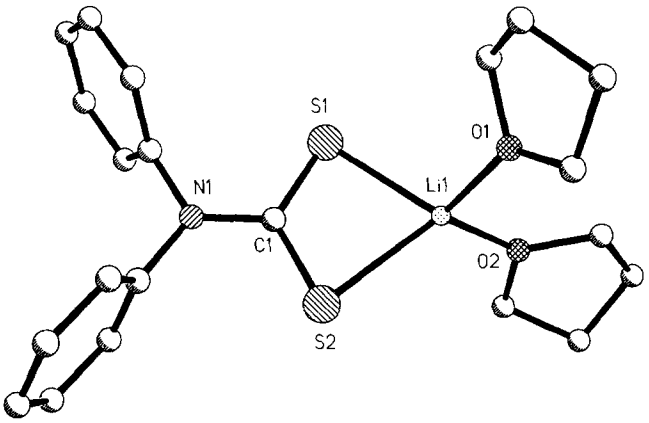


Fig. 3. The molecular structure of $Ph_2NCS_2Li \cdot 2\,thf$.

(0.008 M), increasing to 1.14 ± 0.08 with increasing concentration (0.018 M). Unusually, distinct resonances are observable close to room temperature in ^7Li NMR solution spectra. For a 0.048 M solution at 10 °C, there are two dominant singlets at $\delta = -1.38$ and -1.82 (relative to PhLi as external standard in benzene) and a much smaller one at $\delta = -2.08$. The same three signals occur at lower concentration (0.012 M) at 10 °C ($\delta = -1.36$, -1.80, -2.16), but the lowest frequency one ($\delta = -2.16$) is the largest. Therefore we assign this resonance to monomeric $\mathbf{3a} \cdot$ tmeda. This assignment, and others, are supported by variable-temperature studies on the more concentrated solution. Thus at 25 °C, the highest frequency signal (now at $\delta = -1.42$) has diminished and the other two (at $\delta = -1.87$, -2.10) have grown. By 45 °C, only these latter two resonances (now at $\delta = -1.90$, -2.17) are present. The highest frequency signal can therefore be attributed to dimeric $\mathbf{3a} \cdot$ tmeda. The intermediate resonance (at about $\delta = -1.8$) is possibly due to an "open-dimer" (as detected recently for certain lithium amides[10]) formed by cleavage of one Li–O bond in the dimer and thus the intermediate stage between monomer and dimer, that is, $(tmeda)Li^+ - OC(NPh_2)O - Li(tmeda) - OC(NPh_2)O^-$.

We return finally to the question of how the CO_2 unit in a lithium carbamate—or indeed the CS_2 unit in a lithium dithiacarbamate—might direct the position of a second lithiation (step **3** → **4** in Scheme 1). Our results show that the suggested[3e] "chelation" of added $(t\text{BuLi})_n$ ($n = 4$ in the solid[11]) by a complexed R_2NCX_2Li monomer or by a complexed $(R_2NCX_2Li)_2$ dimer (X = O or S) is unlikely. Any complexation of $(t\text{BuLi})_n$ would need to be external to the CX_2Li chelate ring in the former (as found in solid $Ph_2NCS_2Li \cdot 2\,thf$, Fig. 3) or to the larger $(CX_2Li)_2$ ring in the latter [as found in solid $(\mathbf{3a} \cdot \text{tmeda})_2$, Fig. 2a]. Indeed, this is a crucial point. It is precisely such *external* initial complexation of added $(t\text{BuLi})_n$ to a (merely two-coordinate) O center of, for example, dimeric $(\mathbf{3a} \cdot \text{tmeda})_2$ (see Fig. 2a, O2, O3) which would hold this reagent (presumably with $n < 4$) close to aromatic α-CH units (C22, C42). However, while such a scenario seems fine in theory, we have obtained some puzzling experimental results in attempting to carry out a second lithiation. Thus, treatment of THF solutions of $(\mathbf{3} \cdot \text{thf})_n$ and of $(\mathbf{3a} \cdot \text{tmeda})_n$ with $(t\text{BuLi})_n$ give solutions from which it has proved impossible to isolate any dilithiated products, even at room temperature (note from Scheme 1 that conversion **3** → **4** is held to occur at −20 °C). To explore this further, a solution of $(\mathbf{3} \cdot \text{thf})_n$ was prepared in $[D_8]$THF. To one half of this was added two equivalents of *t*BuLi (that is, two moles of *t*BuLi as a monomer to every one mole of **3** · thf as a monomer) at −70 °C, and this mixture was then transferred to a chilled

NMR tube. ^{1}H NMR spectra were recorded from $-60\,^\circ$C to $60\,^\circ$C. There was no discernible reaction. All eight aromatic protons of **3** · thf (including both α-CH protons) remained intact, and two *t*Bu singlets ($\delta = 0.94$, 0.90) of relative integrals for 9H and 9H (that is, 2 *t*BuLi) were apparent at all temperatures. To the other half of the solution of **3** · thf at $-70\,^\circ$C were added two equivalents of *t*BuLi *and* one of Me_3SiCl. ^{1}H NMR monitoring shows that now reaction does occur, starting at $-60\,^\circ$C: the α-CH proton resonances begin to diminish (fewer than 2H) as do the two singlet *t*Bu ones (fewer than 18H), and several Me_3Si singlets are apparent (total relative integral for 9H). At $60\,^\circ$C, α-Me_3Si substitution of **3** · thf appears complete: aryl resonances sum to 7H, *t*BuLi ones to 9H (that is, one of the two added equivalents of *t*BuLi remains) and there is one Me_3Si singlet (9H, $\delta = 0.36$). Remarkably, therefore, it seems that **3** will not react to any significant extent with *t*BuLi alone, but that the presence of the electrophile (here, Me_3SiCl) is needed. The deduction is that steps **3** → **4** and **4** → **5** in Scheme 1 are not consecutive, but are in some way interdependent. Explanations must be speculative, but include 1) that $(t\text{BuLi})_n$, held in **3** between an O atom of the CO_2 unit and an α-CH, is first complexed further by added Me_3SiCl (through Cl), which reduces the degree of aggregation *n* further and increases its reactivity; 2) that $(t\text{BuLi})_n$ reacts with Me_3SiCl to produce a "mixed-anion" lithiating reagent[12] of general form $(t\text{BuLi} \cdot \text{ClLi})_{n'}$, again of enhanced reactivity; or 3) that **3** does react with $(t\text{BuLi})_n$ to give **4**, but only in trace amounts, and the equilibrium **3** ⇌ **4** is driven forward by a fast reaction between **4** and added Me_3SiCl. We are investigating these possibilities.

Experimental Procedure

Synthesis of **2** · 3thf: Solid **1** (0.496 g, 2.5 mmol) was dissolved under nitrogen in dry THF (6 mL), the solution chilled in an acetone/dry ice bath, and *n*BuLi solution (2.5 mmol in hexane) added. The resulting orange solution and precipitate was heated to 60 °C to dissolve the solid. After cooling to room temperature over 2 h large orange crystals of **2a** · 3thf were isolated. First batch yield 0.48 g, 45%; m.p. > 300 °C; satisfactory analysis for $C_{24}H_{32}LiNO_3S$, ^{1}H NMR (C_6D_6, 250 MHz, 25 °C): $\delta = 6.95$ (t, 4H), 6.6 (t, 4H), 3.5 (m, 12H, THF), 1.3 (m, 12H THF).

Synthesis of **3** · thf: An orange solution of **2** · 3thf was chilled in an acetone/dry ice bath and CO_2 gas bubbled through for two minutes, which caused decolorisation to pale yellow. Removal of solvent and addition of toluene (8 mL) gave a pale yellow solution. After storage at room temperature for 1 d, small white crystals of **3** · thf were isolated. First batch yield 0.46 g, 57%; m.p. > 250 °C; satisfactory analysis for $C_{17}H_{16}LiNO_3S$; ^{1}H NMR (C_6D_6, 250 MHz, 25 °C): $\delta = 7.1$–6.6 (m, 8H), 3.35 (s, 4H, THF), 1.37 (s, 4H, THF).

Synthesis of **3a** · tmeda: Solid **1a** (0.423 g, 2.5 mmol) was dissolved under nitrogen in dry THF (6 mL), the solution chilled, and *n*BuLi solution (2.5 mmol, in hexane) added. The resulting pale yellow solution was warmed to room temperature before being chilled in an acetone/dry ice bath. CO_2 gas was bubbled through the solution for two minutes, causing decolorization. Removal of solvent under reduced pressure, followed by addition of toluene (5 mL), hexane (5 mL), and TMEDA (0.38 mL, 2.5 mmol), gave a pale yellow solution, which was refrigerated at $-20\,^\circ$C for 7 d, whereupon small white crystals of **3a** · tmeda were isolated. First batch yield 0.65 g, 77%; m.p. 117–120 °C; satisfactory analysis for $C_{19}H_{26}LiN_3O_2$, ^{1}H NMR (C_6D_6, 360 MHz, 10 °C): $\delta = 7.4$ (m, 3H), 7.1 (m, 4H), 6.9 (m, 3H), 2.1 (s, 4H, $Me_2N(CH_2)_2NMe_2$), 2.0 (s, 12H, $Me_2N(CH_2)_2NMe_2$).

Synthesis of Ph_2NCS_2Li · 2thf: A solution of **1a** (0.846 g, 5 mmol) in dry THF (6 mL) was chilled, and *n*BuLi solution (5 mmol, in hexane) added. The resulting pale yellow solution was warmed to room temperature before being slightly chilled. CS_2 (0.3 ml, 5 mmol) was then added, giving a thick orange precipitate. Removal of solvent, addition of toluene (10 mL), and gentle heating gave an orange solution. After cooling to room temperature over 2 h a large crop of small orange crystals of Ph_2NCS_2Li · 2thf was isolated. First batch yield 1.52 g, 77%; m.p. 290–295 °C; satisfactory analyis for $C_{21}H_{26}LiNO_2S_2$, ^{1}H NMR (C_6D_6, 250 MHz, 25 °C): δ = 7.7 (d, 6H), 7.12 (d, 2H), 6.97 (d,2H), 3.6 (m, 8H, THF), 1.3 (m, 8H, THF).

Received: November 2, 1994 [Z 7447 IE]
German version: *Angew. Chem.* **1995**, *107*, 1002

Keywords: electrophilic substitution · heterocycles · lithiation · lithium compounds

[1] a) M. Fieser, *Reagents for Organic Synthesis, Vol. 15*, Wiley-Interscience, New York, **1990**; b) B. J. Wakefield, *Organolithium Methods*, Academic Press, New York, **1988**; c) L. Brandsma, H. D. Verkruijsse, *Preparative Polar Organometallic Chemistry, Vol. 1*, Springer, Berlin, **1987**.

[2] a) W. Setzer, P. von R. Schleyer, *Adv. Organomet. Chem.* **1985**, *24*, 353–451; b) D. Seebach, *Angew. Chem.* **1988**, *100*, 1685–1715; *Angew. Chem. Int. Ed. Engl.* **1988**, *27*, 1624–1654; c) R. E. Mulvey, *Chem. Soc. Rev.* **1991**, *20*, 167–209; d) K. Gregory, P. von R. Schleyer, R. Snaith, *Adv. Inorg. Chem.* **1991**, *37*, 47–142; e) E. Weiss, *Angew. Chem.* **1993**, *105*, 1565–1587; *Angew. Chem. Int. Ed. Engl.* **1993**, *32*, 1501–1523.

[3] a) A. R. Katritzky, K. Akutagawa, *Tetrahedron Lett.* **1985**, *26*, 5935–5938; b) *Tetrahedron* **1986**, *42*, 2571–2574; c) A. R. Katritzky, L. M. Vazquez de Miguel, G. W. Rewcastle, *Synthesis* **1988**, 215–217.

[4] a) X-ray crystal data for **2** · 3thf: $C_{24}H_{32}LiNO_3S$, $M = 421.51$, monoclinic, space group $P2_1/n$, $a = 8.612(2)$, $b = 15.848(3)$, $c = 17.013(3)$ Å, $\beta = 98.88(3)°$, $V = 2294.2(8)$ Å^3, $F(000) = 904$, $\lambda(Mo_{K\alpha}) = 0.71073$ Å, $\mu(Mo_{K\alpha}) = 0.165$ mm^{-1}, $T = 153(2)$ K, $Z = 4$, $\rho_{calcd} = 1.220$ Mg m^{-3}. Data were collected on a Stoe-Siemens diffractometer in the range $3.51° \le \theta \le 22.50°$ (3104 reflections collected, 2990 independent reflections). The structure was solved by direct methods and refinement, based on F^2, was by full-matrix least-squares techniques (SHELX92, G.M. Sheldrick, Universität Göttingen; all non-hydrogen atoms were refined anisotropically and hydrogen atoms were included in calculated positions) to $R_1 = 0.0687$, $wR_2 = 0.1888$ for 2259 unique reflections [$I > 2\sigma(I)$]. [b] Further details of this and other crystal structure investigations reported here are available on request from the Director of the Cambridge Crystallographic Data Centre, 12 Union Road, Cambridge CB2 1EZ (UK), on quoting the full journal citation.

[5] X-ray crystal data for (**3a** · tmeda)$_2$: $C_{38}H_{52}Li_2N_6O_4$, $M = 670.74$, monoclinic, space group $P2_1/n$, $a = 10.652(2)$, $b = 19.037(4)$, $c = 19.146(4)$ Å, $\beta = 99.95(3)°$, $V = 3824.1(13)$ Å^3, $F(000) = 1440$, $\lambda(Mo_{K\alpha}) = 0.71073$ Å, $\mu(Mo_{K\alpha}) = 0.075$ mm^{-1}, $T = 153(2)$ K, $Z = 4$, $\rho_{calcd} = 1.165$ Mg m^{-3}. Data were collected on a Stoe-Siemens diffractometer in the range $2.61° \le \theta \le 22.51°$ (5131 reflections collected, 4968 independent reflections). The structure was solved and refined as in [4] to $R_1 = 0.0721$, $wR_2 = 0.1789$ for 2831 unique reflections [$I > 2\sigma(I)$].

[6] G. Smith, E. J. O'Reilly, C. H. L. Kennard, *Acta Crystallogr. Sect. C* **1986**, *42*, 1329; H. Küppers, *ibid.* **1988**, *44*, 2093; X.-M. Chen, T. C. W. Mak, *J. Crystallogr. Spectrosc. Res.* **1993**, *23*, 291.

[7] H. Albrecht, D. Kornetzky, *Synthesis*, **1988**, 775–777.

[8] X-ray crystal data for Ph_2NCS_2Li · 2thf: $C_{21}H_{26}LiNO_2S_2$, $M = 395.49$, monoclinic, space group $P2_1/c$, $a = 10.261(2)$, $b = 13.615(3)$, $c = 14.824(3)$ Å, $\beta = 96.05(3)°$, $V = 2059.4(7)$ Å^3, $F(000) = 840$, $\lambda(Mo_{K\alpha}) = 0.71073$ Å, $\mu(Mo_{K\alpha}) = 0.274$ mm^{-1}, $T = 153(2)$ K, $Z = 4$, $\rho_{calcd} = 1.276$ Mg m^{-3}. Data were collected on a Stoe-Siemens diffractometer in the range $3.56° \le \theta \le 22.49°$ (2554 reflections collected, 2483 independent reflections). The structure was solved and refined as in [4] to $R_1 = 0.0341$, $wR_2 = 0.0742$ for 2049 unique reflections [$I > 2\sigma(I)$].

[9] K. Tatsumi, I. Matsubara, Y. Inoue, A. Nakamura, R. E. Cramer, G. J. Tagoshi, J. A. Golen, J. W. Gilje, *Inorg. Chem.* **1990**, *29*, 4928–4938.

[10] M. P. Bernstein, D. B. Collum, *J. Am. Chem. Soc.* **1993**, *115*, 8008–8018, and references therein.

[11] T. Kottke, D. Stalke, *Angew. Chem.* **1993**, *105*, 619–621; *Angew. Chem. Int. Ed. Engl.* **1993**, *32*, 580–582.

[12] a) P. L. Hall, J. H. Gilchrist, D. B. Collum, *J. Am. Chem. Soc.* **1991**, *113*, 9571–9574; b) F. S. Mair, W. Clegg, P. A. O'Neil, *ibid.* **1993**, *115*, 3388–3389.

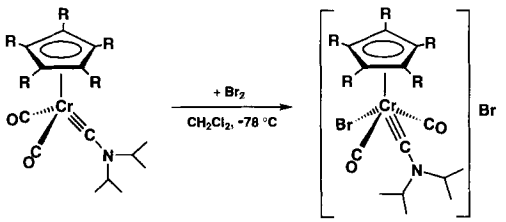
 © *VCH Verlagsgesellschaft mbH, D-69451 Weinheim, 1995* *0570-0833/95/0808-0923 $ 10.00+.25/0*

Aminocarbyne Complexes of Chromium in a High Oxidation State—Synthesis, Structure, and Reactivity**

Alexander C. Filippou,* Bernhard Lungwitz, Klaus M. A. Wanninger, and Eberhardt Herdtweck

In 1975 R. R. Schrock et al. reported the synthesis of [Li(dmp)][(tBuCH$_2$)$_3$Ta≡CtBu] (dmp = *N*,*N*′-dimethylpiperazine), the first carbyne complex of a transition metal in a high oxidation state.[1] Since then numerous second- and third-row transition metal carbyne complexes of this type have been prepared.[2] Among them, the molybdenum and tungsten carbyne complexes [(RO)$_3$M≡CR′] (R,R′ = alkyl, aryl; R′ = amino) have been extensively studied because of their catalytic activity in alkyne metathesis.[3] Two principal methods have been developed for the synthesis of these compounds. The first involves the reaction of Mo^{VI} and W^{VI} halides with alkyllithium compounds,[4] the second is the oxidative decarbonylation of Fischer-type carbyne complexes.[5] In comparison, analogous carbyne complexes of first-row transition metals have not yet been reported. Attempts to prepare Schrock-type carbyne complexes of chromium have so far been unsuccessful owing to the oxidation of alkyl transfer reagents by Cr^{VI} halides[6] or the oxidative cleavage of the chromium–carbon triple bond of Fischer-type carbyne complexes.[7] Here we report the synthesis, structure, and reactivity of the first carbyne complexes of chromium in a high oxidation state.

Oxidation of **1a** and **1b**[8] with bromine in CH_2Cl_2 at −78 °C leads selectively to the cationic aminocarbyne complexes in **2a** and **2b** [Eq. a]. Similarly, the cationic chloro complex in [Cp(Cl)(CO)$_2$Cr≡CN^{i}Pr$_2$]Cl (**2c**) is obtained from **1a** and $PhICl_2$,



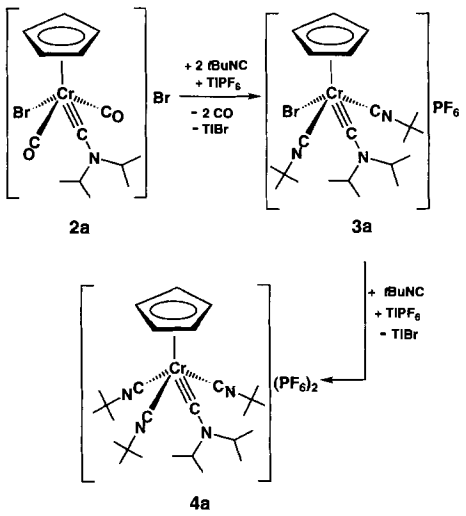
(a)

1a, 1b **2a, 2b**

a: R = H; b: R = Me

while oxidation of the analogous molybdenum and tungsten complexes [(η^5-C$_5$R$_5$)(CO)$_2$M≡CNEt$_2$] with halogens affords the neutral aminocarbyne complexes *cis*-[(η^5-C$_5$R$_5$)(X)$_2$(CO)M≡CNEt$_2$] (R = H, Me; X = Cl, Br, I), bearing one carbonyl ligand.[5b, e, f]

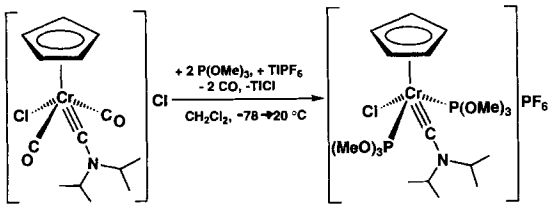
The salts **2a**–**2c** were isolated as ocker-yellow, very thermolabile solids (decomposition of the solids above ca. −50 °C). Their low thermal stability can be ascribed to the labile chromium–carbonyl bonds.[9] Thus, thermal decomposition of these compounds in solution leads after elimination of both CO ligands to blue paramagnetic products of yet unknown structure. However, thermally stable aminocarbyne complexes of chromium in a high oxidation state can be obtained after CO substitution, if the halide counterion of **2a**–**2c** is removed by reaction with TlPF$_6$. Thus, treatment of **2a** with TlPF$_6$ and tBuNC leads to the salt **3a** containing a monocationic aminocarbyne complex, which can be subsequently converted with additional TlPF$_6$ and tBuNC to the dicationic aminocarbyne complex in **4a** (Scheme 1). In contrast, reaction of **2b** with TlPF$_6$ and tBuNC leads directly to the analogous pentamethylcyclopentadienyl (Cp*) derivative [Cp*(tBuNC)$_3$Cr≡CN^{i}Pr$_2$] (PF$_6$)$_2$ (**4b**).



2a **3a** **4a**

Scheme 1.

Similarly, the salt **5** containing a cationic aminocarbyne complex is obtained from **2c** after treatment with TlPF$_6$ and P(OMe)$_3$ [Eq. b]. Also mixed-substituted aminocarbyne derivatives are accessible following this route, as demonstrated by the selective oxidation of **6**[8] with bromine to give the thermolabile, light-brown aminocarbyne complex in **7** (m.p. = ca. −50 °C (decomp.)), followed by the transformation of this complex in **7** to the cation in **8** after treatment with TlPF$_6$ and tBuNC (m.p. = 83 °C (decomp.)) (Scheme 2).



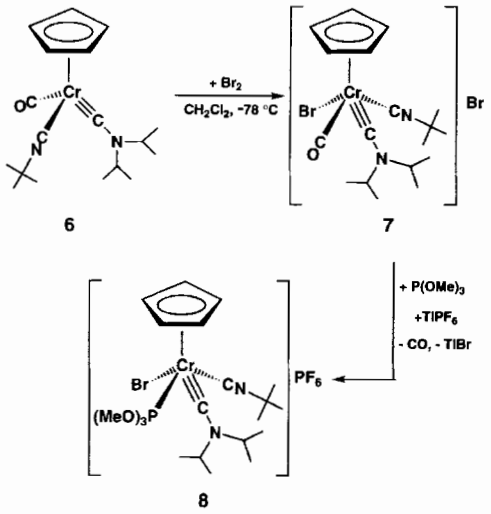
(b)

2c **5**

The amine carbyne complexes of chromium are isolated as yellow (**4a**), orange-red (**3a**, **8**), red (**4b**), and brown (**5**) solids, which, unlike the salts **2a**–**2c**, and **7** with their carbonyl-containing cationic precursor complexes show a surprising thermal stability (m.p.: 83–141 °C (decomp.)). The salts **2a**–**5**, **7**, and **8** were characterized by elemental analyses, IR, NMR, and mass spectra (Table 1). All aminocarbyne

[*] Prof. Dr. A. C. Filippou, Dipl.-Chem. B. Lungwitz
Institut für Anorganische und Allgemeine Chemie der Humboldt-Universität
Hessischestrasse 1–2, D-10115 Berlin (Germany)
Telefax: Int. code + (30)2846 8639
Dipl.-Chem. K. M. A. Wanninger
Max-Planck Institut für Kohlenforschung, Mülheim/Ruhr (Germany)
Dr. E. Herdtweck
Anorganisch-chemisches Institut
der Technischen Universität München (Germany)

[**] This work was supported by the Volkswagen-Stiftung, the Deutsche Forschungsgemeinschaft, and the Fonds der Chemischen Industrie. We thank Professor Dr. E. O. Fischer and Professor Dr. W. A. Herrmann for support.



Scheme 2.

Table 1. Spectroscopic data of **2a–8** [a, b].

2a: IR (CH_2Cl_2, −60 °C): $\tilde{\nu}$[cm^{-1}] = 2101 m, 2070 vs [ν(CO)]; 1634 s [ν(C$_{carbyne}$···N)]; ^{1}H NMR (CD_2Cl_2, −60 °C): δ = 1.48 (d, 12H, 2 × CHMe_2), 3.93 (sept, 2H; 2 × CHMe$_2$), 6.19 (s, 5H; Cp); ^{13}C{^{1}H}-NMR (CD_2Cl_2, −60 °C): δ = 21.1 (CHMe_2), 60.1 (CHMe$_2$), 102.4 (Cp), 213.4 (CO), 318.4 (Cr≡C).

2b: IR (CH_2Cl_2, −60 °C): $\tilde{\nu}$[cm^{-1}] = 2079 m, 2052 vs [ν(CO)]; 1616 s ν(C$_{carbyne}$···N)]; ^{1}H NMR (CD_2Cl_2, −60 °C): δ = 1.44 (d, 12H, 2 × CHMe_2), 2.10 (s, 15H; C_5Me_5), 3.84 (sept, 2H; 2 × CHMe$_2$); ^{13}C{^{1}H} NMR (CD_2Cl_2, −60 °C): δ = 13.3 (C_5Me_5), 22.3 (CHMe_2), 57.2 (CHMe$_2$), 113.6 (C_5Me$_5$), 219.6 (CO), 311.7 (Cr≡C.).

2c: IR (CH_2Cl_2, −60 °C): $\tilde{\nu}$[cm^{-1}] = 2111 m, 2079 vs [ν(CO)]; 1637 s [ν(C$_{carbyne}$···N)].

3a: IR: $\tilde{\nu}$[cm^{-1}] = 2172 vs [ν(C≡NtBu)]; 1593 m [ν(C$_{carbyne}$···N)]; ^{1}H NMR: δ = 1.40 (d, 12H; CHMe_2), 1.58 (s, 18H; Me_3C), 3.60 (sept, 2H; CHMe$_2$), 5.45 (s, 5H; C_5H_5); ^{13}C{^{1}H}-NMR: δ = 23.2 (CHMe_2), 30.2 (Me_3C), 58.7 (CHMe$_2$), 60.3 (Me_3C), 98.8 (Cp), 158.8 (Me_3CNC), 325.8 (Cr≡C); FD-MS: m/z 395 [M − Br]$^+$.

4a: IR (CH_3CN): $\tilde{\nu}$[cm^{-1}] = 2208 s, 2184 vs [ν(C≡NtBu)]; 1630 s [ν(C$_{carbyne}$···N)]; ^{1}H NMR (CD_3CN, 25 °C): δ = 1.38 (d, 12H; CHMe_2), 1.51 (s, 9H; Me_3C), 1.59 (s, 18H; 2 × Me_3C). 3.78 (sept, 2H; 2 × CHMe$_2$), 5.59 (s, 5H; C_5H_5); ^{13}C{^{1}H}-NMR (CD_3CN, 25 °C): δ = 22.8 (CHMe_2), 29.8 (1 × Me_3C), 29.9 (2 × Me_3C), 61.2 (CHMe$_2$), 61.9 (1 × Me_3C), 62.5 (2 × Me_3C), 98.1 (Cp), 149.4 (1 × Me_3CNC), 156.0 (2 × Me_3CNC), 324.1 (Cr≡C); FD-MS (CH_3CN): m/z 395 [M − tBuNC]$^+$.

4b: IR: $\tilde{\nu}$[cm^{-1}] = 2180 s, 2162 vs [ν(C≡NtBu)]; 1608 m [ν(C$_{carbyne}$···N)]; ^{1}H NMR (CD_3CN, 25 °C): δ = 1.37 (d, 12H; 2 × CHMe_2), 1.52 (s, 9H; 1 × Me_3C), 1.61 (s, 18H; 2 × Me_3C), 1.97 (s, 15H; C_5Me_5), 3.78 (sept, 2H; 2 × CHMe$_2$); ^{13}C{^{1}H}-NMR (CD_3CN, 25 °C): δ = 11.9 (C_5Me_5), 22.8 (CHMe_2), 30.0 (Me_3C), 30.4 (2 × Me_3C), 58.8 (CHMe$_2$), 61.7 (Me_3C), 62.1 (2 × Me_3C), 111.0 (C_5Me$_5$), 154.6 (1 × Me_3CNC), 162.9 (2 × Me_3CNC), 315.7 (Cr≡C).

5: IR: $\tilde{\nu}$[cm^{-1}] = 1560 s [ν(C$_{carbyne}$···N)]; ^{1}H NMR (CD_2Cl_2, −10 °C): δ = 1.24 (d, 12H; 2 × CHMe_2), 3.87 (m, ^3J(H,P) = 9.8 Hz; P(OMe)$_3$ and 2 × CHMe$_2$); 5.31 (t, ^3J(P,H) = 3.0 Hz, 5H; C_5H_5); ^{13}C{^{1}H}-NMR (CD_2Cl_2, −10 °C): δ = 21.6 (CHMe_2), 56.3 (pt, ^2J(C,P) = 8.2 Hz; P(OMe)$_3$), 96.7 (Cp), 315.8 (t, ^2J(C,P) = 95.2 Hz; Cr≡C); ^{31}P{^{1}H}-NMR: δ = 161.1.

7: IR (CH_2Cl_2, −60 °C): $\tilde{\nu}$[cm^{-1}] = 2194 s [ν(C≡NtBu)], 2057 vs [ν(CO)], 1621 s [ν(C$_{carbyne}$···N)].

8: IR: $\tilde{\nu}$[cm^{-1}] = 2173 s [ν(C≡NtBu)]; 1589 m, sh, 1575 s [ν(C$_{carbyne}$···N)]; ^{1}H NMR: δ = 1.31 (d, 6H; 2 × CHMe_AMe$_B$), 1.36 (d, 6H; 2 × CHMe$_A$$Me_B$), 1.58 (s, 9H; Me_3C), 3.76 (sept, 2H; 2 × CHMe$_2$), 3.93 (d, ^3J(H,P) = 10.4 Hz, 9H; P(OMe)$_3$), 5.36 (d, ^3J(H,P) = 3.7 Hz, 5H; C_5H_5); ^{13}C{^{1}H}-NMR: δ = 21.8 (2 × CHMe_AMe$_B$), 22.6 (2 × CHMe$_A$$Me_B$), 30.4 ($Me_3$C), 56.0 (d, ^3J(C,P) = 6.1 Hz; 2 × CHMe$_2$), 57.1 (d, ^2J(C,P) = 6.7 Hz; P(OMe)$_3$), 60.3 (Me_3C), 97.6 (Cp), 161.1 (Me_3CNC), 319.6 (d, ^2J(C,P) = 95.2 Hz; Cr≡C); ^{31}P{^{1}H} NMR: δ = 158.7; FD-MS (CH_2Cl_2): m/z 517 [M]$^+$.

[a] Correct elemental analyses were obtained for **3a–5** and **8**. [b] IR spectra (FT-IR spectrometer Perkin Elmer 1650) in CH_2Cl_2 at room temperature, unless otherwise stated; NMR spectra (Jeol-JMX-GX-400 spectrometer) in CD_2Cl_2 at room temperature, unless otherwise stated; the δ_H and δ_C values are referenced to residue solvent signals and the δ_P values to a 85% H_3PO_4 solution (external standard); the ^{3}J(H,H) coupling constant of the N(CHMe$_2$)$_2$ group is 6.1 Hz; mass spectra: m/z values relative to the ^{52}Cr and ^{81}Br isotopes.

complexes of chromium in a high oxidation state are distinguished by an intense IR absorption of the ν(C$_{carbyne}$···N) vibration in the range 1560–1637 cm^{-1} (Table 1). This vibration is slightly lower in frequency than that of the immonium ions [R$_2$C=NR$'_2$]$^+$ (1640–1690 cm^{-1})[10] revealing a strong π conjugation of the amino group with the chromium–carbon triple bond.[8, 9] The ν(C$_{carbyne}$···N) absorption of the aminocarbyne complexes of chromium in a high oxidation state appears at higher wavenumbers than that of the starting materials **1a**, **1b**, and **6** [ν(C···N) = 1519–1552 cm^{-1}].[8] There is a shift of this frequency towards lower wavenumbers in the series **2a**, **2c** > **7** > **3a** > **8** > **5** as a result of the increasing electron density at the metal center and the strengthening of the chromium–carbyne back bonding.[5b–f] The number and relative intensity of the ν(CO) and ν(C≡NtBu) absorptions of the complexes in **2a–2c** and **3a** indicate the diagonal arrangement of these ligands in the coordination sphere. The weak chromium–carbonyl and chromium–isocyanide back bonding in these compounds is displayed by the frequencies of these absorptions. In the ^{1}H NMR spectra of **2a–5** one doublet is observed for the methyl protons and one septet for the methine protons of the aminocarbyne ligand, confirming the C_s symmetry of these complexes and the fast rotation of the amino group about the C$_{carbyne}$–N bond (Table 1).[11] In contrast, two doublets are found in the ^{1}H NMR spectrum of the C_1-symmetric complex in **8** for the diastereotopic methyl protons of the aminocarbyne ligand. The carbyne–carbon resonances of the complexes in **2a–5**, **7**, and **8** appear at a considerably lower field (δ = 311.7–325.8) than those of the starting materials **1a**, **1b**, and **6** (δ = 276.6–281.7).[8] The same trend is observed on comparing Schrock-type with Fischer-type carbyne complexes of molybdenum and tungsten.[2, 5]

The proposed structures of the carbyne complexes in **3a** and **4b** were confirmed by single-crystal X-ray diffraction studies (Figs. 1 and 2).[12] Interesting structural features of **3a** and **4b**

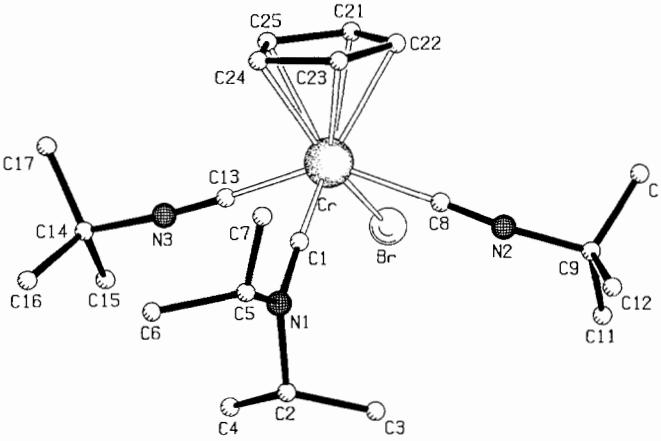


Fig. 1. Structure of the cation in **3a** (PLUTON plot) in the crystal. Selected bond lengths [pm] and angles [°]: Cr-C1 174.5(3), Cr-Br 255.7(1), Cr-Cp$_{centroid}$ 186.2, Cr-C8 197.6(3), Cr-C13 197.4(3), C1-N1 130.0(4); Cr-C1-N1 177.0(3), Br-Cr-C1 109.5(1), Br-Cr-C8 75.0(1), Br-Cr-C13 79.6(1), C1-Cr-C8 81.3(1), C1-Cr-C13 81.4(1), C8-Cr-C13 142.1(1), C8-N2-C9 164.1(3), C13-N3-C14 174.8(3).

are a) the unusual high coordination number observed for half-sandwich chromium complexes bearing a Cp ligand (C.N. = 5, if the complexes in **3a** and **4b** are considered as distorted square pyramids with the Cp or Cp* ligand, respectively, on the apex)[13]; b) the very short Cr–C$_{carbyne}$ bonds of **3a** and **4b** (174.5 and 173.5 pm respectively), which are however of similar

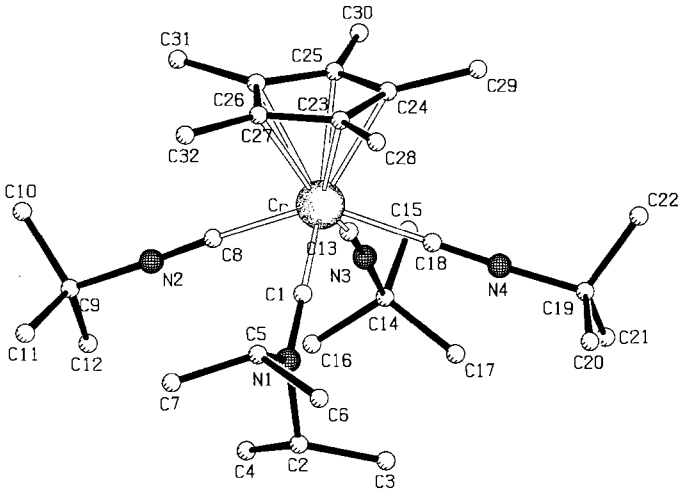


Fig. 2. Structure of the cation in **4b** · CH_3CN (PLUTON plot) in the crystal. Selected bond lengths [pm] and angles [°]: Cr-C1 173.5(4), Cr-$Cp^*_{centroid}$ 186.7, Cr-C8 197.2(4), Cr-C13 199.1(5), Cr-C18 194.9(5), C1-N1 127.8(5); Cr-C1-N1 179.3(4), C1-Cr-C8 78.0(2), C1-Cr-C13 109.5(2), C1-Cr-C18 80.7(2), C8-Cr-C18 141.9(2), C8-N2-C9 176.6(5), C13-N3-C14 174.9(5), C18-N4-C19 177.1(6).

length to the $Cr-C_{carbyne}$ bonds of aminocarbyne complexes of chromium in a low oxidation state;[14] c) the trigonal-planar coordination of the amino-nitrogen atom (the sum of angles around nitrogen is 360° for both **3a** and **4b**), and the short $C_{carbyne}-N$ bonds of 130.0 and 127.8 pm, respectively, which together with the spectroscopic data demonstrate the π-conjugation of the amino group with the chromium–carbon triple bond,[10, 14] and d) the almost perpendicular orientation of the aminocarbyne ligand plane, defined by the atoms C1, N1, C2, and C5, relative to the Cp or Cp* ring plane (dihedral angle between the best planes: **3a** 92.2°; **4b** 93.4°).[11]

The cations in **2a–5**, **7**, and **8** are the first isolated and characterized carbyne complexes of chromium in a high oxidation state. Protonation of these compounds may provide a route to carbene complexes of chromium in a high oxidation state. Further studies are necessary to demonstrate whether the synthetic concept presented here can be extended to Cp-free carbyne complexes of chromium and other first-row transition metals, and to investigate the reactions of these compounds with unsaturated hydrocarbons.

Experimental Procedure

2a: A precooled (−78 °C) solution of Br_2 (0.496 g, 0.16 mL, 3.11 mmol) in CH_2Cl_2 (20 mL) was added dropwise to a solution of **1a** (0.93 g, 3.26 mmol) in CH_2Cl_2 (30 mL) at −78 °C and the reaction mixture stirred for 2 h. The resulting brown-yellow solution was reduced in volume at −78 °C and the product precipitated with a cold (−78 °C) Et_2O/pentane mixture (1/5). The precipitate was washed repeatedly with cold Et_2O (−78 °C). Yield 1.31 g (90%), yellow powder, m.p. = ca. −50 °C (decomp.).

3a: A solution of **2a** (0.93 g, 2.09 mmol) in CH_2Cl_2 (50 mL) was treated at −78 °C with a cold (−78 °C) solution of *t*BuNC (0.698 g, 0.95 mL, 8.40 mmol) in CH_2Cl_2 (10 mL) and $TlPF_6$ (0.90 g, 2.58 mmol). The mixture was then allowed to warm to room temperature and stirred for 1 h. The resulting brown reaction mixture was treated with a small amount of Et_2O and filtered from the insoluble thallium salts. The filtrate was reduced in volume and the product precipitated with a Et_2O/pentane (1/1) mixture. The precipitate was recrystallized from THF/Et_2O. Yield 0.70 g (54%), orange-red, microcrystalline powder, m.p. = 117 °C (decomp.).

4b: A solution of **2b** (0.57 g, 1.11 mmol) in CH_2Cl_2 (50 mL) was treated at −78 °C with a precooled (−78 °C) solution of *t*BuNC (1.25 g, 1.70 mL, 15.04 mmol) in CH_2Cl_2 (20 mL) and $TlPF_6$ (0.77 g, 2.20 mmol). The mixture was allowed to warm to room temperature and stirred for 3 h. The resulting red reaction mixture was treated with a small amount of Et_2O and filtered from the insoluble TlBr. The filtrate was concentrated and the product precipitated with Et_2O. The precipitate was dissolved in a few mL of CH_2Cl_2 and the solution filtered from a small amount of a red-purple by-product. The filtrate was reduced in volume and the product precipitated with Et_2O/pentane. Yield 0.56 g (60%), red, microcrystalline solid, m.p. = 141 °C (decomp.).

Received: December 5, 1994 [Z 7523 IE]
German version: *Angew. Chem.* **1995**, *107*, 1007

Keywords: carbyne complexes · chromium compounds · oxidations

[1] L. J. Guggenberger, R. R. Schrock, *J. Am. Chem. Soc.* **1975**, *97*, 2935.
[2] H. Fischer, P. Hofmann, F. R. Kreissl, R. R. Schrock, K. Weiss, *Carbyne Complexes*, VCH, Weinheim, **1988**, p. 147.
[3] R. R. Schrock, *Acc. Chem. Res.* **1986**, *19*, 342–348.
[4] a) R. R. Schrock, D. N. Clark, J. Sancho, J. H. Wengrovius, S. M. Rocklage, S. F. Pedersen, *Organometallics* **1982**, *1*, 1645–1651; b) L. G. McCullough, R. R. Schrock, J. C. Dewan, J. S. Murdzek, *J. Am. Chem. Soc.* **1985**, *107*, 5987–5998.
[5] a) A. Mayr, G. A. McDermott, *J. Am. Chem. Soc.* **1986**, *108*, 548–549; b) A. C. Filippou, W. Grünleitner, *Z. Naturforsch. B* **1989**, *44*, 1572–1580; c) A. C. Filippou, *Polyhedron* **1989**, *8*, 1285–1291; d) A. C. Filippou, E. O. Fischer, *J. Organomet. Chem.* **1990**, *382*, 143–156; e) A. C. Filippou, E. O. Fischer, W. Grünleitner, *ibid.* **1990**, *386*, 333–347; f) A. C. Filippou, W. Grünleitner, *ibid.* **1991**, *407*, 61–79.
[6] Stable organochromium(VI) complexes can be obtained in some cases, when the oxidative power of chromium(VI) is reduced by good π-donor ligands: a) A. C. Sullivan, G. Wilkinson, M. Motevalli, M. B. Hursthouse, *J. Chem. Soc. Dalton Trans.* **1988**, 53–60; b) N. Meijboom, C. J. Schaverien, A. G. Orpen, *Organometallics* **1990**, *9*, 774–782; c) J. Sundermeyer, K. Weber, H. Pritzkow, *Angew. Chem.* **1993**, *105*, 751–753; *Angew. Chem. Int. Ed. Engl.* **1993**, *32*, 731–733.
[7] E. O. Fischer, A. Ruhs, H. J. Kalder, *Z. Naturforsch. B* **1977**, *32*, 473–475.
[8] A. C. Filippou, K. Wanninger, C. Mehnert, *J. Organomet. Chem.* **1993**, *461*, 99–109.
[9] The aminocarbyne ligand bears, other than alkyl or arylcarbyne ligands, only one low-lying π-acceptor orbital, which is oriented in the plane of the amino group [2]. Therefore only one filled metal-centered orbital of π symmetry is primarily used for the metal-carbyne back bonding in the complexes in **2a–5**, **7**, and **8**. The other π-acceptor orbital of the aminocarbyne ligand is raised in energy due to overlap with the p-type orbital of the amino-nitrogen atom. This orbital interacts in **2a–2c** with the other metal-centered π-orbital, competing with the two π*-acceptor orbitals of the CO ligands. This specific electronic situation is the reason for the lability of the chromium–carbonyl bonds in **2a–2c**, the high frequency of the $\nu(C_{carbyne}\cdots N)$ vibration found in the IR spectra of the aminocarbyne complexes of chromium in a high oxidation state and the "upright" conformation of the aminocarbyne ligand found in the crystal structures of **3a** and **4b**.
[10] C. Sandorfy in *The Chemistry of the Carbon-Nitrogen Double Bond* (Ed.: S. Patai), Interscience, London, **1970**.
[11] Molybdenum and tungsten aminocarbyne complexes of the type *cis*-[(η^5-C_5R_5)$(X)_2(CO)M{\equiv}CNR'_2$] (X = Cl, Br; R = H, Me; R' = Et, *i*Pr, cyclohexyl), which are related with the chromium compounds in **2a–5**, **7** and **8**, show temperature-dependent ^1H NMR spectra due to a restricted rotation of the amino group about the $C_{carbyne}-N$ bond. The free activation enthalpy of ca. 10 kcal mol^{-1} for this rotation, was determined from the coalescence temperature of the inequivalent alkyl groups attached to the amino-nitrogen atom. The rotational barrier is of electronic origin. Thus, EHMO calculations of the model compound $[Cp(Br)_2(CO)W{\equiv}CNH_2]$ show, that the conformer, in which the amino and the Cp ring plane are perpendicular to each other, is more stable (by ca. 10 kcal) than the conformer, in which the amino group is rotated by 90°. The crystal structures of **3a**, **4b**, and [(η^5-C_5Me_4Et)$(Br)_2(CO)W{\equiv}CNEt_2$] show, in full agreement with these calculations, that the amino and the Cp or Cp* ring plane are perpendicular to each other: A. C. Filippou, B. Lungwitz, H. Berke, T. Bürgi, unpublished results.
[12] X-ray structure analysis of **3a**: $C_{22}H_{37}BrCrF_6N_3P$, M = 620.4; orange-red needles (0.36 × 0.08 × 0.04 mm) from CH_2Cl_2/*n*-pentane at −30 °C by diffusion; monoclinic, $P2_1/c$ (no. 14), a = 977.5(1), b = 1328.8(1), c = 2198.2(2) pm, β = 95.93(1)° (25 reflections at high scattering angles, $2\theta_{min/max}$ = 69.8°/94.0°), $V = 2840 \times 10^6$ pm^3, Z = 4, ρ_{calcd} = 1.451 g cm^{-3}; $F(000)$ = 1272; μ = 60.7 cm^{-1}; CAD4, $Cu_{K\alpha}$ radiation, λ = 154.184 pm; $\theta/2\theta$ scan, 8.8° < θ < 70.0°; t_{max} = 90 s. 5951 reflections were collected at $T = -110 \pm 5$ °C. After LP and decay correction (135.5 h, −7.5% decay), and an empirical absorption correction (5 Psi-scan-data, $C_{min/max}$ = 0.902/1.000), 4534 independent reflections remained with R_m = 0.020 (F). Solution of the structure was carried out using a combination of Patterson and difference-Fourier-methods and full matrix least-squares refinement (STRUX-IV, SHELXS-86, SDP). One isopropyl group of the aminocarbyne ligand is disordered in two locations with different probability (2:1). All non-hydrogen atoms except those for the disordered group were refined anisotropically. Hydrogen atoms were calculated on ideal positions (d_{C-H}: 95 pm; B_H: 1.3 B_C) and included in the structure factor calculations. The calculations converged at R = 0.056 and R_w = 0.038 for 3678

reflections with $I > 2\sigma(I)$ and 305 parameters. Subsequent difference-Fourier synthesis led to a final electron density of $e_{min/max} = +0.65/-0.78\ e\text{Å}^{-3}$. Because of the high thermal parameters of the PF_6 anion, the distances P–F seem to be shortened. X-ray structure analysis of **4b** · CH_3CN: $C_{34}H_{59}CrF_{12}N_5P_2$, $M = 879.8$; red needles (crystal dimensions $0.20 \times 0.20 \times 0.60$ mm) from CH_3CN/Et_2O by diffusion at $-30\,^{\circ}C$; orthorhombic, $P2_12_12_1$ (no. 19), $a = 1150.4(1)$, $b = 1663.2(2)$, $c = 2378.6(2)$ pm (48 reflections at high scattering angles, $2\theta_{min/max} = 31.8/37.6^{\circ}$), $V = 4551 \times 10^6$ pm^3, $Z = 4$; $\rho_{calcd} = 1.284$ g cm^{-3}; $F(000) = 1840$; $\mu = 3.8$ cm^{-1}; CAD4; $Mo_{K\alpha}$ radiation, $\lambda = 71.073$ pm; ω scan, $1.0^{\circ} < \theta < 25.0^{\circ}$; $t_{max} = 90$ s. 4468 reflections were collected at $T = -50 \pm 3\,^{\circ}C$. After LP correction 4063 independent reflections remained with ($R_m = 0.020(F)$). Structure solution was carried out using a combination of direct and difference-Fourier methods and full matrix least-squares refinement (STRUX-IV, SHELXS-86, SDP). All non-hydrogen atoms were refined anisotropically. Hydrogen atoms were calculated on ideal positions with $d_{C\ H}$: 95 pm; B_H: 1.3 B_C) and included in the structure factor calculations. All calculations converged at $R = 0.075$ and $R_w = 0.054$ for 3476 reflections with $I > 2.0\,\sigma(I)$ and 470 parameters. Subsequent difference-Fourier synthesis led to a final electron density of $e_{min/max} = +0.65/-0.78\ e\text{Å}^{-3}$. Because of the high thermal parameters of the PF_6 anion, the distances P–F seem to be shortened. Compound **4b** exists also in a solvent-free pseudo-tetragonal brown phase. The chromium atom lies on a fourfold axis, and thus the ligands are highly disordered. Apparently acetonitrile stabilizes the orthorhombic phase. That means high thermal parameters for the PF_6 anions, disordered solvent, and unoccupied sites in the lattice with space for 9 Å^3 and 7 Å^3. It is possible that the solvent does not properly occupy sites in the crystal or is exchanged by Et_2O. Further details of the crystal structure investigations may be obtained from the Fachinformationszentrum Karlsruhe, D-76344 Eggenstein-Leopoldshafen, on quoting the depository number CSD-58816.

[13] Halfsandwich complexes of chromium, bearing a Cp ligand, are mostly four-coordinate. In contrast, only few five-coordinate compounds are known such as the carbonyl complexes $[CpCr(CO)_3X]$ (X = H, halogen Me, $SnPh_3$) and $[CpCr(CO)_2L_2]$ $[CpCr(CO)_3]$ (L_2 = bis(diphenylphosphano)methane (dppm), 1,2-bis(diphenylphosphano)ethane (dppe): a) A. R. Manning, D. J. Thornhill, *J. Chem. Soc. A* **1971**, 637–639; b) N. A. Cooley, K. A. Watson, S. Fortler, M. C. Baird, *Organometallics* **1986**, *5*, 2563–2565; c) N. A. Cooley, P. T. F. McConnachie, M. C. Baird, *Polyhedron* **1988**, *7*, 1965–1972; d) K. H. Theopold, *Acc. Chem. Res.* **1990**, *23*, 263–270; e) S. K. Noh, R. A. Heintz, B. S. Haggerty, A. L. Rheingold, K. H. Theopold, *J. Am. Chem. Soc.* **1992**, *114*, 1892–1893.

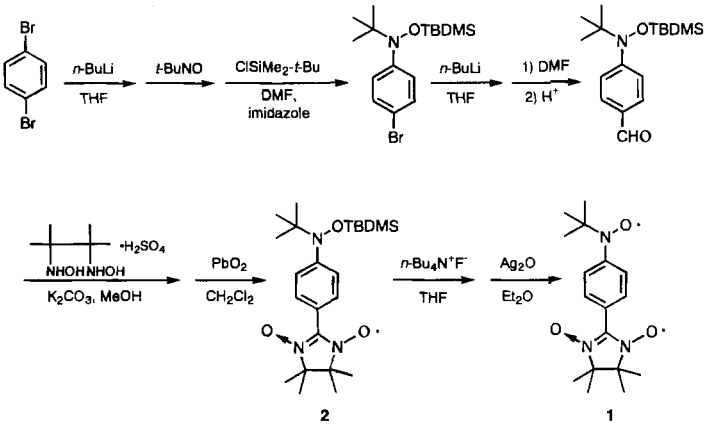
[14] U. Schubert, D. Neugebauer, P. Hoffmann, B. E. R. Schilling, H. Fischer, A. Motsch, *Chem. Ber.* **1981**, *114*, 3349–3365.

2-[*p*-(*N*-*tert*-butyl-*N*-oxyamino)phenyl]-4,4,5,5-tetramethyl-4,5-dihydroimidazol-3-oxide-1-oxyl, a Stable Diradical with a Triplet Ground State**

Katsuya Inoue and Hiizu Iwamura*

Stable triplet diradicals with additional functionalities such as donor/acceptor properties and ligating capabilities to transition metal ions are of great interest for the construction of molecular magnets by assembling electron spins (radical centers) in more than one dimension.[1] Except for Yang's biradical,[2] *meta*-phenylenebis(nitroxide)s,[3] and the stabilized "Schlenk hydrocarbon",[4] there are not very many examples that satisfy both the requirements of kinetic stability and a large energy gap between the triplet ground and singlet excited states. We have prepared the title diradical **1** that, in spite of its formal *para*-substitution pattern of Ullman's nitronyl nitroxide[5] and *tert*-butyl nitroxide moieties, is a stable and robust ground-state triplet species.

p-[*N*-*tert*-Butyl-*N*-(*tert*-butyldimethylsilyloxy)amino]benzaldehyde[6] was condensed with 2,3-bis(hydroxyamino)-2,3-dimethylbutane, and the resulting bis(hydroxylamine) was oxidized with lead dioxide to give oxyl **2**. Deprotection by treatment with tetrabutylammonium fluoride followed by oxidation with silver oxide gave bis(nitroxide) **1** as violet needles (Scheme 1).



Scheme 1. Synthesis of the diradical **1**. TBDMS: *tert*-butyldimethylsilyl, DMF = dimethylformamide.

The results of the X-ray crystal structure analysis of **1**[9] are reproduced in Figure 1. The molecular structure is characterized by the presence of three approximately planar units: the dihydroimidazole ring, the *para*-phenylene ring, and the C, N, O unit of the *tert*-butylnitroxide group. The dihedral angle between the first two planes is about 27° (N_1-C-C-C = 27.5° and N_2-C-C-C = 27.2°) and that of the last two is 22° (C-C-N-O = 21.6°). Typical values for the corresponding dihedral angles in unbiased monoradicals are 35–39° and 30–40°, respectively; that is, **1** is closer to a coplanar structure than these monoradicals. The N–O bonds are slightly elongated. The *para*-phenylene ring appears to deviate from a regular hexagon toward a slightly bond-alternating quinonoidal structure, but only by 0.01–0.02 Å.

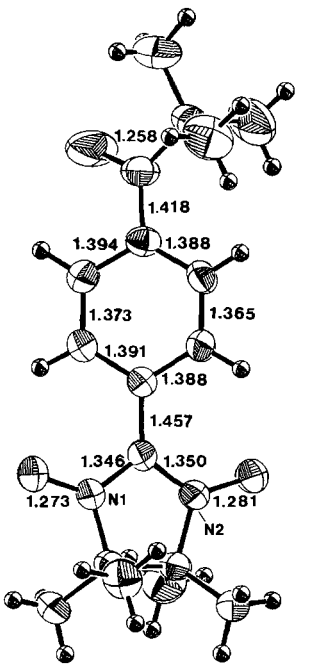


Fig. 1. ORTEP representation of **1** with 50.0% probability ellipsoids [9].

A degassed solution of **1** in 2-methyltetrahydrofuran (MTHF) at room temperature showed a seven line EPR hyperfine structure (a = 3.5 G (2 N) and 4.4 G (1 N) by simulation) at $g = 2.0061$, which suggests that the exchange interaction is greater

[*] Prof. Dr. H. Iwamura, Dr. K. Inoue[+]
Department of Chemistry, Graduate School of Science
The University of Tokyo
7-3-1 Hongo, Bunkyo-ku, Tokyo 113 (Japan)
Telefax: Int. code + (3) 5800-6889

[+] Present address: Department of Chemistry, School of Science
Kitasato University, Kanagawa (Japan)

[**] This work was supported by a Grant-in-Aid for Specially Promoted Research (No. 03102003) from the Ministry of Education, Science and Culture, Japan. We thank the Japan Society for the Promotion of Science for the postdoctoral fellowship given to K. I.

than the hyperfine coupling. A frozen solution of **1** in MTHF gave a broad singlet (width 20.0 G) at $g = 2.0073$ and a $\Delta m_S = \pm 2$ transition at 168 mT, showing that the dipole–dipole interaction between the two unpaired electrons is rather weak. Temperature dependence of the broad $\Delta m_S = \pm 1$ signal followed a Curie law in the range 14–55 K.

The temperature dependence (2–300 K) of the paramagnetic susceptibility of a microcrystalline sample of **1** was measured at 5000 Oe, and the data are expressed by the effective magnetic moment μ_{eff} vs. temperature plot in Figure 2. The μ_{eff} value of

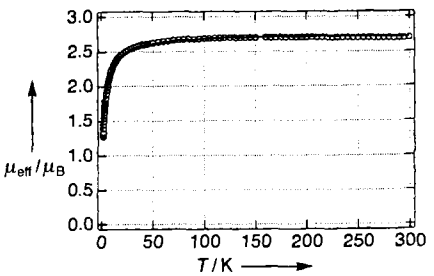


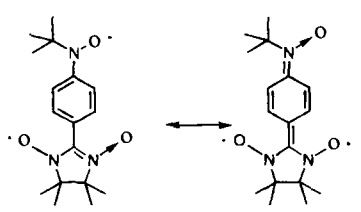
Fig. 2. The temperature dependence of the magnetic moment μ_{eff} of polycrystalline **1** measured at 5000 Oe.

2.71 μ_B at 300 K is close to a theoretical value of 2.83 μ_B for a triplet species. Since there is no specific short contact found between the diradical molecules in the X-ray crystal structure, the contribution of a strong ferromagnetic intermolecular interaction, which is operative even at room temperature, is a remote possibility. The magnetic data were analyzed in terms of a Bleany–Bowers-type singlet–triplet model for the diradical molecule[7] with a weak intermolecular interaction, which is treated by the Weiss field [Eq. 1], in which the magnetic exchange coupling constant J corresponds to a Hamiltonian of the

$$\chi_m = \frac{2fNg^2\mu_B^2}{k_B(T-\theta)\{3 + \exp(-2J/k_BT)\}} \quad (1)$$

form $\mathcal{H} = -2JS_1S_2$. Since μ_{eff} remained constant in the range 100–300 K, only the lower limit of J ($J/k \geq 450$ K) was obtained. By fixing J at 450 K, the other parameters were optimized by means of a least squares analysis to give $\theta = -5.64 \pm 0.063$ K, and f (purity of the diradical) $= 94.9 \pm 0.2\%$.

A preliminary study on the suitability of **1** as a ligand was not satisfactory. Thus when **1** was mixed with $[Mn^{II}(hfac)_2]$, (hfac = hexafluoroacetylacetonato) a two-to-one complex was formed in which only the *tert*-butylnitroxide moiety takes part in complexation.[10] The basicity of the nitronyl nitroxide moiety appears to have decreased somewhat, which supports the canonical structure **1a**. A study employing more acidic transition metal centers is in progress.



1 **1a**

It is concluded that diradical **1** is a kinetically stable and robust triplet diradical. A contribution of resonance structure **1a**, a heteroatom analogue and vinylogue of trimethylenemethane,[2b, 8] may be evoked for the strong intramolecular exchange coupling between the two radical centers separated by several π bonds (about 7 Å), but the bond alternation toward the quinonoidal structure **1a** revealed by the X-ray molecular structure is limited.

Experimental Procedure

Protected nitronyl nitroxide **2** was obtained by condensation of 2,3-dihydroxyamino-2,3-dimethylbutane sulfate with *p*-[*N*-*tert*-butyl-*N*-(*tert*-butyldimethylsiloxy)amino]benzaldehyde [5] in the presence of potassium carbonate followed by oxidation with lead(IV) oxide in dichloromethane at 0 °C. Recrystallization from CH_2Cl_2 gave **2** as black crystals: mp. 140.0–140.8 °C.

1: Compound **2** was deprotected by treatment with tetrabutylammonium fluoride in THF at 0 °C for 30 min. Deprotected **2** was not stable and therefore was oxidized with silver oxide in dichloromethane at 0 °C without purification. Purification of the oxidized crude product by chromatography (SiO_2, CH_2Cl_2/hexane (1:1)) and recrystallization from hexane/ether gave **1** as stable, deep violet needles: m.p. approximately 180 °C (decomp.); UV/Vis [$CHCl_3$, $\lambda(\varepsilon)$] 574.0 (1.30×10^3), 354 nm (3.72×10^4).

Received: September 6, 1994
Revised version: December 9, 1994 [Z 7295 IE]
German version: *Angew. Chem.* **1995**, *107*, 973

Keywords: magnetic properties · nitroxyls · radicals

[1] a) J. S. Miller, A. J. Epstein, W. M. Reiff, *Chem. Rev.* **1988**, *88*, 201; b) *Ferromagnetic and High Spin Molecular Based Materials* (*Mol. Cryst. Liq. Cryst.* **1989**, *176*); c) *Magnetic Molecular Materials* (*NATO ASI Ser. Ser. E* **1991**; d) *Chemistry and Physics of Molecular Based Magnetic Materials* (*Mol. Cryst. Liq. Cryst.* **1993** *232*, *233*); e) J. S. Miller, A. J. Epstein, *Angew. Chem.* **1994**, *106*, 399; *Angew. Chem. Int. Ed. Engl.* **1994**, *33*, 385; f) A. Rajca, *Chem. Rev.* **1994**, *94*, 871.

[2] a) N. C. Yang, A. J. Castro, *J. Am. Chem. Soc.* **1960**, *82*, 6208; b) H. Bock, A. John, Z. Havlas, J. W. Bats, *Angew. Chem.* **1993**, *105*, 416; *Angew. Chem. Int. Ed. Engl.* **1993**, *32*, 416.

[3] a) A. Calder, A. R. Forrester, P. G. James, G. R. Luckhurst, *J. Am. Chem. Soc.* **1969**, *91*, 3724; b) K. Mukai, H. Nagai, K. Ishizu, *Bull. Chem. Soc. Jpn.* **1975**, *84*, 2381; c) T. Ishida, H. Iwamura, *J. Am. Chem. Soc.* **1991**, *113*, 4238; d) F. Kanno, K. Inoue, N. Koga, H. Iwamura, *J. Phys. Chem.* **1993**, *97*, 13267.

[4] a) J. Veciana, C. Rovira, M. I. Crespo, O. Armet, V. M. Domingo, F. Palacio, *J. Am. Chem. Soc.* **1991**, *113*, 2552; b) A. Rajca, S. Utamapanya, *J. Org. Chem.* **1992**, *57*, 1760.

[5] E. F. Ullman, J. H. Osiecki, G. B. Boocock, R. Darcy, *J. Am. Chem. Soc.* **1972**, *94*, 7049.

[6] M. Kitano, N. Koga, H. Iwamura, *Inorg. Chem.* **1994**, *33*, 6012.

[7] B. Bleaney, K. D. Bowers, *Proc. R. Soc. London Ser. A* **1952**, *214*, 451.

[8] H. Kurreck, *Angew. Chem.* **1993**, *105*, 1472; *Angew. Chem. Int. Ed. Engl.* **1993**, *32*, 1409.

[9] X-ray crystal structure analysis: A violet needle single crystal of **1** (approximate dimensions $0.20 \times 0.40 \times 0.70$ mm^3) was mounted on a glass fiber. Diffraction data were obtained with $2\theta_{max.} = 55.1°$ at 22 °C. $C_{17}H_{25}N_3O_3$, $M_r = 319.40$, monoclinic, space group $P2_1/n$ (No. 14), $a = 6.155(2)$, $b = 11.356(2)$, $c = 24.995(2)$ Å, $\beta = 96.48(2)°$, $V = 1735.8(7)$ Å^3, and $\rho_{calcd} = 1.222$ g cm^{-3} for $Z = 4$. All non-hydrogen atoms were refined anisotropically. Refinement converged at $R = 0.052$ and $R_w = 0.055$ for 1982 unique reflections, with $I > 3\sigma(I)$ and 224 variables. Further details of the crystal structure investigation are available on request from the Director of the Cambridge Crystallographic Data Centre, 12 Union Road, GB-Cambridge CB2 1EZ (UK) on quoting the full journal citation.

[10] For one-dimensional ferro- and fern-magnetic chains made up of an alternating array of 1,3-bis(*N*-*tert*-butyl-*N*-oxyamino)benzene and $Mn^{II}(hfac)_2$, see K. Inoue, H. Iwamura, *J. Chem. Soc. Chem. Commun.* **1994**, 2273.

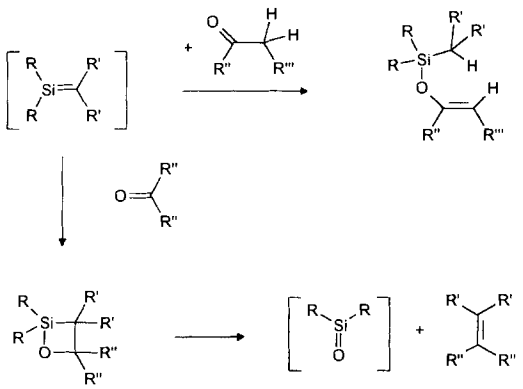
 © VCH Verlagsgesellschaft mbH, D-69451 Weinheim, 1995 0570-0833/95/0808-0928 $ 10.00+.25/0

Reaction of 1,1-Dimethylsilene with Formaldehyde**

Martin Trommer, Wolfram Sander,*
Carl-Henrik Ottosson, and Dieter Cremer*

Dedicated to Professor Paul von Ragué Schleyer on the occasion of his 65th birthday

In contrast to C–C double bonds, Si–C double bonds are strongly polar and labile and thus undergo reactions with polar molecules that are unknown in olefin chemistry.[1] For example, silenes react with carbonyl compounds (in particular aromatic carbonyl compounds) in a Wittig-type reaction to give olefins (Scheme 1).[2–4] 1,2-Oxasiletanes have been postulated, and in some cases demonstrated, as intermediates in the formation of olefins.[4–6] The extremely unstable silanones formed in the fragmentation of the 1,2-oxasiletanes immediately react further to give cyclosiloxanes.



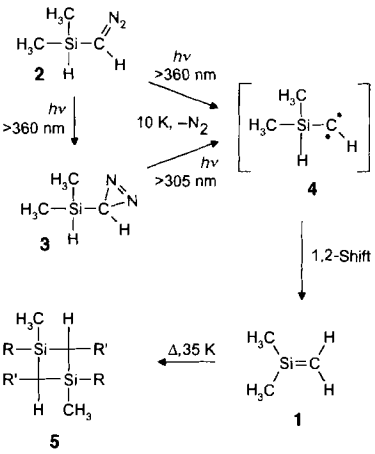
Scheme 1.

According to the results of our CCSD(T)/6-31G(d,p) calculations the reaction of silene with formaldehyde leading to formation of 1,2-oxasiletane is exothermic by 67 kcal mol^{-1}. The overall reaction, including fragmentation to ethene and silanone, is still exothermic by 30 kcal mol^{-1},[6] but the 1,2-oxasiletane lies in such a deep energy well that it can be detected as an intermediate.

The reaction of silenes with carbonyl compounds having an α-H atom follows another route. Here, the main product is a silyl enol ether formed by migration of an H atom (Scheme 1).[1a, 7]

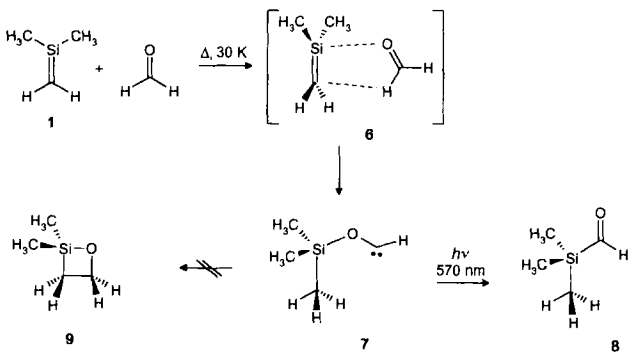
We report here on the reaction of 1,1-dimethylsilene (**1**) with formaldehyde. This silene can be synthesized[8] in high yield by photolysis of (dimethylsilyl)diazomethane (**2**) and is very suitable for the investigation of simple silenes that are not stabilized by bulky substituents (Scheme 2).

Irradiation (λ = 360 nm) of **2** in an argon matrix at 10 K[9] led to formation of the silene **1** and the diazirine **3**. The carbene **4** was too short lived to be detected by IR or UV/Vis spectroscopy, even under conditions of matrix isolation. Irradiation at shorter wavelength (λ > 305 nm) also resulted in elimination of N_2 from **3**, and **1** was formed in almost quantitative yield (IR detection). When the matrix was annealed at 30–40 K, **1** dimerized within a few hours to give disiletane **5** as the main product.[10–13]



Scheme 2.

In the photolysis of **2** (λ > 305 nm, 10 K) in a matrix containing 0.6% formaldehyde, **1** was still formed as the main product, but small amounts of other reaction products were now observed by IR spectroscopy. When the matrix was warmed to 30–35 K after photolysis of **2** at 10 K, the reaction between **1** and CH_2O could then be followed directly by IR spectroscopy: the intensity of the bands of CH_2O and **1** decreased markedly within a few hours, and the new product **7** was formed in addition to small amounts of dimer **5** (Scheme 3). After about 70% conversion the reaction stopped. The new product formed by warming the matrix was extremely photolabile and rearranged quantitatively to 2,2-dimethyl-2-silapropanal (**8**) within a few minutes' irradiation (λ > 570 nm) (Fig. 1). Comparison of the most intense bands at 2624 (aldehyde C–H str.), 1661 (C=O str.), 1252, and 851 cm^{-1} with those of an authentic matrix-isolated sample[8, 14] allowed **8** to be identified.



Scheme 3.

The photolabile compound **7** shows an intense IR absorption at 2605 cm^{-1}, the position and intensity of which resemble that of the OC–H stretching vibration of aldehydes.[15] However, this functional group can be excluded because of the absence of a C=O vibration. Other bands of high intensity are found at 1306, 1254, and 850 cm^{-1} in the range of Si–O and Si–C stretching vibrations. Ab initio calculations of the vibrational spectra of a series of $C_4H_{10}SiO$ isomers carried out at the MP2/6-31G(d,p) level shed light on the identity of **7**. The calculated

[*] Prof. Dr. W. Sander, M. Trommer
Lehrstuhl für Organische Chemie II der Universität
D-44780 Bochum (Germany)
Telefax: Int. code + (234) 709-4353
Prof. Dr. D. Cremer, C.-H. Ottosson
Department of Theoretical Chemistry
University of Göteborg (Sweden)
Telefax: Int. code + (31) 772-2933

[**] This work was supported by the Deutsche Forschungsgemeinschaft, the Fonds der Chemischen Industrie, the Deutschen Akademischen Austauschdienst, the Swedish Natural Science Research Council (NFR), and the Nationellt Superdatorcentrum (NSC), Linköping, Sweden.

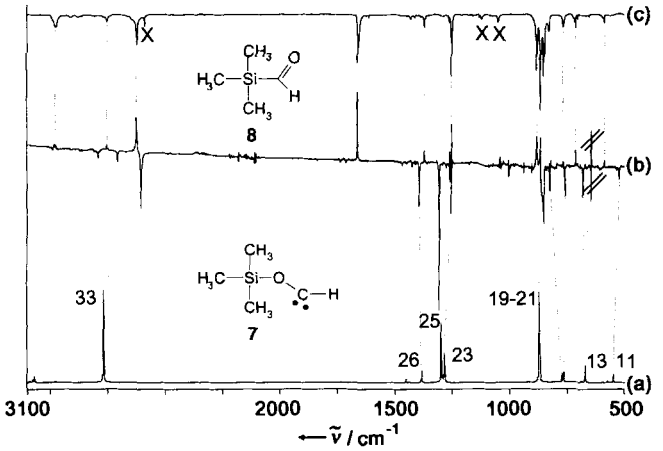
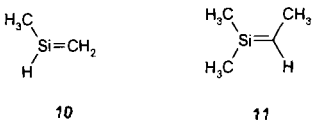


Fig. 1. a) IR spectrum of trimethylsiloxycarbene (7) from ab initio calculations at the MP2/6-31G(d,p) level. b) IR difference spectrum of the photoisomerization **7** → **8** (λ = 570 nm) at 10 K; bands of **7** (pointing downwards) disappear to be replaced by bands of **8** (pointing upwards). c) IR reference spectrum of **8** at 10 K. To match the experimental spectrum, the calculated spectrum was scaled with a factor of 0.95 and simulated with a Lorentz band form with a half-bandwidth of 2 cm^{-1}. Bands marked X are due to residual solvent.

spectrum of trimethylsiloxycarbene was in very good agreement with that of **7** (Fig. 1), whereas no correlation was found for 2,2-dimethyl-1,2-oxasiletane (**9**).

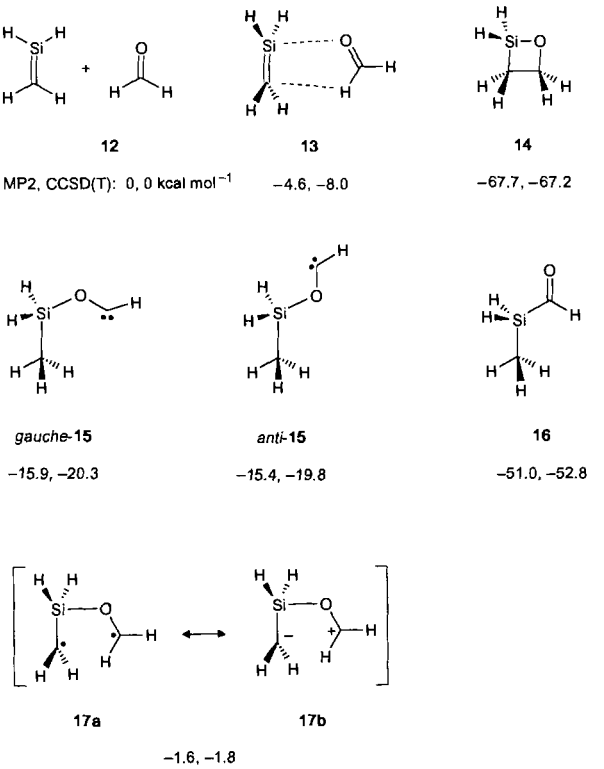
The formation of siloxycarbenes as short-lived intermediates in the irradiation of silylcarbonyl compounds has frequently been postulated,[16, 17] but hitherto only been observed directly in one case by time-resolved spectroscopy.[18, 19] Under the conditions of matrix isolation (T < 40 K) **7** is thermally stable.

For comparison, 2-silapropene (**10**) and 2-methyl-2-sila-2-butene (**11**)[12, 13] were treated with formaldehyde under similar conditions. Whereas the silapropene reacted with formaldehyde analogously to **1**—although quantitatively and markedly faster at 35 K—no thermal reaction was observed with the silabutene. The reactivity of the silene towards formaldehyde therefore drops with increasing number of methyl substituents. Because of the large kinetic isotope effect, reaction of silapropene with [D_2]formaldehyde could not be measured (no reaction after 12 h at 35 K).



Results from CCSD(T)/6-31G(d,p)//MP2/6-31G(d,p) calculations for the system SiH_2CH_2 + CH_2O show that the thermal reaction to form carbene **15** takes place via the van der Waals complex **13** and the intermediate diradical or zwitterion **17** (Scheme 4). The van der Waals complex[20] resembles the complex between silanones and CH_2O,[8] but the bonding is considerably weaker than that in the latter complex (8 kcal mol^{-1}, Scheme 4). Intermediate **17** sits in an extremely shallow well (0.3 kcal mol^{-1} deep) on the energy hypersurface 6.2 kcal mol^{-1} above the van der Waals complex **13**, so that **17** effectively corresponds to a transition state, from which carbene **15** is formed by a proton shift.[21]

The transformation of complex **13** via **17** to carbene **15** also takes place at low temperature, as a result of the excess energy of 8 kcal mol^{-1} and slow dissipation of energy in the argon matrix. On the other hand, the remaining excess energy of the van der Waals complex **13** is insufficient to allow access to the transition state for formation of the oxasiletane **14**, which lies 7.8 kcal mol^{-1} above **13** and is formed by a 90° rotation of the



Scheme 4. Energies of some C_2OSiH_6 isomers, relative to the energy of **12**, calculated at the MP2/6-31G(d,p) and CCSD(T) levels.

CH_2O group in **17**. An energy difference of 1.6 kcal mol^{-1} in the respective barriers is therefore responsible for the fact that carbene **15** is formed rather than silaoxetane **14**.[22]

Carbene **15** can exist as C_1-symmetrical *gauche* or C_s-symmetrical *anti* conformer, although the former is more stable by 0.5 kcal mol^{-1}. The energy barrier for the rearrangement **15** → **16** is 4.7 kcal mol^{-1}; the reaction is exothermic by 33 kcal mol^{-1} and therefore irreversible. The results of the ab initio calculations are consistent with the experimental results and explain the formation of the carbene **15** in place of the anticipated oxasiletane **14**. Further experiments will show to what extent the new type of reaction between silenes and formaldehyde reported here is restricted to a matrix environment or whether it can also take place in solution.

Received: July 8, 1994
Revised version: December 23, 1994 [Z 7111 IE]
German version: *Angew. Chem.* **1995**, *107*, 999

Keywords: ab initio calculations · carbenes · IR spectroscopy · matrix isolation · silenes

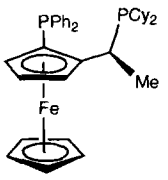
[1] a) N. Wiberg, *J. Organomet. Chem.* **1984**, *273*, 141–177; b) Silenes: A. G. Brook, K. M. Baines, *Adv. Organomet. Chem.* **1985**, *25*, 1–44.
[2] C. M. Golino, R. D. Bush, D. N. Roark, L. H. Sommer, *J. Organomet. Chem.* **1974**, *66*, 29–41.
[3] A. Sekiguchi, W. Ando, *Organometallics* **1987**, *6*, 1857–1860.
[4] NMR spectra of 1,2-silaoxetanes: a) N. Wiberg, G. Preiner, O. Schieda, *Chem. Ber.* **1981**, *114*, 3518–3532; b) W. L. Leigh, G. W. Slugett, *Organometallics* **1994**, *13*, 269–281.
[5] Crystal structure of a 1,2-silaoxetane: A. G. Brook, W. J. Chatterton, D. W. Hughes, K. Vorspohl, *Organometallics* **1987**, *6*, 1246–1256.
[6] S. M. Bachrach, A. J. Streitwieser, *J. Am. Chem. Soc.* **1985**, *107*, 1186–1190.
[7] W. J. Leigh, C. J. Bradaric, G. W. Sluggett, *J. Am. Chem. Soc.* **1993**, *115*, 5332–5333.
[8] M. Trommer, W. Sander, A. Patyk, *J. Am. Chem. Soc.* **1993**, *115*, 11775–11783.
[9] The photolyses were carried out with a 500 W Hg high-pressure lamp in combination with cutoff and interereference filters. The IR spectra were recorded

with a Bruker IFS-66 FT-IR spectrometer in the range 4000–400 cm^{-1} with a resolution of 1 cm^{-1}. Description of the matrix isolation equipment: W. Sander, *J. Org. Chem.* **1989**, *54*, 333–339.
[10] T. J. Drahnak, J. Michl, R. West, *J. Am. Chem. Soc.* **1981**, *103*, 1845–1846.
[11] O. M. Nefedov, A. K. Maltsev, V. N. Khabashesku, V. A. Korolev, *J. Organomet. Chem.* **1980**, *201*, 123–136.
[12] O. L. Chapman, C. C. Chang, J. Kolc, M. E. Jung, J. A. Lowe, T. J. Barton, M. L. Tumey, *J. Am. Chem. Soc.* **1976**, *98*, 7844–7846.
[13] M. R. Chedekel, M. Skoglund, R. L. Kreeger, H. Shechter, *J. Am. Chem. Soc.* **1976**, *98*, 7846–7848.
[14] **8**: IR (Ar, 10 K): $\tilde{\nu}$ = 2974.6 (14, C-H str.), 2912.5 (4, C-H str.), 2752.4 (9, C-H str.), 2624.2 (32, aldehyde C-H str.), 1661.4 (51, C=O str.), 1370.2 (14), 1252.1 (64), 880.8 (58), 864.7 (100), 850.6 (63), 765.5 (14), 711.8 (15), 702.5 (7), 585.3 (9) cm^{-1} (rel. intensity, assignment).
[15] **7**: IR (Ar, 10 K): $\tilde{\nu}$ = 2791 (13, C-H str.), 2706.4 (8, C-H str.), 2604.7 (25, C-H str. carbene), 1393.2 (25, OCH bend), 1306.6 (67), 1254.9 (97), 862.6 (73), 850.5 (100), 759.7 (35), 680.8 (30), 522.1 (7) cm^{-1} (rel. intensity, assignment).
[16] a) J. M. Duff, A. G. Brook, *Can. J. Chem.* **1973**, *51*, 2869–2883; b) R. A. Bourque, P. D. Davis, J. C. Dalton, *J. Am. Chem. Soc.* **1981**, *103*, 697–699.
[17] H. M. Perrin, W. R. White, M. S. Platz, *Tetrahedron Lett.* **1991**, *32*, 4443–4446.
[18] a) W. Kirmse, S. Steenken, M. Guth, unpublished results; b) M. Guth, Dissertation, Universität Bochum, **1993**.
[19] A series of oxycarbenes has been investigated by Sheridan et al.: a) M. A. Kesselmayer, R. S. Sheridan, *J. Am. Chem. Soc.* **1986**, *108*, 99–107; b) *ibid.* **1986**, *108*, 844–845; c) R. S. Sheridan, R. A. Moss, B. K. Wilk, S. Shen, M. Wlostowski, M. A. Kesselmayer, R. Subramanian, G. Kmiecik-Lawrynowicz, K. Krogh-Jespersen, *ibid.* **1988**, *110*, 7563–7564.
[20] A stable complex between a silene and THF with a very short Si–O distance: N. Wiberg, G. Wagner, G. Müller, J. Riede, *J. Organometal. Chem.* **1984**, *271*, 381–391.
[21] An exact description of the strongly zwitterionic compound **17** requires extensive MR-CI calculations (10 electrons, 10 active MOs), which are beyond the scope of the current work.
[22] The concerted [2 + 2] cycloaddition of silaethene and formaldehyde has an energy barrier of 18 kcal mol^{-1} (relative to **13**), according to the results of CCSD(T) calculations.

Strong Electronic Effects on Enantioselectivity in Rhodium-Catalyzed Hydroborations with Novel Pyrazole-Containing Ferrocenyl Ligands

Anita Schnyder, Lukas Hintermann, and Antonio Togni*

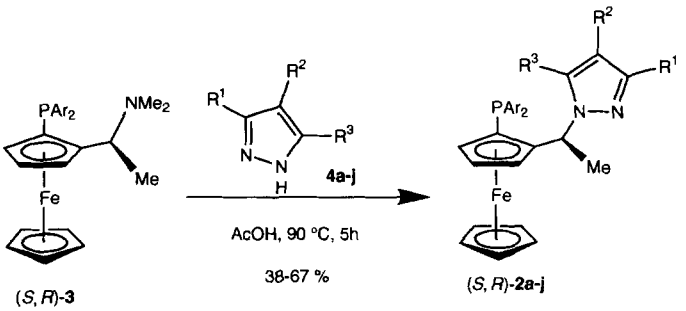
We have recently shown that chiral bidentate ferrocenyl phosphanes of type **1**, which contain two sterically and electronically different ligating fragments, are able to ensure high enantioselectivities in a variety of transition-metal-catalyzed reactions.[1] Our two-step methodology for the synthesis of such ligands allows the incorporation of phosphano groups with virtually no limitations. This ligand system provides an opportunity for studying steric and electronic effects due to the chiral inducing agent on stereoselectivity.



(*S*,*R*)-**1**

We then extended our concept to P,N-ligands[2] of type **2**, incorporating a phosphane and a pyrazole, an unprecedented combination in asymmetric catalysis,[3] and now report their use in the Rh-catalyzed hydroboration of styrenes with catecholborane.[4] The most striking finding relates to the observation of large electronic effects on the enantioselectivity of this reaction.[5] Furthermore, the different electronic properties of the pyrazole and phosphane fragments exert opposite influences: high enantioselectivities are obtained when both the N-ligand is a good σ-*donor* and the P-ligand a good π-*acceptor* (vide infra).

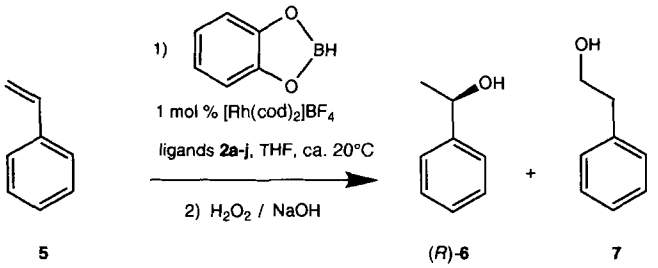
The new ligands **2** were easily prepared in moderate yields starting from ferrocenyl amines of type **3**[6] and the corresponding pyrazoles **4** in glacial acetic acid (Scheme 1). The results of



(*S*,*R*)-**3** (*S*,*R*)-**2a-j**

Scheme 1. Synthesis of pyrazolyl-containing ferrocenyl ligands. Cy = cyclohexyl. For R^1, R^2, R^3, Ar see Table 1.

the catalytic hydroboration experiments (Scheme 2) are summarized in Table 1. The reactions were conducted at room temperature in THF, with 1 mol% of the catalyst (formed in situ from $[Rh(1,5\text{-cod})_2]BF_4$ and 1.1 equiv of the ligand). Complete conversion of the substrate styrene was found to take place within



5 (*R*)-**6** **7**

Scheme 2. The Rh-catalyzed hydroboration of styrene with catecholborane. cod = cyclooctadiene.

3 to 5 h. Workup and product analysis were carried out as previously reported.[1a] Compared to some known systems,[4] our catalysts proved to be less regioselective and afforded relatively high amounts of the achiral linear alcohol. On the other hand, in some cases the enantioselectivity for the desired branched product **6** reaches very high and unprecedented values (up to 98.0% *ee*). Thus, the ligand containing the 3,5-dimethylpyrazolyl fragment (**2a**) affords an *ee* of 95.1% (Table 1, entry 1). Similar values were obtained with ligands **2c** and **2f**, which contain the extra substituent 4-methyl and 4-bromo, respectively (entries 3 and 6). Increasing the size of the groups in positions 3 and 5 from methyl to isopropyl lead to a lower enantioselectivity (91.6%, entry 5); the *steric* properties of those substituents are therefore crucial.

Replacement of the methyl groups by the strong σ-accepting trifluoromethyl fragments at positions 3 and 5 of the pyrazole should engender an *electronic* modification of the ligand, whilst only marginally altering its steric properties.[7] Thus ligand **2b** led to a drastically different stereochemical outcome when used under the exact same conditions. Whereas the regioselectivity dropped by only a few percent (from 66:34 to 61:39 branched to linear), the enantioselectivity dropped to 33.4% *ee* (from

[*] Prof. Dr. A. Togni, Dipl.-Chem. A. Schnyder, L. Hintermann
Laboratorium für Anorganische Chemie der Eidgenössischen Technischen Hochschule
ETH-Zentrum, CH-8092 Zürich (Switzerland)
Telefax: Int. code + (1)632-1090

 © VCH Verlagsgesellschaft mbH, D-69451 Weinheim, 1995 0570-0833/95/0808-0931 $ 10.00+.25/0

Table 1. Rhodium-catalyzed hydroboration of styrene with the ferrocenyl ligands **2**.

	Ligand				Regio-selectivity branched **6**/linear **7**	Enantio-selectivity **6**, % ee (*R*)	Yield [%] [1][a]
	R^1	R^2	R^3	Ar			
2a	Me	H	Me	Ph	66:34	95.1	91
2b	CF_3	H	CF_3	Ph	61:39	33.4	78
2c	Me	Me	Me	Ph	79:21	95.6	90
2d	CF_3	H	Me	Ph	46:54	43.8	79
2e	*i*Pr	H	*i*Pr	Ph	36:64	91.6	55
2f	Me	Br	Me	Ph	65:35	95.7	80
2g	H	H	H	Ph	41:59	65.2	71
2h	Ph	H	Me	Ph	47:53	79.6	92
2i	Me	H	Me	4-CF_3-C_6H_4	60:40	98.0	68
2j	Me	H	Me	4-MeO-C_6H_4	61:39	90.0	61

[a] Not optimized.

95.1% *ee*, entry 2). This corresponds to a difference of more than 1.5 kcal mol^{-1} in $\Delta\Delta G^{\neq}$ for the two diastereomorphous transition states in the reactions with the two different ligands. The 3-trifluoromethyl-5-methyl derivative **2d**, for which it is reasonable to assume electron-donating properties intermediate between those of **2a** and **2b**, also gave an intermediate *ee* of 43.8% (entry 4). A similar comment applies to the result obtained with ligand **2h** (3-phenyl-5-methyl derivative, 79.6% *ee*, entry 8). However, the comparison is not completely justified solely in *electronic* terms, because there is also an important *steric* difference between **2h** and **2a**,**b**,**d**.

Since the 3,5-dimethylpyrazolyl fragment was assumed to be the best suited for the reaction under study both from an electronic and a steric point of view, the electronic properties of the phosphane fragment of this derivative were modified. The introduction of *para*-substituents on the phenyl rings is easily achieved.[6b] Again a significant increase of enantioselectivity is obtained with ligand **2i**, which bears the electron-accepting trifluoromethyl group. The obtained value of 98% *ee* (entry 9) is the highest so far reported for this particular reaction and indicates a gain of about 0.5 kcal mol^{-1} in $\Delta\Delta G^{\neq}$ in going from **2a** to **2i**. When the electron-donating substituent OMe is used instead (ligand **2j**), a loss of enantioselectivity is observed (90.0% *ee*, entry 10). This is comparable, in terms of $\Delta\Delta G^{\neq}$, to the gain mentioned above.[8]

The ligands affording lower selectivities contain pyrazolyl fragments that are relatively electron-poor. Therefore one could argue that the observed low enantioselectivity yielded by, for example, **2b** could be due to partial dissociation of this ligand from rhodium during catalysis. Such dissociation to yield a monodentate phosphane ligand would reduce the selectivity of the catalyst. We addressed the problem of *thermodynamic* stability of the Rh complexes containing the ligands **2a**,**b**,**d**,**g**, and **h** by simple NMR competition experiments. Mixing equivalent amounts of a) $[Rh(1,5\text{-cod})_2]BF_4$ and two different ligands of type **2**, or b) of the complex [Rh(1,5-cod)(ligand 1)]BF_4 and ligand 2, and analyzing the equilibrium mixture by ^1H and ^{31}P NMR allowed us to establish the following relative stability series of the species [Rh(1,5-cod)(**2**)]BF_4, depending on the ligand: **2g** ≈ **2a** > **2h** > **2d** > **2b**. According to these experiments the difference in stability constant for the complexes containing **2g** and **2b** (the most and the least stable, respectively) is at least four orders of magnitude.[9] Thus, stability partially correlates with the observed enantioselectivity. However, we were not able to observe partial dissociation of the pyrazolyl moiety, even upon addition of less than one equivalent of a monodentate phosphane (PEt_3 or PPh_3) to the corresponding complex. The monodentate ligand was incorporated into the complex $[Rh(1,5\text{-cod})(PR_3)_2]BF_4$ quantitatively, thus indicating that under thermodynamic control the ferrocenyl ligands either dissociated completely or not at all. Furthermore, a large excess of the substrate of the catalytic reaction, styrene, is not able to induce any observable dissociation of any of the pyrazolyl ligands under study. From these experiments we conclude that dissociation of the ligands from the catalytically active species most likely is not taking place and that the effects on enantioselectivity we report are indeed predominantly electronic in nature.[10]

Since the effects we observed are ultimately an expression of a subtle change in the electronic structure of the transition metal complexes involved in the catalytic reaction, and hence of their reactivity, they elude any treatment according to current views on electronic effects in organic chemistry.[11] The observed phenomena can be tentatively explained as follows, taking into account a comparison between ligands **2a** and **2b** explicitly: In the two ligands the phosphane group is both a good σ-donor and a moderate π-acceptor. The pyrazolyl nitrogen in **2a** will be a very good σ-donor with almost no π-accepting properties, whereas in **2b** its σ-donor capability will be reduced, in favor of a moderate π-accepting propensity, by virtue of the aromatic system in which it is imbedded. In this respect it will behave similarly to an electron-poor phosphane. Thus, because of the pure σ-character of the Rh–N bond in the complex containing ligand **2a**, this ligand will induce a higher "*electronic asymmetry*" at the metal center than **2b**, which will be reflected in the enhanced enantioselectivity observed. This electronic asymmetry seems to be maximized in ligand **2i**, in terms of further enhancing the π-acceptor qualities of the phosphane, relative to the situation in **2a**. In order to turn these conjectures into a more sound argument, detailed mechanistic and structural studies are required. These are currently in progress and will be reported in due course.

Experimental Procedure

A typical preparation for the pyrazolyl ligands, that of 1-{(*S*)-1-[(*R*)-(diphenylphosphano)ferrocenyl]ethyl}-3,5-di-methylpyrazole (**2a**), is described: A solution of (*S*)-(*R*)-**3** (2.5 g, 5.6 mmol) and 3,5-dimethylpyrazole (0.65 g, 6.8 mmol, 1.2 equiv) in glacial acetic acid (10 mL) was stirred at 90 °C for 3 h. The red reaction mixture was quenched with saturated, aqueous $NaHCO_3$ and extracted with hexane. The combined organic layers were washed with saturated, aqueous NaCl and dried over $MgSO_4$. Removal of the solvent and recrystallization from hexane afforded **2a** as yellow crystals (1.52 g, 55%). m.p. 127 °C (decomp.); $[\alpha]_D^{20} = 329$ ($c = 0.42$, $CHCl_3$); ^1H NMR ($CDCl_3$, 250 MHz): $\delta = 6.68$–7.53 (m, 10H), 5.58 (dq, 2 Hz, 1H), 5.06 (s, 1H), 4.79–4.81 (m, 1H), 4.35–4.37 (m, 1H), 4.05 (s, 5H), 3.72–3.74 (m, 1H), 2.13 (s, 3H), 1.95 (s, 3H), 1.70 (d, 7 Hz, 3H); ^{31}P NMR ($CDCl_3$, 101 MHz): $\delta = -24.1$ (s, PPh_2); elemental analysis: calcd for $C_{29}H_{29}FeN_2P$: C, 70.72; H, 5.94; N, 5.69; found: C, 70.74; H, 6.01; N, 5.59. The ligands **2b**–**j** were prepared analogously.

Received: October 8, 1994
Revised version: February 6, 1995 [Z73851E]
German version: *Angew. Chem.* **1995**, *107*, 996

Keywords: asymmetric syntheses · complexes with P,N ligands · ferrocenyl ligands · hydroborations

[1] a) A. Togni, C. Breutel, A. Schnyder, F. Spindler, H. Landolt, A. Tijani, *J. Am. Chem. Soc.* **1994**, *116*, 4062–4066; b) C. Breutel, P. S. Pregosin, R. Salzmann, A. Togni, *ibid.* **1994**, *116*, 4067–4068; c) A. Togni, C. Breutel, M. C. Soares, N. Zanetti, T. Gerfin, V. Gramlich, F. Spindler, G. Rihs, *Inorg. Chim. Acta* **1994**, *222*, 213–224.

[2] For other successful chiral P,N-ligands recently reported, see a) P. von Matt, A. Pfaltz, *Angew. Chem.* **1993**, *105*, 614–615; *Angew. Chem. Int. Ed. Engl.* **1993**, *32*, 566–567; b) P. von Matt, O. Loiseleur, G. Koch, A. Pfaltz, C. Lefeber, T. Feucht, G. Helmchen, *Tetrahedron: Asymmetry* **1994**, *5*, 573–584; c) J. Sprinz, G. Helmchen, *Tetrahedron Lett.* **1993**, *34*, 1769–1772; d) J. Sprinz, M. Kiefer, G. Helmchen, M. Reggelin, G. Huttner, O. Walter, L. Zsolnai, *ibid.* **1994**, *35*, 1523–1526.

 © VCH Verlagsgesellschaft mbH, D-69451 Weinheim, 1995 0570-0833/95/0808-0932 $ 10.00+.25/0

[3] The first two derivatives of this type have been reported from our laboratory in the context of a new general synthetic approach to chiral ferrocenyl ligands: H. C. L. Abbenhuis, U. Burckhardt, V. Gramlich, A. Togni, A. Albinati, B. Müller, *Organometallics*, **1994**, *13*, 4481–4493. For other enantiomerically pure ligands incorporating two or three pyrazole fragments and their use in asymmetric catalysis see, for example, M. Bovens, A. Togni, L. M. Venanzi, *J. Organomet. Chem.* **1993**, *451*, C28–C31; C. J. Tokar, P. B. Kettler, W. V. Tolman, *Organometallics* **1992**, *11*, 2737–2739; D. D. LeCloux, W. V. Tolman, *J. Am. Chem. Soc.* **1993**, *115*, 1153–1154. For a review on nitrogen ligands in homogeneous catalysis, see A. Togni, L. M. Venanzi, *Angew. Chem.* **1994**, *106*, 517–547; *Angew. Chem. Int. Ed. Engl.* **1994**, *33*, 497–526.

[4] For a recent review, see: K. Burgess, M. J. Ohlmeyer in *Homogeneous Transition Metal Catalyzed Reactions* (*Adv. Chem. Ser.* **1992**, *230*) pp. 163–177, and references cited therein. For a recent report on the use of a chiral chelating P,N-ligand system in Rh-catalyzed hydroboration, see: J. M. Brown, D. I. Hulmes, T. P. Layzell, *J. Chem. Soc. Chem. Commun.* **1993**, 1673–1674.

[5] Electronic effects in asymmetric catalysis with other types of ligands have been recently reported. Rh-catalyzed hydrogenation: a) K. Inoguchi, S. Sakuraba, K. Achiwa, *Synlett* **1992**, 169–178, and references cited therein. b) T. V. Rajan Babu, T. A. Ayers, A. L. Casalnuovo, *J. Am. Chem. Soc.* **1994**, *116*, 4101–4102. Ru-catalyzed hydrogenation with BINAP-type ligands: c) K. Mashima, K. Kusano, N. Sato, Y. Matsumura, K. Nozaki, H. Kumobayashi, N. Sayo, Y. Hori, T. Ishizaki, S. Akutagawa, H. Takaya, *J. Org. Chem.* **1994**, *59*, 3064–3076. Ni-catalyzed hydrocyanation of vinylarenes: d) A. L. Casalnuovo, T. V. RajanBabu, T. A. Ayers, T. H. Warren, *J. Am. Chem. Soc.* **1994**, *116*, 9869–9882. e) T. V. RajanBabu, A. L. Casalnuovo, *Pure Appl. Chem.* **1994**, *66*, 1535–1542. f) *J. Am. Chem. Soc.* **1992**, *114*, 6265–6266. Rh-catalyzed hydroformylation of olefins: g) T. V. RajanBabu, T. A. Ayers, *Tetrahedron Lett.* **1994**, *35*, 4295–4298. Mn-catalyzed epoxidation of nonfunctionalized olefins: h) E. N. Jacobsen in *Catalytic Asymmetric Synthesis* (Ed.: I. Ojima), VCH, New York, **1993**, pp. 159–202, and references therein. Rh-catalyzed hydrosilylation of ketones: i) H. Nishiyama, S. Yamaguchi, M. Kondo, K. Itoh, *J. Org. Chem.* **1992**, *57*, 4306–4309. For electronically controlled stoichiometric reactions of Mo-allyl complexes, see: j) J. W. Faller, K.-H. Chao, *J. Am. Chem. Soc.* **1983**, *105*, 3893-3898. k) J. W. Faller, J. T. Nguyen, W. Ellis, M. R. Mazzieri, *Organometallics*, **1993**, *12*, 1434–1438.

[6] a) T. Hayashi, T. Mise, M. Fukushima, M. Kagotani, N. Nagashima, Y. Hamada, A. Matsumoto, S. Kawakami, M. Konishi, K. Yamamoto, M. Kumada, *Bull. Chem. Soc. Jpn.* **1980**, *53*, 1138–1151. b) T. Hayashi, A. Yamazaki, *J. Organomet. Chem.* **1991**, *413*, 295-302.

[7] For a discussion of the steric bulk of aliphatic groups in terms of cone angles, see a) D. Datta, D. Majumdar, *J. Phys. Org. Chem.* **1991**, *4*, 611–617. b) D. White, N. J. Coville, *Adv. Organomet. Chem.* **1994**, *36*, 95–158. The cone angle of a methyl group is 112°, whereas that of the trifluoromethyl substituent is 135°, identical to the value for isopropyl.

[8] Substrate electronic effects were also observed (see also [4]). Thus, compared to styrene and in the presence of ligand **2a**, *para*-chlorostyrene and *para*-methoxystyrene both gave lower *ee*'s (93.5 and 79.2% *ee*, respectively). With ligand **2b** the same two substrates afforded 13 and 77.6% *ee*, compared to 33.4% *ee* for styrene.

[9] Assuming a conservative NMR detection limit of 100:1 for two different compounds, such a difference in stability constant between the complexes containing **2g** and **2b** is inferred by comparing different pairs of ligands. These stability measurements, carried out on catalyst precursors, do not necessarily reflect the stabilities of the actual complexes involved in the catalytic cycle, but may be reasonably taken as an indication of the trend.

[10] However, the existence of a catalytically active complex containing the ferrocenyl ligand acting in a monodentate fashion under kinetic control cannot be excluded by these experiments.

[11] For general discussions of electronic effects in organic chemistry see, for example, a) J. March, *Advanced Organic Chemistry*; 4th ed., Wiley, New York, **1992**, Chapter 9, pp. 273–292. b) R. D. Topsom, *Progr. Phys. Org. Chem.* **1976**, *12*, 1–20.

 © *VCH Verlagsgesellschaft mbH, D-69451 Weinheim, 1995* *0570-0833/95/0808-0933 $ 10.00+.25/0*

What's in a Name

Instrumental Methods for Determining Elements. By *L. R. Taylor, R. B. Papp* and *B. D. Pollard.* VCH Verlagsgesellschaft, Weinheim/VCH Publishers, New York, 1994. 322 pp., hardcover DM 128.00, $ 51.50.—ISBN 3-527-28096-0/1-56081-038-6

This book is intended for the analytical chemist who has to choose the most suitable method for a given problem. It treats in detail all the most important modern instrumental methods of elemental analysis: atomic absorption spectroscopy (AAS), atomic emission spectroscopy (AES), voltammetry, potentiometry, chromatography, X-ray fluorescence, and combustion methods. For each method there is a brief description of the basic physical principle and the construction of the instrument. This information is intended only as a short introduction, and not as a substitute for a thorough study of the fundamentals of the method concerned. References to detailed specialist literature in the form of monographs or original papers are provided.

The authors then compare the various methods with regard to their practical application, placing special emphasis on the needs of the user who must decide on a particular analytical method for the problem in hand. They consider questions about the sample itself, including the nature of the matrix, sample size, and sample preparation, economic factors such as the capital and running costs of the instrument, its complexity, sample throughput rate, and possibilities for automation. A clear distinction is made between, on the one hand, purely instrumental factors such as limits of detection, sensitivity, operating range, precision, and selectivity, and on the other hand element-related matters such as capabilities for multielement detection, for quantitative analysis, and for distinguishing between different species of the same element. The authors also discuss questions such as how widespread is the use of the instruments concerned (as this affects the availability of information about applications), and whether the method can be used for on-line process analysis. Each chapter is rounded off by giving examples (in the form of tables) of typical applications of the method, and information about the main instrument manufacturers, which is useful for requesting promotional and technical information. As well as the methods mentioned above, the authors also briefly discuss capillary electrophoresis, flow injection analysis, mass-spectrometric techniques, neutron activation analysis, and spectrophotometry.

The detailed discussions of the various methods are helpful to the reader both in choosing suitable analytical methods for specific problems and, if the question arises, in purchasing a new analytical instrument. In this respect the book differs from conventional texts in this field, which are usually confined to treating in detail the theoretical background and the areas of application of each analytical method. *Instrumental Methods for Determining Elements* is therefore a valuable additional resource for the practical analyst.

Nicolas Braun
Hannover (FRG)

Namen- und Schlagwortreaktionen der Organischen Chemie. By *T. Laue* and *A. Plagens.* Teubner, Stuttgart, 1994. 338 pp., paperback DM 36.80.—ISBN 3-519-03526-X

Organic Syntheses Based on Name Reactions and Unnamed Reactions. By *A. Hassner* and *C. Stumer.* Pergamon, Oxford, 1994. 452 pp., paperback £ 28.00.—ISBN 0-08-040279-8

The Noyori homogeneous catalytic reaction for asymmetric hydrogenation will certainly mean something to you. But are you also familiar with the Perkow synthesis of vinyl phosphates? What do you know about the Neber rearrangement? Would you like to be able to quickly find out something about the Stork enamine reaction? The two books reviewed here can help with such questions, rapidly and at little cost. For the average reader it is still just as important as ever to have rapid access to information without using CD-ROM or on-line services. Although summaries of important reactions already exist—for example, in the relevant section of the Merck Index—these two books by Hassner and Stumer and by Laue and Plagens bring together information on important reactions of organic chemistry in a very handy form that is convenient to use. Although they are very similar in layout, some clear differences emerge. The book by Laue and Plagens, in the Teubner series of student textbooks, has a striking external appearance with a somewhat more careful standard of production, the typeface and the formulas being well matched in size and pleasingly arranged. On the other hand the book by Hassner and Stumer, in the Tetrahedron Organic Chemistry Series, is a compilation of pages produced directly from the computer, and one is struck by the large areas of empty space.

The Laue and Plagens book is intended for students of chemistry, pharmacy, and related disciplines, and contains clear descriptions, in alphabetical order, of some 130 important reactions of organic chemistry. These include both important name reactions and others ("Schlagwortreaktionen", key-word reactions) that are known by descriptive names rather than being linked to the name of a scientist, e.g. the di-π-methane rearrangement. As well as classical examples such as the Finkelstein and haloform reactions, which are to be found in any traditional textbook of organic chemistry, the compilation also includes many of more recent origin, such as the Pauson–Khand reaction, the Bergman cyclization, and the Dötz reaction. In each case the title is followed by a one-sentence description of the reaction and a generalized formula scheme. Next there is a brief discussion in which the main emphasis is on the reaction mechanism. Other relevant information is also given; for example, in

This section contains book reviews and a list of new books received by the editor. Book reviews are written by invitation from the editor. Suggestions for books to be reviewed and for book reviewers are welcome. Publishers should send brochures or (better) books to Dr. Ralf Baumann, Redaktion Angewandte Chemie, Postfach 101161, D-69451 Weinheim, Federal Republic of Germany. The editor reserves the right of selecting which books will be reviewed. Uninvited books not chosen for review will not be returned.

 © *VCH Verlagsgesellschaft mbH, D-69451 Weinheim, 1995* *0570-0833/95/0808-0935 $ 10.00+.25/0*

describing the Cope rearrangement it is pointed out that it should not be confused with the Cope elimination reaction. The cross-references to other reactions described in this book are very helpful. The book also contains a short list of selected literature references, giving not only the first publication in which each reaction is described, but also important review articles enabling the reader to find out about a reaction of interest in greater depth. It is pleasing that the authors appear to have made an effort to include some quite recent citations extending into the 1990s. Brief name and subject indexes are provided at the end of the book.

The book by Hassner and Stumer covers about 450 reactions, including some lesser known ones, again arranged alphabetically. In the preface the authors rightly point out that for reasons of space alone it is not possible to include every reaction, and that some whose mechanisms are likely to be well known to every chemist have been purposely omitted. Nevertheless, in view of the fact that many reactions of a highly specialized nature have been included, it is surprising to find no mention of the mechanistically important and highly topical Bergman cyclization. In many cases several closely similar reactions have been included. Each reaction is first described in a single sentence, which is then followed by a formula scheme for a specific example of the reaction, giving the reaction conditions and in many cases also the yield. A few relevant literature references are listed, including the first paper describing the reaction and at least one review article. Lastly the experimental details for carrying out the example reaction are given. At the end of the book are indexes according to names, reagents, and reaction types, as well as a fold-out "Functional Group Transformations Index" similar to those provided in the *Compendium of Organic Synthetic Methods*.

What are the main differences, and which book should be recommended? The book by Laue and Plagens is certainly aimed more at the needs of students, and from that standpoint the inclusion of brief summaries of the mechanistic background is an important advantage. By cleverly limiting the coverage to about 130 reactions the authors have allowed themselves sufficient space to do justice to the didactic quality expected from a book intended for students. The book by Hassner and Stumer is clearly intended rather for the research chemist in academia or industry. For this readership, although it may still be important to give mechanistic information, the main need seems to be for rapid access to typical experimental conditions for the reaction of interest. Whereas Laue and Plagens can best serve to complete the reader's knowledge, Hassner and Stumer on the other hand is more in the nature of a resource for solving preparative problems. For the latter purpose one is not necessarily looking for a named reaction, but it is a fact that many of the most important reactions carry the names of their originators. What is meant in the title by "Unnamed Reactions"? There are none of these in the book—by definition they cannot even appear in the "Names Index". The authors have given every reaction (at least) one name in its heading. Probably the purpose of this part of the book's title is just to attract the attention of potential readers.

Both books are well suited to their different purposes and can be recommended—this reviewer is glad to have them both. However, a word of caution is in order. These books and others like them are eminently suitable for quickly learning about a large number of reactions of organic chemistry, and many readers will certainly find them very useful, for example when preparing for examinations. Nevertheless, both the readers and their teachers must always bear in mind that knowing about a reaction is no substitute for understanding it. These books are not intended as alternatives to more detailed textbooks, but are for quick reference, and are best treated as an extension of the textbooks to be used judiciously. No well-constructed examination can be limited to merely asking about named reactions, and equally the memorizing of a "data bank" of reactions is not sufficient to enable one to succeed as a scientist.

Holger Butenschön
Institut für Organische Chemie
der Universität Hannover (FRG)

Chemical Generation and Reception of Radio- and Microwaves. By *A. L. Buchachenko* and *E. L. Frankevitch*. VCH Verlagsgesellschaft, Weinheim, 1994. 180 pp., hardcover DM 135.00.—ISBN 3-527-89630-9.

"Spin chemistry", i.e. the investigation and utilization of magnetic field effects and spin effects in chemical reactions, enjoys increasing popularity. The authors of the present book like to distinguish between two generations of spin chemistry. The first was concerned with the influence of static magnetic fields, typical examples being magnetic field effects (MFE) or chemically induced dynamic nuclear and electron spin polarizations (CIDNP and CIDEP). In this book the emphasis is on spin chemistry of the second generation, which comprises the interactions with additional oscillating fields. These cause radio-induced magnetic isotope effects (RIMIE), stimulated nuclear polarization (SNP), and microwave-stimulated quantum beats, and are exploited in reaction yield detected magnetic resonance (RYDMR). In addition, the authors deal with the reversal of such processes, namely the emission of coherent microwave radiation from chemically reacting systems.

In the first chapter, "Magnetic Scenario of Chemical Reaction", numerous examples are given to drive home the principle of spin conservation during chemical transformations and thus spin selectivity of chemical reactions. The second chapter is a discussion of the radical pair mechanism, despite its misleading title, "Magnetic Interactions in Chemical Reactions". The title of the third chapter, "Magnetic Effects in Chemical Reactions", also slightly misrepresents its actual content: except for a few introductory sentences, it only deals with spin chemistry of the first generation. "Chemically Induced Radio-Frequency Emission" is only touched upon in the short (15 pp.) fourth chapter, although from the title of the book one would have expected this to be a central topic. Four chapters on RYDMR ("Reaction Yield Detected Magnetic Resonance—RYDMR", "RYDMR in Solids", "RYDMR in Liquid Solutions", and "RYDMR in Photosynthetic Systems") are followed by two others ("Radio-Induced Magnetic Isotope Effect" and "Microwave-Stimulated Nuclear Polarization") about spin chemistry of the second generation. The authors focus on examples and applications rather than on detailed quantitative explanations of the theory of these effects. In Chapter 11 ("Coherence in Spin Dynamics and Chemical Reactivity") quantum beats are discussed. At the end of the volume we find a very short chapter (3 pp.) on "The Action of Electromagnetic Waves on Biological Processes".

The most striking impression one receives when going through the book for the first time is that it is written in alarmingly bad English. A few examples, quoted verbatim, may illustrate this; there are numerous others of this kind. There are frequent misspellings of proper names—"Plank constant" (p. 3), "Schrodinger equation" (p. 18), "Gann-diode" instead of Gunn-diode (p. 76), "Abraham" instead of Abragam (consistently on p. 125 and p. 127), and chemical names—"vinilene" (p. 100), "acetonitryl" (p. 125), "dinucleatide" (p. 130).

 © VCH Verlagsgesellschaft mbH, D-69451 Weinheim, 1995 0570-0833/95/0808-0936 $ 10.00+.25/0

Often though, not only the laws of the English language but also those of logic are violated, and the reader is slowed down trying to figure out the likely meaning: "The term $(1-\Lambda)F$ takes into account the unfavorable chance that the pair, being transformed from triplet to singlet and being ready to react, avoids the reactions since $\Lambda < 1$" (p. 22); "If in the course of the reaction some products may be produced that have the same spin as that of the pair, then the reaction proceeds" (p. 62); "The kinetic scheme gives a qualitatively good picture of a spectrum of resonant variations in the rate constants away from crossing of intermediate pair levels" (p. 113); "The spin of ion radical D^+ at the moment of its recombination was conditioned by its evolution as the spin of the hole while it was in a state M^+ that was a precursor of D^+" (p. 120). The third of the foregoing examples is utterly incomprehensible (at least to the present reviewer), both with and without its context.

At times, the formulations verge on the absurd:—page 11: "Radical pair is a dynamic system from which the radicals can diffuse apart, traveling randomly in space and time, and then return and reencounter"—page 126: "A small internal size of a micelle where radicals can diffuse makes us believe that the prominent part of their lifetime will be spent suffering on exchange interaction".

Looking more closely into the book, one detects a good many errors in figures and formulas. Again, some examples: In Figures 1.1, 2.3, and 5.4 (bottom), vector representations of the triplet states $|T_{+1}\rangle$ and $|T_{-1}\rangle$ are given, in which the phase difference between the two vectors is 180°. On the other hand, in the vector models of Figures 2.2 and 5.4 (top) there is a phase difference of 0°. What is the reader to think if the same state is depicted in two ways that are obviously quite different? But in addition, even within the limitations of vector models, *both* these representations are wrong. In the first, the resultant spin coincides with the z-axis, which is a violation of the uncertainty principle. In the second, combination of two vectors representing spin-1/2 particles would give a vector of wrong total length ($\sqrt{3}\hbar$ instead of $\sqrt{2}\hbar$). The correct way to draw the diagrams for $|T_{+1}\rangle$ and $|T_{-1}\rangle$ is with a 90° phase difference.

For the magnetic moment of the nucleus, we find $\mu_n = -g_n(\beta_n/\hbar)\boldsymbol{J}$, i.e. the wrong sign (p. 4). The same mistake appears in the expression for the z-component of μ_n. On page 13, the dependence of the sign of the electron Zeeman energies on the electron spin state is ignored. In the expression on page 42 for the ratio of the equilibrium populations of adjacent nuclear energy levels, the denominator of the Boltzmann term should have kT instead of $2kT$. Anyone working in the field of magnetic resonance will probably spot these and similar errors at once. However, the book aims at the non-specialist, for instance at chemical physicists and physical organic chemists, as we read on its cover.

In the equation for the $S-T_0$-mixing matrix element (Eq. 2.12 on p. 18), the sign of the second term is wrong. The third term of the expression for the spin-independent probability of geminate recombination (Eq. 2.27 on p. 20) should have p^2 instead of p. Et cetera; it is to be doubted that a reader trying to get acquainted with spin chemistry will detect such errors at a glance.

The later parts of the book contain more than 50 equations, many of them very specialized, and the derivations of most of them are not given. The above examples do not inspire great confidence in their correctness.

Analyzing the references, some 200 in number, and eliminating duplicate entries and conference proceedings that are not generally available, the reviewer found only about 30 publications that were concerned with the main subjects of the book and had appeared after 1987. One cannot help noticing that the most recent reference pertaining to "Chemically Induced Radio-Frequency Emission" dates back to 1983, and that this was itself a review, written by one of the authors of the present book. Obviously, nothing of importance has happened in the latter field during the last ten years, so why review it anew? The cover text "...first critical overview in a decade..." seems almost ironical under these circumstances.

Finally, one puts aside the book with the impression that the efforts of the two authors have not always been well coordinated and that their treatment of the subject matter is somewhat imbalanced. For instance, vector models and intersystem crossing in radical pairs are discussed at the beginning of Chapter 2 and are explained in just as much detail a second time in Chapter 5. Also, many formulas appear in duplicate (Eqs. 2.4 and 2.11, 2.5 and 2.12, 2.6 and 2.34, 2.7 and 2.35, etc.); the contents of Figures 1.1, 2.2 (top), and 5.4(a) are identical, apart from the inconsistencies mentioned above; the same holds for Figures 2.3 and 5.4(b); and so on. Basic concepts which should be known to the group of scientists the book is intended for, such as singlet and triplet states and spin conservation in chemical reactions, are treated at length (three pages of examples to illustrate the latter principle) and repeated frequently. In contrast, throughout the book practically all derivations and details of the calculations are skipped, and there are abrupt jumps to rather specialized results. Is it not one of the very purposes of a monograph to *bridge* the gaps between the fundamentals and the end results?

In summary, this book is probably of little value for a "chemical physicist, physical organic chemist, material scientist, radio- or biophysicist" (press release) in general. Maybe the expert in the field of spin chemistry could profit from it in some points.

Martin Goez
Institut of Physical Chemistry
University of Braunschweig (FRG)

 © *VCH Verlagsgesellschaft mbH, D-69451 Weinheim, 1995* *0570-0833/95/0808-0937 $ 10.00+.25/0*

Combinatorial Synthesis and Multidimensional NMR Spectroscopy: An Approach to Understanding Protein–Ligand Interactions

James K. Chen and Stuart L. Schreiber*

Combinatorial chemistry is a laboratory emulation of natural recombination and selection processes. Strategies in this developing discipline involve the generation of diverse, molecular libraries through combinatorial synthesis and the selection of compounds that possess a desired property. Such approaches can facilitate the identification of ligands that bind to biological receptors, promoting our chemical understanding of cellular processes. This article illustrates that the coupling of combinatorial synthesis, multidimensional NMR spectroscopy, and biochemical methods has enhanced our understanding of a protein receptor used commonly in signal transduction, the Src Homology 3 (SH3) domain. This novel approach to studying molecular recognition has revealed a set of rules that govern SH3–ligand interactions, allowing models of receptor–ligand complexes to be constructed with only a knowledge of the polypeptide sequences. Combining combinatorial synthesis with structural methods provides a powerful new approach to understanding how proteins bind their ligands in general.

Keywords: combinatorial chemistry · molecular recognition · NMR spectroscopy · proteins

1. Introduction

Chemistry has profoundly influenced the development of modern biology. Since the pioneering work of Emil Fischer, chemists have explored the molecular realm of life and reconstructed its basic elements. Biological cofactors, metabolites, and hormones have been characterized and resynthesized using the tools of organic chemistry. Similarly, X-ray crystallography and NMR spectroscopy have been used to elucidate the primary macromolecules of nature: proteins, DNA, and RNA. These advances have transformed our understanding of biology, allowing cellular processes to be analyzed at the molecular level.

The complementary impact that biology has had on chemistry, however, should not be overlooked. Many chemical strategies have been inspired and guided by biological phenomena. This reciprocal relationship between chemistry and biology is exemplified by recent advances in the areas of ligand discovery and molecular recognition. Traditional approaches in these disciplines have utilized the powerful tools of computer modeling and organic synthesis, but have been limited by our incomplete understanding of molecular interactions and the inefficiency of evaluating individual lead compounds. As a result, new strategies for ligand discovery that emulate biological processes have emerged. These approaches draw from the genetic recombination and selection mechanisms that yield specific receptor–ligand interactions in nature. Similar mechanisms regulate the humoral immune response, in which antigen-binding receptors are selected from large combinatorial pools of antibodies. Guided by these biological models, chemists have developed an alternative strategy for ligand discovery: molecular libraries generated by combinatorial synthesis.

Like its biological counterpart, combinatorial chemistry relies on the efficient synthesis of large, diverse libraries of compounds and the facile selection of molecules that have a desired property. Its success as a strategy for ligand discovery also requires the unambiguous characterization of these molecules, which often are present in minute quantities. Significant progress has been made on both fronts, especially in the past five years. Many initial applications of combinatorial synthesis have focused on the discovery of therapeutic agents, paralleling the development of traditional organic synthesis. Medicinally important targets such as the human platelet fibrinogen receptor have been studied with synthetic libraries, providing chemical leads in drug discovery efforts. Indeed, one important objective in combinatorial chemistry is the development of libraries that contain bioavailable compounds and their application in medical research.

Especially when coupled to neighboring disciplines, combinatorial synthesis also has enormous potential to elucidate fundamental problems in basic research. In particular, combinatorial chemistry can advance our understanding of cellular processes, completing the synergistic cycle of chemistry and biology. This review highlights the recent application of combinatorial syn-

[*] Prof. S. L. Schreiber, J. K. Chen
Howard Hughes Medical Institute
Department of Chemistry, Harvard University
Cambridge, MA 02138 (USA)
Telefax: Int. code + (617) 495-0751

 © VCH Verlagsgesellschaft mbH, D-69451 Weinheim, 1995 0570-0833/95/0909-0953 $ 10.00+.25/0

thesis to the study of Src (pronounced "sark") Homology 3 (SH3) domains, a family of protein modules involved in intracellular signal transduction pathways. By combining this technique with multidimensional NMR spectroscopy and site-directed mutagenesis, it has provided insights into the molecular recognition of SH3 domains, revealing a unique biological mechanism for protein association. These advances have culminated in a detailed understanding of SH3–ligand interactions involving two distinct binding modes and allow for the straightforward molecular modeling of SH3–ligand complexes using only a knowledge of polypeptide sequences.

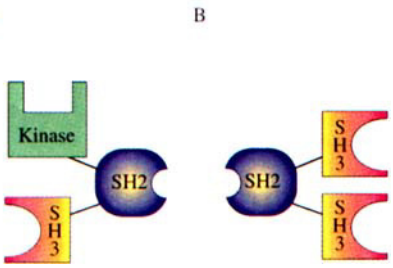


Fig. 1. Schematic representation of two classes of SH3-containing proteins: A) proteins with catalytic domains (e.g. a kinase), B) macromolecular adaptors for protein association.

2. Background

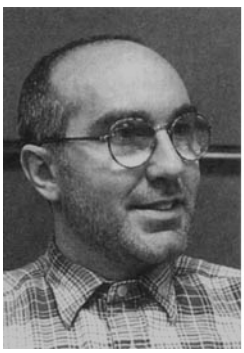
2.1. Biochemical Studies

SH3 domains are small receptor modules of approximately 60 amino acids.[1, 2] Initially observed in the Src family of tyrosine kinases, these conserved domains have been found in a variety of proteins that mediate signal transduction, the biological mechanism by which extracellular molecules influence intracellular events. SH3-containing signaling molecules are structurally and functionally diverse, ranging from phospholipase C-γ (PLC-γ) to the p85 subunit of phosphatidylinositol 3-kinase (PI3K). SH3 domains have also been identified in cytoskeletal proteins and are often accompanied by receptor modules called SH2 domains, which recognize tyrosine-phosphorylated proteins in a sequence-specific manner (Fig. 1). These observations have suggested that SH3 domains mediate protein–protein interactions in signal transduction pathways and cytoskeletal structures (Fig. 2). Biochemical studies have subsequently implicated SH3 domains in subcellular localization,[3] enzymatic regulation,[4] substrate recognition,[5] and the regulation of guanosine triphosphate (GTP) binding proteins.[6]

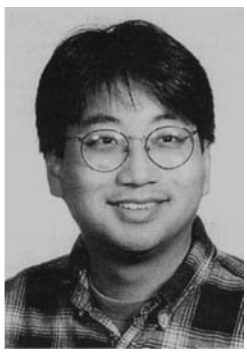
Our investigations have focused on understanding the molecular recognition of SH3 domains, using the cellular Src (c-Src) and PI3K SH3 receptors as model systems. Src is a nonreceptor tyrosine kinase with one SH2 and one SH3 domain, both of which are essential for normal cellular signaling.[7] The mutation or deletion of either domain activates the catalytic and oncogenic potential of Src and abrogates the association of at least one kinase substrate, p110.[4a–c, e, 8] PI3K is a heterodimeric complex composed of a 110 kDa catalytic subunit that contains a lipid (phosphatidyl inositol) kinase domain and an 85 kDa regulatory subunit that contains one SH3 domain, two SH2 domains, and a region with homology to Rho/Rac ("row" and "rack") GTPase-activating proteins (GAPs).[9] The SH2 domains of PI3K mediate its interaction with the phosphorylated cytoplasmic tails of activated growth factor receptors,[9a–c, 10] whereas the cellular function of the SH3 domain is unknown. Like their parent proteins, the SH3 domains of Src and PI3K are structurally diverse, sharing only 21% sequence identity.[2c] The two protein modules contain highly dissimilar regions, including a 15 amino acid insert in PI3K p85 that is absent in the SH3 domain of Src. By studying these two structurally unique SH3 domains, we hoped to elucidate the general principles of SH3–ligand interactions as well as the origins of ligand specificity.

The first insights into the molecular recognition of SH3 domains were provided by Baltimore et al. The SH3-binding proteins 3BP1 and 3BP2 were identified by screening a cDNA expression library, using the Abl ("able") SH3 domain fused to glutathione *S*-transferase (GST) as a probe.[11, 12] Comparative searches of protein sequence data bases revealed that 3BP1 shares homology with the GTPase-activating protein GAP-Rho

Stuart L. Schreiber was raised and educated in Virginia. He obtained a B. A. in chemistry in 1977 at the University of Virginia, and earned his Ph.D. at Harvard University under the direction of R. B. Woodward and Y. Kishi. He is currently an Investigator at the Howard Hughes Medical Institute and a Professor at Harvard University, where he is a Member of the Chemistry Department and an Associate Member of the Department of Molecular and Cellular Biology. His research integrates several disciplines, including synthetic organic chemistry, protein and structural biochemistry, and molecular and cellular biology. His research group has been using chemical methods to understand and control signaling pathways.



S. L. Schreiber



J. K. Chen

James K. Chen was born in Rolla, Missouri in 1969. He received his A. B. degree in 1991 from Harvard University. He is currently a graduate student in Professor Schreiber's research group at Harvard, pursuing the chemistry and biology of immunosuppression, the molecular recognition of SH3 domains, and the development of nonpeptidic combinatorial libraries.

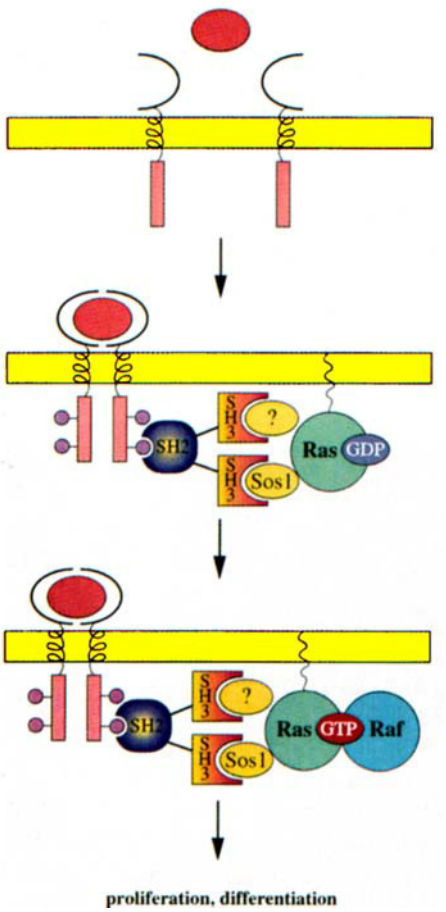


Fig. 2. Schematic representation of the Grb2-mediated activation of Ras, a prototypical signaling cascade involving SH3-containing proteins. In quiescent cells the adaptor protein Grb2, which comprises one SH2 and two SH3 domains, is complexed to the guanine nucleotide exchange factor Sos1 through one or both of its SH3 domains. This complex is recruited to the cellular membrane following stimulation by a growth factor (red) and activates Ras. Purple circles on the activated receptor represent phosphorylated tyrosine residues which are potential docking sites for SH2 domains.

and that 3BP2 contains an SH2 domain. The ability of both 3BP1 and 3BP2 to interact selectively with the Abl SH3 domain was further demonstrated by filter binding assays of GST-3BP1, GST-3BP2-40 (a GST fusion protein containing a 40 amino acid fragment of 3BP2), and several biotinylated GST-SH3 fusion proteins. Colorimetric detection of the 3BP1- and 3BP2-SH3 complexes using streptavidin alkaline phosphatase yielded similar intensities for the SH3 domains of Abl, Src, and Grb2 ("grab-two"), suggesting that they have comparable affinities for the SH3-binding proteins. In contrast, the neural Src, Nck ("nick"), and Crk ("crack") SH3 domains produced much weaker signals. Related experiments also localized the SH3-binding sites of 3BP1 and 3BP2 to the sequences APTMPPPLPP (3BP1-10) and PPAYPPPPVP (3BP2-10), respectively. The proline-rich character of these sequences was intriguing but provided few clues about the molecular origins of SH3–ligand interactions, whereas the absence of conserved non-proline residues in these sequences seemingly contradicted the specificity of 3BP1 and 3BP2. Mutational analysis of 3BP1-10 revealed that only Pro2, Pro7, and Pro10 are essential for Abl SH3 binding, suggesting a PXXXXPXXP consensus motif for SH3 ligands. It was proposed, however, that non-proline residues are still important for SH3–ligand interactions since the Abl SH3 domain cannot bind to a poly-L-proline peptide like Pro_{10}.[12]

This mosaic understanding of SH3–ligand interactions has been gradually clarified in the past two years. In collaboration with George Whitesides and co-workers, we carried out subsequent investigations of 3BP1-10 using affinity capillary electrophoresis,[13] a technique that can quantitatively evaluate receptor–ligand interactions in solution. These studies demonstrated that although the substitution of Pro2 with alanine (P2A) and the P7A and P10A mutations significantly diminish the affinity of the peptide for the Abl SH3 domain, they have little effect on its interactions with the SH3 domain of Src. Moreover, a VPPQ sequence that is C-terminal to 3BP1-10 was found to be critical for Src SH3 binding. These results indicated that 3BP1 has at least two distinct SH3-binding sites, raising the possibility that the PXXXXPXXP motif of 3BP1 and 3BP2 might not be universal for all SH3 ligands. The differential binding of the Abl and Src SH3 domains to 3BP1 was also consistent with the hypothesis that non-proline residues are important determinants of SH3 recognition. These issues were addressed, in part, by the identification of other SH3-binding proteins by affinity chromatography. For example, the motor protein dynamin was isolated from cellular extracts by using affinity columns containing immobilized GST-PI3K SH3 fusion protein[2d, 4d] and the cytoskeletal protein paxillin was similarly extracted with immobilized GST-Src SH3.[14] Both SH3-binding proteins contain proline-rich regions, confirming the general preference of SH3 domains for these motifs. Sequences from these and other reported SH3 ligands, however, failed to elaborate the optimal number of proline residues in SH3-binding motifs or their relative spacing. Analysis of these regions is complicated by the plurality of proline residues, many of which are ostensibly unimportant for SH3 binding. The repetitive, proline-rich nature of these sequences also indicated that these SH3-binding motifs might interact with multiple SH3 domains or contain two or more overlapping binding sites. Accordingly, it has become increasingly apparent that many reported SH3-binding proteins can bind to several different SH3 domains in vitro. Dynamin itself has several overlapping SH3-binding motifs, and at least one of these sites can interact with the SH3 domains of PI3K, PLC-γ, and Grb2.[4d]

The physiological relevance of these particular SH3–ligand associations, therefore, is uncertain. Although they can occur in vitro, several of them involve proline-rich ligands that have low specificities and affinities for their putative SH3 receptors. One SH3-mediated interaction, however, has been shown with certainty to be a component of intracellular signaling pathways. Investigations in several laboratories have elucidated the molecular targets of Grb2, a cytoplasmic protein containing one SH2 domain and two SH3 domains.[6] This signaling protein is representative of the class of SH3-containing proteins that have no catalytic domains and function as molecular adaptors or protein dimerizers. The discovery of its physiological SH3 ligand provided the first cellular model of SH3-mediated events and illustration of non-proline determinants for SH3 binding. As demonstrated by immunoprecipitation and binding studies, either one or both Grb2 SH3 domains bind to Son of sevenless 1 (Sos1, "sauce-one"), a guanine nucleotide exchange factor for the GTPase Ras. Upon growth factor stimulation, this cytosolic complex is recruit-

ed to activated, membrane-bound receptors through Grb2 SH2–phosphotyrosine interactions, thereby localizing Sos1 to the plasma membrane. There, the guanine nucleotide exchange factor can then activate Ras, initiating signaling cascades that promote cellular growth and differentiation (see Fig. 2).

To identify the SH3-binding sites in Sos1, fragments of the nucleotide exchange factor were tested for their ability to bind to the Grb2 protein.[6b, d–f] These experiments localized the SH3-binding region of Sos1 to its C-terminal tail, which contains multiple PX(L/V)PPR motifs. Sos1-derived peptides that contain these residues can inhibit Grb2–Sos1 association in vitro, corroborating their role in SH3 binding. The presence of a conserved C-terminal arginine residue in these regions also suggested that the guanidinium side chain makes specific contacts with the Grb2 SH3 domain(s). Indeed, an arginine-to-lysine mutation in one of these proline-rich peptides abolishes its ability bind Grb2.[6d] Like previously reported SH3-binding motifs, however, the C-terminal region of Sos1 provided few additional insights into the molecular basis of SH3–ligand interactions. Multiple consensus motifs for SH3 ligands were proposed,[4d, 11] but the molecular recognition of proline-rich sequences by SH3 domains remained enigmatic.

2.2. Structural Studies

Sequence alignments of SH3 domains provided early clues about their secondary structure (Fig. 3). The delineation of the SH3 core was facilitated by the independent, modular nature of the domain, which is occasionally located at the extreme N- or C-termini of proteins. Conserved residues in SH3 domains are scattered throughout the primary sequence, including an N-terminal ALYDY motif and several groups of hydrophobic residues. Since many of these hydrophobic amino acids are interspersed with hydrophilic residues, Musacchio et al. initially proposed that SH3 domains are primarily composed of β-strands.[1b] Putative loop regions were also assigned based on the distribution of glycine and proline residues in SH3 sequences. Other attempts to predict the SH3 structure de novo were independently reported by Benner et al.[15] and by Rost and Sander.[16] Although both groups concluded that the domain comprises multiple β-strands and one α-helix, different protein folds were proposed.

The first structural elucidations of two SH3 domains verified many of these conclusions but invalidated others, illustrating the current limitations of de novo structure predictions. The crystal structure of α-spectrin SH3[2a] determined by Saraste et al. and the c-Src SH3 solution structure[2b] determined by Hongtao Yu in our laboratory revealed a conserved topology composed of two three-stranded antiparallel β-sheets that pack against each other at approximately right angles (Fig. 4; an alternative description of the SH3 fold has been proposed by Musacchio et al.,[2a] but the global structures of the two SH3 domains are essentially identical). The interface of these two β-sheets is mediated by several conserved hydrophobic residues, exemplified by Phe86, Leu100, Phe102, Leu108, Ile110, Ile132, and Val137 of Src. Loop regions between the β-strands are conformationally flexible and exhibit a preference for charged residues. Other common motifs in the α-spectrin and Src SH3 domains include a type II β-turn between strands S2 and S3 and a 3_{10} helix after strand S5 that is initiated by a highly conserved proline residue (Pro133 of Src). The general topology of SH3 domains therefore represents a unique protein fold structurally unrelated to the β-sheet- and amphipathic helix-containing SH2 domain.[17] As in SH2 modules, however, the N- and C-termini of SH3 domains

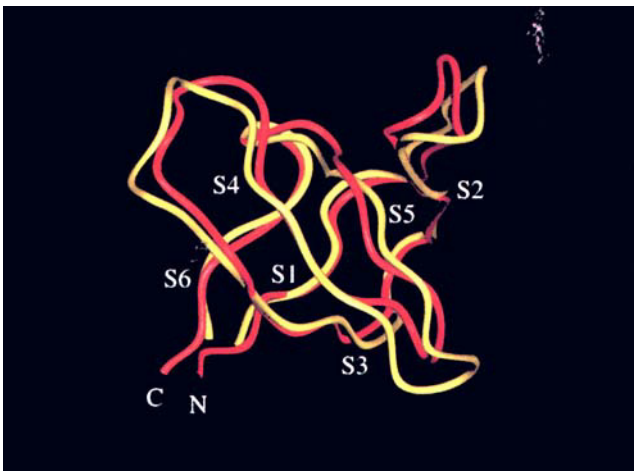


Fig. 4. Superposition of the SH3 domains of Src (yellow) and α-spectrin (red). The α-carbon traces are shown. The β-strands that represent the conserved topology of SH3 domains are labeled S1–S6.



Fig. 3. Sequence alignment of SH3 domains. Conserved residues corresponding to β-strands are colored green, and the C-terminal 3_{10} helix region is violet. Abbreviations for the proteins are based on their species of origin: H (human), C (chicken), V (viral), Ce (*Caenorhabditis elegans*).

converge on one protein face and are relatively disordered. These structural characteristics allow the SH3 domain to exist as an independent entity in proteins with minimal disruption of the surrounding structure.

NMR experiments with ^{15}N-labeled Src SH3 also provided insights into its ligand-binding site.[2b] Several residues exhibited perturbations in their ^{15}N or ^{1}HN chemical shifts upon the addition of 3BP1-derived peptides, suggesting that they either constitute or border the receptor–ligand interface (Fig. 5). One

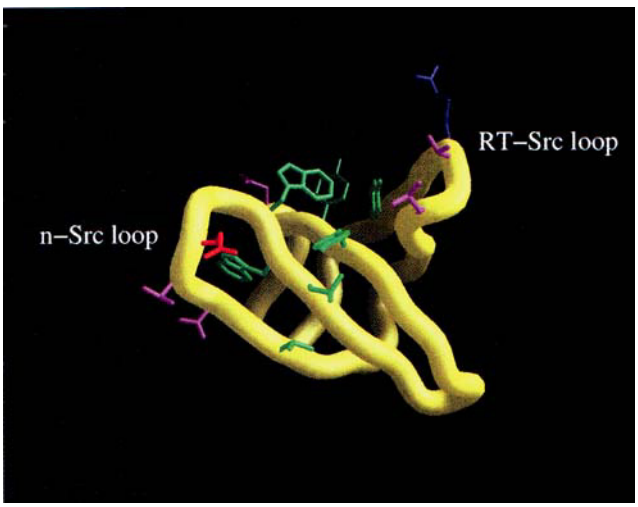


Fig. 5. The α-carbon trace of the Src SH3 domain depicting side chains of residues that show a change in their amide ^{15}N and/or ^{1}HN chemical shifts after the binding of 3BP1-derived peptides. Chemical shifts of the residues Tyr92, Arg95, Thr96, Thr98, Val111, Asn113, Thr114, Glu115, Trp118, Trp119, Leu120, Tyr131, Asn135, and Tyr136 changed by $\Delta\delta > 0.1$ (^{1}H) or > 0.5 (^{15}N) upon peptide binding, whereas others remained unaffected. Hydrophobic residues are shown in green, acidic residues are red, basic residues are blue, and neutral polar residues are purple [51].

subset of these residues (Tyr92, Val111, Trp118, Trp119, Leu120, Tyr131, and Tyr136) forms a smooth, hydrophobic patch on the protein surface that is lined with aromatic side chains. Since many of these amino acids are highly conserved, we were able to propose that this aromatic platform is the core binding site for SH3 ligands. Other perturbed residues (Arg95, Thr96, Thr98, Asn113, Thr114, and Glu115) are not conserved in the SH3 family and are located in variable loop regions. One of these regions, which is located between strands S1 and S2, has been named the RT-Src loop since mutations of either Arg95 or Thr96 cause cell transformation.[4a, b, e] The other ligand-contacting loop is the site of 6 and 17 amino acid insertions that are found in alternatively spliced variants of the Src SH3 domain found in neurons.[18, 19] This region is located between strands S3 and S4 and is commonly called the n-Src loop.

Subsequent investigations of other SH3 domains confirmed the generality of these structural elements.[2e–h] All known SH3 structures share a common global topology although additional β-strands or helices can be tolerated by the SH3 fold. In particular, the residues that correspond to Tyr90, Tyr92, Trp118, and Tyr136 of the Src SH3 domain have a conserved spatial arrangement, with similar side-chain orientations. These four residues are conserved in nearly all SH3 domains and form a gearlike composite surface in the ligand-binding site. In contrast, the RT- and n-Src loops are structurally diverse and can accommodate significant architectural changes. One dramatic example of this structural flexibility is the PI3K SH3 domain, whose structure was shown by Satoshi Koyama in our laboratory to contain a 15 amino acid insert in its n-Src loop, composed of one α-helix and two 3_{10} helices (Fig. 6).[2c] Chemical shift perturbation studies were also conducted on this unique SH3 domain using a proline-rich peptide derived from dynamin.[2d] Although these ex-

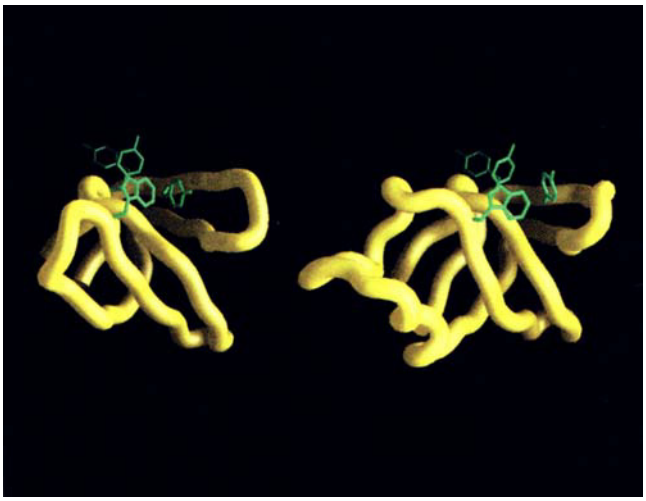


Fig. 6. Comparison of the solution structures of the SH3 domains of Src (left) and PI3K (right). The side chains of the conserved aromatic residues that line the binding site are in green [51]. The residues that are shown are: Tyr90, Tyr92, Trp118, and Tyr136 (Src), and Tyr12, Tyr14, Trp55, and Tyr73 (PI3K).

periments monitored side-chain proton resonances rather than ^{15}N and ^{1}HN chemical shifts of the SH3 backbone, the putative binding site residues of PI3K SH3 are identical or analogous to those elucidated in the Src SH3 perturbation studies. These results supported earlier speculations that the conserved, hydrophobic surface of SH3 domains is a general platform for proline-rich ligands, with specificity conveyed by the RT- and n-Src loops.

Unfortunately, these investigations shed little light on the structure of SH3 ligands. The identification of a putative binding site provided topographical clues, but the bound conformation of SH3 ligands remained a mystery. One major obstacle to further structural studies was the lack of high-affinity SH3-binding peptides. The chemical shift perturbation studies of the Src and PI3K SH3 domains utilized ligands with low specificity and affinity for their respective receptors. For example, the dynamin-derived peptide binds to the PI3K SH3 domain with a dissociation constant (K_D) of 300 μM.[2d] Although these peptides facilitated the delineation of the ligand-binding site (the solution structural studies were carried out at ca. 2 mM concentrations of receptor and ligand), their weak affinity and nonspecific nature precluded a meaningful evaluation of SH3–ligand interactions. Thus, fundamental questions about the molecular recognition of SH3 domains remained unanswered. How do SH3 domains bind proline-rich ligands? Why are certain proline residues critical for SH3 binding? What structural elements in SH3 ligands confer specificity? The remainder of this review will focus on the scientific advances that ultimately resolved these issues. In particular, we will discuss the discovery of SH3 ligands through combinatorial chemistry and the structure elucidation of SH3–

ligand complexes by NMR spectroscopy and X-ray crystallography. The insights provided by these studies will then be used to construct a general model for SH3–ligand interactions.

3. Combinatorial Studies of the PI3K and Src SH3 Domains

Several strategies for ligand discovery that involve combinatorial synthesis and molecular selection have recently emerged.[20] Libraries of peptides,[21] oligonucleotides,[22] and other linear polymers[23] have been synthesized in soluble forms and on a variety of solid supports. Complementary approaches have applied combinatorial synthesis to the generation of benzodiazepines[24] and azinomycin analogues,[20a, 25] demonstrating the compatibility of many synthetic transformations with library construction. Our investigations of the PI3K and Src SH3 domains have utilized combinatorial peptide libraries on beads in analogy to that described by Lam et al.[21d] These libraries are synthesized by a "split-and-pool" procedure[26] which rapidly generates millions of peptides, each covalently attached to a unique bead. Beads that contain high-affinity ligands are then identified by their ability to interact with a labeled receptor. Accordingly, the success of bead-based strategies requires the careful consideration of certain variables: 1) the size and basic structure of the molecular library, 2) the chemical composition of the solid support, 3) the derivatization of the target receptor, 4) the bead selection conditions, and 5) the method of bead characterization. The application of combinatorial libraries to the study of SH3–ligand interactions illustrates the roles of these factors in ligand discovery.

Our initial attempts to discover SH3 ligands used two random libraries: one containing two million linear hexapeptides and another containing two million cyclic heptapeptides.[27] The general structure of the hexapeptide library was XXXXXX, in which X represents any amino acid other than cysteine; the heptapeptide library had the form CXXXXXC and was intramolecularly cyclized by disulfide bond formation. Investigations using these libraries failed to yield suitable SH3 ligands; the amino acid sequences of SH3-binding beads followed general trends, but no clear consensus sequences were apparent. Furthermore, the SH3-binding affinities of synthetic, soluble versions of these ligands were found to be weak ($>100\,\mu M$). These results were both disappointing and puzzling. At the time of these experiments, no SH3 ligands were known and it was uncertain that SH3 domains even recognized polypeptides. The subsequent discovery of 3BP1, 3BP2, and other putative SH3-binding proteins revealed the preference of SH3 domains for proline-rich sequences. Although the minimal consensus motif of SH3 ligands remained elusive and controversial, these proline-rich regions provided the foundation for a modified approach: *biased* combinatorial libraries.

Recognizing that several reported SH3 ligands contain the sequence PPXP, we designed and constructed a biased combinatorial library of the form XXXPPXPXX.[27, 28] The biasing element was incorporated to orient the ligands in a uniform manner and to increase the average affinity of the ligands to the target receptor. Cysteine was again excluded from variable positions to avoid intra- and intermolecular disulfide bonds that would complicate library synthesis and characterization. Analogous to our previous libraries, approximately ten million peptides with this structural bias were synthesized on polydimethylacrylamide beads with a molecular spacer composed of β-alanine, ε-aminocaproic acid, and ethylenediamine. This particular solid support was used since it is well solvated and chemically stable in both the organic solvents necessary for peptide synthesis and the aqueous buffers that solubilize biological receptors. The linker was included to minimize steric interactions between the SH3 domains and the polydimethylacrylamide matrix. The PI3K and Src SH3 domains were then site-specifically derivatized at their N-termini through the coupling of fluorescein thiosemicarbazide to glyoxalamides, which can be introduced to peptides and proteins by cleavage of N-terminal serine residues with sodium periodate (Fig. 7).[29] Fortuitously, the PI3K SH3 domain expressed in *E. coli* already contains an N-terminal serine

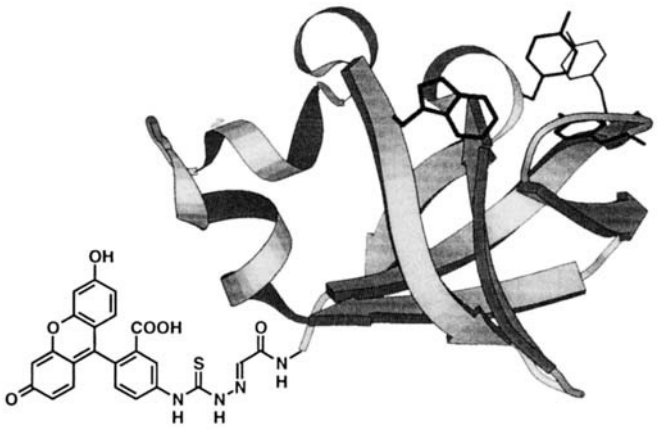


Fig. 7. Ribbon drawing of the N-terminally derivatized, semisynthetic PI3K SH3 domain used to probe the peptide libraries. Conserved aromatic residues that constitute the binding site are outlined with thick lines [52].

since posttranslational modifications remove its initiating methionine. Although this is not the case for the Src SH3 domain, an N-terminal serine was easily incorporated into the protein module by PCR mutagenesis and Factor Xa proteolysis. This selective and mild tagging procedure was chosen since the N-terminus and ligand-binding site of an SH3 domain are on opposite faces of the receptor, thereby preventing any interference with ligand binding by the fluorescent reporter. Aliquots of approximately two million beads from the XXXPPXPXX library were mixed with the fluorescein-conjugated PI3K and Src SH3 domains to allow receptor–ligand complexation, and the matrix was washed extensively with detergent-containing high ionic strength buffers to abrogate nonspecific interactions. SH3 ligand-containing beads were subsequently identified by fluorescence microscopy. In each library screening 60–70 beads were intensely fluorescent, and a subset of the brightest beads were isolated (Fig. 8). Because each bead is approximately $100\,\mu m$ in diameter and contains at least 50 pmol of peptide, resin-bound ligands can then be characterized by automated Edman degradation.

Two distinct classes of SH3 ligands emerged from these library-based studies (Table 1). Class I ligands have the consensus sequence RXLPPΦPXX (Φ represents arginine for PI3K SH3

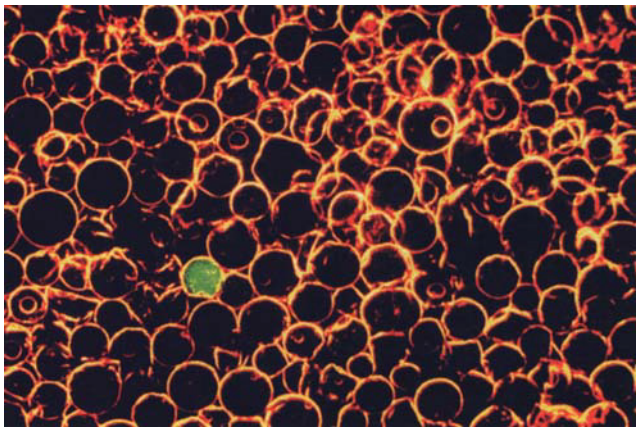


Fig. 8. Random subset of a bead-based library that has been probed with a fluorescein-conjugated SH3 domain. The 100 μm beads were viewed through a microscope using both transmitted light and incident fluorescence.

and leucine for Src SH3; X represents a nonconserved residue), and class II ligands have the consensus XXXPPLPXR. Spectroscopic analysis of several receptor–ligand complexes revealed that the tryptophan fluorescence of SH3 domains changes in intensity and shifts to shorter wavelengths upon ligand binding (Fig. 9). These fluorescence perturbations are presumably caused by ligand-induced desolvation of a conserved tryptophan in the SH3 binding site corresponding to Trp118 of Src. Consequently, representative ligands were synthesized as carboxamide peptides, and their affinities for the SH3 domains were evaluated by fluorescence titration assays (Table 2). Dissociation constants for both classes of ligands are in the micromolar range, with the highest affinity ligands having K_D values that are less than 10 μM. The peptides also bind selectively to their respective receptors, reflecting different residue preferences at certain randomized sites. For example, the PI3K SH3 ligand RKLPPRPSK (RLP1) binds to the PI3K and Src SH3 domains with K_D values of 9.1 and 52 μM, respectively. The Src SH3 ligand RALPPLPRY (RLP2) is somewhat less selective, binding to the PI3K and Src SH3 domains with K_D values of 17 and 7.8 μM, respectively. These affinities are comparable to and in general greater than those reported for peptides derived from SH3-binding proteins. One of the strongest SH3–peptide interactions known to date is that between the N-terminal SH3 domain of Grb2 and a Sos1-derived peptide, VPPPVPPRRR, with a K_D of 5.6 μM (the C-terminal SH3 domain of Grb2 binds to this peptide with a K_D of 39 μM).[27] In comparison, the 3BP1-derived peptide APTMPPPLPP binds to the Abl SH3 domain with a K_D of approximately 37 μM.[13, 30]

Table 1. Amino acid sequences of bead-bound peptides that interact with the SH3 domains of PI3K and Src.

SH3 Domains	Class I		Class II
PI3K SH3	RKLPPRPSK	RMLPPKPRV	PWHPPLPLR
	RDLPPRPAA	RKLPPKPKW	VWKPPLPKR
	RYLPPRPMY	RPLPPHPRR	LNKPPLPKR
	RRLPPRPRR	RALPPHPRF	NRKPPLPAR
	RLLPPRPTF	RKLPPLPKA	
	RKLPPRPAF	RPLPPAPWK	
	PALPPRPHS		
Src SH3	RALPPLPRA	RMLPPLPAW	PYHPPLPRR
	RELPPLPRF	RPLPPLPAW	MMAPPLPRL
	RALPPLPRY	RQLPPLPAF	AFAPPLPRR
	RNLPPLPRI	RRLPPLPQL	
	RALPPLPRW	RDLPPLPHR	
	RTLPPLPRF	RELPPIPVF	
	RALPPLPRI	RPLPPVPMF	
	RPLPPLPTS	RPLPPTPKY	

Table 2. Affinities of peptide ligands to the SH3 domains of PI3K and Src; the dissociation constants K_D of the complexes are given.

SH3 domain	Peptide	K_D (μM)
PI3K	RKLPPRPSK	9.1
	RKLPPRPAF	11
	RYLPPRPMY	13
	LNKPPLPKR	13
	RALPPLPRY	17
Src	RALPPLPRY	7.8
	RELPPLPRF	9.6
	RELPPIPVF	12
	RPLPPTPKY	13
	AFAPPLPRR	59
	RKLPPRPSK	52

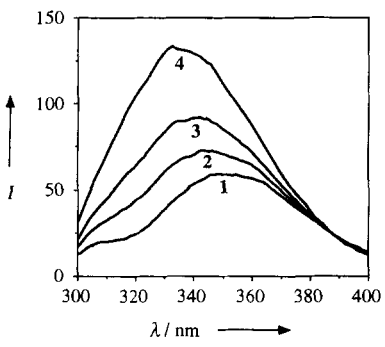


Fig. 9. Effect of ligand binding on the fluorescence spectra of an SH3 domain. 1: = PI3K SH3 (0.5 μM); 2, 3, and 4: PI3K SH3 with 4.3, 13, and 110 equivalents of the peptide RKLPPRPSK, respectively. λ = emission wavelength [nm], I = fluorescence intensity (in arbitrary units).

The discovery of two ligand classes was intriguing because it indicated that SH3–ligand interactions involve two distinct binding modes. Since there is a conserved N-terminal arginine in class I ligands and a conserved C-terminal arginine in class II ligands, we proposed that these peptides bind to SH3 domains in reverse orientations even though we were not aware of any precedent for this behavior in a protein receptor.[27, 28] The preponderance of RXL-containing ligands apparently reflected an inherent preference for class I ligands, yet the tight binding ligand of the N-terminal Grb2 SH3 domain, VPPPVPPRRR, resembles class II peptides and was predicted to bind in a similar manner.[28, 31] These molecular recognition issues were further clarified by mutational analyses of two SH3 ligands (Fig. 10). The class I peptide RLP1[28] and the class II peptide AFAPPLPRR (PLR1)[32] were systematically mutated to determine the relative importance of each residue for SH3 binding. As expected, conserved residues are generally important for SH3 recognition; alanine or glycine substitutions of these amino acids significantly attenuate binding. Nonconserved residues that are not critical for SH3–ligand interactions can be grouped into two categories. One group comprises Lys2 and Pro5 of RLP1, and Pro5 and Arg8 of PLR1, which are interspersed with conserved

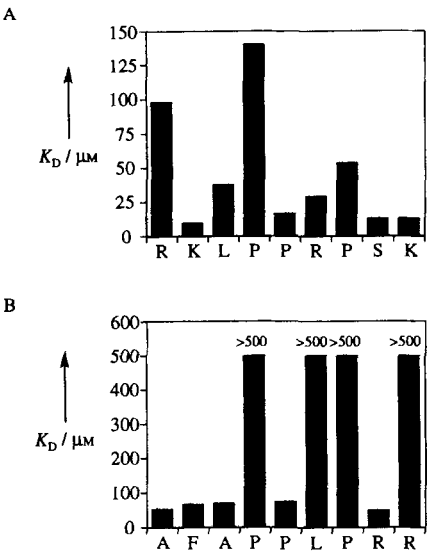


Fig. 10. Mutational analysis of the class I ligand RLP1 and the class II ligand PLR1. A) Effects of alanine substitutions of individual RLP1 residues on the dissociation constant K_D of the PI3K SH3–RLP1 complex. Values for residues Ser8 and Lys9 represent the affinity of the truncated peptide RKLPPRP for the SH3 domain of PI3K. B) Effects of alanine or glycine substitutions (at original alanine sites) of individual PLR1 residues on the dissociation constant K_D of the SrcSH3–PLR1 complex.

SH3-contacting residues. The second group of residues includes terminal amino acids in the two peptides, suggesting that the minimum length of these ligands is approximately seven amino acids. This localization of nonessential residues at the C-terminus of class I ligands and at the N-terminus of class II ligands supported our hypothesis that the two classes of peptides adopt opposite binding orientations. Moreover, we observed a palindromic PXXP motif that is universally conserved; Pro4 and Pro7 of both ligands contribute to SH3 binding. In retrospect, this conserved PXXP motif and the relative spacing of noncontacting residues suggested that SH3 ligands form highly organized structures with an unique spatial relationship between i and $i + 3$ residue positions. These results also revealed why our original molecular libraries failed to contain SH3 ligands. Nonencoded libraries on beads are restricted to five or six random positions owing to synthetic and screening limitations, but SH3 domains require ligands that contain at least seven amino acids. Our proline-rich bias therefore not only incorporated an SH3-binding element, but also allowed for the synthesis of larger ligands which contact the protein receptor more extensively.

Comparative searches of the EMBL/SwissProt data base using class I and class II ligands identified similar proline-rich regions in several cellular and viral proteins. For example, class I-like sequences can be found in the tyrosine kinase v-Fgr,[33] the potassium channel protein HK2,[34] and human proacrosin.[35] Class II-like sequences exist in the proto-oncogene c-Cbl ("sybil"),[36] Sos1,[37] and the N-terminal regulatory domain of the progesterone receptor.[38] Interestingly, there is also a class I-like sequence RPLPVAP in the p85 subunit of PI3K, approximately ten amino acids after the SH3 domain.[9a, b] Recent investigations have determined that the binding of Lyn ("lin") or Fyn ("fin") SH3 domains to this region activates the lipid kinase activity of PI3K.[39] In addition, we have shown that this region can mediate the dimerization of a recombinant p85 fragment in vitro by intermolecularly associating with the SH3 domain.[40] The physiological significance of these putative SH3-binding motifs is uncertain since the length of the PI3K and SrcSH3 ligands precludes the unambiguous identification of endogenous targets. The discovery of these SH3 ligands through combinatorial chemistry, however, laid the groundwork for our structural investigations that would ultimately unravel the molecular basis for SH3–ligand interactions.

4. Structural Studies of SH3–Ligand Complexes

Now equipped with the ligands we sought, we next undertook the structural determination of several SH3–ligand complexes using multidimensional NMR spectroscopy. The PI3K SH3 domain complexed with RLP1[28] and the c-SrcSH3 domain complexed with RLP2 and PLR1[32] were studied by H. Yu and Sibo Feng in our laboratory, revealing a novel molecular architecture for protein–ligand interactions. These studies illustrate how the mode of ligand binding by a protein receptor can be revealed by coupling combinatorial synthesis with protein structure determination techniques. In addition, Musacchio et al. recently reported the crystal structure of the AblSH3–3BP1-10 complex,[30] and Eck et al. determined the provocative structure of an SH3–SH2 fragment of the tyrosine kinase Lck in which the SH2 domain was complexed with a phosphotyrosine peptide.[29] These investigations have yielded valuable insights into the molecular origins of SH3–ligand interactions and the structural determinants of specificity. They also provide fundamental guidelines for the structure-based design of non-peptidic SH3 ligands, which could have important roles in medicinal and biological research.

4.1. Overview of the Structures

The structures of the four SH3–peptide complexes (Figs. 11–16) are generally consistent with early proposals about SH3–ligand interactions and reveal a remarkable structural mechanism for protein–protein interactions. The conserved, hydrophobic patch flanked by the variable RT- and n-Src loops constitutes the ligand-binding site of the SH3 domain, as previously demonstrated by NMR experiments. The overall structure of the SH3 domain does not significantly change upon ligand binding; for example, the root-mean-square deviation of the backbone in the minimized average structures of the free and ligand-bound PI3K SH3 domain is 0.85 Å.[28] Thus, the highly conserved aromatic residues that correspond to Tyr90, Tyr92, Trp118, and Tyr136 of the Src SH3 domain form a preorganized, gearlike template that binds the SH3 ligand. These amino acids and other neighboring residues form three uniformly spaced pockets in the SH3 domain that accommodate specific side chains from the proline-rich ligands. The binding pockets are primarily hydrophobic in character although charged residues from peripheral loops can contribute to the composite receptor surface. Ligand complexation can also significantly retard the cooperative unfolding of the SH3 domain in solution, as exemplified by the observation of eleven slowly exchanging amide protons for the RLP2-bound SH3 domain.[32] Only three are observed in the unbound state.[2b]

The solution structure of the PI3K SH3–RLP1 complex (Fig. 11) clearly revealed that the peptide forms a left-handed polyproline type II (PPII) helix which spans the receptor binding site, and this mode of binding has been confirmed in the three subsequent structures of SH3–peptide complexes. Two complete helical turns contact the SH3 domain, and in the Abl SH3–3BP1-10 complex additional N-terminal residues adopt an extended conformation. This unique PPII helix motif is well suited

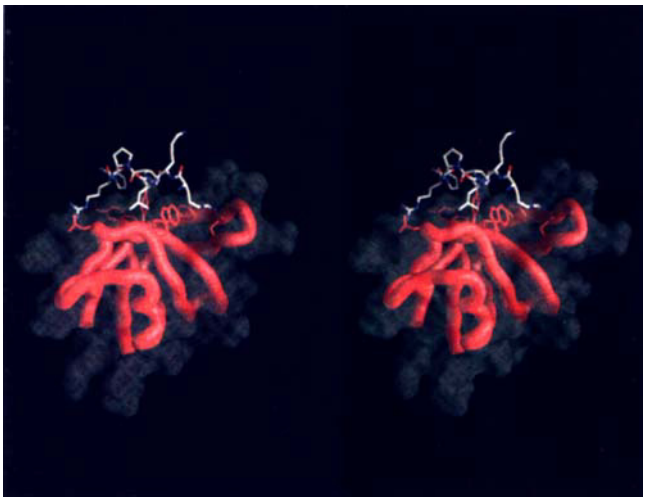


Fig. 11. Stereoview of the PI3K SH3–RLP1 complex. SH3 residues that participate in binding interactions are shown in red [51]. C-terminal ligand residues that do not contact the SH3 domain are omitted.

for the molecular recognition of SH3 domains. Polypeptides in this conformation form an extended molecular scaffold that complements the long, narrow surface of the SH3 ligand-binding site. In comparison, right-handed α-helixes that contain an equivalent number of residues are approximately half the length of these structures. PPII helices in globular proteins are also ideal mediators of protein–protein interactions because these motifs are usually exposed to solvent; lacking internal hydrogen bonds, PPII helices depend on backbone solvation for thermodynamic stability.[41] The most striking features of PPII helices are their left-handedness and their regular, repeating architecture (Fig. 12). There are three residues per helical turn, and amino acids at the i and $i + 3$ positions extend from the same face of the helix with nearly identical orientations. This conformation restricts the peptide to an elongated structure, in which the backbone and side chains form evenly spaced grooves like the threads of a screw. The width and depth of these grooves match the van der Waals surfaces of the aromatic side chains that line the SH3 ligand-binding site. The SH3–ligand complex therefore resembles the mechanical worm gear, in which a threaded, extended shaft interdigitates the teeth of a gearwheel.

Since the side chains of a PPII helix protrude from the peptide backbone every 120° (as viewed along the axis of the helix), one solvent-exposed residue and two adjacent SH3-contacting residues compose each helical turn (Fig. 13). Solvent-exposed amino acids point away from the SH3 ligand-binding site and do not make enthalpic contributions to SH3–ligand interactions. It is these residues in RLP1 (Lys2 and Pro5) and PLR1

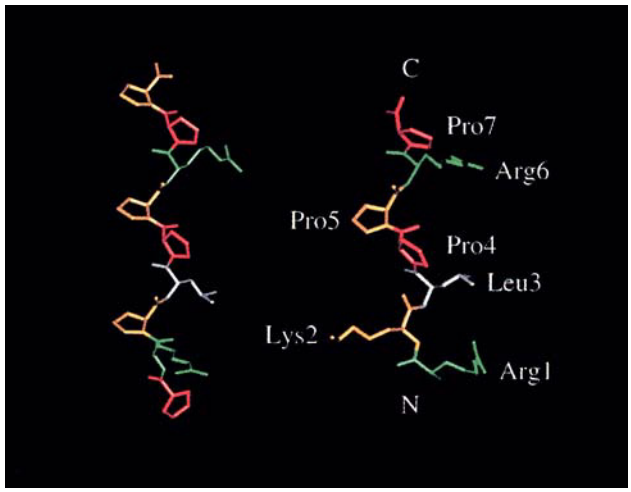
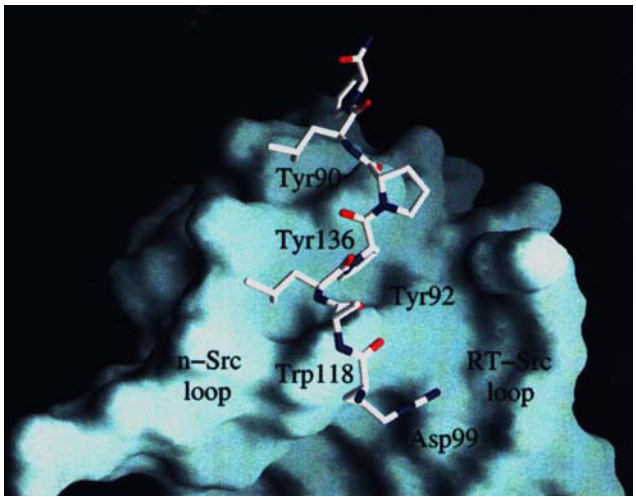


Fig. 12. Comparison of the conformation of bound RLP1 (partial structure RKLP-PRP, right) and a regular PPII helix (left) containing the RLP1 residues critical for SH3 binding. Prolines that contact the SH3 domain are shown in red, non-proline residues that participate in binding interactions are shown in white or green, and residues that do not contact the SH3 domain are shown in yellow.



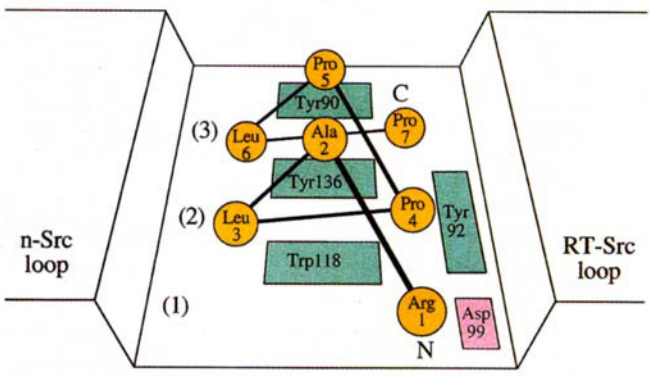


Fig. 13. Detailed view of a representative SH3–ligand complex. Top: Molecular surface of the Src SH3 domain with the bound RLP2 peptide, as viewed along the axis of the PPII helix [51]. Src SH3 residues that are critical for binding are labeled; C-terminal ligand residues that do not contact the SH3 domain are omitted. Bottom: Schematic representation of the Src SH3–RLP2 complex. Numbers in parentheses represent the three hydrophobic pockets in the SH3 binding site.

(Pro5 and Arg8) that can be mutated to alanine without significant attenuation of binding affinity. There is, however, a preference for proline residues in these positions, as demonstrated by

a slight increase in PI3K SH3 binding affinity for a mutant of RLP1 containing a proline residue for lysine at position 2 (the K2P mutant of RLP1, RPLPPRPSK).[28] Although proline residues in these positions do not contact the SH3 domain, they contribute to SH3 binding by conformationally restricting the polypeptide and promoting PPII helix formation. The remaining PPII helix residues interact extensively with the receptor, occupying the three hydrophobic clefts in the ligand-binding site. The first cleft is exemplified by the arginine-binding pocket in the Src SH3–RLP2 complex (see Fig. 15, middle). This pocket is formed by the indole ring of Trp118 and neighboring hydrophobic elements, and accommodates the aliphatic chain of the arginine residue, which caps one end of the PPII helix. (A discussion of the guanidinium-binding component of this pocket follows in Section 4.2.) The second and third binding pockets are also composed of hydrophobic residues in the SH3 domain, corresponding to Tyr90, Tyr92, Trp118, Pro133, and Tyr136 of Src. Each of these aromatic clefts binds an XP dipeptidyl moiety in the PPII helix. A noncontacting residue links these two XP structural elements, yielding the consensus SH3-binding motif **XPXXP**. Thus, the two aromatic pockets and their dipeptidyl ligands provide the structural basis for previous observations of critical PXXP motifs in SH3 ligands.

The molecular basis for the recognition of XP elements is evident from the SH3–ligand complexes. The alkyl substituents of these residues are in close proximity to each other since the $C_\alpha-C_\beta$ bond of X and the $N-C_\delta$ bond of proline are only two backbone bonds apart (Fig. 14). The compact nature of these

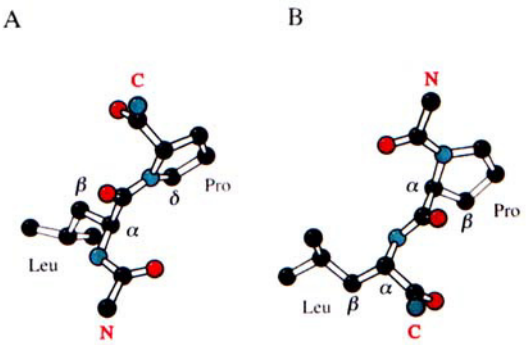


Fig. 14. Comparison of the dipeptidyl moieties XP (A) and PX (B) (X = leucine). Backbone directionality is indicated by N and C in red. Carbon atoms are shown in black, nitrogen atoms are blue, and oxygen atoms are red [52].

XP elements and their spatial relationship in a PPII helix allows them to intercalate between the aromatic residues of the SH3 binding site, maximizing hydrophobic interactions at the protein–ligand interface. In comparison, other dipeptidyl moieties such as XX and PX are less suitable for SH3 binding since their larger composite van der Waals surfaces are not complementary to the receptor binding pockets. Alkyl substituents in these dipeptidyl structures are juxtaposed by the two $C_\alpha-C_\beta$ bonds and are therefore separated by three instead of two backbone bonds. XX and PX elements are also more conformationally flexible than XP dipeptidyl moieties, which are restricted by potential 1,3-allylic interactions involving the $N-C_\delta$ bond of the pyrrolidinyl ring and either the $C_\alpha-C_\beta$ or $N-C_\alpha$ bond of X. Consistent with these observations, when the XP motifs in RLP2 and PLR1 were replaced with PX structural elements, we found that the resultant peptides bind to the Src SH3 domain with significantly diminished affinities.[32] There are, however, special cases in which one or both SH3-contacting moieties has the sequence PP such as in the Abl SH3–3BP1-10 complex. The $C_\alpha-C_\beta$ bond of the N-terminal proline and the $N-C_\delta$ bond of the C-terminal proline are separated by two backbone bonds, and this rigid dipeptidyl element is tolerated by the SH3 binding site. Indeed, recent phage display studies by Rickles et al. have shown that the second hydrophobic pocket of the Abl SH3 domain selectively binds PP elements, whereas the third pocket prefers (I/V)P motifs.[42] Our studies of the Src and PI3K SH3 domains demonstrate that the second and third binding pockets of these SH3 domains have preferences for XP sequences, in which X is an acyclic, aliphatic residue. This propensity for non-proline residues may reflect the ability of N-terminal acyclic residues and C-terminal prolines to form composite binding surfaces that maximize attractive interactions in SH3–ligand complexes.

The SH3–ligand complex therefore represents an extraordinary biological apparatus for protein–protein association. By iteratively combining aromatic and pyrrolidinyl elements, nature has created a molecular framework that is both functional and structurally elegant. In particular, ligands for SH3 domains fully exploit the molecular peculiarities of proline residues, which are structurally compact and conformationally restricted. These unique cyclic amino acids provide a solvent-accessible, hydrophobic surface, and the rigid PPII helix conformation imposed by these residues orients and spaces potential SH3-contacting elements. Such interactive elements have composite surfaces that are both spatially compact and conformationally rigid owing to the $N-C_\delta$ side chain substituents of proline residues. Pyrrolidinyl rings are also apparently ideal structures for contacting aromatic functionalities, as demonstrated by the frequency of proline–arene interactions in protein structures[43] and the selective binding of proline residues by synthetic receptors with aromatic groups.[44] This remarkable optimization of receptor–ligand interactions is the result of molecular evolutionary processes that govern biological systems. It is likely that a similar structural mechanism is involved in the recognition of poly-L-proline (PLP) sequences by the multifunctional receptor profilin. In analogy to SH3 domains, this structurally distinct protein contains an array of conserved aromatic residues that have been recently implicated in PLP binding.[45]

4.2. Ligand Specificity

The core recognition motif of SH3 ligands is the XPXXP sequence, which is functionally equivalent to the phosphotyrosine residue in SH2–ligand interactions. These key recognition elements anchor the ligands in the receptor binding sites, allowing neighboring amino acids to confer binding specificity. In SH2–phosphopeptide complexes, residues that flank the phosphotyrosine extend across the receptor surface and contact specific hydrophobic and electrostatic sites.[2g, 17a, d–f, 46] Similarly, variable residues in and surrounding the XPXXP core confer specificity in SH3–ligand interactions. These differences in receptor-contacting residues parallel topographical and elec-

trostatic variations in SH3 binding sites that are primarily conveyed by the RT- and n-Src loops.

All three hydrophobic pockets in the SH3 domain are subject to structural modifications that alter their ligand preferences (Fig. 15). As demonstrated by our combinatorial studies, the first binding pocket in the PI3K and Src SH3 domains selectively binds arginine residues in proline-rich ligands. The methylene groups of the arginine side chain pack against the surface-exposed cleft composed of hydrophobic residues (including Trp118 in Src and Trp55 in PI3K), whereas the guanidinium group contacts a highly conserved acidic residue in the pocket corresponding to Asp99 of the Src SH3 domain (Asp21 of PI3K). The existence of a salt bridge involving Asp99, which resides at the end of the RT-Src loop, is confirmed by NMR experiments and site-directed mutagenesis. The amide proton chemical shift of Asp99 is significantly perturbed upon ligand binding, and the D99N mutant of the Src SH3 domain binds to RLP2 and PLR1 with greatly diminished affinity.[32] Similar results were observed with the PI3K SH3 domain and RLP1.[28] Phage display[42] and cDNA expression library[11, 12] studies reveal, however, that the analogous binding pocket in the Abl SH3 domain prefers hydrophobic residues such as tyrosine and methionine. This difference in ligand specificity can be attributed to the relatively hydrophobic character of Thr100, which is structurally equivalent to Asp99 of Src.[2c] Indeed, the Abl SH3 domain is unique in its lack of an acidic residue at this site. The absence of a negatively charged residue in the first binding pocket alters its electrostatic potential and enables the Abl SH3 domain to bind aliphatic or aromatic side chains. This structural mechanism for ligand discrimination is reminiscent of the substrate specificity pockets of serine proteases, in which Ser189 and Asp189 modulate the side-chain preferences of chymotrypsin and trypsin, respectively.[47]

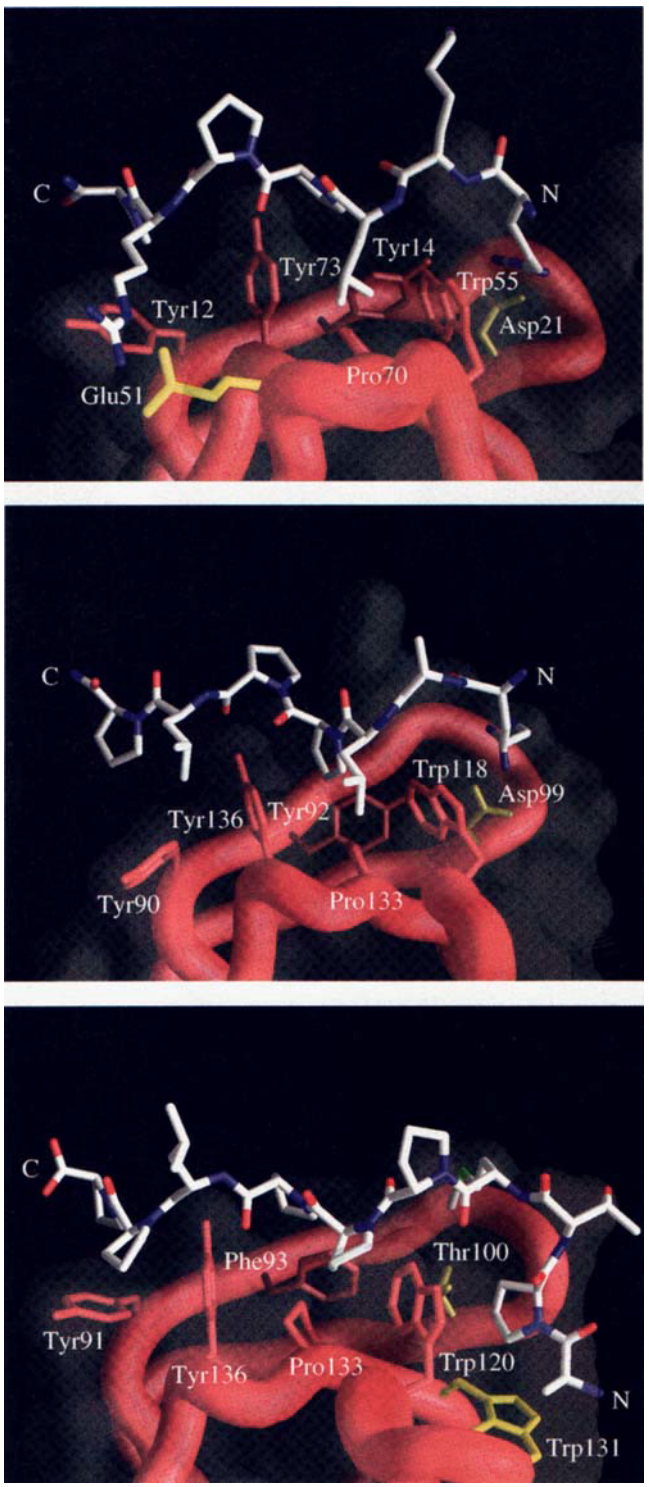


Fig. 15. Molecular determinants of specificity in the PI3K SH3–RLP1 (top), Src-SH3–RLP2 (middle), and Abl SH3–3BP1-10 complexes (bottom). SH3 residues that make conserved contacts in the three complexes are shown in red, and residues that mediate ligand specificity are shown in yellow [51]. C-terminal ligand residues that do not contact the SH3 domains are omitted.

Architectural variations in the second and third SH3 binding pockets regulate other aspects of ligand specificity. Whereas our investigations have revealed that the PI3K and Src SH3 domains prefer LP dipeptidyl moieties in their second binding pockets, complementary studies using phage display libraries have demonstrated that the Abl SH3 domain recognizes PP sequences in this site. The structural basis for this selectivity is not obvious since the SH3 residues in this region are well conserved. It is likely therefore that this binding specificity reflects subtle topographical differences in the SH3 domains, perhaps involving residue changes in the neighboring n-Src loop. Accordingly, the aromatic residues (Trp120 and Tyr136) that form the second binding pocket of the Abl SH3 domain are slightly further apart than the corresponding residues in PI3K and Src, and the n-Src loops of the Abl and Src SH3 domains have different conformations even though they are similar in length. The potential role of this variable loop in ligand discrimination is epitomized by SH3–ligand interactions involving the third binding pockets of the PI3K and Src SH3 domains. Class I ligands selected by the PI3K SH3 domain in combinatorial studies exhibit a preference for arginine residues at the variable site between the prolines (X of PPXP). In contrast, the SH3 domain of Src prefers ligands that contain leucine at this position. These results can be attributed to the 15 amino acid insert in the PI3K SH3 n-Src loop that is absent in the Src SH3 domain. This acidic, helical insert borders the third binding cleft, positioning Glu51 at the end of the pocket. Consequently, the dipeptidyl recognition site-selectively binds RP sequences in class I ligands; the aliphatic portion of the arginine side chain contacts hydrophobic elements in the ligand binding site, while the guanidinium group forms a salt bridge with the carboxylic acid. The importance of this electrostatic interaction for ligand recognition is illustrated by the

E51Q mutant of PI3K SH3, which binds to RLP1 with a threefold loss in affinity.[28] Because the Src SH3 domain lacks this acidic insert, its third binding pocket is primarily hydrophobic and therefore binds LP elements in class I ligands. In comparison, the SH3 domains of neural Src variants contain basic n-Src loop inserts and may prefer ligands containing XP motifs, in which X is aspartic or glutamic acid. One possible target for these neural Src isoforms or structurally related SH3 domains is Burton's tyrosine kinase (Btk), which contains the adjacent proline-rich sequences KPLPPTP and KPLPPEP. The KPLPPTP region binds selectively to the SH3 domains of Fyn, Lyn, and Hck ("hick"), but the KPLPPEP motif interacts weakly with these SH3 receptors.[48] This latter region contains an acidic EP moiety, which might interact specifically with basic residues in the n-Src inserts.

These three binding pockets and their peptidyl ligands represent the core recognition elements of SH3–ligand complexation. A number of studies indicate, however, that additional contacts can be made that increase the affinity and specificity of these interactions. Early mutagenesis experiments on the peptide 3BP1-10 demonstrated that Pro2 in the APTMPPPLPP sequence is essential for Abl SH3 binding,[12] and the Abl SH3–3BP1-10 complex reveals the molecular basis for this structural requirement (Fig. 15, bottom). Although residues Met4–Pro10 adopt a PPII helix conformation, the peptide kinks at Thr3 and places Pro2 in a critical pocket formed by Trp120 and Trp131. Residues in the SH3 family corresponding to or neighboring Trp131 are structurally diverse, suggesting that this general region plays a role in ligand specificity. Phage display studies of several SH3 domains also indicate that additional N-terminal residues in class I-like ligands can contribute to SH3 binding.[42] Based on the known structures of SH3–ligand complexes, these N-terminal residues may be major determinants of molecular specificity since they extend from the conserved aromatic core of the SH3 domain and flank the variable loops. The SH3 domain therefore may contain a fourth binding pocket that is an important mediator of ligand selectivity.

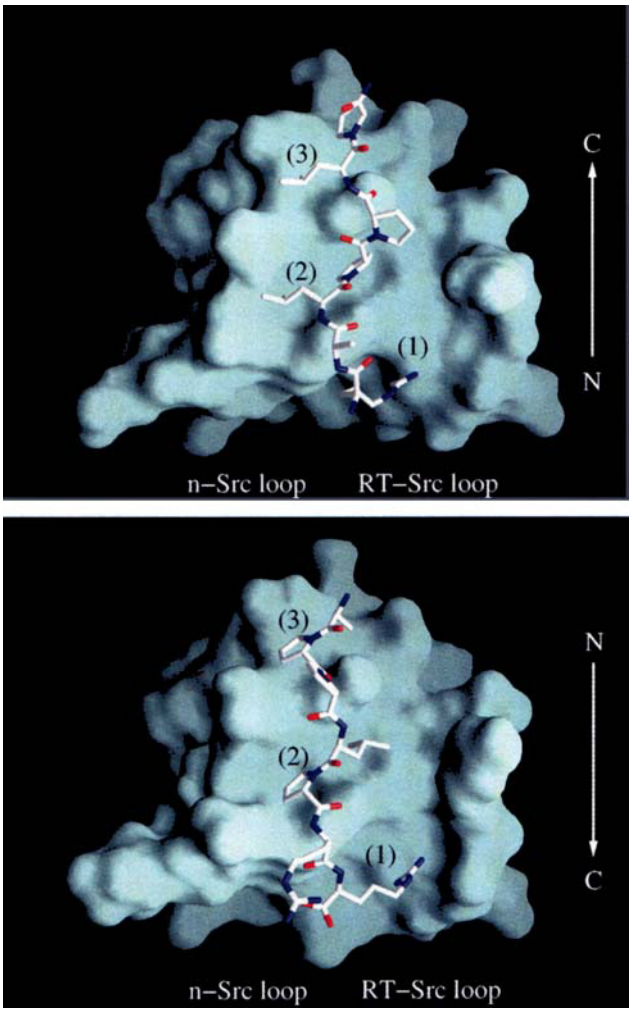


Fig. 16. Two binding modes in SH3–ligand interactions: the Src SH3–RLP2 complex (top) and the Src SH3–PLR1 complex (bottom) [51]. The backbone directionalities of the ligands are denoted by the arrows. Numbers shown on the SH3 domain represent the three hydrophobic pockets in the ligand-binding site. N- and C-terminal ligand residues that do not contact the SH3 domain are omitted.

4.3. Ligand Orientation

The discovery of two SH3 ligand classes through combinatorial synthesis provided the first evidence of dual binding modes. Intrigued by the structural similarities between the two groups of ligands, we initially proposed that SH3 domains can bind proline-rich peptides in two opposing orientations. The structures of the SH3–ligand complexes confirm and elucidate this unprecedented receptor–ligand interaction. The first mode of SH3–ligand interactions is exemplified by the Src SH3–RLP2 complex, in which the peptide amide backbone transverses the ligand binding site with its N-terminus adjacent to Trp118 and its C-terminus adjacent to Tyr90 (Fig. 16, top; see also Fig. 13). The N-terminal Arg1 of RLP2 contacts the first SH3 binding pocket and forms a salt bridge with Asp99 of the Src SH3 domain. The remaining two hydrophobic clefts in the receptor site accommodate LP dipeptidyl moieties from the proline-rich ligand, such that the leucine side chains abut the n-Src loop region of the domain and the proline pyrrolidinyl rings neighbor the RT-Src loop. This binding mode is generally adopted by class I ligands, as demonstrated by the PI3K SH3–RLP1 and Abl SH3–3BP1-10 complexes; peptides in both structures have identical backbone directionalities, and in the PI3K SH3–RLP1 complex the XP structural elements are similarly oriented.

The second mode of binding was uncovered by S. Feng in our laboratory when he determined the structure of the Src SH3 domain complexed with the class II ligand PLR1 (Fig. 16, bottom). The peptides PLR1 and RLP2 interact with the same three binding pockets on the Src SH3 domain, yet the two proline-rich ligands bind with opposite amide backbone directionalities. Thus, SH3 domains can recognize PPII helices in two orientations just as a gear can interdigitate a screw in two directions. The C-terminal Arg9 of PLR1 occupies the first binding cleft and forms a salt bridge with Asp99 of the receptor (again confirmed by mutagenesis and binding studies[32]). The second and third SH3 binding pockets contact XP sequences in PLR1, but the relative positions of non-proline and proline residues in these binding sites are exchanged owing to the reverse orientation of the ligand. Specifically, the acyclic side chains of XP elements face the RT-Src loop, and the pyrrolidinyl rings are

proximal to the n-Src loop in the Src SH3–PLR1 complex and vice versa in the Src SH3–RLP2 complex. The ability of the SH3 domain to accommodate this positional interchange underscores two important aspects of SH3–ligand recognition. First, the second and third binding pockets of the SH3 domain recognize the composite van der Waals surfaces of dipeptidyl XP motifs rather than proline residues alone. Second, the structural tolerance of SH3 domains for both orientations of XP sequences necessitates a mechanism for establishing ligand backbone directionality. Binding mode specificity is apparently mediated by structural asymmetries in the SH3 receptor site. For example, Asp99 of the first Src SH3 binding pocket orients the arginine-containing ligands RLP2 and PLR1. The backbone directionality of the 3BP1-derived ligand APTMPPPLPP is similarly dictated by specific interactions between the Abl SH3 domain and ligand residues N-terminal to the PP recognition elements such as Pro2 and Met4.

It is unclear whether SH3 domains have inherent structural preferences for either binding mode. A bias for class I ligands is suggested by the differential affinities of RLP2 and PLR1 for the Src SH3 domain and the preponderance of RXL-containing ligands in our combinatorial studies. Furthermore, two hydrogen bonds have been proposed in the Abl SH3–3BP1-10 structure based on the intermolecular distances between potential hydrogen bond donors and acceptors: one between the main-chain carbonyl oxygen atom of the ligand residue Met4 and the indole NH group of Trp120 and another involving the carbonyl oxygen atom of Pro7 and the side-chain NH group of Asn135. If real, these attractive interactions could play a role in ligand orientation, although their relative contributions to SH3–ligand interactions are unknown. It is apparent, however, that both classes of ligands can be found in nature. Sequence alignments of reported SH3-binding proteins reveal class I- and class II-like regions, which presumably bind in reverse orientations (Table 3)[4d, 6e, 11, 12, 48, 49]. In order to test our prediction that the Sos1-derived peptide VPPPVPPRRR binds in a class II orientation, we evaluated the ability of VPPPVPPRRR mutants to bind the N-terminal SH3 domain of Grb2.[32] In analogy to Arg9 of PLR1, Arg8 of this Sos1-derived peptide is essential for interactions with the Grb2 SH3 domain.[6d] This C-terminal arginine is expected to form a salt bridge with Glu16 of the Grb2 SH3 domain, which is structurally equivalent to Asp99 of Src.[31] Our additional binding experiments revealed that Pro3 and Pro6 of this peptide are critical for Grb2 SH3 binding, whereas Pro4 and Pro7 can be mutated to alanine with less than a twofold attenuation of affinity.[32] These results strongly support a class II-like binding mode since Pro3 and Pro6 constitute the critical PXXP motif in this orientation and Pro4 and Pro7 correspond to noncontacting prolines that point away from the SH3 domain (Fig. 17). The slight effect of P4A and P7A mutations on SH3 binding is characteristic of ligand proline residues, whose role in complexation is to stabilize the PPII helix conformation without interacting with the receptor.[28, 32] Arg9 and Arg10 of the Sos1-derived peptide also contact the Grb2 SH3 domain, as demonstrated by successive decreases in binding affinity upon their removal.[32] Thus, residues C-terminal to the class II consensus sequence, like residues N-terminal to the class I consensus, can contribute to SH3-binding affinity. Based on the structures of SH3–peptide complexes, these additional N- and C-terminal amino acids probably deviate from the PPII helix conformation in order to contact the SH3 surface. Analogous residues are not well conserved in known SH3 ligands and may be important determinants of ligand specificity.

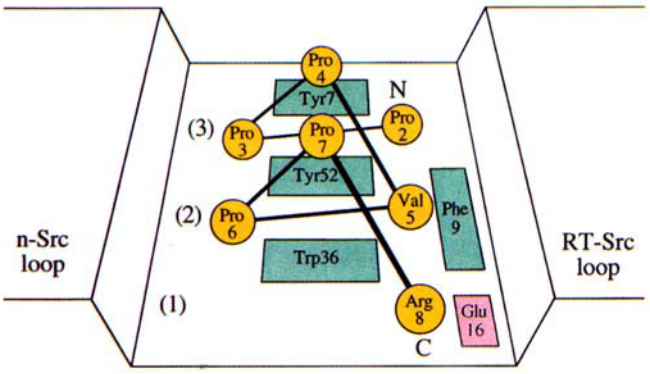


Fig. 17. Schematic representation of the Sos1-derived peptide VPPPVPPRRR bound to the N-terminal SH3 domain of Grb2 in an orientation analogous to that of class II ligands. Numbers in parentheses represent the three hydrophobic pockets in the SH3 binding site.

Table 3. Sequence alignment of SH3-binding motifs [a].

Class I motif	Z	Z	X_1	p	X_2	P	p	X_3	P	Class II motif	X_3'	P	p	X_2'	P	p	X_1'	Z	Z
PI3K library consensus			R	X	L	P	P	R	P	PI3K library consensus	X	P	P	L	P	X	R		
Src library consensus			R	X	L	P	P	L	P	Src library consensus	X	P	P	L	P	X	R		
murine 3BP1 (267–275)	P	T	M	P	P	P	L	P	P	human C3G (608–616) E	P	P	A	L	P	P	K	K	R
murine 3BP2-40 (2–10)	P	A	Y	P	P	P	P	V	P	human dynamin (812–820)	A	P	P	V	P	S	R	P	G
human Btk (184–192)	T	K	K	P	L	P	P	T	P	human $p47^{phox}$ (362–370)	Q	P	A	V	P	P	R	P	S
human Btk (198–206)	L	K	K	P	L	P	P	E	P	murine Sos1 (1153–1161)	P	P	P	V	P	P	R	R	R
human CDC42GAP (250–258)	A	P	K	P	M	P	P	R	P	murine Sos1 (1214–1222)	P	P	L	L	P	P	R	E	P
human dynamin (781–789)	P	Q	R	R	A	P	A	V	P	murine Sos1 (1292–1300)	G	P	P	V	P	P	R	Q	S
human $p22^{phox}$ (151–159)	P	P	S	N	P	P	P	R	P										
human PI3K p85 (91–99)	P	P	R	P	L	P	V	A	P										
human PI3K p85 (303–311)	P	A	P	A	L	P	P	K	P										
human YAP65 (239–247)	V	K	Q	P	P	P	L	A	P										

[a] Capital letters represent amino acid residues in the SH3-binding motifs. X_i and X_i' represent SH3-contacting residues that may confer ligand specificity, Z represents flanking residues that may participate in additional SH3–ligand interactions, and lowercase p represents scaffolding residues, typically proline. Proline residues that are completely conserved are in boxes. In the case of 3BP1, the amino acid position numbers start at the beginning of the partial cDNA sequence reported by Cicchetti et al. [11].

4.4. Insights from the SH3–SH2 Fragment of Lck

Since the discovery of 3BP1 and 3BP2, most studies of SH3 recognition have focused on linear, contiguous epitopes in polypeptide ligands. The structures described above indicate that single peptide chains are optimal SH3 ligands, but it is possible that noncontiguous epitopes in an SH3-binding protein could mimic the hydrophobic and electrostatic elements of a proline-rich peptide. Evidence for such an interaction is provided by the crystal structure of the Lck regulatory domains, in which an SH3–SH2 fragment dimerizes in a bivalent, "head-to-tail" fashion. The SH3 and SH2 domains in this intriguing complex make extensive intermolecular contacts that involve the SH3 binding pockets and SH2 residues flanking the phosphopeptide recognition site (Fig. 18). In particular, the second binding cleft

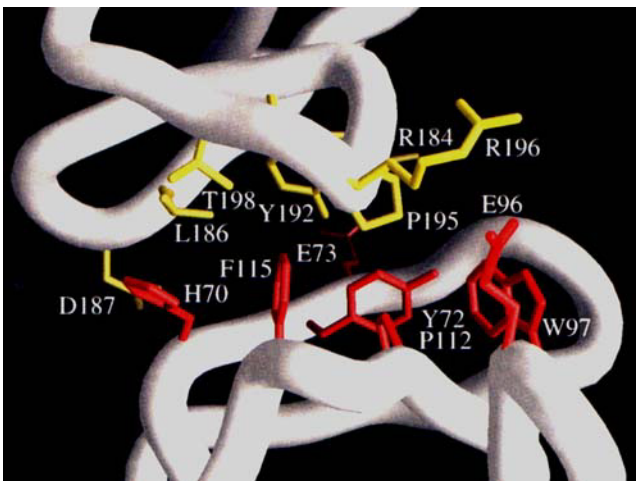


Fig. 18. The intermolecular interface of the Lck SH3–SH2 dimer. The α-carbon traces of the two domains are shown in white. SH3 and SH2 residues that participate in hydrophobic or electrostatic interactions are shown in red and yellow, respectively [51].

of the Lck SH3 domain interacts with Pro195, which protrudes from the SH2 surface. The pyrrolidinyl ring of this residue partially emulates the XP moiety of PPII helix ligands, although its orientation is orthogonal to that of analogous prolines in SH3–peptide complexes. Leu186 and Thr198 of the SH2 domain form another XP mimic and contact the third SH3 binding pocket, while SH2 residue Tyr192 makes additional hydrophobic contacts with aromatic residues in the SH3 domain. Other SH2 and SH3 residues including Glu73, Glu96, Asp187, Arg184, and Arg196 participate in salt-bridge interactions that stabilize the dimer interface. In contrast, intramolecular contacts between the SH3 and SH2 domains are limited to a single hydrogen bond from the backbone NH group of Lys118 in the SH3 domain to the side chain of Glu204 in the SH2 domain and hydrophobic contacts involving Leu69, Ala117, and Pro200.

The crystal structure of the SH3–SH2 fragment complexed to a phosphotyrosyl peptide (sequence TEGQ[pY]QPQPA; pY represents phosphotyrosine) reveals a similar arrangement of domains, in which the SH2 ligand binds at the SH3–SH2 interface (Fig. 19). This phosphorylated peptide corresponds to a region in the Lck C-terminal regulatory tail that presumably in-

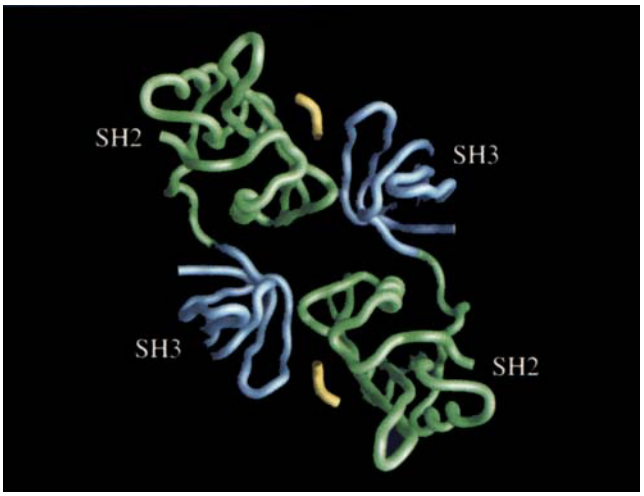


Fig. 19. The Lck SH3–SH2 dimer complexed with a phosphotyrosyl peptide. The α-carbon traces of the SH2 domains are shown in green, the SH3 domains are blue, and the phosphopeptide is yellow [51]. Peptide residues N-terminal to the phosphotyrosine are omitted.

hibits tyrosine kinase activity by intramolecularly binding to the SH2 domain.[4e, 50] The binding of the C-terminal tail appears to stabilize the dimeric complex since the peptide contacts both domains, including the RT-Src loop of the SH3 domain. On the basis of these observations, Harrison et al. have proposed a general model for the regulation of Src-family tyrosine kinases.[2g] In this structural model the SH3–SH2 dimer complexed with the C-terminal region of Lck represents the "closed" catalytically inactive state of tyrosine kinases. The binding sites of SH3 and SH2 domains are thus concealed and unable to recognize heterologous targets. Molecular events that disrupt this dimeric structure may trigger an "open" state and activate the kinase domain, initiating signal transduction cascades. Possible activating events include the dephosphorylation of the regulatory C-terminal tail, the binding of the SH3 or SH2 domains to other endogenous ligands, or mutations in either domain that destabilize the "closed" conformation of tyrosine kinases. The validity of this mechanistic model awaits testing by biochemical methods, since it is possible that the SH3–SH2 dimer is simply the result of crystal packing forces. No association has yet been detected in solution or in cellular lysates. Protein dimerization, however, may occur in intact cells because Src-family tyrosine kinases are localized to the membrane.

5. A General Model for SH3–Ligand Interactions

As demonstrated by combinatorial synthesis and methods of structure elucidation, there are recurring structural features in SH3 domains and their proline-rich ligands. These conserved architectural elements and the structure-based analysis of putative SH3-binding sequences allow for a detailed understanding of SH3–ligand interactions. The molecular recognition of SH3 domains is therefore governed by a common model which we describe below:

1) The SH3 domain contains three core binding pockets formed by conserved hydrophobic residues corresponding to Tyr90, Tyr92, Trp118, Pro133, and Tyr136 of c-Src SH3.

Residues in the RT- and n-Src loop regions contribute to the composite surface of these sites, providing structural elements for binding specificity.

2) SH3 domains recognize PPII helices in two distinct binding modes that differ in the directionality of their amide backbones. Hydrophobic contacts are the primary driving force of complexation, although specific electrostatic and hydrogen bond interactions may also play a role in ligand binding.

3) The core consensus motif for class I ligands is X_1-p-X_2-P-p-X_3-P; the class II consensus motif is X_3'-P-p-X_2'-P-p-X_1' (see Table 3). (X_i and X_i' represent SH3-contacting residues that may confer ligand specificity. The lower case p denotes a scaffolding residue that does not contact the SH3 domain but tends to be proline for PPII helix stabilization.) For both classes of ligands, a critical XPpXP sequence intercalates into the SH3 receptor site. Additional N-terminal residues in class I ligands or C-terminal residues in class II ligands can also contribute to SH3 binding and may play a major role in receptor–ligand specificity.

With these general guidelines, one can predict the molecular structure of an SH3–ligand complex using only the primary sequences of the receptor and ligand. For example, two components of the phagocyte NADPH oxidase complex are associated through an SH3-mediated interaction.[49d] The C-terminal SH3 domain of $p67^{phox}$ specifically binds to a proline-rich region in $p47^{phox}$ (QPAVPPRPS, residues 362–370). Based on the sequences of this SH3 binding motif and the $p67^{phox}$ SH3 domain, we can make the following predictions (Fig. 20). The proline-rich region of $p47^{phox}$ binds to the $p67^{phox}$ SH3 domain as a PPII helix, with its N-terminus adjacent to Phe466 of the receptor and its C-terminus adjacent to Trp494. Arg368 of the ligand contacts the first SH3 binding pocket and forms a salt bridge with Asp475, while dipeptidyl moieties formed by Val365–Pro366 and Gln362–Pro363 interact with the second and third binding clefts, respectively. As in the Sos1-derived ligand VPPPVPPRRR, the two most C-terminal residues (Pro369 and Ser370) may make additional contacts with the SH3 surface, increasing ligand affinity and specificity. Other ligand residues such as Ala364 and Pro367 point away from the SH3–ligand interface and may pack against the surface of $p47^{phox}$. The precise details of these structural predictions are a testament to our current understanding of SH3–ligand interactions. They also illustrate the collective power of combinatorial synthesis and structural methods in receptor–ligand investigations.

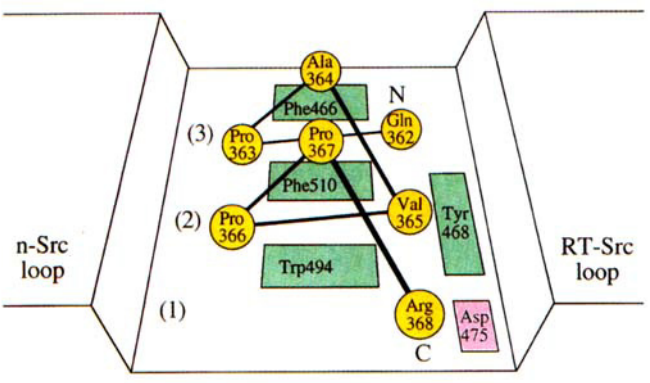


Fig. 20. Schematic representation of the $p47^{phox}$-derived peptide QPAVPPRPS bound to the C-terminal SH3 domain of $p67^{phox}$. Numbers in parentheses represent the three hydrophobic pockets in the SH3 binding site.

6. Summary and Outlook

The determination of the three-dimensional structures of SH3 domains complexed to ligands discovered through combinatorial synthesis has provided a remarkably clear picture of SH3 recognition. In only a short period of time, our view of these receptors has been transformed into one that involves specific molecular interactions between a PPII helix and a spatial array of aromatic SH3 residues. This global understanding of SH3–ligand interactions is the result of a two-step research strategy. Combinatorial synthesis yielded two familes of peptide ligands, filling a critical gap in our knowledge of SH3 recognition. Multidimensional NMR spectroscopy then completed this discovery process, providing a molecular understanding of SH3–ligand complexes that has significant predictive capabilities. The combination of these two techniques embodies a new approach to studying protein–ligand interactions that should be applicable to other systems.

The insights we have obtained through combinatorial synthesis and NMR spectroscopy lead to a number of fundamental questions concerning SH3–ligand interactions. For example, why would nature invent a mechanism for protein–protein association that involves dual orientations? Do individual SH3 domains utilize both binding modes in cellular systems, or do they each have a specific preference for a single class of ligands? The resolution of these biological issues will depend on more traditional strategies, which have gradually dissected the myriad of signal transduction pathways into their molecular components. Fundamental issues of molecular recognition are also highlighted by the structural elucidation of SH3–ligand complexes. In many respects, the PPII helix represents an ideal SH3-recognition motif that has been optimized by countless evolutionary cycles. It is interesting, however, to consider the outcome of selection processes that are not limited to natural amino acids. Can combinations of other functional groups provide suitable SH3 ligands? Will such non-peptidic ligands mimic the structural elements of the PPII helix, or are unique solutions for SH3 binding possible? Answers to these questions await the structure-based design of non-peptidic ligands or perhaps even better, the structure-based design of new combinatorial libraries, including ones that remove the peptide backbone entirely. The chemical leads provided by these strategies, their structural elucidation by NMR spectroscopy or X-ray crystallography, and the redesign of new ligands or libraries constitute an iterative process of discovery that promises to expand our knowledge of molecular recognition and the biological processes it governs.

We would like to thank our friends and colleagues who have contributed to our investigations of SH3 domains. Our success in the application of combinatorial synthesis to SH3 recognition would have been impossible without the patience and efforts of Andrew Brauer of ARIAD Pharmaceuticals, Inc., Bill Lane of the Harvard Microchemistry Facility, and Akito Tanaka of our laboratory. Our accomplishments in the structural elucidation of SH3–ligand complexes are due to the hard work and critical insights of Hongtao Yu, Sibo Feng, and Satoshi Koyama of our laboratory and David Dalgarno of ARIAD Pharmaceuticals, Inc. We would also like to thank Professor George Whitesides and Frank Gomez of Harvard University for their collaboration in our initial studies of SH3–ligand interactions using affinity capillary

electrophoresis. Thanks go out to H. Y., S. F., and Tae Bum Shin for critiquing the manuscript, Professor Stephen Harrison of the Harvard Molecular and Cellular Biology Department for providing coordinates of the SH3–SH2 fragment of Lck, and Andrea Musacchio of EMBL for providing the coordinates of the Abl SH3–3BP1-10 complex. Finally, we are indebted to our colleagues at ARIAD Pharmaceuticals, Inc., including Ricky Rickles and Joan Brugge, and current and former members of the Schreiber group, including T. B. S. and Julian Simon, whose enthusiasm and helpful discussions have made the SH3 project in the laboratory exciting and successful. J. K. C. would like to thank the National Science Foundation, the American Chemical Society Division of Organic Chemistry, and Zeneca for financial support in the form of graduate fellowships. SH3 research in the S. L. S. group is supported by the National Institute of General Medical Sciences (GM-44993) and the Howard Hughes Medical Institute.

Received: October 6, 1994 [A 901E]
German version: *Angew. Chem.* **1995**, *107*, 1041

[1] For reviews see: a) C. A. Koch, D. Anderson, M. F. Moran, C. Ellis, T. Pawson, *Science* **1991**, *252*, 668–674; b) A. Musacchio, T. Gibson, V.-P. Lehto, M. Saraste, *FEBS Lett.* **1992**, *307*, 55–61; c) T. Pawson, J. Schlessinger, *Curr. Biol.* **1993**, *3*, 434–442; d) C. J. Morton, I. D. Campbell, *ibid.* **1994**, *4*, 615–617.

[2] Structures of SH3 domains: a) α-spectrin: A. Musacchio, M. Nobel, R. Pauptit, R. Wierenga, M. Saraste, *Nature* **1992**, *359*, 851–855; b) c-Src: H. Yu, M. K. Rosen, T. B. Shin, C. Seidel-Dugan, J. S. Brugge, S. L. Schreiber, *Science* **1992**, *258*, 1665–1668; c) PI3K: S. Koyama, H. Yu, D. C. Dalgarno, T. B. Shin, L. D. Zydowsky, S. L. Schreiber, *Cell* **1993**, *72*, 945–952; d) PI3K: G. W. Booker, I. Gout, A. K. Downing, P. C. Driscoll, J. Boyd, M. D. Waterfield, I. D. Campbell, *ibid.* **1993**, *73*, 813–822; e) PLC-γ: D. Kohda, H. Hatanaka, M. Odaka, V. Mandiyan, A. Ullrich, J. Schlessinger, F. Inagaki, *ibid.* **1993**, *72*, 953–960; f) Fyn: M. E. M. Noble, A. Musacchio, M. Saraste, S. A. Courtneidge, R. K. Wierenga, *EMBO J.* **1993**, *12*, 2617–2624; g) Lck: M. J. Eck, S. K. Atwell, S. E. Schoelson, S. C. Harrison, *Nature* **1994**, *368*, 764–769; h) Csk: T. V. Borchert, M. Mathieu, J. Ph. Zeelen, S. A. Courtneidge, R. K. Wierenga, *FEBS Lett.* **1994**, *341*, 79–85.

[3] D. Bar-Sagi, D. Rotin, A. Batzer, V. Mandiyan, J. Schlessinger, *Cell* **1993**, *74*, 83–91.

[4] a) J.-Y. Kato, T. Takeya, C. Grandori, H. Iba, J. B. Levy, H. Hanafusa, *Mol. Cell. Biol.* **1986**, *6*, 4155–4160; b) W. M. Potts, A. B. Reynolds, T. J. Lansing, J. T. Parsons, *Oncog. Res.* **1988**, *3*, 343–355; c) S. P. Nemeth, L. C. Fox, M. DeMarco, J. S. Brugge, *Mol. Cell. Biol.* **1989**, *9*, 1109–1119; d) I. Gout, R. Dhand, I. D. Hiles, M. J. Fry, G. Panayotou, P. Das, O. Truong, N. F. Totty, J. Hsuan, G. W. Booker, I. D. Campbell, M. D. Waterfield, *Cell* **1993**, *75*, 25–36; e) G. Superti-Furga; S. Fumagalli, M. Koegl, S. A. Courtneidge, G. Draetta, *EMBO J.* **1993**, *12*, 2625–2634.

[5] C. Seidel-Dugan, B. E. Meyer, S. M. Thomas, J. S. Brugge, *Mol. Cell. Biol.* **1992**, *12*, 1835–1845.

[6] a) M. A. Simon, G. S. Dodson, G. M. Rubin, *Cell* **1993**, *73*, 169–178; b) J. P. Olivier, T. Raabe, M. Henkemeyer, B. Dickson, G. Mbamalu, B. Margolis, J. Schlessinger, E. Hafen, T. Pawson, *ibid.* **1993**, *73*, 179–191; c) L. Buday, J. Downward, *ibid.* **1993**, *73*, 611–620; d) S. E. Egan, B. W. Giddings, M. W. Brooks, L. Buday, A. M. Sizeland, R. A. Weinberg, *Nature (London)* **1993**, *363*, 45–51; e) M. Rozakis-Adcock, R. Fernley, J. Wade, T. Pawson, D. Bowtell, *ibid.* **1993**, *363*, 83–85; f) N. Li, A. Batzer, R. Daly, V. Yajnik, E. Skolnik, P. Chardin, D. Bar-Sagi, B. Margolis, J. Schlessinger, *ibid.* **1993**, *363*, 85–88; g) N. W. Gale, S. Kaplan, E. J. Lowenstein, J. Schlessinger, D. Bar-Sagi, *ibid.* **1993**, *363*, 88–92.

[7] For a review see: J. T. Parsons, M. J. Weber, *Curr. Top. Microbiol. Immunol.* **1989**, *147*, 79–127.

[8] D. S. Wages, J. Keefer, T. B. Rall, M. J. Weber, *J. Virol.* **1992**, *66*, 1866–1874.

[9] a) J. A. Escobedo, S. Navankasattusas, W. M. Kavanaugh, D. Milfay, V. A. Fried, L. T. Williams, *Cell* **1991**, *65*, 75–82; b) E. Y. Skolnik, B. Margolis, M. Mohammadi, E. Lowenstein, R. Fischer, A. Drepps, A. Ullrich, J. Schlessinger, *ibid.* **1991**, *65*, 83–90; c) M. Otsu, I. Hiles, I. Gout, M. J. Fry, F. Ruiz-Larrea, G. Panayotou, A. Thompson, R. Dhand, J. Husan, N. Totty, A. D. Smith, S. J. Morgan, S. A. Courtneidge, P. J. Parker, M. D. Waterfield, *ibid.* **1991**, *65*, 91–104; d) I. D. Hiles, M. Otsu, S. Volinia, M. J. Fry, I. Gout, R. Dhand, G. Panayotou, F. Ruiz-Larrea, A. Thompson, N. F. Totty, J. J. Husan, S. A. Courtneidge, P. J. Parker, M. D. Waterfield, *ibid.* **1992**, *70*, 419–429.

[10] a) L. Varticovski, B. Druker, D. Morrison, L. Cantley, T. Roberts, *Nature (London)* **1989**, *342*, 699–702; b) C. J. McGlade, C. Ellis, M. Reedijk, D. Anderson, G. Mbamalu, A. D. Reith, G. Panayotou, P. End, A. Bernstein, A. Kazlauskas, M. D. Waterfield, T. Pawson, *Mol. Cell. Biol.* **1992**, *12*, 991–997; c) A. Klippel, J. A. Escobedo, W. J. Fantl, L. T. Williams, *ibid.* **1992**, *12*, 1451–1459.

[11] P. Cicchetti, B. J. Mayer, G. Thiel, D. Baltimore, *Science* **1992**, *257*, 803–806.

[12] R. Ren, B. J. Mayer, P. Cicchetti, D. Baltimore, *Science* **1993**, *259*, 1157–1161.

[13] F. A. Gomez, J. K. Chen, A. Tanaka, S. L. Schreiber, G. M. Whitesides, *J. Org. Chem.* **1994**, *59*, 2885–2886.

[14] Z. Weng, J. A. Taylor, C. E. Turner, J. S. Brugge, C. Seidel-Dugan, *J. Biol. Chem.* **1993**, *268*, 14956–14963.

[15] a) S. A. Benner, M. A. Cohen, D. Gerloff, *Nature (London)* **1992**, *359*, 781; b) S. A. Benner, M. A. Cohen, D. Gerloff, *J. Mol. Biol.* **1993**, *229*, 295–305.

[16] B. Rost, C. Sander, *Nature (London)* **1992**, *360*, 540.

[17] Structures of SH2 domains: a) v-Src: G. Waksman, D. Kominos, S. C. Robertson, N. Pant, D. Baltimore, R. B. Birge, D. Cowburn, H. Hanafusa, B. J. Mayer, M. Overduin, M. D. Resh, C. B. Rios, L. Silverman, J. Kuriyan, *Nature (London)* **1992**, *358*, 646–653; b) PI3K, N-terminal: G. W. Booker, A. L. Breeze, A. K. Downing, G. Panayotou, I. Gout, M. D. Waterfield, I. D. Campbell, *ibid.* **1992**, *358*, 684–687; c) Abl: M. Overduin, C. B. Rios, B. J. Mayer, D. Baltimore, D. Cowburn, *Cell* **1992**, *70*, 697–704; d) Lck: M. J. Eck, S. E. Shoelson, S. C. Harrison, *Nature (London)* **1993**, *362*, 87–91; e) PLC-γ1: S. M. Pascal, A. U. Singer, G. Gish, T. Yamazaki, S. E. Shoelson, T. Pawson, L. E. Kay, J. D. Forman-Kay, *Cell* **1994**, *77*, 461–472; f) Syp: C-H. Lee, D. Kominos, S. Jacques, B. Margolis, J. Schlessinger, S. E. Shoelson, J. Kuriyan, *Structure* **1994**, *2*, 423–438.

[18] a) J. B. Levy, T. Dorai, L.-H. Wang, J. S. Brugge, *Mol. Cell. Biol.* **1987**, *7*, 4142–4145; b) R. Martinez, B. Mathey-Prevot, A. Bernards, D. Baltimore, *Science* **1987**, *237*, 411–415.

[19] J. M. Pyper, J. B. Bolen, *Mol. Cell. Biol.* **1990**, *10*, 2035–2040.

[20] For reviews see: a) R. M. Baum, *Chem. Eng. News* **1994**, *72*, 20–26; b) M. A. Gallop, R. W. Barrett, W. J. Dower, S. P. A. Fodor, E. M. Gordon, *J. Med. Chem.* **1994**, *37*, 1233–1251.

[21] a) H. M. Geysen, R. H. Meloen, S. J. Barteling, *Proc. Natl. Acad. Sci. USA* **1984**, *81*, 3998–4002; b) S. F. Parmley, G. P. Smith, *Gene* **1988**, *73*, 305–318; c) S. P. A. Fodor, J. L. Read, M. C. Pirrung, L. Stryer, A. T. Lu, D. Solas, *Science* **1991**, *251*, 767–773; d) K. S. Lam, S. E. Salmon, E. M. Hersh, V. J. Hruby, W. M. Kazmierski, R. J. Knapp, *Nature (London)* **1991**, *354*, 82–84; e) R. A. Houghten, C. Pinilla, S. E. Blondelle, J. R. Appel, C. T. Dooley, J. H. Cuervo, *ibid.* **1991**, *354*, 84–86; f) M. G. Cull, J. F. Miller, P. J. Schatz, *Proc. Natl. Acad. Sci. USA* **1992**, *89*, 1865–1869; g) A. G. Jung, G. Beck-Sickinger, *Angew. Chem.* **1992**, *104*, 375–391; *Angew. Chem. Int. Ed. Engl.* **1992**, *31*, 367–383.

[22] a) C. Tuerk, L. Gold, *Science* **1990**, *249*, 505–510; b) L. C. Bock, L. C. Griffin, J. A. Latham, E. H. Vermaas, J. J. Toole, *Nature (London)* **1992**, *355*, 564–566; c) M. Famulok, J. W. Szostak, *Angew. Chem.* **1992**, *104*, 1001–1011; *Angew. Chem. Int. Ed. Engl.* **1992**, *31*, 979–998; d) M. Sassanfar, J. W. Szostak, *Nature (London)* **1993**, *364*, 550–553; d) R. D. Jenison, S. C. Gill, A. Pardi, B. Polisky, *Science* **1994**, *263*, 1425–1429.

[23] a) R. J. Simon, R. S. Kania, R. N. Zuckermann, V. D. Huebner, D. A. Jewell, S. Banville, S. Ng, L. Wang, S. Rosenberg, C. K. Marlowe, D. C. Spellmeyer, R. Tan, A. D. Frankel, D. V. Santi, F. E. Cohen, P. A. Bartlett, *Proc. Natl. Acad. Sci. USA* **1992**, *89*, 9367–9371; b) C. Y. Cho, E. J. Moran, S. R. Cherry, J. C. Stephans, S. P. A. Fodor, C. L. Adams, A. Sundaram, J. W. Jacobs, P. G. Schultz, *Science* **1993**, *261*, 1303–1305.

[24] a) B. A. Bunin, J. A. Ellman, *J. Am. Chem. Soc.* **1992**, *114*, 10997–10998; b) S. H. Dewitt, J. S. Kiely, C. J. Stankovic, M. C. Schroder, D. M. R. Cody, M. R. Pavia, *Proc. Natl. Acad. Sci. USA* **1993**, *90*, 6909–6913.

[25] A. P. Combs, Dissertation, University of California, Los Angeles, **1994**.

[26] Á. Furka, F. Sebestyén, M. Asgedom, G. Dibó, *Int. J. Pept. Protein Res.* **1991**, *37*, 487–493.

[27] J. K. Chen, W. S. Lane, A. W. Brauer, A. Tanaka, S. L. Schreiber, *J. Am. Chem. Soc.* **1993**, *115*, 12591–12592.

[28] H. Yu, J. K. Chen, S. Feng, D. C. Dalgarno, A. W. Brauer, S. L. Schreiber, *Cell* **1994**, *76*, 933–945.

[29] K. F. Geoghegan, J. G. Stroh, *Bioconjugate Chem.* **1992**, *3*, 138–146.

[30] A. Musacchio, M. Saraste, M. Wilmanns, *Nat. Struct. Biol.* **1994**, *1*, 546–551.

[31] W. A. Lim, F. M. Richards, *Nat. Struct. Biol.* **1994**, *1*, 221–225.

[32] S. Feng, J. K. Chen, H. Yu, J. A. Simon, S. L. Schreiber, *Science* **1994**, *266*, 1241–1247.

[33] G. Naharro, K. C. Robbins, E. P. Reddy, *Science* **1984**, *223*, 63–66.

[34] M. M. Tamkun, K. M. Knoth, J. A. Walbridge, H. Kroemer, D. M. Roden, D. M. Glover, *FASEB J.* **1991**, *5*, 331–337.

[35] T. Baba, K. Watanabe, S. Kashiwabara, Y. Arai, *FEBS Lett.* **1989**, *244*, 296–300.

[36] T. J. Blake, M. Shapiro, H. C. Morse, W. Y. Langdon, *Oncogene* **1991**, *6*, 653–657.

[37] E. Hafen, K. Basler, J. E. Edstroem, G. M. Rubin, *Science* **1987**, *236*, 55–63.

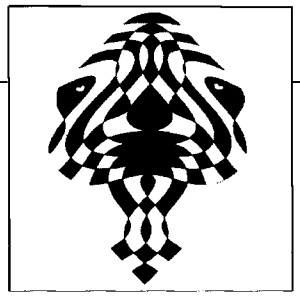
[38] P. Kastner, A. Krust, B. Turcotte, U. Stropp, L. Torn, H. Gronemeyer, P. Cambon, *EMBO J.* **1990**, *9*, 1603–1614.

[39] C. M. Pleiman, W. M. Hertz, J. C. Cambier, *Science* **1994**, *263*, 1609–1612.

[40] J. K. Chen, S. L. Schreiber, *Bioorg. Med. Chem. Lett.* **1994**, *4*, 1755–1760.

[41] A. A. Adzhubei, M. J. E. Sternberg, *J. Mol. Biol.* **1993**, *229*, 472–493.

[42] R. J. Rickles, M. C. Botfield, Z. Weng, J. A. Taylor, O. M. Green, J. S. Brugge, M. J. Zoller, *EMBO J.* **1994**, *13*, 5598–5604.
[43] For examples see: a) bovine pancreatic trypsin inhibitor: W. Bode, P. Schwager, R. Huber, *J. Mol. Biol.* **1978**, *118*, 99–112; b) human carbonic anhydrase II: A. E. Eriksson, T. A. Jones, A. Liljas, *Proteins: Struct. Funct. Genet.* **1988**, *4*, 274–282; c) human retinol binding protein: G. Zanotti, S. Ottonello, R. Berni, H. Monaco, *J. Mol. Biol.* **1993**, *230*, 613–624.
[44] A. Borchardt, W. C. Still, *J. Am. Chem. Soc.* **1994**, *116*, 7467–7468.
[45] a) C. Björkegren, M. Rozycki, C. E. Schutt, U. Lindberg, R. Karlsson, *FEBS Lett.* **1993**, *333*, 123–126; b) W. J. Metzler, A. J. Bell, E. Ernst, T. B. Lavoie, L. Mueller, *J. Biol. Chem.* **1994**, *269*, 4620–4625; c) S. J. Archer, V. K. Vinson, T. D. Pollard, D. A. Torchia, *FEBS Lett.* **1994**, *337*, 145–151.
[46] G. Waksman, S. E. Shoelson, N. Pant, D. Cowburn, J. Kuriyan, *Cell* **1993**, *72*, 779–790.
[47] a) B. W. Matthews, P. B. Sigler, R. Henderson, D. M. Blow, *Nature (London)* **1967**, *214*, 652–664; b) R. M. Stroud, L. M. Kay, R. E. Dickerson, *J. Mol. Biol.* **1974**, *85*, 185–208.
[48] G. Cheng, Z.-S. Ye, D. Baltimore, *Proc. Natl. Acad. Sci. USA* **1994**, *91*, 8152–8155.
[49] a) E. T. Barfod, Y. Zheng, W.-J. Kuang, M. J. Hart, T. Evans, R. A. Cerione, A. Ashkenazi, *J. Biol. Chem.* **1993**, *268*, 26059–26062; b) R. Kapeller, K. V. S. Prasad, O. Janssen, W. Hou, B. S. Schaffhausen, C. E. Rudd, L. C. Cantley, *ibid.* **1994**, *269*, 1927–1933; c) S. Tanaka, T. Morishita, Y. Hashimoto, S. Hattori, S. Nakamura, M. Shibuya, K. Matuoka, T. Takenawa, T. Kurata, K. Nagashima, M. Matsuda, *Proc. Natl. Acad. Sci. USA* **1994**, *91*, 3443–3447; d) P. Finan, Y. Shimizu, I. Gout, J. Hsuan, O. Truong, C. Butcher, P. Bennett, M. D. Waterfield, S. Kellie, *J. Biol. Chem.* **1994**, *269*, 13752–13755; e) K. Seedorf, G. Kostka, R. Lammers, P. Bashkin, R. Daly, W. H. Burgess, A. M. van der Bliek, J. Schlessinger, A. Ullrich, *ibid.* **1994**, *269*, 16009–16014; f) H. Sumimoto, Y. Kage, H. Nunoi, H. Sasaki, T. Nose, Y. Fukumaki, M. Ohno, S. Minakami, K. Takeshige, *Proc. Natl. Acad. Sci. USA* **1994**, *91*, 5345–5349; g) M. Sudol, *Oncogene* **1994**, *9*, 2145–2152.
[50] a) L. C. Cantley, K. R. Auger, C. Carpenter, B. Duckworth, A. Graziani, R. Kapeller, S. Soltoff, *Cell* **1991**, *64*, 281–302; b) R. R. Roussel, S. R. Brodeur, D. Shalloway, A. P. Laudano, *Proc. Natl. Acad. Sci. USA* **1991**, *88*, 10696–10700.
[51] Figures 5, 6, 11, 13, 15, 16, 18, and 19 were generated with the program GRASP: A. Nicholls, K. A. Sharp, B. Honig, *Proteins: Struct. Funct. Genet.* **1991**, *11*, 282–293.
[52] Figures 7 and 14 were generated with the program MOLSCRIPT: P. J. Kraulis, *J. Appl. Crystallogr.* **1991**, *24*, 946–950.



Troubleshooting... with VCH books!

Neuhoff, V.
Scientists in Conference
The Congress Organizer's Handbook
1987. X, 223 pages.
Hardcover. DM 68.00
ISBN 3-527-26579-1

Do you have to organize a conference? Well, sometimes, this can't be avoided. But you don't want to get crushed by the wheels of paperwork? And you want to stay in your budget? Then this handy little book is your survival kit!

Schoenfeld, R.
The Chemist's English
Third, revised edition with Say It in English, Please!
1990. XII, 195 pages with 9 figures.
Hardcover. DM 48.00
ISBN 3-527-28003-0

"Recommended without qualification; and a suitable gift for friends."
Chemical and Engineering News

"The book might well serve as a prescribed text for PhD students."
Nature

Ebel, H.F. /Bliefert, C. / Russey, W.
The Art of Scientific Writing
From Student Reports to Professional Publications in Chemistry and Related Fields
1990. XIX, 493 pages with 27 figures and 16 tables.
Softcover. DM 48.00
ISBN 3-527-26677-1

First of all, here we have a highly readable text on scientific communication - with all its ramifications from writing the most effective text to getting it published. Never before has so much information on scientific writing been assembled in a single book.

To order please contact your bookseller or:
VCH, P.O. Box 10 11 61,
D-69451 Weinheim,
Telefax (0) 62 01 - 60 61 84
VCH, Hardstrasse 10, P.O. Box,
CH-4020 Basel
VCH, 8 Wellington Court,
Cambridge CB1 1HZ, UK
VCH, 303 N.W. 12th Avenue,
Deerfield Beach, FL 33442-1788,
USA
toll-free: 1-800-367-8249 or
fax: 1-800-367-8247
VCH, Eikow Building,
10-9 Hongo 1-chome, Bunkyo-ku,
Tokyo 113

VCH

The Catalytic Oxidative Coupling of Methane

Jack H. Lunsford*

One of the great challenges in the field of heterogeneous catalysis is the conversion of methane to more useful chemicals and fuels. A chemical of particular importance is ethene, which can be obtained by the oxidative coupling of methane. In this reaction CH_4 is first oxidatively converted into C_2H_6, and then into C_2H_4. The fundamental aspects of the problem involve both a heterogeneous component, which includes the activation of CH_4 on a metal oxide surface, and a homogeneous gas-phase component, which includes free-radical chemistry. Ethane is produced mainly by the coupling of the surface-generated $CH_3^{\bullet}$ radicals in the gas phase. The yield of C_2H_4 and C_2H_6 is limited by secondary reactions of $CH_3^{\bullet}$ radicals with the surface and by the further oxidation of C_2H_4, both on the catalyst surface and in the gas phase. Currently, the best catalysts provide 20% CH_4 conversion with 80% combined C_2H_4 and C_2H_6 selectivity in a single pass through the reactor. Less is known about the nature of the active centers than about the reaction mechanism; however, reactive oxygen ions are apparently required for the activation of CH_4 on certain catalysts. There is spectroscopic evidence for surface O^- or O_2^{2-} ions. In addition to the oxidative coupling of CH_4, cross-coupling reactions, such as between methane and toluene to produce styrene, have been investigated. Many of the same catalysts are effective, and the cross-coupling reaction also appears to involve surface-generated radicals. Although a technological process has not been developed, extensive research has resulted in a reasonable understanding of the elementary reactions that occur during the oxidative coupling of methane.

Keywords: catalysis · methane · oxidations · radicals · reaction mechanisms

1. Introduction

Methane, a principal component of natural gas, is an abundant hydrocarbon resource that is mainly used as a relatively inexpensive and clean-burning fuel. Certain chemicals such as methanol are indirectly derived from methane through a reforming reaction, in which methane reacts with water at elevated temperatures to form hydrogen and carbon monoxide. Because of the enormous proven reserves of natural gas in the world (1.4×10^{14} m^3),[1] there is a strong economic incentive to develop a process that would convert methane into more valuable chemicals and fuels. The quest for such a process and the associated scientific challenge has stimulated a large amount of research over the last decade on methods for the direct conversion of methane into ethylene, methanol, formaldehyde, etc. This research has focused on gas-phase reactions (noncatalytic and usually at high pressures),[2, 3] as well as on catalytic reactions in solution and on solid surfaces. The recent report by Lin and Sen[4] describes one of the few homogeneous catalytic systems in which methane has been converted into another organic molecule. In this case, methane was converted into acetic acid over a rhodium complex.

[*] Professor J. H. Lunsford
Department of Chemistry, Texas A & M University
College Station, TX 77843 (USA)
Telefax: Int. code + (409)845-4719

Most of the research on the direct conversion of methane has been devoted to the oxidative coupling reaction, which involves the catalytic conversion of methane and oxygen to ethane and water. The ethane is converted in situ into ethylene, and other sequential reactions produce small amounts of higher hydrocarbons. The hydrocarbon products (ethane, ethylene, and higher hydrocarbons) often are reported as C_{2+} products. The target molecule is ethylene, not only because of price but because of the size of the market. Ethylene is by far the largest volume organic chemical; 6×10^{10} kg was produced in 1992. In addition to these desirable products, CO_x (CO and CO_2) products are formed nonselectively. The conversion of CH_4 to CO_x is undesirable since it represents a reduced yield of hydrocarbons. Moreover the formation of CO_2 is a highly exothermic reaction, and the dissipation of heat would be a formidable engineering problem for commercial operation. The goal of the technical research is to produce, in a single pass through a catalyst, high ethylene selectivity at moderate levels of methane conversion. One might hope to achieve, for example, 90% selectivity for ethylene at 40% methane conversion. As the subsequent sections will show, this goal has certainly not been achieved.

At a more fundamental level the research on the oxidative coupling of methane has provided insight into an unusual type of oxidation catalysis, which involves both surface and gas-phase free-radical chemistry. In many cases the catalysts are uncommon in oxidation catalysis, as they do not contain transi-

 © VCH Verlagsgesellschaft mbH, D-69451 Weinheim, 1995 0570-0833/95/0909-0970 $ 10.00+.25/0

Table 1. Representative oxidative coupling catalysts.

Catalyst	T [°C]	v[a] [mL(min g)$^{-1}$]	C:O:X[b]	$C(CH_4)$[c] [%]	S[%][d] C_{2+}	CO_x	Ref.
Li(5 wt%)/MgO	675	75	78:8:14	9	82	18	[13]
La_2O_3	750	10000	8:2:90	12	67	33	[14]
Sr(1 wt%)La_2O_3	880	3667	91:9:0	16	81	19	[15]
Ba(2 mol%)/MgO	825	2400	42:4:54	17	78	22	[16]
$LiCa_2Bi_3O_4Cl_6$	720	25	20:10:70	42	47 [e]	53	[17]
BiOCl(10 mol%)/Li_2CO_3(10 mol%)/MgO	750	250	20:5:75	18	83	17	[18]
$NaMnO_4$(12 wt%)/MgO	800	84	50:10:40	28	69	31	[19]
Mn(2 wt%)/Na_2WO_4(5 wt%)/SiO_2	800	1320	45:15:39	37	65	35	[20]

[a] v: flow rate. [b] The C:O:X ratio refers to mole percentages of CH_4, O_2, and inert gas in the feed stock; total pressure: 1 atm. [c] $C(CH_4)$: conversion of methane. [d] S: selectivity. [e] The C_2H_4/C_2H_6 ratio was 25.

tion metal ions. Oxidative coupling reactions generally take place at 650–880 °C, at the limits of catalytic combustion where the availability of oxygen largely dictates the C_{2+} selectivity.

In this introduction to oxidative coupling, attention will be given to the mechanistic details and the nature of the centers that are responsible for the activation of methane. The scope of oxidative coupling will be broadened somewhat to include a limited amount of material on cross-coupling reactions; that is, reactions in which a methyl radical couples with another type of hydrocarbon radical. At least two other recent reviews provide a detailed summary of the catalysts that have been employed and the results obtained.[5–6] Likewise, other reviews and at least one book address other aspects of the research and provide alternative viewpoints on oxidative coupling.[7–10]

2. Catalysts and Catalytic Results

The possibility of attaining reasonable C_2 yields through oxidative coupling of CH_4 first became evident with the publication of Baerns and co-workers in 1984[11] and those of Ito et al. in 1985.[12] Baerns achieved 58% C_2 selectivity at 5% CH_4 conversion over a PbO/Al_2O_3 catalyst, whereas Ito et al. reported that a lithium-promoted MgO catalyst (Li/MgO) resulted in 50% C_2 selectivity at 28% conversion. Since these early results were reported, hundreds of catalysts have been found to be more or less active and selective for the coupling reaction. Several of the better catalysts are listed in Table 1, along with the conversions and selectivities that have been achieved.

In earlier studies the goal of the applied research was often to maximize C_2 yield by varying catalyst composition, reagent partial pressures, etc.; however, economic evaluations have shown that C_2 selectivity is more important than yield, provided, of course, one can obtain a modest level of CH_4 conversion. The maximum selectivity and conversion that can be achieved are related, and it is often useful to consider the sum of the two. For the best catalysts known at this time the sum of selectivity and conversion is about 100. Specific activity is a less important factor because of the problems associated with heat removal. Moreover, it often is difficult to ascertain specific activities from published results, because the reactions are carried out under severely oxygen-limited conditions to maximize selectivity. Nevertheless, from the specific flow rates listed in Table 1, one can qualitatively judge the activity. Still another factor in evaluating a catalyst is the need of a diluent. The conversion and selectivity generally increases as the partial pressure of the reagents decreases, but the separation of C_2H_4 from a large excess of a diluent gas is undesirable. Therefore, the better catalysts are capable of promoting high C_{2+} selectivities in the absence of a diluent.

The more effective catalysts may be divided into five groups: a) highly basic pure oxides, of which the early members of the lanthanide oxide series (excluding CeO_2) are the best; b) Group IA or IIA ions supported on basic oxides (for example, Li/MgO, Ba/MgO and Sr/La_2O_3); c) monophasic oxides; d) a few transition metal oxides that contain Group IA ions; and e) any of these materials that are promoted with chloride ions. Dubois and Cameron[21] have concluded that good oxidative coupling catalysts are strongly basic oxides that are p-type semiconduc-



Jack Lunsford, born in 1936 in Houston, Texas, received his undergraduate degree at Texas A & M University (1957) and his Ph.D. degree from Rice University (1962). In 1966 he returned to Texas A & M University as Assistant Professor of Chemistry, and in 1971 he was appointed Professor. He was a Guggenheim Fellow in 1985 and an Alexander von Humboldt Senior Scientist in 1992. He has maintained an active research program in the field of heterogeneous catalysis, with emphasis on the use of spectroscopic techniques to identify active centers and reaction intermediates. His research on surface-generated, gas-phase radicals has provided a basis for understanding the mechanism of oxidative coupling reactions.

tors at elevated temperatures and have oxygen anion mobility. Moreover, they are free of reducible surface cations. Many exceptions to the requirement of strong basicity are now known. For example, the $Mn(2\,wt\%)/Na_2WO_4(5\,wt\%)/SiO_2$ catalyst does not react with CO_2 at elevated temperatures, which usually is taken as measure of strong basicity. It also is surprising that this catalyst is highly selective, because transition metal oxides usually favor the formation of CO_x. We have confirmed the excellent behavior of the $Mn(2\,wt\%)/Na_2WO_4(5\,wt\%)/SiO_2$ catalyst and have found that at a $CH_4:O_2$ ratio of 8:1 without diluent and at 800 °C, the C_{2+} selectivity was 81% at 20% CH_4 conversion.[22] Moreover, as shown in Figure 1, the CH_4 selectivity decreased only a modest amount upon increasing the total

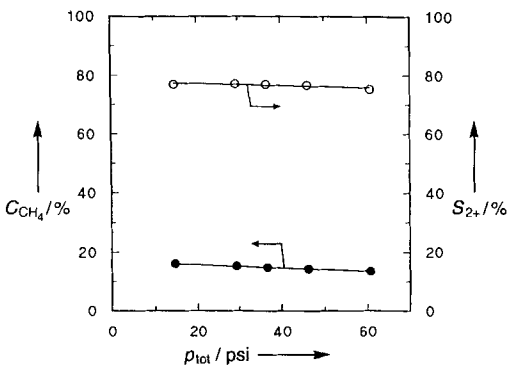


Fig. 1. Oxidative coupling of CH_4 over a $Mn(2\,wt\%)/Na_2WO_4(5\,wt\%)/SiO_2$ catalyst at pressures p greater than 1 atm: 0.1 g (0.22 mL) catalyst, $T = 785$ °C, $p(CH_4)/p(O_2) = 10$, contact time = 0.13 s (1 psi = 6.89 kPa). The y axes represent the methane conversion (C_{CH_4}) and the selectivity with respect to C_{2+} (S_{2+}).

pressure from 1 to 4 atm (1 atm = 101.3 kPa). The mass flow rate was varied so that the residence time of the feed gas in the catalyst bed remained constant at all pressures. This is believed to be the first example of a catalytic system that provides favorable conversions and selectivities at elevated pressures.

The $NaMnO_4/MgO$ catalyst, developed by Sofranko and coworkers,[19] is interesting, because it can be operated either in the usual co-feed or in a cyclic mode. In the latter mode the catalyst is oxidized with air, which eliminates the need for an oxygen separation facility. Moreover, for a given level of conversion, one can achieve approximately 10% greater C_{2+} selectivity. The specific activity for CH_4 conversion, however, is much less in the cyclic mode.

Several mixed-metal monophasic oxides have been studied as coupling catalysts, but these materials are subject to phase separation under the severe conditions employed in the coupling reaction. Of the Ba–Pb, Ba–Bi, and Ba–Sn perovskites that were examined by Dissanayake et al.,[23] only the Ba–Sn perovskite resisted phase separation, and this material was not selective. With the other two catalysts, barium segregated to the surface, and this presumably was the active component. Surface transformation is a common problem with all but the pure oxides, and the loss of an active component can adversely affect the performance. The loss of lithium from Li/MgO or lead from PbO/Al_2O_3 would be a serious impediment to the use of these catalysts in commercial operation.

3. Mechanism

3.1. Methane Activation

Product distributions as a function of residence time in the reactor show that most, if not all, of the initial hydrocarbon produced is C_2H_6, which suggests that ethane is formed by the coupling of $CH_3^{\bullet}$ radicals. This hypothesis is strongly supported by results obtained with a mixture of CH_4 and CD_4 in the reagent stream. Both Nelson et al.[24] and Mims et al.[25] showed that the main product of the coupling reaction was CH_3CD_3. Moreover, there is both qualitative and quantitative evidence for the coupling of the methyl radicals in the gas phase, after activation of CH_4 on the catalyst. Using a matrix isolation electron spin resonance (MIESR) system, we have detected surface-generated, gas-phase radicals over Li/MgO,[26] Li-MgO-Cl,[27] Na/CaO,[28] Na/CeO_2,[29] Sr/La_2O_3,[30] $LiNiO_2$,[31] Li/ZnO,[32] La_2O_3,[33] and other lanthanide oxide catalysts.[34] The results of Figure 2 are typical of the agreement between the $CH_3^{\bullet}$ radical production rate and that of C_2 product formation.

Although the MIESR system normally operates at pressure of about 2 Torr (1 Torr = 133 Pa), it was modified so that both the $CH_3^{\bullet}$ radical production rate and the C_2 production rate over a catalyst could be determined simultaneously at 760 Torr. By locating a leak into the MIESR system at the exit side of a thin catalyst bed, it was possible to minimize coupling within the voids of the bed. The results demonstrated that over a Li/MgO catalyst more than 40% of the C_2H_6 was derived from the coupling of $CH_3^{\bullet}$ radicals in the gas phase.[35] Using an entirely different system based on mass spectrometric detection and photoionization of $CH_3^{\bullet}$ radicals, Gutman and co-workers[36] concluded that greater than 75% of the C_2H_6 resulted from the coupling of $CH_3^{\bullet}$ radicals in the gas phase when the catalyst was Sr/La_2O_3. It may seem unlikely that the gas-phase coupling would exceed the surface coupling; however, one should recall that the binding energy (that is, heat of adsorption) of $CH_3^{\bullet}$ radicals on a closed shell oxide would be small and the entropy factor would favor desorption at the high temperatures used in these reactions.

These results convincingly show the importance of gas-phase reactions in the oxidative coupling reaction. A number of factors influence the production rate of $CH_3^{\bullet}$ radicals, and likewise, the conversion of CH_4 to C_2 products. The results of Figure 2 demonstrate maxima at about 3 wt% Li, whereas in a previous study we reported a maximum at about 13 wt% Li.[26] The difference between the two studies was the temperature at which the Li/MgO was calcined prior to forming $CH_3^{\bullet}$ radicals. By calcining the catalyst at a higher temperature (750 °C) the lithium was apparently more evenly distributed on and in MgO. Thus, less lithium was required to achieve maximum activity. Carbon dioxide likewise has a strong negative effect on $CH_3^{\bullet}$ radical production, but this will be discussed in more detail in Section 3.2.

Once the $CH_3^{\bullet}$ radicals enter the gas phase, they may either couple or enter into chain branching reactions that ultimately result in the formation of CO_x. Several groups have attempted to model these heterogeneous–homogeneous reaction systems with modest success.[37–39] A major difficulty in constructing such a model is in accounting for reactions of radicals or other

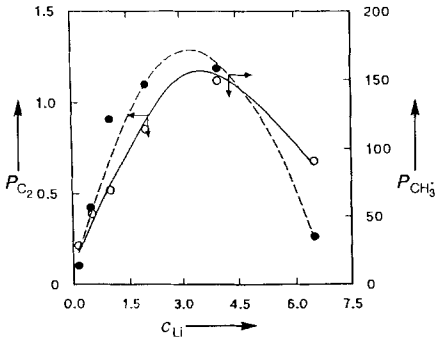


Fig. 2. Variation in C_2 productivity P_{C_2} [μmol m^{-2} s^{-1}] (○) and $CH_3^\bullet$ radical productivity $P_{CH_3^\bullet}$ [arbitrary units m^{-2}] (●) as a function of lithium content c_{Li} [wt%] in a Li/MgO catalyst. The reactions were carried out at 700 °C. The C_2 productivity was determined in a flow of 200 Torr CH_4 and 100 Torr O_2 (1 Torr = 133 Pa); the $CH_3^\bullet$ radical productivity was determined in a flow of 0.2 Torr CH_4 and 0.004 Torr O_2.

intermediates with the surface. For example, the gas-phase reaction (1) is a source of OH$^\bullet$ radicals, which serve as a major chain carrier in the temperature range of interest. But on a surface the facile decomposition reaction (2) occurs, and OH$^\bullet$ radicals do not enter the gas phase.

$$H_2O_2 + M \longrightarrow 2OH^\bullet + M \quad (1)$$

$$H_2O_2 \xrightarrow[\text{surface}]{} H_2O + 1/2\,O_2 \quad (2)$$

A model based on the original scheme proposed by Ito et al.[12] for heterogeneous reactions [Eqs. (3)–(5)] in addition to 156 gas-phase reactions has been used to explain most of the

$$CH_4 + O_s^- \rightarrow CH_3^\bullet + OH_s^- \quad (3)$$

$$2OH_s^- \rightarrow H_2O + O_s^{2-} + \square \quad (4)$$

$$O_s^{2-} + \square + 1/2\,O_2 \rightleftharpoons 2O_s^- \quad (5)$$

kinetic data over the Li/MgO catalyst,[37] including the variation in kinetic isotope effect on changing CH_4 and O_2 partial pressures.[40] The symbol □ denotes an oxide ion vacancy, and the subscript s an adsorbed species. The model can be extended to include N_2O as an oxidant by replacing reaction (5) with (6) and by adding the heterogeneous reactions (7), (8), and (9) as

$$O_s^{2-} + \square + N_2O \longrightarrow 2O_s^- + N_2 \quad (6)$$

$$N_2O + O_s^- \rightarrow O_{2s}^- + N_2 \quad (7)$$

$$N_2O + O_{2s}^- \rightarrow O_{3s}^- + N_2 \quad (8)$$

$$O_{3s}^- \rightleftharpoons O_2 + O_s^- \quad (9)$$

well as relevant gas-phase reactions.[41] Reactions (3) and (7) account for the inhibiting effect that CH_4 has on N_2O decomposition. At a given level of conversion, much greater C_{2+} selectivities were observed with N_2O than with O_2. One might think that this was due to differences in the gas-phase chemistry; however, the model indicates that surface reactions are largely involved. The ozonide ion, formed by reaction (8) or the reverse of reaction (9), might be responsible for the nonselective oxidation of C_2H_4 (see Section 3.3). In general, at temperatures less than 700 °C and at CH_4/O_2 ratios greater than 2, most of the chemistry occurs on the catalytic surface except for the coupling of the $CH_3^\bullet$ radicals.

There have been attempts to model the reaction in terms of Langmuir–Hinshelwood kinetics, which assumes that *adsorbed* CH_4 reacts with some form of surface oxygen,[42] or that $CH_3^\bullet$ radicals couple on the surface.[43] But several studies involving transients have confirmed that CH_4 is not adsorbed on coupling catalysts in the temperature range of interest.[44–46] With the small amount of C_2H_4 and C_2H_6 formed in these transient experiments, it is more difficult to make definitive conclusions about these hydrocarbons, and hence the location for $CH_3^\bullet$ radical coupling. Peil et al.[44] found evidence for a delay in C_2H_6 evolution from Li/MgO at 645 °C, but van der Wiele and co-workers[38] concluded that no C_2H_4 was adsorbed on Li/MgO at 800 °C. Recent studies by Baerns and co-workers,[47] who used a temporal analysis of products (TAP) reactor, confirm that over Sm_2O_3 methyl radicals are formed by the direct reaction of gaseous CH_4 with surface oxygen species in an Eley–Rideal type of mechanism.

Kinetic isotope effect (KIE) studies, first carried out by Cant et al.[48] and more recently by others as well,[49–52] indicate that a C–H bond is broken in the rate-limiting step [reaction (3)], with O_2 as the oxidant. We have found, however, that the KIE for methane conversion over a Li/MgO catalyst was a function of the CH_4/O_2 ratio and perhaps the total pressure.[40] Thus, there is no unique rate-limiting step; reactions (3) and (5) have comparable rates. Only when N_2O is the oxidant is it possible to find evidence for a clearly defined rate-limiting step. At a ratio of $CH_4/N_2O = 0.33$, a value of KIE = 1.1 was observed, which confirms that reaction (6) was rate-limiting.[41]

Our model calculations for the reaction of CH_4 and O_2 over Li/MgO indicate that the orders of reaction are determined by the forward and reverse rates of reaction (5) relative to the rate of reaction (3).[27] One may show analytically that the reaction is first order with respect to CH_4 and half order with respect to O_2 if reaction (3) is rate-limiting and reaction (5) is at equilibrium. As the forward and reverse rates of reaction (5) decrease with respect to the rate of reaction (3), the orders can become half with respect to CH_4 and 1 with respect to O_2. In the limit as the forward reaction (5) becomes rate limiting, the orders will become 0 with respect to CH_4 and 1 with respect to O_2 (or other oxidant). Again, the latter case has been observed only with N_2O as the oxidant.[41]

Another controversial mechanistic question concerns the mode of C–H bond activation. According to reaction (3), the C–H bond is broken homolytically by the abstraction of a hydrogen atom. Other investigators[53–56] focus on the basicity of the catalyst, and propose that the C–H bond is broken heterolytically as indicated in (10) where CH_4 is the acid. For certain catalysts the relationship between C_2 formation and basicity appears to correlate;[56] however, there are many examples for which it does not.

$$CH_4 + M^{n+}{-}O^{2-} \longrightarrow \overset{CH_3^-\ H^+}{M^{n+}{-}O^{2-}} \xrightarrow{O_2} \overset{O_2^-\ H^+}{M^{n+}{-}O^{2-}} + CH_3^\bullet \quad (10)$$

Since hydrogen–deuterium isotopic exchange of reactions among alkanes is believed to occur by heterolytic dissociation of C–H and C–D bonds, the isotopic exchange reaction between

CH_4 and CD_4 can be used independently to probe the circumstances under which the heterolytic dissociation might occur. Lapszewicz and Jiang[55] followed the isotopic exchange reaction between D_2 and CH_4 over Sm_2O_3, MgO, and γ-Al_2O_3, and concluded that no direct correlation exists between C–H bond activation and methane conversion. Moreover, Nelson et al.[57] found that during the oxidative coupling with CH_4/CD_4 mixtures very little hydrogen isotope exchange occurred over a Li/MgO catalyst. We have recently studied both the extent of hydrogen isotope exchange between CH_4 and CD_4 and the conversion of CH_4 during the oxidative coupling reaction over a Ba/MgO catalyst that contained 0.5 mol% Ba.[58] The results of Figure 3 show that the addition of CO_2, which poisons basic sites, has a much greater effect on the exchange reaction than on the activation of CH_4 for coupling. This catalyst apparently contains at least two distinguishable kinds of surface sites. One type is sufficiently basic to promote the heterolytic C–H bond cleavage, but under normal oxidative coupling conditions these would be poisoned by CO_2. The less basic set of sites is capable of catalyzing only the homolytic C–H bond cleavage in methane, directly producing $CH_3^{\bullet}$ radicals that result in C_2H_6 formation.

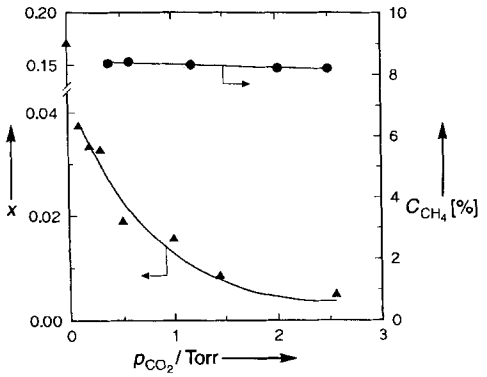


Fig. 3. Effect of CO_2 partial pressure on the isotope exchange between CH_4 and CD_4 (▲) and the oxidation of CH_4 (●) at 850 °C over 0.5 mol% Ba/MgO [58]. x = number of exchanged H or D atoms per molecule.

3.2. Ethene Formation

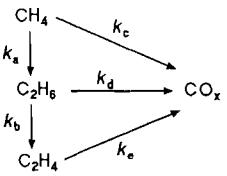
As noted previously, ethene is the desired product in the oxidative coupling of methane, although most mechanistic studies demonstrate that ethane is the initial C_2 product. Hutchings and co-workers[5] have reported that small amounts of C_2H_4 are observed, even at short residence times, but the direct formation of C_2H_4, for example by coupling of CH_2, would only be a minor pathway. Several of the better oxidative coupling catalysts also have been investigated for the oxidative dehydrogenation (OXD) of ethane, and in each case the catalyst has been shown to be effective for this reaction.[59–62] In fact, the best OXD catalysts are also good methane oxidative coupling catalysts. The initial activation step for both CH_4 and C_2H_6 is believed to be the same—the formation of alkyl radicals. The $C_2H_5^{\bullet}$ radicals also have been identified with the MIESR system.[59] The dominant subsequent pathways for methyl and ethyl radicals, however, are different. In the presence of O_2 reaction (11) prevails over coupling or the unimolecular loss of

$$C_2H_5^{\bullet} + O_2 \longrightarrow C_2H_4 + HO_2^{\bullet} \quad (11)$$

$H^{\bullet}$. For $CH_3^{\bullet}$ radicals there is no analogous route to the formation of a stable product. Consequently, the yields of C_2H_4 from the OXD reaction are more than twice as large as those from oxidative coupling of CH_4. Over a Li/MgO catalyst containing chloride ions a C_2H_4 selectivity of 77% has been achieved at a C_2H_6 conversion of 75%, which corresponds to a yield of 58%.[62] Moreover, because the C–H bond strength in C_2H_6 (422 kJ mol^{-1}) is less than that in CH_4 (439 kJ mol^{-1}), the rates of reaction are substantially greater with C_2H_6.

3.3. The Origin and Effects of CO_2

Since the development of a practical oxidative coupling process for methane is limited largely by the undesirable formation of CO_2, it is of interest to determine its origin. Both CO and CO_2 are produced as by-products during CH_4 coupling, but CO is converted into CO_2 over most of the catalysts. These oxides of carbon, which will be collectively referred to as CO_x, may be derived from all of the three hydrocarbons according to the generalized Scheme 1.



Scheme 1.

The three hydrocarbons in Scheme 1 compete for a common set of sites; it is therefore misleading to consider the oxidation of each hydrocarbon separately. The most definitive experiments to determine the origin of CO_x have been carried out by adding $^{13}C_2H_4$ or $^{13}C_2H_6$ to the $^{12}CH_4$ reagent and observing the fraction of $^{13}CO_x$ that appears as a product. Ekstrom et al.[63] were the first to use this method to demonstrate that oxidation of C_2H_6 and C_2H_4 were responsible for much of the CO_x formed over a Sm_2O_3 catalyst. Nelson and Cant[64] carried out similar experiments over Li/MgO catalysts and concluded that at $T > 740$ °C, most of the CO_x is derived from C_2 oxidation, and at $T < 700$ °C most is derived directly from CH_4. In evaluating these results it is important to recognize that both the rate constants (k_c, k_d, or k_e) and the respective hydrocarbon concentrations affect the rate of CO_x production.

It would be useful to separate out the intensive and the extensive factors in the formation of CO_x. In an effort to achieve this, we have defined a parameter R as the ratio of the percentage of ^{13}C in the CO_x products to that in the feed gas.[65] If the amount of CO_x derived from C_2H_6 is small (that is, the conversion of C_2H_6 to C_2H_4 is very selective), R is approximately the ratio of k_e/k_c. In Table 2 values of R are compared for several catalysts over a range of temperatures. Clearly, the values of R are significantly greater than 1. Even at 650 °C over Li/MgO a value of $R = 3.4$ was obtained. Thus, at all temperatures studied CO_x would be derived mainly from C_2H_4, provided the partial pressures of CH_4 and C_2H_4 are comparable. Higher temperatures, however, increase the formation of CO_x from C_2H_4, probably as a result of increased gas-phase oxidation.

Table 2. Origin of CO_x over various catalysts [a].

Catalyst	T [°C]	C_{CH_4} [%] [b]	S_{C_2} [%] [c]	$^{13}C_2H_4$ added [Torr]	CO_x from C_2 cmpds [%]	R
Li/MgO [d]	700	6.7	70.1	2.2	22.5	4.7
Ba/MgO [e]	700	0.7	37.2	4.7	15.6	2.8
	750	2.4	55.5	4.2	26.4	4.3
	800	4.3	71.1	4.4	47.2	5.7
	850	9.7	74.7	4.9	90.8	6.2
Sr/La_2O_3 [e]	700	2.6	33.3	4.1	16.1	2.8
	750	6.1	43.1	3.5	24.9	3.4
	800	9.4	50.8	3.9	40.6	4.0
CeO_2 [f]	800	10.5	3.8	1.1	7.8	7.7

[a] $p(CH_4) = 200$ Torr (1 Torr = 133 Pa); molar ratio $CH_4/O_2 = 10$; balance helium. [b] CH_4 conversion. (c) S_{C_2} = selectivity with respect to C_2 products. [d] 200 mg. [e] 5 mg. [f] 100 mg, diluted to 1 cm^3 with quartz chips.

Nevertheless, when operating at low conversions to achieve high C_2 selectivities, much of the CO_x would be derived directly from CH_4. The mechanism for this direct oxidation should therefore be considered. A simple calculation shows that a $CH_3^{\bullet}$ radical would collide with the surface of the catalyst approximately 10^5 times before it reacts with another $CH_3^{\bullet}$ radical in the gas phase. Some radicals react with species on the surface. By using a modified form of the MIESR system it has been found that for this interaction of $CH_3^{\bullet}$ radicals with selected metal oxides, the reactive sticking coefficients may range between 1×10^{-7} and 2×10^{-5}.[66] Moreover, the reactive sticking coefficients may be directly related to the O_2 pressure.[67] The larger sticking coefficients are found with oxides that have multiple oxidation states, making them accessible to reduction by $CH_3^{\bullet}$ radicals. Thus, reaction may occur through electron transfer, with the concomitant formation of a methoxide ion [Eq. (12)].

$$M^{(n+1)+}O^{2-} + CH_3^{\bullet}(g) \longrightarrow M^{n+}(OCH_3)^- \quad (12)$$

Methoxide ions function as surface intermediates in formation of CO_x under oxidative coupling conditions. Even on nonreducible oxides, which constitute most of the oxidative coupling catalysts, the electron may be transferred to oxide ion vacancies on the surface, forming F-type centers. In the presence of O_2, electron transfer may result in the formation of surface oxide or superoxide ions.

The catalytic behavior of a nonselective oxide (for example, CeO_2) may be completely altered by the addition of an alkali metal ion which forms a surface oxide/carbonate phase. In the case of CeO_2, which reacted extensively with $CH_3^{\bullet}$ radicals and produced only CO_2 during oxidation, the addition of a monolayer of Na_2CO_3 resulted in an active and reasonably selective coupling catalyst.[29, 68] Apparently the Na_2O/Na_2CO_3 layer inhibits electron transfer from $CH_3^{\bullet}$ to the CeO_2, and thus prevents $CH_3^{\bullet}$ radicals from reacting with the surface.

Since the early work of Lin et al.[33, 69] it has been suggested that $CH_3O_2^{\bullet}$ radicals in the gas phase, formed in the equilibrium reaction (13), may be responsible for CO_x formation. This

$$CH_3^{\bullet} + O_2 \rightleftharpoons CH_3O_2^{\bullet} \quad (13)$$

hypothesis is attractive, because the equilibrium $CH_3O_2^{\bullet}$ concentration decreases with increasing temperature, and up to a certain point, the selectivity for C_2 formation increases with temperature. Our model calculation, however, demonstrated that the role of $CH_3O_2^{\bullet}$ in the homogeneous component of the reaction is not important,[37] but it is possible that reactions of $CH_3O_2^{\bullet}$ with the surface may be significant.[64] Even so, it is difficult to understand the effect of O_2 on the reactive sticking coefficient at the low partial pressures of the MIESR experiment. We have suggested that a surface oxygen species, such as O_3^-, may be responsible for the conversion of $CH_3^{\bullet}$ to CO_x,[41] but it also is possible that an electron transfer reaction, analogous to reaction (12), may be involved, but with the reduction of O_2 instead of metal oxide according to reaction (14). Indeed, there was ESR evidence for the O_2^- ions on CeO_2 after the sample had been exposed to $CH_3^{\bullet}$ radicals and O_2.[66]

$$M^{n+}O^{2-} + CH_3^{\bullet}(g) + O_2(g) \longrightarrow M^{n+}(OCH_3)^- + O_2^- \quad (14)$$

At this point we turn our attention to the effect that CO_2 has on activity and selectivity during the catalytic oxidation of methane. The extent of the CO_2 effect depends very much on the basicity of the catalyst. Marcelin and co-workers[70] found that methane conversion over Li/MgO decreased dramatically with the addition of CO_2; however, CO_2 had less effect on methane conversion over Sm_2O_3. Similarly, differences were observed over these same two catalysts with respect to $CH_3^{\bullet}$ radical formation.[71] In poisoning the centers responsible for CH_4 activation, CO_2 has a profound effect on the kinetics of the coupling reaction. For example, over Li/MgO the order of reaction with respect to O_2 is largely determined by the increased amount of CO_2 that is formed.[72] As the O_2 partial pressure is increased, more CO_2 is produced. Moreover, the poisoning effect of CO_2 is manifested in the apparent activation energy for $CH_3^{\bullet}$ radical formation and CH_4 conversion over basic oxide catalysts. Because CO_2 is a poison, the rate equation for $CH_3^{\bullet}$ radical formation may be expressed as shown in Equation (15).[73] If $K[CO_2] \gg 1$, then the conditions in (16) are valid, where λ

$$\frac{d[CH_3^{\bullet}]}{dt} = \frac{k f([CH_4], [O_2])}{1 + K[CO_2]} \quad (15)$$

$$k_a = k/K \quad \text{and} \quad E_a = E + \lambda \quad (16)$$

is the heat of adsorption of CO_2. Upon increasing the amount of added CO_2 from 0 Torr to 0.75 Torr, the activation energy for $CH_3^{\bullet}$ formation increased from 96 kJ mol^{-1} to 201 kJ mol^{-1}, which suggests a value for λ of about 105 kJ mol^{-1} (Fig. 4). A

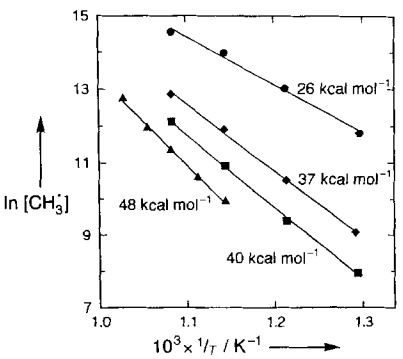


Fig. 4. Arrhenius plots of $CH_3^{\bullet}$ radical formation rate over Li/MgO as a function of the partial pressure of CO_2 added to the reagent stream. $p(CO_2)$: 0 Torr ●, 0.04 Torr ◆, 0.2 Torr ■, 0.75 Torr ▲. The pressures of CH_4 and O_2 were 0.22 and 0.02 Torr, respectively [73].

similar increase in E_a from 134 kJ mol^{-1} to 218 kJ mol^{-1} was found for methane conversion when CO_2 was added to the reagents during oxidative coupling.

The role of CO_2 in improving C_2 selectivity from CH_4, or C_2H_4 selectivity from C_2H_6, is illustrated by the results in Table 3. At a constant level of 5% CH_4 conversion, the C_2 selectivity increased from 45% to 64% upon the addition of

Table 3. Effect of CO_2 poisoning on selectivity S during the partial oxidation of methane and ethane over Li/MgO catalyst.

Hydrocarbon	Cat. [g]	CO_2 added [Torr]	C [%] [a]	S[%] C_2H_6	C_2H_4	CO	CO_2
CH_4 [b]	0.1	0.0 (4.3) [c]	5.3	38.5	6.1	14.5	40.9
CH_4	0.5	0.0 (8.7)	11.2	45.0	11.2	4.9	39.0
CH_4	0.5	23.1 (2.5)	5.2	58.7	5.3	11.5	24.5
C_2H_6 [d]	0.05	0.0 (6.0)	5.6		72.0	9.0	19.0
C_2H_6	0.20	0.0 (13.5)	12.9		75.0	7.0	18.0
C_2H_6	0.20	17.8 (2.5)	5.3		83.8	7.9	8.3

[a] Hydrocarbon conversion. [b] Li content = 4 wt%, $p(CH_4) = 200$ Torr, $p(O_2) = 100$ Torr, total flow rate = 80 mL min^{-1}, T = 650 °C. [c] Numbers in parentheses are the amounts of CO_2 produced by the reaction, in Torr. [d] Li content = 4 wt%, $p(C_2H_6) = p(O_2) = 290$ Torr, total flow rate = 60 mL min^{-1}, $T = 650$ °C.

23 Torr CO_2. MIESR results indicated that CO_2 inhibited secondary reactions between the $CH_3^{\cdot}$ radicals and the Li/MgO catalyst.[71] As the conversion level is increased by increasing the amount of catalyst, and a larger fraction of the CO_2 is derived from C_2H_4, one might expect that the positive effect of CO_2 on C_2 selectivity would become less evident. However, the results of Table 3 clearly show that CO_2 also enhanced the selectivity for C_2H_4 during the OXD of C_2H_6. The origin of this effect is not obvious, but the results suggest that CO_2 may poison sites that are uniquely capable of promoting the further oxidation of C_2H_4 to CO_2.

One of the manifestations of this role of CO_2 is the effect of residence time on selectivity. Usually in oxidation catalysis the conversion increases, but selectivity to a partial oxidation product decreases as the residence time in the catalyst bed increases. But in the oxidative coupling reaction it is often found that short residence times result in low C_2 selectivity because an insufficient amount of CO_2 has been formed. As a result of this effect, comparisons between results obtained in integral and differential reactors can be misleading.

4. Nature of the Active Center

4.1. Surface Oxygen Ions

The diversity of catalysts used in the oxidative coupling reaction makes it unlikely that a single type of center is responsible for the activation of CH_4. Therefore, the potential active centers will be discussed with respect to classes of catalysts. Li/MgO is the most thoroughly investigated. One of the challenges in identifying active centers results from the fact that most characterization methods are applicable only at conditions far removed from those used in the actual catalytic reaction. Nevertheless, rational hypotheses can be made concerning the species that might exist on the surface of a functioning catalyst. With one notable exception, which will be discussed subsequently, the attention has focused on different types of oxygen ions, for example, O^-, O_2^-, O_2^{2-}, or O^{2-} in a state of low coordination. This attention to oxygen ions results because only metal oxides are effective in the coupling reaction and because the CH_4 reactivity is generally much greater in the presence of a gas-phase oxidant (O_2 or N_2O). Even those catalysts that function in a cyclic mode are much more active when CH_4 and O_2 are co-fed to the system.

The effect of the simultaneous presence of CH_4 and O_2 over the catalyst is illustrated by the results of Figure 5, which were obtained over a Mn(2 wt%)/Na_2WO_4(5 wt%)/SiO_2 catalyst

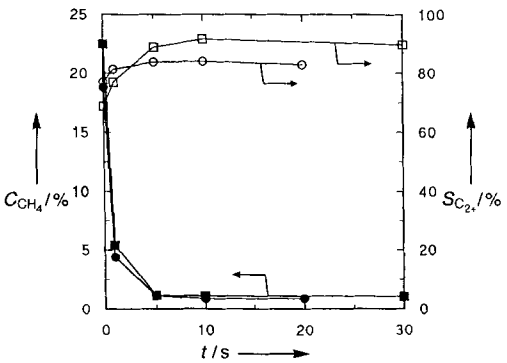


Fig. 5. CH_4 conversion C_{CH_4} and C_{2+} selectivity $S_{C_{2+}}$ obtained during pulse experiments. The time t is the delay between the 1 mL CH_4 pulse and the 0.2 mL O_2 pulse. Catalyst Mn(2 wt%)/Na_2WO_4(5 wt%)/SiO_2 (0.068 g): ● CH_4 conversion, ○ C_{2+} selectivity; catalyst $NaMnO_4$(5 wt%)/MgO (0.133 g): ■ CH_4 conversion □ C_{2+} selectivity.

and a $NaMnO_4$(5 wt%)/MgO catalyst.[22] The latter is similar to the one used in the cyclic experiments described above.[19] The catalysts were first treated with pure O_2 at 800 °C and briefly flushed with a stream of He. The first results, corresponding to zero time, were obtained by passing a pulse of CH_4 and O_2 in a 5:1 ratio over the catalysts. Thereafter a pulse of O_2 was followed by a pulse of CH_4. The periods between the O_2 pulse and the CH_4 pulse are indicated by the times given on the abscissa. During the initial CH_4/O_2 pulse over the $NaMnO_4$(5%)/MgO catalyst, 23% of the CH_4 was converted with a 69% selectivity into C_{2+} products. When the delay between the O_2 pulse and the CH_4 pulse was only one second, the CH_4 conversion decreased to 6%. After a delay of five seconds the conversion decreased to 1% and remained constant at this level. Similar results were obtained for the Mn(2 wt%)/Na_2WO_4(5 wt%)/SiO_2 catalyst. When the CH_4/O_2 mixture was added after several sequential CH_4 and O_2 pulses, the conversion increased to its original high value. These results indicate that a surface form of oxygen is responsible for the activation of CH_4. Bulk lattice oxygen may participate, but it does so at a rate that is slow compared to the rate of CH_4 activation by oxygen derived from the gas phase.

The early discovery of Li/MgO as an effective oxidative coupling catalyst focused attention on [Li^+O^-] centers as possible sites for the activation of CH_4.[26] These centers were known to be present in Li-doped MgO crystals at high temperatures, and they form only in an O_2 atmosphere.[74] Subsequent ESR studies on quenched catalyst samples revealed that [Li^+O^-] centers

were present, but they were mainly in the bulk of the crystallites.[75] It was proposed that surface O^- ions, in equilibrium with bulk $[Li^+O^-]$ centers, were responsible for the activation of CH_4. The $[Li^+O^-]$ centers have also been observed in Li/ZnO catalysts, and the analogous $[Na^+O^-]$ centers have been found in Na/CaO.[32, 69] All three of these catalysts function well at the lower end of the temperature range for oxidative coupling. At least two groups[76, 77] have carried out theoretical studies on the interaction of $[Li^+O^-]$ centers with CH_4, and the most refined calculation indicates a barrier height of only 25 kJ mol^{-1} for the hydrogen atom abstraction reaction, which is considerably less than the experimental value of 96 kJ mol^{-1} for $CH_3^\bullet$ radical formation.[73] The small barrier height is consistent with the gas-phase reaction of O^- ions with CH_4 to form $CH_3^\bullet$ radicals and OH^- ions, which occurs with an 8% probability at 25 °C.[78] Thus, while $[Li^+O^-]$ centers and O_s^- ions undoubtedly exist in and on the surface of Li/MgO catalysts, and they are capable of activating CH_4, it remains to be demonstrated that they are present in sufficient concentrations to account for the oxidative coupling results.

Based upon high resolution electron energy loss spectroscopy (HREELS) of model Li/MgO catalysts, Goodman and coworkers[79] concluded that F-centers (an oxide ion vacancy with two trapped electrons) or F-center aggregates function as the active centers on Li/MgO. Their model catalysts consisted of 20 monolayers of Li/MgO formed on a Mo(100) crystal. After heating the films to progressively higher temperature from 1000 to 1300 K and then cooling to 900 K for the catalytic measurements or 80 K for the HREELS measurements, they found that the activity for C_2H_6 production correlated better with the formation of F-centers and F-center aggregates than with that of $[Li^+O^-]$ centers. It is important to note, however, that the HREELS spectra were obtained after heating the model catalyst in only 5×10^{-7} Torr O_2, whereas the catalytic experiments were carried out in 1 Torr of O_2. Since the $[Li^+O^-]$ concentration is a function of the O_2 pressure,[74] a comparison of spectroscopic and catalytic results obtained after exposing the samples to very different O_2 pressures is problematic.

There also is considerable evidence that peroxide ions play a role in the activation of CH_4 over certain catalysts. It was pointed out by Sinev et al.[80] and Otsuka et al.[81] that Na_2O_2 and BaO_2 are capable of converting CH_4 into C_2H_6 at temperatures above 500 °C. The reactions were stoichiometric rather than catalytic, because both sodium and barium form stable carbonates at these temperatures. Nevertheless the results show that peroxide ions, if they existed at considerably higher temperatures, could activate CH_4. Because of the propensity of sodium to form a stable peroxide, the catalytic behavior of the Na/CeO_2 catalyst, as well as other sodium-promoted lanthanide oxide catalysts, has been explained by the existence of a supported Na_2O_2 phase.[68, 82] But there was no spectroscopic evidence to confirm the presence of this phase.

More recently, both X-ray photoelectron spectroscopy (XPS) and Raman spectroscopy have been used to support the role of BaO_2 in the activation of CH_4. The initial XPS experiment to characterize a barium-containing coupling catalyst was carried out by Yamashita et al.[83], who studied Ba/La_2O_3. From the O(1s) binding energy they concluded that BaO_2 was present on the surface and O_2^- ions, or O^- ions derived from the peroxide, were responsible for the catalytic activity. We subsequently demonstrated that phase separation occurs during catalysis over $BaPbO_3$ and $BaBiO_3$ perovskites (see Section 2) and that the barium-enriched surface contains peroxide ions.[23] Since the O(1s) binding energies in O_2^-, CO_3^{2-} and OH^- are very similar, care must be taken in distinguishing between the three surface species. The contribution from CO_3^{2-} ions can be determined by separately measuring the carbonate C(1s) signal and then evaluating the amount of oxygen from this species. Hydroxide ions generally are removed by a thermal treatment at elevated temperatures, but this may be verified by carrying out an exchange experiment with D_2. If OH_s^- ions are present, HD will be detected in the gas phase.

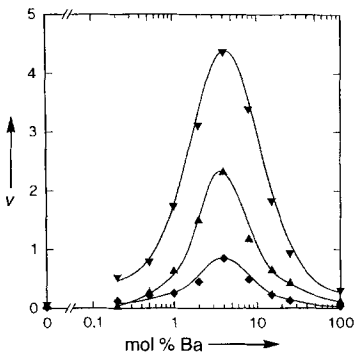


Fig. 6. Specific activities of Ba/MgO catalysts at a $CH_4:O_2$ ratio of 5:1. T = 750 °C ◆, 800 °C ▲, 850 °C ▼ [16]. The y axis represents methane conversion v [mmol min^{-1} m^{-2}].

The relationship between coupling activity and the presence of peroxide ions was even more convincingly shown with a series of Ba/MgO catalysts that contained from 0.2 to 25 mol% Ba.[16] As shown in Figure 6, the catalytic activity reached a maximum at about 4 mol% Ba. The decreasing activity at larger Ba loadings may result from a greater susceptibility to CO_2 poisoning, which indicates that the host oxide may influence the basicity of another surface phase, in this case BaO. The surface compositions for this same set of catalysts are depicted in Figure 7, where it is evident that the percentage of the surface covered by peroxide ions parallels the activity pattern shown in Figure 6.

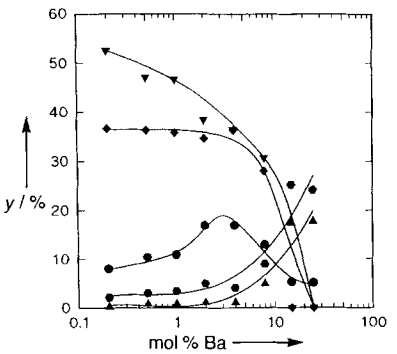


Fig. 7. Surface composition of Ba/MgO catalysts determined by XPS after exposure to a $CH_4:O_2$:He reaction mixture for 1 h at 800 °C and subsequent cooling to 25 °C in an atmosphere of O_2 and He: O^{2-} ▼, O_2^- ●, CO_3^{2-} ▲, Mg^{2+} ◆, and Ba^{2+} ● [16].

Although one might argue that the active centers are actually O^- ions in equilibrium with O_2^- ions, the O–O bond energy in a peroxide ion is about 205 kJ mol^{-1},[84] which is considerably greater than the E_a of 163 kJ mol^{-1} for the coupling reaction over the 4 mol% Ba/MgO catalyst. Moreover, there is evidence that CH_4 reacts with peroxides at relatively low temperatures.

The use of XPS to detect peroxide ions suffers from the fact that it is an ex situ method. By contrast, with Raman spectroscopy results can be obtained in the presence of the reagents and the catalyst at temperatures up to 800 °C. The Raman spectra for the 0.5 mol% Ba/MgO catalyst at progressively higher temperatures are shown in Figure 8.[85] The major band at

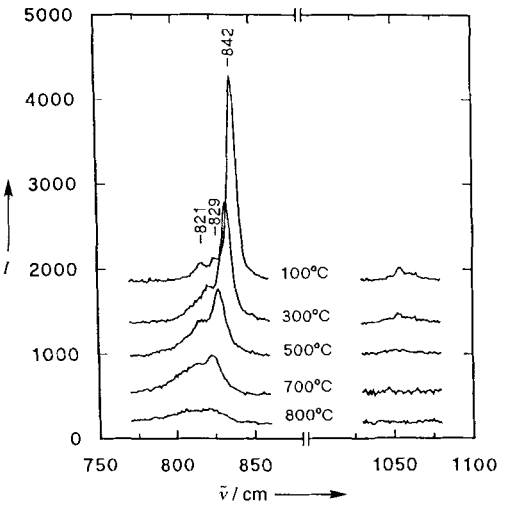


Fig. 8. Raman spectra of Ba(0.5 mol%)/MgO with the sample at the indicated temperatures. The sample had been cooled from 800 °C in a stream of O_2 [85]. *I* in arbitrary units.

842 cm^{-1} is due to the O–O stretch in BaO_2, while the weak band at about 1050 cm^{-1} is due to carbonate ions. The frequency shift with respect to temperature is a well-known phenomenon in Raman spectroscopy of solids, and it is related to the thermal expansion of lattice parameters. Although the Raman signal due to peroxide ions broadens and decreases in area with increasing temperature, there is evidence for the species even at 800 °C. No Raman band was observed around 1150 cm^{-1}, which is the position expected for O_2^- ions. In the presence of CH_4 and O_2 at temperatures greater than 700 °C, the carbonate bands quickly formed as a result of CO_2 produced during reaction, and the peroxide signal decreased below detection limits.

The involvement of peroxide ions in the oxidative coupling of CH_4 over these supported barium catalysts is reasonably convincing; however, the more general role of these ions has yet to be demonstrated. Earlier we reported the presence of a Raman band at 863 cm^{-1} on La_2O_3, which we attributed to O_2^{2-} ions, but subsequent experiments in an externally heated fused-quartz cell failed to reproduce this result.[86] Similarly, XPS results indicate the presence of only oxide ions on La_2O_3, provided the O_2 used to treat the sample is entirely free of H_2O.

4.2. Chloride-Containing Catalysts

The addition of chloride ions to an oxidative coupling catalyst can have a marked effect on its properties, particularly with respect to the C_2H_4/C_2H_6 product ratio. The chlorine may be introduced either initially as part of the catalyst or through organo chlorine compounds that are added to the reagents. Thomas et al.[17] studied a family of alkali-metal bismuth oxychloride catalysts, of which $LiCa_2Bi_3O_4Cl_6$ was an example, and they found C_2H_4/C_2H_6 ratios as great as 35. However, these materials generally lost activity within a few hours, which is a common problem with many of the chlorided catalysts. Typically, the properly chlorided catalysts give C_2H_4/C_2H_6 ratios between 3 and 5, which is still attractive since C_2H_4 is the desired product.

Because chlorine is known to dehydrogenate C_2H_6 in the gas phase, it has been suspected that homogeneous reactions may be responsible for the large C_2H_4/C_2H_6 ratios that are observed in these chlorine-containing systems.[87, 88] Perhaps the most definitive evidence against a substantial gas-phase component is found in the transient studies of Burch and co-workers,[89] who observed that the positive effect of chlorine addition to a catalyst persisted long after the flow of CH_3Cl over the catalyst had ceased. Moreover, we have shown that there is no correlation between the rate of chlorine loss from a Li^+-MgO-Cl^- catalyst and its ethane OXD activity.[90]

Most of the chlorine is lost as HCl in the reaction of water with the catalyst. The rate of chlorine loss can be minimized by operating a catalyst at lower temperatures. For example, Hinson et al.[91] found that a Li^+-MgO-Cl^- catalyst prepared by a sol–gel process was effective for periods up to 238 h at 640 °C; C_2 yields up to 20% and C_2H_4/C_2H_6 ratios of about 5 were achieved.

The favorable C_2H_4/C_2H_6 ratio over the Li^+-MgO-Cl^- catalyst, and presumably over all of the effective chlorided catalysts, results from the fact that the OXD of C_2H_6 is faster than the oxidative coupling of CH_4. In a series of studies on this catalyst we have demonstrated that a separate set of sites is largely responsible for the OXD reaction.[27, 90–92] It has been postulated that these sites consist of Li_2O on a molten film of LiCl. The LiCl modifies the basicity of the catalyst in such a way that neither the CH_4 conversion nor the C_2H_6 conversion is affected by CO_2. This is a particularly nice system with which to obtain kinetic data, because the CO_2 poisoning effect does not complicate the results (Section 3.3). With respect to selectivity, Cl^- ions appear to play the same role as CO_2 did on the Li/MgO catalyst. The unique behavior of the chlorided Li/MgO is found only at Cl/Li ratios ≥ 0.9. At lower Cl/Li ratios Li_2CO_3 is formed and the characteristics of a typical Li/MgO catalyst are observed.

Ruckenstein and Khan[93] found that the addition of pairs of alkali metal chlorides to MgO resulted in good oxidative coupling catalysts; the best additive was 5 mol% NaCl + 5 mol% CsCl on MgO. At 750 °C a C_2 yield of 20% and a C_2H_4/C_2H_6 ratio of 2.2 was attained. Because of the higher reaction temperature, there was a modest decrease in C_2 yield with time on stream. Contrary to the results obtained with the Li^+-MgO-Cl^- catalysts, these authors found that the catalysts promoted with alkali metal chlorides adsorbed CO_2 strongly, and therefore were highly basic. The reason for this large difference in basicity is not evident.

5. Cross-Coupling

If one considers cross-coupling, the scope of methane coupling reactions is considerably expanded. Perhaps the most important of these, and certainly the most thoroughly studied, is

the oxidative coupling of methane with toluene to produce ethylbenzene. While in the catalyst bed, a portion of the ethylbenzene is converted into the desired product, styrene. In addition, small amounts of stilbene, biphenyl, propylbenzene, and xylene are also detected. The initial experiments were carried out by Khcheyan, et al.;[94-96] however, other investigators have continued to pursue the problem.[97-100] Many, though not all, of the CH_4 coupling catalysts are effective for this cross-coupling reaction. For example, Sm_2O_3 is a nonselective catalyst, whereas Li/Sm_2O_3 gave a C_8 (ethylbenzene plus styrene) yield of 16.5%, based on the amount of toulene converted.[99] Khan and Ruckenstein[100] found that the same (Na + Cs)/MgO catalyst that was effective in the CH_4 oxidative coupling reaction also produced the largest C_8 yield (24.2%) in the cross-coupling reaction. They concluded that the superior performance of this catalyst was related to its high (super)basicity.

Although most investigators point out that the mechanism involves the coupling of methyl and benzyl radicals, it is not certain whether the reaction occurs on the surface or in the gas phase. Using the MIESR system, we have identified gas-phase benzyl radicals that were formed when toluene and nitrous oxide were passed over a Li/MgO catalyst.[101] The experimental spectrum and a simulated spectrum are compared in Figure 9. In view of the nonselective reaction over Sm_2O_3, it is significant that mainly $CH_3^{\bullet}$ radicals were produced when toluene and oxygen were passed over this catalyst. Apparently, Sm_2O_3 promotes the breaking of the C–C bond, rather than the abstraction of hydrogen from the methyl group.

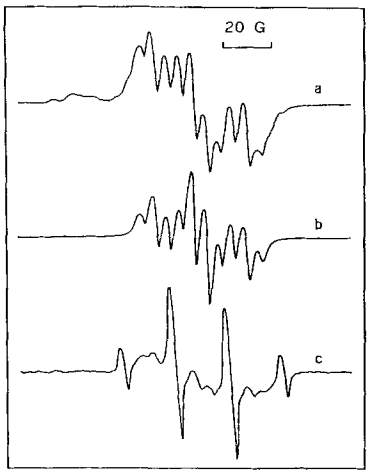


Fig. 9. ESR spectra of gas-phase radicals produced over catalysts: a) experimental spectrum of benzyl radicals formed from toluene over a Li/MgO catalyst, b) simulated spectrum of benzyl radicals, c) experimental spectrum of mainly methyl radicals formed from toluene over a Sm_2O_3 catalyst. Results were obtained with the catalysts at 650 °C in a flow of Ar (4.8 mL min^{-1}), toluene (0.10 mL min^{-1}), and N_2O (0.10 mL min^{-1}), p_{total} = 0.9 Torr [101].

Yet another potentially important cross-coupling reaction occurs when methyl radicals react with allyl radicals formed from propylene. Sodesawa et al.[102] studied the production of C_4 hydrocarbons during the reaction of methane and propylene over several catalysts, including Na/La_2O_3. They concluded that the mechanism involved the oxidative methylation of propylene, followed by the loss of a hydrogen atom. Since the oxidative coupling catalysts are also capable of generating allyl radicals from propylene,[103] it seems more likely that the C_4 products are formed by a radical coupling mechanism. In the allyl radical most of the spin density is on the terminal carbons. Thus it is not surprising that the major C_4 products were linear butenes and butadiene, rather than isobutylene.

6. Summary and Conclusions

Although research on the oxidative coupling of methane has not resulted in a commercial process, it has provided insight into an interesting class of heterogeneous–homogeneous radical reactions. Catalysts have been developed which are capable of generating methyl and other hydrocarbon radicals, but which do not react extensively with these radicals once they are formed. The mechanism for the formation and reactions of these radicals is reasonably well understood; however, less is known about the sites that are responsible for the activation of CH_4 and the hydrocarbon products. The identification of the active forms of surface oxygen on the Group IA and IIA metal oxides remains as one of the significant challenges in this area of research. At a practical level, the oxidation of the desired product, ethylene, must be overcome before larger ethylene yields can be attained. Advances in catalyst development are continuing, but additional research is needed to integrate advanced separation technology with novel reactor designs.

The author is indebted to a large group of graduate students and research associates who contributed significantly to the field of methane oxidation during their time at Texas A & M University. These individuals include K. D. Campbell, S. J. Conway, D. Dissanayake, D. J. Driscoll, M. Hatano, P. G. Hinson, T. Ito, K. C. C. Kharas, C.-H. Lin, W. Martir, E. Morales, C. Shi, Y. Tong, Z. Yu, D. Wang, J.-X. Wang, X. Wang, M. Xu, and H. S. Zhang. In addition, M. P. Rosynek was involved in many aspects of the research. Financial support was provided by the U. S. National Science Foundation and the Gas Research Institute.

Received: June 27, 1994 [A71IE]
German version: *Angew. Chem.* **1995**, *107*, 1059

[1] *Oil Gas J.*, **1993** (*52*), December 27, 37.
[2] P. S. Yarlagadda, L. A. Morton, N. R. Hunter, H. D. Gesser, *Ind. Eng. Chem. Res.* **1988**, *27*, 252.
[3] W. Feng, F. C. Knopf, K. M. Dooley, *Energy Fuels*, **1994**, *8*, 815.
[4] M. Lin, A. Sen, *Nature (London)*, **1994**, *368*, 613.
[5] G. J. Hutchings, M. S. Scurrell in *Methane Conversion by Oxidative Processes* (Ed.: E. E. Wolf) Van Nostrand Reinhold, New York **1992**, pp. 201–258.
[6] A. M. Maitra, *Appl. Catal. A* **1993**, *104*, 11.
[7] *Methane Conversion by Oxidative Processes* (Ed.: E. E. Wolf), Van Nostrand Reinhold, New York **1992**.
[8] O. V. Krylov, *Catal. Today* **1993**, *18*, 209.
[9] J. H. Lunsford, *Struct. Surf. Sci. Catal.* **1993**, *75*, 103.
[10] J. H. Lunsford, *Catal. Today* **1990**, *6*, 235.
[11] W. Hinsen, W. Bytyn, M. Baerns, *Proc. Int. Congr. Catal. 8th 1984*, **1984**, *3*, 581.
[12] T. Ito, J. H. Lunsford, *Nature (London)* **1985**, *314*, 721; T. Ito, J.-X. Wang, C.-H. Lin, J. H. Lunsford, *J. Am. Chem. Soc.* **1985**, 107, 5062.
[13] Z. Yu, J. H. Lunsford, unpublished results.
[14] T. LeVan, M. Chen, M. Kermarec, C. Louis, J. M. Tatibouët, *Catal. Lett.* **1990**, *6*, 395.
[15] H. Mimoun, A. Robine, S. Bonnaudet, C. J. Cameron, *Chem. Lett.* **1989**, 2185.
[16] D. Dissanayake, J. H. Lunsford, M. P. Rosynek, *J. Catal.* **1993**, *143*, 286; D. Dissanayake, Ph.D. thesis, Texas A & M University, **1993**.
[17] J. M. Thomas, W. Ueda, J. Williams, K. D. M. Harris, *Faraday Discuss. Chem. Soc.* **1989**, *87*, 33.
[18] A. Z. Khan, E. Ruckenstein, *J. Catal.* **1992**, *138*, 322.
[19] J. A. Sofranko, J. J. Leonard, C. A. Jones, A. M. Gaffney, H. P. Withers, *Catal. Today* **1988**, *3*, 127.
[20] Z.-C. Jiang, C.-J. Yu, X.-P. Fang, S.-B. Li, H.-L Wang, *J. Phys. Chem.* **1993**, *97*, 12870.
[21] J.-L. Dubois, C. J. Cameron, *Appl. Catal.* **1990**, *67*, 49.
[22] D. Wang, M. P. Rosynek, J. H. Lunsford, unpublished results.
[23] D. Dissanayake, K. C. C. Kharis, J. H. Lunsford, M. P. Rosynek, *J. Catal.* **1993**, *139*, 652.
[24] P. F. Nelson, C. A. Lukey, N. W. Cant, *J. Phys. Chem.* **1988**, *92*, 6176.

[25] C. A. Mims, R. B. Hall, K. D. Rose, G. R. Martin, *Catal. Lett.* **1989**, *2*, 361.
[26] D. J. Driscoll, W. Martir, J.-X. Wang, J. H. Lunsford, *J. Am. Chem. Soc.* **1985**, 107, 58.
[27] J. H. Lunsford, P. G. Hinson, M. P. Rosynek, C. Shi, M. Xu, X. Yang, *J. Catal.* **1994**, *147*, 301.
[28] K. D. Campbell, J. H. Lunsford, *J. Phys. Chem.* **1988**, *92*, 5792.
[29] Y.-D. Tong, M. P. Rosynek, J. H. Lunsford, *J. Phys. Chem.* **1989**, *93*, 2896.
[30] M. Xu, J. H. Lunsford, *Catal. Lett.* **1991**, *11*, 295.
[31] Y. Tong, J. H. Lunsford, *J. Chem. Soc. Chem. Commun.* **1990**, 792.
[32] H. S. Zhang, J.-X. Wang, D. J. Driscoll, J. H. Lunsford, *J. Catal.* **1988**, *112*, 366.
[33] C.-H. Lin, K. D. Campbell, J.-X. Wang, J. H. Lunsford, *J. Phys. Chem.* **1986**, *90*, 534.
[34] K. D. Campbell, H. Zhang, J. H. Lunsford, *J. Phys. Chem.* **1988**, *92*, 750.
[35] K. D. Campbell, E. Morales, J. H. Lunsford, *J. Am. Chem. Soc.* **1987**, 109, 7900.
[36] Y. Feng, D. Gutman, *J. Phys. Chem.* **1991**, *95*, 6556; Y. Feng, J. Niiranen, D. Gutman, *ibid.* **1991**, *95*, 6564.
[37] C. Shi, M. Hatano, J. H. Lunsford, *Catal. Today* ***1992***, 13, 191.
[38] K. van der Wiele, J. W. M. H. Geerts, J. M. N. van Kasteren in [7], pp. 259–319.
[39] J. G. McCarty, A. B. McEwen, M. A. Quinlan in *New Developments in Selective Oxidation* (Eds.: G. Centi, F. Trifiro), Elsevier, New York, **1992**, pp. 405–415.
[40] C. Shi, M. Xu, M. P. Rosynek, J. H. Lunsford, *J. Phys. Chem.* **1993**, *97*, 216.
[41] H. Yamamoto, H. Y. Chu, M. Xu, C. Shi, J. H. Lunsford, *J. Catal.* **1993**, *142*, 325.
[42] J. A. Roos, S. J. Korf, R. H. J. Veehof, J. G. Van Ommen, J. R. H. Ross, *Appl. Catal.* **1989**, *52*, 131.
[43] M. Hatano, K. Otsuka, *J. Chem. Soc. Faraday Trans. 1*, **1989**, *85*, 199.
[44] K. P. Peil, J. G. Goodwin, G. Marcelin, *J. Catal.* **1991**, *131*, 143.
[45] D. J. Stratman, J. T. Gleaves, D. McNamara, P. L. Mills, G. Fornasari, J. R. H. Ross, *Appl. Catal.* **1991**, *77*, 45.
[46] Z. Kalenik, E. E. Wolf, *Catal. Today* **1992**, *13*, 255.
[47] O. V. Buyevskaya, M. Rothaemel, H. W. Zanthoff, M. Baerns, *J. Catal.* **1994**, *146*, 346.
[48] N. W. Cant, C. A. Lukey, P. F. Nelson, R. J. Tyler, *J. Chem. Soc. Chem. Commun.* **1988**, 766.
[49] P. F. Nelson, C. A. Lukey, N. W. Cant, *J. Catal.* **1989**, *120*, 216; N. W. Cant, E. M. Kennedy, P. F. Nelson, *J. Phys. Chem.* **1993**, *97*, 1445.
[50] C. A. Mims, R. B. Hall, K. D. Ross, G. R. Myers, *Catal. Lett.* **1989**, *2*, 361.
[51] K. Otsuka, M. Inaida, Y. Wada, T. Komatsu, A. Morikawa, *Chem. Lett.* **1989**, 1531.
[52] R. Burch, S. C. Tsang, C. Mirodatos, J. G. Sanchez, *Catal. Lett.* **1990**, *7*, 423.
[53] V. R. Choudhary, V. H. Rane, *J. Catal.* **1991**, *130*, 411.
[54] A. M. Maitra, I. Campbell, R. J. Tyler, *Appl Catal. A* **1992**, *85*, 27.
[55] J. A. Lapszewicz, X.-Z Jiang, *Catal. Lett.* **1992**, *13*, 103.
[56] V. D. Sokolovskii, S. M. Aliev, O. V. Buyevskaya, A. A. Davydov, *Catal. Today* **1989**, *4*, 293; O. V. Buyevskaya, A. I. Suleimanov, S. M. Aliev, V. D. Sokolovskii, *React. Kinet. Catal. Lett.* **1987**, *33*, 223.
[57] P. F. Nelson, C. A. Lukey, N. W. Cant, *J. Phys. Chem.* **1988**, *92*, 6176.
[58] D. Dissanayake, J. H. Lunsford, M. P. Rosynek, *J. Catal.* **1994**, *146*, 613.
[59] E. Morales, J. H. Lunsford, *J. Catal.* **1989**, *118*, 255.
[60] S. J. Conway, J. H. Lunsford, *J. Catal.* **1991**, *131*, 513.
[61] S. J. Conway, D. J. Wang, J. H. Lunsford, *Appl. Catal. A* **1991**, *79*, L1.
[62] D. Wang, M. P. Rosynek, J. H. Lunsford, *J. Catal.*, **1995**, *151*, 155.
[63] A. Ekstron, J. A. Lapszewicz, I. Campbell, *Appl. Catal.* **1989**, *56*, L29.
[64] P. F. Nelson, N. W. Cant, *J. Phys. Chem.* **1990**, *94*, 3756.
[65] C. Shi, M. P. Rosynek, J. H. Lunsford, *J. Phys. Chem.* **1994**, *98*, 8371.
[66] Y. Tong, J. H. Lunsford, *J. Am. Chem. Soc.* **1991**, *133*, 4741
[67] M. Xu, T. Ballinger, M. P. Rosynek, J. H. Lunsford, unpublished results.
[68] Y. Tong, M. P. Rosynek, J. H. Lunsford, *J. Catal.* **1990**, *126*, 291.
[69] C.-H. Lin, J.-X. Wang, J. H. Lunsford, *J. Catal.* **1988**, *111*, 302.
[70] K. P. Peil, J. G. Goodwin, G. Marcelin, *Stud. Surf. Sci. Catal.* **1991**, *61*, 73–79.
[71] D. Wang, M. Xu, C. Shi, J. H. Lunsford, *Catal. Lett.* **1993**, *18*, 323.
[72] S. J. Korf, J. A. Roos, N. A. deBruijin, J. G. van Ommen, J. R. H. Ross, *J. Chem. Soc. Chem. Commun.* **1987**, 1433.
[73] M. Xu, C. Shi, X. Yang, M. P. Rosynek, J. H. Lunsford, *J. Phys. Chem.* **1992**, *96*, 6395.
[74] Y. Chen, H. T. Tohver, J. Narayan, M. M. Abraham, *Phys. Rev. Sect. B* **1977**, *16*, 5535.
[75] J.-X. Wang, J. H. Lunsford, *J. Phys. Chem.* **1986**, *90*, 5883.
[76] J. Rodriquez, Y. Aray, R. Ruette, *J. Mol. Struct. (THEOCHEM)* **1990**, *210*, 323.
[77] K. J. Børve, L. G. M. Pettersson, *J. Phys. Chem.* **1991**, *95*, 3214.
[78] D. K. Bohme, F. C. Fehzenfeld, *Can. J. Chem.* **1969**, *47*, 2717.
[79] M.-C. Wu, C. M. Truong, K. Coulter, D. W Goodman, *J. Catal.* **1993**, *140*, 344.
[80] M. Yu. Sinev, V. N. Korchak, O. V. Krylov, *Kinet. Katal.* **1986**, *27*, 1274.
[81] K. Otsuka, Y. Murakami, Y. Wada, A. A. Said, A. Morikawa, *J. Catal.* **1990**, *121*, 122.
[82] A. M. Gaffney, C. A. Jones, J. J. Leonard, J. A. Sofranko, *J. Catal.* **1988**, *114*, 422.
[83] H. Yamashita, Y. Machida, A. Tomita, *Appl. Catal. A* **1991**, *79*, 203.
[84] N. N. Greenwood, A. Earnshaw, *Chemistry of the Elements*, Pergamon, New York, **1984**, p. 720.
[85] J. H. Lunsford, X. Yang, K. Haller, J. Laane, G. Mestl, H. Knözinger, *J. Phys. Chem.* **1993**, *97*, 13810.
[86] G. Mestl, H. Knözinger, J. H. Lunsford, *Ber. Bunsenges. Phys. Chem.* **1993**, *97*, 319.
[87] S. Ahmed, J. B. Moffat, *Appl. Catal.* **1990**, *58*, 83.
[88] B. K. Warren, *Catal. Today* **1992**, *13*, 311.
[89] R. Burch, S. Chalker, S. J. Hibble, *Appl. Catal. A* **1993**, *96*, 289; R. Burch, S. Chalker, P. Louder *Struct. Surf. Sci. Catalysis* **1993**, *75*, 1079–1092.
[90] S. J. Conway, J. H. Lunsford, *J. Catal.* **1991**, *131*, 513.
[91] P. G. Hinson, A. Clearfield, J. H. Lunsford, *J. Chem. Soc. Chem. Commun.* **1991**, 1430.
[92] D. Wang, M. P. Rosynek, J. H. Lunsford, unpublished results.
[93] E. Ruckenstein, A. Z. Khan, *Catal. Lett.* **1993**, *18*, 27.
[94] Kh. E. Khcheyan, O. M. Revenko, A. V. Borisoglebskaya, D. L. Fishman, *Zh. Org. Khim.* **1976**, *12*, 467.
[95] Kh. E. Khcheyan, A. N. Shatalova, O. M. Revenko, L. I. Arginskaya, *Neftekhimiya* **1980**, *20*, 876.
[96] Kh. E. Khcheyan, O. M. Revenko, A. V. Borisoglebskaya, N. I. Yakovich, *Neftekhimiya* **1981**, *21*, 83.
[97] Y. Osada, K. Enomoto, T. Fukushima, S. Ogasawara, T. Shikada, T. Ikariya, *J. Chem. Soc. Chem. Commun.* **1989**, 1156.
[98] K. Otsuka, M. Hatano, T. Amaya, *J. Catal.* **1992**, *137*, 487.
[99] H. Kim, Y. Han, H.-M. Suh, H. Paik, *Appl. Catal. A* **1993**, 105, L135.
[100] A. Z. Khan, E. Ruckenstein, *J. Catal.* **1993**, *143*, 1.
[101] M. Xu, J. H. Lunsford, *J. Chem. Soc. Chem. Commun.*, in press.
[102] T. Sodesawa, M. Matsubara, S. Satoh, F. Nozaki, *Chem. Lett.* **1987**, 1513.
[103] D. J. Driscoll, J. H. Lunsford, *J. Phys. Chem.* **1985**, *89*, 4415.

Filled Buckyballs: Recent Developments from the Endohedral Metallofullerenes of Lanthanides

Frank T. Edelmann*

Over the past several years, significant progress has been made in the exploration of fullerene chemistry, especially that of C_{60}.[1-7] Multifunctionalized fullerenes and transition metal complexes with fullerenes as ligands have become quite common. The extent to which organic fullerene chemistry has already developed is exemplified by recent reports on fullerene sugars,[8] fullerene dendrimers,[9,10] and fullerene-substituted acetylenic polymers.[11] One of the most unusual classes of fullerene derivatives is endohedral metallofullerenes, $M@C_{2n}$, which have been intensively studied for M = lanthanide.[12] Initial evidence for the existence of carbon cages with encapsulated lanthanide ions was first published in 1985.[13,14] However, it was not until 1991 that a "lanthanofullerene", $La@C_{82}$, could be isolated on a macroscopic scale (i.e. a few milligrams!).[15,16] A more detailed investigation of these fascinating molecules was hindered by limited preparative accessibility and low reaction yields. Furthermore, the isolation of pure samples proved to be a major experimental challenge as no method existed for separating endohedral complexes from concurrently formed "empty" fullerenes. In addition, in contrast to metal-free carbon cages, endohedral metallofullerenes were found to be air-sensitive. Several papers published during the past two years are suggestive of a major breakthrough: Not only has it proven possible to dramatically increase the reaction yield,[17] but new procedures for the chromatographic purification have also been devised.[18,19] At last, a full investigation of the chemistry of lanthanofullerenes appears within reach, and one can even start to consider future applications.

The synthesis of endohedral metallofullerenes of encapsulated lanthanides is in principle identical to that employed for the synthesis of empty carbon cages. Mixtures of graphite and lanthanide oxide are pressed into rods and these are then arc-vaporized in a helium atmosphere. Several metallofullerenes of scandium, yttrium, and lanthanum were produced by this technique; unfortunately, the yields were rather low (approximately 0.1% of the produced soot) and the products were found to be contaminated with metal-free fullerenes.[14-16,20-26] In view of the known pronounced oxophilicity of lanthanides, the main reason for the poor yields might be attributed to the use of lanthanide oxides as starting materials; elements such as oxygen and nitrogen are known to also interfere with the synthesis of empty fullerenes using electric arcs.[27] Thus, all physical measurements such as mass spectrometry, ESR spectroscopy as well as EXAFS, and XPS studies had to be carried out initially on mixtures.

The following compounds were identified by mass spectrometry: $Ln@C_{2n}$ (Ln = Sc, Y, La, Ce, Gd; $n = 37-45$), $Ln_2@C_{80}$ (Ln = Sc, La), $Sc_2@C_{2n}$ ($n = 37, 41, 42$), and $Sc_3@C_{82}$. The relative distribution of products varies with the method of preparation; for example, higher ratios of La:C favor the formation of $La_2@C_{80}$,[22] whereas $La@C_{76}$ could only be detected if the samples were isolated under anaerobic conditions.[23] Little has been reported about the colors of isolated metallofullerenes; solutions of $La@C_{82}$ in toluene have been described as greenish-yellow.[16] From a valence-theoretical viewpoint all products with a caged metal atom can be formulated as $Ln^{3+}@C_{2n}^{3-}$.[20,26,28-33]

Scandium derivatives with encapsulated Sc_2 or even Sc_3 moieties are highly remarkable, but have so far been relatively little studied.[30-32] Scandium preferentially forms endohedral fullerene complexes with two atoms trapped inside the fullerene cage ($Sc_2@C_{74}$, $Sc_2@C_{82}$, and $Sc_2@C_{84}$). Other major species that form during the course of the reaction are $Sc@C_{82}$ and $Sc_3@C_{82}$. ESR spectroscopic studies on $Sc_3@C_{82}$ revealed the presence of an encapsulated Sc_3 molecule in which the three Sc atoms form an an equilateral triangle.[30-32] Isolated metallofullerenes of scandium are soluble in benzene, toluene, and CS_2. Surprisingly, these compounds are air-stable in the solid state.[32]

Bandow et al. showed that significant improvements in the yield could be achieved by doping the graphite rods with lanthanum *carbide* instead of the previously employed lanthanum *oxide*.[17] In the case of $La@C_{82}$ this resulted in a tenfold (ca. 1% of the produced soot!) increase in the yield. In the same study, the authors also employed a newly constructed arc generator that allows for the isolation of lanthanofullerenes under anaerobic conditions. Lanthanofullerenes[29] are generally less air-sensitive than most other organolanthanide complexes:[33] for example, $La@C_{82}$ and $Y@C_{82}$ react only slowly with atmospheric oxygen to give insoluble products.[34]

The best-studied lanthanofullerene, $La@C_{82}$, is soluble in a number of solvents such as toluene, CS_2, and pyridine. High-pressure extraction with toluene has proven to be an especially efficient means of separating insoluble soot.[23] Further enrichment of the metallofullerene fraction can be accomplished by extraction with pyridine.[35] This leads to the second major

[*] Prof. Dr. F. T. Edelmann
Chemisches Institut der Universität
Universitätsplatz 2, Gebäude M, D-39106 Magdeburg (Germany)
Telefax: Int. code + (391)5592-131

 © VCH Verlagsgesellschaft mbH, D-69451 Weinheim, 1995 0570-0833/95/0909-0981 $ 10.00+.25/0

problem associated with the isolation of pure lanthanofullerenes, their chromatographic separation and purification. Conventional HPLC techniques are rather demanding when applied to endohedral metallofullerenes and often give pure fractions only after repeated purification steps. The complete separation of empty fullerenes from metallofullerenes is, due to their structural and sterical similarities, barely possible by conventional methods. A method recently developed by Meyerhoff, Francis et al. might provide a solution.[35]

This method has already proven its worth in the separation of polycyclic hydrocarbons.[35, 36] It employs silica-packed HPLC columns in which tetraphenylporphyrin moieties are anchored to the silica surface through carboxyl groups ("CPTPP silica", CPTPP = (*para*-carboxyphenyl)triphenylporphyrin). The tetraphenylporphyrin units are present either as free ligands or as zinc complexes. Using these HPLC columns and with toluene as the mobile phase it was possible to separate $Y@C_{82}$ and $La@C_{82}$ from metal-free fullerenes (C_{60}, C_{70}, C_{76}, C_{78}, C_{82}, and C_{84}) in a single step! The ability of CPTPP silica-gel columns to effect separation of metallofullerenes has been rationalized by Meyerhoff et al. in terms of the three-dimensional interaction between the silica-anchored porphyrin and the fullerenes. As depicted in Figure 1, the four phenyl rings are almost

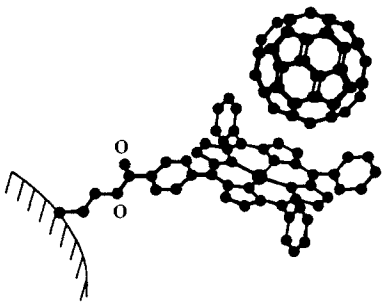


Fig. 1. Interaction between a fullerene (C_{60}) and a silica-anchored zinc(II) tetraphenylporphyrin [35].

perpendicular to the porphyrin ring and form a pocket which can serve as a receptacle for fullerene molecules of up to the size of C_{100}. The formation of C-H π interactions between the fullerene on the one hand and the aromatic rings and the porphyrin system on the other hand provides a plausible explanation for the unusual selectivity of silica-anchored porphyrins for fullerenes and metallofullerenes.

How can one explain the increased retention times of metallofullerenes on CPTPP columns compared to the retention times of metal-free fullerenes of similar size? For example, $La@C_{82}$ has a markedly longer retention time than C_{82}. As previously mentioned, the electronic structure of $La@C_{82}$ can be represented as $La^{3+}@C_{82}^{3-}$. For other lanthanides the transfer of only two electrons from the metal atom to the surrounding carbon framework is conceivable. However, in each case the endohedral metallofullerenes should show a higher π-electron density on the surface than the empty fullerenes. Hence, C–H π interactions with the phenyl rings are strengthened, leading to an increased affinity of the metallofullerenes for the column material and, thus, resulting in longer retention times. The separation is mainly effected by electronic factors and not by size-selectivity of the CPTPP phase.

Another remarkable development in the field of metallofullerenes is the encapsulation of radioactive lanthanide ions in fullerene cages, as recently reported by Kikuchi, Achiba et al.[37] More exactly, this work reports on the encapsulation of nonradioactive lanthanide ions and their subsequent transmutation by neutron activation. In analogy to the yttrium and lanthanum derivatives the novel metallofullerene $Gd@C_{82}$ was first prepared and isolated in pure form by two-stage HPLC. A sample of the crude extract was then irradiated with neutrons (neutron flux: 1.5×10^{12} n cm^{-2} s^{-1}) which by transmutation led to the formation of the isotopes ^{153}Gd, ^{159}Gd, and ^{161}Tb (Scheme 1).

$$^{152}\mathrm{Gd} \xrightarrow{(n,\gamma)} {}^{153}\mathrm{Gd} \xrightarrow[t_{1/2} = 241.6\ \mathrm{d}]{\mathrm{EC}} {}^{153}\mathrm{Tb}$$

$$^{158}\mathrm{Gd} \xrightarrow{(n,\gamma)} {}^{159}\mathrm{Gd} \xrightarrow[t_{1/2} = 18.6\ \mathrm{h}]{\beta^-} {}^{159}\mathrm{Tb}$$

$$^{160}\mathrm{Gd} \xrightarrow{(n,\gamma)} {}^{161}\mathrm{Gd} \xrightarrow[t_{1/2} = 3.2\ \mathrm{min}]{\beta^-} {}^{161}\mathrm{Tb} \xrightarrow[t_{1/2} = 6.90\ \mathrm{d}]{\beta^-} {}^{161}\mathrm{Dy}$$

Scheme 1. Nuclear reactions of Gd isotopes upon neutron activation. EC = electron capture.

Radioactive endohedral metallofullerenes can also be isolated and separated by HPLC. By comparison to normalized solutions the authors were able to show that the C_{82} cage remains intact under the experimental conditions of neutron capture and β decay. These compounds are an unprecedented type of molecular "tracers" with well-defined size and shape. Even though it is still too early to speculate about possible applications, for example in medicine, it is evident that metallofullerenes with encapsulated radioactive metal atoms open up a whole new area of scientific research.

Closely related to fullerenes are the so-called carbon nanotubes.[38, 39] Nanomaterials currently play an ever increasing role in such areas as chemistry, physics, optics, electronics, and material science.[40, 41] Promising applications are found in the manufacture of electronical, optical, and mechanical devices,[40–45] in new methods for the administration of pharmaceuticals,[46] and in the field of bio-encapsulation.[47] Nanotubes are hollow, fiber-like particles with nanometer dimensions. Carbon-based nanotubes are produced in the same way as fullerenes, namely, by arc-vaporization of graphite.[39–41, 48] The nanotubes prepared in this way are generally closed and rounded at the ends. Perfect tubes are expected to comply with Euler's theory, which states that for spherical closure exactly twelve five-membered rings must be present (hence the obvious analogy to fullerenes). Six of these rings should be located at each of the polar caps of these tubes and are thought to be responsible for the observed curvature.[49]

Nanotubes can exhibit considerable structural and electronic variations.[50–57] They can consist of a single or multiple carbon layers and may even exhibit helical symmetry, giving rise to chiral tubes.[49, 54] Single-shell nanotubes typically have diameters of 1–2 nm,[55, 56] whereas multiple-shell tubes are 4–30 nm in diameter, and the tubes can be up to 1 μm in length. It has not yet been possible to control the factors that influence properties such as the number of layers and the tube length. Several tubes

can aggregate to form bundles, threads, or even voluminous nets which cover the inside of the electric arc generator.[57] Depending on the structure, the tubes were found to show semiconducting or metallic conducting properties.[44] Besides tubular arrangements, polyhedral carbon particles with onionlike structure (diameter: 5–20 nm) are also known. Ugarte was able to show that tubes can be transformed into onions by electron bombardment (200 kV).[58] Transmission electron microscopy (TEM) allows for a more detailed characterization of carbon nanotubes. Figure 2 depicts the TEM image of a multilayered tube. The polar caps at the ends and inside the tube are readily discernible.

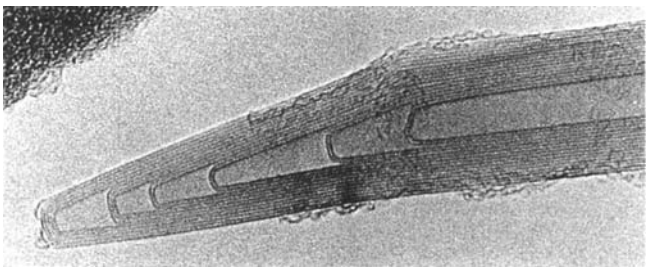


Fig. 2. TEM image of a multi-shell carbon nanotube [70].

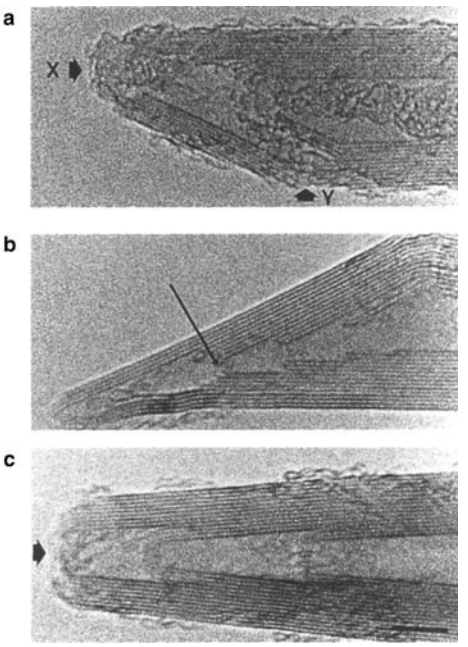


Fig. 3. TEM image of a carbon nanotube after treatment with concentrated nitric acid [70]. a) The attack takes place at positions X and Y; in these positions six-membered rings are not present. b, c) The arrows point to positions where the inside caps of the tubes have been destroyed by treatment with acid.

Macroscopic quantities of carbon nanotubes first became available in 1992.[39] Ever since then researchers have been fascinated by the prospect of opening nanotubes at the ends so as to allow for encapsulation of specific materials in the tubes. Initial experiments met with only limited success. The techniques were either applicable to only a small number of materials or the yields were extremely low. For example, arc-vaporization of metal-doped carbon electrodes resulted in most cases in the formation of free metal carbides as the main product. Only very small amounts of metal or metal carbide were encapsulated in the nanotubes that had concurrently formed.[60–68] In another attempt, nanotubes were heated in air in the presence of molten lead. Closer inspection revealed that under the experimental conditions about 1% of the tubes were opened at the ends and filled with lead. More recently it was found that carbon dioxide[48] or oxygen[69] can selectively oxidize nanotubes at elevated temperatures (ca. 700 °C); the ends of the tubes are removed in these reactions. Again, this procedure only leads to a small amount of uncapped tubes (yield: 2–10%). Also, in oxidative processes such as these the outer carbon layers are attacked, making the resulting tubes thinner and thinner.[48, 69] As an additional complication the nanotubes tend to clog due to the deposition of amorphous carbon.[69]

An extremely simple method to open and fill carbon nanotubes has recently been reported by Green and coworkers.[70a] Uncapped nanotubes were formed in about 80% yield by boiling samples in concentrated nitric acid for 4.5 h at 140 °C. Prolonged heating (24 h) was shown to increase the yield of opened tubes to 90%; however, the formation of amorphous carbon places an upper limit on the reaction time. Figure 3 shows electron micrographs of nanotubes after treatment with nitric acid. Additional studies revealed that the tubes are attacked in places with curvature, that is, those locations where five-membered rings are expected to be present. Interestingly, the caps inside the tubes are also attacked providing particles that are completely open. The high yield of open tubes implies that in most cases opening occurs at both ends.

Filling opened tubes with metals or metal oxides is an amazingly simple process too. Samples containing encapsulated nickel oxide (NiO) (Fig. 4) can be obtained in 60–70% yield (relative to the amount of open nanotubes) by treatment with nitric

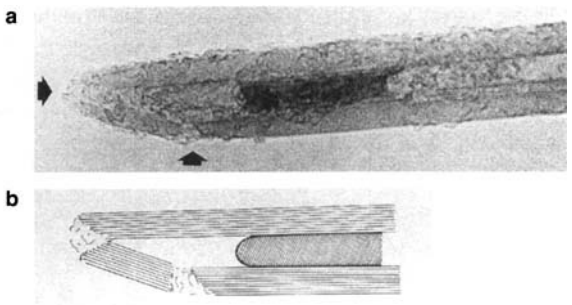


Fig. 4. a) TEM image and b) schematic representation of a nanotube encapsulating NiO [70].

acid in the presence of an aqueous solution of nickel(II) nitrate. NiO crystallites form upon drying and calcination at 450 °C. Most NiO crystallites are typically 10–30 nm long and have diameters of 3–6 nm, and thus almost completely fill the tube cavity wall-to-wall. Incorporation of nickel-containing material in the carbon layers of the tube wall was not observed. The formation of NiO-filled nanotubes can readily be explained by a two-step process: on opening, the tubes fill with a solution of nickel nitrate which upon calcination transforms into crystalline nickel oxide.

The opening and in situ filling of the carbon nanotubes can be easily extended to other metals such as cobalt, iron, and uranium. In another impressive experiment, Green et al. were able to fully reduce the encapsulated metal oxide particles to the corresponding metal (Fe, Co, Ni). Heating the NiO-filled nanotubes to 400 °C for 2 h in a hydrogen atmosphere changed the appearance of the crystallites noticeably. The ends of the particles showed facets typically observed for metal crystals (Fig. 5). This successful production of encapsulated nickel crystals has opened up interesting perspectives for the manufacture of nanomagnets.

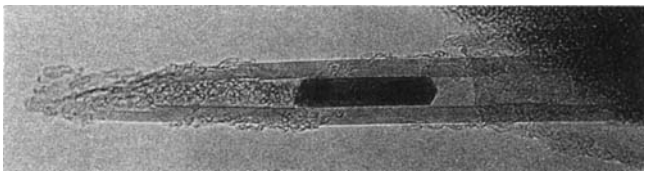


Fig. 5. TEM image of a nanotube after reduction of the encapsulated NiO with hydrogen. The facets are indicative of a nickel single crystal [70].

It should prove possible to extend the approach by Green et al. to other materials. A compelling advantage of this procedure is that the precursors are used directly as aqueous solutions. This work has undoubtedly provided a major thrust to the study of carbon nanotubes.[70b]

The deposition of metals onto the *surface* of carbon nanotubes is another promising area of research. Planeix et al. have recently shown that a novel heterogeneous catalyst is obtained by the deposition of metallic ruthenium onto nanotubes.[71] Tubes with 0.2 wt% of Ru are obtained by treating metal-free nanotubes with a solution of ruthenium acetylacetonate in toluene. The adduct is then dried and the ruthenium is reduced to the metal with hydrogen (3 h, 250 °C). TEM images of this material show the presence of homogeneous ruthenium particles (diameter: 3–7 nm) on the tube surface. These Ru/C nanotubes were shown, for example, to catalyze the hydrogenation of cinnamaldehyde to cinnamyl alcohol (selectivity: 92%). In contrast, a Ru/Al_2O_3 catalyst comprised of ruthenium particles of similar size showed only a selectivity of 20–30%.

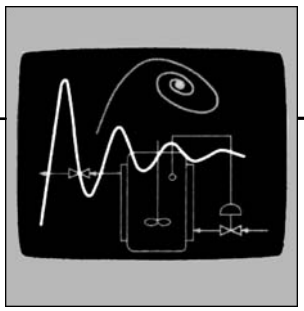
German version: *Angew. Chem.* **1995**, *107*, 1071

Keywords: fullerenes · lanthanide compounds · metallofullerenes · nanotubes

[1] *Fullerenes* (Eds.: G. S. Hammond, V. J. Kuck) *ACS Symp. Ser.* **1992**, *481*.
[2] *Buckminsterfullerenes* (Eds.: W. E. Billups, M. A. Ciufolini), VCH, Weinheim, **1993**.
[3] *The Fullerenes* (Eds.: H. W. Kroto, J. E. Fischer, C. E. Cox), Pergamon, Oxford, **1993**.
[4] *The Fullerenes. New Horizons for the Chemistry, Physics and Astrophysics of Carbon* (Eds.: H. W. Kroto, D. R. M. Watton), Cambridge University Press, Cambridge, **1993**.
[5] A. Hirsch, *The Chemistry of the Fullerenes*, Thieme, Stuttgart, **1994**.
[6] F. Diederich, Y. Rubin, *Angew. Chem.* **1992**, *104*, 1123; *Angew. Chem. Int. Ed. Engl.* **1992**, *31*, 1101.
[7] E. C. Constable, *Angew. Chem.* **1994**, *106*, 2359; *Angew. Chem. Int. Ed. Engl.* **1994**, *33*, 2269.
[8] A. Vasella, P. Uhlmann, C. A. A. Waldraff, F. Diederich, C. Thilgen, *Angew. Chem.* **1992**, *104*, 1383; *Angew. Chem. Int. Ed. Engl.* **1992**, *31*, 1388.
[9] K. L. Wooley, C. J. Hawker, J. M. J. Fréchet, F. Wudl, G. Sradnov, S. Shi, C. Li, M. Kao, *J. Am. Chem. Soc.* **1993**, *115*, 9836.
[10] C. J. Hawker, K. L. Wooley, J. M. J. Fréchet, *J. Chem. Soc. Chem. Commun.* **1994**, 925.
[11] H. L. Anderson, R. Faust, Y. Rubin, F. Diederich, *Angew. Chem.* **1994**, *106*, 1427; *Angew. Chem. Int. Ed. Engl.* **1994**, *33*, 1366.
[12] According to Smalley et al., the symbol @ denotes a moiety that is encapsulated in the fullerene cage. For a recent review on metallofullerenes, see: D. S. Bethune, R. D. Johnson, J. R. Salem, M. S. de Vries, C. S. Yannoni, *Nature* **1993**, *366*, 123.
[13] J. R. Heath, S. C. O'Brien, Q. Zhang, Y. Liu, R. F. Curl, H. W. Kroto, F. K. Tittel, R. E. Smalley, *J. Am. Chem. Soc.* **1985**, *107*, 7779.
[14] H. W. Kroto, J. R. Heath, S. C. O'Brien, R. F. Curl, R. E. Smalley, *Nature* **1985**, *318*, 162.
[15] Y. Chai, T. Guo, C. Jin, R. E. Haufler, L. P. F. Chibante, J. Fure, L. Wang, R. E. Smalley, *J. Phys. Chem.* **1991**, *95*, 7564.
[16] K. Kikuchi, S. Suzuki, Y. Nakao, N. Nakahara, T. Wakabayashi, H. Shiromaru, K. Saito, I. Ikemoto, Y. Achiba, *Chem. Phys. Lett.* **1993**, *216*, 67.
[17] S. Bandow, H. Shinohara, Y. Saito, M. Ohkohchi, Y. Ando, *J. Phys. Chem.* **1993**, *97*, 6101.
[18] C. Tapp, T. D. Wood, A. G. Marshall, J. V. Coe, *J. Am. Chem. Soc.* **1994**, *116*, 4987.
[19] J. Xiao, M. R. Savina, G. B. Martin, A. H. Francis, M. E. Meyerhoff, *J. Am. Chem. Soc.* **1994**, *116*, 9341.
[20] R. D. Johnson, M. S. de Vries, J. Salem, D. S. Bethune, C. S. Yannoni, *Nature* **1992**, *355*, 239.
[21] M. M. Ross, H. H. Nelson, J. H. Callahan, S. W. McElvany, *J. Phys. Chem.* **1992**, *96*, 5231.
[22] E. G. Gillan, C. Yeretzian, K. S. Min, M. M. Alvarez, R. L. Whetten, R. B. Kaner, *J. Phys. Chem.* **1992**, *96*, 6869.
[23] S. Bandow, H. Kitagawa, T. Mitani, H. Inokuchi, Y. Saito, H. Yamaguchi, N. Hayashi, H. Sato, H. Shinohara, *J. Phys. Chem.* **1992**, *96*, 9609.
[24] S. Suzuki, S. Kawata, H. Shinomaru, K. Yamaguchi, K. Kikuchi, T. Kato, Y. Achiba, *J. Phys. Chem.* **1992**, *96*, 7161.
[25] M. Hoinkis, C. S. Yannoni, D. S. Bethune, J. R. Salem, R. D. Johnson, M. S. Crowder, M. S. de Vries, *Chem. Phys. Lett.* **1992**, *198*, 461.
[26] C. S. Yannoni, M. Hoinkis, M. S. de Vries, D. S. Bethune, J. R. Salem, M. S. Crowder, R. D. Johnson, *Science* **1992**, *256*, 52.
[27] T. Belz, H. Werner, F. Zemlin, U. Klengler, M. Wesemann, B. Tesche, E. Zeitler, A. Reller, R. Schlögl, *Angew. Chem.* **1994**, *106*, 1919; *Angew. Chem. Int. Ed. Engl.* **1994**, *33*, 1866.
[28] H. Shinohara, H. Sato, Y. Saito, M. Ohkohchi, Y. Ando, *J. Phys. Chem.* **1992**, *96*, 3571.
[29] J. H. Weaver, Y. Chai, G. H. Kroll, C. Jin, T. R. Ohno, R. E. Haufler, T. Guo, J. M. Alford, J. Conceicao, L. P. F. Chibante, A. Jain, G. Palmer, R. E. Smalley, *Chem. Phys. Lett.* **1992**, *190*, 460.
[30] H. Shinohara, H. Sato, M. Ohkohchi, Y. Ando, T. Komada, T. Shida, T. Kato, Y. Saito, *Nature* **1992**, *357*, 52.
[31] C. S. Yannoni, M. Hoinkis, M. S. de Vries, D. S. Bethune, J. R. Salem, M. S. Crowder, R. D. Johnson, *Science* **1992**, *256*, 1191.
[32] S. Shinohara, H. Yamaguchi, N. Hayashi, H. Sato, M. Ohkohchi, Y. Ando, Y. Saito, *J. Phys. Chem.* **1993**, *97*, 4259.
[33] F. T. Edelmann, *Scandium, Yttrium, and the 4f and 5f Elements, Excluding their Zero Oxidation State Complexes* (*Comprehensive Organometallic Chemistry II, Vol. 4* (Eds.: E. W. Abel, F. G. A. Stone, G. Wilkinson), Pergamon, Oxford, **1995**).
[34] K. Kikuchi, Y. Nakao, S. Suzuki, Y. Achiba, T. Suzuki, Y. Maruyama, *J. Am. Chem. Soc.* **1994**, *116*, 9367.
[35] J. Xiao, M. R. Savina, G. B. Martin, A. H. Francis, M. E. Meyerhoff, *J. Am. Chem. Soc.* **1994**, *116*, 9341.
[36] C. E. Kibbey, M. E. Meyerhoff, *J. Chromatogr.* **1993**, *641*, 49.
[37] K. Kikuchi, K. Kobayashi, K. Sueki, S. Suzuki, H. Nakahara, Y. Achiba, K. Tomura, M. Katada, *J. Am. Chem. Soc.* **1994**, *116*, 9775.
[38] S. Iijima, *Nature* **1991**, *354*, 56.
[39] T. W. Ebbesen, P. M. Ajayan, *Nature* **1992**, *358*, 220.
[40] *Engineering a Small World: From Atomic Manipulation to Microfabrication* (*Science* **1991**, *254*, 1300 (special issue)).
[41] T. W. Ebbesen, H. Hiura, J. Fujita, Y. Ochiai, S. Matsui, K. Tanigaki, *Chem. Phys. Lett.* **1993**, *209*, 83.
[42] G. A. Ozin, *Adv. Mater.* **1992**, *4*, 612.
[43] R. T. Bate, *Sci. Am.* **1988**, *258*, 96.
[44] J. L. Jewell, J. P. Harbison, A. Scherer, *Sci. Am.* **1991**, *265*, 86.
[45] M. H. Devoret, D. Esteve, C. Urbina, *Nature* **1992**, *360*, 547.
[46] R. Gref, Y. Minamitake, M. T. Peracchia, V. Trubetskoy, V. Torchilin, R. Langer, *Science* **1994**, *263*, 1600.
[47] R. Parathasarathy, C. R. Martin, *Nature* **1994**, *369*, 298.
[48] S. C. Tsang, P. J. F. Harris, M. L. H. Green, *Nature* **1993**, *362*, 520.
[49] P. M. Ajayan, T. Ichihashi, S. Iijima, *Chem. Phys. Lett.* **1993**, *202*, 384.
[50] Reviews: a) M. S. Dresselhaus, G. Dresselhaus, R. Saito, *Solid State Commun.* **1992**, *84*, 201; b) M. S. Dresselhaus, G. Dresselhaus, R. Saito, P. C. Eklund, *Elem. Excitations Solids* **1992**, 387; c) R. Saito, M. Fujita, G. Dresselhaus, M. S. Dresselhaus, *Mater. Sci. Engl. B* **1993**, *19*, 387.
[51] H. Hiura, T. W. Ebbesen, J. Fujita, K. Tanigaki, T. Takada, *Nature* **1994**, *367*, 148.

 © VCH Verlagsgesellschaft mbH, D-69451 Weinheim, 1995 0570-0833/95/0909-0984 $ 10.00+.25/0

[52] R. A. Jishi, M. S. Dresselhaus, G. Dresselhaus, *Phys. Rev. B* **1993**, *48*, 11385.
[53] A. W. Fung, M. S. Dresselhaus, M. Endo, *Phys. Rev. B* **1993**, *48*, 14953.
[54] R. A. Jishi, M. S. Dresselhaus, G. Dresselhaus, *Phys. Rev. B* **1993**, *47*, 16671.
[55] S. Iijima, T. Ichibashi, *Nature* **1993**, *363*, 603.
[56] D. S. Bethune, C. H. Kiang, M. S. de Vries, G. Gorman, R. Savoy, J. Vazquez, R. Beyers, *Nature* **1993**, *363*, 605.
[57] P. M. Ajayan, J. M. Lambert, P. Bernier, L. Barbedette, C. Colliex, J. M. Planeix, *Chem. Phys. Lett.* **1993**, *215*, 509.
[58] U. Ugarte, *Z. Phys. D* **1993**, *26*, 150.
[59] M. S. Dresselhaus, *Nature* **1992**, *358*, 195.
[60] R. S. Ruoff, D. C. Lorents, B. Chan, R. Malhotra, S. Subramoney, *Science* **1993**, *259*, 346.
[61] M. Tomita, Y. Saito, T. Hayashi, *Jpn. J. Appl. Phys.* **1993**, *32*, L280.
[62] S. Seraphin, D. Zhou, J. Jiao, J. C. Withers, R. Loufty, *Nature* **1993**, *362*, 503.
[63] Y. Saito, T. Yoshikawa, M. Okuda, M. Ohkohchi, Y. Ando, A. Kasuya, Y. Nishina, *Chem. Phys. Lett.* **1993**, *209*, 72.
[64] Y. Saito, T. Yoshikawa, M. Okuda, N. Fujimoto, K. Sumiyama, K. Suzuki, A. Kasuya, Y. Nishina, *J. Phys. Chem. Solids* **1993**, *54*, 1894.
[65] Y. Saito, M. Okuda, T. Yoshikawa, S. Bandow, S. Yamamuro, K. Wakoh, K. Sumiyama, K. Suzuki, *Jpn. J. Appl. Phys.* **1994**, *33*, L186.
[66] Y. Saito, M. Okuda, N. Fujimoto, T. Yoshikawa, M. Tomita, T. Hayashi, *Jpn. J. Appl. Phys.* **1994**, *33*, L526.
[67] Y. Saito, T. Yoshikawa, *J. Cryst. Growth* **1993**, *134*, 154.
[68] P. M. Ajayan, S. Iijima, *Nature* **1993**, *361*, 333.
[69] P. M. Ajayan, T. W. Ebbesen, T. Ichibashi, S. Iijima, K. Tanigaki, H. Huira, *Nature* **1993**, *362*, 522.
[70] a) S. C. Tsang, Y. K. Chen, P. J. F. Harris, M. L. H. Green, *Nature* **1994**, *372*, 159; b) H. Hiura, T. W. Ebbesen, K. Tanigaki, *Adv. Mater.* **1995**, *7*, 275.
[71] J. M. Planeix, N. Coustel, B. Coq, V. Brotons, P. S. Kumbhar, R. Dutartre, P. Geneste, P. Bernier, P. M. Ajayan, *J. Am. Chem. Soc.* **1994**, *116*, 7935.



Ingham, J. et al.

Chemical Engineering Dynamics

Modelling with PC Simulation

1994. XX, 701 pages with 430 figures.
Hardcover. DM 276.-/
öS 2153.-/ sFr. 256.-.
ISBN 3-527-28577-6

In this book, the reader is guided through the complex study of dynamic chemical engineering systems by the unique combination of a simplified presentation of the fundamental theory (Part 1) and direct hands-on computer experimentation with the provision of 85 accompanying computer-based simulation examples (Part 2) supplied on diskette.

The ISIM digital simulation language is very simple to use and its powerful interactive nature enables the readers to create their own simulations, based on their own specific problems. This powerful dynamic ISIM software is ready to run on any DOS personal computer.

The treatment employed in this book is well tried and tested, based on over 20 years experience in teaching an international post-experience course. Whether for the teacher, the student, the chemist or engineer, this book serves as the key to a greater understanding of chemical engineering dynamics through the fun and enjoyment of active learning.

To order please contact your bookseller or:

VCH, P.O. Box 10 11 61, D-69451 Weinheim, Telefax (0) 62 01 - 60 61 84

VCH, Hardstrasse 10, P.O. Box, CH-4020 Basel

VCH, 8 Wellington Court, Cambridge CB1 1HZ, UK

VCH, 220 East 23rd Street, New York, NY 10010-4606, USA (toll free: 1-800-367-8249)

VCH, Eikow Building, 10-9 Hongo 1-chome, Bunkyo-ku, Tokyo 113 Japan

VCH

Formal Oxidation State versus Partial Charge—A Comment

Martin Kaupp* and Hans Georg von Schnering

In a communication in this journal,[1] Snyder recently claimed that the oxidation state of the copper atom in the square-planar anion $[Cu(CF_3)_4]^-$ is Cu^I, and not Cu^{III} as inferred by Naumann et al.[2] from synthesis and properties, and from structural arguments which up to now have been generally accepted. Snyder based his conclusion on NBO population analysis from ab initio pseudopotential calculations. These gave charges on copper of only $q \approx +1$.

Evidently, there must be a gross misunderstanding. Snyder has confused two important but fundamentally different concepts: the formal oxidation state, and partial charges as obtained, for example, from population analyses. To derive a formal oxidation state, a completely ionic bonding description is chosen deliberately; that is, the bonding electron pairs are assigned exclusively to the more electronegative bonding partner. Thus, if one accepts that the CF_3 ligand is more electronegative than the copper atom, that each CF_3 ligand is bound to the central atom, that there are no additional bonds between the ligands, and that all CF_3 ligands are equivalent, there is no way around an assignment of an oxidation state of III to the copper atom. (An alternative, completely homolytic distribution of the bonding electrons would lead to the unrealistic oxidation state −I.) The validity of none of the above assumptions has been touched in any way by Snyder's calculations.

Snyder's population analysis yields a significant electron population in the $d_{x^2-y^2}$ atomic orbital of copper. This merely tells us that significant covalent interactions contribute to the Cu–C bonds. Therefore, the formal oxidation state III differs appreciably from the calculated partial charge in this case. However, this holds generally true for significantly covalent bonds.

The square-planar structure also clearly supports the original description[2] as a Cu^{III} complex. A four-coordinate Cu^I complex should be tetrahedral. The examples for square-planar Cu^I species erroneously quoted by Snyder turn out to be either obviously Cu^{II} complexes[3] or (slightly distorted) tetrahedrally coordinated systems.[4, 5]

German version: *Angew. Chem.* **1995**, *107*, 1076

[*] Dr. M. Kaupp, Prof. Dr. H. G. von Schnering
Max-Planck-Institut für Festkörperforschung
Heisenbergstrasse 1, D-70569 Stuttgart (Germany)
Telefax: Int. code + (711)689-1562

[1] J. P. Snyder, *Angew. Chem.* **1995**, *107*, 112; *Angew. Chem. Int. Ed. Engl.* **1995**, *34*, 80.
[2] D. Naumann, T. Roy, K.-F. Tebbe, W. Crump, *Angew. Chem.* **1993**, *105*, 1555; *Angew. Chem. Int. Ed. Engl.* **1993**, *32*, 1482.
[3] B. Chiari, O. Piovesana, T. Tarantelli, P. F. Zanazzi, *Inorg. Chem.* **1984**, *23*, 2542.
[4] J. C. Dyason, P. C. Healy, L. M. Engelhardt, C. Pakawatchai, W. A. Patrick, A. H. White, *J. Chem. Soc. Dalton Trans.* **1985**, 839.
[5] M. Hakansson, S. Jagner, M. Nilsson, *J. Organomet. Chem.* **1987**, *336*, 279.

Distinguishing Copper d^8 and d^{10} Configurations in a Highly Ionic Complex; A Nonformal Metal Oxidation State

James P. Snyder*

Since Pauling's introduction of the concept over 40 years ago,[1] assignment of *formal* oxidation numbers and oxidation states has proved to be useful for teaching elementary chemical concepts and for cataloguing trends in the periodic table.[2] Nonetheless, apart from isolated monoatomic ions, designation of a formal oxidation state is entirely arbitrary and often accompanied by assumptions as underscored by Kaupp and von Schnering.[3] Assignment is accomplished by employing one of the many predefined but not entirely consistent electron-counting schemes.[4] Unfortunately, uncritical application of the resulting oxidation values can lead to confusing and physically unrealistic descriptions for organic, organometallic, and inorganic species alike.[5]

The report by Naumann et al.[6] classified the metal in **1** as Cu^{III} and designated it as d^8, suggesting an intimate link between

$[Cu(CF_3)_4]^-$ **1** $[CH_3-Cu-CH_3]^-$ **2**

[*] Prof. Dr. J. P. Snyder
Emerson Center for Scientific Computation
Department of Chemistry, Emory University
1515 Pierce Drive, Atlanta, GA 30322 (USA)
Telefax: Int. code + (404)727-6586
e-mail: snyder@euch4e.chem.emory.edu

 © VCH Verlagsgesellschaft mbH, D-69451 Weinheim, 1995 0570-0833/95/0909-0986 $ 10.00+.25/0

oxidation state and electron distribution. The critical question concerns the filling of copper's d orbitals in the complex. Partial charges alone are not sufficient to address this issue. Among others, atomic and bond orbital populations not dependent on basis set, as provided by natural population analysis (NPA),[7] provide useful additional tools. Two comparisons place our initial analysis[8] in a broader context.

First, both monoanions **1** and **2** exhibit less than 5% (less than 20%) NPA contribution to the localized Cu–C bonding orbitals at the reported[8] MP2 (SCF) levels. The resulting ionic bonding (greater than 80–95%) implies that the valence electrons reside primarily as pairs either with Cu or CF_3/CH_3. The largely ionic character implies further that it should be possible to assign the metal oxidation state in **1** as readily as for monoatomic ions given knowledge of the electron partition. Examination of the total metal d-orbital populations for anions **1** and **2** illustrates that they are very similar (9.7 (9.4) and 9.6 (9.9) electrons, respectively). Accordingly, copper is ascribed a d^{10} configuration and a *nonformal* Cu^{I} oxidation state in both complexes. The calculated charges and orbital populations at the CF_3/CH_3 ligands are fully consistent.

The second comparison concerns the ability of the NPA analysis to treat complexes in which the metal is unambiguously d^8. The square-planar complexes **3**–**5** were treated analogously to **1** and **2** at the MP2/LANL2DZ level of theory.[9] Total d-orbital populations of 8.8, 8.6, and 8.9 electrons were obtained for **3**, **4**, and **5**, respectively. Ligand electron donation gives rise to the metal d^{8+} constitution.

$[RhCl(PH_3)_3]$ **3** $[Pt(NH_3)_4]^{2+}$ **4** $[Ni(CN)_4]^{2-}$ **5**

One qualitative heuristic explanation for the d^{10} result for **1** is to view it as a combination of two complementary effects. First, the crystal field splitting for Cu^{III} is maximized both by the strong-field effect of CF_3 and by its negative charge.[10] Raised to high energy, the $d_{x^2-y^2}$ orbital experiences the transfer of two electron from the surrounding anionic ligands. Second, the electron-depleted CF_3 moieties are internally stabilized by π-type F–X interaction analogous to that for BF_3,[11] CF_3^+,[12] and other fluorinated cations.[13] MO correlation is an alternative but equivalent interpretation in which the square-planar geometry arises from a stabilizing donor–acceptor interaction between the filled $d_{x^2-y^2}$ of Cu^{I} and the four CF_3 ligands sharing three lone electron pairs.[8]

In conclusion, while a broader examination of the ideas outlined herein is required, novel mechanistic insights are already evident from the above analysis. Furthermore, at the very least it can be expected that square-planar tetracoordinate silver and gold centers in anionic complexes will exhibit electronic properties similar to copper in **1**.[14]

German version: *Angew. Chem.* **1995**, *107*, 1076

[1] L. Pauling, *General Chemistry*, 2nd ed., W. H. Freeman, San Francisco, **1954**.

[2] a) D. F. Shriver, P. Atkins, C. H. Langford, *Inorganic Chemistry*, 2nd ed., W. H. Freeman, New York, **1994**; b) G. Wulfsberg, *Principles of Descriptive Inorganic Chemistry*, University Science Books, Mill Valley, CA, USA, **1991**.

[3] M. Kaupp, H. G. von Schnering, *Angew. Chem.* **1995**, *107*, 1076; *Angew. Chem. Int. Ed. Engl.* **1995**, *34*, 986.

[4] J. E. Packer, S. D. Woodgate, *J. Chem. Educ.* **1991**, *68*, 456; J. M. Kauffman, *ibid.* **1986**, *63*, 474; E. M. Holleran, N. D. Jesperson, *ibid.* **1980**, *57*, 670; cf. any introductory chemistry textbook.

[5] a) A. A. Woolf, *J. Chem. Educ.* **1993**, *70*, 691; A. G. Sharpe, *Inorganic Chemistry*, 3rd ed., Longman, New York, **1992**, pp. 449 and 545; A. A. Woolf, *J. Chem. Educ.* **1988**, *65*, 45; H. H. Sisler, C. A. VanderWerf, *ibid.* **1980**, *57*, 42; b) D. A. Summerville, R. D. Jones, B. M. Hoffman, F. Basolo, *ibid.* **1979**, *56*, 1571.

[6] D. Naumann, T. Roy, K.-F. Tebbe, W. Crump, *Angew. Chem.* **1993**, *105*, 1555; *Angew. Chem. Int. Ed. Engl.* **1993**, *32*, 1482.

[7] A. E. Reed, F. J. Weinhold, *Chem. Rev.* **1988**, *88*, 899; *J. Am. Chem. Soc.* **1986**, *108*, 3586; J. E. Carpenter, F. J. Weinhold, *J. Chem. Phys.* **1985**, *92*, 735, 4306; A. E. Reed, F. J. Weinhold, QCPE 504.

[8] J. P. Snyder, *Angew. Chem.* **1995**, *107*, 112; *Angew. Chem. Int. Ed. Engl.* **1995**, *34*, 80.

[9] P. J. Hay, W. R. Wadt, *J. Chem. Phys.* **1985**, *82*, 299; cf. citations in ref. [8].

[10] J. D. Lee, *Concise Inorganic Chemistry*, 4th ed., Chapman & Hall, New York, **1991**, pp. 207–210.

[11] Ref. [2a], pp. 205, 459–460; ref. [10], pp. 385–386.

[12] J. R. Eyler, P. Ausloos, S. G. Lias, *J. Am. Chem. Soc.* **1974**, *96*, 3673.

[13] V. Nguyen, X. Cheng, T. H. Morton, *J. Am. Chem. Soc.* **1992**, *114*, 7127; T. A. Shaler, T. H. Morton, *ibid.* **1991**, *113*, 6771; D. A. Stams, T. D. Thomas, D. C. MacLaren, D. Ji, T. H. Morton, *ibid.* **1990**, *112*, 1427.

[14] J. P. Snyder, unpublished.

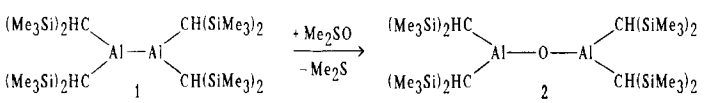
Tetrakis[bis(trimethylsilyl)methyl]dialuminoxane with a Linear Al-O-Al Group**

Werner Uhl, Matthias Koch, Wolfgang Hiller, and Maximilian Heckel*

Dedicated to Professor Peter Paetzold on the occasion of his 60th birthday

Aluminoxanes[1] of general formula $R_2Al\text{-}O\text{-}AlR_2$ or $(RAlO)_n$ are important as cocatalysts in the polymerization of ethene or propene; the investigation of their properties is an area of current interest in organoaluminum chemistry.[1-3] Whilst tetraalkyldialuminoxanes are usually dimers or trimers, the monoalkyl compounds exhibit oligomeric polyhedral structures, and cages with up to nine RAlO formula units have been identified by crystal structure analysis for *tert*-butyl derivatives. Monomeric dialuminoxanes $R_2Al\text{-}O\text{-}AlR_2$ with only twofold coordination of O atoms and threefold coordination of Al atoms were hitherto unknown. The bonding in their Al-O-Al unit is of particular interest on account of the possible π interaction between the unoccupied p orbitals on Al and the free electron pairs on O. Starting with the corresponding dialuminum(4) compound **1**,[4] we recently synthesized derivatives containing Al-S-Al,[5] Al-Se-Al,[6] and Al-Te-Al fragments,[7] which are monomeric in the solid state because of the high steric shielding by four bulky $CH(SiMe_3)_2$ groups. There are no significant π contributions in these derivatives because of the staggered conformation of the substituents and an angle of between 117 and 110° on the central atom.

Tetraalkyldialuminoxane **2** is produced by the reaction of **1** with the oxygen donors trimethylamine oxide, *N*-sulfinylaniline



(H_5C_6—N=S=O), or DMSO.[8] However, the crystals of **2** so obtained include 10–20% of the μ-hydroxo derivative $R_2Al(\mu\text{-}OH)_2AlR_2$, which has already been synthesized as a pure compound by another method,[9] and which could not be removed by recrystallization of **2**. Because DMSO is easy to handle, it was used as the oxygen donor in the subsequent investigations. Pure **2** can be obtained if the raw product is treated with isobutyllithium which traps the hydroxide.[10] The optimum amount of isobutyllithium is determined by ^1H NMR.

[*] Prof. Dr. W. Uhl, M. Koch
Fachbereich Chemie der Universität
Postfach 2503, D-26111 Oldenburg (Germany)
Telefax: Int. code + (441)798-3329
Prof. Dr. W. Hiller, M. Heckel
Anorganisch-chemisches Institut der Technischen Universität München

[**] This work was supported by the Deutsche Forschungsgemeinschaft and the Fonds der Chemischen Industrie.

Compound **2** crystallizes as a monomer in the centrosymmetric space group *C2/c*. The oxygen atom lies on a crystallographic inversion center,[11] and the Al-O-Al group is therefore linear. The frequently observed averaging out of two positions that are in reality separate, thus feigning a linear arrangement of symmetrical atomic groups, can be excluded on account of the low anisotropic displacement parameters of the central atom. To date there are only a few compounds known with a monomeric Al-O-Al group; however, in these the oligomerization is prevented by the coordination of a Lewis base to an Al atom. These include linear[2, 12] and bent[13] molecules, without a discernible correlation between Al-O-Al angles and Al-O bond lengths. In adducts of trimethylamine oxide with **2** ($2\cdot Me_3NO$ and $2\cdot 2Me_3NO$)[9] the linearity is lost, and we observe Al-O-Al angles of 162.30° and 161.4°, respectively. In aluminum suboxide, Al_2O, a linear structure was verified both experimentally and theoretically,[14] and also in $H_2Al\text{-}OR$,[15] which has not yet been synthesized, the approximately linear environment of the oxygen atom has been predicted to give an optimal π overlap of Al and O orbitals.

The very short Al–O bond (168.8 pm) is characteristic for the participation of π interactions (p_π–p_π or n–σ^*);[16, 17] the Al–C distances of 195.6 pm are, as in compounds with Al-S-Al or Al-Te-Al units,[5, 7] shorter than those in the starting material **1** (198.2 pm).[4] The Al atoms in **2** project only 0.6 pm out of the plane of the surrounding atoms. As a result of the interaction of both lone pairs of electrons on the oxygen atom with the Al atoms, the valence electron configuration in **2** would be the same as that of allenes, and the substituents in the 1,3 position should be staggered. This conformation was recently observed in $Cp^*_2Sc\text{-}Te\text{-}ScCp^*_2$, which has an almost linear (172°) Sc-Te-Sc group.[18] In diboroxanes the substituents are also staggered; however, in the gas phase and in the solid state the B-O-B angles range from 144 to 166°.[19] As shown in Figure 1, all the substituents on the Al atoms in **2** are coplanar, which is in agreement with the presence of an inversion center. The α-C–H bonds

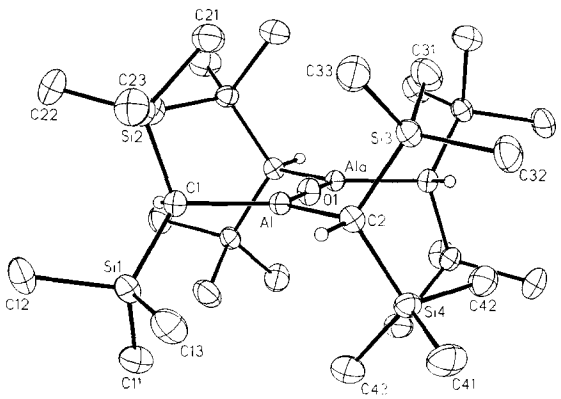


Fig. 1. Molecular structure of **2** in the crystal (vibrational ellipsoids with 40% probability). Only the methine hydrogen atoms are drawn (radius not to scale). The atom Ala is produced by the symmetry operation $-x+0.5, -y+0.5, -z+1$. Selected bond lengths [pm] and angles [°]: Al–O1 168.77(4), Al–C1 195.7(1), Al–C2 195.4(1); Al-O1-Ala 180, O1-Al-C1 117.54(5), O1-Al-C2 119.83(5), C1-Al-C2 122.63(6).

only deviate slightly from the $C_2AlOAlC_2$ plane; each hydrogen atom projects into the space between the two trimethylsilyl groups of the neighboring carbon atom.

The fast rotation about the Al–C bond in solution results in only one NMR signal for the methyl and methine groups. These signals remain virtually unchanged on cooling a solution of **2** in toluene to −80 °C. The methine protons of **2** ($\delta = -0.54$) resonate far upfield from the corresponding protons in the starting material **1** ($\delta = 0.36$), and lie in the range between the values of threefold ($\delta = -0.20$ to -0.45) and fourfold ($\delta < -0.55$) coordinated bis(trimethylsilyl)methylaluminum compounds.[20] The resonance of the C atom bonded to Al ($\delta = 9.0$) also lies at a higher field than that in compounds with Al atoms having threefold coordination (R_2Al-S-AlR_2:[5] $\delta = 16.6$; R_2Al-Te-AlR_2:[7] $\delta = 17.3$); this corresponds to an increase of the charge density on the Al atoms. In analogy to the situation in organoboron compounds (Me_2BOR or Me_2BNR_2),[21] these data possibly verify the participation of a mesomeric structure with Al–O π interactions between the lone pairs of electrons on oxygen and the empty p orbitals on Al.[16]

Experimental Procedure

1 (1.24 g, 1.8 mmol) was dissolved under argon in *n*-hexane (50 mL, freshly distilled over butyllithium) and treated with dimethyl sulfoxide (0.127 mL, 1.8 mmol, distilled over BaO) at room temperature with vigorous stirring. After about 30 min the solution had completely decolorized. The volume of the solution was reduced by half (in vacuo) and the optimal amount of isobutyllithium added (experimentally predetermined; here: 0.84 mL (0.72 mmol) of a 0.857 M solution in *n*-pentane). Colorless crystals of **2** were obtained on cooling to −50 °C. Yield: 0.95 g (75%). M.p. (under Ar): 173 °C; M_r (cryoscopically determined in benzene) [g mol^{-1}]: found 683, calcd 707.6. ^{1}H NMR (C_6D_6): $\delta = 0.30$ (72 H, $SiMe_3$), −0.54 (4 H, AlCH); ^{13}C NMR (C_6D_6): $\delta = 9.0$ (AlC), 4.8 ($SiMe_3$). IR (Nujol, CsBr plates): $\tilde{\nu}$ [cm^{-1}] = 1262 s, 1248 s δCH_3; 1017 s δCH; 930 m, 909 m, 843 vs, 777 s, 756 s, 748 s, 731 m ρCH_3(Si); 704 w, 687 m, 673 s ν_{as}SiC; 642 w, 611 w ν_sSiC; 559 vw, 534 w, 500 w νAlC; 376 vw, 339 vw, 316 vw δSiC; ν_{as}AlO probably lies hidden under the ρCH_3 absorptions.

Received: September 20, 1994
Revised version: November 30, 1994 [Z 7330IE]
German version: *Angew. Chem.* **1995**, *107*, 1122

Keywords: dialuminoxane · π interactions · steric shielding

[1] S. Pasynkiewicz, *Polyhedron* **1990**, *9*, 429–453.
[2] M. R. Mason, J. M. Smith, S. G. Bott, A. R. Barron, *J. Am. Chem. Soc.* **1993**, *115*, 4971–4984.
[3] C. J. Harlan, M. R. Mason, A. R. Barron, *Organometallics* **1994**, *13*, 2957–2969.
[4] W. Uhl, *Z. Naturforsch. B* **1988**, *43*, 1113–1118.
[5] W. Uhl, A. Vester, W. Hiller, *J. Organomet. Chem.* **1993**, *443*, 9–17.
[6] W. Uhl, R. Gerding, unpublished.
[7] W. Uhl, U. Schütz, *Z. Naturforsch. B* **1994**, *49*, 931–934.
[8] Compound **1** does not react with a stoichiometric amount of oxygen, whilst excess oxygen destroys the starting material. Bis(trimethylsilyl)peroxide, dinitrogen monoxide, and cyclohexene oxide do not react with **1**; benzophenone and trialkylphosphane oxide gave indeterminate product mixtures. We also attempted to synthesize **2** from the corresponding dialkylaluminum chloride R_2Al-Cl with Ag_2O, Li_2O, hexamethyldisiloxane, and R_2Al-O-$SiMe_3$ [9] but there was no reaction, even in a melt.
[9] W. Uhl, M. Koch, unpublished results.
[10] The product from hydroxide and isobutyllithium can be separated during recrystallization as the more readily soluble component. It shows eight signals of equal intensity in the $SiMe_3$ region of the ^{1}H NMR spectrum. Its constitution is still unknown, but deprotonation of the μ-hydroxo derivative does not occur.
[11] Single crystals obtained by recrystallization from *n*-pentane; $C_{28}H_{76}Al_2OSi_8$; diffractometer CAD 4; $Mo_{K\alpha}$ radiation; −60 °C; SHELXTL PLUS REL 4.1 and SHELXL-93 programs; monoclinic; $C2/c$; $a = 2297.9(2)$, $b = 959.3(1)$, $c = 2078.1(1)$ pm, $\beta = 98.99(1)°$, $V = 4525 \times 10^6$ pm^3; $Z = 4$, $\rho_{calcd} = 1.039$ g cm^{-3}; crystal dimensions: $0.7 \times 0.5 \times 0.3$ mm^3; θ–2θ scan; measured range: $6 \le 2\theta \le 54°$; 4891 independent reflections; 4275 reflections $F > 4\sigma(F)$; 190 parameters; $R = 0.038$ and $wR^2 = 0.089$ (all measured reflections); max. residual electron density: 0.29×10^{30} e m^{-3}. Further details of the crystal structure investigation may be obtained from the Fachinformationszentrum Karlsruhe, D-76344 Eggenstein-Leopoldshafen (Germany) on quoting the depository number CSD-58779.
[12] R. Kumar, H. Rahbarnoohi, M. J. Heeg, D. G. Dick, J. P. Oliver, *Inorg. Chem.* **1994**, *33*, 1103–1108; Y. Kushi, Q. Fernando, *J. Am. Chem. Soc.* **1970**, *92*, 91–96; K. J. Wynne, *Inorg. Chem.* **1985**, *24*, 1339–1343.
[13] P. L. Gurian, L. K. Cheatham, J. W. Ziller, A. R. Barron, *J. Chem. Soc. Dalton Trans.* **1991**, 1449–1456; G. Johansson, *Acta Chem. Scand.* **1966**, *20*, 505–515; U. Kliebisch, U. Klingebiel, D. Stalke, G. M. Sheldrick, *Angew. Chem.* **1986**, *98*, 921–922; *Angew. Chem. Int. Ed. Engl.* **1986**, *25*, 915–916.
[14] M. Cai, C. C. Carter, T. A. Miller, V. E. Bondybey, *J. Chem. Phys.* **1991**, *95*, 73–79; A. I. Boldyrev, P. von R. Schleyer, *J. Am. Chem. Soc.* **1991**, *113*, 9045–9054; A. V. Nemukhin, F. Weinhold, *J. Chem. Phys.* **1992**, *97*, 3420–3430.
[15] A. R. Barron, K. D. Dobbs, M. M. Francl, *J. Am. Chem. Soc.* **1991**, *113*, 39–43.
[16] M. D. Healy, M. B. Power, A. R. Barron, *Coord. Chem. Rev.* **1994**, *130*, 63–135.
[17] A. Haaland in *Coordination Chemistry of Aluminium* (Ed.: G. H. Robinson) VCH, Weinheim, **1993**.
[18] W. E. Piers, L. R. MacGillivray, M. Zaworotko, *Organometallics* **1993**, *12*, 4723–4725.
[19] G. Gundersen, H. Vahrenkamp, *J. Mol. Struct.* **1976**, *33*, 97–105; C. J. Cardin, H. E. Parge, J. W. Wilson, *J. Chem. Res. (M)* **1983**, 801–809; L. Cynkier, N. Furmanova, *Cryst. Struct. Commun.* **1980**, *9*, 307–308; H. Borrmann, A. Simon, H. Vahrenkamp, *Angew. Chem.* **1989**, *101*, 182–183; *Angew. Chem. Int. Ed. Engl.* **1989**, *28*, 180–181; T. Fjeldberg, G. Gundersen, T. Jonvik, H. M. Seip, S. Säbö, *Acta Chem. Scand. A* **1980**, *34*, 547–565; a planar molecular framework with a bent B-O-B group in $[(X_2N)(XNH)B]_2O$ (X = Me_3Si): K. J. L. Paciorek, R. H. Kratzer, P. F. Kimble, J. H. Nakahara, K. J. Wynne, C. S. Day, *Inorg. Chem.* **1988**, *27*, 2432–2433.
[20] W. Uhl, M. Koch, A. Vester, *Z. Anorg. Allg. Chem.* **1993**, *619*, 359–366.
[21] H.-O. Kalinowski, S. Berger, S. Braun, *^{13}C-NMR-Spektroskopie*, Thieme, Stuttgart, **1984**, p. 230ff.

Synthesis of an RGD-Sialyl-Lewis^X Glycoconjugate: A New Highly Active Ligand for P-Selectin**

Ulrich Sprengard, Gerhard Kretzschmar,* Eckart Bartnik, Christoph Hüls, and Horst Kunz*

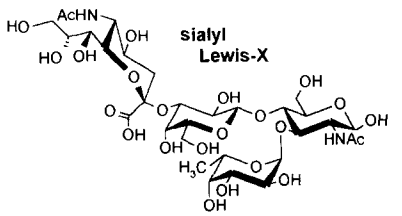
Dedicated to Professor Richard R. Schmidt on the occasion of his 60th birthday

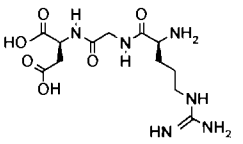
The circulation of blood cells such as leucocytes, neutrophils, granulocytes, and monocytes is a multistep, complex process at the molecular level, and only some steps are known.[1] Current research results show that the molecular mechanism of lymphocyte circulation, which is vital for immune control, and the mechanism of localization of neutrophils and monocytes at sites of inflammation are very similar. During acute and chronic inflammation processes this leads to adhesion of leucocytes to endothelial cells, and to migration to the site of inflammation or to the secondary lymphatic organs.

Many specific signaling molecules, such as interleukins, leukotrienes, tumor necrosis factor (TNF-α), and especially tissue-specific adhesion molecules, are involved in these process-

[*] Dr. G. Kretzschmar, Dipl.-Chem. U. Sprengard
Zentralforschung der Hoechst AG
D-65926 Frankfurt am Main (Germany)
Telefax: Int. code + (69) 331320
Prof. Dr. H. Kunz, Dipl.-Chem. U. Sprengard
Institut für Organische Chemie der Universität
D-55099 Mainz (Germany)
Telefax: Int. code + (6131) 39-4786
Dr. E. Bartnik, Dr. C. Hüls
Werk Kalle-Albert der Hoechst AG

es and are recognized by receptors. In addition to integrins and glycoproteins of the immunoglobulin superfamily, the selectins (E-, P- and L-selectin)[2] are amongst the most important adhe-

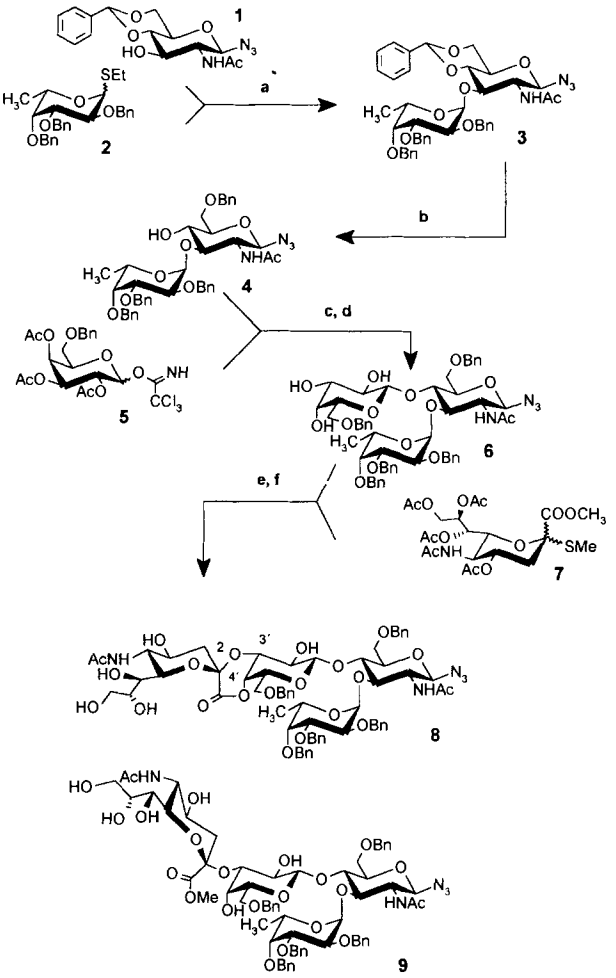




sion molecules, playing a vital role in the initial phases of leucocyte adhesion. It is generally recognized that the tetrasaccharide sialyl Lewis^X,[3] which occurs as a partial structure of glycosphingolipids and glycoproteins on cell membranes, functions as a ligand with a weak affinity for all three selectins in cell culture assays.[4]

The tripeptide Arg-Gly-Asp (RGD) corresponds to the minimal sequence of many adhesion molecules, including the α-chain of fibrinogen that binds to integrin receptor GpIIb/IIIa, and it frequently serves as a model structure for antiadhesive peptide mimetics.[5] However, no peptido- or glycomimetics are known that bind with a high affinity to selectins. Here we describe the synthesis of the adhesion hybrid **14**, which combines the structural elements of the RGD motif with those of the sialyl Lewis^X ligand and is a highly active ligand for P-selectin in cell assays. During the synthesis of **14**, a partially blocked sialyl Lewis^X unit is produced on a multigram scale through a coordinated protective-group strategy, and this is finally converted into **14** by using the presynthesized peptide:[6] a) The azido functional group acts as an anomeric protective group for the glucosamine unit during the saccharide synthesis. It can be selectively reduced to the β-glycosylamine. b) Condensation of only partially O-protected oligosaccharide amines with C-terminal deblocked peptides enables an efficient synthesis of the conjugate, whereby the anomeric amino groups are selectively acylated in the presence of free OH functions by modern peptide chemistry linkage methods. c) The lactone of neuraminic acid **8** is used as an internal protective group to mask the carboxyl function, which renders blocking of the methyl ester superfluous. d) The coordinated protective-group protocol enables mild terminal deblocking of the glycopeptide by catalytic hydrogenation.

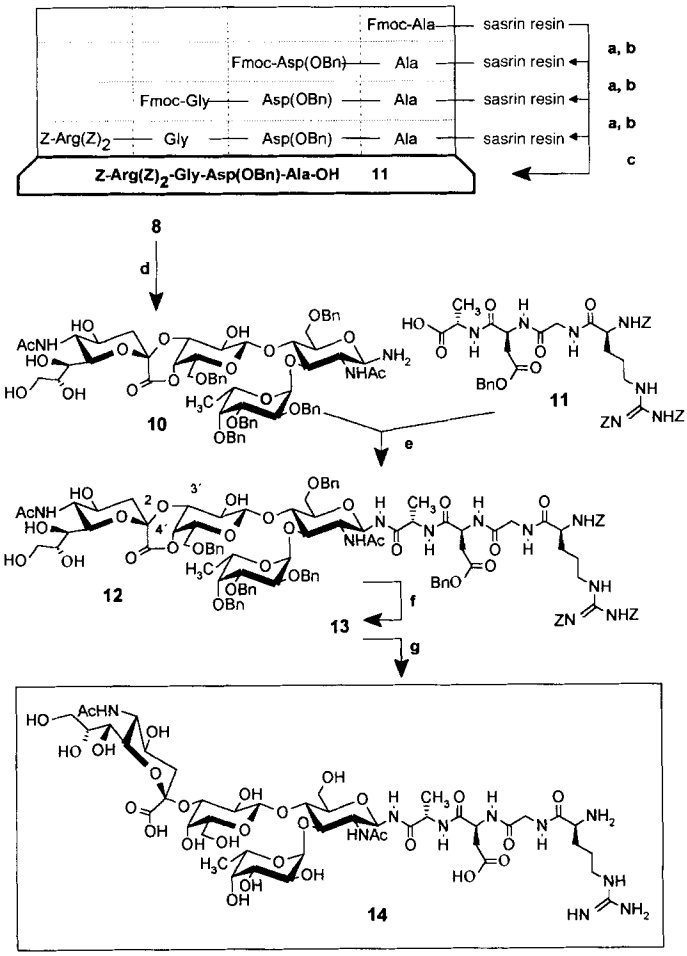
Glycosylation of the 4,6-(benzylidene)-protected *N*-acetylglucosaminylazide **1**[7, 8] with the perbenzylated thiofucoside **2** and tetrabutylammonium bromide/copper (II) bromide[9] stereoselectively produces α-glycoside **3** (Scheme 1) with 92% yield. Regioselective opening of the benzylidene acetal ring is achieved with sodium cyanoborohydride/HCl.[10] However, the yield of 81% is only obtained by titrimetric addition of HCl in ether, because of the acid lability of the fucose. Linkage of the disaccharide **4** with the galactosyl trichloracetimidate **5**[11] on the sluggishly reactive, sterically hindered 4-OH function followed by Zemplen hydrolysis produces β-glycoside **6** in 44% yield. Because of the acetamide group a large amount of Lewis acid is required, which promotes side reactions. Alternatively, trisaccharide **6** can be synthesized with a yield of 16% from **4** and methylthiogalactoside with *N*-iodosuccinimide (NIS)/trifluoromethanesulfonic acid (TfOH). Following deacetylation, the Lewis^X trisaccharide **6** can be derivatized at the galactose unit. Sialylation is performed with the methylthioglycoside of neuraminic acid **7**[12] (1.8 equiv) at -40°C in dichloromethane/acetonitrile, in the presence of methylsulfenyl bromide (MSB)/silver



Scheme 1. a) **2** (1.4 equiv), $Bu_4NBr/CuBr_2$, CH_2Cl_2/DMF (1:1), molecular sieve 3 Å, **3**: 92%; b) $NaCNBH_3$, HCl/Et_2O, molecular sieve 4 Å, **4**: 81%; c),d) **5** (1.5 equiv), TMSOTf (0.15 equiv), CH_2Cl_2; $NaOCH_3$ in MeOH, Amberlite IR 120, **6**: 44%; e),f) MSB/AgOTf, CH_2Cl_2/CH_3CN (5:1), molecular sieves 3 Å, -40°C; $NaOCH_3$ in MeOH, Amberlite H^+ IR 120, **8**: 42% relative to **6**.

trifluoromethanesulfonate as promoter.[13, 14] The sialylation products can be separated chromatographically following deacetylation of the crude products on a multigram scale, and the unconverted trisaccharide can be recovered. The partially deblocked sialyl Lewis^X **8** is formed by intramolecular esterification to give the 1-4′-lactone and can be isolated as the main product with a yield of 42% (based on **6**).[15] The 1-2′-lactone and the methyl ester **9** of the tetrasaccharide can only be detected in trace amounts.[16] The lactone remains as an internal protective group to mask the carboxyl function during subsequent synthesis of the saccharide–peptide conjugate. It can be hydrolyzed using mild conditions, which reduces the risk of racemization during subsequent deblocking.[14, 17, 18] Hydrogenation of the anomeric azide over neutral, washed Raney nickel in isopropyl alcohol/water (9:1) produces the sialyl Lewis^X amine unit **10** (Scheme 2).[19] Alternative methods in which the glycosyl amine is generated from the anomeric unprotected oligosaccharide often lead to salt-containing products.[20]

The second synthetic unit, the RGDA peptide in the form of the C-terminal deblocked Z-Arg (Z_2)-Gly-Asp(OBn)-Ala-OH **11**, is synthesized using the Fmoc solid-phase strategy[21] on acid-labile sasrin resin (Scheme 2).[22] Fragment condensation of the sialyl Lewis^X amine unit **10** with the RGDA peptide **11** using TBTU/HOBT/DIPEA[23] produces the *N*-glycosyl-



Scheme 2. a) 20% piperidine in DMF; b) 3 equiv amino acid, TBTU/HOBT/DIPEA 3 equiv each, DMF; c) 1% TFA in CH_2Cl_2, yield after cleavage from sasrin resin and purification: 49%; d) Raney nickel (neutral washed), 2-propanol (10% H_2O), 1 h, 95%; e) **11** (1.25 equiv), TBTU/HOBT/DIPEA (3:1.25:0.25 equiv), DMF, **12**: 65%; f) H_2, Pd on activated charcoal, methanol/dioxane/acetic acid (2:1:1); g) NaOH in methanol/water pH 10, Amberlite H^+ IR 120, **14**: 66%.

RGDA conjugate **12** in 65% yield.[24] This process enables complex saccharide–peptide conjugates to be accessed whilst the 4′-lactone is maintained as a stable internal protective group for neuraminic acid derivatives. Hydrogenolytic cleavage of the benzyl ether groups over Pd/C to give the 4′-lactone **13**[25] is followed by lactone opening by mild hydrolysis with sodium hydroxide solution. The sialyl-Lewis^X-RGDA glycopeptide **14** was purified by gel chromatography on Biogel P2 and characterized by NMR spectra and FAB mass spectra.[26]

In a cell adhesion test in which competitive binding of **14** was measured on recombinant human P-selectin-immunoglobulin fusion proteins (P-selectin-IgG)[27] relative to tumor cells (HL 60), **14** proved to be the most active synthetic ligand in this test system to date[28], with an IC_{50} value of 26 μM. Three alternative recognition models are discussed for the binding of carbohydrate ligands to selectins.[2] In the Carbohydrate Recognition Model, discrete saccharide structures are assumed to be recognition regions. The Cluster Model assumes that polyvalent carbohydrate clusters are ligands, which bind to neighboring selectins with high avidity. For glycoproteins, the binding epitope can be made up of a carbohydrate and a protein portion, which is considered in the Carbohydrate Protein Recognition Model. The IC_{50} value in the submillimolar region observed for **14** relative to P-selectin suggests the involvement of the N-glycosidically linked peptide in the binding of sialyl Lewis^X to P-selectin. Investigation of further variants of glycopeptide ligands should lead to even more active and selective inhibitors of leucocyte adhesion.

Received: January 12, 1995 [Z 7630 IE]
German version: *Angew. Chem.* **1995**, *107*, 1104

Keywords: biochemistry · glycopeptides · selectins · sialyl Lewis^X

[1] T. A. Springer, *Cell* **1994**, *76*, 301–314.
[2] R. B. Parekh, C. J. Edge, *Tibtech* **1994**, 339–345.
[3] Syntheses of sialyl Lewis^X: a) A. Kameyama, H. Ishida, M. Kiso, A. Hasegawa, *Carbohydr. Res.* **1991**, *209*, C1–C4; b) K. C. Nicolaou, C. W. Hummel, N. J. Bockovich, C.-H. Wong, *J. Chem. Soc. Chem. Commun.* **1991**, 870–872; c) S. J. Danishefsky, J. Gervay, J. M. Peterson, F. E. McDonald, K. Koseki, T. Oriyama, D. A. Griffith, *J. Am. Chem. Soc.* **1992**, *114*, 8329–8331; d) A. Hasegawa, T. Ando, A. Kameyama, M. Kiso, *J. Carbohydr. Chem.* **1992**, *11*, 645–658; e) A. Hasegawa, K. Fushimi, H. Ishida, M. Kiso, *ibid.* **1993**, *12*, 1203–1216.
[4] A. Giannis, *Angew. Chem.* **1994**, *106*, 188–191; *Angew. Chem. Int. Ed. Engl.* **1994**, *33*, 188–191.
[5] J. Gante, *Angew. Chem.* **1994**, *106*, 1780–1802; *Angew. Chem. Int. Ed. Engl.* **1994**, *33*, 1699–1720.
[6] Compound **8** was prepared in a 13 g batch as stable, storable substance.
[7] H. Kunz, C. Unverzagt, *Angew. Chem.* **1988**, *100*, 1763–1765; *Angew. Chem. Int. Ed. Engl.* **1988**, *27*, 1697–1699.
[8] C. Unverzagt, H. Kunz, *J. Prakt. Chem.* **1992**, *334*, 570–578.
[9] S. Sato, M. Mori, Y. Ito, T. Ogawa, *Carbohydr. Res.* **1986**, *155*, C6–C10.
[10] a) H. Ohle, H. Hultberg, S. Wallin, *Carbohydr. Res.* **1982**, *108*, 97; b) R. Johansson, B. Samuelsson, *J. Chem. Soc. Perkin Trans.* **1984**, 2371–2074; c) P. J. Garreg, H. Hultberg, S. Wallin, *Carbohydr. Res.* **1982**, *108*, 97–101.
[11] R. R. Schmidt, J. Michel, *Angew. Chem.* **1980**, *92*, 763–764; *Angew. Chem. Int. Ed. Engl.* **1980**, *19*, 731–732.
[12] A. Hasegawa, H.Ohki, T. Nagahama, H. Ishida, M. Kiso, *Carbohydr. Res.* **1991**, *212*, 277–281.
[13] According to F. Dasgupta, P. J. Garegg, *Carbohydr. Res.* **1988**, *177*, C13–C17, methylenesulfenyltriflate (MST) is thus formed in situ, which activates the thioglycoside.
[14] W. Stahl, U. Sprengard, G. Kretzschmar, H. Kunz, *Angew. Chem.* **1994**, *106*, 2186–2188; *Angew. Chem. Int. Ed. Engl.* **1994**, *33*, 2096–2098.
[15] **8**: ^{1}H NMR (300 MHz, CD_3OD): $\delta = 1.06$ (d, $J_{6,5} = 6.64$ Hz, 3H, 6-H^{Fuc}), 1.78 (dd, $J_{3ax,3eq} = 13.05$, $J_{3ax,4} = 11.22$ Hz, 1H, 3-H^{NeuNAc}), 1.94, 2.00 (s, 6H, NHAc), 2.49 (dd, $J_{3eq,3ax} = 13.05$, $J_{3eq,4} = 5.49$ Hz, 1H, 3-H^{NeuNAc}), 3.32 (dd, 1-H, 2-H^{Gal}), 4.02 (dd, 1H, 3-H^{Gal}), 4.37 (m, 2H, 4-H^{NeuNAc}), 4.68 (d, $J_{1,2} = 12.36$ Hz, 1H, 1-H^{Gal}), 5.28 (d, $J_{1,2} = 3.66$ Hz, 1H, 1-H^{Fuc}), 5.32 (dd, $J = 4.17$ Hz, 1H, 4-H^{Gal}); ^{13}C NMR (75.4 MHz, CD_3OD): $\delta = 17.12$ (6-C^{Fuc}), 22.89, 23.55 (NHAc), 42.19 (3-C^{NeuNAc}), 90.51 (1-C^{GluNAc}), 97.59 (2-C^{NeuNAc}), 98.29 (1-C^{Fuc}), 102.67 (1-C^{Gal}).
[16] The methyl ester **9** and the 2′-lactone were identified by FAB mass spectrometry and NMR spectroscopy.
[17] Hydrolysis of the 4′-lactone is achieved by addition of a sodium hydroxide solution within a few minutes at pH 10.
[18] For synthesis of the antigenic glycopeptide of the human blood group M, Ogawa et al. also used a protected 4′-lactone:
[19] H. Kunz, C. Unverzagt, *Angew. Chem.* **1988**, *100*, 1763–1765; *Angew. Chem. Int. Ed. Engl.* **1988**, *27*, 1697–1699.
[20] L. Likhoshertov, O. Novikova, V. Derevitskaja, N. Kochtekov, *Carbohydr. Res.* **1986**, *146*, C1–C5; S. Y. C. Wong, G. R. Guile, T. W. Rademacher, R. A. Dwek, *Glycoconjugate J.* **1993**, *10*, 227–234.
[21] Linkage of the protected amino acid derivatives (Z-Arg(Z$_2$)-OH, Fmoc-Gly-OH, Fmoc-Asp(Bn)-OH, Fmoc-Ala-OH, 3 equiv) is carried out in DMF under the influence of TBTU, HOBT, DIPEA [23] (3 equiv each). Deblocking of the Fmoc protective group takes place with piperidine (20% in DMF). Mild cleavage of the partially protected peptide is obtained with 1% TFA in dichloromethane.
[22] M. Mergler, R. Tanner, J. Gosteli, P. Grogg, *Tetrahedron Lett.* **1988**, *29*, 4005–4008.
[23] HOBt = 1-hydroxybenzotriazole; TBTU = *O*-(benzotriazol-1-yl)-1,1,3,3-tetramethyluronium tetrafluoroborate; DIPEA = *N*-ethyldiisopropylamine; TSTU = *O*-(*N*-succinimidyl)-1,1,3,3-tetramethyluronium tetrafluoroborate.
[24] Use of TSTU/DIPEA for slower reactions leads to unsatisfactory yields.
[25] **13**: ^{1}H NMR (300 MHz, D_2O): $\delta = 1.11$ (d, $J_{6,5} = 6.9$ Hz, 3H, 6-H^{Fuc}), 1.37 (d, $J_{\beta,\gamma} = 7.2$ Hz, 3H, β-H^{Ala}), 1.69 (m, 1H, γ-H$_a^{Arg}$), 1.79 (m, 1H, β-H$_b^{Arg}$), 1.82 (dd, 1H, 3-H^{NeuNAc}), 2.0, 2.05 (s, 6H, NHAc), 2.58 (dd, $J_{3eq,3ax} = 13.1$, $J_{3eq,4} = 5.6$ Hz, 1H, 3-H^{NeuNAc}), 2.66 (m, 2H, β-H^{Asp}), 3.23 (dd, $J = 6.7$ Hz, 2H, δ-H$_{a,b}^{Arg}$), 3.37 (dd, $J_{2,1} = 8.0$, $J_{2,3} = 9.5$ Hz, 1H, 2-H^{Gal}), 3.81 (m, 1H, 5-H^{NeuNAc}), 4.24 (d, $J_{1,2} = 7.3$ Hz, 1H, α-H^{Ala}), 4.29 (m, 1H, 4-H^{NeuNAc}), 4.34 (dd, $J_{3,2} = 9.5$, $J_{3,4} = 3.9$ Hz, 1H, 3-H^{Gal}), 4.59 (d, 1H, 1-H^{Gal}), 4.62 (dd, 1H, α-H^{Asp}), 5.1 (d, $J_{1,2} = 4$ Hz, 1H, 1-H^{Fuc}), 5.13 (d, $J_{1,2} = 8.2$ Hz, 1H, 1-H^{GluNAc}), 5.35 (dd, $J_{4,3} = 4.2$ Hz, 1H, 4-H^{Gal}); ^{13}C NMR (75.4 MHz, D_2O): $\delta = 17.99$ (6-C^{Fuc}), 19.3 (β-H^{Ala}), 24.9, 25.04 (NHAc), 101.53 (1-C^{Fuc}), 103.67 (1-C^{Gal}).

[26] **14**: ^{1}H NMR (300 MHz, D_2O): $\delta = 1.19$ (d, $J_{6,5} = 6.56$ Hz, 3H, 6-H^{Fuc}), 1.37 (d, $J_{\beta,\alpha} = 6.72$ Hz, 3H, β-H^{Ala}), 1.71 (m, 1H, γ-H_a^{Arg}), 1.8 (dd, $J_{3ax,3eq} = 12.3$ Hz, 1H, 3-H^{NeuNAc}), 1.97 (m, 1H, β-H_b^{Arg}), 1.99, 2.04 (2s, 6H, NH*Ac*), 2.68 (m, 2H, β-H^{Asp}), 2.76 (dd, $J_{3eq,3ax} = 12.3$, $J_{3eq,4} = 4.35$ Hz, 1H, 3-H^{NeuNAc}), 3.25 (dd, $J = 6.6$ Hz, 2H, δ-$H_{a,b}^{Arg}$), 3.54 (dd, $J_{2,1} = 7.8$, $J_{2,3} = 9.6$ Hz, 1H, 2-H^{Gal}), 3.71 (m, 1H, 4-H^{NeuNAc}), 4.09 (dd, 1H, 3-H^{Gal}), 4.12 (dd, 1H, α-H^{Arg}), 4.25 (d, $J_{1,2} = 7.2$ Hz, 1H, α-H^{Ala}), 4.58 (dd, 1H, α-H^{Asp}), 5.11 (d, $J_{1,2} = 4.21$ Hz, 1H, 1-H^{Fuc}); ^{13}C NMR (75.4 MHz, D_2O): $\delta = 18.15$ (6-C^{Fuc}), 19.34 (β-H^{Ala}), 101.48 (1-C^{Fuc}), 102.56 (2-C^{NeuNAc}), 104.55 (1-C^{Gal}); FAB-MS: $m/z = 1219.5$ ($M + H^+$).

[27] A. Aruffo, W. Kolanus, G. Walz, P. Fredman, B. Seed, *Cell* **1991**, *67*, 35–44; Testsystem in Analogie zu: B. M. C. Chan, M. J. Elices, E. Murthy, M. E. Hemler, *J. Biol. Chem.* **1992**, *267*, 8366–8370.

[28] An analogous nonglycosylated RGD peptide that was examined as a control in the cell adhesion test gave an IC_{50} value greater than 800 μM for P-selectin and E-selectin.

Synthesis and Structure of Tetra- and Octanuclear Chelate Complexes—Exohedral Guest Exchange in Tetrahemispheraplexes **

Rolf W. Saalfrank,* Roman Burak, Stefan Reihs, Norbert Löw, Frank Hampel, Hans-Dietrich Stachel, Jochen Lentmaier, Karl Peters, Eva-Maria Peters, and Hans Georg von Schnering

Dedicated to Professor Paul von Ragué Schleyer on the occasion of his 65th birthday

Biomimetic processes have gained significance over the past few years. One of the topics with relevance to this field is that of tailor-made host compounds, which in solution selectively bind complementary guest molecules or incorporate them in concave cavities, similar to biological receptors or enzymes. In the process, host–guest complexes that depend on the formation of ion pairs or on hydrogen bonding require a smaller conformational adjustment of the receptor (induced fit) than systems that are based on van der Waals or charge-transfer interactions between π-electron donors and π-electron acceptors. In addition to studies of the special bonding between host and guest, the specific catalytic properties that characterize these systems as synthetic enzymes are of particular interest.[1]

Tetranuclear adamantanoid chelate complexes are well suited to be tetrahemispherands. The complexes $[(Mg_4L_6^1 \cap (4NH_4)]$ (**1**) and $[(Co_4L_6^1 \cap (4NH_4)]$ (**3**) are not salts in the usual sense, but tetrahemispheraplexes. This is confirmed pictorially by the crystal structure of **3**:[2] The four imaginary tetrahedral surfaces of the tetranuclear adamantanoid framework of **3** are not planar, but each form a half shell. In the center of each shell are three keto oxygen atoms in ideal positions to bind an ammonium ion through three hydrogen bonds (Fig. 1). The length of the hydrogen bonds range from 1.928 to 2.021 Å.

We were then interested in replacing the four exohedrally bound ammonium ions in **1** by alkylammonium groups to influence the physical and chemical properties of the "spherical surface" in $[(Mg_4L_6^1 \cap (4H_3NR)]$ (**2**). The exchange of the ammonium in **1** for alkylammonium to form the new tetrahemispheraplexes **2** (yield: 70–90%, see experimental section) is achieved by addition of alkylamines **4** in excess. Ammonia is set free. The assumption that no structural change takes place on exchange

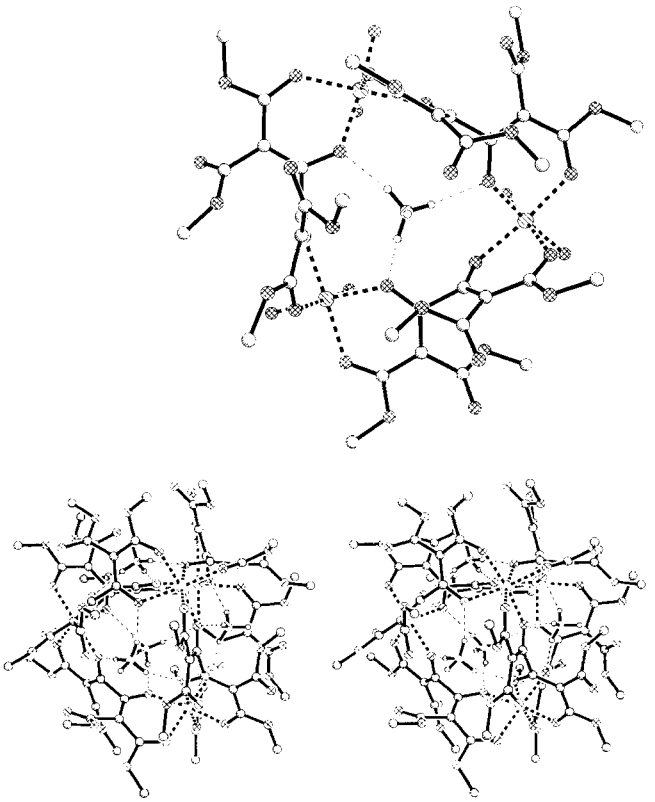


Fig. 1. Top: View into a concave half-shell of **3** with an ammonium ion held in the center by hydrogen bonds (thin dashed lines) to three keto oxygen atoms in ideal geometric positions. For clarity only one "tetrahedral face" with three cobalt ions is represented, and the H atoms have been omitted. Bottom: Stereoview of **3** (H atoms of the ligands omitted; O atoms: ⊗; N atoms: ⊘; H atoms of the NH_4^+ ion: ○.

[*] Prof. Dr. R. W. Saalfrank, Dr. R. Burak, Dipl.-Chem. S. Reihs, Dipl.-Chem. N. Löw, Dr. F. Hampel
Institut für Organische Chemie der Universität Erlangen-Nürnberg
Henkestrasse 42, D-91054 Erlangen (Germany)
Telefax: Int. code + (9131)85-6864
Prof. Dr. H.-D. Stachel, LM-Chem. J. Lentmaier
Institut für Pharmazie und Lebensmittelchemie der Universität München
Dr. K. Peters, E. M. Peters, Prof. H. G. von Schnering[+]
Max-Planck-Institut für Festkörperforschung, Stuttgart

[+] Single-crystal X-ray structure of **8d**.

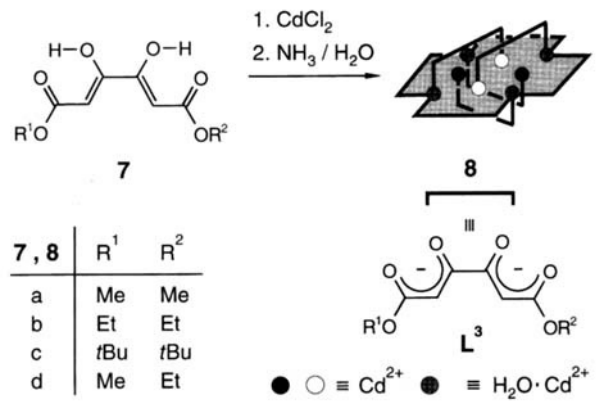
[**] "Adamantanoid" Chelate Complexes, Part 5. This work was supported by the Deutsche Forschungsgemeinschaft and the Fonds der Chemischen Industrie. We thank Prof. Dr. F. Vögtle and Dr. S. Schuth, University of Bonn, Prof. Dr. K.-P. Zeller, University of Tübingen, and Dr. R. Fröbe, University of München, for the FAB mass spectra. Part 4: [3].

of the four ammonium ions in **1** for four alkylammonium groups in the formation of **2** is clearly confirmed by the NMR data of **2**. For example, the ^1H and ^{13}C NMR spectra of **2b** and **1** are virtually superimposable, except for the additional signals that are attributable to the pentyl groups in **2b**. The explanation is that the two compounds have the same chelate (4−) ions that show only two ^1H and six ^{13}C NMR signals on account of the high molecular symmetry (T in an idealized view). A characteristic difference between free and bound pentylammonium is the appearance of two multiplets at $\delta = 2.74$ and 2.45 for the two α-aminomethylene protons, since these protons become diastereotopic when the pentylammonium guest is fixed to the chiral chelate framework and therefore form an AB system.

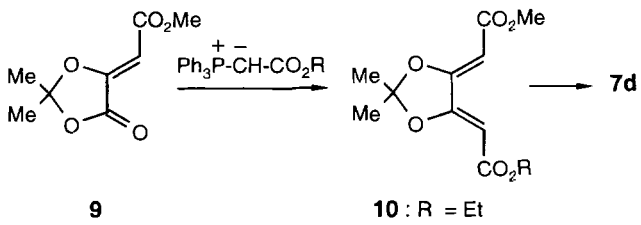
However, reaction of **1** with 1,ω-diaminoalkanes instead of primary alkylamines yields microcrystalline products, which are virtually insoluble in common organic solvents and which are also tetrahemispheraplexes according to solid-state NMR studies. The microanalysis of these complexes proves that the ratio of host to guest is exactly 1:2. This finding indicates the formation of three-dimensional, diamandoid polymers in which the tetranuclear chelate (4−) ions serve as bridgeheads.

The tetrahemispheraplexes **1**–**3** and the mixed-valent endoreceptor complex $[NH_4 \subset Fe_4L_6^1]$ **(5)**[3] are interesting from the point of view of their cage architecture as well as their electrochemistry. We therefore intended to tune both the structure and the properties of the anticipated tetranuclear chelate complexes by varying the ligands. The one-pot process with the *intermolecular* coupling of two malonate anions through oxalyl chloride as key step which allowed the synthesis of the complexes **1**, **3**, and **5** could not be extended to acetylacetonate. We did not succeed in linking two acetylacetonate ions *intermolecularly* with oxalyl chloride to form the required bridging ligand. In general with 1,3-diketones and oxalyl chloride in the presence of catalytic amounts of magnesium chloride we obtained furan-2,3-diones through *intramolecular* ring closure.[4] Consequently we changed our synthesis strategy for the construction of tetranuclear chelate complexes. The required bis(bidentate) chelate ligand has now been generated directly from the tetramethyl 2,2′-terephthaloyldimalonate by double deprotonation with sodium hydride. This chelate ligand forms the spacer complex $[Fe_4L_6^2]$ **(6)**[5] with iron(III) chloride solution.

Our attempts to prepare spacer-free tetranuclear systems of the type **1**–**3** and **5** analogously starting from the ketipinic acid esters **7a**–**c**,[6] have so far remained unsuccessful. Instead, after workup we obtained colorless (**8a, c**) or yellow (**8b**) crystals on treatment of the dialkyl ketipinate **7** with aqueous ammonia and cadmium chloride solution. According to the microanalysis and FAB-MS data (FAB = fast atom bombardment), the resulting products **8** are octanuclear cadmium chelate complexes of the composition $[Cd_8L_8^3] \cdot 4H_2O$ (see experimental section).



The ^1H and ^{13}C NMR spectra of **8** (S_4 symmetry, **8a**: nine ^1H and sixteen ^{13}C NMR signals) indicate that in each case four ligands in these complexes are identical. The two halves of each ligand are in different magnetic environments. For an unambiguous characterization of **8** we tried to grow crystals suitable for X-ray analysis. This was unsuccessful for **8a**–**c**.[7] To obtain a crystal structure nevertheless, based on more favorable packing effects, we synthesized the C_s-symmetric, mixed ethyl methyl ketipinate (**7d**) from 1,3-dioxolane (**9**)[8] and ethoxycarbonylmethylenetriphenylphosphorane via the ketipinic acid derivative **10** and thus prepared the corresponding octanuclear complex **8d**.



It is remarkable that from the resulting mixture of isomers (see experimental section) one pure isomer could be obtained as single crystals suitable for X-ray analysis.[9] The results show that isomer **8d** exists as tetrahydrate $[Cd_8L_8^3] \cdot 4H_2O$ in the crystal (Fig. 2). Of the eight cadmium ions, four are crystallographically identical and form the corners of two squares of different sizes, which have the same center. The smaller square is turned 45° relative to the larger one. The four outer cadmium ions are linked in a μ_1 fashion through the two ester carbonyl

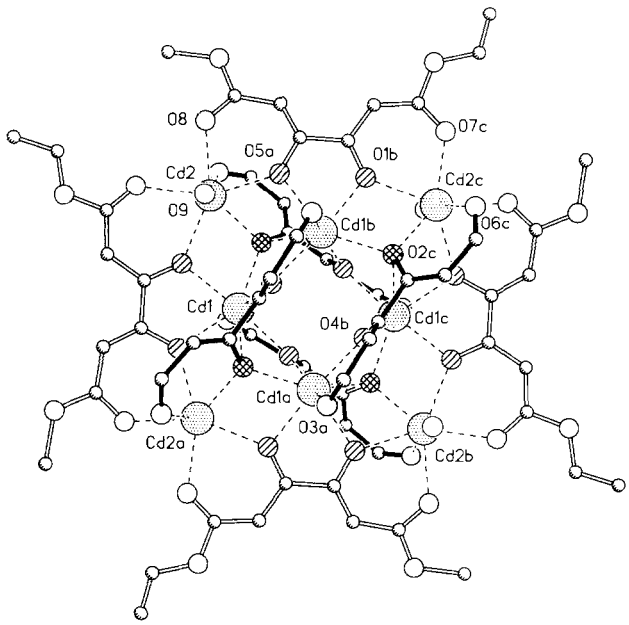


Fig. 2. Structure of **8d** in the crystal. View along the crystallographic S_4 axis: μ_1-bound ester carbonyl atoms empty, μ_2-bound keto oxygen atoms hatched, μ_3-bound oxygen atoms double hatched, cadmium ions dotted. For clarity the H atoms were omitted and the methoxy and ethoxy groups included only on the ligands lying in the illustrated plane.

 © VCH Verlagsgesellschaft mbH, D-69451 Weinheim, 1995 0570-0833/95/0909-0994 $ 10.00+.25/0 Angew. Chem. Int. Ed. Engl. 1995, 34, No. 9

oxygen atoms of a set of four ketipinic acid diester dianions, which lie almost in a plane (E^1). The two keto oxygen atoms of these four ligands are μ_2-bound and bridge inner and outer cadmium ions. Furthermore, a water molecule is coordinated to each of the four outer cadmium ions alternately above and below E^1. In two sets of parallel planes above and below E^1 and perpendicular to it lie four ligands, which are shifted pairwise relative to each other such that $[(E^2 \parallel E^3) \perp (E^4 \parallel E^5)]$. These four ketipinic acid diester dianions are each bound in a μ_1 fashion through the ester carbonyl oxygen atoms to one outer and one inner cadmium ion. One of the keto oxygen atoms forms a μ_2 bridge between two inner cadmium ions, and the other a μ_3 bridge to two inner and an outer cadmium ion. Thus all eight cadmium ions are sevenfold coordinated.

Cadmium is one of the physiologically important metals whose ions, for example, stimulate a reactivation of latent *Herpes simplex* viruses.[10] Suitable chelate-forming species could block this effect.

Experimental Procedure

2: General procedure: An excess of amine **4** (**4a**: 6 mmol (0.35 g); **4b**, **c**: 3 mmol (0.26 g, 0.56 g)) was added to a solution of **1** (0.5 mmol, 1.03 g) [2] in dichloromethane (50 mL) and stirred for 5 h at about 40 °C. The volatile components were removed in a rotary evaporator (30 °C, water-jet vacuum). The unchanged remainder of the amines **4a**, **b** evaporated without leaving any residue. Amine **4c** was removed by washing three times with 50 mL portions of diethyl ether. The crude product was recrystallized from chloroform/hexane (1:1) and dried under vacuum (oil pump). All new compounds gave correct elemental analyses. However, no interpretable FAB mass spectra have yet been recorded for **2a**–**c**. – **2a**: yield: 0.86 g (78%) colorless microcrystals; decomp. above 166 °C; IR ($CHBr_3$): $\tilde{\nu} = 1710\ cm^{-1}$ (C=O), 1650 (C=C); ^1H NMR (400 MHz, $CDCl_3$): $\delta = 7.87$ (br., 8H; NH_3), 7.68 (br., 4H; NH_3), 3.79, 3.55 (s, each 36H, OCH_3), 2.66, 2.43 (m, 4H, NCH_A; NCH_B), 1.30 (m, 8H; CH_2), 0.56 (m, 12H, CH_3); ^{13}C NMR (100.5 MHz, $CDCl_3$): $\delta = 184.3$, 170.9, 167.2 (24 C=O, 12 C=O), 95.3 (12 =C), 52.0, 51.2 (24 OCH_3), 42.7 (4 NCH_2), 20.0 (4 CH_2), 11.1 (4 CH_3). – **2b**: yield: 1.08 g (92%) colorless microcrystals; Decomp. above 181 °C; IR ($CHBr_3$): $\tilde{\nu} = 1710\ cm^{-1}$ (C=O), 1640 (C=C); ^1H NMR (400 MHz, $CDCl_3$): $\delta = 7.69$ (br., 12H; NH_3), 3.78, 3.59 (s, each 36H; OCH_3), 2.74, 2.45 (m, 4H; NCH_A, NCH_B), 1.31, 1.04, 0.91 (m, each 8H; CH_2), 0.75 (t, 12H; CH_3); ^{13}C NMR (100.5 MHz, $CDCl_3$): $\delta = 184.4$, 170.9, 167.2 (24 C=O, 12 C=O), 95.4 (12=C), 51.9, 51.2 (24 OCH_3), 41.6 (4 NCH_2), 29.0, 25.9, 21.6 (12 CH_2), 13.7 (4 CH_3). – **2c**: yield: 0.87 g (68%) colorless microcrystals; Decomp. above 197 °C; IR ($CHBr_3$): $\tilde{\nu} = 1690\ cm^{-1}$ (C=O), 1630 (C=C); ^1H NMR (400 MHz, $CDCl_3$): $\delta = 7.68$ (br., 12H; NH_3), 3.78, 3.55 (s, each 36H; OCH_3), 2.73, 2.45 (m, 4H; NCH_A, NCH_B), 1.29–0.99 (m, 80H; CH_2), 0.87 (t, 12H; CH_3); ^{13}C NMR (100.5 MHz, $CDCl_3$): $\delta = 184.4$, 170.8, 167.3 (24 C=O, 12 C=O), 95.3 (12 =C), 52.0, 51.2 (24 OCH_3), 41.5 (4 NCH_2), 31.9, 29.7, 29.6, 29.4, 29.3, 28.7, 26.9, 26.3, 22.7 (36 of 40 CH_2, two signals per alkylamino group overlap), 14.1 (4 CH_3).

7: **7a**–**c** according to ref. [6]. **7d**: **10** (2 mmol) was stirred in conc. H_2SO_4 (5 mL) for 1 h at room temperature. The solution was then diluted with diethyl ether (100 mL) and stirred into 100 mL of water. The organic phase was separated, washed several times with water, and dried over sodium sulfate. The solvent was removed under vacuum. yield: 0.15 g (35%) colorless crystals (from diethyl ether); M.p. 77 °C; IR (KBr): $\tilde{\nu} = 1646\ cm^{-1}$ (C=O); ^1H NMR (400 MHz, $CDCl_3$): $\delta = 11.66$, 11.57 (s, each 1H; OH), 5.30 (s, 2H; =CH), 4.19 (q, $^3J(H,H) = 7$ Hz, 2H; OCH_2), 3.75 (s, 3H; OCH_3), 1.25 (t, $^3J(H,H) = 7$ Hz, 3H; CH_3); EI-MS (70 eV): $m/z = 216\ [M^+]$.

8: General procedure: Aqueous ammonia (12%) was added dropwise to a solution of cadmium chloride (0.5 mmol, 92 mg) and the appropriate dialkyl ketipinate **7a**–**d** (0.5 mmol) in ethanol (1:1, 100 mL) until no more turbidity formed. The precipitates were filtered off, dried under vacuum (oil pump), and recrystallized from hot methanol (**8a**) or ethanol (**8b**–**d**). yield: 133 mg (83%) colorless needles; Decomp. above 220 °C; IR (KBr): $\tilde{\nu} = 3400\ cm^{-1}$ (OH), 1640 (C=O), 1620 (C=C); ^1H NMR (400 MHz, $CDCl_3$): $\delta = 5.44$, 5.32, 5.10, 4.94 (s, each 4H, =CH), 3.75, 3.73, 3.57, 3.46 (s, each 12H, OCH_3), 1.88 (s, 8H; H_2O); ^{13}C NMR (100.5 MHz, $CDCl_3$): $\delta = 177.66$, 175.17, 175.10, 174.26, 173.89, 173.20, 172.74 (32 C=O, two signals overlap), 87.82, 87.73, 84.42, 83.35 (16 =CH), 51.52, 50.79, 50.68, 50.43 (16 OCH_3); FAB-MS (3-nitrobenzyl alcohol matrix = *m*-NBA): m/z 2500 $[Cd_8L_8^{3a}]$.

8b: yield: 145 mg (83%) yellow crystals; Decomp. above 210 °C; IR (KBr): $\tilde{\nu} = 3400\ cm^{-1}$ (OH), 1630 (C=O), 1620 (C=C); ^1H NMR (400 MHz, $CDCl_3$): $\delta = 5.43$, 5.30, 5.10, 4.95 (s, each 4H; =CH), 4.27–4.07 (m, 8H; OCH_2) [11], 4.21 (q, $^3J(H,H) = 6.9$ Hz, 8H; OH_2) [12], 4.07–3.94 (m, 8H; OCH_2) [11], 3.80 (q, $^3J(H,H) = 7.2$ Hz, 8H; OCH_2) [12], 2.47 (br. s, 8H; H_2O), 1.39, 1.28, 1.19, 1.11 (t, each 12H, CH_3); ^{13}C NMR (100.5 MHz, $CDCl_3$): $\delta = 177.99$, 177.06, 175.21, 174.26, 173.84, 173.16, 172.47 (32 C=O, two signals overlap), 88.74, 88.34, 84.92, 83.75 (16 =CH), 59.96, 59.60, 59.38, 59.27 (16 OCH_2), 14.63, 14.54, 14.32, 14.20 (16 CH_3); FAB-MS (*m*-NBA): m/z 2724 $[Cd_8L_8^{3b}]$. – **8c**: yield: 126 mg (62%) colorless microcrystals; Decomp. above 230 °C; IR (KBr): $\tilde{\nu} = 3450\ cm^{-1}$ (OH), 1645 (C=O), 1635 (C=C); ^1H NMR (400 MHz, $CDCl_3$): $\delta = 5.75$, 5.40, 5.25, 5.10 (s, each 4H, =CH), 2.36 (br. s, 8H; H_2O), 1.58, 1.44, 1.32, 1.26 (s, each 36H; CH_3); ^{13}C NMR (100.5 MHz, $CDCl_3$): $\delta = 177.38$, 177.13, 175.37; 173.97, 173.87, 173.51, 173.27, 172.56 (32 C=O), 90.09, 89.83, 85.91, 85.12 (16 =CH), 79.95, 79.36, 78.78, 78.51 (16 O–C), 28.68, 28.30, 28.21, 28.12 (48 CH_3); FAB-MS (*m*-NBA): m/z 3173 $[Cd_8L_8^{3c}]$. – **8d**: Only as single crystal from ethanol was **8d** obtained isomerically pure. The following data refer to a mixture of isomers. yield: 111 mg (66%) colorless microcrystals; Decomp. above 208 °C; IR (KBr): $\tilde{\nu} = 3445\ cm^{-1}$ (OH), 1652 (C=O), 1636 (C=C); ^1H NMR (400 MHz, $CDCl_3$): $\delta = 5.45–4.90$ (m, 16H; =CH), 4.22–3.90 (m, 16H; OCH_2), 3.74–3.45 (m, 24H; OCH_3), 1.74 (br. s, 8H; H_2O), 1.31–1.10 (m, 24H; CH_3); ^{13}C NMR (100.5 MHz, $CDCl_3$): $\delta = 178.46$, 178.42, 178.17, 178.08, 177.22, 177.18, 177.04, 175.26, 175.14, 174.39, 174.30, 174.09, 173.75, 173.42, 173.05, 172.92, 172.63, 172.29 (C=O), 88.43, 88.37, 88.30, 88.17, 87.70, 84.85, 84.61, 84.42, 84.35, 83.68, 83.51, 83.29 (=CH), 59.98, 59.60, 59.30 (OCH_2), 51.41, 50.83, 50.66, 50.39 (OCH_3), 14.71, 14.65, 14.62, 14.54, 14.49, 14.30, 14.21 (CH_3); FAB-MS (*m*-NBA): m/z 2612 $[Cd_8L_8^{3d}]$.

10: **9** (9.3 g, 0.05 mol) [8] was heated for 24 h with ethoxycarbonylmethylenetriphenylphosphorane (0.15 mol) in xylene (100 mL) under reflux. The solvent was removed under vacuum, and the residue was taken up in ethyl acetate, and purified by column chromatography [column 2 × 15 cm, silica gel (Merck); hexane/ethyl acetate (1:1), $R_f = 0.51$]. yield: 2.53 g (20%) colorless crystals (from diisopropyl ether); M.p. 84 °C; IR (KBr): $\tilde{\nu} = 1724\ cm^{-1}$ (C=O), 1652 (C=C); ^1H NMR (400 MHz, $CDCl_3$): $\delta = 5.38$ (s, 2H; =CH), 4.13 (q, $^3J(H,H) = 7$ Hz, 2H; OCH_2), 3.67 (s, 3H; OCH_3), 1.66 (s, 6H; CH_3), 1.22 (t, $^3J(H,H) = 7$ Hz, 3H; CH_3); EI-MS (50 eV): $m/z = 256\ [M^+]$.

Received: October 26, 1994
Revised: February 4, 1995 [Z 7429 IE]
German version: *Angew. Chem.* **1995**, *107*, 1085

Keywords: cadmium complexes · chelate complexes · host–guest chemistry · self-assembly

[1] See: a) *Frontiers in Supramolecular Organic Chemistry and Photochemistry* (Eds.: H.-J. Schneider, H. Dürr), VCH, Weinheim, **1991**; b) J.-M. Lehn in ref. [1a], p. 1–28; H.-J. Schneider, T. Blatter, U. Cuber, R. Juneja, T. Schiestel, U. Schneider, I. Theis, P. Zimmermann in ref. [1a], p. 29–56; D. J. Cram, J. M. Cram in *Container Molecules and Their Guests* (Eds.: J. F. Stoddart), Royal Society of Chemistry, Cambridge, **1994**, Chap. 2.4, p. 28ff; F. Vögtle in *Supramolekulare Chemie* (Eds.: C. Elchenbroich, F. Hensel, H. Hopf), Teubner, Stuttgart, **1989**, Chap. 4.2, p. 162ff.; C. F. Martens, R. J. M. Klein Gebbink, M. C. Feiters, R. J. M. Nolte, *J. Am. Chem. Soc.* **1994**, *116*, 5667–5670.

[2] R. W. Saalfrank, A. Stark, M. Bremer, H.-U. Hummel, *Angew. Chem.* **1990**, *102*, 292–294; *Angew. Chem. Int. Ed. Engl.* **1990**, *29*, 311–314. In ref. [2] for clarity in the structure of complex **3**, only the adamantanoid tetranuclear framework without the four ammonium guests were depicted. See also: R. W. Saalfrank, A. Stark, K. Peters, H. G. von Schnering, *ibid.* **1988**, *100*, 878–880 and **1988**, *27*, 851–853.

[3] R. W. Saalfrank, R. Burak, A. Breit, D. Stalke, R. Herbst-Irmer, J. Daub, M. Porsch, E. Bill, M. Müther, A. X. Trautwein, *Angew. Chem.* **1994**, *106*, 1697–1699; *Angew. Chem. Int. Ed. Engl.* **1994**, *33*, 1621–1623.

[4] R. W. Saalfrank, T. Lutz, *Angew. Chem.* **1990**, *102*, 1064–1065; *Angew. Chem. Int. Ed. Engl.* **1990**, *29*, 1041–1042.

[5] R. W. Saalfrank, B. Hörner, D. Stalke, *Angew. Chem.* **1993**, *105*, 1223–1225; *Angew. Chem. Int. Ed. Engl.* **1993**, *32*, 1179–1182.

[6] H.-D. Stachel, *Arch. Pharm. Ber. Dtsch. Pharm. Ges.* **1962**, *295*, 735–744; H.-D. Stachel, M. Jungkenn, C. Koser-Gnoss, H. Poschenrieder, J. Redlin, *Liebigs Ann. Chem.* **1994**, 961–964.

[7] **8a**: Needles from methanol; **8b**: twins from ethanol; **8c**: microcrystals from ethanol.

[8] G. Schwenker, K. Stiefvater, *Arch. Pharm. (Weinheim Ger.)* **1991**, *324*, 307–311.

[9] **8d**: $C_{72}H_{80}O_{48}Cd_8 \cdot 4H_2O$, $M = 2764.76$. Crystal dimensions: $0.15 \times 0.25 \times 0.1\ mm^3$, tetragonal, space group $I4_1/a$, $a = 2860.0(4)$, $c = 1258.2(3)$ pm, $V = 10291(3) \times 10^6\ pm^3$, $Z = 16$, $\rho_{calcd} = 1.784\ g\,cm^{-3}$. Diffractometer: Siemens R3m/V. $Mo_{K\alpha}$ radiation, $\lambda = 71.073$ pm, $T = 293$ K. Program system: Siemens SHELXTL-PLUS; monochromator: graphite. Measurement details: Wyckoff scan; range $1.75° \le \omega \le 25.0$ °C; section of the reciprocal lattice: $h = 0$ to 34, $k = h$, $l = 0$ to 14. Number of the measured intensities 4964; number of independent reflections 4530; number of reflections with $F > 3\sigma(F)$ 2772. Linear absorption coefficient $1.71\ mm^{-1}$. Absorption correction: θ scan. Ratio of F/parameters 9.80, $R = 0.082$, $Rw = 0.063$, $w = 1/\sigma^2(F)$. Further details of the crystal structure investigation may be obtained from the Fachinformationszentrum Karlsruhe, D-76344 Eggenstein-Leopoldshafen (Germany) on quoting the depository number CSD-401364.

[10] R. L. Fawl, B. Roizman, *J. Virol.* **1993**, *67*, 7025–7031.

[11] Diastereotopic methylene protons in E^2–E^5.

[12] Enantiotopic methylene protons in E^1.

Synthesis and Structural Characterization of a Stereospecific Dinuclear Gallium Triple Helix: Use of the *trans*-Influence in Metal-Assisted Self-Assembly

Eric J. Enemark and T. D. P. Stack*

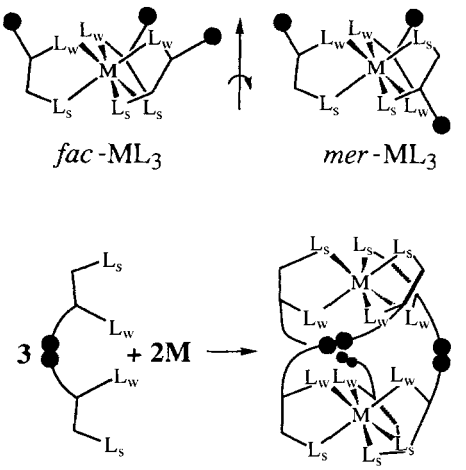
A great interest exists in metal-assisted self-assembly of helical supramolecular complexes because of the prevalence of this structural motif in nature and the cooperative behavior in such systems.[1, 2] The most successful and efficient systems have relied on a labile metal center and well-designed, semi-rigid, polynucleating ligands.[3–6] The lability of the metal allows a system to readily achieve the most thermodynamically stable state, while ligand design is necessary to exploit the stereochemical preferences of such metals to align the organic fragments in a self-complementing framework. Entropy provides a principle driving force to discrete complexes, which maximize the number of particles.

Though supramolecular helical complexes are intrinsically chiral, most investigations have focused on racemic mixtures because of the achiral nature of the polynucleating ligands and the lability of the metals used in their assembly.[7–9] Stereospecific triple[10–12] and double[13] helices have been obtained from labile metals either by the use of enantiomerically pure ligands[10, 13] or by spontaneous resolution during crystallization.[11, 12] The former approach provides additional energetic differentiation between products that would not be possible under racemic or achiral conditions.[13]

To date, most of the ligating subunits used in metal-assisted self-assembling systems have been effectively electronically symmetric, aromatic nitrogenous ligands.[3, 4, 6, 14] Electronic asymmetry within bidentate ligating subunits can potentially provide additional enthalpic drive to discrete, dinuclear triple-helical species. This enhanced thermodynamic bias results from an electronic organizational preference of ligating atoms on an octahedral metal, a phenomenon known as the *trans*-influence.[15] Assuming no steric constraints, the ligand with the stronger donor properties (the "stronger ligand") will orient *trans* to that with the weaker donor properties, lengthening the weaker ligand's bond to the metal.

For a monomeric tris-chelate complex of three electronically nonsymmetric bidentate ligands, two configurations, *fac* and *mer*, are possible (see Scheme 1). Only in the *fac* configuration are all the stronger donors (s) *trans* to the weaker ones (w). The *fac* configuration is enthalpically preferred, generating inherent structural directionality in the complex not possible with electronically symmetric, bidentate ligands. Incorporation of two electronically nonsymmetric, bidentate units in a twofold symmetric, dinucleating tetradentate ligand yields a system that should be enthalpically and entropically biased towards assembly of a 2:3 metal:ligand complex (see Scheme 1, bottom). Cooperative behavior[16] of such systems is a consequence of the ligand design.

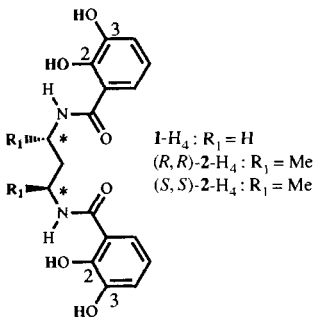
A well-characterized type of nonsymmetric, bidentate ligand is the 2,3-dihydroxybenzamide **L** (catecholamide), a chelating agent found in many bacterial siderophores.[17] The 3-hydroxyl group



Scheme 1. Top: *fac* and *mer* isomers of a mononuclear ML_3 complex. The arrow indicates the direction of the pseudo-C_3 axis. L_w = weak donor ligand, L_s = stronger donor ligand. Bottom: Formation of a dinuclear triple helix.

is a stronger donor than the 2-hydroxyl group as reflected in the difference in their pK_a values (pK_a(2-OH) ≈ 7, pK_a(3-OH) ≈ 12).[18] Spectroscopic studies of a $[GaL_3]^{3-}$ complex have suggested that a *fac* configuration predominates in solution.[19]

The bis-catecholamide ligands used in this study are presented in Scheme 2 and differ only in the nature of the bridging propyl



Scheme 2.

unit. These ligands are designed to bind two separate metals because the bridges do not allow a single metal to be ligated in a tetradentate fashion. The ^{1}H NMR spectra in D_2O and [D$_6$]DMSO of the reaction mixture of three equivalents of **1**, (*R*,*R*)-**2**, or (*S*,*S*)-**2** with two equivalents of Ga^{3+} and twelve equivalents of base (KOH or R_4NOH) are consistent with the formation of a single, D_3-symmetric species. ^{1}H NMR titrations of basic solutions of **1** or (*R*, *R*)-**2** with incremental addition of Ga^{3+} are consistent with the presence of only two species, free ligand and the 2:3 complex. The absence of other species in the presence of excess ligand indicates that the gallium atoms are bound cooperatively.

$(Et_4N)_6[Ga_2\{(R,R)\text{-}2\}_3]\cdot 2.25\,H_2O$ **3**

The structure of **3** confirms the existence of a stereospecific dinuclear triple helix. A simple line drawing of the structure is presented in Figure 1. Views of the hexaanion both perpendicular and parallel to the pseudo-threefold axis are presented in Figures 2 and 3. Each metal is bound by a pseudo-octahedral array of oxygen atoms provided by three catecholamide groups, and the metals are separated by 10.78 Å. Twist angles[20] of

[*] Dr. T. D. P. Stack, E. J. Enemark
Department of Chemistry, Stanford University
Stanford, CA 94305-5080 (USA)
Telefax: Int. code + 415/723-4817
Bitnet: Stack@Leland.Stanford.edu

[**] We thank the NSF (CHE-9118845) and the Stanford Office of Technology and Licensing for financial support of this research.

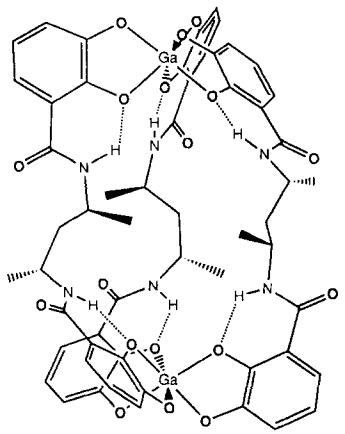


Fig. 1. Line diagram view of the hexaanion of **3** perpendicular to the pseudo-threefold axis. Lengths of the Ga–O3 bonds [Å]: 1.95(1), 1.97(1), 2.00(1), 1.97(1), 1.96(1), 1.98(1); average 1.97(2). Lengths of the Ga–O2 bonds [Å]: 1.99(1), 2.00(1), 2.00(1), 2.00(1), 1.99(1), 1.98(1); average: 1.99(1). O3-Ga-O2 bond angles [°]: 168(1), 162(1), 168(1), 168(1), 168(1), 165(1), 174(1). The standard deviations in parentheses are crystallographically determined except for those of the averages, which are standard deviations of the average. O2 and O3 refer to the 2- and 3-hydroxyl oxygen atoms.

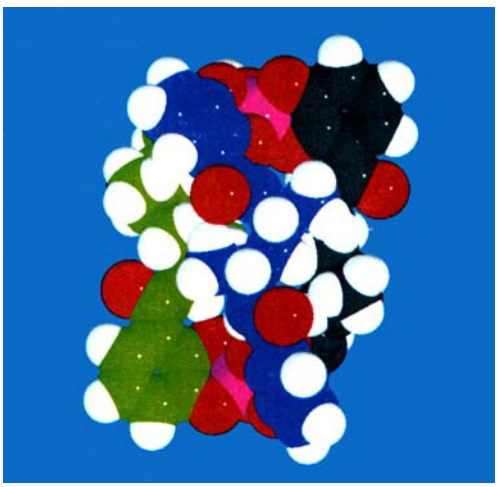


Fig. 2. Space-filling model of the hexaanion of **3**; view perpendicular to the pseudo-threefold axis. Individual ligands are color-coded.

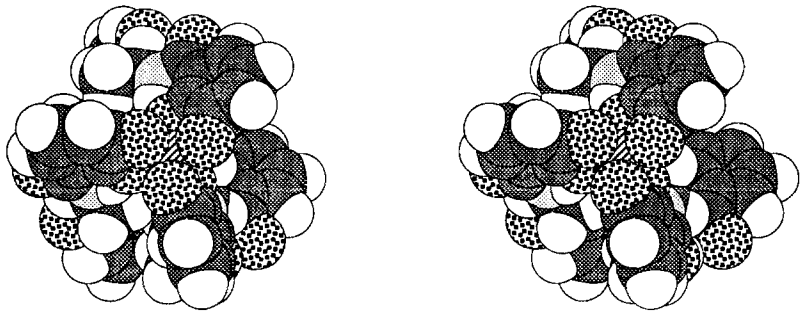


Fig. 3. Stereoview of the hexaanion of **3**, parallel to the pseudo-threefold axis.

44(4)° and 48(3)° at the metal centers are consistent with other characterized gallium catecholate structures.[21–23] The molecule has a 59(1)° helical pitch.[24] Presumably, the large gallium–gallium distance and the near-perfect staggering of the coordination spheres minimize charge repulsion between the formally triply negative metal coordination spheres. Strong hydrogen bonds are maintained between amide protons and deprotonated 2-hydroxyl oxygens, generating planar catecholamide subunits as previously observed in other metal structures.[22, 23, 25, 26] The gallium–oxygen bond lengths range from 1.96 to 2.00 Å; the average Ga–O3 distance is slightly shorter than that of Ga–O2 (Fig. 1). A comparison of the six pairs of *trans*-related ligating oxygens show that all the Ga–O3 distances are equal to or shorter than the Ga–O2 distances, consistent with a *trans*-influence. The distortion of the overall structure from threefold symmetry is apparent from the stereoview (Fig. 3). This distortion results primarily from the attempt of the bridging units to fill the void between the two metal coordination spheres. One of the six methyl groups is rotated inward and affects the positions of the other chains. The result is that one groove of the helix is more open than the other two.

The most interesting feature of **3** is its helical nature; both metal centers have the same absolute configuration, *Λ*, as defined by the absolute chirality of the enantiomerically pure diamine used in the synthesis of ligand **2**.[27] Assessing whether the metals retain this *Λ,Λ* configuration in solution by circular dichroism spectroscopy is not possible, because gallium lacks the necessary optical transitions. The distinct and sharp ^{1}H NMR resonances in the methyl and methylene regions of **3** in D_2O and [D_6]DMSO suggest either the existence of a single species in which both metals adopt the same configuration, or rapid racemization at the metal centers. The ^{1}H NMR spectrum of the less sterically demanding $[Ga_2(\mathbf{1})_3]^{6-}$ complex shows that the methylene protons adjacent to the amide nitrogens are diastereotopic, which is only possible if the metals do not racemize faster than the NMR time scale. Thus, the anion of **3** must retain its helical structure in solution.

To probe the importance of enantiomeric purity on stereospecific helix formation, the product distribution of a 2:3 metal–ligand complex from racemic **2** and Ga^{3+} was examined. Initially, the ^{1}H NMR resonances in D_2O correspond to the statistically predicted 3:1 mixture of heterochiral and homochiral isomers, respectively.[28] An equilibrium mixture of about 6:1 (heterochiral:homochiral) is attained after several hours at 297 K, indicating that the heterochiral isomer is energetically more stable by about 1.0 kcal mol^{-1}. The same equilibrium ratio is observed after mixing equal molar amounts of the preformed, enantiomerically pure triple helices, $[Ga_2\{(R,R)\text{-}\mathbf{2}\}_3]^{6-}$ and $[Ga_2\{(S,S)\text{-}\mathbf{2}\}_3]^{6-}$. These ligand exchange reactions show that these metal–ligand systems are at thermodynamic equilibrium, a fact not evident when enantiomerically pure or achiral ligands are used. This data further supports the idea that **3** exists as a single, stereospecific *Λ,Λ*-helix in solution and that *Δ,Δ*-side-by-side[13] and *Δ,Δ*-helical configurations are each energetically destablized by at least 2.0 kcal mol^{-1} at 297 K.[29]

This study of chiral and achiral dinucleating catecholamide ligands with gallium reveals a number of interesting aspects of metal-assisted self-assembly. First, cooperative polynucleating ligands can be rationally designed to utilize the thermodynamic preferences present in mononuclear species, such as a *trans*-influence. Secondly, enantiomerically pure polynucleating ligands can greatly constrain helical direction producing a stereospecific helix even when the ligand is relatively flexible.

Experimental Procedure

The ligands were synthesized as previously described from an activated form of 2,3-dimethoxybenzoic acid and half an equivalent of diamine followed by deprotection with BBr_3 [22]. The enantiomerically pure diamines used in the syntheses of (*R,R*)-**2** and (*S,S*)-**2** were prepared and resolved according to literature procedures [30].

 © VCH Verlagsgesellschaft mbH, D-69451 Weinheim, 1995 0570-0833/95/0909-0997 $ 10.00+.25/0

Crystal data for **3**: The complex crystallized by slow diffusion of ether into an acetonitrile solution in space group $P2_1$ (no. 4) with the following cell constants based on 25 reflections ($19° < 2\theta < 36°$): $a = 15.029(3)$, $b = 18.050(2)$, $c = 26.561(4)$ Å, $\beta = 94.55(2)°$, $V = 5830(1)$ Å^3, $Z = 2$. A total of 9160 reflections ($\pm h, +k, +l$) were collected at 203 K using ω scans on an Enraf–Nonius CAD4 diffractometer with graphite-monochromated $Mo_{K\alpha}$ radiation ($\lambda = 0.71069$ Å), $5° < 2\theta < 47°$, of which 9015 were unique. The structure was solved by the Patterson method. The water molecules were disordered, and modeled by oxygen atoms at reduced occupancies. Four of the tetraethylammonium ions were well-defined, but the remaining two were significantly disordered and were modeled with additional carbon atoms at reduced occupancies. All gallium and nitrogen atoms were refined anisotropically. Oxygen atoms in the anion were refined anisotropically, and oxygen atoms present as solvent were refined isotropically. All carbon atoms were refined isotropically. Full matrix refinement of 768 variables based on 4757 reflections ($|F_o| > 3\sigma(F_o)$, $8.24° < 2\theta < 47°$) and sigma weights converged with final residuals of $R = 0.072$, $R_w = 0.063$. The absolute configuration of the space group was assigned by the chirality of the ligand (*R,R*)[27]. Inversion of the structure and refinement significantly increased the residuals supporting this assignment. All calculations were performed using the teXsan crystallographic software package of Molecular Structure Corporation. Further details of the crystal structure investigation may be obtained from the Director of the Cambridge Crystallographic Data Centre, 12 Union Road, GB-Cambridge CB2 1EZ (UK), on quoting the full journal citation.

1-H_4: ^{1}H NMR (400 MHz, [D$_6$]DMSO): $\delta = 8.84$ (t, ^3J(H,H) = 5.4 Hz, 2H; NH), 7.28 (d, ^3J(H,H) = 8.4 Hz, 2H; H_a), 6.91 (d, ^3J(H,H) = 7.6 Hz; H_c), 6.69 (t, ^3J(H,H) = 7.8 Hz, 2H; H_b), 3.35 (quart, ^3J(H,H) = 6.4 Hz, 4H, HN–CH_2–CH_2), 1.82 (quin, ^3J(H,H) = 7 Hz, 2H; CH_2–CH_2–CH_2); FAB$^+$-MS: *m/z*: 347.13 (calcd), 347.1 (found).

[Ga_2(**1**)$_3$]$^{6-}$: ^{1}H NMR (200 MHz, D_2O): $\delta = 6.78$ (d, ^3J(H,H) = 8 Hz, 2H; H_a), 6.42 (d, ^3J(H,H) = 6.8 Hz; H_c), 6.25 (t, ^3J(H,H) = 7.6 Hz, 2H; H_b), 3.02 (d, ^2J(H,H) = 13.5 Hz, 2H, HN–CH_2–CH_2), 2.48 (m, 2H; HN–CH_2–CH_2), 0.096 (s, 2H; CH_2–CH_2–CH_2).

(*R,R*)-**2**-H_4: ^{1}H NMR (200 MHz, [D$_6$]DMSO): $\delta = 8.47$ (d, ^3J(H,H) = 7.8 Hz, 2H; NH), 7.31 (d, ^3J(H,H) = 7.8 Hz, 2H; H_a), 6.90 (d, ^3J(H,H) = 7.4 Hz, 2H; H_c), 6.67 (t, ^3J(H,H) = 7.8 Hz, 2H; H_b), 4.10 (quart, ^3J(H,H) = 6.6 Hz, 2H; CH–N), 1.82 (t, ^3J(H,H) = 6.9 Hz, 2H; CH–CH_2–CH), 1.16 (d, ^3J(H,H) = 6.4 Hz, 6H; CH_3); FAB$^+$-MS: *m/z*: 375.16 (calcd); 375.1 (found); $[\alpha]_D^{25} = -74.7$ (*c* = 0.5, MeOH).

(*S,S*)-**2**-H_4: $[\alpha]_D^{25} = +74.5$ (*c* = 0.5, MeOH).

[Ga_2{(*R,R*)-**2**}$_3$]$^{6-}$: ^{1}H NMR (400 MHz, D_2O): $\delta = 6.82$ (d, ^3J(H,H) = 8 Hz, 2H; H_a), 6.44 (d, ^3J(H,H) = 6.8 Hz; H_c), 6.27 (t, ^3J(H,H) = 7.6 Hz, 2H; H_b), 3.80 (d, ^3J(H,H) = 5.2 Hz, 2H, HN–CH_2–CH_2), 1.50 (s, 2H; CH–CH_2–CH), 0.075 (d, ^3J(H,H) = 6.0 Hz, 6H; CH_3).

Received: August 27, 1994 [Z 7272 IE]
German version: *Angew. Chem.* **1995**, *107*, 1082

Keywords: asymmetric syntheses · gallium compounds · helices · self-assembly · supramolecular chemistry

[1] K. P. Meurer, F. Vögtle, *Top. Curr. Chem.* **1985**, *127*, 1–76.
[2] J.-M. Lehn, *Angew. Chem.* **1990**, *102*, 1347–1362; *Angew. Chem. Int. Ed. Engl.* **1990**, *29*, 1304–1319.
[3] **J.-M. Lehn, A. Rigault, *Angew. Chem.* 1988**, *100*, 1121–1122; *Angew. Chem. Int. Ed. Engl.* **1988**, *27*, 1095–1097.
[4] **C. Piguet, G. Bernardinelli, B. Bocquet**, A. Quattropani, A. F. Williams, *J. Am. Chem. Soc.* **1992**, *114*, 7440–7451.
[5] **C. Piguet, J. Bunzli, G. Bernardinelli**, G. Hopfgartner, A. F. Williams, *J. Am. Chem. Soc.* **1993**, *115*, 8197–8206.
[6] E. C. Constable, *Tetrahedron* **1992**, *48*, 10013–10059.
[7] A. F. Williams, C. Piguet, G. Bernardinelli, *Angew. Chem.* **1991**, *103*, 1530–1533; *Angew. Chem. Int. Ed. Engl.* **1991**, *30*, 1490–1492.
[8] **G. Bernardinelli, C. Piguet, A. F. Williams, *Angew. Chem.* 1992**, *104*, 1626–1629; *Angew. Chem. Int. Ed. Engl.* **1992**, *31*, 1622–1624.
[9] **L. J. Charbonniere, G. Bernardinelli, C. Piguet, A. M.** Sargeson, A. F. Williams, *J. Chem. Soc. Chem. Commun.* **1994**, 1419–1420.
[10] J. Libman, Y. Tor, A. Shanzer, *J. Am. Chem. Soc.* **1987**, *109*, 5880–5881.
[11] R. C. Scarrow, D. L. White, K. N. Raymond, *J. Am. Chem. Soc.* **1985**, *107*, 6540–6546.
[12] **R. Kramer, J.-M. Lehn, A. Decian, J. Fischer, *Angew. Chem.* 1993**, *105*, 764–768; *Angew. Chem. Int. Ed. Engl.* **1993**, *32*, 703–706.
[13] W. Zarges, J. Hall, J.-M. Lehn, C. Bolm, *Helv. Chim. Acta* **1991**, *74*, 1843–1852.
[14] J.-M. Lehn, A. Rigault, J. Siegel, J. Harrowfield, B. Chevrier, D. Moras, *Proc. Natl. Acad. Sci. USA* **1987**, *84*, 2565.
[15] The *trans*-influence, a thermodynamic phenomenon, concerns the ground state effects of ligands that are *trans* to another, while the better known *trans*-effect is a kinetic phenomenon. See T. G. Appleton, H. C. Clark, L. E. Manzer, *Coord. Chem. Rev.* **1973**, *10*, 355–422.
[16] A. Pfeil, J.-M. Lehn, *J. Chem. Soc. Chem. Commun.* **1992**, 838–840.
[17] B. F. Matzanke, G. Müller-Matzanke, K. N. Raymond in *Iron Carriers and Iron Proteins, Vol. 5* (Ed.: T. M. Loehr), VCH, New York, **1989**, pp. 1–121.
[18] L. D. Loomis, K. N. Raymond, *Inorg. Chem.* **1991**, *30*, 906–911.
[19] ^{1}H NMR spectra (D_2O, CD_3CN, or [D$_6$]DMSO) of mononuclear [Ga**L**$_3$]$^{3-}$ (**L** = 2,3-dihydroxymethylbenzamide) demonstrate solution compositions of about 85% *fac*, 15% *mer*. The *trans*-influence can conservatively be estimated to enthalpically stabilize the *fac* isomer by 7 kJ mol^{-1} (1.7 kcal mol^{-1}) over the *mer* isomer.
[20] D. L. Kepert in *Inorganic Stereochemistry, Vol. 6* (Ed.: D. L. Kepert), Springer, Berlin, **1982**, pp. 92–132.
[21] B. A. Borgias, S. J. Barclay, K. N. Raymond, *J. Coord. Chem.* **1986**, *15*, 109–123.
[22] T. B. Karpishin, T. D. P. Stack, K. N. Raymond, *J. Am. Chem. Soc.* **1993**, *115*, 6115–6125.
[23] T. B. Karpishin, T. D. P. Stack, K. N. Raymond, *J. Am. Chem. Soc.* **1993**, *115*, 184–192.
[24] The helical pitch reported is the twist angle between the two triangles defined by the mean position of the two oxygen atoms of each catecholate ring. For the definition of a twist angle see ref. [20].
[25] T. B. Karpishin, T. M. Dewey, K. N. Raymond, *J. Am. Chem. Soc.* **1993**, *115*, 1842–1851.
[26] T. D. P. Stack, T. B. Karpishin, K. N. Raymond, *J. Am. Chem. Soc.* **1992**, *114*, 1512–1514.
[27] F. Mizukami, H. Ito, J. Fujita, K. Saito, *Bull. Chem. Soc. Jpn.* **1971**, *44*, 3051–3055.
[28] Excluding each metal's coordination configuration, four possible 2:3 (M:L) isomers exist with racemic **2**. Two isomers that are D_3-symmetric enantiomers, *R,R,R* and *S,S,S* will be referred to as homochiral. The homochiral isomers display a single set of ^{1}H NMR resonances. The two isomers that are C_2-symmetric enantiomers, *R,R,S* and *S,S,R*, will be referred to as heterochiral. The heterochiral isomers display three sets of ^{1}H NMR resonances consistent with the C_2 symmetry. In a statistical mixture, the heterochiral isomers are present at three times the concentration of the homochiral isomers.
[29] Assuming that purity of 97% can be assessed by a "clean" NMR spectrum.
[30] B. Bosnich, J. M. Harrowfield, *J. Am. Chem. Soc.* **1972**, *94*, 3425–3438.

The First Sulfur(VI)–Nitrogen–Phosphorus Macrocycles**

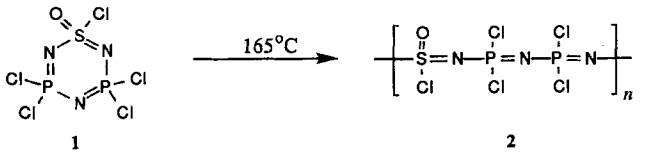
Yizeng Ni, Alan J. Lough, Arnold L. Rheingold, and Ian Manners*

Dedicated to Professor Peter Paetzold on the occasion of his 60th birthday

Cyclic compounds which contain skeletons of inorganic elements are of considerable interest with respect to structure and bonding, solid-state properties, and use as precursors to new polymer systems.[1–6] Over the past two decades six-membered cyclic thionylphosphazenes such as **1** (1,3,3,5,5-pentachloro-1λ^6,2,4,6,3λ^5,5λ^5-thiatriazadiphosphophorin-1-one) have been well-studied, and the skeleton present in these compounds, which consists of four-coordinate sulfur(VI), nitrogen, and phosphorus atoms, has been shown to be robust and stable.[2] We have recently described the thermal ring-opening polymerization of **1** to yield **2**, the first member of the potentially extensive poly(thionylphosphazene) system.[5, 6] These sul-

[*] Prof. I. Manners, Y. Ni, Dr. A. J. Lough
Department of Chemistry, University of Toronto
80 St. George St., Toronto M5S 1A1, Ontario (Canada)
Telefax: Int. code + (416)978-8775
Prof. A. L. Rheingold
Department of Chemistry and Biochemistry, University of Delaware
Newark (USA)

[**] This work was supported by the Natural Sciences and Engineering Research Council of Canada. I.M. is grateful to the Alfred P. Sloan Foundation for a Research Fellowship (1994–96).



1 2

fur–nitrogen–phosphorus polymers show interesting differences from classical polyphosphazenes[7] in terms of material properties, substitution patterns, and the types of polymer structures that are accessible.[6, 8] In this paper we report on our attempts to identify the by-products formed during the polymerization of **1**, which have yielded the first examples of macrocyclic species with a sulfur(VI)–nitrogen–phosphorus skeleton.[9, 10]

A ^{31}P NMR spectrum (in CH_2Cl_2) of the reaction products derived from heating **1** for 4 h at 165 °C is shown in Figure 1a.

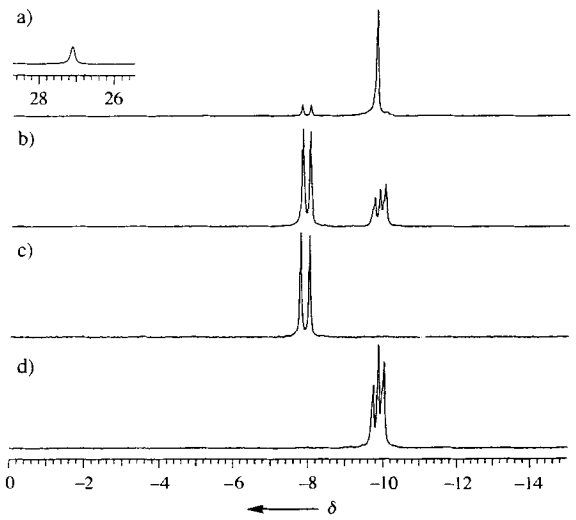
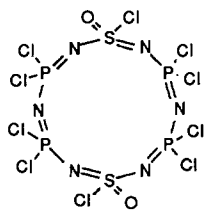


Fig. 1. ^{31}P NMR spectra (121.4 MHz) of the reaction products from the thermolysis of **1** (in CH_2Cl_2).

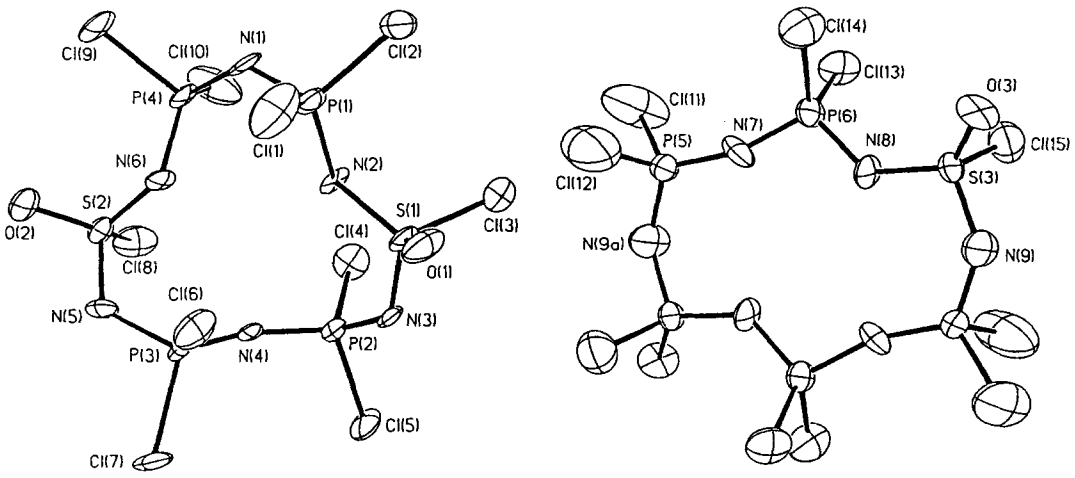
The singlet resonances at $\delta = 27.08$ and $\delta = -9.77$ are assigned to unchanged **1** and the poly(thionylphosphazene) **2**, respectively.[5] In order to isolate the by-product(s) giving rise to the resonances at $\delta = -7.76$ and $\delta = -8.00$, the polymer **2** and then the unreacted **1** were sequentially removed by precipitation and by vacuum sublimation, respectively. The remaining moisture-sensitive products gave the ^{31}P NMR spectrum shown in Figure 1b with the desired resonances at $\delta = -7.76$ and $\delta = -8.00$ (ratio 1.1 to 1.0) and, in addition, a group of poorly resolved peaks at higher field clustered around the original location of the singlet resonance for **2** at $\delta = -9.77$. Analysis by Fast Atom Bombardment (FAB) mass spectrometry indicated that this mixture consisted of the 12-, 18-, 24-, 30-, and 36-membered rings $[(NSOCl)(NPCl_2)_2]_x$ ($x = 2$–6); the strong peaks detected corresponded to the molecular ion minus a chlorine atom for each species.[11] Careful vacuum sublimation of this mixture yielded a white crystalline solid, which afforded the ^{31}P NMR spectrum (in CH_2Cl_2) shown in Figure 1c. The mass spectrum identified this product as the 12-membered ring **3**. The presence of two singlet ^{31}P NMR resonances suggested that both *cis* and *trans* isomers were present.

A block shaped crystal of **3** was selected for a single-crystal X-ray diffraction study.



3

The X-ray analysis showed that the crystals comprised a 2:1 mixture of the *cis* and *trans* isomers of the symmetrical 12-membered ring **3**. Molecules of the *trans* isomer were located at crystallographic inversion centers.[12, 13] The molecular structures of **3a** (*cis*) and **3b** (*trans*) are shown in Figure 2. The sulfur(VI)–nitrogen–phosphorus rings in each isomer are significantly nonplanar, and the bond angles and bond lengths are different. The most dramatic difference in geometry between the 12-membered rings and the six-membered ring **1** is in the P-N-P bond angles, which are substantially expanded to values of 134.1(16)–163.4(13)° in the former relative to the value of

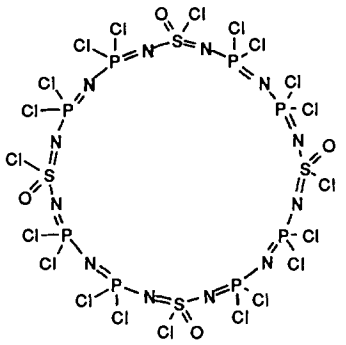


3a 3b

Fig. 2. Molecular structures of the isomers of **3**: **3a** (*cis*) and **3b** (*trans*). Selected bond lengths [Å] and angles [°] (estimated standard deviations in parentheses). **3a** (*cis*): S1-N3 1.554(18), N3-P2 1.583(13), P2-N4 1.544(14), N4-P3 1.526(17), P3-N5 1.632(17), N5-S2 1.531(22), S2-N6 1.543(13), N6-P4 1.592(20), P4-N1 1.530(13), N1-P1 1.578(19), P1-N2 1.543(20), N2-S1 1.602(18); S1-N3-P2 126.3(13), N3-P2-N4 120.3(9), P2-N4-P3 149.4(11), N4-P3-N5 116.9(10), P3-N5-S2 122.9(10), N5-S2-N6 109.7(8), S2-N6-P4 132.5(11), N6-P4-N1 113.9(10), P4-N1-P1 134.1(16), N1-P1-N2 112.3(9), P1-N2-S1 128.5(8), N2-S1-N3 109.6(8). **3b** (*trans*): N9-S3 1.555(17), S3-N8 1.558(19), N8-P6 1.562(13), P6-N7 1.557(26), N7-P5 1.470(25), P5-N9A 1.575(26); P5A-N9-S3 128.6(18), N9-S3-N8 109.2(12), S3-N8-P6 131.9(13), N8-P6-N7 106.2(10), P6-N7-P5 163.4(13), N7-P5-N9a 118.8(11).

122.0(2)° in the latter.[14] The S-N-P angles are also slightly larger in the 12-membered rings **3** (122.9(10)–132.5(11)° compared to an average of 120.9(2) in **1**). In contrast, the N-S-N angles are significantly smaller in **3** (109.2(12)–109.7(8)°) than in **1** (115.2(2)°), whereas the N-P-N angles are similar (106.2(10)–120.3(9)° in **3**, 116.7(2)° in **1**). The 12-membered ring **3** possesses S–N and P–N bond lengths that range from 1.53(2) to 1.60(2) Å and from 1.47(3) to 1.63(2) Å, respectively. The ranges include the values found in **1** (S–N 1.557(3)–1.559(3) Å, P–N 1.571(3)–1.613(3) Å), and the bond lengths are closer to those expected for double rather than single bonds.[15]

After the separation of the 12-membered ring **3**, the remaining products in CH_2Cl_2 gave the ^{31}P NMR spectrum shown in Fig. 1d. Bearing in mind the results of the mass spectrometric analysis mentioned above,[11] this multiplet suggested that the products giving rise to the ^{31}P NMR resonance clustered at $\delta \approx -9.7$ to -10.0 in Figure 1b and d are the higher cyclics $[NSOCl(NPCl_2)_2]_x$ ($x > 2$). Fractional recrystallization from hexanes over three weeks yielded colorless crystals. Analysis of these by mass spectrometry showed a molecular ion minus chlorine for the 24-membered ring **4**, whereas removal of solvent from the mother liquors yielded a mixture of mainly 18-, 24-, and 30-membered rings. One of the crystals of **4** proved to be suitable for an X-ray diffraction study.[16]



4

The single crystal X-ray diffraction analysis indeed identified **4** as a 24-membered ring (Fig. 3), and this molecule is, to our knowledge, the largest discrete inorganic heterocycle to be crystallographically characterized to date.[17] The crystal contained only the *cis*, *trans*, *cis*, *trans* isomer although the molecule was rotationally disordered.[18] Interestingly, the sets of two P–Cl bonds at each phosphorus atom are alternately exo- and endocyclic, whereas in the 12-membered ring **3** all of the P–Cl bonds are exocyclic. This is probably a consequence of the larger cavity in **4** than in **3**. The P-N-P angles in **4**, which vary from 134.8(6) to 138.9(5)°, are similar to the smallest values found in the 12-membered ring **3** and are substantially larger than those in the six-membered ring **1**. The S-N-P, N-S-N, and N-P-N angles vary from 119.9(7) to 131.5(6)°, 109.9(6) to 112.8(9)°, and 109.0(5)° to 114.0(5), respectively. These values are similar to those found in **3** and are not dramatically different from the values found in **1**. The spread in the S–N and P–N bond lengths in **4** is similar to that found in the isomers of **3**, and the ranges contain the values found in **1**. Inspection of the bond-length and bond-angle data for **3**, **4**, and **1** therefore suggests that the ring strain in **1**, which presumably provides the thermodynamic driving force for the ring-opening polymerization to yield **2**, is mainly manifest in a structurally enforced contraction of the P-N-P angles.

The formation of macrocycles, which only correspond to oligomers of the six-membered ring **1**, during the polymerization of this species contrasts with the situation for the ring-opening polymerization of the cyclic phosphazene $[NPCl_2]_3$ which yields mainly the eight-membered ring $[NPCl_2]_4$ together with

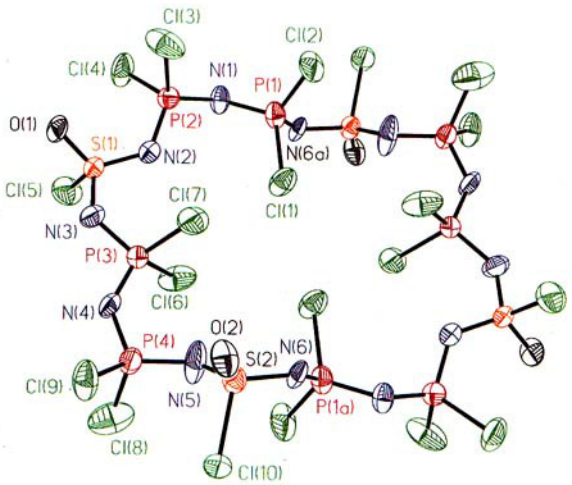


Fig. 3. Molecular structure of **4**. Selected bond lengths [Å] and angles [°] (estimated standard deviations in parentheses): P1-N1 1.570(8), N1-P2 1.538(7), P2-N2 1.595(11), N2-S1 1.532(8), S1-N3 1.546(11), N3-P3 1.575(11), P3-N4 1.541(10), N4-P4 1.566(11), P4-N5 1.579(9), N5-S2 1.617(10), S2-N6 1.551(13), N6-P1A 1.653(13); N6A-P1-N1 106.1(5), P1-N1-P2 138.9(5), N1-P2-N2 114.0(5), P2-N2-S1 127.4(7), N2-S1-N3 110.7(5), S1-N3-P3 131.5(6), N3-P3-N4 106.9(5), P3-N4-P4 134.8(6), N4-P4-N5 113.7(5), P4-N5-S2 130.8(7), N5-S2-N6 109.9(6), S2-N6-P1A 128.1(8).

very small quantities of higher cyclics $[NPCl_2]_x$ ($x = 5$, 6 etc.) in addition to the high polymer $[NPCl_2]_n$.[19] Furthermore, the isolation of 12- and 24-membered rings that exclusively possess SNPNPN sequences provides excellent evidence that molecules of **1** can add to both themselves and to molecules of **3** in a regioselective manner under the thermolysis conditions. The large macrocycles are possible models for the conformations of polymers such as **2** and are also of possible interest as inorganic crown ether type ligands for the complexation of metal ions. In addition, an investigation of the polymerization behavior of the macrocycles should provide additional insight into the processes that can occur when cyclic thionylphosphazenes are heated at elevated temperatures.

Experimental Procedure

3: Monomer **1** (10.0 g) was heated in an evacuated Pyrex tube at 165 °C for 4 h. The tube contents were then dissolved in approximately 40 mL of CH_2Cl_2. The solution was concentrated to about 10 mL, and then added dropwise to 200 mL of stirred hexanes by cannula. Polymer **2** precipitated out of the solution. The polymer was reprecipitated twice, and the mother liquors from all three precipitations were collected, and the solvent removed to leave a white solid (2.1 g). Unconverted **1** was removed from the products by high vacuum sublimation (55–60 °C, 0.008 mmHg, 24 h). The residue was redissolved in hexanes, filtered, and the solvent removed. Small additional amounts of unreacted **1** were removed by vacuum sublimation under the same conditions. High vacuum sublimation at higher temperature (80 to 85 °C, 0.008 mmHg) for 48 h yielded a white crystalline sublimate (**3**). The residue was dissolved in hexanes, the resulting solution filtered, and the solvent removed. Another sublimation under the same conditions yielded a small additional amount of **3**. Total yield of **3**, 0.27 g (3%). ^{31}P NMR: $\delta = -7.76$, -8.00 (1.1:1.0). MS (EI, 70 eV): *m/z* (%): 623 (100, $[M^+ - Cl]$, correct isotope pattern for 9 Cl atoms), 588 (6, $[M^+ - 2\,Cl]$), 553 (85, $[M^+ - 3\,Cl]$), 516 (55 $[M^+ - 4\,Cl]$).

4: The oily residue remaining after the removal of **3** by vacuum sublimation was dissolved in warm hexanes. This solution was filtered and cooled to -14 °C for 24 h. The resulting oily precipitate was redissolved in warm hexanes. At ambient temperature a white powder precipitated over 24 h period. This was isolated and redissolved in warm hexanes. Colorless crystals of **4** formed over 3 weeks at ambient temperature. Yield 15 mg. ^{31}P NMR: $\delta = -9.86$. MS (EI, 70 eV): *m/z* (%): 1282 (100, $[M^+ - Cl]$, correct isotope pattern for 19 Cl atoms), 1210 (38, $[M^+ - 3\,Cl]$), 1140 (15, $[M^+ - 5\,Cl]$), 1068 (7, $[M^+ - 7\,Cl]$). Removal of the solvent from the mother

 © VCH Verlagsgesellschaft mbH, D-69451 Weinheim, 1995 0570-0833/95/0909-1000 $ 10.00+.25/0

liquors yielded an oily residue. ^{31}P NMR: $\delta = -9.76, -9.86, -9.96, -10.01$. MS: m/z 1615, 1282, 952 assigned to $[M^+ - Cl]$ for the 30-, 24-, and 18-membered rings, respectively.

Received: December 12, 1994 [Z 7541 IE]
German version: *Angew. Chem.* **1995**, *107*, 1079

Keywords: heterocycles · nitrogen compounds · phosphazenes · phosphorus compounds · sulfur compounds

[1] See, for example a) T. Chivers, S. S. Kumaravel, A. Meetsma, J. C. van de Grampel, A. van der Lee, *Inorg. Chem.* **1990**, *29*, 4592; b) P. P. Power, *Angew. Chem.* **1990**, *102*, 527; *Angew. Chem. Int. Ed. Engl.* **1990**, *29*, 449; c) N. Burford, B. W. Royan, P. S. White, *J. Am. Chem. Soc.* **1989**, *111*, 3746; d) K. Bestari, A. W. Cordes, R. T. Oakley, K. M. Young, *ibid.* **1990**, *112*, 2249; e) R. Hasselbring, H. W. Roesky, M. Noltemeyer, *Angew. Chem.* **1992**, *104*, 613; *Angew. Chem. Int. Ed. Engl.* **1992**, *31*, 601; f) P. Paetzold, C. von Plotho, E. Niecke, R. Rüger, *Chem. Ber.* **1983**, *116*, 1678; g) A. H. Cowley, R. A. Jones, *Angew. Chem.* **1989**, *101*, 1235; *Angew. Chem. Int. Ed. Engl.* **1989**, *28*, 1208; h) *The Chemistry of Inorganic Homo and Heterocycles* (Eds.: I. Haiduc, D. B. Sowerby), Academic Press, Toronto, **1987**; i) D. A. Dixon, W. B. Farnham, W. Heilemann, R. Mews, M. Noltemeyer, *Heteroat. Chem.* **1993**, *4*, 287.

[2] J. C. van de Grampel, *Rev. Inorg. Chem.* **1981**, *3*, 1; b) *Coord. Chem. Rev.* **1992**, *112*, 247.

[3] a) H. W. Roesky, M. Lücke, *J. Chem. Soc. Chem. Commun.* **1989**, 748; b) D. C. Ngo, J. S. Rutt, H. R. Allcock, *J. Am. Chem. Soc.* **1991**, *113*, 5075; c) M. Cypryk, Y. Gupta, K. Matyjaszewski, *ibid.* **1991**, *113*, 1046; d) R. West, S. Hayase, T. Iwahara, *J. Inorg. Organomet. Polym.* **1991**, *4*, 545; e) J. E. Mark, H. R. Allcock, R. West, *Inorganic Polymers*, Prentice Hall, **1992**; f) P. F. Brandt, T. B. Rauchfuss, *J. Am. Chem. Soc.* **1992**, *114*, 1926.

[4] a) D. A. Foucher, B. Z. Tang, I. Manners, *J. Am. Chem. Soc.* **1992**, *114*, 6246; b) I. Manners, *Adv. Mater.* **1994**, *6*, 68; c) *Adv. Organomet. Chem.* **1995**, *37*, 131.

[5] M. Liang, I. Manners, *J. Am. Chem. Soc.* **1991**, *113*, 4044.

[6] a) Y. Ni, A. Stammer, M. Liang, J. Massey, G. J. Vancso, I. Manners, *Macromolecules* **1992**, *25*, 7119; b) I. Manners, *Coord. Chem. Rev.* **1994**, *137*, 109; c) R. Jaeger, J. Lagowski, I. Manners, G. J. Vancso, *Macromolecules* **1995**, *28*, 539.

[7] For work on "classical" polyphosphazenes $(R_2P{=}N)_n$ see for example a) H. R. Allcock, *Chem. Engl. News* **1985**, *63*(11) 22; b) *J. Inorg. Organomet. Polym.* **1992**, *2*, 197; c) *Adv. Mater.* **1994**, *6*, 106; d) R. H. Neilson, P. Wisian-Neilson, *Chem. Rev.* **1988**, *88*, 541; e) R. A. Montague, K. Matyjaszewski, *J. Am. Chem. Soc.* **1990**, *112*, 6721.

[8] For work on other polymers with main group element/nitrogen/phosphorus backbones, see a) H. W. Roesky, M. Lücke, *Angew. Chem.* **1989**, *101*, 480; *Angew. Chem. Int. Ed. Engl.* **1989**, *28*, 493; b) I. Manners, G. Renner, H. R. Allcock, O. Nuyken, *J. Am. Chem. Soc.* **1989**, *111*, 5478; c) H. R. Allcock, S. M. Coley, I. Manners, G. Renner, O. Nuyken, *Macromolecules* **1991**, *24*, 2024; d) J. A. Dodge, I. Manners, G. Renner, H. R. Allcock, O. Nuyken, *J. Am. Chem. Soc.* **1990**, *112*, 1268; e) H. R. Allcock, J. A. Dodge, I. Manners, *Macromolecules* **1993**, *26*, 11.

[9] van de Grampel has made a brief report of the preparation of the eight-membered ring $NSOCl(NPCl_2)_3$; see C. Voswijk, J. C. van de Grampel, *Recl. Trav. Chim. Pays-Bas* **1974**, *93*, 120. Apart from this example, to our knowledge, only six-membered S(VI)-N-P rings have been reported.

[10] Chivers and co-workers have previously reported the formation by cyclodimerization of 12-membered rings containing three-coordinate sulfur(IV), nitrogen, and phosphorus atoms. See, T. Chivers, M. N. S. Rao, J. F. Richardson, *Inorg. Chem.* **1984**, *23*, 1531.

[11] MS (FAB): m/z (%): 1941 (1, $[M^+ - Cl]$ for $x = 6$), 1611 (2, $[M^+ - Cl]$ for $x = 5$), 1281 (2, $[M^+ - Cl]$ for $x = 4$), 952 (5, $[M^+ - Cl]$ for $x = 3$), 623 (28%, $[M^+ - Cl]$ for $x = 2$), 294 (100, $[M^+ - Cl]$ for $x = 1$). Correct isotope patterns for the number of Cl atoms present were detected in all cases.

[12] a) For **3**: $a = 10.430(3)$, $b = 10.482(3)$, $c = 17.030(6)$ Å, $\alpha = 89.33(3)$, $\beta = 73.96(2)$, $\gamma = 60.80(2)^\circ$; $V = 1545.1(8)$ Å^3; $Z = 3$, $\rho_{calcd} = 2.123$ g cm^{-3}, $P\bar{1}$; crystal dimensions $0.16 \times 0.24 \times 0.34$ mm^3; $T = 295$ K; measuring range $4.0 < 2\theta < 42^\circ$; 3319 independent reflections, 1694 observed with $F > 5\,\sigma(F)$, 323 refined parameters $R = 0.0699$, $R_w = 0.0866$. b) Further details of the crystal structure investigation may be obtained from the Director of the Cambridge Crystallographic Data Centre, 12 Union Road, GB-Cambridge CB2 1EZ (UK), on quoting the full journal citation.

[13] a) The terms *cis* and *trans* refer to the relative orientation of the S=O groups to the best plane of the twelve-membered ring. b) The ^{31}P NMR spectrum of the crystals of **3** consisted of singlet resonances at $\delta = -7.76$ and -8.00 in a 2:1 ratio which indicated that the former resonance arises from the *cis* isomer **3a** and the latter from the *trans* isomer **3b**.

[14] F. van Bolhuis, J. C. van de Grampel, *Acta Crystallogr. Sect. B* **1976**, *32*, 1192.

[15] The S–N and P–N single bonds in H_3NSO_3 and $H_3NPO_3^-$ are 1.76 Å and 1.77 Å long, respectively: see ref. [14]. The S=N bonds in sulfur diimides are about 1.53 Å long: see *Sulfur in Organic and Inorganic Chemistry Vol. 4* (Ed.: A. Senning), Marcel Dekker, New York, **1982**. The lengths of the P=N bonds are approximately 1.56 Å. N. N. Greenwood, A. Earnshaw, *Chemistry of the Elements*, 1st ed., Pergamon, Oxford, England, **1984**.

[16] For **4**: $a = 13.543(5)$, $b = 13.570(3)$, $c = 12.077(3)$ Å, $\beta = 112.41(2)^\circ$, $V = 2051.8(13)$ Å^3; $Z = 2$, $\rho_{calcd} = 2.132$ g cm^{-3}, $P2_1/C$; crystal dimensions $0.35 \times 0.26 \times 0.18$ mm^3; $T = 173$ K; measuring range $6.0 < 2\theta < 60^\circ$; 5897 independent reflections, 3447 observed with $F > 6.0\,\sigma(F)$, 273 refined parameters $R = 0.0950$, $R_w = 0.1603$ [12b].

[17] Two 20-membered rings have been crystallographically characterized: a) S_{20}, see T. Debaerdemaeker, E. Hellner, A. Kutoglu, M. Schmidt, E. Wilhelm, *Naturwissenschaften* **1973**, *60*, 300; b) in the heterocyclic ion $[P_{10}O_{30}]^{10-}$ see M. Bagieu-Beucher, A. Durif, J. C. Guitel, *Solid State Chem.* **1982**, *45*, 159.

[18] The structure was disordered with two molecules of the *cis,trans,cis,trans* isomer of **4** in a 57:43 ratio differing b a 90° rotation about the axis perpendicular to the best plane of the ring.

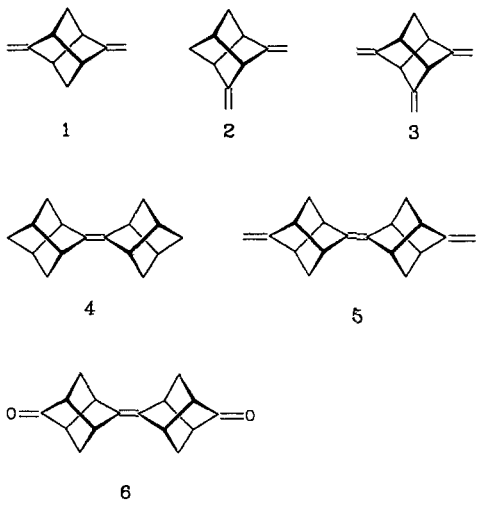
[19] a) H. R. Allcock, *Phosphorus-Nitrogen Compounds*, Academic Press, New York, **1972**. b) The 12-membered ring $[(NCCl)(NPCl_2)_2]_2$ has been identified as a by-product during the thermal ring-opening polymerization of the cyclic carbophosphazene $(NCCl)(NPCl_2)_2$. See H. R. Allcock, S. M. Coley, I. Manners, K. B. Visscher, M. Parvez, *Inorg. Chem.* **1993**, *32*, 5088. c) The crystallographically characterized 12-membered metallophosphazene ring $[(NRe(NAr)_2)(NPPh_2)_2]_2$ is believed to form by cyclodimerization of the six-membered ring $[(NRe(NAr)_2)(NPPh_2)_2]$. See ref. [1e].

Synthesis of Rodlike Distellenes**

Rolf Gleiter* and Oliver Borzyk

Dedicated to Professor Franz Effenberger on the occasion of his 65th birthday

The interaction of nonconjugated π systems can be described either by a through-space or a through-bond mechanism.[1] The latter is of interest with respect to long-range electron transfer processes.[2] In our studies on exomethylene derivatives of tricyclo[3.3.0.0^{3,7}]octane (stellenes) such as **1**–**3**[3] we realized that

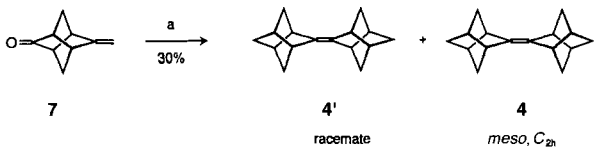


[*] Prof. Dr. R. Gleiter, Dr. O. Borzyk
Organisch-Chemisches Institut der Universität
Im Neuenheimer Feld 270, D-69120 Heidelberg (Germany)
Telefax: Int. code + (6221) 564205

[**] This work was supported by the Volkswagenstiftung, the Fonds der Chemischen Industrie, and the BASF Aktiengesellschaft, Ludwigshafen.

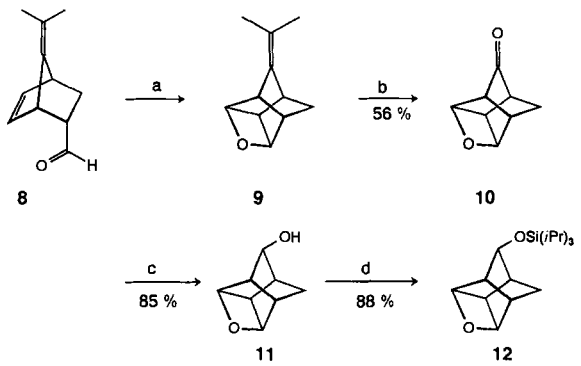
not only the twisted six-membered ring but also the whole tricyclo[3.3.0.0^{3,7}]octane (stellane) skeleton can provide a good relay for through-bond interactions. We therefore concluded that two or more stellane units are not only good building blocks for rodlike molecules but might be of interest with respect to electron transfer processes when they can be placed between acceptor and donor groups. In this paper we report on the synthesis of the rodlike molecules **4**–**6** which incorporate two stellane units (distellenes).

Compound **4** was synthesized by coupling the known ketone **7**[4] with the titanium trichloride/dimethoxyethane (DME) complex described by McMurry et al. (Scheme 1).[5] The starting



Scheme 1. a) $TiCl_3 \cdot DME/Zn-Cu/DME$, 40 °C, 19 h.

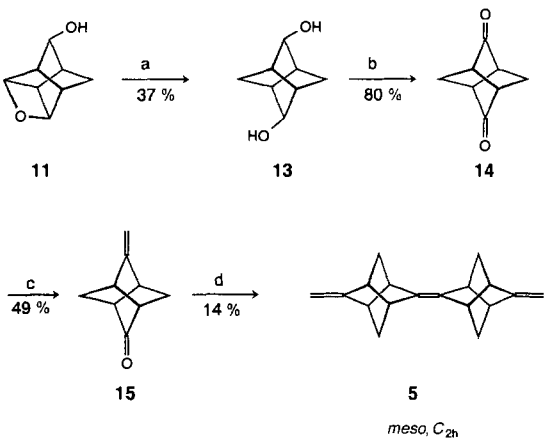
compound **8** for the synthesis of **5** and **6** could be prepared readily by the Diels–Alder addition of acrolein to 6,6-dimethylfulvene.[6] Conversion of **8** to the oxetane **10** was accomplished by irradiation and subsequent ozonization (Scheme 2). The re-



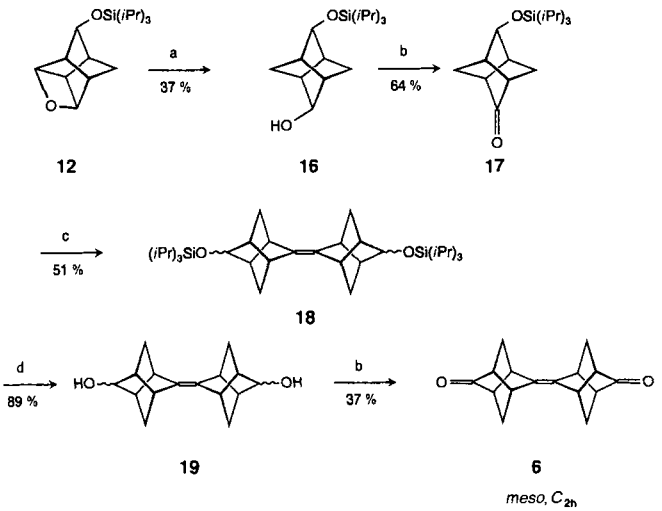
Scheme 2. a) *hν* (285 nm)/Et_2O; b) $O_3/CH_2Cl_2/DMS$; c) $LiEt_3BH/THF$; d) TIPS triflate/CH_2Cl_2.

gioselective reduction of **10** yielded **11** which could be converted to **12** by reaction with triisopropylsilyl (TIPS) triflate. The oxetane rings in **11** and **12** were cleaved as described by Sauers et al.[7] with Li in ethylenediamine (EDA) to yield the alcohols **13** (Scheme 3) and **16** (Scheme 4), respectively. The next steps in the route to **5** were a Swern[8] oxidation (**13** → **14**) and a Wittig reaction (**14** → **15**). This route also comprises a new and efficient synthesis of compounds **14** and **15**.[9] The McMurry coupling of **15** afforded **5**. The preparation of distellene **6** (Scheme 4) relied on the same procedures as in Scheme 3. The key reactions were also the Swern oxidation[8] of **16** to **17** and **19** to **6**.

A salient feature of the synthetic approach to **5** and **6** was the discovery of an efficient high-yielding synthesis of alcohols **13** and **16** by the reductive cleavage of the oxetane rings in **11** and **12**. This reaction sequence is part of a seven-step synthesis of **15** and **17** which provides these key intermediates in gram quantities (Scheme 3 and 4). A previous synthesis yielding small amounts of **14** and **15** required several additional steps.[9]



Scheme 3. a) Li/EDA; b) $(COCl)_2/DMSO/NEt_3$; c) $[Ph_3PCH_3]Br/NaNH_2/THF$; d) $TiCl_3 \cdot DME/Zn-Cu/DME$.



Scheme 4. a) Li/EDA; b) $(COCl)_2/DMSO/NEt_3$; c) $TiCl_3 \cdot DME/Zn-Cu/DME$; d) nBu_4NF/THF.

Three stereoisomers (*meso*, C_{2h}-symmetric; racemate, D_2-symmetric) are possible for compounds **4**, **5**, and **6**. The isomers of **4** (racemate **4'** and *meso* **4**) could be separated on an analytical cyclodextrin column. The ratio of the isomers **4'**:**4** was found to be 5:1. The assignments of the NMR signals are based

Table 1. Selected physical and spectroscopic data of **4**–**6**.

4': Isolation by flash chromatography, colorless needles, m.p. 30 °C; ^1H NMR (300 MHz, $CDCl_3$): δ = 2.46–2.44 (m, 4H), 2.26–2.25 (m, 4H), 1.38–1.21 (m, 8H); ^{13}C NMR (75.47 MHz, $CDCl_3$): δ = 130.80 (s), 45.87 (t), 44.54 (t), 38.22 (d), 35.81 (d)

4: Isolation by flash chromatography, colorless needles, m.p. 30 °C; ^1H NMR (300 MHz, $CDCl_3$): δ = 2.51–2.50 (m, 4H), 2.32–2.31 (m, 4H), 1.38–1.21 (m, 8H); ^{13}C NMR (75.47 MHz, $CDCl_3$): δ = 130.88 (s), 45.74 (t), 44.35 (t), 38.30 (d), 35.85 (d)

5: Isolation by flash chromatography, colorless crystals, m.p. 111 °C; ^1H NMR (300 MHz, $CDCl_3$): δ = 4.34 (s, 4H), 2.59–2.57 (m, 4H), 2.48–2.47 (m, 4H), 1.47–1.33 (m, 8H); ^{13}C NMR (75.47 MHz, $CDCl_3$): δ = 163.86 (s), 131.50 (s), 91.88 (t), 44.49 (t), 41.95 (d), 38.79 (d); PE: $I_{v,1}$ = 7.73 eV (π_i), $I_{v,2}$ = 8.87 eV (π_0^-), $I_{v,3}$ = 9.30 eV (π_0^+)

6: Isolation by flash chromatography, colorless crystals, m.p. 177 °C; ^1H NMR (300 MHz, $CDCl_3$): δ = 2.86 (4H, d, J = 1.3 Hz), 2.28 (4H, dd, J_1 = 5.4, J_2 = 2.6 Hz), 1.74 (4H, dd, J_1 = 11.1, J_2 = 1.5 Hz), 1.53 (4H, dd, J_1 = 11.1, J_2 = 2.5 Hz); ^{13}C NMR (75.47 MHz, $CDCl_3$): δ = 212.08 (s), 131.64 (s), 43.08 (d), 38.64 (t), 37.72 (d); IR ($CDCl_3$): $\tilde{\nu}$[cm^{-1}] = 1751 (vs, br.); PE: $I_{v,1}$ = 8.63 eV (n^+), $I_{v,2}$ = 8.91 eV (n^-), $I_{v,3}$ = 9.02 eV (π_i)

 © VCH Verlagsgesellschaft mbH, D-69451 Weinheim, 1995 0570-0833/95/0909-1002 $ 10.00+.25/0

on this ratio. Separation of the isomers of **5** and **6** has not yet been achieved. Relevant spectroscopic data of **4**–**6** are presented in Table 1.

To elucidate the relay properties of the stellane skeleton we recorded the photoelectron (PE) spectra of **5**, **6**, and **14**. In **14**, in which the oxygens are separated by five bonds (5.6 Å), the first two ionization energies I_v are found at 8.86 and 9.90 eV. These two peaks are assigned to ionizations from the two linear combinations of the two 2p AOs at the oxygen centers and the σ skeleton ($6b_3(n^+)$ and $6b_2(n^-)$; Fig. 1). It is evident that the

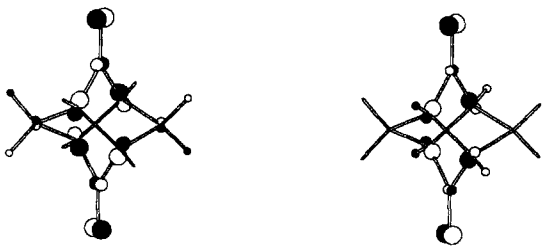


Fig. 1. Drawing of the two highest occupied MOs of **14**; left: $6b_3(n^+)$, right: $6b_2(n^-)$.

2p–σ interaction in $6b_3(n^+)$ is larger than in $6b_2(n^-)$. In **5** the split between the ionization energies from the terminal π bonds (π_o^+, π_o^-) amounts to 0.43 eV (Table 1). In **6** the energy difference between the first two bands (n^+, n^- linear combination) amounts to 0.28 eV (Table 1). Similar efficient relay properties were encountered with the bicyclo[1.1.1]pentane skeleton.[10]

Received: December 7, 1994 [Z 7528 IE]
German version: *Angew. Chem.* **1995**, *107*, 1094

Keywords: distellenes · hydrocarbons · through-bond interactions

[1] Review: R. Gleiter, W. Schäfer, *Acc. Chem. Res.* **1990**, *23*, 369.
[2] Review: M. N. Paddon-Row, K. D. Jordan in *Modern Models of Bonding and Delocalization* (Eds.: J. F. Liebman, A. J. Greenberg), VCH, Weinheim, **1988**, p. 115; *Photoinduced Electron Transfer* (Eds.: M. A. Fox, M. Chanon), Elsevier, Amsterdam, **1988**; *Photoinduced Electron Transfer, Vol. I–IV (Top. Curr. Chem.* **1991**).
[3] B. Kissler, R. Gleiter, *Tetrahedron Lett.* **1985**, *26*, 185; *ibid.* **1987**, *28*, 6151; R. Gleiter, B. Kissler, C. Ganter, *Angew. Chem.* **1987**, *99*, 1292; *Angew. Chem. Int. Ed. Engl.* **1987**, *26*, 1252; R. Gleiter, C. Sigwart, B. Kissler, *ibid.* **1989**, *101*, 1561 and **1989**, *28*, 1525.
[4] R. R. Sauers, K. W. Kelly, B. R. Sickles, *J. Org. Chem.* **1972**, *37*, 537.
[5] J. E. McMurry, M. P. Fleming, *J. Am. Chem. Soc.* **1974**, *96*, 4708; J. E. McMurry, T. Lectka, J. G. Rico, *J. Org. Chem.* **1989**, *54*, 3748.
[6] C. Sigwart, Dissertation, Universität Heidelberg, **1992**.
[7] R. R. Sauers, W. Schinski, M. M. Mason, E. O'Hara, B. Byrne, *J. Org. Chem.* **1973**, *38*, 642.
[8] A. J. Mancuso, D. Swern, *Synthesis* **1981**, *165*.
[9] M. Nakazaki, K. Naemura, H. Harada, H. Narutaki, *J. Org. Chem.* **1982**, *47*, 3470; Review: K. Naemura in *Carbocyclic Cage Compounds* (Eds.: E. Osawa, O. Yonemitsu), VCH, Weinheim, **1992**, p. 61.
[10] R. Gleiter, K.-H. Pfeifer, G. Szeimies, U. Bunz, *Angew. Chem.* **1990**, *102*, 418; *Angew. Chem. Int. Ed. Engl.* **1990**, *29*, 413.

Al,Ti Avoidance in the Microporous Titanoaluminosilicate ETAS-10**

M. W. Anderson,* A. Philippou, Z. Lin, A. Ferreira, and J. Rocha

Recently the structure of the microporous, crystalline titanosilicate ETS-10 was solved and found to be highly disordered.[1, 2] The framework can be described in terms of an intergrowth of two end member structures termed polymorphs A and B, both of which consist of a three-dimensional 12-ring structure. Polymorph A belongs to a chiral space group and like zeolite β possesses a spiral channel. ETS-10, therefore, constitutes a very interesting new microporous material with wide pores and a chemical composition very different from that of zeolites.

The structure of ETS-10 contains corner-sharing TiO_6 octahedra and corner-sharing SiO_4 tetrahedra. Consequently, in the anionic framework every titanium atom is associated with a -2 change in the structure. This charge is compensated by cations not in the framework, which in the case of the ETS-10 produced by the method described here is a mixture of Na^+ and K^+ ions. It appears that the K^+ ions are the most important components for directing the synthesis towards ETS-10 rather than towards other titanosilicate phases. The anhydrous formula of ETS-10 is $M^{m+}_{2/m}TiSi_5O_{13}$, where M is a cation with charge m. The cation density in ETS-10 is, therefore, approximately equivalent to that in a zeolite with Si/Al = 2.5 such as zeolite Y. This makes ETS-10 potentially a very interesting material both for cation exchange and catalysis. With regards to catalysis, the high framework charge and cation exchange ability should impart basic properties. On the other hand, acidic properties could be introduced by forming bridging hydroxyl groups such as Ti-(OH)-Si. To improve the acid chracteristics further, aluminum may be incorporated into tetrahedral silicon sites, thus generating sites for zeolite-type acidity. The formation of ETAS-10 (*E*ngelhard *t*itano*a*luminos*i*licate) has already been described.[3, 4] We have synthesized a number of different ETAS-10 samples and report here on the location of the aluminum atoms and general considerations for titanoaluminosilicates.

When aluminum is incorporated in tetrahedral framework sites in a zeolite, a negative framework charge is introduced. Owing to this negative charge and the consequent electrostatic repulsion, the Al atoms, tend to avoid each other. This behavior is described by the Al, Al avoidance principle of Loewenstein's rule.[5] This precludes the existence of Al-O-Al linkages, and implies that all Al atoms have the same chemical environment, Al(4Si). When Loewenstein's rule holds, Si/Al ratios in the frameworks of structurally simple zeolites such as zeolite may be calculated from ^{29}Si magic-angle spinning (MAS) NMR spectra according to Equation (a).[6] Here $I_{Si}(n\text{Al})$ is the integrated intensity of the resonance corresponding to silicon atoms bonded through oxygen to n Al neighbors.

$$\text{Si/Al} = \frac{\sum_{n=0}^{4} I_{\text{Si}(n\text{Al})}}{0.25 \sum_{n=0}^{4} n I_{\text{Si}(n\text{Al})}} \qquad \text{(a)}$$

[*] Dr. M. W. Anderson, A. Philippou
Department of Chemistry, UMIST
PO Box 88, Manchester M601QD (UK)
Telefax: Int. code + (61)236-7677
Z. Lin, A. Ferreira, J. Rocha
Department of Chemistry, University of Aveiro
P-3800 Aveiro (Portugal)

[**] We thank the European Commission, Joule II program, for a fellowship for A.F., Shell for partial support for A.P., and the EPSRC.

One consequence of Loewenstein's rule is that the lowest Si/Al ratio possible is 1, and strict alternation of silicon and aluminum atoms in the framework must apply (such as in zeolite A and sodalite). Interestingly, it was shown recently[7] that in pyrolytically prepared ultramarines (with the sodalite structure) disorder of the aluminum atoms results in breaking of Loewenstein's rule. However, in hydrothermally prepared sodalites Loewenstein's rule is obeyed. We wondered whether titanoaluminosilicates follow such avoidance rules, in other words whether Al-O-Ti units are found exclusively.

Figure 1 shows the framework connectivity for ETS-10 as reported previously.[1] For the ensuing arguments the choice of

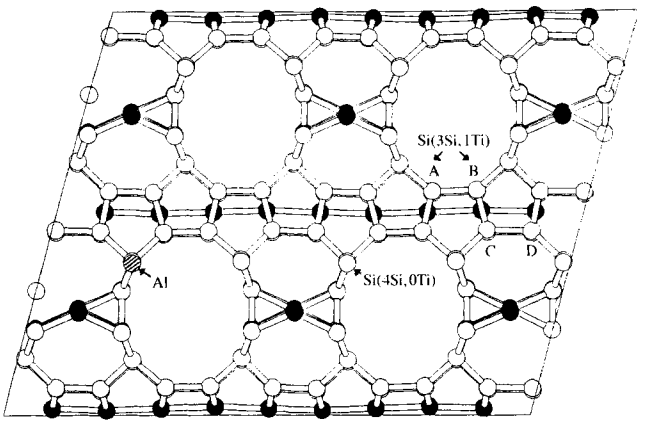


Fig. 1. Framework of ETS-10 (Si: white, Ti: black). Oxygen atoms are not shown; they lie approximately in the middle of the atom connections. One aluminum atom is shown (shaded) incorporated at a tetrahedral site which avoids neighboring titanium.

polymorph is irrelevant as is the disorder in ETS-10; in all cases local environment of the tetrahedral sites remains unaffected. There are only two types of chemical environment for silicon atoms in ETS-10, Si(3Si, 1Ti) and Si(4Si, 0Ti). The ratio of these two environments is 4:1; this can be seen in the structure (Fig. 1) and is supported experimentally in the ^{29}Si MAS NMR spectrum (Fig. 2a). This spectrum reveals a further crystallographic splitting of the Si(3Si, 1Ti) environment into three or four sites, which are labeled A–D in Figure 1. For most of the following discussion this crystallographic inequivalence can be ignored, in other words, it suffices when only chemical environments are considered.

The ^{29}Si and ^{27}Al MAS NMR spectra of ETAS-10 are shown in Figures 2b and 2c, respectively. The ^{27}Al NMR spectrum reveals that 98% of the aluminum is incorporated in tetrahedral sites ($\delta = 60$ relative to $[Al(H_2O)_6]^{3+}$). A small contribution from aluminum centers in octahedral sites (ca. 2%) is evidenced by resonances between $\delta = 0$ and $\delta = -10$, which could be due to aluminum atoms within or not in the framework of ETAS-10. The ^{29}Si MAS NMR spectrum is more complicated. First, the resonances for ETAS-10 are all considerably broader than for ETS-10. Such a phenomenon is also observed in zeolites and is generally regarded to be due to second nearest neighbor effects. Second, all the resonances for ETS-10 appear in the spectrum for ETAS-10, but there is an additional set of resonances roughly 4 ppm downfield from the Si(3Si, 1Ti) signal. We ascribe these signals to Si(2Si, 1Al, 1Ti) environments. A 4 ppm downfield shift is expected upon exchange of a silicon neighbor by aluminum.[6] Importantly, though, there is no signal 4 ppm downfield fom the Si(4Si,0Ti) signal, indicating that there is no aluminum substitution neighboring this silicon site. These arguments are summarized in Scheme 1. This is direct proof of Al, Ti avoidance in ETAS-10. Aluminum only substitutes into

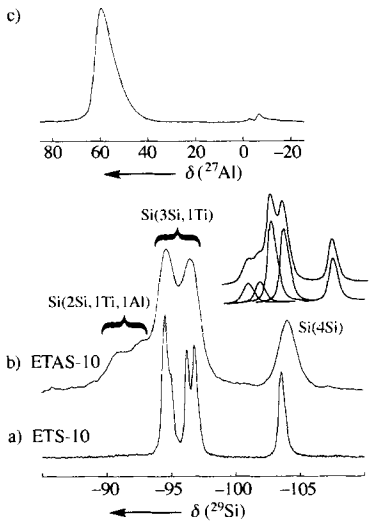
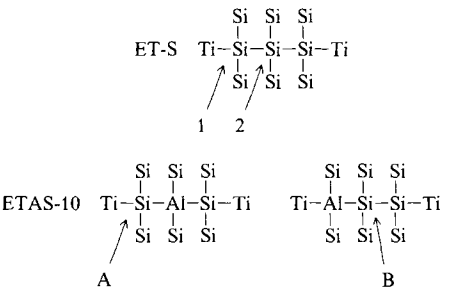


Fig. 2. ^{29}Si MAS NMR spectra of a) ETS-10 and b) ETAS-10. Inset shows deconvolution of the overlapping signals. c) ^{27}Al MAS NMR spectrum of ETAS-10.



Scheme 1. In the representation of ETS-10 the arrows labeled 1 and 2 point to silicon centers having different chemical environments. In the representation of ETAS-10 the arrow labeled A points to a silicon center Si(2 Si, 1 Ti, 1 Al) which gives rise to an NMR signal; the arrow labeled B points to a silicon center Si(3 Si, 1 Al) which does not give rise to an NMR signal.

Si(4Si, 0Ti) sites, thereby avoiding neighboring titanium (O atoms are discounted). The ^{27}Al MAS NMR spectrum also supports this conclusion, as only one signal for an aluminum environment is observed with a chemical shift similar to that found for Al(4Si) sites in zeolites.

Detailed analysis of signal intensities in the spectra, which will be reported in full separately, allows framework Si/Al and Si/Ti ratios to be calculated with Equations (b) and (c), respectively. These calculations reveal that at higher concentrations of aluminum, slight deviations from the Al, Ti avoidance rule are observed. For the sample reported in this study Si/Al = 20.3 and Si/Ti = 4.8 is found. This is in close agreement with the results of an independent chemical analysis by ICP atomic emission spectroscopy.

$$\mathrm{Si/Al} = \frac{\sum_{n=0}^{4-m}\sum_{m=0}^{4-n} I_{\mathrm{Si}(n\mathrm{Al},m\mathrm{Ti})}}{0.25\sum_{n=0}^{4-m}\sum_{m=0}^{4-n} nI_{\mathrm{Si}(n\mathrm{Al},m\mathrm{Ti})}} \qquad \text{(b)}$$

 © VCH Verlagsgesellschaft mbH, D-69451 Weinheim, 1995 0570-0833/95/0909-1004 $ 10.00+.25/0

$$\mathrm{Si/Ti} = \frac{\sum_{n=0}^{4-m}\sum_{m=0}^{4-n} I_{\mathrm{Si}(n\mathrm{Al},m\mathrm{Ti})}}{0.25\sum_{n=0}^{4-m}\sum_{m=0}^{4-n} mI_{\mathrm{Si}(n\mathrm{Al},m\mathrm{Ti})}} \qquad (c)$$

It is too early to say whether Al, Ti avoidance is a general phenomenon in titanoaluminosilicates; however, it seems logical that, when possible, aluminum and titanium will not be neighbors. This has implications for aluminum incorporation in ETS-4.[3] Although a full structural study has not been performed on ETS-4, the structure is believed to be related to that of zorite.[8] All silicon sites in the structure of zorite neighbor titanium, and consequently aluminum atoms cannot avoid being adjacent to titanium atoms. We have been unsuccessful in our attempts to incorporate aluminum into ETS-4, possibly because the Al,Ti avoidance principle holds.

In conclusion ETAS-10 displays Al, Ti avoidance when low to medium concentrations of aluminum are incorporated. This preference of certain sites for aluminum is maintained at higher aluminum concentrations, although the avoidance rule does not hold strictly.

Experimental Procedure

ETAS-10 with Si/Al = 20: An alkaline solution was made by mixing 11.78 g sodium silicate solution (Na_2O: 8 wt%, SiO_2: 27 wt%), 2.5 g H_2O, 0.48 g NaOH, and 0.45 g KF. A mixed Ti/Al solution was made by adding 5.72 g $TiCl_3$ (1.9 M solution of $TiCl_3$ in 2.0 M HCl) to a solution made from 5.08 g H_2O, 0.48 g NaOH, 0.46 g KF, 0.49 g KCl, and 0.36 g $NaAlO_2$. The alkaline silicate solution and the mixed Ti/Al solution were combined with thorough stirring. A seed crystal of ETS-10 (0.1 g) was added to the resulting gel. The gel with a Ti/Al molar ratio of 2 was autoclaved under autogenous pressure for six days at 200 °C. The crystalline product was filtered, washed with distilled water at room temperature, and dried at 120 °C. ^{29}Si MAS NMR: $\delta = -90.8$ [Si(1Al, 1Ti)], -92.9 [Si(1Al, 1Ti)], -94.8 [Si(0Al, 1Ti)], -96.7 [Si(0Al, 1Ti)], -104.4 [Si(0Al, 0Ti)]. The Si(1Al, 1Ti) and Si(0Al, 1Ti) sites are crystallographically distinct. MAS NMR spectra were recorded on a Bruker MSL400 spectrometer. For ^{29}Si NMR spectra a 3.5 μs 45° pulse was used with an interpulse delay of 35 s. For the ^{27}Al NMR spectrum a 0.6 μs π/18 pulse was used with an interpulse delay of 0.5 s.

Received: September 17, 1994
Revised version: November 18, 1994 [Z 7325 IE]
German version: *Angew. Chem.* **1995**, *107*, 1115

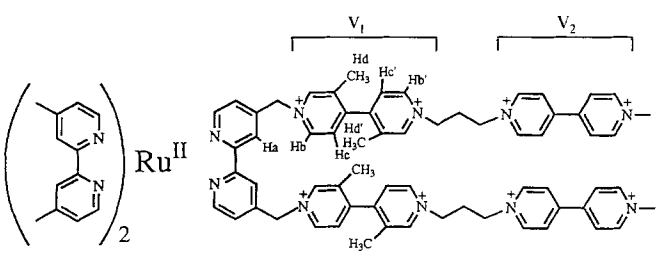
Keywords: aluminum compounds · microporosity · silicon compounds · titanium compounds · zeolites

[1] M. W. Anderson, O. Terasaki, T. Ohsuna, A. Philippou, S. P. MacKay, A. Ferreira, J. Rocha, S. Lidin, *Nature* **1994**, *367*, 347.
[2] M. W. Anderson, O. Terasaki, T. Ohsuna, P. J. O'Malley, A. Philippou, S. P. MacKay, A. Ferreira, J. Rocha, S. Lidin, *Philos. Mag.*, in press.
[3] S. M. Kuznicki, US-A 4 853 202 (**1989**).
[4] S. M. Kuznicki, A. K. Thrush, EP-A-0405978A1 (**1990**).
[5] W. Loewenstein, *Am. Mineral.* **1953**, *39*, 92.
[6] E. Lippmaa, M. Mägi, A. Samoson, G. Engelhardt, A.-R. Grimmer, *J. Am. Chem. Soc.* **1980**, *102*, 4889.
[7] J. Klinowski, S. W. Carr, S. E. Tarling, P. Barnes, *Nature* **1987**, *330*, 56.
[8] P. A. Sandormiskii, N. V. Belov, *Sov. Phys. Crystallogr. (Engl. Transl.)* **1979**, *24*, 686.

Effective Charge Separation in Intermolecular Complexes of an Electron Donor and a Doubly Branched Triad Assembly: A Model System for Environmental Effects Controlling Electron Transfer**

Eran Zahavy, Martin Seiler, Sharon Marx-Tibbon, Ernesto Joselevich, Itamar Willner,* Heinz Dürr, Donald O'Connor, and Anthony Harriman

Photosensitized electron transfer in diad, triad, and tetrad assemblies has been extensively examined as a model of the photosynthetic reaction center.[1–3] It was found that charge separation and stabilization of the intermediate redox products occurs by stepwise vectorial electron transfer within the multiacceptor triads and tetrads. Recently, we showed that effective photoinduced electron transfer takes place in donor–photosensitizer–acceptor assemblies stabilized by intermolecular charge transfer interactions.[4] The protein in which the photosynthetic reaction center is embedded plays a major role in controlling electron transfer and charge separation.[5] Alignment of the electron acceptors within the protein spatially separates the photogenerated photoproducts, thereby supporting efficient charge separation. Similarly, the protein backbone facilitates the vectorial electron transfer through the L-branch within the almost symmetrical M,L-branched photosynthetic reaction center.[6, 7] We report here on the photoinduced electron transfer reactions in a difunctionalized photosensitizer–triad assembly which serves as a functional model for the photosynthetic reaction center. We recently prepared the triad assembly **1** (Cl^- counterion),[8] in which a tris(4,4′-di-



1

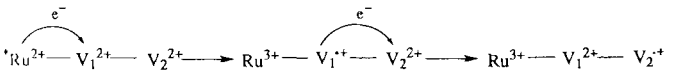
methyl-2,2′-bipyridine)ruthenium(II) component functions as a light-harvesting center. In this triad one of the bipyridine ligands is linked covalently to two acceptor units. We found that formation of intermolecular complexes between the triad and an externally added electron donor such as **3** substantially affects the charge separation within the supramolecular assembly. In this way the electron donor mimics possible effects of protein-linked electron donor units on the charge separation in the photosynthetic reaction center.

[*] Prof. I. Willner, E. Zahavy, S. Marx-Tibbon, E. Joselevich
Institute of Chemistry and Farkas Center for Light-Induced Processes
The Hebrew University of Jerusalem
Jerusalem 91904 (Israel)
Telefax: Int. code + (2)6527715
M. Seiler, Prof. D. Dürr
Universität des Saarlandes, Organische Chemie, Fachbereich 11.2
Saarbrücken (Germany)
Dr. D. O'Connor, Prof. A. Harriman
Center for Fast Kinetics Research, The University of Texas at Austin
Austin, TX (USA)

[**] This research project was supported by the Bundesministerium für Forschung und Technology (BMFT).

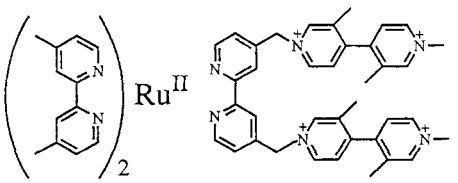
 © VCH Verlagsgesellschaft mbH, D-69451 Weinheim, 1995 0570-0833/95/0909-1005 $ 10.00+.25/0

The components in the difunctional triad **1** were chosen such that their reduction potentials are in the appropriate order for a vectorial stepwise electron transfer. The cyclic voltammogram of triad **1** in the potential range -1.6 to $+2.0$ V (vs. Ag/AgCl) reveals four quasi-reversible reduction waves at -0.405, -0.61, -0.75, and -0.97 V, corresponding to the stepwise reduction of the triad Ru^{2+}-V_1^{2+}-V_2^{2+} (V = electron acceptor unit, see structural formula) to the species Ru^{2+}-V_1^{2+}-$V_2^{\bullet+}$, Ru^{2+}-$V_1^{\bullet+}$-$V_2^{\bullet+}$, Ru^{2+}-$V_1^{\bullet+}$-V^0, and Ru^{2+}-V_1^0-V_2^0, respectively.[9] Since the redox potential of excited Ru^{II} center is -0.638 V (vs. Ag/AgCl), the stepwise vectorial electron transfer summarized in Scheme 1 is feasible.



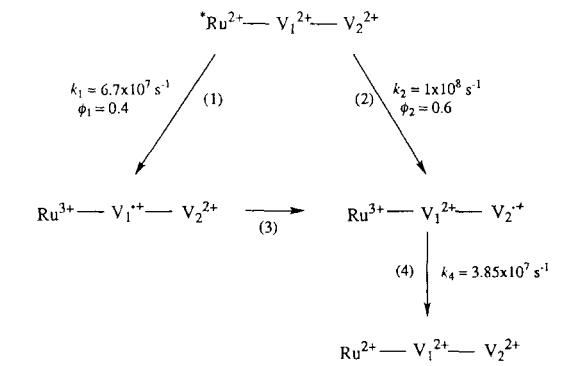
Scheme 1. Vectorial electron transfer in triad **1**.

Photoexcitation of the Ru^{II}–polypyridine center of **1** results in an emission with a lifetime of 6 ± 0.1 ns. For comparison, the lifetime of tris(4,4′-dimethyl-2,2′-bipyridine)ruthenium(II) dichloride is 0.33 μs. Thus, effective quenching of the excited state occurs in the difunctional triad assembly **1**. Further examination of the reference diad assembly **2** reveals that the excited Ru^{II} center has a lifetime of 15 ± 0.3 ns. The shorter lifetime of the excited state of **1** implies that an additional quenching route is operating (Scheme 2).



2

Assuming that electron transfer from the Ru^{II} center in **1** to the first acceptor (V_1) has a similar rate constant to that of the reference compound **2**, $k_1 = (6.7 \pm 0.1) \times 10^7\ s^{-1}$, then the direct electron transfer from Ru^{II} to the second electron acceptor (V_2) proceeds with a rate constant of $k_2 = (1 \pm 0.1) \times 10^8\ s^{-1}$.[10] The quenching of the luminescence ϕ_L of the excited Ru^{II} complex results only in a redox product that corresponds to the charge-separated triad Ru^{3+}-V_1^{2+}-$V_2^{\bullet+}$. This implies that the intermediate redox product Ru^{3+}-$V_1^{\bullet+}$-V_2^{2+} decays to Ru^{3+}-V_1^{2+}-$V_2^{\bullet+}$ [Eq. (3) in Scheme 2] faster than it forms. The charge-separated triad Ru^{3+}-V_1^{2+}-$V_2^{\bullet+}$ decays by back electron transfer to the ground state [Eq. (4) in Scheme 2]. Figure 1 shows the decay of the photogenerated radical cation intermediate Ru^{3+}-V_1^{2+}-$V_2^{\bullet+}$ ($\lambda = 620$ nm) to the ground state. The decay curve is monoexponential and corresponds to a lifetime of 26 ± 0.5 ns. Thus, the recombination rate constant in the triad assembly is $k_4 = (3.8 \pm 0.1) \times 10^7\ s^{-1}$. The species Ru^{3+}-V_1^{2+}-$V_2^{\bullet+}$ was characterized by its transient absorption spectrum; the absorption bands characteristic of the $V_2^{\bullet+}$ unit were identical to those of *N,N′*-dialkyl-4,4′-bipyridinium radical cations.



Scheme 2. Vectorial electron transfer and back-reaction in triad **1**.

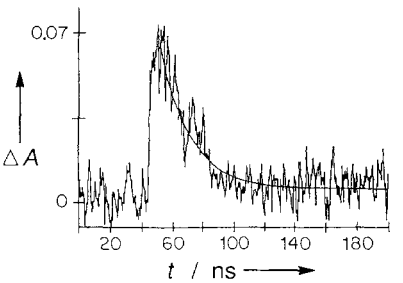
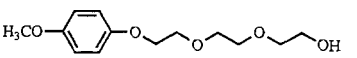


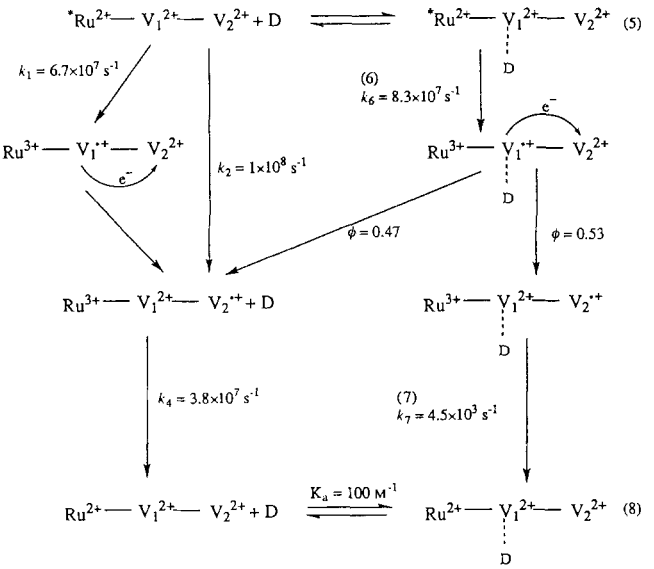
Fig. 1. Transient decay of the photogenerated redox product, Ru^{3+}-V_1^{2+}-$V_2^{\bullet+}$. In this system **1**, $c = 1.5 \times 10^{-4}$ M, $\lambda_{exc} = 532$ nm, $\lambda_{analysis} = 620$ nm.

Addition of 8-(4-anisoxy)-3,6-dioxaoctane-1-ol (**3**), $c = (2.2 \pm 0.2) \times 10^{-2}$ M, to the difunctional triad **1**, $c = 1.5 \times 10^{-4}$ M, substantially influences the electron transfer within the supra-



3

molecular assembly. Dialkoxybenzenes are known to form intermolecular donor–acceptor complexes with *N,N′*-dialkyl-4,4′-bipyridinium salts,[4, 11, 12] and hence the formation of such a supramolecular assembly could structurally distort the difunctional triad. The emission curve of photoexcited **1** in the presence of **3** exhibits a biexponential decay, implying two distinct populations of excited species that are being quenched (Scheme 3).[13]



Scheme 3. Vectorial electron transfer, back-reactions, and charge separation in triad **1** in the presence of added **3**.

 © VCH Verlagsgesellschaft mbH, D-69451 Weinheim, 1995 0570-0833/95/0909-1006 $ 10.00+.25/0

One population (25%) has a lifetime of 6 ± 0.1 ns, identical to that of **1** in the absence of added electron donor. The second population (75%) has a lifetime of 12 ± 0.1 ns. Thus, we suggest that in the presence of **3** the difunctional triad exists in two configurations [Eq. (5) in Scheme 3]. The free triad $*Ru^{2+}$-V_1^{2+}-V_2^{2+} decays within 6 ns, whereas the supramolecular donor–triad complex $*Ru^{2+}$-V_1^{2+}(···D)-V_2^{2+} decays within 12 ns.[14] The redox products detected after the laser pulse contain, however, the oxidized Ru^{3+} center and the reduced second acceptor $V_2^{\bullet+}$ as a radical cation. Figure 2a shows the depletion of the reduced acceptor $V_2^{\bullet+}$ by the intramolecular back-reaction. The decay curve is monoexponential with a time constant τ of 26 ns,

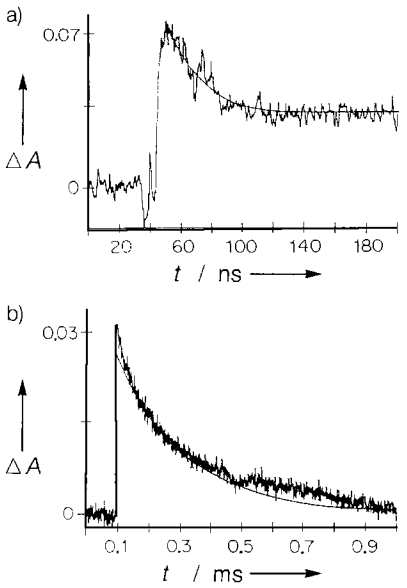
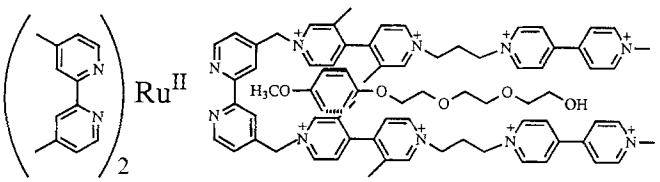


Fig. 2. Transient decay of the photogenerated redox product, Ru^{3+}-V_1^{2+}-$V_2^{\bullet+}$ in the presence of added **3**. $c = 2.25 \times 10^{-2}$ M. a) Transient for fast recombination. b) Transient for slow recombination.

identical to that of the Ru^{3+}-V_1^{2+}-$V_2^{\bullet+}$ radical cation in the absence of **3**. Nonetheless, on this time scale the decay curve of the redox photoproduct does not reach zero, and 40% of the initial redox intermediate remains. Figure 2b shows the decay curve of this stabilized fraction. *We see that this redox intermediate has a lifetime of 220 μs. Thus, in the presence of* **3**, *40% of the generated redox product is stabilized by a factor of roughly* 10^4 *as compared to the redox photoproduct* Ru^{3+}-V_1^{2+}-$V_2^{\bullet+}$ *in the absence of* **3**. We attribute the slow decay to a redox product consisting of the radical cation triad intermolecularly associated with the electron donor **3** [Eq. (7) in Scheme 3].[15]

Previous studies revealed that stable intermolecular complexes are formed between electron donors such as xanthene dyes[16] or dialkoxybenzene[11, 12] and layered bipyridinium salts. Intercalation of **3** between the two bipyridinium branches of triad **1** provides the driving force for the formation of such an intermolecular complex. Further insight into the structure of the intermolecular complex formed between **1** and **3** was obtained by ^{1}H NMR spectroscopy. The ^{1}H NMR spectrum of **1** (400 MHz) was fully analyzed, and the signals of all of the protons associated with the difunctional triad branches were assigned. The two branches are symmetrical. When different concentrations of donor **3** are added to triad **1** in D_2O, the ^{1}H NMR spectra indicate that the symmetry of the triad branches is retained. The signal of proton H_a of the bipyridine ligand is shifted downfield, whereas the signals of protons H_b, $H_{b'}$, H_c, $H_{c'}$, H_d, and $H_{d'}$, associated with the first electron acceptor V_1^{2+}, are shifted upfield. It should be noted that the signals of the protons of the second electron acceptor V_2^{2+} are not affected by the addition of **3**. From the ^{1}H NMR shifts and the titration curves a 1:1 stoichiometry is deduced for the intermolecular complex of **1** and **3**, and the association constant $K_a = 100\ M^{-1}$ was derived.[17] Thus, we suggest that the electron donor intercalates into the groove formed by the photosensitizer ligand and the two electron acceptor units as schematically outlined in structure **4**. The



4

resulting intermolecular complex is stabilized by donor–acceptor charge transfer interactions.[11, 12, 16] The reduction potentials of the electron acceptors indicate that association of the electron donor **3** to the second bipyridinium electron-relay V_2^{2+} should be favored. We believe that the photosensitizer bipyridine ligand acts synergetically in the association of **3** with the less favored position by secondary π–π interactions.

We have found that the formation of the intermolecular complex between **3** and the difunctional triad **1** controls the photoinduced charge separation within the supramolecular assembly. The resulting redox products are 10^4 times more stable to back electron transfer than the system lacking **3**. It is reasonable to assume that the flexibility of the difunctional triad allows the redox centers in Ru^{3+}-V_1^{2+}-$V_2^{\bullet+}$ to be closer together, thus enhancing back electron transfer. The association of the electron donor **3** with the difunctional triad could rigidify the conformation of the triad and align it in a stretched structure, whereby the increased distance between the generated redox species retards back eletron transfer. Such a mechanism could also operate in the natural photosynthetic reaction center. Intermolecular complexes between protein donor units such as histidine or tyrosine and the electron acceptors involved with the reaction center could be aligned in an optimal conformation for effective charge separation.

Received: September 26, 1994
Revised version: December 14, 1994 [Z 7357 IE]
German version: *Angew. Chem.* **1995**, *107*, 1112

Keywords: electron transfer · luminescence · photochemistry · ruthenium compounds

[1] a) D. Gust, T. A. Moore, A. L. Moore, G. Seely, P. Liddell, D. Barrett, L. O. Harding, X. C. Ma, S. J. Lee, F. Gao, *Tetrahedron* **1989**, *45*, 4867; b) D. Gust, T. A. Moore, *Top. Curr. Chem.* **1991**, *159*, 103.

[2] a) D. Gust, T. A. Moore, *Science* **1989**, *244*, 35; b) in *Supramolecular Photochemistry* (Ed.: V. Balzani), Reidel, Dordrecht, The Netherlands, **1987**, p. 267; c) in *Protein Structure, Molecular and Electron Reactivity* (Eds.: R. Austin, E. Buhks, B. Chance, D. De Vault, P. L. Dutton, H. Fraunfelder, V. I. Goldanskii), Springer, Berlin, **1987**, p. 389; d) T. J. Meyer, *Acc. Chem. Res.* **1989**, *22*, 163.

[3] a) J. S. Conolly, J. R. Bolton in *Photoinduced Electron Transfer, Part D* (Eds.: M. A. Fox, M. Chanon), Elsevier, Amsterdam, **1988**, p. 303; b) M. R. Wasielewski, *Chem. Rev.* **1992**, *92*, 435.

[4] a) S. Bossmann, M. Seiler, H. Dürr, *J. Phys. Org. Chem.* **1992**, *5*, 63; b) H. Dürr, S. Bossmann, G. Heppe, R. Schwarz, U. Thiery, H. P. Trierweiler, *Proc. Indian Acad. Sci.* **1993**, *105*, 435; c) M. Seiler, H. Dürr, I. Willner, E. Joselevich, A. Doron, J. F. Stoddart, *J. Am. Chem. Soc.* **1994**, *116*, 3399; d) H. Dürr, S. Bossmann, R. Schwarz, *J. Inf. Rec. Mater.* **1994**, *21*, 471; e) H. Dürr, S. Bossmann, R. Schwarz, M. Kropf, R. Hayo, N. J. Turro, *J. Photochem. Photobiol. A* **1994**, *80*, 341; f) M. Seiler, H. Dürr, *Liebigs Ann.* **1995**, *407*.

[5] S. Kartha, R. Das, J. R. Norris, *Ions Biol. Syst.* **1991**, *27*, 323.
[6] a) C. H. Chang, D. M. Tiede, J. Tang, U. Smith, J. R. Norris, M. Schiffer, *FEBS Lett.* **1986**, *205*, 82; b) J. P. Allen, G. Feher, T. O. Yeates, H. Komiya, D. C. Rees, *Proc. Natl. Acad. Sci. USA* **1987**, *84*, 5730.
[7] a) M. Bixon, M. E. Michel-Beyerle, J. Jortner, *Isr. J. Chem.* **1988**, *28*, 155; b) W. W. Parson, A. Warshel, S. Creighton, *J. Phys. Chem.* **1988**, *92*, 2696; c) E. V. Kitzing, H. Kuhn, *J. Phys. Chem.* **1990**, *94*, 1699.
[8] M. Seiler, H. Dürr, *Synthesis* **1994**, 83; M. Seiler, Dissertation, Universität des Saarlandes, Saarbrücken, **1994**.
[9] The reduction waves were assigned to the corresponding redox intermediates by comparison of the cyclic voltammogram of **1** to that of tris(4,4'-dimethyl-2,2'-bipyridine)ruthenium(II) and reference compound **2**.
[10] Although V_2 is spatially separated from the excited Ru^{II} center, electron transfer to the second acceptor is slightly faster than to the first acceptor V_1. This is attributed to the higher free energy associated with the electron transfer to the second acceptor (V_2) ($\Delta G^\circ = -22.5\ kJ\,mol^{-1}$).
[11] a) P. R. Ashton, R. A. Bissell, D. Philip, N. Spencer, J. F. Stoddart in *Supramolecular Chemistry* (Eds.: V. Balzani, L. De Cola), Kluwer, Dordrecht, The Netherlands, **1991**; b) B. Odell, M. V. Reddington, A. M. Z. Slawin, N. Spencer, J. F. Stoddart, D. J. Williams, *Angew. Chem.* **1988**, *100*, 1605; *Angew. Chem. Int. Ed. Engl.* **1988**, *27*, 1547; c) P. R. Ashton, B. Odell, M. V. Reddington, A. M. Z. Slawin, J. F. Stoddart, D. J. Williams, *ibid.* **1988**, *100*, 1611 and **1988**, *27*, 1550; d) P. R. Ashton, T. T. Goodnow, A. E. Kaifer, M. V. Reddington, A. M. Z. Slawin, N. Spencer, J. F. Stoddart, C. Vincent, D. J. Williams, *Angew. Chem.* **1989**, *101*, 1404; *Angew. Chem. Int. Ed. Engl.* **1989**, *28*, 1396.
[12] a) P. L. Anelli, P. R. Ashton, N. Spencer, A. M. Z. Slawin, J. F. Stoddart, D. J. Williams, *Angew. Chem.* **1991**, *103*, 1052; *Angew. Chem. Int. Ed. Engl.* **1991**, *30*, 1036; b) P. L. Anelli, N. Spencer, J. F. Stoddart, *J. Am. Chem. Soc.* **1991**, *113*, 5131; c) P. R. Ashton, R. Ballardini, V. Balzani, M. T. Gandolfi, D. J.-F. Marquis, L. Perez-Garcia, L. Prodi, J. F. Stoddart, D. J. Williams, *J. Chem. Soc. Chem. Commun.* **1994**, 177; d) S. Bossmann, M. Seiler, H. Dürr, *J. Phys. Org. Chem.* **1992**, *5*, 63; e) P. R. Ashton, D. Philip, N. Spencer, J. F. Stoddart, D. J. Williams, *J. Chem. Soc. Chem. Commun.* **1994**, 181.
[13] All experiments were performed in H_2O at 298 K. No quenching of **2** or of the reference compound tris(4,4'-dimethylbipyridine)ruthenium(II) by **3**, $c = 2.2 \times 10^{-2}$ M, could be detected.
[14] Using the value of the association constant ($K_a = 100\ M^{-1}$) for the complex and the respective concentrations of **1** and **3** (150-fold excess), we estimate the ratio of the ground state reactants Ru^{2+}-V_1^{2+}-V_2^{2+} and Ru^{2+}-V_1^{2+}(···D)-V_2^{2+} to be 3:7. This ratio is very similar to the populations of the quenched photosensitizers **1** and **4**, respectively. Thus, the association constant between **3** and excited **1** has a similar value to the ground state association constant. The quenching rate constant for $^*Ru^{2+}$-V_1^{2+}(···D)-V_2^{2+} is identical to that observed for reference compound **2**. Accordingly, the primary electron transfer in the supramolecular triad–donor complex occurs only to the first acceptor (V_1^{2+}) to generate Ru^{3+}-$V_1^{\bullet+}$(···D)-V_2^{2+}.
[15] Note that although 75% of the excited triad in the supramolecular assembly $^*Ru^{2+}$-V_1^{2+}-V_2^{2+} undergoes electron transfer quenching, only 40% of the photoproduct recombines by the slow route through the intermolecular complex intermediate Ru^{3+}-V_1^{2+}(···D)-$V_2^{\bullet+}$. This is attributed to the fact that the primary electron transfer product is Ru^{3+}-$V_1^{\bullet+}$(···D)-V_2^{2+}. In this intermediate the donor **3** is poorly associated to the triad owing to reduction of one of the bipyridinium components that stabilize the complex. Hence, dissociation of the complex structure competes with the intermolecular vectorial electron transfer, whereby the supramolecular complex is restabilized. Thus, the enriched fraction of Ru^{3+}-V_1^{2+}-$V_2^{\bullet+}$ originates from the dissociation of the complex Ru^{3+}-$V_1^{\bullet+}$(···D)-V_2^{2+} that competes with intramolecular electron transfer generating the stable intermediate, Ru^{3+}-V_1^{2+}(···D)-$V_2^{\bullet+}$ (Scheme 3).
[16] I. Willner, Y. Eichen, M. Rabinovitz, R. Hoffmann, S. Cohen, *J. Am. Chem. Soc.* **1992**, *114*, 637.
[17] C. S. Wilcox in *Frontiers in Supramolecular Chemistry and Photochemistry* (Eds.: H.-J. Schneider, H. Dürr), VCH, New York, **1991**.

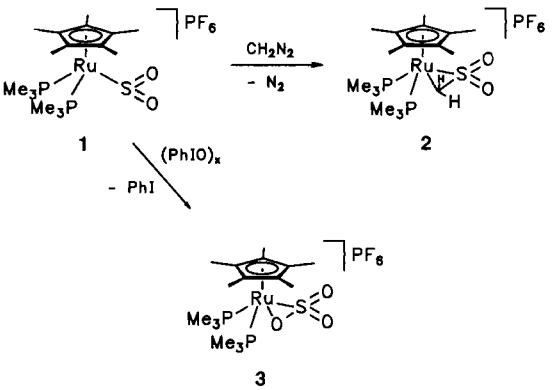
$[Cp^*(Me_3P)_2Ru(\eta^2\text{-}O{=}SO_2)]PF_6$, the First Complex between a Transition Metal and Sulfur Trioxide**

Eberhard Dombrowski and Wolfdieter A. Schenk*

Dedicated to Professor Peter Paetzold on the occasion of this 60th birthday

The reactivity of unsaturated molecules is distinctly modified by coordination to transition metal fragments. This aspect of the coordination chemistry of sulfur dioxide has also attracted increasing attention.[1, 2] Nucleophilic additions at sulfur[3, 4] on one hand, and reduction to SO and other species[2, 5] on the other have been priorities in these studies. Now we report an oxidation of metal-coordinated sulfur dioxide that leads to the first example of a transition metal complex of sulfur trioxide.

Recently we obtained complex **2**,[4b] a stable complex of sulfene, which cannot exist in the free state, from $[Cp^*Ru(PMe_3)_2(SO_2)]PF_6$ (**1**) by nucleophilic methylene transfer. It therefore seemed feasible to synthesize an SO_3 complex in an analogous way. As reagent we selected iodosobenzene, which has previously proved useful for nucleophilic oxygen transfers to coordinated CO and CH_2.[6] From **1** the ionic compound **3** is indeed obtained (Scheme 1) and could be identified as the first sulfur trioxide complex by spectroscopy and X-ray structure analysis.[7]



The structure of **3** (Fig. 1) clearly underscores the close relationship to the sulfene complex **2**.[4b] Thus, **2** and **3** have nearly

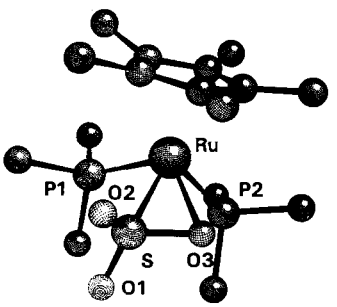


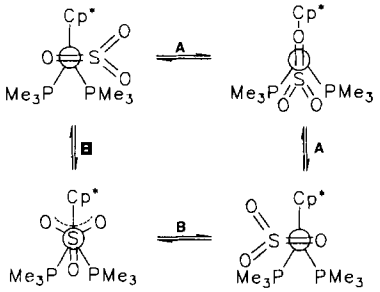
Fig. 1. Structure of the cation of **3** · Me_2CO. Bond lengths [pm]: Ru-P1 237.0(1), Ru-P2 238.1(1), Ru-S 227.15(8), Ru-O3 218.2(2), Ru-Cp (ring centroid) 192.4(0), S-O1 144.1(3), S-O2 145.4(3), S-O3 152.3(3); bond angles [°]: P1-Ru-P2 86.81(3), P1-Ru-S 87.00(3), P1-Ru-O3 118.02(8), P2-Ru-S 103.15(3), P2-Ru-O3 80.26(7), S-Ru-O3 39.94(8), O1-S-O2 113.7(2), O1-S-O3 112.4(2), O2-S-O3 112.7(2).

[*] Prof. Dr. W. A. Schenk, Dipl.-Chem. E. Dombrowski
Institut für Anorganische Chemie der Universität
Am Hubland, D-97074 Würzburg (Germany)
Telefax: Int. code + (931)888-4605

[**] Sulfur(IV) Compounds as Ligands, Part 22. This work was supported by the Fonds der Chemischen Industrie. Part 21: W. A. Schenk, J. Frisch, W. Adam, F. Prechtl, *Angew. Chem.* **1994**, *106*, 1699; *Angew. Chem. Int. Ed. Engl.* **1994**, *33*, 1609.

equal Ru–S lengths, the Ru–O distance of **3** is 15 pm smaller than the Ru–C distance of **2**, which approximately corresponds to the difference between the covalent radii of O and C. The S–O(3) bond is 10 pm longer than in uncoordinated SO_3 (142.0 pm[8]) but still distinctly shorter than a S–O single bond (for example, 158 pm in sulfonic acid esters[9]). The difference between endocyclic and exocyclic S–O distances in **3** equals that in η^2-SO_2 complexes, for example in $[Mo(CO)_2(PMe_3)_3(\eta^2\text{-}O{=}SO)]$.[10] Accordingly the bonding in **3** can best be described in terms of the Dewar–Chatt–Duncanson model as a side-on coordination of a S–O double bond of SO_3 to a 16-valence electron complex. Thus, sulfur trioxide can, unexpectedly,[1] act as a ligand in transition metal complexes despite its pronounced Lewis acidity.

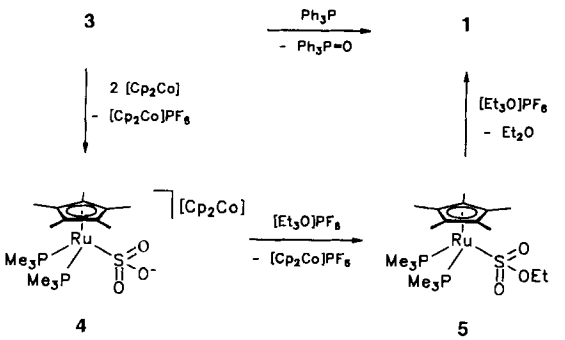
In solution **3** exhibits dynamic behavior: its ^1H and ^{31}P NMR signals are broadened by an exchange process ($\Delta G^{\neq}$ = 61 kJ mol^{-1}) which renders the two PMe_3 ligands magnetically equivalent. Two different processes might be envisioned, a rotation of the SO_3 ligand by 180° (route A, Scheme 1), or a 60°



Scheme 1. Exchange processes leading to equivalence of the PMe_3 ligands in the ^1H and ^{31}P NMR spectra.

rotation concomitant with a 1,2-shift of the metal atom (route B).

Preliminary investigations into the reactivity of **3** document the facile reducibility of the coordinated sulfur trioxide. With a stoichiometric amount of triphenylphosphane, **3** is converted



back into the starting material **1**. An excess of phosphane has to be avoided since this would cause decomposition with phosphane exchange and further reduction of the coordinated SO_2.

Cobaltocene reduces **3** to the sulfito complex **4**; this can be converted back into the starting material **1** by double alkylation via the ethylsulfito complex **5**. Hence the identity of **3** has also been unequivocally proved by chemical means.

Experimental Procedure

3: To a solution of **1** (95 mg, 0.16 mmol) in dichloromethane (5 mL) was added iodosobenzene (88 mg, 0.40 mmol) at −20 °C. After 5 h at 20 °C the slightly turbid brown solution was filtered through celite, and the product precipitated on addition of hexane (15 mL) at 0 °C. Yield 86 mg (88%), yellow-brown crystalline powder (correct elemental analysis for C, H, and S). IR (Nujol) $\tilde{\nu}$(SO) = 1224, 1124 cm^{-1}. ^1H NMR ([D$_6$]acetone, 400 MHz) δ = 1.82 (vt, N = 11.2 Hz, PCH_3), 1.93 (t, J = 0.7 Hz, CCH_3); ^{31}P NMR (CD_2Cl_2, 162 MHz, −70 °C) δ = 9.6, 7.6 (AB system, J(AB) = 55 Hz).

1 from **3**: **3** (7 mg, 11 μmol) was dissolved in CD_2Cl_2 (0.5 mL) in an NMR tube and treated with PPh_3 (2.6 mg, 10 μmol). After 30 min at 20 °C the ^{31}P NMR spectrum consisted predominantly of the signals of **1** (δ = 0.8) and Ph_3PO (δ = 27.5).

4: To a solution of **3** (74 mg, 0.12 mmol) in THF (15 mL) was added cobaltocene (46 mg, 0.24 mmol) at 20 °C. After 3 h the solvent was removed under vacuum, and the residue extracted with benzene. The product was isolated from the evaporated extract by crystallization from dichloromethane/ether. Yield 52 mg (66%), yellow crystalline powder. IR (Nujol) $\tilde{\nu}$(SO) = 1154, 1036 cm^{-1}. ^1H NMR (CD_2Cl_2, 400 MHz) 1.43 (vt, N = 8.9 Hz, PCH_3), 1.71 (s, $C_5(CH_3)_5$), 5.72 (s, $(C_5H_5)_2Co$). ^{31}P NMR (CD_2Cl_2, 162 MHz): δ = 9.3 (s).

1 from **4**: To a solution of **4** (52 mg, 0.08 mmol) in dichloromethane (20 mL) was added Et_3OPF_6 (40 mg, 0.16 mmol) at 20 °C. The yellow solution discolored immediately; precipitation with diethyl ether yielded 45 mg (95%) of **1**.

Received: December 15, 1994
Revised version: February 10, 1995 [Z 7553 IE]
German version: *Angew. Chem.* **1995**, *107*, 1098

Keywords: complexes with sulfur ligands · ruthenium compounds · sulfur trioxide

[1] W. A. Schenk, *Angew. Chem.* **1987**, *99*, 101; *Angew. Chem. Int. Ed. Engl.* **1987**, *26*, 98, and references therein.
[2] G. J. Kubas, *Acc. Chem. Res.* **1994**, *27*, 183, and references therein.
[3] a) W. A. Schenk, U. Karl, *Z. Naturforsch. B* **1989**, *44*, 993; b) W. A. Schenk, P. Urban, T. Stährfeldt, E. Dombrowski, *ibid.* **1992**, *47*, 1493.
[4] a) W. A. Schenk, P. Urban, *J. Organomet. Chem.* **1991**, *411*, C27; b) W. A. Schenk, P. Urban, E. Dombrowski, *Chem. Ber.* **1993**, *126*, 679.
[5] a) A. Neher, L.-P. Lorenz, *Angew. Chem.* **1989**, *101*, 1389; *Angew. Chem. Int. Ed. Engl.* **1989**, *28*, 1342; b) O. Heyke, L.-P. Lorenz, *Phosphorus Sulfur Silicon Relat. Elem.* **1992**, *71*, 139; c) G. B. Karet, C. C. Stern, D. M. Norton, D. F. Shriver, *J. Am. Chem. Soc.* **1993**, *115*, 9979.
[6] a) A. T. Patton, C. E. Strouse, C. B. Knobler, J. A. Gladysz, *J. Am. Chem. Soc.* **1983**, *105*, 5804; b) W. E. Buhro, A. T. Patton, C. E. Strouse, J. A. Gladysz, F. B. Mc Cormick, M. C. Etter, *ibid.* **1983**, *105*, 1056; c) J. K. Shen, Y. L. Shi, Y. C. Gao, O. Z. Shi, F. Basolo, *Organometallics* **1988**, *7*, 531.
[7] X-ray structure analysis of **3** · Me_2CO: crystals from acetone/ether. Triclinic, a = 873.3(8), b = 1176.5(3), c = 1404.7(3) pm, α = 83.97(2), β = 80.02(4), γ = 86.24(4)°, Z = 2, ρ_{calcd} = 1.581 mg mm^{-3}. Space group $P\bar{1}$ (no. 2), 4732 intensities recorded, 4072 of which were symmetry-independent and 3962 classified as observed with $I_o > 3\sigma(I_o)$, R = 0.027, R_w = 0.034. Further details of the crystal structure determination can be obtained from Fachinformationszentrum Karlsruhe, D-76344 Eggenstein-Leopoldshafen, on quoting the depository number CSD-58842.
[8] *Gmelin Handbuch der Anorganischen Chemie (Schwefel, Ergänzungsband 3)*, 8th ed., Springer, Berlin, **1980**.
[9] H. Basch, T. Hoz in *The Chemistry of Sulfonic Acids, Esters and their Derivatives* (Eds.: S. Patai, Z. Rapoport), Wiley, New York, **1991**, p. 1.
[10] F. E. Baumann, C. Burschka, W. A. Schenk, *Z. Naturforsch. B* **1986**, *41*, 1211.
[11] M. J. S. Dewar, *Bull. Soc. Chim. Fr.* **1951**, *18*, C71; J. Chatt, L. A. Duncanson, *J. Chem. Soc.* **1953**, 2939.

 © *VCH Verlagsgesellschaft mbH, D-69451 Weinheim, 1995* *0570-0833/95/0909-1009 $ 10.00+.25/0*

The First Mixed-Metal Borole Cluster; Stabilization of Formally 14e Pd Centers in the Re_2Pd_2 Electron-Deficient $[\{[(\eta^5\text{-}C_4H_4BPh)(CO)_3Re]Pd\}_2]$ Cluster**

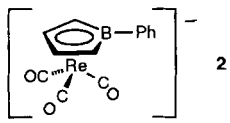
Pierre Braunstein,* Ulli Englert,
Gerhard E. Herberich,* and Mark Neuschütz

Carbonylmetalates have long been used for the synthesis of metal cluster complexes and have proved particularly useful in mixed-metal cluster chemistry. The HOMO of 18-electron reagents such as $[CpMo(CO)_3]^-$ ($Cp = \eta\text{-}C_5H_5$) has mostly metal d orbital character, accounting for its propensity to form metal–metal bonds. For the isosteric reagent $[CpMn(CO)_2(CN)]^-$, in contrast, the HOMO is centered on the cyano nitrogen atom, which explains the tendency of this anion to form linear Mn-CN-M′ arrays.[1] In 1990 we found that this cyanometalate is simultaneously involved in both Mn-CN-Pd and direct Mn–Pd bonding in the unprecedented octanuclear, double-helix-type cluster **1**.[2] We have begun an investigation of the reactivity of electronically related borole-containing metalates such as **2**, where the negative charge is very much delocalized, and **3**, where it is mostly associated with the cyano ligand.[3] We also hoped that these compounds would allow the synthesis of the first cluster complexes containing a borole ligand. This was actually achieved and we present here our first results with anion **2** and the characterization of an unprecedented Re_2Pd_2 cluster **4**.

$[\{(\eta^5\text{-}C_5H_4Me)(CO)_2Mn(CN)Pd\}_4]$ **1** $[(\eta^5\text{-}C_4H_4BPh)Re(CO)_3]^-$ **2**

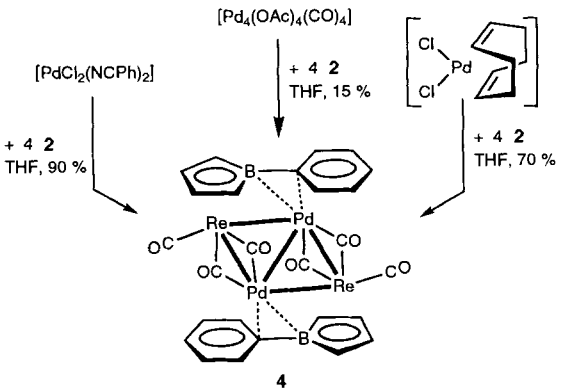
$[(\eta^5\text{-}C_4H_4BPh)Fe(CO)_2(CN)]^-$ **3**

In contrast to the strong nucleophile $[Re(CO)_5]^-$, **2** showed surprisingly little reactivity towards Pt^{II}, Pd^{II}, or Pd^{I} complexes. Neither with *cis*-$[PtCl_2(PEt_3)_2]$, $[PtBr_2(\gamma\text{-picoline})_2]$, $[PtCl_2(NCPh)_2]$, $[PtCl_2(cod)]$ (cod = 1,5-cyclooctadiene), nor $[Pd_2Cl_2(\mu\text{-dppm})_2]$ (dppm = bis(diphenylphosphano)methane) or $[PdCl_2(PPh_3)_2]$ was any product formed and no decomposition of **2** was observed. However, the reactions of **2** with *cis*-$[PdCl_2(NCPh)_2]$, $[PdCl_2(cod)]$, or $[Pd_4(\mu\text{-}OAc)_4(\mu\text{-}CO)_4]$ always afforded the same product **4**. This compound is deep blue-green, owing to the presence of a strong absorption band in the visible region at 640 nm, and is soluble in THF but only slightly soluble in toluene and dichloromethane. It is suprisingly air stable, even in solution. This complex was identified as the Re_2Pd_2 title cluster **4**, in which the palladium centers are in the formal oxidation state +1.



2

The metal core of **4** consists of a planar, triangulated rhombus with an inversion center in the middle of the Pd–Pd′ bond



4

(Fig. 1).[4] This bond is rather long (2.899(2) Å) when compared with those in other clusters,[5–8] in particular the series of planar, triangulated clusters **5**, in which the Pd–Pd′ distance ranges from

$[\{Cp(CO)_3MPd(PEt_3)\}_2]$ **5**, M = Cr, Mo, W

2.573(3) (M = W) to 2.582(1) Å (M = Mo).[5b] The fact that one of the Pd–Re bonds in **4** is very short (2.666(1) Å) is most probably because it is doubly spanned by carbonyl ligands. An average Pd–Re bond length of 2.872 Å has been found in the only other structurally characterized Pd–Re cluster known to us.[9]

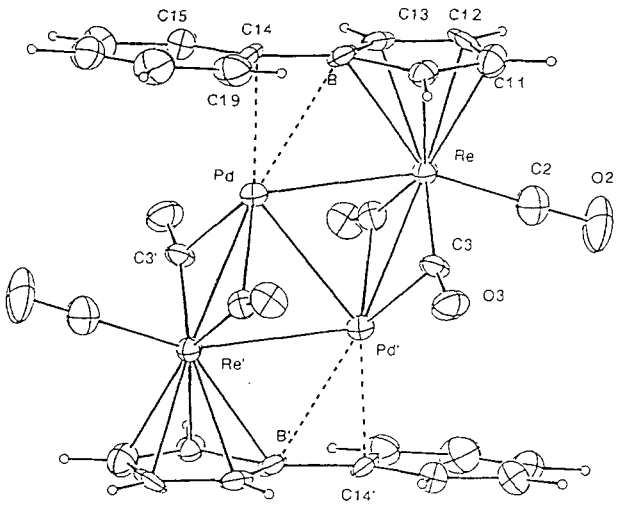


Fig. 1. Structure of **4** in the crystal [4] (thermal ellipsoids for 30% probability). Selected interatomic distances [Å] and angles [°]: Re-Pd 2.866(1), Re-Pd′ 2.666(1), Pd-Pd′ 2.899(2), Re-C1 1.96(1), O1-C1 1.17(1), Re-C2 1.92(1), O2-C2 1.14(1), Re-C3 1.99(1), O3-C3 1.15(1), Re-B 2.43(1), Re-C10 2.29(1), Re-C11 2.23(1), Re-C12 2.22(1), Re-C13 2.26(1), C10-B 1.54(2), C10-C11 1.37(2), C11-C12 1.41(2), C12-C13 1.40(2), C13-B 1.55(2), C14-B 1.57(2), C14-C15 1.41(2), C15-C16 1.39(2), C16-C17 1.35(2), C17-C18 1.41(2), C18-C19 1.37(2), C14-C19 1.42(2), Pd-C1′ 2.19(1), Pd-C3′ 2.22(1), Pd-C14 2.27(1), Pd-B 2.59(2); Re-Pd-Pd′ 55.07(3), Re-Pd-Re′ 116.91(3), Pd-Re-Pd′ 63.09(3), Re-Pd′-Pd 61.83(4), Pd-C14-B 82.9(7), Re-Pd-C14 89.4(2), Re′-Pd-B 169.4(2), Pd-Re-C1 77.4(3), Pd-Re-C2 156.5(5), Pd-Re-C3 77.9(4), C1-Re-C2 90.0(6), C1-Re-C3 108.3(6), C2-Re-C3 87.5(6), Re-C1-O1 161(1), Re-C2-O2 179(1), Re-C3-O3 163(1), C11-C10-B 111(1), C10-C11-C12 108(1), C11-C12-C13 112(1), C12-C13-B 108(1), C10-B-C13 100(1).

[*] Dr. P. Braunstein, Dr. M. Neuschütz
Laboratoire de Chimie de Coordination, URA 416 CNRS
Université Louis Pasteur
4, rue Blaise Pascal, F-67070 Strasbourg Cédex (France)
Telefax: Int. code + 88 41 60 30
e-mail: braunst@chimie.u-strasbg.fr
Prof. Dr. G. E. Herberich, Dr. U. Englert
Institut für Anorganische Chemie der Technischen Hochschule
Professor-Pirlet-Strasse 1, D-52074 Aachen (Germany)
Telefax: Int.code + (241)8888-288

[**] This work is based on the Ph.D. thesis of M. N. We are grateful to the Deutsche Akademische Austauschdienst for a grant to M. N., the Centre National de la Recherche Scientifique (Paris) for financial support, and Johnson Matthey PLC for a generous loan of $PdCl_2$.

A remarkable feature of the crystal structure of **4** is the short distance between the *ipso* carbon atom of the phenyl ring and the corresponding palladium atom (2.27(1) Å), which is, however, not accompanied by a pyramidalization of this carbon. The p(π) orbital at C14, which is perpendicular to the phenyl ring and points toward the palladium atom, must be involved in this interaction. Very few crystal structures contain aryl rings η^1-coordinated to a transition metal center in which all the C atoms are sp^2-hybridized.[10] Neither the interaction of the phenyl group with Pd nor the short Pd–B distance of 2.59(2) Å lead to an important slip distortion (0.07 Å).[11] The slight folding of the borole ligand about the C10–C13 axis shifts the boron atom away from the rhenium atom, but its distance to the best plane passing through the borole carbon atoms is only 0.10 Å. These values may be taken as evidence for η^5-coordination of the borole ligand to rhenium and the interaction of the palladium atom with both the boron and the phenyl *ipso* carbon atom.

Whereas the planar, triangulated cluster anion $[Re_4(CO)_{16}]^{2-}$[12] with 62 cluster valence electrons (CVE) satisfies both Wade–Mingos and the Effective Atomic Number (EAN) rules, clusters containing platinum or palladium generally have fewer CVEs. For example the planar, triangulated cluster **5**, M = Mo, has 58 CVE corresponding to five metal–metal bonds between 16-electron palladium and 18-electron molybdenum centers.[5a, b] A localized electron count was not possible, and the $CpMo(CO)_3$ fragment was best considered as a 3e donor metalloligand. The structural similarity (and differences) between Mo_2Pd_2 cluster **5** and **4** ($CpMo(CO)_3$ and (η^5-C_4H_4BPh)$Re(CO)_3$ are isoelectronic fragments) emphasize the origin of the electronic unsaturation in our new Re_2Pd_2 54 CVE cluster **4** (neglecting the Pd-B-C14 interaction): the two electron donor phosphane ligands present in the Mo_2Pd_2 cluster **5** are "missing" in **4**. The fragment (η^5-C_4H_4BPh)$Re(CO)_3$ should be considered as formally donating 3e to the Pd_2 unit, which results in formally 14e Pd centers. The nature and stabilizing role of the interaction of these Pd centers with the B–Ph σ bonds is being further analyzed.[13]

$$2 \times 18(Re) + 2 \times 14(Pd) = 54(CVE) + 5 \times 2\ (2c\text{–}2e\ bonds)$$

Preliminary extended Hückel calculations on **4**[14] give a MO scheme with a small HOMO–LUMO gap (0.676 eV) and a much larger gap between the LUMO and the next unoccupied orbital (1.409 eV). This confirms that cluster **4** is electron deficient and is consistent with the cyclic voltammogram of **4** (THF/TBAH, platinum electrode), which shows two reduction steps, at −0.47 V and −0.85 V vs. SCE, but no oxidation up to +1.0 V. In contrast, the related 58 CVE planar, triangulated clusters **5** and **6** are difficult to reduce (−0.85 V to −1.57 V vs. SCE) but are easily oxidized to dications.[15]

$[\{Cp(CO)_3MPt(PEt_3)\}_2]$ **6**, M = Cr, Mo, W

Experimental Procedure

Reactions were performed under purified nitrogen, using standard Schlenk techniques. Satisfactory elemental analyses were obtained for all complexes. Experiments were carried out in both [D_8]THF (to determine the yields by ^{1}H NMR spectroscopy with NMe_4^+ as internal standard) and toluene.

4: Toluene was added to a mixture of $NMe_4 \cdot$ **2** [3] and the corresponding palladium complex. The reaction mixture was stirred, the deep blue suspension of **4** was filtered and the solvent removed under vacuum.

Reaction of **2** with *cis*-$[PdCl_2(NCPh)_2]$: A solution of $NMe_4 \cdot$ **2** (16 mg, 0.03 mmol) and *cis*-$[PdCl_2(NCPh)_2]$ (6 mg, 0.015 mmol) in [D_8]toluene (0.3 mL) was stirred at ambient temperature for 10 min. The dark blue residue of **4** was identified by NMR spectroscopy (yield by spectroscopy: ca. 90%).

The reactions of **2** with $[PdCl_2(1,5\text{-cod})]$ (stirring at 60 °C for 45 min) and $[Pd_4(OAc)_4(CO)_4]$ (stirring at ambient temperature for 5 min) afforded **4** in yields of ca. 70% and 15%, respectively, by NMR spectroscopy. Monitoring of the reactions by NMR showed that one equivalent of **2** was used to reduce the Pd^{II} complexes to Pd^{I} species, the second equivalent to form cluster **4**.

Selected data for **4**: IR (toluene): $\tilde{\nu}$(CO) = 1978(s), 1894(s) cm^{-1}; IR (KBr): $\tilde{\nu}$(CO) = 1961(s), 1888(s) cm^{-1}; FIR (polyethylene): $\tilde{\nu}$ = 488(m), 478(s), 466(s), 437(m), 413(s), 370(m), 329(m), 296(m) cm^{-1}; UV (THF): λ = 640 nm; ^{1}H NMR (300 MHz, [D_8]toluene): δ = 7.74, 7.47 (m, 10H; phenyl), 4.87 (m, 4H, $N = {}^3J_{23} + {}^4J_{24} = 6.4$ Hz; 3,4-borole), 3.83 (m, 4H, $N = 6.4$ Hz; 2,5-borole); ^{1}H NMR (80 MHz, [D_8]THF): δ = 7.57, 7.02 (m, 10H; phenyl), 5.39 (m, 4H, $N = 6.4$ Hz; 3,4-borole), 3.89 (m, 4H, $N = 6.4$ Hz; 2,5-borole); MS (SIMS, DMBA): *m/z* (%): 1034 (13) [M^-], 950 (4) [$M^- - 3CO$], 411 (100) [**2**]$^-$.

Received: October 19, 1994
Revised version: December 8, 1994 [Z 7411 IE]
German version: *Angew. Chem.* **1995**, *107*, 1090

Keywords: borole ligands · electron-deficient compounds · palladium compounds · rhenium compounds

[1] P. Braunstein in *Perspectives in Coordination Chemistry* (Eds.: A. F. Williams, C. Floriani, A. E. Merbach), Helvetica Chimica Acta/VCH, Basel, **1992**, pp. 67–107.

[2] P. Braunstein, B. Oswald, A. Tiripicchio, M. Tiripicchio Camellini, *Angew. Chem.* **1990**, *102*, 1206–1209; *Angew. Chem. Int. Ed. Engl.* **1990**, *29*, 1140–1143.

[3] a) G. E. Herberich, B. J. Dunne, B. Hessner, *Angew. Chem.* **1989**, *101*, 798–800; *Angew. Chem. Int. Ed. Engl.* **1989**, *28*, 737; b) G. E. Herberich, T. Carstensen, D. P. J. Köffer, N. Klaff, R. Boese, I. Hyla-Kryspin, R. Gleiter, M. Stephan, H. Meth, U. Zenneck, *Organometallics* **1994**, *13*, 619–630, c) I. Hyla-Kryspin, R. Gleiter, G. E. Herberich, M. Bénard, *ibid.* **1994**, *13*, 1795–1805.

[4] a) Crystal structure determination of **4**. ENRAF-Nonius CAD4; $Mo_{K\alpha}$ radiation, graphite monochromator; numerical absorption correction; intensity data were collected with the ω scan mode at 258 K. $C_{26}H_{18}B_2O_6Pd_2Re_2$: blue-green transparent platelet with approximate dimensions 0.42 × 0.28 × 0.02 mm, orthorhombic, space group *Pbca* (No. 61); a = 8.427(3), b = 15.923(3), c = 19.493(2) Å, V = 2616(1) Å^3, Z = 4, ρ_{calcd} = 2.627 g cm^{-3}, $\mu(Mo_{K\alpha})$ = 107.5 cm^{-1}, $F(000)$ = 1896; 2040 reflections in the scan range $3 < \theta < 25°$, 1564 independent reflections with $I > 0.5\,\sigma(I)$ used in structure solution and refinement [4b] for 172 parameters; point symmetry of the molecule is $\bar{1}$; R = 0.049, R_w = 0.039, $w^{-1} = 1/\sigma^2(F_o)$, GOF = 1.141; anisotropic refinement for non-hydrogen atoms, hydrogen atoms in idealized geometry. Highest residual electron density 1.3 e Å^{-3} close (1.0 Å) to Re; b) B. Frenz, SDP-PLUS, Version 1.1 (1984) and VAXSDP, Version 2.2 (1985); c) Further details of the crystal structure investigation may be obtained from the Fachinformationszentrum Karlsruhe, D-76344 Eggenstein-Leopoldshafen (Germany), on quoting the depository number CSD-401557.

[5] a) R. Bender, P. Braunstein, Y. Dusausoy, J. Protas, *Angew. Chem.* **1978**, *90*, 637–638; *Angew. Chem. Int. Ed. Engl.* **1978**, *17*, 596–597; b) R. Bender, P. Braunstein, J. M. Jud, Y. Dusausoy, *Inorg. Chem.* **1983**, *22*, 3394–3407; c) *ibid.* **1984**, *23*, 4489–4502.

[6] a) I. I. Moiseev, T. A. Stromnova, M. N. Vargaftig, G. J. Mazo, L. G. Kuz'mina, Y. T. Struchkov, *J. Chem. Soc. Chem. Commun.* **1978**, 27–28; b) T. A. Stromnova, I. N. Busygina, S. B. Katser, A. S. Antsyshkina, M. A. Porai-Koshits, I. I. Moiseev, *ibid.* **1988**, 114–115.

[7] a) P. Braunstein, M. A. Luke, A. Tiripicchio, M. Tiripicchio Camellini, *Angew. Chem.* **1987**, *99*, 802–803; *Angew. Chem. Int. Ed. Engl.* **1987**, *26*, 768–770; b) *New J. Chem.* **1988**, *12*, 429–433.

[8] L. Brunet, F. Mercier, L. Ricard, F. Mathey, *Angew. Chem.* **1994**, *106*, 812–816; *Angew. Chem. Int. Ed. Engl.* **1994**, *33*, 742–745.

[9] T. J. Henly, S. R. Wilson, J. R. Shapley, *Inorg. Chem.* **1988**, *27*, 2551–2553.

[10] a) S. A. MacLaughlin, A. J. Carty, N. J. Taylor, *Can. J. Chem.* **1982**, *60*, 87–90; b) K. Shelly, D. C. Finster, Y. J. Lee, W. R. Scheidt, C. A. Reed, *J. Am. Chem. Soc.* **1985**, *107*, 5955–5959; c) R. A. Bartlett, H. Chen, P. P. Power, *Angew. Chem.* **1989**, *101*, 325; *Angew. Chem. Int. Ed. Engl.* **1989**, *28*, 316–317; d) P. H. M. Budzelaar, P. W. N. M. van Leeuwen, C. F. Roobeck, A. G. Orpen, *Organometallics* **1992**, *11*, 23–25; e) L. R. Falvello, J. Forniés, R. Navarro, V. Sicilia, M. Tomas, *Angew. Chem.* **1990**, *102*, 952–954; *Angew. Chem. Int. Ed. Engl.* **1990**, *29*, 891–893; *J. Chem. Soc. Dalton Trans.* **1994**, 3143–3148.

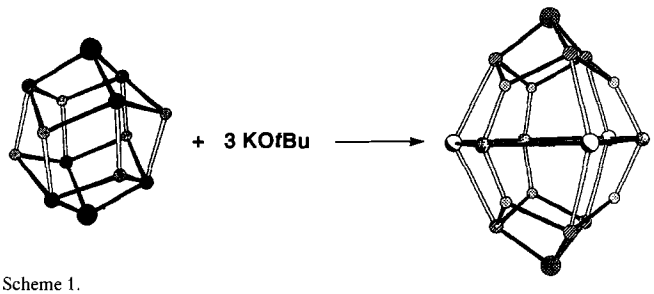
[11] The slip distortion is the distance between the geometric center of the projection of the borole ligand on the best plane defined by carbon atoms 10–13 and the projection of the coordinated metal on the same best plane.

[12] R. Bau, B. Fontal, H. D. Kaesz, M. R. Churchill, *J. Am. Chem. Soc.* **1967**, *89*, 6374–6376.

[13] Considering the B–C14 bond as a 2e donor toward the Pd center, as suggested by a reviewer, would of course lead to 16e Pd, but this does not appear justified on the basis of the ligand geometry and preliminary extended Hückel calculations.

[14] a) The calculations were performed using the extended Hückel method [14b] with a weighted H_{ij} approximation [14c]. The programs used were FORTICON [14d] for the complete molecule and CACAO [14e] for the naked cluster. The geometry used corresponds to the structure of **4** in the crystal, the values for the H_{ii}s and orbital exponents were taken from literature [14f–h], and the Hückel constant was set to 1.75. b) R. Hoffmann, *J. Chem. Phys.* **1963**, *39*, 1397–1412; c) J. H. Ammeter, H.-B. Bürgi, J. C. Thibeault, R. Hoffmann, *J. Am. Chem. Soc.* **1978**, *100*, 3686–3692; d) J. Howell, A. Rossi, D. Wallace, K. Haraki, R. Hoffmann, *QCPE* **1977**, *11*, 344; e) C. Mealli, D. M. Proserpio, *J. Chem. Educ.* **1990**, *67*, 399–402; f) A. Dedieu, T. A. Albright, R. Hoffmann, *J. Am. Chem. Soc.* **1979**, *101*, 3141–3151; g) K. Tatsumi, R. Hoffmann, A. Yamamoto, J. K. Stille, *Bull. Chem. Soc. Jpn.* **1981**, *54*, 1857–1867; h) H. Basch, H. B. Gray, *Theor. Chim. Acta* **1966**, *4*, 367–376.

[15] a) R. Jund, P. Lemoine, M. Gross, R. Bender, P. Braunstein, *J. Chem. Soc. Chem. Commun.* **1983**, 86–88; b) *J. Chem. Soc. Dalton Trans.* **1985**, 711–716; c) P. Zanello, *Struct. Bonding (Berlin)* **1992**, *79*, 101–214.



Scheme 1.

A low-temperature crystallographic study[5] shows **1** to be a twenty-membered polyhedral cage in which a central planar $[K(\mu_2\text{-}OtBu)]_3$ ring is sandwiched between the intact neutral halves of the parent cage $[\{(cyNLi)_3Sb\}_2]$ (Fig. 1, top).[1] Two of the K^+ ions (K(2) and K(3)) within the core are loosely π-bonded to toluene ligands and two additional toluene ligands are found within the lattice, giving a total of four toluene molecules ($x = 4$) for each molecule of **1** (Fig. 1, bottom). This composi-

Cage Expansion of $[\{(cyNLi)_3Sb\}_2]$; Synthesis and Structure of the Trimetallic Complex $[\{(cyNLi)_3Sb\}_2(tBuOK)_3 \cdot x\,C_6H_5CH_3]$**

Donald Barr, Andrew J. Edwards, Michael A. Paver, Paul R. Raithby, Moira-Ann Rennie, Christopher A. Russell, and Dominic S. Wright*

A range of polyamidoantimony anionic cage complexes can be prepared by "mixed-metalation" reactions of dimethylamidoantimony complexes with monometalated primary amines (RNHM).[1, 2] For instance, an $[Sb(NR)_3]^{3-}$ ion is present in the $[\{(PhCH_2CH_2NLi)_3Sb(thf)\}_2]$ complex, produced by the reaction of $Sb(NMe_2)_3$ with $[PhCH_2CH_2NHLi]_n$.[1] The complex has a fourteen-membered polyhedral $[Sb_2N_6Li_6]$ core, which can be regarded as being constructed from an "iminolithium-like" Li_6N_6 core capped at the open Li_3N_3 faces by two Sb atoms.[3] These polyamidoantimony anions can be used as durable ligands for other metals. Thus, the transmetalation reaction of $[Sb_2(Ncy)_4]_2Li_4$ with CuCl produces the mixed-metal complex $[Sb_2(Ncy)_4]_2Cu_4$ in which two $[\{Sb_2(Ncy)_4\}_2]^{2-}$ dianions coordinate to a central planar Cu_4 unit.[4]

We describe here an unexpected alternative in the coordination chemistry of these species towards other salts. Simply mixing the bimetallic $[\{(cyNLi)_3Sb\}_2]$ complex with KO*t*Bu results in cocomplexation of the neutral components. The product is the remarkable trimetallic complex **1** in which cage expansion of the bimetallic precursor to a twenty-membered cage has occurred (Scheme 1).

$[\{(cyNLi)_3Sb\}_2(KOtBu)_3 \cdot x\,C_6H_5CH_3]$ **1**

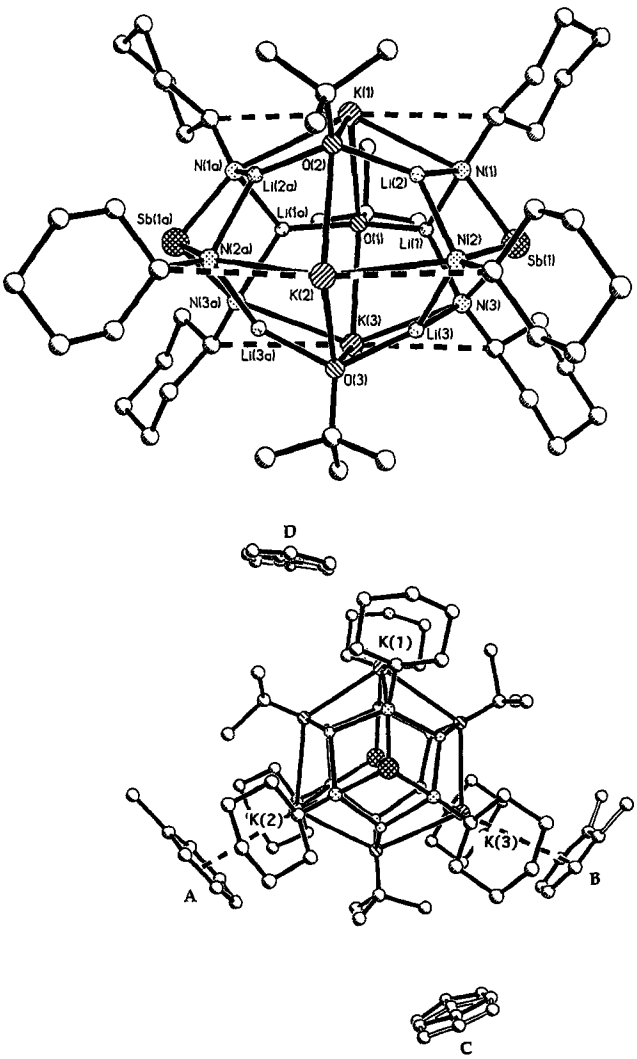


Fig. 1. Top: Molecular structure of **1**. Hydrogen atoms have been omitted for clarity. Selected average bond lengths [Å] and angles [°]: Sb–N 2.063, N–Li 2.01, K–N 2.854, K–O 2.90 (range 2.83–3.05), Li-O 1.90, cy α-C···K from 3.21(1) to 3.352(9); N-Sb-N 91.3, O-K-O 112.3, K-O-K 127.7, N-K-N 125.5, Li-O-Li 125.3, O-K-N 75.2. Bottom: Solvation of **1** by toluene. The disorder in rings B, C, and D was modeled with 50% occupancy in each of the sites indicated (K(2)···A(centroid) 3.43 Å, K(3)···B(centroid) 3.78 Å).

[*] Dr. D. S. Wright, Dr. A. J. Edwards, M. A. Paver, Dr. P. R. Raithby, M.-A. Rennie, C. A. Russell
University Chemical Laboratory
Lensfield Road, GB-Cambridge CB21EW (UK)
Telefax: Int. code + (223)336362

Dr. D. Barr
Associated Octel Co., Ellesmere Port, South Wirral (UK)

[**] We gratefully acknowledge the Science and Engineering Research Council (A.J.E., M.A.P., P.R.R., C.A.R., D.S.W.), the Associated Octel Company, (M.A.P., D.S.W.), the Royal Society (P.R.R., D.S.W.), the Nuffield Foundation (D.S.W.), and the Cambridge Crystallography Data Centre (M.-A.R.) for financial support. cy = cyclohexyl.

 © VCH Verlagsgesellschaft mbH, D-69451 Weinheim, 1995 0570-0833/95/0909-1012 $ 10.00+.25/0

tion is consistent with analytical data on bulk samples of **1**, which indicate that there are about 3.5–4.0 molecules of toluene for each molecular unit. Although tripodal amide complexes of various main group metals[6] have been investigated, the structure of **1** and the cage expansion reaction involved in its formation are unpecedented.

Apart from a small compression in the N-Sb-N angles, the structure of the $[(cyN)_3Sb]^{3-}$ fragments of **1** are similar to that observed in $[\{(PhCH_2CH_2NLi)_3Sb(thf)\}_2]$ (average bond lengths and angles: Sb–N 2.063 Å, N-Sb-N 91.3° in **1**; Sb–N 2.063 Å, N-Sb-N 94.5° in $[\{(PhCH_2CH_2NLi)_3Sb(thf)\}_2]$[1]). A more noticeable difference is seen in the N–Li distances which are significantly shorter in **1** (average 2.01 Å in contrast to 2.10 Å in $[\{PhCH_2CH_2NLi)_3Sb(thf)\}_2]$[1]). Neither the K–O bonds nor the angles within the equatorial $[K(\mu\text{-}OtBu)]_3$ ring are completely symmetrical/average values: K–O 2.904 Å, O-K-O 112.3° and K-O-K 127.7°). This ring is planar, and attached symmetrically to the two $[(cyNLi)_3Sb]$ fragments by both K–N (average: 2.854 Å) and O–Li (average: 1.90 Å) bonds. Thus the terminal $[(cyNLi)_3Sb]$ units act both as donors and as acceptors in stabilizing this ring. The presence of a K_3O_3 fragment is a rare feature in the structure of **1**. Such a ring is seen in the salt complex $[(KNCS)_3 \cdot 5HMPA]$ (HMPA = hexamethylphosphoric triamide), which has a cage structure formed from the oxygen atoms of three HMPA ligands and three K^+ ions, capped by two μ_3-O atoms from HMPA ligands.[7]

All the K^+ ions in **1** are pseudo square-pyramidally surrounded by the O centers of the K_3O_3 ring and the N centers of the two $[(cyNLi)_3Sb]$ fragments (average angles: N-K-N 125.5°, Li-O-Li 125.3°, O-K-N 75.2°). This geometry leaves the K^+ ions open to loose coordination by toluene in the equatorial plane of the cage. The ion–dipole interaction of aromatic ligands with K^+ ions is now well-documented: typical $arene_{(centroid)} \cdots K^+$ distances lie in the range 3.18–3.59 Å[8] (cf. 3.43 and 3.79 Å for the π-bonded $C_6H_5CH_3$ ligands in **1**). Additionally, moderately short agostic interactions between cyclohexyl α-C-H and K^+ apparently further satisfy the coordination sphere of the K^+ centers of **1** (range α-C $\cdots$ K 3.21(1)–3.352(9) Å). These lengths are typical for organopotassium complexes.[9]

The unusual cocomplexation of $[\{cyNLi)_3Sb\}_2]$ and [KO*t*Bu] producing **1** is presumably driven largely by the formation of strong Li–O bonds. We are investigating other reactions of $[\{(cyNLi)_3Sb\}_2]$ and related polyamidoantimony complexes with alkoxides and amides of main group metal and transition metals.

Experimental Procedure

$[\{(cyNLi)_3Sb\}_2]$ was prepared by step-wise metalation of $cyNH_2$ (8.91 g, 90 mmol) in $C_6H_5CH_3$ (50 mL) with first *n*BuLi (56.25 mL, 1.6 mol L^{-1} in hexanes, 90 mmol) and then $Sb(NMe_2)_3$ (7.59 g, 30 mmol) at 20 °C. After filtration of the yellow solution and reduction in vacuo (to about 10 mL), the complex was isolated as a light yellow powder (yield 10.4 g, 80%). To a white slurry of $[\{(cyNLi)_3Sb\}_2]$ (2.165 g, 2.5 mmol) in $C_6H_5CH_3$ (20 mL) was added KO*t*Bu (Aldrich, 0.841 g, 7.5 mmol). Stirring at 20 °C (0.5 h) produced a red-orange solution. The remaining solid was then filtered off, and the solution was reduced to about 5 mL under vacuum. The yellow solid that precipitated was heated back in to solution, and storage at 5 °C (24 h) produced yellow crystalline blocks in low, though reproducible, yield (0.20 g first batch, 10%; although we believe that the low yield is a consequence of the high solubility of **1** in toluene, the possibility of side reactions or equilibria cannot be discounted); the crystals darken at 155 °C and melt at 178–180 °C with liberation of toluene; ^1H NMR (C_6D_6, +25 °C): $\delta = 7.10$ (m, aryl C–H, $C_6H_5CH_3$), 3.63 (m, α-C-H of cyN), 2.10 (s, CH_3 of $C_6H_5CH_3$) 0.7–3.0 (br. m, CH_2 of cyN), 1.25 (*t*BuO); relative integrals could not be obtained due to the overlapping of the *t*BuO, CH_2 (from cyN), and CH_3 (from toluene) resonances; elemental analyses (C, H, N) confirm that ca. 3.5–4.0 $C_6H_5CH_3$ molecules are present per molecule of **1**.

Received: November 11, 1994
Revised version: February 11, 1995 [Z 7470 IE]
German version: *Angew. Chem.* **1995**, *107*, 1088

Keywords: antimony compounds · cage compounds · lithium compounds · potassium compounds

[1] A. J. Edwards, M. A. Paver, M.-A. Rennie, P. R. Raithby, C. A. Russell, D. S. Wright, *Angew. Chem.* **1994**, *106*, 1334; *Angew. Chem. Int. Ed. Engl.* **1994**, *33*, 1277.

[2] R. Alton, D. Barr, A. J. Edwards, M. A. Paver, M.-A. Rennie, P. R. Raithby, C. A. Russell, D. S. Wright, *J. Chem. Soc. Chem. Commun.* **1994**, 1481.

[3] a) R. E. Mulvey, *Chem. Soc. Rev.* **1991**, *20*, 167; b) K. Gregory, P. von R. Schleyer, R. Snaith, *Adv. Inorg. Chem.* **1991**, *37*, 47.

[4] D. Barr, A. J. Edwards, S. Pullen, M. A. Paver, M.-A. Rennie, P. R. Raithby, C. A. Russell, D. S. Wright, *Angew. Chem.* **1994**, *106*, 1960; *Angew. Chem. Int. Ed. Engl.* **1994**, *33*, 1875.

[5] Crystal data for **1**: $C_{76}H_{125}K_3Li_6N_6O_3Sb_2$, $M_r = 1573.26$, monoclinic, space group $P2_1/m$, 13.022(3), $b = 19.661(4)$, $c = 16.686(3)$ Å, $\beta = 99.86(3)°$, $V = 4209(2)$ Å^3, $Z = 2$, $\rho_{calcd} = 1.241$ Mg m^{-3}, $F(000) = 1556$, $\lambda = 0.71073$ Å, $T = 153(2)$ K, $\mu(Mo_{K\alpha}) = 0.835$ mm^{-1}. Stoe AED diffractometer using an oil-coated rapidly cooled crystal mounted directly from solution (technique from T. Kottke, D. Stalke, *J. Appl. Crystallogr.* **1993**, *26*, 615), dimensions $0.35 \times 0.35 \times 0.26$ mm; θ/ω method ($7.20 \le 2\theta \le 45.00$). Of a total of 5689 collected reflections, 5659 were unique. The structure was solved by direct methods (SHELXTL PLUS) and refined by full-matrix least-squares on F^2 (SHELXL-93; G. M. Sheldrick, Göttingen, **1993**) to $R1 = 0.072$ and $wR2 = 0.195$ [$F > 4\sigma(F)$] and $R1 = 0.093$ and $wR2 = 0.232$ (all data) [$R1 = \Sigma \| F_o| - |F_c\| / \Sigma |F_o|$, $wR2 = \sqrt{\{\Sigma w(F_o^2 - F_c^2)^2 / \Sigma w F_o^4\}}$, $w = 1/[\sigma^2(F_o^2) + (xP)^2 + yP]$, $P = (F_o^2 + 2F_c^2)/3$]. Largest features in the final difference map: 1.949 and -0.910 e Å^{-3}. Toluene molecules A and B (Fig. 1b) are 3.43 and 3.78 Å from K(2) and K(3) respectively, and toluene B exhibits disorder of the -CH_3 group over two sites with an occupancy of 50% in each site. In addition, both lattice-bound toluenes C and D exhibit disorder overlapping over two sites with 50% occupancy in each site; for clarity this is shown schematically in the structure at the bottom of Fig. 1. Further details of the crystal structure investigation are available on request from the Director of the Cambridge Crystallographic Data Centre, 12 Union Road, GB-Cambridge CB21EZ (UK), on quoting the full journal citation.

[6] L. Zsolnai, G. Huttner, M. Driess, *Angew. Chem.* **1993**, *105*, 1549–1551; *Angew. Chem., Int. Ed. Engl.* **1993**, *32*, 1439–1440; D. J. Brauer, H. Bürger, G. L. Liewald, J. Wilke, *J. Organomet. Chem.* **1985**, *287*, 305–320; D. J. Brauer, H. Bürger, G. L. Liewald, *ibid.* **1986**, *308*, 119–130; M. Veith, *Adv. Organomet. Chem.* **1990**, *31*, 269; M. Veith, A. Spaniol, J. Pöhlmann, F. Gross, V. Huch, *Chem. Ber.* **1993**, *126*, 2625–2635.

[7] D. Barr, M. J. Doyle, S. R. Drake, P. R. Raithby, R. Snaith, D. S. Wright, *Inorg. Chem.* **1989**, *28*, 1767.

[8] a) C. J. Schavevien, J. B. van Mechelen, *Organometallics* **1991**, *10*, 1704; b) G. R. Fuentes, P. S. Coan, W. E. Streih, K. G. Caulton, *Polyhedron* **1991**, *10*, 2371; c) M. J. Geary, R. H. Cayton, K. Folting, J. C. Huffman, K. G. Caulton, *ibid.* **1992**, *11*, 1369; d) P. B. Hitchcock, M. F. Lappert, G. A. Lawless, B. Royo, *J. Chem. Soc. Chem. Commun.* **1993**, 554.

[9] C. Schade, P. von R. Schleyer, *Adv. Organomet. Chem.* **1987**, *27*, 169.

 © *VCH Verlagsgesellschaft mbH, D-69451 Weinheim, 1995* *0570-0833/95/0909-1013 $ 10.00+.25/0*

Structure Determination of Vitamin A Acetate Isomers through Coupled HPLC and ^{1}H NMR Spectroscopy**

Klaus Albert,* Götz Schlotterbeck, Ulrich Braumann, Heidrun Händel, Manfred Spraul, and Gerhard Krack

Vitamin A (retinol) plays an important role in the human body as a growth and protection factor; after oxidation to the corresponding aldehyde (retinal), it is also an active component in rhodopsin. In the vision process the isomerization of 11-*cis*-retinal to all-*trans*-retinal is one of the important biochemical processes in the rhodopsin cycle. Naturally occurring vitamin A (all-*trans*-retinol) and synthetic vitamin A acetate often coexist with their *cis*–*trans* isomers (Fig. 1).[1, 2] Fast and unequivocal structure

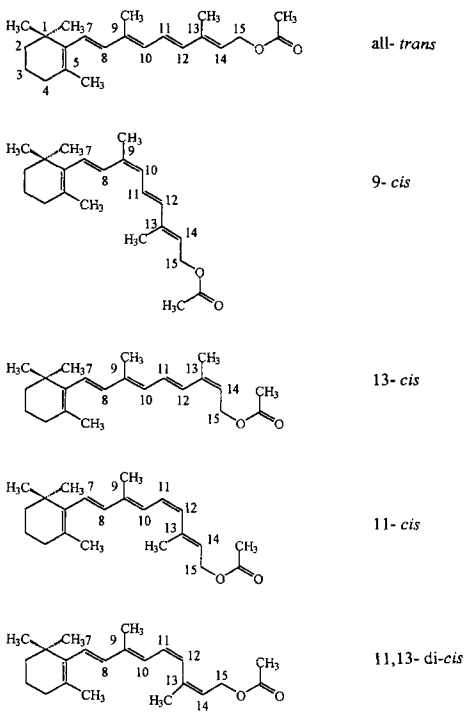


Fig. 1. Major isomers of vitamin A acetate.

determination of vitamin A acetate isomers prepared by different methods is of increasing importance because of the widespread use of these vitamins. Retinol and its derivatives are applied in medicine because of their antioxidative properties[3] and in tumor therapy because of their cytostatic activity.[4] In addition, these compounds are used as nutritional additives and in cosmetics. The separation of *cis*–*trans* isomers of carotinoids, in particular of vitamin A acetate, is possible by high-performance liquid chromatography (HPLC) with cyanopropyl- or *n*-alkyl-modified silica gel as the stationary phase.[5–7] Only hints to the structures of the separated isomers are given by the routine monitoring of the chromatographic separation by UV spectroscopy. Capacity factors derived from the chromatographic separation are not well suited for structure elucidation.[8] Structure assignment may be possible by comparative measurements, which require many experiments and are very time-consuming. Applying HPLC coupled with mass spectrometry for the present application is not feasible because the *cis*–*trans* isomers of vitamin A acetate have the same fragmentation pattern. Therefore we attempted to elucidate the structures of the different isomers by coupled HPLC and ^{1}H NMR spectroscopy.[9–15]

The vitamin A acetate isomers used as model compounds were prepared by briefly heating all-*trans* vitamin A acetate to 160 °C. Figure 2 shows the ^{1}H NMR spectrum (400 MHz) of the isomer mixture. Structure elucidation of distinct compounds is not possible because of signal overlap. Five main compounds are evident in the UV chromatogram for the separation of the isomer mixture on a cyanopropyl-modified silica gel phase with *n*-heptane as eluent (Fig. 3). Under the applied conditions (see Experimental Procedure) peaks 1 and 2 are not fully separated.

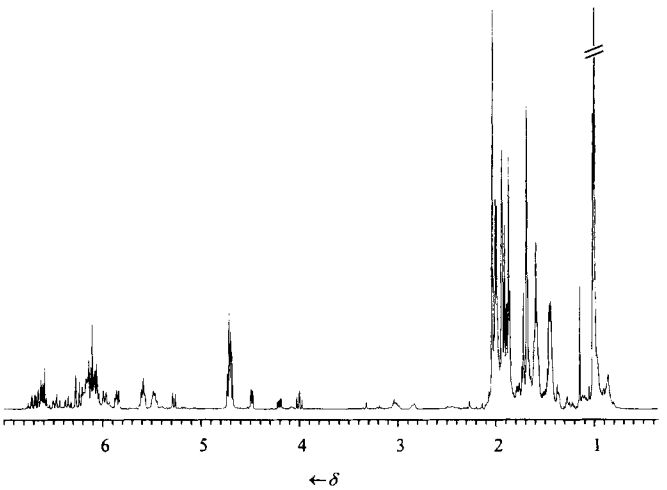


Fig. 2. ^{1}H NMR spectrum (400 MHz) of a mixture of vitamin A acetate isomers.

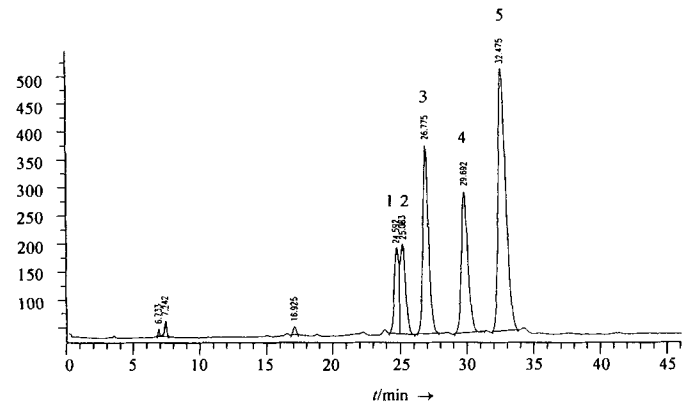


Fig. 3. UV chromatogram of a separation of a mixture of vitamin A acetate isomers. (1: 11,13-di-*cis*, 2: 11-*cis*, 3: 13-*cis*, 4: 9-*cis*, 5: all-*trans* vitamin A acetate).

[*] Priv.-Doz. Dr. K. Albert, Dipl.-Chem. G. Schlotterbeck, Dipl.-Chem. U. Braumann, Dr. H. Händel
Institut für Organische Chemie der Universität
Auf der Morgenstelle 18, D-72076 Tübingen (Germany)
Telefax: Int. code + (7071) 29-5246
Dr. M. Spraul
Bruker Analytische Messtechnik, Silberstreifen, Rheinstetten (Germany)
Dr. G. Krack
BASF AG, Physikalische Analytik, ZAX/PS, E 210, Ludwigshafen (Germany)

[**] This work was funded by Bruker, Karlsruhe, and by BASF AG, Ludwigshafen. We thank Mrs. Brigitte Kloster for her help in the acquisition and interpretation of spectra. Throughout this article the name vitamin A acetate is used instead of the recommended IUPAC name, retinyl acetate.

 © VCH Verlagsgesellschaft mbH, D-69451 Weinheim, 1995 0570-0833/95/0909-1014 $ 10.00+.25/0

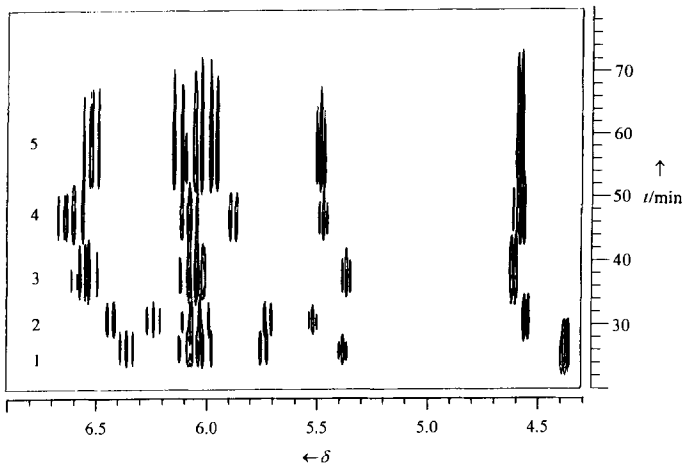


Fig. 4. Contour plot of the on-line HPLC NMR separation of a mixture of vitamin A acetate isomers (for parameters see Experimental Procedure). (1: 11,13-di-*cis*, 2: 11-*cis*, 3: 13-*cis*, 4: 9-*cis*, 5: all-*trans* vitamin A acetate).

Since *n*-heptane is used as eluent, the ^{1}H NMR signals of the aliphatic protons are not accessible for structure determination. Nevertheless, the contour plot (Fig. 4) of the on-line HPLC–NMR separation displays interesting details. Here the ^{1}H NMR signals of the olefinic protons of the separated compounds (x axis = ^{1}H chemical shift) are plotted against the retention times (y axis). The structure assignments will not be discussed in detail, but the two isomers (peaks 1 and 2), which were only poorly distinguished in the UV chromatogram, can be identified by their different ^{1}H NMR spectra.

The structures of the separated isomers were assigned based on the coupling constants, chemical shifts, and integration ratios from the continuous-flow ^{1}H NMR spectra. Figure 5 displays the olefinic region of the continuous-flow ^{1}H NMR spectra of the separated isomers recorded at the peak maximum. Routine and continuous-flow NMR spectra show the same resolution. The analysis of chemical shifts, coupling constants, and intergration ratios, which are not displayed because of lack of space, results in the structure assignments in Table 1.

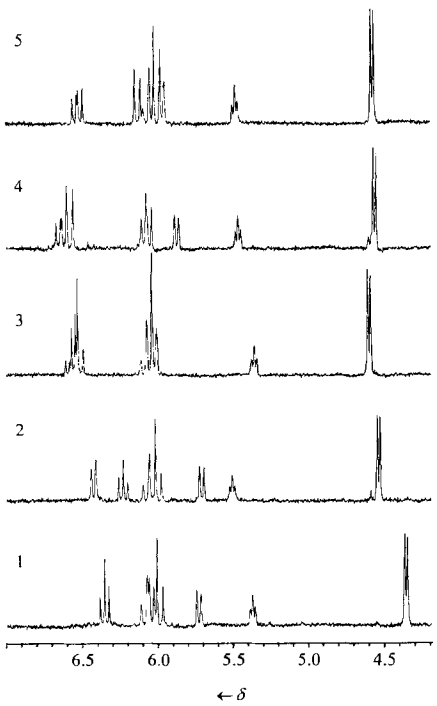


Fig. 5. Continuous-flow ^{1}H NMR spectra (400 MHz) of the separated vitamin A acetate isomers (1: 11,13-di-*cis*, 2: 11-*cis*, 3: 13-*cis*, 4: 9-*cis*, 5: all-*trans* vitamin A acetate).

Table 1. ^{1}H NMR spectroscopic data for vitamin A acetate isomers in *n*-heptane.

Isomer	Peak	Chemical shifts δ of the olefinic protons 7	8	10	11	12	14	Coupling constants J [Hz] ^3J (7,8)	^3J (10,11)	^3J (11,12)
11,13-di-*cis*	1	6.10	6.00	6.05	6.36	5.74	5.38	16.0	12.3	11.3
11-*cis*	2	6.08	6.00	6.43	6.24	5.71	5.51	15.8	11.7	11.7
13-*cis*	3	6.09	6.03	6.03 [a]	6.57 [a]	6.52 [a]	5.36	15.0	11.0 [a]	14.1 [a]
9-*cis*	4	6.09	6.58	5.88	6.64	6.06	5.47	16.1	11.7	14.1
all-*trans*	5	6.07	6.01	5.97	6.53	6.13	5.48	16.1	11.4	15.1

[a] ABX system, $^4J(10,12) < 0.3$ Hz.

Differences between these chemical shifts and previously reported values[16, 17] can be explained by the different solvents used, in our study, *n*-heptane. Whereas chemical shifts and coupling constants can be derived directly from the spectra of 11,13-di-*cis* and 9-*cis* isomers, the all-*trans*, 11-*cis*, and 13-*cis* isomers display more complex spectra. In these three isomers H7 and H8 are an AB system, and in the 13-*cis* isomer H10, H11, and H12 an ABX system. Assignment of the olefinic protons was confirmed by homonuclear correlated spectra (H,H COSY) acquired in the stopped-flow mode. Chemical shifts and coupling constants of the ABX system were determined with the simulation program WIN-DAISY.[18]

Our study of vitamin A acetate isomers shows that under unfavorable chromatographic conditions such as high concentrations[19] and slow flow rates, even coeluting compounds can be characterized unequivocally within a short analysis time. The great advantage of directly coupled HPLC and NMR spectroscopy is quite obvious. Due to the introduction of a second dimension, the ^{1}H NMR frequencies (chemical shifts and coupling constants), safe and unequivocal structure assignment is possible even when overlapping peaks are seen in conventional UV chromatograms.

Experimental Procedure

Two analytical Nucleosil 5 CN columns were connected for the separation of vitamin A acetate isomers. The original separation [20] was performed with a flow rate of 1 mL min^{-1}. From the viewpoint of NMR spectroscopy a lower rate is favorable: with a slower flow rate the number of coadded transients at a given sample volume is higher, which results in an improved signal/noise ratio (S/N). Taking into account a constant S/N and the same number of coadded transients, the number of spectra per peak elution volume can be increased. On the other hand, a reduced flow rate is below the optimal values derived from the van Deemter equation. As a practical compromise the normal flow rate of 1 mL min^{-1} was used at the beginning of the separation, and prior to the appearance of the peaks in the UV detector the flow rate was reduced to 0.2 mL min^{-1}, a more favorable rate for NMR measurements; generally longer retention times resulted.

For extended NMR measurements (e.g. stopped-flow experiments for homonuclear or inverse correlated spectra) a deuterium signal, typically from the deuterated solvent, is recommended for field-frequency stabilization. For economic reasons it is not possible to add enough deuterated eluent for a sufficiently intense deuterium signal. Therefore [D$_6$]benzene was added, because it neither alters the applied chromatographic separation conditions severely nor affects the absorption of the olefinic system at the detection wavelength of 325 nm, and [D$_6$]benzene yields a sufficient lock signal even at a concentration of only 1%.

Chromatographic parameters: Pump: Bruker LC 22; two columns: Macherey-Nagel 250 × 4.6 mm, Nucleosil 5 CN, 5 μm; eluent: *n*-heptane (dried over 0.3 nm molecular sieves); flow rate: 20 min at 1.0 mL min^{-1} (130 bar), later 0.2 mL min^{-1} (30 bar); UV detector: Hewlett Packard 1050, detection wavelength 325 nm. A

 © VCH Verlagsgesellschaft mbH, D-69451 Weinheim, 1995 0570-0833/95/0909-1015 $ 10.00+.25/0

solution of 5 mg of the vitamin A acetate mixture in 50μL of *n*-heptane (10% solution) was used for the chromatographic separation.

NMR parameters: Bruker ARX 400 spectrometer, 120μL continuous-flow probe with an rf coil arrangement for inverse $^{13}C/^{1}H$ spectroscopy; 48 transients per FID; 8K time domain data points (TD2) with a spectral width (SW2) of 5618 Hz, acquisition time (AQ) = 0.73 s per transient, pulse width 90°, solvent presaturation over 0.5 s (alternating irradiation at the heptane signals at $\delta = 0.82$ and 1.22 for 5 ms each); 128 FIDs (TD1) with an acquisition time per FID of 60 s were recorded during the separation.

Data were treated like a 2D NMR matrix (t_1 direction = retention time) and processed with UXNMR software [21]; a phase-sensitive Fourier transformation was performed only in the t_2 direction: zero filling in t_2 to 32K data points; multiplication with a sine square apodization function.

Received: December 6, 1994 [Z7525IE]
German version: *Angew. Chem.* **1995**, *107*, 1102

Keywords: chromatography · HPLC–^{1}H NMR coupling · NMR spectroscopy · vitamin A

[1] B. Stancher, F. Zonta, *J. Chromatogr.* **1982**, *238*, 217–225.
[2] M. E. Cullum, M. H. Zile, *Anal. Biochem.* **1986**, *153*, 23–32.
[3] M. Hiramatsu, L. Packer, *Methods Enzymol.* **1990**, *190*, 273–280.
[4] R. Lotan, D. Lotan, P. G. Sacks, *Methods Enzymol.* **1990**, *190*, 100–110.
[5] B. Stancher, F. Zonta, *J. Chromatogr.* **1982**, *234*, 244–248.
[6] J. Deli, Z. Matus, P. Molnár, G. Tóth, *Helv. Chim. Acta* **1993**, *76*, 952.
[7] L. C. Sander, K. E. Sharpless, N. E. Craft, S. A. Wise, *Anal. Chem.* **1994**, *66*, 1667–1674.
[8] F. Derguini, K. Nakanishi, J. Buck, U. Hämmerling, F. Grün, *Angew. Chem.* **1994**, *106*, 1954–1956; *Angew. Chem. Int. Ed. Engl.* **1994**, *33*, 1837–1839.
[9] H. C. Dorn, *Anal. Chem.* **1984**, *56*, 747A–758A.
[10] D. A. Laude, Jr., C. L. Wilkins, *TrAC Trends Anal. Chem. (Pers. Ed.)* **1986**, *5*, 230–235.
[11] K. Albert, E. Bayer, *TrAC Trends Anal. Chem. (Pers. Ed.)* **1988**, *7*, 288–293.
[12] K. Albert, Habilitationsschrift, Universität Tübingen, **1988**.
[13] K. Albert, E. Bayer in *HPLC Detection Newer Methods* (Ed.: G. Patonay), VCH, New York, **1992**, p. 197.
[14] M. Spraul, M. Hofmann, P. Dvortsak, J. K. Nicholson, I. D. Wilson, *Anal. Chem.* **1993**, *65*, 327–330.
[15] J. K. Roberts, R. J. Smith, *J. Chromatogr. A* **1994**, *667*, 385–389.
[16] W. Vetter, G. Englert, N. Rigassi, U. Schwietel in *Carotenoids* (Ed.: O. Isler), Birkhauser, Basel, **1971**, pp. 218–225.
[17] R. W. Curley, W. Fowble, *Magn. Res. Chem.* **1989**, *27*, 707–709.
[18] WIN-DAISY, Bruker Analytische Meßtechnik GmbH.
[19] Separation and structure assignment is even possible at concentration levels at which UV detection fails. The detection limit of all-*trans* vitamin A acetate under stopped-flow conditions was determined to be 1.2 μg within the flow-cell with a signal/noise ratio of 4:1 for the doublet of H15 at $\delta = 4.8$. Solutions of different concentrations were directly injected into the flow-cell, and 512 transients were accumulated for each measurement. The *n*-heptane signals were suppressed by application of the above-mentioned presaturation sequence. Spectra were processed without using any filter function.
[20] H. Steuerle, *J. Chromatogr.* **1981**, *206*, 319–326.
[21] UXNMR, Bruker, Analytische Meßtechnik GmbH.

4c/3e Radical Cations with Cage-Directed Configurations**

Georg Gescheidt,* Rainer Herges,* Helfried Neumann, Jürgen Heinze,* Markus Wollenweber, Markus Etzkorn, and Horst Prinzbach*

Dedicated to Paul von Ragué Schleyer on the occasion of his 65th birthday

On the reaction coordinate of the symmetry-forbidden ethylene/ethylene [2 + 2]cycloaddition[1] with imposed D_{2h} symmetry, cyclobutane is the sole minimum ($r = 1.584$ Å, Fig. 1). What

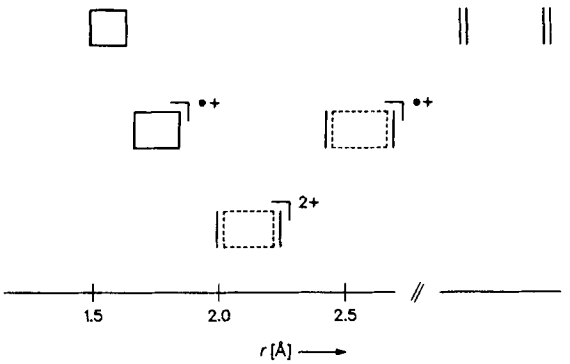


Fig. 1. Minima on the D_{2h} reaction coordinate of the cycloadditions ethylene/ethylene, ethylene/ethylene$^{\bullet+}$, and ethylene$^{\bullet+}$/ethylene$^{\bullet+}$ (ab initio 3-21G). r = distance between the ethylene units.

happens, when one electron is removed from the system? The [2 + 1]addition remains symmetry-forbidden, the activation barrier is lowered, however, in this case two minima exist: a π-complex-like ($r = 2.6$ Å, "extended") and a cyclobutanoid ($r = 1.75$ Å, "tight") species.[2] When a second electron is removed, there is only one (σ-bishomoaromatic) minimum[3] for the symmetry-allowed [1 + 1]addition—with $r = 2.15$ Å almost exactly at a distance where the two forbidden additions show their energy maximum. These nonclassical four-center–three-electron (4c/3e) and 4c/2e configurations are found not to be energy minima in calculations without symmetry restrictions; they are therefore only experimentally observable if structural provisions prohibit their transition into the respective global minimum configurations (open, localized ions).[4]

[*] Dr. G. Gescheidt
Institut für Physikalische Chemie der Universität
Klingelbergstrasse 80, CH-4056 Basel (Switzerland)
Priv.-Doz. Dr. R. Herges, Dipl.-Chem. H. Neumann
Institut für Organische Chemie der Universität
Henkestrasse 42, D-91054 Erlangen (Germany)
Prof. Dr. J. Heinze
Institut für Physikalische Chemie der Universität
Albertstrasse 21, D-79104 Freiburg (Germany)
Prof. Dr. H. Prinzbach, Dr. M. Wollenweber, Dipl.-Chem. M. Etzkorn
Institut für Organische Chemie und Biochemie der Universität
Albertstrasse 21, D-79104 Freiburg (Germany)
Telefax: Int. code + (761) 203-5987

[**] This project has been supported by the Deutsche Forschungsgemeinschaft, the Fonds der Chemischen Industrie and the BASF AG. G. G. thanks the Freiwilligen Akademischen Gesellschaft, Basel, for a Treubel Stipendium. We thank R. Schmidlin for low-temperature measurements, Prof. T. Bally and Prof. E. Haselbach (University of Fribourg, Switzerland) for access to the ^{60}Co source.

 © VCH Verlagsgesellschaft mbH, D-69451 Weinheim, 1995 0570-0833/95/0909-1016 $ 10.00+.25/0

The rigid hydrocarbon cages of the (*iso*)pagodanes ([1.1.1.1]; [2.2.1.1]) and (bisseco-, seco)dodecahedradienes offer such "steric protection" and in addition allow the gradual modulation of the geometrical situation (r) in the central 4c core[5, 6] (cf. the PE spectroscopic characterization of "early" and "late" points on the D_{2h} reaction coordinate[7]). In this communication it is demonstrated that the radical cations generated from the [2.2.1.1] skeletons **1(2)**[2, 8] and the *iso*-skeletons **3(4)**[9]—one molecular half of **1(2)** is rotated by 90°—represent nonclassical, yet different configurations ("tight" and "extended", respectively); in contrast to the findings with the [1.1.1.1]skeletons,[2] the [2.2.1.1]pagodane cage stabilizes the "tight", and the [2.2.1.1]*iso*pagodane cage the "extended" minimum of the [2 + 1] reaction coordinate. MM2 calculations for the neutral molecules had suggested a relative preference for the *iso*-diene **4** ($\Delta\Delta H_f^\circ$ **1** → **2** = +15.0, **3** → **4** = +1.8 kcal mol^{-1});[10] this was confirmed by ab initio 3-21G calculations (Fig. 2).

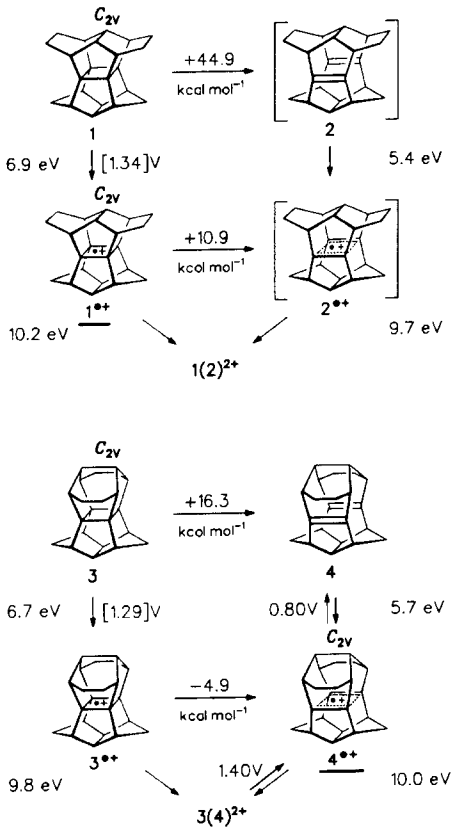


Fig. 2. Calculated nonvertical ionization energies [eV], reaction enthalpies (ab initio 3-21G, [kcal mol^{-1}]), and measured oxidation potentials ([E_p], E_o [V]) of the [2.2.1.1]structures **1(2)** and **3(4)**.

The course of the electrochemical oxidation[11] of **1** and **3** is strikingly different, as characterized by the cyclic voltammograms in Figure 3: For **1** even at very high scan rates and at temperatures as low as −70 °C only an irreversible wave is registered; after reversal of the scan no reduction is observed. For **3**, after a single scan, two oxidation waves, and after reversal of the scan, two reduction waves are revealed. In a multisweep experiment an additional oxidation wave appears which gains intensity at the expense of the first oxidation wave; a cyclic voltammogram has finally evolved which is identical with the one independently obtained from **4** and which, notably, demonstrates reversibility for the second oxidation step. In line with the reaction enthalpies (Fig. 2), the "tight" radical cation **1**$^{\bullet+}$ is not stabilized by opening to **2**$^{\bullet+}$ (speculations can be made about the nature of the obviously very fast follow-up reaction(s)), whilst **3**$^{\bullet+}$ rapidly expands to **4**$^{\bullet+}$. The latter is reversibly reduced to the diene **4** and oxidized to the dication **3(4)**$^{2+}$ (ECE process, the lifetime of **3(4)**$^{2+}$ in CH_2Cl_2, the most persistent σ-bishomoaromatic dication known to date, is about 0.8 s[12]).

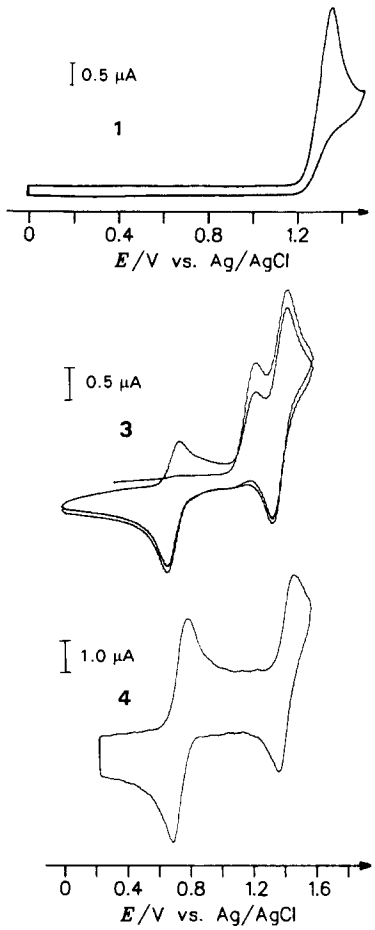


Fig. 3. Cyclic voltammograms of **1** (v = 200 mV s^{-1}), **3** (v = 1 V s^{-1}), and **4** (v = 5 V s^{-1}) in CH_2Cl_2/0.1 M nBu_4NPF_6 at 0 °C.

In agreement with the results of the cyclic voltammetric studies, the deeply colored radical cations generated under high vacuum from **1** and **3** in CH_2Cl_2 by electrolysis or with electron transfer reagents (tris(*p*)bromophenyl)-ammoniumyl-hexachloroantimonate, $AlCl_3$) are found to be of vastly different persistence: The ion from **1** (λ_{max} = 610 nm[13]) exists at −60 °C only for about 30 minutes, the ion from **3** (λ_{max} = 586 nm[13]), however, even at room temperature for more than 24 hours. The ESR spectra, registered at −40 °C in CH_2Cl_2 (Fig. 4), underscore the discrepancy: The spectrum of **1** is dominated by two ^{1}H-hyperfine coupling constants (a_H) of 1.76 and 0.96 mT for two sets of four β-protons. Additional a_H (6 sets) observed in the ENDOR spectrum are not resolved; an assignment cannot be made because of their similar and very small size and unknown multiplicity. The spectrum of **3** with its quintet splitting exhibits a large coupling constant of 1.63 mT for four equivalent β-protons. The multiplicities of the a_H which are additionally detected in the ENDOR spectrum can be determined by simulation of the ESR spectrum; an assignment remains unreliable because of their similar size. In ESR spectra measured after γ-irradiation (^{60}Co) of **1** and **3** at −196 °C in a Freon matrix ($CFCl_3$),[14] the a_H values are practically unchanged—the structures of both radical cations are static (C_{2v} symmetry) within the hyperfine time scale. With estimated dihedral angles between the (hypothetical[15]) $2p_z$ axis of the central C atoms and the C_β–H bonds of the [2.2] molecular parts of 10–0° for **1**$^{\bullet+}$ and **2**$^{\bullet+}$ and of 90–80° for **3**$^{\bullet+}$ and **4**$^{\bullet+}$ (the angles for the [1.1] molecular parts are 15–25° and 10–0°, respectively), however, like in the case of *iso* [1.1.1.1] ions,[2] only the "upper" ([2.2], 1.76, <0.08 mT)/"lower" ([1.1], 0.96, 1.63 mT) differentiation is unambiguous. Particularly in view of the varying hybridization of the quaternary C centers in the "tight" and "extended" configurations further interpretations on the basis of the McConnell equation are problematic.[2, 16]

 © VCH Verlagsgesellschaft mbH, D-69451 Weinheim, 1995 0570-0833/95/0909-1017 $ 10.00+.25/0

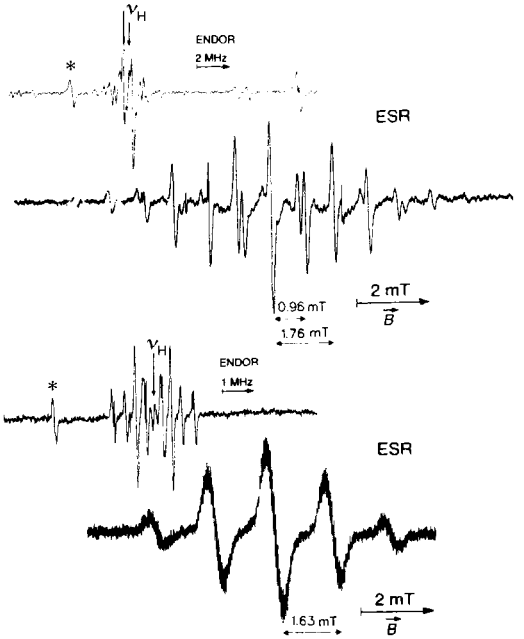
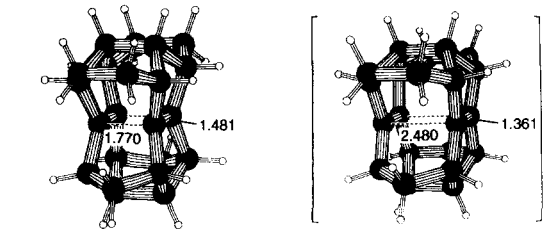
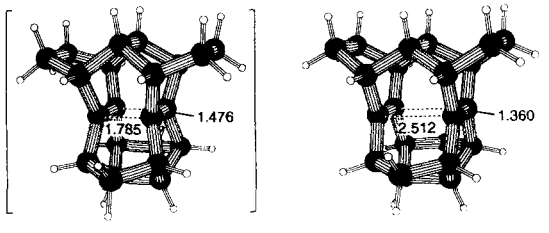


Fig. 4. ESR and ENDOR spectra of the radical cations generated from **1** (above) and **3** (below) ($AlCl_3$, CH_2Cl_2, $-40\,^{\circ}C$). a_H values determined from the ENDOR spectra are: $\mathbf{1}^{\bullet+}$ 1.76 (4H), 0.96 (4H), 0.18, 0.09, 0.07, 0.04, 0.03, 0.01 mT; $\mathbf{4}^{\bullet+}$: 1.63 (4H), 0.18 (2H), 0.13 (2H), 0.08 (6H), 0.04 (4H), 0.03 (2H), 0.01 (4H) mT. *: "mirrored signal".



1·+ ("tight")				2·+ ("extended")
-34.7	:	ϕ	:	-4.1
12.8	:	E_{rel}	:	23.7
1.66/1.02	:	$a_H\beta$(calc.)	:	1.35/1.64
1.76/0.96	:	$a_H\beta$(exp.)	:	-



3·+ ("tight")				4·+ ("extended")
-27.5	:	ϕ	:	2.3
4.9	:	E_{rel}	:	0.0
-0.01/1.03	:	$a_H\beta$(calc.)	:	0.01/1.73
	:	$a_H\beta$(exp.)	:	<0.08/1.63

Fig. 5. Structures of the radical cations $\mathbf{1}^{\bullet+}$–$\mathbf{4}^{\bullet+}$ optimized by ab initio (UHF/3-21G) calculations. Bond lengths and transannular distances in [Å], olefinic pyramidalization Φ in [°], ((−)/(+) inside (outside)), energies E_{rel} (relative to the most stable isomer $\mathbf{4}^{\bullet+}$) in [kcal mol^{-1}], and ESR coupling constants ($a_H\beta$) in [mT] (in each case the first value is for the [2.2] side).

The designation of the short-lived radical cation derived from **1** as "tight" ($\mathbf{1}^{\bullet+}$) and that of the longer lived ion from **3**(**4**) as "extended" ($\mathbf{4}^{\bullet+}$) is again[2, 5] corroborated by ab initio[18] and INDO[19] calculations. The geometries were optimized at the UHF/3-21G level and confirmed as minima by harmonic frequency analysis. The ESR coupling constants (a_H) calculated with the INDO method are based on the geometries determined by ab initio calculations (Fig. 5). According to these calculations both [2.2.1.1]pagodanes exhibit two minima (bond-length isomers $\mathbf{1}^{\bullet+}$, $\mathbf{2}^{\bullet+}$ and $\mathbf{3}^{\bullet+}$, $\mathbf{4}^{\bullet+}$)—for the pagodane cage the "tight" ($\mathbf{1}^{\bullet+}$), for the *iso*pagodane cage the "extended" structure ($\mathbf{4}^{\bullet+}$) is the more stable isomer. Indeed, the agreement between observed and calculated ESR coupling constants is better for $\mathbf{1}^{\bullet+}$ and $\mathbf{4}^{\bullet+}$.[19] The symmetrical (concerted) transition "tight" → "extended" is forbidden since both species in each system have different state symmetries ($\mathbf{1}^{\bullet+}$: $^2B_{2u}$; $\mathbf{2}^{\bullet+}$: $^2B_{1u}$; $\mathbf{3}^{\bullet+}$: $^2B_2$; $\mathbf{4}^{\bullet+}$: $^2B_1$). Nevertheless, the reaction may have a low barrier of activation through a symmetry-breaking process (e.g. a trapezoidal transition structure).[20]

Received: December 10, 1994 [Z 7538 IE]
German version: *Angew. Chem.* **1995**, *107*, 1109

Keywords: ab initio calculations · caged ions · cyclic voltammetry · EPR spectroscopy · pagodanes

[1] R. B. Woodward, R. Hoffmann, *Angew. Chem.* **1969**, *81*, 797; *Angew. Chem. Int. Ed. Engl.* **1969**, *8*, 781.
[2] H. Prinzbach, M. Wollenweber, R. Herges, H. Neumann, G. Gescheidt, R. Schmidlin, *J. Am. Chem. Soc.* **1995**, *117*, 1439; H. Prinzbach, G. Gescheidt, H.-D. Martin, R. Herges, J. Heinze, G. K. Surya Prakash, G. A. Olah, *Pure Appl. Chem.*, in press.
[3] G. K. Surya Prakash, V. V. Krishnamurthy, R. Herges, R. Bau, H. Yuan, G. A. Olah, W.-D. Fessner, H. Prinzbach, *J. Am. Chem. Soc.* **1988**, *110*, 7764; R. Herges, P. von R. Schleyer, M. Schindler, W.-D. Fessner, *ibid.* **1991**, *113*, 3649.
[4] Review: H. D. Roth, *Top. Curr. Chem.* **1992**, *163*, 131; N. L. Bauld, *Hole and Electron Transfer Catalyzed Pericyclic Reactions* in *Advances in Electron Transfer Chemistry, Vol.2*, (Ed.: P. S. Mariano), JAI Press, Greenwich (Connecticut), **1992**; P. Jungwirth, T. Bally, *J. Am. Chem. Soc.* **1993**, *115*, 5789; T. Bally, *Chimia* **1994**, *48*, 378; cf. the recently achieved characterization of the quadricyclane radical cation: K. Ishiguro, I. V. Khudyakov, P. F. McGarry, N. J. Turro, H. D. Roth, *J. Am. Chem. Soc.* **1994**, *116*, 6933.
[5] H. Prinzbach, B. A. R. C. Murty, W.-D. Fessner, J. Mortensen, J. Heinze, G. Gescheidt, F. Gerson, *Angew. Chem.* **1987**, *99*, 488; *Angew. Chem. Int. Ed.: Engl.* **1987**, *26*, 45; K. Weber, H. Prinzbach, R. Schmidlin, F. Gerson, G. Gescheidt, *ibid.* **1993**, *105*, 907 and **1993**, *32*, 875; H. Prinzbach, K. Weber, *ibid.* **1994**, *106*, 2329 and **1994**, *33*, 2239.
[6] Cf. the stabilization of the (planar) $C^{\bullet+}(CH)_4$ radical cations in the structurally similar alkaplane cages: J. E. Lyons, D. R. Rasmussen, M. P. McGrath, R. H. Nobes, L. Radom, *Angew. Chem.* **1994**, *106*, 1722; *Angew. Chem. Int. Ed. Engl.* **1994**, *33*, 1667.
[7] D. Elsässer, H.-D. Martin, B. Mayer, G. Lutz, H. Prinzbach, *Chem. Ber.* **1991**, *124*, 2863; H.-D. Martin, B. Mayer, K. Weber, H. Prinzbach, *Chem. Ber.* unpublished; cf. H.-D. Martin, B. Mayer, *Angew. Chem.* **1983**, *95*, 281; *Angew. Chem. Int. Ed. Engl.* **1983**, *22*, 283; R. Gleiter, R. Schäfer, *Acc. Chem. Res.* **1990**, *23*, 369.
[8] Diene **2** is not yet available; typically for the different reactivity of the (*iso*)pagodanes, the isomerization **1** → **2** can be brought about neither following the conditions repeatedly applied to the [1.1.1.1] structures (addition/elimination of bromine) nor by photo electron transfer (PET), as successfully utilized for the isomerization **3** → **4** (see ref. [19]).
[9] M. Wollenweber, R. Pinkos, H. Prinzbach, *Angew. Chem.* **1994**, *106*, 84; *Angew. Chem. Int. Ed. Engl.* **1994**, *33*, 117.
[10] M. Wollenweber, dissertation, University of Freiburg, **1993**.
[11] J. Heinze, *Angew. Chem.* **1984**, *96*, 823; *Angew. Chem. Int. Ed. Engl.* **1984**, *23*, 831; D. H. Evans, *Acc. Chem. Res.* **1977**, *10*, 313.
[12] According to recent results by Olah, Prakash, and Herges both isomers **3** (**4**)—like **1**[3]—are rapidly oxidized in SbF_5/SO_2ClF (−78 °C) to give the σ-bishomoaromatic dication $(\mathbf{3(4)})^{2+}$ (NMR, IGLO).
[13] The absorption spectra were recorded simultaneously with the ESR signal (range: 400–780 nm), see: G. Gescheidt, *Rev. Sci. Instr.* **1994**, *65*, 2145.
[14] T. Shida, T. Haselbach, T. Bally, *Acc. Chem. Res.* **1994**, *17*, 180.
[15] The $2p_z$ axis is defined as the extension of the longer C···C distance in the cyclobutane core.
[16] C. Heller, H. M. McConnell, *J. Chem. Phys.* **1960**, *32*, 1535; for a similar example see M. Guerra, *J. Am. Chem. Soc.* **1992**, *114*, 2077.

 © VCH Verlagsgesellschaft mbH, D-69451 Weinheim, 1995 0570-0833/95/0909-1018 $ 10.00+.25/0

[17] Gaussian 92, Revision B: M. J. Frisch, G. W. Trucks, M. Head-Gordon, P. M. W. Gill, M. W. Wong, J. B. Foresman, B. G. Johnson, H. B. Schlegel, M. A. Robb, E. S. Repogle, R. Gomperts, J. L. Andres, K. Raghavachari, J. S. Blinkley, C. Gonzalez, R. L. Martin, D. J. Fox, D. J. Defrees, J. Baker, J. J. P. Stewart, J. A. Pople, Gaussian, Inc., Pittsburgh PA, **1992**. Spin projection method: H. B. Schlegel, *J. Chem. Phys.* **1986**, *84*, 4530.

[18] J. A. Pople, D. L. Beveridge: *Approximate Molecular Orbital Theory*, McGraw-Hill, New York, **1970**.

[19] A "chemical" hint to the existence of a "tight" 4c/3e configuration is the finding that the dication produced from [1.1.1.1]*iso*pagodane [2] is reduced by methanol to the starting hydrocarbon (not to the [1.1.1.1]*iso*diene); the [2.2.1.1] dication $3(4)^{2+}$—like the [1.1.1.1] dication [3]—adds methanol (G. A. Olah, G. K. S. Prakash, personal communication). Remarkably, [2.2.1.1]isopagodane **3** (→ **4** [8]), but not [1.1.1.1]*iso*pagodane, can be transformed by PET into the respective diene (T. Voss, dissertation, University of Freiburg, **1995**).

[20] Note added in proof (March 11, 1995): The "tight" [1.1.1.1] radical cation [2] has recently been observed by FDMR (fluorescence detected magnetic resonance) in *n*-hexane (190 K – room temperature); at a lifetime of 0.2 μs at 293 K it is isomerized into the "extended" form. The measured $a_H\beta$ is remarkably close to the one calculated by the ab initio methods applied in this paper (1.02 vs. 1.05 mT) (A. D. Trifunac, D. Werst, personal communication).

Polar Interactions between Stacked π Systems in Fluorinated 1,8-Diarylnaphthalenes: Importance of Quadrupole Moments in Molecular Recognition**

Franco Cozzi,* Francesco Ponzini, Rita Annunziata, Mauro Cinquini, and Jay S. Siegel*

Interactions between aromatic units are invoked to rationalize a variety of molecular processes, such as stereoselective organic transformations[1] and molecular recognition,[2] and to explain the structure of many biologically relevant molecules.[3] Molecular recognition involving simple benzene derivatives has been modeled through a multicomponent equation with a strong electrostatic contribution to the energy of interaction,[4] and the experimentally observed effects are consistent with the quadrupole of the benzene ring playing an important part.[5] The sensitivity of phenyl stacking interactions to substitution can be revealed through a study of the dynamics of 1,8-diarylnaphthalenes.[6, 7] From this study, a simple model arises in which the electrostatic interaction between two benzene rings in the parallel stacked geometry is distinctly repulsive and sensitive to ring substitution such that electron donors heighten the electrostatic repulsion between the rings and electron acceptors diminish it.

A straightforward test for the electrostatic model, and an extension of the general analysis, is to reverse the charge distribution in the quadrupole of the ring and look for a commensurate change in the relative dynamics. Benzene and perfluorobenzene have quadrupole moments of similar magnitudes; however, in contrast to benzene, the individual bond dipoles of fluorobenzene point outward, to the highly electronegative fluorine atoms, resulting in a quadrupole in which the outer torus is negative.[8] Therefore, the electrostatic interaction between benzene and perfluorobenzene in the parallel stacked arrangement should be attractive and the substituent effects should be reversed.[9]

Continuing our investigations into 1,8-diphenylnaphthalene systems, we prepared three new series of 1,8-diphenylnaphthalenes (Fig. 1). In two series an "electron-rich" phenyl ring (ring A, phenyl or tolyl) was held constant as the variable ring (ring B) became progressively more fluorinated (**1a–d** and **2a–e**). In the third series ring A was made "electron-deficient" by perfluorination and ring B varied by different monosubstitutions (**3a–e**).[10] Standard Ullmann coupling methods were used to prepare these compounds.[11] The dynamics of phenyl group rotation were monitored by 2D EXSY NMR experiments;[12, 13] for compounds **2a, b** and **2d, e** barriers were estimated from both ^1H and ^{19}F exchange data.

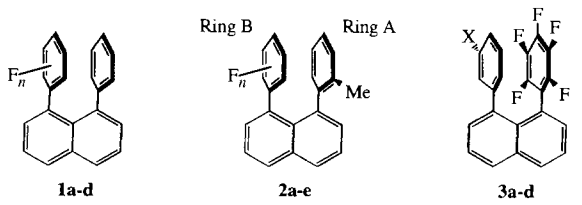


Fig. 1. Structure of compounds **1a–d**, **2a–e**, and **3a–d**; ring A is the phenyl ring on the right.

The barriers determined for **1a–d** and **2a–e** are in line with fluorine's general action as an electron-withdrawing group (Table 1). Progressive addition of fluorine to one phenyl ring correlates with an increase in the barrier to rotation, indicating a decrease in the stacked repulsion due to a removal of electron density from the center of the ring. The effect is approximately additive at 0.5 kcal mol^{-1} per fluorine atom; thus, the direction and magnitude of the slope as a function of Hammett parameter are in accord with our earlier work. In series **2a–e**, *syn*/*anti* isomerism occurs. The ratio of isomers is constant across the series, and *syn*–*anti* barriers are correspondingly 0.5 kcal mol^{-1} lower than *anti*–*syn* barriers. This effect shifts the line but does not change the nature of the correlation.

Table 1. Barriers to rotation for compounds **1a–d** (at 24 °C), **2a–e** (at 120 °C), and **3a–d** (at 80 °C).

Compound	Substituent	Position	ΔG^* [a]
1a	F	2	17.1
1b	F	2,3	17.6
1c	F	2,5	17.7
1d	F	2,3,4	18.1
2a	F	2	21.9 (21.8)
2b	F	2,3	22.3 (22.5)
2c	F	2,4	22.4
2d	F	2,5	22.0 (22.2)
2e	F	2,3,4	22.6 (22.6)
3a	NO_2	3	19.5
3b	CO_2Me	3	19.8
3c	Me	3	20.2
3d	NH_2	3	–

[a] Determined from ^1H NMR spectra; the values in parentheses were determined from ^{19}F NMR spectra.

In the series **3a–d**, ring A is perfluorinated and the electron donor/acceptor character of a single substituent on ring B varies. The symmetry of the perfluorinated ring mandates that

[*] Prof. F. Cozzi, Dr. F. Ponzini, Dr. R. Annunziata, Dr. M. Cinquini
Dipartimento di Chimica Organica e Industriale
Università di Milano
Via Golgi 19, 20133 Milano (Italy)
Telefax: Int. code + (392) 236-4369
Prof. J. S. Siegel
Department of Chemistry and Biochemistry
University of California, San Diego
La Jolla, CA 92093-0358 (USA)
Telefax: Int. code + (619) 534-5383

[**] This work was supported by the U. S. National Science Foundation (CHE-9307582), the Italian Consiglio Nazionale delle Ricerche, NATO, and the Alfred P. Sloan Foundation (J. S. S).

ring B be substituted in an unsymmetrical manner in order to make 2D NMR EXSY analysis possible. Because of the variability of steric effects from substituents in the 2-position, the 3-position was derivatized. The amino compound **3d** was not sufficiently stable to withstand the long times necessary to run the EXSY experiment.

For the series **3a–c**, the highest barrier is observed when methyl occupies the 3-position of ring B; the lowest barrier is observed for the nitro derivative. A plot of $\Delta G^{\ddagger}$ vs. $\Sigma\sigma_n$ displays a negative slope for the series **3a–c** (Fig. 2), in contrast to the

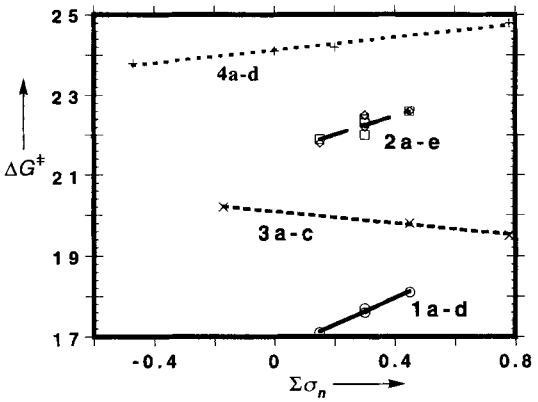
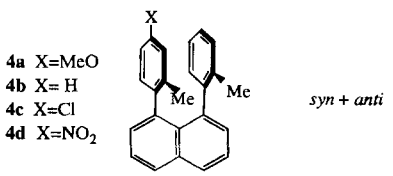


Fig. 2. Plot of the free energy of activation for phenyl group rotation vs. $\Sigma\sigma_n$ for 1,8-diarylnaphthalenes **1a–d**, **2a–e**, **3a–c**, and **4a–d**. For *syn*/*anti* mixtures the thermodynamic ratio of conformers is constant over all substituents; the barriers to the conversion of the *anti* to the *syn* conformer are plotted.

positive slope manifest by **1a–d**, **2a–e**, and the previously investigated series of 1,8-ditolylnaphthalenes **4a–d**. The trend for **3a–c** is exactly the reverse of that seen for the simple phenyl series, but completely compatible with the simple quadrupole



moment model.[14] Thus, from comparison of the trends from these three series with the trend from series **4a–d** (Fig. 2) one can conclude that a) a progressive depletion of the negative core of the benzene ring is associated with consecutive fluorine substitutions, and b) perfluorination can reverse the orientation of the benzene ring quadrupole, and therefore, reverse the electronic interaction with a given molecular electrostatic probe.

The present observations redirect existing avenues in the design of new molecular complexands and synthetic reagents by clearly pointing out the electronic prerequisites for two phenyl rings to interact with either a favorable π-stacked or T-shaped arrangement.[15] Indeed, if this model holds true, perfluorinated molecular hosts should be capable of complexing even unsubstituted benzene. Hosts prepared from a combination of both fluorinated and unfluorinated arenes should be capable of capitalizing on polar π interactions through the face and edge of an aromatic guest simultaneously, thus inducing a favored binding orientation as well as free energy.[16] Control of the degree and orientation of attraction between receptor and substrate translates to control of selectivity in reagent chemistry. Given the ease with which perfluorinated arenes can be prepared, we see this as a rich area for further exploration.

Received: December 1, 1994 [Z7516IE]
German version: *Angew. Chem.* **1995**, *107*, 1092

Keywords: fluorine compounds · molecular recognition · stacking interactions

[1] a) B. M. Trost, D. O'Krongly, J. L. Belletire, *J. Am. Chem. Soc.* **1980**, *102*, 7595–7596; b) D. A. Evans, K. T. Chapman, J. Bisaha, *ibid.* **1988**, *110*, 1238–1256; c) S. C. Siegel, E. R. Thornton, *Tetrahedron Lett.* **1988**, *29*, 5225–5228; d) J. A. Tucker, K. Houk, B. M. Trost, *J. Am. Chem. Soc.* **1990**, *112*, 5465–5471; e) J. M. Hawkins, S. Loren, M. Nambu, *ibid.* **1994**, *116*, 1657–1660; f) B. Mezrheb, F. Dumas, J. d'Angelo, C. Riche, *J. Org. Chem.* **1994**, *59*, 500–503; g) J. F. Maddaluno, N. Gresh, C. Giessner-Prettre, *ibid.* **1994**, *59*, 793–802.

[2] a) T. Benzing, T. Tjivikua, J. Wolfe, J. Rebek, *Science* **1988**, *242*, 266; b) F. Diederich, *Angew. Chem.* **1988**, *100*, 372–396; *Angew. Chem. Int. Ed. Engl.* **1988**, *27*, 362–386; c) A. V. Muehldorf, D. Van Egen, J. C. Warner, A. D. Hamilton, *J. Am. Chem. Soc.* **1988**, *110*, 6561–6562; d) S. C. Zimmermann, Z. Zeng, W. Wu, D. E. Richert, *ibid.* **1991**, *113*, 183–196; e) S. B. Ferguson, E. M. Sanford, E. M. Seward, F. Diederich, *ibid.* **1991**, *113*, 5410–5419; f) C. A. Hunter, *C. Chem. Soc. Chem. Commun.* **1991**, 749–751; g) J. E. Cochran, T. J. Parrot, B. H. Whitlock, H. W. Whitlock, *J. Am. Chem. Soc.* **1992**, *114*, 2269–2270; h) J. Zhang, J. S. Moore, *ibid.* **1992**, *114*, 9701–9702; i) S. Paliwal, S. Geib, C. S. Wilcox, *ibid.* **1994**, *116*, 4497–4498; j) L. F. Newcomb, S. H. Gellman, *ibid.* **1994**, *116*, 4993–4994.

[3] a) W. Saenger, *Principles of Nucleic Acid Structures*, Springer, New York, **1984**, p. 132; b) S. K. Burley, G. A. Petsko, *Science* **1985**, *229*, 23; c) C. A. Hunter, J. Singh, J. M. Thornton, *J. Mol. Biol.* **1991**, *218*, 837–846.

[4] a) C. A. Hunter, J. K. M. Sanders, *J. Am. Chem. Soc.* **1990**, *112*, 5525–5534; b) W. L. Jorgensen, D. L. Severance, (*ibid.* **1990**, *112*, 4768–4774; c) P. Hobza, H. L. Selzle, E. W. Schlag, *ibid.* **1994**, *116*, 3500–3506; d) C. A. Hunter, *Angew. Chem.* **1993**, *105*, 1653–1655); *Angew. Chem. Int. Ed. Engl.* **1993**, *32*, 1584–1586; e) T. Dahl, *Acta Chem. Scand.* **1994**, *48*, 95–106; f) C. A. Hunter, *Chem. Soc. Rev.* **1994**, *23*, 101–109.

[5] a) M. Claessens, L. Palombini, M.-L. Stein, J. Reisse, *New J. Chem.* **1982**, *6*, 595–601; b) J. Vrbancich, G. L. D. Ritchie, *J. Chem. Soc. Faraday Trans. 2* **1980**, *76*, 648–659; c) J. M. Steed, T. A. Dixon, W. Klemperer, *J. Chem. Phys.* **1979**, *70*, 4940–4946.

[6] a) F. Cozzi, M. Cinquini, R. Annunziata, J. S. Siegel, *J. Am. Chem. Soc.* **1993**, *115*, 5330–5331; b) F. Cozzi, M. Cinquini, R. Annunziata, T. Dwyer, J. S. Siegel, *ibid.* **1992**, *114*, 5729–5733.

[7] For other studies on the interactions between π systems in the 1- and 8-positions of naphthalenes, see: H. M. Nugent, M. Rosenblum, P. Klemarczyk, *J. Am. Chem. Soc.* **1993**, *115*, 3848–3849, and references therein; b) K. Komatsu, R. Tsuji, Y. Inoue, K. Takeuchi, *Tetrahedron Lett.* **1993**, *34*, 99–102, and references therein; c) M. Kurada, J. Nakayama, M. Hoshino, N. Furusho, S. Ohba, *Tetrahedron* **1993**, *49*, 3735–3748, and references therein.

[8] M. R. Battaglia, A. D. Buckingham, J. H. Williams, *Chem. Phys. Lett.* **1981**, *78*, 421–423.

[9] a) Evidence for the attractive interaction of stacked benzene and perfluorobenzene molecules can be seen in the crystal structure of their 1:1 complex, see: J. H. Williams, J. K. Cockcroft, A. N. Fitch, *Angew. Chem.* **1992**, *104*, 1666–1669; *Angew. Chem. Int. Ed. Engl.* **1992**, *31*, 1655–1657. b) For a general discussion of benzene–perfluorobenzene complexes see: T. Dahl, *Acta Chem. Scand. Ser. A* **1988**, *42*, 1–7; *Acta Crystallogr. Sect. B.* **1990**, *46*, 283–288.

[10] All products were fully characterized. For full spectroscopic details, see: R. Annunziata, F. Ponzini, L. Raimondi, *Mag. Reson. Chem.*, in press.

[11] For a review of the Ullmann coupling, see: E. Fanta, *Synthesis* **1974**, 9–21.

[12] For a review on the use of 2D EXSY NMR spectroscopy to measure chemical dynamics, see: C. L. Perrin, T. J. Dwyer, *Chem. Rev.* **1990**, *90*, 935–967.

[13] Because of the logarithmic relationship between k and $\Delta G^{\ddagger}$, the major contribution to the error in determining $\Delta G^{\ddagger}$ is the error in the temperature. Thus a liberal estimate of the error is 0.3 kcal mol^{-1}.

[14] Other rationales for the variance of the barrier with respect to σ have been eliminated by methods similar to that described in ref. [6].

[15] For examples of how this model has been implemented successfully, see: a) D. A. Dougherty, D. A. Stauffer, *Science* **1990**, *250*, 1558–1560; C. T. Chen, J. S. Siegel, *J. Am. Soc.* **1994**, *116*, 5959–5960.

[16] For a discussion of the importance of arene quadrupole interactions in receptor design see: a) G. Klebe, F. Diederich, *Philos. Trans. R. Soc. London A.* **1993**, *345*, 37–48; M. Luhmer, K. Bartik, A. Dejaegere, P. Bovy, J. Reisse, *Bull. Soc. Chim. Fr.* **1994**, *131*, 603–606.

 © VCH Verlagsgesellschaft mbH, D-69451 Weinheim, 1995 0570-0833/95/0909-1020 $ 10.00+.25/0

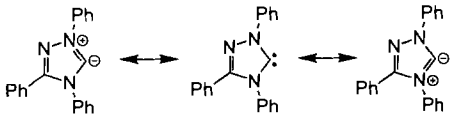
Preparation, Structure, and Reactivity of 1,3,4-Triphenyl-4,5-dihydro-1*H*-1,2,4-triazol-5-ylidene, a New Stable Carbene**

Dieter Enders,* Klaus Breuer, Gerhard Raabe, Jan Runsink, J. Henrique Teles,* Johann-Peter Melder, Klaus Ebel, and Stefan Brode

Carbenes are among the most intensively investigated reactive species in organic chemistry.[1] For many decades chemists accustomed to the quadrivalence of carbon were intrigued by their divalent nature, so there were many attempts to prepare carbenes and to "store them in bottles".[2] Despite this effort, access to these compounds was impossible for a long time because of their high reactivity. The isolation of carbenes was only seldom accomplished in inert matrices at low temperatures.

However, Bertrand et al.[3] and Arduengo et al.[4] recently reported the preparation of compounds stable at ambient temperature, which can be formulated as carbenes.[5] Yet doubts were raised about the extent of the carbene character of Bertrand's phosphinocarbene,[6] since it reacts distinctly like a phosphaacetylene.[7]

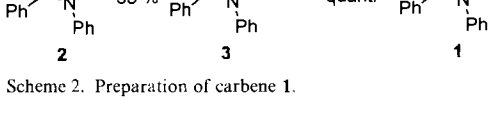
We wish to report a new heterocyclic carbene, the 1,3,4-triphenyl-4,5-dihydro-1*H*-1,2,4-triazol-5-ylidene (**1**, Scheme 1), which is stable up to 150 °C—according to DSC/TG experiments (DSC/TG = differential scanning calorimetry/thermogravimetry) unspecific decomposition begins at 150 °C—and has the typical reactivity of a nucleophilic carbene stabilized by heteroatoms in the 1,3-positions.[1, 8]



1

Scheme 1. Triazolinylidene **1** and its resonance structures.

Carbene **1** was prepared by reaction of 1,3,4-triphenyl-1,2,4-triazolium perchlorate (**2**) with sodium methoxide in methanol, affording 5-methoxy-1,3,4-triphenyl-4,5-dihydro-1*H*-1,2,4-triazole (**3**). Upon heating to 80 °C **3** decomposes endothermically (ΔH = 33 kJ mol^{-1} by DSC/TG) with concomitant elimination of methanol to form carbene **1** (Scheme 2).



2 **3** **1**

Scheme 2. Preparation of carbene **1**.

[*] Prof. Dr. D. Enders, Dipl.-Chem. K. Breuer, Dr. G. Raabe, Dr. J. Runsink
Institut für Organische Chemie der Technischen Hochschule
Professor-Pirlet-Strasse 1, D-52074 Aachen (Germany)
Telefax: Int. code + (241)8888-127

Dr. J. H. Teles, Dr. J.-P. Melder, Dr. K. Ebel, Dr. S. Brode
BASF AG, Ammoniaklaboratorium
D-67056 Ludwigshafen (Germany)
Telefax: Int. code + (621)60-56116

[**] This work was supported by the Fonds der Chemischen Industrie and the Deutsche Forschungsgemeinschaft (SFB 380, Leibniz-Preis). We are obliged to Dr. Nigel Walker, BASF AG, for the X-ray structure determination of **3**.

In the ^{13}C NMR spectrum of **1** the carbene carbon gives rise to a characteristic[4] strongly low-field shifted signal at δ = 214.[9] The chemical shifts of **1** were calculated by the GIAO-SCF method. For the parent heterocyclic system, the 4,5-dihydro-1*H*-1,2,4-triazol-5-ylidene (**1'**, $C_2N_3H_3$; the three phenyl groups were replaced by hydrogen atoms), a GIAO-MP2 calculation with an extended basis set was carried out.[10] This was used to correct the chemical shifts of the carbon atoms in the heterocyclic moiety, since electron correlation was neglected in the calculation of the chemical shifts of **1**. A very good agreement between experimental and calculated chemical shifts was found (Table 1).

Table 1. Selected experimental and calculated ^{13}C NMR chemical shifts for triazolinylidene **1**.

Carbon atom	δ(HF/dzp) [a]	δ (MP2/tzp-corr.) [b]	δ (exp.)
C1	238.7	213	214.6
C3	149.3	148	152.1
C1A	142.8	–	142.5
C1B	128.2	–	127.3
C1C	140.5	–	139.8

[a] The chemical shifts for **1** were calculated with the GIAO method at the HF/DZP level on an ab initio HF-optimized geometry [10]. [b] The correction was carried out by calculation of the chemical shifts of **1'** with the GIAO method at the HF/DZP level on a HF/DZP-optimized geometry and at the MP2/TZP level using a MP2/TZP-optimized geometry [10]. The difference attributable to electron correlation was subtracted from the corresponding chemical shifts of **1** calculated at the HF/DZP level of theory.

In the ^{1}H NMR spectrum no significant line broadening of the signals of the aromatic hydrogen atoms was found at temperatures as low as −100 °C. The rotation of the phenyl groups appears to be unhindered at this temperature. Yet the HF/SCF optimized geometry of **1** shows that the two adjacent phenyl groups are twisted out of the plane of the triazoline ring, which makes a geared rotation of these phenyl groups likely. Single crystals of **1** suitable for X-ray structure determination were obtained by layering a solution of **1** in toluene with pentane; crystals of **3** were prepared by crystallization from methanol. An ab initio calculation at the MP2(full)/6-31 + G* level of theory[13] was carried out for the parent heterocyclic system **1'** in order to gain some insight into the equilibrium structure of **1** unperturbed by the crystal field.[14] Furthermore, the structure of 1,2,4-triazolium ion **2'** ($C_2N_3H_4^+$) derived from **1'** was determined at the MP2(full)/6-31 + G* level of theory.[15]

The structure of **1** in the solid state (Fig. 1) features a bond angle of about 100° at the carbene carbon C1, which is typical of singlet carbenes.[16] This angle is significantly smaller than the corresponding one calculated for **2'** (105.0°). The phenyl groups at N3 and C2 are twisted out of the plane of the triazoline ring, while the phenyl ring at N1 is virtually coplanar with the heterocyclic ring. The C1–N1 and C1–N3 bond lengths (1.351(3) and 1.373(4) Å, respectively) are considerably shorter than expected for single bonds, which suggests a significant interaction of the occupied 2p orbitals of nitrogen atoms and the unoccupied 2p orbital of the adjacent carbene carbon atom in **1** (see Scheme 1). This stablizing interaction should be rescinded by coordinative saturation of the carbene carbon and should cause a lengthening of the bonds. In fact, the corresponding bonds in **3** (1.443(7) Å for both C2–N3 and C2–N1) are clearly longer (Fig. 2) than those in **1**. On the other hand, the C2–N2 bond (1.304(3) Å) in **2** is only negligibly longer than a typical C–N double bond,[17] be-

 © VCH Verlagsgesellschaft mbH, D-69451 Weinheim, 1995 0570-0833/95/0909-1021 $ 10.00+.25/0

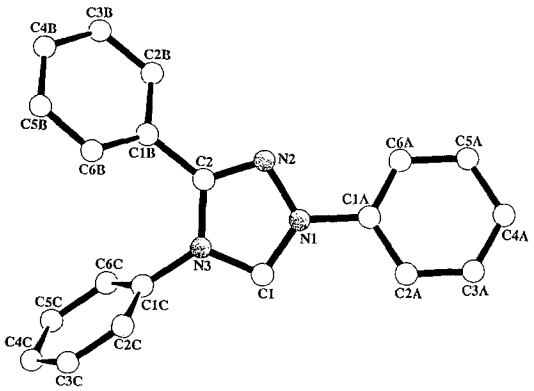


Fig. 1. Crystal structure of **1** (SCHAKAL representation) [11]. Selected bond lengths [Å] and angles [°]: C1–N1 1.351(3), C1–N3 1.373(4), C2–N2 1.304(3), N1–N2 1.398(3), C2–N3 1.391(2), N1-C1-N3 100.6(2).

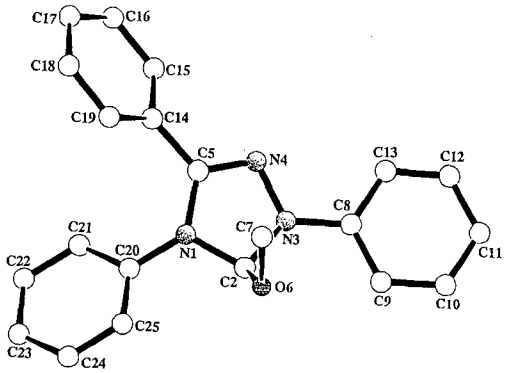
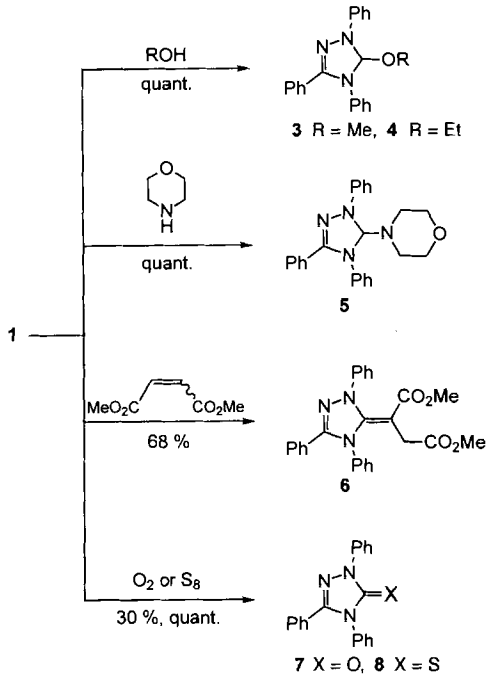


Fig. 2. Crystal structure of **3** (SCHAKAL representation) [12]. Selected bond lengths [Å] and angles [°]: N1–C2 1.443(7), C2–N3 1.443(7), N4–C5 1.296(6), N3–N4 1.394(6), N1–C5 1.391(6), N1-C2-N3 100.1(4).

ing barely longer than the C5–N4 bond in **3** (1.296(6) Å). Furthermore the N1–N2 and C2–N3 bond lengths in **1** are very similar to the corresponding bond lengths in **3**. As a rule, bond lengths determined by X-ray crystallography tend to be apparently shorter than their theoretical values.[18] Provided that this effect is negligible or comparable both for **1** and **3**, one can conclude that the interaction of the C2–N2 bond and the N1-C1-N3 unit in **1** and the corresponding unit in **3** is weak for both systems. Meanwhile the ab initio calculations yield a slightly longer N2–C2 bond for **2'** than for **1'**, while the C1–N1 and the C1–N3 bonds in **2'** are shorter by 0.2–0.3 Å. One should be wary of overrating these results given the positive charge of **2'**, yet they suggest an increased interaction of the lone pairs at the nitrogen atoms with the empty 2p AO at C1. Arduengo et al. attributed the stability of similar systems to kinetic factors, namely, to a hindered attack of nucleophilic species due to the accumulation of electron density at the carbene carbon atom itself and in its vicinity.[19] Neither our crystallographic nor our theoretical results permit us to judge the significance of these factors for the stability of the system examined in this work. Yet the differences between the bond lengths in the N1-C1-N3 unit in **1** and those in the corresponding unit in **3** indicate that 2p–2p interactions between the carbene carbon atom and the adjacent nitrogen atoms play a significant role in the stabilization of carbene **1**.

Triazolinylidene **1** reacts with alcohols such as methanol and ethanol by insertion into the O–H bond to form the 5-alkoxytri-



Scheme 3. Typical reactions of carbene **1**.

azolines **3** and **4** (Scheme 3). Insertion into the N–H bond of amines occurs similarly. Thus the reaction of **1** with morpholine yields the 5-morpholinotriazoline **5**. The carbene **1** reacts with ethyl fumarate or ethyl maleate to give methylenetriazoline **6**.[20] A cyclopropane system is presumably formed as the primary intermediate of the [2 + 1] cycloaddition, leading to the more stable allyl system by ring opening and subsequent 1,2-H shift.[21] The instability inherent in the cyclopropane spiro system can be traced back to the considerable ring strain and the "push–pull"-type substitution pattern of the cyclopropane ring. AM1 calculations[22] yield a strongly negative reaction enthalpy ($\Delta H = -76\ \mathrm{kJ\,mol^{-1}}$) for the rearrangement of the primary cyclic product to the methylenetriazoline **6** and therefore confirm the experimental results. Triazolinylidene **1** also reacts with oxygen with formation of the corresponding triazolinone **7**. Reaction with sulfur analogously leads to the triazolinethione **8**.

The X-ray data, ab initio calculations, and the reactions presented in this work show that compound **1** is a new stable carbene displaying a marked nucleophilic reactivity.

Experimental Procedure

3: Sodium methoxide (1.4 g, 26 mmol) dissolved in methanol (30 mL) was slowly added to a solution of 1,3,4-triphenyl-1,2,4-triazolium perchlorate (10.0 g, 25 mmol) in methanol (150 mL). The methanol was removed under reduced pressure at ambient temperature, and the residue extracted several times with ether. The solvent was removed from the combined ether layers under reduced pressure at ambient temperature. Crystallization from methanol yielded **3** as pale yellow crystals. Yield: 5.2 g (63%); m.p. 80 °C (decomp.); analysis calculated for $C_{21}H_{19}N_3O$: C 76.6, H 5.8, N 12.8, found C 76.5, H 5.8, N 12.6; ^{1}H NMR (300 MHz, C_6D_6, 25 °C, TMS): δ = 7.70–6.80 (m, 15H, arom. H), 6.58 (s, 1H, OC(H)N), 3.02 (s, 3H, OCH_3); ^{13}C NMR (75.4 MHz, C_6D_6, 25 °C, TMS) [23]: δ = 145.1 (C-5), 142.7 (*ipso*-C), 140.7 (*ipso*-C), 129.5 (C_{ar}), 129.2 (C_{ar}), 129.1 (C_{ar}), 128.6 (C_{ar}), 127.8 (C_{ar}), 125.0 (C_{ar}), 123.1 (C_{ar}), 120.5 (C_{ar}), 113.5 (C_{ar}), 101.0 (C2), 46.9 (C7); IR (KBr): $\tilde{\nu}$ = 3049 (m), 3000 (m), 2952 (m), 2928 (m), 2905 (m), 2816 (m), 1597 (s), 1567 (s), 1554 (s), 1505 (s), 1494 (s), 1458 (s), 1446 (m), 1408 (s), 1382 (s), 1358 (s), 1287 (m), 1261 (s), 1160 (m), 1069 (m), 1053 (s), 1038 (s), 1011 (s), 914 (s), 773 (s), 747 (s), 693 (s) cm^{-1}; MS (70 eV): *m/z* (%): 329 (0.21) [M^+], 298 (2.73) [$M^+ - CH_3OH$], 83 (100).

1: **3** (1.0 g, 3.0 mmol) was heated at 80 °C in vacuo for 16 h. Yield: 0.9 g (100%); m.p. 150 °C (decomp.); analysis calculated for $C_{20}H_{15}N_3$: C 80.8, H 5.1, N 14.1, found C 80.5, H 5.2, N 14.0; ^{1}H NMR (500 MHz, C_6D_6, 25 °C, TMS): δ = 8.68 (d,

2H, $^3J(H,H) = 7.5$ Hz), 7.35 (m, 2H), 7.25 (br.t, 2H, $^3J(H,H) = 8$ Hz), 7.21 (m, 2H), 7.06 (tt, 1H, $^3J(H,H) = 7.4$ Hz and $^4J(H,H) = 1.2$ Hz), 6.98–6.89 (m, 6H); ^{13}C NMR (125.6 MHz, C_6D_6, 25 °C, TMS) [24]: $\delta = 214.6$ (C1), 152.2 (C2), 142.5 (C1A), 139.8 (C1C), 129.9 (C4B), 129.5 (C2B, C6B), 129.4 (C3A, C5A), 129.1 (C3C, C5C), 128.6 (C3B, C5B), 127.9 (C4C), 127.3 (C1B), 127.0 (C4A), 126.7 (C2C, C6C), 120.2 (C2A, C6A); IR (KBr): $\tilde{\nu} = 3046$ (w), 1596 (s), 1552 (w), 1494 (s), 1460 (w), 1448 (m), 1359 (s), 1317 (m), 1307 (m), 1215 (m), 1152 (m), 1074 (s), 987 (s), 949 (m), 933 (m), 914 (m), 782 (s), 769 (s), 760 (s), 711 (s), 694 (s) cm^{-1}; MS (70 eV): m/z (%): 297 (56) [M^+], 296 (73) [$M^+ - 1$], 194 (100) [$M^+ - PhNC$], 180 (7), 104 (7), 91 (28), 77 (51); calculated for $C_{20}H_{15}N_3$ [M^+] 297.1266, found 297.1267.

Received: December 27, 1994 [Z 7590 IE]
German version: *Angew. Chem.* **1995**, *107*, 1119

Keywords: carbenes · cycloadditions · heterocycles · insertions

[1] *Methoden Org. Chemie (Houben-Weyl)*, 4th ed., 1952–, Vol. E19b, **1989**, pp. 84.
[2] W. Kirmse, *Carbene, Carbenoide und Carbenanaloga*, 1st ed., Verlag Chemie, Weinheim, **1969**, p. 6 ff.
[3] a) A. Igau, H. Grützmacher, A. Baceiredo, G. Bertrand, *J. Am. Chem. Soc.* **1988**, *110*, 6463; b) A. Igau, A. Baceiredo, G. Trinquier, G. Bertrand, *Angew. Chem.* **1989**, *101*, 617; *Angew. Chem. Int. Ed. Engl.* **1989**, *28*, 621.
[4] a) A. J. Arduengo III, R. L. Harlow, M. Kline, *J. Am. Chem. Soc.* **1991**, *113*, 361; b) A. J. Arduengo III, H. V. R. Dias, R. L. Harlow, M. Kline, *ibid.* **1992**, *114*, 5530.
[5] M. Regitz, *Angew. Chem.* **1991**, *103*, 691; *Angew. Chem. Int. Ed. Engl.* **1991**, *30*, 674.
[6] a) D. A. Dixon, K. D. Dobbs, A. J. Arduengo, III, G. Bertrand, *J. Am. Chem. Soc.* **1991**, *113*, 8782; b) M. Soleilhavoup, A. Baceiredo, O. Treutler, R. Ahlrichs, M. Nieger, G. Bertrand, *ibid.* **1992**, *114*, 10959.
[7] a) G. Sicard, A. Baceiredo, G. Bertrand, J.-P. Majoral, *Angew. Chem.* **1984**, *96*, 459; *Angew. Chem. Int. Ed. Engl.* **1984**, *23*, 459; b) A. Baceiredo, G. Bertrand, J.-P. Majoral, G. Sicard, J. Jaud, J. Galy, *J. Am. Chem. Soc.* **1984**, *106*, 6088; c) R. Dagani, *Chem. Eng. News* **1994**, *72*(18), 20.
[8] a) H.-W. Wanzlick, E. Schikora, *Angew. Chem.* **1960**, *72*, 494; b) H.-W. Wanzlick, *ibid.* **1962**, *74*, 129; *Angew. Chem. Int. Ed. Engl.* **1962**, *1*, 75; c) G. Scherowsky, H. Matloubi, *Liebigs Ann. Chem.* **1978**, 98; d) H. Balli, H. Grüner, R. Maul, H. Schepp, *Helv. Chim. Acta* **1981**, *64*, 648.
[9] The assignment of the corresponding ^{13}C NMR signal was confirmed by ^{13}C labeling of the carbene carbon atom C1.
[10] The geometry optimizations were carried out at the HF/SCF or MP2 level of theory with the parallel version of TURBOMOLE: S. Brode, H. Horn, M. Ehrig, D. Moldrup, J. E. Rice, R. Ahlrichs, *J. Comp. Chem.* **1993**, *14*, 1142. Optimized SV-, SVP-, DZ-, DZP- and TZP basis sets were used: A. Schaefer, H. Horn, R. Ahlrichs, *J. Chem. Phys.* **1992**, *97*, 2571. The chemical shifts were calculated by means of the GIAO method: J. Gauss, *Chem. Phys. Lett.* **1992**, *191*, 614; *J. Chem. Phys.* **1993**, *99*, 3629.
[11] Crystal data for **1**: $C_{20}H_{15}N_3$, $M_r = 297.36$, crystal size $0.3 \times 0.4 \times 0.8$ mm, monoclinic, space group $P2_1/a$ (No. 14), $a = 15.796(2)$, $b = 5.622(2)$, $c = 18.832(2)$ Å, $\beta = 111.386(4)°$. For a cell volume $V = 1557.2$ Å^3 and $Z = 4$ the density $\rho_{calcd} = 1.268$ g cm^{-3} is obtained. Total number of electrons per unit cell $F(000) = 624$. The data was collected on an Enraf-Nonius CAD4 diffractometer, $\Omega/2\theta$ scans, $T = 293$ K, graphite monochromator, $\lambda(Cu_{K\alpha}) = 1.54179$ Å, $\mu = 5.63$ cm^{-1}, 3899 measured and 3310 independent reflections (h: $-19 \leftrightarrow 18$, k: $0 \leftrightarrow 6$, l: $0 \leftrightarrow 23$), 2480 observed ($I \geq 2\sigma(I)$), $R_m = 0.017(14)$, $\theta_{max} = 73.2°$. The structure was solved by direct methods (GENSIN, GENTAN from XTAL 3.2, *XTAL 3.2 Reference Manual* (Eds.: S. R. Hall, H. D. Flack, J. M. Stewart), Universities of Western Australia, Geneva, Maryland, Lamb, Perth, **1992**). The hydrogen atoms were located by the difference Fourier method and isotropically refined. Refinement on F, 269 parameters, $R = 0.053$ and $R_w = 0.054$ for $I \geq 2\sigma(I)$, Zachariasen parameter $r^* = 3239$, residual electron density $-0.2/+0.5$ e Å^{-3}. See [12b].
[12] a) Crystal data for **3**: $C_{21}H_{19}N_3O$, $M_r = 329.40$, crystal size $0.50 \times 0.50 \times 0.38$ mm, monoclinic, space group C_c (No. 9, acentric, nonchiral), $a = 11.656(2)$, $b = 15.479(2)$, $c = 38.166(4)$ Å, $\beta = 92.82(1)°$. For a cell volume $V = 6877.7$ Å^3 and 16 molecules in the unit cell ($Z = 4 \times 4$) the density $\rho_{calcd} = 1.272$ g cm^{-3} is obtained. Total number of electrons in the unit cell $F(000) = 2784$. The data was collected on a Siemens P4 diffractometer, $\theta/2\theta$ scans, $T = 203$ K, graphite monochromator, $\lambda(Cu_{K\alpha}) = 1.54179$ Å, $\mu = 6.34$ cm^{-1}, 5784 measured and 5308 independent reflections (h: $-1 \leftrightarrow 12$, k: $-1 \leftrightarrow 16$, l: $-41 \leftrightarrow 41$), 4810 observed ($I \geq 2\sigma(I)$), $R_m = 0.051$, $\theta_{max} = 56.1°$. The structure was solved by direct methods (SHELXTL-Plus, G. M. Sheldrick, Siemens Analytical X-Ray Instruments, Inc., Madison, Wisconsin, USA). The positions of the hydrogen atoms were calculated in ideal positions. Refinement on F^2, 986 parameters, $R = 0.055$ and $R_w = 0.136$ for $I \geq 2\sigma(I)$, extinction coefficient 0.00031, residual electron density $-0.2/+0.4$ e Å^{-3}. Absolute structure parameter 0.26(36) and therefore not significant. b) Further details of the crystal structure investigations may be obtained through the Fachinformationszentrum Karlsruhe, D-76344 Eggenstein-Leopoldshafen (Germany), upon quoting depository number CSD-58 839.
[13] The geometry optimizations at the MP2(full)/6-31 + G* level of theory were carried out with GAUSSIAN 92: *Gaussian 92*, Revision D1, M. J. Frisch, G. W. Trucks, M. Head-Gordon, P. M. W. Gill, M. W. Wong, J. B. Foresman, B. G. Johnson, H. B. Schlegel, M. A. Robb, E. S. Replogle, R. Gomperts, J. L. Andres, K. Raghavachari, J. S. Binkley, C. Gonzalez, R. L. Martin, D. J. Fox, D. J. Defrees, J. Baker, J. J. P. Stewart, J. A. Pople, Gaussian, Inc., Pittsburgh PA, **1992**.
[14] The numbering of the ring system is analogous to carbene **1** in Figure 1. Selected bond lengths [Å] and angles [°] of **1'**: ($E_{tot} = -241.535236$ a.u.) C1-N1 1.351, C1-N3 1.376, C2-N2 1.317, N1-N2 1.375, C2-N3 1.370, N1-C1-N3 98.5.
[15] The numbering of the ring system is analogous to carbene **1** in Figure 1. Selected bond lengths [Å] and angles [°] of **2'**: ($E_{tot} = -241.921566$ a.u.) C1–N1 1.331, C1–N3 1.342, C2–N2 1.322, N1–N2 1.353, C2–N3 1.369, N1-C1-N3 105.0.
[16] a) C. W. Bauschlicher, Jr., H. F. Schaefer III, P. S. Bagus, *J. Am. Chem. Soc.* **1977**, *99*, 7106; b) D. A. Dixon, *J. Phys. Chem.* **1986**, *90*, 54; c) D. A. Dixon, A. J. Arduengo III, *ibid.* **1991**, *95*, 4180.
[17] The C–N bond length in formaldehyde oxime was determined to be 1.276 Å: I. N. Levine, *J. Chem. Phys.* **1963**, *38*, 2326; the C–N bond length in formaldehyde imine was calculated at the MP2(full)/6-31 + G* level of theory to be 1.283 Å: G. Raabe, unpublished results.
[18] C. K. Johnson, H. A. Levy, *International Tables for X-Ray Crystallography, Vol. IV*, 1st ed., Kluwer, Dordrecht, **1989**, p. 311.
[19] A. J. Arduengo III, H. V. R. Dias, D. A. Dixon, R. L. Harlow, W. T. Klooster, T. F. Koetzle, *J. Am. Chem. Soc.* **1994**, *116*, 6812.
[20] Only one set of signals was found in the ^{13}C NMR spectrum of compound **6**. Since the double bond in **6** bears substituents in a capto-dative way, rotation around it is probably virtually unhindered. Extremely low rotational barriers were previously found for similar systems: H. Kessler, *Chem. Ber.* **1970**, *103*, 973.
[21] The formation of open-chain products upon cyclopropanation with nucleophilic carbenes has been reported: a) W. M. Jones, M. E. Stowe, E. E. Wells, Jr., E. W. Lester, *J. Am. Chem. Soc.* **1968**, *90*, 1849; b) D. Nikolaus, PhD Thesis, University of Kaiserslautern, **1982**.
[22] MOPAC, Version 6.0, J. J. P. Stewart, QCPE 455 (1990), Indiana University, Bloomington, IN.
[23] Numbering analogous to Figure 1.
[24] Numbering analogous to Figure 2.

First Dynamic Kinetic Resolution of Racemic α-Amino Aldehydes**

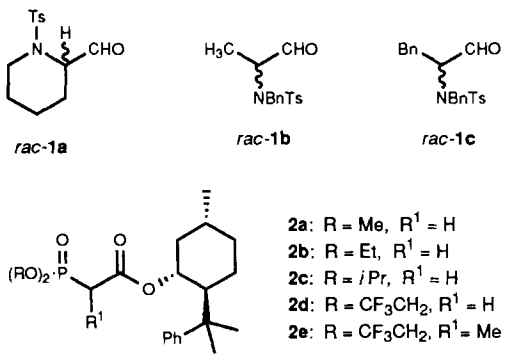
Tobias Rein,* Reinhard Kreuder, Paultheo von Zezschwitz, Christian Wulff, and Oliver Reiser*

The versatility of α-amino aldehydes in synthesis of biologically important compounds has been amply documented.[1] Nevertheless, because α-amino aldehydes are easily racemized, special precautions are necessary for their synthesis, handling, and storage.[2] This undesirable property might be turned to advantage, however, since it offers possibilities for converting racemic α-amino aldehydes to enantiomerically pure derivatives by means

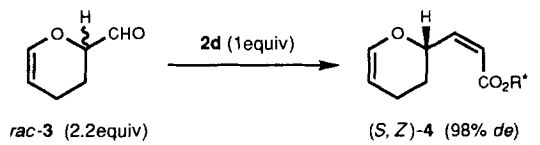
[*] Dr. T. Rein
Organic Chemistry, Royal Institute of Technology
S-10044 Stockholm (Sweden)
Telefax: Int. code + (8)791-2333
e-mail: trein@orgchem.kth.se
Dr. O. Reiser, Dipl.-Chem. R. Kreuder,[+] P. von Zezschwitz,[+] C. Wulff[+]
Institut für Organische Chemie der Universität
Tammannstrasse 2, D-37077 Göttingen (Germany)
Telefax: Int. code + (551)39-9475
e-mail: oreiser@gwdg.de
[+] Exchange students at the Royal Institute of Technology

[**] Financial support from Deutscher Akademischer Austauschdienst (313/S-PPP), the Swedish National Sciences Research Council, Pharmacia AB, Deutsche Forschungsgemeinschaft (Re 948/1), Fonds der Chemischen Industrie, Dr. Otto Röhm Foundation, and the Erasmus program for student exchange are gratefully acknowledged. We thank Raschig AG, Ludwigshafen, for generous gifts of chemicals.

of a chiral reagent that reacts at different rates with the two enantiomers under conditions in which the aldehyde is configurationally unstable.[3] We report here that such dynamic kinetic resolutions can be successfully achieved by treating racemic aldehydes *rac*-**1** (Bn = CH_2Ph, Ts = $H_3CC_6H_4SO_2$) with the chiral phosphonates **2** in the presence of a slight excess of base.



To date, relatively few reports on dynamic kinetic resolutions by chemical[4] methods have appeared, whereas this principle has more frequently been successfully applied to enzymatic[5] methods. Recently, dynamic resolution of 2-substituted cycloalkanones by reaction with a chiral phosphonate derived from mannitol has been demonstrated.[6] We previously reported that classical kinetic resolution of aldehyde *rac*-**3** by reaction with appropiate phosphonates **2a–d** could give either (*S*,*Z*)-**4** (R* = (−)-8-phenylmenthyl) or the corresponding (*R*,*E*)-alkene with good *E*/*Z* selectivity and diastereoselectivities [Eq. (1)].[7]



(1)

In these reactions, use of at least two equivalents of the aldehyde substrate was necessary, since compound **3** epimerizes only slowly in the presence of base. As an extension of these studies, we investigated asymmetric Horner–Wadsworth–Emmons (HWE) reactions with α-amino aldehydes *rac*-**1**,[8, 9] to find reaction conditions under which (*R*)-**1** and (*S*)-**1** would be in fast equilibrium, thus making dynamic resolution possible. Moreover, the corresponding HWE products appeared to be attractive precursors to non-proteinogenic amino acids[10] as well as to various alkaloids.

To establish whether dynamic resolution was possible in these reactions, we performed both classical kinetic resolutions (≥2 equiv aldehyde) and, for comparison, experiments in which only 1.3–1.4 equivalents of the aldehyde substrate were used, either with or without an excess of base over the amount of phosphonate reagent (Table 1). The results from classical resolutions of *N*-tosyl-protected aldehyde **1a**[11] (nos. 1, 2, and 4) showed, as expected, that phosphonates **2a–c** mainly gave the *E* product **5a**[12] (**2c** afforded the highest diastereoselectivity: no. 4), while reagents **2d** and **2e** predominantly gave the *Z* alkenes **6a**[12] and **8a**, respectively (nos. 8 and 12).[12] The experiments in which an excess of base was used (nos. 3, 5, 7, 9, 11, 14) then provided evidence that dynamic resolution is possible with all four reagents **2b–e**. A comparison of the classical resolutions and the reactions in which no excess of base and less than two equivalents of substrate were used (nos. 6, 10, 13) shows that selectivities as high as in the classical resolutions, or even higher, were generally observed when an excess of base was used. This becomes especially evident by comparison of nos. 8–11: While the (*Z*)-alkene (*S*)-**6a** is formed with a diastereoselectivity of 5:1 with 2.2 equivalents of **1a** without an excess of base, the selectivity dramatically improves to 16:1 in the presence of a slight excess of potassium hexamethyldisilazide (KHMDS), with either 2.2 equivalents (no. 9) or only 1.3 equivalents (no. 11) of **1a**. Without excess base, however, interconversion of (*R*)-**1a** and (*S*)-**1a** is too slow to allow dynamic resolution to operate. This is reflected in decreased *E*/*Z* selectivity and diastereoselectivity (no. 10). Under dynamic resolution conditions (*E*)-alkene

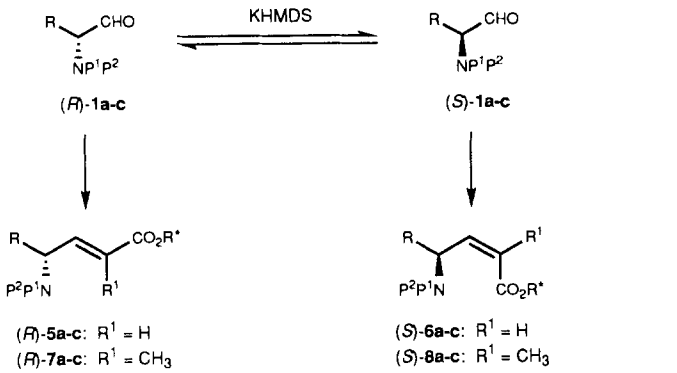
Table 1. Reactions of phosphonates **2** with racemic aldehydes **1**.

Entry	Aldehyde (equiv)	Phosphonate (equiv)	KHMDS (equiv)	(*E*)/(*Z*), crude[b]	(*E*)-Alkene	Diast. ratio (*E*)[b]	Yield,(*E*) [%][c]	(*Z*)-Alkene	Diast. ratio (*Z*)[b]	Yield,(*Z*) [%][c]
1	**1a**(2.2)	**2a**(1.1)	1.0	78:22	**5a**	79:21	68	**6a**	90:10	22
2	**1a**(2.2)	**2b**(1.1)	1.0	98:2	**5a**	81:19	96	–	–	–
3	**1a**(1.3)	**2b**(1.0)	1.2	97:3	**5a**	84:16	61	**6a**	75:25	1
4	**1a**(2.2)	**2c**(1.1)	1.0	≧99:1	**5a**	87:13	87	–	–	–
5	**1a**(2.2)	**2c**(1.0)	1.2	≧99:1	**5a**	84:16	86	–	–	–
6	**1a**(1.4)	**2c**(1.1)	1.0	≧99:1	**5a**	77:23	94	–	–	–
7	**1a**(1.4)	**2c**(1.0)	1.2	≧99:1	**5a**	85:15	78	–	–	–
8	**1a**(2.2)	**2d**(1.1)	1.0	16:84	**5a**	91:9	18[d]	**6a**	83:17	81
9	**1a**(2.2)	**2d**(1.0)	1.2	13:87	**5a**	78:22	15[d]	**6a**	94:6	73
10	**1a**(1.3)	**2d**(1.1)	1.0	28:72	**5a**	93:7	29[d]	**6a**	80:20	62
11	**1a**(1.3)	**2d**(1.0)	1.2	15:85	**5a**	81:19	13[d]	**6a**	94:6	64
12	**1a**(2.2)	**2e**(1.1)	1.0	17:83	**7a**	62:38	20[d]	**8a**	95:5	69
13	**1a**(1.0)	**2e**(1.1)	1.0	23:77	**7a**	76:24	13[d]	**8a**	94:6	56
14	**1a**(1.3)	**2e**(1.0)	1.2	15:85	**7a**	53:47	15[d]	**8a**	97:3	60
15	**1b**(2.2)	**2d**(1.1)	1.0	6:94	**5b**	81:19	16[d]	**6b**	52:48	78
16	**1b**(1.3)	**2d**(1.1)	1.0	6:94	**5b**	80:20	12[d]	**6b**	52:48	86
17	**1b**(1.3)	**2d**(1.0)	1.2	5:95	**5b**	82:18	14[d]	**6b**	52:48	81
18	**1c**(2.2)	**2d**(1.1)	1.0	10:90	**5c**	86:14	13[d]	**6c**	95:5	81
19	**1c**(1.3)	**2d**(1.1)	1.0	16:84	**5c**	91:9	20[d,e]	**6c**	90:10	69
20	**1c**(1.3)	**2d**(1.0)	1.2	10:90	**5c**	87:13	10[d]	**6c**	95:5	77

[a] General conditions: aldehyde **1**, phosphonate **2**, potassium hexamethyldisilazide (KHMDS), [18]crown-6 (5 equiv), 0.01–0.02 M in THF. [b] Determined by ^{1}H NMR at 400 MHz or 500 MHz (integrals of olefin protons). In general, the diastereomeric ratios before and after chromatography differed very little. [c] Isolated yields, after chromatography (>95% pure by NMR and TLC, unless otherwise stated). [d] Mixture of *E* and *Z* products, containing mainly *E*. [e] This fraction also contained some unchanged aldehyde **1c**.

 © VCH Verlagsgesellschaft mbH, D-69451 Weinheim, 1995 0570-0833/95/0909-1024 $ 10.00+.25/0

(*R*)-**5a** could be obtained with 70% *de*, and the (*Z*)-alkenes (*S*)-**6a** and (*S*)-**8a** with 88 and 94% *de*, respectively. In analogy to our results from reactions with *rac*-**3**, the diastereoselectivities and yields obtained in nos. 10 and 13 can only be explained by the fact that the major diastereomers of **5a** and **6a**, and **7a** and **8a**, respectively, must have opposite absolute configuration at the allylic stereocenter (cf. Scheme 1).

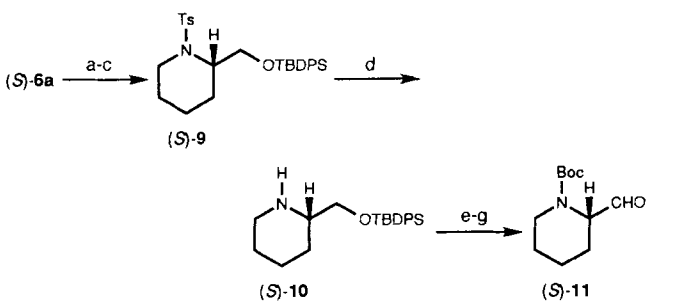


Scheme 1. Dynamic kinetic resolution of aldehydes *rac*-**1** by reaction with chiral phosphonates **2** in the presence of a small excess of base. With **2a–c** the major products are (*R*)-**5a–c**, with **2d–e** (*S*)-**6a–c** and (*S*)-**8a–c**, respectively. P^1, P^2 = protecting group; R* = (−)-8-phenylmenthyl.

To confirm that the improved selectivities were indeed due to dynamic kinetic resolution rather than to subsequent equilibration of the products, samples of **5a** or **6a** of low diastereomeric purity in mixture with *rac*-**1a** were subjected to KHMDS under the same reaction conditions. In no case was a change of the diastereomeric ratio observed.

Also in our studies of reactions with acyclic α-amino aldehydes, the choice of protecting group for the amino functionality turned out to be important. Of the alternatives investigated so far, the combination of one *N*-benzyl and one *N*-tosyl group was the best. Nevertheless, reactions of the alaninal derivative *rac*-**1b** with phosphonate **2d** gave disappointing results (nos. 15–17): while high *Z*:*E* ratios were observed, the *Z* product **6b** was formed with almost no diastereoselectivity, either under classical or under dynamic resolution conditions. To our delight, however, reactions of **2d** with aldehyde *rac*-**1c**, derived from phenylalanine,[13] gave (*S*)-**6c**[12] with diastereoselectivities up to 90% *de* (nos. 18–20). Again, excess of KHMDS not only allowed a decrease of the amount of aldehyde to 1.3 equivalents but also significantly improved the diastereoselectivity by a factor of 2.

The absolute configurations of *Z* products (*S*)-**6a** and (*S*)-**8a** were determined by correlation with the known compound (*S*)-*N*-Boc-piperidine-2-carbaldehyde[14] (**11**; Scheme 2). In analogy with these assignments, the major *Z* diastereomer produced from **1c** is tentatively assigned as (*S*)-**6c**.



Scheme 2. Determination of absolute configuration for compound (*S*)-**6a** by correlation with the known aldehyde (*S*)-**11**: a) OsO_4, NMO (73%). b) 1. H_5IO_6; 2. $NaBH_4$ (80%). c) 1. KHMDS; 2. *tert*-Butyldiphenylsilyl chloride (TBDPSCl) (78%). d) $NaC_{10}H_{10}$ (80%). e) Boc_2O (73%). f) Bu_4NF (97%). g) $(COCl)_2$, DMSO (83%).

To conclude, we have demonstrated that dynamic kinetic resolution of aldehydes *rac*-**1** by reaction with the chiral phosphonates **2** in the presence of a slight excess of base can give selectivities as high as, or even higher than the corresponding classical kinetic resolutions. Use of only 1.3–1.4 equivalents of the aldehyde substrate is sufficient, and both disubstituted and trisubstituted alkenes are accessible with high diastereoselectivities. Furthermore, this technique will also allow the synthesis of compounds derived from amino acids with unnatural configuration. The strategy described should be useful not only in HWE reactions, but should also be of general importance for the use of amino aldehydes in doubly stereodifferentiating reactions. Further extensions of this methodology are currently under investigation.

Experimental Procedure

The dynamic kinetic resolutions were performed as follows: To a solution of the phosphonate reagent **2** (1.0 equiv, 0.01–0.02 M) and [18]crown-6 (5 equiv) in THF at −78 °C under argon was added $KN(SiMe_3)_2$ (1.2 equiv, 0.5 M in toluene). After 30 min the resulting reaction mixture was added by cannula to a precooled (−78 °C) solution of *rac*-**1** (1.3–1.4 equiv) in THF. The reaction mixture was stirred for 2–19 h at −78 °C (monitoring by TLC) and then quenched with water or phosphate buffer (pH 7). Extractive workup (ethyl acetate), drying ($MgSO_4$), and concentration gave the crude condensation product, which was purified by flash chromatography or MPLC [15] on silica gel with EtOAc in hexanes (for example, **6a**: $R_f = 0.18$ in hexanes:ethyl acetate 9:1; **5a**: $R_f = 0.13$ in hexanes:ethyl acetate 9:1).

Received: August 20, 1994
Revised version: February 16, 1995 [Z 7254 IE]
German version: *Angew. Chem.* **1995**, *107*, 1099

Keywords: amino aldehydes · asymmetric syntheses · chiral auxiliaries · enantiomeric resolution · Horner–Wadsworth–Emmons reaction

[1] Reviews: a) M. T. Reetz, *Angew. Chem.* **1991**, *103*, 1559–1573; *Angew. Chem. Int. Ed. Engl.* **1991**, *30*, 1531–1546, and references therein; b) J. Jurczak, A. Golebiowski, *Chem. Rev.* **1989**, *89*, 149–164, and references therein.

[2] See, for example, H. Maeda, T. Maki, H. Ohmori, *Tetrahedron Lett.* **1992**, *33*, 1347–1350.

[3] For an excellent discussion on the use of configurationally unstable compounds in reactions with chiral reagents, see R. W. Hoffmann, M. Julius, F. Chemla, T. Ruhland, G. Frenzen, *Tetrahedron* **1994**, *50*, 6049–6060.

[4] a) K.-I. Nunami, H. Kubota, A. Kubo, *Tetrahedron Lett.* **1994**, *35*, 8639–8642; b) J. P. Genet, X. Pfister, V. Ratovelomana-Vidal, C. Pinel, J. A. Laffitte, *Tetrahedron Lett.* **1994**, *35*, 4559–4562; c) M. Kitamura, M. Tokunaga, R. Noyori, *J. Am. Chem. Soc.* **1993**, *115*, 144–152; d) R. Stürmer, *Angew. Chem.* **1990**, *102*, 62; *Angew. Chem. Int. Ed. Engl.* **1990**, *29*, 59; e) D. Hoppe, O. Zschage, *Angew. Chem.* **1989**, *101*, 67–69; *Angew. Chem. Int. Ed. Engl.* **1989**, *28*, 69; f) T. Hayashi, M. Konishi, K. Fukushima, K. Kanehira, T. Hioki, M. Kumeda, *J. Org. Chem.* **1983**, *48*, 2195; g) A. Tai, H. Watanabe, T. Harada, *Bull. Chem. Soc. Jpn.* **1979**, *52*, 1468–1472.

[5] See, for example, Y. Kawai, K. Hida, K. Nakamura, A. Ohno, *Tetrahedron Lett.* **1995**, *36*, 591–592, and references therein.

[6] K. Narasaka, E. Hidai, Y. Hayashi, J.-L. Gras, *J. Chem. Soc. Chem. Commun.* **1993**, 102–103.

[7] T. Rein, N. Kann, R. Kreuder, B. Gangloff, O. Reiser, *Angew. Chem.* **1994**, *106*, 597–599; *Angew. Chem. Int. Ed. Engl.* **1994**, *33*, 556–558.

[8] For HWE reactions with amino aldehydes: M. T. Reetz, D. Röhrig, *Angew. Chem.* **1989**, *101*, 1732–1734; *Angew. Chem. Int. Ed. Engl.* **1989**, *28*, 1706–1709.

[9] While this paper was under revision, a classical kinetic resolution of *N*,*N*-dibenzylalaninal by reaction with **2a** was reported, which gave up to 60% *de*. T. Furuta, M. Iwamura, *J. Chem. Soc. Chem. Commun.* **1994**, 2167–2168.

[10] C. Bubert, J. Voigt, S. Biasetton, O. Reiser, *Synlett* **1994**, 675–677.

[11] The *N*-tosyl-protected aldehyde *rac*-**1a** gave considerably higher selectivities than the corresponding *N*-Boc- or *N*-methyl-protected derivatives.

[12] Spectroscopic and analytical data (^1H and ^{13}C NMR, IR, MS, elemental analysis) in accordance with the assigned structure were obtained for this compound.

[13] For preparation of (*S*)-**1c**: S. G. Pyne, M. J. Hensel, P. L. Fuchs, *J. Am. Chem. Soc.* **1982**, *104*, 5719–5728.

[14] D. Romo, S. D. Meyer, D. D. Johnson, S. L. Schreiber, *J. Am. Chem. Soc.* **1993**, *115*, 7906–7907.

[15] P. Baeckström, K. Stridh, L. Li, T. Norin, *Acta Chem. Scand. Ser. B* **1987**, *41*, 442–447.

 © VCH Verlagsgesellschaft mbH, D-69451 Weinheim, 1995 0570-0833/95/0909-1025 $ 10.00+.25/0

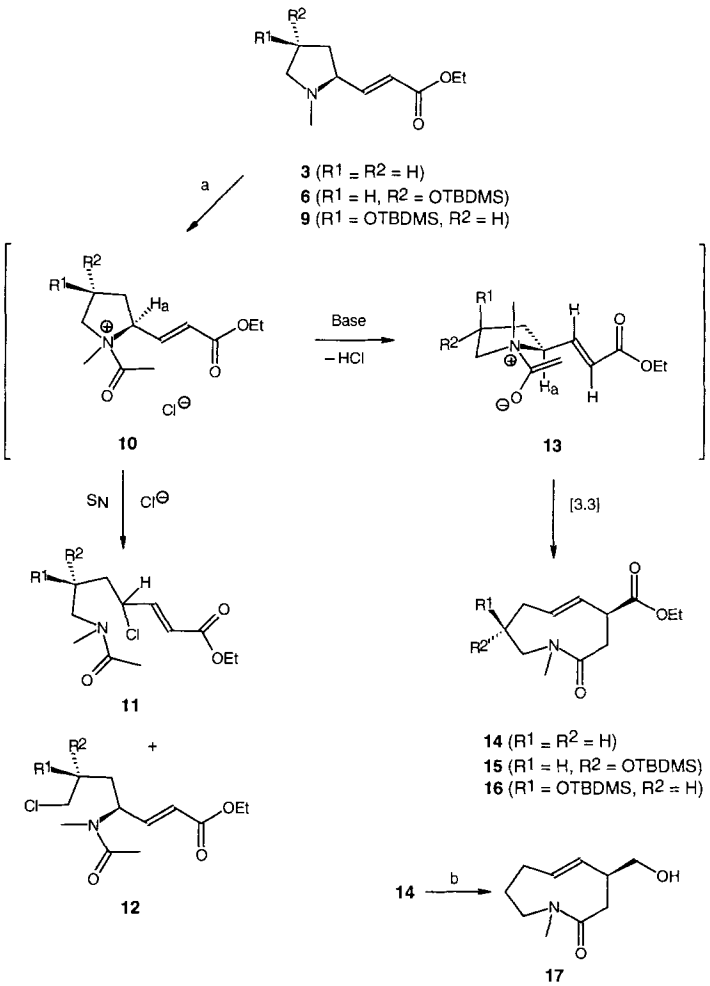
Synthesis of Optically Active Nine-Membered Ring Lactams by a Zwitterionic Aza-Claisen Reaction**

Michel Diederich and Udo Nubbemeyer*

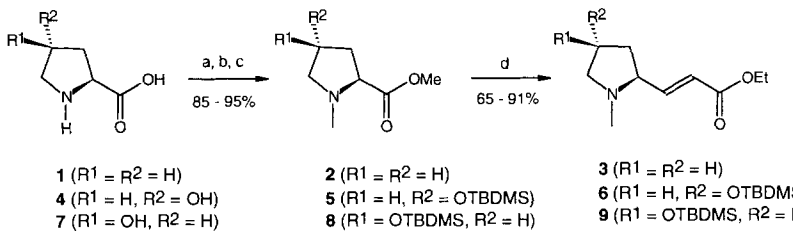
The ketene-Claisen reaction was first described by D. Belluš in 1978 as an intermolecular variant of the [3.3] sigmatropic rearrangement of allyl and thioallyl ethers.[1] Recently, it was reported that allyl sulfides, in particular, can be rearranged under very mild conditions chemoselectively with the expected 1,3-chirality transfer from the C–S to a C–C bond. Furthermore, excellent 1,2-asymmetric induction was found when an optically active C–O functionality was located α to the nascent C–C bond.[2] The reaction was also employed in the syntheses of medium-sized rings (7–13 ring atoms).[3] Until now the rearrangement was restricted to activated ketenes like chloroalkyl- and dichloroketene. Allyl amines have been used in ketene-Claisen reactions only rarely. The few reported cases focused on conformationally fixed bicyclic systems or amines bearing an unhindered terminal olefinic unit.[4] Here, we report on the synthesis of optically active[5] hexahydroazoninones by a zwitterionic aza-Claisen reaction with complete 1,3-chirality transfer from chiral allyl amines.[5]

As starting compounds we used the allyl amines **3**, **6**, and **9**. The proline methyl ester **2** was synthesized from L-(−)-proline (**1**) by Clarke–Eschweiler methylation[6] and subsequent esterification (Scheme 1).[7] In a one-pot reaction **2** was reduced with diisobutylaluminum hydride (DIBAH) in situ to give the aldehyde; Horner olefination provided amino ester **3**. Amino esters **6** and **9** were prepared by analogous sequences starting from *trans*- and *cis*-4-hydroxy-L-proline (**4**) and (**7**), respectively. Prior to the one-pot reduction/chain extension reaction, the free OH group was protected as a *tert*-butyldimethylsilyl (TBDMS) ether in **5** and **8**.[8] The diastereomeric purity of amino esters **3**, **6**, and **9** was determined by ^1H and ^{13}C NMR spectroscopy (see Table 1) and by HPLC analysis.[9]

Special two-phase conditions were developed for the Claisen rearrangement of allyl amines **3**, **6**, and **9**. A slurry of the amine and solid potassium carbonate in anhydrous chloroform at 0 °C was treated with acetyl chloride and 20 to 30 mol% of trimethylaluminium. The corresponding partially hydrogenated azoninones **14**, **15**, and **16** were isolated in 65 to 84% yield (Scheme 2).



Scheme 2. Zwitterionic aza-Claisen reaction: a) AcCl, K_2CO_3, Me_3Al, $CHCl_3$, 0 °C, 72 h (65–85%). Selective reduction of the ester function: b) $NaBH_4$, *t*BuOH, MeOH, reflux, 2 h (46%).



Scheme 1. Synthesis of amino esters **3**, **6**, and **9**. a) 98% HCO_2H, 37% CH_2O/H_2O, reflux, 7 h; b) $SOCl_2$, MeOH, reflux, 6 h; c) **4** and **7**: TBDMSCl, imidazole, CH_2Cl_2, 20 °C, 12 h; d) 1. DIBAH, Et_2O, −78 °C, 16 h, 2. $(EtO)_2P(O)CH_2CO_2Et/NaH$, Et_2O, −78 → 20 °C, 4 h.

In considering the reaction mechanism it seemed reasonable to assume that the acyl ammonium salt **10** forms initially. This intermediate could be attacked either by the nucleophilic halide ion in a von Braun type S_N reaction[10] generating the chlorides **11** and/or **12**, or by a base (e.g. the chloride ion) which could deprotonate the α-position of the activated carbonyl group. The resulting zwitterionic intermediate **13** could then undergo [3.3] sigmatropic rearrangement resulting in the azoninones **14** to **16**.

The postulated reaction path via **10** and **13** is based on the following observations.

1) Acyl ammonium salt **10** was detected in the reaction mixture at low temperatures by ^1H and ^{13}C NMR spectroscopy.

2) Halides of type **11** and **12** were isolated in yields of 0 to 10% and characterized as by-products of the rearrangement. Apparently the reaction path taken is determined by the bulk of the alkyl substituent on acyl ammonium salt **10**: N-benzylated amino esters underwent the von Braun reaction to yield amides **11** and **12**, whereas the N-methylated esters **3**, **6**, and **9** rearranged as described above.[11]

3) The chloride ion served as the essential base under the reaction conditions. After the generation of acyl ammonium salt

[*] Dr. U. Nubbemeyer, M. Diederich
Institut für Organische Chemie der Freien Universität
Takustrasse 3, D-14195 Berlin (Germany)
Telefax: Int. code + (30)838-5163

[**] This work was supported by the Deutsche Forschungsgemeinschaft and by the Fonds der Chemischen Industrie.

10 with acetyl trifluoroacetate[12] the rearrangement was started by the addition of tetraalkylammonium chloride. Acetic anhydride did not react. Numerous bases (Li and K amides, alcoholates, amidines, etc.) destroyed the acyl ammonium salt regenerating the allyl amines **3**, **6**, and **9**.

4) Ketenes did not react with **3**, **6**, and **9** under widely varied reaction conditions,[13] since ketenes are apparently not electrophilic enough to attack the allyl amines.[14]

5) The Lewis acid increases the acidity of the α-protons by interacting with the carbonyl group of the acyl ammonium salt **10** and/or stabilizing the zwitterionic intermediate **13**, thus suppressing the elimination of ketene.[15] Without Lewis acid the reaction rate decreased severely (ca. 25% conversion after three days); von Braun type substitution products were isolated in yields of 20 to 50%.

If the azoninones are formed by the postulated path, acyl ammonium salt **10** might be (partly) racemized, because the acidity of H_a is increased by the ester group (and the Lewis acid) and the ammonium function. The structure assignments of lactams **14**–**16** proved the complete chirality transfer from the C–N to the C–C bond. Furthermore the results support the mechanism proposed by Pombo-Villar et al.[4b] in which a [3.3] sigmatropic rearrangement is postulated as the key step. The alternate mechanism, formation of an allyl cation followed by attack of the enolate, seems to be disfavored. On the one hand, generation of a cation adjacent to an acceptor function is improbable; on the other hand, rearrangement of amino esters **6** and **9** should result in mixtures of diastereomers because of increased rotational freedom after the cleavage of the C–N bond.

The ester group of lactam **14** was reduced selectively with $NaBH_4$ in *tert*-butyl alcohol and methanol to give alcohol **17**,[16] which was protected as a Mosher ester.[17] According to HPLC analysis, and ^1H and ^{13}C NMR spectra of the derivative, only one diastereomer had formed, which indicates that the enantiomeric purity of **17** is >90%.

That the 1,3-chirality transfer was complete could be proved directly by analyzing the structures of lactams **15** and **16**. The *syn*-configurated amino ester **9** gave exclusively the *syn* azoninone **16**. The relative configuration was determined unequivocally by NOE difference spectroscopic analysis. Because the double bond and the amide function of azoninone **16** fix the ring system in one conformation at room temperature, all protons are in fixed positions and could be assigned exactly to the ^1H NMR signals.

The configuration of azoninone **15** (synthesized from the *anti* amino ester **6**) was determined only indirectly owing to the occurrence of two stable conformations at 23 °C. In the ^1H NMR spectrum in DMSO at 130 °C complete coalescence was not achieved. Two nonoverlapping peaks were evident by HPLC analysis, but preparative separation by HPLC failed. After separation the two fractions had the same distribution of the compounds as that originally found by HPLC. However, since both conformers of azoninone **15** are distinctly different from lactam **16**, epimerization of the chiral center can be excluded (complete 1,3-chirality transfer!). Relevant spectroscopic data are given in Table 1.

The zwitterionic aza-Claisen reaction allows the stereospecific rearrangement of allyl amines such as **3**, **6**, and **9** to the corresponding γ,δ-unsaturated lactams **14**, **15**, and **16** under very mild conditions. Thus this reaction offers the following advantages:

1) The high temperatures (>120 °C) of the Johnson, Eschenmoser, and the amide enolate reactions are not necessary.[18]

2) Superbases (LDA, etc.) like that employed in the Ireland type process are avoided.[19]

3) The reaction is not restricted to activated ketenes, which are essential in the rearrangement of thioallyl ethers.[2]

Table 1. Spectroscopic data for compounds **3**, **9**, **14**, and **16**.

	IR (KBr) (neat) $\tilde{\nu}_{max}$	MS (70 eV) (EI) M/z	^1H NMR (270 MHz, $CDCl_3$) (20 °C, TMS, J in Hz) δ	^{13}C NMR (67.9 MHz, $CDCl_3$) (20 °C) δ
3	1721 (CO) 1655 (C=C)	(50 °C): 183 (M^+) 154, 138, 110	6.75 (dd, J = 9.0, J = 18.0, 1H), 5.9 (d, J = 18.0, 1H), 4.15 (q, J = 7, 2H), 3.1 (m, 1H), 2.65 (d, br, J = 9.0, 1H), 2.2 (s, 3H), 2.15 (dd, J = 9.0, J = 12.0, 1H), 2.0 (m, 4H), 1.25 (t, J = 7.0, 3H)	166.1 (s), 149.8 (d), 122.0 (d), 67.5 (d), 60.1 (t), 56.7 (t), 40.4 (q), 31.6 (t), 22.5 (t), 14.1 (q)
9	1711 (CO) 1650 (C=C)	(50 °C): 313 (M^+) 284, 256, 130	6.8 (dd, J = 9.4, J = 15.6, 1H), 5.85 (d, J = 15.6, 1H), 4.3 (m, 1H), 4.15 (q, J = 7.5, 2H), 3.1 (m, 1H), 2.9 (d, br, J = 12.0, 1H), 2.7 (q, J = 9, 1H), 2.45 (m, 1H), 2.35 (m, 1H), 2.15 (s, 3H), 1.6 (m, 1H), 1.2 (t, J = 7.5, 3H), 0.8 (s, 9H), −0.1 (s, 6H)	166.0 (s), 149.3 (d), 122.4 (d), 70.6 (d), 67.4 (d), 65.7 (t), 60.1 (t), 43.3 (t), 40.4 (q), 25.7 (q), 18.0 (s), 14.0 (q), −4.8 (q), −4.9 (q)
14	1734 (CO) 1621 (CO)	(100 °C): 225 (M^+) 197, 179, 172, 121	5.5 (dd, J = 9.8, J = 15.7, 1H), 5.2 (ddd, J = 4.0, J = 11.3, J = 15.7, 1H), 3.95 (q, J = 7, 2H), 3.4 (ddd, J = 5.0, J = 9.5, J = 14, 1H), 3.1 (dt, J = 4.2, J = 10.0, 1H), 2.9 (dd, br, J = 5.0, J = 14, 1H), 2.65 (s, 3H), 2.45 (m, 2H), 2.2 (m, 1H), 1.9 (m, 1H), 1.7 (m, 2H), 1.1 (t, J = 7.0, 3H)	172.9 (s), 171.2 (s), 131.7 (d), 131.3 (d), 60.9 (t), 48.9 (t), 46.4 (d), 40.6 (t), 33.8 (q), 31.5 (t), 27.4 (t), 14.1 (q)
16	1725 (CO) 1618 (CO)	(120 °C): 355 (M^+) 298, 282, 181, 130	5.65 (dd, J = 9.4, J = 15.6, 1H), 5.1 (ddd, J = 3.5, J = 9.4, J = 15.6, 1H), 4.0 (q, J = 7.5, 2H), 3.85 (m, 1H), 3.65 (m, 1H), 3.2 (dt, J = 3.0, J = 12.0, 1H), 2.85 (, 1H), 2.8 (s, 3H), 2.65 (m, 1H), 2.55 (m, 2H), 1.95 (m, 1H), 1.15 (t, J = 7.5, 3H), 0.7 (s, 9H), −0.05 (s, 6H)	172.3 (s), 170.7 (s), 133.2 (d), 127.3 (d), 70.0 (d), 60.8 (t), 57.6 (t), 46.8 (q), 42.4 (t), 40.3 (t), 34.6 (d), 25.6 (q), 17.7 (s), 14.0 (q), −4.7 (q), −5.0 (q)

The method described allows the generation of optically active nine-membered ring lactams in high yields in only five or six steps (three steps with isolated products). The reaction can be carried out in the presence of acidic protons without epimerization.[20] This easy approach to hexahydroazoninones should encourage their application in the synthesis of pharmaceutically active compounds and natural products.[21]

Experimental Procedure

1) One-pot procedure for the DIBAH reduction and Horner olefination: A solution of 50 mmol of amino ester **2**, **5**, or **8** in 50 mL of anhydrous Et_2O under argon was cooled to −78 °C. During the addition of 1.3 equiv of DIBAH (20% in toluene) the temperature was kept below −75 °C. After 16 h at −78 °C, the reaction mixture was treated with 60 mmol of triethyl phosphonoacetate (deprotonated with NaH) in 100 mL of anhydrous THF. The mixture was stirred for 5 h and allowed to warm to room temperature. Then the reaction was quenched with 5 mL of MeOH. After 15 min 10 g of K/Na tartrate was added, and after a further 15 min the mixture was hydrolyzed with 30 mL of 10% aqueous $NaHCO_3$. The organic layer was decanted and the residue extracted with EtOAc. The combined organic phases were dried ($MgSO_4$) and concentrated to dryness. The resulting crude material was purified by column chromatography on silica gel.

2) Aza-Claisen reaction: A suspension of 50 mmol of dry Na_2CO_3 in 200 mL of anhydrous $CHCl_3$ under argon was treated with 60 mmol of amino ester **3**, **6**, or **9**. The reaction mixture was cooled to 0 °C and 90 mmol of AcCl was added with stirring. After a further 20 min, 10–20 mmol of Me_3Al (2 M in hexane) was injected by syringe. The reaction was stopped after 2–5 d by careful hydrolysis of Me_3Al with ice water. The layers were separated and the aqueous phase was extracted with $CHCl_3$. The combined organic phases were dried ($MgSO_4$) and concentrated to dryness. The resulting crude product, **14**, **15**, or **16**, was purified by column chro-

matography on silica gel. Note: When more than 10 to 20% of the amino ester remained after the workup, the crude material was subjected to the reaction conditions again. After the second cycle the reaction was complete without a decrease in the yield.

Received: November 9, 1994 [Z7461IE]
German version: *Angew. Chem.* **1995**, *107*, 1095

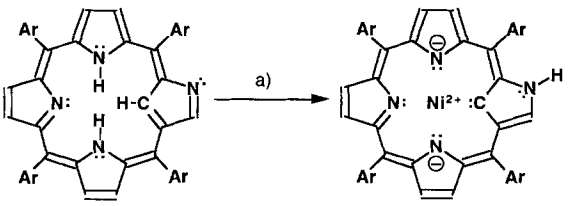
Keywords: aza-Claisen reaction · azoninones · chirality transfer · lactams

[1] a) R. Malherbe, D. Belluš, *Helv. Chim. Acta* **1978**, *61*, 3096; b) R. Malherbe, G. Rist, D. Belluš, *J. Org. Chem.* **1983**, *48*, 860.
[2] a) R. Öhrlein, R. Jeschke, B. Ernst, D. Bellusý, *Tetrahedron Lett.* **1989**, *30*, 3517; b) U. Nubbemeyer, R. Öhrlein, J. Gonda, B. Ernst, D. Belluš, *Angew. Chem.* **1991**, *103*, 1533; *Angew. Chem. Int. Ed. Engl.* **1991**, *30*, 1465.
[3] a) G. Rossini, G. Spineti, E. Foresti, G. Pradella, *J. Org. Chem.* **1981**, *46*, 2228; b) E. Vedejs, R. A. Buchanan, *ibid.* **1984**, *49*, 1840; c) M. Ishida, H. Muramaru, S. Kato, *Synthesis* **1989**, 562.
[4] a) E. D. Edstrom, *J. Am. Chem. Soc.* **1991**, *113*, 6690; b) M. M. Cid, E. Pombo-Villar, *Helv. Chim. Acta* **1993**, *76*, 1591; c) M. M. Cid, U. Eggnauer, H. P. Weber, E. Pombo-Villar, *Tetrahedron Lett.* **1991**, *32*, 7233.
[5] E. Edstrom [4a] described the synthesis of an hexahydroazoninone without a chiral center.
[6] R. N. Icke, B. B. Wisegarver, G. A. Alles, *Org. Synth. Coll. Vol. 3*, **1955**, 723.
[7] L. F. Tietze, T. Eicher, *Reaktionen und Synthesen im Organisch-Chemischen Praktikum*, 2nd ed., Thieme, Stuttgart **1991**, p. 135.
[8] E. J. Corey, A. Venkatesvarlu, *J. Am. Chem. Soc.* **1972**, *94*, 6190.
[9] All attempts at selectively reducing the ester function to avoid racemization in the rearrangement failed; the resulting allyl alcohol was always contaminated with 20 to 50% of the saturated compound. Because of the difficult separation of these products and the low yield of the desired material this sequence was abandoned. Cf. T. Moriwake, S.-I. Hamano, S. Saito, S. Torii, *Chem. Lett.* **1987**, 2085.
[10] H. A. Hagemann, *Org. React.* **1953**, *7*, 158.
[11] The reaction conditions described by Edstrom [4a] afforded exclusively the von Braun type products and decomposed material.
[12] E. C. Bourne, M. Stacey, J. C. Tatlow, R. Worall, *J. Chem. Soc.* **1954**, 2006.
[13] a) E. Valenti, M. A. Pericas, F. Serratosa, D. Maha, *J. Chem. Res. Syn.* **1990**, 118; b) W. T. Brady, Y.-F. Giang, A. P. Marchand, A.-H. Wu, *J. Org. Chem.* **1987**, *52*, 3457; c) R. J. Clemens, J. A. Hyatt, *ibid.* **1985**, *50*, 2431; d) W. T. Brady, R. A. Owens, *Tetrahedron Lett.* **1976**, 1553; e) G. H. Olah, A.-H. Wu, O. Farooq, *Synthesis* **1989**, 568.
[14] Only with dichloroketene could an analogous azoninone be isolated in low yield. (Belluš et al. [1,2] obtained the same results with allyl sulfides.) a) W. T. Brady, W. L. Vaughn, H. G. Liddell, *J. Org. Chem.* **1966**, *31*, 626, b) M. Diederich, Diplomarbeit, Berlin **1992**
[15] E. Vedejs, M. Gringas, *J. Am. Chem. Soc.* **1994**, *116*, 579.
[16] K. Soai, H. Oyamada, A. Okawa, *Synth. Commun.* **1982**, *12*, 463.
[17] D. A. Dale, D. L. Dull, H. S. Mosher, *J. Org. Chem.* **1969**, *34*, 2543.
[18] a) F. E. Ziegler, *Chem. Rev.* **1988**, *88*, 1429; b) W. S. Johnson, L. Werthemann, W. R. Bartlett, T. J. Brocksom, T. Li, D. J. Faulkner, M. R. Petersen, *J. Am. Chem. Soc.* **1970**, *92*, 741; c) D. Felix, K. Gschwend-Steen, A. E. Wick, A. Eschenmoser, *Helv. Chim. Acta* **1969**, *52*, 1030; d) T. Tsunoda, M. Sakai, O. Sakai, Y. Sako, Y. Honda, S. Ito, *Tetrahedron Lett.* **1992**, *33*, 1651.
[19] a) R. E. Ireland, R. H. Mueller, A. K. Willard, *J. Am. Chem. Soc.* **1976**, *98*, 2868; b) R. E. Ireland, R. H. Mueller, *ibid.* **1972**, *94*, 5897.
[20] **2**: $[\alpha]_D^{22} = -70.8$ ($c = 3.3$, $CHCl_3$); **3**: $[\alpha]_D^{22} = -70.6$ ($c = 2.9$, $CHCl_3$); **5**: $[\alpha]_D^{22} = -33.7$ ($c = 3.52$, $CHCl_3$); **6**: $[\alpha]_D^{22} = -38.9$ ($c = 8.1$, $CHCl_3$); **8**: $[\alpha]_D^{22} = 46.7$ ($c = 5.6$, $CHCl_3$); **9**: $[\alpha]_D^{22} = 51.2$ ($c = 2.0$, $CHCl_3$); **14**: $[\alpha]_D^{22} = 86.3$ ($c = 3.1$, $CHCl_3$); **15**: $[\alpha]_D^{22} = 17.0$ ($c = 1.8$, $CHCl_3$); **16**: $[\alpha]_D^{22} = -116.1$ ($c = 3.6$, $CHCl_3$); **17a**: $[\alpha]_D^{22} = -15.0$ ($c = 1.6$, $CHCl_3$, Mosher ester).
[21] B. Lüning, C. Lundin, *Acta Chem. Scand.* **1967**, *21*, 2136.

N-Confused Porphyrins and Singlet Carbenes: Is There a Connection?**

Abhik Ghosh*

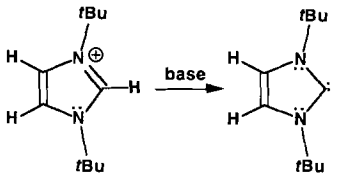
The isolation of 2-aza-21-carba-5,10,15,20-tetraarylporphyrins as by-products of a standard preparative method for tetraarylporphyrins was an important and unexpected development in porphyrin chemistry.[1, 2] Interest in these novel compounds (e.g. **1**), also dubbed N-confused porphyrins, centers on their remarkable ability to act as tetracoordinate ligands and form complexes (e.g. **2**) with metal–carbon bonds (Scheme 1).[1]



Scheme 1. Ar = *p*-tolyl; a) $NiCl_2 \cdot 6H_2O$, $CHCl_3$/EtOH, reflux, 0.5 h.

However, neither the original report[1] on this discovery nor a critical commentary[3] on these compounds proposed a rationale for the unexpectedly labile central C–H bond of **1**.

Here we point out a striking analogy between the remarkable carbon acidity of N-confused porphyrins and the properties of completely different organic compounds, namely stable "bottleable" carbenes such as **4** synthesized by Arduengo et al. by the deprotonation of *N*,*N*-dialkylimidazolium ions **3**.[4] Thus, complex **2** may be formally regarded as a nickel(II)-stabilized carbene. In addition, we propose that the stability and aromaticity of the ligand in **2** may account for the hitherto unexplained carbon acidity of **1** and its N-protonated form, **1**-H$^+$.

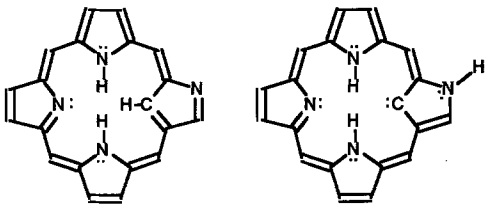


Our proposal, if essentially correct, should have far-reaching implications for the electronic structure and chemical reactivity of N-confused porphyrins. Accordingly, we carried out high-quality ab initio[5] and local density functional (LDF)[6] calculations on compounds **5**–**9** to test the validity of the proposed analogy as well as to develop the first theoretical picture of the electronic structure of N-confused porphyrins. Compounds **5** and **8** are the unsubstituted analogues of **1** and **2**, respectively. Species **6** is the free base form of the ligand in complex **8** and the carbenic tautomer of **5**. The zinc complex **7** was selected for studying the interaction of the carbenic ligand **6** with a closed-

[*] Dr. Ghosh
Department of Chemistry and Minnesota Supercomputer Institute (MSI)
University of Minnesota
Minneapolis MN 55455 (Chemistry) and 55415 (MSI) (USA)
Present address:
Department of Chemistry, University of California
Riverside, CA 92521 (USA)
Telefax: Int. code + (909)787-4713
e-mail: mf10105@sc.msc.edu or mf10105@sk.msc.edu.

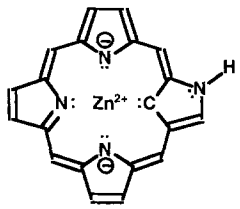
[**] This work supported by the MSI and Prof. Jan Almlöf.

 © VCH Verlagsgesellschaft mbH, D-69451 Weinheim, 1995 0570-0833/95/0909-1028 $ 10.00+.25/0

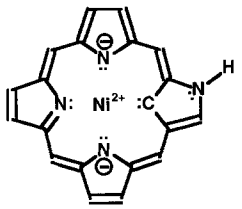


5

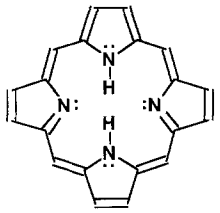
6



7



8



9

shell Lewis acid such as a Zn^{2+} ion. LDF calculations on **5**–**8**, including geometry optimizations, used double-zeta plus polarization (DZP) basis sets, the von Barth–Hedin exchange-correlation functional,[7] and a C_s symmetry constraint. Ab initio calculations using Hartree–Fock (HF) and second-order Møller–Plesset perturbation theories were carried out on LDF-optimized geometries of the organic molecules **5** and **6** and the unsubstituted free base porphyrin **9** with generally contracted double-zeta (DZ) basis sets[8, 9] and direct electronic structure methods[10] that obviate the need for storing prohibitive volumes of electron repulsion integrals. In the optimized geometry of **6** the C-C-C angle subtended at the carbenic center is only 104.2°, which is extremely small for dicoordinate carbon and highly characteristic of singlet carbenes. Table 1 presents the calculated Hartree–Fock orbital energies of the six highest occupied molecular orbitals (MOs) of the purely organic compounds **5**, **6**, and **9**. Table 2 presents calculated LDF values of the lowest singlet–triplet energy gaps (ΔE_{S-T}) for both the lowest $\pi^1\pi^{*1}$ and $\sigma^1\pi^{*1}$ triplet states, and the lowest σ and π ionization potentials (IPs) of **5**–**8**.

Table 1. Sign-reversed HF orbital energies [eV] of the six highest occupied MOs of **5**, **6**, and **9**.

5	**6**	**9**
10.41 (π)	9.74 (π)	10.25 (π)
10.31 (π)	9.11 (π)	10.20 (π)
9.55 (π)	8.54 (σ)	9.30 (π)
8.99 (π)	8.44 (π)	9.07 (π)
6.66 (π)	6.54 (π)	6.52 (π)
6.40 (π)	5.63 (π)	6.20 (π)

Table 1 shows that the values of the HF orbital energies of **5** and **9** are extremely similar,[11] at least for the six lowest IPs (according to Koopmans' theorem, KT), while the values of **6** are considerably different. Thus, none of the six lowest IPs of **5** and **9** corresponds to σ ionization, whereas the fourth lowest HF-KT IP of **6** corresponds to a σ-ionized final state. LDF calculations (using the ΔSCF method) also show that the lowest σ-IP of **6** is relatively low at approximately 7.31 eV compared to the lowest π-IP of 6.65 eV and to the lowest σ-IPs of **5** and **9** (for which the HF-KT values listed in Table 1 may serve as estimates). An LDF calculation on the lowest energy σ-ionized $^2A'$ state of **6** shows that the majority ($\approx 80\%$) of the unpaired spin density is localized in the region of the carbenic lone pair. This is indeed what one expects of a stable nucleophilic carbene of the type synthesized by Arduengo et al.[12] For instance, the lowest σ-IP of **4**, corresponding largely to ionization from the carbenic lone pair, is 7.68 eV,[12] which is quite close to the LDF value of 7.31 eV for **6**. One difference between **4** and **6** is that the aromatic framework of **6** may be regarded as a large annulene whose highest occupied π MOs have rather higher orbital energies (i.e. lower HF-KTs) than the π HOMOs of imidazole. Thus, it is understandable that the lowest LDF IP of **6** (7.31 eV, which corresponds to a π ionization) is significantly smaller than the lowest IP (7.68 eV) of **4**, which corresponds to σ ionization.

Conceptually, the lowest ΔE_{S-T} values of **5**–**8** are not directly comparable to the ΔE_{S-T} values of known carbenes, since the lowest triplet states of **5**–**8** do not arise through electronic excitation from the carbenic lone pair, but rather have have $\pi^1\pi^{*1}$ configurations. The LDF values of the lowest ΔE_{S-T} values of **6**–**8** range from 26.4 to 31.0 kcal mol^{-1}. As Table 2 shows, the lowest $\sigma^1\pi^{*1}$ triplet states of **6**–**8** are even higher in energy. These ΔE_{S-T} values may be compared to calculated values of 45 kcal mol^{-1} for CF_2,[13] a prototypical singlet carbene, and 79.4 kcal mol^{-1} for unsubstituted imidazol-2-ylidene.[14] Thus, the ΔE_{S-T} values of **6**–**8**, while substantial, are significantly lower than those of the stable imidazol-2-ylidene-type carbenes. Once again, this is a consequence of the relatively low energy of the lowest $\pi^1\pi^{*1}$ states of large-ring aromatic compounds such as porphyrins.

Table 2. LDF values of ΔE_{S-T} [kcal mol^{-1}] and lowest σ- and π-IPs [eV].

Molecule	Lowest ΔE_{S-T}		Lowest IP	
	$\pi^1\pi^{*1}$ triplet	$\sigma^1\pi^{*1}$ triplet	σ	π
5	[a]	[a]	[a]	7.22
6	26.4	41.2	7.31	6.65
7	29.6	34.9	6.96	6.76
8	31.0	56.3	7.79	7.72

[a] These values are not available since the calculations on the pertinent, highly excited states could not be converged.

Although **6** exhibits the salient structural and electronic attributes of a stabilized singlet carbene, it is still higher in energy than **5** by a substantial margin—30.4, 32.8, and 42.2 kcal mol^{-1} at the LDF, HF, and MP2 levels, respectively.[15] In view of the significant energy difference between tautomers **5** and **6**, how can we account for the activation of the central C–H bond in **1** (the known analogue of **5**) by a reagent as mild as $NiCl_2$? To probe this issue, we examined the interaction of **6** with a Zn^{2+} ion (a closed-shell Lewis acid) and with a Ni^{2+} ion by performing calculations on **7** and **8**, respectively.[16] Table 2 shows that the lowest σ-IPs of **6** and **7** are similar, as are the energies of the lowest $\sigma^1\pi^{*1}$ triplet states relative to the ground states. However, unlike the lowest cationic $^2A'$ (i.e. σ-ionized) state of **6**, the unpaired electron spin in the lowest $^2A'$ state of **7** is delocalized rather evenly on the carbenic carbon, the three central nitrogen atoms, and the zinc ion, suggesting a certain stabilization of the carbenic lone pair by covalent interactions with the zinc center.

The results on **8** are drastically different from those on **6** and **7**. Thus, the energies of both the lowest $\sigma^1\pi^{*1}$ triplet and cationic $^2A'$ states of **8**, relative to the neutral ground state, are much higher than the corresponding values for **6** and **7**. Indeed, in the lowest energy cationic $^2A'$ state of **8**, the nickel ion carries nearly all the unpaired spin density, leaving negligible spin density at the carbenic center. In other words, the carbenic lone pair does not contribute to the highest occupied σ MO of **8**, but to an MO with an even lower orbital energy. An examination of the high-lying σ MOs of **8** reveals that the stability of **2** or **8** stems significantly from a highly favorable covalent interaction between the carbenic lone pair and the empty d_σ atomic orbital of an Ni^{2+} ion (d^8) placed in a strong square-planar ligand field as well as from a metal–ligand π bond.

Both Arduengo-type carbenes and the carbenic tautomers of N-confused porphyrins feature a carbenic lone pair in the nodal plane of a highly stable aromatic π system. This stereoelectronic feature results in a substantial singlet–triplet energy gap. As in the case of Arduengo-type carbenes, significant fractions of the unpaired spin density in the lowest σ-ionized states of **6** and **7** reside on the carbenic center. The lowest σ IPs of **6** and **7** are also close to the lowest σ IPs of the imidazol-2-ylidene-based carbenes. Thus, our calculations lend strong support to the proposal that **6** is indeed an Arduengo-type aromatic carbene. The specially favorable covalent interactions between **6** and the Ni^{2+} ion provides additional insight into the surprising ease with which N-confused porphyrins form metal–carbon bonds.

Received: November 24, 1994 [Z7496IE]
German version: *Angew. Chem.* **1995**, *107*, 1117

Keywords: ab initio calculations · carbenes · LDF calculations · porphyrinoids

[1] P. J. Chmielewski, L. Latos-Crażyński, K. Rachlewicz, T. Glowiak, *Angew. Chem.* **1994**, *106*, 805; *Angew. Chem. Int. Ed. Engl.* **1994**, *33*, 779.
[2] H. Furuta, T. Asano, T. Ogawa, *J. Am. Chem. Soc.* **1994**, *116*, 767.
[3] J. Sessler, *Angew. Chem.* **1994**, *106*, 1410; *Angew. Chem. Int. Ed. Engl.* **1994**, *33*, 1348.
[4] a) A. J. Arduengo, R. L. Harlow, M. Kline, *J. Am. Chem. Soc.* **1991**, *113*, 361; b) A. J. Arduengo III, H. V. R. Dias, R. L. Harlow, M. Kline, *ibid.* **1992**, *114*, 5530; c) N. Kuhn, T. Kratz, *Synthesis* **1993**, 561.
[5] Computer program used: J. Almlöf, K. Faegri, M. W. F. Feyereisen. T. Fischer, K. Korsell, H. P. Lüthi: DISCO, a direct SCF and MP2 code.
[6] The LDF calculations were carried out with the program DMOL, using methods described in a) B. Delley, *J. Chem. Phys.* **1990**, *92*, 508; b) *ibid.* **1991**, *94*, 7245.
[7] U. von Barth, L. Hedin, *J. Phys. C\ Solid State Phys.* **1972**, *5*, 1629.
[8] General contraction: a) R. C. Raffeneti, *J. Chem. Phys.* **1973**, *58*, 4452; b) M. W. Schmidt; K. Ruedenberg, *ibid.* **1979**, *71*, 3951.
[9] The basis sets for C, N, and H were (6s3p)/[3s2p], (6s3p)/[3s2p], (3s)/[2s], respectively, and were obtained from F. B. van Duijneveldt, *IBM Research Report* RJ945, **1971**. The hydrogen exponents were multiplied by a scaling factor of 1.44
[10] a) Direct SCF calculation: J. Almlöf, K. Faegri, K. Korsell, *J. Comput. Chem.* **1982**, *3*, 385; b) Direct MP2 calculation: S. Saebø, J. Almlöf, *Chem. Phys. Lett.* **1989**, *154*, 521.
[11] For recent ab initio calculations on porphyrinic molecules: a) A. Ghosh, J. Almlöf, P. G. Gassman, *Chem. Phys. Lett.* **1991**, *186*, 113; b) P. G. Gassman, A. Ghosh, J. Almlöf, *J. Am. Chem. Soc.* **1992**, *114*, 9990; c) A. Ghosh, J. Almlöf, *Chem. Phys. Lett.* **1993**, *213*, 519; d) J. Almlöf, T. Fischer, P. G. Gassman, A. Ghosh, M. Häser, *J. Phys. Chem.* **1993**, *97*, 10964; e) A. Ghosh, P. G. Gassman, J. Almlöf, *J. Am. Chem. Soc.* **1994**, *116*, 1932; f) M. Merchán, E. Ortí, B. Roos, *Chem. Phys. Lett.* **1994**, *221*, 136; g) *ibid.* **1994**, *226*, 27; h) A. Ghosh, *J. Phys. Chem.* **1994**, *98*, 11004; i) A. Ghosh, J. Fitzgerald, P. G. Gassman, J. Almlöf, *Inorg. Chem.* **1994**, *33*, 6057; j) A. Ghosh, J. Almlöf, *J. Phys. Chem.* **1995**, *99*, 1073. A. Ghosh, *J. Am. Chem. Soc.* **1995**, *117*, in press.
[12] A. J. Arduengo III, H. Bock, H. Chen, M. Denk, D. A. Dixon, J. C. Green, W. A. Herrmann, N. L. Jones, M. Wagner, R. West, *J. Am. Chem. Soc.* **1994**, *116*, 6641.
[13] H. F. King, A. Komornicki, *J. Chem. Phys.* **1986**, *84*, 5465.
[14] D. A. Dixon, A. J. Arduengo III, *J. Phys. Chem.* **1991**, *95*, 4180.
[15] At the LDF level compound **5** is roughly 16.5 kcal mol^{-1} higher in energy than **9**. This energy difference should be regarded as an upper limit, since the optimization of **5** used a C_s symmetry constraint, which is an approximation.
[16] For an extensive list of reference on Lewis acid complexes of Arduengo-type carbenes, see: A. J. Arduengo III, H. V. R. Dias, D. A. Dixon, R. L. Harlow, W. T. Klooster, T. F. Koetzle, *J. Am. Chem. Soc.* **1994**, *116*, 6812.

Silicon Analogues of Grignard Compounds: Synthesis and Structure of Amine-Stabilized Trimethylsilylmagnesium Halides**

Richard Goddard, Carl Krüger, Nazmi A. Ramadan, and Alfred Ritter*

Dedicated to Professor Hubert Schmidbaur on the occasion of his 60th birthday

For a long time it has been suspected[1] that triorganosilyl Grignard compounds play a role as intermediates in the reaction of halo(triorgano)silanes with elemental magnesium to give hexaorganodisilanes. However, all attempts to synthesize members of this class of compounds in analogy to the classical methods of preparing carbon Grignard reagents have been unsuccessful.

Indirect evidence for the existence of triorganosilylmagnesium halides in ether has been recently obtained by Oehme and coworkers[2] during the metal exchange reaction of tris(trimethylsilyl)silyllithium $(Me_3Si)_3SiLi \cdot 3THF$ with magnesium bromide. The assumed intermediate, tris(trimethylsilyl)silylmagnesium bromide $(Me_3Si)_3SiMgBr$, was not isolated but immediately underwent further reaction in ether solution.

We have now synthesized Grignard analogous trimethylsilylmagnesium compounds easily as complexes with amine chelating ligands, directly from halo(trimethyl)silanes and magnesium, using the highly reactive pyrophoric magnesium (Mg*) of Bogdanović et al.[3]

So far we have observed that only bromo(trimethyl)silane and iodo(trimethyl)silane and not the usual chloro(trimethyl)silane react under our chosen reaction conditions to give trimethylsilyl Grignard compounds. In contrast to the classical Grignard synthesis, the reaction cannot be carried out in oxygen-containing solvents such as tetrahydrofuran or diethyl ether because of quantitative ether cleavage during the course of the reaction. Hence the reactions were carried out in dried toluene in the presence of tetramethylethylenediamine or pentamethyldiethylenetriamine as complexing ligands.

[*] Dr. A. Ritter, Prof. Dr. N. A. Ramadan[+]
Max-Planck-Institut für Strahlenchemie
Postfach 10 13 65, D-45413 Mülheim an der Ruhr (Germany)
Telefax: Int. code + (208) 306-3951
Dr. R. Goddard, Prof. Dr. C. Krüger
Max-Planck-Institut für Kohlenforschung
D-45470 Mülheim an der Ruhr (Germany)
[+] Permanent address: Egyptian Petroleum Research Institute
Nasr City, 7th Region, Cairo (Egypt)

[**] We thank Prof. Dr. M. Demuth and Dr. J. Leitich for valuable discussions, Mr. P. Bayer and Mr. K. H. Claus for experimental assistance, as well as Prof. Dr. K. Schaffner for his kind support. N. A. R. thanks the DFG for financial support for his stay at the MPI für Strahlenchemie in 1992 and 1994.

Under these conditions it has been possible to isolate the trimethylsilylmagnesium compounds **1**–**4** as solids. Crystals of **1** and **2** suitable for X-ray structure analysis have also been obtained.

$$Me_3Si{-}Hal + Mg^* \xrightarrow{tert.\ amine} \underset{\mathbf{1-4}}{Me_3Si{-}Mg{-}Hal \cdot tert.\ amine}$$

$Me_3Si{-}Mg{-}Br \cdot Me_2N{-}CH_2{-}CH_2{-}NMe_2$ **1**

$Me_3Si{-}Mg{-}Br \cdot MeN(CH_2{-}CH_2{-}NMe_2)_2$ **2**

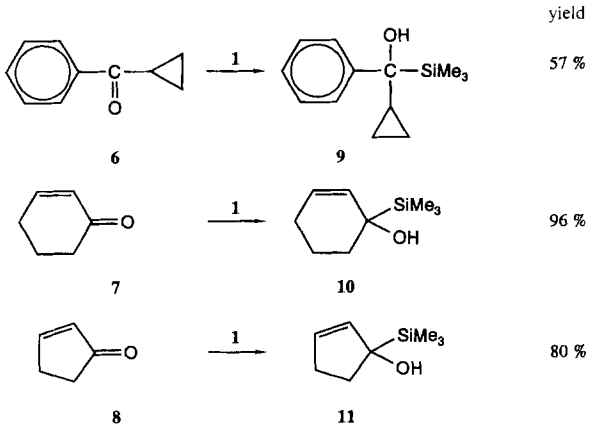
$Me_3Si{-}Mg{-}I \cdot Me_2N{-}CH_2{-}CH_2{-}NMe_2$ **3**

$Me_3Si{-}Mg{-}I \cdot MeN(CH_2{-}CH_2{-}NMe_2)_2$ **4**

The only by-product from the preparation of **1** is the known pyrophoric bis(trimethylsilyl)magnesium · tetramethylethylenediamine (**5**).[4] Bis(trimethylsilyl)magnesium is also known to form complexes with other ligands.[5] Compound **5** is evidently formed as a consequence of a Schlenk equilibrium.[6]

$Me_3Si{-}Mg{-}SiMe_3 \cdot Me_2N{-}CH_2{-}CH_2{-}NMe_2$ **5**

As first examples of the uses of **1**–**4**, **1** was treated with the ketone **6** and the enones **7** and **8** in toluene at −70 °C, and the compounds **9**, **10**,[7] and **11** were formed after hydrolysis. Replacement of **1** by trimethylsilyllithium in the reaction with **7** does not lead to **10**, but yields exclusively 3-(trimethylsilyl)cyclohexanone.[8]



The results of the crystal structure analysis of **1** are summarized in Figure 1.[15] It is particularly noteworthy that in the crystal **1** exists neither as a monomer nor as a symmetrically Br-bridged dimer, but rather as an associated complex. The complex lies on a crystallographic inversion center, but the two independent Mg–Br distances in **1** differ significantly from one another, in contrast to other Br-bridged Grignard compounds.[9–13] Whereas one of the Mg–Br bond lengths of 2.534(4) Å lies between the value observed in the monomeric ethyl((−)-isosparteine)magnesium bromide (2.506 Å)[14] and that in the symmetrical Br-bridged dimeric ethyl(triethylamine)magnesium bromide complex[11] (average 2.567 Å), the other Mg–Br* distance of 3.220(4) Å is clearly longer. It is 0.6 Å larger than the sum of the ionic radii of Mg^{2+} and Br^- (2.60 Å) and thus indicates no interaction between these atoms. Closer inspection of the local geometry of the Mg atoms reveals, however, that the geometry of the monomeric subunit deviates from the expected idealized C_s symmetry of the free monomer. The Mg atom is situated

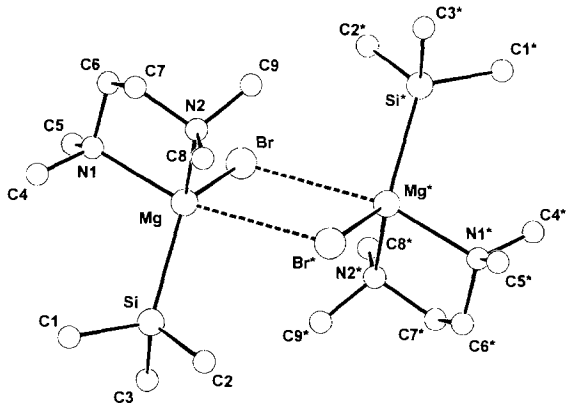


Fig. 1. Molecular structure of **1** in the crystal. Selected bond lengths [Å], angles [°], and torsion angles [°]: Mg-Si 2.630(4), Mg-Br 2.534(4), Mg–Br* 3.220(4), Mg-N1 2.265(8), Mg-N2 2.190(9), Si-C1 1.87(1), Si-C2 1.81(2), Si-C3 1.91(2), N1-C4 1.37(2), N1-C5 1.42(2), N1-C6 1.49(2), N2-C7 1.48(2), N2-C8 1.47(2), N2-C9 1.49(2), C6-C7 1.54(3); Br-Mg–Br* 81.0(1), Mg-Br–Mg* 99.0(1), Br-Mg-Si 128.7(2), Si-Mg–Br* 86.7(1), Br-Mg-N1 95.2(3), Br-Mg-N2 107.5(3), Si-Mg-N1 106.5(2), Si-Mg-N2 121.0(3), N1-Mg-N2 82.1(4), Si-Mg-Br–Br* -78.4(4) [15].

0.27 Å towards Br* from the mean plane through Br, Si, and the midpoint between N1 and N2. Apart from possible steric effects on the Mg atom, the influence of the neighboring Br* atom on the arrangement of the ligands around the Mg atom cannot be ignored. Whether the tendency to dimerize is caused by the acceptor ability of the Si atom cannot be judged without structural information on a corresponding alkyl Grignard compound. Crystal structures have been reported for [{η^5-1,2,4-tris(trimethylsilyl)cyclopentadienyl}magnesium bromide] · tetramethylethylenediamine[16] and the related (η^5-cyclopentadienyl)magnesium · tetraethylethylenediamine,[17] which each contain a π-bonded cyclopentadienyl ligand, but not from the corresponding alkyl Grignard compound with tetramethylethylenediamine as ligand. Ethyl((−)-isosparteine)magnesium bromide[14] is, however, monomeric in the crystal, and this has been attributed to the bulky isosparteine ligand. Interestingly, the Mg–Br bonds of bis-[(μ_2-bromo)(2-methoxymethyl-*o*-phenylene-*C*,*O*)(tetrahydrofuran-*O*)magnesium],[13] in which the Mg atom is pentacoordinate, differ in length [2.509(3) and 2.705(2) Å], but the difference is much smaller than that observed for **1**. The Mg–Si distance of 2.630(4) Å in **1** resembles that in bis(trimethylsilyl)magnesium · tetramethylethylenediamine.[4] Here the bond lengths are 2.624(4) and 2.631(4) Å [average 2.628(5) Å]. The Si-Mg-Br angle in **1** [128.7(2)°] is significantly larger than the Si-Mg-Si angle in bis(trimethylsilyl)magnesium [115.3(1)°].[4]

The molecular structure of **2** is depicted in Figure 2. The molecule is monomeric in the crystal and lies on a crystallographic mirror plane passing through Mg, Br, Si, C1, N2, and C7. Three coordination sites of the pentacoordinate Mg atom are occupied by the pentamethyldiethylenetriamine ligand. The Mg–Br and Mg–Si distances of 2.599(4) and 2.651(6) Å, respectively, are slighly longer than the corresponding distances in **1**, but the Si-Mg-Br angle is considerably smaller [105.0(2)°]. This may be a result of the larger steric requirements of the triamine ligand. Compounds **1** and **2** are the first examples of crystal structures of Si analogues of Grignard compounds.

Experimental Procedure

For the preparation of **1**, pyrophoric Mg* [3] (4.4 g, 0.183 mol), which was obtained by dehydrogenation of catalytically prepared (Ti catalyst) MgH_2, were placed under argon in a three-necked flask fitted with a reflux condensor, three-way tap, dropping funnel, and magnetic stirrer, and covered with 30 mL dried toluene. Then bro-

 © VCH Verlagsgesellschaft mbH, D-69451 Weinheim, 1995 0570-0833/95/0909-1031 $ 10.00+.25/0

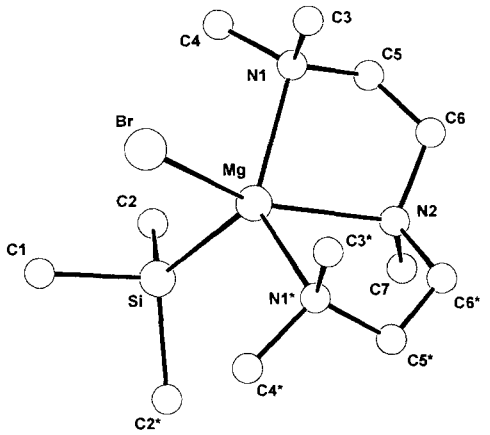


Fig. 2. Molecular structure of **2** in the crystal. Selected bond lengths [Å] and angles [°]: Mg-Si 2.651(6), Mg-Br 2.599(4), Mg-N1 2.251(8), Mg-N2 2.35(1), Si-C1 1.81(2), Si-C2 1.85(1), N1-C3 1.49(1), N1-C4 1.49(2), N1-C5 1.41(2), N2-C6 1.44(2), N2-C7 1.46(2), C5-C6 1.47(2); Si-Mg-Br 105.0(2), Br-Mg-N1 92.8(3), Br-Mg-N2 151.8(4), Si-Mg-N1 113.4(2), Si-Mg-N2 103.2(4), N1-Mg-N2 76.0(4), N1-Mg-N1* 129.5(4) [18].

mo(trimethyl)silane (Fluka, 28.1 g, 0.184 mol) in dried toluene (65 mL) was added dropwise while stirring. A solution of tetramethylethylenediamine (21.3 g, 0.184 mol) in dried toluene (65 mL) was added dropwise over about 2 h. The reaction mixture was maintained at 50 °C for 24 h and then for a further 110 h at 70 °C. The flocculent, dark grey precipitate of $MgBr_2$·amine so formed was filtered off under argon on a glass scinter, washed 3 × with 20 mL portions of dry toluene, and the complete filtrate was dried under oil-pump vacuum. Repeated extractions of the residue with dry pentane and evaporation of the extracts to dryness yielded 7.06 g (13.5%) **5** as a white, air-flammable solid. The deposit that had been freed of **5** by elution of the residue with pentane was analytically pure **1** (20.41 g, 38%) with m.p. 135 °C [19]. Compound **1** decomposes in damp air with loss of trimethylsilane. Correct elemental analysis. MS (70 eV): *m/z*: 219 [*M*−$SiMe_3$], 213 [*M*−Br], 116, 73, 58. ^{1}H NMR (400 MHz, [D_8]toluene): δ = 0.35 (s, 9H, $Si(CH_3)_3$); 1.8–2.1 (br. s at 1.83, 1.92, 2.0, 16H, NCH_2, NCH_3); ^{13}C NMR (100 MHz, [D_8]toluene): δ = 6.1 ($Si(CH_3)_3$), 46.67–46.78 (br. d, $N(CH_3)_x$), 55.91 (NCH_2). All NMR spectra were recorded at room temperature.

The compounds **2**, **3**, and **4** were synthesized by the same experimental method as **1**. Deviations from this procedure were the reaction time of 20 h for **3** and **4** and the reaction temperature of 40 °C. **2**: Yield 15%; m.p. 159–161 °C [19]. Correct elemental analysis. MS (70 eV): *m/z*: 276 [*M*−$SiMe_3$], 270 [*M*−Br], 73. Compound **2** shows complex temperature-dependent NMR spectra, which indicate dynamic processes and equilibria between many species. ^{1}H NMR (400 MHz, C_6D_6): δ = 0.3–0.75 (br.), 0.48 (s, $Si(CH_3)_3$), 1.6–2.5 (many multiplets of differing intensity, among others a strong broad singlet at δ = 2.31 (NCH_3 and NCH_2); ^{13}C NMR (100 MHz, C_6D_6, BB-decoupled and DEPT): δ = 4.0–6.0 (br.), 7.25 (s, $Si(CH_3)_3$), 44.0–48.0 (br., NCH_3), 56.3, 56.5 (each s, NCH_2).

3: Yield 39%; m.p. 100–102 °C [19]. Correct elemental analysis. MS (70 eV): *m/z*: 340 [M^+], 325 [*M*−15], 267 [*M*−$SiMe_3$], 73. ^{1}H NMR (400 MHz, [D_8]toluene): δ = 0.32 (s, 9H, $Si(CH_3)$), 1.97–2.01 (br., 16H, NCH_3, NCH_2); ^{13}C NMR (100 MHz, [D_8]toluene): δ = 5.55 ($Si(CH_3)_3$), 47.23 (NCH_3), 56.39 (NCH_2).

4: Yield about 10%; m.p. 220–225 °C (decomposition) [19].
MS (70 eV): *m/z*: 324 [*M*−$SiMe_3$], 73.

9: MS (70 eV): *m/z*: 219 [*M*−H], 205 [*M*−CH_3], 147 [*M*−$SiMe_3$], 77, 75, 73. The constitution was established by analyses, NMR spectra (^{1}H, ^{13}C-BB, -DEPT, -gated, C/H-COSY), in particular in the aliphatic region from the C–H coupling constants of 147–163 Hz and the geminal H–H coupling constants of 4.8 Hz, which show the presence of the cyclopropane ring.

11: MS (70 eV): *m/z*: 155 [*M*−H], 83 [*M*−$SiMe_3$], 73. The constitution was established by analyses, NMR spectra (^{1}H, ^{13}C-BB, -DEPT, -gated, C/H-COSY).

Received: December 19, 1994 [Z 7554 IE]
German version: *Angew. Chem.* **1995**, *107*, 1107

Keywords: Grignard compounds · magnesium compounds · silicon compounds · structure elucidation

[1] H. J. Emeléus, A. G. Maddock, C. Reid, *J. Chem. Soc.* **1941**, 353; E. R. Van Artsdalen, J. Gavis, *J. Am. Chem. Soc.* **1952**, *74*, 3196; C. Eaborn, *J. Chem. Soc.* **1949**, 2755; T. G. Selin, R. West, *Tetrahedron* **1959**, *5*, 97; W. Steudel, H. Gilman, *J. Am. Chem. Soc.* **1960**, *82*, 6129; L. Rösch, W. Erb, H. Müller, *Z. Naturforsch. B* **1976**, *31*, 281.

[2] C. Krempner, H. Reinke, H. Oehme, *Angew. Chem.* **1994**, *106*, 1709; *Angew. Chem. Int. Ed. Engl.* **1994**, *33*, 1615.

[3] E. Bartmann, B. Bogdanović, N. Janke, S. Liao, K. Schlichte, B. Spliethoff, J. Treber, U. Westeppe, U. Wilczok, *Chem. Ber.* **1990**, *123*, 1517.

[4] D. W. Goebel, Jr., J. L. Hencher, J. P. Oliver, *Organometallics* **1983**, *2*, 746.

[5] A. R. Claggett, W. H. Ilsley, T. J. Anderson, M. D. Glick, J. P. Oliver, *J. Am. Chem. Soc.* **1977**, *99*, 1797; L. Rösch, *Angew. Chem.* **1977**, 89, 257; *Angew. Chem. Int. Ed. Engl.* **1977**, *16*, 247; L. Rösch, J. Pickardt, S. Imme, U. Börner, *Z. Naturforsch. B* **1986**, *41*, 1523.

[6] W. Schlenk, W. Schlenk, Jr., *Ber. Dtsch. Chem. Ges.* **1929**, *62*, 920.

[7] G. Altnau, L. Rösch, G. Jas, *Tetrahedron Lett.* **1983**, *24*, 45.

[8] W. C. Still, *J. Org. Chem.* **1976**, *41*, 3063.

[9] P. R. Markies, O. S. Akkerman, F. Bickelhaupt, W. J. J. Smeets, A. L. Spek, *Adv. Organometallic Chem.* **1991**, *32*, 147.

[10] P. R. Markies, G. Schat, O. S. Akkerman, F. Bickelhaupt, W. J. J. Smeets, A. J. M. Duisenberg, A. L. Spek, *J. Organomet. Chem.* **1989**, *375*, 11.

[11] J. Toney, G. D. Stucky, *J. Chem. Soc. Chem. Commun.* **1967**, 1168.

[12] A. L. Spek, P. Voorbergen, G. Schat, C. Blomberg, F. Bickelhaupt, *J. Organomet. Chem.* **1974**, *77*, 147.

[13] P. R. Markies, G. Schat, S. Griffioen, A. Villena, O. S. Akkerman, F. Bickelhaupt, W. J. J. Smeets, A. L. Spek, *Organometallics* **1991**, *10*, 1531.

[14] H. Kageyama, K. Miki, Y. Kai, N. Kasai, Y. Okamoto, H. Yuki, *Acta Cryst. Sect. B: Struct. Crystallogr. Cryst. Chem.* **1982**, *38*, 2264; H. Kageyama, K. Miki, Y. Kai, N. Tanaka, N. Kasai, Y. Okamoto, H. Yuki, *Bull. Chem. Soc. Jpn.* **1983**, *56*, 1319.

[15] Crystal structure analysis of **1**: $[C_9H_{25}BrMgN_2Si]_2$, M = 587.2 g mol^{-1}, crystal size 0.16 × 0.29 × 0.40 mm, a = 13.094(3), b = 7.963(1), c = 16.200(3) Å, β = 108.01(1), V = 1606.3(5) Å^3, T = 293 K, ρ_{calcd} = 1.21 g cm^{-3}, μ = 26.2 cm^{-1}, $F(000)$ = 616 e, Z = 2, monoclinic, space group $P2_1/n$ (No. 14), Enraf-Nonius CAD4 diffractometer, λ = 0.71069 Å, scan method ω-2θ, 8136 measured reflections ($\pm h, \pm k, +l$), $[(\sin\theta)/\lambda]_{max}$ = 0.65 Å^{-1}, analytical absorption correction (min.: 1.504; max.: 2.112), 3671 independent (R_{av} = 0.07) and 1638 observed reflections [$I \geq 2\sigma(I)$], 212 refined parameters; heavy atom method, H atom positions calculated, twinned (twinning ratio: 0.67/0.33 transformation matrix: [100,0−10,001]), R = 0.089, wR = 0.234 ($\sum w[F_o^2 - F_c^2]^2$ minimized), $w = 1/[\sigma^2(F_o^2) + (0.056(F_o^2 + 2F_c^2))^2 + 0.144(F_o^2 + 2F_c^2)]$, S = 1.02. Δ/σ = 0.00, $-1.25 \leq \rho \leq 0.74$ e Å^{-3}. See also [18b].

[16] C. P. Morley, P. Jutzi, C. Krüger, J. M. Wallis, *Organometallics* **1987**, *6*, 1084.

[17] C. Johnson, J. Toney, G. D. Stucky, *J. Organomet. Chem.* **1972**, *40*, C11.

[18] a) Crystal structure analysis of **2**: $C_{12}H_{32}BrMgN_3Si$, M = 350.7 g mol^{-1}, crystal size 0.22 × 0.30 × 0.24 mm, a = 8.895(1), b = 13.558(2), c = 16.549(2) Å, V = 1995.8(4), T = 293 K, ρ_{calcd} = 1.17 g cm^{-3}, μ = 21.2 cm^{-1}, $F(000)$ = 744 e, Z = 4, crystal system orthorhombic, space group *Pnma* (No. 62), Enraf-Nonius CAD4 diffractometer, λ = 0.71069 Å, scan method ω-2θ, 5469 measured reflections ($\pm h, \pm k, \pm l$), $[(\sin)\theta/\lambda]_{max}$ = 0.70 Å^{-1}, analytical absorption correction (min.: 1.485, max.: 1.780), 1595 independent (R_{av} = 0.07) and 787 observed reflections [$I \leq 2\sigma(I)$], 91 refined parameters; heavy atom method, H atom positions calculated, R = 0.094, wR = 0.199 ($\sum w[F_o^2 - F_c^2]^2$ minimized), $w = 1/[\sigma^2(F_o^2) + (0.010(F_o^2 + 2F_c^2))^2 + 4.835(F_o^2 + 2F_c^2)]$, S = 1.13. Δ/σ = 0.00, $-0.84 \leq \rho \leq 0.30$ e Å^{-3}. b) Further details of the crystal structure analyses can be obtained from the Fachinformationszentrum Karlsruhe, D-76344 Eggenstein-Leopoldshafen (Germany) on quoting the deposite elucidation number CSD-58892.

[19] All melting points were determined under argon in sealed capillaries.

Corrigenda

A reinvestigation (Y. Yarovoy, M. M. Labes, *Mol. Cryst. Lig. Cryst.* **1995**, *264*, 201) of the cholesteric pitch data supporting the effect of cholesteric twisting on the chiral properties of solutes dissolved in liquid crystal solvents revealed that the effects reported in two publications are irreproducible (M. M. Labes, W. Shang, *J. Am. Chem. Soc.* **1991**, *113*, 2773; M. M. Green, D. Weng, W. Shang, M. M. Labes, *Angew. Chem. Int. Ed. Engl.* **1992**, *31*, 88). Therefore the authors withdraw the above-mentioned publication in *Angewandte Chemie*. The central hypothesis raised there remains unsupported by experiment.

In the communication "Formation and Structures of New Metallo- and Metallapolysulfanes, $[MS_y]^+$ (y = 2–16)" by I. Dance, K. Fisher, and G. Willett (*Angew. Chem. Int. Ed. Engl.* **1995**, *105*, 201) the phrase "that is, after all of the Mn^+ has reacted" should be deleted from the legend to Figure 1.

Mature Methods

Chemistry of Non-Stoichiometric Compounds. By *K. Kosuge*. Oxford University Press, Oxford, 1994. 262 pp., hardcover £ 55.00.—ISBN 0-19-855555-5

In this monograph Koji Kosuge, Professor of Solid-State Chemistry at Kyoto University, reviews a subject that is of fundamental importance to chemistry. It is only through understanding the internal processes of solid materials, i.e. the nature and behavior of the relevant particles or chemical stimuli, that one can apply chemistry to solids in analogy to the successes of the acid–base or redox concepts of "wet chemistry". The appearance of a book on this subject is therefore to be welcomed. Regrettably, however, it does not succeed very well in its aims.

The choice of topics seems promising at first. The starting point is the thermodynamics of mixtures, which is then applied to the equilibrium of defects, first in dilute systems, then in more concentrated systems, and finally in those that deviate greatly from the concentration of the ordered phase. However, there is no treatment of chemical diffusion. (In this book the term "diffusion coefficient" is used only in the sense of a tracer diffusion coefficient.) The last chapter can be recommended, dealing with extended defects, shear structures, Vernier structures, micro-twin structures, intergrowth structures, and adaptive structures, and containing a wealth of information that is chiefly useful to the chemist interested in crystallography. Unfortunately high-temperature superconductors, which would have nicely completed this chapter, are not covered.

The first of the three chapters, making up at least half the book, cannot be recommended. There are numerous inaccuracies and errors which will spoil the pleasure of reading the book. A few examples follow.

The nomenclature is not in accordance with conventions in the literature. Moreover, there is confusion between absolute and relative charges, and worse still, the symbols for these are confused. On page 45 the regular electronic state is denoted by "eh", whereas on page 85 it is correctly identified by the symbol "0" in the building elements notation. In the case of ionic equilibria a mixture of structure elements and building elements is used. The introduction to chemical equilibria and the configurational enthalpy (Ch. 1.2) is clumsy and often inaccurate. One could perhaps tolerate the frequent switching between differences and differentials, but not the identification of $-(\Delta G^0-\Delta G)/RT$ as an equilibrium constant. In the discussion of the formation of defects (p. 18) there is no mention of the vibrational entropy, which has an important influence on the free enthalpy of formation, especially in high-temperature chemistry. The fact that the temperature dependence of the equilibrium constant for the band–band transition is determined by the band gap is explained by the following curious statement: "The rate of ionization is believed to be roughly equal to that of the dissociation of water ... and therefore we put [eh] = 1." (?). This is just a small selection. The most annoying aspect of the errors is that they destroy the reader's faith in those parts of the text that are properly written.

Joachim Maier
Max-Planck-Institut
für Festkörperforschung
Stuttgart (FRG)

This section contains book reviews and a list of new books received by the editor. Book reviews are written by invitation from the editor. Suggestions for books to be reviewed and for book reviewers are welcome. Publishers should send brochures or (better) books to Dr. Ralf Baumann, Redaktion Angewandte Chemie, Postfach 101161, D-69451 Weinheim, Federal Republic of Germany. The editor reserves the right of selecting which books will be reviewed. Uninvited books not chosen for review will not be returned.

Principles of Electron Spin Resonance. (Physical Chemistry Series.) By *N. M. Atherton*. Ellis Horwood, Chichester, 1994. 585 pp., hardcover $ 127.00.—ISBN 0-13-721762-5

This book is a revised and updated version of *ESR—Theory and Applications* which appeared in 1973, and the change in the title reflects the author's aim of placing greater emphasis on the fundamentals of ESR spectroscopy. Rapid changes are currently occurring in the experimental methods used in ESR spectroscopy, summed up by the key phrase "pulsed ESR spectroscopy", opening up entirely new possibilities in time-resolved and multidimensional measurements. In turning back to basic principles at this time the author is tapping a great potential but also running some risks.

As is to be expected for a method that has reached maturity, the literature contains a wide variety of notations for the treatment of special cases, making it difficult for students and users to relate the techniques to their specific problems by analogy with methods that are already familiar. Here we undoubtedly find one of the strengths of the book, as the author consistently treats spectral calculations and relaxation processes at a level suitable for the average reader. He also helpfully "translates" even very recently published papers, so that the reader who works consistently through the book gains a comprehensive insight into topical problems. However, the discussion of the possibilities opened up by pulsed ESR spectroscopy is less successful. Only 80 pages are devoted to recently developed methods such as pulsed ENDOR, 2D ESR spectroscopy, and optical spin polarization, and these are treated essentially at an introductory level, in contrast to the first ten chapters (440 pp.) which deal with continuous-wave (CW) forms of ESR and ENDOR spectroscopy, explaining their capabilities and describing many examples of a nontrivial kind.

A work that has the word "principles" in its title invites comparison with other books that make similar claims. Examples are: *Principles of Magnetic Resonance in One and Two Dimensions* (Ernst, Bodenhausen and Wokaun), *Principles of Magnetic Resonance* (Slichter), *Principles of Nuclear Magnetism* (Abragam), and *EPR of Transition Ions* (Abragam and Bleaney), all of which undoubtedly have the character of handbooks. In my view the present book is instead more accurately described as a "comprehensive introduction", although this classification in no

way detracts from its value and usefulness.

Against the background of constantly shrinking library budgets, one must look at any new book and ask whether its purchase is really essential. Here the needs of the specialists are less important than those of the advanced students who, in the course of their work, need to find quick solutions to practical problems without first having to make a deep and detailed study of the methods. This book offers a very good foundation for that purpose. It has the advantages of a detailed subject index and an up-to-date bibliography (although it is difficult to understand why, in the age of computer-aided text processing, all the umlauts have been consistently omitted from names such as Schrödinger, Hückel, and Möbius). To sum up, the book fulfills its aim of providing students and scientists whose main field is physical chemistry with an up-to-date and comprehensive basis for understanding ESR spectroscopy.

Klaus-Peter Dinse
Institut für Physikalische Chemie
der Technischen Hochschule Darmstadt
(FRG)

Computer Simulations of Biomolecular Systems. Theoretical and Experimental Applications. Vol. 2. Edited by *W. F. van Gunsteren, P. K. Weiner* and *A. J. Wilkinson*. ESCOM, Leiden (Netherlands), 1993, 589 pp., hardcover HFl 415.00.—ISBN 90-72199-15-4

About 18 years ago when J. A. McCammon, B. R. Gelin, and M. Karplus published the first molecular dynamics simulation of a protein (*Nature* **1977**, *267*, 585), the accepted picture of a biological molecule was essentially that of a rigid body. The molecular structures of several proteins and of DNA had already been successfully determined by X-ray crystallography, and the results were represented by a rigid wire model. The dynamic aspects that play an important role in all biological processes could not, and still cannot, be directly observed experimentally, at least down to atomic-scale resolution. When the results of molecular dynamics calculations first began to appear, it became possible to follow the molecular motions as if in a ciné film. These calculations were restricted to relatively small molecules, and the time intervals that could be simulated were very short, in the order of picoseconds. However, such simulations made an important contribution to revising the ideas based on the rigid wire model.

The book reviewed here shows how simulation methods have developed during the last 18 years and reflects the present-day importance of the subject. In 25 chapters, introduced in a very detailed preface by Martin Karplus, various authors review simulation techniques, force fields, and applications. The contents list alone occupies more space than is available for this review, and it will only be possible here to pick out some of the topics covered.

The first two sections of the book are concerned with fundamentals, namely simulation techniques (algorithms for molecular dynamics and Monte Carlo calculations) and force fields. A force field should on the one hand approximate as closely as possible to the real quantum-mechanical situation, while on the other hand allowing rapid and efficient calculations. Because of the need to keep the computing time within reasonable bounds, compromises are always necessary. Simplified force fields are necessary in order to study slow processes such as protein folding. However, even more detailed force fields are still only approximations, and it is important for the user to know how this can affect the results of the calculations.

One of the most important applications of molecular dynamics simulations is the calculation of free energies. The book offers an excellent introduction to this topic, with particular emphasis on possible difficulties and sources of error. Several examples of successful free energy calculations are given. On the other hand it is also clearly explained why the predictions from the calculations may not always be correct.

The three chapters on the use of molecular dynamics calculations in refining molecular structural data from X-ray crystallography and NMR spectroscopy can be regarded to some extent as occupying a special position in the book. Here one is using the molecular dynamics algorithm not to investigate the dynamics of a molecule but as an optimization method for the solution of a difficult nonlinear problem. The excellent convergence properties of the molecular dynamics method have revolutionized the process of structure refinement. The occasions when individual steps must be performed laboriously by hand are now increasingly rare, and the end result, the refined structure, is reached much more quickly than in the past. However, the close connection that exists between molecular dynamics and NMR spectroscopy especially is also mentioned here.

I learned much from reading this book, and it can be recommended as a thorough introduction to the simulation of macromolecules. It is a valuable source of practical information and an indispensable work of reference. In a multiauthor work such as this some degree of non-uniformity is perhaps unavoidable, as also is a certain amount of overlapping in chapters on related topics. However, I regard the latter as an advantage, since it means that important topics are seen from different points of view. All the aspects of the simulation of macromolecules discussed in the book are active areas of research, and as is made clear in the preface many questions still remain to be finally answered, even with regard to the methods. It is pleasing that many of the authors are able to view their own work critically from a distance. It is very useful, especially for a newcomer to the field, to be made aware of problems in the application of these methods.

Michael Nilges
European Molecular Biology Laboratory
Heidelberg (FRG)

Ideas in Chemistry. A History of the Science. By *D. Knight*. Athlone Press, London, 1992. 213 pp., hardcover £ 38.00.—ISBN 0-485-11390-2

What a splendid title! It promises a much needed book on the intellectual content of chemistry, and on its trade: by insemination, as with "reaction", borrowed in part from the action/reaction pair in physics; by dissemination, as with "affinity" or "catalysis," terms and concepts that have entered common language too; or as with "complementarity", which spawned molecular biology.

Is it because of the inheritance from alchemy? Chemistry is a conceptual science, rooted in material operations. Other sciences (astronomy, biology, or physics) do not transform their subject matter as a matter of course. But chemistry intellectualizes its metamorphoses, to an extent that is astounding, given the huge distance from the macroscopic to the microscopic that it entails: to think and to talk of molecular *objects*, reaction *paths*, molecular *orbitals*, atomic *hardness*, etc. demands temerity and insight.

What is needed is a thesaurus of key chemical notions. There are two or three dozen central concepts, such as acidity or coordination, plus a hundred or so more peripheral but also necessary notions, such as steric hindrance or chain reaction. Someone should provide such a compendium, with present-day definitions, capsule histories, and illustrative quotations.

 © VCH Verlagsgesellschaft mbH, D-69451 Weinheim, 1995 0570-0833/95/0909-1034 $ 10.00+.25/0

Professor Knight of Durham University indeed takes as his scope the whole of the history of chemistry. Not to worry, he has the scholarship to match! However, besides the misleading book title, which the subtitle corrects to some extent, the chapter titles are other irritants. Each chapter corresponds to a historical period, and is labeled in the manner of those books of yesteryear which had names such as "The Age of Enlightenment", "The Age of Revolutions", and so on. Here, chapters bear names such as "A teachable science", "A deductive science", etc. Of course each such label is questionable. Some—"A service science" for present-day chemistry—raise the blood pressure.

The philosophical bases appear as a little weak, for a book of this sort which aims at providing an intellectual history. Chapter 7, "The experimental science", is not one of the best. Somehow, it fails to convey what "thinking with one's hands" entails. "Experimental science" has two meanings. The jaded meaning is sociological, that of professionals spending their time in the laboratory and somehow, theorizing from their observations, producing novel knowledge. The stronger meaning is philosophical: the methodology, which we owe to Boyle and Bacon, of questioning matter through experiments, the results of which raise new questions, leading in turn to new experiments, so that truth is approached inquisitively rather than speculatively. Hence, some naive statements such as "observation with instruments is remote and theory-laden compared with the working with test-tubes and bottles, and seems somehow unchemical" are questionable.

This is a delightful introduction to the history of chemistry. The tone combines simplicity, down-to earthness, some of the flavor of speech, and erudition, worn lightly. It resembles in these respects some of the outstanding science programs of the BBC, never condescending, always explanatory. David Knight succeeds in making this slim historical volume into a popularization of chemistry. His trick is to talk to the layman as if he too were a layman. Here is just one example of such felicitous writing: "the texture of things get into the memory: the viscosity, mobility and viscidity of different liquids, and the gritty, unctuous or glassy feel of solids; the undescribable but unforgettable smell of things."

One can learn a lot from Professor Knight's learned conversation, and I did: Richard Watson's description of saturnism at the end of the eighteenth century; Lyon Playfair's 1852 prophetic tirade on recycling; or the phrase *glyptic formulae* to describe what we nowadays call molecular modeling.

The insularity is not totally unexpected. Sometimes the constant hagiography of British scientists rubs raw. But it is involuntary and unsystematic, for instance Laurent's ideas and methodology get the rich praise they deserve. A minor irritant is the abysmal typesetting, swarming with typos. Conversely, the jacket design is admirable. All in all, a highly recommended book, which any chemist would be well advised to own.

Pierre Laszlo
Laboratoire de chimie
École polytechnique
Palaiseau (France)

Transition Metals in the Synthesis of Complex Organic Molecules. By *L. S. Hegedus*. University Science Books, Mill Valley, CA (USA), 1994. 358 pp., paperback £ 27.95.—ISBN 0-935702-28-8

The use of transition metals has revolutionized organic synthesis in various ways. In many cases reactions that would otherwise have been simply classified as "impossible" can be carried out using transition metal compounds. Moreover, much of the modern armory of the preparative chemist, especially with regard to chemo-, regio-, and stereoselective methods, is based on transition metal-assisted reactions, so that synthetic chemistry without these has now become unthinkable. This situation has already been well recognized by the excellent treatment in Part III (*Applications to Organic Synthesis*) of the book *Principles and Applications of Organotransition Metal Chemistry* (2nd Edition), by J. P. Collman, L. S. Hegedus, J. R. Norton, and R. G. Finke (University Science Books, Mill Valley, 1987). The development of synthetically relevant organometallic processes has continued apace in recent years, and many new applications of transition metal-assisted reactions in the synthesis of complex organic molecules have been published, and therefore this updated survey by L. S. Hegedus, covering the literature up to January 1993, is very welcome.

The main contents of the book are arranged according to the well proven system used in Chapters 13–20 of Collman, Hegedus, Norton, and Finke. These are preceded by two short, well structured chapters (45 pp. in total) on formalisms, bonding situations, and organometallic reaction mechanisms, which equip the reader with the essential tools for understanding the following chapters on synthetic applications. Chapter 3 (transition metal hydrides) is mainly concerned with homogeneous hydrogenation reactions, now also including enantioselective reductions using ruthenium-BINAP catalysts. Chapter 4, on complexes containing metal–carbon σ-bonds, has been extensively revised (with over 100 new references), and gives the reader good insights into modern organocopper chemistry and the fascinating synthetic possibilities now opened up by palladium-catalyzed processes such as enyne cycloisomerizations, cross-couplings, and Heck reactions. The chapter also includes a new section on reductive cyclodimerizations of alkenes and alkynes based mainly on zirconium chemistry. In Chapter 5 (carbonyl complexes) the sections on coupling reactions, carbonylations, and decarbonylations correspond fairly closely to those in Collman et al., but the chapter also includes some more recent applications of chiral non-racemic metal acyl enolates. In contrast Chapter 6 (carbene complexes) consists almost entirely of recent examples of the various uses of electrophilic and nucleophilic transition metal carbene complexes in organic synthesis, with over 100 new references. Cyclopropanations, Dötz reactions, photochemical generation and subsequent reactions of ketene complexes, as well as metal-catalyzed decompositions of diazo compounds followed by insertion into C–H or X–H bonds or formation of ylides, are all described in detail. This chapter ends with a brief section on carbonyl-olefination using Schrock-type carbene complexes. Many new references also appear in Chapter 7 (alkene, diene, and dienyl complexes). The use of palladium(II) complexes to assist the attack on alkenes by O-, N-, and C-nucleophiles is thoroughly discussed, including cyclization-induced rearrangements. Other topics highlighted in this chapter are the use of iron complexes to protect alkenes and 1,3-dienes, and the regio- and stereoselective formation of carbon–carbon bonds by nucleophilic attack on molybdenum diene complexes, and especially on iron dienyl complexes. Chapter 8 (alkyne complexes) discusses the use of cobalt complexes for the protection of the alkyne function, and in this connection describes new applications of the Nicholas reaction and subsequently takes a closer look at the Pauson–Khand reaction. Cobalt-catalyzed cyclo-oligomerizations of alkynes provide another major topic of this chapter, which ends with a completely new section on zircono benzyne complexes. Chapter 9 (η^3-allyl complexes) begins with the telomerization of 1,3-dienes, with

special attention to recently developed intramolecular processes catalyzed by palladium, iron, or nickel. This is followed by a long section concerned mainly with regio- and stereoselective reactions of π-allyl palladium complexes using C-, N-, and O-nucleophiles, their reduction to olefins, and their elimination reactions yielding 1,3-dienes. Also covered in this chapter and supported by a wealth of new literature references are allylic alkylations using vinyl or aryl tin compounds, palladium ene reactions and cascades based thereon, and formal [3 + 2]-cycloadditions via trimethylenemethane intermediates. The chapter ends with a survey of other η^3-allyl metal complexes (of Mo, W, Fe, Co, and especially Ni). Chapter 10 (arene complexes) gives an up-to-date review of the synthetic applications of arene-chromium tricarbonyl complexes, including nucleophilic substitutions of aryl halides, regio- and stereoselective additions of C-nucleophiles, along with possible types of follow-on reactions, ring lithiations, and reactions involving activation of the benzylic position. Also the potential for using alternative metals that have not yet been thoroughly investigated in this context (Fe, Ru, Mn) is briefly considered at the end of this chapter.

With this updated survey of transition metal-assisted methods the author has succeeded in producing an independent and highly stimulating book, whose particular strengths lie in the carefully chosen examples, the excellent figures, and the succinct explanations. Apparently as a result of limiting the coverage to reactions of compounds containing transition metal–carbon bonds, as in Collman et al. (see p. 6), the enormously important catalytic epoxidations and dihydroxylations are unfortunately not included. Nevertheless, this book, which is intended both as the basis for a one-semester course for upper-level students and as an overview for practicing chemists, sets a new standard in the treatment of this subject matter. It is emphatically recommended for use by advanced students and by all academic and industrial chemists concerned with synthesis.

Peter Metz
Organisch-chemisches Institut
der Universität Münster (FRG)

Bioinorganic Chemistry. Edited by *I. Bertini, H. B. Gray, S. J. Lippard* and *J. S. Valentine.* University Science Books, Mill Valley, CA (USA), 1994. 611 pp., hardcover £ 28.95.—ISBN 0-935702-57-1

Although this work is in fact a textbook on bioinorganic chemistry, it does not aim to compete in quite the same market as other recent introductory textbooks by W. Kaim and B. Schwederski, by J. A. Cowan, and by S. J. Lippard and J. M. Berg. It consists of nine chapters by a total of 15 authors, covering a wide variety of topics, mostly in considerable detail. The reader will not find here an introduction addressing the question "What is bioinorganic chemistry?", nor a systematic treatment of the basic principles of coordination chemistry, biochemistry, and physical methods. Instead the book aims to fill the gap between introductory textbooks (such as those mentioned above) and highly specialized review articles. The level of the contents would be more accurately reflected by a title such as "*Advanced* Bioinorganic Chemistry".

The chapters are of a fairly uniform length, with the exception of Chapter 1, a much shorter one in which E. C. Theil and K. N. Raymond give a clear and understandable description of the storage, transport, and biomineralization of transition metals (including zinc). In the second chapter I. Bertini and C. Luchinat discuss the reactions of zinc enzymes. Taking carbonic anhydrase as an example, they illustrate the importance of NMR spectroscopy and protein crystallography in this field. For some important zinc enzymes the authors describe possible catalytic cycles. The chapter also includes a short section on coenzyme and vitamin B_{12}.

The wide-ranging importance of calcium in the regulation of cell functions is recognized by devoting a separate chapter to this topic. After a short introduction (in which we also learn about the calcium content of a "good" beer), S. Forsén and J. Kördel describe the methods used to measure the concentration and distribution of calcium in cells. This is followed by sections on the transport and regulation of Ca^{2+} ions in higher organisms and on Ca^{2+} receptor proteins in cells. In Chapter 4 G. B. Jameson and J. A. Ibers contribute a review of both biological and synthetic dioxygen-transporting molecules. They begin by describing the thermodynamics of dioxygen transport and the biomolecules hemoglobin, hemocyanin, and hemerythrin, then go on to discuss some aspects of the chemistry of molecular oxygen, iron, copper, and cobalt. The chapter ends by describing the structural characteristics of dioxygen-binding biomolecules and synthetic complexes.

Chapter 5, by J. S. Valentine, is concerned with the reactions of the O_2 molecule that are of biological importance. After dealing with the chemistry and toxicity of O_2, the author discusses the relevant enzymes, namely cytochrome *c* oxidase, oxygenase, catalase, peroxidase, and Cu,Zn superoxide dismutase. Chapter 6 is devoted to electron transfer processes. H. B. Gray and W. R. Ellis Jr. describe the various electron transfer proteins and the types of biological processes in which electron transfer plays a part (e.g. photosynthesis). The emphasis is on theoretical aspects, especially with regard to long-range electron transfer in proteins.

In Chapter 7 E. I. Stiefel and G. N. George discuss proteins containing metal sulfide centers. They begin with iron sulfur proteins, concentrating appropriately on relevant (model) complexes of low molecular mass. Hydrogenases and nitrogenases are then discussed (including the recent crystal structure study by J. Kim and D. C. Rees). Chapter 8, by J. K. Barton, deals with interactions and reactions of metal ions and their complexes with nucleic acids. Topics covered include tris(phenanthroline) metal complexes, zinc-finger proteins, the MerR protein, and Fe^{II}-bleomycin.

In the last chapter S. J. Lippard discusses practical applications of bioinorganic chemistry, concentrating on the uses of metal compounds in medical diagnostics and chemotherapy. Cisplatin is treated at length (over 50 pages) as a case study. This chapter is also of interest in that the author broadens the discussion to include aspects beyond basic research, for example in drawing parallels between protagonists of new inorganic drugs and Hollywood film producers.

The inclusion of color plates and about 2000 (!) literature references add to the appeal of this excellent book, and there are few textual errors. It is unfortunate, however, that the IUPAC recommendation to enclose formulas of coordination compounds in square brackets has only been followed consistently in Chapter 9. I feel it is especially important in a student textbook to stick to the accepted rules of nomenclature.

Anyone who already has an elementary knowledge of bioinorganic chemistry, even if only from an introductory lecture course, will find this book useful and

 © VCH Verlagsgesellschaft mbH, D-69451 Weinheim, 1995 0570-0833/95/0909-1036 $ 10.00+.25/0

readily understandable. It should be in every departmental library, and I hope that it will also find its way into many personal collections, helped by the reasonable price.

Henry Strasdeit
Fachbereich Chemie
der Universität Oldenburg (FRG)

Destruction of Hazardous Chemicals in the Laboratory. 2nd edition. By *G. Lunn* and *E. B. Sansone*. Wiley, Chichester, 1994. 501 pp., hardcover £ 66.00.—ISBN 0-471-57399-X

It has always been one of the chemist's regular tasks to convert residues that are toxic, reactive, or harmful to the environment into products that can safely be disposed of. The methods for achieving this are becoming increasingly important as a consequence of strict legislation governing the handling of dangerous substances and properly disposing of them in environmentally acceptable ways. Although there is nowadays general agreement that certain substances should no longer be used in some situations, such as in teaching chemistry at elementary level, in modern research it is often impossible to avoid using reagents that present severe problems. This book contains over sixty short articles (an increase of about a third since the first edition in 1990), each giving well tested laboratory procedures for dealing with a particular substance or compound class, including critical evaluations of alternative methods. Substances with cytotoxic, anti-neoplastic, and enzyme-inhibiting properties, pharmacological products, and histological staining substances are included, so that the book also covers typical problems encountered in biochemical, microbiological, and medical laboratory practice.

The book begins with a very useful introduction which clearly explains the basic philosophy of appropriate reactions for destroying chemicals. Since many of the breakdown reagents used, which are mostly oxidizing or reducing agents, are themselves hazardous substances, and some of the reactions can become dangerously exothermic if not carefully controlled, the authors emphasize that the work must be carried out by people trained in chemistry or chemical engineering, in a properly equipped laboratory. Each article is well set out according to the following scheme: a) explanation of the potential risks, b) chemical principles of both well-known and new conversion methods, c) detailed laboratory procedures for carrying out recommended conversion reactions for large and small quantities and for dealing with spillages, d) instructions and recommendations for analyzing to check the success of the reaction, with limits of detection, e) mutagenicity assays of the end-products, where appropriate, f) suitability of the method for related compounds not specifically covered, g) an extensive bibliography. In addition there are four appendices as follows: a table of recommended solvents for obtaining samples from contaminated surfaces, methods for drying solvents without the use of highly reactive reagents, recommended safe procedures for using potassium permanganate, and recent developments in techniques for dealing with waste materials in biomedical research.

The substances included are listed in the alphabetical index under their systematic names, and also under synonyms, acronyms, and trade names. Dyes and biochemical compounds are also listed under the corresponding alphanumeric codes. One can also search for a compound via its molecular formula or CAS number. For example, under the heading "Halogenated Compounds" one finds a table listing alkyl halides, halogenated carboxylic acids, alcohols, and arenes (35 compounds altogether) with toxicological information supported by literature references. The recommended breakdown reactions are reductive dehalogenation by a Raney-nickel catalyst in alkaline solution, and substitutive dehalogenation in alcoholic NaOH. Tables giving the percentage conversion, as determined by GC analysis, are also provided. With this information it should be relatively easy for a chemist to choose the best method, even for compounds not listed in the book.

The authors work in a laboratory of the US National Cancer Institute, and the book has therefore been written from the standpoint of experience in American research organizations, where an agreed safety concept that meets the detailed requirements and is supported by expert opinion can be put into practice with less formalization and bureaucratic justification than under the rules of the European Union. Consequently the introduction contains only one brief mention of internal regulations. Thus, for example, the frequently appearing phrase "the decontaminated solution is discarded" should not necessarily be taken to mean that the end-product can safely be poured into the drain or the waste bin; instead one should proceed according to the regulations in one's own situation. Within the European Union one needs to set out formal instructions for carrying out the destruction reaction, and the necessary data must be obtained from elsewhere, as in all other procedures in a laboratory.

This professionally written and information-packed book should prove to be very useful in biomedical as well as chemical laboratories. The only qualification is that in the latter case, since the destruction process usually results in a rather large final volume, one would often prefer direct disposal as special waste for incineration. The book should be available as a standard work of reference in every library, and many laboratories should also have a copy to hand, a purpose for which it is well suited, especially in view of its stout binding.

Andreas Merz
Institut für Organische Chemie
der Universität Regensburg (FRG)

 © *VCH Verlagsgesellschaft mbH, D-69451 Weinheim, 1995* *0570-0833/95/0909-1037 $ 10.00+.25/0*

Ligand-Accelerated Catalysis

David J. Berrisford, Carsten Bolm, and K. Barry Sharpless*

The search for new metal-catalyzed asymmetric reactions has provided some fascinating insights into the effects imposed on the metal catalysts by chiral ligands. A practical consequence is the discovery of ligand-accelerated catalysis (LAC). Thus, an existing catalyzed process is improved by the addition of a specific ligand, which leads to a faster, "ligand-accelerated" reaction. Both homogeneous and heterogeneous catalysts are known to exhibit this behavior. The concept is especially valuable in reactions catalyzed by early transition metals, where dynamic ligand exchange processes require an efficient in situ self-selection of a highly reactive catalyst from a variety of thermodynamically dictated assemblies. Results of detailed mechanistic studies will be presented, and the significance of LAC phenomena in transformations catalyzed by early and late transition metals will be discussed.

Keywords: asymmetric syntheses · catalysis · dihydroxylations · epoxidations · titanium compounds

1. Introduction

More than a decade has passed since the discovery of the titanium-catalyzed asymmetric epoxidation (AE) of allylic alcohols.[1] The efforts to understand and develop this process have led to mechanistic insights,[2] many of which have extended its synthetic utility.[3] Discovery of the AE demonstrated that an abiotic catalyst could overcome the limitations on substrate that are often characteristic of the exquisite selectivity of enzymes (the lock-and-key phenomenon). More recently, another catalyst system has captured our imagination. The osmium tetraoxide catalyzed asymmetric dihydroxylation[4, 5] (AD) of olefins has, at first sight, little in common with asymmetric epoxidation save the obvious modus operandi—enantiofacially selective addition of heteroatoms to prochiral olefins. However, one factor irrevocably links the AE and the AD—they are both manifestations of, and owe their success to, ligand-accelerated catalysis (LAC).

The purpose of this review is to discuss these and other significant examples in which ligand-acceleration effects are essential for a catalyzed reaction to occur in a rapid and highly enantioselective manner. A simple picture of the LAC phenomenon is presented in Section 2.

[*] Prof. Dr. K. B. Sharpless
The Scripps Research Institute, Department of Chemistry
10666 North Torrey Pines Road, La Jolla, CA 92037 (USA)
Telefax: Int. code + (619) 554-6406
Dr. D. J. Berrisford
Department of Chemistry, University of Manchester
Institute of Science and Technology
Manchester (UK)
Prof. Dr. C. Bolm
Fachbereich Chemie der Universität Marburg (Germany)

2. General Concept

In ligand-accelerated catalysis the addition of a ligand increases the reaction rate of an already existing catalytic transformation (Scheme 1). Both the ligand-accelerated and the basic catalytic process operate simultaneously and in competition with each other.

$$A + B \xrightarrow[k_0]{\text{catalyst}} \text{product}^* \xleftarrow[k_1]{\text{catalyst / ligand}^*} A + B$$

Scheme 1. Ligand acceleration. * = optically active.

Of course, the nature of the ligands bound to a metal center or complex almost always affects the selectivities and rates of the organic transformations catalyzed by such a species. When a ligand is bound, the rate of product formation can either be slowed down ($v_{ML} < v_M$, where v_{ML} is the overall rate of product formation in the presence of the ligand, and v_M is the rate of the reference reaction in the absence of the ligand in question), remain the same ($v_{ML} = v_M$), or be increased ($v_{ML} > v_M$). The latter, the accelerated process, offers a powerful approach to increasing reaction efficiency.[6]

The simplest definition of ligand acceleration is given in Equation (1a). The rate comparison should be performed for reactions giving a product common to the reference reaction and the ligand-accelerated version. Ligand deceleration then can obviously be defined by Equation (1b).

$$v_{ML}/v_M > 1 \quad (1a)$$

$$v_{ML}/v_M < 1 \quad (1b)$$

In processes with rapidly exchanging ligands both the relative microscopic rate constants (k_0 and k_1) and the magnitude of the catalyst/ligand binding constant (expressed by K_{eq}) are important to the overall ligand-acceleration effect (LAE). In terms of these quantities (and assuming no change in the rate law), the LAE can be defined by Equation (2). Particularly attractive pos-

$$k_1 K_{eq}[\text{ligand}]/k_0 > 1 \quad (2)$$

sibilities are offered, when the accelerating ligand also affects the stereochemical outcome.[7] Thus, use of chiral ligands[8] generates asymmetric catalysts.[9] If the reaction rate is increased upon ligand binding, the stereoselective pathway can dominate over the nonselective one. Although a mixture of several different reactive species—selective and nonselective ones—are present in solution, enantioselectivity can be achieved. Even with a relatively modest acceleration effect, useful levels of selectivity may be reached. In general, we regard a ligand-accelerated pathway to be potentially viable for asymmetric synthesis when the value of the expression in Equation 2 is greater than or equal to 20. The ligand-derived process is then responsible for 95% or more of the conversion (thus producing $\geq 95\%$ *ee* in ideal cases for which the ligand provides perfect enantioselection).

For the majority of asymmetric processes, however, no significant reactivity enhancement is observed; that is, $v_{ML} \leq v_M$. The creation of an effective chiral environment often results in extra steric crowding around the binding/catalytic site, which leads to rate *deceleration*. Useful levels of asymmetric induction then require high ligand concentrations—a situation not conducive to efficient catalysis.

Significant selectivity in organic transformations can only be achieved in reactions that proceed through highly organized transition states. In principle, the creation of a single reactive species (reactant or catalyst) is desirable to avoid participation of intermediates that react with different selectivity.[10] In many organometallic reactions this goal is accomplished by tight metal-to-ligand binding. For example, in the most widely studied asymmetric reaction, the metal-catalyzed hydrogenation of olefins, bidentate phosphane ligands possessing high binding constants for the transition metal complexes provide the asymmetric bias.[8–11] Such ligands do not dissociate under the reaction conditions, which ensures the structural integrity of the asymmetric environment during the catalysis.

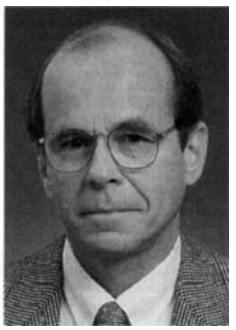
In reactions with early transition metals, however, a variety of metal complexes often exist in solution.[12] These molecular assemblies form spontaneously, and the composition of the mixtures depends only on thermodynamic factors. Dynamic ligand exchange processes result in complex solution equilibria. Unraveling of the mechanism of the AE has revealed that even though the coordination chemistry of early transition metal complexes is capricious, an appropriate conjunction of metal, ligand, and correct stoichiometry may, even in such complex systems, lead to the discovery of new catalysts for efficient asymmetric reactions.[13] The goal of channeling the catalysis



D. J. Berrisford



C. Bolm



K. B. Sharpless

David J. Berrisford studied for his PhD (1990) at the University of Sheffield (UK) under the supervision of Dr. J. F. Stoddart, working on chiral lithium amides. He then took up a SERC–NATO Postdoctoral Fellowship with Prof. K. B. Sharpless, then at Massachusetts Institute of Technology, Boston (USA). After returning to the UK, he joined the research group of Dr. I. Paterson in Cambridge (1992–1993). In January 1994 he was appointed lecturer in Chemistry at the Institute of Science and Technology of the University of Manchester and continues research into asymmetric catalysis with metals (conjugate addition, chiral Lewis acids) and bifunctional organic systems.

Carsten Bolm, born in 1960, studied chemistry in Braunschweig (Germany) and at the University of Wisconsin, Madison (USA). He completed his doctorate with Prof. M. T. Reetz in Marburg (Germany) on chiral catalysts for enantioselective C–C coupling. After a postdoctoral stay with Prof. K. B. Sharpless at the Massachusetts Institute of Technology, Boston (USA), he worked with Prof. B. Giese in Basel (Switzerland), obtaining his habilitation on enantioselective catalysis with chiral ligand–metal complexes. Since 1993 he has been Professor of Organic Chemistry at the University of Marburg (Germany). His awards include the Heinz-Maier-Leibnitz prize, the ADUC-Jahrespreis for habilitands, and the annual prize for Chemistry of the Akademie der Wissenschaften zu Göttingen.

K. Barry Sharpless, born in 1941, obtained his doctorate at Stanford University (USA) with Prof. E. E. Tamelen. After postdoctoral years at Stanford with Prof. J. P. Collman and at Harvard University with Prof. K. Bloch, he joined the faculty at the Massachusetts Institute of Technology, Boston (USA). In 1990 he moved to the Scripps Research Institute, La Jolla, CA (USA). Finding new metal-catalyzed transformations of use in organic synthesis is the main goal of his research.

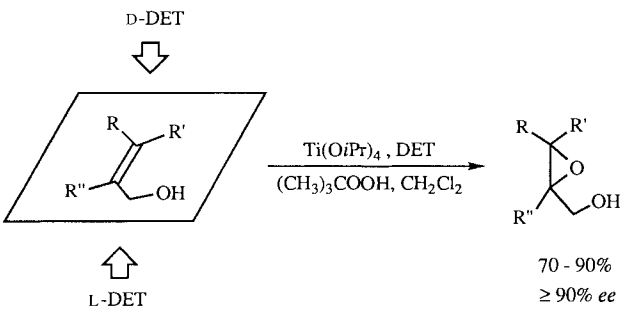
through one particular complex is usually achieved by an overwhelming *kinetic activity* favoring that one complex over the many other complexes which assemble in solution.[14] *For ligand-accelerated processes with early transition metal complexes, this in situ selection* of a highly reactive (and selective) metallic complex from a variety of thermodynamically dictated assemblies *is a crucial requirement.*

Our understanding of LAC phenomena has required detailed mechanistic studies. In the following paragraphs significant results will be presented, focusing in particular on ligand-acceleration effects in early and late transition metal-catalyzed asymmetric reactions.

3. Ligand-Acceleration in Early Transition Metal Catalysis

3.1 Asymmetric Oxidations

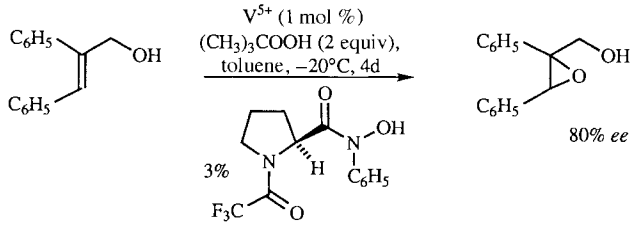
The discovery of titanium-catalyzed asymmetric epoxidation was, in hindsight, dependent on ligand acceleration. A remarkable consequence of the coordination chemistry[12, 15] of early transition metals is the extreme sensitivity of epoxidation catalysts to varying combinations of ligand and metal. The unsuccessful experiments prior to the discovery of the titanium/tartrate AE[3, 16] (Scheme 2) did not foresee, or allow for, either the complexity surrounding the coordination chemistry of early transition metals or the phenomenon of LAC.



Scheme 2. Catalytic asymmetric epoxidation (AE) of allylic alcohols with D-(−)- and L-(+)-diethyltartrate (D- and L-DET).

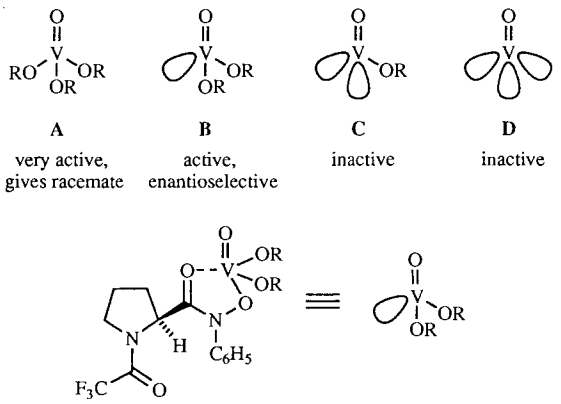
Of the twenty-five metals that were eventually found to catalyze the epoxidation of allylic alcohols by *tert*-butylhydroperoxide (TBHP), catalysis by all but one is either stopped or strongly inhibited by adding tartrate.[17] With tartrate esters as ligands, vanadium and molybdenum alkoxides[1d, 18, 19] are the runner-up catalysts, but they fall far behind titanium alkoxides in both rate and enantioselectivity.

To set the stage for discussing LAC reactions, it is instructive to begin with the catalytic asymmetric epoxidations effected by chiral vanadium hydroxamate complexes reported in 1977[1d, 18, 19] (Scheme 3). The significant deactivation of the catalyst upon binding of the chiral ligand to the metal (that is, ligand deceleration), along with the occurrence of dynamic ligand exchange processes, made it impossible to develop useful catalysts in this system.



Scheme 3. Asymmetric epoxidation with a chiral hydroxamatovanadium catalyst.

Whereas the vanadium-catalyzed reaction in the absence of the hydroxamic acid ligand is over in less than one day, the enantioselective reaction under the optimized conditions requires four days. As shown in Scheme 4, progressive replacement of the three alkoxide groups (-OR in **A**) by the chiral bidentate ligand first reduces and then destroys the activity of the complexes so produced. Exchange of more than one alkoxide group leads to inactive complexes, because the mechanism for these metal-catalyzed epoxidations of allylic alcohols requires that at least two such groups be present and in adjacent positions.[2]



Scheme 4. Activity of vanadium alkoxide complexes in epoxidations.

Ligand exchange in vanadium(v) alkoxides is rapid.[12] Even supposing that complex **B** (Scheme 4) represents the major species in solution, it is still in equilibrium with complexes **A** and **C**. While **C** is inactive, racemate-producing complex **A** is a more active species than **B**. To avoid the racemic pathway (with complex **A**), one must maintain all the vanadium in the inactive forms (complexes **C** and **D**) and depend on the occasional disproportionation of **C** into **B** and **D** to generate some of the desired enantioselective catalyst (**B**). Hence, an excess of hydroxamic acid is necessary. The cost of completely suppressing the presence of catalyst **A** is to have essentially all the vanadium bound within the inactive complexes. Consequently, with rising ligand concentration the enantiomeric excess increases to a plateau, whereas the reaction rate decreases steadily (Fig. 1).

In the vanadium case, dynamic ligand exchange generates a mixture of vanadium–ligand species in which only two complexes are significantly active. In general, however, all complexes formed in solution have to be considered as potential catalysts, even though they may only exist in minor quantities. Given this fact, it is clear that LAC offers an appealing, and perhaps a

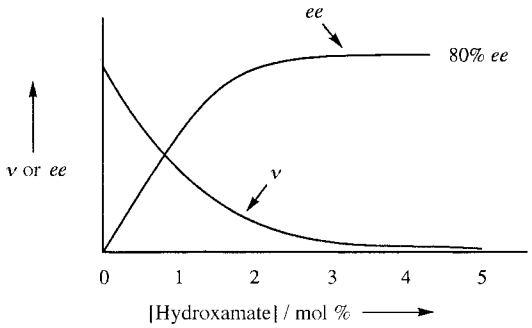


Fig. 1. Asymmetric epoxidation with chiral vanadium hydroxamate catalysts: the dependence of the rate v and enantioselectivity *ee* [%] on ligand concentration. Mol% of ligand corresponds to number of equivalents, since 1 mol% of vanadium catalyst was used.

unique, means for simultaneously achieving both high rates and enantioselectivities.

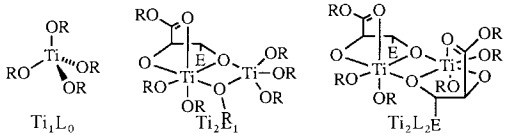
In the asymmetric epoxidation catalyzed by titanium complexes, the ability of titanium(IV) alkoxides to exchange ligands rapidly makes the reaction mixture difficult to characterize. Exchange of bound monoalkoxide ligands (including allylic alkoxide, "spectator" alkoxides such as isopropoxide, epoxy alkoxide, and alkylhydroperoxide) between metals via oligomeric intermediates and with free alcohols in solution is rapid in most cases. Therefore, a mixture of complexes involving various alkoxides is expected to be present, subject only to thermodynamic factors. In equimolar mixtures of titanium tetraalkoxides and dialkyltartrates, more than one complex may be present, and individual oligomeric complexes may have nonequivalent amounts of metal and tartrate ligand (Table 1). Many of these are potential epoxidation catalysts, each of which would be expected to operate with a different profile with respect to rate, enantioselectivity, and facial selectivity.

Table 1. Titanium/tartrate species in solution (Ti = titanium, L = tartrate; species are in boldface if there is evidence for their existence from either NMR spectroscopy, mass spectrometry, or X-ray diffraction).

	L_0	L_1	L_2	L_3	L_4	$L_5 \rightarrow L_n$
T_1	**Ti_1L_0**	Ti_1L_1	Ti_1L_2	Ti_1L_3	Ti_1L_4	Ti_1L_5
T_2	**Ti_2L_0**	**Ti_2L_1**	**Ti_2L_2**	**Ti_2L_3**	Ti_2L_4	Ti_2L_5
T_3	Ti_3L_0	**Ti_3L_1**	Ti_3L_2	**Ti_3L_3**	Ti_3L_4	Ti_3L_5
T_4	Ti_4L_0	Ti_4L_1	Ti_4L_2	Ti_4L_3	**Ti_4L_4**	Ti_4L_5
T_5	Ti_5L_0	Ti_5L_1	Ti_5L_2	Ti_5L_3	Ti_5L_4	Ti_5L_5
↓						
T_m						

Studies on the solution-phase structures of titanium/tartrate mixtures indicate that one major species of 1:1 stoichiometry is present in the reaction mixture along with at least two minor components.[2] Kinetic experiments using different ratios of $[Ti(OiPr)_4]$ to (+)-diisopropyltartrate [(+)-DIPT] revealed that the major species (a dimeric complex) is the catalyst that dominates the epoxidation activity. One minor component identified as a 2:1 Ti:tartrate species, as well as other oligomeric species with more tartrate ligands than titanium atoms, proved to be sluggish epoxidation catalysts. Thus, a comparison of the epoxidation rates of different titanium alkoxides (Table 2)

Table 2. Estimated fractions of the three main epoxidation catalysts present in a 1:1 mixture of $[Ti(OiPr)_4]$ and DIPT (R = *i*Pr, E = CO_2iPr), their approximate relative epoxidation rates, and the enantioselectivity of the epoxidation of (*E*)-2-hexen-1-ol in CH_2Cl_2.



	Ti_1L_0	Ti_2L_1	Ti_2L_2E
fraction in solution[%]	ca. 10	ca. 10	ca. 80
relative epoxidation rate	1.4	1.0	3.6
enantioselectivity	none	low	high

showed that the reaction rate with a mixture of $[Ti(OiPr)_4]$ and 50 mol% tartrate (forming the $[Ti_2(DIPT)(OiPr)_6]$ complex as the major species) was significantly *lower* than that of free $[Ti(OiPr)_4]$ alone—an example of ligand deceleration. In contrast, substantial *rate acceleration* was observed for the 1:1 $[Ti(OiPr)_4]$:tartrate ratio known to favor formation of the most active dimeric complex, $[Ti(DIPT)(OiPr)_2]_2$.

The kinetic data presented in Table 2 only represent the lower limits for the rate acceleration, since the rate laws for epoxidation of the competing species are different. Taking into account the number of exchangeable ligand sites per metal center, the $[Ti_2L_2]$ complex is approximately ten times more active than $[Ti(OiPr)_4]$.[2b] In addition, the standard AE recipe calls for a 20% excess of tartrate (that is, Ti:L = 1:1.2) which shifts all the equilibria involving the complexes in Table 1, with the consequence that the unwanted epoxidation catalysts $[TiL_0]$ and $[Ti_2L_1]$ are elimininated.

The use of a 2:1 ratio of $[Ti(OR)_4]$ to tartrate under otherwise standard stoichiometric epoxidation conditions results in epoxidation of the "predicted" olefinic face in reduced enantiomeric excess. For example, a 2:1 ratio of $[Ti(OiPr)_4]$ to (*R*,*R*)-diethyltartrate yields the (2*S*)-epoxy alcohol of (*E*)-α-phenylcinnamyl alcohol in 80% *ee*, compared to more than 98% *ee* for a 1.0:1.2 ratio of reagents.[2a] We have also found that the addition of electron-withdrawing monodentate additives (such as *p*-nitrophenol or hexafluoroisopropanol) to this 2:1 Ti:tartrate system results in a reversal of enantioselectivity in epoxidation of allylic alcohols; for example, in the presence of *p*-nitrophenol, (*E*)-α-phenylcinnamyl alcohol gives the (2*R*)-epoxy alcohol in 80–85% *ee*. Thus, the potential exists for many manifolds of reactivity in the titanium/tartrate system.

We have since found, in experiments that involved pairing approximately 50 tartrate analogues with titanium and other neighboring transition metal alkoxide epoxidation catalysts,[17] that tartrate and titanium are perfectly matched. Slight deviations in ligand structure and/or a change in the metal catalyst severely reduce the rate and/or enantioselectivity.[3] Ligand deceleration of catalysis seems to be the dominant phenomenon. Fortunately, in the titanium/tartrate-catalyzed epoxidation of allylic alcohols the major species present in solution is not only the most reactive but probably also the most enantioselective.

Titanium/tartrate mixtures different from 1:1 stoichiometry have also been found to mediate other oxidation reactions. For example, catalysts for the chlorohydroxylation of allylic alcohols[20] and the kinetic resolution of β-amino alcohols[21] have

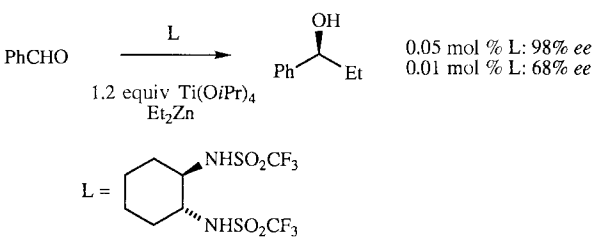
been developed that utilize a 2:1 Ti:tartrate formulation. The former reaction provides chlorohydrin derivatives by opening of the intermediate epoxides with enantiofacial selection opposite to that of the "parent" AE system.

The in situ selfselection of a highly reactive and enantioselective catalyst from a variety of titanium-containing species is also important in sulfide oxidations. Kagan et al. discovered a water-modified titanium reagent consisting of [Ti(O*i*Pr)$_4$], diethyltartrate (DET), and water in a 1:2:1 ratio.[22] With TBHP as oxidant, optically active sulfoxides with high enantiomeric excesses were obtained from sulfides by asymmetric oxidation. The titanium-mediated pathway is almost 200 times faster than the uncatalyzed oxidation with TBHP. Use of cumene hydroperoxide allowed the development of a catalytic process.[23] Catalyst loading can be reduced to 20 mol% while retaining good enantioselectivity. In the absence of water a larger excess of DET with respect to [Ti(O*i*Pr)$_4$] has a beneficial effect on enantioselectivity.[24] Uemura et al. studied a similar sulfide oxidation system prepared from [Ti(O*i*Pr)$_4$] and binaphthol (BINOL).[25] Again, added water is essential for high enantioselectivity. With 2.5 mol% of the titanium complex, aqueous TBHP as oxidant, and an excess of water, about 50% *ee* was achieved in the oxidation of aryl methyl sulfides to the corresponding sulfoxides. Titanium-catalyzed kinetic resolution following the asymmetric sulfide oxidation provides chiral sulfoxides with over 90% enantiomeric excess.

3.2 Asymmetric Nucleophilic Additions

The significant effort devoted over the years to achieving asymmetric nucleophilic additions to carbonyls has yielded some spectacular successes.[26] Ligand acceleration also plays an important role in these reactions. Again titanium chemistry provides excellent examples.[27–29]

Yoshioka, Ohno et al. have demonstrated the utility of Ti-mediated organozinc additions to aldehydes (Scheme 5).[28] Here one sees an extraordinary effect of a chelating, and relative to the other ligands present within the mixture, highly electron-withdrawing ligand coordinated to the titanium. In favorable cases, very small quantities of the chiral ligand still afford high *ee*'s (Scheme 5). For example, the alkyl transfer from diethylzinc to benzaldehyde is effected by 1.2 equivalents of [Ti(O*i*Pr)$_4$] and 0.05 mol% of the chiral ligand (Ti:L = 2400:1) to give the addition product in 98% *ee*. Reducing the catalyst loading still further (0.01 mol%; Ti:L = 12000:1) has a significant effect on the *ee* which, for benzaldehyde, decreases to 68%.[28] However, even this case is remarkable in that a preequilibrium Ti:L ratio

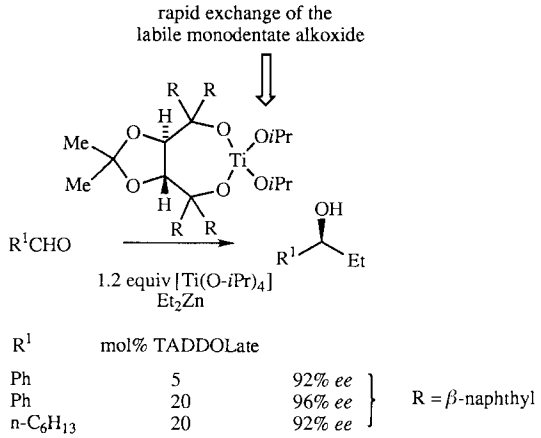


Scheme 5. Titanium-catalyzed asymmetric addition of dialkylzinc compounds to aldehydes.

of 12000 still provides two out of every three product molecules from the asymmetric pathway! This reaction dramatically illustrates the virtues of ligand-accelerated catalysis; a very practical process results when only a trace of the chiral ligand is used.

A significant recent extension of this chemistry is the observation that a variety of functionalized organometallics[30] may also be employed to provide access to a broad range of chiral synthons.[31]

Ligand acceleration in titanium-catalyzed processes is not limited to the straightforward (but valuable!) effects of Lewis acidity. The α,α,α′,α′-tetraaryl-1,3-dioxolane-4,5-dimethanol (TADDOL) ligands[26, 32] pioneered by Seebach[29] form a class of titanium complexes (Ti–TADDOLates) that catalyze asymmetric addition of organozincs to aldehydes (Scheme 6). Comprehensive studies indicate that the highly hindered TADDOLate complexes are more active than [Ti(O*i*Pr)$_4$]. Such activity is necessary as [Ti(O*i*Pr)$_4$] is present in excess (greater than one equivalent). The steric hindrance of the chiral complex ensures that oligomerization of the catalyst is minimized.[33] In turn, this effect allows rapid exchange of the monodentate ligands on the active, monomeric complex.[29d] The reactivity *increases* in parallel with the steric demand of the anterior part of the TADDOL ligands (R = Me < R = Ph < R = β-naphthyl; Scheme 6).[33]



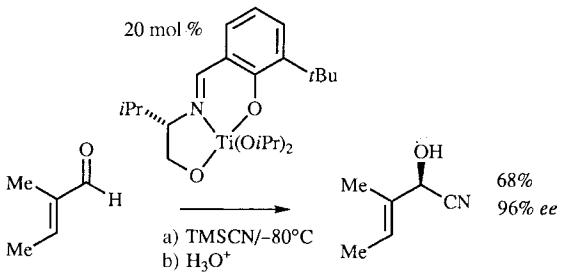
Scheme 6. Ti-TADDOLate catalyzed additions [29] of organozinc compounds to aldehydes.

Oligomerization of [Ti(OR)$_4$] causes a marked decrease in the catalytic efficiency for the racemic pathway.[34] This large difference in activity of the chiral and achiral complexes allows efficient asymmetric induction at low catalyst loading. For example, with only 5 mol% of TADDOLate (R = β-naphthyl) the *ee* in the diethylzinc addition to benzaldehyde decreases by just 4% from the ceiling value at 20 mol% catalyst loading (Scheme 6). The ligand-accelerated asymmetric pathway is around 23 times faster than the racemic route, even though the ratio of chiral titanium complex to free [Ti(O*i*Pr)$_4$] is 1:24.

Allylation of aldehydes is also catalyzed by titanates.[35–38] Enantioselective catalysis in the presence of BINOL has recently been achieved by three independent groups. It is interesting to note that there appears to be a very specific structural requirement for the ligand. An Italian group reports[35] that [TiCl$_2$(O*i*Pr)$_2$] is less active than [TiCl$_2$(binol)], a result which

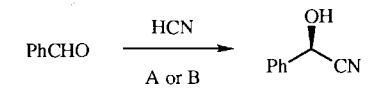
could be explained by the relative acidities[32, 39] of the ligands. An excess of $[TiCl_2(OiPr)_2]$ relative to binol decreases the enantioselectivity.[35, 36c] In a cleaner demonstration of LAC, $[Ti(OiPr)_4]$ is inactive by itself but allylation using allylstannanes is very selectively promoted by $[Ti(OR)_2(binol)]$.[36] Other ligands with comparable acidity, like tartrate esters, or higher acidity than to binol, like the bistriflamide of *trans*-1,2-diaminocyclohexane, are ineffective.[40, 41] Mikami has also utilized $[TiCl_2(binol)]$ to promote asymmetric ene reactions,[39, 42] aldol reactions,[43] and cycloadditions.[44] As with the allylation chemistry promoted by this Lewis acid, coordination of the binol ligand appears to enhance the reactivity relative to $[TiCl_2(OiPr)_2]$.[39e, 41]

Dynamic ligand exchange behavior also gives rise to profound effects in other transformations involving titanium alkoxides. Trimethylsilylcyanation and hydrocyanation of aldehydes can be catalyzed by a number of chiral titanium-based Lewis acids.[45] Recently Oguni et al. have found a very selective process (Scheme 7) using an amino alcohol derived Schiff base ligand and and $[Ti(OiPr)_4]$.[46] The catalyst is formed in situ from titanium/ligand mixtures, and the cyanation is accelerated in the presence of the chiral ligand when compared to the reference $[Ti(OiPr)_4]$ catalyzed reaction. This acceleration makes the asymmetric reaction viable at low catalyst loadings. Similar ligand-acceleration effects were noted in the asymmetric addition of TMSCN to epoxides.[47]



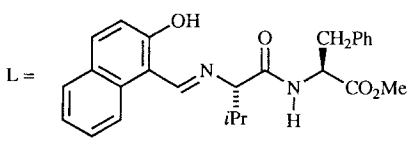
Scheme 7. Titanium-catalyzed trimethylsilylcyanation of aldehydes.

A related series of ligands (Scheme 8) was investigated by Inoue et. al.,[48] who found that the rate of hydrocyanation catalyzed by Ti and Zr alkoxides was enhanced by the presence of amide groups on the Schiff base–peptide ligands. This observation led to a development of an asymmetric process[49] that retains the ligand-acceleration effect, as demonstrated by the increased yield in the presence of the ligand (Scheme 8).



A) –20°C/10 mol % $[Ti(OiPr)_4]$ 43%

B) –20°C/10 mol % $[Ti(OiPr)_4/L]$ 94%, 78% *ee*



Scheme 8. Titanium-catalyzed hydrocyanation of aldehydes [49b].

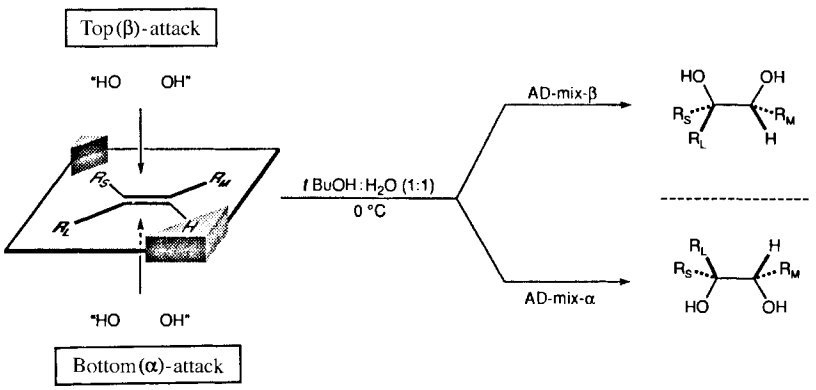
In this review on ligand acceleration in nucleophilic addition reactions only a few contributions have been highlighted, and our discussion is based on published information that refers explicitly to rate enhancements conferred by the chiral ligand. Undoubtedly, ligand-acceleration effects will be revealed in many more asymmetric transformations involving early transition metals. A detailed knowledge of mechanism—often unavailable—is necessary for the understanding and rational design of new ligand-accelerated processes.

4. Ligand-Acceleration in Late Transition Metal Catalysis

4.1 Asymmetric Oxidations

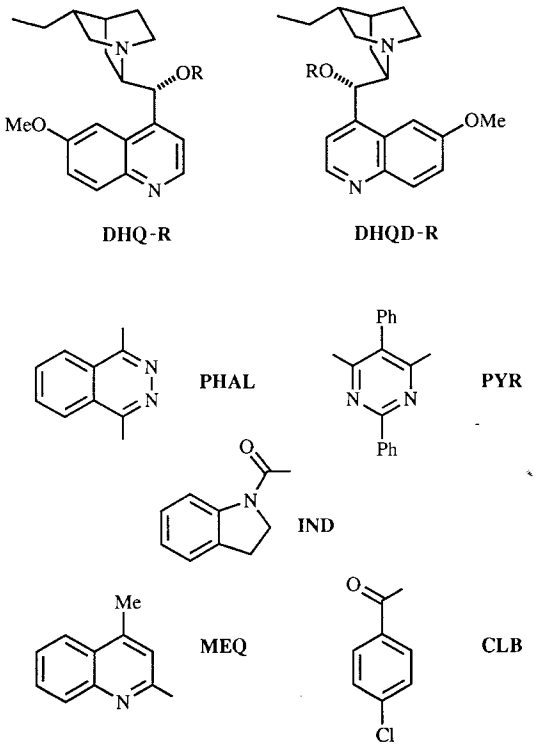
The discovery[5] of the catalytic asymmetric dihydroxylation of olefins (AD) (Scheme 9) has been equally instructive regarding ligand-acceleration effects. Again, ligand acceleration is central to the efficiency and selectivity of this catalytic process.

Historically, the first documented example of a ligand-accelerated reaction emerged from the pioneering study[50] by Criegee. This investigation demonstrated that the addition of pyridine led to a marked increase in the rate of formation of cyclic osmate esters from alkenes and OsO_4. Criegee's ligand-acceleration effect was the direct inspiration for the discovery of the stoichiometric version of the AD.[4] The AD in its present form[51–53] is the result of many incremental improvements, since the catalytic version of the reaction was first uncovered.[5a] The synthetic utility[53] of the AD is now comparable with, or perhaps surpasses that of the titanium-catalyzed asymmetric epoxidation.

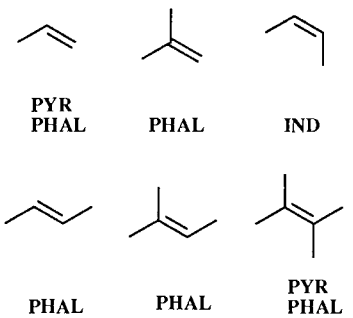


Scheme 9. Asymmetric catalytic dihydroxylation (AD) of olefins: the diagram allows prediction of the face selectivity (R_L, R_M, and R_S are respectively, the large, medium, and small olefinic substituents).

By judicious selection of the alkaloid ligand (Scheme 10), enantioselectivities of greater than 95% are achievable for members of five out of the six olefin classes (Scheme 11). Highly enantioselective dihydroxylation of generic *cis*-di- and tetrasubstituted olefins remains elusive, however. Modification of the cinchona alkaloid ligand has led to remarkable levels of enan-



Scheme 10. Ligand structures and their abbreviations. The ligands consist of one or two alkaloid units and a mono- or divalent group R. DHQ-R = dihydroquinine (R = H), DHQD-R = dihydroquinidine (R = H). R: PHAL = 1,4-phthalazinediyl, PYR = 2,5-diphenylpyrimidinediyl, IND = 1-indolinyl, MEQ = 4-methyl-2-quinolinyl, CLB = 4-chlorobenzoyl). See also ref. [53].



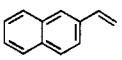
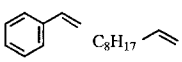
Scheme 11. Optimum ligand recommendations (only the R group is given, see Scheme 10) for the six olefin classes.

tioselectivity, undreamed of at the time of the original discovery,[4, 5] and has also helped delineate other profound effects that the ligands have on the reaction.

A feature common to both the catalytic AD and the parent stoichiometric process[4] is the facilitation of the osmylation step by the nitrogen donor ligand—the Criegee effect. Rate accelerations are always observed in the presence of the alkaloid.[55] For example, the second order rate constant k_0 for formation of the osmate ester from 2-vinylnaphthalene at 25 °C in *tert*-butanol in the *absence* of ligand is only 2.41 L mol^{-1} min^{-1}.[55a] In the presence of (DHQD)$_2$PHAL the reaction becomes extremly rapid, and a saturation rate constant (k_c) of 35600 L mol^{-1} min^{-1} has been measured for the dihydroxylation of 2-vinylnaphthalene with OsO_4.[55a] In the catalytic version the turnover-limiting step is often hydrolysis of the intermediate osmate ester, not the ligand-accelerated oxidative process. Thus, in the case of 2-vinylnaphthalene in the homogeneous acetone/water system with *N*-methylmorpholine-*N*-oxide (NMO) and (DHQD)$_2$PHAL a turnover number of 3000 min^{-1} at 25 °C was determined.[55c] This turnover number would be much higher if the hydrolysis step were not rate-limiting.

It is instructive to explore the rate accelerations induced by the ligand on the osmylation step in isolation from the effects of turnover. We have evaluated a series of ceiling rate constants (k_c) for the ligand-accelerated reaction of OsO_4 with various olefins under pseudo first-order conditions.[55a] At this high concentration of ligand all of the reaction is funneled through the ligand-mediated pathway. The ratio of rate constants $k_c:k_0$ (where k_0 is the background rate constant in the absence of the ligand) is a measure of the ligand-acceleration effect for the osmylation step (Table 3). These figures confirm that there is marked acceleration (up to 10^4) of the reaction in the presence of the ligand. The data also reveal that the rate accelerations are significantly greater with the alkaloid derivatives than with quinuclidine; that is, the rate accelerations are not directly related to the ground state binding energy between the ligand and OsO_4, a feature that we shall return to. Furthermore, the rate accelerations are dependent on the substrate; for example, 2-vinylnaphthalene reacts 19 times faster under these conditions (PHAL ligand, 25 °C, *t*BuOH) than 1-decene. However, the rates of osmylation of these two olefins are virtually identical when quinuclidine is used as the ligand (Table 3). In general, aromatic olefins are more sensitive to the structure of the ligand, but even 1-decene shows substantial rate accelerations specifically with the alkaloid ligands. These rate ratios amply demonstrate the unique effectiveness of the alkaloid ligand's structure in facilitating the osmylation step of the AD.

Table 3. Ratio of the rate constants k_c/k_0 in *t*BuOH at 25 °C for the reaction of OsO_4 with olefins [55a] in the presence of various ligands. k_c = rate as ligand concentration $\rightarrow \infty$, k_0 = rate with no ligand (see Fig. 2).

Ligand			
(DHQD)$_2$PHAL	14771	4182	770	341
DHQD-CLB	791	622	238	139
quinuclidine	61	75	55	–

Clearly, the rate enhancement [Eq. (2)] will depend on the ligand concentration and the OsO_4–ligand binding constant (K_{eq}). The K_{eq} for quinuclidine[55a, 56] is 2630 L mol^{-1} (*t*BuOH, 25 °C), a value which should be compared with that for the (DHQD)$_2$PHAL ligand of 27.7 L mol^{-1} (*t*BuOH, 25 °C). However, there is no correlation between the binding constant of a particular ligand and the observed rates of the osmylation reaction. The ratio of binding constants for quinuclidine:(DHQD)$_2$PHAL is approximately 95:1. However, the (DHQD)$_2$PHAL promoted reaction occurs between about 240 (2-vinylnaphthalene) and about 14 (1-decene) times *faster* than the reaction in the presence of quinuclidine (Table 3). Under the standard (potassium hexacyanoferrate(III)) catalytic AD conditions, all olefins exhibit rates greater than or equal to those in the absence of the ligand. This is because the ligand accelerates the addition step and does not retard the hydrolysis step.[57] For those olefins (for example, terminal olefins) producing osmate esters that are rapidly hydrolyzed, the rate acceleration in the addition step results in increased rates of catalysis. However, for

the more substituted olefins, osmate ester hydrolysis is often slow enough to partially or completely obscure the acceleration of the rate by the ligand in the addition step. As already mentioned for 2-vinylnaphthalene, even a terminal olefin can reach the turnover-limiting hydrolysis barrier if the ligand concentration is raised above the low levels used in the standard AD procedures. At higher ligand concentrations, one climbs the saturation-rate curve, and for "good" substrates like 2-vinylnaphthalene, the ligand-accelerated addition step soon outpaces even a fairly rapid hydrolysis step, since the latter is largely unaffected by the higher ligand concentration. This analysis offers a clear objective for improving the AD process: for many substrates, the catalytic efficiency will be increased if yet better ways to increase the rate of osmate ester hydrolysis can be found. One key discovery has already been made in this context:[51a] The hydrolysis of the Os^{VI}-glycolate product can be significantly accelerated by $MeSO_2NH_2$. Thus, for some substrates the reaction time is as much as 50 times shorter in the presence of this additive.

In a catalytic asymmetric process, rate and enantioselectivity are the important criteria for synthetic chemists. In the AD the enantiomeric excess approaches its maximum value[5b] at much lower alkaloid concentrations than the onset of rate saturation. In Figure 2 data for the asymmetric dihydroxylation of (*E*)-stilbene under the original conditions (DHQD-CLB/NMO) are depicted. Similar results have been obtained with the $(DHQD)_2PHAL$ ligand giving the corresponding diol with much higher enantiomeric excess.

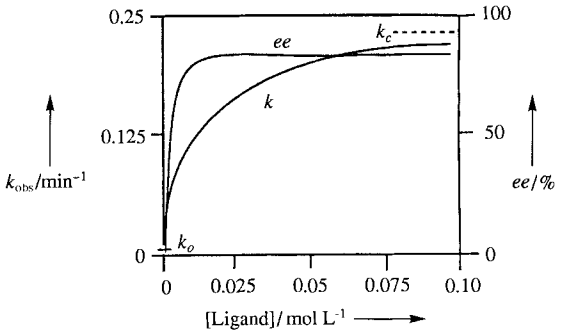


Fig. 2. Plot of concentration of the DHQD-CLB ligand against observed rate constant k_{obs} and against *ee* [%] for the AD of (*E*)-stilbene under original conditions (with NMO) [5b].

A consequence of this particular relationship between *ee*, rate, and ligand concentration is that extremely low levels of ligand can be employed while retaining optimal enantioselectivity. For terminal, disubstituted, and trisubstituted olefinic substrates, a standard AD protocol[58] calls for 0.2–0.4 mol% of osmium and 1 mol% of ligand (PHAL or PYR). Moreover, in the AD of stilbene[51a] [$(DHQD)_2PHAL$, 0 °C], the amount of ligand can be reduced 100-fold to 0.01 mol% when 0.2 mol% of osmium is used. Under these conditions there is only a slight reduction in enantioselectivity from over 99% (1 mol% ligand) to 96% (0.01 mol% ligand). This outcome translates to a ratio of rates for the enantioselective to the racemic reaction ($R_{Os\cdot L}:R_{Os}$) of 24:1 (Equation 1). Given the osmium-to-ligand ratio of 20:1 in this 0.01 mol% ligand experiment, the approximate ratio of the rate constants $k_1:k_0$ must be 480:1. Expressed in a different way, in a mixture of 10000 molecules of stilbene, 20 molecules of OsO_4 and *1 molecule* of chiral ligand, only 400 stilbene molecules are dihydroxylated by unbound osmium tetraoxide. The remaining 9600 stilbene molecules are enantioselectively oxidized through the OsO_4/ligand-assisted process.

The present ligand recommendations[51, 53] have arisen through an extended process of screening experiments. The presence of oxygenation at C-9 of the alkaloid and the nature of the substituent on the oxygen are of paramount importance in determining the enantioselectivity and the reaction rate. An extended aromatic moiety, provided by the C-9 ether substituents of the PHAL and PYR ligands, is a crucial structural feature. Other structure–activity relationships are more subtle,[59] and yet more are manifest[55a] in the binding of the ligand to the osmium. Our recent kinetic studies[55a] indicate that transition-state stabilization is an important factor in determining the rate and enantioselectivity of the AD. Given the differential rate effects between substrates (Table 3), especially the rapidity of the reaction with aromatic olefins, we believe that the contribution[60] of stabilizing, attractive[61–63] transition-state stacking interactions and solvophobic effects[64] are significant. Although of lower magnitude, the rate enhancements observed with alkyl-substituted olefins indicate that similar effects[64, 65] are active for these substrates too. The alkaloid ligands always outpace quinuclidine (Table 3), presumably because of the large aromatic moieties specific to the alkaloids. In particular, the PHAL ligand exhibits some unique effects, which we ascribe[55] to the presence of a "binding pocket", created by the phthalazine spacer and the methoxyquinoline group of the bystander alkaloid moiety. In the year following the centenary of Emil Fischer's lock-and-key analogy, it is worth noting that the AD responds to subtle variations in the substrate's shape, particularly when a ligand possessing a binding pocket is used.[53, 66]

Attractive transition-state interactions should manifest themselves in both the rate and enantioselectivity of the process. Indeed, an intriguing relationship exists between the enantioselectivities and the ceiling rate constants (k_c) for the osmylation. The measurements of k_c were correlated with the *ee* values in a series of experiments conducted with a range of ligands (Table 4). In-

Table 4. Comparison of enantioselectivity and ceiling rate constants k_c (measured at 0 °C) for various olefin/ligand combinations [55].

Ligand	$C_8H_{17}CH=CH_2$		$PhCH=CH_2$	
	ee[%]	k_c[L mol^{-1} min^{-1}]	*ee*[%]	k_c[L mol^{-1} min^{-1}]
DHQD-CLB	45[a]	331	74	1089
DHQD-MEQ	65	335	87	1210
$(DHQD)_2PHAL$	84	1065	97	7320

[a] The AD reaction was carried out at room temperature.

creases in k_c and the enantioselectivity in the AD of, for example, 1-decene and styrene, occur in concert. These concurrent trends provide additional support for the proposed attractive transition-state interactions.

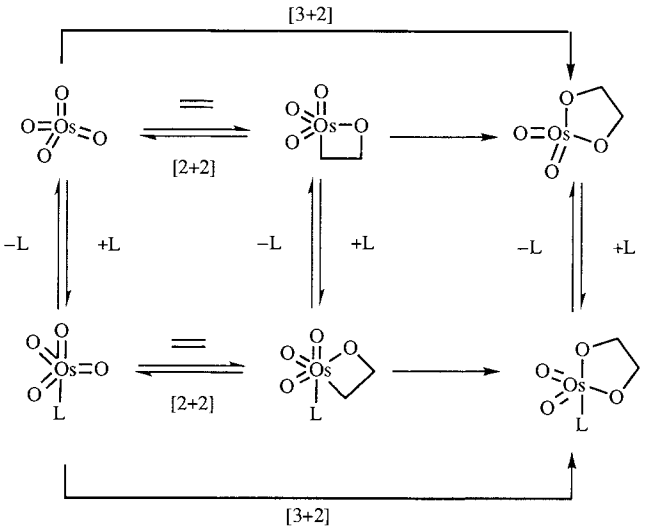
In summary, a balance must be struck in the binding ability of the ligand. The ligand must mediate the asymmetry-inducing step but must also allow efficient turnover to occur. This is where the many bidentate chiral amine ligands recently intro-

duced for asymmetric dihydroxylation fail.[54] They yield stable octahedral osmate ester complexes, and catalytic turnover is blocked. Ligand acceleration of the osmylation step by monodentate amines offers the unique opportunity for effective catalysis to be realized. By definition, ligand-accelerated reactions are less prone to the deleterious rate reductions usually encountered when architecturally complex ligands are used. In fact, in the AD the more complex ligands actually enhance the reactivity!

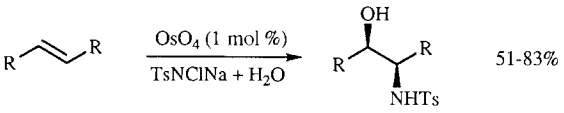
The origin of the acceleration effect is irrevocably linked with the remaining uncertainties about the mechanism of the osmylation step (Scheme 12). Kinetic studies[55, 67] on the AD do not prescribe whether a [3+2][68] or a [2+2][69] pathway is involved. Nonetheless, temperature effects,[70] Gable's strong evidence for an intermediate in the extrusion of olefins from rhenium glycolates,[71] and theoretical studies[55, 72] encourage us in our preference for the metallaoxetane [2+2] pathway.

Given the often near perfect enantioselection of the AD, the enforced proximity of the ligand and olefin in the [2 + 2] mechanism is a powerful argument in favor of that pathway. The significant rate accelerations documented here may be attributed to either a) the formation of an osmium tetraoxide–alkaloid complex which is more reactive[68] than unbound osmium tetraoxide, or b) the trapping of a transitory[73] metallaoxetane[74] by the alkaloid ligand and subsequent oxygen insertion into the metal–carbon bond.[75] We believe that our evidence[70] for a process with at least two enantioselectivity-determining steps (weighted differentially according to temperature) lends credence to the latter rationale.

A close relative of the dihydroxylation reaction is the vicinal oxyamination[76] of olefins (Scheme 13). It seems likely that the mechanisms, and therefore also the ligand-acceleration effects, operating in both processes are intimately linked. Oxyamination can be performed either using stoichiometric quantities of trioxo(*tert*-butylimido)osmium[77] or catalytic amounts of osmium



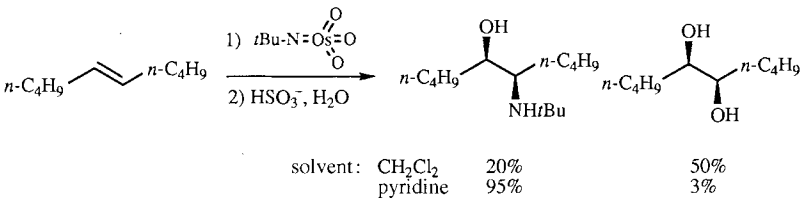
Scheme 12. Plausible mechanistic pathways for the AD of olefins (shown for ethylene).



Scheme 13. Catalytic oxyamination of olefins [78].

tetraoxide in the presence of Chloramine-T or argentochlorocarbamates.[78]

Investigation of the stoichiometric reactions with trioxo(*tert*-butylimido)osmium revealed[76] remarkable effects upon addition of a ligand (Scheme 14). In the absence of pyridine or quinuclidine, a major competing pathway is the formation of *cis* diols. In a noncoordinating solvent, reaction[76] of trioxo(*tert*-butylimido)osmium with (*E*)-5-decene affords a 5:2 ratio of diol:amino alcohol. When pyridine is the solvent, the ratio swings dramatically to 3:95 in favor of the amino alcohol. The ligand completely alters the reaction path, enhancing the



Scheme 14. Effect of the ligand on stoichiometric oxyamination of (*E*)-5-decene [76].

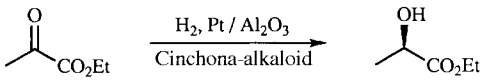
formation of amino alcohol. In addition, the overall reaction rate is increased.

Unlike the asymmetric dihydroxylation (AD), asymmetric oxyamination (AOA) is virtually unexplored,[79] but up to 92% *ee* has been achieved[80, 81] in a stoichiometric reaction of trioxo(*tert*-butylimido)osmium with stilbene in the presence of DHQD-CLB at ambient temperature. The catalytic process with an argentochlorocarbamate[80] gives a 63% *ee* with stilbene. However, turnover in these catalytic asymmetric oxyaminations is very slow, and unless it can be improved they will not be of interest in organic synthesis.

4.2 Asymmetric Hydrogenations

Ligand-accelerated processes require the in situ selection of a catalyst from many possible interconverting structures. When ligands are strongly bound to the metal, in situ selection becomes irrelevant. This is the case in catalyzed homogeneous hydrogenations[11] when bidentate phosphane ligands[8, 9] are used. They have uniformly high binding constants for the transition metal. Hence it is impossible for ligand-acceleration to be involved, and the concept of LAC is not applicable. However, a striking example of ligand-accelerated catalysis has been discovered in an important *heterogeneous* hydrogenation process.

Blaser and co-workers at Ciba-Geigy developed a remarkably effective process for the enantioselective hydrogenation of α-ketoesters (Scheme 15).[82–85] This reaction had first been described by Orito et al.[82] who investigated the use of cinchona-modified heterogeneous platinum catalysts for asymmetric reductions. Reactivity and enantioselectivity are strongly de-



Scheme 15. Heterogeneous asymmetric hydrogenation.

pendent on catalyst pretreatment and on the presence of various additives in the reaction mixture.

Catalysts modified with cinchona alkaloids were up to 100 times more active than ligand-free catalysts used as the reference.[83b] Only small amounts of cinchonidine were needed to give optimal enantioselectivity. As in the asymmetric dihydroxylation, higher alkaloid concentrations were required to obtain rate saturation (Fig. 3).

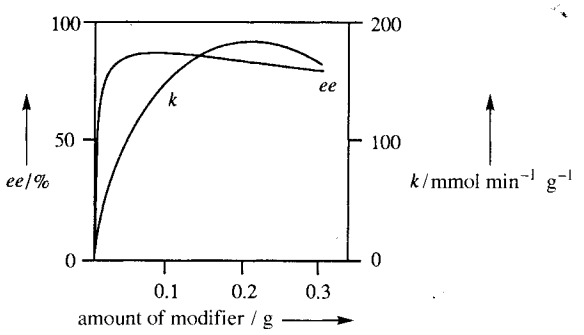


Fig. 3. Heterogeneous asymmetric hydrogenation: dependence of enantiomeric excess *ee* [%] and rate *k* [mmol min^{-1} g^{-1}] on concentration of the alkaloid modifier [g] [83b].

No correlation was found between enantioselectivity and total or metal surface area.[83b] Although the rate acceleration tends to depend on the basicity of the additive,[84] the cinchona alkaloids show a stronger effect than additives of comparable pK_a. A kinetic model describing the effect of the alkaloid modifier on *ee* and reaction rate was developed.[83a, 85] Analysis of the model predicts the linear relationship between the enantiomeric excess and the reciprocal of the rate that was indeed observed. Reversible adsorption of the alkaloid on the metal surface is thought to promote an interaction with the prochiral α-ketoesters leading to enantioselection and enhanced activity of the modified metal centers or active sites. Apparently, alkaloids do *not* block unselective catalyst sites (a negative effect) as proposed for modifiers in related heterogeneous hydrogenation catalysts containing nickel tartrate.[86] Stereoselectivity and enhanced catalytic activity may result from well-defined interactions between the platinum surface and individual cinchona molecules[85] or, as suggested by Thomas,[87] from a highly ordered, well-spaced array of modifier molecules in the sorbed layer. For higher alkaloid concentrations the observed effects were rationalized by invoking two- and three-site models.[85, 88, 89]

5. Summary and Outlook

Given the enormous variety offered by the periodic table and especially the dominance of metallic elements along with their special ability to enhance reactivity, metal-catalyzed reactions would seem to be pivotal in the development of viable synthetic strategies. The powerful phenomenon of ligand-accelerated catalysis offers great promise. No doubt serendipity will play a significant role in further discoveries, since predictions regarding catalysis are often wrong. We recall with humility the unproductive foray into the synthesis and application of tridentate chiral ligands for vanadium-catalyzed asymmetric epoxidation.[1c] This, of course, was prior to our realization that this approach is irrelevant for the reasons outlined in this article. The appeal of ligand-accelerated catalysis, albeit extremely rare and difficult to find, is the arresting efficiency it can possess. Not to be overlooked is the often unique window on fundamental aspects of mechanism that is afforded by the discovery of a ligand-accelerated variant of a reaction. We look forward to the new selective catalysts, still lying undiscovered, that all of us will be able to share.

We are especially grateful to the colleagues and friends who gave us excellent advice and help during writing of this review. We particulary thank Professors M. G. Finn (Charlottesville), R. W. Hoffmann (Marburg), E. N. Jacobsen (Cambridge), and Drs. P.-O. Norrby (Copenhagen), S. Loren (La Jolla), P. T. Ho (La Jolla), H. Kolb (Basel), and H.-U Blaser (Basel) for their suggestions, comments and helpful discussions. K.B.S. thanks the National Institutes of Health (GM-28384), the National Science Foundation (CHE-9296055), and the W. M. Keck Foundation for financial support. D.J.B. and C.B. thank SERC-NATO and the Fonds der Chemischen Industrie, respectively, for funding and fellowships.

Received: September 12, 1994 [A 83 IE]
German version: *Angew. Chem.* **1995**, *107*, 1159

[1] a) T. Katsuki, K. B. Sharpless, *J. Am. Chem. Soc.* **1980**, *102*, 5974; b) K. B. Sharpless, *Chem. Brit.* **1986**, *22*, 38; c) *Proc. Robert A. Welch Found. Conf. Chem. Res.* **1984**, *27*, 59; d) *CHEMTECH* **1985**, *15*, 692.

[2] a) M. G. Finn, K. B. Sharpless in *Asymmetric Synthesis, Vol. 5* (Ed.: J. D. Morrison), Academic Press, New York, **1985**, p. 247; b) S. S. Woodard, M. G. Finn, K. B. Sharpless, *J. Am. Chem. Soc.* **1991**, *113*, 106; c) M. G. Finn, K. B. Sharpless, *ibid.* **1991**, *113*, 113.

[3] a) R. A. Johnson, K. B. Sharpless in Ref. [9b], S. 103; b) B. E. Rossiter in *Asymmetric Synthesis, Vol. 5* (Ed.: J. D. Morrison), Academic Press, New York, **1985**, S. 193; c) A. Pfenninger, *Synthesis* **1986**, 89; d) Y. Gao, R. M. Hanson, J. M. Klunder, S. Y. Ko, H. Masamune, K. B. Sharpless, *J. Am. Chem. Soc.* **1987**, *109*, 5765; e) V. S. Martin, S. S. Woodward, T. Katsuki, Y. Yamada, M. Ikeda, K. B. Sharpless, *ibid.* **1981**, *113*, 6237; f) S. Y. Ko, H. Masamune, K. B. Sharpless, *J. Org. Chem.* **1987**, *52*, 667; g) S. Y. Ko, K. B. Sharpless, *ibid.* **1986**, *51*, 5413; h) J. M. Klunder, S. Y. Ko, K. B. Sharpless, *ibid.* **1986**, *51*, 3710; i) C. H. Behrens, S. Y. Ko, K. B. Sharpless, F. J. Walker, *ibid.* **1985**, *50*, 5687; j) C. H. Behrens, K. B. Sharpless, *ibid.* **1985**, *50*, 5696; k) M. Caron, K. B. Sharpless, *ibid.* **1985**, *50*, 1557; l) J. M. Chong, K. B. Sharpless, *ibid.* **1985**, *50*, 1560; m) C. E. Adams, F. J. Walker, K. B. Sharpless, *ibid.* **1985**, *50*, 420.

[4] S. G. Hentges, K. B. Sharpless, *J. Am. Chem. Soc.* **1980**, *102*, 4263.

[5] a) E. N. Jacobsen, I. Markó, W. S. Mungall, G. Schröder, K. B. Sharpless, *J. Am. Chem. Soc.* **1988**, *110*, 1968; b) E. N. Jacobsen, I. Markó, M. B. France, J. S. Svendsen, K. B. Sharpless, *ibid.* **1989**, *111*, 737.

[6] The activation of a stoichiometric reagent by a ligand is considered as "ligand acceleration". To be a *ligand-accelerated catalysis* (LAC) a catalytically active species (other than the ligand) must be present.

[7] For a very well studied example of a ligand-accelerated stereoselective reaction, see W. Klute, R. Dress, R. W. Hoffmann, *J. Chem. Soc. Perkin Trans 2*, **1993**, 1409.

[8] a) H. Brunner, W. Zettlmeier, *Handbook of Enantioselective Catalysis, 2 Vols.*, VCH, Weinheim, **1994**; b) H. Brunner, *Top. Stereochem.* **1988**, *18*, 129.

[9] a) R. Noyori, *Asymmetric Catalysis in Organic Synthesis*, Wiley, New York, **1994**; b) *Catalytic Asymmetric Synthesis* (Ed.: I. Ojima), VCH, New York, **1993**; c) R. Noyori, M. Kitamura in *Modern Synthetic Methods, Vol. 5* (Ed.: R. Scheffold), Springer, Berlin, **1989**, p. 115; d) R. Noyori, *Chem. Soc. Rev.* **1989**, *18*, 187; e) H. Brunner, *Pure Appl. Chem.* **1990**, *62*, 589; f) R. Noyori, *Science* **1990**, *248*, 1194; g) H. Brunner, *Synthesis* **1988**, 645; h) D. A. Evans, *Science* **1988**, *240*, 420; i) J. M. Brown, S. G. Davies, *Nature (London)* **1989**, *342*, 631; j) I. Ojima, N. Clos, C. Bastos, *Tetrahedron* **1989**, *45*, 6901.

[10] R. Noyori, H. Takaya, *Chem. Scr.* **1985**, *25*, 83.
[11] a) R. Noyori, H. Takaya, *Acc. Chem. Res.* **1990**, *23*, 345; b) H. Takaya, T. Ohta, R. Noyori in Ref. [9b], p. 1; c) R. Noyori, *CHEMTECH* **1992**, 360; d) *Tetrahedron* **1994**, *50*, 4259; e) K. Mashima, K. Kusano, N. Sato, Y. Matsumura, K. Nozaki, H. Kumobayashi, N. Sayo, Y. Hori, T. Ishizaki, S. Akutagawa, H. Takaya, *J. Org. Chem.* **1994**, *59*, 3064.
[12] a) D. C. Bradley, R. C. Mehrotra, D. P. Gaur, *Metal Alkoxides*, Academic Press, New York, **1978**, Kap. 4; b) R. J. H. Clark, *The Chemistry of Titanium and Vanadium*, Elsevier, Amsterdam, **1968**; c) T. J. Boyle, N. W. Eilerts, J. A. Heppert, F. Takusagawa, *Organometallics* **1994**, *13*, 2218.
[13] K. B. Sharpless, *Chem. Scr.* **1987**, *27*, 521.
[14] If the in situ self-assembly leads to more than one catalytically active chiral species, cooperative or counteracting stereochemical effects may result. Even in the worst cases, ligand acceleration can enable the desired transformation to occur in a rapid and highly stereoselective manner.
[15] a) I. D. Williams, S. F. Pedersen, K. B. Sharpless, S. J. Lippard, *J. Am. Chem. Soc.* **1984**, *106*, 6430; b) S. F. Pedersen, J. C. Dewan, R. R. Eckman, K. B. Sharpless, *ibid.* **1987**, *109*, 1279.
[16] For the catalytic version of the asymmetric epoxidation, see R. M. Hanson, K. B. Sharpless, *J. Org. Chem.* **1986**, *51*, 1922.
[17] K. B. Sharpless, *Tetrahedron* **1994**, *50*, 4235.
[18] a) R. C. Michaelson, R. E. Palermo, K. B. Sharpless, *J. Am. Chem. Soc.* **1977**, *99*, 1990; b) K. B. Sharpless, T. R. Verhoeven, *Aldrichim. Acta* **1979**, *12*, 63.
[19] a) K. Tani, M. Hanafusa, S. Otsuka, *Tetrahedron Lett.* **1979**, 3017; b) S. Yamada, T. Mashiko, S. Terashima, *J. Am. Chem. Soc.* **1977**, *99*, 1988.
[20] a) L. D.-L. Lu, R. A. Johnson, M. G. Finn, K. B. Sharpless, *J. Org. Chem.* **1984**, *49*, 728; b) R. Choukroun, *Inorg. Chim. Acta* **1981**, *58*, 121.
[21] S. Miyano, L. D.-L. Lu, S. M. Viti, K. B. Sharpless, *J. Org. Chem.* **1983**, *48*, 3608.
[22] a) H. B. Kagan in ref. [9b], p. 203; b) H. B. Kagan, F. Rebière, *Synlett* **1990**, 643; c) P. Pitchen, E. Duñach, M. N. Deshmukh, H. B. Kagan, *J. Am. Chem. Soc.* **1984**, *106*, 8188.
[23] a) S. H. Zhao, O. Samuel, H. B. Kagan, *Tetrahedron* **1987**, *43*, 5135; b) S. Zhao, O. Samuel, H. B. Kagan, *Org. Synth.* **1989**, *68*, 49.
[24] F. Di Furia, G. Modena, R. Seraglia, *Synthesis* **1984**, 325.
[25] N. Komatsu, M. Hashizume, T. Sugita, S. Uemura, *J. Org. Chem.* **1993**, *58*, 4529, 7624.
[26] a) K. Narasaka, *Synthesis* **1991**, 1; b) D. Seebach, *Angew. Chem.* **1990**, *102*, 1363; *Angew. Chem. Int. Ed. Engl.* **1990**, *29*, 1320; c) R. Noyori, S. Suga, K. Kawai, S. Okada, M. Kitamura, *Pure Appl. Chem.* **1988**, *60*, 1597; d) K. Marouka, H. Yamamoto in ref. [9b], p. 413; e) *Comprehensive Organic Synthesis, Vols. 1, 2* (Eds.: B. M. Trost, I. Fleming), Pergamon, Oxford, **1991**. See also ref. [8, 9].
[27] For an excellent review on chiral titanium reagents and catalysts, see R. O. Duthaler, A. Hafner, *Chem. Rev.* **1992**, *92*, 807.
[28] a) M. Yoshioka, T. Kawakita, M. Ohno, *Tetrahedron Lett.* **1989**, *30*, 1657; b) H. Takahashi, T. Kawakita, M. Yoshioka, S. Kobayashi, M. Ohno, *ibid.* **1989**, *30*, 7095; c) H. Takahashi, T. Kawakita, M. Ohno, M. Yoshioka, S. Kobayashi, *Tetrahedron* **1992**, *48*, 5691.
[29] a) B. Schmidt, D. Seebach, *Angew. Chem.* **1991**, *103*, 100; *Angew. Chem. Int. Ed. Engl.* **1991**, *30*, 99; b) D. Seebach, L. Behrendt, D. Felix, *ibid.* **1991**, *103*, 991 and **1991**, *30*, 1008; c) B. Schmidt, D. Seebach, *ibid.* **1991**, *103*, 1383 and **1991**, *30*, 1321; d) D. Seebach, D. A. Plattner, A. K. Beck, Y. M. Wang, D. Hunziker, W. Pettner, *Helv. Chim. Acta* **1992**, *75*, 2171; e) J. L. von dem Bussche-Hünnefeld, D. Seebach, *Tetrahedron* **1992**, *48*, 5719; f) D. Seebach, A. K. Beck, B. Schmidt, Y. M. Wang, *ibid.* **1994**, *50*, 4363; g) B. Weber, D. Seebach, *ibid.* **1994**, *50*, 7473.
[30] a) M. J. Rozema, A. Sidduri, P. Knochel, *J. Org. Chem.* **1992**, *57*, 1956; b) W. Brieden, R. Ostwald, P. Knochel, *Angew. Chem.* **1993**, *105*, 629; *Angew. Chem. Int. Ed. Engl.* **1993**, *32*, 582; c) M. J. Rozema, C. Eisenberg, H. Lütjens, R. Ostwald, K. Belyk, P. Knochel, *Tetrahedron Lett.* **1993**, *34*, 3115; d) S. Nowotny, S. Vettel, P. Knochel, *ibid.* **1994**, *35*, 4539; e) C. Eisenberg, P. Knochel, *J. Org. Chem.* **1994**, *59*, 3760; f) R. Ostwald, P.-Y. Chavant, H. Stadtmüller, P. Knochel, *ibid.* **1994**, *59*, 4143. For a review of functionalized organozinc reagents, see g) P. Knochel, R. D. Singer, *Chem. Rev.* **1993**, *93*, 2117. Functionalized organozincs have been used in the amino alcohol catalyzed reaction: h) W. Oppolzer, R. N. Radinov, *Tetrahedron Lett.* **1991**, *32*, 5777; i) *Helv. Chim. Acta* **1992**, *75*, 170; j) *J. Am. Chem. Soc.* **1993**, *115*, 1593.
[31] The normal catalyst loadings are 8 mol% for the additions of the functionalized organozinc complexes [30a–g].
[32] a) N. Iwasawa, Y. Hayashi, H. Sakurai, K. Narasaka, *Chem. Lett.* **1989**, 1581; b) K. Narasaka, K. Hayashi, Y. Hayashi, *Tetrahedron* **1994**, *50*, 4507, and references therein.
[33] β-Naphthyl appears optimal; α-naphthyl is too hindered, and both the rate and *ee* suffer [29]. A similar effect was reported by Oguni in the enantioselective opening of *meso* epoxides by Me_3SiN_3 catalyzed by titanium/tartrate mixtures. The complex derived from di-*tert*-butyltartrate ester effected enantioselective catalysis, whereas the catalyst prepared with the diisopropyl ester was only effective under stoichiometric conditions: M. Hayashi, K. Kohmura, N. Oguni, *Synlett* **1991**, 774.
[34] Use of a more hindered alkoxide, for example $[Ti(OtBu)_4]$, in stoichiometic quantities disrupts the relative rates of exchange between chiral and achiral complexes and has a deleterious effect on *ee*. Related effects have been noted in the kinetic resolution of allylic alcohols by titanium alkoxide/tartrate mixtures: B. H. McKee, T. H. Kalantar, K. B. Sharpless, *J. Org. Chem.* **1991**, *56*, 6966.
[35] A. L. Costa, M. G. Piazza, E. Tagliavini, C. Trombini, A. Umani-Ronchi, *J. Am. Chem. Soc.* **1993**, *115*, 7001.
[36] G. E. Keck, K. N. Tarbet, L. S. Geraci, *J. Am. Chem. Soc.* **1993**, *115*, 8467; b) G. E. Keck, D. Krishnamurthy, M. C. Grier, *J. Org. Chem.* **1993**, *58*, 6543; c) G. E. Keck, L. S. Geraci, *Tetrahedron Lett.* **1993**, *34*, 7827.
[37] S. Aoki, K. Mikami, M. Terada, T. Nakai, *Tetrahedron* **1993**, *49*, 1783.
[38] For reviews on allylation and related topics, see: a) T. Bach, *Angew. Chem.* **1994**, *106*, 433; *Angew. Chem. Int. Ed. Engl.* **1994**, *33*, 417; b) Y. Yamamoto, N. Assao, *Chem. Rev.* **1993**, *93*, 2207.
[39] a) K. Mikami, M. Terada, T. Nakai, *J. Am. Chem. Soc.* **1990**, *112*, 3949; b) K. Mikami, S. Narisawa, M. Shimizu, M. Terada, *ibid.* **1992**, *114*, 6566; c) K. Mikami, M. Terada, *Tetrahedron* **1992**, *48*, 5671; d) K. Mikami, S. Matsukawa, *Tetrahedron Lett.* **1994**, *35*, 3133; e) K. Mikami, M. Terada, S. Narisawa, T. Nakai, *Synlett* **1992**, 255. Review: f) K. Mikami, M. Shimizu, *Chem. Rev.* **1992**, *92*, 1021.
[40] I. Paterson, D. J. Berrisford, University of Cambridge, unpublished results.
[41] G. E. Keck, University of Utah, unpublished results; K. Mikami, Tokyo Institute of Technology, unpublished results.
[42] For recent results with a μ-oxo-titanium complex, see M. Terada, K. Mikami, *J. Chem. Soc. Chem. Commun.* **1994**, 833.
[43] K. Mikami, S. Matsukawa, *J. Am. Chem. Soc.* **1993**, *115*, 7039.
[44] K. Mikami, Y. Motoyama, M. Terada, *J. Am. Chem. Soc.* **1994**, *116*, 2812, and references therein.
[45] For recent reviews on asymmetric synthesis of cyanohydrins, see: a) M. North, *Synlett* **1993**, 807; b) F. Effenberger, *Angew. Chem.* **1994**, *106*, 1609; *Angew. Chem. Int. Ed. Engl.* **1994**, *33*, 1555.
[46] a) M. Hayashi, T. Inoue, Y. Miyamoto, N. Oguni, *Tetrahedron* **1994**, *50*, 4385; b) M. Hayashi, Y. Miyamoto, T. Inoue, N. Oguni, *J. Org. Chem.* **1993**, *58*, 1515; c) *J. Chem. Soc. Chem. Commun.* **1991**, 1752; d) M. Hayashi, T. Matsuda, N. Oguni, *ibid.* **1990**, 1364; e) *J. Chem. Soc. Perkin Trans. 1* **1992**, 3135.
[47] M. Hayashi, M. Tamura, N. Oguni, *Synlett* **1992**, 663.
[48] A. Mori, S. Inoue, *Chem. Lett.* **1991**, 145.
[49] a) H. Nitta, D. Yu, M. Kudo, A. Mori, S. Inoue, *J. Am. Chem. Soc.* **1992**, *114*, 7969; b) A. Mori, H. Nitta, M. Kudo, S. Inoue, *Tetrahedron Lett.* **1991**, *32*, 4333; c) H. Abe, H. Nitta, A. Mori, S. Inoue, *Chem. Lett.* **1992**, 2443; d) H. Ohno, H. Nitta, K. Tanaka, A. Mori, S. Inoue, *J. Org. Chem.* **1992**, *57*, 6778.
[50] a) R. Criegee, *Justus Liebigs Ann. Chem.* **1936**, *522*, 75; b) *Angew. Chem.* **1937**, *50*, 153; c) *Angew. Chem.* **1938**, *51*, 519; d) R. Criegee, B. Marchand, H. Wannowias, *Justus Liebigs Ann. Chem.* **1942**, *550*, 99, and references therein.
[51] a) K. B. Sharpless, W. Amberg, Y. L. Bennani, G. A. Crispino, J. Hartung, K.-S. Jeong, H.-L. Kwong, K. Morikawa, Z.-M. Wang, D. Xu, X.-L. Zhang, *J. Org. Chem.* **1992**, *57*, 2768; b) G. A. Crispino, K.-S. Jeong, H. C. Kolb, Z.-M. Wang, D. Xu, K. B. Sharpless, *ibid.* **1993**, *58*, 3785.
[52] Reports of other catalytic ADs: a) T. Oishi, M. Hirama, *Tetrahedron Lett.* **1992**, *33*, 639; b) Y. Imada, T. Saito, T. Kawakami, S.-I. Murahashi, *ibid.* **1992**, *33*, 5081.
[53] For recent process improvements and synthetic applications for the AD, see H. C. Kolb, M. S. VanNieuwenhze, K. B. Sharpless, *Chem. Rev.* **1994**, *94*, 2483.
[54] a) M. Tokles, J. K. Snyder, *Tetrahedron Lett.* **1986**, *27*, 3951; b) T. Yamada, K. Narasaka, *Chem. Lett.* **1986**, 131; c) K. Tomioka, M. Nakajima, K. Koga, *J. Am. Chem. Soc.* **1987**, *109*, 6213; d) R. Annunziata, M. Cinquini, F. Cozzi, L. Raimondi, S. Stefanelli, *Tetrahedron Lett.* **1987**, *28*, 3139; e) T. Oishi, M. Hirama, *J. Org. Chem.* **1989**, *54*, 5834; f) E. J. Corey, P. D. Jardine, S. Virgil, P.-W. Yuen, R. D. Connell, *J. Am. Chem. Soc.* **1989**, *111*, 9243; g) K. Tomioka, M. Nakajima, K. Koga, *Tetrahedron Lett.* **1990**, *31*, 1741; h) K. Fuji, K. Tanaka, H. Miyamoto, *ibid.* **1992**, *33*, 4021; i) S. Hanessian, P. Meffre, M. Girard, S. Beaudoin, J.-Y. Sancéau, Y. Bennani, *J. Org. Chem.* **1993**, *58*, 1991; j) M. Nakajima, K. Tomioka, Y. Iitaka, K. Koga, *Tetrahedron* **1993**, *49*, 10793; k) D. Tanner, P. G. Anderson, A. Harden, P. Somfai, *Tetrahedron Lett.* **1994**, *35*, 4631.
[55] a) H. C. Kolb, P. G. Andersson, K. B. Sharpless, *J. Am. Chem. Soc.* **1994**, *116*, 1278; b) P.-O. Norrby, H. C. Kolb, K. B. Sharpless, *ibid.* **1994**, *116*, 8470; c) D. W. Nelson, K. B. Sharpless, The Scripps Research Institute, unpublished results.
[56] K_{eq}(quinuclidine) = 80000 L mol^{-1} (toluene): H. C. Kolb, K. B. Sharpless, The Scripps Research Institute, unpublished results. Binding constants for the alkaloids DHQ and DHQD are greater in toluene than in *t*BuOH. The stoichiometric osmylations with bidentate chiral amines [54] are generally run at low temperature in toluene.
[57] a) The effect of tertiary amine ligands on the catalytic turnover in the original AD process with NMO as the oxidant in a homogeneous acetone/water system is quite different from that seen in the new two-phase AD process with potassium hexacyanoferrate(III) as the oxidant. In the NMO system, quinuclidine strongly inhibits the catalysis at concentrations above 0.01 M [5a], and even the

alkaloid ligands DHQ and DHQD begin to show inhibition at concentrations greater than 0.5 M [5b]. These effects are probably due to "second-cycle problems" [5b, 57b], which will not be discussed here since they are absent in the now favored potassium hexacyanoferrate(III)-based AD system. b) Y. Ogino, H. Chen, H.-L. Kwong, K. B. Sharpless, *Tetrahedron Lett.* **1991**, *32*, 3965.

[58] The commercial AD mixes use 0.4 mol% OsO_4 to ensure reproducible results. With slower reacting olefins the OsO_4 loading should be increased to 1 mol%.

[59] For example, the presence of the methoxy group on the quinoline ring (the difference between the quinine and cinchonine series) imparts an approximately twofold rate increase (k_c) for 2-vinylnaphthalene [55a].

[60] For a similar earlier proposal, see B. B. Lohray, V. Bhushan, *Tetrahedron Lett.* **1992**, *33*, 5113.

[61] a) J. M. Hawkins, A. Meyer, *Science* **1993**, *260*, 1918; b) J. M. Hawkins, A. Meyer, M. Nambu, *J. Am. Chem. Soc.* **1993**, *115*, 9844.

[62] Stacking interactions have been invoked as stereocontrolling elements in asymmetric Diels–Alder reactions: a) J. M. Hawkins, S. Loren, *J. Am. Chem. Soc.* **1991**, *113*, 7794; b) J. M. Hawkins, S. Loren, M. Nambu, *ibid.* **1994**, *116*, 1657; c) E. J. Corey, T.-P. Loh, T. D. Roper, M. D. Azimioara, M. C. Noe, *ibid.* **1992**, *114*, 8290; d) D. A. Evans, K. T. Chapman, D. T. Hung, A. T. Kawaguchi, *Angew. Chem.* **1987**, *99*, 1197; *Angew. Chem. Int. Ed. Engl.* **1987**, *26*, 1184; e) J. A. Tucker, K. N. Houk, B. M. Trost, *J. Am. Chem. Soc.* **1990**, *112*, 5465. Stacking interactions have also been invoked to rationalize the regioselectivity in asymmetric hydroformylation: f) L. A. Castenguay, A. K. Rappé, C. J. Casewit, *J. Am. Chem. Soc.* **1991**, *113*, 7177.

[63] For recent examples in which attractive van der Waals interactions play an important role, see: a) T. Harada, I. Wada, J. J. Uchimura, A. Inoue, S. Tanake, A. Oku, *Tetrahedron Lett.* **1991**, *32*, 1219; b) T. Harada, A. Oku, *Synlett* **1994**, 95; c) U. Berg, I. Pettersson, *J. Org. Chem.* **1987**, *52*, 5177.

[64] For leading references on stacking interactions, see: a) D. B. Smithrud, F. Diederich, *J. Am. Chem. Soc.* **1990**, *112*, 339; b) W. L. Jorgensen, D. L. Severance, *ibid.* **1990**, *112*, 4768; c) F. Cozzi, M. Cinquini, R. Annuziata, J. S. Siegel, *ibid.* **1993**, *115*, 5330; d) C. A. Hunter, *Chem. Soc. Rev.* **1994**, *23*, 101; e) G. Liang, R. Tribolet, H. Sigel, *Inorg. Chem.* **1988**, *27*, 2877; for π-dicarbonyl interactions, see: f) J. K. Whitesell, J. N. Younathon, J. R. Hurst, M. A. Fox, *J. Org. Chem.* **1985**, *50*, 5499.

[65] The attractive interactions are also manifest in the application of the device (Scheme 9) that aids prediction of the AD face selectivity. Predictions for 1,1-disubstituted olefins can seem ambiguous because one must know which of the substituents prefers to occupy the attractive SW quadrant [53]. The order of occupancy is aryl > alkyl > Me ≈ CH_2OR: cf. K. J. Hale, S. Manaviazar, S. A. Peak, *Tetrahedron Lett.* **1994**, *35*, 425.

[66] H. Becker, P. T. Ho, H. C. Kolb, S. Loren, P.-O. Norrby, K. B. Sharpless, *Tetrahedron Lett.* **1994**, *35*, 7315.

[67] H.-L. Kwong, Dissertation, Massachusetts Institute of Technology, Boston, USA, **1993**.

[68] a) K. A. Jørgensen, R. Hoffmann, *J. Am. Chem. Soc.* **1986**, *108*, 1867; b) E. J. Corey, M. C. Noe, S. Sarshar, *ibid.* **1993**, *115*, 3828.

[69] a) K. B. Sharpless, A. Y. Teranishi, J.-E. Bäckvall, *J. Am. Chem. Soc.* **1977**, *99*, 3120; b) A. K. Rappé, W. A. Goddard, *ibid.* **1982**, *104*, 3287.

[70] T. Göbel, K. B. Sharpless, *Angew. Chem.* **1993**, *105*, 1417; *Angew. Chem. Int. Ed. Engl.* **1993**, *32*, 1329.

[71] a) K. P. Gable, T. N. Phan, *J. Am. Chem. Soc.* **1993**, *115*, 3036; b) *ibid.* **1994**, *116*, 833.

[72] a) P.-O. Norrby, H. C. Kolb, K. B. Sharpless, *Organometallics* **1994**, *13*, 344; b) A. Veldkamp, G. Frenking, *J. Am. Chem. Soc.* **1994**, *116*, 4937. The [3 + 2] mechanism is being examined by a theoretical approach: S. Niwayama, K. N. Houk, University of California, Los Angeles, unpublished results.

[73] a) To be observed the metallacycle must be formed rapidly and rearrange slowly. For X-ray crystallographic analysis of metallaoxetanes, see: a) Mo: G. C. Bazan, R. R. Schrock, M. B. O'Regan, *Organometallics* **1991**, *10*, 1062; b) Cr: J. Sundermeyer, K. Weber, H. Pritzkow, *Angew. Chem.* **1993**, *105*, 751; *Angew. Chem. Int. Ed. Engl.* **1993**, *32*, 731; ref.[44]. However, we have not observed metallaoxetanes in the osmylation using matrix isolation techniques: D. V. McGrath, G. D. Brabson, L. Andrews, K. B. Sharpless, The Scripps Research Institute, unpublished results.

[74] K. A. Jørgensen, B. Schiøtt, *Chem. Rev.* **1990**, *90*, 1483.

[75] Norbornene undergoes ring-opening metathesis polymerization with OsO_4, an observation that can be rationalized by invoking a metallaoxetane: J. G. Hamilton, O. N. D. Mackey, J. J. Rooney, D. G. Gilheany, *J. Chem. Soc. Chem. Commun.* **1990**, 1600.

[76] K. B. Sharpless, D. W. Patrick, L. K. Truesdale, S. A. Biller, *J. Am. Chem. Soc.* **1975**, *97*, 2305.

[77] S. G. Hentges, K. B. Sharpless, *J. Org. Chem.* **1980**, *45*, 2257.

[78] a) K. B. Sharpless, A. O. Chong, K. Oshima, *J. Org. Chem.* **1976**, *41*, 177; b) E. Herranz, K. B. Sharpless, *ibid.* **1978**, *43*, 2544; c) E. Herranz, S. A. Biller, K. B. Sharpless, *J. Am. Chem. Soc.* **1978**, *100*, 3596.

[79] B. B. Hassine, M. Gorsane, J. Pecher, R. H. Martin, *Bull. Soc. Chim. Belg.* **1985**, *94*, 759.

[80] C. Burns, D. Gilheany, C. Y. Park, K. B. Sharpless, The Scripps Research Institute, unpublished results.

[81] For a recent investigation, see H. Rubinstein, J. S. Svendsen, *Acta Chem. Scand.* **1994**, *48*, 439.

[82] a) Y. Orito, S. Imai, S. Niwa, G.-H. Nguyen, *Yuki Gosei Kagaku Kyokaishi* **1979**, *37*, 173; b) Y. Orito, S. Imai, S. Niwa, *Nippon Kagaku Kaishi* **1979**, 118; c) *ibid.* **1980**, 670; d) *ibid.* **1982**, 137; e) I. M. Sutherland, A. Ibbotson, R. B. Moyes, P. B. Wells, *J. Catal.* **1990**, *125*, 77.

[83] a) M. Garland, H.-U. Blaser, *J. Am. Chem. Soc.* **1990**, *112*, 7048; b) H.-U. Blaser, H. P. Jalett, D. M. Monti, J. F. Reber, J. T. Wehrli, *Stud. Surf. Sci. Catal.* **1988**, *41*, 153; c) H.-U. Blaser, H. P. Jalett in *Heterogeneous Catalysis and Fine Chemicals III* (Ed.: M. Guisnet), Elsevier, Amsterdam, **1993**, p. 139; d) J. T. Wehrli, A. Baiker, D. M. Monti, H.-U. Blaser, H. P. Jalett, *J. Mol. Catal.* **1989**, *57*, 245; e) J. T. Wehrli, A. Baiker, D. M. Monti, H.-U. Blaser, *ibid.* **1990**, *61*, 207.

[84] H.-U. Blaser, H. P. Jalett, J. Wiehl, *J. Mol. Catal.* **1991**, *68*, 215.

[85] H.-U. Blaser, M. Garland, H. P. Jallet, *J. Catal.* **1993**, *144*, 569.

[86] a) M. Bartok, *Stereochemistry in Heterogeneous Metal Catalysis*, Wiley, New York, **1985**, p. 511; b) H.-U. Blaser, *Tetrahedron: Asymmetry* **1991**, *2*, 843; c) H.-U. Blaser, M. Müller, *Stud. Surf. Sci. Catal.* **1991**, *59*, 73.

[87] a) J. M. Thomas, *Angew. Chem. Adv. Mater.* **1989**, *101*, 1105; *Angew. Chem. Int. Ed. Engl. Adv. Mater.* **1989**, *28*, 1079; b) *Angew. Chem.* **1994**, *106*, 963; *Angew. Chem. Int. Ed. Engl.* **1994**, *33*, 913.

[88] H.-U. Blaser, Ciba Geigy AG, Basel, unpublished results.

[89] For a recent study describing enhanced hydrogenation rates with novel alkaloid-modified Pt catalysts, see: S. P. Griffiths, P. Johnston, W. A. H. Vermeer, P. B. Wells, *J. Chem. Soc. Chem. Commun.* **1994**, 2431.

On the Synthesis of the FeMo Cofactor of Nitrogenase: Gene-Controlled in Nature versus Laboratory-Produced by Man

Achim Müller* and Eugen Krahn

One of the primary challenges of chemistry is the controlled synthesis of compounds with tailor-made structures and properties. Natural products serve as inspiration in this quest, ranging from biocatalysts with optimal selectivity and activity to "inorganic materials" with exceptional properties, whose generation can be described by the term biomineralization. It is of fundamental importance to comprehend the courses of events at the interface between gene expression and the subsequent processes of epigenesis that are no longer under gene control. Chemistry has been able to achieve many goals; however, in the area of controlled syntheses of highly complex, tailor-made metal clusters, there is a lack of fundamental theories and principles. This is especially true for the fascinating metal–sulfur cluster of nitrogenase, which, in this enzyme, functions as the active center for the N_2 reduction and, so far, has eluded all attempts to be synthesized in the laboratory. To understand the biosynthesis of this cluster, information from genetics *and* chemistry must be combined.

Keywords: bioinorganic chemistry · biosynthesis · iron–molybdenum cofactor · iron–sulfur cluster · nitrogenases · nitrogen fixation

The fixation of nitrogen from the air will be one of the great discoveries, which are awaiting the ingenuity of chemists.
Sir William Crookes, 1898[**]

1. Introduction

In spite of innumerable attempts, it has not yet been possible to synthesize the iron–molybdenum cofactor (FeMo cofactor) that is central to the bacterial fixation of nitrogen by the nitrogenase enzyme system. This synthesis would be a groundbreaking contribution to the efforts made to adapt the "natural Haber–Bosch process", that is, the action of biological nitrogen fixation, which, together with photosynthesis, is the most important natural process for food production. The desire to gain a deeper understanding of this fundamental metabolic process stems from the dream to improve the extremely energy-intensive industrial procedure. In contrast, however, it is virtually impossible to prevent the formation of chemically similar clusters, particularly those with an $[Fe_4S_4]^{2+}$ core, once the basic constituents are present. What is the reason for this apparent contradiction? Exciting results from genetic investigations, which, in chemical circles, have not received as much attention as those obtained from crystallographic studies, have begun to yield an emerging picture of how nature proceeds with the synthesis of this cluster. The analysis of the results of genetic studies, however, could be of prime importance for the successful synthesis "in the test-tube", as they yield hints regarding the special conditions employed for the stepwise synthesis: the in vivo synthesis of the FeMo cofactor of the nitrogenase enzyme system is so far the only biosynthesis of an inorganic cluster known to proceed by enzymatically catalyzed intermediate steps.

The numerous attempts to synthesize chemically the FeMo cofactor were hampered for a long time by the fact that only the approximate composition, and not the exact structure of this cluster was known.[1] In this context, the limits of current chemical understanding became apparent, as it proved to be impossible to determine the structure of this cluster, which is relatively small from the standpoint of a chemist, despite the application of all modern chemical knowledge, especially in combination with the availability of virtually all imaginable spectroscopic data.

Then a report came that spread like wildfire among scientists—and even appeared in the daily newspapers: based on X-ray crystal structure analyses, it was possible to successfully model the spatial structure of both components of nitrogenase, including the almost legendary cluster centers. This structural analysis also made known the exact position and the protein environment of the clusters in the MoFe protein (Fig. 1).[2] The so-called Kim model of the FeMo cofactor showed—much to the disappointment of chemists—that none of the previous models exhibited the determined structure; however, a fascinating chemistry was developed, stimulated by the endeavor to obtain the FeMo cofactor synthetically (see below). The struc-

[*] Prof. Dr. A. Müller, E. Krahn
Fakultät für Chemie der Universität
Lehrstuhl für Anorganische Chemie I
Postfach 100131, D-33501 Bielefeld (Germany)
Telefax: Int. code + (521)106-6003

[**] The gist of a statement made by Sir William Crookes in response to the doomsday saying at the end of the 19th century: "England and all civilized nations are facing the mortal danger of not having enough food."

 © *VCH Verlagsgesellschaft mbH, D-69451 Weinheim, 1995* *0570-0833/95/1010-1071 $ 10.00+.25/0*

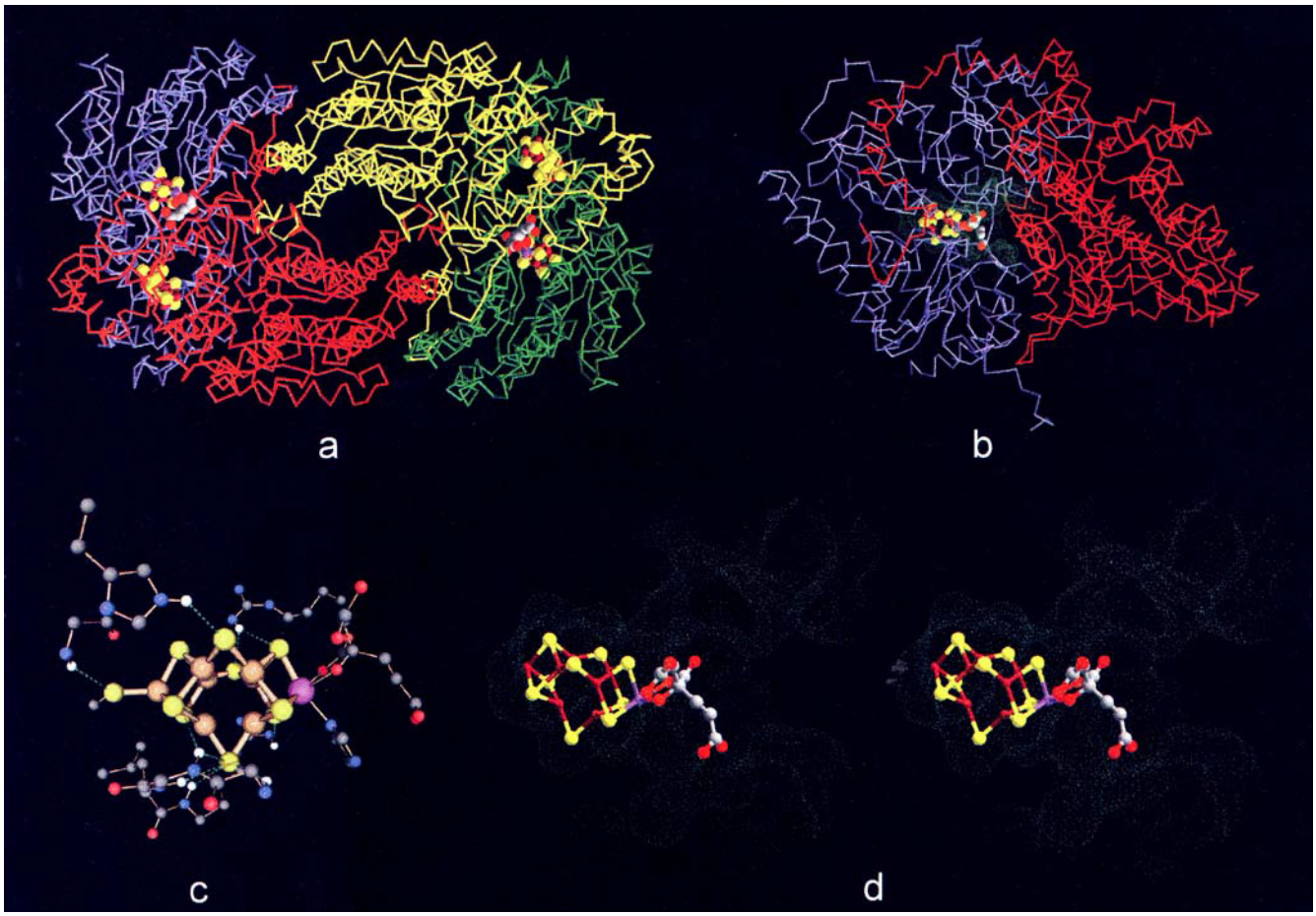


Fig. 1. a) Protein chains (only α-carbon atoms are shown) and cluster centers of the MoFe protein (α-subunits: blue and green; β-subunits: yellow and red). b) Protein chains (only α-carbon atoms) of one α and one β-subunit, including the FeMo cofactor and its protein environment within the α-subunit (represented as a segment of the water-accessible surface (see text) of the α-subunit). c) Structure of the FeMo cofactor including amino acid side chains from its protein environment, which are coordinatively bound or form hydrogen bonds to it (hydrogen bonds: green, dashed lines; Fe: brown, S: yellow, Mo: violet, C: gray, O: red, N: blue). d) Stereoscopic view of the FeMo cofactor and the water-accessible surface of its protein environment.

ture of the cofactor (Fig. 1c, d) formally consists of an Fe_4S_3 and a $MoFe_3S_3$ cubane fragment, which are linked by three (inorganic) sulfide ligands. The composition $MoFe_7S_9$/homocitrate and its unusual structure—particularly the six Fe centers that are in a nearly trigonal environment and, hence, are coordinatively unsaturated—make the FeMo cofactor the largest and most complex metal cluster in the biosphere that is known to exist in enzymes.

In spite of the above-mentioned detailed structural information, many essential features of the nitrogenase enzyme system are



Achim Müller, born in 1938 in Detmold, studied chemistry and physics at the University of Göttingen and received his Ph. D. (1965) and his Habilitation (1967) there under the supervision of O. Glemser. He is now Professor of Inorganic Chemistry at the University of Bielefeld. He is a member of several scientific academies, including the Deutsche Akademie für Naturforscher (Leopoldina) and the Polish Academy of Sciences. His research interests range from problems of molecular physics (theory of mass influence on molecular constants), vibrational spectroscopy (matrix isolation spectroscopy, band contour analysis, resonance Raman effect, metal isotope effects), bioinorganic chemistry (model compounds and biological nitrogen fixation by free-living organisms), and molecular metal chalcogenide complexes and clusters (synthesis, geochemical relevance, electronic and molecular structure, topological and supermolecular aspects, and use in heterogeneous catalysis) to aspects of natural philosophy. He has published, besides numerous original papers, more than 30 reviews in these areas and is coeditor of eight books.

not yet understood.[8] Only very little is known about the mechanism of the catalysis. Even the question of the binding sites of the various substrates remains unanswered, as well as the one concerning the structure of reaction intermediates. In addition to the mechanistic aspects, the following are of interest:

- How does the biosynthesis of the cluster occur, that is, where are the elements that constitute the FeMo cofactor (Fe^{n+}, Mo^{n+}, S^{2-}, and homocitrate) introduced into the biosynthetic pathway? Are there any preassembled units involved and which intermediates occur?
- How does nature stabilize the structure of the FeMo cofactor—especially with regard to the six coordinatively unsaturated Fe centers—and the possible intermediates in the biosynthesis? Is an in vitro synthesis fundamentally impossible or has it only not yet been achieved? Which new concepts are required to mimic nature in this context?

The answers to these questions are also of a more general relevance, as they will certainly be able to provide contributions towards the understanding of the in vivo formation of metal clusters that occur in the active center of other enzymes. There are very few details known about the biosynthesis of a number of different binary FeS clusters with the compositions $\{Fe_2S_2\}$, $\{Fe_3S_4\}$, $\{Fe_4S_4\}$,[9] and $\{Fe_6S_6\}$.[10, 11] The same is true for the Mn_xO_y cluster of photosystem II.[12]

2. Why Is the Cluster Synthesis of the FeMo Cofactor In Vitro so Difficult?

The one-pot synthesis of MoFeS clusters, especially those containing only one Mo atom is a non-trivial problem. The difficulties most encountered are as follows:

- maintaining the desired oxidation states—in particular for the molybdenum centers—in the presence of redox-active ligands such as S^{2-};[13]
- controlling the configuration, for example during the formation of a *fac*-environment around the Mo center;
- avoiding the formation of polynuclear Mo species, a tendency favored by the inclination of the S^{2-} and O^{2-} ligands to form bridges and of molybdenum in low oxidation states to form metal–metal bonds;
- generating specific low coordination numbers at the metal and sulfur centers;
- bypassing the formation of cubane-type systems if non-cubane structures—like the FeMo cofactor—are desired.

The most stable FeS clusters are those of the type Fe_4S_4. Bridged cubane systems, are also accessible (compare for example the synthesis of $[(Fe_4S_4Cl_3)_2S]^{4-}$[14]). The first reported MoFeS species that were synthesized as model compounds for the active center of the MoFe protein were prepared by "strict self-assembly" (SSA), given the appropriate reaction conditions. These compounds are mostly heteroatom analogues or derivatives of the more readily accessible binary FeS clusters mentioned above. The resulting compounds are, for instance, of the double-cubane type $[(MoFe_3S_4)_2(SR)_3]$.[15] It took several years of intensive work from the first synthesis of a double-cubane type species to the successful preparation of the corresponding monocubane type species—containing only one $MoFe_3S_4$ center—by solvent-induced cleavage of a double-cubane system.[16] This long delay stemmed primarily from the difficulties mentioned above, particularly from the strong tendency of the Mo centers to form metal–metal bonds. In addition to the Fe_4S_4 core, Fe_2S_2, Fe_3S_4, and (probably) Fe_6S_6 centers, all of which are known from iron–sulfur chemistry, can be found within metalloenzymes. Due to the comparatively lower formation tendency of these clusters, their syntheses require that specific conditions are maintained.[17] A reaction type that seems to be important for considerations on the course of the FeMo cofactor biosynthesis is the interconversion (Fig. 2a) of the cluster types Fe_4S_4, Fe_3S_4, and MFe_3S_4, which has been successfully performed in vitro in metalloproteins and with model compounds.[18] During capping-type reactions, additional metal centers are coordinated to or removed from suitably oriented metal–sulfur fragments. The $Fe_3(\mu_3\text{-}S)(\mu_2\text{-}S)_3$ fragment **1** (Fig. 2a) acts hereby formally as tridentate η^3-ligand.[19] Compounds of the prismane type, that is, those with a central $[Fe_6S_6]^{n+}$ unit (**3** Fig. 2b; compare also the analogous heteroprismane cluster anion $[MoFe_5S_6L_6]^{n-}$)[14] presumably also represent an intermediate during the reaction leading to compounds with the unit $[Fe_8S_6]^{4+}$ (**4**, Fig. 2b; M = Fe).[20] During this reaction, capping of the Fe_3S_3 faces occurs, which act—in analogy to the Fe_3S_4 fragment—as η^3-ligands, but with a $(\mu_3\text{-}S)_3$ arrangement. The capping of an $L_6Fe_6S_6$ structure with a $MoL_3(solv)_3$ fragment yields clusters of the type $[(MoL_3)_mFe_6S_6L_6']^{n-}$ (m = 1, 2) (**4**, Fig. 2b; M = Mo).[14]

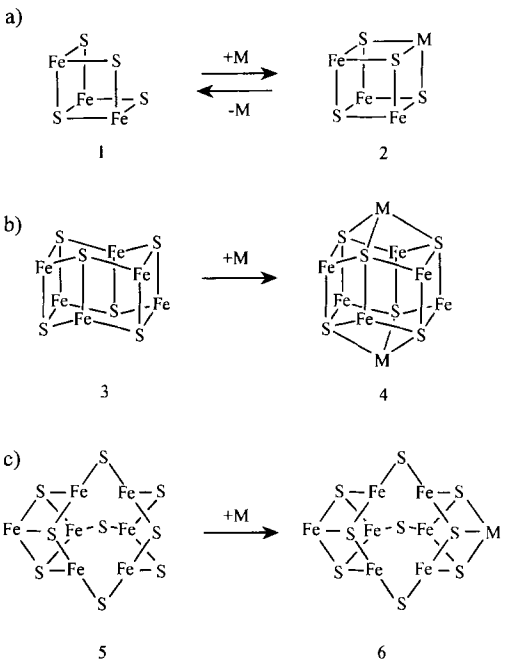


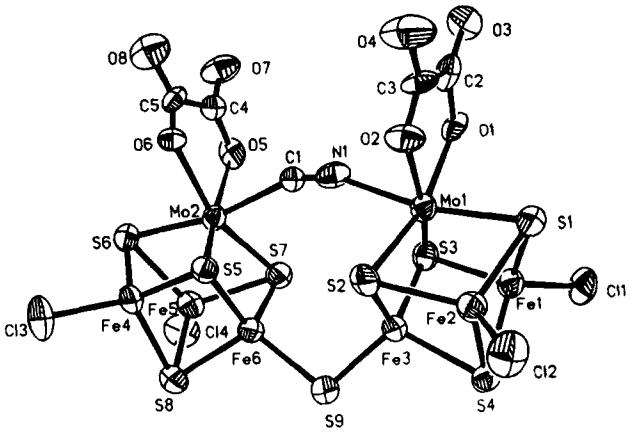
Fig. 2. Schematic representation of the transformation of cluster centers by complexation of metal ions by sulfur-containing cluster fragments. a) An Fe_3S_4 unit (**1**) binds a metal cation M using the three μ_2-sulfur centers, thereby forming a MFe_3S_4 cluster core (**2**). b) Capping of the Fe_6S_6 cluster **3**. c) A possible terminal reaction step within the nifEN protein during the biosynthesis of the FeMo cofactor: capping the Fe_7S_9 fragment **5** analogous to a) leads to the FeMo cofactor cluster core structure MFe_7S_9 **6** (M = Mo). A preceding formation of **5** from **6** (M = Fe) is also possible, as the cofactor pocket of the MoFe protein—and, therefore presumably in the nifEN protein as well—leaves only one of the two "ends" of the cluster unprotected (see Fig. 1b, d).

The driving force for the capping reaction can be found in the tendency to increase the coordination number of the sulfide ligands, corresponding to the sequence μ_2-S to μ_3-S or μ_3-S to μ_4-S, respectively. This tendency increases significantly with a decreasing oxidation state of the cluster, expressed, for instance, by the ratio of Fe^{II} to Fe^{III} centers which can be seen from the following series of core cluster units:[21]

$$[Fe_2^{III}(\mu_2\text{-}S)_2]^{2+} / [Fe_2^{II}Fe_2^{III}(\mu_3\text{-}S)_4]^{2+} / [Fe_8^{II}(\mu_4\text{-}S)_6]^{4+}$$

This indicates that the μ_2-sulfur centers of the FeMo cofactor are more readily formed in a relatively highly oxidized cluster intermediate.

Meanwhile, compounds with bridged, cubane-type $MoFe_3S_4$ units without significant Mo–Mo interactions are accessible by multistep syntheses. The cluster anion $[\{(MoFe_3S_4Cl_2)(C_2O_4)\}_2(\mu_2\text{-}S)(\mu_2\text{-}CN)]^{5-}$ (Fig. 3 top) is a relevant example. The synthesis of analogous compounds containing one $MoFe_3S_4$ and one Fe_4S_4 unit, has, however, so far not been achieved.



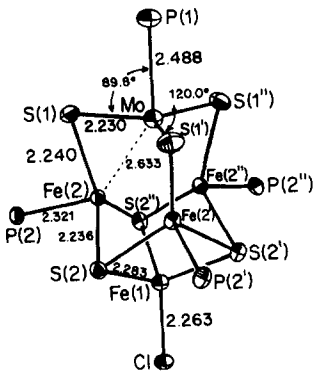


Fig. 3. Top: ORTEP representation of the cluster anion $[\{(MoFe_3S_4Cl_2)(C_2O_4)\}_2(\mu_2\text{-}S)(\mu_2\text{-}CN)]^{5}$ (see K. D. Demadis, D. Coucouvanis, *Inorg. Chem.* **1995**, *34*, 436–448). Bottom: Structure of the cluster $[MoFe_4S_6(PEt_3)_4Cl]$ [22a]. The distances are given in Å; the Mo···Fe(1) distance is 4.343 Å.

A recently published compound, namely the cluster $[MoFe_4S_6(PEt_3)_4Cl]$ (Fig. 3 bottom),[22] obtained by strict self-assembly in a nonpolar solvent, is notable in this context, as the $Fe_4(\mu_3\text{-}S)_3(\mu_2\text{-}S)_3$ fragment in this molecule represents the largest partial structure of the Kim model obtained so far. The Fe_4S_3 unit, which has an inverted Fe_3S_4 core structure, has until now only been known to exist in the anion of the black Roussin salt and some of its derivatives.[23] The $(\mu_2\text{-}S)_3$ arrangement in the $MoFe_4S_6$ cluster is, however, probably determined and stabilized by a $(PEt_3)MoS_3$ fragment, as the side product is an Fe_6S_6-type prismane cluster instead of a compound with an $(Fe_4S_3)(\mu_2\text{-}S)_3(Fe_4S_3)$ core (**6**, Fig. 2c; M = Fe). In contrast to the trigonal coordinated Fe centers in the FeMo cofactor, the four Fe atoms of this compound are coordinatively saturated by the PEt_3 groups acting as fourth ligands. The results summarized above give an outline of the closest approximations to nature achieved by inorganic model systems so far.

In view of these results, a key to the biosynthesis of the FeMo cofactor must lie in the linking of preorganized fragments according to the principles laid out below, as the FeMo cofactor is obviously not formed by a single strict self-assembly process. Therefore, a chemical synthesis should apply a basic principle of nature, namely to create small building blocks that contain within them the relevant information for the (later) formation of the complex structure.[24] For instance, an $[OMoS_3]^{2-}$ unit—as a fragment of a distorted cube—in the presence of soft metal centers leads to the formation of cubane structures, such as $[(CuCl)_3(OMoS_3)]^{2-}$ (Fig. 4).[25] The anion $[OMoS_3]^{2-}$ represents half a cube, with the oxygen ligand exhibiting less affinity towards Cu^+ than the sulfur ligands. The information contained in the $[OMoS_3]^{2-}$ fragment that is necessary for the generation of the target structure is read by the coordination algorithm of the copper atoms.[24] An example for the guidance of a further linkage of such cubane fragments is the formation of the prismane-shaped compound $[(OMoS_3)_2(CuPPh_3)_4]$ from two equal precursors, namely $OMoS_3(CuPPh_3)(Cu(PPh_3)_2)$ units (Fig. 5). After the PPh_3 moiety, one of the archetypal protecting groups for cluster fragments, is cleaved off in solution, the "dimerization" to form the target compound takes place.[25]

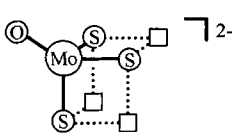


Fig. 4. Schematic representation of the cubane-like cluster anion $[(CuCl)_3(OMoS_3)]^{2-}$. Each square represents one CuCl moiety.

The contribution of inorganic chemistry can be summarized as follows: even though the hunt for the FeMo cofactor has so far been in vain, the hunting party has brought forth a fascinating multitude of compounds.[14, 18]

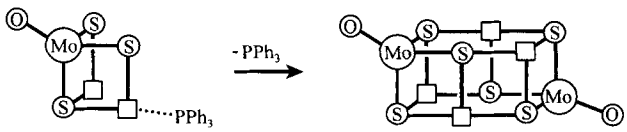


Fig. 5. Schematic representation of the formation of the prismane-shaped compound $[(OMoS_3)_2(CuPPh_3)_4]$ by the "dimerization" of two $[OMoS_3(CuPPh_3)(Cu(PPh_3)_2)]$ units. Each square represents one $CuPPh_3$ moiety.

3. How Does Nature Control the Biosynthesis of the FeMo Cofactor?

Nature is to be considered as a system of steps, each of which is necessarily born out of the previous one.

G. W. F. Hegel

3.1. Functions of the Participating Gene Products

Nearly unnoticed by chemists, geneticists have accumulated a lot of material describing the molecular tools that achieve the assembly of the FeMo cofactor in nitrogen-fixing microorgan-

isms. Bacteria require more than twenty genes for the process of nitrogen fixation. The biochemical characterization of mutants, in which these so-called *nif* genes[26] were selectively inactivated, has led to evidence that at least six gene products (*nif* genes E, N, Q, V, B, and H) participate in the biosynthesis of the FeMo cofactor.[27, 28] This indicates that essential aspects of the synthesis of the inorganic cofactor are genetically controlled. The central question is: how do gene products, that is, proteins, prepare and clear the pathway through the cell for the elements that make up the FeMo cofactor, namely Fe, S, and Mo?

Two genes, *nifE* and *nifN*, show a clear homology (similarities in their sequences) to *nifD* and *nifK*, which are the structural genes that code for the protein chains of the MoFe protein. Accordingly, the gene products of *nifE* and *nifN* also form a tetrameric protein.[29] In addition, bacterial strains containing inactive forms of these genes produce a cofactor-free apo-MoFe protein. This protein can be activated by the addition of the previously isolated FeMo cofactor in the so-called reconstitution test.[30] These results support the conclusion that the nifEN protein forms a template for a crucial step of the FeMo cofactor biosynthesis. In addition, it is assumed that the Fe protein binds also to the nifEN protein and provides electrons for reductive steps.[29]

A decisive hint for the function of the nifB protein within the iron processing system came from the observation that the *nifB* gene is essential for the two alternative nitrogenase systems as well.[31, 32] This is in contrast to the other above-mentioned genes, which are unique for all three systems. The group of P. Ludden succeeded in making a further breakthrough by the recent isolation of the cofactor of the nifB protein (nifB cofactor), which is the only intermediate of the FeMo cofactor biosynthesis known so far.[33] This group at the University of Wisconsin in Madison has been working for some time on an in vitro system for the FeMo cofactor biosynthesis.[34] The initial basis was cell-free extracts of two bacterial strains, deficient in *nifB* and *nifEN*, respectively. While both strains can only form cofactor-free apo-MoFe protein, a combination of the two extracts yields the complete machinery for the cofactor synthesis. Using this system, it proved possible, about six years ago, to integrate into the MoFe protein modified forms of the cofactor, in which homocitrate[2] was replaced by similar organic species. This system has been used as an "activity test" for the enrichment and purification of the nifB and nifEN proteins. The crucial aspect is that nifB cofactor, which, according to current knowledge, is an FeS cluster, can replace the nifB protein in the in vitro system.[33]

In addition, the characterization of the nifS protein[35] has apparently yielded the synthetic equivalent for the inorganic sulfide ligands, which cannot be present in the cell in an unbound state owing to their toxicity. This enzyme activates the cysteine sulfur for biosynthesis by the formation of a protein-bound persulfide moiety. The proposed mechanism is of general relevance for the biosynthesis of FeS clusters.[35]

The element molybdenum is taken up by the cells in the form of $[MoO_4]^{2-}$ or $[MoO_3(OH)]^-$ ions. Therefore, the Mo processing must contain the following steps: 1) a change of the ligand environment (to soft S ligands and homocitrate), 2) an increase in the coordination number from 4 to 6, and 3) a reduction of the Mo center (the oxidation state in the FeMo cofactor appears to be IV).[36]

The participation of the nifQ protein in the Mo processing is illuminated by the following results: the inactivation of this gene has no influence on the activity of the alternative (Mo-independent) nitrogenase systems[31] and does not manifest itself phenotypically in the presence of high concentrations of $[MoO_4]^{2-}$ ions or cysteine in the environment of the organisms. In addition, experiments with $[^{99}MoO_4]^{2-}$ and tritium-labeled homocitrate show that molybdenum atoms and homocitrate enter the pathway of the FeMo cofactor synthesis relatively early.[27]

In vivo measurements using ^{99}Mo TDPAC spectroscopy (TDPAC = *t*ime *d*ifferential *p*erturbed *a*ngular *c*orrelation), allow the gathering of information about the Mo processing. This method is based on the determination of the interaction of the nuclear quadrupole moment and the electric field gradient caused by the electron shell, that is, the obtained frequency data are basically comparable to those of nuclear quadrupole resonance spectroscopy. The results mean that, in principle, information about the nature of intermediate Mo species can be gained. We performed measurements on mutant strains, in which the FeMo cofactor biosynthesis had been interrupted at different stages by the inactivation of one or several of the involved genes. We have so far been able to detect the completed MoFe protein and a Mo storage protein.[37]

3.2. The Assembly of the Fragments

The results from genetic studies clearly indicate that the FeMo cofactor biosynthesis is a multistep process. Obviously, this information cannot be directly derived from the structural model of the cluster itself. The nifEN protein apparently acts as the site of the completion of the FeMo cofactor. An "FeS" fragment (nifB cofactor) is taken up and subsequently fused with a molybdenum-containing fragment (Fig. 6), yielding the

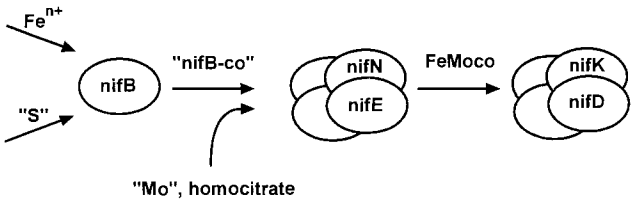


Fig. 6. Simplified schematic representation of the introduction of the "ingredients" Fe^{n+}, "S", "Mo", and homocitrate into the biosynthetic pathway of the FeMo cofactor. NifX denotes the gene product (protein or protein subunit) of the *nifX* gene, co the cofactor.

complete FeMo cofactor. Further conclusions regarding the function of the nifEN protein are made possible by a comparison of the amino acid sequences of the MoFe and the nifEN protein together with a subsequent correlation of the "observed" particularities with the function of amino acids derived from their spatial arrangement within the Kim/Rees structure of the MoFe protein.[38]

The information presented so far leads to two possible scenarios for the course of the FeMo cofactor biosynthesis.

1) The linking of an "Fe_4" fragment with a "$MoFe_3$" cluster fragment occurs within the nifEN protein. (The formation of such a $MoFe_n$ fragment could proceed with the participation of

a MoS precursor, which could—in analogy to the above-mentioned $OMoS_3$ fragment—determine the environment of one of the corners of the cluster.[39]

2) The nifB cofactor forms the entire iron–sulfur part of the FeMo cofactor (**5**, Fig. 2), and the capping of the η^3-S arrangement (analogous to the $Fe_3S_4 \rightarrow MFe_3S_4$ conversion, **1** → **2**, Fig. 2) with a Mo-homocitrate moiety within the nifEN protein occurs as the terminal step in the FeMo cofactor synthesis (**5** → **6**, Fig. 2). The molecular recognition of molybdate in the cell is done by homocitrate, thereby forming a complex of the type MoO_n/homocitrate. This complex is then captured and positioned by the nifEN protein.[41] The subsequent in situ reduction of molybdenum(VI) increases the basicity of the metal center, which in turn facilitates the protonation of terminal oxygen ligands, thereby increasing the lability of the ligand sphere. In addition, the reduction of the molybdenum center increases its affinity for "soft" sulfur ligands, which facilitates the capping of the Fe_7S_9 fragment. The generation of such a fragment within the nifB protein would require that the fragment is stabilized in a relatively highly oxidized state in order to form the μ_2-sulfur centers. (The reduction steps necessary for the capping reaction could occur in the nifEN protein, with the participation of the Fe protein.)

3.3. How Does the Completed FeMo Cofactor Get Incorporated into the MoFe Protein?

The question now arises, how does the cofactor, after its synthesis in the nifEN protein, get into the apo-MoFe protein, and how is the higher affinity achieved that the target protein must possess compared to the synthesis template? The fact that the apo-MoFe protein can be reconstituted with isolated FeMo cofactor in the presence of the Fe protein[36] indicates that during the transition, the FeMo cofactor is present in the cytosole of the cell in a more or less "free" state—that is, not bound by proteins. Additionally, we were able to demonstrate that newly synthesized FeMo cofactor is taken up in vivo by the apo-"MoFe" protein of a previously expressed alternative nitrogenase system[42] (cf. in particular Fig. 5 in ref. [43]). This requires at least a certain kinetic stability of the cluster outside the protein environment. (The slightly different ESR spectrum indicates that the FeMo cofactor is present outside the protein in a marginally modified form.[36])

A number of further proteins play a role in the "relocation" of the FeMo cofactor. For example, the Fe protein has a so far unknown function during the insertion of the FeMo cofactor into the apo-MoFe protein. The apo-MoFe protein is also associated with a helper protein (nifY), which assumably stabilizes a conformation that facilitates the uptake of the cofactor.[28] For this uptake, an insertion channel must be opened up, as, surprisingly, the structure of the MoFe protein determined by Rees et al. does not show any permanently present openings for a possible cofactor insertion.[5]

In order to study this problem in more detail, we calculated with a molecular modeling program,[45] based on the structural data of the MoFe protein obtained by D. C. Rees et al., the water-accessible surface[46] of the α-subunit (Fig. 1b, d). One can clearly discern a hollow which "houses" the cofactor. This cavity exhibits an opening, which, in the MoFe protein, is completely closed off by the β-subunit in a lidlike manner (Fig. 1b). An insertion of the cofactor through this channel would require an at least partial dissociation of the α-subunit.[38] Potential deviations of the protein structure in solution from that of the crystallographically determined structure are of fundamental interest. Therefore we are investigating solutions of the MoFe protein with dynamic light scattering techniques. Preliminary results indicate that the hydrodynamic volume of the MoFe protein is slightly larger than that implied by the structure in the crystal lattice. (The experimentally determined diffusion coefficient is about 10–15% higher than the one obtained by hydrodynamic calculations based on the crystallographic data.) The sequence comparison has yielded new clues that the extent of the interactions between the α and β-subunits is smaller in the nifEN protein than in the MoFe protein. Hence, the insertion channel is more readily opened up in the nifEN protein.[47] In this context, it is also important that in the nifEN protein, there is an asparagine residue at the corresponding site where the MoFe protein possesses a histidine residue that coordinates the molybdenum atom.[29] This certainly leads to a destabilized binding of the cofactor compared to the MoFe protein. An amide nitrogen is much less basic than an imidazole nitrogen atom, and thus is a much weaker ligand. These results have therefore yielded reasonable indications about the manner in which the completed cofactor can "escape" from its nifEN synthesis template and how, once integrated into the MoFe protein, it is firmly held in place at its final position.

4. Perspectives: What Can Chemists Learn from Nature?

The completed structure was nowhere preexistent as such. Its design plan, however, did already exist in its basic components.

J. Monod

The formation of larger "cluster" aggregates, like the FeO core of ferritin, shows, in addition to a nucleation process, evidence of a growth phase dominated by self-assembly processes.[48] In contrast, the *stepwise* synthesis of the FeMo cofactor appears to be controlled to a large extent by protein templates. This can be compared with some of the template-directed syntheses in inorganic host–guest chemistry.[49] The active centers of the template proteins carry the secret discussed herein: *the blueprint for the synthesis of the FeMo cofactor is written in the language of proteins.* Proteins can solve many of the problems that chemists have a difficult time tackling. The control of the redox processes is performed in the example discussed herein in part by the enzymatic control over the sulfide ligands, that is, by the nifS protein. The formation of polynuclear Mo species of the double-cubane or prismane types—clearly favored in in vitro reactions—is inhibited by the provision of well-defined cavities, specific interactions, such as hydrogen bonds, as well as by charge compensation. In this manner, the type of linkage formed between the fragments is controlled and shielding from "destructive" molecules (e.g., nucleophiles) is achieved.

The FeMo cofactor structure is stabilized within special cavities of the proteins. Hydrogen bonds, especially those to the less stable μ_2-sulfur ligands (Fig. 1c), play a decisive role.

In this context it becomes clear why no template proteins have been found for the synthesis of Fe_4S_4 protein centers, which are ubiquitous in the biosphere. These species have such a strong tendency of formation by self-assembly processes that they are formed directly within enzyme pockets that contain a preformed set of ligands.[50] This is probably also true for Fe_2S_2 centers, which are somewhat less thermodynamically favored.[51] $\{Fe_4S_4\}^{2+}$ clusters can be found in the phylogenetically oldest organisms, for example, the N_2-fixing chlostridia, a fact that appears plausible also because of the relatively high Fe^{2+} content of this compound type. These clusters could have readily formed in the reducing atmosphere of the early earth from Fe^{2+} and S^{2-} ions in the presence of an electron acceptor, which could have been traces(!) of O_2—stemming maybe from the radiolysis of H_2O.[52]

A final word on the central question: how would a tailor-made "synthetic" host have to look to function as the template for an in vitro synthesis of the FeMo cofactor? Such a host would certainly have to reflect the threefold symmetry of the cofactor and contain a cavity that is suitable with respect to shape, size, and hydrophobicity. Additionally, the host should—in a truly biomimetic approach—contain a thiolate function as a ligand for the *exo*-iron atom, hydrogen-bond-forming centers to stabilize the μ_2-S^{2-} ligands, as well as (basic) groups to compensate the negative charge of the potential guest. Such a "synthetic" host could of course also be used for the complexation of the isolated FeMo cofactor. Another interesting case would be to preprogram a "molecular receptor"[24, 49] which is not preorganized and formed under the auspices of the FeMo cofactor by self-organization from several building blocks, following a given algorithm. The fact that even a cluster synthesis and the concomitant formation of an envelope from several fragments is possible as an interdependent and synergistic overall process is demonstrated by the synthesis of the polyoxo anion $[V_{34}O_{82}]^{10-}$. This anion contains at its center a cubane-like $[V_4O_4O'_4]$ cluster which serves as template for the formation of its host structure. The formation of this core cluster itself, however, is not independent of the assembly of the "outer shell".[53]

The long-range goal of this concept, of course, is to achieve the in vitro synthesis of the FeMo cofactor using a host–guest complex—perhaps even in the sense of a not completely preexisting host structure like in the $[V_{34}O_{82}]^{10-}$ case—and thereby to enable the reduction of N_2 "in the test-tube". In that case, chemistry would have once again—after the development of the Haber–Bosch process—acted in accordance with the statement of Sir William Crookes, but this time in cooperation with other scientific disciplines, especially by incorporating results from genetics.

We wish to thank Priv.-Doz. Dr. Werner Klipp, Bielefeld, for the fruitful cooperation in the context of a project of the Forschergruppe: "Biosynthese, Struktur und Wirkungsweise einiger der am N-Stoffwechsel beteiligten Enzyme mit besonderem Bezug zur N_2-Fixierung und Photosynthese" which was funded by the Deutsche Forschungsgemeinschaft. We also thank Prof. Dr. D. C. Rees, Los Angeles, for providing crystallographic data. This project was funded by the Fonds der Chemischen Industrie and the Deutsche Forschungsgemeinschaft.

Received: October 26, 1994 [A 1001E]
German version: *Angew. Chem.* **1995**, *107*, 1172
Translated by Dr. W. C. Wilisch, Ansbach, Germany

[1] *Nitrogen Fixation* (Eds.: A. Müller, W. E. Newton), Plenum Press, New York, **1983**; cf. especially B. E. Smith, pp. 23–62.
[2] The nitrogenase enzyme system consists of two components: The Fe protein is a γ_2-dimer with a molecular mass of about 60000 Da, and, in an ATP-dependent reaction, transfers electrons to the MoFe protein, which is the site of the nitrogen reduction. The MoFe protein is an $\alpha_2\beta_2$ tetramer and has a molecular mass of about 240000 Da. The FeMo cofactor is situated in the α-subunit and covalently linked to the protein by two amino acid side chains (a cysteine and a histidine residue). In addition, several hydrogen bonds exist between the protein and various sulfur ligands of the cofactor. The molybdenum atom is coordinated in a bidentate fashion by the hydroxyl and a carboxyl group of a homocitrate anion (Fig. 1c, d). The MoFe protein contains, in addition to the FeMo cofactor, also another type of metal–sulfur aggregate (P clusters) (Fig. 1a). For these clusters, two structural models are currently under consideration: 1) two Fe_4S_4 cubanes linked through an S–S bond involving one S atom from each unit [3–5] or 2) two Fe_4S_3 fragments that are linked by a hexacoordinated sulfur atom [6,7]. The two P clusters form bridges between the α and β-subunits; they are linked by three cysteine residues to each subunit. One of these three cysteine sulfur atoms links the two halves of the cluster, the other two function as terminal ligands for the "outer" Fe atoms of the cluster [3–7].
[3] J. Kim, D. C. Rees, *Science* **1992**, *257*, 1677–1682; *Nature (London)* **1992**, *360*, 553–560.
[4] M. K. Chan, J. Kim, D. C. Rees, *Science* **1993**, *260*, 792–794.
[5] D. C. Rees, M. K. Chan, J. Kim, *Adv. Inorg. Chem.* **1993**, *40*, 89–119.
[6] J. Chen, J. Christiansen, N. Campobasso, J. T. Bolin, R. C. Tittsworth, B. J. Hales, J. J. Rehr, S. P. Cramer, *Angew. Chem.* **1993**, *105*, 1661–1663; *Angew. Chem. Int. Ed. Engl.* **1993**, *32*, 1592–1594.
[7] J. T. Bolin, A. E. Ronco, T. V. Morgan, L. E. Mortenson, N.-H. Xuong, *Proc. Natl. Acad. Sci. USA* **1993**, *90*, 1078-1082; J. Chen, J. Christiansen, S. J. George, J. van Elp, R. Tittsworth, B. J. Hales, S. Al-Ahmad, D. Coucouvanis, N. Campobasso, J. T. Bolin, S. P. Cramer, in ref. [8], pp. 231-241.
[8] *Molybdenum Enzymes, Cofactors and Model Systems* (Eds.: E. I. Stiefel, D. Coucouvanis, W. E. Newton), American Chemical Society, Washington, D. C., **1993**.
[9] H. Beinert, *FASEB J.* **1990**, *4*, 2483–2491.
[10] I. Moura, P. Tavares, J. J. G. Moura, N. Ravi, B. H. Huynh, M.-Y. Liu, J. LeGall, *J. Biol. Chem.* **1992**, *267*, 4489–4496.
[11] A. J. Pierik, R. G. B. Wolbert, P. H. A. Mutsaers, W. R. Hagen, C. Veeger, *Eur. J. Biochem.* **1992**, *206*, 697–704; A. J. Pierik, W. R. Hagen, W. R. Dunham, R. H. Sands, *ibid.* **1992**, *206*, 705–719.
[12] K. Wieghardt, *Angew. Chem.* **1994**, *106*, 765–768; *Angew. Chem. Int. Ed. Engl.* **1994**, *33*, 725–728.
[13] A. Müller, *Polyhedron* **1986**, *5*, 323–340.
[14] D. Coucouvanis, in ref. [8], pp. 304–331, and references therein.
[15] T. E. Wolff, J. M. Berg, C. Warrick, K. O. Hodgson, R. H. Holm, R. B. Frankel, *J. Am. Chem. Soc.* **1978**, *100*, 4630–4632; G. Christou, C. D. Garner, F. E. Mabbs, T. J. King, *J. Chem. Soc. Chem. Commun.* **1978**, 740–741.
[16] T. E. Wolff, J. M. Berg, R. H. Holm, *Inorg. Chem.* **1981**, *20*, 174–180.
[17] A. Müller, K. Knüttel, E. Krickemeyer, A. Hildebrand, H. Bögge, K. Schneider, A. Armatage, *Naturwissenschaften* **1991**, *78*, 460–462.
[18] R. H. Holm, *Adv. Inorg. Chem.* **1992**, *38*, 1–71.
[19] A. Müller, V. P. Fedin, E. Diemann, H. Bögge, E. Krickemeyer, D. Sölter, A. M. Giuliani, R. Barbieri, P. Adler, *Inorg. Chem.* **1994**, *33*, 2243–2247.
[20] S. Pohl, U. Opitz, *Angew. Chem.* **1993**, *105*, 950–952; *Angew. Chem. Int. Ed. Engl.* **1993**, *32*, 863–864.
[21] A. Müller, N. Schladerbeck, *Chimia* **1985**, *39*, 23–24.
[22] a) E. Nordlander, S. C. Lee, W. Cen, Z. Y. Wu, C. R. Natoli, A. Di Cicco, A. Filipponi, B. Hedman, K. O. Hodgson, R. H. Holm, *J. Am. Chem. Soc.* **1993**, *115*, 5549–5558; b) W. Cen, F. M. MacDonnell, M. J. Scott, R. H. Holm, *Inorg. Chem.* **1994**, *33*, 5809–5818.
[23] M. J. Scott, R. H. Holm, *Angew. Chem.* **1993**, *105*, 621–623; *Angew. Chem. Int. Ed. Engl.* **1993**, *32*, 564–566.
[24] P. Baxter, J.-M. Lehn, A. De Cian, J. Fischer, *Angew. Chem.* **1993**, *105*, 92-95; *Angew. Chem. Int. Ed. Engl.* **1993**, *32*, 69; R. Krämer, J.-M. Lehn, A. De Cian, J. Fischer, *ibid.* **1993**, *105*, 764-767 and **1993**, *32*, 703, and references therein.
[25] A. Müller, U. Schimanski, J. Schimanski, *Inorg. Chim. Acta* **1983**, *76*, L245–L246.
[26] A number of these *nif* genes (*nif*: *n*itrogen *f*ixation) have been sequenced, which allows the determination of the amino acid sequences of the corresponding gene products. The structural genes for the α and β-protein chains of the MoFe protein are termed *nifD* and *nifK*, the γ-subunit of the Fe protein is encoded by *nifH* (cf. D. R. Dean, M. R. Jacobsen in *Biological Nitrogen Fixation* (Eds.: G. Stacey, R. H. Burris, H. J. Evans), Chapman and Hall, New York, **1992**; J. Erfkamp, A. Müller, *Chem. Unserer Zeit* **1990**, *6*, 267–279, and references therein). The product of the *nifV* gene catalyzes the synthesis of the homocitrate ligand (reviewed in [27]). The use of genetics enables the comprehension of numerous aspects of biological nitrogen fixation. This includes, apart from the cluster synthesis, also the regulation of the *nif* gene expression by ammonium ions and other nitrogen-containing compounds, as well as by molyb-

date ions and O_2. The transfer of *nif* genes to plants is obviously of general interest.

[27] P. W. Ludden, V. K. Shah, G. P. Roberts, M. Homer, R. Allen, T. Paustian, J. Roll, R. Chatterjee, M. Madden, J. Allen, in ref. [8], pp. 196–215.

[28] D. R. Dean, J. T. Bolin, L. Zheng, *J. Bacteriol.* **1993**, *175*, 6737–6744.

[29] K. E. Brigle, M. C. Weiss, W. E. Newton, D. R. Dean, *J. Bacteriol.* **1987**, *169*, 1547–1553.

[30] V. K. Shah, W. J. Brill, *Proc. Natl. Acad. Sci. USA* **1977**, *74*, 3249–3253.

[31] In addition to the conventional Mo-dependent nitrogenase, there are two other, so-called "alternative" nitrogenase systems. These are encoded by separate genetic systems and their cofactors contain vanadium (FeV cofactor) and iron centers (FeFe cofactor), respectively, instead of the molybdenum atom. R. N. Pau in *Biology and Biochemistry of Nitrogen Fixation* (Eds.: M. J. Dilworth, A. R. Glenn), Elsevier, Amsterdam, **1991**, pp. 37–57.

[32] K. Schüddekopf, S. Hennecke, U. Liese, M. Kutsche, W. Klipp, *Mol. Microbiol.* **1993**, *8*, 673-684, and references therein.

[33] V. K. Shah, J. R. Allen, N. J. Spangler, P. W. Ludden, *J. Biol. Chem.* **1994**, *269*, 1154–1158.

[34] V. K. Shah, J. Imperial, R. A. Ugalde, P. W. Ludden, W. J. Brill, *Proc. Natl. Acad. Sci. USA* **1986**, *83*, 1636–1640.

[35] L. Zheng, R. H. White, V. L. Cash, D. R. Dean, *Biochemistry* **1994**, *33*, 4714–4720.

[36] B. K. Burgess, *Chem. Rev.* **1990**, *90*, 1377–1406; this review includes important background information on the isolation, spectroscopic properties, and biosynthesis of the FeMo cofactor; see also an interesting older review: W. H. Orme-Johnson, *Ann. Rev. Biophys. Biophys. Chem.* **1985**, *14*, 419–459.

[37] P. Mottner, T. Butz, A. Lerf, J. Erfkamp, K. Schneider, A. Müller, *Biochim. Biophys. Acta*, **1993**, *1164*, 311–318; A. Lerf, T. Butz, *Angew. Chem.* **1987**, *99*, 113–130; *Angew. Chem. Int. Ed. Engl.* **1987**, *26*, 110–126. In principle, scanning tunneling microscopy (STM) can be used in addition to TDPAC spectroscopy to study mutants with defects in genes coding for gene products, which are involved in the Mo processing. So far we could visualize the gross metal cluster organization in the MoFe protein using this technique (E. Diemann, A. Branding, A. Müller, *Naturwissenschaften.* **1992**, *79*, 267).

[38] A. Müller, E. Krahn, U. Gollan, W. Suer, K. Schneider, unpublished results.

[39] In connection with the outlined problem of the synthesis of a $MoFe_3S_4$ fragment, a comparison of the amino acid sequences of the so far known nifEN and MoFe proteins (of different N_2-fixing organisms) yields a further notable characteristic: All nifEN proteins exhibit, compared to the MoFe protein, homogeneous deviations in the region corresponding to the P cluster bonding site in the MoFe protein. Of the corresponding cysteine residues, which bind the P cluster in the MoFe protein [2], the two terminal cysteine residues in the β-subunit are missing. The remaining ones form a complete set of ligands for an Fe_4S_4 cluster, or even its synthesis. The 3:1 differentiation among the iron centers [18,40] (3 α-cys, 1 β-cys) could also enable a conversion like $Fe_4S_4 \rightarrow Fe_3S_4 \rightarrow MoFe_3S_4$ in this particular environment [38].

[40] G. P. F. van Strijdonck, J. A. E. H. van Haare, J. G. M. van der Linden, J. J. Steggerda, R. J. M. Nolte, *Inorg. Chem.* **1994**, *33*, 999–1000.

[41] In the MoFe protein, a glutamine residue interacts with one of the carboxyl groups of homocitrate [3]. The corresponding site in the nifEN protein is occupied by a lysine residue [29]. This leads—compared to the MoFe protein—to an additional electrostatic interaction, which could be involved in the capture and the alignment of the homocitrate ion (or a Mo-homocitrate intermediate) [38]. Homocitrate is negatively charged under physiological conditions.

[42] We have been able to demonstrate that the addition of molybdate ions to a growing bacterial culture, which has already expressed the alternative "FeFe" nitrogenase, leads to the formation of a "hybrid" enzyme. This was shown to consist of the "alternative" apo-protein, which has incorporated the "conventional" cofactor (FeMo cofactor), instead of the FeFe cofactor, by spectroscopic and catalytic characterization. The addition of $[MoO_4]^{2-}$ stimulates the biosynthesis of the FeMo cofactor on the one hand; on the other hand, the presence of molybdate ions also induces the expression of protein components for the conventional nitrogenase system. In order to prevent the formation of the MoFe protein, mutants were employed in which the genes coding for the structural proteins of the conventional system had been deactivated [43]. These results [43,44] indicate that the alternative cofactors [31]—for which, compared to the FeMo cofactor, there is much less structural information available—are structurally very similar to the FeMo cofactor.

[43] U. Gollan, K. Schneider, A. Müller, K. Schüddekopf, W. Klipp, *Eur. J. Biochem.* **1993**, *215*, 25–35.

[44] R. N. Pau, M. E. Eldridge, D. J. Lowe, L. A. Mitchenall, R. R. Eady, *Biochem. J.* **1993**, *293*, 101–107.

[45] CERIUS 3.2 Molecular Modelling Package, Molecular Simulations, Cambridge, Burlington, **1993**.

[46] M. L. Connolly, *Science* **1983**, *221*, 709–713.

[47] The α-β arrangement of the MoFe protein is stabilized by seven salt bridges (ionic interactions between charged amino acid residues). In addition, the N-terminal of the β-subunit is "wrapped" around the α-subunit (Fig. 1b) [3]. A comparison of the sequences of *nifDK* and *nifEN* (from *azotobacter vinelandii*) shows that the first 52 amino acids in the *nifN*-coded β-subunit are missing [29]. The β-branch of the MoFe protein, which is missing at the corresponding site in the nifEN protein, carries three of these salt bridge forming residues. Two additional (of the seven) salt bridges appear to be absent in the nifEN protein [38]. The changes in the region that corresponds to the P cluster binding site in the MoFe protein [39] can also contribute to the destabilization of the α-β complex in the nifEN protein.

[48] K. L. Taft, G. C. Papaefthymiou, S. J. Lippard, *Inorg. Chem.* **1994**, *33*, 1510–1520, and references therein.

[49] Review: A. Müller, H. Reuter, S. Dillinger, *Angew. Chem.* in press.

[50] F. Bonomi, S. Pagani, B. M. Kurtz Jr., *Eur. J. Biochem.* **1985**, *148*, 67–73.

[51] S. Pagani, F. Bonomi, P. Cerletti, *Eur. J. Biochem.* **1984**, *142*, 361–366.

[52] A. Müller, N. H. Schladerbeck, *Naturwissenschaften.* **1986**, *73*, 669–670; A strong tendency towards the formation of this species is also indicated by the fact that clusters like $[Fe_4S_4(SH)_4]^{2-}$ (the simplest model system for Fe_4S_4 proteins) can be isolated (A. Müller, N. H. Schladerbeck, H. Bögge, *J. Chem. Soc. Chem. Commun.* **1987**, 35; A. Müller, N. H. Schladerbeck, E. Krickemeyer, H. Bögge, K. Schmitz, E. Bill, A. X. Trautwein, *Z. Anorg. Allg. Chem.* **1989**, *570*, 7) as well as by the observation that crystals containing the anion $[Fe_4S_4(SPh)_4]^{2-}$ can be obtained from the MoFe protein by treatment with *N*-methylformamide and the addition of various cations and thiophenol (A. Müller, K. Knüttel, E. Krickemeyer, A. Hildebrand, H. Bögge, K. Schneider, A. Armatage, *Naturwissenschaften.* **1991**, *78*, 460-462).

[53] A. Müller, R. Rohlfing, J. Döring, M. Penk, *Angew. Chem.* **1991**, *103*, 575–577; *Angew. Chem. Int. Ed. Engl.* **1991**, *30*, 588–590.

Self-Assembly of Molecular-Sized Boxes

C. A. Hunter*

Molecular recognition of guests by synthetic hosts is a rapidly developing field, and many of the basic principles that govern the efficiency and selectivity of intermolecular complexation have been elucidated.[1] The following requirements have emerged for the design of an effective receptor for a particular target molecule:

1. The host should be polymacrocyclic and contain a large cavity in which the number of interactions with the bound guest can be maximized.

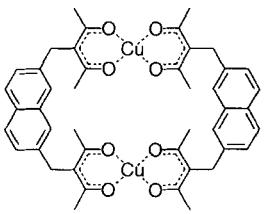
2. The van der Waals surfaces and electrostatic potential surfaces of the host and guest should be complementary.

3. The host should be relatively rigid so that the loss of conformational entropy on binding a guest is minimized.

While these principles are clear, the realization of rigid polymacrocyclic structures is a difficult synthetic challenge. The use of high-dilution conditions is one way to encourage macrocyclization and reduce polymer formation, but yields can be low, and chromatographic separation of mixtures of linear and cyclic oligomers with similar properties can be difficult. Template-directed synthesis has proved to be a very successful method for generating macrocycles.[2] Since it works well when the interactions between the template and the acyclic precursor are strong, its use has been restricted to metal ion/ligand interactions and the construction of hosts for ionic or coordinating guests. Templating is not a viable approach for the construction of macrocyclic hosts for neutral organic guests where the individual interactions between the template and the acyclic precursor are orders of magnitude weaker.

Thus new techniques are needed for the construction of polymacrocyclic structures. Over the last few years, self-assembly has emerged as a very promising approach to the generation of compounds with large molecular-sized cavities. Self-assembled complexes are discrete, structurally well-defined species composed of at least two molecular units connected by noncovalent interactions.[3] The use of noncovalent interactions to generate macrocyclic structures is particularly attractive since the cyclization is under thermodynamic control. Provided that the design of the components is sufficiently accurate, entropically unfavorable polymerization is avoided. Moreover, the self-assembly process should become increasingly favorable as the complexity of the structure increases from simple macrocyclic to polymacrocyclic architectures. There are obvious parallels in nature where large three-dimensional cavities are almost always generated by the self-assembly of many proteins, for example in the coats of viruses.

The first self-assembled macrocyclic host (**1**) was reported in 1986 by Maverick et al.[4] This work showed how coordination chemistry could be used to generate cyclic structures in good yield by simply mixing the appropriate components in solution. **1** also functioned as a host: it selectively complexed 1,4-diazabicyclo[2.2.2]octane in chloroform ($K = 220\ M^{-1}$).



1

An appealing design for a host molecule is a regular box shape—construction in three dimensions is conceptually simpler if we use three orthogonal axes, in other words, if we use right angles in our building blocks. An attractive feature of inorganic complexes is that they afford a range of 90° linkages for the construction of macrocyclic boxes. The square-planar geometry of platinum(II) and palladium(II) complexes makes them ideal building blocks, and in 1990, Fujita et al. first demonstrated the utility of palladium(II) in the self-assembly of a large macrocyclic cavity (Fig. 1).[5] The thermodynamic cyclization resulted in a quantitative yield of the macrocycle, which also formed a stable 1:1 complex ($K = 750\ M^{-1}$) with 1,3,5-trimethoxybenzene in water.

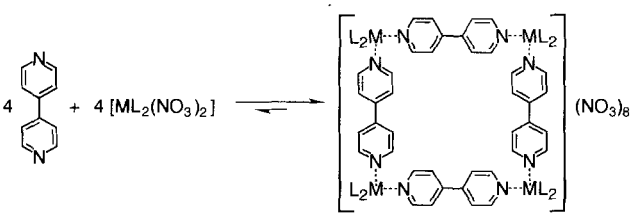
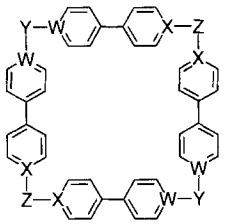


Fig. 1. Fujita and Ogura's box forms in quantitative yield on mixing the components [5]. M = Pd^{II}, L_2 = ethylenediamine.

Stang and others have recently produced several variations on this basic idea (**2** and **3**).[6] These structures are obtained in high yields by simply mixing the components. Interestingly, covalent analogues of these macrocycles are known (**4** and **5**).[7] These require multistep syntheses concluding with a low-yielding macrocyclization reaction which produces large quantities of acyclic oligomers. The similarity between these self-assembled

[*] Dr. C. A. Hunter
Department of Chemistry, University of Sheffield
GB-Sheffield S3 7HF (UK)
Telefax: Int. code + (114)273-8673

 © VCH Verlagsgesellschaft mbH, D-69451 Weinheim, 1995 0570-0833/95/1010-1079 $ 10.00+.25/0



2, W = X = N; Y = Z = $M(NH_2CH_2CH_2NH_2)_2$, $M(Ph_2PCH_2CH_2CH_2PPh_2)_2$
3, W = N; X = C; Y = $M(Ph_2PCH_2CH_2CH_2PPh_2)_2$; Z = I^+
4, W = X = C; Y = Z = I^+
5, W = X = N^+; Y = Z = CH_2

M = Pt, Pd

macrocycles and Stoddart's "big blue box" (**5**) suggests that they will have a bright and colorful future in supramolecular chemistry.

Fujita and Ogura have now extended this work to the construction of a three-dimensional cavity (Fig. 2).[8] This self-assembly process is significantly less efficient than that in Figure 1 because the ligands are more flexible; less than 60% of the molecules exist as the macrobicyclic complex which is in equilibrium with other oligomers. However, addition of a complementary guest such as sodium 4-methoxyphenylacetate shifts the equilibrium dramatically such that only the cage complex can be detected. Guests that are too large to fit inside the cage can still bind but shift the equilibrium in the opposite direction, in favor of open oligomers.

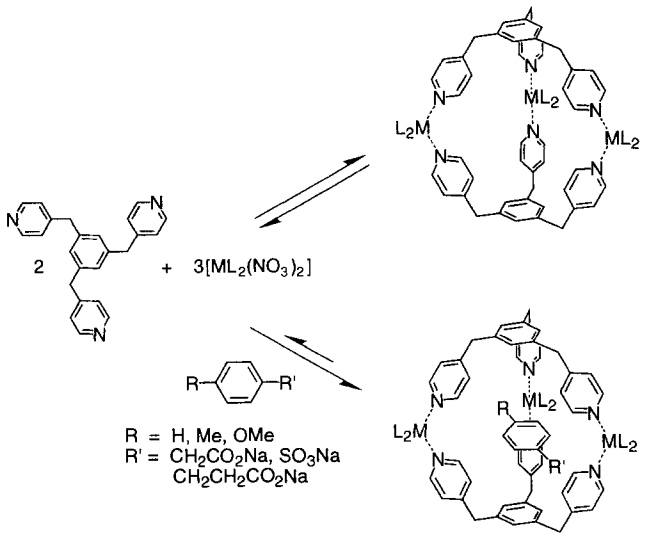


Fig. 2. This macrobicyclic structure does not assemble efficiently unless a complementary guest is added to the mixture [8]. M = Pd^{II}, L_2 = ethylenediamine.

Three-dimensional macrobicyclic assemblies have also been described by Baxter et al. and by Saalfrank et al. The Lehn group used the coordination of copper(I) by 2,2'-bipyridyl derivatives to generate a large cylindrical box (Fig. 3a).[9] In total, five ligands are complexed by six metal centers in this singularly impressive example of the power of self-assembly to generate polymacrocyclic architectures. Saalfrank et al. have developed the coordination chemistry of iron with malonic acid derivatives to produce tetrahedral tetranuclear complexes which enclose cavities of variable dimensions (Fig. 3b).[10] The smallest structure encapsulates cations such as ammonium. Both of these systems use bifunctional chelating ligands rather than pyridyl ligands: the cylinder in Figure 3a is generated by a distorted tetrahedral metal center and the tetrahedron in Figure 3b is generated by an octahedral metal center.

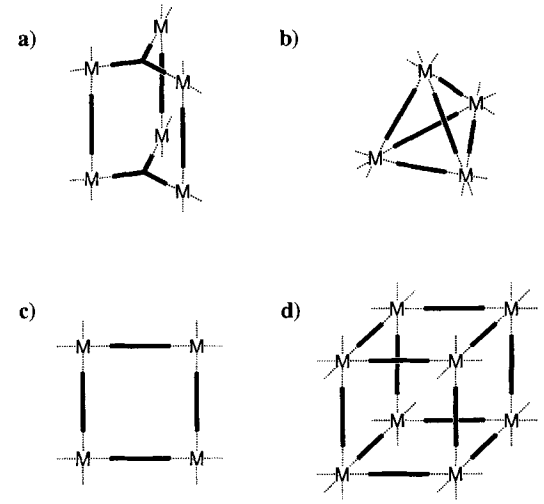


Fig. 3. Schematic representations of cavities assembled on metal centers. a) Lehn's cylindrical box based on copper(I) and coordination of 2,2'-bipyridine [9]. b) Saalfrank's tetrahedral iron–malonate assembly [10]. c) Fujita and Ogura's square box, which could be extended into a cube (d) by using an octahedral metal center [5].

In principle, such three-dimensional assemblies should be more stable than simple macrocycles since the number of interactions per component is larger. It remains to be seen whether the two-dimensional self-assembly of square boxes based on pyridyl ligands and square-planar metal centers can be extended into three-dimensional cubic structures by the use of octahedral metal centers (Fig. 3c and d).

Self-assembly of macrocyclic hosts is not restricted to metal complexes, and macrocyclic hosts have been reported in which hydrogen bonding alone controls the assembly process.[11] The most striking example is Rebek's "tennis ball".[11c] Two self-complementary molecules form a three-dimensional spherical cavity, which complexes small nonpolar guests such as methane in organic solvents.

Self-assembly appears to be an extremely promising method for the construction of polymacrocyclic structures and will facilitate the construction of large cavities for use in molecular recognition. An interesting feature of these systems is that assembly of the host structure may itself be coupled with guest recognition such that the host only exists in the presence of the guest. The structures generated to date all have a high degree of symmetry, which may limit the range of substrates that can be recognized, but strategies for avoiding symmetry have yet to be explored.

German version: *Angew. Chem.* **1995**, *107*, 1181

Keywords: molecular recognition · noncovalent interactions self-assembly

 © VCH Verlagsgesellschaft mbH, D-69451 Weinheim, 1995 0570-0833/95/1010-1080 $ 10.00+.25/0

[1] J. M. Lehn, *Angew. Chem.* **1988**, *100*, 91–116; *Angew. Chem. Int. Ed. Engl.* **1988**, *27*, 89–112; D. J. Cram, *ibid.* **1988**, *100*, 1041–1052 and **1988**, *27*, 1009–1020.
[2] S. Anderson, H. L. Anderson, J. K. M. Sanders, *Acc. Chem. Res.* **1993**, *26*, 469–475; R. Hoss, F. Vögtle, *Angew. Chem.* **1994**, *106*, 389–398; *Angew. Chem. Int. Ed. Engl.* **1994**, *33*, 375–384.
[3] J. S. Lindsey, *New J. Chem.* **1991**, *15*, 153–180.
[4] A. W. Maverick, S. C. Buckingham, Q. Yao, J. R. Bradbury, G. G. Stanley, *J. Am. Chem. Soc.* **1986**, *108*, 7430–7431.
[5] M. Fujita, J. Yazaki, K. Ogura, *J. Am. Chem. Soc.* **1990**, *112*, 5645–5647.
[6] P. J. Stang, D. H. Cao, *J. Am. Chem. Soc.* **1994**, *116*, 4981–4982; P. J. Stang, K. Chen, *ibid.* **1995**, *117*, 1667–1668; M. Fujita, S. Nagao, M. Iida, K. Ogata, K. Ogura, *ibid.* **1993**, *115*, 1574–1576; H. Rauter, E. C. Hillgeris, A. Erxleben, B. Lippert, *ibid.* **1994**, *116*, 616–624; P. J. Stang, J. A. Whiteford, *Organometallics* **1994**, *13*, 3776–3777; C. M. Drain, J. M. Lehn, *J. Chem. Soc. Chem. Commun.* **1994**, 2313–2315; see also A. W. Schwabacher, J. Lee, H. Lei, *J. Am. Chem. Soc.* **1992**, *114*, 7597–7598; R. Rüttimann, G. Bernardinelli, A. F. Williams, *Angew. Chem.* **1993**, *105*, 432–434; *Angew. Chem. Int. Ed. Engl.* **1993**, *32*, 392–394; C. A. Hunter, L. D. Sarson, *ibid.* **1994**, *106*, 2424–2426 and **1994**, *33*, 2313–2316; P. Klüfers, J. Schuhmacher, *ibid.* **1994**, *106*, 1925–1927 and **1994**, *33*, 1863–1865.
[7] P. J. Stang, V. V. Zhdankin, *J. Am. Chem. Soc.* **1993**, *115*, 9808–9809; P. R. Ashton, C. L. Brown, E. J. T. Chrystal, T. T. Goodnow, A. E. Kaifer, K. P. Parry, A. M. Z. Slawin, N. Spencer, J. F. Stoddart, D. J. Williams, *Angew. Chem.* **1991**, *103*, 1055–1061; *Angew. Chem. Int. Ed. Engl.* **1991**, *30*, 1039–1042.
[8] M. Fujita, S. Nagao, K. Ogura, *J. Am. Chem. Soc.* **1995**, *117*, 1649–1650.
[9] P. Baxter, J. M. Lehn, A. DeCian, J. Fischer, *Angew. Chem.* **1993**, *105*, 92–95; *Angew. Chem. Int. Ed. Engl.* **1993**, *32*, 69–72.
[10] R. W. Saalfrank, B. Hörner, D. Stalke, J. Salbeck, *Angew. Chem.* **1993**, *105*, 1223–1225; *Angew. Chem. Int. Ed. Engl.* **1993**, *32*, 1179–1182; R. W. Saalfrank, R. Burak, A. Breit, D. Stalke, R. Herbst-Irmer, J. Daub, M. Porsch, E. Bill, M. Müther, A. X. Trautwein, *ibid.* **1994**, *106*, 1697–1699 and **1994**, *33*, 1621–1623; R. W. Saalfrank, R. Burak, S. Reihs, N. Löw, F. Hampel, H.-D. Stachel, J. Lentmaier, K. Peters, E. M. Peters, H. G. von Schnering, *ibid.* **1995**, *107*, 1085–1088 and **1995**, *34*, 993–995.
[11] a) M. Kim, G. W. Gokel, *J. Chem. Soc. Chem. Commun.* **1987**, 1686–1688; b) C. M. Drain, R. Fischer, E. G. Nolen, J. M. Lehn, *ibid.* **1993**, 243–245; c) R. Wyler, J. de Mendoza, J. Rebek, Jr., *Angew. Chem.* **1993**, *105*, 1820–1821; *Angew. Chem. Int. Ed. Engl.* **1993**, *32*, 1699–1701; d) N. Branda, R. Wyler, J. Rebek, *Science* **1994**, *263*, 1267–1268.

Does the Death Knell Toll for the Metallic Bond?**

J. Christian Schön*

"There is an appointed time for everything under the heavens—a time to be born, and a time to die." Judging from two recent publications,[1, 2] the latter fate awaits the concept of the metallic bond. Based on two somewhat different trains of thought, the authors conclude that the metallic bond is a disposable quantity in descriptions of bonding in solids, and should be subsumed into the supposedly better established concepts of the covalent and ionic bond.

Analyzing their arguments in more detail, we notice that Allen et al.[1] base their conclusion on an attempt to quantify the so-called van Arkel–Ketelaar triangle.[3, 4] They suggest that a configuration energy (CE) should be defined as an average "valence shell energy", in other words, the average energy needed to remove a single valence electron. Here, it is assumed that the remaining valence electrons remain in their original states during this "ionization" process. Thus, according to Koopman's theorem, these valence shell energies correspond to the one-particle energies in the Hartree–Fock approximation.[5][***] For a compound composed of A and B, Allen et al. then identify CE_A and CE_B with the diagonal elements of the interaction matrix within the approximation of the extended Hückel theory (EHT).[1, 2] Using a common approximation for the off-diagonal matrix elements,[6] $H_{ij} = 1/2(H_i + H_j)$, they find that $H_{AB} = (CE_A + CE_B)/2$ holds. Since the off-diagonal matrix elements explain (within the context of the EHT, at least) the Peierls distortion,[7, 8] which accompanies the change from "metallic" to "covalent" band structures, Allen et al. conclude that $(CE_A + CE_B)/2$ is a natural coordinate along the metallic → covalent edge of the van Arkel–Ketelaar triangle.

The second coordinate in the description of the triangle would have to reflect the degree of ionicity in the bonds. Here, Allen et al.[9] refer to the classical concept of the difference in electronegativities for the characterization of the polarity of the bond. Within their model, this concept is most easily implemented by employing the difference in configuration energies, $(CE_A - CE_B)/2$.[*] From these considerations it follows that the three traditional bonding concepts should be expressed in a natural way through the two "coordinates" derived from the configuration energy.[**]

At the same time, Anderson, Burdett, and Czech[2] (= ABC) have addressed the issue that certain materials should not necessarily be described in terms of typical metallic bonding, although they show macroscopic metallic behavior. Examples are doped molecular crystals and ionic systems, for instance fullerenes and compounds related to the high-temperature superconductors, respectively. The band structures of such "metals" can be determined within the tight-binding (TB) approach,[5, 11] and it is not necessary to invoke the metallic bond with its somewhat vague concept of delocalized vs. localized electrons to explain the metallike behavior. Thus, ABC suggest that one should reevaluate the concept of metallic bonding in light of the current understanding of theoretical models of the bonding in solids. They point out that most of the properties associated with metallic behavior are related to the position of the Fermi surface in the band approximation[11] for the theoretical analysis of the

[*] Dr. J. C. Schön
Institut für Anorganische Chemie der Universität
Gerhard-Domagk-Strasse 1, D-53121 Bonn (Germany)
Telefax: Int. code + (228)73-5660
e-mail: unc419@ibm.rhrz.uni-bonn.de

[**] I would like to thank Prof. Dr. M. Jansen, Bonn, for many valuable comments and discussions.

[***] The interpretation of the one-particle energies is subtle: the total energy of the solid is not the sum of all one-particle energies, since we are dealing with an interacting system. In particular, a one-particle energy is in general *not* identical with the standard ionization energy.

[*] Based on these considerations, Allen draws the conclusion that CE should be used as a general characteristic quantity for the chemical behavior of an atom on the same level as its position in the periodic table.

[**] For an alternative approach to go beyond the van Arkel–Ketelaar triangle by applying quantum mechanical concepts, see the work by Urland [10].

electronic degrees of freedom in the solid. In metals, the bands are filled only partly, and thus no energy gap exists for the promotion of a (quasi-)electron into a conducting state. With statistical mechanics it can be shown that this lack of a gap explains many of the characteristic properties of a metal.[12]

It is known[5, 11] that within the context of the one-electron band approximation the eigenfunctions of the corresponding one-particle Hamiltonian for a periodic lattice are Bloch functions of the form $\Psi_n(\vec{k};\vec{r}) = \exp(i\vec{k}\vec{r})\,u_n(\vec{k};\vec{r})$. The function u_n reflects the periodicity of the crystal lattice, such that $u_n(\vec{k};\vec{r}) = u_n(\vec{k};\vec{r}+\vec{R}_i)$, where $\vec{R}_i$ is any translation vector of the lattice. Since these Bloch functions are obviously "delocalized", any description of the electronic degrees of freedom of the crystal relying on this approximation refers to delocalized (quasi)-particles. On the other hand, it is always possible to choose any complete orthogonal basis of functions, including rather localized bases, and express the Bloch functions in this basis. One should notice here that nothing has been said about the actual method used to calculate the band structure. The reason is that plane-wave expansions (NFE, OPW, etc.),[5, 11] expansions using atomic/molecular orbitals including ionization states (TB, LCAO, etc.),[5, 11] and also the "cell-methods" (APW, KKR, etc.)[5, 11] are in principle applicable to all band structures and all types of chemical bonding.[5] Only the ease of computation for a given system and property favors one method over the others.

Next, ABC point out that because of the high degree of degeneracy a Fermi surface is subject to instabilities, which in a partly filled band can lead to the opening of an energy gap in the density of states.[8] Slight distortions of the arrangement of the ion cores away from a high-symmetry configuration can remove this degeneracy (= Peierls distortion in analogy to the Jahn–Teller effect,[8] its strength should be related to the electron-phonon interaction). Similar effects can be produced by a modulation of the electron distribution, in other words, charge density waves.[8] This removal of the degeneracy can result in the opening of an energy gap at the Fermi surface. This would be of importance in a metal, since the band gap would cause a change to an insulator/semiconductor. Whether this actually occurs depends on whether the ground state energy of the symmetric (undistorted) structure lies above or below that of the distorted structure, a fact that can be influenced, for instance, by the application of external pressure.[13] As was pointed out earlier, within the EHT one can estimate the relative stability of the Peierls distortion in compounds by considering the off-diagonal elements. Thus the considerations of ABC lead to the same classification of the metallic → covalent bond transition as those of Allen et al.,[1] who started from the calculation of the configuration energy.

Finally, ABC suggest that one might define the metallic bond to apply to those systems within the one-electron approximation for which the interpretation of Wannier functions[5] as single-electron wave functions is inappropriate. Since the (relatively localized) Wannier functions are not eigenfunctions of the one-particle Hamiltonian (in contrast to the Bloch functions, which can be transformed into Wannier functions by a type of Fourier transform), their Slater determinant may be interpreted as a many-electron state only if all the Bloch states within a band are filled and present in the determinant. Recalling that metals are essentially defined by the property of having a partly filled energy band, one can conclude that metallic bonds are just bonds in metals; no special attributes belong to the metallic bond itself.

Adding to this their analysis of the transition from metallic to covalent bonds, ABC draw the conclusion that the traditional concept of a metallic bond as such, as an individual type essentially different from other bonds, is no longer necessary. It might even be disadvantageous to maintain this concept, since it hides the more fundamental aspects of the bonding situation as reflected in the (calculated) band structures.

Now, while the arguments of Allen and ABC against the metallic bond as an entity completely separate and distinct from other types of bonds are very interesting, one should not overlook that the concept of metallic bonding is first and foremost a qualitative one based on the prominence of certain features of the wave function(s) describing a solid. In this sense, the metallic bond is not different from other types of bonds that stress other properties of the wave function. They all serve the same purpose of allowing a first qualitative characterization of a solid and its behavior. Similarly, as pointed out above, in the context of quantum mechanical band structure calculations, covalent or ionic bonds are no more special than metallic ones (and neither are the use of localized or delocalized bases for the expansion of the Hamiltonian). Thus, the arguments of both ABC and Allen et al. carried to their final conclusion actually imply that not only the concept of the metallic bond should vanish, but so should all the traditional concepts of bonds in solids!

Has a major change of paradigm thus occurred in solid-state chemistry? Not really. The seemingly radical conclusion we have just reached should come as no surprise, since it is known that any solid is composed of strongly interacting particles, namely ion cores and electrons. Thus any more detailed understanding of its properties will always involve studying the collective behavior of its constituents, which implies that local concepts like bonds will only be of limited value.[*] However, the necessity of having to solve the full quantum mechanical problem first is a certain disadvantage over more simple classification procedures, although it seems quite likely that with the increasing availability of powerful computers and sophisticated algorithms the concepts of metallic or ionic bonds will become more quantitative.[**]

As a consequence, the boundaries between bonding regimes will become less sharp than a more qualitative heuristic picture of bonds in solids usually implies. Nevertheless, the extreme cases of the ideal covalent, ionic, or metallic bond will retain their usefulness, as long as one is always aware of their limitations. Thus, we expect the different concepts of bonds in solids, including the metallic one, to keep their place in the tool box of the solid-state scientist. The time has not yet come for the metallic bond to pass into oblivion.

German version: *Angew. Chem.* **1995**, *107*, 1183

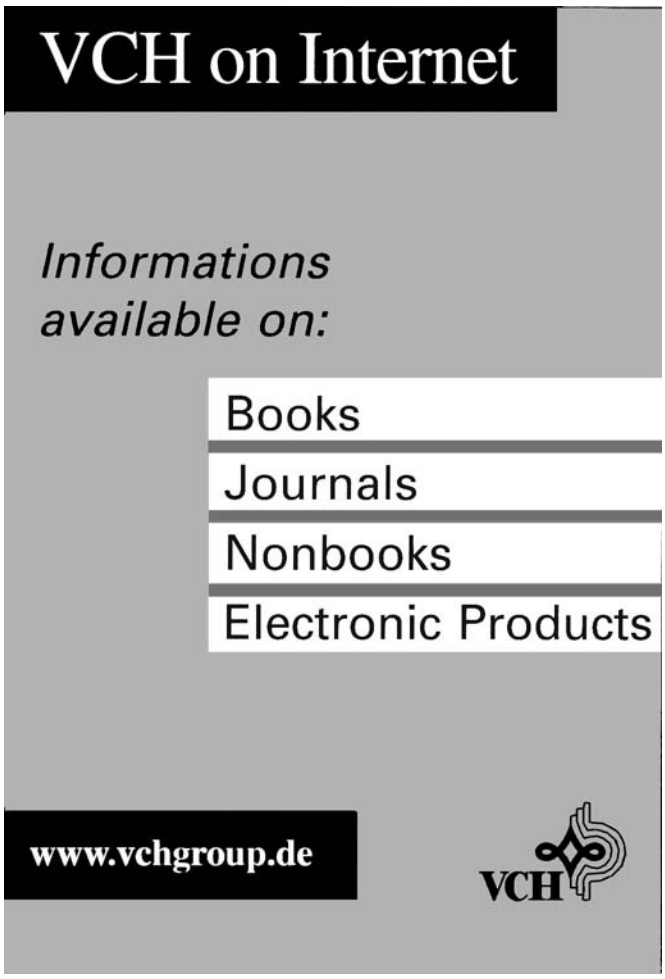
Keywords: bond theory · metallic bond · solid-state chemistry

[*] Compare, however, the fruitful concept of quasi-particles introduced by Landau [5].

[**] Such a direct classification method has been recently proposed by Silvi and Savin [14]. They suggest employing the electron localization function(s) (ELF) [15, 16] for a more rigorous definition of quantities like ionicity or metallicity of a compound. Clearly, their procedure points the way towards a quantum mechanical classification of the types of bonds prevalent in a given chemical compound, thus providing us with definitions that would allow us to speak with confidence about the metallic, covalent, and/or ionic character of bonds.

 © VCH Verlagsgesellschaft mbH, D-69451 Weinheim, 1995 0570-0833/95/1010-1082 $ 10.00+.25/0

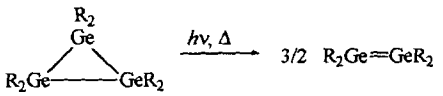
[1] L. C. Allen, J. F. Capitani, *J. Am. Chem. Soc.* **1994**, *116*, 8810.
[2] W. P. Anderson, J. K. Burdett, P. T. Czech, *J. Am. Chem. Soc.* **1994**, *116*, 8808–8809.
[3] J. A. A. Ketelaar, *Chemical Constitution. An Introduction to the Theory of the Chemical Bond*, Elsevier, Amsterdam, **1958**.
[4] A. E. van Arkel, *Molecules and Crystals in Inorganic Chemistry*, Wiley, Interscience, New York, **1956**.
[5] J. Callaway, *Quantum Theory of the Solid State*, Academic Press, New York, **1974**.
[6] M. Wolfsberg, L. J. Helmholz, *J. Chem. Phys.* **1952**, *20*, 837.
[7] J. K. Burdett, S. Lee, *J. Am. Chem. Soc.* **1983**, *105*, 1079–1083.
[8] E. Canadell, M.-H. Whangbo, *Chem. Rev.* **1991**, *91*, 965–1034.
[9] L. C. Allen, *J. Am. Chem. Soc.* **1989**, *111*, 9003–9014.
[10] W. Urland, *Angew. Chem.* **1987**, *99*, 1316–1318; *Angew. Chem. Int. Ed. Engl.* **1987**, *26*, 1275–1277.
[11] F. Bassani, G. P. Parravicini, *Electronic States and Optical Transitions in Solids*, Pergamon, New York, **1975**.
[12] R. K. Pathria, *Statistical Mechanics*, Pergamon, New York, **1978**.
[13] J. K. Burdett, *Prog. Solid State Chem.* **1984**, *15*, 173.
[14] B. Silvi, A. Savin, *Nature* **1994**, *371*, 683–686.
[15] R. F. Bader, M. E. Stephens, *J. Am. Chem. Soc.* **1975**, *97*, 7391–7399.
[16] A. D. Becke, K. E. Edgecombe, *J. Chem. Phys.* **1990**, *92*, 5397–5403.



Reactions of Hexa-*tert*-butylcyclotrigermane: Isolation of an Enantiomerically Pure 1,3-Diiodotrigermane**

Manfred Weidenbruch,* Annette Hagedorn, Karl Peters, and Hans Georg von Schnering

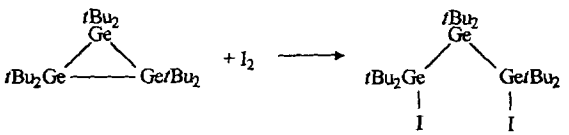
The hexaarylcyclotrigermanes **1**, which have been known since 1982, can be photochemically and thermally converted to tetraaryldigermenes (tetraaryldigermaethenes) **2**.[1] These, in turn, undergo a large variety of addition and cycloaddition reactions,[7] for example with chalcogens,[2-6] alkynes,[4, 6] and azides.[4, 6]



1 **2**

R = 2,6-$Et_2C_6H_3$, 2,6-$iPr_2C_6H_3$ etc.

Hexa-*tert*-butylcyclotrigermane **3**,[8] the only known hexaalkylcyclotrigermane[1] to date, behaves rather differently, reacting with the heavier chalcogens by cleavage of just one Ge–Ge bond to give the ring-expanded thia-, selena-,[9] and telluratrigermetanes.[10] We have now found that the reaction with iodine also occurs with the cleavage of one Ge–Ge bond and results in the formation of the strained open-chain hexa-*tert*-butyl-1,3-diiodotrigermane **4**.



3 **4**

According to the crystal structure analysis,[11] **4** assumes the *gauche-trans* conformation. The Ge–Ge bonds are of different lengths (266.0 and 262.2 pm) and considerably stretched in comparison to the normal bond length of 244 pm.[17] This length is only exceeded by the Ge–Ge bond in hexa-*tert*-butyldigermane (d = 271.0 pm).[8] Trigermane **4** is thus analogous to the structurally related hexa-*tert*-butyl-1,3-diiodotrisilane,[12] which also contains extended Si–Si bonds of different lengths.

[*] Prof. Dr. M. Weidenbruch, A. Hagedorn
Fachbereich Chemie der Universität
Carl-von-Ossietzky-Strasse 9–11, D-26111 Oldenburg (Germany)
Telefax: Int. code + (441) 798-3329
Dr. K. Peters, Prof. Dr. H. G. von Schnering
Max-Planck-Institut für Festkörperforschung, Stuttgart (Germany)

[**] Compounds of Germanium and Tin, Part 15. This work was supported by the Deutsche Forschungsgemeinschaft and the Fonds der Chemischen Industrie. Part 14: M. Weidenbruch, A. Stilter, J. Schlaefke, K. Peters, H. G. von Schnering, *J. Organomet. Chem.* in press.

Whereas the Si analogue of **4** crystallizes as a racemate,[12] **4** forms a conglomerate of enantiomerically pure crystals on slow cooling to −25 °C. The absolute configuration of the single crystal that was selected and investigated was determined by the anomalous scattering of X-rays and is shown in Figure 1.

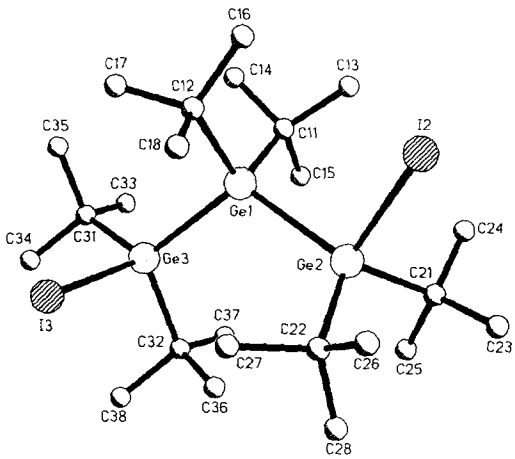
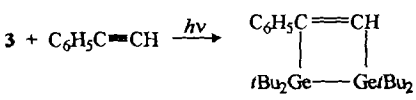


Fig. 1. Molecular structure of *P*-**4** in the crystal (H atoms not shown). Selected bond lengths [pm] and angles [°]: Ge1-Ge2 266.0(1), Ge1-Ge3 262.2(1), Ge2-I2 261.0(1), Ge3-I3 260.5(1); Ge2-Ge1-Ge3 115.4(1).

Although several hundred conglomerates have been described since their initial discovery by Pasteur,[13] the enantiomers isolated from these almost all owe their chirality to the presence of stereogenic centers.[14] In contrast, the chirality in **4** is based on a helical arrangement of the germanium and iodine atoms, in which the conformers form either a right-handed or a left-handed helix. This is the first case known to us in which a simple molecular compound made from heavier elements of Group 14 (fourth main group) undergoes spontaneous enantiomeric resolution on crystallizing. Intermolecular contacts that could be significant for the formation of the conglomerate are not observed, since the I···I and I···Ge distances of >450 pm are too long for bonding interactions.

Further proof of the presence of a conglomerate is provided by the melting points of **4**; the melting point of the racemate is 21 K lower than that of the pure enantiomers. In solution, **4** may have a symmetrical structure with unhindered rotation around the Ge–Ge bonds, as the very simple ^1H and ^{13}C NMR spectra do not reflect the different Ge–Ge bond lengths nor the different orientations of the *tert*-butyl groups observed in the crystal.

Whereas **3** reacts differently in the absence of light than the cyclotrigermanes **1**, it undergoes photochemically induced bond cleavage to give tetra-*tert*-butyldigermene. This can be trapped,



5

 © VCH Verlagsgesellschaft mbH, D-69451 Weinheim, 1995 0570-0833/95/1010-1085 $ 10.00+.25/0

for example, by [2 + 2] cycloaddition with phenylacetylene leading to 1,2-digermacyclobutene **5**, the constitution of which has been confirmed by the X-ray structure analysis (Fig. 2).[11]

This manner of reaction is not self-evident, since the only tetraalkyldigermene $R_2Ge{=}GeR_2$ ($R = CH(SiMe_3)_2$) known to date, although stable in the crystal, reacts in solution exclusively as singlet germylene (germanediyl).[15]

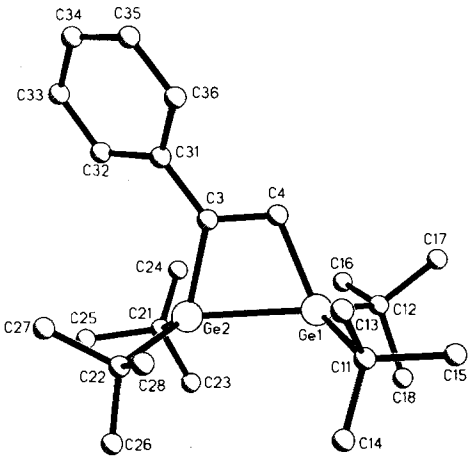


Fig. 2. Molecular structure of **5** in the crystal (H atoms not shown). Selected bond lengths [pm] and angles [°]: Ge1-Ge2 253.1(6); Ge1-Ge2-C3 73.0(3), Ge2-C3-C4 107.0(6), C3-C4-Ge1 107.8(6), C4-Ge1-Ge2 72.2(3).

Experimental Procedure

4: A solution of **3** (100 mg, 0.18 mmol) in *n*-hexane (50 mL) was cooled to −78 °C and a solution of iodine (46 mg, 0.18 mmol) in *n*-hexane (30 mL) added dropwise. The mixture was allowed to warm to room temperature and solvent removed under reduced pressure to give 30 mL of solution. After cooling to −25 °C, colorless needles of **4** (120 mg, 83% yield) were obtained. M.p. (enantiomers) 122 °C, m.p. (racemate) 101 °C. ^{1}H NMR (300 MHz, C_6D_6): $\delta = 1.44$ (s, 36H, 1.57 (s, 18H); ^{13}C NMR (75.44 MHz, $CDCl_3$): $\delta = 33.13$ (C_p), 34.46 (C_q), 37.02 (C_q), 37.34 (C_q); MS (CI, isobutane): *m/z* (%): 687 (54, $M^+ - I$). Correct C, H, I elemental analyses.

5: A solution of **3** (150 mg, 0.27 mmol) and phenylacetylene (73 mg, 0.71 mmol) in *n*-hexane (70 mL) was irradiated at −25 °C with a high-pressure mercury lamp (Heraeus TQ150) until **3** was no longer detectable by TLC (about 4 h). After exchanging *n*-hexane with toluene and cooling to −25 °C, yellow crystals of **5** (36 mg, 27%) were obtained. M.p. 96 °C. ^{1}H NMR (300 MHz, $CDCl_3$): $\delta = 1.30$ (s, 18), 1.33 (s, 18H), 7.27 (m, 5H), 7.82 (s, 1H); ^{13}C NMR (75.44 MHz, $CDCl_3$): $\delta = 29.99$ (C_q), 30.07 (C_q), 32.18 (C_p), 32.25 (C_p), 126.78, 126.99, 128.16, 142.46, 152.29, 173.43; MS (CI, isobutane): *m/z* (%): 476 (28, $M^+ - t$Bu). Correct C, H elemental analyses.

Received: January 20, 1995 [Z 7649 IE]
German version: *Angew. Chem.* **1995**, *107*, 1187

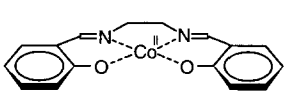
Keywords: germanium compounds · enantiomeric resolution · trigermanes

[1] Reviews: T. Tsumuraya, S. A. Batcheller, S. Masamune, *Angew. Chem.* **1991**, *103*, 916; *Angew. Chem. Int. Ed. Engl.* **1991**, *30*, 902; T. Tsumuraya, Y. Kabe, W. Ando, *J. Organomet. Chem.* **1994**, *482*, 131.
[2] S. Masamune, S. A. Batcheller, J. Park, W. M. Davis, *J. Am. Chem. Soc.* **1989**, *111*, 1888.
[3] T. Tsumuraya, S. Sato, W. Ando, *Organometallics* **1988**, *7*, 2015.
[4] S. A. Batcheller, S. Masamune, *Tetrahedron Lett.* **1988**, *27*, 3383.
[5] T. Tsumuraya, Y. Kabe, W. Ando, *J. Chem. Soc. Chem. Commun.* **1990**, 1159.
[6] W. Ando, T. Tsumuraya, *Organometallics* **1988**, *7*, 1882; T. Tsumuraya, S. Sato, W. Ando, *ibid.* **1990**, *9*, 2061.
[7] Review: Y. Kabe, W. Ando, *Adv. Strain Org. Chem.* **1993**, *3*, 59.
[8] M. Weidenbruch, F.-T. Grimm, M. Herrndorf, A. Schäfer, K. Peters, H. G. von Schnering, *J. Organomet. Chem.* **1988**, *341*, 335.
[9] M. Weidenbruch, A. Ritschl, K. Peters, H. G. von Schnering, *J. Organomet. Chem.* **1992**, *438*, 39.
[10] M. Weidenbruch, A. Ritschl, K. Peters, H. G. von Schnering, *J. Organomet. Chem.* **1992**, *437*, C25.
[11] **4**: $C_{24}H_{54}Ge_3I_2$, $M_r = 814.27$, orthorhombic, space group $P2_12_12_1$, $a = 1794.3(6)$, $b = 1982.3(5)$, $c = 903.5(3)$ pm, $V = 3214(2) \times 10^6$ pm^3, $Z = 4$, $\rho_{calcd} = 1.683$ g cm^{-3}, $Mo_{K\alpha}$ radiation, graphite monochromator, $2\theta_{max} = 55°$, Wyckoff scan, 7382 independent reflections, 6649 observed independent reflections ($F > 3\sigma(F)$), F_0/parameter ratio = 25.2. Solved using direct methods and refined using the Siemens SHELXTL-Plus Program system, $R = 0.048$, $R_w = 0.044$. Due to the systematic evaluation of the reflections *hkl* and $\overline{hkl}$ and the heavy atoms in **4**, it was possible to determine the absolute configuration using "Hamilton's Ratio Test [16]. **5**: $C_{25}H_{42}Ge_2$, $M_r = 475.78$, triclinic, space group $P\bar{1}$, $a = 1166(2)$, $b = 1355(3)$, $c = 826(2)$ pm, $\alpha = 93.1(2)$, $\beta = 91.3(2)$, $\gamma = 105.4(2)°$, $V = 1256(5) \times 10^6$ pm^3, $Z = 2$, $\rho_{calcd} = 1.258$ g cm^{-3}, $Mo_{K\alpha}$ radiation, graphite monochromator, $2\theta_{max} = 55°$, Wyckoff scan, 5763 independent reflections, 4546 observed independent reflections ($F > 3\sigma(F)$), F_0/parameter ratio = 19.3. Solved using direct methods and refined using the Siemens SHELXTL-Plus Program system, $R = 0.077$, $R_w = 0.063$. Further details of the crystal structure investigations may be obtained from the Fachinformationszentrum Karlsruhe, D-76344 Eggenstein-Leopoldshafen (Germany) on quoting the depository numbers CSD-401472 (**5**) and CSD-401473 (**4**).
[12] M. Weidenbruch, B. Flintjer, K. Peters, H. G. von Schnering, *Angew. Chem.* **1986**, *98*, 1090; *Angew. Chem. Int. Ed. Engl.* **1986**, *25*, 1129.
[13] L. Pasteur, *C. R. Hebd. Seances Acad. Sci.* **1848**, *26*, 535.
[14] Reviews: A. Collet, M.-J. Brienne, J. Jacques, *Chem. Rev.* **1980**, *80*, 215; J. Jacques, A. Collet, S. H. Wilen, *Enantiomers, Racemates, and Resolutions*, Wiley, New York, **1981**; E. L. Eliel, S. H. Wilen, L. N. Mander, *Stereochemistry of Organic Compounds*, Wiley, New York, **1994**.
[15] P. B. Hitchcock, M. F. Lappert, S. J. Miles, A. J. Thorne, *J. Chem. Soc. Chem. Commun.* **1984**, 480.
[16] D. Rogers, *Acta Crystallogr. Sect. A* **1981**, *37*, 734.
[17] Average value for the Ge–Ge bonds with sterically undemanding substituents on the germanium atoms. The value corresponds to twice the covalent radius.

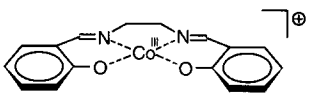
Complexation of [*N*,*N*′-Bis(salicylidene)-ethylenediiminato]cobalt(III)$^+$ by Anilines in Dimethylformamide**

Bernd Speiser* and Hartmut Stahl

[*N*,*N*′-Bis(salicylidene)ethylenediiminato]cobalt(II), [Co^{II}(salen)] **1**, binds oxygen reversibly and is employed as an oxygenation catalyst for the transfer of one or two O atoms to organic substrates.[2–5] It is assumed that a hypothetical ternary complex of **1**, O_2, and a substrate molecule is formed. In investigations of the catalyst in solvent mixtures[6] we have shown that axial ligands in neutral Co^{II} as well as in Co^{III} complexes (having a single positive charge) and with **2** as the central unit can be



1

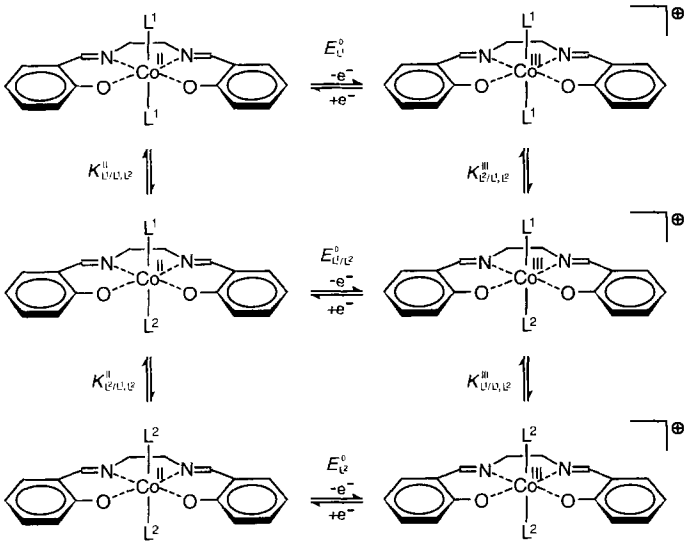


2

exchanged in two steps. A total of six redox-active species are linked together by three electron transfer and four ligand exchange equilibria ("ladder scheme", Scheme 1). We report here that this not only applies when both ligands are solvent molecules, but also that solvent molecules (L^1) can be exchanged by

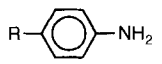
[*] Priv.-Doz. Dr. B. Speiser, Dipl.-Chem. H. Stahl
Institut für Organische Chemie der Universität
Auf der Morgenstelle 18, D-72076 Tübingen (Germany)
Telefax: Int. code + (7071) 29-6205

[**] Electrochemistry of Oxygenation Catalysts, Part 5. This work was supported by the Volkswagen-Stiftung and the Fonds der Chemischen Industrie. B. S. would like to thank the Deutsche Forschungsgemeinschaft for a Heisenberg fellowship. Part **4**: [1].



Scheme 1. Ladder scheme with electron transfer and ligand exchange reactions of [Co(salen)]; for the nomenclature of the equilibrium constants see [8].

substrate molecules (L^2). We also present the equilibrium constants determined by electrochemistry and by NMR spectroscopy for the binding of anilines **3** to $[Co^{III}(salen)]^+$ in dimethylformamide (dmf), a solvent commonly used for oxygenation reactions. The kinetics and thermodynamics of the binding of these substrates to the catalyst may play an important role in the oxygen transfer reaction.



3

a	R=N(CH$_3$)$_2$	**e**	R=Cl
b	R=OCH$_3$	**f**	R=Br
c	R=CH$_3$	**g**	R=CF$_3$
d	R=H	**h**	R=NO$_2$

In dmf the Co^{III} complex, present as $[Co^{III}(salen)(dmf)_2]^+$, is reduced in a quasi-reversible one-electron transfer (formal potential $E^0 = -0.450 \pm 0.007$ V, cyclic voltammogram[7] in Fig. 1a, curve 1). If 4-methoxyaniline (**3b**) is added (Fig. 1a, curve 2, and Fig. 1b) a further reduction peak appears ($E_p \approx -0.7$ V). The intensity of the original peak ($E_p \approx -0.5$ V) is greatly decreased already for a deficit of aniline compared to the complex (Fig. 1a, curve 2), and with a tenfold excess (Fig. 1b, curve 1) this peak disappears. At the same time a new reduction peak at $E_p \approx -1.0$ V appears, which, with a 30-fold excess of aniline, dominates the voltammogram (Fig. 1b, curve 2). In these voltammograms, the oxidation peak remains virtually unchanged.

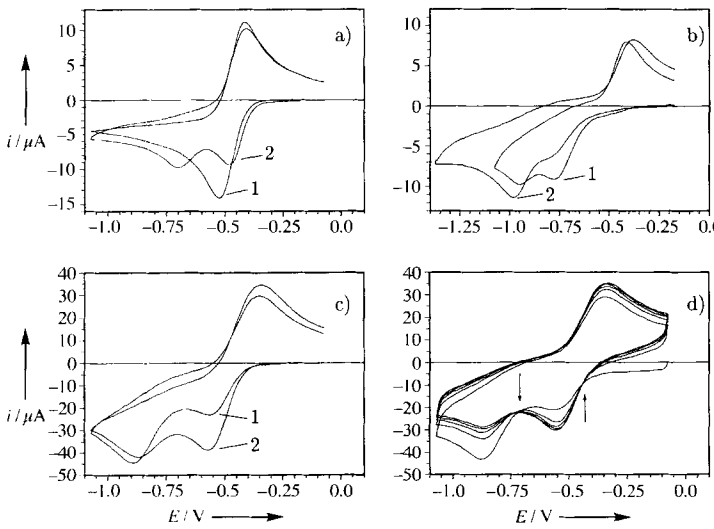


Fig. 1. Cyclic voltammograms of **2**-ClO_4 in dmf. a) Before (curve 1) and after addition of **3b** ($c = 0.24$ mM) (curve 2): c(complex) = 0.45 mM, $v = 0.5$ Vs^{-1}. b) After addition of **3b** [curve 1: $c = 5.02$ mM; curve 2: $c = 15.02$ mM]; c(complex) = 0.45 mM, $v = 0.5$ Vs^{-1}). c) After addition of **3b** [curve 1, c(complex) = 0.75 mM] and **3c**, respectively [curve 2, c(complex) = 0.79 mM]; c(aniline) = 0.75 mM, v = 5.1 Vs^{-1}. d) Current/potential curve with isopotential points (arrows), c(**3b**) = 0.39 mM, c(complex) = 0.73 mM, $v = 5.1$ Vs^{-1}, multicycle experiment.

This behavior is consistent with the presence of a ladder scheme for the exchange of dmf by **3b** [Scheme 1 (L^1 = dmf, L^2 = **3b**)]. As the concentration of **3b** increases, the equilibria on the right-hand side of Scheme 1 shift from top to bottom; starting from $[Co^{III}(salen)(dmf)_2]^+$, a mixed complex $[Co^{III}(salen)(dmf)(\mathbf{3b})]^+$ (reduction at -0.7 V), and then a bis(aniline) species $[Co^{III}(salen)(\mathbf{3b})_2]^+$ (reduction at -1.0 V) are observed. As in the case of the solvent system dmf/pyridine[1] the exchange reactions for the Co^{II} complexes are fast and their equilibria are shifted less to the side of complexes containing L^2. Therefore, because of the large excess of dmf compared to **3b** we find only *one* oxidation peak, which corresponds to the electron transfer $[Co^{II}(salen)(dmf)_2] - e^- \rightarrow [Co^{III}(salen)(dmf)_2]^+$. As in the case of dmf/pyridine, isopotential points are observed here (Fig. 1d). Thus reactions apart from those constituting the ladder scheme can be excluded.[1] Experiments with a number of substituted anilines resulted in analogous cyclic voltammograms. However, it can be seen from Figure 1c that for example 4-methylaniline (**3c**) (curve 2) under almost identical concentration conditions is less strongly bound than **3b** (curve 1).

The ratios of the reduction peak currents in the cyclic voltammograms are independent of the experimental time scale when the sweep rates are larger than $v = 2.0$ Vs^{-1}. Here, the rate of the reactions in the Co^{III} oxidation state is already so small compared to v that the peak currents are measures of the equilibrium concentrations of the individual species. The concentration of free aniline can be determined from its oxidation peak current at more positive potentials (not shown in the cyclic voltammograms in Fig. 1). These concentrations were used to determine the equilibrium constants according to Equation (a)

$$K^{III}_{dmf/dmf,\,3} = \frac{c([Co^{III}(salen)(dmf)(\mathbf{3})]^+) \cdot c(dmf)}{c([Co^{III}(salen)(dmf)_2]^+) \cdot c(\mathbf{3})} \qquad (a)$$

(Table 1)[8] [c(dmf) = 13.0 M]. Nearly all the investigated anilines are capable of displacing dmf from the complex. However, in the case of R = CF_3 (**3g**) the bonding is weak, and for R = NO_2 (**3h**) complexation cannot yet be detected even with an

Table 1. Equilibrium constants for the exchange of axially bound dmf on **2** by anilines **3a**-**3g**.

Aniline	$K^{III}_{dmf/dmf,\,3}$ [a]	$K^{III}_{dmf/dmf,\,3}$ [b]	$K^{III}_{3/dmf,\,3}$ [b]
3a	$2.7 \pm 0.2 \times 10^5$		
3b	$6.1 \pm 1.5 \times 10^4$	$6 \pm 2 \times 10^4$ [c]	1220 ± 90
3c	$1.5 \pm 0.2 \times 10^4$	$1.6 \pm 0.7 \times 10^4$ [c]	290 ± 5
3d	$4.2 \pm 0.4 \times 10^3$	-	-
3e	$1.4 \pm 0.1 \times 10^3$	-	-
3f	980 ± 60	1042 ± 5	43.3 ± 0.3
3g	37 ± 4	-	-

[a] Determined by cyclic voltammetry. [b] Determined by ^{1}H NMR spectroscopy. [c] Error limits determined from the standard deviations of the concentrations (averaged from data from several signals in a spectrum) by using the Gaussian law of error propagation. All the other error limits correspond to standard deviations from several (cyclic voltammetry) or two experiments (^{1}H NMR spectroscopy).

 © VCH Verlagsgesellschaft mbH, D-69451 Weinheim, 1995 0570-0833/95/1010-1087 $ 10.00+.25/0

excess of **3h/2** of roughly 100. Values for the equilibrium constants for the exchange of the second dmf molecule by **3** cannot be obtained from the cyclic voltammograms because several currents are superimposed.

The exchange of the solvent molecules by anilines was also investigated by ^{1}H NMR spectroscopy for three examples (**3b**, **3c**, **3f**).[9] Four species may be present simultaneously in solution: $[Co^{III}(salen)([D_7]dmf)_2]^+$, $[Co^{III}(salen)([D_7]dmf)(\mathbf{3})]^+$, $[Co^{III}(salen)(\mathbf{3})_2]^+$ and free **3**. By recording spectra of solutions of the components **2** and **3** (each separately in $[D_7]$dmf) as well as of solutions with various concentration ratios between **2** and **3**, all the ^{1}H NMR signals can be assigned to the respective species.

Figure 2 shows the changes in the ^{1}H NMR spectra in the regions of the N=CH protons (Figs. 2a–c) and the protons of

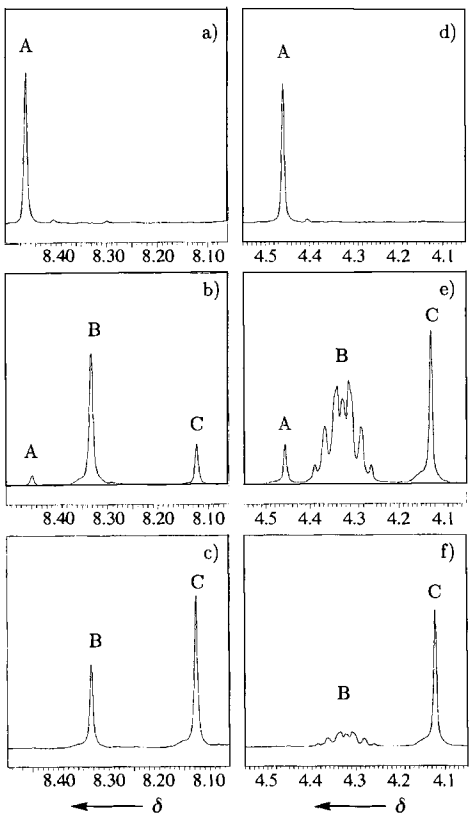


Fig. 2. Parts of the ^{1}H NMR spectra of **2**-ClO_4 in $[D_7]$dmf. a) and d) Without added **3b**; b) and e) concentration ratio **2**:**3b** = 1:1.18; c) and f) concentration ratio **2**:**3b** = 1:1.81.

the ethylene bridge (Figs. 2d–f) in the salen ligands with different concentrations of **3b**. Initially, the azomethine protons give rise to only one signal (δ(A) = 8.45, bis($[D_7]$dmf) complex), while at higher concentrations of **3b** several singlets are observed. The intensity of signal B (δ = 8.33, mixed complex) increases and then decreases, whilst signal C (δ = 8.13, $[Co^{III}(salen)(\mathbf{3b})_2]^+$) becomes more intense with increasing aniline concentration. The signals of the H atoms of the ethylene bridge behave analogously. In the spectrum of the mixed complex, in contrast to the other species, however, there is a multiplet (AA'BB' system). Similar multiplets were observed for Co^{III} Schiff base complexes substituted with two different axial ligands.[10, 11] We explain this coupling pattern in $[Co^{III}(salen)(dmf)(\mathbf{3})]^+$ by a nonplanar, flexible conformation of the N-CH_2-CH_2-N bridge in the salen ligand. We obtained analogous spectra for **3c** and **3f**.

The integration of the signals in the ^{1}H NMR spectra and the total weighted amounts of **2**-ClO_4 and **3** were used to determine the amounts of the equilibrium partners present, and from those the equilibrium constants (Table 1). The values obtained for $K^{III}_{dmf/dmf,3}$ are in very good agreement with those determined electrochemically. In addition, we succeeded in evaluating $K^{III}_{3/dmf,3}$, the equilibrium constant for the exchange of the second solvent molecule by **3**. The values for $K^{III}_{3/dmf,3}$ are smaller than the values of $K^{III}_{dmf/dmf,3}$ by several orders of magnitude (see Table 1) due to statistical[12] and electronical reasons.

The equilibrium constants $K^{III}_{dmf/dmf,3}$ determined electrochemically correlate linearly with the σ_p substituent constants:[13] $K^{III}_{dmf/dmf,3} = 3.64 - 3.28\,\sigma_p$ (r = 0.984). The σ_p^- and the σ_p^0 series give—in contrast to σ_p^+—only slightly inferior correlations. The more electron-rich the aniline, the more sucessfully it can displace dmf from the $Co^{III}(dmf)_2$ complex. However, the effect is not completely parallel to the basicity of the anilines which, at least in water, is best represented by the σ_p^- constants.[14]

Therefore, we have succeeded in characterizing the thermodynamics of the interaction of $[Co^{III}(salen)]^+$ **2** with anilines **3** by two methods and have obtained concurrent results. The displacement of dmf by **3**, as given by the equilibrium constants found here, is part of the ladder scheme which is decisive for the redox reactions of [Co(salen)] **1** in dmf in the presence of anilines. The exchange of ligands considerably shifts the redox potentials of the complexes. Although at least the electrochemical experiments were conducted with exclusion of oxygen, the results are also fundamental for the comprehension of oxygenation reactions with Co Schiff base catalysts. Redox reactions at the Co center are part of the oxygenation.[15] Basic axial ligands favor the complexation of oxygen thermodynamically.[4, 16] Furthermore, axially bound bases increase the rate of the O_2 uptake by Co–tetrahydrosalen complexes with simultaneous dehydrogenation.[17] Finally, the ease with which the anilines coordinate to $[Co^{III}(salen)]^+$ **2** in dmf is parallel to the ease and yield of their preparative oxygenation.[18] Thus the reaction steps characterized here must be a central part of the oxygenation mechanism.

Received: November 17, 1994
Revised version: February 27, 1995 [Z 7480 IE]
German version: *Angew. Chem.* **1995**, *107*, 1222

Keywords: anilines · cobalt compounds · oxygenations · Schiff base complexes

[1] E. Eichhorn, B. Speiser, *J. Electroanal. Chem. Interfacial Electrochem.* **1994**, *365*, 207–212.
[2] T. Matsuura, *Tetrahedron* **1977**, *33*, 2869–2905.
[3] A. E. Martell, D. T. Sawyer, Jr., *Oxygen Complexes and Oxygen Activation by Transition Metals*, Plenum, New York, **1988**.
[4] A. Sobkowiak, D. T. Sawyer, *J. Am. Chem. Soc.* **1991**, *113*, 9520–9523.
[5] A. Nishinaga, S. Förster, E. Eichhorn, B. Speiser, A. Rieker, *Tetrahedron Lett.* **1992**, *33*, 4425–4428.
[6] E. Eichhorn, A. Rieker, B. Speiser, *Angew. Chem.* **1992**, *104*, 1246–1248; *Angew. Chem. Int. Ed. Engl.* **1992**, *31*, 1215–1217.
[7] All potentials are reported versus the ferrocene/ferrocenium ion standard redox couple [19] in dmf. Cyclic voltammetry was carried out in a full glass cell under argon with a three-electrode system [working electrode: Pt electrode tip (Metrohm) with an electroactive surface A = 0.076 cm^2; counterelectrode: Pt wire; reference electrode: Ag/Ag^+ (0.01 M) in CH_3CN/0.1 M NBu_4PF_6, connected to the working electrode with a Haber–Luggin capillary; Pt wire [20] placed in parallel to reduce interference]. dmf was dried over activated molecular sieves (3 Å) and fractionally distilled four times. $[Co^{III}(salen)]ClO_4$ was synthesized as the dihydrate or as the bis(dmf) complex [1]. The anilines were purified by distillation or sublimation.
[8] The superscript specifies the oxidation state of the complex in which the ligand exchange takes place; in the subscript the axial ligand remaining bonded to the central atom is given first then the two exchanging ligands in order of increasing basicity.
[9] Solvent: $[D_7]$dmf; spectrometer: Bruker AMX 400; chemical shifts are referenced to tetramethylsilane.

[10] C. Floriani, M. Puppis, F. Calderazzo, *J. Organomet. Chem.* **1968**, *12*, 209–223.
[11] H. A. O. Hill, K. G. Morallee, G. Pellizer, *J. Chem. Soc. A* **1969**, 2096–2101.
[12] F. A. Cotton, G. Wilkinson, *Anorganische Chemie – eine zusammenfassende Preparation for Fortgeschrittene*, 3rd ed., Verlag Chemie, Weinheim, **1974**, p. 687.
[13] O. Exner, *Correlation Analysis of Chemical Data*, Plenum, New York, **1988**.
[14] Ref. [13], p. 71.
[15] F. Basolo in *Facets of Coordination Chemistry* (Eds.: B. V. Agarvala, K. N. Munshi), World Scientific, Singapore, **1993**, Chapter 3, pp. 24–45.
[16] M. J. Carter, D. P. Rillema, F. Basolo, *J. Am. Chem. Soc.* **1974**, *96*, 392–400.
[17] A. Böttcher, H. Elias, E.-G. Jäger, H. Langfelderova, M. Mazur, L. Müller, H. Paulus, P. Pelikan, M. Rudolph, M. Valko, *Inorg. Chem.* **1993**, *32*, 4131–4138.
[18] S. Förster, A. Rieker, Tübingen, personal communication.
[19] G. Gritzner, J. Kůta, *Pure Appl. Chem.* **1984**, *56*, 461–466.
[20] B. Gollas, B. Krauss, B. Speiser, H. Stahl, *Curr. Sep.* **1994**, *13*, 42–44.

$(Nb,Ta)_9(S,Te)_5$, a Metal-Rich Chalcogenide with a Microporous Metal Substructure**

Thomas Degen and Bernd Harbrecht*

Niobium and tantalum form several metal-rich chalcogenides of complex structure. Compounds such as $Nb_{21}S_8$,[1] Nb_5Se_4,[2] or Ta_6S[3] have been known for many years; others such as Ta_6S (triclinic),[4] Ta_3S_2,[5] Ta_2Se,[6] $Nb_{4.7}Te_5$,[7] Ta_2Te_3,[8] and Ta_6Te_5[9] have been characterized very recently. A striking feature of these compounds is the structural heterogeneity which, as a matter of fact, is not only due to variation in composition. The pronounced variety is also based on the fact that the structures of the sulfides, selenides, and tellurides differ significantly, as do the structures of the niobium- and tantalum-rich chalcogenides. Thus, compounds with the same number of valence electrons, for example Ta_2S,[10] Ta_2Se,[6] and Nb_2Se,[11] form unique structures. Whereas the metal partial structure of the sulfide comprises interpenetrating and interconnecting Ta_{13} icosahedra, the structures of the selenides contain fragments of the metal bcc structure. Such bcc fragments extend in three dimensions in Nb_2Se, but are confined to two dimensions in Ta_2Se.

The structural diversification caused by both components, metal and chalcogen, evidently holds a remarkable potential for syntheses: Structurally modified phases such as $Ta_{6-x}V_xS$,[12] $AuTa_5S$,[13] or $Ta_2S_{1-x}Se_x$[14] are accessible by partial substitution at the metal or chalcogen atom sites in phases of known stoichiometry. Moreover, ternary phases of new compositions and structural types such as $Au_xTa_{15-x}S_2$,[13] $Ta_n(S,Se)_4$ ($n = 9$, 10),[14b] and $(Nb,Ta)_nS_4$ ($n = 10-12$)[15] have been characterized. In some cases such phases exhibit only small, islandlike homogeneity ranges in the three-component systems. Here we report a new phase[16] existing in the quaternary system Nb-Ta-S-Te. It is formed by reduction of a mixture of niobium dichalcogenides by the elemental metals in sealed tantalum ampoules (1870 K to 1470 K, 12 h). The phase occurred in form of a black wad containing a few needles, up to 50 μm thick. EDX analyses proved that the needlelike crystals and the fibrous product of a batch do not noticeably differ in composition. Phases of different batches had nearly constant ratios n_S/n_{Te} (about 2) even when starting mixtures containing equimolar amounts of dichalcogenides were used. In contrast, the metal ratios n_{Nb}/n_{Ta} could vary significantly: examples so far varied from about 1 to 3.

The structure[17] (Fig. 1) contains—like numerous structures of niobium-rich chalcogenides and pnictides—fragments of the bcc arrangement of the element (see Fig. 2). A striking new feature is that those complex columnar bcc fragments (Fig. 1, bottom) are connected through extended metal-metal bonding regions—indicated by numerous M–M distances in the range of 283–342 pm—to a remarkable microporous metal partial structure. The remaining valences on the inner surfaces of the pores are saturated by chalcogen atoms. In accord with their surface-covering function, these chalcogen atoms are coordinated on one side by four, five, or six metal atoms. The chalcogen atoms themselves enclose channels that in principal could serve as hosts for small metal atoms.

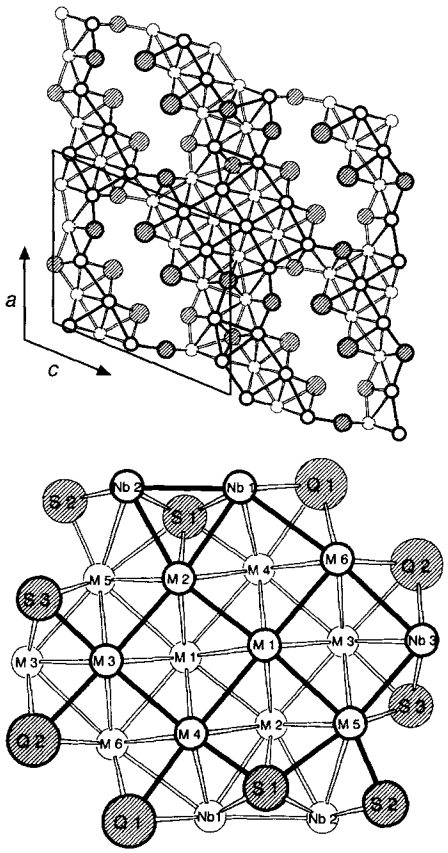


Fig. 1. Section of the structure of $(Nb,Ta)_9(S,Te)_5$ shown as a projection along *b*. Top: Four unit cells. Bottom: Double asymmetric unit. All atoms are in mirror planes perpendicular to *b* at $y = 1/4$ and 3/4 modulo 1; atoms from neighboring layers are symmetry-related by 2_1 screw axes; different depths are indicated by outlines of different thickness for the circles; for occupation factors of the positions M1–M6 and Q1, Q2 with mixed occupation, see text.

The seemingly arbitrary coordination figures of the chalcogenides are based on a common construction principle: They are fragments of a tetrakaidecahedron, a regular body with 14 planes, built up of nine metal atoms located at the vertices of a tricapped trigonal prism. In accordance with the topological concept that was developed for the boranes,[18] the coordination figure about S3 (see Fig. 1, bottom) with the coordination number six (average distance: 254.5 pm) is a *hypho* fragment. The polyhedra that cover the five-coordinate positions with mixed occupation represented by the symbols for chalcogens Q1 (80(1)% Te, 20% S, 291.1 pm) and Q2 (74(1)% Te, 26% S, 289.3 pm) correspond to

[*] Prof. Dr. B. Harbrecht, Dipl.-Chem. T. Degen
Institut für Anorganische Chemie der Universität
Gerhard-Domagk-Strasse 1, D-53121 Bonn (Germany)
Telefax: Int. code + (228) 73-5660

[**] This work was supported by the Deutsche Forschungsgemeinschaft, the Fonds der Chemischen Industrie, and the Ministerium für Wissenschaft und Forschung des Landes Nordrhein-Westfalen. We wish to thank Dr. M. Nieger for the measurement of the single crystal data.

a sub-*hypho* fragment. S2 is only fourfold coordinated (249.2 pm). S1 has a special function playing a decisive role in the aggregation of the bcc fragments. The nine surrounding metal atoms (262.1 pm) form a *closo*-cluster which is otherwise found only in the most metal-rich sulfides, for example $Au_xTa_{15-x}S_2$ (265.6 pm).[13] As expected, the average distances correlate with the coordination numbers of the chalcogen atoms and for a given coordination geometry, reflect slight differences in S/Te occupations. Neighboring chalcogen atoms (shortest distances: 339.8 pm (S2–S3), 341.6 pm (*b* lattice constant)) are in van der Waals contact.

The analysis of electron density leads to two (out of five) chalcogen positions with mixed occupation (Q1, Q2) if we assume that all 14 distinct positions are fully occupied. At the metal sites, six (M1–M6) out of nine are statistically occupied. Nevertheless the specific distribution of the metal atoms is more likely driven by a minimization of enthalpy than by maximization of entropy. Like in the case of the mixed sulfides $(Nb,Ta)_nS_4$,[5] tantalum preferably accumulates at the central positions of the bcc fragments, in accordance with its cohesive energy that is higher than that of niobium. M1 at the center, most enriched with tantalum (67.4(9)%), is surrounded primarily by metal atoms only (six plus eight). The chemically similar atoms M2 (50.5(9)%), M3 (49.1(9)%), and M4 (48.7(9)%) each have two chalcogen atoms in the 14-fold coordination. Considerably less tantalum is found at M5 (24.3(9)%) and M6 (9.6(9)%). At these sites, 4 out of 14 and 13 neighbors, respectively, are chalcogen atoms. Nb1 and Nb3 occupy peripheral positions of the bcc fragments. They are, like Nb2, primarily coordinated by five chalcogen atoms.

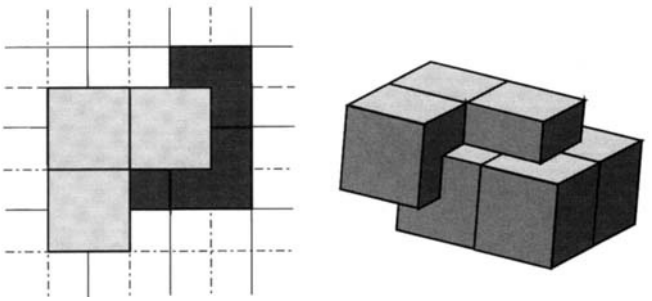


Fig. 2. Schematic representation of the columnar bcc fragments of $(Nb,Ta)_9(S,Te)_5$ as sections of 4^4 nets (left) and interpenetrating cubes (right).

Because of the larger number of Nb–Q contacts, such a partitioning pattern is also favored if the affinity of chalcogen is larger toward niobium than toward tantalum. This sequence in the affinities is also indicated by the higher decomposition pressure above Ta_2S/Ta_6S than above $Nb_{21}S_8/Nb_{14}S_5$ at a given high temperature.[19] Extended Hückel calculations, however, point to stronger Ta–S interactions than Nb–S interactions.[20] If these calculations were correct and if the M–Q interactions were the deciding factor for the occupation, tantalum should accumulate at the periphery of the fragments. All results known so far reject this distribution (see also ref. [15]). The partition of the metal atoms is obviously dominated by the differences between the cohesive energies of the metals.

The compound $(Nb,Ta)_9(S,Te)_5$ gives rise to the idea that phases with more marked, perhaps even zeolite-like, porosity may be hidden in the metal-rich regions of multicomponent chalcogen-containing systems. We think it is worthwhile to track down such phases.

Received: October 12, 1994 [Z 7396 IE]
German version: *Angew. Chem.* **1995**, *107*, 1226

Keywords: chalcogen compounds · niobium compounds · solid-state structures · tantalum compounds

[1] H. F. Franzen, T. A. Beineke, B. R. Conard, *Acta Crystallogr. Sect. B* **1968**, *24*, 412.
[2] K. Selte, A. Kjekshus, *Acta Chem. Scand.* **1963**, *17*, 2560.
[3] H. F. Franzen, J. G. Smeggil, *Acta Crystallogr. Sect. B* **1970**, *26*, 125.
[4] B. Harbrecht, *J. Less-Common Met.* **1988**, *138*, 225; H. Nozaki, H. Wada, S. Takekawa, *J. Phys. Soc. Jpn.* **1991**, *60*, 3510.
[5] a) H. Wada, M. Onoda, *Mater. Res. Bull.* **1989**, *24*, 191; b) S. J. Kim, K. S. Nanjundaswamy; T. Hughbanks, *Inorg. Chem.* **1991**, *30*, 159; c) K. Ahn, T. Hughbanks, *J. Solid State Chem.* **1993**, *102*, 446; d) T. Degen, B. Harbrecht, *Acta Crystallogr. Sect. C*, in press.
[6] B. Harbrecht, *Angew. Chem.* **1989**, *101*, 1696; *Angew. Chem. Int. Ed. Engl.* **1989**, *28*, 1660.
[7] R. Dronskowski, A. Simon, P. Plambeck-Fischer, *Z. Kristallogr.* **1992**, *198*, 101.
[8] M. Conrad, B. Harbrecht, *J. Alloys Compd.* **1992**, *187*, 181.
[9] M. Conrad, B. Harbrecht, *IVth Eur. Conf. Solid State Chem.*, Dresden, **1992**, p. 324.
[10] H. F. Franzen, J. G. Smeggil, *Acta Crystallogr. Sect. B* **1969**, *25*, 1736.
[11] B. R. Conard, L. J. Norrby, H. F. Franzen, *Acta Crystallogr. Sect. B* **1969**, *25*, 1729.
[12] B. Harbrecht, H. F. Franzen, *Z. Anorg. Allg. Chem.* **1987**, *551*, 74.
[13] a) V. Wagner, Dissertation, Universität Dortmund, **1994**; b) B. Harbrecht, V. Wagner, *Z. Anorg. Allg. Chem.* **1994**, *620*, 969.
[14] a) K. S. Nanjundaswamy, T. Hughbanks, *J. Solid State Chem.* **1992**, *98*, 278; b) B. Harbrecht, T. Degen, *7. Tagung Festkörperanalytik*, Chemnitz, **1993**, p. 136.
[15] a) X. Yao, H. F. Franzen, *J. Solid State Chem.* **1990**, *86*, 88; b) X. Yao, H. F. Franzen, *J. Am. Chem. Soc.* **1991**, *113*, 1426; c) X. Yao, H. F. Franzen, *Z. Anorg. Allg. Chem.* **1991**, *598/599*, 353.
[16] $(Nb,Ta)_9(S,Te)_5$ together with another metal-rich phase with completely different structure, $Ta_5(S,Te)_2$, $C2/c$, $Z = 16$, $a = 1547.5(6)$ pm, $b = 1421.3(4)$ pm, $c = 1041.1(4)$ pm, $= 108.65(3)°$, $R(F_0) = 0.045$, was presented at a conference: T. Degen, B. Harbrecht, 5. Vortragstagung der Fachgruppe Festkörperchemie, Bonn (Germany), **1994**.
[17] Data of the crystal structure analysis of $(Nb,Ta)_9(S,Te)_5$: $Mo_{K\alpha}$ radiation, CAD 4 diffractometer, SDP Plus (Enraf Nonius), crystal dimensions: $0.03 \times 0.03 \times 0.30$ mm^3, space group: $P2_1/m$, $Z = 2$, $a = 1226.4(3)$, $b = 341.6(1)$, $c = 1355.2(3)$ pm, $\beta = 112.52(2)°$, ω–2θ scans, $\theta_{max} = 32°$, 3782 reflections, 983 unique reflections with $I_o > 3\sigma(I_o)$, absorption correction (psi scans), $R_{int}(F) = 0.045$, 94 variables, $R(F_0)/R_w(F_0) = 0.061/0.074$, composition as determined by X-ray crystal structure analysis: $Nb_{6.50}Ta_{2.50(5)}S_{3.46}Te_{1.54(2)}$; further details of the crystal structure investigation may be obtained from the Fachinformationszentrum Karlsruhe, D-76344, Eggenstein-Leopoldshafen (Germany), on quoting the depository number CSD-58765.
[18] a) W. N. Lipscomb, *Boron Hydrides*, Benjamin, New York, 1963; b) R. W. Rudolph, *Acc. Chem. Res.* **1976**, *9*, 67; c) R. E. Williams, *Adv. Inorg. Chem. Radiochem.* **1976**, *18*, 67; d) K. Wade, *ibid.* **1976**, *18*, 1.
[19] Only vapor pressures above the tantalum-rich sulfides are detectable by means of the Knudsen effusion method in the temperature range 1500 K–1950 K with an accuracy sufficient to determine meaningful thermodynamic values: B. Harbrecht, S. R. Schmidt, H. F. Franzen, *J. Solid State Chem.* **1984**, *53*, 113.
[20] a) X. Yao, G. J. Miller, H. F. Franzen, *J. Alloys Comp.*, **1992**, *183*, 7; b) X. Yao, G. Marking, G. J. Miller, *Ber. Bunsenges. Phys. Chem.*, **1992**, *96*, 1552.

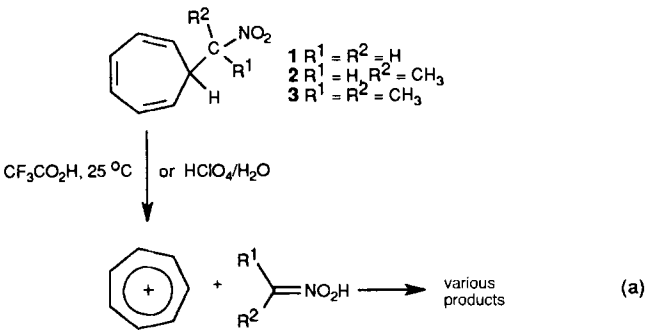
 © VCH Verlagsgesellschaft mbH, D-69451 Weinheim, 1995 0570-0833/95/1010-1090 $ 10.00+.25/0

Formation of Nitronic Acids by Ring Opening of Nitrocyclopropanes by a Concerted, Acid-Catalyzed Mechanism**

Weiguo Cao, Ihsan Erden,* and James R. Keeffe*

Tautomerism of aldehydes, ketones, and nitroalkanes has played a central role in the development of our ideas about acid- and base-catalyzed reactions. Unlike the interconversion of keto and enol isomers, the nitroalkane–nitronic acid prototropy is not acid-catalyzed;[1] this is presumably a consequence of the very poor basicity of the nitro group coupled with its ability to permit C–H cleavage by bases as weak as water itself.[2]

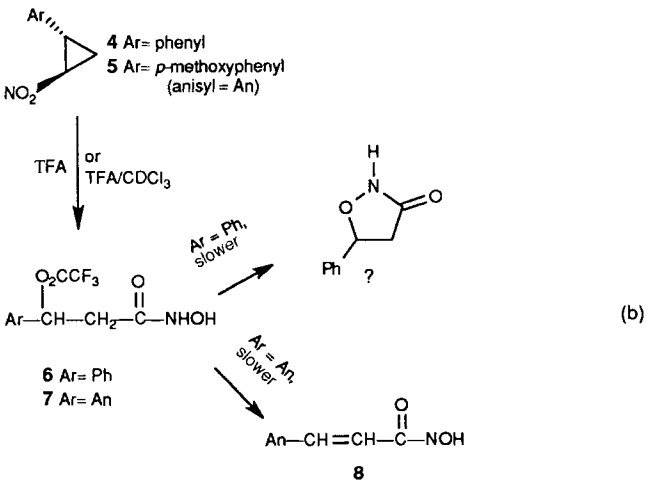
Recently we reported on the formation of nitronic acids from nitroalkanes **1**–**3** under acid catalysis.[3] In these reactions [Eq. (a)] the departing electrofuge is not a proton, but the highly



(a)

stable tropylium cation (Tr^+), which can depart from the protonated nitroalkane in a unimolecular fashion (no base needed).

In this communication we show that relief of ring strain is a powerful factor which also enables acid-catalyzed cleavage of a C–C bond in nitroalkanes. Compounds **4** and **5** undergo ready ring opening at or below room temperature in CF_3CO_2H (TFA), or (more slowly) in 4 M TFA in $CDCl_3$,[4] to give the products shown in Equation (b).



(b)

Compounds **6**–**8** were synthesized independently and subjected to the reaction conditions. The ^1H NMR spectra of these synthesized compounds were identical to the spectra of the reaction solution corresponding to Equation (b) and also indicated the slower formation of secondary products from **6** and **7**.[5] The spectra for reactions in deuterated and non-deuterated TFA were identical. Even after the starting material had disappeared, there was no evidence of deuterium incorporation, as would be found if protonation of the cyclopropane ring had occurred.[6] Hydroxamic acids are, in fact, the products expected from the generation of nitronic acids, $RCH{=}NO_2H$, in strongly acidic media.[1, 3, 7]

Compound **5** reacts with TFA much more rapidly than **4** does. The reaction of **4** in TFA and in 4 M TFA in $CDCl_3$ showed excellent first-order kinetics.[8] The rate constants for the reaction of compounds **1**–**5** are listed in Table 1. Although it was

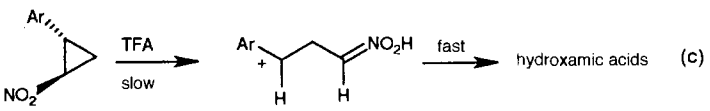
Table 1. Rate constants k for acid-catalyzed cleavage of tropylnitroalkanes **1**–**3** and 1-nitro-2-arylcyclopropanes **4** and **5** in CF_3CO_2H.

Compound	$k \times 10^3$ [s^{-1}] TFA	T [°C]	$k \times 10^3$ [s^{-1}] 4 M TFA/$CDCl_3$	T [°C]
1	0.0335 [a]	25	–	–
2	0.590 [a]	25	–	–
3	11.8 [a]	25	–	–
4	1.08, 0.51 [b]	18–20	0.0117	18–20
5	–	18–20	>23	18–20

[a] Ref. [3]. [b] In [D]TFA corrected for contribution from 2 mol% TFA.

not possible with our NMR method to determine accurately the rate of reaction of **5**, we could obtain a lower limit in the TFA/$CDCl_3$ medium. The rate constant of **5** is more than 2000 times greater than that of **4**, which allows an estimate of the reaction constant, $-\rho^+ \geq 4$. ρ values of this magnitude are common for reactions leading to carbocation-like transition states from tetracoordinate precursors.[9]

A solvent kinetic hydrogen isotope effect $k_{TFA}/k_{[D]TFA}$ of 2.1 ± 0.1 was determined for the reaction of **4**. Based on this result and the large *para*-substituent effect, we propose that protonation of the nitro group and cleavage of the C1–C2 bond are *concerted* [Eq. (c)]. As in aqueous solutions, preequilibrium



(c)

protonation followed by a rate-controlling step, is revealed in TFA by an inverse solvent kinetic isotope effect.[10] To the best of our knowledge no other examples of protonation at a heteroatom concomitant with C–C bond cleavage have been demonstrated. We suggest that relief of ring strain enabled by incipient protonation is the causal factor.

Experimentally observed primary kinetic isotope effects for proton transfer between heteroatoms are not common, but have been reported by several groups.[11] Maxima in k_H/k_D ranging from roughly 2.5 to 4.3 have been found; such maxima appear to require a close match of the pK_a values of the proton donor and acceptor. The magnitude of the effect drops off rapidly as ΔpK_a deviates from the optimum. These smaller values signify either a variable isotope effect on the proton transfer step itself and/or partial rate control by preceeding or succeeding steps: encounter and association of reactants, or separation of the

[*] Prof. Dr. I. Erden, Prof. Dr. J. R. Keeffe, W. Cao
Department of Chemistry and Biochemistry
San Francisco State University
San Francisco, CA 94132 (USA)
Telefax: Int. code + (415)338-2384

[**] This work was supported by the National Institutes of Health and the National Science Foundation. We thank Dr. Scott Gronert, San Francisco State University, for valuable discussions.

conjugate acid/conjugate base pair. At first glance it does not appear that the pK_a values can be similar in the present case. A protonated nitroalkane should be much more acidic than TFA. We postulate that nitrocyclopropanes, especially if activated by donors at C2, are effectively more basic than expected owing to electron release from the C1–C2 bond. Since this mode of release opens the ring, protonation produces a nitronic acid rather than a protonated nitroalkane. The transition state might be further stabilized by interaction at C2 with the solvent. In another scenario the transferred proton is not part of the reaction coordinate but always lies in a stable potential well.[12] A hydrogen-bonded TFA–nitrocyclopropane complex first forms, then the C1–C2 bond starts to break. During the bond cleavage the NO_2 oxygen atoms become more basic until the pK_a values of the donor and acceptor nearly match. The proton then moves to the NO_2 group in an altered hydrogen-bonded complex. The isotope effect arises as a consequence of a reduced zero-point energy difference for the hydrogen bond in the transition state relative to that in the initial TFA–nitrocyclopropane complex.[13]

Semiempirical MO calculations (AM1[14] and PM3[15]) support the possibility of a concerted ring opening for **4** and **5**. Although conjugate acids $\mathbf{4H^+}$ and $\mathbf{5H^+}$ are found to be stable, transition states for the succeeding reaction are only 2.5–3.9 kcal mol^{-1} higher in energy. By contrast cleavage of protonated tropylnitroalkanes $\mathbf{1H^+}$–$\mathbf{3H^+}$ is calculated to require another 12 kcal mol^{-1} of activation.

Finally, we wish to quantify the effect of ring strain in these C–C heterolyses. Despite the enormous difference in stability between tropylium ion ($pK_R^+ = 4.7$)[16] and $PhCHR^+$ (estimated $pK_R^+ = -15.3$),[9] compounds **2** and **4** react with TFA at similar rates to yield monoalkylnitronic acids $RCH{=}NO_2H$ (Table 1). The ΔpK_R^+ of approximately 20 units corresponds to 27 kcal mol^{-1} at room temperature, which is also the strain energy of a cyclopropane ring.[17] The two compounds present an interesting case in which the development of carbocation character at the transition state, a factor favoring the reaction of **2**, is almost exactly balanced by relief of ring strain favoring **4**!

Received: November 23, 1994 [Z 7493 IE]
German version: *Angew. Chem.* **1995**, *107*, 1206

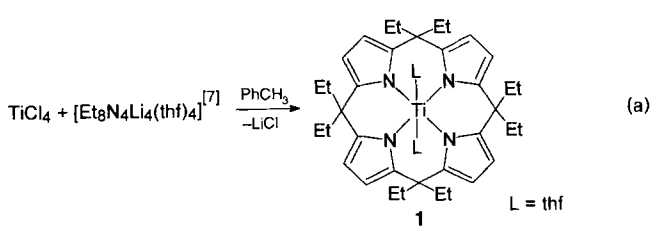
Keywords: cyclopropanes · hydroxamic acids · nitronic acids · reaction mechanisms · ring strain

[1] J. T. Edward, P. H. Tremaine, *Can. J. Chem.* **1971**, *49*, 3483, 3489, 3493.
[2] The pK_{BH^+} value of nitromethane is about −12 (E. M. Arnett in *Progress in Physical Organic Chemistry* (Eds.: S. G. Cohen, A. Streitwieser, R. N. Taft), Wiley-Interscience, New York, **1963**, p. 223); that of acetone is about −3.1 (A. Bagno, G. Scorrano, R. A. More O'Ferrall, *Rev. Chem. Intermed.* **1987**, *7*, 313; A. Bagno, V. Lucchini, G. Scorrano, *Bull. Soc. Chim. Fr.* **1987**, 563). Rate constants for deprotonation by water (25 °C) are 4.3×10^{-8} s^{-1} for nitromethane (D. Turnbull, S. H. Maron, *J. Am. Chem. Soc.* **1943**, *65*, 212) and 4.6×10^{-10} s^{-1} for acetone (R. Stewart, R. Srinivasan, *Can. J. Chem.* **1981**, *59*, 957).
[3] I. Erden, J. R. Keeffe, F.-P. Xu, J.-B. Zheng, *J. Am. Chem. Soc.* **1993**, *115*, 9834.
[4] Compounds **4** and **5** were synthesized according to J. Asunskis, H. Shechter *J. Org. Chem.* **1968**, *33*, 1164.
[5] Compounds **6**–**8** were generated in situ by addition of the corresponding 3-aryl-3-hydroxyhydroxamic acids to TFA (or TFA/$CDCl_3$) containing an equivalent of trifluoroacetic anhydride (TFAA). Compounds **6** and **7** form from the alcohols almost immediately: K. B. Wiberg, D. J. Wasserman, E. J. Martin, M. A. Murcko, *J. Am. Chem. Soc.* **1985**, *107*, 6019. Subsequent formation of **8** from **7**, and of the postulated cyclic hydroxamate ester from **6** is slower. The 3-aryl-3-hydroxyhydroxamic acids **6** and **7**, as well as compound **8** were synthesized from their methyl or ethyl esters: C. R. Hauser, W. B. Renfrow, Jr., *Org. Synth. Coll., Vol. 2*, **1943**, 67–68.
[6] The addition of TFA to phenylcyclopropane with ring opening is at least ten times slower than the addition of TFA to **4**. The products are 1-phenylpropyl trifluoroacetate and the Friedel–Crafts dimers (1-phenylpropyl)phenylcyclopropane (*o*:*m*:*p* = 1:1:2).
[7] N. Kornblum, R. A. Brown, *J. Am. Chem. Soc.* **1965**, *87*, 1742.
[8] The disappearance of **4** was monitored by ^{1}H NMR spectroscopy (each of three different signals) over three to five half-lives. For the studies on the solvent isotope effect identical media (except for the isotope) were prepared by addition of 0.98 equivalents of H_2O (D_2O) to TFAA. In both media a substrate concentration of 0.45 M was used.
[9] J. P. Richard, M. E. Rothenberg, W. P. Jencks, *J. Am. Chem. Soc.* **1984**, *106*, 1361.
[10] C. M. Brennan, I. Hunt, T. C. Jarvis, C. D. Johnson, P. D. McDonnell, *Can. J. Chem.* **1990**, *68*, 1780.
[11] N.-Å. Bergman, Y. Chiang, A. J. Kresge, *J. Am. Chem. Soc.* **1978**, *100*, 5954; M. M. Cox, W. P. Jencks, *ibid.* **1978**, *100*, 5956; A. J. Kresge, *Pure Appl. Chem.* **1981**, *53*, 189; B. G. Cox, N. V. Truong, H. Schneider, *J. Chem. Soc. Perkin Trans. 2* **1983**, 515.
[12] C. G. Swain, D. A. Kuhn, R. L. Schowen, *J. Am. Chem. Soc.* **1965**, *87*, 1553; R. Eliason, M. M. Kreevoy, *ibid.* **1978**, *100*, 7037.
[13] In support of this picture are the low fractionation factors observed and modeled for hydrogen-bonded complexes by Kreevoy and Liang: M. M. Kreevoy, T. M. Liang, *J. Am. Chem. Soc.* **1980**, *102*, 3315. For a recent discussion of the vibrational behavior and kinetic advantages of "low-barrier hydrogen bonds" see: W. W. Cleland, M. M. Kreevoy, *Science* **1994**, *264*, 1887. For an application to serine protease action see: P. A. Frey, S. A. Whitt, J. B. Tobin, *ibid.* **1994**, *264*, 1927.
[14] M. J. S. Dewar, E. G. Zoebisch, E. F. Healy, J. J. P. Stewart, *J. Am. Chem. Soc.* **1985**, *107*, 3902.
[15] J. J. P. Stewart, *J. Comput. Chem.* **1989**, *10*, 221.
[16] W. von E. Doering, L. H. Knox, *J. Am. Chem. Soc.* **1954**, *76*, 3203.
[17] A. de Meijere, *Angew. Chem.* **1979**, *91*, 867; *Angew. Chem. Int. Ed. Engl.* **1979**, *18*, 809; K. B. Wiberg, *Angew. Chem.* **1986**, *98*, 312; *Angew. Chem. Int. Ed. Engl.* **1986**, *25*, 312.

A Li_2Ti_2-Substituted Acetylene Formed from Ethylene by Reaction with (*meso*-Octaethylporphyrinogen)titanium**

Stefania De Angelis, Euro Solari, Carlo Floriani,* Angiola Chiesi-Villa, and Corrado Rizzoli

The chemistry of metal carbides is dramatically expanding in a number of directions.[1] These compounds include those in which linear carbon chains bridge different organometallic building blocks.[2] In particular, complexes with a C_2 bridge, which can be obtained readily from acetylene,[3] are a rapidly developing class of compounds.[4] We report here the one-step synthesis of a complex with C_2 bridge directly from ethylene. The "naked" C_2 unit is confined in a square-planar array of two titanium and two lithium cations supported by two *meso*-octaethylporphyrinogen tetraanions ($Et_8N_4^{4-}$).[5] The starting material $[Et_8N_4Ti(thf)_2]$ **1** was obtained by the established procedure[5] according to Equation (a) and its structure shown in Figure 1.[6]



(a)

1

[*] Prof. Dr. C. Floriani, S. De Angelis, Dr. E. Solari
Institut de Chimie Minérale et Analytique
Université de Lausanne
BCH 3307, CH-1015 Lausanne (Switzerland)
Telefax: Int. code + (21) 692-3905
Prof. Dr. A. Chiesi-Villa, Dr. C. Rizzoli
Dipartimento di Chimica, Università di Parma (Italy)

[**] This work was supported by the Fonds National Suisse de la Recherche Scientifique (grant. no. 20-40268.94) and Ciba-Geigy (Basel, Switzerland).

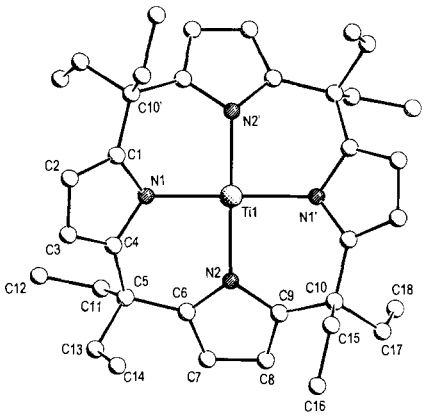
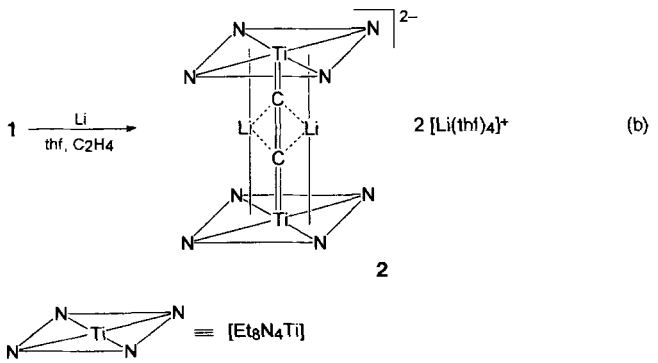


Fig. 1. Crystal structure of complex **1** (SCHAKAL). Selected bond lengths [Å] (O1 and O2 are the oxygen atoms on the axial thf ligands on Ti1 which are not shown): Ti1-O1 2.113(3), Ti1-O2 2.091(3), Ti1-N1 2.036(2), Ti1-N2 2.034(2). Selected bond angles [°]: N1-Ti1-N2 89.9(1), O1-Ti1-O2 180.0(1), N2-Ti1-N2' 178.6(11), N1-Ti1-N2' 90.1(8), N1-Ti1-N1' 178.6(11). Primed atoms derived by a transformation of 0.5 $- x, y, -z$.

The complex possesses a crystallographically imposed C_2 axis passing through the titanium cation and the oxygen atoms of the two thf molecules. The η^1-η^1-η^1-η^1-bound porphyrinogen[5g] has a saddle-shaped conformation; the pyrrole rings are tilted up and down alternately relative to the N_4 core, forming dihedral angles of 149.5(1)° and 149.8(1)° for N1,C1–C4 and N2,C6–C9, respectively. The Ti–N bond lengths are in the lower end of the range found for Ti^{IV}–N bonds in such compounds.[5]

Reduction of **1** in thf under a C_2H_4 atmosphere with an excess of Li metal at room temperature led to the formation of red crystals of **2** [Eq. (b)]. This reaction may have promise as a



general route to metal carbides or μ-hydrocarbon complexes directly from the corresponding hydrocarbon skeleton. Complex **2** is a paramagnetic species with $\mu_{eff} = 1.80\ \mu_B$ per titanium center at 290 K. The lithium cations are sandwiched between two $[Et_8N_4Ti]$ moieties (A and B; the values referring to the B moiety are given in square brackets) in which the titanium centers are bound through σ bonds to all the pyrrolyl rings (Fig. 2).[8] This arrangement creates a square-planar Li_2Ti_2[9] array about the C_2 unit. The titanium centers lie out of the N_4 mean plane by 0.585(2) Å [0.563(2) Å]. The two N_4 planes are parallel (dihedral angle 0.8(2)°) and rotated with respect to each other by 18.5(2)°. The Ti1A-C37-C38-Ti1B vector is perpendicular to the N_4 planes, and the dihedral angle it forms with the normal to the N_4 plane is 1.0(2)° [1.3(1)°]. The Ti–N distances within the porphyrinogen complex are significantly longer (Ti–N_{av} 2.120(5) Å) that those in **1** (2.033(2) Å) for the same

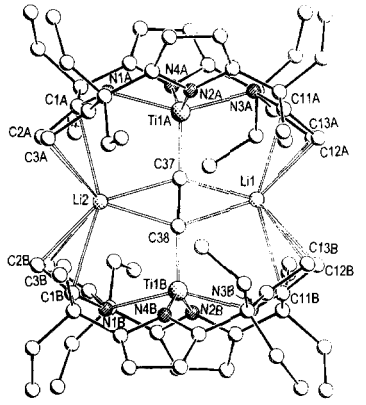


Fig. 2. Crystal stucture of the anion in complex **2** (SCHAKAL). Disorder omitted for clarity. Bond lengths [Å] for the A [B] unit: Ti1A-C37 1.809(9), Ti1B-C38 1.757(7), Li1-C37 2.221(25), Li1-C38 2.292(25), Li2-C37 2.304(25), Li2-C38 2.266(24), C37-C38 1.301(11), Ti1-N1 2.113(9) [2.115(10)], Ti1-N2 2.127(11) [2.133(10)], Ti1-N3 2.115(9) [2.140(10)], Ti1-N4 362.122(11) [2.091(12)]. Bond angles [°]: Ti1A-C37-C38 178.7(9), Ti1B-C38-C37 178.7(8).

bonding mode of the ligand. The lithium cations are bound η^3-fashion to both porphyrinogen moieties[5] (assuming that interactions for distances greater than 2.8 Å can be disregarded).[10] The major feature in the structure is the Ti-C-C-Ti skeleton, which is linear within experimental error. The Ti–C bonds (1.809(9) and 1.757(7) Å) are much shorter than those in the Ti–C≡C–R fragments in both **3**[11] [Ti–C, 2.056(11) Å] and **4**[12] [Ti–C 2.051(2) Å]. Consequently the C–C bond length

$[\{Cp_2Ti-C\equiv C-SiMe_3\}_2]$ **3**

$[Cp_2(Me_3P)Ti-C\equiv C-Ti(PMe_3)Cp_2]$ **4**

[C37–C38 1.301(11) Å] is significantly longer than in complexes **3** [1.253(15) Å][11] and **4** [1.253(2) Å][12] and in many other complexes with bridging acetylide ligands. The bond lengths we determined are much closer to those expected for a sequence of double bonds.[4] Curiously, the magnetic moment of **2** is much better accounted for by a bridging acetylide. We should emphasize that this sort of bridging C_2 unit is unprecedented in metal complexes of macrocycles, although related C_1 bridges in porphyrin[13a] and phthalocyanine complexes[13b] are known.

The formation of **2** can be interpreted as a consequence of both the very electron-rich nature of the titanium under the reducing conditions employed and the coordination environment, since the bifunctional porphyrinogens can bind the lithium cation at their periphery.[5] Both of these factors are believed to contribute to the stabilization of the C_2 unit. The extension of such synthetic methods to complexes with bridging hydrocarbon species and explorations of the chemistry of the C_2 moiety is in progress.

Experimental Procedure

1: $[TiCl_4(thf)_2]$ (8.90 g, 26.8 mmol) and $[Et_8N_4Li_4(thf)_2]$ [6] (22.88 g, 2.68 mmol) were added to toluene (350 mL). The resulting dark green-black solution was stirred at room temperature for 1 d, then LiCl was removed by filtration. After evaporation of the solvent and trituration of the residue with pentane (120 mL) a dark green solid was filtered off and dried in vacuo (12.0 g, 62%). Recrystallization from benzene gave crystals suitable for X-ray analysis. Anal. calcd for $C_{44}H_{64}N_4O_2Ti$: C 72.50, H 8.85, N 7.69; found: C 72.69, H 8.93, N 7.89; ^1H NMR (C_6D_6, 25 °C): δ = 5.98 (s, 8H, C_4H_2N), 3.40 (m, 8H, thf), 1.93 (q, 16H, CH_2), 1.18 (m, 8H, thf), 0.90 (t, 24H, CH_3).

2: Lithium sand (0.100 g, 14.0 mmol) was added to a solution of **1** (2.40 g, 3.30 mmol) in thf (100 mL) under ethylene, and the mixture was stirred at room temperature for 3 d. After removal of excess lithium from the dark red solution, the solvent was evaporated and the residue triturated with *n*-hexane (30 mL) and collected (1.3 g, 44%). Recrystallization of the powder from thf/*n*-hexane gave crystals suitable for X-ray analysis. Anal. calcd for $C_{53}H_{80}Li_2N_4O_4Ti$: C 70.78, H 8.97, N 6.23; found: C 70.33, H 9.50, N 6.48.

Received: December 2, 1994 [Z7520IE]
German version: *Angew. Chem.* **1995**, *107*, 1200

Keywords: acetylene complexes · bridging ligands · titanium compounds · porphyrinogens

[1] H. W. Kroto, A. W. Allaf, S. P. Balm, *Chem. Rev.* **1991**, *91*, 1213–1235; B. C. Guo, K. P. Kerns, A. W. Castelman, Jr., *Science* **1992**, *255*, 1411–1413; B. C. Guo, S. Wei, J. Purnell, S. Buzza, A. W. Castleman, Jr., *ibid.* **1992**, *256*, 515–516; S. Wei, B. C. Guo, J. Purnell, S. Buzza, A. W. Castleman, Jr., *ibid.* **1992**, *256*, 818–820; S. F. Cartier, Z. Y. Chen, G. J. Walder, C. R. Sleppy, A. W. Castleman, *Jr., ibid.* **1993**, *260*, 195–196.

[2] a) H. Lang, *Angew. Chem.* **1994**, *106*, 569–572; *Angew. Chem. Int. Ed. Engl.* **1994**, *33*, 547–550, and references therein; b) J. A. Ramsden, W. Weng, A. M. Arif, J. A. Gladysz, *J. Am. Chem. Soc.* **1992**, *114*, 5890–5891; c) W. Weng, J. A. Ramsden, A. M. Arif, J. A. Gladysz, *ibid.* **1993**, *115*, 3824–3825; d) Y. Zhou, J. W. Seyler, W. Weng, A. M. Arif, J. A. Gladysz, *ibid.* **1993**, *115*, 8509–8510; e) W. Weng, T. Bartik, J. A. Gladysz, *Angew. Chem.* **1994**, *106*, 2269–2272; *Angew. Chem. Int. Ed. Engl.* **1994**, *33*, 2199–2202; f) K. Sonogashira, S. Kataoka, S. Takahashi, N. Hagihara, *J. Organometal. Chem.* **1978**, *160*, 319–327; A. Wong, P. C. W. Kang, C. D. Tagge, D. R. Leon, *Organometallics* **1990**, *9*, 1992–1994; H. B. Fyfe, M. Mlekuz, D. Zargarian, N. J. Taylor, T. B. Marder, *J. Chem. Soc. Chem. Commun.* **1991**, 188–190; P. J. Stang, R. Tykwinski, *J. Am. Chem. Soc.* **1992**, *114*, 4411–4412; R. Crescenzi, C. Lo Sterzo, *Organometallics* **1992**, *11*, 4301–4305; T. Rappert, O. Nürnberg, H. Werner, *ibid.* **1993**, *12*, 1359–1364; N. Le Narvor, C. Lapinte, *J. Chem. Soc. Chem. Commun.* **1993**, 357–359.

[3] M. Appel, J. Heidrich, W. Beck, *Chem. Ber.* **1987**, *120*, 1087–1089; J. Heidrich, M. Steimann, W. Beck, J. R. Phillips, W. C. Trogler, *Organometallics* **1990**, *9*, 1296–1300; M. Akita, M. Terada, S. Oyama, Y. Moro-oka, *ibid.* **1990**, *9*, 816–825; K. G. Frank, J. P. Selegue, *J. Am. Chem. Soc.* **1990**, *112*, 6414–6416; H. Ogawa, K. Onitsuka, T. Joh, S. Takahashi, Y. Yamamoto, H. Yamazaki, *Organometallics* **1988**, *7*, 2257–2260; J. A. Davies, M. El-Ghanam, A. A. Pinkerton, D. A. Smith, *J. Organomet. Chem.* **1991**, *409*, 367–376.

[4] W. Beck, B. Niemer, M. Wieser, *Angew. Chem.* **1993**, *105*, 969–995; *Angew. Chem. Int. Ed. Engl.* **1993**, *32*, 923–949, and references therein; G. A. Koutsantonis, J. P. Selegue, *J. Am. Chem. Soc.* **1991**, *113*, 2316–2317; F. R. Lemke, D. J. Szalda, R. M. Bullock, *ibid.* **1991**, *113*, 8466–8477.

[5] a) D. Jacoby, C. Floriani, A. Chiesi-Villa, C. Rizzoli, *J. Chem. Soc. Chem. Commun.* **1991**, 220–222. 790–792; b) *J. Am. Chem. Soc.* **1993**, *115*, 3595–3602, 7025–7026; c) S. DeAngelis, E. Solari, C. Floriani, A. Chiesi-Villa, C. Rizzoli, *J. Am. Chem. Soc* **1994**, *116*, 5691–5701, 5702–5713; d) E. Solari, F. Musso, C. Floriani, A. Chiesi-Villa, C. Rizzoli, *J. Chem. Soc. Dalton Trans.* **1994**, 2015–2017.

[6] a) Crystal structure analysis of **1**: $C_{44}H_{64}N_4O_2Ti \cdot 1/2C_6H_6$, $M_r = 885.1$, monoclinic, space group $I2/a$, $a = 17.330(2)$, $b = 12.820(2)$, $c = 22.732(2)$ Å, $\beta = 101.47(1)$, $V = 4949.5(11)$ Å^3, $Z = 4$, $\rho_{calcd} = 1.188$ g cm^{-3}, $F(000) = 1912$, $Cu_{K\alpha}$ radiation ($\lambda = 1.54178$ Å, $\mu(Cu_{K\alpha}) = 17.87$ cm^{-1}: crystal dimensions $0.23 \times 0.35 \times 0.45$ mm. The structure was solved by the heavy-atom method and anisotropically refined for all non-hydrogen atoms. The hydrogen atoms were found from a difference Fourier map and introduced as fixed contributors in the last stage of refinement ($U_{iso} = 0.08$ Å^2). 2775 Unique observed reflections [$I > 2\sigma(I)$] were collected at $T = 295$ K on a Rigaku AFC6S diffractometer ($6 < 2\theta < 140°$) and corrected for absorption; $R = 0.051$ ($wR2 = 0.153$ for 4625 total unique reflections). All calculations were carried out on an IBM PS2/80 personal computer and on an Encore 91 computer. b) Further details of the crystal structure investigation may be obtained from the Director of the Cambridge Crystallographic Data Centre, 12 Union Road, GB-Cambridge CB2 1EZ (UK), on quoting the full journal citation.

[7] S. DeAngelis, E. Solari, C. Floriani, A. Chiesi-Villa, C. Rizzoli, *J. Chem. Soc. Dalton Trans.* **1994**, 2467–2469.

[8] Crystal structure analysis of **2**: $C_{74}H_{96}Li_2N_8Ti_2 \cdot 2(C_{16}H_{32}LiO_4)$, $M_r = 1798.0$, triclinic, space group $P\bar{1}$, $a = 16.648(2)$, $b = 22.144(3)$, $c = 15.948(2)$ Å, $\alpha = 97.97(1)$, $\beta = 108.95(1)$, $\gamma = 79.02(1)°$, $V = 5440.2(13)$ Å^3, $Z = 2$, $\rho_{calcd} = 1.098$ g cm^{-3}, $F(000) = 1944$, $Cu_{K\alpha}$ radiation ($\lambda = 1.54178$ Å, $\mu(Cu_{K\alpha}) = 16.51$ cm^{-1}: crystal dimensions $0.22 \times 0.26 \times 0.38$ mm. The structure was solved by the heavy-atom method (Patterson and Fourier synthesis) and anisotropically refined for all non-hydrogen atoms. Some ethyl chains and six thf molecules of the two independent Li(thf)$_4$ cations were disordered. The disorder was solved by splitting the atoms in two positions and refining isotropically with the site occupation factors given in the supplementary material. All the hydrogen atoms of the porphyrinogens except for those attached to the disordered atoms were located in difference Fourier maps and introduced as fixed contributors in the last stage of refinement ($U_{iso} = 0.12$ Å^2). The hydrogen atoms of the thf molecules were ignored. 5277 Unique observed reflections [$I > 2\sigma(I)$] were collected at room temperature ($6 < 2\theta < 140°$) and corrected for absorption; $R = 0.092$ ($wR2 = 0.244$). All calculations were carried out with the SHELX-76 and SHELXL-92 programs on an Encore 91 computer [6b].

[9] Li1-Ti1B 3.304(21), Ti1B-Li2 3.229(21), Li2-Ti1A 3.328(21), Ti1A-Li1 3.206(21) Å; Ti1-Li1-Ti1B 96.116, Li1-Ti2B-Li2 83.5(6), Ti1B-Li2-Ti1A 96.8(6), Li2-Ti1A-Li1 83.7(6)°.

[10] The Li–C distances [Å] for the A [B] unit are: Li1–C11 2.688(24) [2.735(22)], Li1 ··· C12 2.402(26) [2.433(24)], Li1 ··· C13 2.565(24) [2.567(29)], Li2 ··· C1 2.731(23) [2.664(22)], Li2–C2 2.398(24) [2.454(26)], Li2–C3 2.605(23) [2.635(28)].

[11] G. L. Wood, C. B. Knobler, M. F. Hawthorne, *Inorg. Chem.* **1989**, *28*, 382–384.

[12] P. Binger, P. Müller, P. Philipps, B. Gabor, R. Mynott, A. T. Herrman, F. Langhauser, C. Krüger, *Chem. Ber.* **1992**, *125*, 2209–2212.

[13] a) D. Mansuy, M. Lange, J.-C. Chottard, P. Guerin, P. Morlière, D. Brault, M. Rougée, *J. Chem. Soc. Chem. Commun.* **1977**, 648–649; D. Mansuy, J.-P. Lecomte, J.-C. Chottard, J.-F. Bartoli, *Inorg. Chem.* **1981**, *20*, 3119–3121; b) G. Rossi, V. L. Goedken, C. Ercolani, *J. Chem. Soc. Chem. Commun.* **1988**, 46–47; C. Ercolani, M. Gardini, V. L. Goedken, G. Pennesi, G. Rossi, U. Russo, P. Zanonato, *Inorg. Chem.* **1989**, *28*, 3097–3099.

Electrochemistry and Ab Initio Study of the Dimetallofullerene $La_2@C_{80}$**

Toshiyasu Suzuki,* Yusei Maruyama, Tatsuhisa Kato, Koichi Kikuchi, Yasuhiko Nakao, Yohji Achiba, Kaoru Kobayashi, and Shigeru Nagase*

Metallofullerenes are fullerene derivatives that contain some metals inside their cages.[1] Although their structures, including the cage structures and the positions of the metals, have not yet been determined, the recent development of methods for purifying metallofullerenes allows more advanced studies of these new molecules.[2–10] Theoretical calculations suggest that their electronic structures are significantly changed by electron transfer from highly electropositive metals to the electronegative carbon cages.[11, 12] Very recently, we reported that $La@C_{82}$ and $Y@C_{82}$ showed almost identical electrochemical properties,[6, 7] in accord with the ab initio calculations.[12e] It is interesting to see how redox properties of the metallofullerene change when *two* lanthanide atoms are present in the cage. Encapsulating two lanthanide atoms is expected to result in an increase in total charge transfer from the two metals to the cage and in the interaction between the two metals. Since the first detection of $La_2@C_{80}$ by mass spectrometry in 1991,[13] there has been little information about the electronic structure. Unlike $La@C_{82}$, $La_2@C_{80}$ is EPR-silent. We report here the electrochemistry of $La_2@C_{80}$, which significantly differs from those of empty fullerenes and monometallofullerenes, and the ab initio study of $La_2@C_{80}$ at the HF level.

$La_2@C_{80}$ was obtained as a by-product in the synthesis of $La@C_{82}$ and isolated in pure form by HPLC.[14] The cyclic voltammogram (CV) of $La_2@C_{80}$ in 1,2-dichlorobenzene shows two reversible oxidations and two reversible reductions (Fig. 1 and Table 1). The differential pulse voltammogram (DPV) displays four well-defined peaks with the same current intensities as well as an additional ill-defined peak at -2.13 V (Fig. 1).

[*] Dr. T. Suzuki
Fundamental Research Laboratories, NEC Corporation
34, Miyukigaoka, Tsukuba 305 (Japan)
Telefax: Int. code + (298)56-6136
Prof. S. Nagase, K. Kobayashi
Department of Chemistry, Faculty of Education,
Yokohama National University
Yokohama 240 (Japan)
Prof. Y. Maruyama, Prof. T. Kato
Institute for Molecular Science, Myodaiji, Okazaki 444 (Japan)
Prof. K. Kikuchi, Y. Nakao, Prof. Y. Achiba
Tokyo Metropolitan University (Japan)

[**] This work was supported by the Ministry of Education, Science and Culture of Japan (No. 06224230).

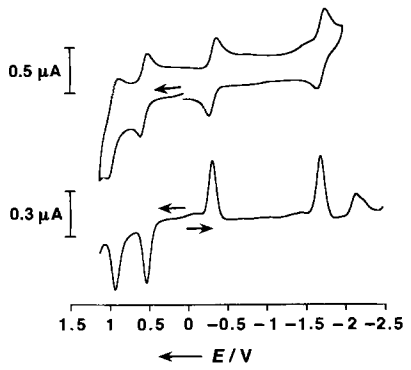


Fig. 1. CV (top) and DPV (bottom) of $La_2@C_{80}$ at 20 mVs^{-1} in 1,2-dichlorobenzene containing 0.1 M nBu_4NPF_6.

When the CV scan is continued beyond this potential, the second reduction also becomes irreversible. The first reduction potential of $La_2@C_{80}$ is anodically shifted relative to those of $La@C_{82}$-A[6] and -B[8] (major and minor isomers, respectively), suggesting that the dimetallofullerene is a stronger electron acceptor than the monometallofullerenes (Table 1). The first oxidation potential of $La_2@C_{80}$ is much more anodic than those of $La@C_{82}$-A and -B, implying that $La_2@C_{80}$ is a weaker electron donor than the $La@C_{82}$ isomers.[15] Also, $La_2@C_{80}$ has a remarkably narrow HOMO–LUMO gap compared to the empty fullerenes such as C_{60}[16] and C_{76}[17] ($E_{ox}1-E_{red}1$: $La_2@C_{80}$, 0.87; C_{60}, 2.33; C_{76}, 1.75 V).

Table 1. Redox potentials of metallofullerenes and empty fullerenes[a].

Compound	$E_{ox}2$	$E_{ox}1$	$E_{red}1$	$E_{red}2$	$E_{red}3$	$E_{red}4$
$La_2@C_{80}$	+0.95	+0.56	−0.31	−1.71	−2.13[b]	–
$La@C_{82}$-A	+1.07[b]	+0.07	−0.42	−1.37	−1.53	−2.26
$La@C_{82}$-B	+1.08[b]	−0.07	−0.47	−1.40[c]	–	−2.01
C_{60}	–	+1.21[b]	−1.12	−1.50	−1.95	−2.41
C_{76}	+1.25	+0.81	−0.94	−1.26	−1.72	−2.13

[a] Half-cell potentials unless otherwise stated. Values are in volts relative to ferrocene/ferrocenium couple. [b] Irreversible. Values were obtained by DPV. [c] Two-electron process.

To understand the redox behavior of $La_2@C_{80}$, we carried out ab initio theoretical calculations.[18] Among the seven C_{80} isomers that obey the isolated-pentagon rule,[19] we chose the most symmetrical cage structure, I_h-C_{80}, which was first proposed by Whetten et al.[15] As shown in Figure 2, the La_2 dimer is placed inside the I_h-C_{80} cage along the C_2 axis that passes through the centers of two six-membered rings. This endohedral structure has D_{2h} symmetry. The Hückel molecular orbital calculations suggest that I_h-C_{80} has fourfold degenerate HOMOs occupied by two electrons and fourfold degenerate LUMOs.[20] In Figure 3, two electrons are added to the a_g orbital for convenience. In the ab initio calculations, the energy level of the a_g orbital becomes lower than those of the other three orbitals (b_{1g}, b_{2g}, and b_{3g}).[21] Upon endohedral doping, the HOMOs are fully occupied by six electrons from La_2 and stabilized at a La–La distance of 3.45 Å. Because the LUMO levels of C_{80} are not significantly affected by endohedral doping, the low-lying empty $6s\sigma_g$ orbital of La_2 becomes the LUMO of $La_2@C_{80}$. Interestingly, this is not the case for $La@C_{82}$, in which the energy levels of the empty 5d and 6s atomic orbitals are higher than those of the unoccupied orbitals derived from the C_{82}.[12a] Upon electroreduction of $La_2@C_{80}$, the first electron goes to the LUMO (a_g) which is mostly localized on La_2. This process is favored, and the a_g orbital is lowered from −2.6 to −4.4 eV. The first reduction potential observed is very positive because the energy level of the LUMO is relatively low. The second electron goes to the same orbital (a_g), and not to b_{2u} or b_{3u}. This process costs much energy because of the unfavorable electrostatic repulsion between the two electrons on the LUMO.[22] Unlike electroreduction, the oxidation processes would take place on the C_{80} cage. The electron–electron repulsion is expected to be larger on the relatively small La_2 orbitals than on the delocalized fullerene orbitals. This may explain why the potential difference between the two reductions is much larger than that between the two oxidations (1.40 and 0.39 V, respectively).

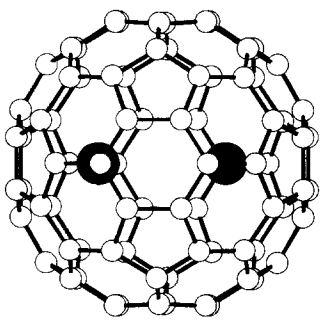


Fig. 2. View of $La_2@C_{80}$ with the I_h-C_{80} cage.

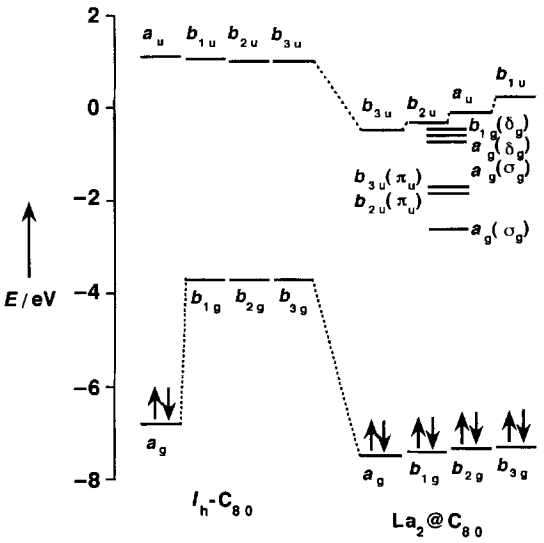


Fig. 3. The orbital energy levels [eV] of I_h-C_{80} and $La_2@C_{80}$ at the HF level..

In summary, in the first electrochemical study of the pure dimetallofullerene we have shown that $La_2@C_{80}$ is a stronger electron acceptor than monometallofullerenes such as $La@C_{82}$-A and -B and has a remarkably narrow HOMO–LUMO gap compared to empty fullerenes. The theoretical calculations predict that upon electroreduction, at least the first two electrons go to the lanthanum atoms, not to the C_{80} cage. Because only small amounts of the materials are available, electrochemistry is a quite useful method for characterizing metallofullerenes, especially, the EPR-silent ones.

Experimental Procedure

Cyclic (CV) and differential pulse voltammograms (DPV) were recorded on a BAS-B/W electrochemical analyzer. A three-electrode configuration was used throughout. All measurements were performed at ambient temperature under an argon atmosphere in 0.1 M 1,2-dichlorobenzene solution of nBu_4NPF_6. The concentration of $La_2@C_{80}$ was 10^{-4} M. IR compensation was employed throughout. A platinum working electrode (1 mm diameter) was polished with 0.05 μm alumina before measurements. A platinum wire was used as the counter electrode. The reference electrode was a Ag/0.01 M $AgNO_3$ electrode filled with 0.1 M nBu_4NClO_4 in CH_3CN. All potentials are referenced to the ferrocene/ferrocenium couple (Fc/Fc^+) as the

internal standard. CV: scan rate, 20 mVs^{-1}. DPV: pulse amplitude, 50 mV; pulse width, 50 ms; pulse period, 200 ms; scan rate, 20 mVs^{-1}.

Received: November 21, 1994 [Z 74871E]
German version: *Angew. Chem.* **1995**, *107*, 1228

Keywords: ab initio calculations · electrochemistry · lanthanide compounds

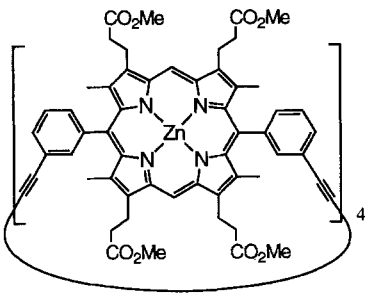
[1] For a recent review on metallofullerenes, see: D. S. Bethune, R. D. Johnson, J. R. Salem, M. S. de Vries, C. S. Yannoni, *Nature* **1993**, *366*, 123.
[2] K. Kikuchi, S. Suzuki, Y. Nakao, N. Nakahara, T. Wakabayashi, H. Shiromaru, K. Saito, I. Ikemoto, Y. Achiba, *Chem. Phys. Lett.* **1993**, *216*, 67.
[3] K. Yamamoto, H. Funasaka, T. Takahashi, T. Akasaka, *J. Phys. Chem.* **1994**, *98*, 2008.
[4] a) H. Shinohara, H. Yamaguchi, Y. Hayashi, H. Sato, M. Ohkochi, Y. Ando, Y. Saito, *J. Phys. Chem.* **1993**, *97*, 4259; b) H. Shinohara, N. Hayashi, H. Sato, Y. Saito, X.-D. Wang, T. Hashizume, T. Sakurai, *ibid.* **1993**, *97*, 13438.
[5] R. Beyers, C.-H. Kiang, R. D. Johnson, J. R. Salem, M. S. de Vries, C. S. Yannoni, D. S. Bethune, H. C. Dorn, P. Burbank, K. Harich, S. Stevenson, *Nature* **1994**, *370*, 196.
[6] Suzuki, T.; Maruyama, Y.; Kato, T.; Kikuchi, K.; Achiba, Y. *J. Am. Chem. Soc.* **1993**, *115*, 11006.
[7] K. Kikuchi, Y. Nakao, S. Suzuki, Y. Achiba, T. Suzuki, Y. Maruyama, *J. Am. Chem. Soc.* **1994**, *116*, 9367.
[8] K. Yamamoto, H. Funasaka, T. Takahashi, T. Akasaka, T. Suzuki, Y. Maruyama, *J. Phys. Chem.* **1994**, *98*, 12831.
[9] S. Hino, H. Takahashi, K. Iwasaki, K. Matsumoto, T. Miyazaki, S. Hasegawa, K. Kikuchi, Y. Achiba, *Phys. Rev. Lett.* **1993**, *71*, 4261.
[10] D. M. Poirier, M. Knupfer, J. H. Weaver, W. Andreoni, K. Laasonen, M. Parrinello, D. S. Bethune, K. Kikuchi, Y. Achiba, *Phys. Rev. B* **1994**, *49*, 17403.
[11] K. Laasonen, W. Andreoni, M. Parrinello, *Science* **1992**, *258*, 1916.
[12] a) S. Nagase, K. Kobayashi, T. Kato, Y. Achiba, *Chem. Phys Lett.* **1993**, *201*, 475; b) S. Nagase, K. Kobayashi, *ibid.* **1993**, *214*, 57; c) S. Nagase, K. Kobayashi, *ibid.* **1994**, *228*, 106; d) S. Nagase, K. Kobayashi, *ibid.* **1994**, *231*, 319; e) S. Nagase, K. Kobayashi, *J. Chem. Soc., Chem. Commun.* **1994**, 1837.
[13] M. M. Alvarez, E. G. Gillan, K. Holczer, R. B. Kaner, K. S. Min, R. L. Whetten, *J. Phys. Chem.* **1991**, *95*, 10561.
[14] For experimental details, see ref. [2]. Retention times for $La_2@C_{80}$: 490 min (polystyrene column, JAIGEL Co., CS_2 eluant) and 9.4 min (Buckyclucher I column, Regis Co., toluene eluant).
[15] On the basis of the mass spectrometric studies, Whetten et al. suggested that: 1) $La_2@C_{80}$ has an ionization potential higher than $La@C_{82}$, and 2) $La_2@C_{80}$ has an electron affinity higher than known fullerenes. These observations are consistent with our electrochemical results. C. Yeretzian, K. Hansen, M. M. Alvarez, K. S. Min, E. G. Gillan, K. Holczer, R. B. Kaner, R. L. Whetten, *Chem. Phys. Lett.* **1992**, *196*, 337.
[16] D. Dubois, K. M. Kadish, S. Flanagan, L. J. Wilson, *J. Am. Chem. Soc.* **1991**, *113*, 7773.
[17] Q. Li, F. Wudl, C. Thilgen, R. L. Whetten, F. Diederich, F. *J. Am. Chem. Soc.* **1992**, *114*, 3994.
[18] Computational details: Calculations were carried out using Hartree–Fock (HF) molecular orbital method and the Gaussian 92/DFT program. The effective core potential and basis set developed by Hay and Walt were used on La but the outermost core electrons in the $5s^25p^6$ configuration were explicitly treated as valence electrons [18a]. The basis set of La was (5s5p3d)/[4s4p3d] in standard notation. The split-valence 3-21G basis set was used for C [18b]. These give 782 contracted Gaussian functions for $La_2@C_{80}$. The geometry optimized with the AM1 method was used for the C_{80} cage [18c]. a) P. J. Hay, W. R. Wadt, *J. Chem. Phys.* **1985**, *82*, 299; b) J. S. Binkley, J. A. Pople, W. J. Hehre, *J. Am. Chem. Soc.* **1980**, *102*, 939; c) M. J. S. Dewar, E. G. Zoebisch, E. F. Healy, J. J. P. Stewart, *ibid.* **1985**, *107*, 3902.
[19] The ab initio calculations by Nakao et al. suggest that I_h-C_{80} has the largest bond energy among the seven C_{80} isomers. K. Nakao, N. Kurita, M. Fujita, *Phys. Rev. B* **1994**, *49*, 11415.
[20] a) P. W. Fowler, *Chem. Phys. Lett.* **1986**, *131*, 444. b) P. W. Fowler, D. E. Manolopoulos, *Nature* **1992**, *355*, 428.
[21] Because we keep the I_h symmetry of the C_{80} cage during our calculations, this is not due to the Jahn–Teller distortion.
[22] In this case, the a_g orbital is raised from −4.4 to −0.1 eV.

Assembly and Crystal Structure of a Photoactive Array of Five Porphyrins**

Sally Anderson,* Harry L. Anderson, Alan Bashall, Mary McPartlin,* and Jeremy K. M. Sanders*

The investigation of conformationally homogeneous porphyrin assemblies is essential for the better understanding of energy and electron transfer in natural photosynthetic reaction centers.[1] This area of research has been stimulated by the characterization of natural photosynthetic reaction centers by Deisenhofer, Huber, and Michel,[2] and by the theoretical work of Marcus.[3] Structures containing many porphyrin chromophores are of particular interest as models for light-harvesting antennae; only a few antennae models containing more than three porphyrin units have been studied,[4] and all of these structures are rather flexible, which hampers understanding of their photophysical properties. The structure of the five-porphyrin complex presented in this communication is exceptionally well defined; its conformation in solution, deduced by NMR, is essentially identical to that in the solid state, as determined by single-crystal X-ray diffraction. It should be straightforward to vary the structure of this complex systematically, because the central porphyrin is inserted in the last step with strong but reversible noncovalent binding interactions.

Corey–Pauling–Koltun (CPK) models of the cyclic zinc porphyrin tetramer[5] Zn_4-**1** indicate that it is rather flexible, and NMR spectroscopy confirms that the molecule exists in several conformations, which interchange slowly on the chemical shift time scale.[5c, 6] One possible conformer is shown schematically in Figure 1. When *meso*-tetra(4-pyridyl)porphyrin H_2-Py_4P is added to a solution of cyclic tetramer Zn_4-**1**, a strong 1:1 complex forms, which is in slow exchange with excess of either component on the ^{1}H NMR chemical shift time scale and runs on a silica column as a single band. The H_2-Py_4P ligand locks the tetramer in a single symmetrical conformation: the signals of the ester methyl (Me_a) and ring methyl (Me_b) groups each give rise to two singlets of equal intensity separated by $\Delta\delta = 0.28$ and 0.05, respectively, which rules out the D_{4h} conformation shown schematically in Figure 1. Similar splittings are also observed in the ^{13}C NMR spectrum. Molecular mechanics calculations and CPK models indicate that the



Zn$_4$-1

[*] Dr. S. Anderson,[+] Dr. H. L. Anderson,[+] Dr. J. K. M. Sanders
Cambridge Centre for Molecular Recognition
University Chemical Laboratory
Lensfield Road, GB-Cambridge CB2 1EW (UK)
Telefax: Int. code + (1223) 336913
Prof. M. McPartlin, A. Bashall
School of Chemistry, University of North London
Holloway Road, GB-London N7 8DB (UK)
Telefax: Int. code + (171) 753-5402
[+] Current address: Dyson Perrins Laboratory
South Parks Road, GB-Oxford OX1 3QY (UK)
Telefax: Int. code + (1865) 275674

[**] This work was supported by the Science and Engineering Research Council (UK), Rhône Poulenc Rorer, Magdalene College Cambridge, and Trinity College Cambridge. We are grateful to Prof. F. Diederich (ETH Zürich, Switzerland) for generously providing facilities for fluorescence measurements.

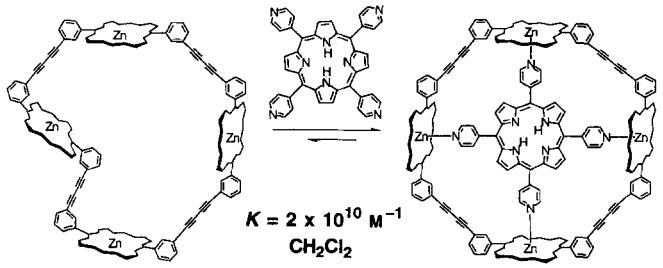


Fig. 1. One possible conformer of cyclic tetramer Zn_4-**1**, and the complex formed with H_2-Py_4P.

complex H_2-$Py_4P \cdot Zn_4$-**1** prefers to adopt a tub-shaped geometry reminiscent of cyclooctatetraene (Fig. 2). This D_{2d} symmetry is consistent with the ^1H and ^{13}C NMR spectra.[7] Split signals result from the two pyrrole environments shown in Figure 2.

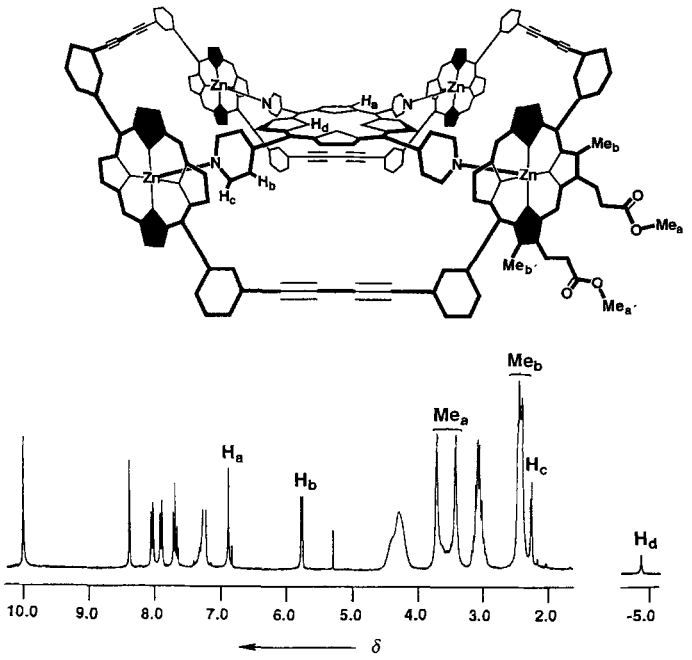


Fig. 2. Idealized structure and ^1H NMR spectrum of the H_2-$Py_4P \cdot Zn_4$-**1** complex. Most functional groups have been omitted for clarity. Axial pyrrole units are shaded black and equatorial units unshaded.

The H_c and H_b pyridine protons of H_2-Py_4P appear in the complex as sharp doublets at $\delta = 2.26$ and 5.77, respectively. The H_c protons are shifted upfield by $\Delta\delta = 6.81$ and the H_b protons by $\Delta\delta = 2.41$ on complexation to the cyclic tetramer. The magnitude of these upfield shifts, when compared with those in other pyridine–zinc porphyrin complexes,[8] shows that all four porphyrins of Zn_4-**1** must be bound simultaneously. The N–H signal of the ligand is shifted upfield by $\Delta\delta = 2.9$ to $\delta = -4.8$, as would be expected from the additive effect of four porphyrin ring currents perpendicular to the ligand plane and in close proximity.

The symmetry of the tetrazinc complex H_2-$Py_4P \cdot Zn_4$-**1** in the solid state is consistent with that observed in solution. X-ray structure analysis[9] of a well-formed, but very poorly diffracting crystal established the structure shown in Figure 3 with exact crystallographic S_4, and idealized D_{2d} symmetry. The four zinc porphyrin rings are orthogonal to the central H_2-Py_4P porphyrin unit (dihedral angle between N_4 planes 91.2°) and highly bowed. The bonds from the central porphyrin pyridyl nitrogen atoms to the surrounding zinc atoms, responsible for the conformational homogeneity of the tetramer, are equal by symmetry, with a Zn–N length of 2.20(2) Å. The N_4 donor set is planar to within 0.06 Å; the zinc atom lies 0.29 Å out of the plane towards the pyridyl group.

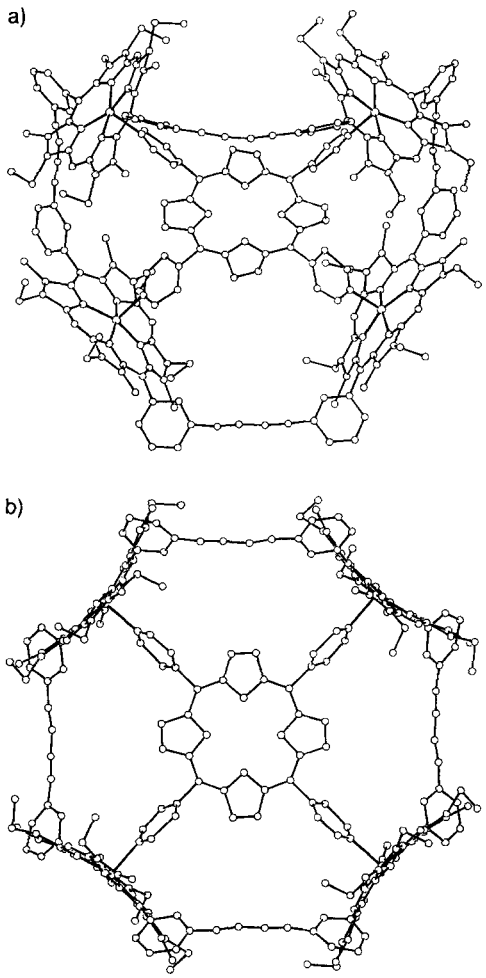


Fig. 3. Crystal structure of the tetrameric zinc porphyrin complex H_2-$Py_4P \cdot Zn_4$-**1**. a) Side view. b) A view perpendicular to the central porphyrin plane showing the crystallographic S_4 symmetry and the orthogonal orientation of the four peripheral zinc porphyrins of the Zn_4-**1** unit.

In the solid state the tetramer molecules form infinite stacks, parallel to the *c* axis, and each alternate molecule is rotated relative to its neighbors along this axis as shown in Figure 4a. Large channels parallel to the *a* and *b* axes (shown in cross section in Fig. 4a) lie between adjacent molecules. The stacks do not adopt a close-packed arrangement, but pack to leave large, square channels running the length of the crystal (Fig. 4b) in the *c* direction. Apparently, π–π interactions between porphyrins from adjacent stacks determine this arrangement; the minimum interporphyrin distance is 3.66 Å and the offset between the porphyrin centers 4.49 Å. Extended regions of electron density are consistent with occupation of the three sets of mutually perpendicular channels by randomly oriented solvent molecules. Similar large channels running the length of the crystal, and accommodating a large number of solvent molecules, were also found in a related trinuclear zinc porphyrin,[10] and both structures are reminiscent of the "porphyrin sponges" reported for tetraarylporphyrins.[11]

 © VCH Verlagsgesellschaft mbH, D-69451 Weinheim, 1995 0570-0833/95/1010-1097 $ 10.00+.25/0

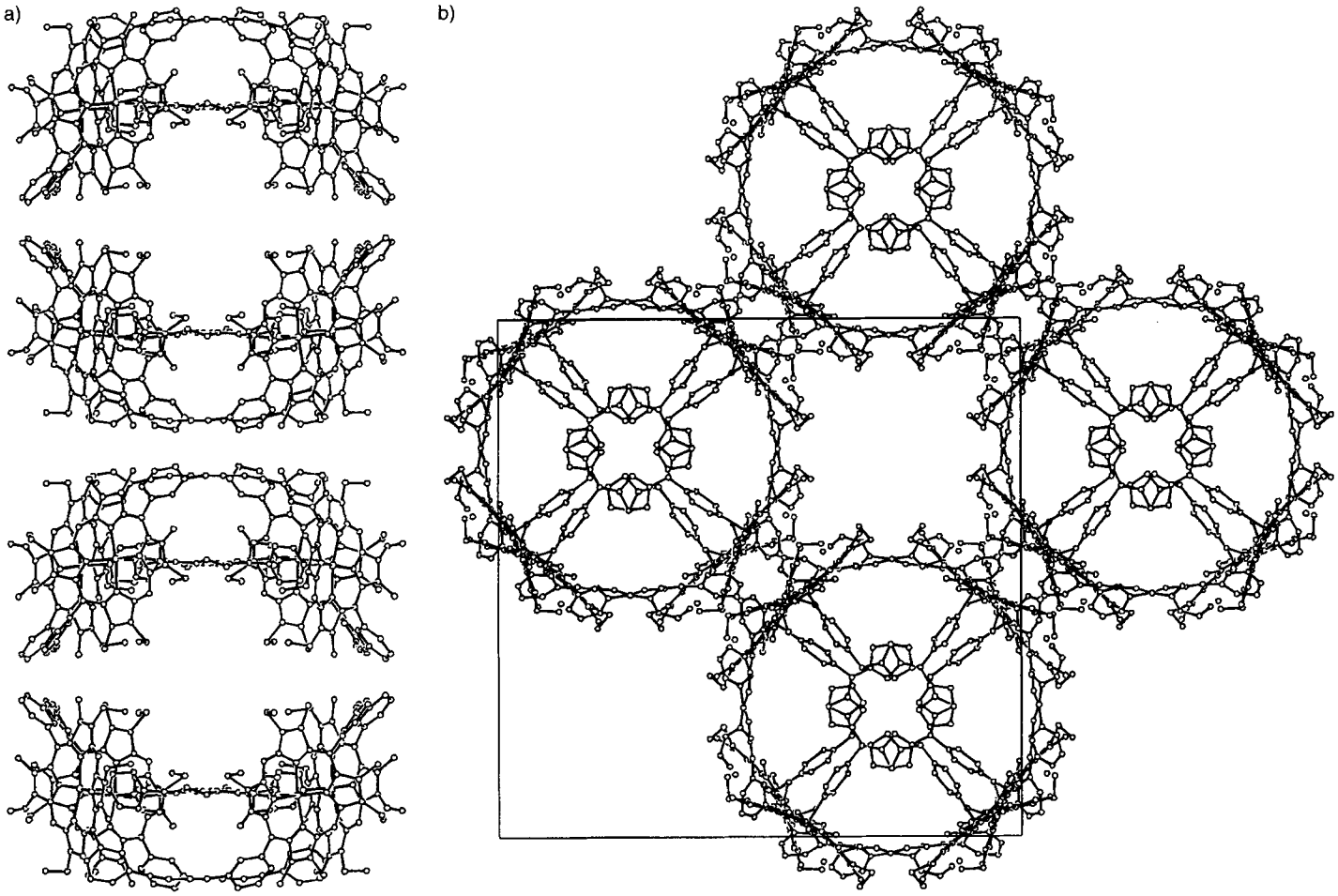


Fig. 4. a) The stacks of H_2-$Py_4P \cdot Zn_4$-**1** molecules parallel to the *c* axis, showing a cross section of the channels running parallel to the *b* axis (identical channels parallel to the *a* axis are generated by symmetry). b) A view down the stacks of H_2-$Py_4P \cdot Zn_4$-**1** showing the square cross section of the large channels that run parallel to the *c* axis.

The association constant between Zn_4-**1** and H_2-Py_4P was found to be $2 \pm 1 \times 10^{10}\,M^{-1}$ at 30 °C in dichloromethane by using UV/visible spectroscopy (Fig. 5).[12] Although this is a very strong binding constant, it is much lower than would be expected by extrapolation from the binding constants of the cyclic dimer for 4,4′-bipyridyl ($6 \times 10^{8}\,M^{-1}$) and the cyclic trimer for tris(4-pyridyl)triazine ($1 \times 10^{9}\,M^{-1}$).[8] Presumably the entropy and enthalpy associated with locking the conformation of the cyclic tetramer into a tub geometry are unfavorable.

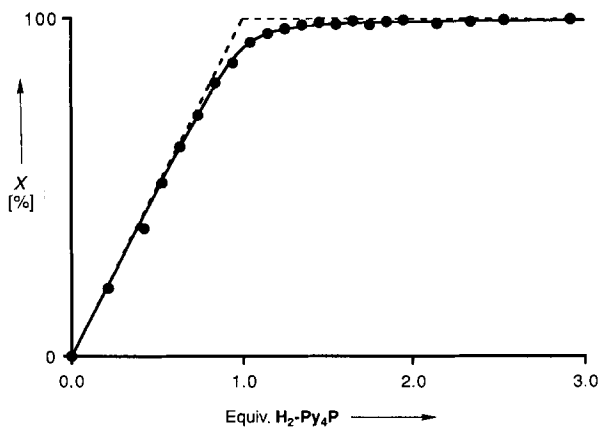


Fig. 5. Binding curve for cyclic tetramer binding to H_2-Py_4P. Experimental points on the calculated curve for $K = 2 \times 10^{10}\,M^{-1}$. Dashed curve shows strong-binding limit. X = fraction of bound H_2-Py_4P.

The absorption spectrum of the H_2-$Py_4P \cdot Zn_4$-**1** complex is essentially the sum of the absorption spectra of the two component parts. However, the fluorescence emission spectrum of the complex is around 1000 times less intense than that of either component; even the residual fluorescence of the 1:1 mixture can mainly be accounted for by traces of the dissociated components (Fig. 6). Similar fluorescence quenching is observed in the Zn-$Py_4P \cdot Zn_4$-**1** complex, where the central tetrapyridylporphyrin has been metalated with zinc. This behavior is much more dramatic than that observed in Lindsey's five-porphyrin array, where the fluorescence of only the peripheral zinc porphyrins was quenched.[4d] A possible explanation for the fluorescence quenching in our system is that photoinduced electron transfer occurs, as in natural photosynthetic reaction centers, followed by nonradiative decay of the charge-separated state.

This is one of the most conformationally homogeneous and well-characterized mimics of the photosynthetic reaction center, and it is also one of the most versatile. Reversible interactions leading to noncovalent bonds are often thought of as more flexible than covalent bonds, but this system demonstrates that many cooperative weak interactions can yield a well-defined supramolecular object. It should be possible to insert a range of tetrapyridylporphyrin ligands into the cyclic tetramer to give a variety of models for photosynthetic reaction centers with iden-

 © VCH Verlagsgesellschaft mbH, D-69451 Weinheim, 1995 0570-0833/95/1010-1098 $ 10.00+.25/0

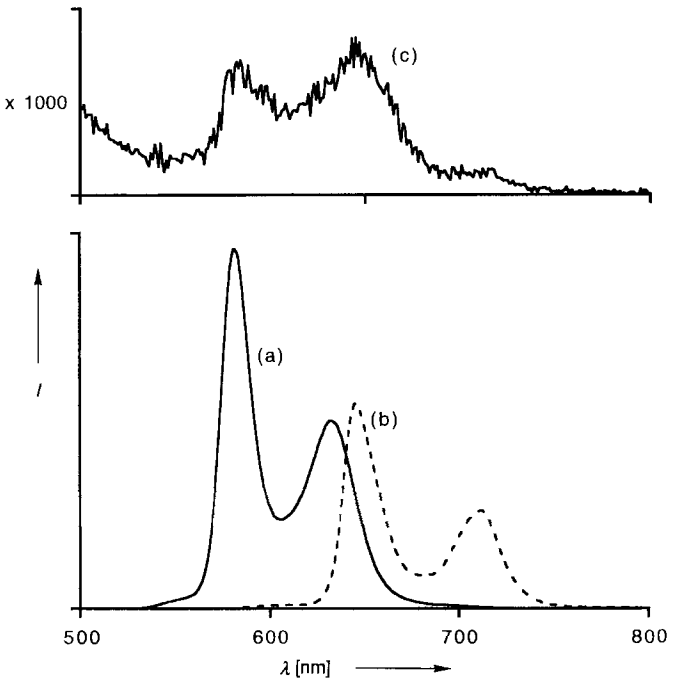


Fig. 6. Fluorescence emission (I) plotted against wavelength at 1 μM in dichloromethane for a) Zn_4-**1** (solid line), b) H_2-Py_4P (dashed line), and c) H_2-$Py_4P \cdot Zn_4$-**1** (expansion times 1000).

tical geometries but different electronic properties; this will provide a valuable tool for analyzing the photophysics of such systems.

Experimental Procedure

Binding studies: A solution of H_2-Py_4P (1.0 μM in CH_2Cl_2, also containing 6.0 nM Zn_4-**1**) was titrated into a solution of Zn_4-**1** (6.0 nM in CH_2Cl_2) in a 10 mm quartz cuvette kept at 30 C. The absorptions at 412 and 427 nm were recorded; the absorption at 412 nm was subtracted from the absorption at 427 nm to remove errors due to the slow drift in the baseline. The results were reproduced twice. A Perkin Elmer Lambda 2 spectrophotometer was used, which can reliably record absorption changes of 1×10^{-4}.

Fluorescence measurements: All spectra were recorded on a Spex 1680 0.22-m Double Spectrometer in emission mode exciting at 411 nm at 1 μM concentration in argon-saturated dichloromethane.

Received: December 27, 1994 [Z 7587 IE]
German version: *Angew. Chem.* **1995**, *107*, 1196

Keywords: host–guest chemistry · photosynthesis · porphyrinoids

[1] a) J. A. Cowan, J. K. M. Sanders, G. S. Beddard, R. J. Harrison, *J. Chem. Soc. Chem. Commun.* **1987**, 55–58; b) D. Gust, T. A. Moore, A. L. Moore, S.-J. Lee, E. Bittersmann, D. K. Luttrull, A. A. Rehms, J. M. DeGraziano, X. C. Ma, F. Gao, R. E. Belford, T. T. Trier, *Science* **1990**, *248*, 199–201; c) M. R. Wasielewski, *Chem. Rev.* **1992**, *92*, 435–461; d) A. Osuka, S. Nakajima, K. Maruyama, N. Mataga, T. Asahi, I. Yamazaki, Y. Nishimura, T. Ohno, K. Nozaki, *J. Am. Chem. Soc.* **1993**, *115*, 4577–4589; e) J. L. Sessler, V. L. Capuano, A. Harriman, *ibid.* **1993**, *115*, 4618–4628; f) J.-C. Chambron, A. Harriman, V. Heitz, J.-P. Sauvage, *ibid.* **1993**, *115*, 6109–6114; g) J. L. Sessler, B. Wang, A. Harriman, *ibid.* **1993**, *115*, 10418–10419; h) V. S.-Y. Lin, S. G. DiMagno, M. J. Therien, *Science* **1994**, *264*, 1105–1111.

[2] a) J. Deisenhofer, O. Epp, K. Miki, R. Huber, H. Michel, *Nature* **1985**, *318*, 618–624; b) R. Huber, *Angew. Chem.* **1989**, *101*, 849–871; *Angew. Chem. Int. Ed. Engl.* **1989**, *28*, 848–869; c) J. Deisenhofer, H. Michel, *ibid.* **1989**, *101*, 872–892 and **1989**, *28*, 829–847.

[3] R. A. Marcus, *Angew. Chem.* **1993**, *105*, 1161–1172; *Angew. Chem. Int. Ed. Engl.* **1993**, *32*, 1111–1121.

[4] a) J. Davila, A. Harriman, L. R. Milgrom, *Chem. Phys. Lett.* **1987**, *136*, 427–430; b) O. Wennerström, H. Ericsson, I. Raston, S. Svensson, W. Pimlott, *Tetrahedron Lett.* **1989**, *30*, 1129–1132; c) T. Nagata, A. Osuka, K. Maruyama, *J. Am. Chem. Soc.* **1990**, *112*, 3054–3059; d) S. Prathapan, T. E. Johnson, J. S. Lindsey, *ibid.* **1993**, *115*, 7519–7520; e) R. W. Wagner, J. S. Lindsey, *ibid.* **1994**, *116*, 9759–9760.

[5] The cyclic porphyrin tetramer Zn_4-**1** was synthesized with *meso*-tetra(4-pyridyl)porphyrin (H_2-Py_4P) as a template, as described previously: a) S. Anderson, H. L. Anderson, J. K. M. Sanders, *Angew. Chem.* **1992**, *104*, 921–924; *Angew. Chem. Int. Ed. Engl.* **1992**, *31*, 907–910; b) S. Anderson, H. L. Anderson, J. K. M. Sanders, *Acc. Chem. Res.* **1993**, *26*, 469–475; c) H. L. Anderson, R. P. Bonar-Law, L. G. Mackay, S. Nicholson, J. K. M. Sanders, *Proc. NATO Science Forum on Supramol. Chem.*, Kluwer, **1992**, 359–374; d) S. Anderson, H. L. Anderson, J. K. M. Sanders, unpublished.

[6] The conformers of the cyclic tetramer interconvert slowly relative to the ^1H NMR chemical shift time scale in $C_2D_2Cl_4$ up to 100 °C.

[7] NMR spectra consistent with D_{2d} symmetry are observed, because tautomerism of the H_2-Py_4P N–H protons is fast on the NMR time scale.

[8] a) H. L. Anderson, J. K. M. Sanders, *J. Chem. Soc. Chem. Commun.* **1989**, 1714–1715; b) H. L. Anderson, J. K. M. Sanders, *Angew. Chem.* **1990**, *102*, 1478–1480; *Angew. Chem. Int. Ed. Engl.* **1990**, *29*, 1400–1403.

[9] Crystal data for H_2-$Py_4P \cdot Zn_4$-**1** $\cdot 5C_6H_{12} \cdot 3CHCl_3$, $C_{207}H_{289}Cl_9N_{24}O_{32}Zn_4$, $M_r = 5287.26$, tetragonal, space group $P4/nnc$ (No. 126), $a = 35.860(8)$, $c = 29.244(6)$ Å, $Z = 4$, $V = 37606.02$ Å^3, $\rho_{calcd} = 0.934$ g cm^{-3}, $F(000) = 11072$, $\mu(Mo_{K\alpha}) = 0.37$ mm^{-1}. Crystals of H_2-$Py_4P \cdot Zn_4$-**1** were very fragile and rapidly lost solvent in air, so data were collected for a crystal sealed with mother liquor in a Lindemann tube. 16183 (7562 unique) data were collected in the θ range of 3–19° using a Phillips PW 1100 diffractometer with ω–2θ scans. The structure was solved with difficulty by direct methods [SHELXS-86]; the center of the molecule lies on a site of S_4 symmetry, and the main skeleton of the structure was only slowly revealed during many subsequent difference-Fourier syntheses. Only the first two carbon atoms of each methyl propanoate side chain (that is, the two carbon atoms closest to the zinc porphyrins) were located, and there was an unresolved region of extended electron density near to the terminal atom of each two atom chain. The presence of approximately three chloroform and five cyclohexane molecules per tetramer was indicated by analysis of the ^1H NMR spectrum of crystals of H_2-$Py_4P \cdot Zn_4$-**1** in CD_2Cl_2 (that is, 103.5 e per asymmetric unit). No recognizable solvent molecules could be identified, but many regions of extended electron density were located in the channels running parallel to the three cell axes. The highest residual maxima were included in the refinement as carbon atoms with their population parameters adjusted to correspond to the expected total-solvent and side-chain electron density. The structure was refined on F^2 [SHELXL-93] using all 7562 independent refelections. Due to the paucity of data, geometrical restraints were applied to chemically equivalent bonds and to make the phenyl and pyridyl groups planar. $wR_2 = [\sum w(F_o^2 - F_c^2)/\sum F_o^2]^{1/2} = 0.471$, $R_1 = \sum ||F_o| - |F_c|| / \sum F_o = 0.167$ [for 1202 refections with $F_o^2 > 2\sigma(F_o^2)$], goodness of fit on $F^2 = 0.893$ on 532 parameters. Further details of the crystal structure investigation are available on request from the Director of the Cambridge Crystallographic Data Centre, 12 Union Road, GB-Cambridge CB2 1EZ (UK) on quoting the full journal citation.

[10] H. L. Anderson, A. Bashall, K. Henrick, M. McPartlin, J. K. M. Sanders, *Angew. Chem.* **1994**, *106*, 445–447; *Angew. Chem. Int. Ed. Engl.* **1994**, *33*, 429–431.

[11] M. P. Byrn, C. J. Curtis, I. Goldberg, Y. Hsiou, S. I. Khan, P. A. Sawin, S. K. Tendick, C. E. Strouse, *J. Am. Chem. Soc.* **1991**, *113*, 6549–6557.

[12] Both host and guest absorb in the same region of the UV spectrum. This does not hinder the measurement of binding constants since the extinction coefficients for the absorbing ligand are known, but rather allows an internal check on the ligand concentration.

Electronic Energy Transfer Across Ethynyl-Bridged Ru^{II}/Os^{II} Terpyridyl Complexes**

Vincent Grosshenny, Anthony Harriman,* and Raymond Ziessel*

Current interest in the design of materials for applications in molecular electronics has focused, in part, on the identification of molecules having spatially remote, redox-active subunits in good electronic communication.[1, 2] In turn, this requires the synthesis of multicomponent molecular systems with highly restricted conformational mobility and well-defined and logically placed structural subunits. For the construction of linear molecules with extended bridges separating terminal redox-active subunits, it is appropriate to consider alkenes,[3] alkynes,[4-6] and polyphenyls[7] as potential spacer moieties. Such bridging units facilitate long-range electronic coupling between terminal subunits and, at least with alkynes and polyphenyls, do not pose problems with stereoisomerism. Indeed, compounds have been described recently in which alkenes[8] and polyphenyls[7] promote through-bond photoinduced energy or electron transfer over considerable distances (i.e. 20 Å).

It has also been proposed that alkynes can be used as effective bridges for electron donor/acceptor systems[9] and for the fabrication of novel chromophoric materials.[10] The incorporation of alkynes is also a simple strategy for enhancing the triplet lifetime of metal bis(terpy) complexes (terpy = 2,2′:6′,2″-terpyridine) and, in the case of bis(terpy)ruthenium(II) **1**, converting a poor photosensitizer into a much more effective one.[10] Here, we report that alkyne bridges allow for rapid intramolecular triplet energy transfer from a bis(terpy)ruthenium(II) to a bis(terpy)osmium(II) unit at both 295 and 77 K, as reported previously for the molecular systems with spacers formed from one or two phenyl rings,[7] from a single 1,4-bis(ethynyl)bicyclo-[2.2.2]octane unit,[11a] or from a 1,4-bis(ethenyl)bicyclo[2.2.2]-octane unit.[11b]

The PF_6^- salts of the ethynyl-bridged monoruthenium(II) complexes **3** and **4** (Fig. 1) were synthesized by reacting alkyne-linked terpy ligands with $[Ru^{II}(terpy)(dmso)Cl_2]$ (dmso = dimethyl sulfoxide) and anion exchange with NH_4PF_6 as described previously.[5, 12] The PF_6^- salts of the heterodinuclear Ru^{II}/Os^{II} compounds **5** and **6** were prepared by reaction of $[Os(terpy)(O)_2(OH)](NO_3)\cdot 2H_2O$ with complexes **3** and **4** in THF/H_2O with hydrazine hydrate as a reducing agent.[13] The compounds were purified by chromatography on alumina followed by recrystallization from CH_2Cl_2/hexane (53% yield for **5**-PF_6 and 23% yield for **6**-PF_6). All new compounds were characterized by UV/Vis, emission, and FT-IR spectroscopy, FAB mass spectrometry, and elemental analysis.

Absorption spectra recorded for **5** and **6** in acetonitrile solution retain the essential characteristics of the corresponding molecular components (i.e., **2** + **3** and **2** + **4**, respectively), although there is considerable overlap of absorption transitions associated with the individual subunits in the 400–500 nm region. Excitation at 600 nm, where bis(terpy)Os^{II} is the dominant if not sole chromophore, results in luminescence centered around 750 nm, which is characteristic of the bis(terpy)Os^{II} chromophore.[14] The luminescence quantum yields Φ_L and lifetimes τ_L recorded in acetonitrile solution at 295 K and in an ethanol glass at 77 K are comparable to those recorded for bis-(terpy)Os^{II} **2** under identical conditions (Table 1). Slight variations in these parameters and in the luminescence maxima λ_{em} can be attributed to the ethynyl substituents in compounds **5**

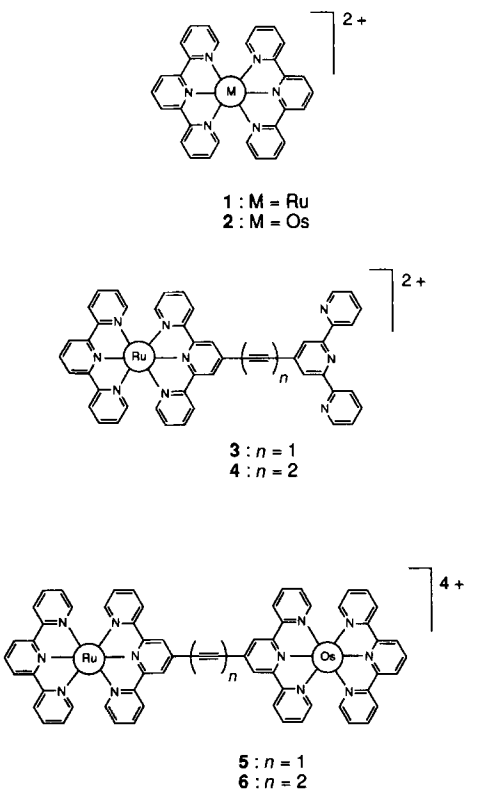


Fig. 1. Structures of the ethynyl-substituted mono- and dinuclear complexes in this work and their mononuclear reference compounds. In all cases the counterion is PF_6^-.

Table 1. Photophysical properties for the various complexes in deoxygenated acetonitrile at 295 K and in ethanol at 77 K [a].

Cmpd.	"Os^{II} center"			"Ru^{II} center"		
	Φ_L	τ_L	λ_{em} [nm]	Φ_L	τ_L	λ_{em} [nm]
			295 K			
1	–	–	–	<0.0002 [b]	0.56 ns	640
2	0.014 [b]	270 ns	718	–	–	–
3	–	–	–	0.0003	55 ns	690
4	–	–	–	0.0006	170 ns	710
5	0.016	225 ns	746	<0.0001	0.020 ns [c] 0.014 ns [d]	–
6	0.013	200 ns	760	<0.0001	0.027 ns [c] 0.020 ns [d]	–
			77 K			
1	–	–	–	0.48 [b]	11.0 μs	600
2	0.12 [b]	3.9 μs	690	–	–	–
3	–	–	–	0.55	14.0 μs	635
4	–	–	–	0.52	13.6 μs	645
5	0.10	2.4 μs	730	0.0005	0.72 ns	640
6	0.09	2.2 μs	745	0.0003	1.07 ns	650

[a] Φ_L = luminescence quantum yield, ±15%; τ_L = luminescence lifetime; λ_{em} = luminescence maximum, ±10 nm. [b] From ref. [2]. [c] Time-resolved luminescence, ±10%. [d] Laser flash photolysis, ±20%.

[*] Prof. A. Harriman
Center for Fast Kinetics Research
The University of Texas at Austin
Austin, TX 78712 (USA)
Telefax: Int. code + (512)471-6095
Dr. R. Ziessel, V. Grosshenny
Laboratoire de Chimie, d'Electronique et de Photonique Moléculaires
Ecole Européenne de Hautes Etudes des Industries Chimiques de Strasbourg
IPCMS, URM 46
1, rue Blaise Pascal, F-67008 Strasbourg (France)
Telefax: Int. code + 88 41 68 25

[**] This work was supported by the NIH and the CNRS.

and **6**, as described previously for the corresponding Ru^{II} analogues.[10] Both the energy and the lifetime of the triplet state decrease with increasing number of ethynyl units. Furthermore, relative to related bis(terpy)Os^{II} complexes of comparable triplet energy[2] the compounds reported here exhibit a small but significant enhancement in triplet lifetime at both 295 and 77 K.[15] Such findings appear to be entirely in accord with selective population of the substituted terpyridine ligand and subsequent delocalization of the electron over an extended π^* orbital following excitation at 600 nm.[10, 16]

Upon excitation of **5** and **6** in acetonitrile solution at 295 K or in an ethanol glass at 77 K with light at 440 nm it was very difficult to detect luminescence characteristic of the bis(terpy)Ru^{II} unit. At this excitation wavelength the bis(terpy)Ru^{II} unit absorbs roughly 60% of the incident photons, as judged from studies made with the reference compounds. Comparison with the corresponding mononuclear bis(terpy)Ru^{II} complexes, **3** and **4**, indicates that for these units in **5** and **6** Φ_L is less than 0.0001 (Table 1). On the basis of highly sensitive single-photon counting studies it was concluded that the luminescent lifetimes of the bis(terpy)Ru^{II} units in **5** and **6** are approximately 10^4 times shorter than those observed for the corresponding mononuclear complexes **3** and **4** (Table 1). Triplet lifetimes were also determined by transient absorption spectroscopy following excitation of **5** and **6** in acetonitrile solution at 295 K with a 1-ps laser pulse at 295 nm and monitoring recovery of the ground state at 450 nm (Table 1). It can be seen that the triplet lifetimes measured by the two techniques are quite similar (Table 1), although, because of the temporal resolution of these instruments, we consider those recorded by transient absorption spectroscopy to be the more reliable values.

In marked contrast, emission from the bis(terpy)Os^{II} units in **5** and **6** was clearly apparent following excitation of the bis(terpy)Ru^{II} unit at 440 nm. By comparison to the appropriate reference compounds, it appears that triplet energy transfer from bis(terpy)Ru^{II} to the appended bis(terpy)Os^{II} unit is quantitative for the two compounds at both 295 and 77 K. Photophysical properties measured for the bis(terpy)Os^{II} units are insensitive to the excitation wavelength, while the corrected excitation spectra were found to be in good agreement with the absorption spectral profiles recorded across the visible region. The spectroscopic triplet energy gaps ΔE measured in solution and in ethanol glass are consistent with the proposed triplet energy transfer (Table 2).

Efficient intramolecular triplet energy transfer across binuclear metal complexes has been observed in many other cases,[2, 11, 17] although kinetic data for short separations are scarce. We determined rate constants[18] for triplet energy transfer across one and two ethynyl bonds from the transient absorption and time-resolved luminescence studies at 295 and 77 K (Table 2). For both **5** and **6** there is a moderate (i.e., 50-fold) decrease in rate at the lower temperature, while at both temperatures the rate of energy transfer is slightly faster for **5** than for **6**. The magnitude of the decrease in the rate of energy transfer upon insertion of the second ethynyl bond, in fact, is surprisingly small, even when compared to the rates obtained for complexes with alkene[19] and phenyl[20] spacer groups. Such findings might be used to argue that polyalkynes are especially effective at promoting long-range electronic coupling between remote subunits.

It is instructive to consider the mechanism by which intramolecular triplet energy transfer occurs in these compounds. Studies with closely related binuclear systems have provided support for a through-bond electron exchange (i.e., Dexter-type) mechanism.[2, 11] A schematic description of the overall process is shown in Figure 2. In our case, the 50-fold decrease in rate of triplet energy transfer observed upon changing from

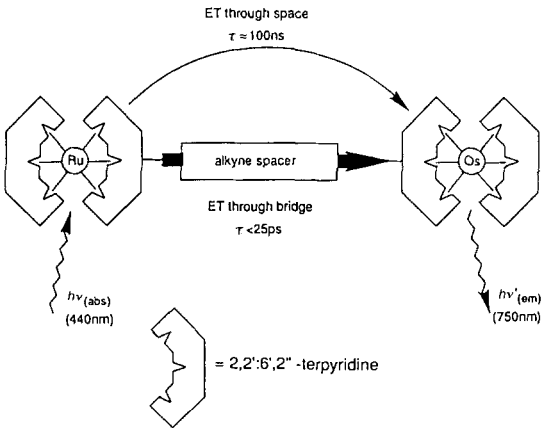


Fig. 2. Representation of energy transfer across one ($k = 7.1 \times 10^{10}\ s^{-1}$) and two ($k = 5 \times 10^{10}\ s^{-1}$) alkyne groups at room temperature. The rate of energy transfer through space ($k = 1 \times 10^{7}\ s^{-1}$) is calculated from the Förster expression for a single ethynyl spacer.

fluid solution to a frozen glass appears to be more consistent with a Dexter mechanism than with dipole–dipole (i.e., Förster-type) transfer.[21] Furthermore, the small decrease in rate observed for **6** relative to that of **5** corresponds roughly to an R^{-2} dependence rather than the R^{-6} dependence (where R is the metal–metal distance in the binuclear complexes) that is required for transfer by means of the Förster mechanism.[22] The rate constants for triplet energy transfer occurring by the Förster mechanism (k_F) can be estimated by Equation (a). Here Φ_L and τ_L refer to the photophysical properties of the appropri-

$$k_F = 8.8 \times 10^{-25} \Phi_L J_F K^2 / n^4 \tau_L R^6 \quad \text{(a)}$$

ate mononuclear bis(terpy)Ru^{II} complex, n is the refractive index of the solvent, J_F is the spectroscopic overlap integral ($J_F = 1 \times 10^{-13}\ cm^6\ mol^{-1}$), and K is the orientation factor ($K^2 = 0.67$). At 77 K the calculated k_F values are $1.2 \times 10^7\ s^{-1}$ and $4.4 \times 10^6\ s^{-1}$ for complexes **5** and **6**, respectively. Even allowing for errors in the measured values, it is clear that dipole–dipole transfer cannot account for the observed rates of triplet energy transfer.

The rate constant for Dexter-type triplet energy transfer (k_D) is expressed by Equations (b) and (c), where V is the electronic

$$k_D = (2V^2/h)(\pi^3/\lambda k_B T)^{1/2} \exp[-\Delta G^{\ddagger}/k_B T] \quad \text{(b)}$$

$$\Delta G^{\ddagger} = [(\lambda - \Delta E)^2/4\lambda] \quad \text{(c)}$$

matrix coupling element, λ is the reorganization energy accompanying energy transfer, and ΔE is the difference in energy between donor and acceptor. Values for ΔE can be estimated from the luminescence spectra (Table 2), while λ has been estimated to be 0.15 eV from the relevant Stokes' shift.[23] Based on these values and the assumption that triplet energy transfer does indeed occur exclusively by an electron exchange mechanism, the magnitude of V is estimated to be about $7\ cm^{-1}$ at room temperature. The rate of energy transfer is expected to decrease exponentially with increasing metal–metal distance (R), as described by Equation (d).[24] As such, the decreased rate of energy

$$k_D = A \exp[-\beta R] \quad \text{(d)}$$

transfer for **6** relative to **5** corresponds to an attenuation factor β of $0.17 \pm 0.04\ Å^{-1}$. Comparison of this derived parameter to the

 © VCH Verlagsgesellschaft mbH, D-69451 Weinheim, 1995 0570-0833/95/1010-1101 $ 10.00+.25/0

Table 2. Parameters for triplet energy transfer for the mono- and diethynyl bridged heterodinuclear Ru/Os complexes [a].

Cmpd.	T [K]	ΔE [b] [eV]	$k/10^{10}$ [s^{-1}]
5	295	0.13	7.1 [c]
	77	0.25	0.14 [d]
6	295	0.11	5.0 [c]
	77	0.26	0.09 [d]

[a] ΔE = triplet energy gap, ±15%; k = rate constant for triplet energy transfer. [b] Calculated by using **3** and **4** to estimate the triplet energy of bis(terpy)Ru^{II}units. [c] From transient absorption spectroscopy, ±20%. [d] From time-resolved luminescence spectroscopy, ±10%.

corresponding values obtained for electron transfer through alkenes ($\beta = 0.06$ Å^{-1}),[8] aromatic hydrocarbons ($\beta = 0.4$ Å^{-1}),[25] proline groups ($\beta = 0.7$ Å^{-1}),[26] fused alkanes ($\beta = 0.6-1.0$ Å^{-1}),[27] DNA ($\beta = 0.9$ Å^{-1}),[28] and proteins ($\beta = 1.7$ Å^{-1})[29] confirms the high efficacy of electronic coupling along alkyne spacers. It is important to realize, however, that the rate of intramolecular (through-bond!) triplet energy transfer observed for **6** at 295 K ($k = 5 \times 10^{10}$ s^{-1}) is less than that reported[2, 7] for the corresponding binuclear system with a biphenyl spacer ($k > 5 \times 10^{10}$ s^{-1}), even though the metal–metal distance in **6** is 3.5 Å less and correspondingly the β value is smaller. This suggests that electronic coupling between terpyridine and alkyne groups, but not between adjacent alkynes, is relatively ineffective, probably due to symmetry restrictions.

Experimental Procedure

Preparation of **5**-PF_6 and **6**-PF_6: To a stirred solution of compounds **3** and **4** (30 mg, 0.027 mmol) in THF/H_2O (1/1, 20 mL) was added dropwise a solution of [Os(terpy)$(O)_2$(OH)]$(NO_3)\cdot 2H_2O$ [13] (18 mg, 0.033 mol) in H_2O (5 mL). After the reaction mixture was heated at 45 °C for 15 min. three drops of hydrazine hydrate were added. Complexation was evidenced by development of a deep brown color. The reaction mixture was allowed to stand for ca. 12 h before an aqueous solution (10 mL) of NH_4PF_6 (22 mg, 0.135 mmol) was added, resulting in the precipitation of the crude product. The salts were purified by chromatography (alumina standard, 1–6% CH_3OH/CH_2Cl_2, $R_f = 0.57$ for **5**-PF_6 and $R_f = 0.52$ for **6**-PF_6 in CH_2Cl_2/CH_3OH 9/1). The resulting red-brown salts were recrystallized from CH_2Cl_2/hexane.

5: 57% yield; UV/Vis (CH_3CN): λ_{max} (ε) = 266 (63800), 302 (67300), 476 (18300), 536 nm (sh, 7200); FT-IR (KBr pellets): $\tilde{\nu} = 2070$ (C≡C), 1638, 1450, 1385, 1262, 1087, 1048, 844 cm^{-1}; FAB-MS (*meta*-nitrobenzylalcohol as matrix): *m/z* 1536/1538 [$M^+ - 2PF_6$], 1391/1393 [$M^+ - 3PF_6$], 1246/1248 [$M^+ - 4PF_6$]; anal. calcd. for $C_{62}H_{42}N_{12}P_4F_{24}RuOs$ (M_r = 1826.233): C 40.78, H 2.32, N 9.20; found C 40.50, H 2.09, N 8.93.

6: 23% yield; UV/Vis (CH_3CN): λ_{max} (ε) = 266 (118600), 301 (94400), 478 (24600), 539 nm (sh, 11500); FT-IR (KBr pellets): $\tilde{n} = 2081$ (C≡C), 1604, 1450, 1386, 1262, 1089, 1048, 844 cm^{-1}; FAB-MS (*meta*-nitrobenzylalcohol as matrix): *m/z* 1560/1562 [$M^+ - 2PF_6$], 1415/1417 [$M^+ - 3PF_6$], 1270/1272 [$M^+ - 4PF_6$]; anal. calcd. for $C_{64}H_{42}N_{12}P_4F_{24}RuOs$ (M_r = 1850.255): C 41.55, H 2.29, N 9.08; found C 41.37, H 2.03, N 8.96.

Methods: Luminescence lifetimes were measured by time-correlated, single-photon counting methods after excitation with a synchronously pumped, cavity-dumped dye laser. Rhodamine 6G (for excitation at 600 nm) and frequency-doubled Styryl-9 (for excitation at 440 nm) dye lasers were used. After application of global analysis techniques to the deconvoluted decay profiles, the temporal resolution of this instrument was around 15 ps. Transient absorption studies were made with a frequency-doubled, mode-locked Nd:YAG laser (pulse width 30 ps, Raman shifted to 598 nm, 2 mJ per pulse) or a frequency-doubled Rhodamine 6G dual-jet dye laser (pulse width 1 ps, 295 nm, 450 μJ per pulse). Kinetic measurements were made by following the recovery of the ground-state absorption band at 450 nm (bis(terpy)Ru^{II}) or 650 nm (bis(terpy)Os^{II}).

Received: December 9, 1994 [Z75351E]
German version: *Angew. Chem.* **1995**, *107*, 1211

Keywords: electronic energy transfer · osmium compounds · photochemistry · ruthenium compounds

[1] V. Balzani, F. Scandola, *Supramolecular Photochemistry*, Horwood, Chichester, **1991**.
[2] J. P. Sauvage, J. P. Collin, J. C. Chambron, S. Guillerez, C. Coudret, V. Balzani, F. Barigelletti, L. De Cola, L. Flamigni, *Chem. Rev.* **1994**, *94*, 993.
[3] A. Slama-Schwok, M. Blanchard-Desce, J. M. Lehn, *J. Phys. Chem.* **1990**, *94*, 3894.
[4] V. Grosshenny, R. Ziessel, *J. Chem. Soc. Dalton Trans.* **1993**, 817.
[5] V. Grosshenny, R. Ziessel, *J. Organomet. Chem.* **1993**, *453*, C19.
[6] L. R. Khundkar, A. E. Stiegman, J. W. Perry, *J. Phys. Chem.* **1990**, *94*, 1224.
[7] F. Barigelletti, L. Flamigini, V. Balzani, J.-P. Collin, J.-P. Sauvage, A. Sour, E. C. Constable, A. M. W. Cargill Thompson, *J. Chem. Soc. Chem. Commun.* **1993**, 942; *J. Am. Chem. Soc.* **1994**, *116*, 7692.
[8] A. C. Benniston, V. Goulle, A. Harriman, J. M. Lehn, B. Marczinke, *J. Phys. Chem.* **1994**, *98*, 7798.
[9] A. E. Steigman, V. M. Miskowski, J. W. Perry, D. R. Coulter, *J. Am. Chem. Soc.* **1987**, *109*, 5884.
[10] A. C. Benniston, V. Grosshenny, A. Harriman, R. Ziessel, *Angew. Chem.* **1994**, *106*, 1956; *Angew. Chem. Int. Ed. Engl.* **1994**, *33*, 1884.
[11] a) F. Vögtle, M. Frank, M. Nieger, P. Belser, A. von Zelewsky, V. Balzani, F. Barigelletti, L. De Cola, L. Flamigni, *Angew. Chem.* **1993**, *105*, 1706; *Angew. Chem. Int. Ed. Engl.* **1993**, *32*, 1643; b) L. De Cola, V. Balzani, F. Barigelletti, L. Flamigni, P. Belser, A. von Zelewsky, M. Frank, F. Vögtle, *Inorg. Chem.* **1993**, *32*, 5228.
[12] V. Grosshenny, R. Ziessel, *Tetrahedron Lett.* **1992**, *33*, 8075.
[13] D. W. Pipes, T. J. Meyer, *Inorg. Chem.* **1986**, *25*, 4042.
[14] J. N. Demas, G. A. Crosby, *J. Am. Chem. Soc.* **1971**, *93*, 2841.
[15] The best comparison is between **5** and the binuclear system having a single phenyl linkage: the triplet energies are identical but the triplet lifetimes differ.
[16] S. Boyde, G. F. Stroude, W. E. Jones, Jr., T. J. Meyer, *J. Am. Chem. Soc.* **1990**, *112*, 7395.
[17] M. T. Indelli, C. A. Bignozzi, A. Harriman, J. R. Schoonover, F. Scandola, *J. Am. Chem. Soc.* **1994**, *116*, 3768.
[18] The rate constant for triplet energy transfer was calculated as $k = (1/\tau_i) - (1/\tau_o)$ where τ_i is the lifetime of the bis(terpy)Ru^{II} unit in compound **5** or **6**, measured by transient absorption spectroscopy, and τ_o is the corresponding lifetime for the reference compound **4** or **5**, measured by time-resolved luminescence spectroscopy.
[19] J. E. Sutton, H. Taube, *Inorg. Chem.* **1981**, *20*, 3125.
[20] J. P. Collin, P. Lainé, J. P. Launay, J. P. Sauvage, A. Sour, *J. Chem. Soc. Chem. Commun.* **1993**, 434.
[21] The primary reason for expecting a slower rate of Förster-type energy transfer at 77 K compared to 295 K is due to the increase in refractive index when a solution is frozen. Inserting appropriate values into the Förster expression indicates that the rate will decrease by a factor of ca. 5 on changing from solution to glass, provided there is no change in orientation.
[22] Based on metal–metal distances of 13.8 and 16.2 Å from CPK models of **5** and **6**, respectively, the average decrease in rate with increasing separation corresponds to an $R^{-2.2}$ dependence.
[23] V. Balzani, F. Bolletta, F. Scandola, *J. Am. Chem. Soc.* **1980**, *102*, 2152.
[24] M. N. Paddon-Row, *Acc. Chem. Res.* **1994**, *27*, 18.
[25] A. Osuka, K. Maruyama, N. Mataga, T. Asahi, I. Yamazaki, N. Tamai, *J. Am. Chem. Soc.* **1990**, *112*, 4958.
[26] A. Vassilian, J. F. Wishart, B. van Hemelryck, H. Schwarz, S. S. Isied, *J. Am. Chem. Soc.* **1990**, *112*, 7278.
[27] M. N. Paddon-Row, M. J. Shephard, K. D. Jordan, *J. Phys. Chem.* **1993**, *97*, 1743.
[28] A. M. Brun, A. Harriman, *J. Am. Chem. Soc.* **1992**, *114*, 3656.
[29] D. N. Beratan, J. N. Betts, J. N. Onuchic, *Science* **1991**, *252*, 1285.

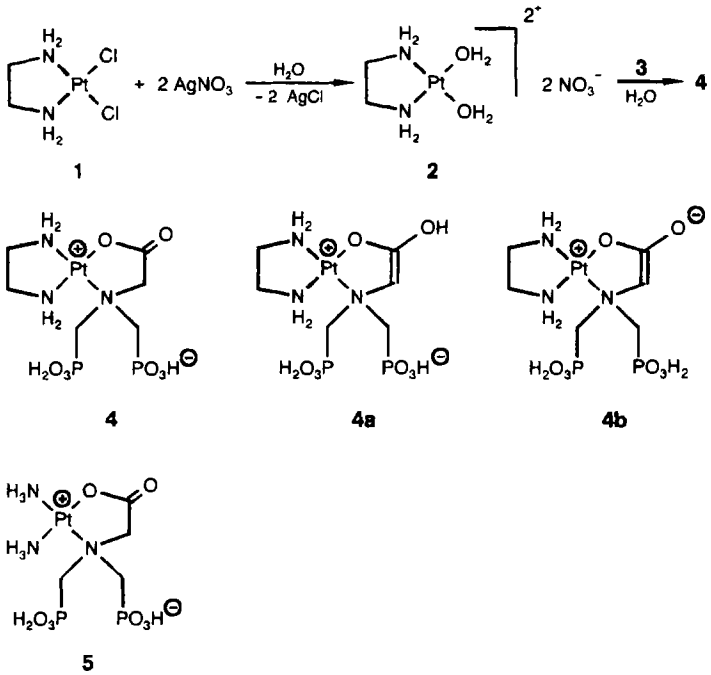
 © VCH Verlagsgesellschaft mbH, D-69451 Weinheim, 1995 0570-0833/95/1010-1102 $ 10.00+.25/0

First Isolation of an Enol of a Carboxylic Acid by Complexation to an (Ethane-1,2-diamine)-platinum(II) Fragment**

Markus Galanski, Bernhard Klaus Keppler,* and Bernhard Nuber

Enol isomers of simple aldehydes and ketones have been known for a long time,[1] but very little is known about the enols of other carbonyl compounds such as carboxylic acids and carbonic acid esters. On account of the high thermodynamic instability with respect to the carboxylic acid isomer it has so far not been possible to isolate a geminal enediol or its metal derivative. Only a few enols of carboxylic acids in solution are known. These include the two sterically hindered derivatives of enolizated acetic acid,[2] 2,2-bis(pentamethylphenyl)ethane-1,1-diol and 2,2-bis(mesityl)ethane-1,1-diol, the enol of amygdalic acid,[3] fulvene-6,6-diol,[4] the enol of α-cyano-α-phenylacetic acid,[5] and the enols of various indene carboxylic acids.[6] The synthesis of geminal enediols in all cases was carried out by hydration of the corresponding ketenes. Dilithium and organomagnesium derivatives of 1,1-enediols so far have only been prepared in solution as reactive intermediates and reacted in situ.

The synthesis of osteotropic (bone-seeking) analogues[7] of *cis*-diamminedichloroplatinum(II), cisplatin,[8] one of the most successful drugs in the treatment of malignant tumors, led to not only ethane-1,2-diamine[(bis(phosphonatomethyl)amino)acetato(2−)-O^1,N^1]platinum(II) (**4**) (Scheme 1) but also to the enol tautomer **4a** (see Fig. 1).[9] Thus a geminal enediol derivative



Scheme 1. Synthesis of **4** as well as enol and keto isomers of the complexed α-amino carboxylic acid and the possible zwitterions **4a** and **4b** of the enol isomer.

[*] Doz. Dr. Dr. B. K. Keppler, Dipl.-Chem. M. Galanski, Dr. B. Nuber
Anorganisch-chemisches Institut der Universität
Im Neuenheimer Feld 270, D-69120 Heidelberg (Germany)
Telefax: Int. code + (6221)56-4955

[**] This work was supported by the European Community within the HCM and COST programs (COST Action D1, project D1-92-002), by the Deutsche Krebshilfe, Dr. Mildred-Scheel-Stiftung für Krebsforschung, Bonn, and by the Fonds der Chemischen Industrie, Frankfurt/Main.

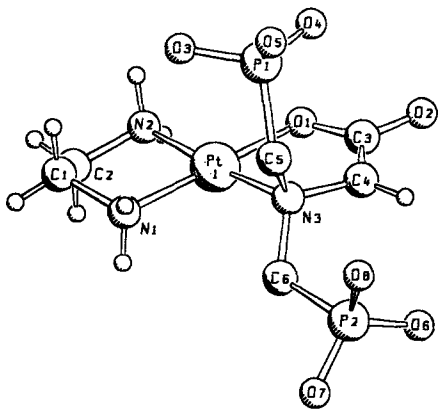


Fig. 1. Molecular structure of **4a** in the crystal. Selected distances [pm] and angles [°]: Pt1–N1 203.1(12), Pt1–N2 205.0(13), Pt1–N3 205.9(12), Pt1–O1 198.9(10), O1–C3 129.9(19), O2–C3 127.8(20), C3–C4 138.6(22), P1–O3 154.0(10), P1–O4 146.8(12), P1–O5 152.1(12), P2–O6 150.1(12), P2–O7 150.1(13), P2–O8 151.6(12); N1-Pt1-N2 84.0(5), N1-Pt1-N3 98.2(5), N2-Pt1-O1 93.7(5), N3-Pt1-O1 84.2(4), O3-P1-O4 114.4(6), O3-P1-O5 105.3(6), O4-P1-O5 113.3(6), O6-P2-O7 113.8(7), O6-P2-O8 110.5(6), O7-P2-O8 112.4(7); O1-C3-C4-N3 8.54, Pt1-O1-C3-C4 0.24.

of a carboxylic acid was isolated for the first time in the solid state.

Activation of the dichloro complex **1** with silver nitrate gives the aqua complex **2**, which is treated in situ with *N*,*N*-bis(phosphonomethyl)aminoacetic acid (BPMAA) (**3**) (Scheme 1) to give **4**. Complex **4** is precipitated with acetone as a white solid. In the recrystallization from water (pH = 1), a colorless clear crystal was obtained after four weeks. In addition to the crystal structure analysis, an IR spectrum was recorded with a fragment of the crystal.

Since we determined the crystal structure of the keto isomer[7, 10] *cis*-diammine[(bis(phosphonatomethyl)amino)acetato(2−)-O^1,N^1]platinum(II) (**5**) (see Fig. 2) previously, the complexation of **3** to the *cis*-diam(m)ineplatinum(II) fragments thus makes it possible to directly compare the structures of the two isomers of the keto–enol equilibrium of a carboxylic acid.

As expected, the ligands are arranged in a square-planar fashion about the platinum centers; sum of angles: 360.1° for **4a** and 360° for **5**. The N1-Pt1-N2, N1-Pt1-N3, and O1-Pt1-N3 angles (84.0(5)–98.2(5)°) deviate markedly from the ideal value of 90°. The Pt–N (203.1(12)–208.0(7) pm) and Pt–O bond lengths (198.9(10)–201.5(5) pm) lie in the usual range. As expected, the sum of angles in the Pt1-N1-C1-C2-N2 five-membered ring of **4a** (513.7°), differs markedly from the sum of angles in a planar five-membered ring (540°). Values between 13.4 and 56.3° were

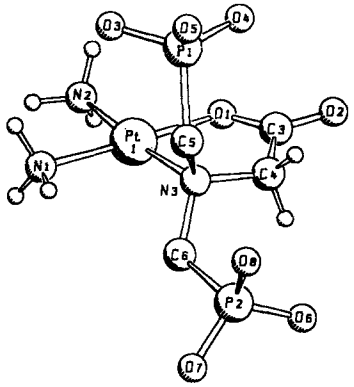


Fig. 2. Molecular structure of **5** in the crystal. Selected distances [pm] and angles [°]: Pt1–N1 205.4(7), Pt1 N2 204.3 (8), Pt1–N3 208.0(7), Pt1–O1 201.5(5), O1–C3 129.9(10), O2–C3 121.5(10), C3–C4 150.1(13), P1–O3 155.1(6), P1–O4 150.9(6), P1–O5 153.9(7), P2–O6 153.9(9), P2–O7 154.1(7), P2–O8 152.0(6); N1-Pt1-N2 88.7(3), N1-Pt1-N3 97.1(3), N2-Pt1-O1 89.0(3), N3-Pt1-O1 85.2(2), O3-P1-O4 113.6(4), O3-P1-O5 106.8(3), O4-P1-O5 113.4(3), O6-P2-O7 112.0(4), O6-P2-O8 110.1(3), O7-P2-O8 113.1(4); O1-C3-C4-N3 16.45, N3-Pt1-O1-C3 1.69.

determined for the dihedral angles. The sum of angles in the Pt1-O1-C3-C4-N3 five-membered ring of **4a** is 538.7° with dihedral angles of 0.2–11.9°; that in the five-membered ring of **5** is 538.1° with dihedral angles of 1.7–16.5°.

The unexpectedly short C3–C4 bond length of **4a** (138.6(22) pm) corresponds to a double bond. In contrast, the length of the C3–C4 bond of **5** (150.1(13) pm) reveals the presence of a single bond. In the case of a double bond, the ideal dihedral angle is expected to be 0°; however, in the crystal structure of **4a**, it is 8.5°, that is the bond is slightly twisted. This can be attributed to the complexation to the platinum through the N3 nitrogen if the fact that Pt1, O1, C3, and C4 are in a coplanar arrangement (dihedral angles 0.2°!) is taken into account. The difference to the O1-C3-C4-N3 dihedral angle of **5** at the C3–C4 single bond (16.5°) is very marked; in this case, the atoms N3, Pt1, O1, and C3 lie almost in a single plane (dihedral angle 1.7°).

The presence of the enol isomer **4a** is confirmed by the comparison of the IR spectra of **4** and **4a**. Complex **4** shows a strong carbonyl band at 1655 cm^{-1}, while **4a** shows two sharp bands at 1633 and 1603 cm^{-1}. The band at 1633 cm^{-1} is assigned to the stretching vibration of the enolic double bond,[2] the absorption at 1603 cm^{-1} to the N–H deformation vibration.

A direct statement as to whether the zwitterion **4a** or **4b** (Fig. 1) is present in the crystal cannot be made on the basis of structure analysis. A comparison of the bond lengths and bond angles of the two phosphonic acid groups with the data of phosphonic acid (P–O 154 pm, P=O 147 pm; O–P=O 113° and 116°, O-P-O 102°) and that of a bis(diethylphosphonate) derivative (P–O 154 and 153 pm, P=O 144 pm; O–P=O 116°, O-P-O 101 and 102°) suggests structure **4a**. The crystal structure data of **4a** shows that for charge equalization with respect to platinum, the phosphonic acid group P2 is singly deprotonated.

Experimental Procedure

All reactions were carried out in distilled water and in the absence of light.

4: To a suspension of **1** (946 mg, 2.90 mmol) in water (40 mL) was added silver nitrate (937 mg, 5.52 mmol), and the mixture was stirred for one day at room temperature. The silver chloride formed was removed by filtration, and the volume of the remaining yellow solution was reduced to 10 mL. Thereafter **3** (750 mg, 2.85 mmol) was added, and the solution was stirred for one hour at 50 °C and subsequently for one day at room temperature. Complex **4** was precipitated with acetone, filtered, and dried under high vacuum. Yield: 77.3% (based on the amount of silver nitrate used). If **4** is contaminated with free ligand, it can be purifed by recrystallization from water.

4: ^1H NMR (D_2O, 25 °C, 200 MHz): δ = 2.42 (m, 4H, N–CH_2CH_2–N), 3.1–3.6 (m, 4H, 2 CH_2–P), 4.04 (s, 2H, CH_2–COO), 5.0–6.0 (2 broad signals, 2 NH_2); ^{13}C NMR (D_2O, 25 °C, 50 MHz, [D_6]acetone): δ = 47.1, 47.8, 61.7 (d, ^1J(C,P) = 149 Hz, 2C), 66.2, 184.5; ^{31}P NMR (D_2O, 25 °C, 81 MHz, 85% H_3PO_4): δ = 11.73; IR (KBr): $\tilde{\nu}$ = 1655 cm^{-1} (C=O); correct C,H,N analysis.

Received: December 22, 1994 [Z 7571 IE]
German version: *Angew. Chem.* **1995**, *107*, 1220

Keywords: enediols · keto–enol tautomerism · platinum compounds

[1] H. Hart, *Chem. Rev.* **1979**, *79*, 515; B. Capon, B.-Z. Guo, F. C. Kwok, A. R. Siddhanta, C. Zucco, *Acc. Chem. Res.* **1988**, *21*, 135; Z. Rappoport, S. E. Biali, *ibid.* **1988**, *21*, 442; A. J. Kresge, *ibid.* **1990**, *23*, 43.

[2] P. O'Neill, A. F. Hegarty, *J. Chem. Soc. Chem. Commun.* **1987**, 744; B. M. Allen, A. F. Hegarty, P. O'Neill, M. T. Nguyen, *J. Chem. Soc. Perkin Trans. 2* **1992**, 927.

[3] Y. Chiang, A. J. Kresge, P. Pruszynsky, N. P. Schepp, J. Wirz, *Angew. Chem.* **1990**, *102*, 810; *Angew. Chem. Int. Ed. Engl.* **1990**, *29*, 792.

[4] B. Urwyler, J. Wirz, *Angew. Chem.* **1990**, *102*, 807; *Angew. Chem. Int. Ed. Engl.* **1990**, *29*, 790.

[5] J. Andraos, Y. Chiang, A. J. Kresge, I. G. Pojarlieff, N. P. Schepp, J. Wirz, *J. Am. Chem. Soc.* **1994**, *116*, 73.

[6] J. Andraos, Y. Chiang, C.-G. Huang, A. J. Kresge, J. C. Scaiano, *J. Am. Chem. Soc.* **1993**, *115*, 10605.

[7] T. Klenner, P. Valenzuela-Paz, F. Amelung, H. Münch, H. Zahn, B. K. Keppler, H. Blum in *Metal Complexes in Cancer Chemotherapy* (Ed.: B. K. Keppler), VCH, Weinheim, **1993**, p. 85.

[8] J. Reedijk, P. H. M. Lohman, *Pharm. Weekbl.* **1985**, *7*, 173; S. J. Lippard, *Science* **1982**, *218*, 1075.

[9] a) Crystal data for **4a**: crystal dimensions [mm]: 0.5 × 0.7 × 0.9, monoclinic, space group *C*2/*c* (no. 15), a = 18.83(2), b = 10.029(8), c = 14.41(1) Å, β = 94.57(8)°, V = 2708.9 Å^3, Z = 8, ρ_{calcd} = 2.60 g cm^{-3}. F(000) = 2008: 3808 reflections with 3 < 2θ < 57.5°, reflections with I > 2.0 $\sigma(I)$ not determined. Structure solution and refinement with 2830 independent reflections with I > 2.5 $\sigma(I)$ for 91 parameters. Absorption correction empirical, 9 reflections, 8.0 < 2θ < 51.0°. R = 0.068, R(w) = 0.064. Residual electron density max. 6.50, min. −3.30 e Å^{-3}, very high residual electron density at the platinum caused by the strong absorption of the heavy metal. SynTex-R3 diffractometer, $Mo_{K\alpha}$ radiation (λ = 0.71073 Å), graphite monochromator. Structure solution and refinement was carried out on a microvax II with SHELXTL PLUS release 4.11/V and Patterson–Fourier methods. Hydrogen atoms were placed in their calculated positions (HFIX). b) Further details of the crystal structure investigation may be obtained from the Fachinformationszentrum Karlsruhe, D-76344 Eggenstein-Leopoldshafen (Germany), on quoting the depository number CSD-58895.

[10] Crystal data for **5**: crystal dimensions [mm]: 0.17 × 0.17 × 0.51, monoclinic, space group *C*2/*c* (no. 15), a = 18.386(8), b = 9.978(3), c = 14.385(4) Å, β = 103.64(3)°, V = 2564.58 Å^3, Z = 8, ρ_{calcd} = 2.67 g cm^{-3}. F(000) = 1976: 4031 reflections with 3 < 2θ < 60.0°, for 3066 of which I > 2.0 $\sigma(I)$. Structure solution and refinement with 2857 independent reflections with I > 2.5 $\sigma(I)$ for 178 parameters. Absorption correction empirical, 8 reflections, 5.8° < 2θ < 51.4°. R = 0.034, R(w) = 0.036. Residual electron density max. 2.4, min. −1.54 e Å^{-3}. SynTex-R3 diffractometer. $Mo_{K\alpha}$ radiation (λ = 0.71073 Å), graphite monochromator. Structure solution and refinement was carried out on a microvax II with SHELXTL PLUS release 4.11/V and Patterson–Fourier methods. Hydrogen atoms were placed in their calculated positions (HFIX) [9b].

Stereoselective Syntheses of Peptide Derivatives with 2-Acetamido-3,4,6-tri-*O*-acetyl-1-amino-2-deoxy-β-D-glucopyranose by Four-Component Condensation

Stefan Lehnhoff, Matthias Goebel, Rosa Maria Karl, Roland Klösel, and Ivar Ugi*

Dedicated to Professor Miklos Bodanszky

Syntheses that feature the simultaneous reaction of several reactants in a one-pot procedure are called multicomponent reactions (MCRs). In 1850 A. Strecker[1] discovered a reaction, subsequently named after him, which in our nomenclature is formulated as S-3CR, and in which ammonia, carbonyl compounds, and hydrogen cyanide react to form α-aminoalkyl cyanides that can be hydrolyzed to the corresponding amino acids. Since 1934 α-amino acids have been obtained by the Bucherer–Bergs reaction (BB-4CR),[2] one of the very first 4CRs.

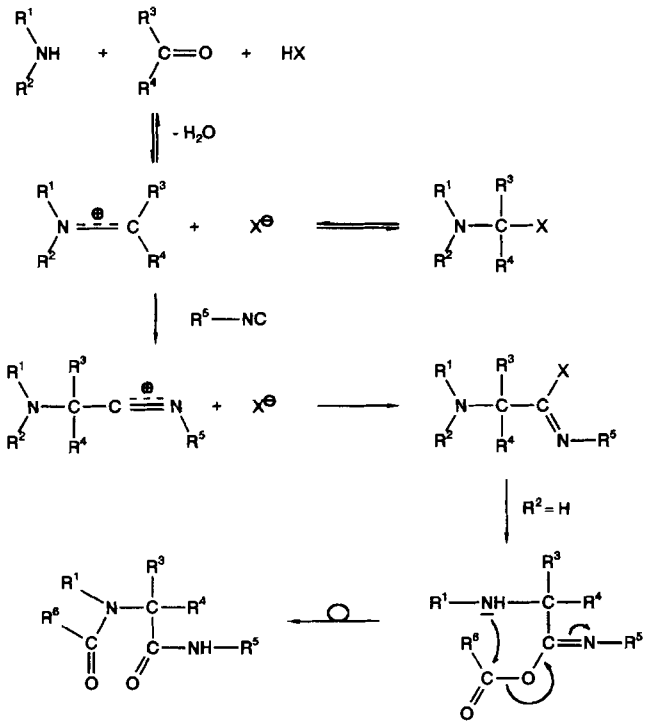
Hellmann and Opitz[3] recognized that many 3CRs are of the same basic type of reaction, namely an α-aminoalkylation of nucleophiles (HO-3CR). In 1921 Passerini[4] discovered that carboxylic acids, isocyanides, and carbonyl compounds form α-imino esters, which rearrange irreversibly thereafter. Other acids, such as HN_3 undergo analogous reactions.[5]

Although isocyanides have been available since 1867,[6] this P-3CR was their only significant application in organic syntheses until 1958 when their preparation was notably simplified

[*] Prof. Dr. I. Ugi, Dr. S. Lehnhoff, Dr. M. Goebel, Dr. R. M. Karl, Dr. R. Klösel
Institut für Organische Chemie und Biochemie
der Technischen Universität München
Lichtenbergstrasse 4, D-82747 Garching (Germany)
Telefax: Int. code + (89)32093290

 © VCH Verlagsgesellschaft mbH, D-69451 Weinheim, 1995 0570-0833/95/1010-1104 $ 10.00+.25/0

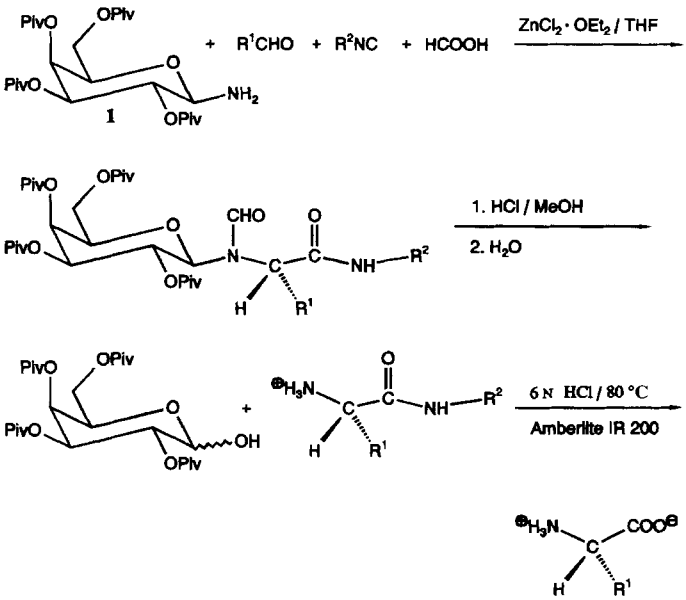
(dehydratation of *N*-formyl amides).[7, 8] The four-component condensation U-4CR was discovered in 1959, and most variants of this reaction followed within a few weeks (HX = H_2O, $H_2S_2O_3$, H_2Se, HN_3, HNCO, HNCS, RCO_2H).[9–11] The U-4CR is by far the most versatile of all multicomponent reactions. It is not only the starting point of all higher MCRs such as the AU-7CR[12] but also an ideal system for stereoselective reaction planning such as that necessary for the preparation of peptide derivatives. This point was made by M. Bodanszky and A. Ondetti in 1966.[13] Preparatively, the most important kind of U-4CR is the reaction with carboxylic acids[8, 11] (Scheme 1). Thereby, for instance, β-lactam antibiotics, α-amino acids, peptide derivatives, and various other types of compounds became available.[11, 14]



Scheme 1. U-4CR with X = R^6COO.

In the meantime, the rather complex reaction mechanisms have been described well by mathematical models,[15] resulting in the successful development of stereoselective U-4CRs by using α-aminoalkylferrocenes as chiral templates.[16] These chiral auxiliaries prepared by the Herrmann reaction (He-3CR) could be cleaved from the peptide formed in the U-4CR under mild conditions and recycled as well.[17] Besides *de* values that were not completely satisfactory, the disadvantages of this procedure are relatively low yields and limited stability of the ferrocene derivatives.

During the last decade many methods of syntheses of α-amino acids and their derivatives have been developed, but all these procedures are multistep syntheses consisting of, in some cases, up to ten steps.[18] Kunz et al. used 1-amino-2,3,4,6-tetra-*O*-pivaloyl-β-D-galactopyranose (**1**) as a chiral template in the U-4CR to form N-formylated derivatives of α-D-amino acids from various aldehydes with *tert*-butyl isocyanide and formic acid. Acidolysis at high temperatures followed by amide cleavage gave α-D-amino acids in more than 90% *ee*[19, 20] (Scheme 2). Other acids besides formic acid have not been used, since only

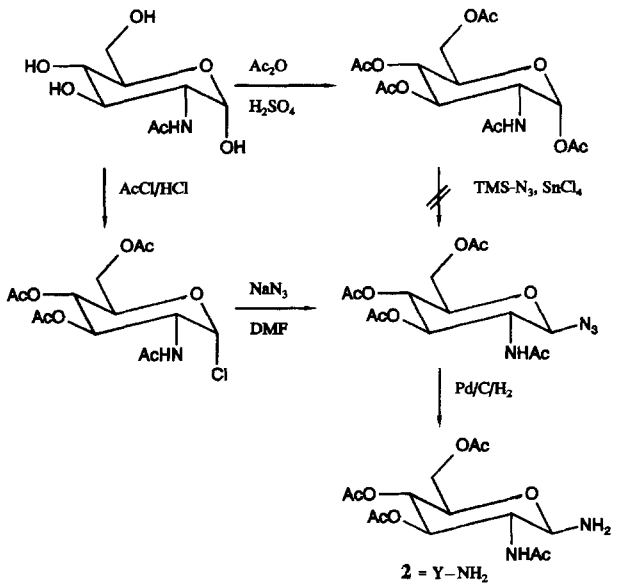


Scheme 2. Stereoselective synthesis of α-amino acids with 1-galactopyranosyl amines by Kunz et al.; R^2 = *t*Bu.

the N-formyl derivatives are cleavable by this rather drastic method. Therefore, peptides were not accessible.

These results motivated us to employ *O*-alkylated 1-aminopyranoses in a similar way, and in this case several peptide derivatives could be synthesized, since the glycosidic template could be removed by mild acidolysis with various, often sulfur-containing, nucleophiles.[21] The stereoselectivity reached was at a level similar to that obtained by Kunz et al.; however, the yields of these fragmentations were mostly low and the uniformity of the products often dissatisfying.

A major improvement was achieved by the use of the acetylated aminoglucopyranose **2**.[22] This compound is easy to prepare from readily available "*N*-acetyl glucosamine" in three simple steps[23, 24] (Scheme 3). The imine obtained from an aldehyde and the amine **2** forms a rigid complex with zinc chloride, which,

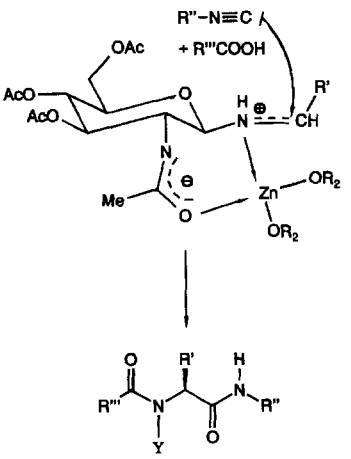


Scheme 3. Synthesis of the acetylated 1-aminoglucopyranose **2**. TMS = trimethylsilyl.

 © VCH Verlagsgesellschaft mbH, D-69451 Weinheim, 1995 0570-0833/95/1010-1105 $ 10.00+.25/0

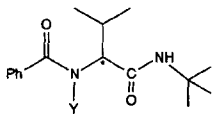
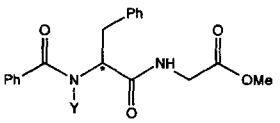
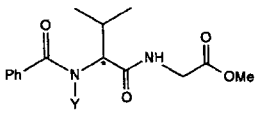
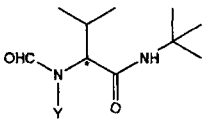
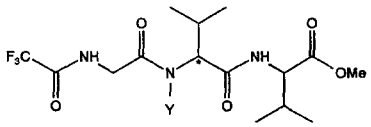
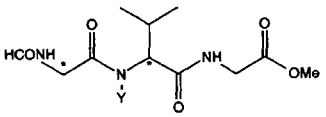
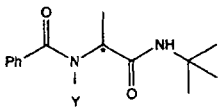
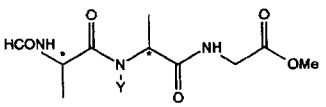
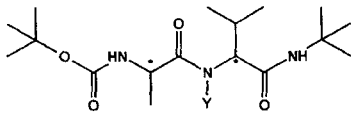
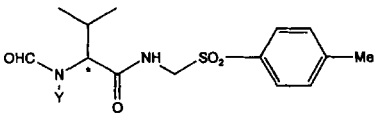
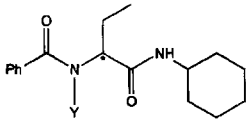
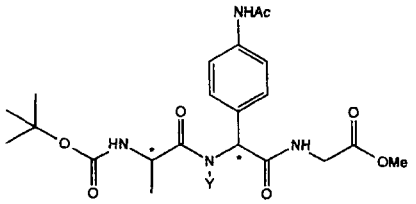
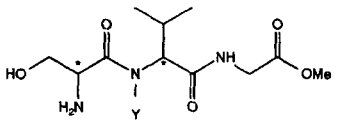
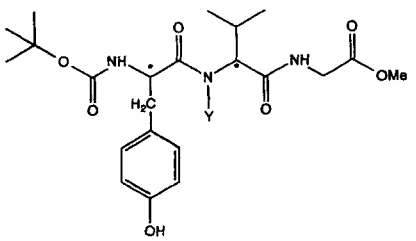
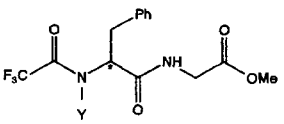
together with a clearly favored *trans* configuration of the imine, results in restricting the nucleophilic attack of the isocyanide to the back side at sufficiently low temperatures (Scheme 4). The diastereoisomeric excesses achieved thereby are above 99% in most cases, as a matter of fact, the second diastereoisomer could not be found. Small amounts of the second diastereoisomer were detected only for the smallest aldehydes, namely acetaldehyde and propionic aldehyde, (*de* = 89 and 94%, respectively, Table 1).

While the stereochemical inductivity of the templates used by Kunz et al. relied heavily on type and steric position of the chosen acyl groups on the pyranosyl system, these factors had no influence when using template **2**. Therefore, simple acetyl groups and the inexpensive glucopyranose system could be used. Significantly, there is no stereoselectivity, when **2** is used without the zinc catalyst, which also catalyses the formation of



Scheme 4. Mechanism of the stereoselective U-4CR with the amine **2**. R = Et, Y = sugar group (see Scheme 3).

Table 1. Selection of condensation products that were obtained with the amine **2** according to the reaction given in Scheme 2; in the formulas the newly formed stereocenters (all D configurated) are labeled with an asterisk; the amino acid derivatives used were all L configurated.

Compound	Maximum yield (%)	Maximum *de* (%)	Compound	Maximum yield (%)	Maximum *de* (%)
	85	>99		80	99
	80	>99		90	>99
	82	>99		5	–
	81	89		17	92
	79	>99		10	–
	72	94		7	–
	50	>99		83	>99
	50	98			

 © VCH Verlagsgesellschaft mbH, D-69451 Weinheim, 1995 0570-0833/95/1010-1106 $ 10.00+.25/0

the imine. Other metal salts, like $MgBr_2$, show similar effects, but none as convincingly as zinc chloride dietherate. Typical yields are in the range of 80% (Table 1) with best yields obtained at $-40\,^{\circ}C$ in most cases, while optimal stereoselectivity was always achieved at $-75\,^{\circ}C$. Much lower optical and chemical yields are obtained at temperatures above $0\,^{\circ}C$.

Possible acid components are all soluble acids that are not too strongly acidic. For example, trifluoroacetic acid already leads to a rather uncertain mixture of by-products, while excellent results were obtained with formic acid. Aromatic or heteroaromatic aldehydes do not form stable imino chelates, which differs from our experiences concerning alkylated 1-amino pyranoses. Isocyanides have to be sufficiently nucleophilic, otherwise reaction times will be very long. Tests with (*para*-toluenesulfonyl)methyl isocyanide, for instance, gave yields of less than 10% after 10 days reaction time. THF and methanol are suitable solvents for these reactions, whereas halogen-containing solvents strongly favor the P-3CR, making them as unsuitable as nonpolar solvents (amine will not dissolve!) or solvents that show a high viscosity at the temperatures employed. At $-75\,^{\circ}C$, reaction times including the time for the precondensation of the imine are roughly six days. Other limitations were not found. All compounds in Table 1 were made by this simple one-pot procedure without special adaptations. Syntheses of longer peptide structures are currently under investigation as are preparations of cyclopeptides. We are also developing a template for the preparation of the analogous L derivatives. An important feature of the amine **2** is its ability to form dihydrooxazoles, which should make cleaving the chiral template easier. We have already been able to realize an acidolytic and a reductive fragmentation process. However, since yields and overall reproductivity have yet to be optimized, this work will be reported at a later date. One aspect herein, is the possible variation of the amide group at C2 of **2** in order to get better fragmentation and also to improve the diastereoselectivity at higher temperatures.

Experimental Procedure

General procedure for the stereoselective U-4CR: To the amine **2** (10 mmol) and the chosen aldehyde (10 mmol), dissolved in THF or methanol (90 mL) at the chosen temperature (standard value is $-75\,^{\circ}C$), molecular sieves (4 Å) (2.5 g) and catalyst ($ZnCl_2$ in Et_2O) (11 mmol) were added under an argon atmosphere. This mixture was stirred for several hours until complete formation of the imine. Then the isocyanide (10.4 mmol), dissolved in precooled solvent (5 mL), and subsequently the acid component (10.4 mmol), dissolved or suspended in precooled solvent (5 mL), were added. The mixture was stirred at a constant temperature until no amine was detectable by TLC. The reaction mixture was then filtered swiftly through a layer of celite (1 cm) and this was additionally washed with dichloromethane (20 mL). Under vigorous stirring a mixture of saturated aqueous sodium hydrogen carbonate solution (15 mL) and methanol (65 mL) was poured into the reaction mixture. After five minutes of additional stirring, the resulting suspension was filtered and the solvent removed. The sometimes oily, often foamy residue was taken up in dichloromethane (100 mL) and the remaining isocyanide was removed by extraction with aqueous tartaric acid (for *tert*-butyl isocyanide) or by treatment with acetic acid (for involatile isocyanides). This was followed by extraction with water, saturated sodium hydrogen carbonate, and water again (each 250 mL). The mixture was then dried over sodium sulfate and the solvent evaporated. In most cases, after several hours at high vacuum a crystalline foam was obtained, which was often found to be already analytically pure. Otherwise it was purified by recrystallization and/or chromatography.

Received: December 14, 1994
Revised version: February 15, 1995 [Z 7551 IE]
German version: *Angew. Chem.* **1995**, *107*, 1208

Keywords: asymmetric syntheses · chiral auxiliaries · peptide syntheses · four-component reactions

[1] A. Strecker, *Ann. Chem. Pharm.* **1850**, *75*, 27.
[2] H. Bergs, *Chem. Zentralbl.* **1933**, *27*, 1001; H. T. Bucherer, W. Steiner, *Z. Prakt. Chem.* **1934**, *140*, 291.
[3] H. Hellmann, G. Opitz, *α-Aminoalkylierung*, Verlag Chemie, Weinheim, **1960**.
[4] M. Passerini, *Gazz. Chim. Ital.* **1921**, *51 II*, 126,181; *ibid.* **1926**, *56*, 826; M. Passerini, G. Ragni, *ibid.* **1931**, *61*, 964.
[5] I. Ugi, *Isonitrile Chemistry*, *Vol.20*, Academic Press, New York, **1971**; I. Ugi, S. Lohberger, R. Karl in *Comprehensive Organic Chemistry: Selectivity for Synthesis Efficiency*, *Vol.20*, (Eds.: B. M. Trost, C. H. Heathcock), Pergamon, Oxford **1991**, p. 1083.
[6] A. Gautier, *Ann. Chem. Pharm.* **1867**, *142*, 289; *ibid.* **1867**, *144*, 114; *Ann. Chim. Phys.* **1869**, *17*, 103,203.
[7] I. Ugi, C. Steinbrückner, *Angew. Chem.* **1960**, *72*, 267; *ibid.* **1962**, *74*, 9; *Angew. Chem. Int. Ed. Engl.* **1962**, *1*, 6.
[8] I. Ugi, C. Steinbrückner, *Chem. Ber.* **1961**, *94*, 2802.
[9] C. Steinbrückner, Dissertation, Universität München, **1961**.
[10] I. Ugi, R. Meyer, U. Fetzer, C. Steinbrückner, *Angew. Chem.* **1959**, *71*, 386.
[11] C. Steinbrückner, *Chem. Ber.* **1961**, *94*, 2814.
[12] I. Ugi, A. Dömling, W. Hörl, *GIT Fach. Lab.* **1994**, *38*, 340; *Endeavour* **1994**, *18*, 115.
[13] M. Bodanszky, M. A. Ondetti in *Peptide Synthesis* (Ed.: G. A. Olah), Wiley Interscience, New York **1966**, p. 127.
[14] G. Neyer, J. Achatz, B. Danzer, I. Ugi, *Heterocycles* **1990**, *20*, 863.
[15] I. Ugi, G. Kaufhold, *Justus Liebigs Ann. Chem.* **1967**, *709*, 11.
[16] F. Siglmüller, R. Herrmann, I. Ugi, *Tetrahedron* **1986**, *42*, 5931.
[17] R. Herrmann, G. Hübener, F. Siglmüller, I. Ugi, *Liebigs Ann. Chem.* **1986**, 251.
[18] R. M. Williams, *Synthesis of Optically Active α-Aminoacids*, *Vol 7*, Pergamon, Oxford, **1989**; J. Mulzer, H.-J. Altenbach, M. Braun, K. Krohn, H.-U. Reissig, *Organic Synthesis Highlights*, VCH, Weinheim, **1991**; D. Seebach, R. Imwinkelried, T. Weber, *Mod. Synth. Methods* **1986**, *4*; U. Schöllkopf, *Pure Appl. Chem.* **1983**, *55*, 1799-1806; *α-Amino Acid Synthesis*, (Ed.: M. J. O'Donnel), *Tetrahedron* **1988**, *44*, 5253-5614.
[19] H. Kunz, W. Sager, *Angew. Chem.* **1987**, *99*, 595; *Angew. Chem Int. Ed. Engl.* **1987**, *26*, 557.
[20] H. Kunz, W. Pfrengle, *J. Am. Chem. Soc.* **1988**, *110*, 651; *Tetrahedron* **1988**, *44*, 5487.
[21] M. Goebel, I. Ugi, *Synthesis* **1991**, 1095.
[22] S. Lehnhoff, Dissertation Technische Universität München, **1994**.
[23] F. Micheel, A. Klemer, *Adv. Carbohydr. Chem.* **1961**, *16*, 95.
[24] W. Pfleiderer, E. Bühler, *Chem. Ber.* **1966**, *99*, 3022.

Novel Genetically Engineered Tetracenomycins**

Heinrich Decker, Sabine Haag, Györgyi Udvarnoki, and Jürgen Rohr*

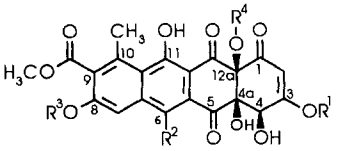
Chemically untreatable diseases as well as increasing numbers of bacteria,[1] viruses, parasites, and cancer cells resistant to chemotherapy demand innovative concepts to find new molecules, which might serve as lead structures for pharmaceutically useful drugs. Natural products have proven to be a primary basis for novel bioactive molecules. Since the pioneering experiments of Hopwood et al. in 1985, genetically engineered hybrid microorganisms[2] with modified genes have also been discussed as a possible source of new natural products.[3] Even though this method has been highlighted as a major step forward in biotechnology,[3c] there are no other examples of genetically engineered hybrid compounds except for some macrolide derivatives.[4] Re-

[*] Priv.-Doz. Dr. J. Rohr, Dipl.-Ing. G. Udvarnoki
Institut für Organische Chemie der Universität
Tammannstrasse 2, D-37077 Göttingen (Germany).
Telefax: Int. code + (551)39-9660
e-mail: jrohr@gwdg.de
Dr. H. Decker, Dipl.-Biol. S. Haag
Institut für Biologie II der Universität Tübingen (Germany)

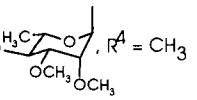
[**] This work was supported by the Deutsche Forschungsgemeinschaft and the Fonds der Chemischen Industrie. We also thank Dipl.-Chem. R. Machinek for the H,H-NOESY NMR spectrum, and Dr. J. Metzger (Universität Tübingen) for the electron spray, and Dr. G. Remberg (Universität Göttingen) for all other mass spectra.

cently, however, Khosla et al. have proven the general concept to be prosperous, since the interspecies exchange of polyketide synthase genes of different producers of multicyclic aromatic polyketides resulted in the production of several new metabolites.[5] Consequently, more and various types of hybrid products should be expected in the future. Polyketides occur in most organisms (bacteria, fungi, plants) and are an extremely rich family of bioactive molecules (antibiotics, antitumor agents, immunosuppressants, etc.). The biosynthetic pathways of many polyketides have been elucidated and the analysis of the genetics of polyketide production is under intense investigation.[2b] Therefore, this group of natural products seems to be the most promising one to be approached by genetic engineering for the production of novel hybrid compounds,[2c] as the current examples show.[3–5] Our strategy in this context was to combine genes of two well-studied producers of related types of multicyclic, aromatic polyketides in order to enhance the chance for detection of novel hybrid products. The first results of our studies are three novel tetracenomycins isolated from two hybrid strains, which were made by transferring the tetracenomycin biosynthesis genes from *Streptomyces glaucescens* GLA. O[6] and elloramycin biosynthesis genes from *Streptomyces olivaceus* Tü 2353,[6] into the urdamycin-producer *Streptomyces fradiae* Tü 2717.[7]

The tetracenomycins (tetracenomycin C **1**) and the related elloramycins[6] (elloramycin A **2**) as well as the urdamycins[7] (urdamycin A **3**) are examples of biosynthetically well-studied polyketide antibiotics. In addition, since the elloramycins and urdamycins are glycosylated during the biosynthesis, the producing strains contain, besides the biosynthetic genes coding for the polyketide synthase, the genes necessary for the biosynthesis of the special carbohydrate moieties as well as for the glycosylation of the polyketide-derived aglycon moieties. Thus, from a combination of the biosynthetic genes of both parent *Streptomyces* species, one could expect as possible hybrid products not only those derived from a hybrid polyketide synthase, but also those that result from intercombining the polyketide biosynthesis with the post-polyketide biosynthesis apparatus of the other parent, for instance the enzymes of the carbohydrate biosynthesis, including the glycosyl transferase activities. Biosynthetic enzymes for middle or late biosynthetic steps, for example methyltransferases and oxygenases, may be expected also to contribute by acting on the other strains intermediates or end products. The success of this approach depends mainly on the substrate specificity of the enzymes involved in the biosynthesis of the different polyketide compounds. To inspect this general possibility, we introduced the entire tetracenomycin (*tcm*) gene cluster (pWHM3 with a 12.5 kb DNA insert = pWHM1026[8a]) and part of the elloramycin (*elm*) gene cluster (pKC505[8b] with a 25 kb DNA insert = 16F4[8c]) into the urdamycin producer *Streptomyces fradiae* Tü 2717 by transformation.[8c] Most of the metabolites in the fermentation broth of the two hybrid strains were recognized as tetracenomycin-, elloramycin-, or urdamycin-related natural products through their UV spectra (HPLC/diode array detector).[9a] Three of the compounds did not match with any known products and their subsequent isolation and structure elucidation revealed the presence of novel tetracenomycin derivatives, namely 6-hydroxytetracenomycin C (**4**) from *Streptomyces fradiae* Tü2717(pWHM1026), and 3,8-didemethyltetracenomycin C (**5**) and 8-β-D-olivosyl-8-demethyltetracenomycin C (**6**) from *Streptomyces fradiae* Tü2717(16F4). The structures could be determined from the analyses of the NMR (Tables 1 and 2) and mass spectra by comparison with that of tetracenomycin C (**1**). The characteristic NMR features of **4** are the missing 6-H signal (Table 1) and the additional chelated OH group ($\delta = 12.68$; Table 2) in the ^{1}H NMR spectrum, and the quarternary C-6 in the ^{13}C NMR spectrum (attached proton test (APT); Table 1). The molecular formula $C_{23}H_{20}O_{12}$ (488.4) follows from the electron spray (ES) MS (*m/z* 556.5 (100%)

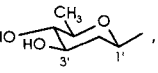


1, $R^1 = CH_3$, $R^2 = H$, $R^3 = CH_3$, $R^4 = H$

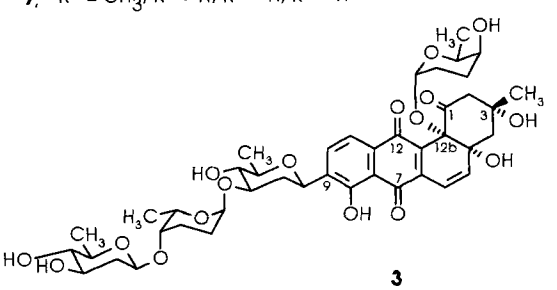
2, $R^1 = CH_3$, $R^2 = H$, R^3 =  , $R^4 = CH_3$

4, $R^1 = CH_3$, $R^2 = OH$, $R^3 = CH_3$, $R^4 = H$

5, $R^1 = H$, $R^2 = H$, $R^3 = H$, $R^4 = H$

6, $R^1 = CH_3$, $R^2 = H$, R^3 =  , $R^4 = H$

7, $R^1 = CH_3$, $R^2 = H$, $R^3 = H$, $R^4 = H$



3

Table 1. ^{13}C NMR Data of the novel tetracenomycin derivatives **4**, **5**, and **6** compared with that of **1** (relative to TMS, 125.7 MHz; δ, multiplicity (APT)).

	1[a]	**4**[a]	**5**[b]	**6**[a, c]
C-1	190.8 s	190.6 s	190.8 s	190.3 s
C-2	99.7 d	100.0 d	98.0 d	100.0 d
C-3	175.3 s	174.9 s	187.0 s	175.0 s
3-OCH_3	57.2 q	57.4 q	–	57.3 q
C-4	70.3 d	71.0 d	74.4 d	70.5 d
C-4a	85.2 s	84.0 s	86.0 s	79.2 s
C-5	194.1 s	196.7 s	196.3 s	193.9 s
C-5a	141.2 s	106.3 s[d]	141.8 s	141.1 s
C-6	120.7 d	161.9 s	120.6 d	121.3 d
C-6a	129.0 s	134.1 s	129.7 s	129.1 s
C-7	108.4 d	102.9 d	112.0 d	112.1 d
C-8	158.3 s	158.8 s	158.0 s	156.0 s
8-OCH_3	56.6 q	56.8 q	–	–
C-9	129.6 s	131.5 s	129.9 s	131.0 s
9-C=O	167.5 s	167.9 s	168.0 s	167.9 s
9-OCH_3	52.8 q	52.8 q	52.9 q	52.8 q
C-10	137.9 s	138.9 s	139.5 s	138.4 s
10-CH_3	21.1 q	21.0 q	21.1 q	21.0 q
C-10a	121.0 s	123.0 s	120.8 s	122.0 s
C-11	168.0 s	167.9 s	170.2 s	168.0 s
C-11a	109.8 s	106.5 s[d]	109.6 s	110.2 s
C-12	197.9 s	199.5 s	199.5 s	197.9 s
C-12a	83.6 s	82.9	82.5 s	83.6 s

[a] In [D_6]acetone, the carbon atoms were further assigned through long-range C,H couplings (2D-COLOC or HMBC). [b] In CD_3OD, assignments in analogy to **1**. [c] Sugar moiety signals: 97.8 (d, C-1'), 39.6 (t, C-2'), 71.6 (d, C-3'), 78.0 (d, C-4'), 73.3 (d, C-5'), 18.2 (q, C-6'). [d] Assignments interchangeable.

 © VCH Verlagsgesellschaft mbH, D-69451 Weinheim, 1995 0570-0833/95/1010-1108 $ 10.00+.25/0

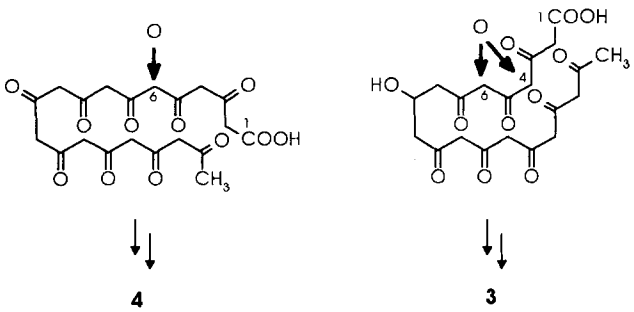
Table 2. ^{1}H NMR data of the novel tetracenomycin derivatives **4**, **5**, and **6** compared with that of **1**, (relative to TMS, 500 MHz, δ, multiplicity).

	1[a]	**4**[a]	**5**[b]	**6**[a]
2-H	5.61 s, br.	5.61 s	[m]	5.61 s, br.
3-OCH_3	3.83 s	3.83 s	–	3.81 s
4-H	5.05 d[c]	5.02 s	4.82 s	5.04 s[c]
4-OH	4.95 d[c, d]	5.12 s[d, e]	[m]	4.94 d[c, d]
4a-OH	5.16 s[d, e]	5.29 s[d, e]	[m]	5.11 s[d, e]
6-H	8.00 s	–	7.14 s	7.99 s
6-OH	–	12.68 s[d]	–	–
7-H	7.60 s	7.80 s	7.80 s	7.76 s
8-OCH_3	4.00 s	4.05 s	–	–
8-OH	–	–	[m]	–
9-$COOCH_3$	3.90 s	3.95 s	3.94 s	3.93 s
10-CH_3	2.80 s	2.78 s	2.81 s	2.82 s
11-OH	13.98 s[d]	13.92 s[d]	[m]	14.01 s[d]
12a-OH	5.73 s[d, e]	5.72 s[d, e]	[m]	5.76 s[d, e]
1′-H	–	–	–	5.57 dd[f]
2′-H_a	–	–	–	1.75 ddd[g]
2′-H_e	–	–	–	2.32 ddd[h]
3′-H	–	–	–	3.71 m
3′-OH	–	–	–	4.25 s[d, i]
4′-H	–	–	–	3.05 dd[j]
4′-OH	–	–	–	4.30 s[d, i]
5′-H	–	–	–	3.66 dq[k]
6′-H_3	–	–	–	1.32 d[l]

[a] In [D_6]acetone. [b] In CD_3OD. [c] Broad, $J = 7$ Hz, not always observable. [d] Broad, exchangeable with D_2O. [e] Assignments interchangeable. [f] $J = 10$, 2 Hz. [g] $J = 12$, 12, 10 Hz. [h] $J = 12$, 5, 2 Hz. [i] Assignments interchangeable. [j] $J = 9$, 9 Hz. [k] $J = 9$, 6 Hz. [l] $J = 6$ Hz. [m] Not observeable because of H/D exchange.

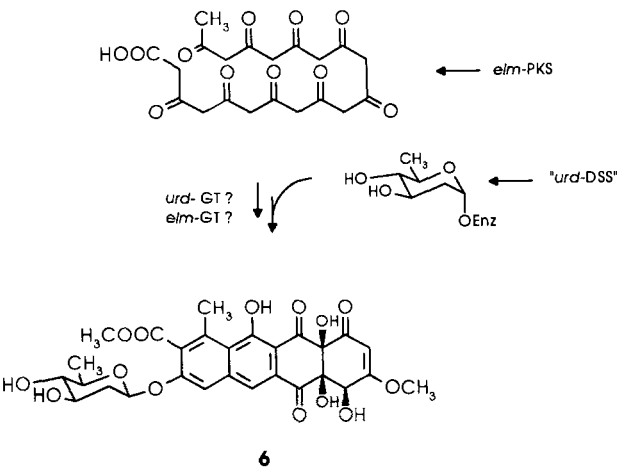
$[M + 3\,Na]$) as well as from the highly resolved molecular peak of the EI-MS (488.0954). The molecular formula $C_{21}H_{15}O_{11}$ (443.3) and structure of **5** were derived from the ES-MS (*m/z* 466.5 (100%) $[M + Na]$) and the NMR spectra, containing only one OCH_3 group and the additional keto group at $\delta = 187.0$. The position of the remaining OCH_3 group at C-9 could be deduced from its chemical shift in the NMR spectra (Tables 1 and 2) in comparison with that of the corresponding group in **1**. The compound is obtained after workup (pH 7) as the sodium salt of the anion and has the 1,3-diketo structure, in which one of the acidic 2-H atoms is removed. The compound resembles 3-demethylelloramycinone, a hydrolysis derivative of **2**.[6a] The NMR spectra of the third novel compound **6** show the structural elements of the 8-demethyltetracenomycin C aglycon plus one D-olivose moiety. Its molecular formula $C_{28}H_{28}O_{14}$ (588.5) could be deduced from negative ion FAB-MS (*m/z* 587 (100%) $[M-H^-]$). The assignment of the position of the sugar moiety was complicated, since no helpful $^3J_{C-H}$ coupling could be detected in the HMBC or COLOC spectrum. Although a significant upfield shift of C-4a in **6** (in comparison with the chemical shifts of this carbon in **1**, **4** and **5**, Table 1) seems to indicate a variation of the molecule in this region, it could be unambigously concluded that 8-O is the linkage position of the sugar moiety. This was deduced from the ^{1}H NMR spectrum (all other OH groups are free, see Table 2), the UV data (the UV spectrum of the compound at pH > 7 does not show the typical absorption at 315 nm, caused from the 8-OH group, which is, for example, observed in elloramycinone[6d]), and finally from the H,H-NOESY NMR spectrum, in which a significant NOE effect is observed inter alia between 1′-H and 7-H. The β-glycosidic linkage follows from the coupling pattern of the 1′ and 2′-H_a signals in the ^{1}H NMR spectrum, the absolute stereochemistry of the sugar moiety from the $[\alpha]_D$ value of its liberated α-methylglycoside (+133, $c = 0.08$, EtOH, 21 °C).[9b]

We demonstrated the co-production of tetracenomycin C (**1**) and its biosynthetic intermediate 8-demethyltetracenomycin C (**7**) in the urdamycin-producer *Streptomyces fradiae* Tü 2717 (pWHM1026) and *S. fradiae* Tü2717(16F4), respectively. Furthermore three novel compounds were produced by the hybrid strains, namely a minor product **5**, and two major products **4** and **6** (production ca. 10 mg L^{-1}). 8-demethyltetracenomycin C (**7**) has previously been isolated by Yue et al.[10a] from a mutant of *Streptomyces glaucescens* impaired in the 8-*O*-methylation step. The plasmid conferring tetracenomycin C (pWHM1026) production is well-characterized and all *tcm* genes on this plasmid have been sequenced and analyzed.[10b] Since there is no indication for an enzyme in the *tcm* cluster catalyzing the 6-hydroxylation of **1**, this activity has to arise from an enzyme present in *Streptomyces fradiae*. Therefore, **4** could be formed by one of the oxygenases of urdamycin biosynthesis through which oxygens in the 12 and the 12b positions are introduced[11] at carbons 4 and 6, respectively, of its initial decaketide. The 6-position of the tetracenomycins corresponds to the carbon 6 of its initial decaketide precursor (Scheme 1). 6-hydroxytetracenomycin (**4**) is the **1**-analog of elloramycin F (6-hydroxyelloramycin A), known as a minor side product (production 0.01 mg L^{-1}) of the elloramycin-producer *S. olivaceus*.[12]



Scheme 1. Decaketide precursors of **4** and **3**.

The plasmid carrying some of the elloramycin biosynthetic genes (16F4)[8c] is less well characterized than pWHM1026. It confers resistance to elloramycin (**2**) and tetracenomycin C (**1**), and introduction of 16F4 into *Streptomyces fradiae* Tü 2717 or *Streptomyces lividans* TK24 by transformation results in the production of 8-demethyltetracenomycin C (**7**).[8c] In addition, *Streptomyces fradiae*(16F4) produced 3,8-didemethyltetracenomycin C (**5**) and 8-β-D-olivosyl-8-demethyltetracenomycin C (**6**). Compound **5**, a minor side product (1 mg L^{-1}), seems to be the result of an incomplete aglycon biosynthesis in which 3-*O*-methylation did not occur. The occurrence of compound **5** can be considered an indicator that the methylation sequence for the biosynthesis of **1**, as outlined by Hutchinson et al.,[6c, 10a] can be curtailed in some instances. In contrast, **6** is a true hybrid molecule, because the 2,6-dideoxy sugar olivose is normally only produced for urdamycin biosynthesis; it occurs twice in urdamycin A (**3**). Elloramycin (**2**) bears a permethylated L-rhamnose moiety, also linked at 8-O. The genes for the biosynthesis of the permethylated L-rhamnose moiety are not present on 16F4.[8c] Thus, the hybrid strain *Streptomyces fradiae*(16F4) must use glycosyl transferase activity to link the dideoxy sugar β-D-olivose and the elloramycin polyketide backbone resulting in the hybrid product **6** (Scheme 2). We cannot exclude the possibility that there is a glycosyl transferase present on 16F4; therefore this reaction may either be catalyzed by an enzyme present on 16F4 or by an enzyme of the urdamycin producer. That **6** can only be obtained through transferring the genes into *Streptomyces fradiae* and not by simple microbial transformation[13]



6

Scheme 2. PKS = Polyketide synthase; "DSS" = "deoxy sugar synthase", that is, genes necessary for the biosynthesis of the deoxysugar olivose from glucose; GT = glycosyl transferase; Enz = enzyme.

was shown by a control experiment: Feeding of **7** to a growing culture of the urdamycin-producing wild-type strain did not yield any olivosyltetracenomycin (**6**). This indicates that the glycosyltransferase from the urdamycin producer either does not work on **7** but on a different biosynthetic intermediate, or that there is an unidentified glycosyl transferase present on 16F4 that catalyzes the linkage of the sugar moiety.[14]

Our initial experiments indicate that co-expression of two different polyketide pathways in one hybrid strain is a promising tool to create new natural products in reasonable yields (10 mg L^{-1}). We have not yet detected any novel urdamycin derivatives or novel types of polyketides derived from the activity of a hybrid polyketide synthase.[5] Therefore, the expression of engineered hybrid polyketide synthases in a heterologous host as demonstrated by Khosla et al.[5] should be done to obtain further hybrid compounds.

Experimental Procedure

Bacterial strains and plasmids: *S. fradiae* Tü 2717 was transformed with 16F4 and pWMH1026 by protoplast fusion and protoplasts were regenerated on R2YE agar plates [15]. Plasmid pWHM1026 carrying the entire *tcm* cluster was described previously [8a]. 16F4 consists of the cosmid vector pKC505 [8b] that contains a 25 kb DNA fragment isolated from the elloramycin-producer *S. olivaceus* Tü 2353 [8c]. This plasmid contains all the genes necessary for the production of **7** [8c].

Cultivation of the recombinant strains: *S. fradiae* Tü2717(16F4) and *S. fradiae* Tü2717(pWHM1026) were grown for 96 h in a production medium (2% soybean meal, 2% glucose, pH 7.2 [7]) with 25 μg mL^{-1} apramycin and 10 μg mL^{-1} thiostrepton, respectively.

Isolation of the novel products: The culture was extracted twice with ethyl acetate at pH 7 and evaporated to dryness. The ethyl acetate residue was disolved in CH_2Cl_2 and further purified on silica gel saturated with oxalic acid (silica gel SI 60, Merck, Germany). The silica gel column was washed with CH_2Cl_2 and the compounds were eluted with CH_2Cl_2/MeOH (95:5, 9:1, and 8:2). Fractions containing different urdamycin and tetracenomycin metabolites were pooled, evaporated to dryness, and further purified on Sephadex LH 20 (MeOH). The final purification was performed by HPLC (preparative column, Nucleosil 100 C-18, particle size 10 μm), elution with water/MeOH (gradient 40% to 100% MeOH in 15 min).

Instruments: All NMR spectra were recorded on a Varian VXR 500 spectrometer at a field strength of 11.7 Tesla, except the HMBC spectra and the NOESY spectrum which were recorded on a Bruker AMX 300 at a field strength of 7.1 Tesla. Details see Tables 1 and 2. All mass spectra (except ES- MS, see below) were obtained on a Finnigan MAT 95 spectrometer, for the FAB-MS 3-nitrobenzyl alcohol was used as the matrix. The electron spray mass spectra (ES-MS) were recorded on a API III Taga 6000 E equipped with an ion spray source (Sciex, Thornhill, Canada).

Received: December 27, 1994 [Z 7577 IE]
German version: *Angew. Chem.* **1995**, *107*, 1214

Keywords: biosynthesis · gene technology · polyketides · tetracenomycins

[1] a) N. C. J. Strynadka, S. E. Jensen, K. Johns, H. Blanchard, M. Page, A. Matagne, J.-M. Frère, M. N. G. James, *Nature* **1994**, *368*, 657–660, and references therein; b) H. C. Neu, *Science* **1992**, *257*, 1064–1073, and references therein; c) J. Travis, E. Culotta, R. Nowak, S. Kingman, R. Stone, *ibid.* **1994**, *264*, 360–367; d) L. L. Silver, K. A. Bostian, *Antimicrob. Agents Chemother.* **1993**, *37*, 377–383; e) V. Webb, J. Davies, *ibid.* **1993**, *37*, 2379–2384.

[2] a) C. R. Hutchinson, *Med. Res. Rev.* **1988**, *8*, 557–567; b) L. Katz, S. Donadio, *Annu. Rev. Microbiol.* **1993**, *47*, 875–912; c) D. E. Cane, *Science* **1994**, *263*, 338–340, and references therein.

[3] a) D. A. Hopwood, F. Malpartida, H. M. Kieser, H. Ikeda, J. Duncan, I. Fujii, B. A. Rudd, H. G. Floss, S. Ōmura, *Nature* **1985**, *314*, 642–644; b) S. Ōmura, H. Ikeda, F. Malpartida, H. M. Kieser, D. A. Hopwood, *Antimicrob. Agents Chemother.* **1986**, *29*, 13–19; c) A. L. Demain, *Nature* **1985**, *314*, 577–578.

[4] a) J. M. Weber, J. O. Leung, S. J. Swanson, K. B. Idler, J. B. McAlpine, *Science* **1991**, *252*, 114–117; b) S. Donadio, M. J. Staver, J. B. McAlpine, S. J. Swanson, L. Katz, *ibid.* **1991**, 675–679; c) S. Lai, Y. Shizuri, S. Yamamura, K. Kawai, H. Furukawa, *Bull. Chem. Soc. Jpn.* **1991**, *64*, 1048–1050; d) S. Donadio, J. B. McAlpine, P. J. Sheldon, M. Jackson, L. Katz, *Proc. Natl. Acad. Sci. USA* **1993**, *90*, 7119–7123; e) J. K. Epp, M. L. B. Huber, J. R. Turner, T. Goodson, B. E. Schoner, *Gene* **1989**, *85*, 293–301; f) O. Hara, C. R. Hutchinson, *J. Bacteriol.* **1992**, *174*, 5141–5144.

[5] a) R. McDaniel, S. Ebert-Khosla, D. A. Hopwood, C. Khosla, *Science* **1993**, *262*, 1546–1550; b) R. McDaniel, S. Ebert-Khosla, D. A. Hopwood, C. Khosla, *J. Am. Chem. Soc.* **1993**, *115*, 11671–11675; c) H. Fu, S. Ebert-Khosla, D. A. Hopwood, C. Khosla, *Ibid.* **1994**, *116*, 4166–4170; d) H. Fu, S. Ebert-Khosla, D. A. Hopwood, C. Khosla, *Ibid.* **1994**, *116*, 6443–6444; e) H. Fu, R. McDaniel, D. A. Hopwood, C. Khosla, *Biochemistry* **1994**, *33*, 9321–9326.

[6] a) J. Rohr, A. Zeeck, *J. Antibiot.* **1990**, *43*, 1169–1178, and references therein; b) J. Rohr, S. Eick, A. Zeeck, P. Reuschenbach, H. Zähner, H. P. Fiedler, *ibid.* **1988**, *41*, 1066–1073; c) H. Decker, H. Motamedi, C. R. Hutchinson, *J. Bacteriol.* **1993**, *175*, 3876–3886, and references therein; d) H. Drautz, P. Reuschenbach, H. Zähner, J. Rohr, A. Zeeck, *J. Antibiot.* **1985**, *38*, 1291–1301; e) G. Udvarnoki, C. Wagner, R. Machinek, J. Rohr, *Angew. Chem.* **1995**, *107*, 643–645; *Angew. Chem. Int. Ed. Engl.* **1995**, *34*, 565–567; f) W. Weber, H. Zähner, J. Siebers, K. Schröder, A. Zeeck, *Arch. Microbiol.* **1979**, *121*, 111–116.

[7] J. Rohr, M. Schönewolf, G. Udvarnoki, K. Eckardt, G. Schumann, C. Wagner, J. M. Beale, S. D. Sorey, *J. Org. Chem.* **1993**, *58*, 2547–2551, and references therein.

[8] a) H. Decker, C. R. Hutchinson, *J. Bacteriol.* **1993**, *175*, 3887–3892 b) M. A. Richardson, S. Kuhstoss, P. Solenberg, N. A. Schaus, R. Nagaraja Rao, *Gene* **1987**, *61*, 231–241. c) H. Decker, J. Rohr, H. Motamedi, H. Zähner, C. R. Hutchinson, *Gene*, submitted.

[9] a) H. P. Fiedler, *Nat. Prod. Lett.* **1993**, *2*, 119–128, and references therein; b) T. Henkel, J. Rohr, J. M. Beale, L. Schwenen, *J. Antibiot.* **1990**, *43*, 492–503, and references therein.

[10] a) S. Yue, H. Motamedi, E. Wendt-Pienkowsky, C. R. Hutchinson, *J. Bacteriol.* **1986**, *167*, 581–586. b) C. R. Hutchinson, H. Decker, H. Motamedi, B. Shen, R. G. Summers, E. Wendt-Pienkowsky, W. Wessel, in *Genetics and Molecular Biology of Industrial Microorgansims* (Eds.: R. H. Baltz, T. Ingolia, G. Hegeman), American Society for Microbiology, Washington, DC, **1993**, p. 203–216.

[11] G. Udvarnoki, T. Henkel, R. Machinek, J. Rohr, *J. Org. Chem.* **1992**, *57*, 1274–1276.

[12] H. P. Fiedler, J. Rohr, A. Zeeck, *J. Antibiot.* **1986**, *39*, 856–859.

[13] R. Thiericke, J. Rohr, *Nat. Prod. Rep.* **1993**, *10*, 265–289, and references therein.

[14] It also cannot be completely ruled out that **7** is unable to penetrate the cell membrane of *S. fradiae*. But this is unlikely, since we observed a decreasing concentration of **7** after the feeding experiment.

[15] D. A. Hopwood, M. J. Bibb, K. F. Chater, T. Kieser, C. J. Bruton, H. M. Kieser, D. J. Lydiate, C. P. Smith, J. M. Ward, H. Schrempf, *Genetic manipulation of Streptomyces. A Laboratory Manual*, The John Innes Foundation, Norwich UK **1985**.

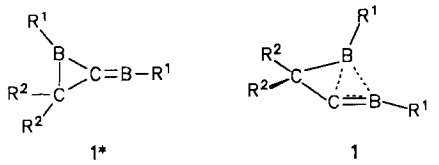
 © *VCH Verlagsgesellschaft mbH, D-69451 Weinheim, 1995* *0570-0833/95/1010-1110 $ 10.00+.25/0*

Dicobalt and Diplatinum Complexes of Diborylcarbenes**

Anuradha Gunale, Hans Pritzkow, Walter Siebert,* Dirk Steiner, and Armin Berndt*

Dedicated to Professor Paul von Ragué Schleyer on the occasion of his 65th birthday

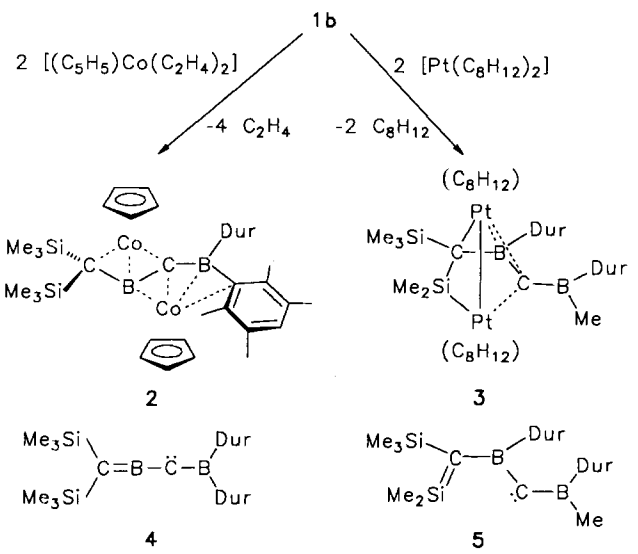
The nonclassical structure **1** of boriranylideneboranes[1] (the classical formulation is **1***[2]) was predicted by Schleyer[3] and others[4] years before proof was provided by an X-ray structure determination of **1a**.[5] Among the versatile reactions of **1b**, **c**[6] several occur with cleavage of bonds in the three-membered ring and migration of substituents.



1* 1

a: R^1 = 2,3,5,6-tetramethylphenyl (Dur), R^2 = $GeMe_3$
b: R^1 = Dur, R^2 = $SiMe_3$
c: R^1 = 2,4,6-trimethylphenyl (Mes), R^2 = $SiMe_3$

Here we show that **1b** reacts with $[Co(C_5H_5)(C_2H_4)_2]$ and $[Pt(C_8H_{12})_2]$ to yield **2** and **3**. During the formation of **2** a duryl group migrates from one boron to the other; in the case of **3** a methyl group migrates from silicon to boron. They can be viewed as the first examples of complex-stabilized diborylcarbenes **4** and **5**.



[*] Prof. Dr. W. Siebert, A. Gunale, Dr. H. Pritzkow
Anorganisch-chemisches Institut der Universität
Im Neuenheimer Feld 270, D-69120 Heidelberg (Germany)
Telefax: Int. code + (6221)56-5609
Prof. Dr. A. Berndt, Dipl.-Chem. D. Steiner
Fachbereich Chemie der Universität
Hans-Meerwein-Strasse, D-35032 Marburg (Germany)
Telefax: Int. code + (6421)28-8917

[**] This work was supported by the Deutsche Forschungsgemeinschaft (SFB 247) and the Fonds der Chemischen Industrie.

Two equivalents of $[Co(C_5H_5)(C_2H_4)_2]$[7] react with **1b** in hexane with evolution of ethene. Chromatographic workup gives a dark green diamagnetic compound in 46% yield; its mass spectrum is in agreement with the formula $[(CpCo)_2C_2B_2(SiMe_3)_2Dur_2]$. In the ^1H NMR spectrum two singlets for the CpCo moieties, two singlets of the $Si(CH_3)_3$ groups, and eight signals for the methyl groups of the duryl substituents indicate an unsymmetrical complex. Its unusual constitution was determined by an X-ray structure analysis (Fig. 1).[8]

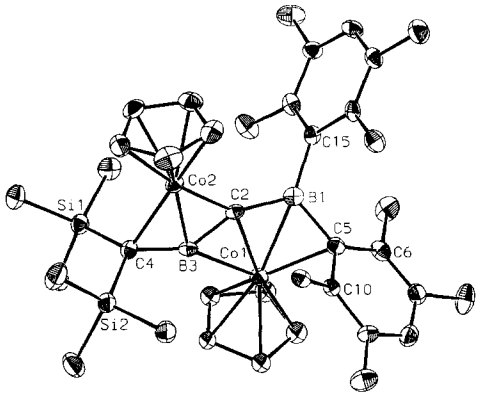


Fig. 1. Structure of **2** in the crystal. Selected bond lengths [Å] and angles [°]: Co1-B1 2.276(6), Co1-C2 2.009(6), Co1-B3 2.081(8), Co1-C5 2.180(7), Co1-C10 2.554(9), Co1-C6 3.06, Co2-C2 1.887(6), Co2-B3 1.973(7), Co2-C4 2.114(6), B1-C2 1.522(10), C2-B3 1.474(9), B3-C4 1.483(10), B1-C5 1.601(10); B1-C2-B3 150.3(6), C2-B3-C4 138.0(6).

The C-B-C part of the C-B-C-B chain in **2** is *trihapto*-coordinated to a CpCo moiety. The distances between the atoms Co2, C4, and B3 show structural similarity to the CpCo(CO) complex of an aminomethyleneborane.[10] The second CpCo fragment is bonded *tetrahapto* to the other side of the ligand through the B-C-B atoms as well as one duryl substituent (to C5 and weakly to C10; see also the temperature-dependent ^{13}C NMR shifts). The dinuclear complex with a bridging B–C group has short Co1–C2 and Co2–C2 distances, which may be compared with the length of a C=Co bond [1.881(6) Å] of a cyclopentadienylidene cobalt complex.[11] The Co–B distances fall within normal bonding ranges,[12, 13] although Co1–B1 [2.276(8) Å] is somewhat long.

The ^{13}C NMR chemical shifts of one duryl ring [δ = 146.3 (*i*-C), 132.9, 133.4, 135.5, 136.0 (*o*- and *m*-C), 130.9 (*p*-C)] are essentially temperature-independent ($\Delta\delta$ = 0.1 to 0.3). In contrast, the second duryl ring shows signals that are clearly shifted to higher and lower field (to δ = 97.2 and δ = 155.6). These signals are of varying broadness and are temperature-dependent ($\Delta\delta$ = 1.6–10.5, Table 1).

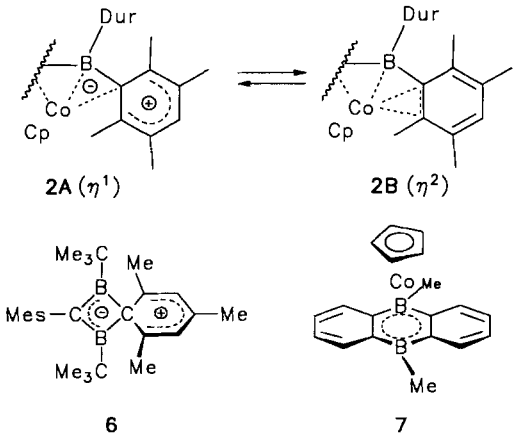
Table 1. ^{13}C NMR chemical shifts [δ] of selected C atoms in **2** at various temperatures.

T [K]	193	233	273	298	$\Delta\delta$ (298–193)
CSi_2	29.1	28.9	27.2	[a]	
i-C	97.2	97.9	100.9	105.5	+8.3
o-C	120.9	124.2	128.0	131.4	+10.5
m-C	131.4	131.5	130.8	129.8	−1.6
p-C	134.4	134.9	136.0	137.4	+3.0
m'-C	141.2	140.4	139.3	138.0	−3.2
o'-C	151.9	152.7	154.1	155.6	+3.7
CB_2	196.5	194.5	189.9	[a]	

[a] Not observed.

 © VCH Verlagsgesellschaft mbH, D-69451 Weinheim, 1995 0570-0833/95/1010-1111 $ 10.00+.25/0

This finding can be explained as a dynamic equilibrium in solution between the complex **2A** with η^1 interaction and the valence isomer complex **2B** with η^2 interaction. It is expected that the Co1-bound C atom of the coordinated duryl ring in **2B** (η^2) has a similar chemical shift as in complex **7** [δ = 103 (*i*-C), 128.3 (*o*-C), 137.2 (*m*-C)[14]]. Compound **2A**, however, should be similar to **6** [δ = 113.4 (*i*-C), 160.4 (*o*-C), 129.3 (*m*-C), 146.1 (*p*-C)[15]]. The weighted averaging has an especially strong effect on the chemical shifts of the *i*-C and *o*-C atoms of the duryl ring in **2**. Similar equilibria $\eta^1 \rightleftarrows \eta^2$ have been postulated for Re–aryl complexes.[16]



The atoms of the C4-B3-C2-B1 chain and the two Co atoms lie in a plane. The plane through Si1-C4-Si2 is perpendicular to this plane and that through C5-B1-C15 forms an angle of approximately 30° to it. The C2 carbon atom is planar-coordinated (sum of angles = 359.9°) by four electron-poor centers.[17] Its ^{13}C NMR resonance at 194.5 shows that it is notably deshielded. Similar deshielding of carbene-C atoms appears in other dinuclear carbene complexes.[18] The C-B-C-B chain is bent (C4-B3-C2 = 138.0° and B3-C2-B1 = 150.3°). The bonds C4–B3 and B3–C2 are quite short [1.483(10) and 1.474(9) Å, respectively] and are in the range of coordinated B=C bonds.[10] The C2–B1 bond [1.522(10) Å] is a bit shorter than a B–C single bond (1.55–1.60 Å). Both Co centers in the μ_2,η^3,η^4-dinuclear complex **2** have a closed-shell configuration. The 14 VE fragment CpCo of Co2 interacts with the atoms C4–B3 (C=B as 2e donor) and with μ-C2, which as a carbene carbon atom forms a 3c–2e Co2-C2-Co1 bond. Co1 completes its 18 VE configuration through this 3c–2e bonding and the interaction with the duryl group.

The addition of one equivalent of [Pt(η^4-C_8H_{12})$_2$] to **1b** in toluene at room temperature led unexpectedly to the diplatinum compound **3**. An optimized synthesis of red-orange crystalline **3** occurs in 63% yield. An analysis of its ^{1}H NMR spectrum demonstrates the migration of a methyl group from silicon to boron. The two ^{11}B NMR signals (δ = 41 and 65) indicate that the interaction of platinum with one boron atom is strong while that with the other is weak. This is confirmed by the X-ray structure (Fig. 2).[8] The complex is best described as a five-membered ring (made up of Si1, Pt2, C2, B3, and C4) which is *tetrahapto*-bonded to Pt1. Unusual is the *dihapto*-complexation of the C_8H_{12} ligand to Pt2.

In contrast to the *anti* arrangement of the CpCo moieties in **2**, the platinum atoms in **3** are adjacent. Although the Pt–Pt distance of 2.864(2) Å is slightly longer than normal for a Pt–Pt bond (2.6–2.8 Å), it is considered a real interaction. The platinum atoms are bridged by the carbene carbon atom. Similar structural features have been reported for di- and triplatinum complexes.[19] The Pt1 atom can be assigned an 18 VE configuration (C_8H_{12} as a η^4-ligand, σ-bonds to C4 and Pt2, and a 3c–2e bond Pt1-C2-Pt2).[20] On this basis Pt2 formally has a 16 VE configuration, since it is only *dihapto*-coordinated to its C_8H_{12} ligand.

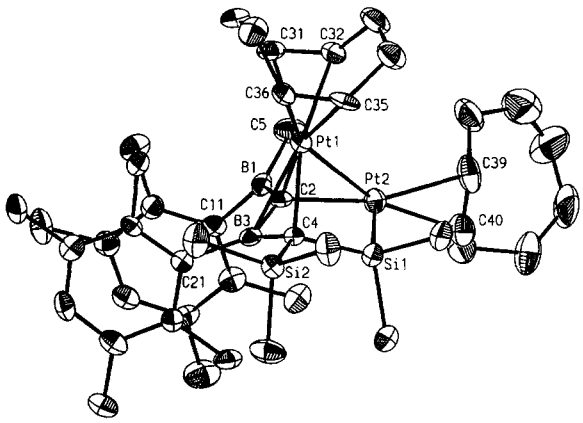


Fig. 2. Structure of **3** in the crystal. Selected bond lengths [Å] and angles [°]: Pt1-C2 2.118(10), Pt1-B3 2.409(12), Pt1-C4 2.166(10), Pt1-Pt2 2.864(2), Pt2-C2 2.084(10), Pt2-Si1 2.304(4), B1-C2 1.58(2), C2-B3 1.53(2), B3-C4 1.56(2); C2-B3-C4 107.4(9), B3-C4-Si1 105.3(7), C4-Si1-Pt2 102.9(4), Si1-Pt2-C2 81.2(3), Pt2-C2-B3 122.5(8).

Our results show that though the complexes **2** and **3** are structurally very different, the formation of both involves cleavage of the C–C bond in **1b** as well as migration of a substituent (either Dur or Me) to a boron atom.

Experimental Procedure

2: A mixture of **1b** (0.310 g, 0.68 mmol) and [Co(C_5H_5)(C_2H_4)$_2$] (0.380 g, 2.1 mmol) in 15 mL hexane was stirred for 3 h. Chromatographic workup of the brown solution on Al_2O_3 with hexane provided an orange fraction (excess [Co(C_5H_5)(C_2H_4)$_2$]) and dark green **2**; 230 mg (46%), m.p. 183 °C (from hexane). ^{1}H NMR (500 MHz, [D$_8$]THF, −40 °C): δ = 0.21, 0.29 (each s, 2 × 9 H; Si(CH_3)$_3$), 0.57, 2.16, 2.20, 2.24, 2.25, 2.30, 2.32, 2.39 (each s, 8 × 3 H; *o*- and *m*-CH_3), 4.07, 4.18 (each s, 2 × 5 H, C_5H_5), 7.00, 7.12 (each s, 2 × 1 H, *p*-H). ^{13}C NMR (125 MHz, [D$_8$]THF, −40 °C): δ = 5.4, 5.6 (2 q, Si(CH_3)$_3$), 20.0, 20.1, 20.6, 20.7, 20.9, 21.2, 22.4, 29.3 (8 q, *o*- and *m*-CH_3), 28.9 (br. s, CSi_2), 80.1, 83.8 (2 d, C_5H_5), 97.9 (br. s, *i*-C(B-Dur-Co)), 124.2 (br), 131.5, 132.9, 133.4, 135.5, 136.0, 140.4, 152.7 (7 s, *o*- and *m*-C), 130.9, 134.9 (2 d, *p*-C), 146.5 (br. s, *i*-C(B)), 194.5 (br. s, CB_2). ^{11}B NMR (96 MHz, [D$_8$]THF, 25 °C): δ = 41; EI-MS: *m*/*z* (%) = 706 ([*M*$^+$], 39), 632 ([*M*$^+$ − Si(CH_3)$_3$ − H], 5), 582 ([*M*$^+$ − Co(C_5H_5)], 100), 567 ([*M*$^+$ − Co(C_5H_5) − CH_3], 3), 517 ([*M*$^+$ − Co(C_5H_5)$_2$], 9).

3: A solution of **1b** (0.225 g, 0.49 mmol) in a mixture of hexane (6 mL) and toluene (1 mL) was added at 0 °C to [Pt(η^4-C_8H_{12})$_2$] (0.405 g, 0.98 mmol) and stirred for 3 h at 20 °C. Chromatographic workup on Al_2O_3 with hexane eluent provided a yellow fraction (**1b**) and uncharacterized side products. Elution with hexane/toluene (1:1) provided red-orange **3**, 330 mg (63%), m.p. 165 °C (decomp.). ^{1}H NMR (200 MHz, CD_2Cl_2): δ = −0.12 (s, 9H; Si(CH_3)$_3$), 0.37, 0.48 (2 s, 2 × 3 H, *J*(Pt,H) = 42 Hz; Si(CH_3)$_2$), 0.81 (s, 3 H; BCH_3), 1.56, 1.66, 1.72, 1.75, 2.03, 2.08, 2.28, 2.35 (8 s, 8 × 3 H; CCH_3), 1.95–2.70 (m, br, 16 H; CH_2), 4.05–4.35 (m, br, 2 H; −CH=), 5.10–6.10 (m, br, 6 H; −CH=), 6.41 (s, 2 H; *p*-H). ^{11}B NMR (96 MHz, CD_2Cl_2, 25 °C): δ = 41, 65. ^{13}C NMR (50.3 MHz, CD_2Cl_2): δ = 2.9 (Si(CH_3)$_3$), 5.4, 5.7 (Si(CH_3)$_2$), 18.7, 19.3, 19.4, 19.5, 19.8, 20.9, 21.5, 22.4 (CCH_3), 27.9, 29.0, 29.2, 29.5, 29.6, 30.8, 31.1, 33.2 (CH_2), 80.8, 81.8, 88.2, 89.1, 89.3, 93.5 (Pt-coordinated −CH=), 128.0, 128.5, 129.2, 130.0 (uncoordinated −CH= and *p*-H), 130.9, 131.0, 131.1, 131.2, 131.4, 131.6, 133.8, 134.5 (CCH_3), carbon atoms adjacent to boron were not observed. EI-MS: *m*/*z* (%) = 761 ([*M*$^+$ − Pt(C_8H_{12})], 0.23), 746 ([*M*$^+$ − Pt(C_8H_{12})−CH_3], 0.7), 703 ([*M*$^+$ − Pt(C_8H_{12})−CH_3], 0.7), 703 ([*M*$^+$ − Pt(C_8H_{12})−Si(CH_3)$_2$], 0.2), 653 ([*M*$^+$ − Pt(C_8H_{12})$_2$], 0.9), 476 (**1b**·H_2O^+, 6) 134 ([$C_6(CH_3)_4H_2$]$^+$, 65), 119 ([$C_6(CH_3)_3H_2$]$^+$, 100), 73 ([Si(CH_3)$_3$]$^+$, 99).

Received: December 27, 1994,
Revised: February 28, 1995 [Z 7574 IE]
German version: *Angew. Chem.* **1995**, *107*, 1194

Keywords: boron compounds · carbene complexes · cobalt compounds · platinum compounds

[1] H. Klusik, A. Berndt, *Angew. Chem.* **1983**, *95*, 895–896; *Angew. Chem. Int. Ed. Engl.* **1983**, *22*, 877–878.

[2] The star signifies the nonexistent, but classical structure of the non-classical compound, as in ref. [6].

[3] P. H. M. Budzelaar, P. von R. Schleyer, K. Krogh-Jespersen, *Angew. Chem.* **1984**, *96*, 809–810; *Angew. Chem. Int. Ed. Engl.* **1984**, *23*, 825–827; P. H. M. Budzelaar, K. Krogh-Jespersen, T. Clark, P. von R. Schleyer, *J. Am. Chem. Soc.* **1985**, *107*, 2773–2779.

[4] G. Frenking, H. F. Schaefer III, *Chem. Phys. Lett.* **1984**, *109*, 521–524.

[5] C. Wieczorek, J. Allwohn, G. Schmidt-Lukasch, R. Hunold, W. Massa, A. Berndt, *Angew. Chem.* **1990**, *102*, 435–436; *Angew. Chem. Int. Ed. Engl.* **1990**, *29*, 398–399.

[6] A. Berndt, *Angew. Chem.* **1993**, *105*, 1034–1058; *Angew. Chem. Int. Ed. Engl.* **1993**, *32*, 985–1009.

[7] K. Jonas, C. Krüger, *Angew. Chem.* **1980**, *92*, 513–531; *Angew. Chem. Int. Ed. Engl.* **1980**, *19*, 520–537.

[8] Crystal structure analyses: Siemens-Stoe-AED2 diffractometer ($Mo_{K\alpha}$ radiation, ω scan, $T = -55\,^{\circ}C$), empirical absorption correction, structure analyses with direct methods (SHELXLS 86 [9]), refinement with SHELXL 93 [9] (non-hydrogen atoms anisotropic, H atoms in calculated positions or as part of a rigid group). **2**: rhombohedral, $P2_12_12_1$, $a = 8.960(6)$, $b = 17.187(10)$, $c = 24.08(2)$ Å, $V = 3708$ Å^3, $Z = 4$; 4327 measured reflections ($2\theta_{max} = 50°$, 3036 with $I > 2\sigma_I$), $wR2 = 0.102$ (all reflections), $R1(F > 4\sigma(F)) = 0.047$, 395 parameters. **3**: triclinic, $P\bar{1}$, $a = 11.650(6)$, $b = 13.020(6)$, $c = 15.921(8)$ Å, $\alpha = 102.83(4)$, $\beta = 97.91(3)$, $\gamma = 96.04(4)°$, $V = 2309$ Å^2, $Z = 2$; 6937 reflections ($2\theta_{max} = 48°$, 4733 with $I > 2\sigma_I$), $wR2 = 0.102$ (all reflections), $R1(F > 4\sigma(F)) = 0.045$, 507 parameters. Further details of the crystal structure investigations may be obtained from the Fachinformationszentrum Karlsruhe, D-76344 Eggenstein-Leopoldshafen (Germany) on quoting the depository numbers CSD-401 952 (**2**) and CSD-401 953 (**3**).

[9] G. M. Sheldrick, SHELXLS 86, Universität Göttingen, **1986**; SHELXL 93, Universität Göttingen, **1993**.

[10] S. W. Helm, G. Linti, H. Nöth, C. Channareddy, P. Hofmann, *Chem. Ber.* **1992**, *125*, 73–86.

[11] H. Wadepohl, H. Pritzkow, *Angew. Chem.* **1987**, *99*, 132–134; *Angew. Chem. Int. Ed. Engl.* **1987**, *26*, 127–128.

[12] L. G. Sneddon, D. Voet, *J. Chem. Soc. Chem. Commun.* **1976**, 118–119.

[13] J. R. Pipal, R. N. Grimes, *Inorg. Chem.* **1977**, *16*, 3255–3262.

[14] P. Müller, B. Gangnus, H. Pritzkow, H. Schulz, M. Stephan, W. Siebert, *J. Organomet. Chem.* **1995**, *487*, 235–243.

[15] M. Pilz, J. Allwohn, W. Massa, A. Berndt, *Angew. Chem.* **1990**, *102*, 436–438, *Angew. Chem. Int. Ed. Engl.* **1990**, *29*, 399–401.

[16] J. R. Sweet, W. A. G. Graham, *J. Am. Chem. Soc.* **1983**, *105*, 305–306; *Organometallics* **1983**, *2*, 135–140.

[17] For compounds with planar, tetracoordinated carbon atoms, see: M. Albrecht, G. Erker, C. Krüger, *Synlett* **1993**, 441–448, and references therein.

[18] M. G. Richmond, J. K. Kochi, *Organometallics* **1987**, *6*, 777–788.

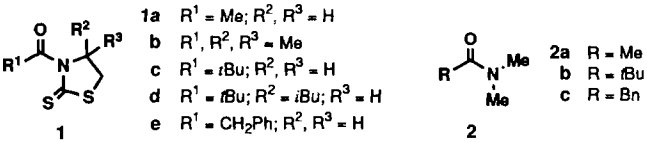
[19] J. C. Jeffrey, I. Moore, M. Murray, F. G. A. Stone, *J. Chem. Soc. Dalton Trans.* **1982**, 1741–1747; T. V. Ashworth, M. Berry, J. A. K. Howard, M. Laguna, F. G. A. Stone, *ibid.* **1980**, 1615–1624.

[20] R. Adams, *Chem. Rev.* **1989**, *89*, 1703–1712.

Relationship between C(O)–N Twist Angles and ^{17}O NMR Chemical Shifts in a Series of Twisted Amides**

Shinji Yamada*

The structure and spectroscopic properties of twisted amides[1] have received considerable attention not only in organic chemistry but also in biochemistry.[2] The influence of the rotation about the C(O)–N bond on IR,[3] UV,[4] and ^1H,[5] ^{13}C,[6] ^{15}N[7] NMR, and ESCA[8, 9] spectroscopic data has been studied. However, no investigations on the dependence of the ^{17}O NMR chemical shift on the C(O)-N twist angle have been carried out, although it has been recognized that the chemical shift of the ^{17}O NMR signal is more sensitive to structural variation than the shifts of the ^{13}C and ^{15}N NMR signals.[10] Here we describe the relationships between the C(O)–N twist angles[11] and the ^{17}O and ^{13}C NMR chemical shifts of the 3-acyl-1,3-thiazolidine-2-thiones **1a–e** (Scheme 1). Furthermore, the relationship with the amide resonance, which on the basis of calculated electron populations has been challenged recently,[12] is also described.



Scheme 1. Structural formulas of the twisted amides **1a–e** and those of the dimethyl amides **2a–c**.

We previously reported[13] that the C(O)–N bond of 3-pivaloyl-1,3-thiazolidine-2-thione (**1c**) is highly twisted, whereas, that of 3-acetyl-1,3-thiazolidine-2-thione (**1a**) is almost planar; both results were confirmed by X-ray crystallographic analysis. A series of derivatives with different substituents at the C-4 atom and the acyl carbon atom were synthesized to give a variety of twist angles between 0–90°. Amides **1b**, **1d**, and **1e** were newly prepared by the acylation of the corresponding 1,3-thiazolidine-2-thiones with acetyl, pivaloyl, and phenylacetyl chloride, respectively. Table 1 shows the structural parameters of the C(O)–N twist angle τ, and the bond lengths r(C=O) and r(C(O)–N) of **1a–e**. The value of the twist angles τ lies in the range of 10° to 75°. The carbonyl group and the 1,3-thiazolidine-2-thione ring of **1a** and **1e** are coplanar, whereas, those of **1c** and **1d** are nearly orthogonal because of their steric repulsion between the bulky *t*Bu and C=S groups. In amide **1b** the two *gem*-dimethyl groups at the C-4 atom twist the C(O)–N bond to produce a twist angle of 36.5°, which is almost half the value of that of **1c**. An increase in the twist angle lengthens the C(O)–N bond, while the C=O bond lengths remain virtually unchanged. The independence of C=O bond lengths on twist angles has also been observed in bicyclic amides.[7]

Table 1. Selected structure parameters of **1a–e**.

Compd.	τ [°]	r(C(O) – N) [Å]	r(C=O) [Å]	Ref.
1a	20.1	1.413(9)	1.21(1)	[13]
1b	36.5	1.432(3)	1.210(3)	[17]
1c	74.3	1.448(4)	1.196(4)	[13]
1d	65.5	1.466(5)	1.195(5)	[17]
1e	10.2	1.415(6)	1.203(7)	[17]

To examine the relationships of ^{17}O and ^{13}C NMR chemical shifts with twist angles, ^{17}O NMR spectra of the compounds were acquired in natural abundance in CD_3CN (2–3 M solution) at 54.1 MHz at 23 °C; the chemical shifts were referenced to external H_2O. Table 2 shows the ^{17}O NMR chemical shifts[14] for **1a–e** and their partial structures **2a–c**. In order to compensate for the substituent effects around the carbonyl groups the $\Delta\delta(^{17}O)$ values are given as the differences in the ^{17}O chemical shifts of the compounds **1a–e** and the corresponding dimethyl amides **2a–c**. The range of $\Delta\delta(^{17}O)$ values is 100–173 ppm. As shown in Figure 1a, a linear relationship was observed between

[*] Dr. S. Yamada
Department of Chemistry
Faculty of Science, Ochanomizu University
Otsuka, Bunkyo-ku, Tokyo 112 (Japan)
Telefax: Int. code + (3)3942-2815

[**] The author gratefully acknowledges Haruka Yamada at Kanagawa University for her helpful assistance in obtaining the NMR spectra.

[1] H. Klusik, A. Berndt, *Angew. Chem.* **1983**, *95*, 895–896; *Angew. Chem. Int. Ed. Engl.* **1983**, *22*, 877–878.

[2] The star signifies the nonexistent, but classical structure of the non-classical compound, as in ref. [6].

[3] P. H. M. Budzelaar, P. von R. Schleyer, K. Krogh-Jespersen, *Angew. Chem.* **1984**, *96*, 809–810; *Angew. Chem. Int. Ed. Engl.* **1984**, *23*, 825–827; P. H. M. Budzelaar, K. Krogh-Jespersen, T. Clark, P. von R. Schleyer, *J. Am. Chem. Soc.* **1985**, *107*, 2773–2779.

[4] G. Frenking, H. F. Schaefer III, *Chem. Phys. Lett.* **1984**, *109*, 521–524.

[5] C. Wieczorek, J. Allwohn, G. Schmidt-Lukasch, R. Hunold, W. Massa, A. Berndt, *Angew. Chem.* **1990**, *102*, 435–436; *Angew. Chem. Int. Ed. Engl.* **1990**, *29*, 398–399.

[6] A. Berndt, *Angew. Chem.* **1993**, *105*, 1034–1058; *Angew. Chem. Int. Ed. Engl.* **1993**, *32*, 985–1009.

[7] K. Jonas, C. Krüger, *Angew. Chem.* **1980**, *92*, 513–531; *Angew. Chem. Int. Ed. Engl.* **1980**, *19*, 520–537.

[8] Crystal structure analyses: Siemens-Stoe-AED2 diffractometer ($Mo_{K\alpha}$ radiation, ω scan, $T = -55\,^{\circ}C$), empirical absorption correction, structure analyses with direct methods (SHELXLS 86 [9]), refinement with SHELXL 93 [9] (non-hydrogen atoms anisotropic, H atoms in calculated positions or as part of a rigid group). **2**: rhombohedral, $P2_12_12_1$, $a = 8.960(6)$, $b = 17.187(10)$, $c = 24.08(2)$ Å, $V = 3708$ Å^3, $Z = 4$; 4327 measured reflections ($2\theta_{max} = 50°$, 3036 with $I > 2\sigma_I$), $wR2 = 0.102$ (all reflections), $R1(F > 4\sigma(F)) = 0.047$, 395 parameters. **3**: triclinic, $P\bar{1}$, $a = 11.650(6)$, $b = 13.020(6)$, $c = 15.921(8)$ Å, $\alpha = 102.83(4)$, $\beta = 97.91(3)$, $\gamma = 96.04(4)°$, $V = 2309$ Å^2, $Z = 2$; 6937 reflections ($2\theta_{max} = 48°$, 4733 with $I > 2\sigma_I$), $wR2 = 0.102$ (all reflections), $R1(F > 4\sigma(F)) = 0.045$, 507 parameters. Further details of the crystal structure investigations may be obtained from the Fachinformationszentrum Karlsruhe, D-76344 Eggenstein-Leopoldshafen (Germany) on quoting the depository numbers CSD-401 952 (**2**) and CSD-401 953 (**3**).

[9] G. M. Sheldrick, SHELXLS 86, Universität Göttingen, **1986**; SHELXL 93, Universität Göttingen, **1993**.

[10] S. W. Helm, G. Linti, H. Nöth, C. Channareddy, P. Hofmann, *Chem. Ber.* **1992**, *125*, 73–86.

[11] H. Wadepohl, H. Pritzkow, *Angew. Chem.* **1987**, *99*, 132–134; *Angew. Chem. Int. Ed. Engl.* **1987**, *26*, 127–128.

[12] L. G. Sneddon, D. Voet, *J. Chem. Soc. Chem. Commun.* **1976**, 118–119.

[13] J. R. Pipal, R. N. Grimes, *Inorg. Chem.* **1977**, *16*, 3255–3262.

[14] P. Müller, B. Gangnus, H. Pritzkow, H. Schulz, M. Stephan, W. Siebert, *J. Organomet. Chem.* **1995**, *487*, 235–243.

[15] M. Pilz, J. Allwohn, W. Massa, A. Berndt, *Angew. Chem.* **1990**, *102*, 436–438, *Angew. Chem. Int. Ed. Engl.* **1990**, *29*, 399–401.

[16] J. R. Sweet, W. A. G. Graham, *J. Am. Chem. Soc.* **1983**, *105*, 305–306; *Organometallics* **1983**, *2*, 135–140.

[17] For compounds with planar, tetracoordinated carbon atoms, see: M. Albrecht, G. Erker, C. Krüger, *Synlett* **1993**, 441–448, and references therein.

[18] M. G. Richmond, J. K. Kochi, *Organometallics* **1987**, *6*, 777–788.

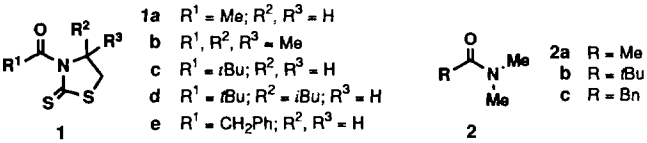
[19] J. C. Jeffrey, I. Moore, M. Murray, F. G. A. Stone, *J. Chem. Soc. Dalton Trans.* **1982**, 1741–1747; T. V. Ashworth, M. Berry, J. A. K. Howard, M. Laguna, F. G. A. Stone, *ibid.* **1980**, 1615–1624.

[20] R. Adams, *Chem. Rev.* **1989**, *89*, 1703–1712.

Relationship between C(O)–N Twist Angles and ^{17}O NMR Chemical Shifts in a Series of Twisted Amides**

Shinji Yamada*

The structure and spectroscopic properties of twisted amides[1] have received considerable attention not only in organic chemistry but also in biochemistry.[2] The influence of the rotation about the C(O)–N bond on IR,[3] UV,[4] and ^1H,[5] ^{13}C,[6] ^{15}N[7] NMR, and ESCA[8, 9] spectroscopic data has been studied. However, no investigations on the dependence of the ^{17}O NMR chemical shift on the C(O)-N twist angle have been carried out, although it has been recognized that the chemical shift of the ^{17}O NMR signal is more sensitive to structural variation than the shifts of the ^{13}C and ^{15}N NMR signals.[10] Here we describe the relationships between the C(O)–N twist angles[11] and the ^{17}O and ^{13}C NMR chemical shifts of the 3-acyl-1,3-thiazolidine-2-thiones **1a–e** (Scheme 1). Furthermore, the relationship with the amide resonance, which on the basis of calculated electron populations has been challenged recently,[12] is also described.



Scheme 1. Structural formulas of the twisted amides **1a–e** and those of the dimethyl amides **2a–c**.

We previously reported[13] that the C(O)–N bond of 3-pivaloyl-1,3-thiazolidine-2-thione (**1c**) is highly twisted, whereas, that of 3-acetyl-1,3-thiazolidine-2-thione (**1a**) is almost planar; both results were confirmed by X-ray crystallographic analysis. A series of derivatives with different substituents at the C-4 atom and the acyl carbon atom were synthesized to give a variety of twist angles between 0–90°. Amides **1b**, **1d**, and **1e** were newly prepared by the acylation of the corresponding 1,3-thiazolidine-2-thiones with acetyl, pivaloyl, and phenylacetyl chloride, respectively. Table 1 shows the structural parameters of the C(O)–N twist angle τ, and the bond lengths r(C=O) and r(C(O)–N) of **1a–e**. The value of the twist angles τ lies in the range of 10° to 75°. The carbonyl group and the 1,3-thiazolidine-2-thione ring of **1a** and **1e** are coplanar, whereas, those of **1c** and **1d** are nearly orthogonal because of their steric repulsion between the bulky *t*Bu and C=S groups. In amide **1b** the two *gem*-dimethyl groups at the C-4 atom twist the C(O)–N bond to produce a twist angle of 36.5°, which is almost half the value of that of **1c**. An increase in the twist angle lengthens the C(O)–N bond, while the C=O bond lengths remain virtually unchanged. The independence of C=O bond lengths on twist angles has also been observed in bicyclic amides.[7]

Table 1. Selected structure parameters of **1a–e**.

Compd.	τ [°]	r(C(O) – N) [Å]	r(C=O) [Å]	Ref.
1a	20.1	1.413(9)	1.21(1)	[13]
1b	36.5	1.432(3)	1.210(3)	[17]
1c	74.3	1.448(4)	1.196(4)	[13]
1d	65.5	1.466(5)	1.195(5)	[17]
1e	10.2	1.415(6)	1.203(7)	[17]

To examine the relationships of ^{17}O and ^{13}C NMR chemical shifts with twist angles, ^{17}O NMR spectra of the compounds were acquired in natural abundance in CD_3CN (2–3 M solution) at 54.1 MHz at 23 °C; the chemical shifts were referenced to external H_2O. Table 2 shows the ^{17}O NMR chemical shifts[14] for **1a–e** and their partial structures **2a–c**. In order to compensate for the substituent effects around the carbonyl groups the $\Delta\delta(^{17}O)$ values are given as the differences in the ^{17}O chemical shifts of the compounds **1a–e** and the corresponding dimethyl amides **2a–c**. The range of $\Delta\delta(^{17}O)$ values is 100–173 ppm. As shown in Figure 1a, a linear relationship was observed between

[*] Dr. S. Yamada
Department of Chemistry
Faculty of Science, Ochanomizu University
Otsuka, Bunkyo-ku, Tokyo 112 (Japan)
Telefax: Int. code + (3)3942-2815

[**] The author gratefully acknowledges Haruka Yamada at Kanagawa University for her helpful assistance in obtaining the NMR spectra.

Table 2. ^{17}O NMR chemical shifts for **1a–e** and **2a–c**.

Compd.	$\delta(^{17}O)$ [a]	Compd.	$\delta(^{17}O)$ [a]	$\Delta\delta(^{17}O)$
1a	438.4	**2a**	338.1	100.3
1b	475.6	**2a**	338.1	137.5
1c	506.1	**2b**	340.2	165.9
1d	513.0	**2b**	340.2	172.8
1e	436.1	**2c**	335.3	100.8

[a] Recorded at 54.1 MHz in CD_3CN. Chemical shifts are referenced to external H_2O.

Table 3. ^{13}C NMR chemical shifts for **1a–e** and **2a–c**.

Compd.	$\delta(^{13}C)$ [a]	Compd.	$\delta(^{13}C)$ [a]	$\Delta\delta(^{13}C)$
1a	171.34	**2a**	170.61	0.73
1b	174.29	**2a**	170.61	3.68
1c	187.80	**2b**	177.50	10.30
1d	188.95	**2b**	177.50	11.45
1e	172.75	**2c**	171.03	1.72

[a] Recorded at 100.4 MHz in $CDCl_3$. Chemical shifts are referenced to internal tetramethylsilane.

the $\Delta\delta(^{17}O)$ and the τ values; increasing the twist angle causes an increase in the $\Delta\delta(^{17}O)$ value. The influence of the structure of the NC(S)S ring on the chemical shift of the carbonyl groups seems to be very small because the NC(S)S and carbonyl groups are not very close together. Since these amides have similar structures, the influence on the chemical shift arising from structural differences should also be negligible. In general, ^{17}O NMR chemical shifts are thought to be essentially dependent upon the paramagnetic term which is proportional to the charge density. Therefore, the changes in the $\Delta\delta(^{17}O)$ values are largely ascribed to the changes in the charge density of the O atom during C(O)–N bond rotation. The ^{13}C chemical shifts of the carbonyl carbon for **1a–e** and **2a–c**, and their difference $\Delta\delta(^{13}C)$ are listed in Table 3. The plot of the $\Delta\delta(^{13}C)$ against the τ values was also found to be almost linear (Fig. 1b). These relationships can

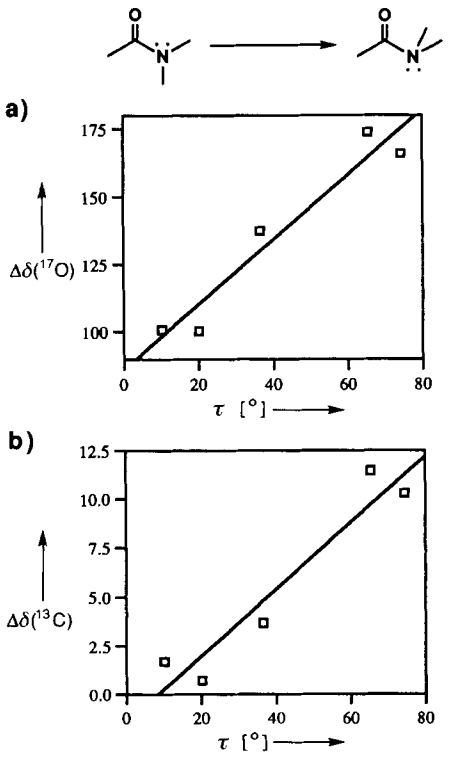
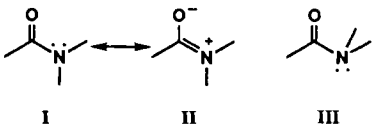


Fig. 1. Plot of the relationship between the $\Delta\delta(^{17}O)$ and the τ values (a) as well as between the $\Delta\delta(^{13}C)$ and the τ values (b).

be explained by the classical amide resonance model (Scheme 2). Thus, for the small twist angle the contribution of the form **II** leads to shielding of the O atom. The rotation of the C(O)–N bond disturbs this contribution, which leads to weakening of the shielding effects. A similar explanation can be adopted for the results observed for the ^{13}C chemical shifts.



I **II** **III**

Scheme 2. Structures of the planar amide **I**, the form **II**, and the twisted amide **III**.

Wiberg and Laidig made a prediction[12] concerning the amide resonance based on a comparison of the C, N, O electron populations in planar **I** and in twisted **III** amides (Scheme 2) calculated with Bader's method.[15] They describe that the electron population of carbon and nitrogen are opposite of what would be expected from the resonance model and that of oxygen is not dependent on the rotation of the C(O)–N bond. In connection with this prediction a number of theoretical studies were undertaken;[16] however, only a few experimental approaches have been carried out.[7, 9] The results described above seem inconsistent with the analysis, because the $\Delta\delta(^{17}O)$ value, which is closely related to the electron population of the O atom, is dependent on the C(O)–N twist angle as shown in Figure 1a. Furthermore, the relationship of $\Delta\delta(^{13}C)$ value with the twist angles in Figure 1b is opposite to that predicted from the reported analysis. However, the relative independence of the C=O bond length on the twist angle compared to the C(O)–N still remains to be explained.

Further investigations of the C(O)–N rotational effect on other spectra and the relation with the amide resonance are currently in progress.

Received: August 27, 1994
Revised version: December 8, 1994 [Z 7274 IE]
German version: *Angew. Chem.* **1995**, *107*, 1224

Keywords: amides · NMR spectroscopy · structure elucidation · thiones

[1] Review: A. Greenberg, *Mol. Struct. Energ.* **1988**, *7*, 139.
[2] M. K. Rosen, R. F. Standaert, A. Galat, M. Nakatsuka, S. L. Schreiber, *Science* **1990**, *248*, 863; M. W. Albers, C. T. Walsh, S. L. Schreiber, *J. Org. Chem.* **1990**, *55*, 4984; M. K. Rosen, S. L. Schreiber, *Angew. Chem.* **1992**, *104*, 413; *Angew. Chem. Int. Ed. Engl.* **1992**, *31*, 384.
[3] M. Tichy, E. Duskova, K. Blaha, *Tetrahedron Lett.* **1974**, 237; A. Greenberg, Y.-Y. Chiu, J. L. Johnson, J. F. Liebman, *Struct. Chem.* **1991**, *2*, 117.
[4] H. Pracejus, M. Kehlen, H. Kehlen, H. Matschiner, *Tetrahedron* **1965**, *21*, 2257.
[5] F. Bernardi, L. Lunazzi, P. Zanirato, G. Cerioni, *Tetrahedron* **1977**, *33*, 1337.
[6] C. W. Fong, H. G. Grant, *Aust. J. Chem.* **1981**, *34*, 2307.
[7] A. J. Bennet, V. Somayaji, R. S. Brown, B. D. Santarsiero, *J. Am. Chem. Soc.* **1991**, *113*, 7563.
[8] L. Treschanke, P. Rodemacher, *J. Mol. Struct.* **1985**, *122*, 47.
[9] A. Greenberg, T. D. Thomas, C. R. Bevilacqua, M. Coville, D. Ji, J.-C. Tsai, G. Wu, *J. Org. Chem.* **1992**, *57*, 7093.
[10] W. G. Klemperer, *Angew. Chem.* **1978**, *90*, 258; *Angew. Chem. Int. Ed. Engl.* **1978**, *17*, 246; D. W. Boykin, A. L. Baumstark, *Tetrahedron* **1989**, *45*, 3613; D. W. Boykin, A. L. Baumstark in *^{17}O NMR Spectroscopy in Organic Chemistry* (Ed.: D. W. Boykin), CRC, Boca Raton, **1991**, S. 39–94.
[11] The twist angles of C(O)–N bonds were determined by X-ray crystallographic analysis according to the definition by Winkler and Dunitz. See: F. K. Winkler, J. D. Dunitz, J. Mol. Biol. **1971**, *59*, 169.

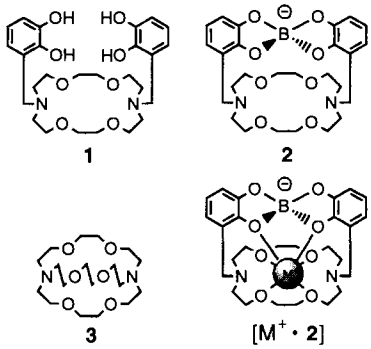
[12] K. B. Wiberg, K. E. Laidig, *J. Am. Chem. Soc.* **1987**, *109*, 5935.
[13] S. Yamada, *Angew. Chem.* **1993**, *105*, 1128; *Angew. Chem. Int. Ed. Engl.* **1993**, *32*, 1083.
[14] Linewidths at half heights are as follows: **1a**, 270 Hz; **1b**, 260 Hz; **1c**, 540 Hz; **1d**, 780 Hz; **1e**, 490 Hz; **2a**, 87 Hz; **2b**, 180 Hz; **2c**, 360 Hz.
[15] R. F. W. Bader, T. T. Nguyen-Dang, *Adv. Quantum Chem.* **1981**, *14*, 63.
[16] R. F. W. Bader, K. E. Cheeseman, K. E. Laidig, K. B. Wiberg, C. M. Breneman, *J. Am. Chem. Soc.* **1990**, *112*, 6530; C. M. Breneman, K. B. Wiberg, *J. Comput. Chem.* **1990**, *11*, 361; C. L. Perrin, *J. Am. Chem. Soc.* **1991**, *113*, 2865; A. Greenberg, Y.-Y. Chiu, J. L. Johnson, J. F. Liebman, *Struct. Chem.* **1991**, *2*, 117; K. E. Laidig, R. F. W. Bader, *J. Am. Chem. Soc.* **1991**, *113*, 6312; K. B. Wiberg, C. M. Breneman, *ibid.* **1992**, *114*, 831; A. Greenberg, C. A. Venanzi, *ibid.* **1993**, *115*, 6951; K. B. Wiberg, P. R. Rablen, *ibid.* **1993**, *115*, 9234; R. D. Bach, I. Mintcheva, *J. Org. Chem.* **1993**, *58*, 6135; F. J. Luque, M. Orozco, *ibid.* **1993**, *58*, 6397.
[17] This work. Full details of the crystal structure will be published elsewhere.

Binding of Boron and Alkali Metal Cations by a Pseudocryptand**

Ernest Graf,* Mir Wais Hosseini,* Romain Ruppert, Nathalie Kyritsakas, André De Cian, Jean Fischer, Christine Estournès, and Francis Taulelle

Since the discovery of cryptands, in particular the [2.2.2] macrobicyclic ligand **3**, some 25 years ago by Dietrich, Lehn, and Sauvage[1] and of the crown ethers by Pedersen[2] an exciting new field of research named supramolecular chemistry has opened to inorganic, organic, and physical chemists.[3–5] Whereas at the outset much attention was focused on the selective binding of spherical monoatomic alkali metal and alkaline-earth metal cations, very rapidly considerable achievements were reported with regard to the recognition of molecular cations.[6] Many aspects of supramolecular chemistry remain to be developed, for example, new materials based on self-assembly may be targeted by using weak interactions.[7]

The early design of cryptands involved the construction of cage molecules capable of binding cationic substrates within their cavities leading to the formation of cryptates. Since the [2.2.2]cryptand **3** is neutral, for the sake of charge neutrality the cationic cryptate complex must be accompanied by a counter anion. In order to overcome the problems associated with the presence of the anion, we designed a cryptand bearing a negative charge within its framework. Inspired by the naturally occurring antibiotics such as boromycin[8] and aplasmomycin,[9] which both bear a borate ester moiety, we synthesized the pseudocryptand **1**.[10] This compound combines the [2.2] macrocyclic core[11] of the [2.2.2]cryptand with two bidentate dianionic catecholate units. A similar concept was previously reported for podands and coronands bearing two catechol units linked by polyethyleneglycol chains.[12] Compounds bearing the [2.2] macrocycle and two bipyridine moieties are known and their ability to bind both transition and alkaline metal cations has been described.[13] Triaza and tetraaza macrocycles bearing three and four pendant catecholate units, respectively,[14] as well as macrobicyclic tris-catecholate ligands that serve as siderophore analogues have also been reported.[15]



Compound **1** may also be regarded as a binucleating ligand capable of binding two cations. Indeed, the binding of a main group element such as boron by **1** would lead to the negatively charged pseudocryptand **2**, a complex of the Böeseken type[16] found in boromycin[8] and in aplasmomycin.[9] In turn, this complex should bind an alkali metal cation, affording the neutral cryptate [$M^+ \cdot$ **2**]. Although the design and synthesis of binuclear complexes have been extensively studied over the past twenty years,[17] only recently has considerable effort been invested in the synthesis of heterobinuclear complexes bearing both a hard alkali or alkaline-earth metal cation and a soft transition metal cation.[18]

Treatment of **1**[10] in EtOH with one equivalent of $B(OH)_3$ and one equivalent of MOH in H_2O at room temperature led exclusively to the formation of the [$M^+ \cdot$ **2**] complex. A single recrystallization of the raw material afforded the pure [$M^+ \cdot$ **2**] complex (M = Li, Na, K, Rb, Cs, NH_4).

The binding ability of **2** towards alkali metal cations was studied in solution by NMR spectroscopy in $CDCl_3$ and in CD_3OD. In $CDCl_3$, the ^1H NMR spectrum of the parent compound **1** in the region $\delta = 2$–4.5 showed two triplets at $\delta = 2.82$ and 3.69 for CH_2N and NCH_2CH_2O, respectively, and two singlets at $\delta = 3.61$ and 3.81 for OCH_2CH_2O and the benzylic CH_2N protons, respectively (Fig. 1a). The coordination of boron in **1**, caused dramatic changes in the ^1H NMR spectrum. In particular, the benzylic CH_2N protons in **2** give rise to an AB quartet. Furthermore, the chemical shift values in the ^1H NMR spectrum appear to be strongly dependent on the nature of the cation complexed in the cavity. This was especially true for the benzylic CH_2 protons for which the observed chemical shift difference ($\delta_A - \delta_B$) varied from about 375 Hz for Na^+ to about 554 Hz for K^+ (Fig. 1). For the complex [$K^+ \cdot$ **2**] all ^1H and ^{13}C signals were assigned based on a ^1H–^{13}C correlation experiment. For the other complexes the same assignment was assumed to be correct. Since the positions of the ^1H signals for the [$M^+ \cdot$ **2**] complexes appeared to be cation-dependent, the selectivity and stability were studied by ^1H NMR spectroscopy. The stability of [$M^+ \cdot$ **2**] complexes (M = Na^+, K^+, Cs^+) was investigated by competition experiments with [2.2.2]cryptand **3** in CD_3OD. Addition of less than one equivalent of **3** to a solution of [$Na^+ \cdot$ **2**] caused partial decomplexation of the Na^+ ion leading to a mixture of [$Na^+ \cdot$ **2**] and [$Na^+ \cdot$ **3**] complexes. Complete

[*] Dr. E. Graf, Prof. Dr. M. W. Hosseini, Dr. R. Ruppert
Laboratoire de Chimie de Coordination Organique (URA au CNRS 422)
Université Louis Pasteur, Institut Le Bel
4, rue Blaise Pascal, F-67000 Strasbourg (France)
Telefax: Int. code +88416266
N. Kyritsakas, Dr. A. De Cian, Prof. Dr. J. Fischer
Laboratoire de Christallochimie et Chimie Structurale (URA au CNRS 424)
Université Louis Pasteur, Institut Le Bel, Strasbourg (France)
Dr. C. Estournès, Dr. F. Taulelle
Laboratoire de RMN et Chimie du Solide (UMR au CNRS 50)
Université Louis Pasteur, Institut Le Bel, Strasbourg (France)

[**] This work was supported by the CNRS and by the Institut Universitaire de France. The first publication about [2.2.2]cryptands by B. Dietrich, J.-M. Lehn, and J.-P. Sauvage appeared in 1969 (ref. [1]); this work is dedicated to them.

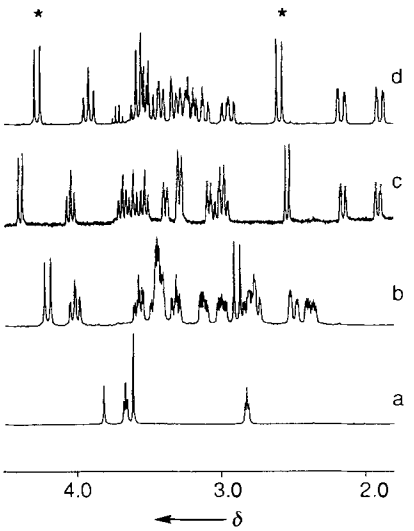


Fig. 1. Selected regions ($\delta = 1.8-4.5$) in the ^{1}H NMR spectra ($CDCl_3$): a) free ligand **1**, b) $[Na^+ \cdot \mathbf{2}]$, c) $[K^+ \cdot \mathbf{2}]$, and d) $[Cs^+ \cdot \mathbf{2}]$. The quartet in Fig. 1d at $\delta = 3.72$ is attributed to residual EtOH. The quartet of AB benzylic protons are indicated with an *.

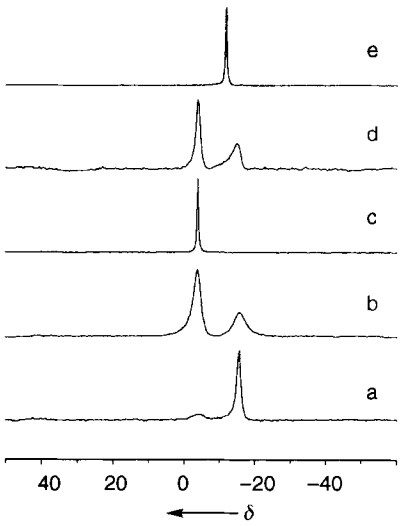


Fig. 2. ^{23}Na NMR spectra (105 MHz, CD_3OD, 25 °C). a) $[Na^+ \cdot \mathbf{2}]$, b) $[Na^+ \cdot \mathbf{2}] + 1$ equiv NaI, c) $[Na^+ \cdot \mathbf{2}] + 1$ equiv KI, d) $[Na^+ \cdot \mathbf{2}] + 1$ equiv CsBr, e) $[Na^+ \cdot \mathbf{2}] + 1$ equiv **3**. 5 M NaCl in D_2O was used as external reference.

removal of Na^+ from **2** was attained by addition of more than one equivalent of **3**, indicating that the $[Na^+ \cdot \mathbf{2}]$ complex was less stable than the $[Na^+ \cdot \mathbf{3}]$ complex. On the other hand, addition of up to 100 equivalents of **3** to the $[K^+ \cdot \mathbf{2}]$ complex did not lead to the removal of the K^+ ion from **2**, indicating that the $[K^+ \cdot \mathbf{2}]$ complex was at least two orders of magnitude more stable than the $[K^+ \cdot \mathbf{3}]$ complex. In other words, since the binding constant K_s for the $[K^+ \cdot \mathbf{3}]$ complex in methanol was initially estimated to be greater than 10^7 L mol^{-1},[19] and subsequently determined to be $10^{10.49}$ in methanol in the presence of 0.5 M NEt_4ClO_4,[20] for the $[K^+ \cdot \mathbf{2}]$ complex this K_s value should be greater than $10^{12.5}$ L mol^{-1}. However, owing to the high stability of the $[K^+ \cdot \mathbf{2}]$ complex we have so far been unable to determine its binding constant accurately using conventional methods. The selectivity of **2** towards Na^+, K^+, and Cs^+ ions was likewise investigated by competition experiments in CD_3OD. Whereas addition of less than one equivalent of KI to the $[Na^+ \cdot \mathbf{2}]$ complex led to a mixture of both $[Na^+ \cdot \mathbf{2}]$ and $[K^+ \cdot \mathbf{2}]$ complexes, upon addition of one equivalent of KI, only the characteristic ^{1}H NMR pattern of the $[K^+ \cdot \mathbf{2}]$ complex was observed. These findings indicated a stronger binding of K^+ than Na^+ by **2**. Further confirmation of this was obtained from the following experiment. Addition of up to 10^3 equivalents of NaI to the $[K^+ \cdot \mathbf{2}]$ complexes led to no changes in the ^{1}H NMR spectrum, indicating that the selectivity factor between Na^+ and K^+ lay in the favor of the latter by at least a factor of 10^3. For comparison, a selectivity factor of about 300:1 for K^+/Na^+ was reported in methanol for the cryptand [2.2.2] (**3**).[20] Analogous competition experiments between Cs^+ and K^+ revealed that **2** binds K^+ more strongly than Cs^+ with a selectivity factor greater than 10^2.

The binding ability of **2** towards alkali metal cations was also studied by ^{23}Na NMR spectroscopy (Fig. 2). In CD_3OD, the $[Na^+ \cdot \mathbf{2}]$ complex gave a major signal at $\delta = -15.7$ with a line width of 113 Hz; and a minor signal at $\delta = -4.1$ is attributed to some sodium contamination (5 M NaCl in D_2O was used as external reference) (Fig. 2a). For NaI under the same conditions values of $\delta = -3.91$ and line width = 16.1 Hz were observed. For the $[Na^+ \cdot \mathbf{3}]$ cryptate the ^{23}Na NMR signal occurs at $\delta = -11.4$ and the line width $\Delta\nu$ is 29 Hz in CD_3OD/D_2O: 95/5.[21] Since **2** is considerably less symmetrical than **3**, the increase in the line width values from 29 Hz for the $[Na^+ \cdot \mathbf{3}]$ complex to 113 Hz for the $[Na^+ \cdot \mathbf{2}]$ complex may be expected because of the nuclear quadrupolar moment of ^{23}Na ($I = 3/2$). Upon addition of one equivalent of NaI (Fig. 2b) to the solution containing the $[Na^+ \cdot \mathbf{2}]$ complex, two signals were observed at $\delta = -15.4$ and -3.7 with line widths of 238 and 192 Hz, respectively; this indicates a slow exchange process between the free and the complexed Na^+ at 25 °C ($T_c = 55$ °C, $k_c = 2.7 \times 10^3$ s^{-1}, $\Delta G^+ = 15.5$ kcal mol^{-1}). The addition of one equivalent of KI to this solution restored the signal at $\delta = -3.9$ with a line width of 18.9 Hz corresponding to free Na^+ ions (Fig. 2c). This thus confirmed the results of the ^{1}H NMR investigations namely that the K^+ ion was more strongly complexed by **2** than the Na^+ ion. Furthermore, addition of one equivalent of CsBr to a solution of the $[Na^+ \cdot \mathbf{2}]$ complex gave two signals at $\delta = -15.5$ and -4.0, which are assigned to the free and complexed sodium, indicating that the affinity of **2** for Na^+ and Cs^+ was in the same range (Fig. 2d). Finally, addition of the [2.2.2]cryptand **3** to a solution of the $[Na^+ \cdot \mathbf{2}]$ complex led to a single signal at $\delta = -11.8$ with a line width of 21.3 Hz. This signal corresponds to the $[Na^+ \cdot \mathbf{3}]$ complex, confirming the results of the ^{1}H NMR studies according to which **3** showed a higher affinity for the Na^+ ion than **2** (Fig. 2e).

Although X-ray data were collected for the $[M^+ \cdot \mathbf{2}]$ complexes with $M = K^+$, Cs^+, and NH_4^+, only the crystal structure of $[K^+ \cdot \mathbf{2}]$ is reported here.[22] The X-ray crystal structure analysis of the racemic potassium complex (Fig. 3) showed that K^+ is

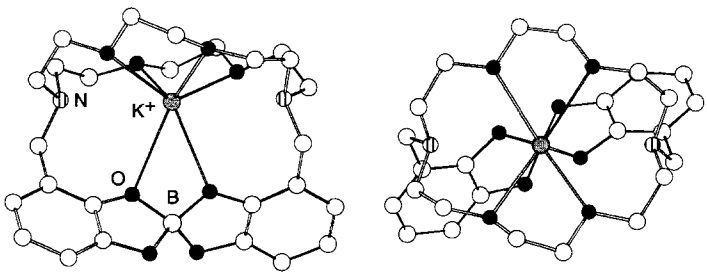


Fig. 3. X-ray structure of the $[K^+ \cdot \mathbf{2}]$ complex. The enantiomer shown is arbitrary. Side view (left) and view along the boron–potassium axis (right). Selected bond lengths [Å] and angles [°] (average values given): K-O 2.82, K-N 3.15, B-O 1.48; O-B-O 105.0 and 109.9, N-K-N 179.

 © VCH Verlagsgesellschaft mbH, D-69451 Weinheim, 1995 0570-0833/95/1010-1116 $ 10.00+.25/0

located within the cavity formed by the negatively charged cryptand **2**. The coordination geometry around the boron atom is indeed tetrahedral with two sets of O-B-O angles of about 105 and 109.9°, and an average B–O distance of about 1.48 Å. As expected, because of the tetrahedral coordination around the boron atom, *R* and *S* isomers are present in the unit cell. The lone pairs of the two nitrogen atoms are oriented towards the interior of the cavity (*in,in* conformation) and the K^+ ion is located at position that is almost equidistant from the two bridgehead nitrogen atoms (N–K distance ca. 3.15 Å); the N-K-N angle is 179°. Among the eight oxygen atoms present in **2**, only six of them, namely the four oxygen atoms of the ether junctions and two borate oxygen atoms, are localized within a bonding distance of K^+ (average distance of ca. 2.82 Å). The coordination polyhedron of the K^+ ion in the [K^+ · **2**] complex, in which the K^+ ion is surrounded by six oxygen and two nitrogen atoms at distances of 2.82–3.15 Å, is irregular. The average K–O distance of about 2.82 Å is considerably shorter than the average K–N distance of about 3.15 Å. In contrast the K^+ ion in [K^+ · **3**] is located almost in the center of the cage with average K–O and K–N distances of about 2.78 Å and 2.87 Å, respectively.[23]

In conclusion, we have demonstrated that the pseudocryptand **1** participates in a cascade-type complexation process. Indeed, binding of the boron atom by both catecholate moieties in **1** leads to the borate ester **2**, thus creating a preorganized cavity bearing one negative charge. Compound **2** acts as a cryptand and binds an alkali metal cation, leading to a neutral [M^+ · **2**] complex. To our knowledge, both the estimated binding constant of about $10^{12.5}$ mol L^{-1} for the potassium complex in methanol and the selectivity factor of the ligand **2** for K^+ over Na^+ and Cs^+ cations of more than 10^3 and 10^2, respectively, are the highest values obtained to date for artificial K^+ receptors.

Received: December 27, 1994 [Z 7580 IE]
German version: *Angew. Chem.* **1995**, *107*, 1204

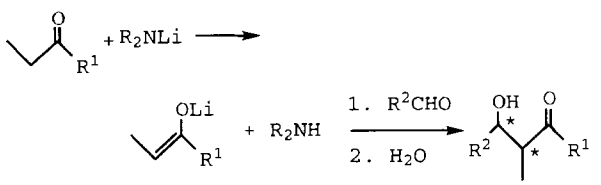
Keywords: alkali metal compounds · boron compounds · cryptands · macrocycles · molecular recognition

[1] B. Dietrich, J.-M. Lehn, J.-P. Sauvage, *Tetrahedron Lett.* **1969**, 2885, 2889.
[2] C. J. Pedersen, *J. Am. Chem. Soc.* **1967**, *89*, 2495, 7017.
[3] C. J. Pedersen, *Angew. Chem.* **1988**, *100*, 1053; *Angew. Chem. Int. Ed. Engl.* **1988**, *27*, 1021.
[4] D. J. Cram, *Angew. Chem.* **1988**, *100*, 1041; *Angew. Chem. Int. Ed. Engl.* **1988**, *27*, 1009.
[5] J.-M. Lehn, *Angew. Chem.* **1988**, *100*, 91; *Angew. Chem. Int. Ed. Engl.* **1988**, *27*, 89.
[6] F. Vögtle, *Supramolecular Chemistry*, Wiley, Chichester, **1991**; G. Gokel, *Crown Ethers and Cryptands*, Royal Society of Chemistry, Cambridge, **1991**; D. J. Cram, J. M. Cram, *Container Molecules and Their Guests*, Royal Society of Chemistry, Cambridge, **1994**; B. Dietrich, P. Viout, J.-M. Lehn, *Macrocyclic Chemistry*, VCH, Weinheim, **1993**.
[7] J.-M. Lehn, *Angew. Chem.* **1990**, *102*, 1347; *Angew. Chem. Int. Ed. Engl.* **1990**, *29*, 1304; G. M. Whitesides, J. P. Mathias, T. Seto, *Science* **1991**, *254*, 1312; J. S. Lindsey, *New J. Chem.* **1991**, *15*, 153.
[8] R. Hütter, W. Keller-Schierlein, F. Knüsel, V. Prelog, G. C. Rodgers, P. Sutter, G. Vogel, W. Voser, H. Zähner, *Helv. Chim. Acta* **1967**, *50*, 1533; J. D. Dunitz, D. M. Hawley, D. Miklos, D. N. J. White, Y. Berlin, R. Marusic, V. Prelog, *ibid.* **1971**, *54*, 1709, W. Marsh, J. D. Dunitz, D. N. J. White, *ibid.* **1974**, *57*, 10.
[9] T. Okazaki, T. Kitahara, Y. Okami, *J. Antibiot.* **1975**, *28*, 176; T. J. Stout, J. Clardy, I. C. Pathirana, W. Fenical, *Tetrahedron* **1991**, *47*, 3511.
[10] E. Graf, M. W. Hosseini, R. Ruppert, *Tetrahedron Lett.* **1994**, *35*, 7779.
[11] B. Dietrich, J.-M. Lehn, J.-P. Sauvage, J. Blanzat, *Tetrahedron* **1973**, *29*, 1629; B. Dietrich, J.-M. Lehn, J.-P. Sauvage, *ibid.* **1973**, *29*, 1647.
[12] Y. Kobuke, Y. Sumida, M. Hayashi, H. Ogoshi, *Angew. Chem.* **1991**, *103*, 1513; *Angew. Chem. Int. Ed. Engl.* **1991**, *30*, 1496.
[13] T. Nabeshima, T. Inaba, T. Sagae, N. Furukawa, *Tetrahedron Lett.* **1990**, *31*, 3919.
[14] F. L. Weitl, K. N. Raymond, *J. Am. Chem. Soc.* **1980**, *102*, 2289; K. N. Raymond, G. Müller, B. F. Matzanke, *Top. Curr. Chem.* **1984**, *123*, 49.
[15] K. Wolfgang, F. Vögtle, *Angew. Chem.* **1984**, *96*, 712; *Angew. Chem. Int. Ed. Engl.* **1984**, *23*, 714; P. Stutte, W. Kiggen, F. Vögtle, *Tetrahedron* **1987**, *43*, 2065; T. J. McMurry, S. J. Rodgers, K. N. Raymond, *J. Am. Chem. Soc.* **1987**, *109*, 3451; T. J. McMurry, M. W. Hosseini, T. M. Garrett, F. E. Hahn, Z. E. Reyes, K. N. Raymond, *ibid.* **1987**, *109*, 7196; T. M. Garrett, T. J. McMurry, M. W. Hosseini, Z. E. Reyes, F. E. Hahn, K. N. Raymond, *ibid.* **1991**, *113*, 2965.
[16] J. Böeseken, *Adv. Carbohydr. Chem.* **1949**, *4*, 189.
[17] J.-M. Lehn in *Frontiers of Chemistry, IUPAC* (Ed.: K. J. Laidler), Pergamon, Oxford, **1982**, S. 265; R. M. Izatt, K. Pawlak, J. S. Bradshaw, *Chem. Rev.* **1991**, *91*, 1721; P. Zanello, S. Tamburini, P. A. Vigato, G. A. Mazzocchin, *Coord. Chem. Rev.* **1987**, *77*, 165; D. C. Smith, H. B. Gray, *Chem. Rev.* **1990**, *90*, 169.
[18] F. C. J. M. Van Veggel, W. Verboom, D. N. Reinhoudt, *Chem. Rev.* **1994**, *94*, 279.
[19] J.-M. Lehn, J.-P. Sauvage, *J. Am. Chem. Soc.* **1975**, *97*, 6700.
[20] H. J. Buschmann, *Inorg. Chim. Acta* **1986**, *125*, 31.
[21] J.-P. Kintzinger, J.-M. Lehn, *J. Am. Chem. Soc.* **1974**, *96*, 3313.
[22] Crystal data for [K^+ · **2**] complex: $C_{26}H_{34}BN_2O_8K \cdot CH_2Cl_2$, $M_r = 637.4$, monoclinic, space group $P2_1/c$, $a = 11.813(3)$, $b = 15.576(4)$, $c = 17.205(5)$ Å, $\beta = 106.12(2)°$, $V = 3041.2$ Å^3, $\rho_{calcd} = 1.392$ g cm^{-3}, $Z = 4$, $\mu(Cu_{K\alpha}) = 36.177$ cm^{-1} (graphite monochromator). A total of 3646 reflections were collected using a Philips PW1100/16 automatic diffractometer. Quantitative data were obtained at −100 °C using a self-made gas flow device. The resulting data set was analyzed with the Enraf-Nonius SDP/VAX package. The structure was solved with MULTAN and refined to $R(F) = 0.032$ ($Rw(F) = 0.050$) using 2410 reflections with $I > 3\sigma(I)$. Further details of the crystal structure investigation are available on request from the Director of the Cambridge Crystallographic Data Centre, 12 Union Road, GB-Cambridge CB2 1EZ (UK), on quoting the full journal citation.
[23] D. Moras, B. Metz, R. Weiss, *Acta Crystallogr. Sect. B* **1973**, *29*, 383.

Synthesis and Characterization of the First Mixed Alkali Metal Enolate Containing Amine Ligands: A Novel "Open-Stack" Structure and Its Implications for Aldol Addition**

Kenneth W. Henderson, Paul G. Williard,* and Peter R. Bernstein

During the past two decades there has been an increasing awareness of the role that aggregation plays in the reactions of lithium enolates.[1] This focus has been created by interest in the aldol reaction and in particular in the possibility of forming chiral materials from simple ketones [Eq. (a)].[2] The synthetic



(a)

utility of this carbon–carbon bond-forming reaction has proved itself in numerous natural product syntheses, leading to an evolution in its methodology. Generally, lithium amides such as lithium diisopropylamide (LDA) or lithium hexamethyldisi-

[*] Prof. P. G. Williard, Dr. K. W. Henderson
Department of Chemistry, Brown University
Providence, RI 02912 (USA)
Telefax: Int. code. +(401) 863-2594
Dr. P. R. Bernstein
Zeneca Pharmaceuticals

[**] This work was funded by Zeneca Pharmaceuticals strategic research fund, grant no. 235. P. G. W. wishes to thank the NIH for grant no. GM-35982.

lazide (LHMDS) are used as strong bases to perform the deprotonation reaction, producing the corresponding amine and lithium enolate.

Much of the attention on enantioselective aldol syntheses has concentrated on the use of chiral amide bases and amines as chiral catalysts.[1-3] Of fundamental importance is the role the chiral moiety plays in the reaction. Despite this, no direct structural evidence has been reported for an enolate bonded to its reprotonated secondary amine. Seebach et al.[4] have studied in detail the interaction of lithium enolates with the chelating secondary amine *N,N,N'N'*-trimethylethylenediamine (triMEDA). This revealed an interaction between the enolate moiety and the hydrogen of the N–H bond. Typically, however, external donor bases such as THF or *N,N,N',N'*-tetramethylethylenediamine (TMEDA) have been used to mimic the action of the chiral moiety.

Only a handful of enolates of the heavier alkali metals have been structurally characterized, which is surprising considering these species offer different selectivities to their lithium counterparts.[5] To our knowledge no studies, either synthetic or theoretical, have been performed for simple mixed-cation enolate systems.[6] This contrasts to the growing documentation on mixed-anion systems.[7] We now outline the characterization of the first mixed alkali metal enolate, which furthermore contains a secondary amine formed by protonation of the amide base as donor ligand.

Specific categories of mixed alkali metal systems, such as superbases,[8] amides,[9] and imides,[10] have recently received an increasing degree of attention because their reactivity and structures are different from that of their homometallic analogs. We were interested in obtaining structural details of mixed alkali metal enolate complexes. Reaction of sodium diisopropylamide (NDA) and LDA with 3,3-dimethyl-2-butanone (pinacolone) yields crystals of $[Li_2Na_4\{OC(=CH_2)tBu\}_6 \cdot (iPr_2NH)_2]$ (**1**) [Eq. (b)].

$$4\,iPr_2NNa + 4\,iPr_2NLi \xrightarrow{8\,tBuCOMe} \mathbf{1} + 6\,iPr_2NH + 2\,[LiOC(=CH_2)tBu] \quad \text{(b)}$$

A single-crystal X-ray structural analysis of **1** revealed a triple-layered stack of one NaONaO ring dimer sandwiched between two LiONaO dinuclear rings (Fig. 1).[11] Stack structures, either tetrameric (cubane) or hexameric (consisting of two stacked trimers), have been found for a number of alkali metal compounds, including imides ($R_2C{=}N^-$), alkynyls ($RC{\equiv}C^-$), alkoxy/aryloxy (RO^-), and enolates $[RC(=CR_2)O^-]$.[12] The triple-layered stack unit found for **1** is rather unusual, and only two such structures have been reported,[10] namely the bimetallic imides **2** and **3**, which interestingly also contain both sodium and lithium. Higher oligomeric stacks have been found for lithium alkynides[13] and also for sodium amides.[14]

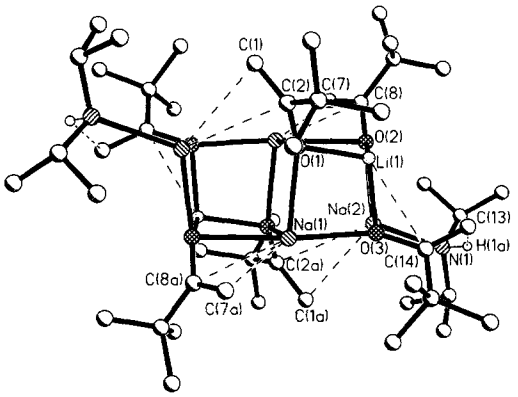


Fig. 1. Molecular structure of **1** (hydrogen atoms, except H(1a), omitted for clarity). Key bond lengths [Å] and angles [°] not in text: Na(1)-O(1) 2.366(7), Na(1)-O(1a) 2.418(7), Na(2)-O(2) 2.288(7), Li(1)-O(2) 1.87(2), Li(1)-O(3), 1.93(2); O(1)-Li(1)-O(2) 108.7(7), O(1)-Li(1)-O(3) 102.7(7), O(3)-Na(1)-O(1a) 95.8(2), O(1a)-Na(1)-O(2a) 80.3(2), O(2)-Na(2)-O(1a) 84.5(2), O(3)-Na(2)-O(1a) 81.6(2), Li(1)-O(1)-Na(1) 83.8(5), Li(1)-O(1)-Na(1a) 83.5(5), Li(1)-O(2)-Na(1a) 85.3(5), Na(2)-O(2)-Na(1a) 97.2(2), Li(1)-O(3)-Na(1) 88.1(5), Na(1)-O(3)-Na(2) 99.3(3).

$[Li_4Na_2\{N{=}C(NMe_2)_2\}_6]$ **2**

$[Li_{4-x}Na_{2+x}\{N{=}C(Ph)tBu\}_6]$ **3**

A clear difference between **1** and the imides **2** and **3** is the ratio of metals present. Both **2** and **3** are lithium rich (4 Li:2 Na), while **1** is sodium rich (2 Li:4 Na). The stoichiometry of metal atoms in **1** deviates from the 1:1 ratio of reactants used. Similar situations have been found to arise commonly for mixed-metal systems containing alkali metals, where the stability of the structural arrangement determines which products are isolable.[15] Even when the mixture of starting materials contains more lithium (2 LDA:1 NDA), only **1** was isolated. This implies that a soluble lithium enolate species is present in solution; lithium pinacolate is known to be highly soluble in hydrocarbons.[16]

Also unique to **1** is its structural form, in which two edges of the face-sharing cubes are absent. The distance between Na(2)–O(1a) and Na(2a)–O(1), that is, the "open" edges, is 2.875 Å. This contrasts sharply with the lengths of the shorter closed edges Na(1)–O(3) and Na(1)–O(2a) of 2.242 Å and 2.420 Å, respectively (and Li(1)–O(1) at 1.96 Å). Short contacts are apparent between the $H_2C{=}C$ units of the central NaONaO enolate ring and the terminal sodium atoms (Na(2)–C(1a) 2.778 Å; Na(2)–C(2a) 2.873 Å). Even shorter contacts are observed between the central sodium atoms and the π bond of the outer enolate residues (Na(1)–C(8a) 2.702 Å; Na(1)–C(7a) 2.716 Å). Similarly Li(1)–C(14) is short (2.74 Å), but Li(1)–C(13) is longer than 3 Å. This feature also manifests itself on comparison of the bond angles. The angles of the central dimeric ring are not unusual (93.7° at sodium and 86.3° at oxygen), whereas the outer rings are very distorted from square (106.8° at lithium, 81.4° at sodium, 88.0° at O2, and 83.8° at O3). Each closed side of the stack is more linear (O(3)-Na(1)-O(2a) 174.6°) than the sides with an "open" edge (Li(1)-O(1)-Na(2a) is 162.6°).

Several factors may combine to give the framework of **1**. The disparity in size between the lithium and sodium atoms causes significant distortion of the structure.[9, 10] Interactions between the π bonds of the enolates and the metals amplifies the distortion, resulting in two "open" edges of the stack. An "open-stack" arrangement has not been noted for any prior alkali metal complexes in the solid state, although Jackman et al. suggested such structures as intermediates in transesterification reactions.[17] Also of note is the mixed-cation imide **4** that can be described as a "broken-cube".[18] A number of "open-dimers" have been proposed both as solution aggregates and as important reaction intermediates.[19] Structures such as **1** can be considered close cousins to open dimers.

$[\{Sb_2Li_2\{N(C_6H_{11})\}_4\}_2]$ **4**

The final component of **1** is a coordinated diisopropylamine at each of the outer sodium atoms; the Na(2)–N(1) bond length

is 2.558 Å. Previously, tertiary or secondary amines were added as cosolvents to alkali metal enolates in order to study the interaction of the free base with the salt.[1-4] Compound **1** represents a new and important stage after full enolization has taken place: the enolate is immediately solvated by free amine. Although much attention has been paid to using amides as chiral additives in the aldol reaction, the role the base plays has not yet been fully defined. We now have direct evidence that the free base can form a coordination complex with the metal enolate. This implies that the amine, and not only the metalated amide, may influence the regioselectivities of an incoming reactant in the formation of chiral materials. Such a suggestion is supported by synthetic results, which show a correlation between enantioselectivity and stoichiometry of the chiral amine.[3] Each amino hydrogen is directed towards a terminal carbon atom of an enolate residue (C(13)–H(1a) 3.006 Å), but does not lie on the N(1)–C(13) vector (N(1)–C(13) 3.646 Å). This is reminiscent of the geometry involved in the enolization reaction.[4]

In conclusion, we have reported the synthesis and structure of the first mixed alkali metal enolate. It adopts a unique "open-stack" arrangement in the crystal and contains a secondary amine formed during protonation as ligand. The triple-stack motif is unprecedented for alkali metal enolates. Such structures should now be considered when conducting theoretical or NMR studies of the aldol reaction.

Experimental Procedure

A vigorously stirred mixture of *n*-butyllithium (1 mmol) and *n*-butylsodium (1 mmol) in 2 mL of pentane, under a protective nitrogen blanket, was treated at 0 °C with diisopropylamine (2.2 mmol). After warming to 20 °C, the mixture was placed in an ultrasound bath for 5 minutes. The homogeneous suspension was cooled to 0 °C and pinacolone (2.2 mmol) added over a 5 minute period. The now near clear solution was filtered through a glass frit and the clear colorless filtrate kept at 0 °C. Colorless cubic crystals of X-ray diffraction quality of **1** were deposited after 12 hours. Yield of first crop of crystals (based on *n*BuNa) 22%; m.p. 207–210 °C; ^{1}H NMR (400 MHz, C_6D_6, 300 K): 0.25 (br.s., 2H; NH), 0.94 (d, 24H; $(CH_3)_2CH$), 1.20 (s, 54H; $(CH_3)_3C$), 2.74 (oct, 4H; $(CH_3)_2CH$), 3.43 (br.s., 6H; $C=CH_2$), 3.77 (br.s., 6H; $C=CH_2$).

Received: December 22, 1994 [Z 7569 IE]
German version: *Angew. Chem.* **1995**, *107*, 1218

Keywords: aldol reactions · alkali metal compounds · enolates

[1] D. Seebach, R. Amstutz, J. D. Dunitz, *Helv. Chim. Acta*, **1981**, *64*, 2622; E. M. Arnett, F. J. Fisher, M. A. Nichols, A. A. Ribeiro, *J. Am. Chem. Soc.* **1990**, *112*, 801; *ibid.* **1989**, *111*, 748; L. M. Jackman, N. M. Szeverenyi, *ibid.* **1977**, *99*, 4954; P. G. Williard in *Comprehensive Organic Synthesis, Vol. 1* (Eds.: B. M. Trost, I. Flemming), Pergamon, New York, **1991**, Chapter 1.

[2] C. H. Heathcock in *Asymmetric Synthesis, Vol. 3* (Ed.: J. D. Morrison), Academic Press, New York, **1984**; S. Masamune, W. Choy, J. S. Peterson, L. R. Sita, *Angew. Chem.* **1985**, *97*, 1; *Angew. Chem. Int. Ed. Engl.* **1985**, *24*, 1; I. Paterson, J. M. Goodman, M. A. Lister, R. C. Schumann, C. K. McKlure, R. D. Norcross, *Tetrahedron* **1990**, *46*, 4663; for a comprehensive list of reviews, see W. R. Roush, *J. Org. Chem.* **1991**, *56*, 4151.

[3] E. Juaristi, A. K. Beck, J. Hansen, T. Matt, T. Mukhopadhyay, M. Simson, D. Seebach, *Synthesis* **1993**, 1271, and references therein.

[4] T. Laube, J. D. Dunitz, D. Seebach, *Helv. Chim. Acta.* **1985**, *68*, 1373.

[5] C. A. Maryanoff, K. L. Sorgi, A. M. Zientek, *J. Org. Chem.* **1994**, *59*, 237; R. T. Jacobs, P. R. Bernstein, L. A. Cronk, E. P. Vacek, L. F. Newcomb, D. Aharony, C. K. Buckner, E. J. Kusner, *J. Med. Chem.* **1994**, *37*, 1282.

[6] An aggregate containing Li^+, K^+, *t*-butyl alcoholate, and pinacolate has been reported: P. G. Williard, G. J. MacEwan, *J. Am. Chem. Soc.* **1989**, *111*, 7671.

[7] F. E. Romesberg, D. B. Collum, *J. Am. Chem. Soc.* **1994**, *116*, 9187, 9198; P. G. Williard, M. J. Hintze, *ibid.* **1990**, *112*, 8602; *ibid.* **1987**, *109*, 5539; Y. Hasegawa, H. Kawasaki, K. Koga, *Tetrahedron Lett.* **1993**, *34*, 1963.

[8] M. Schlosser, *J. Organomet. Chem.* **1967**, *8*, 9; W. Bauer, L. Lochmann, *J. Am. Chem. Soc.* **1992**, *114*, 7482; S. Harder, A. Streitwieser, *Angew. Chem.* **1993**, *105*, 1108; *Angew. Chem. Int. Ed. Engl.* **1993**, *32*, 1066.

[9] D. R. Baker, W. Clegg, L. Horsburgh, R. E. Mulvey, *Organometallics* **1994**, *13*, 4170.

[10] N. D. R. Barnett, R. E. Mulvey, W. Clegg, P. A. O'Neil, *Polyhedron* **1992**, *11*, 2809; D. Barr, W. Clegg, R. E. Mulvey, R. Snaith, *J. Chem. Soc. Chem. Commun.* **1989**, 57.

[11] Crystal data for **1**: $C_{24}H_{48}LiNa_2NO_3$, monoclinic, space group $c2/c$, $a = 19.730(5)$, $b = 12.664(3)$, $c = 23.960(7)$ Å, $\beta = 99.76(2)°$, $V = 5900(3)$ Å^3, $Z = 8$, $\rho_{calcd} = 1.017$ g cm^{-3}, $Mo_{K\alpha}$-radiation, $\lambda = 0.71073$ Å, $2\theta_{max} = 45°$, θ-2θ scan, $T = 253$ K, 4659 measured reflections, 3815 independent reflections, 3811 used in the refinement; no σ limits, no absorption corrections, Lorentz polarization corrections; structure solved by direct methods (SHELXTL), all non-hydrogen atoms anisotropic (280 parameters), H atoms were refined in idealized positions, $R = 8.91$, $wR = 18.26$, full-matrix least-squares on F^2 (SHELXL-93), largest peak and hole in the final difference map 0.363 and -0.252 e Å^{-3}; further details of the crystal structure investigation are available on request from the Director of the Cambridge Crystallographic Data Centre, 12 Union Road, GB-Cambridge CB2 1EZ (UK), on quoting the full journal citation.

[12] Reviews: E. Weiss, *Angew. Chem.* **1993**, *105*, 1565; *Angew. Chem. Int. Ed. Engl.* **1993**, *32*, 1501; K. Gregory, P. von R. Schleyer, R. Snaith, *Adv. Inorg. Chem.* **1991**, *37*, 47; R. E. Mulvey, *Chem. Soc. Rev.* **1991**, *20*, 167.

[13] N. P. Lorenzen, J. Kopf, F. Olbrich, U. Schümann, E. Weiss, *Angew. Chem.* **1990**, *102*, 1481; *Angew. Chem. Int. Ed. Engl.* **1990**, *29*, 1441.

[14] M. Geissler, J. Kopf, B. Schubert, E. Weiss, W. Neugebauer, P. von R. Schleyer, *Angew. Chem.* **1987**, *99*, 569; *Angew. Chem. Int. Ed. Engl.* **1987**, *26*, 587.

[15] W. Clegg, K. W. Henderson, R. E. Mulvey, P. A. O'Neil, *J. Chem. Soc. Chem. Commun.* **1994**, 769.

[16] P. G. Williard, G. B. Carpenter, *J. Am. Chem. Soc.* **1986**, *108*, 462.

[17] L. M. Jackman, M. M. Petrei, B. D. Smith, *J. Am. Chem. Soc.* **1991**, *113*, 3451.

[18] R. A. Alton, D. Barr, A. J. Edwards, M. A. Paver, P. R. Raithby, M. A. Rennie, C. A. Russell, D. S. Wright, *J. Chem. Soc. Chem. Commun.* **1994**, 1481.

[19] L. A. Paquette, W. Bauer, M. R. Sivik, M. Bühl, M. Freigel, P. von R. Schleyer, *J. Am. Chem. Soc.* **1990**, *112*, 8776; L. M. Jackman, E. F. Rakiewicz, *ibid.* **1991**, *113*, 1202; F. E. Romesberg, J. H. Gilchrist, A. T. Harrison, D. J. Fuller, D. B. Collum, *ibid.* **1991**, *113*, 5751; N. A. Petasis, K. A. Teets, *ibid.* **1992**, *114*, 10328; P. G. Williard, Q.-Y. Lui, *ibid.* **1993**, *115*, 3380.

Photonic Molecular Devices: Reversibly Photoswitchable Fluorophores for Nondestructive Readout for Optical Memory**

Gerasimos M. Tsivgoulis and Jean-Marie Lehn*

Systems that allow the reversible modulation of a given electronic property like conjugation by an external trigger such as light constitute basic components for the development of molecular and supramolecular devices.[1] This is the case for organic photochromic compounds,[2-10] some of which exhibit remarkable properties for use in optical memory media,[2-4] for example low fatigue and/or very good thermal stability. However, photochromic materials must fulfill many criteria for practical applications in optical information storage systems.[2] A major problem arises from readout unstability. Some possible solutions have been proposed,[3, 5, 8, 10] but the development of a nondestructive readout method remains a challenging problem.[2, 3]

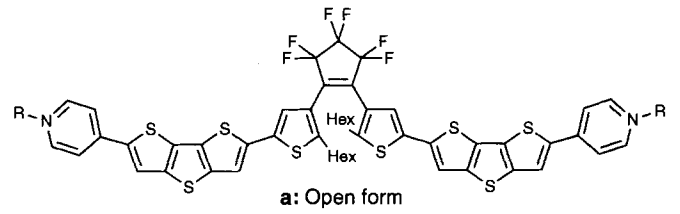
Diarylethenes, notably bis(thien-3-yl) systems, display excellent photochromic properties[6-8] and can be reversibly inter-

[*] Prof. Dr. J.-M. Lehn, Dr. G. M. Tsivgoulis
Collège de France
Chimie des Interactions Moléculaires, UPR No. 285, CNRS
11, place Marcelin Berthelot, F-75231 Paris Cedex 05 (France)
Telefax: Int. code +(1) 44 27 13 56

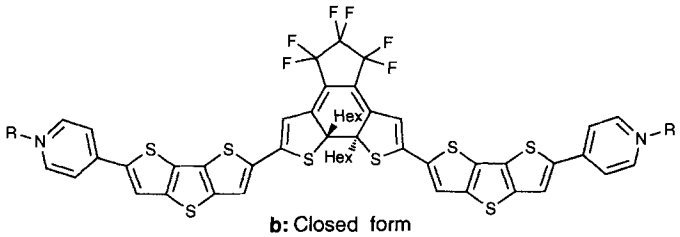
[**] This research was financially supported by the EEC Human Capital and Mobility Program. We thank S. Gilat and Dr. S. H. Kawai for helpful discussions.

converted between a nonplanar, colorless, open form and a planar, colored, closed form in which extended conjugation over the whole molecule is possible.[7] Thus, properties depending on changes in the π system (electrical, optical) as well as structural changes (solubility, chirality, recognition) may be strongly altered by the form of the system.

We have designed and synthesized (as delineated in Scheme 1[11]) two photoswitching units **1** and **2**, in which extensive conjugation between two condensed dithieno(thiophene)

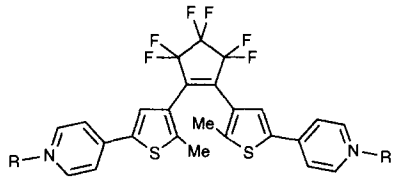


>600 nm ⇌ 330-365 nm

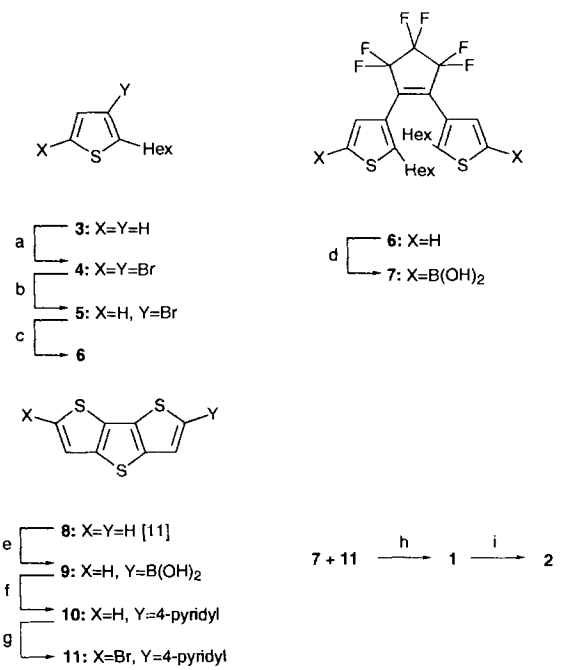


1: R = lone pair

2: R = CH_3^+, anion = $CF_3SO_3^-$



12: R=CH_3^+, anion= $CF_3SO_3^-$



Scheme 1. Synthesis of compounds **1** and **2**. a) Br_2, $CHCl_3$/AcOH (52%); b) *n*BuLi, Et_2O (−78 °C) then MeOH (92%); c) *n*BuLi, *n*-C_5H_{12} (−78 °C) then THF, C_5F_8 (55%); d) *n*BuLi, Et_2O/cat. LDA then $B(OBu)_3$; e) *n*BuLi, Et_2O (−78 °C) then $B(OBu)_3$ (83%); f) 4-bromopyridine, $Pd(PPh_3)_4$, aq. Na_2CO_3/THF (72%); g) *N*-bromosuccinimide, $CHCl_3$/AcOH (90%); h) $Pd(PPh_3)_4$, aq. Na_2CO_3/THF (40–55%); i) CF_3SO_3Me, CH_2Cl_2 (81%); Hex = *n*-hexyl.

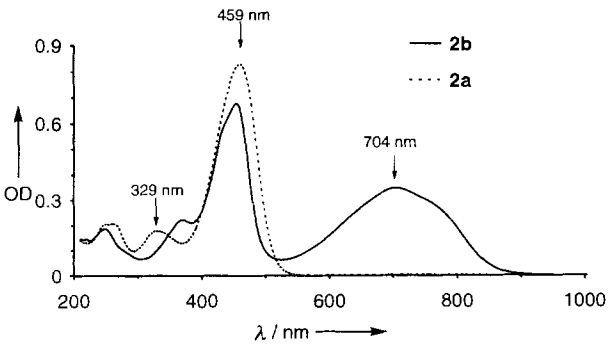


Fig. 1. Absorption spectra of forms **2a** and **2b** (1×10^{-5} M in methanol).

units is possible, in order to: a) extend the concept of a switchable molecular wire,[7] b) introduce new absorption bands and study their behavior with regards to the "switch" action, and c) bathochromically shift the UV/Vis absorbance bands relative to those of related systems. We report here the optical properties of the novel unit **2** which meets many of the criteria for practical applications of organic photochromic compounds, notably thermal stability, fatigue resistance, sensitivity to diode laser wavelength, close to quantitative reversible interconversion, and in particular nondestructive readout capability.

The photochemical interconversion properties of compound **2** were studied by irradiating methanolic solutions (1×10^{-5} M and 2×10^{-6} M in a 1×1 cm quartz cell) under a variety of conditions. The UV/Vis spectra of the open **2a** and closed **2b** forms are shown in Figure 1. Irradiation of the main band of the open form **2a** ($\lambda_{max} = 459$ nm, $\varepsilon = 92800\ M^{-1}cm^{-1}$) at 400–500 nm through a window filter[12] gave no change, whereas in related compounds,[7, 8] as well as in the parent compound **1**, irradiation of the main bands of the open forms gave the closed forms in nearly quantitative yields. The main band of the open form **1a** is so active that very fast, quantitative conversion to the closed form **1b** occurs simply on exposure to daylight. Conversion of **2a** to the closed form **2b** (in 92% yield) can be achieved only by irradiation at wavelengths less than 400 nm; backconversion occurs (>98%) on irradiation of **2b** at $\lambda > 600$ nm[13] for roughly 30 min. Under the conditions used, irradiation times of about 10 min were sufficient to give conversions of 70–75% in both directions. The ring closure was not quantitative but reached around 92% conversion. To confirm that this reaction corresponds to a photostationary equilibrium, solutions of the closed form **2b** were irradiated at 365 nm, giving **2a** exponentially with a maximum conversion of around 8%.

The closed form **2b** presents an intense ($\varepsilon = 41000\ M^{-1}cm^{-1}$ in MeOH and $\varepsilon = 43300\ M^{-1}cm^{-1}$ in CH_3CN) broad absorption band at $\lambda_{max} = 704$ nm, which is red-shifted by roughly 45 nm and is about 2.7 times more intense than the corresponding band[7] of compound **12** ($\lambda_{max} = 662$ nm, $\varepsilon = 16000\ M^{-1}cm^{-1}$ in CH_3CN). Minimal solvatochromism is observed; in MeOH,

 © VCH Verlagsgesellschaft mbH, D-69451 Weinheim, 1995 0570-0833/95/1010-1120 $ 10.00+.25/0

CH_3CN, and DMSO, $\lambda_{max} = 704$, 707, and 724 nm, respectively. This sensitivity in the 650–830 nm region is of much interest for practical applications.[2]

The absorption spectrum of **2a** presents at least three bands ($20000 < \varepsilon < 26000$) in the region between 210 and 400 nm (Fig. 1). To find out which band is active in the closing process, **2a** was irradiated with light of different wavelengths between 250 and 400 nm (using the monochromator of the fluorimeter). We found that only the band at $\lambda_{max} = 329$ nm led to conversion to **2b**. Similar results were obtained by irradiating samples of **2a** with three UV lamps of equal power (6 W) at 365, 312, and 254 nm (Table 1).

Table 1. Conversion of the open form **2a** to the closed form **2b** by irradiation in methanol for 1, 2, 4, and 6 min at different wavelengths λ.

	Conversion of **2a** to **2b** [%]			
	1 min	2 min	4 min	6 min
365 nm	9.5	19.0	36.5	50.0
312 nm	8.0	17.0	32.5	44.5
254 nm	3.0	6.5	12.0	18.0

The thermal stability of **2a** and **2b** was investigated by storing methanolic solutions of both in the dark a) at room temperature for more than 15 days and b) at 60 °C for five hours. In both cases no change was observed in the UV/Vis spectra. Also, no decomposition was detected when compound **2a** was exposed to daylight in air for two to three days. Nevertheless, irradiation experiments were always conducted under an inert atmosphere (N_2). Under these conditions, ten photocycles[14] did not cause any change in the UV/Vis spectra.

It was mentioned above that the strong band of **2a** at 459 nm was found to be inactive. In the same region the closed form **2b** also displays a weakly active band only 19% lower in intensity and at nearly the same wavelength ($\lambda_{max} = 454$ nm). These two bands may be assigned to the [pyridyl–dithieno(thiophene)–thiophene] units, as indicated by comparison of the spectra of **2a** and **2b** with that of the isolated unit. However, because of the small difference between their absorption coefficients, these bands are of little interest for nondestructive readout capability. Therefore, attempts were made to find other properties related to these bands.

The open form **2a** was found to present a strong emission at 589 nm when excited in the 400–500 nm region (Fig. 2). In contrast, the closed form **2b** displays only a weak fluorescence (less than 3% of the intensity of **2a**) that seems to be due, at least in part, to contamination from the open form.[15, 16] It is not possible at present to determine which structural and/or conjugation effects are responsible for this dramatic change in fluorescence.

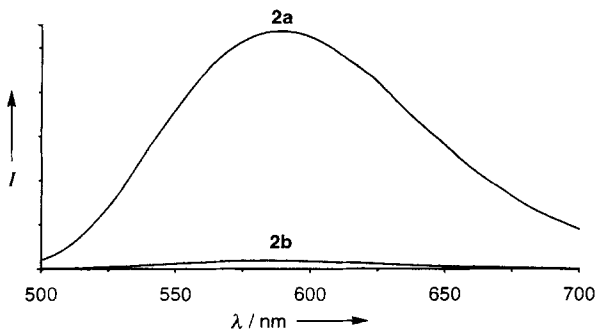


Fig. 2. Emission spectra of forms **2a** and **2b** (2×10^{-6} M in methanol; excitation at 459 nm).

Of special interest is the fact that the absorption bands of both **2a** and **2b**, which by excitation give a fluorescence discrimination, are photochemically almost inactive, while two other absorption bands can be used to interconvert the open and closed forms. Ideally, the bands in the 400–500 nm region must be completely inactive to irradiation for achieving a nondestructive readout capability. As already mentioned, the band of the open form at 459 nm is inactive, while the analogous band of the closed form ($\lambda_{max} = 454$ nm) appears to have low activity when irradiated at 400–500 nm with a 300 W tungsten lamp; a slow conversion of less than 10% per hour is observed. In order to evaluate the fluorescence properties of compounds **2** irradiations were performed with a narrow range of excitation wavelengths. The results (Table 2) show that indeed the "switch position" remains almost unaffected (less than 1%) after 1 h excitation at 459 nm (1 nm excitation width); a broader excitation range (2.5 nm width) gave only a very slow change.

Table 2. Interconversion between the open (**2a**) and closed form (**2b**) in MeOH under different conditions.

λ (conditions)	Conversion after 30 min radiation [%]	
	2a → **2b**	**2b** → **2a**
> 610 nm (cutoff filter) [13]	0	> 98
365 nm (UV lamp)	ca. 92 (max.)	ca. 8
400–500 nm (window filter) [12]	< 0.5	ca. 5
459 nm (2.5 nm width)	< 0.5	2
459 nm (1.0 nm width)	–	< 0.5

In conclusion, the photochromic unit **2** acts as an optical switch presenting a light-triggered fluorescence by excitation of absorption bands that have almost no effect on the switch process. Since excitation at 459 nm leaves the fluorescent open form **2a** unchanged and affects the nonfluorescent closed form **2b** only very little (1% after 1 h) the interconversion between **2a** and **2b** may be used for writing and erasing, while reading can be performed on either form by means of the fluorescent/nonfluorescent contrast. A very large number of fluorescence readings can in principle[17] be performed on **2a** before any significant change takes place. The combination of these properties can offer a promising route towards nondestructive readout capability in optical memory media.

Received: December 27, 1994 [Z 7575 IE]
German version: *Angew. Chem.* **1995**, *107*, 1188

Keywords: fluorescence · molecular switches · optical readout · photochromism

[1] J.-M. Lehn, *Angew. Chem.* **1988**, *100*, 91; *Angew. Chem. Int. Ed. Engl.* **1988**, *27*, 89; *ibid.* **1990**, *102*, 1347 and **1990**, *29*, 1304.

[2] a) J. Whittal in *Photochromism, Molecules and Systems* (Eds.: H. Dürr, H. Bouas-Laurent), Elsevier, Amsterdam, **1990**, p. 467; b) M. Irie, *Mol. Cryst. Liq. Cryst.* **1993**, *227*, 263; B. L. Feringa, W. F. Jager, B. de Lange, *Tetrahedron* **1993**, *49*, 8267.

[3] Y. Yokoyama, T. Yamane, Y. Kurita, *J. Chem. Soc. Chem. Commun.* **1991**, 1722.

[4] S. Nakamura, M. Irie, *J. Org. Chem.* **1988**, *53*, 6136; H. G. Heller, *Chem. Ind. (London)* **1978**, 193.

[5] M. Irie, O. Miyatake, K. Uchida, *J. Am. Chem. Soc.* **1992**, *114*, 8715; M. Irie, O. Miyatake, K. Uchida, T. Eriguchi, *ibid.* **1994**, *116*, 9894; M. Irie, O. Miyatake, R. Sumiya, M. Hanazawa, Y. Horikawa, K. Uchida, *Mol. Cryst. Liq. Cryst.* **1994**, *246*, 155.

[6] M. Irie, M. Mohri, *J. Org. Chem.* **1988**, *53*, 803; M. Irie, *Jpn. J. Appl. Phys.* **1989**, *28*, Suppl. 28-3, 215; K. Uchida, Y. Nakayama, M. Irie, *Bull. Chem. Soc. Jpn.* **1990**, *63*, 1311; Y. Nakayama, K. Hayashi, M. Irie, *ibid.* **1991**, *64*, 789; M. Hanazawa, R. Sumiya, Y. Horikawa, M. Irie, *J. Chem. Soc. Chem. Commun.*

 © VCH Verlagsgesellschaft mbH, D-69451 Weinheim, 1995 0570-0833/95/1010-1121 $ 10.00+.25/0

1992, 206; S. Iwata, Y. Ishihara, C.-P. Qian, K. Tanaka, *J. Org. Chem.* **1992**, *57*, 3726; T. Saika, M. Irie, T. Shimidzu, *J. Chem. Soc. Chem. Commun.* **1994**, 2123.
[7] S. L. Gilat, S. H. Kawai, J.-M. Lehn, *J. Chem. Soc. Chem. Commun.* **1993**, 1439.
[8] S. H. Kawai, S. L. Gilat, J.-M. Lehn, *J. Chem. Soc. Chem. Commun.* **1994**, 1011.
[9] J.-F. Zhi, R. Baba, K. Hashimoto, A. Fujishima, *Chem. Lett.* **1994**, 1521; J. Huuskonen, J. Schulz, E. Kolehmainen, K. Rissanen, *Chem. Ber.* **1994**, *127*, 2267.
[10] M. Irie, K. Sayo, *J. Phys. Chem.* **1992**, *96*, 7671; F. Tatezono, T. Harada, Y. Shimizu, M. Ohara, M. Irie, *Jpn. J. Appl. Phys. Part 1* **1993**, *32*, 3987.
[11] Details regarding the syntheses as well as spectroscopic and electrochemical properties of compounds **1** and **2** will be published in a forthcoming paper. All new compounds were characterized by spectroscopy and microanalysis; compounds **1a**, **b** gave correct microanalyses and FAB mass spectra; for **2a**, **b** only the FAB mass spectra were obtained. The synthesis of the dithieno(thiophene) **8** was described: F. de Jong, M. J. Janssen, *J. Org. Chem.* **1971**, *36*, 1645. Compound **1** is soluble in many common organic solvents like $CHCl_3$, CH_2Cl_2, acetone, THF, and higher alcohols, and is even slightly soluble in hexane. On the other hand, compound **2** carrying two positive charges, is insoluble in solvents of low or medium polarity like hexane, $CHCl_3$, CH_2Cl_2, and acetone, but soluble in solvents of high polarity like CH_3CN, DMSO, DMF, and MeOH.
[12] Characteristics of the window filter: 425–475 nm, transmittance = 68%; $\lambda < 400$ nm and $\lambda > 500$ nm, transmittance < 3%.
[13] Characteristics of the cutoff filter: $\lambda > 620$ nm, transmittance = 83%; $\lambda < 585$ nm, transmittance < 1%.
[14] Conversion to the closed form was limited to 70–75% (10 min irradiation) during these photocycles, while the opening was carried to completion (ca. 30 min irradiation) to check for any change in the spectra. In contrast to experiments in methanol, irradiation of **2a** in aprotic solvents like DMSO or CH_3CN at wavelengths less than 400 nm resulted in partial decomposition.
[15] The only possibility of obtaining pure **2b** is by synthesis from **1b** because the photochemical ring closure of **2a** reaches a maximum of 92% conversion. Contamination by the open form is also indicated by the similar λ_{max} and shape of the emission bands of the two forms.
[16] As in the case of **2**, solutions of the open form **1a** in *n*-pentanol present strong emission bands (at 465 and 444 nm; excitation at 395 nm), whereas the closed form **1b** is only weakly (ca. 1%) luminescent.
[17] Supposing that irradiation for 1 s is necessary for a fluorescence reading (actually this can be much shorter), then over 10^4 readings of the weakly photoactive closed form **2b** can be performed with less than 10% backreaction to the open form.

Synthesis, Structure, and Properties of Dinuclear and Trinuclear Rack-Type Ru^{II} Complexes**

Garry S. Hanan, Claudia R. Arana, Jean-Marie Lehn,* and Dieter Fenske

The design of organic and inorganic programmed systems that self-assemble into well-defined architectures is a major current research theme in supramolecular chemistry.[1, 2] Ligands containing suitable binding sites in a correct arrangement may be read by metal ions following the algorithm defined by their coordination geometry, thus spontaneously generating as output the desired inorganic architecture. In the area of self-assembled inorganic complexes our work has been concerned with several types of systems: double-[3, 4] and triple-helical[5] complexes, helicates, based on tetrahedral and octahedral metal centers, respectively, multicomponent cylindrical cage complexes,[6] and grid-type arrays of metal ions.[7]

[*] Prof. Dr. J.-M. Lehn, G. S. Hanan, Dr. C. R. Arana
Laboratoire de Chimie Supramoléculaire
Institut Le Bel, Université Louis Pasteur
4, rue Blaise Pascal, F-67000 Strasbourg (France)
Telefax: Int. code + 88 41 10 20
Prof. Dr. D. Fenske
Institut für Anorganische Chemie der Universität Karlsruhe (Germany)

[**] G. S. H. thanks the NSERC (Canada) for a doctoral fellowship. C. R. A. thanks the Jubiläum Stiftung and the Chateaubriand Program for postdoctoral fellowships.

The latter grid structure belongs to a broad class of ordered inorganic architectures comprising, in sequence of increasing complexity, two-dimensional geometries that may be termed racks [*n*]R, ladders [2*n*]L, and grids [*m* × *n*]G (Fig. 1), where [*n*], [2*n*], and [*m* × *n*] specify the number of metal atoms in the R, L, and G structures, and *n* (for a square grid) represents their rank. Extension into three-dimensional structures is conceivable.

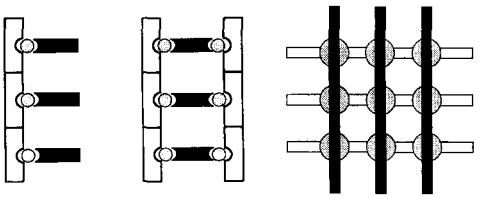
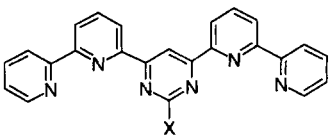


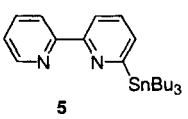
Fig. 1. Inorganic architectures of rack (left), ladder (center), and grid type (right).

Such inorganic architectures may be assembled from either tetrahedral metal ions and bidentate ligands such as 2,2′-bipyridyl (bpy) or from octahedral metal ions and tridentate ligands such as 2,2′:6′,2″-terpyridyl (tpy). In addition to serving as centers for ligand binding and positioning, the metal ions also introduce electrochemical, photochemical, and reactivity properties, thus conferring functionality to the final architectures for development towards inorganic molecular devices.[1, 8]

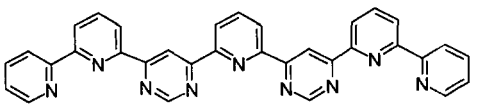
We now report the synthesis of the linear ligands **1** and **2**, which contain two and three binding sites, respectively, of tpy



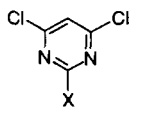
1a X = H
b X = 9-anthryl =



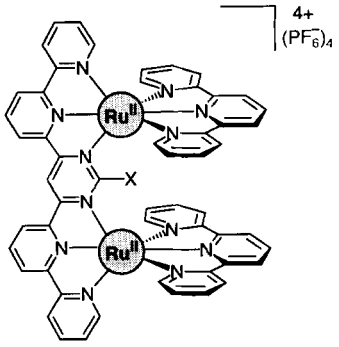
5



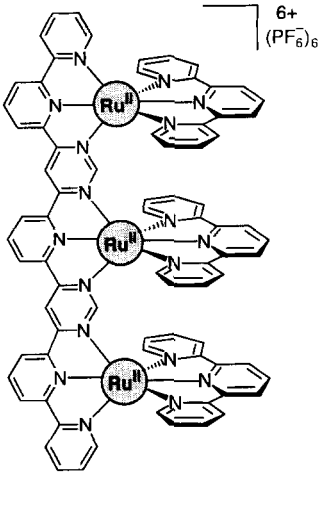
2



6a X = H
b X = 9-anthryl



[2]R; **3a** X = H
b X = 9-anthryl



[3]R; **4**

type, and the formation of the corresponding rack complexes [2]R **3** and [3]R **4** by coordination of these ligands to $Ru(tpy)^{2+}$ centers.

The synthesis[9] of the bis(bipyridyl)pyrimidines **1a, b** involved the Pd^{II}-catalyzed cross-coupling[10] of 6-tributylstannyl-2,2′-bipyridine (**5**)[11] with the 2-substituted 4,6-dichloropyrimidines **6a, b**[12] in DMF. After column chromatography (alumina, CH_2Cl_2; R_F: **1a** 0.06, **1b** 0.48) **1a** was obtained as a white solid in 49% yield (m.p. 233–235 °C) and **1b** as a yellow solid in 65% yield (m.p. 270–272 °C). Bis(bipyridylpyrimidyl)pyridine **2** was prepared as described elsewhere.[13] The reaction of **1a** with 2.5 equivalents of $[Ru(tpy)Cl_3]$[14] in refluxing ethanol/water (1:1) proceeded smoothly giving a deep green solution, from which the green dinuclear complex $[\{Ru(tpy)\}_2(\mathbf{1a})][PF_6]_4$ **3a** precipitated upon addition of excess NH_4PF_6. The complex was chromatographed on neutral alumina eluting with 2:1 acetonitrile/toluene, and the green fraction was collected and recrystallized from acetonitrile/diethyl ether affording the pure complex **3a** in 72% yield. The complexes $[\{Ru(tpy)\}_2(\mathbf{1b})][PF_6]_4$ **3b** and $[\{Ru(tpy)\}_3(\mathbf{2})][PF_6]_6$ **4** were synthesized in an analogous fashion from refluxing ethylene glycol in the presence of *N*-ethylmorpholine. The products were purified by precipitation out of acetone solution by addition of diethyl ether followed by recrystallization from acetonitrile/toluene, affording the green complexes **3b** and **4** in 51% and 58% yield, respectively.

In the crystal structure of complex **3b**[15] (Fig. 2), the azaheterocyclic backbone of ligand **1b** is slightly distorted from planarity; the anthryl moiety is orthogonal to this main plane.

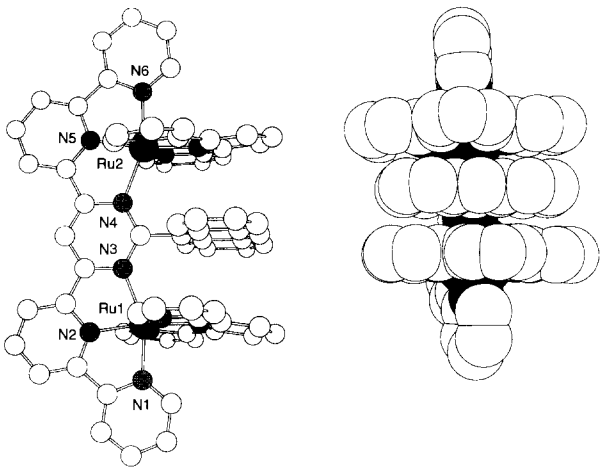


Fig. 2. Left: Ball-and-stick representation of the molecular structure of **3b** with numbered nitrogen and ruthenium sites; the hydrogen atoms, and labels for the carbon and tpy nitrogen atoms have been omitted for clarity. Selected bond lengths [Å] and angles [°]: Ru1-N1 2.067(4), Ru1-N2 2.001(5), Ru1-N3 2.151(4), Ru2-N4 2.148(4), Ru2-N5 1.980(5), Ru2-N6 2.064(4); N1-Ru1-N2 78.9(2), N1-Ru1-N3 156.7(2), N2-Ru1-N3 77.8(2), N4-Ru2-N5 78.3(2), N4-Ru2-N6 157.8(2), N5-Ru2-N6 79.5(2). Right: Space-filling model of **3b** showing van der Waals contact distances.

The ruthenium cations display octahedral coordination to three nitrogen atoms in each of the two tridentate sites of the bridging ligand and to the three nitrogen atoms of the ancillary tpy ligands. The Ru–N bond lengths are comparable with those observed in other ruthenium complexes with azaheterocyclic ligands,[16] although the Ru–N(pyrimidine) bond lengths are slightly longer in **3b**.[17] The ruthenium centers are separated by 6.404 Å, and the carbon atom (C_2) of the pyrimidine unit almost lies on the axis joining the two metal atoms (Ru1-C_2-Ru2 = 174.9°).

As observed in many metal–tpy complexes,[18] the terminal pyridine rings of both tridentate ligands in **3b** as well as those of the ancillary tpys are pulled in toward the metal atoms. The N3-Ru1-N (N atom of the middle pyridine ring in tpy) angle (110.0°) is larger than those in similar complexes,[19, 20] presumably due to the longer Ru–N(pyrimidine) bond and steric interactions between the anthryl moiety and the ancillary tpys, which are stacked at van der Waals contact distances of 3.24 to 3.40 Å.[21] A similar structure persists in solution; ROESY experiments show NOE interactions between the anthracene and tpy hydrogen atoms and inter-ring interactions along the backbone of ligand **1b** in complex **3b**. Until the crystal structure of the trinuclear complex formed by **2** can be determined, its structure may be extrapolated from that of the dinuclear complex **3b**. The schematic representation of **4** is in accord with its ^1H and ^{13}C NMR and mass spectra as well as with its electrochemical behavior.

The degree of metal–metal interaction in polynuclear complexes is highly dependent on the nature of the bridging ligands[22] and of the ancillary ligands.[23] The new complexes **3** and **4** are redox active (Table 1). In cyclic voltammetric studies

Table 1. Electrochemical data for complexes **3a**, **3b**, and **4** [a].

Complex	$E^{\circ\prime}$ (Ox) [V vs SCE]	$\Delta E^{\circ\prime}$ (Ox) [mV]	$E^{\circ\prime}$ (Red) [V vs SCE]
			−0.43 [60]
3a	+1.41 [60]	160	−1.03 [60]
	+1.57 [60]		−1.40 [b]
			−1.50 [c]
			−1.59 [c]
			−0.45 [60]
3b	+1.41 [60]	170	−1.07 [50]
	+1.58 [60]		−1.42 [b]
			−1.52 [c]
			−1.58 [c]
			−0.33 [60]
			−0.56 [60]
	+1.47 [70] [d]		−1.08 [60]
4	+1.88 [70]		−1.28 [60]
			−1.38 [b]
			−1.62 [c] [d]

[a] Recorded in acetonitrile solution; scan rate 100 mVs^{-1}; 0.1 M $TBAPF_6$. [b] Stripping peak. [c] Irreversible peak. [d] Two-electron process.

solutions of **3a** in acetonitrile undergo reversible oxidations of the Ru centers at +1.41 and +1.57 V (vs. SCE). Two ligand-based reductions at −0.43 and −1.03 V are ascribed to the sequential reductions of the bridging pyrimidine group. Reduction of the tpy ligands at −1.50 and −1.59 V leads to the adsorption of the formally neutral complex on the electrode surface, as shown by the sharp stripping peak observed at −1.40 V. The redox behavior of **3b** is similar to that observed for **3a** (Table 1), indicating that the presence of the 9-anthryl group does not significantly affect the electrochemical properties. The comproportionation constants for **3a** and **3b**, $K_c = 510$ and 750, respectively, are slightly higher than that of a dimetallic Ru complex incorporating bipyrimidine as the bridging ligand and bpy groups as ancillary ligands ($K_c = 110$).[24]

The cyclic voltammogram of the trimetallic complex **4** exhibits a two-electron oxidation at +1.47 V and a one-electron oxidation at +1.88 V, which are attributed to the terminal Ru sites and the central Ru site, respectively. Since the latter is located between two doubly charged centers, it is expected to be more difficult to oxidize. At negative potentials four one-electron processes are observed between −0.33 and −1.28 V, which are ascribed to sequential reduction of the two bridging pyrim-

 © VCH Verlagsgesellschaft mbH, D-69451 Weinheim, 1995 0570-0833/95/1010-1123 $ 10.00+.25/0

idine groups. The large wave at -1.62 V (irreversible) corresponds to adsorption of the formally neutral complex and is ascribed to the reduction of the ancillary tpys. The three Ru^{II} complexes **3a**, **3b**, and **4** have an unusual green color that may be related to both the nature of the ligand and the interaction between the metal sites.[25]

The present results demonstrate the generation of ordered rack-type metal complexes displaying rigid linear arrangements of the metal centers which may communicate through the bridging groups. Extension of these racks, modification of the bridging units (for instance replacing N by C^- sites), and generation of extended arrays of homo- and heterometallic centers will provide a range of novel linear and rigid electroactive and photoactive coordination architectures suitable for incorporation as components of inorganic supramolecular devices.

Received: December 27, 1994 [Z 7611 IE]
German version: *Angew. Chem.* **1995**, *107*, 1191

Keywords: complexes with nitrogen ligands · ruthenium compounds · self-assembly · supramolecular chemistry

[1] J.-M. Lehn, *Angew. Chem.* **1988**, *100*, 91; *Angew. Chem. Int. Ed. Engl.* **1988**, *27*, 89.
[2] J.-M. Lehn, *Angew. Chem.* **1990**, *102*, 1347; *Angew. Chem. Int. Ed. Engl.* **1990**, *29*, 1304.
[3] J.-M. Lehn, A. Rigault, *Angew. Chem.* **1988**, *100*, 1121; *Angew. Chem. Int. Ed. Engl.* **1988**, *27*, 1095.
[4] J.-M. Lehn, A. Rigault, J. Siegel, J. Harrowfield, B. Chevrier, D. Moras, *Proc. Natl. Acad. Sci. USA* **1987**, *84*, 2565.
[5] R. Krämer, J.-M. Lehn, A. DeCian, J. Fischer, *Angew. Chem.* **1993**, *105*, 764; *Angew. Chem. Int. Ed. Engl.* **1993**, *32*, 703.
[6] P. Baxter, J.-M. Lehn, A. DeCian, J. Fischer, *Angew. Chem.* **1993**, *105*, 92; *Angew. Chem. Int. Ed. Engl.* **1993**, *32*, 69.
[7] P. Baxter, J.-M. Lehn, J. Fischer, M.-T. Youinou, *Angew. Chem.* **1994**, *106*, 2432; *Angew. Chem. Int. Ed. Engl.* **1994**, *33*, 2284.
[8] V. Balzani, F. Scandola, *Supramolecular Photochemistry*, Ellis Horwood, Chichester, **1991**.
[9] All new compounds described were characterized by ^1H NMR, ^{13}C NMR, and IR spectroscopy, mass spectrometry, elemental analyses, and/or X-ray crystallographic studies.
[10] J. Solberg, K. Undheim, *Acta Chem. Scand.* **1989**, *43*, 62.
[11] Bipyridine **5** was synthesized by quenching a solution of 6-lithio-2,2'-bipyridine in THF with tributyltin chloride at -70 °C. For the analogous synthesis of 2-tributylstannylpyridine see: C. Bolm, M. Erwald, M. Felder, G. Schingloff, *Chem. Ber.* **1992**, *125*, 1169.
[12] Pyrimidine **6b** was synthesized from 9-lithioanthracene and 4,6-dichloropyrimidine in an analogous way: D. B. Harden, M. J. Mokrosz, L. Strekowski, *J. Org. Chem.* **1988**, *53*, 4137.
[13] G. S. Hanan, J.-M. Lehn, N. Kyritsakas, J. Fischer, *J. Chem. Soc. Chem. Commun.*, in press.
[14] B. P. Sullivan, J. M. Calvert, T. J. Meyer, *Inorg. Chem.* **1980**, *19*, 1404.
[15] Crystals of **3b** suitable for X-ray diffraction were grown by slow diffusion of diethyl ether into an acetonitrile/acetone solution of the complex. X-ray data for **3b**: $C_{71}H_{52}F_{24}N_{12}OP_4Ru_2$, $M = 1871.33$, green crystals, triclinic, $a = 12.446(5)$, $b = 13.236(5)$, $c = 23.046(8)$ Å, $\alpha = 102.25(2)$, $\beta = 97.87(2)$, $\gamma = 102.30(2)°$, $V = 3558(2)$ Å^3, $Z = 2$, $\rho_{calcd} = 1.747$, $\mu = 0.600$ mm^{-1}, space group $P\bar{1}$ (No. 2). 15730 Reflections were collected on a STOE IPDS instrument at 203(2) K ($\lambda = 0.71069$ Å); $2\theta_{max} = 60°$ and two unique sets of data were collected. Final $R(F) = 0.0689$. Further details of the structure investigation may be obtained from the Director of the Cambridge Crystallographic Data Centre, 12 Union Road, GB-Cambridge CB2 1EZ (UK), on quoting the full journal citation.
[16] D. P. Rillema, D. S. Jones, C. Woods, H. A. Levy, *Inorg. Chem.* **1992**, *31*, 2935.
[17] The Ru–N(pyrimidine) bond lengths found for **3b** are 2.148 and 2.151 Å; they are between 2.062 and 2.072 Å for Ru(bipyrimidine)$_3$ [16].
[18] E. C. Constable, *Adv. Inorg. Chem. Radiochem.* **1986**, *30*, 69.
[19] E. C. Constable, A. M. W. C. Thompson, *New J. Chem.* **1992**, *16*, 855.
[20] N. Gupta, N. Grover, G. A. Neyhart, P. Singh, H. H. Thorp, *Inorg. Chem.* **1993**, *32*, 310.
[21] Steric interactions are minimized by the slight bend of the central pyridine ring of the ancillary tpys away from the 9-anthryl moiety (see Fig. 2).
[22] P. J. Steel, *Coord. Chem. Rev.* **1990**, *106*, 227.
[23] G. Giuffrida, S. Campagna, *Coord. Chem. Rev.* **1994**, *135/136*, 517.
[24] D. P. Rillema, G. Allen, T. J. Meyer, D. Conrad, *Inorg. Chem.* **1983**, *22*, 1617.
[25] Absorption bands in the visible region: $\lambda_{max}(\varepsilon) = 454$ (19000), 550 (11000), 616 (11000) for **3a**; 443 (24000), 560 (15000), 617 (17000) for **3b**; 447 (43000), 539 (29000), 621 (31000) for **4** (in CH_3CN); the absorption spectra will be described in more detail elsewhere.

Synthesis of a Stable Arenesulfenic Acid Bearing a Bowl-Shaped Macrobicyclic Cyclophane Skeleton**

Kei Goto, Norihiro Tokitoh, and Renji Okazaki*

While there have been a great number of reports on functionalized macrocycles that utilize their cavities as a complexing site, far fewer studies have been carried out on the use of those well-defined microenvironments as a reaction field for a functionality fixed on its inside.[1] If a functional group is embedded in a large, shallow molecular bowl with a rigid framework (Fig. 1), the

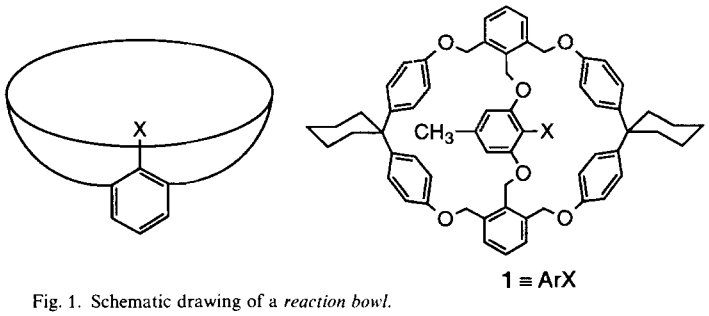


Fig. 1. Schematic drawing of a *reaction bowl*.

cavity will serve as a reaction field with unique and unprecedented properties. Such a molecule, which we refer to as a *reaction bowl*, is expected to inhibit the approach of functional groups on molecules of the same type, while not preventing different molecules from reacting with it. Thus, for example when a chemical species, which normally dimerizes readily and is therefore unstable, is introduced into the concave environment, it could be stabilized kinetically by the bowl-shaped framework without diminution of its intrinsic reactivity toward other molecules.

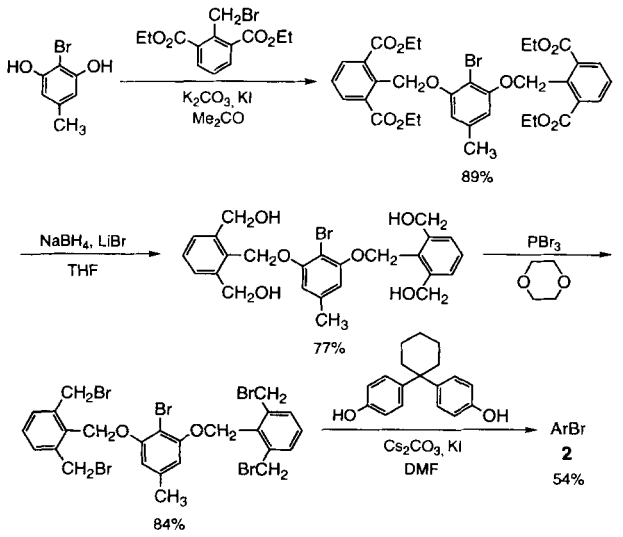
In this paper, we report the synthesis of the first kinetically stabilized arenesulfenic acid, for which we have taken advantage of a novel molecular bowl based on a macrobicyclic cyclophane skeleton. In spite of the well-known importance of sulfenic acids in organosulfur chemistry,[2–4] they have proved difficult to synthesize due to the ready self-condensation and most of the sulfenic acids isolated to date have been stabilized by their electronic properties and intramolecular hydrogen bonding,[4] which inevitably perturb the properties of the SOH group. However, a reaction bowl environment would enable us to stabilize such species without perturbing their properties and intrinsic reactivities. While two alkanesulfenic acids have been isolated by kinetic stabilization,[5] no stable arenesulfenic acid has been obtainable even with extremely bulky substituents such as 2,4,6-tri-*tert*-butylphenyl or 2,4,6-triisopropylphenyl groups.[6]

In order to embody the concept mentioned above, we designed the novel bicyclic cyclophane **1** (Fig. 1) based on an aryl benzyl ether framework,[7, 8] which we were able to synthesize readily as the bromide **2** (Scheme 1). The structure of **2** was determined by X-ray crystallography (Fig. 2).[9] The figure clearly shows that **2** is a shallow bowl-shaped molecule; its diameter is about 13 Å.

[*] Prof. Dr. R. Okazaki, Dr. K. Goto, Prof. Dr. N. Tokitoh
Department of Chemistry, Graduate School of Science
The University of Tokyo
7-3-1 Hongo, Bunkyo-ku, Tokyo 113 (Japan)
Telefax: Int. code + (3)5800-6899

[**] This work was partly supported by a Grant-in-Aid for Scientific Research (No. 06453062) from the Ministry of Education, Science and Culture, Japan. We also thank Tosoh Akzo Co., Ltd. for the generous gift of alkyllithium compounds.

 © VCH Verlagsgesellschaft mbH, D-69451 Weinheim, 1995 0570-0833/95/1010-1124 $ 10.00+.25/0



Scheme 1. Synthesis of the bromide **2**.

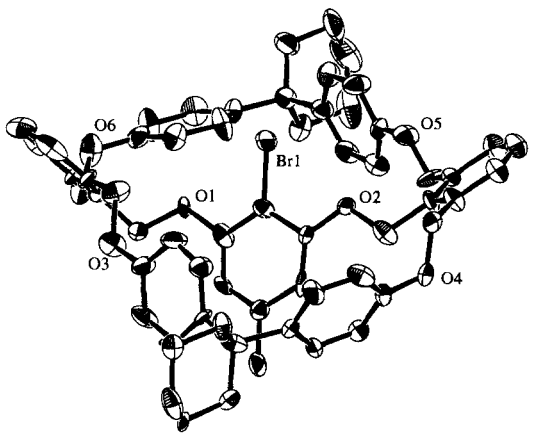
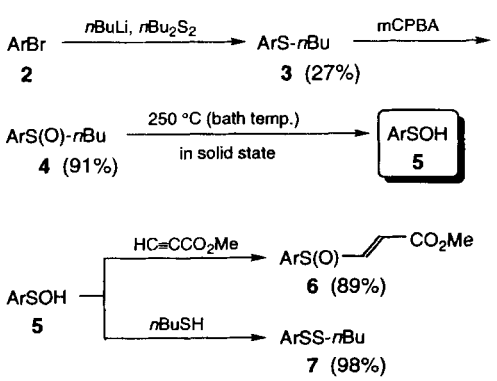


Fig. 2. ORTEP drawing of the structure of **2** with thermal ellipsoid plot (40% probability).

Lithiation of **2** with butyllithium followed by quenching with dibutyl disulfide afforded the butyl sulfide **3**, which was readily oxidized by mCPBA (mCPBA = *meta*-chloroperbenzoic acid) to give the sulfoxide **4** (Scheme 2). Its solid-state pyrolysis gave the sulfenic acid **5** as a crystalline solid (90% based on conversion of **4**). The ^{1}H NMR ($CDCl_3$) spectrum showed the signal of the hydroxyl proton at $\delta = 3.26$ (readily exchangeable with D_2O), which is very close to the reported values for the alkanesulfenic



Scheme 2. Synthesis and reactions of the sulfenic acid **5**.

acids isolated by kinetic stabilization.[10] In the IR spectrum (CH_2Cl_2) the OH stretching bands were observed at 3685 (m), 3600 (w), and 3494 (m) cm^{-1}. These spectral data are fully consistent with the formulation of **5** as a sulfenic acid. The reaction of **5** with methyl propiolate afforded the corresponding vinyl sulfoxide **6** in 89% yield (Scheme 2), which lent further confirmation to the structure of **5**. Unfortunately we have thus far been unable to obtain a crystal of **5** suitable for an X-ray study.

The sulfenic acid **5** is stable at room temperature in air for several weeks. Upon heating at 80 °C for 12 h in [D_8]toluene **5** underwent only slight decomposition, indicating its remarkable thermal stability. While the IR absorption at 3685 cm^{-1} is unambiguously assigned to a free hydroxyl group, the band at 3494 cm^{-1} suggests the intramolecular hydrogen bonding between the OH group and the oxygen atoms at the *ortho*-positions.[11] It is not likely, however, that this hydrogen bonding is responsible for the high stability of **5**, since it has been reported that hydrogen bonding with such an ether functionality alone cannot render a sulfenic acid stable enough to be isolated.[4] Thus, the noticeable stability of **5** is most reasonably explained in terms of the steric inhibition of the self-condensation by the bicyclic cyclophane skeleton, where the brim of the bowl surrounds the SOH group from all sides. Therefore, **5** can be regarded as the first kinetically stabilized arenesulfenic acid.

Oxidation of thiols to disulfides is one of the most important reactions of thiols from a biological point of view.[12] It is assumed that sulfenic acids are transient intermediates in the reaction, but the evidence is circumstantial.[13–15] The reaction of the sulfenic acid **5** with a large excess of 1-butanethiol afforded the disulfide **7** as a single product almost quantitatively (Scheme 2). This is the first conclusive demonstration of disulfide formation from the reaction of a sulfenic acid with a thiol. At the same time this result validates the concept of the reaction bowl, namely that a functional group in its inside is stabilized, yet capable of undergoing an intermolecular reaction with an appropriate molecule.

The stabilization of a sulfenic acid realized in the present study is reminiscent of the formation of stable sulfenic acid intermediates from cysteine in the active sites of some enzymes,[3] where the structural features of the environment around the SOH group are believed to prevent its self-condensation. An exploration of the wider application of this new concept is currently in progress.

Experimental Procedure

Fine powders of **4** (28.7 mg, 0.029 mmol) were loaded into a glass tube of 1 mm diameter and 80 mm long, and the tube was sealed in vacuo and soaked in an oil bath heated at 250 °C for 5 s. About one third of the sulfoxide **4** reacted and the sulfenic acid **5** was obtained in more than 90% yield (by ^{1}H NMR). Compound **5** was isolated by preparative TLC (silica gel/dichloromethane) as a crystalline solid (27%) in addition to recovered **4** (70%). **5**: colorless crystals, m.p. 174 °C (decomp.); ^{1}H NMR (500 MHz, $CDCl_3$): $\delta = 1.50$ (br. s, 4H), 1.54 (br. s, 8H), 2.14 (br. s, 8H), 2.28 (s, 3H), 3.26 (s, 1H; OH), 5.10 (s, 4H), 5.20 (s, 8H), 6.40 (s, 2H), 6.77–6.80 (m, 8H), 6.94–6.97 (m, 8H), 7.42–7.46 (m, 2H), 7.55–7.57 (m, 4H); ^{13}C NMR (125 MHz, $CDCl_3$): $\delta = 22.1$ (q), 23.0 (t; cyclohexyl), 26.5 (t; cyclohexyl), 36.6 (t; cyclohexyl), 37.4 (t; cyclohexyl), 45.7 (s), 63.9 (t), 68.9 (t), 107.8 (d), 115.0 (d), 116.2 (s; *ipso* to SOH), 128.3 (d), 129.0 (d), 129.6 (d), 131.6 (s), 138.1 (s), 141.2 (s), 141.7 (s), 156.6 (s), 156.9 (s); IR (CH_2Cl_2): $\tilde{\nu}$(OH) = 3685 (m), 3600 (w), 3494 (m) cm^{-1}.

Received: January 4, 1995 [Z 7605 IE]
German version: *Angew. Chem.* **1995**, *107*, 1202

Keywords: cyclophanes · kinetic stabilization · sulfenic acids

 © *VCH Verlagsgesellschaft mbH, D-69451 Weinheim, 1995* *0570-0833/95/1010-1125 $ 10.00+.25/0*

[1] a) U. Lüning, *Liebigs Ann. Chem.* **1987**, 949–955; b) U. Lüning, R. Baumstark, C. Wangnick, M. Müller, W. Schyja, M. Gerst, M. Gelbert, *Pure Appl. Chem.* **1993**, *65*, 527–532; c) U. Lüning, H. Baumgartner, *Synlett* **1993**, 571–572; d) U. Lüning, M. Müller, M. Gelbert, K. Peters, H. G. von Schnering, M. Keller, *Chem. Ber.* **1994**, *127*, 2297–2306, and references therein.

[2] For reviews on the chemistry of sulfenic acids see: D. R. Hogg in *The Chemistry of Sulfenic Acids and Their Derivatives* (Ed.: S. Patai), Wiley, New York, **1990**, p. 361; J. L. Kice, *Adv. Phys. Org. Chem.* **1980**, *17*, 65–181.

[3] For leading references on the biological reactions of sulfenic acids see: a) W. S. Allison, *Acc. Chem. Res.* **1976**, *9*, 293–299; b) A. Claiborne, H. Miller, D. Parsonage, R. P. Ross, *FASEB J.* **1993**, *7*, 1483–1490.

[4] F. A. Davis, L. A. Jenkins, R. L. Billmers, *J. Org. Chem.* **1986**, *51*, 1033–1040, and references therein.

[5] a) N. Nakamura, *J. Am. Chem. Soc.* **1983**, *105*, 7172–7173; b) T. Yoshimura, E. Tsukurimichi, S. Yamazaki, S. Soga, C. Shimasaki, K. Hasegawa, *J. Chem. Soc. Chem. Commun.* **1992**, 1337–1338.

[6] a) F. A. Davis, R. H. Jenkins, Jr., S. Q. A. Rizvi, S. G. Yocklovich, *J. Org. Chem.* **1981**, *46*, 3467–3474; b) F. A. Davis, S. B. Awad, R. H. Jenkins, Jr., R. L. Billmers, L. A. Jenkins, *ibid.* **1983**, *48*, 3071–3074.

[7] A related compound is described in K. Goto, N. Tokitoh, M. Goto, R. Okazaki, *Tetrahedron Lett.* **1993**, *34*, 5605–5608.

[8] Recently, Lüning et al. reported a series of bowl-type acids and bases; the intention was to improve the selectivities of those reagents by concave shielding [1]. However their cavities are too congested for the present purpose.

[9] Crystallographic data for **2**: $C_{61}H_{59}O_6Br$, $M = 968.04$, monoclinic, space group $P2_1/n$, $a = 16.35(1)$, $b = 8.141(9)$, $c = 36.20(1)$ Å, $\beta = 98.15(4)^\circ$, $V = 4769(6)$ Å^3, $Z = 4$, $\rho_{calcd} = 1.348$ g cm^{-3}, $\mu = 9.19$ cm^{-1}. The sample was placed in a glass capillary and intensity data were collected on a Rigaku AFC7R diffractometer with graphite monochromated $Mo_{K\alpha}$ radiation ($\lambda = 0.71069$ Å). The structure was solved by heavy-atom Patterson methods and expanded using Fourier techniques. The non-hydrogen atoms were refined anisotropically. The final cycle of full-matrix least-squares refinement was based on 3183 observed reflections [$I > 3.00\,\sigma(I)$] and 613 variable parameters with $R(R_w) = 0.086$ (0.058). Further details of the crystal structure investigation are available on request from the Director of the Cambridge Crystallographic Data Centre, 12 Union Road, GB-Cambridge CB21EZ (UK), on quoting the full journal citation.

[10] $\delta = 3.20$ for 9-triptycenesulfenic acid [5a] and $\delta = 3.29$ for *trans*-decalin-9-sulfenic acid [5b].

[11] The assignment of the band at 3600 cm^{-1} is not definite at present but it may possibly be attributed to an intramolecular interaction such as an OH-π interaction.

[12] a) P. C. Jocelyn, *Biochemistry of the SH Group*, Academic Press, London, **1972**, p. 94; b) G. Capozzi, G. Modena in *The Chemistry of the Thiol Group* (Ed.: S. Patai), Wiley, New York, **1974**, p. 785.

[13] For the reactions of a transient sulfenic acid with a thiol see: a) R. D. Allan, D. H. R. Barton, M. Girijavallabhan, P. G. Sammes, M. V. Taylor, *J. Chem. Soc. Perkin Trans. 1* **1973**, 1182–1187; b) F. A. Davis, R. H. Jenkins, Jr., *J. Am. Chem. Soc.* **1980**, *102*, 7967–7969.

[14] F. A. Davis, R. L. Billmers, *J. Am. Chem. Soc.* **1981**, *103*, 7016–7018.

[15] The reaction of ethanethiol with isolated 1,3,6-trimethyllumazine-7-sulfenic acid was reported without description of the conditions and the yield, although in this compound the properties of the SOH group are considered to be electronically perturbed: A. Heckel, W. Pfleiderer, *Tetrahedron Lett.* **1983**, *24*, 5047–5050.

Synthesis, Structure, and Decay of In_4Br_7**

Richard Dronskowski*

In the In/Br binary system, the phases InBr, In_5Br_7 ($\equiv InBr_{1.4}$), In_2Br_3 ($\equiv InBr_{1.5}$), $InBr_2$, and $InBr_3$ have been recently characterized by crystallographic structure determination.[1] The reduced binary indium bromides in particular are of interest to theoretical chemistry because of their relatively low chemical stability (e.g. toward air and moisture), their weak In^+-Br^- bonds, and their slight electrophilic tendency.[2]

More than 30 years ago, two independent thermoanalytical investigations had suggested the existence of an additional phase, In_4Br_7 ($\equiv InBr_{1.75}$).[3] Due to the unusual sensitivity of In_4Br_7, the first structure determination of In_4Br_7 has only now been accomplished. In_4Br_7 shows not only the typical sensitivity to air and moisture for a reduced indium bromide, but also exhibits the signs of decay due to the influence of light[4] and mechanical stress.

In_4Br_7 can be prepared quantitatively by synproportionation of a stoichiometric melt of $InBr_3$ and metallic indium, followed by slow cooling (2 °C h^{-1}) to room temperature. The nearly colorless product exhibits a slight, pale greenish-yellow tint. In the temperature gradient of 120/210 °C, single crystals appear within two months; however, these crystals tend to macroscopically grow together, thus making isolation of individual single crystals difficult due to the sensitivity of the compound to physical manipulation (see above). Nevertheless, the intensity data of an imperfectly shaped crystal (taken without exposing it to light) allowed the solution of the structure by direct methods. The following structural description is based on a Rietveld refinement of powdery, pure In_4Br_7.[5] Such a refinement is insensitive to absorption errors and problems of twinning.

At room temperature, the crystal structure of In_4Br_7 may be characterized in the trigonal space group $R\bar{3}m$, the crystal chemical formula is $(In^{3+})_3(In^+)_5(Br^-)_{14} = In_8Br_{14} = 2 \times In_4Br_7$.[6] Along the long c axis (4658 pm) are a total of five distinct coordination polyhedra stacked on top of each other. The two trivalent indium cations are found both in an approximately octahedrally shaped polyhedron, In(1), and also in an approximately tetrahedrally shaped polyhedron, In(2), coordinated through Br^- ions; the average bond lengths of $In^{3+}-Br^-$ are 267 and 247 pm, respectively.[7] Both polyhedra are already known from the structures of $InBr_3$ (octahedron) and $InBr_2$ (tetrahedron) with very similar distances of 267 and 250 pm. In comparison, the univalent indium cations exhibit very different and enlarged types of coordination polyhedra (Fig. 1), as a consequence of the special electronic configuration of In^+.[2] The In^+-Br^- bond lengths cover a typically greater range between 330–440 pm, and none of these three polyhedra has been observed up to now in the known structures of the reduced indium bromides. Simple counting of the bromide ions gives the following coordination numbers: for In(3) $3+1+6=10$, for In(4) $3+6+3=12$, and for In(5) likewise $6+6=12$. Furthermore, with aid of the recently optimized bond length–bond strength parameter ($r_0 = 266.7$ pm)[2] for the In^+-Br^- combination, the empirical valences for the different univalent indium atoms are deter-

[*] Dr. R. Dronskowski
Max-Planck-Institut für Festkörperforschung
Heisenbergstrasse 1, D-70569 Stuttgart (Germany)
Telefax: Int. code + (711)689 1010
e-mail: drons@simix.mpi-stuttgart.mpg.de

[**] My heartfelt thanks are due to Dr. Horst Borrmann and Dr. Rainer Pöttgen for their helpful assistance with the X-ray investigations. For friendly support and financial assistance with my research efforts I would also like to thank Prof. Dr. Arndt Simon.

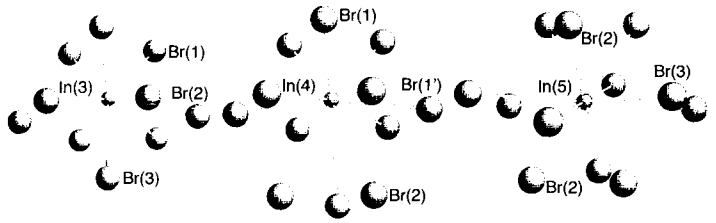


Fig. 1. Coordination of univalent indium cations in In_4Br_7. The interatomic distances [pm] are for In(3), left, 3×327.6 (−Br(1), head), 1×340.9 (−Br(3), foot), and 6×390.6 (−Br(2), waist); for In(4), middle, 3×337.6 (−Br(1), head), 6×382.0 (−Br(1'), waist), and 3×436.4 (−Br(2), foot); for In(5), right, 6×350.6 (−Br(2), head and foot) and 6×439.2 (−Br(3), waist). The standard deviations for the interatomic distances are about 0.5 pm.

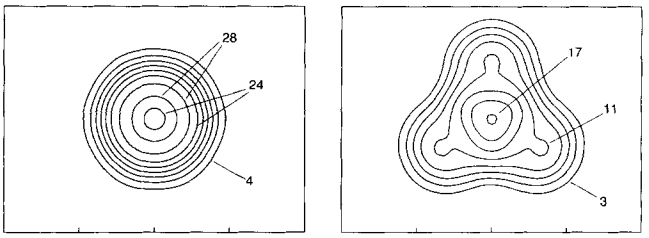


Fig. 3. Difference Fourier synthesis for In_4Br_7 at 90 K (single crystal data, $Mo_{K\alpha}$ radiation) based on the phases of the atoms In(1–4) and Br(1,2). Shown are cuts (400×300 pm^2) parallel to the *ab* plane, in the direct neighborhood of In(5), left, and Br(3), right. The contours of the electron density are given in multiples of e Å^{-3}.

mined to be 0.92, 0.74, and 0.68 for In(3), In(4), and In(5), respectively. An unusual bonding situation is already apparent from this classical description since the sums of the bond orders of the univalent indium cations are too low most noticably for In(5). Self-consistent, semiempirical calculations of the band structure[8] indeed prove that the average In^+-Br^- overlap populations are slightly lower than that of the typical In^+-Br^- interactions of +0.07[2] with values of +0.066 for In(3), +0.061 for In(4), and most significantly the value of +0.049 for the strongly reduced In(5). The shortest indium–indium interaction ($In(1)^{3+}-In(3)^+$ = 397 pm) is weakly antibonding (−0.051), which is consistent with an electrostatic interpretation.

The previously mentioned chemical and physical sensitivity of In_4Br_7 can be explained by a theoretical analysis. A calculation of atomic reactivity increments[9] makes it clear that In(5) is mainly responsible for the additionally reduced absolute electronic hardness of only 1.97 eV, compared to all other reduced indium bromides;[10] one origin for the sensitivity of this phase can thus be spatially localized in the crystal. The simple reason for this lies in the lowest lying unoccupied crystal orbital (LUCO), which is almost completely centered at the univalent In(5) ion, and which possesses $5p_{x,y}$ character (Fig. 2). The small energy gap of this LUCO from the occupied levels of the density of states leads, in connection with the weak In^+-Br^- bonding and the local symmetry $\bar{3}m$, to structural consequences:

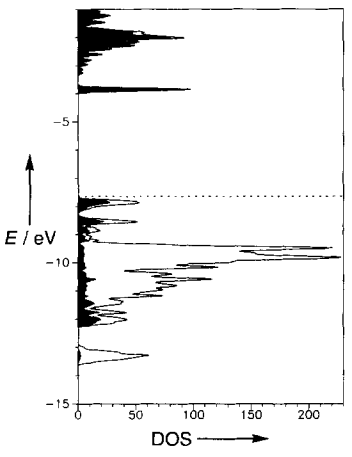


Fig. 2. Density of states (DOS) for In_4Br_7 with local projections of the univalent indium cations in black. The peak at −3.8 eV possesses nearly exclusively In(5)-$5p_{x,y}$ character.

The first low-temperature crystallographic studies prove that at 90 K In(5) is no longer found on the special position 3*a* (i.e. on the threefold rotoinversion axis), but moves away from the center of its coordination polyhedron by around 40 pm (!) (Fig. 3). As already theoretically predicted,[2] such a distortion can be easily understood as a consequence of second-order Jahn–Teller instability. This second-order effect is exactly what would be expected if the mixing of a formerly unoccupied orbital or energy band with *p*-character is possible by an atomic displacement under energy reduction. This result is achieved for In(5) at very low temperatures. Additionally, Br(3), which lies nearly in the same plane, is affected by this unprecedented structural instability of In^+ (Fig. 3).

However, a similar effect may be observed already at room temperature under different conditions. In Rietveld refinements on In_4Br_7, which continuously undergoes decay due to light and stress, and whose primary decomposition product can easily be identified and refined as $InBr_2$ (in superb agreement with the previously published data[11]), greatly enlarged displacement parameters result for In(5) and Br(3), indicating the very high mobility of these atoms in their coordination polyhedra. It is very likely that it is at this specific point that the decay of In_4Br_7 to $InBr_2$ begins through the exuding of amorphous indium. In accordance with this, an expected enhanced chemical reactivity of solid In_4Br_7 could be observed in the first attempts at reactions with likewise solid organic substances at room temperature. Currently, we are investigating these reactions which occur in just seconds or minutes.

Received: November 11, 1994 [Z 7472 IE]
German version: *Angew. Chem.* **1995**, *107*, 1230

Keywords: bromine compounds · indium compounds · Jahn–Teller distortion · solid-state structures

[1] T. Staffel, G. Meyer, *Z. Anorg. Allg. Chem.* **1987**, *552*, 113; *ibid.* **1988**, *563*, 27; H. P. Beck, *Z. Naturforsch. B* **1987**, *42*, 251; H. Bärnighausen, *Z. Kristallogr.* **1989**, *186*, 16; R. E. Marsh, G. Meyer, *Z. Anorg. Allg. Chem.* **1990**, *582*, 128.

[2] R. Dronskowski, *Inorg. Chem.* **1994**, *33*, 6201.

[3] P. H. L. Walter, J. Kleinberg, E. Griswold, *J. Inorg. Nucl. Chem.* **1961**, *19*, 223; W. Morawietz, H. Morawietz, G. Brauer, *Z. Anorg. Allg. Chem.* **1962**, *316*, 220.

[4] Also the yellow low-temperature modification of the related phase InCl decomposes under light: W. Klemm, *Z. Anorg. Chem.* **1926**, *152*, 262.

[5] X-ray diffraction at room temperature was performed on a calibrated STOE powder diffractometer (0.3 mm capillary; $Cu_{K\alpha 1}$ radiation; $10.00 \le 2\theta \le 89.90°$; step rate 0.02°); Rietveld refinement carried out with the program DBW9006 (School of Physics, Georgia Institute of Technology, Atlanta, GA 30322, USA) and a pseudo-Voigt profile function (1 instrumental parameter, 5 profile parameters, 1 parameter for preferred orientation, 1 asymmetry parameter, 1 overall scale parameter, 2 parameters for the lattice constants, 8 positional parameters, 3 isotropic displacement parameters, and atomic form factors of the neutral atoms). The residual values and the goodness of fit are $R_p = 0.033$, $R_{wp} = 0.042$, $R_{Bragg}(I) = 0.057$ and GooF = 0.76 for 283 Bragg reflections (3996 data points) and 22 variable parameters. Further details of the crystal structure investigation may be obtained from the Fachinformationszentrum Karlsruhe, D-76344 Eggenstein-Leopoldshafen (Germany) on quoting the depository number CSD-401451.

[6] The lattice constants are $a = 757.75(2)$ and $c = 4657.7(2)$ pm, the obtained positions (oxidation numbers as superscripts) in space group $R\bar{3}m$ (No. 166) are $In(1)^{3+}$ in 3*b*; $In(2)^{3+}$ in 6*c* with $z = 0.7100(1)$; $In(3)^+$ in 6*c* with $z = 0.4148(1)$; $In(4)^+$ in 6*c* with $z = 0.1443(1)$; $In(5)^+$ in 3*a*; $Br(1)^-$ in 18*h* with $x = 0.1665(5)$, $z = 0.4672(1)$; $Br(2)^-$ in 18*h* with $x = 0.5120(4)$, $z = 0.3947(1)$; $Br(3)^-$ in 6*c* with $z = 0.6584(1)$. The isotropic displacement parameter *B* amounts to 1.3(1), 3.0(1), and 2.94(8) Å^2 for In^{3+}, In^+, and Br^-, respectively.

 © VCH Verlagsgesellschaft mbH, D-69451 Weinheim, 1995 0570-0833/95/1010-1127 $ 10.00+.25/0

[7] The individual interatomic distances [pm] are 6 × 266.6 (– Br(1)) for In(1) and 1 × 240.3 (– Br(3)) and 3 × 249.0 (– Br(2)) for In(2), with standard deviations of approximately 0.5 pm.

[8] The three-dimensional band structure calculations were performed with the help of a charge self-consistent extended Hückel–Hamiltonian and a weighted WH-approximation following in all particulars (basis sets, start and iteration parameters) as stated in its entirety in ref. [2]. The diagonalization was done at 48 *k* points within the irreducible part of the trigonal Brillouin zone with the help of a modified EHMACC program. Self-consistency was reached after 22 cycles.

[9] Atomic reactivity increments as well as increments of electrophilicity and nucleophilicity can be computed for any structures (molecules, crystals) through a mathematical decomposition of the absolute electronic hardness [10]. The technique is based on a partitioning of the total energy into atomic contributions: R. Dronskowski, *J. Am. Chem. Soc.* **1992**, *114*, 7230.

[10] The absolute electronic hardness is a quantitative measure of the electronic resistance of a system (molecule, crystal) against outer chemical perturbation (attack of a reaction partner): R. G. Parr, R. G. Pearson, *J. Am. Chem. Soc.* **1983**, *105*, 7512.

Miller, R.J.D. (ed.)

Surface Electron Transfer Processes

1995. XII, 368 pages
with 137 figures and 3 tables.
Hardcover. DM 128.00.
ISBN 1-56081-036-X
(VCH, New York)

This book gives an extensive theoretical treatment of its theme. The emphasis is on electronic coupling of molecular potentials to conducting band states. The essential role of surface electron transfer in catalysis, electrochemistry, photo imaging, and virtually all charge transfer solid state devices make this process one of the most important single chemical events.

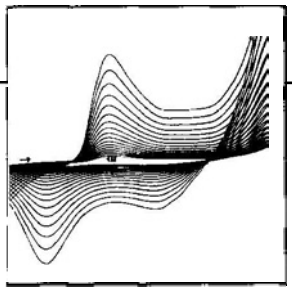
Sandifer, J. R.

Ion-Transfer Kinetics

1995. X, 142 pages with
38 figures and 16 tables.
Hardcover. DM 165.00.
ISBN 1-56081-508-6
(VCH, New York)

In six concise, well-referenced chapters, this book covers the essentials of ion-transfer principles and applications, including computer simulation techniques for ion-transfer kinetics models.

It is addressed to chemists in academia and industry, to physical chemists and to chemical engineers.



ELECTRO CHEMISTRY

To order please contact your bookseller or:

VCH, P.O. Box 10 11 61,
D-69451 Weinheim,
Telefax (0) 62 01 - 60 61 84

VCH, Hardstrasse 10, P.O. Box,
CH-4020 Basel

VCH, 8 Wellington Court,
Cambridge CB1 1HZ, UK

VCH, 303 N.W. 12th Avenue,
Deerfield Beach, FL 33442-1788, USA
toll-free: 1-800-367-8249
or fax: 1-800-367-8247

VCH, Eikow Building,
10-9 Hongo 1-chome, Bunkyo-ku,
Tokyo 113, Japan

VCH

 © VCH Verlagsgesellschaft mbH, D-69451 Weinheim, 1995 0570-0833/95/1010-1128 $ 10.00+.25/0

Mechanistic Heyday

The Adventure Playground of Mechanisms and Novel Reactions. (Series: Profiles, Pathways, and Dreams. Series editor: *J. I. Seeman.*) By *R. Huisgen.* American Chemical Society, Washington, 1994. 279 pp., hardcover $ 24.95.—ISBN 0-8412-1832-3

This book is one of a series in which chemists who have had an important influence on chemistry during the postwar years look back over their life's work; 22 have contributed to the series so far. For each of these authors the award of a Nobel Prize (if that had not occurred already) would come as no surprise to the scientific world. Remarkably, the list includes only one German chemist, Rolf Huisgen. This book therefore has a special importance, since it was Huisgen above all others who, through his fundamental work on reaction mechanisms which gained worldwide recognition, played a decisive role in establishing the high standing of German chemistry in the immediate postwar period.

One approaches the book with curiosity to discover which aspects of Huisgen's research he regards in retrospect as the most important and elaborates on. There are the classical studies which established arynes as important reactive intermediates. Then there are the chapters on azoles, azides, and azomethynimines, work which pointed the way to studies of 1,3-dipolar cycloadditions. At the time when the concept of the conservation of orbital symmetry in pericyclic reactions was being developed by Havinga and Oosterhoff and by Woodward and Hoffmann, it had scarcely been formulated when Huisgen tested it in the field of electrocyclic reactions applied to cyclooctatrienes, aziridines, and many other substrates. This is followed by chapters on [2+2]-cycloadditions, mainly applied to ketenes and to donor- and acceptor-substituted alkenes. Equally interesting is the insight into the beginnings of Huisgen's research, which was in the area of azo and diazo compounds and prepared the way for mechanistic studies in free radical chemistry. Of all the work described, only that in the chapter on effects in medium-sized rings no longer seems to find an echo in present-day research topics, but here too, as in all the rest of the chapters, we find physical organic chemistry in its purest form. The skillful exploitation of the physical properties of compounds to facilitate their analysis, and the masterly way in which kinetic studies are used to analyze reaction mechanisms, are hallmarks of Huisgen's research which stand out very clearly in this book. From Husigen's school there emerged a whole generation of German university teachers, and their contributions during that period are impressively described here. No less than thirteen of Huisgen's students hold, or have held, professorial chairs in German universities. This contribution that the researches summarized in this book have made to the intellectual standing now enjoyed by organic chemistry in the universities of the Federal Republic cannot be overstated.

The book is literally a historic document of the history of the period concerned. On the one hand Huisgen documents, in his characteristically perfectionist style, the milestones of his research career, and evaluates their significance in the context of the state of knowledge and the ideas of other research groups at that time. On the other hand the book also describes the heyday of mechanistic organic chemistry in Germany, before it was superseded by other lines of research. How quickly time has passed on can be seen from the way in which present-day textbooks treat arynes and 1,3-dipolar cycloadditions, citing well-established principles and giving just one or two representative examples. Huisgen's book describes the considerable intellectual and experimental efforts that were originally needed to arrive at these clear and unambiguous statements.

Nevertheless, after reading this book one's curiosity remains unsatisfied in some respects. What was the information that led to a start being made on a new area of study? What key development prompted the thoughts that eventually parted the fog and led to a clear understanding of a particular reaction mechanism? If these insights emerged from each chapter the book would give us a clearer understanding of Rolf Huisgen's enquiring mind. But Huisgen concentrates so much on thoroughly analyzing a problem and presenting the result in a polished form that the researcher himself, learning from the lessons of false trails as the work proceeds, remains hidden, despite the inclusion of many of the author's personal experiences. One hardly expects anecdotes about a scientist of these qualities—although, on the other hand, perhaps there ought to be some for that very reason.

The book is well worth reading, not only for those who have lived through the period described and wish to be reminded of the adventures in the "playground of mechanisms and novel reactions". It is equally important that it should be read by those who wish to gain a brief insight, through these examples, into how results that now belong to the established canon of knowledge in organic chemistry were arrived at. Furthermore, since there is now a renewal of interest in the study of reaction mechanisms, this book has an important function in showing where the connections to the past are to be made.

Reinhard W. Hoffmann
Fachbereich Chemie
der Universität Marburg (FRG)

This section contains book reviews and a list of new books received by the editor. Book reviews are written by invitation from the editor. Suggestions for books to be reviewed and for book reviewers are welcome. Publishers should send brochures or (better) books to Dr. Ralf Baumann, Redaktion Angewandte Chemie, Postfach 101161, D-69451 Weinheim, Federal Republic of Germany. The editor reserves the right of selecting which books will be reviewed. Uninvited books not chosen for review will not be returned.

 © *VCH Verlagsgesellschaft mbH, D-69451 Weinheim, 1995* *0570-0833/95/1010-1129 $ 10.00+.25/0*

Stereospecific Olefin Polymerization with Chiral Metallocene Catalysts

Hans H. Brintzinger,* David Fischer, Rolf Mülhaupt, Bernhard Rieger, and Robert M. Waymouth

Dedicated to all those excellent graduate students who are the true heroes of this story

Current studies on novel, metallocene-based catalysts for the polymerization of α-olefins have far-reaching implications for the development of new materials as well as for the understanding of basic reaction mechanisms responsible for the growth of a polymer chain at a catalyst center and the control of its stereoregularity. In contrast to heterogeneous Ziegler–Natta catalysts, polymerization by a homogeneous, metallocene-based catalyst occurs principally at a single type of metal center with a defined coordination environment. This makes it possible to correlate metallocene structures with polymer properties such as molecular weight, stereochemical microstructure, crystallization behavior, and mechanical properties. Homogeneous catalyst systems now afford efficient control of regio- and stereoregularities, molecular weights and molecular weight distributions, and comonomer incorporation. By providing a means for the homo- and copolymerization of cyclic olefins, the cyclopolymerization of dienes, and access even to functionalized polyolefins, these catalysts greatly expand the range and versatility of technically feasible types of polyolefin materials.

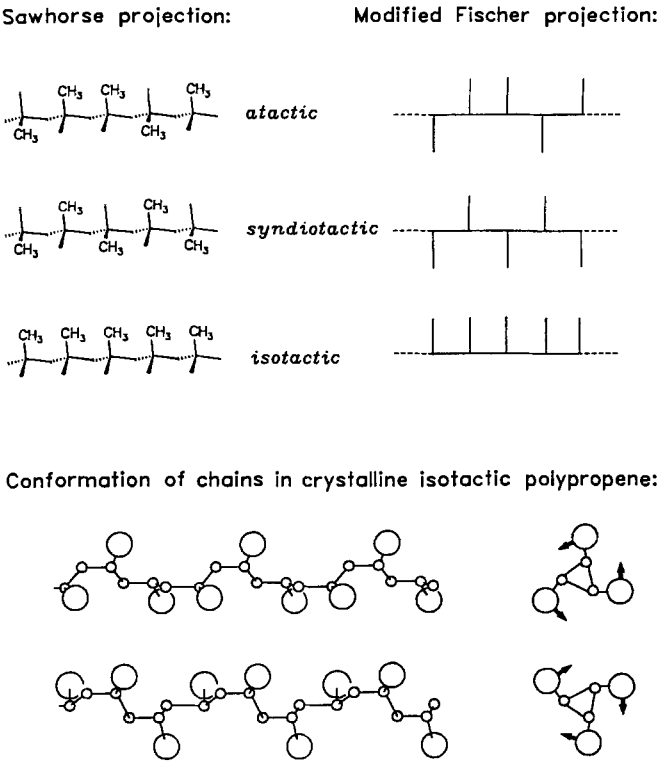
Keywords: alkenes · catalysis · metallocenes · polymerizations

1. Introduction

Forty years after Karl Ziegler's invention of transition metal catalyzed polyinsertion and Giulio Natta's discovery of the stereoselective polymerization of α-olefins,[1–4] we are witnessing the evolution of new generations of catalysts and polyolefin materials, which originate from studies on homogeneous, metallocene-based polymerization catalysts. In the following, we will attempt to review some of these recent developments.[5–7]

Research on metallocene-catalyzed olefin polymerization has derived much of its impetus from the desire to model the reaction mechanisms of heterogeneous polymerization catalysts. In the evolution of Ziegler–Natta catalysis, an empirical approach has proven highly successful. Modern $MgCl_2$-supported catalysts have tremendous activities for the production of polypropene and other polyolefins; at the same time, they are

[*] Prof. Dr. H. H. Brintzinger
Fakultät für Chemie der Universität
D-78434 Konstanz (Germany)
Telefax: Int. code +(7531) 883137
Dr. D. Fischer
BASF AG, Abteilung ZKP
Ludwigshafen (Germany)
Prof. Dr. R. Mülhaupt
Institut für Makromolekulare Chemie der Universität Freiburg (Germany)
Dr. B. Rieger
Institut für Anorganische Chemie der Universität Tübingen (Germany)
Prof. Dr. R. M. Waymouth
Department of Chemistry, Stanford University (USA)



Scheme 1. Structure of isotactic, syndiotactic, and atactic polypropene in sawhorse and modified Fischer projections [107] (top), and conformation of the chains in crystalline isotactic polypropene, determined by Natta and Corradini [2] (bottom).

 © *VCH Verlagsgesellschaft mbH, D-69451 Weinheim, 1995* *0570-0833/95/1111-1143 $ 10.00+.25/0*

highly stereoselective, forming practically only the isotactic, most useful stereoisomer of the polymer[8] (Scheme 1). Still unsatisfactory, however, is our understanding of the reaction mechanisms that are the basis of this advanced catalyst technology. Plausible hypotheses concerning these mechanisms have certainly been advanced, most notably Cossee's model of polymer chain growth by *cis*-insertion of α-olefins into a Ti–C bond on the surface of crystalline $TiCl_3$.[9, 10] Based on Natta's early ideas about the role of chiral surface sites in the formation of isotactic polyolefins,[6, 11] very adequate models were proposed to explain the induction of stereoregular polymer growth by the chiral environment of the catalyst centers[9b, 12] (Scheme 2).

The relationship between the properties of a particular catalyst and the coordination geometry of its reaction centers, however, leaves many questions open,[8g, h] due to the notorious nonuniformity of active sites in these heterogeneous catalysts and the limited experimental access to their structural details. In a review written in 1980, Pino and Mülhaupt summarized this shortcoming:[4b] "Up to now, there is no direct proof for the structures proposed; most of them are the result of speculations or derived from indirect experimental indications."

In this situation, related developments in other fields of catalysis nourished the hope that homogeneous organometallic catalysts capable of stereoselective olefin polymerization might eventually allow more direct observations on the catalyst species



H.-H. Brintzinger



D. Fischer



R. Mülhaupt



B. Rieger



R. M. Waymouth

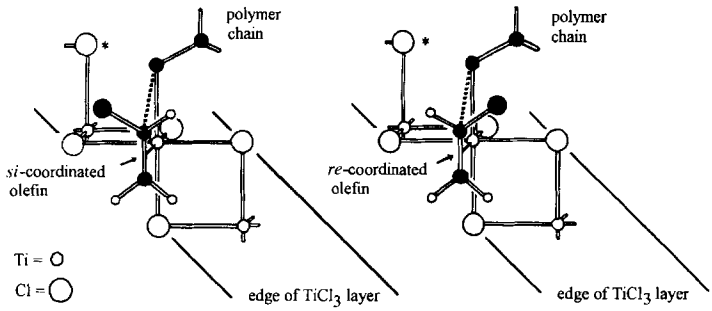
Hans-Herbert Brintzinger, born in Jena, Germany, in 1935, studied chemistry in Basel, where he received his Ph.D. in 1960 with Hans Erlenmeyer and his Habilitation in 1964. After teaching chemistry at the University of Michigan for several years, he moved to the University of Constance in 1972, where he holds a professorship for General Chemistry and Coordination Chemistry. His fields of interest are organometallic chemistry and reaction mechanisms in homogeneous catalysis.

David Fischer, born 1963 in Cologne, Germany, studied chemistry at the University of Cologne. After earning his diploma in physical chemistry, he joined Rolf Mülhaupt's group at the University of Freiburg as a graduate student. He received his Ph.D. in 1992 for studies on propene polymerization with homogeneous zirconocene catalysts. After a postdoctoral period with Robert Waymouth at Stanford, he joined the plastics laboratory of BASF AG in 1993, where he is still working on stereospecific propene polymerization with metallocene catalysts.

Rolf Mülhaupt was born in Waldshut-Tiengen, Germany, in 1954. From 1973 to 1978 he studied chemistry in Freiburg; he received his Ph.D. in 1981 with Professor Pino at the Laboratory for Technical Chemistry at the ETH in Zürich. Following industrial research positions at the Central Research and Development Experimental Station of Dupont in Wilmington, Delaware, from 1981 to 1985 and at Ciby-Geigy AG in Marly, Switzerland, from 1985 to 1989, he was appointed professor of Macromolecular Chemistry at the University of Freiburg in 1989. Since 1992 he has been director of the Material Research Center in Freiburg. His research interests include, besides transition metal catalyzed polymerization, new polymer structural materials, material compounds, dispersions and specialty polymers.

Bernhard Rieger was born in Augsburg, Germany, in 1959. He studied chemistry at the University of Munich and received his Ph.D. in 1988 for studies on enantioselective hydrogenations with rhodium–phosphane catalysts. After research appointments at the Institute for Polymer Science and Engineering of the University of Massachusetts at Amherst and in the plastics laboratory of BASF AG, he received his Habilitation in 1995 at the University of Tübingen, where he presently holds a faculty position in chemistry.

Robert M. Waymouth was born in Warner Robins, Georgia (USA), in 1960. He received bachelor's degrees in mathematics and chemistry at Washington and Lee University and his Ph.D. from California Institute of Technology in 1987, where he worked with Professor R. Grubbs. Following a year's postdoctoral appointment at the ETH in Switzerland with Professor Pino, he joined the faculty at Stanford in 1988, where he is now an Associate Professor of Chemistry. His research interests are in stereoselective catalysis.



Scheme 2. Model for the stereospecific polymerization of propene at a chiral Ti center on the edge of a $TiCl_3$ crystal, as proposed by Corradini and co-workers [12b]. The growing polymer chain occupies the open sector of the chiral coordination sphere; the olefin adopts that enantiofacial orientation which places the olefin substituent *trans* to the polymer chain at the incipient C–C bond (left); a *cis* orientation of olefin substituent and polymer chain is disfavored (right).

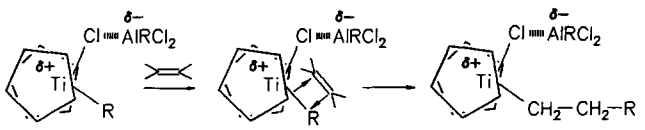
involved and, hence, on the mechanisms of polymer growth and its stereochemical control.[13] This sentiment was expressed, for example, by Boor in the concluding chapter of his book on Ziegler–Natta catalysts.[3c]

Particularly attractive as model systems of this kind appeared alkylaluminum-activated metallocene complexes of the Group 4 transition metals, which have been known since 1955 to catalyze the polymerization of ethene[14, 15] and have since been the topic of many studies. The simple coordination geometry of Group 4 metallocene complexes—only two reactive, *cis*-positioned ligand sites—promised opportunities for identifying and characterizing essential intermediates of homogeneous polymerization catalysts and providing more direct experimental verification for some of the hypotheses in the field of Ziegler–Natta catalysis.

2. Activation of Metallocene Halides for α-Olefin Polymerization

In 1957, patents and publications by Breslow and Newburg[14] at the Hercules Research Center and by Natta, Pino, and their co-workers[15] reported that homogeneous reaction mixtures of dicyclopentadienyltitanium dichoride (Cp_2TiCl_2) and diethylaluminum chloride (Et_2AlCl) catalyze the formation of polyethene under conditions similar to those used with heterogeneous Ziegler catalysts. Numerous subsequent studies were aimed at the identification of reaction intermediates and reaction mechanisms of this homogeneous catalysis. The results obtained have been summarized previously;[4a, b, 16] some are particularly noteworthy in the context of the following discussion.

Formation of (alkyl)titanocene complexes Cp_2TiRCl (R = Me or Et) by ligand exchange with the alkylaluminum cocatalyst, polarization of the Cp_2Ti–Cl bond by Lewis-acidic aluminum centers in an adduct of the type $Cp_2Ti(R)$–$Cl \cdot AlRCl_2$, and insertion of the olefin into the Cp_2Ti–R bond of this (or some closely related) electron-deficient species, had been deduced by 1960 from spectroscopic, kinetic, and isotope labeling studies done at the Hercules laboratories by Breslow, Newburg, and Long and by Chien[17, 18] (Scheme 3). These early metallocene studies contributed to the ideas put forth by Cossee[9a] with regard to the mechanisms of heterogeneous Ziegler–Natta catalysis.



Scheme 3. Polymerization of ethene by *cis*-insertion into the Ti–C bond of an alkylaluminum halide activated titanocene complex, as proposed by Breslow, Newburg, and Long [17].

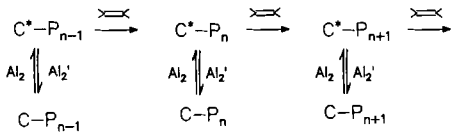
2.1. Metallocene Cations in the Polymerization of Ethene

An interesting question remained unresolved by this early research: does olefin insertion occur in a bimetallic species, in which an alkyl group or a halogen bridges the titanium and aluminum centers, as advocated by Natta and his group,[19] by Patat and Sinn,[20] by Reichert and co-workers,[21] and by Henrici-Olivé and Olivé?[22] Or does it require the formation of a truly ionic species $[Cp_2TiR]^+$ by abstraction of a halide anion and its incorporation into an anion $R_xCl_{4-x}Al^-$, as proposed by Shilov, Dyachkovskii, and Shilova?[23]

Crystal structures of complexes that were occasionally isolated from reaction mixtures containing Cp_2TiCl_2 and an alkylaluminum chloride[24, 25] were not conclusive in this regard, as they represented degradation products, which require either reoxidation[17] or renewed alkyl exchange with alkylaluminum cocatalysts[4a] for reactivation. In 1986, however, Jordan and co-workers isolated the tetraphenylborate salts of cations such as $[Cp_2ZrCH_3 \cdot THF]^+$ and $[Cp_2ZrCH_2Ph \cdot THF]^+$ and demonstrated their capability to polymerize ethene without addition of any activator.[26] These and related findings in the groups of Bochmann,[27] Teuben,[28] and Taube[29] and by Hlatky and Turner at Exxon[30] lent general credence to the proposal that (alkyl)metallocene cations are crucial intermediates in homogeneous polymerization catalysis.

A useful concept for the description of alkylaluminum-activated metallocene catalyst systems goes back to kinetic studies in Reichert's group.[21] During the growth of a polymer chain, each metal–polymer species appears to alternate between a "dormant" state and a state in which it actively grows. This "intermittent-growth" model was further elaborated by Fink[31] and by Eisch[32] and their co-workers in extensive kinetic and reactivity studies. Consecutive equilibria appear to convert alkylaluminum and (alkyl)metallocene halides first into Lewis acid–base adducts equivalent to inner (or contact) ion pairs and then into dissociated (or separated) ion pairs. In these highly dynamic equilibria, only the cation of a separated ion pair appears to be capable of interacting with an olefin substrate and, hence, of contributing to polymer growth.[33] Contact ion pairs, which appear to dominate in these equilibria, can then be termed "dormant" in this regard[34, 35] (Scheme 4).

This model would explain the inability of metallocenes activated by alkylaluminum halides to catalyze the polymerization of propene and higher olefins[4a, 36] by the insufficient capability of the more weakly coordinating, substituted α-olefins to form



Scheme 4. "Intermittent-growth" model involving equilibria between polymer-bearing, but inactive primary complexes (C–P$_n$) and active catalyst species (C*–P$_n$), generated by excess alkylaluminum halide, as proposed by Fink and co-workers [31]. $Al_2 = (AlEtCl_2)_2$, $Al_2' =$ unknown, $P_n =$ polymer chain with n monomer units; C–P$_n$ here $Cp_2TiP_nCl \cdots AlCl_2Et$.

reactive, olefin-separated ion pairs by displacement of an aluminate anion from the metal center. At any rate, the limitation of homogeneous catalyst systems to the polymerization of only ethene was a crucial obstacle for progress in this field for many years. Fortunately, this impediment was overcome by a series of serendipitous observations,[37–39] which led, around 1980, to the discovery by Kaminsky, Sinn, and co-workers that metallocenes are activated for the catalytic polymerization of propene and higher olefins by methyl aluminoxanes.[4a, 39]

2.2. Polymerization of Propene and Higher Olefins

Water, which had long been considered to be a "poison" for Ziegler–Natta catalysts, was first reported by Reichert and Meyer to cause a surprising increase in the rate of ethene polymerization by the catalyst system $Cp_2TiEtCl/AlEtCl_2$.[37] Subsequent studies by Long and Breslow on the effects of water in the otherwise inactive system Cp_2TiCl_2/Me_2AlCl led to the notion that formation of a dimeric aluminoxane, ClMeAl–O–AlClMe, by partial hydrolysis of Me_2AlCl might generate an exceptionally strong Lewis acid and, hence, a potent activator for $Cp_2TiMeCl$ toward ethene polymerization.[38]

While studying halogen-free systems such as $Cp_2ZrMe_2/AlMe_3$, Sinn and Kaminsky noticed that addition of water imparts to this otherwise inactive reaction system a surprisingly high activity for ethene polymerization which was, furthermore, unprecedentedly constant over extended reaction times.[39a, b] Sinn and Kaminsky observed that an interaction between Cp_2ZrMe_2 and $AlMe_3$ occurred only when water had been added. The suspected formation of methyl aluminoxane (MAO) by partial hydrolysis of $AlMe_3$ was subsequently supported by its direct synthesis and characterization as a mixture of oligomers of approximate composition $(MeAlO)_n$. Activation of Cp_2ZrMe_2 and Cp_2ZrCl_2 with preformed MAO did indeed yield exceedingly active catalysts for the polymerization of ethene.[39b] Similar activities were obtained with MAO-activated Cp_2TiCl_2; however, at temperatures above 0 °C this catalyst system is rapidly deactivated, most likely by reduction to the Ti^{III} stage.[40]

Sinn, Kaminsky, and co-workers noticed furthermore that MAO-activated homogeneous metallocene catalysts were—in contrast to previously studied metallocene catalysts activated by aluminum halides—capable of polymerizing propene and higher olefins.[4a, 39c–g] Although the achiral metallocene catalysts were still lacking the stereoselectivity of heterogeneous Ziegler–Natta systems, aluminoxane-activated metallocene catalysts now came to be most promising as model systems.

While oligomeric alkyl aluminoxanes have been known for more than 30 years, for example as initiators for the polymerization of oxiranes,[41] their exact composition and structure are still not entirely clear. When the hydrolysis of $AlMe_3$, which is highly exothermic (and indeed potentially dangerous[39j, 42b]), is conducted under controlled conditions, it appears to generate mostly oligomers $Me_2Al–[O-AlMe]_n–OAlMe_2$ with $n \approx 5–20$.[39j]

Investigations in quite a number of research groups by cryoscopy, UV, vibrational and NMR spectroscopy, chromatography, and other means[38, 39j, 42–50c] yield the following picture for aluminoxane solutions. Residual $AlMe_3$ in MAO solutions[42b, 43] seems to participate in equilibria that interconvert different MAO oligomers[42b, 43–46] and possibly also cyclic and branched oligomers.[39e–j, 46] Cross-linking by methyl-free oxoaluminum centers has been proposed to generate a microphase with an Al_xO_y core.[47] Aluminoxane clusters $[RAl(\mu_3\text{-}O])_n$, with R = *tert*-butyl and $n = 4$, 6, or 9, have been isolated and structurally characterized by Barron and his group.[48a] Complexes with four-coordinate Al centers seem to predominate in MAO solutions[48a, 49] and might contain intramolecular $Al_2O \rightarrow Al$ or $Al–CH_3 \rightarrow Al$ bridges.[42b] The presence of three-coordinate Al centers in MAO solutions has been deduced by Siedle and co-workers from ^{27}Al NMR data.[50b, c] While species of exceptional Lewis acidity are certainly present in MAO solutions, their exact composition and structure is still not adequately understood.[51]

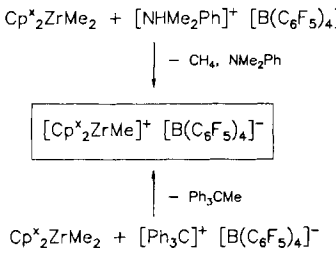
When toluene solutions of Cp_2ZrCl_2 are treated with MAO, a fast, initial ligand exchange reaction generates primarily the monomethyl complex $Cp_2ZrMeCl$;[39i, 44b] excess MAO leads to Cp_2ZrMe_2.[39i] These systems become catalytically active when the concentration of excess MAO is raised to Al:Zr ratios of about 200:1 or higher.[39] The ways in which excess MAO induces this activity have been investigated largely by spectroscopic methods.[39i, 50–52, 53a] It is generally assumed that some of the Al centers in MAO have an exceptionally high propensity to abstract a CH_3^- ion from Cp_2ZrMe_2 and to sequester it in a weakly coordinating ion $CH_3–MAO^-$. A fast, reversible transfer of $^{13}CH_3$ groups from Cp_2ZrMe_2 to the Al centers of a MAO activator was observed by Siedle et al.[50b, c] Barron and coworkers[48b] obtained NMR spectroscopic evidence that Cp_2ZrMe_2 and alumoxane clusters like $(\mu_3\text{-}O)_6Al_6tBu_6$ form complexes of the type $[Cp_2ZrMe^+ \cdots (\mu_3\text{-}O)_6Al_6(tBu)_6Me^-]$ in $[D_8]$toluene solution, which polymerize ethene. The tendency of four-coordinate Al centers in these aluminoxane clusters to abstract a methyl anion is ascribed by these authors to the relief of ring strain upon formation of the methyl complex.

^{91}Zr and ^{13}C NMR spectra of Cp_2ZrMe_2/MAO solutions[50b, c] and solid-state XPS[52] and ^{13}C NMR[53a] studies indicate formation of a cation $[Cp_2ZrR]^+$, which is most likely stabilized by coordinative contact with its $CH_3–MAO^-$ counterion, for example through bonding like that in $Al_2O \rightarrow Zr$ or $Al–CH_3 \rightarrow Zr$. These contacts appear to give way, in the presence even of substituted olefins, to olefin-separated ion pairs $[Cp_2ZrR(olefin)]^+ CH_3–MAO^-$, the presumed prerequisite for olefin insertion into the Zr–R bond. This hypothesis—that the unusually low coordinating capability of the anion A^- in the ion pair $[Cp_2ZrMe]^+ A^-$ is crucial for catalytic activity[50e]—led to the discovery of a series of highly active cationic metallocene

catalysts for the polymerization of propene and higher α-olefins.

Even for large, weakly coordinating anions such as $(C_6H_5)_4B^-$ and $C_2B_9H_{12}^-$ fairly strong interactions have been observed with cationic (alkyl)zirconocene species.[30, 53b, 58a] Reaction systems containing $[Cp_2ZrMe]^+$ together with $(C_6H_5)_4B^-$, $C_2B_9H_{12}^-$, or other carborane anions thus polymerize propene only at low rates, if at all.[26f, g, j, 27–30]

A breakthrough in this regard was the introduction of perfluorinated tetraphenylborate as a counterion by Hlatky and Turner[54] and by Marks and co-workers.[53b] An ion pair $[Cp^x_2ZrMe]^+(C_6F_5)_4B^-$ (where Cp^x is some substituted Cp or indenyl ligand) is formed by reaction of $Cp^x_2ZrMe_2$ with dimethylanilinium tetrakis(perfluorophenyl)borate or by abstraction of CH_3^- from a (dimethyl)zirconocene complex by trityl tetrakis(perfluorophenyl)borate[55, 56] (Scheme 5). These were the first well-defined zirconocene catalysts capable of polymerizing propene and higher olefins at high rates without addition of a further activator. Similar activities for propene polymerization were subsequently observed also with other base-free or weakly stabilized[53, 57, 58] (alkyl)metallocene cations. Cations obtained by abstraction of CH_3^- from a (dimethyl)zirconocene complex by the powerful Lewis acid $B(C_6F_5)_3$ were likewise found to be highly active catalysts for α-olefin polymerization.[59, 60]



Scheme 5. Alternative ways to generate a propene-polymerizing (alkyl)zirconocene cation (associated with the weakly coordinating $B(C_6F_5)_4^-$ anion) as reported by Hlatky, Upton, and Turner [54], by Marks and co-workers [53b], by Ewen and Elder [55], and by Chien and co-workers [56]. Cp^x represents a variety of substituted and/or bridged cyclopentadienyl and indenyl ligands (see Section 3.1).

Crystal structures obtained by Marks and co-workers,[60] for example that of $[(Me_2C_5H_3)_2ZrCH_3^+ \cdots H_3C-B(C_6F_5)_3^-]$, reveal residual coordinative contacts between the cationic Zr center and its counterion (Fig. 1). This contact appears to resemble those yet unidentified interactions that stabilize an (alkyl)-metallocene cation in contact with a H_3C-MAO^- counterion.

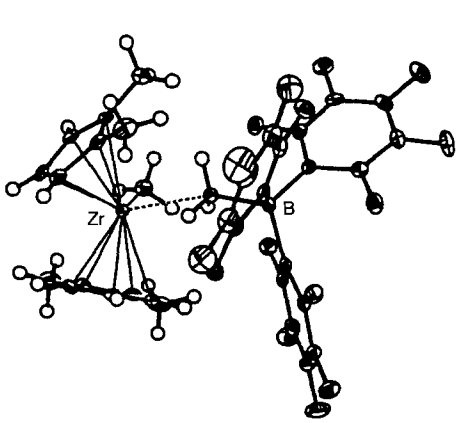


Fig. 1. Crystal structure of the zirconocene catalyst $[(Me_2C_5H_3)_2ZrCH_3^+ \cdots H_3C-B(C_6F_5)_3^-]$, as determined by Marks and co-workers [60]. The bridging $Zr \cdots CH_3B$ bond is substantially longer (255 pm) than the terminal $Zr-CH_3$ bond (225 pm).

In both cases, a fast methyl exchange occurs between the cationic and anionic complex moieties;[50, 60] most importantly, both types of contacts appear to be weak enough to allow an α-olefin to displace the anion from its coordination site at the Zr center.

Cationic metallocene complexes, particularly those that arise by in situ activation of a stable zirconocene precursor,[56] yield catalysts with very high activities. They are easily deactivated, however, probably by minute traces of impurities. Addition of $AlMe_3$ or $AlEt_3$ has been shown to stabilize these cationic metallocene catalysts[55, 56b] by formation of AlR_3 adducts.[57d]

Of even greater simplicity, at least conceptionally, are catalysts based on an (alkyl)metallocene complex containing a Sc^{III}, Y^{III}, or a trivalent lanthanide center. As shown by Ballard et al.[61] and by Watson et al.,[62] neutral complexes of the type $Cp_2M^{III}R$ act as single-component catalysts for the oligomerization of α-olefins.[63, 64] While generally more difficult to prepare and to handle than the Group 4 metallocene catalyst systems described above, catalysts such as $(C_5Me_5)_2ScR$ (R = Me, Et) provided Bercaw and his co-workers detailed information on the rates and mechanisms of individual olefin insertion steps.[63] The results of these studies lent additional support to the concept that an analogous olefin insertion into the isoelectronic species $[Cp_2ZrR]^+$ is responsible for the growth of polymer chains in zirconocene-based catalyst systems.

2.3. Kinetics and Mechanisms of α-Olefin Polymerization

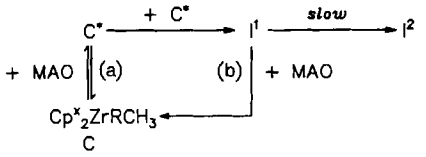
Because of many practical advantages, activation of zirconocene dichloride derivatives by methyl aluminoxane still appears to be the generally favored route to homogeneous polymerization catalysts. Substantial efforts have been made, therefore, to identify intermediates arising in the resulting, relatively complex reaction systems and to clarify the kinetics of the polymer chain growth they induce.

At propene pressures of 1–2 bar and ambient temperatures these reaction systems produce roughly 100–1000 kg polypropene per hour and mol of Cp_2ZrCl_2. This corresponds to about 2000–10000 olefin insertions per hour at each Zr center. T is equivalent to the production of 500–5000 polymer chains with average molecular weights on the order of $M_n = 200–2000$. Ethene is polymerized by these catalyst systems with still higher turnover numbers of 10–100 insertions per second, which approach those of C–C bond forming enzymes.[39b, c, g]

Attempts to identify the species involved in the rate-determining step of the polymerization process by kinetic methods (i.e. by determining the rate of polymer formation as a function of the concentrations of zirconocene, MAO, and olefin reagents) have been hampered by the complex time-dependence of the catalytic reaction. Relatively high initial values, reached shortly after the components are mixed, decrease to much lower steady-state values.[65–69] This decrease occurs within minutes at temperatures of 40–60 °C; at lower temperatures, it can take hours until the steady-state rate is reached.

In kinetic studies, Fischer and Mülhaupt[69a, b] describe the steady-state activity of a Cp_2ZrCl_2/MAO catalyst system as a sequence of reversible and irreversible processes. A reactive species C* appears to be generated in a fast equilibrium reaction

involving excess MAO and an (alkyl)zirconocene complex C (Scheme 6).[70] Another, slower reaction, which shows a second-order dependence on the concentration of the active species C*, converts C* to some inactive species I^1. This inactive species I^1 is constantly reconverted to the catalyst species C and C* by reaction with excess MAO; this was demonstrated by the effects of MAO additions on the catalytic activity of a system that had already reached steady-state conditions.[69c] A further, still slower reaction converts I^1 to another inactive species I^2 from which C* is not regenerated in these reaction systems. Since the transformation of C* to I^1 is bimolecular, the steady-state fraction of the inactive species I^1 decreases at low concentrations of C*. Accordingly, specific activities are observed to increase at lower zirconocene concentrations.[39, 69]



Scheme 6. Dual effect of MAO on the steady-state activity of a zirconocene-based polymerization catalyst, derived from kinetic studies by Mülhaupt and Fischer [69a, b]. (a) Generation of active species C* in a fast equilibrium with a (dialkyl)zirconocene complex and (b) reactivation of an inactive intermediate I^1 arising from a second-order deactivation reaction of C*; I^1 slowly decays to another inactive species I^2, from which the active catalyst is not regenerated.

The reaction that converts C* to I^1 is undoubtedly connected with the known propensity of (methyl)zirconocene cations to react with a wide variety of C–H units by means of σ-bond metathesis and release of CH_4.[26d–f, 28, 30, 50, 71] Kaminsky and co-workers have indeed observed a steady liberation of CH_4 from MAO-activated zirconocene catalysts, which reached up to 50 molecules of CH_4 per Zr center.[39i] The inactive, dominant steady-state species is proposed to be a binuclear complex with CH_2 bridges between a Zr and an Al center. Binuclear species with C_2H_4 bridges between two Zr centers were isolated by the same authors from ethene-polymerizing catalyst systems.[4a, 39] Regeneration of active polymerization catalysts from these binuclear, C_xH_y-bridged deactivation products by MAO is proposed to occur by alkyl exchange reactions, for instance between a $Zr-CH_2-Al$ species and the alkylaluminum activator;[72] the latter will thus be consumed gradually under formation of $Al-CH_2-Al$ units. Evidence for the formation of binuclear cations of the type $[Cp_2ZrMe(\mu\text{-}CH_3)MeZrCp_2]^+$ is now firmly established.[53a, 57d, 60a, 73, 120e, 132b] Further insights with regard to their identity and their involvement in deactivation processes[74] can be expected from studies on MAO-free, cationic zirconocene catalysts.

The question of why such a huge excess of MAO is required to induce catalytic activity for α-olefin polymerization is still unanswered. Catalytic activities are found to decline dramatically for MAO concentrations below an Al:Zr ratio of roughly 200–300:1. Even at Al:Zr ratios greater than 1000:1, steady-state activities increase with rising MAO concentrations,[75] approximately as the cube root of the MAO concentration.[39d, 69b] MAO appears to be involved in a fast equilibrium $C + MAO \rightleftharpoons C^{*+} + CH_3-MAO^-$ as well as in the slower reactivation process $I^1 + MAO \rightarrow C^*$. The concentration of the most Lewis-acidic Al centers must be related, furthermore, to the total MAO concentration through complicated equilibria. To date, it has not been possible to model the overall effects of MAO concentrations on catalytic reaction rates by a plausible, comprehensive system of kinetic equations.

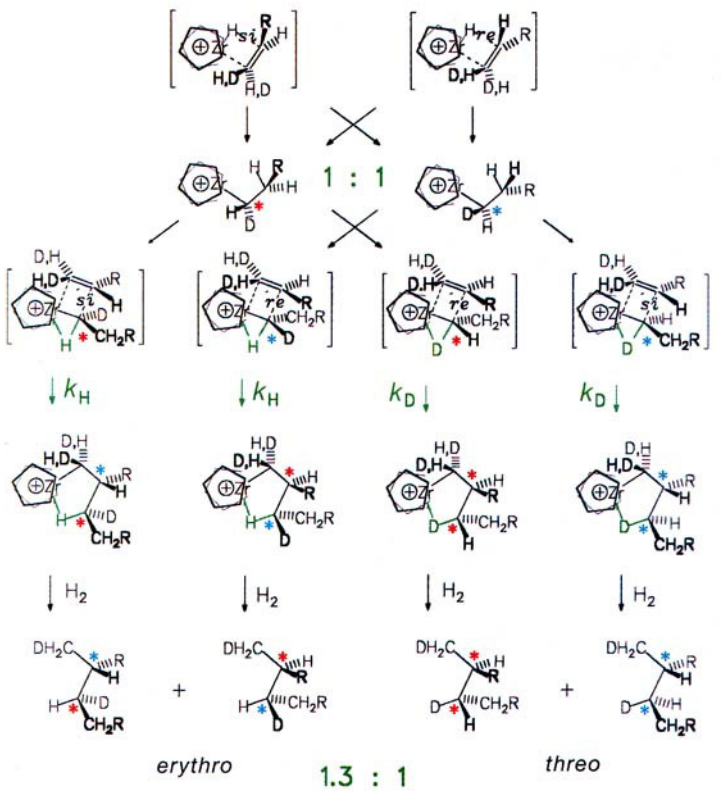
The effect of olefin concentration on the reaction rates is likewise complicated by catalyst deactivation. Since the reactive species appears to be stabilized by excess olefin, rates of polymer production under steady-state conditions are not proportional to propene concentrations, but approximately to $c(\text{olefin})^{1.3}$.[69b] Related observations (see for example refs. [50b, c]) that polymerization rates depend on olefin concentration to a fractional order between 1 and 2 have led to the proposal that two olefin molecules are involved in the insertion transition state.[76] While initial rates of polymer production, determined before the onset of catalyst deactivation, have been reported in two instances to increase in proportion to ethene[65c] or propene concentration[69b] (i.e. as $c(\text{olefin})^{1.0}$), this point requires further clarification (see Section 3.3).

For the present we will assume, in accord with general opinion, that the productive reaction complex in MAO-activated zirconocene catalysts is a cationic alkyl(olefin)zirconocene complex of the type $[Cp_2ZrR(\text{olefin})]^+H_3C-MAO^-$, which is generated by displacement of an anion H_3C-MAO^- from its $[Cp_2ZrR]^+$ counterion by an olefin molecule.

The reaction step by which such an alkyl(olefin)zirconocene cation is finally converted to the olefin-insertion product has been further characterized by kinetic isotope effects. Laverty and Rooney,[77] and Brookhart and Green[78] had proposed that an agostic interaction of one of the α-H atoms of the metal-bound alkyl chain with the metal center of a Ziegler–Natta catalyst[79] facilitates the insertion of an olefin into the metal–alkyl bond. To test this hypothesis, Krauledat and Brintzinger[80] investigated the catalytic hydrodimerization of α-deuterated hexenes to the *threo* and *erythro* diastereomers of $5\text{-}CH_2D\text{-}6\text{-}[D]$-undecane by MAO-activated Cp_2ZrCl_2. Diastereomer ratios in accord with a value of $k_H/k_D \approx 1.3$ were observed with *cis* and *trans* α-deuterated 1-hexene. This indicates—along a line of reasoning developed earlier by Grubbs and co-workers[81]—that the transition state for the insertion of hexene into the Zr–C bond of the initially formed $Zr-CHD-(CH_2)_4CH_3$ unit involves considerable weakening either of its α-C–H or of its α-C–D bond. In other reaction systems agostic interactions with H atoms have been shown to be preferred over those with D atoms by a factor of about 1.2–1.5.[79a] The stereokinetic isotope effect $k_H/k_D \approx 1.3$ associated with the insertion of an α-olefin into the metal–CHD–R unit of a MAO-activated zirconocene catalyst can thus be regarded as evidence that this reaction requires the agostic interaction of one of the α-H atoms with the metal center (Scheme 7).

Similar results were obtained by Piers and Bercaw[82] in studies on hydrocyclizations and hydrodimerizations induced by single-component scandocene catalysts. It remains to be tested whether this notion can be generalized or whether olefin insertions into metal–alkyl species might occasionally occur without agostic assistance.[83]

Olefin insertion into the metal–alkyl bond of a cationic metallocene complex of the type $[Cp_2MMe(\text{olefin})]^+$ (M = Ti,



Scheme 7. Stereokinetic isotope effects in the $(C_5H_5)_2ZrCl_2$/MAO-catalyzed hydrodimerization of (*E*)- and (*Z*)-1-[D]-1-hexene (R = *n*-C_4H_9) favor the *erythro* over the *threo* products in a ratio of 1.3:1 [80]. While the achiral starting compounds must give the Zr–CHD–CH_2R enantiomers in a 1:1 ratio, the second olefin insertion is influenced by α-agostic interactions. A H–C(α) bond is weakened in the formation of the *erythro* isomers, a D–C(α) bond in the formation of the *threo* isomers of the hydrodimer product.

Zr) has been the subject of numerous theoretical studies.[84–89] Calculations with ab initio and density functional methods depict the transition state as a planar[84e,g,85,87,88] or slightly puckered[84f,86] four-membered ring with Ti–C and Zr–C distances of 2.1–2.3 and 2.3–2.5 Å, respectively, an incipient alkyl–olefin C···C distance of 2.1–2.3 Å, and a slightly increased olefin C=C bond length of roughly 1.4 Å[84e–g,85–88] (Fig. 2).

Most of these studies concur with the view that in the insertion transition state one α-H atom of the migrating Zr–CH_2–R

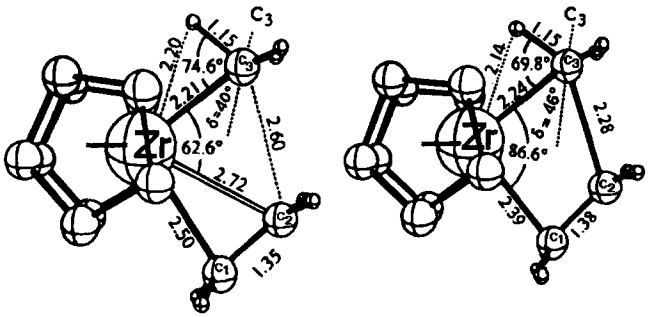


Fig. 2. Structures of a cation $[(C_5H_5)_2ZrMe(C_2H_4)]^+$ (left) and of the transition state for insertion of the ethene ligand into the Zr–Me bond (right), as determined by Ziegler and co-workers by density functional methods [87]. A shortening of the agostic Zr–H(α) contact helps align the C_3 axis of the CH_3 group for interaction with the ethene π* orbital.

group is in close proximity to the metal center and that this Zr–H interaction is due to an α-agostic bond.[86–88] An Extended-Hückel MO study[89] indicates that the α-agostic interaction of a Zr–CH_2–R unit with the Zr center is linked to the increasing electron deficiency of the reaction complex as it progresses along the olefin-insertion coordinate from a 16-electron to a 14-electron species. The size of the contribution of the agostic interaction to the stabilization of the olefin-insertion transition state is still a matter of debate.[89]

These studies also indicate that the Zr–*n*-propyl unit at the end of the insertion path is stabilized by the agostic interaction of one of its γ-C–H bonds with the Zr center.[84g,85–89] A yet more stable structure appears to be a product in which one of the β-C–H bonds of the Zr–*n*-propyl unit interacts with the electron-deficient Zr center.[85–88] The γ-agostic species initially arising from the insertion process is thus likely to rearrange into a structure with a β-agostic bond;[79] the latter probably represents something like a resting state for a $[Cp_2Zr–alkyl]^+$ ion (see ref. [63]). Theoretical studies indicate that the $\gamma \rightarrow \beta$ rearrangement might be relatively slow.[85b,87b]

Effects of the solvent and counterions, neglected so far in these theoretical studies, might be of more than peripheral concern. In an ion-cyclotron resonance study, Richardson and co-workers[74] showed that $[Cp_2TiCH_3]^+$ and C_2H_4 react in vacuo to form the allyl complex $[Cp_2TiC_3H_5]^+$ and H_2, rather than the insertion product $[Cp_2TiC_3H_7]^+$. It remains to be clarified which interactions induce the more useful course to polymers in the analogous condensed-phase reaction systems.

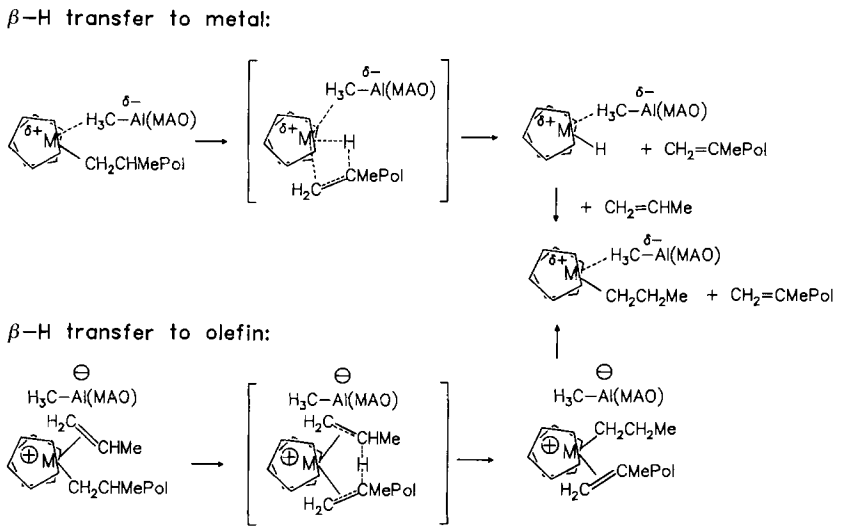
2.4. Molecular Weights and Chain Termination Reactions

An important aspect in which homogeneous olefin polymerization by metallocene catalysts differs from heterogeneous Ziegler–Natta catalysis is the narrow molecular weight distribution of homogeneously produced polymers. While polyolefins obtained with heterogeneous catalysts have broad molecular weight distributions with large polydispersities of $M_w/M_n \approx 5–10$,[8] homogeneous catalysts produce polymers with polydispersities M_w/M_n close to 2.[39f] A polydispersity of 2 is predicted by Schulz–Flory statistics[90] for polymers arising from identical catalyst centers with fixed rates of chain propagation and chain termination, v_P and v_T. A polydispersity of 2 is thus regarded as evidence that only a single catalyst species contributes to polymer growth in a homogeneous catalyst system. Even though the deactivation and reactivation reactions discussed above are likely to generate a diversity of complex species in these catalyst systems under steady-state conditions, only one of these species, presumably the cation $[Cp_2Zr–alkyl(olefin)^+]$, appears to contribute to polymer growth.

While ethene is polymerized by MAO-activated or cation-type Cp_2Zr-based catalysts to give polymers with high molecular weights in the range of 100 000 to 1 000 000,[39] propene polymers obtained at room temperature with these catalysts have rather low degrees of polymerization, with molecular weights in the range of 200–1000.[39e,g,69b] The relatively low molecular weights of the polymer products must be due either to an increased rate of chain termination or to a decreased rate of olefin insertion (or both), since the average degree of polymerization

P_N is determined by the ratio of the rates of chain propagation and chain termination, $P_N \approx v_P/v_T$.[90]

^1H and ^{13}C NMR analyses show that polypropene chains produced with zirconocene-based catalysts bear *n*-propyl and 2-propenyl end groups.[91] The 2-propenyl end groups could arise by transfer of a β-H atom from the polymer chain to the metal center (Scheme 8). The Zr–H unit generated by this process can then react with propene to form a Zr–*n*-propyl unit, from which a new polymer chain can start to grow.[96] Another conceivable chain termination mechanism is the transfer of a β-H atom from the Zr-bound polymer chain directly to the β-C atom of a coordinated olefin molecule. In this case, the 2-propenyl-terminated polymer chain and a new Zr–*n*-propyl unit are generated without the intermediacy of a Zr–H species (Scheme 8).



Scheme 8. Chain termination by β-H transfer to the metal (top) and to a coordinated olefin (bottom). A polymer chain with a 2-propenyl end and a metallocene complex with a *n*-propyl chain result from both of these processes, but the rate of the latter increases with olefin concentration in parallel to that of olefin insertion, while the rate of the former is olefin-independent. Molecular weights of the polymers will thus increase with olefin concentration in the case of β-H transfer to the metal, while molecular weights independent of olefin concentration indicate β-H transfer to an olefin ligand.

Evidence for direct β-H transfer to a coordinated olefin was obtained by Kashiwa and co-workers[97] from studies on ethene–propene copolymers. A Zr–H intermediate would be expected to react at least as fast with ethene to give a Zr–ethyl unit as with propene to give a Zr–propyl unit; ethyl end groups should thus be found at the head of a polymer chain with the same frequency as *n*-propyl ends. In fact, very few ethyl ends were formed at comparable concentrations of ethene and propene. The most plausible explanation for this observation is that β-H transfer to a coordinated propene molecule occurs more often than that to a coordinated ethene molecule, since the rate of insertion of propene into a Zr–polymer bond is lower than that of ethene.[97]

This mechanism does not appear compatible, on the other hand, with observations that polymer molecular weights increase linearly with ethene[65c] or propene[69b] concentrations. For chain termination by β-H transfer to a coordinated monomer one would expect v_T like v_P to depend linearly on monomer concentration. In this case, the mean degree of polymerization, $P_N \approx v_P/v_T$, is expected to be independent of the monomer concentration. This discrepancy obviously needs to be readdressed; we will return to it in the discussion of stereoselective polymerization catalysis in Section 3.3.

Molecular weights of polyolefins obtained with MAO-activated zirconocene systems generally increase with the concentration of the MAO cocatalyst,[39, 69b, 98] in parallel with increased rates of chain growth. Effects of zirconocene concentrations on polymer molecular weights again parallel those on catalytic activities: molecular weights increase substantially as zirconocene concentrations are decreased.[39, 69b, 98] This might be due to dilution effects favoring the dissociated or olefin-separated ion pairs C* relative to their associated precursors C, and hence the rate of chain propagation over that of chain termination.[99] As an alternative, Kaminsky and co-workers[39, 98] advocate that a bimolecular reaction of the active complex with a second zirconocene species terminates growth of the polymer chain in a manner possibly related to the second-order deactivation process discussed in Section 2.3. Further clarification of these questions can be expected from future studies on MAO-free, cationic metallocene polymerization catalysts.

3. Stereoregular Polymers from Chiral Metallocene Catalysts

The discovery of homogeneous catalysts capable of polymerizing propene and higher α-olefins around 1980 revived a long-standing question:[13] Would it be possible to induce these homogeneous polymerizations in a stereoregular fashion, so as to produce isotactic polymers, by using suitably designed chiral metallocenes as catalysts?

Chiral metallocenes suitable for this purpose[100] became available, not quite accidentally[101] just at that time. Using ethylene-bridged ligands,[102] Wild and Brintzinger[103] obtained ethylenebis(indenyl)- and ethylenebis(tetrahydroindenyl)titanium complexes, *rac*-(en)(ind)$_2$TiCl$_2$ and *rac*-(en)(thind)$_2$TiCl$_2$, and their zirconium analogues. The conformationally constrained indenyl and tetrahydroindenyl ligands give these complexes chiral structures (Fig. 3) which

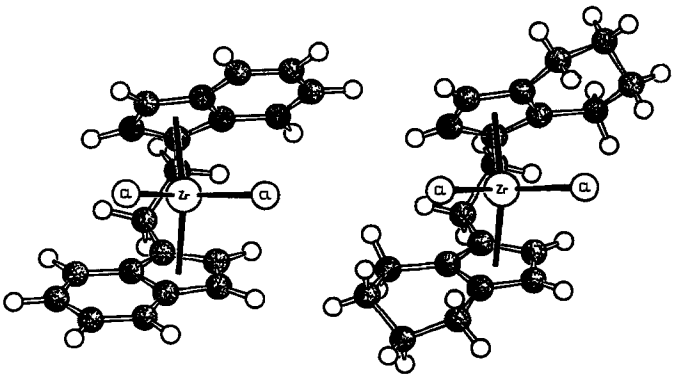


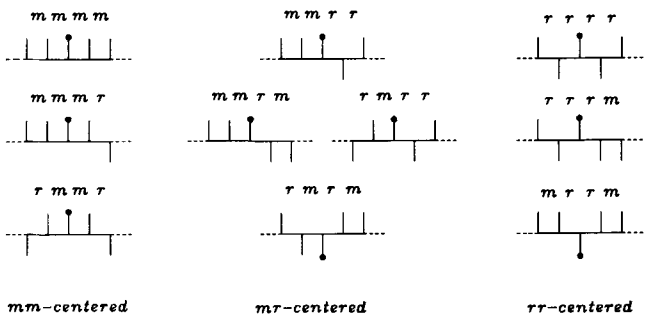
Fig. 3. Prototypical *ansa*-zirconocene complexes prepared by Wild et al. [103]: *rac*-(en)(ind)$_2$ZrCl$_2$ (left) and *rac*-(en)(thind)$_2$ZrCl$_2$ (right).

could be expected to be retained even under catalysis conditions. When activated with MAO in the manner described above, these *ansa*-metallocenes[104] were indeed found, in independent studies by Ewen with (en)(thind)$_2$TiCl$_2$/MAO[105] and by Kaminsky and Külper with *rac*-(en)(thind)$_2$ZrCl$_2$/MAO,[106] to polymerize propene and other α-olefins to give highly isotactic polymers. These findings led to extensive exploration of the mechanisms by which these catalysts control the stereochemistry of polymer growth and the effects of different metallocene structures on the tacticities and other properties of the polymers produced.

3.1. Catalyst Structures and Stereoselectivities

Polypropene produced by MAO-activated chiral *ansa*-zirconocenes such as *rac*-(en)(ind)$_2$ZrCl$_2$ or *rac*(en)(thind)$_2$ZrCl$_2$ has similar isotacticity to polymers produced with heterogeneous Ziegler–Natta catalysts. For a more quantitative discussion of these relations, we consider briefly the ^{13}C NMR spectroscopic methods[107] currently used to characterize the stereoregularity of poly(α-olefins).

The ^{13}C NMR signals of a polymer are most conveniently related to its microstructure by a stereochemical notation developed by Bovey.[107a] Relative configurations of neighboring units (or "dyads") are designated as *m* (*meso*) for equally and *r* (*racemo*) for unequally positioned substituents in a Fischer-type projection of the polymer chain. In polypropene, the ^{13}C NMR shift of each CH_3 group is determined by the configurations of two neighboring repeat units on either side;[108] each CH_3 signal is thus assignable to a particular "pentad" pattern, represented by the four consecutive *m* or *r* designators framing the CH_3 group under consideration (Scheme 9). All ten possible



Scheme 9. The ten possible stereochemical pentads of a polyolefin [107].

pentad signals (*mmmm*, *mmmr*, *rmmr*, *mmrr*, *mmrm*, *rmrr*, *rmrm*, *rrrr*, *rrrm*, and *mrrm*)[109] are observed for the randomly configurated repeat units of atactic polypropene[110] (Fig. 4). Isotactic polypropene, on the other hand, is ideally characterized by a single ^{13}C NMR signal for *mmmm* pentads, since its repeat units have identical configuration over long segments of the polymer chain.

The degree of isotacticity of such a polymer is usually expressed as the ratio of the *mmmm* pentad integral to the integral sum of all pentad signals observed; it will be designated in the following as [*mmmm*].[111] Isotactic polypropene produced by modern heterogeneous Ziegler–Natta catalysts[8] is highly

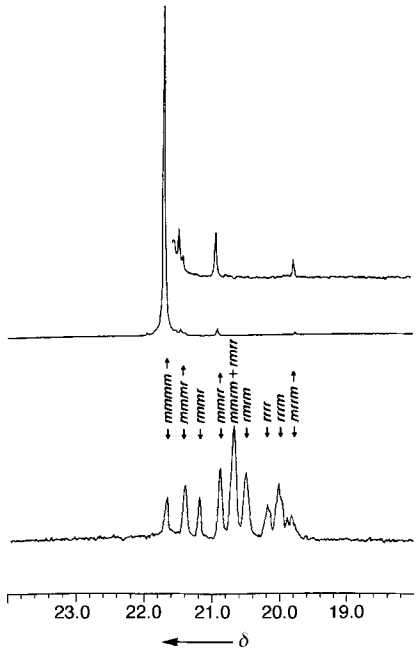


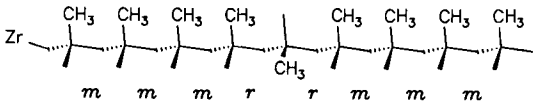
Fig. 4. ^{13}C NMR spectra of isotactic polypropene (CH_3 region) with [*mmmm*] > 90% obtained with *rac*-Me$_2$Si(1-benz[*e*]indenyl)$_2$ZrCl$_2$/MAO [117h, 120d] (top), and of atactic polypropene with random pentad distribution obtained with the *meso* isomer of the same catalyst (bottom).

stereoregular with [*mmmm*] > 0.95. At ambient temperatures, typical MAO-activated chiral *ansa*-metallocene catalysts yield polypropene with stereoregularities of [*mmmm*] ≈ 0.8–0.9.[106, 112, 113] At increased polymerization temperatures, however, most of these homogeneous catalysts are distinctly less stereoselective than typical heterogeneous Ziegler–Natta catalysts.[114a]

The ^{13}C NMR signals associated with occasional stereoerrors in the isotactic polymers produced by metallocene catalysts indicate that stereoregularity is controlled by the chirality of the metallocene catalyst and not by the asymmetry of the last inserted unit: Such "chain-end" control would give rise to the single-inversion pentad *mmrm* as a main error signal, since an occasionally inverted chain-end configuration would generally be followed by units of the same configuration. For this chain-end control one would expect an error pentad ratio close to *mmmr*:*mmrr*:*mmrm*:*mrrm* = 1:0:1:0. In fact, an error pentad distribution close to *mmmr*:*mmrr*:*mmrm*:*mrrm* = 2:2:0:1 is observed for these polymers (Scheme 10). As previously established for heterogeneous catalysts,[12] this pentad pattern is expected when olefin insertion is indeed under "catalytic-site" control.[105, 115] In this case, *r* dyads due to stereoinversions will occur in pairs, since a catalyst center of fixed chirality forces the enantiofacial orientation of subsequent olefin insertions to return to the previous preference immediately after an occasional mistake (Scheme 10).

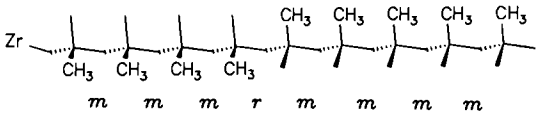
How the stereoselectivities of chiral catalysts depend on the structure of the complex, in particular on different bridging units and substituent patterns, has been the subject of comparative studies in several research groups.[116–120] In investigations of this kind, it is crucial to take into account the polymerization temperature T_p.[121] Even an unbridged metallocene catalyst with unsubstituted ring ligands, Cp_2TiPh_2/MAO, has been

Catalytic–site control



mmmr : *mmrr* : *mmrm* : *mrrm* = 2 : 2 : 0 : 1

Chain–end control



mmmr : *mmrr* : *mmrm* : *mrrm* = 1 : 0 : 1 : 0

Scheme 10. Pentad distributions of stereoerrors in isotactic polypropene characteristic for catalytic-site stereocontrol (top; see also insert in Fig. 4) and for chain-end stereocontrol (bottom).

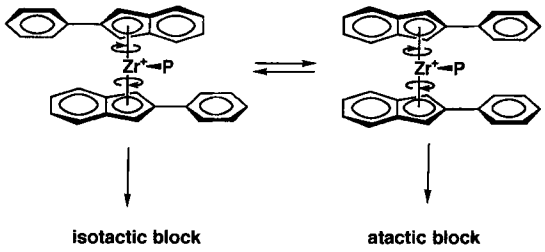
shown by Ewen[105] to yield partially isotactic polypropene with [*mmmm*] ≈ 0.5 at temperatures below −40 °C. In this case, the nearly equal intensities of the *mmmr* and *mmrm* pentad signals indicate a chain-end control mechanism.[105, 122]

Similar observations were reported by Erker and co-workers[123] for unbridged zirconocenes with substituents containing an asymmetric C atom; these were found to give isotactic polymers with [*mmmm*] ≈ 0.4–0.8 at polymerization temperatures of −50 °C or lower. This partial control by the configuration of the last inserted unit over the stereochemistry of the next olefin insertion is almost completely lost at ambient temperatures. Apparently, insufficiently restricted rotations of the C_5 ring ligands and their substituents and the increasing conformational mobility of the growing polymer chain abolish this stereocontrol mechanism at ambient temperatures.

An unbridged, chiral zirconocene that produces an isotactic polymer even at T_P = 60 °C was described by Razavi and Atwood.[124] MAO-activated (1-methylfluorenyl)$_2$ZrCl$_2$ generates polypropene with [*mmmm*] = 0.83 and a catalytic site controlled pentad distribution. The fluorenyl ligands of this complex are chirally disposed, due to their methyl substituents, and apparently so strongly hindered in their mutual rotation that the enantiomers of this complex are not interconverted during the growth of a polymer chain.

Waymouth and co-workers recently reported on an unbridged metallocene catalyst, (2-phenylindenyl)$_2$ZrCl$_2$/MAO, which appears to isomerize, by restricted rotation of its indenyl ligands, between chiral and achiral coordination geometries during chain growth; this catalyst yields a highly stretchable atactic–isotactic stereoblock polypropene with elastomeric properties (Scheme 11).[125]

A short interannular bridge will necessarily restrict rotation of the C_5 ring ligands. Accordingly, high stereoselectivities are found for all chirally substituted *ansa*-metallocene catalysts with one-atom or two-atom bridges,[116–120] at least at lower polymerization temperatures. At temperatures of 50–70 °C, typical for technical polymerizations, stereoselectivities are often substantially decreased. Incorporation of the ethylene bridge of (en)(ind)$_2$ZrCl$_2$ (which can fluctuate between δ and λ chelate ring conformers[126a]) into a carbocyclic system[127] or its replacement by a one-atom silanediyl or germanediyl bridge[114b, 116c, 117b] increases stereoselectivities, but only to a limited extent.[117g] Even in metallocenes with a short Me_2Si bridge, the ZrX_2 and ligand framework moieties appear to retain substantial degrees of mobility.[126b] Molecular mechanics studies indicate that much of this mobility is restricted by substituents placed in α-position to the bridgehead atom.[126b] Chirally substituted *ansa*-zirconocene catalysts with α-CH_3 groups at each C_5 ring do indeed show increased stereoselectivities.[118–120]

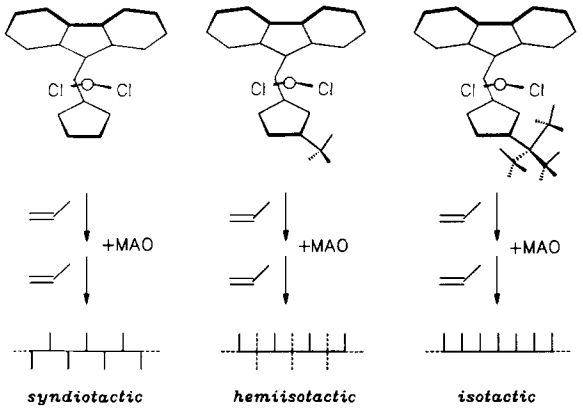


Scheme 11. Reversible isomerization of an unbridged zirconocene catalyst between chiral and achiral geometries found by Waymouth and co-workers [125] to yield isotactic and atactic blocks alternating along each polymer chain. The resulting polypropene is an elastomer.

Most interesting with respect to their effects on polymer stereoregularities, however, are the substituents in β-position to the bridgehead atom of an *ansa*-zirconocene. These β-substituents are in close proximity to the coordination sites at which the growing polymer chain and the α-olefin substrate are bound. In the chiral complexes (en)(ind)$_2$ZrCl$_2$, (en)(thind)$_2$ZrCl$_2$, and Me_2Si(ind)$_2$ZrCl$_2$, CH or CH_2 groups of the annelated C_6 ring function as β-substituents and flank each of the adjacent coordination sites. If the β-substituents are very bulky, as in Me_2Si(2-Me-4-*t*Bu-C_5H_2)$_2$ZrCl$_2$[120a, b] or in Bercaw's [Me_2Si(2-$SiMe_3$-4-*tert*-butyl-C_5H_2)$_2$YH]$_2$,[144] or particularly protruding, as in Spaleck's Me_2Si(2-methyl-4-aryl-1-indenyl)$_2$ZrCl$_2$,[117h] polypropenes with stereoregularities of [*mmmm*] > 0.95 are generated even at polymerization temperatures of 70–80 °C.

Chiral *ansa*-zirconocene complexes with two identical ligand moieties have C_2 symmetry. Both coordination sites of such a C_2-symmetric complex are thus equivalent; each is framed by the β-substituents in such a manner that olefin insertions at the Zr center occur with equal enantiofacial preference at both sites. *Unilateral* coverage of each coordination site is essential for this stereoselectivity; this is documented by the observation that atactic polypropene is produced if both coordination sites are flanked by *two* β-substituents, as in C_2H_4(3-methyl-1-indenyl)$_2$ZrCl$_2$/MAO or in its silyl-bridged analogue Me_2Si(3-methyl-1-indenyl)$_2$ZrCl$_2$/MAO.[116c, 117h] The bilateral coverage of each coordination site in these complexes, by a CH and a CH_3 group, appears to render them indifferent with respect to the enantiofacial orientation of an entering olefin. The same result, production of essentially atactic polymers, was also observed for the *meso* isomers of each *ansa*-metallocene catalyst.[105]

The relationship between the stereoselectivity of *ansa*-metallocene catalysts and the spatial disposition of their β-sub-



Scheme 12. Relationship between catalyst structure and stereoselectivity discovered by Ewen and co-workers [116d–h]. Syndiotactic polypropene is produced by $Me_2C(C_5H_4)$(9-fluorenyl)$ZrCl_2$/MAO; introduction of a β-CH_3 group on the C_5 ring results in formation of hemiisotactic polymer in which every other repeat unit is randomly configurated; introduction of a β-*tert*-butyl group gives highly isotactic polypropene.

stituents has been most elegantly utilized by Ewen and co-workers in a series of studies on Me_2C-bridged fluorenyl complexes (Scheme 12).[116d–h] The complex Me_2C(Cp)(9-fluorenyl)-$ZrCl_2$, for example, is not a C_2-symmetric but a C_s-symmetric structure with one unsubstituted C_5 ring ligand and, in its fluorenyl ligand, one C_5 ring ligand with *two* β-substituents.[124b, c] In the presence of MAO or cationic activators this complex produces highly syndiotactic polypropene.[116d–g, 117d]

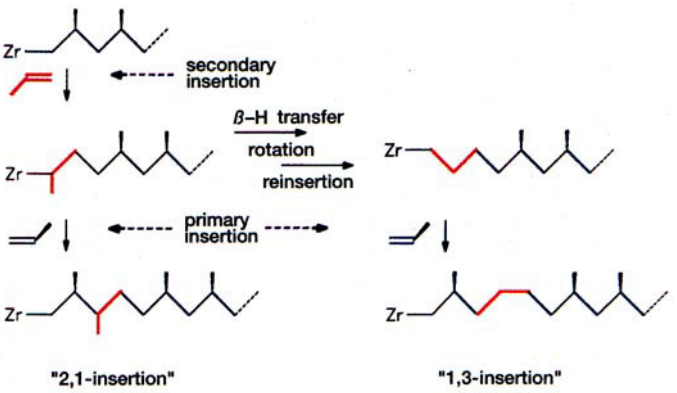
Syndiotactic polypropene is ideally characterized by a ^{13}C NMR spectrum with a single *rrrr* pentad signal, as configurations alternate here from one repeat unit to the next.[128] Ewen's syndiospecific catalyst provided this polypropene isomer for the first time in substantial quantities, with stereoregularities of [*rrrr*] > 0.9 and with a pentad intensity distribution in accord with catalytic-site control.[116d] The alternating enantiofacial orientation of subsequent olefin insertions, which gives rise to this particular tacticity, is undoubtedly due to the fact that the two coordination sites in this C_s-symmetric complex are no longer homotopic, as in a complex with C_2 symmetry, but enantiotopic.[129c]

The correlation between the substituent pattern of a metallocene and the stereoregularity of its polymer products is further extended by Ewen's finding that still another polypropene stereoisomer is formed with MAO-activated $Me_2C(3\text{-}MeC_5H_3)$-(9-fluorenyl)$ZrCl_2$.[116e–g, 117d] This catalyst, with one coordination site framed by one β-substituent and one by two β-substituents (Scheme 12), produces hemiisotactic polypropene[129] in which every other repeat unit is of identical configuration while the remaining units are randomly configurated. By totally blocking one of the coordination sites in the catalyst $Me_2C(3\text{-}t\text{Bu}C_5H_3)$(9-fluorenyl)$ZrCl_2$/MAO with a *tert*-butyl group and a fluorenyl C_6 ring, while keeping the other site unilaterally framed by the other fluorenyl C_6 ring, Ewen and Elder finally obtained isotactic polypropene again.[116h]

The stereoselectivity of a C_2-symmetric isotactic polymerization catalyst such as $Me_2Si(ind)_2ZrCl_2$ is practically independent of zirconocene and MAO concentrations[131] and essentially unaffected even by the replacement of MAO by a borane or borate activator.[116f, g, 132a, b] The C_s-symmetric syndiospecific catalyst Me_2C(Cp)(9-fluorenyl)$ZrCl_2$/MAO, however, behaves differently in this regard: its syndiotactic polymers show more frequent *rmrr* errors when either MAO or olefin concentrations are decreased.[116e, f, 132a]

Ewen et al.[116f] and Herfert and Fink[132a] showed that this dependence must indeed result from a crucial requirement for syndiotactic polymerization: each olefin insertion has to occur at the coordination site opposite to the previous one. This requirement can only be met when the polymer chain remains at the coordination site of the previous olefin unit until the next olefin insertion occurs. Stereoerrors with single-*m* dyads must result whenever the polymer chain moves to the opposite coordination site before the next olefin inserts. Such an event[133] will become more likely when the rate of olefin insertion is decreased by low olefin or MAO concentrations. Similar changes in the stereoregularity of hemiisotactic polypropene, recently reported by Herfert and Fink[132c] and by Farina and co-workers,[129b] and of partly isotactic polypropene obtained with several asymmetric catalysts,[130] underscore the importance of the relative rates of olefin insertion and chain migration between coordination sites for these non-C_2-symmetric metallocene catalysts.

While olefin insertion in metallocene-based homogeneous catalysts, as in heterogeneous Ziegler–Natta systems,[10, 12] generally occurs with 1,2-regioselectivity so as to generate primary Zr–alkyl units, polyolefins produced with metallocene-based catalysts contain varying fractions of regioinverted units.[114a, 135, 136] Depending on the polymerization temperature and on the metallocene catalyst used, one finds either head-to-head concatenations resulting from primary olefin insertion into regioinverted secondary Zr–alkyl units, or tetramethylene units (1,3-insertions). The latter arise from an isomerization of a secondary Zr–alkyl unit to one with a terminal Zr–alkyl bond prior to insertion of the next olefin[114a, 136] (Scheme 13).



Scheme 13. Alternative sequences arising from a secondary olefin insertion [114a, 136]. A (relatively slow) primary insertion gives the tail-to-tail and head-to-head pattern typical of a 2,1-insertion; rearrangement of the secondary Zr–alkyl unit into its terminal isomer, followed by a primary insertion, yields a tetramethylene or 1,3-insertion unit.

Different zirconocene catalysts produce the regioirregularities in different ratios:[69b] only 1,3-misinsertions (ca. 1%) are found in polymers made with (en)(thind)$_2ZrCl_2$/MAO; with (en)(ind)$_2ZrCl_2$/MAO both types of misinsertions are present; and $Me_2Si(ind)_2ZrCl_2$/MAO forms polymers with only 2,1-misinsertions (ca. 0.6%) at 40 °C. With "fast" catalysts, misin-

sertions are generally of the 2,1-type; slower catalysts produce mainly 1,3-misinsertions.[117h, 120d] Effects of these misinsertions on catalyst activities will be considered in Section 3.3.

The irregularities introduced into a polypropene chain by 2,1- or 1,3-misinsertions decrease its melting point considerably (see Section 3.4); these misinsertions are thus of practical concern. Their frequency seems to depend mainly on the steric demands of the substituents on the C_5 ring. Rather frequent misinsertions are found for metallocenes with bulky β-substituents, while α-methyl substituents appear to suppress these regioirregularities.[120a–c]

Steric relationships in a metallocene complex can be described by its "coordination-gap aperture", the largest possible angle spanned by two planes through the metal center which touch the van der Waals surfaces of the β-substituents at the C_5 ring ligands, and by its "lateral extension angle", which is limited by the two α-substituents protruding into the coordination gap (Fig. 5).[137a]

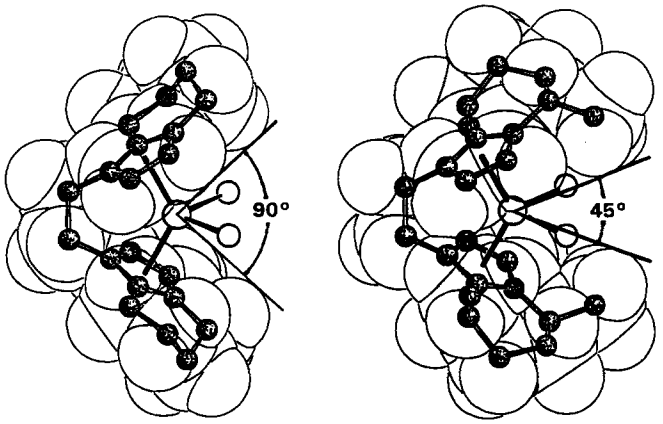


Fig. 5. Right: Narrow coordination gap aperture [137] of *rac*-C_2H_4(4,7-dimethyltetrahydroindenyl)$_2ZrCl_2$ was found by Spaleck and co-workers [117i] to produce unusually large fractions (ca. 24%) of 1,3-misinsertions (molecular model). Left: Crystal structure of unsubstituted *rac*-C_2H_4(tetrahydroindenyl)$_2ZrCl_2$ [103] for comparison (see Fig. 3).

A secondary olefin insertion (2,1-insertion) is expected—due to the lateral orientation of the olefin substituent—to require less space in the aperture direction but more space in the lateral direction than a regular 1,2-insertion. Regioinversions are thus favored by those zirconocene catalysts whose β-substituents strongly limit the gap aperture, provided that the lateral extension angle is not restricted also by α-substituents protruding into the coordination gap.[137b, c] Polypropene with an unusually high fraction of 1,3-misinsertions has been reported by Spaleck and co-workers[117i] to arise from the catalyst C_2H_4(4,7-dimethyl-thind)$_2ZrCl_2$/MAO, whose *endo*-oriented 4-methyl groups severely restrict the coordination gap aperture (Fig. 5).

3.2. Mechanisms of Stereochemical Control

The mechanisms by which chiral *ansa*-metallocenes control the stereochemistry of polymer growth are reasonably well-understood today. As usual, stereochemical analysis affords more reliable information on a reaction mechanism than most other methods. This analysis is simplified, furthermore, by the observation that the stereoregularity of isotactic polymers is rather insensitive to MAO or zirconocene concentrations[120c, 132a] (see, however, ref. [131]) and even to the type of activator used to generate the reactive cationic species.[116f, g, 132b, 151b]

First important clues as to the factors governing the stereoselectivity of C_2-symmetric, chiral metallocene catalysts came from ^{13}C NMR studies of Zambelli and co-workers. These authors followed the course of propene and 1-butene insertions into ^{13}C-enriched CH_3 and CH_2CH_3 end groups, which were introduced into a MAO-activated (en)(ind)$_2TiMe_2$ catalyst by alkyl exchange with Al($^{13}CH_3$)$_3$ or Al($^{13}CH_2CH_3$)$_3$.[138] The results of these studies can be summarized as follows:

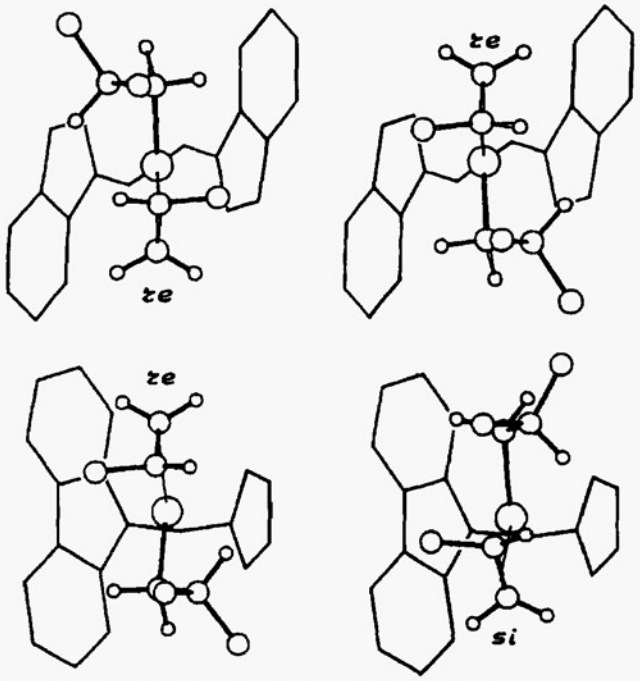
1. Propene inserts into (en)(ind)$_2$Ti–$^{13}CH_3$ bonds without significant stereoselectivity, as shown by signals of diastereomeric end groups with almost equal intensity.
2. Butene insertion into (en)(ind)$_2$Ti–$^{13}CH_3$ bonds occurs with slight (2:1) selectivity.
3. Complete stereoselectivity prevails when either propene or butene inserts into (en)(ind)$_2$Ti–$^{13}CH_2CH_3$ bonds.
4. All these results resemble those obtained before with analogously activated heterogeneous polymerization catalyst systems.[12]

Efficient control of the chiral catalyst over the enantiofacial orientation of the entering olefin is thus clearly contingent on the presence of a metal–alkyl segment with at least two C atoms. This segment appears to act as a sort of lever in transmitting the effects of the β-substituents on the orientation of the prochiral α-olefin.

The nature of this stereocontrol mechanism was clarified by molecular mechanics calculations by Corradini, Guerra, and co-workers.[139] As previously proposed for heterogeneous Ziegler–Natta catalysis,[12b] repulsive interactions were shown to force an olefin into that enantiofacial approach to the metal–alkyl unit which places the olefin substituent *trans* to (i.e. away from) the β-C atom of the metal-bound alkyl chain. The metal–alkyl chain, in turn, was proposed to favor an orientation in which its C(α)–C(β) segment is in the most open sector of the chiral *ansa*-metallocene ligand framework (Scheme 14). Subsequent model studies in other groups by means of more elaborate force field and ab initio methods[85, 86] support this proposal.

Analogous considerations hold for stereocontrol mechanisms for *ansa*-metallocene derivatives that produce syndiotactic and hemiisotactic polymers.[116e–g, 139e, g–i, 140] In each case, the C(α)–C(β) segment of the polymer chain appears to orient itself so as to avoid interaction with the C_5 ring substituents in β-position adjacent to its coordination site (Scheme 15); an entering olefin is then forced into that orientation in which the two alkyl substituents at the incipient C···C bond are *trans* to each other.[141]

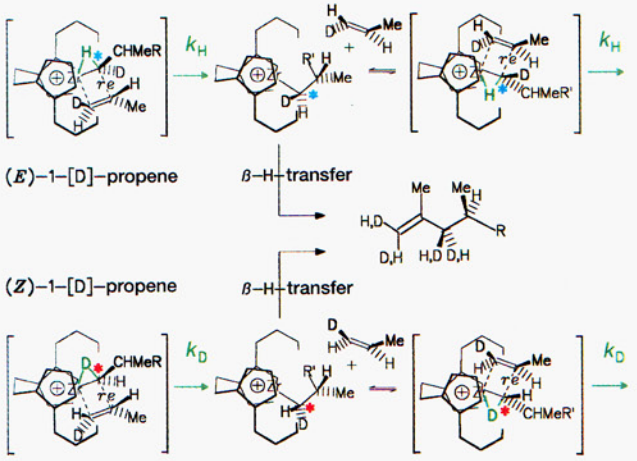
Experimental proof for this catalytic-site control by means of chain-segment orientation was provided by Pino and co-workers.[142] Chiral hydrotrimers and hydrotetramers with the predicted absolute configurations were obtained when propene was hydrooligomerized[143a] with enantiomerically pure[103, 125] (en)(thind)$_2ZrMe_2$ activated by MAO in the presence of H_2. Formation of asymmetric oligomers with olefinic end groups in similar reaction systems without H_2 were studied by Kaminsky and co-workers[143b] and found to follow the same rules.



Scheme 14. Models for the stereocontrol of olefin insertions in *ansa*-zirconocene catalysts, proposed by Corradini, Guerra, and co-workers [139]. The growing alkyl chain occupies an open sector of the ligand framework; the olefin enters the reaction complex with its substituent *trans* to the C(α)–C(β) chain segment. For C_2-symmetric complexes identical enantiofacial olefin orientation at both coordination sites results in isotactic polymer formation (top); for C_s-symmetric complexes the enantiofacial orientation alternates between coordination sites and leads to syndiotactic polymers (bottom).

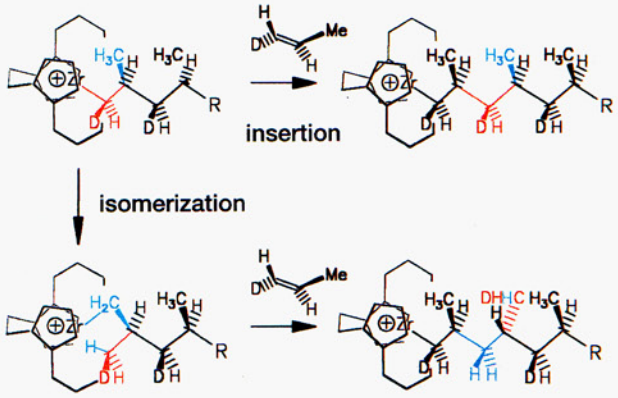
The origin of stereoselectivity in *ansa*-metallocene catalysts was further examined by use of α-deuterated olefins. In studies similar to those previously reported for achiral zirconocene and scandocene catalyst systems,[80, 82] stereokinetic isotope effects of $k_H/k_D \approx 1.4$ were observed for hydrodimerization of (*E*)- and (*Z*)-1-[D_1]-1-hexene by chiral *ansa*-zirconocene and scandocene catalyst systems.[144–146] This indicates that the insertion reaction favors a transition state in which the α-H and not the α-D atom of initially formed Zr–CHD–R unit is in a position suitable for α-agostic interaction with the metal center. Recently stereokinetic isotope effects of $k_H/k_D \approx 1.3$ were determined directly for isotactic propene polymerizations catalyzed by (en)(thind)$_2$ZrCl_2/MAO and other chiral *ansa*-zirconocene catalysts from the mean chain lengths of polymers produced from either (*E*)- or (*Z*)-1-[D_1]-propene (Scheme 15).[145b] These results indicate that α-agostic interactions control the stability of alternative transition states for the insertion of an olefin into a metal–alkyl bond.

These α-agostic interactions can thus be considered to be the origin of the stereoselectivity of chiral *ansa*-metallocene catalysts. Of the two alternative Zr–C(α)–C(β) orientations resulting from binding one of the α-H atoms to the metal center, one orientation is sterically inaccessible since it would cause the growing chain to collide with a β-substituent of the chiral ligand framework; the other one is sterically unencumbered and in fact practically indistinguishable from that proposed by Corradini and co-workers[139] on the basis of nonbonding van der Waals repulsions alone (see Scheme 14). The α-agostic model would thus describe the *re* or *si* orientation of an inserting olefin as being controlled by the required placement of the β-C atom of the growing chain in the more open of the two possible positions at a rigid three-membered Zr–H(α)–C(α) ring.



Scheme 15. Stereokinetic isotope effects in isotactic polypropene formation indicate α-agostic interactions in the olefin insertion transition state [145]. Chain growth with (*E*)-1-[D]-propene proceeds faster, due to its Zr ← H–C(α)-stabilized transition state, than that with (*Z*)-1-[D]-propene, which proceeds via a transition state with a Zr ← D–C(α) interaction; this is manifested in polymer chain lengths that are ca. 1.3 times longer for (*E*)- than for (*Z*)-1-[D]-propene.

The exclusion of one of the possible Zr–H(α) interactions implied by this model raises questions as to the origin of the stereoerrors produced by homogeneous catalysts especially at higher reaction temperatures. Increased stereoerror frequencies at decreased olefin concentrations, recently observed by Cipullo and Busico, and by Resconi and co-workers,[131] were ascribed to an epimerization of the last inserted unit, which competes with olefin insertion. Direct evidence for stereoerror formation by chain-end isomerization was obtained by Leclerc and Brintzinger from a study of D-label distributions in isotactic polypropene obtained from (*E*)- or (*Z*)-[D_1]-propene with chiral *ansa*-zirconocene catalysts.[145b] The appearance of CH_2D instead of CH_3 groups in the *mrrm* stereoerror positions indicates that most of these errors arise from the isomerization represented in Scheme 16. *ansa*-Zirconocene catalysts with par-



Scheme 16. Formation of stereoerrors by chain-end isomerization [145]. Isolated (*mrrm*-framed) stereoerrors are associated with CH_2D instead of CH_3 groups in isotactic polypropene made from (*E*)- or (*Z*)-1-[D]-propene with (en)(thind)$ZrCl_2$/MAO. The stereoinverted CH_2D groups must originate from the α-CHD olefin terminus by an isomerization process, the exact mechanism of which is still being debated [131a, b].

ticularly high stereoselectivity[117h, i, 120b, d] thus appear to owe this property to their suppression of chain-end isomerization relative to olefin insertion.

3.3. Activities of *ansa*-Zirconocene Catalysts

The rate of a reaction is normally expected to decrease when it is made stereoselective by imposing steric restrictions on some of its possible reaction modes. Yet even the first studies on propene polymerization with the chiral *ansa*-zirconocene catalyst *rac*-(en)(thin)$_2$ZrCl$_2$/MAO showed its catalytic activity to be substantially higher than that of the stereochemically unselective, unsubstituted catalyst Cp$_2$ZrCl$_2$/MAO.[106, 107g] Even the sterically strongly congested chiral catalyst *rac*-Me$_2$Si(2-Me-4-*t*Bu-C$_5$H$_2$)$_2$ZrCl$_2$/MAO produces polypropene at higher rates than Cp$_2$ZrCl$_2$/MAO system.[120c]

Apparently, some favorable effects compensate for the steric congestion of a β-substituted *ansa*-metallocene. β-Substituents might favor formation of active, olefin-separated ion pairs at the expense of the presumably dormant contact ion pairs or, alternatively, facilitate access to an α-agostic insertion transition state by destabilizing the β-agostic interactions that otherwise compete.

With regard to the effects of different bridging units linking the C$_5$ ring ligands, one finds that zirconocenes with the one-atom bridge Me$_2$Si yield somewhat more active catalysts than otherwise comparable complexes with the two-atom bridge C$_2$H$_4$,[116f, 117g] most likely because such a short bridge widens the coordination-gap aperture.[137] Zirconocenes with three-atom or four-atom bridges have so far all been found to be practically inactive for propene polymerization in the presence of MAO.[117b, 148–150a] The same is true for chiral zirconocenes containing two Me$_2$Si bridges.[150b] Structural studies on these inactive complexes reveal that the geometrical constraints of their interannular bridges place at least one and, in some cases, two of the substituents on the C$_5$ ring in a central position close to the meridional centroid–Zr–centroid plane (Fig. 6). Substituents in this position appear to interfere with the course of the otherwise facile insertion of an α-olefin into the Zr-bound alkyl chain, most probably by colliding with the alkyl substituent of the olefin substrate, which has to be close to this meridional position in the insertion transition state. In accord with this view, these propene-inactive catalysts are generally found to be active in the polymerization of ethene, which is unobstructed by a substituent.[117b, 150, 151a]

Different ring substituents also affect catalyst activities to a substantial degree. Low activities in MAO-activated propene polymerization are obtained with the *tert*-alkyl-substituted *ansa*-zirconocenes Me$_2$Si(2-Me-4-R-C$_5$H$_2$)$_2$ZrCl$_2$ with R = *tert*-butyl or 1-methyl-cyclohexyl.[120c] A kinetic study by Fischer and Mülhaupt revealed, however, that these catalyst systems show even higher initial activities than some of the most productive bis(benzindenyl) catalysts, but differ from these by a very fast deactivation to rather low levels of residual steady-state activity.[69d]

Annelation of further six-membered rings as in Me$_2$Si-(benz[*e*]indenyl)$_2$ZrCl$_2$ results in three- to fourfold increases in productivity.[117h, i, 120d] These high activities are likely to stem

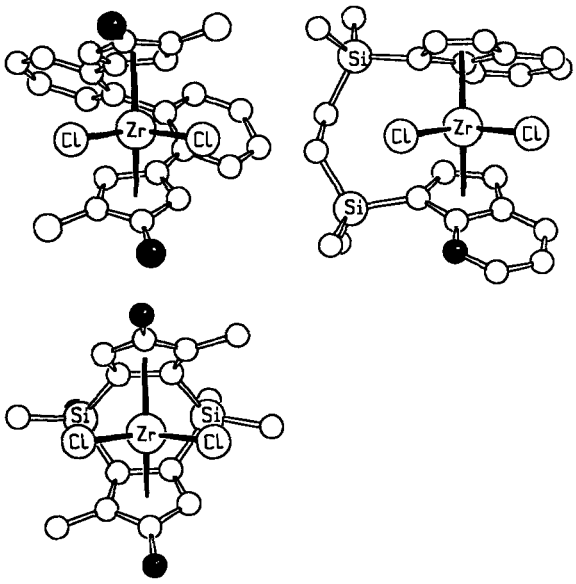


Fig. 6. Crystal structures of *ansa*-zirconocene complexes that are inactive for propene polymerization in the presence of MAO [117b, 150]. A substituent on the C$_5$ ring close to the meridional centroid–Zr–centroid plane appears to block the insertion of propene (but not that of ethene).

from steric or electronic shielding of the cationic reaction center against coordination of MAO-bound anions or other metallocene units by the extended annelated ring systems. Overall, little is known about the effects of electronic factors on catalyst activities.[119b, 152]

Isospecific metallocene catalysts usually polymerize propene at rates four to five times slower than those for ethene.[132a] This preference for ethene is less pronounced, however, than that observed with the unsubstituted system Cp$_2$ZrCl$_2$/MAO.[39e, f] Ewen's C_s-symmetric, syndiospecific catalyst is unique in that it polymerizes propene with higher activity than ethene.[132a] Higher α-olefins such as 1-butene[106] and 1-hexene,[50c] and even α-olefins branched at their 4-position such as 4-methyl-1-hexene[152] are polymerized by *ansa*-metallocene catalysts at rates only moderately lower than those for propene. The rather low degree of chemoselectivity of these catalysts is essential for their properties as copolymerization catalysts (cf. Section 4.1).

Studies with chiral olefins such as 4-methyl-1-hexene have shown that an enantiomeric catalyst center—both in homogeneous[152] and in heterogeneous catalyst systems[153a]—tends to incorporate preferentially one of the olefin enantiomers into the growing polymer chain.[153b, c]

With α-olefins branched in 3-position such as 3-methyl-1-pentene, *ansa*-zirconocene catalysts generally have negligible activities.[154] Styrene, formally also an olefin branched in 3-position, has not yet been polymerized at any worthwhile rate by MAO-activated metallocene catalysts.[36] The CpTiR$_3$/MAO systems that catalyze this reaction[7b] appear to polymerize styrene through a 2,1-concatenation, that is, by formation of secondary insertion products.[138b, 155] Apparently, the regioselectivity of *ansa*-zirconocene-based polymerization catalysts for 1,2-insertions is incompatible with the preference of styrene for 2,1-insertion.

Occasional regioerrors appear to inhibit the polymerization of normal α-olefins by MAO-activated metallocene catalysts

significantly.[114, 120, 136, 156, 157] Kashiwa, Tsutsui, and co-workers[156] found that the rates of propene and butene polymerization by (en)(ind)$_2$ZrCl$_2$/MAO increase in the presence of H_2 roughly 10- and 60-fold, respectively. These polymers were found to be free of misinserted units; hydrogenolysis apparently eliminates the slowly inserting 2,1-units and allows the start of a new, fast-growing polymer chain.

Busico, Cipullo, and Corradini[157] determined the frequency with which oligomers having primary and secondary end groups are liberated from zirconocene centers by hydrogenolysis in propene hydrooligomerization catalyzed by (en)(ind)$_2$ZrCl$_2$/MAO. Their data indicate that insertion of propene into a secondary Zr–alkyl unit is about 100 times slower than into a primary one.[158] As a consequence, 2,1-insertions with an incidence frequency of only 1% are sufficient to tie up about 90% of the catalyst in secondary Zr–alkyl units when polymerizations are conducted in the absence of H_2. Based on Busico's estimate, substantially increased activities can be expected for a catalyst that would be unimpeded by occasional 2,1-misinsertions.

Activities of chiral zirconocene catalysts are also affected by MAO concentrations. Increasing activation occurs at Al:Zr ratios of up to roughly 1–5000:1, while inhibition is observed at still higher Al:Zr ratios.[75, 132a] For propene polymerization with (en)(thind)$_2$ZrCl$_2$/MAO,[106, 116b] Me$_2$Si(ind)$_2$ZrCl$_2$/MAO,[116c, 117c] or Me$_2$C(Cp)(9-fluorenyl)ZrCl$_2$/MAO activity maxima are found at Al:Zr ratios between about 1000:1 and 10000:1.[116d–f] Apparently, yet unknown types of equilibria interconnect a diversity of species in these reaction systems.

Puzzling is also the dependence of catalyst activities on the monomer concentration. In several recent studies[69c, 120d, 132c] polymerization rates have been observed to increase more than linearly with olefin concentrations, for example, as [olefin]$^{1.4-1.7}$. Whether these observations indicate the participation of more than one olefin molecule in the insertion transition state[76]—a notion diverging from most of the current thinking about this reaction—or whether they arise from the participation of a second olefin in another reaction step that augments the overall activity of the catalyst, such as reactivation following a 2,1-insertion,[156, 157] remains to be clarified.

3.4. Polymer Chain Lengths and Crystallinity

Molecular weight is another property of polyolefins that is strongly influenced by the metallocene catalyst employed. Initial studies with (en)(ind)$_2$ZrCl$_2$/MAO and (en)(thind)$_2$ZrCl$_2$/MAO yielded polypropene with molecular weights ranging from $M_w \approx 50000\ g\,mol^{-1}$ at ambient polymerization temperatures down to $M_w \approx 10000\ g\,mol^{-1}$ at 60–70 °C.[106, 112, 114, 116c, 117g] These molecular weights are almost two orders of magnitude higher than those of the atactic polypropene obtained under otherwise identical conditions with Cp$_2$ZrCl$_2$/MAO. This effect is probably due, at least in part, to an increased rate of chain propagation v_P for *ansa*-metallocene catalysts.[117g] In addition to an increased v_P, β-substituents in these complexes might also cause a decreased rate of chain termination v_T, for example by sterically hindering the tertiary β-CH group of the growing chain in its approach to the Zr center. Bulky β-*tert*-butyl substituents as in Me$_2$Si(2-Me-4-*t*Bu-C$_5$H$_2$)$_2$ZrCl$_2$/MAO lead to rather low molecular weights at elevated temperatures[69b, 120a–c] A relatively high fraction of isopropyl end groups indicates that chain growth is frequently terminated here by transfer of the polymer chain to an Al center, presumably of the trimethylaluminum component of the MAO cocatalyst.[120c]

The molecular weights initially accessible with metallocene-based catalysts were far lower than those obtained with heterogeneous Ziegler–Natta catalysts. Higher molecular weight polymers were obtained with the analogous hafnium complexes (en)(ind)$_2$HfCl$_2$/MAO and (en)(thind)$_2$HfCl$_2$/MAO, albeit at the expense of substantially decreased catalytic activities.[116b, c, 135] Further studies revealed that additional α-methyl substituents at each C$_5$ ring ligand increase molecular weights of the polymers produced by factors of 3 to 5.[118, 120a–c] With α-methylated complexes such as Me$_2$Si(2-Me-ind)$_2$ZrCl$_2$ and Me$_2$Si(2-Me-benzind)$_2$ZrCl$_2$, polypropene can be obtained at $T_P = 50$ °C with molecular weights of $M_w = 100000–400000\ g\,mol^{-1}$.[117f, h, 120d] Polypropene with M_w close to $1000000\ g\,mol^{-1}$ is accessible with the catalyst Me$_2$Si(2-methyl-4-naphthyl-1-indenyl)$_2$ZrCl$_2$/MAO developed by Spaleck and co-workers.[117h]

β-Hydride transfer from the growing polymer chain directly to a coordinated olefin (see Scheme 8) has been implied as a dominant chain termination process by studies on end-group distributions in ethene–propene copolymers[97] and on hydrooligomer distributions at different olefin concentrations.[157c] In *ansa*-zirconocene catalysts without α-methyl substituents, direct β-H transfer from the growing polymer chain to a coordinated olefin does indeed appear to predominate, as indicated by a near-constancy of molecular weights with increasing olefin concentration.[120d, 157c] For *ansa*-metallocene catalysts with α-methyl substituents, however, a strong increase of molecular weight almost proportional to olefin concentration[117h, 120d] indicates that the remaining chain termination arises almost exclusively from β-H transfer to the metal. α-Methyl substituents thus appear to block a relatively large fraction of chain terminations that would otherwise arise from β-H transfer directly to a coordinated olefin.

Narrow molecular weight distributions, as measured by polydispersity ratios of $M_w/M_n \approx 2$,[105, 106, 112, 114, 117g, 118, 120] are as typical for these stereoregular polyolefins as for the atactic polymers produced with MAO-activated Cp$_2$ZrCl$_2$.[39e, g] Substituted *ansa*-zirconocene catalysts thus also appear to induce the growth of their respective polymer products at a single type of active center.

A polydispersity of $M_w/M_n \approx 1$, which indicates a "living" polymerization system (i.e. polymer chains permanently attached to the metal centers on which they simultaneously start to grow),[90] are typically observed for ring-opening metathesis[159, 160] and group-transfer polymerization catalysts,[161a, b] but so far not with either heterogeneous Ziegler–Natta catalysts or with zirconocene-based catalysts for normal α-olefin polymerization. Polymerization systems with a finite life span have been obtained with scandium-based metallocene catalysts.[62] Their utilization for the formation of ethene–methacrylate block copolymers as well as partially living polymerizations of cycloolefins with zirconocene-based catalysts will be discussed

in Sections 4.1 and 4.2, respectively. Development of truly living α-olefin polymerization systems remains a challenge.[162]

Stereoregularity, regioregularity, and chain length of a polypropene all appear to influence its crystallinity as well as its melting behavior and mechanical properties. Heterogeneously produced isotactic polypropenes normally crystallize in a regular packing of parallel helices, the classical α-modification.[163] In contrast, isotactic polypropenes produced by homogeneous, C_2-symmetric *ansa*-zirconocene catalysts often crystallize from their melts with sizeable fractions of a heretofore infrequently observed[164] γ-modification,[114, 165–167b] which was found by Brückner and co-workers to contain alternate layers of helices oriented at an angle of 81° to each other.[166] For a given polypropene sample, the fraction of this γ-modification, as measured by wide-angle X-ray diffraction (WAXD), appears to be inversely related to the average length of isotactic chain segments, n_{iso}, if one takes into account that stereoerrors as well as regioinversions and chain ends limit the length of the isotactic segments.[69b, d, 168]

Statistical factor analysis has been used to correlate the melting points of isotactic polypropenes with the substituent patterns of the *ansa*-zirconocene catalysts used, without differentiating between effects of regio- and stereoerrors and chain lengths variation.[169a] Melting points and total crystallinity both appear to be directly correlated with the average length of isotactic chain segments in these polyolefins.[69d] A finite fraction of noncrystalline segments within each polypropene chain appears to augment the toughness of the polymer materials.[117e, 169b] These segments apparently function as flexible links between the crystalline polymer domains (Fig. 7).

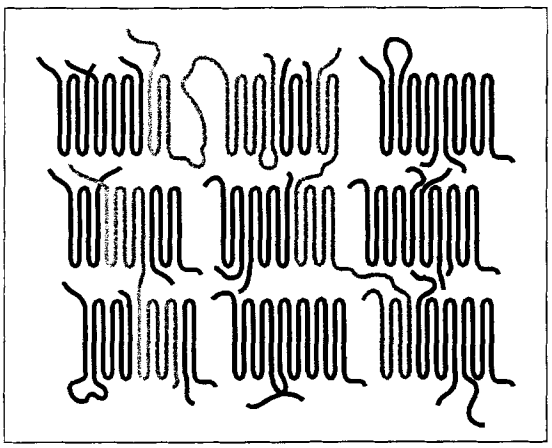


Fig. 7. Noncrystalline segments within longer polymer chains act as flexible links; they connect the crystalline polymer domains and render the polymer tougher (less brittle).

Several crystal modifications have now also been characterized for the syndiotactic polypropenes formed with C_2-symmetric metallocene catalysts.[167c, 170–173] Their crystallinity appears to correlate again with the length of uninterrupted syndiotactic chain segments;[174] a large proportion of an amorphous phase, together with a small crystallite size, appears to cause the high transparency of this material.[169b] Syndiotactic polypropene can slowly form highly crystalline solids with a melting point of about 160 °C when kept just slightly below the melting temperature.[171b] Correlations between the structures of polyolefin materials produced with different homogeneous catalysts and their respective thermal, mechanical, and optical properties are presently being studied in more detail than can be accounted for within the limits of this review.[167, 175]

4. Olefin Copolymerization and New Polyolefin Materials

While the development of homogeneous, chiral metallocene catalysts can be seen mainly as an opportunity for in-depth studies on the fundamental principles of stereoselective α-olefin polymerizations, two examples of homogeneously produced polymers encountered already, syndiotactic and hemiisotactic polyolefins, are inaccessible with heterogeneous Ziegler–Natta catalysts. In the following chapter, we summarize additional examples for the formation of polyolefin materials by homogeneous metallocene catalysts which extend beyond the capabilities of classical heterogeneous polymerization catalysts.

4.1. Copolymers from Ethene and Higher Olefins

Olefin copolymers, especially those of ethene with propene and/or another α-olefin, are of great practical interest; their total production volume is comparable to that of the homopolymers. New possibilities for controlling the properties of olefin copolymers with metallocene-based catalysts have recently caught the interest of industrial chemists and will thus be summarized here.

Linear polyethene with short-chain branches, which has low crystallinity and, hence, low density (*l*inear *l*ow-*d*ensity *poly*ethene, LLDPE) is obtained by copolymerization of ethene with 1-butene, 1-hexene, and/or 1-octene.[176] Its mechanical properties, which differ from those of the long-chain branched LDPE (*l*ow-*d*ensity *poly*ethene) produced by high-pressure radical polymerization, make LLDPE one of the largest volume polyolefin products. Copolymerization of propene with small amounts of ethene gives copolymers of lower crystallinity;[177] increased fractions of ethene lead to amorphous materials with rubber-like elasticity (EP-rubbers). Blending of these EP-rubbers with the stiffer but brittle polypropene yields heterophase materials with balanced toughness–stiffness properties which have opened new ranges of practical applications for these polyolefin blends.[178, 179]

Mechanical, thermal, and optical properties of these copolymers obviously depend on their comonomer content; however, to a significant degree they also depend on the distribution of the comonomers between and within individual polymer chains. If a catalyst distributes the comonomers randomly along each chain, an amorphous polymer is to be expected, whereas partially crystalline polymers are likely to result when the monomers are collected into separate blocks.

The comonomer selectivity of a given catalyst, in other words its tendency to insert one of two competing monomers into each type of metal–chain-end bonds, is expressed by its copolymerization parameters r_1 and r_2 (the subscripts specify the monomer).[176a, 180] These are defined as $r_i = k_{ii}/k_{ij}$, the ratio of

the rate constant for a homopolymerization step (k_{ii}) over that for a copolymerization step (k_{ij}).[181, 182] The product r_1r_2 is an indicator for the distribution of two monomers along each chain.[176] Values of $r_1r_2 > 1$ indicate that a catalyst tends to collect at least one of the comonomers into separate blocks, while a catalyst with $r_1r_2 < 1$ tends to alternate isolated comonomer units along each chain.[183]

Values of $r_1r_2 > 1$ are typical for ethene–propene copolymers made with heterogeneous polymerization catalysts[177b, 184b] (Table 1) and indicate that these catalysts tend to collect each

Table 1. Copolymerization parameters r_1 and r_2 for ethene and a second α-olefin. For heterogeneous catalysts (entries 1–3) values of $r_1r_2 > 1$ indicate that the monomers are incorporated in blocks; for metallocene-based catalyst systems (entries 4–9), random or alternating monomer sequences are indicated by values of $r_1r_2 \leq 1$.

Entry	Catalyst	r_1	r_2	r_1r_2
1	δ-$TiCl_3$/$AlEt_3$ [176c]	7.3	0.76 [a]	5.5
2	$MgCl_2$/$TiCl_4$/$AlEt_3$ [184a]	–	– [a]	4
3	SiO_2/$MgCl_2$/$TiCl_4$/$AlEt_3$ [184a]	5–10	0.2–0.34 [a]	1.9
4	$(C_5H_5)_2ZrCl_2$/MAO [190]	48	0.015 [a]	0.72
5	$C_2H_4(ind)_2ZrCl_2$/MAO [194a]	2.57	0.39 [a]	1.0
6	$C_2H_4(thind)_2ZrCl_2$/MAO [194a]	2.90	0.28 [a]	0.81
7	$Me_2C(Cp)(flu)ZrCl_2$/MAO [197]	1.3	0.20 [a]	0.26
8	$C_2H_4(thind)_2ZrCl_2$/MAO [193]	59	0.012 [b]	0.71
9	$Me_2Si(ind)_2ZrCl_2$/MAO [193]	25	0.016 [b]	0.4

[a] Ethene/propene. [b] Ethene/1-hexene.

type of monomer into separate blocks. In addition, the nonuniform centers of heterogeneous polymerization catalysts have in general different copolymerization characteristics.[6, 176b, 185] Analysis of the copolymer products by *t*emperature-*r*ising *e*lution *f*ractionation (TREF) and cross-fractionation[186] (Fig. 8) shows that the higher α-olefin is preferentially incorporated at the centers that produce shorter chains; higher olefins are thus enriched in the low molecular weight fractions of these copolymers.[187] This increases the content of extractables and tends to make these materials sticky, two generally undesirable properties.

In their early studies on chiral, metallocene-based catalysts such as (en)$(thind)_2ZrCl_2$/MAO, Kaminsky and co-workers had noticed that these catalysts polymerize propene or 1-butene with only modestly lower rates than ethene.[39c–h, 188] Accordingly, copolymers obtained with these catalysts contain larger fractions of higher olefins than those obtained with heterogeneous catalysts under comparable conditions.[176, 177] These and additional studies,[189–193] particularly by the groups of Zambelli,[122, 136b] Chien,[194] Soga,[195] and Kashiwa,[66, 97] showed that copolymers produced by metallocene-based catalysts consist of uniform chains with narrow molecular weight distributions typical of single-site catalysts. The copolymer chains contain the comonomers in nearly random placement,[196] as indicated by copolymerization-factor products of $r_1r_2 \approx 1$ (Table 1); their TREF characteristics (Fig. 8) show that comonomer distributions are essentially independent of chain lengths, an important aspect for applications of these copolymers, for instance in films or sealant layers.

The copolymerization characteristics of metallocene-based catalysts vary with the metallocene complex used.[197] Higher

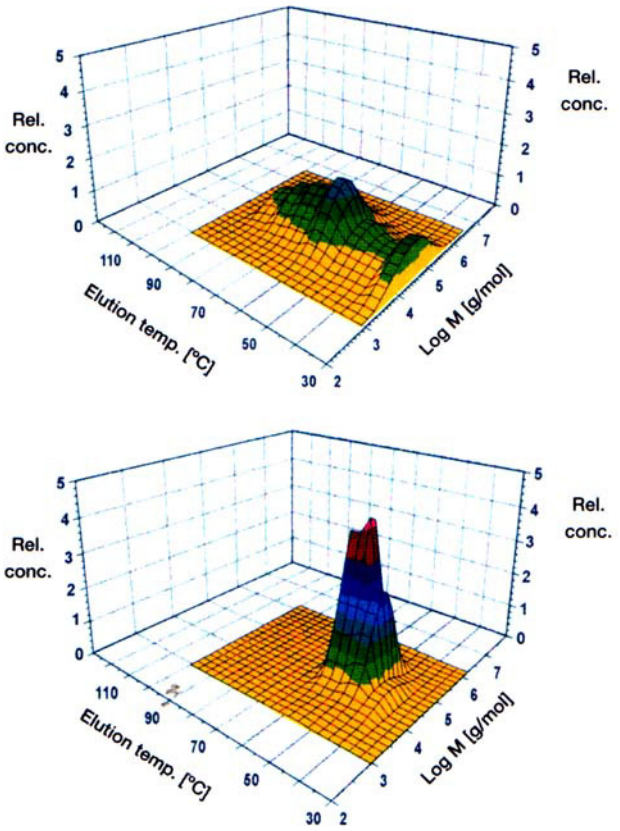


Fig. 8. Holtrup cross-fractionation of a conventional (top) and a metallocene-derived (bottom) ethene–butene random copolymer (LLDPE). Whereas LLDPE produced by classical heterogeneous catalysts contains a mixture of polymer chains with different composition and chain lengths, LLDPE produced by metallocene catalysts shows chemical uniformity and a very narrow molecular weight distribution.

α-olefins are taken up more readily by isospecific, chiral *ansa*-metallocenes than by unbridged complexes. An even greater tendency for the incorporation of higher α-olefins is evident for the syndiospecific catalyst $Me_2C(Cp)$(fluorenyl)$ZrCl_2$/MAO. This trend reflects the rising activities in this series of catalysts for the homopolymerization of higher α-olefins as compared to that of ethene.[132a] But even monomers that are not homopolymerized by metallocene catalysts, for example isobutene,[188f] styrene, and 1,3-dienes,[188e, 191] are incorporated, albeit in minor amounts, into various copolymers.[39c, 188, 189d, 191, 194d]

Even less restricted than the metallocene-based catalysts with regard to comonomer selection are monocyclopentadienyl complexes such as MAO-activated dimethylsilyl-bridged amidocyclopentadienyltitanium complexes.[7a, 189c, 198] These catalysts (Fig. 9) incorporate into their polymer products even the vinylic end groups of polymer chains terminated by β-hydrogen transfer; they can thus generate copolymers with long-chain branches, in contrast to the strictly linear LLDPE copolymers produced by metallocene-based catalysts.[189c, 198a] These catalysts can also copolymerize styrene with ethene;[7a] styrene units in these copolymers are mostly isolated and of low regioregularity. Whether styrene–ethene and styrene–1,3-diene copolymers can be obtained also with the unbridged titanium system $CpTiCl_3$/MAO,[199–201] which catalyzes the syndiotactic homopolymerization of styrene,[7b] needs further clarification.[202]

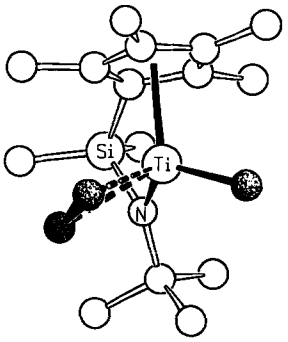
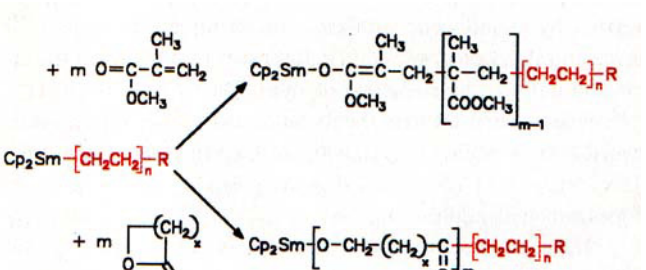


Fig. 9. Monocyclopentadienyltitanium complex with an Me_2Si-bridged alkylamido ligand framework [7a] which catalyzes, in the presence of MAO, formation of long-chain branched copolymers [198] (ab initio model for the C_2H_4 complex of $Me_2Si(Me_4C_5)(tBuN)Ti-CH_3^+$) [87b, 88b].

A long-standing goal in olefin polymerization catalysis is the copolymerization of ethene or propene with olefins bearing polar functional groups such as acrylate esters or vinyl ethers. Copolymers of this type might endow polyolefins with some of the useful properties of polyvinyl esters or ethers such as their adhesiveness. While most metallocene-based polymerization catalysts appear to be as sensitive to oxygen-containing functional groups as their heterogeneous predecessors, advances toward the goal of incorporating olefins with polar functional groups into Ziegler–Natta polymerization systems have recently been made and will be discussed in Section 4.3.

Living polymerizations, briefly mentioned in Section 3.4, would allow the formation of block copolymers, with polar olefins as well as with other alkenes. Advances in this regard—catalyst systems with polymer chains bound to the central metal atom for at least some minutes—have recently been reported. Ethene–propene block copolymers, prepared by Turner and Hlatky with cationic hafnocene catalysts at lower temperatures, indicate that Hf–polymer bonds have a finite lifetime at these temperatures.[203] Yasuda and co-workers[204] utilized the persistence of lanthanide–alkyl bonds[62] to prepare ethene copolymers with polar polyacrylate or polyester blocks. They first polymerized ethene with a samarocene catalyst and used this system then to initiate the polymerization of the polar monomer by group-transfer polymerization or by ring-opening polymerization of a lactone (Scheme 17).



Scheme 17. Block copolymers from ethene and polar monomers obtained by Yasuda and co-workers [204] with a samarocene catalyst. A living Sm–polyethene system is utilized to initiate group-transfer or ring-opening polymerizations of unsaturated or cyclic esters.

Studies on ^{13}C NMR characteristics of ethene–propene copolymers have led to rather complete assignments of their repeat patterns and end group signals.[97, 205] Isospecific *ansa*-zirconocene catalysts generate copolymers with mainly *m*-oriented side chains, as expected from their stereoselectivity.[197] Studies by Zambelli and co-workers on propene copolymers with ^{13}C-labeled ethene showed furthermore that the stereoselectivity of the catalyst system is undiminished by incorporation of ethene, thus proving that this stereoselectivity is indeed caused by the chirality of the metallocene centers and not by that of the last inserted monomer unit.[122]

End group distributions in ethene–propene copolymers were studied by Kashiwa and co-workers by ^{13}C NMR spectroscopy.[97] The strong prevalence of *n*-propyl ends and the near-absence of ethyl end groups were taken as evidence that chain termination occurs mainly by β-H transfer directly to a coordinated propene molecule rather than to the metal followed by monomer insertion into the Zr–H bond, as discussed in Section 2.4.

As with heterogeneous Ziegler–Natta catalysts,[176b] a distinct comonomer effect is generally observed with MAO-activated zirconocenes.[66, 182, 188, 206] Under otherwise identical conditions, the rate of copolymerization of ethene with higher α-olefins often exceeds that of the homopolymerization of ethene. This effect is difficult to reconcile with the fact that homopolymerization rates are higher for ethene than for other α-olefins and that ethene is always preferentially incorporated into the copolymer. It remains to be clarified whether these comonomer effects are due to increased rates of ethene insertion into a $Zr-CH_2-CHR-$ rather than into a $Zr-CH_2-CH_2-$polymer bond (e.g. by destabilization of a β-agostic resting state of the former[26i, 63, 89, 120a]), to cooperative effects of both olefins (e.g. in insertion transition states involving two olefins[76]), or simply to a higher solubility of a copolymer in the reaction medium[206b] (which might allow for higher rates of diffusion of the monomers to the catalyst centers).

4.2. Cycloolefin Polymerization and Diolefin Cyclopolymerization

A distinctive property of homogeneous, metallocene-based polymerization catalysts is their capability to induce the polymerization of cyclic olefins without inducing ring-opening metathesis, which is characteristic of those heterogeneous Ziegler–Natta catalyst systems that polymerize cycloolefins.[4a] As noted by Kaminsky and co-workers,[207a] cyclobutene, cyclopentene, norbornene, and dimethanooctahydronaphthalene but not cyclohexene (Scheme 18) are polymerized with remarkably high activities by chiral *ansa*-zirconocene catalysts such as $(en)(ind)_2ZrCl_2$/MAO and its Me_2Si-bridged analogue.

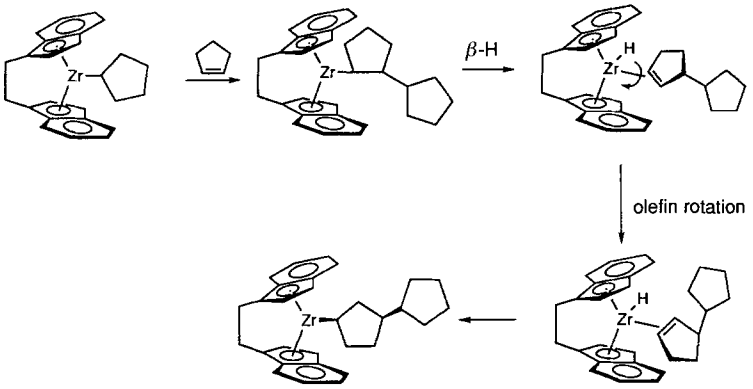
The homopolymers obtained from these reactions are highly crystalline with melting points around or above 400 °C,[207] close to their respective decomposition temperatures. Structural assignments for these polymers are rendered difficult by their



DMON

Scheme 18. Cyclic olefins used by Kaminsky and co-workers [207] in ring-preserving polymerization reactions with *rac*-$(en)(ind)_2ZrCl_2$/MAO or *rac*-$Me_2Si(ind)_2ZrCl_2$/MAO.

insolubility in all common solvents. Instead of a 1,2-enchainment as originally proposed by Kaminsky and co-workers for polymers of cyclopentene,[207b] a 1,3-enchainment was revealed in a recent study by Collins and Kelly[208a] on the corresponding zirconocene/MAO-catalyzed hydrooligomerization. The mechanism proposed for this enchainment—1,2-insertion followed by β-H elimination, olefin rotation, and reinsertion—is analogous to that assumed to lead to the minor fraction of 1,3-inserted propene units in propene polymerization with these catalysts.[114, 136a, b, 208b] Apparently, the intermediate derived from 1,2-insertion of cyclopentene is sterically too demanding to permit insertion of another cyclopentene and has to isomerize before another olefin inserts (Scheme 19). This system is an interesting example for an insertion–isomerization type of polymerization with metallocene-based catalysts.[209]

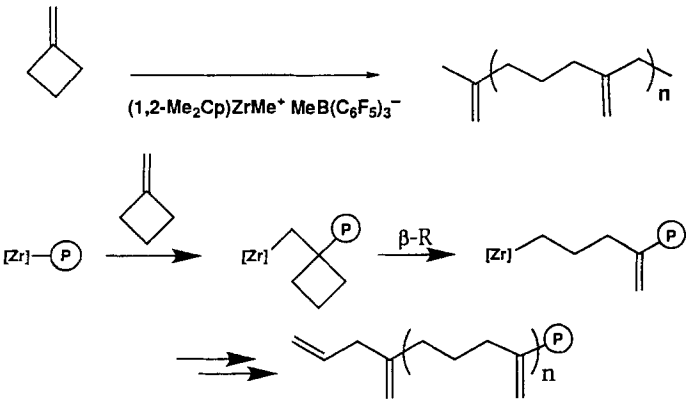


Scheme 19. Mechanism for the formation of 1,3-linked polycyclopentene proposed by Collins and co-workers [208].

The cycloolefin polymers prepared with chiral (en)(ind)$_2$-$ZrCl_2$/MAO as catalyst are undoubtedly stereoregular;[208, 209] whether they have an isotactic structure like that of the other olefin polymers produced by this catalyst could not yet be established unequivocally.

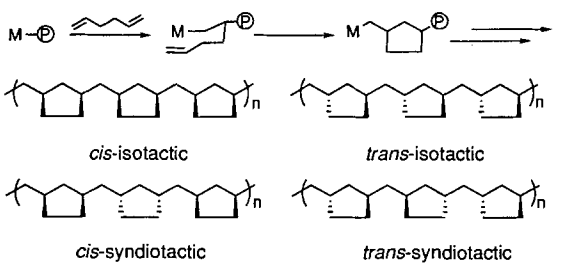
Studies on the copolymerization of cyclic monomers with ethene or propene[207, 210] showed that all of the cycloolefins mentioned above, as well as cycloheptene and cyclooctene, are incorporated into copolymers. While ethene is vastly more reactive than cyclopentene in the catalyst system (en)(ind)$_2$$ZrCl_2$/MAO, with a comonomer selectivity factor of $r_1 = 80-300$, norbornene is quite readily incorporated, with $r_1 = 1.5-3.2$, such that a broad range of ethene/norbornene copolymers can be obtained with this system.[207] The cycloolefin copolymers are mostly amorphous (rather than crystalline like the respective homopolymers) and have a relatively high glass transition temperature. A 1,2-enchainment, rather than a 1,3-enchainment has been determined for the copolymers of cyclopentene and ethene.[207] Apparently, insertion of ethene is faster than isomerization of the cyclopentyl group at the zirconium center. In contrast to cyclopentene homopolymers, these copolymers are mostly amorphous; however, they often have relatively high glass transition temperatures.

An interesting ring-opening polymerization, which contrasts the ring-preserving polymerizations of internal cycloolefins discussed above, was recently reported by Marks and co-workers,[211] who observed that polymerization of exomethylenecyclobutane by [(1,2-$Me_2C_5H_3)_2$-$ZrMe^+ \cdots MeB(C_6F_5)_3^-$] yields a polymer with mainly ring-opened 2-methylene-1-buten-4-yl rather than the expected 1-methylenecyclobutan-1-yl units (Scheme 20). Apparently, insertion of the disubstituted olefin into a Zr–alkyl unit with a quarternary β-C atom is so slow that rearrangement of the latter by β-alkyl transfer to give a secondary Zr–alkyl unit is the preferred process. Kinetic data indicate that insertion of the disubstituted olefin into the latter—rather than the β-alkyl transfer—still limits the overall rate of this process, which has turnover numbers of about 400 h^{-1} at 25 °C.



Scheme 20. Ring-opening polymerization of methylenecyclobutane reported by Marks and co-workers [211]. Ring-opening β-alkyl transfer appears to be faster than insertion of methylenecyclobutane into the sterically hindered cyclobutylmethyl–Zr bond.

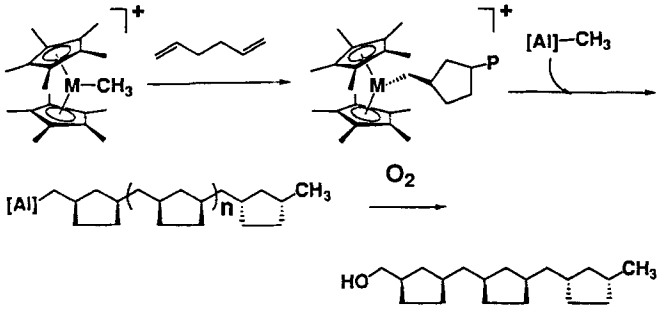
Another polymerization process that leads to 1,3-cycloalkanediyl units, connected this time by methylene groups, is the cyclopolymerization of nonconjugated dienes.[93, 95b, 212–217] It involves 1,2-insertion of one of the vinyl functions into a metal–carbon bond followed by an intramolecular cyclization (Scheme 21). The microstructure of the resulting polymers concerns the *cis*/*trans* stereochemistry of the rings and the relative stereochemistry between rings. The latter, i.e. the tacticity of the polymer, is determined by the enantiofacial selectivity of the metallocene catalyst in the first insertion step; the *cis*/*trans* stereochemistry of the rings, on the other hand, arises from the diastereoselectivity of the cyclization step.



Scheme 21. Cyclopolymerization of nonconjugated dienes studied by Waymouth and co-workers [93, 95, 213–217]. The *trans*-isotactic form represents an effectively chiral polymer; polymers with substantial molar optical rotations are obtained with *R*- or *S*-(en)(thind)$_2$$ZrCl_2$/MAO.

While the *cis/trans* diastereoselectivity can hardly be controlled with heterogeneous catalysts,[212] it is strongly influenced by substituents at the cyclopentadienyl ligands in metallocene-based catalysts.[93] Cyclopolymerization of 1,5-hexadiene by MAO-activated $(C_5H_5)_2MX_2$ (M = Ti, Zr, Hf; X = Cl, CH_3) leads to polymers containing predominantly *trans* rings, while cyclopolymerization with the more hindered catalyst $(C_5Me_5)_2MX_2$/MAO yields predominantly *cis* rings.

The melting points of the resulting polymers proved to be quite sensitive to the *cis/trans* ratio of the carbocycles.[213] *trans* Polymers are waxes with melting points $\leq 70\,^{\circ}C$; polymers containing $>90\,\%$ *cis* rings are crystalline and melt at 189 °C. Cyclopolymerization of unsymmetrical dienes such as 2-methyl-1,5-hexadiene with catalysts such as $Cp_2^*ZrMe_2$/MAO or with $[Cp_2^*ZrMe^+\cdots X^-]$ (X = $B(C_6F_5)_4$ or $H_3CB(C_6F_5)_3$) affords highly regioregular cyclopolymers.[215] The perfectly alternating head-to-tail microstructure must arise from the regioselective insertion of the less hindered terminus of the diene into the metal–polymer bond, which is sterically encumbered by its quarternary β-C atom. Cyclization of the disubstituted olefin yields a methylene-1-methylcyclopentan-3-yl intermediate (Scheme 22). This insertion appears to be greatly facilitated by its intramolecular nature; intermolecular insertions of disubstituted olefins into Zr–alkyl bonds are at best quite sluggish.



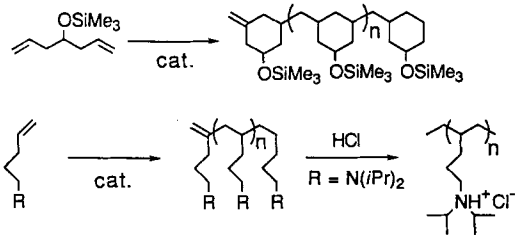
Scheme 22. Hydroxy-terminated cyclopolymers formed by alkyl exchange with a methylaluminum activator [95b].

Cyclopolymerization of 1,5-hexadiene generates polymers with substantially higher molecular weights than polymerization of 1-hexene with the same catalysts,[93] undoubtedly due to some hindrance of the β-H transfer that normally terminates growth of a polymer chain. For the cyclopolymerization of 1,5-hexadiene with a $Cp_2^*ZrCl_2$/MAO catalyst at $-25\,^{\circ}C$, chain transfer to aluminum was found to be the only chain termination process.[95b] The resulting poly(methylene–cyclopentane) was shown to bear an alkylaluminum end group, which could be oxidized with O_2 to give hydroxy-terminated polymers (Scheme 22). Cyclopolymerization of 2-methyl-1,5-hexadiene with the catalysts $[Cp_2^*ZrMe^+\cdots X^-]$ (X = $B(C_6F_5)_4$ or $H_3CB(C_6F_5)_3$), for which neither β-H transfer nor chain transfer to aluminum are feasible, gave a polymer with end groups derived from a β-CH_3 transfer process.[95b]

Although optically active olefin oligomers of low molecular weight can be obtained with enantiomerically pure *ansa*-metallocene catalysts,[140, 141b, 143b] stereoregular polyolefins of high molecular weight contain an effective mirror plane perpendicular to the molecular axis in the middle of the molecule and are thus achiral.[107c] Chiral polymers have now become available by metallocene-catalyzed cyclopolymerization of 1,5-hexadiene. Coates and Waymouth recognized that the *trans*-isotactic form of poly(methylene-1,3-cyclopentane) is chiral.[213, 217] Using MAO-activated, resolved (1*R*)-(en)(thind)$_2$Zr-binaphtholate as a catalyst, they obtained optically active poly(methylene-1,3-cyclopentane) with a molar optical rotation of $[\Phi]_D^{20} = +51.0$ ($c = 0.8$ in $CHCl_3$). Cyclopolymerization with the (1*S*) enantiomer of the catalyst gave the enantiomeric polymer. Cyclopolymers of 1,5-hexadiene obtained with (en)(thind)$_2$Zr-derived catalysts contain a mixture of *cis* and *trans* rings. Despite the presence of roughly 32 % *cis* rings, the molar optical rotation of the polymer ($[\Phi]_D^{20} = +22.8$) is considerably higher than that of the model compound *trans*-(1*R*,3*R*)-1,3-dimethylcyclopentane ($[\Phi]_D^{20} = +3.1$), presumably due to the presence of helical polymer conformations in solution. Interesting insights in this regard might come from X-ray diffraction studies on these chiral polymers. A ^{13}C NMR analysis of the microstructure of the polymer at tetrad resolution provided an estimate of 91 % for the enantiofacial selectivity of this cyclopolymerization reaction.[217]

4.3. Functionalized Polyolefins

Advances toward the goal of polymerizing polar monomers by Ziegler–Natta catalysis have recently been made with cationic metallocene catalysts. Waymouth and co-workers found that these catalysts are considerably more tolerant of functional groups than either conventional heterogeneous catalysts or homogeneous catalysts activated by MAO. Catalysts of the type $[Cp_2^*ZrMe^+\cdots X^-]$ (X^- = $B(C_6F_5)_4^-$ or $H_3CB(C_6F_5)_3^-$) are indeed capable of polymerizing a variety of functionalized α-olefins and dienes such as 4-*tert*-butyldimethylsiloxy-1-pentene, 5-*N*,*N*-diisopropylamino-1-pentene, and 4-trimethylsiloxy-1,6-heptadiene[218] (Scheme 23).



Scheme 23. Formation of polymers with O- or N-functional groups by use of borane-activated zirconocene catalysts reported by Waymouth and co-workers [218, 219]. R = $NiPr_2$, OTBDMS; cat = $[Cp_2^*ZrMe^+MeB(C_6F_5)_3^-]$.

Activities for the polymerization of 4-*tert*-butyldimethylsiloxy- and 5-*N*,*N*-diisopropylamino-1-pentene by the catalyst $[(C_5Me_5)_2ZrMe^+\cdots X^-]$ were lower than for 1-hexene, with average turnover numbers (at ca. 40–50 % conversion) ranging from 2700 h^{-1} for 1-hexene to 190 h^{-1} for 4-*tert*-butyldimethyl-siloxy-1-pentene and 130 h^{-1} for 5-*N*,*N*-diisopropylamino-1-pentene. Chiral $[rac$-(en)(thind)$_2$ZrMe$^+\cdots$X$^-]$ catalysts are active for the polymerization of 5-*N*,*N*-diisopropylamino-1-pentene, but not for that of 4-*tert*-butyldimethyl-

siloxy-1-pentene. Preliminary ^{13}C NMR analysis of poly-(5-*N*,*N*-diisopropylamino-1-pentene) obtained in this manner indicates an isotactic microstructure.[219]

Another approach toward functionalized polyolefins is the generation of α-olefin polymers capped by polar end groups. Polymers of this kind are principally accessible through living polymerizations. Living polymers of α-olefins have been obtained so far only in rare instances, at low temperatures[220, 221] (see Section 4.1). Complete transfer of polymer chains to aluminum centers of the cocatalyst, also useful for this purpose, has been observed in only one special case, again at temperatures below ambient.[95b]

In contrast to heterogeneous polymerization catalysts, which afford shorter propene oligomers only in the presence of H_2, that is, only with saturated chain ends, metallocene catalysts give easy access to propene oligomers with olefinic end groups, which can be converted to various other functional groups.[222, 223] Thiol-terminated oligopropenes have been used as chain transfer reagents in methacrylate polymerization to form poly(propene-*block*-methylmethacrylate). A new class of polymers containing pendant polypropene chains such as polymethylmethacrylate-*graft*-polypropene is derived from methacrylate-terminated oligopropene macromonomers, which are copolymerized with various acrylic esters, acrylonitrile, or styrene.[224a]

These polypropene block and graft copolymers are efficient blend compatibilizers. By enhancing the dispersion of otherwise incompatible polymers and improving their interfacial adhesion, these copolymers allow the formation of "alloys" of isotactic polypropene, for example, with styrene–acrylonitrile or polyamides.[224b, c] Polymer blends of this type afford property synergisms such as improved stiffness combined with improved toughness. They are obtained by way of the short isotactic polypropene chains with unsaturated end groups formed by the *ansa*-metallocene catalyst $Me_2Si(2\text{-}Me\text{-}4\text{-}t\text{Bu-}C_5H_2)_2ZrCl_2$/MAO.

5. Perspectives

The most remarkable aspect of metallocene-based catalysts appears to be that they can produce an unprecedented variety of polyolefins. The range of stereo- and regioregularities, molecular weights, and polydispersities of copolymers and cyclopolymers available with these catalysts exceeds that accessible with classical heterogeneous Ziegler–Natta catalysts and opens new possibilities for producing tailored polyolefin materials.

Much of our knowledge in this area has been acquired by application of rational conceptional models to the design of new metallocene structures and catalyst activators. Some traits of these catalysts, in particular their stereoselectivity, are now close to being predictable, based on our understanding of the essential elementary reaction steps in these homogeneous reaction systems. Other traits such as the formation of cyclic or functionalized polyolefins have been and continue to be discovered by testing our understanding of the basic reaction mechanisms of these catalysts against increasingly demanding tasks. This approach derives substantial support from the rapidly advancing methods for modeling even large metallocene reaction systems by ab initio and density functional methods.[84–88] These methods can also provide a calibration for useful molecular mechanics models for these catalysts,[86, 139, 225] which may eventually allow estimates of steric effects on the course of essential reaction steps, for example on competing insertion and chain termination reactions.

The evolution of advanced catalysts and catalytic processes based on rational model hypotheses is now beginning to carry over to heterogeneous Ziegler–Natta catalysis as well. Practical application of metallocene catalysts requires their preadsorption on solid supports such as alumina or silica gels.[189c, 200, 226–228] Instead of the polymer dust produced by a homogeneously dissolved metallocene catalyst, the solid catalyst particles generate coherent polymer grains.[117e, 229] As with classical heterogeneous catalysts, these grains appear to be enlarged replicas of the catalyst particles[117e, 228] (Fig. 10). Metallocene catalysts that are heterogenized, for example on a silica gel support, can thus be readily used in existing Ziegler–Natta production facilities, for instance in solvent-free slurry or gas-phase reaction systems.[227, 228]

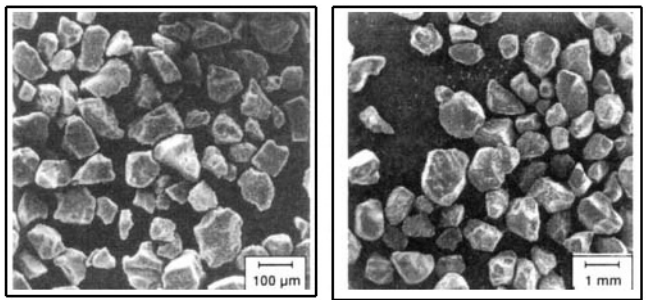


Fig. 10. Catalyst grains containing $Me_2Si(2\text{-}Me\text{-}benz[e]indenyl)_2ZrCl_2$/MAO on a silica gel support (left) and polymer grains grown on these in a gas-phase reactor at 70 °C (right, note different scale) [228].

Detailed guidelines have been developed for the selection of supports with optimal composition, particle size, pore size distribution, and surface OH group density, and for their treatment with various alkyl aluminum and aluminoxane activators[227, 228] prior or subsequent to adsorption of the metallocene complex. The more advanced of these protocols require only limited excess ratios of alkylaluminum activators per zirconocene unit; Al:Zr ratios of roughly 100–400:1, much below those used for homogeneous catalyst systems, appear to give entirely satisfactory activities for these surface-supported metallocene catalysts.[228, 230] In contrast to modern $MgCl_2$-supported heterogeneous Ziegler–Natta catalysts, silica gel supported metallocene catalysts are practically free of chlorine. This could be an advantage from a ecological standpoint when the chemical or thermal recycling of polymer products reaches a larger scale.[231]

Despite the practical advantages of supported catalysts, interactions between support materials and catalyst complexes are only partly understood on a molecular level. Based on the generally close resemblance of the polymer microstructures produced by a metallocene catalyst in homogeneous solutions and on solid supports, even in solvent-free gas phase systems,[228, 232] it appears likely that the active catalysts are quite

similar, in other words that the (presumably cationic) metallocene catalyst is only physisorbed on the alkylaluminum-pretreated (possibly anionic) catalyst surface. Based on this model, "microreactors" might be fabricated by immobilizing different types of single-site metallocene catalysts—or even catalyst cascades[193]—on suitable supports for in situ production of novel polyolefin blends and other environmentally friendly polyolefin materials.

Polymers with properties distinctly different from those produced in homogeneous solution—with unusually high molecular weights—have recently been obtained by fixing a metallocene catalyst on unpretreated supports[233] and by synthesizing covalently linked *ansa*-metallocenes directly on a SiO_2 support.[234] These observations are probably connected with the site-isolation effects, that is, with the strict suppression of all binuclear reaction intermediates, known to arise from linking catalyst centers covalently to a solid support.[235] If methods become available for a controlled synthesis of such covalently supported metallocenes and for their structural characterization, one could imagine another round of developments toward novel metallocene-based Ziegler–Natta catalysts that are heterogeneous, like their predecessors discovered forty years ago, yet endowed with wider process and product variability and with superior environmental properties.

We thank Dr. A. Reinmuth and Ms. S. Kyncl for checking the text and the references of this article and for help in composing the table and figures. We are grateful to BASF AG for providing graphs and figures, and for financial support.

Received: September 29, 1994 [A 85 IE]
German version: *Angew. Chem.* **1995**, *107*, 1255–1283

[1] K. Ziegler, E. Holzkamp, H. Breil, H. Martin, *Angew. Chem.* **1955**, *67*, 541; K. Ziegler, *Angew. Chem.* **1964**, *76*, 545.

[2] G. Natta, P. Corradini, *Atti Accad. naz. Lincei Mem. Cl. Sci. Fis. Mat. Nat. Sez. II* **1955**, *5*, 73; G. Natta, *Angew. Chem.* **1956**, *68*, 393; *ibid.* **1964**, *76*, 553.

[3] a) *History of Polyolefins* (Eds.: R. B. Seymour, T. Cheng), Reidel, Dordrecht, **1986**; b) J. J. Eisch, *J. Chem. Educ.* **1983**, *60*, 1009; c) J. Boor, *Ziegler-Natta Catalysts and Polymerizations*, Academic Press, New York, **1979**.

[4] a) H. Sinn, W. Kaminsky, *Adv. Organomet. Chem.* **1980**, *18*, 99; b) P. Pino, R. Mülhaupt, *Angew. Chem.* **1980**, *92*, 869; *Angew. Chem. Int. Ed. Engl.* **1980**, *19*, 857.

[5] Recent reviews: M. Aulbach, F. Küber, *Chem. Unserer Zeit* **1994**, *28*, 197; P. C. Möhring, N. J. Coville, *J. Organomet. Chem.* **1994**, *479*, 1; K. B. Sinclair, R. B. Wilson, *Chem. Ind. (London)* **1994**, 857; W. Kaminsky, *Catal. Today* **1994**, *20*, 257; J. C. W. Chien in ref. [6g], p. 199.

[6] Conference proceedings: a) *Catalytic Polymerization of Olefins* (Eds.: T. Keii, K. Soga), Kodansha Elsevier, Tokyo, **1986**; b) *Transition Metals and Organometallics as Catalysts for Olefin Polymerization* (Eds.: W. Kaminsky, H. Sinn), Springer, Berlin, **1988**; c) *Catalysis in Polymer Synthesis* (Eds.: E. J. Vandenberg, J. C. Salamone) (*ACS Symp. Ser.* **1992**, *496*); d) *Proc. Int. Conf. Polyolefins VIII*, Soc. Plast. Eng., Houston, **1993**; e) *Advances in Olefin, Cycloolefin and Diolefin Polymerization* (Eds.: A. Guyot, R. Spitz) (*Makromol. Chem. Macromol. Symp.* **1993**, *66*); f) *Catalyst Design for Tailor-Made Polyolefins* (Eds.: K. Soga, M. Terano), Kodansha Elsevier, Tokyo, **1994**; g) *Ziegler Catalysts* (Eds.: G. Fink, R. Mülhaupt, H. H. Brintzinger), Springer, Berlin, **1995**; h) *Synthetic, Structural and Industrial Aspects of Stereospecific Polymerization* (Eds.: I. Tritto, U. Giannini) (*Makromol. Chem. Macromol. Symp.* **1995**, *89*).

[7] The present review is focused on metallocene-based catalysts for the stereoselective polymerization of α-olefins; it will thus not deal in detail with a) recent work on ethene polymerization, e.g. by monocyclopentadienyl (Cp) "constrained-geometry" catalysts (P. J. Shapiro, E. Bunel, W. P. Schaefer, J. E. Bercaw, *Organometallics* **1990**, *9*, 867; P. J. Shapiro, W. D. Cotter, W. P. Schaefer, J. A. Labinger, J. E. Bercaw, *J. Am. Chem. Soc.* **1994**, *116*, 4623; D. D. Devore, *Eur. Pat. Appl.* **1991**, 514828; J. C. Stevens, F. J. Timmers, D. R. Wilson, G. F. Schmidt, P. N. Nickias, R. K. Rosen, G. W. Knight, S. Y. Lay, *ibid.* **1990**, 416815; J. C. Flores, J. C. W. Chien, M. D. Rausch, *Organometallics* **1994**, *13*, 4140, and b) on styrene polymerization by CpTi complexes (N. Ishihara, T. Seimiya, M. Kuramoto, M. Uoi, *Macromolecules* **1986**, *19*, 2464; *ibid.* **1988**, *21*, 3356; N. Ishihara, N. Kuramoto in ref. [6f], p. 339; N. Ishihara in ref. [6h], p. 553; C. Pellecchia, P. Longo, A. Proto, A. Zambelli, *Makromol. Chem. Rapid Commun.* **1992**, *13*, 265; T. E. Ready, R. O. Day, J. C. W. Chien, M. D. Rausch, *Macromolecules* **1993**, *26*, 5822; R. Quyoum, Q. Wang, M. J. Tudoret, M. C. Baird, D. J. Gillis, *J. Am. Chem. Soc.* **1994**, *116*, 6435), or c) by Cp-free homogeneous catalysts (T. Miyatake, K. Mizunuma, M. Kakugo, in ref. [6e], p. 203; T. Dall'Occo, F. Sartori, G. Vecellio, U. Zucchini, A. Maldotti, *Makromol. Chem.* **1993**, *194*, 151).

[8] Third-generation Ziegler–Natta catalysts: a) N. Kashiwa, *Polymer* **1980**, *12*, 603; N. Kashiwa, J. Yoshitake, *Makromol. Chem.* **1984**, *185*, 1133; b) B. L. Goodall, *J. Chem. Educ.* **1986**, *63*, 191; c) P. Galli, P. C. Barbè, L. Noristi, *Angew. Makromol. Chem.* **1984**, *120*, 73; P. Galli, J. C. Haylock, *Prog. Polym. Sci.* **1991**, *16*, 443; *Makromol. Chem. Macromol. Symp.* **1992**, *63*, 19; P. Galli in ref. [6h], p. 13; d) T. Simonazzi, G. Cecchin, S. Mazzullo, *Prog. Polym. Sci.* **1991**, *16*, 303; e) J. C. W. Chien in ref. [6c], p. 27; f) U. Zucchini, in ref. [6e], p. 25; g) A. Guyot, R. Spitz, C. Journard, O. Eisenstein in ref. [6h], p. 39; h) E. Albizatti, U. Giannini, G. Morini, M. Galimberti, L. Barino, R. Scordamaglia in ref. [6h], p. 73.

[9] a) P. Cossee, *Tetrahedron Lett.* **1960**, 12, 17; *J. Catal.* **1964**, *3*, 80; b) E. J. Arlman, *ibid.* **1964**, *3*, 89; E. J. Arlman, P. Cossee, *ibid.* **1964**, *3*, 99.

[10] *cis*-Insertion stereochemistry was documented by use of deuterated α-olefins: G. Natta, M. Farina, M. Peraldo, *Chim. Ind. (Paris)* **1960**, *42*, 255; T. Miyazawa, Y. Ideguchi, *J. Polym. Sci. Part B* **1963**, *1*, 389; A. Zambelli, M. G. Giongo, G. Natta, *Makromol. Chem.* **1968**, *112*, 183.

[11] G. Natta, P. Pino, G. Mazzanti, R. Lanzo, *Chim. Ind. (Paris)* **1957**, *39*, 1032.

[12] a) Experimental evidence for "enantiomorphic-site control" of olefin insertion stereochemistry: A. Zambelli, G. Gatti, C. Sacchi, W. O. Crain, Jr., J. D. Roberts, *Macromolecules* **1971**, *4*, 475; W. O. Crain, Jr., A. Zambelli, J. D. Roberts, *ibid.* **1971**, *4*, 330; A. Zambelli, C. Tosi, *Adv. Polym. Sci.* **1974**, *15*, 31; *ibid.* **1974**, *25*, 32. b) Olefin insertion under "chain-segment mediated" enantiomorphic-site control, molecular models: P. Corradini, V. Barone, R. Fusco, G. Guerra, *Eur. Polym. J.* **1979**, *15*, 1133; P. Corradini, G. Guerra, R. Fusco, V. Barone, *ibid.* **1980**, *16*, 835; P. Corradini, V. Barone, R. Fusco, G. Guerra, *J. Catal.* **1982**, *77*, 32; P. Corradini, V. Barone, G. Guerra, *Macromolecules* **1982**, *15*, 1242. c) Evidence from ^{13}C NMR spectroscopy: A. Zambelli, M. C. Sacchi, P. Locatelli, G. Zannoni, *ibid.* **1982**, *15*, 211; A. Zambelli, P. Locatelli, M. C. Sacchi, I. Tritto, *ibid.* **1982**, *15*, 831; A. Zambelli, P. Ammendola, M. C. Sacchi, P. Locatelli, *NMR and Macromolecules* (Ed.: J. C. Randall) (*ACS Symp. Ser.* **1984**, *247*, p. 223).

[13] F. Patat, H. Sinn, *Angew. Chem.* **1958**, *70*, 496.

[14] D. S. Breslow, *US Pat. Appl.* **1955**, 537039; D. S. Breslow, N. R. Newburg, *J. Am. Chem. Soc.* **1957**, *79*, 5072.

[15] G. Natta, P. Pino, G. Mazzanti, U. Giannini, E. Mantica, M. Peraldo, *Chim. Ind. (Paris)* **1957**, *39*, 19; G. Natta, P. Pino, G. Mazzanti, U. Giannini, *J. Am. Chem. Soc.* **1957**, *79*, 2975.

[16] a) B. A. Krentsel', L. A. Nekhaeva, *Russ. Chem. Rev. (Engl. Transl.)* **1990**, *59*, 1193; b) J. Skupinska, *Chem. Rev.* **1991**, *91*, 613.

[17] D. S. Breslow, N. R. Newburg, *J. Am. Chem. Soc.* **1959**, *81*, 81; W. P. Long, *ibid.* **1959**, *81*, 5312; W. P. Long, D. S. Breslow, *ibid.* **1960**, *82*, 1953.

[18] J. C. W. Chien, *J. Am. Chem. Soc.* **1959**, *81*, 86.

[19] G. Natta, G. Mazzanti, *Tetrahedron* **1960**, *8*, 86.

[20] H. Sinn, F. Patat, *Angew. Chem.* **1963**, *75*, 805.

[21] a) K. H. Reichert, E. Schubert, *Makromol. Chem.* **1969**, *123*, 58; b) K. H. Reichert, J. Berthold, V. Dornow, *ibid.* **1969**, *121*, 258; c) K. Meyer, K. H. Reichert, *Angew. Makromol. Chem.* **1970**, *12*, 175; d) K. H. Reichert, *ibid.* **1970**, *13*, 177.

[22] G. Henrici-Olivé, S. Olivé, *Angew. Chem.* **1967**, *79*, 764; *Angew. Chem. Int. Ed. Engl.* **1967**, *6*, 790; *Kolloid Z. Z. Polym.* **1968**, *228*, 43; *J. Organomet. Chem.* **1969**, *16*, 339; *Polymerization*, Verlag Chemie, Weinheim, **1969**.

[23] A. K. Zefirova, A. E. Shilov, *Dokl. Akad. Nauk SSSR* **1961**, *136*, 599; *Dokl. Chem. (Engl. Transl.)* **1961**, *136*, 77; F. S. Dyachkovskii, A. K. Shilova, A. E. Shilov, *J. Polym. Sci. Part C* **1967**, *16*, 2333.

[24] G. Natta, P. Corradini, I. W. Bassi, *J. Am. Chem. Soc.* **1958**, *80*, 755.

[25] W. Kaminsky, J. Kopf, H. Sinn, H. J. Vollmer, *Angew. Chem.* **1976**, *88*, 688; *Angew. Chem. Int. Ed. Engl.* **1976**, *15*, 629, and references therein.

[26] a) R. F. Jordan, W. E. Dasher, S. F. Echols, *J. Am. Chem. Soc.* **1986**, *108*, 1718; b) R. F. Jordan, C. S. Bajgur, R. Willett, B. Scott, *ibid.* **1986**, *108*, 7410; c) R. F. Jordan, R. E. LaPointe, C. S. Bajgur, S. F. Echols, R. Willett, *ibid.* **1987**, *109*, 4111; d) R. F. Jordan, C. S. Bajgur, W. E. Dasher, A. L. Rheingold, *Organometallics* **1987**, *6*, 1041; e) R. F. Jordan, *J. Chem. Educ.* **1988**, *65*, 285; f) R. F. Jordan, R. E. LaPointe, P. K. Bradley, N. Baenziger, *Organometallics* **1989**, *8*, 2892; g) R. F. Jordan, P. K. Bradley, R. E. LaPointe, D. F. Taylor, *New J. Chem.* **1990**, *14*, 505; h) R. F. Jordan, P. K. Bradley, N. C. Baenziger, R. E. LaPointe, *J. Am. Chem. Soc.* **1990**, *112*, 1289; i) R. F. Jordan, R. E. LaPointe, N. Baenziger, G. D. Hinch, *Organometallics* **1990**, *9*, 1539; j) R. F. Jordan, *Adv. Organomet. Chem.* **1991**, *32*, 325; k) D. J. Crowther, S. L.

Borkowsky, D. Swenson, T. Y. Meyer, R. F. Jordan, *Organometallics* **1993**, *12*, 2897.
[27] M. Bochmann, L. M. Wilson, *J. Chem. Soc. Chem. Commun.* **1986**, 1610; M. Bochmann, L. M. Wilson, M. B. Hursthouse, R. L. Short, *Organometallics* **1987**, *6*, 2556; M. Bochmann, L. M. Wilson, M. B. Hursthouse, M. Motevalli, *ibid.* **1988**, *7*, 1148; M. Bochmann, A. J. Jaggar, J. C. Nicholls, *Angew. Chem.* **1990**, *102*, 830; *Angew. Chem. Int. Ed. Engl.* **1990**, *29*, 780; M. Bochmann, A. J. Jaggar, *J. Organomet. Chem.* **1992**, *424*, C5; M. Bochmann, S. J. Lancaster, *ibid.* **1992**, *434*, C1.
[28] J. J. W. Eshuis, Y. Y. Tan, J. H. Teuben, *J. Mol. Catal.* **1990**, *62*, 277; b) J. J. W. Eshuis, Y. Y. Tan, A. Meetsma, J. H. Teuben, J. Renkema, G. G. Evens, *Organometallics* **1992**, *11*, 362.
[29] R. Taube, L. Krukowka, *J. Organomet. Chem.* **1988**, *347*, C9.
[30] G. G. Hlatky, H. W. Turner, R. R. Eckman, *J. Am. Chem. Soc.* **1989**, *111*, 2728; H. W. Turner, *Eur. Pat. Appl.* **1988**, 277004; *Chem. Abstr.* **1989**, *110*, 58290a; H. W. Turner, G. G. Hlatky, *Eur. Pat. Appl.* **1988**, 277003; *Chem. Abstr.* **1989**, *110*, 58291b; G. G. Hlatky, R. R. Eckman, H. W. Turner, *Organometallics* **1992**, *11*, 1413.
[31] D. Schnell, G. Fink, *Angew. Makromol. Chem.* **1974**, *39*, 131; G. Fink, R. Rottler, *ibid.* **1981**, *94*, 25; G. Fink, R. Rottler, C. G. Kreiter, *ibid.* **1981**, 96, 1; G. Fink, D. Schnell, *ibid.* **1982**, *105*, 15, 31, 39; G. Fink, W. Zoller, *Makromol. Chem.* **1981**, *182*, 3265; G. Fink, W. Fenzl, R. Mynott, *Z. Naturforsch. B* **1985**, *40*, 158; R. Mynott, G. Fink, W. Fenzl, *Angew. Makromol. Chem.* **1987**, *154*, 1.
[32] J. J. Eisch, A. M. Piotrowski, S. K. Brownstein, E. J. Gabe, F. L. Lee, *J. Am. Chem. Soc.* **1985**, *107*, 7219; J. J. Eisch, M. P. Boleslawski, A. M. Piotrowski in ref. [6b], p. 371; J. J. Eisch, K. R. Caldwell, S. Werner, C. Krüger, *Organometallics* **1991**, *10*, 3417; J. J. Eisch, S. I. Pombrik, G. X. Zheng in ref. [6e], p. 109; *Organometallics* **1993**, *12*, 3856; J. J. Eisch, S. I. Pombrik, S. Gürtzgen, R. Rieger, W. Uzick in ref. [6f], p. 221; J. J. Eisch, S. I. Pombrik, X. Shi, S.-C. Wu in ref. [6h], p. 221.
[33] Since an olefin complex of the type $[Cp_2MR(olefin)]^+$ (M = Ti, Zr) has not been observed by spectroscopic or kinetic means so far [32], it is doubtful whether it should be regarded as a reaction intermediate.
[34] These "dormant" species might still be quite reactive, however, with regard to other important transformations, such as chain termination or catalyst deactivation reactions.
[35] Reagents such as $^{131}I_2$, ^{14}CO or CH_3OT, which are used to determine the number of active sites in a given reaction system [18], react also with these "dormant" sites; these methods will thus count all transition metal alkyl species as "active": P. J. T. Tait, B. L. Booth, M. O. Jejelowo, *Makromol. Chem. Rapid Commun.* **1988**, *9*, 393; P. J. T. Tait in ref. [6b], p. 309.
[36] Besides ethene, styrene has been reported to be polymerized by Cp_2TiCl_2/$AlEt_2Cl$ catalyst systems (C. G. Overberger, F. S. Diachkovsky, P. A. Jarovitzsky, *J. Polym. Sci.* **1964**, *A2*, 4113; C. G. Overberger, P. A. Jarovitzsky, *ibid.* **1965**, *A3*, 1483); it cannot be excluded that the presence of minor amounts of mono-Cp titanium compounds in these reaction systems are responsible for this catalysis (cf. ref. [7b]). Recently, polymerization of styrene has been found to occur also with $CH_2(C_5H_4)_2TiCl_2$/MAO: A. Miyashita, M. Nabika, T. Suzuki, *Abstr. Int. Symp. Synthetic, Structural and Industrial Aspects of Stereoselective Polymerization* (Ed.: L. Porri), Milan, **1994**, p. 88.
[37] K. H. Reichert, K. R. Meyer, *Makromol. Chem.* **1973**, *169*, 163.
[38] W. P. Long, D. S. Breslow, *Liebigs Ann. Chem.* **1975**, 463.
[39] a) A. Andresen, H. G. Cordes, J. Herwig, W. Kaminsky, A. Merck, R. Mottweiler, J. Pein, H. Sinn, H. J. Vollmer, *Angew. Chem.* **1976**, *88*, 689; *Angew. Chem. Int. Ed. Engl.* **1976**, *15*, 630; b) H. Sinn, W. Kaminsky, H. J. Vollmer, R. Woldt, *ibid.* **1980**, *92*, 396 and **1980**, *19*, 396; c) W. Kaminsky, *Nachr. Chem. Tech. Lab.* **1981**, *29*, 373; d) W. Kaminsky, *MMI Press Symp. Ser.* **1983**, *4*, 225; e) J. Herwig, W. Kaminsky, *Polym. Bull. (Berlin)* **1983**, *9*, 464; f) W. Kaminsky, M. Miri, H. Sinn, R. Woldt, *Makromol. Chem. Rapid Commun.* **1983**, *4*, 417; g) W. Kaminsky, *Naturwissenschaften* **1984**, *71*, 93; h) W. Kaminsky, *Angew. Makromol. Chem.* **1986**, *145/146*, 149; i) W. Kaminsky, R. Steiger, *Polyhedron* **1988**, *7*, 2375; R. Steiger, Dissertation, Universität Hamburg, **1990**; W. Kaminsky, A. Bark, R. Steiger, *J. Mol. Catal.* **1992**, *74*, 109; j) H. Sinn, J. Bliemeister, D. Clausnitzer, L. Tikwe, H. Winter, O. Zarncke in ref. [6b], p. 257; J. Bliemeister, W. Hagendorf, A. Harder, B. Heitmann, I. Schimmel, E. Schmedt, W. Schnuchel, H. Sinn, L. Tikwe, N. von Thienen, K. Urlass, H. Winter, O. Zarncke in ref. [6g], p. 57; O. Zarncke, Dissertation, Universität Hamburg, **1991**.
[40] Similar but less pronounced reductions to the Zr^{III} stage have been reported also for Cp_2ZrCl_2/MAO catalyst systems, especially in the presence of ethene: D. Cam, F. Sartori, A. Maldotti, *Macromol. Chem. Phys.* **1994**, *195*, 2817.
[41] E. J. Vandenberg, *J. Polym. Sci.* **1960**, *47*, 486.
[42] a) N. Piccolrovazzi, P. Pino, G. Consiglio, A. Sironi, M. Moret, *Organometallics* **1990**, *9*, 3098; b) N. Piccolrovazzi, Dissertation, Eidgenössische Technische Hochschule Zürich, **1989**.
[43] L. Resconi, S. Bossi, L. Abis, *Macromolecules* **1990**, *23*, 4489.
[44] a) D. Cam, E. Albizzati, P. Cinquina, *Makromol. Chem.* **1990**, *191*, 1641; b) D. Cam, U. Giannini, *ibid.* **1992**, *193*, 1049.
[45] S. Pasynkiewicz, *Polyhedron* **1990**, *9*, 429.
[46] E. Giannetti, G. M. Nicoletti, R. Mazzocchi, *J. Polym. Sci. Polym. Chem. Ed.* **1985**, *23*, 2117.
[47] S. Lasserre, J. Derouault, *Nouv. J. Chim.* **1983**, *7*, 659.
[48] a) M. R. Mason, J. M. Smith, S. G. Bott, A. R. Barron, *J. Am. Chem. Soc.* **1993**, *115*, 4971; C. J. Harlan, M. R. Mason, A. R. Barron, *Organometallics* **1994**, *13*, 2957; b) C. J. Harlan, S. G. Bott, A. R. Barron, *J. Am. Chem. Soc.* **1995**, *117*, in press.
[49] L. A. Nekhaeva, G. N. Bondarenko, S. V. Rykov, A. I. Nekhaev, B. A. Krentsel, V. P. Mar'in, L. I. Vyshinskaya, I. M. Khrapova, A. V. Polonskii, N. N. Korneev, *J. Organomet. Chem.* **1991**, *406*, 139.
[50] a) A. R. Siedle, R. A. Newmark, W. M. Lamanna, J. N. Schroepfer, *Polyhedron* **1990**, *9*, 301; b) A. R. Siedle, W. M. Lamanna, J. M. Olofson, B. A. Nerad, R. A. Newmark, *Selectivity in Catalysis* (Eds.: M. E. Davis, S. L. Suib) (*ACS Symp. Ser.* **1993**, *517*, 156); c) A. R. Siedle, W. M. Lamanna, R. A. Newmark, J. Stevens, D. E. Richardson, M. Ryan in ref. [6e], p. 215; d) A. R. Siedle, R. A. Newmark, D. E. Richardson, M. F. Ryan, C. R. Landis, J. Wright, D. Root, M. G. Hill, K. R. Mann, *Proc. MetCon, Houston* **1993**, 351; e) A. R. Siedle, R. A. Newmark, *J. Organomet. Chem.* **1995**, in press; A. R. Siedle, B. Hanggi, R. A. Newmark, K. R. Mann, T. Wilson, in ref. [6h], p. 299.
[51] Catalytic activities of titanocene and zirconocene complexes for the polymerization of propene, comparable to those attainable with MAO, have also been induced by mixtures of $AlMe_3$ and $AlMe_2F$: A. Zambelli, P. Longo, A. Grassi, *Macromolecules* **1989**, *22*, 2186; P. Longo, L. Oliva, A. Grassi, C. Pellecchia, *Makromol. Chem.* **1989**, *190*, 2357.
[52] P. G. Gassman, M. R. Callstrom, *J. Am. Chem. Soc.* **1987**, *109*, 7875.
[53] a) C. Sishta, R. M. Hathorn, T. J. Marks, *J. Am. Chem. Soc.* **1992**, *114*, 1112; b) X. Yang, C. L. Stern, T. J. Marks, *Organometallics* **1991**, *10*, 840.
[54] G. G. Hlatky, D. J. Upton, H. W. Turner, *US Pat. Appl.* **1990**, 459921; *Chem. Abstr.* **1991**, *115*, 256897v.
[55] J. A. Ewen, M. J. Elder, *Eur. Pat. Appl.* **1991**, 426637, 426638; *Chem. Abstr.* **1991**, *115*, 136987c, 136988d; in ref. [6e], p. 179.
[56] J. C. W. Chien, W. M. Tsai, M. D. Rausch, *J. Am. Chem. Soc.* **1991**, *113*, 8570; J. C. W. Chien, W. M. Tsai in ref. [6e], p. 141.
[57] a) M. Bochmann, S. J. Lancaster, *Organometallics* **1993**, *12*, 633; b) M. Bochmann, *Nachr. Chem. Tech. Lab.* **1993**, *41*, 1220; c) M. Bochmann, S. J. Lancaster, M. B. Hursthouse, K. I. M. Abdul Malik, *Organometallics* **1994**, *13*, 2235; d) M. Bochmann, S. J. Lancaster, *Angew. Chem.* **1994**, *106*, 1715; *Angew. Chem. Int. Ed. Engl.* **1994**, *33*, 1634.
[58] a) A. D. Horton, J. H. G. Frijns, *Angew. Chem.* **1991**, *103*, 1181; *Angew. Chem. Int. Ed. Engl.* **1991**, *30*, 1152; b) A. D. Horton, A. G. Orpen, *Organometallics* **1991**, *10*, 3910; c) A. D. Horton, *J. Chem. Soc. Chem. Commun.* **1992**, 185.
[59] J. A. Ewen, M. J. Elder, *US Pat. Appl.* **1989**, 419017; *Chem. Abstr.* **1991**, *115*, 136998g.
[60] a) X. Yang, C. L. Stern, T. J. Marks, *J. Am. Chem. Soc.* **1991**, *113*, 3623; *ibid.* **1994**, *116*, 10015; b) related permethyl zirconocene hydride complexes: X. Yang, C. L. Stern, T. J. Marks, *Angew. Chem.* **1992**, *104*, 1406; *Angew. Chem. Int. Ed. Engl.* **1992**, *31*, 1375.
[61] D. G. H. Ballard, A. Courtis, J. Holton, J. McMeeking, R. Pearce, *J. Chem. Soc. Chem. Commun.* **1978**, 994.
[62] P. L. Watson, *J. Am. Chem. Soc.* **1982**, *104*, 337; P. L. Watson, D. C. Roe, *ibid.* **1982**, *104*, 6471; P. L. Watson, G. W. Parshall, *Acc. Chem. Res.* **1985**, *18*, 51.
[63] G. Parkin, E. Bunel, B. J. Burger, M. S. Trimmer, A. van Asselt, J. E. Bercaw, *J. Mol. Catal.* **1987**, *41*, 21; B. J. Burger, M. E. Thompson, W. D. Cotter, J. E. Bercaw, *J. Am. Chem. Soc.* **1990**, *112*, 1566.
[64] G. Jeske, H. Lauke, H. Mauermann, P. N. Swepston, H. Schumann, T. J. Marks, *J. Am. Chem. Soc.* **1985**, *107*, 8091.
[65] a) D. T. Mallin, M. D. Rausch, J. C. W. Chien, *Polym. Bull. (Berlin)* **1988**, *20*, 421; b) J. C. W. Chien, A. Razavi, *J. Polym. Sci. Part A* **1988**, *26*, 2369; J. C. W. Chien, B. P. Wang, *ibid.* **1988**, *26*, 3089; *ibid.* **1989**, *27*, 1539; c) *ibid.* **1990**, *28*, 15.
[66] T. Tsutsui, N. Kashiwa, *Polym. Commun.* **1988**, *29*, 180.
[67] P. J. T. Tait, B. L. Booth, M. O. Jejelowo in ref. [6c], p. 78.
[68] B. W. S. Kolthammer, D. J. Mangold, D. R. Gifford, *J. Polym. Sci. Part A* **1992**, *30*, 1017.
[69] a) D. Fischer, R. Mülhaupt, *J. Organomet. Chem.* **1991**, *417*, C7; b) D. Fischer, Dissertation, Universität Freiburg, **1992**; c) D. Fischer, S. Jüngling, R. Mülhaupt in ref. [6e], p. 191; d) D. Fischer, R. Mülhaupt, *Makromol. Chem.* **1994**, *195*, 1433; e) S. Jüngling, Dissertation, Universität Freiburg, **1995**.
[70] Such an equilibrium explains that increasing MAO concentrations cause further increases in activity even though ^{14}CO or CH_3OT radio-tagging methods represent most of the Zr centers as "active", i.e. as carrying a polymer chain, even in homogeneous catalyst systems with moderate MAO concentrations [18, 35, 65, 67].
[71] A. D. Horton, A. G. Orpen, *Organometallics* **1992**, *11*, 8; *Angew. Chem.* **1992**, *104*, 912; *Angew. Chem. Int. Ed. Engl.* **1992**, *31*, 876; A. D. Horton, *Organometallics* **1992**, *11*, 3271.
[72] Added $AlMe_3$ increases the steady-state activities in reaction systems of this kind: S. Srinivasa Reddy, G. Shashidhar, S. Sivaram, *Macromolecules* **1993**,

26, 1180; I_1 might thus be reconverted to C by alkyl exchange with the $AlMe_3$ content of MAO.

[73] a) M. Bochmann, S. J. Lancaster, *J. Organomet. Chem.* **1992**, *434*, C1; b) *Angew. Chem.* **1994**, *106*, 1715; *Angew. Chem. Int. Ed. Engl.* **1994**, *33*, 1634.

[74] Formation of a zirconocene allyl cation from $[Cp_2ZrMe]^+$ and C_2H_4 has been observed in the gas phase: C. S. Christ, J. R. Eyler, D. E. Richardson, *J. Am. Chem. Soc.* **1988**, *110*, 4038.

[75] A decrease of activities with increasing MAO concentrations is occasionally observed at very high Al:Zr ratios: J. C. W. Chien, R. Sugimoto, *J. Polym. Sci. Part A* **1991**, *29*, 459; and ref. [132a].

[76] M. Ystenes, *J. Catal.* **1991**, *129*, 383; in ref. [6e], p. 71.

[77] D. T. Laverty, J. J. Rooney, *J. Chem. Soc. Faraday Trans. 1* **1983**, *79*, 869.

[78] M. Brookhart, M. L. H. Green, *J. Organomet. Chem.* **1983**, *250*, 395; M. Brookhart, M. L. H. Green, L. Wong, *Prog. Inorg. Chem.* **1988**, *36*, 1.

[79] Experimental and theoretical investigations on agostic interactions: a) R. B. Calvert, J. R. Shapley, *J. Am. Chem. Soc.* **1978**, *100*, 7726; b) S. Obara, N. Koga, K. Morokuma, *J. Organomet. Chem.* **1984**, *270*, C33; N. Koga, S. Obara, K. Morokuma, *J. Am. Chem. Soc.* **1984**, *106*, 4625; c) O. Eisenstein, Y. Jean, *ibid.* **1985**, *107*, 1177; d) M. J. Calhorda, J. A. M. Simoes, *Organometallics* **1987**, *6*, 1188; e) K. Tatsumi, A. Nakamura, *J. Am. Chem. Soc.* **1987**, *109*, 3195; *Organometallics* **1987**, *6*, 427; K. Mashima, A. Nakamura, *J. Organomet. Chem.* **1992**, *428*, 49; f) A. Shiga, J. Kojima, T. Sasaki, Y. Kikuzono, *ibid.* **1988**, *345*, 275; g) R. F. Jordan, P. K. Bradley, N. C. Baenziger, R. E. LaPointe, *J. Am. Chem. Soc.* **1990**, *112*, 1289; Z. Guo, D. C. Svenson, R. F. Jordan, *Organometallics* **1994**, *13*, 1424.

[80] H. Krauledat, H. H. Brintzinger, *Angew. Chem.* **1990**, *102*, 1459; *Angew. Chem. Int. Ed. Engl.* **1990**, *29*, 1412.

[81] L. Clawson, J. Soto, S. L. Buchwald, M. L. Steigerwald, R. H. Grubbs, *J. Am. Chem. Soc.* **1985**, *107*, 3377.

[82] W. E. Piers, J. E. Bercaw, *J. Am. Chem. Soc.* **1990**, *112*, 9406.

[83] While hydrocyclization of 1,6-$[D_2]$-1,5-hexadiene with a scandocene catalyst gave a stereokinetic isotope effect of $k_H/k_D \approx 1.25$ [82, 144], the analogous reaction with Cp_2ZrCl_2/MAO did not [80].

[84] a) D. R. Armstrong, P. G. Perkins, J. J. P. Steward, *J. Chem. Soc. Dalton Trans.* **1972**, *1972*; b) J. W. Lauher, R. Hoffmann, *J. Am. Chem. Soc.* **1976**, *98*, 1729; c) D. L. Thorn, R. Hoffmann, *ibid.* **1978**, *100*, 2079; d) O. Novaro, E. Blaisten-Barojas, E. Clementi, G. Giunchi, M. E. Ruiz-Vizcaya, *J. Chem. Phys.* **1978**, *68*, 2337; e) H. Fujimoto, T. Yamasaki, H. Mizutani, N. Koga, *J. Am. Chem. Soc.* **1985**, *107*, 6157; f) A. Shiga, H. Kawamura, T. Ebara, T. Sasaki, Y. Kikuzono, *J. Organomet. Chem.* **1989**, *366*, 95; g) C. A. Jolly, D. S. Marynick, *J. Am. Chem. Soc.* **1989**, *111*, 7968.

[85] H. Kawamura-Kuribayashi, N. Koga, K. Morokuma, *J. Am. Chem. Soc.* **1992**, *114*, 8687; *Chem. Rev.* **1991**, *91*, 823; T. Yoshida, N. Koga, K. Morokuma, *Organometallics* **1995**, *14*, 746; N. Koga, T. Yoshida, K. Marokuma in ref. [6g], p. 275.

[86] a) L. A. Castonguay, A. K. Rappé, *J. Am. Chem. Soc.* **1992**, *114*, 5832; b) J. R. Hart, A. K. Rappé, *ibid.* **1993**, *115*, 6159.

[87] a) T. K. Woo, L. Fan, T. Ziegler, *Organometallics* **1994**, *13*, 432, 2252; in ref. [6g], p. 291; b) L. Fan, D. Harrison, T. K. Woo, T. Ziegler, *ibid.*, **1995**. *14*, 2018.

[88] a) H. Weiss, M. Ehrig, R. Ahlrichs, *J. Am. Chem. Soc.* **1994**, *116*, 4919; b) H. Weiss, private communication; c) R. J. Meier, G. H. J. van Doremaele, S. Iarlori, F. Buda, *J. Am. Chem. Soc.* **1994**, *116*, 7274; S. Iarlori, F. Buda, G. van Doremaele, R. J. Meier in ref. [6h], p. 369.

[89] M. H. Prosenc, C. Janiak, H. H. Brintzinger, *Organometallics* **1992**, *11*, 4036. This study yields a—probably exaggerated—estimate of ca. 20 kJ mol^{-1} for the agostic stabilization of the insertion transition state.

[90] P. J. Flory, *Principles of Polymer Chemistry*, Cornell University Press, Ithaca, **1986**, p. 317.

[91] Other end groups, which arise from β-alkyl transfer to the Zr centers [58, 92–94], from σ-bond metathesis with the olefin substrate [50b, c], or from alkyl exchange between Zr and Al centers [43, 65c, 95], are occasionally observed, in particular with sterically strongly hindered (e.g. permethyl) metallocene catalysts (cf. G. Sini, S. A. Macgregor, O. Eisenstein, J. H. Teuben, *Organometallics* **1994**, *13*, 1049). These reactions do not appear to contribute significantly to chain termination in propene polymerization by MAO-activated Cp_2ZrCl_2 systems.

[92] E. Bunel, B. J. Burger, J. E. Bercaw, *J. Am. Chem. Soc.* **1988**, *110*, 976; S. Hajela, J. E. Bercaw, *Organometallics* **1994**, *13*, 1147.

[93] L. Resconi, R. M. Waymouth, *J. Am. Chem. Soc.* **1990**, *112*, 4953; L. Resconi, U. Giannini, E. Albizzati, F. Piemontesi, T. Fiorani, *Polym. Prepr. (Am. Chem. Soc. Div. Polym. Chem.)* **1991**, *32*, 463; L. Resconi, F. Piemontesi, G. Franciscono, L. Abis, T. Fiorani, *J. Am. Chem. Soc.* **1992**, *114*, 1025.

[94] T. Mise, A. Kageyama, S. Miya, H. Yamazaki, *Chem. Lett.* **1991**, 1525.

[95] a) A. L. Mogstad, L. Resconi, R. M. Waymouth, *Polym. Prepr. (Am. Chem. Soc. Div. Polym. Chem.)* **1991**, *32*, 160; b) A. L. Mogstad, R. M. Waymouth, *Macromolecules* **1992**, *25*, 2282.

[96] Such an *n*-propyl unit is observed at the head of most polypropene chains, except for a small fraction, which is initially formed by propene insertion into the $Zr-CH_3$ units generated during activation of Cp_2ZrCl_2 by the MAO cocatalyst [97].

[97] T. Tsutsui, A. Mizuno, N. Kashiwa, *Polymer* **1989**, *30*, 428.

[98] W. Kaminsky, K. Külper, S. Niedoba, *Makromol. Chem. Macromol. Symp.* **1986**, *3*, 377.

[99] This would imply that v_T is not significantly affected by MAO concentrations, i.e. that chain terminations arise predominantly) from "dormant" (i.e. associated) zirconocene ion pairs. Facile olefin isomerizations with Schwartz's hydrozirconation reagent Cp_2ZrHCl indicate that olefin extrusion from neutral zirconocene alkyl species is fairly fast: J. Schwartz, J. A. Labinger, *Angew. Chem.* **1976**, *88*, 402; *Angew. Chem. Int. Ed. Engl.* **1976**, *15*, 333.

[100] Previously prepared chiral titanocene and zirconocene complexes: H. Brunner, H. D. Schindler, *J. Organomet. Chem.* **1973**, *55*, C71; J. Tirouflet, A. Dormond, J. C. Leblanc, F. Le Moigne, *Tetrahedron Lett.* **1973**, 257; J. Besancon, F. Huq, M. Colette, *J. Organomet. Chem.* **1975**, *96*, 63; P. Renaut, G. Tainturier, B. Gautheron, *ibid.* **1978**, *148*, 43; J. C. Leblanc, C. Moise, J. Tirouflet, *ibid.* **1978**, *148*, 171; S. Couturier, B. Gautheron, *ibid.* **1978**, *157*, C61; E. Cesarotti, H. B. Kagan, R. Goddard, C. Krüger, *ibid.* **1978**, *162*, 297.

[101] Studies on metallocene-based polymerization catalysts in Kaminsky's group [39a, b] as well as syntheses of chiral *ansa*-metallocenes in Brintzinger's group (H. Schnutenhaus, H. H. Brintzinger, *Angew. Chem.* **1979**, *91*, 837; *Angew. Chem. Int. Ed. Engl.* **1979**, *18*, 777) were supported from 1973 to 1978 by Deutsche Forschungsgemeinschaft through a special program for research in homogeneous catalysis.

[102] Fixation of ligand geometries by an ethanediyl bridge had been found to be beneficial for other types of stereoselective homogeneous catalysts, see e.g.: M. D. Fryzuk, B. Bosnich, *J. Am. Chem. Soc.* **1978**, *100*, 5491; B. Bosnich, M. D. Fryzuk, *Top. Stereochem.* **1981**, *12*, 119.

[103] a) F. R. W. P. Wild, L. Zsolnai, G. Huttner, H. H. Brintzinger, *J. Organomet. Chem.* **1982**, *232*, 233; F. R. W. P. Wild, M. Wasiucionek, G. Huttner, H. H. Brintzinger, *ibid.* **1985**, *288*, 63; b) more recent syntheses and structural studies: J. A. Ewen, L. Haspeslagh, J. L. Atwood, H. Zhang, *J. Am. Chem. Soc.* **1987**, *109*, 6544; R. M. Waymouth, F. Bangerter, P. Pino, *Inorg. Chem.* **1988**, *27*, 758; S. Collins, B. A. Kuntz, N. J. Taylor, D. G. Ward, *J. Organomet. Chem.* **1988**, *342*, 21; S. Collins, W. J. Gauthier, D. A. Holden, B. A. Kuntz, N. J. Taylor, D. G. Ward, *Organometallics* **1991**, *10*, 2061; R. B. Grossman, R. A. Doyle, S. L. Buchwald, *ibid.* **1991**, *10*, 1501; G. M. Diamond, S. Rodewald, R. F. Jordan, *ibid.* **1995**, *14*, 5; F. Piemontesi, I. Camurati, L. Resconi, D. Balboni, A. Sironi, M. Moret, R. Zeigler, N. Piccolrovazzi, *ibid.* **1995**, *14*, 1256.

[104] The prefix *ansa* (lat. ansa = bent, handle), first used for compounds with an alkane bridge across an arene ring (A. Lüttringhaus, H. Gralheer, *Justus Liebigs Ann. Chem.* **1942**, *550*, 67), was adopted as a short notation for metallocene derivatives with an interannular bridge (J. A. Smith, J. von Seyerl, G. Huttner, H. H. Brintzinger, *J. Organomet. Chem.* **1979**, *173*, 175).

[105] J. A. Ewen, *J. Am. Chem. Soc.* **1984**, *106*, 6355.

[106] W. Kaminsky, K. Külper, H. H. Brintzinger, F. R. W. P. Wild, *Angew. Chem.* **1985**, *97*, 507; *Angew. Chem. Int. Ed. Engl.* **1985**, *24*, 507.

[107] a) F. A. Bovey, *High Resolution NMR of Macromolecules*, Academic Press, New York, **1972**; A. Zambelli, P. Locatelli, G. Bajo, F. A. Bovey, *Macromolecules* **1975**, *8*, 687; F. A. Bovey, *Chain Structure and Conformation of Macromolecules*, Academic Press, New York, **1982**; b) J. C. Randall, *Polymer Sequence Determination by the Carbon 13 NMR Method*, Academic Press, New York, **1977**; in *Polymer Characterization by NMR and ESR* (Eds.: A. E. Woodward, F. A. Bovey) (*ACS Symp. Ser.*; **1980**, *142*); c) M. Farina, *Top. Stereochem.* **1987**, *17*, 1; d) A. E. Tonelli, *NMR Spectroscopy and Polymer Microstructure*, VCH, Weinheim, **1989**; e) J. L. Koenig, *Spectroscopy of Polymers*, American Chemical Society, Washington, **1991**.

[108] Today, polymer NMR spectra can be analyzed at even higher resolution levels: A. E. Tonelli, F. C. Schilling, *Acc. Chem. Res.* **1981**, *14*, 233; T. Hayashi, Y. Inoue, R. Chujo, T. Asakura, *Polymer* **1988**, *29*, 138; A. De Marco, P. Sozzani, G. Di Silvestro, M. Farina, *Macromolecules* **1989**, *22*, 2154; M. Farina, G. Di Silvestro, P. Sozzani, *Prog. Polym. Sci.* **1991**, *16*, 219.

[109] The *mmrm* and *rmrr* pentad signals have identical chemical shifts.

[110] Essentially atactic polypropylene was first obtained with a homogeneous catalyst containing VCl_4 and $AlClEt_2$ at $-78\,^\circ C$ (G. Natta, A. Zambelli, G. Lanzi, I. Pasquon, E. R. Mognaschi, A. L. Segre, P. Cantola, *Makromol. Chem.* **1965**, *81*, 161). Strictly atactic polypropene is obtained from isotactic polypropene by epimerization with Pd catalysts at elevated temperatures: U. W. Suter, P. Neuenschwander, *Macromolecules* **1981**, *14*, 528.

[111] Alternative measures for polyolefin stereoregularity are the relative triad probabilities $[mm] = [mmmm] + [mmmr] + [rmmr]$, $[mr] = [mmrr] + [mmrm] + [rmrr] + [rmrm]$ and $[rr] = [rrrr] + [rrrm] + [mrrm]$, and the average lengths of isotactic and syndiotactic sequences, $n_{iso} = 2[mm]/[mr] + 1$ and $n_{syn} = 2[rr]/[mr] + 1$ [107]. For typical isotactic polymers with $[mmmm] \approx 0.95$, the mean length of an isotactic sequence is $n_{iso} \approx 100$ units.

[112] T. Tsutsui, N. Ishimaru, A. Mizuno, A. Toyota, N. Kashiwa, *Polymer* **1989**, *30*, 1350.

[113] Since [*mmmm*] > 0.9 corresponds to a diastereomer excess of > 95% for each insertion step, these homogeneous polymerization catalysts are roughly comparable to the most highly stereoselective organometallic catalysts employed for other C-C coupling reactions: H. Brunner, *Top. Stereochem.* **1988**, *18*, 129; *Synthesis* **1988**, 645; D. Seebach, *Angew. Chem.* **1990**, *102*, 1363; *Angew. Chem. Int. Ed. Engl.* **1990**, *29*, 1320.

[114] a) B. Rieger, J. C. W. Chien, *Polym. Bull. (Berlin)* **1989**, *21*, 159; B. Rieger, X. Mu, D. T. Mallin, M. D. Rausch, J. C. W. Chien, *Macromolecules* **1990**, *23*, 3559; b) Y. X. Chen, M. D. Rausch, J. C. W. Chien, *Organometallics* **1994**, *13*, 748.

[115] a) H. N. Cheng, M. A. Bennett, *Makromol. Chem.* **1987**, *188*, 135; H. N. Cheng, J. A. Ewen, *ibid.* **1989**, *190*, 1931; H. N. Cheng, G. N. Babu, R. A. Newmark, J. C. W. Chien, *Macromolecules* **1992**, *25*, 6980; H. N. Cheng, *Makromol. Chem. Theory Simul.* **1993**, *2*, 561. b) Recently, the term "catalytic-site control", which is applicable also to metal centers of C_s symmetry, appears to be used more frequently instead of the previously used term "enantiomorphic-site control".

[116] a) J. A. Ewen, in ref. [6a], p. 271; b) J. A. Ewen, L. Haspeslagh, J. L. Atwood, H. Zhang, *J. Am. Chem. Soc.* **1987**, *109*, 6544; c) J. A. Ewen, L. Haspeslagh, M. J. Elder, J. L. Atwood, H. Zhang, H. N. Cheng, in ref. [6b], p. 281; d) J. A. Ewen, R. L. Jones, A. Razavi, J. D. Ferrara, *J. Am. Chem. Soc.* **1988**, *110*, 6255; e) J. A. Ewen, M. J. Elder, R. L. Jones, S. Curtis, H. N. Cheng, *Stud. Surf. Sci. Catal.* **1990**, *56*, 439; f) J. A. Ewen, M. J. Elder, R. L. Jones, L. Haspeslagh, J. L. Atwood, S. G. Bott, K. Robinson, *Makromol. Chem. Macromol. Symp.* **1991**, *48/49*, 253; g) J. A. Ewen, M. J. Elder in ref. [6e], p. 179; h) J. A. Ewen, M. J. Elder, *Eur. Pat. Appl.* **1993**, EP-A 0537130; in ref. [6g], p. 99; J. A. Ewen in ref. [6h], p. 181.

[117] a) M. Antberg, L. L. Böhm, V. Dolle, H. Lüker, J. Rohrmann, W. Spaleck, A. Winter, *44th Southwest Reg. Meet. Am. Chem. Soc.* **1988**, Abstr. No. 48; b) W. A. Herrmann, J. Rohrmann, E. Herdtweck, W. Spaleck, A. Winter, *Angew. Chem.* **1989**, *101*, 1536; *Angew. Chem. Int. Ed. Engl.* **1989**, *28*, 1511; c) W. Spaleck, M. Antberg, V. Dolle, R. Klein, J. Rohrmann, A. Winter, *New J. Chem.* **1990**, *14*, 499; d) M. Antberg, V. Dolle, R. Klein, J. Rohrmann, W. Spaleck, A. Winter, *Stud. Surf. Sci. Catal.* **1990**, *56*, 501; e) M. Antberg, V. Dolle, S. Haftka, J. Rohrmann, W. Spaleck, A. Winter, H. J. Zimmermann, *Makromol. Chem. Macromol. Symp.* **1991**, *48/49*, 333; f) W. Spaleck, M. Antberg, J. Rohrmann, A. Winter, B. Bachmann, P. Kiprof, J. Behm, W. A. Herrmann, *Angew. Chem.* **1992**, *104*, 1373; *Angew. Chem. Int. Ed. Engl.* **1992**, *31*, 1347; g) W. Kaminsky, R. Engehausen, K. Zoumis, W. Spaleck, J. Rohrmann, *Makromol. Chem.* **1992**, *193*, 1643; h) W. Spaleck, F. Küber, A. Winter, J. Rohrmann, B. Bachmann, M. Antberg, V. Dolle, E. F. Paulus, *Organometallics* **1994**, *13*, 954; i) W. Spaleck, M. Antberg, M. Aulbach, B. Bachmann, V. Dolle, S. Haftka, F. Küber, J. Rohrmann, A. Winter in ref. [6g], p. 83; W. Spaleck, M. Aulbach, B. Bachmann, F. Küber, A. Winter in ref. [6h], p. 237.

[118] S. Miya, T. Yoshimura, T. Mise, H. Yamazaki, *Polym. Prepr. Jpn.* **1988**, *37*, 285; T. Mise, S. Miya, H. Yamazaki, *Chem. Lett.* **1989**, 1853; S. Miya, T. Mise, H. Yamazaki, *Stud. Surf. Sci. Catal.* **1990**, *56*, 531.

[119] a) S. Collins, W. J. Gauthier, D. A. Holden, B. A. Kuntz, N. J. Taylor, D. G. Ward, *Organometallics* **1991**, *10*, 2061; b) I. M. Lee, W. J. Gauthier, J. M. Ball, B. Iyengar, S. Collins, *ibid.* **1992**, *11*, 2115.

[120] a) W. Röll, H. H. Brintzinger, B. Rieger, R. Zolk, *Angew. Chem.* **1990**, *102*, 339; *Angew. Chem. Int. Ed. Engl.* **1990**, *29*, 279; b) B. Rieger, A. Reinmuth, W. Röll, H. H. Brintzinger, *J. Mol. Catal.* **1993**, *82*, 67; c) A. Reinmuth, Dissertation, Universität Konstanz, **1992**; d) U. Stehling, J. Diebold, R. Kirsten, W. Röll, H. H. Brintzinger, S. Jüngling, R. Mülhaupt, F. Langhauser, *Organometallics* **1994**, *13*, 964; e) T. Haselwander, S. Beck, H. H. Brintzinger in ref. [6g], p. 181.

[121] Comparison of results from different laboratories is difficult not only because of variations in T_p and other catalysis parameters, but also because of inexplicit corrections of signal intensities for contributions from various end group and regio-irregularity signals and by use of different stereoregularity measures [111].

[122] A. Zambelli, P. Ammendola, A. Grassi, P. Longo, A. Proto, *Macromolecules* **1986**, *19*, 2703; A. Zambelli, P. Longo, P. Ammendola, A. Grassi, *Gazz. Chim. Ital.* **1986**, *116*, 731; A. Zambelli, P. Ammendola in ref. [6b], p. 329.

[123] G. Erker, R. Nolte, Y. H. Tsay, C. Krüger, *Angew. Chem.* **1989**, *101*, 642; *Angew. Chem. Int. Ed. Engl.* **1989**, *28*, 628; G. Erker, R. Nolte, R. Aul, S. Wilker, C. Krüger, R. Noe, *J. Am. Chem. Soc.* **1991**, *113*, 7594; G. Erker, C. Fritze, *Angew. Chem.* **1992**, *104*, 204; *Angew. Chem. Int. Ed. Engl.* **1992**, *31*, 199; G. Erker, B. Temme, *J. Am. Chem. Soc.* **1992**, *114*, 4004; G. Erker, M. Aulbach, C. Krüger, S. Werner, *J. Organomet. Chem.* **1993**, *450*, 1; G. Erker, M. Aulbach, M. Knickmeier, D. Wingbermühle, C. Krüger, M. Nolte, S. Werner, *J. Am. Chem. Soc.* **1993**, *115*, 4590; G. Erker, C. Mollenkopf, *J. Organomet. Chem.* **1994**, *483*, 173.

[124] a) A. Razavi, J. L. Atwood, *J. Am. Chem. Soc.* **1993**, *115*, 7529; b) A. Razavi, U. Thewalt, *J. Organomet. Chem.* **1993**, *445*, 111; c) A. Razavi, J. Ferrara, *ibid.* **1992**, *435*, 299; A. Razawi, D. Vereecke, L. Peters, K. Den Dauw, L. Nafpliotis, J. L. Atwood in ref. [6g], p. 111; A. Razawi, L. Peters, L. Nafpliotis, D. Vereecke, K. Den Dauw, J. L. Atwood, U. Thewald in ref. [6h], p. 345.

[125] G. W. Coates, R. M. Waymouth, *Science* **1995**, *267*, 217.

[126] a) A. Schäfer, E. Karl, L. Zsolnai, G. Huttner, H. H. Brintzinger, *J. Organomet. Chem.* **1987**, *328*, 87; b) P. Burger, J. Diebold, S. Gutmann, H. U. Hund, H. H. Brintzinger, *Organometallics* **1992**, *11*, 1319.

[127] B. Rieger, *J. Organomet. Chem.* **1992**, *428*, C33.

[128] Predominantly syndiotactic polypropene was first obtained with vanadium-based catalyst systems at low temperatures: G. Natta, J. Pasquon, A. Zambelli, *J. Am. Chem. Soc.* **1962**, *84*, 1488; Y. Doi, J. Kinoshita, A. Morinaga, T. Keii, *J. Polym. Sci.* **1975**, *13*, 2491. There, it arises from a 2,1 olefin insertion, which is stereocontrolled by the configuration of the secondary chain end: A. Zambelli, G. Allegra, *Macromolecules* **1980**, *13*, 42.

[129] a) Previously prepared by host–guest inclusion polymerization of 2-methyl-1,3-pentadiene and subsequent hydrogenation: M. Farina, G. Di Silvestro, P. Sozzani, *Macromolecules* **1982**, *15*, 1451; M. Farina, G. Di Silvestro, P. Sozzani, B. Savaré, *ibid.* **1985**, *18*, 923; G. Silvestro, P. Sozzani, B. Savaré, M. Farina, *ibid.* **1985**, *18*, 928; b) stereoerror statistics: M. Farina, G. Di Silvestro, P. Sozzani, *ibid.* **1993**, *26*, 946; c) M. Farina, G. Di Silvestro, A. Terragni, *Macromol. Chem. Phys.* **1995**, *196*, 353.

[130] Polymers with microstructures intermediate between isotactic and atactic structures, which resemble the hemiisotactic structures discussed above in being sensitive to monomer concentrations, have also been obtained with other *ansa*-metallocene catalysts lacking C_2 or C_s symmetry: D. T. Mallin, M. D. Rausch, Y. G. Lin, S. Dong, J. C. W. Chien, *J. Am. Chem. Soc.* **1990**, *112*, 2030; G. Hidalgo Llinas, S. H. Dong, D. T. Mallin, M. D. Rausch, Y. G. Lin, H. H. Winter, J. C. W. Chien, *Macromolecules* **1992**, *25*, 1242; J. C. W. Chien, G. Hildago Llinas, M. D. Rausch, Y. G. Lin, H. H. Winter, J. L. Atwood, S. G. Bott, *J. Polym. Sci. Part A* **1992**, *30*, 2601; M. A. Giardello, M. S. Eisen, C. L. Stern, T. J. Marks, *J. Am. Chem. Soc.* **1993**, *115*, 3326; B. Rieger, R. Fawzi, M. Steimann, *Chem. Ber.* **1992**, *125*, 2373; B. Rieger, G. Jani, R. Fawzi, M. Steinmann, *Organometallics* **1994**, *13*, 647.

[131] Decreased stereoregularities have recently been observed for polypropylene obtained at low olefin concentrations even with *rac*-(en)(thind)$_2$ZrCl$_2$/MAO and other C_2-symmetric catalysts [69e]: a) V. Busico, R. Cipullo, *J. Am. Chem. Soc.* **1994**, *116*, 9329; V. Busico in ref. [6h], p. 277; b) G. Balbontin, A. Fait, F. Piemontesi, L. Resconi, H. Rychlicki in *Abstr. Internat. Symp. Synthetic, Structural and Industrial Aspects of Stereoselective Polymerization* (Ed.: L. Porri), Milan **1994**, p. 205; L. Resconi, A. Fait, F. Piemontesi, M. Colonnesi, H. Rychlicki, R. Zeigler, *J. Am. Chem. Soc.* **1995**, *117*, in press.

[132] a) N. Herfert, G. Fink, *Makromol. Chem.* **1992**, *193*, 1359; b) *Makromol. Chem. Rapid Commun.* **1993**, *14*, 91; in ref. [6e], p. 157; c) G. Fink, N. Herferth, P. Montag in ref. [6g], p. 159.

[133] Exchange of a CH_3 ligand between the coordination sites of a zirconocene methyl cation: NMR spectroscopic studies [50a, d, e]; calculations by EHMO [84b] and ab initio methods [85, 86, 134].

[134] E. P. Bierwagen, J. E. Bercaw, W. A. Goddard III, *J. Am. Chem. Soc.* **1994**, *116*, 1481.

[135] *ansa*-Hafnocene catalysts, such as MAO-activated (en)(ind)$_2$HfCl$_2$ and (en)(thind)$_2$HfCl$_2$ have similar stereoselectivities as their Zr analogues [118a, b, 119g]: A. Toyota, T. Tsutsui, N. Kashiwa, *J. Mol. Catal.* **1989**, *56*, 237; M. Kioka, T. Tsutsui, T. Ueda, N. Kashiwa, *Stud. Surf. Sci. Catal.* **1990**, *56*, 483.

[136] a) K. Soga, T. Shiono, S. Takemura, W. Kaminsky, *Makromol. Chem. Rapid Commun.* **1987**, *8*, 305; b) A. Grassi, A. Zambelli, L. Resconi, E. Albizzati, R. Mazzocchi, *Macromolecules* **1988**, *21*, 617; A. Grassi, P. Ammendola, P. Longo, E. Albizzati, L. Resconi, R. Mazzocchi, *Gazz. Chim. Ital.* **1988**, *118*, 539; c) T. Tsutsui, A. Mizuno, N. Kashiwa, *Makromol. Chem.* **1989**, *190*, 1177; d) T. Asakura, N. Nakayama, M. Demura, A. Asano, *Macromolecules* **1992**, *25*, 4876.

[137] a) K. Hortmann, H. H. Brintzinger, *New J. Chem.* **1992**, *16*, 51; b) P. Burger, K. Hortmann, H. H. Brintzinger, *Makromol. Chem. Macromol. Symp.* **1993**, *66*, 127.

[138] a) P. Longo, A. Grassi, C. Pellecchia, A. Zambelli, *Macromolecules* **1987**, *20*, 1015; b) A. Zambelli, C. Pellecchia, L. Oliva, *Makromol. Chem. Macromol. Symp.* **1991**, *48/49*, 297; c) A. Zambelli, C. Pellecchia in ref. [6e], p. 1.

[139] a) P. Corradini, G. Guerra, M. Vacatello, V. Villani, *Gazz. Chim. Ital.* **1988**, *118*, 173; P. Corradini, V. Busico, G. Guerra in ref. [6b], p. 337; b) L. Cavallo, G. Guerra, L. Oliva, M. Vacatello, P. Corradini, *Polym. Commun.* **1989**, *30*, 16; c) V. Venditto, G. Guerra, P. Corradini, R. Fusco, *Polymer* **1990**, *31*, 530; d) L. Cavallo, P. Corradini, G. Guerra, M. Vacatello, *ibid.* **1991**, *32*, 1329; e) *Macromolecules* **1991**, *24*, 1784; f) L. Cavallo, G. Guerra, M. Vacatello, P. Corradini, *Chirality* **1991**, *3*, 299; g) P. Corradini, G. Guerra, *Prog. Polym. Sci.* **1991**, *16*, 239; h) P. Corradini, V. Busico, L. Cavallo, G. Guerra, M. Vacatello, V. Venditto, *J. Mol. Catal.* **1992**, *74*, 433; i) P. Corradini in ref. [6e], p. 11; j) G. Guerra, L. Cavallo, V. Venditto, M. Vacatello, P. Corradini, *Makromol. Chem. Macromol. Symp.* **1993**, *69*, 237; k) G. Guerra, L. Cavallo, G. Moscardi, M. Vacatello, P. Corradini, *J. Am. Chem. Soc.* **1994**, *116*, 2988; l) P. Corradini, G. Guerra, L. Cavallo, G. Moscardi, M. Vacatello in ref. [6g], p. 237; m) G. Guerra, P. Corradini, L. Cavallo, M. Vacatello in ref. [6h], p. 307.

[140] T. Asanuma, Y. Nishimori, M. Ito, T. Shiomura, *Makromol. Chem. Rapid Commun.* **1993**, *14*, 315; *ibid.* **1994**, *15*, 723.

[141] Weak direct interactions between the olefin substituent and the chiral ligand framework appear to reinforce this olefin orientation for an isospecific *ansa*-metallocene catalyst, while opposing it for a syndiospecific catalyst: P. Longo, A. Proto, A. Grassi, P. Ammendola, *Macromolecules* **1991**, *24*, 4624.

[142] P. Pino, P. Cioni, J. Wei, *J. Am. Chem. Soc.* **1987**, *109*, 6189; P. Pino, P. Cioni, M. Galimberti, J. Wei, N. Piccolrovazzi in ref. [6b], p. 269.

[143] a) W. Kaminsky, H. Lüker, *Makromol. Chem. Rapid Commun.* **1984**, *5*, 225; b) W. Kaminsky, A. Ahlers, N. Möller-Lindenhof, *Angew. Chem.* **1989**, *101*, 1304; *Angew. Chem. Int. Ed. Engl.* **1989**, *28*, 1216; W. Kaminsky, A. Ahlers, O. Rabe, W. König in *Proc. 4. Symp. Organic Synthesis via Organometallics 1992* (Eds.: D. Enders, H. J. Gais, W. Keim), Vieweg, Braunschweig, **1993**, p. 151.

[144] a) E. B. Coughlin, J. E. Bercaw, *J. Am. Chem. Soc.* **1992**, *114*, 7606; b) B. J. Burger, W. D. Cotter, E. B. Coughlin, S. T. Chacon, S. Hajela, T. A. Herzog, R. O. Köhn, J. P. Mitchell, W. E. Piers, P. J. Shapiro, J. E. Bercaw in ref. [6g], p. 317.

[145] M. Leclerc, H. H. Brintzinger, *J. Am. Chem. Soc.* **1995**, *117*, 1651.

[146] Appropriate corrections have to be made for the stereoselectivity of the first olefin insertion into the Zr–H bond [147], which affects the resulting diastereomer ratios in a sense opposite for *cis*- and *trans*-deuterated olefins.

[147] P. Pino, M. Galimberti, *J. Organomet. Chem.* **1989**, *370*, 1; P. Pino, M. Galimberti, P. Prada, G. Consiglio, *Makromol. Chem.* **1990**, *191*, 1677; R. Waymouth, P. Pino, *J. Am. Chem. Soc.* **1990**, *112*, 4911.

[148] W. Röll, L. Zsolnai, G. Huttner, H. H. Brintzinger, *J. Organomet. Chem.* **1987**, *322*, 65; J. A. Ewen, personal communication.

[149] J. A. Volpy, M. L. H. Green, I. M. Gardiner, K. Prout, *J. Chem. Soc. Dalton Trans.* **1991**, 2207.

[150] a) M. E. Huttenloch, J. Diebold, U. Rief, H. H. Brintzinger, A. M. Gilbert, T. J. Katz, *Organometallics* **1992**, *11*, 3600; M. E. Huttenloch, Dissertation, Universität Konstanz, **1994**; b) W. Mengele, J. Diebold, C. Troll, W. Röll, H. H. Brintzinger, *Organometallics* **1993**, *12*, 1931; W. Mengele, Dissertation, Universität Konstanz, **1993**.

[151] a) J. C. W. Chien, J. C. Vizzini, W. Kaminsky, *Makromol. Chem. Rapid Commun.* **1992**, *13*, 479; b) J. C. Vizzini, J. C. W. Chien, G. N. Babu, R. A. Newmark, *J. Polym. Sci. Part A* **1994**, *32*, 2049; c) J. C. W. Chien, W. Song, M. D. Rausch, *ibid.* **1994**, *32*, 2387.

[152] H. J. R. de Boer, B. W. Royan, *J. Mol. Catal.* **1994**, *90*, 171.

[153] a) G. Natta, P. Pino, G. Mazzanti, P. Corradini, U. Giannini, *Rend. Accad. naz. Lincei Cl. Sci. Fis. Mat. Nat. Rend. (VIII)* **1955**, *19*, 397; P. Pino, F. Ciardelli, G. P. Lorenzi, G. Natta, *J. Am. Chem. Soc.* **1962**, *84*, 1487; P. Pino, F. Ciardelli, G. Montagnoli, *J. Polym. Sci. Part C* **1969**, *16*, 3256; C. G. Overberger, G. Khattab, *J. Polym. Sci. Polym. Chem. Ed.* **1969**, *7*, 217; Y. Atarashi, *ibid.* **1970**, *8*, 3359; F. Ciardelli, C. Carlini, G. Montagnoli, *Macromolecules* **1969**, *2*, 296; C. Carlini, R. Nocci, F. Ciardelli, *J. Polym. Sci. Polym. Chem. Ed.* **1977**, *15*, 767; A. Zambelli, P. Ammendola, M. C. Sacchi, P. Locatelli, G. Zannoni, *Macromolecules* **1983**, *16*, 341; A. Zambelli, P. Ammendola, A. J. Sivak, *ibid.* **1984**, *17*, 461; A. Zambelli, P. Ammendola, P. Locatelli, M. C. Sacchi, *ibid.* **1984**, *17*, 977; P. Ammendola, G. Guerra, V. Villani, *Makromol. Chem.* **1984**, *185*, 2599; P. Corradini, G. Guerra, V. Villani, *Macromolecules* **1985**, *18*, 1401; A. Zambelli, P. Ammendola, P. Longo, A. Grassi, *Gazz. Chim. Ital.* **1987**, *117*, 579; A. Zambelli, A. Proto, P. Longo in ref. [6g], p. 217; b) for the stereochemistry of the polymers obtained from 4-methyl-1-hexene with the syndiospecific catalyst $Me_2C(Cp)(9\text{-fluorenyl})ZrCl_2$/MAO [116d–g] cf. A. Zambelli, A. Grassi, M. Galimberti, G. Perego, *Makromol. Chem. Rapid Commun.* **1992**, *13*, 269, 467; c) a polymerization in which one of the olefin enantiomers is incorporated into a polymer at a higher rate than its antipode has been termed "stereo-elective": P. Pino, F. Ciardelli, G. P. Lorenzi, *J. Polym. Sci. Part C* **1962**, *4*, 21; F. Ciardelli, C. Carlini, A. Altomare in ref. [3c], p. 448.

[154] Polymerization of 3-methyl-1-butene by the syndiospecific catalyst $Me_2C(Cp)(9\text{-fluorenyl})ZrCl_2$/MAO [116d–g] has been reported by Kashiwa and co-workers (Jap. Pat. Appl. 338220 to Mitsui Toatsu Chem. Inc.); low activities for the polymerization of 3-methyl-1-butene and 3-methyl-1-pentene have been observed with the catalyst $Me_2Si(benzind)_2ZrCl_2$/MAO [120d].

[155] C. Pellecchia, P. Longo, A. Grassi, P. Ammendola, A. Zambelli, *Makromol. Chem. Rapid Commun.* **1987**, *8*, 277; P. Longo, A. Grassi, A. Proto, P. Ammendola, *Macromolecules* **1988**, *21*, 24; A. Zambelli, C. Pellecchia, L. Oliva, *ibid.* **1989**, *22*, 2129; A. Zambelli, C. Pellecchia, L. Oliva, P. Longo, A. Grassi, *Makromol. Chem.* **1991**, *192*, 223.

[156] T. Tsutsui, N. Kashiwa, A. Mizuno, *Makromol. Chem. Rapid Commun.* **1990**, *11*, 565; M. Kashiwa, M. Kioka, *Polym. Mat. Sci. Eng.* **1991**, *64*, 43; M. Kioka, A. Mizuno, T. Tsutsui, N. Kashiwa in ref. [6c], p. 72.

[157] a) V. Busico, R. Cipullo, P. Corradini, *Makromol. Chem. Rapid Commun.* **1992**, *13*, 15; b) *ibid.* **1992**, *13*, 21; c) *ibid.* **1993**, *14*, 97.

[158] A recent molecular modeling study finds that an agostic Zr–C–H(α) interaction is impossible in the transition state for the insertion of propene into a secondary Zr–alkyl unit [139k, l]; this might be an explanation for the low rate of this reaction.

[159] B. M. Novak, R. H. Grubbs, *J. Am. Chem. Soc.* **1988**, *110*, 960, 7542; H. Grubbs in *Proceedings 3. Symposium on Organic Syntheses via Organometallics 1990* (Eds.: K. H. Dötz, R. W. Hoffmann), Vieweg, Braunschweig, **1991**, p. 1.

[160] K. Knoll, R. R. Schrock, *J. Am. Chem. Soc.* **1989**, *111*, 7989; R. S. Saunders, R. E. Cohen, R. R. Schrock, *Macromolecules* **1991**, *24*, 5599; H. H. Fox, R. R. Schrock, *Organometallics* **1992**, *11*, 2763.

[161] a) O. W. Webster, W. R. Hertler, D. Y. Sogah, W. B. Farnham, T. V. Rajan-Babu, *J. Am. Chem. Soc.* **1983**, *105*, 5706; O. W. Webster, *Science* **1991**, *251*, 887; b) S. Collins, D. G. Ward, *J. Am. Chem. Soc.* **1992**, *114*, 5460.

[162] Polyethenes with M_w/M_n values of ca. 1.1 have been obtained at temperatures between −20 and −60 °C with reaction systems containing CpTa(butadiene)Me_2 or its heptamethyl analogue in the presence of MAO: K. Mashima, S. Fujikawa, A. Nakamura, *J. Am. Chem. Soc.* **1993**, *115*, 10990; *J. Chem. Soc. Chem. Commun.* **1994**, 1623.

[163] G. Natta, P. Corradini, M. Cesari, *Rend. Accad. naz. Lincei Cl. Sci. Fis. Mat. Nat.* **1956**, *21*, 365.

[164] E. J. Addink, J. Beintema, *Polymer* **1961**, *2*, 185; A. Turner-Jones, J. M. Aizlewood, D. R. Beckett, *Makromol. Chem.* **1964**, *75*, 134; D. R. Morrow, *J. Macromol. Sci. Part B* **1969**, *3*, 53; A. Turner-Jones, *Polymer* **1971**, *12*, 487; G. P. Giuidetti, P. Busi, I. Giulianelli, R. Zannetti, *Eur. Polym. J.* **1983**, *19*, 757; V. Busico, P. Corradini, C. De Rosa, E. Di Benedetto, *ibid.* **1985**, *21*, 239; M. Avella, E. Martuscelli, G. Della Volpe, A. Segre, E. Rossi, T. Simonazzi, *Makromol. Chem.* **1986**, *187*, 1927.

[165] a) B. Lotz, S. Graff, J. C. Wittmann, *J. Polym. Sci. Part B* **1986**, *24*, 2017; b) B. Lotz, S. Graff, C. Straupé, J. C. Wittmann, *Polymer* **1991**, *32*, 2902.

[166] a) S. Brückner, S. V. Meille, *Nature (London)* **1989**, *340*, 455; b) S. V. Meille, S. Brückner, W. Porzio, *Macromolecules* **1990**, *23*, 4114; c) S. Brückner, S. V. Meille, P. Sozzani, G. Torri, *Makromol. Chem. Rapid Commun.* **1990**, *11*, 55; d) S. Brückner, S. V. Meille, V. Petraccone, B. Pirozzi, *Prog. Polym. Sci.* **1991**, *16*, 361; S. V. Meille, D. R. Ferro, S. Brückner, *Polym. Pepr. (Am. Chem. Soc. Dir. Polym. Chem.)* **1992**, *33*, 268; S. V. Meille, D. R. Ferro, S. Brückner in ref. [6h], p. 499; e) structure of the β-modification: S. V. Meille, D. R. Ferro, S. Brückner, A. J. Lovinger, F. J. Padden, *Macromolecules* **1994**, *27*, 2615.

[167] a) A. Marigo, C. Marega, R. Zannetti, G. Paganetto, E. Canossa, F. Coletta, F. Gottardi, *Makromol. Chem.* **1989**, *190*, 2805; b) A. Marigo, C. Marega, R. Zannetti, G. Paganetto, S. Schmidt, H. G. Zachmann, *ibid.* **1990**, *191*, 1967; c) A. Marigo, C. Marega, R. Zannetti, A. Celli, G. Paganetto, *Macromol. Rapid Commun.* **1994**, *15*, 225.

[168] As the mean length of isotactic sequences approaches a value of $n_{iso} \approx 100$, polypropene tends to crystallize predominantly in the α-modification [69b, d].

[169] a) T. J. Burkhardt, M. Murata, R. J. Vaz in ref. [6h], p. 321; b) K. B. Sinclair, in ref. [6d].

[170] a) G. Natta, M. Peraldo, G. Allegra, *Makromol. Chem.* **1964**, *75*, 215; b) P. Corradini, G. Natta, P. Ganis, P. A. Temussi, *J. Polym. Sci.* **1967**, *C-16*, 2477.

[171] a) B. Lotz, A. J. Lovinger, R. E. Cais, *Macromolecules* **1988**, *21*, 2375; A. J. Lovinger, B. Lotz, D. D. Davis, *Polymer* **1990**, *31*, 2253; A. J. Lovinger, D. D. Davis, B. Lotz, *Macromolecules* **1991**, *24*, 552; A. J. Lovinger, B. Lotz, D. D. Davis, *Polym. Preprints* **1992**, *33*, 270; A. J. Lovinger, B. Lotz, D. D. Davis, F. J. Padden Jr., *Macromolecules* **1993**, *26*, 3494; G. Balbontin, D. Dainelli, M. Galimberti, G. Paganetto, *Makromol. Chem.* **1992**, *193*, 693; P. Sozzani, R. Simonutti, M. Galimberti, *Macromolecules* **1993**, *26*, 5782; b) J. Rodriguez-Arnold, A. Zhang, S. Z. D. Cheng, A. J. Lovinger, E. T. Hsieh, P. Chu, T. W. Johnson, K. G. Honell, R. G. Geerts, S. J. Palackal, G. R. Hawley, M. B. Welch, *Polymer* **1994**, *35*, 1884; A. J. Lovinger, B. Lotz, D. D. Davis, M. Schumacher, *Macromolecules* **1994**, *27*, 6603; W. Stocker, M. Schumacher, S. Graff, J. Lang, J. C. Wittmann, A. J. Lovinger, B. Lotz, *ibid.* **1994**, *27*, 6948; M. Schumacher, A. J. Lovinger, P. Agarwal, J. C. Wittmann, B. Lotz, *ibid.* **1994**, *27*, 6956; R. Thomann, C. Wang, J. Kressler, S. Jüngling, R. Mülhaupt, *Polymer* **1995**, in press.

[172] Y. Chatani, H. Maruyama, K. Noguchi, T. Asanuma, T. Shiomura, *J. Polym. Sci. Part C: Polym. Lett.* **1990**, *28*, 393.

[173] a) C. De Rosa, P. Corradini, *Macromolecules* **1993**, *26*, 5711; b) F. Auriemma, C. De Rosa, P. Corradini, *ibid.* **1993**, *26*, 5719.

[174] Since these syndiotactic polypropenes show no regioirregularities and rather high molecular weights [69b, d, 116e–f, 132b, c], the length of stereoregular chain segments, n_{syn}, is primarily limited here by *mm* triad and single-*m* dyad stereoerrors.

[175] F. de Candia, R. Russo, V. Vittoria, *Makromol. Chem.* **1988**, *189*, 815; S. Haftka, K. Könnecke, *J. Macromol. Sci. Part B* **1991**, *30*, 319; A. Galambos, M. Wolkowicz, R. Zeigler, M. Galimberti, *Polym. Mat. Sci. Eng.* **1991**, *64*, 45; A. Galambos, M. Wolkowicz, R. Zeigler in ref. [6c], p. 104; G. Balbontin, D. Dainelli, M. Galimberti, G. Paganetto, *Makromol. Chem.* **1992**, *193*, 693; P. Sozzani, R. Simonutti, M. Galimberti, *Macromolecules* **1993**, *26*, 5782.

[176] a) P. J. T. Tait, I. G. Berry in *Comprehensive Polymer Science, Vol. 4* (Eds.: G. C. Eastmond, A. Ledwith, S. Russo, P. Sigwalt), Vol. 4, Pergamon Press, Oxford, **1989**, p. 575; b) Encyclopedia of Polymer Science and Engineering (Eds.: H. F. Mark, N. B. Bikales, C. G. Overberger, G. Menges, J. I. Kroschwitz), Vol. 6, John Wiley & Sons, New York **1986**, p. 429 (LLDPE), p. 522 (EPDM); c) *ibid.*, Vol. 13, **1988**, p. 500.

[177] a) G. P. Guidetti, P. Busi, I. Giulianelli, R. Zannetti, *Eur. Polym. J.* **1983**, *19*, 757; b) V. Busico, P. Corradini, C. De Rosa, E. Di Benedetto, *ibid.* **1985**, *21*, 239; c) M. Avella, E. Martuscelli, G. D. Volpe, A. Segre, E. Rossi, T. Simonazzi, *Makromol. Chem.* **1986**, *187*, 1927; d) D. S. Davis, *Proc. Annu. Tech. Conf. Reinf. Plast. Compos. Inst. Soc. Plast. Ind.* **1992**, *50*, 628; e) J. Zimmermann, *J. Macromol. Sci.* **1993**, *B32*, 141.

[178] a) F. M. Mirabella, Jr., *Polym. Mater. Sci. Eng.* **1992**, *67*, 303; b) *Polymer* **1993**, *34*, 1729; c) H. Schwager, *Kunststoffe* **1992**, *82*, 499; d) L. D'Orazio, C. Mancarella, E. Martuscelli, G. Sticotti, P. Massari, *Polymer* **1993**, *34*, 3671.

[179] Elastomers are also available by terpolymerization of ethene, propene, and small amounts of a diene (EPDM); residual double bonds remaining in the Ziegler–Natta polmyerization products are used for their subsequent vulcanization [176].

[180] a) F. R. Mayo, C. Walling, *Chem. Rev.* **1950**, *46*, 191; b) A. E. Hamielec, J. F. Macgregor, A. Penlidis in *Comprehensive Polymer Science, Vol. 3* (Eds.: G. C. Eastmond, A. Ledwith, S. Russo, P. Sigwalt), Pergamon, Oxford, **1989**, p. 17.

[181] Equation $r_1 = k_{11}/k_{12}$ thus pertains to a catalyst center which had previously inserted monomer 1, $r_2 = k_{22}/k_{21}$ to one with monomer 2 as the last inserted unit.

[182] For the metallocene-catalyzed copolymerization of ethene and 1-hexene Fink and Herfert observed deviations from this "terminal model"; these authors report that the probabilities of inserting either one of the comonomers depend on the last two previously inserted units ("penultimate effect"), ref. [132d]; N. Herfert, G. Fink, *Polym. Mater. Sci. Eng.* **1992**, *67*, 31; N. Herfert, P. Montag, G. Fink, *Makromol. Chem.* **1993**, *194*, 3167; N. Herfert, Dissertation, Universität Düsseldorf, **1992**; cf. also ref. [69e].

[183] In the case of $r_1 r_2 = 1$, the probability of inserting either monomer is independent of the last inserted unit; the comonomer distribution along each chain will then correspond to a Bernoullian random distribution.

[184] a) S. van der Ven, *Studies in Polymer Science, Vol. 7*, Dekker, New York, **1989**, 221; b) Y. V. Kissin in *Handbook of Polymer Science and Technology* (Ed.: N. P. Cheremisinoff), Marcel Dekker, New York, **1989**, *1*, p. 103.

[185] a) H. N. Cheng, *Polym. Mater. Sci. Eng.* **1992**, *67*, 61; b) Y. V. Kissin, T. E. Nowlin, R. I. Mink, *Macromolecules* **1993**, *26*, 2151; Y. V. Kissin in ref. [6h], p. 113; c) M. W. van der Burg, J. C. Chadwick, O. Sudmeijer, H. J. A. F. Tulleken, *Makromol. Chem. Theory Simul.* **1993**, *2*, 399.

[186] L. Wild, C. Blatz, *Polym. Mater. Sci. Eng.* **1992**, *67*, 153; M. G. Pigeon, A. Rudin, *J. Appl. Polym. Sci.* **1994**, *51*, 303.

[187] a) T. Usami, Y. Gotoh, S. Takayama, *Macromolecules* **1986**, *19*, 2722; b) F. Defoor, G. Groeninckx, P. Schouterden, B. van der Heijden, *Polymer* **1992**, *33*, 3878; c) A. A. Montagna, J. C. Floyd, *Proc. MetCon Houston* **1993**, 172.

[188] a) W. Kaminsky, M. Miri, *J. Polym. Sci. Polym. Chem. Ed.* **1985**, *23*, 2151; b) M. Miri, Dissertation, Universität Hamburg, **1985**; c) W. Kaminsky, *Stud. Surf. Sci. Catal.* **1986**, *25*, 293; d) W. Kaminsky, M. Miri, *Proc. Int. Symp. Relat. Heterog. Homog. Catal.*, VNU Science, Novosibirsk, **1986**; e) W. Kaminsky, M. Schlobohm, *Makromol. Chem. Macromol. Symp.* **1986**, *4*, 103; f) W. Kaminsky, A. Bark, R. Spiehl, N. Möller-Lindenhof, S. Niedboda in ref. [6b], p. 291; g) H. Drögemüller, K. Heiland, W. Kaminsky, *ibid.*, p. 303; h) W. Kaminsky, H. Drögemüller, *Makromol. Chem. Rapid Commun.* **1990**, *11*, 89; i) K. Heiland, W. Kaminsky, *Makromol. Chem.* **1992**, *193*, 601.

[189] a) D. van der Sanden, R. W. Halle, *Proc. Annu. Tech. Conf. Reinf. Plast. Compos. Inst. Soc. Plast. Ind.* **1992**, *50*, 154; b) B. C. Trudell, C. S. Speed, F. C. Stehling, *ibid.* **1992**, *50*, 613; c) G. W. Knight, S. Lai in ref. [6d], p. 226; d) A. B. Furtek, *Proc. MetCon Houston* **1993**, 126; e) J. Koivumäki, J. V. Seppälä, *Polym. Commun.* **1993**, *34*, 1958.

[190] J. A. Ewen, *Stud. Surf. Sci. Catal.* **1986**, *25*, 271.

[191] M. Galimberti, E. Albizatti, L. Abis, G. Bacchilega, *Makromol. Chem.* **1991**, *192*, 2591.

[192] R. Mani, C. M. Burns, *Polymer* **1993**, *34*, 1941.

[193] Formation of LLDPE by simultaneous oligomerization of ethene with a nickel catalyst and polymerization by an *ansa*-metallocene catalyst: Ch. Denger, U. Haase, G. Fink, *Makromol. Chem. Rapid Commun.* **1991**, *12*, 697.

[194] a) J. C. W. Chien, D. He, *J. Polym. Sci. Part A* **1991**, *29*, 1585; b) *ibid.* **1991**, *29*, 1595; c) *ibid.* **1991**, *29*, 1603; d) *ibid.* **1991**, *29*, 1609; e) J. C. W. Chien, T. Nozaki, *J. Polym. Sci. Part A: Polym. Chem.* **1993**, *31*, 227; f) J. C. W. Chien, B. Xu, *Makromol. Chem. Rapid Commun.* **1993**, *14*, 109.

[195] T. Uozumi, K. Soga, *Makromol. Chem.* **1992**, *193*, 823.

[196] Ethene–olefin copolymers prepared with catalysts of this type have been commercialized by Dow Chemicals ("Insite"-LLDPE) and by Exxon ("Exxact"-LLDPE): R. D. Leaversuch, *Modern Plastics International* November **1993**, 12; *ibid.* October **1993**, 8; *Plastics Week* March 22, **1993**, 3; G. Lancaster, *Eur. Chem. News* **1993**, 35; *Eur. Plast. News* **1993**, 19; *Modern Plastics International* October **1993**, 99; *Plastic Week* November 8, **1993**, 6.

[197] V. Busico, L. Mevo, G. Palumbo, A. Zambelli, *Makromol. Chem.* **1983**, *184*, 2193; A. Zambelli, A. Grassi, M. Galimberti, R. Mazzocchi, F. Piemontesi, *Makromol. Chem. Rapid Commun.* **1991**, *12*, 523.

[198] a) S.-Y. Lai, J. R. Wilson, G. W. Knight, J. C. Stevens, WO-93/08221, **1992**; b) J. Stevens, *Proc. MetCon Houston* **1993**, 157; in ref. [6f], p. 277; c) K. W. Swogger, Che-I Kao in ref. [6d], p. 13; K. W. Swogger, G. M. Lancaster in ref. [6h], p. 285; d) B. Story, *Proc. MetCon Houston* **1993**, 111.

[199] a)L. Oliva, P. Longo, A. Grassi, P. Ammendola, C. Pellecchia, *Makromol. Chem. Rapid Commun.* **1990**, *11*, 519; b) P. Longo, A. Grassi, L. Oliva, *Makromol. Chem.* **1990**, *191*, 2387; c) G. Ricci, S. Italia, A. Giarrusso, L. Porri, *J. Organomet. Chem.* **1993**, *451*, 67; d) L. Porri, A. Giarrusso, G. Ricci in ref. [6e], p. 231.

[200] K. Soga, J. R. Park, T. Shiono, *Polym. Commun.* **1991**, *10*, 310.

[201] C. Pellecchia, A. Proto, A. Zambelli, *Macromolecules* **1992**, *25*, 4450; A. Zambelli, C. Pellecchia, *Proc. MetCon Houston* **1993**, 378.

[202] P. Aaltonen, J. Seppälä, *Eur. Polym. J.* **1994**, *30*, 683.

[203] H. Turner, G. Hlatky WO-91/12285, **1991**.

[204] H. Yasuda, H. Yamamoto, K. Yokota, S. Miyake, A. Nakamura, *J. Am. Chem. Soc.* **1992**, *114*, 4908; b) H. Yasuda, N. Furo, H. Yamamoto, A. Nakamura, S. Miyake, N. Kibino, *Macromolecules* **1992**, *25*, 5115; H. Yasuda, H. Yamamoto, M. Yamashita, K. Yokota, A. Nakamura, S. Miyake, Y. Kai, N. Tanehisa, *ibid.* **1993**, *26*, 7134; H. Yasuda, E. Ihara, S. Yoshioka, M. Nodono, M. Morimoto, M. Yamashita in ref. [6f], p. 237.

[205] H. N. Cheng, D. A. Smith, *Macromolecules* **1986**, *19*, 2065.

[206] a) J. V. Seppälä, J. Koivumäki, X. Liu, *J. Polym. Sci. Part A: Polym. Chem.* **1993**, *31*, 3447; b) J. Koivumäki, J. V. Seppälä, *Macromolecules* **1993**, *26*, 5535.

[207] a) W. Kaminsky, A. Bark, M. Arndt, *Makromol. Chem. Macromol. Symp.* **1991**, *47*, 83; b) W. Kaminsky, A. Bark, I. Däke in ref. [6a], p. 425; c) W. Kaminsky, R. Spiehl, *Makromol. Chem.* **1989**, *190*, 515; W. Kaminsky, *Shokubai* **1991**, *33*, 536; W. Kaminsky, A. Noll in ref. [6g], p. 149.

[208] a) S. Collins, W. M. Kelly, *Macromolecules* **1992**, *25*, 233; W. M. Kelly, N. J. Taylor, S. Collins, *ibid.* **1994**, *27*, 4477; *Proc. MetCon Houston* **1994**, 1. b) The *trans*-connection of part of the 1,3-cyclopentandiyl units observed in these hydroligomers is not in accord with the stereochemistry of normal olefin insertions; its mechanism deserves further study.

[209] A strictly alternating insertion–isomerization mechanism has been determined for nickel-based olefin polymerization catalysts: V. M. Möhring, G. Fink, *Angew. Chem.* **1985**, *97*, 982; *Angew. Chem. Int. Ed. Engl.* **1985**, *24*, 1001; G. Fink, V. Möhring, A. Heinrichs, C. Denger in ref. [6c], p. 88.

[210] M. Brekner, F. Osan, J. Rohrmann, M. Antherg, *Eur. Pat. Appl.* **1992**, 485893.

[211] X. Yang, L. Jia, T. J. Marks, *J. Am. Chem. Soc.* **1993**, *115*, 3392.

[212] Cyclopolymerization of 1,5-hexadiene with heterogeneous Ziegler catalysts: C. S. Marvel, J. K. Stille, *J. Am. Chem. Soc.* **1958**, *80*, 1740; H. S. Makowski, B. K. Shim, Z. W. Wilchinsky, *J. Polym. Sci. Part A* **1964**, *2*, 5149; H. N. Cheng, N. P. Khasat, *J. Appl. Polym. Sci.* **1988**, *35*, 825.

[213] L. Resconi, G. W. Coates, A. Mogstad, R. M. Waymouth, *J. Macromol. Sci. Chem. Ed.* **1991**, *A 28*, 1225.

[214] G. W. Coates, R. M. Waymouth, *J. Am. Chem. Soc.* **1991**, *113*, 6270; *J. Mol. Catal.* **1992**, *76*, 189.

[215] M. R. Kesti, R. M. Waymouth, *J. Am. Chem. Soc.* **1992**, *114*, 3565.

[216] L. Cavallo, G. Guerra, P. Corradini, L. Resconi, R. M. Waymouth, *Macromolecules* **1993**, *26*, 260.

[217] G. W. Coates, R. M. Waymouth, *J. Am. Chem. Soc.* **1993**, *115*, 91; S. H. Miller, R. M. Waymouth in ref. [6g], p. 441; G. Ruiz de Ballesteros, F. Auriemma, L. Cavallo, V. Venditto, G. Guerra, L. Resconi, R. M. Waymouth in *Abstr. Internat. Symp. Stereoselective Polymerization*, (Ed.: L. Porri), Milan, **1994**, p. 282.

[218] M. R. Kesti, G. W. Coates, R. M. Waymouth, *J. Am. Chem. Soc.* **1992**, *114*, 9679.

[219] K. Stein, R. M. Waymouth, unpublished results.

[220] Y. Doi, T. Keii, *Adv. Polym. Sci.* **1986**, *73/74*, 201; Y. Doi, S. Suzuki, F. Nozawa, K. Soga, *Stud. Surf. Sci. Catal.* **1986**, *25*, 257; Y. Doi, S. Suzuki, G. Hizal, K. Soga, *Transition Metal Catalyzed Polymerizations* (Ed.: R. P. Quirk), Cambridge University Press, Cambridge, **1988**, p. 182; Y. Doi, N. Tokuhiro, M. Nunomura, H. Miyake, S. Suzuki, K. Soga in ref. [6b], p. 379.

[221] T. Shiono, K. Yoshida, K. Soga, *Makromol. Chem. Rapid Commun.* **1990**, *11*, 169.

[222] R. Mülhaupt, T. Duschek, B. Rieger, *Makromol. Chem. Macromol. Symp.* **1991**, *48/49*, 317.

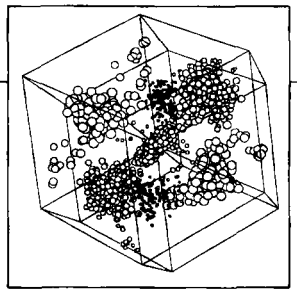
[223] T. Shiono, K. Soga, *Makromol. Chem. Rapid Commun.* **1992**, *13*, 371.

[224] a) T. Duschek, R. Mülhaupt, *Polym. Prepr.* **1992**, *33*, 170; T. Duschek, Dissertation, Universität Freiburg, **1993**; b) R. Mülhaupt, T. Duschek, D. Fischer, S. Setz, *Polym. Adv. Technol.* **1993**, *4*, 439; R. Mülhaupt, T. Duschek, J. Rösch, *ibid.* **1993**, *4*, 465.

[225] a) T. N. Doman, C. R. Landis, B. Bosnich, *J. Am. Chem. Soc.* **1992**, *114*, 7264; T. K. Hollis, J. K. Burdett, B. Bosnich, *Organometallics* **1993**, *12*, 3385; B. Bosnich, *Chem. Soc. Rev.* **1994**, 387; T. N. Doman, K. T. Hollis, B. Bosnich, *J. Am. Chem. Soc.* **1995**, *17*, 1352; b) K. Angermund, A. Hanuschik, M. Nolte in ref. [6g], p. 251; c) U. Höweler, R. Mohr, M. Knickmeier, G. Erker, *Organometallics* **1994**, *13*, 2380.

[226] M. Kaminaka, K. Soga, *Makromol. Chem. Rapid Commun.* **1991**, *12*, 367; K. Soga, M. Kaminaka, *ibid.* **1992**, *13*, 221; *ibid.* **1994**, *15*, 593.

[227] H. F. Herrmann, B. Bachmann, B. Hierholzer, W. Spaleck, *Eur. Pat. Appl.* **1993**, 563917 A1; T. J. Burkhardt, M. Murata, W. B. Brandley, WO-93/23439, **1993**.
[228] K. D. Hungenberg, J. Kerth, F. Langhauser, P. Müller in ref. [6f], p. 373; K. D. Hungenberg, J. Kerth, F. Langhauser, B. Marczinke, R. Schlund in ref. [6g], p. 363.
[229] Particle forming kinetics for homogeneous and heterogeneous polymerization catalysts: H. F. Herrmann, L. L. Böhm, *Polym. Commun.* **1991**, *32*, 58.
[230] The overall productivities of these heterogenized metallocene catalysts, per g of support and catalyst, are about 50% of those of recent heterogeneous, $MgCl_2$-supported catalysts [228].
[231] a) E. Otto, *Kunststoffe* **1993**, *83*, 188; b) K. Wagemann, *Nachr. Chem. Tech. Lab.* **1994**, *42*, 28.
[232] T. Tsutsui, N. Kashiwa, *Polymer* **1991**, *32*, 2671.
[233] W. Kaminsky, F. Renner, *Makromol. Chem. Rapid Commun.* **1993**, *14*, 239; W. Kaminsky in ref. [6h], p. 203.
[234] K. Soga, H. J. Kim, T. Shiono, *Makromol. Chem. Rapid Commun.* **1994**, *15*, 139; *Makromol. Chem. Phys.* **1994**, *195*, 3347; K. Soga in ref. [6f], p. 307; K. Soga, M. Kaminaka, H. J. Kim, T. Shiono in ref. [6g], p. 333; K. Soga in ref. [6h], p. 249.
[235] R. Grubbs, C. P. Lau, R. Cukier, C. Brubaker, Jr., *J. Am. Chem. Soc.* **1977**, *99*, 4517; C. U. Pittman, Jr., *Polymer-supported Reactions in Organic Synthesis* (Eds.: P. Hodge, D. C. Sherrington), Wiley, New York, **1980**, p. 24.



Y. Ohashi (ed.)

Reactivity in Molecular Crystals

1993. XII, 348 pages. Hardcover. DM 198.00.
ISBN 3-527-29098-2

Do you need to design syntheses that are
- highly selective
- fast
- enantioselective with quantitative enantiomeric yield?

This book describes in detail how best to exploit the enormous synthetic potential of solid state reactions. Written by leading experts, it provides in depth information on
- the theoretical and physico-chemical approach to solid state reactions
- solid-to-solid organic reactions
- stereoselective solid state photoreactions
- reactivity and crystal structure

An ideal companion to Bürgi and Dunitz's *Structure Correlation*, this book will be highly useful to synthetic organic chemists, stereochemists, crystallographers, and solid-state chemists.

To order please contact your bookseller or:

VCH, P.O. Box 10 11 61,
D-69451 Weinheim,
Telefax (0) 62 01 - 60 61 84
VCH, Hardstrasse 10,
P.O. Box, CH-4020 Basel
VCH, 8 Wellington Court, Cambridge
CB1 1HZ, UK
VCH, 220 East 23rd Street,
New York, NY 10010-4606, USA
(toll free: 1-800-367-8249)
VCH, Eikow Building,
10-9 Hongo 1-chome,
Bunkyo-ku, Tokyo 113, Japan

VCH

Basic Principles of Thermoanalytical Techniques and Their Applications in Preparative Chemistry

Heiko Karl Cammenga* and Matthias Epple*

The investigation of thermodynamic properties and reactivity yields interesting insights into the chemistry of newly synthesized substances. With thermal analysis extensive information can be gained from small samples (often only a few milligrams). In addition, the data obtained by thermal analysis can be used to plan and optimize a synthesis. Among the most important applications are identification and purity analysis, and the determination of characteristic temperatures and enthalpies of phase transitions (melting, vaporization), phase transformations, and reactions. Investigations into the kinetics of consecutive reactions and decomposition reactions are also possible. With the instruments available today such analyses can usually be performed quickly and easily. In this review the fundamentals of thermoanalytical methods are described and illustrated with selected examples of applications to low and high molecular weight compounds.

Keywords: analytical methods · phase transformations · kinetics · thermal analysis

1. Introduction

In general, thermal analysis describes the examination of temperature-dependent properties of materials. In this respect a feature of thermoanalytical methods is the large variety of possibilities. Common fields of application range from the generation of thermodynamic and kinetic parameters in basic research, through the characterization of materials, to routine quality control and maintenance in industrial practice.

As thermally induced processes (phase changes, phase transitions, reactions, decompositions) and temperature-dependent material properties (heat capacity, thermal stability, mechanical properties) are very important in chemistry, the potential amount of information is substantial. For this reason increasing numbers of chemists are using thermal analysis. The extensive range of commercially available instruments and their easy operation are further reasons for the growing popularity of thermal analysis. Unfortunately the potential from the information extracted from the recorded graphs is often not fully exploited.

Thermal analysis has had only a minor impact on preparative chemistry so far. This is probably because scientists active in the field of synthesis are not familiar with the many and diverse possibilities of these methods. In this article, therefore, the basic principles and potential applications will be expounded. The user should also know the limits of the methodology, because the computer-assisted data processing commonly used today often leads to wrong conclusions and thus to incorrect results, which could have been avoided had the basic principles behind the program for evaluation been known.

An important aid that thermal analysis can offer preparative chemists is, for instance, the rapid determination of purity, phase state, and stability of newly synthesized substances as well as of adduct formation with the solvent. Such information can often be obtained easily from a single measurement. Different polymorphous forms of solids can be identified. Table 1 collates

Table 1. Some of the variables obtainable from thermoanalytical measurements.

Variable or Process	Symbol [a]	Method [b]
melting point	T_{fus}	DTA, DSC
enthalpy of fusion	$\Delta_{fus}H$	DSC
mixed melting point	T_{fus}^{mix}	DTA, DSC
boiling point	T_{vap}	DTA, DSC, TG
enthalpy of vaporization	$\Delta_{vap}H$	DSC
decomposition temperature	T_{dec}	DTA, DSC, TG
enthalpy of decomposition	$\Delta_{dec}H$	DSC
purity	x_1	DSC
enantiomeric purity	% *ee*	DSC
heat capacity	$C_p(T)$	DSC
expansion coefficient	α	TMA, thermal X-ray
phase transition temperature	T_{trs}	DTA, DSC, TMA
phase transition enthalpy	$\Delta_{trs}H$	DSC
glass transition	T_g, $\Delta C_{p,g}$	DSC, TMA, DMA
enthalpy of reaction	Δ_rH	DSC
reaction kinetics	E_A, $\lg(k_\infty)$, n [c]	DTA, DSC, TG, TOA, thermal X-ray

[a] The physical quantity determined directly or indirectly. [b] The abbreviations are explained in the text. [c] From these variables deductions on the mechanism can be made.

[*] Prof. Dr. H. K. Cammenga
Institut für Physikalische und Theoretische Chemie der Technische Universität
Hans-Sommer-Strasse 10, D-38106 Braunschweig (Germany)
Telefax: Int. code + (531)391-5832

Dr. M. Epple
Institut für Anorganische und Angewandte Chemie der Universität
Martin-Luther-King-Platz 6, D-20146 (Germany)
Telefax: Int. code + (40)4123-6348

 © *VCH Verlagsgesellschaft mbH, D-69451 Weinheim, 1995* *0570-0833/95/1111-1171 $ 10.00+.25/0*

a number of variables that can be obtained from thermodynamic measurements.

Apart from thermodynamic parameters (heat capacities, phase transition temperatures, enthalpies), kinetic data (rates of transition, reaction, and decomposition) can often also be obtained from the quantitative evaluation of the data. The precise evaluation of the shape of a melting peak can enable the determination of the total concentration of impurities even in a range below 1 mol%, a concentration range in which the usual analytical methods (for example spectrometric methods) reach their limits. The examination of the enantiomeric purity of newly synthesized pharmaceuticals is an important application.

Applications in the extensive field of the chemistry of high molecular weight substances (polymers) include, for instance, the determination of thermal and mechanical properties in addition to the measurement of the degree of crystallinity and of the kinetics of polymerization, crystallization, and decomposition. An interesting branch of thermal analysis is biocalorimetry. In this field the thermal behavior of living beings (from protozoa to large mammals, even humans) is examined. The change in the rate of heat generation of living cultures can be employed, for instance, in screening procedures to test the effectiveness of pharmaceuticals.

2. Basic Principles of Methods of Thermal analysis

In this section the basic principles of thermal analysis will be introduced briefly. Detailed information can be found in a series of more recent monographs.[1-11]

The German Industrial Standard (DIN) 51005 defines thermal analysis as follows:

> Thermal analysis (TA): Generic term for methods in which the physical and chemical properties of a substance, a mixture of substances, and/or reaction mixtures are measured as a function of temperature or time, for which the sample is subjected to a controlled temperature program.[12]

This definition also includes isothermal temperature programs (that is, measurements at constant temperature) and the observation of free (that is, unregulated) heating and cooling processes. In almost all cases, however, measurements are carried out at a constant heating rate $\beta = dT/dt$ (scanning mode), which strictly speaking also includes isothermal measurements ($\beta = 0$).[14]

For a given sample property a potentially large number of variables may be considered. The most common methods follow the mass m (thermogravimetry TG), the temperature difference ΔT (differential thermal analysis DTA), the change in enthalpy dH/dt (differential scanning calorimetry DSC),[18] and the linear expansion of a sample l (dilatometry and thermomechanical analysis TMA).

These four most important methods are illustrated in Figure 1. In the case of thermogravimetry (TG, Fig. 1a) the change in the weight of a sample is measured as a function of time and/or temperature (example: monitoring the thermal decomposition of a hydrated salt). The sample masses lie in the mg to g range depending on the particular instrument and problem. Typically 10 to 20 mg of a substance is sufficient. As a rule it is



H. K. Cammenga



M. Epple

Heiko K. Cammenga, born 1938 in Bremen, studied chemistry in Braunschweig and Helsinki. Following his doctorate on precision measurements of low vapor pressures at the Technische Hochschule Braunschweig in 1967, he first became assistant, then senior assistant there at the "Institut für Physikalische Chemie". From 1970 to 1971 he visited the University of Rochester, NY, USA, as assistant professor on the invitation of Professor K. C. D. Hickman. There he worked on a project of the U. S. Office of Saline Water on the basic principles of sea water desalination processes. In 1973 he habilitated in physical chemistry with studies on the kinetics of vaporization and sublimation. Since 1977 he has been professor and director of the Department of Applied Physical Chemistry at Braunschweig. Since its foundation in 1985 he has also been a member in the collaborative project SFB 179 "Water and Matter Dynamics in Agro-Ecosystems". His areas of research are many and diverse. Main focuses are the kinetics and mechanisms of reactions of (above all organic) solids, kinetics of phase transition processes, chemistry of and damaging processes in building materials, development and improvement of analytical methods, and ecological-chemical processes. He is author or coauthor of several books and more than 120 contributions to journals. In 1988 he received the prize of the "Schweizer Gesellschaft für Thermoanalytik und Kalorimetrie".

Matthias Epple, born 1966 in Reutlingen, studied chemistry from 1984 to 1989 at the Technische Universität Braunschweig. In 1992 he completed his doctorate under the supervision of Professor H. K. Cammenga on the investigation of the kinetics of the solid-state reactions and of solid–solid phase transitions by time- and temperature-resolved X-ray diffraction. During 1993 he was postdoctorate fellow with Professor J. C. Berg at the Department of Chemical Engineering at the University of Washington in Seattle, USA, and worked in the area of recycled paper fiber recovery by flotation processes. Since January 1994 he has been working on his habilitation (chemistry of organic solids) at the "Institut für Anorganische und Angewandte Chemie der Universität Hamburg" with Professor A. Reller.

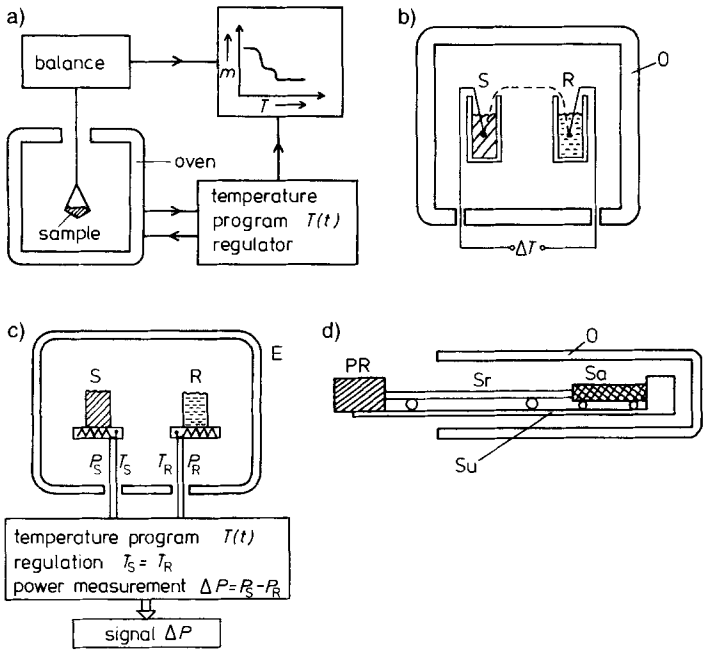


Fig. 1. The four most commonly used methods of thermal analysis presented schematically. a) Thermogravimetry (TG). b) Differential thermal analysis (DTA): S sample, R reference sample, O oven, ΔT temperature difference between sample and reference sample. c) Differential scanning calorimetry (DSC): S sample, R reference sample, E environment, T_S sample temperature, T_R reference sample temperature, P_S electrical heating power supplied to sample, P_R electrical heating power supplied to reference sample, ΔP difference in power. d) Thermomechanical analysis (TMA): Sa sample, O oven, Sr steering rod, Su support, PR displacement recorder (from refs. [1, 19]).

possible to detect changes in relative weight in the order of parts per thousand without difficulty. The purge gas in the sample chamber can usually be varied, and measurements in inert or reactive gases and even measurements in a vacuum are possible. Temperatures of approximately 1500 °C are attained, and in specially designed equipment more than 2000 °C are possible. With cooling systems low-temperature measurements to −150 °C can be conducted.

Differential thermal analysis (DTA, Fig. 1b) is based on the measurement of the temperature difference between the test sample *S* and an inert sample (reference *R*) during a temperature program. Both samples are placed as symmetrically as possible in an oven *O*. The temperatures of the test and reference samples can be measured either directly inside the samples or near the samples. At thermal equilibrium, the oven and the test and reference samples should have the same temperature. If the oven is heated at a constant rate, a constant temperature difference ΔT, which is smaller the more symmetric the experimental setup, is established following an initial transition period caused by the thermal lag within the system. In general, ideal thermal symmetry is not possible because of different heat capacities of the test and reference samples and the asymmetries caused by instrument design. As a result the temperature difference does not reach zero but is constant (stationary state). This results in a constant signal from the calorimeter (giving rise to the base line, see Section 3.1 and ref. [20]).

To reach the stationary state the system requires a certain amount of time during which the signal approaches the base line asymptotically. Such transient processes also always occur on changing the heating rate during the course of a measurement program and at the beginning of a measurement in every case (see for example, Figs. 10 and 12). Under no circumstances may they be confused with thermal events or even integrated!

If a thermal event (change in heat capacity, melting, boiling, phase transformation, reaction) now occurs in the test sample, the stationary state will be disturbed. The temperature of the test sample is then higher than (exothermic reaction) or lower than (endothermic reaction) the temperature of the reference sample; in other words, the signal recorded deviates from the base line. The temperature difference is plotted against time or temperature. Depending on the design of the calorimeter the recorded signal ΔT can be evaluated qualitatively or quantitatively. For DTA the feasible temperature range is approximately −190 to 3000 °C.

Differential scanning calorimetry (DSC, Fig. 1c) is based on a related principle for measurement. In this case the temperature difference arising from thermal activity is balanced by two independent compensatory heaters, which are positioned underneath the test sample and the reference sample. The heater power required to compensate for the temperature difference is recorded. In this arrangement the heat used or released (q) is obtained directly. Differential scanning calorimetry conducted with this type of setup is therefore described as "power-compensated DSC" (temperature range approximately between −180 and 800 °C).[23]

For DSC measurements the samples are filled into small containers ("crucibles"; made for example from aluminum, high-grade steel, gold, or glass), so that the measurements are not dependent on the different sample forms (heat radiation and dissipation varies depending on sample surface and form) and also to prevent a reaction between the sample and calorimeter (corrosion!). Attention must, however, be paid to possible reactions between the sample and crucible material, such as, for instance, an attack by acids and bases on the frequently used aluminum crucibles. A compilation of the compatibility of important calibration substances (see below) with crucible materials has been published.[24] Special high-pressure crucibles are also available for several instruments. In general the required sample quantity is only a few mg.

In dilatometry and thermomechanical analysis (TMA, Fig. 1d) the sample length is the property examined. The simplest procedure consists of heating the sample in an oven and measuring only the change in length. Expansion coefficients can be determined and transformations detected (for example, the glass transition in polymers). Whilst in dilatometry as little pressure as possible is applied to the sample, a constant force is applied in thermomechanical analysis (usually one of pressure, more rarely one of tension).

In an extension of the method, namely dynamic mechanical analysis (DMA), the applied force is changed with time, for instance sinusoidally. The mechanical response of the sample to the change is observed. Important viscoelastic sample characteristics (storage modulus E', loss modulus E'', $\tan\delta = \tan(E'/E'')$) can be calculated from the penetration depth of the test plunger and the time delay. DMA plays a particularly important role in the characterization of polymers.

Besides these four classical techniques a large number of procedures are based on monitoring the temperature dependence of other variables. Some of these are listed here as examples:

- Thermooptical analysis (TOA)[7, 25] is based on following the optical properties of a sample (absorption, emission of radiation). Thermomicroscopy is a special case, which can be used to gain important supplementary information.[26–31] Changes in grain size (structural alterations), phase changes, phase transitions, nucleation processes, precipitation processes in solids, recrystallizations and solid-state reactions are often investigated with thermomicroscopy. In thermophotometry, the temperature dependence of optical properties (for example, IR, VIS, UV, index of refraction, polarization, luminescence) is measured.[7, 32]
- In evolved gas analysis (EGA) the gases released by a sample are detected and, if applicable, analyzed quantitatively, for example by gas chromatography/mass spectrometry or FTIR-spectroscopy.[7, 33] Evolved gas analysis is often applied simultaneously with thermogravimetry.
- Emanation thermal analysis (ETA)[34, 35] concerns the detection of the release of radioactive radon from samples that have been appropriately pre-treated. With this method, for instance, structural changes of a sample (microscopic cracking, phase transformations, sintering, melting) can be detected with high sensitivity.
- Thermoconductometry[7] involves the measurement of the temperature-dependence of electrical conductivity. It is particularly suitable for the detection of phase transformations in the solid state.
- Thermal X-ray methods[36–42] involve the study of the X-ray diffraction pattern of a sample. This method enables numerous conclusions to be drawn about solid–solid phase transitions and solid-state reactions. This method can be applied to powders as well as single crystals (with synchrotron radiation).[43] Expansion coefficients can also be determined.[2]

Thermoanalytical methods are often combined. Such procedures are described as simultaneous methods. For example, the widespread, simultaneous analysis of a sample by TG and DTA enables a specific change in mass to be attributed to a thermal event. In contrast, comparative measurements are often limited when two different methods are used in succession because of the different conditions under which they are performed (sample container, oven type, temperature sensor allocation, atmosphere, etc.). Sample-to-sample variations that generally occur in solids can be avoided. A disadvantage of simultaneous methods is that the sensitivity of the measurement system is frequently reduced relative to (optimized) single methods. All other procedures which may contribute towards the characterization of a sample are described as supplementary methods. This term covers, in particular, the more rarely applied thermoanalytical methods listed above.

Finally, a brief comment on the calibration of thermoanalytical instruments is necessary. As in virtually all procedures the temperature is not directly measured at the sample site, a certain doubt arises over the "true" temperatures that should be attributed to the processes observed. These can be determined by examining well-known reference materials (with known melting temperatures, phase transition temperatures, heat capacities, expansion coefficients, heats of melting etc.; see for example, reference [44]) by the method concerned and correlating the temperatures measured with the thermodynamic equilibrium temperatures. A calibration function calculated from the observed deviations[45] can be used to correct the measured temperatures.

3. Measurements on Low Molecular Weight Materials

The preparative chemist is primarily interested in the properties of low molecular weight materials. Thermoanalysis enables the determination of diverse thermodynamic and kinetic data, which can, for instance, be used for the identification of synthesized materials and the optimization of syntheses (see Table 1). This section will highlight and, using representative examples, demonstrate the different applications.

3.1. Phase Transformations and Phase Transitions of Pure Substances

Knowledge of phase transition temperatures and enthalpies is important for the design of syntheses and for industrial manufacture. In particular, phase transition processes are exploited in purification processes (distillation, sublimation, crystallization). It is important to avoid the decomposition of a substance in the process and to achieve as good a separation as possible.

The determination of phase transition temperatures counts among the oldest applications of thermal analysis (construction of phase diagrams from cooling curves). The DSC instruments available today enable a quick and precise analysis when using temperature programs. Only a little time is required for an overview. Characteristic temperatures and enthalpies of thermally induced processes count primarily among the information accessible.

DSC is generally used for the determination of thermodynamic parameters. Figure 2 shows a typical melting peak. The change in heat capacity on melting generally gives rise to a change in the base line, and accordingly, an interpolation must be carried out.[20] From the shape of the peak the five temperatures T_i (initial peak temperature), T_e (extrapolated peak-onset temperature), T_p (maximum peak temperature), T_c (extrapolated peak-offset temperature) and T_f (final peak temperature) can

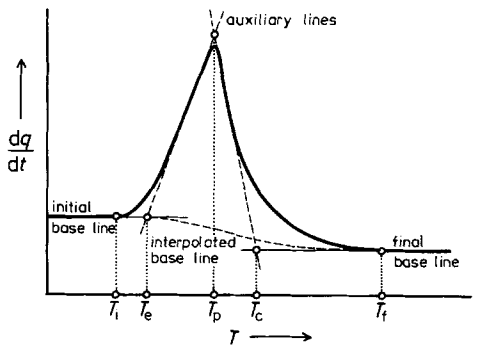


Fig. 2. An endothermic peak as obtained by the melting of a pure substance by DSC. The five characteristic temperatures T_i, T_e, T_p, T_c, and T_f can be determined from the peak shape; refer to text (from ref. [46]).

be deduced. For the characterization of melting and phase transformation temperatures the peak-onset temperature T_e is generally recommended.[46] This temperature is defined as the intersection of the tangent to the ascending peak slope and the linearly extrapolated initial base line. The peak-onset temperature is (in contrast to T_p) almost independent of the heating rate and the sample quantity, and is easier to determine than the initial peak temperature T_i.

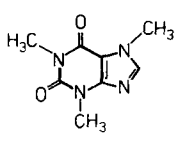
The enthalpies related to the phase changes and transitions can easily be obtained by integration of the appropriate peak (the product of heat flow and time gives a quantity of heat). This procedure naturally presents the problem of the base line construction underneath the peak.[20] A linear interpolation is usually undertaken; however, other constructions may also be appropriate.[22]

In routine operation, melting points of pure materials can usually be reproduced to within 0.5 K; enthalpies can be accurately measured to within several percent, depending on the quality of the instrument and the calibration performed.[22] For the determination of boiling points the normally sealed DSC crucibles may be pierced with a fine needle in order to enable the evolved vapor to escape. To limit the extent of vaporization below the boiling temperature, a small ball may be placed on the perforation to act as a "valve" which "opens" when the boiling point is reached, thus giving rise to sharper boiling peaks. The variation of boiling point with pressure of the environment can be ascertained by performing DSC at different selected pressures.[50, 51] The enthalpy of vaporization can be calculated from the vapor pressure curve obtained by this method and the Clausius–Clapeyron equation.

Liquid crystalline phases are primarily formed by long, asymmetric molecules. Their properties lie between those of crystalline and liquid phases. To investigate transitions between the different liquid-crystalline phases, DSC, temperature-resolved X-ray diffraction (often with synchrotron radiation), and polarization microscopy (TOA) may be used to advantage.[48, 49]

Solid–solid phase transitions occur quite often.[5, 52, 53] Different orders of transitions are recognized. According to Ehrenfest a phase transition is of the same order as the lowest derivative of Gibbs energy G that exhibits a discontinuity at the transformation. For example, G is continuous in a first-order transition, while the derivatives of G with respect to T and p are discontinuous (for example, S, V, H). The enthalpy–temperature curve of a first-order transition therefore exhibits a discontinuity at the transition temperature (examples: melting, vaporization). Among other characteristics, higher order transitions have $C_p(T)$ curves that often increase long before the transformation, ending in a maximum at the transition temperature (examples: λ transformation, magnetic transformation).

Figure 3 shows a DSC curve of caffeine (**1**). The low-temperature phase, β-caffeine, is converted into the high-temperature phase, α-caffeine, at 141 ± 2 °C in a first-order phase transition ($\Delta_{trs}H$ = 4.1 ± 0.2 kJ mol^{-1}). α-Caffeine melts at 236.0 ± 0.2 °C ($\Delta_{fus}H$ = 21.6 ± 0.5 kJ mol^{-1}).[1, 54, 55] The phase transition peak is not as "sharp" as the melting



1

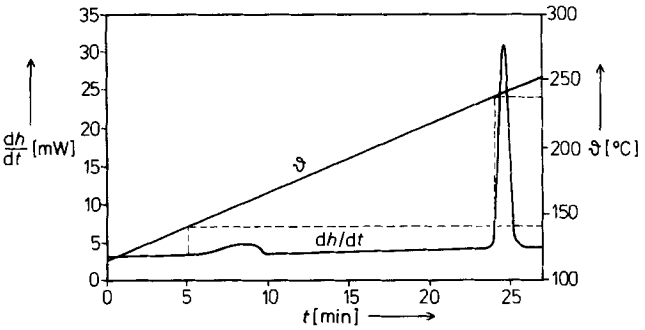


Fig. 3. DSC curve of caffeine (**1**, heating rate 5 K min^{-1}). At 141 °C the phase transition $\beta \rightarrow \alpha$ occurs and at 236 °C the melting process. The temperature is plotted on the right, the heat flow on the left (endothermic peaks point upwards, exothermic peaks downwards).

peak, as nucleation processes during a phase transition in the solid state require time. Dilatometric measurements were performed to establish whether this transition was first order. Figure 4 shows the change in length l with temperature of a pressed pellet of β-caffeine. There is a distinct discontinuity in l at the transition temperature; in other words, it is a first-order transition.

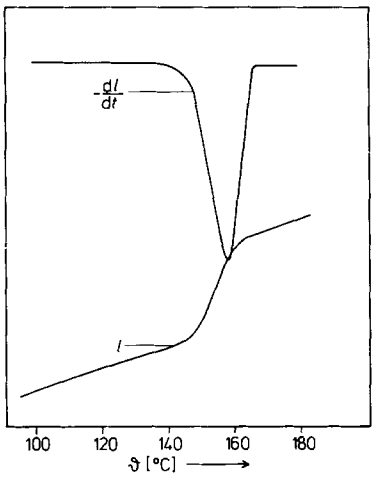


Fig. 4. Graph showing the linear expansion of a β-caffeine pellet with increase in temperature. The lower curve shows the change in length l, the upper curve the differentiation of the lower curve with time dl/dt. At approximately 140 °C the phase transition $\beta \rightarrow \alpha$ begins. The heating rate was 1 K min^{-1} (from ref. [1, 54]).

Phenanthrene undergoes a higher order transition between 72 and 74 °C. Figure 5a illustrates a DSC curve, and Figure 5b the lattice parameters determined by temperature-resolved X-ray diffraction. In both methods the transformation already begins to show at low temperatures and comes to an end with a sharp rise in the transformation rate between 72 and 74 °C. The nature of this transformation was elucidated by X-ray structure determination on single crystals at elevated temperatures.[56] The transition is one of order–disorder, in which the individual phenanthrene molecules have two different orientations in the high-temperature phase (Fig. 6). At room temperature all phenanthrene molecules lie in the orientation drawn in black. In the high-temperature phase the positions drawn in white and in black are taken up with the same probability; in other words,

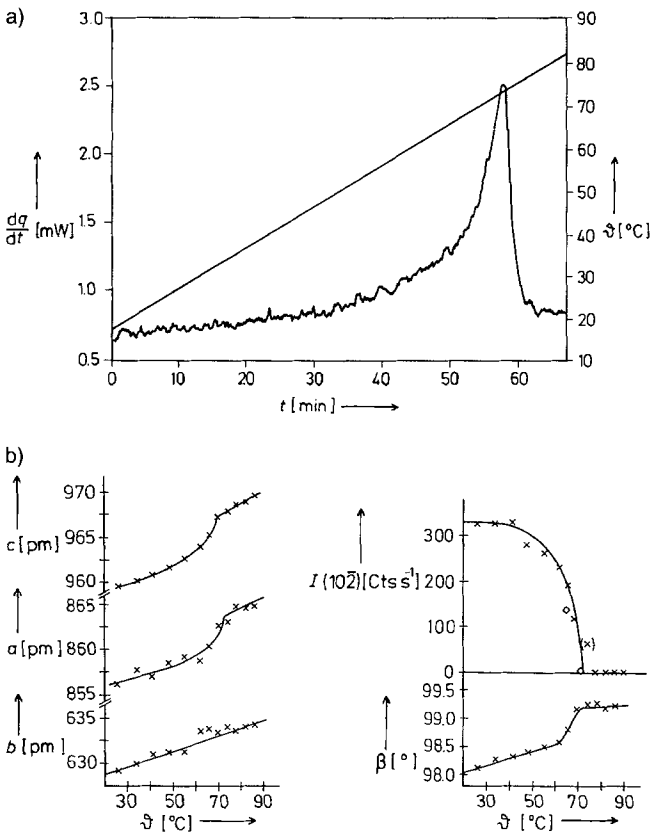


Fig. 5. Graph showing the solid–solid phase transition of phenanthrene. a) DSC curve (heating rate 1 K min^{-1}; according to ref. [1]). b) Crystallographic monitoring of the lattice parameters a, b, c, and β, and X-ray reflection (10$\bar{2}$) characteristic of the transition (temperature program: isothermal steps). The values for the (10$\bar{2}$) reflection gathered from examinations of single crystals [56] are plotted as ◇ (from ref. [41]).

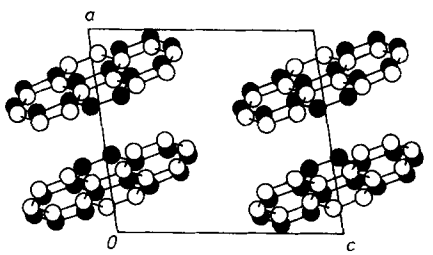
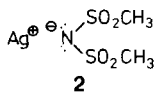


Fig. 6. Projection of the arrangement of phenanthrene molecules in a crystal onto the a/c plane. In the high temperature phase the molecules lie with the same probability either in the black or the white orientation (from ref. [56]).

the structural symmetry of the individual phenanthrene molecule in the crystal increases.

If the samples to be examined exhibit a more complex thermal behavior, or if nothing is known about the samples, the information from DSC is often insufficient, because DSC only yields the rather unspecific variable "enthalpy change". It is not possible to differentiate clearly between an endothermic phase transition, a melting process, and an endothermic reaction by DSC alone. Supplementary methods of measurement must be employed in cases that are not clear-cut. In particular the examination of solids could prove to be difficult due to the widespread appearance of polymorphism: approximately one third of organic solids have two or more polymorphic forms. Other thermoanalytical procedures can be used as additional methods (see Section 2). This approach was demonstrated here for the analyses of caffeine (Fig. 4, use of dilatometry) and phenanthrene (Fig. 5, use of temperature-resolved X-ray methods).

Cases where only small changes in enthalpy, no change in mass, and little change in length are associated with the events in progress (for example, some solid–solid phase transitions) present problems. This situation arises in a solid–solid phase transition of higher order in anhydrous silver dimesylamide (**2**), which takes place with only very small thermal effect, shows no discontinuity in its thermal expansion behavior, and is, of course, not associated with a mass loss.[57]



2

Thermoconductometry and temperature-resolved X-ray diffraction were therefore the methods chosen for this investigation. In Figure 7 the logarithm of conductivity is plotted against the reciprocal temperature. The kink at about 142 °C pointing to a phase transformation is clearly visible. The measurements carried out by X-ray diffraction enabled the quantitative determination of this higher order transition.[58]

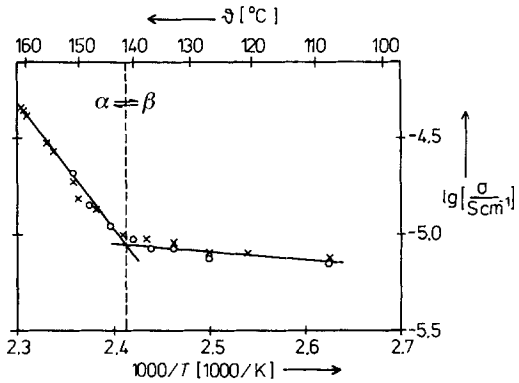


Fig. 7. Thermoconductometric study of the phase transformation $\alpha \rightleftharpoons \beta$ in anhydrous **2** (pressed pellet, 2000 Hz). The quarter hydrate **2**·1/4H2O was the starting material, which was dehydrated by heating. The subsequent cooling curve (○) and second heating(×) were recorded.

3.2. Determination of Phase Diagrams of Mixtures

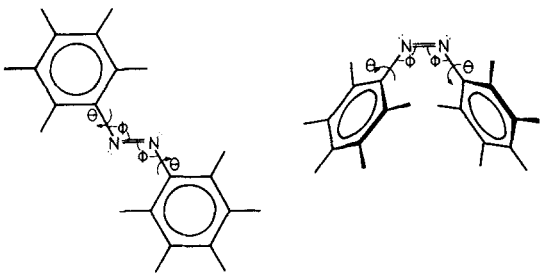
As already mentioned, a classical application of thermal analysis is the determination of phase diagrams of mixtures or alloys from cooling curves (monitoring the temperature while allowing the sample to cool freely). Knowledge of the phase state is also important in syntheses, because the materials obtained are often more or less contaminated.

One of the simplest methods for checking the identity and purity is the determination of the mixed melting point T_{fus}^{mix}, which can easily be obtained from a DSC measurement. The classical van't Hoff method for the determination of purity provides more extensive information. This method is based on the lowering of the melting or freezing point, which occurs if a pure substance is contaminated with an impurity (cryoscopy). A tacit condition for this procedure is the existence of a eutectic phase diagram (cf. physical chemistry textbooks), in which the contamination of a pure component always leads to depression of

the melting point. If however a solid solution is formed between the two components (mixed crystals), the melting point of the mixture always lies between the melting temperatures of the pure substances; in other words, the method of melting temperature depression cannot be used. This situation is not rare, but is often not considered.

Such simple, and even more complex, phase diagrams can easily be determined using thermoanalytical methods. For this purpose different compositions of mixtures of pure materials are examined. DSC is the method normally used for these measurements. For more complicated problems, X-ray diffraction (if necessary temperature-resolved), thermooptical methods, and temperature-dependent measurements of electrical conductivity or electrode potential[59] are also often used.

The pseudo-binary phase diagram of *cis*- and *trans*-azobenzene will be used to demonstrate the procedure. At elevated temperature *cis*-azobenzene (**3b**) is slowly transformed into *trans*-azobenzene (**3a**) in the solid state as well as in the melt.[60-63]



3a, *trans* **3b**, *cis*

By repeatedly melting a sample of pure *cis*-azobenzene, allowing partial isomerization in the melt, and then cooling, the entire phase diagram can be established in small stages. In addition of course, mixtures can also be weighed out and measured.

Melting curves of some *cis*/*trans*-azobenzene mixtures with different compositions are shown in Figure 8. The change in the melting peaks for the pure substances as well as the eutectic peak for a mixture containing different portions of the components is clearly visible. The phase diagram shown in Figure 9 can be constructed from the melting temperatures of the mixtures. The eutectic of *cis*- and *trans*-azobenzene containing 52% of *trans*-azobenzene melts at 41.4 °C. When quenching molten mixtures of *cis*- and *trans*-azobenzene presumably a further modification of *cis*-azobenzene occurs, which also forms a eutectic with *trans*-azobenzene (eutectic temperature 36.7 °C). The melting temperature of the *cis*-azobenzene is also lowered (broken liquidus curve).[61-63] The agreement with additional data obtained by TOA[62] and by the Kofler contact method[30] is good. This example shows that unexpectedly complex phenomena can also occur in (seemingly) simple systems.

3.3. Identification and Determination of Purity

The purity of synthesized substances is often of crucial importance for the subsequent synthetic step. While the previous section dealt with larger quantities of foreign substances (impurities), this section outlines the calorimetric determination of small concentrations of impurities.

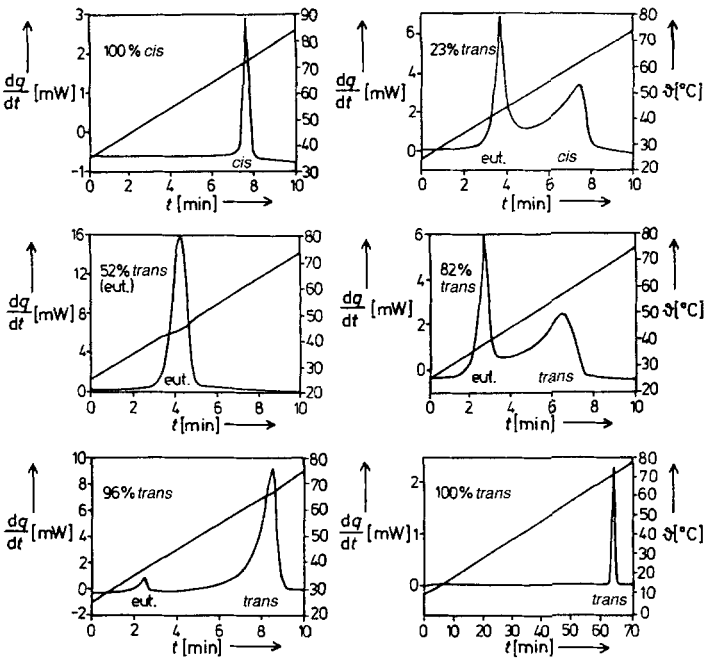


Fig. 8. Melting curves of some mixtures of *cis*- and *trans*-azobenzene (**3**). The melting temperature of the eutectic (eut.) is 41.4 °C, of *cis*-azobenzene (**3b**) 71.6 °C, and of *trans*-azobenzene (**3a**) 68.3 °C.

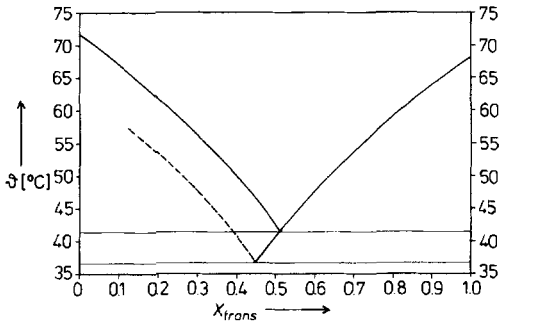


Fig. 9. The pseudo-binary phase diagram of *cis*- and *trans*-azobenzene (**3**). For details see text.

A DSC curve of a sample can be recorded quickly. The purity can already be roughly estimated by visual inspection of the shape of a melting peak. Figure 10 exhibits melting curves of naphthalene which was definitely contaminated with *trans*-azobenzene. Pure naphthalene has a very sharp melting peak with a very steeply ascending left slope. The melting peak becomes broader and flatter with increasing concentration of contaminant (the peak area remains approximately constant!). The extrapolated peak-onset temperature (described here as T_m) decreases. This effect is due to the increasing depression in melting temperature with increasing concentration of contaminant according to the Schröder–van-Laar equation and the van't Hoff law [Eq. (a)], where T_0 is the melting point of pure substance A

$$T_0 - T_m = \frac{R T_0 T_m}{\Delta_{fus} H_A} \ln x_A \approx \frac{R T_0^2}{\Delta_{fus} H_A} x_B = \frac{R T_0^2}{\Delta_{fus} H_A} x_B^* \frac{1}{F_m} \qquad (a)$$

(naphthalene in example), T_m the melting point of contaminated substance A, x_A the fraction of main component A in the liquid phase (melt), x_B the fraction of contaminant B (*trans*-azoben-

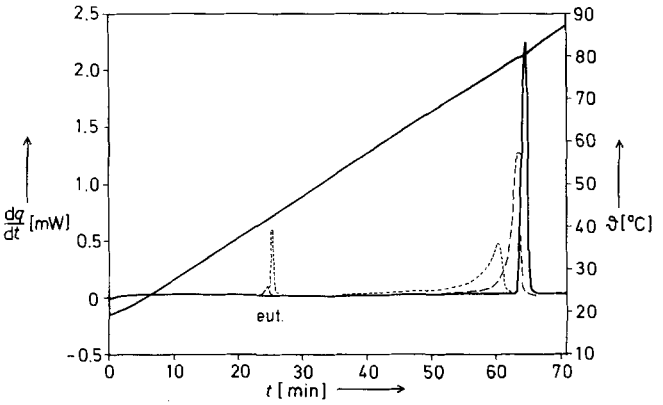


Fig. 10. The effect of contaminant concentration x_{3a} on the DSC melting curve of naphthalene. The solid curve represents zone refined (highly pure) naphthalene, the broken curve naphthalene containing 0.98 mol% **3a**, and the dotted curve naphthalene containing 5.01 mol% **3a** (from ref. [1]). eut. = eutectic.

zene in example) in the liquid phase, and $\Delta_{fus}H_A$ the enthalpy of fusion of pure substance A. The basic prerequisite for the use of this equation is the formation of a eutectic between A and B. In addition, this equation is only valid under certain conditions (see ref. [66]), which primarily include an adequately low concentration x_B, thermal stability of the components even after melting, and thermodynamic equilibrium (neither temperature nor concentration gradients). The last of these requirements results in the use of a low heating rate β (normally 1 to 2 K min^{-1}) and a small sample quantity (a few mg). As a rule of thumb, a substance is of high purity if the ascending (left) side of the melting peak is steeper than the descending (right) side.

Quantitative analysis of the melting peak shape provides more precise values for purity. In this method it is assumed that the eutectic of A and B initially melts. The pure component A (in this case naphthalene) then gradually dissolves in the eutectic with increasing temperature, and as a result the concentration of B (in this case *trans*-azobenzene) steadily decreases. Thus one moves along the solubility curve of B in A, which is approximately given by the van't Hoff equation. When all of A has melted, the melt has a contaminant concentration of x_B.

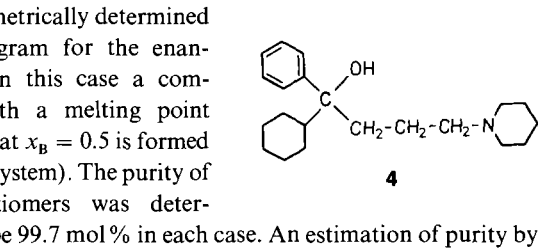
By suitable plotting of the melting temperature versus the corresponding fraction that has melted (F_m), which can easily be determined from the ratio of the integral of the curve up to the particular melting temperature to the integral of the whole curve, the fraction x_B^* of contamination in the original sample can be calculated by linearization: the gradient gives the contaminant concentration x_B^*. The intercept of the extrapolated line with the temperature axis yields the melting temperature of pure component A.[1, 64, 65] The small but measurable total concentration of contaminants (less than 0.1 mol%), which can often no longer be quantitatively determined by the usual procedures such as NMR, UV, IR, and MS, is a particular advantage of this method.

As the reduction in melting temperature, being a colligative property, depends not on the type of dissolved particles but on their number only, the concentration of contaminant x_B must be regarded as a summated variable. All foreign substances which form eutectics with the main component are detected together. This feature differentiates this method from other sensitive methods (GC, HPLC, etc.), which can only detect individual impurities but do not directly yield the purity of the sample. The requirement that all components behave ideally in the melt limits the safely detectable concentration range to $x_B \approx 5$ mol% (for an estimation of the error resulting from approximations associated with the van't Hoff and Schröder–van Laar equations, see ref. [66]).

Another method that so far has hardly been used is based on a mathematical simulation of a measured curve by allocating suitable thermal resistances and time constants for the calorimeter and calculating the rate of enthalpy change in the sample.[66, 67] In this procedure calculated melting curves are compared with an experimentally obtained melting curve. The concentration of contaminant is mathematically varied in the simulation process until optimal agreement between the calculated and measured curves has been reached.

An important practical application of the calorimetric purity analysis is the determination of enantiomeric purity of newly synthesized substances. This type of analysis is particularly important for pharmaceuticals. In these cases calorimetric analysis can provide valuable results.[68–71]

The example of the selective antimuscarine agent 1-cyclohexyl-1-phenyl-4-piperidino-1-butanol (hexahydro-difenidol, **4**) will be used to illustrate this application. Figure 11 exhibits the calorimetrically determined phase diagram for the enantiomers. In this case a compound with a melting point maximum at $x_B = 0.5$ is formed (dystectic system). The purity of the enantiomers was determined to be 99.7 mol% in each case. An estimation of purity by melting point determination alone would lead to completely incorrect results here. The course of the curve between the melting temperatures of the pure enantiomers and the eutectics was calculated with the unsimplified Equation (a) (Schröder–van-Laar equation; middle partial equation). The course of the curve between the two eutectics arises from the Prigogine–Defay equation $\ln 4x_B(1 - x_B) = \Delta_{fus}H_{rc}(1/T_{max} - 1/T)$ Enantiomeric purities are frequently quoted as %*ee*. The relation to molar fraction is $\%ee = 100(2x - 1)$.[68, 70]



4

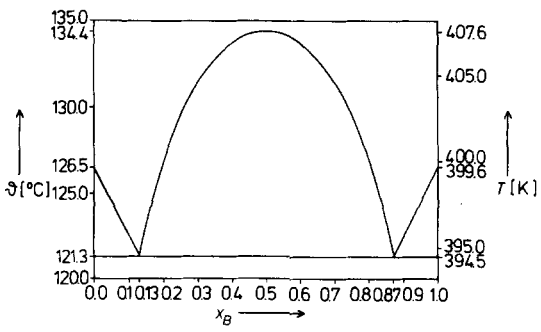


Fig. 11. The calorimetrically determined phase diagram of the two enantiomers of **4**. Both components form a dystectic (from ref. [70]).

3.4. Determination of Thermochemical Parameters

Besides the properties of pure, thermally unreactive materials, the measurement of which was discussed in the previous three sections, chemical reactions can also easily be examined with

thermoanalytical methods. These methods enable thermodynamic data (heat capacity change $\Delta_r C_p$, enthalpy of reaction $\Delta_r H$, equilibrium constant K_p, and Gibbs energy $\Delta_r G$) as well as kinetic data to be determined. The study of reaction kinetics is discussed extensively in the separate Section 3.5 because of the large significance of this field of application.

Differential scanning calorimetry (DSC) on small sample quantities (2–4 mg) can provide a general analysis of an unidentified or newly synthesized material within a few hours. An analysis by this method provides information on phase transformations and on reactions, among these also decomposition reactions. Although the temperature and enthalpy values obtained are usually still rather inaccurate, valuable conclusions on the identity, purity, and stability of the sample can still be drawn.[72–74] Unexpected effects such as phase transitions and reactions are often found. These easily obtainable results should be of interest to the preparative chemist in particular. Experience shows that a quantitative determination of the effects taking place requires a larger number of measurements. However, a quantitative description of the system is not always necessary, depending on the specific research task.

The determination of different thermochemical parameters is demonstrated here with the silver dimesylamide quarter-hydrate ($\mathbf{2}\cdot 1/4\,H_2O$) as example. Figure 12 shows the DSC curve of a

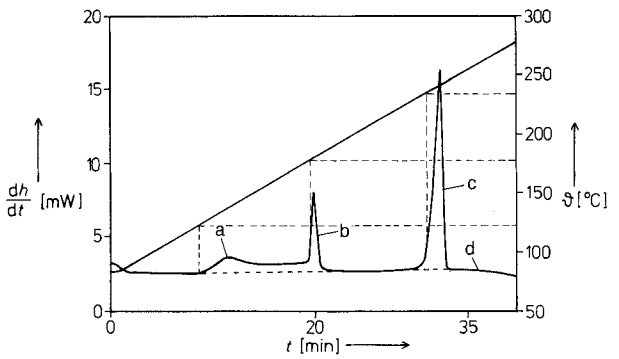


Fig. 12. DSC curve of $\mathbf{2}\cdot 1/4\,H_2O$. The dehydration a begins above 100 °C and ends with a very rapidly occurring phase transition b at 174 °C. At 238 °C the now anhydrous substance melts (c). In the melt, exothermic decomposition d occurs. The heating rate was 5 K min^{-1} (from reference [75]).

heating event. Dehydration a appears above 120 °C as a broad, endothermic peak. At 174 °C the dehydration is concluded by a rapid phase transition, during which the remainder of the water of hydration is released (sharp endothermic peak b). The sum of the enthalpy of dehydration and phase transformation was calculated by integration to be +18.42 kJ mol^{-1}.[75] After the dehydration and phase transition the substance is yellow because the crystals shatter into many small fragments while maintaining the external morphology.[75]

From the fusion peak c the melting temperature can be calculated to be 237.7 °C. The calorimetrically determined purity of the sample is 99.6 mol% (enthalpy of melting 26.48 kJ mol^{-1}). Exothermic decomposition d begins only in the melt and is seen in the falling base line.

At this point it becomes clear how information obtained from thermal analysis data can be useful in the planning of a synthesis. Silver dimesylamide is used as a starting material for further syntheses and must be available in an anhydrous form; in other words, it must be dehydrated.[58] The optimal dehydration temperature lies approximately between 180 and 190 °C, as the entire amount of water of crystallization is released quickly at this temperature without decomposition. Thermal analysis also shows that the yellow coloration after dehydration is not due to decomposition, as may have been assumed upon superficial examination. Knowledge of the high purity is of considerable value for further synthesis planning.

3.5. Kinetic Parameters from Thermoanalytical Measurements

The variables measurable by thermoanalytical methods can often be correlated with the progress of reaction. In the case of thermogravimetry the quotient from the loss in mass $\Delta m(t)$ at time t with the total mass loss $\Delta m(t = \infty)$ equals the proportion which has reacted so far, the degree of conversion. The degree of conversion is generally defined by using the extent of reaction ξ and is described as α [Eq. (b), see physical chemistry textbooks]. For a reaction proceeding to completion the degree of conversion lies between 0 and 1. The relationship between the degree of conversion and loss in mass is given by Equation (c), where $\Delta m(t)$ is the mass loss by time t, $\Delta m(t = \infty)$

$$\alpha = \frac{\xi}{\xi_{max}} \tag{b}$$

$$\alpha(t) = \frac{\Delta m(t)}{\Delta m(t = \infty)} = \frac{m(t = 0) - m(t)}{m(t = 0) - m(t = \infty)} \tag{c}$$

the total mass loss at the end of the reaction, $m(t)$ the sample mass at time t, $m(t = 0)$ the sample mass before reaction, and $m(t = \infty)$ the sample mass at the end of the reaction.

This simple equation is, of course, only valid for one-step reactions proceeding to completion ($\alpha(t = \infty) = 1$) in which the starting material used has not yet undergone decomposition ($\alpha(t = 0) = 0$). An example is the thermal decomposition of $Li_2SO_4\cdot H_2O$, which takes place without the formation of lower hydrates.[76] For the dehydration of $CuSO_4\cdot 5\,H_2O$ to $CuSO_4$, which is known to have intermediate steps, this equation must be applied to the individual steps.

A similar equation applies to DSC for the relationship between the enthalpy of reaction and degree of conversion. In this case the partial area of the reaction peak up to time t is compared with the total peak area [Eq. (d)], where $\Delta_r H(t)$ is the

$$\alpha(t) = \frac{\Delta_r H(t)}{\Delta_r H} = \frac{\int_{t_i}^{t}\left(\frac{dH}{dt}\right)dt}{\int_{t_i}^{t_f}\left(\frac{dH}{dt}\right)dt} \tag{d}$$

enthalpy of reaction (= partial peak area) up to time t, $\Delta_r H$ the total enthalpy of reaction (= total peak area between t_i and t_f), t_i the initial peak time (temperature T_i), t_f peak-end time (temperature T_f), and dH/dt enthalpy change (= heat flow) at time t.

Besides those conditions mentioned for thermogravimetry, additional conditions apply to DSC. No other thermal event (phase transition, melting, evaporation) may take place during

the reaction, and furthermore the enthalpy of reaction, which is dependent on the amount of material, must be independent of the degree of conversion. This means, for instance, that the enthalpy changes by the same amount when the degree of conversion changes from $\alpha = 0$ to $\alpha = 0.1$ as it does when the degree of conversion changes from $\alpha = 0.6$ to $\alpha = 0.7$.

Thermogravimetry and DSC are the methods most frequently used for the determination of kinetic data. Other methods such as thermooptical analysis, evolved gas analysis, and X-ray diffraction can also be used in kinetic measurements.

A particular feature of thermoanalytical methods is their suitability for the study of the kinetics of nonisothermal reactions. Conventionally, kinetic measurements are performed isothermally at different temperatures. The calculated rate constants are plotted according to Arrhenius ($\ln(k)$ versus $1/T$) to give the activation energy and collision factor (providing the plot forms a straight line). This procedure can be time consuming and requires substantial amounts of material.

Nonisothermal measurements enable, in principle, the activation parameters E_A and $\lg(k_\infty)$ to be determined from a single experiment.[25, 78–80] This procedure considerably reduces the measurement time. Although some procedures for evaluation have been available for over thirty years, this method of analysis is used comparatively seldom and is therefore unfamiliar to many chemists. For this reason the most important procedure for the evaluation of nonisothermally obtained data (the Borchardt and Daniels method),[81] which is also frequently included in the commercially marketed TA program packages, will be introduced briefly here. The rate of reaction is defined by using the previously introduced degree of conversion α [Eq. (e)],

$$\frac{d\alpha}{dt} = k(T)f(\alpha) \qquad (e)$$

where $d\alpha/dt$ is the rate of reaction, $k(T)$ the temperature-dependent rate constant, and $f(\alpha)$ a function characteristic of the reaction mechanism. For a first-order reaction, for instance, $f(\alpha) = 1-\alpha$; for an nth order reaction $f(\alpha) = c_0^{n-1} \times (1-\alpha)^n$, where c_0 is the initial concentration.[82]

For determining the temperature dependence of the rate constant k the Arrhenius equation [Eq. (f)] is applied. k_∞ is the collision factor (preexponential factor, often also denoted as k_0, A, or Z) and E_A the activation energy.

The combination of the two equations gives Equation (g). Equation (h) is thus valid for an nth order reaction. By taking logarithms the Equation (i) is obtained.

$$k(T) = k_\infty \exp\left(-\frac{E_A}{RT}\right) \qquad (f)$$

$$k(T) = \frac{d\alpha/dt}{f(\alpha)} = k_\infty \exp\left(-\frac{E_A}{RT}\right) \qquad (g)$$

$$k(T) = \frac{d\alpha/dt}{c_0^{n-1}(1-\alpha)^n} = k_\infty \exp\left(-\frac{E_A}{RT}\right) \qquad (h)$$

$$\ln k(T) = \ln(d\alpha/dt) - (n-1)\cdot\ln(c_0) - n\cdot\ln(1-\alpha) = \ln k_\infty - \frac{E_A}{RT} \qquad (i)$$

In the most favorable case the order n of the reaction is known. In this situation $k(T)$ can be calculated from the variables $d\alpha/dt$, c_0, and α for all temperatures. The value of $\ln(k(T))$ is plotted versus $1/T$, and after linear regression the activation energy E_A can be calculated from the gradient and the collision factor k_∞ from the intercept, providing n has been chosen correctly. If the order of reaction n is not known, an optimal fit of the three parameters E_A, k_∞, and n can be achieved by multiple linear regression (MLR) or nonlinear regression.[84, 85]

This procedure is demonstrated in Figure 13. The thermally induced rearrangement of (diphenylsilyl)methyl benzoate (**5a**)

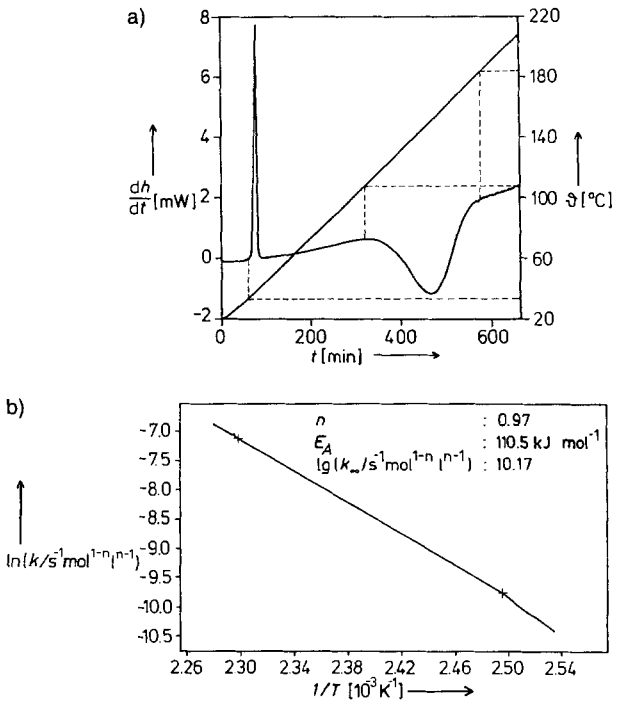
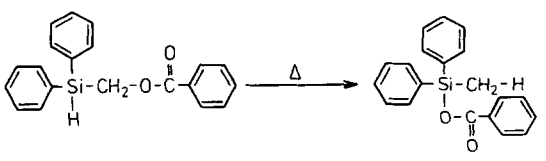


Fig. 13. Determination of the kinetics of the rearrangement of benzoic acid ester **5a** to **5b** by DSC. a) DSC curve (heating rate 0.3 K min^{-1}). At 39.4 °C the substance melts (sharp endothermic melting peak). Between 105 and 180 °C the exothermic rearrangement reaction takes place. b) Kinetic plot, obtained by multiple linear regression (MLR) for an n-th order reaction. The calculated fit parameters are included. The crosses mark the range used for MLR. The reaction only starts at elevated temperatures. Even ten cycles of melting and resolidification do no lead to any conversion.

was studied. This compound melts at 39.4 °C (enthalpy of fus $\Delta_{fus}H = 25.74$ kJ mol^{-1}). Rearrangement to the silyl ester **5b** takes place in the melt in the temperature region between 105 and 180 °C. The enthalpy of reaction calculated as described in Section 3.4 is $\Delta_r H = -169.1$ kJ mol^{-1}. Kinetic analysis of the exothermic reaction peak by multiple linear regression resulted in a first-order reaction ($n = 0.97$) with an activation energy E_A of 110.5 kJ mol^{-1} and a collision factor $\lg(k_\infty/s^{-1}\,mol^{1-n}\,l^{n-1}) \approx \lg(k_\infty/s^{-1})$ of 10.17. These results agree well with the



5a **5b**

results obtained by conventional methods (NMR, isothermal) and by theoretical calculations.[86, 87]

Besides the Borchardt and Daniels method, a series of other methods for the evaluation of nonisothermal measurements exist. The following categories of procedures can be differentiated:[1, 25]

- *Direct methods* employ the degree of conversion α and the rate of reaction $d\alpha/dt$. They are particularly suitable for DTA and DSC measurements in which the signal recorded is proportional to $d\alpha/dt$. The most important method is that of Borchardt and Daniels.[81]
- *Integral methods* employ only the degree of conversion α.[88–90] They are particularly suitable for the thermogravimetric and temperature-resolved X-ray diffraction methods, as in these cases the signal recorded (mass, intensity) is directly related to the degree of conversion.
- *Differential methods* involve the derivative of the reaction rate $d\alpha/dt$ with respect to time or temperature.[91–93] These methods naturally react very sensitively to noisy curves and are therefore not applicable in many cases except after curve smoothing.
- Some methods make use only of *specific points* on the experimental curve, such as the maximum in the rate of reaction $d\alpha/dt$.[94–100] Usually several measurements with different heating rates are necessary. These methods are often based on simplifying assumptions, which are not always justified.

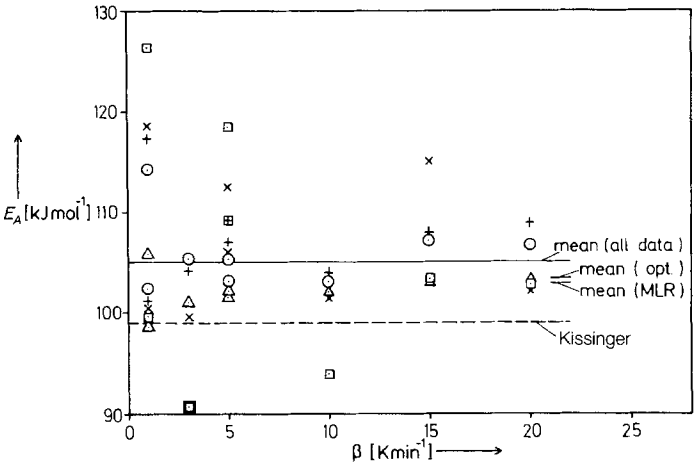


Fig. 14. Isomerization of *cis*-azobenzene **3b** in the melt analyzed by DSC with different methods of data processing. The calculated isomerization activation energy (first-order reaction) is plotted against the heating rate, β. The points ⊙ were determined by the Borchardt and Daniels method [81], × by the Ellerstein method [92], + by the Coats and Redfern method [88], △ by multiple linear regression [84], and ⊡ by the Freeman and Carroll method [91]. In addition, the values determined by the Kissinger method [96] and by discontinuous (isothermal) spectrophotometric measurements [60] are also plotted. The mean values from multiple linear regression and the mean of all non-isothermal measurements are also included (from ref. [102]). Very recently Flammersheim and Eckert, using samples we provided, obtained $E_A = 103 \pm 1$ kJ mol^{-1} by multivariate nonlinear regression (heating rate 1–40 K min^{-1}). The reaction and its data may thus be used as a kinetic reference.

As these methods always deal only with different mathematical variants of the same basic kinetic equations (see above), they should, in principle, produce identical activation energies and collision factors for a given reaction. However, the chosen method of evaluation may depend on the heating rate β as a result of different approximations made when differentiating the equations and of varying signal-to-noise ratios. Nonlinear methods of curve fitting are therefore being increasingly used (for consecutive, equilibrium, and parallel reactions as well), which perform a numerical optimization without approximations.[101] However, caution is advised here if the process investigated is not well known. Clearly, the more variables (i.e., kinetic parameters of assumed partial stages of a reaction) that are fitted to a curve, the better the mathematical fit will be. This should, however, not encourage a noncritical acceptance of the calculated activation parameters and reaction mechanisms.

Different methods of evaluation were applied to the example of the thoroughly investigated thermal isomerization of *cis*- to *trans*-azobenzene in the melt (**3b** → **3a**; enthalpy of isomerization according to DSC: $\Delta_{iso}H^{\ominus}_{298} = -48.2$ kJ mol^{-1}).[61–63] DSC measurements were performed at six different heating rates. The results for the activation energy obtained are depicted in Figure 14.[102] Besides the results determined by the methods of Borchardt and Daniels,[81] Ellerstein,[92] Coats and Redfern,[88] Freeman and Carroll,[91] and Kissinger,[96] and by multiple linear regression from the DSC curves, results arising from isothermally performed spectrophotometric measurements (discontinuous, classical Arrhenius evaluation)[60] are also plotted.

The "classically" performed optical measurements conform well to the mean value from the calorimetric measurements. It is, however, clear that the methods always produce slightly differing results. At low heating rates the signal-to-noise ratio of the DSC curve increases, which manifests itself in a greater scatter of the activation energies obtained. The differential procedures of Ellerstein, and also of Freeman and Carroll, react particularly sensitively to the increasing noise. The selected heating rate can therefore have considerable impact on the result.

In summary, the nonisothermal methods deliver results consistent with those from isothermal measurements. In each individual case the heating rate must always be varied and the calculated kinetic data analyzed critically to avoid serious errors in conclusions. This is all the more important because programs for kinetic data processing with a convenient and easy operation that can lead to an all too uncritical handling of the data are offered by instrument manufacturers today.

The examples given so far concern homogenous chemical reactions. In general the applicability of kinetic procedures and their agreement with results obtained by "classical isothermal" methods is good in these cases.[63, 78, 86, 102] The examination of heterogenous reactions (for instance, when at least one participant in the reaction is a solid) proves to be more difficult.

Whilst the possible mechanisms for homogenous reactions (expressed by the functions $f(\alpha)$[82]) are usually zeroth, first, or second order, the circumstances surrounding the reactions of solids are completely different. Because of the fixed orientation of the molecules or atoms, nucleation, diffusion, and thermal conduction phenomena play crucial roles. The resulting rate laws are often complicated even though numerous simplifications were involved in their derivation.[82] Selection and verification of the "correct" reaction mechanism is difficult. As yet no successful unified theory for solid-state reactions has been developed, despite extensive theoretical and practical efforts. The basic principles of the kinetics of these reactions as understood today can be found in several monographs.[5, 103–108]

The significance of the kinetic parameters E_A and k_∞ in the solid-state reactions is controversial.[109–113] Increasingly, the

view is taken that the calculated variables are artifacts; in other words, they have no physical significance.[114] In fact, the concept of an "activation energy" was originally developed for collision-induced reactions in the gas phase and is already not valid without reservation in liquid phases.

The extensive characterization of solid-state reactions is considerably more difficult (and therefore more laborious) than that of a homogeneous reaction. Additional analyses by optical, electrical,[59] and diffraction methods, amongst others, must usually be performed.

Figure 15 illustrates an example of the application of a supplementary method to a solid-state reaction. Lithium sulphate

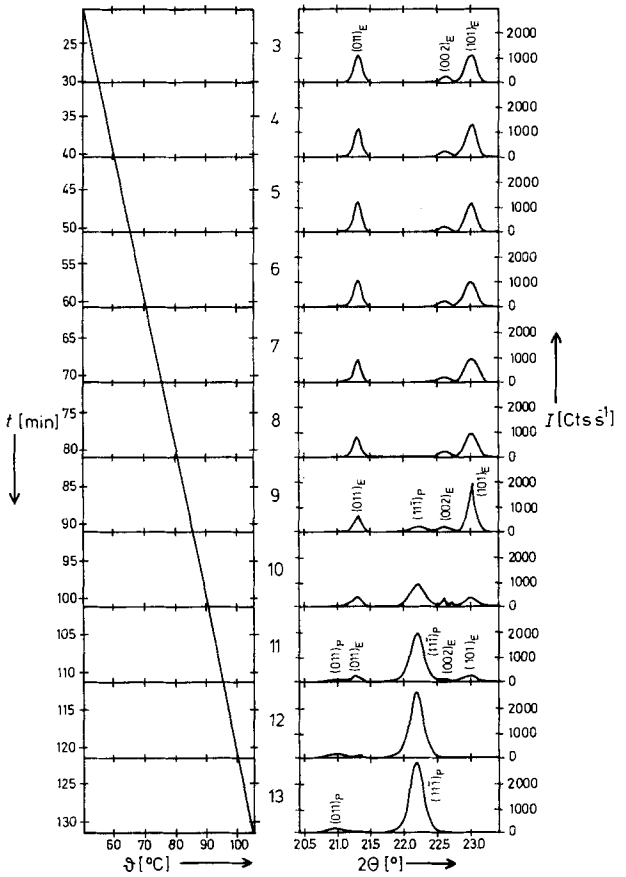


Fig. 15. Analysis of the dehydration of lithium sulphate monohydrate by temperature-resolved X-ray diffraction (TXRD). On the left the temperature is plotted against time; on the right the recorded diffractograms (scans 3 to 13) are portrayed. The heating rate was + 0.5 K min^{-1}, the angular velocity relative to 0.3° 2θ min^{-1}. The reflections from starting material E (= $Li_2SO_4 \cdot H_2O$) and product P (= Li_2SO_4) are marked (from ref. [77]).

monohydrate was discussed as a potential kinetic standard for solid-state reactions.[76] Here we discuss the study of the dehydration of lithium sulphate monohydrate by time- and temperature-resolved X-ray powder diffraction.[77] During the heating process performed at a constant heating rate, powder diffractograms of the sample are recorded continually. During dehydration the reflections of the hydrate (E) become smaller until they have completely disappeared. The reflections of the anhydride (P) develop concurrently. The reflections could be indexed.[115] The quantitative ratio of hydrate to anhydride can be calculated from the intensities of the reflections, from which the degree of conversion can be determined.[41] It is then possible to draw conclusions on the kinetics of the solid-state reaction from the temperature- and time-dependent degree of conversion data. The data recorded point to a nucleation mechanism A_2 according to Avrami–Erofeev.[82]

However, the X-ray reflections of the hydrate do not decrease monotonically as would be expected. Instead, for instance, the intensity of the (101) reflection suddenly increases in scan 9, and decreases again in the following scan. Such effects can also be observed with other hydrate reflections. They indicate that during the dehydration, processes are taking place that cannot be explained by simple kinetic models. Neither DSC nor TG measurements gave any indication of such processes.[77] Such observations show that solid-state reactions involve very complicated processes that can only be explained after analysis by as many methods as possible (see for example, ref. [116]).

For this reason nonisothermal kinetic measurements should preferably be performed in a homogeneous (liquid) phase. In this case DSC is usually the method of choice. In favorable cases all energetic and kinetic parameters of a reaction can be determined from very few measurements by this method with mg quantities, as shown in Sections 3.4 and 3.5. Naturally, the nonisothermal procedure can also be applied advantageously to other techniques (for example, the large variety of spectrometric methods[117, 118]), an option that unfortunately has only been used very sporadically as yet.

4. Measurements on High Molecular Weight Substances (Polymers)

An important field for the application of thermoanalysis is the examination of high molecular weight substances.[10, 119–122] The main methods used are DSC, thermogravimetry, and thermomechanical procedures. The processes and variables examined include glass transition temperatures (DSC, TMA, DMA), degrees of crystallinity and melting processes (DSC), rates of polymerization (DSC), heat capacities (DSC), rates of crystallization (TOA), softening processes (TMA, DMA), mechanical variables such as expansion coefficient, elasticity, storage modulus, loss modulus (TMA, DMA), thermal stability (TG, DSC), and the determination of the composition and compatibility of multicomponent mixtures (DSC, TG, TMA, DMA). In the following examples will be used to illustrate these applications.

Glass transitions appear as a shift in the base line (in an endothermal direction, change in heat capacity ΔC_p) during a DSC measurement. The glass transition in polyethylene terephthalate (PET) is illustrated in Figure 16 (78.7–83.7 °C). Knowledge of glass transition temperatures is important for the assessment of elastic properties and estimation of the compatibility of the individual components in polymer mixtures (polymer blends).

The exothermic crystallization of amorphous regions (peak temperature 157.6 °C) and the melting process (peak-onset temperature 239.6 °C) can also be seen in Figure 16. By comparing the measured enthalpy of melting with the enthalpy of melting tabulated for an entirely crystalline polymer, the crystalline fraction of the sample can be estimated (polymers generally contain crystalline as well as amorphous regions).

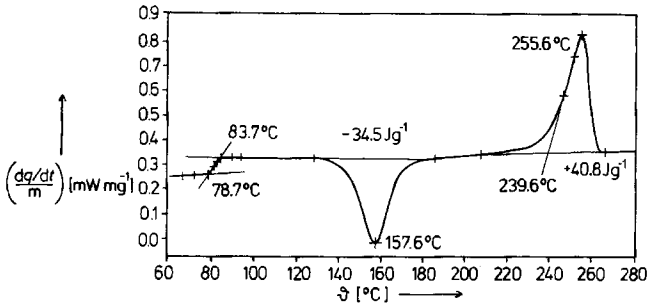


Fig. 16. Melting curve of PET by DSC. From 78 to 84 °C the glass transition appears as an endothermic step. At a peak temperature of 158 °C exothermic recrystallization takes place (enthalpy of crystallization $-34.5\ J\,g^{-1}$), at a temperature of 240 °C (onset) and 256 °C (maximum) melting takes place (enthalpy of melting $+40.8\ J\,g^{-1}$). The heating rate was $10\ K\,min^{-1}$ (from ref. [123]).

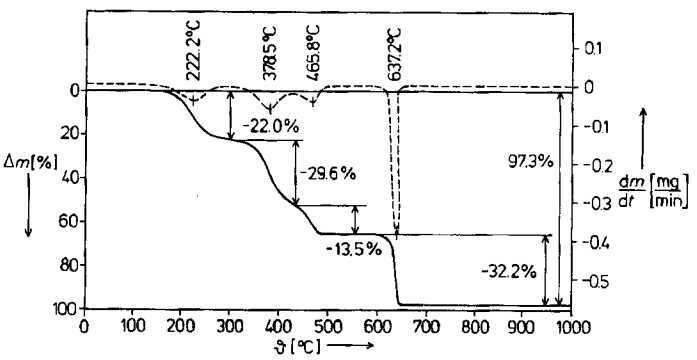


Fig. 17. TG curve of the decomposition of a natural rubber/ethylene–propylene copolymer blend. The solid line illustrates the mass curve (lefthand scale, Δm), the broken line the differential mass signal dm/dt (righthand scale). For details see text (from ref. [126]).

The ratio of the glass transition temperature T_g to the melting temperature T_{fus} can provide information on the type of polymer. For highly symmetrical, highly crystalline homopolymers made from very small monomer components (for example, polyethylene, polyoxymethylene), T_g/T_{fus} lies below 0.5; for certain unsymmetrical polymers T_g/T_{fus} lies above 0.76. For the large majority of polymers the ratio T_g/T_{fus} is approximately 2/3.[123]

Rates of polymerization can be accurately measured by DSC.[124] Important information on the treatment necessary for complete curing (length of time, temperature, type and quantity of catalyst) can be gained from the position and shape of the normally exothermic reaction peak. In addition, the reaction peak can be analyzed by the kinetic methods of evaluation introduced in Section 3.5.

TMA and DMA are used to measure the temperature-dependent mechanical properties.[125] Besides the expansion coefficient, the response of a sample to the application of a force that is changed with time (for example, a sinusoidal oscillation) can also be measured. Glass transition temperatures can often be recorded more clearly by this method than by DSC (the elasticity increases markedly when the polymer is heated beyond the glass transition temperature).

The thermal stability of polymers can be estimated by DSC or TG measurements. Decomposition manifests itself as an exothermic or endothermic peak during DSC analysis or as mass loss in thermogravimetric analysis. An important application of this thermal decomposition of polymeric materials is the determination of the composition of samples containing several components. Thermogravimetry is the selected method of analysis. By quantitative analysis of the dependence of the mass loss on temperature and type of purge gas, the mass fractions of the individual components are determined. This procedure can, for example, be used for quality control of polymers.

Figure 17 portrays the TG curve of the decomposition of a mixture of natural rubber and an ethylene–propylene copolymer. The measurement is begun in a stream of nitrogen. Between approximately 150 °C and 300 °C the plasticizer (a low-boiling ester of adipic acid) is given off (22.0 wt%). Pyrolysis of the rubber (29.6 wt%) and the ethylene–propylene copolymer (13.5 wt%) follows. At 600 °C the purge gas is switched from nitrogen to air. A sharp peak corresponds to the combustion of the soot contained in the sample (32.2 wt%). An occasional residue (here: 2.7 wt%) consists of ash and filler, in this case of zinc oxide ZnO.

The individual components can be determined with good accuracy. Naturally the method has its limits if the decomposition reactions of the individual components overlap strongly. Reducing the heating rate in this instance often gives a better separation of the peaks. If even this measure does not lead to success, other methods of analysis (for example, simultaneous TG/DTA, EGA with mass spectrometry or FTIR) must be used.

5. Possible Applications of Thermal Analysis in Industry

The potential applications of thermal analysis in industrial production and routine analysis are manifold. Possibilities are quality control of raw materials on delivery, continuous control of production by analysis of aliquots, and the examination of products for quality assurance.[111] The methods of analysis used essentially are:

- differential scanning calorimetry (DSC) for the determination of melting point, boiling point, vapor pressure, purity, heat capacity, heat of reaction, thermal stability
- thermogravimetry (TG) for the determination of moisture content, fractions of volatile components, and thermal stability, as well as the released gases and remaining residues after combustion or pyrolysis (if necessary coupled with gas chromatography, FTIR, or mass spectrometry)
- dilatometric methods of analysis (dilatometry, TMA, DMA), for the determination of mechanical behavior (expansion coefficients, glass transition temperatures, elasticity, plasticity), especially of polymers (see Section 4).

Besides production control and quality assurance, thermal analysis can provide important information on the potential hazards of decomposable materials.[127–132] The data obtained by these methods are not only important for large scale production, but also for the preparative chemist, as the prevention of accidents in pilot plants and even in the laboratory is imperative. The following text gives a brief summary of the possibilities for technical safety.

Exothermic decomposition reactions present a considerable risk. Potentially hazardous organic compounds are, for example, nitrenes, isocyanates, azo and hydrazo compounds, azides, amino-halide compounds (for example, halogen-substituted anilines), oximes, epoxides, peroxides, and *N*-oxides. The danger

arises from the high exothermic decomposition energy resulting from the formation of small, very stable molecules (N_2, H_2O, CO_2). Most decompositions of this type are also autocatalytic.

The enthalpy of decomposition $\Delta_{dec}H$ (p = constant) can be determined by DTA and DSC measurements. It can, in many cases, also be calculated from the tabulated thermodynamic enthalpies of formation, which, however, always involves uncertainty about the assumed reaction products and the complete conversion required. For organic compounds an approximate calculation by incremental methods is usually possible. In ref. [129] the chemical structure is compared with the decomposition energy $\Delta_{dec}U$ (V = constant), enabling an approximate estimation. The enthalpy of decomposition is expediently related to the mass of the chemical substance and is given in $J\,g^{-1}$. Typical values are, for instance, $-1740\,J\,g^{-1}$ for nitrobenzene, $-1882\,J\,g^{-1}$ for 4-nitroaniline, $-800\,J\,g^{-1}$ for azobenzene, $-830\,J\,g^{-1}$ for 3,5-dimethoxyaniline, $-920\,J\,g^{-1}$ for maleic anhydride, $-406\,J\,g^{-1}$ for glucose, and $-835\,J\,g^{-1}$ for sodium azide.[128]

The adiabatic temperature rise ΔT_{ad}, which is defined as the quotient of the enthalpy of decomposition and heat capacity, is more significant [Eq. (j)]. An adiabatic temperature rise of 50 to

$$\Delta T_{ad} = -\frac{\Delta_{dec}H}{C_p} \qquad \text{(j)}$$

100 K is generally regarded as safe.[127] If the heat capacity C_p is not known, the approximation $C_p \times \rho \approx 1.7\,J\,cm^{-3}\,K^{-1}$ (ρ is the density in $g\,cm^{-3}$) can be used for organic materials.[127] C_p can also be determined by DSC or approximately calculated by incremental methods.[10]

Nonexplosive materials can easily be examined by DSC and TG for the risk of an exothermic decomposition. A quick general analysis scanned at $10\,K\,min^{-1}$ to approximately 500 °C is performed. If the DSC analysis reveals no exothermic peak and the TG analysis no great loss in mass, the substance may be regarded as safe.[127]

If an exothermic peak appears, the hazard potential must be further assessed by performing additional investigations (measurements using a low heating rate, adiabatic thermal storage experiments, estimation of the adiabatic temperature rise and adiabatic induction time).[127, 128] Conclusions on the long-term storage behavior of unstable materials can be drawn by performing adiabatic temperature experiments, in Dewar flasks for example.

In this context it is interesting that the heat transfer behavior of a $2\,m^3$ agitated reactor is approximately the same as that of a $500\,cm^3$ Dewar flask.[133] A powder exhibiting similar heat transfer behavior as reactor occupies an even smaller volume of $0.1\,m^3$.[127] This makes it clear how quickly dangers resulting from difficulties with heat dissipation can arise when scaling up chemical syntheses from the laboratory to industrial production (or even only on storage of chemicals).

The decomposition temperature may be considerably lowered by additives and impurities. Figure 18, which portrays DTA curves of 3-nitrobenzoic acid in a pure form and with different additives, makes this point clear. A shift of the decomposition peak to lower temperatures results, especially following the addition of heavy metals.

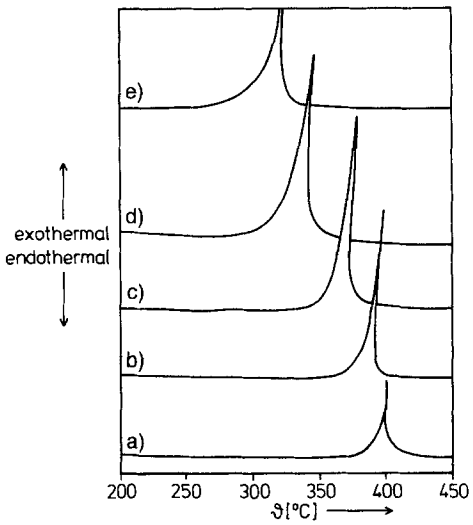


Fig. 18. DTA curves of the decomposition of 3-nitrobenzoic acid contaminated with different salts. a) Pure substance, b) 3-nitrobenzoic acid contaminated with 1.6 wt.% NaCl, curve c) 3-nitrobenzoic acid contaminated with 1.3 wt.% $FeCl_3$, d) 3-nitrobenzoic acid contaminated with 1.5 wt.% VCl_3, and e) 3-nitrobenzoic acid contaminated with 1.6 wt.% $MoCl_5$. In contrast to the other figures, the exothermic signal points upwards (from ref. [128]).

6. Biocalorimetry

Biocalorimetry involves the use of calorimetric methods for the study of biological processes. The application of calorimetry to living organisms is already very old. As far back as 200 years ago Lavoisier and Laplace examined the heat production of guinea-pigs with their newly developed ice calorimeter.[3] As heat exchange with the environment belongs to the fundamental characteristics of living systems, biocalorimetry with its methods of measurement, which meanwhile have become considerably more sensitive, today offers applications for the examination of a wide variety of subjects ranging from microorganisms, through plants and insects, to man.[134–137]

An example taken from the examination of microorganisms demonstrates the potential for the application of this method. Figure 19 illustrates the growth of a strain of *Escherichia coli* bacteria without and with the addition of antibacterial agents. The addition of amoxycillin and clavulinic acid causes strong bacterial growth inhibition, which manifests itself in a drop in heat generation. Control experiments showed that the addition of amoxycillin or clavulinic acid alone had no effect on bacterial growth.[138, 139] Such measurements can produce important contributions towards judging the effectiveness of pharmaceuticals.[138, 140]

7. Summary and Outlook

We hope we have shown that the reputation of thermal analysis as merely a qualitative method for measurement is unjustified. Providing investigations are performed carefully and the data evaluated critically, thermal analysis can provide quantitative results on material properties, thermodynamics, and kinetics. As is the case with all analytical methods, a certain basic knowledge of the operation of instruments, algorithms, and programs for

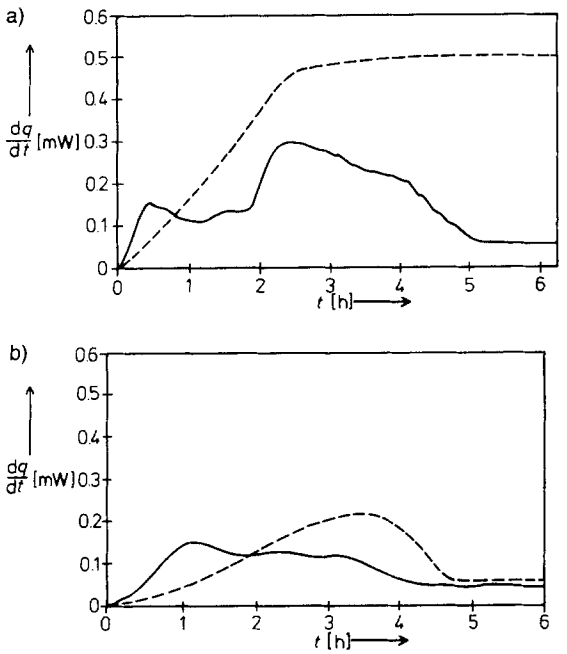


Fig. 19. Heat flow–time diagrams of the growth of *Escherichia coli* bacteria (solid line: heat evolution, broken line: growth curve). a) Undisturbed growth. b) Inhibited growth following the addition of antibacterial agents (amoxycillin, clavulinic acid) (from to ref. [138, 139]).

the data processing is required. Thermal analysis is a method for the measurement of thermodynamic and kinetic properties of materials that is easy to operate. The four most frequently applied methods, thermogravimetry, differential thermal analysis, differential scanning calorimetry, and dilatometry can be used in many different ways to characterize synthesized materials. The range of possible applications in technical practice is extensive. Special advantages are the speed and small samples required.

Besides these established methods, an increasing number of other methods are being developed. As virtually all physical methods of measurement can also (at least potentially) be performed with temperature programming, this trend will certainly continue. Investigations into kinetics in particular should profit from such new developments. Although most procedures of this type are (still?) not commercially available, we have purposely included a series of examples to demonstrate the variety of results obtainable. In addition, the intention was to expound the limits beyond which results obtainable by current methods are no longer reliable for a definite characterization.

We would like to thank Henning Arnecke, Sigurd Bauerecker, Dr. Heino Bothe, Dr. N. Eckardt, Dr. Sabine Eligehausen, Prof. Dr. Claus Führer, Dr. Peter Gabel, Dietmar Hamann, Erwin Kaisersberger, Dr. Kerstin Martin, Gerlind Öhlschläger, Dr. Joachim Reichelt, Dr. Stefan M. Sarge, Petra B. Schneider, Axel Steer, Dr. Ingeborg Steppuhn, Manfred Steppuhn, Prof. Dr. R. Tacke, Dr. Uwe Ulbrich, and Martin Welzel for their contributions towards this study as well as the Fonds der Chemischen Industrie, the Deutsche Forschungsgemeinschaft, and the Arbeitsgemeinschaft Industrieller Forschungsvereinigungen (AIF) for their financial support.

Received: January 11, 1993
Revised: February 5, 1994 [A941IE]
German version: *Angew. Chem.* **1995**, *107*, 1284–1301
Translated by Ms. Sigrid Robson, London (UK)

[1] W. F. Hemminger, H. K. Cammenga, *Methoden der Thermischen Analysen*, Springer, Berlin, **1989**.
[2] K. Heide, *Dynamische thermische Analysenmethoden*, 2nd ed., VEB Deutscher Verlag for Grundstoffindustrie, Leipzig, **1982**.
[3] W. Hemminger, G. Höhne, *Grundlagen der Kalorimetrie*, Verlag Chemie, Weinheim, **1979**; *Calorimetry – Fundamentals and Practice*, Verlag Chemie, Weinheim, **1984**.
[4] M. J. Pope, M. D. Judd, *Differential Thermal Analysis*, Heyden, London, **1977**.
[5] J. Šesták, *Thermophysical Properties of Solids—Their Measurements and Theoretical Thermal Analysis*, Elsevier, Amsterdam, **1984**.
[6] W. Smykatz-Kloss, *Differential Thermal Analysis, Applications and Results in Mineralogy*, Springer, Berlin, **1984**.
[7] W. W. Wendlandt, *Thermal Analysis*, 3rd ed., Wiley, New York, **1986**.
[8] G. Widmann, R. Riesen, *Thermoanalyse – Anwendungen, Begriffe, Methoden*, 3rd ed., Hüthig, Heidelberg, **1990**.
[9] M. E. Brown, *Introduction to Thermal Analysis*, Chapman and Hall, London, **1988**.
[10] B. Wunderlich, *Thermal Analysis*, Academic Press, San Diego, **1990**.
[11] E. L. Charsley, S. B. Warrington, *Thermal Analysis – Techniques and Applications*, Royal Society of Chemistry, Cambridge, **1992**.
[12] The standard valid in Germany is German Industrial Standard (DIN) 51005 "thermal analysis (TA), concepts" dated August 1993. Further standards relevant here are DIN 51004 (determination of melting temperature by DTA), DIN 51006 (thermogravimetry), DIN 51007 (differential thermal analysis), and DIN 51045 (thermal expansion in solids) (in part initially published as preliminary paper). The German standards can be obtained from Beuth Verlag, Berlin. Definitions and instructions were also published by the "International Confederation for Thermoanalysis and Calorimetry" (ICTAC) and the "American Society for Testing and Materials" (ASTM) [13]. Important ASTM instructions are E473-85 (definition of concepts in TA), E472-86 (presentation of thermoanalytical data), E1142-90 (terminology), E967-83 and 968-83 (calibration of DSC), E914-83 and E1131-86 (thermogravimetry), E793-85 and E794-85 (melting and solidification), E831-86 (thermal expansion), E928-85 (determination of purity by TA), E537-86 and E487-79 (thermal stability), E698-79 (kinetics), D3417-83 (melting and solidification of polymers), and D3418-32 (phase transformations of polymers).
[13] J. O. Hill, *For Better Thermal Analysis and Calorimetry*, 3rd ed., ICTAC, **1991**.
[14] Besides the generally used temperature programs with a constant heating rate (including isothermal measurements) there are a series of other temperature–time programs. Of some significance are stepwise isothermal temperature programs, during which the oven temperature is increased in a series of stages and held constant at each temperature for a predetermined period of time [15]. Specifically developed for the study of reactions were the quasi-isothermal temperature control and the establishing of a constant rate of reaction, which often enable a better kinetic evaluation of reactions of solids [15, 16, 17]. Furthermore, most instruments also offer heating–cooling programs as well as the cycling of temperature programs (important in investigations into the reversibility of processes). A newly developed version of DSC is oscillating DSC (ODSC), also called modulated DSC (MDSC) in which an oscillating (for instance, sinusoidal) temperature profile is superimposed on a constant heating rate. This results in better resolution of reversible and irreversible phenomena, especially in polymers and polymer blends. P. J. Gill, S. R. Sauerbrunn, M. Reading, *J. Therm. Anal.* **1993**, *40*, 931–939.
[15] O. T. Sørensen, *Thermochim. Acta* **1981**, *50*, 163–175; *J. Therm. Anal.* **1992**, *38*, 213–228.
[16] F. Paulik, J. Paulik, *J. Therm. Anal.* **1992**, *38*, 197–211; J. Paulik, F. Paulik, *Simultaneous Thermoanalytical Examination by Means of the Derivatograph (Compr. Anal. Chem. 1959–*, **1981**, *12*).
[17] J. Rouquerol, *Thermochim. Acta* **1989**, *144*, 209–224; J. Málek, J. Šesták, F. Rouquerol, J. Rouquerol, J. M. Criado, A. Ortega, *J. Therm. Anal.* **1992**, *38*, 71–87; J. Rouquerol, S. Bordère, F. Rouquerol, *Thermochim. Acta* **1992**, *203*, 193–202.
[18] The common acronym DSC will be used throughout this review.
[19] W. F. Hemminger, H. K. Cammenga, *Labo* **1990**, *21*(4), 7–19.
[20] For instruments used in scanning operations a differentiation must be made in thermoanalysis between the zero line (German standardized term: Nullinie), the reference line (German: Grundlinie), and the base line (German: Basislinie). The signal blank, that is, when the instrument does not contain a sample crucible, is described as the zero line. The reference line is the signal recorded when the instrument contains an empty sample crucible. The signal recorded during a period of measurement in which no thermal event takes place is described as the base line. In the case of a single peak as illustrated in Figure 2, the base line before and after the thermal event is known. Naturally, the base line cannot be measured during the thermal event and must therefore be constructed. Different methods have been developed for this purpose [1, 21, 22]. Normally only a linear interpolation is used as the simplest method in the construction of a base line.
[21] S. M. Sarge, *Thermochim. Acta* **1992**, *187*, 323–334; W. F. Hemminger, S. M. Sarge, *J. Therm. Anal.* **1991**, *103*, 1455–1478.

[22] S. M. Sarge, E. Gmelin, G. W. H. Höhne, H. K. Cammenga, W. F. Hemminger, W. Eysel, *PTB-Mitt.* **1993**, 491–512; *Thermochim. Acta* **1994**, *247*, 129–168.

[23] The likewise frequently encountered "heat flux DSC" or "quantitative DTA" is based on a measurement principle similar to that of DTA. The specific design here ensures that the temperature difference is proportional to the difference between the flow of heat to each sample. By assuming a constant flow of heat to the reference sample the thermal flow $\dot{q}$ from or to the sample can then be calculated from the signal ΔT; in other words, a quantitative measurement of the change in enthalpy is possible, as it is in power-compensated DSC. The maximal attainable temperatures of 1500 °C are considerably higher than they are in power-compensated DSC. Whether this method can be classified as DTA or DSC is a question of definition (see for example, ref. [1] for more details).

[24] H. K. Cammenga, W. Eysel, E. Gmelin, W. Hemminger, G. W. H. Höhne, S. M. Sarge, *PTB-Mitt.* **1992**, *102*, 13–18; *Thermochim. Acta* **1993**, *219*, 333–342.

[25] E. Koch, *Non-isothermal Reaction Analysis*, Academic Press, London, **1977**.

[26] L. Kofler, A. Kofler, *Thermo-Mikro-Methoden*, Verlag Chemie, Weinheim, **1954**.

[27] W. C. McCrone, *Fusion Methods in Chemical Microscopy*, Wiley, New York, **1957**.

[28] M. G. Lozinskij, *High Temperature Metallography*, Pergamon, New York, **1961**.

[29] H. H. Emons, H. Keune, H. Seyfarth, *Chemische Mikroskopie*, VEB Deutscher Verlag für Grundstoffindustrie, Leipzig, **1973**.

[30] M. Kuhnert-Brandstätter, *Thermomicroscopy of Organic Compounds* (*Compr. Anal. Chem. 1959–*, **1982**, *16*).

[31] H. K. Cammenga, W. F. Hemminger, *Labo* **1990**, *21*(6), 7–19.

[32] D. J. Johnson, D. A. C. Compton, P. L. Canale, *Thermochim. Acta* **1992**, *195*, 5–20.

[33] G. Szekely, M. Nebuloni, L. F. Zerilli, *Thermochim. Acta* **1992**, *196*, 511–532.

[34] V. Balek, J. Tolgyessy, *Emanation Thermal Analysis and other Radiometric Emanation Methods* (*Compr. Anal. Chem.* **1984**, *12*, *Part C*).

[35] V. Balek, *Thermochim. Acta* **1991**, *192*, 1–17.

[36] N. Gérard, *J. Phys. E* **1974**, *7*, 509–510.

[37] B. Baumgartner, Dissertation, Technische Hochschule Darmstadt, **1987**.

[38] J. Plevert, J. P. Auffredic, M. Louer, D. Louer, *J. Mater. Sci.* **1989**, *24*, 1913–1918.

[39] N. Eisenreich, W. Engel, *J. Therm. Anal.* **1989**, *35*, 577–584; V. Kolarik, M. Juez-Lorenzo, N. Eisenreich, W. Engel, *ibid.* **1992**, *38*, 649–655; A. Deimling, W. Engel, N. Eisenreich, *ibid.* **1992**, *38*, 843–853; W. Engel, N. Eisenreich, M. Alonso, V. Kolarik, *ibid.* **1993**, *40*, 1017–1024.

[40] M. Epple, H. K. Cammenga, *J. Therm. Anal.* **1992**, *38*, 619–626.

[41] M. Epple, H. K. Cammenga, *Ber. Bunsenges. Phys. Chem.* **1992**, *96*, 1774–1778.

[42] M. Epple, *J. Therm. Anal.* **1994**, *42*, 559–593.

[43] For the application of synchrotron radiation to different problems, including time- and temperature-dependent phenomena, see B. Lengeler, *Adv. Mater.* **1990**, *2*, 123–131; *Synchrotron-Radiation in Chemistry and Biology I–II* (Ed.: E. Mandelkow), *Top. Current. Chem. Vol. 145*, **1988**, *Vol. 147*, **1988**, *Vol. 151*, **1989**, Springer; A. k. Cheetham, A. P. Wilkinson, *Angew. Chem.* **1992**, *104*, 1594–1608; *Angew. Chem. Int. Ed. Engl.* **1992**, *31*, 1557–1570.

[44] *Recommended Reference Materials for the Realization of Physicochemical Properties* (Ed.: K. N. Marsh), Blackwell Scientific Publications, Oxford, **1987**.

[45] Substances which were selected as fixed points on the International Temperature Scale of 1990 (ITS-90) are particularly suitable for temperature calibration. A procedure for temperature calibration for DTA and DSC is suggested in ref. [46,24]. Ref. [24] contains a selection of recommended materials for calibration in the temperature range 120 K to 1350 K. See ref. [47] for ITS-90. Besides the temperature calibration, a mass calibration can be performed for TG instruments, a heat calibration and heat flow calibration for DSC instruments, and a length calibration for dilatometers. The procedure for heat calibration and heat flow calibration of DSC instruments recommended by the Gesellschaft für thermische Analysis (GEFTA) is illustrated in ref. [22]. Factors influencing the calibration of heat flux calorimeters are discussed, for example, in H. K. Cammenga, A. Steer, *Thermochim. Acta* **1993**, *229*, 15–25.

[46] G. W. H. Höhne, H. K. Cammenga, W. Eysel, E. Gmelin, W. Hemminger, *PTB-Mitt.* **1990**, *100*, 25–31; *Thermochim. Acta* **1990**, *160*, 1–12.

[47] H. Preston-Thomas, *Metrologia* **1990**, *27*, 3–10; W. Blanke, *PTB-Mitt.* **1989**, *99*, 411–418.

[48] P. Laggner, *Top. Curr. Chem.* **1988**, *145*, 173–202; in *Subcellular Biochemistry, Vol. 23* (Eds.: H. J. Hilderson, G. B. Ralston), Plenum, New York, **1994**, pp. 451–491.

[49] M. Caffrey, *Annu. Rev. Biophys. Biophys. Chem.* **1989**, *18*, 159–186.

[50] K. Blankenhorn, G. W. H. Höhne, *Thermochim. Acta* **1991**, *187*, 219–224.

[51] H. G. Wiedemann, *Thermochim. Acta* **1991**, *187*, 245–256.

[52] C. N. R. Rao, K. J. Rao, *Phase Transitions in Solids*, McGraw-Hill, New York, **1978**; E. K. H. Salje, *Phase Transitions in Ferroelastic and Co-Elastic Crystals*, Cambridge, **1990**.

[53] I. Prigogine, R. Defay, *Chemische Thermodynamik*, VEB Deutscher Verlag for Grundstoffindustrie, Leipzig, **1962**.

[54] H. Bothe, Dissertation, Technische Universität Braunschweig, **1980**. H. Bothe, H. K. Cammenga, *J. Therm. Anal.* **1979**, *16*, 267–275.

[55] H. Bothe, H. K. Cammenga, *Z. Phys. Chem. (Frankfurt am Main)* **1981**, *127*, 193–206; M. Epple, H. K. Cammenga, S. M. Sarge, R. Diedrich, V. Balek, *Thermochim. Acta* **1995**, *250*, 29–39.

[56] V. Petříček, I. Cisařová, L. Hummel, J. Kroupa, B. Březina, *Acta Crystallogr. Sect. B* **1990**, *46*, 830–832.

[57] H. K. Cammenga, M. Epple, B. Baumgartner, *J. Chim. Phys. Phys. Chim. Biol.* **1990**, *87*, 1249–1256.

[58] M. Näveke, P. G. Jones, A. Blaschette, D. Schomburg, H. K. Cammenga, M. Epple, *Z. Anorg. Allg. Chem.* **1993**, *619*, 1027–1036.

[59] H. J. Seifert, G. Thiel, *Thermochim. Acta* **1986**, *100*, 81–107.

[60] E. Wolf, H. K. Cammenga, *Z. Phys. Chem. (Frankfurt am Main)* **1977**, *107*, 21–38.

[61] S. Eligehausen, Dissertation, Technische Universität Braunschweig, **1988**.

[62] S. Eligehausen, S. M. Sarge, G. Öhlschläger, H. K. Cammenga, *J. Therm. Anal.* **1989**, *35*, 515–526.

[63] H. K. Cammenga, S. M. Sarge, S. Eligehausen, *Solid State Ionics* **1989**, *32/33*, 625–629.

[64] *Purity Determination by Thermal Methods* (Eds.: R. L. Blaine, C. K. Schoff), ASTM STP 838, American Society for Testing and Materials, Philadelphia, **1984**.

[65] E. E. Marti, *Thermochim. Acta* **1972**, *5*, 173–220.

[66] S. Bauerecker, S. M. Sarge, H. K. Cammenga, *J. Therm. Anal.* **1989**, *35*, 527–539. This method has recently been extended with considerable success to mixed crystal systems in collaboration with R. Stosch of our group (unpublished results).

[67] S. Sarge, S. Bauerecker, H. K. Cammenga, *Thermochim. Acta* **1988**, *129*, 309–324.

[68] J. Jaques, A. Collet, S. H. Wilen, *Enantiomers, Racemates and Resolutions*, Wiley, New York, **1981**.

[69] R. Tacke, H. Linoh, L. Ernst, E. Lambrecht, U. Moser, E. Mutschler, S. Sarge, H. K. Cammenga, *Chem. Ber.* **1987**, *120*, 1229–1237.

[70] R. Tacke, C. Strohmann, S. Sarge, H. K. Cammenga, D. Schomburg, E. Mutschler, G. Lambrecht, *Liebigs Ann. Chem.* **1989**, 137–143.

[71] C. Strohmann, S. Bauerecker, H. K. Cammenga, P. G. Jones, E. Mutschler, G. Lambrecht, R. Tacke, *Liebigs. Ann. Chem.* **1991**, 523–527.

[72] M. Yalpani, W. R. Scheidt, K. Seevogel, *J. Am. Chem. Soc.* **1985**, *107*, 1684–1690.

[73] M. Yalpani, R. Köster, M. Boese, M. Sulkowski, *Chem. Ber.* **1989**, *122*, 9–17.

[74] T. S. A. Hor, L. T. Phang, L. K. Liu, Y. S. Wen, *J. Organomet. Chem.* **1990**, *397*, 29–39.

[75] H. K. Cammenga, M. Epple, A. Blaschette, M. Näveke, *Thermochim. Acta* **1989**, *151*, 171–178.

[76] The dehydration of lithium sulphate monohydrate proceeds in one stage without the formation of intermediates according to measurements carried out to date. Other hydrates are not known. For this reason it was considered for a while as a kinetic reference material for solid-state reactions by the "Kinetics Committee" of the ICTAC. For more recent measurements on lithium sulphate regarding kinetics, see V.B. Okhotnikov, N. A. Simakova, B. I. Kidyakov, *React. Kinet. Catal. Lett.* **1989**, *39*, 345–350; H. Tanaka, N. Koga, J. Šesták, *Thermochim. Acta* **1992**, *203*, 203–220; A. K. Galwey, N. Koga, H. Tanaka, *J. Chem. Soc. Faraday Trans.* **1990**, *86*, 531–537; J. Huang, P. K. Gallagher, *Thermochim. Acta* **1991**, *192*, 35–45; M. E. Brown, A. K. Galwey, A. Wan Po, *ibid.* **1992**, *203*, 221–240; *ibid.* **1993**, *220*, 131–150; ref. [77].

[77] M. Epple, H. K. Cammenga, *Solid State Ionics* **1993**, *63–65*, 307–311.

[78] E. Koch, *Angew. Chem.* **1983**, *95*, 185–201; *Angew. Chem. Int. Ed. Engl.* **1983**, *22*, 225–240.

[79] N. Sbirrazzuoli, D. Brunel, L. Elegant, *J. Therm. Anal.* **1992**, *38*, 1509–1524.

[80] J. H. Flynn, *Thermochim. Acta* **1992**, *203*, 519–526.

[81] H. J. Borchardt, F. Daniels, *J. Am. Chem. Soc.* **1957**, *79*, 41–46.

[82] Reactions in homogeneous phase are predominantly simple n-th order, in which $f(\alpha) = (1-\alpha)n$, where n is the order of reaction. The introduction of the function $f(\alpha)$ is primarily justified by the fact that considerably more complex time laws appear in the kinetics of heterogeneous reactions, which may be due to nucleation or diffusion processes, for example. For three-dimensional diffusion (Jander equation), the function is, for instance: $f(\alpha) = [1-(1-\alpha)^{1/3}]^{-1}(1-\alpha)^{2/3}$. The different equations for the rates of heterogeneous reactions are quoted (ref. [1, 7]) or derived (refs. [2, 83, 105, 107]) in several papers.

[83] A. Fevre, M. Murat, *J. Therm. Anal.* **1975**, *7*, 429–443, 445–463.

[84] H. Wyden, G. Widmann in *Angewandte Chemische Thermodynamik and Thermoanalytik* (Eds.: E. Marti, H. R. Oswald, H. G. Wiedemann), Birkhäuser, Basel, **1979**, p. 284–290.

[85] S. Boy, K. Böhme, *Thermochim. Acta.* **1978**, *27*, 390–392.

[86] R. Tacke, F. Wiesenberger, B. Becker, R. Rohr-Aehle, P. S. Schneider, U. Ulbrich, S. M. Sarge, H. K. Cammenga, T. Kosłowski, W. von Niessen, *Chem. Ber.* **1992**, *125*, 591–605.

[87] S. Sarge, H. K. Cammenga, B. Becker, R. Rohr-Aehle, R. Tacke, *J. Therm. Anal.* **1988**, *33*, 1185–1192.
[88] A. W. Coats, J. P. Redfern, *Nature (London)* **1964**, *201*, 68–69.
[89] C. D. Doyle, *J. Appl. Polym. Sci.* **1961**, *5*, 285–292.
[90] A. J. Kassman, *Thermochim. Acta* **1985**, *84*, 89–99.
[91] E. S. Freeman, B. Carroll, *J. Phys. Chem.* **1958**, *62*, 394–397.
[92] S. M. Ellerstein in *Analytical Chemistry* (Eds.: R. S. Porter, J. F. Johnson), Plenum, New York, **1968**, p. 279–287.
[93] J. Vachuška, M. Vobořil, *Thermochim. Acta* **1971**, *2*, 379–392.
[94] D. W. van Krevelen, C. van Heeren, F. J. Huntjens, *Fuel* **1951**, *30*, 253–259.
[95] P. Murray, J. White, *Trans. Br. Ceram. Soc.* **1955**, *54*, 204–238.
[96] H. E. Kissinger, *J. Res. Natl. Bur. Stand. (U.S.)* **1956**, *57*, 217–221; *Anal. Chem.* **1957**, *29*, 1702–1706. An ASTM standard for kinetics is based on these studies: ANSI/ASTM-Norm E 698-79, **1979**, p. 1–8.
[97] H. H. Horowitz, G. Metzger, *Anal. Chem.* **1963**, *35*, 1464–1468.
[98] R. N. Rogers, L. C. Smith, *Thermochim. Acta* **1970**, *1*, 1–9.
[99] T. Ozawa, *Bull. Chem. Soc. Jpn.* **1965**, *38*, 1881.
[100] T. Ozawa, *Thermochim. Acta* **1992**, *203*, 159–165.
[101] J. Opfermann, E. Kaisersberger, *Thermochim. Acta* **1992**, *203*, 167–175.
[102] H. K. Cammenga, S. M. Sarge, unpublished. For a comparison of deconvolution methods for nonisothermal measurements, see U. Ulbrich, H. K. Cammenga, *Thermochim. Acta* **1993**, *229*, 53–67, and references therein.
[103] J. A. Hedvall, *Einführung in die Festkörperchemie*, Vieweg, Braunschweig, **1952**.
[104] D. A. Young, *Decomposition of Solids*, Pergamon, London. **1966**.
[105] B. Delmon, *Introduction à la Cinétique Hétérogène*, Editions Technip, Paris, **1969**.
[106] H. Schmalzried, *Festkörperreaktionen*, Verlag Chemie, Weinheim, **1971**; *Solid State Reactions*, Academic Press, New York, **1974**; *Chemical Kinetics of Solids*, VCH, Weinheim, **1995**.
[107] W. E. Brown, D. Dollimore, A. K. Galwey, *Compr. Chem. Kinet. 1969–*, **1980**, *22*.
[108] V. V. Boldyrev, M. Bulens, B. Delmon, *The Control of the Reactivity of Solids*, Elsevier. Amsterdam, **1983**.
[109] J. Šesták, *J. Therm. Anal.* **1979**, *16*, 503–520.
[110] J. H. Flynn, M. Brown, J. Šesták, *Thermochim. Acta* **1987**, *110*, 101–112.
[111] J. Šesták, *J. Therm. Anal.* **1988**, *33*, 1263–1265.
[112] J. H. Flynn, M. Brown, E. Segal, J. Šesták, *Thermochim. Acta* **1989**, *148*, 45–47.
[113] J. H. Flynn, *J. Therm. Anal.* **1990**, *36*, 1579–1593.
[114] M. Maciejewski, A. Reller, *Thermochim. Acta* **1987**, *110*, 145–152; M. Maciejewski, *J. Therm. Anal.* **1988**, *33*, 1269–1277; *ibid.* **1992**, *38*, 51–70.
[115] *Structure Reports, Vol. 53A* (Ed.: G. Ferguson, J. Trotter), International Union of Crystallography, **1988**; *Crystal Structures, Vol. 3* (Eds.: R. W. G. Wyckoff) 2nd ed., Wiley, New York, **1965**.
[116] E. V. Boldyreva, *React. Solids* **1990**, *8*, 269–282; *J. Therm. Anal.* **1992**, *38*, 89–97; V. V. Boldyrev, *ibid.* **1993**, *40*, 1041–1062.
[117] F. M. Mirabella, Jr., M. J. Shankernarayanan, *Microbeam Anal.* **1988**, *23*, 233–235.
[118] M. E. E. Harju, J. Valkonen, U. A. Jayasooriya, *Spectrochim. Acta Ser. A* **1991**, *47*, 1395–1398.
[119] E. A. Turi, *Thermal Characterization of Polymeric Materials*, Academic Press, Orlando, FL, USA, **1981**.
[120] P. J. Haines, *Thermochim. Acta* **1989**, *148*, 365–373.
[121] D. W. van Krevelen, *Properties of Polymers*. 3rd ed., Elsevier, Amsterdam, **1990**.
[122] Y. K. Godovsky, *Thermophysical Properties of Polymers*, Springer, Heidelberg, **1992**.
[123] E. Kaisersberger et al., *DSC an Polymerwerkstoffen, Vol. 1*, Netzsch-Jahrbücher für Wissenschaft and Praxis, Selb, **1991**; *TA für die Polymertechnik – DSC · TG · DMA, Vol. 2*, Selb **1992**, *TA für die Polymertechnik – DSC · TG · DMA · TMA, Vol. 3*, Selb **1994**.
[124] H. J. Flammersheim, N. Eckardt, J. Opfermann, *Thermochim. Acta* **1993**, *229*, 281–287.
[125] J. B. Henderson, W.-D. Emmerich, *J. Therm. Anal.* **1991**, *37*, 1825–1831.
[126] H. Möhler, A. Stegmayer, E. Kaisersberger, *Thermische Analyse in der Polymerindustrie*, Firmenschrift, Netzsch-Gerätebau, Selb.
[127] T. Grewer, H. Klusacek, U. Löffler, R. L. Rogers, J. Steinbach, *DECHEMA Monogr.* **1988**, *111*; *J. Loss Prev. Process Ind.* **1989**, *2*, 215–223.
[128] T. Grewer, O. Klais, *Exotherme Zersetzung. Untersuchung der charakteristischen Stoffeigenschaften* (Schriftenreihe *Humanisierung des Arbeitslebens, Vol. 84*), VDI-Verlag, Düsseldorf, **1988**; T. Grewer, *Thermal Hazards of Chemical Reactions*, Elsevier, Amsterdam, **1994**.
[129] T. Grewer, *Thermochim. Acta* **1991**, *187*, 133–149.
[130] L. D. Tuma, *Thermochim. Acta* **1991**, *192*, 121–128.
[131] R. Raemy, *J. Therm. Anal.* **1992**, *38*, 437–443.
[132] A special volume of *Thermochimica Acta* deals exclusively with safety: *Safety Techniques* (*Thermochim. Acta* **1993**, *225*, 143–301).
[133] R. L. Rogers, T. K. Wright, *Inst. Chem. Eng. Symp. Ser.* **1986**, *97*, 121.
[134] *Application of Calorimetry in Life Sciences* (Proceedings of the International Conference in Berlin 1976) (Eds.: I. Lamprecht, B. Schaarschmidt), Walter de Gruyter, Berlin, **1977**.
[135] *Biological Microcalorimetry* (Ed.: A. E. Beezer), Academic Press, London, **1980**.
[136] I. Wadsö in *Thermal and Energetic Studies of Cellular Biological systems* (Ed.: A. M. James), Wright, **1987**, p. 34–67.
[137] A comprehensive overview of biocalorimetry has been published: Special issue: *Calorimetry in the Biological Sciences* (*Thermochim. Acta* **1991**, *193*); *Biological Calorimetry* (*Thermochim. Acta* **1990**, *172*, 1–266).
[138] G. Buckton, S. J. Russell, A. E. Beezer, *Thermochim. Acta* **1991**, *193*, 195–214.
[139] E. Semenitz, P. A. Casey, W. Pfaller, G. Gstraunthaler, *Chemotherapy (Basel)* **1983**, *29*, 192–207.
[140] B. Chowdhry, A. E. Beezer, E. J. Greenhow, *Talanta* **1983**, *30*, 208–243.

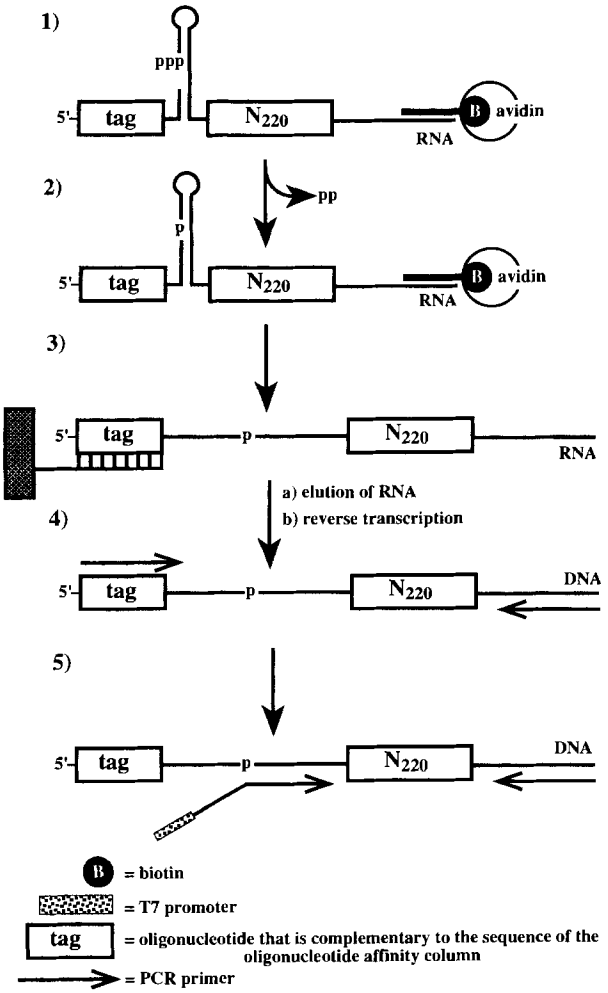
Synthetic Ribozymes and the First Deoxyribozyme**

Petra Burgstaller and Michael Famulok*

The principal aims of the early stages of protein engineering were limited to understanding how enzymes work. Today's greatest challenge is the de novo design of synthetic enzymes. Since the discovery of natural catalytic RNAs more than ten years ago,[1] however, progress in this field is no longer limited just to proteins. The development of methods for in vitro selection and in vitro evolution have made it possible not only to alter and improve the functionality and specificity of natural ribozymes, but also to develop RNA catalysts with new functionalities. The strategies by which this is achieved differ—with one exception[2]—from those used, for instance, to isolate catalytic antibodies. In this case, antibodies that specifically bind to transition state analogues (TSAs) are isolated. Such antibodies contain a binding site that fits better to the structure of the transition state of a particular chemical reaction than to the structures of the products or starting materials, and hence catalyze the corresponding reaction.[3] In contrast to this, catalysts based on nucleic acids are isolated by the method of "direct selection", whereby a randomized, highly complex pool of nucleic acids is subjected to a competitive situation in which only those molecules survive that can catalyze a particular reaction. The principles applied are similar to those that play a role in Darwinian evolution, and are based on in vitro selection and in vitro evolution, techniques whose function has been described several times, also in this journal.[4] In this highlight we will present some of the newest, most exciting results in this field, which is developing at a truly astonishing rate.

Bartel and Szostak made a major step forward two years ago. They succeeded in isolating ribozymes from a synthetic RNA pool which were capable of ligating an oligonucleotide to their 5'-end with cleavage of pyrophosphate.[5] The mechanism of this reaction corresponds to the mode of action of RNA-dependent RNA polymerases. The selection strategy started with a pool with a very long randomized synthetic sequence of 220 nucleotides. This length was chosen to increase the probability of isolating catalytically active sequences (Scheme 1).

To bring the 3'-hydroxyl group of the oligonucleotide in proximity to the triphosphate at the 5'-end of the RNA pool, a sequence in the constant region of the 5'-primer was constructed such that the substrate oligonucleotide could hybridize to the 5'-end of the pool. Catalytically active molecules were enriched



Scheme 1. Selection strategy for the isolation of an RNA ligase ribozyme. 1) The defined region at the 5'-end of a synthetic RNA pool with 220 randomized nucleotides forms a hairpin structure which allows binding of the oligonucleotide to be ligated. This binding reaction brings the 3'-end of the oligonucleotide into close proximity to the triphosphate unit (ppp) at the 5'-end of the RNA pool. To prevent aggregation of the RNA molecules, they are immobilized on streptavidin agarose by hybridization of the 3'-primer binding site of the pool to a biotinylated oligonucleotide. 2) After successful ligation and release of pyrophosphate (pp), the pool is enriched in two steps. 3) First, the ligated tag sequence is hybridized to an immobilized, complementary oligonucleotide, whereby ligated and unligated sequences are separated. After removal of unligated sequences from the oligonucleotide affinity column by washing, the bound sequences are eluted by denaturation, and reverse-transcribed. 4) A further enrichment follows, using PCR with a primer which is also complementary to the ligated region. 5) By means of a second PCR the original unligated sequence is regenerated, and the T7 promoter for the subsequent in vitro transcription is added. Transcription with T7 RNA polymerase (not shown) adds a triphosphate group to the 5'-end of the RNA pool, and the resulting RNA can then be subjected to a further selection cycle.

[*] Dr. M. Famulok, Dipl.-Chem. P. Burgstaller
Institut für Biochemie der Universität
Würmtalerstrasse 221, D-81375 München (Germany)
Telefax: Int. code + (89) 74017-448
e-mail: famulok@lmb.uni-muenchen.de

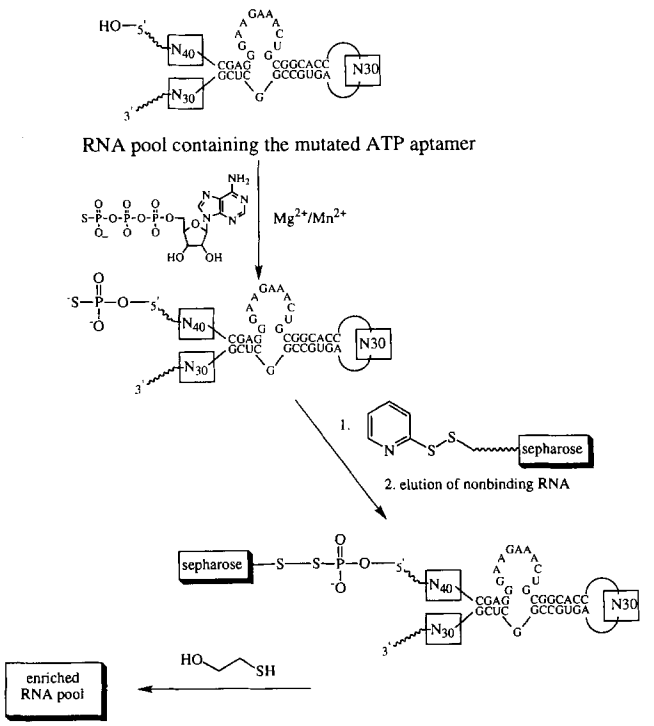
 © VCH Verlagsgesellschaft mbH, D-69451 Weinheim, 1995 0570-0833/95/1111-1189 $ 10.00+.25/0

in two steps. Following incubation with the oligonucleotide, the pool was purified by passage through an oligonucleotide affinity column, to which only successfully ligated sequences could bind. These were then eluted, reverse transcribed, and amplified in a PCR reaction with a primer that was complementary to the sequence of the ligated oligonucleotide. In a second PCR reaction the original, unligated structure was then regenerated, from which an enriched RNA pool was transcribed for the next round of selection. Three of the ten selection rounds contained a mutagenic PCR step, so that "worse" catalysts had the chance to develop into "better" ones. This strategy led to an increase in the ligation rate from $3 \times 10^{-6}\,h^{-1}$, for the uncatalyzed rate, to $8\,h^{-1}$.

A characteristic trait of many enzymatic catalysis mechanisms is their specific substrate recognition and their cofactor requirements. In order to study whether RNA can also carry out a substrate- or cofactor-dependent catalysis, Lorsch and Szostak started from a specific ATP-binding RNA, which had been previously selected by affinity chromatography on ATP agarose,[6] and used this as the basis for the evolution of an ATP-dependent oligonucleotide kinase[7] (Scheme 2). An RNA pool was synthesized in which the central sequence of the ATP binder had been 15% randomized and was surrounded by three completely randomized sequences of a total of 100 bases. This pool was incubated with ATP-γ-S. RNAs onto which the γ-thiophosphate group of the ATP had been transferred could be separated from the rest of the pool on activated thiopropyl agarose, since they specifically formed a disulfide bond between the thiophosphate group and the agarose. These covalently bound RNAs were then eluted by washing with an excess of 2-mercaptoethanol, amplified, and reselected.

After thirteen cycles of selection, seven classes of ribozymes were characterized which catalyzed various reactions. Five of these RNA classes catalyzed the transfer of the γ-thiophosphate onto their own 5′-hydroxyl group and are therefore 5′-kinases. The other two classes phosphorylated the 2′-hydroxyl groups of specific internal base positions. Starting from one of these sequences, a ribozyme was developed which can phosphorylate oligonucleotides at their 5′-end in an intermolecular reaction. In this way a multiple, ATP-dependent transfer reaction could also be demonstrated, and it was shown that the kinetics of the catalysis followed the Michaelis–Menten equation.

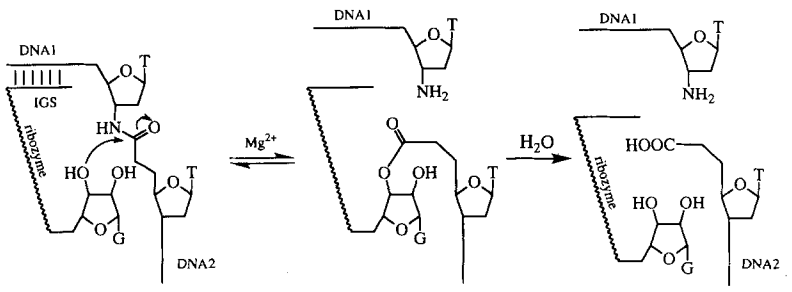
The novel synthetic ribozymes developed up to now all carry out phosphodiester transfer reactions and hydrolyses, as do all known natural, catalytically active RNA molecules. However, Joyce et al. recently demonstrated a far broader catalytic potential for RNA, by describing a ribozyme that catalyzes the cleavage of an amide bond.[8] For this purpose a DNA-cleaving RNA molecule was chosen that had previously been isolated by in vitro evolution from a pool of variants of the *Tetrahymena* ribozyme.[9] It was assumed that the DNA-cleaving ribozyme should also be capable of hydrolyzing an amide bond, since the transition state of amide hydrolysis corresponds exactly to the tetrahedral structure of the phosphate group. In addition, Piccirilli et al. had previously shown that the wild-type group I intron from *Tetrahymena* can also catalyze the hydrolysis



Scheme 2. Selection of a ribozyme with polynucleotide kinase activity. The RNA pool, which is based on the ATP-binding aptamer [6] of Sassanfar and Szostak, is incubated with ATP-γ-S. Molecules that have been successfully thiophosphorylated bind to activated thiopropylsepharose by formation of a disulfide bond and can be separated by chromatography. The disulfide bond is then cleaved with an excess of β-mercaptoethanol, so that the molecules can be amplified and subjected to the next round of selection.

of a carboxylic ester if this is presented as substrate to the ribozyme in the form of an aminoacyl-oligonucleotide.[10] The substrate used for the amide hydrolysis was an oligonucleotide (DNA1), which contained an amide group and could hybridize to a particular region of the ribozyme, the "internal guide sequence" (IGS). The ribozyme contained 17 mutations in comparison with the wild-type sequence of the *Tetrahymena* intron and catalyzed the amide cleavage, whereas the wild-type sequence was inactive (Scheme 3).

Although the reaction rate of the hydrolysis in the presence of the ribozyme was only $10^{-6}\,min^{-1}$, this nonetheless corresponds to a 100-fold acceleration over the uncatalyzed reaction. The cleavage is independent of the nature of the substituents on the amide group, which was tested with four different sub-

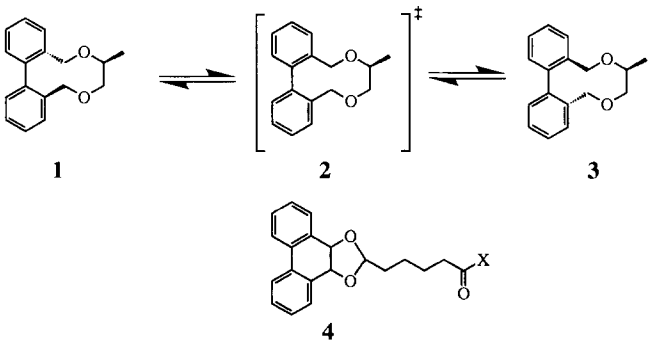


Scheme 3. Mechanism for the RNA-catalyzed cleavage of an amide bond. The region upstream of the amide bond (DNA1) is complementary to the internal guide sequence (IGS) of a DNA-cleaving variant of the *Tetrahymena* ribozyme. The amide bond is thereby brought close to the guanosine at the 3′-end of the ribozyme, and the 2′-hydroxyl group can carry out a nucleophilic attack of the amide bond. Spontaneous hydrolysis of the resulting ester bond regenerates the ribozyme and releases DNA2.

 © VCH Verlagsgesellschaft mbH, D-69451 Weinheim, 1995 0570-0833/95/1111-1190 $ 10.00+.25/0

strates, DNA1-methionine and DNA1-(arginine)$_n$ ($n = 1$, 2, or 3). All four substrates were hydrolyzed selectively at the amide group immediately following DNA1. Peptide bonds within the (arginine)$_2$ or (arginine)$_3$ moieties were not attacked.

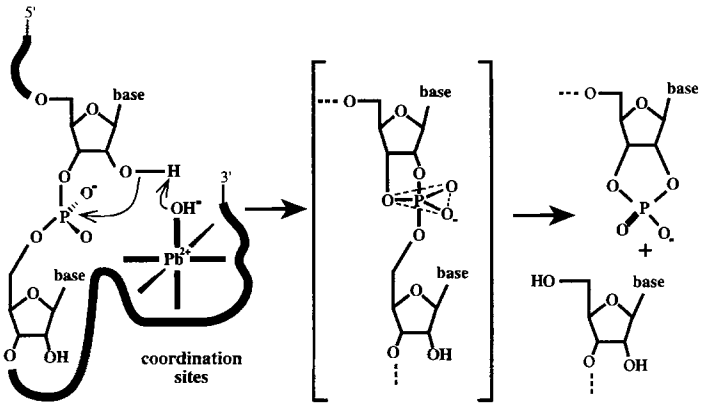
An indirect selection of ribozymes is also possible, as has been shown by Prudent et al.[2] They isolated RNA aptamers that could bind specifically to the TSA **4** of the isomerization of an asymmetrically substituted biphenyl derivative. The selection was performed by affinity chromatography of a randomized pool on the TSA immobilized on agarose. A selection scheme of this nature has already been applied in several cases in order to isolate RNA aptamers for various molecular ligands.[6, 11] After seven rounds of selection, the RNA pool was able to bind to the TSA column. Of the 20 sequenced clones, one sequence made up 75% of the selected pool and was able to accelerate the reaction by a factor of 100 over the uncatalyzed reaction (Scheme 4).



Scheme 4. Isomerization reaction of the biphenyl derivative **1** to its diastereomer **3**. This reaction is catalyzed by a ribozyme that was selected by binding to TSA **4**, which mimics the planar transition state **2** of this reaction.

The kinetic study showed that a Michaelis–Menten complex is formed initially, followed by the isomerization reaction and release of the reaction product. The reaction was completely inhibited by the planar TSA **4**. This strategy is analogous to the principle that has been used successfully many times for the isolation of catalytic antibodies. The isolation of ribozymes by selection of TSA-binding RNAs constitutes a highly efficient method for investigating the diversity of available chemical reactions that can be catalyzed by RNA. In a very recent publication, however, RNA aptamers are described which bind to the TSA of a Diels–Alder reaction but are not able to catalyze the corresponding reaction.[12]

A new departure in the development of nucleic acid based catalysts was made by Breaker and Joyce, who recently reported the isolation of the first deoxyribozyme.[13] This proof that DNA can also catalyze chemical reactions is not completely unexpected, especially since it was shown shortly after the development of the in vitro selection technique that single-stranded DNA molecules can also be selected to bind to a variety of ligands.[14] However, the selection technique used by Breaker and Joyce is remarkable. Their aim was the isolation of a DNA enzyme that could specifically cleave the phosphodiester bond of a ribonucleotide. The DNA pool synthesized for this purpose contained a single ribonucleotide at a specific position within a primer binding site, in order to avoid a possible effect of RNA on the catalysis. In addition, they assumed that a DNA-dependent RNA cleavage at pH 7 would require a cofactor, possibly a metal ion. All ribozymes whose reaction mechanisms have been studied are metalloenzymes. Metal ions such as Mg^{2+}, Mn^{2+}, or even Pb^{2+} in the case of the self-cleaving yeast tRNA^{Phe} were always involved in the catalytic mechanism and also served to maintain the correct folding of the RNA. Pan and Uhlenbeck had shown that new ribozymes with Pb^{2+}-dependent phosphodiesterase activity could be isolated from a randomized pool of tRNA^{Phe} molecules.[15] The specificity of the reaction depends on the coordination of a Pb^{2+} ion to a defined position within the RNA (Scheme 5).

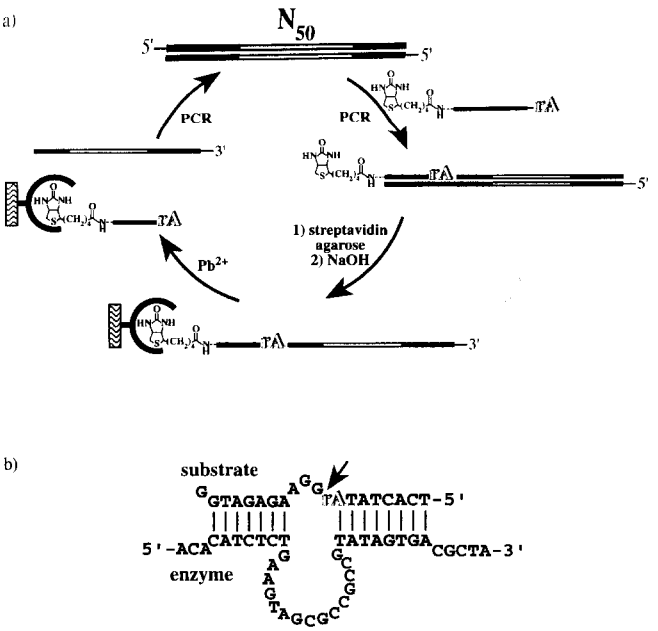


Scheme 5. Possible mechanism of RNA cleavage by Pb^{2+} ions. The $Pb(OH)^+$ ion is brought close to the 2'-hydroxyl group by specific coordination to the RNA. Abstraction of the H^+ ion of the 2'-hydroxyl group facilitates nucleophilic attack of the oxygen atom on the neighboring phosphorus atom. This leads to a transition state with a fivefold coordinated phosphorus atom with trigonal-bipyramidal coordination, which in turn generates a 2',3'-cyclic phosphate and a 5'-hydroxyl group.

Breaker and Joyce also used Pb^{2+} as the cofactor in their selection. They generated a pool of about 10^{14} double-stranded DNAs with a randomized region of 50 nucleotides. One of the strands contains a biotin group at the 5'-end, followed by a defined 43-mer base sequence containing a ribose adenosine unit at position 28. The double-stranded DNA was immobilized on streptavidin agarose, and the non-biotinylated strand was removed by increasing the pH. The immobilized single-stranded DNA was then incubated in Pb^{2+}-containing buffer. In active sequences this led to cleavage of the phosphodiester bond to the ribose phosphate group, and hence to loss of the covalent attachment to the biotin-bearing 5'-end. The catalytically active sequences were thereby specifically eluted from the column, and were subsequently amplified and selected once more (Scheme 6a). Five rounds of selection afforded a population of single-stranded DNAs that could catalyze the Pb^{2+}-dependent cleavage of the ribose residue. These DNAs also showed similarities in their sequences. Like the hammerhead and hairpin ribozymes, they contain two conserved, unpaired regions between two sequences which can pair with bases upstream and downstream of the splice site. This structural motif served as the basis for the construction of a shortened version of the catalytic and substrate domains.

In this way, it was shown that the 38-nucleotide long catalytic domain could cleave the 21-mer substrate specifically and with high turnover rates. The deoxyribozyme is, however, not capable of cleaving a pure RNA substrate, although the substrate

 © VCH Verlagsgesellschaft mbH, D-69451 Weinheim, 1995 0570-0833/95/1111-1191 $ 10.00+.25/0



Scheme 6. a) In vitro selection of a deoxyribozyme that cleaves the phosphodiester bond of a ribonucleotide group. PCR is used to introduce a single ribonucleotide (rA) into the defined region at the 5'-end of a synthetic DNA pool with 50 randomized nucleotides, and also a biotin group on the same strand. By immobilization on streptavidin agarose and raising the pH, a single-stranded pool is obtained, which is subsequently incubated in the presence of Pb^{2+} ions. Sequences that are cleaved at the rA are eluted, amplified by PCR, and subjected to the next cycle. b) Secondary structure of a shortened DNA enzyme that cleaves the phosphodiester bond of a ribonucleotide in an intermolecular reaction, based on one of the selected sequences.

binding to the enzyme is ensured with two longer base-paired regions. These are interrupted by three unpaired bases immediately after the splicing site (Scheme 6b). It is planned, however, to achieve this in further experiments by in vitro evolution.[9, 16]

The development of the deoxyribozyme reported by Breaker and Joyce brings medical applications to mind. A deoxyribozyme that uses less toxic metal ions than Pb^{2+}, for example Mg^{2+} or Ca^{2+}, could cleave specific mRNA targets under physiological conditions, thereby constituting an alternative to antisense and ribozyme techniques.[17]

The man-made ribo- and (now also) dexyribozymes, which have been created, or at least given birth to, catalyze a remarkable spectrum of chemical reactions. They will certainly be applicable in some diagnostic, technical, or medical purposes, where it is advantageous that they are based not on proteins but on nucleic acids. We will not go so far as to maintain that nucleic acid enzymes could catalyze as broad a variety of reactions as protein enzymes can. The examples presented here show, however, that they have far greater potential than merely the storage of information. Prebiotic evolution may possibly have included a phase of the "RNA world", in which primitive organisms existed whose metabolism and replication were controlled by RNA enzymes, and which then led into the DNA–RNA–protein world. It is unclear whether we will ever know how an RNA world may have looked, or how it began. Experiments of the type described may soon, however, allow us to develop a plausible scenario.

German version: *Angew. Chem.* **1995**, *107*, 1303–1306

Keywords: catalysis · DNA enzymes · in vitro selection · metalloenzymes · ribozymes

[1] K. Kruger, P. J. Grabowski, A. J. Zaug, J. Sands, D. E. Gottschling, T. R. Cech, *Cell* **1982**, *31*, 47–157; C. Guerrier-Takada, K. Gardiner, T. Marsh, N. Pace, S. Altman, *ibid.* **1983**, *35*, 849–857.
[2] J. R. Prudent, T. Uno, P. G. Schultz, *Science* **1994**, *264*, 1924–1927.
[3] See for example: D. Hilvert, *Curr. Opin. Struct. Biol.* **1994**, *4*, 612–617.
[4] Reviews in: M. Famulok, J. W. Szostak, *Angew. Chem.* **1992**, *104*, 1001–1011; *Angew. Chem. Int. Ed. Engl.* **1992**, *31*, 979–988; G. F. Joyce, *Curr. Opin. Struct. Biol.* **1994**, *4*, 331–336; R. R. Breaker, G. F. Joyce, *Trends Biotechnol.* **1994**, *12*, 268–275; K. B. Chapman, J. W. Szostak, *Curr. Opin. Struct. Biol.* **1994**, *4*, 618–622; A. D. Ellington, *Curr. Biol.* **1994**, *4*, 427; S. J. Klug, M. Famulok, *Mol. Biol. Rep.* **1994**, *20*, 97–107.
[5] D. P. Bartel, J. W. Szostak, *Science* **1993**, *261*, 1411–1418.
[6] M. Sassanfar, J. W. Szostak, *Nature* **1993**, *364*, 550.
[7] J. R. Lorsch, J. W. Szostak, *Nature* **1994**, *371*, 31–36.
[8] X. Dai, A. De Mesmaeker, G. F. Joyce, *Science* **1995**, *267*, 237–240.
[9] A. A. Beaudry, G. F. Joyce, *Science* **1992**, *257*, 635.
[10] J. A. Piccirilli, T. S. McConnell, A. J. Zaug, H. F. Noller, T. R. Cech, *Science* **1992**, *256*, 1420.
[11] A. D. Ellington, J. W. Szostak, *Nature* **1990**, *346*, 818–822; M. Famulok, J. W. Szostak, *J. Am. Chem. Soc.* **1992**, *114*, 3990–3991; J. Lorsch, J. W. Szostak, *Biochemistry* **1994**, *33*, 973–982; R. D. Jenison, S. C. Gill, A. Pardi, B. Polisky, *Science* **1994**, *263*, 1425–1429; M. Famulok, *J. Am. Chem. Soc.* **1994**, *116*, 1698–1706; P. Burgstaller, M. Famulok, *Angew. Chem.* **1994**, *6*, 1163–1166; *Angew. Chem. Int. Ed. Engl.* **1994**, *33*, 1084–1087; C. T. Lauhon, J. W. Szostak, *J. Am. Chem. Soc.* **1995**, *117*, 1246–1257.
[12] K. N. Morris, T. M. Tharasow, C. M. Julin, S. L. Simons, D. Hilvert, L. Gold, *Proc. Natl. Acad. Sci. USA* **1994**, *91*, 13028–13032.
[13] R. R. Breaker, G. F. Joyce, *Chem. & Biol.* **1994**, *1*, 223–229.
[14] A. D. Ellington, J. W. Szostak, *Nature* **1992**, *355*, 850–852; L. C. Bock, L. C. Griffin, J. A. Latham, E. H. Vermaas, J. J. Toole, *ibid.* **1992**, *355*, 564–566; D. E. Huizenga, J. W. Szostak, *Biochemistry* **1995**, *34*, 656–665.
[15] T. Pan, O. C. Uhlenbeck, *Nature* **1992**, *358*, 560–563; T. Pan, O. C. Uhlenbeck, *Biochemistry* **1992**, *32*, 3887–3895.
[16] N. Lehman, G. F. Joyce, *Nature* **1993**, *361*, 182–185.
[17] J. J. Rossi, *Curr. Opin. Biotechnol.* **1992**, *3*, 3–7.

 © VCH Verlagsgesellschaft mbH, D-69451 Weinheim, 1995 0570-0833/95/1111-1192 $ 10.00+.25/0

The Structure of the *D. gigas* [NiFe] Hydrogenase and the Nature of the Hydrogenase Nickel Complex

Malcolm A. Halcrow*

The enzyme hydrogenase is central to the metabolisms of many classes of bacteria and archaebacteria, acting as an energy transducer to allow the controllable generation and disposal of electrons and protons by reversible catalysis of the oxidation of H_2 [Eq. (a)].[1, 2] The protons produced by H_2 oxidation can be

$$H_2 \rightleftharpoons H^+ + 2e^- \qquad (a)$$

used for the maintenance of proton gradients for ATP synthesis, for example, while the electrons may be channeled to the reduction of electron transport co-factors such as flavins, cytochromes, and NAD^+, and thus fed into one of several respiratory chains. The mode of action of this enzyme is therefore of interest to chemical engineers as well as to biochemists and microbiologists, because it allows the organism to utilize H_2 as a fuel source in aqueous conditions using cheap metals, namely iron and nickel, as catalysts.

By far the most common hydrogenases are the [NiFe] enzymes which contain one equivalent of Ni and varying amounts of Fe and S^{2-} per active site. A subset of these also contain one equivalent of Se per Ni, in the form of selenocysteine which is ligated to the Ni ion, and are therefore termed the [NiFeSe] hydrogenases. A small class of Fe-only hydrogenases is also known, which show very different properties from those of the [NiFe] enzymes. Despite wide variations in metal content and subunit and cofactor inventories between enzymes,[1a] it is thought that the structure of the Ni-containing site is similar in all [NiFe] hydrogenases and that this Ni center forms the H_2 oxidation site of the enzyme.

The Ni site of [NiFe] hydrogenases exhibits a complex chemistry, which may be summarized as follows.[1, 2] The enzymes are generally isolated in one of two, or as a mixture of both inactive states (termed "Ni-A" and "Ni-B"), which show EPR spectra typical of a Ni^{III} ion with a $d_{z^2}^1$ ground state. Incubation of this enzyme with H_2 or other reductants leads to the disappearance of the Ni-A and Ni-B spectra and the successive formation of an EPR-silent "silent intermediate" form, a form ("Ni-C") showing an EPR spectrum ascribable to either a Ni^{III} or Ni^{I} species with a $d_{z^2}^1$ ground state, and a fully reduced form ("Ni-R") again showing no EPR signals attributable to Ni. The silent intermediate and the Ni-C and Ni-R forms are active toward H_2 oxidation and proton reduction; the EPR spectrum of the Ni-C form has been observed in intact bacteria. Low-temperature photolysis of the Ni-C form and its incubation with CO both lead to the reversible formation of new EPR-active species which can be interconverted. The Ni-A, Ni-B, and Ni-C EPR spectra show splittings at very low temperatures consistent with coupling to a nearby paramagnetic center; all the above EPR signals are observed in addition to those arising from the iron–sulfur clusters that form an electron-transport chain to and from the active site.

The structure of the Ni hydrogenase complex and the assignment of the different redox states shown by this unusual biologically active metal center have been debated for over a decade. A plethora of EPR and XAS (X-ray absorption spectroscopy) data have generally favored two structural models for the hydrogenase Ni site: isolated Ni ions with square-planar or square-pyramidal coordination as in $[Ni(cys)_4L]^{2-}$, cysH = cysteine, L = vacant coordination site or N/O donor (Fig. 1, A), or (pseudo-) trigonal-bipyramidal coordination as in $[Ni(cys)_2(N/O)_3L]$ and $[Ni(Secys)(cys)(N,O)_3L]$, SecysH = selenocysteine (Fig. 1, B).[1, 2] Some authors have also suggested the presence of a $[Fe_4S_4]$ cluster covalently bound to the Ni ion through a cysteinyl or S^{2-} bridging ligand (Fig. 1, C).[3a]

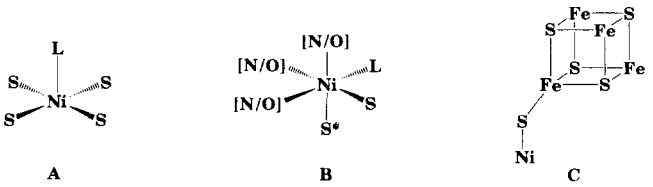


Fig. 1. Previously proposed structural models for the Ni complexes in hydrogenase. The starred S donor corresponds to that proposed to be replaced by Se in [NiFeSe] hydrogenases. L = N/O donor or vacant coordination site.

The assignment of the Ni-C EPR signal to a Ni^{III} or Ni^{I} center, which has an important bearing on the mechanism of enzyme catalysis, has been similarly controversial.[1, 2] Indeed, a thorough XAS study of one hydrogenase questioned the involvement of Ni in any of these redox processes.[3] Now, Volbeda et al. have shed some light on the matter with the first reported single-crystal X-ray structural characterization of a hydrogenase, namely the [NiFe] hydrogenase from *D. gigas* in the (probably Ni^{III}-containing) Ni-A state.[4] Hydrogenase thus has the distinction of being the first of the four known Ni-containing enzymes to be crystallized.

In view of the aforementioned hypotheses regarding the active site of hydrogenase (Fig. 1) the structure described by Volbeda et al.[4] is both surprising and tantalizing (Fig. 2). The Ni ion in the hydrogenase is clearly in a binuclear metal site. It is ligated by four cysteine S atoms in a distorted geometry that may be described as a square pyramid lacking one basal ligand, or as an octahedron with two *cis* coordination vacancies. Two of the basal thiolato ligands form a bridge to a second metal ion M 2.7 Å from the Ni ion; M is further ligated by three non-proteinaceous donors modeled as water, in a geometry approximating octahedral with one missing vertex. The vacant coordination sites at Ni and M correspond to a third bridging position

[*] Dr. M. A. Halcrow[+]
Department of Chemistry, University of Cambridge
Lensfield Road, GB-Cambridge CB2 1EW (UK)
Telefax: Int. code + (1223)336-362

[+] The author is a Royal Society University Research Fellow.

 © VCH Verlagsgesellschaft mbH, D-69451 Weinheim, 1995 0570-0833/95/1111-1193 $ 10.00+.25/0

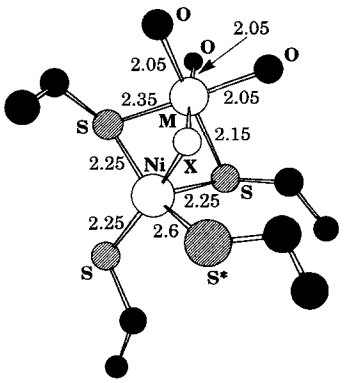


Fig. 2. The NiM site in the *D. gigas* hydrogenase as described by Volbeda et.al. X is the vacant coordination site common to Ni and M, and the starred S donor corresponds to that replaced by Se in [NiFeSe] hydrogenases. Bond lengths are in Å.

between the two ions (X in Fig. 2). Although the identity of M is unclear, the strong anomalous scattering properties of this atom in the Fourier difference map rule out Ni, Cu, Zn, Ca, and Mg. According to ICP analyses Co, Mn, V, and Mo also seem unlikely because of the zero or near-zero content of these metals in the enzyme samples. The most likely metal ion M is therefore an Fe ion, an assignment consistent with the previously reported Fe analysis for this enzyme and apparently supported by very recent EXAFS results.[4] Unfortunately, large temperature factors for the atoms in the active site may indicate some disorder in the structure, which could be related to the fact that the sample employed, while predominantly in the Ni-A form, contained approximately 15% of the Ni-B form. Hence, despite the reasonable resolution of the reported structure (2.85 Å, $R = 0.18$), structural parameters derived from the refinement must be interpreted with care.

Only two thiolato-bridged Ni–Fe complexes have appeared in the literature, namely the tetranuclear species $[\{Ni(BME\text{-}DACO)FeCl\}_2(\mu\text{-}Cl)_2]$, (BME-DACO)$H_2$ = *N*,*N*′-bis(2-mercaptoethyl)-1,5-diazacyclooctane (Fig. 3, A) and $[\{Ni(dmpn)\}_3Fe]^{2+}$, (dmpn)H_2 = *N*,*N*′-dimethyl-*N*,*N*′-bis(2-mercaptoethyl)-1,3-diaminopropane (Fig. 3, B).[5, 6] While it is tempting to compare the Ni–S and Fe–S bond lengths in these and other Ni and Fe complexes with those of the NiM cluster in the hydrogenase structure, the caveats regarding the structural refinement, the ambiguity about the identity of M, and the lack of structural data on relevant Ni^{III} model complexes[2] prevent firm conclusions about the electronic character of the NiM site from being drawn. The Ni···M distance of 2.7 Å is at the low end of the 2.6–3.9 Å range of Ni···Ni distances observed for synthetic $[Ni_2(\mu\text{-}SR)_2]^{2+}$ complexes[2] and suggests pre-organization of the NiM center for the inclusion of a third bridging ligand.

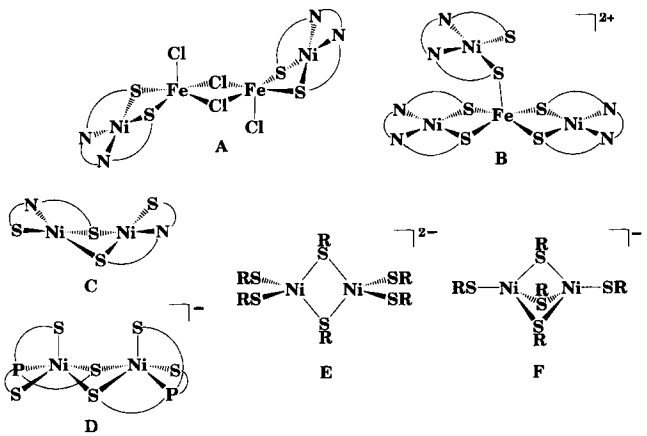


Fig. 3. Schematic structures of the model complexes referred to in the text. A: $[\{Ni(BME\text{-}DACO)FeCl\}_2(\mu\text{-}Cl)_2]$; B: $[\{Ni(dmpn)\}_3Fe]^{2+}$; C: $[Ni_2(memta)_2]$ and $[Ni_2(pdmt)_2]$; D: $[Ni_2\{P(2\text{-}SC_6H_4)_3\}_2]^-$; E: $[Ni_2(SC_4H_9)_6]^{2-}$; F: $[Ni_2(S\text{-}2,4,5\text{-}i\text{Pr}_3C_6H_2)_5]^-$.

A large number of dimers with two thiolato bridges and Ni^{II} ions with square-planar coordination have been reported, some of which are redox active.[2] In particular, Maroney and co-workers have reported that $[Ni_2(memta)_2]$, (memta)H_2 = $(HSC_2H_4)_2NC_2H_4SMe$ (Fig. 3, C), exhibits a chemically reversible one-electron oxidation at $E_{1/2} = -0.35$ V versus the ferrocene/ferrocenium couple (+ 0.05 V vs SCE) to form a mixed-valence species $[Ni_2(memta)_2]^+$.[7] The EPR spectrum of this oxidized species is comparable to the spectra of the Ni-A and Ni-B forms, unlike the EPR spectra of mononuclear Ni^{III} thiolates,[8] while experiments with ^{61}Ni-enriched samples of a closely related oxidized product indicate a valence-delocalized $[Ni_2^{2.5}]^+$ electronic structure.[9] By contrast, however, Krüger and Holm have reported that the structurally related $[Ni_2(pdmt)_2]$, (pdmt)H_2 = 2,6-bis(mercaptomethyl)pyridine (Fig. 3, C), shows a chemically reversible one-electron *reduction* at $E_{1/2} = -1.21$ V versus SCE to form a valence-delocalized species $[Ni_2^{1.5}(pdmt)_2]^-$.[10] The reason for the difference in behavior between these two complexes is unclear, and it is therefore impossible to predict the redox chemistry expected for the $[Ni(\mu\text{-}SR)_2Fe]$ complex proposed by Volbeda et al.

Perhaps the most relevant model compound for the NiM center is the valence-delocalized complex $[Ni_2\{P(2\text{-}SC_6H_4)_3\}_2]^-$, described by Millar and co-workers as containing a doubly thiolato-bridged core, $[Ni_2^{2.5}(\mu\text{-}SR)_2]^{3+}$, with Ni–($\mu$-S) = 2.251(2)–2.260(2) Å and Ni···Ni = 2.501(2) Å.[11] The square-pyramidal Ni ions and are also coordinated by one basal and one apical thiolato ligand ($Ni\text{-}S_{ba} = 2.115(2)$, $Ni\text{-}S_{ap} = 2.373(2)$ Å) and one basal phosphano ligand (Fig. 3, D). While this compound demonstrates the viability of a binuclear $[Ni^{III}(\mu\text{-}S)_2M]$ cluster, it is a poor model for the reductive activation of the NiM site of Volbeda et al., since the parent complex $[Ni_2\{P(2\text{-}SC_6H_4)_3\}_2]^{2-}$ is a dimer of square-planar Ni^{II} ions spanned by arms of the tris(2-mercaptophenyl)phosphano ligands. Finally, it should be stressed that several other structural models also exist for low-nuclearity Ni^{II} thiolate complexes. Of particular relevance to the NiM structure are the complexes $[Ni_2(SC_4H_9)_6]^{2-}$ (Fig. 3, E) and $[Ni_2(S\text{-}2,4,5\text{-}i\text{Pr}_3C_6H_2)_5]^-$ (Fig. 3, F), which are dimers of Ni^{II} ions with distorted tetrahedral coordination bridged by two and three thiolato ligands, respectively.[12] All redox studies performed on these and other tetrahedral Ni^{II} thiolates have shown only irreversible behavior, however.

The structure determination of the binuclear NiM center raises as many questions as it answers. Firstly, the relationship between this structure in the *inactive* form of the enzyme and that in the reduced, active species is unclear. An obvious possibility for the activation reaction would be insertion of a ligand into the vacant site common to Ni and M. But the nature of this putative ligand, which is unlikely to be proteinaceous but could be derived from H_2O or S^{2-}, and the site of the reductive transition are not known. Secondly, the interpretation of the Ni-A, Ni-B, and Ni-C EPR spectra, for which the Ni center has been treated as an isolated Ni^{III} or Ni^{I} paramagnet and which is fundamental to previous discussions of the Ni site, must now be reassessed. In particular, given the probable assignment

 © VCH Verlagsgesellschaft mbH, D-69451 Weinheim, 1995 0570-0833/95/1111-1194 $ 10.00+.25/0

of M (Fig. 2) as Fe, it is interesting that the EPR spectrum of the Ni-A form does not show hyperfine coupling to ^{57}Fe even in ^{57}Fe-enriched enzyme.[13] Thirdly, it is unclear whether a heterobinuclear site can account for the Ni XAS data of Maroney and co-workers, which are inconsistent with large changes in electron density at Ni between the different redox states of hydrogenase.[3] The structure of the NiM site has evidently presented inorganic coordination chemists and spectroscopists with a new series of challenges!

While the reported structure clearly shows potential electron and proton transport pathways to and from the NiM center (Fig. 4),[4] little light has been shed on the mechanism of H_2 oxidation by this complex. It is known that H_2 oxidation by

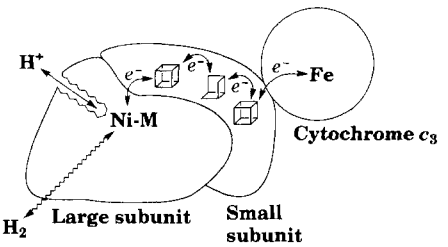


Fig. 4. Schematic diagram showing the relationship of the hydrogenase subunits and the proposed docking site of cytochrome c_3, the arrangement of the NiM and Fe–S clusters within the polypeptide, and the proposed electron and proton transfer pathways to and from the NiM center [4].

hydrogenase involves heterolytic rather than homolytic H–H cleavage, although the nature of the proton and hydride acceptors at the active site is unclear. In proposed mechanisms a Ni hydride is formed in either the + 3 or +1 oxidation states from a Ni^{II} precursor, with concomitant electron transfer and protonation of a neighboring base.[1, 2] In addition to the Ni-bound thiolates, there are several groups in the active site pocket of the *D. gigas* hydrogenase that may act as external bases for the H–H cleavage step; these include nearby arginine and histidine residues and the putative third bridging ligand if this were OH^-. Alternatively, if the third bridging ligand were S^{2-}, this could act as hydride acceptor, as has been shown in several synthetic metal sulfide clusters.[14]

It is noteworthy, however, that Ni-substituted rubredoxin, which contains a well-defined tetrahedral $[Ni(cys)_4]^{2-}$ unit, also catalyzes H_2 oxidation through a reaction that shows some kinetic similarities to that exhibited by hydrogenase.[15] A small number of mononuclear Ni thiolate complexes have also been reported to interact directly with H_2 or to reduce protons.[16] Hence, it seems that in principle the activation of H_2 by Ni thiolate complexes does not require a second metal ion or a S^{2-} bridging ligand, and it is interesting to speculate what the role of M in the NiM site might be.

German version: *Angew. Chem.* **1995**, *107*, 1307–1310

Keywords: bioinorganic chemistry · hydrogenases · nickel compounds

[1] a) A. F. Kolodziej, *Prog. Inorg. Chem.* **1994**, *41*, 493–597; b) J. A. Kovacs, *Adv. Inorg. Biochem.* **1994**, *9*, 173–218; c) R. P. Hausinger, *Biochemistry of Nickel*, Plenum, New York, **1993**.
[2] M. A. Halcrow, G. Christou, *Chem. Rev.* **1994**, *94*, 2421–2481.
[3] a) M. J. Maroney, G. J. Colpas, C. Bagyinka, N. Baidya, P. K. Mascharak, *J. Am. Chem. Soc.* **1991**, *113*, 3962–3972; b) C. Bagyinka, J. P. Whitehead, M. J. Maroney, *ibid.* **1993**, *115*, 3576–3585; c) J. P. Whitehead, R. J. Gurbiel, C. Bagyinka, B. M. Hoffmann, M. J. Maroney, *ibid.* **1993**, *115*, 5629–5635.
[4] A. Volbeda, M.-H. Charon, C. Piras, E. C. Hatchikian, M. Frey, J. C. Fonticella-Camps, *Nature (London)* **1995**, *373*, 580–587.
[5] D. K. Mills, Y. M. Hsiao, P. J. Farmer, E. V. Atnip, J. H. Reibenspies, M. Y. Darensbourg, *J. Am. Chem. Soc.* **1991**, *113*, 1421–1423.
[6] G. J. Colpas, R. O. Day, M. J. Maroney, *Inorg. Chem.* **1992**, *31*, 5053–5055.
[7] M. Kumar, R. O. Day, G. J. Colpas, M. J. Maroney, *J. Am. Chem. Soc.* **1989**, *111*, 5974–5976.
[8] a) S. Fox, Y. Wang, A. Silver, M. Millar, *J. Am. Chem. Soc.* **1990**, *112*, 3218–3220; b) N. Baidya, P. K. Mascharak, D. W. Stephan, C. F. Campagna, *Inorg. Chim. Acta* **1990**, *177*, 233–238.
[9] S. B. Choudhury, M. A. Pressler, S. A. Mirza, R. O. Day, M. J. Maroney, *Inorg. Chem.* **1994**, *33*, 4831–4839.
[10] H.-J. Krüger, R. H. Holm, *Inorg. Chem.* **1989**, *28*, 1148–1155.
[11] J. D. Franolic, W. Y. Wang, M. Millar, *J. Am. Chem. Soc.* **1992**, *114*, 6587–6588.
[12] a) A. Silver, M. Millar, *J. Chem. Soc. Chem. Commun.* **1992**, 948–949; b) A. Müller, G. Henkel, *Z. Naturforsch. B*, in press.
[13] H.-J. Krüger, B. H. Huynh, P. O. Ljungdahl, A. V. Xavier, D. V. DerVartanian, I. Moura, H. D. Peck Jr., M. Teixeira, J. J. G. Moura, J. LeGall, *J. Biol. Chem.* **1982**, *257*, 14620–14623.
[14] M. Rakowski Dubois, *Chem. Rev.* **1989**, *89*, 1–9.
[15] P. Saint-Martin, P. A. Lespinat, G. Fauque, Y. Berlier, J. LeGall, I. Moura, M. Teixeira, A. V. Xavier, J. J. G. Moura, *Proc. Natl. Acad. Sci. USA* **1988**, *85*, 9378–9380.
[16] a) A. Vlcek, Jr., A. A. Vlcek, *Inorg. Chim. Acta* **1980**, *41*, 123–131; b) M. Zimmer, G. Schulte, X.-L. Luo, R. H. Crabtree, *Angew. Chem.* **1991**, *103*, 205–207; *Angew. Chem. Int. Ed. Engl.* **1991**, *30*, 193–194; c) M. J. Ashcroft, D. Collison, C. D. Garner, *J. Inorg. Biochem.* **1993**, *51*, 34; d) C. A. Marganian, H. Vazir, N. Baidya, M. M. Olmstead, P. K. Mascharak, *J. Am. Chem. Soc.* **1995**, *117*, 1584–1594.

$^3_\infty[(CoCp_2) \subset Fe(\mu\text{-}CNSnMe_3NC)_3]$: A Purely Organometallic Channel Inclusion Compound**

Peter Schwarz, Eric Siebel, R. Dieter Fischer,*
David C. Apperley, Nicola A. Davies,
and Robin K. Harris*

Inclusion compounds with metallocene guest components are of interest not only in fundamental research, but also increasingly in materials science.[1, 2] So far, metal dichalcogenide intercalates[1] and zeolite–metallocene host–guest compounds[3] have been of particular interest.[3] Yet to our knowledge, no crystals of such a zeolite derivative suitable for X-ray structural analysis have been obtained.[3f] As early as 1988 we postulated that merely by grinding the supramolecular organotin(IV) polymer **1** (which may, alternatively, be formulated as $[(Me_3Sn)_3Fe(CN)_6]$

$^3_\infty[Fe^{III}(\mu\text{-}CNSn^{IV}Me_3NC)_3]$ **1**

$^3_\infty[(Fe^{III}Cp_2) \subset Fe^{II}(\mu\text{-}CNSn^{IV}Me_3NC)_3]$ **2**

$^3_\infty[(Co^{III}Cp_2) \subset Fe^{II}(\mu\text{-}CNSn^{IV}Me_3NC)_3]$ **3**

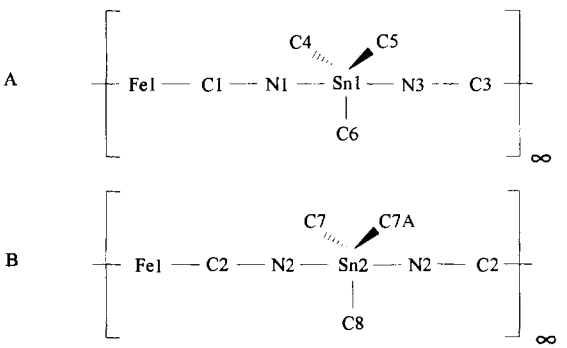
or $Fe(CN_3)\cdot 3Me_3SnNC$[4]) with ferrocene would produce the zeolite-like host–guest compound **2** in the form of an X-ray amorphous powder.[5] Here we present the first insights into the static and dynamic structure of the homologous cobaltocenium compound **3**,[6] which readily crystallizes, as we have found recently, when prepared by spontaneous self-assembly in H_2O [Eq. (a)].

$$[CoCp_2]ClO_4 + K_4[Fe(CN)_6] \xrightarrow[(H_2O)]{3\,Me_3SnCl} \mathbf{3}\downarrow + 4K^+ + 3Cl^- + ClO_4^- \quad (a)$$

A crystal structure analysis[8] shows that **3** strongly resembles **4**, the Co^{III} homologue of **1**,[4] in that it contains an extensively

$^3_\infty[Co^{III}(\mu\text{-}CNSnMe_3NC)_3]$ **4**

porous, three-dimensional (3D) host framework, built up of corner-sharing octahedral $[Fe(\mu\text{-}CN)_6]$ and trigonal-bipyramidal $[SnMe_3(\mu\text{-}NC)_2]$ constituents (with equatorial Me ligands). In an alternative view, two unique, infinite chains **A** (nonlinear, I_{rel}: 2) and **B** (quasi linear, I_{rel}:1) turn out to span the 3D network found in **3** (Scheme 1).



Scheme 1. Topology of the chains **A** and **B** (H atoms have been omitted). Atomic distances [pm] and angles [°], **A**: Sn1-N1 230.4(6), Sn1-N3 236.2(6); C1-N1-Sn1 148.4(5), C3-N3-Sn1 134.5(5), C1-Fe1-C3 91.8(3), C4-Sn1-C5 119.5(4), C5-Sn1-C6 114.8(4), C6-Sn1-C4 125.6(4), **B**: Sn2-N2 230.2(6); C2-N2-Sn2 173.2(5), C2-Fe1-C2A 180.0(1), C7-Sn2-C8 121.1(3), C7-Sn2-C7A 117.7(5).

The average Sn–N distance in **3** (232.3 pm) lies between the corresponding values for $[Me_3SnNCS]$ (215 pm[9]) and polymeric $[Me_3SnCN]$ (249 pm[10]). The formation of unusually large channels in **3** and **4** argues against the presence of a real ionic lattice, which would be expected to be more compact. Stacks of $[CoCp_2^+]$ guest ions extend in the direction of the *c* axis in **3** (the shortest intermolecular ring–plane distance: 240–245 pm). Surprisingly, the channels in **3** contain two $(CoCp_2^+)_n$ stacks alternating with solely Me ligands from the Sn atoms (Fig. 1). The Cent-Co-Cent′ axes (Cent: Cp center) do not lie

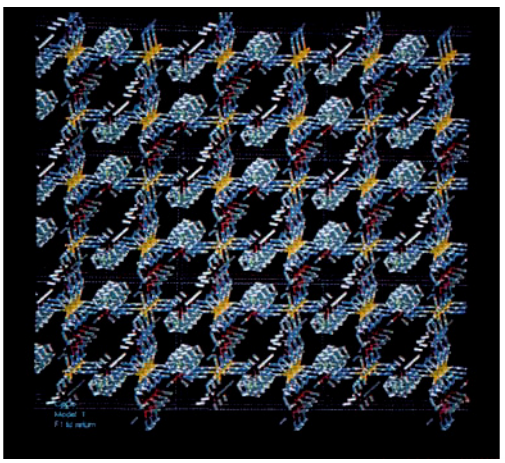


Fig. 1. View of the 3D network in **3** along the *c* axis in the direction of the main channels. The type **B** chains run horizontally (seen in projection!) (red Sn, yellow Fe, green Co, gray C).

strictly parallel to the *c* axis (Fig. 2). The average Co–C(Cp) distance (199.0 pm)[11] is slightly shorter than that in conventional cobaltocenium salts (about 202.9 pm).[12] However, the formula volume $V_f = 0.602 \times V/Z = M_r/\rho_{calcd}$ of **3** (520 $cm^3\,mol^{-1}$), as determined from the X-ray data, exceeds

[*] Prof. Dr. R. D. Fischer, Dr. P. Schwarz, Dipl.-Chem. E. Siebel
Institut für Anorganische und Angewandte Chemie der Universität
Martin-Luther-King-Platz 6, D-20146 Hamburg (Germany)
Telefax: Int. code + (40)4123-2893
Prof. Dr. R. K. Harris, Dr. D. C. Apperley, N. A. Davies, M. Sc.
University of Durham, Department of Chemistry
South Road, Durham DH1 3LE (UK)
Telefax: Int. code + (191)3861127

[**] The authors thank the Deutscher Akademischer Austauschdienst and the British Council for support of this collaboration within the framework of an ARC program, as well as the Deutsche Forschungsgemeinschaft (P. S., R. D. F) and the U. K. Engineering and Physical Sciences Research Council (for access to the National Solid-State NMR Service (R. K. H., D. C. A., and N. A. D.).

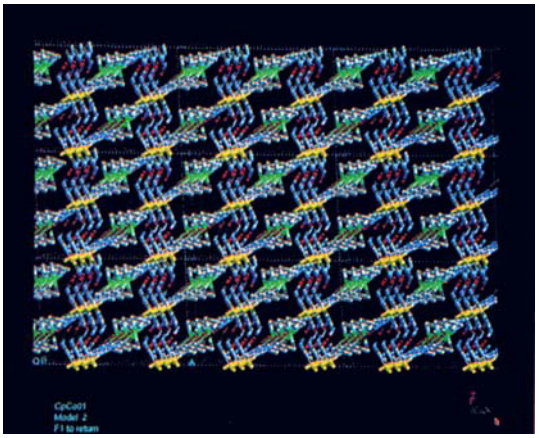


Fig. 2. View of the 3D network in **3** approximately along the *b* axis. The main channels run vertically, the type **B** chains diagonally (red Sn, yellow Fe, green Co, gray C).

that of **4** by approximately half the V_f value of crystalline $FeCp_2$ (123 $cm^3 mol^{-1}$).[13] At room temperature neither the $[CoCp_2^+]$ ion (Fig. 3) nor the methyl C atoms of the two nonequivalent Me_3Sn components are disordered. The calculated[14] X-ray powder diagram of **3** corresponds excellently with the experimental diffraction pattern.[15]

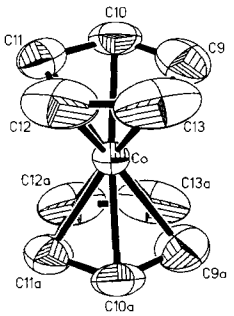


Fig. 3. SHELXTL PLUS drawing of the $[CoCp_2^+]$ guest ion in **3** (ellipsoids represent 30% probability).

The unambiguous X-ray diffraction data make the diamagnetic compound **3**, preferably when enriched with the ^{15}N isotope, a promising candidate for a detailed comparison with cross polarization magic angle spinning (CP/MAS) solid-state NMR data. The ^{13}C, ^{15}N, and ^{119}Sn nuclei of the $[Fe(CNSn_{0.5})_6]$ framework show (already at about 25 °C) exactly as many resonance signals as would be expected for the asymmetric unit deduced from the X-ray structure (see Scheme 1; three singlets each for the ^{13}C and ^{15}N nuclei and two singlets for the ^{119}Sn nucleus).[16] The chemical shifts δ for **3** correspond to those of the homologous host–guest compound **5** with Et_4N^+ instead of the $[CoCp_2^+]$ guest ions.[6]

$^3_\infty[(Et_4N) \subset Fe(\mu\text{-}CNSnMe_3NC)_3]$ **5**

$[(Me_3Sn)_4Fe(CN)_6]$ **6**

However, in the structurally different polymers **4**[4] and **6**, certain framework nuclei exhibit significantly shifted δ values (Table 1). The extremely low frequencies of the ^{119}Sn resonance signals for **3** and **5** are also noteworthy.[17]

The ^{13}C NMR spectra of all the Me and Cp ligands suggest a dynamic behavior. The sharp methyl ^{13}C singlet[18] (only one line at 25 °C) splits into the pair of signals expected for the two nonequivalent, but still freely rotating, Me_3Sn groups at about −60 °C (Fig. 4). The appearance of five lines in the spectrum measured at −140 °C corresponds to the number of signals predicted by the asymmetric unit.[20] Interestingly, also in the case of **4** three methyl ^{13}C singlets, instead of nine, indicating three crystallographically nonequivalent but labile Me_3Sn groups, were seen at −60 °C. At −20 °C only two signals occurred.[4] Occupation of the cavities in **3** by guest ions

Table 1. Solid-state NMR data (^{13}C, ^{15}N, ^{119}Sn; room temperature) of the framework atoms in **3**–**6** [16].

	3	**5**	**6**	**4** [b]
$^{13}C(CN)$ [a]	166.4	171.0	169.6	
	175.0		175.2	ca. 132
	179.5	175.5	178.9	
$^{15}N(CN)$ [a]	−112.0	−116	−109	−116
	−121.5	−123	−124	−119
	−123.2	−125	−166	−123
^{119}Sn [a]	−189 [c]	−181 [c]	−108	−118 [c]
	−139	−159	46	−88

[a] δ values are referenced to $SiMe_4$ (^{13}C), NH_4NO_3 (NO_3 signal, ^{15}N), $SnMe_4$ (^{119}Sn); for further experimental details see Ref. [4,16]. [b] Without ^{15}N enrichment. [c] ^{119}Sn NMR signals of lower intensity.

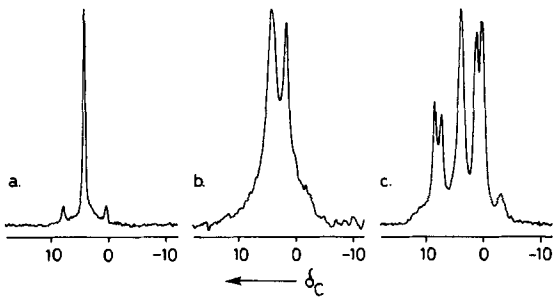


Fig. 4. CP/MAS ^{13}C NMR spectra (75.4 MHz) of the methyl C atoms in **3**: a) 25 °C, b) −60 °C, c) −140 °C (nominal temperature). Contact time: 1 ms; recycle delay: 10 s; number of acquisitions: 120 (a,b), 180 (c); rotation frequency: 3.23, 3.33, 3.00 kHz.

should lead, as in the case of **6**,[16, 19] to increased restriction of rotation. Conversely, from the considerably expanded lattice of **3** (for example, when compared with that of **4**), a substantial opposite effect may be expected. At 25 °C the Cp ligands display rotation about their C_5 axes (only one singlet at $\delta = 85.9$ is seen).[21] This rotation would probably be "frozen out" at about −140 °C; however, instead of the five expected signals, only three are resolved ($\delta = 81.8, 84.4, 88.2$).[20] A resonance signal for the quadrupolar ^{59}Co nucleus was not observed. A possible reason for this could be the strongly anisotropic surroundings of the $[CoCp_2^+]$ ion (see Figs. 1 and 2).

Experimental Procedure

3: An aqueous solution of Me_3SnCl (234.4 mg, 1.176 mmol) and $[CoCp_2]ClO_4$ (135.8 mg, 0.047 mmol) was added dropwise to a stirred, saturated aqueous solution of $K_4[Fe(CN)_6]\cdot 3H_2O$ (165.6 mg, 0.392 mmol) (total volume 35 mL H_2O). After filtration and repeated washing with a little H_2O, the precipitate was dried in vacuo (oil pump vacuum at room temperature) to provide 135.8 mg (0.356 mmol = 91%) of analytically pure **3** (correct C, H, N, Co, Fe, Sn analyses). Orange color, m.p. = 280 °C (decomp.; blackening), ν(CN) frequencies in cm^{-1}: 2044, 2061, 2077 (IR); 2066, 2083, 2124 (Raman). Single crystals were grown as described above, but with the following amounts: 28.3 mg (0.067 mmol) $K_4[Fe(CN)_6]\cdot 3H_2O$, 46.1 mg (0.23 mmol) Me_3SnCl, and 22.5 mg (0.078 mmol) $[CoCp_2]ClO_4$ in a total of 75 mL H_2O. After 2–3 days suitably sized crystals were obtained (correct C, H, N analyses). The preparation of **3** with 50% ^{15}N enrichment was analogous to that of **3** with the use of $K_4[Fe(CN)_6]\cdot 3H_2O$ and $K_4[Fe(C^{15}N)_6]\cdot 3H_2O$ [16] in a 1:1 molar ratio (correct C, H, N analyses).

Received: December 15, 1994 [Z 7552 IE]
German version: *Angew. Chem.* **1995**, *107*, 1311–1313

Keywords: cobalt compounds · host–guest chemistry · inclusion compounds · iron compounds · zeolites

[1] Intercalation compounds: a) P. Palvadeau, L. Coic, J. Rouxel, F. Ménil, L. Forn's, *Mater. Res. Bull.* **1981**, *16*, 1055; b) C. A. Formstone, E. T. FitzGerald, P. A. Cox, D. O'Hare, *Inorg. Chem.* **1990**, *29*, 3860; c) D. O'Hare, J. S. O. Evans, P. J. Wiseman, C. K. Prout, *Angew. Chem.* **1991**, *103*, 1175; *Angew. Chem. Int. Ed. Engl.* **1991**, *30*, 1156; d) D. G. Clerc, D. A. Cleary, *Chem. Mater.* **1994**, *6*, 13; e) H.-V. Wong, J. S. O. Evans, S. Barlow, S. J. Mason, C. O'Hare, *Inorg. Chem.* **1994**, *33*, 5515; f) J. S. O. Evans, S. Barlow, H.-V. Wong, D. O'Hare, *Adv. Mater.* **1995**, *7*, 136.

[2] Further inclusion complexes (excluding zeolite derivatives [3]): a) E. Hough, D. G. Nicholson, *J. Chem. Soc. Dalton Trans.* **1978**, 15; b) B. Klingert, G. Rihs, *ibid.* **1991**, 2749.

[3] See also a) P. K. Dutta, R. E. Zaykoski, M. A. Thomson, *Zeolites* **1986**, *6*, 423; b) A. Mahay, G. Lemay, A. Adnot, I. M. Szöghy, S. Kaliaguine, *J. Catal.* 1987, *103*, 480; c) G. A. Ozin, J. Godber, *J. Phys. Chem.* **1989**, *93*, 878; d) G. A. Ozin, C. Gil, *Chem. Rev.* **1989**, *89*, 1749; e) K. J. Balkus, Jr., S. Shepelev, *Microporous Mater.* **1993**, 1, 383; f) Note added in proof (March 31, 1995): In the meantime the first successful crystal structure analysis of a "cobaltocenium-clathrasil" system has been carried out: G. van de Goor, C. C. Freyhardt, P. Behrens, *Z. Anorg. Allg. Chem.* **1995**, *621*, 311.

[4] See also U. Behrens, A. K. Brimah, T. M. Soliman, R. D. Fischer, D. C. Apperley, N. A. Davies, R. K. Harris, *Organometallics* **1992**, *11*, 1718.

[5] P. Brandt, A. K. Brimah, R. D. Fischer, *Angew. Chem.* **1988**, *100*, 1578; *Angew. Chem. Int. Ed. Engl.* **1988**, *27*, 1521.

[6] Regarding alternative syntheses, see ref. [7].

[7] See also S. Eller, P. Brandt, A. K. Brimah, P. Schwarz, R. D. Fischer, *Angew. Chem.* **1989**, *101*, 1274; *Angew. Chem. Int. Ed. Engl.* **1989**, *28*, 1263.

[8] Crystal data for **3**: $C_{25}H_{37}N_6FeCoSn_3$, $M_r = 892.46$, monoclinic, $C2/c$; $a = 1799.5(2)$, $b = 1557.0(3)$, $c = 1236.0(2)$ pm, $\beta = 92.60(2)^\circ$, $V = 3459.5(9) \times 10^6$ pm^3, $Z = 4$, $\rho_{calcd} = 1.71$ Mg m^{-3}, $F(000) = 1580$. Syntex-$P2_1$ four-circle diffractometer, $T = 23\,^\circ$C, 2θ range: 4.5–45°. Symmetry-independent reflections: 3666 (total: 3996); portion used for refinement($E > 4.0\sigma(E)$): 2913. Independent parameters: 165; direct methods, SHELXTL PLUS (VMS). DIFABS correction. $R = 0.0480$, $R_w = 0.0494$. Visualization with CERIUS from Molecular Simulations, Inc. Further details of the crystal structure investigation may be obtained from the Fachinformationszentrum Karlsruhe, D-76344 Eggenstein-Leopoldshafen (Germany) on quoting the depository number CSD-58447.

[9] R. A. Forder, G. M. Sheldrick, *J. Organomet. Chem.* **1970**, *21*, 115.

[10] E. O. Schlemper, D. Britton, *Inorg. Chem.* **1966**, *5*, 507.

[11] Determined Co-C distances [pm]: Co-C9 199.7(18), Co-C10 199.2(11), Co-C11 201.0(15), Co-C12 198.7(17), Co-C13 196.6(17). The comparatively favorable thermal ellipsoids found here even for the guest ion are shown in Fig. 3 (for delicate problems in the structure determination of guest component see ref. [1c]).

[12] See also R. D. W. Kemmitt, D. R. Russell in *Comprehensive Organometallic Chemistry, Vol. 5* (Ed. G. Wilkinson, F. G. A. Stone, E. W. Abel), Pergamon, Oxford, **1982**, 245.

[13] Calculated with data from P. Seiler, J. D. Dunitz, *Acta Crystallogr. Sect. B* **1979**, *35*, 2020.

[14] Calculated with the program SHELXTL/XPOW; relevant 2θ-range: 0–45°.

[15] Even the X-ray powder diagrams for the Ru and Os homologues of **3**, which we also prepared, showed good agreement with that of **3**: "Co⊂Ru", "Co⊂Os" and "Fe⊂Ru" (in each case, the first metal atom belongs to the guest ion component).

[16] See also S. Eller, P. Schwarz, A. K. Brimah, R. D. Fischer, D. C. Apperley, N. A. Davies, R. K. Harris, *Organometallics*, **1993**, *12*, 3232.

[17] Compare with the positive $\delta(^{119}Sn)$ values for two betaine-like organotin(IV) complexes with Sn coordination numbers ≥ 5 and a charge of +1 or +2 in B. Wrackmeyer, G. Kehr, R. Boese, *Angew. Chem.* **1991**, *103*, 1374; *Angew. Chem. Int. Ed. Engl.* **1991**, *30*, 1370.

[18] $^1J(^{119}Sn, ^{13}C) = 565$ Hz (from the observed coupling satellites; see Fig. 4a).

[19] For further examples of related compounds with Me_3Sn groups showing free rotation about their threefold N-Sn-N axes (on the NMR time scale) see: a) R. K. Harris, D. C. Apperley, N. A. Davies, R. D. Fischer, *Bull. Magn. Reson.* **1993**, *15*, 22; b) R. K. Harris, M. M. Sünnetçioglu, R. D. Fischer, *Spectrochim. Acta Part A*, **1994**, *50*, 2069.

[20] A DSC investigation of **3** between −95 and about 30 °C did not give any evidence for a phase transformation. We thank Dipl.-Chem. U. Gloistein and Professor H. K. Cammenga (Braunschweig) for the measurements.

[21] $\delta(^{13}C)$ value of dissolved $[CoCp_2]ClO_4$: 85.89; see J. E. Sheats, *J. Organomet. Chem. Libr.* **1979**, *7*, 461.

AlMepO-α: A Novel Open-Framework Aluminum Methylphosphonate with Organo-Lined Unidimensional Channels

Kazuyuki Maeda,* Junji Akimoto,
Yoshimichi Kiyozumi, and Fujio Mizukami

Microporous crystals such as zeolites are important materials for molecular sieves, shape-selective catalysts, ion-exchangers and many other applications.[1, 2] An ultimate goal in the syntheses of these compounds is the control of size, shape, and (hydrophilic or hydrophobic) character of micropores. Our aim was to design a pore system in which organic groups formed parts of the framework. Most organic phosphonates of various metals have layered structures[3, 4] with few exceptions, and such molecularly engineered layered structures are promising as optical and intercalation materials, and solid catalysts, etc.[5, 6] They are closely related to purely inorganic layered phosphates.[3, 4] We expected to be able to substitute phosphate groups in the microporous aluminophosphates[7–9] (ALPOs) by methylphosphonate groups to produce novel open frameworks. Recently, we reported on a microporous aluminum methylphosphonate (AlMepO-β) synthesized under hydrothermal conditions.[10] AlMepO-β has a framework composition of $Al_2(CH_3PO_3)_3$ and unidimensional channels formed from intertwined fused four-ring chains.[11] Here we report the synthesis and structural analysis of another microporous aluminum methylphosphonate (AlMepO-α), which has the same composition as AlMepO-β.

AlMepO-α crystallizes in the trigonal space group $P31c$ with $a = 13.9949(13)$ and $c = 8.5311(16)$ Å. The structure is based on a three-dimensional net in which aluminates and methylphoshonates alternate like in ALPOs (Fig. 1). ALPOs are generally composed of only 4-connected nets, while AlMepO-α includes four-coordinate but also topologically 3-connected phos-

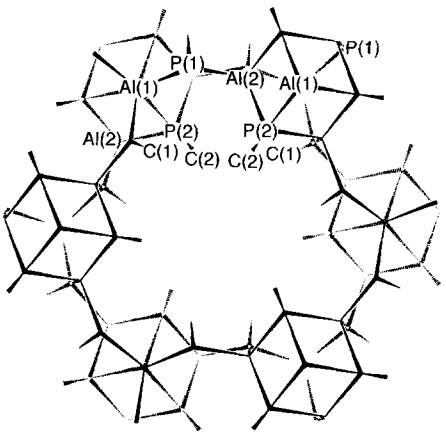


Fig. 1. Schematic drawing of the framework of AlMepO-α projected along the c axis. Oxygen and hydrogen atoms are omitted. Wedged lines locate structural features above the plane of the paper and wedged hashed lines locate those below the plane of the paper. The thicker end of the wedged lines denotes the upper side. Threefold rotation axes parallel to the c axis both along the center of the channel and through the position where every Al(1) atom locates.

[*] K. Maeda, Dr. J. Akimoto, Y. Kiyozumi, Dr. F. Mizukami
Surface Chemistry Division
National Institute of Materials and Chemical Research
1-1 Higashi, Tsukuba, Ibaraki 305 (Japan)
Telefax: Int. code + (298)54-4709
e-mail: maeda@nimc.go.jp

 © VCH Verlagsgesellschaft mbH, D-69451 Weinheim, 1995 0570-0833/95/1111-1199 $ 10.00+.25/0

phorus owing to terminal methyl groups. To compensate the framework charge, one of the three oxygen atoms in each CH_3PO_3 group is bound to a six-coordinate aluminum atom [Al(1)], the other two oxygen atoms are bound to four-coordinate aluminum atoms [Al(2)]. This mode of connectivity is the same as that predicted from MAS-NMR results for AlMepO-β.[10] The three-dimensional framework is based on aluminate and methylphosphonate layers, which alternate along the c axis (Fig. 2). This suggests that the initial layered structure of boehmite is essentially retained throughout the hydrothermal reaction.

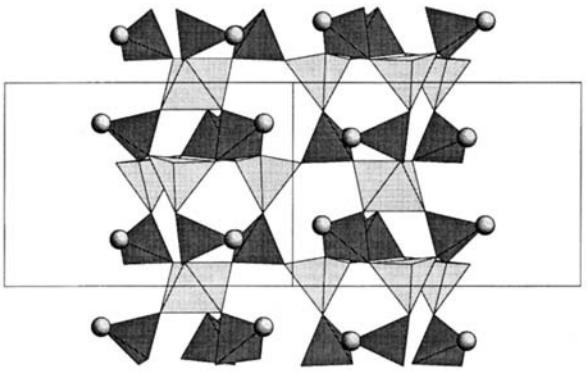


Fig. 2. Polyhedra model of the channel wall of AlMepO-α viewed along the [110] axis. Dark gray tetrahedra with spheres (methyl group) denote $[CH_3PO_3]$, the other pale gray tetrahedra denote $[AlO_4]$, and the octahedra denote $[AlO_6]$. Methylphosphonate and aluminate layers alternate along the c axis.

The most remarkable feature of AlMepO-α is the existence of unidimensional channels running parallel to the c axis. All of the methyl groups point toward the centers of the channels. Figure 3 shows that the channels are almost completely lined by the methyl groups, and that the cross section of a channel is close to an equilateral triangle (side length ca. 7.0 Å). The inorganic framework forming the basis of a channel is made up of 18-rings composed of a sequence of [P(1)-Al(1)-P(1)-Al(2)-P(2)-Al(2)]$_3$. Similar 18-rings were found also in AlMepO-β, whose framework is composed of ladderlike polymeric chains.[11] Besides AlMepO-β, only β-Cu(CH_3PO_3)[13] reported recently, as far as we know, has unidimensional channels lined with organic groups among reported metal organophosphonates. Similar unidimensional channels lined with hydrogen atoms bound to phosphorus atoms are reported in several metal phosphites, $M_2(HPO_3)_3$ (M = Fe,[14] Al,[15] Ga[15]) and $M_{11}(HPO_3)_8(OH)_6$ (M = Zn,[16] Mn,[17] Fe[17]). Unidimensional channels lined with both hydrogen (P–H) and terminal OH groups are reported in $Zn(H_2PO_3)_2 \cdot 3H_2O$.[18] Since the largest rings that make up the inorganic frameworks of these compounds are 12-rings, however, there is not sufficient space in the channels to allow small molecules to enter. Although there are also 6-rings between the channels in AlMepO-α, no small molecule probably can pass through the holes because they are partly covered by methyl groups (Fig. 2). The structure of AlMepO-α is related to that of the AFI framework[19] such as that in ALPO-5. Replacement of the three aluminum atoms of every other 6-ring in the framework of ALPO-5 by a six-coordinate aluminum atom located in the center of the triangle formed by the replaced aluminum atoms can generate a framework of the same topology as AlMepO-α.

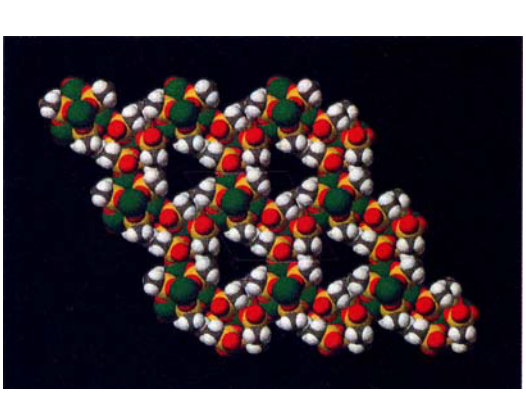


Fig. 3. The structure of AlMepO-α viewed along the c axis. Green: aluminum; yellow: phosphorus; red: oxygen; gray: carbon; white: hydrogen. The central rhombus denotes a unit cell ($a = b = 13.995$ Å). van der Waals radii of 1.7 Å for C and 1.2 Å for H were used to draw the figure [12].

According to X-ray diffraction, ^{13}C, and ^{31}P NMR studies, thermal treatment at 500 °C under vacuum causes no substantial change of the AlMepO-α framework structure and its methyl groups. AlMepO-α degassed at 400 °C adsorbed 2,2-dimethylpropane, for which a kinetic diameter of 6.2 Å was reported.[20] This result shows that the molecules fit well into the triangular-shaped channels and demonstrates the flexibility of the methyl groups forming the channel wall.

Experimental Procedure

Single crystals of AlMepO-α suitable for an X-ray structural analysis were obtained from an unstirred aqueous mixture (Al:P:H_2O = 1:1:40) of methylphosphonic acid (Aldrich, 98 wt.%) and pseudo-boehmite powder (PURAL SCF from Condea Chemie, 74.4 wt.% Al_2O_3, 25.6 wt.% water). The mixture was hydrothermally treated at 220 °C for 48 h without stirring under an autogeneous pressure using an autoclave with a Teflon sleeve. Subsequently, crystals floating on the liquid phase were separated from boehmite-derived solid at the bottom of the vessel. The air-dried product gave an approximate composition of $Al_2(CH_3PO_3)_3 \cdot nH_2O$ ($n = 0$–1.5) from elemental analyses.

Single-crystal X-ray diffraction data were collected on $0.1 \times 0.1 \times 0.6$ mm crystal with $Mo_{K\alpha}$ radiation ($\lambda = 0.71069$ Å) using a Rigaku AFC-5 four-circle diffractometer. A total of 5272 reflections were collected; of the 1795 unique reflections, 1712 had $F_o^2 > 2\sigma(F_o^2)$. Although initial survey suggested a hexagonal cell with the lattice parameters described above, attempts to derive crystallographically meaningful structural models based on several possible space groups expected from the systematic extinction ($l = 2n$ for hhl) were unsuccessful. The adoption of the space group $P31c$ in trigonal system with the same cell parameters led to a plausible framework structure by using direct methods [21]. The isotropic refinement based on F_o^2 using SHELXL-93 [22] on the assumption of the twinning [23] of the reciprocal lattice by a rotation operation along the [110] axis [24] resulted in a drop of $R_w(F^2)$ to 0.205, otherwise $R_w(F^2)$ was 0.537. The final refinement included anisotropic thermal displacement parameters for all non-hydrogen atoms and a rotating rigid group model for hydrogen atoms (104 parameters). The structure was refined by full-matrix least squares to $R_w(F^2) = 0.108$ (for all 1795 reflections) and $R_w(F) = 0.046$ ($F > 4.0\sigma$). Further details of the crystal structure investigation may be obtained from the Fachinformationszentrum Karlsruhe, D-76344 Eggenstein-Leopoldshafen (Germany), on quoting the depository number CSD-58862.

Received: December 30, 1994 [Z 7599 IE]
German version: *Angew. Chem.* **1995**, *107*, 1313–1315

Keywords: aluminophosphates · channel structures · zeolite analogues

[1] R. Szostak, *Molecular Sieves*, Van Nostrand Reinhold, New York, **1989**.
[2] M. E. Davis, R. F. Lobo, *Chem. Mater.* **1992**, *4*, 756.
[3] G. Cao, H.-G. Hong, T. E. Mallouk, *Acc. Chem. Res.* **1992**, *25*, 422.
[4] Y. P. Zhang, A. Clearfield, *Inorg. Chem.* **1992**, *31*, 2821.
[5] M. E. Thompson, *Chem. Mater.* **1994**, *6*, 1168.
[6] D. L. King, M. D. Cooper, W. A. Sanderson, C. M. Schramm, J. D. Fellmann, *Stud. Surf. Sci. Catal.* **1991**, *63*, 247.
[7] S. T. Wilson, B. M. Lok, C. A. Messina, T. R. Cannan, E. M. Flanigen, *J. Am. Chem. Soc.* **1982**, *104*, 1146.

 © VCH Verlagsgesellschaft mbH, D-69451 Weinheim, 1995 0570-0833/95/1111-1200 $ 10.00+.25/0

[8] E. M. Flanigen, B. M. Lok, R. L. Patton, S. T. Wilson in *New Developments in Zeolite Science and Technology* (Eds.: Y. Murakami, A. Iijima, J. W. Ward), Elsevier, Amsterdam, **1986**, p. 103.
[9] J. M. Bennett, W. J. Dytrych, J. J. Pluth, J. W. Richardson, Jr., J. W. Smith, *Zeolites* **1986**, *6*, 349.
[10] K. Maeda, Y. Kiyozumi, F. Mizukami, *Angew. Chem.* **1994**, *106*, 2427; *Angew. Chem. Int. Ed. Engl.* **1994**, *33*, 2335.
[11] K. Maeda, J. Akimoto, Y. Kiyozumi, F. Mizukami, *J. Chem. Soc. Chem. Commun.* in press.
[12] A. Bondi, *J. Phys. Chem.* **1964**, *68*, 443.
[13] J. Le Bideau, C. Payen, P. Palvadeau, B. Bujoli, *Inorg. Chem.* **1994**, *43*, 4885.
[14] M. Sghyar, J. Durand, L. Cot, M. Rafiq, *Acta Crystallogr. Sect. C* **1991**, *47*, 2515.
[15] R. E. Morris, M. P. Attfield, A. K. Cheetham, *Acta Crystallogr. Sect. C* **1994**, *50*, 473.
[16] M. D. Marcos, P. Amoros, A. LeBail, *J. Solid State Chem.* **1993**, *107*, 250.
[17] M. P. Attfield, R. E. Morris, A. K. Cheetham, *Acta Crystallogr. Sect. C* **1994**, *50*, 981.
[18] C. Y. Ortiz-Avila, P. J. Squattrito, M. Shieh, A. Clearfield, *Inorg. Chem.* **1989**, *28*, 2608.
[19] W. M. Meier, D. H. Olson, *Atlas of Zeolite Structure Types*, 3rd ed., Butterworth-Heinemann, London, **1992**.
[20] D. W. Breck, *Zeolite Molecular Sieves*, Wiley, New York, **1974**, p. 636.
[21] G. M. Sheldrick, *Acta Crystallogr. Sect. A* **1990**, *46*, 467.
[22] G. M. Sheldrick, *J. Appl. Crystallogr.* in press.
[23] G. B. Jameson, *Acta Crystallogr. Sect. A* **1982**, *38*, 817.
[24] Y. L. Page, J. D. H. Donnay, G. Donnay, *Acta Crystallogr. Sect. A* **1984**, *40*, 679.

Galloxane and Alumoxane Hydroxides: $[Ga_{12}tBu_{12}(\mu_3\text{-}O)_8(\mu\text{-}O)_2(\mu\text{-}OH)_4]$ and $[Al_6tBu_6(\mu_3\text{-}O)_4(\mu\text{-}OH)_4]$**

Christopher C. Landry, C. Jeff Harlan, Simon G. Bott, and Andrew R. Barron*

In contrast to the extensive oxide and oxide-hydroxide chemistry observed for aluminum and indium,[1] there are relatively few studies of the analogous chemistry of gallium. A recent ^{71}Ga NMR spectral study has indicated the formation of the unstable cationic cluster, $[Ga_{13}O_4(OH)_{24}(H_2O)_{12}]^{7+}$, whose structure is proposed to be identical to that of the aluminum analog.[2] Similarly, the first organogallium-oxo compound reported, $[t\text{BuGa}(\mu_3\text{-O})]_9$, was determined by mass spectrometry and NMR spectroscopy to also be isostructural to its aluminum analog.[3] The first reported examples of apparent diversification between the chemistry of aluminum and gallium oxide and oxide-hydroxide clusters was for the hexagallium compounds $[Ga_6Mes_6O_4X_4]$, Mes = mesityl, X = F,[4] OH[5] for which the equivalent aluminum compounds did not exist. We now report the structural characterization of the largest galloxane hydroxide isolated thus far, as well as the aluminum analog of $[Ga_6R_6O_4(OH)_4]$.

Oxidation of $[t\text{Bu}_2\text{Ga(Spy)}]$ (H-Spy = 2-mercaptopyridine),[6] followed by atmospheric hydrolysis yields colorless crystals with a composition corresponding to $[Ga_{12}tBu_{12}O_{10}(OH)_4]$ (**1**). Single crystals of **1** suitable for X-ray structure analysis[7] were obtained from Et_2O and four molecules of solvent are present in the formula unit. While the Et_2O molecules of solvation are disordered, the O···O distances are within the range expected for weak hydrogen bonding interaction. The molecular structure of **1** is shown in Figure 1. Each of the gallium atoms and bridging O atoms (Ga-O-Ga) lie on a mirror plane. The cage structure consists of twelve fused six-membered rings. Each gallium atom is coordinated to one carbon and three oxygens, while there are two types of oxygen atom sites; six oxygens bridging two galliums [O(1)], and eight oxygens capping three galliums [O(2)]. However, the structure may also be considered to consist of an oxo-cube [O(2)], with each face capped by a [tBuGa(μ-X)GatBu] unit, X = O or OH.

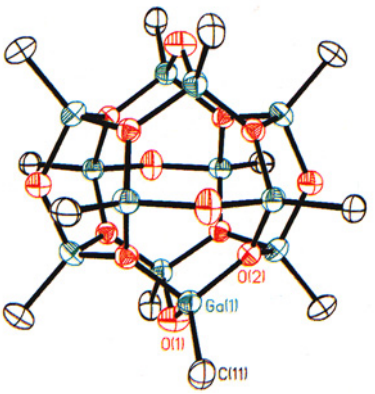


Fig. 1. Molecular structure of **1**. The methyl groups have been omitted for clarity. The bridging oxygen atom, O(1), exists as a 40:60 disorder of an oxo and a hydroxo ligand. Selected bond lengths [Å] and angles [°]: Ga(1)–O(1) 1.911(5), Ga(1)–O(2) 1.878(1), Ga(1)–C(11) 1.98(1); O(1)-Ga(1)-O(2) 98.4(2), O(2)-Ga(1)-O(2a) 106.7(2), O(1)-Ga(1)-C(11) 114.6(5), O(2)-Ga(1)-C(11) 117.6(2), Ga(1)-O(1)-Ga(1a) 129.1(1), Ga(1)-O(2)-Ga(1a) 119.6(1).

Based upon charge balance and ^{1}H NMR spectroscopy the actual formula of **1** is $[Ga_{12}tBu_{12}(\mu_3\text{-}O)_8(\mu\text{-}O)_2(\mu\text{-}OH)_4]$. Thus, the oxygen atoms bridging two galliums are a disorder of two oxo and four hydroxo ligands. In line with this, the Ga–O(1) distances [1.911(5) Å] are a weighted average of the values expected for a gallium-oxide (1.87–1.89 Å) and a gallium-hydroxide (2.21–2.45 Å). The Ga–O(2) distance [1.878(1) Å] is exactly as expected for a gallium-oxide interaction. The higher esd's in the Ga–O(1) bond lengths and the thermal parameters for O(1), as compared to O(2), is consistent with the presence of a disorder, however, the high symmetry of the molecule precluded refinement of this disorder.

A similar disorder between oxo and hydroxo ligands is observed in the structure of $[Al_6tBu_6(\mu_3\text{-}O)_4(\mu_3\text{-}OH)_4]$ (**2**), (Fig. 2).[7] Compound **2**, prepared from the hydrolysis of $[t\text{BuAl}(\mu_3\text{-O})]_6$,[8] is isostructural to $[Ga_6Mes_6O_4X_4]$ (X = F, OH). As with the gallium compounds, **2** can be described as an octahedron of aluminum atoms, with each face capped by either a μ_3-O or μ_3-OH moiety.[9] An alternative description is that compound **2** is a cube of oxygen atoms face-capped by six AltBu units, and as such a structural relationship between **1** and **2** may be drawn. Like the gallium compounds, the oxide and hydroxide sites in **2** are disordered. The Al(1)–O(1) distance [1.900(8) Å] is within the range of values we have previously reported for Al–OH [1.84–1.90 Å] interactions, while the Al(1)–O(2) distances [1.87(1)–1.95(1) Å] cover the range for both Al–O [1.78–1.88 Å] and Al–OH distances.[10] This is obviously a result of the high symmetry of the $[Al$$t$$Bu]_6$ core.

[*] Prof. Dr. A. R. Barron, C. C. Landry, Dr. C. J. Harlan
Department of Chemistry, Harvard University
12 Oxford Street, Cambridge, MA 02138 (USA)
Telefax: Int. code: (617)496-7402
Prof. Dr. S. G. Bott
Department of Chemistry, University of North Texas, Denton (USA)

[**] This work was supported by the Office of Naval Research, Akzo Nobel, the Welch Foundation, and the University of North Texas Research Office.

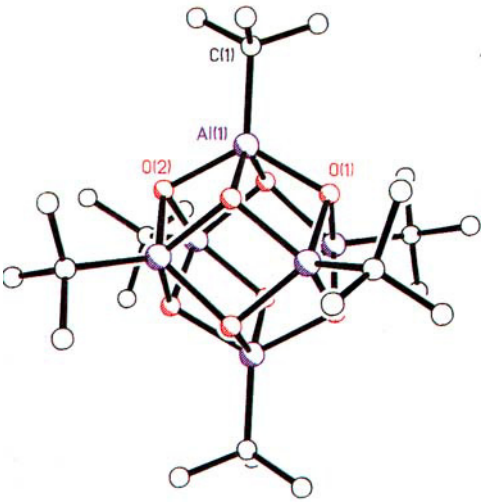
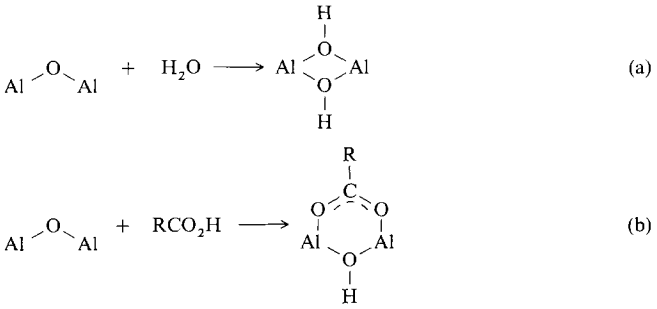


Fig. 2. Molecular structure of **2**. The hydrogen atoms have been omitted for clarity. Both O(1) and O(2) exist as a 50:50 disorder of an oxo and a hydroxo ligand. Selected bond lengths [Å] and angles [°]: Al(1)–O(1) 1.900(8), Al(1)–O(2) 1.95(1), Al(1)–O(2a) 1.88(1), Al(1)–O(2b) 1.87(1), Al(1)–C(1) 1.910(9); O(1)-Al(1)-O(2) 74.8(3), O(1)-Al(1)-O(2a) 76.4(3), O(1)-Al(1)-O(2b) 122.1(3), O(1)-Al(1)-C(1) 116.6(6), O(2)-Al(1)-O(2a) 125.3(3), O(2)-Al(1)-O(2b) 77.9(3), Al(1)-O(1)-Al(1a) 103.7(9), Al(1)-O(2)-Al(1a) 102.5(9).

A rational for the formation of **2** from $[t\mathrm{BuAl}(\mu_3\text{-O})]_6$ is the addition of H_2O to an Al–O bond [Eq. (a)]. We have observed a similar reaction during the formation of alumoxane carboxylates from the aluminum oxides [Eq. (b)].[11]



Given that several workers have postulated the existence of five-coordinate aluminum in alumoxanes,[12] it is important to note that compound **2** represents the first structural characterization of an alkylalumoxane in which the aluminum centers are five-coordinate.

Finally, we note that **1** is unusual when compared to previous group 13–16 cluster compounds or solid-state phases, in that while several chalcogenide cages are made entirely of six-membered cycles, this represents the first example of an oxygen derivative with such a structure.[1] Thus, **1** consists of twelve vertex-sharing tetrahedra (Fig. 3), while other alumoxanes, galloxanes, and indoxanes consist of edge- as well as vertex-sharing tetrahedra. Furthermore, **1** has a cavity of about 2.4 Å in diameter in which the shortest centroid-cage distance is to O(2) (1.3 Å); sufficiently large to accommodate a variety of different cations. In this regard **1** represents the first example of a group 13–16 cage in which inclusion may occur in a manner analogous to that observed for vanadium phosphates.[13]

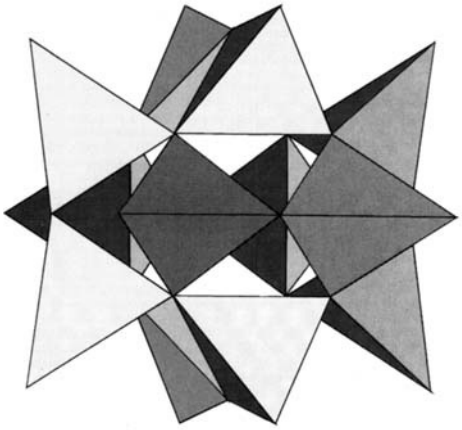


Fig. 3. Polyhedral structure of **1**. The methyl groups have been omitted for clarity.

Experimental Procedure

1: A solution of $[t\mathrm{Bu_2Ga(Spy)}]$ (0.501 g, 1.71 mmol) in toluene (30 mL) was exposed to an atmosphere of dry oxygen, upon which a white precipitate formed from the yellow solution. Filtration, followed by crystallization from Et_2O in air allowed the isolation of **1**. Isolated yield: about 70%. ^{1}H NMR (C_6D_6): $\delta = 1.10$ (4 H, br, s; OH), 1.06 [36 H, s; $C(CH_3)_3$], 1.02 [72 H, s; $C(CH_3)_3$]; IR (cm^{-1}): $\tilde{\nu} = 3600$ (OH).

2: To a solution of $[t\mathrm{BuAl}(\mu_3\text{-O})]_6$ (0.415 g, 0.691 mmol) in hexane (20 mL) was added wet β-lactone (0.056 g, 0.65 mmol). The reaction was stirred overnight at room temperature. An insoluble white precipitate formed. Filtration and cooling of the supernatant resulted in the crystallization of compound **2**. Isolated yield: about 9%. ^{1}H NMR (C_6D_6): $\delta = 2.48$ (4 H, s; OH), 1.02 [54 H, s; $C(CH_3)_3$]. IR (cm^{-1}): $\tilde{\nu} = 3424$ (OH).

Received: December 27, 1994
Revised version: February 20, 1995 [Z 7582 IE]
German version: *Angew. Chem.* **1995**, *107*, 1315–1317

Keywords: aluminum compounds · cage compounds · coordination · gallium compounds

[1] For a review see, A. R. Barron, *Comments Inorg. Chem.* **1993**, *14*, 123.
[2] S. M. Bradley, R. A. Kydd, R. Yamdagni, *J. Chem. Soc. Dalton Trans.* **1990**, 1911.
[3] M. B. Power, J. W. Ziller, A. R. Barron, *Organometallics* **1992**, *11*, 2783.
[4] B. Neumüller, F. Gahlmann, *Angew. Chem.* **1993**, *105*, 1770; *Angew. Chem. Int. Ed. Engl.* **1993**, *32*, 1701.
[5] J. Storre, T. Belgardt, D. Stalke, H. W. Roesky, *Angew. Chem.* **1994**, *106*, 1365; *Angew. Chem. Int. Ed. Engl.* **1994**, *33*, 1244.
[6] C. C. Landry, A. Hynes, I. Haiduc, A. R. Barron, *Polyhedron* in press.
[7] X-ray structure analysis of $\mathbf{1}\cdot 4(Et_2O)$ space group $Pm\bar{3}n$, $a = 15.972(1)$ Å, $V = 4074.5(6)$ Å^3, $\rho_{calcd} = 1.665$ g cm^{-3}, $\lambda(\mathrm{Mo_{K\alpha}}) = 0.7107$ Å, $T = 25$ °C, range of data $= 2 < 2\theta < 44°$, 560 unique reflections, 295 observed ($I > 6\sigma(I)$), $R = 0.0339$, $R_w = 0.0412$, data to parameter ratio = 8.2. X-ray structure analysis of **2** space group $R\bar{3}$, $a = 10.611(1)$, $c = 29.736(3)$ Å, $V = 2899.6(5)$ Å^3, $\rho_{calcd} = 1.094$ g cm^{-3}, $\lambda(\mathrm{Mo_{K\alpha}}) = 0.7107$ Å, $T = 25$ °C, range of data $= 2 < 2\theta < 44°$, 1122 unique reflections, 353 observed ($I > 6\sigma(I)$), $R = 0.0756$, $R_w = 0.0748$, data to parameter ratio = 6.4. Structure solution was by SHELXT. Further details of the crystal structure investigation may be obtined from the Director of the Cambridge Crystallographic Data Centre, 12 Union Road, Cambridge, CB2 1EZ (UK) on quoting the full journal citation.
[8] M. R. Mason, J. M. Smith, S. G. Bott, A. R. Barron, *J. Am. Chem. Soc.* **1993**, *115*, 4971.
[9] Although unusual, trifurcated hydroxide groups have previously been structurally characterized for aluminum compounds, see A. W. Apblett, A. C. Warren, A. R. Barron, *Chem. Mater.* **1992**, *4*, 167.
[10] C. J. Harlan, M. R. Mason, A. R. Barron, *Organometallics* **1994**, *13*, 2957.
[11] C. C. Landry, N. Pappé, M. R. Mason, A. W. Apblett, A. N. Tyler, A. N. MacInnes, A. R. Barron, *J. Mater. Chem.* **1995**, *5*, 33.
[12] See, S. Pasynkiewicz, *Polyhedron* **1990**, *9*, 429, and references therein.
[13] J. Salta, Q. Chen, Y. Chang, J. Zubieta, *Angew. Chem.* **1994**, *106*, 781; *Angew. Chem. Int. Ed. Engl.* **1994**, *33*, 757, and references therein.

 © VCH Verlagsgesellschaft mbH, D-69451 Weinheim, 1995 0570-0833/95/1111-1202 $ 10.00+.25/0

Six Interpenetrating Quartz-Like Nets in the Structure of $ZnAu_2(CN)_4$**

Bernard F. Hoskins, Richard Robson,* and Nicola V. Y. Scarlett

Infinite frameworks composed of tetrahedral centers linked together by 2-connecting units often adopt a topology related to that of diamond. In SiO_2 where silicon is tetrahedral and oxygen is 2-connecting, the diamond-related topology, β-cristobalite, is thermodynamically less stable than the alternative 4-connected topology of quartz. It is therefore perhaps a little surprising how few classes of substances are known with the quartz topology. Examples generally involve a single atom bridge between two tetrahedral centers as in $GaPO_4$,[1] BeF_2,[2] and stuffed structures such as eukryptite, $LiAlSiO_4$.[3] We report here an example in which tetrahedral centers linked together by polyatomic connectors adopt a quartz-like topology.[4] The range of structural types for infinite cyano-bridged networks, especially those involving cadmium(II), is remarkable and continuously expanding.[5] We[6] and others[7] have started to explore the possibility that this structural diversity may be further enriched by using $[M(CN)_2]^-$ (M = Au, Ag, and possibly Cu) as an extended, approximately linear 2-connector in place of CN^-.

Aqueous solutions containing zinc nitrate and potassium dicyanoaurate deposit crystals of composition $ZnAu_2(CN)_4$, whose structure we have determined by single-crystal X-ray diffraction. The hexagonal unit cell is shown in Figure 1. All zinc centers are equivalent as are all gold centers. Two types of cyano units occur in slightly different environments. The zinc atoms are in an approximately tetrahedral environment of four nitrogen atoms (∢ N-Zn-N, 106.3, 107.3, 109.6, and 112.1°) from $[Au(CN)_2]^-$ units, which act as approximately linear zinc-to-zinc connectors (∢ Zn-N-C: 166 and 172°; ∢ N-C-Au 178 and 173°; ∢ C-Au-C, 174.6°). The 3D net generated thereby has a topology identical to that of quartz, in which each tetrahedral Si atom is replaced by a Zn atom and each Si-O-Si connection by Zn-CN-Au-CN-Zn (Zn ··· Zn, 10.041 Å). A consequence of this lengthening of the connections is that there is room for the interpenetration of six identical but independent nets. Fragments of these six independent nets can be seen in the unit cell in Figure 1.

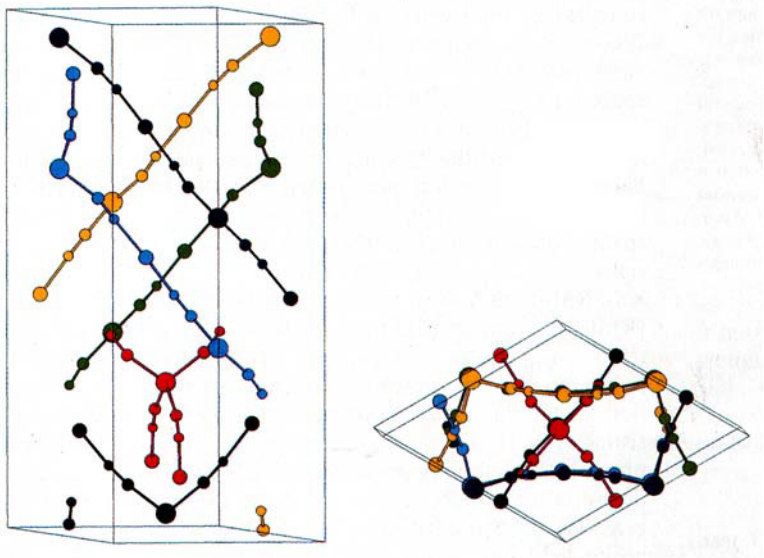


Fig. 1. The hexagonal unit cell of $ZnAu_2(CN)_4$ viewed perpendicular to the c axis (left) which here is vertical and from an angle slightly displaced from the c direction (right). Circles in order of decreasing size represent Zn, Au, N, and C. Fragments of six independent infinite networks are represented by different colours.

A single extended net is represented in Figure 2. The quartz-like connectivity is immediately evident. The six independent nets consist of three pairs, the members of any particular pair being related to each other by a translation along the sixfold c axis of approximately $c/4$ or 5.20 Å. The pairs are color-coded for easy identification in Figure 1: yellow/green, red/black, and dark blue/pale blue. Figure 3 shows how the three pairs interpenetrate (paired colors as in Figure 1).

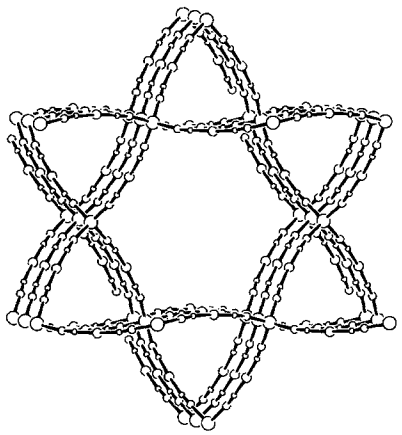


Fig. 2. A view from an angle slightly displaced from the c direction, of a single quartz-like net in the structure of $ZnAu_2(CN)_4$ which contains six such independent nets.

Like the quartz prototype, $ZnAu_2(CN)_4$ is enantiomorphic. All six nets have the same handedness; in the particular crystal studied, the absolute configuration of the threefold helices within each net is that of a righthanded screw.

The closest approach between nets is a Au ··· Au contact of 3.11 Å, examples of which can be seen in Figure 1 between yellow and dark blue frameworks and between green and light blue frameworks; these and other analogous Au ··· Au contacts can also be seen in Figure 3. The bowing in the Zn-NC-Au-CN-Zn links apparent in Figures 1b and 3 is suggestive of an attractive Au–Au interaction. Schmidbaur has previously presented convincing evidence for the reality of such Au^I–Au^I bonding interactions, which he notes are comparable in strength with hydrogen bonds and, like hydrogen bonds, may be "conformation determining";[8a] homoatomic d^{10}–d^{10} interactions, in general, have been reviewed by Jansen.[8b]

The basic structural type reported here would appear to lend itself to considerable variation in composition, and it remains to be seen how many related $[M(CN)_2]^-$-derived materials with this topology can be generated. It may also be possible to incorporate chiral guest molecules of appropriate size and shape in order to generate materials with fewer than six individual quartz-like nets.

[*] Dr. Robson, Dr. B. F. Hoskins, N. V. Y. Scarlett
School of Chemistry, University of Melbourne
Parkville, 3052 Victoria (Australia)
Telefax: Int. code +(3) 347-5180

[**] This work was supported by the Australian Research Council.

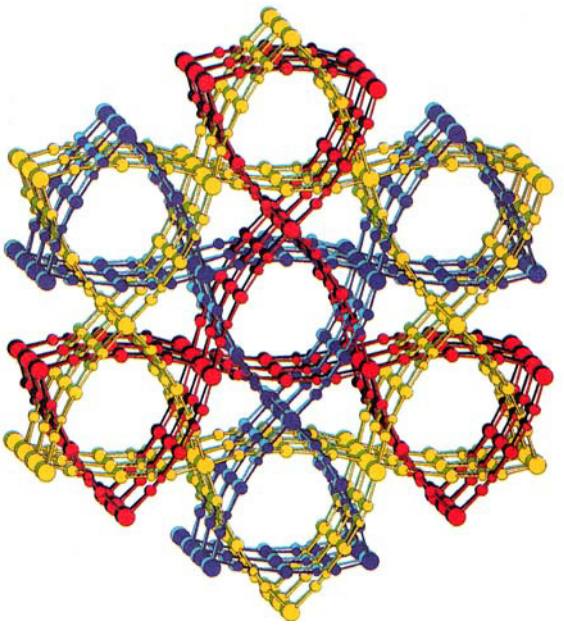


Fig. 3. Extended structure of $ZnAu_2(CN)_4$ showing the six independent, interpenetrating quartz-like nets.

Experimental Procedure

To a solution of $K[Au(CN)_2]$ (8.6 mg, 0.029 mmol) in H_2O (2 mL) was added a solution of $Zn(NO)_3 \cdot 6H_2O$ (25.0 mg, 0.087 mmol) in H_2O (2 mL). A small amount of very fine, cloudy white precipitate was formed immediately and settled on standing. Within 24 h, large, colorless, air-stable crystals of $ZnAu_2(CN)_4$ grew, many in the form of brilliant hexagonal bipyramids.

Crystal data: $ZnAu_2(CN)_4$, $M = 563.4$, hexagonal, space group $P6_422$ (No. 181), $a = 8.4520(10)$, $c = 20.622(11)$ Å, $V = 1275.8(7)$ Å^3, $Z = 6$, approximate crystal dimensions $0.21 \times 0.21 \times 0.29$ mm, $\rho_{calcd} = 4.400$ g cm^{-1}, $F(000) = 1440$, 2959 reflections measured, 757 unique reflections, $2\theta_{max} = 50°$. Intensity data were measured at 293(2) K with $Mo_{K\alpha}$ radiation (graphite crystal monochromator) on an Enraf-Nonious CAD-4MachS diffractometer with the $\omega/2\theta$-scan method; corrections for Lorentz, polarization, and absorption effects were applied ($\mu(Mo_{K\alpha}) = 37.146$ mm^{-1}, min/max transmission = 0.0221 and 0.0463). The structure was solved with a combination of Patterson map, direct methods, and difference synthesis (SHELX-76 [9] and SHELXS-86 [10]). A full-matrix least-squares refinement method based on F^2 (SHELXL-93 [11]) was employed, and anisotropic thermal parameters assigned to all atoms. For the space group $P6_422$ (No. 180), $R_1 = 0.0551$ and $wR_2 = 0.0858$. The absolute structure (Flack) parameter indicated that the true space group was $P6_422$ (No. 181). This was confirmed by refinement in this space group which yielded $R_1 = 0.0459$ and $wR_2 = 0.0616$ (for all data). $R_1 = \sum||F_o| - |F_c||/\sum|F_o|$ and $wR_2 = [\sum[w(F_o^2 - F_c^2)^2]/\sum[w(F_o^2)^2]]^{0.5}$. Further details of the crystal structure investigation may be obtained from the Fachinformationszentrum Karlsruhe, D-76344 Eggenstein-Leopoldshafen (Germany), on quoting the depository number CSD-58823.

Received: January 2, 1995 [Z 7601 IE]
German version: *Angew. Chem.* **1995**, *107*, 1317–1318

Keywords: cyano complexes · gold compounds · solid-state structures · zinc compounds

[1] O. Baumgartner, A. Preisinger, P. W. Krempi, H. Mang, *Z. Kristallogr.* **1984**, *168*, 83.
[2] A. F. Wright, A. N. Fitch, A. C. Wright, *J. Solid State Chem.* **1988**, *73*, 298.
[3] H. G. F. Winkler, *Acta Crystallogr.* **1948**, *1*, 27.
[4] We are indebted to one referee for drawing our attention to the fact that the structure described here is essentially that of $CoAu_2(CN)_4$ (S. C. Abrahams, L. E. Zyontz, J. L. Bernstein, *J. Chem. Phys.* **1982**, *76*, 5485), although these authors made no reference to the quartz-related topology nor to the presence of six independent nets.
[5] T. Kitazawa, T. Kikuyama, M. Takahashi, M. Takeda, *J. Chem. Soc. Dalton Trans.* **1994**, 2933, and references therein.
[6] B. F. Hoskins, R. Robson, N. V. Y. Scarlett, *J. Chem. Soc. Chem. Commun.* **1994**, 2025.
[7] T. Soma, H. Yuge, T. Iwamoto, *Angew. Chem.* **1994**, *106*, 1746; *Angew. Chem. Int. Ed. Engl.* **1994**, *33*, 1665.
[8] a) H. Schmidbaur, W. Graf, G. Müller, *Angew. Chem.* **1988**, *100*, 439; *Angew. Chem. Int. Ed. Engl.* **1988**, *27*, 417; b) M. Jansen, *ibid.* **1987**, *99*, 1136 bzw. **1987**, *26*, 1098.
[9] G. M. Sheldrick, SHELX-76, A Program for Crystal Structure Determination, Cambridge, United Kingdom, **1976**.
[10] G. M. Sheldrick, SHELX-86, A Program for Crystal Structure Determination, in *Crystallographic Computing 3* (Eds.: G. M. Sheldrick, C. Krüger, R. Goddard), Oxford University Press, Oxford, **1985**, p. 175.
[11] G. M. Sheldrick, SHELX-93, A Program for Crystal Structure Determination, Göttingen, **1993**.

Hyperbolic Lone Pair Structure in $RhBi_4$

Yuri Grin, Ulrich Wedig, and
Hans Georg von Schnering*

With studies of the electronic structure of several low valence tin compounds, SnSe, SnP_3, and SrSnP Wagner[1] shows that even SrSnP, with formal Sn^I, exhibits a strong tendency to form lone pairs. Thus, the Sn–Sn bonds in this compound are considerably weaker than the Ga–Ga bonds in the isostructural compound CaGaN. Compounds such as $PdGa_5$,[2,3] $PtPb_4$,[2] $PdSn_3$,[2] and $RhBi_4$ have been found to be suitable for the investigation of similar phenomena in classic intermetallic phases. The electronic structure of $RhBi_4$, presented here, is remarkable because of its extraordinary topology.

The crystal structure of $RhBi_4$ has been known for a long time.[4] Cubic $RhBi_4$ is built of two independent crystallographic sites, one occupied by Rh and the other by Bi, and is described as a packing of tetragonal antiprisms.[5] A special peculiarity of this structure is the arrangement of the Rh atoms and subsequently, the condensed ($RhBi_{8/2}$) polyhedra, which form the so-called V* framework as described by Hellner et al. (Fig. 1). It consists of two interpenetrating chiral $3^2.10^4$ nets, which are enantiomorphic.[6] From our experience, the separation of space into regions of different interaction types is particularly evident in chemical structures that have interpenetrating atomic nets.[8] In the $RhBi_4$ structure, these regions are defined, on one hand, by the two interpenetrating chiral $3^2.10^4$ nets of condensed ($RhBi_{8/2}$) antiprisms and, on the other hand, by the spaces between the nets. Therefore this separation should be reflected in the electronic structure.

In $RhBi_4$, each three slightly distorted tetragonal antiprisms, ($RhBi_{8/2}$), are condensed through the square faces of a common (empty) trigonal Bi_6 prism (Fig. 1). Thus, both frameworks of polyhedra not only show the characteristics of a V* framework, but also the characteristics of the so-called Y** framework consisting of the three-connected nodes in the centers of the trigonal prisms.[6] The periodic nodal surface (PNS) I_2-Y**[9] perfectly describes the hyperbolic organization of the entire $RhBi_4$ structure. The PNS is defined only by the symmetry of the space group $Ia\bar{3}d$ and can be easily calculated.[10] It envelops both interpenetrating polyhedral frameworks and separates them from the embedding empty space (Fig. 1). This space has the topology of the hyperbolic PNS Y**[9] and of Schoen's[11] minimal surface "gyroid", representing a non-Euclidean mirror.

[*] Prof. Dr. H. G. von Schnering, Dr. Yu. Grin, Dr. U. Wedig
Max-Planck-Institut für Festkörperforschung
Heisenbergstrasse 1, D-70569 Stuttgart (Germany)
Telefax: Int. code + (711)689-1562

 © VCH Verlagsgesellschaft mbH, D-69451 Weinheim, 1995 0570-0833/95/1111-1204 $ 10.00+.25/0

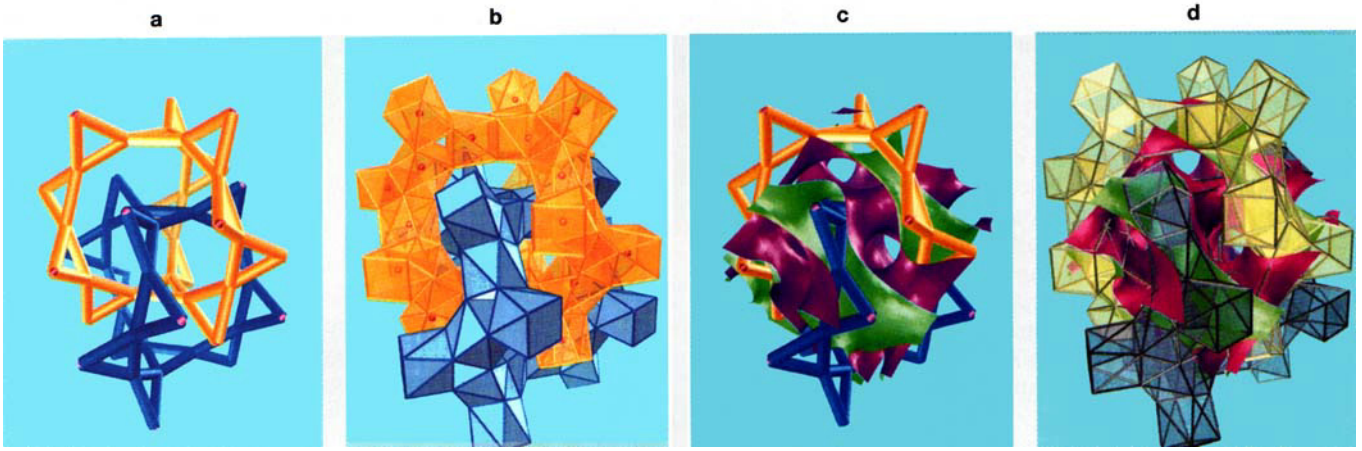


Fig. 1. a) Two enantiomorphic chiral ($3^2.10^4$) nets [7] form the V* framework according to Hellner et al. [6]. Each four-connected node (here Rh) belongs to two three-membered and four ten-membered rings. b) The two chiral nets of condensed ($RhBi_{8/2}$) polyhedra with Rh (red/pink) situated in the centers and Bi on the vertices of the tetragonal antiprisms. c) and d): The periodic nodal surface I_2-Y** envelops both parts (V* framework (c), framework of polyhedra (d)) and separates them. There are two separated interpenetrating labyrinths (green) and one common hyperbolic space (violet).

The electronic structure of $RhBi_4$ was determined with the tight-binding-LMTO program[12] using the local density functional approach (LDA) with the exchange correlation potential taken from reference [13]. The partial waves were derived from the solutions of the radial scalar-relativistic Dirac equation. Interstitial spheres (E1–E5) had to be added to reduce the overlap of the atomic spheres when using the atomic spheres approximation (ASA, corrections according to [14]). The volume of the empty spheres amounts to 27.8% of the unit cell volume, indicating an open structure. The radii of the atomic spheres are: Rh 1.533 Å, Bi 1.714 Å, E1 1.223 Å, E2 1.208 Å, E3 1.110 Å, E4 0.947 Å, E5 0.867 Å.

Within the density functional theory, the electron localization function (ELF)[15] was calculated from the Pauli local kinetic energy density $t_p(r)$,[16] where $t_p(r)$ is that part of the local kinetic energy density $t(r)$, which is due to the Pauli principle. At each point r, the ELF is related to the value $t_{p,h}(\rho(r))$ for the homogeneous electron gas with the density $\rho(r)$. The ELF falls between values of 0 to 1;[15] the higher ELF values indicating regions of high localization such as bonds or lone pairs.

The results are shown in Figure 2. The isosurface of $\rho(r) = 0.035\ e a_0^{-3}$ (in blue) was selected to represent the electron density, and the isosurface of ELF(r) = 0.7 (in red) was taken for the electron localization function. Since only the valence electron bands were used for the calculation, the density minima were obtained at the position of the atomic nuclei. The difference between the distribution of electron density and ELF is remarkable:

- The isosurface of $\rho(r)$ around the Bi atoms is spherical and possesses tubelike connections to the Rh atoms in the centers of the ($RhBi_{8/2}$) polyhedra. This gives the impression of continuous electronic nets that link the Rh and Bi atoms.
- The ELF of the valence electrons, however, indicates maxima exclusively at the Bi atoms but situated outside the polyhedra and directed into the space between the polyhedral nets. No appreciable localization has been found between Rh and Bi atoms, nor in the peripheral regions of possible Bi–Bi interactions (two- or three-center bonds).

Therefore, the ELF maxima cannot be attributed to covalent bonds, but obviously show the lone pairs of the Bi atoms. All electrons in the regions of Rh–Bi bonds are strongly delocalized

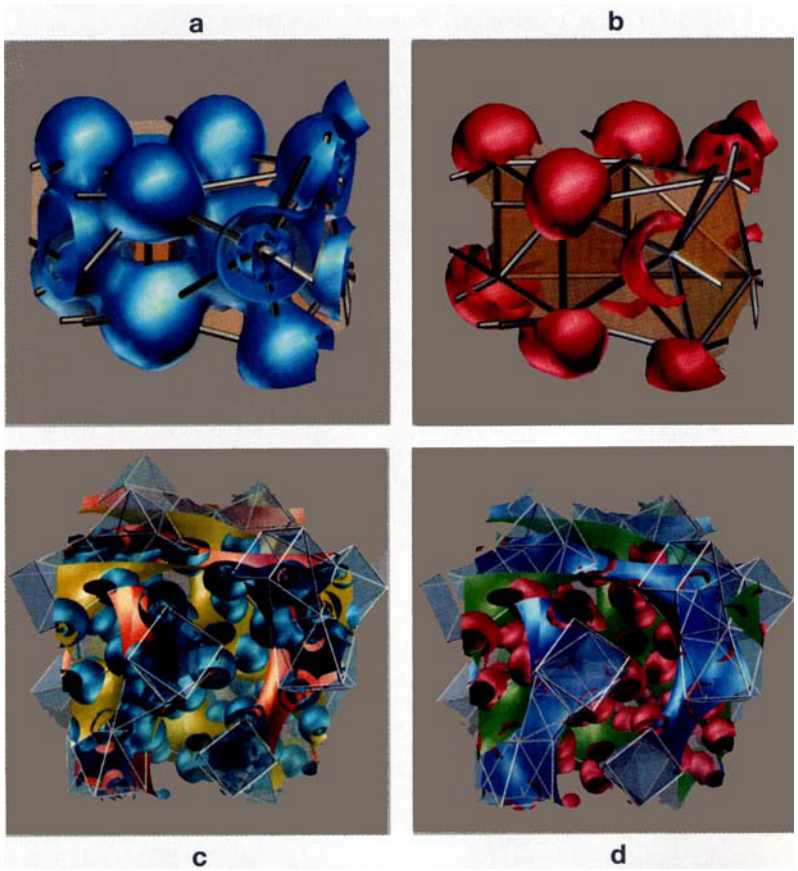


Fig. 2. a) Valence electron density $\rho(r)$ (isosurface of $r = 0.035\ e a_0^{-3}$; blue) shows a spherical form at the Bi atoms and pronounced tubes around Rh–Bi bonds. b) In contrast, ELF exclusively shows the localization of the lone pairs of Bi atoms on the periphery of the polyhedral nets (isosurface of ELF = 0.7: red). c) Polyhedral nets and $\rho(r)$ together with the PNS I_2-Y**. d) Polyhedral nets and ELF together with the PNS I_2-Y**. The common space between the nets (green) represents a hyperolic layer of lone pairs.

 © VCH Verlagsgesellschaft mbH, D-69451 Weinheim, 1995 0570-0833/95/1111-1205 $ 10.00+.25/0

indicating metallic character. The hyperbolic PNS I_2-Y** bounds regions with very different degrees of valence electron localization, that is of different bonding character. One has the impression that the metallically conducting $3^2.10^4$ nets are separated by insulating hyperbolic layers.

The cubic phase $RhBi_4$ as a whole is isotropic. Nevertheless, the atomic distribution and electronic structure show intrinsically a strongly anisotropic, layerlike structure. However, due to the hyperbolic (non-Euclidean[8]) form of these layers, all anisotropic components are compensated in the crystal.

The formation of regions with very different localization of the valence electrons and the resulting microscopic anisotropy should influence the electro-kinetical properties and may correlate to the superconductivity of the compound (T_c = 2.9–3.4 K[17]).

Received: December 9, 1994 [Z 7566 IE]
German version: *Angew. Chem.* **1995**, *107*, 1318–1320

Keywords: electron localization function · intermetallic phases · periodic nodal surface · polyhedral nets

[1] F. Wagner, Dissertation, Universität Saarbrücken, **1993**.
[2] Yu. Grin, U. Wedig, H. G. von Schnering, *11th Intern. Conf. Solid Compounds of Transition Elements*, Abstracts, Wrocław, **1994**, p. 39.
[3] Yu. Grin, U. Wedig, F. Wagner, A. Savin, H. G. von Schnering, *J. Alloys Comp.*, submitted.
[4] V. P. Glagoleva, G. S. Zhdanov, *Zh. Eksp. Teor. Fiz.* **1956**, *30*, 248, *Sov. Phys. JETP (Engl. Trans.)* **1956**, *3*, 155.
[5] P. I. Kripiakevich, *Structure types of intermetallic compounds* (Russian), Nauka, Moskau, **1977**, p. 118.
[6] E. Hellner, E. Koch, A. Reinhardt, *Phys. Daten / Phys. Data* **1981**, 16-2, define the frameworks using crystallographic point configurations of the space groups. The connection of all positions of the site 24*c* (1/8 0 1/4) of the space group $Ia\bar{3}d$ (No. 230) leads to *two* interpenetrating nets consisting of four-connected nodes. The nets are called $^{+}$V and $^{-}$V, both together—V*. Each of the four-connected nodes belongs to six rings, two three-membered and four ten-membered: $3^2.10^4$ according to Wells [7].
[7] A. F. Wells, *Three-Dimensional Nets and Polyhedra*, Wiley, New York, **1977**, p. 74ff.
[8] H. G. von Schnering, R. Nesper, *Angew. Chem.* **1987**, *99*, 1097; *Angew. Chem. Int. Ed. Engl.* **1987**, *26*, 1059.
[9] H. G. von Schnering, R. Nesper, *Z. Phys. B. Condens. Matter* **1991**, *83*, 407; H. G. von Schnering, M. Oehme, G. Rudolf, *Acta Chem. Scand.* **1991**, *45*, 873.
[10] The PNS I_2-Y** represents the zero points of the Fourier series built using geometrical structure factors $|S(112)| = |S(220)| = 1$ and their phases $\alpha(112) = \alpha(220) = 0$ as coefficients under the consideration of the permutations of the space group $Ia\bar{3}d$. The reduced form is (c = cos, s = sin, $X = 2\pi x$, $Y = 2\pi y$, $Z = 2\pi z$): $0 = -2[s2X\,cY\,sZ + sX\,s2Y\,cZ + cX\,sY\,s2Z] + c2X\,c2Y + c2Y\,c2Z + c2X\,c2Z$. The description I_2-Y** uses the symbols according to [6] and shows that the point configurations I_2 and Y** were separated by this PNS [8]. All 16 points of the twofold body-centred lattice I are placed in one labyrinth, which separates two other enantiomorph labyrinths. The 2 × 8 points of the nets $^{+}$Y* + $^{-}$Y* = Y** are located in the last two labyrinths.
[11] A. H. Schoen, NASA Technical Note D-5541, Washington, D. C., **1970**.
[12] G. Krier, M. van Schilfgaarde, T. A. Paxton, O. Jepsen, O. K. Andersen, Program TB-LMTO, unpublished.
[13] U. Barth, L. Hedin, *J. Phys. C* **1972**, *5*, 1629.
[14] O. K. Andersen, Z. Pawlowska, O. Jepsen, *Phys. Rev. B: Condens. Matter* **1986**, *34*, 5253.
[15] A. Savin, A. D. Becke, J. Flad, R. Nesper, H. Preuss, H. G. von Schnering, *Angew. Chem.* **1991**, *103*, 421; *Angew. Chem. Int. Ed. Engl.* **1991**, *30*, 409.
[16] A. Savin, O. Jepsen, J. Flad, O. K. Andersen, H. Preuss, H. G. von Schnering, *Angew. Chem.* **1992**, *104*, 186; *Angew. Chem. Int. Ed. Engl.* **1992**, *31*, 187.
[17] N. E. Alekseevskii, G. S. Zhdanov, N. N. Zhuravlev, *Zh. Eksp. Teor. Fiz.* **1955**, *28*, 237.

Optical Activity of Chiral Dendritic Surfaces**

Johan F. G. A. Jansen, H. W. I. Peerlings, Ellen M. M. de Brabander-Van den Berg, and E. W. Meijer*

Macroscopic, nanoscopic, and mesoscopic chirality are among the intriguing new key words in the studies of chiral clusters, associated complexes, homo- and heterogeneous catalysts, and of many polymers.[1] Major drawbacks for these studies are, generally, the complexity of the materials under investigation and their lack of long-range order. Therefore, comprehensive studies of macroscopic chirality are primarily performed on single crystals and synthetic bilayers.[2] However, for a better understanding of the chiroptical features of non-ordered structures, well-defined materials are required. Dendrimers are promising candidates for the preparation of well-defined chiral materials with nanoscopic dimensions.[3] To the best of our knowledge only chiral dendrimers of lower generations have been prepared and no irregularities in the chiroptical properties of these enantiomerically pure dendrimers are reported.[4–9] Newkome et al.[4] modified an amine-terminated dendrimer with enantiomerically pure tryptophane, whereas Seebach et al.[5] prepared some dendrimers with a chiral core and Chow et al.[6] prepared dendrimers with a chiral spacer. Hudson and Damha[7] synthesized a nucleic acid based chiral dendrimer, Mitchell[8] a glutamic acid based dendrimer, while Denkewalter disclosed a number of dendrimeric structures based on amino acids.[9]

Larger chiral dendrimers with a more dense packing of functional groups in the shell have not been studied so far. Recently, we successfully prepared chiral structures of nanometer dimensions based on poly(propylene imine) dendrimers (DAB-*dendr*-$(NH_2)_{64}$)[10] that are terminated with amino acid derivatives and we presented evidence that these compounds are useful as dendritic "boxes" (DAB-*dendr*-(NH-*t*-BOC-L-Phe)$_{64}$; Fig. 1).[11] Due to the dense packing of the shell and the presence of internal cavities, we are able to encapsulate a variety of guests into these dendritic boxes; guests that are physically locked. The synthesis of this and other amino acid modified dendrimers is summarized in Scheme 1. Here we report on the peculiar chiroptical properties of these dendritic boxes and discuss the structure of highly curved chiral dendritic surfaces.

The investigation presented here was triggered by the observation that the specific optical rotation of the DAB-*dendr*-(NH-*t*-BOC-L-Phe)$_x$ decreases to almost zero on going from dendrimers of the first generation ($[\alpha]_D = -11$; $c = 1$, $CHCl_3$) with four end groups to dendrimers of the fifth generation ($[\alpha]_D = -0.1$; $c = 1$, $CHCl_3$) with 64 end groups. A more thorough investigation employing a variety of different amino acid derivatives reveals that this decrease of optical rotation with increasing generation is a general phenomenon for all the amino acids studied (Table 1). The most striking results are found for the DAB-*dendr*-(NH-*t*-BOC-ε-*Z*-L-Lys)$_x$, in which the $[\alpha]_D$ value decreases from −28 ($c = 1$, $CHCl_3$) for the first generation dendrimer ($x = 4$) to 0 ($c = 1$, $CHCl_3$) for the fifth generation den-

[*] Prof. Dr. E. W. Meijer, Dr. J. F. G. A. Jansen, Ir. H. W. I. Peerlings
Laboratory of Organic Chemistry
Eindhoven University of Technology
P. O. Box 513, NL-5600 MB Eindhoven (The Netherlands)
Telefax: Int. code + (40)451036

Dr. E. M. M. de Brabander - Van den Berg
DSM Research, P. O. Box 18, NL-6160 MD Geleen (The Netherlands).

[**] We would like to thank Prof. M. M. Green, Prof. M. Lahav, and Prof. R. J. M. Nolte, as well as Dr. E. E. Havinga and Dr. M. H. P. van Genderen for valuable discussions.

 © VCH Verlagsgesellschaft mbH, D-69451 Weinheim, 1995 0570-0833/95/1111-1206 $ 10.00+.25/0

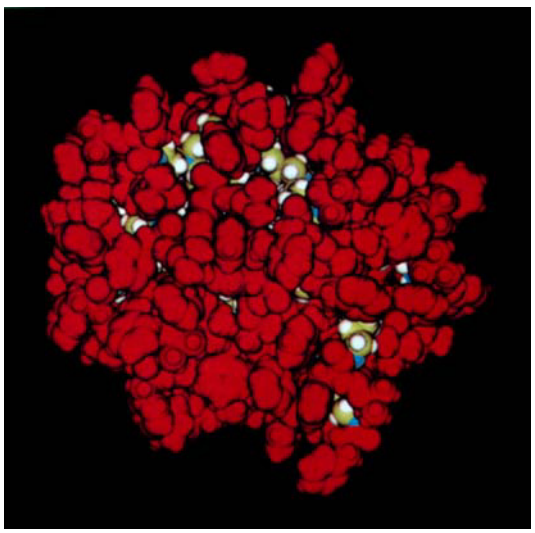


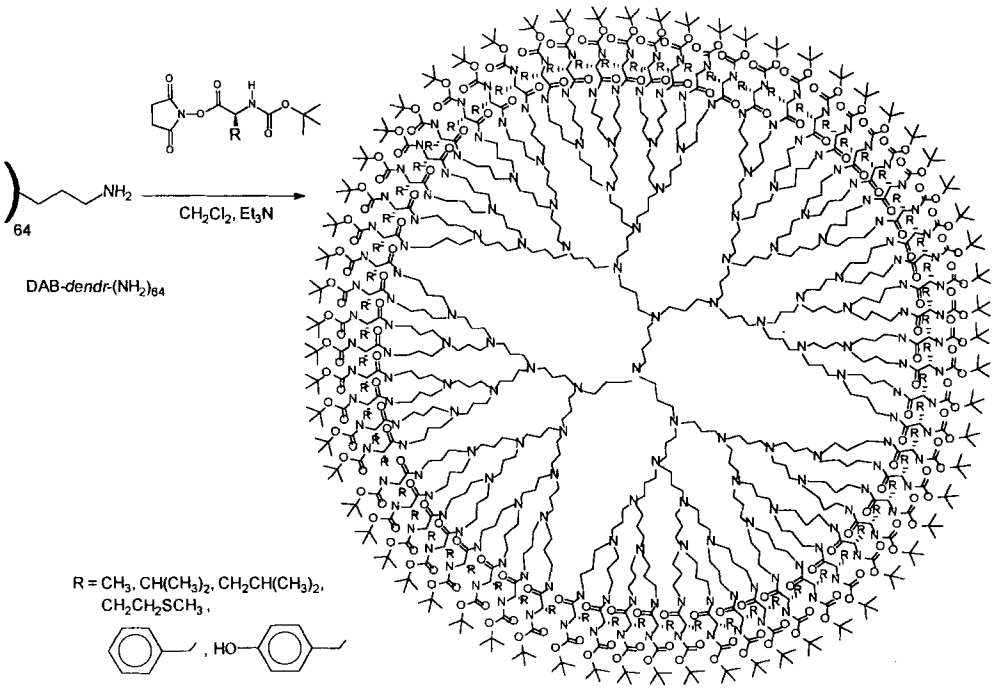
Fig. 1. Space-filling model of DAB-*dendr*-(NH-*t*-BOC-L-Phe)$_{64}$; the *t*-BOC-L-Phe end groups are given in red, while the core atoms are given in green, white, and blue.

Table 1. Selected specific rotations of modified poly(propylene imine) dendrimers.

Number of end groups (generation)	4 (1)	8 (2)	16 (3)	32 (4)	64 (5)
BOC amino acid $c = 1$ (solvent)	$[\alpha]_D$	$[\alpha]_D$	$[\alpha]_D$	$[\alpha]_D$	$[\alpha]_D$
L-alanine (L-Ala) ($CHCl_3$)	−24	−25	−26	−33	−14
L-valine (L-Val) ($CHCl_3$)	−39	−31	−27	−28	−22
L-leucine (L-Leu) ($CHCl_3$)	−28	−23	−21	−13	−10
L-methionine (L-Met) ($CHCl_3$)	−16	−12	−11	−10	−2
L-(*S*)-benzylcysteine ($CHCl_3$)	+56	+42	+26	+13	+5
ε-(*Z*)-L-lysine ($CHCl_3$)	−28	−8	−3	−1	0.0 [a]
L-phenylalanine (L-Phe) ($CHCl_3$)	−11	−7	−2	−1	−0.1 [a]
D-phenylalanine (D-Phe) ($CHCl_3$)	+10 [b]	+7	+2	+1	+0.1 [a]
L-tyrosine (L-Tyr) (DMSO)	+19 [c]	+9	+1	−0.2	−0.1[a]

[a] Error approximately ±0.2. [b] In DMSO $[\alpha] = -13$. [c] In $CHCl_3$ $[\alpha] = +15$.

drimer ($x = 64$). Dramatic changes are also observed for L-(*S*)-benzylcysteine and the L-tyrosine derivatives. For the smaller amino acids (Ala, Val and Leu) the decrease in optical rotation is less pronounced. As the number of chiral end groups per weight unit is roughly independent of the generation (in each new generation both the number of end groups and the molecular weight double), the decrease in the $[\alpha]_D$ values with increasing generation is not due to the reduction of chiral chromophores.[1,2] Furthermore neither concentration nor temperature effects are responsible for this decrease in optical activity, as nearly identical rotations are observed for $c = 0.1$, 1, and 4 in chloroform at temperatures of 20 and 55 °C in the L-Phe dendrimer series. However, a significant solvent dependency of the specific rotations was noticed for the lower generations and was investigated in detail for the model compound *N*-*t*-BOC-L-Phe-propylamide. Specific optical rotations were dependent on the dielectric constant of the solvent, varying from $[\alpha]_D = 7.3$ ($c = 1$, toluene) to $[\alpha]_D = -6.4$ ($c = 1$, acetonitrile) for the model compound. The behavior of the corresponding dimeric model compound from diaminobutane and two L-Phe residues deviated remarkably from all other ones. The dimer is only slightly soluble, indicative of intermolecular hydrogen bonding, and the optical rotation is large ($[\alpha]_D = 22$, $c = 1$, $CHCl_3$; see Fig. 4). The peculiar behavior of symmetric dipeptides is the subject of many recent studies.[13] Finally, we have demonstrated that the protected amino acids do not undergo racemization in the coupling method employed; analysis of the amino acids after acid-catalyzed hydrolysis of the modified dendrimers by HPLC using chiral stationary phases revealed an enantiomeric excess of greater than 96%.



Scheme 1. Synthesis of the dendritic "box", DAB-*dendr*-(NH-*t*-BOC-L-Phe)$_{64}$ and other amino acid derivatives.

Circular dichroism (CD) and optical rotatory dispersion (ORD) studies in conjunction with UV/Vis absorption spectroscopy have been performed to gain a better insight into the peculiar chiroptical effects observed. The restricted solubility of the dendritic boxes hampers the use of the entire spectral range. Most of the Cotton effects (CEs) present in the CD spectra of the lower generations decrease with generation; the results of the L- and D-Phe series are given in Figure 2. Both the CE of the car-

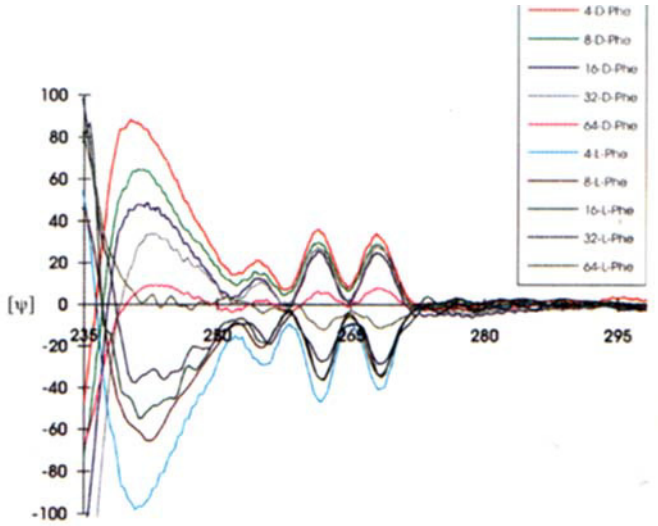


Fig. 2. Dependence of the specific ellipticity ψ [deg cm^2 g^{-1}] on the wavelength for D- and L-Phe modified dendrimers in $CHCl_3$.

bamate chromophore at $\lambda_{max} = 240$ nm and the CEs of the phenyl chromophore at $\lambda = 250-270$ nm are influenced strongly by the generation, while some (diminished) residual optical activity remains for the amide chromophore.[14] The decrease in the CEs is accompanied by some small changes in the UV/Vis spectra, indicative of changes in conformation. Similar chiroptical effects are observed for dendrimers modified with other amino acids. Since the L-Tyr series has limited solubility, ORD spectra are taken in dimethylsulfoxide (DMSO) and compared with those of the 4- and 64-L-Phe derived dendrimer (Fig. 3: note the change of sign in the rotation of the L-Phe series; negative in $CHCl_3$ and positive in DMSO)

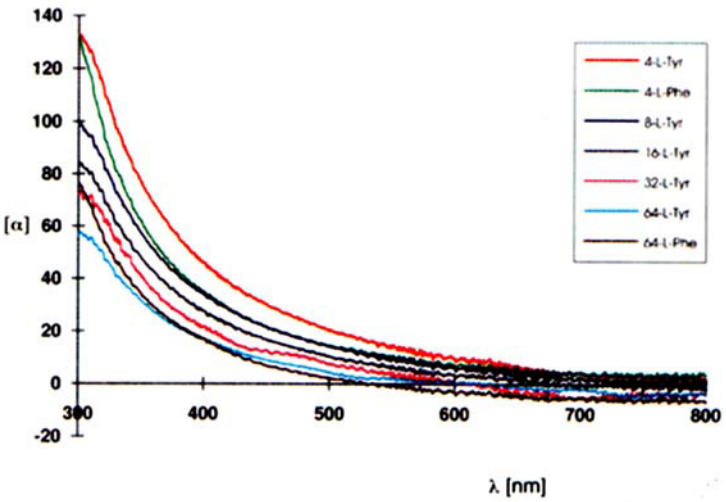


Fig. 3. Dependence of the specific rotation [α] [deg cm^2 g^{-1}] on the wavelength for the L-Tyr modified dendrimers in DMSO.

The optical behavior of the amino acid modified dendrimers is in sharp contrast with the optical rotations found for chiral dendrimers with more rigid end groups. The rigid dendritic camphor sulfonamides (Fig. 4) and camphanic amides have almost identical rotations ($[\alpha]_D \approx 23$; $c = 1$, $CHCl_3$ and $[\alpha]_D \approx -18$;

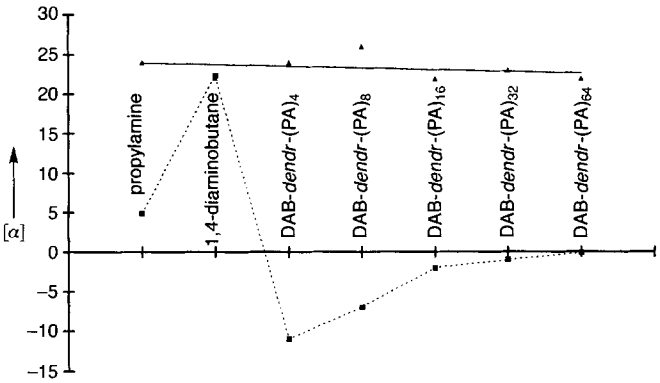


Fig. 4. Specific optical rotation of camphor sulfonic acid modified dendrimers (▲) and L-Phe modified dendrimers (■), both measured in $CHCl_3$ ($c = 1$).

$c = 1$, $CHCl_3$, respectively) for all generations. Furthermore, the corresponding *N*-propyl camphor sulfonamide model compound showed a specific rotation independent of solvent ($[\alpha]_D \approx 25$; $c = 1$, $CHCl_3$).

A number of phenomena other than trivial ones, like racemization or concentration effects, can explain the remarkable observations presented above for the amino acid modified dendrimers. A decreasing/vanishing optical activity of dendrimers is observed for dendrimers with chiral end groups; whose optical activity is susceptible to changes in the local environment. We are prompted to propose an explanation based on the fact that the outer surface (shell) of these dendrimers exhibit a highly dense solidlike packing in solution, as has been demonstrated by ^{13}C NMR relaxation measurements.[11] The rigidity of the shell is probably enhanced by multiple hydrogen bonding of the amide and carbamate groups in the shell. This rigid, close packing will lead to a number of conformations that are frozen. Due to the sensitivity of the chiroptical properties of the amino acid derivatives to the molecular environment and, hence, to conformational disorder, it is hypothesized that an internal compensation effect of different chiral conformers in the dendritic surface causes the vanishing or decreasing optical activity of the dendrimers. Chiral conformers with a non-equilibrium conformation are formed, forced by the dense packing in the shell. This explanation is related to the discussions by Green and Garetz on how the configurational stereochemistry of polymers can lead to vanishing optical activities by compensation among diastereomeric states.[15]

As these dendritic structures are highly organized, it is tempting to suggest that the conformational disorder in the shell is limited to the presence of only two frozen conformations with a kind of pseudo-enantiomeric relationship and almost opposite CD and ORD for both pseudo-enantiomers. It is well documented that the density of racemic crystals is higher than that of conglomerates[16] and the most dramatic differences are found for amino acid derivatives.[17] A pseudo mirror-image relation of conformers of enantiomerically pure compounds has been observed in X-ray studies of a number of crystals.[18] We have performed a variety of preliminary studies using scalemic mixtures to evaluate this pseudo-enantiomer hypothesis, but a detailed interpretation is lacking.[19] However, it is apparent from our results that the highly curved surface does not allow the packing of all amino acid derivatives into their preferred lowest energy conformations. This effect is probably strengthened by multiple hydrogen bonding.[20]

The constant optical rotation of the camphor sulfonamide and camphanic amide dendrimers of different generations is in

 © VCH Verlagsgesellschaft mbH, D-69451 Weinheim, 1995 0570-0833/95/1111-1208 $ 10.00+.25/0

full agreement with the insensitivity of its rotation with respect to changes in the molecular environment. The constant $[\alpha]_D$ value does not imply that the camphor sulfonamide and camphanic amide shells are not densely packed nor that they do not possess frozen-in conformations. However, in these densely packed surfaces the frozen-in conformations all have the same optical activity and no internal compensation effects are operative here. Also the number and strength of the hydrogen bonds in these cases will be lower than in the case of the amino acid derived dendrimers. Further research to elucidate the reasons for the observations presented here are in progress. It is foreseen that research on chiral dendrimers with highly packed shells will yield important information for this type of curved structures; structures that are so prominently present in nature.

Received: November 8, 1994
Revised version: January 26, 1995 [Z 7459 IE]
German version: *Angew. Chem.* **1995**, *107*, 1321–1324

Keywords: chirality · chiroptical studies · circular dichroism · dendrimers · stereochemistry

[1] a) F. Ciardelli, *Encyclopedia of Polymer Science and Enginering*, *Vol 10*, Wiley, New York, **1987**, p 463; b) J. M. Lehn, *Angew. Chem.* **1988**, *100*, 91–116; *Angew. Chem. Int. Ed. Engl.* **1988**, *27*, 89–112; c) M. Kitamura, S. Okada, S. Suga, R. Noyori, *J. Am. Chem. Soc.* **1989**, *111*, 4028–4036; d) M. Kitamura, R. Noyori, *Angew. Chem.* **1991**, *103*, 34–55; *Angew. Chem. Int. Ed. Engl.* **1991**, *30*, 49–76; e) T. Katsuki, K. B. Sharpless, *J. Am. Chem. Soc.* **1980**, *102*, 5974–5976; f) D. K. Mitchell, J.-P. Sauvage, *Angew. Chem.* **1988**, *100*, 985–987; *Angew. Chem. Int. Ed. Engl.* **1988**, *27*, 930–933; g) H. Ringsdorf, B. Schlarb, J. Venzmer, *ibid.* **1988**, *100*, 117–162 and **1988**, *27*, 113–158; h) D. Seebach, *ibid.* **1990**, *102*, 1363–1409 and **1990**, *29*, 1320–1366.

[2] a) L. Addadi, Z. Berkovitch-Yellin, I. Weissbuch, M. Lahav, L. Leiserowitz, in *Top. Stereochem.* **1986**, *16*, 1; b) T. Kunitake, N. Nakashima, S. Hayashida, K. Yonemori, *Chem. Lett.* **1979**, 1413; c) T. Kunitake, N. Nakashima, M. Shimomura, Y. Okahata, K. Kano, T. Ogawa, *J. Am. Chem. Soc.* **1980**, *102*, 6642; d) N. Nakashima, R. Ando, T. Muramtsu, T. Kunitake, *Langmuir* **1994**, *10*, 232.

[3] a) D. A. Tomalia, A. Naylor, W. A. Goddard, *Angew. Chem.* **1990**, *102*, 119–157; *Angew. Chem. Int. Ed. Engl.* **1990**, *29*, 138–175; b) G. R. Newkome, C. N. Moorfield, G. R. Baker, A. L. Johnson, R. K. Behera, *J. Org. Chem.* **1992**, *57*, 358–362; c) Z. Xu, J. S. Moore, *Angew. Chem.* **1993**, *105*, 1394–1396; *Angew. Chem. Int. Ed. Engl.* **1993**, *32*, 1354–1357; d) C. Wörner, R. Mülhaupt, *ibid.* **1993**, *105*, 1367–1370 and **1993**, *32*, 1306–1308 e) K. L. Wooley, C. J. Hawker, J. M. J. Fréchet, *J. Am. Chem. Soc.* **1991**, *113*, 4252–4261; f) K. L. Wooley, C. J. Hawker, J. M. J. Fréchet, *Angew. Chem.* **1994**, *106*, 123–126; *Angew. Chem. Int. Ed. Engl.* **1994**, *33*, 82–85; g) T. M. Miller, T. X. Neenan, E. W. Kwock, S. M. Stein, *J. Am. Chem. Soc.* **1993**, *115*, 356–357; h) J. Issberner, R. Moors, F. Vögtle, *Angew. Chem.* **1994**, *106*, 2507–2514; *Angew. Chem. Int. Ed. Engl.* **1994**, *33*, 2413–2420.

[4] G. R. Newkome, X. Lin, C. D. Weis, *Tetrahedron Asymmetry* **1991**, *2*, 957–960.

[5] a) D. Seebach, J.-M. Lapierre, K. Skobridis, G. Greiveldinger, *Angew. Chem.* **1994**, *106*, 457–458; *Angew. Chem. Int. Ed. Engl.* **1994**, *33*, 440–442; *Helv. Chim. Acta* **1994**, *77*, 1673–1688.

[6] a) H.-F. Chow, L. F. Fok, C. C. Mak, *Tetrahedron Lett.* **1994**, *35*, 3547–3550; b) H.-F. Chow, C. C. Mak, *J. Chem. Soc. Perkin Trans. 1* **1994**, 2223.

[7] R. H. E. Hudson, M. J. Damha, *J. Am. Chem. Soc.* **1993**, *115*, 2119–2124.

[8] L. W. Twyman, A. E. Beezer, J. C. Mitchell, *Tetrahedron Lett.* **1994**, *35*, 4423.

[9] a) R. G. Denkewalter, J. F. Kolc, W. J. Lukasavage, *US-A* 4410688, **1983** [*Chem. Abstr.* **1984**, *100*, 103907p]; b) R. G. Denkewalter, J. F. Kolc, W. J. Lukasavage, *US-A* 4289872, **1981** [*Chem. Abstr.* **1985**, *102*, 79324q].

[10] E. M. M. den Brabander-van den Berg, E. W. Meijer, *Angew. Chem.* **1993**, *105*, 1370–1372; *Angew. Chem. Int. Ed. Engl.* **1993**, *32*, 1308–1311.

[11] J. F. G. A. Jansen, E. M. M. den Brabander-van den Berg, E. W. Meijer, *Science*, **1994**, *266*, 1226–1229.

[12] The $[\alpha]_D$ values of the dendrimers of all generations are comparable to the specific optical rotation per chiral group. In the class of chiral dendrimers with a chiral core and achiral branches it is obvious that the optical rotation decreases with generation [5].

[13] D. Q. McDonnald, W. C. Still, *J. Am. Chem. Soc.* **1994**, *116*, 11550–11553; b) S. H. Gellman, G. P. Dado, G.-B. Liang, B. R. Adams, *J. Am. Chem. Soc.* **1991**, *113*, 1164.

[14] A similar decrease in optical activity, although not as pronounced, is found for the amide absorption in trifluoroethanol. In this solvent, however, neither the aromatic nor the carbamate absorption could be detected with CD.

[15] M. M. Green, B. A. Garetz, *Tetrahedron Lett.* **1984**, *25*, 2831.

[16] O. Wallach, *Justus Liebigs Ann. Chem.* **1895**, *286*, 90–143

[17] C. P. Brock, W. B. Schweizer, J. Dunitz, *J. Am. Chem. Soc.* **1991**, *113*, 9811–9820

[18] I. Weissbuch, F. Frolow, L. Addadi, M. Lahav, L. Leiserowitz, *J. Am. Chem. Soc.* **1990**, *112*, 7718–7724.

[19] In order to discriminate between disorder and pseudo-centrosymmetry, we performed experiments using scalemic mixtures of D-Phe and L-Tyr in the formation of the fifth-generation box. In sharp contrast to the $[\alpha]_D$ values of 0 for the pure D-Phe or L-Tyr, we found $[\alpha]_D = +16$ ($c = 1$, DMSO) for the 50:50 scalemic mixture of D-Phe and L-Tyr, and optical rotations between +16 and 0 for the other mixtures studied. The trend observed is indicative for some kind of pseudo-centrosymmetric ordering in the shell, in which in the case of the 50:50 scalemic mixture both units can adopt their preferred conformation and still the most dense packing is formed.

[20] This conclusion seems at first glance to be in contrast with "la coupe du roi" in which both chiral halves are of the same handedness, however a chiral dendritic surface possesses molecular chirality while "la coupe du roi" has only macroscopic chirality, see K. Mislow, *Bull. Soc. Chim. Fr.* **1994**, *131*, 534-538.

Facile Synthesis and Solid-State Structure of a Benzylic Amide [2]Catenane**

Andrew G. Johnston, David A. Leigh,* Robin J. Pritchard, and Michael D. Deegan

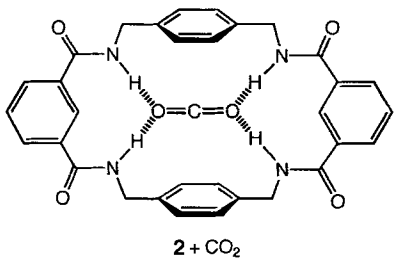
The synthesis of interlocked molecular rings, *catenanes*, is one of the greatest challenges in preparative chemistry.[1–3] Large macromolecular catenane structures (10^5 D) are found in DNA, where they appear to act as intermediates during the replication, transcription, and recombination processes,[4, 5] and are probably formed in small quantities in some polymerization reactions by the chance threading of growing molecular chains through large rings.[6] Recently the structural characteristics of smaller catenanes (10^3 D) have earmarked them, together with their relatives the rotaxanes, as key elements in the development of components for nanoscale electronic devices and molecular machines such as molecular shuttles, switches, and information storage systems.[3, 7] Here we report the serendipitous formation of a new amide-based [2]catenane (**1**) prepared in one step from two commercially available starting materials (see Scheme 2). The catenane is obtained in 20% yield (remarkable for an eight-molecule condensation) following a chromatography-free purification procedure simple enough to be performed in a well-equipped high school or undergraduate laboratory. The structure of **1** has been confirmed by NMR spectroscopy, mass spectrometry, and, in particular, by X-ray crystallography, which reveals a beautiful self-assembled system held together by networks of inter- and intramolecular hydrogen bonds and perfectly tessellating π-stacking interactions between four aromatic rings. Each catenane consists of two identical, interlocked, 26-membered rings with an internal cavity of 4×6 Å, making **1** the smallest interlocked ring system yet isolated.

[*] Dr. D. A. Leigh, A. G. Johnston, Dr. R. J. Pritchard
Department of Chemistry
University of Manchester Institute of Science and Technology
Sackville St., Manchester M60 1QD (UK)
Telefax: Int. code + (161) 200-4539

M. D. Deegan
Gas Research Centre, British Gas PLC
Loughborough (UK)

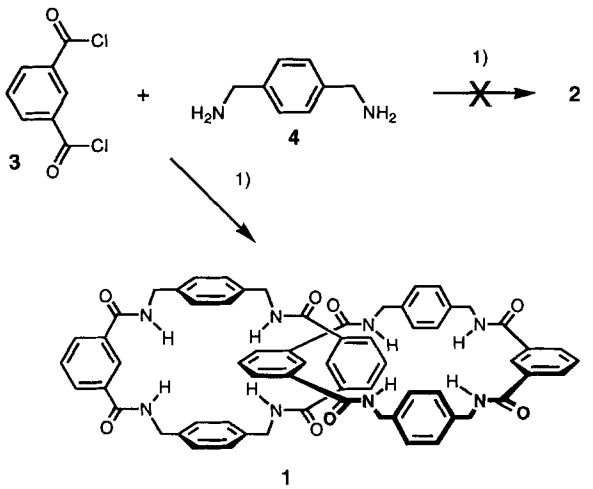
[**] We thank Dr. J. P. Smart for useful discussions and advice, and S. Davey, M. Bolgar, and Prof. S. Gaskell for mass spectral data. This work was carried out through the support of a British Gas Scholarship award (to A. G. J).

As part of a program to prepare chemical sensors for small gas molecules we identified the simple amide macrocycle **2** as a potential molecular receptor for carbon dioxide. Molecular modeling indicated a favorable mode and enthalpy of interaction of **2** with CO_2 (Scheme 1),[8] and the synthesis was attempted by means of a direct [2 + 2] condensation (Scheme 2). Upon addition of equimolar quantities of isophthaloyl dichloride (**3**) and *para*-xylylenediamine (**4**) to a solution of triethylamine in chloroform, a precipitate began to form almost immediately. After 24 h the precipitate was removed by filtration, and the filtrate was washed with acid, base, and water, and concentrated to dryness to give a white solid which proved to be a single compound. ^1H and ^{13}C NMR spectra in [D_6]dimethylsulfoxide (Figs. 1a and 1b) and the low molecular weight mass spectrum (< 1000 Da, Fig. 1c) were consistent with the anticipated macrocyclic structure. However, in complexation experiments the material showed no signs of binding CO_2.



2 + CO_2

Scheme 1. Structure of an amide macrocycle designed to bind to CO_2.



Scheme 2. One step, eight-molecule condensation to give the [2]catenane **1**. 1) Et_3N, anhydrous $CHCl_3$.

Single crystals were obtained (by slow diffusion of acetone vapor into a methanolic solution of the material) which proved suitable for structural investigation by X-ray crystallography (Figs. 2–4). The crystal study revealed why CO_2 binding did not occur; the [2 + 2] macrocycle formed was not in fact a discrete molecule but rather the [2]catenane **1** with a second macrocycle threaded tightly through the cavity of the first!

Octaamide [2]catenanes derived from a hindered aniline have been independently reported by Hunter et al.[9–11] and Vögtle et al.,[12] and characterized by extremely elegant NMR experiments and mass spectrometry. However, **1** is the first amide-based catenane for which the structure has been determined by X-ray crystallography. The solid-state ensemble is dominated by inter- and intramolecular hydrogen bonding interactions together with π-stacks composed of four aromatic rings.

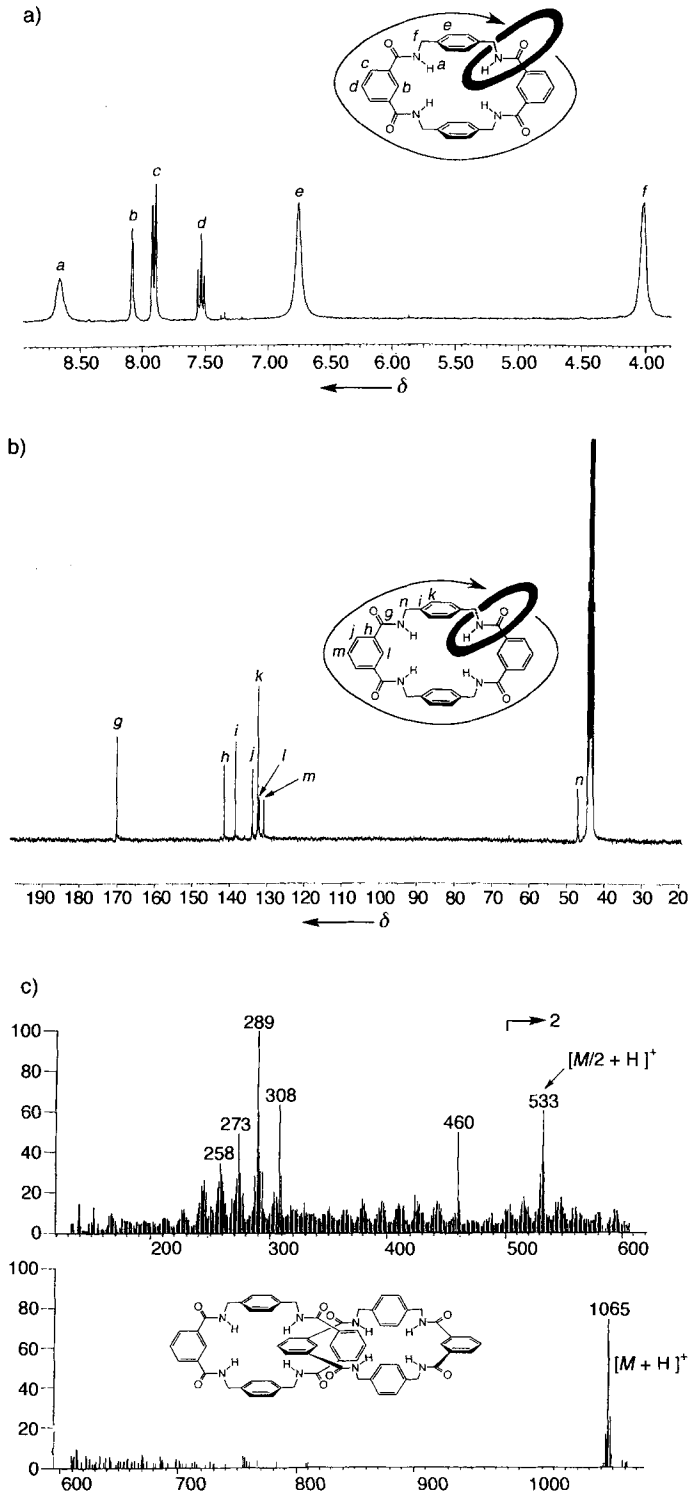


Fig. 1. Selected spectroscopic data for **1**: a) ^1H NMR and b) ^{13}C NMR spectra in [D_6]DMSO at room temperature (298 K). The second macrocycle is represented by the heavy ring. The simple NMR spectra indicate that the macrocyclic rings of **1** rotate rapidly on the NMR timescale at room temperature in DMSO, but the signals for protons *e* and *f* are still broad. c) Fast atom bombardment mass spectrum using *meta*-nitrobenzyl alcohol as matrix.

 © VCH Verlagsgesellschaft mbH, D-69451 Weinheim, 1995 0570-0833/95/1111-1210 $ 10.00+.25/0

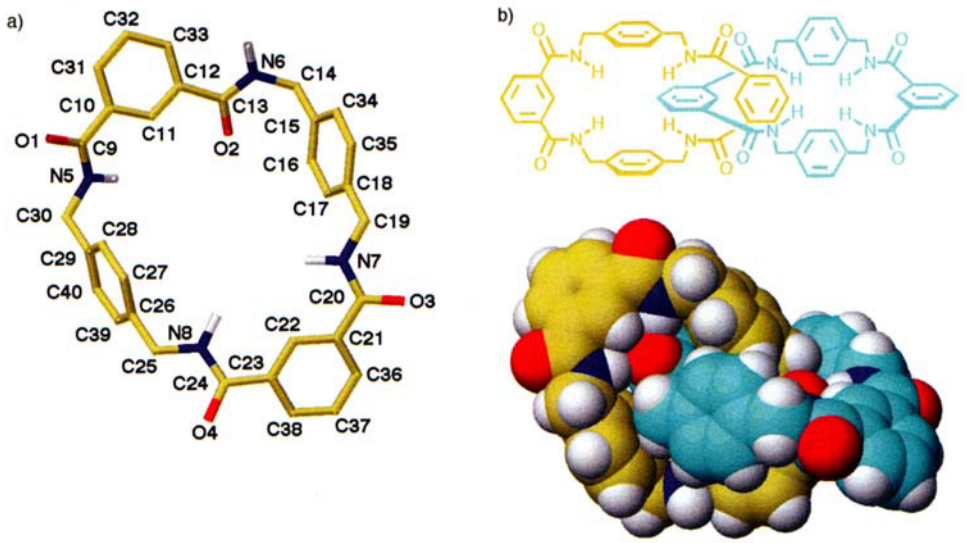


Fig. 2. Solid-state structure of [2]catenane **1** as determined by X-ray crystallography (for clarity, carbon atoms of one macrocyclic ring of a catenane are shown in blue and those of the other in yellow; oxygen atoms are red, nitrogen atoms purple, and hydrogen atoms white). a) A single macrocyclic ring (the minimum repeating unit in the crystal structure), maximum internal diameter 4 × 6 Å. Selected bond lengths [Å]: O1-C9 1.261, O2-C13 1.226, O3-C20 1.241, O4-C24 1.224, N5-C9 1.321, N5-C30 1.466, N6-C13 1.353, N6-C14 1.472, N7-C19 1.453, N7-C20 1.336, N8-C24 1.339, N8-C25 1.449. Selected bond angles [°]: O1-C9-C10 119.218, O1-C9-N5 122.150, O2-C13-C12 119.349, O2-C13-N6 122.677, O3-C20-C21 119.916, O3-C20-N7 120.218, O4-C24-C23 121.674, O4-C24-N8 121.191, N5-C9-C10 118.630, N5-C30-C29 115.287, N6-C13-C12 117.569, N6-C14-C15 116.266, N7-C20-C21 119.855, N7-C19-C18 113.918, N8-C24-C23 117.091, N8-C25-C26 113.913. Selected dihedral angles [°]: C11-C10-C9-N5 −27.081, C11-C10-C9-O1 152.343, C10-C9-N5-C30 173.748, C9-N5-C30-C29 109.880, N5-C30-C29-C28 63.120, C11-C12-C13-N6 −150.140, C11-C12-C13-O2 22.751, C12-C13-N6-C14 179.816, C13-N6-C14-C15 −77.409, N6-C14-C15-C34 −85.918, C22-C21-C20-N7 −18.619, C22-C21-C20-O3 160.175, C21-C20-N7-C19 178.022, C20-N7-C19-C18 139.509, N7-C19-C18-C17 −30.022, C22-C23-C24-N8 25.692, C22-C23-C24-O4 −151.932, C23-C24-N8-C25 178.325, C24-N8-C25-C26 −152.766, N8-C25-C26-C39 91.121. b) Representation of **1** with 100% van der Waals radii.

The macrocyclic rings of each catenane are structurally and, in the solid state, conformationally identical (Fig. 2a), bearing close resemblance to the conformation determined for the Hunter catenane in $CDCl_3/CD_3OD$ solution.[9] Each macrocycle adopts a chairlike conformation with a single carbonyl group pointing into the macrocyclic cavity (i.e. each macrocyclic ring contains one *endo*- and three *exo*-carbonyl groups). The two isophthaloyl rings of each macrocycle are parallel to each other and form roughly an 80° angle with the mutually parallel xylylene units of the same macrocycle (Figs. 2a and b).

The two macrocyclic rings of each catenane are held in a fixed orientation in the solid state by a total of six hydrogen bonds, including two sets of bifurcated hydrogen bonds between the amide hydrogens of the cisoid isophthaloyldiamide unit of each macrocycle and the *exo*-carbonyl group of the transoid isophthaloyldiamide unit of the other macrocycle (i.e. N7···O1′···N8 and N7′···O1···N8′, Fig. 3). The fixed orientation of the macrocyclic rings within a catenane confers chirality upon the individual catenanes (adjacent molecules in the crystal structure form enantiomeric pairs, Fig. 3).

The crystal lattice has a fascinating layered structure. In both directions within each layer the catenanes assemble to maximize both inter- and intramolecular π-stacking interactions. Each stack consists of four units in three different catenanes in an ABCD sequence (Fig. 4). The four aromatic rings in each stack are close to parallel and offset from each other in the classic manner which maximizes favorable electrostatic interactions within the stack.[13] Every aromatic ring in every catenane is involved in one of these π-stacks, which pack perfectly to form a single layer.

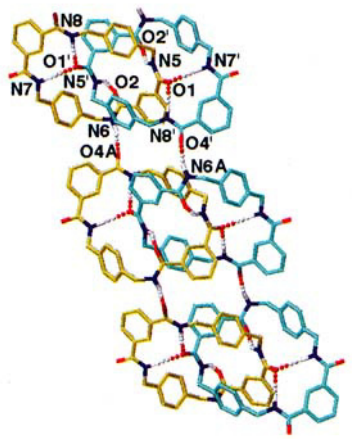


Fig. 3. Interlayer packing in the crystal structure of **1** in which all three modes of hydrogen bonding (two intra- and one intermolecular) are clearly shown. The layers are held together by an exquisite hydrogen bonding array in which four intramolecular hydrogen bonds per catenane hold the macrocyclic rings of an individual molecule in a fixed orientation and two intermolecular hydrogen bonds per catenane pair hold adjacent layers in place. Note that only the protons of the "inverted" amide groups are available for intermolecular hydrogen bonding. Distances for these intracatenane hydrogen bonds [Å]: O1-N7′ (= O1′-N7) 3.264, O1-N8′ (= O1′-N8) 3.119, O2-N5′ (= O2′-N5) 3.052; distance for the hydrogen bond between the catenanes: O4A-N6 (= N6′A-O4′) 2.913.

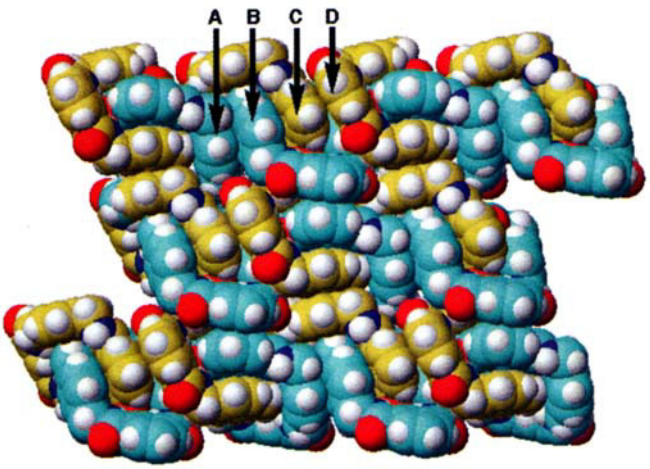


Fig. 4. Intralayer packing in the crystal structure showing tessellation of the π-stacks of four aromatic units to form discrete layers within the crystal. A is a xylylene group bearing one *exo*- and one *endo*-carbonyl group; B is a xylylene group bonded to two *exo*-carbonyl groups of a second, adjacent catenane; C is the transoid isophthaloyldiamide unit of the other macrocycle of the second catenane; and D is the cisoid isophthaloyldiamide unit of a third catenane, adjacent to the second and one-removed from the first. Distances between the centroids of the rings forming a π-stack [Å]: A···B 3.874, B···C 4.033, C···D 4.239.

 © VCH Verlagsgesellschaft mbH, D-69451 Weinheim, 1995 0570-0833/95/1111-1211 $ 10.00+.25/0

The catenane layers, in turn, are held together by van der Waals interactions and two intermolecular hydrogen bonds between each catenane and its nearest neighbors in the layers above and below (Fig. 3). The interlayer hydrogen bonds are formed between the amide hydrogen atoms of the inverted amide groups and the carbonyl groups of the cisoid isophthaloyldiamide units. The remaining amide hydrogen atoms and carbonyl groups (N5′ and O2; N5 and O2′) appear, by the positioning of the heavy atoms, to be connected through an unusual hydrogen bonding architecture in which the amide proton either binds to the π-cloud of the O=C bond or binds in a nonlinear arrangement to the oxygen atom. Since the H atoms are not resolved in the structure, these two possibilities cannot currently be distinguished.

The X-ray crystal structure supports the proposal that the driving force for catenane formation is hydrogen bonding between the newly formed 1,3-diamide units and carbonyl groups on the acid chloride or other intermediates. The stacking of the electron-rich xylylene and electron-poor isophthaloyl rings may also play a supporting role. *In the manner first introduced with the Stoddart catenanes, the formation of new functional groups in this reaction controls the self-assembly of a topologically complex product.*[3]

The following communication[17] shows that **1** is not an isolated example of a [2]catenane, but rather the simplest of a diverse family of catenanes derived in one step from aromatic 1,3-dicarbonyl compounds and benzylic diamines. Self-assembly processes currently provide the only viable route to these kinds of topologically complex molecules which exhibit, in both solution and the solid state, a range of structural and dynamic properties not available to topologically trivial molecules.

Experimental Procedure[18]

To a stirred solution of triethylamine (1.19 g, 18.9 mmol) in anhydrous chloroform (130 mL, stabilized with amylenes not ethanol) [19] under argon were added **3** (0.87 g, 4.3 mmol) in anhydrous chloroform (130 mL) and **4** (0.58 g, 4.3 mmol) in anhydrous chloroform (130 mL) simultaneously, over 30 min by means of motor-driven syringe pumps. The mixture was allowed to stir for about 12 h and then filtered. The filtrate was washed with 1 M aqueous hydrochloric acid (3 × 200 mL), then 5% aqueous sodium hydroxide (3 × 200 mL), and finally water (3 × 200 mL). The organic layer was then dried over anhydrous magnesium sulfate and concentrated under reduced pressure to afford 0.23 g (20.1%) of [2]catenane **1**. M.p. 315 °C (decomp); ^{1}H NMR (300 MHz, [D$_6$]DMSO): δ = 4.01 (br. s, 16H, CH$_2$), 6.75 (br. s, 16H, *p*-xylyl H), 7.50 (t, $J_{4,5} = J_{5,6} = 8$ Hz, 4H, isophthaloyl 5-H), 7.88 (dd, $J_{4,5} = 8$ Hz, $J_{2,4} = 1$ Hz, 8H, isophthaloyl 4-H and 6-H), 8.05 (d, $J_{2,4} = 1$ Hz, 4H, isophthaloyl 2-H), 8.62 (s, 8H, CONH); ^{13}C NMR (75 MHz, [D$_6$]DMSO): δ = 46.98, 130.03, 130.81, 132.40, 133.78, 138.40, 141.35, 168.94; FAB-MS (*m*NBA matrix): m/z 1065 [$(M + H)^+$], 533 [$(M/2 + H)^+$]. The precipitate from the reaction contains polymers, larger macrocycles, and catenanes (as indicated by FAB-MS and NMR analysis) which have not yet been completely characterized.

Received: January 9, 1995 [Z 7610 IE]
German version: *Angew. Chem.* **1995**, *107*, 1324–1327

Keywords: catenanes · macrocycles · structure elucidation

[1] G. Schill, *Catenanes, Rotaxanes and Knots*, Academic Press, New York, **1971**.
[2] For a representative paper from the Strasbourg group see J.-F. Nierengarten, C. O. Dietrich-Buchecker, J.-P. Sauvage, *J. Am. Chem. Soc.* **1994**, *116*, 375–376.
[3] For a representative paper from the Birmingham group see D. B. Amabilino, P. R. Ashton, C. L. Brown, E. Córdova, L. A. Godínez, T. T. Goodnow, A. E. Kaifer, S. P. Newton, M. Pietraszkiewicz, D. Philp, F. M. Raymo, A. S. Reder, M. T. Rutland, A. M. Z. Slawin, N. Spencer, J. F. Stoddart, D. J. Williams, *J. Am. Chem. Soc.* **1995**, *117*, 1271-1293.
[4] M. A. Gellert, *Annu. Rev. Biochem.* **1981**, *50*, 879–910.
[5] J. C. Wang, *J. Biol. Chem.* **1991**, *266*, 6659–6662.
[6] J. E. Mark, *New J. Chem.* **1993**, *17*, 703–709.
[7] R. A. Bissell, E. Córdova, A. E. Kaifer, J. F. Stoddart, *Nature (London)* **1994**, *369*, 133–137.
[8] Molecular modeling calculations (carried out on a CAChe Tektronix workstation with an MM2 forcefield) and semiempirical quantum mechanical calculations (MOPAC 6.0; AM1 parameterization) indicate favorable enthalpies for the interaction of **2** and CO_2. The complexation properties of a derivative of **2** with CO_2 will be reported elsewhere.
[9] C. A. Hunter, *J. Am. Chem. Soc.* **1992**, *114*, 5303–5311.
[10] C. A. Hunter, D. H. Purvis, *Angew. Chem.* **1992**, *104*, 779–782; *Angew. Chem. Int. Ed. Engl.* **1992**, *31*, 792–795.
[11] F. J. Carver, C. A. Hunter, R. J. J. Shannon, *J. Chem. Soc. Chem. Commun.* **1994**, 1277–1280.
[12] F. Vögtle, S. Meier, R. Hoss, *Angew. Chem.* **1992**, *104*, 1628–1631; *Angew. Chem. Int. Ed. Engl.* **1992**, *31*, 1619–1622.
[13] C. A. Hunter, J. K. M. Sanders, *J. Am. Chem. Soc.* **1990**, *112*, 5525–5534.
[14] Crystal data for **1**: $C_{32}H_{28}O_4N_4$, M = 1065.2, orthorhombic, space group *Pbcn* (No. 60), a = 17.510(4), b = 12.632(4), c = 23.834(8) Å, V = 5272(5) Å^3, ρ_{calcd} = 1.342 g cm^{-3}, Z = 8; 4171 reflections measured, 765 with $I > 2\sigma(I)$. Diffractometer Rigaku AFC6S, $2\theta_{max} = 50°$, $Mo_{K\alpha}$ radiation, λ = 0.71069 Å, T = 296. The structure was solved by direct methods (SHELLXS-86 [15]) and subjected to least-squares refinement (TEXSAN [16]) to yield final residuals of R = 0.062 and R_w = 0.063 for 161 parameters. All hydrogen atoms were placed in chemically reasonable positions. Further details of the crystal structure investigation may be obtained from the Director of the Cambridge Crystallographic Data Centre, 12 Union Road, GB-Cambridge CB2 1EZ (UK), on quoting the full journal citation.
[15] G. Sheldrick, SHELLXS-86, Crystallographic Computing 3 175, OUP, Oxford, **1985**.
[16] Molecular Structure Corporation, TEXSAN, Texray Structure Analysis Package, **1985**, MSC 3200A Research Forest Drive, The Woodlands, TX 77381, USA.
[17] A. G. Johnston, D. A. Leigh, L. Nezhat, J. P. Smart, M. D. Deegan, *Angew. Chem.* **1995**, *107*, 1327–1331; *Angew. Chem. Int. Ed. Engl.* **1995**, *34*, 1212–1216.
[18] Few examples of self-assembly processes are straightforward enough to be introduced into undergraduate laboratories. The synthesis of **1** is an exception and has been successfully incorporated into the first-year organic chemistry course at the University of Manchester Institute of Science and Technology.
[19] The use of chloroform that has not been rigorously dried or contains ethanol gives lower yields of the [2]catenane and, more problematically, produces byproducts arising from the partial hydrolysis of the starting acid chloride. These are not removed in the above workup procedure. However, in this case the [2]catenane can be obtained pure by carefully washing the end product with cold chloroform.

Structurally Diverse and Dynamically Versatile Benzylic Amide [2]Catenanes Assembled Directly from Commercially Available Precursors**

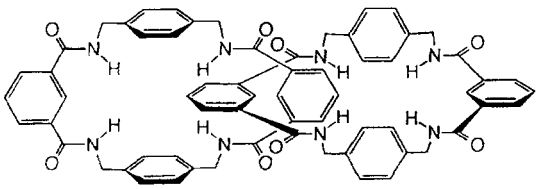
Andrew G. Johnston, David A. Leigh,* Lida Nezhat, John P. Smart, and Michael D. Deegan

The unique architectures and structural characteristics of catenanes and rotaxanes have identified them as attractive targets in the search for nanoscale devices and molecular electronic applications.[1] Accordingly, following the pioneering work of Stoddart et al.[2] and Sauvage et al.,[3] there is great interest in the development of new catenane systems that can be obtained in high yield[4–10] and especially syntheses that are tolerant towards structural variations which can be used to control the dynamic properties of the catenanes. In 1992 Hunter and Vögtle et al. reported the first amide-based catenanes,[4, 5]

[*] Dr. D. A. Leigh, A. G. Johnston, Dr. L. Nezhat, Dr. J. P. Smart
Department of Chemistry
University of Manchester Institute of Science and Technology
Sackville St., Manchester M60 1QD (UK)
Telefax: Int. code + (161) 200-4539
M. D. Deegan
Gas Research Centre, British Gas PLC
Loughborough (UK)

[**] This work was carried out through the support of a British Gas Scholarship award (to A. G. J) and the EPSRC IPS initiative (GR/J/88579).

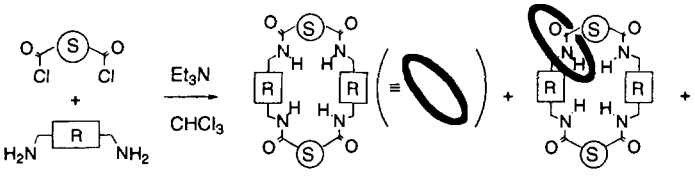
which relied on a hindered anilide structure. However, both groups found that the catenane assembly process was not tolerant to some simple modifications in the aromatic 1,3-dicarbonyl unit (5-nitrobenzene 1,3-dicarboxylic acid dichloride (Vögtle) and pyridine 2,5-diamidyl precursors (Hunter)). Furthermore, the steric demand of the spacer prevents the macrocyclic components of these catenanes from rotating. The preceeding communication describes the serendipitous formation of the first benzylic amide [2]catenane (**1**).[11] Here we report that benzylic

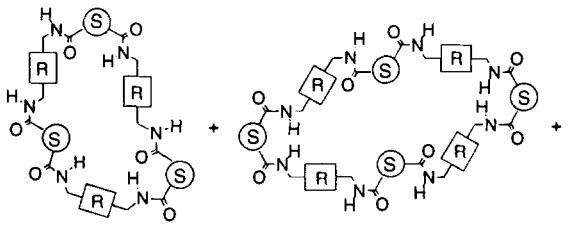


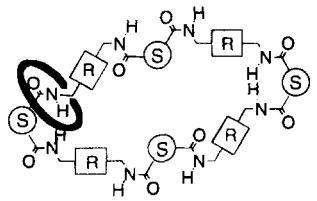
1

amide catenanes form a readily accessible and functionally diverse [2]catenane system, allowing the self-assembly of catenanes with differing conformational and dynamic properties in good yields. Commercially available and other readily accessible dicarboxylic acid dichlorides and benzylic diamines serve as starting materials.

The generality of the catenane-forming reaction described in ref. [11] was examined in detail (Scheme 1, Table 1). Variations in both the aromatic 1,3-dicarbonyl compound (five-membered rings (**11**), six-membered rings (**1**–**10**, **12**–**15**), thiophenes (**11**), pyridines (**12**, **13**), with nitro groups (**9**), alkyl groups (**2**, **3**), alkenes (**4**, **14**, **15**), ethers (**4**–**7**, **14**, **15**), halogens (**8**, **10**)) and the







+ higher cyclic oligomers, catenanes and polymers

Scheme 1. Possible products from the reaction of aromatic 1,3-dicarboxylic acid dichlorides with benzylic amides. The benzylic amide [2]catenanes ((2+2+2+2) catenanes) **1**–**15** (Table 1) are formed by eight-molecule condensations.

Table 1. Products and yields (either of isolated material or, in the case of very insoluble or difficult-to-purify products, by HPLC) from the condensation of equimolar quantities of various aromatic 1,3-dicarboxylic acid dichlorides and benzylic diamines in dry chloroform in the presence of triethylamine according to Scheme 1.

S	R	(2+2) Macrocycle [%]	(2+2+2+2) Catenane [%]	(3+3) Macrocycle [%]	(4+4) Macrocycle [%]	(4+4+2+2) Catenane [%]
		– [a]	20 (**1**)	– [a]	– [a]	– [a]
H_3C		22 (**16**)	20 (**2**)	3	10 (**17**)	5
*t*Bu		25	18 (**3**)	trace	10	5
		20	18 (**4**)	–	5	–
$C_6H_{11}O$		20	21 (**5**)	trace	3	trace
$C_8H_{17}O$		19	20 (**6**)	–	trace	–
$C_{18}H_{37}O$		22	15 (**7**)	–	5	–
Br		20	20 (**8**)	–	7	trace
O_2N		22	18 (**9**)	–	5	–
Br		25 [b]	15 [b] (**10**)	–	5 [b]	–
S		25 (**18**)	25 (**11**)	trace	2	–
N		20	27 (**12**)	–	6	trace
N		21	20 (**13**)	–	5	trace
		21	18 (**14**)	trace	6	–
		19	19 (**15**)	–	5	–
F, F, F		20	–	–	5	–

[a] The very poor solubility of these products made their analysis impossible, even by HPLC.
[b] Mixtures of diastereomers and, in the case of the [2]catenane, topological enantiomers.

benzylic spacer (1,4-phenylene (**1**–**13**), 2,6-naphthalenediyl (**14**), 4,4′-biphenylene (**15**)) were well tolerated, in all cases but one, giving rise to [2]catenanes in yields of 15–27%. The exception was 2,4,5,6-tetrafluorobenzene 1,3-dicarboxylic acid dichloride, which failed to produce detectable amounts of catenane with any of the benzylic diamines.

Also formed in each reaction were the topologically trivial macrocycles arising from (2+2), (4+4), and higher condensations (the macrocycle from the (3+3) condensation was usually formed only in trace amounts); however, these could not always be isolated as pure compounds due to their poor solubilities. The (2+2+2+2) catenane and (2+2) macrocycle were invariably the most abundant reaction products. With the exception of catenane **1**, whose trivial isolation is reported in ref. [11], all of the products required purification by careful column chromatography (silica gel, 1–15% methanol in dichloromethane as eluent); in each case the (2+2+2+2) catenane was the first compound eluted.

The macrocycles and catenanes were distinguished by FAB mass spectrometry and ^1H and ^{13}C NMR spectroscopy (Figs. 1–3). FAB mass spectra of the catenanes show features characteristic of interlocked molecules such as the lack of fragmenta-

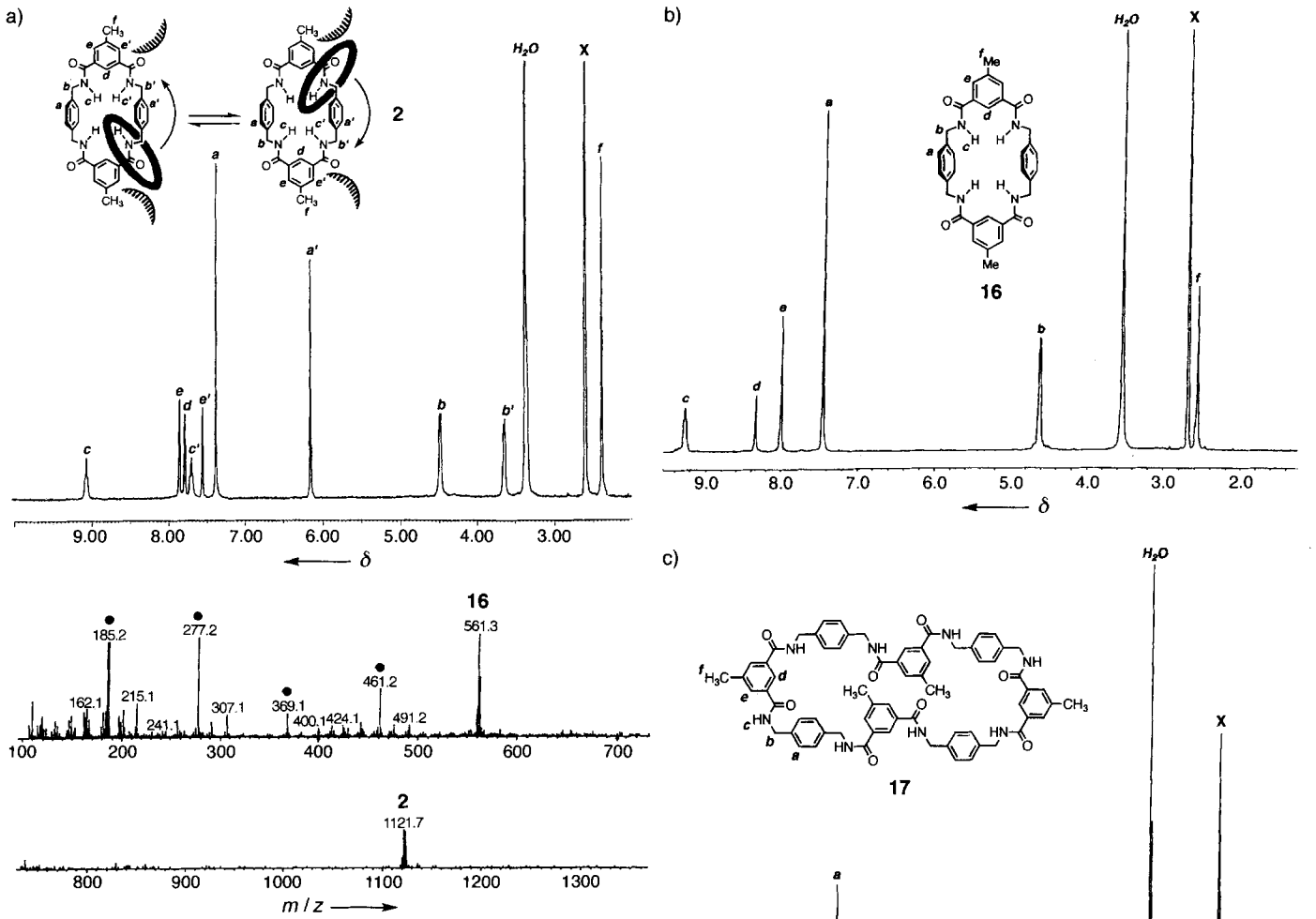


Fig. 1. Room-temperature ^{1}H NMR spectra (300 MHz, [D$_6$]DMSO, X = residual solvent peak) of a) the catenane **2** (along with its FAB mass spectrum; • = peaks arising from the matrix), b) the (2+2) macrocycle **16**, and c) the (4+4) macrocycle **17**. In the formula of **2** the unringed side of the catenane is on the left. The two xylylene, rather than the (5-methylisophthaloyl) units, of the constituent macrocycles of **2** are in different chemical environments on the NMR timescale. Inspection of CPK models reveals that the methyl groups prevent rotation of either macrocycle around the other giving rise to this phenomenon. Heating the sample does not bring about coalescence of these signals. As a catenane that cannot spin, this molecule may be considered a kind of "cyclic rotaxane" [12]. Somewhat suprisingly, however, the mass spectrum still shows no fragmentation peaks between M and $M/2$.

tion between M + H and $M/2$ + H (upon cleavage of a macrocyclic bond in the spectrometer the catenane unthreads to two components of $m/z \leq M/2$ + H).

The self-assembly process is clearly very tolerant to structural and functional variations in the reactants (indeed even the yields of the catenanes are remarkably similar). However, NMR spectroscopy reveals that the functional and structural changes impart varied dynamic and conformational properties to the different catenanes in solution.

The substituents on the isophthaloyl units of catenanes **2**–**10**, **14**, and **15** prevent complete circumvolution (also termed "circumrotation"; the spinning of one macrocyclic ring through the other), thereby locking the two sides (i.e. the two *para*-xylylene units) of each macrocycle in different chemical environments. This reduction in symmetry is evident in the ^{1}H NMR spectra of catenane **2** (Fig. 1a), which has two signals for most protons. The exceptions are protons *d* and *f* which lie on the axis separating the "ringed" and "unringed" halves of each macrocycle. The signals arising from the "ringed" half of the macrocycle (labeled with primed letters) are shifted to higher field, owing to the shielding effects of the aromatic rings of the "ringing" macrocycle. In contrast to the catenane **2**, both the (2+2) and (4+4) macrocycles (**16** and **17**, respectively) give simple NMR spectra with no doubling of resonances, and which remain simple even upon cooling in [D$_4$]methanol. Indeed, the ^{1}H NMR spectra of the (2+2) and (4+4) macrocycles are very similar (Fig. 1b and c). The largest chemical shift difference is that of H-2 (*d*) of the isophthaloyl rings, which is attributable to the greater flexibility (open and closed conformations) of the (4+4) macrocycle.[10]

Catenanes **1**, **11**, and **13**, which bear unsubstituted aromatic rings in the dicarbonyl unit, rotate rapidly on the NMR timescale at room temperature in [D$_6$]DMSO, giving rise to simple time-averaged ^{1}H NMR spectra. Catenane **11**, for example, yields only four signals for its 48 hydrogen atoms (Fig. 2a). In these cases the ^{1}H NMR spectra of the catenanes resemble those of the (2+2) and (4+4) macrocycles in terms of the number of signals. However, comparison of the ^{1}H NMR spectrum of catenane **11** with that of the corresponding (2+2) macrocycle **18** (Fig. 2b) shows that the catenane signals are all shifted considerably further upfield from the signals of the macrocycle, again due to the shielding effect of the aromatic

 © VCH Verlagsgesellschaft mbH, D-69451 Weinheim, 1995 0570-0833/95/1111-1214 $ 10.00+.25/0

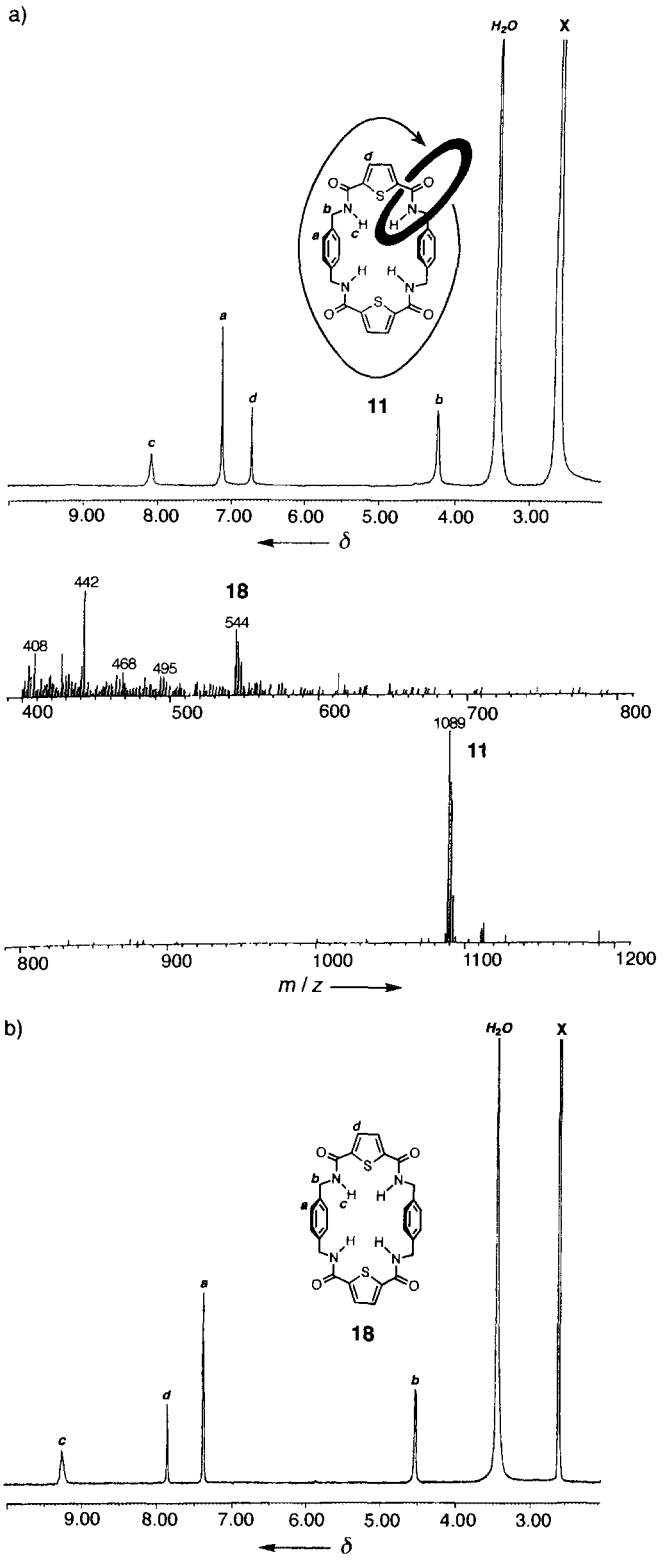


Fig. 2. Room-temperature ^{1}H NMR spectra (300 MHz, [D$_6$]DMSO) recorded of a) the catenane **11** (along with its FAB mass spectrum) and b) the (2+2) macrocycle **18**.

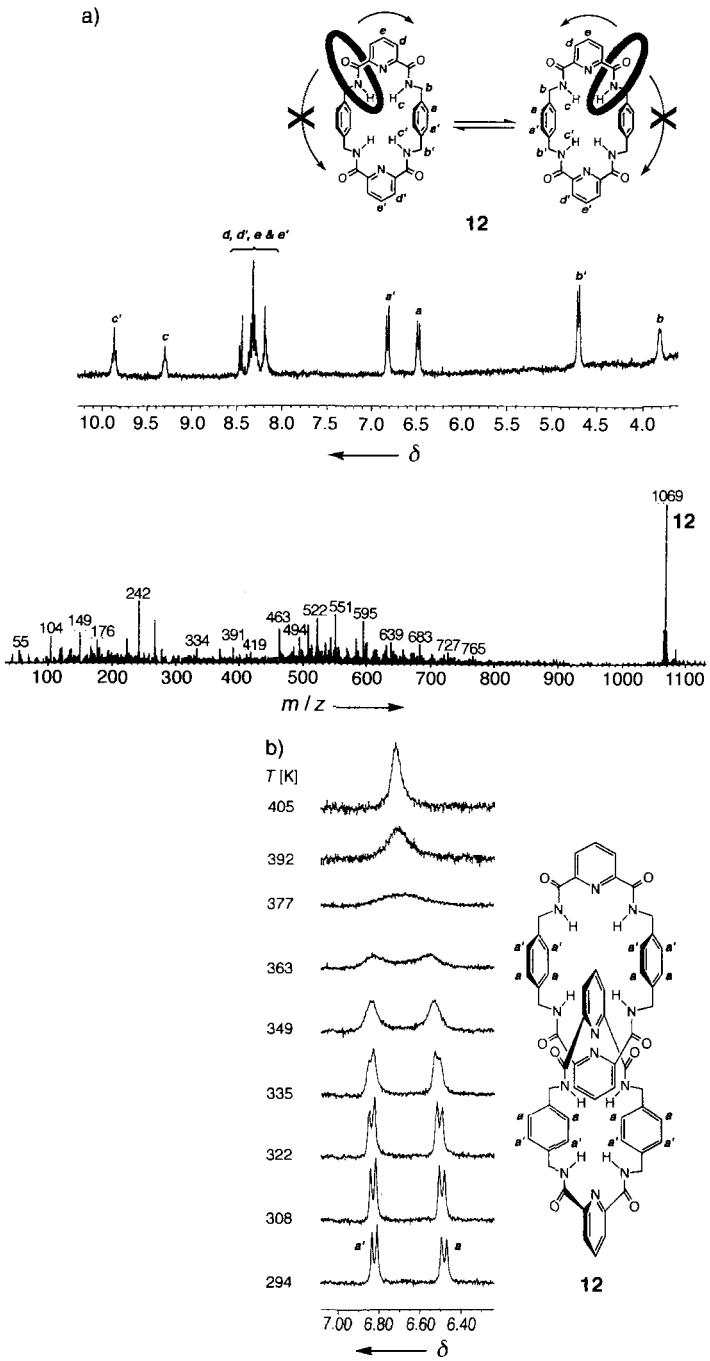


Fig 3. ^{1}H NMR spectra (300 MHz, [D$_6$]DMSO) of the catenane **12** at a) room temperature (along with its FAB mass spectrum) and b) of the phenylene units of **12** at elevated temperatures. The unprimed signals (especially *a*, *b*, *c*) in the ^{1}H NMR spectrum are broad at room temperature because the passage of the macrocyclic ring over the pyridine unit also has an appreciable energy barrier. In the formulas of **12** in a) the ringed part is on the top, and the unringed part is on the bottom.

rings of the rapidly spinning macrocycles. In this way, in particular, the (4+4) macrocycles and their isomeric, fast rotating (2+2+2+2) catenanes can be readily distinguished.

Catenane **12** is extraordinary in that the circumvolution of its macrocyclic ring is slow on the NMR timescale (giving rise to a symmetry-reduced spectrum, Fig. 3), although **12** does not have any substituents on the 1,3-dicarbonyl unit! Furthermore, the ^{1}H NMR spectrum shows that it is the two pyridine units (top and bottom halves) of each macrocycle that are in different environments, whereas the single set of signals for the two *para*-xylylene sides of the macrocycles (an AA'BB' system) indicate that the two sides of each macrocycle are chemically equivalent. Clearly, in this catenane the macrocyclic rings do not pass over the xylylene spacers rapidly on the NMR timescale and are effectively isolated on individual pyridine units. Upon heating, the primed and unprimed phenylene signals coalesce (Fig. 3b) as

the rate of macrocyclic ring circumvolution increases and the process becomes rapid on the NMR timescale.

Comparison with the [D_6]DMSO ^{1}H NMR spectra of both **1** and **13** recorded at room temperature indicates that this hindrance to circumvolution is peculiar to **12** and therefore must be governed wholly by the electronic nature of the pyridine unit rather than by the steric requirements of the catenane components. The X-ray crystal structure of **1** suggests that circumvolution of benzylic amide catenanes is restricted primarily by the two sets of intramolecular, intermacrocyclic hydrogen bonds between the cisoid 1,3-diamide hydrogen atoms and the amide carbonyl groups (Fig. 4). Remarkably, even in a solvent that

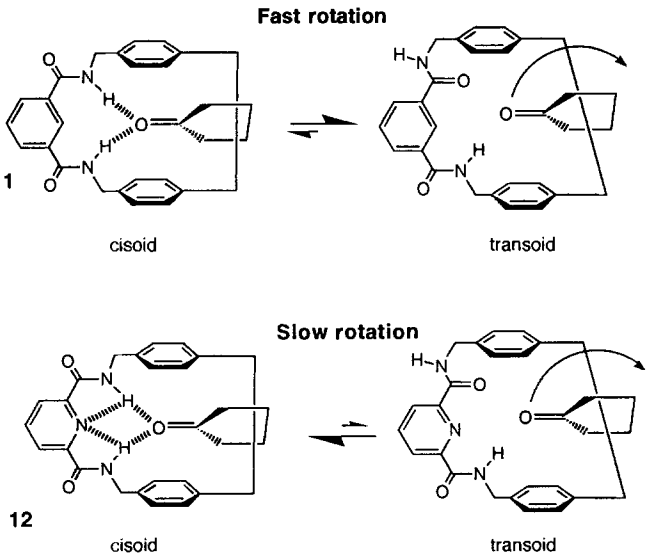


Fig. 4. Circumvolution of the catenanes involves the breaking and subsequent reforming of the intramolecular hydrogen-bonding networks between the two macrocyclic components. Rotation is achieved more easily when the 1,3-dicarbonyl moiety is attached to a benzene ring (e.g. **1**, top) rather than a pyridine unit (e.g. **12**, bottom), since the lowest energy conformation of the isophthaloyl group has the diamide in a transoid orientation, which releases the hydrogen-bonded carbonyl of the other macrocyclic ring. In the minimum energy conformation of the pyridine unit of **12** the diamide is in a cisoid orientation. This can be explained by the hydrogen bonding of the amide hydrogens to the pyridine nitrogen and/or electrostatic repulsions between the pyridine lone pair and the carbonyl group in the pyridine-2,6-dicarbonyl system. This leads to strong bifurcated hydrogen bonds between the two rings, fixing them in position and preventing macrocyclic ring rotation.

can form hydrogen bonds such as DMSO the circumvolution of catenane **12** is slow on the NMR timescale at temperatures below 100 °C! Since catenanes **13**, **1**, and **11** do not display this slow rotation behavior in DMSO, the phenomenon can be attributed to the greater propensity for pyridine-2,6-dicarbamido units to adopt the cisoid conformation necessary for strong binding to a carbonyl group.[10] Conversely, in macrocyclic components of catenanes **1**, **11**, and **13** the lack of binding sites for strong bonds with carbonyl groups allows unhindered, and consequently rapid, circumvolution to occur.

The synthesis of benzylic amide based catenanes is remarkably tolerant to significant variations in both the diamine and the dicarboxylic acid dichloride starting materials. The resulting catenanes display rotational properties associated with an intricate intramolecular network of hydrogen bonding interactions, which can be controlled both electronically and sterically. These fascinating molecules are clearly well suited for the construction of *revolutionary* nanoscale molecular devices.

Experimental Procedure

The optimum conditions for the catenane-forming reaction described in ref. [11] were worked out by systematic variations in reactant concentration, solvent, and temperature. The ideal concentration for catenane formation is ca. 0.02 M; more dilute solutions decrease the yield of [2]catenane in favor of the (2+2) macrocycle, more concentrated solutions lead preferentially to polymeric products. Nonaromatic, unpolar, ethereal, and halogenated solvents (in particular, chloroform) are amongst the best solvents for catenane formation. Reactions in toluene and chlorobenzene generally have lower yields, possibly due to inhibition of π-stacking interactions which may play a supporting role in catenane formation. Polar solvents such as acetone, dimethylformamide, and methanol inhibited the catenane self-assembly process almost completely, probably because of competitive hydrogen bonding between key intermediates and solvent molecules. Lowering the reaction temperature increases the yield of [2]catenane only at very dilute concentrations where solubility of the intermediates and products is not an important factor. At a concentration of 0.02 M, 298 K appears to be close to the optimal temperature for [2]catenane formation.

Received: January 9, 1995 [Z 7616 IE]
German version: *Angew. Chem.* **1995**, *107*, 1327–1331

Keywords: catenanes · macrocycles · self-assembly

[1] F. Vögtle, W. M. Müller, U. Müller, M. Bauer, K. Rissanen, *Angew. Chem.* **1993**, *105*, 1356–1358; *Angew. Chem. Int. Ed. Engl.* **1993**, *32*, 1295–1297; T. Lu, L. Khang, G. W. Gokel, A. E. Kaifer, *J. Am. Chem. Soc.* **1993**, *115*, 2542–2543.
[2] D. Philp, J. F. Stoddart, *Synlett* **1991**, 445–458, and references therein.
[3] J.-P. Sauvage, *Acc. Chem. Res.* **1990**, *23*, 319–325, and references therein.
[4] C. A. Hunter, *J. Am. Chem. Soc.* **1992**, *114*, 5303–5311.
[5] F. Vögtle, S. Meier, R. Hoss, *Angew. Chem.* **1992**, *104*, 1628–1631; *Angew. Chem. Int. Ed. Engl.* **1992**, *31*, 1619; S. Ottens-Hildebrandt, S. Meier, W. Schmidt, F. Vögtle, *ibid.* **1994**, *106*, 1818–1821, and **1994**, *33*, 1767–1770.
[6] M. J. Gunter, M. R. Johnston, *J. Chem. Soc. Chem. Commun.* **1992**, 1163–1165; M. J. Gunter, D. C. R. Hockless, M. R. Johnston, B. W. Skelton, A. H. White, *J. Am. Chem. Soc.* **1994**, *116*, 4810–4823.
[7] M. Momenteau, F. Le Bras, B. Loock, *Tetrahedron Lett.* **1994**, *35*, 3289–3292.
[8] J.-G. M. Gruter, F. J. J. de Kanter, P. R. Markies, T. Nomoto, O. S. Akkerman, F. Bickelhaupt, *J. Am. Chem. Soc.* **1993**, *115*, 12179–12180.
[9] M. Fujita, F. Ibukuro, H. Hagihara, K. Ogura, *Nature (London)* **1994**, *367*, 720–723.
[10] C. A. Hunter, D. H. Purvis, *Angew. Chem.* **1992**, *104*, 779–782; *Angew. Chem. Int. Ed. Engl.* **1992**, *31*, 792–795.
[11] A. G. Johnston, D. A. Leigh, R. J. Pritchard, M. D. Deegan, *Angew. Chem.* **1995**, *107*, 1324–1327; *Angew. Chem. Int. Ed. Engl.* **1995**, *34*, 1209–1212.
[12] C. O. Dietrich-Buchecker, J.-P. Sauvage, J. Weiss, *Tetrahedron Lett.* **1986**, *27*, 2257–2260.

A Stable Aquairon(III) Complex with $S = 1$: Structure and Spectroscopic Properties**

Michael J. Bartos, Christopher Kidwell, Karl E. Kauffmann, Scott W. Gordon-Wylie, Terrence J. Collins,* George C. Clark, Eckard Münck,* and Susan T. Weintraub

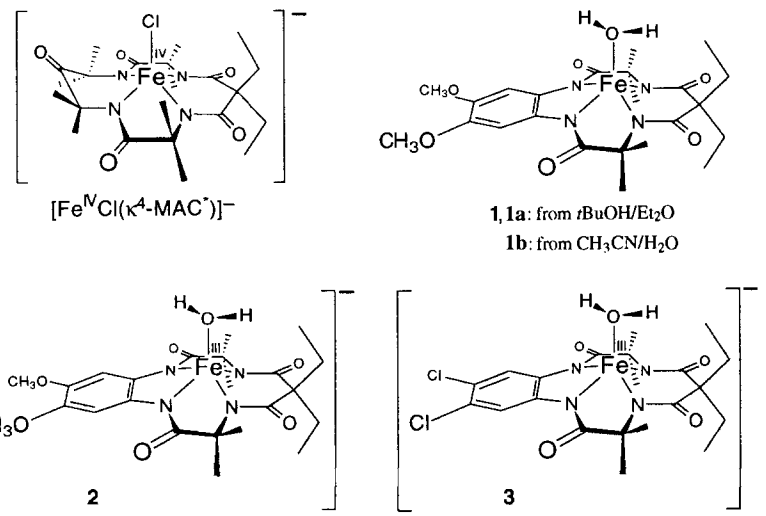
The importance of iron in biological oxidations continues to attract widespread attention to the chemistry of high-valent iron complexes. We have developed macrocyclic tetraamides that stabilize iron compounds in high oxidation states; resistance to oxidative degradation and strong donor capacities are the essen-

[*] Prof. T. J. Collins, Prof. E. Münck, M. J. Bartos, C. Kidwell, K. E. Kauffmann, S. W. Gordon-Wylie
Department of Chemistry, Carnegie Mellon University
4400 Fifth Avenue, Pittsburgh, PA 15206 (USA)
Telefax: Int. code + (412)268-6897
Prof. G. C. Clark
University of Auckland (New Zealand)
Prof. S. T. Weintraub
University of Texas Health Science Center at San Antonio (USA)

[**] This work was supported by the U. S. National Institutes of Health (Grant GM44867 to T. J. C. and GM22701 to E. M.).

tial criteria in ligand design.[1] One such ligand, $(\kappa^4\text{-MAC*})^{4-}$, has been used to make two novel Fe^{IV} compounds, a five-coordinate, high-spin ($S = 2$) complex with an axial chloro ligand[2] and a six-coordinate complex ($S = 1$) with two axial isocyanide ligands.[3] In these studies, we have aimed at producing oxidized iron complexes with biologically significant oxygen ligands. Here we report on an oxidized iron complex with the biologically important aqua ligand. The five-coordinate complex **1** is derived by oxidation of the identically ligated, intermediate-spin ($S = 3/2$) iron complex **2**. We show that the oxidation is ligand-centered in a manner that is both reminiscent of heme redox chemistry[4] and indicative[5] of a further source of stable non-porphyrinic iron compounds in high oxidation states.

Compound **2** was prepared by employing metal-insertion procedures developed for the macrocyclic tetraamides.[1] While **2** has not been structurally characterized, its Mössbauer and EPR data are very similar to those of **3**, a structurally characterized analogue with chlorine substituents on the aromatic ring in place of the methoxy groups (unpublished results). Compound **1** can be prepared by oxidation of **2** with Ag^I salts or with $Ce(NH_4)_2(NO_3)_6$. The complex is slightly soluble in water (< 0.5 mM), in which it shows a one-electron reduction with well-defined isosbestic points giving **2** (Fig. 1); complex **2** can be reoxidized to **1** with $Ce(NH_4)_2(NO_3)_6$. The cyclic voltammogram of **2** in water shows a reversible oxidation wave (+ 0.46 vs. SSCE, glassy carbon electrode, 0.1 M KPF_6). Depending upon the isolation conditions, **1** is produced in different crystal forms. Form **1a**, isolated from tBuOH/Et_2O, has been characterized by X-ray crystallography (Fig. 2). The average Fe–N distance in **1a** is 1.871 Å. The four N atoms are nearly planar (maximum displacement from mean plane 0.025 Å) with the Fe atom 0.362 Å above the N_4 plane. The Fe–O(H_2O) distance is 2.068(3) Å. The coordination of the O7 atom of the aqua ligand appears to deviate from ideal sp^3 hybridization. While experimental uncertainties in the O–H distances are large, one O–H distance is long (O7–HO7B, 0.92(6) Å); the H atom forms a strong hydrogen bond with an amide oxygen atom of a neighboring anion (HO7B···O2, 1.86 Å). The second more isolated O–H bond is short (O7–HO7A, 0.72(6) Å) with long distances to the O atoms of the methoxy substituents in the other macrocyle of the complex dimer (HO7A···O5′ 2.47 Å; HO7A···O6′, 2.57 Å). Short O–H bonds (< 0.8 Å) with similar experimental uncertainties have been found for other aquairon complexes.[9–11]



The zero-field Mössbauer spectrum of crystalline **2** (Fig. 3A) consists of a doublet with $\Delta E_Q = 4.19(4)\ mm\,s^{-1}$ and $\delta_{Fe} = 0.14(2)\ mm\,s^{-1}$ at 4.2 K. These parameters are similar to those observed for the $S = 3/2$ complex **3** ($\Delta E_Q = 4.01\ mm\,s^{-1}$, $\delta_{Fe} = 0.12\ mm\,s^{-1}$). Aqueous solutions of **2** (0.1–0.5 mM) at 2 K exhibit broad EPR spectra ($S = 3/2$) with resonances at $g = 4.5$ and 3.3; the region near $g = 2$ was obscured partially by signals of a contaminant. The zero-field Mössbauer spectrum of polycrystalline **1a**, recorded at 4.2 K (Fig. 4A), exhibits a sharp doublet with $\Delta E_Q = 3.97(2)\ mm\,s^{-1}$ and $\delta_{Fe} = 0.14(1)\ mm\,s^{-1}$. Remarkably, the isomer shifts of **1a** and **2** are the same. Since δ values are generally quite sensitive to the oxidation state of the metal atom, this observation suggests that the oxidation of **2** is essentially ligand-based rather than metal-centered. In the following we will pursue this suggestion.

Figure 3B shows a Mössbauer spectrum of crystalline **2** recorded in an 8.0 T applied field. We have analyzed spectra recorded at 4.2 K and 1.5 K in fields of 2.0, 4.0, 6.0, and 8.0 T with the Hamiltonian given in Equation (a) ($S = 3/2$), allowing

$$\mathcal{H} = \boldsymbol{D}[\boldsymbol{S}_z^2 - S(S+1)/3] + \boldsymbol{E}(\boldsymbol{S}_x^2 - \boldsymbol{S}_y^2) + \boldsymbol{S}\cdot\boldsymbol{g}\cdot\boldsymbol{H} + \boldsymbol{S}\cdot\boldsymbol{A}\cdot\boldsymbol{I} + \boldsymbol{I}\cdot\boldsymbol{P}\cdot\boldsymbol{I} - g_n\beta_n\boldsymbol{H}\cdot\boldsymbol{I} \quad \text{(a)}$$

that the magnetic hyperfine tensor, **A**, and the quadrupole tensor, **P**, are rotated relative to the zero-field splitting (ZFS) tensor by Euler angles $(\alpha_A,\beta_A,\gamma_A)$ and $(\alpha_P,\beta_P,\gamma_P)$, respectively. Figure 3B shows a representative simulated spectrum obtained with the parameters listed in Table 1. Figure 4 shows 8.0 T spectra of **1a** obtained from crystalline powder (Fig. 4B) and frozen aqueous solution (Fig. 4C). The spectra are typical of those obtained for complexes with integer electronic spin. We have analyzed a series of spectra of the solution sample in applied fields by applying Equation (a) for $S = 1$; a representative fit is shown in Figure 4C (solid line). The choice of spin state $S = 1$ is based on magnetization data of **1b** (crystallized from MeCN/H_2O), which has the same δ_{Fe} and ΔE_Q as the solution sample that yielded the spectrum shown in Figure 4C.[12] Data recorded at 2 to 300 K in fields up to 5.0 T show that μ_{eff} is nearly

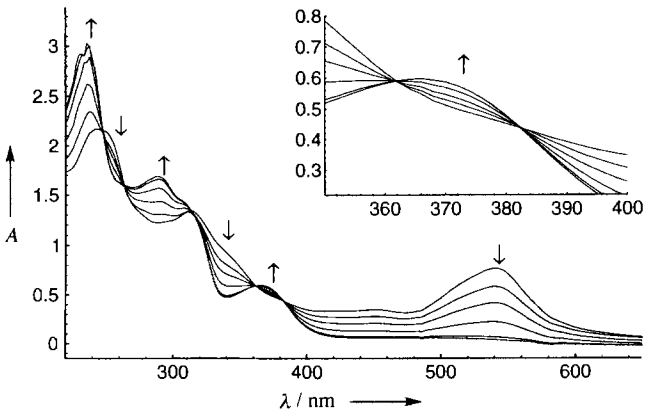


Fig. 1. UV/Vis spectra showing one-electron reduction of **1** with $[Ru^{II}(NH_3)_6]Cl_2$ in water. The concentration of **1** [λ_{max} (ε): 539 (9240)] decreases upon addition of five aliquots of $[Ru^{II}(NH_3)_6]Cl_2$ (0.2 equiv per aliquot) to give the spectrum of the pure **2** [366 (6740)].

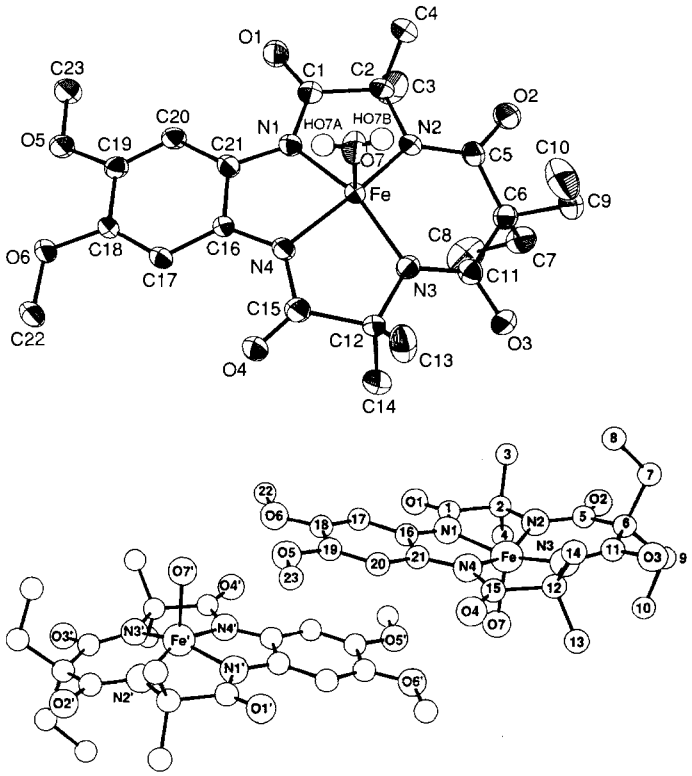


Fig. 2. Crystal structure of **1a**. Top: monomer; bottom: dimer. Selected bond lengths [Å] and bond angles [°]: Fe-N1 1.867(3), Fe-N2 1.887(3), Fe-N3 1.8855(3), Fe-N4 1.875(3), N4-C16 1.374(5), C16-C17 1.419(5), C17-C18 1.368(5), C18-C19 1.441(5), C19-C20 1.367(5), C20-C21 1.416(5), C21-C16 1.436(5), C18-O6 1.338(4), O6-C22 1.463(5), C19-O5 1.352(4), O5-C23 1:421(5); O7-Fe-N4 98.3(1), N1-Fe-N4 81.9(1), N2-Fe-N3 99.2(1), HO7A-O7-HO7B 82.8, HO7A-O7-Fe 132.3, HO7B-O7-Fe 117.4. N1, N3, and N4 amido-*N* ligands are distorted from planarity: Dunitz amide nonplanarity parameters [6–8]: $amide_{N1}$: $\bar{\tau} = -15°$, $\chi_N = -4°$, $\chi_C = -1°$; $amide_{N2}$: $\bar{\tau} = -2°$, $\chi_N = -2°$, $\chi_C = 2°$; $amide_{N3}$: $\bar{\tau} = 12°$, $\chi_N = 8°$, $\chi_C = 3°$; $amide_{N4}$: $\bar{\tau} = 11°$, $\chi_N = 5°$, $\chi_C = -3°$.

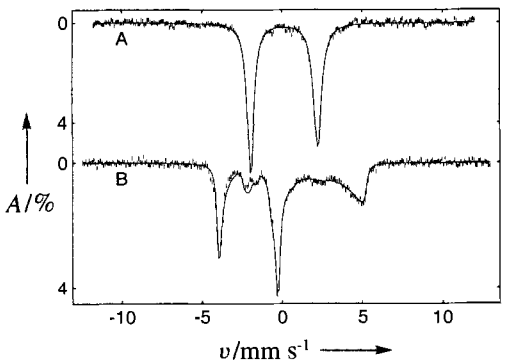


Fig. 3. Mössbauer spectra of the Fe^{III} complex **2** with $S = 3/2$ recorded at 4.2 K in zero field (A) and in an 8.0 T parallel applied field (B). The solid line in B is a simulation based on Eq. (a) using the parameters in Table 1.

constant above 50 K and $\approx 3.0\ \mu_B$, which is close to the spin-only value of 2.83 for an $S = 1$ system.

Crystalline **1a** behaves at 4.2 K like a diamagnet even in a field of 8.0 T (Fig. 4B). However, 8.0 T spectra taken at temperatures greater than 15 K reveal paramagnetic hyperfine structure, suggesting that molecules in the crystal interact in pairs by intermolecular exchange. We have fitted the solution parameters of **1a** (Fig. 4B) with a model that considers intermolecular antiferromagnetic exchange of two monomers with $S_1 = S_2 = 1$,

Table 1. Mössbauer parameters of **1** and **2**.

	D [cm^{-1}]	E/D	A_x, A_y, A_z [MHz]	β_A [°]	ΔE_Q [$mm\,s^{-1}$]	η	β_P[a] [°]	δ[b] [$mm\,s^{-1}$]
1	+9.2	0.10	−32, −28, +11	55	+3.72	0.23	65	0.14
2	+2–3	0.04	−31, −22, +11	90	+4.29	0.20	90	0.14

[a] Because the ZFS-, ***P***-, and ***A***-tensors are nearly axial, the spectra are quite insensitive to Euler angles α and γ. [b] Isomer shift is given relative to Fe metal at 298 K.

$\boldsymbol{H} = j\boldsymbol{S}_1 \cdot \boldsymbol{S}_2$, with $j \approx 20\ cm^{-1}$.[13] Similar intermolecular couplings have been reported, for instance, for porphyrins.[4] Inspection of the structure of the dimers (Fig. 2, bottom) suggests a likely exchange pathway through the aromatic rings of the ligands. Thus, within isolated pairs, segments of the aromatic rings of the ligands touch at van der Waals distances (C16–O5′ 3.34, C16–C19′ 3.49, C20–C18′ 3.40, C21–C18′ 3.50 Å).

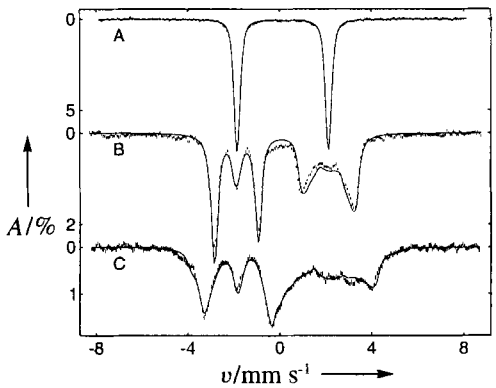


Fig. 4. Mössbauer spectra of **1** recorded at 4.2 K in zero field (A) and in an 8.0 T parallel applied field (B and C). The spectra in A and B were obtained for **1a**. The solid line in A is a least-squares fit to a doublet with $\Delta E_Q = 3.97\ mm\,s^{-1}$ and $\delta_{Fe} = 0.14\ mm\,s^{-1}$. The solid line in B is a spectral simulation assuming that two monomers with $S_1 = S_2 = 1$ are coupled by $\boldsymbol{H} = j\boldsymbol{S}_1 \cdot \boldsymbol{S}_2$ with the parameters listed in Table 1. The spectrum in C was obtained for an aqueous solution containing 0.4 mM ^{57}Fe-enriched (> 90%) **1**. The sample contained 10% of **2**; its contribution was simulated and is included in the theoretical curve. The solid line in C is the result of fitting a group of spectra to Eq. (a) for $S = 1$.

The similarity of the parameter sets (Table 1) obtained for **1** and **2** is remarkable. Thus, both compounds have nearly axial ZFS tensors. The ***A***- and ***P***-tensors are nearly collinear for each compound. The z-axes of both tensors are tilted by $\beta \approx 90°$ (for **2**) and $\beta \approx 60°$ (for **1**) away from the z-axis of the ZFS tensor. The striking similarity of the fine and hyperfine structure parameters of **1** and **2**, especially the identical δ-values, indicates that both complexes have Fe^{III} centers. This suggests a description of the $S = 1$ state of **1** by antiferromagnetic coupling ($\boldsymbol{H} = J\boldsymbol{S}_1 \cdot \boldsymbol{S}_R$, $J > 0$) of the spin of the Fe^{III} site with $S_1 = 3/2$ to a ligand-based radical with $S_R = 1/2$. In this coupling model, the ***A***- and ***D***-tensors of the $S = 1$ system are very similar to those of the $S = 3/2$ system and are related to those of the Fe^{III} site by $\boldsymbol{A} = (5/4)\boldsymbol{A}(Fe^{III})$ and $\boldsymbol{D} = (3/2)\boldsymbol{D}(Fe^{III})$.[14] The interpretation of **1** as an Fe^{III} complex containing a ligand-based radical[15] is supported by the X-ray structure of **1a**, which suggests that the locus of the oxidation is centered on the aromatic portion of the macrocycle. If **1** were an Fe^{IV} complex, the C_φ–N distances

 © VCH Verlagsgesellschaft mbH, D-69451 Weinheim, 1995 0570-0833/95/1111-1218 $ 10.00+.25/0

should be those of single bonds, in this case close to 1.4 Å.[1] The observed C–N distances from the aromatic ring to N1 (1.356 Å) and N4 (1.374 Å) are noticeably shorter, consistent with a semiquinone-like ligand and an Fe^{III} formulation. Moreover, two of the C–C bonds in the aromatic ring (C17–C18, C19–C20) are significantly shorter than the other four. Finally, the methyl groups of the methoxy substituents lie in the plane of the aromatic diamide unit, suggesting that oxygen π-donor interactions are important, as would be expected for an oxidized aromatic ring. A Hückel treatment (assuming C_s symmetry) suggests that the pattern of bond length changes results from removing an electron from an A' molecular orbital of the ligand.

These high-field Mössbauer studies of **1** and **2** and the crystal structure of **1a** delineate the electronic structure of **1**. The values of ΔE_Q, δ, and μ_{eff} for **1**, taken alone, could easily mislead one to suggest an Fe^{IV} complex with $S = 1$. The oxidation of **2** to give **1** is fundamentally different from that reported for $[Fe^{III}Cl(\kappa^4\text{-}MAC^*)]^{2-}$, a tetraamide complex lacking the aromatic ring in the macrocycle.[2] As noted, oxidation of the latter is metal-centered and produces a high-spin Fe^{IV} complex. With two axial *tert*-butylisocyanides, the $(\kappa^4\text{-}MAC^*)^{4-}$ ligand stabilizes a complex with an $S = 1$ state and an Fe^{IV} ion ($\delta_{Fe} = -0.04$ mm s^{-1}).[3] Thus, the spin state depends on the axial ligation, and the location of the oxidation can be locked at the metal by ligand design or freed to range over ligand fragments with delocalized electrons that remain in intimate contact with the metal. We are particularly interested in understanding how these details of electronic structure can be exploited in reactivity and are currently exploring deprotonation procedures for **1** to obtain stable oxidized hydroxo- and oxoiron complexes.

Experimental Procedure

2: $[Et_4N]_2[Fe^{III}Cl(\kappa^4\text{-}L)]$ (L = tetramido ligand in **1** and **2**) (500 mg, 0.6 mmol), prepared by standard techniques [16], was dissolved in deionized H_2O (40 mL) and the mixture was filtered. A solution of $[PPh_4]Cl$ in H_2O (1.2 g, 3.2 mmol, 10 mL) was added and the solution was stirred (24 h). The burgundy precipitate was collected and washed with deionized water (2 × 10 mL). Yield: 255 mg (50%). IR (Nujol): 1610 (ν(CO)amide), 1562 (ν(CO)amide), 1546 cm^{-1} (ν(CO)amide). Separate analyses on three different samples gave satisfactory, reproducible data for $C_{47}H_{52}N_4FeO_7P_1 \cdot H_2O$. Anal. calcd: C 63.44, H 6.12, N 6.30; found: C 63.28, H 6.00, N 6.25. ESI-MS: $[Ph_4P]$**2** in CH_3CN: m/z 514 [**2** – H_2O] (base peak), 573 [**2** + CH_3CN].

1: $[Et_4N]_2[Fe^{III}Cl(\kappa^4\text{-}L)]$ (600 mg, 0.7 mmol) was dissolved in deionized water (20 mL). A solution of $AgBF_4$ (720 mg, 3.7 mmol) in H_2O (5 mL) was added and the mixture was stirred (3 h). The solid was collected and extracted into CH_3CN (20 mL). The mixture was filtered (celite), water was added (10 mL), and the CH_3CN was removed under reduced pressure. The resulting purple crystalline solid was collected (160 mg, 0.3 mmol, 43% yield). **1** was chromatographed (silica gel, Davison Chemical, CH_2Cl_2, 10 cm × 1.5 cm column, 7.5% MeOH in CH_2Cl_2, 200 mL) and the solvent removed under reduced pressure. The resulting purple solid was recrystallized from CH_3CN/H_2O giving **1b**. IR (Nujol): 3667 (sharp), 3332 (br.), 3175 (br.) ν(OH)H_2O, 1680, 1599, 1578, 1542 cm^{-1} ν(CO)amide. Anal. calcd for $C_{23}H_{32}N_4FeO_7 \cdot H_2O$: C 50.19, H 6.23, N 10.18; found: C 50.33, H 6.20, N 10.18.

1a · 0.4(C_2H_5)$_2$O: Crystals of **1b** · 0.4$(C_2H_5)_2O$ were recrystallized from *tert*-butyl alcohol/ether. IR (Nujol): 3525 (sharp), 3365 (br.) ν(OH)H_2O, 1688, 1673, 1599, 1582, 1580, 1540 cm^{-1} ν(CO)amide. Crystal structure: tetragonal, space group $I4_1/a$, $a = 35.697(8)$, $c = 10.052(3)$ Å, $V = 3775(3)$ Å^3, $T = -100$ °C, $Z = 16$, $\rho_{calcd} = 1.17$ g cm^{-3}, $\rho_{obs} = 1.20(1)$ g cm^{-3}, $\mu = 5.32$ cm^{-1}; 6144 unique reflections ($2° < 2\theta < 56°$) collected using $\omega/2\theta$ scans with graphite-monochromated $Mo_{K\alpha}$ radiation ($\lambda = 0.71069$ Å). Hydrogen atoms were located in a difference map. Methyl hydrogen atoms were refined as rigid rotors; all other hydrogen atoms, including those on the coordinated water, were refined individually. The crystal studied contained a poorly resolved diethyl ether molecule of solvation which had a purely space-filling role. Its occupancy refined to 0.40. Refinement converged with R_1 (based on F) = 0.058 for 4434 observed reflections [$I > 3\sigma(I)$]. Further details of the crystal structure investigation may be obtained from the Director of the Cambridge Crystallographic Data Centre, 12 Union Road, GB-Cambridge CB2 1EZ (UK), on quoting the full journal citation.

Received: January 9, 1995 [Z 7612 IE]
German version: *Angew. Chem.* **1995**, *107*, 1345–1348

Keywords: complexes with oxygen ligands · electronic structure · iron compounds · macrocycles · oxidations

[1] T. J. Collins, *Acc. Chem. Res.* **1994**, *27*, 279, and references therein.
[2] K. L. Kostka, B. G. Fox, M. P. Hendrich, T. J. Collins, C. E. F. Rickard, L. J. Wright, E. Münck, *J. Am. Chem. Soc.* **1993**, *115*, 6746.
[3] T. J. Collins, B. G. Fox, Z. G. Hu, K. L. Kostka, E. Münck, C. E. F. Rickard, L. J. Wright, *J. Am. Chem. Soc.* **1992**, *114*, 8724.
[4] C. E. Schulz, H. Song, Y. J. Lee, J. U. Mondal, K. Mohanrao, C. A. Reed, F. A. Walker, W. R. Scheidt, *J. Am. Chem. Soc.* **1994**, *116*, 7196, and references therein.
[5] E. Vogel, S. Will, A. Schulze-Tilling, L. Neumann, J. Lex, E. Bill, A. X. Trautwein, K. Wieghardt, *Angew. Chem.* **1994**, *106*, 771; *Angew. Chem. Int. Ed. Engl.* **1994**, *33*, 731, and references therein.
[6] J. D. Dunitz, F. K. Winkler, *J. Mol. Biol.* **1971**, *59*, 169.
[7] J. D. Dunitz, F. K. Winkler, *Acta Crystallogr. Sect. B* **1975**, *31*, 251.
[8] T. J. Collins, R. J. Coots, T. T. Furutani, J. T. Keech, G. T. Peake, B. D. Santarsiero, *J. Am. Chem. Soc.* **1986**, *108*, 5333.
[9] W. R. Scheidt, I. A. Cohen, M. E. Kastner, *Biochemistry* **1979**, *18*, 3546.
[10] E. Herdtweck, *Z. Anorg. Allg. Chem.* **1983**, *501*, 131.
[11] P. Garge, R. Chikate, P. Subhash, J.-M. Savariault, P. de Loth, J.-P. Tuchagues, *Inorg. Chem.* **1990**, *29*, 3315.
[12] Since the axial water ligand is hydrogen-bonded to neighboring ions in **1a**, it is not surprising that ΔE_Q of the solution sample differs slightly from that of **1a**.
[13] Mössbauer studies of polycrystalline **1b** have also revealed dimer interactions. However, these interactions are much weaker ($j \approx 3$ cm^{-1}) than those of **1a**. Calculations show that for $j \approx 3$ cm^{-1} and $D \approx 10$ cm^{-1}, μ_{eff} is independent of D and j for $T \geq 50$ K. For this reason, we have chosen **1b** rather than **1a** for the magnetization studies.
[14] A. Bencini, D. Gatteschi, *Electron Paramagnetic Resonance of Exchange Coupled Systems*, Springer, Berlin, **1990**, see Table 3.3.
[15] While exchange coupling seems plausible, more information is needed to decide on the most appropriate description of the electronic structure. Magnetization studies above 200 K will be sensitive to the population of the putative $S = 2$ manifold for $J < 300$ cm^{-1}. While our preliminary data indicate the presence of such a state, our samples do not yet have the desired purity for presenting a convincing case.
[16] T. J. Collins, R. D. Powell, C. Slebodnick, E. S. Uffelman, *J. Am. Chem. Soc.* **1991**, *113*, 8419.

Diastereo- and Enantioselective Synthesis of 1,2-Amino Alcohols from Glycol Aldehyde Hydrazones; Asymmetric Synthesis of (*R*,*R*)-Statin**

Dieter Enders* and Ulrich Reinhold

Dedicated to Professor Franz Dallacker on the occasion of his 70th birthday

The 1,2-amino alcohol unit **A** is found in many important natural products and drugs.[1] In this context diastereo- and enantiomerically pure amino alcohols are becoming increasingly important in the development of enzyme inhibitors. γ-Amino-β-hydroxycarboxylic acids of type **B** such as statin (R = *i*Bu), 3-amino-2-hydroxy-5-phenylpentanoic acid AHPPA (R = CH_2Ph = Bn), and cyclohexylstatin (R = $CH_2C_6H_{11}$) are important examples of peptide mimetics.[2] Statin and AHPPA are essential components of pepstatin[3] and aphatinin,[4] respec-

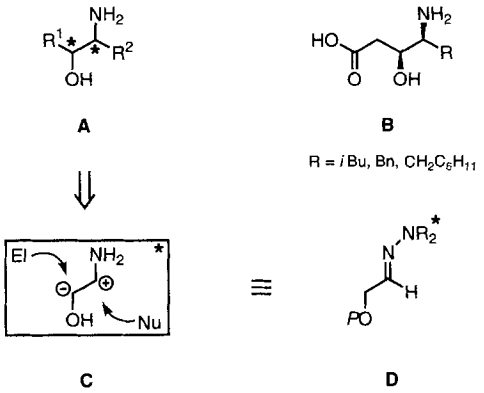
[*] Prof. Dr. D. Enders, Dipl.-Chem. U. Reinhold
Institut für Organische Chemie der Technischen Hochschule
Professor-Pirlet-Strasse 1, D-52074 Aachen (Germany)
Telefax: Int. code + (241) 8888127

[**] This work was supported by the Deutsche Forschungsgemeinschaft (Sonderforschungsbereich 380 and Leibniz Prize) and by the Fonds der Chemischen Industrie. We thank the companies Degussa AG, BASF AG, Bayer AG, Hoechst AG, and Wacker Chemie for the donation of chemicals.

tively, both natural peptidic inhibitors of acidic proteases such as renin and HIV-1-protease.

Despite the previously known syntheses of optically active amino alcohols, in most cases from naturally occurring amino acids, there is still demand for new, efficient, flexible, and highly stereoselective methods; asymmetric synthesis, in particular, has become increasingly important recently.[1, 5, 6]

Our retrosynthetic analysis of the amino alcohol **A** leads to the 1,2-amino alcohol synthon **C**, which has a^1 reactivity with regard to the amino group and d^1 reactivity with regard to the hydroxyl function and to the corresponding nucleophile (Nu) und electrophile (El). An enantiomerically pure protected glycol aldehyde hydrazone **D** (P = protecting group) can serve as a

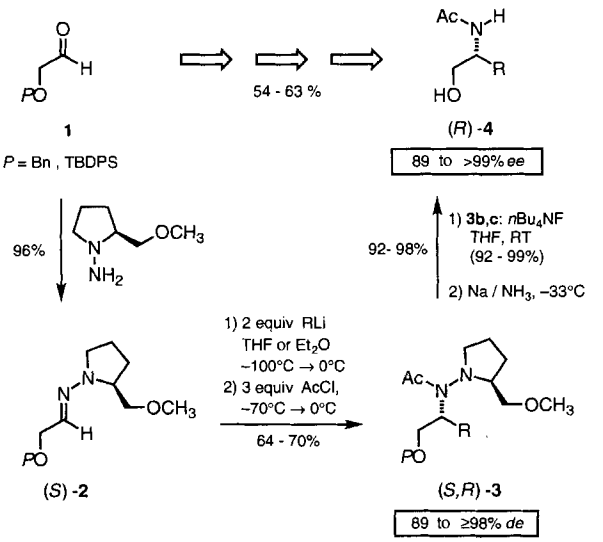


synthetic equivalent of **C**. In principle, aldehydes can be both electrophilically alkylated in the α-position and transformed into optically active amines by nucleophilic 1,2-addition to the C=N bond with high diastereo- and enantioselectivities by the SAMP/RAMP hydazone method.[7]

We now wish to report a C–C bond forming, flexible, *syn*-diastereo- and enantioselective synthesis of N-acetyl-protected amino alcohols **A** (R^1 = allyl, H; R^2 = alkyl, allyl, benzyl). Ozonolysis of a previously introduced alkenyl group and removal of the protecting groups opens up a new diastereo- and enantioselective approach to (*R,R*)-statin.

Starting from cheap and readily accessible benzyl- (Bn) or *tert*-butyldiphenylsilyl- (TBDPS) protected glycol aldehyde **1**, reaction with the chiral auxiliary (*S*)-1-amino-2-methoxymethylpyrrolidine (SAMP)[7a–e] yields the corresponding SAMP hydrazones (*S*)-**2** (Scheme 1). These are treated with two equivalents of an organolithium reagent at low temperature, and the lithium hydrazide formed was trapped with three equivalents of acetyl chloride.[8] After aqueous workup and purification by chromatography the N-acetyl-protected hydrazides (*S,R*)-**3** are obtained in good yields (64–70%) and with high to very high diastereomeric excesses (89–≥98% *de*; Table 1).[20] The silyl-protected acetyl hydrazides **3b** and **3c** are desilylated with tetra-*n*-butylammonium fluoride prior to cleavage of the N–N bond.[9] Reductive N–N bond cleavage with concomitant removal of the benzyl protecting group of (*S,R*)-**3a** is carried out with sodium in ammonia.[7h, 10] N-Acetyl-protected amino alcohols (*R*)-**4** are obtained without racemization after column chromatography in good yields (92–98%) and with high enantioselectivities (89 to >99% *ee*; Table 1).[20]

Enantiomeric excesses were determined by gas chromatography (GC) with chiral stationary phases (CSP) and by ^{1}H NMR shift experiments.[11] The chiral amine auxiliary (*S*)-2-methoxymethylpyrrolidine (SMP) can be recovered.[12] In a repre-



Scheme 1. Enantioselective synthesis of *N*-acetyl-1,2-amino alcohols (*R*)-**4**. RT = room temperature.

Table 1. N-Acetyl-protected 1,2-amino alcohols **4** prepared by 1,2-addition to hydrazones **2**.

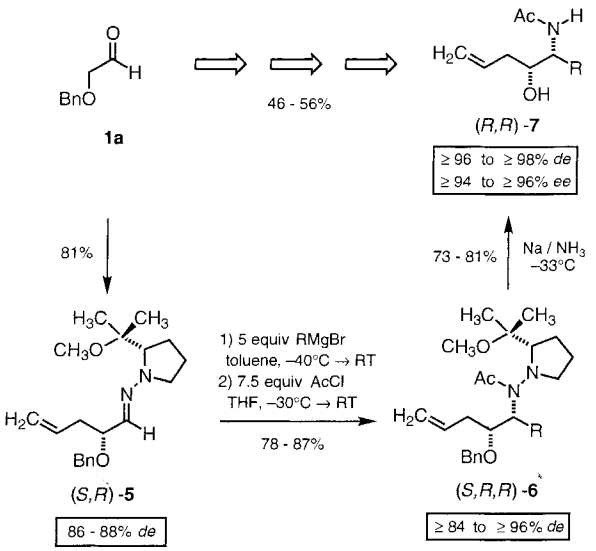
3, 4	*P*	R	3		4			
			Yield [a] [%]	*de* [b] [%]	Yield [%]	*ee* [c] [%]	$[\alpha]_D^{RT}$ (*c*, $CHCl_3$)	Config.
a [d]	CH_2Ph	Me	66 (51)	96 (>99)	96 (97)	95 (>99)	+21.7 [e] (3.24)	(*R*) [f]
b	TBDPS	*n*Bu	64	89	98	89	+27.9 (0.85)	(*R*) [f]
c	TBDPS	Allyl	70	≥98	92	>99	−15.0 (0.67)	(*R*)

[a] THF was used as solvent for **2a,b**, diethyl ether for **2c**. [b] *de* Values were determined by gas chromatography for **3a** (SE-30, FID), and by ^{13}C NMR spectroscopy for **3b,c**. [c] Based on GC analysis with a chiral stationary phase and NMR shift experiments [11]. [d] Values in parentheses for yields after separation of the diastereomers of **3a** (SiO_2, diethyl ether/petroleum ether 1:1). [e] Optical rotation of the enantiomerically pure compound **4a**. [f] Determined by comparison of the optical rotation with the literature data [13].

sentative example, (*S,R*)-**3a** was obtained diastereomerically pure (>99% *de*) by column chromatography and converted to the enantiomerically pure protected 1,2-amino alcohols (*R*)-**4a** (>99% *ee*). The absolute configurations of **4a** and **4b** were determined by comparing their optical rotations to literature data.[10] The total yield (**1** → (*R*)-**4**) over three or four steps is 54–63%.

Scheme 2 shows the successive introduction of two vicinal stereogenic centers starting from benzyl-protected glycol aldehyde **1a** by α-alkylation and 1,2-addition to afford the amino alcohols (*R,R*)-**7**. The known α-alkylation of **1a** provides (*R,S*)-**5** in very good yield (81%, two steps) and with high asymmetric inductions (86–88% *de*) with (*S*)-1-amino-2-(1-methyl-1-methoxyethyl)pyrrolidine (SADP)[14] as chiral auxiliary.[7e] The SADP hydrazone (*S,R*)-**5** is subsequently treated with five equivalents of Grignard reagent in toluene[15] and then acetyl chloride to give the *syn*-configurated *N*-acetyl hydrazides (*S,R,R*)-**6** in 78–87% yield (Table 2)[20]. The diastereoselectivities achieved with regard to the newly generated stereogenic center are greater than 98%. In addition to the directing effect of the chiral hydrazone function, this very high induction can be explained by the influence of the α-stereogenic center, which should favor the same configuration according to the chelation model.[7g–i] Hydrazide **6b** (R = Bn) is obtained with ≥98% *de* after simple purification by column chromatography. After N–N bond cleavage and simultaneous removal of the benzyl protecting group with Na/NH_3, the functionalized N-protected

 © VCH Verlagsgesellschaft mbH, D-69451 Weinheim, 1995 0570-0833/95/1111-1220 $ 10.00+.25/0 Angew. Chem. Int. Ed. Engl. 1995, 34, No. 11



Scheme 2. *syn*-Diastereo- and enantioselective synthesis of 1,2-amino alcohols (*R,R*)-7.

amino alcohols (*R,R*)-**7** are obtained with high optical purity (≥96% *de*; ≥94% *ee*; Table 2) after separation of the diastereomers by flash column chromatography.

Table 2. N-Acetyl-protected 1,2-amino alcohols **7** prepared by nucleophilic 1,2-addition to **5**.

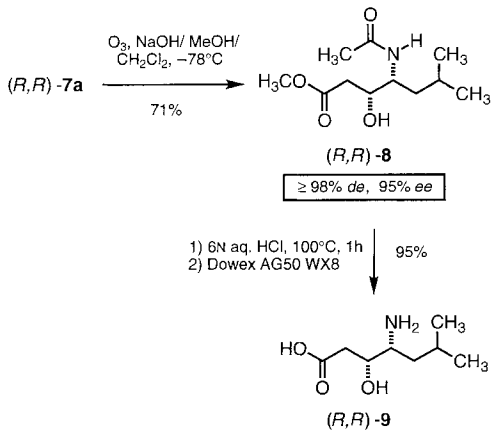
6, 7	R	6		7				
		Yield [%]	*de* [a] [%]	Yield [b] [%]	*de* [a] [%]	*ee* [c] [%]	$[\alpha]_D^{RT}$ (*c*, $CHCl_3$)	Config. [d]
a	*i*Bu	86	≥84	81	≥98 [e]	≥96	+50.3 (0.78)	(*R,R*)
b	CH_2Ph	78	≥96 [f]	73	≥96	≥94	+37.5 (1.85)	(*R,R*)
c	$CH_2C_6H_{11}$	87	≥84	75	≥98 [e]	96	+52.3 (0.65)	(*R,R*)

[a] Determined by ^{13}C NMR spectroscopy. [b] Contained 3–11% impurites (NMR, GC) after purification by column chromatography due to reduction of the allyic residue and Birch reduction of the aromatic ring. [c] Determined by ^1H NMR spectroscopy after esterification with (*S*)- or (*R*)-α-methoxy-α-trifluoromethylphenylacetic acid (MTPA) [16]. [d] Determined by comparison of the optical rotation of **9** with literature data [19] and on the basis of earlier α-alkylations and 1,2-additions with SAMP or SADP hydrazones [7e,f]. [e] After flash column chromatography (SiO_2, diethyl ether). [f] After purification by column chromatography (SiO_2, diethyl ether, petroleum ether 1:3).

The 1,2-amino alcohols (*R,R*)-**7**, accessible in four steps with yields of 46–56%, are precursors of (*R,R*)-statin (R = *i*Bu), AHPPA (R = Bn), and cyclohexylstatin (R = $CH_2C_6H_{11}$). The *N*-acetyl amino alcohol (*R,R*)-**7a** can be transformed to the methyl ester (*R,R*)-**8** by oxidative cleavage of the C=C bond with ozone in basic methanol/dichloromethane in good yield (71%) without racemization.[17] The acid hydrolysis of the methyl ester and the acetamide function proceeds at 100 °C in 6N aqueous hydrochloric acid within one hour quantitatively, yielding statin hydrochloride (*R,R*)-**9**·HCl. After ion exchange chromatography free (*R,R*)-statin (**9**) is obtained in a total yield of 38% over six steps[18] (Scheme 3).

Compounds **6**–**9** are assigned the (*R,R*) configuration by comparison of the optical rotation of the synthesized statin with literature data,[19] given the (*R*) configuration in the α-alkylation[7e] and assuming a uniform reaction course. The natural *syn*-(*S,S*)-statin is analogously accessible by the use of the auxiliary (*R*)-1-amino-2-(1-methoxy-1-methylethyl)pyrrolidine (RADP)[14] instead of SADP.

The method described here opens up a new *syn*-diastereo- and enantioselective route to N-acetyl-protected functionalized vicinal amino alcohols. The particular advantage is the high flexibility through variation of the nucleophilic and the electrophilic component. As was shown for statin and its analogues, this procedure should facilitate the asymmetric synthesis of a multitude of optically active 1,2-amino alcohols in the scope of natural product and drug synthesis.



Scheme 3. Diastereo- and enantioselective synthesis of (*R,R*)-statin (**9**).

Experimental Procedure

(*S,R*)-**3**: To a solution of 10 mmol of hydrazone (*S*)-**2** in 40 mL of THF (Et_2O for R = allyl) was added dropwise 20 mmol of the organolithium solution at −100 °C (for R = Me, −70 °C) with stirring. The solution was allowed to warm to 0 °C over 12 h. The solution was then cooled to −70 °C, 30 mmol of AcCl was added, and the mixture was stirred for 1 h at this temperature and for a further 0.5–2 h at 0 °C. It is advisable to monitor the reaction by thin-layer chromatography to avoid reduced yields. For hydrolysis 80 mL of saturated $NaHCO_3$ solution was added and the reaction mixture extracted three times with ether. The combined extracts were dried over $MgSO_4$ and the ether was removed in vacuo. After purification of the yellow-brown crude products by flash column chromatography (SiO_2, diethyl ether/petroleum ether 1:1 to 1:2), colorless or pale yellow liquids were obtained.

(*S,R,R*)-**6**: To a solution of 10 mmol of hydrazone (*S,R*)-**5** in 500 mL of toluene under argon was added dropwise at −40 °C with stirring 50 mmol of RMgBr (2N in diethyl ether). This solution was then allowed to warm to room temperature over 12 h. THF (100 mL) was added, the solution was cooled to −30 °C, and then 75 mmol of AcCl was added dropwise. The solution was warmed to room temperature over 2 h and then stirred for a further 2 h (tlc control). Finally workup was carried out as above to afford, after column chromatography (SiO_2, diethyl ether/petroleum ether 1:3 to 1:4), colorless to pale yellow liquids. **6b** precipitated as a colorless crystalline solid.

(*R*)-**4** and (*R,R*)-**7**: To 25 mL of liquid ammonia at −70 °C was added dropwise a solution of 1 mmol of acetyl hydrazide **3a** and **6** (**3b** and **3c** were previously desilylated with 1.5 equiv *n*-Bu_4NF in THF at room temperature) in 6 mL of THF, and then 10 mmol of Na was added. The solution was warmed to reflux (−33 °C). Upon complete consumption of starting material (tlc control) 1.5 g of NH_4Cl was added. The ammonia was evaporated, and the solid residue was extracted three times with 30 mL of dichloromethane. The combined extracts were filtered, and the solvent was removed in vacuo. Purification by flash column chromatography (SiO_2, diethyl ether or diethyl ether/MeOH 6:1 to 15:1) afforded either a colorless liquid or solid.

Received: February 4, 1995 [Z7695 IE]
German version: *Angew. Chem.* **1995**, *107*, 1332–1334

Keywords: amino alcohols · asymmetric syntheses · hydrazones · nucleophilic additions · statins

[1] Reviews on the synthesis and applications of 1,2-amino alcohols: a) R. Henning, *Nachr. Chem. Tech. Lab.* **1990**, *38*, 460–464; b) M. T. Reetz, *Angew. Chem.* **1991**, *103*, 1559–1573; *Angew. Chem. Int. Ed. Engl.* **1991**, *30*, 1531–1545; c) Y. Ohfune, *Acc. Chem. Res.* **1992**, *25*, 360–366; d) T. Yokomatsu, Y. Yuasa, S. Shibuya, *Heterocycles* **1992**, *33*, 1051–1078; e) A. Golebiowski, J. Jurczak, *Synlett* **1993**, 241–245; f) T. Kunieda, T. Ishizuka in *Studies in Natural Products Chemistry, Vol. 12* (Ed.: Atta-ur-Rahman), Elsevier, New York, **1993**, p. 411.

[2] Review: a) D. H. Rich in *Comprehensive Medicinal Chemistry, Bd. 2* (Ed.: C. Hansch, P. G. Sammes, J. B. Taylor), Pergamon, New York, **1990**, p. 391; b) J. Gante, *Angew. Chem.* **1994**, *106*, 1780–1802; *Angew. Chem. Int. Ed. Engl.* **1994**, *33*, 1699–1720.

 © VCH Verlagsgesellschaft mbH, D-69451 Weinheim, 1995 0570-0833/95/1111-1221 $ 10.00+.25/0

[3] a) H. Umezawa, T. Aoyagi, H. Morishima, M. Matsuzaki, M. Hamada, T. Takeuchi, *J. Antibiotics* **1970**, *23*, 259–265; b) H. Morishima, T. Takita, T. Aoyagi, T. Takeuchi, H. Umezawa, *ibid.* **1970**, *23*, 263–265.

[4] a) D. H. Rich, E. T. Sun, *J. Med. Chem.* **1980**, *23*, 27–33; b) S. Omura, N. Imamura, K. Kawakita, Y. Mori, Y. Yamazaki, R. Masuma, Y. Takahachi, H. Tanaka, L.-Y. Huang, H. B. Woodruff, *J. Antibiot.* **1986**, *39*, 1079–1085.

[5] Asymmetric syntheses: a) D. Enders, U. Jegelka, B. Dücker, *Angew. Chem.* **1993**, *105*, 423–425; *Angew. Chem. Int. Ed. Engl.* **1993**, *32*, 423–425; b) S. Kanemasa, T. Mori, A. Tatsukawa, *Tetrahedron Lett.* **1993**, *34*, 8293–8296; c) A. G. M. Barrett, M. A. Seefeld, *Tetrahedron* **1993**, *49*, 7857–7870; d) K. Hattori, H. Yamamoto, *ibid.* **1994**, *50*, 2785–2792; e) M. E. Brunnage, A. J. Burke, S. G. Davies, C. J. Goodwin, *Tetrahedron: Asymmetry* **1994**, *5*, 203–206; f) A. M. Kanazawa, J.-N. Denis, A. E. Greene, *J. Org. Chem.* **1994**, *59*, 1238–1240; asymmetric syntheses of primary 1,2-amino alcohols: g) Y. Ukaji, K. Kume, T. Watai, T. Fujisawa, *Chem. Lett.* **1991**, 173–176; h) J. Schwerdtfeger, D. Hoppe, *Angew. Chem.* **1992**, *104*, 1547–1549; *Angew. Chem. Int. Ed. Engl.* **1992**, *31*, 1505–1508; i) S. Matsubara, H. Ukita, T. Kodama, K. Utimoto, *Chem. Lett.* **1994**, 831–834; j) O. Lingibe, B. Graffe, M.-C. Sacquet, G. Lhommet, *Heterocycles* **1994**, *37*, 1469–1472.

[6] Review on statin synthesis: a) J. Mulzer, H.-J. Altenbach, M. Braun, K. Krohn, H.-U. Reissig, *Organic Synthesis Highlights*, VCH, Weinheim, **1991**, p. 365; b) ref. [1d]; recent statin syntheses: c) A. Bernardi, F. Micheli, D. Potenza, C. Scolastico, R. Villa, *Tetrahedron Lett.* **1990**, *31*, 4949–4952; d) D. Misti, G. Zappa, *ibid.* **1990**, *31*, 7359–7362; e) T. Ohta, S. Shiokawa, R. Sakamoto, S. Nozoe, *ibid.* **1990**, *31*, 7329–7332; f) K. Shinozaki, K. Mizuno, H. Oda, Y. Masaki, *Chem. Lett.* **1992**, 2265–2268; g) Y. Lu, C. Miet, N. Kunesch, J. E. Poisson, *Tetrahedron: Asymmetry* **1993**, *4*, 893–902; h) J. W. B. Cooke, S. G. Davis, A. Naylor, *Tetrahedron* **1993**, *49*, 7955–7966; i) U. Schmidt, B. Riedl, G. Haas, H. Griesser, A. Vetter, S. Weinbrenner, *Synthesis* **1993**, 216–220, and references therein; j) K. Otsuka, T. Ishizuka, K. Kimura, T. Kunieda, *Chem. Pharm. Bull.* **1994**, *42*, 748–750; asymmetric syntheses of statin: l) T. Ishizuka, S. Ishibuchi, T. Kunieda, *Tetrahedron* **1993**, *49*, 1841–1852 and references therein; m) L. Bertelli, R. Fiaschi, E. Napolitano, *Gazz. Chim. Ital.* **1993**, *123*, 521–524; n) K.-J. Hwang, C.-M. Yu, N.-K. Choi, K.-H. Park, *Bull. Korean Chem. Soc.* **1994**, *15*, 525–526.

[7] Reviews on the SAMP/RAMP method: a) D. Enders in *Asymmetric Synthesis, Vol. 3 B* (Ed.: J. D. Morrison), Academic Press, Orlando, **1984**, p. 275; b) D. Enders, P. Fey, H. Kipphardt, *Org. Synth.* **1987**, *65*, 173–202; c) D. Enders, M. Klatt in *Encyclopedia of Reagents for Organic Synthesis* (Hrsg.: L. A. Paquette), Wiley, New York, **1995**, in press; examples of α-alkylation: d) D. Enders, J. Tiebes, N. de Kimpe, M. Keppens, C. Steens, G. Smagghe, O. Betz, *J. Org. Chem.* **1993**, *58*, 4881–4884; e) D. Enders, U. Reinhold, *Synlett* **1994**, 792–795; for 1,2-additions to hydrazones see: f) D. Enders, J. Schankat, M. Klatt, *ibid.* **1994**, 795–797 and references therein; for 1,2-additions to α-hydroxyaldehyde hydrazones see: g) D. A. Claremon, P. K. Lumma, B. T. Philips, *J. Am. Chem. Soc.* **1986**, *108*, 8265–8266; h) C. Nübling, Dissertation, Technische Hochschule, Aachen, **1987**; i) W. R. Baker, S. L. Condon, *J. Org. Chem.* **1993**, *58*, 3277–3284.

[8] Allyllithium was prepared by transmetalation of allyl-tri-*n*-butylstannane with *n*-butyllithium in diethyl ether and used without further purification.

[9] S. Hanessian, P. Lavallee, *Can. J. Chem.* **1975**, *53*, 2975–2977.

[10] S. E. Denmark, O. Nicaise, J. P. Edwards, *J. Org. Chem.* **1990**, *55*, 6219–6223.

[11] Chiral stationary phases: heptakis(2,3,6-tri-*O*-methyl)-β-cyclodextrin/polysiloxane (25 m, 0.25 mm internal diameter (ID)) for **4a**; heptakis(2,6-di-*O*-methyl)-β-cyclodextrin/polysiloxane (25 m, 0.25 mm ID) for **4b**. (−)-(*R*)-1-(9-Anthryl)-2,2,2-trifluoroethanol was used as chiral cosolvent in the NMR experiments.

[12] D. Enders, R. Funk, M. Klatt, G. Raabe, *Angew. Chem.* **1993**, *105*, 418–420; *Angew. Chem. Int. Ed. Engl.* **1993**, *32*, 418–420.

[13] S. Fernández, R. Brieva, F. Rebolledo, V. Gotor, *J. Chem. Soc. Perkin Trans. 1* **1992**, 2885–2889.

[14] D. Enders, H. Kipphardt, P. Gerdes, L. J. Breña-Valle, V. Bushan, *Bull. Soc. Chim. Belg.* **1988**, *97*, 691–704.

[15] a) A. Alexakis, N. Lensen, J.-P. Tranchier, P. Mangeney, *J. Org. Chem.* **1992**, *57*, 4563–4565. b) Lower inductions were achieved for the 1,2-addition of Grignard reagents in toluene to hydrazones **2** in comparison with that of organolithium compounds (< 90% *de*).

[16] a) J. A. Dale, D. L. Dull, H. S. Mosher, *J. Org. Chem.* **1969**, *34*, 2543–2549; b) J. A. Dale, H. S. Mosher, *J. Am. Chem. Soc.* **1973**, *95*, 512–519.

[17] J. A. Marshall, A. W. Garofalo, *J. Org. Chem.* **1993**, *58*, 3675–3680.

[18] For removal of the protecting group and subsequent ion exchange chromatography (Dowex AG50 WX8, 0.1 M pH 5 buffer (acetic acid/pyridine)): a) R. Steulmann, H. Klostermeyer, *Liebigs Ann. Chem.* **1975**, 2245–2250; b) W.-S. Liu, S. C. Smith, G. I. Glover, *J. Med. Chem.* **1979**, *22*, 577–579.

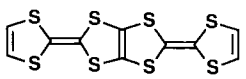
[19] (*R,R*)-9: $[\alpha]_D^{25} = +18.4$ ($c = 0.43$ in H_2O), $[\alpha]_D^{RT} = +19$ to $+20$ ($c = 0.55$–1.0 in H_2O) [18b] and references cited therein (RT = room temperature); m.p. 198–199 °C (decomp, H_2O/acetone), 200–202 °C, 234–236 °C [18b], and references cited therein.

[20] All new compounds gave correct spectroscopic data (IR, NMR, MS) and correct microanalyses or high-resolution mass spectra (HRMS).

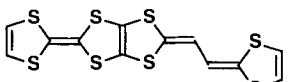
(DTEDT)[Au(CN)$_2$]$_{0.4}$: An Organic Superconductor Based on the Novel π-Electron Framework of Vinylogous Bis-Fused Tetrathiafulvalene**

Yohji Misaki,* Natsuko Higuchi, Hideki Fujiwara, Tokio Yamabe,* Takehiko Mori,* Hatsumi Mori,* and Shoji Tanaka

Highly conducting and superconducting organic solids have attracted much attention in the fields of organic chemistry, physical chemistry, and solid-state physics, amongst others.[1] The most appropriate strategy to stabilize the metallic state down to low temperature and to reach the superconducting transition has been thought to be the formation of a two-dimensional (2D) electronic structure, which is usually attained by use of TTF with "capped" dichalcogeno groups, such as bis(ethylenedithio)tetrathiafulvalene (BEDT-TTF).[1, 2] We have now found that a bis-fused TTF, 2,5-bis(1,3-dithiol-2-ylidene)-1,3,4,6-tetrathiapentalene (BDT-TTP),[3] tends to produce 2D "metals" without such substituents.[4] The extended π-conjgation systems of BDT-TTP (bis-fused donors containing extended TTFs[5, 6]), which have received much attention recently, are of considerable interest in the search for new donors for organic superconductors. We report herein the synthesis of the first vinylogous BDT-TTP, DTEDT, **1a**, which contains one 2,2′-ethanediylidenebis(1,3-dithiole) (**2**).[6] Furthermore, we have found that the present donor produces a superconducting Au(CN)$_2$ salt, as well as many metallic cation radical salts stable to liquid helium temperature.



BDT-TTP



DTEDT **1a**

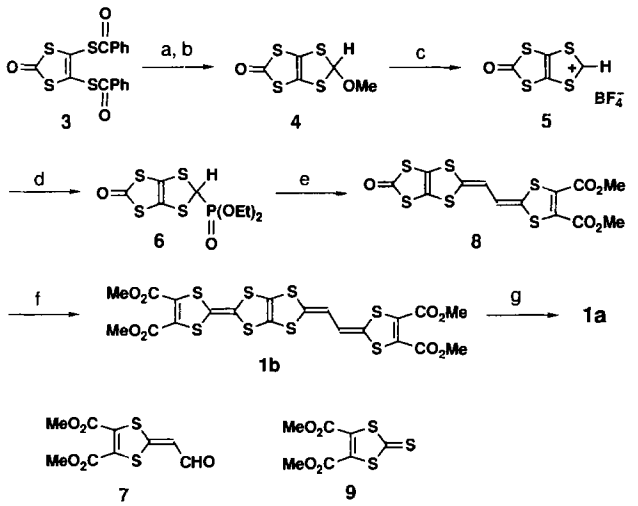
The synthesis of DTEDT was achieved as shown in Scheme 1. Treatment of 1,3-dithiol-2-one **3** with sodium methoxide, and then with α,α-dichloromethyl methyl ether afforded **4**. This one-pot reaction was carried out in acetone to avoid reaction of α,α-dichloromethyl methyl ether with usual solvent (methanol). The reaction of **4** with aqueous hydrofluoroboric acid gave the corresponding 1,3-dithiolium salt **5**, which was converted to a phosphonate **6** by treatment with triethylphosphite in the presence of sodium iodide. The compound **6** was allowed to react with lithium diisopropylamide in the presence of 2-formylmethylidene-4,5-bis(methoxycarbonyl)-1,3-dithiole (**7**)[6a] to give **8**. The cross-coupling reaction between **8** and 4,5-bis(methoxy-

[*] Dr. Y. Misaki, Prof. Dr. T. Yamabe, N. Higuchi, H. Fujiwara
Division of Molecular Engineering, Graduate School of Engineering
Kyoto University, Yoshida, Kyoto 606-01 (Japan)
Telefax: Int. code + (75) 751-7279

Dr. T. Mori
Department of Organic and Polymeric Materials
Faculty of Engineering, Tokyo Institute of Technology
O-okayama, Tokyo 152 (Japan)
Telefax: Int. code + (3) 5734-2876

Dr. H. Mori, Dr. S. Tanaka
International Superconductivity Technology Center
Shinonome, Tokyo 135 (Japan)
Telefax: Int. code + (3) 3536-5717

[**] This work was partially supported by a Grant-in-Aid for Scientific Research on Priority Area "Molecular Conductors" (No. 06243215) from the Ministry of Education, Science, and Culture of Japan. DTEDT = 2-(1,3-dithiol-2-ylidene)-5-(2-ethanediylidene-1,3-dithiole)-1,3,4,6-tetrathiapentalene, TTF = tetrathiafulvene.



Scheme 1. a) NaOMe (2 equiv), acetone, room temperature, 30 min; b) Cl_2CHOMe (2 equiv), 30 min (59%), c) 42% aqueous HBF_4 (2 equiv), CH_2Cl_2/Ac_2O (4/1), 0 °C, 30 min (92%); d) $P(OEt)_3$ (2 equiv), NaI (2 equiv), acetone, room temperature, 12 h (83%); e) LDA (1 equiv), **7** (1 equiv), THF, −78 °C, 20 min (57%); f) **9** (2 equiv), $P(OMe)_3$ (100 equiv), toluene, 110 °C, 2 h (76%); g) $LiBr \cdot H_2O$ (20 equiv), HMPA, 90 °C, 1 h, 130 °C, 30 min (88%).

carbonyl)-1,3-dithiole-2-thione (**9**) with a large excess of trimethylphosphite afforded the tetrakis(methoxycarbonyl) derivative **1b**. The target molecule **1a** was obtained by heating **1b** with an excess of $LiBr \cdot H_2O$ in HMPA. DTEDT forms as yellow orange stable microcrystals,[7] which are less soluble in organic solvents than BEDT-TTF and BDT-TTP.

The cyclic voltammograms of **1a, b** exhibit four pairs of single-electron redox waves at +0.37, +0.50, +0.81, and +1.05 V (vs. SCE, in PhCN at 25 °C) for **1a**, and +0.56, +0.70, +1.07, and +1.30 V for **1b**. The E_1 value of **1a** is 0.07 V lower than that of BDT-TTP (+0.44 V)[3b] measured under the identical conditions. However, it is 0.08 V higher than that of **2** (+0.29 V) and is comparable to that of TTF (+0.35 V). The donor ability thus becomes weaker in spite of the apparent extension of the π-conjugation, as is also the case for BDT-TTP. On the other hand, $E_2 - E_1$ value (0.13 V) is smaller than those of BDT-TTP (0.18 V), TTF (0.42 V), and **2** (0.20 V), which suggests that the Coulomb repulsion has decreased in the dication.

The MNDO molecular orbital calculations of DTEDT revealed that in the highest occupied molecular orbital (HOMO) the phases of the sulfur atoms in the terminal vinylogous 1,3-dithiole ring are reversed with respect to the other sulfur atoms (Fig. 1).[8] This feature together with the crooked structure of DTEDT is anticipated to diminish the effectiveness of the transverse interaction both sterically and electronically in the charge transfer salts relative to the strip-like BDT-TTP in which all sulfur atoms have the same phase.[9]

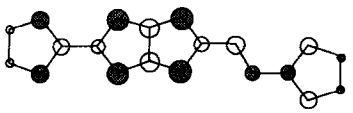


Fig. 1. The highest occupied molecular orbital (HOMO) of DTEDT (**1a**).

Cation radical salts of DTEDT were prepared by electrochemical oxidation in the presence of the corresponding tetra-*n*-butylammonium salts under a constant current of 0.3–1 $\mu A\,cm^{-2}$ in chlorobenzene or 1,1,2-trichloroethane at 50 °C. The I_3 salt was obtained by using the diffusion technique with n-Bu_4NI_3 in chlorobenzene at 50 °C. Table 1 shows their electrical properties measured by the four-probe technique on single crystals. Surprisingly, most of the salts obtained so far show metallic conducting behavior down to low temperature (1.4–4.2 K) regardless of the counteranion. Figure 2 shows conducting behavior of the $Au(CN)_2$ salt. It shows an abrupt drop of resistivity at 4 K, which is characteristic of the onset of the superconducting transition. However, the resistivity remained nonzero even at 2 K probably because of non-superconducting domains in the crystal. The superconductivity was also confirmed by magnetic susceptibility measurements with a SQUID susceptometer (Fig. 3). The diamagnetic shielding at 2 K amounts to 10% of the perfect diamagnetism, suggesting bulk superconductivity. Both zero-field cooled data (ZFC) and field cooled data (FC) start to decrease at 4 K, which agrees with the transition temperature obtained from the resistivity measurement.

Table 1. Composition and electrical conductivity of DTEDT salts (DTEDT · A_x).

Anion A	x[a]	σ[$S\,cm^{-1}$][b]	Behavior
ClO_4	0.67(Cl)	830	metallic[c]
BF_4	–[d]	540	metallic[c]
ReO_4	0.39(Re)	900	metallic ≥1.4 K
$GaCl_4$	0.48(Ga)	50	metallic ≥1.4 K
PF_6	0.39(P)	170	metallic ≥4.2 K
AsF_6	0.54(As)	90	metallic ≥1.4 K
SbF_6	0.57(Sb), 0.33[e]	80	metallic ≥1.4 K
I_3	0.34(I)	670	metallic ≥1.4 K
$Au(CN)_2$	0.39(Au), 0.4[e]	15	T_c = 4 K[f]

[a] Determined by the energy dispersion spectroscopy (EDS) from the ratio of sulfur and the elements designated in the parentheses. [b] Conductivity at room temperature measured by four-probe technique on a single crystal. [c] The resistivity increases a little at low temperatures, but the compound is essentially metallic down to 1.4 K. [d] The content of light elements such as B and F were not reliably determined by EDS. [e] Determined from X-ray structure analysis. [f] T_c designates critical temperature of superconducting transition.

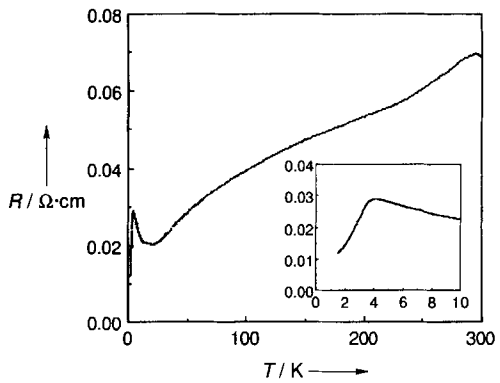


Fig. 2. Temperature dependence of resistivity of $(DTEDT)[Au(CN)_2]_{0.4}$. The inset shows the resistivity in the range of 1.4–10 K.

The crystal structure of this $Au(CN)_2$ salt was determined by X-ray structure analysis.[10] The donors form conducting sheets parallel to the *ac* plane (Fig. 4). They are stacked face-to-face, with ring-over-bond type overlap (Fig. 5). Because the present salt crystallizes in space group $P\bar{1}$ and there is only one DTEDT molecule in the unit cell, the donors are arranged in such a way that the stacking and transverse directions are parallel. Since DTEDT has a crooked structure and the phase of the sulfur atoms in the HOMO is reversed at the terminal vinylogous 1,3-dithiole, such a parallel arrangement results in the most

 © VCH Verlagsgesellschaft mbH, D-69451 Weinheim, 1995 0570-0833/95/1111-1223 $ 10.00+.25/0

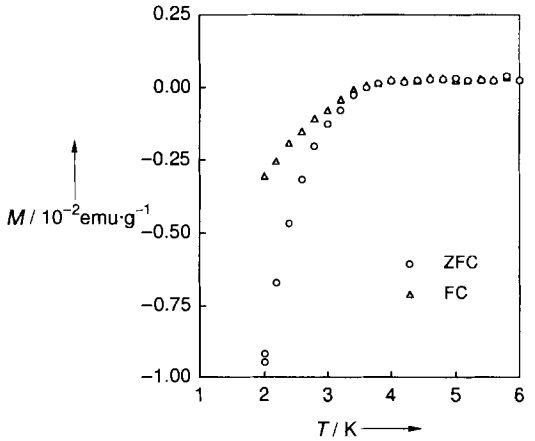


Fig. 3. Temperature dependence of magnetization at an applied magnetic field of 2 mT.

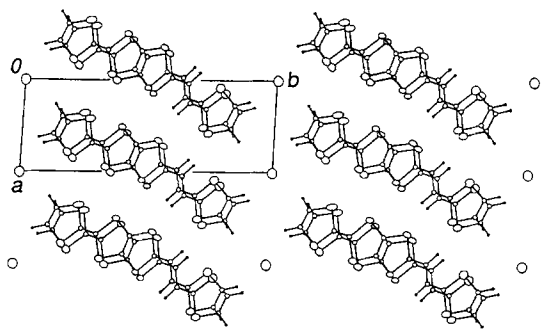


Fig. 4. Crystal structure of (DTEDT)$[Au(CN)_2]_{0.4}$. Projection onto the *ab* plane.

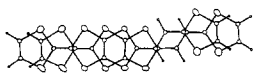


Fig. 5. Projection onto the plane of the molecule showing ring-over-bond type overlap of the donor molecules in (DTEDT)$[Au(CN)_2]_{0.4}$.

effective intermolecular interaction both sterically and electronically. Population analysis indicates that the ratio of DTEDT to $Au(CN)_2$ is 1:0.4. The linear anion, $Au(CN)_2$, is aligned along the *c* axis, and exists in every other unit cell with 80% population. This is in good agreement with the result of energy dispersion spectroscopy (D:A = 1:0.39). The arrangement of donors resembles that of β-(BEDT-TTF)$_2$X (X = I_3, IBr_2, AuI_2 etc.) (Fig. 6).[2] However, the donors form completely uniform stacks in (DTEDT)$[Au(CN)_2]_{0.4}$, whereas they exist as dimers in β-type BEDT-TTF salts. The interplanar distances is 3.51 Å. Such a uniform β-type arrangement of donors is also observed in (BDT-TTP)$_2$X (X = ClO_4, SbF_6)[4] and (DTEDT)$_3SbF_6$.[11]

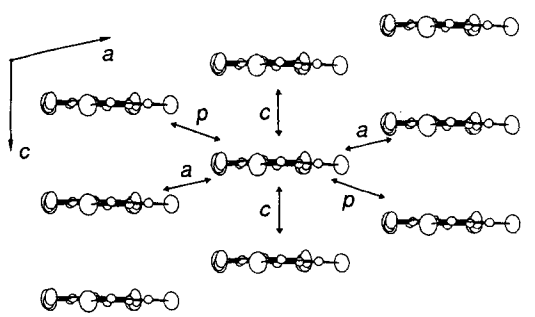


Fig. 6. Donor sheet structure of (DTEDT)$[Au(CN)_2]_{0.4}$.

The fact that both the SbF_6 and $Au(CN)_2$ salts have isostructural 2D arrays of donors regardless of the counteranions indicates that DTEDT has a strong tendency to form a 2D array in spite of its unsymmetrical and crooked structures.

The band structure calculated by the tight-binding method is shown in Figure 7. A fairly large overlap in the stack ($c = -18.3 \times 10^{-3}$) corresponds to a large bandwidth of 0.9 eV. On the other hand, the interstack overlap is about one third of the intrastack interaction. Such a comparatively large interstack interaction gives a closed Fermi surface, although one-dimensional character along the stacking direction is dominant.

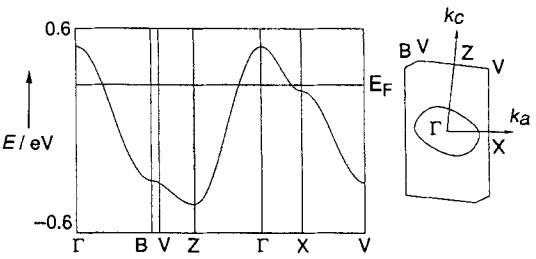


Fig. 7. Energy band structure and Fermi surface of (DTEDT)$[Au(CN)_2]_{0.4}$. The intermolecular overlap integrals are $a = -1.5$, $c = -18.3$, $p = -5.0 \times 10^{-3}$ (see also Fig. 6). E_F = Fermi energy.

In conclusion, we have synthesized an organic superconductor using a novel π-electron framework. DTEDT is the first vinylogous component for organic superconductors; however, the role of vinylogous TTF moiety is not clear at the present time. The further investigations on physical properties of the salt are in progress.

Received: January 27, 1995
Revised: March 8, 1995 [Z 7669/7670 IE]
German version: *Angew. Chem.* **1995**, *107*, 1340–1343

Keywords: organic conductors · superconductors · tetrathiafulvalenes

[1] a) Proc. ICSM'92 (Göteborg), *Synth. Meth.* **1993**, *55–57*; b) *The Physics and Chemistry of Organic Superconductors* (Eds.: G. Saito, S. Kagoshima), Springer, Berlin, Heidelberg, **1990**.

[2] a) J. M. Williams, J. R. Ferraro, R. J. Thorn, K. D. Carlson, U. Geiser, H. H. Wang, A. M. Kini, M.-H. Whangbo, *Organic Superconductors*, Prentice Hall, New Jersey, **1992**; b) T. Ishiguro, K. Yamaji, *Organic Superconductors*, Springer, Berlin, Heidelberg, **1990**.

[3] a) Y. Misaki, H. Nishikawa, K. Kawakami, S. Koyanagi, T. Yamabe, M. Shiro, *Chem. Lett.* **1992**, 2321; b) Y. Misaki, T. Matsui, K. Kawakami, H. Nishikawa, T. Yamabe, M. Shiro, *ibid.* **1993**, 1337; c) Y. Misaki, K. Kawakami, T. Matsui, T. Yamabe, M. Shiro, *J. Chem. Soc. Chem. Commun.* **1994**, 459; T. Mori, Y. Misaki, T. Yamabe, *Bull. Chem. Soc. Jpn.* **1994**, *67*, 3187, and references therein.

[4] a) Y. Misaki, H. Fujiwara, T. Yamabe, T. Mori, H. Mori, S. Tanaka, *Chem. Lett.* **1994**, 1653; b) T. Mori, Y. Misaki, H. Fujiwara, T. Yamabe, *Bull. Chem. Soc. Jpn.* **1994**, *67*, 2685.

[5] See, for example: a) Y. Yamashita, Y. Kobayashi, T. Miyashi, *Angew. Chem.* **1989**, *101*, 1090; *Angew. Chem. Int. Ed. Engl.* **1989**, *28*, 1052; b) K. Takahashi, T. Nihira, K. Tomitani, *J. Chem. Soc. Chem. Commun.* **1993**, 1617; c) T. K. Hansen, M. V. Lakshmikantham, M. P. Cava, R. E. Niziurski-Mann, F. Jensen, J. Becher, *J. Am. Chem. Soc.* **1992**, *114*, 5035; d) A. S. Benahmed-Gasmi, P. Frère, B. Garrigues, A. Gorgues, M. Jubault, R. Carlier, F. Texier, *Tetrahedron Lett.* **1992**, *33*, 6457; e) A. Belyasmine, P. Frère, A. Gorgues, M. Jubault, G. Duguay, P. Hudhomme, *ibid.* **1993**, *34*, 4005.

[6] See, for example: a) Z. Yoshida, T. Kawase, H. Awaji, I. Sugimoto, T. Sugimoto, S. Yoneda, *Tetrahedron Lett.* **1983**, *24*, 3469; b) T. Sugimoto, H. Awaji, I. Sugimoto, Y. Misaki, T. Kawase, S. Yoneda, Z. Yoshida, T. Kobayashi, H. Anzai, *Chem. Mater.* **1989**, *1*, 535; c) V. Y. Khodorkovskii, L. N. Veselova, O. Y. Neiland, *Khim. Geterotsikl. Soedin.* **1990**, 130; d) A. J. Moore, M. R. Bryce, D. J. Ando, M. B. Hursthouse, *J. Chem. Soc. Chem. Commun.* **1991**, 320; e) T. K. Hansen, M. V. Lakshmikantham, M. P. Cava, R. M. Metzger, J. Becher, *J. Org. Chem.* **1991**, *56*, 2720; f) A. J. Moore, M. R. Bryce, *Tetrahedron Lett.* **1992**, *33*, 1373; g) M. Sallé, A. J. Moore, M. R. Bryce, M. Jubault, *ibid.* **1993**, *34*, 7475.

[7] Selected physical and spectral data of DTEDT **1a**: M.p. 197 °C (decomp.); IR (KBr): $\tilde{\nu}$ = 3059, 1504, 1283, 1261, 805 cm^{-1}; UV ($CHCl_3$): λ_{max} (lg ε) = 402 (4.54), 345 (4.46), 283 (4.23) nm; ^1H NMR (90 MHz, CS_2/C_6D_6, 25 °C, TMS): δ = 6.04 (s, 4H), 5.69 (s, 2H); MS (70 eV): *m/z*: 406 [M^+].

[8] The molecular orbital calculation was carried out with the Gaussian 90 program: M. J. Frisch, M. Head-Gordon, G. W. Trucks, J. B. Foresman, H. B. Schlegel, D. J. Defrees, D. J. Fox, R. A. Whiteside, R. Seeger, C. F. Melius, J. Baker, R. L. Martin, L. R. Kahn, J. J. P. Stewart, S. Topiol, J. A. Pople, *Gaussian 90, Revision F*, Gaussian Inc., Pittsburgh, PA, **1990**.

[9] S. Kawauchi, H. Nishikawa, Y. Misaki, T. Yamabe, unpublished results.

[10] Crystal data of $(DTEDT)[AuCN)_2]_{0.4}$: M_r = 506.31, triclinic, space group *P*1, *a* = 6.322(1), *b* = 17.211(3), *c* = 3.857(1) Å, α = 95.25(2), β = 95.52(2), γ = 93.75(1)°, *V* = 414.8(2) Å^3, *Z* = 1, ρ_{calcd} = 2.027 g cm^{-3}, Rigaku AFC-5R diffractometer, graphite monochromator, $Mo_{K\alpha}$ radiation (λ = 0.71073 Å), ω-2θ scan mode (2θ < 55°), 1206 independent reflections, ($|F_o| > 3\sigma(F_o)$), absorption correction, $\mu(Mo_{K\alpha})$ = 45.407 cm^{-1}. The structure was solved by direct methods (SHELXS86: G. M. Sheldrick, *Crystallographic Computing 3*, Oxford University Press, **1985**, pp. 175–189), and was refined by a block-diagonal, least-squares procedure (UNICS III; $\omega = [\sigma(F_o)^2 + (0.015F_o)^2]^{-1}$). Anisotropic thermal parameters were adopted for all non-hydrogen atoms, whereas the hydrogen atoms were refined isotropically. *R* (R_w) = 0.079 (0.081). Further details of the crystal structure investigation may be obtained from the Director of the Cambridge Crystallographic Data Centre, 12 Union Road, CB-Cambridge CB2 1EZ (UK) on quoting the full journal of citation.

[11] Y. Misaki, N. Higuchi, T. Ohta, H. Fujiwara, T. Yamabe, T. Mori, H. Mori, S. Tanaka, unpublished results.

Reactions of Carbocations with π Nucleophiles: Polar Mechanism and No Outer Sphere Electron Transfer**

Matthias Patz, Herbert Mayr,* Junichi Maruta, and Shunichi Fukuzumi*

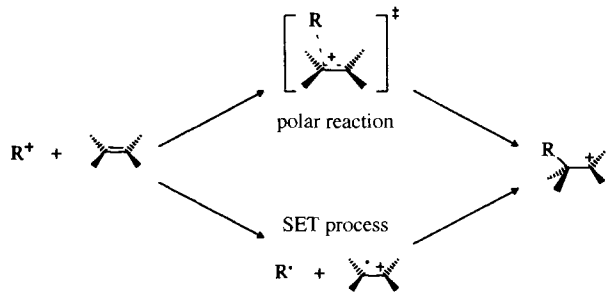
Dedicated to Professor Paul von Ragué Schleyer on the occasion of his 65th birthday

The importance of electron transfer processes has been recognized in many areas of organic chemistry. Numerous reactions, previously described by "movements of electron pairs" by the familiar "curved-arrow" mechanisms are now understood as processes, in which an initial electron transfer step produces a pair of radical ions, which successively react with formation of a new bond.[1]

Consequently, for the reactions of cationic electrophiles R^+ with neutral π nucleophiles two different mechanisms have to be considered. In the polar mechanism depicted in the upper route of Scheme 1, the carbocation approaches the π system of the nucleophile, and the charge transfer is associated with the formation of the new carbon–carbon σ bond. In the alternative outer sphere electron transfer mechanism at the bottom of Scheme 1, rate-determining electron transfer (single electron transfer, SET) produces a radical and a radical cation which may combine to give the same cation produced by the polar reaction.

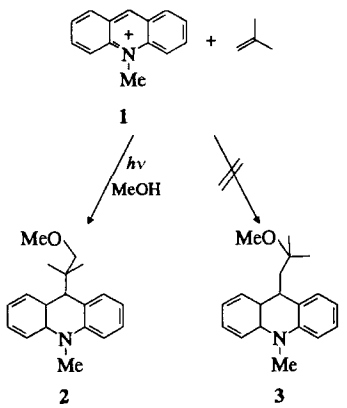
[*] Prof. Dr. H. Mayr, Dr. M. Patz
Institut für Organische Chemie der Technischen Hochschule
Petersenstrasse. 22, D-64287 Darmstadt (Germany)
Telefax: Int. code + (6151) 16 5591
Prof. Dr. S. Fukuzumi, J. Maruta
Department of Applied Chemistry, Faculty of Engineering
Osaka University
Suita Osaka 565 (Japan)
Telefax: Int. code + (6)876-4754

[**] We thank the Deutsche Forschungsgemeinschaft for financial support, and we are grateful to the Fonds der chemischen Industrie for the award of a Kekulé-stipend (M. P.).



Scheme 1. Polar (top) and electron transfer mechanism (bottom) of the reaction of cationic electrophiles R^+ with neutral π nucleophiles.

Both mechanisms do not necessarily give identical products, however. As expected from their reactivity parameters,[2] isobutene and the *N*-methylacridinium ion **1** do not react by a polar mechanism at room temperature (estimated rate constant from Equation (1), $k_2 = 2 \times 10^{-7}$ L $mol^{-1} s^{-1}$). When the electron transfer was induced photochemically, the anti Markovnikov product **2** was produced exclusively, while the product expected from a polar mechanism (**3**) could not be detected.[3] The fact that only Markovnikov adducts have been observed in a manifold of reactions of carbenium ions with alkenes[4] thus provides a hint against the operation of electron transfer processes. We now confirm this suspicion on the basis of linear free energy relationships.



Two of us (H. M. and M. P.) recently demonstrated that the rates of reactions of cationic electrophiles with uncharged nucleophiles can be described by Equation 1 which relates the second-order rate constants with the nucleophile-specific constants *s* and *N* and with the electrophilicity parameter *E*.[2]

$$\lg k = s\,(E + N) \qquad (1)$$

There is a rough correlation between the one-electron oxidation potentials of a variety of π nucleophiles[5] and their nucleophilicity parameters *N*[2] (Table 1; Fig. 1), where the *N* value increases with a decrease in E_{ox} [Eq. (2); correlation coefficient r = 0.89; standard deviation of *N*, s_N = 1.6; number of data, n = 20].

$$N = -8.0\,E_{ox} + 14.2 \qquad (2)$$

As shown in Figure 2, the reduction potentials E_{red} (vs. saturated calomel electrode (SCE) in acetonitrile) of a variety of cations correlate fairly well with their electrophilicity parameters *E* [Eq. (3); correlation coefficient r = 0.98; standard deviation of *E*, s_E = 1.7; number of data, n = 7].

$$E = 12.1\,E_{red} - 0.6 \qquad (3)$$

 © VCH Verlagsgesellschaft mbH, D-69451 Weinheim, 1995 0570-0833/95/1111-1225 $ 10.00+.25/0

Table 1. One-electron oxidation potentials E_{ox} and nucleophilicity parameters N of π nucleophiles.

Nucleophile	E_{ox}[a][V]	N[b]
	0.90[c]	9.49
	1.30[c]	5.58
1,3,5-$(MeO)_3C_6H_3$	1.36	3.40
1,3-$(MeO)_2C_6H_4$	1.36	2.40
	1.39[c]	0.84
	1.48	0.02
	1.50[c]	1.62
	1.50	−0.96
	1.79	0.20
	1.81	0.64
	1.81	0.71
	1.83	0.20
	1.88	0.78
	1.88	0.20
	1.98	−0.12
1,3-$Me_2C_6H_4$	2.02	−3.31
	2.04	−1.93
	2.14	−1.82
	2.24	−2.39
MeC_6H_5	2.20	−4.22
C_6H_6	2.35	−6.29

[a] vs. SCE (MeCN), determined by SHACV [5]. [b] From ref. [2]. [c] From ref. [6].

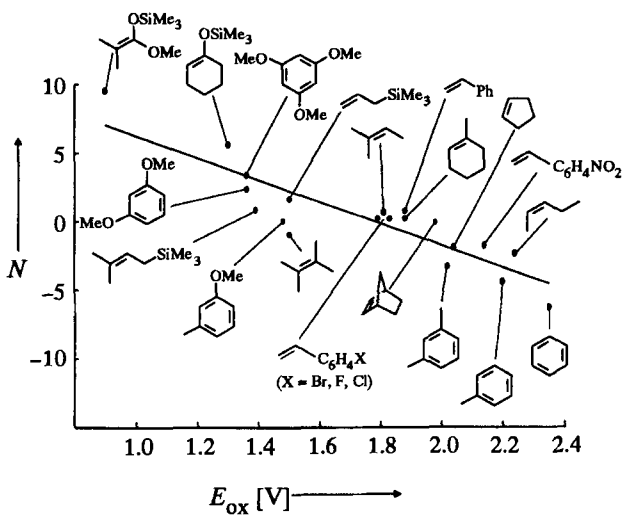


Fig. 1. Correlation between the one-electron oxidation potentials of π nucleophiles and the nucleophilicity parameter N.

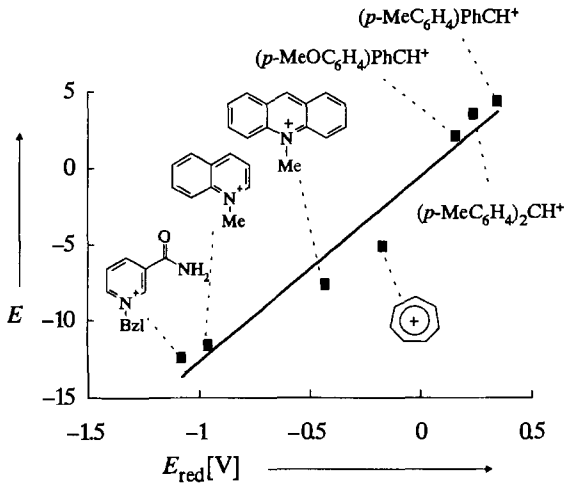
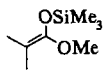


Fig. 2. Correlation between the reduction potentials [7] of electrophiles and the electrophilicity parameters E.

As a consequence of Equations 1 and 3, there is also a linear correlation between the activation-controlled electrophilic reactivities of carbocations and their reduction potentials as shown for the reactions with the silylketene acetal **4** in Figure 3 (left-curve ■).

One of us (S. F.) recently studied the kinetics of electron transfer processes from electron-rich π systems to one-electron oxidants.[6] The rate constants reported for the reactions of one-electron oxidants with the silylketene acetal **4** are considerably smaller (Fig. 3, right curve ▲) than the rate constants of the reactions of **4** with electron-pair acceptors of the same reduction potential (Fig. 3, left curve ■). The existence of two discrete correlations in Figure 3 thus provides an argument that two different mechanisms have to operate for the electron-pair acceptors on the left side and the one-electron oxidants on the right. Thus, an outer sphere electron transfer process cannot



4

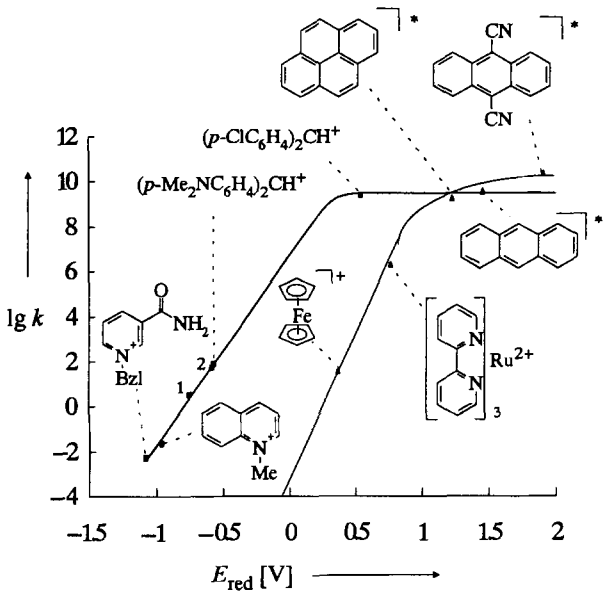


Fig. 3. Relationship between the rate constants of the reactions of various electron-pair acceptors (■) and one-electron oxidants (▲) with the silylketene acetal **4** (data from refs. [2, 6]). Points 1 and 2 correspond to pyronin G and the acridinium ion. E_{red} calculated from Equation 3 if not known experimentally.

 © VCH Verlagsgesellschaft mbH, D-69451 Weinheim, 1995 0570-0833/95/1111-1226 $ 10.00+.25/0 Angew. Chem. Int. Ed. Engl. 1995, 34, No. 11

account for the rate constants observed for the reactions of the electron-pair acceptors, and the higher reactivity (10 orders of magnitude!) of the oxidants corresponding to the left graph is most readily explained by a mechanism in which electron transfer is accompanied by the formation of a new σ bond. It can alternatively be called an inner sphere electron transfer process or a polar mechanism.

A similar conclusion can be derived for the reactions with other π nucleophiles. The actual rate constant for the reaction of an electrophile with a nucleophile is given by Equation (4), which follows from Equations (1)–(3).

$$\lg k_{\text{polar}} = s\,(13.6 + 12.1E_{\text{red}} - 8.0\,E_{\text{ox}}) \quad (4)$$

Since ΔG^0 of the electron transfer step is given by Equation (5) and $\Delta G^{\neq} \geq \Delta G^0$, one can derive the maximum rate of the electron transfer processes from Equation 6,[8] which follows from Equation (5) and the Eyring equation.

$$\Delta G^0 = F\,(E_{\text{ox}} - E_{\text{red}}) \quad (5)$$

$$\lg k_{\text{ET}} \leq \lg(k_{\text{B}}T/h) - F(E_{\text{ox}} - E_{\text{red}})/(2.303\,RT) = 12.8 - 17.2\,E_{\text{ox}} + 17.2\,E_{\text{Red}} \quad \text{(at 20 °C)} \quad (6)$$

Subtraction of Equation 6 from Equation 4 yields $\lg k_{\text{polar}} - \lg k_{\text{ET}}$, that is, the ratio between the actual rate constant for the electrophile–nucleophile combinations and the maximum rate constant for the outer sphere electron transfer process under the condition that none of these reactions is diffusion controlled.

If we assume $s = 1.1$, the typical value for the nucleophiles shown in Figure 1, $\lg k_{\text{polar}} - \lg k_{\text{ET}}$ is given by Equation 7.

$$\lg k_{\text{polar}} - \lg k_{\text{ET}} \geq 2.2 + 8.4\,E_{\text{ox}} - 3.9\,E_{\text{red}} \quad (7)$$

According to Equation 7 the minimum value of $\lg k_{\text{polar}} - \lg k_{\text{ET}}$ is 8.2 for the electrophile–nucleophile combinations employed in this study ($E_{\text{ox}} \geq 0.9$ V, $E_{\text{red}} \leq 0.4$ V). Thus, the actual rates of the reactions of cationic carbon electrophiles with uncharged π nucleophiles are at least 10^8 times greater than the maximum rates calculated for the electron transfer processes.[9]

Apart from cases, where the rate of the polar reaction is reduced by steric effects, there are two situations in which an outer sphere electron transfer process may compete with the polar reaction. Such a case may be encountered with ethylenes substituted by strong donor groups in positions 1 *and* 2 or with arenes substituted by strong donors in *o*- or *p*-position. In these systems only one of the donors can stabilize the carbenium ion produced in the polar reaction and thus accelerate the polar reaction, while both donor groups will reduce the oxidation potential and thus increase the rate of the electron transfer process. The second case is indicated in Figure 3: Since the diffusion limit for electron transfer processes is found to be higher than for polar reactions, systems where $E_{\text{ox}} - E_{\text{red}}$ is smaller than -0.2 V can also be expected to proceed by SET processes.

Received: February 3, 1995 [Z7688IE]
German version: *Angew. Chem.* **1995**, *107*, 1351–1353

Keywords: carbocations · electron transfer reactions · electrophilic additions · linear free energy relationships · reaction mechanisms

[1] a) E. C. Ashby, *Acc. Chem. Res.* **1988**, *21*, 414–421; b) A. Pross, *ibid.* **1985**, *18*, 212-219; c) J.-M. Savéant, *Adv. Phys. Org. Chem.* **1990**, *26*, 1–130; d) M. Chanon, M. L. Tobe, *Angew. Chem.* **1982**, *94*, 27–49, *Angew. Chem. Int. Ed. Engl.* **1982**, *21*, 1–23; e) F. G. Bordwell, J. A. Harrelson Jr., *J. Org. Chem.* **1989**, *54*, 4893–4898; f) L. E. Eberson, *Electron transfer reactions in organic chemistry; Reactivity and structure, Vol. 25*, Springer, Heidelberg, **1987**; g) J. K. Kochi, *Angew. Chem.* **1988**, *100*, 1331–1372; *Angew. Chem. Int. Ed. Engl.* **1988**, *27*, 1227–1258; h) S. Fukuzumi, J. K. Kochi, *J. Am. Chem. Soc.* **1981**, *103*, 7240–7252; h) E. M. Arnett, L. G. Whitesell Jr., K. Amarnath, J. P. Cheng, E. Marchot, *Makromol. Chem., Macromol. Symp.* **1988**, *13/14*, 21–31; i) T. Lund, H. Lund, *Acta Chem. Scand. B* **1986**, *40*, 470-485.

[2] a) H. Mayr, M. Patz, *Angew. Chem.* **1994**, *106*, 990–1010; *Angew. Chem. Int. Ed. Engl.* **1994**, *33*, 938–957; b) H. Mayr, R. Pock, *Chem. Ber.* **1986**, *119*, 2473–2496; c) R. Pock, H. Mayr, *Chem. Ber.* **1986**, *119*, 2497–2509; H. Mayr, R. Schneider, B. Irrgang, C. Schade, *J. Am. Chem. Soc.* **1990**, *112*, 4454–4459.

[3] M. Fujita, S. Fukuzumi, *J. Chem. Soc. Perkin Trans. 2* **1993**, 1915–1921.

[4] H. Mayr, *Angew. Chem.* **1990**, *102*, 1415–1428; *Angew. Chem. Int. Ed. Engl.* **1990**, *29*, 1371–1384.

[5] The E_{ox} values were determined by using the second harmonic ac voltammetry (SHACV) measurements in deaerated MeCN containing 0.10 M $N\!n\text{Bu}_4\text{ClO}_4$ as a supporting electrolyte at 298 K. The SHACV components are symmetrical and appear as mirror images about the zero current axis. The E_{ox} values are obtained from the intersection values, see: E. Ahlberg, V. D. Parker, *Acta Chem. Scand. B* **1980**, *34*, 91–96. The details will be published elsewhere.

[6] S. Fukuzumi, M. Fujita, J. Otera, Y. Fujita, *J. Am. Chem. Soc.* **1992**, *114*, 10271–10278.

[7] E_{red} from: a) H. Volz, W. Lotsch, *Tetrahedron Lett.* **1969**, *27*, 2275–2278; b) S. Fukuzumi, S. Koumitsu, K. Hironaka, T. Tanaka, *J. Am. Chem. Soc.* **1987**, *109*, 305–316; c) B. A. Sim, P. H. Milne, D. Griller, D. D. M. Wayner, *ibid.* **1990**, *112*, 6635–6638.

[8] Because of the small reorganization energies, the actual values of k_{ET} will only be slightly smaller than the maximal values used for our calculations.

[9] A similar method has been employed to differentiate electron transfer and classical S_N2 mechanisms for the reactions of anionic nucleophiles with alkyl halides by comparing observed rate constants and those expected for the electron transfer process: a) T. Lund, H. Lund, *Acta Chem. Scand. B* **1986**, *40*, 470–485; b) *Tetrahedron Lett.* **1986**, *27*, 95–98; c) *Acta Chem. Scand. B*, **1988**, *42*, 269–279.

Relative and Absolute Configuration of Filipin III**

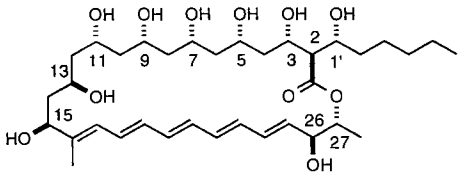
Scott D. Rychnovsky* and Timothy I. Richardson

Filipin belongs to a class of natural products known as the polyene macrolide antibiotics. There are over 200 known representatives of this class, most of which are produced by soil actinomycetes belonging to the genus *Streptomyces*.[1] Although structural formulas for many polyene macrolides are known, the complete stereochemical assignments have been made in only a handful of cases.[2] In cell biology, filipin has become a popular probe for cholesterol and has even been used to quantitate cholesterol in cell membranes.[3] Filipin complex is also used in the study and clinical diagnosis of Type C Niemann-Pick disease.[4] More recently, the use of filipin as a probe for cholesterol has been questioned.[5] The development of detailed models for the interaction of cholesterol with filipin has not been possible because, until now, the configuration of filipin III was unknown. We report herein the complete absolute stereochemical assignment of filipin III (**1**, Scheme 1).

[*] Prof. S. D. Rychnovsky, T. I. Richardson
Department of Chemistry, University of Minnesota
207 Pleasant Street SE, Minneapolis, MN 55455 (USA)
Telefax: Int. code + (612)626-7541

[**] Support was provided by the National Institutes of Health, the Camille and Henry Dreyfus Foundation Teacher-Scholar Award, and the Alfred P. Sloan Foundation. Additional support was provided by American Cyanamid, Bristol-Myers Squibb, Pfizer, and Zeneca. The generous donation of filipin complex by the Upjohn Company is gratefully acknowledged.

 © VCH Verlagsgesellschaft mbH, D-69451 Weinheim, 1995 0570-0833/95/1111-1227 $ 10.00+.25/0

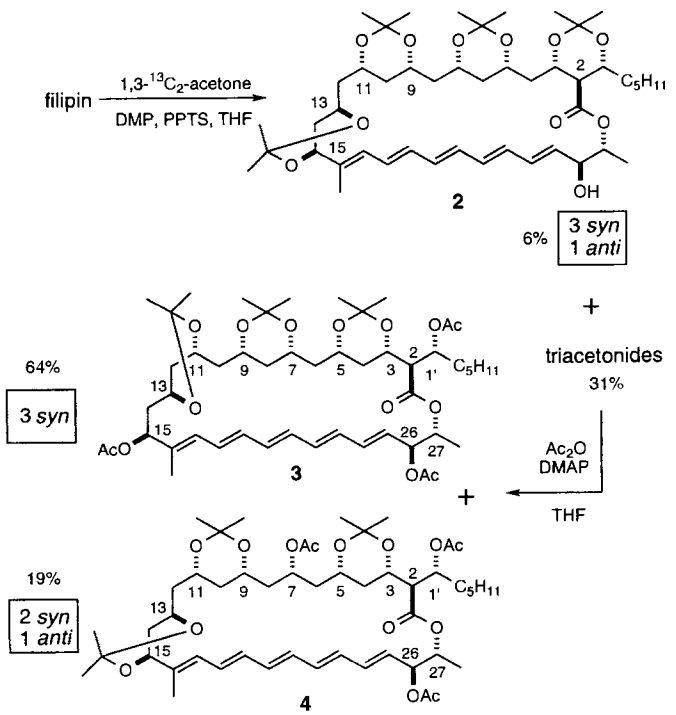


1

Scheme 1. Configuration of natural filipin III (**1**).

Filipin was isolated in 1955 from *Streptomyces filipinensis* found in a sample of Philippine soil.[6] Much later filipin was shown to be a mixture of four components—filipin I (4%), II (25%), III (53%), and IV (18%).[7] The connectivity of filipin III, the major component of the filipin complex, was assigned in a series of degradation studies.[8] Filipin I, which has been difficult to characterize, is probably a mixture of several components having two hydroxyl groups fewer than filipin III.[9] Filipin II is 1′-deoxy-filipin III.[9-10] Filipin IV is isomeric to filipin III and is probably epimeric at C1′ or C3.[11]

We have shown that *syn* and *anti* 1,3-diols can be easily distinguished by ^{13}C NMR analysis of the corresponding acetonides: the *syn* isomers have methyl resonances at $\delta \approx 20$ and 30, whereas the *anti* isomers have methyl resonances at $\delta \approx 25$ ppm.[12] This analysis was used to determine the relative configuration of filipin III. Initial attempts to prepare an acetonide derivative of filipin III with *p*-toluenesulfonic acid showed that the molecule is acid sensitive. Treatment of filipin complex[13] (Sigma) with the mild acid catalyst, pyridinium *p*-toluenesulfonate (PPTS), in a 2:1 mixture of acetone and 2,2-dimethoxypropane (DMP), followed by silica gel chromatography gave tetraacetonide **2** in 6% yield and a mixture of triacetonides in 31% yield (Scheme 2, Table 1). A highly purified sample of filipin III gave the same mixture of products when subjected to the reaction conditions, confirming that these derivatives arise from the major component of the complex. The mixture of triacetonides was acetylated and separated to give triacetonide **3** in 64% yield and triacetonide **4** in 19% yield. The structures of triacetonides **3** and **4**, including the positions of the acetyl groups, were established with ^1H NMR and COSY data.[14] The acetylation of the hydroxyl groups was carried out with 50% enriched 1,3-$^{13}C_2$-acetone to simplify detection and identification of the acetonide methyl signals in the ^{13}C NMR spectra.



Scheme 2. Preparation of filipin III acetonide derivatives **2**–**4**. DMAP = 4-dimethylaminopyridine.

Table 1. Physical data for compounds **2**-**4**.[a]

2: ^1H NMR (500 MHz, C_6D_6): $\delta = 6.78-6.67$ (m, 2H), 6.57–6.51 (m, 2H), 6.48–6.42 (m, 2H), 6.37–6.25 (m, 2H), 5.87 (dd, $J = 5.0$, 15.3 Hz, C25), 4.89 (dq, $J = 6.0$, 6.4 Hz, C27), 4.48 (dt, $J = 2.6$, 10.0 Hz, C1′), 4.42–4.36 (m, 2H), 4.28–4.22 (m, 2H), 4.06–4.01 (m, 2H), 3.90–3.84 (m, 1H), 3.75 (ddd, 1H, $J = 4.1$, 6.0, 7.4 Hz, C26), 2.49 (t, 1H, $J = 10.1$ Hz, C2), 2.26 (d, 1H, $J = 13.8$ Hz), 2.12–1.20 (m, 19H), 1.85 (s, 3H), 1.543 (s, 3H), 1.538 (s, 3H), 1.50 (s, 3H), 1.49 (s, 3H), 1.46 (s, 3H), 1.43 (s, 3H), 1.34 (s, 3H), 1.212 (s, 3H), 1.206 (d, 3H, $J = 6.4$ Hz), 0.869 (t, 3H, $J = 6.9$ Hz); HR-MS (FAB): found: 814.5239, calcd ($C_{47}H_{74}O_{11}$): 814.5233

3: ^1H NMR (500 MHz, C_6D_6): $\delta = 6.51$ (dd, 1H, $J = 10.4$, 13.6 Hz), 6.45–6.30 (m, 4H), 6.27–6.21 (m, 2H), 6.13 (dd, 1H, $J = 10.6$, 15.1 Hz), 5.81 (dd, 1H, $J = 5.8$, 15.6 Hz, C25), 5.69 (ddd, 1H, 3.0, 6.25, 10.0 Hz, C1′), 5.62 (dd, 1H, $J = 4.6$, 10.6 Hz, C15), 5.37 (dd, 1H, $J = 6.0$, 9.3 Hz, C26), 5.31 (dq, 1H, $J = 6.0$, 6.1 Hz, C27), 4.29 (ddd, 1H, $J = 2.1$, 8.6, 10.8 Hz), 4.12–4.07 (m, 1H), 4.06–3.99 (m, 1H), 3.90–3.81 (m, 2H), 3.77–3.70 (m, 1H), 3.11 (dd, 1H, $J = 6.1$, 8.0 Hz, C2), 2.25 (ddd, 1H, $J = 3.4$, 10.1, 13.5 Hz), 2.10–1.16 (m, 19H), 1.78 (s, 3H), 1.73 (s, 3H), 1.66 (s, 6H), 1.55 (s, 3H), 1.54 (s, 3H), 1.45 (s, 3H), 1.43 (s, 3H), 1.30 (s, 3H), 1.22 (s, 3H), 1.15 (d, 3H, $J = 6.1$ Hz), 0.861 (t, 3H, $J = 6.9$ Hz); HR-MS (FAB): found: 900.5226, calcd ($C_{50}H_{76}O_{14}$): 900.5237

4: ^1H NMR (500 MHz, C_6D_6): $\delta = 6.91$ (dd, 1H, $J = 11.5$, 14.3 Hz), 6.74 (dd, 1H, $J = 11.1$, 14.5 Hz), 6.66–6.55 (m, 2H), 6.50–6.34 (m, 3H), 6.28 (dd, 1H, $J = 11.3$, 14.1 Hz), 6.09 (dd, 1H, $J = 4.9$, 14.6 Hz, C25), 5.70 (ddd, 1H, $J = 2.8$, 7.4, 10.1 Hz, C1′), 5.49 (dd, 1H, $J = 5.0$, 9.6 Hz, C26), 5.33 (dq, 1H, $J = 5.0$, 6.3 Hz, C27), 5.33–5.27 (m, 1H, C7), 4.54–4.51 (m, 1H), 4.39 (d, 1H, $J = 5.6$ Hz), 4.28 (ddd, 1H, $J = 2.4$, 7.3, 11.4 Hz), 3.91–3.84 (m, 2H), 3.76–3.72 (m, 1H), 3.16 (t, 1H, $J = 7.4$ Hz, C2), 2.63 (d, 1H, $J = 14.1$ Hz), 2.04–1.21 (m, 19H), 1.87 (s, 3H), 1.85 (s, 3H), 1.77 (s, 3H), 1.67 (s, 3H), 1.56 (s, 3H), 1.52 (s, 3H), 1.43 (s, 3H), 1.39 (s, 3H), 1.33 (s, 3H), 1.28 (s, 3H), 1.19 (d, 3H, $J = 6.3$ Hz), 0.840 (t, 3H, $J = 7.0$ Hz); HR-MS (FAB): found: 900.5150, calcd ($C_{50}H_{76}O_{14}$): 900.5237

[a] The NMR and MS data are reported for samples with natural ^{13}C abundance.

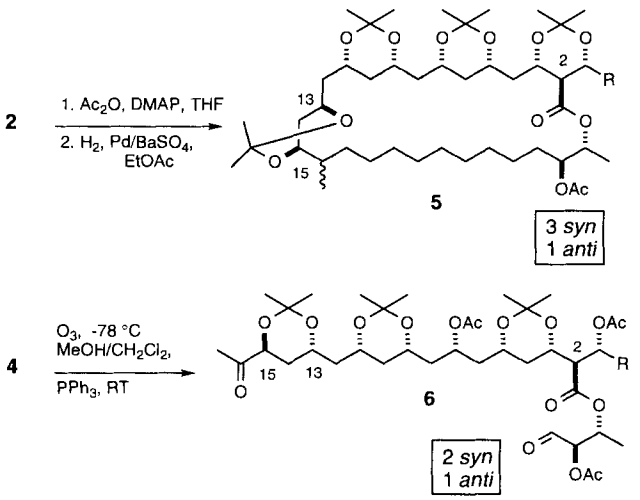
The signals in the ^{13}C NMR spectrum of tetraacetonide **2** at $\delta = 31.00, 30.65, 30.50, 30.13, 24.82, 19.97$, and 19.54 (×2) were assigned to methyl groups of three *syn* acetonide groups and one further acetonide group with methyl peaks at $\delta \approx 30$ and 24.82. The ^{13}C NMR spectrum of triacetonide **3** showed methyl resonances at $\delta = 30.76, 30.70, 30.02, 19.93, 19.82$, and 19.41 that correspond to three *syn* acetonide groups. The methyl resonances in the ^{13}C NMR spectrum of triacetonide **4** at $\delta = 30.46, 30.15, 30.05, 24.74, 19.03$, and 18.97 belong to two *syn* acetonide groups and an additional acetonide group with methyl peaks at $\delta \approx 30$ and 24.74. The acetonide rings from the compounds **2**, **3**, and **4** span all the potential 1,3-diol relationships in the C1′ to C15 segment of filipin III.

Both compounds **2** and **4** show a very unusual set of methyl peaks for one of the acetonide rings. Over 200 acetonide rings were analyzed in a previous paper, and none of them showed a pair of methyl peaks at these positions.[12c] One compound that shows similar ^{13}C chemical shifts for the acetonide methyl groups is 2,2,4,4,6-pentamethyl-1,3-dioxane. This heterocycle is known to adopt a chair conformation because of the quaternary center at C4, and the chemical shift of the C2 axial methyl group is $\delta = 24.93$ and that of the C2 equatorial methyl group 32.04.[15] These are very close to the observed values in compounds **2** ($\delta \approx 30$ and 24.82) and **4** ($\delta \approx 30$ and 24.74). The signal at $\delta \approx 24$ is characteristic of an axial acetonide methyl group that has another axial substituent at the C4 or C6 atom, and can best be attributed to an *anti* acetonide that adopts a chair conformation. Apparently the macrocyclic ring of **2** and **4** biases the *anti* 1,3-diol acetonide group to adopt a chair conformation rather than the more stable twist-boat conformation. The chair conformation, although still energetically

 © VCH Verlagsgesellschaft mbH, D-69451 Weinheim, 1995 0570-0833/95/1111-1228 $ 10.00+.25/0

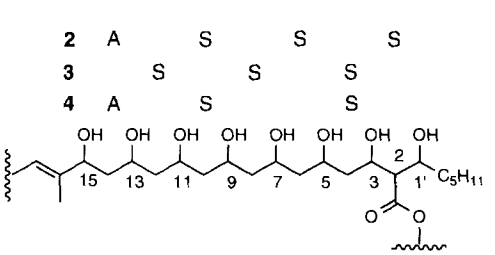
unfavorable, is more accessible for an alkene-substituted acetonide than for an alkyl-substituted acetonide,[16] and so the most likely position of the *anti* acetonide is at C13–C15.

To test this hypothesis we degraded compounds **2** and **4** as shown in Scheme 3. Acetylation, followed by hydrogenation of **2** gave the saturated macrocycle **5**, which showed methyl signals



Scheme 3. Preparation of compounds **5** and **6**. These compounds are instrumental in confirming the C13–C15 position of the *anti* acetonide ring in derivatives **2** and **4**. RT = room temperature.

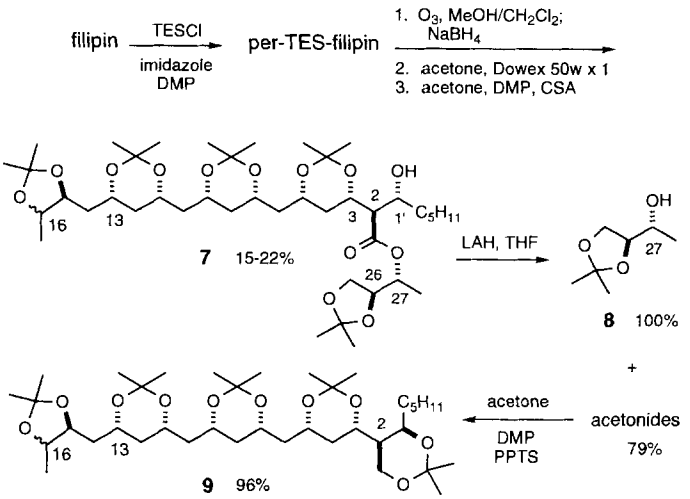
at $\delta = 30.75$, 30.69, 30.14, 25.69, 24.78, 19.95 ($\times 2$), and 19.45 in the ^{13}C NMR spectrum. The new methyl peaks at $\delta = 25.69$ and 24.78 fall in the expected range for a saturated *anti* acetonide. Triacetonide **4** was ozonized and reduced with triphenylphosphane to give a 43% yield of triacetonide **6**, whose methyl groups resonate at $\delta = 30.50$, 30.30, 25.94, 24.32, 19.57 and 19.29. The new methyl peaks at $\delta = 25.94$ and 24.32 clearly represent an *anti* 1,3-diol acetonide. More significantly, the difference $\Delta\delta = 1.62$ between the two peaks is larger than one would expect for a saturated *anti* 1,3-diol acetonide but is in line with an acyl-substituted *anti* acetonide.[12c] Thus the *anti* acetonide ring in both **2** and **4** is located at C13–C15, and the relative configurations for the other alcohol stereogenic centers in the C1′ to C15 section are as shown in Scheme 4.



Scheme 4. The relative configuration of filipin III in the C1′–C15 section. The relative stereochemistry at each acetonide position is listed as either S (*syn*) or A (*anti*) for compounds **2**–**4**.

The acetonide ring at C1′–C3 adopts a chair conformation in tetraacetonide **2**. The signal of the C2 proton in the ^1H NMR spectrum of tetraacetonide **2** is a triplet with a coupling constant of 10.1 Hz. This coupling constant is only consistent with an equatorial ester; therefore the configuration at C2 is *anti* with respect to C1′ and C3.

The configuration of filipin III at the C26 and C27 stereogenic centers was determined by another degradation sequence (Scheme 5). Per-TES-filipin prepared from filipin complex (Upjohn or Sigma) was ozonized and then reduced with $NaBH_4$.



Scheme 5. Degradation of filipin to determine the absolute configuration of filipin III. Advanced Mosher analysis of **7** identified the absolute configuration at C1′ as *R*. Compound **8** was identified as the enantiomer of an authentic sample prepared from D-mannitol.

The triethylsilyl (TES) protecting groups were exchanged for acetonides to give 15–22% of pentaacetonide **7** as a mixture of diastereomers at C16. The position of the lone hydroxyl was identified by COSY analysis of acetylated **7**. Reduction of **7** with $LiAlH_4$ (LAH) gave a quantitative yield of *anti*-1,2-di-*O*-isopropylidene-1,2,3-butanetriol (**8**) that was identified by direct comparison (^1H NMR spectroscopy, GC) with an authentic sample.[17] The absolute configuration of **8** was identified as (2*S*,3*R*) by comparison of the *R* and *S* Mosher's esters of **8** with those prepared from an authentic sample of (2*R*,3*S*)-1,2-di-*O*-isopropylidene-1,2,3-butanetriol.[17] The reduction of **7** also gave a mixture of acetonides that was treated with acetone and acid to give pentaacetonide **9** in 76% yield. The ^{13}C NMR spectrum of **9** showed four *syn* 1,3-diol acetonide rings and a mixture of *syn* and *anti* 1,2-diol acetonide rings, which provides independent support for the relative configurations proposed in Scheme 5.[18]

The last question to be resolved is the absolute stereochemistry of the C1′ to C15 fragment. An advanced Mosher's ester analysis[19] of C1′ alcohol **7** led to $\Delta\delta_H$ ($= \delta_S - \delta_R$) values (reported as Hz at 500 MHz in $CHCl_3$) of −58 (H3), −8.5 (H2), −10 (H1′), +5 (H2′), and +25 (H3′). These values indicate an *R* configuration at C1′, and complete the structure assignment of filipin III. Thus the configurations of the stereogenic centers in filipin III are 1′*R*, 2*R*, 3*S*, 5*S*, 7*S*, 9*R*, 11*R*, 13*R*, 15*S*, 26*S*, and 27*R*. It must be emphasized that the relative configurations for the nine stereogenic centers in the top half of the structural formula **1** of filipin were initially identified from just three acetonide derivatives, **2**, **3**, and **4**, arising from a two-step protection sequence. Subsequent experiments confirmed the analysis. The stereochemical assignment of filipin III will facilitate rational modeling of filipin–cholesterol interactions.

Received: January 11, 1995 [Z7619IE]
German version: *Angew. Chem.* **1995**, *107*, 1355–1358

Keywords: antibiotics · filipin · macrolides · polyenes · structure elucidation

[1] S. Omura, H. Tanaka in *Macrolide Antibiotics: Chemistry, Biology and Practice* (Ed.: S. Omura), Academic Press, New York, **1984**, p. 351.

[2] Configurational assignment by X-ray analysis: a) amphotericin B: W. Mechlinski, C. P. Schaffner, P. Ganis, G. Avitable, *Tetrahedron Lett.* **1970**, 3873; b) roxaticin: H. Maehr, R. Yang, L.-N. Hong, C.-M. Liu, M. H. Hatada, L. J. Todaro, *J. Org. Chem.* **1989**, *54*, 3816; configurational assignment by degradation, NMR analysis, and synthesis of partial units: mycoticin: c) S. L. Schreiber, M. T. Goulet, *Tetrahedron Lett.* **1987**, *28*, 6001; d) S. L. Schreiber, M. T. Goulet, T. Sammakia, *ibid.* **1987**, *28*, 6005; e) *J. Am. Chem. Soc.* **1987**, *109*, 8120; Nystatin: f) J.-M. Lancelin, J.-M. Beau, *Tetrahedron Lett.* **1989**, *30*, 4521; g) J. Prandi, J.-M. Beau, *ibid.* **1989**, *30*, 4517; h) K. C. Nicolaou, K. H. Ahn, *ibid.* **1989**, *30*, 1217; partial structure of lienomycin: i) J. Pawlak, K. Nakanishi, T. Iwashita, E. Borowski, *J. Org. Chem.* **1987**, *52*, 2896; roflamycoin: j) S. D. Rychnovsky, G. Griesgraber, R. Schlege, *J. Am. Chem. Soc.* **1994**, *116*, 2623; pentamycin: k) T. Oishi, *Pure Appl. Chem.* **1989**, *61*, 427; l) T. Nakata, N. Hata, T. Suenaga, T. Oishi, *Tennen Yuki Kagobuton Toronkai Koen Yoshishu 30th 1988* (*Chem. Nat. Prod. Symp. Pap.*), Fukuoka, **1988**, 540; configurational assignment by NMR spectroscopy: pimaricin: m) J.-M. Lancelin, J.-M. Beau, *J. Am. Chem. Soc.* **1990**, *112*, 4060; Candidin: n) J. Pawlak, P. Sowinski, E. Borowski, P. Gariboldi, *J. Antibiot.* **1993**, *46*, 1598.

[3] a) J. Bolard, *Biochim. Biophys. Acta* **1986**, *865*, 257; b) O. Behnke, J. Tranum-Jensen, B. Van Deurs, *Eur. J. Cell Biol.* **1984**, *35*, 189.

[4] R. A. Coxey, P. G. Pentchev, G. Campbell, E. J. Blanchette-Mackie, *J. Lipid Res.* **1993**, *34*, 1165.

[5] a) J. Milhaud, J. Mazerski, E. J. Dufourc, *Eur. Biophys. J.* **1989**, *17*, 151; b) M. A. R. B. Castanho, M. J. E. Prieto, *Eur. J. Biochem.* **1992**, *207*, 125.

[6] a) G. B. Whitefield, T. D. Brock, A. Ammann, D. Gottlieb, H. E. Carter, *J. Am. Chem. Soc.* **1955**, *77*, 4799; b) A. Ammann, D. Gottlieb, H. E. Carter, *Plant Dis. Rep.* **1955**, *39*, 219.

[7] M. E. Bergy, T. E. Eble, *Biochemistry* **1968**, *7*, 653.

[8] a) B. Berkoz, C. Djerassi, *Proc. Chem. Soc. London* **1959**, 316; b) C. Djerassi, M. Ishikawa, H. Budzikiewicz, J. N. Shoolery, L. F. Johnson, *Tetrahedron Lett.* **1961**, 383; c) B. T. Golding, R. W. Rickards, M. Barber, *ibid.* **1964**, 2615; d) O. Ceder, R. Ryhage, *Acta Chem. Scand.* **1964**, *18*, 558.

[9] R. C. Pandey, K. L. Rinehart, *J. Antibiot.* **1970**, *23*, 414.

[10] D. M. F. Edwards, *J. Antibiot.* **1989**, *42*, 322.

[11] R. C. Pandey, N. Narasimhachari, K. L. Rinehart, D. S. Millington, *J. Am. Chem. Soc.* **1972**, *94*, 4306.

[12] a) S. D. Rychnovsky, D. J. Skalitzky, *Tetrahedron Lett.* **1990**, *31*, 945; b) D. A. Evans, D. L. Rieger, J. R. Gage, *ibid.* **1990**, *31*, 7099; c) S. D. Rychnovsky, B. Rogers, G. Yang, *J. Org. Chem.* **1993**, *58*, 3511.

[13] Filipin complex was obtained from Sigma (F-9765) as a crude mixture containing about 50% filipin III or from Upjohn (Lot 2923-DEV-39) containing about about 8% filipin III. It can be purified by reversed-phase preparative HPLC.

[14] The location of the C1′ acetates in **3** and **4** were determined by their cross-peak in the COSY spectra with the readily identifiable C2 proton. The C15 acetate in **3** was identified by the simplicity of its coupling pattern. The location of the C7 acetate in **4** is less secure, and was assigned from the COSY spectrum. The second acetate in **4** must be at either at C7 or C11, and its location does not affect the stereochemical analysis. The assignments for these protons are listed in Table 1.

[15] K. Pihlaja, M. Kivimaki, A.-M. Myllyniemi, T. Nurmi, *J. Org. Chem.* **1982**, *47*, 4688.

[16] S. D. Rychnovsky, G. Yang, J. P. Powers, *J. Org. Chem.* **1993**, *58*, 5251.

[17] J. Mulzer, A. Angermann, W. Münch, G. Schlichthörl, A. Hentzschel, *Liebigs Ann. Chem.* **1987**, 7.

[18] **9**: ^{13}C NMR (125 MHz, C_6D_6), 1,2-diolacetonide mixture: δ = 29.03, 27.76, 27.61, 26.10; 1,3-diolacetonide: δ = 30.81, 30.69, 30.66, 30.22, 20.04, 19.92, 19.83, 19.00.

[19] I. Ohtani, T. Kusumi, Y. Kashman, H. Kakisawa, *J. Am. Chem. Soc.* **1991**, *113*, 4092.

Competing Pathways in the Reaction of Bis(pentafluorophenyl)borane with Bis(η^5-cyclopentadienyl)dimethylzirconium: Methane Elimination versus Methyl–Hydride Exchange and an Example of Pentacoordinate Carbon**

Rupert E. von H. Spence, Daniel J. Parks, Warren E. Piers,* Mary-Anne MacDonald, Michael J. Zaworotko, and Steven J. Rettig

The combination of group 4 bent metallocene compounds with group 13 Lewis acids often leads to catalysts capable of polymerizing olefinic substrates by ring opening metathesis[1] or Ziegler–Natta type mechanisms.[2] The activation in the latter systems commonly involves treatment of dichloro metal complexes $[Cp_2MCl_2]$ with an excess of methylaluminoxane (MAO) which leads to $[Cp_2MCH_3]^+[MAO]^-$, the cation of which is generally accepted to be the active species in these catalysts.[3] Alternatively, the reaction of $[Cp_2ZrR_2]$ derivatives (R = H, alkyl) with equimolar amounts of $B(C_6F_5)_3$[3b,4] has proven to be an effective means of producing active centers by alkyl abstraction, minimizing the need for excessive amounts of cocatalyst.

Spurred by these discoveries, we have developed synthetic routes to the electrophilic borane $HB(C_6F_5)_2$ (**1**)[5] as a reagent for incorporating the $B(C_6F_5)_2$ moiety into the structural framework of ancillary ligands which support soluble Ziegler–Natta catalysts. During these studies, we found borane **1** to be reactive towards simple alkylzirconium complexes as exemplified by its reaction with $[Cp_2Zr(CH_3)_2]$ (**2**). In addition to methyl-hydrogen exchange pathways,[6] **1** was found to induce methane elimination from **2**, ultimately leading to an intriguing compound containing a rare example of pentacoordinate carbon. The chemistry reported herein is summarized in Scheme 1.

The reaction of **1** with one equivalent of **2** in benzene, led to an intractable mixture of several zirconium- and/or $B(C_6F_5)_2$-containing products. Conversely, the same reaction in hexanes resulted in the evolution of methane (confirmed by ^{1}H NMR spectroscopy) and isolation of a single product, a brick red solid, **3**, in 86% yield.

The product **3** decomposed at room temperature in benzene over one to two hours to give several species but could be stabilized with PMe_3 with which it forms a 1:1 adduct **3**·PMe_3. Spectroscopic data indicated that **3** contained a four-coordinate boron[7] (^{11}B NMR, $\delta = -1.1$), a Zr-H-B arrangement (^{1}H NMR, $\delta = -0.75$, broad; IR, $\tilde{\nu} = 1602\ cm^{-1}$), and a deshielded methylene group bonded to boron as evidenced by quadrupolar broading of the ^{1}H NMR signal (^{1}H NMR, $\delta = 5.30$). These data are consistent with the structure shown

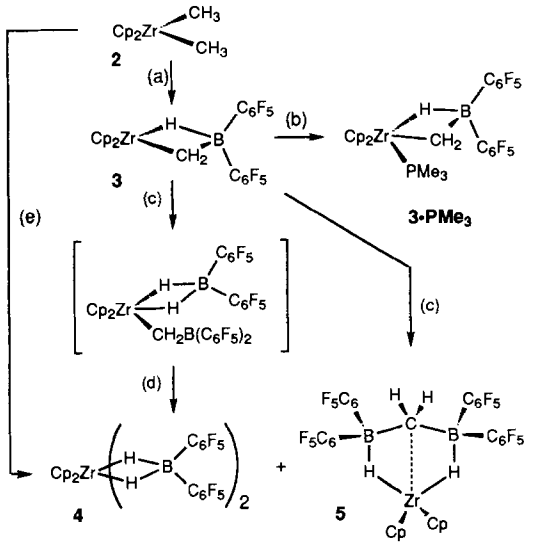
[*] Prof. W. E. Piers, Dr. R. E. von H. Spence, D. J. Parks
Guelph-Waterloo Centre for Graduate Work in Chemistry
Guelph Campus, Department of Chemistry and Biochemistry
University of Guelph
Guelph, Ontario, N1G 2W1 (Canada)
Telefax: Int. code + (519) 766 1499

M.-A. MacDonald, Prof. M. J. Zaworotko
Department of Chemistry, Saint Mary's University
Halifax, Nova Scotia (Canada)

Dr. S. J. Rettig
Department of Chemistry, University of British Columbia
Vancouver, British Columbia (Canada)

[**] Financial support for this work was provided by the Novacor Research and Technology Corporation of Calgary, Alberta and by the Natural Sciences and Engineering Council of Canada in the form of a Postgraduate Scholarship for D. J. P.

 © VCH Verlagsgesellschaft mbH, D-69451 Weinheim, 1995 0570-0833/95/1111-1230 $ 10.00+.25/0



Scheme 1. Reactions of $HB(C_6F_5)_2$ (**1**) with $[Cp_2Zr(CH_3)_2]$ (**2**). a) **1**, hexane; $-CH_4$; b) PMe_3; c) **1**; d) 2 **1**, $-CH_2[B(C_6F_5)_2]_2$; e) 4 **1**, benzene; $-CH_4$, $-CH_3B(C_6F_5)_2$ and $-CH_2[B(C_6F_5)_2]_2$; **4**:**5** ≈ 1:2.

for **3** in Scheme 1, a species which may formally be described as a zirconocene methylidene unit in a state of arrested hydroboration, stabilized by $HB(C_6F_5)_2$ in a similar bonding arrangement to that found in $[Cp_2Ti(\mu\text{-}CH_2)(\mu\text{-}Cl)AlMe_2]$, Tebbe's reagent.[8]

This formulation was confirmed by an X-ray crystallographic analysis of **3**·PMe_3 (Fig. 1).[9, 10] The PMe_3 ligand occupies an *exo* coordination site, quenching the electron deficiency of the zirconium center in unligated **3**. The methylene unit resides in the central position and is shielded by the PMe_3 ligand as evidenced by the upfield shift of its signal in the ^1H NMR spectrum relative to the corresponding signal of **3** ($\delta = 0.93$). The Zr–C1 and C1–B distances of 2.300(7) and 1.586(12) Å, respectively, are typical of single bonds for these bonding partners. While the position of the μ-H ligand had to be calculated, the spectroscopic and structural evidence is clearly indicative of a four-membered Zr-C-B-H[11] unit in **3**·PMe_3 and presumably also in **3**.

When $[Cp_2Zr(CH_3)_2]$ was treated with an excess of borane **1** in benzene, two zirconium-containing products, **4** and **5**, were formed in a ratio of approximately 1:2. The minor product was identified as the bis(dihydroborate) complex $[Cp_2Zr\{H_2B(C_6F_5)_2\}_2]$ (**4**) by NMR spectroscopy, characteristic IR absorptions for the Zr-(μ-H)$_2$-B units[12] at 2184, 2110, and 2028 cm^{-1} (Zr-(μ-D)$_2$-B, $\tilde{\nu} = 1597\ cm^{-1}$), and its synthesis by a separate route from $[Cp_2ZrH_2]$[13] and two equivalents of **1**.

The major product in the reaction, **5**, apparently arises from complexation of **3** with a further equivalent of borane. The ^1H NMR spectrum of **5** consists of singlets at $\delta = 5.23$, 2.29 (broad), and -2.05 (very broad) in a 10:2:2 ratio, suggesting retention of the methylene unit to form a complex of stoichiometry $[Cp_2ZrH_2 \cdot CH_2\{B(C_6F_5)_2\}_2]$. Four-coordinate boron was implied by the ^{11}B chemical shift at about $\delta = 0.0$.[7] The signal for the methylene carbon was not detected with standard pulse sequences, but by using the HMQC experiment[14] a broad signal at $\delta = 0.5$ was identified ($^1J_{C-H} = 120$ Hz).

These spectral features of **5** were consistent with the general formulation given above but an X-ray analysis[15, 10] of the compound as a benzene solvate revealed a unique bonding arrangement in which the methylene carbon is five coordinate by virtue of a bonding contact with the zirconium center (Fig. 2).

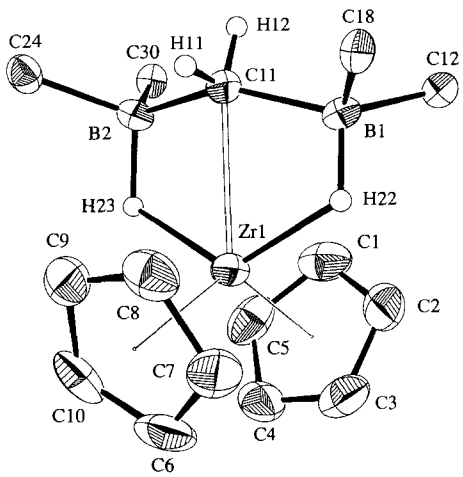


Fig. 2. Molecular structure of **5**; noncyclopentadienyl hydrogens were located and refined. The C_6F_5 groups have been omitted for clarity. Selected bond lengths [Å] and angles [°]: Zr1–C11 2.419(4), Zr1–H22 1.97(3), Zr1–H23 1.94(3), C11–B1 1.697(7), C11–B2 1.693(7), B1–H22 1.13(3), B2–H23 1.27(3), Zr1–$Cp1_{cent}$ 2.19, Zr1–$Cp2_{cent}$ 2.19; H22-Zr1-H23 126(1), B1-C11-B2 149.3(4), B1-C11-Zr1 76.6(2), B2-Zr1-C11 78.0(2), Zr1-H22-B1 112(2), Zr1-H23-B2 110(2), C12-B1-C18 108.4(4), C24-B2-C30 106.0(4); $Cp1_{cent}$-Zr1-$Cp2_{cent}$ 128.6.

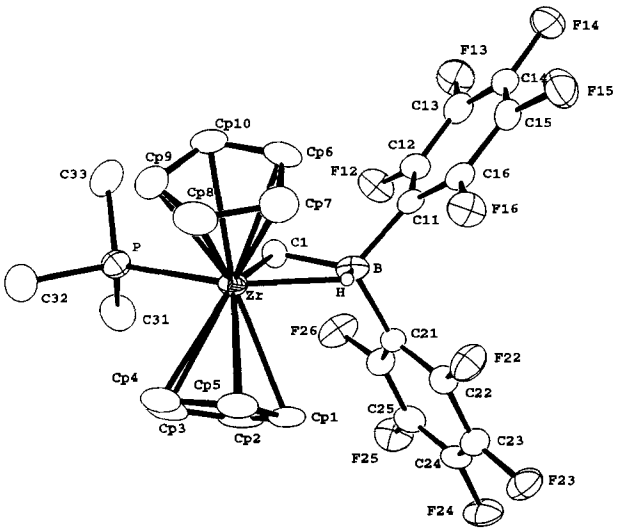


Fig. 1. Molecular structure of **3**·PMe_3. Selected bond lengths [Å] and angles [°]: Zr–P 2.726(3), Zr–C1 2.300(7), B–C1 1.586(12), B–H 1.51(5), Zr–H 1.99(5), Zr–$Cp1_{cent}$ 2.232, Zr–$Cp2_{cent}$ 2.225; P-Zr-C1 72.83(19), Zr-C1-B 85.0(4), C1-B-C11 116.7(7), C1-B-C21 116.4(7), C11-B-C21 108.5(7), Zr-H-B 98(3); $Cp1_{cent}$-Zr-$Cp2_{cent}$ 131.4.

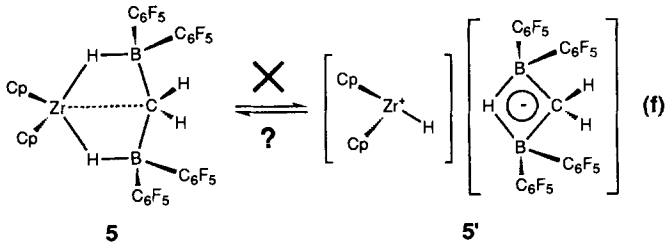
The Zr1–C11 distance is 2.419(4) Å, only slightly longer than the distances of about 2.27 Å for **2**[16] and Zr–C1 in **3**·PMe_3. Both the H22-Zr1-H23 (126(1)°) and B1-C11-B2 (149.3(4)°) angles are significantly greater than expected values,[17, 18] allowing for interaction between Zr1 and C11, which is approximately trigonal bipyramidal in geometry. The unusual coordination environment around C11 is reflected in its upfield chemical shift in the $^{13}C\{^1H\}$ NMR spectrum, compared to chemical shifts of $\delta > 30$ which we have observed for the B-C-B carbons in "free" chelating boranes of general formula $[RCH_2CH\{B(C_6F_5)_2\}_2]$.[5]

 © VCH Verlagsgesellschaft mbH, D-69451 Weinheim, 1995 0570-0833/95/1111-1231 $ 10.00+.25/0

The sum of the angles between C11 and the three atoms in the equatorial plane is 358° but the atoms are not in an ideal trigonal arrangement, that is the Zr1-C11-H11 angle of 107(2)° is decidely more acute than the Zr1-C11-H12 angle of 149(2)°. No evidence, however, was found for an agostic interaction in the solution NMR data. Previous examples of five-coordinate carbon involved either the three-center, two-electron bonding type of an alkyl ligand bridging two transition metals,[19] or "ate" complexes with lithium counterions.[20] If one views **5** formally as a complex of $[Cp_2Zr]^{2+}$ and the dianion $[CH_2\{HB(C_6F_5)_2\}_2]^{2-}$, one might expect negative charge localization on the methylene carbon which is donated to the electrophilic zirconium center; computational studies are required to define this interaction more precisely.

A plausible means of formation of **5** would involve complexation of **1** with the Tebbe-type complex **3** if the borane approaches from the μ-methylene side of the metallocene wedge. Interestingly, when **3** is treated with excess borane **1**, *both* **4** and **5** are formed, again in a ratio of approximately 1:2, suggesting that approach from the μ-hydride side is also occuring. This approach would produce the intermediate shown in square brackets in Scheme 1. We have not isolated this species, but signals in the ^{1}H NMR spectrum of the reaction of **3** plus one equivalent of **1** at $\delta = 4.95$ (Cp) and $\delta = 2.81$ (CH_2) are assignable to this compound. Further reaction with **1** resulted in the disappearance of these signals and growth of resonances for **4**.[21] Another pathway by which **4** may be formed from **1** and **2** involves methyl-hydride exchange[6] and complexation of further equivalents of **1** to Zr–H units. The identification of the compound $CH_3B(C_6F_5)_2$[4] in the product mixture of reaction (e) in Scheme 1 is consistent with this scenario.

Complex **5** is also significant because of its *inactivity* as an ethylene polymerization catalyst under ambient conditions. On the basis of recent disclosures by Marks et. al.[22] one might expect an isomer, **5'**, to be accessible and function as a highly active catalyst [Eq. (f)]. The implications of structure **5** for the



(f)

5 **5'**

use of counterions of general formula $[RCH_2CH\{B(C_6F_5)_2\}_2(\mu\text{-}H)]^-$ in homogenous Ziegler–Natta catalysts remain to be determined but if the isomers depicted in Equation f are interconvertible under realistic polymerization conditions, some attenuation of catalyst activity may be expected. We are currently exploring these issues further as well as the mechanistic details of the reactions of **1** with dialkylzirconium complexes.

Experimental Procedure

All NMR spectra were performed in C_6D_6 on a Varian Unity 400 instrument.

3: Hexane (15 mL) was condensed into a vessel containing **1** (115 mg, 0.33 mmol) and **2** (84 mg, 0.33 mmol) at −78 °C. The reaction was allowed to warm to room temperature. After stirring and sonicating for 1 hour a red precipitate was isolated by filtration. Yield 164 mg, 0.28 mmol, 86%. ^{1}H NMR: $\delta = 5.70$ (10H; C_5H_5), 5.30 (2H; CH_2), −0.75 (1H, br; Zr-H-B); ^{19}F NMR (referenced to $CFCl_3$ at $\delta = 0.0$): $\delta = -132.3$, −160.4, −165.2; ^{11}B NMR (referenced to $BF_3 \cdot Et_2O$ at $\delta = 0.0$): $\delta = -1.1$. IR (KBr, Nujol, cm^{-1}): $\tilde{\nu} = 1640$ m, 1602 w (B-H-Zr), 1509 m, 1305 w, 1282 w, 1374 w, 1094 s, 1017 s, 967 s, 810 s, 775 m.

3·PMe_3: To a frozen suspension of **3** (147 mg, 0.25 mmol) in benzene (3 mL) at −78 °C was condensed excess PMe_3 (1.5 equivalents). The reaction mixture was warmed to room temperature and filtered; hexane (15 mL) was added to precipitate the product as a lime green solid which was isolated by filtration. Yield, 113 mg, 0.17 mmol, 68%. Crystals were obtained by recrystallization from benzene ^{1}H NMR: $\delta = 5.07$ (d, 10H, J(P,H) = 2.4 Hz; C_5H_5), 0.93 (dd, 2H, ^3J(P,H) = 12.7 Hz, ^3J(H,H) = 3.9 Hz; CH_2), 0.54 (d, 9H, ^2J(P,H) = 6.4 Hz; PCH_3), −1.9 (br, 1H; Zr-*H*-B). ^{13}C{^{1}H} NMR (referenced to benzene at $\delta = 128.0$, HMQC [14]): $\delta = 105.1$ (C_5H_5), 33.0 (CH_2, ^1J(C,H) = 128 Hz), 15.6 (d, ^1J(P,C) = 24.4 Hz, PCH_3); ^{11}B NMR: $\delta = -30.3$; ^{19}F NMR: $\delta = -131.8$, −162.1, −165.9; ^{31}P{^{1}H} NMR (referenced to 85% H_3PO_4 at $\delta = 0.0$): δ −3.0.

4·C_6H_6: Benzene (25 mL) was condensed into a vessel containing $[Cp_2ZrH_2]$ (44.5 mg, 0.2 mmol) and **1** (138 mg, 0.4 mmol) at −78 °C. The reaction mixture was heated to reflux; on cooling, white crystalline needles of **4** appeared. The crystals were isolated by filtration and dried under vacuum. Yield: 122 mg, 0.13 mmol, 67%. Recrystallization from benzene gave clear cubes of the benzene solvate of **4**. ^{1}H NMR: $\delta = 5.42$ (s, C_5H_5); 0.38 (br, μ-H); ^{11}B NMR: $\delta = -12.9$ (t, ^1J(H,B) = 64 Hz); ^{19}F NMR: $\delta = -133.0$, −156.8, −163.4. Elemental analysis: calcd. for $C_{34}H_{14}F_{20}B_2Zr \cdot C_6H_6$: C 48.36, H 2.03; found (separate samples): C 47.61, 47.71; H 1.77, 1.81. IR (KBr, Nujol, cm^{-1}): $\tilde{\nu} = 2184$ w (br), 2110 w (br), 2028 w (br), 1645 m, 1514 s, 1288 m, 1260 m, 1114 m, 1094 m, 957 s, 826 m.

5·C_6H_6: Benzene (7 mL) was added to a flask containing **2** (126 mg, 0.5 mmol) and **1** (346 mg, 1 mmol). Upon stirring, the reaction mixture became dark red and gas evolution was observed. After 30 minutes, the reaction mixture was heated to reflux; on cooling, colorless crystals formed which were isolated by filtration, washed with benzene, and dried in vacuo. Yield 225 mg, 0.22 mmol, 45%. ^{1}H NMR: $\delta = 5.23$ (s, 10H; C_5H_5), 2.29 (s, 2H; CH_2), −2.05 (br, 2H; Zr-H-B); ^{13}C{^{1}H} (HMQC): $\delta = 111.1$ (C_5H_5), 0.5 (CH_2, ^1J(C,H) = 120 Hz); ^{19}F NMR: $\delta = -132.4$, −157.2, −163.4. ^{11}B NMR: 0.0 (fwhm, 135 Hz). IR (Nujol mull, KBr): $\tilde{\nu} = 1937$ w, 1902 w, 1857 m, 1822 w, 1779 w, 1644 m, 1516 s, 1284 m, 1128 w, 1098 s, 1025 m, 1015 w, 978 s, 895 w, 883 w, 855 w, 838 w, 824 m, 818 m, 793 w, 766 w, 754 w, 744 w, 702 w, 647 m. Elemental analysis: calcd for $C_{41}H_{20}B_2F_{20}Zr$: C 49.35, H 2.35; found: C 49.49, H, 2.14.

Received: January 10, 1995 [Z 7621 IE]
German version: *Angew. Chem.* **1995**, *107*, 1337–1340

Keywords: boranes · catalysis · five-coordinate carbon · sandwich complexes · zirconium compounds

[1] R. H. Grubbs, W. Tumas, *Science* **1989**, *243*, 907.
[2] H. Sinn, W. Kaminsky, *Adv. Organomet Chem.* **1980**, *18*, 99.
[3] a) J. J. Eisch, A. M. Piortrowski, S. K. Brownstein, E. J. Gabe, F. L. Lee, *J. Am. Chem. Soc.* **1985**, *107*, 7219; b) X. Yang, C. L. Stern, T. J. Marks, *ibid.* **1991**, *113*, 3623; c) T. J. Marks, *Acc. Chem. Res.* **1992**, *25*, 57; d) R. F. Jordan, *Adv. Organomet. Chem.* **1991**, *32*, 325; e) P. G. Gassman, M. R. Callstrom, *J. Am. Chem. Soc.* **1987**, *109*, 7875.
[4] X. Yang, C. L. Stern, T. J. Marks, *J. Am. Chem. Soc.* **1994**, *116*, 10015.
[5] D. J. Parks, R. E. von H. Spence, W. E. Piers, *Angew. Chem.* **1995**, *107*, 895; *Angew. Chem. Int. Ed. Engl.* **1995**, *34*, 809.
[6] J. A. Marsella, K. G. Caulton, *J. Am. Chem. Soc.* **1982**, *104*, 2361.
[7] R. G. Kidd in *NMR of Newly Accessible Nuclei, Vol. 2* (Ed.: P. Laszlo), Academic Press, New York, **1983**.
[8] F. N. Tebbe, G. W. Parhsall, G. S. Reddy, *J. Am. Chem. Soc.* **1978**, *100*, 3611.
[9] Crystal data for **3**·PMe_3: $C_{26}H_{22}F_{10}BPZr$, 0.40 × 0.60 × 0.70 mm, monoclinic, $P2_1/n$, $a = 10.884(4)$, $b = 16.002(5)$, $c = 15.312(6)$ Å, $\beta = 103.71(3)°$, $V = 2590.8(16)$ Å^3, $Z = 4$, $\rho_{calcd} = 1.686$ mg m^{-3}, $2\theta_{max} = 50°$, $Mo_{K\alpha}$ radiation, $\lambda = 0.70930$ Å, ω-scan, $T = 298$ K, 4731 measured reflections, 4552 independent, 3129 reflections with $I_{net} > 3.0\sigma(I_{net})$, $\mu = 0.55$ mm^{-1}, min/max transmission = 0.735 and 0.999, $R(F) = 0.057$, $R_w = 0.052$, GOF = 4.31, no. of parameters = 356. After anisotropic refinement of all non-hydrogen atoms, planar and methylene hydrogen atoms were placed in calculated positions ($D_{C-H} = 1.00$ Å and 1.08 Å) and methyl hydrogen atoms were located by inspection of a difference Fourier map. All hydrogens were given temperature factors based upon the atom to which they are bonded and fixed during least squares refinement. All crystallographic calculations were conducted with the PC version of the NRCVAX program package locally implemented on an IBM compatible 80486 computer: E. J. Gabe, Y. Le Page, J.-P. Charland, F. L. Lee, P. S. White *J. Appl. Crystallogr.* **1989**, *22*, 384.
[10] Further details of the crystal structure investigations are available on request from the Director of the Cambridge Crystallographic Data Centre, 12 Union Road, GB-Cambridge CB2 1EZ (UK) on quoting the full journal citation.
[11] R. T. Baker, D. W. Ovenall, J. C. Calabrese, S. A. Westcott, N. J. Taylor, I. D. Williams, T. B. Marder, *J. Am. Chem. Soc.* **1990**, *112*, 9399.
[12] W. K. Kot, N. M. Edelstein, A. Zalkin, *Inorg. Chem.* **1987**, *26*, 1339.
[13] P. C. Wailes, H. Weigold, *J. Organomet. Chem.* **1970**, *24*, 405.
[14] a) V. J. Robinson, A. D. Bain, *Magn. Reson. Chem.* **1993**, *31*, 865; b) A. Bax, S. Subramanian, *J. Magn, Reson.* **1986**, *67*, 565.

[15] Crystal data for $5 \cdot 1.5C_6H_6$: $C_{44}H_{23}F_{20}B_2Zr$, $0.15 \times 0.30 \times 0.50$ mm, triclinic, $P\bar{1}$ (no. 2), $a = 14.8025(8)$, $b = 14.9622(7)$, $c = 9.8708(7)$ Å, $\alpha = 93.972(8)$, $\beta = 108.340(7)$, $\gamma = 94.416(8)°$, $V = 2058.8(3)$ Å^3, $Z = 2$, $\rho_{calcd} = 1.685$ mg m^{-3}, $2\theta_{max} = 55$, $Mo_{K\alpha}$ radiation, $\lambda = 0.71069$ Å, ω-scan, $T = 294$ K, 9839 measured reflections, 9467 independent, 3885 reflections with $I_{net} > 3.0\sigma(I_{net})$, $\mu = 3.91$ cm^{-1}, min/max transmission = 0.9023 and 1.0000, $R(F) = 0.039$, $R_w = 0.032$, GOF = 1.60, no. of parameters = 620. The structure was solved by the Patterson method and was refined by full-matrix least-squares procedures. All non-hydrogen atoms were refined with anisotropic thermal parameters and the B-H and methylene C-H hydrogen atoms were refined with isotropic thermal parameters. The remaining hydrogen atoms were fixed in calculated positions with C-H = 0.98 Å and B(H) = 1.2 B(bonded atom). All calculations were performed on a Silicon Graphics Indigo Workstation using the *teXsan* Crystal Structure Analysis Package: Molecular Structure Corporation, The Woodlands, TX, USA **1992**.

[16] a) W. E. Hunter, D. C. Hrncir, R. Vann Bynum, R. A. Penttila, J. L. Atwood, *Organometallics* **1983**, *2*, 750. b) R. F. Jordan, C. S. Bajgur, R. Willett, B. Scott, *J. Am. Chem. Soc.* **1986**, *108*, 7410.

[17] MM2 minimization of $CH_2[B(C_6F_5)_2]_2$ lead to a B-C-B angle of about 122°.

[18] Typical L-Zr-L values for Zr^{IV} metallocenes are about 95°: D. J. Cardin, M. F. Lappert, C. L. Raston, P. I. Riley, in *Comprehensive Organometallic Chemistry*, *Vol. 3* (Ed.: G. Wilkinson, F. G. A. Stone, E. W. Abel), Pergamon, New York, **1982**, p. 551.

[19] J. Holton, M. F. Lappert, R. Pearce, P. I. W. Yarrow, *Chem. Rev.* **1983**, *83*, 135.

[20] a) D. L. Clark, J. C. Gordon, J. C. Huffman, J. G. Watkin, B. D. Zwick, *Organometallics* **1994**, *13*, 4267; b) R. J. Morris, G. S. Girolami, *ibid.* **1989**, *8*, 1478; c) W. J. Evans, T. A. Ulibarri, J. W. Ziller, *ibid.* **1991**, *10*, 134.

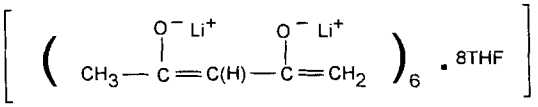
[21] A broad methylene resonance at about $\delta \approx 3.1$ is consistent with the presence of free $CH_2[B(C_6F_5)_2]_2$, which must be produced in these reactions.

[22] L. Jia, X. Yang, C. Stern, T. J. Marks, *Organometallics* **1994**, *13*, 3755.

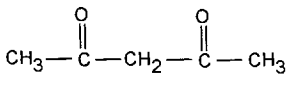
Crystal Structure of Dilithioacetylacetone: A Twenty-Four Vertex Li-O Cage Molecule with Limited Li–C(terminal) Bonding and Selective THF Solvation**

William Clegg, Lynne Horsburgh, Robert E. Mulvey,* and Michael J. Ross

Dienolate anions generated by double metallation of a β-diketone with alkali metals are important building blocks in organic chemistry.[1] In reality these are dimetallo intermediates, whose precise identities are normally concealed by the in situ manner of their utilization. Here we report the isolation and crystallographic characterization of the representative dilithium dienolate **1**. Though derived from the simplest 1,3-diketone,



1



2

acetylacetone (acac), **2**, its structure is surprisingly complicated, containing twelve Li^+ ions in an odd cage architecture, which is totally out of line with the regular dimeric, tetrameric, or hexameric aggregates generally adopted by lithium enolates.[2]

THF solvation proved to be the key to capturing the dilithioacetylacetone in a crystalline form suitable for X-ray diffraction study. However, despite the availability of excess THF in the reaction solution, solvation is incomplete with only eight of the twelve Li^+ ions carrying a THF ligand.

The implication of the THF-deficiency, that the doubly charged acac anions form a robust aggregate with the Li^+ ions, is confirmed by the crystal structure (Fig. 1a).[3] Possessing

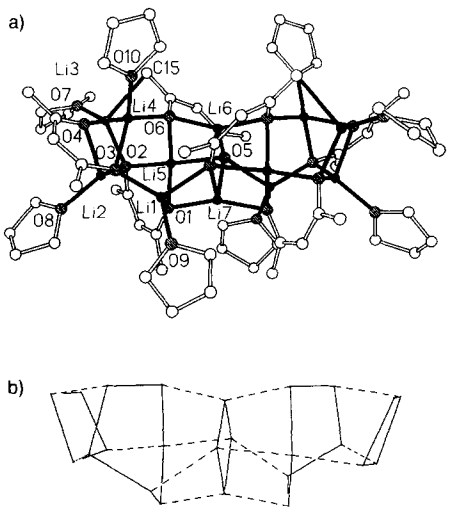


Fig. 1. a) Crystal structure of **1** (excluding hydrogen atoms). Principal distances [Å]: Li1–O1 1.947(7), Li1–O3 1.883(7), Li1–O5a 2.071(7), Li1–O9 2.009(7), Li2–O2 1.969(7), Li2–O3 1.961(7), Li2–O4 2.003(7), Li2–O8 2.037(7), Li3–O2 1.915(7), Li3–O4 1.853(7), Li3–O7 1.924(7), Li3–C15 2.429(8), Li4–O3 2.015(6), Li4–O4 1.984(7), Li4–O6 1.912(6), Li4–O10 1.945(7), Li5–O1 1.920(7), Li5–O2 1.906(6), Li5–O5 2.049(6), Li5–O6 1.980(7), Li6–O5 2.011(5), Li6–O6 1.912(3), Li7–O1 1.853(3), Li7–O5 2.165(9); angles at Li atoms in range 86.1(3)–159.7(8)°. b) Line drawing of the quintuple-decker sandwich core of **1** showing the Li–O rhomboid and six-membered boat layers with solid lines and connections between these layers as dashed lines; the view direction is as for a).

crystallographic C_2 symmetry about the Li6···Li7 axis, the molecule's irregular appearance can be made more intelligible if its Li–O(acac) core is viewed as a quintuple-decker sandwich (Fig. 1b): a central unique rhomboid Li6-O5-Li7-O5a sits between two identical, distorted boats Li4-O3-Li1-O1-Li5-O6 and its symmetry equivalent. Two identical, rhomboids Li2-O2-Li3-O4 and its symmetry equivalent form the outer layers. The unique "bridging" rhomboid forms η^4-contacts with the boats on either side, while the other rhomboids bind to them in a "terminal" η^3 manner. These latter rhomboids additionally interact with a terminal carbon atom of acac (C15/C15a).

Two of the three crystallographically distinct acac dianions **A** and **B** each participate in six Li–O contacts in total (three per O atom; Fig. 2). Such μ_3O–Li bonding is commonplace in higher aggregates, for example, the hexameric enolate derived from pinacolone.[4] In contrast, the third dianion **C** takes part in seven Li–O contacts, the odd number stemming from a novel μ_4-bonding stance assumed by O5. This extra coordination leads to long Li–O5 bonds (2.011–2.165 Å; mean 2.074 Å). In comparison, other Li–O(anionic) bonds have mean lengths below 2 Å (range of mean lengths, 1.907–1.953 Å). Figure 2 shows how the attached Li^+ centers are oriented with respect to

[*] Dr. R. E. Mulvey, M. J. Ross
Department of Pure and Applied Chemistry, University of Strathclyde
GB-Glasgow G1 1XL (UK)
Telefax: Int. code + (141) 552 0876
Prof. W. Clegg, L. Horsburgh
Department of Chemistry, University of Newcastle (UK)

[**] This work was supported by the UK Engineering and Physical Science Research Council.

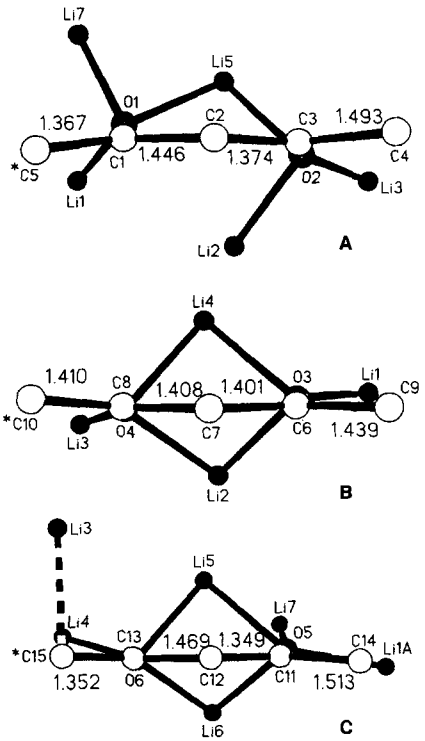


Fig. 2. The three distinct acac dianions **A** (top), **B** (middle), and **C** (bottom) edge on, with their connected lithium centers and C–C bond lengths; each terminal CH_2 group is marked with an asterisk. C–O bond lengths [Å]: C1–O1 1.352(5), C3–O2 1.318(5), C6–O3 1.338(4), C8–O4 1.335(4), C11–O5 1.342(4), C13–O6 1.341(4).

the mean acac ligand planes. Only in the case of dianion **A** do the O atoms (O1, O2) lie significantly out of the mean C-C(O)-C-C(O)-C plane (deviations 0.235 and −0.235 Å, respectively, cf., 0.079 and −0.093 in **B** and 0.080 and −0.080 Å in **C**).

Tetracoordination of Li^+ is usual in enolate structures.[2] In **1** it occurs in three distinct ways. Embedded close to the center of the cage, the group of Li5, Li6, and Li7 atoms attain it exclusively through coordination to acac O centers. Another trio of atoms, Li1, Li2, and Li4, positioned more towards the end of the cage, are only three-coordinate with respect to these centers, but have room to form a fourth bond with a THF solvent molecule. With the exception of the Li1–O(THF) bond, whose length (2.009(7) Å) implies that Li1 is the least sterically accessible of the ligated atoms, these terminal Li–O(neutral) bonds are comparable in length (1.937, 1.945 Å) to the bridging Li–O(anionic) type discussed above. Two acac O atoms, one THF O atom, and one terminal $C(H_2)$ atom make up the unique coordination of the Li3 atom. The bonds to these O atoms are comparatively short (1.853(7), 1.915(7) and 1.924(7) Å, respectively). Indicative of a modest degree of keto character, the Li3-C15 interaction (2.429(8) Å) is marginally shorter than that observed in the dimeric monolithium dienolate of 2,2,5,6,6-pentamethylhept-4-en-3-one[5] (2.50 Å). As shown both experimentally[6] and theoretically[7] by Schleyer et al., Li–C bonding makes a much more substantial contribution to "Y-conjugated" dilithium derivatives of α,α′-keto dianions.

The intricate nature of the Li–O/Li–C core bonding is communicated to the three coordinatively distinct acac dianions as evidenced by the profound variations in their dimensions (Fig. 2). Most significantly, dianion **B** is decidedly more symmetrical on account of its greater overall charge delocalization, for example, C–C bonds involving the terminal methyl and methylene groups differ in length by only 0.029 Å, in comparsion to 0.126 and 0.161 Å in **A** and **C**, respectively. This finding appears to be linked to the nature, solvated or unsolvated, of the attached Li^+ ions, as **B** interacts exclusively with the former, whereas **A** and **C** form contacts with both types. Although twofold disorder of dianion **B** could produce the apparent near-symmetry as an artefact, we do not believe this is the case here, since all six hydrogen atoms for each dianion were clearly located in difference syntheses, so that terminal CH_3 and CH_2 groups are distinguished. Also noteworthy is the insensitivity of the C–O bond lengths (C–O5 1.342 and C–O6 1.341 Å) to the electronic imbalance created by the Li–C(terminal) bonding found in **C**. Since these O atoms have different coordination numbers (five and four, respectively), this may be coincidental, given that the bond angles involved do vary significantly (C14-C11-O5, 115.1°; C15-C13-O6, 122.6°).

Herein we have demonstrated that dilithiation of a 1,3-dicarbonyl compound can lead to an extremely complicated contact ion pair aggregate. As an aid to establishing structure–reactivity correlations, our next targets are to ascertain the structure of the mixed Li–Na analogue, since it has been previously reported that it exhibits different chemical behavior,[8] and to investigate the solution structures of both building blocks.

Experimental Procedure

1: The preparation was performed in a Schlenk tube, under anaerobic and anhydrous conditions. Acetylacetone (20 mmol) was doubly deprotonated by action of LDA (40 mmol: prepared in situ in hexane/THF from *n*BuLi and diisopropylamine). The solution (initially chilled), was stirred for two hours at ambient temperature to ensure reaction completion. The best medium for crystallization of pale yellow **1** proved to be a 5/1, hexane/THF mixture, maintained at ambient temperature. Yield (without refinement), 41%. M.p. 106–108 °C. Satisfactory C, H, Li, N analyses. Single crystals suitable for X-ray crystallography were examined and mounted under an inert oil.

Received: December 13, 1995 [Z7543IE]
German version: *Angew. Chem.* **1995**, *107*, 1353–1355

Keywords: cage compounds · enolates · lithium compounds · structure elucidation

[1] For typical examples see: E. M. Kaiser, J. D. Petty, P. L. A. Knutson, *Synthesis* **1977**, 509; T. M. Harris, C. M. Harris, *Org. React.* **1969**, *17*, 155; J. S. Hubbard, T. M. Harris, *J. Org. Chem.* **1981**, *46*, 2566; R. M. Sandifer, A. K. Bhattacharya, T. M. Harris, *J. Org. Chem.* **1981**, *46*, 2260.

[2] D. Seebach, *Angew. Chem.* **1988**, *100*, 1685; *Angew. Chem. Int. Ed. Engl.* **1988**, *27*, 1624.

[3] **1**: $M_r = 1248.7$, monoclinic, $C2/c$, $a = 17.846(6)$, $b = 19.945(8)$, $c = 20.167(6)$ Å, $\beta = 94.56(4)°$, $V = 7155(5)$ Å^3, $Z = 4$, $\rho_{calcd} = 1.159$ g cm^{-3}, $F(000) = 2672$, $Mo_{K\alpha}$ radiation, $\lambda = 0.71073$ Å, $\mu = 0.081$ mm^{-1}. The structure was determined by direct methods and refined on F^2 using all 4686 independent reflections measured at 160 K with a Stoe-Siemens diffractometer ($2\theta_{max} = 45°$), with anisotropic atomic displacement parameters and with constrained isotropic H atoms: $R' = [\Sigma\{w(F_o^2 - F_c^2)^2\}/\Sigma\{w(F_o^2)^2\}]^{0.5} = 0.2002$, conventional R [on F values for 3254 reflections with $F_o^2 > 2\sigma(F_o^2)$] = 0.0645, S (on F^2 for all data) = 1.033 for 434 parameters. Further details of the crystal structure determination can be obtained from the Director of the Cambridge Crystallographic Data Centre, 12 Union Road, GB-Cambridge CB2 1EZ (UK), on quoting the full journal citation.

[4] P. G. Williard, G. B. Carpenter, *J. Am. Chem. Soc.* **1985**, *107*, 3345; *ibid.* **1986**, *108*, 462.

[5] R. Amstutz, J. D. Dunitz, T. Laube, W. B. Schweizer, D. Seebach, *Chem. Ber.* **1986**, *119*, 434.

[6] H. Dietrich, W. Mahdi, D. Wilhelm, T. Clark, P. von R. Schleyer, *Angew. Chem.* **1984**, *96*, 623; *Angew. Chem. Int. Ed. Engl.* **1984**, *23*, 621.

[7] A. J. Kos, T. Clark, P. von R. Schleyer, *Angew. Chem.* **1984**, *96*, 622; *Angew. Chem. Int. Ed. Engl.* **1984**, *23*, 620.

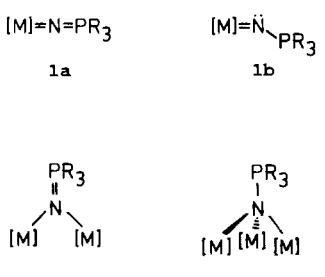
[8] K. G. Hampton, J. J. Christie, *J. Org. Chem.* **1975**, *40*, 3887.

 © VCH Verlagsgesellschaft mbH, D-69451 Weinheim, 1995 0570-0833/95/1111-1234 $ 10.00+.25/0

Phosphorane Iminato Complexes of Manganese and Cobalt with Heterocubane Structure**

Hans-Joachim Mai, Rolf Meyer zu Köcker, Sigrid Wocadlo, Werner Massa, and Kurt Dehnicke*

The phosphorane iminato ligand $[NPR_3]^-$, which is among others isoelectronic to the siloxy ligand $[OSiR_3]^-$, displays a diverse coordination chemistry. The mode of coordination realized depends on the transition metal fragment [M] as well as on the substituents bonded to the phosphorus atom. Electron-poor transition metals in high oxidation states prefer type **1** with M-N-P bond angles between 180 and 130°.[1] An example for this type is the ionic tantalum complex **4**.[2] In electron-rich metal complex fragments the μ_2-bridging type **2**, for example found in **5**,[3] and the μ_3-bridging type **3** found in the nickel complex **6**[4] have been observed. Phenyl groups bonded to the phosphorus atom stimulate the formation of **1**, alkyl groups promote the μ_3-N type **3**.



1a **1b** **2** **3**

Here we report the first phosphorane iminato complexes of manganese(II) (**10**) and cobalt(II) (**11**) with heterocubane structure, in which the bridging type **3** is found. Heterocubane complexes of manganese with μ_3-N atoms are unknown; however, manganese complexes with μ_3-OH, μ_3-OR groups, and μ_3-chalcogen atoms[5] have been reported. Cobalt preferably forms heterocubanes with phosphido and arsenido groups.[5] The only heterocubane of cobalt with a μ_3-N imido ligand is the nitrosyl complex **7**.[6]

$[Ta(NPPh_3)_4]^+[TaCl_6]^-$ **4** $[\{FeCl_2(\mu_2\text{-}NPPh_3)\}_2]$ **5**

$[(\mu_3\text{-}NH)(\mu_3\text{-}NPMe_3)(NiClPMe_3)_3]$ **6** $[\{Co(NO)(\mu_3\text{-}N\text{-}t\text{Bu})\}_4]$ **7**

We obtained the phosphorane iminato complexes of manganese(II) and cobalt(II) by reaction of the anhydrous metal halides MnI_2 and $CoCl_2$ with the silylated phosphorane imine $Me_3SiNPEt_3$. The reactions first yield the surprisingly stable monomeric donor–acceptor complexes **8** and **9**, in which according to the X-ray structure analysis[7] the N atoms of the phosphorane iminato ligands act as donor atoms. The Si–N interatomic distances in both complexes are 2–3 pm shorter than the comparable distances in the noncoordinating phosphorane imine $Me_3SiNPMe_3$.[8] This explains the thermal stability of **8** and **9**. Only heating to above 200 °C brings about the cleavage of trimethylsilyl halide and the formation of the heterocubanes **10** and **11** [Eqs. (a), (b)]. Considerable amounts of **10** could only be obtained after the addition of potassium fluoride.

$$4[MnI_2(Me_3SiNPEt_3)_2] + 4\,KF \quad (a)$$
8
$$\longrightarrow [\{MnI(NPEt_3)\}_4] + 4\,FSiMe_3 + 4\,KI + 4\,Me_3SiNPEt_3$$
10

$$4[CoCl_2(Me_3SiNPEt_3)_2] \quad (b)$$
9
$$\longrightarrow [\{CoCl(NPEt_3)\}_4] + 4\,ClSiMe_3 + 4\,Me_3SiNPEt_3$$
11

After the extraction of the solidified melt with dichloromethane the complexes are isolated as shiny red (**10**) and green (**11**) crystals, respectively. Intensive signals are observed for the molecular ions of the tetrameric units in the EI mass spectra (70 eV). The remarkably intense color of **9** is caused by three charge-transfer(CT) bands. Their maxima at 520, 462, and 365 nm (in dichloromethane) are located in the visible range of the spectrum and are missing in the starting material **8**. The measurement of the magnetic susceptibility of **10** at 20 °C gave a magnetic moment of $\mu_{eff} = 3.1$ B.M. per manganese atom. This value is considerably lower than the value of 5.92 B.M. which would be expected for a d^5 high-spin configuration and indicates the presence of spin-spin interactions between the manganese atoms in the heterocubane. In contrast to this, a magnetic moment of $\mu_{eff} = 3.2$ B.M. is found for the cobalt complex **11** at 20 °C, a value which is only slightly lower than the spin-only value for Co^{II} (3.87 B.M.).

The IR spectra of **10** and **11** show the characteristic stretching vibration of the phosphorane iminato ligand at 1035 and 1053 cm^{-1}, respectively. These frequencies are in agreement to the crystallographic findings of short P–N bonds.

According to the X-ray structure analyses[9] **10** and **11** are not isotypic; however, they form very similar heterocubanes (Figs. 1 and 2). Their inside bond angles differ only slightly from 90°, thus almost ideal cubane structures exist. The Co complex **11** exhibits C_2 symmetry, the Mn cubane **10** is without symmetry. The differences are caused mainly by the arrangements of the PEt_3 groups. The metal–nitrogen interatomic distances suggest single bonds.[10] In this respect it is remarkable that the Co–N interatomic distances in **11** (204.8 pm) are about 10 pm shorter

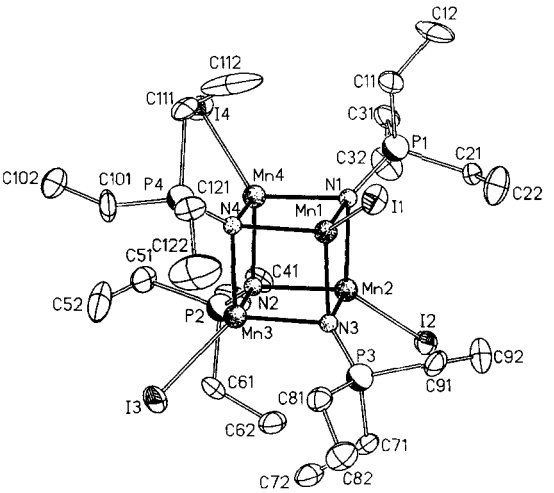


Fig. 1. Molecular structure of **10**. Selected interatomic distances [pm] and angles [°] (standard deviations in parentheses): Mn-I 265.83(9), Mn-N 213.7(5), P-N 159.2(5), Mn···Mn 296.1(1); Mn-N-Mn 88.5(2), N-Mn-N 92.2(2).

[*] Prof. Dr. K. Dehnicke, Dipl.-Chem. H.-J. Mai,
Dipl.-Chem. R. Meyer zu Köcker, S. Wocadlo, Prof. Dr. W. Massa
Fachbereich Chemie der Universität Marburg
Hans-Meerwein-Strasse, D-35032 Marburg (Germany)
Telefax: Int. code +(6421) 288917

[**] This work was supported by the Deutsche Forschungsgemeinschaft and by the Fonds der Chemischen Industrie.

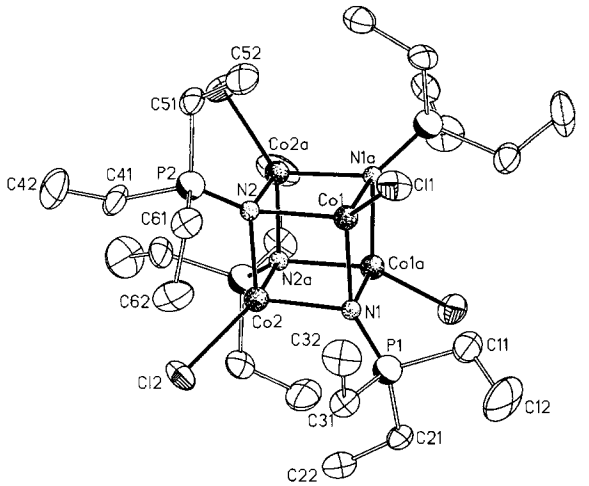


Fig. 2. Molecular structure of **11**. Selected interatomic distances [pm] and angles [°] (standard deviations in parentheses): Co-Cl 222.9(2), Co-N 204.8(5), P-N 159.6(6), Co···Co 280.5(1); Co-N-Co 86.5(2), N-Co-N 93.4(2).

than the Mn–N interatomic distances in **10**. This leads to relatively short Co···Co interactions (280.5 pm) in **11** compared to the value observed for the Mn···Mn interactions (296.1 pm) in **10**. This trend continues for phosphorane iminato complexes of 3d elements containing μ_3-N bridges; in the nickel complex **6** Ni–N interatomic distances of 195.3(6) pm[4] and in the hexameric copper cluster **12**[11] interatomic distances of 191.7(8) are

$[Cu_6Br_6(\mu_3\text{-}NPMe_3)_4]$ **12**

observed. These shortenings of interatomic distances are only partially caused by the contraction of the radii of the M^{2+} ions. The P–N interatomic distances in the heterocubanes **10** and **11** (159.2 pm and 159.6 pm) are equal within the standard deviation. They correspond to the expected values for double bonds (160–164 pm[10, 12]) which can be described as σ- and polar bonds according to type **3**.

The reactions of the heterocubanes **10** and **11** with organolithium compounds lead to hexane-soluble, highly reactive pyrophoric organometallic heterocubanes of the general formula $[\{M(R)(NPEt_3)\}_4]$, which are capable of undergoing various subsequent reactions.

Experimental Procedure

All reactions require the strict absence of oxygen and moisture.

10: A mixture of MnI_2 (2.05 g, 6.63 mmol), KF (1.05 g, 18.10 mmol), and $Me_3SiNPEt_3$ (2.93 mL, 13.25 mmol) [13] was heated to 230 °C for 4 h, then CH_2Cl_2 (40 mL) was added to the cooled mixture and KF/KI was removed by filtration. The solvent was removed under vacuum and the remaining solid was recrystallized with CH_3CN (20 mL). Yield: 2.83 g (34%). Single crystals were obtained by cooling the saturated solution to 4 °C. $C_{24}H_{60}Mn_4N_4P_4$ (1256.00 g mol^{-1}); elemental analysis: found C 21.71, H 4.20, N 4.20%; calc. C 23.41, H 4.87, N 4.54%.

11: A mixture of $CoCl_2$ (1.10 g, 8.5 mmol) and $Me_3SiNPEt_3$ (2.0 mL, 9.1 mmol) was heated to 150 °C for 2 h, then CH_2Cl_2 (10 mL) was added to the cool melt and insoluble material was removed by filtration. The solvent was removed under vacuum until about 4 mL of solution remained. The mixture was left to stand at 20 °C (Yield: 0.83 g single crystals (43%). $C_{24}H_{60}Cl_4Co_4N_4P_4$ (906.21 g mol^{-1}); elemental analysis: found C 31.84, H 6.47, N 5.99, Co 26.63, Cl 16.37%; calc. C 31.81, H 6.67, N 6.18, Co 26.04, Cl 15.65%.

Received: January 11, 1995 [Z 7622 IE]
German version: *Angew. Chem.* **1995**, *107*, 1349–1350

Keywords: cobalt compounds · heterocubanes · manganese compounds · phosphorane iminato complexes

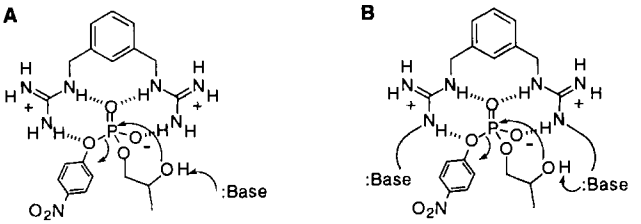
[1] K. Dehnicke, J. Strähle, *Polyhedron* **1989**, *8*, 707.
[2] D. Nusshär, F. Weller, A. Neuhaus, G. Frenking, K. Dehnicke, *Z. Anorg. Allg. Chem.* **1992**, *615*, 86.
[3] H. W. Roesky, U. Seseke, M. Noltemeyer, G. M. Sheldrick, *Z. Naturforsch. B* **1988**, *43*, 1130.
[4] H.-F. Klein, S. Haller, H. König, M. Dartiguenave, Y. Dartiguenave, M. J. Menu, *J. Am. Chem. Soc.* **1991**, *113*, 4673.
[5] Heterocubanes of manganese: S. B. Copp, S. Subramanian, M. J. Zaworotko, *J. Am. Chem. Soc.* **1992**, *114*, 8719; M. D. Clerk, S. B. Copp, S. Subramanian, M. J. Zaworotko, *Supramol. Chem.* **1992**, *1*, 7; S. B. Copp, S. Subramanian, M. J. Zaworotko, *Angew. Chem.* **1993**, *105*, 755; *Angew. Chem. Int. Ed. Engl.* **1993**, *32*, 706; D. N. Hendrickson, G. Christou, E. A. Schmitt, E. Libby, J. S. Bashkin, S. Wang, H.-L. Tsai, J. B. Vincent, P. D. W. Boyd, J. C. Huffman, K. Folting, Q. Li, W. E. Streib, *J. Am. Chem. Soc.* **1992**, *114*, 2455; M. W. Wemple, H.-L. Tsai, K. Folting, D. N. Hendrickson, G. Christou, *Inorg. Chem.* **1993**, *32*, 2025; H.-O. Stephan, C. Chen, G. Henkel, K. Griesar, W. Haase, *J. Chem. Soc. Chem. Commun.* **1993**, *886*; H.-O. Stephan, G. Henkel, *Angew. Chem.* **1994**, *106*, 2422; *Angew. Chem. Int. Ed. Engl.* **1994**, *33*, 2322; K. L. Taft, A. Caneschi, L. E. Pence, C. D. Delfs, G. C. Papaefthymiou, S. J. Lippard, *J. Am. Chem. Soc.* **1993**, *115*, 11753. – Heterocubanes of cobalt: G. L. Simon, L. F. Dahl, *ibid.* **1973**, *95*, 2175; E. Röttinger, H. Vahrenkamp, *J. Organomet. Chem.* **1981**, *213*, 1; D. Fenske, R. Basoglu, J. Hachgenei, F. Rogel, *Angew. Chem.* **1984**, *96*, 160; *Angew. Chem. Int. Ed. Engl.* **1984**, *23*, 160; J. A. Bertrand, T. C. Hightower, *Inorg. Chem.* **1973**, *12*, 206; Yu. A. Simonov, G. S. Matuzenko, M. M. Botoshanskii, M. A. Yampol'skaya, N. V. Gerbeleu, T. I. Malinovskii, *Zh. Neorg. Khim.* **1982**, *27*, 407; K. Dimitrou, K. Folting, W. E. Streib, G. Christou, *J. Am. Chem. Soc.* **1993**, *115*, 6432.
[6] R. S. Gall, N. G. Connelly, L. F. Dahl, *J. Am. Chem. Soc.* **1974**, *96*, 4017.
[7] R. Meyer zu Köcker, G. Frenzen, B. Neumüller, K. Dehnicke, J. Magull, *Z. Anorg. Allg. Chem.* **1994**, *620*, 431; H.-J. Mai, K. Harms, K. Dehnicke, unpublished.
[8] R. Meyer zu Köcker, A. Behrendt, K. Dehnicke, D. Fenske, *Z. Naturforsch. B* **1994**, *49*, 301.
[9] Crystallographic data of **10** (– 80 °C): space group $P2_12_12_1$, $a = 1346.7(1)$, $b = 1442.6(1)$, $c = 2295.3(1)$ pm, $Z = 4$, four-circle diffractometer Enraf-Nonius CAD4, $Mo_{K\alpha}$-radiation, graphite-monochromator, ω-scan, $\theta = 2.3–25.0°$, 6661 independent reflections [$R_{int} = 0.0201$], 6149 with $I > 2\sigma(I)$, semiempirical absorption correction (φ-scans), $\mu(Mo_{K\alpha}) = 40.39$ cm^{-1}. Crystal dimensions $0.3 \times 0.3 \times 0.2$ mm, calculated density 1.871 g cm^{-3}, transmission range 0.466–0.390, programs SHELXS-86, SHELXL-93. The structure was solved by Patterson and Difference Fourier methods and refined with all reflections (F^2-data). All H atoms could be located; however, they were included using a riding model. Their isotropic thermal parameters were assumed to be the 1.2-fold or 1.5-fold (for methyl groups) of the U_{eq} value of the appropriate C atom. Anisotropic thermal parameters were used for all other atoms. $wR_2 = 0.066$, $R = 0.026$ ($I > 2\sigma(I)$), goodness of fit: 1.085 (F^2, 376 refined parameters), residual electron density: 0.49 e Å^{-3}. – **11** (– 50 °C: space group $C2/c$, $a = 2076.3(3)$, $b = 1094.4(2)$, $c = 1958.0(5)$ pm, $\beta = 115.80(1)°$, $Z = 4$, four-circle diffractometer Siemens P4, $Mo_{K\alpha}$-radiation, graphite monochromator, ω-scan, $\theta = 2.2–23.0°$, 2253 independent reflections [$R_{int} = 0.0576$], 1377 with $I > 2\sigma(I)$, without absorption correction, $\mu(Mo_{K\alpha}) = 20.75$ cm^{-1}. Crystal dimensions $0.25 \times 0.2 \times 0.18$ mm, calculated density 1.503 g cm^{-3}, programs SHELXS-86, SHELXL-93. The structure was solved, refined and the thermal parameters were used as described for **10**, H atoms on calculated positions. $wR_2 = 0.101$, $R = 0.040$ ($I > 2\sigma(I)$), goodness of fit: 0.838 (F^2, 182 refined reflections), residual electron density: 0.49 e Å^{-3}. Further details of the crystal structure investigations may be obtained from the Fachinformationszentrum Karlsruhe, D-76344 Eggenstein-Leopoldshafen (Germany) on quoting the depository number CSD-58868.
[10] A. F. Wells, *Structural Inorganic Chemistry*, Clarendon Press, Oxford, **1984**.
[11] R. Meyer zu Köcker, K. Dehnicke, D. Fenske, *Z. Naturforsch. B* **1994**, *49*, 987.
[12] L. G. Hoard, R. A. Jacobson, *J. Chem. Soc. A* **1966**, 1203.
[13] H. Schmidbaur, W. Wolfsberger, *Chem. Ber.* **1967**, *100*, 1000.

 © VCH Verlagsgesellschaft mbH, D-69451 Weinheim, 1995 0570-0833/95/1111-1236 $ 10.00+.25/0

Acceleration of a Phosphate Diester Transesterification Reaction by Bis(alkylguanidinium) Receptors Containing an Appended General Base**

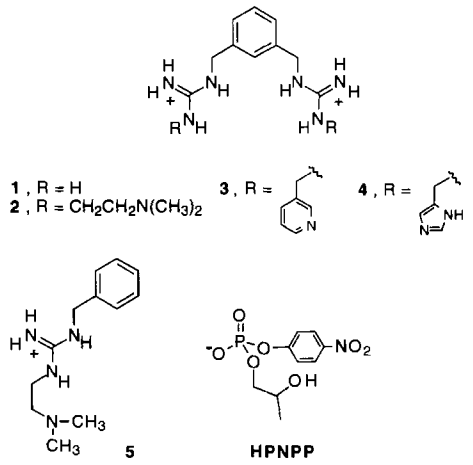
Vrej Jubian, Andrea Veronese, Robert P. Dixon, and Andrew D. Hamilton*

There is considerable interest in designing synthetic catalysts that can hydrolyze phosphate diesters[1-3] since such artificial nucleases have potential applications as novel antiviral and anticancer therapeutic agents.[4-6] An important strategy for developing artificial enzymes is to incorporate, into a synthetic framework, functional groups known to be present in the enzyme's active site and that are essential for maintaining catalytic activity. The DNA and RNA hydrolyzing enzyme, staphylococcal nuclease (SN), contains two key arginine residues, Arg35 and Arg87, in its active site.[7] Site directed mutagenesis studies have established[8-10] that only one arginine residue (Arg35) binds to the monoanionic substrate, but both residues are required for phosphate ester hydrolysis. In an attempt to exploit this important feature of SN, we[11] and others[12-18] have designed mono- and bis(guanidinium) derivatives that bind with phosphate diesters in organic solvents. We have shown that certain bis(guanidinium) receptors can mimic SN and accelerate the transesterification of phosphate diesters. A key requirement for these guanidinium receptors[19] and related systems[2, 20, 21] is the addition of a general base (e.g. lutidine, tetramethylguanidine, imidazole) to deprotonate the hydroxyl nucleophile (Scheme 1, A). In an attempt to design a receptor that contains

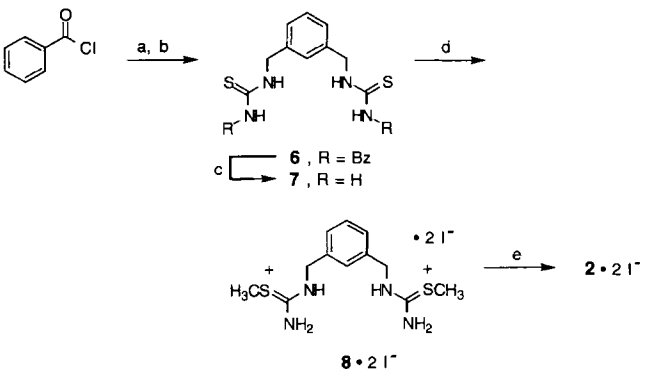


Scheme 1. Transesterification of HPNPP mediated by bis(guanidinium) receptors and an added base (A) and by a bis(guanidinium) receptor with an appended basic group (B).

all the necessary components for catalysis, we have linked general base groups to the bis(guanidinium) receptors. The receptor design is based on bis(alkylguanidinium) derivatives that remain protonated in the presence of a wide range of basic groups. These receptors can potentially accelerate phosphate ester cleavage by providing a hydrogen-bonding cleft to increase the electrophilicity and facilitate nucleophilic attack on phosphorus upon binding in the manner depicted in Scheme 1, B. In this paper we report a series of alkylguanidinium ions **1**–**5** containing appended nitrogen bases and compare their efficiencies in accelerating the transesterification reaction of the RNA model, 2-hydroxypropyl-*para*-nitrophenylphosphate (HPNPP).[22, 23]



All the *N,N'*-disubstituted guanidinium receptors were prepared from the reaction of a thiouronium salt with an appropriate diamine following the general method for the synthesis of substituted guanidines.[24, 25] The method involves in situ generation of benzoyl isothiocyanate (from ammonium thiocyanate and benzoyl chloride) and reaction with 1,3-bis(aminomethyl)-benzene to form the corresponding bis(benzoylthiourea) **6** (Scheme 2). Hydrolysis of **6** in 10% sodium hydroxide solution



Scheme 2. a) NH_4SCN, acetone, reflux; b) 1,3-$(H_2NCH_2)_2C_6H_4$, reflux; c) NaOH (10%), 80 °C; d) MeI, MeOH, reflux; e) $NH_2CH_2CH_2N(CH_3)_2$, *t*BuOH, reflux.

affords the bis(thiourea) **7**, which upon treatment with methyl iodide in methanol gives the desired thiouronium salt **8**. Treatment of **8** with various amines in refluxing *tert*-butyl alcohol affords the receptors **1**–**4**. Salts containing the bis(alkylguanidinium ion **1** were prepared in a single step from 1,3-bis(aminomethyl)benzene and pyrazole-1-carboxamidine hydrochloride.[26]

The phosphoryl transfer reaction of HPNPP gave, in the presence of the guanidinium receptors, the cyclic phosphate ester and *para*-nitrophenol as confirmed by ^{31}P NMR spectroscopy and HPLC, respectively. The rate of the transesterification reaction of HPNPP follows Michaelis–Menten kinetics showing saturation behavior as the concentration of receptor increases (Fig. 1). Eadie–Hofstee plots give values for k_{cat} and K_m (Table 1). When fully bound to receptor **1** with monosubstituted guanidinium groups, the phosphate ester undergoes cleavage ($k_{cat} = 5.5 \times 10^{-6}\ s^{-1}$) 14 times faster than the background reaction ($k_{uncat} = 3.8 \times 10^{-7}\ s^{-1}$). Receptors **2**–**4** with appended general base groups show increased efficiency for phosphate ester cleavage.

[*] Prof. A. D. Hamilton, Dr. V. Jubian, A. Veronese, Dr. R. P. Dixon
Department of Chemistry, University of Pittsburgh
Pittsburgh, PA 15217 (USA)
Telefax: Int. code +(412) 624-8552

[**] This work was supported by the U.S. Office of Naval Research.

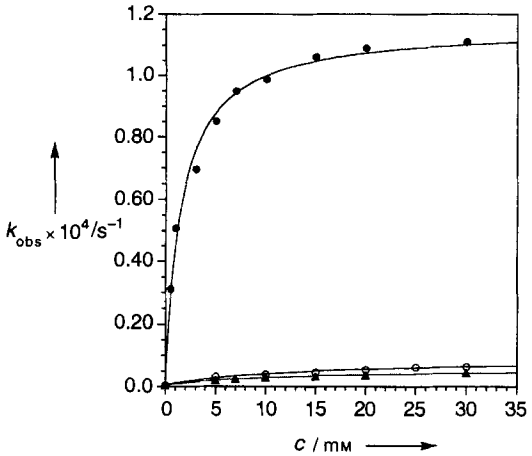


Fig. 1. Plot of the reaction rate versus the receptor concentration for **2** (●), **5** (○), and **1** (▲) for the accelerated transesterification of HPNPP.

The most efficient catalyst is the trialkylamine receptor **2**. At a concentration of 5 mM **2** ($k_{obs} = 8.5 \times 10^{-5}\ s^{-1}$) accelerates the cleavage of HPNPP by a factor of 45 relative to the rate with **1** ($k_{obs} = 1.9 \times 10^{-6}\ s^{-1}$) and displays an acceleration of 290-fold over the rate of the uncatalyzed reaction (Table 1). The efficiency of **2** stems in part from the increased basicity of its internal base relative to that in **3** and **4**. The basicity of the functional groups present in **3** (pyridine) and **4** (imidazole) are comparable with that of lutidine. At a concentration of 5 mM **3** ($k_{obs} = 7.3 \times 10^{-6}\ s^{-1}$) and **4** ($k_{obs} = 1.2 \times 10^{-5}\ s^{-1}$) display up to a sixfold increase in the rate of HPNPP transesterification compared to that of **1** with lutidine. The dimethylethylamine group in **2** is more basic than the nitrogen bases in **3** and **4** and hence **2** is the most efficient in accelerating the phosphoryl transfer reaction. However, the basicity of the amine in **2** is much weaker than simple trialkylamines due to the electron-withdrawing effect of the guanidinium groups and their tendency to form hydrogen bonds. As a consequence, compound **5** was used as a control because its basicity should be comparable to that in **2**.

Table 1. Rate constants for the transesterification of HPNPP accelerated by guanidinium receptors **1**, **2**, and **5** [a].

Receptor	K_m [mM]	k_{cat} [s^{-1}]	k_{cat}/k_{uncat}
2	1.6	1.1×10^{-4}	290
5	13.8	8.5×10^{-6}	22
1 [b]	12.6	5.5×10^{-6}	14

[a] In CH_3CN, HPNPP (1×10^{-4} M) at 25 °C. [b] With lutidine (1.25×10^{-2} M).

The first-order rate constant for HPNPP cleavage promoted by the "half receptor" **5** (10 mM) is $4.0 \times 10^{-6}\ s^{-1}$, whereas receptor **2**, at half the concentration (5 mM), increases the rate of the reaction by an additional 20-fold ($k_{obs} = 8.5 \times 10^{-5}\ s^{-1}$) (Fig. 1). Thus, the binding arrangement provided by both guanidiniums in **2** is crucial for obtaining large rate enhancements. The two guanidinium groups can work cooperatively to stabilize the dianionic trigonal-bipyramidal intermediate by means of four hydrogen bonds with concomitant charge neutralization.

The binding constant K_a of **2** ($625\ M^{-1}$) is higher than that of **1** in the presence of added lutidine ($K_a = 80\ M^{-1}$). Addition of excess lutidine lowers the binding affinity of the receptor, presumably reflecting the increased polarity of the medium. Binding studies were performed by ^{31}P NMR titrations of **2** and **5** with diethyl phosphate (Fig. 2). The binding isotherms for **2** and **5** are markedly different; the inflections are indicative of multiple binding equilibria.[13, 27, 28] The binding isotherm for **2** shows a downfield shift of the ^{31}P NMR signal ($\Delta\delta > 0$) for the 1:2 receptor/diethyl phosphate complex followed by a shift to higher field ($\Delta\delta < 0$) for the 1:1 complex, whereas for **5** a downfield shift for the 1:1 complex and a smaller downfield shift for the 2:1 complex are seen. The contrasting shapes of the two titration curves demonstrate the dramatically different microenvironments provided for the phosphate diester by **2** and **5**. At high host/guest ratios (2–4) the chemical shift of the bound phosphate differs by more than 2 ppm. This indicates that **2** forms a strong 1:1 complex with both guanidinium groups binding to the phosphate, while **5** forms a much weaker 2:1 complex of guanidinium and diethyl phosphate. These differences in complex structure are translated into the efficiency of the receptors in accelerating phosphoryl transfer reactions. Kinetic experiments were carried out with a large excess of receptor relative to the phosphate diester. Under these conditions, the bis(guanidinium) receptors will bind to only one phosphate ester substrate (Scheme 1, B).

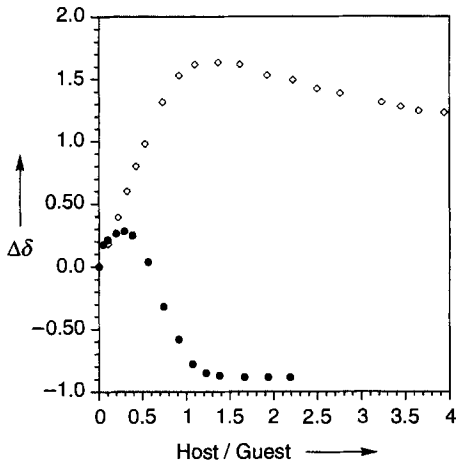


Fig. 2. Relative changes in the positions of the ^{31}P NMR resonances of diethyl phosphate (guest) at increasing concentrations of receptor (host) **2** (●) and **5** (○) in CD_3CN.

In summary we have taken an important step in the development of artificial nucleases by combining two key catalytic elements into a synthetic receptor. Substantial rate enhancements in a phosphoryl transfer reaction are shown by bis(guanidinium) receptors containing appended general base groups. The large accelerations are achieved by the provision of an intramolecular general base group and electrostatic complementarity of the binding site to the trigonal-bipyramidal intermediate in the phosphoryl transfer reaction.

Experimental Procedure

The intramolecular reactions of HPNPP were monitored by following the absorption of released 4-nitrophenol at 324 nm. The receptors were used as their tetraphenylborate salts. The reactions were carried out in acetonitrile under pseudo-first-order conditions with an initial concentration of HPNPP of 1×10^{-4} M and with the receptor (3–30 mM) and, if necessary, lutidine (1.25×10^{-2} M) in excess. In a typical kinetics experiment, 2 mL of a solution of the receptor (5 mM) in CH_3CN and 50 μL of a 0.5 M CH_3CN stock solution of lutidine (if necessary) were added to a cuvette. The reaction was initiated by adding 20 μL of a 0.01 M CH_3CN solution

 © VCH Verlagsgesellschaft mbH, D-69451 Weinheim, 1995 0570-0833/95/1111-1238 $ 10.00+.25/0

of HPNPP [29]. The rate constants were obtained by fitting at least three half-lives of the reaction according to a first-order kinetics equation. For slower reactions, rate constants were calculated from the initial rates. First-order rate constants were calculated from the slopes of the linear plots of absorbance versus time by converting to concentration units of the phosphate ester ($\varepsilon = 4500\ M^{-1}cm^{-1}$) and dividing by the initial phosphate ester concentration. All kinetic experiments were run at least twice and were reproducible within 5% error.

Received: November 29, 1994
Revised version: February 21, 1995 [Z 7508 IE]
German version: *Angew. Chem.* **1995**, *107*, 1343–1345

Keywords: enzyme mimics · guanidines · transesterifications

[1] Reviews: D. S. Sigman, A. Mazumder, D. M. Perrin, *Chem. Rev.* **1993**, *93*, 2295–2316; J. R. Morrow, *Adv. Inorg. Biochem.* **1994**, *9*, 41–74; J. Chin, *Acc. Chem. Res.* **1991**, *24*, 145–152; M. W. Göbel, *Angew. Chem.* **1994**, *106*, 1201–1203; *Angew. Chem. Int. Ed. Engl.* **1994**, *33*, 1141–1143.
[2] J. Smith, K. Ariga, E. V. Anslyn, *J. Am. Chem. Soc.* **1993**, *115*, 362–364.
[3] For recent examples see: J. K. Bashkin, E. I. Frolova, U. Sampath, *J. Am. Chem. Soc.* **1994**, *116*, 5981–5982; M. Wall, R. C. Hynes, J. Chin, *Angew. Chem.* **1993**, *105*, 1696–1697; *Angew. Chem. Int. Ed. Engl.* **1993**, *32*, 1633–1635; D. Wahnon, R. C. Hynes, J. Chin, *J. Chem. Soc. Chem. Commun.* **1994**, 1441–1442; B. K. Takasaki, J. Chin, *J. Am. Chem. Soc.* **1993**, *115*, 9337–9338; *ibid.* **1994**, *116*, 1121–1122; D. Magda, R. A. Miller, L. Sessler, B. L. Iverson, *ibid.* **1994**, *116*, 7439–7440.
[4] C. A. Stein, J. S. Cohen, *Cancer Res.* **1988**, *48*, 2659–2668.
[5] E. Uhlmann, A. Peyman, *Chem. Rev.* **1990**, *90*, 543–584.
[6] J. F. Milligan, M. D. Matteucci, J. C. Martin, *J. Med. Chem.* **1993**, *36*, 1923–1937.
[7] F. A. Cotton, E. E. J. Hazen, M. J. Legg, *Proc. Natl. Acad. Sci. USA* **1979**, *76*, 2551.
[8] D. J. Weber, A. K. Meeker, A. S. Mildvan, *Biochemistry* **1991**, *30*, 6103–6114.
[9] E. H. Serpersu, D. Shortle, A. S. Mildvan, *Biochemistry* **1987**, *26*, 1289–1300.
[10] A. S. Mildvan, E. H. Serpersu, *Met. Ions Biol. Syst.* **1989**, *25*, 309–334.
[11] R. P. Dixon, S. J. Geib, A. D. Hamilton, *J. Am. Chem. Soc.* **1992**, *114*, 365–366.
[12] K. Ariga, E. V. Anslyn, *J. Org. Chem.* **1992**, *57*, 417–419.
[13] D. M. Kneeland, K. Ariga, V. Lynch, C. Huang, E. V. Anslyn, *J. Am. Chem. Soc.* **1993**, *115*, 10042–10055.
[14] R. Gross, J. W. Bats, M. W. Göbel, *Liebigs Ann. Chem.* **1994**, 205–210.
[15] P. Schiessl, F. P. Schmidtchen, *J. Org. Chem.* **1994**, *59*, 509–511.
[16] F. P. Schmidtchen, *Tetrahedron Lett.* **1989**, *30*, 4493–4496.
[17] A. Galan, E. Pueyo, A. Salmeron, J. de Mendoza, *Tetrahedron Lett.* **1991**, *32*, 1827–1830.
[18] B. Dietrich, T. M. Fyles, J. M. Lehn, L. G. Pease, D. L. Fyles, *J. Chem. Soc. Chem. Commun.* **1978**, *21*, 934–936.
[19] V. Jubian, R. P. Dixon, A. D. Hamilton, *J. Am. Chem. Soc.* **1992**, *114*, 1120–1121.
[20] M. W. Göbel, J. W. Bats, G. Dürner, *Angew. Chem.* **1992**, *104*, 217–218; *Angew. Chem. Int. Ed. Engl.* **1992**, *31*, 207–209.
[21] R. Gross, G. Dürner, M. W. Göbel, *Liebigs Ann. Chem.* **1994**, 49–58.
[22] D. M. Brown, D. A. Usher, *J. Chem. Soc.* **1965**, 6558–6564.
[23] For a discussion on using activated esters see: F. M. Menger, M. Ladika, *J. Am. Chem. Soc.* **1987**, *109*, 3145–3146.
[24] C. R. Rasmussen, F. J. J. Villani, L. E. Weaner, B. E. Reynolds, A. R. Hood, L. R. Hecker, S. O. Nortey, A. Hanslin, M. J. Costanzo, E. T. Powell, A. J. Molinari, *Synthesis* **1988**, 456–459.
[25] C. R. Rasmussen, F. J. J. Villani, B. E. Reynolds, J. N. Plampin, A. R. Hood, L. R. Hecker, S. O. Nortey, A. Hanslin, M. J. Costanzo, R. M. J. Howse, A. J. Molinari, *Synthesis* **1988**, 460–465.
[26] M. S. Bernatowicz, Y. Wu, G. R. Matsueda, *J. Org. Chem.* **1992**, *57*, 2497–2502.
[27] L. S. Flatt, V. Lynch, E. V. Anslyn, *Tetrahedron Lett.* **1992**, *33*, 2785–2788.
[28] F. Chu, L. S. Flatt, E. V. Anslyn, *J. Am. Chem. Soc.* **1994**, *116*, 4194–4204.
[29] [18]Crown-6 (1 equiv) and water (8×10^{-5} M) were added to the stock solution of the barium salt of HPNPP in CH_3CN to increase solubility.

Chemoenzymatic Synthesis of a Modified Pentasaccharide as a Specific Substrate for a Sensitive Assay of α-Amylase by Fluorescence Quenching**

Nathalie Payre, Sylvain Cottaz, and Hugues Driguez*

Most living species such as microorganisms, higher plants, and animals generate energy by the metabolism of starch. The enzymes involved in the degradation of starch include α-amylase (1,4-α-D-glucan glucanohydrolase) [EC 3.2.1.1], an endoglycanase, and exoglucanases such as glucoamylase [EC 3.2.1.3] and β-amylase [EC 3.2.1.2].[1]

The detection and the determination of α-amylase activity are not only necessary for catalysis studies but also important for technological and medical applications, for example for monitoring fermentation processes and for diagnosing diseases like parotitis (mumps) and acute pancreatitis. The assay of amylases usually requires specific substrates to distinguish between the endo- and exoglucanases, which both act on the α-(1 → 4)-glycosidic bond in D-Glc-α-(1 → 4)-D-Glc units. A survey of the literature from the mid-1980s shows the considerable amount of work that has been directed toward this goal.[2]

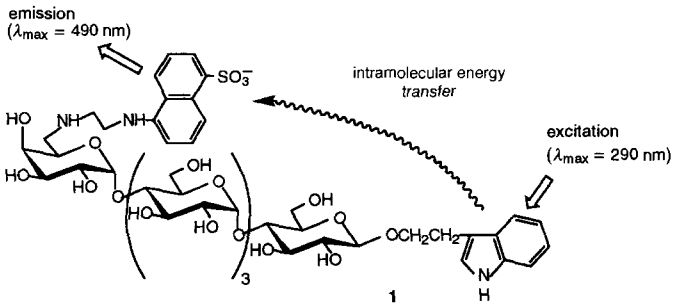
The specific substrates can be divided into two groups: substrates with a single chromophore or fluorophore, which are used in most of the commercially available diagnostic kits, and substrates with an additional fluorescence-quenching group. The chromogenic substrates are usually nitrophenylmaltooligosaccharides bearing blocking groups at the nonreducing end to prevent action of exoenzymes. The nitrophenyl group and the blocking substituent are introduced by demanding multiple-step reactions and/or low-yielding procedures, either by chemical synthesis from maltodextrins with an appropriate degree of polymerization,[3] or by chemoenzymatic transformations of modified linear or cyclic dextrins.[4] Since the enzymatic hydrolysis of these substrates never occurs at the reducing unit, α-glucosidase or β-glucosidase and glucoamylase have to be added during the assay to liberate nitrophenol from the residual nitrophenylmaltooligosaccharides. Not only are these drawbacks costly but complications may also arise from the multitude of possible side reactions.

These problems may be overcome by the use of specific substrates that display intramolecular fluorescence quenching, in which the variation of fluorescence between a fluorophore/quencher pair on the same molecule can be monitored by using the intramolecular resonance energy transfer effect.[5] This strategy is analogous to that developed for the specific assay of proteases,[6] and for glycanases this was first achieved by Omishi and Ikenaka, who prepared a disubstituted maltopentaoside by a complex chemoenzymatic synthesis.[7] In a very recent paper, Bock et al. described the preparation of acylated maltotriosides which appeared to be pH sensitive and poor substrates for α-amylases.[8]

The merit of substrates that display intramolecular fluorescence quenching is confirmed here by the specific detection of α-amylase activities with micromolar concentrations of the sub-

[*] Dr. H. Driguez, N. Payre, Dr. S. Cottaz
Centre de Recherches sur les Macromolécules Végétales (CERMAV-CNRS)
BP 53 X, F-38041 Grenoble cedex 9 (France)
Telefax : Int. code +76547203
e-mail : hdriguez@cermav.grenet.fr

[**] This work was supported by the Centre National de la Recherche Scientifique (France) and by the European Biotech Program (1994–1996). We thank Prof. P. Jardon (U. J. F. Grenoble) for providing his help in recording the fluorescence spectra.



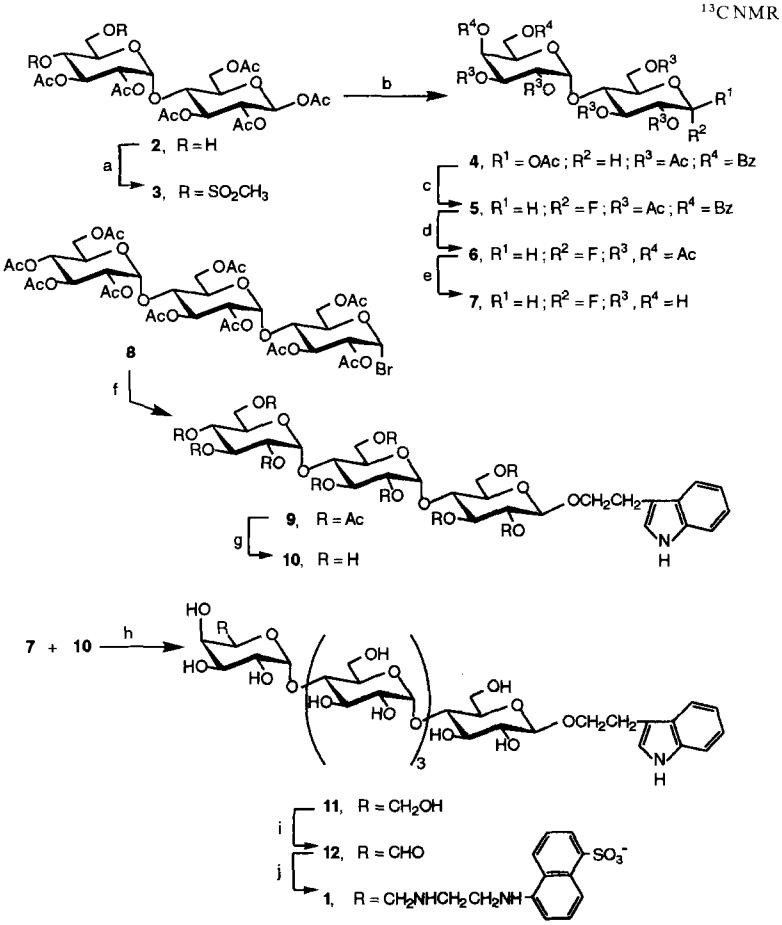
Scheme 1. Fluorescence quenching and intramolecular energy transfer in **1**. After irradiation of **1** at 290 nm, fluorescence at 490 nm was observed.

strate indolylethyl- and 5-(2-aminoethylamino)-1-naphthalenesulfonate-substituted maltopentaoside **1** (Scheme 1).

The design of **1** was based on several observations: maltopentaose is the best substrate for our model enzyme, porcine pancreatic α-amylase (PPA),[9] and the emission band of excited 3-(2-hydroxyethyl)indole (indolylethanol) (λ_{max} = 345 nm) and the absorption band of 5-(2-aminoethylamino)-1-naphthalenesulfonate (EDANS) (λ_{max} = 340 nm) show excellent overlap. Despite the relatively short lifetime of excited indolylethanol (2 ns), the efficiency of the fluorescence quenching is satisfactory.[5] The EDANS/indolylethanol pair was also chosen based on synthetic considerations. Our strategy requires one fluorophore with an amino function that can form an amino linkages with the oligosaccharide, and the other fluorophore with an aliphatic hydroxyl group that can form an ether linkage. These two linkages are much more stable than an ester bond during the enzymatic assay.[8]

Compound **1** was prepared chemoenzymatically (Scheme 2); this approach is very valuable for the synthesis of regiospecifically modified oligosaccharides.[10] The key steps of the synthesis of **1** are the α-amylase-catalyzed coupling of a modified α-maltosyl fluoride donor **7** with an indolylethylmaltotrioside **10**, and the oxidation of pentasaccharide **11** by galactose oxidase [EC 1.1.3.9], such that EDANS can be introduced regiospecifically at the nonreducing end of the oligosaccharide. α-D-Galactosyl-(1 → 4)-α-D-glucosyl fluoride **7** and indolylethylmaltotrioside **10** were obtained by conventional chemical modifications from known hexa-*O*-acetyl maltose **2**[11] and maltotriosyl bromide **8**[12] (Table 1).

The glycosylation of **10** with **7** was achieved by using conditions originally described by Kobayashi et al. for the enzymatic



Scheme 2. Preparation of pentasaccharide **1**. a) $MeSO_2Cl$, pyridine, 0 °C to room temperature, 94%; b) sodium benzoate, hexamethylphosphoric triamide, 110 °C, 52%; c) HF/pyridine, 0 °C, 86%; d) NaOMe/MeOH, then Ac_2O, pyridine, 90%; e) NaOMe/MeOH, quant.; f) 3-(2-hydroxyethyl)indole, $Hg(CN)_2$, $HgBr_2$, toluene/$MeNO_2$, 44%; g) NaOMe/MeOH, quant.; h) α-amylase (*Aspergillus oryzae*), MeOH/phosphate buffer, 59%; i) galactose oxidase (*Dactylium dendroides*), catalase (bovine liver), phosphate buffer, 37 °C; j) EDANS, MeOH, reflux, then $NaBH_3CN$, i)–j) 54% overall.

Table 1. Physical and spectroscopic data for **1**, **3**–**6**, **9**, and **11**. NBA = 3-nitrobenzyl alcohol.

3: M.p. 197–199 °C; $[\alpha]_D^{25} = +50$ ($c = 0.5$ in $CHCl_3$); ^{1}H NMR (300 MHz, $CDCl_3$): $\delta = 5.80$ (d, ^3J(H-1^1,H-2^1) = 8.04 Hz, 1H; H-1^1), 5.36 (d, ^3J(H-1^2,H-2^2) = 4.02 Hz, 1H; H-1^2), 3.00 (s, 6H; 2 × CH_3SO_2), 2.00 (m, 18H; 6 × CH_3CO); ^{13}C NMR (75.4 MHz, $CDCl_3$): $\delta = 95.50$ (C-1^1), 91.00 (C-1^2), 38.50 and 37.50 (2 × CH_3SO_2); $C_{26}H_{38}O_{21}S_2$ (750.5): calcd: 41.61, H 5.10, S 8.54; found: C 41.46, H 5.08, S 8.48.

4: M.p. 165–166 °C; $[\alpha]_D^{25} = +62$ ($c = 0.49$ in $CHCl_3$); ^{1}H NMR (300 MHz, $CDCl_3$): $\delta = 8.05$–7.50 (m, 10H; Ph), 5.83 (dd, ^3J(H-3^2,H-4^2) = 3.2 Hz, ^3J(H-4^2,H-5^2) < 1 Hz, 1H; H-4^2), 5.73 (d, ^3J(H-1^1,H-2^1) = 8.1 Hz, 1H; H-1^1), 5.55 (d, ^3J(H-1^2,H-2^2) = 3.7 Hz, 1H; H-1^2), 5.40 (dd, 1H; H-3^2), 5.30 (t, ^3J(H-2^1,H-3^1) = ^3J(H-3^1,H-4^1) = 9.5 Hz, 1H; H-3^1), 5.23 (dd, ^3J(H-2^2,H-3^2) = 7.3 Hz, 1H; H-2^2), 4.95 (dd, 1H; H-2^1), 4.53 (dd, ^2J(H-6a^1,H-6b^1) = 12.3 Hz, ^3J(H-5^1,H-6b^1) = 2.5 Hz, 1H; H-6b^1), 4.48 (dd, ^2J(H-6a^2,H-6b^2) = 9.3 Hz, 1H; H-6b^2), 4.42 (ddd, 1H; H-5^2), 4.26 (dd, ^3J(H-5^2,H-6a^2) = 4.0 Hz, 1H; H-6a^2), 4.20 (dd, ^3J(H-5^1,H-6a^1) = 4.6 Hz, 1H; H-6a^1), 4.05 (t, ^3J(H-4^1,H-5^1) = 9.5 Hz, 1H; H-4^1), 3.80 (ddd, 1H; H-5^1), 2.07–1.93 (m, 18H; CH_3CO); $C_{38}H_{42}O_{19}$ (802.7): calcd: C 56.86, H 5.27; found: C 56.65, H 5.25.

5: M.p. 113–114 °C; $[\alpha]_D^{25} = +91$ ($c = 0.5$ in $CHCl_3$); ^{13}C NMR (75.4 MHz, $CDCl_3$): δ = 170.62, 169.93, 169.76, 169.56 (5 × CO, acetates), 165.52, 165.26 (2 × CO, benzoates), 103.4 (d, ^1J(C-1^1,F) = 229 Hz; C-1^1), 96.0 (C-1^2), 20.66, 20.45, 20.39, 20.29, 20.18 (5 × CH_3CO); $C_{36}H_{39}FO_{17}$ (762.7): calcd: C 56.69, H 5.15, F 2.49; found: C 56.39, H 5.10, F 2.50.

6: M.p. 117 °C; $[\alpha]_D^{25} = +109$ ($c = 0.5$ in $CHCl_3$); ^{13}C NMR (75.4 MHz, $CDCl_3$): δ = 170.64–169.51 (7 × CO, acetates), 103.4 (d, ^1J(C-1^1, F) = 229 Hz; C-1^1), 95.9 (C-1^2), 20.61–20.21 (7 × CH_3CO); $C_{26}H_{35}FO_{17}$ (638.6): calcd: C 48.91, H 5.52, F 2.98; found: C 48.77, H 5.52, F 2.91.

9: $[\alpha]_D^{25} = +58.5$ ($c = 0.9$ in $CHCl_3$); ^{13}C NMR (75.4 MHz, $CDCl_3$): δ = 170.33–169.19 (10 × CO, acetates), 135.94, 122.04, 121.66, 119.06,118.43, 112.12, 110.88 (indole), 99.97 (C-1^1), 95.46 (C-1^2, C-1^3), 62.84, 62.15, 61.19 (C-6^1, C-6^2, C-6^3), 25.32 (OCH_2CH_2), 20.61–20.19 (10 × CH_3CO); FAB-MS (NBA + KCl, positive-ion mode): *m/z*: 1067 [M^+]; $C_{48}H_{61}NO_{26}$ (1068.0) = calcd: C 53.98, H 5.76, N 1.31; found: C 53.90, H 6.04, N 1.45.

11: $[\alpha]_D^{25} = +99$ ($c = 0.54$ in H_2O); ^{1}H NMR (500 MHz, D_2O): δ = 7.63–7.08 (m, 5H; indole), 5.27, 5.25, 5.24, 5.22 (each d, 4H; H-1^2, H-1^3, H-1^4, H-1^5), 4.26 (d, ^3J(H-1^1,H-2^1) = 8.04 Hz, 1H; H-1^1); FAB-MS (NBA + KCl, positive-ion mode): *m/z*: 972 [M^+].

1: $[\alpha]_D^{25} = +87$ ($c = 0.42$ in DMSO); ^{1}H NMR (500 MHz, D_2O): δ = 8.20–6.75 (m, 11H; H arom.), 5.20 (d, ^3J(H-1^2,H-2^2) = 3.83 Hz, 1H; H-1^2), 5.16 (d, ^3J(H-1^3,H-2^3) = 3.83 Hz, 1H; H-1^3), 5.05 (d, ^3J(H-1^4,H-2^4) = 3.97 Hz, 1H; H-1^4), 4.94 (d, ^3J(H-1^5,H-2^5) = 3.28 Hz, 1H; H-1^5), 4.73 (d, J = 2.25 Hz, 1H; H-4^5), 4.10 (d, ^3J(H-1^1,H-2^1) = 7.95 Hz, 1H; H-1^1); FAB-MS (positive-ion mode): *m/z*: 1246.364, calcd. for $C_{52}H_{72}N_3NaO_{28}S$ [$M - H_2O + Na^+$]: 1246.371.

 © VCH Verlagsgesellschaft mbH, D-69451 Weinheim, 1995 0570-0833/95/1111-1240 $ 10.00+.25/0

polymerization of α-maltosyl fluoride with α-amylase as catalyst.[13] Under these conditions **11** was obtained in 78% yield (determined by HPLC, 59% isolated yield). The epimerization at the 4'-position in the formation of **4** is beneficial for two reasons. Firstly, **7** is accepted by the α-amylase as a donor, but neither **7** nor **11** are acceptors because of the axial 4-OH at the nonreducing end unit. Therefore only one disaccharide is added and **11** is obtained in good yield. Secondly, the nonreducing galactosyl residue at the C-6 position in **11** can be oxidized regiospecifically by the galactose oxidase/catalase system to give aldehyde **12**.[14] In the final step the EDANS group can be introduced by reductive amination, giving **1** in 54% isolated yield (Table 1).

The intramolecular fluorescence quenching in **1** was demonstrated in preliminary experiments at concentrations of 10 μM. When **1** was excited at 290 nm, the EDANS fluorescence emitted at 490 nm was 12 times more intense than that of free EDANS. We also detected a fivefold decrease in the intensity of the indolylethyl emission at 345 nm. At this concentration we can assume that variation of fluorescence intensity due to collisional quenching is negligible. In fact a 2% increase in fluorescence intensity at 490 nm was observed for solutions of free EDANS with indolylethylpentasaccharide **11** when the EDANS concentration was increased from 10 to 20 μM.

When a 5 μM solution of **1** was incubated with PPA, the intensity of the fluorescence at 490 nm decreased rapidly. After 6 min the substrate was completely hydrolyzed (Fig. 1). At this stage,

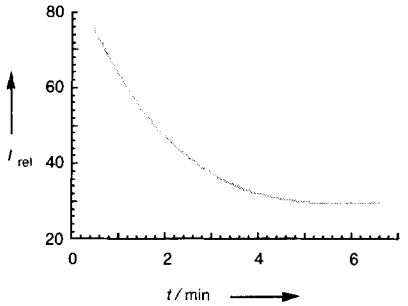


Fig. 1. Progress of the PPA-catalyzed hydrolysis of **1** monitored by steady-state fluorescence based on the relative fluorescence intensity I_{rel} at 490 nm. A 5 μM solution of **1** in phosphate buffer (0.02 M, pH 7) was incubated with PPA (Sigma, 100 U L^{-1}) at 30 °C [16].

HPLC analysis of the reaction mixture confirmed the complete conversion of **1** into two shorter oligosaccharides (EDANS-galactosyl-α-(1 → 4)-maltose and indolylethylmaltoside; the retention times were compared to those of authentic standards prepared independently).

When the same experiment was conducted with different concentrations of α-amylase, a linear relationship was found for the initial rate of hydrolysis of **1** and the concentration of the enzyme. In contrast, even under optimal conditions, α-galactosidase, β-amylase, α-glucosidase, and glucoamylase were inactive.[15]

Compound **1** is thus the first specific, sensitive, and readily available substrate for the in vitro assay of human salivary and pancreatic α-amylases (HSA and HPA). Further studies on **1** and the preparation of new substrates with improved performances are under way.

Received: December 28, 1994 [Z 7591 IE]
German version: *Angew. Chem.* **1995**, *107*, 1361–1364

Keywords: α-amylase assay · chemoenzymatic syntheses · enzymes · fluorescence · oligosaccharides

[1] a) D. French in *Biochemistry of Carbohydrates, Serie one, Vol. 5* (Ed. W. J. Whelan), Butterworths, London, **1975**, p. 267; b) P. J. Reilly, *Food Sci. Technol.* **1985**, *14*, 101–142.
[2] See for example: a) K. Omishi, T. Ikenaka, *J. Biochem.* **1985**, *97*, 977–982; b) S. Satomura, T. Iwata, Y. Sakata, *Carbohydr. Res.* **1988**, *176*, 107–115; c) S. Satomura, K. Omishi, T. Ikenaka, *ibid.* **1988**, *180*, 137–146; d) E. O. Hägele, M. Kratzer, E. Schaich, E. Rauscher, *Clin. Chem. (Winston-Salem NC)* **1989**, *35*, 188–189; e) K. Ogawa, H. Matsui, T. Usui, *Biosci. Biotechnol. Biochem.* **1992**, *56*, 1933–1936; f) K. Ogawa, Y. Taki, H. Ishida, Y. Yamagata, S. Satomura, M. Kiso, A. Hasegawa, *ibid.* **1993**, *57*, 821–828; g) S. Tokutake, T. Oguma, K. Tobe, K. Kotani, K. Saito, N. Yamaji, *Carbohydr. Res.* **1993**, *238*, 193–213; h) K. Ozawa, Y. Yamagata, S. Satomura, H. Ishida, M. Kiso, A. Hasegawa, *ibid.* **1994**, *262*, 137–145.
[3] See refs. [2c,d, f–h].
[4] See refs. [2a, b, e, g].
[5] R. H. Fairclough, C. R. Cantor, *Methods Enzymol.* **1978**, *48*, 347–379.
[6] a) A. Yaron, A. Carmel, E. Katchalski-Katzir, *Anal. Biochem.* **1979**, *95*, 228–235; b) E. D. Matayoshi, G. T. Wang, G. A. Krafft, J. Erickson, *Science* **1990**, *247*, 954–958.
[7] K. Omishi, T. Ikenaka, *J. Biochem.* **1986**, *99*, 291–294.
[8] V. Ferro, M. Meldal, K. Bock, *J. Chem. Soc. Perkin Trans. 1* **1994**, 2169–2176.
[9] C. Seigner, E. Prodanov, G. Marchis-Mouren, *Biochim. Biophys. Acta* **1987**, *913*, 200–209.
[10] a) D. G. Drueckhammer, W. J. Hennen, R. L. Pedersen, C. F. Barbas III, C. M. Gautheron, T. Krack, C.-H. Wong, *Synthesis* **1990**, 499–525, and references therein; b) S. Cottaz, C. Apparu, H. Driguez, *J. Chem. Soc. Perkin Trans. 1* **1991**, 2235–2241; c) C. Simiand, S. Cottaz, C. Bosso, H. Driguez, *Biochimie* **1992**, *74*, 75–79; d) B. Evers, P. Mischnick, J. Thiem, *Carbohydr. Res.* **1994**, *262*, 335–341.
[11] K. Takeo, K. Shinmitsu, *Carbohydr. Res.* **1984**, *133*, 135–145.
[12] K. Takeo, K. Mine, T. Kuge, *Carbohydr. Res.* **1976**, *48*, 197–208.
[13] S. Kobayashi, J. Shimada, K. Kashiwa, S.-I. Koda, *Macromolecules* **1992**, *25*, 3237–3241.
[14] a) G. Avigad, D. Amaral, C. Asensio, B. L. Horecker, *J. Biol. Chem.* **1962**, *237*, 2736–2743; b) R. A. Schlegel, C. M. Gerbeck, R. Montgomery, *Carbohydr. Res.* **1968**, *7*, 193–199.
[15] For the glucoamylase used (Sigma) low hydrolytic activity was detected but attributed to contamination by α-amylase (sigma).
[16] α-amylase activity was previously determined with the Sigma Amylase Diagnostic Kit by using nitrophenyl 4,6-ethylidenemaltoheptaoside as substrate.

The Synthesis of Tris(perfluoroalkyl)-phosphanes**

Joel J. Kampa, John W. Nail, and Richard J. Lagow*

Many papers and review articles have dealt with the synthesis, characterization, and reactions of highly fluorinated phosphanes.[1, 2] Much attention has been drawn to the fact that fluorinated phosphanes form complexes with transition metals. Phosphorus trifluoride (PF_3), the first member of the fluorophosphane family, has been shown to be an analogue of carbon monoxide. In its reactions with transition metals, PF_3 closely resembles CO electronically. Other highly fluorinated phosphorus(III) compounds similar to PF_3 exhibited similar reaction chemistry. Recent work in our laboratory has shown that $P(CF_3)_3$ forms complexes with numerous transition metals.[3]

Tris(trifluoromethyl)phosphane, $P(CF_3)_3$,[4] has been known for years; however, its preparation from trifluoromethyl iodide

[*] Prof. R. J. Lagow, Dr. J. J. Kampa, Dr. J. W. Nail
Department of Chemistry, University of Texas at Austin
Austin, TX 78712 (USA)
Telefax: Int. code + (512)471-8648

[**] This research was supported by the Air Force Office of Scientific Research (F49620-92-0104) and the U.S. Department of Energy (DE-FG05-91ER12119).

 © VCH Verlagsgesellschaft mbH, D-69451 Weinheim, 1995 0570-0833/95/1111-1241 $ 10.00+.25/0

is not applicable to the larger perfluoroalkyl groups. Synthesis of phosphanes by this route has not produced trisubstituted products with larger alkyl groups. Only dialkylated products are produced, and in low yield.[5, 6] Occasionally, a perfluorinated trialkylphosphane such as $[(CF_3)_2PCF(CF_3)_2]$ does appear in the literature;[7–9] however, the methods described are, in general, unsuitable for a wide range of compounds.

The preparation of numerous difluorotris(perfluoroalkyl)-phosphoranes of various structural types has been achieved by direct elemental fluorination in solution. The development of methodologies for safely treating organic substrates with elemental fluorine has made it possible to prepare complex and unique new materials.[10] The most recent advance in this technology is the use of inert solvents to reduce fragmentation and side reactions and thus to enhance the selectivity of the reaction further.[11] Organophosphanes have been subjected to direct elemental fluorination in Freon to produce a series of difluorotris(perfluoroalkyl)phosphoranes (**1**–**7**) in good yield.

Results of ^{19}F NMR experiments are shown in Table 1. Peak locations, multiplicity, and intensities are all consistent with the structures indicated.[12] Spin–spin coupling between the ^{31}P and ^{19}F nuclei provides definitive structural information. The two fluorine atoms bound to the phosphorus center in **1**–**7** are equivalent, as are the three perfluoroalkyl groups. This indicates a trigonal bipyramidal configuration with the σ-bound fluorine atoms in the axial positions and the alkyl groups in the equatorial positions.[13] No fluxional behavior was observed on the NMR time scale. In the ^{31}P NMR spectra of **1**–**7** (Table 1) each signal appears as a triplet of septets (Fig. 1 shows the spectrum of **1**). The triplet is due to ^1J coupling of about 1000 Hz. Each of the peaks of the triplet is split into a septet by the ^2J coupling of about 125 Hz between the phosphorus and the six fluorine atoms bound to the α-carbon atoms of the three alkyl groups.

Mass spectral analysis of these perfluorophosphoranes provides additional evidence for the proposed formulas. The general

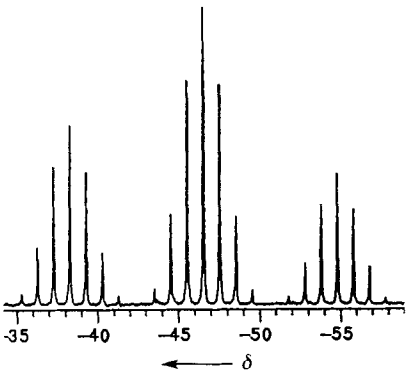


Fig. 1. ^{31}P NMR spectrum of difluorotris(pentafluoroethyl)phosphorane (**1**).

Table 1. The spectral data of phosphoranes **1**–**7**.

Compound	^{19}F NMR		^{31}P NMR	HR-MS [a]	
	$\delta(^{19}F)$	J [Hz]	$\delta(^{31}P)$	calcd	found
$F_2P(CF_2CF_3)_3$ *a b c* **1**	*a*: −51.1 (d of m) *b*: −115.1 (d) *c*: −83.5 (s)	$^1J_{PF} = 1002$ $^2J_{FCP} = 122$	−45.6	406.948215	406.950753
$F_2P(CF_2CF_2CF_3)_3$ *a b c d* **2**	*a*: −47.5 (d of m) *b*: −110.3 (d) *c*: −125.7 (s) *d*: −82.2 (s)	$^1J_{PF} = 1041$ $^2J_{FCP} = 124$	−41.8	556.938635	556.937623
$F_2P(CF_2CF_2CF_2CF_3)_3$ *a b c d e* **3**	*a*: −47.0 (d of m) *b*: −109.4 (d) *c*: −121.9 (s) *d*: −127.6 (s) *e*: −83.3 (s)	$^1J_{PF} = 1050$ $^2J_{FCP} = 126$	−39.6	706.929054	706.929362
$F_2P(CF_2CF_2CF_2CF_2CF_3)_3$ *a b c d e f* **4**	*a*: −46.8 (d of m) *b*: −108.8 (d) *c*: −120.7 (s) *d*: −123.4 (s) *e*: −127.4 (s) *f*: −82.5 (s)	$^1J_{PF} = 1050$ $^2J_{FCP} = 126$	−37.6	856.919474	856.918693
$F_2P(CF_2CF_2CF_2CF_2CF_2CF_3)_3$ *a b c d e f g* **5**	*a*: −47.0 (d of m) *b*: −109.4 (d) *c*: −121.1 (s) *d*: −123.3 (s) *e*: −124.5 (s) *f*: −128.3 (s) *g*: −83.6 (s)	$^1J_{PF} = 1051$ $^2J_{FCP} = 123$	−40.0	1006.909893	1006.908234
$F_2P(CF_2CF_3)_2(CF_2CF_2CF_2CF_3)$ *a b c d e f g* **6**	*a*: −49.8 (d of m) *b*: −114.8 (d) *c*: −83.6 (s) *d*: −110.3 (d) *e*: −121.7(s) *f*: −127.8 (s) *g*: −83.5 (s)	$^1J_{PF} = 1017$ $^2J_{FCP} = 122$ $^2J_{FCP} = 127$	−43.8	506.941828	506.941224
$[(CF_3CF_2P(F)_2CF_2]_2$ *a b c d* **7**	*a*: −82.4 (s) *b*: −113.9 (d) *c*: −48.4 (d of m) *d*: −107.3 (d)	$^2J_{FCP} = 121$ $^1J_{PF} = 1030$ $^2J_{FCP} = 123$	−43.0	694.904415	694.907036

[a] The values are relative to the $[M^+ - F]$ fragment.

 © VCH Verlagsgesellschaft mbH, D-69451 Weinheim, 1995 0570-0833/95/1111-1242 $ 10.00+.25/0

Table 2. The spectral data of the phosphanes **8**–**14**.

Compound	^{19}F NMR $\delta(^{19}F)$	J [Hz]	^{31}P NMR $\delta(^{31}P)$	HR-MS [a] calcd	found
$P(CF_2CF_3)_3$ *a b* **8**	*a*: −107.9 (d) *b*: −84.5 (d)	$^2J_{PCF} = 48$ $^3J_{PCCF} = 16$	13.7	387.948726	387.949812
$P(CF_2CF_2CF_3)_3$ *a b c* **9**	*a*: −103.2 (d) *b*: −122.7 (d) *c*: −81.0 (s)	$^2J_{PCF} = 37$ $^3J_{PCCF} = 30$	23.3	537.942122	537.940232
$P(CF_2CF_2CF_2CF_3)_3$ *a b c d* **10**	*a*: −103.3 (d) *b*: −120.1 (d) *c*: −128.0 (s) *d*: −83.7 (s)	$^2J_{PCF} = 32$ $^3J_{PCCF} = 30$	23.7	687.930651	687.930651
$P(CF_2CF_2CF_2CF_2CF_3)_3$ *a b c d e* **11**	*a*: −103.1 (d) *b*: −119.3 (s) *c*: −124.2 (s) *d*: −128.2 (s) *e*: −83.5 (s)	$^2J_{PCF} = 31$	26.8	837.921532	837.921071
$P(CF_2CF_2CF_2CF_2CF_2CF_3)_3$ *a b c d e f* **12**	*a*: −102.8 (d) *b*: −118.8 (d) *c*: −123.2 (s) *d*: −124.3 (s) *e*: −128.0 (s) *f*: −83.2 (s)	$^2J_{PCF} = 25$ $^3J_{PCCF} = 11$	25.0	987.913714	987.911490
$P(CF_2CF_3)_2(CF_2CF_2CF_2CF_3)$ *a b c d e f* **13**	*a*: −107.4 (d) *b*: −83.2 (d) *c*: −103.5 (d) *d*: −119.8 (d) *e*: −127.6 (s) *f*: −84.1 (s)	$^2J_{PCF} = 48$ $^3J_{PCCF} = 12$ $^2J_{PCF} = 40$ $^2J_{PCF} = 40$	7.6	488.950608	488.951250
$(CF_3CF_2)_2PCF_2CF_2P(CF_2CF_3)_2$ *a b c* **14**	*a*: −84.0 (d) *b*: −107.2 (d) *c*: −107.1 (d)	$^3J_{PCCF} = 23$ $^2J_{PCF} = 48$ $^2J_{PCF} = 48$	4.7	638.917668	638.917030

[a] The values are relative to the $[M^+ - F]$ fragment.

fragmentation pattern observed coincides with the thermaldecomposition pattern observed by Mahler for $F_2P(CF_3)_3$.[14] High resolution mass spectra (HR-MS) on the $[M^+ - F]$ fragments confirms their elemental composition (Table 1).

The careful reduction of these phosphorus(v) compounds **1**–**7** to the phosphorus(III) compounds **8**–**14** by selective removal of the two axial fluorine atoms directly bound to phosphorus yields the previously inaccessible (perfluoroalkyl)-phosphanes. Previous work has shown trimethylsilyldiphenylphosphane to be an effective reducing agent for the fluorophosphoranes.[15] Trimethylsilylfluoride is produced as an easily removable volatile by-product. Tris(trimethylsilyl)phosphane was used as the reducing agent for these studies. During the reaction a black, nonvolatile material of undetermined composition is produced; it is assumed to be a trimethylsilyl-substituted polyphosphane.

The identities of the tris(perfluoroalkyl)phosphanes **8**–**14** were determined by NMR spectroscopy and mass spectrometry (Table 2). The doublet of complex multiplets indicative of the axial fluorine atoms of the phosphorane starting materials **1**–**7** is no longer present. In addition, the resonance of the α-fluorine atoms of the perfluoroalkyl group is shifted downfield slightly. Table 2 shows the ^{19}F and ^{31}P chemical shifts for the compounds under investigation along with their coupling constants.

In the case of tris(pentafluoroethyl)phosphane (**8**), the ^{31}P NMR spectrum was simulated with the $^2J_{PCF}$ and $^3J_{PCCF}$ values (48 Hz and 16 Hz, respectively) obtained from the ^{19}F NMR spectrum. The overlapping resonances with the appropriate intensities would give a 28 peak pattern, each 16 Hz apart, with a relative intensity ratio of 1:9:36:90:180:342:603:927:1305:1785:2286:2664:2961:3195:3195:2961:2664:2286:1785:1305:927:603:342:180:90:36:9:1. Neglecting the four outside peaks on each side yields a 20 peak pattern with relative intensities of 1:1.9:3.3:5.2:7.2:10:12.8:15:16.7:17.8:17.8:16.7:15:12.8:10:7.2:5.2:3.3:1.9:1 (Fig. 2). The ^{31}P spectra of perfluorophosphanes **9**–**14** do not have the same serendipitous overlap of coupling constants.

In contrast to the phosphorane starting materials, each of **8**–**14** produce a positive parent ion under electron impact conditions with surprisingly little fragmentation. High resolution spectra of the parent ion of the (perfluoroalkyl)phosphanes under investigation confirms their elemental composition (Table 2).

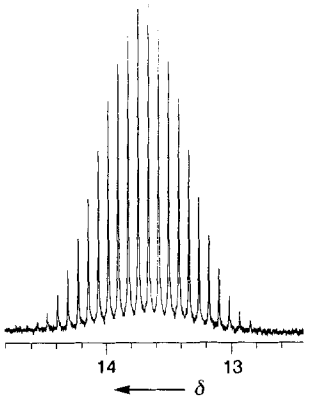


Fig. 2. ^{31}P NMR spectrum of tris(pentafluoroethyl)phosphane (**8**).

Experimental Procedure

The mass spectra were recorded on the following mass spectrometers: HR-MS: analytical ZAB2-E; CI-MS: Finnigan MAT TSQ-70; and EI-MS: Bell and Howell 21-491 (70 eV). ^{19}F NMR analysis was performed on a Nicolet NT-360 spectrometer. Samples were handled anaerobically and sealed in Teflon tubes for NMR experiments. All spectra are references to external $CFCl_3$ ($\delta = 0.0$); higher field was

designated as negative. ^{31}P NMR spectra were obtained on a General Electric (QE-300 spectrometer operating at 121.5 MHz, and are referenced to external 85% aqueous H_3PO_4 ($\delta = 0.0$). The spectral parameters were such that the digital resolution was at least one data point per Hz.

Alkylphosphanes: The trialkylphosphane precursors were synthesized by the action of three equivalents of the corresponding alkyl Grignard compound on PCl_3. PEt_2Bu was prepared from Et_2PCl (prepared by the method of Issleib et al. [16]) and subsequent reaction with BuLi (2.5 M in hexanes; Aldrich). This was followed by work-up in the usual manner and purification by distillation. 1,2-Bis(diethylphosphano)ethane (Strem) was used as received.

1–7: Fluorination of the alkylphosphanes was carried out in a solution phase reactor, which has been fully described elsewhere [17]. The reactor was charged with a mixture of Freon 11 and 113 (1:1), then cooled to −60 °C, and purged with 100 $cm^3 min^{-1}$ of helium overnight. After this period of deoxygenation, typically 5 g of the organophosphane was injected into the reactor and fluorinated under the conditions outlined in Table 3. The contents of the reactor were then filtered and excess Freon removed by passing dry argon over the surface of the solution.

Table 3. Conditions for the fluorination of the alkylphosphanes **1–7**.

t [h]	F_2 [$cm^3 min^{-1}$]	He [$cm^3 min^{-1}$]	T [°C]
12	0	100	−60
4	5	50	−60
8	10	50	−40
12	15	50	−20
12	15	15	0
12	15	15	+25
12	0	15	[a]

[a] Room temperature.

The reducing agent, $P(SiMe_3)_3$, was synthesized by slightly adapted literature methods [22] and purified by a single distillation.

8–14: Routinely difluorophosphorane (5 mmol) was treated with an excess (20%) of $P(SiMe_3)_3$. The reagents were stirred vigorously (by magnetic stirrer) in the absence of any solvents and heated to 100 °C in an oil bath. In the absence of agitation the two materials quickly separated, and the more dense fluorinated materials formed a clear lower phase. The by-product $(CH_3)_3SiF$ was occasionally vented from the reaction tube to avoid excessive pressure build-up. The formation of trimethyl-silyl fluoride was confirmed by ^1H and ^{19}F NMR, EI-MS, and IR analysis. Reaction times were increased as the length of the perfluoroalkyl chain increased. Compound **8** was completely reduced in about 3 days. One day was added for each additional carbon in the alkyl chain. Compound **12** was therefore heated for a full week. Upon completion of the reaction stirring was stopped, and the two immiscible phases allowed to separate. The lower perfluorophosphane phase, which was >90% pure (NMR), was then removed from the black, nonvolatile residue of the reducing agent.

Received: September 14, 1994 [Z 7315/7316 IE]
German version: *Angew. Chem.* **1995**, *107*, 1334–1337

Keywords: fluorine compounds · mass spectrometry · NMR spectroscopy · phosphorus compounds

[1] J. F. Nixon, *Adv. Inorg. Chem. Radiochem.* **1970**, *13*, 363.
[2] J. F. Nixon, *Adv. Inorg. Chem. Radiochem.* **1985**, *29*, 41.
[3] S. L. Battle, PhD Thesis, University of Texas at Austin, **1993**.
[4] F. W. Bennett, H. J. Emeleus, R. N. Hazeldine, *J. Chem. Soc.* **1953**, 1565.
[5] T. Mahmood, J. M. Shreeve, *Inorg. Chem.* **1986**, *25*, 3128.
[6] H. J. Emeleus, J. D. Smith, *J. Chem. Soc.* **1959**, 375.
[7] A. Haas, C. Limberg, S. R. Sterlin, *J. Fluorine Chem.* **1991**, *53*, 71.
[8] K. G. Sharp, I. Schwager, *Inorg. Chem.* **1976**, *15*, 1697.
[9] P. Cooper, R. Fields, R. N. Hazeldine, G. H. Mitchell, S. N. Nona, *J. Fluorine Chem.* **1982**, *21*, 317.
[10] a) N. J. Maraschin, R. J. Lagow, *Inorg. Chem.* **1973**, *12*, 1459; b) T.-Y. Lin, PhD Thesis, University of Texas at Austin, **1992**; c) E. K. S. Liu, R. J. Lagow, *J. Organomet. Chem.* **1978**, *145*, 167; d) *Inorg. Chem.* **1978**, *17*, 618; e) W. H. Lin, R. J. Lagow, *J. Fluorine Chem.* **1990**, *50*, 15; f) T. E. Mlsna, PhD Thesis, University of Texas at Austin, **1992**.
[11] a) S. Modena, P. Calini, G. Gregorio, G. Moggi, *J. Fluorine Chem.* **1988**, *40*, 349; b) F. R. Feher, P. W. Foerst, P. H. Liu, D. J. Kalots, J. S. McConaghy, Jr., *Eur. Pat. Appl.* 332601, **1989**; c) A. C. Sievert, W. R. Tong, M. J. Nappa, *J. Fluorine Chem.* **1991**, *53*, 397; d) G. B. Rutherford, MA Thesis, University of Texas at Austin, **1990**.
[12] C. H. Dungan, J. R. VanWazer, *Compilation of Reported F-19 NMR Chemical Shifts – 1951–1967*, Wiley, New York, **1970**.
[13] R. G. Cavell, J. A. Gibson, K. I. The, *J. Am. Chem. Soc.* **1977**, *99*, 7841.
[14] W. Mahler, *Inorg. Chem.* **1963**, *2*, 230.
[15] G. V. Roschenthaler, J. A. Gibson, R. Schmutzler, *Chem. Ber.* **1977**, *110*, 611.
[16] K. Issleib, W. Seidel, *Chem. Ber.* **1959**, *92*, 2681.
[17] J. J. Kampa, PhD Thesis, University of Texas at Austin, **1992**.
[18] G. W. Parshall, R. V. Lindsey, Jr., *J. Am. Chem. Soc.* **1959**, *81*, 6273.

C–C Coupling Reactions as a Novel Synthetic Route to π-Allyl- and π-Butadienylrhodium Complexes**

Ralf Wiedemann, Justin Wolf, and Helmut Werner*

Dedicated to Professor Manfred Hesse on the occasion of his 60th birthday

Transition-metal complexes containing vinylidene ligands have not only been discussed as important intermediates in homogeneous and heterogeneous catalytic reactions[1] but have also been considered as useful starting materials in organic and organometallic synthesis.[2] Our interest in the chemistry of the already thoroughly studied compounds of the type **A** (cf. **1–3**)[3, 4] has recently been focussed upon the question whether by

trans-[RhX(=C=CHR)($PiPr_3$)$_2$]

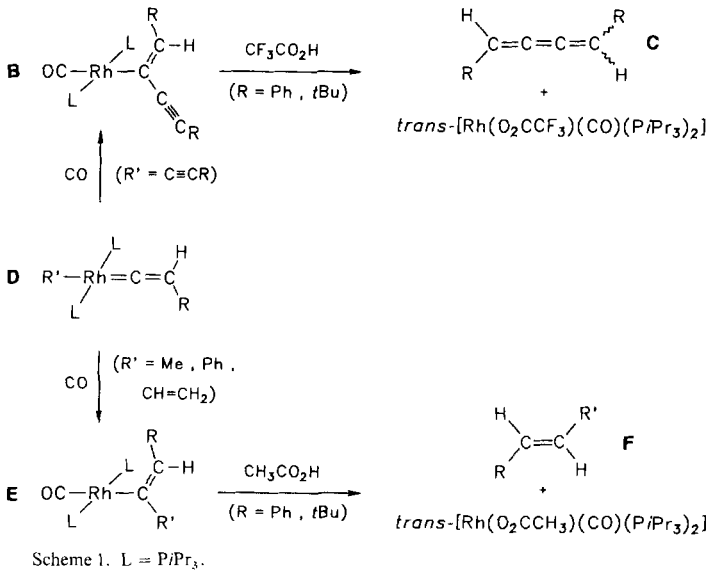
A, X = Cl, OAc; R = H, alkyl, aryl

substitution of the chloro or acetato ligand corresponding organorhodium derivatives **D** (cf. **4–6**, and **10**, **11**) would be accessible and could be used for metal-assisted C–C coupling reactions. One of the first successes was achieved on reacting the compounds **D** with CO, which led, by migration of the group R′ to the α-carbon atom of the vinylidene ligand, to the formation of σ-vinylrhodium complexes **B** and **E** (see Scheme 1). Subsequent treatment of these isolated and structurally characterized products with acetic or trifluoroacetic acid yielded butatrienes **C** (or enynes, respectively) or the (*E*) isomers of disubstituted ethenes **F**.[5, 6] In continuation of this work we have now found that a coupling of the C-bonded ligands of the organo(vinylidene)rhodium compounds **D** is even possible *without* the presence of a supporting substrate and that this opens up a novel synthetic route to π-allyl and π-butadienyl metal complexes.[7]

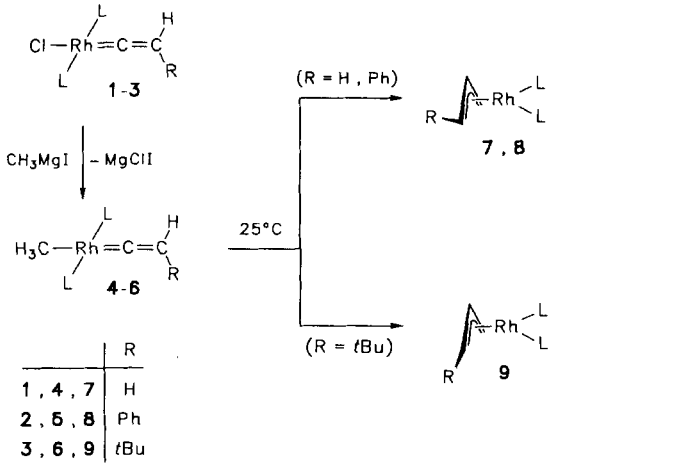
The methyl(vinylidene) complexes **4**, **5**,[6] and **6** are obtained from the well-known precursors **1–3**[3] upon reaction with Grignard reagent (CH_3MgI) in benzene/ether at 10 °C (see Scheme 2). The deep-blue or dark violet compounds **4–6**, isolated in 80% yield, react slowly (12 h) in benzene at room temperature to give the π-allylrhodium complexes **7–9** (yellow or orange air-sensitive solids) of which the parent derivative **7** has also been prepared in a different way.[8] It is most noteworthy that from **5** the allylic ligand is formed in the *syn* (**8**) and from **6** in the *anti* configuration (**9**),[9] and that compound **9** even after

[*] Prof. Dr. H. Werner, Dipl.-Chem. R. Wiedemann, Dr. J. Wolf
Institut für Anorganische Chemie der Universität
Am Hubland, D-97074 Würzburg (Germany)
Telefax: Int. code +(931) 888-4605

[**] This work was supported by Volkswagen-Stiftung, the Deutsche Forschungsgemeinschaft (SFB 347) and Degussa AG.



Scheme 1. L = P*i*Pr$_3$.



Scheme 2. L = P*i*Pr$_3$.

stirring for 24 h in benzene does not rearrange to the thermodynamically more stable *syn* isomer. With regard to earlier studies[10] we assume that initially a 14-electron species of the composition **G** (analogous to **H**)[8] is formed as an intermediate which by β-H shift reacts to give a four-coordinate (η^2-allene)hydrido metal derivative. This generates the final product by a hydride transfer from the metal to the central carbon atom of the allene ligand.

$[Rh(\eta^1\text{-}C(CH_3)=CHR)(PiPr_3)_2]$ **G**

$[Rh(\eta^1\text{-}CH_2Ph)(PiPr_3)_2]$ **H**

The vinyl(vinylidene)rhodium complexes **10**[6] and **11** (violet crystalline solids), which are prepared in a similar way to the compounds **4**–**6**, also undergo isomerization reactions. The most remarkable feature is that *in solution* and in the *solid state* different products are formed. Whereas the reaction of **10** and **11** in benzene (3 h, 45–50 °C) exclusively affords the η^3-2,3,4-*trans*-butadienyl complexes **12** and **13**, respectively, on storing the solid compounds under argon (10–14 days, 25 °C) the alkynyl(ethene) metal derivatives **14** and **15**, respectively, are obtained. The latter have previously been prepared from

Table 1. Selected spectroscopic data of the allyl and butadienyl complexes **8**, **9**, **12**, and **13** (without the ^{1}H and ^{13}C NMR data for the phosphane ligands and the phenyl groups; assignment: C^1 (carrying H^1) is always the substituted carbon atom of the allyl or butadienyl ligand; C^2, C^3, C^4 in continuing order; H^3 in *syn* and H^4 in *anti* position to H^2).

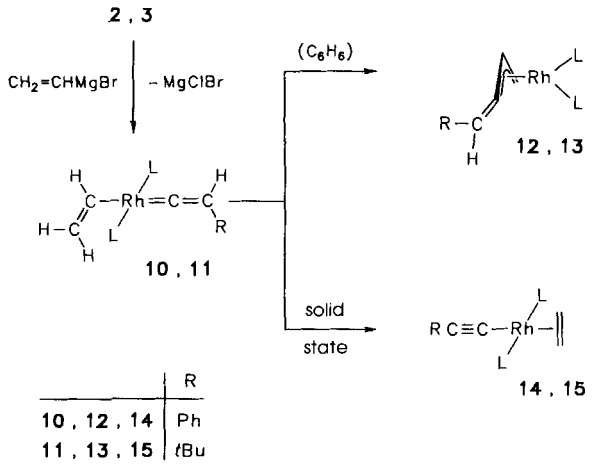
8: ^{1}H NMR (400 MHz, C_6D_6): δ = 5.28 [ddd, $J(H^2H^4)$ = 12.2, $J(H^1H^2)$ = 10.7, $J(H^2H^3)$ = 6.7 Hz, H^2], 3.40 [dd, $J(H^1H^2)$ = 10.7, $J(PH)$ = 7.7 Hz, H^1], 3.12 [ddd, $J(H^2H^3)$ = 6.7, $J(PH)$ = 3.8 and 2.2 Hz, H^3], 2.09 [dd, $J(H^2H^4)$ = 12.2, $J(PH)$ = 5.6 Hz, H^4]; ^{13}C NMR (100.6 MHz, C_6D_6): δ = 99.90 (m, C^2), 65.03 [ddd, $J(RhC)$ = 27.6, $J(PC)$ = 6.9 and 2.7 Hz, C^1], 46.24 [ddd, $J(RhC)$ = 21.0, $J(PC)$ = 9.4 and 5.2 Hz, C^3]; ^{31}P NMR (162.0 MHz, C_6D_6): δ = 56.51 [dd, $J(RhP)$ = 198.0, $J(PP)$ = 22.0 Hz], 46.20 [dd, $J(RhP)$ = 189.5, $J(PP)$ = 22.0 Hz]

9: ^{1}H NMR (400 MHz, C_6D_6): δ = 4.86 [dddd, $J(RhH)$ = 2.1, $J(H^2H^4)$ = 12.6, $J(H^1H^2)$ = 8.2, $J(H^2H^3)$ = 8.0 Hz, H^2], 3.86 [m, in the $^1H\{^{31}P\}$ ddd, $J(H^1H^2)$ = 8.2, $J(PH)$ = 3.6 and 3.6 Hz, H^1], 2.74 [m, in the $^1H\{^{31}P\}$ d, br., $J(H^2H^3)$ = 8.0 Hz, H^3], 2.05 [dd, br., $J(H^2H^4)$ = 12.6, $J(PH)$ = 8.2 Hz, H^4]; ^{13}C NMR (100.6 MHz, C_6D_6): δ = 95.06 [ddd, $J(RhC)$ = 5.7, $J(PC)$ = 1.2 and 1.2 Hz, C^2], 76.62 [ddd, $J(RhC)$ = 25.9, $J(PC)$ = 10.6 and 4.4 Hz, C^1], 45.04 [ddd, $J(RhC)$ = 29.9, $J(PC)$ = 8.3 and 5.2 Hz, C^3], 35.18 [dd, $J(RhC)$ = 0.9, $J(PC)$ = 3.3 Hz, $C(CH_3)_3$], 34.40 [d, $J(PC)$ = 1.9 Hz, $C(CH_3)_3$]; ^{31}P NMR (162.0 MHz, C_6D_6): δ = 49.02 [dd, $J(RhP)$ = 206.7, $J(PP)$ = 19.1 Hz], 47.85 [dd, $J(RhP)$ = 211.8, $J(PP)$ = 19.1 Hz]

12: ^{1}H NMR (400 MHz, C_6D_6): δ = 6.34 (m, H^1), 4.71 (m, H^2), 3.13 [ddd, $J(H^2H^3)$ = 7.4, $J(PH)$ = 2.5 and 2.5 Hz, H^3), signal of H^4 obscured by PCH-resonance; ^{13}C NMR (100.6 MHz, C_6D_6): δ = 171.23 (m, C^2), 111.81 (s, C^1), 78.74 [d, $J(RhC)$ = 3.9 Hz, C^3], 47.94 [ddd, $J(RhC)$ = 25.1, $J(PC)$ = 5.9 and 4.9 Hz, C^4]; ^{31}P NMR (162.0 MHz, C_6D_6): δ = 52.80 [dd, $J(RhP)$ = 197.0, $J(PP)$ = 21.9 Hz], 46.80 [dd, $J(RhP)$ = 160.5, $J(PP)$ = 21.9 Hz]

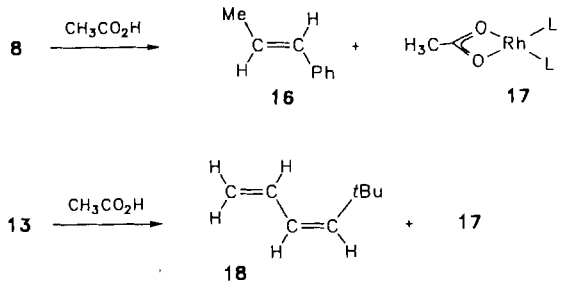
13: ^{1}H NMR (400 MHz, C_6D_6): δ = 5.14 (m, H^1), 4.50 (m, H^2), 2.98 [ddd, $J(H^2H^3)$ = 8.0, $J(PH)$ = 2.6 and 2.6 Hz, H^3], 1.93 [dd, $J(H^2H^4)$ = 11.7, $J(PH)$ = 6.7 Hz, H^4], 1.30 (s, $C(CH_3)_3$); ^{13}C NMR (100.6 MHz, C_6D_6): δ = 160.96 [ddd, $J(RhC)$ = 43.8, $J(PC)$ = 18.3 and 9.2 Hz, C^2], 120.26 (s, C^1), 76.99 [d, $J(RhC)$ = 4.0 Hz, C^3], 47.55 [ddd, $J(RhC)$ = 26.4, $J(PC)$ = 6.9 and 5.7 Hz, C^4], 34.19 [d, $J(PC)$ = 5.6 Hz, $C(CH_3)_3$], 31.24 (s, $C(CH_3)_3$); ^{31}P NMR (162.0 MHz, C_6D_6): δ = 52.24 [dd, $J(RhP)$ = 196.8, $J(PP)$ = 20.9 Hz], 48.03 [dd, $J(RhP)$ = 164.6, $J(PP)$ = 20.9 Hz]

$[Rh(\eta^3\text{-}CH_2Ph)(PiPr_3)_2]$ and HC≡CR (R = Ph, *t*Bu) under an atmosphere of ethene.[4c] The ^{13}C NMR data of **12** and **13**, in particular, which are in good agreement with those of other η^3-2,3,4-butadienyl metal compounds[11] support the structural proposal shown in Scheme 3.



Scheme 3. L = P*i*Pr$_3$.

As already mentioned,[6] the reaction of **5** with CO yields the η^1-vinylrhodium complex **E**, R = Ph, R′ = Me which reacts with acetic acid to give **16**.[6] This olefin is also formed almost quantitatively upon treatment of **8** with acetic acid (Scheme 4). The corresponding reaction of **13** with acetic acid affords regioselectively the butadiene derivative **18**.[12] The exclusive for-



Schema 4. L = $PiPr_3$.

mation of the (*Z*) isomer supports the assumption that in compound **13** (and probably also in **12**) the substituents at the non-coordinated C=C double bond are arranged *cis*. The rhodium-containing product of the reaction of **8** or **13** with acetic acid is the chelate complex **17**,[8] which can be reconverted in two steps [a) reaction with HC≡CR to give **I**;[4b] b) "chromatography" of **I** on chloride-containing Al_2O_3[13]] to the starting materials **2** and **3**. In this way a cyclic process can be established by which, from HC≡CR, R'MgX, and CH_3CO_2H and assisted by the metal, an olefin RCH=CHR' (R = Ph, *t*Bu; R' = Me, $CH=CH_2$) is *regio- and stereoselectively* formed.

trans-[RhH(C≡CR)(η^2-O_2CCH_3)($PiPr_3$)$_2$] **I**

Preliminary attempts indicate that the "metallabutatrienes" **J**[14] behave similarly towards Grignard reagents as the vinylidene complexes **1**–**3** and that the corresponding vinyl metal derivatives **K** undergo isomerization reactions as well. Therefore, the expectation is that even higher unsaturated hydrocarbons than **18** could be accessible by a rhodium-assisted C–C coupling procedure.

trans-[RhCl(=C=C=CR_2)($PiPr_3$)$_2$] **J**

trans-[Rh($CH=CH_2$)(=C=C=CR_2)($PiPr_3$)$_2$] **K**

Received: January 19, 1995 [Z 7642 IE]
German version: *Angew. Chem.* **1995**, *107*, 1359–1361

Keywords: allyl complexes · carbon–carbon coupling · isomerization · vinylidene complexes

[1] a) R. Mahé, Y. Sasaki, C. Bruneau, P. H. Dixneuf, *J. Org. Chem.* **1989**, *54*, 1518–1523; b) V. C. Gibson, G. Parkin, J. E. Bercaw, *Organometallics* **1991**, *10*, 220–231; c) B. M. Trost, J. A. Flygare, *J. Am. Chem. Soc.* **1992**, *114*, 5476–5477.

[2] a) A. G. M. Barrett, J. Mortier, M. Sabat, M. A. Sturgess, *Organometallics* **1988**, *7*, 2553–2561; b) S. Feracin, H.-U. Hund, H. W. Bosch, E. Lippmann, W. Beck, H. Berke, *Helv. Chim. Acta* **1992**, *75*, 1305–1312; c) B. M. Trost, J. A. Martinez, R. J. Kulawiec, A. F. Indolese, *J. Am. Chem. Soc.* **1993**, *115*, 10402–10403; d) C. Bianchini, L. Glendenning, M. Peruzzini, A. Romerosa, F. Zanobini, *J. Chem. Soc. Chem. Commun.* **1994**, 2219–2220.

[3] Chloro complexes: a) H. Werner, F. J. Garcia Alonso, H. Otto, J. Wolf, *Z. Naturforsch. B* **1988**, *43*, 722–726; b) H. Werner, U. Brekau, *ibid.* **1989**, *44*, 1438–1446; c) T. Rappert, O. Nürnberg, N. Mahr, J. Wolf, H. Werner, *Organometallics* **1992**, *11*, 4156–4164; d) T. Rappert, O. Nürnberg, H. Werner, *ibid.* **1993**, *12*, 1359–1364; e) H. Werner, M. Baum, D. Schneider, B. Windmüller, *ibid.* **1994**, *13*, 1089–1097.

[4] Acetato complexes: a) M. Schäfer, J. Wolf, H. Werner, *J. Chem. Soc. Chem. Commun.* **1991**, 1341–1343; b) *J. Organomet. Chem.* **1995**, *485*, 85–100; c) M. Schäfer, Dissertation, Universität Würzburg, **1994**.

[5] M. Schäfer, N. Mahr, J. Wolf, H. Werner, *Angew. Chem.* **1993**, *105*, 1377–1379; *Angew. Chem. Int. Ed. Engl.* **1993**, *32*, 1315–1317.

[6] R. Wiedemann, P. Steinert, M. Schäfer, H. Werner, *J. Am. Chem. Soc.* **1993**, *115*, 9864–9865.

[7] The formation of an allylic unit by transfer of a bridging methyl group to an iridium-bonded vinylidene ligand has already been reported: M. D. Fryzuk, L. Huang, N. T. McManus, P. Paglia, S. J. Rettig, G. S. White, *Organometallics* **1992**, *11*, 2979–2990.

[8] H. Werner, M. Schäfer, O. Nürnberg, J. Wolf, *Chem. Ber.* **1994**, *127*, 27–38.

[9] For the nomenclature and the thermodynamic stabilities of the *syn*/*anti* isomers see: a) G. Wilke, B. Bogdanovic, P. Hardt, P. Heimbach, W. Keim, M. Kröner, W. Oberkirch, K. Tanaka, E. Steinrücke, D. Walter, H. Zimmermann, *Angew. Chem.* **1966**, *78*, 157–172; *Angew. Chem. Int. Ed. Engl.* **1966**, *5*, 151–166; b) K. Vrieze, H. C. Volger, P. W. N. M. van Leeuwen, *Inorg. Chim. Acta, Rev.* **1969**, 109–129; c) R. P. Hughes in *Comprehensive Organometallic Chemistry, Vol. 5* (Eds.: G. Wilkinson, F. G. A. Stone, E. W. Abel), 1st ed., Pergamon, Oxford, **1982**, p. 492–540.

[10] J. Wolf, H. Werner, *Organometallics* **1987**, *6*, 1164–1169.

[11] S. A. Benyunes, R. J. Deeth, A. Fries, M. Green, M. McPartlin, C. B. M. Nation, *J. Chem. Soc. Dalton Trans.* **1992**, 3453–3465, and references therein.

[12] Characterization by comparison of the NMR data: A. L. Segre, L. Zetta, A. Di Corato, *J. Mol. Spectrosc.* **1969**, *32*, 296–308.

[13] H. Werner, M. Schäfer, J. Wolf, K. Peters, H. G. von Schnering, *Angew. Chem.* **1995**, *107*, 213–215; *Angew. Chem. Int. Ed. Engl.* **1995**, *34*, 191–194.

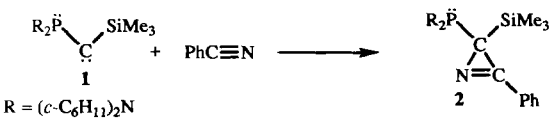
[14] a) H. Werner, *Nachr. Chem. Tech. Lab.* **1992**, *40*, 435–444; b) H. Werner, T. Rappert, R. Wiedemann, J. Wolf, N. Mahr, *Organometallics* **1994**, *13*, 2721–2727.

Synthesis of a 2*H*-Azirine by [1+2] Cycloaddition of a Phosphinocarbene with a Nitrile and Its Ring-Expansion to a 1,2λ^5-Azaphosphete**

Gilles Alcaraz, Ulrich Wecker, Antoine Baceiredo, Françoise Dahan, and Guy Bertrand*

Whether carbene, germylene, and silylene are justifiable terms for stabilized versions[1–4] of the reactive species is a very debatable question.[5] Calculations[6] and an X-ray diffraction study[1d] have clearly shown that phosphinocarbenes are best formulated as phosphorus-vinyl ylides. However, for synthetic chemists, the most important issue is to know whether these stable species show the reactivity of transient carbenes. The formation of azaphospholidines upon thermolysis (intramolecular carbene insertion into a carbon–hydrogen bond),[1a] cyclopropanations,[1b] and [1+1] addition to isocyanides giving keteneimines[1b,c] are nice examples of the carbene behavior of phosphinocarbenes. Here we report another carbene-type reaction, which has never been described with transient carbenes, namely the formation of a 2*H*-azirine by a [1+2] cycloaddition. We also report the first example of a ring expansion reaction of an azirine to a four-membered ring system with four π electrons.

The phosphinocarbene **1**[1e] reacts with a large excess of benzonitrile in toluene, at room temperature, to afford compound **2** (Scheme 1) in 85% isolated yield. According to ^{31}P NMR spec-



Scheme 1.

[*] Dr. G. Bertrand, G. Alcaraz, Dr. U. Wecker, Dr. A. Baceiredo, Dr. F. Dahan
Laboratoire de Chimie de Coordination du CNRS
205, route de Narbonne, F-31077 Toulouse Cédex (France)
Telefax: Int. code + 61 55 30 03

[**] This work was supported by the Alexander von Humboldt Foundation in the form of a Feodor-Lynen grant (U.W.), and by the Centre National de la Recherche Scientifique.

troscopy, the reaction was complete after 18 hours, and no intermediate was detected. Multinuclear NMR spectroscopy and mass spectrometry as well as elemental analysis showed that compound **2** was a 1,1-adduct of **1** with benzonitrile,[7] and an X-ray diffraction study[8] demonstrated that **2** was a 2*H*-azirine. The molecular structure of **2** is shown in Figure 1. Note, the typical[9] very long C1–N1 bond [1.629(4) Å]; for comparison, in diazirines the value of the C–N bond length is around 1.46 Å.[10]

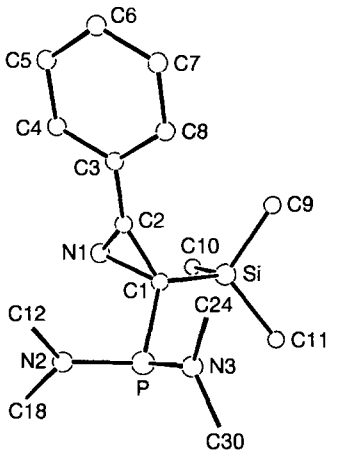
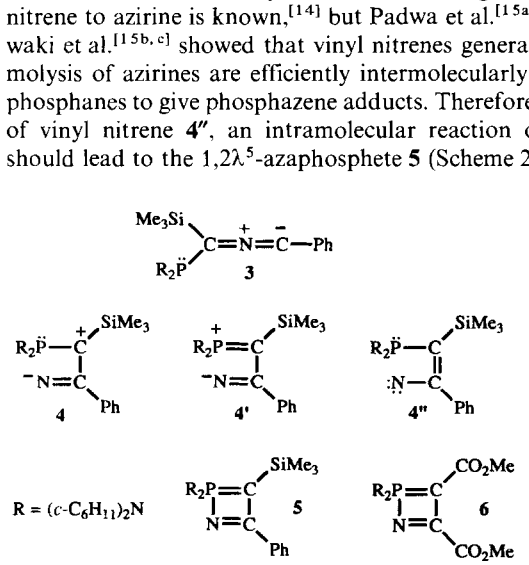


Fig. 1. Structure of **2** (ORTEP view). The cyclohexyl groups on N2 and N3 are omitted for clarity. Selected bond lengths [Å] and bond angles [°]: P-C1 1.870(3), P-N2 1.692(2), P-N3 1.705(2), C1-C2 1.468(3), C1-N1 1.630(3), C1-Si 1.899(2), C2-N1 1.254(4), C2-C3 1.452(4), P-C1-Si 118.1(1), P-C1-C2 125.9(2), P-C1-N1 111.5(2), N1-C1-C2 47.4(2), C1-N1-C2 59.5(2), N1-C2-C1 73.1(2), N1-C2-C3 137.6(3), C1-C2-C3 149.2(3).

Formally, azirine **2** results from a [1 + 2] cycloaddition of the carbene **1** to the nitrile. Electrophilic carbenes are known to react with nitriles giving transient[11] or even stable nitrile ylides.[12] Phosphinocarbenes have never shown any electrophilic character, and the ring closure of nitrile ylides into 2*H*-azirines is quite unlikely;[11–13] thus the nitrile ylide **3** cannot be the intermediate in the reaction leading to **2**. A stepwise mechanism, first involving the nucleophilic attack of the carbene at the carbon atom of the nitrile would lead to the 1,3-dipole **4**. However, it should be noted that **4** can also be regarded as azabetaine **4′**, or vinyl nitrene **4″**. The ring closure of vinyl nitrene to azirine is known,[14] but Padwa et al.[15a] and Nishiwaki et al.[15b,c] showed that vinyl nitrenes generated by thermolysis of azirines are efficiently intermolecularly trapped by phosphanes to give phosphazene adducts. Therefore, in the case of vinyl nitrene **4″**, an intramolecular reaction of this type should lead to the 1,2λ^5-azaphosphete **5** (Scheme 2).



Scheme 2.

Interestingly, addition of a catalytic amount of dichloro(*p*-cymene)ruthenium(II)[16] to a solution of **2** in dichloromethane at room temperature led to the 1,2λ^5-azaphosphete **5** in 95% yield! The four-π-electron four-membered heterocycle **5** has been fully characterized,[7] and the NMR data compared very well with those of the recently reported 1,2λ^5-azaphosphete **6**[17] ($\delta^{31}P = +52.3$ (**5**), +52.6 (**6**); $\delta^{13}C\alpha$ and $\beta = +84.9$ and +192.4 (**5**), +92.4 and 181.7 (**6**)).

These results as a whole suggest that either the formation of azirine **2** results from a concerted [1 + 2] cycloaddition, or that **2** is the kinetic product of the stepwise reaction of the stable carbene **1** with benzonitrile; the 1,2λ^5-azaphosphete **5** is the thermodynamic product. Whatever the mechanism, these findings should open a new route to the synthesis of a variety of 2*H*-azirines from transient nucleophilic carbenes.[18] More generally, after having used well-known reactions of transient species to demonstrate the existence of their stabilized versions, now, it is probably time to use the stabilized derivatives to discover new reactions applicable to the transient species.

Received: January 9, 1995 [Z 7613 IE]
German version: *Angew. Chem.* **1995**, *107*, 1358–1359

Keywords: carbenes · cycloadditions · heterocycles · phosphorus compounds

[1] a) A. Igau, H. Grützmacher, A. Baceiredo, G. Bertrand, *J. Am. Chem. Soc.* **1988**, *110*, 6463; b) A. Igau, A. Baceiredo, G. Trinquier, G. Bertrand, *Angew. Chem.* **1989**, *101*, 617; *Angew. Chem. Int. Ed. Engl.* **1989**, *28*, 621; c) G. Gillette, A. Igau, A. Baceiredo, G. Bertrand, *ibid.* **1990**, *102*, 1486 and **1990**, *29*, 1429; d) M. Soleilhavoup, A. Baceiredo, O. Treutler, R. Ahlrichs, M. Nieger, G. Bertrand, *J. Am. Chem. Soc.* **1992**, *114*, 10959; e) G. Alcaraz, R. Reed, A. Baceiredo, G. Bertrand, *J. Chem. Soc. Chem. Commun.* **1993**, 1354.

[2] a) A. J. Arduengo, R. L. Harlow, M. Kline, *J. Am. Chem. Soc.* **1991**, *113*, 361; b) A. J. Arduengo, H. V. R. Dias, R. L. Harlow, M. Kline, *ibid.* **1992**, *114*, 4430; c) A. J. Arduengo, H. V. R. Dias, D. A. Dixon, R. L. Harlow, W. T. Klooster, T. F. Koetzle, *ibid.* **1994**, *116*, 6812; d) A. J. Arduengo, D. A. Dixon, K. K. Kumashiro, C. Lee, W. P. Power, K. W. Zilm, *ibid.* **1994**, *116*, 6361; e) A. J. Arduengo, H. Bock, H. Chen, M. Denk, D. A. Dixon, J. C. Green, W. A. Herrmann, N. L. Jones, M. Wagner, R. West, *ibid.* **1994**, *116*, 6641.

[3] W. A. Herrmann, M. Denk, J. Behm, W. Scherer, F. R. Klingan, H. Bock, B. Solouki, M. Wagner, *Angew. Chem.* **1992**, *104*, 1489; *Angew. Chem. Int. Ed. Engl.* **1992**, *31*, 1485.

[4] M. Denk, R. Lennon, R. Hayashi, R. West, A. V. Belyakov, H. P. Verne, A. Haaland, M. Wagner, N. Metzler, *J. Am. Chem. Soc.* **1994**, *116*, 2691.

[5] a) R. Dagani, *Chem. Eng. News* **1994**, *72* (18), 20; b) *ibid.* **1991**, *69* (4), 19; c) M. Regitz, *Angew. Chem.* **1991**, *103*, 691; *Angew. Chem. Int. Ed. Engl.* **1991**, *30*, 674.

[6] a) D. A. Dixon, K. D. Dobbs, A. J. Arduengo, G. Bertrand, *J. Am. Chem. Soc.* **1991**, *113*, 8782; b) M. T. Nguyen, M. A. McGinn, A. F. Hegarty, *Inorg. Chem.* **1986**, *25*, 2185; c) O. Treutler, R. Ahlrichs, M. Soleilhavoup, *J. Am. Chem. Soc.* **1993**, *115*, 8788.

[7] **2**: M.p. 105 °C; ^{31}P NMR ($CDCl_3$): $\delta = 69.3$; ^{13}C NMR ($CDCl_3$): $\delta = 165.5$ (s, C=N); ^{29}Si-NMR ($CDCl_3$): $\delta = 4.3$ (d, $^2J(P,Si) = 51.7$ Hz); IR (CH_2Cl_2): $\tilde{\nu} = 2019, 1726\ cm^{-1}$; MS: *m/z*: 580 [$M^+$]. **5**: yellow oil; ^{31}P-NMR ($CDCl_3$): $\delta = 52.3$; ^{13}C NMR ($CDCl_3$): $\delta = 192.4$ (d, $^2J(P,C) = 46.7$ Hz, C=N), 139.0 (d, $^3J(P,C) = 55.7$ Hz, C_i), 130.7, 128.8, 128.7 (s, $C_{o,m,p}$), 84.9 (d, $^1J(P,C) = 42.9$ Hz, PC), 58.3 (d, $^2J(P,C) = 4.9$ Hz, CH), 34.3, 34.1, 27.8, 27.7, 26.4 (s, CH_2), 3.5 (d, $^3J(P,C) = 3.9$ Hz, CH_3Si); MS: *m/z*: 580 [M^+].

[8] X-ray data for **2**: $C_{35}H_{58}N_3SiP$, monoclinic, space group *Cc* (No 9) with $a = 19.308(1)$, $b = 10.429(1)$, and $c = 18.028(2)$ Å, $\beta = 106.93(1)°$, $V = 3472.8$ Å^3 and $\rho_{calc} = 1.909\ g cm^{-3}$ for $Z = 4$. Data were collected on an Enraf-Nonius CAD4 at 293 K with ω-2θ scans with $Mo_{K\alpha}$ radiation ($\lambda = 0.71073$ Å). A total of 6072 reflections were collected up to $2\theta = 50°$, of which 4258 were observed [$F_o^2 > 2\sigma(F_o^2)$]. The solution and refinement on F_o^2, with SHELXL-93, of the structure gave R(obs) = 0.034, [R(all) = 0.082] and Rw(obs) = 0.082 [Rw(all) = 0.090]. Further details of the crystal structure investigation may be obtained from the Fachinformationszentrum Karlsruhe, D-76344 Eggenstein-Leopoldshafen (Germany) on quoting the depository number CSD-58847.

[9] N. Kanehisa, N. Yasuoka, N. Kasai, K. Isomura, H. Taniguchi, *J. Chem. Soc. Chem. Commun.* **1980**, 98.

[10] a) A. Linden, T. S. Cameron, M. T. H. Liu, S. M. Anand, *J. Org. Chem.* **1988**, *53*, 1085; b) S. Cameron, P. K. Bakshi, B. Borecka, *J. Am. Chem. Soc.* **1992**, *114*, 1889.

 © VCH Verlagsgesellschaft mbH, D-69451 Weinheim, 1995 0570-0833/95/1111-1247 $ 10.00+.25/0

[11] A. Padwa, S. F. Hornbuckle, *Chem. Rev.* **1991**, *91*, 263.
[12] E. P. Janulis, Jr., S. R. Wilson, A. J. Arduengo, *Tetrahedron Lett.* **1984**, *25*, 405.
[13] D. Griller, L. Hadel, A. S. Nazran, M. S. Platz, P. C. Wong, T. G. Savino, J. C. Scaiano, *J. Am. Chem. Soc.* **1984**, *106*, 2227.
[14] a) M. Sakurai, K. Noguchi, K. Isomura, R. Tanaka, H. Taniguchi, *Heterocycles* **1992**, *33*, 519; b) G. L'abbé, *Angew. Chem.* **1975**, *87*, 831; *Angew. Chem. Int. Ed. Engl.* **1975**, *14*, 775; c) A. Hassner in *Azides and Nitrenes* (Ed.: E. F. V. Scriven), Academic Press, New York, **1984**, pp. 35–95.
[15] a) A. Padwa, J. Smolanoff, A. Tremper, *J. Org. Chem.* **1976**, *41*, 543; b) T. Nishiwaki, A. Nakano, H. Matsuoko, *J. Chem. Soc. C* **1970**, 1825; c) T. Nishiwaki, F. Fugiyama, *J. Chem. Soc. Perkin Trans. 1* **1972**, 1456.
[16] M. A. Bennett, A. K. Smith, *J. Chem. Soc. Dalton Trans.* **1974**, 233.
[17] a) J. Tejeda, R. Réau, F. Dahan, G. Bertrand, *J. Am. Chem. Soc.* **1993**, *115*, 7880; b) K. Bieger, J. Tejeda, R. Réau, F. Dahan, G. Bertrand, *ibid.* **1994**, *116*, 8087.
[18] R. A. Moss, *Acc. Chem. Res.* **1980**, *13*, 58.

 © VCH Verlagsgesellschaft mbH, D-69451 Weinheim, 1995 0570-0833/95/1111-1248 $ 10.00+.25/0

Trends and Controversies

Redox Mechanisms in Inorganic Chemistry. (Ellis Horwood Series in Inorganic Chemistry.) By *A. G. Lappin*. Ellis Horwood, Chichester, 1994. 285 pp., hardcover £ 56.50.—ISBN 0-13-770751-7

This is a very timely and urgently needed book by an author who is well known for his contributions to the understanding of electron transfer reactions in inorganic chemistry. The author makes it clear in the preface that this is not a book on kinetics and mechanisms, nor on electron transfer or the theory of electron transfer reactions. The focus of the book is an examination of trends in mechanisms that are found in inorganic electron transfer reactions. And that is exactly what the book offers, a detailed account of available literature data and the trends that can be seen in these data.

As one would expect, the main topics covered, following a general introductory chapter, are the outer-sphere mechanism, the inner-sphere mechanism, intramolecular electron transfer, and multiple electron transfer. The author has devoted an impressive effort to compiling the available literature data and pointing out the trends observed. The individual chapters are excellent reviews on the topics, with the advantage that they are all written by the same author, resulting in a consistent style of presentation. At the end of each chapter a series of questions are given that enable the reader to check the insight gained into the topic treated. In addition, a detailed list of references to the original sources of the data is provided for each chapter.

The quality of production is good, except for the aspect referred to at the end of this review. Data are summarized in tables and correlations are summarized in figures. This method of presentation avoids excessive text and makes it easy for the reader to find the desired data. Reaction schemes and details of intermediate species are presented in a very clear manner, which all adds to the convenience and readability of the book.

The book will be of great help to anyone involved in the study of inorganic electron transfer reactions, since it is an up-to-date presentation of the available literature data. Furthermore, it identifies areas in which there is scope for further investigation and theoretical treatment of the data. All in all, it will be a standard text for students and researchers involved in the study of inorganic electron transfer processes.

It is rather unfortunate that there are quite a number of very obvious typing errors, especially in the first chapter of the book. It is the responsibility of the publisher, and to some extent the author, to eliminate such errors, which detract from the quality of the book and fail to do justice to the author's diligent efforts. Notwithstanding this, the book is highly recommended for everyone interested in inorganic electron transfer reactions.

Rudi van Eldik
University of Erlangen-Nürnberg (FRG)

The Organic Chemistry of Aliphatic Nitrogen Compounds. (International Series of Monographs on Chemistry, Vol. 28.) By *B. R. Brown*. Clarendon Press, Oxford, 1994. 767 pp., hardcover £ 145.00.—ISBN 0-19-855783-3

The author's aim in this well set out work was to provide a comprehensive survey of the organic chemistry of classical nitrogen compounds. The title is intended to indicate that heterocyclic systems are not in general covered, although aziridines and β-lactams are in fact included. The 22 chapters deal in varying degrees of detail with the following compound types: amines (Ch. 1), enamines and ynamines (Ch. 2), imines, iminium salts, ketenimines, and keteniminium salts (Ch. 3), nitriles, together with acyl nitriles and trimethylsilyl cyanide (Ch. 4), *N*-oxides, nitrones, and nitrile oxides (Ch. 5), isonitriles (Ch. 6), cyanates, isocyanates, and their sulfur analogs (Ch. 7), amides (especially dimethylformamide and its acetals), thioamides, carbamates, and sulfonamides (Ch. 8), urea derivatives and carbodiimides (Ch. 9), amidines (Ch. 10), nitro and nitroso compounds (Chs. 11 and 12, respectively), diazoalkanes (Ch. 13), hydroxylamines and oximes (Ch. 14), hydrazines (Ch. 15), azo and azoxy compounds (Ch. 16), azides (Ch. 17), nitrates, nitrites, and nitramines (Chs. 18 and 19), β-aminoalcohols (Ch. 20), aziridines (Ch. 21), and β-lactams (Ch. 22).

The main emphasis is on the synthesis of the various classes of compounds, including details of several reactions in each case, although these are not always the most important from a preparative standpoint. Each chapter begins with a very brief description of the structural properties of the compounds under discussion. Not all these introductions reflect the latest research results, and the selection of original papers that are cited is often idiosyncratic and sometimes incomplete. The frequent use of the abbreviation "F. & F." betrays the fact that the principal literature source used was the standard work by Fieser and Fieser. Altogether there are more than 1800 literature citations, mainly from the period 1960–1985. More recent citations (up to 1990) are found only occasionally. Some important original publications by well-known contributors to the field of nitrogen chemistry, such as Arnold, Böhme, and Viehe, are noticeably absent. By providing better coverage of recent reviews (including at least references to the *more recent* volumes in the Patai series), the author could have made it easier for the reader to gain access to the original literature. Moreover, the many typographical errors in authors' names, some of which are quite grotesque, are an annoying distraction.

The book is provided with a comprehensive subject index, but some random tests indicate that it does not always give the interested reader the required information. For example, the chapter on

This section contains book reviews and a list of new books received by the editor. Book reviews are written by invitation from the editor. Suggestions for books to be reviewed and for book reviewers are welcome. Publishers should send brochures or (better) books to Dr. Ralf Baumann, Redaktion Angewandte Chemie, Postfach 101161, D-69451 Weinheim, Federal Republic of Germany. The editor reserves the right of selecting which books will be reviewed. Uninvited books not chosen for review will not be returned.

enamines includes a section devoted to 1-chloro-*N*,*N*-2-trimethylpropenylamine, which is correctly described as having reactions typical of a keteniminium salt; however, this fact is not mentioned in the index, nor in the chapter on keteniminium salts. To give another example, the Vilsmeier reagent appears in the chapter on iminium salts, but its reactions are covered in the chapter on dimethylformamide, with no cross-reference. Inconsistencies of this kind make it rather difficult to use the book. Regrettably, the author (who died in September 1992) was unable to complete the manuscript himself.

I have some reservations about recommending that one should buy this book. It undoubtedly offers a clearly written and well illustrated guide to a wealth of interesting literature on nitrogen chemistry. However, as it is not very up-to-date and because of the shortcomings mentioned above, it can only serve as an introduction to the field and—with some reservations—as a reference source. As one would expect, it is not an alternative to the more comprehensive standard works such as "Houben-Weyl" and "Patai".

Ernst-Ulrich Würthwein
Institut für Organische Chemie
der Universität Münster (FRG)

Talking Back to Prozac: What Doctors Aren't Telling You about Today's Most Controversial Drug. By *P. R. Breggin* and *G. R. Breggin*. St. Martin's Press, New York, 1994. XIV, 273 pp., hardcover $ 19.95.—ISBN 0-312-11486-9

Audiatur et altera pars! (Let the other side also be heard!) In many ways this book is the mirror image of Peter D. Kramer's controversial best-seller *Listening to Prozac* (Viking, 1993; for a review see G. B. Kauffman, *American Scientist* **1995**, *83*, 90–91). Both books were written by practicing psychiatrists; both deal with the mechanism of operation of antidepressants, particularly the class of selective serotonin reuptake inhibitors (SSRIs) to which Prozac, hailed by many as the antidepressant drug of choice of the 1990s, belongs; both recount the development and testing of Prozac and present detailed personal case studies and accounts of positive and negative effects of the drug; both consider the ethics of administering the drug as a "mood brightener", what Kramer himself called "cosmetic psychiatry"; and both, although replete with extensive documentation, were written for a popular audience. But here the similarity ends.

Peter R. Breggin, M.D., who wrote the first medical books on the brain-damaging effects of electroshock and psychiatric drug treatment, is a leading medical critic of biological psychiatry. His efforts at reform have included numerous articles and books, and U.S. media appearances on "Sixty Minutes," "20–20", and "Dan Rather Reports". His wife, Ginger Ross Breggin, is Director for Research and Education at her husband's non-profit Center for the Study of Psychiatry and is his coauthor of the forthcoming book, *The War Against Children*, a critical examination of the growing psychiatric movement to increase medication of pre-school children and minorities, with Prozac joining Ritalin as the drug of choice. Dr. Breggin, who has been called "the conscience of American psychiatry", states: "I wrote *Talking Back to Prozac* because of my compassion for the hundreds of thousands of people who suffer from depression, and for the many people who are being misled by the current emphasis on antidepressants as safe and effective treatments." He claims to be "one of the few psychiatric drug experts in the country without ties to the pharmaceutical companies, and can therefore speak openly about Prozac."

The Breggins' book is an urgently needed antidote to Kramer's book, which, they state: "has misled hundreds of thousands of readers and millions more who have heard its message of better living through chemistry." The Breggins argue that Kramer "bases his theory of Prozac-induced personality transformation on nothing more than a handful of his own cases, ... shows a naive reliance on the manufacturer of Prozac, Eli Lilly, in his discussion of the drug's impact on the brain, ... shows too little awareness of the pharmacological mechanisms that could cause the opposite of Prozac's intended effect, ... gives no credence to the Prozac survivor movement, ... [and] sprinkles his book with moral considerations, but does not seem to take them seriously."

In contrast to most books about psychiatric drugs, which provide the kind of information drug advocates and pharmaceutical companies want the public to have, the Breggins' book "provides information not readily available, even to most experts in the field, much of it ... systematically withheld from physicians and patients alike." Among other topics, they discuss in detail: the supposed selectivity of Prozac; the fact that Prozac was tested in trials of only four to six weeks before receiving U.S. Food and Drug Administration (FDA) approval; the difficulty that Eli Lilly had in proving its efficacy during these tests; the side effects that the FDA failed to include in its final labeling requirements; Prozac's short-term and long-term impacts on the brain; how Prozac acts as a stimulant similar to the addictive drugs cocaine and amphetamines; the economic and political forces ("the medical-industrial complex") backing promotion of the drug; the dangers of possible Prozac addiction, abuse, and withdrawal symptoms; the seriousness and frequency of Prozac's side effects; the growing evidence from case study after case study that Prozac can cause violence and suicide; the avalanche of lawsuits against Eli Lilly involving Prozac; and the social and workplace implications of using drugs, not to cure depression, but to change personality and enhance performance.

The authors also disclose the intricate web of cozy connections between the FDA, the drug companies, and the psychiatric community (what they call the "psycho-pharmaceutical complex"); the close ties that existed between Eli Lilly and both former U.S. President George Bush and former U.S. Vice-President Dan Quayle; and the FDA ban on the food supplement L-tryptophan, which forces people to use SSRIs instead. They decry the flooding of the country with propaganda in favor of taking drugs—"a technological shortcut for people who want to find their real personalities the fast-food way"—for conditions such as depression, which, in many cases, may be part of the human condition and a normal concomitant of an empathic life. They explore the positive side of depression and state: "To the degree that a human being is capable of suffering deeply, to that same degree the human being is capable of a full, rich, exciting, and creative life." They describe the resounding success achieved by more humane non-drug alternatives to the "National Prescription Drug" for the treatment of depression. In their copious notes the Breggins provide an extensive bibliography listing every author, article, or project mentioned in the book, and in the appendix they give useful information about the Psychiatric Reform Movement and the Prozac Survivors Support Group, including addresses and telephone numbers. They also provide a form and full directions for filing an adverse drug reaction report with the FDA.

This fact-packed book is a gold mine of valuable data for practicing scientists, science educators, pychiatrists, historians of science, policy makers, and those concerned with the relations between government regulatory agencies and pharmaceutical companies. On a more personal level,

 © VCH Verlagsgesellschaft mbH, D-69451 Weinheim, 1995 0570-0833/95/1111-1250 $ 10.00+.25/0

it is intended for anyone taking Prozac, considering taking it, or wanting to stop taking it, as well as for the families and physicians of anyone suffering from depression. It deserves to be as well known as or even better known than Kramer's book, which has received an incredible amount of publicity. Because the two books are complementary, they should be read together. Caveat aeger! (Let the patient beware!)

George B. Kauffman
Department of Chemistry
California State University
Fresno, CA (USA)

Synthesis of Sulphones, Sulphoxides and Cyclic Sulphides. Edited by *S. Patai* and *Z. Rappoport*. Wiley, Chichester, 1994. 720 pp., hardcover £ 175.00.—ISBN 0-471-93970-6

The book reviewed here belongs to the series *The Chemistry of Functional Groups*, which began over 30 years ago and is of great importance to synthetic chemists. As noted by the editors in the preface, this volume is the last in the current series of updated versions. It contains seven chapters by well-recognized authors, dealing mainly with synthetic aspects of open-chain and cyclic sulfones and sulfoxides, as well as cyclic sulfides. Three of the chapters (Ch. 1: "Synthesis of Open-Chain Sulfones", by K. Schank; Ch. 3: "Synthesis of Sulphoxides", by J. Drabowicz, P. Kielbasinski and M. Mikolajczyk); Ch. 5: "Cyclic Sulfones and Sulfoxides", by U. Zoller) are identical with Chapters 7–9 of the volume *The Chemistry of Sulphones and Sulphoxides*, published in the same series in 1988 (review: J. Voss, *Angew. Chem. Int. Ed. Engl.* **1989**, *28*, 1070). The latest developments in these areas (since 1986) are covered in the form of appendices (Chapters 2, 4, and 6). These follow the same structure as Chapters 1, 3, and 5, and the numbering system for the reaction equations, tables, and literature references continues directly on from the preceding chapters, so that one can easily compare the two and quickly find out about the latest research. The literature up to 1992 is covered thoroughly, extending in some cases up to early 1993. The lengths of these "appendix" chapters are clear evidence of the rapid developments in the last few years on many aspects of the chemistry of sulfones and sulfoxides. This is seen especially in Chapter 4, which is largely concerned with the use of chiral sulfoxides for asymmetric syntheses. All the authors have aimed at a concise but well-balanced treatment. Unavoidably, the monograph *Sulphones in Organic Synthesis*, by N. S. Simpkins, published in 1993 by Pergamon Press, appeared too late to be cited in the bibliography.

The last chapter, "Cyclic Sulfides", by G. Capozzi, S. Menichetti, and C. Nativi, seems to me to be of special importance and a very welcome part of this book for several reasons. Firstly, cyclic sulfides are in many cases indispensable precursors for the synthesis of cyclic sulfoxides and sulfones, reactions for which a wide variety of effective oxidizing agents for different situations are now available. Secondly, the most important characteristic properties of sulfur heterocycles with three- to eight-membered rings, mainly saturated, are here summarized in a single chapter. The authors have concentrated mainly on developments since 1980, while not neglecting earlier results of fundamental importance. In addition the comprehensive bibliography to this chapter (698 references) allows rapid access to earlier publications.

A minor point, but one that is unusual in a monograph, is that the authors have each been allowed to use their preferred spellings "sulphur" or "sulfur" in the names of the compounds discussed.

The volume contains a total of 3037 literature references and has carefully prepared author and subject indexes, which contribute to giving it the true quality of a handbook. It will be an extremely useful source of information, not exclusively for "sulfur chemists", and should therefore be available in every chemistry library.

Eberhard Wenschuh
Berlin (FRG)

Carbon-13 NMR Chemical Shifts in Structural and Stereochemical Analysis. (Series: Methods in Stereochemical Analysis. Series editor: *A. P. Marchand.*) By *K. Pihlaja* and *E. Kleinpeter*. VCH Publishers, New York, 1994. 379 pp., hardcover DM 150.00.—ISBN 0-89573-332-3

In the early 1970s, when ^{13}C NMR spectroscopy was approaching its full maturity, the effects of substituents on chemical shifts (substituent chemical shifts—SCSs) were important as an empirical aid in the interpretation of spectra, and thus in determining the structures of organic molecules. Since that time the importance of empirical correlations has declined as new one-dimensional and multi-dimensional experimental techniques have become available. These yield "hard" information (e.g., on scalar spin–spin couplings or on the nuclear Overhauser effect), making the "softer" information based on chemical shift considerations largely superfluous. This is a welcome development, as it puts structure determination onto a firmer basis and reduces the necessity for interpretations that rely on probabilities. Therefore, one might well ask whether it is still appropriate to bring out a book such as this one by the Finnish-German team of Pihlaja and Kleinpeter, which aims to stimulate an interest in ^{13}C NMR chemical shifts and to convince the reader of the usefulness of such data in structural analysis. The answer to the question is a definite yes, because the book is mainly concerned with the stereochemical aspects of ^{13}C chemical shifts, and the most recent major reviews on this subject appeared a considerable time ago, for example the articles in *Topics in Stereochemistry* by Wilson and Stothers in 1974 and by Duddeck in 1986.

The introductory chapter deals with practical considerations, including a discussion of the assignment of ^{13}C NMR spectra. The advice given to the reader seems somewhat arbitrarily chosen; the tips are occasionally trivial (e.g., "peak picking is strongly recommended"), and owing to the shortness of the chapter its value is rather limited. There is an error on page 2, where it is stated that the improvement in signal-to-noise ratio using quadrature detection compared with single-phase detection is a factor of $\sqrt{n}$ (where n is the number of accumulations); the correct factor is $\sqrt{2}$. In the section on "Referencing the Spectrum" it is of little help to give only the chemical shifts of undeuteriated solvents, and the information that deuterium isotope effects can be as large as 1 ppm does not improve matters. In the spectra shown in Figures 1.5 and 1.6 the numbering of the peaks does not entirely correspond to that in the structural formula. The list of literature references for Chapter 1 contains many errors, especially in the names of authors, which will immediately catch the reader's eye without even having to look up the references: "Breitmeier" for Breitmaier, "Hull" for Hill, "Schoolery" for Shoolery, "Bedall" for Bendall, "Submarian" for Subramanian, and so on. The references attached to the later chapters also show a lack of care.

The short second chapter deals in a general way with additivity relationships for SCSs (and deviations therefrom), and with the use of SCSs in structure determination and stereochemical assignments. Chapter 3 then discusses in greater detail

 © VCH Verlagsgesellschaft mbH, D-69451 Weinheim, 1995 0570-0833/95/1111-1251 $ 10.00+.25/0

how SCSs (classified according to the effects of monosubstitution at α, β-, γ-, and δ-positions, vicinal disubstitution, polysubstitution, and buttressing effects) are related to molecular constitution and geometry. The arrangement of the subject matter in this chapter is not always ideal. In Chapters 4 (A–C) and 5, which form the major part of the book, the authors discuss in detail the ^{13}C chemical shifts for alicyclic compounds with four to seven atoms in the ring and for heterocyclic compounds with boron, nitrogen, oxygen, phosphorus, and sulfur as the heteroatom. An impressive amount of information is collected together in these chapters. The choice of material reflects the authors' research interests to some extent; for example, it contains a substantial collection of 54 methyl-substituted tetrahydro-1,3-oxazines (with up to five methyl groups) from Pihlaja's laboratory. The best part of the book in my opinion is Chapter 5, dealing with ^{13}C chemical shifts as probes for configurational and conformational analysis. Examples from a wide variety of compound types are discussed, showing how ^{13}C NMR spectroscopy is able to give answers to many different questions of stereochemistry. These include *endo/exo* isomerism in annelated norbornanes, configurations of diastereomeric pyranoses, conformations of hydroanthracenes and hydrophenanthrenes, configurations of olefins, conformational equilibria in cyclohexane derivatives and their hetero-analogs, steric perturbation of conjugated systems, stereochemically relevant deuterium isotope effects, relative configurations in compounds with several chiral centers, absolute configurations in chiral ketones and secondary alcohols, and conformations and tautomerism in the solid phase. The book is completed by three rather short chapters: one on dynamic ^{13}C NMR spectroscopy, one on configurational and conformational studies of natural products, organometallic compounds, and synthetic polymers, and a third on additional NMR parameters (δ_H, J_{HH}, J_{CH}, NOE, T_1) that can be combined with ^{13}C chemical shift data to yield information about configurations or conformations. Finally there is a fairly comprehensive subject index, but no author index.

This is in itself a very useful work, but as well as the defects already mentioned there is one more, which should not be exaggerated but nevertheless deserves to be mentioned. There were some long sections (probably written by only one of the two authors) in which I found the style very irritating. Typical faults were a lack of clarity, unnecessarily complicated sentence constructions, and occasionally modes of expression that might have been used in musty offices long ago. Moreover, the impression persists that in the translation (self-translation?) from this author's mother tongue into English there has been some sacrifice of clarity, which could put the reader into a state of "selective excitement" (quoted from p. 19). A more thorough language-polishing job by the publishers would have improved the book. When I read out some selected passages to an English colleague he found them incomprehensible. I will avoid prolonging this review by quoting examples. In fairness it must be added that the reader's irritation with these passages will quickly subside on reaching parts of the text that are clearly the work of the other author. I recommend that one should consider buying copies of this book by Pihlaja and Kleinpeter for the departmental library and/or for the NMR laboratory.

Ludger Ernst
NMR-Laboratorium der
Chemischen Institute
Technische Universität Braunschweig
(FRG)

Free Atoms, Clusters, and Nanoscale Particles. By *K. J. Klabunde*. Academic Press, London, 1994. 311 pp., hardcover DM 177.00.—ISBN 0-12-410760-5

Fourteen years after the appearance of the monograph *Chemistry of Free Atoms and Particles* (Academic Press, 1980), in which the fundamentals of the generation and use of such species were presented for the first time, a second monograph on the subject has appeared from the same author, well known as one of the pioneers in this area. The current state of development in the chemistry of high temperature (HT) particles is presented in this volume.

After the initial rapid development phase of this chemistry in the 60s and 70s, in which the main emphasis was on matrix isolation studies and later increasingly on the molecular chemistry of such highly reactive particles, interest has now turned to new topics during the 80s and early 90s. In addition to the use of free atoms as synthetic building blocks in complex and organometallic chemistry, *Free Atoms, Clusters and Nanoscale Particles* also deals with studies of naked and ligand-stabilized (metal) clusters and particles. In addition to these main themes, the author, as hinted at in the title, devotes particular attention to the synthesis of new materials in the nano range by the use of free atoms and particles, as well as the study and characterization of the frequently unusual material properties of the nanoparticles thus prepared.

With regard to the organization of material, the author retains the trusted classification used in the earlier book mentioned above. After a brief introduction to the chemistry of highly reactive particles (first chapter), the second chapter (the only one that is completely new) deals with techniques and apparatus added since 1980 to the synthetic arsenal for the generation of free (metal) atoms, (metal) clusters, and also heterogeneous metal catalysts. In the whole section the reader is introduced, with the help of clear and precise diagrams, to the construction and mode of operation of the apparatus for the generation of these species. Thus, for example, the *S*olvated *M*etal *A*tom *D*ispersion (SMAD) technique for the preparation of supported heterogeneous catalysts is discussed in detail. Then, in 280 pages and eight chapters, subdivided according to the periodic system of the elements (Groups 1 and 2, 3–7, 8–10, 11, and 12, 13, 14, 15, and 16, together with lanthanides and actinides), the author discusses the chemistry of the individual HT species of the respective elements. Each chapter concludes with a summary of the relevant literature. Within the individual chapters there is a further subdivision into free atoms, free clusters, and molecular species of the elements in question. Each chapter closes with a generally brief report on the generation and properties of thin films of the elements in the group. In particular the first two subdivisions are further subdivided into a) preparation and occurrence, b) physical properties, and c) chemical reactions of these species.

The fact that the organization of the contents is almost identical to that in the earlier book—*Chemistry of Free Atoms and Particles*—might lead the reader to suspect that the work has only been superficially brought up to date. However, that is clearly not the case. The collection of almost 1300 references, mainly from the period 1980–1993, of which only a tiny portion appeared in the first work, refutes this impressively and, in addition, shows the amount of work that has gone into preparing the references. In particular, researchers active in the area of highly reactive particles will find a highly valuable source and reference for their own work in the detailed literature references in the individual chapters. The literature citations will provide those entering the field of HT

 © VCH Verlagsgesellschaft mbH, D-69451 Weinheim, 1995 0570-0833/95/1111-1252 $ 10.00+.25/0

particles as newcomers with a survey of almost the whole range of topics covered during the period 1980–1993.

In spite of the extensive literature references in the individual chapters, a few important investigations are unfortunately missing. Two examples from organometallic chemistry and heterogeneous catalysis will illustrate this. Thus, there is no reference in Chapter 3 to the preparation of sterically hindered Group II metallocenes by the use of atomic alkaline earth elements such as $Ca(^0)$, $Ba(^0)$, and $Sr(^0)$ (year of publication 1986). Similarly, in Chapter 10, there is no reference to investigations into ethene dimerization on heterogeneous $Sm(^0)$ and $Yb(^0)$ catalysts prepared according to the SMAD method (published 1989).

With regard to the content, in each of the eight chapters in the book the new developments within the individual areas of the main- and sub-groups of the Periodic Table are described concisely, but in sufficient detail where appropriate. The author avoids detailed repetition of topics that have already been adequately covered in the earlier work, referring the reader to that instead.

Chapter 8 (hydrocarbon groups) is the one that has been extended most in comparison with the earlier work. The reason for this is the newly added treatment of fullerenes, in which their preparation, bonding characteristics, and chemistry are discussed. The concise overviews on physical and spectroscopic studies of fullerenes, the preparation of fullerenes with encapsulated metal atoms (endohedral fullerenes), and the compilation of properties of thin films generated from C_{60} and C_{70} fullerenes, given in clearly arranged tabular form and again presented with a multitude of useful literature citations, are extremely useful. However, I feel that the reactions of fullerenes, in so far as they do not directly involve HT processes, could have been omitted without compromising the topicality of the book in this area. The reader who needs a more detailed account of the chemistry of the fullerenes can make use of the specialist monographs devoted to this topic.

The remaining criticisms are limited to a few formal matters. Thus, it is evident that the index is incomplete for efficient use of the book, because the organization is too brief to allow specific points to be found quickly or even at all. A little more detail in this respect would have helped the book a great deal. Also, although collecting the literature references together at the end of each chapter has some merits, it has the disadvantage that cross-references are difficult to follow up without tedious searching through the volume.

Regarding the visual presentation, it is a pity that most of the molecular structures, in particular those of the complex compounds presented, convey no spatial or perspective impression of the molecules. This is particularly evident in Chapters 4 ("Early Transition Metal Elements") and 5 ("Late Transition Metal Elements").

In spite of these rather formal criticisms, the reviewer has an overall positive impression of the book. It is a successful account of the developments in the chemistry of HT species, starting from 1980 up to the most recent past. In addition, it represents the sole currently available up-to-date summary of this topic. Using it in combination with the author's earlier monograph, one has an overview both of the basics and of the most recent developments and trends in the chemistry of HT species, which can be expressly recommended without hesitation to everyone interested in this area.

For the researcher already working on the chemistry of HT particles, *Free Atoms, Clusters and Nanoscale Particles* will, exactly as its predecessor—*Chemistry of Free Atoms and Particles*—quickly become an indispensable compendium on the chemistry of HT particles, despite of the rather high price. For the newcomer who wants a compact overview of this special area, the high price will discourage personal purchase, so that for this group of potential users the monograph may only be available by way of a well-stocked library.

Jörg J. Schneider
Institut für Anorganische Chemie
der Universität-Gesamthochschule
Essen (FRG)

Vibrational Spectroscopy in Supercritical Fluids: From Analysis and Hydrogen Bonding to Polymers and Synthesis**

Martyn Poliakoff,* Steven M. Howdle, and Sergei G. Kazarian

Supercritical fluids are beginning to be used widely in chemistry. Applications range from extraction and chromatography in analytical chemistry to solvents for reaction chemistry and preparation of new materials. Spectroscopic monitoring is important in much of supercritical chemistry, and vibrational spectroscopy is particularly useful in this context because the vibrational spectrum of a given molecule is usually quite sensitive to the environment of that molecule. Thus, vibrational spectra are excellent probes of conditions within the fluid. In this review, we describe a variety of techniques and cells for IR and Raman spectroscopy in supercritical fluids and illustrate the breadth of applications in supercritical fluids. The examples include: the use of supercritical Xe as a spectroscopically transparent solvent for chemistry and for supercritical fluid chromatography with FTIR detection of analytes; Raman spectroscopy as a monitor for gases dissolved in supercritical CO_2; the effect of solvent density on hydrogen bonding in supercritical fluids and the formation of reverse micelles; IR as a monitor for the supercritical impregnation/extraction of polymers and the reactions of organometallic compounds impregnated into polymers; reactions of organometallic compounds in supercritical fluids; and finally, the use of miniature flow reactors for laboratory-scale preparative chemistry. Overall, our aim is to provide a starting point from which individual readers can judge whether such measurements might usefully be applied to their own particular problems.

Keywords: analytical chemistry · IR spectroscopy · photochemistry · Raman spectroscopy · supercritical fluids

1. Introduction

Supercritical fluids are currently the subject of major research projects in both academic and industrial chemistry.[1] The fluids have already had a significant impact on traditional analytical chemistry[2] and may well transform wide areas of chemistry. The systematic study of supercritical fluids is therefore a matter of both urgency and interest.

In its broadest sense, the term supercritical fluid can be applied to any gas that is compressed to a pressure greater than its critical pressure, p_c, and heated to a temperature above its critical temperature, T_c (Table 1). In practice, the definition is generally restricted either to gases close to their critical temperatures or, if the temperature is far above T_c, to those gases compressed to densities close to their critical densities, ρ_c. The behavior of such gases is so far from ideal that supercritical fluids have been a source of continuing scientific interest since the middle of the nineteenth century. In recent years, this interest has been significantly increased by the possibility of using supercritical fluids for a wide range of extraction processes and chemical reactions, applications which exploit the almost counter-intuitive power of supercritical fluids to dissolve solid substances.[1] The result has been a general shift in focus of research

[*] Prof. M. Poliakoff, Dr. S. M. Howdle
Department of Chemistry, University of Nottingham
Nottingham, NG7 2RD (UK)
Telefax: Int. code + (115) 951 3563
e-mail: Martyn.Poliakoff@Nottingham.ac.uk
Present address:
Dr. S. G. Kazarian
Georgia Institute of Technology
Atlanta, GA 30332-0100 (USA)

[**] Throughout this review the abbreviation sc is used to indicate the supercritical state, for example $scCO_2$.

Table 1. Critical data for selected substances [a].

Substance	T_c/K	p_c/MPa	ρ_c/g mL^{-1}
Ar	150.9	4.898	0.536
CH_4	190.5	4.604	0.162
Kr	209.4	5.50	0.919
C_3H_4	282.3	5.041	0.214
Xe	289.7	5.84	1.110
C_2F_6	293.0	3.06	0.622
CHF_3	299.3	4.858	0.528
$CClF_3$	302.0	3.870	0.579
CO_2	304.1	7.375	0.468
C_2H_6	305.4	4.884	0.203
N_2O [b]	309.6	7.255	0.452
SF_6	318.7	3.77	0.735
H_2S	373.2	8.94	0.346
$C_2H_4(NH_2)_2$	593	6.27	0.29
H_2O	647.1	22.06	0.322

[a] For critical data of other substances, see the excellent compilation by Reid et al [112]. [b] **Safety warning**: N_2O has similar critical parameters and rather better solvent properties than $scCO_2$ but there have been reports [113] of potentially disastrous explosions when scN_2O has been used with even small amounts of organic compounds. Therefore, scN_2O should only be used with extreme caution.

from pure fluids to the behavior of more complex supercritical solutions. Traditionally, most investigations of supercritical fluids have involved macroscopic phenomena (phase changes, thermodynamics, etc) but the complexity of these mixtures has led to the need for more detailed information on a molecular level. It is the purpose of this review to show how vibrational spectroscopy, both infrared and Raman, is now providing molecular information relevant to a wide range of processes in supercritical fluids.

The application of vibrational spectroscopy to the investigation of supercritical fluids is relatively new. In this review, we outline the scope of the technique and highlight how it has been applied to problems of chemical interest. We also discuss the main technical problems and indicate how they have been overcome. Mostly, we consider fluids whose critical temperatures lie in the range close to room temperature (i.e. from scC_2H_4 with $T_c = 9\,^{\circ}C$ to $scSF_6$ with $T_c = 46\,^{\circ}C$) since these have had the widest impact on both synthetic and analytical chemistry.[1, 2] scH_2O is only briefly discussed, not because scH_2O is less interesting (it has considerable potential for the oxidation of toxic materials and environmental contaminants[3]) but because the high temperature and pressure ($T_c = 374\,^{\circ}C$ and $p_c = 218$ atm) render most of the technical problems quite different. Our review complements Buback's excellent summary of near-IR spectroscopy in supercritical fluids,[4] and the reader's attention is drawn to a number of recent multiauthored books[2, 5] which, together, constitute an excellent introduction to the current state of supercritical science and its applications to chemistry. In Section 2, we describe a number of designs of high-pressure cells for IR and Raman spectroscopy. Then, in Section 3, we describe the use of scXe as a solvent for both spectroscopy and chromatography and compare its properties with those of $scCO_2$. In Section 4, we outline the role of Raman spectroscopy and show how it can be applied to the study of supercritical fluid/gas mixtures. Sections 5–7 give an illustrative range of applications to hydrogen bonding (5), to polymers (6), and to organometallic chemistry (7). Finally, in Section 8, we show how IR spectroscopy is playing an important role in the development of laboratory-scale flow-reactors.



M. Poliakoff



S. M. Howdle



S. Kazarian

Martyn Poliakoff was born in 1947 in London (UK), studied chemistry at Cambridge University (BA, 1969) and received his Ph.D. for work on the matrix isolation of large molecules under the supervision of J. J. Turner, with whom he has subsequently had a long and productive scientific collaboration. In 1972 he moved to the University of Newcastle upon Tyne and in 1979 to the University of Nottingham, where he is currently Professor of Chemistry and holder of an EPSRC Fellowship in Clean Technology. For the past eight years his research has focussed increasingly on the chemical and analytical applications of supercritical fluids. He has been awarded the Meldola Medal (1976) and Tilden Medal (1990) of the Royal Society of Chemistry and has held a Nuffield Foundation University Fellowship (1988/9) and a Royal Society Leverhulme Trust Senior Fellowship (1993/4). He has longstanding scientific connections with Germany; Stipendiat of the Alexander von Humboldt Stiftung (Laserforschung in Garching), 1978 and 1979, and fruitful collaborations with the Max-Planck-Institut für Strahlenchemie, Mülheim, and the University of Würzburg.

Steve Howdle was born in 1964 in Rotherham, Yorkshire. He studied chemistry at the University of Manchester (1986) and then moved to Nottingham to study for his Ph.D. (1989) under the supervision of M. Poliakoff. For the next two years, he extended his Ph.D. work on chemical reactions in supercritical fluids, as BP Venture Research Fellow at Nottingham. In 1991, he was awarded a Royal Society University Research Fellowship, which he has held at Nottingham. Over the past three years, he has investigated the supercritical impregnation of polymers porous solids and his interests have broadened to encompass the preparation and characterization of biocompatible coatings. Recently, he and M. Poliakoff have built up a strong and extremely fruitful collaboration with research groups in Russia.

Sergei Kazarian born in 1958 in East Kazakhstan (USSR), studied physics at the Novosibirsk State and Yerevan State Universities. After completing his diploma in physics (1980) he moved into physical chemistry and received his doctorate in 1987 under the supervision of B. V. Lokshin at the Nesmeyanov Institute of Organoelement Compounds (Moscow) for the work on the interactions of transition metal complexes with proton donors in liquefied noble gases. In 1988, he moved to the Institute of Spectroscopy in Troitzk, where he continued this work. He spent six months at the Max-Planck-Institut für Strahlenchemie, Mülheim and from 1991–1994 he worked as Visiting Researcher in M. Poliakoff's group at the University of Nottingham (UK). Currently, he is a Research Associate with C. A. Eckert at Georgia Institute of Technology, Atlanta (USA). His research interests include the spectroscopic study of intermolecular interactions in liquid xenon, supercritical fluids, and polymers.

2. The Design of High-Pressure Cells

2.1. General Considerations

The design of the high-pressure cell needed for a particular IR experiment clearly depends on the nature of that experiment. Important points include the maximum operating pressure and temperature, the optical pathlength required, the particular range of the IR spectrum, which will restrict the choice of window material and, finally, whether the contents of the cell need to be stirred. There is also a number of more subjective questions: Are the measurements to be strictly quantitative? Is it likely the cell will have to be dismantled frequently (for example, to remove reaction products)?

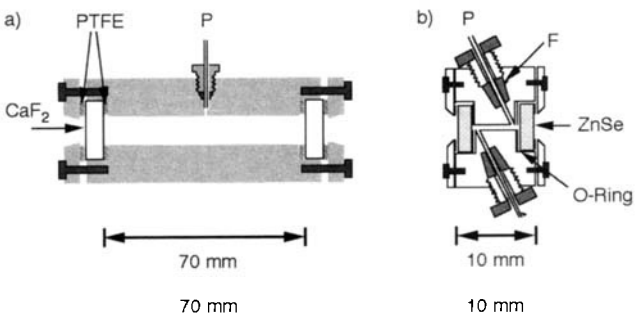
Although the pressures involved in experiments in supercritical fluids (usually less than 300 atm) are sometimes considered to be modest by those who specialize in "high-pressure" chemistry, the gaslike nature of the fluids impose quite severe constraints on the design of the cells. As far as we are aware, there are few, if any, cells which are commercially available. However, a considerable variety of designs for high-pressure cells for use with supercritical fluids have already been published[6] including some elegant designs in Buback's review.[4] All of these cells share a number of general features. Clearly, the cell has to be safe for high-pressure operation, there has to be at least one IR transparent window, although most designs accommodate two, and at least one port for filling/venting the fluid.

In general, the IR transparent windows are mechanically the weakest part of any cell and sealing these windows to the cell body is usually the most difficult engineering task. Sherman and Stadtmuller have provided a very detailed discussion of the design of high-pressure cells, although much of their book[7] is devoted to pressures greatly in excess of those required for supercritical fluids, and Whyman has reviewed the design of high-pressure IR cells for conventional solvents.[8] Both the book and the review discuss, in some detail, the safety margins needed for the IR windows. Three of the key parameters are the ratio of the total area of window to the unsupported area (i.e. the area through which the IR light passes), the thickness of the window, and the rupture modulus of the window material. By applying the appropriate formulae, one finds that surprisingly thin windows, only 2 or 3 mm thick, are required for miniature cells with very small unsupported areas, such as the chromatography cell shown in Figure 1b. All modern Fourier transform (FT) IR instruments have a circular IR beam profile so it is no longer necessary to use rectangular windows,[9] which improved the performance of high-pressure cells in older dispersive IR spectrometers. Even so, it should be borne in mind that most commercial suppliers have a range of standard diameters for IR windows and apparently minor changes in design can alter the cost of a cell disproportionately, depending on whether the windows are standard or non-standard sizes.

Sherman and Stadtmuller have described a number of approaches to the design of the pressure seal between optical windows and the cell body,[7] two of which are most appropriate for supercritical fluids. Both approaches work well but each has problems. The more straightforward approach, the "opposed force" method, involves sealing the cell body to the inner face of the window (i.e the face which is in contact with the fluid) with a gasket, O-ring, or similar. The main drawback is that windows often break during assembly; most window materials are brittle, and mechanical pressure must be applied to the window to make the seal. Supercritical fluids can cause swelling in some polymers and, in smaller cells, the swelling of polymer O-rings can be sufficient to shatter the windows. The alternative approach, the "Poulter" method, has been pioneered for liquefied gases by Bulanin in Russia.[10] This approach involves sealing a window on its planar outer surface; the internal pressure of the fluid then forces the window into the seal, and leaks are less frequent. However, it is often difficult with this design to avoid crevices and dead-volumes which can be more easily penetrated by supercritical fluids than by conventional liquids. Such crevices preclude quantitative measurements and, in evacuable cells, additional precautions are needed to prevent atmospheric pressure pushing the windows inwards away from their seals. We now describe a selection of cells that illustrate these general design principles.

2.2. Selected Cell Designs for IR Spectroscopy

The cell shown in Figure 1a was developed by Johnston and Kim for investigating solvatochromism and hydrogen bonding[11] (see Section 5). The pathlength is long (70 mm) because the cell is intended for use with dilute solutes in fluids (e.g. $scSF_6$ or $scCO_2$) which do not themselves absorb in the region of interest. Since the studies were to be quantitative, the overriding requirement was to eliminate dead volumes where undissolved solute might accumulate. Thus, the windows are sealed on their inside edges, and a mechanical stirrer is provided to ensure that the contents of the cell are homogeneous. An absence of dead volume is also a crucial requirement for the cell shown in Figure 1b. This cell, developed by Jenkins et al. is intended for FTIR identification of analytes separated by capillary supercritical fluid chromatography (cSFC,[12] see Section 3). The volumes of fluid involved in such a separation are very small, because the capillary is only 50–100 μm in diameter, so the internal volume of the cell has to be extremely small to preserve the separation of the analytes. At the same time, the optical



70 mm 10 mm

Fig. 1. Two high-pressure IR cells for use with supercritical fluids, both with windows sealed by the "opposed force" method. a) Schematic cross-section of a stainless steel cell designed by Johnston and Kim for studying solvatochromism and hydrogen bonding [11]. P = fill port; PTFE = polymer seals; CaF_2 = calcium fluoride windows. The cell has two electric cartridge heaters (not shown) embedded in the walls for raising the temperature of the cell. b) A brass cell for cSFC-FTIR measurements [12]. P = ports connected to a silica capillary tube (50 μm i.d.); F = graphite ferrule for sealing the capillary to the cell body; O-ring = Viton seals; ZnSe = zinc selenide windows. Note that the two parts of the Figure are drawn to different scales. The cell a) has an internal volume of about 5 mL, while cell b) has a volume of only 500 nL.

pathlength must be as long as possible to give increased sensitivity and good limits of detectability. The design is therefore a carefully engineered compromise between these conflicting requirements: Although the internal volume of the cSFC cell in Figure 1b is 500 nL, 10^{-4} times that of Johnston's cell,[11] the pathlength of the cell is 4.4 mm, that is only 1/16th of that of Johnston's. With appropriate beam condensing lenses on the cSFC cell,[12] the optical throughputs of the two cells are remarkably similar.

Figure 2 illustrates a completely different approach adopted by Smith and co-workers for the study of reverse micelles in supercritical and near-critical solution.[13] In this case, the optical pathlength needed to be short because the mixtures under

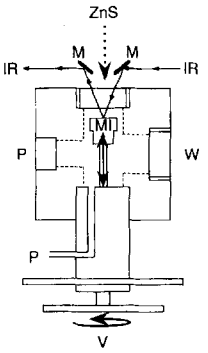


Fig. 2. Variable pathlength IR reflectance cell devised by Smith and co-workers. P = fill ports; IR = beam of FTIR interferometer; M = external mirrors; MI = internal mirror, which can be moved up and down to vary the pathlength by rotating the handle of the modified high-pressure valve V; ZnS = zinc sulfide window; W = observation window; from ref. [13].

study were highly IR absorbing but, at the same time, the vessel itself had to be relatively large so that the components could be properly mixed. The design satisfies these requirements in that the spectra are measured in reflectance rather than in transmission, with a single IR-transparent window and a highly polished steel mirror, which can be moved to adjust the optical pathlength. Although this design worked well for their particular experiments, quantitative measurements are quite difficult to make in such a cell because one has to correct for the effect of the light which is reflected from the outside face of the window without passing through the solution.

The three cells described so far were designed, at least initially, for very specific experiments. A much simpler and more general design is shown in Figure 3. This cell, developed at Nottingham, is specifically designed to be easy to dismantle and reassemble.[14] The windows are therefore sealed on their outer

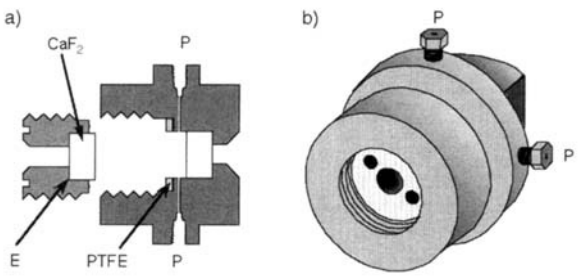


Fig. 3. Cross-section (a) and external view (b) of a stainless steel general purpose high-pressure IR cell. P = fill ports, threaded for standard 1/16th inch o.d. pipe fittings; E = epoxy resin, which is used to seal the CaF_2 windows (15 mm diameter, 10 mm thickness) by the "Poulter principle"; PTFE = principal seal between the two parts of the cell, which is made metal → metal. For further details, see ref. [14].

edges (one into the body of the cell and the other into the removable holder), and the main seal is made between metal surfaces and a PTFE spacer. Unlike the Smith cell (see Fig. 2), the pathlength cannot be varied during an experiment, but a selection of different pathlengths is available merely by using a number of different holders, each with the window held at a different depth. The simplicity of the cell means that it can easily be adapted for experiments as varied as impregnation of polymers (Section 6) or photochemistry of organometallic compounds (Section 7). The cell is however too small to allow effective stirring, although it can be used as a component of flow systems (see Section 8).

Any of these cells can be heated and varying the temperature of the fluid is frequently a key feature in supercritical experiments. It should, however, be remembered that even quite modest rises in temperature can cause substantial rises in pressure. In general, it is more difficult to cool IR cells than to heat them. The Russian cell designs, described in some detail by Bulanin[10] have usually included cooling, largely because the cells were primarily intended for spectroscopy in liquid solution at cryogenic temperatures. Figure 4 shows a relatively simple miniature

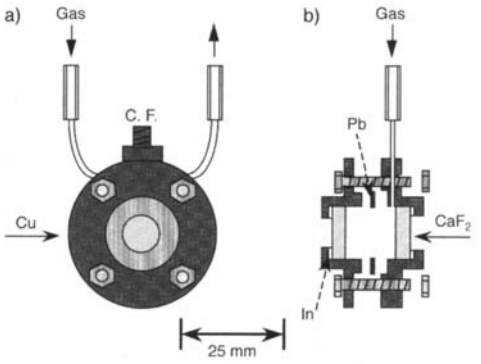


Fig. 4. External view (a) and cross-section (b) of a miniature high-pressure IR cell, made of copper and capable of being cooled to cryogenic temperatures. C. F. = mounting stud for cold finger of cryogenic cooler; In = indium metal which seals the CaF_2 window to the Cu cell body by the "Poulter Principle"; Pb = main lead seal between the two halves of the cell; ↑ and ↓ = gas fill ports.

high-pressure cell,[15] small enough to mount directly on a closed cycle-cryogenic cooler, and suitable for use in the temperature range 30–300 K. This design will allow fluids with a critical temperature T_c well below room temperature to be studied close to their critical points as well as at ambient temperatures.

2.3. Cells for Raman Spectroscopy

A number of IR cells have been based on high-pressure T- or X-pieces,[16] adapted so that the ports can take IR windows rather than pipes. This design approach has also been taken in the construction of cells for Raman spectroscopy, where the optical and geometric requirements are somewhat different from those of IR. Briefly, Raman experiments in supercritical fluids usually involve excitation of the sample by a focussed and relatively intense laser beam; the scattered light is then detected in a direction perpendicular to the laser beam. Raman scattering is a relatively weak effect and so this scattered light has to be

collected efficiently which is difficult to achieve in practice. Thus, the number of published Raman studies on supercritical systems is much smaller than that for the corresponding IR studies. Ben-Amotz and co-workers have designed an elegant cell with a single window;[17] the scattered light is collected at 180° to the incident laser beam. Although similar in concept to Smith's design for IR cells (see Fig. 2), the Raman cell does not require a mirror since Raman scattering occurs in all directions. A number of groups have used optic fibers to introduce the laser light and this considerably simplifies the Raman experiment. Figures 5a and b show two such designs; a) is a cell intended for

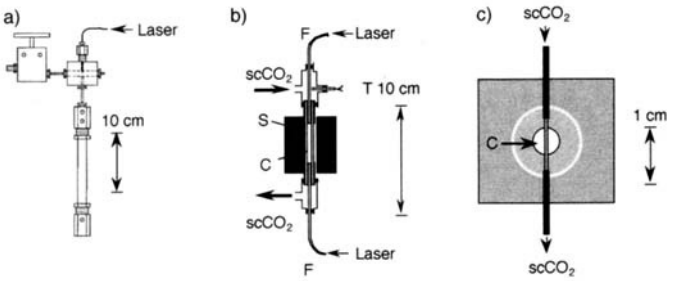


Fig. 5. Three high-pressure cells for Raman spectroscopy of supercritical fluids. a) Cell for studying reactions in scH_2O. The laser beam enters the cell through an optic fiber, and a parallel fiber is used to collect the scattered light; from ref. [18]. b) A cell, based on high-pressure capillary tubing, C, for Raman measurements with an Ar ion (visible wavelength) laser. The cell is mounted directly between the entrance slits S of the spectrometer. F = optic fibers for the input of laser light; T = thermocouple; $scCO_2$ = ports for the supercritical fluid (for more complete diagrams, see ref. [19]). c) Cell for FT Raman, based on a capillary, C, similar to that in Fig. 5b. The opaque polyimide coating of the capillary, (thick black bar) is removed at the point where the near-IR laser irradiates the cell (similarly, the coating is removed in cell b). The capillary is mounted directly in the holder supplied with the Perkin-Elmer System 2000 FT Raman instrument, which has a silvered reflector designed to optimize collection of the scattered light. (Note the different scales of the drawings of the three cells.)

experiments in scH_2O, fibers are used both for laser excitation and collection of the scattered light[18] and b) is a sub-miniature capillary cell,[19] devised by Howdle et al. for studying gases dissolved in $scCO_2$. Raman spectroscopy has distinct advantages over IR spectroscopy for experiments in scH_2O, largely because the fluid is highly absorbing over much of the range of the IR spectrum and so corrosive that most IR window materials are rapidly destroyed. The ultimate in simplicity is achieved by the cell for FT-Raman[20] shown in Figure 5c. This cell is made merely by removing the polyimide coating from standard silica capillary tubing of the type normally used for chromatography. The small diameter of these capillary cells ensures that the scattered light can be collected extremely efficiently and, furthermore, one does not need to worry about cleaning the cell since it is essentially disposable!

Safety Note: All of the illustrations in Figures 1 to 5 are purely schematic and should not be regarded as engineering drawings for the construction of safe high-pressure cells. Those wishing to build such equipment for themselves must carry out their own safety evaluation.

3. Supercritical Xenon

Ever since the classic work by Andrews on the critical point,[21] a huge proportion of the published research on super critical fluids has involved $scCO_2$, most recently because of its potential as an environmentally acceptable substitute for organic solvents in extraction and in synthetic chemistry.[1, 2] From the spectroscopic standpoint, $scCO_2$ has the distinct disadvantage that a number of key regions in the IR spectrum are completely obscured by absorptions of $scCO_2$ itself. This problem has led to considerable interest in liquefied and supercritical noble gases[10b] which constitute a unique set of solvents for spectroscopy, totally transparent throughout the spectrum from vacuum-UV to far-IR.

The first systematic IR studies in liquid noble gas solution were initiated in Leningrad by Bulanin and co-workers over 20 years ago.[10a] Their primary interests have centered on cryogenic noble gas solutions, an area which they have recently reviewed in some detail[10b, 22] but, as mentioned in Section 2, some of their cells had a sufficiently high-pressure rating (i.e. > 60 atm) to be used with supercritical xenon scXe. Maier et al. also developed the use of liquid noble gases in the USA but his equipment could not be used for supercritical fluids because it was not suitable for use at pressures above 20 atm.[9]

scXe is a fascinating material. Its critical temperature, 16.7 °C (see Table 1), is very close to ambient temperature, making scXe a convenient medium for investigations of the spectroscopic effects associated with the transition from the liquid to the supercritical state. The critical density ρ_c, $1.11\,g\,mL^{-1}$, is greater than the density not only of water but also of many common organic compounds, both liquid and solid. scXe is a moderately good solvent for nonpolar compounds and, although there have been few quantitative comparisons, the solubility in scXe is somewhat higher than in $scCO_2$, in at least some cases (e.g. polycyclic aromatic compounds).[23, 24] In general, the solvent properties of scXe are comparable to but not quite as good as those of hexane or other alkanes. scXe can therefore be used as a solvent for chemical reactions and for chromatographic separations. For a given compound, solubility is nearly always greater in scXe near room temperature than in liquid Xe (LXe) at cryogenic temperatures; this increase in solubility is probably due more to the higher temperature of the scXe rather than to some inherent solvent property of the fluid itself. Whatever its cause, the effect is substantial. For example, $[(\eta^6\text{-}C_6H_6)Cr(CO)_3]$ is virtually insoluble in LXe even at −30 °C, but usable concentrations can be obtained[25] in solution in scXe at 25 °C, even in the presence of "antisolvents" such as H_2 or N_2. As with other supercritical fluids, solubility of a compound in scXe at a particular temperature increases with increasing pressure and hence density. This property is a key factor in the use of scXe for chromatography[12, 23] but it can complicate some studies such as the investigation of hydrogen bonding (see Section 5).[16]

Liquid Xe (LXe) has been extremely successful as a solvent for studying weak intermolecular interactions,[10b] for example for proton donors,[22] or for stabilizing highly labile organometallic compounds.[26] This success largely derives from the cryogenic temperatures of LXe, a property which clearly cannot be matched by scXe, although scXe still retains the chemical inertness of LXe. Nevertheless, IR spectra of stable solutes reveal few differences between the properties of LXe and scXe. Some IR bands, for example, ν(C–O) vibrations of transition metal carbonyl compounds are significantly broader in

scXe than in cryogenic LXe, possibly a consequence of the lower viscosity of scXe. On the other hand, inherently broader bands,[27] for example the ν(H–H) band of $[W(CO)_5(\eta^2\text{-}H_2)]$, can have identical FWHM (full width half maximum) values in scXe at 25 °C and LXe at −90 °C. The transition through the critical point from LXe → scXe has almost no effect on some vibrational properties. For example, Moustakas and Weitz found[28] that the rate of vibrational relaxation of HCl ($v = 1 \rightarrow v = 0$) in Xe is unchanged on heating at constant density from 289 K (liquid phase) to 291 K (supercritical), possibly because bimolecular encounters HCl + HCl are not a major relaxation pathway.

In general, as shown in Figure 6, the IR bands of a particular solute in scXe are slightly narrower than the bands of the same

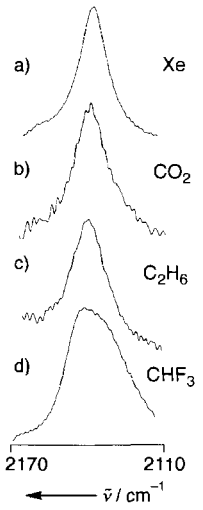


Fig. 6. Comparison of the IR bands of $[Cp^*Ir(CO)(H)_2]$ ($Cp^* = \eta^5\text{-}C_5Me_5$) dissolved in different supercritical fluids, all of which are doped with H_2: a) Xe, b) CO_2, c) C_2H_6, and d) CHF_3. In each case, $[Cp^*Ir(CO)(H)_2]$ was generated in situ by irradiation of $[Cp^*Ir(CO)_2]$ with UV light in the presence of H_2. The IR band illustrated is in the ν(Ir–H) region and corresponds to the unresolved a′ and a″ vibrations of the H-Ir-H moiety; from ref. [29].

solute dissolved in other supercritical fluids at the same temperature.[29] As might be expected the width of the bands is dependent on the polarity of the fluid; the broadest band in Figure 6 is observed in the most polar fluid CHF_3, although it is possible that some form of hydrogen bonding could be occurring in this case. The overriding advantages of scXe remain its inertness and its transparency (lack of absorption bands) which can transform IR spectroscopy into a surprisingly sensitive and versatile tool for structural chemistry. This transparency of scXe has also been a key factor in its use as a mobile phase for supercritical fluid chromatography (SFC).

SFC is a relatively specialized chromatographic technique that shares features of both gas and liquid chromatography (GC and LC). The techniques of SFC have been described in detail elsewhere[30] but in principle they are quite simple. In its capillary form (cSFC), separation occurs on a microbore silica column suitably coated on the inside surface with a stationary phase similar to that used for capillary GC. The supercritical fluid mobile phase flows down the column and then through an extremely narrow bore restrictor which throttles the flow of the fluid sufficiently to maintain a high pressure in the column. To carry out a separation, the fluid is made to flow through the column at a relatively low pressure and the mixture of analytes is injected onto the column so that the components partition between the mobile and stationary phases. The pressure of the fluid, and hence its density, is then gradually increased under computer control, and the various components of the mixture elute from the end of the column sequentially, with the most soluble compound eluting first. Thus, unlike GC, the whole separation is carried out isothermally and cSFC is particularly suited to separating thermally labile compounds of high molecular weight (e.g. polyglycerides).[31] One of the attractions of cSFC over LC is that one can use most of the detectors normally used for GC (i.e. FTIR, flame ionization, etc).[31a, 32] Such detectors are not easily used with LC because signals from the liquid mobile phase swamp those due to the analytes. cSFC-FTIR, therefore, offers excellent opportunities not only to separate but also to fingerprint the components of a complex mixture and Novotny and co-workers were the first to suggest that the IR transparency of scXe would make it preferable to $scCO_2$ as a mobile phase for cSFC-FTIR.[33]

The general requirements of a high-pressure IR cell for cSFC-FTIR were discussed in Section 2. The differences between the cell designs from different groups have lain in the volume and beam optics rather than in the overall concept but it is these differences which have determined the sensitivity and detection limits of the various cells.[12, 23, 34] The more sensitive cells can be used to record spectra "on the fly" so that spectra of all of the components in a mixture can be obtained in a single run.

Figure 7 shows a chromatogram for the separation of a mixture of polycyclic aromatic compounds (PAH) and the FTIR

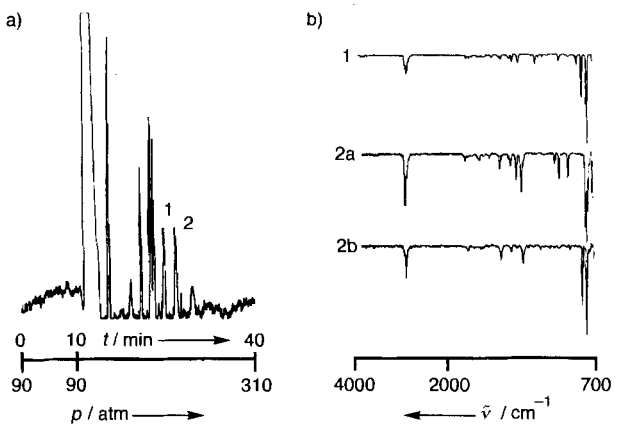


Fig. 7. cSFC-FTIR separation of a test mixture of eight polycyclic aromatic compounds (PAH) (10 mg mL^{-1} in CH_2Cl_2) using scXe as a mobile phase. a) Chromatogram, reconstructed from the total IR absorption spectrum; the first peak is due to the solvent CH_2Cl_2, and the other peaks are due to the different PAH compounds which elute from the column in order of increasing molecular weight. b) IR spectra corresponding respectively to peak 1 and to the leading (2a) and trailing edges (2b) of peak 2 of the chromatogram; the spectra are readily identifiable as those of chrysene (1), 9,10-diphenylanthracene (2a), and perylene (2b). Spectra were recorded in 15 s using the cell illustrated in Fig. 1b; from ref. [12].

spectra corresponding to some of the peaks.[12] In this case, the most characteristic bands of the different PAH compounds lie below 800 cm^{-1}, a region which is obscured in $scCO_2$ by absorptions of the CO_2 itself. On the other hand, the absorptions of CO_2 mask relatively limited regions of the spectrum (3800–3500, 2250–2100, and < 800 cm^{-1}, see Fig. 9a) and, for many compounds, spectra adequate for identification can be obtained with $scCO_2$ as eluent. A quite detailed comparison has been made between scXe and $scCO_2$ as mobile phases.[35] The conclu-

sion was that there are minor differences. Analytes do not necessarily elute in precisely the same order; the more polar analytes taking longer to elute in scXe than in $scCO_2$. There are modest shifts in the wavenumbers of IR bands of solutes as the density of the fluid is increased but the effect is similar in magnitude for both fluids. These shifts present problems when analytes are to be identified by matching the observed spectra against a library of spectra, which are unlikely to have been recorded under supercritical conditions.[36, 37] It seems, however, that particular classes of bands (e.g. ν(C–O) bands of ketones) all display comparable shifts and so it should be relatively simple to adapt the standard algorithms for library searching to allow for these supercritical shifts.

The sensitivity of the cSFC-FTIR method is surprisingly high and, outside the regions where $scCO_2$ absorbs, there is little difference between scXe and $scCO_2$. Using the cell illustrated in Figure 1b, the minimum detectable injected quantity of caffeine in $scCO_2$ is only 95 pg. and the cell gives a linear response over a wide range of concentrations[36] (Fig. 8). Over the past decade, the price of Xe has been highly volatile but, in recent years, the price has stabilized at a level which permits scXe to be used in the laboratory whenever cSFC-FTIR data are required over the entire region. cSFC columns have a very small volume and Cook and co-workers quote a usage of about 3 mL scXe per day[23] (although they did not define how many separations constituted a "day"). With larger scale usage, there is always the possibility of recycling the Xe, for example, as is done by Bulanin and co-workers.[10] Fortunately, cSFC-FTIR equipment can easily be switched between $scCO_2$ and scXe so that the chromatographer can choose the more appropriate mobile phase for a particular separation.

tection, there are some experiments where it is a distinct advantage, particularly those where the properties of pure fluids are to be probed. In such cases, the IR absorption bands associated with the fundamental vibrations of the molecules (CO_2, C_2H_6, etc) are so intense that extraordinarily short optical pathlengths would be needed for usable measurements. This difference can be seen clearly in Figure 9, where the Raman and FTIR spectra of $scCO_2$ are compared.

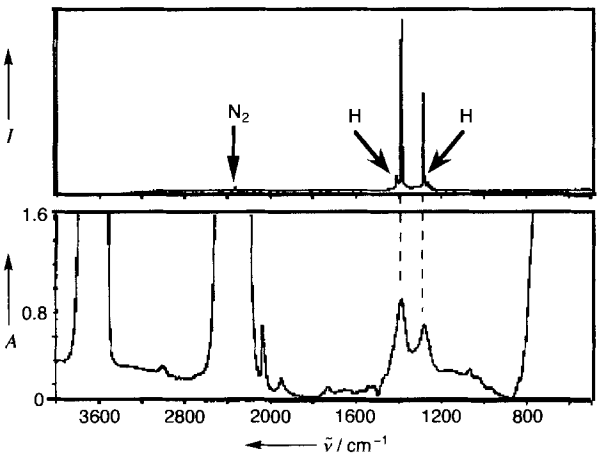


Fig. 9. Comparison of the FTIR spectrum (bottom) and the FT Raman (top) spectrum of $scCO_2$. The IR spectrum was recorded in the cSFC cell (Fig. 1b) at 250 bar pressure and ca. 32 °C with a 4.4 mm optical pathlength, while the Raman spectrum was recorded at ca. 100 bar pressure in the cell constructed from high-pressure capillary tubing (Fig. 5c). The dotted lines indicate the two Fermi resonance bands in the IR spectrum which coincide with the principal bands in the FT Raman spectrum. The two weak features, labeled H in the Raman spectrum, are due to hot bands, while the band labeled N_2 is due to atmospheric nitrogen in the light path of the FT Raman spectrometer.

4. Raman Spectroscopy in Supercritical Fluids

Raman scattering is a relatively weak effect compared to IR absorption. Although this weakness can create problems in detection, there are some experiments where it is a distinct advantage, particularly those where the properties of pure fluids are to be probed. In such cases, the IR absorption bands associated with the fundamental vibrations of the molecules (CO_2, C_2H_6, etc) are so intense that extraordinarily short optical pathlengths would be needed for usable measurements. This difference can be seen clearly in Figure 9, where the Raman and FTIR spectra of $scCO_2$ are compared.

There have been a number of Raman investigations where changes in either the contour or the position of Raman bands have been measured as a function of fluid density and these changes have then been related to the intermolecular interactions within fluids such as $scCO_2$,[38] scC_2H_6,[17] and recently, near-critical H_2S.[39] Figure 10 shows data obtained by Ben-Amotz et al. for C_2H_6 just below its critical point, a regime where the fluid compressibility is already anomalously high.[17] The data are striking because they show that the behavior of two vibrational modes of the same molecule can be substantially different under identical conditions. Nevertheless, their behavior can be modeled reasonably well by using a hard sphere model and the differences between the modes is ascribed to the fact that the ν(C–H) vibration is more polarizable than the ν(C–C). Ben-Amotz makes the interesting point that these differences might be reflected in a chemical reaction with two or more possible products. If branching in such a reaction were to involve sig-

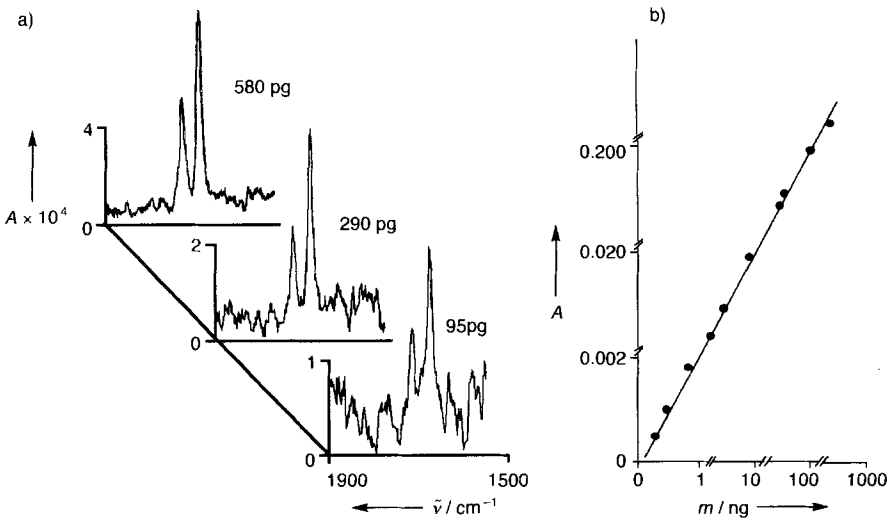


Fig. 8. a) Spectra illustrating the sensitivity of the cSFC-FTIR method with $scCO_2$ as the mobile phase and using the 500 nL IR cell illustrated in Fig. 1b. ν(C–O) region of the spectrum recorded for injections of solutions containing respectively 580, 290, and 95 pg of caffeine. b) Beer's Law plot (IR peak absorbance vs. injected concentration) for caffeine in $scCO_2$. Note that, somewhat unusually, both axes have been split so as to accommodate the very large range of concentration (95 pg–170 ng) on a single Figure; from ref. [36].

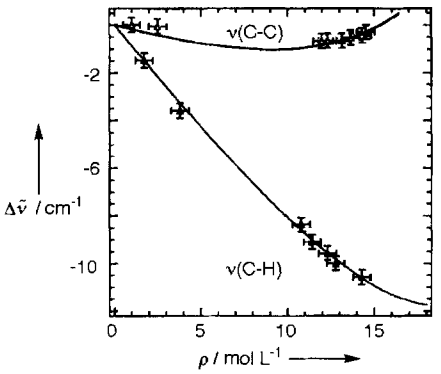


Fig. 10. The shifts in frequency $\Delta\tilde{\nu}$ of two vibrational modes with increasing density ρ of sub-critical C_2H_6 at 26 °C. The lines show the shifts computed with a hard fluid model; from ref. [17]

nificantly different vibrational coordinates, changes in fluid density might change the relative yields of the products. Density effects have been observed in a number of reactions, most dramatically for the photodimerization of isophorone,[40] but the changes in product distribution have been explained satisfactorily on the basis of solvation effects in bimolecular intermediates. Thus, Ben-Amotz's intriguing prediction remains to be verified experimentally.

An alternative approach to studying interactions is to use Raman spectroscopy to monitor bands of solute molecules dissolved within the fluid. The problem is one of sensitivity; relatively concentrated solutions must be used. Elegant Raman spectroscopic work has been carried out by Akimoto and Kajimoto in acetone and acetonitrile, both of which have quite high solubility in a variety of fluids ($scCO_2$, $scCF_3Cl$, etc).[41] They monitored the position of the $\nu(C{=}O)$ and $\nu(C{\equiv}N)$ bands as a function of fluid density and interpreted the shifts of these bands in terms of the solute–fluid interaction potential. In general, however, such studies are often easier to carry out by IR spectroscopy, as can be seen from the spectra in Figure 11, comparing the effects of scC_2H_6 and scC_2F_6 on the ν_2 (bending vibration) band of CO_2. These spectra were recorded by Yee et al. as part of an investigation[42] aimed at establishing whether the high solubility of fluorocarbons in $scCO_2$ (see Section 5) might be due to a strong $C{-}F\cdots CO_2$ interaction. However, the similarity of the spectra of CO_2 in scC_2H_6 and in scC_2F_6 shows that, in this case at least, there is no exceptional $C{-}F\cdots CO_2$ interaction.

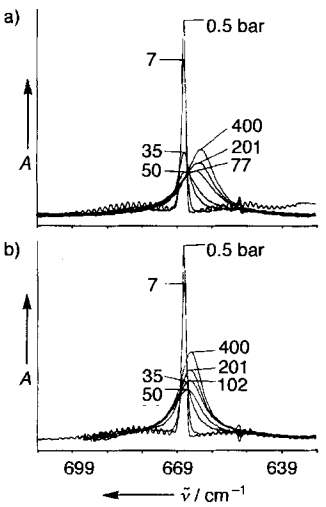


Fig. 11. IR spectra showing the effect of fluid pressure on the $\nu_2(O{=}C{=}O)$ bending vibration of CO_2 (0.02 M) in a) C_2H_6 and b) C_2F_6 from 0.5 bar (pure CO_2 gas) to 400 bar; from ref. [42].

Even a cursory glance at Figure 9 reveals the consequences of the centrosymmetric structure of CO_2 and the mutual exclusion principle of IR- and Raman-active bands; regions of the spectrum which are obscured by IR absorptions of $scCO_2$ (Fig. 9 bottom) are essentially free of bands in the Raman spectrum (Fig. 9 top). The only exception is in the region, 1400–1200 cm^{-1}, where two bands, formally forbidden in IR spectroscopy, become allowed at high pressures and are observed as relatively weak, pressure-dependent absorptions. (The presence of these two bands can cause some difficulty in cSFC-FTIR with $scCO_2$ as the mobile phase but the bands can be removed from the spectra of the analytes by the appropriate computer subtraction of "blank" spectra of $scCO_2$ itself.[36]) A detailed FTIR study[43] of these bands has recently been published. The advantage of mutual exclusion can be seen in the Raman spectrum of naphthalene in $scCO_2$ (Fig. 12), which shows two bands in a region which would be obscured in the IR spectrum.[19] Unfortunately, the low sensitivity of most Raman experiments means that spectra of solutes can only be recorded in relatively concentrated solutions. A more detailed Raman study[44] of naphthalene/$scCO_2$ was carried out by Zerda et al. who deduced from the shifts in the wavenumbers of three different bands of naphthalene that there was a modest anisotropic interaction between naphthalene and CO_2. Their calculations suggested that this interaction might be due to the quadrupole–quadrupole $CO_2/C_{10}H_8$ interaction ($U^{QQ} = 19.1$ kJ mol^{-1}) shown in **1**. These conclusions have been supported by recent MINDO/3 calculations from Dean and co-workers.[45]

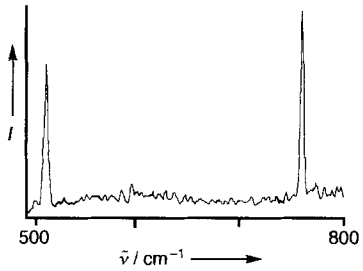
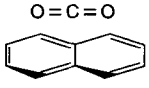
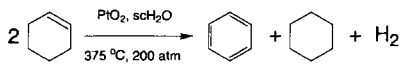


Fig. 12. Part of the Raman spectrum, ν_9 and ν_8 vibrations, of a saturated solution of naphthalene in $scCO_2$ (165 atm and 39 °C) recorded with 488 nm excitation (30 mW) and using the cell shown in Fig. 5b. Note that this region of the IR spectrum would be totally obscured by intense absorptions of $scCO_2$ itself; from ref. [19].



1

A more practical application of Raman spectroscopy is for monitoring reaction mixtures. Some Raman spectroscopic studies[18, 46] have been reported for scH_2O, where technical problems preclude the use of IR spectroscopy; apart from the absence of IR windows which are not corroded rapidly by scH_2O, high temperatures can cause problems in FTIR, and scH_2O itself has extremely intense absorptions over much of the mid-IR region. Masten et al. have followed the decomposition of N_2H_4 in near-critical and scH_2O,[46] while, using the cell shown in Figure 5a, Kolis and co-workers were able to monitor the catalytic dehydrogenation of cyclohexene given in Equation (a) (ca. 12% in scH_2O; Fig. 13).[18]



(a)

The complete miscibility of H_2 and N_2 with supercritical fluids can be exploited for a variety of new or more efficient reactions (see Section 7). Raman spectroscopy is proving to be the most convenient method of detecting these gases;[19, 20] the vi-

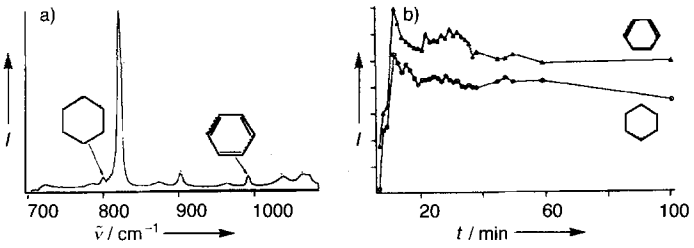


Fig. 13. a) Raman spectrum recorded during the catalytic reaction of cyclohexene in scH_2O, see Equation (a). The unlabeled bands are due to unconverted cyclohexene, those marked are due to cyclohexane and benzene. The intensity of the bands for cyclohexane and benzene are recorded as a function of time in Fig. 13 b; from ref. [18].

bration of an isolated homonuclear diatomic does not give rise to an IR absorption and, even though the vibrations may become IR active in solution or at high pressures, only very weak IR absorptions can be observed.[25] The vibrational Raman bands[19] of both N_2 and H_2 show modest shifts and broadening on going from the pure gas at high pressure to a mixture of the gas with $scCO_2$ at a similar pressure (Fig. 14a). The broadening, however, is considerably more dramatic and highly pressure-dependent for the rotational bands of H_2 in near- and supercritical CO_2 (see Fig. 14b); this broadening has been tentatively attributed to clustering of the solvent around the H_2 "solute".[47]

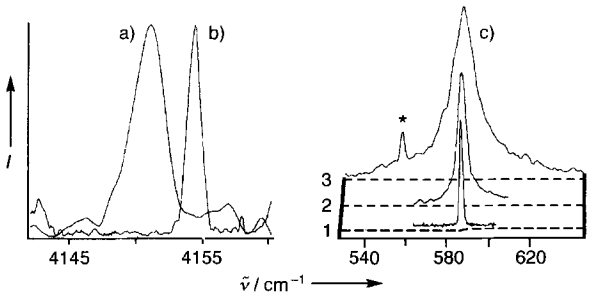


Fig. 14. Raman spectra showing how the $Q_1^{(1)}$ vibrational band of H_2 is broadened and shifted to lower frequency in $scCO_2$ (a) (23 °C and 175 atm; mole ratio H_2:CO_2, 1:4.8) compared to the same band (b) of H_2 gas at the same total pressure (175 atm). By contrast, there is almost no frequency shift in the $S_1^{(1)}$ rotational band (c) but there is a strong pressure dependence in width; 1: pure H_2 gas (87 atm); H_2 gas dissolved in $scCO_2$ at 60 atm (2) and 160 atm (3). The band marked with an * is a laser plasma line; from ref. [19].

Solute/solvent clustering[48] (sometimes also referred to as "Charisma"[48]) in supercritical systems is still a subject of much debate.[49] Near the critical point, local fluctuations of density undoubtedly occur even in pure fluids and give rise to the well-known effect of "critical opalescence". This can cause such strong scattering of light that the fluid is rendered opaque even in the IR region. The scientific debate, however, centers on whether clustering can occur specifically around solute molecules. Evidence for clustering comes largely from UV/Vis fluorescence measurements where fluorescence lifetimes are extremely sensitive to the concentration of the fluorescer; unexpectedly short lifetimes close to the critical point are taken to indicate a local increase in the concentration of solute. In fluorescence studies, the behavior of solute molecules is monitored in dilute solution and, for precisely this reason, effects due to clustering are relatively easy to detect.[50, 51] By contrast, Raman studies generally involve observation of the spectrum of a pure fluid or very concentrated solution. Thus, the spectra will be dominated by features from the bulk of the fluid, and the effects of clustering may be difficult or impossible to observe. Thus, it is not surprising that Raman studies such as that by Ben-Amotz et al. do not show evidence for clustering.[17]

Solute/solvent clustering is discussed further in Section 5 in the context of hydrogen bonding, but first we highlight a promising application of Raman spectroscopy to the study of dissociation processes in supercritical fluids. One of the most fascinating features of supercritical fluids is that phenomena can be studied as a function of solvent density, from gaslike to liquidlike values. Homolytic dissociation of molecules and the subsequent recombination of radicals (or atoms) is a process which is likely to be heavily influenced by solvent density; at high densities, geminate recombination within the solvent cage should be significant but, at low densities, the process is highly improbable. Ravi et al. have modeled the effects of solvent density on the dissociation of Br_2 in noble gas solvents.[52]

Clearly, geminate recombination is an extremely rapid process. Recently, Knopf and co-workers have begun experiments[53a] aimed at detecting vibrationally excited I_2 formed by geminate recombination in $scCO_2$ on a picosecond timescale [Eq. (b).]

$$I_2(v = 0) \xrightarrow[scCO_2]{h\nu} 2I^{\bullet} \longrightarrow I_2(v \gg 1) \longrightarrow I_2(v = 0) \qquad \text{(b)}$$

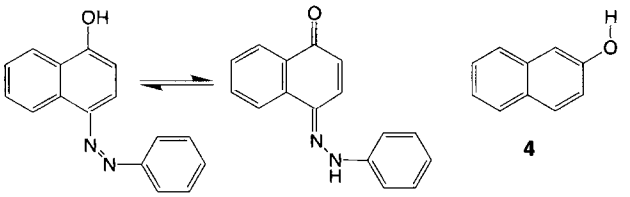
In principle, the requisite sensitivity can be achieved because the dissociation is completely reversible and spectra can be accumulated over many shots at 200 Hz. Preliminary experiments in cyclohexane have been successful, revealing the generation of very highly excited I_2 ($v < 52$); work on $scCO_2$ solutions is in progress. The dynamics of the geminate recombination itself have been studied in scAr on much shorter (i.e. sub-picosecond) timescales by Zewail and co-workers[53b] using UV/Vis detection which has much higher inherent sensitivity than Raman spectroscopy but which cannot provide as detailed information as Raman spectroscopy on the vibrational distribution in condensed phases.

5. Hydrogen Bonding

5.1. The Need for IR Monitoring

The original impetus for studying hydrogen bonding in supercritical fluids was twofold; first, the possibility of establishing whether equilibria involving hydrogen bonding were sensitive to solvent density and, second, the fact that hydrogen bonding is frequently a key factor in the action of so-called "modifiers", compounds added to supercritical fluids to enhance the solubility of particular solutes.[54] It is occasionally possible to use UV/Vis spectroscopy for monitoring equilibria of compounds with hydrogen bonds. This has obvious advantages because UV spectrometers have high sensitivity and few, if any, of the common supercritical fluids absorb in the UV range. Thus, the absorption spectra of the two tautomers in equibrium, **2** and **3**, are significantly different.[55] In scC_2H_6 (and in liquid higher alkanes), the azo tautomer, **2**, predominates at all fluid densities

while, in $scCO_2$, increased fluid density increases the concentration of hydrazone **3** relative to that of **2**, to a point where the concentrations of the two tautomers are almost equal. This effect is attributed to a quadrupolar interaction of **3** with CO_2 (analogous to the interaction between naphthalene and CO_2 in **1**). By contrast, **3** is favored at all densities in the more polar fluid $scCHF_3$, presumably because a hydrogen bond between the solvent and solute ($F_3C-H\cdots O=C$), can stabilize **3** relative to **2**.



2 **3** **4**

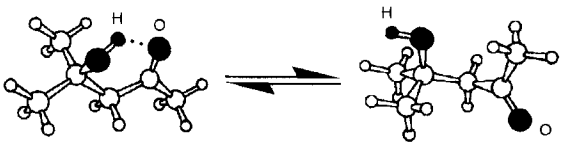
On the other hand, significant hydrogen bonding has been excluded by Tomasko et al. as a possible explanation of their fluorescence experiments[51] with **4** and related compounds in pure and modified $scCO_2$. In general, however, hydrogen bonding cannot be detected by UV spectroscopy and vibrational spectroscopy is needed.

5.2. Hydrogen Bonding and IR Spectroscopy

Unlike UV/vis spectroscopy, IR spectroscopy is widely applicable for studing hydrogen bonding. Thus, in compounds with O–H groups, hydrogen bonding causes the ν(O–H) band, typically at 3600 cm^{-1}, to broaden, increase in intensity, and to shift down in wavenumber;[56] both qualitatively and semiquantitatively, the stronger the interaction the greater the increase in intensity and the greater the wavenumber shift.[57] Most studies of hydrogen bonding in supercritical fluids have been carried out with alcohols and have involved measuring the change in equilibrium constant as a function of temperature, pressure, or density for a particular equilibrium [Eq. (c)].

$$RO-H + B \rightleftharpoons RO-H-B \qquad K_c = \frac{[RO-H-B]}{[RO-H][B]} \tag{c}$$

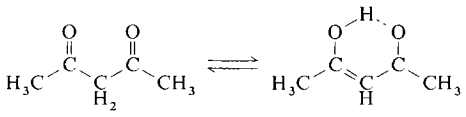
However, the variation in intensity of the ν(O–H) band of hydrogen-bonded O–H groups makes it difficult to measure the concentrations of both the alcohol [ROH] and that of the hydrogen-bonded complex [RO–H–B]. To circumvent this problem, quantitative studies have often been made with the total concentration of alcohol constant (i.e. [ROH] + [RO–H–B] = constant) whereupon it is only necessary to monitor the amount of free alcohol [ROH] by way of the ν(O–H) band. Unfortunately, $scCO_2$ has a strong IR combination band in precisely the region where this ν(O–H) band occurs (see Fig. 9 bottom), and ν(O–H) vibrations are poor Raman scatterers so that Raman spectroscopy is not a viable alternative in this case. A number of strategies have been tried to overcome this difficulty. One approach,[16] tried by Ikawa and Fujita, is to use scXe which has no IR absorptions there (see Section 3). They studied 4-hydroxy-4-methyl-pentan-2-one, one rotamer of which has intramolecular hydrogen bonding [Eq. (d)].



(d)

Although the ν(O–H) region of the spectrum contained no solvent absorptions in scXe, the bands of the free and hydrogen-bonded rotamers overlapped so that computer subtraction was still required to disentangle the spectra. Furthermore, the solubility of the compound increased dramatically with increasing density of scXe so that spectra required additional normalization. Nevertheless, their results reveal a striking change in partial molar volume associated with the rotamerization close to the critical point, changes which are over two orders of magnitude larger than those observed in conventional solvents. This anomaly was attributed to solvent/solute clustering.

Surprisingly, no such clustering effects were observed by Saito and co-workers,[58] who investigated the tautomerism of 2,4-pentanedione in $scCO_2$, which also involves intramolecular hydrogen bonding [Eq. (e)]. The ratio of tautomers was measured based on the ν(C=O) region of the spectrum, where $scCO_2$ does not absorb significantly. Increasing density was found to favor the keto (non-H-bonded) tautomer, although the enol form remained predominant at all densities. This decrease in hydrogen bonding (intra- or intermolecular) as the fluid density increases appears to occur in nearly all of the systems studied so far.



(e)

5.3. Hydrogen Bonding of Methanol

The most extensive work on hydrogen bonding in supercritical fluids has been carried out by the groups of Johnston and his collaborators and of Smith, using the cells illustrated in Figures 1a and 2, respectively. Much of their attention has been focussed on CH_3OH which is the most commonly used modifier for $scCO_2$; indeed, chromatographers often use commercial cylinders of CO_2 premixed with CH_3OH.[59] Smith and coworkers[60, 61] overcame the difficulty of observing ν(O–H) vibrations in $scCO_2$ by using deuterated CH_3OD which has its ν(O–D) band in the region, about 2600 cm^{-1}, unobscured by absorptions of $scCO_2$ (Fig. 15). They were helped by the design of their cell which allowed high concentrations of CH_3OD to be used, because the use of low concentrations of deuterated alcohols in metal apparatus is frequently plagued by D/H exchange with residual traces of H_2O. Some of their results are shown

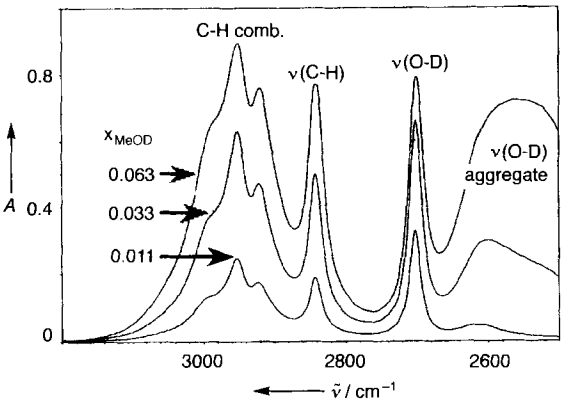


Fig. 15. The FTIR spectrum of CH_3OD in $scCO_2$, illustrating the strategy by Smith and co-workers of using deuterated alcohols to avoid the spectral regions obscured by absorptions of $scCO_2$. The spectrum was recorded in the cell shown in Fig. 2 at 40 °C and 400 bar. The band marked "C-H comb." is a composite absorption resultng from several ν(C-H) combinations; from ref. [61].

schematically in Figure 16. The phase diagram shown there indicates that it is possible for higher concentrations of CH_3OD to be dissolved in the single supercritical phase than in the gas phase at the same temperature.[61] Thus, supercritical mixtures of $scCO_2$ and CH_3OH can contain predominantly hydrogen-bonded alcohol. Surprisingly, their experiments showed that there was relatively little difference in aggregation between any of the $CH_3(CH_2)_nOH$ alcohols $0 < n < 9$. Figure 16 illustrates

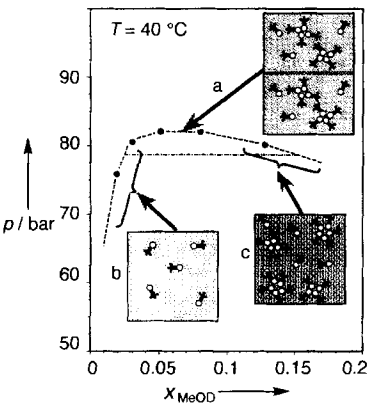


Fig. 16. Phase diagram (pressure p vs. mole fraction x) for CH_3OD in CO_2 at 40 °C, with schematic representations of the aggregation of CH_3OD in the vapor, liquid, and single phase regions of the diagram. a = critical point; b = vapor phase; c = liquid phase; from ref. [61].

two further points: First it is extremely important in such studies, indeed in any supercritical study, to know the precise phase behavior of the system in question. Second the self-association of CH_3OH and other alcohols consists of a series of coupled equilibria [Eq. (f)], which are complicated, if not impossible, to separate for quantitative study.

$$n\,ROH \rightleftharpoons (ROH)_2 + (n-2)ROH \rightleftharpoons (ROH)_3 + (n-3)ROH \ldots \rightleftharpoons (ROH)_n \quad (f)$$

Gupta et al. largely avoided this problem of self association of CH_3OH by using a considerable excess of the base Et_3N.[62] They then tried to use the equilibrium in Equation (g) for

$$CH_3OH + Et_3N \rightleftharpoons CH_3O\text{-}H\text{-}NEt_3 \quad (g)$$

investigating the effect of solvent density on hydrogen bonding in $scCO_2$. The results were encouraging; increased solvent density appeared to shift the equilibrium in favor of the unbonded species. This study was made with $scSF_6$ which, unlike $scCO_2$, has no IR bands in the ν(O–H) region so that undeuterated CH_3OH could be used. The ν(O–H) bands of both the free and the hydrogen-bonded alcohol could also be monitored, but the extinction coefficient of the band of hydrogen-bonded complex was difficult to calibrate. More importantly, the vapor pressures of CH_3OH and NEt_3 were sufficiently low that care was needed to keep the $CH_3OH/NEt_3/CO_2$ mixture as a single phase.

5.4. Hydrogen Bonding of Perfluorinated Alcohols

Smith and co-workers were the first to use perfluoroalcohols in the study of hydrogen bonding in supercritical systems.[42] These alcohols had been used in related studies in the non-supercritical range over a number of years prior to this,[22b] particularly because they are much more acidic than their nonfluorinated analogues[63] and therefore form stronger hydrogen bonds and can be used in greater dilution in the supercritical solution. In $scCO_2$, fluoroalcohols have the added attraction that they are considerably more soluble than the corresponding nonfluorinated compounds. Studies of the type illustrated in Figure 11, suggest that there is no enhanced interaction between CO_2 and C–F bonds. Smith and his co-workers therefore proposed that the reason for the high solubility lay in the formation of weaker hydrogen bonds by the fluoroalcohols than by the nonfluorinated alcohols.[42] However, this suggestion does not explain why other fluorocarbons that are not alcohols also show enhanced solubility in $scCO_2$. Whatever the reason, the phenomenon is quite widespread and has considerable promise, as shown by DeSimone et al., for the synthesis of fluoropolymers[64] and by Wai et al., for the extraction of metals with fluorinated chelating agents in supercritical fluids.[65]

Smith's experiments on hydrogen bonding were performed with unbranched perfluoroalcohols,[42] which retain the propensity to aggregate and therefore the equilibria are just as complicated as those of the unfluorinated compounds. By contrast, branched perfluoroalcohols such as perfluoro-*tert*-butyl alcohol (PFTB), $(CF_3)_3COH$, have a very small degree of self-aggregation,[22b] even at low temperature in cryogenic solvents. This means that PFTB has quite a low boiling point and vapor pressure (ca. 40 Torr at room temperature) relatively high in comparison to the unbranched alcohols. In collaboration with Gupta and Johnston, we have exploited the volatility of PFTB to study its hydrogen bonding to $(CH_3)_2O$, an even more volatile base (vapor pressure at room temperature ca. 4 atm).[66] With PFTB and $(CH_3)_2O$ in the cell shown in Figure 1a, it was possible to obtain the required concentrations of acid and base in the gas phase *without* any added fluid. We were therefore able to study the effect of fluid density on this equilibrium between the components without and with hydrogen bonds from zero up to liquidlike densities. Again $scSF_6$ was used as the fluid because it has no significant IR absorptions above 2500 cm^{-1} even with an optical pathlength of 7 cm. As pointed out by Inomata et al.,[67] the key problem in such studies is that IR extinction

coefficients of solutes can vary with fluid density and, furthermore, the effect is not necessarily linear[66] nor is it the same for different solutes. Thus, for the PFTB/$(CH_3)_2O$/SF_6 system, a considerable amount of calibration was required to allow for the nonlinear variation of IR extinction coefficients with fluid density and to avoid spectroscopic artefacts. Spectra, such as those in Figure 17, fully supported the results of earlier workers,

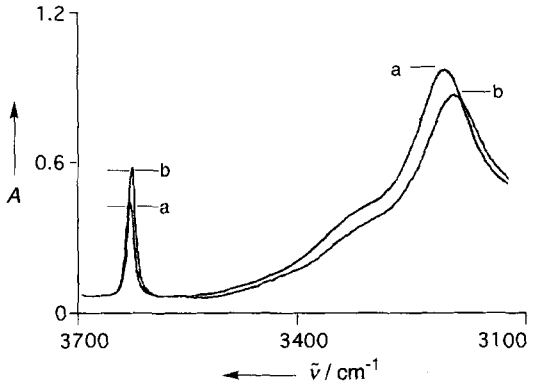


Fig. 17. IR absorption spectra in the ν(O–H) region showing the effect of adding SF_6 to a mixture of $(CF_3)_3COH$ and $(CH_3)_2O$ at 50 °C. Trace a was recorded after addition of 560 psi of SF_6 and trace b with 645 psi total pressure of SF_6. The increase in pressure causes a reduction in intensity of the broad band of the complex with hydrogen bonds with a concomitant increase in the sharp band of the free $(CF_3)_3COH$. The spectra were recorded in the cell shown in Fig. 1a; from ref. [66].

namely that increased solvent density shifts the equilibrium in favor of the free acid and base. It can be seen from these spectra that, close to the critical pressure, even quite modest changes in pressure can cause a significant shift in equilibrium. Gupta et al. have outlined the thermodynamics behind this shift.[62] Very tritely, their explanation can be summarised as stating that solvation energies become increasingly important as the density of the fluid increases, and that the solvation energy of the complex with hydrogen bonds is less than the sum of the solvation energies of the free alcohol and free base. This behavior has been successfully modeled and $\ln K_c$ decreases almost linearly with increasing fluid density (Fig. 18 left). Perhaps the most interesting finding was the observation of nonlinear behavior of $\ln K_c$ of the PFTB/$(CH_3)_2O$/SF_6 system at temperatures close to critical (Fig. 18 right). This deviation was attributed to enhanced solute/solute interaction, probably mediated by solute/solvent

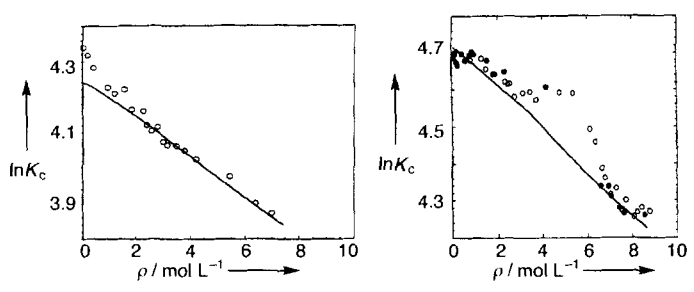


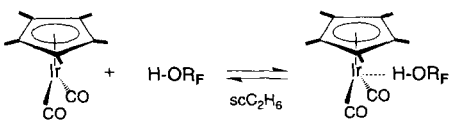
Fig. 18. Plots for the $(CF_3)_3COH/(CH_3)_2O$ system, showing the variation of $\ln K_c$ with density of SF_6 at *constant temperature*. See Equation (c) for definition of K_c. Left: 60 °C, [PFTB] 1.2 mM, $[(CH_3)_2O]$ 30 mM; right: 50 °C, points marked ○ [PFTB] 2.0 mM, $[(CH_3)_2O]$ 16 mM and those marked ●, [PFTB] 1.5 mM, $[(CH_3)_2O]$ 25 mM. In both parts of the Figure, the solid lines indicate the predictions of the modified lattice fluid hydrogen bonding model; from ref. [66].

clustering.[66] As in other studies, it was important to establish whether the presence of PFTB and $(CH_3)_2O$ affected the critical point of SF_6. It was shown that T_c was unaffected within experimental error by PFTB (ca. 1 mM) and $(CH_3)_2O$ (ca. 30 mM) using the relatively uncommon method of measuring the velocity of sound in the fluid.[66] The acoustic properties of a fluid change very substantially in the region of the critical point and, hence, even small changes in T_c and p_c can be detected.[20a, 68] The method promises to have quite widespread applications.

Recently, Ochel and Schneider[69] have monitored the hydrogen bonding and solubility of polar organic acids and esters in $scCClF_3$. In an elegant application of near-IR spectroscopy, they used the 2 × ν(O–H) bands to quantify the amount of hydrogen bonding and the 2 × ν(C–H) bands, which are essentially unaffected by hydrogen bonding to measure the total amount of solute in the fluid. Their conclusion was that the more important factors for determining solubility were molecular size, polarity, and self-association.

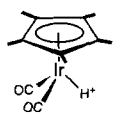
5.5. Hydrogen Bonding and Protonation of Organometallic Compounds

Kazarian et al.[63] made a qualitative study in scC_2H_6 of the interaction between $(CF_3)_2CHOH$ and $[Cp^*Ir(CO)_2]$ ($Cp^* = C_5Me_5$) [Eq. (h)]. The effect of fluid density was similar to that for other systems; increased density disfavors hydrogen bonding. Equilibrium (h) is interesting, however, because it is one of the rare cases where such an equilibrium has been monitored by way of the base rather than the acid, using the extremely intense ν(C–O) bands of the metal compound.



(h)

A similar study[70] in scXe of the interaction of $[Cp^*Ir(CO)_2]$ with the stronger proton donor HCl produced an unexpected result; the IR spectra showed only the known bands of the protonated ion **5**.[70] No IR absorptions which could be assigned to a counter anion were observed but Cl^- does not absorb IR radiation, and the bands of $[HCl_2]^-$ would probably have been much weaker than the ν(C–O) bands of **5**, which themselves were very weak in this experiment. Although the observation of ionic species in a nonpolar fluid is unusual, Lokshin et al. reported some years ago that protonation of neutral organometallic compounds can lead to ionic species in LXe solution at cryogenic temperatures[22b, 71] and, presumably, such charged species are present as ion pairs or small aggregates in both LXe and scXe. Therefore, it is not entirely surprising that solutions of **5** in scXe proved to be unstable, with the ν(C–O) IR bands disappearing within a few minutes of the HCl being added, possibly because of precipitation or further reaction with HCl.



5

5.6. Reverse Micelles in Supercritical Fluids

Very recent, and as yet unpublished, work by Eckert and co-workers[72] has shown that phase transfer catalysts can transport ions into $scCO_2$. However, most of the research effort to solubilize ionic compounds in supercritical fluids has involved surfactants and reverse micelles. Indeed, much of the IR work of Smith's group has been aimed directly or indirectly at the study of reverse micelles in supercritical fluids.[73] Apart from $scCHF_3$, most fluids with a critical temperature T_c close to room temperature are nonpolar. This means that a vast range of hydrophilic and ionic compounds cannot be dissolved or processed in these fluids. Smith and co-workers have shown that some of these compounds (e.g. cytochrome c) can be solubilized by adding surfactants which allow reverse micelles to form in the supercritical fluid.[74] Such micelles have been observed in scC_2H_6, in near-critical and scC_3H_8, and in scXe[74, 75] but crucially no suitable surfactant has yet been found which can form reverse micelles in $scCO_2$. The search for such a surfactant has been intense because, once identified, it will open up whole new areas of chemistry in $scCO_2$. Unfortunately, as Smith and co-workers wryly remark,[73c] "the list of conventional (ionic) surfactants that are insoluble in CO_2 is indeed impressive but not surprising because these (surfactants) have been developed for 'oil' phases of much different character". Therefore, FTIR studies of hydrogen bonding have been an important tool in the search for non-ionic surfactants for $scCO_2$. The role of IR spectroscopy has been twofold, to estimate the degree of aggregation of the surfactants and to establish whether water has indeed been incorporated into the aggregates. Smith and co-workers[73c] have used the approach already outlined above, namely their variable path IR cell and deuterated alcohols, to compare hydrogen bonding of polyethylene glycol dodecyl ethers in scC_2H_6 (where reverse micelles have already been observed) and in $scCO_2$ (where they have not). Their results indicate that, in the absence of added water, the solubility of these surfactants is higher in $scCO_2$ than in scC_2H_6 but that there is less aggregation of the molecules in $scCO_2$ than in scC_2H_6. Clearly, a tendency to aggregate is an important factor in the formation of reverse micelles and so the difference between $scCO_2$ and scC_2H_6 is consistent with the lack of micelles in $scCO_2$.

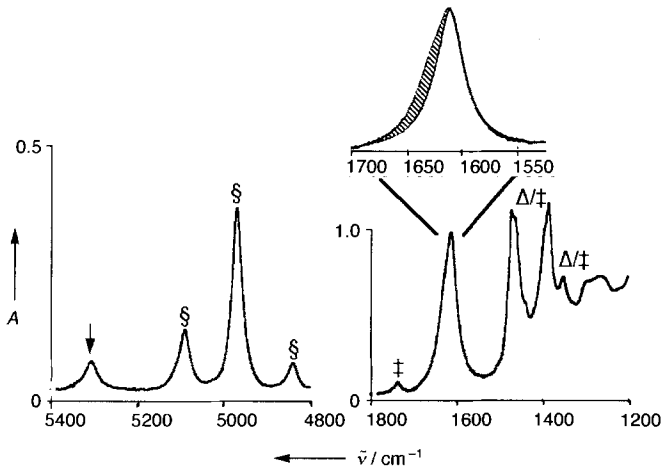


Fig. 19. FTIR spectra of a mixture containing 2.5% surfactant, 6.0% pentanol and H_2O in $scCO_2$ at 60 °C and 5000 psi pressure. The absorption bands of H_2O are the weak combination band (arrowed) and the stronger band, ca. 1600 cm^{-1}, shown separately with an expanded wavenumber scale. This band is broader in the presence of surfactant than in pure $scCO_2$, as indicated by the shading. Other bands are labeled as follows: §: $scCO_2$; Δ: pentanol; ‡, surfactant; from ref. [76].

In a similar study, McFann et al. investigated the non-ionic surfactant,[76] pentaethylene glycol *n*-octyl ether, dissolved in $scCO_2$/*n*-pentanol/H_2O. FTIR spectra recorded in the presence of the surfactant showed an unresolved broadening to high wavenumber of the band at approximately 1600 cm^{-1}, compared to spectra recorded in the absence of surfactant (Fig. 19). This broadening is attributed to water within surfactant aggregates but the level of water present in the surfactant/$scCO_2$ phase did not appear to be much higher than that found in the absence of the surfactant.

6. Impregnation and Extraction of Polymers

Supercritical fluid extraction (SFE) is one of the major uses of $scCO_2$ both on the industrial scale[1] and in the analytical laboratory,[31a] where it is rapidly replacing more traditional extraction (e.g. Soxhlet) in many "standard" methods. Analytical SFE not only eliminates the use of potentially toxic organic solvents but also it is usually faster than conventional extraction techniques. Equally important, SFE delivers the extracted analytes free of solvent for subsequent analysis, allowing measurement to be made from smaller samples than could be handled by conventional means.

One of the major problems with any analytical extraction method lies in knowing when an extraction is complete. Of course, one can deliberately "spike" a matrix with some material and then establish how well the spike is recovered. However, one cannot know, by definition, how much analyte is contained in an "unknown" sample; all that can be done is to compare the amounts of analyte extracted from the same sample by different methods. SFE appears to be efficient; there have even been occasions when SFE has extracted *more* analyte from a certified sample than that sample was supposed to contain. Nevertheless, Clifford and co-workers are attempting to develop models[77] that will allow analysts to use the accumulated results of several sequential extractions to estimate the probable total content of the sample.

There is clearly a need to test such models. Spectroscopic monitoring of extraction requires high sensitivity because the extracted analyte is usually present in the fluid at relatively low concentrations. The aim is to monitor the levels of both the extracted analyte in solution and of the residual analyte in the matrix. FTIR spectroscopy is probably a better method than UV/Vis spectroscopy for carrying out this monitoring because IR absorption bands are usually more sensitive to environment than are UV/Vis bands but the detection limits of IR spectroscopy are much worse. Although attempts are being made to couple FTIR detection to SFE,[32] the technique is less developed than the cSFC-FTIR method (see Section 3). Nevertheless, progress is being made. Hawthorne and co-workers have reported the use of IR optic fibers for monitoring SFE[32b] and recent work at Nottingham[54b, 78] has shown that FTIR spectroscopy can be used for monitoring the extraction of transition metal carbonyl compounds, for example $[CpMn(CO)_3]$

($Cp = \eta^5$-C_5H_5), with supercritical phases from and impregnation into polymers. The important feature of this work is that such compounds have unusually narrow and intense ν(C–O) IR bands, the precise wavenumbers of which are particularly sensitive to the environment. Thus, one can easily distinguish between the IR absorptions of $[CpMn(CO)_3]$ in $scCO_2$ solution and those of $[CpMn(CO)_3]$ isolated within a polymer matrix. Using a cell similar to that in Figure 3, Howdle and co-workers[78] have shown that FTIR spectroscopy can be used to follow the impregnation of $[CpMn(CO)_3]$ into polyethylene (PE) and its subsequent extraction (Fig. 20). So far, the technique has only been used with static extraction (i.e. in a closed cell without any flow of $scCO_2$) but even in these circumstances there is potential for accumulating useful data.

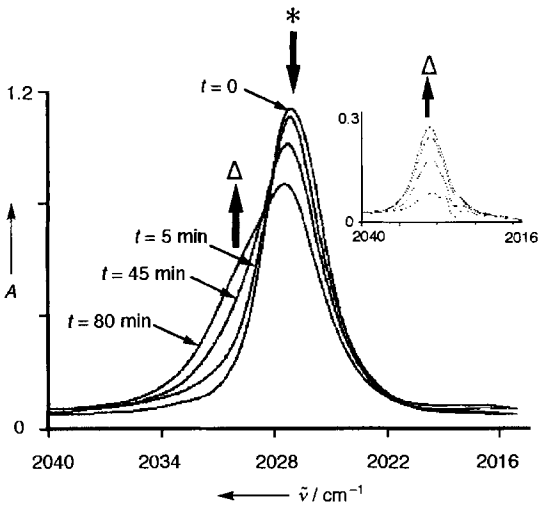


Fig. 20. "Real-time" FTIR monitoring of extraction of $[CpMn(CO)_3]$ from polyethylene (PE) with supercritical $scCO_2$. The extraction can be monitored because the ν(C–O) bands of $[CpMn(CO)_3]$ have slightly higher wavenumber when the compound is dissolved in $scCO_2$ solution than when it is in a PE matrix. The spectra were obtained by placing four pieces of PE film (total thickness 1 mm) in a cell and then pressurising with $scCO_2$ (200 atm 32 °C). The absorption due to $[CpMn(CO)_3]$ in $scCO_2$ grows as a shoulder, marked with a Δ, on the side of the band due to $[CpMn(CO)_3]$ within the PE, labeled with an *. The spectra in the inset were obtained by computer subtraction and show the growth of the band of "free" $[CpMn(CO)_3]$ dissolved in $scCO_2$; from ref. [78].

The impregnation of organometallic compounds into a polymer matrix with supercritical phases leaves no solvent residues within the polymer because the CO_2 for example can easily diffuse out. This diffusion process can also be monitored by FTIR spectroscopy but Briscoe and co-workers have devised ultrasonic methods that are considerably more sensitive.[79] Once impregnated into the polymer, the organometallic compounds can be induced to react with the polymer itself without any side reactions with solvent residues. One such reaction,[80] the C–H activation of PE by $[Cp^*Ir(CO)_2]$ is illustrated schematically in Figure 21. This photochemical reaction can be followed easily by FTIR spectroscopy because reactant and product have substantially different spectra in the ν(C–O) region, where PE itself does not absorb significantly. Furthermore, the fact that the product is bound to the polymer was established by showing that excess reactant can be extracted by $scCO_2$, while the product cannot. Unfortunately, this reaction

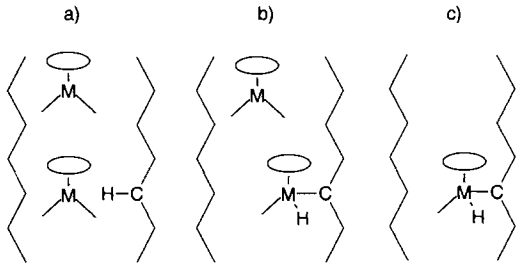
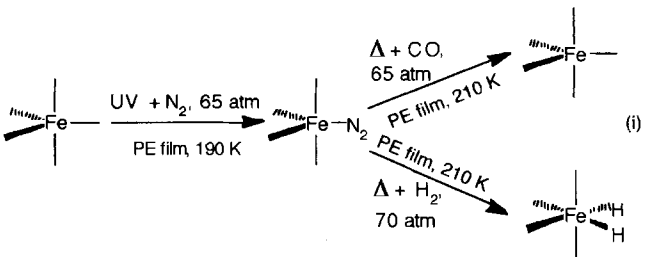


Fig. 21. Schematic representation of the three stages of the C–H activation of polyethylene (PE), the chains of which are represented by zigzag lines, by $[Cp^*Ir(CO)_2]$. a) Impregnation of $[Cp^*Ir(CO)_2]$ into PE using $scCO_2$; b) C–H activation by UV irradiation of the impregnated film, and c) extraction of unconverted $[Cp^*Ir(CO)_2]$ by $scCO_2$. The whole experiment was carried out in a cell similar to that shown in Fig. 3; from ref. [80].

suffers from the same limitation as the C–H activation of lighter hydrocarbons by $[Cp^*Ir(CO)_2]$; once $[Cp^*Ir(CO)H(R)]$ has been formed, it is extremely difficult to develop the chemistry by exploiting the activated C–H bond to make new organic compounds.[81] Interestingly, hydrogen bonding of the Ir center by $(CF_3)_3COH$ was found to reduce significantly the efficiency of the C–H activation.[82] It is not clear, however, whether this reduction in efficiency is due to the change in the electron density on the metal center or merely due to a reduction in the UV extinction of the complex with hydrogen bonds, leading to less UV light absorbed in a given irradiation time. Clearly, the impregnation of other organometallic compounds into polymers offers considerable possibilities for the modification or tailoring of both bulk and surface properties of the polymers.

Over the past decade, Rest and co-workers have pioneered the use of impregnated polymer films as a substitute for frozen noble gases in matrix isolation experiments,[83] to create what they rather self-depreciatively describe as "infra-dig" matrices. Impregnation using supercritical fluids extends the possibilities of Rest's technique because some of his original experiments were bedevilled by problems of solvent residues. Recently, the high-pressure/low-temperature cell, illustrated in Figure 4, has been used[15a] to synthesize the highly unstable molecule $[Fe(CO)_4N_2]$ from $[Fe(CO)_5]$ impregnated into PE and then to follow its subsequent thermal reaction with H_2. Both the photochemical and thermal steps were followed by FTIR spectroscopy [Eq. (i)].



(i)

The same high-pressure/low-temperature cell has also been used by Kazarian et al. to investigate the reaction of HCl with $[Cp^*Ir(CO)_2]$ in PE.[15b] This reaction led to the formation of $[Cp^*Ir(CO)_2H]^+$, again with no detectable counterion, but unlike scXe solution at room temperature (see Section 5),

$[Cp^*Ir(CO)_2H]^+$ was quite stable in PE at 250 K. More surprisingly, venting the HCl and warming the impregnated PE film back to room temperature caused up to 70% regeneration of the neutral $[Cp^*Ir(CO)_2]$ [Eq. (j)]. Under these conditions,

$$[Cp^*Ir(CO)_2] \underset{290\ K}{\overset{+HCl,\ 250\ K,\ PE\text{-}Film}{\rightleftharpoons}} [Cp^*Ir(CO)_2H]^+ \qquad (j)$$

$[Cp^*Ir(CO)_2]$ appears to be isolated within PE and its ν(C–O) bands are only slightly broader than those observed in alkane solution. Thus, the fact that the protonation of $[Cp^*Ir(CO)_2]$ in PE is largely reversible strongly suggests that $[Cp^*Ir(CO)_2H]^+$ is present as ion pairs rather than as large aggregates.

A rather different non-spectroscopic study involving ions, polymers, and $scCO_2$ has just been reported by Sullenberger et al., who fabricated two platinum microelectrodes, embedded next to each other in the end of a glass rod.[84] The electrodes were then covered with a 50 μm film of polyethylene oxide (PEO) doped with an appropriate electrolyte (i.e. $LiCF_3SO_3$). The coated electrode assembly was then mounted in a high-pressure cell, filled with $scCO_2$ containing dissolved anthracene or benzoquinone. The aromatic compound was thus impregnated into the polymer where it be could be oxidized or reduced electrochemically. When the PEO film was additionally doped with $[Ru(bpy)_3]^{2+}$, there was evidence for the electrochemical activation of CO_2 and its reaction with benzoquinone.

7. Reactions of Organometallic Compounds

For over three decades, IR spectroscopy has played a central role in the mechanistic study of photochemical reactions of organometallic compounds, particularly of transition metal carbonyls.[85] Techniques such as frozen hydrocarbon glasses, matrix isolation, liquefied noble gases, and time-resolved IR spectroscopy, have been developed and optimized through such studies, sometimes exclusively so. The emphasis on metal carbonyls and the closely related dinitrogen and nitrosyl compounds derives partly from inherent chemical interest but equally importantly from the enormous amount of structural information that can be derived merely from recording IR spectra in the ν(C–O), ν(N–N), and ν(N–O) regions. Molecular geometries, bond angles and, on occasions, even estimates of bond lengths can be derived from these spectra. Improved instrumentation, particularly FTIR instruments, has allowed at least some of these techniques to be extended in recent years to non-carbonyl organometallic compounds.[86]

The original impetus for studying photochemical reactions of organometallic compounds in supercritical fluids arose from the very low solubility of some substituted metal carbonyl compounds in liquid xenon.[87] Thus, even though $[Ru(CO)_4(PPh_3)]$ is virtually insoluble in LXe, it has modest solubility in scXe at 25 °C. Figure 22 illustrates spectra recorded by Upmacis et al. during the reaction of $[Ru(CO)_4(PPh_3)]$ with H_2 in scXe, one of the first reactions of organometallic compounds to be carried out in supercritical fluid solution.[87] The reaction product, $[H_2Ru(CO)_3(PPh_3)]$ had previously only been observed by Whyman[88a] in a thermal reaction in heptane under very much harsher conditions, 100 °C and 300 atm H_2. Once generated[87]

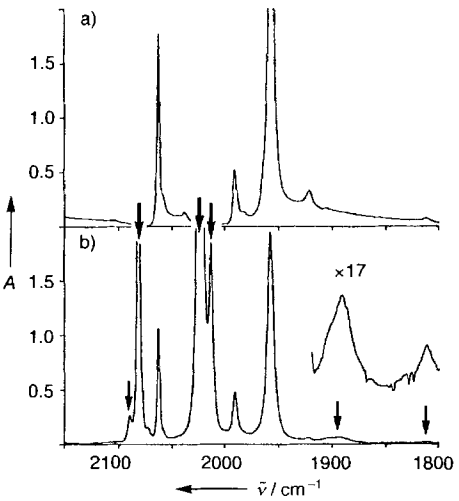


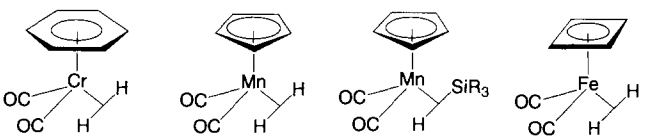
Fig. 22. FTIR spectra showing the photochemical synthesis of $[H_2Ru(CO)_3(PPh_3)]$ by irradiation of $[Ru(CO)_4(PPh_3)]$ and H_2 with UV light in scXe at 25 °C; a) spectrum before irradiation; b) spectrum after 9 min photolysis. Bands due to $[H_2Ru(CO)_3(PPh_3)]$ are marked with arrows. The ν(Ru–H) region of the spectrum is shown with a 17-fold expansion of the absorbance scale; from ref. [87].

in scXe, $[H_2Ru(CO)_3(PPh_3)]$ decayed over a period of about six hours even under a high pressure of H_2, possibly by reaction with the photoejected CO. This reactivity is considerably greater than that of $[H_2Ru(CO)_2(PPh_3)_2]$ which had been isolated many years earlier.[88b]

This reaction of $[Ru(CO)_4(PPh_3)]$ led to the realization that the irradiation of metal carbonyl compounds with UV light in supercritical solution in the presence of H_2 might be a relatively general route to either dihydrogen or dihydrido complexes, depending on the particular metal center[25] [Eq. (k)].

$$[L_nM(CO)_x] + H_2 \underset{-CO}{\overset{h\nu}{\longrightarrow}} [L_nM(CO)_{x-1}(\eta^2\text{-}H_2)] \quad \text{or} \quad [L_nM(CO)_{x-1}(H)_2] \qquad (k)$$

Using this route, Howdle et al. generated a series of compounds, including the half-sandwich dihydrogen complexes, **6**–**8**, formed from the corresponding $[(\eta^n\text{-}C_nH_n)M(CO)_3]$ compounds in scXe solution.[25] Such compounds should, in



6 **7** **7'** **8**

principle, have a weak IR band within the region 3400–2400 cm^{-1}, associated with the ν(H–H) vibration of the η^2-H_2 group.[89] Although the ν(H–H) band of $[W(CO)_5(\eta^2\text{-}H_2)]$ has been observed[27] in scXe using a cell similar to that in Figure 3, no band was found for any of the compounds, **6**–**8**, presumably because the bands were extremely weak. Nevertheless, there was sufficient circumstantial evidence to confirm that each of these compounds did indeed contain an η^2-H_2 group. The compounds **6**–**8** are of interest because **7** was the first nonclassical dihydrogen complex of manganese to be identified, and **8** was the first

dihydrogen compound of iron also to contain a coordinated olefin or diene ligand. Compound **7** appeared to be relatively stable even after the H_2 had been vented (see Section 8). The arrested oxidation of the Mn center is not unprecedented in view of the extensive series of known η^2-H–SiR_3 complexes of Mn (e.g **7'**).[90]

H_2 is significantly less soluble than other gases (e.g. N_2, CO, etc) in conventional organic solvents. However, H_2 is completely miscible with a supercritical solvent, such as scXe, since the fluid is merely a dense gas. Thus, if properly mixed with the fluid (see Section 8), a given pressure of H_2 will give an effective concentration of "dissolved" H_2 nearly an order of magnitude higher than in a conventional solvent under a similar pressure of H_2. The predominant reaction pathway for labile dihydrogen complexes appears to involve dissociative loss of the η^2-H_2 group and so this very high concentration of H_2 can increase the lifetime of such complexes in scXe solution.[25] Nevertheless, even under a such pressure of H_2, **8** reacted further within a few minutes, possibly through transfer of H_2 to the C_4H_4 ring, while **6** decayed only slowly under the same conditions.

The miscibility of H_2 and scXe has an additional benefit namely that, in a closed vessel, the concentration of dissolved H_2 is independent of temperature. By contrast, the solubility of H_2 in a conventional solvent will show a temperature dependence as dictated by Henry's Law. Howdle et al.[25] exploited this constant concentration of H_2 in scXe to investigate the kinetics of the reaction of CO with $[(\eta^6\text{-}C_6H_5Me)Cr(CO)_2(\eta^2\text{-}H_2)]$ [Eq. (l)]. The reaction was monitored via the a″

$$[(\eta^6\text{-}C_6H_5Me)Cr(CO)_2(\eta^2\text{-}H_2)] \underset{+H_2}{\overset{-H_2}{\rightleftharpoons}} [(\eta^6\text{-}C_6H_5Me)Cr(CO)_2] \xrightarrow{CO} [(\eta^6\text{-}C_6H_5Me)Cr(CO)_3] \quad (l)$$

ν(C–O) band of $[(\eta^6\text{-}C_6H_5Me)Cr(CO)_2(\eta^2\text{-}H_2)]$; it showed pseudo-first order kinetics with an activation energy of 70 ± 5 kJ mol^{-1} over the temperature range 11 to 80 °C (Fig. 23). If loss of H_2 is assumed to be the rate-determining step, this activation energy can be taken as an estimate of the Cr–$(\eta^2$-$H_2)$ bond dissociation energy and, perhaps fortuitously, the value is almost identical to that estimated by photoacoustic and calorimetric techniques for related Cr–$(\eta^2$-$H_2)$ bonds.[91]

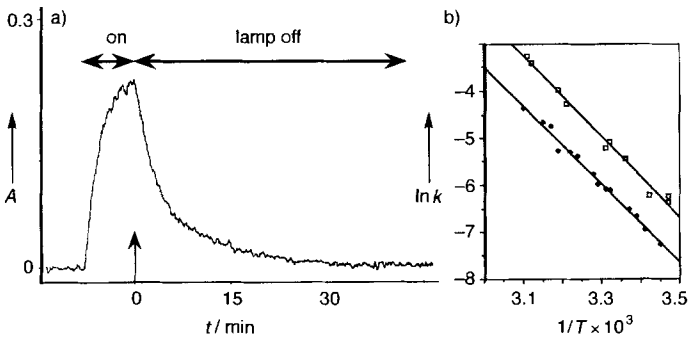


Fig. 23. a) An IR kinetic trace showing the photochemical generation and thermal decay of $[(\eta^6\text{-}C_6H_5Me)Cr(CO)_2(\eta^2\text{-}H_2)]$ in scXe/H_2 at 70 °C, see Equation (l). The decay follows pseudo-first order kinetics. b) Arrhenius plot for the rate of decay of $[(\eta^6\text{-}C_6H_5Me)Cr(CO)_2(\eta^2\text{-}H_2)]$ measured in the presence of two concentrations of added CO. Note that, within experimental error, the two curves have the same gradient, corresponding to an activation energy of 70 kJ mol^{-1}; from ref. [25].

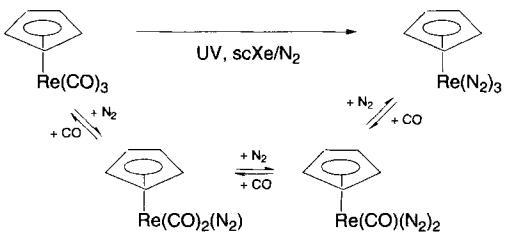
Equation (l) is, perhaps, slightly misleading because there is increasing evidence that reaction intermediates such as $[(\eta^6\text{-}C_6H_5Me)Cr(CO)_2]$ are not genuinely coordinatively unsaturated but are weakly solvated by a molecule of solvent acting as a "token" ligand in the otherwise vacant coordination site.[85] Even solvents, apparently as inert as Xe, can act as token ligands and the strength of the M–Xe interaction has been estimated for the group 6 metals in gaseous and liquid Xe.[92] In recent experiments we have begun using nanosecond time-resolved IR spectroscopy to monitor these interactions in scXe and $scCO_2$.[93]

The high concentrations of H_2 in supercritical solution have since been exploited by other groups. Rathke and co-workers[94] reported a series of elegant experiments where thermal hydroformylation reactions catalyzed by $[Co_2(CO)_8]$ in $scCO_2$ were monitored by NMR spectroscopy. The product distribution was rather different from that found in conventional solvents and a patent has been granted on the process.[94c] The very low viscosity of supercritical solvents is of considerable benefit for NMR spectroscopy and nuclei with spin ≥ 1 have shorter correlation times and correspondingly sharper resonances under supercritical conditions.

Very recently, Noyori and co-workers[95] have reported the catalytic hydrogenation of $scCO_2$ itself [Eq. (m)]. This experiment has aroused considerable excitement, not because the product (formic acid) is any way different from that in THF solution but because the reaction is over an order of magnitude faster in $scCO_2$. Presumably, this acceleration is the result of the greater concentration of H_2 in the supercritical fluid.

$$CO_2 + H_2\,(85\text{ atm}) \xrightarrow[scCO_2,\ p_{tot.} = 205\text{ atm},\ 50\,^\circ C]{[Ru(PMe_3)_4H_2] + NEt_3} HCOOH \quad (m)$$

N_2 is also miscible with supercritical fluids, and Howdle et al. have again exploited this for the generation of new compounds. Their most striking reaction[96a] was the total substitution of CO by N_2 in the molecule $[CpRe(CO)_3]$ to generate $[CpRe(N_2)_3]$ [Eq. (n)]. As with many of the reactions described previously,



(n)

this substitution reaction was followed by FTIR spectroscopy but this time in the ν(N–N) region (Fig. 24). The assignment of the bands was confirmed by comparison with earlier experiments in solid N_2 matrices doped with $^{15}N_2$ at 20 K. Neither $[CpRe(CO)(N_2)_2]$ nor $[CpRe(N_2)_3]$ had been observed previously at room temperature. However, once generated $[CpRe(N_2)_3]$ was remarkably stable, persisting for more than 24 h in scXe solution under a pressure of N_2, and then taking nearly 1 h to react with added CO at room temperature. $[CpRe(CO)(N_2)_2]$ was even more robust and, although only spectroscopic amounts were generated, the experiments suggested that $[CpRe(CO)(N_2)_2]$ might be air stable.[29]

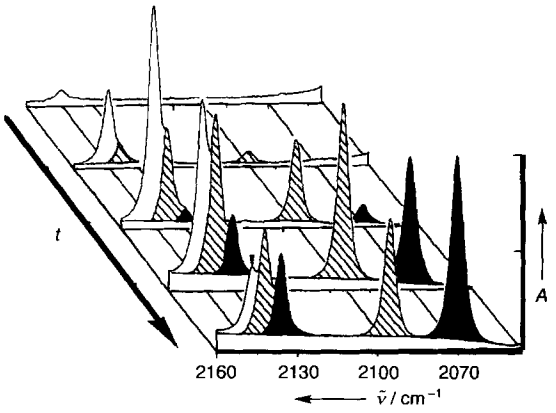
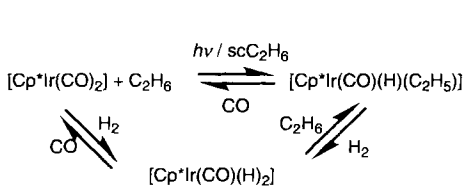


Fig. 24. FTIR spectra in the ν(N–N) region recorded during the UV photolysis of $[CpRe(CO)_3]$ in $scXe/N_2$ (total pressure 2600 psi). The spectra show the sequential formation of $[CpRe(CO)_2(N_2)]$ (white bands), $[CpRe(CO)(N_2)_2]$ (shaded bands) and, finally, $[CpRe(N_2)_3]$ (black bands). The total irradiation time was 2 h but subsequent experiments with more powerful lamps show that the reaction can be carried out far more rapidly; from ref. [96a].

A number of other dinitrogen compounds have been generated by a similar route but there are limitations; UV photolysis of $[(C_5H_4Me)Mn(CO)_2(PR_3)]$ compounds with N_2 in supercritical solution leads to considerable loss of the PR_3 ligand and, only with PMe_3, were significant amounts of the $[(C_5H_4Me)Mn(CO)(N_2)(PR_3)]$ compound observed.[96b]

Apart from Noyori's hydrogenation experiment[95] with $scCO_2$, most attempts to activate $scCO_2$ have been disappointing.[97] In fact, $scCO_2$ is a remarkably inert solvent and Jobling et al. have taken advantage of this inertness[98] to use $scCO_2$ for photochemical activation of C–H bonds by $[Cp^*Ir(CO)_2]$. C–H activation of alkanes is an area of considerable research activity but one continuing problem has been to find suitably inert solvents in which to carry out activation of light alkanes such as CH_4 or C_2H_6. Graham and co-workers were successful in using fluorocarbon solvents[81] and Bergman and co-workers used LXe[99] but neither solvent was ideal. Jobling et al.[98] showed that photochemical C–H activation of scC_2H_6 could be carried out satisfactorily in $scCO_2$. It quickly became apparent, however, that the $scCO_2$ was superfluous because the critical temperature of C_2H_6 is so close to that of CO_2 (see Table 1). Thus, scC_2H_6 could be used as both solvent and reactant but the C–H activation did not proceed far because a photostationary state was established rapidly (Fig. 25a). Surprisingly, addition of high pressures of H_2 to the mixture not only promoted formation of $[Cp^*Ir(CO)(H)_2]$ but led to greatly increased amounts of C–H activation [Fig. 25b and Eq. (o)].



(o)

Since the critical pressure of C_2H_6 is considerably lower than that of CO_2 (see Table 1), it was possible to use much higher pressures of H_2 with C_2H_6 without exceeding the pressure rating of the cell shown in Figure 3, and even to reach approximately

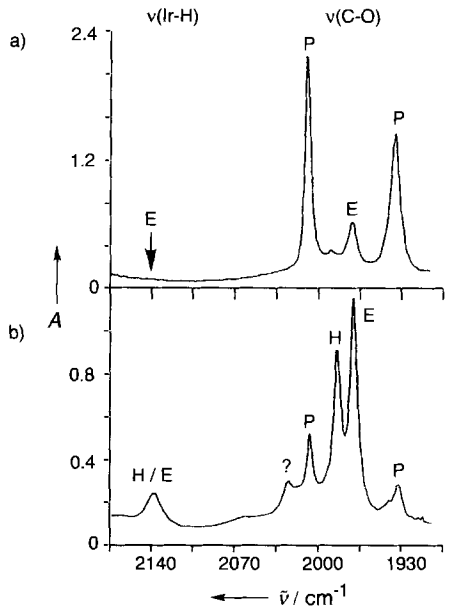
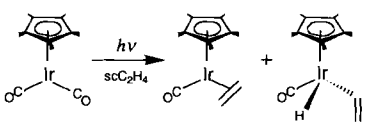


Fig. 25. FTIR spectra illustrating the dramatic effect of H_2 on the C–H activation of scC_2H_6 by $[Cp^*Ir(CO)_2]$. a) IR spectrum recorded after 3 minutes UV irradiation of $[Cp^*Ir(CO)_2]$ in scC_2H_6 (68 atm); b) IR spectrum showing the strikingly different result of 10 minutes UV photolysis of $[Cp^*Ir(CO)_2]$ in scC_2H_6 (50 atm) with added H_2 to give a total pressure of 179 atm. The bands are labeled as follows: E = $[Cp^*Ir(CO)(H)(C_2H_5)]$; H = $[Cp^*Ir(CO)(H)_2]$; P = residual $[Cp^*Ir(CO)_2]$; ? = an unidentified labile photoproduct; from ref. [98].

equimolar concentrations of H_2 and C_2H_6 in the solution. The effect of H_2 on C-H activation is chemical rather than physical because high pressures of He are ineffective; experiments with D_2 indicated that no deuterium was incorporated into $[Cp^*Ir(CO)H(Et)]$. Sequential experiments in $scCO_2$ (addition of H_2 to generate $[Cp^*Ir(CO)(H)_2]$ followed by addition C_2H_6) showed that C–H activation by $[Cp^*Ir(CO)(H)_2]$ is more efficient than by $[Cp^*Ir(CO)_2]$ itself. The reason for this still remains unclear but the overall effect is dramatic.

CH_4 has its critical temperature at 190.5 K well below that of C_2H_6. Nevertheless, it is possible to dissolve small amounts of $[Cp^*Ir(CO)_2]$ in $scCH_4$ at temperatures close to ambient, provided that the pressure is sufficiently high to give a fluid density close to ρ_c, 0.162 g mL^{-1}. This density can be achieved at a pressure of about 3750 psi at 297 K. Under these conditions,[100] UV irradiation of $[Cp^*Ir(CO)_2]$ leads to activation of CH_4 and formation of $[Cp^*Ir(CO)H(CH_3)]$, identifiable by comparison with IR data from low temperature matrices.

Irradiation of $[Cp^*Ir(CO)_2]$ in scC_2H_4 leads to two processes,[29] substitution of CO by C_2H_4 and C–H activation to generate a hydrido(vinyl) complex [Eq. (p)]. As in the other C–H activation experiments, both compounds were identified by FTIR spectroscopy; scC_2H_4 has strong IR bands which obscure considerable regions of the spectrum but, fortuitously, it has a series of "windows" in each of the regions, ν(Ir–H), ν(C–O), ν(C=C), and δ(C–H), needed to characterize $[Cp^*Ir(CO)H(\eta^1\text{-}C_2H_3)]$.



(p)

These experiments are interesting not only because C_2H_6 or C_2H_4 can be activated but also because the reaction products can be recovered. Product recovery has been a substantial problem in C–H activation experiments in conventional solvents; attempts to remove the solvent frequently lead to decomposition of the compound. By contrast, a reduction in applied pressure will result in precipitation of solid compounds from supercritical solution. Figure 26 shows how such precipitation can be

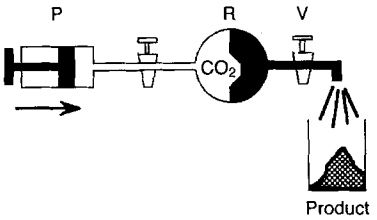


Fig. 26. Schematic illustration of how small quantities of reaction product can be recovered from a cell, R (such as that shown in Fig. 3). A syringe pump P forces $scCO_2$ through the system to flush the reaction mixture (shown black) through an expansion valve V. The reduction in pressure across the expansion valve causes the dissolved solids to precipitate from solution allowing collection.

achieved in a controlled manner by pumping $scCO_2$ to flush the contents of the reaction cell through an expansion valve.[93a] In this way, it was possible to recover sufficient [Cp*Ir(CO)H(R)] (R = Et or η^1-C_2H_3) for ^{1}H NMR confirmation of the structures, already identified by IR spectroscopy. Alternatively, the compounds can be redissolved in scXe to obtain IR spectra free from interfering IR absorptions of the solvent.[29] This method of precipitating a product from supercritical solution is a key feature of the miniature flow reactors under development for continuous reactions in supercritical fluids.

IR spectroscopy can be used, of course, to monitor a much wider range of processes than just reactions of organometallic compounds. Buback describes a number of applications of IR and near-IR spectroscopy for following polymerization reactions.[4] Saito and co-workers[101] have recently reported the use of IR spectroscopy for monitoring Diels–Alder reactions between isoprene and methyl acrylate, which has relatively intense ν(C=O) bands. In fact, most reactant/product combinations are likely to have absorption bands somewhere within the mid-IR region, suitable for spectroscopic monitoring. However, the particular advantage of IR spectroscopy in reactions of organometallic compounds is both the high sensitivity provided by the ν(C–O) bands and the possibility of identifying previously unknown compounds with a considerable degree of certainty merely from their IR spectra.

8. Reactions with Supercritical Fluids on a Preparative Scale

The ultimate objective of many chemists is to harness new techniques to make new compounds on a preparative scale. However, most of the reactions and processes described in the previous sections of this review have been carried out in dilute solutions and on a relatively small scale. These reactions, therefore, need to be scaled up. Vibrational spectroscopy is playing a key role in the scale-up of reactions of organometallic compounds in supercritical fluids.

Apart from any safety considerations, the scale-up of reactions in supercritical fluids presents a number of unusual problems. Most substrates have critical temperatures far higher than that of CO_2 and so to maintain supercritical conditions reactions must either be run in very dilute solution or at high temperatures. However, dilute solutions prevent the processing of large quantities of material unless the reaction vessel is extremely large. High temperatures are often undesirable because reaction products, if labile, may degrade. Furthermore, many of the more interesting phenomena associated with supercritical fluids occur relatively close to the critical point (see for example, Fig. 18). In addition, the composition of a reaction mixture changes as the reaction proceeds and so the critical point will also change, making it difficult to maintain the desired near-critical reaction conditions.

These problems can be minimized, if not removed completely, by use of a continuous flow reactor because at any particular point in such a reactor the composition remains constant throughout the reaction. Equally, the gaslike nature of supercritical fluids (low viscosity, good heat transfer, etc) readily lends itself to flow reactors. Pickel and Steiner[102] have pioneered the use of flow reactors for industrial-scale processes in the pharmaceutical industry, particularly catalytic hydrogenation. Their use of such reactors in one process has resulted in a 1/250 reduction in reactor volume compared to the batch process in conventional solvents.

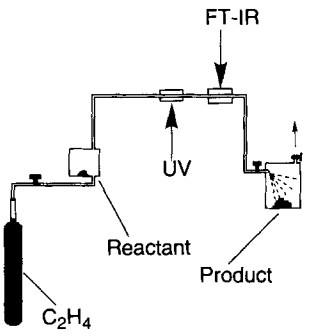


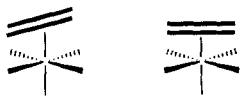
Fig. 27. A schematic diagram of the flow reactor used for the synthesis [103] of $[Cr(CO)_5(C_2H_4)]$. scC_2H_4 is pumped through a reservoir containing solid $[Cr(CO)_6]$, which dissolves in the scC_2H_4. The supercritical solution then passes through a UV irradiation cell (a modified version of that in Fig. 3) where reactant is converted into product, through an IR cell for FTIR monitoring and finally through an expansion valve (analogous to Fig. 26) to precipitate the product as a dry solid.

At Nottingham, we are developing miniature flow reactors for laboratory-scale preparative reactions. Our prototype reactor was designed for reactions in scC_2H_4, where the fluid acted both as solvent and as one of the reactants.[103] Figure 27 shows a schematic view of the reactor; a solid organometallic compound is dissolved in scC_2H_4, converted into product by UV irradiation, monitored by IR spectroscopy, and finally precipitated as a fine powder, all as a single continuous process. Once the fluid pump is running, reactant is converted into product automatically, while the operator uses IR monitoring to optimize the reaction conditions. Using this reactor, it was possible to isolate $[Cr(CO)_5(C_2H_4)]$ (>80% purity) directly from the reaction of $[Cr(CO)_6]$ and scC_2H_4 at a rate of approximately 40 mg h^{-1} [Eq. (q)].

$$[Cr(CO)_6] \xrightarrow[scC_2H_4]{UV} [Cr(CO)_5(C_2H_4)] \quad (q)$$

Although $[Cr(CO)_5(C_2H_4)]$ was already known in solution,[104] previous attempts to isolate it had been thwarted by

the lability of the C_2H_4; removal of the solvent also removed the ligand. Expansion of scC_2H_4 is more rapid than conventional solvent evaporation; thus the solution does not need to be heated and a high concentration of the free ligand C_2H_4 is maintained right up to the moment at which the solid is formed. Once precipitated, $[Cr(CO)_5(C_2H_4)]$ appears to be moderately stable in the solid state.[103] The relative intensities of the ν(C–O) IR bands of $[Cr(CO)_5(C_2H_4)]$ suggest that the C_2H_4 group is aligned parallel to a *trans* pair of CO groups (as in **9** not **10**) as found by Grevels and co-workers in the crystal structure of the related compound $[Cr(CO)_4(C_2H_4)_2]$.[104b]



9 **10**

Success with $[Cr(CO)_5(C_2H_4)]$, encouraged us to build a more complex reactor using H_2 mixed with $scCO_2$ (Fig. 28) for the isolation on a larger scale of the dihydrogen compounds which we had previously made only on a spectroscopic scale (see Section 7).[105] In this case, the mixing of the

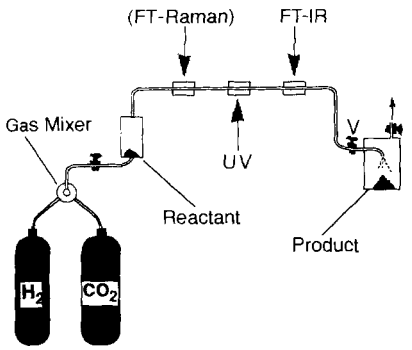
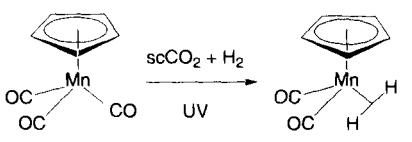


Fig. 28. A simplified schematic diagram of the flow reactor used for photochemical reactions of organometallic compounds in $scCO_2/H_2$ mixtures. Initially, high-pressure H_2 and $scCO_2$ are mixed. The organometallic compound (e.g. $[CpMn(CO)_3]$) is then dissolved in the mixture and the H_2 content can be verified, as necessary, by FT Raman spectroscopy using the cell shown in Fig. 5c. After UV irradiation, the fluid is monitored by FTIR spectroscopy and finally the product is precipitated, as in Figs. 26 and 27, by expansion through a high-pressure valve.

H_2 and $scCO_2$ is monitored in-line by FT-Raman spectroscopy using the cell shown in Figure 5c, and the photochemistry is followed by FTIR spectroscopy, as before. This reactor has been used successfully to prepare **7**[106] [Eq. (r)]. This com-



(r)

7

pound has never been isolated before and transpires to be remarkably robust; it is a pale yellow solid that melts to a brownish liquid at room temperature. The thermal stability contrasts with the relative lability of many other dihydrogen complexes.[89]

9. Conclusions

Supercritical fluids have a range of properties that are qualitatively different from those found in conventional solvents, including "tunable" density, high solubility of gases, low viscosity, etc. High-pressure conditions make chemistry in supercritical fluids necessarily more complicated than in conventional solvents, although the technology for microscale reactions is rapidly becoming simpler. We remind readers, however, that false expectations have sometimes been aroused in the past by over-optimistic articles and patents. There are many things which supercritical fluids cannot do. They are not magic solvents that will dissolve materials which have defied all other attempts to dissolve them. Of course, there are unexpected surprises such as the ability of $scCO_2$ to dissolve fluoropolymers but such cases are exceptions. Similarly, the behavior of supercritical fluids cannot contravene fundamental laws of thermodynamics, although the different solvation properties may alter the precise energetics of a process. Nevertheless, it is clearly important to identify those areas of chemistry where the special properties of supercritical fluids bring real benefits. Fortunately, diagnostic tools and laboratory techniques have now developed to the point where chemists can place their investigations on a systematic basis.

This review has shown that vibrational spectroscopy already plays a significant role in a very varied range of chemistry in supercritical fluids and clearly the range will become still broader in the future. In some areas the role of spectroscopy is central to the whole investigation while, in others, the role is to provide diagnostics for optimizing a process. In selecting our examples, we have not tried to be encyclopaedic but rather we hope to have described a sufficient number of applications for individual readers to judge whether such measurements might usefully be applied to their own particular problems. It is important, however, to repeat the fact that we have largely ignored those areas already covered in Buback's review.[4] Neither have we had the space to discuss the applications of UV/Vis spectroscopy and also some important areas of chemistry in supercritical fluids where vibrational spectroscopy has not yet been exploited fully. For example, supercritical fluids permit the use of enzymes in an essentially non-aqueous environment for reactions such as esterification.[107] Sievers and co-workers have shown that supercritical fluids have considerable promise for the deposition of thin films and coatings because their use eliminates the need for solvents which might leave residues and contaminate the resulting film.[108] Furthermore, the solvent power of supercritical fluids increases the range of possible precursor molecules for MOCVD (metal organic chemical vapor deposition because molecules can be induced into the gas phase at relatively low temperatures.[109] Lynch and co-workers have found that $scCO_2$ can be used for removal of solvent from thin films, originally deposited by wet chemistry, without destroying the integrity of the film.[110] Finally, we have not described the chemical possibilities of fluids with critical points at rather higher temperatures. For example, recent work by Wood et al. has shown that previously unknown metal sulfide complexes can be synthesized relatively simply from K_2S_4 and $[W(CO)_6]$ in supercritical ethylene diamine ($T_c = 320\,^{\circ}C$).[111]

We hope that our review has shown how many of the boundaries in traditional chemistry, analytical/spectroscopy/polymer/synthetic become blurred in supercritical chemistry or, like the liquid/gas boundary, may even disappear completely. The study of supercritical fluids should not be considered as the exclusive preserve of physical chemists and chemical engineers. When chemists have collaborated with scientists working with supercritical fluids, for example, Fox and Johnston, the outcome has been extremely successful.[140] There are now many laboratories throughout the world with expertise in handling supercritical fluids and we urge synthetic chemists to begin collaborating with them. Exciting new science will emerge.

We thank our co-workers, colleagues, and technical staff at Nottingham and our UK and overseas collaborators for their contribution to our work described within this review. We gratefully acknowledge financial support for this work from EPSRC Chemistry and Clean Technology (Grant nos. GR/H95464 and GR/J95065), from EC Human Capital and Mobility and COST programs, the Volkswagen Stiftung, Perkin-Elmer, BP International, BP Chemicals, Zeneca, NATO Laboratory Linkage Program and particularly to the Royal Society for providing a Leverhulme Senior Research Fellowship to M. P., a University Research Fellowship to S. M. H., and a Visiting Fellowship to S. G. K.

Received July 6, 1994 [A 72 IE]
German version: *Angew. Chem.* **1995**, *107*, 1409–1432

[1] M. A. McHugh, V. J. Krukonis, *Supercritical Fluid Extraction: Principles and Practice*, 2nd ed., Butterworth-Heinemann, Boston, **1994**.
[2] a) *Supercritical Fluid Technology* (Eds.: F. V. Bright, M. E. P. McNally) (*ACS Symp. Ser.* **1992**, *488*); b) *Extraction of Natural Products Using Near-Critical Solvents* (Eds.: M. B. King, T. R. Bott), Chapman & Hall, Glasgow, **1993**.
[3] R. W. Shaw, T. B. Brill, A. A. Clifford, C. A. Eckert, E. U. Franck, *Chem. Eng. News* **1991**, *69*, 26.
[4] M. Buback, *Angew. Chem.* **1991**, *103*, 658; *Angew. Chem. Int. Ed. Engl.* **1991**, *30*, 641.
[5] a) *Supercritical Fluid Science and Technology* (Eds.: K. P. Johnston, J. M. L. Penninger) (*ACS Symp. Ser.* **1989**, *406*); b) *Supercritical Fluid Engineering Science: Fundamentals and Applications* (Eds.: E. Kiran, J. F. Brennecke) (*ibid.* **1993**, *541*); c) *Supercritical Fluids – Fundamentals for Applications* (Eds.: E. Kiran, J. M. H. Sengers) (*NATO ASI Ser. Ser. E* **1994**, *273*).
[6] See C. J. Gregg, F. P. Stein, C. K. Morgan, M. Radosz, *J. Chem. Eng. Data* **1994**, *39*, 219.
[7] W. F. Sherman, A. A. Stadtmuller, *Experimental Techniques in High-Pressure Research*, Wiley, London, **1987**.
[8] R. Whyman in *Techniques for Vibrational Spectroscopic Measurements under High Pressures*, in *Laboratory Methods in Vibrational Spectroscopy* (Eds.: H. L. Willis), Wiley, London, **1987**, p. 281.
[9] W. H. Beattie, W. B. Maier, R. F. Holland, S. M. Freund, B. Stewart, *Proc. SPIE Int. Soc. Opt. Eng.* **1978**, *158*, 113.
[10] a) M. O. Bulanin, *J. Mol. Struct.* **1973**, *19*, 59; b) V. V. Bertsev in *Molecular Cryospectroscopy, Advances in Spectroscopy* (Eds.: R. J. H. Clark, R. E. Hester), Wiley, London, **1994**, chapter 1.
[11] S. Kim, K. P. Johnston, *Ind. Eng. Chem. Res.* **1987**, *26*, 1206.
[12] M. A. Healy, T. J. Jenkins, M. Poliakoff, *TrAC Trends Anal. Chem. Pers. Ed.* **1991**, *10*, 92.
[13] G. G. Yee, J. L. Fulton, J. P. Blitz, R. D. Smith, *J. Phys. Chem.* **1991**, *95*, 1403.
[14] a) S. M. Howdle, M. A. Healy, M. Poliakoff, J. M. Whalley in *Proc. Int. Symp. Supercrit. Fluids* (Eds.: M. Perrut), Societe Francaise de Chimie, Paris, **1988**, p. 967; b) S. M. Howdle, M. Poliakoff, *Supercritical Fluids – Fundamentals for Applications* (Eds.: E. Kiran, J. M. H. Sengers) (*NATO ASI Ser. Ser. E* **1994**, *273*, 527).
[15] a) A. I. Cooper, M. Poliakoff, unpublished; b) S. G. Kazarian, A. I. Cooper, M. Poliakoff, *Opt. Spectrosc.* **1994**, *76*, 242.
[16] See S. Ikawa, Y. Fujita, *J. Phys. Chem.* **1993**, *97*, 10607.
[17] D. Ben-Amotz, F. LaPlant, D. Shea, J. Gardecki, D. List, *ACS Symp. Ser.* **1992**, *488*, 18.
[18] M. L. Myrick, J. Kolis, E. Parsons, K. Chilke, M. Lovelace, W. Scrivens, *J. Raman Spectrosc.* **1994**, *25*, 59.
[19] S. M. Howdle, K. Stanley, V. K. Popov, V. N. Bagratashvili, *Appl. Spectrosc.* **1994**, *48*, 214.
[20] a) V. N. Bagratashvili, V. K. Popov, D. G. Robertson, S. M. Howdle, M. Poliakoff, M. W. George, E. Walsh, *Third Int. Symp. Supercrit. Fluids*, Strasbourg, France, **1994**, *1*, 337; b) D. G. Robertson, S. M. Howdle, unpublished.
[21] T. Andrews, *Proc. R. Soc. London* **1875**, *24*, 455.
[22] a) S. G. Kazarian, B. V. Lokshin, Y. M. Kimelfeld, R. B. Materikova, *Izv. Acad. Nauk SSSR Ser. Khim.* **1986**, 2603; b) B. V. Lokshin, S. G. Kazarian, A. G. Ginzburg, *J. Mol. Struct.* **1988**, *174*, 29.
[23] M. W. Raynor, G. F. Shilstone, K. D. Bartle, A. A. Clifford, M. Cleary, B. W. Cook, *J. High Resolut. Chromatogr.* **1989**, *12*, 301.
[24] V. J. Krukonis, M. A. McHugh, A. J. Seckner, *J. Phys. Chem.* **1984**, *88*, 2687.
[25] S. M. Howdle, M. A. Healy, M. Poliakoff, *J. Am. Chem. Soc.* **1990**, *112*, 4804.
[26] M. Poliakoff, J. J. Turner, in ref. [10b], Chapter 8.
[27] J. J. Turner, M. Poliakoff, S. M. Howdle, S. A. Jackson, J. G. McLaughlin, *Faraday Discuss. Chem. Soc.* **1988**, *86*, 271.
[28] A. Moustakas, E. Weitz, *Chem. Phys. Lett.* **1992**, *191*, 264.
[29] M. Jobling, PhD Thesis, University of Nottingham, UK, **1992**.
[30] R. M. Smith, *Supercritical Fluid Chromatography*, Royal Society of Chemistry, London, **1988**.
[31] a) *Analytical Supercritical Fluid Chromatography and Extraction* (Eds.: M. L. Lee, K. E. Markides), Chromatography Conferences, Provo, UT, **1990**; b) *Applications of Supercritical Fluids in Industrial Analysis* (Hrsg.: J. R. Dean), Chapman & Hall, Glasgow, **1993**; c) *Analysis with Supercritical Fluids: Extraction and Chromatography* (Ed.: B. Wenclawiak), Springer, Berlin, **1992**.
[32] a) *Hyphenated Techniques in Supercritical Fluid Chromatography and Extraction* (Ed.: K. Jinno) (*J. Chromatogr. Libr.* **1992**, *53*); b) D. L. Heglund, D. C. Tilotta, S. B. Hawthorne, D. J. Miller, *Anal. Chem.* **1994**, *66*, 3543.
[33] a) S. B. French, M. Novotny, *Anal. Chem.* **1986**, *58*, 164; b) S. V. Olesik, S. B. French, M. Novotny, *Chromatographia* **1984**, *18*, 489.
[34] S. Shah, M. Ashraf-Khorassani, L. T. Taylor, *Chromatographia* **1988**, *25*, 631; L. T. Taylor, E. M. Calvey, *Chem. Rev.* **1989**, *89*, 321.
[35] T. J. Jenkins, G. Davidson, M. A. Healy, M. Poliakoff, *J. High Resolut. Chromatogr.* **1992**, *15*, 819.
[36] T. J. Jenkins, M. Kaplan, G. Davidson, M. A. Healy, M. Poliakoff, *J. Chromatogr.* **1992**, *53*, 626.
[37] P. Morin, C. Beccard, M. Caude, R. Rosset, *HRC & CC J. High Resolut. Chromatogr. Chromatogr. Commun.* **1988**, *11*, 697.
[38] Y. Garrabos, V. Chandrasekharan, M. A. Echargui, F. Marsault-Herail, *Chem. Phys. Lett.* **1989**, *160*, 250.
[39] F. Salmoun, J. Dubessy, Y. Garrabos, F. Marsault-Herail, *J. Raman Spectrosc.* **1994**, *25*, 281.
[40] B. J. Hrnjez, A. J. Mehta, M. A. Fox, K. P. Johnston, *J. Am. Chem. Soc.* **1989**, *111*, 2662.
[41] S. Akimoto, O. Kajimoto, *Chem. Phys. Lett.* **1993**, *209*, 263.
[42] G. G. Yee, J. L. Fulton, R. D. Smith, *J. Phys. Chem.* **1992**, *96*, 6172.
[43] Y. Yagi, H. Tsugane, H. Inomata, S. Saito, *J. Supercrit. Fluids* **1993**, *6*, 139.
[44] T. W. Zerda, X. Song, J. Jonas, *Appl. Spectrosc.* **1986**, *40*, 1194.
[45] P. Battersby, J. R. Dean, S. M. Hitchen, W. R. Tomlinson, P. M. Myers, *J. Comput. Chem.* **1994**, *15*, 580.
[46] D. A. Masten, B. R. Foy, D. M. Harradine, R. B. Dyer, *J. Phys. Chem.* **1993**, *97*, 8557.
[47] S. M. Howdle, V. N. Bagratashvili, *Chem. Phys. Lett.* **1993**, *214*, 215.
[48] C. A. Eckert, B. L. Knutson, *Fluid Phase Equilib.* **1993**, *83*, 93.
[49] a) R.-S. Wu, L. L. Lee, H. D. Cochran, *Ind. Eng. Chem. Res.* **1990**, *29*, 977; b) C. B. Roberts, J. E. Chateauneuf, J. F. Brennecke, *J. Am. Chem. Soc.* **1992**, *114*, 8455; c) Y.-P. Sun, *ibid.* **1993**, *115*, 3340; c) J. Zagrobelny, F. V. Bright, *ibid.* **1992**, *114*, 7821; d) K. P. Johnston, S. Kim, *AIChE J.* **1987**, *33*, 1603; e) J. A. O'Brien, T. W. Randolph, C. Carlier, S. Ganapathy, *ibid.* **1993**, *39*, 1061; f) C. Carlier, T. W. Randolph, *ibid.* **1993**, *39*, 876; g) T. W. Randolph, J. A. O'Brien, S. Ganapathy, *J. Phys. Chem.* **1994**, *98*, 4173; h) A. Morita, O. Kajimoto, *ibid.* **1990**, *94*, 6420; i) P. G. Debenedetti, *Chem. Eng. Sci.* **1987**, *42*, 2203; k) P. G. Debenedetti, I. B. Petsche, R. S. Mohamed, *Fluid Phase Equilib.* **1989**, *52*, 347.
[50] a) J. F. Brennecke, D. L. Tomasko, J. Peshkin, C. A. Eckert, *Ind. Eng. Chem. Res.* **1990**, *29*, 1682; b) J. F. Brennecke, C. A. Eckert, *ACS Symp. Ser.* **1989**, *406*, 14; c) Y. P. Sun, G. Bennett, K. P. Johnston, M. A. Fox, *Anal. Chem.* **1992**, *64*, 1763; d) Y.-P. Sun, M. A. Fox, *J. Phys. Chem.* **1993**, *97*, 282; e) D. L. Tomasko, B. L. Knutson, J. M. Coppom, W. Windsor, B. West, C. A. Eckert, *ACS Symp. Ser.* **1993**, *541*, 220; f) J. Zagrobelny, T. A. Betts, F. V. Bright, *J. Am. Chem. Soc.* **1992**, *114*, 5249; g) J. Zhang, F. V. Bright, *J. Phys. Chem.* **1992**, *96*, 5633.
[51] D. L. Tomasko, B. L. Knutson, F. Pouillot, C. L. Liotta, C. A. Eckert, *J. Phys. Chem.* **1993**, *97*, 11823.
[52] R. Ravi, L. E. S. deSouza, D. Ben-Amotz, *J. Phys. Chem.* **1993**, *97*, 11835.
[53] a) F. C. Knopf, X. Xu, S.-C. Yu, R. Lingle in *Second Int. Symp. Supercrit. Fluids* (Ed.: M. A. McHugh), Johns Hopkins University, Baltimore, **1991**, p. 154; b) C. Lienau, J. C. Williamson, A. H. Zewail, *Chem. Phys. Lett.* **1993**, *213*, 289.

[54] a) J. M. Walsh, M. D. Donohue, *Fluid Phase Equilib.* **1989**, *52*, 397; b) A. I. Cooper, S. M. Howdle, C. Hughes, M. Jobling, S. G. Kazarian, M. Poliakoff, L. A. Shepherd, K. P. Johnston, *Analyst* **1993**, *118*, 1111.

[55] K. E. O'Shea, K. M. Kirmse, M. A. Fox, K. P. Johnston, *J. Phys. Chem.* **1991**, *95*, 7863.

[56] G. C. Pimentel, A. L. McClellan, *The Hydrogen Bond*, Freeman, San Francisco. **1960**.

[57] a) *Intermolecular Forces: an Introduction to Modern Methods and Results* (Eds.: P. L. Huyskens, W. A. P. Luck, T. Zeegers-Huyskens), Springer, Berlin, **1991**; b) A. V. Iogansen, G. A. Kurkchi, V. M. Furman, V. P. Glazunov, S. E. Odinokov, *Zh. Prikl. Spectrosk.* **1980**, *33*, 460.

[58] Y. Yagi, S. Saito, H. Inomata, *J. Chem. Eng. Jpn.* **1993**, *26*, 116.

[59] J. Via, L. T. Taylor, F. K. Schweighardt, *Anal. Chem.* **1994**, *66*, 1459.

[60] J. L. Fulton, G. G. Yee, R. D. Smith, *J. Am. Chem. Soc.* **1991**, *113*, 8327.

[61] J. L. Fulton, G. G. Yee, R. D. Smith, *ACS Symp. Ser.* **1993**, *541*, 175.

[62] R. B. Gupta, J. R. Combes, K. P. Johnston, *J. Phys. Chem.* **1993**, *97*, 707.

[63] S. G. Kazarian, P. A. Hamley, M. Poliakoff, *J. Am. Chem. Soc.* **1993**, *115*, 9069.

[64] J. M. DeSimone, Z. Guan, C. S. Elsbernd, *Science* **1992**, *257*, 945.

[65] a) K. E. Laintz, C. M. Wai, C. R. Yonker, R. D. Smith, *J. Supercrit. Fluids* **1991**, *4*, 194; b) Y. Lin, R. D. Brauer, K. E. Laintz, C. M. Wai, *Anal. Chem.* **1993**, *65*, 2549.

[66] S. G. Kazarian, R. G. Gupta, M. J. Clarke, K. P. Johnston, M. Poliakoff, *J. Am. Chem. Soc.* **1993**, *115*, 11099.

[67] H. Inomata, Y. Yagi, M. Saito, S. Saito, *J. Supercrit. Fluids* **1993**, *6*, 237.

[68] V. K. Popov, J. A. Banister, V. N. Bagratashvili, S. M. Howdle, M. Poliakoff, *J. Supercrit. Fluids* **1994**, *7*, 69.

[69] H. Ochel, G. M. Schneider, *Ber. Bunsenges. Phys. Chem.* **1994**, *98*, 610.

[70] S. G. Kazarian, M. Jobling, M. Poliakoff, *Mendeleev Commun.* **1993**, 148.

[71] B. V. Lokshin, S. G. Kazarian, A. G. Ginzburg, *Izv. Akad. Nauk SSSR Ser. Khim.* **1988**, 333.

[72] C. A. Eckert, D. Suleiman, C. L. Liotta, D. L. Boatwright, unpublished.

[73] a) R. D. Smith, J. P. Blitz, J. L. Fulton, *ACS Symp. Ser.* **1989**, *406*, 1; b) J. P. Blitz, J. L. Fulton, R. D. Smith, *Appl. Spectrosc.* **1989**, *43*, 812; c) G. G. Yee, J. L. Fulton, R. D. Smith, *Langmuir* **1992**, *8*, 377.

[74] R. D. Smith, J. L. Fulton, J. P. Blitz, J. M. Tingey, *J. Phys. Chem.* **1990**, *94*, 781.

[75] J. L. Fulton, J. P. Blitz, J. M. Tingey, R. D. Smith, *J. Phys. Chem.* **1989**, *93*, 4198.

[76] G. J. McFann, K. P. Johnston, S. M. Howdle, *AIChE J.* **1994**, *40*, 543.

[77] a) K. D. Bartle, A. A. Clifford, S. B. Hawthorne, J. J. Lagenfield, D. J. Miller, R. Robinson, *J. Supercrit. Fluids* **1990**, *3*, 143; b) K. D. Bartle, T. Boddington, A. A. Clifford, N. J. Cotton, C. J. Dowle, *Anal. Chem.* **1991**, *63*, 2371; c) K. D. Bartle, T. Boddington, A. A. Clifford, S. B. Hawthorne, *J. Supercrit. Fluids* **1992**, *5*, 207.

[78] S. M. Howdle, J. M. Ramsay, A. I. Cooper, *J. Polym. Sci. Part B: Polym. Phys.* **1994**, *32*, 541.

[79] B. J. Briscoe, S. Zakaria, *Polymer* **1990**, *31*, 440.

[80] M. Jobling, S. M. Howdle, M. Poliakoff, *J. Chem. Soc. Chem. Commun.* **1990**, 1762.

[81] R. G. Ball, W. A. G. Graham, D. M. Heinekey, J. K. Hoyano, A. D. McMaster, B. M. Mattson, S. T. Michel, *Inorg. Chem.* **1990**, *29*, 2023.

[82] A. I. Cooper, S. G. Kazarian, M. Poliakoff, *Chem. Phys. Lett.* **1993**, *206*, 175.

[83] a) A. J. Rest, *J. Mol. Struct.* **1990**, *222*, 87; b) A. K. Campen, A. J. Rest, K. Yoshihara, *J. Photochem. Photobiol. A* **1991**, *55*, 301.

[84] E. V. Sullenberger, S. F. Dressman, A. C. Michael, *J. Phys. Chem.* **1994**, *98*, 5347.

[85] J. J. Turner in *Photoprocesses in Transition Metal Complexes, Biosystems and other Systems* (Ed.: E. Kochanski), Kluwer, Dordrecht, **1992**, p. 113.

[86] R. N. Perutz, *Chem. Soc. Rev.* **1993**, *22*, 361.

[87] R. K. Upmacis, M. Poliakoff, J. J. Turner, *J. Am. Chem. Soc.* **1986**, *108*, 3645.

[88] a) R. Whyman, *J. Organomet. Chem.* **1973**, *56*, 339; b) F. L'Eplattenier, F. Calderazzo, *Inorg. Chem.* **1968**, *7*, 1290.

[89] *Transition Metal Hydrides* (Ed.: A. Dedieu), VCH, New York, **1992**.

[90] For a recent review on silane compexes: U. Schubert, *Adv. Organomet. Chem.* **1990**, *30*, 151.

[91] a) A. A. Gonzalez, K. Zhang, S. P. Nolan, R. L. Vega, S. L. Mukherjee, C. D. Hoff, G. J. Kubas, *Organometallics* **1988**, *7*, 2429; b) A. A. Gonzalez, C. D. Hoff, *Inorg. Chem.* **1989**, *28*, 4295.

[92] a) J. R. Wells, E. Weitz, *J. Am. Chem. Soc.* **1992**, *114*, 2783; b) B. H. Weiller, *ACS Symp. Ser.* **1993**, *530*, 164.

[93] a) M. Poliakoff, S. M. Howdle, M. Jobling, M. W. George, *Second Int. Symp. Supercrit. Fluids* (Ed.: M. A. McHugh), Johns Hopkins University, Baltimore. **1991**, p. 189; b) M. W. George, M. Poliakoff, J. J. Turner, *Analyst* **1994**, *119*, 551; c) S. G. Kazarian, R. B. Gupta, K. P. Johnston, M. J. Clarke, M. W. George, M. Poliakoff, *Third Int. Symp. Supercrit. Fluids*, Strasbourg, France **1994**, *1*, 343.

[94] a) J. W. Rathke, R. J. Klingler, T. R. Krause, *Organometallics* **1991**, *10*, 1350; b) *ibid.* **1992**, *11*, 585; c) J. W. Rathke, R. J. Klingler ■firm■, US-A 5198589, **1994**; d) R. J. Klingler, J. W. Rathke, *J. Am. Chem. Soc.* **1994**, *116*, 4772.

[95] P. G. Jessop, T. Ikariya, R. Noyori, *Nature (London)* **1994**, *368*, 231.

[96] a) S. M. Howdle, P. Grebenik, R. N. Perutz, M. Poliakoff, *J. Chem. Soc. Chem. Commun.* **1989**, 1517; b) J. A. Banister, M. W. George, S. Grubert, S. M. Howdle, M. Jobling, F. P. A. Johnston, S. L. Morrison, M. Poliakoff, U. Schubert, J. R. Westwell, *J. Organomet. Chem.*, **1994**, *484*, 129.

[97] An exception, for example, is the reaction of hex-3-yne with $scCO_2$ catalyzed by a nickel complex: M. T. Reetz, W. Könen, T. Strack, *Chimia* **1993**, *47*, 493.

[98] M. Jobling, S. M. Howdle, M. A. Healy, M. Poliakoff, *J. Chem. Soc. Chem. Commun.* **1990**, 1287.

[99] M. B. Sponsler, B. H. Weiller, P. O. Stoutland, R. G. Bergman, *J. Am. Chem. Soc.* **1989**, *111*, 6841.

[100] A. I. Cooper, M. Poliakoff, unpublished.

[101] a) Y. Ikushima, N. Saito, M. Arai, *J. Phys. Chem.* **1992**, *96*, 2293; b) *Bull. Chem. Soc. Jpn.* **1991**, *64*, 282.

[102] a) „Drucksachen; ein Rundgang durch das Druck- und Hydrierlabor Roche Kaiseraugst", *Roche Magazin* **1992**, *41*, 2; b) K. H. Pickel, K. Steiner, *Third Int. Symp. Supercrit. Fluids*, Strasbourg, France, **1994**, *3*, 25.

[103] J. A. Banister, S. M. Howdle, M. Poliakoff, *J. Chem. Soc. Chem. Commun.* **1993**, 1814.

[104] a) M. F. Gregory, S. A. Jackson, M. Poliakoff, J. J. Turner, *J. Chem. Soc. Chem. Commun.* **1986**, 1175; b) F.-W. Grevels, J. Jacke, S. Ozkar, *J. Am. Chem. Soc.* **1987**, *109*, 7536; c) B. H. Weiller, E. R. Grant, *ibid.* **1987**, *109*, 1252.

[105] S. M. Howdle, M. Poliakoff, *J. Chem. Soc. Chem. Commun.* **1989**, 1099.

[106] M. Poliakoff, J. A. Banister, P. D. Lee in *XVIth Organomet. Chem. Conf. 1994*, U.K; *Organometallics*, in press.

[107] a) S. V. Kamat, B. Iwaskewycz, E. J. Beckman, A. J. Russell, *Proc. Natl. Acad. Sci. USA* **1993**, *90*, 2940; b) O. Aaltonen, M. Rantakyla, *CHEMTECH* **1991**, 240; c) A. J. Russell, E. J. Beckman, A. K. Chaudhary, *ibid.* **1994**, 33.

[108] B. N. Hansen, B. M. Hybertson, R. M. Barkley, R. E. Sievers, *Chem. Mater.* **1992**, *4*, 749.

[109] V. K. Popov, V. N. Bagratashvili, S. M. Howdle, O. A. Louchev, E. A. Antonov, G. V. Mishakov, *Third Int. Symp. Supercrit. Fluids*, Strasbourg, France, **1994**, *3*, 369.

[110] L. T. Canham, A. G. Cullis, C. Pickering, O. D. Dosser, T. I. Cox, T. P. Lynch, *Nature (London)* **1994**, *368*, 133.

[111] a) P. T. Wood, W. T. Pennington, J. W. Kolis, B. Wu, C. J. O'Connor, *Inorg. Chem.* **1993**, *32*, 129; b) P. T. Wood, W. T. Pennington, J. M. Kolis, *J. Chem. Soc. Chem. Commun.* **1993**, 235.

[112] R. C. Reid, J. M. Prausnitz, B. E. Poling, *The Properties of Gases and Liquids*, 4th ed., McGraw-Hill, New York, **1986**.

[113] See, for example: D. E. Raynie, *Anal. Chem.* **1993**, *65*, 3127.

Recent Trends in Photoaffinity Labeling

Florence Kotzyba-Hibert, Isabelle Kapfer, and Maurice Goeldner*

Dedicated to the memory of Christian Hirth

Investigation of receptor–ligand interactions remains an inexhaustible challenge for chemists and biologists. Structural exploration of biological receptors is the starting point for a better understanding of how they function. Photoaffinity labeling is a biochemical approach to identify and characterize receptors targeting further structural investigations. The primary structure of a receptor protein was typically obtained by reverse genetics after exhaustive purification and sequencing of the N-terminal peptide, which allowed the design of the corresponding oligonucleotide probes. Synthesis of these oligonucleotide probes then led to identification of cDNA clones by hybridization. Following this strategy, several membrane neurotransmitter receptors and constituent polypeptides, present in very small quantities in the central nervous system, were identified and their sequence deduced from the cDNA sequence. Since photoaffinity labeling implies the formation of a covalent bond between a radiolabeled ligand analogue and a receptor binding site, it becomes theoretically possible to isolate and sequence radiolabeled peptides and then synthesize the corresponding oligonucleotide probes. Photoaffinity labeling might avoid the critical solubilization and purification steps of the classical approach. To our knowledge, no such example of primary structure determination based on photoaffinity labeling experiments has been reported. However, the extraordinary developments in gene cloning technologies, in particular homology cloning and expression cloning, have made this approach obsolete and raised the question of new perspectives for photoaffinity labeling technology. In this article we present an update on selected original developments, as well as new challenges for this method. Photoaffinity labeling not only gives access to structural elements but is also a potential tool for the investigation of functional aspects of biological receptors, for example their role in signal transduction mechanisms.

Keywords: amino acids · photoaffinity labeling · proteins · reactive intermediates · structure elucidation

1. Introduction

Discovered over thirty years ago by Westheimer et al.,[1] photoaffinity labeling has evolved considerably, although the basic principle remains unchanged. Photoaffinity labeling requires the use of a photoactivatable but chemically inert ligand analogue, which by the action of light produces a highly reactive species that binds irreversibly to the biological receptor at the site of interaction. Figure 1 illustrates the different levels of structural information that can be expected from such labeling studies. Photoaffinity labeling has been thoroughly reviewed,[2–4] and a complete study of the photochemical reagents as well as an analysis of the photolabeling experiments can be found in Bayley's monograph.[5a]

Several hundred recent articles refer to photoaffinity labeling as a tool for labeling polypeptides with photoactivatable ligand analogues. In many cases these radiolabeled ligands allowed the characterization of functional proteins on sodium dodecylsulfate (SDS) gels. However, only a few of these experiments led to the identification of the amino acid residues labeled by the photosensitive probes (Fig. 1). This ultimate step gives important structural information, the position of the binding site on the primary structure of a receptor and precise data on the ligand–receptor interaction. Other, more chemically oriented articles describe new photosensitive functional groups for potential application in photoaffinity labeling. In some cases, efforts have been made to understand the photochemical reaction by studying the reactivity of the photogenerated species.

The present article concentrates on a few types of photoaffinity reagents: fluoroaryl azides, because of their promising photolabeling potential, and aryldiazonium salts and trifluoromethylaryldiazirines, because of their efficient photocoupling properties to proteins. With respect to the biochemical aspects of photoaffinity labeling, this article also highlights the contribution of the target protein in photoaffinity labeling reactions.

[*] Prof. M. Goeldner, Dr. F. Kotzyba-Hibert, Dr. I. Kapfer
Laboratoire de Chimie Bio-organique, URA 1386 CNRS, Faculté de Pharmacie
Université Louis Pasteur Strasbourg
BP 24, F-67401 Illkirch Cédex (France)
Telefax: Int. code + 8867-8891

 © VCH Verlagsgesellschaft mbH, D-69451 Weinheim, 1995 0570-0833/95/1212-1297 $ 10.00+.25/0

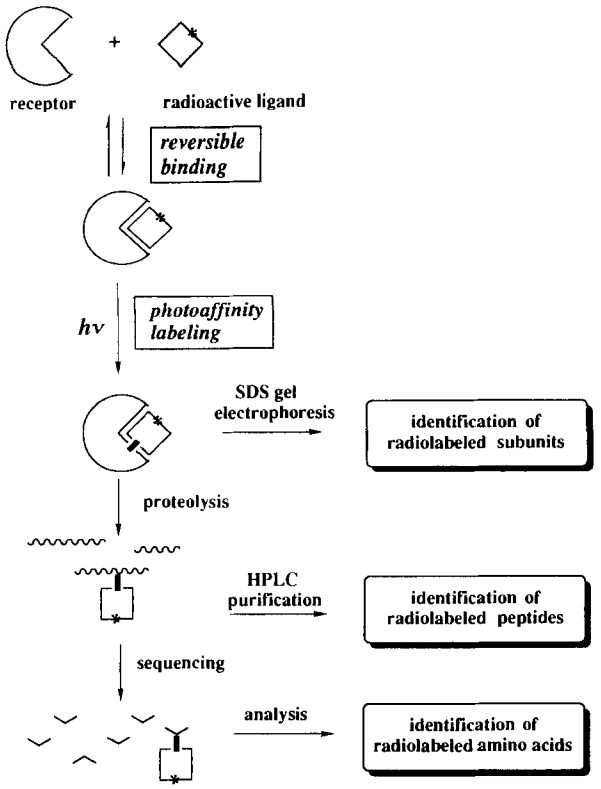
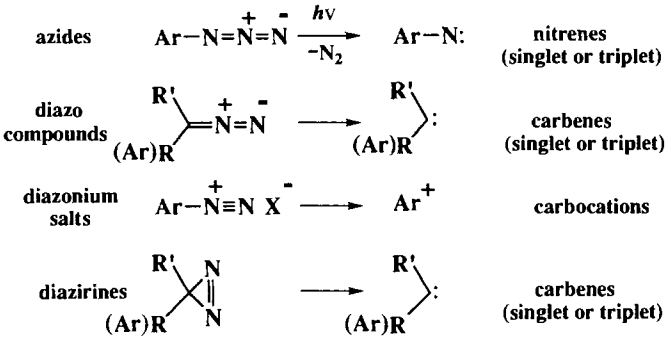


Fig. 1. Photoaffinity labeling: principle and successive steps for the identification of amino acids.

2. The Search for Ideal Photoaffinity Probes

Much time has been devoted to elaborating new chemical functions that could be used in photoaffinity labeling experiments. This search was mainly directed towards analogues of previously described photosensitive chemicals rather than towards finding truly new chemical functions. This is not surprising when one considers that the photochemical generation of a highly reactive species is generally accompanied by the production of a stabilized counterpart, ideally a gaseous compound. This is the criterion that has restricted the area of investigation. Photochemical fragmentations that induce the release of nitrogen make up the majority of documented examples, since nitrogen is an inert gas and several chemical functions can serve as precursors, for example azido, diazo, and azo groups, diazirines, and diazonium ions. These functional groups serve as precursors of reactive species such as nitrenes, carbenes, radicals, and carbocations (Scheme 1). Among these probes, aryl azides are by far the most frequently used photoaffinity labels. This popularity is more related to their chemical stability in the dark and their ready synthesis rather than to their intrinsic photochemical properties.



Scheme 1. Typical compounds used as precursors of reactive species in photoaffinity labeling.

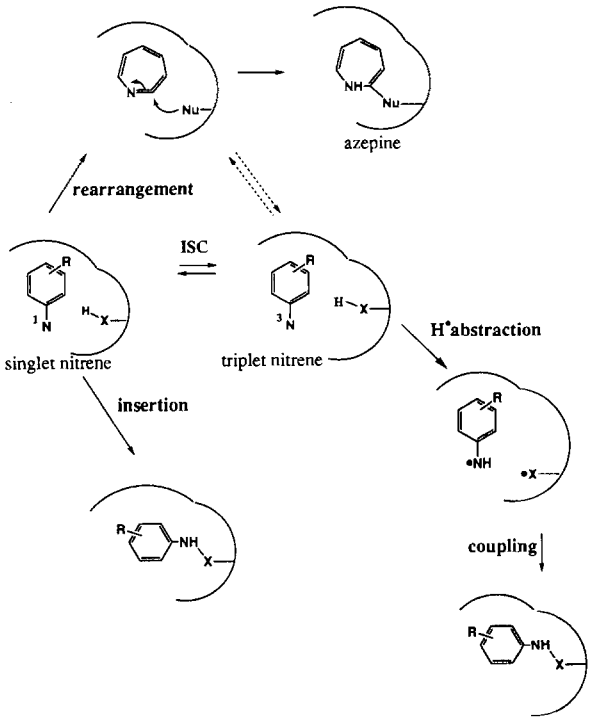
2.1. The Aryl Azide Series

2.1.1. Towards a Better Understanding of the Photochemical Reaction

The photochemistry of aryl azides has often been considered confusing essentially because of the contradictory results obtained with different aryl azides in photoaffinity labeling experiments. Since their discovery in 1969 by Knowles et al.,[6] many substituted aryl azides have been developed such as nitro-substituted derivatives,[7] which can be activated at wavelengths beyond the protein absorption region. It has now been shown that the nature of the substituent on the aromatic ring influences the photochemical reaction and thus the chemical reactivity of the photogenerated intermediate.[8] Recent photochemical studies, mainly from the groups of Schuster and Platz, have elucitated these photochemical reactions.[9] Upon irradiation, an azide is promoted to a singlet excited state which either loses nitrogen to form singlet nitrene or undergoes intersystem crossing (ISC) to triplet azide, which in turn can lose nitrogen to form triplet nitrene. A simplified picture (Scheme 2) starts with singlet nitrene, which can either insert into a carbon–hydrogen or



Maurice Goeldner was born in 1945 in Strasbourg, France, where he studied chemistry at the Université Louis Pasteur. He received his doctorate in 1972 under the direction of Dr. J. F. Biellmann, and during this time he conducted research at the Centre National de la Recherche Scientifique in Strasbourg. After postdoctoral studies with Prof. S. Wolfe (Kingston, Canada) and Prof. A. Eschenmoser (ETH, Zürich, Switzerland), he returned to Strasbourg to codirect, with his friend Christian Hirth, the Laboratoire de Chimie Bio-organique. In 1983 Goeldner was appointed Professor of Organic Chemistry at the Faculté de Pharmacie. His research interests focus on bioorganic chemistry, in particular, the structural determinants of membrane receptors investigated by site-directed labeling methods.



Scheme 2. Possible mechanisms for the coupling of arylnitrenes to biological receptors. ISC = intersystem crossing.

heteroatom–hydrogen bond, rearrange to the corresponding didehydroazepine, or undergo intersystem crossing to triplet nitrene. These intermediates lead to different reactions in photoaffinity labeling experiments:

a) A quasi-nondiscriminative insertion reaction with any amino acid residue or with the solvent is expected in the case of singlet nitrene.

b) A reaction with an appropriate nucleophile may follow formation of the didehydroazepine; possible nucleophiles are cysteinyl and histidinyl residues, while side chains with hydroxyl groups and the protonated lysine side chain are probably not sufficiently nucleophilic. For example, it has been shown that methanol does not react with didehydroazepines.[10]

c) Triplet nitrene leads to less predictable radical chemistry (see Section 2.3).

With few exceptions, such as the fluorinated aryl azide and the azidonucleotides (see Sections 2.1.2 and 2.1.3), aryl azides either rearrange to the corresponding didehydroazepines or convert to the triplet nitrene; insertion reactions of singlet nitrene are not observed.[8] Schuster et al. have clearly demonstrated the influence of the substituent on the aromatic ring on the photochemical reaction (Table 1). The complexity of the reaction is demonstrated by the completely opposite reactivity of the *para*-chloro- and the *para*-dimethylaminophenyl azides. Irradiation of *para*-chlorophenyl azide in cyclohexane in the presence of diethylamine as nucleophile gave the azepine in 100% yield, whereas *para*-dimethylaminophenyl azide led to compounds arising from radical chemistry. Thus, for photoaffinity labeling experiments using aryl azides, the course of the labeling reaction depends not only on the nature of the substituents on the aromatic ring but also on the presence of a nucleophilic residue in the binding site. Therefore, predictions

Table 1. Yields of the products formed by irradiation of aryl azides $XC_6H_4N_3$ in cyclohexane alone and in the presence of diethylamine [8]. The azo compounds and the anilines arise from triplet nitrene coupling, the azepines from singlet nitrene coupling.

X	Azo compound [%]	^3H-Azepine [%][a]	Aniline [%][a]
H	15	80	–
p-Ph	55	71	10
p-SMe	71	51	18
p-OMe	80	27	30
p-NMe_2	92	0	44
p-CO_2H	–	70	15
p-$CONMe_2$	70	74	trace
p-$COCH_3$	87	70	30
p-CN	74	68	10
m-NO_2	50	10	30
p-NO_2	73	<3	80
p-Cl	80	100	–
p-Br	80	71	trace
p-I	96	34	12

[a] Photolysis in the presence of Et_2NH.

concerning the course of photoaffinity labeling experiments using aryl azides are practically impossible.

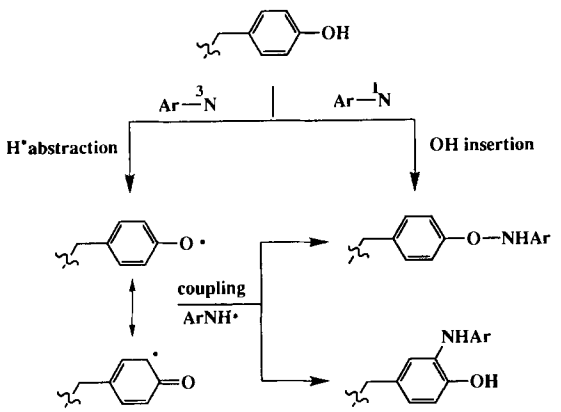
For the photochemical coupling of aryl azides to receptors, nucleophilic addition to the didehydroazepine might be of limited use since the azepines obtained are not always stable to the proteolytic conditions typically used for peptide and amino acid identification. On the other hand, many successful labeling reactions with aryl azides reacting as triplet nitrenes have been observed. Radical chemistry involves a multistep process for the coupling reaction between the ligand and the receptor. The abstraction of a hydrogen radical from the protein by the triplet nitrene and combination of the newly formed radicals to give the covalent bond are shown in Scheme 2. In the context of the receptor, this reaction raises the question of which amino acid residues are likely to form stabilized radicals (see Section 2.3).

An interesting observation made by Platz et al.[11] is that low-temperature photochemistry (77 K) favors the formation of triplet nitrene by preventing the rearrangement of singlet nitrene into didehydroazepine. This could be applied to *meta*-azidophenyl-substituted acylchymotrypsin; irradiation at 77 K led to increased irreversible photolytic inactivation of the enzyme. This phenomenon, however, could not be applied successfully to the inactivation of the estrogen receptor.[12]

2.1.2. *Azidonucleotides*

Azidonucleotides are an interesting category of aryl azides. They are very often excellent nucleotide analogues with a minimum of chemical modification since the azido group is incorporated on the heterocyclic ring. They have been used successfully in many photoaffinity labeling studies. In particular, radiolabeled 2-azido-ATP,[13, 14] 2-azido-ADP,[15–17] 8-azido-ATP,[18, 19] 8-azido-GTP,[20] and 8-azido-cAMP[21] allowed the characterization of the labeled amino acid residues on the target receptor's binding site. By considering the different amino acid residues that have been labeled by these purinergic azido probes (Tyr, Trp, Lys, Thr, Leu, Ile, and Pro; see Section 4, Table 7), it is not possible to associate clearly singlet or triplet reactivity with the corresponding photogenerated nitrene. The reactivity of either singlet or triplet nitrene could account for the observed

results. Nucleophilic addition on the nucleotide-derived didehydroazepine seems unlikely, unless tyrosinate ions are involved. Scheme 3 illustrates the possible insertion mechanisms on the tyrosine side chain by both nitrene species; tyrosine is the amino acid most frequently labeled with these purinergic azido probes (15 examples of tyrosine labeling are listed in Table 7). A structural analogy with carbonyl azide, known to generate highly



Scheme 3. Possible reaction mechanisms for the insertion of singlet or triplet nitrenes in the tyrosine side chain.

reactive nitrenes,[22] has been proposed for the nucleotide azides.[5b] It is certain that precise kinetic data and in particular the determination of the lifetime of the corresponding singlet nitrene, as well as the rates of rearrangement to didehydroazepine and to triplet nitrene, would be very valuable for a clearer understanding of the photochemical reactions involving these azidonucleotides.

2.1.3. *Fluorinated Aryl Azides*

The fluorinated aryl azides constitute by far the most promising development in the aryl azide series for photoaffinity labeling. In early findings, Banks et al.[23] described the thermolysis of fluorinated aryl azides and demonstrated C–H insertion in mesitylene and trimethoxybenzene. A detailed study of the photochemical reaction reported by Platz et al.[10, 24–27] led to the conclusion that singlet fluorinated arylnitrene rearranges more slowly to the corresponding didehydroazepine than the unsubstituted species, thus allowing this intermediate to react with most chemical bonds, including C–H bonds, by formal insertion (Table 2). New functionalized fluorinated aryl azides have been synthesized as potential photoaffinity probes.[28, 29] Few examples of photochemical cross-linking[30] and photoaffinity labeling[12, 31–33] using such derivatives have been published. Comparative photoaffinity labeling studies between fluorinated and non-fluorinated arylazido photoaffinity probes led to contradictory results. In one case labeling results were comparable with the two probes,[12] while in the second case the fluorinated probe was more effective.[34] Care should be taken in analyzing these results, especially in the absence of data demonstrating analogous positioning of these probes within the target binding site. A recent study on fluorinated aryl azides substituted in different positions on the aromatic ring established a precise correlation between the reactivity and the substitution pattern.[35] The 4-substituted 2,6-difluorophenyl azides demonstrate maximum reactivity with minimum fluorine substitution. It is suggested that these derivatives are able to react as singlet nitrene in an hydrophobic environment, while hydroxylated solvents catalyze intersystem crossing to triplet nitrene. Considering the implications for photoaffinity labeling, the authors claimed these reagents to be effective only in a hydrophobic environment through efficient insertion reactions in single bonds by means of the corresponding singlet nitrenes. They suggested that triplet nitrene reactivity in a hydrophilic environment leads to cleavage of the polypeptide rather than coupling to the biological receptor. However, this latter proposal can be questioned, when one considers the numerous successful examples of photoaffinity labeling experiments involving triplet nitrenes (see Section 2.3 and Table 7 for typical radical-issued photoaffinity labeling examples).

Table 2. Yield of singlet and triplet nitrene adducts formed on photolysis of pentafluorophenyl azide in various solvents RH (as trapping agent) [27].

Solvent	C_6F_5NHR [%]	$C_6F_5NH_2$ [%][a]	*trans*-$(C_6F_5)_2N_2$ [%][a]
cyclohexane	22	2	0
cyclopentane	28	0	0
cyclopentane[b]	4	12	5
tetramethylethylene	49	[c]	[c]
benzene	39	5	0
benzene[b]	0	6	32
toluene	51	12	0
toluene[b]	10	26	6
tetrahydrofuran	41	3	0
dimethyl sulfide	12	[c]	[c]
dimethyl sulfoxide	41	[c]	[c]
diethylamine	58	22	0

[a] Triplet nitrene adduct. [b] Triplet sensitized. [c] The yield was not determined, but the product was formed in only minor amounts.

Although fluorinated aryl azides can be activated only by light with wavelengths less than 300 nm, which might be harmful for sensitive proteins, these compounds fulfill most of the criteria of effective photoaffinity labeling reagents and should gradually replace the other commonly used aryl azides. In particular, phospholipidic probes incorporating fluorinated aryl azides are promising tools for the structural investigation of membrane receptors. The predicted singlet nitrene reactivity[35] should lead to insertion into C–H bonds, which is a prerequisite for efficient labeling of the hydrophobic amino acid residues of membrane proteins. Finally, the elaboration of synthetic strategies allowing the incorporation of radiolabeled isotopes in fluorinated aryl azide reagents[36, 37] should guarantee enormous success for these probes.

2.2. Efficient Photoaffinity Probes

In addition to the aryl azides, a great variety of other photosensitive compounds have been described as potential probes for photoaffinity labeling.[5a] We will describe two classes of very powerful probes, aryldiazonium salts and trifluoromethylaryldiazirines. Their remarkable ability to couple to proteins will be discussed in Section 5. We briefly summarize here their chemical and photochemical properties.

2.2.1. *Aryldiazonium Salts*

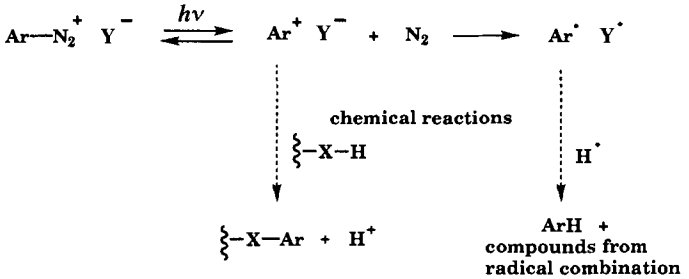
Aryldiazonium salts are often considered to be difficult to isolate and handle. This is certainly true for diazonium salts with electron-withdrawing substituents, which are unstable species under nonacidic conditions. On the other hand, electron-donating substituents in *ortho* and *para* position confer sufficient stability and also interesting photochemical properties to these species such as high quantum yields[38] and absorption at wavelengths greater than 300 nm (Table 3). Thus these derivatives are good candidates for photoaffinity probes.

Table 3. Absorption maxima λ_{max}, molar extinction coefficients ε, and quantum yields ϱ for several *para*- and *meta*-substituted diazonium ions $XC_6H_4N_2^+$.

X	λ_{max}[nm]	ε[$M^{-1}cm^{-1}$]	ϱ
p-NMe_2	379[a]	37500[a]	0.59[a]
p-OCH_3	313[a]	23500[a]	0.46[a]
p-I	326[a]	12500[a]	–
p-OH	350[b]	–	0.54[b]
p-N(Me)COMe	340[a]	16600[a]	–
m-OCH_3	273[a]	7300[a]	–
m-SO_3H	260[c]	11500[c]	–
m-NO_2	232[b]	–	0.17[b]

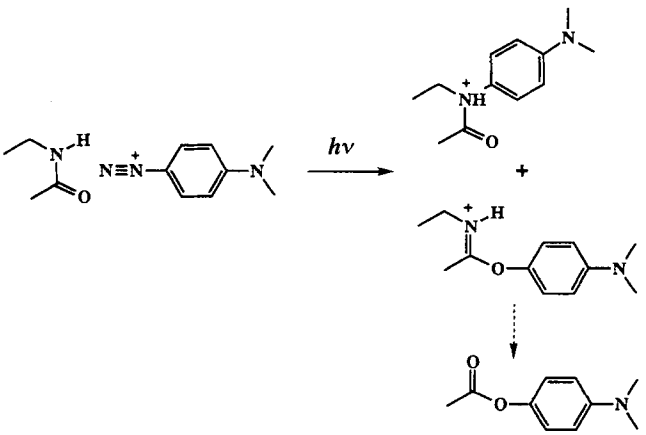
[a] Ref. [45]. [b] Ref. [38]. [c] Ref. [181].

The primary process in the photochemical decomposition is the formation of the corresponding aryl cation, which can undergo further photochemical reduction to give the corresponding aryl radical (Scheme 4). These transient species lead to different chemical reactions. Put simply, the presence of electron-withdrawing groups on the aromatic ring favors the electronic photoreduction process, whereas electron-donating substituents stabilize the cationic species by resonance. For instance, the photochemical reaction of *para*-nitrophenyldiazonium salts in alcohol gives nitrobenzene as the major product, while the *para*-dimethylamino derivative gives almost exclusively the corresponding ether derivative.[38]



Scheme 4. Photochemical reactivity of aryldiazonium salts $ArN_2^+Y^-$ and subsequent reactions. X = heteroatom, CR_2.

Aryl cations are highly reactive species,[39] whose lifetime has not yet been determined accurately. The lifetime of the phenyl cation in water has been determined indirectly by laser flash techniques to be less than 500 ps.[40] A direct study of the photochemical decomposition of aryl cations in hydrocarbon solvents, in which the C–H bond serves as a reference bond, is difficult due to the insolubility of these cations in such media. Nevertheless, a few examples of intramolecular reactions with C–H bonds have been described.[41, 42] In an original approach Speranza et al. generated an unsolvated aryl cation by radiolysis of tritiated benzene.[43] Several interesting aspects of the reactivity of the free aryl cation could be observed, including several efficient reactions with C–H bonds. The photochemical reaction of the *para*-dimethylaminophenyldiazonium ion (DDF) with the amide bond in *N*-ethylacetamide, as a model of a peptide bond, was tested.[44] Over 90% of the reaction led to an O- or N-alkylation process which was expected from the solvation of the charged moiety of the diazonium salt by the oxygen and nitrogen atoms (Scheme 5).

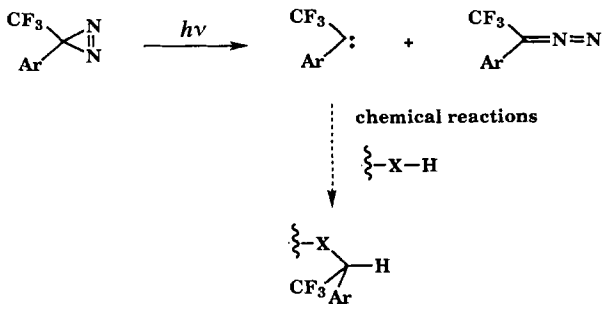


Scheme 5. Analysis of the photochemical reaction of the *p*-(*N*,*N*-dimethylamino)-phenyldiazonium ion with *N*-ethylacetamide [44].

Aryldiazonium salts with electron-donating substituents meet all the criteria of potential photoaffinity probes,[45] and we have used them extensively in our group for the labeling of cholinergic proteins; the binding site for the quaternary ammonium group could be efficiently probed by the charged diazonium species. Several examples will be described in detail in Sections 4 and 5.

2.2.2. *Trifluoromethylaryldiazirines*

Aryldiazirine derivatives were initially described by Smith and Knowles[46] as potential photoaffinity probes. The search in this series for powerful reagents led to the discovery of trifluoromethylaryldiazirines,[47] which show favorable photochemical properties in addition to excellent chemical stability. On irradiation the diazirine either undergoes fragmentation to the corresponding carbene or isomerizes to a linear diazo compound (Scheme 6). The rearrangement products are long-lived species under the diazirine irradiation conditions and have led to undesired alkylation reactions in the dark.[48] This problem was overcome with trifluoromethylaryldiazirines. Photolysis in cyclohexane gives C–H insertion products in satisfactory yields,[49] whereas in alcohols O–H insertion reactions are the main reactions; both reactions are attributed to the singlet reactivity of the carbene. Other reactions involving triplet carbenes have been observed during the photolysis in alcohols[50] (Table 4).



Scheme 6. Photochemical reactivity of diazirines and subsequent reactions. X = heteroatom, CR_2.

Table 4. Distribution of products obtained on photolysis of two 3-trifluoromethyl-3-aryl-3*H*-diazirines in organic solvents [49a].

Ar	c[mM]	Solvent	Product	Yield[%]
C_6H_5	3	MeOH	$ArCH(OCH_3)CF_3$	95
	3	C_6H_{12}	$ArCH(OC_6H_{11})CF_3$	55
$C_6H_4CH_2CH(CP_2CH_3)$-NHCP$_2$*t*Bu	2	EtOH	$ArCH(OC_2H_5)CF_3$	73
			$ArCOCF_3$	17
			$ArCH_2(OH)CF_3$	6
			$ArCH_2CF_3$	5

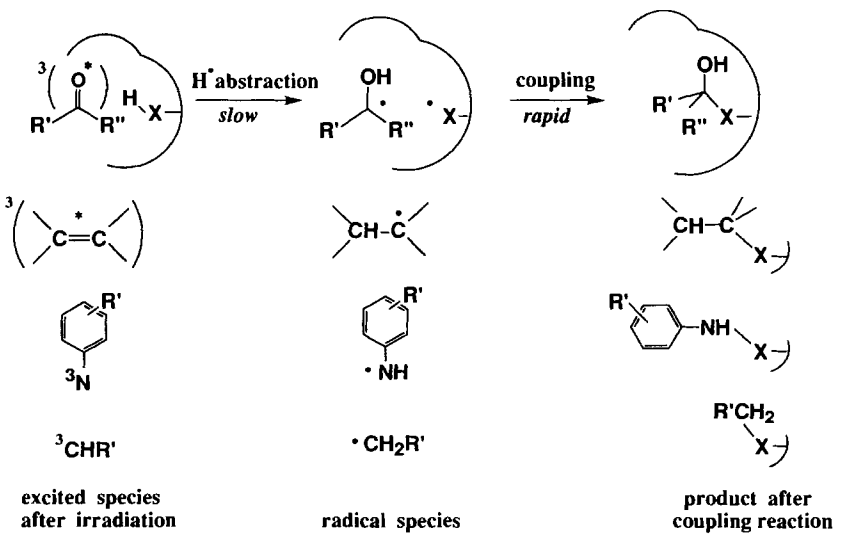
3-Trifluoromethyl-3-*meta*-iodophenyl-3*H*-diazirine (TID) synthesized by incorporation of [^{125}I] is an outstanding photoactivatable probe.[51] This reagent has been used successfully for hydrophobic labeling of membrane proteins,[49a] illustrating in particular the ability of the photogenerated carbene to react with nonactivated amino acid side chains. More recently,[52] TID has been used as a true photoaffinity probe by interaction with the noncompetitive blocker binding site of the nicotinic acetylcholine receptor. The observed outstanding photochemical labeling results will be described in Section 5.

2.3. Radical Reactions in Photoaffinity Labeling

Photochemically generated free radicals may couple with receptors in two different ways, either to the peptide backbone or to the amino acid side chains. Diradicals (triplet states from nitrenes, carbenes, excited ketones and alkenes) probably abstract a hydrogen radical from the receptor, and the two newly created radicals combine rapidly[5c] (Scheme 7). In the case of monoradical species, photogenerated for instance from aromatic halides, the coupling process is less obvious, since the hydrogen abstraction reaction results in the disappearance of the initially formed radical. Nevertheless, a delayed coupling between two radical species can always be postulated. Finally, a last type of radical mechanism might occur during the cleavage of disulfide bonds leading to the formation of stabilized thiol radicals, which ultimately combine with another radical species.

Acetophenones and benzophenones have been used extensively for photoaffinity labeling experiments and are typical examples of precursors of photogenerated radicals. The properties of the excited-state radicals generated from these aromatic ketones are well understood.[58] The physicochemical requirements for photoaffinity labeling using such aromatic ketones are fulfilled: the reactive triplet state does not rearrange, is easily generated at long wavelengths ($\lambda \geq 320$ nm), avoiding significant damage to aromatic amino acids of proteins,[53] and is able to insert into C–H bonds. Abstraction–addition reactions of the triplet radicals of aromatic ketones were first used for the selective introduction of functional groups at methylene positions in steroids and long-chain alcohols[55–57] and for photoaffinity labeling of the binding sites of peptide hormones.[58] Triplet radicals of aromatic ketones do not react efficiently with water,[59] a property claimed to be useful for photoaffinity labeling experiments.[54] However, reactive species not quenched by the solvent may lead to nonspecific labeling (Section 3).

At which sites do free radicals react with the protein, and which amino acid residues are involved in these reactions? The α-carbon radicals generated on the peptide backbone are stabilized through the synergistic effect of captodative substituents with opposite polarity.[60] However, this effect could not be experimentally determined in measurements of the thermodynamic reaction and activation parameters for the formation of α-cyano-α-methoxyalkyl radicals.[61] Preferential reactivity of glycine residues in free radical reactions with peptide model compounds has been observed and attributed to selective hydrogen atom abstraction from the α-carbon of the glycine moiety. This preference was unexpected, as glycine affords secondary radicals by homolysis of the C_α–H bond, whereas the analogous reaction on other amino acid derivatives produces thermodynamically favored tertiary radicals. This peculiar stability of the glycyl radical has been studied by Easton et al.[62–64] using the reactivity of NBS towards *N*-acylglycine derivatives. The stability has been attributed to a favorable conformation of the radical, which is planar and relatively free of nonbonding interactions, thus allowing maximum delocalization of the unpaired electron. In the presence of C_α-substituents unfavorable nonbonding interactions arise (Table 5). The preferential reactivity of glycine residues has also been demonstrated with a model



Scheme 7. Radical coupling of photogenerated triplet species to biological receptors through H' abstraction.

Table 5. Relative rate k_{rel} of the reaction of *N*-bromosuccinimide (NBS) with three amino acid derivatives $PhCONHCHRCO_2CH_3$ [62, 63].

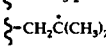
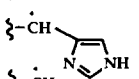
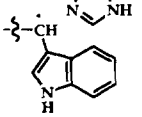
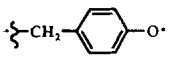
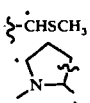
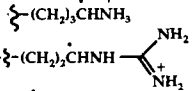
R	Corresponding amino acid	k_{rel}[a]
$(CH_3)_2CH$	valine	1
CH_3	alanine	7.7 ± 1.1
H	glycine	23 ± 3.5

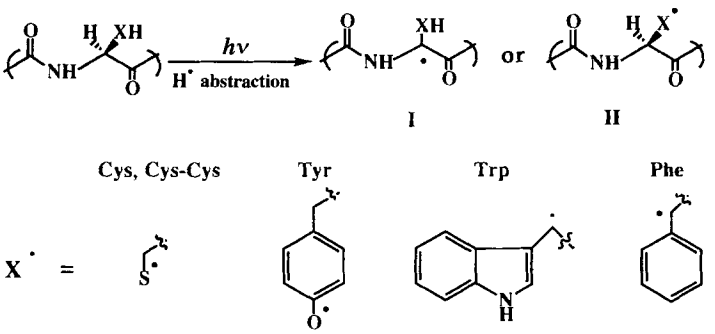
[a] Irradiation under nitrogen in refluxing carbon tetrachloride.

reaction, the oxidative cleavage of a C-terminal peptide with nickel oxide,[64] and with photoalkylation reactions of some synthetic glycine-containing polypeptides with 1-butene or toluene.[65] Yet, a protein is a complex polypeptide and the degree of selectivity depends on the location of the glycine residue in the peptide (i.e its accessibility) as well as on the conformation of the peptide.[66]

Table 6 contains bond dissociation energies[67, 68] for a series of compounds, which can be correlated to the relative energies required for hydrogen abstraction (or disulfide dissociation) from amino acid side chains. Clearly the disulfide dissociation reaction is by far the least energetic process and should lead to the efficient radical-induced cleavage of disulfide bridges in the protein. For the other amino acid side chains, hypotheses can be forwarded concerning the stabilization of derived radicals. The functional groups that are presumed targets for photogenerated radicals, based on the bond dissociation energies listed in Table 6, are shown in Scheme 8. Stabilized radicals such as phenoxyl radical for Tyr, benzylic radicals for Trp, Phe, and His, and thiolate radical for Cys are likely candidates. Also radicals α to heteroatoms (O in Ser and Thr, N in Arg, Lys, Pro) and α to carbonyl groups (Asp, Glu, Asn, Gln) are stabilized and could be formed by hydrogen abstraction. Finally, even some tertiary alkyl radicals (Val, Leu, Ile) can be envisaged as arising from hydrogen abstraction. As a consequence, practically all the amino acid side chains could be involved in radical chemistry through hydrogen abstraction reactions.

Table 6. Bond dissociation energies E_{diss} determined with model compounds for amino acid side chains [67, 68].

Amino acid	Side-chain radical	Model compound	E_{diss}[kcal mol^{-1}] [67]
Ala		CH_3CH_2-H	98
Val		$(CH_3)_3C-H$	91
Leu			
Ile			
Phe		$C_6H_5CH_2-H$	85
His			
Trp			
Tyr		C_6H_5O-H	86.5[68]
Ser		$CH_3CH(OH)-H$	90
Thr			
Cys		CH_3S-H	88
Cys–Cys	"	CH_3S-SCH_3	69
Met			
Pro			
Lys			
Arg			
Asp		CH_3COCH_2-H	92
Glu			
Asn			
Gln			



Scheme 8. Radical reactivity of peptides: radicals in the peptide backbone (I) and stabilized radicals in the side chains (II).

The existence of other radical species has been demonstrated recently by γ-irradiation of protein and protein–DNA complexes.[69] The major radical species formed under these conditions by electron loss have been identified by ESR as N radicals in the peptide backbone and not carbon-centered radicals as proposed in previous work; side-chain radical cations such as $Trp^{\bullet+}$ and $Tyr^{\bullet+}$ have been found in relatively low yields.[70] Nevertheless, such a process does not occur under classical irradiation conditions. Finally, photodestruction of proteins most probably proceeds through formation of radicals and involves several amino acid residues, especially those sensitive to light such as Cys–Cys, Trp, Phe, and Tyr.[71]

3. Nonspecific Labeling: A Major Problem in Photoaffinity Labeling

Probes directed at the active site are generally used to study the interactions between ligands and biological macromolecules. This strategy requires the replacement of a weak and reversible ligand–receptor interaction, as indicated by the transient character of the complex, by formation of a stable covalent bond. To be valuable, this chemical reaction must be site specific, that is, it must occur exclusively at the binding site of the target molecule and not at any other protein domain or on any other material in the incubation mixture. This problem of nonspecific labeling occurs often in photoinduced labeling studies, since highly reactive species are generated in the vicinity of the proteins. The higher the ligand excess during the labeling

reaction (low-affinity probe), the greater the extent of nonspecific labeling. Another case of nonspecific labeling was demonstrated for photogenerated species having a longer lifetime, for which pseudophotoaffinity labeling can occur.[72] The use of radical scavengers has been recommended and used successfully to trap reactive intermediates in the outer medium, restricting the chemical reaction to the binding site.[5d] Obviously, most successful photoaffinity labeling experiments (Table 7) were performed with purified proteins available in large quantities. This permitted the photochemical reaction to be conducted at high receptor concentrations, thereby reducing the ligand excess and the resulting nonspecific labeling. How can nonspecific labeling be minimized when the labeling receptors are present in very small quantities within a preparation?

3.1. The Historical Example

The labeling of α-chymotrypsin by diazoacetylchymotrypsin[1] was indeed a clever example of site-directed labeling in which the photoreactive species was generated exclusively at the active site. The chemical stability of the acylated enzyme was sufficient for the removal of the unreacted photosensitive substrate, *p*-nitrophenyl diazoacetate, thus allowing an efficient photolabeling reaction on a stoichiometrically modified enzyme.[73, 74] Beyond the problems encountered due to the rearrangement of the diazoacetyl probe, this experiment was a remarkable example of selective photoactivation within the active site which thus avoided nonspecific labeling.

3.2. Photochemical Cross-Linking of Long-Lived Complexes

The use of ligand analogues having very high affinity for a binding site is the simplest way to avoid the use of an excess of ligand in the labeling reaction and thus reduce nonspecific labeling. High affinity corresponds generally to a very slow dissociation rate of the ligand–receptor complex and generally allows excellent labeling conditions. When highly dilute ligand solutions are used, for example, quasi-stoichiometric receptor–ligand complexes are formed after an appropriate incubation time. The success of the photolabeling reaction becomes exclusively dependent on the intrinsic reactivity of the photogenerated species.

Neurotoxins are an extraordinary group of very specific ligands showing extremely high affinities for a number of neuroreceptors (affinity constants of up to 10^{-12} M)[75] and giving rise to typical examples of long-lived complexes. Because neurotoxins form an almost irreversible interaction with the receptor in the absence of light, radiolabeled toxin derivatives are required for further analyses under denaturating conditions. Generally, the toxins are modified specifically (i.e. at cysteine or lysine residues) by using photochemical cross-linking reagents.[5e] Snake venom neurotoxins acting on the nicotinic acetylcholine receptor have been modified by bifunctional reagents and have been used extensively to probe this receptor.[76–81] The relatively large surface of these neuropeptide probes (M_w from 70 to 80 kDa) offers many possible sites for probe–receptor interactions. Thus, several derivatives modified at different positions can be designed to study different areas of the receptor. These photoaffinity labeling probes limit the nonspecific labeling and provide powerful tools for structural investigations. The determination of the three-dimensional structure of membrane receptors is at an early stage, especially for heterooligomeric polypeptide assemblies for which only low-resolution (9 Å), low-temperature, electronic microscopy data are available.[82] Therefore, labeling results obtained with these toxin derivatives might be a sophisticated method for characterizing the quaternary organization of the receptor polypeptides.[76–81]

3.3. Photosuicide Labeling

It is clear that modified neurotoxins are highly elaborate tools that are not always available to the scientist. Therefore, the development of a method that minimizes nonspecific labeling and is applicable to more commonly used derivatives is of general interest. Photosuicide inhibitors are ligand analogues whose selective photodecomposition is triggered by the intrinsic properties of the target protein.[83] This method, which is an extrapolation of the more conventional suicide or k_{cat} enzyme inactivation,[84] combines the high reactivity of photogenerated probes with a selective mode of activation within a binding site.

Three methods have been described for the preferential photoactivation of a ligand when it is bound to a receptor site. In the first, nitrosamine derivatives in the hydrophobic environment of the binding site are photoactivated preferentially.[85] The second method consists of an enzymatic-induced shift of the absorption band of the chromophore, allowing the selective photoactivation of the enzyme-bound reaction product.[86] The third approach relies on the photoactivation of a ligand having an appropriate chromophore by tryptophan-mediated energy transfer (Fig. 2).[87] This type of photoactivation requires the presence of a tryptophan residue in the binding site or its vicinity, as well as a probe with appropriate spectroscopic properties. In particular, these probes should have minimal absorption at the Trp excitation wavelength ($\lambda \approx 290$ nm) and maximum absorption at the Trp emission wavelength (λ_{max}(probe) $\approx$ 320–340 nm). Three types of molecules having the appropriate photosensitive chromophores are shown in Scheme 9. The improvement of the labeling reaction by energy transfer photoactiva-

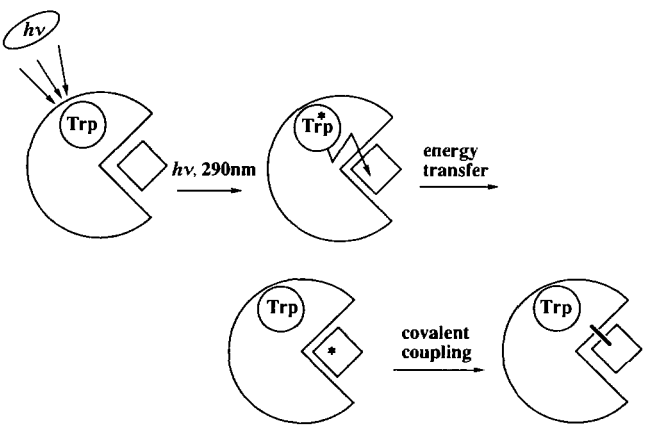
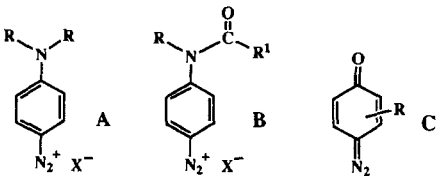


Fig. 2. Photolabeling by tryptophan-mediated energy transfer.

tion ($\lambda_{exc} \approx 290$ nm) over the usual photolabeling reaction ($\lambda_{exc} \approx \lambda_{max}$(probe)) was first demonstrated with the inactivation of acetylcholinesterase by an aryldiazonium derivative (compound **A**, Scheme 9).[87] This method should be applicable in many cases, and several other successful examples of receptor labeling by tryptophan-mediated photoactivation have already been described.[88-92]



λ_{max} [nm]	ca. 380	ca. 340	ca. 350
ε [L mol^{-1}cm^{-1}]	> 35 000	ca. 15 000	> 25 000

Scheme 9. Spectroscopic properties of aryldiazonium and diazo compounds **A**–**C**, which are suitable for photoactivation by tryptophan-mediated energy transfer. R, R^1 = alkyl.

4. Identification of Labeled Amino Acid Residues

Numerous amino acid residues labeled in photoaffinity labeling experiments have been identified recently. This success can be related to a) the increasing number of known protein sequences deduced from the corresponding cloned genes,[93,94] which obviously facilitates the sequencing of peptides and the identification of amino acids; and b) recent progress in microsequencing technology, which facilitates the sequencing of very small quantities of peptides.[95]

These identification studies have several consequences. First they allow the location of a ligand binding site along the protein sequence and the eventual deduction of important information on the receptor–ligand interaction. In addition, if the three-dimensional structure of the target receptor is known, it is extremely important for crystallographers to have access to additional structural data not accessible in the solid state. Secondly, the identified amino acid residues are suitable targets for site-directed mutagenesis experiments. Clearly, the greater the number of residues identified, the more information obtained on the structure in solution.

Table 7 summarizes successful photoaffinity labeling experiments that identified labeled amino acid residues and lists the probes and target receptors used. Several comments can be made:

a) In most of the examples proteins available in purified form and in appreciable quantities were used. Remarkable exceptions are the β-adrenergic,[96] GABA,[97] and vasopressin[98] receptors.

b) Many different photosensitive probes have been used, ranging from the classical aryl azides to diazirines, diazoketones, aryldiazonium salts, and aromatic halides. The fact that aryl azides are the most frequently listed reflects frequent usage rather than better labeling properties of the generated species. The list includes also nonphotoactivatable probes such as unmodified nucleotides,[99-102] nicotine,[103] physostigmine,[104] and d-tubocurarine.[105] The use of such probes as site-directed photochemical inactivators is indeed a convenient alternative to photoaffinity labeling, but the actual mechanism by which the coupling reaction to the protein occurs remains undefined.

c) Of the different probes, only a few could be used to label several amino acid residues within the binding site. *para*-Dimethylaminobenzenediazonium tetrafluoroborate (DDF; **A**, R = CH_3, X = BF_4; Scheme 9)[89-92] showed exceptional reactivity, in particular for the nicotinic acetylcholine receptor;[106,107] eight different amino acid residues could be identified on the receptor α-subunit: Cys 192, Cys 193, Tyr 93, Tyr 151, Tyr 190, Tyr 198, Trp 86, and Trp 149. Also the monochlorophenothiazine derivative chlorpromazine[108-110] could be photoincorporated, although very weakly, on seven different amino acids belonging to putative channel-forming M2 segments of the nicotinic acetylcholine receptor (αSer 248, βSer 254, βLeu 257, γThr 253, γSer 257, γLeu 260, δSer 262). A remarkable diversity of labeling was observed with the reagent [^{125}I]TID,[49b] which allowed extensive labeling of the nicotinic acetylcholine receptor. Eight different residues (βLeu 257, δLeu 265, βVal 261, δVal 269, βSer 250, βSer 254, δSer 258, δSer 262) on the channel-forming M2 segments from the β- and δ-subunits[52] could be identified. Considering the lipid–protein interface of *Torpedo*, the labeling results are even more impressive: five residues (Cys 412, Cys 418, Met 415, Thr 422, Val 425) from the hydrophobic M4 segment of the α-subunit[111] and sixteen residues (3 Phe, 3 Met, 3 Ile, 2 Ser, 2 Asn, Gly, Val, Leu) from the M_3 segment of the β-, γ-, and δ-subunits.[112] A few other probes listed in Table 7 showed a similar trend but to a much lesser extent.

d) Each of the twenty amino acids has been labeled at least once. Tyr and Cys are most frequently labeled. These residues can be labeled by different types of probes generating nitrenes, carbenes, aryl cations, or even undefined reactive species. Surprisingly, the nucleophilic His residue, which is often labeled by specific protein modification reagents[113] and by affinity reagents,[114] has been identified only twice in photoaffinity labeling experiments. Other amino acids with functionalized side chains are frequently encountered (Met, Trp, Lys, Glu, Ser, Thr), while a few hydrophobic residues could be labeled occasionally (Leu, Ile, Pro, Phe, Ala, Val). It is noteworthy that the labeling of the hydrophobic residues is mainly achieved with probes that generate particularly reactive species such as carbenes and aromatic cations (Section 2.2).

The survey in Table 7 shows firstly that most of these residue identifications result from recently published photoaffinity labeling experiments, which reflects technical progress in this research area. Secondly, it seems that no evident connection can be made between the nature of the labeled residues and the reactivity of the photoprobes; such a relationship is even more difficult to evaluate because of the lack of quantitative results for irreversible labeling in many publications. Finally, the molecules that can be used for the efficient labeling of several amino acid residues are potentially powerful probes for the investigation of the topology of membrane receptors, a topic of growing interest. This point will be discussed in detail in the following section.

Table 7. Amino acids in biological receptors that have been identified by photolabeling; the amino acids are listed in order of decreasing frequency.

Amino acid	Radioactive probe	Target receptor	Ref.
Tyr	2-azido-[α-^{32}P]ADP	beef heart mitochondrial F_1 ATPase (β-subunit)	[15]
	[^{3}H]SAM, [*methyl*-^{3}H]AdoMet	guanidinoacetate methyltransferase	[101]
	2-azido-[β,γ-^{32}P]ATP	chloroplast F_1 ATPase (β-subunit)	[14]
	2-azido-[β,γ-^{32}P]ADP		
	2-azido-[β,γ-^{32}P]ATP	beef heart F_1 ATPase (β-subunit)	[16]
	8-azido-[α-^{32}P]ATP	recA protein from *E.coli*	[18]
	8-azido-[α-^{32}P]cAMP	cAMP-dependent protein kinase	[21, 127]
	[^{14}C]Gly-Pro-Arg-*N*-(4-azido-2-nitrophenyl)-Lys-NH_2	fibrin (γ-chain)	[117]
	[^{32}P]azidonitrophenylphosphate	mitochondrial F_1 ATPase	[118]
	[^{3}H]DDF[a]	*Torpedo* nicotinic acetylcholine receptor	[106, 107]
	[^{3}H]nicotine	*Torpedo* nicotinic acetylcholine receptor	[103]
	[^{3}H]2,4-dinitrophenyl azide	anti dinitrophenyl antibody myeloma protein 460	[130b]
	[^{3}H]azidonevirapine	virus type 1 reverse transcriptase	[141]
	[^{32}P]$_2$-azido-NAD^+	lactate dehydrogenase (LDH)	[142]
	3′-*O*-(4-benzoyl)benzoyl-ATP	chloroplast coupling factor 1	[139]
Cys	[^{3}H]DDF[a]	*Torpedo* nicotinic acetylcholine receptor	[106]
	[^{3}H]GTP	tubulin (β-subunit)	[102]
	[^{32}P]dTTP	*E.coli* ribonucleotide reductase	[138]
	arylazido-β-[3-^{3}H]alanyl-NAD^+	D-(−)-β-hydroxybutyrate dehydrogenase	[119]
	[^{3}H]nicotine	*Torpedo* nicotinic acetylcholine receptor	[103]
	[^{125}I]TID[b]	*Torpedo* nicotinic acetylcholine receptor	[111]
	ε-(4-azido-2-nitrophenyl)-L-lysine	rabbit antibody	[134]
	arylazido-β-[3-^{3}H]alanyl-NAD^+	rabbit muscle glycerinaldehyde-3-phosphate dehydrogenase	[143]
	[^{3}H]promegestone	rat glucocorticoid receptor	[144]
	[^{3}H]dTPP	*E.coli* ribonucleotide reductase (β1-subunit)	[145]
	8-azido-2′-*O*-[^{14}C]dansyl-ATP	rabbit muscle adenylate kinase	[150]
Met	[^{14}C]azidoatrazine	reaction center of photosystem 2	[116]
	peptides containing [^{3}H]*p*-benzoylphenylalanine	calmodulin	[120]
	[^{125}I]TID[b]	*Torpedo* nicotinic acetylcholine receptor	[111, 112]
	peptide containing [^{3}H]*p*-benzoyl-L-phenylalanine	cAMP-dependent protein kinase	[133]
	[^{3}H]promegestone	human progestin receptor	[144]
	[^{3}H]promegestone	rat glucocorticoid receptor	[144]
	Δ^6-[^{3}H]testosterone, Δ^6-[^{3}H]estradiol	human sex hormone binding globulin	[148]
Trp	2-azido-[^{3}H]ATP	skeletal myosin	[17]
	[^{3}H]NANDP[c]	skeletal myosin	[115]
	8-azido-[α-^{32}P]cAMP	cAMP-dependent protein kinase	[21]
	[^{3}H]DDF[a]	*Torpedo* acetylcholinesterase	[92, 124]
	[^{3}H]DDF[a]	*Torpedo* nicotinic acetylcholine receptor	[106, 107]
	[^{125}I]iodocyanopindololdiazirine	β-adrenergic receptor	[96]
	[^{125}I]iodoazidobenzylpindolol	turkey erythrocyte	
	[^{3}H]d-tubocurarine	*Torpedo* nicotinic acetylcholine receptor	[105]
Lys	8-azido-[α-^{32}P]GTP, 8-azido-[γ-^{32}P]GTP	glutamate dehydrogenase	[20]
	[^{3}H]physostigmine	*Torpedo* nicotinic acetylcholine receptor	[104b]
	[^{3}H]2,4-dinitrophenyl alanyl diazoketone	anti dinitrophenyl antibody myeloma protein 460	[130a]
	4-maleimidobenzophenone[d]	troponin I	[140]
	[^{3}H]azido-*N*-β-ADP	pterin binding site of phenylalanine hydroxylase	[146]
	[*methyl*-^{3}H]dTPP	heterodimeric reverse transcriptase of HIV-1	[147]
Glu	[^{3}H]ADP	gizzard myosin	[99]
	[^{3}H]UDP	gizzard myosin	[100]
	[^{3}H]*m*-diazirinophenyl derivative of retinal	bacteriorhodopsin	[123]
	[^{14}C]*m*-diazirinophenyl derivative of phospholipids	glycophorin A	[128]
	diazoacyl trypsin	trypsin	[137]
	[^{32}P]$_2$azido-NAD^+	glutamate dehydrogenase (GDH)	[142]
Ser	[^{14}C]3′(2′)-*O*-(4-benzoyl)benzoyl-ATP	rabbit skeletal myosin	[122]
	[^{3}H]chlorpromazine	nicotinic acetylcholine receptor	[108, 110]
	[^{3}H]*m*-diazirinophenyl derivative of retinal	bacteriorhodopsin	[123]
	[^{14}C]uridine-2′(3′),5′-diP(pUp)	RNase	[129]
	[^{3}H]trimethylphenylphosphonium ion	*Torpedo* nicotinic acetylcholine receptor	[131]
	[^{125}I]TID[b]	*Torpedo* nicotinic acetylcholine receptor	[52, 112]
Thr	2-azido-[α-^{32}P]ATP	uncoupling protein from brown adipose tissue	[13]
	8-azido-[α-^{32}P]ATP	uncoupling protein from brown adipose tissue	[19]
	[^{3}H]chlorpromazine	*Torpedo* nicotinic acetylcholine receptor	[108]
	[^{14}C]uridine-2′(3′),5′-diP(pUp)	RNase	[129]
	[^{125}I]TID[b]	*Torpedo* nicotinic acetylcholine receptor	[111]
	8-lysyl-ε-*N*-amidino-4-azidophenylvasopressin	vasopressin receptor	[98]
Leu	2-azido-[α-^{32}P]ADP	beef heart mitochondrial F_1 ATPase (β-subunit)	[15]
	[^{3}H]chlorpromazine	*Torpedo* nicotinic acetylcholine receptor	[108]
	[^{3}H]DDF[a]	*Torpedo* acetylcholinesterase	[126]
	[^{125}I]TID[b]	*Torpedo* nicotinic acetylcholine receptor	[52, 112]
	8-azido-2′-*O*-[^{14}C]dansyl-ATP	rabbit muscle adenylate kinase	[150]

[a] DDF = *p*-(*N*,*N*-dimethylamino)phenyldiazonium tetrafluoroborate. [b] TID = 3-trifluoromethyl-3-*meta*-iodophenyl-3*H*-diazirine. [c] NANDP = 2-[(4-azido-2-nitrophenyl)amino]ethyl diphosphate. [d] A cross-linker.

Table 7. (continued).

Amino acid	Radioactive probe	Target receptor	Ref.
Arg	[^{3}H]NANDP[c]	scallop myosin	[125]
	[^{3}H]quinacrine azide	*Torpedo* nicotinic acetylcholine receptor	[132]
	8-lysyl-ε-*N*-amidino-4-azidophenylvasopressin	vasopressin receptor	[98]
	4-maleimidobenzophenone[d]	troponin I	[140]
Ile	2-azido-[α-^{32}P]ADP	beef heart mitochondrial F_1 ATPase(β-subunit)	[15]
	[^{32}P]azidonitrophenylphosphate	mitochondrial F_1 ATPase	[118]
	[^{14}C]uridine-2′(3′),5′-diP(pUp)	RNase	[129]
	[^{125}I]TID[b]	*Torpedo* nicotinic acetylcholine receptor	[112]
Pro	2-azido-[α-^{32}P]ADP	beef heart mitochondrial F_1 ATPase(β-subunit)	[15]
	[^{14}C]3′(2′)-*O*-(4-benzoyl)benzoyl-ATP	gizzard myosin	[121]
	4-maleimidobenzophenone[d]	troponin I	[140]
	[^{3}H]quinacrine azide	*Torpedo* nicotinic acetylcholine receptor	[132]
Gly	peptide containing [^{3}H]*p*-benzoyl-L-phenylalanine	cAMP-dependent protein kinase	[133]
	N-2,4-dinitrophenyl-*p*-aminobenzoate	anti dinitrophenyl antibody	[135,136]
	[^{125}I]TID[b]	*Torpedo* nicotinic acetylcholine receptor	[112]
Phe	[^{3}H]DDF[a]	*Torpedo* and electric eel acetylcholinesterase	[44,124]
	[^{3}H]muscimol	bovine cortex GABA receptor	[97]
	[^{125}I]TID[b]	*Torpedo* nicotinic acetylcholine receptor	[112]
Ala	ε-(4-azido-2-nitrophenyl)-L-lysine	rabbit antibody	[134]
	diazoacyltrypsin	trypsin	[137]
Asp	3′-*O*-(4-benzoyl)benzoyl-ATP	chloroplast coupling factor 1	[139]
	Δ^6-testosterone-agarose	Δ^5-3-ketosteroid Δ^5-Δ^4-isomerase	[151]
His	*N*-2,4-dinitrophenyl-*p*-aminobenzoate	anti dinitrophenyl antibody	[135,136]
	[α-^{32}P]dTPP	*E.coli* DNA polymerase I (Pol I)	[149]
Asn	[^{125}I]TID[b]	*Torpedo* nicotinic acetylcholine receptor	[112]
Gln	[^{32}P]azidonitrophenylphosphate	mitochondrial F_1 ATPase	[118]
Val	[^{125}I]TID[b]	*Torpedo* nicotinic acetylcholine receptor	[52,111,112]

[a] DDF = *p*-(*N*,*N*-dimethylamino)phenyldiazonium tetrafluoroborate. [b] TID = 3-trifluoromethyl-3-*meta*-iodophenyl-3*H*-diazirine. [c] NANDP = 2-[(4-azido-2-nitrophenyl)amino]ethyl diphosphate. [d] A cross-linker.

5. Topographical Mapping

5.1. Definition

Topographical mapping can be defined as a labeling pattern that involves the full environment of a ligand within a binding site. This mapping can be established either on a macromolecular level by labeling different subunits defining the receptor binding site or can be defined on a molecular level by labeling and identifying amino acids that surround the binding site (Fig. 3). It is clear that topographical mapping is necessarily related to the intrinsic chemical reactivity of the photogenerated species. Probes with the highest possible reactivity ("universal reactivity") are required, since they should be able to map the entire surroundings of the ligand by reacting with all amino acid residues, including those with chemically inert alkyl side chains. Consequently, these probes should react not only with nucleophilic residues, which would lead to a partial mapping of the binding site. The best way to estimate the reactivity of the probe is to measure the lifetime of the photogenerated species in different media, from water to hydrocarbons. The probe should be able to react efficiently with a C–H bond (for instance from the solvent), since the C–H bond can be considered to represent any particular bond in the ligand binding site of a receptor.

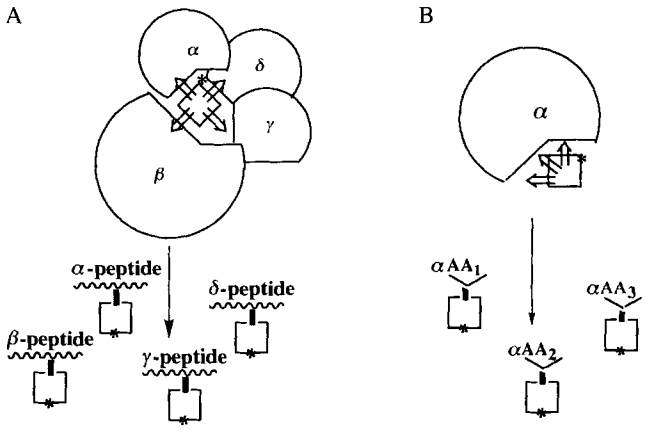


Fig. 3. Definitions in topographic mapping A) at the macromolecular level: labeling of all peptide subunits α–δ defining the binding site; b) at the molecular level: labeling of all amino acid residues that compose the binding site.

5.2. Limitations

The use of highly reactive probes is not enough to ensure topographical mapping. Different situations that might occur during photoaffinity labeling experiments are represented in Figure 4. For instance the photoactivated probe might be rapidly quenched by surrounding water molecules if the environment of the bound probe is hydrophilic (Fig. 4A). We described the example of labeling on one receptor binding site existing in two different conformations by using a highly reactive photoactivatable probe. We observed that very efficient labeling occurred in one conformation, while labeling was nonexistent in the other conformation, possibly because the reactive moiety was oriented towards the aqueous medium.[89] Another possible limitation to full topographical mapping is the use of a probe showing very high affinity for a binding site. These probes generally (although

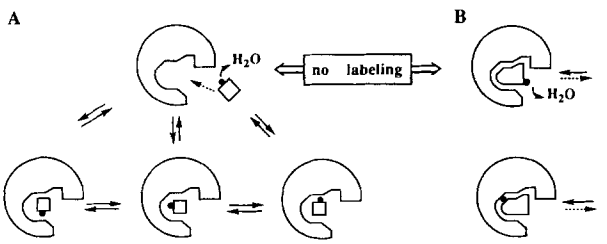


Fig. 4. Differences in receptor mapping with highly reactive photoaffinity probes having moderate (A) and high (B) binding affinity. A) Topographical mapping through dynamic interaction (fast dissociation) of the probe and the binding site. B) Specific but partial mapping through "static" interaction (slow dissociation) of the probe and the binding site.

not necessarily) dissociate very slowly from the binding site. This is likely to correspond to a static interaction between the photoactivated ligand and a limited area of the binding site (Fig. 4B). This situation is typically encountered during the slow photochemical coupling of modified neurotoxins or hormone peptides (Section 3.2). In contrast, topographical mapping requires dynamic interaction, allowing the probe to adopt different positions in the binding site. The extreme reactivity of the excited species guarantees efficient labeling of all the areas of the binding site. Hence, by definition, the best topographical probes show a rather moderate binding affinity for their recognition site, leading to an efficient dynamic labeling process. Theoretically, the use of probes showing moderate binding affinities should lead to increased nonspecific labeling (Section 3). However, in this case, nonspecific labeling is usually limited, due to efficient quenching of the photogenerated species by the solvent.

5.3. Expected Consequences

Oligomeric protein complexes are frequently encountered in biology and raise the question of the precise localization of a binding site within the multisubunit protein complex. Recent descriptions of highly organized quaternary structures of several membrane receptors such as neurotransmitter-gated receptors[152] require appropriate tools to identify the ligand binding sites. As an example, the five constituent subunits of the ion channel on the nicotinic acetylcholine receptor were labeled by using photosensitive channel blocker derivatives.[109, 110, 131, 153] Topographical probes are best adapted to labeling receptor sites located on different receptor subunits. Many publications describe the labeling of one subunit in a multisubunit complex, but interpretations that tend to localize the binding site on the singly labeled subunit may be misleading. A more reactive topographical probe might extend the labeling to residues belonging to other subunits.

Of the probes listed in Table 7 (see also Sections 2.2 and 4), only two molecules might be considered as topographical probes: the aryldiazonium salt DDF[90, 106, 107] and the diazirine derivative TID.[49b, 52, 111] Both compounds generate highly reactive species and lead to high yields of irreversible labeling on the nicotinic acetylcholine receptor, which allowed the identification of several binding site residues. Their binding affinities are rather low (K_i = 200 μM for DDF on the acetylcholine binding site[90] and 6.5 μM for TID on the noncompetitive binding site[52]). The remarkable labeling pattern obtained with DDF on the α-subunit of the nicotinic acetylcholine receptor can be explained by the combination of the high reactivity of the photogenerated aryl cation (lifetime in water ≤ 0.5 ns[40]) and the ideal replacement of the quaternary ammonium group of acetylcholine with the charged diazonium group of the photoreactive moiety. Figure 5 shows an overview of the labeling results obtained with different probes tested on the acetylcholine binding site of the nicotinic receptor. The efficiency of DDF as a topographical probe is apparent.

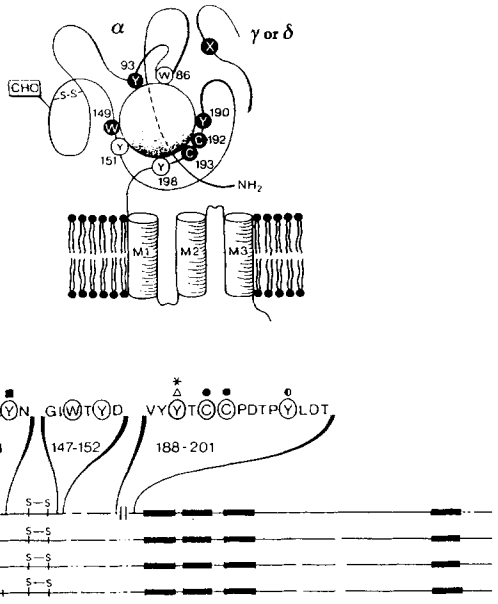


Fig. 5. Amino acids in the cholinergic binding area of the nicotinic acetylcholine receptor from *Torpedo* [157] localized by: chemical affinity labeling with 4-(*N*-maleimido)benzyltrimethylammonium (iodide; MBTA) [154] (●), lophotoxin [155] (△), and acetylcholine isothiocyanate [156] (■); photoaffinity labeling with DDF [90, 106, 107] (○), d-tubocurarine [105] (*), and nicotine [103] (◐).

Extensive labeling of membrane protein domains with hydrophobic probes can be considered an extension of the topographical mapping of a binding site to the lipid–protein interface. Again, an outstanding result was obtained with [^{125}I]TID:[112] 16 different amino acid residues were identified from the M_3 transmembrane segments of the nicotinic acetylcholine receptor, which led to interesting topographical analyses of the membrane components.

6. Site-Directed Labeling and Site-Directed Mutagenesis

Both site-directed labeling and site-directed mutagenesis are designed to investigate functional proteins but in different ways. The first objective in site-directed labeling experiments is to gain as much structural information on ligand binding sites as possible by identifying amino acid residues belonging to these sites. As emphasized in this article, topographical mapping is the most efficient method in this respect. Site-directed mutagenesis addresses the same problem by identifying amino acid residues for which mutations alter the functional properties of the

biological receptor. The evaluation of this change in function is used to interpret the structure–function relationship. In contrast, the functional properties are totally lost during site-directed labeling experiments. Mutational analyses of the amino acid residues identified by labeling experiments represent an evident link between the two methods. It is clear that site-directed mutagenesis requires structural information. Ideally, X-ray data, in particular for protein–ligand complexes, are available. Another way to identify sites that might determine functional properties is to find sequence alignments within protein families.[158] The aim of the search for sequence alignments, apart from implications on evolution, is to locate the conserved regions that might be essential for function and to identify more precisely the highly conserved amino acid residues. This method has become particularly attractive for recently cloned and sequenced membrane receptors,[159] for which structural determinations of sufficient resolution are still lacking. An enormous amount of information has been and will be generated by site-directed mutagenesis on these receptors.[160] However, it is clear that many of the mutations that induce functional alterations do not result from direct changes in interactions within the binding site. Many examples in the literature refer to somatic mutations which induce long-range effects on ligand binding properties as proven by X-ray data.[161–164] Finally, the lipid–protein interface, which might play an important role in the regulation of allosteric transitions of membrane receptors,[165, 166] cannot be probed by classical mutation and requires adapted photochemical labeling experiments.[49a] In summary, both methods have their own advantages and drawbacks; ideally one would like to support data obtained from mutagenesis studies with biochemical techniques and vice versa.

7. Future Trends in Photoaffinity Labeling

7.1. Photoaffinity Labeling of Recombinant Receptors

Photoaffinity labeling of recombinant receptors is the ideal answer to a series of issues raised recently by molecular biologists. In particular, molecular heterogeneity of a series of receptors has been demonstrated by the isolation of genes coding for many isoforms, especially in the neurobiological field.[167] This heterogeneity leads to the presence of several receptor subtypes having a high degree of homology within an organ; the complexity correspondingly increases when heterooligomeric receptors are considered.[168, 169] Recombinant receptors, which are expressed in cell lines not normally expressing this receptor following transfection with the cDNAs encoding the chosen receptor subunits, overcome the heterogeneity problem. The legitimate question of the physiological relevance of such expressed receptors is not a major drawback for photoaffinity labeling experiments as long as the functional properties, in particular the ligand binding properties, are retained. Photoaffinity labeling studies on such recombinant receptors[170, 171] were first achieved to establish molecular identity with the native receptors, emphasizing the relevance of such biological material. A photoaffinity labeling study on several recombinant *N*-methyl-D-aspartic acid (NMDA) receptors was described recently by using a highly specific [^{125}I]iodoarylazido-NMDA antagonist.[172] Different labeling patterns revealed by autoradiography on sodium dodecylsulfate gels were obtained according to the subunit composition, underscoring the value of such an approach in analyzing structural heterogeneity. The successful photoaffinity labeling of a cloned purinergic receptor was also reported[173] and raised the question of the existence of specific binding sites for ATP and UTP on this receptor.

The step following photoaffinity labeling on recombinant receptors is the identification of the binding sites on the polypeptides. As mentioned in Sections 4 and 5, amino acid identification is best achieved when efficient probes (topographical probes) are used on purified material available in appreciable quantities. This in turn requires an efficient system of expression for the recombinant receptors of interest. The use of insect cells infected with baculovirus proved to be very efficient for the overexpression of a number of receptors,[174] and it is certain that this and/or other efficient expression systems will be used frequently in the future.

7.2. Photoaffinity Labeling and Signal Transduction Mechanisms

There are two basic types of receptor transducing systems: intracellular receptors which upon activation by their effector interact directly with DNA and alter the genetic program of a cell, and membrane-bound receptors which are generally activated at the cell surface by the appropriate hormone or neurotransmitter and transmit their signal inside the cell. These membrane-bound receptors have been divided into three main classes, each having several subtypes.[152] Typical structural features of selected receptors in these three classes are shown in Figure 6: a) the ligand-stimulated tyrosine kinases or guanylate cyclases which are monomers or dimers of polypeptides having a single hydrophobic domain, b) the G-protein linked receptors formed by a polypeptide which typically has seven hydrophobic transmembrane domains, and c) the transmitter-gated ion channels, which form (hetero)oligomeric complexes and for which four postulated transmembrane helices on each polypeptide are predicted to span the membrane.

How can photoaffinity labeling be used to investigate the function of such biological receptors? As already mentioned, a direct link can be made by site-directed mutagenesis of the amino acid residues that were previously identified by photoaffinity labeling and that are directly involved in ligand recognition. Such mutations should induce changes in the ligand binding properties, depending on the nature of the mutation. Another way to relate structural elements and functions is to use photoaffinity probes to visualize receptor sites in different conformations. As mentioned earlier, topographical probes are appropriate tools for such studies. The cholinergic antagonist DDF was used to probe the structural changes that occur upon desensitization of the acetycholine receptor; the labeled amino acid residues were identified in both resting and desensitized states of the receptor.[175] Similarly, TID[52] has been used to probe channel-forming regions of the nicotinic receptor of *Torpedo* in resting and desensitized conformations.

The interconversion of the resting state to the desensitized state proceeds via a transitory active state, in which the ionic

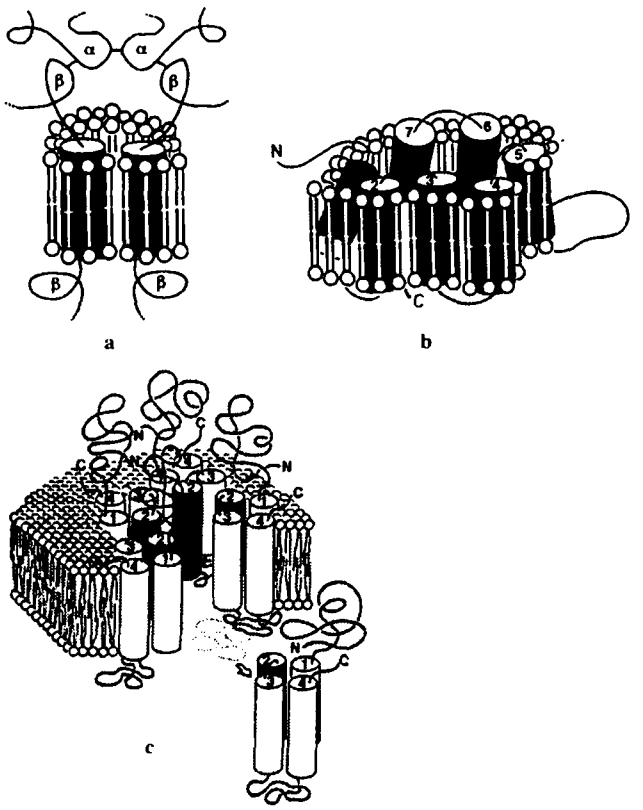
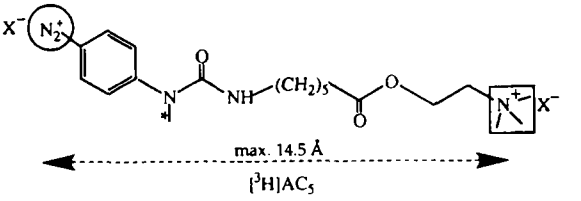


Fig. 6. Three classes of membrane-bound receptors: a) polypeptides having a single hydrophobic transmembrane domain (ligand-stimulated tyrosine kinases and guanylate cyclases); b) peptides with seven hydrophobic transmembrane domains (G-protein linked receptors); c) peptides with four hydrophobic transmembrane domains (transmitter-gated ion channels).



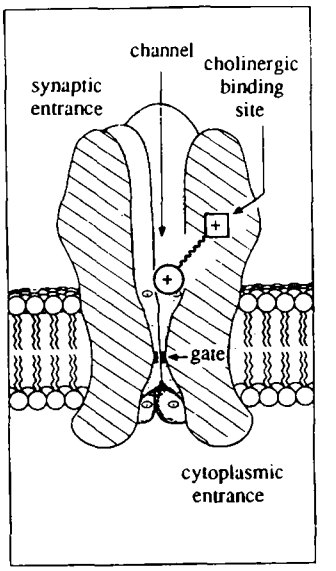


Fig. 7. The photoactivatable agonist AC_5 and its hypothetical position in the cholinergic binding side of the nicotinic acetylcholine receptor.

channel remains open for a short (≈ 10 ms) period of time. This rapid transduction signaling process,[176, 177] triggered by the binding of an agonist, was analyzed by trapping the transient conformation and requires adapted analytical methods. In particular, it requires rapid mixing techniques (stopped-flow equipment) and appropriate photochemical procedures (time-resolved flash photolysis).[178] Such experiments require the design and the synthesis of photoactivatable agonists having the photochemical properties of a topographical probe to ensure that the light-induced coupling reactions are faster than the conformational transitions of the receptor. The analysis of these time-dependent labeling reactions on the receptor should allow characterization of the structural transitions that occur during a physiological process. For the nicotinic acetylcholine receptor, we have developed different photosensitive agonists to probe the conformational transitions of this heterooligomeric receptor upon agonist binding.[179, 180] The analysis can be conducted at a macroscopic level by probing the entire protein complex with an agonist bearing a remote photoactivatable moiety. In the photosensitive compound AC_5 (Fig. 7), for example, the ammonium group of the choline moiety is separated from the photosensitive diazonium by up to 14.5 Å in an extended conformation. The flexible spacer confers sufficient mobility on this ligand such that all the subunits of the pentameric nicotinic acetylcholine receptor complex can be proved. Successive transitions of the receptor complex from the resting state to the desensitized state could be visualized by use of the radiolabeled probe $[^3H]AC_5$. The radioactivity incorporated into the different subunits of the receptor under two different sets of experimental conditions (with flash photolysis after 30 ms preincubation and at equilibrium) were determined[180] (Fig. 8). In similar analysis at a molecular level a photoactivatable agonist of appropriate size would be used to probe the agonist binding site directly. In this investigation the labeled amino acid residues would be identified after photolytic experiments, again after appropriate time-controlled agonist mixing and subsequent flash photolysis. To our knowledge, such a study has not yet been conducted. It should allow the identification of amino acid residues specifically involved in conformational transitions of receptors and might provide key structural information for the understanding of receptor functioning.

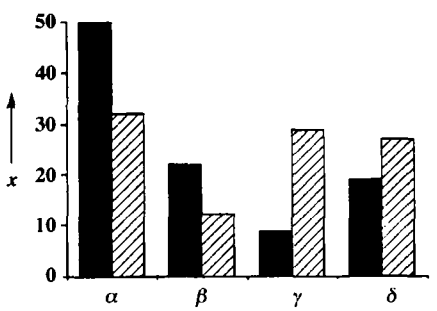


Fig. 8. Labeling pattern obtained by photoaffinity labeling with $[^3H]AC_5$ on all four subunits α-δ of the nicotinic acetylcholine receptor in two conformational states, the mainly resting state (preincubation time 30 ms) (■) and the desensitized state) (▨) [180]. x = relative amount of specific incorporated radioactivity.

8. Summary and Outlook

Although over thirty years old, photoaffinity labeling is a useful and reliable method for the structural investigation of receptor binding sites. It remains a classical research area for chemists who design and synthesize new photoactivatable reagents; biochemists and biologists then use these reagents to identify and characterize the target receptors. In the present article we did not try to review or update these aspects; Bayley's monograph[5a] is still the best reference work. Instead, we emphasized the importance of the identification of amino acid residues belonging to the target binding sites which might lead to further insight into ligand–receptor interactions. We presented an update on the different amino acid residues that have been identified on the different biological receptors by means of photoaffinity labeling, and emphasized mainly the photochemical probes that permitted extensive labeling of a binding site. Finally, we discussed new perspectives for photoaffinity labeling. The possibility of studying ligand–receptor interactions in a dynamic fashion, in particular, makes this method even more attractive and opens up a new field of investigation, the study of rapid physiological events.

Photoaffinity labeling remains, however, a labor-intensive method, from the radiosynthesis of the probes to the sequencing of the receptor peptides. In contrast, site-directed mutagenesis can usually be carried out more rapidly. In this last case, much information can be obtained on the subsequent functional alterations of these mutations. However, in the absence of appropriate structural information, great care should be taken to avoid hasty interpretation of such results in a direct structure–function relationship. Photoaffinity labeling therefore remains a reliable method which should be considered complementary to rather than in competition with site-directed mutagenesis.

Many of the results reported here were obtained during the last decade by collaborators from our laboratory; we are very grateful to all of them. The authors thank Drs. M. Hibert and B. Winsor for critical reading of the manuscript.

Received: March 9, 1994
Revised version: July 1, 1994 [A 541E]
German version: *Angew. Chem.* **1995**, *107*, 1391–1408

[1] A. Singh, E. R. Thornton, F. H. Westheimer, *J. Biol. Chem.* **1962**, *237*, 3006–3008.
[2] V. Chowdhry, F. H. Westheimer, *Annu. Rev. Biochem.* **1979**, *48*, 293–325.
[3] H. Bayley, J. R. Knowles, *Methods Enzymol.* **1977**, *46*, 69–114.
[4] D. I. Schuster, W. C. Probst, G. K. Ehrlich, G. Singh, *Photochem. Photobiol.* **1989**, *49*, 785–804.
[5] a) H. Bayley in *Photogenerated Reagents in Biochemistry and Molecular Biology* (Eds.: T. S. Work, R. H. Burdon), Elsevier, Amsterdam, **1983**; b) in ref. [5a], p. 32; c) in ref. [5a], p. 15; d) in ref. [5a], p. 107; e) in ref. [5a], p. 116.
[6] G. W. J. Fleet, R. R. Porter, J. R. Knowles, *Nature (London)* **1969**, *224*, 511–512.
[7] J. R. Knowles, *Acc. Chem. Res.* **1972**, *5*, 155–160.
[8] Y.- Z. Li, J. P. Kirby, M. W. George, M. Poliakoff, G. B. Schuster, *J. Am. Chem. Soc.* **1988**, *110*, 8092–8098.
[9] For a review see G. B. Schuster, M. S. Platz, *Adv. Photochem.* **1992**, *17*, 69–143.
[10] N. Soundararajan, M. S. Platz, *J. Org. Chem.* **1990**, *55*, 2034–2044.
[11] K. Kanakarajan, R. Goodrich, M. J. T. Young, S. Soundararajan, M. S. Platz, *J. Am. Chem. Soc.* **1988**, *110*, 6536–6541.
[12] K. G. Pinney, K. E. Carlson, B. S. Katzenellenbogen, J. A. Katzenellenbogen, *Biochemistry* **1991**, *30*, 2421–2431.
[13] P. Mayinger, M. Klingenberg, *Biochemistry* **1992**, *31*, 10536–10543.
[14] Z. Xue, C. G. Miller, J.- M. Zhou, P. D. Boyer, *FEBS Lett.* **1987**, *223*, 391–394.
[15] J. Garin, F. Boulay, J.- P. Issartel, F. Lunardi, P. V. Vignais, *Biochemistry* **1986**, *25*, 4431–4437.
[16] R. L. Cross, D. Cunningham, C. G. Miller, Z. Xue, J.-M. Zhou, P. D. Boyer, *Proc. Natl. Acad. Sci. USA* **1987**, *84*, 5715–5719.
[17] J. C. Grammer, H. Kuwayama, R. G. Yount, *Biochemistry* **1993**, *32*, 5725–5732.
[18] K. L. Knight, K. McEntee, *J. Biol. Chem.* **1985**, *260*, 10185–10191.
[19] E. Winkler, M. Klingenberg, *Eur. J. Biochem.* **1992**, *203*, 295–304.
[20] M. T. Shoemaker, B. E. Haley, *Biochemistry* **1993**, *32*, 1883–1890.
[21] J. Bubis, J. J. Neitzel, L. D. Saraswat, S. S. Taylor, *J. Biol. Chem.* **1988**, *263*, 9668–9673.
[22] G. B. Schuster, *NATO ASI Ser. Ser. C*, **1989**, *272*, 31–41.
[23] R. E. Banks, N. D. Venayak, T. A. Hamor, *J. Chem. Soc. Chem. Commun.* **1980**, 900–901.
[24] M. J. T. Young, M. S. Platz, *Tetrahedron Lett.* **1989**, *30*, 2199–2202.
[25] M. J. T. Young, M. S. Platz, *J. Org. Chem.* **1991**, *56*, 6403–6406.
[26] R. Poe, J. Grayzar, M. J. T. Young, E. Leyva, K. A. Schnapp, M. S. Platz, *J. Am. Chem. Soc.* **1991**, *113*, 3209–3211.
[27] R. Poe, K. Schnapp, M. J. T. Young, J. Grayzar, M. S. Platz, *J. Am. Chem. Soc.* **1992**, *114*, 5054–5067.
[28] J. W. F. Keana, S. X. Cai, *J. Org. Chem.* **1990**, *55*, 3640–3647.
[29] M. Golinski, M. Heine, D. S. Watt, *Tetrahedron Lett.* **1991**, *32*, 1553–1556.
[30] P. J. Crocker, N. Imai, K. Rajagopalan, M. A. Boggess, S. Kwiatkowski, L. D. Dwyer, T. C. Vanaman, D. S. Watt, *Bioconjugate Chem.* **1990**, *1*, 419–424.
[31] K. G. Pinney, J. A. Katzenellenbogen, *J. Org. Chem.* **1991**, *56*, 3125–3133.
[32] R. R. Drake, J. T. Slama, K. A. Wall, M. Abramova, C. D'Souza, A. D. Elbein, P. J. Crocker, D. S. Watt, *Bioconjugate Chem.* **1992**, *3*, 69–73.
[33] I. Kapfer, J. E. Hawkinson, J. E. Casida, M. P. Goeldner, *J. Med. Chem.* **1994**, *37*, 133–140.
[34] I. Kapfer, P. Jacques, H. Toubal, M. Goeldner, *Bioconjugate Chem.* **1995**, *6*, 109–114.
[35] K. A. Schnapp, R. Poe, E. Leyva, N. Soundararajan, M. S. Platz, *Bioconjugate Chem.* **1993**, *4*, 172–177.
[36] a) S. X. Cai, J. F. W. Keana, *Tetrahedron Lett.* **1989**, *30*, 5409–5412; b) S. X. Cai, D. J. Glenn, J. W. F. Keana, *J. Org. Chem.* **1992**, *57*, 1299–1304.
[37] M. Golinski, M. Heine, D. J. Orlicky, T. A. Fitz, D. S. Watt, *Eicosanoids* **1992**, *5*, 87–97.
[38] "Photochemistry of the Diazonium and Diazo Groups": W. Ando in *The Chemistry of Diazonium and Diazo Groups, Part 1* (Ed.: S. Patai), Wiley, Chichester, **1978**, p. 355.
[39] H. B. Ambroz, T. J. Kemp, *Chem. Soc. Rev.* **1979**, *8*, 353–365.
[40] J. C. Scaiano, K. T. Nguyen, *J. Photochem.* **1983**, *23*, 269–276.
[41] R. W. Stumpe, *Tetrahedron Lett.* **1980**, *21*, 4891–4892.
[42] R. Huisgen, W. D. Zahler, *Chem. Ber.* **1963**, *96*, 736–746.
[43] a) M. Speranza, *Tetrahedron Lett.* **1980**, *21*, 1983–1986; b) G. Angelini, C. Sparapani, M. Speranza, *Tetrahedron* **1984**, *40*, 4865–4871.
[44] B. Kieffer, M. Goeldner, C. Hirth, R. Aebersold, J.-Y. Chang, *FEBS Lett.* **1986**, *202*, 91–96.
[45] B. Kieffer, M. P. Goeldner, C. G. Hirth, *J. Chem. Soc. Chem. Commun.* **1981**, 398–399.
[46] R. A. G. Smith, J. R. Knowles, *J. Am. Chem. Soc.* **1973**, *95*, 5072–5073.
[47] J. Brunner, H. Senn, F. M. Richards, *J. Biol. Chem.* **1980**, *255*, 3313–3318.
[48] A. H. Ross, R. Radhakrishnan, R. J. Robson, H. G. Khorana, *J. Biol. Chem.* **1982**, *257*, 4152–4161.
[49] a) J. Brunner, *Methods Enzymol.* **1989**, *172*, 628–687; b) *Trends Biochem. Sci.* **1981**, 44–46.
[50] M. Nassal, *J. Am. Chem. Soc.* **1984**, *106*, 7540–7545.
[51] J. Brunner, G. Semenza, *Biochemistry* **1981**, *20*, 7174–7182.
[52] B. H. White, J. B. Cohen, *J. Biol. Chem.* **1992**, *267*, 15770–15783.
[53] N. J. Turro, *Modern Molecular Photochemistry*, Benjamin/Cummings, Menlo Park, CA, **1978**, p. 374.
[54] G. E. Galardy, L. C. Craig, M. P. Printz, *Nature (London)* **1973**, *242*, 127–128.
[55] R. Breslow, S. W. Baldwin, *J. Am. Chem. Soc.* **1970**, *92*, 732–734.
[56] R. Breslow, *Acc. Chem. Res.* **1980**, *13*, 170–177.
[57] J. E. Baldwin, A. K. Bhatnagar, R. W. Harper, *J. Chem. Soc. Chem. Commun.* **1970**, 659–661.
[58] R. E. Galardy, L. C. Craig, J. D. Jamieson, M. P. Printz, *J. Biol. Chem.* **1974**, *249*, 3510–3518.
[59] C. Hélène, *Photochem. Photobiol.* **1972**, *16*, 519–522.
[60] a) H. G. Viehe, R. Merényi, L. Stella, Z. Janousek, *Angew. Chem.* **1979**, *91*, 982–997; *Angew. Chem. Int. Ed. Engl.* **1979**, *18*, 917–932; b) H. G. Viehe, Z. Janousek, R. Merényi, L. Stella, *Acc. Chem. Res.* **1985**, *18*, 148–154.
[61] a) H. Birkhofer, J. Hädrich, H.-D. Beckhaus, C. Rüchardt, *Angew. Chem.* **1987**, *99*, 592–594; *Angew. Chem. Int. Ed. Engl.* **1987**, *26*, 573–575; b) H. D. Beckhaus, C. Rüchardt, *ibid.*, **1987**, *99*, 807–808 and **1987**, *26*, 770–771.
[62] C. J. Easton, M. P. Hay, *J. Chem. Soc. Chem. Commun.* **1986**, 55–57.

[63] V. A. Burgess, C. J. Easton, M. P. Hay, *J. Am. Chem. Soc.* **1989**, *111*, 1047–1052.
[64] C. J. Easton, S. K. Eichinger, M. J. Pitt, *J. Chem. Soc. Chem. Commun.* **1992**, 1295–1296.
[65] a) J. Sperling, D. Elad, *J. Am. Chem. Soc.* **1971**, *93*, 967–971; b) *ibid.* **1971**, *93*, 3839–3842.
[66] R. B. Johns, F. D. Looney, D. J. Whelan, *Biochim. Biophys. Acta* **1967**, *147*, 369–380.
[67] J. A. Kerr, *Chem. Rev.* **1966**, *66*, 465–500.
[68] J. Lind, X. Shen, T. E. Eriksen, G. Merényi, *J. Am. Chem. Soc.* **1990**, *112*, 479–482.
[69] a) G. D. D. Jones, J. S. Lea, M. C. R. Symon, F. A. Taiwo, *Nature (London)* **1987**, *330*, 772–773; b) P. M. Cullis, G. D. D. Jones, M. C. R. Symon, J. S. Lea, *ibid.* **1987**, *330*, 773–774.
[70] F. G. Liming, W. Gordy, *Proc. Natl. Acad. Sci. USA* **1968**, *60*, 795–806.
[71] K. C. Smith, P. C. Hanawalt in *Molecular Biology—Inactivation and Recovery* (Eds.: B. Horecker, N. O. Kaplan, J. Marmur, H. A. Scheraga), Academic Press, New York, **1969**, p. 85.
[72] A. E. Ruoho, H. Kiefer, P. E. Roeder, S. J. Singer, *Proc. Natl. Acad. Sci. USA* **1973**, *70*, 2567–2571.
[73] J. Shafer, P. Baronowsky, R. Laursen, F. Finn, F. H. Westheimer, *J. Biol. Chem.* **1966**, *241*, 421–427.
[74] C. S. Hexter, F. H. Westheimer, *J. Biol. Chem.* **1971**, *246*, 3928–3933.
[75] Y. Ishikawa, A. Menez, H. Hori, H. Yoshida, N. Tamiya, *Toxicon* **1977**, *15*, 477–488.
[76] V. Witzemann, D. Muchmore, M. A. Raftery, *Biochemistry* **1979**, *18*, 5511–5518.
[77] F. Hucho, *FEBS Lett.* **1979**, *103*, 27–32.
[78] N. M. Nathanson, Z. W. Hall, *J. Biol. Chem.* **1980**, *255*, 1698–1703.
[79] B. Chatrenet, O. Tremeau, F. Bontems, M. P. Goeldner, C. G. Hirth, A. Ménez, *Proc. Natl. Acad. Sci. USA* **1990**, *87*, 3378–3382.
[80] R. A. Myers, G. C. Zafaralla, W. R. Gray, J. Abbott, L. J. Cruz, B. M. Olivera, *Biochemistry* **1991**, *30*, 9370–9377.
[81] M. Hervé, L. Pillet, P. Humbert, O. Tremeau, F. Ducancel, C. Hirth, A. Ménez, *Eur. J. Biochem.* **1992**, *208*, 125–131.
[82] N. Unwin, *J. Mol. Biol.* **1993**, *229*, 1104–1124.
[83] M. P. Goeldner, C. G. Hirth, B. Kieffer, G. Ourisson, *Trends Biochem. Sci.* **1982**, *7*, 310–312.
[84] K. Bloch, *Acc. Chem. Res.* **1969**, *2*, 193–202.
[85] P. Eid, M. P. Goeldner, C. G. Hirth, P. Jost, *Biochemistry* **1981**, *20*, 2251–2256.
[86] L. Ehret-Sabatier, B. Kieffer, M. P. Goeldner, C. G. Hirth, *NATO ASI Ser. Ser. C*, **1989**, *272*, 107–122.
[87] M. Goeldner, C. G. Hirth, *Proc. Natl. Acad. Sci. USA* **1980**, *77*, 6439–6442.
[88] M. P. Goeldner, C. G. Hirth, B. Rossi, G. Ponsio, M. Lazdunski, *Biochemistry* **1983**, *22*, 4685–4690.
[89] F. Kotzyba-Hibert, J. Langenbuch-Cachat, A. Jaganathen, M. Goeldner, C. Hirth, *FEBS Lett.* **1985**, *198*, 297–301.
[90] J. Langenbuch-Cachat, C. Bon, C. Mulle, M. Goeldner, C. Hirth, J.-P. Changeux, *Biochemistry* **1988**, *27*, 2337–2345.
[91] B. Ilien, C. Hirth, *Eur. J. Biochem.* **1989**, *183*, 331–337.
[92] I. Schalk, L. Ehret-Sabatier, F. Bouet, M. Goeldner, C. Hirth, *Eur. J. Biochem.* **1994**, *219*, 155–159.
[93] K. Moriyoshi, M. Masu, T. Ishii, R. Shigemoto, N. Mizuno, S. Nakanishi, *Nature (London)* **1991**, *354*, 31–37.
[94] N. Nakayama, T. Yokota, K.-I. Arai, *Curr. Opin. Biotechnol.* **1992**, *3*, 497–505.
[95] J. Fernandez, M. DeMott, D. Atherton, S. M. Mische, *Anal. Biochem.* **1992**, *201*, 255–264.
[96] S. K.-F. Wong, C. Slaughter, A. E. Ruoho, E. M. Ross, *J. Biol. Chem.* **1988**, *263*, 7925–7928.
[97] G. B. Smith, R. W. Olsen, *J. Biol. Chem.* **1994**, *269*, 20380–20387.
[98] E. Kojro, P. Eich, G. Gimpl, F. Fahrenholz, *Biochemistry* **1993**, *32*, 13537–13544.
[99] T. E. Garabedian, R. G. Yount, *Biochemistry* **1991**, *30*, 10126–10132.
[100] T. E. Garabedian, R. G. Yount, *J. Biol. Chem.* **1990**, *265*, 22547–22553.
[101] Y. Takata, M. Fujioka, *Biochemistry* **1992**, *31*, 4369–4374.
[102] B. D. Shivanna, M. R. Mejillano, T. D. Williams, R. H. Himes, *J. Biol. Chem.* **1993**, *268*, 127–132.
[103] R. E. Middleton, J. B. Cohen, *Biochemistry* **1991**, *30*, 6987–6997.
[104] a) A. Schrattenholz, T. Coban, B. Schröder, K. O. Okonjo, J. Kuhlmann, E. F. Pereira, E. X. Albuquerque, A. Maelicke, *J. Recept. Res.* **1993**, *13*, 393–412; b) A. Shrattenholz, J. Godovac-Zimmermann, H.-J. Schäfer, E. X. Albuquerque, A. Maelicke, *Eur. J. Biochem.* **1993**, *216*, 671–677.
[105] J. B. Cohen, M. P. Blanton, D. C. Chiara, S. D. Sharp, B. H. White, *Abstr. Pap. Soc. Neurosci.* **1993**, *19*, T003.
[106] M. Dennis, J. Giraudat, F. Kotzyba-Hibert, M. Goeldner, C. Hirth, J. Y. Chang, C. Lazure, M. Chrétien, J.-P. Changeux, *Biochemistry* **1988**, *27*, 2346–2357.
[107] J.-L. Galzi, F. Revah, D. Black, M. Goeldner, C. Hirth, J.-P. Changeux, *J. Biol. Chem.* **1990**, *265*, 10430–10437.
[108] F. Revah, J.-L. Galzi, J. Giraudat, P.-Y. Haumont, F. Lederer, J.-P. Changeux, *Proc. Natl. Acad. Sci. USA* **1990**, *87*, 4675–4679.
[109] J. Giraudat, M. Dennis, T. Heidmann, J.-Y. Chang, J.-P. Changeux, *Proc. Natl. Acad. Sci. USA* **1986**, *83*, 2719–2723.
[110] J. Giraudat, M. Dennis, T. Heidmann, P.-Y. Haumont, F. Lederer, J.-P. Changeux, *Biochemistry* **1987**, *26*, 2410–2418.
[111] M. P. Blanton, J. B. Cohen, *Biochemistry* **1992**, *31*, 3738–3750.
[112] M. P. Blanton, J. B. Cohen, *Biochemistry* **1994**, *33*, 2859–2872.
[113] R. L. Lundblad, C. M. Noyes, *Chemical Reagents for Protein Modification*, CRC, Boca Raton, FL, **1984**, p. 105.
[114] R. F. Roberta in *Protein Function. A Practical Approach* (Ed.: T. E. Creighton), IRL, Oxford, **1989**, p. 77.
[115] Y. Okamoto, R. G. Yount, *Proc. Natl. Acad. Sci. USA* **1985**, *82*, 1575–1579.
[116] J. P. Whitelegge, P. Jewess, M. G. Pickering, C. Gerrish, P. Camilleri, J. R. Bowyer, *Eur. J. Biochem.* **1992**, *207*, 1077–1084.
[117] K. Yamazumi, R. F. Doolittle, *Proc. Natl. Acad. Sci. USA* **1992**, *89*, 2893–2896.
[118] J. Garin, L. Michel, A. Dupuis, J. P. Issartel, J. Lunardi, J. Hoppe, P. Vignais, *Biochemistry* **1989**, *28*, 1442–1448.
[119] M. Yamaguchi, S. Chen, Y. Hatefi, *Biochemistry* **1986**, *25*, 4864–4868.
[120] K. T. O'Neil, S. Erickson-Viitanen, W. F. DeGrado, *J. Biol. Chem.* **1989**, *264*, 14571–14578.
[121] D. G. Cole, R. G. Yount, *J. Biol. Chem.* **1990**, *265*, 22537–22546.
[122] R. Mahmood, M. Elzinga, R. G. Yount, *Biochemistry* **1989**, *28*, 3989–3995.
[123] K.-S. Huang, R. Radhakrishnan, H. Bayley, H. G. Khorana, *J. Biol. Chem.* **1982**, *257*, 13616–13623.
[124] M. Harel, I. Schalk, L. Ehret-Sabatier, F. Bouet, M. Goeldner, C. Hirth, P. Axelsen, I. Silman, J. L. Sussman, *Proc. Natl. Acad. Sci. USA* **1993**, *90*, 9031–9035.
[125] B. A. Kerwin, R. G. Yount, *Bioconjugate Chem.* **1992**, *3*, 328–336.
[126] I. Schalk, L. Ehret-Sabatier, F. Bouet, M. Goeldner, C. Hirth in *Multidisciplinary Approaches to Cholinesterase Functions* (Eds.: A. Shafferman, B. Velan), Plenum, New York, **1992**, p. 117.
[127] A. R. Kerlavage, S. S. Taylor, *J. Biol. Chem.* **1980**, *255*, 8483–8488.
[128] A. H. Ross, R. Radhakrishnan, R. J. Robson, H. G. Khorana, *J. Biol. Chem.* **1982**, *257*, 4152–4161.
[129] A. Havron, J. Sperling, *Biochemistry* **1977**, *16*, 5631–5635.
[130] a) C.-L. Hew, J. Lifter, M. Yoshioka, F. F. Richards, W. H. Konigsberg, *Biochemistry* **1973**, *12*, 4669–4673; b) J. Lifter, C.-L. Hew, M. Yoshioka, F. F. Richards, W. H. Konigsberg, *ibid.* **1974**, *13*, 3567–3571.
[131] F. Hucho, W. Oberthür, F. Lottspeich, *FEBS Lett.* **1986**, *205*, 137–142.
[132] A. Karlin, *Harvey Lect.* **1991**, *85*, 71–107.
[133] W. T. Miller, E. T. Kaiser, *Proc. Natl. Acad. Sci. USA* **1988**, *85*, 5429–5433.
[134] G. W. Fleet, J. R. Knowles, R. R. Porter, *Biochem. J.* **1972**, *128*, 499–508.
[135] J. G. Lindemann, D. K. Woodard, M. E. Woehler, G. E. Chism, R. E. Lovins, *Immunochemistry* **1975**, *12*, 849–854.
[136] L. E. Cannon, D. K. Woodard, M. E. Woehler, R. E. Lovins, *Immunology* **1974**, *26*, 1183–1194.
[137] R. J. Vaughan, F. H. Westheimer, *J. Am. Chem. Soc.* **1969**, *21*, 217–218.
[138] B. Kierdaszuk, S. Eriksson, *Biochemistry* **1988**, *27*, 4952–4956.
[139] A. Admon, G. G. Hammes, *Biochemistry* **1987**, *26*, 3193–3197.
[140] J. Leszyk, J. H. Collins, *Biochemistry* **1987**, *26*, 7042–7047.
[141] K. A. Cohen, J. Hopkins, R. H. Ingraham, C. Pargellis, J. C. Wu, D. E. H. Palladino, P. Kinkade, T. C. Warren, S. Rogers, J. Adams, P. R. Farina, P. M. Grob, *J. Biol. Chem.* **1991**, *266*, 14670–14674.
[142] H. Kim, B. Haley, *Bioconjugate Chem.* **1991**, *2*, 142–147.
[143] S. Chen, T. D. Lee, K. Legesse, J. E. Shively, *Biochemistry* **1986**, *25*, 5391–5395.
[144] P.-E. Strömstedt, A. Berkenstam, H. Jörnvall, J.-Å. Gustafsson, J. Carlstedt-Duke, *J. Biol. Chem.* **1990**, *265*, 12973–12977.
[145] S. Eriksson, B.-M. Sjöberg, H. Jörnvall, M. Carlquist, *J. Biol. Chem.* **1986**, *261*, 1878–1882.
[146] B. Shuster Gibbs, S. J. Benkovic, *Biochemistry* **1991**, *30*, 6795–6802.
[147] N. Cheng, B. M. Merrill, G. R. Painter, L. W. Frick, P. A. Furman, *Biochemistry* **1993**, *32*, 7630–7634.
[148] C. Grenot, A. de Montard, T. Blachère, M. R. de Ravel, E. Mappus, C. Y. Cuilleron, *Biochemistry* **1992**, 31, 7609–7621.
[149] V. N. Pandey, K. R. Williams, K. L. Stone, M. J. Modak, *Biochemistry* **1987**, *26*, 7744–7748.
[150] H. Chuan, J. Lin, J. H. Wang, *J. Biol. Chem.* **1989**, *264*, 7981–7988.
[151] M. Hearne, W. F. Benisek, *Biochemistry* **1985**, *24*, 7511–7516.
[152] E. A. Barnard, *Trends Biochem. Sci.* **1992**, *17*, 368–374.
[153] F. Kotzyba-Hibert, A. Jaganathen, M. Goeldner, C. Hirth, in *Sigma and Phencyclidine Compounds as Molecular Probes in Biology* (Eds.: E. F. Domino, J.-M. Kamenka), NPP Books, Ann Arbor, **1988**, p. 223.
[154] P. N. Kao, A. J. Dwork, R. R. J. Kadalny, M. L. Silver, J. Widemann, J. Stein, A. Karlin, *J. Biol. Chem.* **1984**, *259*, 11662–11665.
[155] S. N. Abramson, Y. Li, P. Curver, P. Taylor, *J. Biol. Chem.* **1989**, *264*, 12666–12672.
[156] J. B. Cohen, S. D. Sharp, W. S. Liu, *J. Biol. Chem.* **1991**, *266*, 23354–23364.

[157] J.-L. Galzi, J.-P. Changeux in *Membrane Proteins: Structures, Interactions and Models* (Ed.: A. Pullman), Kluwer, Dordrecht, **1992**, p. 127.
[158] M. Delarue, O. Poch, N. Tordo, D. Moras, P. Argos, *Protein Eng.* **1990**, *3*, 461–467.
[159] W. C. Probst, L. A. Snyder, D. I. Schuster, J. Borsius, S. C. Sealfon, *DNA Cell Biol.* **1992**, *11*, 1–20.
[160] T. M. Savarese, C. M. Fraser, *Biochem. J.* **1992**, *283*, 1–19.
[161] N. C. Chien, V. A. Roberts, A. M. Giusti, M. D. Scharff, E. D. Getzoff, *Proc. Natl. Acad. Sci. USA* **1989**, *86*, 5532–5536.
[162] T. B. Lavoie, W. N. Drohan, S. J. Smith-Gill, *J. Immunol.* **1992**, *148*, 503–513.
[163] J. Foote, G. Winter, *J. Mol. Biol.* **1992**, *224*, 487–499.
[164] G. Bucht, E. Artursson, B. Häggström, A. Osterman, K. Hjalmarsson in *Multidisciplinary Approaches to Cholinesterase Functions* (Eds.: A. Shafferman, B. Velan), Plenum, New York, London, **1992**, pp. 185–188.
[165] T. M. Fong, M. G. McNamee, *Biochemistry* **1987**, *26*, 3871–3880.
[166] F. J. Barrantes, *Crit. Rev. Biochem. Mol. Biol.* **1989**, *24*(5), 437–478.
[167] N. L. Novere, A. Bessis, C. Léna, M. Piccioto, M. Zoli, *Médecine/Sciences* **1993**, *9*, 41–49.
[168] H. Lüddens, W. Wisden, *Trends Pharmacol. Sci.* **1991**, *12*, 49–51.
[169] D. R. Burt, G. L. Kamatchi, *FASEB J.* **1991**, *5*, 2916–2923.
[170] C. D. Ulrich, D. I. Pinon, E. M. Hadac, E. L. Holicky, A. Chang-Miller, L. K. Gates, L. J. Miller, *Gastroenterology* **1993**, *105*, 1534–1543.
[171] K. Touhara, K. A. Lerro, B. C. Bonning, B. D. Hammock, G. D. Prestwich, *Biochemistry* **1993**, *32*, 2068–2075.
[172] T. Marti, D. Benke, S. Mertens, R. Heckendorn, M. Pozza, H. Allgeier, C. Angst, D. Laurie, P. Seeburg, H. Möhler, *Proc. Natl. Acad. Sci. USA* **1993**, *90*, 8434–8438.
[173] L. Erb, K. D. Lustig, D. M. Sullivan, J. T. Turner, G. A. Weisman, *Proc. Natl. Acad. Sci. USA* **1993**, *90*, 10449–10453.
[174] D. B. Carter, D. R. Thomsen, W. B. Im, D. J. Lennon, D. M. Ngo, W. Gale, H. K. Im, P. H. Seeburg, M. W. Smith, *Bio/Technology* **1992**, *10*, 679–681.
[175] J.-L. Galzi, F. Revah, F. Bouet, A. Ménez, M. Goeldner, C. Hirth, J.-P. Changeux, *Proc. Natl. Acad. Sci. USA* **1991**, *88*, 5051–5055.
[176] H. Prinz, A. Maelicke, *J. Biol. Chem.* **1983**, *258*, 10273–10282.
[177] T. Heidmann, J.-P. Changeux, *Eur. J. Biochem.* **1979**, *94*, 255–279.
[178] T. Heidmann, J.-P. Changeux, *Biochemistry* **1986**, *25*, 6109–6113.
[179] B. Chatrenet, F. Kotzyba-Hibert, C. Mulle, J.-P. Changeux, M. P. Goeldner, C. Hirth, *Mol. Pharmacol.* **1992**, *41*, 1100–1106.
[180] B. Chatrenet, *Etudes topographiques des sites agonistes du récepteur nicotinique de l'acétylcholine*, Thèse, Université Louis Pasteur, Strasbourg, **1990**.
[181] M.-J. Bouchet, A. Rendon, C. G. Wermuth, M. Goeldner, C. Hirth, *J. Med. Chem.* **1987**, *30*, 2222–2227.

Sulfuric Acid from Sulfur Trioxide and Water—A Surprisingly Complex Reaction**

Ralf Steudel*

Sulfuric acid is not only one of the longest known and utilized chemicals but also one of the most important compounds of all; the annual worldwide production varied in the last four years between 135 and 152 million tons depending on the economic situation.[1] Under these circumstances it is surprising that the structure of the free H_2SO_4 molecule was experimentally determined only in 1981: microwave spectroscopy of gaseous H_2SO_4[2] showed that the molecule has C_2 symmetry; the two hydrogen atoms are situated *anti* to one another (Fig. 1). Previously, a somewhat more symmetric conformation with the hydrogens in *trans* positions (symmetry C_{2v}) had been assumed since the vibrational spectra of H_2SO_4 vapor had been assigned in this point group. In the meantime the C_2 conformation of H_2SO_4 has been confirmed as the most stable structure by various ab initio MO calculations.[3–6] These findings demonstrate once more that the structure of highest symmetry is not always the most stable one, as is often claimed.

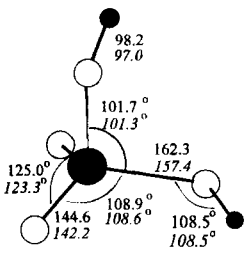


Fig. 1. Structure of the H_2SO_4 molecule in the vapor phase (bond lengths in pm). The geometrical parameters were obtained by ab initio MO calculations [4]; values in italics from microwave spectroscopy [2].

Industrially, sulfuric acid is produced from sulfur trioxide and water. However, the direct reaction of these reagents is not practical for several reasons. First, reaction (a) is highly exothermic, which results in high temperatures and thereby leads to problems with corrosion. Second, the very hygroscopic sulfuric acid molecules formed would react with water vapor to give a mist of $H_2SO_4 \cdot n H_2O$ droplets which are difficult to precipitate. Therefore, the gas prepared by the contact process and containing SO_3 as well as S_3O_9 is washed with concentrated sulfuric acid (98%) resulting in polysulfuric acids; these are then hydrolyzed by water[7] [Eqs. (b)–(e)].

$$SO_3(g) + H_2O(g) \longrightarrow H_2SO_4(g) \quad \Delta H_6^\circ = -92\ kJ\,mol^{-1} \qquad (a)$$

$$3\,SO_3 \rightleftharpoons S_3O_9 \qquad (b)$$

$$SO_3 + H_2SO_4 \rightleftharpoons H_2S_2O_7 \qquad (c)$$

$$S_3O_9 + H_2SO_4 \rightleftharpoons H_2S_4O_{13} \qquad (d)$$

$$H_2O + H_2S_2O_7 \rightleftharpoons 2\,H_2SO_4 \qquad (e)$$

Nevertheless, the simple reaction according to Equation (a) is also of considerable interest, for example, in context with the formation of sulfuric acid in the earth's atmosphere, where H_2SO_4 mainly results from SO_2. To a large extent the latter is of anthropogenic origin, resulting in the phenomenon of acid rain in certain regions of the northern hemisphere. However, as recent results show, the pathway from SO_2 to H_2SO_4 is rather complex, although very interesting. In the atmosphere SO_2 is mainly oxidized by $OH^\bullet$ radicals which are generated photochemically from electronically excited oxygen atoms and water[8] [Eqs. (f)–(h)]. The resulting $HOSO_2^\bullet$ radicals react rapidly and exothermically with dioxygen to give SO_3[9] [Eq. (i)]

$$O_3 \xrightarrow{h\nu} O_2 + O(^1D) \qquad (f)$$

$$O(^1D) + H_2O \longrightarrow 2\,OH^\bullet \qquad (g)$$

$$OH^\bullet + SO_2\,(+\,M) \longrightarrow HOSO_2^\bullet\,(+\,M) \qquad (h)$$

$$HOSO_2^\bullet + O_2 \longrightarrow HO_2^\bullet + SO_3 \qquad (i)$$

(M = collision partner). Since reaction (h) is slower than reaction (i), it is rate determining. The $HO_2^\bullet$ radicals react with NO to give NO_2 and $OH^\bullet$ thus regenerating the latter.

Because of the low SO_3 partial pressure in the atmosphere the equilibrium (b) is of no importance. It therefore may seem that SO_3 and H_2O can simply combine according to Equation (a) to give H_2SO_4. However, this reaction occurs in several steps and only under certain conditions. Initially, the Lewis acid SO_3 and the Lewis base H_2O react, analogously to other reactions of SO_3 with bases, to give an adduct $SO_3 \cdot H_2O$ [Eq. (j)]. This adduct

$$H_2O + SO_3 \rightleftharpoons \overset{(+)}{H_2O}\text{–}\overset{(-)}{SO_3} \qquad (j)$$

[*] Prof. Dr. R. Steudel
Institut für Anorganische und Analytische Chemie der
Technischen Universität
D-10623 Berlin (Germany)
Telefax: Int. code + (30)314 265 19
e-mail steudel@ wap0204.chem.tu-berlin.de

[**] Sulfur Compounds, Part 189. The assistance of Dr. Yana Drozdova in the preparation of Figures 1–4 is gratefully acknowledged. Part 188: M. Pridöhl, R. Steudel, J. Buschmann, P. Luger, *Z. Anorg. Allg. Chem.*, in press.

 © VCH Verlagsgesellschaft mbH, D-69451 Weinheim, 1995 0570-0833/95/1212-1313 $ 10.00+.25/0

was first detected in matrix isolation experiments by vibrational spectroscopy.[10, 11] The spectra showed that the product has a H_2O-SO_3 bond rather than a hydrogen-bonded structure, $HOH\cdots OSO_2$. A precise structural characterization was achieved by high-level ab initio MO calculations (Fig. 2).[3-5] The most accurate of these calculations showed the SO_3 group slightly pyramidalized; the "intermolecular" S–O bond length

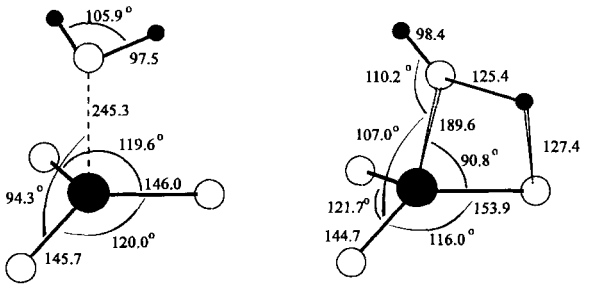


Fig. 2. Left: Structure of the adduct $H_2O\cdot SO_3$ according to ab initio MO calculations (distances in pm). The two hydrogen atoms are almost eclipsed by two oxygen atoms of SO_3 (overall symmetry C_s). The intermolecular H···O distance is larger than the intermolecular S···O distance. Therefore, the proton migration requires a considerable activation energy [4]. Right: Transition state of the reaction $H_2O\cdot SO_3 \rightarrow H_2SO_4$ according to ab initio MO calculations [4].

between the two components is 254 pm.[4] Surprisingly, the hydrogen atoms have no close contacts to the oxygen atoms of the SO_3 group but point slightly in the oposite direction; the angle between the two molecular planes is 22°.[4] Very recently the rotational spectrum of $H_2O\cdot SO_3$ was measured by FT microwave spectroscopy[12] but only a few molecular parameters could be determined. Assuming that d_{OH} and α_{HOH} have the same values as in free H_2O molecules, the "intermolecular" S–O bond length was determined as 243.2(3) pm. The SO_3 fragment is in fact slightly pyramidal; the angle between the two molecular planes is 13°. The torsional angle around the "intermolecular" S–O bond could not be determined.[12]

Previously it had been assumed that $H_2O\cdot SO_3$ can isomerize to H_2SO_4 by a simple proton migration; however, in 1985 it was already demonstrated by MO calculations that this isomerization requires a rather large activation energy.[3] Very recent ab initio MO calculations,[4] performed at the very high level MP4SDQ/6-311+G(2df,p)//RMP2(fu)/6-31+G* (taking the zero point energy calculated at level RMP2(fu)/6-31G* into account) yielded an activation energy of 114 kJ mol^{-1} for the reaction $H_2O\cdot SO_3 \rightarrow H_2SO_4$ at 0 K. This energy has to be compared with the reaction enthalpy of reaction (j) which is only -33 kJ mol^{-1}. Therefore, it has to be concluded that any activation of $H_2O\cdot SO_3$ would result in dissociation rather than isomerization. In other words, the formation of H_2SO_4 by this route is impossible! If the thermal energy at 25 °C is taken into account the free reaction enthalpy for reaction (j) is found to be $\Delta G^0_{298} = 0$ kJ mol^{-1} (because of the negative reaction entropy), from which the equilibrium constant $K = \exp(-\Delta G^0_{298}/RT) = 1$ is obtained. The free activation enthalpy $\Delta G^{\neq}_{298}$ of the isomerization $H_2O\cdot SO_3 \rightarrow H_2SO_4$ is 119.6 kJ mol^{-1}.[4]

This picture changes dramatically if a second water molecule is added. In the vapor phase H_2O is in equilibrium with its dimer, the structure of which is well known [Eq. (k)]. There are now two possibilities: either H_2O can react with $H_2O\cdot SO_3$ or

$$2H_2O \rightleftharpoons (H_2O)_2 \qquad (k)$$

$(H_2O)_2$ attacks SO_3 directly. In both cases this results in the formation of the adduct $(H_2O)_2\cdot SO_3$, the structure of which has been determined by ab initio methods (Fig. 3 left).[5] This structure indicates that a proton migration should be much easier since the $HOH\cdots OSO_2$ distance of 210.8 pm is considerably smaller than in the case of $H_2O\cdot SO_3$ (> 250 pm). However, the formation of H_2SO_4 from $(H_2O)_2\cdot SO_3$ requires the synchronized migration of *two* protons in the corresponding hydrogen bonds. The transition state structure (Fig. 3 right) is character-

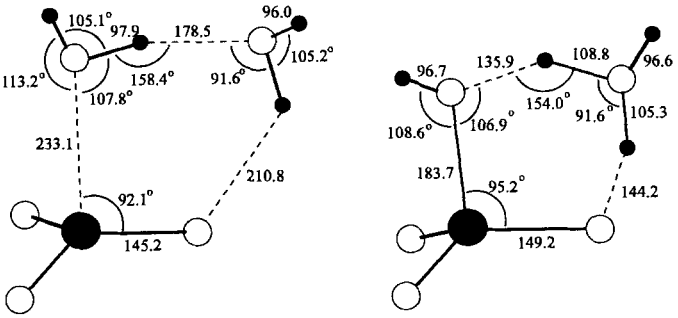


Fig. 3. Left: Structure of the adduct from SO_3 and $(H_2O)_2$ according to ab initio MO calculations (distances in pm) [5]. The intermolecular S···O distance (233.1 pm) is smaller than that in $SO_3\cdot H_2O$ (245.3 pm). Right: Transition state of the isomerization $(H_2O)_2\cdot SO_3 \rightarrow H_2SO_4\cdot H_2O$. The two protons in the almost linear hydrogen bonds move synchroneously and clockwise towards their new bonding partners [5]. The structure may be interpreted as a cyclic ion pair, $H_3O^+HSO_4^-$. The final product $H_2O\cdot H_2SO_4$ is not an ion pair.

ized by a six-membered ring; this lies about 96 kJ mol^{-1} higher in energy than the adduct $(H_2O)_2\cdot SO_3$, the formation of which from $2H_2O$ and SO_3 is exothermic by 110 kJ mol^{-1}. In other words, in this case the activation energy is *smaller* than the dissociation energy, and the isomerization $H_2O\cdot SO_3 \rightarrow (H_2O)\cdot H_2SO_4$ may proceed without problems. The energy profiles of reactions (a) and (l) are shown in Figure 4.

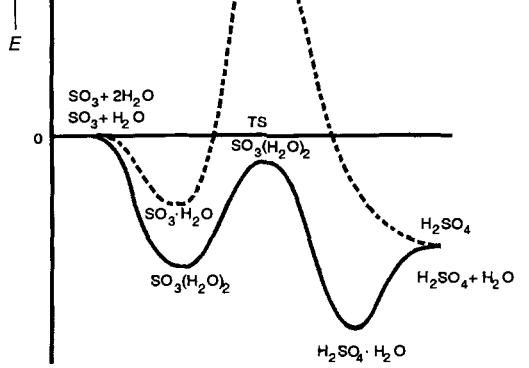


Fig. 4. Energy profiles for the reactions of SO_3 with H_2O via $H_2O\cdot SO_3$ to H_2SO_4 and of SO_3 with $(H_2O)_2$ via $(H_2O)_2SO_3$ to $H_2O\cdot H_2SO_4$. The x axis is the reaction coordinate; TS = transition state.

 © VCH Verlagsgesellschaft mbH, D-69451 Weinheim, 1995 0570-0833/95/1212-1314 $ 10.00+.25/0

Recent kinetic measurements[13] support the idea of a second-order reaction with respect to H_2O [Eq. (l)]. Such measurements are all but trivial, since wall reactions have to be suppressed.

$$2H_2O + SO_3 \longrightarrow H_2SO_4 + H_2O \quad (l)$$

Using a reactor with turbulent flow, designed to minimize wall reactions, it could be demonstrated that SO_3 on mixing with water vapor at 22 °C disappears in a reaction of order 2.04 with respect to the H_2O concentration. Reaction (l) proceeds in two steps: dimerization of H_2O according to Equation (k) and reaction of the dimer with SO_3 to give H_2SO_4 and H_2O. Because of the slightly exothermic pre-equilibrium (k), the rate of reaction (l) increases with decreasing temperature.[13] The concentration of $(H_2O)_2$ in the atmosphere has been estimated to be approximately 10^{14} cm^{-3} at ground level and approximately $10^4 cm^{-3}$ at an altitude of 40 km. These concentrations are sufficient to allow the formation of significant amounts of H_2SO_4 by reaction (l).[13] It should however be pointed out that about 50% of the atmospheric SO_2 is oxidized as an aqueous solution, that is dissolved in the droplets of clouds, rather than in a homogeneous gas phase reaction. Suitable oxidants for the dissolved SO_2 are ozone and hydrogen peroxide, but in addition peroxoacetic acid, methyl hydroperoxide, and peroxoacetylnitrate are discussed. The relative importance of these reagents depends on pH and temperature.[8]

Besides SO_2 tremendous amounts of carbonylsulfide (COS) and dimethylsulfide (DMS) are released into the atmosphere. DMS is of biological origin, produced mainly by marine phytoplankton, and together with its oxidation products and COS it yields the "background" of sulfur compounds in the atmosphere. The oxidative degradation of DMS is complex but among its products also yields SO_2 as in the case of COS.[14]

Finally, it should be mentioned that the sulfuric acid formed in the atmosphere causes a variety of effects. H_2SO_4 molecules attract water molecules and form droplets of less than 1 μm diameter (the size depends on the humidity). These droplets absorb atmospheric ammonia and form what is called a liquid "sulfate aerosol". This aerosol not only reduces the visibility but also increases the earth's albedo. As a consequence, the reflection of sunlight is enhanced and it is most probably this effect that partly compensates the global warming resulting from the greenhouse effect in industrialized areas.[15, 16] Approximately 90% of the anthropogenic SO_2 emissions occur in the northern hemisphere. The half-lifes of SO_2 and H_2SO_4 in the atmosphere are only a few days. Therefore, these compounds are not transported to the southern hemisphere, in contrast to CO_2, COS, CH_4, N_2O, and fluorochloro hydrocarbons. These facts possibly explain why most of the global warming has been observed in the southern hemisphere although most of the air pollution is generated in the northern hemisphere.[15]

As acid rain, H_2SO_4 causes well-known damage, but at the same time serves as a nutrient for plants which depend on the availability of sulfate ions for the synthesis of sulfur-containing amino acids. There are good reasons to demand a rigorous reduction of SO_2 emissions; however, this will result in an increased need for sulfur-containing fertilizers for sulfur-deficient farm land.

German version: *Angew. Chem.* **1995**, *107*, 1433–1435

Keywords: atmospheric chemistry · hydrogen bonds · structure elucidation · sulfur compounds · sulfuric acid

[1] *Sulphur* **1994**, *235* (Statistical Suppl., Table 4).
[2] R. L. Kuczkowski, R. D. Suenram, F. J. Lovas, *J. Am. Chem. Soc.* **1981**, *103*, 2561.
[3] T. S. Chen, P. L. Moore Plummer, *J. Phys. Chem.* **1985**, *89*, 3689.
[4] M. Hofmann, P. von R. Schleyer, *J. Am. Chem. Soc.* **1994**, *116*, 4947.
[5] K. Morokuma, C. Muguruma, *J. Am. Chem. Soc.* **1994**, *116*, 10316.
[6] Thiosulfuric acid has the analogous structure: K. Miaskiewicz, R. Steudel, *Angew. Chem.* **1992**, *104*, 87; *Angew. Chem. Int. Ed. Engl.* **1992**, *31*, 58.
[7] H. Müller, U. Sander, U. Rothe, R. Kola, *Ullmanns Encycl. Ind. Chem.* **1994**, *25*, 635.
[8] J. G. Calvert, A. Lazrus, G. L. Kok, B. G. Heikes, J. G. Walega, J. Lind, C. A. Cantrell, *Nature* **1985**, *317*, 27.
[9] J. F. Gleason, A. Sinha, C. J. Howard, *J. Phys. Chem.* **1987**, *91*, 719; J. F. Gleason, C. J. Howard, *ibid.* **1988**, *92*, 3414; W. R. Stockwell, J. G. Calvert, *Atmos. Environ.* **1983**, *17*, 2231.
[10] T.-L. Tso, E. K. C. Lee, *J. Phys. Chem.* **1984**, *88*, 2776; L. Schriver, D. Carrere, A. Schriver, K. Jaeger, *Chem. Phys. Lett.* **1991**, *181*, 505.
[11] V. E. Bondybey, J. H. English, *J. Mol. Spectrosc.* **1985**, *109*, 221.
[12] J. A. Phillips, M. Canagaratna, H. Goodfriend, K. R. Leopold, *J. Phys. Chem.* **1995**, *99*, 501.
[13] C. E. Kolb, J. T. Jayne, D. R. Worsnop, M. J. Molina, R. F. Meads, A. A. Viggiano, *J. Am. Chem. Soc.* **1994**, *116*, 10314.
[14] G. S. Tyndall, A. R. Ravishankara, *Int. J. Chem. Kinet.* **1991**, *23*, 483; A. A. Turnipseed, A. R. Ravishankara in *Dimethylsulfide: Oceans, Atmosphere and Climate* (Eds.: G. Restelli, G. Angeletti), Kluwer, Dordrecht, **1993**, p. 185; I. Barnes, K. H. Becker, I. Patroescu, *Geophys. Res. Lett.* **1994**, *21*, 2389.
[15] R. J. Charlson, T. M. L. Wigley, *Sci. Am.* **1994**, Nr. 2, 28.
[16] Clouds reflect about 30% of the sun's radiation. Most recent results indicate that clouds absorb more energy than previously assumed: R. D. Cess, M. H. Zhang, P. Minnis, L. Corsetti, E. G. Dutton, B. W. Forgan, D. P. Garber, W. L. Gates, J. J. Hack, E. F. Harrison, X. Jing, J. T. Kiehl, C. N. Long, J.-J. Morcrette, G. L. Potter, V. Ramanathan, B. Subasilar, C. H. Whitlock, D. F. Young, Y. Zhou, *Science* **1995**, *267*, 496; V. Ramanathan, B. Subasilas, G. J. Zhang, W. Conant, R. D. Cess, J. T. Kiehl, H. Grassl, L. Shi, *ibid.* **1995**, *267*, 499.

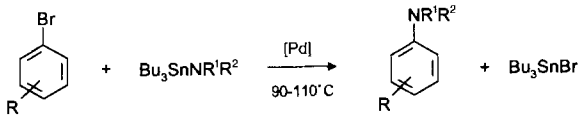
 © *VCH Verlagsgesellschaft mbH, D-69451 Weinheim, 1995* *0570-0833/95/1212-1315 $ 10.00+.25/0*

Palladium-Catalyzed Amination of Aryl Halides—Catalysts on New Routes to Known Targets

Matthias Beller*

"The discovery of truely *new* reactions is likely to be limited to the realm of transition-metal organic chemistry, which will almost certainly provide us with additional "miracle reagents" in the years to come", was predicted by D. Seebach in 1990.[1] No other area of classic synthetic chemistry today still offers such innovative possibilities as metal-catalyzed processes. Transition metal catalyzed reactions are becoming increasingly more significant not only for the synthesis of complex building blocks, but also for structurally simpler, industrially important intermediates. Since the inception of the Wacker–Hoechst oxidation[2] and the Heck reaction,[3] palladium-catalyzed processes, in particular, have aroused the interests both of the synthetic chemist in the laboratory and also of the industrial chemist. Based on the almost unique range of catalytic activity of palladium complexes, whose use however is often limited by low selectivities and deactivations during the reactions, a multitude of palladium-supported syntheses were discovered or developed further in the the last few years.[4] So far, the research has focussed on methods for C–C coupling. Because of the significance of unsymmetrically substituted ethers and amines in organic synthesis, the transferability of catalysis by palladium complexes of C–C couplings to the equally important C–O and C–N couplings are of general interest.

Against this background new methodic developments for hetero-Heck-reactions by Hartwig et al. and Buchwald et al. are noteworthy,[5] the simple, palladium-catalyzed aminations of aryl bromides to give arylamines with aminostannanes[6] described in 1994 (Scheme 1).

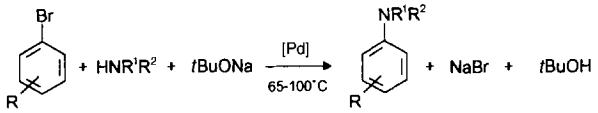


Scheme 1. [Pd] = $[PdCl_2(P(o\text{-tolyl})_3)_2]$. Selected substituents: R = 4-$CO_2C_2H_5$, 4-$(CH_3)_2N$, 3-OCH_3, 3-CH_3; R^1 = $C_6H_5CH_2$, $C_{18}H_{37}$, C_6H_5; R^2 = H, CH_3, $CH_2CH_2C_6H_5$.

Palladium(0) or palladium(II) compounds are used as catalyst precursors in the presence of tri-*o*-tolylphosphane as ligand. According to investigations by Hartwig et al. the actual active species seems to be a palladium(0)bis(tri-*o*-tolylphosphane) complex, which in the catalytic cycle initially inserts oxidatively into the aryl–halogen bond. The resulting arylpalladium(II) complex then reacts with the tin amide under transmetalation; this step is postulated to be rate determining. The subsequent reductive elimination leads back to the palladium(0) catalyst. Very recent investigations show that in addition to tri-*o*-tolylphosphane complexes, simpler arylpalladium(II)-bis(triphenylphosphane) complexes can also react with alkali metal amides to form amido complexes, which can be converted by reductive elimination to give arylamines.[7]

By clever coupling of a transamination reaction of tributyl-*N*,*N*-diethylaminostannane with higher boiling amines with Pd catalysis, Buchwald and Guram succeeded in extending the method.[5b] It was shown that secondary aliphatic and aromatic amines react with substituted aryl bromides to afford the corresponding arylamines in good yields. As in the classic Heck reaction, depending on the substitution pattern of the arene, electron acceptor substituents promote the reactivity of the aryl bromide.

The use of stoichiometric amounts of organo tin compounds is the main disadvantage of this method both for ecological reasons and with regard to practicability. Thus, from an industrial point of view the aim was to replace the tin amides by simpler amino sources, ideally the amines themselves.[8] Independently, Buchwald et al.[9] and Hartwig et al.[10] reported the first catalytic aminations of aryl bromides with free amines. The palladium-catalyzed reactions occur in the presence of stoichiometric amounts of a sterically hindered base such as NaO*t*Bu in toluene or tetrahydrofuran at temperatures of 65–100 °C (Scheme 2).



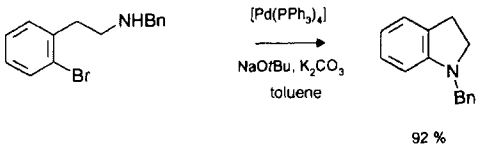
Scheme 2. [Pd] = $[PdCl_2(P(o\text{-tolyl})_3)_2]$. Selected substituents: R = 4-C_4H_9, 4-CF_3, 4-C_6H_5, 4-$(CH_3)_2N$; R^1 = C_6H_5, C_6H_{13}; R^2 = H, CH_3; R^1–R^2 = $H_2C(CH_2)_3CH_2$, $H_2CCH_2N(CH_3)CH_2CH_2$.

The arylamines are generally formed in good yields (67–89%). Dehalogenation products are the only by-products that occur, which probably arise from base-induced β-hydride elimination of the amido arylpalladium complex and subsequent reduction. The base employed has a decisive influence on the course of the reaction. In the amination of 1-bromo-4-*n*-butylbenzene with free amines in the presence of silyl amides as base—in contrast to the coupling with tin amides—the rate-determining step in the catalytic cycle is the oxidative addition of bis(tri-*o*-tolylphosphane)palladium(0) to the aryl halide. However, when LiO*t*Bu is used as base, the formation and reductive elimination of the amido arylpalladium complex is decisive for the rate of the reaction. In the presence of NaO*t*Bu both reaction steps seem to take place at similar rates.[10]

Extending the intermolecular coupling, dihydroindoles (Scheme 3), dihydroquinolines, and other N-heterocycles were successfully synthesized by simple intramolecular trapping reactions, starting from alkylamino substituted aryl bromides.[9] Intramolecular amination can be achieved in the presence of tetrakis(triphenylphosphane)palladium as catalyst and stoi-

[*] Dr. M. Beller
Hoechst AG, Zentralforschung
D-65926 Frankfurt am Main (Germany)

 © VCH Verlagsgesellschaft mbH, D-69451 Weinheim, 1995 0570-0833/95/1212-1316 $ 10.00+.25/0



Scheme 3. Intramolecular variant of the palladium-catalyzed amination of aryl halides.

chiometric amounts of base in toluene. The best results are obtained with mixtures of NaO*t*Bu and potassium carbonate.

The quality of the catalysts applied with turnover numbers of up to 200 and turnover frequencies of up to 100 h^{-1} does not yet satisfy industrial demands. Nevertheless the publications by Buchwald and Hartwig are noteworthy in that they demonstrate the general applicability of the Heck reaction and its Stille and Suzuki variants to C–N couplings and open up new possibilites for Tandem processes. Thus, they show the way to further catalytic carbon–heteroatom couplings.[11] Furthermore, it becomes evident that there is a need for alternative synthetic methods also for apparently structurally trivial molecules such as arylamines. The future will show that in this respect organometallic chemistry and catalysis offers manifold possibilities.

German version: *Angew. Chem.* **1995**, *107*, 1436–1437

Keywords: aminations · arylamines · catalysis · Heck reactions

[1] D. Seebach, *Angew. Chem.* **1990**, *102*, 1363; *Angew. Chem. Int. Ed. Engl.* **1990**, *29*, 1320.
[2] J. Tsuji in *Comprehensive Organic Synthesis, Vol. 7* (Eds.: S. V. Ley), Pergamon, Oxford, **1991**, p. 449.
[3] Reviews: a) R. F. Heck, *Palladium Reagents in Organic Synthesis*, Academic Press, London, **1985**; b) A. de Meijere, F. Meier, *Angew. Chem.* **1994**, *106*, 2473; *Angew. Chem. Int. Ed. Engl.* **1994**, *33*, 2379; c) R. F. Heck in *Comprehensive Organic Synthesis, Vol. 4* (Eds.: B. M. Trost, I. Fleming, M. F. Semmelhack), Pergamon, Oxford, **1991**, p. 833; d) W. Cabri, I. Candiani, *Acc. Chem. Res.* **1995**, *28*, 2.
[4] Several recent examples: a) B. M. Trost, *Angew. Chem.* **1995**, *107*, 285; *Angew. Chem. Int. Ed. Engl.* **1995**, *34*, 259; b) S. C. A. Nefkens, M. Sperrle, G. Consiglio, *ibid.* **1993**, *105*, 1837 and **1993**, *32*, 1719; c) W. Oppolzer, *Pure Appl. Chem.* **1990**, *62*, 1941; d) Y. Ben-David, M. Portnoy, D. Milstein, *J. Am. Chem. Soc.* **1989**, *111*, 8742; e) Y. Sato, S. Nukui, M. Sodeoka, M. Shibasaki, *Tetrahedron* **1994**, *50*, 371; f) L. F. Tietze, R. Schimpf, *Angew. Chem.* **1994**, *106*, 1138; *Angew. Chem. Int. Ed. Engl.* **1994**, *33*, 1089; g) E. Drent, J. A. M. van Broekhooven, M. J. Doyle, *J. Organomet. Chem.* **1991**, *417*, 235; h) G. Dyker, *Angew. Chem.* **1994**, *106*, 117; *Angew. Chem. Int. Ed. Engl.* **1994**, *33*, 103; i) T. Ohishi, J. Yamada, Y. Inui, T. Sakaguchi, M. Yamashita, *J. Org. Chem.* **1994**, *59*, 7521; j) T. I. Wallow, B. M. Novak, *ibid.* **1994**, *59*, 5034; k) H. M. R. Hoffmann, A. R. Otte, A. Wilde, *Angew. Chem.* **1992**, *104*, 224; *Angew. Chem. Int. Ed. Engl.* **1992**, *31*, 2379.
[5] a) F. Paul, J. Patt, J. F. Hartwig, *J. Am. Chem. Soc.* **1994**, *116*, 5969; b) A. S. Guram, S. L. Buchwald, *ibid.* **1994**, *116*, 7901.
[6] M. Kosugi, M. Kameyama, T. Migata, *Chem. Lett.* **1983**, 927.
[7] M. S. driver, J. F. Hartwig, *J. Am. Chem. Soc.* **1995**, *117*, in press.
[8] Reactions of aryl halides with amines in the presence of stoichiometric amounts of palladium compounds have been known for some time: D. L. Boger, S. R. Duff, J. S. Panek, M. Yasuda, *J. Org. Chem.* **1985**, *50*, 5782.
[9] A. S. Guram, R. A. Rennels, S. L. Buchwald, *Angew. Chem.* **1995**, *107*, 1456; *Angew. Chem. Int. Ed. Engl.* **1995**, *34*, 1348.
[10] J. Louie, J. F. Hartwig, *Tetrahedron Lett.* **1995**, in press.
[11] For further carbon–heteroatom coupling reactions see D. Baranano, J. Hartwig, *J. Am. Chem. Soc.* **1995**, *117*, 2937, and references therein.

 © *VCH Verlagsgesellschaft mbH, D-69451 Weinheim, 1995* *0570-0833/95/1212-1317 $ 10.00+.25/0*

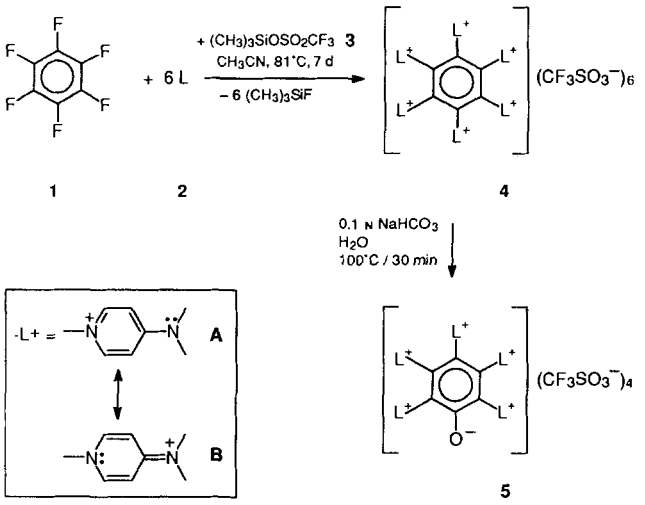
First-Ever Per(onio) Substitution of Benzene: The Role of the Counterion

Robert Weiss,* Bernd Pomrehn, Frank Hampel, and Walter Bauer

In earlier studies we have shown that the transition from neutral to cationic sets of substituents by poly(onio) substitution (POS) with main group element derivatives and nonaromatic organic π systems generally leads to a marked increase in Lewis acidity and electron affinity.[1–6] At the same time, novel reaction pathways are observed for redox and substitution reactions with appropriate reagents.[5, 6] This is attributed primarily to the electrostatic field effect (pole effect)[7] of the cationic substituents. Since electrostatic effects are not, in principle, subject to any saturation effect, but are instead additive in nature, it is of particular interest to introduce the maximum number of onio substituents structurally possible at a basic core unit. In this context, we have now turned our attention to the example of an aromatic π system and report herein on the synthesis, structure, and some properties of the first hexakis(onio)-substituted benzene derivative.[8]

In 1993 Streitwieser et al. reported on an unsuccessful attempt at synthesizing one such hexacationic substituted benzene derivative.[9] Upon reaction of hexafluorobenzene (**1**) with 4-dimethylaminopyridine (DMAP, **2**), an S_NAr sequence gave the corresponding 1,4-bis(onio)-substituted benzene derivative, which was obtained in 20% yield and structurally characterized. An attempt at synthesizing the corresponding per(onio)-substituted salt starting from **1** and DMAP led, after a reaction time of three and a half months, to a higher substituted product in extremely low yield. This was identified on the basis of spectroscopic data as the corresponding pentakis(onio)-substituted benzene. The last fluorine substituent could not, however, be displaced, even under elevated pressure.

The low reactivity of this bis(onio)-substituted and particularly the pentakis(onio)-substituted benzene is at variance with the expectation that the electrophilicity of π systems should be enhanced with an increase in the number of onio substituents. To explain the results of Streitwieser et al., we assume that contacts between the electrophilic countercation and the liberated fluoride ions lead to inhibition of any further nucleophilic substitution. A number of possibilities may be discussed regarding the nature of these contacts, for example the formation of kinetically stable ion clusters or even the formation of stable Meisenheimer complexes (more likely with higher levels of onio substitution). Exchange of fluoride ion for a more strongly nucleofugic anion should then hold the key to successful per(onio) substitution in the benzene system. This simple approach met with complete success and led to the thermodynamically particularly favorable variant of poly(onio) substitution depicted in Scheme 1.



Scheme 1. Synthesis and hydrolysis of **4**.

The desired per(onio) substitution product **4**, the sole reaction product, was obtained in virtually analytically pure form in 92% yield as a sparingly soluble salt. It is clear that the reaction is greatly facilitated by the combination of the S_NAr substitution sequence with the formation of the extremely stable Si–F bond. We do not rule out an assisting intervention by **3** at a relatively early stage of the substitution sequence. The exclusive formation of **4**, even upon addition of **2** and **3** in a molar ratio of 1:1:1, underlines most explicitly the electrophilic autoactivation of the π system through increasing onio substitution and confirms our interpretation of the results of Streitwieser et al.[9]

Remarkably, **4** can be recrystallized from hot water without decomposition. This allowed us to obtain colorless needles suitable for X-ray structure analysis,[10] the results of which are depicted in Figure 1 (for clarity four of the triflate ions located at a greater distance from the hexacation are omitted).

The following structural features are noteworthy:

- With a torsion angle of 80.0°, the pyridine rings are almost orthogonal to the benzene ring, whereas the corresponding angle in hexaphenylbenzene amounts to about only 65°.[11] MNDO calculations give an average torsion angle of 83° for

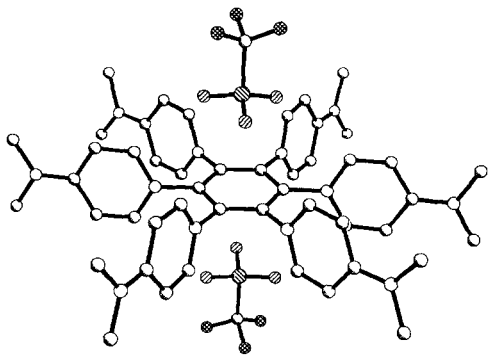


Fig. 1. Crystal structure of **4**.

[*] Prof. Dr. R. Weiss, Dipl.-Chem. B. Pomrehn, Dr. F. Hampel, Dr. W. Bauer
Institut für Organische Chemie der Universität Erlangen-Nürnberg
Henkestrasse 42, D-91054 Erlangen (Germany)
Telefax: Int. code + (9131)85-9132

 © VCH Verlagsgesellschaft mbH, D-69451 Weinheim, 1995 0570-0833/95/1212-1319 $ 10.00+.25/0

the cation in **4**. The bond lengths in the onio substituents attest to a considerable contribution from resonance structure **B** (Scheme 1)—a charge-stabilizing effect generally found for onio systems derived from **2**.[1, 4, 9, 12]

- Whereas four of the six triflate ions occupy peripheral positions relative to the polycation (in the outer region of the pyridinio substituents), the remaining two triflate ions are located directly above and below the plane of the benzene π system. Thus, the two planes through the oxygen atoms in the triflate groups are almost parallel to that of the benzene ring. Clearly, the hexacation is partially neutralized—in the primary sphere, so to speak—by two electrostatically strongly bound counterions, whereas the remaining four counterions form a distinctly more weakly bound secondary anion sphere. The resulting central triple-decker ion cluster is a completely novel structural element. To the best of our knowledge, this positioning of anions relative to an aromatic π system seen here has not been observed previously. The interplanar distance of 3.2 Å here points to purely ionic interactions. Weak bonding contacts between the oxygen centers and the α-hydrogen atoms of the pyridinio substituents are also evident (mean O–H distance 2.2–2.5 Å).

Cyclic voltammetric investigations of **4** yielded one quasi-reversible reduction at -0.80 V and a second, irreversible one at -1.14 V.[13] This corresponds to an increase in redox potential of 2.55 V relative to that of benzene,[14] which, because of the extensive out-of-plane torsion of the pyridinio substituents, must be essentially electrostatic in origin. The poly(onio)-substituted salts 1,3,5-tris(4-dimethylamino-1-pyridinio)benzene tris(trifluoromethanesulfonate) (**6**) and 1,2,3,4,5-pentakis(4-dimethylamino-1-pyridinio)benzene pentakis(trifluoromethanesulfonate) (**7**), which we synthesized in analogy to **4**, exhibit (irreversible) $E_{1/2}$ values of -1.34 and -0.88 V, respectively.[13] Figure 2 shows a plot of the redox potentials of the compounds investigated versus the number of pyridinio substituents.

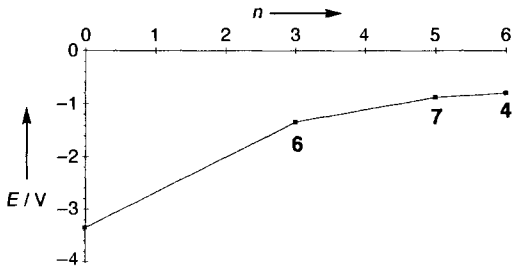


Fig. 2. Dependence of the redox potentials of substituted benzenes on the number n of 4-dimethylaminopyridinio substituents.

It can be seen that the first three onio substituents, arranged alternately, increase the electron affinity of the benzene system much more efficiently than those following. This deviation from the additivity of the substituent effect may be a consequence of the $-$M effect of the pyridinio substituents, which, due to the conformationally restricted conjugation in **4** and **7**, can only be realized for **6**. That the redox potential of **4** lies only slightly above that of **7** can be attributed to an increasingly nonlinear contribution from the dimethylamino groups. The importance of the iminium structure **B** (Scheme 1) increases with increasing electrophilicity of the template such that the positive charge is increasingly shifted to the periphery of the molecule. This hypothesis is supported by the observation that this effect is found only with dimethylaminopyridinio substituents and not with pyridinio substituents.[15, 16]

The ^{13}C NMR spectrum of **4** in solution (CD_3NO_2/CF_3COOD) shows, as expected, only one signal for the benzene ring and one set of signals for the onio substituents. Thus, in solution, (averaged) D_{6h} symmetry can be inferred for the poly(onio) system. In the crystal, on the other hand, **4** is present with a lower degree of symmetry. The asymmetric unit consists of a "half" molecule of **4**, with three carbon atoms of the benzene ring, three onio substituents, and three counterions. Consequently, the ^{13}C CP/MAS solid-state NMR spectrum[17] contains three sets of signals for the cation in **4**. The smallest differences in the δ values are shown by the signals for C2/C6 of the substituents ($\Delta\delta \approx 0.6$). For the carbon atoms of the benzene ring and carbon atoms C3/C5 of the substituents, the difference is larger ($\Delta\delta \approx 2.7$ and 2.5, respectively).

The electrostatic activation of **4** is likewise illustrated by its hydrolysis. Whereas hexafluorobenzene is stable at normal pressure to aqueous sodium hydroxide solution,[18] **4** undergoes hydrolysis within 30 min in refluxing 0.1 N $NaHCO_3$ solution to give the corresponding pentakis-substituted phenolate **5** virtually quantitatively. The analogous introduction of a hydroxyl group under comparably mild conditions is also observed with hexacyanobenzene.[19] Apparently the almost purely electrostatic activation of this reaction through the set of cationic substituents in **4** is as effective as the $-$M activation of the cyano groups in hexacyanobenzene.

The reactions of **4** with reducing agents and nucleophiles are being investigated currently.

Experimental Procedure

4: To a solution of **1** (0.20 mL, 1.73 mmol) in anhydrous CH_3CN (30 mL) under N_2 was added **3** (2.50 mL, 13.8 mmol) and **2** (2.00 g, 16.4 mmol), and the solution was then stirred at reflux. After 7 d the resulting white precipitate was filtered off, washed first with CH_3CN (2 × 5 mL) and then CH_2Cl_2 (3 × 5 mL), and dried under high vacuum for 12 h. Yield: 2.71 g (92.1%). The use of stoichiometric quantities of **2** and **3** afforded significantly lower yields, even after longer reaction times. Single crystals of **4** were obtained by boiling briefly in water followed by slow cooling. Correct C,H,N-analysis; ^{1}H NMR (399.65 MHz, CD_3NO_2/CF_3COOD, 20 °C, TMS): $\delta = 8.21$ (d, ^3J(H,H) = 8.0 Hz, 12H; H-2/H-6), 7.02 (d, ^3J(H,H) = 8.0 Hz, 12H; H-3/H-5), 3.31 (s, 36H; CH_3); ^{13}C NMR (100.4 MHz, CD_3NO_2/CF_3COOD, 20 °C, TMS): $\delta = 157.79$ (s; C4, DMAP), 141.12 (s; C2/C6, DMAP), 140.99 (s, benzene), 121.48 (q, ^1J(C,F) = $-$ 317.0 Hz; CF_3), 111.07 (s; C3/C5, DMAP), 41.66 (s; CH_3); ^{19}F NMR (470.4 MHz, D_2O/HCl, 20 °C, C_6F_6): $\delta = -79.6$ (s; CF_3); IR (KBr): $\tilde{\nu}$[cm^{-1}] = 3060w, 3050w, 1650s, 1600m, 1480w, 1440m, 1410w, 1350vw, 1330vw, 1260vs, 1230s, 1150s, 1060vw, 1030s, 810m, 790w, 750vw, 630s.

5: A suspension of **4** (1.00 g, 0.59 mmol) in aqueous $NaHCO_3$ solution (0.1 N, 30 mL) was heated for 30 min at reflux. The solution was then cooled to 5 °C and the resulting pale yellow precipitate filtered off, washed with cold water (1 × 5 mL) followed by CH_2Cl_2 (2 × 5 mL), and then dried under high vacuum for 12 h. Yield: 0.72 g (94.2%). Correct C,H,N-analysis; ^{1}H NMR (400.05 MHz, CD_3CN, 20 °C, TMS): $\delta = 8.25$ (d, ^3J(H,H) = 7.57 Hz, 2H; H-2/H-6), 8.19 (d, ^3J(H,H) = 7.33 Hz, 4H; H-2/H-6), 8.03 (d, ^3J(H,H) = 7.57 Hz, 4H; H-2/H-6), 6.87 (d, ^3J(H,H) = 7.57 Hz, 4H; H-3(H-5), 6.78 (d, ^3J(H,H) = 7.33 Hz, 4H; H-3/H-5), 6.72 (d, ^3J(H,H) = 7.57 Hz, 2H; H-3/H-5), 3.17 s (12H; CH_3), 3.13 s (12H; CH_3), 3.12 s (6H; CH_3); ^{13}C NMR (100.50 MHz, CD_3CN, 20 °C, TMS): $\delta = 164.56$ (s; C1, phenol), 157.51 (s; C4, DMAP), 157.34 (s; C4, DMAP), 157.25 (s; C4, *p*-DMAP), 144.23 (s; C2/C6, *p*-DMAP), 143.86 (s; C2/C6, DMAP), 141.96 (s; C2/C6, DMAP), 137.50 (s; C3/C5, phenol), 132.31 (s; C2/C6, phenol), 121.93 (q, ^1J(C,F) = $-$ 321.4 Hz; CF_3), 113.70 (s; C4, phenol), 109.51 (s; C3/C5, DMAP), 109.48 (s; C3/C5, *p*-DMAP), 108.95 (s; C3/C5, DMAP), 41.09 (s; CH_3), 41.04 (s; *p*-CH_3), 40.87 (s; CH_3); IR (KBr): $\tilde{\nu}$[cm^{-1}] = 3050w, 1650vs, 1580m, 1540m, 1440w, 1405m, 1270s, 1220s, 1150s, 1030s, 820w, 750vw, 720vw, 630s.

Compound **5** may be protonated with trifluoromethanesulfonic acid in CH_2Cl_2 to give pentakis(4-dimethylamino-1-pyridinio)phenol pentakis(trifluoromethanesulfonate).

6: To a solution of 1,3,5-trifluorobenzene (0.30 mL, 2.90 mmol) in anhydrous chlorobenzene (20 mL) under N_2 was added **3** (2.00 mL, 11.1 mmol) and **2** (1.60 g, 13.1 mmol), and the solution was then stirred at reflux. After 9 d the resulting white precipitate was filtered off, washed with Et_2O (2 × 5 mL), and then dried under high vacuum for 12 h. Yield 1.06 g (41.1%, unoptimized). Correct C,H,N-analysis; ^{1}H NMR (400.05 MHz, CD_3CN, 20 °C, TMS): $\delta = 8.44$ (d, ^3J(H,H) = 7.93 Hz, 6H; H-2/H-6), 8.01 (s, 3H; C-H, benzene), 7.10 (d, ^3J(H,H) = 7.93 Hz, 6H; H-3/H-5), 3.30 (s, 18H; CH_3); ^{13}C NMR (100.50 MHz, CD_3CN, 20 °C, TMS):

δ = 157.93 (s; C4, DMAP), 144.74 (s; C1/C3/C5, benzene), 141.85 (s; C2/C6, DMAP), 122.05 (q, ^1J(C,F) = − 319.5 Hz; CF_3), 121.17 (s, C2/C4/C6, benzene), 109.18 (s; C3/C5, DMAP), 41.22 (s; CH_3); IR (KBr): $\tilde{\nu}$[cm^{-1}] = 3060w, 1650vs, 1640vs, 1605s, 1570s, 1530w, 1450m, 1400m, 1350w, 1260s, 1160s, 1090w, 1030s, 830m, 820m, 730w, 630s.

7: To a solution of pentafluorobenzene (0.10 mL, 0.91 mmol) in anhydrous CH_3CN (20 mL) under N_2 was added **3** (0.95 mL, 5.26 mmol) and **2** (0.800 g, 6.55 mmol), and the solution was then stirred at reflux. After 8 d the reaction mixture was concentrated to dryness and the resulting white solid suspended in CH_2Cl_2 (20 mL), filtered off, washed with CH_2Cl_2 (3 × 5 mL), and then dried under high vacuum for 12 h. Yield 0.808 g (62.1%, unoptimized). Correct C,H,N-analysis; ^{1}H NMR (400.05 MHz, CD_3CN, 20 °C, TMS): δ = 8.65 (s, 1H; benzenel), 8.13 (d, ^3J(H,H) = 7.94 Hz, 4H; H-2/H-6), 8.07 (d, ^3J(H,H) = 8.67 Hz, 2H, H-2/H-6), 8.02 (d, ^3J(H,H) = 8.06 Hz, 4H; H-2/H-6), 7.01 (d, ^3J(H,H) = 7.94 Hz, 4H; H-3/H-5), 6.91 (d, ^3J(H,H) = 8.06 Hz, 4H; H-3/H-5), 6.88 (d, ^3J(H,H) = 8.67 Hz, 2H; H-3/H-5); 3.25 (s, 12H; CH_3), 3.21 (s, 12H; CH_3), 3.20 (s, 6H; CH_3); ^{13}C NMR (100.50 MHz, CD_3CN, 20 °C, TMS): δ = 158.00 (s; C4, DMAP), 157.67 (s; C4, DMAP), 157.63 (s; C4, DMAP), 142.40 (s; C1/C5, benzene), 141.43 (s; C2/C6, DMAP), 140.97 (s; C2/C6, DMAP), 138.31 (s; C3, benzene), 137.96 (s; C2/C4, benzene), 132.88 (s; C6, benzene), 121.83 (q, ^1J(C,F) = − 319.8 Hz; CF_3), 110.65 (s; C3/C5, DMAP), 110.55 (s; C3/C5, DMAP), 109.81 (s; C3/C5, DMAP), 41.44 (s; CH_3), 41.37 (s; CH_3); IR (KBr): $\tilde{\nu}$[cm^{-1}] = 3100s, 2980w, 1660s, 1580s, 1510s, 1450s, 1350m, 1270vs, 1170s, 1060m, 1030s, 940m, 830s, 790m, 750m, 740w, 730w, 710w, 630s.

Received: September 23, 1994
Revised version: March 14, 1995 [Z 7346 IE]
German version: *Angew. Chem.* **1995**, *107*, 1446–1448

Keywords: arenes · nucleophilic aromatic substitution · polycations

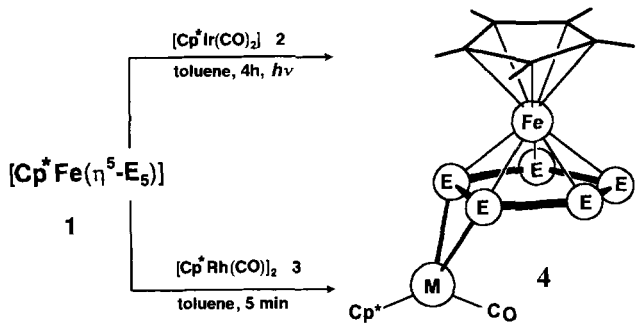
[1] R. Weiss, N. J. Salomon, G. E. Miess, R. Roth, *Angew. Chem.* **1986**, *98*, 925; *Angew. Chem. Int. Ed. Engl.* **1986**, *25*, 917.
[2] R. Weiss, R. Roth, *J. Chem. Soc. Chem. Commun.* **1987**, 317.
[3] R. Weiss, R. Roth, *Synthesis* **1987**, 870.
[4] R. Weiss, R. Roth, R. H. Lowack, M. Bremer, *Angew. Chem.* **1990**, *102*, 1164; *Angew. Chem. Int. Ed. Engl.* **1990**, *29*, 1132.
[5] R. Weiss, J. Seubert, *Angew. Chem.* **1994**, *106*, 900; *Angew. Chem. Int. Ed. Engl.* **1994**, *33*, 891.
[6] R. Weiss, J. Seubert, F. Hampel, *Angew. Chem.* **1994**, *106*, 2038; *Angew. Chem. Int. Ed. Engl.* **1994**, *33*, 1952.
[7] R. W. Taft, R. D. Topsom, *Prog. Phys. Org. Chem.* **1987**, *16*, 6.
[8] The first hexacationically substituted benzene derivative was reported by R. Breslow et al. (R. Breslow, G. A. Crispino, *Tetrahedron Lett.* **1991**, *32*, 601). The sixfold alkylated hexakis(4-pyridyl)benzene described therein has onio centers in the periphery of the ligands, and therefore cannot be generated, as in our case, by a substitution sequence at the central benzene ring but only by a multistep synthesis. Reduction potentials for this compound have not yet been published.
[9] A. S. Koch, A. S. Feng, T. A. Hopkins, A. Streitwieser, *J. Org. Chem.* **1993**, *58*, 1409.
[10] Crystal structure analysis for **4**: $C_{54}H_{60}F_{18}N_{12}O_{18}S_6$, M = 1699.50, monoclinic, in crystal **4** has centrosymmetry, space group $P2(1)/c$, a = 12.749(8), b = 22.03(2), c = 13.513(8) Å, β = 107.42(5)°, V = 3621(4) Å^3, Z = 2, ρ_{calcd} = 1.559 mg m^{-3}, $F(000)$ = 1740, T = 298(2) K. Data collection was carried out with a Nicolet R3mV automatic four-circle diffractometer with graphite-monochromated $Mo_{K\alpha}$ radiation (λ = 0.71073 Å) in the region 4.00 ≤ 2θ ≤ 50.0° (7293 measured reflections of which 6467 are independent). Structure solution with direct methods (SHELXTL Plus V4.11), refinement with full matrix against F^2 according to the least squares process (SHELXL93: G. M. Sheldrick, Göttingen, 1993). All non-hydrogen atoms were refined anisotropically. The CF_3SO_3 units were refined with distance restraints for the resolution of positional disorder; the disorder positions of the oxygen atoms could be resolved with an occupational probability of only ca. 70:30. The hydrogen atoms were fixed in ideal positions in isotropic refinements using the riding model. 6467 Reflections were used to refine 479 parameters and 13 restraints. R-values for 2157 reflections with $I > 2\sigma(I)$: $R1$ = 0.1104, $wR2$ = 0.3560 (all reflections, $R1 = \Sigma||F_o| - |F_c||/\Sigma|F_o|$, $wR2 = [\Sigma w(F_o^2 - F_c^2)^2/\Sigma w(F_o^2)^2]^{0.5}$); residual electron density 0.78 e Å^{-3}; GOF = 0.847. Further details of the crystal structure investigation may be obtained from the Director of the Cambridge Crystallographic Data Centre, 12 Union Road, GB-Cambridge CB2 1EZ (UK), upon quoting the full journal citation.
[11] J. C. J. Bart, *Acta Crystallogr. Sect. B* **1968**, *24*, 1277.
[12] H. Bock, S. Nick, J. W. Bats, *Tetrahedron Lett.* **1992**, *33*, 5941.
[13] The electrochemical investigations were carried out at room temperature under N_2 with ferrocene as an internal standard in a 0.1 N NEt_4BF_4/CH_3CN conducting electrolyte. A saturated Ag/AgCl electrode immersed in a 0.1 N NEt_4Cl/CH_3CN solution was used; working and supporting electrodes were platinum.
[14] K. Meerholz, J. Heinze, *J. Am. Chem. Soc.* **1989**, *111*, 2325.
[15] R. König, Dissertation, Universität Erlangen-Nürnberg, **1992**.
[16] B. Pomrehn, Diplomarbeit, Universität Erlangen-Nürnberg, **1993**.
[17] C. Fyfe, *Solid State NMR for Chemists*, C.F.C. Press, Guelph, Ontario, Canada, **1983**.
[18] J. M. Birchall, R. N. Haszeldine, *J. Chem. Soc.* **1959**, 13.
[19] K. Friedrich, S. Oeckl, *Chem. Ber.* **1973**, *106*, 2361.

η^5:η^2 Coordination of a *cyclo*-E_5 Ligand, E = P, As**

Michaela Detzel, Gabriele Friedrich, Otto J. Scherer,* and Gotthelf Wolmershäuser

Dedicated to Professor Manfred Regitz on the occasion of his 60th birthday

In the extensive literature[1] on ferrocene and its derivatives there is to our knowledge no example in which in addition to η^5 coordination, the η^2-side-on coordination to one of the two parallel five-membered rings has been achieved. In lanthanoid complexes with bent sandwich structures, a (μ-η^5:η^2-C_5H_5) structural unit is found in $[(C_5H_5)_3La]_n$,[2a] a type of coordination which is also discussed in $[Cp^*_2Sm(\mu\text{-}C_5H_5)SmCp^*_2]$.[2b] We have now been able to show that the sandwich complexes **1** (**1a**: E = P;[3] **1b**: E = As[4]), which are iso(valence)electronic and isolobal to ferrocene $FeCp_2$, can be converted to the complexes **4** in which the unusual μ-η^5:η^2-*cyclo*-E_5 coordination (**4a**: E = P; **4b**: E = As) is realized. So far only terminal η^1 coordination of 16 VE complex fragments could be verified both in sandwich complexes with five-membered rings consisting of P(As) and CR building blocks[5a] as well as in **1**.[5b]



Compound **4a** forms brown crystals that can be manipulated in air for short periods, **4b** dark brown crystals that are air and moisture sensitive. They are sparingly soluble in pentane and dissolve well in toluene and dichloromethane. The five P atoms of the *cyclo*-P_5 ligand give rise in the ^{31}P NMR spectrum to an

[*] Prof. Dr. O. J. Scherer, Dipl.-Chem. M. Detzel, Dipl.-Chem. G. Friedrich, Dr. G. Wolmershäuser[+]
Fachbereich Chemie der Universität
D-67663 Kaiserslautern (Germany)
Telefax: Int. code + (631) 205-3200
[+]X-ray crystal structure analyses.

[**] This work was supported by the Fonds der Chemischen Industrie and by the Graduiertenkolleg (M. D.) "Phosphorchemie als Bindeglied verschiedener chemischer Disziplinen".

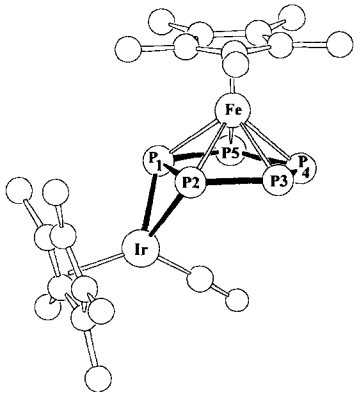


Fig. 1. Crystal structure of **4a**. Selected bond lengths [Å] and angles [°]: P1-P2 2.359(2), P2-P3 2.134(3), P1-P5 2.132(3), P3-P4 2.117(3), P4-P5 2.112(3), Ir-P1 2.375(2), Ir-P2 2.378(2), Fe-P1 2.381(2), Fe-P2 2.399(2), Fe-P3 2.320(2), Fe-P5 2.317(2), Fe-P4 2.380(2), Ir-$Cp^*_{(centroid)}$ 1.94, Fe-$Cp^*_{(centroid)}$ 1.72; P1-Ir-P2 59.50(6), P2-P1-P5 104.97 (10), P1-P2-P3 105.25(10), P2-P3-P4 109.15(12), P3-P4-P5 110.31(11), P1-P5-P4 109.54(11).

ABB′XX′ spin system,[6] whose ^1J(P,P) coupling constants for the four short P–P bonds (−391 to −433 Hz) lie in the expected range.[7] In contrast, a ^1J(P,P) coupling constant of −211 Hz is found for the significantly longer P1–P2 bond (Fig. 1); however, this value is considerably larger than the ^2J(P,P) value of −41 Hz in the IrP_5 six-membered ring (P···P 2.64 Å)[8] of the complex **5**.

$[\{Cp^*Fe\}\{Cp^*_2(CO)_2\overline{Ir_2}\}\{\overline{P_5}Ir(CO)Cp^*\}\{Ir(CO)Cp^*\}]$ **5**

Among the selected MS data[6] the fragments $[Cp^*FeE_5MCp^*]^+$ and $[Cp^*FeE_3MCp^*]^+$ (E = P, M = Ir; E = As, M = Rh), which give rise to intense signals, are particularly noteworthy, since they could possibly be assigned to 31VE and 29VE triple-decker cations, respectively.

The crystal structure analyses[9] reveal **4a** (Fig. 1) and **4b** (Fig. 2) to be sandwich complexes with μ-η^5:η^2 coordination of

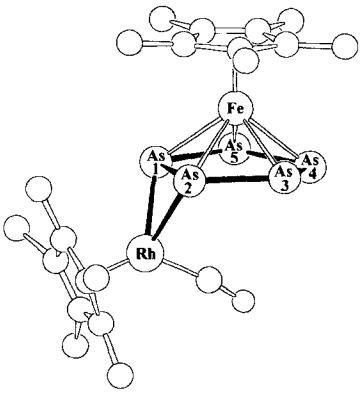


Fig. 2. Crystal structure of **4b**. Selected bond lengths [Å] and angles [°]: As1-As2 2.502(2), As2-As3 2.356(2), As1-As5 2.345(2), As3-As4 2.317(2), As4-As5 2.315(2), Rh-As1 2.486(2), Rh-As2 2.486(2), Fe-As1 2.550(2), Fe-As2 2.558(2), Fe-As3 2.447(2), Fe-As5 2.463(2), Fe-As4 2.528(2), Rh-$Cp^*_{(centroid)}$ 1.91, Fe-$Cp^*_{(centroid)}$ 1.71; As1-Rh-As2 60.44(5), As2-As1-As5 106.57(7), As1-As2-As3 105.04(6), As2-As3-As4 109.30(7), As3-As4-As5 109-54(8), As1-As5-As4 108.63 (7).

the *cyclo*-E_5 ligand (E = P, As). As expected, the additional η^2-side-on coordination of a 16VE Cp*(CO)M fragment (M = Ir, Rh) to the starting materials **1a** and **1b** leads to a significant lengthening of the respective E–E bonds. However, the P1–P2 distance (2.36 Å) is considerably shorter than the 2.46 Å found for the side-on coordinated intact P_4 edge in the $[RhCl(\eta^2\text{-}P_4)(PPh_3)_2]$ complex.[10] P–P bonds of comparable length are present in $P_2(BR)_2$ (2.35 Å)[11a] and $P_2(SiR_2)_2$ (2.34 Å),[11b] molecules with butterfly skeletons (R = 2,2,6,6-tetramethylpiperidino, mesityl); a structural subunit, which is also formed by the atoms Fe,P1,P2,Ir in **4a**. In **4b** the As1–As2 distance (2.50 Å) is likewise longer than the other As–As bonds; however, for example, in realgar, As_4S_4 (2.59 Å)[12a] and in $As_2(SiMestBu)_2$ (2.60 Å)[12b] the As–As bonds are even longer. The average values of 2.12 and 2.33 Å found for the remaining four P–P and As–As distances of the respective five-membered rings can be divided into two pairs (Figs. 1 and 2). These values do not differ or scarcely differ from those in the starting material **1a** (2.12 Å)[13] and $[(C_5Me_4Et)Fe(As_5)]$ (2.32 Å).[4] In **4a** and **4b** Ir,P1,P2 and Rh,As1,As2, respectively, form an almost equilateral triangle. P4 and As4 are tilted below the plane of the ring by 8.6 and 6°, respectively, which, as expected, leads to a slight reduction in the sum of the angles in the *cyclo*-P_5 (539.2°) and the *cyclo*-As_5 (539.0°) unit. The plane of the four remaining P and As atoms is arranged almost parallel (deviation: **4a** 0.7°, **4b** 2.1°) to the plane of five-membered ring of the Fe-Cp* ligand. The dihedral angles of the Fe,P1,P2,Ir and Fe,As1,As2,Rh "butterfly" structural subunits are 158.5 and 152°, respectively.

In the synthesis of **4a** the isomer **6a** is formed as a by-product. Unlike **4a**, **4b** can isomerize to give **6b** (see Experimental Procedure). The M(CO)Cp* ligand is not η^2 (as in **4**) but η^1 bound in the complexes **6**.

$[Cp^*Fe(\mu\text{-}\eta^{5:1}\text{-}E_5)\{M(CO)Cp^*\}]$ **6**

6a: E = P, M = Ir; **6b**: E = As, M = Rh

Experimental Procedure

Improved synthetic method for **1a** [3]: $[Cp^*Fe(CO)_2]_2$ (1.0 g, 2.02 mmol), P_4 (1.0 g, 8.07 mmol), decalin (250 mL), were heated to reflux for 3h. After the decalin had been removed under vacuum, the brown residue was transferred to a column (25 × 3 cm) packed with SiO_2 (2% H_2O)/petroleum ether. Elution with petroleum ether gave a green fraction of **1a** (840 mg, 60%).

4a: **1a** (132 mg, 0.38 mmol) and **2** (364 mg, 0.95 mmol) [14] (excess used for yield optimization) were dissolved in toluene (80 mL) and irradiated for approximately 4 h (150 W-Hg lamp, water cooled, Ar stream) and monitored by IR spectroscopy. The red-brown solution was evaporated to dryness under vacuum, the residue dissolved in dichloromethane (ca. 5 mL), and dried with basic Al_2O_3 (1 g, 2% H_2O). Column chromatographic workup (column: 20 × 1.5 cm, Al_2O_3, petroleum ether), initially gave excess **2** (160 mg, 44%) with petroleum ether as a pale yellow fraction. A pale brown fraction of **4a** (122 mg, 45% based on **1a**) was obtained with petroleum ether/toluene. Red-brown **6a** (95 mg; 36% based on **1a**) was eluted with pure toluene. The product contained small amounts of phosphorus-containing impurities.

4b: **1b** (150 mg, 0.26 mmol) [4] and **3** [70 mg, 0.13 mmol) [15] were each dissolved in toluene (15 mL) and mixed at room temperature. A reaction took place (color change to brown) immediately, which, according to IR spectroscopy, was completely finished after 5 min. Workup as for **4a**. A sand-colored fraction of **4b** was obtained with petroleum ether/toluene (3:1). Yield 55 mg (25%), pale brown powder, which was recrystallized (0 °C) from a toluene/hexane mixture (1:10). Small amounts of a mixture of products that could not be characterized were eluted with CH_2Cl_2.

6b: **4b** (100 mg, 0.12 mmol) was warmed to 110 °C in toluene (ca. 20 mL) for 150 min (^{1}H NMR control indicates quantitative isomerization). After recrystallization (0 °C) **6b** (70 mg; 70%) was obtained as a brown-black microcrystalline powder from toluene/hexane (ca. 1:5).

Received: January 18, 1995
Revised version: March 23, 1995 [Z 7638 IE]
German version: *Angew. Chem.* **1995**, *107*, 1454–1456

Keywords: arsenic compounds · complexes with arsenic ligands · complexes with phosphorus ligands · phosphorus compounds · sandwich complexes

[1] a) For example C. Elschenbroich, A. Salzer, *Organometallics. A Concise Introduction*, 2nd ed. VCH, Weinheim **1991**; b) *Comprehensive Organometallic Chemistry* (Eds.: G. Wilkinson, F.G. A. Stone, E. W. Abel), Pergamon, Oxford, **1982**; c) A. J. Deeming in [1 b], Vol. 4, p. 475; d) W. E. Watts in [1 b], *Vol. 8*, p. 1013; e) M. Drössmar-Wolf in *Gmelin, Handbook of Inorganic Chemistry, Organoiron Compounds, Part A, Ferrocene*, Springer, Heidelberg, **1989**.

[2] a) S. H. Eggers, J. Kopf, R. D. Fischer, *Organometallics* **1986**, *5*, 383–385; b) W. J. Evans, T. A. Ulibarry, *J. Am. Chem. Soc.* **1987**, *109*, 4292–4297.

[3] O. J. Scherer, T. Brück, *Angew. Chem.* **1987**, *99*, 59; *Angew. Chem. Int. Ed. Engl.* **1987**, *26*, 59; O. J. Scherer, T. Brück, G. Wolmershäuser, *Chem. Ber.* **1988**, *121*, 935–938; for an improved method of synthesis see Experimental Procedure.

[4] O. J. Scherer, C. Blath, G. Wolmershäuser, *J. Organomet. Chem.* **1990**, *387*, C21–C24.

[5] Recent reviews: a) F. Mathey, *Coord. Chem. Rev.* **1994**, *137*, 1–52; b) O. J. Scherer, *Angew. Chem.* **1990**, *102*, 1137–1155; *Angew. Chem. Int. Ed. Engl.* **1990**, *29*, 1104–1122.

[6] ^{1}H NMR (200/400 MHz, C_6D_6, 298 K, C_6H_6 int.): **4a**: $\delta = 1.52$ (s, 15H), 1.64 (s, 15H); **4b**: $\delta = 1.49$ (s, 15H), 1.70 (s, 15H); **6a**: $\delta = 1.40$ (s, 15H), 1.81 (s, 15H); **6b**: $\delta = 1.67$ (s, 15H), 1.89 (s, 15H). ^{31}P NMR (162 MHz, C_6D_6, 298 K, 85% H_3PO_4 ext.): **4a**: ABB'XX' spin system (A≡P4, BB'≡P3P5, XX'≡P1P2): $\delta = 110.5$ (P_A, „tt"), 95.1 ($P_{BB'}$,m), 30.5 ($P_{XX'}$,m), $^1J_{AB} = -431$, $^1J_{AB'} = -433$, $^1J_{BX} = -392$, $^1J_{B'X'} = -391$, $^1J_{XX'} = -211$, $^2J_{AX} = 44$, $^2J_{AX'} = 43$, $^2J_{BB'} = 39$, $^2J_{BX'} = 10$, $^2J_{B'X} = 9$ Hz; **6a**: AMNXY spin system: $\delta = 131.1$ (P_A, „t"), 30.8 ((P_M,m), 29.8 (P_N,m), −53.7 (P_X,m), −56.4 (P_Y,m), $^1J_{AX} = -336$, $^1J_{MN} = -386$, $^1J_{NY} = -410$, $^1J_{MX} = -394$, $^1J_{AY} = -316$, $^2J_{AM} = 9$, $^2J_{MY} = 43$, $^2J_{AN} = 7$, $^2J_{NX} = 35$, $^2J_{XY} = -3$ Hz; accuracy for $J = \pm 5$ Hz. Spectra simulation: PERCH program, R. Laatikainen, M. Niemitz, Version 1994, University of Kuopio, Finland. IR(toluene): **4a**: ν(CO) [cm^{-1}] = 1967 (s, br), 1935 (sh); **4b**: 1980 (s); **6a**: 2015 (s); **6b**: 1935 (s). MS (70 eV): **4a**: *m/z* (%) 674 (100) [M^+ − CO], 612(93) [M^+ − CO − 2P]; **4b**: 804 (100) [M^+ − CO], 654 (67) [M^+ − CO − 2As] and other peaks; **6a**: 702 (0.3) [M^+], 674 (0.7) [M^+ − CO], 136 (100) [Cp*H]; **6b**: 832 (12%) [M^+], 804 (100) [M^+ − CO] and other peaks.

[7] J. Hahn in *Phosphorus-31NMR-Spectroscopy in Stereochemical Analysis* (Eds.: J. G. Verkade, L. D. Quin), VCH Publishers, Deerfield Beach, FL, USA), **1987**, p. 339.

[8] M. Detzel, T. Mohr, O. J. Scherer, G. Wolmershäuser, *Angew. Chem.* **1994**, *106*, 1142–1144; *Angew. Chem. Int. Ed. Engl.* **1994**, *33*, 1110–1112.

[9] **4a** [**4b**] $C_{21}H_{30}FeIrOP_5$ [$C_{21}H_{30}As_5FeORh$], molecular weight [g mol^{-1}] 701.35 [831.81], crystal system monoclinic [monoclinic], space group $P2_1/c$ [$P2_1/c$], cell parameters $a = 17.150(4)$ [18.951(4)], $b = 8.9015(11)$ [8.889(2)], $c = 17.111(4)$ [16.018(3)] Å, $\beta = 100.412(4)$ [98.67(3)]°, $V = 2569.3(9)$ [2667.5(10)] Å^3, $Z = 4$ [4], crystal dimensions $0.47 \times 0.20 \times 0.05$ [$0.50 \times 0.20 \times 0.10$] mm^3, $T = 293(2)$ [273(2)] K, $Mo_{K\alpha}$ radiation, Enraf-Nonius CAD 4 diffractometer for **4a**, [Siemens P4 for **4b**], λ 0.71073 Å, measured θ range 2.41–27.41 [2.17–27.50]°, $2\theta_{max}$ 54.82 [55.00]°, scan mode ω scan $\rho_{calcd} = 1.813$ [2.071] mg m^{-3}, absorption coefficient 6.061 [7.329] mm^{-1}, number of observed reflections 6813 [7580], number of unique reflections 5838/R(int) = 0.0288 [6091/R(int) = 0.0546], absorption correction semiempirical from Ψ scan, max. and min. Transmission 0.168/0.269 [0.101/0.056], structure solution by direct methods, SHELXS-86 (Sheldrick, 1990), full-matrix least squares refinement against F^2, SHELXL-93 (Sheldrick, 1993), data/parameter 5837/274 [6090/274], idealized hydrogen atom positions calculated geometrically. Riding model refined with a common temperature factor, final R values ($I > 2\sigma I$). $R1 = 0.041$ [0.0609], $wR2 = 0.0661$ [0.0992], R values (all data); $R1 = 0.0879$ [0.1813], $wR2 = 0.0791$ [0.1417], residual electron density (largest maxima and minima) 0.901/−0.854 [0.986/−0.688] e Å^{-3}. Further details of the crystal structure investigations may be obtained from the Fachinformationszentrum Karlsruhe, D-76344 Eggenstein-Leopoldshafen (Germany) on quoting the depository number CSD-401767/401768.

[10] A. P. Ginsberg, W. E. Lindsell, K. J. McCullough, C. R. Sprinkle, A. J. Welch, *J. Am. Chem. Soc.* **1986**, *108*, 403–416.

[11] a) P. Kölle, G. Linti, H. Nöth, K. Polborn, *J. Organomet. Chem.* **1988**, *355*, 7–18; b) M. Driess, A. D. Fanta, D. Powell, R. West, *Angew. Chem.* **1989**, *101*, 1087–1088; *Angew. Chem. Int. Ed. Engl.* **1989**, *28*, 1038–1039.

[12] a) E. J. Porter, G. M. Sheldrick, *J. Chem. Soc. Dalton Trans.* **1972**, 1347–1349; b) M. Driess, R. Janoscheck, H. Pritzkow, *Angew. Chem.* **1992**, *104*, 449–451; *Angew. Chem. Int. Ed. Engl.* **1992**, *31*, 460–462.

[13] R. Blom, T. Brück, O. J. Scherer, *Acta Chem. Scand.* **1989**, *43*, 458–462.

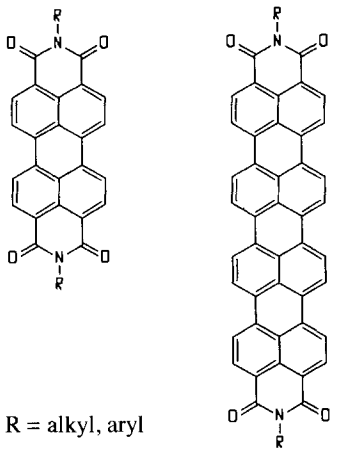
[14] J. W. Kang, K. Moseley, P. M. Maitlis, *J. Am. Chem. Soc.* **1969**, *91*, 5970–5977.

[15] W. A. Herrmann, J. Plank, C. Bauer, M. L. Ziegler, E. Guggolz, R. Alt, *Z. Anorg. Allg. Chem.* **1982**, *487*, 85–110.

Quaterrylenebis(dicarboximides)**

Heribert Quante and Klaus Müllen*

Perylene-3,4:9,10-bis(dicarboximides) **1** are important chromophores in dye chemistry.[1] They are characterized, above all, by their chemical, thermal, and photochemical inertness.[2, 3] Because of their absorption between 530 and 590 nm and their high fluorescence quantum yield,[3] compounds like **1** have wide technical applications both as pigments and as soluble dyes. In recent years the electrooptical properties of **1** have received more attention, and the use of **1** in reprographic processes,[4] fluorescence solar collectors,[5] photovoltaic processes,[6] and molecular switches[7] has been reported.



1 **2**

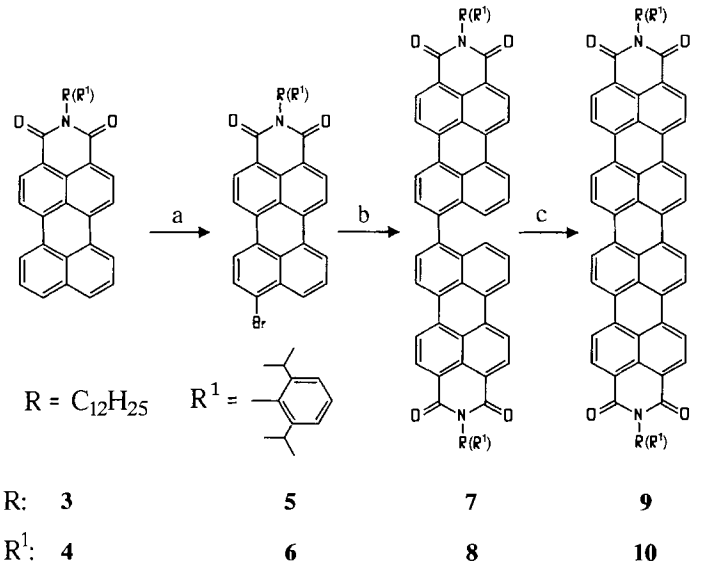
A particular challenge in current, in particular nontextile, dye chemistry is the generation of stable dyes that absorb at the limits of the visible spectrum or even in the near-infrared region.[8] In view of the advantages shown by **1**, it is reasonable to make use of this structural type in the search for "highly colored" chromophores.[8]

We describe here the synthesis and attractive optical properties of quaterrylenebis(dicarboximides) **2**. Depending on its structure, the new chromophore **2** may be a pigment or a soluble dye, which leads to a wide range of applications as well as the development of even larger chromophoric systems.

The key units in our synthetic approach (Scheme 1) are the perylene derivatives **3** and **4** functionalized on one side only. The preparation of these intermediates in the case of the N-alkylated species **3** was achieved by the known procedure of decarboxylating perylenetetracarboxylic monoimide monoanhydride.[9, 10] Subsequent bromination gave the monobromo derivatives **5** and **6** in yields of over 90%. Coupling to form the biperylenyl compounds **7** and **8** was a considerable challenge. Coupling by means of an Ullmann reaction, as suggested by Misono and Nagao,[11] is limited to N-alkylated derivatives with a maximum chain length of four C atoms and, in addition, gives only low yields. Because of the moderate solubility of the resulting biperylenyls, their isolation and characterization can be accomplished only with great difficulty. Yamamoto coupling[12] with [Ni(cod)$_2$] (cod = 1,5-cyclooctadiene) proved to be the method of choice for the preparation of N-alkyl- and N-arylbiperylenyls in yields of 83–89%. The subsequent cyclization to provide the target compounds **9** and **10** was achieved in the conventional manner by heating in molten KOH with an added oxidizing agent.[13] Compound **9** synthesized in this manner (see Table 1 for spectroscopic data for this and other compounds) is regarded as a pigment since it is insoluble in all organic solvents. Compound **10**, on the other hand, is moderately soluble in chlo-

[*] Prof. Dr. K. Müllen, Dr. H. Quante
Max-Planck-Institut für Polymerforschung
Ackermannweg 10, D-55128 Mainz (Germany)
Telefax: Int. code + (6131) 379-350

[**] This work was supported by BASF AG.



Scheme 1. Synthesis of quaterrylenebis(dicarboximides) **9** and **10**. Reagents, conditions, and yields: a) **3**: Br_2/CH_2Cl_2, reflux, 94%, **4**: Br_2/C_6H_5Cl, 50 °C, 98%; b) $[Ni(cod)_2]$/DMF, 60 °C, 2 d, **7**: 89%, **8**: 83%; c) KOH/EtOH/ox., **9**: 37%, **10**: 83%.

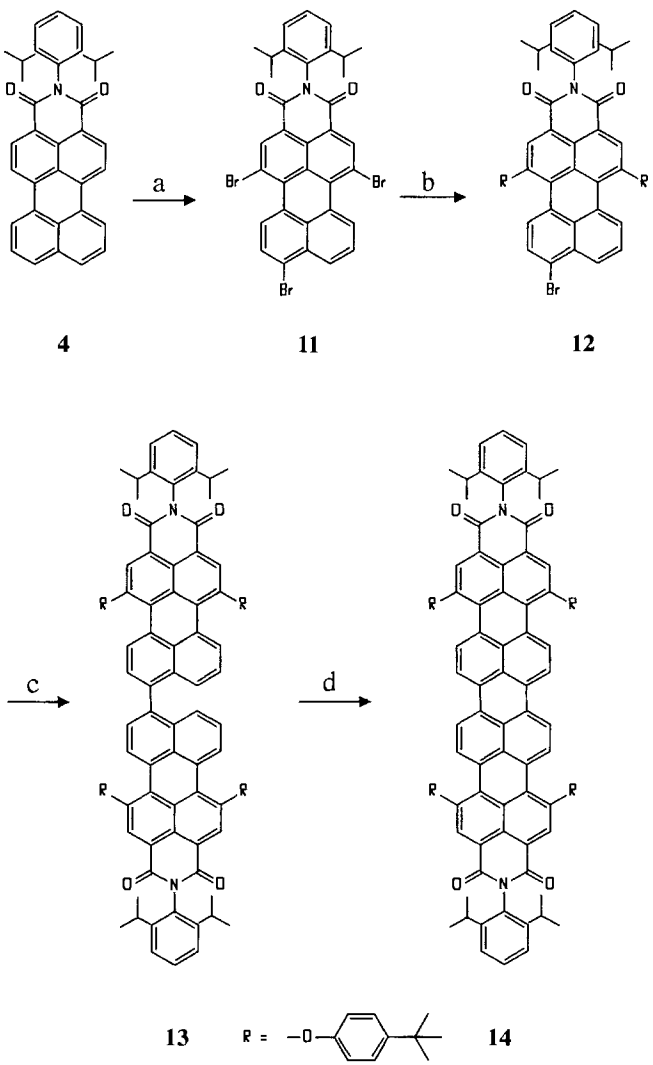
Table 1. Selected spectroscopic data for compounds **9**, **10**, and **14** [a].

9: m.p. >300 °C; IR: $\tilde{\nu}$[cm^{-1}] = 1690 (C=O), 1650 (C=O); UV/VIS [H_2SO_4/oleum (57%) (4:1)]: $\lambda_{max}(\varepsilon)$ = 281 (524288), 323 (57659), 784 (34367), 876 (337000) nm.

10: m.p. >300 °C; ^{1}H NMR (300 MHz, $C_2D_2Cl_4$, 135 °C): δ = 8.68 (d, 4H), 8.68 (d, 4H), 8.63 (d, 4H), 8.56 (d, 4H), 7.42 (dd, 2H), 7.29 (d, 4H), 2.80 (m, 4H), 1.19 (d, 24H). IR: $\tilde{\nu}$[cm^{-1}] = 1702 (C=O), 1659 (C=O); UV/VIS (CH_2Cl_2): $\lambda_{max}(\varepsilon)$ = 264 (97377), 274 (100124), 317 (9195), 375 (14689), 764 (162024) nm; UV/VIS [H_2SO_4/oleum (57%) (4:1)]: $\lambda_{max}(\varepsilon)$ = 281 (698994), 326 (58801), 783 (83173), 876 (654705) nm.

14: m.p. >300 °C; ^{1}H NMR (500 MHz, $CDCl_3$): δ = 9.09 (d, 4H), 8.32 (s, 4H), 7.76 (d, 4H), 7.41 (t, 2H), 7.34 (d, 8H), 7.28 (d, 4H), 7.00 (d, 8H), 2.76 (m, 4H), 1.26 (s, 36H), 1.13 (d, 24H); ^{13}C NMR (125 MHz, $CDCl_3$): δ = 162.99, 153.55, 152.93, 147.00, 145.75, 131.24, 130.85, 130.80, 129.40, 129.19, 128.87, 127.73, 127.47, 127.17, 126.42, 125.24, 124.32, 123.94, 122.53, 121.63, 117.39, 34.37, 31.44, 29.23, 24.10; IR: $\tilde{\nu}$[cm^{-1}] = 1707 (C=O), 1669 (C=O); UV/VIS (CH_2Cl_2): $\lambda_{max}(\varepsilon)$ = 262 (95819), 271 (97645), 382 (12895), 709 (71931), 781 (166571) nm.

[a] The FD mass spectra of all compounds contain the correct M^+ peaks. IR: KBr pellet.



Scheme 2. Synthesis of (tetraphenoxy)quaterrylenebis(dicarboximide) **14**. Reagents, conditions, and yields: a) $Br_2/CHCl_3$, reflux, 91%; b): *p-tert*-butylphenol/K_2CO_3/*N*-methyl-2-pyrrolidinone, 33%; c) $[Ni(cod)_2]$/DMF, 60 °C, 2 d, 88%; d) KOH/EtOH/ox., 87%.

rinated hydrocarbons but very soluble in boiling tetrachlorethane, nitrobenzene, and pyridine. Since each step in the synthesis of **10** is high yielding and chromatographic procedures are not required, technical production should be possible.

Quaterrylenebis(dicarboximides) with very good solubility (15–25 gL^{-1}, $CHCl_3$) may be prepared by introducing phenoxy substituents into the bay reaction (Scheme 2). This is achieved by brominating **4** under drastic conditions to afford tribromide **11**, which is converted to **12** with *p-tert*-butylphenol/K_2CO_3. Coupling and cyclization as in Scheme 1 leads to the (tetraphenoxy)quaterrylenebis(dicarboximide) **14**.

All the quaterrylene derivatives synthesized were characterized by FD mass spectrometry, and IR and UV/VIS spectroscopy. ^{1}H NMR spectra were obtained for **10** and **14**, but a ^{13}C NMR spectrum was obtained only for **14**.

In the electronic absorption spectra (Fig. 1) of **10** (λ_{max} (ε) = 762 (162024) nm) and **14** ($\lambda_{max}(\varepsilon)$ = 781 (166571) nm) the wavelength of the end absorption increases considerably owing to the greater size of the chromophore. Compared to the UV/VIS spectrum of perylenebis(dicarboximide) **1**, **10** shows a bathochromic shift of 250 nm and a considerable increase in the absorption coefficient. The distinct bathochromic shift of **14** can be ascribed to the introduction of the phenoxy groups and corresponds to the related bands in the equivalent phenoxy-substituted perylenebis(dicarboximides).[5] All the quaterrylenebis-

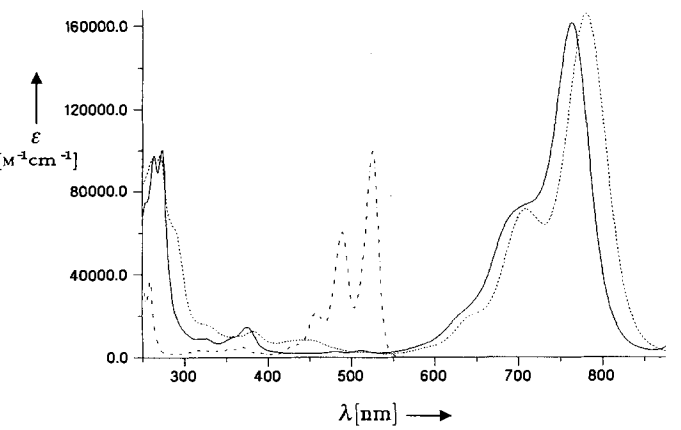


Fig. 1. Electronic absorption spectra of **1**, R = 2,6-diisopropylphenyl (– · · · –), **10** (—), and **14** (– – –) in CH_2Cl_2.

 © VCH Verlagsgesellschaft mbH, D-69451 Weinheim, 1995 0570-0833/95/1212-1324 $ 10.00+.25/0

(dicarboximides) are green both in the solid state and in concentrated solutions. At the concentrations required for UV spectroscopy, $c = 10^{-5}$ M, the solutions are largely colorless. Similarly, films of **14** spin-coated onto quartz are also colorless. To compare the aryl- and alkyl-substituted quaterrylenes **9** and **10**, their spectra were measured in sulfuric acid/oleum. Both compounds have unusual but identical UV spectra in the NIR region with only a single very sharp peak (*J*-band[14]). Particularly remarkable is the extremely high extinction ($\varepsilon = 654705$) of the band at 876 nm (**10**, Fig. 2). The identical behavior of **9** and **10** may be used as supporting evidence for the structure of the alkyl derivatives which are not soluble in organic solvents.

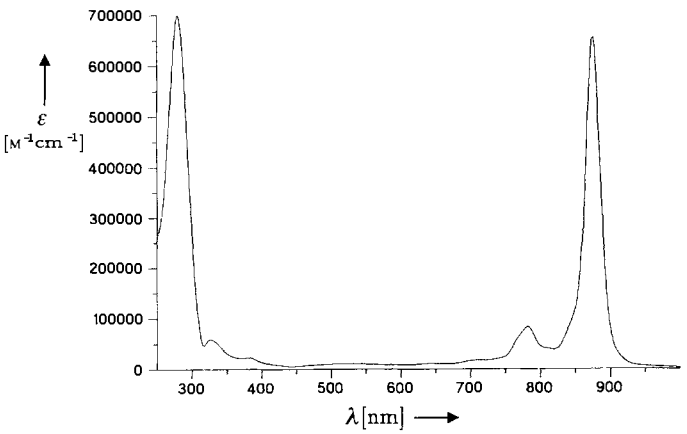


Fig. 2. Electronic absorption spectrum of **10** in H_2SO_4/oleum (57%) (4:1).

According to thermogravimetric investigations, the stabilities of **9**, **10**, and **14** (no decomposition up to 480 °C) correspond to those of the known perylenebis(dicarboximides). The important contributor to the thermal stability of the perylenebis(dicarboximides) is only, therefore, the type of N-substitution; the mass loss determined corresponds exactly to the loss of the substituent on the N atom.

The marked absorption in the region 764 to 782 nm in this system has particular advantages since it can be used in many optical applications in conjunction with commercially available GaAlAs lasers which emit at 780 nm. This is a necessary prerequisite, for example, for applications in optical data storage systems. Future investigations will aim at extending applications to semiconductors and thermal liquid crystal displays.

Received: January 20, 1995 [Z 7647 IE]
German version: *Angew. Chem.* **1995**, *107*, 1487–1489

Keywords: arenes · carboximides · dyes · perylenes · UV spectroscopy

[1] F. Graser, E. Hädicke, *Liebigs. Ann. Chem.* **1980**, 1994; *ibid.* **1984**, 483.
[2] Y. Nagao, T. Misono, *Dyes Pigm.* **1984**, *5*, 171.
[3] A. Rademacher, S. Märkle, H. Langhals, *Chem. Ber.* **1982**, *115*, 2927.
[4] H. O. Loutfy, A. M. Hor, P. Kazmaler, M. Tam, *J. Imaging Sci.* **1989**, *33*, 151.
[5] G. Seybold, G. Wagenblast, *Dyes Pigm.* **1989**, *11*, 303. H. Langhals, *Nachr. Chem. Tech. Lab.* **1980**, *28*, 716.
[6] D. Schlettwein, D. Wöhrle, E. Karmann, U. Melville, *Chem. Mater.* **1994**, *6*, 3.
[7] M. P. O'Neil, M. P. Niemczyk, W. A. Svec, D. Gosztola, G. L. Gaines III, M. R. Wasielewski, *Science* **1992**, *257*, 63.
[8] J. Fabian, R. Zahradnik, *Angew. Chem.* **1989**, *101*, 693; *Angew. Chem. Int. Ed.* **1989**, *28*, 677.
[9] Y. Nagao, T. Misono, *Bull. Chem. Soc. Jpn.* **1981**, *54*, 1191.
[10] We would like to thank BASF AG for donating a sample of *N*-(2,6-diisopropylphenyl)-3,4-perylenedicarboximide (**4**).
[11] Y. Nagao, Y. Abe, T. Misono, *Dyes Pigm.* **1991**, *16*, 19.
[12] T. Yamamoto, A. Morita, Y. Miyazaki, T. Maruyama, H. Wakayama, Z. Zhou, Y. Nakamura, T. Kanbara, *Macromolecules* **1992**, *25*, 1214.
[13] W. Bradley, F. W. Pexton, *J. Chem. Soc.* **1954**, 4432.
[14] The *J*-band results from the formation of aggregates and is observed for polymethine dyes, in particular. In the case of quaterrylenebis(dicarboximides) this behavior can be explained by protonation of the chromophore. a) G. Scheibe, *Kolloid-Z.* **1938**, 1. b) K. Norland, A. Ames, T. Taylor, *Phot. Sci. Engl.* **1970**, *14*, 295.

The First Clusters with a Y-Shaped Arrangement of Ligands at Three-Coordinate Rh^I Atoms in the Solid State: $[M^1M^2\{\mu\text{-}P(C_6H_{11})_2\}(CO)_8Rh(PPh_3)]$ (M^1, M^2 = Mn, Re)**

Hans-Günther Beckers, Ulrich Flörke, and Hans-Jürgen Haupt*

According to kinetic studies by Halpern et al.,[1] during the homogeneously catalyzed hydrogenation of alkenes, complex fragments are formed from the Wilkinson catalyst [RhCl(P$Ph_3)_3$] by dissociation that contain three-coordinate Rh^I atoms. Corresponding species should also be produced in solution during the thermal decomposition (−70 °C) of [RhH(N_2)($PR_3)_2$] complexes with sterically demanding phosphane ligands (R = Bu, cyclohexyl (Cy)) by the release of $N_{2(g)}$.[2] In the solid state, however, a coordination number of 3 for a central d^8 rhodium(I) atom is unusual and has only been described for the diamagnetic, red complex cation $[Rh(PPh_3)_3]^+$ in salts with various anions (ClO_4^-, [*nido*-7-(1-*closo*-1,2-$C_2B_{10}H_{11}$)-7,8-$C_2B_9H_{11}]^-$).[3, 4] According to the X-ray structure analysis, the three covalent Rh–P bonds are arranged in a T formation. For the perchlorate salt, this ground state geometry is stabilized by the attractive Rh···H interactions with a concomitant weakening of the Lewis acid strength of the central atom.[3, 5] Futhermore, the rigidity of the cation in non-coordinating solvents was verified by ^{31}P DNMR spectroscopy.[6] Spin coupling data between ^{103}Rh and ^{31}P from temperature-dependent experiments indicate that an intramolecular exchange of the phosphane ligands takes place. This would occur, in agreement with MO calculations, via a Y-shaped intermediate (C_{3v}).[7, 8] Instead of using sterically demanding ligands we attempted to produce threefold coordination by the inclusion of a ligand-stabilized Rh^I center into a bond system capable of mesomerism. In the light of our work on π-bonding properties of *cyclo*-M_3 and *tetrahedro*-M_4 clusters, we decided to join suitable anionic phosphido-bridged binuclear complexes with rhodium(I) complex cations using a so-called redox condensation.[5, 7, 8]

The title compounds **3** and **4** were obtained from hydridophosphido-bridged binuclear complexes of metals from group nine [9, 10, 12] in a three-step synthesis as summarized in Scheme 1: 1) deprotonation by a non-nucleophilic base, 2) "redox condensation", and 3) selective oxidative removal of a Rh-bound CO ligand. The analogous Mn_2Rh cluster **5** was obtained

[*] Prof. Dr. H.-J. Haupt, Dipl.-Chem. H.-G. Beckers, Dr. U. Flörke
Anorganische und Analytische Chemie der Unversität–Gesamthochschule
Warburger Strasse 100, D-33098 Paderborn (Germany)
Telefax: Int. code + (5251)603-423

 © VCH Verlagsgesellschaft mbH, D-69451 Weinheim, 1995 0570-0833/95/1212-1325 $ 10.00+.25/0

$[M^1M^2(\mu\text{-H})(\mu\text{-PCy}_2)(CO)_8]$

1) 1. DBU, THF, 20°C; 2. PPh_4Br

$PPh_4[M^1M^2(\mu\text{-PCy}_2)(CO)_8]$ $M^1 = Mn$, $M^2 = Re$, **1**; $M^1 = M^2 = Re$

2) 1. $[Rh(CO)(PPh_3)_2]Cl$ / $CO(g)$, THF, 0°C; 2. $TlPF_6$, THF, 0–20°C

$[M^1M^2(\mu\text{-PCy}_2)(CO)_8Rh(CO)_2PPh_3]$ $M^1 = Mn$, $M^2 = Re$, **2**; $M^1 = M^2 = Re$

3) Me_3NO, THF, 20°C; $-CO_2(g)$, $-CO(g)$

$[M^1M^2(\mu\text{-PCy}_2)(CO)_8Rh(PPh_3)]$ $M^1 = Mn$, $M^2 = Re$, **3**; $M^1 = M^2 = Re$, **4**

Scheme 1.

by a somewhat modified synthesis.[12] On swapping Rh^I for Ir^I, reaction step 3 did not produce any corresponding clusters of the title compounds. The molecular structures of the two precursors $[M^1M^2(\mu\text{-PCy}_2)(CO)_8Rh(CO)_2(PPh_3)]$, namely the *cyclo*-$Re_2Rh$ cluster ($M^1 = M^2 = Re$) and **2** ($M^1 = Mn$, $M^2 = Re$), have been established by single-crystal X-ray diffraction.[8, 12] They differ in that one of the terminal CO groups on the Rh^I atom in the Re_2Rh cluster is in a semi-bridging position towards the manganese atom in compound **2**.

The molecular structures of **3**–**5** were solved by single-crystal X-ray analysis[13] (Fig. 1). The central molecular fragment is a three-membered ring consisting of MnReRh in **3**, Re_2Rh in **4**, and Mn_2Rh in **5**. The Rh^I atom coordinates with both metal atoms of group nine to give an acute bond angle (69.59(2)° in **3**, 68.93(3)° in **4**, and 68.80(3)° in **5**) and with the phosphorus atom in the PPh_3 ligands to give differing obtuse bond angles (P(2)-Rh-M(1) 135.4(1), P(2)-Rh-M(2) 153.7(1)° in **3**; 136.2(1), 151.7(1)° in **4**; 135.9(1), 154.0(1)° in **5**). Such varying bond angles are also found in precursors with five-coordinate Rh^I atoms[8, 12] and are therefore independent of the coordination number. Consequently, the Rh^I atom in the three structurally analogous *cyclo*-M_3 clusters is, in each case, coordinated in a distorted Y-shaped, almost planar manner; the smaller of the two exocyclic bond angles always occurs on the longer Rh–transition metal bond. This differentiation leads to a quasi *trans* positioning of the Rh–P bond towards the shorter Rh–M bond in **4** and **5** (a thermodynamic *trans* effect). The resulting significant shortening of the Rh–M bond is 0.025(1) Å in **3**, 0.015(1) Å in **4**, and 0.038(1) Å in **5**. Because compounds **3**–**5** do not show any unusual distances between neighboring ligands along the two Rh–M bonds, and they crystallize in different crystal systems, the Y-shaped coordination geometry at the Rh^I atom is not influenced by either repulsive interactions of neighboring ligands or by packing effects. In contrast to the ideal D_{3h} geometry of a $[Rh^IL_3]$ complex, both this new Y-shaped as well as the previously described T-shaped coordination geometry (ideally C_{2v}) at the Rh^I atom allows the removal of the degeneracy of the e' orbital set that is occupied by two valence electrons. This explains the diamagnetism of compounds **3**–**5**. Not only the P atom of the bridging dicyclohexylphosphido group but also the Y-coordinated Rh^I atom is a component of an edge-sharing coordination dioctahedron of the two transition metal atoms. There are no distortions of the coordination geometry when compared to the structures of similar heteronuclear *cyclo*-M_3 clusters.[7, 8, 10] From this, it follows that in the molecular fragment $[M^1M^2(\mu\text{-PCy}_2)(CO)_8]$ (M^1–M^2, d^7–d^7) of the *cyclo*-M_3 cluster the covalent bonds to the Rh^I atom are formed over centered as well as over edge-sharing frontier orbitals, as was already postulated by MO calculations on related complexes.[14] If the fragment is considered to be an anionic two-electron donor ligand, the Rh^I atom (d^8) with the PPh_3 ligand has the same number of donor electrons, that is formally only 12 valence electrons as opposed to the usual 14 and 16 valence electrons in the compounds known to date. This obvious electron deficiency on the Rh atom is compensated by π-electron delocalization along the two Rh–M bonds. Therefore these are shorter than the corresponding covalent single bonds. This is demonstrated by the following comparisons which, on the one hand, show a shortening of the Rh–M bonds in **3**–**5** compared to σ bonds, and on the other hand, a lengthening compared to π bonds in other similar compounds. Thus, in **4** the Rh–Rh distance is 2.827(1) Å (average value), whilst for $[(PCy_2)_2ReH(\mu\text{-PCy}_2)_2Rh(1,5\text{-cod})][BF_4]$ (cod = cyclooctadiene) with diphosphido-bridged metal centers, a Re–Rh distance of 2.9361(8) Å[15] for a σ bond is observed. In the hydridosulfido-bridged compound $[RhRe(CO)_3(\mu\text{-H})(\mu\text{-SEt})(dppm)_2]$ (dppm = bis(diphenylphosphano)methane) the Re–Rh σ bond length is 2.9697(8) Å.[16] In comparison, the Re–Rh π bond in $[Re_2Rh(\mu\text{-CO})_2(\mu\text{-PCy}_2)(CO)_6(PPh_3)_2]$ is 2.681(1) Å.[8] Likewise, the Mn–Rh bond in **5** (mean 2.708(1) Å) is shorter than the Mn–Rh σ bond in $[MnRh(CO)_4(dppm)_2]$ (2.843(1) Å)[17] and longer than the Mn–Rh π bond in $[ReMnRh(\mu\text{-CO})_2(\mu\text{-PCy}_2)(CO)_6(PPh_3)_2]$ (2.585(2) Å).[12] Therefore, the Rh–M bond lengths found for the title compounds lie in the range of a bond order of 1.5, which corresponds to a π-electron delocalization in the M^1-Rh-M^2 ring. This effect undoubtedly reduces the strength of the M^1–M^2 bond, so that the M^1–M^2 bonds in **3**,

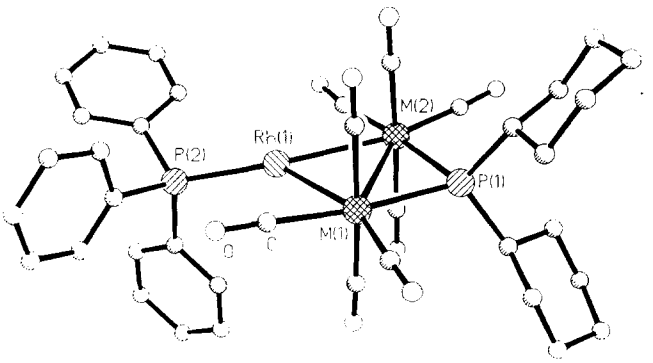


Fig. 1. Molecular structure of **3** ($M^1 = M^2 = Mn,Re$), **4** ($M^1 = M^2 = Re$) and **5** ($M^1 = M^2 = Mn$). Important bond lengths [Å] and angles [°]: for **3**: M1-M2 3.164(1), M1-Rh 2.785(1), M2-Rh 2.760(1), M1-P1 2.375(2), M2-P1 2.391(2); M1-Rh-M2 69.59(2), M1-Rh-P2 135.42(5), M2-Rh-P2 153.65(5), Rh-M1-M2 54.83(2), Rh-M2-M1 55.58(2), M1-P1-M2 83.20(6); for **4**: Re1-Re2 3.199(1), Re1-Rh 2.834(1), Re2-Rh 2.819(1), Re1-P1 2.435(2), Re2-P1 2.443(2); Re1-Rh-Re2 68.93(3), Re1-Rh-P2 151.65(5), Re2-Rh-P2 136.20(5), Rh-Re1-Re2 55.32(2), Rh-Re2-Re1 55.75(2), Re1-P1-Re2 81.96(6); for **5**: Mn1-Mn2 3.060(2), Mn1-Rh 2.727(1), Mn2-Rh 2.689(1), Mn1-P1 2.301(2), Mn2-P1 2.310(2); Mn1-Rh-Mn2 68.80(3), Mn1-Rh-P2 135.88(5), Mn2-Rh-P2 153.96(5), Rh-Mn1-Mn2 55.02(3), Rh-Mn2-Mn1 56.17(3), Mn1-P1-Mn2 83.17(6).

 © VCH Verlagsgesellschaft mbH, D-69451 Weinheim, 1995 0570-0833/95/1212-1326 $ 10.00+.25/0 Angew. Chem. Int. Ed. Engl. 1995, 34, No. 12

4, and **5** are longer than the corresponding bonds in compounds of the type $[M^1M^2(\mu\text{-H})(\mu\text{-PCy}_2)(CO)_8]$.[9] Similar results have been found for the mercury atom in the *cyclo*-M_3 compound $[ReMo(\eta\text{-}C_5H_5)(\mu\text{-PCy}_2)(CO)_6HgW(CO)_3(\eta\text{-}C_5H_5)]$.[10]

Because the rhodium(I) atom in **3**–**5** has one or two free coordination sites for two-electron donors, we were also interested in the homogeneous catalytic properties of these compounds. However, attempts at homogeneous catalytic hydrogenation with **4** or **5** as the catalyst in dioxane were unsucessful (10 bar H_2, 1-hexene, 100 °C, 12 h); only metal deposition was observed in each case. Consequently, the transitions between 16 and 18 valence electrons, which are typical for a catalytic hydrogenation cycle with Rh^I complexes, cannot be obtained with the title compounds because the activation barrier is too high. Therefore, the three-coordinate Rh^I atom only appears to be an active homogeneous catalyst if it is not a particularly strong Lewis acid. This argumentation is supported by our observations that the similar *cyclo*-M_3 cluster $[M^1M^2(\mu\text{-PCy}_2)Rh(\mu\text{-CO})_2(PPh_3)(CO)_8]$ (M^1, M^2 = Mn, Re) with (4 + 2)-fold coordination of the Rh^I atom is catalytically active under analogous reaction conditions (THF, 3 bar H_2, 3 bar CO, 60 °C, 1-hexene).[12] For example, TON values of approximately 100 h^{-1} were obtained with an Mn_2Rh compound in an oxo reaction.[12] To date, this could not be even nearly achieved with a soluble heteronuclear Rh cluster as the catalyst.[18, 19] The Rh^I atom shows in the cited *cyclo*-M_3 clusters a rarely observed (4 + 2) coordination.[8] Therefore, in the Rh^I complex fragments bound in the clusters the decisive factor for the interplay between 16 and 18 valence electron species in the catalytic cycle and for the catalytic efficiency is not the threefold coordination of the Rh^I atom, but the type of ligands and the symmetry of their spatial arrangement. Such considerations are important for the development of new Rh^I catalysts.

Experimental Procedure

FT-IR spectra (Nicolet P510) of the new compounds were recorded, unless otherwise stated, in CH_2Cl_2 in the range 2200 to 1600 cm^{-1} for ν(CO) absorption bands. ^{31}P NMR spectra (Bruker AMX 300) were recorded in $CDCl_3$ with 85% H_3PO_4 as the external standard. Solvents used were distilled twice, dried, and stored under argon. All reactions were carried out under argon.

1: $[MnRe(\mu\text{-H})(\mu\text{-PCy}_2)(CO)_8]$ (663 mg, 1 mmol) [9] in THF (20 mL) was deprotonated with 1,8-diazabicyclo[5.4.0]undec-7-ene (DBU) (300 mL, 2 mmol) at 20 °C in 4 h. To isolate the product, the solvent was evaporated, the residue dissolved in C_2H_5OH (10 mL), and PPh_4Br (545 mg, 1.3 mmol) added. Compound **1** was precipitated by addition of oxygen-free water (50 mL), filtered off, and washed with water (3 × 15 mL) followed by *n*-hexane (3 × 15 mL). Yield: 940 mg (94%) of air-stable, yellow complex salt.

2: Equimolar amounts of **1** (100 mg, 0.1 mmol) and $[RhCO(PPh_3)_2]Cl$ (69 mg, 0.1 mmol) were dissolved in CO-saturated THF at 0 °C and $TlPF_6$ (419 mg, 1.2 mmol) was added as a halogen trap. The reaction solution immediately turned deep red and was allowed to warm to 20 °C over 2 h in a weak flow of $CO_{(g)}$. To isolate the product, the THF was removed and the solid residue dissolved in CH_2Cl_2, the solution was filtered through Celite and the components separated by thick layer chromatography using CH_2Cl_2/*n*-hexane (1/3) as the eluent. Yield: 74 mg (69%) of red solid.

3: **2** (108 mg, 0.1 mmol) in THF (15 mL) was treated with Me_3NO (8.3 mg, 0.11 mmol) at 0 °C and the reaction mixture was allowed to warm to 20 °C over 2 h, during which time the color of the solution changed from red to yellow. To isolate the product the THF was removed, the solid residue dissolved in a small amount of acetone, the solution filtered through basic Al_2O_3 and the product separated chromatographically and crystallized with CH_2Cl_2/hexane (1/5). Yield: 83 mg (80%) of yellow product.

4: In an analogous procedure to that used for **1** from $[Re_2(\mu\text{-H})(\mu\text{-PCy}_2)(CO)_8]$ (794 mg, 1 mmol) [10], DBU (450 mL, 3 mmol), and PPh_4Br (545 mg, 1.3 mmol) produced $PPh_4[Re_2(\mu\text{-PCy}_2)(CO)_8]$ (1008 mg, 95%). The reaction of this salt (113 mg, 0.1 mmol) with $[Rh(CO)(PPh_3)_2]Cl$ (69 mg, 0.1 mmol)[11] under the same conditions applied for complex **2**, gave $[Re(\mu\text{-PCy}_2)(CO)_8Rh(CO)_2(PPh_3)]$ [8]. Treatment of the latter (118 mg, 0.1 mmol) with Me_3NO (8.3 mg, 0.1 mmol) in an analogous way to that used for **3** gave the pale yellow product **4** (99 mg, 85%).

Compounds **1**–**4** and $PPh_4[Re_2(\mu\text{-PCy}_2)(CO)_8]$ gave correct C,H analysis (Automat PE 240). IR (CH_3COCH_3): **1**: $\tilde{\nu}$(CO) = 2039 m, 1971 s, 1936 vs, 1905 s, 1888 s; 1871 s cm^{-1}; **2**: $\tilde{\nu}$(CO) = 2079 w, 2035 m, 2015 s, 1998 vs, 1946 s, 1898 m (br.) cm^{-1}; **3**: $\tilde{\nu}$(CO) = 2013 s, 1973 vs, 1944 s, 1921 s cm^{-1}; $PPh_4[Re_2(\mu\text{-PCy}_2)(CO)_8]$: $\tilde{\nu}$(CO) = 2042 m, 1988 m, 1936 vs, 1911 m, 1888 s, 1873 s cm^{-1}; **4**: $\tilde{\nu}$(CO) = 2033 s, 1977 vs, 1950 s, 1921 s cm^{-1}; UV-Vis (Perkin-Elmer-Lambda-15, CH_2Cl_2): **3**: $\lambda_{max}(\varepsilon)$ = 338 (817), 392 nm (359 m^2mol^{-1}); **4**: $\lambda_{max}(\varepsilon)$ = 323 (773), 359 (522 m^2mol^{-1}); ^{31}P-NMR ($CDCl_3$): **1**: δ = 156.7 (s, μ-P), 23.7 (s, PPh_4); **2**: δ = 215.1 (s, μ-P), 35.1 (d, ^1J(P,Rh) = 147 Hz); **3**: δ = 177.9 (s, μ-P), 18.5 (d, ^1J(P,Rh) = 322 Hz); $PPh_4[Re_2(\mu\text{-PCy}_2)(CO)_8]$: δ = 101.4 (s, μ-P), 23.7 (s, PPh_4); **4**: δ = 124.5 (s, μ-P), 21.1 (d, ^1J(P,Rh) = 352 Hz).

Received: January 28, 1995 [Z7671IE]
German version: *Angew. Chem.* **1995**, *107*, 1464–1466

Keywords: catalysis · clusters · coordination · rhodium compounds

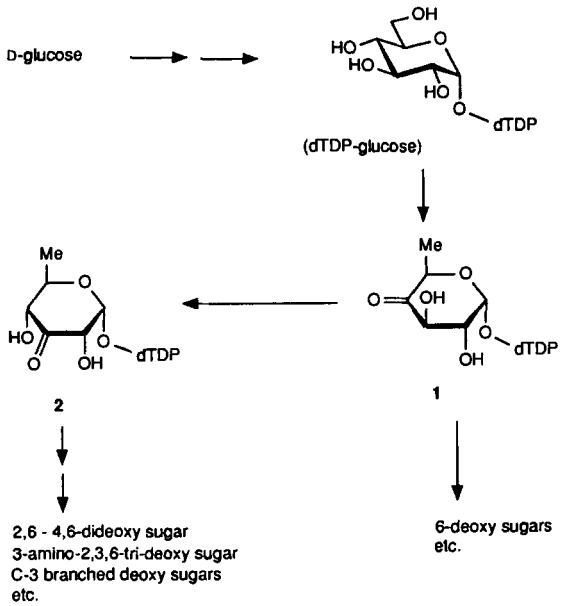
[1] H. Aria, J. Halpern, *J. Chem. Soc. Chem. Commun.* **1971**, 1571–1573; P. Meakin, J. P. Jesson, C. A. Tolman, *J. Am. Chem. Soc.* **1972**, *94*, 3240–3242.
[2] T. Yoshida, T. Okano, S. Otsuka, *J. Chem. Soc. Chem. Commun.* **1978**, 855–856.
[3] Y. W. Yared, S. L. Miles, R. Bau, C. A. Reed, *J. Am. Chem. Soc.* **1977**, *99*, 7076–7078.
[4] C. B. Knobler, T. B. Marder, E. A. Mizusawa, R. G. Teller, J. A. Long, P. E. Behnken, M. F. Hawthorne, *J. Am. Chem. Soc.* **1984**, *106*, 2990–3004.
[5] H.-J. Haupt, P. Balsaa, U. Flörke, *Angew. Chem.* **1988**, *100*, 280–281; *Angew. Chem. Int. Ed. Engl.* **1988**, *27*, 263–264; H.-J. Haupt, U. Flörke, H. Schnieder, *Acta Crystallogr. Sect. C* **1991**, *47*, 2531–2535, 2304–2307.
[6] A. R. Siedle, R. A. Newmark, R. D. Howells, *Inorg. Chem.* **1988**, *27*, 2473–2478.
[7] H.-J. Haupt, C. Heinekamp, U. Flörke, *Inorg. Chem.* **1990**, 2955–2963; *Chem. Ber.* **1991**, *124*, 2191–2195.
[8] H.-J. Haupt, U. Flörke, H.-G. Beckers, *Inorg. Chem.* **1994**, *33*, 3481–3486.
[9] U. Flörke, H.-G. Beckers, H.-J. Haupt, *Z. Kristallogr.*, in press.
[10] A. Merla, U. Flörke, H.-J. Haupt, *Z. Anorg. Allg. Chem.* **1994**, *62*, 994–1005.
[11] J. R. Shapley, R. R. Schrock, J. A. Osborn, *J. Am. Chem. Soc.* **1969**, *91*, 2816–2817.
[12] H.-G. Beckers, Dissertation, Universität-Gesamthochschule Paderborn, **1995**.
[13] Crystal structure analysis of **3**: orange-red crystal, 0.39 × 0.44 × 0.50 mm, monoclinic, space group $P2_1/n$, a = 11.122(3), b = 12.929(3), c = 28.761(8) Å, β = 99.69(2)°, V = 4077(2) Å^3, Z = 4, ρ_{calcd} = 1.674 g cm^{-3}, μ = 3.79 mm^{-1}, $3 \le 2\theta \le 55°$, $Mo_{K\alpha}$ radiation, λ = 0.71073 Å, $\omega/2\theta$ scan, 298 K, 9508 measured reflections, 9333 independent, of which 6637 with $F > 4\sigma(F)$, empirical absorption correction with ψ-scans, min./max. transmission 0.680/0.956, structure solved by direct and conventional Fourier methods, full matrix least-squares refinement based on F^2 and 458 parameters, all non-hydrogen atoms anisotropic, H atoms in idealized positions (riding model), Re and Mn are disordered on the metal positions M1: 0.46 Re, 0.54 Mn and M2: = 0.54 Re, 0.46 Mn, one cyclohexyl group is disordered over two positions each with an occupation factor of 0.5, $R1(F)$ = 0.053, $wR2(F^2)$ = 0.166. Crystal structure analysis of **4**·0.5$(CH_3)_2CO$: yellow crystal, 0.35 × 0.43 × 0.52 mm, triclinic, space group $P\bar{1}$, a = 10.438(4), b = 14.385(5), c = 14.619(5) Å, α = 107.01(2), β = 90.22(2), γ = 97.23(2)°, V = 2080(1) Å^3, Z = 2, ρ_{calcd} = 1.896 g cm^{-3}, μ = 6.39 mm^{-1}, data collection as for **3**, 9954 measured reflections, 9585 independent, of which 7698 with $F > 4\sigma(F)$, correction as above, min./max. transmission 0.666/0.896, structure solved and refined as above, 488 parameters, $R1(F)$ = 0.047, $wR2(F^2)$ = 0.124. Crystal structure analysis of **5**: yellow crystal, 0.20 × 0.33 × 0.45 mm, monoclinic, space group $P2_1/n$, a = 11.023(2), b = 12.918(4), c = 28.534(7) Å, β = 99.70(2)°, V = 4005(2) Å^3, Z = 4, ρ_{calcd} = 1.487 g cm^{-3}, μ = 1.156 mm^{-1}, data collection as for **3**, 9387 measured reflections, 9212 independent, of which 5063 with $F > 4\sigma(F)$, corrections as above, min./max. transmission 0.743/0.867, structure solved and refined as above, 471 parameters, one carbonyl and one cyclohexyl group are disordered over two positions, each with an occupation factor of 0.5, $R1(F)$ = 0.061, $wR2(F^2)$ = 0.173. Programs used: SHELXTL-Plus,[20] SHELXL-93 [21]. Further details of the crystal structure investigations may be obtained from the Fachinformationszentrum Karlsruhe, D-76344 Eggenstein-Leopoldshafen (Germany) on quoting the depository numbers CSD-401484 (**3**), CSD-401485 (**4**), and CSD-401486 (**5**).
[14] T. A. Albright, S.-K. Kang, A. M. Arif, A. M. Bord, R. J. Jones, J. K. Leland, S. T. Schwab, *Inorg. Chem.* **1988**, *27*, 1246–1253.
[15] R. T. Baker, J. C. Calabrese, T. E. Glassman, *Organometallics* **1988**, *7*, 1889–1891.
[16] D. M. Antonelli, M. Cowie, *Inorg. Chem.* **1990**, *29*, 3339–3345.
[17] D. M. Antonelli, M. Cowie, *Organometallics* **1990**, *9*, 1818–1826.
[18] J. S. Bradley, *Clusters and Colloids – From Theory to Applications* (Ed.: G. Schmid), VCH, Weinheim, **1994**, p. 523–524.
[19] R. D. Adams, *The Chemistry of Metal Cluster Complexes* (Hrsg.: D. F. Shriver, H. D. Kaesz, R. D. Adams), VCH, Weinheim, **1990**, p. 121–165.
[20] G. M. Sheldrick, SHELXTL-Plus, Siemens Analytical X-ray Instruments, Madison, WI, USA, **1991**.
[21] G. M. Sheldrick, SHELXL-93, Program for Crystal Structure Refinement, Universität Göttingen, **1993**.

 © VCH Verlagsgesellschaft mbH, D-69451 Weinheim, 1995 0570-0833/95/1212-1327 $ 10.00+.25/0

Thymidine Diphospho-6-deoxy-α-D-*ribo*-3-hexulose—Synthesis of a Central Intermediate in the Biosynthesis of Di- and Trideoxysugars**

Thomas Müller and Richard R. Schmidt*

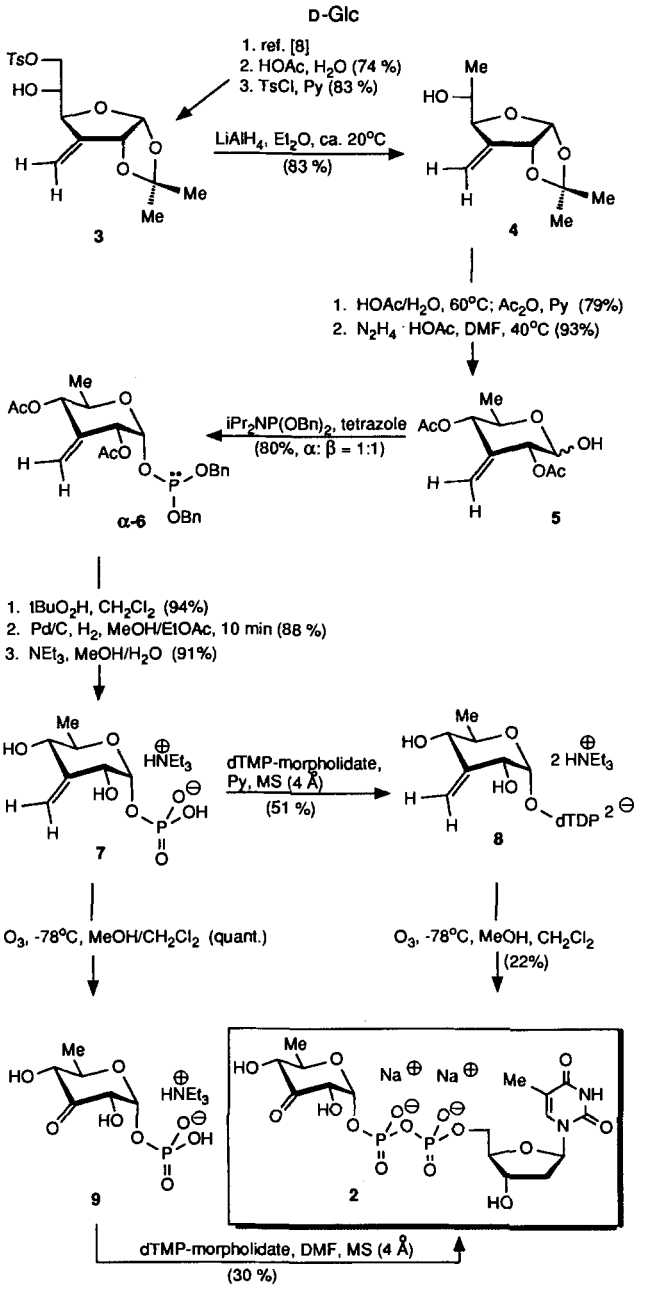
Many antibiotics contain deoxy-, aminodeoxy-, and C-branched deoxysugar units. Elucidation of their biosynthesis is far from complete.[1, 2] An important initial intermediate in this biosynthetic pathway is dTDP-6-deoxy-D-*xylo*-4-hexulose (**1**), made from dTDP-glucose (Scheme 1) by NAD-dependent



Scheme 1.

dTDP-glucose-4,6-dehydratase (e.g. from *E. coli*); **1** is a precursor for, amongst other rare sugars, the commonly occurring 6-deoxysugars.[1-3] An isomerase apparently converts **1** into the corresponding 3-hexulose **2**,[2] the compound mentioned in the title, which serves as the next key intermediate (with pyridoxamine phosphate as cofactor) for preparation of the important dideoxy-, aminodeoxy-, and C-branched sugars.[2, 4] Since the 6-deoxy-3-hexulose intermediate **2** has not yet been isolated,[2] its synthesis is very important for elucidation of the biosynthesis of di- and trideoxysugars (e.g. with 4,6-dehydratase- or isomerase-deficient mutants).[2] The synthesis of **2** is particularly difficult due to the hydrolytic instability of nucleoside diphosphates of deoxysugars[5] and the tendency of 3-ulosides to undergo β-elimination of the nucleoside diphosphate group.[6] We report here on a first efficient synthesis of **2**,[7] which is based on removal of all protecting groups (in the penultimate or last reaction step) and introduction of the 3-oxo function by ozonolysis of the corresponding methylene group.

Firstly, D-glucose was converted to the 1,2:5,6-di-*O*-isopropylidene-3-methylene derivative by published methods;[8] selective cleavage of the 5,6-*O*-isopropylidene group with 50% acetic acid, and subsequent regioselective 6-*O*-tosylation resulted in compound **3** (Scheme 2). The 6-deoxy compound **4** was produced in 83% yield by reaction with $LiAlH_4$ in ether at room temperature. Treatment with 80% acetic acid at 60 °C resulted



Scheme 2.

in cleavage of the isopropylidene group; subsequent acetylation with acetic anhydride in pyridine, and selective cleavage of the 1-*O*-acetyl group with hydrazine acetate[9] in DMF at 40 °C produced the pyranose derivative **5** in high overall yield. Phosphite **6** was obtained as a 1:1 α/β mixture[11] by reaction with the monofunctional phosphitylation reagent bis(benzyloxy)-diisopropylaminophosphane[10] in the presence of tetrazole. Compound **6** proved to be sufficiently stable for separation by flash chromatography on silica gel (petroleum ether/

[*] Prof. Dr. R. R. Schmidt, Dipl.-Chem. T. Müller
Fakultät Chemie der Universität
Postfach 5560 M 725, D-78434 Konstanz (Germany)
Telefax: Int. code + (7531)88-3135

[**] This work was supported by the Deutsche Forschungsgemeinschaft and by the Fonds der Chemischen Industrie.

EtOAc = 10:1 + 1% NEt_3). The compound **α-6** thus obtained (Table 1) was converted almost quantitatively by oxidation with *tert*-butylhydroperoxide to the corresponding phosphate, which was much less stable than the phosphite **α-6**. The phosphate was chemoselectively debenzylated by brief hydrogenation with palladium on carbon as catalyst without removal of the methylene group. Deacetylation was performed with NEt_3 in methanol/water, and thus the important intermediate **7** was obtained in high overall yield as the completely unprotected triethylammonium salt.

Table 1. Selected physical data for **2**, **α-6**, and **7**–**9**. Coupling constants in Hz.

2: ^{1}H NMR (250 MHz, D_2O): $\delta = 1.05$ (d, $J_{5'',6''} = 5.8$, 3H, 6″-H), 1.73 (s, 3H, CH_3), 2.14–2.18 (m, 2H, $2'_a$-H, $2'_c$-H), 3.93–4.07 (m, 5H, 4′-H, $5'_a$-H, $5'_c$-H, 4″-H, 5″-H), 4.41–4.56 (m, 2H, 3′-H, 2″-H), 5.67 (dd, $J_{1'',P} = 7.1$, $J_{1'',2''} = 4.3$, 1H, 1″-H), 6.13 (dd, $J_{1',2'a} = 6.6$, $J_{1',2'c} = 6.9$, 1H, 1′-H), 7.55 (s, 1H, 6-H); ^{31}P NMR (161.7 MHz, D_2O): $\delta = -10.64$ (d, $J_{P,P'} = 22.5$, 1P), -6.02 (d, $J_{P,P} = 22.5$, 1P); FAB-MS (70 eV, negative-ion mode): *m/z* (%): 545 (27) $[M-H^+]^-$

α-6: ^{1}H NMR (250 MHz, $CDCl_3$): $\delta = 1.16$ (d, $J_{5,6} = 6.2$, 3H, 6-H), 1.97, 2.17 (2 s, 6H, 2 × OAc), 3.99 (dq, $J_{4,5} = 9.8$, $J_{5,6} = 6.2$, 1H, 5-H), 4.86–4.94 (m, 4H, 2 × CH_2Ph), 4.95–5.11 (m, 3H, 4-H, methylene-H), 5.41 (dd, $J_{1,2} = 3.5$, $J_{2,4} = 1.1$, 1H, 2-H), 5.68 (dd, $J_{1,P} = 8.3$, $J_{1,2} = 3.5$, 1H, 1-H), 7.24–7.38 (m, 10H, 2 × Ph); ^{31}P NMR (161.7 MHz, $CDCl_3$): $\delta = 138.85$ (s, P)

7: ^{1}H NMR (250 MHz, D_2O): $\delta = 1.05$ (t, $J = 7.3$, 9H, $N(CH_2CH_3)_3$), 1.07 (d, $J_{5,6} = 5.4$, 3H, 6-H), 2.97 (q, $J = 7.3$, 6H, $N(CH_2CH_3)_3$), 3.52–3.62 (m, 2H, 4-H, 5-H), 4.08 (m, 1H, 2-H), 4.83–5.01 (m, 2H, methylene-H), 5.24 (dd, $J_{1,P} = 6.5$, $J_{1,2} = 3.7$, 1H, 1-H); ^{13}C NMR (62.9 MHz, D_2O): $\delta = 9.16$ (s, 3C, $N(CH_2CH_3)_3$), 18.11 (s, 1C, 6-C), 47.61 (s, 3C, $N(CH_2CH_3)_3$), 70.89 (d, $J_{2,P} = 8.9$, 1C, 2-C), 71.80–73.40 (2 s, 2C, 4-C, 5-C), 95.48 (d, $J_{1,P} = 6.3$, 1C, 1-C), 105.58 (s, 1C, 3-C), 146.30 (s, 1C, methylene-C); ^{31}P NMR (161.7 MHz, D_2O): $\delta = 3.97$ (s, P); FAB-MS (70 eV, negative-ion mode): *m/z* (%): 239 (100) $[M-H^+]^-$

8: ^{1}H NMR (250 MHz, D_2O): $\delta = 1.05$ (d, $J_{5'',6''} = 5.8$, 3H, 6″-H), 1.07 (t, $J = 7.3$, 18H, 2 × $N(CH_2CH_3)_3$), 1.73 (s, 3H, CH_3), 2.13–2.18 (m, 2H, 2′a-H, 2′e-H), 2.97 (q, $J = 7.3$ Hz, 12H, 2 × $N(CH_2CH_3)_3$), 3.61–3.63 (m, 2H, 4″-H, 5″-H), 3.95–3.97 (m, 3H, 4′-H, 5′-H, 5″-H), 4.08 (m, 1H, 2″-H), 4.42 (m, 1H, 3′-H), 4.97–5.04 (m, 2H, methylene-H), 5.37(dd, $J_{1'',P} = 7.0$, $J_{1'',2''} = 3.7$, 1H, 1″-H), 6.16 (dd, $J_{1',2'a} = 6.8$, $J_{1',2'c} = 7.1$, 1H, 1′-H), 7.52 (d, $J = 0.9$, 1H, 6-H); ^{13}C NMR (62.9 MHz, D_2O), $\delta = 9.17$ (s, 6C, 2 × $N(CH_2CH_3)_3$), 12.59 (s, 1C, CH_3), 18.20 (s, 1C, 6″-C), 39.56 (s, 1C, 2′-C), 47.63 (s, 6C, 2 × $N(CH_2CH_3)_3$), 66.32 (d, $J_{5',P} = 5.2$, 1C, 5′-C), 71.07 (d, $J_{2'',P} = 9.1$, 1C, 2″-C), 71.82–73.44 (m, 3C, 3′-C, 4″-C, 5″-C), 85.92 (s, 1C, 1′-C), 86.35 (d, $J_{4',P} = 9.1$, 1C, 4′-C), 96.25 (d, $J_{1'',P} = 6.4$, 1C, 6″-C), 105.62 (s, 1C, 3″-C), 112.62 (s, 1C, 5-C), 138.33 (s, 1C, 6-C), 164.54 (s, 1C, methylene-C), 152.60 (s, 1C, 2-C), 167.40 (s, 1C, 4-C); ^{31}P NMR (161.7 MHz, D_2O): $\delta = -12.35$ (d, $J_{P,P'} = 22.5$, 1P), -10.81 (d, $J_{P,P'} = 22.5$, 1P); FAB-MS (70 eV, negative-ion mode): *m/z* (%): 543 (31) $[M-H^+]^-$

9: ^{1}H NMR (250 MHz, D_2O): $\delta = 1.09$ (t, $J = 7.3$, 9H, $N(CH_2CH_3)_3$), 1.23 (d, $J_{5,6} = 5.8$, 3H, 6-H), 3.00 (q, $J = 7.3$, 6H, $N(CH_2CH_3)_3$), 3.86–3.99 (m, 2H, 4-H, 5-H), 4.44 (m, 1H, 2-H), 5.58 (dd, $J_{1,P} = 6.7$, $J_{1,2} = 4.3$, 1H, 1-H); ^{13}C NMR (62.9 MHz, D_2O): $\delta = 13.82$ (s, 3C, $N(CH_2CH_3)_3$), 23.98 (s, 1C, 6-C), 51.16 (s, 3C, $N(CH_2CH_3)_3$), 77.70–83.52 (2 s, 2C, 4-C, 5-C), 81.71 (d, $J_{2,P} = 5.2$, 1C, 2-C), 103.06 (d, $J_{1,P} = 4.3$, 1C, 1-C), 199.54 (s, 1C, 3-C); ^{31}P NMR (161.7 MHz, D_2O): $\delta = -1.44$ (s, P); FAB-MS (70 eV, negative-ion mode): *m/z* (%): 241 (100) $[M-H^+]^-$

Two routes were used to synthesize the target molecule **2** from **7**. First, the thymidine diphospho derivative **8** was produced using thymidine phosphomorpholidate[12] in pyridine and 4 Å molecular sieves. Compound **8** was obtained with 51% yield by preparative HPLC (5% CH_3CN in 0.5 M $HNEt_3^+$ HCO_3^-) as the bis(triethylammonium) salt; as expected, it was stable at pH 7. It is also of interest for biological investigations as the methylene analogue of **2**. To obtain the 3-ulose structure, a methanolic solution of **8** at $-78\,^\circ C$ was mixed with a dichloromethane solution saturated with ozone at $-78\,^\circ C$, and the reaction mixture was separated by subsequent reversed-phase HPLC on RP-18 (3% CH_3CN in 0.5 M $HNEt_3^+$ HCO_3^-); following lyophilization the target molecule **2** was obtained in 22% yield as the bis(triethylammonium) salt along with recovered starting material. Due to low hydrolytic stability of this salt (half-life ca. 1 h at pH 7), the disodium salt of **2** was obtained by ion exchange (Amberlite IR-120, Na^+ form), which, as expected,[13] was much more stable. Surprisingly, a higher overall yield was obtained for the synthesis of **2** from **7** by changing the order of the reaction steps. The 3-ulose phosphate **9** was obtained in almost quantitative yield by direct ozonolysis of **7** at $-78\,^\circ C$. In spite of the greater instability of **9**, the target molecule **2** was obtained in 30% yield by the morpholidate method,[12] when the procedure described above was used for purification.[14] The target molecule **2** was thus obtained in a pure form (30 mg), and its structure was confirmed by NMR (^{1}H, ^{13}C, ^{31}P) and FAB-MS data, as were the structures of the intermediate compounds **3**–**9** (for **2**, **α-6**, **7**–**9**, see Table 1). The synthetic strategy presented here is apparently variable and suitable for production of further interesting nucleoside derivatives of deoxysugars;[7] it should make an important contribution to the elucidation of their biosynthesis.

Received: February 2, 1995 [Z 7683 IE]
German version: *Angew. Chem.* **1995**, *107*, 1467–1468

Keywords: carbohydrates · deoxysugars · ketosugars · nucleoside diphosphate sugars

[1] H. Griesebach, *Adv. Carbohydr. Chem. Biochem.* **1978**, *35*, 81–126; V. N. Shibaev, *ibid.* **1986**, *44*, 277–339.
[2] J. S. Thorson, S. F. Lo, H.-W. Liu, C. R. Hutchinson, *J. Am. Chem. Soc.* **1993**, *115*, 6993–6994; H.-W. Liu, J. S. Thorson, *Annu. Rev. Microbiol.* **1994**, *48*, 223–256, and references therein.
[3] R. Okazaki, T. Okazaki, J. L. Strominger, A. M. Michelson, *J. Biol. Chem.* **1962**, *237*, 3014–3026; C. E. Snipes, G. U. Brillinger, L. Sellers, L. Mascaro, H. G. Floss, *ibid.* **1977**, *252*, 8113–8117.
[4] C. E. Snipes, C. Chang, H. G. Floss, *J. Am. Chem. Soc.* **1979**, *101*, 701–706; H. G. Floss in *The Antibiotics, Vol. 4* (Ed.: J. W. Corcoran), Springer, Berlin, **1981**, pp. 215–235; J. J. Lee, J. P. Lee, P. J. Keller, C. E. Cottrell, C.-J. Chang, *J. Antibiotics* **1986**, *39*, 1123–134.
[5] E. Heinz, H.Schmidt, M. Hoch, K.-H. Jung, R. R. Schmidt, *Eur. J. Biochem.* **1989**, *184*, 445–453; M. Hoch, E. Heinz, R. R. Schmidt, *Carbohydr. Res.* **1989**, *193*, 33–47; R. R. Schmidt, B. Wegmann, K.-H. Jung, *Liebigs Ann. Chem.* **1991**, 121–124.
[6] T. Eisele, R. R. Schmidt, unpublished; T. Eisele, Diplomarbeit, Universität Konstanz, 1993.
[7] T. Müller, unpublished.
[8] O. T. Schmidt in *Methods in Carbohydrate Chemistry, Vol. II* (Eds.: R. L. Whistler, M. L. Wolfrom), Academic Press, New York, **1963**, pp. 318–325; W. Sowa, G. M. S. Thomas, *Can. J. Chem.* **1966**, *44*, 836–838; A. Mazur, B. E. Tropp, R. Engel, *Tetrahedron* **1984**, *44*, 3949–3956.
[9] G. Excoffier, D. Gagnaire, J.-P. Utille, *Carbohydr. Res.* **1975**, *39*, 368–373.
[10] W. Bannwarth, A. Trzeciak, *Helv. Chim. Acta* **1987**, *70*, 175–183.
[11] Attempts to perform acid-catalyzed anomerization **β-6** → **α-6** resulted in decomposition.
[12] S. Roseman, J. J. Distler, J. G. Moffat, H. G. Khorana, *J. Am. Chem. Soc.* **1961**, *83*, 659–663; J. G. Moffat, *Methods Enzymol.* **1966**, *8*, 136–142.
[13] R. R. Schmidt, K. Frische, *Bioorg. Med. Chem. Lett.* **1993**, *3*, 1747–1750; K. Frische, R. R. Schmidt, *Liebigs Ann. Chem.* **1994**, 297–303.
[14] Purification on a strongly basic anion exchange resin (Dowex 2 × 8 $[Cl^-]$) by elution with aqueous LiCl solution resulted in decomposition of compound **2**.

 © VCH Verlagsgesellschaft mbH, D-69451 Weinheim, 1995 0570-0833/95/1212-1329 $ 10.00+.25/0

S_7NH and S_7NCH_3 as Novel Chelating Ligands in $[(\eta^5\text{-}C_5H_5)_2Ti]$ Complexes: Synthesis of Medium-Sized Sulfur–Nitrogen Rings by Ligand Transfer**

Klaus Bergemann, Monika Kustos, Per Krüger, and Ralf Steudel*

A vast number of sulfur–nitrogen compounds is known.[1] These may be classified as saturated or unsaturated depending on whether the nitrogen is two- or three-coordinate. The remarkable properties of the linear polymer $(SN)_x$, a superconductor at temperatures below 0.26 K, have considerably stimulated the interest in this class of compounds.[1] Most of the cyclic species contain small rings and only very few compounds with rings containing more than eight atoms are known. Examples are the unsaturated cation $S_5N_5^+$[1b] and the saturated twelve-membered S_8N_4 ring in $S_8(NSO_2CF_3)_4$.[2] For quite some time we have been investigating the sulfur homocycles S_6–S_{20}, most of which have been prepared as pure materials.[3] The results of the studies on these rings suggest that cyclic sulfur imides of the type S_nNR (R = H, organic group; $n > 7$) should also be stable. However, so far only derivatives with $n = 7$ have been prepared, which is explained by the lack of synthetic routes for the planned preparation of saturated SN rings with more than eight ring atoms. Since the preparation of sulfur homocycles has profited enormously from the application of $[(\eta^5\text{-}C_5H_5)_2TiS_5]$ as a ligand transfer reagent,[3] we have tried to find a similar access to SN heterocycles by preparing a titanocene complex containing a sulfur–nitrogen ligand.

Here we report on the syntheses and structures of two titanocene complexes with sulfur–nitrogen ligands and on the preliminary results on the application of these compounds in ligand transfer reactions to synthesize S_8NCH_3 and S_9NCH_3. Titanocene dicarbonyl reacts with elemental sulfur[4] as well as with organic di- and trisulfanes [4b, 5] at 20 °C with insertion of the Cp_2Ti unit in a sulfur–sulfur bond and liberation of carbon monoxide. In an analogous way, we have obtained the complexes **1** and **2** by reaction of $[Cp_2Ti(CO)_2]$ (Cp = η^5-C_5H_5) with S_7NH and S_7NCH_3, respectively, in *n*-hexane at 20 °C [Eq. (a)].

$$[Cp_2Ti(CO)_2] + S_7NR \longrightarrow [Cp_2Ti(S_7NR)] + 2\,CO \qquad \text{(a)}$$

1: R = H
2: R = CH_3

$[Cp_2TiS_5]$ and $[Cp_4Ti_2S_4]$ are observed as minor products in these reactions.

Compounds **1** and **2** are the first titanocene complexes with exclusively sulfur-bound SN ligands.[6] Both compounds form black crystals stable at 20 °C in air. Solutions of the complexes for example in CH_2Cl_2 or CS_2 are intense violet (**1**) or green (**2**), respectively. In solution complexes **1** and **2** slowly decompose. On heating the solid compounds to 115–120 °C $[Cp_2TiS_5]$ is formed. The complexes **1** and **2** were characterized by single-crystal X-ray structural analyses,[7] which surprisingly showed that **1** contains a disulfide and a pentasulfide bridging ligand (Fig. 1), while **2** exhibits a trisulfide and a tetrasulfide bridge (Fig. 2). In principle, insertion of a Cp_2Ti unit in one of the S–S bonds of S_7NH or S_7NCH_3 can result in *three* isomeric products in both cases. At present, we cannot explain why only *one* isomer is formed in each case and why the coordination in **1** is $[Cp_2Ti(\mu\text{-}S_2)(\mu\text{-}S_5)NH]$, while that in **2** is $[Cp_2Ti(\mu\text{-}S_3)(\mu\text{-}S_4)NCH_3]$. This differing behavior is not attributed to either recognizable steric or electronic reasons. We confirmed that both samples are homogeneous by high-resolution HPLC (one peak only);[8] in addition, the ^1H NMR spectrum of **2** shows only one signal for the methyl protons, and X-ray powder diffraction measurements on a representative sample of **2** showed lines at positions in accordance with those calculated from the single-crystal diffraction data.[9]

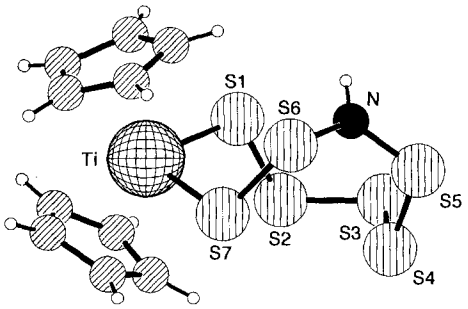


Fig. 1. Structure of **1** in the crystal. Selected distances [pm] and angles [°]: Ti–S1 242.3(5), Ti–S7 242.2(5), S1–S2 207.3(6), S2–S3 201.2(8), S3–S4 206.7(8), S4–S5 204.7(8), S5–N 165.1(14), S6–S7 205.3(6), S6–N 168.9(14); S5-N-S6 122.5(8), S1-Ti-S7 96.9(2); S7-Ti-S1-S2 73.6(2), Ti-S1-S2-S3 −121.2(3), S1-S2-S3-S4 78.6(3), S2-S3-S4-S5 −110.4(3), S3-S4-S5-N 78.9(6), S4-S5-N-S6 78.8(9), S5-N-S6-S7 − 79.7(9), N-S6-S7-Ti −70.4(5), S6-S7-Ti-S1 61.7(2).

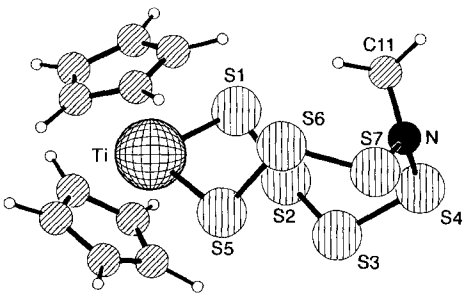


Fig. 2. Structure of **2** in the crystal. Selected distances [pm] and angles [°]: Ti–S1 242.6(2), S1–S2 204.2(2), S2–S3 204.9(3), S3–S4 204.1(3), S4–N 170.3(7), Ti–S5 241.4(2), S5–S6 207.6(2), S6–S7 202.3(3), S7–N 171.6(7), N–C 144(1); S1-Ti-S5 95.44(6), S4-N-S7 117.7(4), S4-N-C 117.8(5), S7-N-C 117.7(5); S5-Ti-S1-S2 65.5(1), Ti-S1-S2-S3 −67.7(1), S1-S2-S3-S4 −80.5(1), S2-S3-S4-N 86.6(3), S3-S4-N-S7 60.4(4), S1-Ti-S5-S6 61.73(9), Ti-S5-S6-S7 −126.4(1), S5-S6-S7-N 88.6(3), S6-S7-N-S4 −110.0(4), S3-S4-N-C −90.0(6), S6-S7-N-C 40.4(6).

Despite the differing connectivities of **1** and **2** the conformations of the nine-membered rings[11] are comparable. The motifs (the signs of the torsional angles) are in both cases the same:

[*] Prof. Dr. R. Steudel, Dipl.-Chem. K. Bergemann, Dr. M. Kustos, Dipl.-Chem. P. Krüger
Institut für Anorganische und Analytische Chemie
der Technischen Universität, Sekr. C 2
D-10623 Berlin (Germany)
Telefax: Int. code + (30)3142-6519
e-mail: steudel@wap0204.chem.tu-berlin.de

[**] Sulfur Compounds, Part 185. This work was supported by the Deutsche Forschungsgemeinschaft. Part 184: Y. Drozdova, R. Steudel, *Chem. Eur. J.* **1995**, *1*, 193.

+ − + − + + − − + (starting from the Ti atom). The values of the torsional angles at the S–S bonds range from 67 to 126°; consequently, the S–S internuclear distances are in the range 201.2–207.6 pm. These conformations may be compared to that of *cyclo*-S_9 for which an experimental structure determination is not available yet. However, density functional calculations have shown that the most stable form of S_9 has C_2 symmetry[12] with exactly the same motif as the nine-membered rings in **1** and **2**.

In solution the metallacycle of **1** seems to undergo pseudorotation (ring inversion) at 20 °C, since only one Cp signal is observed in the ^{1}H NMR spectrum in CS_2/[D_6]acetone or in [D_8]THF. However, at −57 °C two Cp signals (at $\delta = 6.49$, 6.47) are observed. In contrast, **2** yields two well-separated Cp signals already at 25 °C (in CS_2/[D_6]acetone). Evidently, either the methyl group hinders the pseudorotation or the presence of four neighboring S–S bonds as in **1** is a prerequisite for pseudorotation (assuming that the torsional barriers at the Ti–S and S–N bonds are considerably higher than those at S–S bonds[13]); **2** has only three neighboring S–S bonds.

To check whether the novel complexes are suitable reagents for ligand transfer reactions, we treated **2** with SCl_2 and S_2Cl_2.[14] The new imides S_8NCH_3 (**3**) and $S_9N(CH_3)$ (**4**) were isolated as yellow oils [Eq. (b)]. Compounds **3** and **4** were detect-

$$\underset{\mathbf{2}}{[Cp_2Ti(S_7NCH_3)]} + S_nCl_2 \longrightarrow [Cp_2TiCl_2] + \underset{\begin{array}{l}\mathbf{3}\ (n=1)\\ \mathbf{4}\ (n=2)\end{array}}{S_{7+n}NCH_3} \qquad (b)$$

ed as molecular ions in the EI mass spectra. The retention times of **3** and **4** in HPLC analysis[15] together with that of S_7NCH_3 yield a linear regression of the type $\ln k' = a + bn$ (k' = capacity factor) as is typical for homologous series of compounds. Heterocycles of this kind should make it possible to study the conformation of sulfur-rich rings in solution by temperature-dependent NMR spectroscopy (^{1}H, ^{15}N). We expect that pseudorotation will be frozen in at low temperatures making it possible to indirectly detect the nonequivalent ring atom positions present in homocycles like S_9 and S_{10} by spectroscopy. In addition, the large and ever increasing number of inorganic and organic sulfur compounds prepared by ligand transfer from $[Cp_2TiS_5]$[16] makes it likely that **1** and **2** will also become precursors for numerous novel compounds not accessible by other routes.

Experimental Procedure

1: Under an inert atmosphere $[Cp_2Ti(CO)_2]$ (85 mg, 0.36 mmol) in *n*-hexane (15 mL) was added dropwise within 30 min to S_7NH (87 mg, 0.36 mmol) in *n*-hexane (70 mL) at 20 °C and stirred for an additional 2.5 h. The black precipitate formed was isolated and extracted with CS_2 in a Soxhlet apparatus. The extracts were reduced in volume resulting in black crystals which were recrystallized from CH_2Cl_2. Yield 65 mg (41%). Correct C,H,N analysis. ^{1}H NMR (200 MHz, CS_2/[D_6]acetone, 25 °C): $\delta = 6.44$, 6.45 (Cp). UV/VIS (methanol): $\lambda_{max} = 209$, 230, 313, 575 nm (diode array detector).

2: As in the case of **1**, $[Cp_2Ti(CO)_2]$ (234 mg, 1 mmol) in *n*-hexane (30 mL) was added to S_7NCH_3 (235 mg, 1 mmol) in *n*-hexane (150 mL) at 20 °C and stirred for 24 h. Workup as for **1**. Yield: 215 mg (50%). Correct C,H,N analysis. ^{1}H NMR (200 MHz, CS_2/[D_6]acetone, 25 °C): $\delta = 6.47$ (s, 5H), 6.37 (s, 5H), 3.27 (s, 3H); UV/VIS (methanol): $\lambda_{max} = 206$, 231, 290, 390, 578 nm (diode array detector).

Received: February 4, 1995 [Z 7694 IE]
German version: *Angew. Chem.* **1995**, *107*, 1481–1483

Keywords: ligand transfer · nitrogen compounds · sulfur compounds · titanium compounds

[1] a) H. G. Heal, *The Inorganic Heterocyclic Chemistry of Sulfur, Nitrogen and Phosphorus*, Academic Press, London, **1980**; b) T. Chivers, in *The Chemistry of Inorganic Homo- and Heterocycles, Vol. 2*, (Eds.: I. Haiduc, D. B. Sowerby), Academic Press, London, **1987**, p. 793; c) T. Chivers, in *Encyclopedia of Inorganic Chemistry, Vol. 7*, (Ed.: R. B. King), Wiley, Chichester, **1994**.

[2] B. Krebs, M. Hein, M. Diehl, H. W. Roesky, *Angew. Chem.* **1978**, *90*, 825; *Angew. Chem. Int. Ed. Engl.* **1978**, *17*, 778.

[3] R. Steudel, *Top. Curr. Chem.* **1982**, *102*, 149; R. Steudel, in *The Chemistry of Inorganic Homo- and Heterocycles, Vol. 2*, (Eds.: I. Haiduc, D. B. Sowerby), Academic Press, London, **1987**, p. 737.

[4] a) G. Müller, J. L. Peterson, *J. Org. Chem.* **1974**, *111*, 91; b) U. Westphal, R. Steudel, *Phosphorus Sulfur Silicon* **1992**, *65*, 151.

[5] A. Shaver, S. Morris, *Inorg. Chem.* **1991**, *30*, 1926; G. Facchinetti, C. Floriani, *J. Chem. Soc. Dalton Trans.* **1974**, 2433.

[6] The reaction of $[Cp_2Ti(CO)_2]$ with S_4N_4 yielded $[Cp_2Ti(NSN)_2S]$ and $[Cp_2Ti(NSN)SS]$; C. M. Marcellus, R. T. Oakley, W. T. Pennington, A. W. Cordes, *Organometallics* **1986**, *5*, 1395. Review on metal complexes with sulfur–nitrogen ligands: P. F. Kelly, J. D. Woollins, *Polyhedron* **1986**, *5*, 607.

[7] Crystal structure analyses: **1**: 0.45 × 0.25 × 0.1 mm, monoclinic, $P2_1/n$, $Z = 4$. $a = 825.6(3)$, $b = 1089.7(7)$, $c = 1744(2)$ pm, $\beta = 93.87(5)°$, $V = 1565(2) \times 10^6$ pm^3, $\rho_{calcd} = 1.772(2)$ g cm^{-3}, $2\theta_{max} = 55°$, $Mo_{K\alpha}$ radiation, $\lambda = 71.069$ pm, ω-2θ scan, $T = 298$ K, 3960 measured, 3517 independent and 1545 observed reflections, criterium: $I \geq 2\sigma(I)$, no absorption correction, structure solved by direct method (program: SHELXS 86), refined versus F^2 (program: SHELXL 93) with anisotropic temperature factors for all non-hydrogen atoms, positions of hydrogen atoms calculated, $R = 0.0097$ with 172 refinded parameters, residual electron density (max/min): 0.69/−0.66 e Å^{-3}. **2**: 0.3 × 0.4 × 0.15 mm, monoclinic, $P2_1/n$, $Z = 4$, $a = 858.8(2)$, $b = 1555.1(5)$, $c = 1239.8(3)$ pm, $\beta = 90.04(2)°$, $V = 1655.7(7) \times 10^6$ pm^3, $\rho_{calcd} = 1.731$ g cm^{-3}, $2\theta_{max} = 55°$, $Mo_{K\alpha}$, $\lambda = 71.069$ pm, ω-2θ scan, $T = 298$ K, 4195 measured, 3041 independent and 2497 observed reflections with $I \geq 2\sigma(I)$, $\mu = 1.35$ mm^{-1}, absorption correction (DIFABS) (T_{min}/T_{max}) 0.857/1.100, solved by direct method (SHELXS 86), refinement (SHELX 76) versus F^2 with anisotropic temperature factors, hydrogen atoms calculated, free parameters 182, $R = 0.057$, $R_w = 0.057$, residual electron density (max/min): 0.522/−0.477 e Å^{-3}. Further details on the crystal structure investigations are available on request from the Fachinformationszentrum Karlsruhe, D-76344 Eggenstein-Leopoldshafen (Germany), on quoting the depository numbers CSD-401514 (**1**) or CSD-401515 (**2**).

[8] Two C18-columns in line ($l = 2 \times 10$ cm; 10 µm and 5 µm particle diameter), eluant: methanol. In the case of the isomeric complexes $[Cp_2Ti(\mu\text{-}S_2)(\mu\text{-}S_2)AsCH_3]$ and $[Cp_2Ti(\mu\text{-}S)(\mu\text{-}S_3)AsCH_3]$ the retention times differ considerably; see B. Holz, Dissertation, Technische Universität Berlin, **1991**.

[9] Simulation of the powder diffractogram with the program LAZY PULVERIX. Measurement in the angle range $2\theta = 9–27°$ with a Siemens apparatus D5000. We thank Dipl.-Chem. U. Stege for this measurement.

[10] In free S_7NH the N atom has a planar or nearly planar coordination; see H.-J. Hecht, R. Reinhardt, R. Steudel, H. Bradaczek, *Z. Anorg. Allg. Chem.* **1976**, *426*, 43. The structure of S_7NCH_3 is unknown.

[11] The same ring size occurs in $[Cp_2TiS_8]$: ref. [4b] and U. Westphal, Dissertation, Technische Universität Berlin, **1994**.

[12] D. Hohl, R. O. Jones, R. Car, M. Parrinello, *J. Chem. Phys.* **1988**, *89*, 6823.

[13] The torsion barrier at cumulated S–S bonds is about 27 (*trans*-barrier) or 32 (*cis*-barrier) kJ mol^{-1}; see Y. Drozdova, K. Miaskiewicz, R. Steudel, *Z. Naturforsch. Part B* **1995**, *50*, 889.

[14] Equimolar amounts of **2** and SCl_2 or S_2Cl_2, respectively, were allowed to react with each other at 20 °C in CS_2. After removal of the solvent in vacuo **3** and **4** were extracted with *n*-pentane. Compounds **3** and **4** were obtained as yellow oils from the extracts, the HPLC analyses of which show small portions of homologous rings S_nNCH_3. MS (EI, 70 eV, 90 °C): B^+ 160 (S_5), M^+ 285 (S_8NCH_3), and 317 (S_9NCH_3), respectively.

[15] Column: C18, 10 µm; eluant: methanol. For HPLC analysis of SN compounds see R. Steudel, D. Rosenbauer, *J. Chromatogr.* **1981**, *216*, 399.

[16] R. Steudel, in *The Chemistry of Inorganic Ring Systems*, (Ed. R. Steudel), Elsevier, Amsterdam, **1992**, p. 233.

 © VCH Verlagsgesellschaft mbH, D-69451 Weinheim, 1995 0570-0833/95/1212-1331 $ 10.00+.25/0

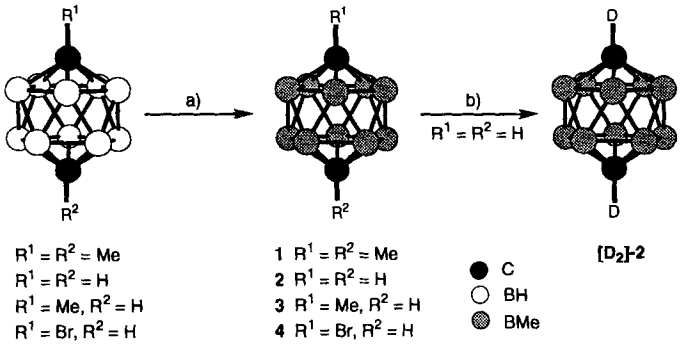
A Camouflaged Icosahedral Carborane: Dodecamethyl-1,12-dicarba-*closo*-dodecaborane(12) and Related Compounds**

Wei Jiang, Carolyn B. Knobler, Mark D. Mortimer, and M. Frederick Hawthorne*

The selective placement of substituents on the boron vertices of the three isomeric icosahedral $C_2B_{10}H_{12}$ carboranes remains as a major target of synthetic strategies.[1] At the same time, the attachment of functional groups to the carbon vertices and their subsequent conversion is relatively well developed[2, 3] since the CH vertices of the parent carboranes may be deprotonated with strong bases and the resulting carbanions employed as nucleophilic reagents. The principal mode of reaction of the BH vertices has been attack by electrophilic reagents leading to halogenation, metalation, or alkylation.[1, 2] The nature of the products that result from these electrophilic substitution reactions are very dependent upon the identity of the carborane isomer employed as the substrate.

The three isomeric icosahedral $C_2B_{10}H_{12}$ carboranes are frequently suggested as structural components for molecular scaffolding[4] and supramolecular constructs.[5] These applications of carboranes might be better served if the BH and CH vertices were converted to their chemically stable and hydrophobically enhanced BCH_3 and CCH_3 counterparts. Completely sheathing an icosahedral carborane with methyl groups would provide a form of camouflage for the underlying polyhedral borane framework and produce a molecule whose exterior resembles a hydrocarbon, but whose superstructure is that of a polyhedral borane. Consequently, one might expect the external $(CH_3)_{12}$ sheath to reduce the reactivity characteristic of the carborane skeleton[1, 2] while at the same time presenting opportunities for typical hydrocarbon reactions in an unusual environment. Such compounds would also be expected to exhibit the excellent thermal stability characteristic of carboranes and unsurpassed hydrophobicity. Until now, no successful syntheses have been reported leading to fully alkylated icosahedral carboranes, although a few low-yielding routes are known for the smaller carboranes,[6] and partial substitution of icosahedral carboranes leads to mixtures of isomers which can be difficult or impossible to separate. We here report high-yielding syntheses of 1,12-dicarba-*closo*-dodecaborane(12) derivatives in which all boron vertices are methylated and one or both carbon vertices are either methylated or remain as CH vertices available for lithiation and further reactions.

Permethylated 1,12-dicarba-*closo*-dodecaborane(12) (**1**) was obtained in 91% isolated yield by reaction of 1,12-dimethyl-1,12-dicarba-*closo*-dodecaborane(12)[7a] with neat methyl trifluoromethanelsulfonate (methyl triflate) and small quantities of trifluoromethanesulfonic acid (triflic acid) acting as a catalyst at reflux for 20 h (Scheme 1). The identity of **1** was clearly indicated by the presence of a single signal in the ^{11}B NMR spectrum with no coupling to hydrogen. The crude reaction products when subjected to GC/MS analysis revealed that the reaction had gone to completion; no species having less than twelve methyl groups was present. Similarly, reaction of 1,12-dicarba-*closo*-dodecaborane(12) with methyl triflate and triflic acid as described above gave deca-*B*-methyl-carborane **2** in 89% yield. As with compound **1**, the presence of only one singlet peak in the ^{11}B NMR spectrum unequivocally demonstrated full methylation of all the boron vertices. Analysis of the crude reaction mixture by GC/MS revealed small amounts (ca. 5%) of a compound with a mass suggesting the presence of eleven methyl groups, which was assumed to be undecamethylcarborane **3** (vide infra), formed by attack of the methylating agent on a carbon vertex. Thus the reaction is essentially chemoselective towards the boron vertices.



Scheme 1. Methylation reactions of 1,12-dicarba-*closo*-dodecaboranes(12): a) CF_3SO_3Me, CF_3SO_3H, reflux 10–24 h; b) PhLi (10 equiv.), C_6H_6, reflux 10 h; D_2O.

In order to provide a single free carbon vertex as a potential site for further reactions, 1-methyl-1,12-dicarba-*closo*-dodecaborane(12)[7b] was reacted with methyl triflate under the usual conditions to afford undecamethylcarborane **3** in 60% yield. Compound **3** exhibited two signals in the ^{11}B NMR spectrum, one arising from the boron atoms adjacent to the CH vertex, and the other from those adjacent to the CCH_3 vertex. Two BCH_3 signals were also distinguishable in the ^1H NMR spectrum, in addition to CH and CCH_3 peaks. A derivative with a single CBr vertex was also prepared, giving the molecule another potential functionality; 1-bromo-deca-*B*-methyl-carborane **4** was formed in 55% yield by reaction of 1-bromo-1,12-dicarba-*closo*-dodecaborane(12)[7b,c] with methyl triflate and triflic acid. Like compound **3**, **4** showed two singlets in its ^{11}B NMR spectrum, and signals for two sets of BCH_3 groups and a CH moiety in the ^1H NMR spectrum.

In previous work by Plešek et al. with 1,2-dicarba-*closo*-dodecaborane(12) derivatives,[8] it was proposed that initial alkylation of carboranes under electrophilic conditions activates the cluster to further substitution in a manner analogous to that seen with aromatic hydrocarbons. However, these reactions did not proceed to completion, presumably due to increasing steric hindrance and the lack of reactivity of the BH vertices closest to the two adjacent CH vertices. The use of a very reactive methylating agent and catalyst combined with a substrate in which no vertex is strongly deactivated has overcome this problem.

Compounds **2**, **3**, and **4** have CH cage vertices still available for further reaction, but due to the electron-donating effect of the methyl groups, it was expected that the acidity of these positions would be reduced compared to the corresponding vertices of 1,12-dicarbaborane. While the 1,12 isomer is significantly less acidic than the 1,2 and 1,7 isomers,[9] it is possible to completely deprotonate the CH vertices by reaction with two molar equivalents of butyllithium in diethyl ether at room temperature for two hours. However, a similar reaction with **2** which was quenched with D_2O revealed only 25–30% C-deuteration, as estimated from ^1H NMR spectroscopy. Under more forcing conditions (ca. 10 mol equiv PhLi in benzene heat-

[*] Prof. M. F. Hawthorne, W. Jiang, Dr. C. B. Knobler, Dr. M. D. Mortimer
Department of Chemistry and Biochemistry
University of California
Los Angeles, CA 90095 (USA)
Telefax: Int. code + (310) 825-5490

[**] This work was supported by the National Science Foundation (Grant CHE 9314037).

ed at reflux for 24 h followed by treatment with D_2O), [D_2]-**2** could be formed in 95% yield.

Our ability to fully deprotonate the CH vertices of **2** suggested that derivatives should be accessible. However, attempts to convert **2** into **1** by deprotonation of the CH vertices of **2** followed by reaction with methyl triflate met with only limited success. Analysis of the reaction products by mass spectrometry proved them to be a mixture of **1**, **2**, and **3** in a ratio of roughly 1:1:3. While distinguishable by GC/MS, these mixtures were not easily separated on a large scale. The difficulty in forcing this reaction to completion must be due to the relative lack of reactivity of the CH vertices present in **2**, which is exacerbated by the steric protection afforded to each CH vertex by the methyl groups of the five surrounding BCH_3 vertices.

The results of the structural studies carried out on **1** and **2**[10] are shown in Figures 1 and 2, respectively. Compound **1** showed

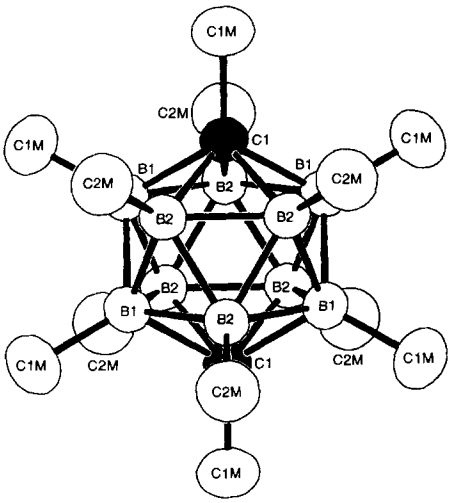


Fig. 1. Crystal structure of **1** (ORTEP representation) along the S_6 axis, showing the crystallographic numbering scheme. Hydrogen atoms are omitted. The molecule has crystallographically imposed S_6 symmetry. One of the two unique icosahedral atoms is described as carbon with one-third occupancy and boron with two-thirds occupancy. Two arbitrarily chosen vertices of the six are shaded and labeled C1, whilst the other four positions are labeled B1. The other unique icosahedral atom, B2, is refined as a boron atom. Selected bond lengths: C1–B1 1.735(6), C1–B2 1.757(6), B2–B2 1.763(6), C1–C1M 1.575(6), B2–C2M 1.583(6) Å.

no unusual features, although the structure exhibits crystallographically imposed symmetry which prohibited assignment of the carbon atoms within the cage. The icosahedral structure of **2** was found to have an interesting distortion in which the methyl groups are displaced slightly towards the C1–C1 axis. This was measured by comparing the angle between a line drawn from a boron vertex to the center of the molecule and the C1–C1 axis with the angle between a line drawn from the carbon of the respective methyl group to the center and the same axis (average C1-midpoint-B 64.0°, average C1-midpoint-C_{Me} 61.6°). The displacement of the methyl groups is accompanied by a compression of the cage at the CH poles, shown by a markedly short C1–C1 distance of 3.014(5) Å as compared with that of other structurally characterized 1,12-dicarbaboranes (3.065(5)–3.219(14) Å).[4a, 11] Both observations are attributed to a "roll-over" effect on the sp-hybridized boron orbitals in the cage due to steric repulsions between the methyl groups accompanied by a corresponding displacement of tangential p orbitals in the icosahedral surface. Similar distortions have been noted in the recent structural characterization[11] of deca-*B*-iodo-1,12-

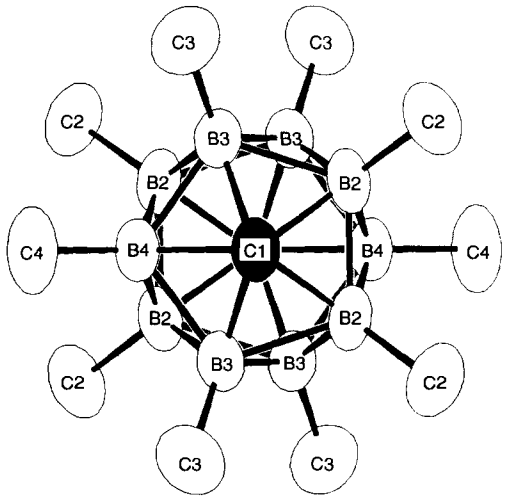


Fig. 2. Crystal structure of **2** (ORTEP representation) along the C1–C1 axis, showing the crystallographic numbering scheme. Hydrogen atoms are omitted. Compound **2** has crystallographically imposed C_{2h} symmetry. Selected bond lengths: B–C range 1.701(5)–1.712(7) average 1.707(4), B–B range 1.767(6)–1.798(5) average 1.785(7), B–C_{Me} range 1.577(5)–1.588(6) average 1.583(5). C1–C1 cross cage distance 3.014(5) Å.

dicarba-*closo*-dodecaborane(12),[12] whose structure resembles that of **2**.

Despite the diminished accessibility of the carbon vertices of the derivatives of deca-*B*-methyl-1,12-dicarba-*closo*-dodecaborane(12) described here, preliminary studies suggest that some further reactions are possible at these positions. Alternatively, the introduction of suitable groups to the carbon vertices prior to methylation of the boron vertices provides synthetic possibilities. Radical halogenation of the methyl groups might form the foundation of a fascinating chemistry formulated around a reactive "sphere" of organic functional groups. We are currently exploring these and other approaches directed towards a new class of carborane-based multifunctionalized compounds.

Experimental Procedure

General laboratory procedures were as described previously [11]. All reactions were carried out under N_2. It was generally found that yields were maximized when the smallest possible volume of experimental apparatus was used.

1: A solution of 1,12-dimethyl-1,12-dicarba-*closo*-dodecaborane(12) (50 mg, 0.35 mmol) in neat methyl triflate (0.4 mL, 3.5 mmol) and triflic acid (0.1 mL, 0.06 mmol) was heated at reflux for 20 h. After cooling, a saturated solution of sodium chloride in water was added (10 mL) and the product was extracted with diethyl ether (3 × 10 mL). The ethereal solution was dried over anhydrous magnesium sulfate and then solvent was removed in vacuo. The crude product was taken up in 5 mL of pentane and passed through a bed of silica gel. Removal of solvent under reduced pressure yielded **1** as a white solid (83 mg, 91%). M.p. 347–348 °C (sealed capillary); ^1H NMR (360 MHz, $CDCl_3$): $\delta = 0.79$ (s, 6H, CCH_3), −0.09 (br s, 30H, BCH_3); $^{13}C\{^1H\}$ NMR (90.5 MHz, $CDCl_3$): $\delta = 76.4$ (CCH_3), 13.1 (CCH_3), −4.0 (vbr, BCH_3); ^{11}B NMR (160.5 MHz, Et_2O): $\delta = -7.4$ (BCH_3); HRMS (EI) (*m/z*), calcd. 312.3820, found 312.3822 (M^+).

2: In a similar fashion, a solution of 1,12-dicarba-*closo*-dodecaborane(12) (100 mg, 0.7 mmol) in methyl triflate (0.8 mL, 7.0 mmol) and triflic acid (0.1 mL, 0.06 mmol) was heated at reflux for 10 h. Workup as for **1** afforded **2** as a white solid (176 mg, 89%). M.p. 232–233 °C (sealed capillary); ^1H NMR (360 MHz, $CDCl_3$): $\delta = 2.01$ (br s, 2H, CH), 0.05 (br s, 30H, BCH_3); $^{13}C\{^1H\}$ NMR (90.5 MHz, $CDCl_3$): $\delta = 74.5$ (CH), −3.7 (vbr, BCH_3); ^{11}B NMR (160.5 MHz, Et_2O): $\delta = -8.8$ (BCH_3); HRMS (EI) (*m/z*), calcd. 284.3507, found 284.3508 (M^+).

3: In a similar fashion, a solution of 1-methyl-1,12-dicarba-*closo*-dodecaborane(12) (43 mg, 0.27 mmol) in methyl triflate (0.3 mL, 2.7 mmol) and triflic acid (0.1 mL, 0.06 mmol) was heated at reflux for 10 h. Workup as for **1** afforded **3** as a white solid (49 mg, 60%). M.p. 308–309 °C (sealed capillary); ^1H NMR (360 MHz, $CDCl_3$): $\delta = 1.98$ (br s, 1H, CH), 0.77 (s, 3H, CCH_3), 0.04, −0.09 (br s, 2 × 15H, BCH_3); $^{13}C\{^1H\}$ NMR (90.5 MHz, $CDCl_3$): $\delta = 76.2$ (CCH_3), 73.7 (CH), 13.1 (CCH_3), −3.0, −3.8 (vbr, BCH_3); ^{11}B NMR (160.5 MHz, Et_2O): $\delta = -7.6$, −9.0 (5B, BCH_3); HRMS (EI) (*m/z*), calcd. 298.3663, found 298.3660 (M^+).

4: In a similar fashion, a solution of 1-bromo-1,12-dicarba-*closo*-dodecaborane(12) (100 mg, 0.45 mmol) in methyl triflate (0.5 mL, 4.5 mmol) and triflic acid (0.1 mL, 0.06 mmol) was heated under reflux for 10 h. Workup as for **1** afforded **4** as a white solid (145 mg, 89%). M.p. 251 °C (decomp) (sealed capillary); ^{1}H NMR (360 MHz, $CDCl_3$): δ = 2.11 (br s, 1H, CH), 0.04, 0.09 (br s, 2 × 15H, BCH_3); $^{13}C\{^1H\}$ NMR (90.5 MHz, $CDCl_3$): δ = 76.2 (CH), 72.7 (CBr), −2.3, −3.6 (vbr, BCH_3); ^{11}B NMR (160.5 MHz, Et_2O): δ = −7.2, −9.7 (5B, BCH_3); HRMS (EI) (*m/z*), calcd. 364.2591, found 364.2602 (M^+).

Received: January 12, 1995 [Z 7629 IE]
German version: *Angew. Chem.* **1995**, *107*, 1470–1473

Keywords: alkylations · boron compounds · carboranes · electrophilic substitutions

[1] a) V. I. Bregadze, *Chem. Rev.* **1992**, *92*, 209–223; b) V. V. Grushin, V. I. Bregadze, V. N. Kalinin, *J. Organomet. Chem. Lib. 20* **1988**, *20*, 1–68, and references therein.

[2] R. N. Grimes, *Carboranes*, Academic Press, New York, **1970** pp. 54–180, and references therein.

[3] F. A. Gomez, M. F. Hawthorne, *J. Org. Chem.* **1992**, *57*, 1384–1390.

[4] a) X. Yang, W. Jiang, C. B. Knobler, M. F. Hawthorne, *J. Am. Chem. Soc.* **1992**, *114*, 9719–9721; b) J. Müller, K. Baše, T. F. Magnera, J. Michl, *ibid.* **1992**, *114*, 9721–9722.

[5] a) X. Yang, C. B. Knobler, Z. Zheng, M. F. Hawthorne, *J. Am. Chem. Soc.* **1994**, *116*, 7142–7159; b) I. T. Chizhevsky, S. E. Johnson, C. B. Knobler, F. A. Gomez, M. F. Hawthorne, *ibid.* **1993**, *115*, 6981–6982; c) W. Clegg, W. R. Gill, J. A. H. McBride, K. Wade, *Angew. Chem.* **1993**, *105*, 1402–1403; *Angew. Chem. Int. Ed. Engl.* **1993**, *32*, 1328–1329.

[6] a) R. Köster, G. W. Rotermund, *Tetrahedron Lett.* **1964**, 1667–1670; b) P. Binger, *ibid.* **1966**, 2675–2680.

[7] a) V. I. Stanko, A. I. Klimova, A. N. Kashin, *Zh. Obshch. Khim.* **1969**, *39*, 1895; b) V. I. Stanko, G. A. Anorova, T. V. Klimova, *ibid.* **1969**, *39*, 2143–2144; c) V. I. Stanko, A. I. Klimova, *ibid.* **1969**, *39*, 1896.

[8] J. Plešek, Z. Plzák, J. Štuchlík, S. Heřmánek, *Collect. Czech. Chem. Commun.* **1981**, *46*, 1748–1763.

[9] L. I. Zakharkin, V. N. Kalinin, L. S. Podvisotskaya, *Izv. Akad. Nauk SSSR Ser. Khim.* **1968**, 2661.

[10] Crystallographic data for **1**: $C_{14}H_{36}B_{10}$, M = 312.60, cubic, space group $Pa3$, a = 12.859(1) Å, V = 2126 Å^3, Z = 4 (1/6 molecule per asymmetric unit), ρ_{calcd} = 0.98 g cm^{-3}, T = 25 °C, μ = 3.0 cm^{-1}. Data were collected on a Syntex P$\bar{1}$ diffractometer using $Cu_{K\alpha}$ radiation (λ = 1.5418 Å) to a maximum 2θ = 115°, giving 484 unique reflections, of which 370 reflections with $I > 3\sigma(I)$ were retained for structure analysis. The data were corrected for Lorentz and polarization effects and for secondary extinction but not for absorption. The structure was solved by direct methods. All non-hydrogen atoms were refined anisotropically. Hydrogen atoms were included in calculated positions. The final discrepancy index was R = 0.085, R_w = 0.110. Because of the high symmetry required by this space group for the molecule, there is disorder, and one of the two unique icosahedral atoms has been described as carbon with 1/3 occupancy and boron with 2/3 occupancy and with both carbon and boron constrained to the same values of x, y, z, and displacement parameters. The largest peak on a final difference electron density map was 0.9 e Å^{-3}. Crystallographic data for **2**: $C_{12}H_{32}B_{10}$, M = 284.54, orthorhombic, space group $Ccmb$ (No. 64, standard setting $Ccma$), a = 13.930(3), b = 15.440(3), c = 9.089(3) Å, V = 1954.9(8) Å^3, Z = 4, ρ_{calcd} = 0.97 g cm^{-3}, T = 25 °C, μ = 2.90 cm^{-1}. Data were collected on a Rigaku AFC5 diffractometer using $Cu_{K\alpha}$ radiation (λ = 1.5418 Å) to a maximum 2θ = 110°, giving 650 unique reflections, of which 488 reflections with $I > 3\sigma(I)$ were retained for structure analysis. The data were corrected for Lorentz and polarization effects and for secondary extinction but not for absorption. The structure was solved by direct methods. All non-hydrogen atoms were refined anisotropically. Methyl hydrogen atoms were included in calculated positions, and the carboranyl hydrogen atom was included in the located position. The final discrepancy index was R = 0.077, R_w = 0.119. The largest peak on a final difference electron density map was 0.11 e Å^{-3}. Further details of the crystal structure investigations may be obtained from the Director of the Cambridge Crystallographic Data Centre, 12 Union Road, GB-Cambridge CB2 1EZ (UK), on quoting the full journal citation.

[11] W. Jiang, C. B. Knobler, C. E. Curtis, M. D. Mortimer, M. F. Hawthorne, *Inorg. Chem.*, in press.

[12] R. R. Srivastava, D. S. Wilbur, Abstracts of Papers, 208th National Meeting of the American Chemical Society, Washington DC, American Chemical Society, Washington DC, **1994**, p. 208.

Bis(hypersilyl)tin and Bis(hypersilyl)lead, Two Electron-Rich Carbene Homologs**

Karl Wilhelm Klinkhammer* and Wolfgang Schwarz

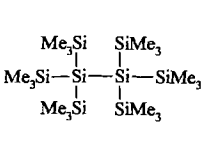
Dedicated to Professor Peter I. Paetzold on the occasion of his 60th birthday

Molecular compounds of divalent tin and lead (stannylenes and plumbylenes, respectively) with solely electropositive σ-bonded substituents tend to oligomerize or to disproportionate, respectively. It has previously been possible to stabilize such systems by introduction of sterically demanding groups or additional coordinative saturation of the central atom. Typical examples are bis(trimethylsilyl)methyl and bis(trimethylsilyl)-amino derivatives,[1, 2] stannylenes and plumbylenes bearing aryl substituents,[3, 4] or intermolecularly donor-stabilized compounds such as $Sn[P(CMe_3)_2]_2$[5a] or $Sn[E(SiMe_3)_2]_2$ (E = P, As).[5b, c] Furthermore, several heteroleptic plumbylenes and stannylenes are known.[6] In the solid state the homoleptic stannylenes are either dimeric or monomeric, in the gas phase those studied to date have only been monomeric. The corresponding lead compounds were observed as monomers in all aggregate states.[7] Stannylenes and plumbylenes with stronger electropositive substituents were to date unknown. The synthesis and the structural characterization of two such derivatives, namely bis(hypersilyl)tin (**1**), and bis(hypersilyl)lead (**2**), is the subject of this communication.

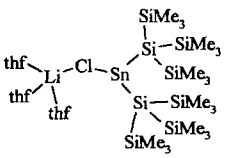
$Sn[Si(SiMe_3)_3]_2$ **1**

$Pb[Si(SiMe_3)_3]_2$ **2**

Geanangel et al. reported in 1992 on the attempt to synthesize **2** from lead(II) chloride and the thf solvate of hypersilyllithium. However, in the course of a redox process they obtained 1,1,1,4,4,4-hexamethyl-2,2,3,3-tetrakis(trimethylsilyl)tetrasilane (**3**) and lead only.[8] It also proved not possible to synthesize the corresponding stannylene **1** by this process;[9a] however, a product that could be described as an LiCl adduct of **1** was isolated, namely the heteroleptic lithium stannanide **4**.[9b]



3



4

Recently, during the synthesis of a hypersilylthallium compound we avoided similiar problems by replacing thallium chloride with thallium bis(trimethylsilyl)amide.[10] Thus, we tried to apply the same method to synthesizing the desired tin(II) and lead(II) compounds.

If lead bis[bis(trimethylsilyl)amide] is treated with the hypersilyl derivative of a heavy alkali metal[11] in *n*-pentane at −60 °C, a clear blue solution is produced together with an al-

[*] Dr. K. W. Klinkhammer, Dr. W. Schwarz
Institut für Anorganische Chemie der Universität
Pfaffenwaldring 55, D-70550 Stuttgart (Germany)
Telefax: Int. code + (711) 685-4241
e-mail: karl.klinkhammer@rus.uni-stuttgart.de

[**] We thank Prof. Dr. G. Becker for his splendid support. – For the term "hypersilyl" see citation 5 in ref. [10].

most colorless crystal paste. From this solution black, coffin-lid shaped crystals precipitate on concentration and cooling to $-60\,^{\circ}C$.

The correct elemental analysis and the molecular ion identified as the heaviest ion by mass spectrometry confirm the identity of the compound as **2**. ^{1}H, and ^{13}C NMR spectra of freshly prepared solutions of the diamagnetic compound show the expected singlets. After a short while, however, one observes the appearance of further resonances, which according to reference samples originate mostly from silane **3**. An absorption measurement in the UV/Vis range showed in addition to some intensive bands which are also found in other hypersilyl derivatives in the areas below 350 nm, two further, less intensive absorptions at 578 ($\varepsilon = 620$) and 1056 nm ($\varepsilon = 370$).

A reaction carried out in an analogous way with tin bis[bis(trimethylsilyl)amide] gave initially a green, and then later a violet-brown solution[12] from which, small black quadratic crystal platelets crystallized at $-60\,^{\circ}C$. Here too the elemental analysis gave correct results and the molecular ion could be identified by mass spectrometry as that for **1**. While as expected a singlet appears in the ^{1}H and ^{13}C NMR spectra of the diamagnetic[13] compound, it was not possible to obtain any satisfying ^{29}Si or ^{119}Sn NMR spectra in the temperature range between -60 and $+30\,^{\circ}C$. Therefore, at present it is not possible to make any statements concerning aggregation in solution by NMR spectroscopy. The UV/Vis spectrum is similiar to that of **2**. However, the absorption maxima (559 nm ($\varepsilon = 580$) and 838 nm ($\varepsilon = 120$)) are shifted to shorter wavelengths as could be expected. As no further absorptions occur even with more concentrated samples, the tin compound **1** is assumed to be largely monomeric in solution as is the lead compound **2**. A cryoscopic molar mass determination confirmed these presumptions.

The crystal structure analyses carried out to elucidate the constitution of the compounds show them to be the expected bis(hypersilyl)lead (**2**) and bis(hypersilyl)tin (**1**). While the lead compound is monomeric,[7a] bis(hypersilyl)tin dimerizes in the solid state to the distannene, tetrakis(hypersilyl)ditin (*Sn–Sn*) $(\mathbf{1})_2$.

The molecules of compound **2** (Fig. 1), like the other structurally characterized molecular lead(II) compounds, are bent

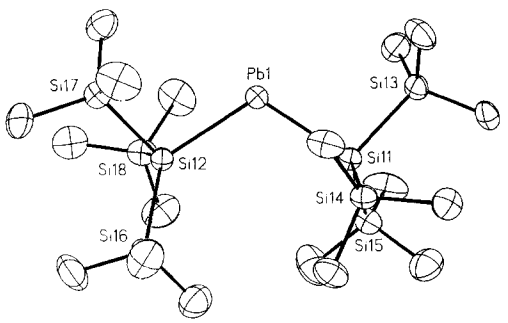
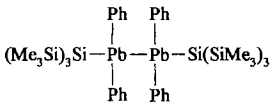


Fig. 1. Molecular structure of **2** in the crystal (thermal ellipsoids at 50% probability level). Selected bond lengths [pm] and angles [°] of one of four symmetry-independent molecules: Pb1–Si11 270.0(3), Pb1–Si12 270.4(3), Si11-Pb1-Si12 113.56(10), Pb1-Si11-Si13 99.6(2), Pb1-Si11-Si14 104.8(2), Pb1-Si11-Si15 125.0(2), Pb1-Si12-Si16 129.2(2), Pb1-Si12-Si17 98.3(2), Pb1-Si12-Si18 101.62(2).

monomers. The Si-Pb-Si angles determined lie between 113.6 and 115.7° and are therefore considerably more obtuse than in other plumbylenes[8] studied so far. The Pb–Si bond lengths vary only slightly between 268 and 271 pm and are about 5 pm longer than those in bis[(hypersilyl)diphenyllead](*Pb–Pb*) (**5**),[15] the only structurally characterized silyl-substituted lead compound to date.



5

That overloading of the central atom in **2** with the very voluminous hypersilyl substituents has a distinct influence on the geometry of the molecule can be recognized by a considerable tilting of this substituent towards the Pb–Si bond axis. Thus, in addition to two Pb-Si-Si angles compressed to nearly 90°, one angle is widened up to 130°. A similiar although less pronounced variance is observed for the Si-Si-Si angles.

The $Si_2Sn–SnSi_2$ backbone (Fig. 2a) of the bis(hypersilyl)tin dimer $(\mathbf{1})_2$ (Fig. 2b) shows a unique strongly distorted *trans*-

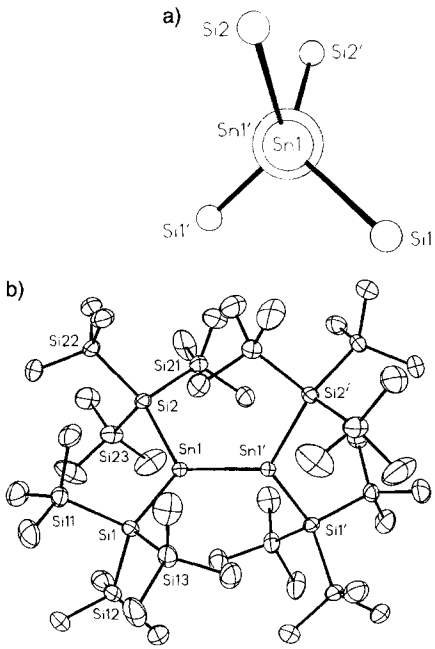
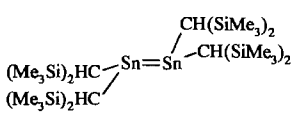


Fig. 2. a) Newman projection of the Sn_2Si_4-framework of $(\mathbf{1})_2$. b) Molecular structure of $(\mathbf{1})_2$ in the crystal (thermal ellipsoids at 50% probability level). Selected bond lengths [pm] and angles [°]: Sn1–Sn1' 282.47(6), Sn1–Si1 266.67(11), Sn1–Si2 267.81(11), Si1-Sn1-Sn1' 108.25(3), Si2-Sn1-Sn1' 123.25(3), Si1-Sn1-Si2 120.46(4), Sn1-Si2-Si21 106.19(5), Sn1-Si2-Si22 131.88(6), Sn1-Si2-Si23 99.78(5), Sn1-Si1-Si11 112.06(5), Sn1-Si1-Si12 115.51(5), Sn1-Si1-Si13 112.35(5).

bent conformation (crystallographic *C*2 symmetry). The dihedral angle (τ) between the planes defined by a tin atom and the central silicon atoms of the bound hypersilyl group is 63.2°, the angle (κ) between these planes and the Sn–Sn bond 28.6°. In the only structurally characterized stannylene dimer to date, the bis(trimethylsilyl)methyl derivative **6**,[1] Lappert et al observed the theoretically expected[7b] undistorted *trans*-bent arrangement ($\tau = 0°$; $\kappa = 41°$). Torsions about the central element–element bond, although considerably less pronounced, have so far only been detected in related sterically strongly loaded alkenes, disilenes, and digermenes.[16] As expected, the Sn–Sn distance in $(\mathbf{1})_2$[7b] is longer than in **6** and lies with 282 pm in the range of "normal" Sn–Sn single bonds in distannanes.[17] The Sn–Si bond lengths and the Si-Sn-Si angle in $(\mathbf{1})_2$ do not differ much from the values of the lithium stannanide **3** synthesized by Cowley et al.[9b]



6

Experimental Procedure

1: A solution of $Sn[N(SiMe_3)_2]_2$ (1.53 g, 3.49 mmol) in *n*-pentane at $-60\,^{\circ}C$ was quickly added to a thoroughly stirred suspension of $KSi(SiMe_3)_3$ (2.00 g, 6.97 mmol) [11] in *n*-pentane (20 mL). The resulting lime green mixture was stirred for 1 h at this temperature and then for 30 min at $0\,^{\circ}C$. The resulting violet-brown solution was pipetted off from the colorless crystal paste and concentrated to 10 mL by removal of the solvent under vacuum. After 15 h at $-60\,^{\circ}C$ black crystal platelets of $(\mathbf{1})_2$ precipitated from the solution (1.22 g, 1.99 mmol, yield 57%). Decomp. $130\,^{\circ}C$; correct elemental analysis; ^1H NMR (250.133 MHz, [D$_6$]benzene, $27\,^{\circ}C$, TMS): $\delta = 0.60$, $^2J(Si,H) = 6.1$ Hz; ^{13}C NMR (62.896 MHz, [D$_6$]benzene, $27\,^{\circ}C$, TMS): $\delta = 5.5$; EI-MS (70 eV; sample 360 K; source 510 K): *m/z* (%): 73 (100) $[Me_3Si^+]$, 247 (7) $[(Me_3Si)_3Si^+]$, 541 (2.7) $[M^+ - 73]$, 614 (1.3) $[M^+]$.

2: The reaction was carried out in a way similar to that for $(\mathbf{1})_2$ [$KSi(SiMe_3)_3$ (2.00 g, 6.97 mmol) and $Pb[N(SiMe_3)_2]_2$ (1.84 g, 3.49 mmol], however, because of the better solubility of the product the solution should be concentrated to 5 mL. After 15 h at $-60\,^{\circ}C$, black, coffin-lid shaped crystals of **2** (1.83 g, 2.60 mmol, 75%) were isolated. Decomp. $152\,^{\circ}C$; correct elemental analysis; ^1H NMR (250.133 MHz, [D$_6$]benzene, $27\,^{\circ}C$, TMS): $\delta = 0.54$, $^2J(Si,H) = 6.6$ Hz; ^{13}C NMR (62.896 MHz, [D$_6$]benzene, $27\,^{\circ}C$, TMS): $\delta = 8.5$, $^1J(Si,C) = 44.5$; EI-MS (70 eV; sample 350 K; source 400 K): *m/z* (%): 73 (100), 247 (19), 455 (4) $[(Me_3Si)_3SiPb^+]$, 702.2 (1.7) $[M^+]$.

Received: February 1, 1995 [Z7706IE]
German version: *Angew. Chem.* **1995**, *107*, 1448–1451

Keywords: distannenes · hypersilyl derivatives · plumbylenes · stannylenes

[1] T. Fjeldberg, A. Haaland, B. E. R. Schilling, M. F. Lappert, A. J. Thorne, *J. Chem. Soc. Dalton Trans.* **1986**, 1551.

[2] C. D. Schaeffer, Jr., J. J. Zuckerman, *J. Am. Chem. Soc.* **1974**, *96*, 7160; D. E. Goldberg, D. H. Harris, M. F. Lappert, K. M. Thomas, *J. Chem. Soc. Chem. Commun.* **1976**, 261; M. F. Lappert, P. P. Power, M. J. Slade, L. Hedberg, V. Schomaker, *ibid.* **1979**, 369.

[3] H. Grützmacher, H. Pritzkow, F. T. Edelmann, *Organometallics* **1991**, *10*, 23; S. Brooker, J.-K. Buijink, F. T. Edelmann, *ibid.* **1991**, *10*, 25.

[4] M. Weidenbruch, J. Schlaefke, A. Schäfer, K. Peters, H. G. von Schnering, H. Marsmann, *Angew. Chem.* **1994**, *106*, 1938; *Angew. Chem. Int. Ed. Engl.* **1994**, *33*, 1846.

[5] a) W.-W. du Mont, H.-J. Kroth, *Angew. Chem.* **1977**, *89*, 832; *Angew. Chem. Int. Ed. Engl.* **1977**, *16*, 792; b) S. C. Goel, M. Y. Chiang, D. J. Rauscher, W. E. Buhro, *J. Am. Chem. Soc.* **1993**, *115*, 160; c) M. Westerhausen, M. M. Enzelberger, W. Schwarz, *J. Organomet. Chem.* **1995**, *485*, 185.

[6] Review: M. F. Lappert, *Main Group Met. Chem.* **1994**, *17*, 183.

[7] For ab initio calculations on the stability of dimers see for example: a) G. J. Trinquier, *J. Am. Chem. Soc.* **1990**, *112*, 1039; b) T. L. Windus, M. S. Gordon, *J. Am. Chem. Soc.* **1992**, *114*, 9559.

[8] S. P. Mallela, I. Bernal, R. A. Geanangel, *Inorg. Chem.* **1992**, *31*, 1626.

[9] S. P. Mallela and R. A. Geanangel claimed the isolation of a colorless(!) THF adduct of **1** [*Inorg. Chem.* **1990**, *29*, 3525]. Our own results (**1** forms a brown THF solution) and the reported extreme ^{119}Sn *highfield* shift led us to doubt its identity. b) A. A. Arif, A. H. Cowley, T. M. Elkins, *J. Organomet. Chem.* **1987**, *325*, C11.

[10] S. Henkel, K. W. Klinkhammer, W. Schwarz, *Angew. Chem.* **1994**, *106*, 721; *Angew. Chem. Int. Ed. Engl.* **1994**, *33*, 681. For earlier usage of bis(trimethylsilyl)amides in the syntheses of stannylenes and plumbylenes see for example ref. [6].

[11] K. W. Klinkhammer, W. Schwarz, *Z. Anorg. Allg. Chem.* **1993**, *619*, 1777; K. W. Klinkhammer, W. Schwarz, *J. Am. Chem. Soc.*, submitted.

[12] The reaction of bis[bis(trimethylsilyl)amides] with hypersilanides is strongly dependent on the temperature and the solvent. Larger quantities of unknown paramagnetic compounds are formed in pentane above $-30\,^{\circ}C$. In the presence of toluene additional interesting products are found: At temperatures below $-30\,^{\circ}C$ mainly solvated alkali metal tris[tris(trimethylsilyl)silyl]stannanides or -plumbanides are obtained in addition to **1** and **2**, respectively. At higher temperatures the main products are alkali metal derivatives of benzylbis[tris(trimethylsilyl)silyl]stannane or -plumbane.

[13] a) How much distannene $(\mathbf{1})_2$ is already present in the triplet state at room temperature remains an unclarified question. In the EPR spectrum of the solid, no triplet resonances were observed in the temperature range between 4 and 300 K. However, ab initio calculations performed on the model system $(H_3Si)_2Sn-Sn(SiH_3)_2$ reveal only a small energy difference of about 25 kJ mol^{-1} in favor of the singlet state [13b] in the observed $Si_2Sn-SnSi_2$ backbone conformation in the solid, so that a measurable population of the triplet state at room temperature cannot be excluded. b) MP2; quasi-relativistic pseudopotentials on Sn(46e core) and Si(10e core) and appropriate basis sets from G. Igel-Mann, H. Stoll, H. Preuss, *Mol. Phys.* **1988**, *65*, 1321; basis sets for H from T. H. Dunning, *J. Chem. Phys.* **1970**, *19*, 553.

[14] Crystal structure analyses: $(\mathbf{1})_2$: $a = 27.884(3)$ $b = 13.106(1)$, $c = 23.173(2)$ Å, $\beta = 126.203(6)^{\circ}$, $V = 6833.5(1)$ Å^3, $Z = 4$, monoclinic, space group $C2/c$ (no. 15), $F(000) = 2592$, $\rho_{calcd} = 1.194$ g cm^{-3}, $\mu = 1.03$ mm^{-1}, four-circle diffractometer $P2_1$ (Syntex), $3^{\circ} < 2\theta < 56^{\circ}$, $Mo_{K\alpha}$, Wyckoff scan, $T = -100\,^{\circ}C$, $N(hkl) = 8519$, from which $7364 > -1\sigma(I)$, Lorenz- and polarization correction, no absorption correction. The structure was solved by direct methods (SHELXS-86) refined with full-matrix least squares based on F_o^2 values (SHELXL93) ($(\mathbf{1})_2$ surprisingly crystallizes isotypically to tetrakis(hypersilyl)dithallium(*Tl–Tl*) which comprises two valence electrons less [10]). Sn, Si, and C atoms were refined anisotropically; the hydrogen atoms, except those which belong to a disordered trimethylsilyl group were found und their positional parameters were freely refined. The tin atom is slightly disordered; the occupation factor for the major position refined to 0.9812(9). 433 parameters, 57 restraints, residual electron density: 0.776/−0.621 e Å^{-3}, $R1[F_o > 4\sigma(F_o)] = 0.044$, $wR2 = 0.091$, GOF = 1.10. **2**: $a = 16.222(3)$, $b = 22.130(3)$, $c = 22.380(4)$ Å, $\alpha = 110.61(3)$, $\beta = 100.57(3)$, $\gamma = 100.35(3)^{\circ}$, $V = 7127(1)$ Å^3, $Z = 8$, triclinic, space group $P\bar{1}$ (no. 2), $F(000) = 2848$, $\rho_{calcd} = 1.309$ g cm^{-3}, $\mu = 5.04$ mm^{-1}, four-circle diffractometer $P2_1$ (Syntex), $6.5^{\circ} < 2\theta < 45^{\circ}$, $Mo_{K\alpha}$, Wyckoff scan, $T = -100\,^{\circ}C$, $N(hkl) = 18628$, from which $18406 > -3\sigma(I)$, Lorenz and polarization correction, empirical absorption correction (ψ scan, min./max. transmission: 0.63/0.99). All the examined crystals were twinned about (1 0 $\bar{1}$) by pseudomeroedry. In the individual used for the final structure solution, the refined volume proportion of the minority component was however very small [0.0131(5)]. The structure was solved by direct methods (SHELXS-86) refined with full-matrix least squares based on F_o^2 values (SHELXL93). Pb, Si, and C atoms were refined anisotropically; the hydrogen atoms were calculated at ideal positions and included in the refinement according to a riding model (AFIX 137) with fixed isotopic displacement parameters. In two out of four symmetry independent molecules the lead atom shows a positional disorder which was carried by a split model calculation. 1068 parameters, 64 restraints, residual electron density: 1.874/−1.074 e Å^{-3}, $R1[F_o > 4\sigma(F_o)] = 0.067$, $wR2 = 0.141$, GOF = 1.10. Further details of the crystal structure investigations may be obtained from the Fachinformationszentrum Karlsruhe, D-76344 Eggenstein-Leopoldshafen (Germany), on quoting the depository numbers CSD-141531 $(\mathbf{1})_2$ and CSD-141530 (**2**).

[15] S. P. Mallela, R. A. Geanangel, *Inorg. Chem.* **1993**, *32*, 602.

[16] For examples see: M. Kira, T. Maruyama, C. Kabuto, K. Ebata, H. Sakurai, *Angew. Chem.* **1994**, *106*, 1575; *Angew. Chem. Int. Ed. Engl.* **1994**, *33*, 1489, and references therein.

[17] See for example: S. P. Mallela, R. A. Geanangel, *Inorg. Chem.* **1993**, *32*, 5623.

Transition Metal Catalyzed Diboration of Vinylarenes**

R. Thomas Baker,* Paul Nguyen, Todd B. Marder,* and Stephen A. Westcott*

Dedicated to Dr. George W. Parshall on the occasion of his 65th birthday

Following the discovery of rhodium-catalyzed hydroboration of alkenes and alkynes,[1] subsequent studies have investigated analogous metal-mediated additions of boron–heteroatom bonds.[2] Although tetraalkoxydiboranes cannot be added to C–C multiple bonds by conventional reactions,[3] a report published by Suzuki et al. in 1993 described a platinum-catalyzed variant using a bis(pinacolate) derivative.[2d] Unfortunately,

[*] Dr. R. T. Baker
Central Research and Development
Dupont Science and Engineering Laboratories
Experimental Station, Wilmington, DE 19880-0328 (USA)
Telefax: Int. code + (302)695-8281

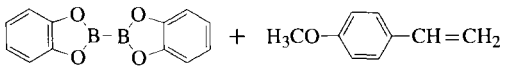
Prof. T. B. Marder, P. Nguyen
Department of Chemistry, University of Waterloo
Waterloo, Ontario N2L 3G1 (Canada)

Dr. S. A. Westcott
Department of Chemistry, University of North Carolina
Chapel Hill, NC 27514 (USA)

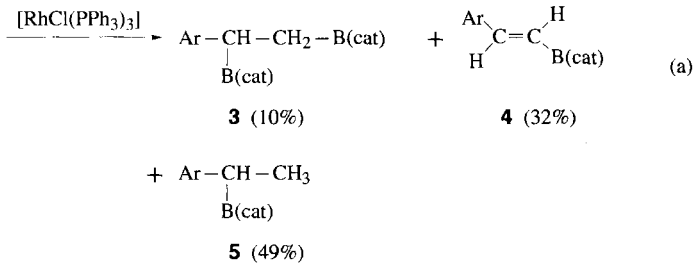
[**] Contribution No. 6936 from Central Research and Development, Dupont Science and Engineering Laboratories. We thank Todd W. Hunt, John Nguyen, and Fred Davidson for expert technical assistance. T. B. M. acknowledges support from the Natural Sciences and Engineering Research Council (NSERC) of Canada. P. N. and S. A. W. thank the NSERC for their respective predoctoral and postdoctoral fellowships.

this catalyst system was limited to the diboration of alkynes; alkenes failed to react. The catalyzed diboration of alkenes to 1,2-bis(boronate) esters could provide a new route to a wide variety of 1,2-bifunctional organic compounds.[4] Reactivity studies of bis(boryl)rhodium complexes[5a] and the observation of B–B oxidative addition to Rh^I centers[5b] prompted us to investigate the Rh-catalyzed diboration of vinylarenes using $B_2(cat)_2$ (**1**) (cat = 1,2-$O_2C_6H_4$).[6] We report herein the first examples of metal-catalyzed addition of B–B bonds to C=C bonds.

Metal-catalyzed addition of **1** to 4-vinylanisole (**2**) was monitored by ^1H and ^{13}C NMR spectroscopy.[7] With typical rhodium hydroboration catalysts such as [$RhCl(PPh_3)_3$], the products consisted mostly of alkenyl- and alkylboronate esters (**4** and **5**) resulting from β-H elimination [Eq. (a)];[8] only 10% of the



1 **2**

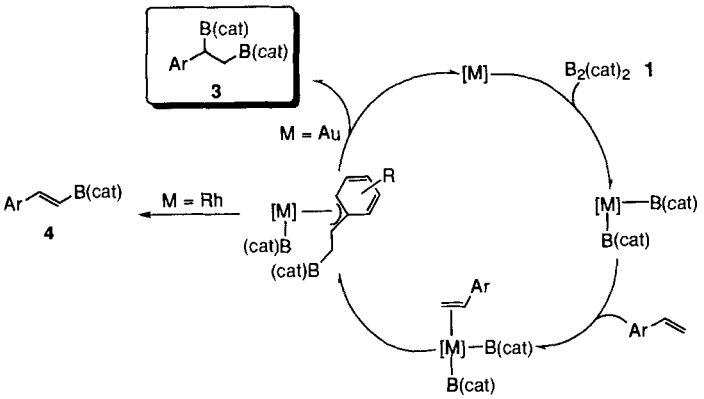


3 (10%) **4** (32%) **5** (49%) (a)

desired 1,2-bis(boronate) ester (**3**) was observed.[9] Previous studies indicated that competing β-H elimination pathways could be avoided by use of a rhodium complex with a chelating bis(phosphane) ligand.[10, 11] Indeed, the more active zwitterionic catalyst precursor [Rh(dppb){η^6-(cat)B(cat)}][11] (dppb = butane-1,4-diylbis(diphenylphosphane)) gave the highest yield of **3** observed for any rhodium catalyst (44%). Unfortunately, even this catalyst system suffered from competing β-H elimination (23% **5**, 22% $ArCH_2C[B(cat)]_3$ **6**[7]).[12]

One approach to prevent β-H elimination is to find a catalyst system in which the alkylmetal intermediate is stabilized relative to the alkene metal hydride. As alkenegold complexes are known to be labile and there are no known mononuclear gold hydrides,[13] we examined diborations catalyzed by phosphanegold complexes. In initial studies the complexes [$AuCl(PR_3)_n$] (R = Et, Ph and n = 2, 3) showed little activity, even at 80 °C. We recently reported the preparation of new gold(I) complexes containing bulky, electron-rich bis(phosphane) ligands.[14] Addition of two equivalents of dcpe (ethane-1,2-diylbis(dicyclohexylphosphane)) to commercially available [$AuCl(PEt_3)$] generates a catalyst system that gives *exclusive* formation of the 1,2-bis(boronate) ester.[15]

This new catalyst system reacts selectively with vinylarenes, including electron-poor (4-$CF_3C_6H_4$)CH=CH_2 and some activated alkenes such as allylbenzene.[7] While polar solvents such as *N*,*N*-dimethylformamide increased diboration rates, competing degradation of **1** was also observed. Although we have not yet conducted mechanistic studies, we presume that the electron-rich phosphane is needed for reversible B–B bond activation[2d, 5b, 16] by the monovalent gold center (Scheme 1). Further studies are in progress to elucidate this mechanism and to increase the activity of these phosphanegold catalyst precursors for this new selective route to 1,2-bis(boronate) esters.



Scheme 1. Proposed cycle for metal-catalyzed diborations and the competing β-H elimination when M = Rh.

Experimental Procedure

In a typical Rh-catalyzed diboration reaction, a solution of **2** (34 mg, 0.25 mmol) in 0.5 mL of [D_8]THF was added to a suspension of **1** (60 mg, 0.25 mmol) and 0.01 mmol of catalyst in 0.5 mL of [D_8]THF. The mixture was stirred for 20 h, at which time the ^1H, ^{13}C, and ^{11}B NMR spectra were recorded. In several instances the ^1H NMR spectrum was rerecorded 4–6 weeks later. No significant changes in product distributions were observed. Product distributions were verified by comparison of the intensities of the OMe resonances in the ^1H and ^{13}C NMR spectra. The 2,2,2-tris(boronate) ester **6** was prepared independently by catalyzed diboration of vinylboronate ester **4**; full details will be published elsewhere.

Diborations using gold complex catalysts were conducted at 80 °C in [D_8]THF for 48 h with 8 mol% catalyst, 1.5 equiv **1**, and 1 equiv vinylarene.

Received: October 24, 1994
Revised version: March 24, 1995 [Z74251E]
German version: *Angew. Chem.* **1995**, *107*, 1451–1452

Keywords: boron compounds · catalysis · diborations · gold compounds

[1] D. Männig, H. Nöth, *Angew. Chem.* **1985**, *97*, 854; *Angew. Chem. Int. Ed. Engl.* **1985**, *24*, 878.

[2] a) K. Nozaki, K. Wakamatsu, T. Nonaka, W. Tuckmantel, K. Oshima, K. Utimoto, *Tetrahedron Lett.* **1986**, *27*, 2007; b) S. Sharma, A. C. Oehlschlager, *ibid.* **1988**, *29*, 261; c) T. Ishiyama, K. Nishijima, N. Miyaura, A. Suzuki, *J. Am. Chem. Soc.* **1993**, *115*, 7219; d) T. Ishiyama, N. Matsuda, N. Miyaura, A. Suzuki, *ibid.* **1993**, *115*, 11018.

[3] Reactions of tetrahalodiboranes with unsaturated C–C bonds have been reported previously, but the difficulty in handling these compounds limits their application to organic synthesis. a) P. Ceron, A. Finch, J. Frey, J. Kerrigan, T. Parsons, G. Urry, H. I. Schlesinger, *J. Am. Chem. Soc.* **1959**, *81*, 6368; b) T. Onak, *Organoborane Chemistry*, Academic Press, New York, **1975**, pp. 38–40, and references therein; c) L. Ahmed, J. Castillo, D. A. Saulys, J. A. Morrison, *Inorg. Chem.* **1992**, *31*, 706.

[4] For utility of organoboranes in organic synthesis see: A. Pelter, K. Smith, H. C. Brown, *Borane Reagents*, Academic, New York, **1988**.

[5] a) R. T. Baker, J. C. Calabrese, S. A. Westcott, P. Nguyen, T. B. Marder, *J. Am. Chem. Soc.* **1993**, *115*, 4367; b) P. Nguyen, G. Lesley, N. J. Taylor, T. B. Marder, N. Pickett, W. Clegg, M. R. J. Elsegood, N. C. Norman, *Inorg. Chem.* **1994**, *33*, 4623.

[6] C. N. Welch, S. G. Shore, *Inorg. Chem.* **1968**, *7*, 225.

[7] Spectroscopic data for **3**–**5** are given elsewhere [5a, 11]. Selected NMR data for **6** in [D_8]THF: $\delta(^1H)$ = 3.66 (s, OMe), 3.92 (s, CH_2); $\delta(^{13}C)$ = 55.32 (OMe), 33.9 (C_α); the C_β signal was not observed due to quadrupolar broadening from the boron nuclei. ^1H NMR data for (4-$CF_3C_6H_4$)CH[B(cat)]CH_2[B(cat)]: δ = 1.87 (dd, J = 16.5, 7 Hz, 1H, CH_2), 2.22 (dd, J = 16.5, 9.5 Hz, 1H, CH_2), 3.46 (dd, J = 9.5, 7 Hz, CH). ^1H NMR data for $PhCH_2CH$[B(cat)]-CH_2[B(cat)]: δ = 3.21 (dd, J = 13.5, 6 Hz, 1H, $PhCH_2$), 2.88 (dd, J = 13.5, 9 Hz, 1H, $PhCH_2$), 2.27 (dddd, J = 9, 8.5, 6.5, 6 Hz, CH), 1.57 (dd, J = 16.5, 8.5 Hz, 1H, CH_2), 1.48 (dd, J = 16.5, 6.5 Hz, 1H, CH_2).

[8] Alkenylborane and alkenylboronate ester products in transition metal mediated processes are believed to arise from insertion of the starting alkene into an M–B bond. For examples see: a) T. Davan, E. W. Corcoran, Jr., L. G. Sneddon, *Organometallics* **1983**, *2*, 1693; b) K. Burgess, W. A. van der Donk, S. A. Westcott, T. B. Marder, R. T. Baker, J. C. Calabrese, *J. Am. Chem. Soc.* **1992**, *114*, 9350; c) J. M. Brown, G. C. Lloyd-Jones, *ibid.* **1993**, *115*, 866.

[9] Roughly 10% of the products of the rhodium-catalyzed reactions were additional boronate esters; full details will be presented elsewhere.
[10] S. A. Westcott, T. B. Marder, R. T. Baker, *Organometallics* **1993**, *12*, 975.
[11] S. A. Westcott, H. P. Blom, T. B. Marder, R. T. Baker, *J. Am. Chem. Soc.* **1992**, *114*, 8863.
[12] Other metal complexes were also examined. For example, $[CpCo(\eta^2\text{-}C_2H_4)_2]$, $[Pd(PPh_3)_4]$, $[Pd(PPh_3)_4$/DiPPE, $[Pt(PPh_3)_3]$, and $PtBr_2$ gave negligible reactions at 80 °C (conversion <20%).
[13] a) H. Schmidbaur, *Organogold Compounds, Gmelin Handbuch der Anorganischen Chemie*, Springer, Berlin **1980**; b) R. J. Puddephatt in *Comprehensive Organometallic Chemistry, Vol. X* (Eds.: G. Wilkinson, F. G. A. Stone, E. W. Abel), Pergamon, Oxford, **1982**, Chapter 15, pp. 765–821.
[14] R. T. Baker, J. C. Calabrese, S. A. Westcott, *J. Organomet. Chem.*, in press.
[15] Catalyst lifetime was limited for less bulky bis(phosphane) ligands $(R_2PCH_2)_2$ (R = Et, *i*Pr).
[16] Oxidative addition of $B_2(cat)_2$ to organoplatinum compounds has been reported recently: C. N. Iverson, M. R. Smith, III, *J. Am. Chem. Soc.* **1995**, *117*, 4403.

1,5-Anhydrohexitol Nucleic Acids, a New Promising Antisense Construct**

Arthur Van Aerschot,* Ilse Verheggen, Chris Hendrix, and Piet Herdewijn

Antisense oligodeoxyribonucleotides (ODNs) can be considered a new class of potential therapeutic agents that function by preventing the synthesis of specific proteins by either physical blockage of the translation process or by inducing RNase H mediated cleavage of the mRNA. The major obstacles to the use of these constructs are their low metabolic stability and problems in cellular uptake.[1] It is clear this therapeutic approach could benefit from the availability of modified oligonucleotides that efficiently block translation by formation of very stable complexes with their target.

Of the many modifications in the ODN structure,[2] only few give an increase in duplex stability.[3] Among these, the most stable (albeit triple helix forming) are polyamide linked acyclic nucleic acids or PNAs; however, these also suffer from low solubility in water and limited uptake.[4] A more recent finding are the N3′ → P5′ phosphoramidates, which increase the melting temperature T_m of the duplexes by an average of 2 °C per base pair versus RNA.[5]

Because pyranose ODNs are energetically favored over furanose ODNs (smaller change in entropy during duplex formation), various pyranoses have already been studied.[6] In view of the structural similarity of 1,5-anhydrohexitol nucleoside analogues **1** (Fig. 1) with natural 2′-deoxynucleosides,[7] we have investigated ODNs made of monomers of type **1**. An extra methylene group is inserted between the base moiety and the ring oxygen atom, affording a much less flexible tetrahydropyran skeleton.

The synthesis of 1,5-anhydro-2-(adenin-9-yl)-2,3-dideoxy-D-*arabino*-hexitol (**2**, hA), and its congeners **3** (hT) and **4** (hG) has been described previously.[7] These monomeric units were incorporated into oligomers using phosphoramidite chemistry and standard protecting groups (A: benzoyl, G: isobutyryl); long-chain alkylamine controlled pore glass (CPG) was used as the support.[8, 9]

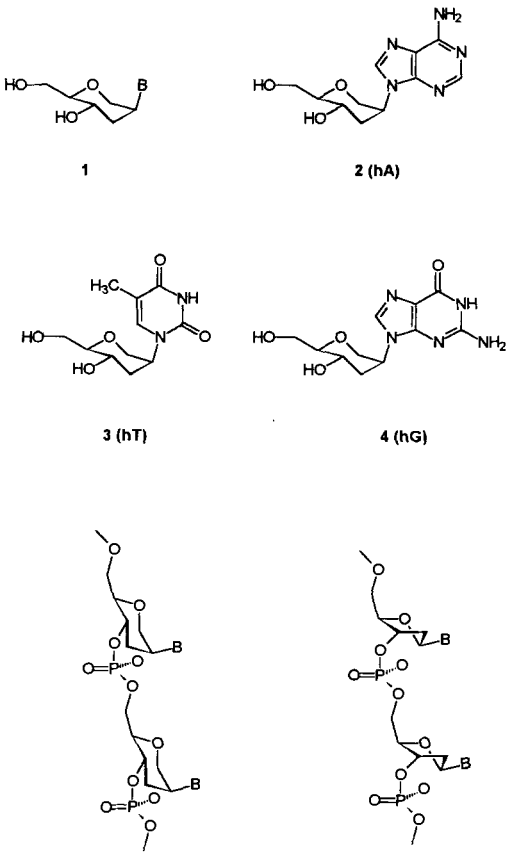


Fig. 1. Structural formulas of the anhydrohexitol monomers, and comparison of the structure of natural DNA (right) and 1,5-anhydrohexitol oligomers (left).

From Table 1 it is clear that incorporation of hA into an oligo(dA) gives nearly the same helix–coil transitions as insertion of a natural dA. Substitution of thymidine by hT into the oligo(dT) gives a substantial decrease in melting temperature, but there is no alteration in base pairing specificity with the 1,5-anhydrohexitol nucleosides.

Table 1. Melting temperatures T_m [°C] for the duplexes formed by oligonucleotides **5**, **6** and **7**, **8** and their respective complementary sequences $(dA)_6N(dA)_6$ and $(dT)_6N(dT)_6$, in which the internal A or T residue Ts scrambled to evaluate base pairing specificity; N = G, C, A, or T (0.1 M NaCl, 20 mM KH_2PO_4, pH 7.5, 0.1 mM EDTA, strand concentration 4 μM of each).

Sequence	T_m			
	G	C	A	T
5	20.0	17.9	18.5	34.0
6	20.2	17.1	17.7	31.9
	G	C	T	A
7	21.0	20.7	21.3	34.0
8	15.1	15.2	18.3	28.6

While adenine–adenine pairing has been described in homo-DNA,[10] we could not observe helix–coil transitions below 90 °C for either **10** or **12** under the physiological conditions studied here (Fig. 2). By measuring the thermal stability of homopolymer mixtures **12**·**7** and **10**·**5** (Table 2), we observed the

[*] Dr. A. Van Aerschot, Dr. I. Verheggen, Dr. C. Hendrix, Prof. Dr. P. Herdewijn
Laboratory of Medicinal Chemistry
Rega Institute, Katholieke Universiteit Leuven
Minderbroedersstraat 10, B-3000 Leuven (Belgium)
Telefax: Int. code + (16)337340
e-mail: Arthur.VanAerschot@Rega.KULeuven.ac.be

[**] This work was supported by a grant from the Fonds voor Geneeskundig Wetenschappelijk Onderzoek. A. V. A. is a Research Associate of the Belgian National Fund of Scientific Research. We thank Guido Schepers for his efficient technical assistance.

$(dA)_{13}$ **5** $(dA)_6hA(dA)_6$ **6** $(dT)_{13}$ **7**

$(dT)_6hT(dT)_6$ **8** $(hT)_2(dT)_9(hT)_2$ **9** $(hT)_{13}$ **10**

$(hA)_2(dA)_9(hA)_2$ **11** $(hA)_{13}$ **12**

6′-h(AGGAGA) **13** 5′-d(AGGAGA) **14**

6′-h(AGGGAGAGGAGA) **15**

5′-d(AGGGAGAGGAGA) **16**

Fig. 2. Formulas of the oligonucleotides discussed in the text.

Table 2. T_m values [°C] (hyperchromicity H [%]) of melting curves (260 nm) of modified ODNs ($c = 4\,\mu M$) in 0.1 M NaCl buffer and their enzymatic stability ($t_{\frac{1}{2}}$[min]).

Sequence	Complement	T_m (H)	$t_{1/2}$ [a]
9	**5**	27.6 (32)	>120
10	**5**	45.4 (49) [b]	S [c]
11	**7**	30.3 (33)	>120
12	**7**	21.0 (49)	S [c]
10	**12**	76.3 (ND) [d]	
7	**5**	34.0 (35)	4

[a] Determined by hyperchromicity (260 nm) at 37 °C in 1 mL of 200 mM Tris · HCl, pH 8.6, 200 mM NaCl, 28 mM $MgCl_2$ with 0.04 U of SV PDE (*Crotalus Adamanteus* venom, Pharmacia) for 0.4 OD_{260}. [b] Measured at 284 nm. [c] Completely stable under the reaction conditions for 24 h. [d] Could not be determined due to the high melting temperature.

formation of complexes between a completely modified hexitol nucleic acid (HNA) and natural DNA. Respective melting temperatures of 21 and 45 °C were observed for the two homopolymer mixtures, in comparison with a T_m of 34 °C for the control duplex **7**·**5**. The T_m of **10** was determined at 284 nm, because the thermal behavior of the complex at 260 nm indicated that the oligo(hT)·oligo(dA) association does not have a classical helix structure. The UV absorption first decreases at 260 nm, shows a minimum at 46 °C, and then increases (Fig. 3).

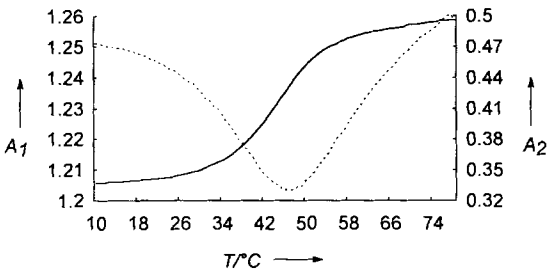


Fig. 3. T_m values of the duplex **10**·**5** in 0.1 M NaCl as determined at 260 nm (solid curve) (A_1) and at 284 nm (dashed line) (A_2). Both curves show an inflection point at 45–46 °C. A = absorption with 4 μM **10** and 4 μM **5**.

The modified oligonucleotides **10** and **12** are completely stable against snake venom phosphodiesterase (SV PDE), while the natural oligonucleotides **5** and **7** are degraded within minutes (Table 2). Substitution with two hA monomers at either end as in **11**, likewise afforded very stable ODNs. SV PDE is a 3′-exonuclease, and 3′-exonuclease activity is the major cause of degradation of ODNs in serum.[11]

A hexamer and a dodecamer (Table 3) consisting of a mixed purine sequence containing hA and hG clearly provide more stable duplexes with both DNA and RNA than their natural counterparts do. The observed T_m values are not the result of

Table 3. T_m values [°C] (hyperchromicity [%]) of fully modified oligonucleotides ($c = 4\,\mu M$) in 0.1 M NaCl, 20 mM KH_2PO_4 pH 7.5, 0.1 mM EDTA. Duplexes were formed with either DNA or RNA complementary sequences.

Sequence	DNA complement	RNA complement
13	31.2 (9.5) [a]	44.8 (13)
14	10.0 [a, b]	10.5 [b]
15	64.8 (14)	84.0 (>15 [b])
16	49.0 (19)	47.6 (15)

[a] Determined in 1 M NaCl. [b] Could not be determined due to the either low or high melting temperature.

self-association of the HNAs, since they do not display any hyperchromicity alone under these conditions. For the HNA–DNA duplex an increase in the T_m value of 16 °C for dodecamer **15** and 21 °C for hexamer **13** was noticed. The ΔT_m value per base pair is clearly dependent on the sequence. For HNA–RNA duplex formation, the increase relative to the DNA–RNA control duplex is even more pronounced: 36 °C for the dodecamer and 34 °C for the hexamer. An HNA–RNA duplex is thus more stable than an HNA–DNA duplex, which further underlines the potential of HNAs as antisense ODNs. The increase in the T_m value of 3 °C to 5.5 °C per base pair indicates the very strong interaction of these HNAs with complementary oligoribonucleotides.

These results indicate that ODNs containing 1,5-anhydrohexitol building blocks form very stable complexes with DNA and RNA and are enzymatically stable. Therefore these new constructs fulfill at least two requirements of an ideal antisense construct.

Received: February 8, 1995 [Z 7703 IE]
German version: *Angew. Chem.* **1995**, *107*, 1483–1485

Keywords: antisense oligonucleotides · DNA · nucleic acids · polyalcohols · RNA

[1] For a review, see E. Uhlmann, A. Peyman, *Chem. Rev.* **1990**, *90*, 543–584.
[2] S. L. Beaucage, R. P. Iyer, *Tetrahedron* **1993**, *49*, 6123-6194; R. S. Varma, *Synlett* **1993**, 621–637; N. T. Thuong, C. Hélène, *Angew. Chem.* **1993**, *105*, 697–723; *Angew. Chem. Int. Ed. Engl.* **1993**, *32*, 666–690.
[3] Y. S. Sanghvi, P. D. Cook, *Carbohydrate Modifications in Antisense Research*, (Eds.: Y. S. Sanghvi, P. D. Cook), *ACS Symp. Series* **1994**, *580*, 1.
[4] M. Egholm, O. Buchardt, P. E. Nielsen, R. H. Berg, *J. Am. Chem. Soc.* **1992**, *14*, 1895–1897; P. E. Nielsen, M. Egholm, R. H. Berg, O. Buchardt, *Science* **1991**, *254*, 1497–1500.
[5] S. Gryaznov, J.-K. Chen, *J. Am. Chem. Soc.* **1994**, *116*, 3143–3144.
[6] A. Eschenmoser, *Pure Appl. Chem.* **1993**, *65*, 1179–1188; K. Augustyns, A. Van Aerschot, C. Urbanke, P. Herdewijn, *Bull. Soc. Chim. Belg.* **1992**, *101*, 119–129; K. Augustyns, F. Vandendriessche, A. Van Aerschot, R. Busson, C. Urbanke, P. Herdewijn, *Nucleic Acids Res.* **1992**, *20*, 4711–4716; K. Augustyns, G. Godard, C. Hendrix, A. Van Aerschot, J. Rozenski, T. Saison-Behmoaras, P. Herdewijn, *ibid.* **1993**, *21*, 4670–4676.
[7] I. Verheggen, A. Van Aerschot, S. Toppet, R. Snoeck, G. Janssen, P. Claes, J. Balzarini, E. De Clercq, P. Herdewijn, *J. Med. Chem.* **1993**, *36*, 2033–2040.
[8] R. Pon, N. Usman, K. Ogilvie, *BioTechniques* **1988**, *6*, 768–771.
[9] Standard protocols for oligonucleotide synthesis were used for all protections, chain extensions (ABI 392), and deprotections. Products were purified by by fast protein, peptide, and polynucleotide liquid chromatography (FPLC) on a Mono Q column at pH 12 (see also ref. [6b]).
[10] J. Hunziker, H.-J. Roth, M. Böhringer, A. Giger, U. Diederichsen, M. Göbel, R. Krishnan, B. Jaun, C. Leumann, A. Eschenmoser, *Helv. Chim. Acta* **1993**, *76*, 259–352.
[11] J.-P. Shaw, K. Kent, J. Bird, J. Fishback, B. Froehler, *Nucleic Acids Res.* **1991**, *19*, 747–750.

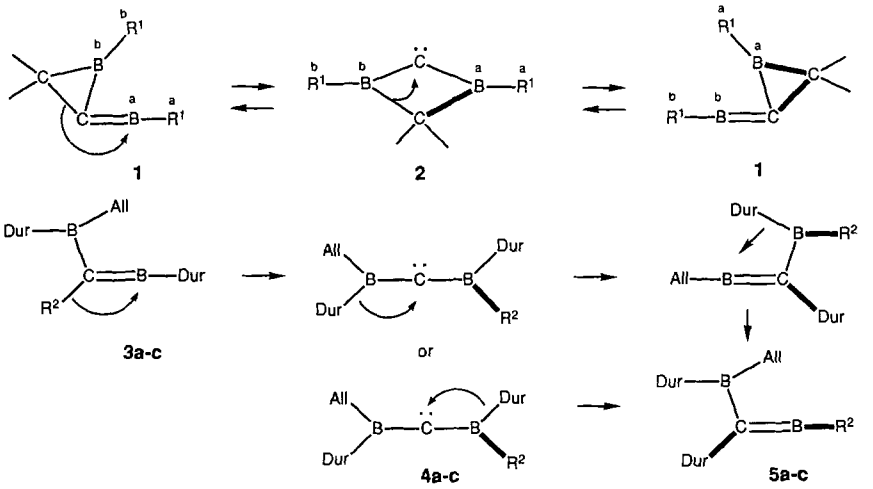
 © VCH Verlagsgesellschaft mbH, D-69451 Weinheim, 1995 0570-0833/95/1212-1339 $ 10.00+.25/0

Diborylcarbenes as Reactive Intermediates in Double 1,2-Rearrangements with Low Activation Enthalpies**

Matthias Menzel, Heinz Jürgen Winkler, Tesfay Ablelom, Dirk Steiner, Stefan Fau, Gernot Frenking, Werner Massa, and Armin Berndt*

Dedicated to Professor Karl Dimroth on the occasion of his 85th birthday

The topomerization of boriranylideneboranes **1**,[1] according to calculations by Schleyer et al.,[2] occurs via cyclic diborylcarbenes **2** as reactive intermediates. A C–C and a C–B bond of the skeleton (Scheme 1, see arrows, double 1,2-rearrangement) are broken under very mild conditions ($\Delta G^{\neq}$ = 11–13 kcal mol^{-1}).



R^1 = tBu, Mes = 2,4,6-trimethylphenyl, Dur = 2,3,5,6-tetramethylphenyl

R^2 = Me (**a**), Et (**b**), neopentyl (**c**) All = 1-alkyl-3,3-bis(trimethylsilyl)allenyl

Scheme 1. For clarity π and σ delocalizations in **1**–**5** are not shown in the diagram; bonds newly formed by 1,2 rearrangement are drawn in boldface.

Here we report on facile isomerizations of borylmethyleneboranes **3a–c** via open-chain diborylcarbenes **4a–c** to **5a–c**. The 1,2-migration of substituents (Scheme 1, see bent arrows) here replaces the breaking of bonds in the skeleton as in **1** and **2**. This interpretation is supported by the results of MP2/6-31G* calculations for tetramethylborylmethyleneborane **3d** and tetramethyldiborylcarbene **4d**.

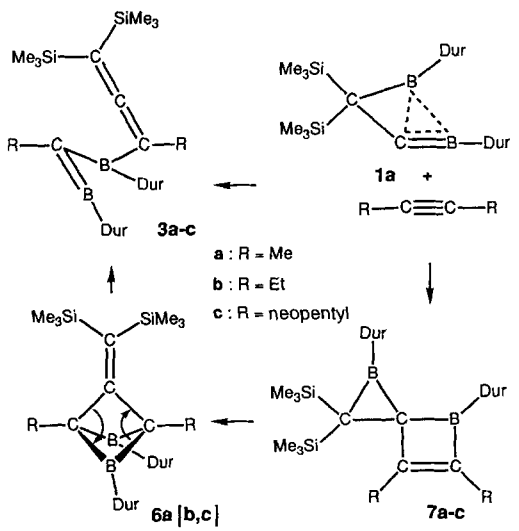
The formation of allenylborylmethyleneboranes[1b,3] **3a–c** in the reaction of **1a** with alkynes can be easily explained by cycloreversion (Scheme 2, see arrows) of a four-membered ring in the intermediates **6a–c**. These are formed readily from **7a–c**, the primary products[4] of the reaction of **1a–c** and alkynes, as shown recently for the rearrangement of **7a** into **6a**.[5]

The primary rearrangement product of **6a** at 25 °C is **3a** as shown by trapping with acetone to yield **9**. The probable intermediate **8** undergoes a hydride shift to form **9** (Scheme 3),[6] which has been characterized by NMR spectroscopy (Table 1).

In the absence of a trapping reagent, the rearrangement product of **6a** is not **3a** but the isomer **5a**. The ^{13}C NMR spectra of **5a** show a boron-bound methyl group (broad signal at δ = 2.2) and a carbon-bound duryl group (sharp signal of the *ipso*-carbon atom at δ = 142.9). This indicates that a methyl group has migrated from a carbon to a boron atom, and a duryl group from a boron to a carbon atom. During the isomerization **6a** → **3a** → **5a**, at 25 °C, **3a** can not be detected by NMR spectroscopy. Therefore, the second step (**3a** → **5a**) of the reaction must be faster than the first (**6a** → **3a**), but slower than the trapping reaction (**3a** → **9**, see above). Compound **3b** is formed at −10 °C from **7b** and can be characterized by NMR spectroscopy; signals for **6b** can not be detected. Compound **3b** isomerizes to form **5b** at 30 °C in one hour. X-ray structural analysis of **5b** shows an ethyl group at the boron atom B1, and a duryl group at the carbon atom C1 between the two boron atoms (see Fig. 2 bottom). The isomerization of **3c** into **5c** is so slow that **3c** can be isolated by working quickly at low temperatures. The structure of **3c** has been confirmed by X-ray structural analysis (see Fig. 2 top). The free activation enthalpies of the isomerizations **3** → **5** are determined to be 23.0 for **3c** → **5c**, and 22.0 kcal mol^{-1} for **3b** → **5b**. Thus, $\Delta G^{\neq}$ for the isomerization **3a** → **5a** is concluded to be less than 22.0 kcal mol^{-1}.

MP2/6-31G* calculations[7,8] indicate that the diborylcarbene **4d** is 23.1 kcal mol^{-1} higher in energy than the borylmethyleneborane **3d** (Fig. 1).[9]

We conclude that the rearrangements of **3a–c** → **5a–c** proceed via diborylcarbenes, assuming that the barriers to rearrangement for the diborylcarbenes **4a–c** into the reactants **3a–c** or into the products **5a–c** are low. For the prototype diborylcarbene and for **4d** this assumption has been con-



Scheme 2.

[*] Prof. Dr. A. Berndt, Dr. M. Menzel, Dipl.-Chem. H.-J. Winkler, Dipl.-Chem. S. Fau, Prof. Dr. G. Frenking, Prof. Dr. W. Massa, T. Ablelom, Dipl.-Chem. D. Steiner
Fachbereich Chemie der Universität
D-35032 Marburg (Germany)
Telefax: Int. code + (6421)288917

[**] This work was supported by the Deutsche Forschungsgemeinschaft and the Fonds der Chemischen Industrie.

Table 1. Some physical properties of compounds **3b,c**, **5a–c**, **7b**, and **9**.

3b: Yield: quantitative by NMR spectroscopy. ^{1}H NMR (400 MHz, $CDCl_3$, 30 °C): δ = 0.14 (s, 18H, $SiMe_3$), 1.04 (br. 6H, CH_2-CH_3), 2.08, 2.28 (each s, each 12H, *o*- and *m*-CH_3), 6.92 (s, 2H, *p*-H). No signal was observed for the CH_2 groups. The equivalence of the duryl groups indicates the rapid shift of the allenyl group from the tricoordinate- to the dicoordinate-boron atom. ^{13}C NMR (100 MHz, $CDCl_3$, −40 °C): δ = 0.3 (q, 6C, $SiMe_3$), 13.4, 16.0, 19.7, 20.6, 21.3, 22.3, 23.7 (some are br., 12C, *o*- and *m*-CH_3 and CH_2-CH_3), 79.9 (s, 1C, CSi_2), 89.9 (br. s, 1C, CB of allene), 103.0 (br. s, 1C, CB_2), 127.6, 137.7 (each br. s, each 1C, *i*-C)), 129.5, 136.3 (each d, each 1C, *p*-C), 131.7, 132.9, 135.6, 143.5 (each s, each 2C, *o*- and *m*-C), ca. 214.0 (1C, middle allene-C). Additionally, at −40 °C the following signals are detected, which we attribute to a rotation isomer of **3b**: 0.5 ($SiMe_3$), 79.4 (CSi_2), 96.1 (br., CB).

3c: colorless crystals, m.p. 58 °C, yield: 55%. ^{1}H NMR (500 MHz, $CDCl_3$, −30 °C): δ = 0.17 (s, 18H, $SiMe_3$), 0.83, 0.93 (each s, each 9H, $C(CH_3)_3$), 1.72, 2.56 (each s, each 2 H, CH_2), 1.85, 2.02, 2.19, (each s, 24H, *o*- and *m*-CH_3), 6.43, 6.89 (each s, each 1H, *p*-H); ^{13}C NMR (125 MHz, $CDCl_3$, −30 °C): δ = 0.7 (q, 6C, $SiMe_3$), 19.7, 20.7, 21.1, (each q, 8C, *o*- and *m*-CH_3), 29.8, 30.1 (each q, each 3C, $C(CH_3)_3$), 32.5, 32.8 (each s, each 1C, $C(CH_3)_3$), 43.5, 44.1 (each t, each 1C, CH_2), 77.6 (s, 1C, CSi_2), 86.5 (br.s, 1C, CB of allene), 98.4 (br.s, 1C, CB_2), 128.3, 144.3 (each br.s, each 1C, *i*-C), 129.8, 135.6 (each d, each 1C, *p*-C), 131.9, 132.8, 136.7, 142.8 (each s, each 2C, *o*- and *m*-C), 213.7 (s, 1C, middle allene-C). ^{11}B NMR (96 MHz, $CDCl_3$, 25 °C): δ = 60.

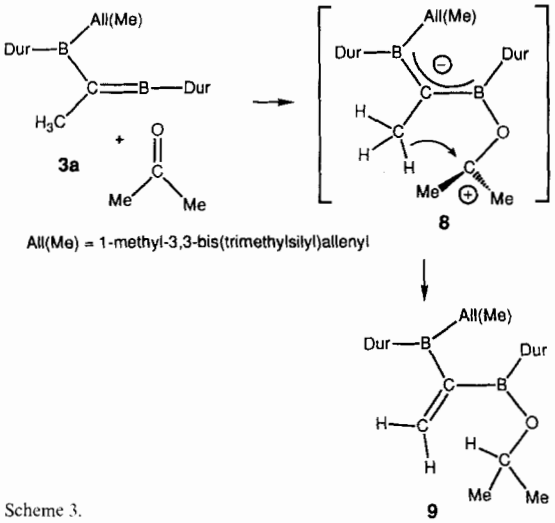
5a: white solid, m.p. 93 °C, yield: 55%. ^{1}H NMR (500 MHz, $CDCl_3$, −40 °C): δ = 0.25, 0.28 (each s, each 9H, $SiMe_3$), 0.72, 1.67 (each s, each 3H, CH_3), 1.98, 2.00, 2.11, 2.16, 2.25 (each s, 24H, *o*- and *m*-CH_3), 6.68, 6.83 (each s, each 1H, *p*-H); ^{13}C NMR (125 MHz, $CDCl_3$, −40 °C): δ = 1.0, 1.3 (each q, each 3C, $SiMe_3$), 2.2 (br.q, 1C, CH_3(B)), 16.1 (q, 1C, CH_3(C)), 17.2, 20.2, 20.3, 20.6, 21.2, 21.3 (each q, 8C, *o*- and *m*-CH_3), 63.6 (s, 1C, CSi_2), 71.9 (s, 1C, CB of allene), 126.4, 129.9 (each d, each 1C, *p*-C), 128.7, 132.4, 132.9, 134.2, 136.7 (each s, 8C, *o*- and *m*-C), 139.0 (br.s, 1C, *i*-C(B)), 142.9 (s, 1C, *i*-C(C)), 166.4 (br.s, 1C, CB_2), 214.1 (s, 1C, middle allene-C); ^{11}B NMR (96 MHz, $CDCl_3$, 25 °C): δ = 27.

5b: white solid, m.p. 95 °C, yield: 50%. ^{1}H NMR (500 MHz, $CDCl_3$, −40 °C): δ = 0.21, 0.29 (each s, each 9H, $SiMe_3$), 0.99, 1.06 (each t, each 3H, CH_3(Et)), 1.11–1.16, 1.21–1.24 (each m, each 1H, CH_2(Et)), 1.81–1.85, ca. 2.10 (each m, each 1H, CH_2(Et)), 1.96, 2.03, 2.07, 2.14, 2.17, 2.21 (each s, 24H, *o*- and *m*-CH_3), 6.65, 6.08 (each s, each 1H, each *p*-H); ^{13}C NMR (125 MHz, $CDCl_3$, −40 °C): δ = 0.9, 1.0 (each q, each 3C, $SiMe_3$), 10.8 (q, 1C, CH_3(Et)), 11.9 (br.t, 1C, CH_2(B)), 13.2 (q, 1C, CH_3(Et)), 17.2, 20.1, 20.5, 21.1, 21.2 (each q, 8C, *o*- and *m*-CH_3), 21.6 (t, 1C, CH_2(C)), 66.2 (s, 1C, CSi_2), 77.6 (s, 1C, CB of allene), 125.9, 129.7 (each d, each 1C, *p*-C), 128.4, 131.9, 132.7, 133.9, 136.6 (each s, 8C, *o*- and *m*-C), 139.7 (br.s, 1C, *i*-C(B)), 142.8 (s, 1C, *i*-C(C)), 164.3 (br. s, 1C, CB_2), 212.8 (s, 1C, middle allene-C); ^{11}B NMR (96 MHz, $CDCl_3$, 25 °C): δ = 28.

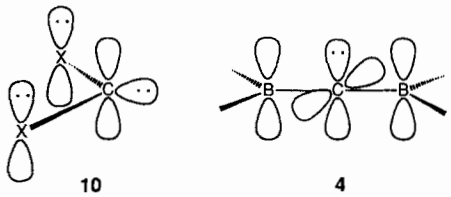
5c: Oil, after crystallization the product contains decomposition products, yield: quantitative by NMR spectroscopy. ^{1}H NMR (500 MHz, $CDCl_3$, −40 °C): δ = −0.07 (s, 18H, $SiMe_3$), 0.62, 0.69 (each s, each 9H, $C(CH_3)_3$), 0.28, 1.61 (each s, each 2H, CH_2), 1.99, 2.20, 2.22, 2.43 (each s, each 6H, *o*- and *m*-CH_3), 6.70, 6.05 (each s, each 1H, *p*-H); ^{13}C NMR (125 MHz, $CDCl_3$, −40 °C): δ = 0.7 (q, 6C, $SiMe_3$), 18.4, 20.1, 20.6, 21.2, (each q, 8C, *o*- and *m*-CH_3), 29.4, 30.7 (each q, each 3C, $C(CH_3)_3$), 31.2, 32.4 (each s, each 1C, $C(CH_3)_3$), 40.8 (br.t, 1C, CH_2(B), 41.8 (t, 1C, CH_2), 79.9 (s, 1C, CSi_2), 85.8 (br. s, 1C, CB of allen), 123.9 (br. s, 1C, *i*-C(B)), 126.0, 137.5 (each d, each 1C, *p*-C), 128.6, 131.9, 133.6 (each s, 6C, *o*- and *m*-C), 141.2 (s, 1C, *i*-C(C)), 151.1 (s, 2C, *o*-C), 211.9 (s, 1C, middle allene-C), the signal of the carbon atom that is bound to both boron atoms could not be observed; ^{11}B NMR (96 MHz, $CDCl_3$, 25 °C): δ = 43.

7b: yellow solid, yield: quantitative by NMR spectroscopy. ^{13}C NMR (100 MHz, $CDCl_3$, −30 °C): δ = 2.7, 3.6 (each q, each 3C, $SiMe_3$), 12.3, 14.2 (each q, each 1C, CH_3(Et)), 19.3, 20.0, 21.1, 22.5 (each q, 8C, *o*- and *m*-CH_3), 20.4, 20.7 (each t, each 1C, CH_2(Et)), 24.8 (s, 1C, CSi_2), 47.9 (br.s, 1C, CB_2), 130.2, 133.4 (each d, each 1C, *p*-C), 132.5, 132.6, 132.7, 135.4, 136.5, 139.5 (each s, 6C, *o*- and *m*-C), 144.5 (br.s, 2C, *o*-C at the three-membered ring), 149.5 (br.s, 1C, *i*-C), 162.7 (s, 1C, =C), 166.2 (br.s, 1C, =CB).

9: pale pink solid, m.p. 106 °C, yield: 59%. ^{1}H NMR (300 MHz, $CDCl_3$, 25 °C): δ = 0.23 (s, 18H, $SiMe_3$), 1.17 (d, 6H, CH_3-*i*Pr), 1.91 (s, 3H, CH_3), 2.16, 2.30 (each s, total 24H, *o*- and *m*-CH_3), 4.14 (m, 1H, C-H-*i*Pr), 5.99, 6.29 (each d, ^2J(H,H) = 5.8 Hz, each 1H, =CH_2), 6.91, 6.97 (each s, each 1H, *p*-H); ^{13}C NMR (75 MHz, $CDCl_3$, 25 °C): δ = 0.5 (q, 6C, $SiMe_3$), 16.4 (q, 1C, CH_3), 19.4 (q, 2C, CH_3-*i*Pr), 20.0, 24.1 (each q, 8C, *o*- and *m*-CH_3), 70.1 (d, ^1J(C,H) = 143 Hz, 1C, C-H-*i*Pr), 77.7 (s, 1C, CSi_2), 87.9 (br. s, 1C, CB of allene), 129.5, 130.6 (each d, each 1C, *p*-C), 132.1, 132.2, 132.7, 134.1 (each s, 8C, *o*- and *m*-C), 140.3, 147.6 (each br. s, each 1C, *i*-C), 143.7 (t, ^1J(C,H) = 154 Hz, =CH_2), 159.6 (br. s, 1C, =CB), 215.2 (s, 1C, middle allene-C); ^{11}B NMR (96 MHz, $CDCl_3$, 25 °C): δ = 49, 70.



Scheme 3.



Scheme 4.

firmed by calculations: the barriers for rearrangement of H_2B-$\dot{C}$-BH_2 and **4d** are 0.4[10] and > 0.1 kcal mol^{-1}, respectively.

The energy difference between **3d** and **4d** shows that diborylcarbenes **4** are not as high in energy as one may expect, given the three neighboring electron-deficient centers. In contrast to familiar carbenes **10**[11] with π-donor/σ-acceptor substituents (Goddard et al.[12]) diborylcarbenes **4** have π-acceptor/σ-donor substituents (Scheme 4). Following Bent's rule,[13] the σ-acceptor substituents in **10** form a small angle with the carbene-carbon atom, and the lone pair is localized in a low-energy σ orbital with high s character.

The σ-donor substituents in **4** lead to high s character in the bonds to the boron atoms. The lone pair at the carbene-carbon atom in the p orbital parallel to the p orbitals at the boron atoms is stabilized by π delocalization. This is reflected in the short (143.9 pm) B–C(B) bonds of **4d**. The empty p orbital at the carbene-carbon atom lying in the plane of the molecule strongly

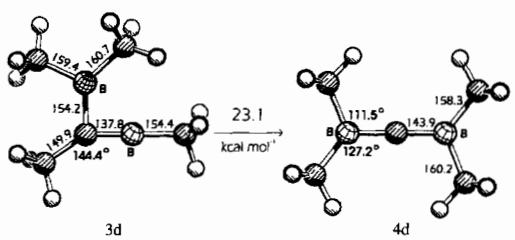


Fig. 1. Calculated geometries (distances in pm) and energy difference of **3d** and **4d**.

interacts with only one of the two B–CH_3 σ bonds of each of the two dimethylboryl substituents. This is reflected in small and large C-B-CH_3 angles (111.5° and 127.2°) and the elongated B–CH_3 distances (160.2 pm)[14] of the bonds which belong to the small angles. Preference for one of two equivalent σ bonds is characteristic[1b] of electron-deficient centers that interact strongly with neighboring σ bonds.

Figure 2 shows the X-ray crystal structures[15] of **3c** and **5b**. The structure of **5a** corresponds to that of **5b**, be-

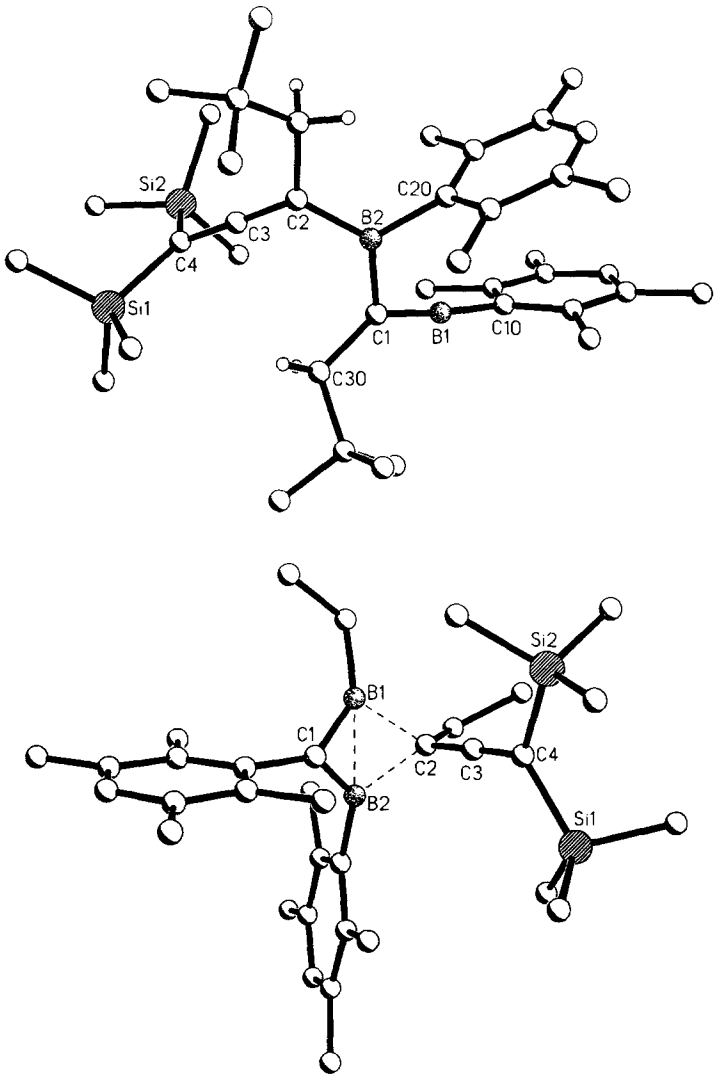
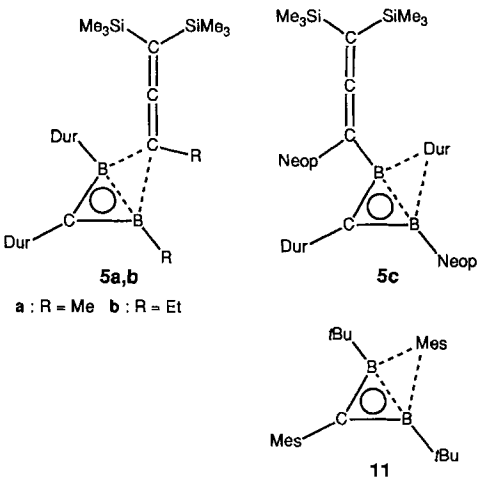


Fig. 2. Crystal structures of **3c** (top) and **5b** (bottom). Selected distances [pm] and angles [°]: **3c**: B1-C1 139.1(3), C1-B2 152.9(3), B2-C2 157.3(3), C2-C3 131.7(3), C3-C4 130.9(3); B1-C1-B2 104.3(2), B1-C1-C30 128.0(2), C30-C1-B2 127.3(2); B1-C1-B2-C2 156.3(2); **5b**: B1-C1 145.0(3), C1-B2 146.1(3), B2-C2 167.5(3), C2-B1 173.1(3), B1-B2 185.1(3), C2-C3 134.5(3), C3-C4 127.3(3); B1-C1-B2 79.0(2), B1-C2-B2 65.8(1), C1-B1-B2-C2, -148.5(2).

cause the chemical shifts of the skeleton atoms of **5a** and **5b** are similar ($\delta^{11}B = 27$ and 28, respectively; $\delta^{13}C = 166.4$ and 164.3, respectively). In contrast to the α-agostically distorted boryl-methyleneborane **3c** (with a B-C-B angle of 104.3°, cf. 91.0° in **3d**), **5a** and **5b** are bridged β-agostically[1b] by allenyl groups (Scheme 5).

The NMR data of the isomerization product of **3c** indicate the presence of the duryl-bridged structure **5c**:



Scheme 5.

the ^{11}B NMR signal at $\delta = 43$ corresponds to that ($\delta = 42$) in mesityl-bridged **11**.[16]

Received: February 6, 1995 [Z7696IE]
German version: *Angew. Chem.* **1995**, *107*, 1476–1479

Keywords: ab initio calculations · boron compounds · carbenes · electron-deficient compounds · rearrangements

[1] a) H. Klusik, A. Berndt, *Angew. Chem.* **1983**, *95*, 895–896; *Angew. Chem. Int. Ed. Engl.* **1983**, *22*, 877–878; b) A. Berndt, *ibid.* **1993**, *105*, 1034–1058 and **1993**, *32*, 985–1009, and references cited therein.

[2] P. H. M. Budzelaar, P. von R. Schleyer, K. Krogh-Jespersen, *Angew. Chem.* **1984**, *96*, 809–810; *Angew. Chem. Int. Ed. Engl.* **1984**, *23*, 825; P. H. M. Budzelaar, K. Krogh-Jespersen, T. Clark, P. von R. Schleyer, *J. Am. Chem. Soc.* **1985**, *107*, 2773–2779.

[3] D. Steiner, H.-J. Winkler, S. Wocadlo, S. Fau, W. Massa, G. Frenking, A. Berndt, *Angew. Chem.* **1994**, *106*, 2172–2175, *Angew. Chem. Int. Ed. Engl.* **1994**, *33*, 2064–2067.

[4] C. Balzereit, C. Kybart, H.-J. Winkler, W. Massa, A. Berndt, *Angew. Chem.* **1994**, *106*, 1579–1581, *Angew. Chem. Int. Ed. Engl.* **1994**, *33*, 1487–1489.

[5] M. Menzel, C. Wieczorek, S. Mehle, J. Allwohn, H.-J. Winkler, M. Unverzagt, M. Hofmann, P. von R. Schleyer, S. Berger, W. Massa, A. Berndt, *Angew. Chem.* **1995**, *107*, 728–731; *Angew. Chem. Int. Ed. Engl.* **1995**, *34*, 657–660.

[6] The product of the trapping reaction of **3a** with 2-butyne and the subsequent reaction will be described elsewhere together with related reactions.

[7] The calculations have been carried out using GAUSSIAN 92 [8]. The geometries are fully optimized at the MP2/6-31G* level. The structures have been characterized as minima or transition states by calculation of the harmonic frequencies. The zero point energy (ZPE) corrections have been scaled by a factor of 0.90. The relative energies include the scaled ZPEs.

[8] GAUSSIAN 92, Revision A, M. J. Frisch, G. W. Trucks, M. Head-Gordon, P. M. W. Gill, M. W. Wong, J. B. Foresman, H. B. Schlegel, K. Raghavachari, M. A. Robb, J. S. Binkley, C. Gonzalez, R. Martin, D. J. Fox, D. J. DeFrees, J. Baker, J. J. P. Stewart, J. A. Pople, Gaussian Inc., Pittsburgh, PA, **1992**.

[9] The (orthogonal) triplet state of **4d** is a minimum on the potential energy hypersurface; it lies 16.6 kcal mol^{-1} higher in energy than the (planar) singlet state (MP2/6-31G* + 0.90 × ZPE).

[10] S. Fau, G. Frenking, *THEOCHEM*. **1995**, in press.

[11] A. J. Arduengo III, H. V. R. Dias, R. L. Harlow, M. Kline, *J. Am. Chem. Soc.* **1992**, *114*, 5530–5534, and references cited therein.

[12] K. K. Irikura, W. A. Goddard III, J. L. Beauchamp, *J. Am. Chem. Soc.* **1992**, *114*, 48–51.

[13] H. A. Bent, *Chem. Rev.* **1961**, *61*, 275–313.

[14] In **2** the corresponding interaction of the formally empty orbital at the carbene center, with the strained B–CH_2 σ bonds, leads to their elongation to 168.8 pm [2]. This stronger interaction explains—at least partially—the smaller energy difference between **2** and **1** (10–12 kcal mol^{-1}) compared to that between **4** and **3** (21–23 kcal mol^{-1}).

[15] Crystal structure determinations: yellow crystals of **3c** and colorless crystals of **5b** have been studied on a four-circle diffractometer (CAD4, Enraf-Nonius) at −60 °C (**3c**) and −80 °C (**5b**) with $Cu_{K\alpha}$ radiation ($\lambda = 154.178$ pm). **3c**: $C_{40}H_{66}B_2Si_2$, crystal dimensions 0.6 × 0.5 × 0.5 mm^3, monoclinic, space group

$P2_1/n$, $Z = 4$, $a = 1712.0(3)$, $b = 1520.2(3)$, $c = 1776.3(4)$ pm, $\beta = 115.22(3)°$, $V = 4182 \times 10^{-30}$ m^3, $\rho_{calcd} = 0.992$ g cm^{-3}; in the range to $2\theta = 110°$ 5463 reflections have been measured by ω scans; 5244 of the 5251 independent reflections were used after LP corrections; no absorption correction ($\mu = 9.2$ cm^{-1}). The structure was solved by using direct methods and refined against the F_o^2 data using the full matrix. Some H atoms could be localized by difference Fourier synthesis, the others were calculated; they were included riding on their bond partners with groupwise commonly refined temperature factors. For all other atoms anisotropic temperature factors were used. This gave $wR_2 = 0.160$, corresponding to $R = 0.058$ for 4679 reflections with $I > 2\sigma(I)$; the residual electron density was max. 0.32 e Å^{-1}. **5b**: $C_{34}H_{54}B_2Si_2$, crystal dimensions $0.5 \times 0.5 \times 0.3$ mm^3, triclinic, space group $P\bar{1}$, $Z = 2$, $a = 931.1(2)$, $b = 1285.5(3)$, $c = 1636.4(3)$ pm, $\alpha = 70.37(3)$, $\beta = 89.26(3)$, $\gamma = 71.71(3)$, $V = 1742.2 \times 10^{-30}$ m^3, $\rho_{calcd} = 1.030$ g cm^{-3}; in the range to $2\theta = 149°$ 7454 reflections have been measured by $\omega/2\theta$ scans; 7112 of the 7123 independent reflections were used after LP corrections; no absorption correction ($\mu = 10.4$ cm^{-1}). Treatment analogous to **3c** gave $wR_2 = 0.2375$, corresponding to $R = 0.071$ for 5686 reflections with $I > 2\sigma(I)$; the residual electrou density was max. 0.58 e Å^{-1}. Further details of the crystal structure investigations can be obtained from the Fachinformationszentrum Karlsruhe, D-76344 Eggenstein-Leopoldshafen (Germany), on quoting the depository number CSD-58927.

[16] M. Pilz, J. Allwohn, W. Massa, A. Berndt, *Angew. Chem.* **1990**, *102*, 436–438; *Angew. Chem. Int. Ed. Engl.* **1990**, *29*, 399–401.

Ring Expansion of the Fullerene Core by Highly Regioselective Formation of Diazafulleroids**

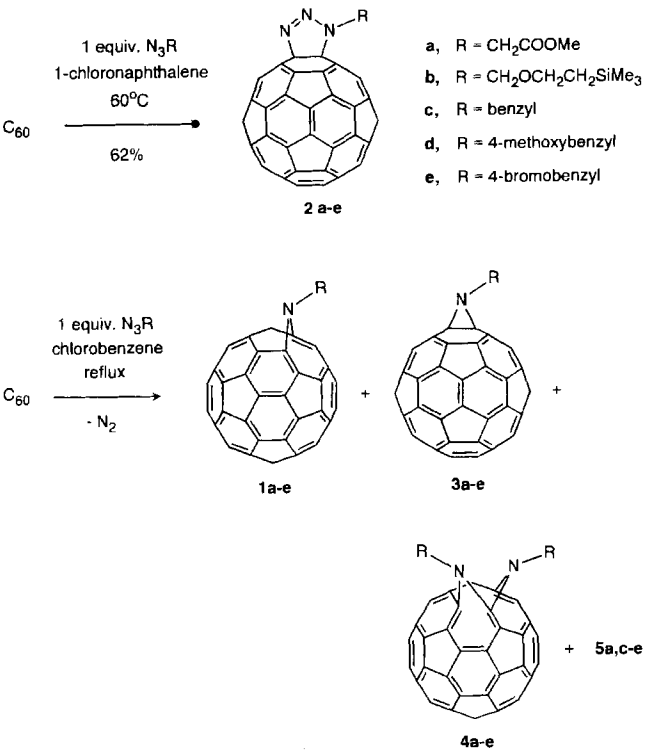
Thomas Grösser, Maurizio Prato,* Vittorio Lucchini,* Andreas Hirsch,* and Fred Wudl*

Investigations on the regioselectivity of multiple additions to C_{60} are currently at the forefront of organic fullerene chemistry.[1] The first step in cycloadditions is always the attack of a double bond common to two six-membered rings (6-6 bonds) of the fullerene framework.[2] Multiple additions to 6-6 bonds show some degree of regioselectivity.[1] Subsequent additions to *e*-positions (octahedral sites), for example, allow the synthesis of highly symmetric hexaadducts.[1d–f] Addition of diazo compounds or azides[4] to C_{60} followed by extrusion of N_2 of the initially formed 6-6-bridged pyrazolines or triazolines leads also to ring-opened 5-6 adducts (fulleroids). In fulleroids $C_{61}R_2$ and $C_{60}NR$ the π-electron system of C_{60} remains intact and the fullerene core contains a bridged nine-membered ring.[3, 4] The expansion or opening of a ring in the C_{60} framework could be a key step for the systematic synthesis of endohedral C_{60} compounds. In this paper we report for the first time on the regiochemistry of additions to fulleroids. We show that diazafulleroids with a further ring expansion (three seven-membered and one eleven-membered ring in the fullerene core) are formed in an extraordinary regioselective pathway. In addition, intermediate triazoline adducts leading to azafulleroids have been isolated.

[*] Prof. Dr. A. Hirsch, T. Grösser
Institut für Organische Chemie
Richard-Willstätter-Allee 2, D-76131 Karlsruhe (Germany)
Telefax: Int. code + (721) 698-305
Prof. Dr. M. Prato
Dipartimento di Scienze Farmaceutiche, Trieste (Italy)
Prof. Dr. V. Lucchini
Dipartimento di Scienze Ambientali, Venezia (Italy)
Prof. Dr. F. Wudl
Institute for Polymers and Organic Solids, Santa Barbara (USA)

[**] This work was supported by the Deutsche Forschungsgemeinschaft (DFG), the Bundesministerium für Forschung und Technologie (BMFT), and Hoechst AG. M. P. thanks the Consiglio Nazionale delle Richerche for a travel grant. F. W. wishes to thank National Science Foundation for support (grant DMR91-22536).

We had first synthesized azafulleroids by allowing C_{60} to react with an equimolar amount of azide in chlorobenzene at reflux.[4] As major products we obtained the azafulleroids **1** together with more polar compounds, which were not further characterized. The intermediate triazolines **2** cannot be obtained by this procedure since they readily lose N_2 at elevated temperatures. We have now found that treatment of a concentrated solution of C_{60} in 1-chloronaphthalene with an equimolar amount of methyl azidoacetate at 60 °C yields triazoline **2a** in 62% yield (Table 1). When **2a** is heated in *o*-dichlorobenzene at 100 °C, **1a** is obtained as the major product (24%) together with C_{60} (22%), compound **3a** with an intact 6-6 bond (4%), and bisadduct **4a** (13%). In **4a** two neighboring, open 5-6 bonds are imino bridged. Besides **4a** we obtained only a small amount of another bisadduct **5a**, whose exact structure is not yet known. Bisadducts **4** and **5** are also accessible by the direct synthesis of azafulleroids from C_{60}; these compounds are the more polar side products, which we mentioned earlier.[4] The black microcrystalline compounds **1**–**4** were isolated by flash chromatography. Both **4a** and **5a** are stable in *o*-dichlorobenzene at 100 °C.



The addition of azide to C_{60} seems to be general, as analogous compounds were formed when other azides, for instance substituted benzyl azides RN_3 (R = benzyl, 4-methoxybenzyl, 4-bromobenzyl), were used. The addition of trimethylsilylethoxy methyl azide ($SEMN_3$) to C_{60} is a special case: **4b** is the exclusive bisaddition product. When a dilute solution of C_{60} and excess $SEMN_3$ in chlorobenzene was heated to reflux for approximately 12 h, **4b** formed as the main product (60% based on reacted C_{60}) along with **2b** (30%) and **3b** (10%). The presence of exclusively these three compounds was proved by the ^{1}H NMR spectrum of the crude mixture and by chromatographic separation of the three adducts in the same ratios.

Table 1. Selected spectroscopic data of the new compounds **1a**, **2a**, **3a**, **4a,b**, and **6a**.

1a: ^{1}H NMR (CS_2/C_6D_6 4/1, 250 MHz): δ = 4.43 (s, 2H), 3.72 (s, 3H); ^{13}C NMR (CS_2/C_6D_6 4/1, 62.9 MHz): δ = 167.89, 147.96, 145.47, 145.33, 144.99, 144.94, 144.78, 144.60, 144.46, 144.35, 144.18, 143.90, 143.72, 143.51, 143.41, 143.35, 143.20, 143.12, 142.89, 141.63, 141.10, 140.81, 139.60, 138.83, 138.49, 138.13, 137.30, 137.14, 136.45, 135.57, 133.98, 52.73 (CH_2), 52.04 (CH_3); UV/Vis (Et_2O): λ_{max} [nm] = 532 (br), 432 (sh), 332, 260, 218; FD-MS: *m/z*: 807 (M^+).

2a: ^{1}H NMR (CS_2/C_6D_6 4/1, 250 MHz): δ = 4.99 (s, 2H), 3.62 (s, 3H); ^{13}C NMR (CS_2/C_6D_6 4/1, 62.9 MHz): δ = 168.23, 147.79, 147.59, 146.43, 146.40, 146.25, 146.21, 146.09, 145.96, 145.63, 145.34, 144.82, 144.64, 144.52, 144.11, 143.32, 143.19, 143.05, 142.88, 142.80, 142.73, 142.37, 142.28, 142.26, 142.10, 140.98, 140.90, 140.34, 137.03, 136.45, 80.67, 52.30 (CH_2), 48.55 (CH_3); UV/Vis (cyclohexane): λ_{max} [nm] = 687, 677, 461, 425, 315, 255, 211; FAB-MS (3-nitrobenzyl alcohol (NBA)): *m/z*: 836 (M^+ + H).

3a: ^{1}H NMR (CS_2/C_6D_6 4/1, 250 MHz): δ = 4.31 (s, 2H), 3.78 (s, 3H); ^{13}C NMR (CS_2/C_6D_6 4/1, 100.6 MHz): δ = 167.85, 145.44, 145.38, 145.00, 144.84, 144.78, 144.04, 143.43, 143.32, 143.07, 142.50, 142.37, 141.11, 83.94, 52.12 (CH_2), 51.22 (CH_3); UV/Vis (Et_2O): λ_{max} [nm] = 483, 422, 410, 323, 256; FD-MS: *m/z*: 807 (M^+).

4a: ^{1}H NMR (CS_2/C_6D_6 4/1, 250 MHz): δ = 5.20 (AB-q, *J* = 17 Hz, 1H), 4.32 (AB-q, *J* = 17 Hz, 1H), 3.69 (s, 3H); ^{13}C NMR (CS_2/C_6D_6 4/1, 62.9 MHz): δ = 169.81, 161.00, 147.83, 147.20, 145.82, 145.59, 145.29, 145.25, 144.95, 144.92, 144.58, 144.51, 144.39, 144.30, 144.11, 143.85, 143.70, 142.85, 142.60, 142.02, 141.89, 140.04, 139.93, 139.33, 137.60, 135.61, 134.93, 132.71, 132.53, 131.35, 52.30 (CH_2), 51.83 (CH_3); UV/Vis (cyclohexane): λ_{max} [nm] = 702 (br), 538 (br), 456 (sh), 435 (sh), 327, 259, 212; FD-MS: *m/z*: 894 (M^+).

4b: ^{1}H NMR ($CDCl_3$, 600 MHz): δ = 5.56 (AB-q, 1H, *J* = 9.4 Hz), 5.41 (AB-q, 1H, *J* = 9.4 Hz), 4.14 (td, 1H, *J* = 9.5, 7.1), 3.98 (td, 1H, *J* = 9.5, 7.1), 1.67 (m, 2H), 0.15 (s, 9H); ^{13}C NMR (125 MHz, $CDCl_3$): δ = 160.19 (1C), 147.45 (2C), 147.09 (2C), 145.54 (1C), 145.36 (2C), 144.96 (2C), 144.86 (2C), 144.62 (2C), 144.59 (2C), 144.21 (6C), 144.10 (1C), 144.00 (2C), 143.77 (2C), 143.59 (2C), 143.45 (2C), 142.83 (2C), 142.33 (2C), 141.81 (2C), 141.74 (2C), 140.28 (2C), 139.59 (2C), 139.42 (2C), 139.15 (2C), 138.71 (2C), 136.74 (2C), 135.36 (2C), 134.66 (2C), 132.12 (2C), 132.93 (1C), 130.54 (2C), 82.89 (NCH_2O), 66.56 (OCH_2), 18.21 (CH_2Si), −1.24 ($Si(CH_3)_3$); UV/Vis (CH_2Cl_2): λ_{max} [nm] = 545, 430, 331, 261; FAB-MS: *m/z*: 1011 (M^+).

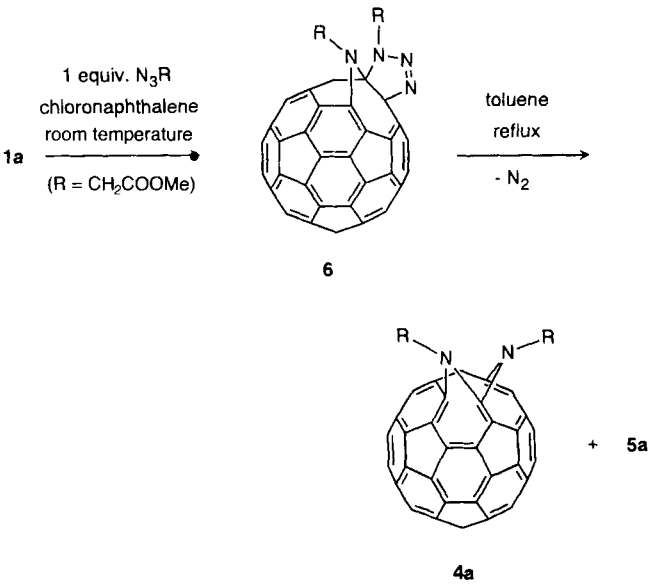
6a: ^{1}H NMR (CS_2/C_6D_6 4/1, 250 MHz): δ = 5.19 (AB-q, *J* = 17 Hz, 1H), 5.08 (AB-q, *J* = 17.4 Hz, 1H), 4.88 (AB-q, *J* = 17.4 Hz, 1H), 4.53 (AB-q, *J* = 17 Hz, 1H), 3.77 (s, 3H), 3.71 (s, 3H); UV/Vis (cyclohexane): λ_{max} [nm] = 694, 558 (sh), 497 (sh), 320, 253, 214; FAB-MS (NBA): *m/z*: 924 (M^+ + 2H).

Bisadduct **4b** is not stable in refluxing chlorobenzene. Heating **4b** for about 12 h resulted in quantitative conversion to a 7:1 mixture of **1b** and **3b**.

The unique structure of **4** was established by means of ^{1}H, ^{13}C, ^{15}N, and HMQC NMR techniques (Fig. 1, Table 1). The ^{1}H and ^{13}C spectra of bisadducts **4** exhibit some striking features: 1) The signal pattern is highly symmetrical; the two R groups are magnetically equivalent and the methylene hydrogens α to nitrogen are diasterotopic and give rise to well-resolved AB quartets. 2) In the ^{13}C spectra only 32 signals are observed for the fullerene core; the integrations of 28 signals (2C each) are twice that of the other four (1C each). This suggests C_s symmetry for compounds **4**, with the mirror plane crossing the four carbon atoms of two 6-6 junctions. 3) The presence of a ^{13}C signal at δ = 160 (1C) is common to all compounds **4**. The correct assignment of this peak and the definitive structural determination is based on the analysis of the multiplets at about δ = 160 in [^{15}N]**4b**, which was obtained from $SEMN_3$ labeled with ^{15}N (50%) at each terminal nitrogen atom; three isotopomers resulted with no, one, and two ^{15}N atoms. Three signals can be detected for these compounds: a singlet at δ = 160.19, a doublet at δ = 160.17 (J_{CN} = 6.9 Hz), and a triplet at δ = 160.14 (J_{CN} = 6.9 Hz) in an approximate 1:2:1 ratio. The signals can be assigned readily to the carbon atom bonded directly to both nitrogen atoms in [^{15}N]**4b**, which is labeled with none, one, amd two ^{15}N atoms, respectively, in statistical isotopomeric ratios. This assignment, which also explains the strong downfield shift of these peaks, is further substantiated by the coupling of this C atom with the α-methylene protons over three bonds (by multiple HMQC spectroscopy). In [^{15}N]**4b** the signal at δ = 138.71 (2C) is split into a singlet at δ = 138.71 and a doublet at δ = 138.69 (J_{CN} = 7.3 Hz) in a 1:1 ratio; these signals are assigned to the equivalent C_{60} carbon atoms bound to a single nitrogen atom. In compounds **4** the R groups are equivalent, but the α-methylene protons are diastereotopic. The two imino bridges are on adjacent 5-6 junctions and the nitrogen atoms would remain chiral, even if rapid pyramidal inversion would take place.

The ^{1}H NMR spectrum of **5** shows one quartet for the diastereotopic α-methylene protons, which indicates C_s symmetry. A possible structure could be the isomer in which two opened 5-6 bonds within the same six-membered are bridged by the imino groups. This is supported by the shift of the center of gravity of the methylene proton resonances by 0.7 ppm to lower field. In this structure, due to hindered inversion, the most favorable location of the R groups is above the five-membered rings, which leads to deshielding.[3d, e]

To obtain further information on the very regioselective formation of these bisadducts starting from **1**, we treated a concentrated solution of **1a** with methyl azidoacetate at room temperature. Under these conditions, in addition to a small amount of **4a** and **5a**, only one mixed triazoline/azafulleroid isomer **6** was



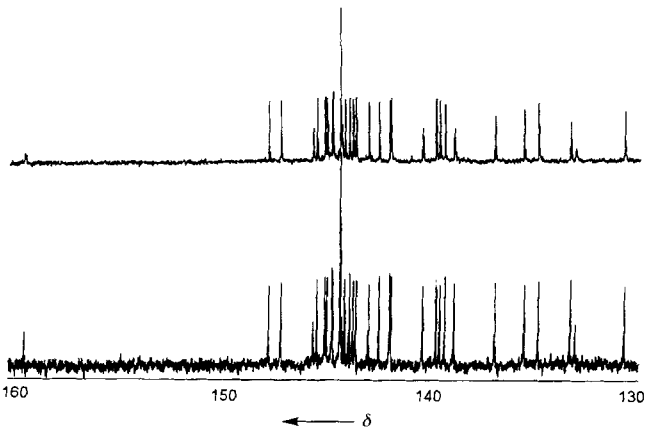


Fig. 1. ^{13}C NMR spectra (125 MHz, $CDCl_3$) of [^{15}N]**4b** (top) and **4b** (bottom).

 © VCH Verlagsgesellschaft mbH, D-69451 Weinheim, 1995 0570-0833/95/1212-1344 $ 10.00+.25/0

formed (HPLC, NMR), which was isolated by flash chromatography. The ^{1}H NMR spectrum for **6a** shows two quartets for two sets of diastereotopic methylene protons and two singlets for the methyl groups (Table 1). The exclusive formation of **6a** is explained by the fact that **1** behaves as a strained electron-poor enamine. The significantly highest positive Mulliken charge of 0.06 (AM1) is at C-1 and C-6, and the lowest of -0.07 at C-2 and C-5 (Fig. 2). Enhanced Mulliken charges are also located at C-8 (0.03) and C-10 (-0.02). All other carbon atoms of the fullerene core exhibit Mulliken charges of 0.00 ± 0.01. The most negatively polarized N atom of the azide (AM1) is that bearing R (Fig. 2). A kinetically controlled attack of the azide, therefore, leads predominantly to **6**. Already at room temperature **6** rearranges slowly to give **4a** and **5a** in a 6:1 ratio.

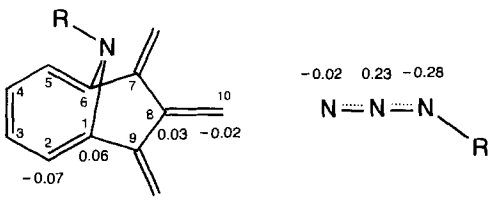


Fig. 2. Mulliken charges (AM1) near the imino bridge in **1a** and in N_3R ($R = CH_2COOMe$).

We are currently investigating the possibility of further ring expansions of fullerenes by the regioselective synthesis of tri- and tetraazafulleroids. Larger holes in the C_{60} framework could provide windows for the penetration of noble gases without the need for destructive reaction conditions at high temperatures.[5]

Experimental Procedure

2a: A solution of C_{60} (500 mg, 0.694 mmol) and methyl azidoacetate (80 mg, 0.695 mmol) in 1-chloronaphthalene (15 mL) was stirred overnight at 60 °C. The reaction mixture was then separated by flash chromatography (SiO_2, toluene) to give C_{60} (270 mg, 0.375 mmol), traces of **1a** and **3a**, and **2a** (165 mg, 0.198 mmol, 62% based on consumed C_{60}).

Thermolysis of **2a**: A solution of **2a** (200 mg, 0.239 mmol) in *o*-dichlorobenzene (15 mL) was stirred at 100 °C for 25 min. The reaction mixture was then separated by flash chromatography (SiO_2, toluene) to give C_{60} (38 mg, 22%), **1a** (53 mg, 24%), **3a** (8 mg, 4%), **4a** + **5a** (32 mg, 15%), and higher adducts (12 mg).

1a: A solution of C_{60} (516 mg, 0.7166 mmol) and 1.5 equiv of methyl azidoacetate (123.6 mg, 1.075 mmol) in 1-chloronaphthalene (15 mL) was stirred at 60 °C for ca. 12 h. The reaction mixture was then diluted with toluene to 400 mL and refluxed for 25 min. Separation by flash chromatography (SiO_2, toluene) yielded C_{60} (378.2 mg), **3a**, **1a** (92.2 mg, 59.7% based on consumed C_{60}), and **4a** + **5a**.

6a: A solution of **1a** (100 mg, 0.124 mmol) and methyl azidoacetate (14.5 mg, 0.126 mmol) in 1-chloronaphthalene (6 mL) was stirred for 3 d at room temperature. The reaction mixture was separated by flash chromatography (SiO_2, toluene) to give **1a** and traces of **4a** and **5a**. **6a** (17.2 mg, 15%) was then eluted with toluene/ethyl acetate (9:1).

Received: January 20, 1995 [Z 7648 IE]
German version: *Angew. Chem.* **1995**, *107*, 1462–1464

Keywords: azides · fullerenes · nitrogen compounds

[1] a) J. M. Hawkins, A. Meyer, T. A. Lewis, U. Bunz, R. Nunlist, G. E. Ball, T. W. Ebbesen, K. Tanigaki, *J. Am. Chem. Soc.* **1992**, *114*, 7954; b) A. Hirsch, I. Lamparth, H. R. Karfunkel, *Angew. Chem.* **1994**, *106*, 453; *Angew. Chem. Int. Ed. Engl.* **1994**, *33*, 437; c) C. C. Henderson, R. A. Assink, P. A. Cahill, *ibid.* **1994**, *106*, 803 and **1994**, *33*, 786; d) A. Hirsch, I. Lamparth, T. Grösser, H. R. Karfunkel, *J. Am. Chem. Soc.* **1994**, *116*, 9385; e) L. Isaacs, R. F. Haldimann, F. Diederich, *Angew. Chem.* **1994**, *106*, 2435; *Angew. Chem. Int. Ed. Engl.* **1994**, *33*, 2434; f) B. Kräutler, J. Maynollo, *ibid.* **1995**, *107*, 66 and **1995**, *34*, 87.

[2] A. Hirsch, *The Chemistry of the Fullerenes*, Thieme, Stuttgart, New York, **1994**.

[3] a) T. Suzuki, Q. Li, K. C. Khemani, F. Wudl, Ö. Almarsson, *Science* **1991**, *254*, 1186; b) F. Wudl, *Acc. Chem. Res.* **1992**, *25*, 157; c) T. Suzuki, Q. Li, K. C. Khemani, F. Wudl, *J. Am. Chem. Soc.* **1992**, *114*, 7301; d) M. Prato, V. Lucchini, M. Maggini, E. Stimpfl, G. Scorrano, M. Eiermann, T. Suzuki, F. Wudl, *ibid.* **1993**, *115*, 8479; e) F. Diederich, L. Isaacs, D. Philip, *Chem. Soc. Rev.* **1994**, 243.

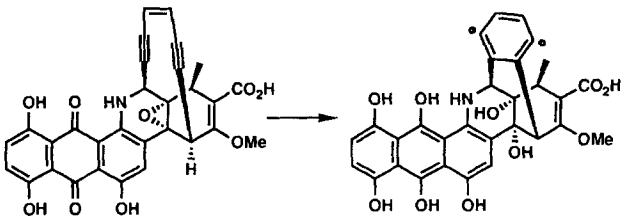
[4] M. Prato, Q. Li, F. Wudl, V. Lucchini, *J. Am. Chem. Soc.* **1993**, *115*, 1148.

[5] a) M. Saunders, H. A. Jimenez-Vazquez, R. J. Cross, S. Mroczkowski, D. I. Freedberg, F. A. L. Anet, *Science* **1994**, *367*, 256; b) M. Saunders, H. A. Jimenez-Vazquez, R. J. Cross, S. Mroczkowski, M. L. Gross, D. E. Giblin, R. J. Poreda, *J. Am. Chem. Soc.* **1994**, *116*, 2193.

Synthesis of a Dynemicin A Analogue and Its Bergman-Type Cycloaromatization**

Takashi Takahashi,* Yasuharu Sakamoto, Haruo Yamada, Shuji Usui, and Yoshimasa Fukazawa

Dynemicin A (**1**) is a potent antibacterial and anticancer agent of the enediyne class[1] isolated from the fermentation broth of *Micromonospora chersina*.[2] The biological activity of **1** is attributed to its ability to undergo cycloaromatization to give the highly reactive benzenoid diradical **2**, which initiates



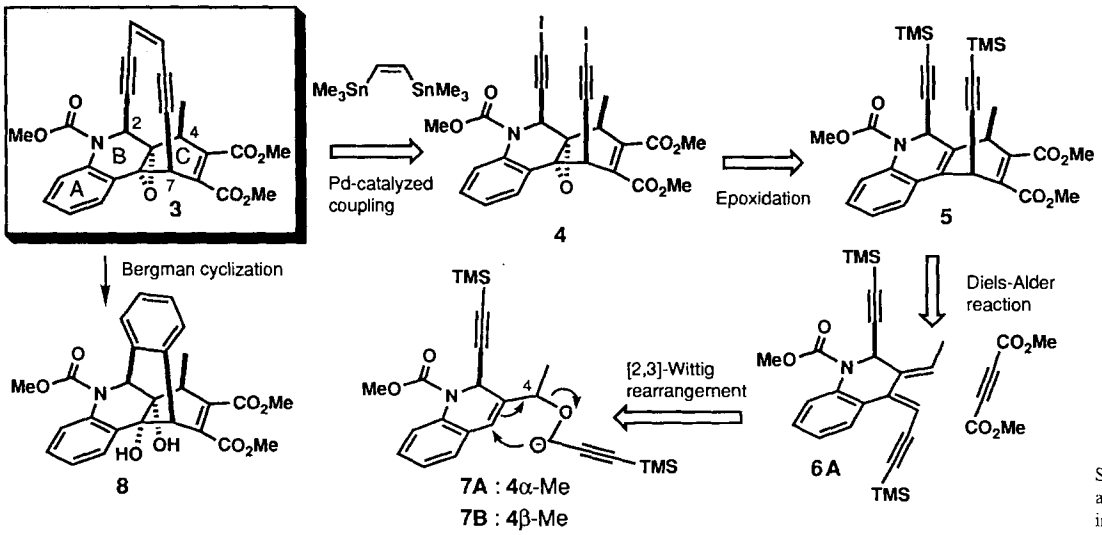
1 **2**

DNA cleavage through hydrogen abstraction from the deoxyribose backbone of DNA.[3a] It is presumed[3b–g] that the cycloaromatization of dynemicin A is induced by bioreduction of its anthraquinone moiety, opening of the epoxide, and Bergman cyclization. Its unique molecular structure and potent antitumor activity have stimulated extensive research on both the mechanism of action[4] and synthesis of model systems[5, 6] to mimic the action of dynemicin A. In this communication, we report the synthesis of dynemicin A model **3** and its Bergman-type cycloaromatization giving **8**.

Our retrosynthetic analysis is summarized in Scheme 1.[7] One key reaction is the palladium-catalyzed coupling reaction of bis(iodoalkyne) **4** with (*Z*)-bis(trimethylstannyl)ethylene,[6] which provides the highly strained enediyne unit in **3** directly. A second key reaction is the Diels–Alder reaction of diene **6A** with

[*] Prof. Dr. T. Takahashi, Y. Sakamoto, Dr. H. Yamada
Department of Chemical Engineering, Tokyo Institute of Technology
Ookayama, Meguro, Tokyo 152 (Japan)
Telefax: Int. code + (3) 5734-2884
Prof. Dr. S. Usui,[+] Prof. Dr. Y. Fukazawa[+]
Department of Chemistry, Hiroshima University
Higashi-Hiroshima, Hiroshima 724 (Japan)
[+] X-ray crystallographic analysis.

[**] This work was supported by Grants-in-Aid for Scientific Reseach on Priority Areas (nos. 05234102 and 06240104) from the Ministry of Education, Science and Culture, Japan.



Scheme 1. Retrosynthesis of **3** and its Bergman cyclization giving **8**. TMS = trimethylsilyl.

dimethyl acetylenedicarboxylate. In this way, we are able to introduce the required all-*cis* relative configuration for the diethynyl side chains at C(2), C(7) (dynemicin numbering) and the C(4) methyl group in **5**. Simultaneously, the 1,4-hexadiene moiety is formed, in which the [3(8)] double bond can be used to introduce the α-epoxy function that serves as the "trigger". The (*Z*,*Z*) diene system in **6A** is constructed by the [2,3]-Wittig rearrangement[8] of allyl ether **7** and subsequent β-elimination of the resulting propargyl hydroxyl group. By this route the 10-membered ring enediyne system including the epoxide "trigger" can be prepared in four steps from the (*Z*,*Z*) diene **6A**.

The diaxial orientation of the diethynyl side chains at C(2) and C(7) in **4** is essential for the success of the palladium-catalyzed cyclization (**4** → **3**). Molecular modeling based on MM2 calculations has proved to be useful in the design of the key intermediates.[9] Thus, conformational analysis of bis(alkyne) **9**, a model of bis(iodoalkyne) **4**, was conducted by using the Monte Carlo conformational search[10] and the MM2* force field in MacroModel.[11] Sixteen unique lower energy conformations of **9** were found within 3.0 kcal mol^{-1} of the global minimum. Figure 1 shows the lowest energy conformations **9A** and **9B**, which have a diaxial and an axial–equatorial orientation of the diethynyl side chains, respectively. These calculations and a Boltzmann distribution based on the energy differences of the 16 conformations predict that the palladium-catalyzed coupling reaction of the bis(iodoalkyne) **4** should proceed through its diaxial conformation to give the double coupling product **3** preferentially.

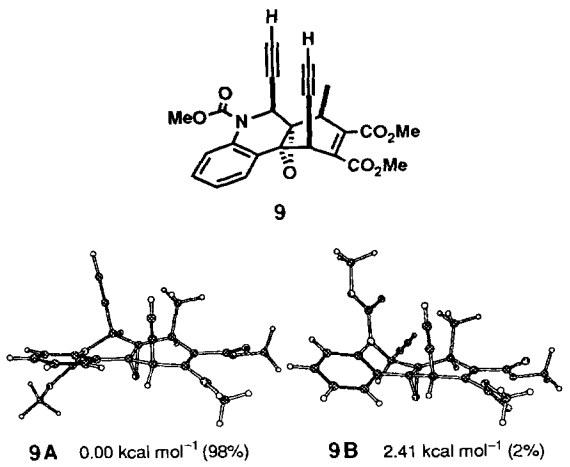
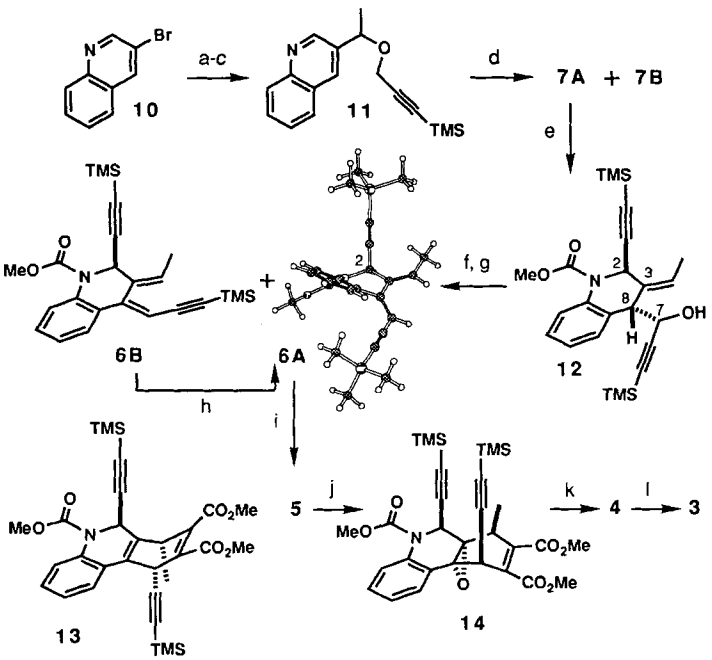


Fig. 1. Results of the conformational analysis of **9** based on MM2* calculations.

Synthesis of the precursor of **4**, bis(trimethylsilylalkyne) **14**, was carried out as follows (Scheme 2): Addition of the lithium derivative of **10**[12] to acetaldehyde, O-alkylation of the resulting secondary alcohol with propargyl bromide, and protection of the terminal alkyne with trimethylsilyl chloride gave the propargyl ether **11** in 78% overall yield. Addition of methyl chloroformate[13] to a mixture of (trimethylsilyl)ethynylmag-



Scheme 2. Synthesis of enediyne **3** and the structure of diene **6A** based on MM2* calculations. a) *n*BuLi, Et_2O, −78 °C, then acetaldehyde, 92%; b) NaH, THF, 0 °C, then propargyl bromide, hexamethylphosphoric triamide, 25 °C, 91%; c) EtMgBr, THF, 0 °C, then trimethylsilyl chloride, 93%; d) (trimethylsilyl)-ethynylmagnesium bromide, THF, −78 °C, then $ClCO_2Me$, −78 °C, then −15 °C, 91%; e) *t*BuLi, THF, −78 °C, 73%; f) mesyl chloride, Et_3N, CH_2Cl_2, 0 °C; g) diazabicycloundecene, benzene, 25 °C, 65% from **12**; h) I_2, benzene, 25 °C, 98%; i) dimethyl acetylenedicarboxylate, toluene, 140 °C, 80%; j) *meta*-chloroperbenzoic acid, $NaHCO_3$, CH_2Cl_2, 25 °C, 88%; k) $AgNO_3$, *N*-iodosuccinimide, acetone, 25 °C, 81%; l) **4**, 10 mol% $[Pd(PPh_3)_4]$, DMF, 60 °C, addition of (*Z*)-bis(trimethylstannyl)ethene in DMF, 1.5 h, 67%.

 © VCH Verlagsgesellschaft mbH, D-69451 Weinheim, 1995 0570-0833/95/1212-1346 $ 10.00+.25/0

nesium bromide and **11** afforded a 78:22 mixture of ether **7A** having 4α-methyl group and its β-isomer **7B**. Ether **7A** was subjected to the [2,3]-Wittig rearrangement to give alcohol **12** as a single isomer. The configuration of the [3(4)] double bond (*Z*) and the *trans* configurational relationship between alkynyl groups at C(2) and C(8) in **12** were established by NMR spectra and nOe studies; however, we have not yet assigned the stereochemistry at C(7). Mesylation of alcohol **12** followed by treatment with DBU gave a 45:55 mixture[14] of the (*Z*,*Z*) diene **6A** and the (*Z*,*E*) diene **6B**, which was converted to the desired **6A** by treatment with I_2. The configurations of dienes **6A** and **6B** were confirmed by NMR spectra and nOe studies (Table 1). The

Table 1. Selected physical data for compound **3**, **4**, **6A**, and **8**.

3: IR (neat): $\tilde{\nu}$ = 2948, 1720, 1492, 1437, 1370, 1322, 1276, 758 cm^{-1}; ^1H NMR (270 MHz, $CDCl_3$): δ = 7.61 (br. d, J = 7.6 Hz, 1H), 7.31–7.48 (m, 1H), 7.34 (ddd, J = 7.9, 7.9, 1.3 Hz, 1H), 7.23 (ddd, J = 7.9, 7.6, 1.3 Hz, 1H), 5.74 (dd, J = 9.9, 1.7 Hz, 1H), 5.69 (br. s, 1H), 5.65 (dd, J = 9.9, 1.7 Hz, 1H), 4.67 (br. s, 1H), 3.833 (s, 3H), 3.827 (s, 3H), 3.78 (s, 3H), 3.57 (br. q, J = 7.4 Hz, 1H), 1.51 (d, J = 7.4 Hz, 3H); ^{13}C NMR (67.8 MHz, $CDCl_3$): δ = 168.0, 165.4, 155.1, 144.9, 136.0, 128.4, 127.8, 126.7, 125.3, 124.7, 124.3, 122.9, 99.8, 94.4, 91.3, 88.4, 70.2, 63.1, 53.7, 52.8, 52.6, 47.1, 38.4, 30.0, 16.8; FAB-MS: m/z 482 [M + Na^+], 460 [M + H^+].

4: IR (neat): $\tilde{\nu}$ = 2944, 2184, 1717, 1437, 1261, 1043, 758 cm^{-1}; ^1H NMR (270 MHz, $CDCl_3$): δ = 7.76 (br. d, J = 7.6 Hz, 1H), 7.23–7.43 (m, 3H), 5.72 (br. s, 1H), 4.69 (s, 1H), 3.82 (s, 3H), 3.81 (s, 3H), 3.72 (br. s, 3H), 3.34 (br. q, J = 7.3 Hz, 1H), 1.64 (d, J = 7.3 Hz, 3H); ^{13}C NMR (67.8 MHz, $CDCl_3$): δ = 167.9, 165.1, 155.3, 142.9, 136.0, 128.7, 127.3, 127.1, 125.6, 125.5, 89.8, 89.1, 70.0, 59.5, 53.7, 52.8, 52.6, 47.4, 38.2, 30.8, 16.6, 4.4, 2.2; FAB-MS: m/z 710 [M + Na^+], 688 [M + H^+]; High-resolution FAB-MS: found: 709.9147 (calc.: 709.9149, $C_{24}H_{19}NO_7I_2Na$).

6A: IR (neat): $\tilde{\nu}$ = 2954, 2170, 2118, 1711, 1484, 1442, 1372, 1321, 1283, 1249, 1027, 907, 847, 760, 734 cm^{-1}; ^1H NMR (270 MHz, $CDCl_3$): δ = 8.27 (dd, J = 7.9, 1.7 Hz, 1H), 7.45 (br. d, J = 7.9 Hz, 1H), 7.30 (ddd, J = 7.9, 7.9, 1.7 Hz, 1H), 7.15 (ddd, J = 7.9, 7.9, 1.3 Hz, 1H), 6.09 (br. s, 1H), 6.03 (dq, J = 1.3, 7.3 Hz, 1H), 5.95 (s, 1H), 3.79 (s, 3H), 1.88 (d, J = 7.3 Hz, 3H), 0.20 (s, 9H), −0.05 (s, 9H); ^{13}C NMR (67.8 MHz, $CDCl_3$): δ = 153.9, 141.9, 138.1, 135.9, 129.0, 128.4, 127.7, 125.2, 124.5, 121.2, 104.4, 102.5, 102.1, 102.0, 87.6, 53.2, 46.3, 14.4, −0.30, −0.34; FAB-MS: m/z 444 [M + Na^+], 422 [M + H^+]; High-resolution FAB-MS: found: 444.1786 (calc.: 444.1791, $C_{24}H_{31}NO_2Si_2Na$).

8: IR (neat): $\tilde{\nu}$ = 3428, 2920, 1712, 1438, 1328, 1264, 1076, 765 cm^{-1}; ^1H NMR (270 MHz, $CDCl_3$): δ = 7.73 (m, 1H), 7.52 (br. d, J = 7.2 Hz, 1H), 7.42 (br. d, J = 7.4 Hz, 1H), 7.05–7.23 (m, 5H), 5.97 (s, 1H), 4.22 (s, 1H), 3.93 (s, 3H), 3.81 (s, 3H), 3.76 (s, 3H), 3.31 (q, J = 7.6 Hz, 1H), 1.21 (d, J = 7.6 Hz, 3H).

Diels–Alder reaction of **6A** with dimethyl acetylenedicarboxylate gave a 60:40 mixture[15] of **5** (from β-side attack) and **13** (from α-side attack). The epoxy function was introduced stereoselectively to the major product **5** giving the α-epoxide **14** in 88% yield. The configuration of **14** was established by X-ray crystallography (Fig. 2).[16] The ethynyl side chains were found to be diaxial, as expected based on MM2* calculations of the bis(alkyne) **9**.

In the next step the bis(trimethylsilylalkyne) **14** was converted to the bis(iodoalkyne) **4** (Table 1).[17] Then, the crucial palladium(0)-catalyzed coupling reaction[18] of **4** with (*Z*)-bis(trimethylstannyl)ethylene[19] gave the dynemicin model **3** (Table 1). In this reaction neither the corresponding homo coupling product of **4** nor the bis(vinyl) compound were obtained. Enediyne **3** was sufficiently stable under the reaction conditions and during purification on silica gel.

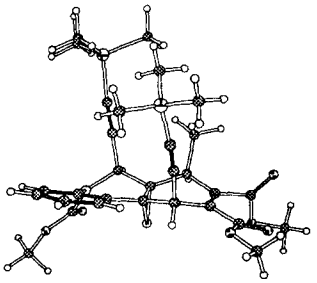


Fig. 2. Chem 3D representation of the X-ray crystal structure of **14**.

Acid-induced Bergman cyclization[5a,c] of enediyne **3** was achieved (Scheme 1) with *p*-TsOH·H_2O in THF in the presence of 1,4-cyclohexadiene at 25 °C to give the aromatized product **8** in 32% yield (Table 1). The formation of **8** can be explained by initial opening of the epoxide to give the corresponding diol, followed by Bergman cyclization and hydrogen abstraction.

In summary, the synthesis of the dynemicin model **3**, which has a 10-membered ring enediyne system and an epoxide "trigger", has been achieved by [2,3]-Wittig rearrangement, Diels–Alder reaction, and palladium-catalyzed coupling reaction. MM2 calculations were useful in the design of the key synthetic intermediate with the desired conformational property. Finally, compound **3** has been shown to undergo acid-induced Bergman cyclization, which suggests its potential as a novel DNA-cleaving molecule.

Received: December 27, 1994 [Z 7579 IE]
German version: *Angew. Chem.* **1995**, *107*, 1443–1446

Keywords: dynemicins · enediynes · semiempirical calculations

[1] Reviews: K. C. Nicolaou, W.-M. Dai, *Angew. Chem.* **1991**, *103*, 1453; *Angew. Chem. Int. Ed. Engl.* **1991**, *30*, 1387.

[2] a) M. Konishi, H. Ohkuma, T. Tsuno, T. Oki, G. D. VanDuyne, J. Clardy, *J. Am. Chem. Soc.* **1990**, *112*, 3715; b) M. Konishi, H. Ohkuma, K. Matsumoto, T. Tsuno, H. Kamei, T. Miyake, T. Oki, H. Kawaguchi, G. D. VanDuyne, J. Clardy, *J. Antibiot.* **1989**, *42*, 1449.

[3] a) Recent review on nonhydrolytic DNA cleavage: G. Pratviel, J. Bernadou, B. Meunier, *Angew. Chem.* **1995**, *107*, 819; *Angew. Chem. Int. Ed. Engl.* **1995**, *34*, 746; b) Y. Sugiura, T. Shiraki, M. Konishi, T. Oki, *Proc. Natl. Acad. Sci. USA* **1990**, *87*, 3831; c) T. Shiraki, Y. Sugiura, *Biochemistry* **1990**, *29*, 9795; d) Y. Sugiura, T. Arakawa, M. Uesugi, T. Shiraki, H. Ohkuma, M. Konishi, *ibid.* **1991**, *30*, 2989; e) T. Shiraki, M. Uesugi, Y. Sugiura, *Biochem. Biophys. Res. Commun.* **1992**, *188*, 584; f) M. F. Semmelhack, J. Gallagher, D. Cohen, *Tetrahedron Lett.* **1990**, *31*, 1521; g) J. P. Snyder, G. E. Tipsword, *J. Am. Chem. Soc.* **1990**, *112*, 4040.

[4] a) K. C. Nicolaou, W.-M. Dai, S. V. Wendeborn, A. L. Smith, Y. Torisawa, P. Maligres, C.-K. Hwang, *Angew. Chem.* **1991**, *103*, 1034; *Angew. Chem. Int. Ed. Engl.* **1991**, *30*, 1032; b) K. C. Nicolaou, W.-M. Dai, S.-C. Tsay, V. A. Estevez, W. Wrasidlo, *Science* **1992**, *256*, 1172; c) K. C. Nicolaou, P. Maligres, T. Suzuki, S. V. Wendeborn, W.-M. Dai, R. K. Chadha, *J. Am. Chem. Soc.* **1992**, *114*, 8890; d) K. C. Nicolaou, W.-M. Dai, *ibid.* **1992**, *114*, 8908.

[5] a) K. C. Nicolaou, C.-K. Hwang, A. L. Smith, S. V. Wendeborn, *J. Am. Chem. Soc.* **1990**, *112*, 7416; b) K. C. Nicolaou, A. L. Smith, S. V. Wendeborn, C.-K. Hwang, *ibid.* **1991**, *113*, 3106; c) J. A. Porco, Jr., F. J. Schoenen, T. J. Stout, J. Clardy, S. L. Schreiber, *ibid.* **1990**, *112*, 7410; d) J. L. Wood, J. A. Porco, Jr., J. Taunton, A. Y. Lee, J. Clardy, S. L. Schreiber, *ibid.* **1992**, *114*, 5898; e) P. A. Wender, C. K. Zercher, *ibid.* **1991**, *113*, 2311; f) P. A. Wender, C. K. Zercher, S. Beckham, E.-M. Haubold, *J. Org. Chem.* **1993**, *58*, 5867; g) T. Nishikawa, M. Isobe, T. Goto, *Synlett* **1991**, 393; h) T. Nishikawa, A. Ino, M. Isobe, T. Goto, *Chem. Lett.* **1991**, 1271; i) T. Nishikawa, A. Ino, M. Isobe, *Tetrahedron* **1994**, *50*, 1449; j) P. Magnus, S. M. Fortt, *J. Chem. Soc. Chem. Commun.* **1991**, 544; k) P. Magnus, *Tetrahedron* **1994**, *50*, 1397; l) T. Yoon, M. D. Shair, S. J. Danishefsky, G. K. Shulte, *J. Org. Chem.* **1994**, *59*, 3752; m) A. G. Myers, M. E. Fraley, N. J. Tom, *J. Am. Chem. Soc.* **1994**, *116*, 11556. Total synthesis: n) J. Taunton, J. L. Wood, S. L. Schreiber, *ibid.* **1993**, *115*, 10378.

[6] For a related cyclization approach to dynemicin analogues, see: M. D. Shair, T. Yoon, S. J. Danishefsky, *J. Org. Chem.* **1994**, *59*, 3755.

[7] T. Takahashi, Y. Sakamoto, H. Yamada, 65th Spring Meeting of the Japan Chemical Society, **1993**, Abstract p. 366.

[8] Reviews: a) K. Mikami, T. Nakai, *Synthesis* **1991**, 594; b) J. A. Marshall in *Comprehensive Organic Synthesis, Vol. 3* (Eds.: B. M. Trost, I. Fleming, G. Pattenden), Pergamon, London, **1991**, p. 975; c) R. Brückner in *Comprehensive Organic Synthesis, Vol. 6* (Eds.: B. M. Trost, I. Fleming, E. Winterfeldt), Pergamon, London, **1991**, p. 873; d) T. Nakai, K. Mikami, *Chem. Rev.* **1986**, *86*, 885; e) R. W. Hoffmann, *Angew. Chem.* **1979**, *91*, 625; *Angew. Chem. Int. Ed. Engl.* **1979**, *18*, 563.

[9] a) K. Takatori, M. Kajiwara, Y. Sakamoto, T. Shimayama, H. Yamada, T. Takahashi, *Tetrahedron Lett.* **1994**, *35*, 5669; b) T. Takahashi, M. Nakazawa, Y. Sakamoto, K. N. Houk, *ibid.* **1993**, *34*, 4075; c) T. Takahashi, H. Tanaka, Y. Hirai, T. Doi, H. Yamada, T. Shiraki, Y. Sugiura, *Angew. Chem.* **1993**, *105*, 1719; *Angew. Chem. Int. Ed. Engl.* **1993**, *32*, 1657; d) T. Takahashi, H. Yokoyama, T. Haino, H. Yamada, *J. Org. Chem.* **1992**, *57*, 3521; e) T. Takahashi, K. Shimizu, T. Doi, J. Tsuji, *J. Am. Chem. Soc.* **1988**, *110*, 2674.

[10] G. Chang, W. C. Guida, W. C. Still, *J. Am. Chem. Soc.* **1989**, *111*, 4379.

 © VCH Verlagsgesellschaft mbH, D-69451 Weinheim, 1995 0570-0833/95/1212-1347 $ 10.00+.25/0

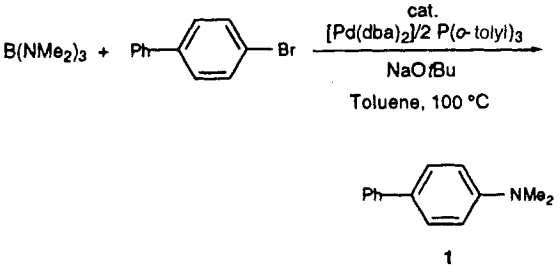
[11] The program MacroModel (version 3.5) was employed for these calculations. We are grateful to Prof. W. C. Still for providing a copy of this program; F. Mohamadi, N. G. J. Richards, W. C. Guida, R. Liskamp, M. Lipton, C. Caufield, G. Chang, T. Hendrickson, W. C. Still, *J. Comput. Chem.* **1990**, *11*, 440.
[12] 3-Bromoquinoline **10** is available from Tokyo Kasei Co., Ltd; for its lithiation, see: H. Gilman, S. M. Spatz, *J. Am. Chem. Soc.* **1940**, *62*, 446.
[13] R. Yamaguchi, Y. Nakazono, M. Kawanishi, *Tetrahedron Lett.* **1983**, *24*, 1801.
[14] Although it was expected that this elimination should provide a single isomer from the pure diastereomer **12**, a partial E_1 elimination through a benzyl anion intermediate resulted in the formation of the mixture of two dienes.
[15] The conformational analysis of **6A** based on MM2* calculations (see Scheme 2) predicts that the dominant conformation (>95%) has a twisted diene moiety and an axial orientation of the alkyne side chain at C(2). Attack of the dienophile from the less hindered convex β-face of the diene can explain the slightly preferential formation of **5**. These calculations also suggest "remote control" of the Diels–Alder reaction of **6A**, in which intermediate binding of the dienophile (acetylenedicarboxylate) to the alkynyl group attached to the diene moiety in **6a**, would help produce compound **5** as the sole product.
[16] Crystal structure data of **14**: monoclinic, space group $P2_1/a$, $a = 11.888(4)$, $b = 27.454(8)$, $c = 10.509(3)$ Å, $\beta = 103.68(2)°$, $V = 3333(2)$ Å^3, $Z = 4$; $\rho_{calcd} = 1.16$ g cm^{-3}; 4705 measured reflections, 2525 classed as observed with $I \geq 3.0\sigma(I)$. Solution of structure by direct methods (Monte-Carlo MULTAN), R = 0.073. Further details of the crystal structure investigation may be obtained from the Director of the Cambridge Crystallographic Data Centre, 12 Union Road, GB-Cambridge CB21EZ (UK), on quoting the full journal citation.
[17] T. Nishikawa, S. Shibuya, S. Hosokawa, M. Isobe, *Synlett* **1994**, 485.
[18] Our first attempt at the Pd^0/Cu^I-catalyzed coupling reaction of a bis(acetylene) derivative of **5** with (*Z*)-dichloroethylene failed. (For palladium-catalyzed coupling reactions for the synthesis of 11-membered ring enediyne systems, see: D. Schinzer, J. Kabbara, *Synlett* **1992**, 766.) During our work an efficient Pd^0 coupling reaction was reported by S. J. Danishefsky et al. (see ref. [6]).
[19] T. N. Mitchell, A. Amamria, H. Killing, D. Rutschow, *J. Organomet. Chem.* **1986**, *304*, 257.

A Simple Catalytic Method for the Conversion of Aryl Bromides to Arylamines**

Anil S. Guram, Roger A. Rennels, and Stephen L. Buchwald*

Arylamines are of considerable importance in a variety of industries. As such, the development of new and more general methods for their preparation is of significant interest.[1, 2] We recently reported that the palladium-catalyzed reactions of aryl bromides with in situ generated aminostannanes provide a general route to a variety of arylamines.[1, 3, 4] While these tin-mediated reactions were efficient, they suffered from relatively long reaction times, non-trivial workup procedures (to remove tin by-products), and were inapplicable to primary aliphatic amines. Furthermore, the use of tin reagents was a concern, particularly for the large-scale preparation of arylamines of pharmaceutical significance. Herein, we describe an improved palladium-catalyzed reaction protocol which ameliorates, to a significant extent, the problems described above.

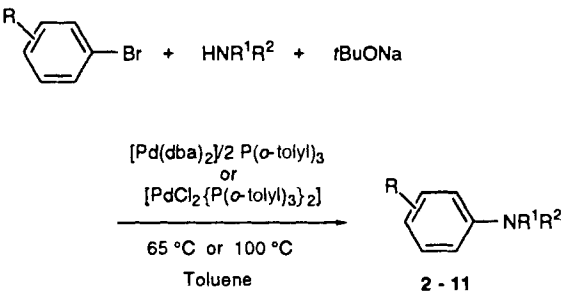
Our initial strategy, based on the well-established boron-mediated C–C bond-forming reactions,[5] focused on the investigation of analogous palladium-catalyzed reactions of aryl halides and aminoboranes. We discovered that tris(dimethylamino)borane ($B(NMe_2)_3$,[6] commercially available from Aldrich) reacts efficiently with 4-bromobiphenyl in the presence of $[Pd(dba)_2]/2\ P(o\text{-tolyl})_3$ (2 mol%; dba = dibenzylideneacetone) and sodium *tert*-butoxide in toluene at 100 °C to afford the arylamine **1** in 85% isolated yield [Eq. (a)]. Moreover,



(a)

$B(NMe_2)_3$ also serves as a precursor for the transfer of other amines.[7] For example, the transamination reaction of $B(NMe_2)_3$ (1.0 equiv) with *N*-methylaniline (3.3 equiv) (in toluene under argon purge), followed by reaction of the in situ generated $B(N(Me)Ph)_3$ with 4-bromobiphenyl under similar conditions afforded 4-(*N*-methylanilino)biphenyl (**2**) in 83% isolated yield.

After some experimentation, we have found that aryl bromides react efficiently with amines in the presence of sodium *tert*-butoxide and a catalytic amount of $[PdCl_2(P(o\text{-tolyl})_3)_2]$ or $[Pd(dba)_2]/2\ P(o\text{-tolyl})_3$ to afford arylamines in good yields [Eq. (b), Table 1]. The experimental procedure simply involves heat-



(b)

ing a mixture of aryl bromide (1 equiv), amine (1.2 equiv), sodium-*tert*-butoxide (1.4 equiv), and the Pd catalyst (≈2 mol%) in toluene at 65–100 °C. An aqueous workup and chromatography on silica gel afford the analytically pure arylamines.

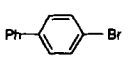
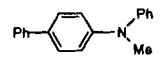
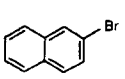
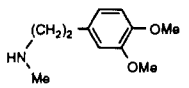
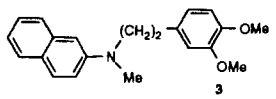
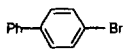
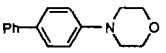
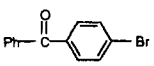
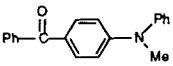
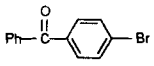
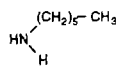
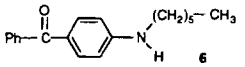
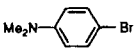
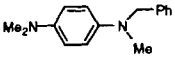
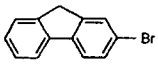
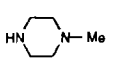
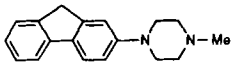
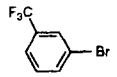
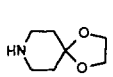
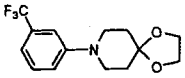
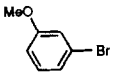
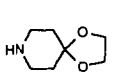
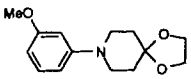
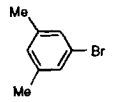
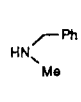
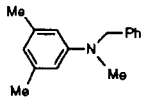
As illustrated in Table 1, the Pd-catalyzed aryl amination reactions provide a general route to a variety of arylamines. Aryl bromides with both electron-withdrawing and electron-donating substituents react efficiently with both primary and secondary amines. Substrates with acid-sensitive functional groups are well tolerated (entries 8 and 9), while those containing base-sensitive functional groups, as anticipated, are not (e.g., attempted amination of 4-bromoacetophenone was unsuccessful).

A side-product, resulting from reduction of the starting aryl bromide, is formed in variable amounts in these reactions. This side-product is readily separated from the arylamine products by flash chromatography. The amount of this side-product is dependent on the steric and electronic properties of both the aryl bromide and amine. In general, reactions involving simple secondary amines and simple aryl bromides with *para* electron-withdrawing substituents resulted in the formation of the least amount of reduced product (entries 1, 3, and 4), whereas reactions involving primary aliphatic amines resulted in the production of larger quantities of reduced product (entry 5).

[*] Prof. Dr. S. L. Buchwald, Dr. A. S. Guram, Dr. R. A. Rennels
Department of Chemistry, Massachusetts Institute of Technology
Cambridge, MA 02139 (USA)
Telefax: Int. code + (617)253-3297
e-mail: SBUCHWAL@MIT.EDU

[**] This work was supported by the National Science Foundation (CHE-9000482) and the National Institutes of Health (GM34917). Additional support from the Dow Chemical Company is gratefully acknowledged. A. S. G. and R. A. R. were NCI Postdoctoral Trainees supported by NIH Cancer Training Grant CI T32CA09112. We thank Professor G. C. Fu for helpful discussions.

Table 1. Palladium-catalyzed reactions of aryl bromides and amines [a,b].

Entry	Aryl bromide	Amine	Arylamine	Yield [%][c]
1			 2	88
2			 3	78
3			 4	86
4			 5	89
5			 6	72
6			 7	71
7			 8	79
8			 9	67
9			 10	81
10			 11	84

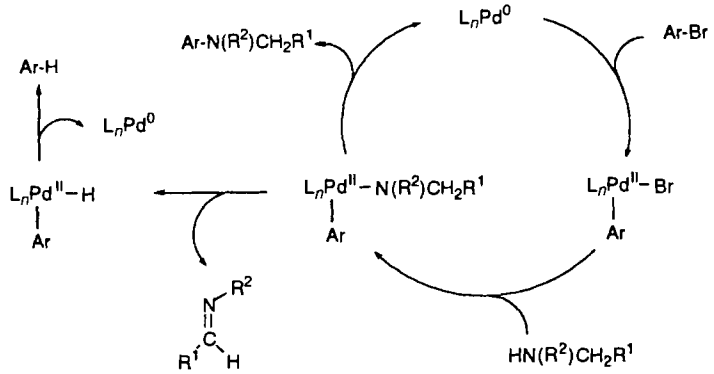
[a] For entries 1 and 10, the catalyst [Pd(dba)$_2$]/2 P(*o*-tolyl)$_3$ and reaction temperature of 65 °C were employed, and for entries 2–9, the catalyst [PdCl$_2$(P(*o*-tolyl)$_3$)$_2$] and reaction temperature of 100 °C were employed. [b] By GC analysis using an internal standard, approximately 8, 12, 5, 6, 27, 24, 8, not determined, 12, 10% of reduced side-product was formed in entries 1–10, respectively. [c] Yields reported correspond to analytically pure, isolated compounds.

The Pd-catalyzed aryl amination reactions most likely proceed by the oxidative addition of the aryl bromide to a Pd^0 species, followed by the formation of an intermediate "Ar–Pd^{II} NCH$_2$R^1(R^2)" species which undergoes reductive elimination to afford the desired arylamine and regenerates the Pd^0 catalyst (Scheme 1).[8, 9] We believe that formation of the reduced side-product occurs, at least in part, as shown in Scheme 1. The "Ar-Pd^{II}-NCH$_2$R^1(R^2)" intermediate can undergo a β-hydride elimination reaction to produce a "Ar-Pd^{II}-H" species which can reductively eliminate to afford the arene side-product and regenerate the Pd^0 catalyst (Scheme 1).[10] Consistent with this notion, when *N*-methylbenzylamine is employed as the amine coupling partner, *N*-methylbenzylidene was detected by GC/MS.

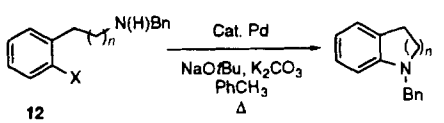
Preliminary studies of the reaction of 1-bromo-3,5-dimethylbenzene with *N*-methylbenzylamine in the presence of a base and a catalytic amount of [Pd(dba)$_2$]/2 phosphanes (100 °C, toluene) indicate that the P(*o*-tolyl)$_3$ ligand is critical to the success of these intermolecular aromatic amination reactions. Related ligands such as PPh$_3$, 1,1′-bis(diphenylphosphano)ferrocene (dppf), and 1,3-bis(diphenylphosphano)propane (dppp) were found to be inefficient. With PPh$_3$ and dppf as ligands, the aryl bromide was completely consumed (< 1 h) with the formation of *m*-xylene as the major product. With dppp as the ligand, the aryl bromide remains mostly unreacted and only a trace of desired arylamine is formed. The Pd-catalyzed aromatic amination reaction is also very sensitive to the nature of base. With NaOMe, the aryl bromide slowly decomposes to *m*-xylene with no formation of the desired arylamine, while with K$_2$CO$_3$, no conversion to product is observed (100 °C, toluene, 3 h).

An obvious application of this methodology was to the intramolecular reaction of an amine with an aryl halide due to the importance of nitrogen heterocycles.[4, 11] We note that a transformation of this type which utilized a stoichiometric quantity of [Pd(PPh$_3$)$_4$] was reported by Boger and co-workers several years ago.[4]

Applying the NaO*t*Bu-mediated palladium-catalyzed procedure to the cyclization of **12** provides good yields of nitrogen heterocycles of ring size 5–7 [Eq. (c)] as shown in Table 2. Although the use of K$_2$CO$_3$ was not found to be essential in these transformations, cleaner reactions were generally observed when it was employed. At 100 °C all reactions proceeded quickly (0.5–6 h) and in excellent yields (entries 1, 3, 4, and 6).



Scheme 1. Postulated mechanism of the Pd^0-catalyzed amination of aryl bromides.



12 (c)

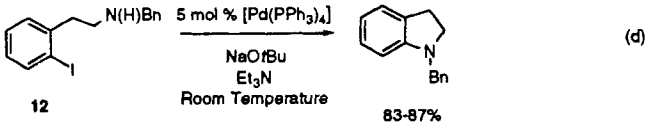
Table 2. Palladium-catalyzed cyclization with sodium *tert*-butoxide [Eq. (c)].

Entry	X	*n*	Catalyst	mol %	*T* [°C]	*t* [h]	yield [%] [a]
1	Br	1	$[Pd(PPh_3)_4]$	1	100	2.5	92
2	Br	1	$[Pd(PPh_3)_4]$	5	65	46	83
3	Br	2	$[Pd(PPh_3)_4]$	1	100	6	87
4	Br	3	$[Pd(PPh_3)_4]$	1	100	6	89
5	Br	2	$[PdCl_2\{P(o\text{-tolyl})_3\}_2]$	10	65	21	75
6	I	1	$[Pd(PPh_3)_4]$	1	100	0.5	93
7	I	1	$[Pd(PPh_3)_4]$	1	65	2	96

[a] Yield of isolated product.

When the temperature was lowered to 65 °C, the reactions of the aryl bromides tend to slow greatly as they approach completion,[12] although good yields are still realized (entries 2 and 5). In contrast to the intermolecular process, aryl iodides proved to be superior substrates. Under the conditions described, aryl iodide **12** (X = I, $n = 1$) reacts rapidly and produces *N*-benzylindoline in excellent yields (entries 6 and 7). In general, the use of $Pd(PPh_3)_4$ proved superior to the procedures employing $P(o\text{-tolyl})_3$ for the intramolecular reactions, in contrast to the results seen for the intermolecular reactions.

The intramolecular aryl amination reaction of aryl iodide **12** (X = I, $n = 1$) has also been accomplished at room temperature using 5 mol% $[Pd(PPh_3)_4]$ and excess triethylamine (20 equiv) in toluene for 40 h, which afforded *N*-benzylindoline in 87% isolated yield [Eq. (d)]. When triethylamine was employed as the



(d)

solvent with 5 mol% $[Pd(PPh_3)_4]$, aryl iodide **12** (X = I, $n = 1$) was consumed in 15 h at room temperature and provided *N*-benzylindoline in 83% isolated yield.

In summary, we have developed a facile and general catalytic method for the conversion of aryl bromides to arylamines, which works well for inter- and intramolecular processes. Particularly noteworthy features of this method include the experimental simplicity, the tin/boron-free conditions, and the broad substrate scope. Efforts to discover improved catalyst systems which operate under milder reaction conditions as well as to employ these methods in synthetic organic chemistry are in progress.[13, 14]

Experimental Procedure

3: A mixture of 2-bromonaphthalene (205 mg, 0.99 mmol), *N*-methylhomoveratrylamine (234 mg, 1.20 mmol), sodium *tert*-butoxide (134 mg, 1.39 mmol) and $[PdCl_2(P(o\text{-tolyl})_3)_2]$ (14 mg, 0.02 mmol) in toluene (8–9 mL) was heated under argon at 100 °C for 3 h. After cooling to room temperature, the reaction mixture was taken up in Et_2O (30–40 mL) and washed with brine (15–20 mL). The organic fraction was dried with $MgSO_4$, and concentrated using a rotary evaporator. The crude material was purified by flash chromatography on silica gel using hexane (100 mL), hexane:EtOAc (10/1, 100 mL), and then hexane:EtOAC (4/1) to afford **1** (249 mg, 78%) as a pale yellow solid. Formation of ca. 12% of naphthalene (reduced side-product) was detected by GC analysis of the crude reaction mixture. ^1H NMR (300 MHz, $CDCl_3$): $\delta = 7.69$ (overlapping d's, $J = 8$ Hz, 2H, ArH), 7.64 (d, $J = 8$ Hz, 1H, ArH), 7.36 (t, $J = 7$ Hz, 1H, ArH), 7.19 (t, $J = 7$ Hz, 1H, ArH), 7.14 (dd, $J = 7$, 2 Hz, 1H, ArH), 6.90 (dd, $J = 2$ Hz, 1H, ArH), 6.80 (d, $J = 7$ Hz, 1H, ArH), 6.77 (dd, $J = 7$ Hz, 1H, ArH), 6.70 (d, $J = 2$ Hz, 1H ArH), 3.86 (s, 3H, OCH_3), 3.84 (s, 3H, OCH_3), 3.67 (t, $J = 8$ Hz, CH_2N), 2.97 (s, 3H, NCH_3), 2.84 (t, $J = 8$ Hz, 2H, NCH_2CH_2). ^{13}C NMR (75 MHz, $CDCl_3$): $\delta = 148.9$, 147.5, 146.8, 135.1, 132.3, 128.8, 127.4, 126.6, 126.2, 126.0, 121.8, 120.7, 115.9, 112.1, 111.3, 106.0, 55.9, 55.8, 55.0, 38.9, 32.7. **M. P.**: 84–85 °C. Anal. Calcd. for $C_{21}H_{23}NO_2$: C 78.47, H 7.21. Found: C 78.41, H 7.29.

***N*-benzylindoline:** To a suspension of NaO*t*-Bu (154 mg, 1.60 mmol), K_2CO_3 (221 mg, 1.60 mmol), and tetrakis(triphenylphosphane)palladium(0) (12 mg, 0.01 mmol) in toluene (3 mL, 0.33 M) under argon was added by syringe *N*-benzyl-*o*-bromophenethylamine (**12**) (290 mg, 1.0 mmol). The reaction mixture was then heated in an oil bath for 2.5 h under argon until GC showed no starting material [12]. After cooling to room temperature, water and ether (5 mL each) were added. After stirring until all the solids were dissolved, the layers were separated and the aqueous layer was extracted with ether (2 × 5 mL). The combined organic fractions were then stirred with 30% hydrogen peroxide (5 mL) for 10 to 20 minutes to oxidize the triphenylphosphane. The hydrogen peroxide was removed and the organic layer was washed with water (10 mL). The combined hydrogen peroxide and water layers were extracted with ether (2 × 20 mL). The combined ether layers were then washed with saturated aqueous ferrous sulfate (10 mL) followed by water (10 mL). The combined ferrous sulfate and water layers were extracted with ether (2 × 20 mL). The combined ether layers were then washed with saturated aqueous sodium chloride and dried ($MgSO_4$). Concentration using a rotary evaporator and flash chromatography on silica gel using 40/1 hexane/ether afforded *N*-benzylindoline as a yellow oil. The product was essentially pure at this point. A small quantity of aliphatic impurity, however, which appeared at $\delta = 1.25$ in the ^1H NMR was removed by Kugelrohr distillation at 100 °C and 0.01 mm Hg to afford 197 mg of *N*-benzylindoline [15] as a clear colorless oil (94%).

Received: January 17, 1995
Revised version: March 13, 1995 [Z 7643 IE]
German version: *Angew. Chem.* **1995**, *107*, 1456–1459

Keywords: arylamines · catalysis · indolines · palladium compounds

[1] A. S. Guram, S. L. Buchwald, *J. Am. Chem. Soc.* **1994**, *116*, 7901–7902.
[2] a) W. ten Hoeve, C. G. Kruse, J. M. Luteyn, J. R. G. Thiecke, H. Wynberg, *J. Org. Chem.* **1993**, *58*, 5101–5106; b) H. Mitchell, Y. Leblanc, *ibid.* **1994**, *59*, 682–687; c) J. V. B. Kanth, M. Periasamy, *ibid.* **1993**, *58*, 3156–3157; d) A. Banfi, M. Bartoletti, E. Bellora, M. Bignotti, M. Turconi, *Synthesis* **1994**, 775–776; e) J. March, *Advanced Organic Chemistry*, 4th ed., Wiley, New York, **1992**, pp 641–677.
[3] For related Pd-catalyzed reactions of aryl bromides and aminostannanes, see a) F. Paul, J. Patt, J. F. Hartwig, *J. Am. Chem. Soc.* **1994**, *116*, 5969–5970; b) M. Kosugi, M. Kameyama, T. Migita, *Chem. Lett.* **1983**, 927–928.
[4] For related tin-free stoichiometric Pd-mediated reactions, see a) D. L. Boger, J. S. Panek, *Tetrahedron Lett.* **1984**, *25*, 3175–3178; b) D. L. Boger, S. R. Duff, J. S. Panek, M. Yasuda, *J. Org. Chem.* **1985**, *50*, 5782–5789; c) *ibid.* **1985**, *50*, 5790–5795.
[5] a) T. Watanabe, N. Miyaura, A. Suzuki, *Synlett* **1992**, 207–210, and references therein; b) N. Miyaura, T. Ishiyama, H. Sasaki, M. Ishikawa, M. Satoh, A. Suzuki, *J. Am. Chem. Soc.* **1989**, *111*, 314–321, and references therein.
[6] K. Niedenzu, J. W. Dawson, *Inorg. Synth.* **1967**, *10*, 135–137.
[7] For early reports of transamination of aminoboranes, see a) K. Niedenzu, P. Fritz, J. W. Dawson, *Inorg. Chem.* **1964**, *3*, 1077–1079; b) W. D. English, A. L. McCloskey, H. Steinberg, *J. Am. Chem. Soc.* **1961**, *83*, 2122–2124.
[8] Base-induced formation of "Pd–N" complexes has been observed previously, M. D. Fryzuk, P. A. MacNeil, S. J. Rettig, A. S. Secco, J. Trotter, *Organometallics* **1982**, *1*, 918–930.
[9] L. A. Villanueva, K. A. Abboud, J. M. Boncella, *Organometallics* **1994**, *13*, 3921–3931.
[10] "Pd-N-CHR_2" complexes can decompose by β-hydride elimination: a) H. E. Bryndza, W. Tam, *Chem. Rev.* **1988**, *88*, 1163–1188; b) S. I. Murahashi, N. Yoshimura, T. Tsumiyama, T. Kojima, *J. Am. Chem. Soc.* **1983**, *105*, 5002–5011.
[11] A variety of methods are available for their synthesis via intramolecular nitrogen-aryl bond formation. a) T. Kametani, K. Takahashi, M. Ihara, K. Fukumoto, *J. Chem. Soc. Perkin 1* **1976**, 389–393; b) T. Kametani, T. Ohsawa, M. Ihara, K. Fukumoto, *ibid.* **1978**, 460–464; c) T. Kametani, T. Ohsawa, M. Ihara, *Heterocycles* **1980**, *14*, 277–280; d) J. Lindley, *Tetrahedron* **1984**, *40*, 1433–1456; e) R. Huisgen, H. König, A. R. Lepley, *Chem. Ber.* **1960**, *93*, 1496–1506; f) J. F. Bunnett, B. F. Hrutfiord, *J. Am. Chem. Soc.* **1961**, *83*, 1691–1697; g) H. Heaney, *Chem. Rev.* **1962**, *62*, 81–97; h) E. Ciganek, *J. Org. Chem.* **1992**, *57*, 4521–4527; i) E. M. Hawes, H. L. Davis, *J. Heterocyclic Chem.* **1973**, *10*, 39–42; j) A. F. Pozharski, A. M. Simonov, V. N. Doronkin, *Russ. Chem. Rev. Engl. Trans.* **1978**, *47*, 1042–1060; k) P. Rocca, F. Marsais, A. Godard, G. Queguiner, *Tetrahedron* **1993**, *49*, 49–64; l) *ibid.* **1993**, *49*, 3325–3342; m) *Tetrahedron Lett.* **1993**, *34*, 2937–2940; n) For a review on transition metal-mediated approaches to the indole nucleus see: L. S. Hegedus, *Angew. Chem.* **1988**, *100*, 1147–1161; *Angew. Chem. Int. Ed. Engl.* **1988**, *27*, 1113–1126.
[12] The products of the aryl bromide cyclizations at 65 °C were isolated prior to reaction completion (ca. 95% conversion by GC).
[13] Amides can also be cyclized under Pd-catalyzed conditions; R. A. Rennels, S. L. Buchwald, unpublished results.
[14] Carbon–nitrogen bond formation has also been achieved by using Pd/C as the catalyst with added phosphane ligands: A. S. Gurum, R. A. Rennels, S. L. Buchwald, unpublished results.
[15] Spectral data of all cyclization products were consistent with those reported: a) T. Kiguchi, N. Kuninobu, Y. Takahashi, Y. Yoshida, T. Naito, I. Ninomiya, *Synthesis* **1989**, 778–781; b) D. Thon, W. Schneider, *Chem. Ber.* **1976**, *109*, 2743–2761.

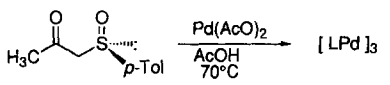
 © VCH Verlagsgesellschaft mbH, D-69451 Weinheim, 1995 0570-0833/95/1212-1350 $ 10.00+.25/0

Enantiomerically Pure Palladacycles Derived from β-Ketosulfoxides**

José L. García-Ruano,* Ana M. González, Isabel López-Solera, José R. Masaguer, Carmen Navarro-Ranninger,* Paul R. Raithby, and Jesús H. Rodríguez

The coordination of the sulfinyl group to transition metal atoms has been extensively investigated with particular reference to whether the ligand bonds through the sulfur or the oxygen atoms.[1] We are currently interested in *ortho*-metalation reactions[2] and the use of optically pure β-ketosulfoxides in asymmetric synthesis.[3] As part of these studies we therefore decided to investigate the behavior of sulfinyls ($RC(O)-CH_2-SO-p$-Tol) toward palladium(II) salts. These compounds contain several possible coordination sites, for example the carbonyl and the sulfinyl oxygen atoms, and one chiral center (sulfinyl sulfur atom). They may be obtained in high optical purity, and the inherent chirality may be transferred to the metal complexes derived from them. In addition, β-ketosulfoxides offer the possibility of forming diastereoisomeric *ortho*-metalated species by the initial insertion of the electrophilic Pd^{II} salts into the strongly acidic H–C bonds flanked by the SO and CO groups,[4] followed by the *ortho*-metalation of the *para*-tolyl ring. Despite the interest in chiral compounds containing a stereogenic sp^3 hybridized C atom directly bonded to the palladium atom, very few are known.[5] In this paper we describe the synthesis and structure of the enantiomerically pure trimer **2**, which exhibits an unprecedented structure of a C-metalated enolate ("palladium C-enolate"), unequivocally demonstrated by X-ray diffraction.

The reaction of $Pd(OAc)_2$ with (*R*)-3-*para*-tolylsulfinyl-2-propanone (**1**)[6] under nitrogen for 48–72 hours, afforded, after chromatographic purification, the complex **2** as a solid in 42% yield. The microanalytical data are consistent with the empirical formula $C_{10}H_{10}O_2SPd$, which indicates the structure $[LPd]_n$, and suggests that acetato ligands are not present. This was confirmed by the IR spectra, which revealed the absence of the two bands (1580 and 1420 cm^{-1}) typical of η^2-acetato ligands.[7] The S=O stretch is tentatively assigned to the strong band at 1127 cm^{-1}, which suggests that the coordination is through sulfur.[8] The C=O stretching absorption appears at 1570 cm^{-1} (139 cm^{-1} lower than in the ligand **1**), which indicates that the carbonyl oxygen must be involved in the coordination; however, the high value observed for $\Delta\tilde{\nu}$ is difficult to explain.[9]



1 **2**

The *ortho*-metalation of the *para*-tolyl ring is evident from the ^1H NMR data (only three aromatic protons), and instead of the methylene proton signal of **1** (δ = 3.83 (m, 2H)), a singlet with an integral corresponding to only one proton appears for the complex **2** (δ = 5.26 (s, 1H)). Both facts suggest the formation of a five-membered palladacycle with two Pd–C σ bonds.

The ^{13}C NMR parameters of **2** reveal the expected deshielding for the carbon atoms bonded to palladium, as well as of those carbon atoms directly connected to the ligand coordination sites. In comparison with previously reported compounds,[10] the observed deshielding effect is larger for the aliphatic carbon atom ($\Delta\delta$(C2) = 13–15) but smaller for the aromatic one ($\Delta\delta$(C11) = 12). These differences are difficult to explain unless we assume significant structural differences with respect to both Pd–C bonds. Finally, the strong deshielding observed for C1 ($\Delta\delta$ = 15.6) is consistent with the structural element Pd–O=C deduced from the IR data.

The structure of **2**, which crystallizes as yellow prisms from ethyl acetate/hexane (1/1), was confirmed by an X-ray structure determination.[11] Views of the molecular structure are shown in Figure 1. The complex is a trimer with crystallographic threefold symmetry. The core of the trimer is a nine-membered ring of alternating S, Pd, and C(H) atoms. The plane defined by the

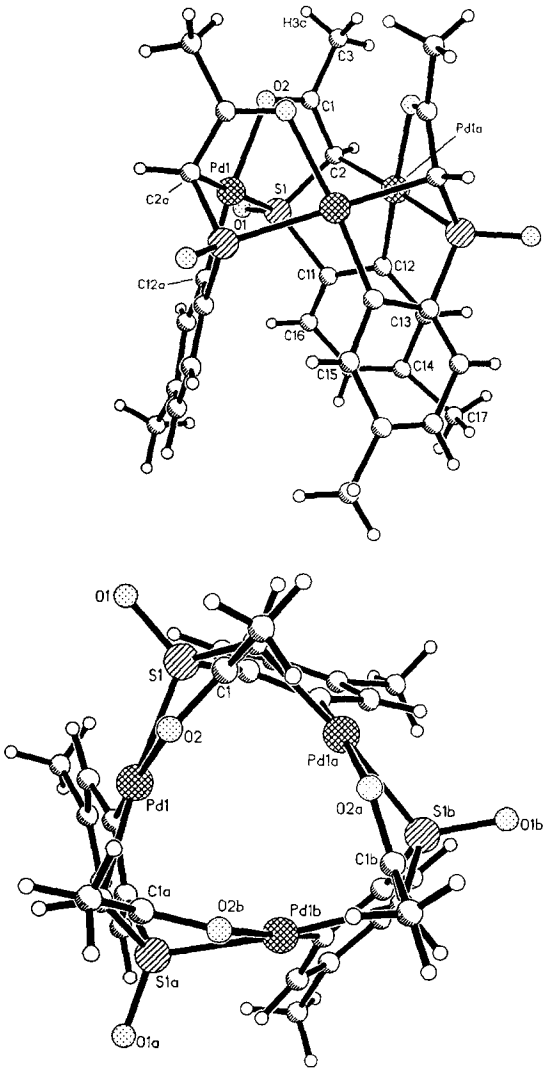


Fig. 1. Two views of the molecular structure of **2**. Selected bond lengths [Å] and angles [°]: Pd1-S1 2.32(6), Pd1-O2 2.16(1), Pd1-C2a 2.10(2), Pd1-C12a 1.95(2), S1-O1 1.44(2), S1-C2 1.82(2), S1-C11 1.80(2), C1-O2 1.24(3), C1-C2 1.49(3); S1-Pd1-O2 80.5(5), S1-Pd1-C12a 94.6(7), C12a-Pd1-C2a 85.2(9), C2a-Pd1-O2 99.4(8). (Symmetry transformation used to generate the equivalent atoms, a: $-y+2, x-y+1, z$). The cavity diameter is 4.04 Å.

[*] Prof. J. L. García-Ruano, Dr. J. H. Rodríguez
Departamento de Química Orgánica, Universidad Autónoma
Cantoblanco E-28049-Madrid (Spain)
Telefax: Int. code + (1) 3973-966
Prof. C. Navarro-Ranninger, A. M. González, Prof. J. R. Masaguer
Departamento de Química Inorgánica, Universidad Autónoma
Cantoblanco E-28049-Madrid (Spain)
Telefax: Int. code + (1) 3974-833
Dr. I. López-Solera, Dr. P. R. Raithby
Department of Chemistry, University of Cambridge (UK)

[**] This work was supported by CICYT Grants PB 93-0257 and SAF 93-1122, HB-059. I. L.-S. thanks the DGICYT for funding.

palladium atoms is sandwiched between two planes, one of them defined by the sulfur atoms and the other by the methyne carbon atoms.

Each ligand is bonded to two palladium atoms. One palladium atom is joined through two dative bonds by using the lone pairs of electrons at the sulfur and carbonyl oxygen, while the other palladium atom is bonded to the ligand through two covalent bonds to the methyne carbon and the *ortho*-carbon of the *para*-tolyl unit. The two five-membered rings supported by each palladium atom (Fig. 2), adopt an envelope shape, in which C2 (− 0.97 Å) and S1 (− 0.84 Å) lie out of the planes defined by the Pd1a, C11, C12, and S1 atoms and the Pd1, O2, C1, and C2 atoms, respectively. The angle between the coordination planes of two adjacent Pd atoms is 62.3°. Figure 1 bottom shows that the trimer forms a cavity, 4.04 Å in diameter. The sulfur atom and the chiral carbon atom are both *R*-configurated. As expected, the two Pd–C bonds are different. The Pd1–C12a bond length is 1.95(2) Å, similar to M–C bonds in other cyclometalated aryl complexes[2] where there is some multiple-bond character because of metal-to-ligand back bonding.[12] The Pd1–C2a bond length is longer (2.10(2) Å) than that for Pd1–C12a, but also similar to other Pd–C(sp^3) σ bonds supporting a sulfur atom in the *trans* position (2.05–2.10 Å).[13] The value of the C1-C2-S1 angle (109(2)°) supports the palladium C-enolate structure of the compound **2**. The Pd1–O2 distance of 2.16(1) Å is indicative of a carbon atom of an aryl group lying in a *trans* position.[14] The Pd1–S1 distance of 2.32(6) Å is slightly longer than those observed for other complexes containing a Pd–S bond (2.19–2.25 Å).[15] The palladacycle containing the two Pd–C σ bonds is almost coplanar with the aromatic ring (angle between them is 3.2°). The sulfinyl oxygen atoms are located outside the central framework of S, Pd, and C(H) atoms, and they form a network of intermolecular hydrogen bonds with the methyl groups joined to the carbonyl groups [H3c···O1 = 2.50(4) Å, C3···O1 = 3.47(4) Å, C3-H3c···O1 = 173(8)°; symmetry: 0.6667 − *x* + *y*, 1.3333 − *x*, 0.3333 + *z*].

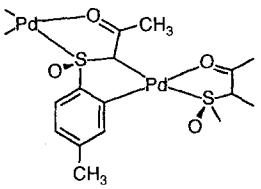


Fig. 2. Section of the structure of **2**, showing the coordination sphere of the palladium atoms.

Compound **2** exhibits a very high specific rotation ($[\alpha]_D^{20}$ = − 486.5; *c* = 0.2 in chloroform). Its absolute configuration was unequivocally established as (*R*,*R*) by X-ray diffraction studies (see above). Taking into account that compound **2** is the only diastereoisomer obtained in the reaction (the NMR spectra of the crude product reveals the presence of only one set of signals corresponding to this kind of diastereoisomer), we can conclude that the sequence involving the insertion of the palladium into the C–H bond (resulting in the formation of the Pd^{II} C-enolate) followed by the *ortho*-metalation is highly stereoselective. This behavior and the fact that the formation of the Pd–$C^*_{sp^3}$ σ bond does not require special activation, suggests that the formation of the palladacycle involving the two σ-Pd–C bonds must take place after the formation of the chelate containing the S–Pd and O–Pd bonds, since this chelation is responsible for the activation of the C–H methylene bonds.

The reactions of other β-ketosulfoxides with Pd^{II} acetate under conditions identical to those for compound **1**, yield complexes with structures similar to that of **2**.

In conclusion we have reported on the synthesis of a new type of enantiomerically pure complex composed of three molecules of ligand and three palladium atoms. The ligand supplies the two lone pairs of electrons to coordinate with Pd^{II} by formation of a stable five-membered ring and the two carbon atoms to form the covalent Pd–C bonds of a five-membered palladacycle. This is the first stable palladium C-enolate unequivocally characterized. The usefulness of this kind of compound as ferroelectric materials is currently under investigation.

Received: February 8, 1995
Revised version: March 19, 1995 [Z 7704 IE]
German version: *Angew. Chem.* **1995**, *107*, 1452–1454

Keywords: complexes with sulfur ligands · *ortho*-metalation · palladium compounds · sulfoxides

[1] E. L. M. Lempers, M. J. Bloemink, J. Reedijk, *Inorg. Chem.* **1991**, *30*, 201–206; S. J. Lippard, *Platinum, Gold and other Metal Chemotherapeutic Agents* (*ACS Symp. Ser.* **1983**, *209*); R. Melanson, C. Chevrotiere, F. Rochon, *Acta Crystallogr. Sect. C* **1985**, *41*, 1428–1431; H. B. Kagan, B. Ronan, *Rev. Heteroat. Chem.* **1992**, *7*, 92–116, and references therein; R. Rüger, W. Rittner, P. Jones, W. Isenberg, G. M. Sheldrick, *Angew. Chem.* **1981**, *93*, 389–390; *Angew. Chem. Int. Ed. Engl.* **1981**, *20*, 382–383.

[2] J. L. García-Ruano, I. López-Solera, J. R. Masaguer, C. Navarro-Ranninger, J. H. Rodríguez, *Organometallics* **1992**, *11*, 3013–3018; A. Alvarez-Valdés, J. L. García-Ruano, I. López-Solera, J. R. Masaguer, C. Navarro-Ranninger, J. H. Rodríguez, *ibid.* **1993**, *12*, 4104–4111.

[3] J. L. García-Ruano, A. M. Martín, J. H. Rodríguez, *J. Org. Chem.* **1994**, *59*, 533–536; I. Alonso, J. C. Carretero, J. L. García-Ruano, *ibid.* **1994**, *59*, 1499–1508; E. Arce, M. C. Carreño, B. Cid, J. L. García-Ruano, *ibid.* **1994**, *59*, 3421–3426.

[4] One immediate precedent of these insertion processes is the reactions of $PtCl_2$ with $(PhCOCH_2)_2SO$, which afforded a complex which contained a puckered four-membered ring with two C–Pt bonds (W. Henderson, R. D. W. Kemmitt, J. Fawcett, L. J. S. Prouse, D. R. Russell, *J. Chem. Soc. Chem. Commun.* **1986**, 1791–1793; W. Henderson, R. D. W. Kemmitt, L. J. S. Prouse, D. R. Russell, *J. Chem. Soc. Dalton Trans.* **1990**, 1853–1859). Similar insertion reactions have been observed starting from β-ketoesters (D. A. Clarke, R. D. W. Kemmitt, M. A. Mazid, P. Mckenna, D. R. Russell, M. D. Schilling, L. J. S. Sherry, *ibid.* **1984**, 1993–2002) and β-ketosulfones (W. Henderson, R. D. W. Kemmitt, L. J. S. Prouse, D. R. Russell, *ibid.* **1989**, 259–266). With some of these ligands (but not for sulfoxides), palladium complexes have also been obtained.

[5] A. Yoneda, T. Hakushi, G. R. Newkome, F. R. Fronczek, *Organometallics* **1994**, *13*, 4912–4918, and references therein.

[6] R. Annunziata, M. Cinquini, F. Lozzi, *J. Chem. Soc. Perkin Trans. 1* **1979**, 1687–1690.

[7] K. Nakamoto, *IR and Raman Spectra of Inorganic and Coordination Compounds*, 3rd ed., Wiley-Interscience, New York, **1978**, p. 232.

[8] J. A. Davies, *Adv. Inorg. Chem. Radiochem.* **1981**, *24*, 115–187; B. R. James, H. R. Morris, *Can. J. Chem.* **1980**, *58*, 399–408.

[9] A similar $\Delta\tilde{\nu}$ value has been observed for the carbonyl group associated to palladium when the α-carbon atom is also bonded to a metal atom [J. Fawcett, W. Henderson, R. D. W. Kemmitt, L. J. S. Prouse, D. R. Russell, *J. Chem. Soc. Dalton Trans.* **1991**, 2595–2599].

[10] A. R. Garber, P. E. Garrou, G. E. Hartwell, M. J. Smas, J. R. Wilkinson, *J. Organomet. Chem.* **1975**, *86*, 219–223.

[11] Crystal data for **2**: $C_{30}H_{30}O_6Pd_3S_3 \cdot H_2O$, rhombohedral, space group *R*3, *a* = 13.935(2), *b* = 13.935(2), *c* = 17.114(2) Å, *V* = 2878.0(8) Å^3, *Z* = 3, ρ_{calcd} = 1.589 g cm^{-3}; *F*(000) = 1356; $\mu(Mo_{K\alpha})$ = 1.591 mm^{-1}, *T* = 153(2) K; 3271 reflections with $5° < 2\theta < 45°$, of which 1660 are independent were collected on a Stoe four-circle diffractometer using graphite monochromated $Mo_{K\alpha}$ (λ = 0.71073 Å) radiation. Three standard reflections were measured every 60 minutes. There was no evidence of crystal decomposition. The data were corrected for absorption. The structure was solved by a combination of Patterson and Fourier difference techniques [SHELXTL PLUS, Program version 4.0, Siemens Analytical X-Ray Instruments, Madison, WI, **1990**] and refined by a full-matrix least-square methodology based on F^2 to *R* = 0.079 with all non-H atoms anisotropic [SHELX 93, Program for Crystal Structure Refinement, G. M. Sheldrick, University of Göttingen, **1993**]; H atoms were placed in idealized positions and allowed to ride on the relevant C atom. Largest peak and hole in the final difference map 0.784 and − 1.658 e Å^{-3}, respectively. A H_2O solvate was located in three disordered positions, and an occupancy factor of 0.33 was assigned according to the height of the Fourier synthesis. Further details of the crystal structure investigation are available on request from the Director of the Cambridge Crystallographic data Centre, 12 Union Road, GB-Cambridge CB2 1EZ (UK), on quoting the full journal citation.

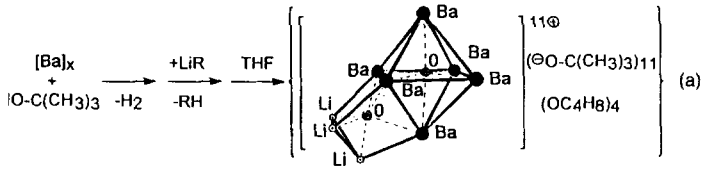
[12] G. Minghetti, M. A. Cinellu, G. Chelucci, S. Gladiali, F. Demartin, M. Manassero, *J. Organomet. Chem.* **1986**, *307*, 107–114; J. Selbin, K. Abboud, S. F. Watkins, M. A. Gutiérrez, F. R. Fronczek, *ibid.* **1983**, *241*, 259–268.
[13] K. Osakada, Y. Ozawa, A. Yamamoto, *Bull. Chem. Soc. Jpn.* **1991**, *64*, 2002–2004; D. L. Reger, D. G. Garza, L. Lebioda, *Organometallics* **1991**, *10*, 902–906; *ibid.* **1992**, *11*, 4285–4292.
[14] A. L. Rheingold, D. L. Staley, *Acta Crystallogr. Sect. C* **1988**, *44*, 572–574; J. Fornies, R. Navarro, M. Tomas, E. P. Urriolabeitia, *Organometallics* **1993**, *12*, 940–943.
[15] R. Ruger, W. Rittner, P. G. Jones, W. Isenberg, G. M. Sheldrick, *Angew. Chem.* **1981**, *93*, 389–390; *Angew. Chem. Int. Ed. Engl.* **1981**, *20*, 382–383; G. Annibale, L. Cattalini, V. Bertolasi, V. Ferretti, G. Gilli, M. L. Tobe, *J. Chem. Soc. Dalton Trans.* **1989**, 1265–1271; B. F. G. Johnson, J. Puga, P. R. Raithby, *Acta Crystallogr. Sect. B* **1981**, *37*, 953–956; S. Y. M. Chooi, P.-H. Leung, F. F. Mok, *Inorg. Chim. Acta* **1993**, *205*, 245–247.

The Lipophilically Wrapped Polyion Aggregate $\{[Ba_6Li_3O_2]^{11+}[^-OC(CH_3)_3]_{11}(OC_4H_8)_3\}$, a Face-Sharing (Octahedron + Prismane) $Ba_6Li_3O_2$ Polyhedron in a Hydrocarbon Ellipsoid: Preparation, Single Crystal Structure Analysis, and Density Functional Calculations**

Hans Bock,* Tim Hauck, Christian Näther,
Notker Rösch,* Markus Staufer,
and Oliver D. Häberlen

Dedicated to Professor Gerhard Ertl

When barium metal is treated with *tert*-butyl alcohol, *n*-butyllithium in *n*-hexane added, the precipitate filtered off, dissolved in tetrahydrofuran, and the resulting solution layered with *n*-hexane, colorless monoclinic prisms of a novel type of cluster crystallize [Eq. (a)]. According to the single crystal structure determination (Fig. 1 center), its nucleus $[Ba_6Li_3O_2]^{11+}$ consists of a Ba_6^{2+} octahedron surrounding an O^{2-} ion and of an analogously O^{2-} centered prismate $Ba_3^{2+}Li_3^+$, formed by connecting three Li^+ centers to one of the triangular faces Ba_3^{2+}. The polyion aggregate with eleven positive charges is lipophilically wrapped by eleven *tert*-butyl alcoholate ions and three tetrahydrofuran solvent molecules. The surface of the distorted ellipsoid is covered by a total $9\times11 + 8\times3 = 123$ hydrogen substituents (Fig. 1 top).



(a)

Crystals of the title compound and other related compounds were first produced serendipitously,[1, 2a] and then also deliberately under well-designed[2b–d] conditions. They will be called "lipophilically wrapped polyion aggregates", which are defined as follows:[3] A cluster nucleus of cations and anions provides the essential contributions to the thermodynamic stability, whereas predominantly the largely impenetrable hydrocarbon skin lends kinetic stability. Other specimens of a different type,[2] prepared shortly thereafter, provided evidence of a wide-spread, generalizable crystallization (self-organization) principle.[3]

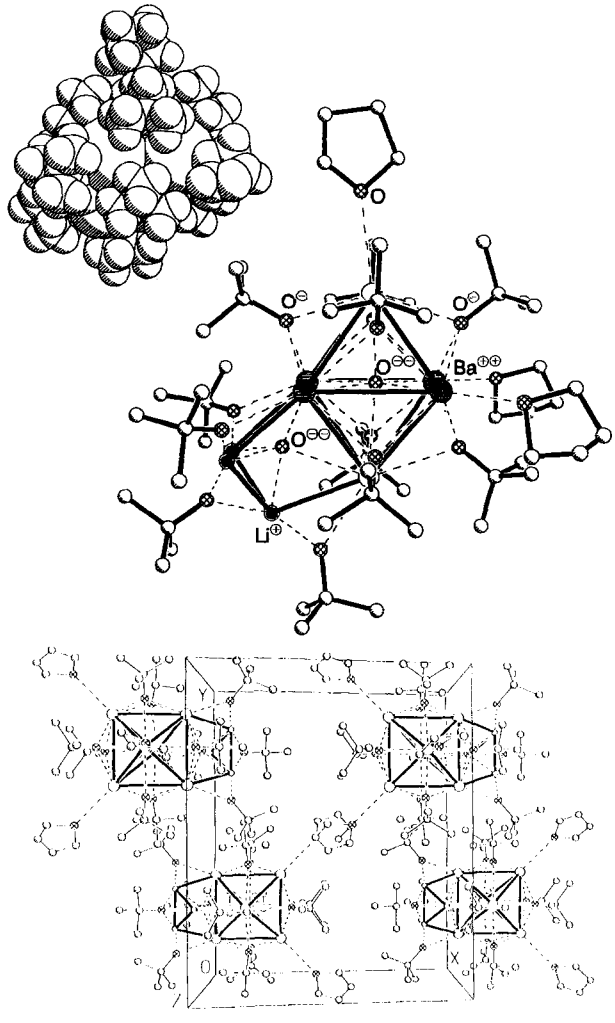


Fig. 1. Single-crystal structure of $\{[Ba_6Li_3O_2]^{11+}[^-OC(CH_3)_3]_{11}(OC_4H_8)_3\}$ at 150 K. Top: Space-filling representation; center: side view; bottom: unit cell (monoclinic, $P2_1/m$, $Z = 2$) viewed along the *z* axis. Selected bond lengths [pm] and angles [°]: BaBa(Ba) 381, BaBa(Li) 373, BaLi 307, LiLi 238; BaBaBa 90 and 60, BaLiLi 103, LiLiLi 60; BaO(Ba) 260, 276, 277, BaO(Li) 266, LiO(Ba) 195, 199, BaO(R) 264 to 278, $BaO(R_2)$ 295, LiO(R) 178 to 191, $OC(R_3)$ 140. An additional THF molecule is disordered in the crystal cavities.

The following structural details are emphasized: The Ba octahedron is slightly distorted, since the interbarium distances are 8 pm shorter on its lithium side [BaBa(Li)]. The O^{2-} center is shifted by about 15 pm out of the center of the octahedron towards the outer Ba_3 triangle and that of the prismane by about 8 pm towards the Li_3 triangular face. Of the eleven *tert*-butyl alcoholate anions, seven are above Ba_3 octahedral faces,

[*] Prof. Dr. H. Bock, Dipl.-Chem. T. Hauck, Dr. C. Näther
Chemische Institute der Universität
Marie-Curie-Strasse 11, D-60439 Frankfurt (Germany)
Telefax: Int. code + (69)5800-9188
Prof. Dr. N. Rösch, M. Staufer, Dr. O. D. Häberlen
Lehrstuhl für Theoretische Chemie der Technischen Universität München
D-85747 Garching (Germany)
Telefax: Int. code + (89)3209-3622

[**] Lipophilically wrapped polyion aggregates, Part 1, and Interactions in Crystals, Part 69. The research project was supported by the Adolf Messer Foundation, the Deutschen Forschungsgemeinschaft, the state of Hesse, and the Fonds der Chemischen Industrie. – Part 68: N. Nagel, C. Näther, H. Bock, *Acta Crystallogr. Sect. C*, **1995**, in print.